ChemComm
FEATURE ARTICLE

Calixpyrroles

Philip A. Gale, Jonathan L. Sessler* and Vladimír Král

Department of Chemistry and Biochemistry, The University of Texas at Austin, Austin, Texas 78712-1167, USA

The calix[4]pyrroles are a class of old but new heterocalixarene analogues that show interesting anion and neutral substrate binding properties. Calix[4]pyrroles are easy to make and functionalize. As such, they have been employed in the production of separation media for anionic and neutral species. Calixpyrroles also provide useful precursors for the generation of novel calixpyridinopyrroles and calixpyridines.

Introduction

This short review article covers the chemistry of systems that resemble calixarenes but are not calixarenes. Specifically, it discusses the synthesis and properties of calixpyrroles and other heterocyclic calixarene analogues. This story starts with Baeyer's publication of his paper on the condensation of pyrrole and acetone[1] which appeared in 1886, some fourteen years after he initiated his first studies of phenol–formaldehyde condensation chemistry.[2]

Although he did not appreciate it at the time, the white crystalline product Baeyer obtained by mixing pyrrole, acetone and hydrochloric acid was an octamethyl substituted form of porphyrinogen **1**. Porphyrinogens are naturally occurring

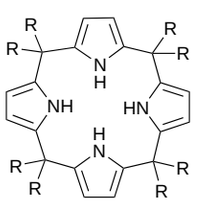

1 R = Me
3 R = Et

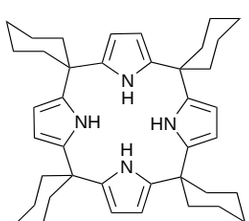

2

colourless macrocycles consisting of four pyrrole rings linked through the α (*i.e.* pyrrolic 2 and 5) or *meso*-like positions by sp^3 hybridized carbon atoms. The chemistry of porphyrinogens containing hydrogen atoms in the *meso*-position is well known as these species readily oxidize to form aromatic porphyrins. However, fully *meso*-substituted porphyrinogens have attracted much less attention, precisely because they do not constitute useful porphyrin precursors. Nonetheless, for reasons outlined in a recent communication,[3] we felt that these materials might be interesting. Specifically, we felt this class of macrocycle was perhaps mis-named and might better be referred to as calix[4]pyrroles. This renaming, which is supported by structural studies (*vide infra*), helps establish an obvious analogy to the calixarenes. It also led us to consider that this class of cyclic tetrapyrroles might display interesting anion binding characteristics. Thus, this exercise in nomenclature provided us with an incentive to begin studying further this venerable set of macrocycles.

As implied above, the chemistry of calix[4]pyrroles goes way back. Indeed, subsequent to the work of Baeyer, Dennstedt and Zimmermann also studied this reaction, using 'chlorzink' as the acid catalyst.[4–6] Thirty years later, during the First World War, Chelintzev and Tronov repeated these reactions and proposed (correctly) a cyclic tetrameric structure for a calix[4]pyrrole.[7] These same authors carried out several other reactions. These included an acid catalysed condensation of pyrrole with methyl ethyl ketone, which yielded a small quantity of a single calix[4]pyrrole configurational isomer. Additionally, methyl ethyl ketone and acetone were co-condensed with pyrrole forming a mixed *meso*-hexamethyldiethylcalix[4]pyrrole of unknown structure.[8] In the 1950s, Rothemund and Gage used methanesulfonic acid as the acid catalyst and obtained improved yields.[9] In the early 1970s, Brown *et al.* reported a refined procedure that permitted them to obtain tetraspirocyclohexylcalix[4]pyrrole **2**,[10] a compound that had previously been reported by Chelintzev, Tronov and Karmanov in 1916,[11] in decent yield. Calixpyrroles with functionalizable groups in the *meso*-positions (chloroalkyl or cyano) were also reported recently by Lehn and co-workers in a book chapter.[12–14] In work that is of a very different character, the transition metal coordination chemistry of deprotonated *meso*-octaalkylcalix[4]pyrroles, particularly *meso*-octaethylcalixpyrrole **3**, has been extensively studied by Floriani and co-workers. This chemistry has recently been highlighted in a Feature Article appearing in this journal.[15] It is, therefore, omitted from this review.

Structural studies

Several crystal structures of calix[4]pyrrole macrocycles (Fig. 1) have been elucidated. Taken in concert, these reveal that the macrocycle adopts a 1,3-alternate conformation in the solid state (*i.e.* adjacent pyrrole moieties are oriented in opposite directions).[3,16] Interestingly, in contradistinction to what is true for calix[4]arenes, in calix[4]pyrroles there is no possibility for the formation of a hydrogen bonded array between the various pyrrolic NH groups. Thus, in the absence of an added substrate there is no propensity for the free macrocycles to adopt the cone conformation, a motif so prevalent in calix[4]arene chemistry.

Anion binding properties

On a track that is very different from that of Floriani (see above), our group in Austin has focused on studying the anion binding properties of the calix[4]pyrroles. Our interest in this line of study, abetted by our renaming process (*vide supra*), came about as the result of our previous work with sapphyrins. Sapphyrin, a pentapyrrolic expanded porphyrin first synthesized by Woodward,[17] is an excellent receptor for anions (particularly fluoride) when diprotonated.[18] Knowing this, we were keen to test whether *neutral* non-aromatic polypyrrolic macrocycles, such as the calix[4]pyrroles, could also serve as anion binding agents.

The solution binding properties of **1** and **2** were studied using ^{1}H NMR titration techniques. Stability constants were then determined using the EQNMR least-squares fitting procedure.[19] The findings, summarized in Table 1, revealed that compounds **1** and **2** are not only effective 1 : 1 anion binding agents in solution, they are also selective. Specifically, they show a marked preference for F^- over other putative anionic guests (*viz.* Cl^-, Br^-, I^-, $H_2PO_4^-$ and HSO_4^-).

X-Ray crystal analyses of the Bu_4NCl complex of calixpyrrole **1** and the Bu_4NF complex of **2** revealed that in both cases the calix[4]pyrrole ligand adopts a cone-like conformation in the solid state such that the four NH protons can hydrogen bond to the halide anion (Fig. 2). While these two structures are similar, in the case of the chloride complex [Fig. 2(*a*)] the nitrogen-to-anion distances are in the range of 3.264(7)–3.331(7) Å, while for the corresponding fluoride complex they are 2.790(2) Å [Fig. 2(*b*)] (the four pyrrole groups are equivalent by symmetry). As a result, in these two complexes the chloride and fluoride anions reside 2.319(3) and 1.499(3) Å above the N_4 root mean square planes of calixpyrroles **1** and **2**, respectively. Thus, the fluoride anion appears to be more tightly bound, at least in the solid state.

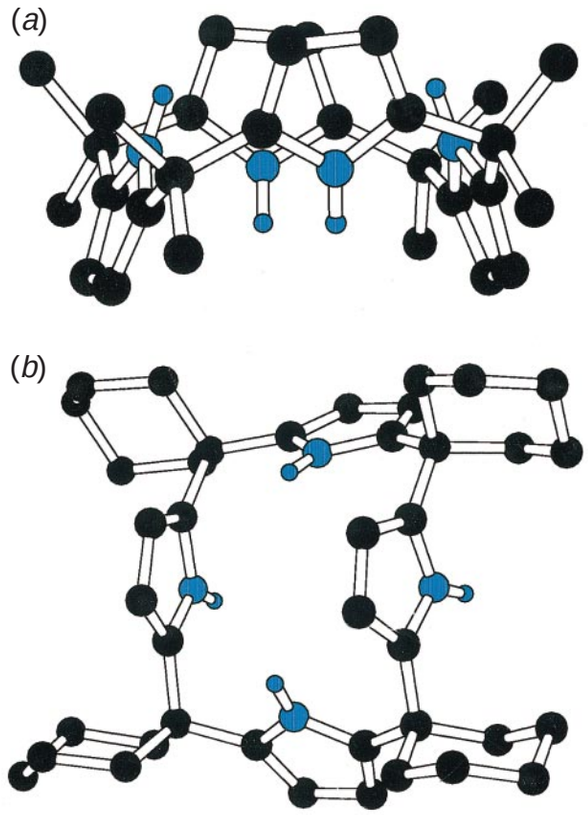

Fig. 1 X-Ray crystal structure of (*a*) **1** and (*b*) **2**·CH_2Cl_2. In (*b*) the solvent is omitted for clarity. Nitrogen and pyrrolic hydrogen atoms are blue. This figure was generated using data originally published in ref. 3.

Table 1 Stability constants for compounds **1** and **2** with anionic substrates[a] in CD_2Cl_2 at 298 K. For further details, see ref. 3

	Stability constant/M^{-1}	
Anion	**1**	**2**
Fluoride[b,c]	17 170 (± 900)	3600 (± 395))
Chloride	350 (± 5.5)	117 (± 4.0)
Bromide	10 (± 0.5)	[d]
Iodide	< 10	[d]
Dihydrogen phosphate[e]	97 (± 3.9)	< 10
Hydrogen sulfate	< 10	[d]

[a] Anions were added as 0.1 M CD_2Cl_2 solutions of their Bu_4N^+ salts to 10 mM solutions of the receptor in CD_2Cl_2, with concentration changes being accounted for by EQNMR. In determining the stability constants, the possible effects of ion pairing (if any) were ignored. [b] Bu_4NF was added as the trihydrate. [c] A repeat titration with compound **1** at 1.0 mM concentration gave concordant results. [d] Not determined. [e] A repeat titration with compound **1** at 100 mM concentration gave concordant results.

In an effort to study the conformational properties of the calix[4]pyrroles in solution, variable temperature ^{1}H NMR studies were carried out on a CD_2Cl_2 solution of **1** in the absence and presence of fluoride anions. In the presence of 3 equiv. of Bu_4NF, the *meso*-methyl resonance splits into two separate signals as the temperature is lowered. By contrast, in the absence of fluoride anions, there is no significant change in the ^{1}H NMR spectrum of compound **1**. The splitting seen in the presence of F^- may be due to the calixpyrrole adopting a cone conformation in solution when bound to this, and presumably other anions. Certainly, such a model is consistent with experiment. This is because it leads to the prediction that in the presence of F^- at low temperature the *meso*-methyl groups will be arranged in either axial or equatorial positions and thus resonating at different frequencies, as is indeed observed.

Surprisingly, the pyrrole NH resonance was also found to split into two peaks as the temperature was lowered in the presence of fluoride (Fig. 3). It was considered that a likely cause for this engendered splitting might be coupling between the NH protons and the ^{19}F nucleus of the bound fluoride anion. To test this supposition, a ^{19}F NMR spectrum of the fluoride complex was acquired at 193 K. The bound fluoride nucleus was found to resonate as a quintet (with a coupling constant of 39.5 Hz), confirming the proposed coupling effect (Fig. 3).

Binding of neutral substrates

In work that was designed to complement the above, it was found that the molecular recognition chemistry of the calix[4]pyrroles is not limited to anionic substrates. Indeed, the coordination of neutral species was explicitly achieved using *meso*-octamethylcalix[4]pyrrole **1**. In this instance, ^{1}H NMR titration experiments in C_6D_6 and subsequent analysis of the titration curves using the EQNMR computer program,[19] revealed that this calix[4]pyrrole forms complexes with neutral species, including short chain alcohols, amides and other oxygen-containing neutral species. Although the binding constants are modest, a clear trend is evident in both the alcohol and

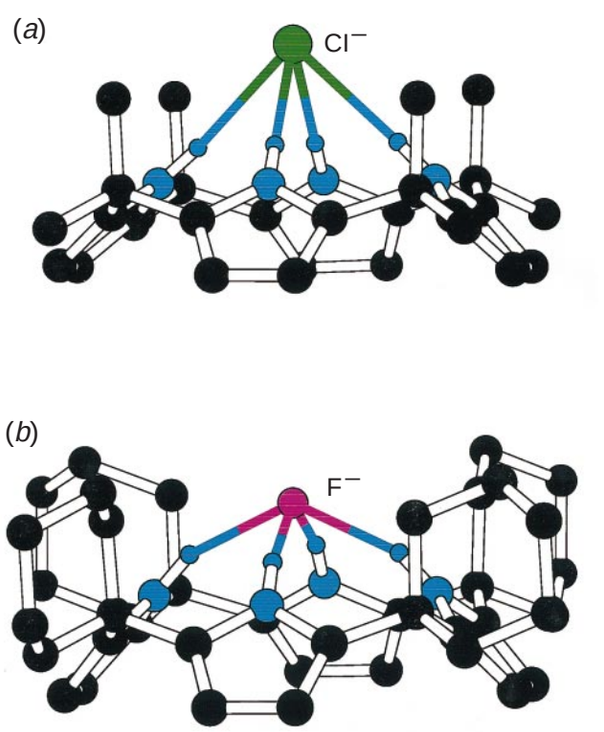

Fig. 2 X-Ray crystal structure of (*a*) the chloride complex of compound **1** and (*b*) the fluoride complex of compound **2**. Nitrogen and pyrrolic hydrogen atoms are blue, chloride is green and fluoride is magenta. This figure was generated using data originally published in ref. 3.

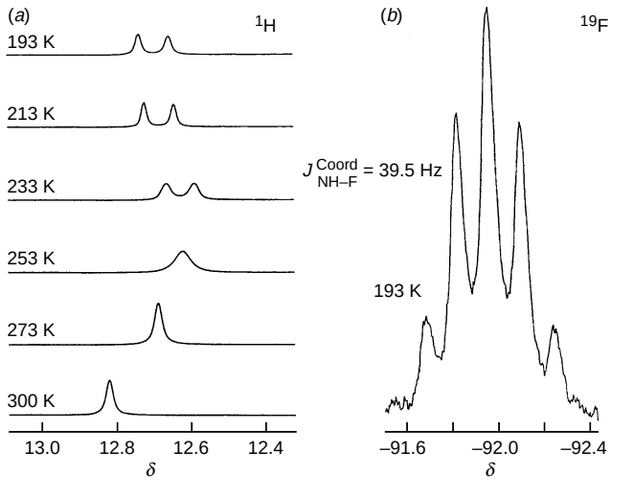

Fig. 3 (*a*) The NH resonance of **1**·F$^-$ splits as the temperature is lowered to 193 K (*b*), indicating coupling to the bound fluoride anion

amide series. Specifically, it was found that the relevant stability constants decrease as the steric bulk around the oxygen atom is increased (Table 2).[20]

The structure of **1** coordinated to two molecules of MeOH was determined by X-ray diffraction analysis. In contrast to the crystal structures of the anion-bound forms of **1** and **2** (discussed above), the calixpyrrole in this neutral substrate complex adopts a 1,3-alternate conformation in the solid state [Fig. 4(*a*)]. The two MeOH molecules are each coordinated to the calixpyrrole *via* two sets of hydrogen bonds involving the pyrrolic moieties [the $N_{pyrrole}$-O_{MeOH} distances are 3.155(4) Å].

The single crystal X-ray structure of the DMF complex of **1** was also solved. As in the bis(methanol) adduct, each of the two DMF molecules was found to be coordinated to a single calix[4]pyrrole macrocycle *via* two hydrogen bonds. However, in the case of the DMF complex the calix[4]pyrrole adopts a 1,2-alternate conformation, wherein each DMF molecule is coordinated to adjacent pyrrole moieties [$N_{pyrrole}$–O_{DMF} = 2.908(2) and 2.924(2) Å]. Each of the DMF molecules lies *ca.* 3.4 Å over the plane of one of the pyrrole rings to which it is not hydrogen bonded. This finding led us to suggest that π–π interactions help stabilize the 1,2-alternate conformation of this particular calix[4]pyrrole-neutral substrate complex [Fig. 4(*b*)].[20]

Table 2 Association constants for **1** with neutral substrates. [a] For further details, see ref. 20

Substrate added	K_a M^{-1}
MeOH	12.7 ± 1.0
EtOH	10.7 ± 0.7
BnOH	9.7 ± 0.7
Pr^{i}OH	7.0 ± 0.4
Bu^{s}OH	6.2 ± 0.4
N-Formylglycine ethyl ester	13.3 ± 1.0
DMF	11.3 ± 0.8
N,*N*-Dimethylacetamide	9.0 ± 0.9
1,1,3,3-Tetramethylurea	2.2 ± 0.1
DMSO	16.2 ± 1.1
1,2-Dimethylimidazole	5.4 ± 0.3
Acetone	2.2 ± 0.2
Nitromethane[b]	—

[a] In C_6D_6 at 298 K. For each titration, the concentration of **1** was held constant (at *ca.* 4 10^{-3} M) as aliquots of the substrate in C_6D_6 (*ca.* 1 M) were added. [b] In this instance, the induced shifts in the NH proton(s) of **1** were too small (< 0.15 ppm) to afford a reliable K_a value.

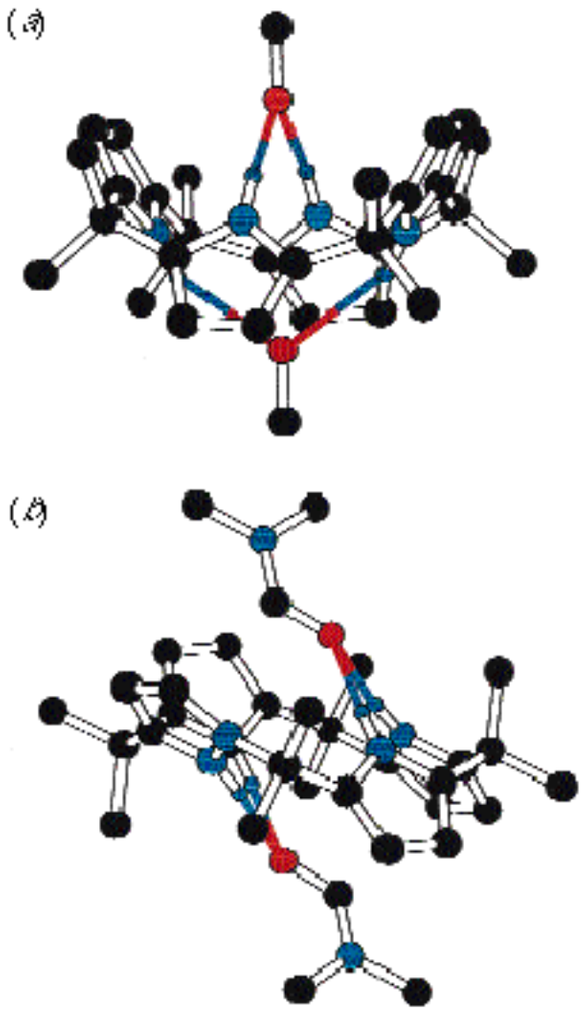

Fig. 4 X-Ray crystal structure of (*a*) **1**·2(MeOH) and (*b*) **1**·2(DMF). Nitrogen and pyrrolic hydrogen atoms are blue and oxygen is red. This figure was generated using data originally published in ref. 20.

Functionalized systems

The introduction of a 'tailed' butanoate group to a calix[4]pyrrole produces an anionic calixpyrrole with interesting self-assembly properties.[21] The requisite '*meso*-hook' calix[4]pyrrole monoester **4** was synthesized by co-condensing methyl 4-acetylbutyrate, cyclohexanone and pyrrole. After column chromatography, the monoester was isolated from a mixture of calixpyrroles containing different numbers of ester functional groups in 12% yield. Subsequent hydrolysis of **4** yielded the monoacid **5**.

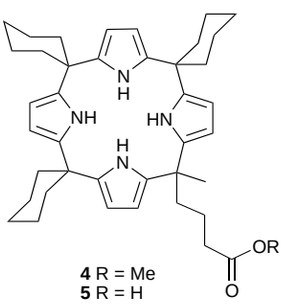

X-Ray quality crystals of the calixpyrrole carboxylate **5** were obtained by slow evaporation of a CH_2Cl_2 solution of **5** in the

presence of excess $Bu_4NF{\cdot}xH_2O$. Interestingly, the crystals did not contain any fluoride anions within the lattice. Rather, this latter was found to be comprised entirely of the tetrabutylammonium calix[4]pyrrole carboxylate salt. The structure of the salt revealed that the calixpyrrole carboxylate self-assembles in the solid state. Specifically, the carboxylate functionality of one calixpyrrole was found to be bound to the pyrrolic array of an adjacent calixpyrrole and *vice versa*. The net result of these interactions is a dimeric cyclic structure as indicated in Fig. 5. In this instance, the calix[4]pyrrole adopts a cone conformation with four hydrogen bonds from the calixpyrrole pyrrole groups serving, as implied above, to bind the carboxylate 'tail' of a second functionalized calixpyrrole unit.[21]

A ROESY NMR spectrum of the trimethylammonium salt of **5** in CD_2Cl_2 provided evidence for aggregation in solution. Two resonances were observed between δ 7.0 and 7.5 corresponding to non-complexed pyrrole NH protons. Another resonance was observed at approximately δ 11. This was assigned to bound pyrrole NH protons, in exchange with the unbound NH resonances. As such, this datum point provides evidence in favour of aggregate formation in solution. The dimer could also be observed using FAB MS techniques.[21] In any event, to the best of our knowledge, this self-assembling calix[4]pyrrole system (**5**) represents the first and only example wherein purely anionic sub-units are seen to self-assemble.

In addition to the above, we have recently described the synthesis of several novel calix[4]pyrrole molecules containing functional groups appended to the carbon- or *C*-rim of the calix[4]pyrrole 'bowl'. Two strategies were pursued in the synthesis of these materials. The first involved a direct condensation approach. Using such a strategy the β-octamethoxy-*meso*-tetraspirocyclohexylcalix[4]pyrrole **6** was prepared *via* the condensation of 3,4-dimethoxypyrrole and cyclohexanone in glacial acetic acid. The resulting calixpyrrole was then isolated in 8% yield after column chromatography.[22]

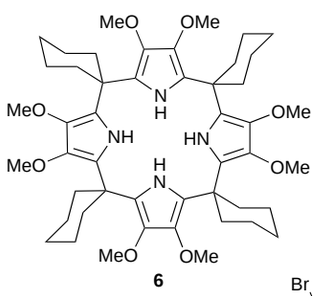

6

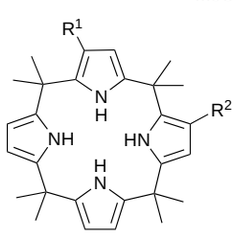

7 $R^1 = CH_2CO_2Et$, $R^2 = H$ (26%)
8 $R^1 = R^2 = CH_2CO_2Et$ (3%)

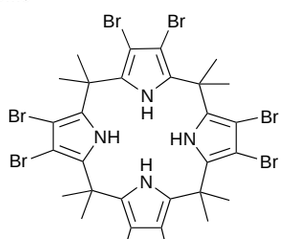

9

The second strategy involved modifying the *C*-rim of a presynthesized calix[4]pyrrole. In this case, *meso*-octamethylcalix[4]pyrrole was dissolved in dry THF and cooled to −78 °C. A solution of *n*-butyllithium in hexanes (4.0 equiv.) was added dropwise to the calixpyrrole solution followed by 4.0 equiv. of ethyl bromoacetate. Purification by column chromatography afforded two isolatable products, a *C*-rim monoester **7** (formed in 26% yield) and a diester **8** (3% yield). Surprisingly ^1H and ^{13}C NMR experiments showed that the diester **8** present in the fraction collected was a single isomer, with the ester groups

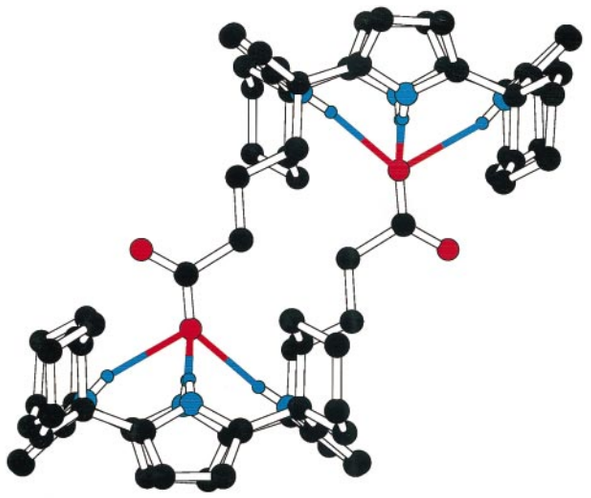

Fig. 5 X-Ray crystal structure of the calix[4]pyrrole carboxylate dimer (**5·5** − $2H^+$). Nitrogen and pyrrolic hydrogen atoms are blue and oxygen is red. This figure was generated using data originally published in ref. 21.

attached to the calixpyrrole in the 2 and 7 positions, as judged from single crystal X-ray diffraction and NMR analyses.[22]

In chemistry somewhat related to the above, β-octabromo-*meso*-octamethylcalix[4]pyrrole **9** was synthesized in 90% yield by reacting *meso*-octamethylcalix[4]pyrrole with *N*-bromosuccinimide in dry THF at reflux. In this instance, an X-ray structure (Fig. 6) revealed the calixpyrrole macrocycle **9** exists in a chair-like flattened 1,2-alternate conformation in the solid state (*i.e.*, the dihedral angles between pyrrole rings and plane through the calixpyrrole *meso*-carbon atoms are 66.8°, 5.8, −66.8 and −5.8°, respectively).[22]

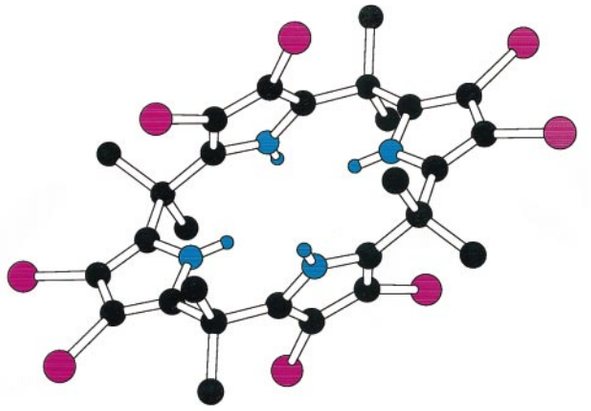

Fig. 6 X-Ray crystal structure of compound **9**. Nitrogen and pyrrolic hydrogen atoms are blue and bromine is magenta. This figure was generated using data originally published in ref. 22.

The solution anion binding properties of the β-octamethoxy derivative **6** and the β-octabromo derivative **9** have been studied in CD_2Cl_2 using ^1H NMR titration techniques (Table 3).[22] Compound **6** displays lower stability constants than the corresponding 'β-free' analogue **2**, presumably due to the electron-donating effects of the methoxy groups (this decreases the acidity of the pyrrole NH protons and therefore lowers the stabilty of the calixpyrrole–anion complex formed). By contrast, compound **9** displays higher stability constants with anions than its 'β-free' control (compound **1**) as a result, presumably, of the electron-withdrawing effect of the bromine substituents.[22]

Higher order systems

While currently the chemistry of calix[4]pyrroles is fairly well worked out, that of higher order systems (*i.e.* calix[*n*]pyrroles

Table 3 Stability constants for compounds **6** and **9** with anionic substrates[a] in CD_2Cl_2 at 298 K. For further details, see ref. 22

	Stability constants/M^{-1}	
Anion added	**6**	**9**
Fluoride	$1.7 (\pm 0.2) \times 10^2$	$2.7 (\pm 0.4) \times 10^4$[b]
Chloride	< 10	$4.3 (\pm 0.6) \times 10^3$
Dihydrogen phosphate	*c*	$6.5 (\pm 0.4) \times 10^2$

[a] Anions were added as 0.3 M CD_2Cl_2 solutions of their Bu_4N^+ salts to 3 mM solutions of the receptor in CD_2Cl_2 with concentration changes being accounted for by EQNMR. In determining the stability constants, the possible effects of ion pairing (if any) were ignored. [b] Estimated value. The NH proton resonance broadened considerably during the titration, forcing the frequency of the resonance to be noted manually. This value should therefore, be treated with caution. [c] Not determined.

with $n > 4$) is still essentially unexplored. While such species may be identified as by-products in condensations leading to the generation of calix[4]pyrroles, they have yet to be isolated cleanly.[3] Recently it occurred to us that a *p-tert*-butylcalix[*n*]arene could be used as a template around which a calix[*n*]pyrrole could form. Such a strategy could prove useful in the synthesis of higher order calix[*n*]pyrroles (*i.e.* those where $n > 4$). As a first step towards this approach, *p-tert*-butylcalix[4]arene tetramethyl ketone[23] was condensed with pyrrole in the presence of methanesulfonic acid. This afforded the cylindrical calix[4]arene-calix[4]pyrrole pseudo-dimer **10** in 32% yield.[24]

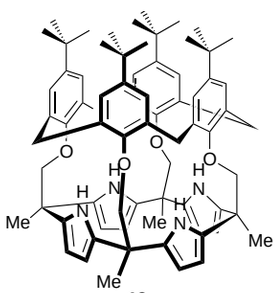

10

The X-ray structure of **10** was solved. It revealed, as expected, that the calixarene adopts a cone conformation. Further, two of the pyrrole NH groups were seen to form hydrogen bonds to the phenolic oxygen atoms at the lower rim of the calixarene (Fig. 7).

The hydrogen bonding between the pyrrole NH groups and phenolic oxygen atoms is maintained in solution, as evidenced by ^{1}H NMR spectroscopic studies.[24] Here, it was found, for instance, that the pyrrole NH protons resonate at δ 11.22. This is consistent with the proposal that they are deshielded as a result of their participation in the suggested hydrogen bonding interactions. Addition of polar solvents such as CD_3OD or anions such as fluoride does not disrupt the hydrogen bonding array. This latter finding thus supports the notion that the molecule adopts a cylindrical conformation in solution.

When *p-tert*-butylcalix[5]arene pentamethyl ketone[25] was condensed with 5 equiv. of pyrrole in the presence of $BF_3{\cdot}OEt_2$, a calix[5]pyrrole-calix[5]arene pseudo-dimer **11** was formed in 10% yield.[26] Compound **11** is, to the best of our knowledge, the first example of an expanded calixpyrrole. The intramolecular hydrogen bonding array in compound **11** appears to be weaker than that of the tetramer. For example, the NH protons resonate at δ 9.88 in the pentamer, and addition of CD_3OD or chloride anions cause shifts in the NH protons.

The use of other templates, such as cyclodextrins, using the same strategy, may lead to the synthesis of new expanded calixpyrroles and porphyrins. This approach is currently being pursued in the authors' laboratory.

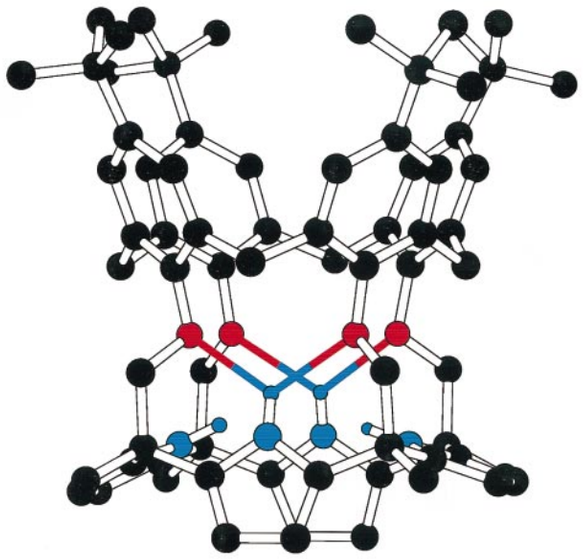

Fig. 7 X-Ray crystal structure of compound **10** showing intramolecular pyrrole NH–phenolic oxygen hydrogen bonding: N(2)···O(1) 2.701(6), N(2)···O(2) 2.739(6) Å. Nitrogen and pyrrolic hydrogen atoms are blue and oxygen is red. This figure was generated using data originally published in ref. 24.

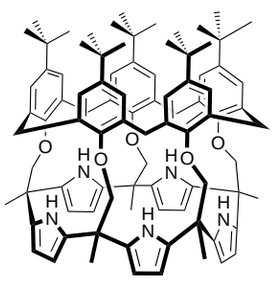

11

Towards possible commercial applications

The fact that calixpyrroles are easy to make has led us to consider that products based on the calixpyrrole technology could be commercially viable. With a view towards testing this hypothesis, we decided to investigate whether calixpyrrole-based solid supports could be used to separate oligonucleotides and other polyanionic substrates. Thus in work that is still ongoing, we have recently attached carboxylic acid functionalized calix[4]pyrroles to aminopropyl silica gel *via* both the *meso*- and β-positions. As determined from HPLC studies,[27] the resulting media allow for the ready separation of mixtures of (i) AMP, ADP, and ATP, (ii) aromatic carboxylates, and (iii) oligonucleotides of varying chain length (Fig. 8) under isochratic conditions. These same media also permit the HPLC-based separation of mixtures of neutral species such as polyfluorobiphenyls.

The synthesis of pyridine-containing macrocycles calixpyrroles as synthetic precursors

While pyridine-containing macrocycles are among the most versatile and important of all those known, in the heterocalixarene analogue area pyridine remains a minor player. Indeed, until the authors' recent contributions,[28] calix[4]pyridine was actually unknown. However a decade ago (1987), Newkome *et al.* did report the synthesis of several interesting calixpyridine analogues including compound **12**.[29]

In work that is of a very different nature, Floriani has succeeded in producing calix[1]pyridino[3]pyrroles and calix[2]pyridino[2]pyrroles. This was done by carrying out an

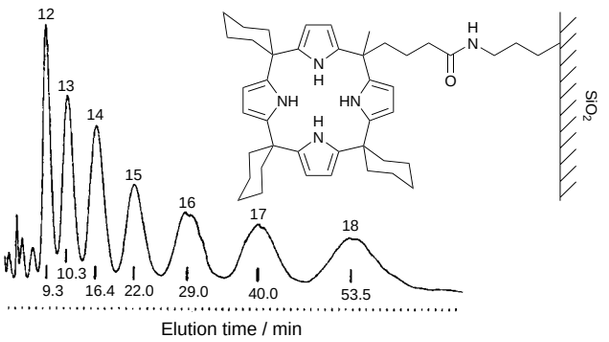

Fig. 8 Separation of $dT_{12–18}$ on calixpyrrole modified silica gel column. Flow rate 0.4 ml min^{-1}, mobile phase MeCN–[aq. NaCl (250 мм) + aq. Na_3PO_4 (50 мм)], 1 : 1 (v/v) (isochratic), pH = 7.0, column temperature 25 °C, UV detection at 265 nm.

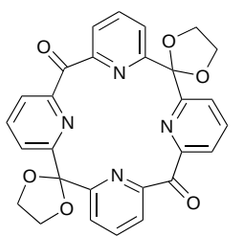

12

homologation of the pyrrole rings effected by reacting the zirconium complex of deprotonated *meso*-octaethylcalix[4]pyrrole with CO.[30]

Recently the present authors have discovered a very versatile and easy entry into the chemistry of calixpyridines. It is predicated on the use of calixpyrroles and dichlorocarbene and, as illustrated in Scheme 1, provides ready access to the previously unknown calix[3]pyridino[1]pyrrole and calix[4]pyridine families.

Our initial synthetic efforts were based on attempts to condense substituted pyridine *N*-oxides in a manner analogous to *p-tert*-butylphenol in calixarene synthesis.[31–33] However, using this approach none of the desired products could be isolated from the reaction mixtures. Our attention then turned on finding a way that would allow us to convert calix[4]pyrroles (*e.g.* **1**) into calix[4]pyridines. Here, we were inspired by the fact that the reaction of dichlorocarbene with pyrrole, imidazole or indole rings will lead to an insertion of the $:CCl_2$ unit (generated *inter alia* by heating sodium trichloroacetate under neutral conditions) into one of the double bonds.[34] In the case of pyrroles, subsequent elimination of HCl and rearrangement produces a 3-chloropyridine ring. We therefore decided to apply this methodology to calix[4]pyrrole and investigate whether a tetrachloro calix[4]pyridine derivative might not be obtainable in this way.

The conversion of *meso*-octamethylcalix[4]pyrrole **1** into tetrachloro-*meso*-octamethylcalix[4]pyridine **13** was attempted in several different solvents using a range of reaction times as well as different (excess) concentrations of sodium trichloroacetate. Using 1,4-dioxane as the solvent, and 15 equiv. of sodium trichloroacetate, a 2.4 : 1 mixture of the mono- and dipyridine macrocycles (**14** and **15**) was formed. Interestingly, when the same reaction conditions were employed using 1,2-dimethoxyethane as the solvent, a mixture of di- (**15**), tri- (**16**) and tetra-pyridine (**13**) species was obtained in a 1 : 1 : 1 ratio. The latter conditions, therefore, allowed us to obtain chlorinated derivatives of two previously unknown heterocalixarene analogues, namely, calix[3]pyridino[1]pyrrole (**16**) and calix[4]pyridine (**13**). Improved yields of the latter products could be obtained by adding separate batches of the dichlorocarbene precursor. In fact, using this approach the

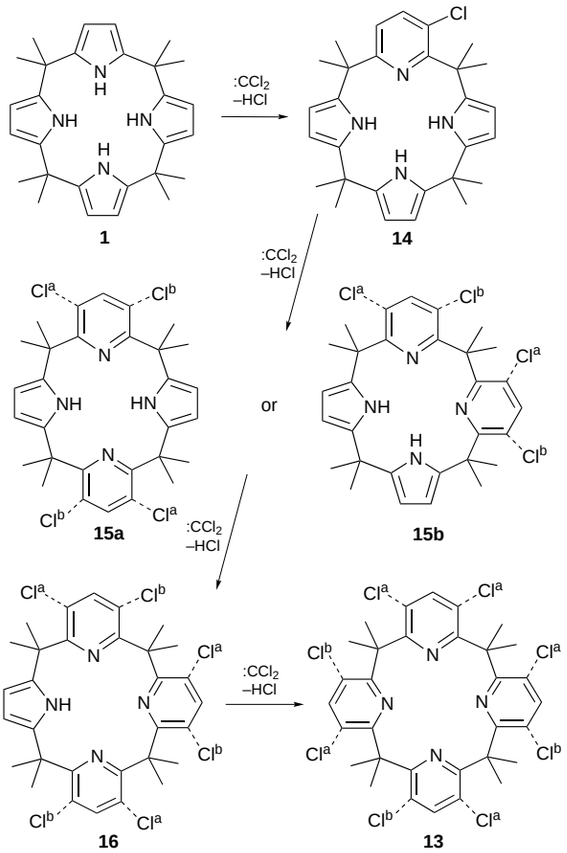

Scheme 1

reaction process could be made to favour, as desired, the formation of either **15** and **16**, or just **13**. The calix[2]pyridino[2]pyrrole, calix[3]pyridino[1]pyrrole, and calix[4]pyridine products prepared in this way can be easily separated by column chromatography (silica gel, CH_2Cl_2–hexane eluent). Thus, it has proved possible, depending on the choice of conditions, to obtain **15**, **16** and **13** in optimized yields of 65, 42 and 26%, respectively. The NMR spectra of the crude products obtained from the above reactions are complicated due to the presence of isomers. This is reflected in Scheme 1 wherein each pyridine ring is bound to either Cl^a or Cl^b (not to both).

The X-ray crystal structure of **15** [Fig. 9(*a*)] reveals that there are two crystallographically distinct molecules in the unit cell. Both adopt the cone conformation in the solid state. The pyrrolic NH groups are oriented near the pyridine nitrogen atoms such that potential NH···N hydrogen bonds may be formed. These hydrogen bonds may influence the conformational properties of the macrocycle.

The X-ray crystal structure of **16** has also been elucidated [Fig. 9(*b*) and (*c*)]. As in the case of **15**, there are two molecules of **16** per asymmetric unit. However unlike **15**, where the two molecules were found to be conformationally equivalent, the two molecules of **16** assume strikingly different conformations. In Fig. 9(*b*), the molecular conformation is similar to that found in compound **13** (see below) wherein alternate rings are either parallel or nearly perpendicular. In this case, the pyrrole NH group is not hydrogen-bonded to any of the pyridine nitrogen atoms. The other molecule [Fig. 9(*c*)] in the asymmetric unit displays a dramatically different conformation.

Finally, in work that is still very recent,[28] the single crystal X-ray structure of the calix[4]pyridine **13** was solved. This structure revealed that the molecule adopts a flattened partial cone conformation in the solid state [Fig. 9(*d*)]. As importantly, by virtue of simply being solved, this structure served to confirm the existence of **13**. As such, it provides a critical proof

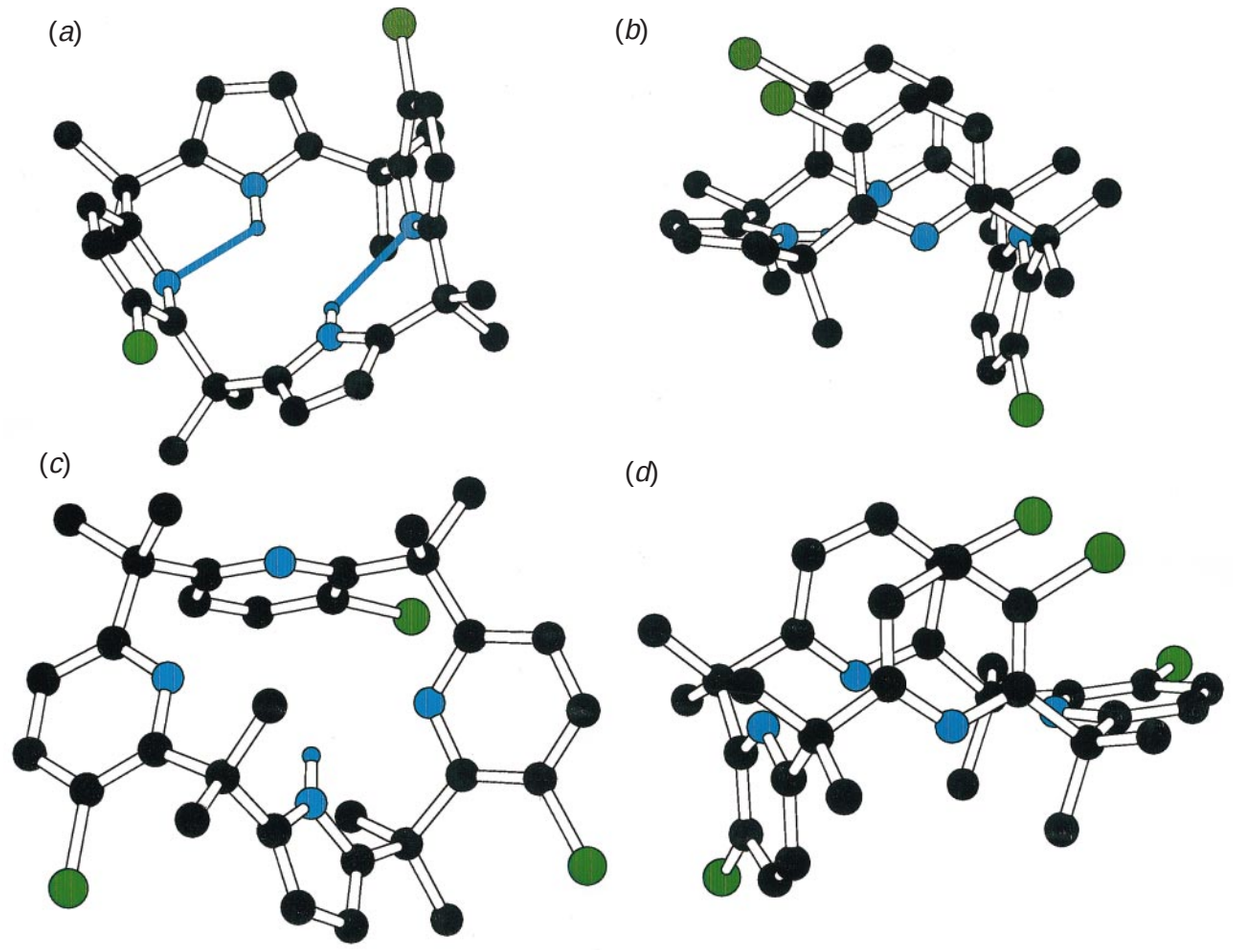

Fig. 9 X-Ray crystal structures of (*a*) bis(chloro)calix[2]pyridino[2]pyrrole **15**, (*b*) and (*c*) tri(chloro)calix[3]pyridino[1]pyrrole **16** in two conformations and (*d*) tetra(chloro)calix[4]pyridine **13**. Nitrogen and pyrrolic hydrogen atoms are blue and chlorine is green.

that calix[4]pyridines can be made and that they are potentially well-organized in the solid state.

Conclusion

The goal of this review has been to summarize the current state of calixpyrrole chemistry and, by implication, highlight the similarities and differences that exist with regard to normal calixarene chemistry. One feature that is particularly noteworthy is the fact that the calixpyrroles act as such effective receptors for neutral and anionic substrates. This finding leads us to suggest that related systems, such as the calixindoles,[35,36] might be worth studying in this regard. Indeed we think the chemistry of heterocalixarenes in general is one that is likely to be blessed with a rich supramolecular future.

Acknowledgements

The authors would like to thank Dr William E. Allen, Andrei Andrievsky, Christopher T. Brown, Andreas Gebauer, John W. Genge, Dr Vincent Lynch, Petra I. Sansom and Nicolai A. Tvermoes, whose work is in part summarized in this article. Their intellectual and experimental contributions to this project are deeply appreciated. This research was supported by the National Institutes of Health (grants AI 33577 to J. L. S. and TW00682 to J. L. S. and V. K.), the National Science Foundation (grants CHE 9122161 and CHE 9725399 to J. L. S.) and the Howard Hughes Medical Institute (J. L. S. and V. K.). V. K. thanks the Grant Agency of the Czech republic for grants 203/97/1099 and 203/96/0740. P. A. G. wishes to thank the Fulbright Commission for a post-doctoral research scholarship. The authors also thank Brent Iverson for producing the excellent cover illustration.

Professor Jonathan L. Sessler was born in Urbana, Illinois, USA on May 20, 1956. He received a BS degree (with highest honors) in Chemistry in 1977 from the University of California, Berkeley. He obtained a PhD in Organic Chemistry from Stanford University in 1982 (supervisor: Professor James P. Collman). He was a NSF-CNRS and NSF-NATO Postdoctoral Fellow with Professor Jean-Marie Lehn at L'Université Louis Pasteur de Strasbourg, France. He was then a JSPS Visiting Scientist in Professor Tabushi's group in Kyoto, Japan. In September 1984 he accepted a position as an Assistant Professor of Chemistry at the University of Texas at Austin. In September 1989 he was promoted to Associate Professor and in September of 1992 was promoted to Full Professor. Professor Sessler has authored or coauthored nearly 200 research publications, written one book (with Dr Steven J. Weghorn), and been an inventor of record on over 45 issued or allowed US Patents. He has been the recipient of a Camille and Henry Dreyfus Foundation Teacher-Scholar Award (1988), a Sloan Foundation Fellowship (1989), Arthur C. Cope Scholar Award (1991) and Senior Visiting Scientist Award of the Alexander von Humboldt Foundation (1993). He is also a cofounder (with Dr Richard A. Miller, MD) of Pharmacyclics Inc., a publicly traded company (pcyc; NASDQ) dedicated to developing various biomedical applications of expanded porphyrins.

Dr Philip A. Gale was born in Liverpool, England on September 24, 1969. In 1992 he graduated with a BA (Hons) in Chemistry from Wadham College, Oxford. He remained in

Oxford (moving to Linacre College) to undertake research in calixarene chemistry under the supervision of Dr P. D. Beer. In 1995 he received an MA and a DPhil and joined Professor Sessler's research group at the University of Texas at Austin as a Fulbright postdoctoral fellow researching the chemistry of the calixpyrroles. In October 1997 he took up a Royal Society University Research Fellowship at the Inorganic Chemistry Laboratory, Oxford.

Dr Vladimír Král was born on December 26, 1949. From 1969 to 1974 he attended the Charles University, Prague where he obtained an honours degree in Chemistry and an RNDr degree in the same year. His doctoral studies were conducted under the supervision of Dr Z. Arnold at the Institute of Organic Chemistry and Biochemistry of the Czechoslovak Academy of Sciences, from where he graduated with a PhD in 1978. From 1978–1991 he worked as a research scientist at the same institute. In 1982 and 1986 he was a visiting scholar at the Zelinski Institute of Organic Chemistry, Academy of Sciences, Moscow, USSR working with Professor L. A. Yanovskaya. In 1983 and 1987 he was a visiting Scholar at the University of Kuopio, Medical School, in Finland working with Professor R. Laatikainen. From 1987 he was the recipient of an Alexander von Humboldt Stiftung, and from 1987 to 1989 worked with Professor H. A. Staab at the Max Planck Institut für Medizinische Forschung. He took up a postdoctoral position in Professor Sessler's group in 1991 where he remained until 1995. From 1995–1996 he worked with Professor F. P. Schmidtchen at the Technische Universitäte München. He is now an Assistant Professor at the Institute of Chemical Technology, Prague.

Footnotes and References

* E-mail: sessler@mail.utexas.edu

1 A. Baeyer, *Ber. Dtsch. Chem. Ges.*, 1886, **19**, 2184.
2 A. Baeyer, *Ber. Dtsch. Chem. Ges.*, 1872, **5**, 1094.
3 P. A. Gale, J. L. Sessler, V. Král and V. Lynch, *J. Am. Chem. Soc.*, 1996, **118**, 5140.
4 M. Dennstedt and J. Zimmerman, *Chem. Ber. Dtsch. Ges.*, 1886, **19**, 2189.
5 M. Dennstedt and J. Zimmermann, *Chem. Ber.*, 1887, **20**, 850.
6 M. Dennstedt, *Ber. Dtsch. Chem. Ges.*, 1890, **23**, 1370.
7 V. V. Chelintzev and B. V. Tronov, *J. Russ. Phys. Chem. Soc.*, 1916, **48**, 105.
8 V. V. Chelintzev and B. V. Tronov, *J. Russ. Phys. Chem. Soc.*, 1916, **48**, 1197.
9 P. Rothemund and C. L. Gage, *J. Am. Chem. Soc.*, 1955, **77**, 3340.
10 W. H. Brown, B. J. Hutchinson and M. H. MacKinnon, *Can. J. Chem.*, 1971, **49**, 4017.
11 V. V. Chelintzev, B. V. Tronov and S. G. Karmanov, *J. Russ. Phys. Chem.*, 1916, **48**, 1210.
12 J. C. Lalloz and J. M. Lehn, unpublished results reported in *Macrocyclic Chemistry*, ed. B. Dietrich, P. Viout and J. M. Lehn, VCH, Weinheim, 1993.
13 J. C. Lalloz, J. M. Lehn and A. K. Willard, unpublished results reported in *Macrocyclic Chemistry*, ed. B. Dietrich, P. Viout and J. M. Lehn, VCH, Weinheim, 1993.
14 M. Cesario and C. Pascard, unpublished results reported in *Macrocyclic Chemistry*, ed. B. Dietrich, P. Viout and J. M. Lehn, VCH, Weinheim, 1993.
15 C. Floriani, *Chem. Commun.*, 1996, 1257.
16 D. Jacoby, C. Floriani, A. Chiesi-Villa and C. Rizzoli, *J. Chem. Soc., Chem. Commun.*, 1991, 790.
17 V. J. Bauer, D. L. J. Clive, D. Dolphin, J. B. Paine, III, F. L. Harris, M. M. King, J. Loder, S.-W. C. Wang and R. B. Woodward, *J. Am. Chem. Soc.*, 1983, **105**, 6429.
18 J. L. Sessler, M. J. Cyr, V. Lynch, E. McGhee and J. A. Ibers, *J. Am. Chem. Soc.*, 1990, **112**, 2810.
19 M. J. Hynes, *J. Chem. Soc., Dalton Trans.*, 1993, 311.
20 W. E. Allen, P. A. Gale, C. T. Brown, V. M. Lynch and J. L. Sessler, *J. Am. Chem. Soc.*, 1996, **118**, 12 471.
21 J. L. Sessler, A. Andrievsky, P. A. Gale and V. Lynch, *Angew. Chem., Int. Ed. Engl.*, 1996, **35**, 2782.
22 P. A. Gale, J. L. Sessler, W. E. Allen, N. A. Tvermoes and V. Lynch, *Chem. Commun.*, 1997, 665.
23 F. Arnaud-Neu, E. M. Collins, M. Deasy, G. Ferguson, S. J. Harris, B. Kaitner, A. J. Lough, M. A. McKervey, E. Marques, B. L. Ruhl, M. J. Schwing-Weill and E. M. Seward, *J. Am. Chem. Soc.*, 1989, **111**, 8681.
24 P. A. Gale, J. L. Sessler, V. Lynch and P. I. Sansom, *Tetrahedron Lett.*, 1996, **37**, 7881.
25 S. E. J. Bell, J. K. Browne, V. McKee, M. A. McKervey, J. F. Malone, M. O'Leary and A. Walker, unpublished work.
26 P. A. Gale, J. W. Genge, V. Král, M. A. McKervey, J. L. Sessler and A. Walker, *Tetrahedron Lett.*, in the press.
27 J. L. Sessler, P. A. Gale and J. W. Genge, unpublished work.
28 V. Král, P. A. Gale, P. Anzenbacher Jr., K. Jursíková, V. Lynch and J. L. Sessler, *Chem. Commun.*, 1998, 9.
29 G. R. Newkome, Y. J. Joo and F. R. Fronczek, *J. Chem. Soc. Chem. Commun.*, 1987, 854.
30 D. Jacoby, S. Isoz, C. Floriani, A. Chiesi-Villa and C. Rizzoli, *J. Am. Chem. Soc.*, 1995, **117**, 2793.
31 C. D. Gutsche and M. Iqbal, *Org. Synth.*, 1990, **68**, 234.
32 C. D. Gutsche and D. R. Stewart, *Org. Prep. Proced. Int.*, 1993, **25**, 137.
33 C. D. Gutsche, B. Dhawan, M. Leonis and D. Stewart, *Org. Synth.*, 1990, **68**, 238.
34 R. L. Jones and C. W. Rees, *J. Chem. Soc.* (*C*), 1969, 2249.
35 D. S. Black, M. C. Bowyer, N. Kumar and P. S. R. Mitchell, *J. Chem. Soc., Chem. Commun.*, 1993, 819.
36 D. S. Black, D. C. Craig and N. Kumar, *Tetrahedron Lett.*, 1995, **36**, 8075.

7/06280J

Calix[4]pyridine: a new arrival in the heterocalixarene family

Vladimír Král,[a,b] Philip A. Gale,[a] Pavel Anzenbacher Jr.,[a,b] Karolina Jursíková,[a] Vincent Lynch[a] and Jonathan L. Sessler*[a]

[a] *Department of Chemistry and Biochemistry, The University of Texas at Austin, Austin, Texas, 78712-1167, USA*
[b] *Institute of Chemical Technology, Department of Analytical Chemistry, Prague, 166 28 Czech Republic*

Reaction of dichlorocarbene with *meso*-octamethylcalix[4]pyrrole causes pyrrole ring expansion, producing chlorocalixpyridinopyrroles and chlorocalixpyridines.

Considerable effort of late has been devoted to synthesizing new macrocycles containing pyridine subunits. While many such systems have been reported, some of considerable elegance,[1] one of the simplest conceivable pyridine-containing macrocycles, calix[4]pyridine, remains unknown.

Currently, close analogues of calix[4]pyridine, in the form of homocalixpyridines[2] and tetrapyridine tetraone[3] macrocycles are known. However, macrocyclic systems with pyridine rings linked in the 2 and 6 positions *via* a single sp^3 hybridized carbon atom have yet to be prepared. We have now discovered a general synthetic strategy that not only allows for the preparation of calix[4]pyridine derivatives (*e.g.* **1**), but also provides access to calix[*n*]pyridino[*n*]pyrroles ($m + n = 4$). While some species related to this latter set of macrocycles are known, namely mixed porphyrin-like pyrrole-pyridine systems and calixpyridinopyrroles containing one or two pyridines,[4] calix[3]pyridine[1]pyrrole derivatives (*e.g.* **4**), as reported here, appear to be without precedent in the literature.

Our initial synthetic efforts were based on attempts to condense substituted pyridine *N*-oxides in a manner analogous to *p-tert*-butylphenol in calixarene synthesis.[5] However none of the desired products could be isolated from the reaction mixtures. Our attention then turned on finding methods that would allow us to convert calix[4]pyrroles[6] (*e.g.* **5**) to calix[4]pyridines. Reaction of dichlorocarbene with pyrrole, imidazole or indole rings has been shown to cause an insertion of the CCl_2 unit into one of the double bonds.[7] In the case of pyrroles, subsequent elimination of HCl and rearrangement produces a 3-chloropyridine ring. We thus attempted the conversion of *meso*-octamethylcalix[4]pyrrole **5** into tetrachloro-*meso*-octamethylcalix[4]pyridine **1** in several different solvents using a range of reaction times as well as different (excess) concentrations of sodium trichloroacetate. Using dioxane as the solvent, and 15 equiv. of sodium trichloroacetate, a 2.4 : 1 mixture of the mono- and di-pyridine macrocycles (**2** and **3**) was formed. Interestingly when the same reaction conditions were employed using 1,2-dimethoxyethane as solvent, a mixture of di-, tri- and tetra-pyridine species **3**, **4** and **1** was obtained in a 1 : 1 : 1 ratio (Scheme 1).† The latter conditions, therefore, offer easy access to chlorinated derivatives of two previously unknown macrocycles, namely, calix[3]pyridino[1]pyrrole **4** and calix[4]pyridine **1**, in the same reaction. In any event, it was found that by adding between 3 and 6 equiv. of the carbene source in a sequential manner, isolated yields of 65, 42 and 26% could be obtained for targets **3**, **4** and **1**, respectively.

X-Ray diffraction-grade single crystals of compound **3** were grown by slow evaporation of a dilute CH_2Cl_2 solution of the macrocycle (Fig. 1).‡ The resulting X-ray structure reveals that there are two crystallographically distinct molecules in the unit cell. Both adopt the cone conformation in the solid state such that potential NH···N hydrogen bonds are formed. These hydrogen bonds may influence the conformation of the macrocycle.

Crystals of the calix[3]pyridino[1]pyrrole were grown from a MeOH–CH_2Cl_2–hexanes solvent mixture.§ As in the structure

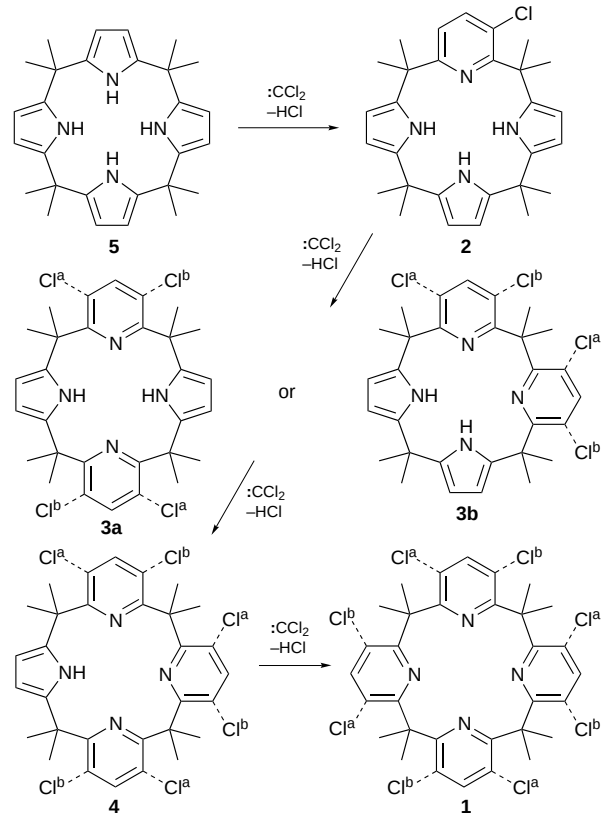

Scheme 1 The chlorine atoms indicated may be present in position 'a' or 'b' but not both. This results in isomers, as discussed in the text.

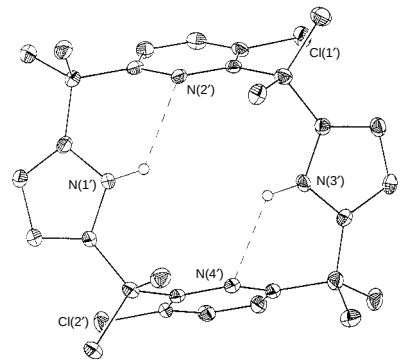

Fig. 1 X-Ray crystal structure of **3**. Intramolecular hydrogen bonds are shown by dotted lines. Thermal ellipsoids are at the 30% probability level.

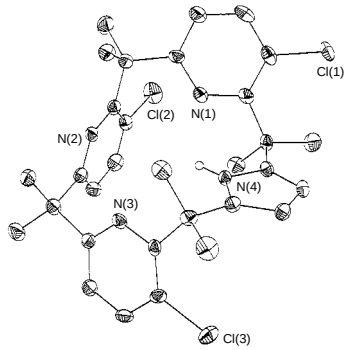

Fig. 2 X-Ray crystal structure of **4**. Only one molecule from the asymmetric unit is shown. Thermal ellipsoids are at the 30% probability level.

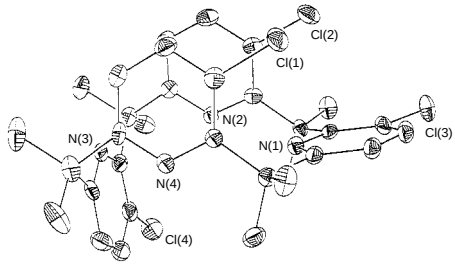

Fig. 3 X-Ray crystal structure of **1**. Intramolecular hydrogen bonds are shown by dotted lines. Thermal ellipsoids are at the 30% probability level.

of compound **3**, there are two molecules of compound **4** per asymmetric unit. The two molecules in the structure of **4** assume strikingly different conformations. For molecule 2, the molecular conformation is similar to that found in the structure of **1** (below) where alternate rings are either nearly parallel or nearly perpendicular. The dihedral angle between ring 2 (as denoted by the nitrogen atom label) and the pyrrole ring 4 is 81.9(2)°. The dihedral angle between ring 1 and ring 3 is 13.4(2)°. The dihedral angles between the rings and the plane through the bridging carbon atoms C(6′), C(12′), C(18′) and C(23′) is 81.6(2)° for ring 1, 74.9(2)° for ring 2, 85.1(2)° for ring 3 and 7.3(3)° for ring 4. Molecule 1 has a dramatically different conformation (Fig. 2). The dihedral angles between the rings and the plane through the bridging carbon atoms of molecule 1 are 51.3(2)° for ring 1, 89.3(2)° for ring 2, 55.5(2)° for ring 3 and 21.5(2)° for ring 4.

Single crystals of the calix[4]pyridine **1** were grown by slow evaporation of a CH_2Cl_2–hexane–MeOH solution of the macrocycle (Fig. 3).¶ The molecule adopts a flattened partial cone conformation in the solid state.

In summary, we have developed a universal and easy synthetic protocol for the preparation of calix[*m*]pyridino-[*n*]pyrrole ($m + n = 4$) and calix[4]pyridine systems based on a non-metal mediated ring expansion of pyrrole. We are currently investigating the molecular recognition properties of these new systems.

This research was supported by the National Institutes of Health (grants AI 33577 to J. L. S., and TW00682 to J. L. S. and V. K.), the National Science Foundation (grant CHE 9725399 to J. L. S) and the Howard Hughes Medical Institute (J. L. S. and V. K.). P. A. G. wishes to thank the Fulbright Commission for a post-doctoral research scholarship.

Footnotes and References

* E-mail: sessler@mail.utexas.edu

† Isomers are present in the reaction mixture, since the intermediate dichlorocarbene formed can insert into either of the two double bonds present in each of the various pyrrole rings under attack.

‡ *Crystal data* for **3**: Colourless plates of $(C_{30}H_{34}N_4Cl_2)_2 \cdot CH_2Cl_2$; triclinic, space group $P\bar{1}$, with a = 12.546(2), b = 15.403(2), c = 16.771(3) Å, α = 63.95(11), β = 82.953(10), γ = 76.937(9)°, V = 2835.3(8) Å^3, Z = 2, μ = 3.51 cm^{-1}, ρ_{calc} = 1.32 g cm^{-3}, M = 1127.95. There are two molecules of $C_{30}H_{34}N_4Cl_2$ along with a partially disordered CH_2Cl_2 solvate molecule per asymmetric unit. The conformations of the two macrocycles are nearly identical. The final $R_w(F^2)$ = 0.215 with a goodness of fit = 1.071, while the conventional $R(F)$ = 0.0844 for 5852 reflections with $F_o > 4[\sigma(F_o)]$.

§ *Crystal data* for **4**: Colourless needle-shaped crystals of $(C_{31}H_{33}N_4Cl_3)_2 \cdot 0.5CH_2Cl_2$ were monoclinic, space group $P2_1/c$, with a = 28.646(5), b = 10.368(2), c = 19.877(3) Å, β = 93.76(1)°, V = 5891(2) Å^3, Z = 4, μ = 3.85 cm^{-1}, ρ_{calc} = 1.33 g cm^{-3}, M = 1178.39. The pyrrolic hydrogen atoms were refined. There are two crystallographically independent molecules per asymmetric unit. The two molecules have markedly different conformations. There is a small amount of disorder of some Cl atoms on the pyridine rings in both molecules. The CH_2Cl_2 solvate molecule is disordered about a crystallographic inversion centre. The final $R_w(F^2)$ = 0.191 with a goodness of fit = 1.004, while the conventional $R(F)$ = 0.0774 for 5037 reflections with $F_o > 4$ [$\sigma(F_o)$].

¶ *Crystal data* for **1**: Colourless needle-shaped crystals of $C_{32}H_{32}N_4Cl_4$ were triclinic, space group $P\bar{1}$, with a = 9.883(2), b = 10.159(2), c = 15.720(3) Å, α = 93.66(2), β = 104.89(2), γ = 98.92(1)°, V = 1498.0(5) Å^3, Z = 2, μ = 4.24 cm^{-1}, ρ_{calc} = 1.36 g cm^{-3}, M = 614.42. The chlorine atoms, Cl(3) and Cl(4), appear to be disordered about two orientations. partial occupancy chlorine atoms appear bound to C(2) and C(16). The final $R_w(F^2)$ = 0.184 with a goodness of fit = 1.049, while the conventional $R(F)$ = 0.0750 for 2440 reflections with $F_o > 4[\sigma(F_o)]$. 182/654.

1 For an early review of pyridine containing macrocycles (along with furan and thiophene) see G. R. Newkome, J. D. Sauer, J. M. Roper and D. C. Hager, *Chem. Rev.*, 1977, **77**, 513. Mixed porphyrin-like pyrrole-pyridine systems are also known; see for instance T. D. Lash and S. T. Chaney, *Chem. Eur. J.*, 1996, **2**, 944; T. Schönemeier and E. Breitmaier, *Synthesis*, 1977, 273. For dodecahydrohexaazakekulene synthesis, see H. A. Staab and F. Diederich, *Chem. Ber.*, 1983, **116**, 3487; H. A. Staab, F. Diederich, C. Krieger and D. Schweitzer, *Chem. Ber.*, 1983, **116**, 3504. For the synthesis of sexipyridines, see J. L. Toner, *Tetrahedron Lett.*, 1983, **24**, 2707; G. R. Newkome and H.-W. Lee, *J. Am. Chem. Soc.*, 1983, **105**, 5956.

2 For a review of homocalixarenes and homocalixpyridines, see G. Brodesser and F. Vögtle, *J. Inclusion Phenom.*, 1994, **19**, 111.

3 G. R. Newkome, Y. J. Joo and F. R. Fronczek, *J. Chem. Soc., Chem. Commun.*, 1987, 854.

4 D. Jacoby, S. Isoz, C. Floriani, A. Chiesi-Villa and C. Rizzoli, *J. Am. Chem. Soc.*, 1995, **117**, 2793.

5 C. D. Gutsche and M. Iqbal, *Org. Synth.*, 1990, **68**, 234.

6 A. Bayer, *Ber. Dtsch. Chem. Ges.*, 1886, **19**, 2184; D. Jacoby, C. Floriani, A. Chiesi-Villa and C. Rizzoli, *J. Chem. Soc., Chem. Commun.*, 1991, 220; P. A. Gale, J. L. Sessler, V. Král and V. Lynch, *J. Am. Chem. Soc.*, 1996, **118**, 5140; P. A. Gale, J. L. Sessler, V. Lynch and P. I. Sansom, *Tetrahedron Lett.*, 1996, **37**, 7881; W. E. Allen, P. A. Gale, C. T. Brown, V. M. Lynch and J. L. Sessler, *J. Am. Chem. Soc.*, 1995, **118**, 12 471; J. L. Sessler, A. Andrievsky, P. A. Gale and V. Lynch, *Angew. Chem., Int. Ed. Engl.*, 1996, **35**, 2782; P. A. Gale, J. L. Sessler, W. E. Allen, N. A. Tvermoes and V. Lynch, *Chem. Commun.*, 1997, 665.

7 C. W. Rees and C. E. Smithen, *J. Chem. Soc.*, 1964, 928; C. W. Rees and C. E. Smithen, *J. Chem. Soc.*, 1964, 938; R. L. Jones and C. W. Rees, *J. Chem. Soc. (C)*, 1969, 2249; R. L. Jones and C. W. Rees, *J. Chem. Soc. (C)*, 1969, 2251; R. L. Jones and C. W. Rees, *J. Chem. Soc. (C)*, 1969, 2255.

Received in Columbia, MO, USA, 18th August 1997; 7/06018A

Templated assembly of a molecular capsule

Joost N. H. Reek,[a] Albert P. H. J. Schenning,[b] Anton W. Bosman,[b] E. W. Meijer[b] and Maxwell J. Crossley*[a]

[a] *School of Chemistry, The University of Sydney, NSW 2006, Australia*
[b] *Laboratory of Organic Chemistry, Eindhoven University of Technology, PO Box 513, NL-5600 MD Eindhoven, The Netherlands*

Two rigid Tröger's base dizinc(II) bis-porphyrin receptor molecules 1 and the first generation of dendrimer tetramine 4 form a 2:1 complex 5, a self-assembled spherical superstructure encapsulating the dendrimer.

Self-assembled molecular capsules have received much attention in supramolecular chemistry. Most of them are based on diphenylglycoluril building blocks in which the formation of eight (or more) hydrogen bonds favours a dimeric structure resembling a 'molecular tennis ball'.[1] These assemblies were able to reversibly encapsulate small guest molecules.[2] Recently larger dimeric structures based on calix[4]arenes have also been described, showing comparable behaviour.[3]

The use of self-assembly in the formation of porphyrin arrays to mimic some aspects of the photosynthetic machinery, has emerged in different supramolecular porphyrin structures. These porphyrin assemblies are based on hydrogen bonding,[4] metal ion coordination,[1,5] and central metal atom coordination.[6] Here, we report the formation of a self-assembled molecular capsule based on metal-to-ligand interactions of two dizinc(II) bis-porphyrins around a tetramine.

Previously we have shown that a rigid Tröger's base-like receptor strongly binds ditopic diamino ligands such as L-histidine esters[7] and α,ω-diaminoalkanes[8] in its cleft which has a Zn···Zn distance of *ca.* 8.5 Å. We have also synthesised the expanded Tröger's base dizinc(II) bis-porphyrin receptor **1**.[9] Models indicate that the Zn···Zn distance in the unbound state is *ca.* 16 Å.

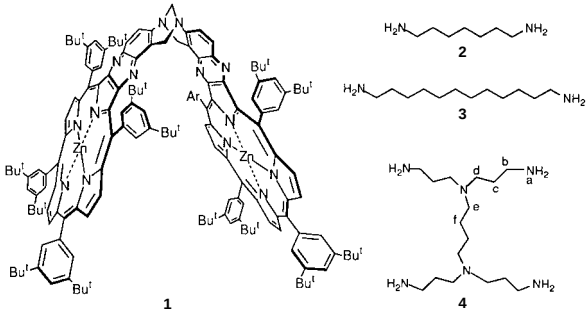

Binding studies, using UV–VIS spectroscopy,† of a series of ditopic α,ω-diaminoalkanes show that 1,7-diaminoheptane **2** is the smallest guest which can bind to the receptor **1** in a ditopic manner giving a 1:1 complex with a high binding constant (1.5×10^6 dm^3 mol^{-1}). This indicates that there is some flexibility in the skeleton of **1** and that the cleft can be contracted to a Zn···Zn distance of 13 Å. The binding strength of the monodentate ligand 1-hexylamine is significantly less (5×10^4 dm^3 mol^{-1}). In the case of 1,6-diaminohexane binding is also significantly weaker and sigmoidal titration curves are observed indicating several competing modes of binding occur. Larger guests, for example 1,12-diaminododecane **3** bind significantly more strongly (7×10^7 dm^3 mol^{-1}), indicating that there is an energy penalty associated with contraction of the binding cleft.

The observation of tight binding of suitably long ditopic ligands to dizinc(II) bis-porphyrin **1** suggested to us that polyamines could be used as ligands to assemble a number of dimetallo bis-porphyrin systems around a ligand core. Dizinc(II) bis-porphyrin **1** and quatratopic ligands such as the first generation of aminodendrimer[10] **4** were expected to give a 2:1 complex by the formation of four Zn–amine bonds. Indeed, the UV–VIS titration curve of **1** with tetramine **4** showed an inflection point at 0.5 equiv. of **4** added, indicating that a 2:1 complex **5** was formed (Fig. 1). The porphyrin Q bands as well as the Soret band were shifted towards the red in the visible spectrum as ligand was added, indicating that the amines of **4** were complexed to the Zn atoms of the porphyrin units of **1**. These shifts were similar to those found for the ditopic ligands **2** and **3** upon full complexation showing that to each Zn atom of **1**, an amine was bound. The only structure which allowed a 2:1 complex and all the Zn atoms to be occupied was the molecular capsule **5** with the tetramine guest **4** inside the spherical dimer (Fig. 2). Although there are two possible forms in which the guest molecule can be bound to the tetramine, either with 9 or 14 atoms between the two Zn atoms of one unit of **1**, molecular modelling‡ studies suggest that the latter form is much more favourable, which is in line with the difference seen in binding of **2** and **3** with receptor **1**.§

In order to explore the stability of the molecular capsule **5** the titration was continued by adding further free ligand **4**. A second inflection point was observed corresponding to the addition of 1 equiv. of **4** (Fig. 1). This indicates that complex **5** dissociates to form 1:1 complexes (two Zn–amine bonds and two free amine groups per complex) at higher ligand concentration. By comparison, a titration curve of **1** with the ditopic guest **3** (or **2**) showed only one inflection point which corresponded to the addition of 1 equiv. of ligand (also two Zn–amine bonds).

To further investigate the structure of the molecular capsule **5**, 400 MHz ^{1}H NMR studies were performed (Fig. 3). To a 2.2 mmol $CDCl_3$ solution of tetramine **4** was added stepwise a 12.6 mmol solution of **1** also containing 2.2 mmol of **4**. Upon the addition of **1** the signals of **4** were broadened and upfield shifted. The NH_2 (protons a in structure **4**), α-CH_2 (protons b) and β-CH_2 (protons c) signals showed the highest shifts, being the closest protons to the porphyrin ring upon complexation. These signals shifted approximately linearly with concentration towards δ −4.68 (NH_2; total shift −5.92 ppm), −2.82 (α-CH_2; total shift −5.50 ppm) and −1.80 (β-CH_2; total shift −3.35 ppm) at 2 equiv. of **1** [Fig. 3(*c*)], indicating that all amino groups were complexed to zinc(II) porphyrins. The addition of more **1**

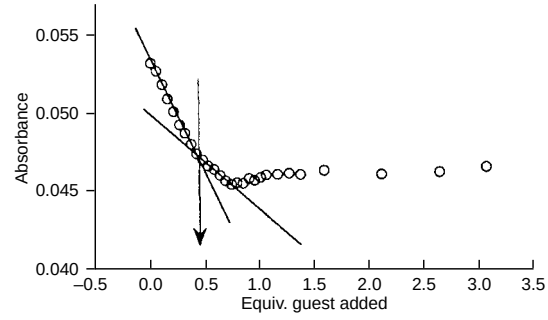

Fig. 1 UV Titration curve (616 nm) of **1** with quatratopic guest **4**

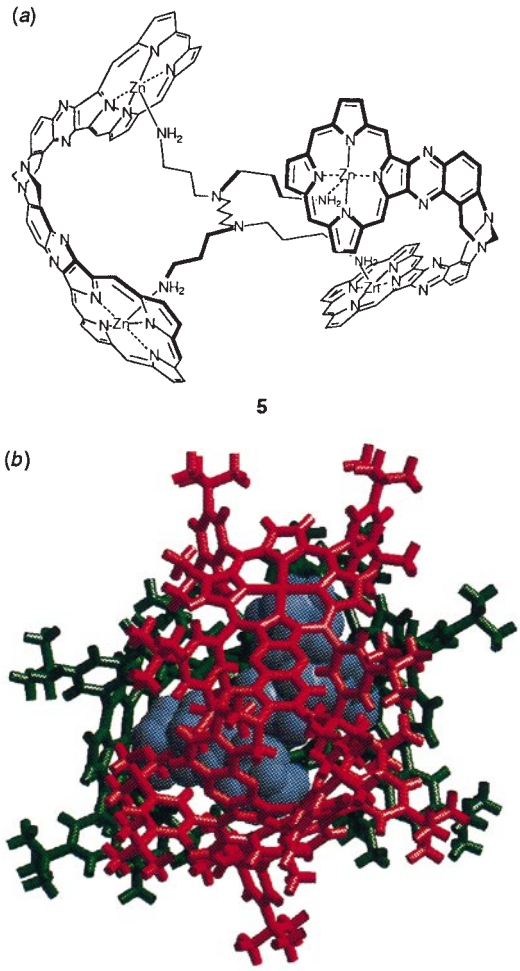

Fig. 2 (*a*) Schematic sideview with sixteen *meso* aryl groups omitted for clarity and (*b*) a modelled structure of the capsule **5** consisting of the two shape complementary receptor molecules **1** assembled around the core guest **4**. The encapsulated guest is in blue (space-filling), the receptors are in dark green and red (stick).

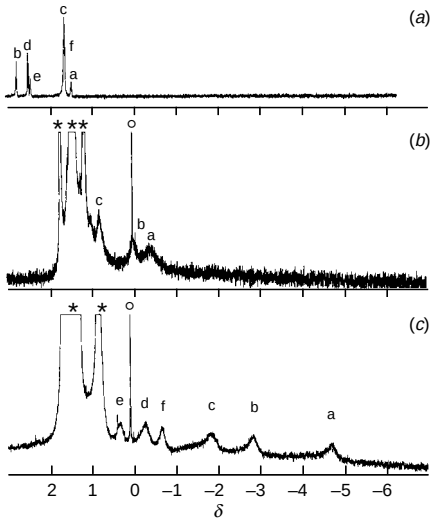

Fig. 3 ^{1}H NMR spectra of (*a*) **4**, (*b*) a 1 : 1 complex of **4** and **1**, (c) molecular capsule **5**. Peaks marked with an asterisk are from the *tert*-butyl protons of the receptor molecule and the $SiMe_4$ resonance is marked with a circle.

(up to 5.4 equiv.) did not result in significant change of chemical shifts of the protons of **4**, indicating that at these concentrations the 2 : 1 complex is stable and no higher complexes are formed. Upon the addition of just 1 equiv. of **1** the shifts of protons a, b and c of **4** [Fig. 3(*b*)] were in between the signals of free **4** [Fig. 3(*a*)] and fully complexed **4** [Fig. 3(*c*)], suggesting that a 1 : 1 complex is formed as an intermediate.

The signals of receptor **1** shifted as well. The signals of the bridging methyl groups and the β-pyrrolic protons of the porphyrin rings shifted to higher field, upon complexation. Adding more than 2 equiv. of **1** resulted in broadening of the signals of the receptor and signals of the bridging methyl groups and the β-pyrrolic protons of the porphyrin rings shifted back to lower field. These data clearly show that a 2 : 1 complex between receptor **1** and quatratopic guest **4** is formed, and that the exchange between the free components and the complex is at coalescence on the NMR timescale. At −50 °C, this equilibrium is slow and the ^{1}H NMR spectrum of a 1 : 4 mixture of **4** and **1** showed signals of the free and the complexed receptor **1**. Although the spectrum was complicated and could not be completely assigned, large downfield shifts were observed for the β-pyrrolic protons of the porphyrin rings and the other aromatic protons of the receptor. These large shifts, which were not observed for ditopic ligands, are in agreement with the structure of molecular capsule **5**.

Studies of porphyrin arrays assembled around larger dendrimers are in progress.

We thank the Australian Research Council for a research grant to M. J. C.

Footnotes and References

* E-mail: m.crossley@chem.usyd.edu.au

† Spectrophotometric titrations were carried out in toluene at 25.0 °C (receptor concentration 2×10^{-6} mol dm^{-3}). The absorption was followed at different wavelengths and the obtained curves were analysed using a Simplex least-squares curve-fitting procedure.[11]

‡ SPARTAN version 4.0, Wavefunction, Inc, Irvine, CA, USA, 1995 and Cerius^{2TM}, which was developed by BIOSYM/Molecular Simulations, were used.

§ The energy difference on the basis of the binding difference of **2** and **3** is estimated to be 19 kJ mol^{-1}.

1 R. Wyler, J. D. Mendoza and J. Rebek Jr., *Angew. Chem., Int. Ed. Engl.*, 1993, **32**, 1699.
2 N. Branda, R. Wyler and J. Rebek Jr., *Science*, 1994, **263**, 1267; J. Kang and J. Rebek Jr., *Nature*, 1996, **382**, 239; R. M. Grotzfeld, N. Branda and J. Rebek Jr., *Science*, 1996, **271**, 487.
3 B. C. Hamann, K. D. Shimizu and J. Rebek Jr., *Angew. Chem., Int. Ed. Engl.*, 1996, **35**, 1326.
4 C. M. Drain, K. C. Russel, J. L. Sessler, B. Wang and A. Harriman, *J. Am. Chem. Soc.*, 1995, **117**, 704; C. M. Drain, K. C. Russell and J.-M. Lehn, *Chem. Commun.*, 1996, 337; Y. Kuroda, A. Kawashima, Y. Hayashi and H. Ogoshi, *J. Am. Chem. Soc.*, 1997, **119**, 4929.
5 C. M. Drain and J.-M. Lehn, *J. Chem. Soc., Chem. Commun.*, 1994, 2313; J.-P. Collin, A. Harriman, V. Heitz, F. Odobel and J.-P. Sauvage, *J. Am. Chem. Soc.*, 1994, **116**, 5679; A. P. H. J. Schenning, F. Benneker, H. P. Geurts, X. Y. Liu and R. J. M. Nolte, *J. Am. Chem. Soc.*, 1996, **118**, 8549.
6 C. A. Hunter and L. D. Sarson, *Angew. Chem., Int. Ed. Engl.*, 1994, **33**, 2313; S. Anderson, H. L. Anderson, A. Bashall, M. McPartlin and J. K. M. Sanders, *Angew. Chem., Int. Ed. Engl.*, 1995, **34**, 1096; H. L. Anderson, S. Anderson and J. K. M. Sanders, *J. Chem. Soc., Perkin Trans. 1*, 1995, 2231.
7 M. J. Crossley, L. G. Mackay and A. C. Try, *J. Chem. Soc., Chem. Commun.*, 1995, 1925.
8 M. J. Crossley, T. W. Hambley, L. G. Mackay, A. C. Try and R. Walton, *J. Chem. Soc., Chem. Commun.*, 1995, 1077.
9 M. J. Crossley, A. C. Try and R. Walton, *Tetrahedron Lett.*, 1996, **37**, 6807.
10 E. M. M. de Brabander-van den Berg and E. W. Meijer, *Angew. Chem., Int. Ed. Engl.*, 1993, **32**, 1308.
11 W. H. Press, B. P. Flannery, S. A. Teukolsky and W. T. Vetterling, *Numerical Recipes in Pascal*, Cambridge University Press, Cambridge, 1989.

Received in Cambridge, UK, 22nd July 1997; revised manuscript received 27th October 1997; 7/07748C

Crystallization of 3-cyanophenyl 4-cyanobenzoate with $AgSbF_6$: a polar coordination network based on the crisscrossing of intertwined helices

Keith A. Hirsch, Scott R. Wilson and Jeffrey S. Moore*

Departments of Chemistry and Materials Science and Engineering, The University of Illinois at Urbana-Champaign, Roger Adams Laboratory, Box 55-5, 600 S. Mathews Avenue, Urbana, IL 61801, USA

Crystallization of 3-cyanophenyl 4-cyanobenzoate 1 with $AgSbF_6$ yields the non-centrosymmetric, fourfold interpenetrated grid structure $[Ag(\mathbf{1})_2]SbF_6$ 2 through the crisscrossing of two-dimensional sheets.

The construction of self-assembled materials through metal coordination is an area of research that has grown tremendously in recent years.[1] The challenge that faces chemists working in this field is to identify packing trends that may allow for the rational design of functional materials. In this vein, we developed a packing model for interpenetrated diamondoid networks that was applied with success to our structures and those in the literature.[2] Also, many interesting structural studies on other coordination networks have been put forth,[3] and some have yielded materials exhibiting novel properties.[4] In order to observe packing trends such that coordination network topology may be better anticipated, systematic structural studies should continue to elucidate the role of variables such as counterion and ligand structure. In time, such studies may allow for the rational construction of materials exhibiting catalytic or nonlinear optical activity. In continuing towards this goal, we report a novel, non-centrosymmetric coordination network based on 3-cyanophenyl 4-cyanobenzoate **1**. Included here is a description of this structure that accounts for its packing in a polar space group.

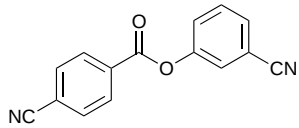

1

3-Cyanophenyl 4-cyanobenzoate **1** was prepared in 92% yield by reaction of 3-cyanophenol (1.0 equiv.) and 4-cyanobenzoyl chloride (1.0 equiv.) in CH_2Cl_2 at room temperature in the presence of DMAP (0.1 equiv.) and NEt_3 (2.4 equiv.). Crystallization of ligand **1** (1.0 equiv.) with $AgSbF_6$ (1.1 equiv.) was achieved by heating and slow cooling from toluene in a programmable oven. The temperature program involved heating from room temperature to 100 °C at a rate of 20 °C h^{-1}, holding at 100 °C for 2 h, and cooling to ambient temperature at a rate of 1.2 °C h^{-1}. Colorless columnar crystals of the complex $[Ag(\mathbf{1})_2]SbF_6$ **2** were obtained and one was selected for X-ray analysis.† The resulting structure crystallizes in the non-centrosymmetric, orthorhombic space group *Ccc*2 and is composed of crisscrossing sheets that form an infinite grid.

In complex **2**, silver(I) adopts a distorted tetrahedral geometry coordinated by four nitrile nitrogen atoms of ligand **1**. The metal ion bonds to nitrile nitrogens of two cyanobenzoyl rings and two cyanophenyl rings. N–Ag–N bond angles about silver(I) range from 100.4(3) to 130.1(4)°. The SbF_6^- ions do not coordinate to silver(I) and are disordered over two sites, each of which is half-occupied. The shortest Ag···F separation is 5.30 Å.

The sheet topology of complex **2** is shown in Fig. 1. Within a sheet, the Ag–**1**–Ag distance is 16.11 Å. Twofold interpenetration is observed to partially fill void space created by a single sheet. This interpenetration may be viewed as the intertwining of two 2/1 helices (Fig. 1). Closest-packing in complex **2** is not achieved by twofold interpenetration. Rather, it results from further interpenetration of twofold interpenetrated sheets that propagate orthogonal to one another. Crisscrossing of orthogonal twofold sheets yields a fourfold interpenetrated grid structure overall (see Fig. 2). π–π Stacking is observed between molecules of ligand **1** that originate from orthogonal sheets [Fig. 2(*b*)]. Specifically, stacking occurs between cyanobenzoyl rings at a plane-to-plane distance of 3.35 Å and between cyanophenyl rings at a plane-to-plane distance of 3.44 Å.

Fourfold interpenetration in complex **2** can be viewed as arising from the crisscrossing of orthogonal pairs of 2/1 helices (see Fig. 3). Orthogonal sheets are mirror images of one another and, therefore, orthogonal helices are of opposite handedness [Fig. 3(*b*)]. The reason that this structure is polar is that helices of opposite handedness propagate orthogonal to one another. Therefore, the opposite twist sense associated with these helices does not cancel. Had helices of opposite handedness propagated

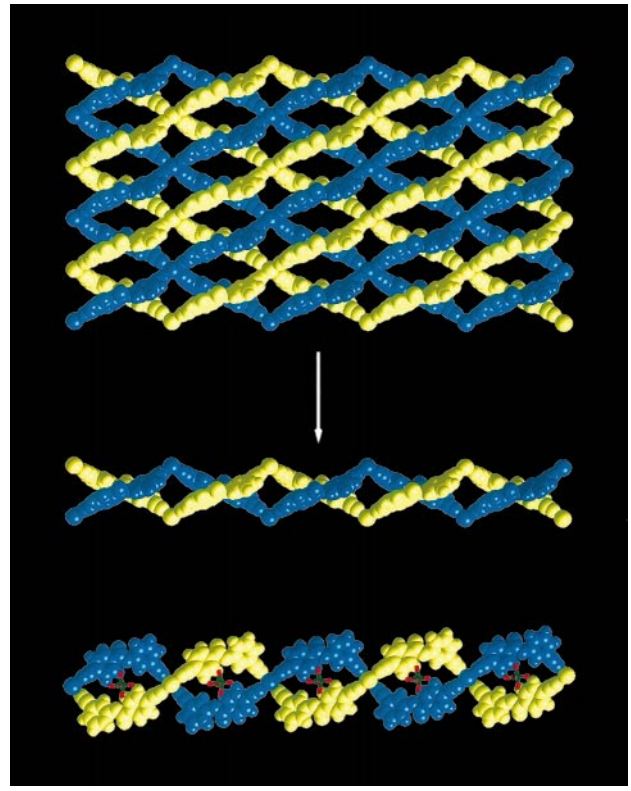

Fig. 1 Twofold interpenetrated sheets as a means to partially fill void space in the grid structure $[Ag(\mathbf{1})_2]SbF_6$ **2**. Interpenetration may be viewed as the intertwining of two 2/1 helices that are derived from the sheets as shown. The projection at the bottom is obtained by rotation of the middle figure by *ca*. 90° about the horizontal axis. The inclusion of counterions is shown in this projection (antimony is green and fluorine is red).

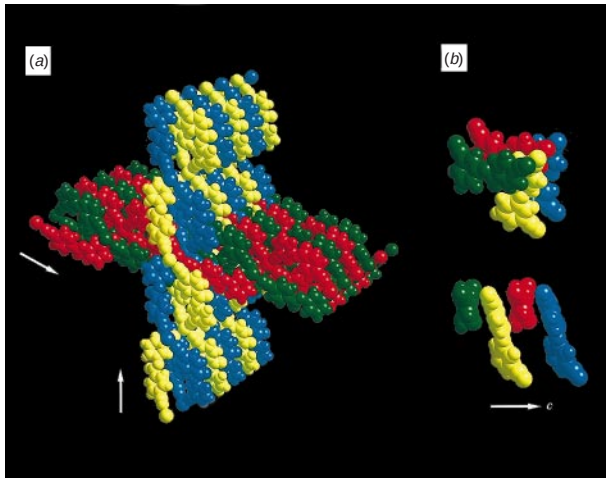

Fig. 2 (*a*) Fourfold interpenetration in $[Ag(\mathbf{1})_2]SbF_6$ **2** resulting from the crisscrossing of an orthogonal pair of twofold interpenetrated sheets. The blue and yellow networks constitute one set of twofold sheets and the red and green networks constitute the other. The arrows indicate the directions of propagation for the orthogonal sheets. Fourfold interpenetration is shown from left to right in a blue–green–yellow–red sequence where the orthogonal sheets cross. (*b*) Two views of π–π stacking of cyanobenzoyl rings of compound **1** as a result of fourfold interpenetration. Stacking occurs between ligands of orthogonal sheets along the polar *c*-axis. The direction of the *c*-axis is indicated for the bottom projection. The plane-to-plane distance for this stacking interaction is 3.35 Å.

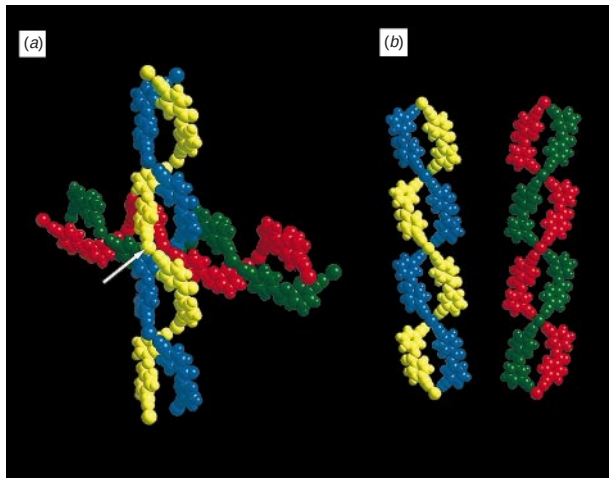

Fig. 3 The crisscrossing of orthogonal pairs of 2/1 helices in $[Ag(\mathbf{1})_2]SbF_6$ **2**. (*a*) Pairs of intertwined helices crisscross to afford fourfold interpenetration. Fourfold interpenetration is indicated by the arrow, which highlights a yellow–red–blue–green sequence of silver(I) ions (balls). Orthogonal helices are of opposite handedness. This point is clarified on the right. (*b*) Two orthogonal pairs of helices separated to reveal mirror symmetry. The blue and yellow helices are left-handed and the red and green helices are right-handed.

along the same direction, a non-polar structure could have formed. Such a packing of helices was observed in the sheet structures $[Ag(3,3'\text{-dicyanodiphenylacetylene})_2]XF_6$ (X = P, As, Sb), which we reported recently.[3a] These structures crystallized in space group $P\bar{1}$ and the topology is twofold interpenetrated sheets that are very similar to those shown in Fig. 1. However, for the 3,3′-dicyanodiphenylacetylene structures, closest-packing arises from the interdigitation of helices of opposite handedness[3a] rather than the crisscrossing of such helices. As a result, left- and right-handed helices propagate along the same axis such that the opposite twist sense associated with these helices cancel out, and the structures are non-polar ($P\bar{1}$). The difference in the packing between the structure presented here and those of 3,3′-dicyanodiphenylacetylene may be a result of the *para*-nitrile group of ligand **1**, which changes the conformation of the 2/1 helix. This comparison demonstrates the value of viewing solid-state packing in terms of helices in order to better understand gross structure. An increased understanding of solid-state packing is essential if self-assembled materials possessing novel properties are to be designed.

We acknowledge the US Department of Energy through the Materials Research Laboratory at the University of Illinois (Grant DEFG02-96ER45439) for financial support of this work. We also thank the School of Chemical Sciences Materials Characterization Laboratory at the University of Illinois for X-ray data collection.

Footnotes and References

* E-mail: moore@aries.scs.uiuc.edu

† *Crystal data* for **2**: orthorhombic, space group *Ccc*2 (no. 37), a = 18.9697(5), b = 21.251 90(10), c = 7.5365(2) Å, U = 3038.21(11) Å^3, D_c = 1.837 g cm^{-3}, Z = 4, M = 840.09, Mo-Kα, L_p corrected, 9596 reflections collected at −75 °C, 3589 unique reflections. The structure was solved using SHELXS and was refined using SHELXTL. 3586 Reflections refined based on F_o^2 by full-matrix least squares; number of parameters = 237; $R_1 = \Sigma||F_o| - |F_c||/\Sigma|F_o| = 0.0570$ (for $F_o > 4\sigma$) and 0.1086 (for all data); $wR_2 = [\Sigma(w|F_o^2 - F_c^2|)/\Sigma w|F_o^2|^2]^{\frac{1}{2}} = 0.0804$ (for $F_o > 4\sigma$) and 0.1042 (for all data); GOF = 1.171. The space group choice was confirmed using the CALC MISSYM option of PLATON (A. L. Spek, *J. Appl. Crystallogr.*, 1988, **21**, 578) as no extra crystallographic symmetry was detected. CCDC 182/684.

1 J. S. Moore and S. Lee, *Chem. Ind.*, 1994, 556; G. A. Ozin and C. L. Bowes, *Adv. Mater.*, 1996, **8**, 13.
2 K. A. Hirsch, S. R. Wilson and J. S. Moore, *Chem. Eur. J.*, 1997, **3**, 765.
3 (*a*) K. A. Hirsch, S. R. Wilson and J. S. Moore, *Inorg. Chem.*, 1997, **36**, 2960; (*b*) K. A. Hirsch, D. Venkataraman, S. R. Wilson, J. S. Moore and S. Lee, *J. Chem. Soc., Chem. Commun.*, 1995, 2199; (*c*) D. Venkataraman, S. Lee, J. S. Moore, P. Zhang, K. A. Hirsch, G. B. Gardner, A. C. Covey and C. L. Prentice, *Chem. Mater.*, 1996, **8**, 2030; (*d*) L. R. MacGillivray, S. Subramanian and M. J. Zaworotko, *J. Chem. Soc., Chem. Commun.*, 1994, 1325; (*e*) L. Carlucci, G. Ciani, D. M. Proserpio and A. Sironi, *J. Am. Chem. Soc.*, 1995, **117**, 4562.
4 G. B. Gardner, D. Venkataraman, J. S. Moore and S. Lee, *Nature*, 1995, **374**, 792; D. Venkataraman, G. B. Gardner, S. Lee and J. S. Moore, *J. Am. Chem. Soc.*, 1995, **117**, 11 600; (*c*) B. F. Hoskins and R. Robson, *J. Am. Chem. Soc.*, 1989, **111**, 5962; (*d*) M. Fujita, Y. J. Kwon, S. Washizu and K. Ogura, *J. Am. Chem. Soc.*, 1994, **116**, 1151; (*e*) O. M. Yaghi, G. Li and H. Li, *Nature*, 1995, **378**, 703.

Received in Columbia, MO, USA, 18th June 1997; Revised Manuscript received 17th October 1997; 7/07574J

Novel supported catalysts: platinum and platinum oxide nanoparticles dispersed on polypyrrole/polystyrenesulfonate particles

Zhigang Qi and Peter G. Pickup*

Department of Chemistry, Memorial University of Newfoundland, St. John's, Newfoundland, Canada A1B 3X7

Platinum and platinum oxide nanoparticles are deposited on electronically and ionically conducting polypyrrole/polystyrenesulfonate particles by the reduction of $Pt(NH_3)_4Cl_2$ with formaldehyde and the oxidation of $Na_6Pt(SO_3)_4$ with H_2O_2, respectively.

Supported metal catalysts play a crucial role in many industrially important chemical reactions.[1] The support enables the metal particles to be highly dispersed and thermostable to retard sintering so that they can be used with high efficiency. This is particularly important with expensive noble metal catalysts such as platinum. The most widely used supports are carbon, SiO_2, Al_2O_3, TiO_2 and zeolites. Carbon is the only electronically conducting support in widespread use.

We introduce here a new type of support, polypyrrole/polystyrenesulfonate, which is both electronically and ionically conductive. The polypyrrole (PPy) provides electronic conductivity that can be controlled either chemically or electrochemically.[2] The polystyrenesulfonate (PSS) counter-ion, incorporated into the PPy during preparation, provides cation exchange sites. When the oxidation state of the polypyrrole is decreased, mobile cations are drawn into the particles to compensate the loss of cationic polymer sites. This causes an increase in the ionic conductivity that can be chemically or electrochemically controlled.[3]

Our primary interest in using PPy/PSS particles as a catalyst support arises from their potential application in proton exchange membrane fuel cells. The ideal catalyst support in such fuel cells would be gas and water permeable, and conduct both protons and electrons.[4] None of the conventional catalyst supports possess all these properties, but PPy/PSS does.

Although using conducting polymers as catalyst supports has been attracting research interest for more than 10 years, the deposition of metal particles has been restricted to the use of electrochemical methods and polymer films.[5] In one case, chemically prepared colloidal Pt particles were dispersed in a polypyrrole film during its electrochemical synthesis,[6] but there are no reports on the deposition of metal particles on conducting polymer particles. We have developed simple methodology that enables the fabrication of size-controllable PPy/PSS particles with dimensions ranging from *ca.* 30 to 1000 nm, and the chemical deposition of highly dispersed Pt on these particles.

The sizes of chemically synthesized PPy/PSS particles were controlled by varying the concentrations of pyrrole and the iron(III) oxidant.[7] The higher the concentration, the smaller the resulting polymer particles. The presence of PSS is essential in the size-control process. In a typical procedure (*i.e.* the preparation of the PPy/PSS particles shown in Fig. 1), a mixture consisting of 7.0 ml of 0.1 M NaPSS(aq) (0.70×10^{-3} mol, Aldrich; *M ca.* 70 000), 150 μl of neat pyrrole (2.1×10^{-3} mol), and 61 ml of water was shaken for 10 min before addition of 12 ml of 0.5 M $FeCl_3$ (6.0×10^{-3} mol) in 0.1 M HCl(aq). Following stirring for 15 min and centrifuging, the PPy/PSS particles were washed five times with water. The average diameter of the PPy/PSS particles produced under these conditions was *ca.* 500 nm, and their electronic conductivity was *ca.* 10^{-2} S cm^{-1}. Based on a model of spherical particles with a density[8] of *ca.* 1.5 g cm^{-3}, the estimated surface area is *ca.* 8 m^2 g^{-1}. The sample shown in Fig. 2 has an estimated surface area of *ca.* 100 m^2 g^{-1}.

The deposition of Pt nanoparticles on PPy/PSS particles was accomplished by the reduction of $Pt(NH_3)_4Cl_2$ with formaldehyde. PPy/PSS was heated at reflux in 60 ml of formaldehyde for 1 h to ensure full dispersion, followed by the addition of 72 mg of $Pt(NH_3)_4Cl_2$ and stirring for 30 min. The mixture was then heated at reflux for 30, 60, 90, 120 or 150 min.

Transmission electron microscopy (TEM) revealed that little Pt deposition occurred during the first 1.5 h, while large quantities of Pt nanoparticles with diameters of *ca.* 4 nm were produced after *ca.* 2 h. The reaction time had little influence on the Pt particle size. Fig. 1 shows a TEM of a Pt/PPy/PSS sample following 2.5 h of reflux. The distribution of Pt nanoparticles is quite homogeneous. Electronic conductivity measurements following Pt deposition revealed a *ca.* three order of magnitude decrease to *ca.* 10^{-5} S cm^{-1}. A similar decrease in conductivity was observed when PPy/PSS particles were treated with formaldehyde alone, suggesting that it is due to irreversible reduction of the polypyrrole.

Deposition of Pt oxide nanoparticles on PPy/PSS particles was also performed.[9] In this case, the PPy/PSS was produced from a mixture consisting of 0.14 M pyrrole, 0.70 M $Fe(NO_3)_3$ and 0.04 M PSS with a 90 min reaction time. The resulting PPy/PSS particles were of an irregular shape, with an average dimension of *ca.* 40 nm. After 0.2000 g of dried PPy/PSS and 0.1695 g of $Na_6Pt(SO_3)_4$[9] were stirred in 80 ml of water for 5

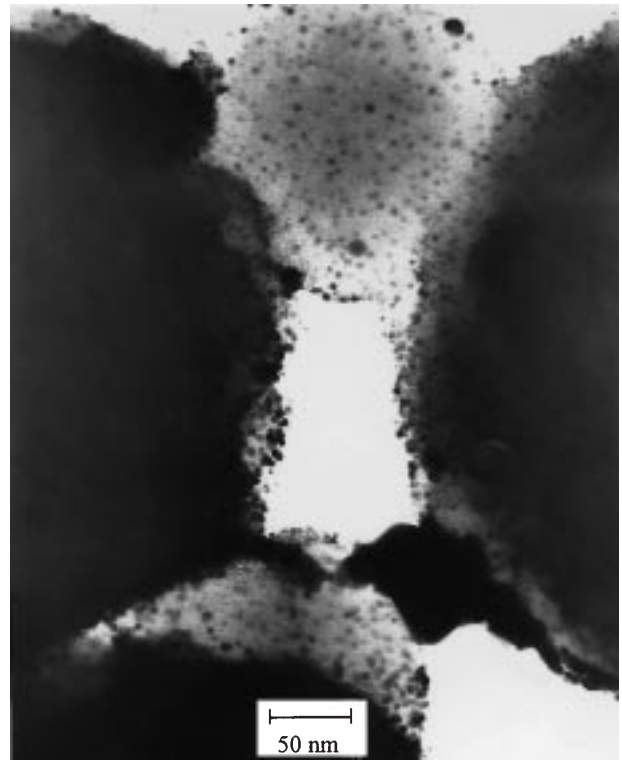

Fig. 1 TEM of Pt nanoparticles dispersed on PPy/PSS particles

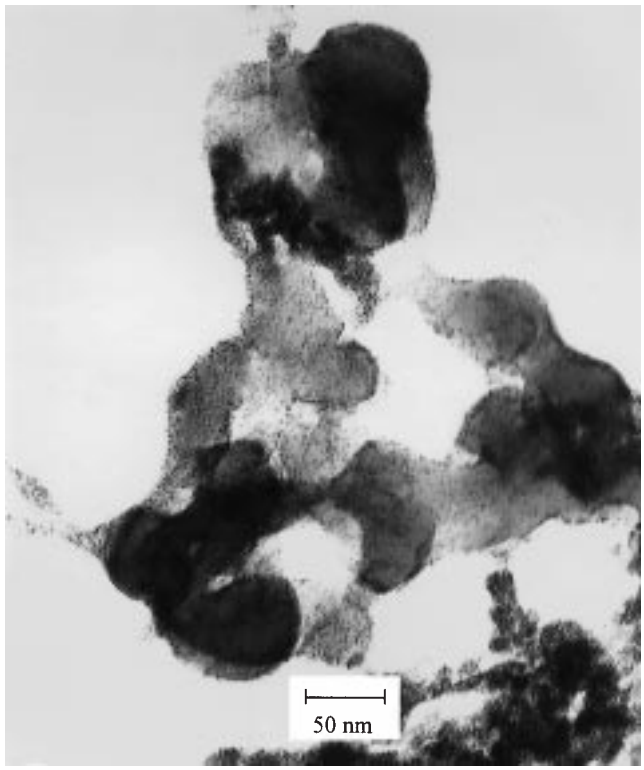

Fig. 2 TEM of Pt oxide nanoparticles dispersed on PPy/PSS particles

min, 1 M H_2SO_4 was added dropwise to adjust the pH from *ca*. 4 to 2.0, followed by the dropwise addition of 0.5 M NaOH to adjust the pH to 3.0. Then 1.00 ml of 30% H_2O_2 was added and the mixture was stirred for 1 h and then boiled. The Pt oxide/PPy/PSS particles were separated from the reaction medium by centrifuging, washed three times with water, and dried under vacuum overnight at room temperature.

Fig. 2 shows a TEM of the resulting Pt oxide/PPy/PSS particles. Pt oxide nanoparticles were *ca*. 2 nm in diameter and evenly distributed on the PPy/PSS particles. Although the exact chemical nature of the Pt oxide particles is unknown, they can be converted to highly catalytic Pt particles simply by heating.[9] This sample exhibited electronic conductivities of *ca*. 3 and 10^{-5} S cm^{-1} before and after Pt oxide deposition, respectively. The decrease in conductivity is presumably due to over-oxidation[10] of the polypyrrole by the H_2O_2.

Preliminary results (Fig. 3) have indicated that the supported catalysts described here are effective for oxygen reduction in

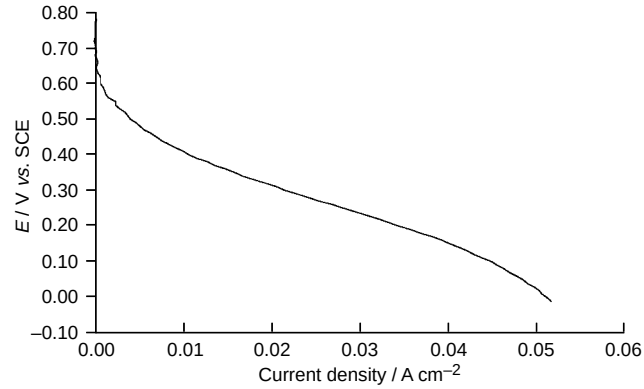

Fig. 3 Polarization curve for oxygen reduction in a C | O_2 (1 atm), PPy/PSS/Pt oxide (0.15 mg Pt cm^{-2}) | Nafion | 1 M H_2SO_4(aq), SCE | Pt cell at ambient temperature. Experimental details are reported elsewhere.[11]

proton exchange membrane fuel cells, despite their low electronic conductivities. However, significantly high conductivities are required to compete with the carbon supported catalysts currently in use.

This work was supported by the Natural Sciences and Engineering Research Council of Canada and Memorial University.

Footnotes and References

* E-mail: ppickup@morgan.ucs.mun.ca

1 *Heterogeneous Catalysis: Principles and Applications*, ed. G. C. Bond, Clarendon Press, Oxford, 2nd edn., 1987.
2 A. F. Diaz and J. Bargon, in *Handbook of Conducting Polymers*, ed. T. A. Skotheim, Marcel Dekker, New York and Basel, 1986, vol. 1, pp. 81–115.
3 X. Ren and P. G. Pickup, *J. Electroanal. Chem.*, 1995, **396**, 359.
4 A. J. Appleby, *Philosophical Transactions of the Royal Society of London Series A—Mathematical Physical and Engineering Sciences*, 1996, **354**, 1681.
5 M. E. G. Lyons, *Analyst*, 1994, **119**, 805.
6 C. S. C. Bose and K. Rajeshwar, *J. Electroanal. Chem.*, 1992, **333**, 235.
7 Z. Qi and P. G. Pickup, *Chem. Mater.*, 1997, in press.
8 M. Salmon, A. F. Diaz, A. J. Logan, M. Krounbi and J. Bargon, *Mol. Cryst. Liq. Cryst.*, 1982, **83**, 265.
9 H. G. Petrow and R. J. Allen, *US Pat.*, 4 044 193, 1977.
10 A. A. Pud, *Synth. Met.*, 1994, **66**, 1.
11 Z. Qi, M. C. Lefebvre and P. G. Pickup, *J. Electroanal. Chem.*, submitted.

Received in Columbia, MO, USA, 22nd October 1997; 7/07648G

Intramolecular coordination of an alkene to a mixed dicyclopentadienyl benzyl zirconium cation studied by NMR spectroscopy

Mikhail V. Galakhov, Georg Heinz and P. Royo*

Departamento de Química Inorgánica, Universidad de Alcalá de Henares, Campus Universitario, E-28871 Alcalá de Henares, Spain

Benzylation of $[Zr(\eta^5\text{-}C_5H_5)\{\eta^5\text{-}C_5H_4SiMe_2(CH_2CH{=}CH_2)\}Cl_2]$ 1 yields $[Zr(\eta^5\text{-}C_5H_5)\{\eta^5\text{-}C_5H_4SiMe_2(CH_2CH{=}CH_2)\}(CH_2C_6H_5)_2]$ 2, which reacts with either $B(C_6F_5)_3$ or $[Ph_3C][B(C_6F_5)_4]$ to generate the same cation, 3^+, which has been fully characterised by ^1H, ^{13}C NMR and ^1H DNMR spectroscopy.

It is generally accepted[1] that a cationic 14-electron alkyl dicyclopentadienylzirconium complex of the type $[ZrCp_2R]^+$ stabilized by coordinative contact with a counter-ion $[R\text{-}MAO]^-$ (MAO = methylalumoxane), $[RB(C_6F_5)_3]^-$ or $[B(C_6F_5)_4]^-$ provides a route to $[ZrCp_2R(alkene)]^+$, a productive, active, cationic polymerization catalyst. Numerous synthetic studies involving the characterization of dicyclopentadienyl alkyl cationic group 4 metal complexes and their catalytic activity in Ziegler–Natta polymerization processes, have recently been reported.[2] Many structural techniques have been used to investigate the formation of cationic species of this type and various theoretical methods[3] have been applied to calculate the kinetic and thermodynamic parameters of their transition states and intermediate species.

However, in spite of the many attempts made,[4] the crucial cationic d^0 metal–alkene complex has only been observed and studied by X-ray diffraction[5] in the zirconium complex $[ZrCp_2(OCMe_2CH_2CH_2CH{=}CH_2)]^+$, in which the alkenic double bond shows a rather weak interaction with the metal center. The isolation of dimethyl titanium[6a] and zirconium[6b] complexes containing the 1-(but-3-enyl)-2,3,4,5-tetramethylcyclopentadienyl ligand has been reported, for which extensive low temperature NMR studies were unable to detect the alkene-coordinated metal complex. An yttrium pentenyl chelate has also been studied,[7] where the exchange between the diastereotopic C_5H_4Me ligands is proposed to occur *via* rapid and reversible alkene dissociation followed by rate limiting inversion of the pyramidal d^0 yttrium center. A related compound reported by Erker[8] was isolated by reaction of the butadiene zirconium complex $[ZrCp_2(C_4H_6)]$ with $B(C_6F_5)_3$, resulting in the formation of a betaine system in which an anionic allyl system is coordinated to the dicyclopentadienyl zirconium cation.

In order to favour alkene coordination we decided to synthesize zirconium complexes containing the more electron-withdrawing di(methyl)(allyl)silyl(cyclopentadienyl) ligand to create a more acidic metal center with a slightly longer and more fluxional pendant chain, owing to the bulkier silicon atom.

As shown in Scheme 1 the dichloro complex $[Zr(\eta^5\text{-}C_5H_5)\{\eta^5\text{-}C_5H_4SiMe_2(CH_2CH{=}CH_2)\}Cl_2]$ **1** was prepared† by reaction of the lithium salt of di(methyl)(allyl)silylcyclopentadiene[9] with stoichiometric amounts of $ZrCpCl_3{\cdot}DME$. Treatment of **1** with $MgBn_2{\cdot}2THF$ yielded the dibenzyl complex **2**.

NMR spectra recorded after mixing 1 equiv. of either $[Ph_3C][B(C_6F_5)_4]$ or $B(C_6F_5)_3$ with 1 equiv. of complex **2** in CD_2Cl_2 at −70 °C demonstrate the formation of the same 14-electron cationic species 3^+. Characteristic methylene resonances of Ph_3CCH_2Ph (δ 3.90) and non-coordinated $[PhCH_2B(C_6F_5)_3]^-$ (δ 2.70, br) were observed, respectively.

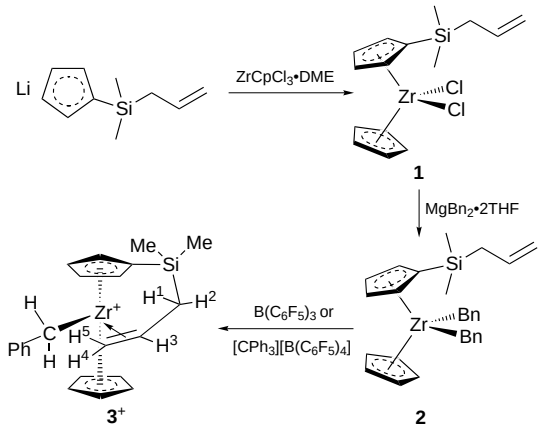

Scheme 1

Stabilization of this 14-electron cationic zirconium species is usually achieved by benzallylic coordination of the benzyl ligand, evidenced by the loss of the C_{2v} symmetry of the phenyl ring and a substantial difference between the ^1H chemical shifts for the two methylenic protons ($\Delta\delta$ = 2.80 ppm) observed[1c] in the solid by X-ray analysis and in solution by NMR spectroscopy at low temperatures. However, this behaviour is not observed in the ^1H NMR spectra of 3^+ at 203 K which shows C_{2v} symmetry for the phenyl ring, an AB spin system (δ_{av} 3.13, $\Delta\delta$ = 0.27 ppm) for the two diastereotopic methylenic protons, two SiMe signals at δ 0.31 and 0.59, and four resonances at δ 5.74, 6.13, 6.35, 7.10 due to the CpSi ring protons, consistent with an asymmetric species. The ^1H NMR spectra of 3^+ did not show a typical vinylic signal between δ 4.9 and 5.6, but instead five new multiplets were observed at δ 1.81, 2.05, 2.13, 2.78, 7.30. Table 1 summarizes the chemical shifts and proton–proton coupling constants for the allyl chain protons of complexes **2** and 3^+.

All of the spin–spin coupling constants for H^3, H^4 and H^5 in complexes **2** and 3^+ are very similar indicating that the sp^2 character of the alkenic carbon atoms is not lost. However the H^3 signal is shifted [$\Delta\delta = \delta(3^+) - \delta(2)$] to low field ($\Delta\delta$ = +1.58 ppm) whereas the terminal H^4 and H^5 signals are displaced to high field ($\Delta\delta$ = −2.08 and −2.83 ppm, respectively); the CH_2Si resonance is split and also displaced to low field ($\Delta\delta$ = +0.38, +0.46 ppm). Similar behaviour is

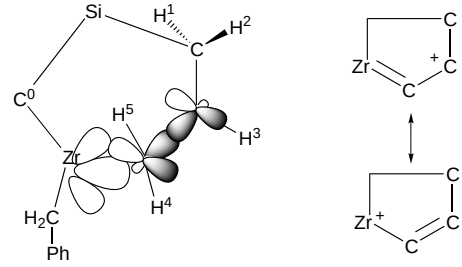

Scheme 2

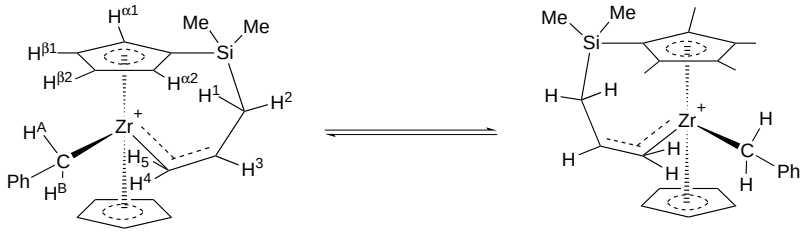

Scheme 3

Table 1 Important ^{1}H NMR data for complexes **2** and **3**$^+$ in CD_2Cl_2 at 203 K

Assignment	δ(SSCC, *J*/Hz) **2**	**3**$^+$
H^1, H^2	1.66 (H^1, H^2–H^3 8.0)	2.05, 2.13 (H^1–H^2 11.5) (H^1–H^3 10.5) (H^2–H^3 5.2)
H^3	5.72 (H^3–H^4 10.5) (H^3–H^5 16.3)	7.30 (H^3–H^4 8.80) (H^3–H^5 16.5)
H^4	4.86 (H^4–H^5 3.8)	2.78 (H^4–H^5 4.0)
H^5	4.83	1.81

observed in the ^{13}C NMR spectra which show $\Delta\delta(CH{=}CH_2)$ = +36.2, $\Delta\delta(CH{=}CH_2)$ = −22.7, $\Delta\delta(CH_2Si)$ = +2.8 and $\Delta\delta(C_{Cp})$ = −3.1 ppm. Displacement of the terminal alkenic CH_2 moiety signals to high field is consistent with its coordination to the metal atom. This interaction is stronger than that reported by Wu and Jordan[5] and may be interpreted as the result of the interaction of the σ-bonding alkene orbital with the vacant $2a_1$ zirconium orbital and simultaneous overlapping of the HOMO π alkene orbital with the vacant zirconium orbital of the same symmetry, b_2.

As shown in Scheme 2 these interactions result in delocalized electron density in the Zr–C–C system, similar to that observed for classical allyl cations, which is favoured by the known silicon effect[9] and can be described in terms of the resonance structures of Scheme 2, where the terminal alkenic carbon is in a well known pentacoordinate situation.[10] This description is consistent with the observed displacement of the CH= and $SiCH_2$ resonances to low field and of CH_2= resonances to high field.

Variable temperature ^{1}H NMR spectra show dynamic behaviour which implies an interchange between the signals of the CH_2Ph, CH_2Si, $(CH_3)_2Si$ and the $H^{\alpha1}$–$H^{\alpha2}$ and $H^{\beta1}$–$H^{\beta2}$ protons of the C_5H_4R ring, with little exchange in the Zr–C–C system. The assignment of the $H^{\alpha1}$–$H^{\alpha2}$ and $H^{\beta1}$–$H^{\beta2}$ signals was made from the results of saturation transfer experiments at 253 K and the spin–lattice relaxation time T_1 values measured at −213 K ($H^{\alpha1}$: δ 6.30, T_1 = 1.67 s; $H^{\alpha2}$: δ = 6.10, T_1 = 1.61 s; $H^{\beta1}$: δ = 7.10, T_1 = 0.96 s; $H^{\beta2}$: δ = 5.70, T_1 = 1.26 s). The signal at δ 7.10 is assigned to the $H^{\beta1}$ proton located near the C_5H_5 moiety since is well known that proton relaxation times depend mainly on the number of adjacent protons and their distances. The $SiCH_2$ resonance is observed at 263 K as one doublet (^3J 8.3 Hz) due to spin–spin coupling with H^3. Coalescences of the $SiMe_2$ and CH_2Ph resonances are observed at 253 K with the same $\Delta G^{\ddagger}$ = 11.7 kcal mol^{-1} (1 cal = 4.184 J) calculated for the collapse of two equally populated singlets and for an AB spin system, respectively. This indicates that both are associated with a unique dynamic process involving interconversion between two enantiomers through a transition state with C_s symmetry.

The kinetic parameters for the process shown in Scheme 3 ($\log A$ = 14.4 ± 0.5, E_a = 13.4 ± 0.54 kcal mol^{-1}, $\Delta H^{\ddagger}$ = 12.9 ± 0.53 kcal mol^{-1}, $\Delta S^{\ddagger}$ = 5.0 ± 2.3 cal K^{-1} mol^{-1} and $\Delta G^{\ddagger}_{298\,K}$ = 11.4 kcal mol^{-1}) obtained from ^{1}H DNMR data for exchange of the $SiMe_2$ groups are consistent with an intramolecular process with negligible variation of entropy and are in good agreement with theoretical data reported by Bercaw and coworkers[11] for $[MCp_2Me]^+$.

Financial support of our work by DGICTY (Project PB-92/0178-C) and CAM(I+D0034/94) is gratefully acknowledged. G. H. is grateful to the University of Alcalá for financial support and the Alexander von Humboldt-Stiftung for a fellowship.

Footnotes and References

* E-mail: proyo@inorg.alcala.es

† Complex **1** was isolated *via* treatment of a THF solution of $(C_5H_5)SiMe_2CH_2CH{=}CH_2$ (8.46 g, 42.0 mmol) with a 1.6 M solution of buthyllithium in hexane (28 ml, 45.0 mmol) for 3 h, and addition of the resulting solution to a suspension of $Zr(C_5H_5)Cl_3$·DME (14.9 g, 42 mmol) in THF (80 ml) and stirring for 18 h at room temp. Complex **2** was prepared as a yellow solid (yield 84%) by stirring a mixture of **1** (853 mg, 2.18 mmol) and $MgBn_2$·2THF (920 mg, 2.62 mmol) in diethyl ether (100 ml) for 18 h at room temp.

1 (*a*) R. F. Jordan, *Adv. Organomet. Chem.*, 1991, **32**, 3235; (*b*) H. H. Brintzinger, D. Fischer, R. Mülhaupt, B. Rieger and R. M. Waymouth, *Angew. Chem., Int. Ed. Engl.*, 1995, **34**, 1143; (*c*) M. Bochmann, *J. Chem. Soc., Dalton Trans.*, 1996, 255.
2 X. Yang, C. L. Stern and T. J. Marks, *J. Am. Chem. Soc.*, 1994, **116**, 10 015; L. Jia, X. Yang, C. Stern and T. J. Marks, *Organometallics*, 1994, **13**, 3755; J. I. Amor, T. Cuenca, M. Galakhov and P. Royo, *J. Organomet. Chem.*, 1995, **497**, 127; L. Jia, X. Yang, A. Ishihara and T. J. Marks, *Organometallics*, 1995, **14**, 3135; Y.-X. Chen, C. L. Stern, S. Yang and T. J. Marks, *J. Am. Chem. Soc.*, 1996, **118**, 12 451; A. H. Horton, *Organometallics*, 1996, **15**, 2675; T. L. Tremblay, S. W. Ewart, M. J. Sarsfield and M. C. Baird, *Chem. Commun.*, 1997, 831; T. Cuenca, M. Galakhov, G. Jiménez, E. Royo, P. Royo and M. Bochmann, *J. Organomet. Chem.*, 1997, in press; J. I. Amor, T. Cuenca, M. Galakhov, P. Gómez-Sal, A. Manzanero and P. Royo, *J. Organomet. Chem.*, 1997, in press; L. Jia, X. Yang, C. L. Stern and T. J. Marks, *Organometallics*, 1997, **16**, 842; A. D. Horton and A. G. Orpen, *Organometallics*, 1992, **11**, 8; C. Pellecchia, A. Immirzi, A. Grassi and A. Zambelli, *Organometallics*, 1993, **12**, 4473.
3 H. Weiss, M. Ehrig and R. Ahlrichs, *J. Am. Chem. Soc.*, 1994, **116**, 4919; T. K. Woo, L. Fan and T. Ziegler, *Organometallics*, 1994, **13**, 2252; J. C. W. Lohrenz, T. K. Woo and T. Ziegler, *J. Am. Chem. Soc.*, 1995, **117**, 12 793; P. Margl, J. C. W. Lohrenz, T. Ziegler and P. E. Blöchl, *J. Am. Chem. Soc.*, 1996, **118**, 4434.
4 J. Okuda, *Nachr. Chem. Tech: Lab.*, 1996, **44**, 135.
5 Z. Wu and R. F. Jordan, *J. Am. Chem. Soc.*, 1995, **117**, 5867.
6 (*a*) J. Okuda, K. E. du Plooy and P. J. Toscano, *J. Organomet. Chem.*, 1995, **495**, 195; (*b*) K. A. Butakoff, D. A. Lemenovskii, P. Mountford, L. G. Kuz'mina and A. V. Churakov, *Polyhedron*, 1996, **15**, 489.
7 C. P. Casey, S. L. Hallenbeck, J. M. Wright and C. R. Landis, *J. Am. Chem. Soc.*, 1997, **119**, 9690.
8 B. Temme, G. Erker, J. Karl, R. Luftmann, R. Fröhlich and S. Kotila, *Angew. Chem.*, 1995, **107**, 1867.
9 J. B. Lambert, *Tetrahedron*, 1990, **46**, 2677.
10 F. J. Fernández, P. Gómez-Sal, A. Manzanero, P. Royo, H. Jacobsen and H. Berke, *Organometallics*, 1997, **16**, 1553.
11 E. P. Bierwagen, J. E. Bercaw and W. A. Goddard, III, *J. Am. Chem. Soc.*, 1994, **116**, 1481.

Received in Liverpool, UK, 8th July 1997; 7/04886F

$Sc(OTf)_3$-Catalyzed three-component reactions of aldehydes, amines and allyltributylstannane in micellar systems. Facile synthesis of homoallylic amines in water

Shū Kobayashi,* Tsuyoshi Busujima and Satoshi Nagayama

Department of Applied Chemistry, Faculty of Science, Science University of Tokyo (SUT), and CREST, Japan Science and Technology Corporation (JST), Kagurazaka, Shinjuku-ku, Tokyo 162, Japan

Three-component reactions of aldehydes, amines and allyltributylstannane proceeded smoothly in water without using any organic solvents, in the presence of a small amount of scandium trifluoromethanesulfonate [$Sc(OTf)_3$] and sodium dodecylsulfate (SDS), to afford the corresponding homoallylic amines in high yields.

The reaction of imines with allyltributylstannane provides a useful route for the synthesis of homoallylic amines.[1] The reaction is generally carried out in the presence of a Lewis acid in organic solvents under strict anhydrous conditions,[2] because most imines, Lewis acids and organotin reagents used are hygroscopic and easily decompose in the presence of even a small amount of water.[3] On the other hand, the utility of aqueous reactions is now generally recognized,[4] and development of carbon–carbon bond-forming reactions that can be carried out in aqueous media is one of the most challenging tasks in organic synthesis. It was believed, however, that the above reaction would remain difficult to perform in water because of the use of water-sensitive imines, Lewis acids and organotin reagents. Recently, we have found that scandium trifluoromethanesulfonate [$Sc(OTf)_3$]-catalyzed aldol reactions[5] and allylations of aldehydes[6] proceed smoothly in the presence of a small amount of a surfactant in water. It was indicated that micelles formed in these reactions and that the excellent hydrophobic reaction fields created realized the aqueous reactions. In the course of our investigations to develop new synthetic reactions in micellar systems, we have found that three-component reactions of aldehydes, amines and allyltributylstannane proceed smoothly in micellar systems using $Sc(OTf)_3$ as a Lewis acid catalyst.†

The reaction of benzaldehyde, aniline and allyltributylstannane was chosen as a model, and several sets of reaction conditions were examined. While the reaction proceeded sluggishly in the presence of $Sc(OTf)_3$ without sodium dodecylsulfate (SDS) or in the presence of SDS without $Sc(OTf)_3$, a 77% yield of the desired homoallylic amine was obtained in the presence of both $Sc(OTf)_3$ and SDS. It was suggested that an imine formed from the aldehyde and the amine rapidly reacted with allyltributylstannane to afford the desired adduct. We also examined the effect of the amount of $Sc(OTf)_3$ and SDS used and the results are summarized in Table 1. When a 70 mM SDS solution (0.4 equiv.) was used, the desired homoallylic amine was obtained in a 79% yield, and the yield remained unchanged with increasing amounts of SDS.‡ On the other hand, it was found that reduction of the amount of $Sc(OTf)_3$ decreased the yield, and that a prolonged reaction time increased the yield. Finally, a satisfactory yield was obtained when 0.2 equiv. $Sc(OTf)_3$ and 35 mM (0.2 equiv.) SDS were used and the reaction was carried out at room temp. for 20 h. No homoallylic alcohol (an adduct between the aldehyde and allyltributylstannane) was produced under these conditions.

Several examples of the present three-component reactions of aldehydes, amines and allyltributylstannane are shown in Table 2. The reactions proceeded smoothly in water without using any organic solvents in the presence of a small amount of $Sc(OTf)_3$ and SDS, to afford the corresponding homoallylic amines in high yields. Not only aromatic aldehydes but also aliphatic, unsaturated and heterocyclic aldehydes worked well. It is known that severe side reactions occur to decrease yields in the reactions of imines having α-protons with allyltributylstannane.[1] It should be noted that aliphatic aldehydes, especially non-branched aliphatic aldehydes, reacted smoothly under these conditions to afford the homoallylic amines in high yields. In all cases, no aldehyde adducts (homoallylic alcohols) were ob-

Table 1 Effect of the amounts of $Sc(OTf)_3$ and SDS[a]

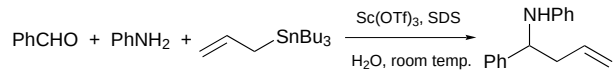

$Sc(OTf)_3$/ mol%	SDS/mM	*t*/h	Yield (%)
20	—	4	trace
—	105[b]	4	trace
20	105	4	77
20	18	4	60
20	35	4	68
20	70	4	79
20	140	4	76
10	35	4	52
5	35	4	37
20	35	10	80
20	35	20	83

[a] PhCHO (1.3 equiv.), $PhNH_2$ (1.0 equiv.) and allyltributylstannane (1.5 equiv.). [b] 0.6 equiv.

Table 2 Three-component reactions of aldehydes, amines and allyltributylstannane

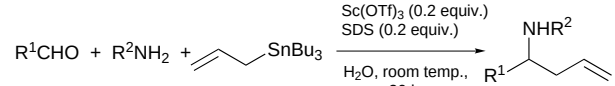

R^1	R^2	Yield (%)
Ph	Ph	83
Ph	*p*-ClPh	90
Ph	*p*-MeOPh	81
p-ClPh	*p*-ClPh	70
2-Furyl	*p*-ClPh	67 (71,[a] 82[c])
2-Thienyl	*p*-ClPh	67[a] (78[c])
$Ph(CH_2)_2$	*p*-ClPh	78
$Me(CH_2)_7$	*p*-ClPh	66
c-C_6H_{11}	Ph	80 (83[b])
c-C_6H_{11}	*p*-MeOPh	74
PhCO	*p*-ClPh	71 (83[c])
(*E*)-PhCH=CH	*p*-ClPh	80 (82[a])

[a] SDS, 0.4 equiv. [b] 0.6 equiv. [c] 1.0 equiv.

tained. It was suggested that the imine formation from aldehydes and amines was very fast in the presence of both $Sc(OTf)_3$ and SDS,[8] and that the selective activation of imines rather than aldehydes was achieved using $Sc(OTf)_3$ as a catalyst.[9] It is also noteworthy that using a small amount of a surfactant created efficient hydrophobic reaction fields[10] and achieved the dehydration and addition reactions in water.

A typical experimental procedure is as follows. To a 35 mM water solution of SDS (3 ml) and $Sc(OTf)_3$ (0.1 mmol) were added the amine (0.5 mmol), allyltributylstannane (0.75 mmol) and the aldehyde (0.65 mmol) successively, and the mixture was stirred at room temp. After 20 h, the mixture was diluted with water and ethyl acetate, and Amberlite IRA96SB was added. After being stirred for 10 min, the resin was filtered and the filtrate was extracted with ethyl acetate. The combined organic layers were dried, filtered and concentrated. The crude adduct was purified by column chromatography on silica gel to afford the pure desired homoallylic amine.

In summary, we have developed $Sc(OTf)_3$-catalyzed three-component reactions between aldehydes, amines and allyltributylstannane in micellar systems. The reactions proceed smoothly in water without using any organic solvents, to afford the corresponding homoallylic amines in high yields. In addition to the synthetic utility of these reactions, it should be noted that reactions using water-sensitive substrates have been successfully carried out in water under the present reaction conditions. Further progress is expected in this field and investigations on these micellar systems including mechanistic aspects are now underway in our laboratories.

This work was partially supported by a Grant-in-Aid for Scientific Research from the Ministry of Education, Science, Sports, and Culture, Japan, and a SUT Special Grant for Research Promotion. S. N. thanks the JSPS fellowship for Japanese Junior Scientists.

Footnotes and References

* E-mail: skobayas@ch.kagu.sut.ac.jp

† We found that $Sc(OTf)_3$, $Y(OTf)_3$ and $Ln(OTf)_3$ (Ln = La, Ce, Pr, Nd, Sm, Eu, Gd, Tb, Dy, Ho, Er, Tm, Yb, Lu) are stable Lewis acids in water (ref. 7).

‡ In some other substrates, yields were improved a little with increasing amounts of SDS (see Table 2).

1 Review: Y. Yamamoto and N. Asao, *Chem. Rev.*, 1992, **93**, 2207.
2 G. E. Keck and E. J. Enholm, *J. Org. Chem.*, 1985, **50**, 147; Y. Yamamoto, T. Komatsu and K. Maruyama, *J. Org. Chem.*, 1985, **50**, 3115; M. A. Ciufolini and G. O. Spencer, *J. Org. Chem.*, 1989, **54**, 4739; C. Bellucci, P. G. Cozzi and A. Umani-Ronchi, *Tetrahedron Lett.*, 1995, **36**, 7289; M. Yasuda, Y. Sugawa, A. Yamamoto, I. Shibata and A. Baba, *Tetrahedron Lett.*, 1996, **37**, 5951.
3 *Cf.* P. A. Grieco and A. Bahsas, *J. Org. Chem.*, 1987, **52**, 1378; H. Nakamura, H. Iwama and Y. Yamomoto, *J. Am. Chem. Soc.*, 1996, **118**, 6641.
4 C.-J. Li, *Chem. Rev.*, 1993, **93**, 2023; A. Lubineau, J. Ange and Y. Queneau, *Synthesis*, 1994, 741; *Structure and Reactivity in Aqueous Solution*, ed. C. J. Cramer and D. G. Truhlar, ACS, Washington, DC, 1994.
5 S. Kobayashi, T. Wakabayashi, S. Nagayama and H. Oyamada, *Tetrahedron Lett.*, 1997, **38**, 4559.
6 S. Kobayashi, T. Wakabayashi and H. Oyamada, *Chem. Lett.*, 1997, 831.
7 S. Kobayashi, *Synlett*, 1994, 689.
8 S. Kobayashi and H. Ishitani, *J. Chem. Soc., Chem. Commun.*, 1995, 1379.
9 S. Kobayashi and S. Nagayama, *J. Org. Chem.*, 1997, **62**, 232.
10 *Cf.* J. H. Fendler and E. J. Fendler, *Catalysis in Micellar and Macromolecular Systems*, Academic Press, London, 1975; *Mixed Surfactant Systems*, ed. by P. M. Holland and D. N. Rubingh, ACS, Washington, DC, 1994; *Surfactant-Enhanced Subsurface Remediation*, ed. by D. A. Sabatini, R. C. Knox and J. H. Harwell, ACS, Washington, DC, 1995.

Received in Cambridge, UK, 5th September 1997; 7/06489E

Stereospecific intramolecular proton transfer in the cyclization of geranylgeranyl diphosphate to (−)-abietadiene catalyzed by recombinant cyclase from grand fir (*Abies grandis*)

Matthew M. Ravn,[a] Robert M. Coates,*[a] Reinhard Jetter[b] and Rodney B. Croteau[c]

[a] *Department of Chemistry, University of Illinois, 600 S. Mathews Avenue, Urbana, IL 61801, USA*
[b] *Lehrstuhl für Botanik der Universität Würzburg, Mittlerer Dallenbergweg 64, D-97082 Würzburg, Germany*
[c] *Institute of Biological Chemistry, Washington State University, Pullman, WA 99164-6340, USA*

The cyclization–rearrangement of deuterated geranylgeranyl diphosphate (GGPP) and (+)-copalyl diphosphate (CPP) catalyzed by recombinant (−)-abietadiene synthase from grand fir proceeds with intramolecular proton transfer from C-19 of GGPP, and from the C-17 pro-*E* position of CPP, to form the C-16 *pro-S* methyl group of (−)-abietadiene.

(−)-Abietic acid **3** is a major component of oleoresin exuded by conifer species, including lodgepole pine (*Pinus contorta*) and grand fir (*Abies grandis*),[1] as a defensive secretion against insect and pathogen attack. This diterpenoid resin acid is biosynthesized by cyclization of geranylgeranyl diphosphate (GGPP, **1**) to (−)-abietadiene **2** and sequential oxidations of the C-18-methyl group (Scheme 1).[2] (−)-Abietadiene synthase (AS) was purified and identified as an 80 kDa protein with general characteristics typical for terpenoid cyclases.[3]

AS from grand fir yielded internal amino acid sequence information from which a PCR-based cloning strategy was developed.[4] A 286 base-pair insert was isolated that encoded an 868-amino acid preprotein bearing a putative plastidial transit peptide. The cDNA encoded preprotein was functionally expressed in *Escherichia coli*, thereby confirming that a single enzyme catalyzes this multistep cyclization. Recent experiments with the recombinant enzyme (rAS) demonstrated that (+)-copalyl diphosphate (CPP, **4**) could serve as an efficient alternative precursor of **2**† whereas none of the four pimaradiene isomers tested were converted to abietadiene. Here we report the use of deuterated substrates to examine the mechanism of the rAS cyclization.

The synthesis of the labelled substrates [19-$^2H_3$]-**1** and (17*E*)-[17-$^2H_1$]-**4** followed analogous procedures in the literature. 19-Nor-7-methoxycarbonylgeranylgeranyl benzyl ether prepared by *Z*-selective phosphonate condensation[5] was converted to [19-$^2H_3$]geranylgeraniol by (a) AlD_3; (b) MsCl, Et_3N, CH_2Cl_2; (c) $LiBEt_3D$, THF; (d) Li, NH_3. (17*E*)-[17-$^2H_1$]Copalol was obtained from (17*E*)-17-bromocopalyl THP ether by lithiation, deuterolysis and deprotection.[6] Diphosphate esters were formed by standard methods[7] and were characterized by ^1H and ^{31}P NMR spectra. Incubation of these labelled substrates and [1-$^2H_2$]-**1** with rAS‡ gave (15*S*)-[14,16-$^2H_2$]-, (15*S*)-[16-$^2H_1$]- and (15*S*)-[16-$^2H_2$]-**2** respectively, with one deuterium located exclusively in the upfield methyl doublet of the isopropyl group according to ^1H NMR integrations and broadening from deuterium coupling (Scheme 2).§ No loss of the deuterium transferred to C-16 could be observed by GC–MS (≤1%). The absence of any detectable [$^2H_1$]abietadiene from a cross-over experiment with [19-$^2H_3$]-**1** and unlabelled **1** establishes that proton or deuteron transfer occurs within one catalytic cycle and rules out an enzyme-bound pimara-7,15-diene intermediate.

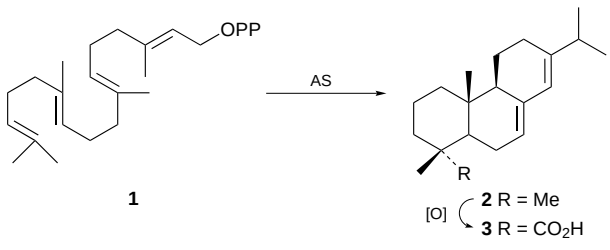

Scheme 1

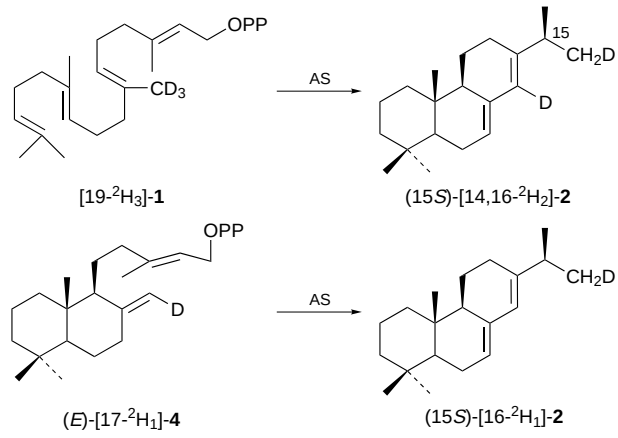

Scheme 2

NMR assignments for the isopropyl methyl groups required unambiguous synthesis of stereospecifically labelled **2** (Scheme 3). Reaction of the tricyclic 8(14)-en-13-one[8] with ethyl lithioacetate·$CeCl_3$ complex provided a mixture of β-hydroxy esters (91%, 3 : 1 α-OH : β-OH) which underwent dehydration (HCl, EtOH, reflux) and saponification to give 7,13-diene acid **5** (65%).¶ Methylation of the ψ-ephedrine amide **6** afforded two diastereomers (94 : 6). The major isomer is assigned the 15*S*

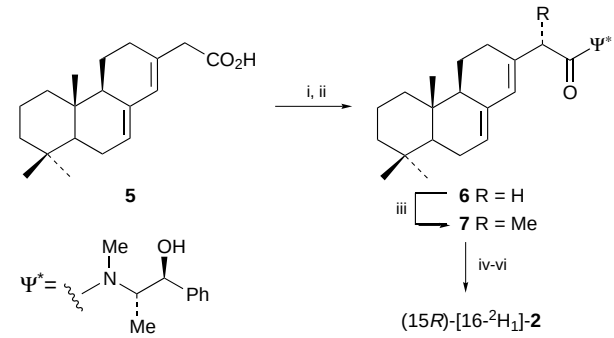

Scheme 3 *Reagents and conditions*: i, $(ClCO)_2$, PhH; ii, (*S*,*S*)-pseudoephedrine, pyridine, THF, 84% from **5**; iii, LDA, LiCl, THF, −78 °C; MeI, −78 °C, 92%; iv, $LiBH_3NH_2$, THF, 73%; v, MsCl, Et_3N, CH_2Cl_2, 0 °C; vi, $LiEt_3BD$, THF, 0 °C, 88% from **7**

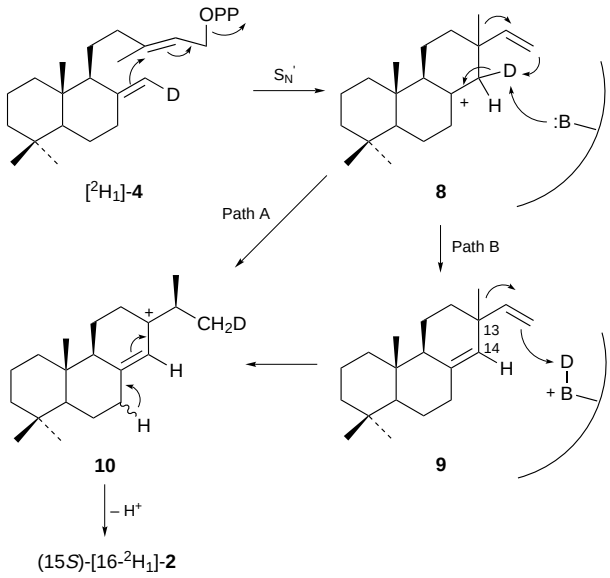

Scheme 4

configuration (**7**) based on the established stereodirecting influence of this chiral auxiliary.[9] $LiBH_3NH_2$ reduction,¶ mesylation and $LiBEt_3D$ displacement gave (15*R*)-[16-$^2H_1$]-**2** (64%). The ^1H NMR spectrum shows deuterium coupling and a characteristic upfield isotope shift for the downfield isopropyl methyl group of unlabelled **2** which is therefore assigned the *pro-R* configuration.§ It follows that rAS effects intramolecular proton transfer to the terminal carbon of the vinyl group which becomes the *pro-S* methyl, and that the methyl migration occurs to the *si* face at C-15 of the putative pimara-9(14),15-diene intermediate.

Intramolecular proton transfers to enzyme-bound polyolefin intermediates have been observed previously in pentalenene and taxadiene biosynthesis.[10] The occurrence of an analogous proton transfer to form the *pro-S* methyl of a presumptive abietadiene intermediate was inferred from the labelling pattern of ginkgolide A biosynthesized from [6,6,6-$^2H_3$]mevalonate in *Ginkgo biloba* cell cultures.[11] The same *si* face selectivity for the methyl migration presumed to occur in the biosynthesis of 12-*O*-methylferruginol and cryptotanshinone was deduced from label distributions resulting from incorporation experiments with [*U*-^{13}C]glucose in *Salvia miltiorhiza* cell cultures.[12]

Two plausible mechanisms for this novel cyclization–rearrangement are presented in Scheme 4. S_N' cyclization of **4** analogous to those involved in the biosynthesis of related pimarane and kaurane diterpenes[6,13] gives the pimaren-8-yl carbocation **8** which can undergo either intramolecular C-14-to-C-16 hydrogen transfer (Path A) or enzyme-mediated proton elimination to form a pimara-8(14),15-diene intermediate **9** that re-incorporates the proton at C-16 (Path B). Further research to elucidate the mechanism of the cyclization–rearrangement, the nature of the intermediate(s), and the identity of the participating enzyme base, if any, is underway.

Footnotes and References

* E-mail: coates@aries.scs.uiuc.edu

† R. Jetter and R. Croteau, manuscript in preparation.

‡ Enzyme incubations conditions: HEPES buffer (30 mM, pH 7.2), rAS (100 μl), dithiothreitol (5 mM), $MgCl_2$ (7.5 mM), $MnCl_2$ (20 μM), 5% glycerol (v/v) and GGPP (20 μM) in 1 ml.

§ *Selected ^1H NMR (500 MHz, C_6D_6 J/Hz) data* for isopropyl methyls of (15*S*)-[14,16-$^2H_2$]-**2**: δ_H 1.003 (br d, *J* 6.8, ≈2H, CDH_2), 1.030 (d, *J* 6.8 Hz, 3 H, CH_3). For (15*R*)-[16-$^2H_1$]-**2**: δ_H 1.014 (br d, *J* 6.8, ≈2 H, CDH_2), 1.020 (d, *J* 6.8, 3 H, CH_3). For **2**: δ_H 1.020 (d, *J* 6.9, 3 H, CH_3) and 1.031 (d, *J* 6.9, 3 H, CH_3). Observed deuterium isotope shift $\Delta\delta$ = −0.017 ppm in each case.

¶ *Selected data* for **5** (di-*n*-amylamine salt): mp, 64–65 °C; λ_{max} 244 nm (ε 19 600 M^{-1} cm^{-1}). For **5**: δ_H(500 MHz, $CDCl_3$, *J*/Hz) 5.48 (dt, *J* 5.0, 2.5, 1 H, C-7 =C*H*), 5.90 (s, 1 H, C-14 =C*H*). For (15*S*)-abietadien-16-ol: δ_H(500 MHz, $CDCl_3$, *J*/Hz) 0.99 (d, *J* 7.0, 3 H, CHCH_3), 3.47 (dABq, *J* 7.8, 10.4, $\Delta\nu_{AB}$ 19 Hz, 2 H, CH_2OH).

1 E. J. Soltes, in *Naval Stores; Production, Chemistry, Utilization*, ed. D. F. Zinkle and J. Russell, Pulp Chemicals Assoc., New York, 1989, pp. 261–345.
2 C. Funk and R. Croteau, *Arch. Biochem. Biophys.*, 1994, **308**, 258.
3 R. E. LaFever, B. Stofer Vogel and R. Croteau, *Arch. Biochem. Biophys.*, 1994, **313**, 139.
4 B. Stofer Vogel, M. R. Wildung, G. Vogel and R. Croteau, *J. Biol. Chem.*, 1996, **271**, 23 262.
5 W. C. Still and C. Gennari, *Tetrahedron Lett.*, 1983, **41**, 4405.
6 R. M. Coates and P. L. Cavender, *J. Am. Chem. Soc.*, 1980, **102**, 6358.
7 A. I. Meyers and E. W. Collington, *J. Org. Chem.*, 1971, **36**, 3044; A. B. Woodside, Z. Huang and C. D. Poulter, *Org. Synth.*, 1993, Coll. vol. VIII, 616.
8 H. Wu, H. Nakamura, J. Kobayashi and M. Kobayashi, *Bull. Chem. Soc. Jpn.*, 1986, **59**, 2495.
9 A. G. Myers, J. L. Gleason, T. Yoon and D. W. Kang, *J. Am. Chem. Soc.*, 1997, **119**, 656.
10 D. E. Cane and S. W. Weiner, *Can. J. Chem.*, 1994, **72**, 118; X. Lin, M. Hezari, A. E. Koepp, H. G. Floss and R. Croteau, *Biochemistry*, 1996, **35**, 2968.
11 M. K. Schwarz and D. Arigoni; unpublished results cited in Dissertation 10951, ETH Zurich, Switzerland, 1994.
12 Y. Tomita, M. Annaka and Y. Ikeshiro, *J. Chem. Soc., Chem. Commun.*, 1989, 108; Y. Tomita and Y. Ikeshiro, *J. Chem. Soc., Chem. Commun.*, 1987, 1311.
13 C. A. West, in *Biosynthesis of Isoprenoid Compounds*, ed. J. W. Porter and S. L. Spurgeon, Wiley, New York, 1981, vol. 1, pp. 375–411.

Received in Corvallis, OR, USA, 22nd August 1997; 7/06202H

A 3 : 1 mixed aggregate of diphenylamidolithium with lithium chloride: crystal structure of [$(Ph_2NLi)_3LiCl\cdot 3tmen$] (tmen = *N,N,N′,N′*-tetramethylethylenediamine)

William Clegg,[a] Andrew J. Edwards,[a] Francis S. Mair*[b] and Philip M. Nolan[c]

[a] *Department of Chemistry, University of Newcastle, Newcastle upon Tyne, UK NE1 7RU*
[b] *Department of Chemistry, UMIST, PO Box 88, Manchester, UK M60 1QD*
[c] *Department of Chemistry, University of Dublin, Trinity College, Dublin 2, Republic of Ireland*

Demonstrating a new structural type in mixed aggregate chemistry, a 3 : 1 mixture of Ph_2NLi and LiCl with 3 equiv. of *N,N,N′,N′*-tetramethylethylenediamine exists in toluene and in the solid state as a Ph_2NLi/LiCl mixed 'dimer' and a $(Ph_2NLi)_2$ homodimer linked only by a Li–Cl coordinate bond, as determined by NMR spectroscopy and X-ray crystallography.

There has been growing interest in the effect of added salts in a wide variety of chemical reactons, focused by a recent treatise on the subject.[1] One of the most intensely investigated phenomena has been the effect of added lithium halides on reactions involving lithium amides.[2] Mixed aggregates have been implicated by NMR[3] and, more recently, by crystallographic,[4] and *ab initio* computational[4d,f,5] analysis. So far for mixtures of lithium amides and lithium halides, of particular importance in modern enolisation reaction methodology, there have been examples of 1 : 1 {the 5,10-dihydrophenazine derivative[4a] [$LiCl\cdot Li(NC_{12}H_8NH)\cdot 4thf$] and the 2,2,6,6-tetramethylpiperidine (tmp) derivative[4d] [$LiBr\cdot Li(tmp)\cdot 3thf$]} and 2 : 1 {*e.g.* [$LiCl\cdot 2LDA\cdot 2tmen$] and isostructural analogues[4b,c,d,f]} aggregates. For 3 : 1 amide/halide aggregates there is no prior evidence; the only structurally characterised 3 : 1 mixed aggregate has been the organolithium heterocubane [$LiBr\cdot 3LiPh\cdot 3thf$], a structure in which the halide occupies one corner of the cube,[6] in retrospect unsurprising in view of the isostructural homo-aggregates $[LiBr\cdot Et_2O]_4$ and $[LiPh\cdot Et_2O]_4$.[7,6] While halides and carbanions are often associated with the ring stacking motif, inclusion of amides in the aggregates precludes this structural type.[8] Halides have previousl been incorporated into ladder structures,[4] including a very recent tetralithium butterfly cluster with μ_4 bromide,[4e] but we here report an alternative way for two dimers to associate *via* a single contact.

We chose the diphenylamido system as the basis for an extensive study of mixed aggregation phenomena since it is a simple model secondary amide amenable to crystallographic study. Prior to our work, only a single structure involving Ph_2NLi had been reported, that of a monomeric 12-crown-4 complex.[9] However, a thorough NMR spectroscopic investigation of the Ph_2NLi/LiBr system was also in the literature. This revealed evidence only of mixed dimeric aggregates.[3a] As this manuscript was in preparation, a further structure report appeared involving Ph_2NLi in a large aggregate with Bu^nLi and dilithiated Ph_2NH.[10]

Crystals of [$(Ph_2NLi)_3LiCl\cdot 3tmen$] **1** were grown from a toluene solution prepared from Ph_2NH, Ph_2NH_2Cl and Bu^nLi in the presence of tmen.† This hydrohalide *in situ* route has proved advantageous over 'direct' or 'ammonium salt' routes in the past for generation of crystalline mixed aggregates.[4b,d,f] Structure determination by X-ray crystallography‡ revealed the elegantly simple structure depicted in Fig. 1. Perhaps the simplest way of rationalising the molecule is to consider it as an adduct of a homodimeric amidolithium and a 1 : 1 mixed dimer. Taken in this way the mixed dimer may be compared with [$LiCl\cdot Li(NC_{12}H_8NH)\cdot 4thf$] in which each lithium is four-coordinate,[4a] as in **1**, but in which the chloride was only two-coordinate. In **1** the chloride is μ_3, as it is in [$LiCl\cdot 2LDAP\cdot 2tmen$],[4b] but in a Y-shaped rather than a T-shaped conformation. This near-planar (sum of angles 356°) Y-shape is rare for chloride. The closest analogy structurally lies in $[(LiCl)_4(pmdeta)_3]$ (pmdeta = *N,N,N′,N″,N″*-pentamethyldiethylenetriamine),[11] where the sum of angles around the three-coordinate chloride is 337°. This structure also provides the closest analogy to the two linked rhomboids of **1**. However, in $[(LiCl)_4(pmdeta)_3]$ the link is supported by a bridging pmdeta ligand.[11]

A more intriguing view of the molecule might be as a frozen analogue of a postulated intermediate in the fluxion of [$LiCl\cdot 2LDA\cdot 2tmen$] in toluene solution.[4f] In this way, inclusion of a further amidolithium unit converts this fluxion intermediate, in which chloride acts as a fulcrum around which the other ligands rotate, into a stable geometry. The retention of the double-ring structure of **1** in solution is proven by the concentration-invariant observation of three signals in a 2 : 1 : 1 ratio in the ^7Li NMR spectrum in toluene. This view of an extra amidolithium unit trapping an opened 2 : 1 aggregate is also relevant to enolisation mechanisms of 2 : 1 LDA/LiCl ag-

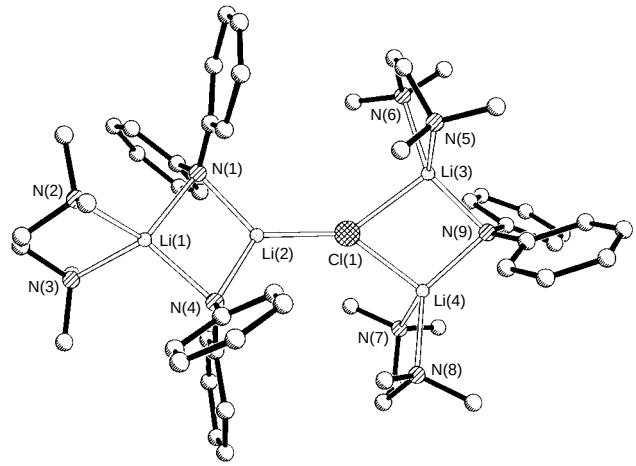

Fig. 1 Molecular structure of compound **1**. Selected bond lengths (Å) and angles (°): Cl(1)–Li(2) 2.242(6), Cl(1)–Li(3) 2.377(7), Cl(1)–Li(4) 2.378(7), Li(1)–N(4) 2.140(7), Li(1)–N(1) 2.151(8), Li(1)–N(3) 2.169(7), Li(1)–N(2) 2.220(7), Li(2)–N(4) 2.004(9), Li(2)–N(1) 2.106(8), Li(3)–N(9) 2.068(8), Li(3)–N(5) 2.130(8), Li(3)–N(6) 2.168(9), Li(4)–N(9) 2.088(7), Li(4)–N(8) 2.135(9), Li(4)–N(7) 2.165(8), Li(2)–Cl(1)–Li(3) 135.9(3), Li(2)–Cl(1)–Li(4) 144.0(3), Li(3)–Cl(1)–Ll(4) 75.8(2), N(4)–Li(1)–N(1) 98.1(3), N(4)–Li(2)–N(1) 107.5(3), N(4)–Li(2)–Cl(1) 127.5(4), N(1)–Li(2)–Cl(1) 124.9(4), N(9)–Li(3)–Cl(1) 97.7(3), N(9)–Li(4)–Cl(1) 97.1(3), Li(2)–N(1)–Li(1) 76.9(3), Li(2)–N(4)–Li(1) 77.4(3), Li(2)–N(9)–Li(4) 89.3(3).

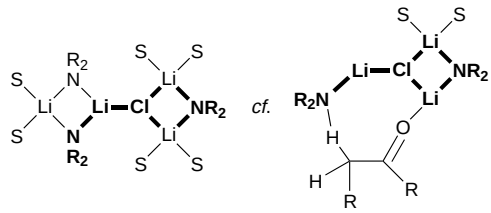

Scheme 1

gregates in solution: it has been proposed that such aggregates react *via* scission of a Li–N bond and coordination of a ketone.[4d] This proposal is further supported by the similarities between the putative opened intermediate and the stable geometry of **1** as shown emboldened in Scheme 1.

Another interesting view of the molecule is as a 'crystallographic snapshot' of the process of amidolithium ladder fragmentation by solvation, as recently discussed by Mulvey and coworkers.[12] By variation of solvent ratio and organic substituent on amido nitrogen, a series of fragmented ladders have been structurally determined, most recently by use of the primary amide PhNHLi and limited amounts of thf.[12] Inclusion of chloride in the aggregate **1** reduces the connectivity of two dimers to its minimal limit.

The success of the Ph_2N anion as a platform for mixed aggregate studies is due in large part to its favour of asymmetric solvation in the dimeric state. One four-coordinate and one three-coordinate lithium are observed in the unmixed tmen complex of this amide, just as in **1**, and in other mixed aggregates that we have structurally characterised. Details of some of these will be found in a forthcoming full paper once their solution behaviour has been fully characterised.[13]

Forbairt (P. M. N., F. S. M.) and the EPSRC (W. C., A. J. E.) are gratefully acknowledged for financial support. We thank Dr J. O'Brien for obtaining NMR spectra.

Footnotes and References

* E-mail: frank.mair@umist.ac.uk

† Compound **1**, mp 151 °C, was obtained as colourless needles in a yield of 51%. A second crop produced a combined yield of 98%. Satisfactory C, H, and N analyses were obtained.

‡ *Crystal data* for **1**: $C_{54}H_{78}ClLi_4N_9$, M = 916.5, monoclinic, space group $P2_1/c$, a = 23.067(3), b = 14.879(2), c = 17.124(2) Å, β = 104.77(2)°, U = 5682.8(12) Å^3, Z = 4, D_c = 1.071 g cm^{-3}, μ = 0.896 mm^{-1} (Cu-Kα, λ = 1.541 78 Å), $F(000)$ = 1976, T = 160 K. Stoe-Siemens diffractometer, crystal size 0.57 × 0.42 × 0.30 mm, θ_{max} 67.5°, 9314 reflections measured, 9266 unique (R_{int} = 0.0772). Structure solution by direct methods, full-matrix least-squares refinement on F^2 for all data, with anisotropic displacement parameters, riding isotropic H atoms, no absorption correction. Final R_w = $\{\Sigma[w(F_o^2 - F_c^2)^2]/\Sigma[w(F_o^2)^2]^{\frac{1}{2}}\}$ = 0.2627 for all data, conventional R = 0.0930 for 6115 data having $F_o^2 > 2\sigma(F_o^2)$, S = 1.032. Final difference map between +0.70 and −0.35 e Å^{-3}. Programs: SHELXTL (G. M. Sheldrick, University of Göttingen, Germany), and local programs. CCDC 182/661.

1 A. Loupy and B. Tchoubar, *Salt Effects in Organic and Organometallic Chemistry*, VCH, Weinheim, 1992.
2 See, for example: D. Seebach, A. Beck and A. Studer, *Mod. Synth. Methods*, 1995, **7**, 1 and references therein.
3 (*a*) J. S. De Pue and D. B. Collum, *J. Am. Chem. Soc.*, 1988, **110**, 5518; (*b*) P. L. Hall, J. H. Gilchrist and D. B. Collum, *J. Am. Chem. Soc.*, 1991, **113**, 9571; (*c*) P. L. Hall, J. H. Gilchrist, A. T. Harrison, D. J. Fuller and D. B. Collum, *J. Am. Chem. Soc.*, 1991, **113**, 9575; (*d*) K. B. Aubrecht and D. B. Collum, *J. Org. Chem.*, 1996, **61**, 8674.
4 (*a*) L. M. Engelhardt, G. E. Jacobsen, A. H. White and C. L. Raston, *Inorg. Chem.*, 1991, **30**, 3979; (*b*) F. S. Mair, W. Clegg and P. A. O'Neil, *J. Am. Chem. Soc.*, 1993, **115**, 3388; (*c*) Z. Duan, V. G. Young and J. G. Verkade, *Inorg. Chem.*, 1995, **34**, 2179; (*d*) K. W. Henderson, A. E. Dorigo, Q.-Y. Liu, P. G. Williard, P. v. R. Schleyer and P. Bernstein, *J. Am. Chem. Soc.*, 1996, **118**, 1339; (*e*) K. W. Henderson, A. E. Dorigo, P. G. Williard and P. R. Bernstein, *Angew. Chem., Int. Ed. Engl.*, 1996, **35**, 1322; (*f*) W. Clegg, J. C. Greer, J. M. Hayes, F. S. Mair, P. M. Nolan and P. A. O'Neil, *Inorg. Chim. Acta*, 1997, **258**, 1.
5 T. Koizumi, K. Morihashi and O. Kikuchi, *Bull. Chem. Soc. Jpn.*, 1996, **69**, 305.
6 H. Hope and P. P. Power, *J. Am. Chem. Soc.*, 1983, **105**, 5320.
7 F. Neumann, F. Hampel and P. v. R. Schleyer, *Inorg. Chem.*, 1995, **34**, 6553.
8 R. E. Mulvey, *Chem. Soc. Rev.*, 1991, **20**, 167.
9 P. P. Power and X. Xiaojie, *J. Chem. Soc., Chem. Commun.*, 1984, 358.
10 R. P. Davies, P. R. Raithby and R. Snaith, *Angew. Chem., Int. Ed. Engl.*, 1997, **36**, 1215.
11 C. L. Raston, B. W. Skelton, C. R. Whittaker and A. H. White, *J. Chem. Soc., Dalton Trans.*, 1988, 987.
12 W. Clegg, L. Horsburgh, F. M. Mackenzie and R. E. Mulvey, *J. Chem. Soc., Chem. Commun.*, 1995, 2011 and references therein.
13 W. Clegg, A. J. Edwards, F. S. Mair and P. M. Nolan, unpublished results.

Received in Cambridge, UK, 12th September 1997; 7/06645G

Iron(III) 2-ethylhexanoate as a novel, stereoselective hetero-Diels–Alder catalyst

David B. Gorman* and Ian A. Tomlinson

The Dow Chemical Company, Midland, Michigan 48674, USA

Iron(III) 2-ethylhexanoate has been used as a novel, mild Lewis acid catalyst for the stereoselective Diels–Alder reaction of ethyl (*E*)-4-oxobutenoate with alkyl vinyl ethers to stereoselectively produce *cis*-2-alkoxy-3,4-dihydro-2*H*-pyran-4-carboxylic acid, ethyl esters with diastereoisomeric excesses (de) as high as 98%.

Since its discovery over 65 years ago,[1] the Diels–Alder reaction has been one of the most versatile reactions for assembling six-membered rings. The use of Lewis acid catalysts has led to improved regio- and stereo-selectivity for many of these reactions. Lanthanide reagents have been used as very mild Lewis acid catalysts for the Diels–Alder reaction of α,β-unsaturated aldehydes or esters with vinyl ethers to give substituted dihydropyrans.[2] In a search for cost-effective alternative catalysts, we have discovered that iron(III) 2-ethylhexanoate **1** is a novel, mild and economical Lewis acid catalyst for carrying out highly stereoselective Diels–Alder reactions between ethyl (*E*)-4-oxobutenoate **2**[3] and alkyl vinyl ethers **3a**–**3c** to give 2,4-disubstituted pyrans **4a**–**c** and **5a**–**c** (Scheme 1).

Based on analogous Diels–Alder transformations to give 2,4-substituted tetrahydropyrans, the major products have been assigned as the *endo* isomers.[4] Effectively an inverse electron demand hetero-Diels–Alder reaction, cyclization occurs selectively through the *endo* transition state, regio- and stereoselectively producing the *cis*-2,4-disubstituted pyrans **4**). This *endo* selectivity is enhanced using **1** as a catalyst (Table 1), giving diastereoisomeric excesses (de) as high as 98% based on relative product peak ratios obtained by gas chromatography. Similar yields and selectivities have been obtained when ethyl, isobutyl, and n-butyl vinyl ethers are used.

The reaction of **2** and **3b** has been examined with varying amounts of **1** at various temperatures (Table 2). Clearly, selectivity and reaction rate were enhanced by the addition of **1** (entry 6 *vs.* entries 7–10). The highest selectivity was seen at room temperature. Increasing reaction temperature shortened the reaction time from a few days to a few hours, but the de decreased from 98% at room temperature to 96% at 60 °C and 90% at 80 °C (entries 2–5 *vs.* entries 7–10 *vs.* entry 15). For reaction mixtures at elevated temperatures, yields could be improved by adding a trace amount of Et_3N as an inhibitor; at levels above 1 wt% Et_3N in the reaction of **2**, yields and selectivity began to decrease, indicating Et_3N was poisoning the catalyst (entries 15–19). Reaction times could also be shortened by adding additional catalyst, but optimal yields of ⩾80% were obtained using 0.20–0.25 equiv. of **1** (entries 3, 8 and 13). Modest yield increases also were realized by increasing the amount of vinyl ether from 6 to 10 equiv. (entries 12 and 14 *vs.* entries 11 and 13).

To isolate gram quantities, the product was removed from the catalyst by selective precipitation followed by column chroma-

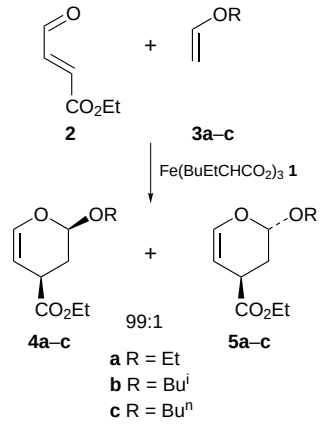

Scheme 1

Table 1 Comparison of vinyl ethers[a]

Entry	Ether	*T*/°C	*t*/d	Yield (%)	De (%)
1	**3a**	23	14	78	98
2	**3b**	23	14	80	98
3	**3c**	23	14	79	98

[a] Each reaction mixture contained ethyl (*E*)-4-oxobutenoate, 6 equiv. of vinyl ether and 0.1 euqiv. of iron(III) 2-ethylhexanoate. Ethyl (*E*)-4-oxobutenoate was inhibited with a trace amount of hydroquinone. Reported yields are GLC yields based on an internal standard. Yields at 66 h were calculated to be 72, 79 and 71% for entries 1, 2 and 3, respectively.

Table 2 Optimization reactions[a]

Entry	*T*/°C	*t*/h	**1** (equiv.)	Yield[b] (%)	De (%)
1	23	96	0	2	—
2	23	96	0.10	66	98
3	23	96	0.25	81	98
4	23	96	0.50	78	98
5	23	96	1.00	70	98
6[c]	60	18	0	13	66
7[c]	60	18	0.10	72	96
8[c]	60	18	0.25	80	96
9[c]	60	18	0.50	79	98
10[c]	60	18	1.00	67	98
11	60	16	0.10	72	96
12[d]	60	16	0.10	75	96
13	60	16	0.20	80	96
14[d]	60	16	0.20	84	96
15[e]	80	20	0.10	64	90
16[e]	80	20	0.10	73	92
17[e]	80	20	0.10	67	90
18[e]	80	20	0.10	56	82
19[e]	80	20	0.10	47	78

[a] Each reaction mixture contained ethyl (*E*)-4-oxobutenoate, isobutyl vinyl ether and iron(III) 2-ethylhexanoate. Ethyl (*E*)-4-oxobutenoate was inhibited with a trace amount of hydroquinone. Unless otherwise specified, 6 equiv. of isobutyl vinyl ether were used. [b] Reported yields are GLC yields based on an internal standard. [c] The reaction mixtures were stirred at room temperature for 18 h before heating to 60 °C for 18 h. [d] 10 equiv. of isobutyl vinyl ether were added instead of 6 equiv. [e] Et_3N was added in the following weight percents relative to **2**: 0% for entry 15, 1% for entry 16, 5% for entry 17, 15% for entry 18 and 25% for entry 19.

Table 3 Comparison of Iron-Based Catalysts[a]

Entry	Catalyst	*T* °C	*t*/h	**2** (%)	Yield[b] (%)	De (%)
1	Iron(III) 2-ethylhexanoate	70	6	15	58	96
2	Iron(II) 2-ethylhexanoate	70	6	29	38	92
3	Iron(III) naphthenate	70	5	21	30	92
4	Iron(III) benzoate	70	5	44	29	86
5	Iron(II) stearate	70	4	59	18	86
6	Iron(III) stearate	70	4	71	14	80
7	—	70	6	71	10	64

[a] All reactions were carried out in sealed glass tubes containing **2**, 6 equiv. of ethyl vinyl ether and 0.1 equiv. of catalyst. [b] Reported yields are GLC yields based on an internal standard.

tography on silica gel which had been deactivated by mixing with Et_3N in CH_2Cl_2 and evaporating to dryness. For larger samples, the product was isolated either by chromatography or wiped-film evaporation.

Although the exact binding nature of the catalyst is unknown, the choice of metal ligands and metal oxidation state is critical to the success of the catalytic reaction. Similar catalysts containing lower metal oxidation states and/or ligands which are bulkier and/or more rigid give lower selectivity, as well as lower reaction yields (Table 3). The bulkier/more rigid ligands may cause steric interference with the ethyl (*E*)-4-oxobutenoate, where complexation is believed to take place. A lower oxidation state may decrease the catalyst electrophilicity enough that it does not coordinate well with any of the oxygens from **2**.

In summary, iron(III) 2-ethylhexanoate is a novel, mild and relatively inexpensive Lewis acid catalyst for the stereoselective Diels–Alder reaction of ethyl (*E*)-4-oxobutenoate with alkyl vinyl ethers to give *cis*-2,4-disubstituted pyrans, extending the range of known catalysts for these types of transformations.

We thank Don Zakett for determining mass spectral data for **4a**–**c** and **5a**–**c**.

Footnotes and References

* E-mail: dbgorman@dow.com

† Iron(III) 2-ethylhexanoate was purchased as a 52% solution in mineral spirits from Johnson Matthey Alfa Aesar. Ethyl (*E*)- 4-oxobutenoate was purchased from Lonza. Representative experimental procedures. (*a*) Purification by chromatography: A mixture of ethyl (*E*)-4-oxobutenoate (2.56 g, 0.02 mol): *n*-butyl vinyl ether (8.65 g, 0.12 mol) and 52% iron(III) 2-ethylhexanoate (1.86 g, 0.002 mol) in mineral spirits was stirred at room temperature for 44 h. The catalyst precipitated after adding 20 ml of 20% MeCN in water. The slurry was filtered through filter agent, rinsing the cake with 20% MeCN in water. The filtrate was saturated with NaCl. The organic layer was separated and dried ($MgSO_4$). The solution was decanted and the MeCN evaporated. The remaining brown oil was flushed through a 0.75″ × 12″ deactivated silica gel column, eluting with hexane, followed by 20% EtOAc in hexane. After concentrating, a clear yellow oil (3.36 g) was obtained, assaying at 97% of **4a** as a single isomer for a calculated yield of 3.26 g (81%).

(*b*) purification by wiped-film evaporation: A mixture of of 52% iron(III) 2-ethylhexanoate (96.5 g) in mineral spirits and (±)-bis(2-ethylhexyl) sebacate (50.3 g) was dripped down a wiped-film still over 2 h operating at a vacuum of 0.05 mmHg, a heating temperature of 60 °C, a condensing temperature of 4 °C and a spinning rate of 300 rpm. The recovered bottoms (99.4 g) were assumed to be 50% catalyst by weight. A mixture of ethyl (*E*)-4-oxobutenoate (25.7 g, 0.20 mol) *n*-butyl vinyl ether (120.4 g, 1.20 mol) Et_3N (0.3 g), hydroquinone (0.026 g), and 50% iron(III) 2-ethylhexanoate in (±)-bis(2-ethylhexyl) sebacate (18.6 g, 0.02 mol) was heated at 60 °C for 12 h. After evaporating excess vinyl ether, the residue was dripped at 1 drop per second down a wiped-film still operating at a vacuum of 0.1 mmHg, a heating temperature of 90 °C, a condensing temperature of 2 °C and a spinning rate of 300 rpm. The overheads (30.2 g) assayed at 93% of **4a** for a calculated yield of 28 g (62%).

1 For selected reviews of the Diels–Alder reaction, see U. Pindur, G. Lutz and C. Otto, *Chem. Rev.*, 1993, **93**, 741; H. B. Kagan and O. Riant, *Chem. Rev.*, 1992, **92**, 1007; G. Desimoni and G. Tacconi, *Chem. Rev.*, 1975, **75**, 651; A. Wasserman, *Diels–Alder Reactions*, Elsevier, New York, 1965; H. L. Holmes, *Org. React.*, 1948, **4**, 60.

2 J.-Y. Merour, A.-S. Bourlot and E. Desarbre, *Tetrahedron Lett.*, 1995, **36**, 3527; I. E. Marko, G. R. Evans, J.-P. Declercq, B. Tinant, J. Feneau-Dupont, *Acros Organics Acta*, 1995, **1**, 2, 63; S. Danishefsky, M. Bednarski, *J. Am. Chem. Soc.*, 1983, **105**, 3716; S. Danishefsky, M. Bednarski, *Tetrahedron Lett.*, 1984, **25**, 721.

3 For preparation of ethyl (*E*)-4-oxobutenoate by ozonolysis of ethyl sorbate, see V. Tarik, L. A. Mitscher and J. K. Dep, *Synthesis*, 1980, **10**, 807.

4 W. G. Dauben and H. O. Krabbenhoft, *J. Org. Chem.*, 1977, **42**, 282.

Received in Corvallis, OR, USA, 25th August 1997; 7/06194C

Preparation and X-ray analysis of novel carbonyltungsten(0) complexes of diphosphinidenecyclobutenes

Masaaki Yoshifuji,* Yoshito Ichikawa, Naoki Yamada and Kozo Toyota

Department of Chemistry, Graduate School of Science, Tohoku University, Aoba, Sendai 980-77, Japan

A sterically protected diphosphinidenecyclobutene 5 bearing a bulky 2,4,6-triisopropylphenyl group is prepared and allowed to react with $W(CO)_5$(thf) to give a doubly tungsten-coordinated complex 8, with chelate- and π-type coordination; the structure of the complex is confirmed by X-ray analysis.

Sterically protected phosphorus-containing multiple bonded compounds with bulky substituents are currently of interest. We have been interested in cumulated and conjugated systems[1,2] involving phosphorus atom(s) in low coordination states, as well as diphosphenes[3] and phosphaethenes.[4] Recently, Appel *et al.*,[5] Märkl *et al.*[6] and ourselves[7–9] have reported the preparation and isolation of diphosphinidenecyclobutenes (**1a**–**c**, Scheme 1) utilizing 2,4,6-tri-*tert*-butylphenyl as a protecting group (Ar), as well as their *E*/*Z* isomerization about the P=C bonds.[7,10] We have also reported on their transition metal complexes, where metals are Cr, Mo, W,[8,11,12] Pt and Pd.[13] We now report a new type of tungsten carbonyl complex ligated with diphosphinidenecyclobutenes carrying the 2,4,6-triisopropylphenyl group[14] (Tip) as well as the Ar group.

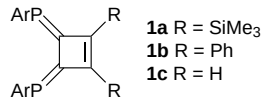

1a R = $SiMe_3$
1b R = Ph
1c R = H

Scheme 1 Ar = $C_6H_2Bu^t_3$-2,4,6

According to a slightly modified procedure employed for the preparation of **1b**, (2-phenylethynyl)(2,4,6-triisopropylphenyl)phosphinous halides **3** were prepared by the reaction of 2-phenylethynylphosphinous dichloride **2**[15] with 2,4,6-triisopropylphenylmagnesium bromide in thf at −78 °C. Then **3** was allowed to react with Bu^tLi at −78 °C or with Zn powder at room temp. to give diphosphane **4** as a diastereomeric mixture (D,L : *meso* = *ca.* 1 : 1) and the mixture was refluxed in thf to give (*E*,*Z*)-1,2-diphenyl-3,4-bis(2,4,6-triisopropylphenylphosphinidene)cyclobutene **5**.† It should be noted that only a trace amount of (*E*,*E*)-**5** was observed by ^{31}P NMR spectroscopy.

In the ^1H NMR spectrum of **5** in [$^2H_8$]toluene, there appeared six types of isopropyl peaks at 295 K. At higher temperatures, only two sets due to the *ortho*-isopropyl groups became coalesced, but the other two sets due to the other *ortho*-isopropyl groups remained magnetically non-equivalent. The remainder of the isopropyl groups assigned to the *para*-isopropyl groups remained unchanged even at 375 K. The fact suggests that one of the Tip groups, probably (*E*)-Tip, taking the steric congestion into account, starts to rotate at 323 K, while (*Z*)-Tip appears not to rotate even at 375 K.

We are now able to obtain a novel class of tungsten complex by the reaction of the diphosphinidenecyclobutene **5** with $W(CO)_5$(thf)[16] in refluxing thf.‡ The reaction gave **8** together with **6** and **7** (Scheme 2).† The ^{31}P NMR chemical shift of **8** appeared at δ_P 57, indicating that the phosphorus atom is strongly shielded compared with the value in the free ligand of either δ_P 164 for (*E*,*E*)-**5** or δ_P 169 and 183 for (*E*,*Z*)-**5**.

The structure of **8** was confirmed by the X-ray analysis§ to reveal a novel coordination type. Fig. 1 depicts an ORTEP drawing of the molecular structure for the bis-tungsten complex **8**. There are observed two WCO moieties, one is tetracarbonyl with chelate type coordination, the other is tricarbonyl with π-coordination. The two phosphorus atoms coordinate doubly on both $W(CO)_4$ and $W(CO)_3$ adopting sp^3 type configuration. The exocyclic P=C bonds are bent strongly from the ring plane [interplanar angle between the plane P(1)P(2)C(3)C(4) and the plane C(1)–C(4) 32.3°] to adopt a good interaction with the 6π system to coordinate on $W(CO)_3$, thus exhibiting a sharp contrast to the regular group 6 metal tetracarbonyl or palladium complexes of diphosphinidenecyclobutenes, where the system is planar with all sp^2 type configuration as exemplified in W,[11] Mo,[12] and Pd complexes.[13]

The P=C bond lengths of **8** [av. 1.763(10) Å] are elongated upon coordination compared to those of (*E*,*E*)-**1a** [1.677(6) Å][12] and (*E*,*E*)-**1b** [1.690(8) Å].[5] The bond length C(1)–C(2) of **8** [1.47(1) Å] is fairly elongated compared to the values of 1.400(9) Å and 1.380(9) Å for (*E*,*E*)-**1a** and (*E*,*E*)-**1b**, respectively. Thus, the interaction between the $W(CO)_3$ group and the ligand is apparently strong, since little change in bond lengths has been observed upon coordination with the chelate.[8,11–13]

Furthermore, in the case of compound (*E*,*E*)-**1c**, carrying the two Ar groups and no substituents on the cyclobutene ring, a doubly coordinated complex **9** was formed under similar conditions using $W(CO)_4(MeCN)_2$ (Scheme 3).[16] Complex **9** seems to have been formed *via* **10** as an intermediate, since **10** reacted with $W(CO)_4(MeCN)_2$ to give **9**.¶ It appeared to require less hindered environment than **1a** or **1b** to obtain double coordination products such as **8** or **9**.

Although Rau and Behrens reported on the formation and the structural analysis of (η^6-dimethylenecyclobutene)tricar-

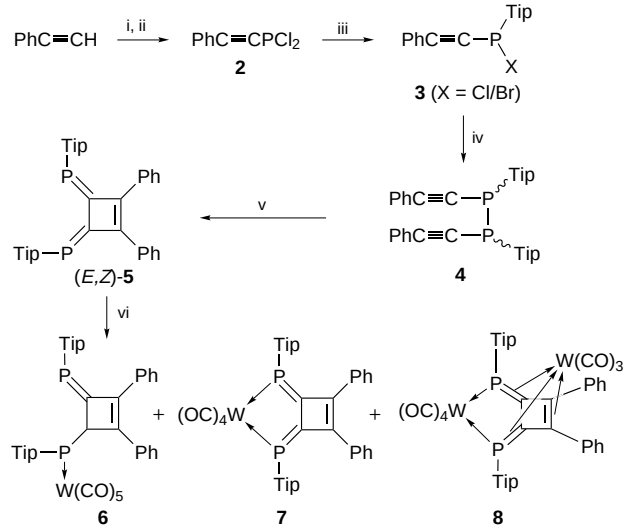

Scheme 2 Tip = $C_6H_2Pr^i_3$-2,4,6. *Reagents and conditions*: i, NEt_3; ii, PCl_3; iii, (Tip)MgBr; iv, Bu^tLi or Zn; v, reflux in thf; vi, $W(CO)_5$(thf), reflux in thf.

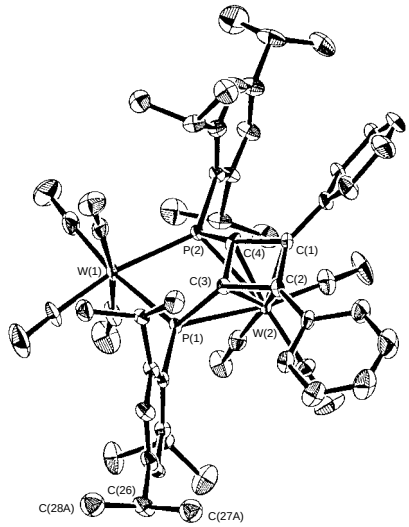

Fig. 1 The molecular structure of bis-tungsten complex **8** showing the atomic labelling scheme; only atoms with dominant occupancy factors are displayed. Important bond lengths (Å) and angles (°): W(1)–P(1) 2.493(3), W(1)–P(2) 2.490(3), W(2)–P(1) 2.679(3), W(2)–P(2) 2.664(3), W(2)–C(1) 2.35(1), W(2)–C(2) 2.321(10), W(2)–C(3) 2.24(1), W(2)–C(4) 2.18(1), P(1)–C(3) 1.788(10), P(2)–C(4) 1.737(9), C(1)–C(2) 1.47(1), C(1)–C(4) 1.49(1), C(2)–C(3) 1.47(1), C(3)–C(4) 1.47(1); P(1)–W(1)–P(2) 73.22(9), P(1)–W(2)–P(2) 67.60(8), C(2)–C(1)–C(4) 90.0(8), C(1)–C(2)–C(3) 90.2(8), C(2)–C(3)–C(4) 90.4(8), C(1)–C(4)–C(3) 89.2(8).

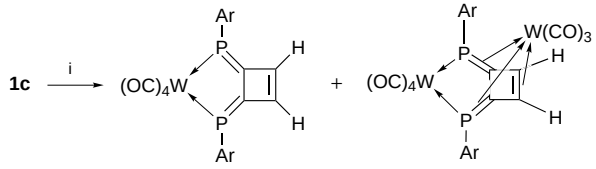

Scheme 3 Ar = $C_6H_2Bu^t_3$-2,4,6. *Reagents and conditions*: i, $W(CO)_4(MeCN)_2$, thf, in the dark.

bonylchromium(0)[17] and (η⁶-diisopropylidenecyclobutene)tricarbonylchromium(0),[18] this is the first example in the diphosphinidenecyclobutene–tungsten carbonyl system, where the ligand is doubly coordinated to tungsten.

This work was supported in part by the Grants-in-Aid for Scientific Research (Nos. 08454193 and 09239101) from the Ministry of Education, Science, Sports and Culture, Japanese Government.

Footnotes and References

* E-mail: yoshifj@mail.cc.tohoku.ac.jp

† *Selected spectroscopic data* (NMR spectra were recorded on either a Bruker AC200P, a JEOL α-500, or a Bruker AM600 spectrometer): (*E,Z*)-**5**: ^{1}H NMR (600 MHz, at 295 K, $CDCl_3$): δ 0.92 (6 H, d, *J* 6.8 Hz, *o*-CH*Me*), 1.00 (6 H, d, *J* 6.8 Hz, *o*-CH*Me*), 1.20 (6 H, d, *J* 6.9 Hz, *p*-CH*Me*$_2$), 1.25 (6 H, d, *J* 6.9 Hz, *p*′-CH*Me*$_2$), 1.32 (6 H, d, *J* 6.8 Hz, *o*′-CH*Me*), 1.39 (6 H, d, *J* 6.8 Hz, *o*′-CH*Me*), 2.75 (1 H, spt, *J* 6.9 Hz, *p*-C*H*Me$_2$), 2.75 (1 H, spt, *J* 6.9 Hz, *p*′-C*H*Me$_2$), 3.21 (2 H, m, *o*-C*H*Me$_2$), 3.72 (2 H, m, *o*′-C*H*Me$_2$); ^{31}P{^{1}H} NMR (81 MHz, $CDCl_3$): δ 168.6, 182.8 (AB, *J* 17.8 Hz). **8**: dark violet crystals, mp 183 °C (decomp.); ^{1}H NMR (600 MHz, $CDCl_3$): δ 1.18 (6 H, d, *J* 6.6 Hz, *o*-CH*Me*), 1.31 (6 H, d, *J* 6.9 Hz, *p*-CH*Me*), 1.31 (12 H, d, *J* 6.9 Hz, *o*-, *p*-CH*Me*), 1.41 (6 H, d, *J* 6.7 Hz, *o*-CH*Me*), 1.43 (6 H, d, *J* 6.6 Hz, *o*-CH*Me*), 2.94 (2 H, spt, *J* 6.9 Hz, *p*-C*H*Me$_2$), 4.35 (2 H, br s, *o*-C*H*Me$_2$), 4.46 (2 H, spt, *J* 6.7 Hz, *o*-C*H*Me$_2$); ^{31}P{^{1}H} NMR (81 MHz, $CDCl_3$): δ 56.7 (satellite d, $^1J_{PW}$ 226 Hz); IR (KBr): ν/cm^{-1} 2033, 1994, 1979, 1923, 1913, 1878, UV–VIS (CH_2Cl_2): λ_{max}(log ε) 254 (sh, 4.87), 272 (sh, 4.75), 321 (4.37), 456 (4.04), 603 nm (sh, 3.51); MS (FAB): *m/z* 1234 (M^+), 1206 (M^+ – CO). **9**: red needles, mp 180–181 °C (decomp.); ^{1}H NMR (500 MHz, $CDCl_3$): δ 1.19 (18 H, s, *p*-Bu^t), 1.65 (18 H, s, *o*-Bu^t), 1.75 (18 H, s, *o*-Bu^t), 4.66 (2 H, m, P=C–CH); ^{31}P{^{1}H} NMR (81 MHz, $CDCl_3$): δ 64.6 (satellite d, $^1J_{PW}$ 227.6 Hz); IR (KBr): ν/cm^{-1} 2033, 1994, 1942, 1900, 1865, 604 cm^{-1}; UV–VIS (*n*-hexane): λ_{max}(log ε) 218 (4.88), 236 (4.71), 380 (3.94), 456 (3.66), 505 (sh, 3.54), 598 nm (3.30); MS (FAB): *m/z* 1166 (M^+), 1138 (M^+ − CO), 968 (M^+ − 7CO − 2). **10**: orange powder, mp 198–199.5 °C (decomp.); ^{1}H NMR (200 MHz, $CDCl_3$): δ 1.34 (18 H, s, *p*-Bu^t), 1.63 (36 H, s, *o*-Bu^t), 6.45 (2 H, dd, $^3J_{PH}$ = $^4J_{PH}$ 3.6 Hz, P=C–CH); ^{31}P{^{1}H} NMR (81 MHz, $CDCl_3$): δ 154.1 (satellite d, $^1J_{PW}$ 250.1 Hz); UV–VIS (*n*-hexane): λ_{max}(log ε) 242 (4.79), 319 (4.12), 413 (4.09), 482 nm (3.45); MS (FAB): *m/z* 898 (M^+), 870 (M^+ − CO).

‡ *Preparative procedure*: **8**: under argon, a solution of phenylethynylphosphonous dichloride **2** (356 mg, 1.8 mmol)[15] in thf (10 ml) was cooled at −78 °C and was allowed to react with triisopropylphenylmagnesium bromide (1.8 mmol) and the mixture was warmed to room temp. to give phenylethynylphosphinous chloride **3** (X = Cl, δ_P 40) together with the bromide **3** (X = Br, δ_P 22) (chloride : bromide = 1 : 0.8). The mixture of the halides **3** (X = Cl, Br) was allowed to react with Zn (261 mg, 4.0 mmol) in thf (7 ml) at room temp. for 3 h to give the corresponding diphosphane **4** as a diastereomeric mixture (δ_P −66, −65); D,L : *meso* = *ca.* 1 : 1. It was then refluxed in thf for 24 h to give (*E,Z*)-**5**. The ligand (*E,Z*)-**5** was allowed to react with $W(CO)_5$(thf) (1.7 mmol) in refluxing thf for 9 h. **8** (62 mg, 0.051 mmol)† was isolated in 6% yield based on **2**, together with **6** [δ_P 114 (satellite d, $^1J_{PW}$ 265 Hz) and 186, AB, $^4J_{PP}$ 8 Hz] and **7** [δ_P 139, $^1J_{PW}$ 251 Hz].

§ *Crystal data* for **8**: recrystallised from ethanol–benzene. $C_{53}H_{56}O_7P_2W_2$, *M* = 1234.67, monoclinic, space group $P2_1/n$, *a* = 10.241(3), *b* = 25.462(4), *c* = 20.219(3) Å, β = 92.61(2)°, *U* = 5266(1) Å^3, *Z* = 4, *T* = 223 K, D_c = 1.557 g cm^{-3}; 9529 reflections with $2\theta \leqslant 50.0°$ were recorded on a four-circle diffractometer using graphite-monochromated Mo-Kα radiation. Of these, 6693 with $I > 3\sigma(I)$ were judged as observed. The structure was solved using SIR92.[19] The non-hydrogen atoms, except for C(27) and C(28), were refined anisotropically. Atoms C(27) and C(28) were disordered and refined isotropically (occupancy factor for the dominant: 0.55). Hydrogen atoms except for those on C(26)–C(28) were included, but their positions were not refined. *R* = 0.054, R_w = 0.064. CCDC 182/653.

¶ *Preparative procedure*: **9** (*E,E*)-**1c** (86 mg, 0.14 mmol) was allowed to react with 0.43 mmol of $W(CO)_4(MeCN)_2$ in refluxing thf (30 ml) for 1.5 h to give 90 mg of **9** in 54% yield.† **10**: a mixture of diphosphinidenecyclobutene (*E,E*)-**1c** (31 mg, 0.051 mmol) and $W(CO)_4(MeCN)_2$ (40 mg, 0.11 mmol) was dissolved in thf (20 ml) and the solution was stirred at room temp. for 21 h to give **10** (20 mg, 43% yield).†

1 M. Yoshifuji, K. Toyota and N. Inamoto, *J. Chem. Soc., Chem. Commun.*, 1984, 689; M. Yoshifuji, K. Toyota, K. Shibayama and N. Inamoto, *Tetrahedron Lett.*, 1984, **25**, 1809; M. Yoshifuji, K. Toyota, H. Yoshimura, K. Hirotsu and A. Okamoto, *J. Chem. Soc., Chem. Commun.*, 1991, 124; M. Yoshifuji, K. Toyota and H. Yoshimura, *Chem. Lett.*, 1991, 491.
2 S. Ito, K. Toyota and M.Yoshifuji, *Chem. Lett.*, 1995, 747.
3 M. Yoshifuji, I. Shima, N. Inamoto, K. Hirotsu and T. Higuchi, *J. Am. Chem. Soc.*, 1981, **103**, 4587; 1982, **104**, 6167.
4 M. Yoshifuji, K. Toyota, I. Matsuda, T. Niitsu, N. Inamoto, K. Hirotsu and T. Higuchi, *Tetrahedron*, 1988, **44**, 1363.
5 R. Appel, V. Winkhaus and F. Knoch, *Chem. Ber.*, 1987, **120**, 243.
6 G. Märkl, P. Kreitmeier, H. Nöth and K. Polborn, *Angew. Chem., Int. Ed. Engl.*, 1990, **29**, 927; G. Märkl and R. Hennig, *Liebigs Ann.*, 1996, 2059.
7 M. Yoshifuji, K. Toyota, M. Murayama, H. Yoshimura, A. Okamoto, K. Hirotsu and S. Nagase, *Chem. Lett.*, 1990, 2195.
8 K. Toyota, K. Tashiro and M. Yoshifuji, *Chem. Lett.*, 1991, 2079.
9 K. Toyota, K. Tashiro, M. Yoshifuji and S. Nagase, *Bull. Chem. Soc. Jpn.*, 1992, **65**, 2297.
10 K. Toyota, K. Tashiro, T. Abe and M. Yoshifuji, *Heteroatom Chem.*, 1994, **5**, 549.
11 M. Yoshifuji, Y. Ichikawa, K. Toyota, E. Kasashima and Y. Okamoto, *Chem. Lett.*, 1997, 87.
12 K. Toyota, K. Tashiro, M. Yoshifuji, I. Miyahara, A. Hayashi and K. Hirotsu, *J. Organomet. Chem.*, 1992, **431**, C35.
13 K. Toyota, K. Masaki, T. Abe and M. Yoshifuji, *Chem. Lett.*, 1995, 221.
14 C. N. Smit, Th. A. van der Knaap and F. Bickelhaupt, *Tetrahedron Lett.*, 1983, **24**, 2031.
15 G. Yu. Mikhailov, I. G. Trostyanskaya, M. A. Kazankova and I. F. Lutsenko, *Zh. Obshch. Khim.*, 1987, **57**, 2636.
16 W. Strohmeier and G. Schönauer, *Chem. Ber.*, 1961, **94**, 1346.
17 D. Rau and U. Behrens, *Angew. Chem., Int. Ed. Engl.*, 1991, **30**, 870.
18 D. Rau and U. Behrens, *J. Organomet. Chem.*, 1993, **454**, 151.
19 A. Altomare, G. Cascarano, C. Giacovazzo, A. Guagliardi, M. C. Burla, G. Polidori and M. Camalli, *J. Appl. Crystallogr.*, 1994, **27**, 435.

Received in Cambridge, UK, 26th September 1997; 7/06963B

Aziridination of naphthalene by 3-acetoxyaminoquinazolin-4(3*H*)-ones

Robert S. Atkinson,*[a]† Emma Barker,[a] Christopher K. Meades[a] and Hassan A. Albar*[b]‡

[a] *Department of Chemistry, University of Leicester, Leicester, UK LE1 7RH*
[b] *Department of Chemistry, King Abdul Aziz University, Jeddah 21413, Saudi Arabia*

Reaction of naphthalene with 3-acetoxyaminoquinazolinones 1, 4 or 8 in the presence of hexamethyldisilazane gives the corresponding mono-aziridine as the major (for 1) or exclusive (for 8) product; on heating in benzene, aziridine 5 acts as an aziridinating agent for alkenes.

Intermolecular non-enzymic reactions of simple naphthalenes which result in exclusive 1,2-addition to a peripheral double bond are uncommon: the remaining 3,4-double bond in the functionalised six-membered ring will usually be more reactive than any bond in the parent naphthalene with the result that bis-addition (1,2 and 3,4) is the major pathway. Thus the reaction of naphthalene with *m*-chloroperoxybenzoic acid[1] or with methyl(trifluoromethyl)dioxirane[2] is reported to give the *trans*-1,2,3,4-bis-epoxide but none of the mono-epoxide. A stereoselective addition to just one double bond would be valuable because subsequent stereoselective addition to the second double bond, using a different reagent, would lead to 1,2,3,4-tetrahydronaphthalene derivatives as single diastereoisomers.

Aziridination of naphthalene (3 equiv.) with 3-acetoxyamino-2-methylquinazolinone **1** (Q^1NHOAc)[3] in the presence of hexamethyldisilazane (HMDS) (3 equiv.) in chloroform gave mono-aziridine **2** (29%) and bis-aziridine **3** (7%) from examination of the crude reaction product by NMR spectroscopy using triphenylmethane as an internal standard (Scheme 1).§ After removal of the bulk of the naphthalene by sublimation (40 °C, ~ 10^{-5} mmHg), the products **2** and **3** were isolated in 17 and 3% yields respectively after chromatography on de-activated silica.

When aziridination of naphthalene was carried out using 3-acetoxyamino-2-isopropylquinazolinone **4** (Q^2NHOAc)[4] under the same conditions, the analogous mono- and bis-aziridines **5** and **6** were present in 26 and 29% yields in the crude reaction product and isolated in 20 and 11% yields respectively (Scheme 1) after chromatography as described above.

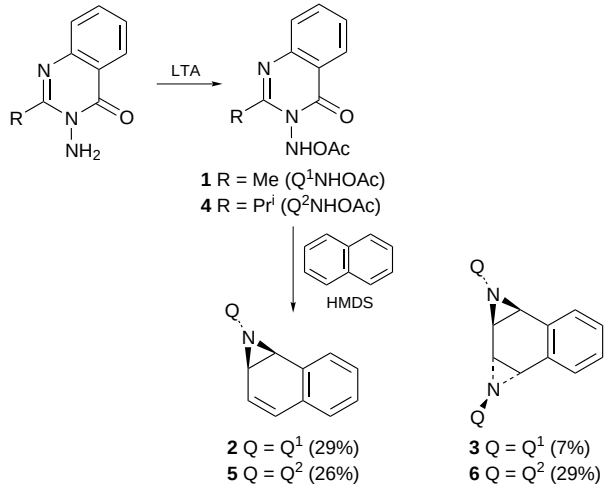

Scheme 1

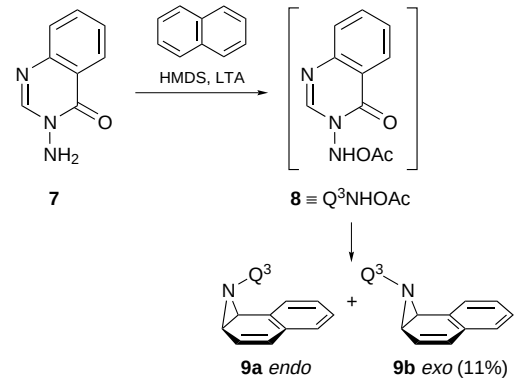

Scheme 2

The presumed 3-acetoxyaminoquinazolinone **8** (Q^3NHOAc) (Scheme 2), unsubstituted in the 2-position, is not stable under the conditions used for the preparation of Q^1NHOAc **1** and Q^2NHOAc **4**. However, *N*-acetoxylation of the corresponding 3-aminoquinazolinone **7** by lead tetraacetate (LTA) in the presence of naphthalene (3 equiv.) and HMDS (3 equiv.) gave the mono-aziridine, isolated as a mixture of *N*-invertomers **9a** (*endo*) and **9b** (*exo*) (11%) after chromatography: examination of the crude reaction product revealed that no bis-aziridine was formed.

Following the course of these aziridinations by NMR spectroscopy at temperatures from −20 °C to ambient is particularly informative and the changes observed can be interpreted as follows (Scheme 3): (a) the kinetically-formed products in each case are, as expected,[3] the *endo*-*N*-invertomers **10** and **11** (Scheme 3) and **9a** (Scheme 2) in which the quinazolinone ring and naphthalene residue are *cis*; (b) for each of the *endo*-invertomers **10** and **11** two *rotamers* around the *N–N* bond are present (ratio 3 : 1 and 5 : 1 respectively): only a single rotamer appears to be present in the case of **9a**; (c) interconversion between the *N–N* bond rotamers in **10** and **11** although slow on the NMR time-scale is fast on the *N*-inversion (*endo*→*exo*) time-scale;¶ (d) bis-aziridines **3** and **6** have the *exo–exo* configuration;‖ if the corresponding *exo–endo* stereoisomers **12** and **13** are intermediates in the formation of **3** and **6**, their concentrations are not sufficiently high for detection; (e) signals for mono-aziridines **2** and **5** (*exo*-invertomers) only become significant in these NMR spectra when signals from the respective aziridinating agents Q^1NHOAc **1** or Q^2NHOAc **4** have almost disappeared;** (f) bis-aziridination takes place predominantly or exclusively from the *exo*-invertomers **2** and **5**.

The competititve or predominant formation of mono-aziridine in these reactions arises as a consequence of (f) above together with a slow rate of *N*-inversion (*endo*→*exo*) for the mono-aziridine. Support for the conclusion in (f) comes from the absence of bis-aziridine as a product from the reaction in Scheme 2 and from the greater ratio of mono- : bis-aziridines **2** : **3** over **5** : **6**. The rates of *N*-inversion (*endo*→*exo*) in these mono-aziridines would be expected to increase in the order **9a** < **10** < **11** and this order correlates with the ratios bis- : mono-

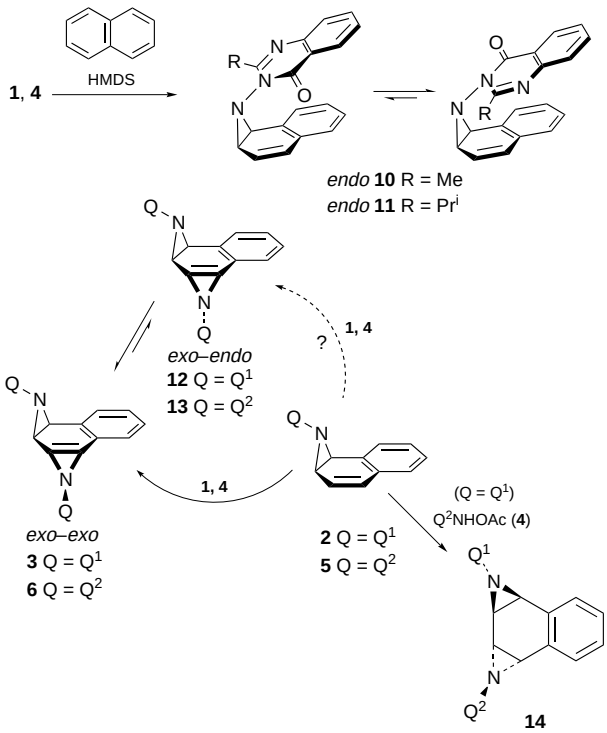

Scheme 3

aziridine obtained. The absence of any bis-aziridine in the reaction in Scheme 2 is because reaction of Q^3NHOAc with naphthalene is complete, and gives only *endo*-invertomer **9a**, before conversion of **9a** to **9b** takes place as the temperature is raised to ambient.††

syn-Addition of these 3-acetoxyaminoquinazolinones to aryl-substituted double bonds to give *endo*-substituted aziridines as kintically-formed products is well known and has been ascribed to an attractive interaction between the quinazolinone and aryl rings in the transition state.[3] Deactivation of the residual 3,4-double bond in the *endo*-configured mono-aziridines **10**, **11** and **9a** presumably arises from a similar interaction in these stereoisomers in which the aziriding ring bonds are now fully formed.

Further functionalisation of the 3,4-double bond in these mono-aziridines is under study: the mono-aziridine **2** reacts with Q^2NHOAc **4** (2 equiv.) to give the bis-aziridine **14** in 68% yield.

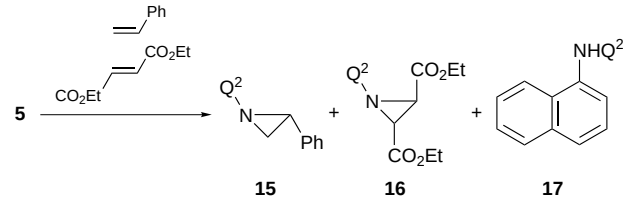

Scheme 4

Heating aziridine **5** in benzene containing a mixture of styrene (3 equiv.) and diethyl fumarate (3 equiv.) gave the corresponding aziridines **15** and **16** and the amine **17** in a 1 : 1 : 2 ratio (Scheme 4). It is likely that the intermediate in this aziridination is the nitrene [$Q^2\ddot{N}$:] since the same selectivity for these two alkenes is found for this species generated by other means.[5]

Footnotes and References

† E-mail: vow@le.ac.uk

‡ E-mail: scf3043@kaau.edu.sa

§ In the absence of HMDS, the major product is 1-(3,4-dihydro-2-methyl-4-oxoquinazolin-3-yl)aminonaphthalene **17** (22%).

¶ As the reactions proceed the concentrations of **10** and **11** are reduced to zero but there is no change in the ratios of their two rotamers.

‖ The two aziridine rings in these bis-aziridines would be expected to be *trans*-disposed based on steric grounds and this assignment is supported by the C_{2v} symmetry present (NMR spectroscopy) in the corresponding bis-aziridine obtained from reaction of naphthalene and 3-acetoxyamino-2-[(1′*S*)-2′,2′-dimethyl-1′-hydroxypropyl]quinazolin-4(3*H*)-one (see R. S. Atkinson, A. P. Ayscough, W. T. Gattrell and T. M. Raynham, *Chem. Commun.*, 1996, 1935).

** The rates of aziridination of *exo*-*N*-invertomers **2** and **5** by Q^1NHOAc **1** and Q^2NHOAc **4** are expected to be faster than that of naphthalene.

†† Further support for the conclusion in (f) is the higher ratio mono- : bis-aziridine **5** : **6** (4 : 1) obtained using the nitrene [$Q^2\ddot{N}$:] derived from Q^2NHOAc **4** and triethylamine (ref. 5): aziridinations of alkenes using [$Q^2\ddot{N}$:] take place at slightly lower temperatures than those using Q^2NHOAc.

1 K. Ishikawa and G. W. Griffin, *Angew. Chem., Int. Ed. Engl.*, 1977, **16**, 171.

2 R. Mello, F. Ciminale, M. Fiorentino, C. Fusco, T. Prencipe and R. Curci, *Tetrahedron Lett.*, 1990, **31**, 6097.

3 R. S. Atkinson, M. J. Grimshire and B. J. Kelly, *Tetrahedron*, 1989, **45**, 2875.

4 R. S. Atkinson, P. E. Edwards and G. A. Thomson, *J. Chem. Soc., Perkin Trans. 1*, 1994, 3209.

5 R. S. Atkinson and E. Barker, *J. Chem. Soc., Chem. Commun.*, 1995, 819.

Received in Liverpool, UK, 27th August 1997; 7/06283D

A porous chiral framework of coordinated 1,3,5-benzenetricarboxylate: quadruple interpenetration of the (10,3)-a network

Cameron J. Kepert and Matthew J. Rosseinsky*

Inorganic Chemistry Laboratory, University of Oxford, South Parks Road, Oxford UK OX1 3QR

The chiral and porous cubic coordination polymer $Ni_3(btc)_2(py)_6(eg)_6{\cdot}xeg\cdot yH_2$O (btc = 1,3,5-benzenetricarboxylate, py = pyridine, eg = ethylene glycol, $x \approx 3$, $y \approx 4$) is based on the interpenetration of four independent (10,3)-a networks, and contains large interconnected cavities with diameter 16 Å which may be desolvated without irreversibly destroying the porous framework structure.

The search for porous chiral solids is driven largely by a desire to perform enantioselective separations and syntheses.[1] The only two chiral zeolites known, zeolite β[2] and the titanosilicate ETS-10,[3] are both polymorphic, and samples currently retain one handedness only over a few crystallographic layers. Chiral, porous solids have very recently been resolved by the formation of single crystals: $NaZnPO_4{\cdot}H_2O$[4] consists of a tetrahedral framework containing water-filled channels, $Co(tn)_3{\cdot}Al_3P_4O_{16}{\cdot}2H_2O$[5] (GTex-2) consists of aluminophosphate layers separated by layers of the template, $Cd(tcm)[B(OMe)_4]{\cdot}x$MeOH[6] ($x \approx 1.6$) consists of sixfold helices containing methanol of solvation, and $Zn_2(btc)(NO_3){\cdot}H_2O{\cdot}5C_2H_5OH$[7] contains a single (10,3)-a network.[8] The last of these, as well as three achiral btc metallate phases,[9] shows structural stability to removal of solvent.

Here, we report the preparation of an air-stable nickel(II) salt of btc with spontaneous resolution from achiral starting materials. The material is novel in containing four interpenetrating (10,3)-a networks of the same handedness, through which lie solvent-filled pores of an unprecedented size. These pores may be desolvated completely at 115 °C to leave a poorly crystalline material with empty chiral cavities. The crystallinity of the interpenetrating lattice may be regenerated by resolvating this material with a variety of solvents.

Batches of single crystals consisting of a 50 : 50 mixture of enantiomers were synthesised by slow diffusion techniques,† and the crystal structure was determined by X-ray diffraction at 150(2) and 295(2) K.‡ $Ni_3(btc)_2(py)_6(eg)_6{\cdot}xeg\cdot yH_2$O is cubic, and is the first molecular material to crystallise in the chiral space group $P4_232$. The chiral network self-assembles due to unique interactions between the ligands in the first coordination sphere of the six-coordinate Ni^{II}. The two axial positions of the octahedron are occupied by tridentate btc anions while the equatorial positions are occupied equally by eg/H_2O and py (Fig. 1). Hydrogen bonding between the non-coordinated oxygen atom of the btc carbonyl group and the equatorial alcohol/H_2O group [O(11)···O(2) 2.60 Å] produces an approximately orthogonal orientation of the *trans* btc groups bound to Ni^{II}. This hydrogen-bonded arrangement, which appears to be highly uncommon, is the structural key to the formation of the chiral framework.

In the (10,3)-a network, chirality arises from the <100> fourfold and <111> threefold helices of the same handedness propagating in all crystallographically equivalent directions. Here the 11.3 Å separation between neighbouring btc prevents interpenetration of networks of opposite chirality (such as that resulting in a racemic crystal in $[Zn(tpt)_{2/3}(SiF_6)(H_2O)_2(MeOH)]$[10]) and four networks of the same handedness interpenetrate in such a way that each is related by unit translation or twofold rotation. Pseudo-tetrahedral cavities between the networks are bounded by the four btc anions per unit cell, and are linked by wide zigzag channels running along the <111> directions and passing through the vertices of the tetrahedra. The cavities are centred about (0,0,0) and (1/2,1/2,1/2) (Fig. 2). Approximately 28.1% of the crystal volume is occupied by free solvent,‡ so that each pore has a volume of *ca.* 600 Å^3, and a maximum diameter of *ca.* 16 Å. With the assumed Ni coordination, each contains three eg and four H_2O molecules, as determined by elemental microanalysis. The pseudo-hexagonal <111> channels have radii in the range 7–10 Å. There are narrower <100> channels with radii in the range 5–8 Å.

With heating to 115 °C, the material undergoes a colour change from blue to green. Thermogravimetry§ and elemental microanalyses§ are consistent with the loss of six eg and one py to leave $Ni_3(btc)_2(py)_5(eg)_3(H_2O)_4$. This is accompanied by a severe broadening of the X-ray powder diffraction (XRPD) pattern.¶ Exposure to eg, EtOH and MeOH vapour at ambient conditions in all cases led to a considerable sharpening of the XRPD pattern¶ indicating a drastic increase in crystallinity with the resolvation of the lattice. This implies that the partially desolvated material, $Ni_3(btc)_2(py)_5(eg)_3(H_2O)_4$, contains large

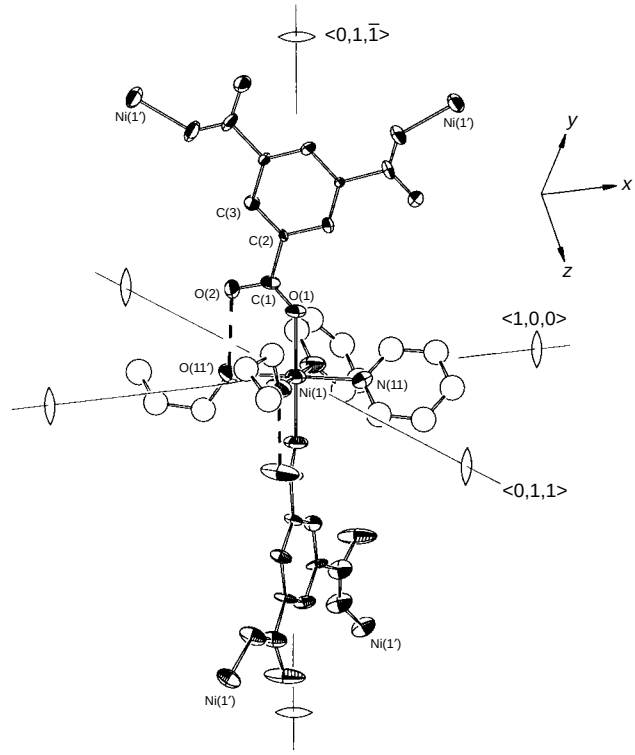

Fig. 1 The linear coordination of 1,3,5-benzenetricarboxylate to Ni^{II}, which is stabilised by hydrogen bonding to equatorial alcohol/H_2O groups (indicated by the dashed lines). The three orthogonal twofold rotation axes passing through the Ni are shown. All atoms are shown with 30% thermal ellipsoids. For clarity, only one orientation of the highly disordered fragment is shown, and hydrogen atoms have been omitted.

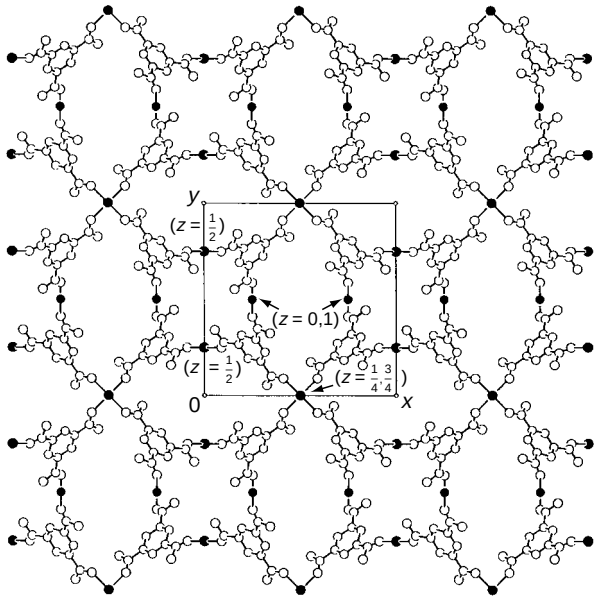

Fig. 2 Axial projection of the structure (for clarity, the equatorial ligands of the Ni^{II} cations and the solvent species occupying the pores have been removed, and only one of the two disordered orientations of the 1,3,5-benzenetricarboxylate is shown). Large, pseudo-tetrahedral solvent-filled cavities are centred about (0,0,0) and (1/2, 1/2, 1/2), and are linked by wide channels along the <111> and <100> directions. A view along (111) is presented as the graphical abstract.

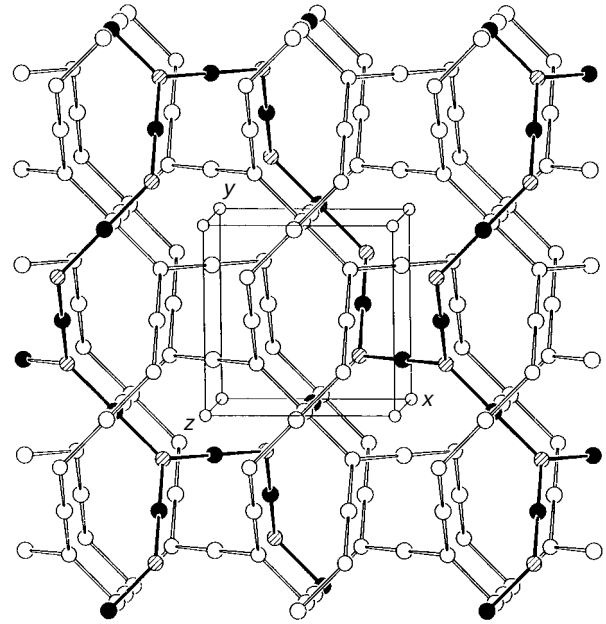

Fig. 3 Conceptual diagram showing the interpenetration of four 'clockwise' (10,3)-a networks. One of the four networks is highlighted such that the blackened circles represent Ni atoms and the hatched circles represent centres of the benzene rings.

empty chiral cavities, and that the relatively inflexible (10,3)-a network structure is retained throughout the cycle.

The chemical significance of the first-sphere hydrogen bonding in orienting the helix-forming btc anions is shown by the formation of isomorphous structures, either by resolvation or direct growth, with MeOH and EtOH replacing eg. The choice of ligands around the metal centre thus promises to greatly influence the chemical nature of the chiral pores in this new framework structure.

C. J. K. thanks Christ Church, Oxford, for a Junior Research Fellowship. We thank Professor C. K. Prout and Dr D. J. Watkin for access to the single crystal X-ray diffractometers (funded by EPSRC) and for useful discussions.

Footnotes and References

* E-mail: {cameron.kepert, matthew.rosseinsky}@chem.ox.ac.uk

† Batches of large, octahedral, clear blue crystals (up to 2 × 2 × 2 mm) were grown under ambient conditions over a period of four weeks by slow diffusion of pyridine (1 mmol) into a stoichiometric 2 : 3 solution of trimesic acid (1,3,5-benzenetricarboxylic acid, 0.10 mmol) and $Ni(NO_3)_2{\cdot}6H_2O$ (0.15 mmol) in ethylene glycol (20 cm^3).

‡ Structural data were collected at 150(2) K on an Enraf-Nonius DIP2000 diffractometer equipped with Mo-Kα radiation, and at 293(2) K on an Enraf-Nonius CAD4 diffractometer equipped with Cu-Kα radiation. The DIP2000 data were reduced with the HKL suite of programs.[11]

Crystal data for $Ni_3(btc)_2(py)_6(eg)_6{\cdot}3eg{\cdot}4H_2O$: $C_{66}H_{98}Ni_3N_6O_{34}$, M = 1695.63, cubic, space group $P4_232$, a = 15.922(1) and 16.025(1) Å, U = 4036.4(4) and 4115.2(4) $Å^3$, D_c = 1.395 and 1.368 Mg m^{-3} at 150(2) and 293(2) K, respectively, Z = 2, crystal dimensions 0.40 × 0.375 × 0.35 mm, $2\theta_{max}$ = 53.46 and 149.38°. Structure solution was by a combination of geometric considerations and Fourier techniques using SHELXL-93.[12] Full-matrix least-squares refinement on F_o^2 for 1445 and 1347 unique data (30 973 and 3320 collected, R_{int} = 0.112 and 0.0363), 124 parameters and 37 restraints converged to $wR2$ = 25.99 and 20.46 (all data), conventional R = 0.0965 and 0.0697 (1070 and 908 data with $F_o > 4\sigma F_o$), with Flack parameters 0.03(11) and −0.04(15). Cavity volumes were calculated within PLATON[13] by summing voxels more than 1.2 Å away from the van der Waals surface of the framework. CCDC 182/641.

§ In the temperature range 90–120 °C the material loses *ca.* 30% of its mass to form $Ni_3(btc)_2(py)_5(eg)_3(H_2O)_4$. In the range 120–380 °C there is a loss of a further 35%, equal to the mass of the remaining neutral species.

¶ Ground samples were sealed in 0.5 mm Lindemann capillaries and mounted on a D5000 Siemens X-ray powder diffractometer. For the [210] reflections at 2θ = 12.3°, FWHM = 0.086, 0.151, 0.165 and 0.095° for the fresh, the two 115 °C desolvated and eg resolvated samples, respectively.

1 S. Allenmark, *Chromatographic Enantioseparations*, Ellis Horwood, New York, 1991; H.-U. Blaser, *Tetrahedron Asymmetry*, 1991, **2**, 843; G. Sundarababu, M. Leibovitch, D. R. Corbin, J. R. Scheffer and V. Ramamurthy, *Chem. Commun.*, 1996, 2159; S. Feast, D. Bethell, P. C. B. Page, F. King, C. H. Rochester, M. R. H. Siddiqui, D. J. Willock and G. J. Hutchings, *J. Chem. Soc., Chem. Commun.*, 1995, 2409; W. Reschetilowski, U. Bohmer and J. Wiehl, *Stud. Surf. Sci. Catal.*, 1994, **84**, 2002.

2 J. M. Newsam, M. M. J. Treacy, W. T. Koetsier and C. B. de Gruyter, *Proc. R. Soc. London, Ser. A.*, 1988, **420**, 375.

3 M. W. Anderson, O. Terasaki, T. Ohsuna, A. Philippou, S. P. MacKay, A. Ferreira, J. Rocha and S. Lidin, *Nature*, 1994, **367**, 347.

4 W. T. A. Harrison, T. E. Gier, G. D. Stucky, R. W. Broach and R. A. Bedard, *Chem. Mater.*, 1996, **8**, 145.

5 D. A. Bruce, A. P. Wilkinson, M. G. White and J. A. Bertrand, *J. Chem. Soc., Chem. Commun.*, 1995, 2059.

6 S. R. Batten, B. F. Hoskins and R. Robson, *Angew. Chem., Int. Ed. Engl.*, 1997, **36**, 636.

7 O. M. Yaghi, C. E. Davis, G. M. Li and H. L. Li, *J. Am. Chem. Soc.*, 1997, **119**, 2861.

8 A. F. Wells, *Structural Inorganic Chemistry*, Clarendon Press, Oxford, 1975.

9 O. M. Yaghi, G. M. Li and H. L. Li, *Nature*, 1995, **378**, 703.; O. M. Yaghi, H. L. Li and T. L. Groy, *J. Am. Chem. Soc.*, 1996, **118**, 9096; M. J. Plater, A. J. Roberts and R. A. Howie, *Chem. Commun.*, 1997, 893.

10 B. F. Abrahams, S. R. Batten, H. Hamit, B. F. Hoskins and R. Robson, *Chem. Commun.*, 1996, 1313.

11 Z. Otwinowski, W. Minor, in *Methods in Enzymology*, ed. C. W. Carter, and R. M. Sweet, Academic Press, New York, 1996, p. 276.

12 G. M. Sheldrick, SHELXL-93 Program for the refinement of crystal structures, Universität Göttingen, 1993.

13 A. L. Spek, *Acta Crystallogr., Sect. A*, 1990, **46**, C34.

Received in Basel, Switzerland, 23rd July 1997; 7/05336C

Phosphonium salts of diacetoxyiodine(I) anions, new reagents for the iodoacetoxylation of alkenes

Andreas Kirschning,* Claus Plumeier and Lars Rose

Institut für Organische Chemie, TU Clausthal, Leibnizstr. 6, D-38678 Clausthal-Zellerfeld, Germany

Novel phosphonium salts of diacetoxyiodine(I) anions 1 add to alkenes like tri-*O*-benzyl galactal 8 affording 1-acetoxy-2-iodopyranoses 12a,b which can efficiently be employed in the synthesis of 2-deoxyglycoside 14.

Stereo- and regio-selective 1,2-additions to alkenic double bonds are one of the most important transformations in organic synthesis.[1] Among this class of reactions, acetoxyiodinations are only rarely used. The α-iodo acetates which are created *via* this transformation can serve as starting materials for the preparation of allyl acetates or α-iodo alcohols with subsequent formation of oxiranes.[2] Current reagent systems in use for the acetoxyiodination of alkenes involve KIO_3 in glacial AcOH at 60 °C,[3] or various heavy metal salts[4] derived from silver(I), thallium(I), copper(II), mercury(II) or bismuth(III), all in the presence of I_2. AcOH and *N*-iodosuccinimide at 60 °C can also be used to form α-iodo acetates from the corresponding alkenes.[5] Due to the harsh reaction conditions employed and environmental problems involved with heavy metals, these methods have not found wide acceptance in reactions with multifunctional alkenes or in natural product synthesis.

Here we describe the preparation of a new class of reagents, the phosphonium salts of diacetoxyiodine(I) **1**,[6] which can be regarded as an acetyl hypoiodite **4** equivalent. Compound **4** has never been isolated, but has been postulated as an intermediate in the Hunsdiecker and Simonini reactions[7] and in the thermal decomposition of diacyliodobenzenes.[8] As is demonstrated, diacetoxyiodine(I) species **1** are ideally suited for promoting acetoxyiodination of alkenes under very mild conditions. Scheme 1 shows that these reagents are conveniently prepared from the corresponding phosphonium iodides **2a** and **2b** and diacetoxyiodobenzene **3** ($CHCl_3$, room temp., 2 h). After addition of Et_2O, the tetraphenylphosphonium salt **1a** precipitates as a light brown amorphous material [mp 145 °C (decomp.)], whereas the methyltriphenylphosphonium salt **1b** separates from the organic layer as a dark brown oil.†

Diacyliodine(I) compounds like **1a** promote acetoxyiodination of alkenes such as cyclohexene **5** or indene **6** in a highly *anti* selective manner (Table 1). α-Iodo acetates **9**[9] and **10** are isolated in good yield. Regiocontrol is determined by the relative stability of the two possible intermediate cations. Acetoxyiodination may further be simplified by *in situ* generation of **1** from **2**,‡ including formation of **1c** from Murahashi's reagent **2c**, in various solvents followed by addition of the alkene. Under these conditions carbohydrate derived enol ethers such as **7** and **8** quantitatively afford 1-acetoxy-2-iodopyranoses **11a**,**b** and **12a**,**b**, respectively, under very mild conditions. Usually, a preference for α-glycosyl acetates is observed. Due to the reduced solubility of

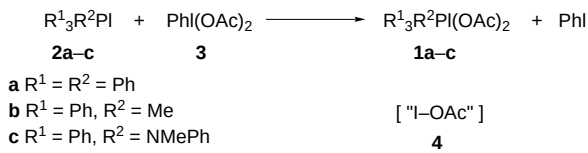

Scheme 1

1a and **2a** in toluene, acetoxyiodination of **7** proceeds sluggishly. This obstacle may be circumvented by accellerating the reaction with catalytic $Me_3SiOSO_2CF_3$. Under these conditions the rare 2-deoxy β-anomer **11b** is formed in substantial amounts. The reaction exclusively furnishes 1,2-*trans* adducts, which can be rationalized by assuming a *trans*-diaxial addition of iodonium cation and acetoxy group to the electron-rich enol ether double bond.§

Table 1 Results of some acetoxyiodinations

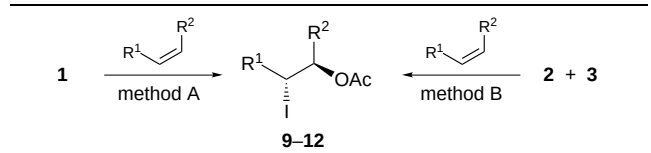

Method[a]	1	Solvent	*t*/h	Ratio[b]	Yield (%)[c]
					
	5			9	
A	**1a**	CH_2Cl_2	36	—	61
	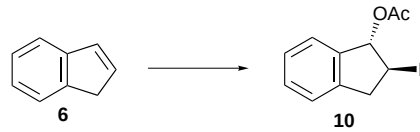				
	6			10	
A	**1a**	CH_2Cl_2	12	—	69
	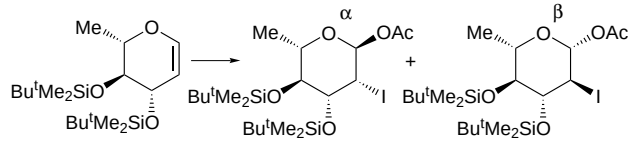				
	7			11a[d]	11b[d]
A	**1a**	CH_2Cl_2	16	1.8 : 1	59
B	**1a**	MeCN	16	2.1 : 1	73
B[e]	**1a**	PhMe	72	1.1 : 1	69
B	**1b**	CH_2Cl_2	24	2.2 : 1	68
B	**1c**	CH_2Cl_2	24	2.7 : 1	72
	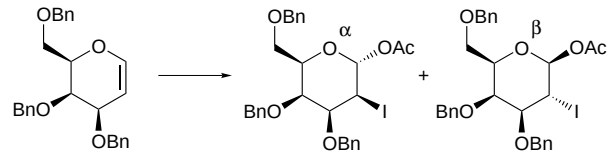				
	8			12a	12b
B	**1b**	MeCN	72	3.5 : 1	67
B	**1b**	PhMe	72	3.5 : 1	74[f]

[a] Method A: Preformed **1a**. Method B: **1a**–**c** generated *in situ*. All reactions carried out at room temp. [b] Determined from ^1H NMR spectra of crude product. [c] Yield of isolated product after column chromatography. [d] See footnote §. [e] Added $Me_3SiOSO_2CF_3$. [f] Crude product was contaminated with **8** (10%).

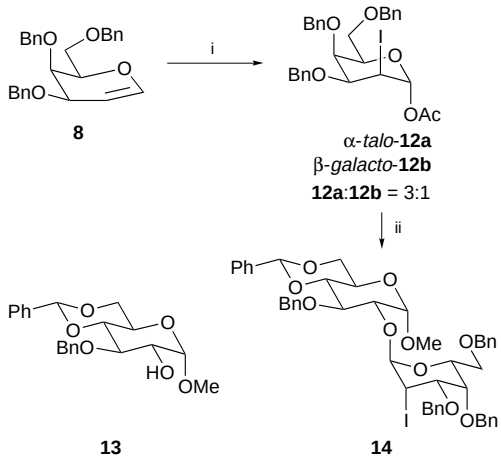

Scheme 2 *Reagents and conditions*: i, **2b**, **3**, CH_2Cl_2, 78%; ii, **12a**, **13**, $Me_3SiOSO_2CF_3$, CH_2Cl_2, −78 °C, 89%

These glycosyl acetates are ideal precursors for the construction of 2-deoxy glycosides, which occur as structural moieties of many bioactive natural products.[10] In glycosidations the 1-acetoxy group has glycosyl donor properties, while the 2-iodo substituent serves as a stereocontrol element in the glycosidation step which can be removed reductively at a later stage. In fact, acetoxyiodination of glycal **8** in CH_2Cl_2 yields glycosyl acetate **12** (α:β = 3.1:1, 78%) (Scheme 2). Separation by column chromatography gave pure α-*talo*-**12** which, after Lewis acid-promoted activation, was glycosidated in the presence of methyl glycoside **13** to afford α(1-2) disaccharide **14** as the only product in excellent yield.

In summary, phosphonium salts of diacetoxyiodine(I) represent a new class of reagents for the facile acetoxyiodination of alkenes. Starting from glycals, 1-acetoxy-2-iodo pyranoses are generated which can efficiently be employed in the synthesis of 2-deoxy glycosides.

The authors thank the Deutsche Forschungsgemeinschaft and the Fonds der Chemischen Industrie for financial support.

Footnotes and References

* E-mail: andreas.kirschning@tu-clausthal.de

† The ^{31}P NMR chemical shifts ($CDCl_3$) measured for **1a** and **1b** were identical with those for the starting iodides **2a** and **2b**. From this it can be concluded that compounds **1** are composed of an ion pair similar to phosphonium iodides **2**.

‡ *Experimental procedure*: A mixture of $PhI(OAc)_2$ **3** (0.966 g, 3.0 mmol) and Ph_3MePI **2b** (1.114 g, 3.0 mmol) in CH_2Cl_2 (15 ml) was stirred for 15 min at rom temp. until the solution turned dark red. Glycal **8** (416 mg, 1.0 mmol) was added and stirring was continued for 72 h. The solution was washed twice with aqueous $NaHSO_3$ and the aqueous phase was extracted four times with CH_2Cl_2. The combined organic extracts were dried ($MgSO_4$) and concentrated under reduced pressure. Column chromatography using light petroleum–EtOAc (4:1) gave two fractions (**12a**:**12b** = 3:1; 470 mg, 78%).

First fraction: β-**12b**; colourless crystals, mp 101 °C; $[\alpha]_D^{20}$ +52.2 (*c* 1.02, $CHCl_3$); δ_H (C_6D_6) 7.42–7.20 (m, 15 H, arom. H), 6.13 (d, 1 H, $J_{1,2}$ 9.6, 1-H), 4.84, 4.50, 4.37, 4.31, 4.26, 4.17 (6d, 6 H, *J* 11.2 and 12.0, CH_2Ph), 4.68 (dd, 1 H, $J_{2,1}$ 9.6, $J_{2,3}$ 11.2, 2-H), 3.78 (br t, 1 H, $J_{5,6} = J_{5,6'}$ = 8.0, 5-H), 3.71 (d, 1 H, $J_{4,3}$ 1.6, 4-H), 3.56 (m, 2 H, 6-H, 6′-H), 3.27 (dd, 1 H, $J_{3,2}$ 11.2, $J_{3,4}$ 1.6, 3-H), 2.10 (s, 3 H, OAc); δ_C ($CDCl_3$) 169.0, 138.0–136.9 and 128.5–127.7, 94.8 (C-1), 83.2, 74.6, 72.5 (C-3, C-4, C-5), 74.7, 73.5, 72.8 (OCH_2Ph), 67.6 (C-6), 30.5 (C-2), 20.8.

Second fraction: α-**12a**; colourless oil, $[\alpha]_D^{19}$ −7.6 (*c* 0.99, $CHCl_3$); δ_H ($CDCl_3$) 7.50–7.25 (m, 15 H, arom. H), 6.57 (d, 1 H, $J_{1,2}$ 2.4, 1-H), 5.08, 4.80, 4.58, 4.53, 4.50, 4.40 (6d, 6 H, *J* 12.0, CH_2Ph), 4.31 (ddd, 1 H, $J_{2,3}$ 4.4, $J_{2,1}$ 2.4, $J_{2,4}$ 0.8, 2-H), 4.19 (dt, 1 H, $J_{5,6} = J_{5,6'}$ = 6.0, $J_{5,4}$ 2.4, 5-H), 4.00 (dd, 1 H, $J_{4,3} = J_{4,5}$ = 2.4, 4-H), 3.70 (m, 2 H, 6-H, 6′-H), 3.49 (dd, 1 H, $J_{3,4}$ 2.4, $J_{3,2}$ 4.4, 3-H), 2.03 (s, 3 H, OAc); δ_C ($CDCl_3$) 168.5, 138.3–137.2 and 128.4–127.4, 95.2 (C-1), 73.5, 73.4, 70.9, 73.4, 73.3, 72.9 (C-3, C- 4, C-5), 68.4 (C-6), 22.4 (C-2), 20.9.

§ The ^1H NMR spectra of the crude products revealed traces of the α-*gluco* isomer, in particular when the reaction was run in toluene for a prolonged time.

1 J. A. Gladysz and J. Boone, *Angew. Chem.*, 1997, **109**, 567; *Angew. Chem., Int. Ed. Engl.*, 1997, **36**, 551; J. Rodriguez and J.-P. Dulcère, *Synthesis*, 1993, 1177.
2 J. W. Cornforth and D. T. Green, *J. Chem. Soc.* (*C*), 1970, 846.
3 L. Mangoni, M. Adinolfi, G. Barone and M. Parrilli, *Tetrahedron Lett.*, 1973, 4485; L. Mangoni, M. Adinolfi, G. Barone and M. Parrilli, *Gazz. Chim. Ital.*, 1975, **105**, 377.
4 L. Birckenbach, J. Goubeau and E. Berninger, *Ber.*, 1932, **65**, 1339; R. B. Woodward and F. V. Brutcher, Jr., *J. Am. Chem. Soc.*, 1958, **80**, 209; R. C. Cambie, D. M. Gash, P. S. Rutledge and P. D. Woodgate, *J. Chem. Soc., Perkin Trans. 1*, 1977, 1157; J. Barluenga, M. A. Rodriguez, P. J. Campos and G. Asenio, *J. Chem. Soc., Chem. Commun.*, 1987, 1491; C. Georgoulis and J. Valery, *Bull. Soc. Chim. Fr.*, 1975, 1431; R. W. Trainor, G. B. Deacon, W. R. Jackson and N. Giunta, *Aust. J. Chem.*, 1992, **45**, 1265.
5 M. Adinolfi, M. Parrilli, G. Barone, G. Laonigro and L. Mangoni, *Tetrahedron Lett.*, 1976, 3661.
6 Iodine(I) complexes were identified with reference to the analogous tetraalkylammonium salts: G. Doleschall and G. Tóth, *Tetrahedron*, 1980, **36**, 1649; C. Szántay, G. Blaskó, M. Bárczai-Beke, P. Péchy and G. Dörnei, *Tetrahedron Lett.*, 1980, **21**, 3509.
7 These salts are analogues of the Simonini complex $[(AcO)_2AgI)]$: A. Simonini, *Monatsh. Chem.*, 1892, **13**, 320.
8 J. E. Leffler and L. J. Story, *J. Am. Chem. Soc.*, 1967, **89**, 2333.
9 R. C. Cambie, R. C. Hayward, J. L. Roberts and P. S. Rutledge, *J. Chem. Soc., Perkin Trans. 1*, 1974, 1858.
10 A. Kirschning, A. Bechthold and J. Rohr, *Top. Curr. Chem.*, 1997, **188**, 1; J. F. Kennedy and C. A. White, *Bioactive Carbohydrates in Chemistry, Biochemistry, and Biology*, Ellis Horwood, Chichester, 1983; S. J. Danishefsky and M. T. Bilodeau, *Angew. Chem.*, 1996, **108**, 1482; *Angew. Chem., Int. Ed. Engl.*, 1996, **35**, 1380.

Received in Liverpool, UK, 28th August 1997; 7/06305I

Oxygen states present at a Ag(111) surface in the presence of ammonia: evidence for a NH_3–$O_2^{\delta-}$ complex

A. F. Carley, P. R. Davies, M. W. Roberts,* K. K. Thomas and S. Yan

Department of Chemistry, University of Wales, Cardiff, UK CF1 3TB

Molecular oxygen states present at Ag(111) surfaces when dioxygen is coadsorbed with ammonia at 80 K are characterised by vibrational loss features at 1488 and 1640 cm^{-1}. The former is suggested to be associated with the $NH_3\cdots O_2^{\delta-}$ complex, a key intermediate in the oxidation pathway.

There is now incontrovertible experimental evidence for the role of specific oxygen states present at single crystal metal surfaces (*e.g.* zinc, copper, nickel) as the active sites in oxydehydrogenation of ammonia.[1–4] In the case of Cu(110)O surfaces the isolated oxygen adatoms, or oxygens at the ends of Cu–O–Cu–O– chains, are the most active[5] but for atomically clean Cu(110) surfaces there is evidence during the coadsorption of oxygen–ammonia mixtures for a dioxygen–ammonia complex being the key intermediate. Both experimental and theoretical[6] work have supported this view and there are strong analogies with the model developed for the oxidation of ammonia when coadsorbed with dioxygen at a Zn(0001) surface at low temperatures.[2] The Ag(111)–dioxygen/ammonia system shows very similar precursor kinetics to that observed with Zn(0001) and for this reason we have searched for spectroscopic evidence, using both X-ray and vibrational electron energy loss spectroscopies (XPS and VEELS), for the presence of dioxygen states present at low temperatures when dioxygen–ammonia mixtures are coadsorbed at Ag(111) at 100 K.

The sticking probability of pure dioxygen at clean Ag(111) surfaces at 120 K is very low (*ca.* 10^{-4}); a peroxo species is observed after 3000 L exposure,[7] as evidenced by VEELS bands at 220 cm^{-1} [$\nu(AgO_2)$] and 670 cm^{-1} [ν(O–O)]. However, when dioxygen and ammonia are coadsorbed the reactivity to dissociative oxygen chemisorption is increased and the chemistry, as reflected by the O 1s and N 1s spectra, indicate that dehydrogenation has occurred. A typical set of kinetic data for the coadsorption of an ammonia–dioxygen mixture is shown in Fig. 1. The 'oxygen' uptake, calculated from the total O1s intensity data, is shown as a function of oxygen exposure in four different experiments at four different temperatures (220, 180, 150 and 120 K) using an O_2–NH_3 (1 : 3) mixture. As well as demonstrating the much increased sticking probability for oxygen adsorption [as observed at Zn(0001) surfaces[2]], these results provide strong circumstantial evidence for dioxygen–ammonia complexes participating in the oxidation pathway; this was the impetus for the VEELS investigation.

Fig. 2 shows a set of VEEL spectra when an atomically clean Ag(111) surface was exposed to an ammonia–dioxygen mixture at 100 K [Fig. 2(*a*)] and then warmed to 210 K [Fig. 2(*b*)]. The main loss features at 100 K are at 250, 700, 1120, 1480, 1640 and 3390 cm^{-1}. The assignments [Fig. 2(*a*)] are as shown; the 250 cm^{-1} feature is attributed to Ag–adsorbate stretch frequencies. A similar experiment, but replacing NH_3 with ND_3, gave rise to the spectra in Fig. 2(*c*), curves (*ii*) and (*iii*); for

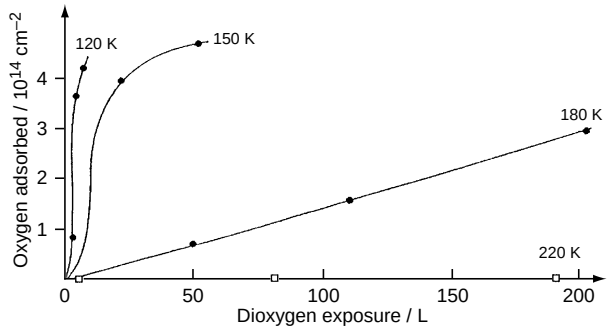

Fig. 1 Exposure of a Ag(111) surface to an O_2–NH_3 (1 : 3) mixture at four different temperatures. The graphs are plots of total concentration of oxygen adsorbed (expressed as atoms) *vs.* equivalent dioxygen exposure. The reaction of pure dioxygen leads to negligible adsorption in this exposure and temperature range.

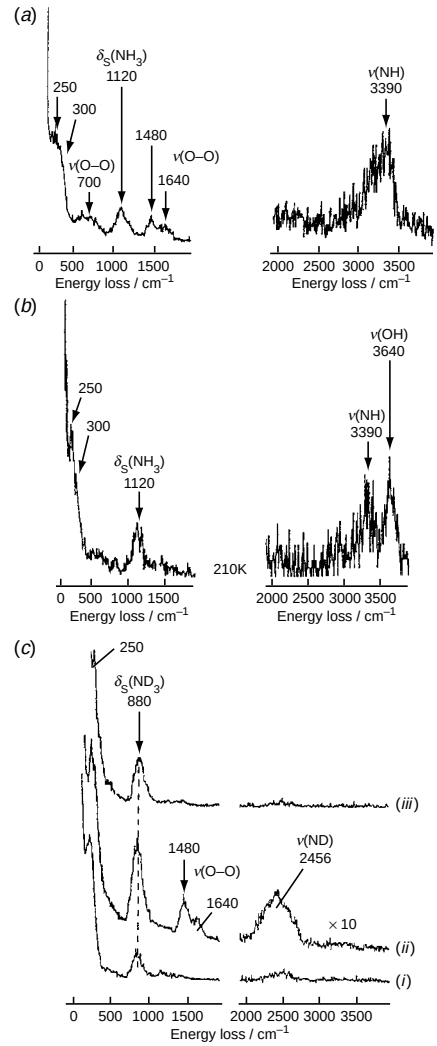

Fig. 2 VEELS spectra for (*a*) exposure of a clean Ag(111) surface to a dioxygen–ammonia mixture at 100 K; (*b*) surface in (*a*) warmed to 210 K and (*c*) VEELS spectra for (*i*) adsorption of ND_3 at Ag(111) at 100 K, (*ii*) adsorption of an O_2–ND_3 mixture at Ag(111) at 100 K and (*iii*) surface in (*ii*) warmed to 210 K

comparison curve (*i*) shows the adsorption of pure ND_3 at Ag(111) at 100 K. The spectra for deuterated ammonia confirm the assignments of the 1480 and 1640 cm^{-1} features in Fig. 2(*a*) for the ammonia–dioxygen mixture as arising from adsorbed dioxygen states. The unusually strong and broad ν(ND) feature at 2456 cm^{-1} [Fig. 2(*c*), curve (*ii*)] is the consequence of hydrogen bonding in the dioxygen–ND_3 complex.

On warming the Ag(111) surface exposed to the dioxygen–NH_3 mixture [spectrum (*a*)] to 210 K [Fig. 2(*b*)] the features assigned to the dioxygen states were not present. There was however spectroscopic evidence, from the loss feature characteristic of $\delta_s(NH_3)$ at 1120 cm^{-1}, for adsorbed ammonia present at low coverage. Also there had developed two features in the high frequency loss region, one at 3390 cm^{-1} assigned to ν(NH) and the other at 3640 cm^{-1} assigned to ν(OH).

The correlation shown to exist[8] between the O–O stretch frequencies and the electronic state of oxygen, suggests that the VEEL spectra for the coadsorbed dioxygen–ammonia system reflect the presence of two different molecular oxygen species [ν(O–O) at 1488 and 1640 cm^{-1}]. One of these (1488 cm^{-1}) is involved in a $NH_3\cdots O_2^{\delta-}$ charge transfer type complex while the other characterised by the higher frequency (1640 cm^{-1}) is a more isolated physisorbed species. There is very little charge associated with this state, its vibrational frequency being close to that reported for the gas phase molecule. It is the former that opens up a low energy oxidation pathway leading to surface OH and NH species [Fig. 2(*b*)]; in contrast, the peroxo state [ν(O–O) at 670 cm^{-1}] observed after the adsorption of pure dioxygen at a Ag(111) surface is unreactive towards ammonia. It is interesting to note that at a Cu(111) surface, exposure of an ND_3 adlayer to dioxygen at 100 K gives rise to a molecularly adsorbed oxygen species[9] characterised by a loss feature at 1500 cm^{-1}.

We acknowledge the support of EPSRC through a CASE Award with ICI to K. T.

Footnote and References

* E-mail: robertsmw@cf.ac.uk

1 A. Boronin, A. Pashusky and M. W. Roberts, *Catal. Lett.*, 1992, **16**, 345; B. Afsin, P. R. Davies, A. Pashusky, M. W. Roberts and D. Vincent, *Surf. Sci.*, 1993, **284,**, 109.
2 A. F. Carley, M. W. Roberts and S. Yan, *J. Chem. Soc., Chem. Commun.*, 1988, 267; *J. Chem. Soc., Faraday Trans.*, 1990, **86**, 2701.
3 G. U. Kulkarni, C. N. R. Rao and M. W. Roberts, *J. Phys. Chem.*, 1995, **99**, 3310.
4 M. W. Roberts, *Chem. Soc. Rev.*, 1996, 437.
5 A. F. Carley, P. R. Davies, M. W. Roberts and D. Vincent, *Top. Catal.*, 1994, **1**, 35; W. W. Crew and R. J. Madix, *Surf. Sci.*, 1996, **356**, 1.
6 M. Neurock, R. A. van Santen, W. Biemolt and A. P. J. Jansen, *J. Am. Chem. Soc.*, 1994, **116**, 6860.
7 A. F. Carley, P. R. Davies, M. W. Roberts and K. K. Thomas, *Surf. Sci.*, 1990, **238**, L467.
8 C. Pettenkoefer, I. Pockrand and A. Otto, *Surf. Sci.*, 1983, **135**, 1.
9 P. R. Davies, M. W. Roberts, N. Shukla and D. J. Vincent, *Surf. Sci.*, 1995, **325**, 50.

Received in Cambridge, UK, 2nd October 1997; 7/07124H

Hydrostannation of C–C multiple bonds with Bu_3SnH prepared *in situ* from Bu_3SnCl and Et_3SiH in the presence of Lewis acid catalysts

Vladimir Gevorgyan, Jian-Xiu Liu and Yoshinori Yamamoto*

Department of Chemistry, Graduate School of Science, Tohoku University, Sendai 980-77, Japan

A number of alkynes 5, allene 11 and alkene 13 smoothly underwent hydrostannation with tributyltin hydride 1, prepared *in situ* from tributylchlorostannane 6 and triethylsilane 7 in the presence of catalytic amounts of Lewis acids.

Since the first synthesis of tributyltin hydride **1** by Finholt *et al.* in 1947,[1] this compound has become one of the most frequently used organometallic reagents in organic synthesis.[2] Along with wide applicability as a hydrogen source in various kinds of reductions,[2] Bu_3SnH is the most popular hydrostannation agent for the synthesis of vinyl-[3] and allyl-stannanes.[4] The latter, due to their great versatility as building blocks, are of increasing importance in modern synthetic organic chemistry.[5] Recently we reported regio- and stereo-selective methods for the synthesis of vinyl- and allyl-tributylstannanes *via* Lewis acid-catalyzed *trans*-hydrostannation of acetylenes[6] and allenes.[7] Although Bu_3SnH is commercially available, it gradually decomposes after storage in a refrigerator for a prolonged period of time;[8] consequently, distillation is needed before use. It occurred to us that *in situ* generation of **1** from stable precursors would be synthetically more convenient for the hydrostannation reaction. The generation of Bu_3SnH *in situ* from more stable stannyl precursors and hydride sources could serve this purpose.[9] In general, the preparation of commercially available tributyltin hydride **1** is carried out by the reduction of tributyltin oxide **2** with hydrosiloxane **3** [reaction (1)].[10]

$$\underset{\mathbf{2}}{n\,(Bu_3Sn)_2O} + 2\,\underset{\mathbf{3}}{(MeSiHO)_n} \xrightarrow{\text{heat}} 2n\,\underset{\mathbf{1}}{Bu_3SnH} + 2\,\underset{\mathbf{4}}{(MeSiO_{1.5})_n} \quad (1)$$

Accordingly, we attempted to employ this method for the *in situ* preparation of **1** under the conditions of the Lewis acid-catalyzed hydrostannation reaction.[6,7] However, no hydrostannation products were detected, instead the starting alkynes were recovered quantitatively. It is probable that, due to the strong affinity of the Lewis acid for the oxygen of either the reactants (**2** and/or **3**) or of the byproduct **4**, it is deactivated and thus not effective as a catalyst in the hydrostannation reaction. Hence, a non-oxygen containing precursor should be employed for the *in situ* preparation of **1**.

Herein we report the first example of the Lewis acid-catalyzed hydrostannation reaction of alkynes with tributyltin hydride **1**, prepared *in situ* from Bu_3SnCl **6** and Et_3SiH **7** [reactions (2) and (4)].

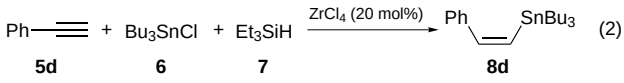

In our initial experiments we found that simple mixing of **6** and **7** in toluene at room temperature did not produce any detectable amount of tin hydride **1**. In contrast, a redistribution took place by the addition of 20 mol% $ZrCl_4$[11] to the same reaction mixture and noticeable amounts of **1** were detected by ^1H NMR analysis of the reaction mixture after one hour [reaction (3)]. Although the mixture contained a large amount of

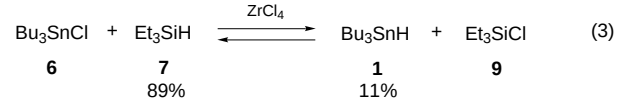

silyl hydride **7** [reaction (3)], it was presumed that, due to the fact that $ZrCl_4$ is not a strong enough Lewis acid to the catalyze hydrosilylation alkynes,[12] this reaction would not compete with the desired hydrostannation process. Motivated by that we applied this method for the *in situ* preparation of **1** and subsequent $ZrCl_4$-catalyzed hydrostannation of phenylacetylene **5d**;[11] as a result the *trans*-addition product (*Z*)-β-(tributylstannyl)styrene **8d** was formed in 52% yield (by ^1H NMR analysis). A brief search for a more efficient Lewis acid catalyst pointed to $B(C_6F_5)_3$. We found that 10 mol% of $B(C_6F_5)_3$ effectively catalyzed the hydrostannation of various alkynes **5** with tributylstannane **1**, generated *in situ* from **6** and **7**, producing the hydrostannation products **8** and **10** in excellent chemical yields [reaction (4), Table 1]. The hydrostannation of

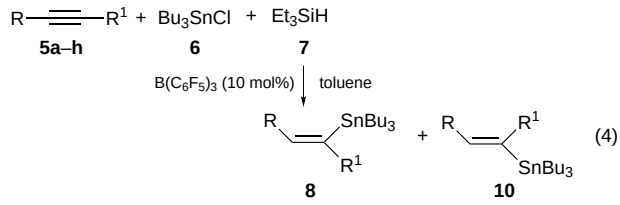

all the monosubstituted alkynes tested (**5a**–**f**) proceeded in a regiospecific manner affording the β-hydrostannation products (**8a**–**f**, **10**) exclusively (entries 1–6, Table 1). Except for the reactions with **5b** and **5g** in which small amounts of the *cis*-addition products were formed (entries 2,7), the reaction was also *trans*-stereoselective (entries 1,3–6,8, Table 1) as was reported for the conventional method for the Lewis acid-catalyzed hydrostannation of alkynes.[6] The preparation of **8a** from **5a** is representative. Tributylstannyl chloride **6** (1.5 mmol), triethylsilane **7** (1.0 mmol) and **5a** (1 mmol) were consecutively added at 0 °C to a solution of $B(C_6F_5)_3$ (0.1 mmol) in dry toluene (0.25 ml) under an argon atmosphere. After being stirred for 40 min at 0 °C the reaction temperature was allowed to warm to 25 °C and the mixture was stirred for another 3 h. The reaction was quenched by adding Et_3N (0.5 mmol) at ambient temperature. Hexane was added and the resulting mixture was filtered through Celite and concentrated under reduced pressure. Purification by column chromatography (aluminium oxide, 90 mesh, *n*-hexane as eluent) gave 220 mg (78%) of **8a**.

Finally, we disclose our initial experiments on the application of this method for the hydrostannation of an allene and alkene. We reported recently that tributyltin hydride **1** in the presence of Lewis acids reacted with a number of allenes affording the corresponding vinylstannanes in good chemical yields.[7] We found that **1**, prepared *in situ* from **6** and **7** in the presence of 10 mol% of $B(C_6F_5)_3$, smoothly reacted with phenylallene **11**

Table 1 $B(C_6F_5)_3$-catalyzed hydrostannation of alkynes with Bu_3SnH generated *in situ* from Bu_3SnCl and Et_3SiH

Entry	R	R^1		Conditions	Yield of **8** + **10**[a] (%)	Ratio **8** : **10**[b]
1	C_6H_{13}	H	**5a**	40 min/0 °C		
				3 h/rt[c]	78	> 95 : 5
2	Cyclohexenyl	H	**5b**	2 h/0 °C	85	86 : 14
3	$PhCH_2$	H	**5c**	4 h/0 °C	85	> 95 : 5
4	Ph	H	**5d**	2.5 h/0 °C	77	> 95 : 5
5	*p*-MeC_6H_4	H	**5e**	2.5 h/0 °C	89	> 95 : 5
6	*p*-$MeOC_6H_4$	H	**5f**	1.5 h/−35 °C	70	> 95 : 5
7	Pentyl	Pentyl	**5g**	40 min/0 °C		
				3 h/rt	90	80 : 20
8	Ph	Ph	**5h**	40 min/0 °C		
				3 h/rt	71	> 95 : 5

[a] Isolated yield. [b] Determined by ^1H NMR analysis of crude reaction mixtures. [c] rt = room temp.

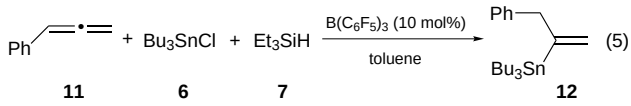

affording the vinylstannane **12** in 51% yield [reaction (5)]. In addition, the same method could be employed for the hydrostannation of alkenes: styrene **13** was converted into the corresponding alkylstannane **14** in 70% isolated yield [reaction (6)]. To the best of our knowledge, reaction (6) is the first

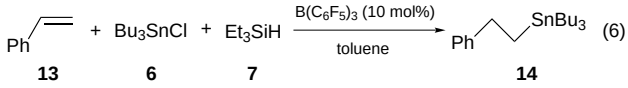

example of the Lewis acid-catalyzed hydrostannation of alkenes.

In conclusion, a synthetically useful and convenient method for the Lewis acid-catalyzed hydrostannation of carbon–carbon multiple bonds with tributyltin hydride **1**, prepared *in situ* from easily handled and cheap chlorostannane **6** and hydrosilane **7**, has been developed. The first example of the Lewis acid-catalyzed hydrostannation of an alkene has been demonstrated.

Footnote and References

* E-mail: yoshi@yamamoto1.chem.tohoku.ac.jp

1 A. E. Finholt, A. C. Bond, K. E. Wilzbach and H. I. Schlesinger, *J. Am. Chem. Soc.*, 1947, **69**, 2693.

2 For a leading review, see W. P. Neumann, *Synthesis*, 1987, 665.

3 H. X. Zhang, F. Guibé and G. Balavoine, *J. Org. Chem.*, 1990, **55**, 1857; Y. Ichinose, H. Oda, K. Oshima and K. Utimoto, *Bull. Chem. Soc. Jpn.*, 1987, **60**, 3468; K. Kikuhawa, F. Umekawa, G. Wada and T. Matsuda, *Chem. Lett.*, 1988, 881; H. Miyake and K. Yamamura, *Chem. Lett.*, 1989, 981.

4 H. G. Kuivila, W. Rahman and R. H. Fish, *J. Am. Chem. Soc.*, 1965, **87**, 2835; M. Koreeda and Y. Tanaka, *Tetrahedron Lett.*, 1987, **28**, 143; Y. Ichinose, K. Oshima and K. Utimoto, *Bull. Chem. Soc. Jpn.*, 1988, **61**, 2693; T. N. Mitchell and U. Schneider, *J. Organomet. Chem.*, 1991, **405**, 195; K. Koerber, J. Gore and J.-M. Vatele, *Tetrahedron Lett.*, 1991, **32**, 1187.

5 (*a*) M. Pereyre, J.-P. Quintard and A. Rahm, *Tin in Organic Synthesis*, Butterworths, London, 1987; (*b*) A. J. Leusink, H. A. Budding and W. Drenth, *J. Organomet. Chem.*, 1967, **9**, 285; 1967, **9**, 295; (*c*) Y. Yamamoto and N. Asao, *Chem. Rev.*, 1993, **93**, 2207; (*d*) J. K. Stille, *Angew. Chem., Int. Ed. Engl.*, 1986, **25**, 508; (*e*) R. F. Heck, *Palladium Reagents in Organic Synthesis*, Academic Press, New York, 1985.

6 N. Asao, J.-X. Liu, T. Sudoh and Y. Yamamoto, *J. Org. Chem.*, 1996, **61**, 4568; N. Asao, J.-X. Liu, T. Sudoh and Y. Yamamoto, *J. Chem. Soc., Chem. Commun.*, 1995, 2405.

7 V. Gevorgyan, J.-X. Liu and Y. Yamamoto, *J. Org. Chem.*, 1997, **62**, 2963.

8 G. Bähr and S. Pawlenko, in *Methoden der Organischen Chemie*, ed. E. Müller and O. Bayer, Thieme Verlag, Stuttgart, 1978, vol. 13/6, p. 181; A. G. Davies and P. J. Smith, in *Comprehensive Organometallic Chemistry*, ed. G. Wilkinson, Pergamon Press, Oxford, 1982, vol. 2, Tin, see also refs. 2, 5(*a*).

9 The reduction of various organic halides with **1** prepared *in situ* from tributyltin chloride and $LiAlH_4$ or $NaBH_4$ has been reported: E. J. Corey and J. W. Suggs, *J. Org. Chem.*, 1975, **40**, 2554; H. G. Kuivila and L. W. Menapace, *J. Org. Chem.*, 1963, **28**, 2165. However, due to the presence of reactive metal hydrides in the reaction mixture, this method could not be applied to the Lewis acid-catalyzed hydrostannation reaction.

10 K. Hayashi, J. Iyoda and I. Shiihara, *J. Organomet. Chem.*, 1967, **10**, 81.

11 Since $ZrCl_4$ was reported to be the best Lewis acid catalyst for *trans*-hydrostannation of alkynes with Bu_3SnH[6] it was chosen for our initial experiments for the *in situ* hydrostannation of alkynes.

12 N. Asao, T. Sudoh and Y. Yamamoto, *J. Org. Chem.*, 1996, **61**, 7654.

Received in Cambridge, UK, 26th August 1997; 7/06187K

Linear tri- and tetra-chromium(II) chains supported by four bis(2-pyridyl)formamidinium ligands

F. Albert Cotton,* Lee M. Daniels, Carlos A. Murillo* and Xiaoping Wang

Department of Chemistry and Laboratory for Molecular Structure and Bonding, Texas A&M University, College Station, TX 77843-3255, USA

Reactions of bis(2-pyridyl)formamidinium ion, $DpyF^-$, with $CrCl_2$ lead to $[Cr_3(DpyF)_4][PF_6]_2$ and $[Cr_4(DpyF)_4Cl_2]Cl_2$, both of which are structurally characterized by X-ray crystallography; the latter contains two Cr–Cr quadruple bonds even though no such bonds were preformed in the starting material ($CrCl_2$).

In our continuing study of compounds with linear chains of metal atoms,[1–3] we have employed the anion of bis(2-pyridyl)formamidine, $DpyF^-$, as a ligand and carried out reactions of the lithium salt with $CrCl_2$ under various conditions, whereby we have obtained† three new and interesting compounds, $[Cr_3(DpyF)_4][PF_6]_2\cdot 4MeCN\cdot 2Et_2O$ (**1**·4MeCN·2Et$_2$O), $[Cr_4(DpyF)_4Cl_2]Cl_2\cdot 5(Me_2CO)$ (**2**·5Me$_2$CO) and a different solvate of **2**, namely, **2**·4MeOH. The crystal structures of all three have been determined‡.

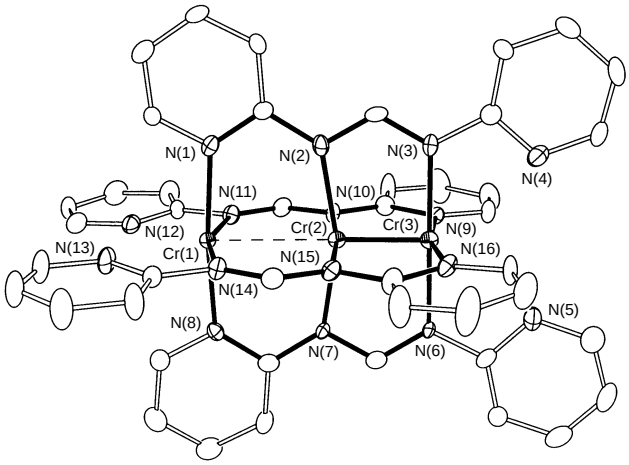

Fig. 1 Perspective view of the cation of **1**. Relevant distances (Å) and angles (°): Cr(1)–Cr(2) 2.738(7), Cr(2)–Cr(3) 1.949(7), Cr(1)–N(1) 2.054(5), Cr(1)–N(11) 2.092(6), Cr(1)–N(14) 2.074(6), Cr(2)–N(2) 2.086(5), Cr(2)–N(7) 2.102(5), Cr(2)–N(10) 2.070(5), Cr(2)–N(15) 2.068(5), Cr(3)–N(3) 2.062(5), Cr(3)–N(6) 2.031(5), Cr(3)–N(9) 2.057(5), Cr(3)–N(16) 2.078(6); Cr(1)–Cr(2)–Cr(3) 179.2(2), N(1)–Cr(1)–N(11) 88.2(2), N(2)–Cr(2)–N(10) 89.7(2), N(3)–Cr(3)–N(9) 90.4(2).

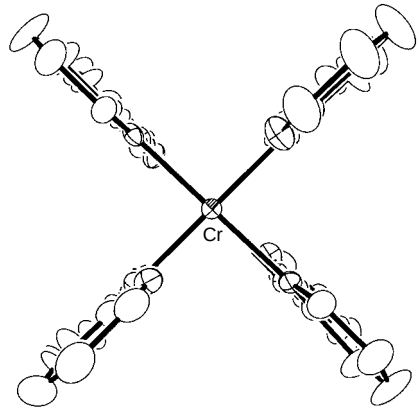

Fig. 2 The $[Cr_3(DpyF)_4]^{2+}$ cation of **1** viewed down the Cr–Cr–Cr direction

The structure of the trinuclear compound **1** is shown in Fig. 1; the Cr_3 chain is not symmetrical and can be qualitatively described as having one pair of chromium atoms quadruply bonded, Cr(2)–Cr(3) 1.949(7) Å, with the third chromium atom not significantly bonded to the central one, Cr(1)–Cr(2) 2.738(7) Å. In comparing the structure of **1** with those previously reported[2] for chromium with dpa^- [dpa^- = anion of bis(2-pyridyl)amine], the most obvious qualitative difference is that the central Cr_3N_{12} core in **1** is essentially untwisted, as shown in Fig. 2, whereas in the dpa compounds there is an overall twist of about 45°. Compound **1** is the first such linear, trinuclear species of any metal§ that is non-helical. The twist in all of the dpa^- compounds is clearly due to the H···H repulsion indicated in **I** while in **II** it is clear that there is no basis for a ligand-imposed twist.

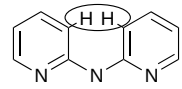

I

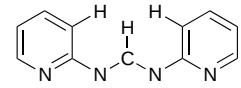

II

As already reported[2] the Cr_3 chains in $Cr_3(dpa)_4X(Y)$ units may be symmetrical (X = Y = Cl, Cr–Cr 2.36 Å) or unsymmetrical (X = Cl, Y = BF_4, Cr–Cr 2.64, 2.00 Å) depending on the axial ligands. In **1** there are no axial ligands. The nearest structural comparison we can make with **1** is the structure of $Cr_3(dpa)_4Cl(BF_4)$ **3**.

To the question of whether absence of helicity is of importance to the electronic structure of the Cr_3^{6+} unit we can offer at least a partial answer at this time. The Cr_3 chain of **1**, like that in **3**, is unsymmetrical. In addition, the Cr–Cr distances in **1**, 1.949(7) and 2.738(7) Å are very similar to those in **3**, 1.995(1) and 2.643(1) Å. In these respects there is no indication that helicity in itself has a qualitative effect on the bonding in the metal atom chain. For the dpa compounds, the structure seems to be tunable, from symmetrical to unsymmetrical, by changing the axial ligands from Cl, Cl to Cl, BF_4. In the case of **1** there are no axial ligands, and thus the unsymmetrical character seems to be inherent in the $[Cr_3(DpyF)_4]^{2+}$ chain.

The cation in **2** is shown in Fig. 3; there are only slight differences between the dimensions in the two crystalline forms. There must, of course, be non-equivalent M–M distances in all M_n chains with $n > 3$. In this case the difference between the central and the outer Cr–Cr distances is very large, *ca*. 2.73 Å *vs*. *ca*. 2.01 Å. It seems reasonable to describe the bonding to a first, and probably good, approximation by saying that there are two Cr–Cr quadruple bonds and little if any bonding between the two inner chromium atoms. The short Cr–Cr distance may be compared to that in the compound $Cr_2(map)_4$[4] (map = anion of 2-amino-6-methylpyridine), where it is 1.870(3) Å. It seems reasonable to attribute the greater length of

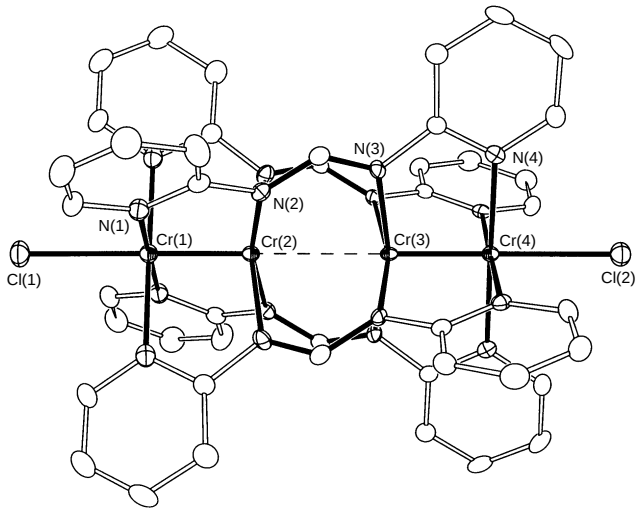

Fig. 3 Perspective view of the cation of **2**·4MeOH. Relevant distances (Å) and angles (°): Cr(1)–Cr(2) 2.013(2), Cr(2)–Cr(3) 2.726(2), Cr(3)–Cr(4) 2.001(2), Cr(1)–N(1) 2.134(4), Cr(2)–N(2) 2.036(3), Cr(3)–N(3) 2.034(4), Cr(4)–N(4) 2.135(4), Cr(1)–Cl(1) 2.545(2), Cr(4)–Cl(2) 2.564(2); Cr(2)–Cr(1)–N(1) 89.7(1), Cr(1)–Cr(2)–N(2) 97.2(1), N(2)–Cr(2)–Cr(3) 82.8(1), Cr(4)–Cr(3)–N(3) 97.3(1), N(3)–Cr(3)–Cr(2) 82.7(1), Cr(3)–Cr(4)–N(4) 90.2(1).

the bonds in **2** to the presence of the axial Cl^- ligands, whereas in $Cr_2(map)_4$ there are no axial interactions.

The observed preference of the chain of three Cr^{2+} ions to form one quadruple bond and the chain of four Cr^{2+} ions to form two separate quadruple bonds rather than to give more delocalized, and therefore evenly spaced arrangements raises the question of how general this tendency may be. It is already known, for both Cr_3 and Co_3 compounds of dpa^- that symmetrical and unsymmetrical structures both occur. In the Cr_4 case, the short–long–short structure makes all the metal chain electrons (MCEs) bonding electrons over short distances where d–d overlaps are very good.¶ It can be hypothesized that in other cases of four metal atoms, especially where MCE counts are higher, more delocalized configurations might be favored. Studies are in progress to examine this.

We acknowledge support by the US National Science Foundation.

Footnotes and References

* E-mail: cotton@tamu.edu; murillo@tamu.edu

† Preparation of $[Cr_3(DPyF)_4][PF_6]_2$ **1** and $[Cr_4(DPyF)_4Cl_2]Cl_2$ **2**. Bis(2-pyridyl)formamidine was prepared by condensation of 2-aminopyridine with triethylorthoformate at 170 °C.[5] An solution of LiDpyF was made by adding 4.0 ml of 1.0 M methyllithium to a solution of HDpyF (0.795 g, 4.0 mmol) in THF (40 ml) at −60 °C. When the LiDpyF solution warmed to ambient temperature, it was transferred to a round-bottom flask containing $CrCl_2$ (0.528 g, 4.3 mmol). A red suspension was obtained after stirring the mixture for 6 h. At this stage, $TlPF_6$ (0.70 g, 2.0 mmol) was added to the suspension. A green solid was produced when it was heated to reflux temperature for 12 h and then cooled to room temp. The supernatant liquid was removed with a syringe and the green solid was washed with THF (15 ml) and CH_2Cl_2 (2 × 20 ml). Extraction with acetone gave a green solution. After layering with hexanes, red crystals of **2**·5Me_2CO were isolated. Yield 0.11 g, 7.7%. The remaining solid was only partially soluble in acetonitrile. After filtration, slow diffusion of diethyl ether into the filtrate changed the color of the solution from green to reddish and gave orange crystals of **1**·4MeCN·2Et_2O, yield 0.44 g, 28%. The remaining solid, which was not soluble in acetone or in acetonitrile, was dissolved in dimethyl sulfoxide to give an emerald green solution. Layering with benzene precipitated a green powder. After filtration, this was washed with diethyl ether and dried under vacuum to yield 0.64 g of green material. Red crystals of **2**·4MeOH were obtained by diffusion of diethyl ether (20 ml) into a saturated green methanol solution (25 ml) of the green powder. The combined yields for **2** are 64%. Crystals of **1** can be redissolved in acetonitrile to produce an orange solution. Red crystals of **2** are not soluble in acetonitrile but can be redissolved in methanol to give a green solution. Compound **1** is paramagnetic, μ_{obs} 4.6 μ_B; **2** is diamagnetic, ^{1}H NMR (CD_3OD, 300 MHz): δ 9.76 (s, 4 H, methine NCHN), 9.48 (d, 8 H, pyridyl CH), 7.83 (m, 16 H, pyridyl CH), 7.09 (t, 8 H, pyridyl CH). UV–VIS (λ/nm): 528, 620 (sh) for **1** in MeCN; 384(sh), 462, 616 for **2** in MeOH.

‡ *Crystal data*: $[Cr_3(DpyF)_4][PF_6]_2$·4MeCN·2Et_2O, **1**·4MeCN·2Et_2O: orange crystal, $C_{60}H_{68}Cr_3F_{12}N_{20}O_2P_2$, M = 1547.28, monoclinic, space group $P2_1/c$, a = 15.006(4), b = 14.993(2), c = 31.238(9) Å. β = 99.79(1)°, U = 6926(3) Å^3, Z = 4, D_c = 1.484 g cm^{-3}, λ = 0.710 73 Å, μ(Mo-Kα) 0.599 mm^{-1}. Intensity data were collected on a CAD4 diffractometer at −100 °C. A ψ-scan absorption correction was made. A total number of 8966 independent reflections were measured, of which 4352 were observed [$I \geqslant 2\sigma(I)$]. The structure was solved by direct methods using SHELXTL and refined using SHELXL-97. During structural refinement, it was found that the chromium atoms were disordered. The final positions of the metal atoms clearly indicate a short Cr–Cr quadruple bond and a long, non-bonded Cr–Cr interaction. The disorder arises since the ligand framework is essentially symmetric, and the short–long bond pair can sit either way in the ligand environment. In the final refinement cycles, the relative occupancy of the two metal-atom groups was refined, and converged with the major orientation having an occupancy of 0.52(1). Final full-matrix least-squares refinement on F^2 of positional and anisotropic thermal parameters for all non-hydrogen atoms converged to R_1 = 0.181, wR_2 = 0.118 for all data; and R_1 = 0.056, wR_2 = 0.102 for data with $I \geqslant 2\sigma(I)$.

$[Cr_4(DPyF)_4Cl_2]Cl_2$·5Me_2CO, **2**·5Me_2CO: red crystal, $C_{59}H_{66}Cl_4Cr_4N_{16}O_5$, M = 1429.08, monoclinic, space group $C2/c$, a = 32.988(4), b = 9.269(1), c = 26.183(7) Å, β = 127.50(1)°, U = 6351(2) Å^3, Z = 4, D_c = 1.491 g cm^{-3}, λ = 0.710 73 Å, μ(Mo-Kα) 0.896 mm^{-1}. Intensity data were collected on a FAST area detector system at −60 °C. A total number of 4145 independent reflections were measured, of which 3660 were observed [$I \geqslant 2\sigma(I)$]. The structure was solved by direct methods using SHELXTL. Full-matrix least-squares refinement on F^2 of positional and anisotropic thermal parameters for all non-hydrogen atoms converged to R_1 = 0.049, wR_2 = 0.111 for all data; and R_1 = 0.041, wR_2 = 0.103 for data with $I \geqslant 2\sigma(I)$.

$[Cr_4(DPyF)_4Cl_2]Cl_2$·4MeOH, **2**·4MeOH: red crystal, $C_{48}H_{52}Cl_4Cr_4N_{16}O_4$, M = 1266.86, tetragonal, space group $P4/n$, a = 12.8063(7), c = 16.326(2) Å, U = 2677.5(4) Å^3, Z = 2, D_c = 1.571 gcm^{-3}, λ = 0.71073 Å, μ(Mo-Kα) 1.050 mm^{-1}. Intensity data were collected on a FAST area detector system at −60 °C. A total number of 1767 independent reflections were measured, of which 1647 were observed [$I \geqslant 2\sigma(I)$]. The structure was solved by direct methods using SHELXTL. During structural refinement, it was found the crystal twinned along the (110) plane. The occupancy of both components were refined and the major component contributed to 59.5% of the structure. Final refinement converged to R_1 = 0.044 and wR_2 = 0.108 for all data, and R_1 = 0.040 and wR_2 = 0.103 for data with $I \geqslant 2\sigma(I)$. CCDC 182/652.

§ $M_3(dpa)_4X_2$ compounds, all of which are helical, have been reported for M = Cr,[2] Co,[3] Ni, Cu and Ru. Full references are found in ref. 3.

¶ Compounds containing two quadruply bonded M_2^{4+} units (M = Mo and W), end-to-end, are also known.[6] In these cases the quadruply bonded dimetal units were already present in the starting material.

1 F. A. Cotton, L. M. Daniels and G. T. Jordan, IV, *Chem. Commun.*, 1997, 421.
2 F. A. Cotton, L. M. Daniels, C. A. Murillo and I. Pascual, *J. Am. Chem. Soc.*, 1997, **119**, 10 233.
3 F. A. Cotton, L. M. Daniels, G. T. Jordan, IV and C. A. Murillo, *J. Am. Chem. Soc.*, 1997, **119**, 10 377.
4 F. A. Cotton, R. H. Niswander and J. C. Sekutowski, *Inorg. Chem.*, 1978, **17**, 3541.
5 R. M. Roberts, *J. Org. Chem.*, 1949, **14**, 277.
6 R. H. Cayton, M. H. Chisholm, J. C. Huffman and E. B. Lobkovsky, *J. Am. Chem. Soc.*, 1991, **113**, 8709; *Angew. Chem., Int. Ed. Engl.*, 1991, **30**, 862; R. H. Cayton, M. H. Chisholm, E. F. Putilina and K. Folting, *Polyhedron*, 1993, **12**, 2627.

Received in Bloomington, IN, USA; 13th August 1997; 7/05940J

A biomimetic methyl transfer from amine to thiol

Masaru Tada,*[a] Tohru Kambe[a] and Yoshinobu Inouye[b]

[a] *Department of Chemistry, Advanced Research Center for Science and Engineering and Materials Research Laboratory for Bioscience and Photonics, Waseda University, Shinjuku, Tokyo 169, Japan*
[b] *Department of Chemistry, University of Tsukuba, Tsukuba, Ibaraki 305, Japan*

A biomimetic methyl transfer, analogous to a tetrahydrofolate-to-homocystein transfer, is simulated by the reaction of methylammonium salts with arylthiolatocobaloxime; the mechanism proposed is an electron transfer from the cobaloxime to the ammonium ion followed by radical substitution of the methyl group.

Biological methyl transfers often occur *via* methionine, $(HO_2C)(NH_2)CHCH_2CH_2SMe$,[1] and methyl coenzyme-M, $^{-}O_3SCH_2CH_2SMe$.[2] Methyl groups in these cofactors originate from N^5-methyl derivatives of tetrahydropteridine, *i.e.* N^5-methyltetrahydrofolic acid **1a**, (R^1 = H, R^2 = CONH–glutamate)[3] and N^5-methyltetrahydromethanopterin **1b**, [R^1 = Me, R^2 = $CH_2(CHOH)_3CH_2OPO_2HOCH(CO_2H)(CH_2)_2CO_2H$].[4]

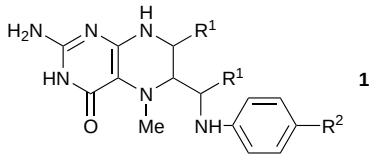

1

These methyl transfers from amine to sulfur are mediated by coenzyme-B_{12} and its congener,[5] but the participation mode of the cobalt complexes has not been clarified as yet.[6,7] The direct methyl transfer from a methyl ammonium salt to a thiolate anion is known[8] but the cobalt mediated biological methyl transfer is much faster than the direct biological methyl transfer from nitrogen to sulfur.[9]

We report here a biomimetic N–S methyl transfer which is assisted by a cobalt complex. Coenzyme-M was originally isolated in the disulfide form.[10] Thiol and disulfide forms both exist in biological systems because they are interconvertible *via* a simple biochemical redox process. We therefore started the model reaction from a disulfide and bis(dimethylglyoximato)(4-*tert*-butylpyridine)cobalt(II) [cobaloxime(II)]. Thus diaryl disulfides **2** were treated with cobaloxime(II) (0.5 equiv.) to produce arylthiolatocobaloxime(III) **3** in fair yields (Scheme 1).

Reaction† of phenylthiolatocobaloxime(III) **3b** with a trimethylanilinium salt **4** gave methyl sulfide **5** in addition to diphenyl disulfide **6**. The reaction of **3b** with a methylpiperidinium salt **7** yielded the corresponding phenyl sulfide **8** and disulfide **6** (Scheme 2).

We then tested the effect of a *para*-substituent on the phenyl group of **3** and the benzyl group of ammonium salt **9**. The ammonium salt **9** having an electron-withdrawing substituent gave higher yields of the products **10** (Scheme 3 and Table 1).

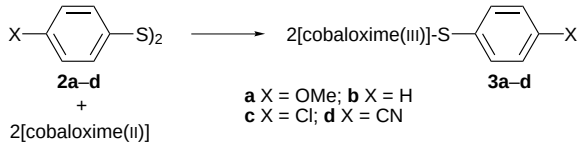

2a–d + 2[cobaloxime(II)] → **3a–d**

a X = OMe; **b** X = H
c X = Cl; **d** X = CN

Scheme 1

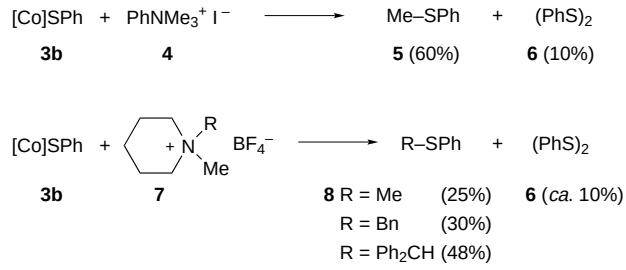

Scheme 2

On the other hand, arylthiolatocobaloxime(III) **3** having an electron-donating substituent showed higher reactivity towards benzyldimethylanilinium salt **11** to yield benzyl sulfide **12** selectively (Scheme 3). Similarly, the reaction with a folate coenzyme model **14**[8] produced methyl sulfide **15**. The time course of the reaction of **3** with benzylammonium salt **11** clearly shows the relationship between the relative rate of product formation and the substituent on **3** (Fig. 1).

The substituent effect envisages nucleophilic attack of the arylthiolate anion at the methyl or benzyl group without the assistance of the cobalt complex, as reported by Hilhorst *et al.*[8] However, the formation of the thiolate anion from arylthiolatocobaloximes **3** must precede the nucleophilic attack, and the electron-withdrawing substituent on **3** is expected to accelerate this heterolysis, contrary to the experimental findings.

If these methyl and benzyl transfer reactions start with the initial homolysis of the sulfur–cobalt bond of **3**,‡ the reactivity

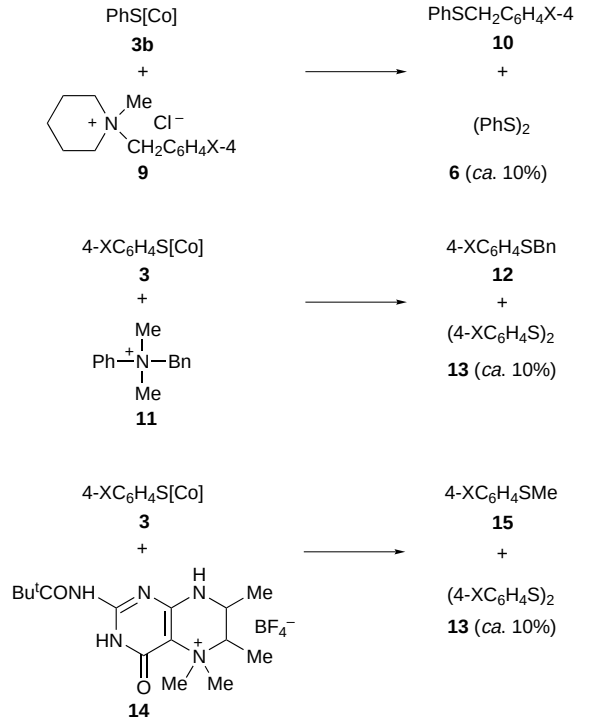

Scheme 3

Table 1 Substituent effect on methyl transfer from an ammonium ion to arylthiolatocobaloximes

Starting material	Ammonium ion	X	Product	Yield (%)
3b	**9a**	OMe	**10**	19
3b	**9b**	H	**10**	30
3b	**9c**	NO_2	**10**	38
3a	**11**	OMe	**12a**	77
3b	**11**	H	**12b**	72
3c	**11**	Cl	**12c**	70
3d	**11**	CN	**12d**	65
3a	**14**	OMe	**15a**	61
3b	**14**	H	**15b**	51
3c	**14**	Cl	**15c**	48
3d	**14**	CN	**15d**	44

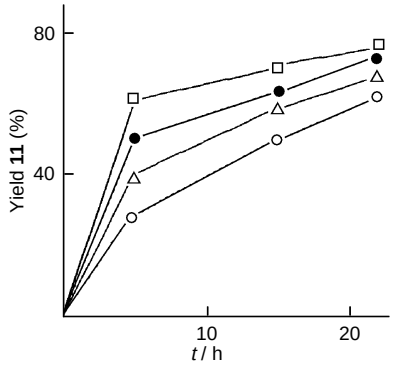

Fig. 1 Time course of the reaction of arylthiolatocobaloximes **3** with benzyldimethylammonium salt **11**: (□) **3a**, (●) **3b**, (△) **3c** and (○) **3d**

of **3** must be inversely proportional to the bond strength and hence the bond distance of the sulfur–cobalt bond. X-Ray crystal analyses[11] determined the Co–S distance of **3** as shown in Table 2. However, this correlation between the oxidation potential (E_{ox}) and the bond distance (d_{Co-S}) breaks down upon moving from **3c** and **3d**. The X-ray analysis unexpectedly showed the Co–S bond in 4-chlorophenylthiolatocobaloxime(III) **3c** to be shorter than the others. As we pointed out earlier,[12] the strength of the cobalt–sulfur bond is a consequence of the donation and back-donation from sulfur to cobalt. Cyclic voltammetry of arylthiolatocobaloximes **3a–d** showed a reversible oxidation wave as shown in Table 2, and the reactivity of the present methyl and arylmethyl group transfer has a trend parallel with the oxidation potential (E_{ox}) of **3a–d**; a lower oxidation potential results in higher reactivity.

The substituent effects on both sides of the reactants suggest a single electron transfer (SET) mechanism. The intermediacy of the arylthiyl radical is supported by the formation of diaryl disulfide in all the reactions. As one of the plausible mechanisms for the methyl transfer, we propose a homolytic substitution by an arylthiyl radical on the methyl group of the zwitterionic species formed by SET [Scheme 4, (*a*)].‡ The migrations of the benzyl and diphenylmethyl groups are considered to proceed *via* a radical coupling mechanism

Table 2 Oxidation potentials and bond lengths of arylthiolatocobaloxime(III) **3**

Compound	X	E_{ox}/V[a]	*d*(Co–S)/Å
3a	OMe	+0.483	2.291
3b	H	+0.542	2.280
3c	Cl	+0.563	2.261
3d	CN	+0.777	2.274[b]

[a] Pt electrodes; voltage *vs.* $Ag/AgNO_3$; **3a–d** (0.2 mmol dm^{-3}), Bu_4NClO_4 (0.1 mol dm^{-3}) in MeCN; scan rate, 0.100 V s^{-1}. The voltages were referenced to ferrocene (E_{ox} = 0.083 V). [b] Mean value of two independent molecules in the asymmetric unit.

(*a*)

$$ArS[Co^{III}] + Me-\overset{+}{N}R_2-Ar \xrightarrow{SET} ArS^{\bullet} + Me-\overset{+}{N}R_2-Ar^{\bullet -}$$

$$\downarrow$$

$$ArS-Me + R_2NAr + [Co^{III}]^+$$

(*b*)

$$ArS[Co^{III}] + R_3\overset{+}{N}-CH_nPh_{3-n} \longrightarrow ArS^{\bullet} + R_3\overset{+}{N}-CH_nPh_{3-n}^{\bullet -} + [Co^{III}]^+$$

$$\downarrow$$

$$ArS-CH_nPh_{3-n} + NR_3 + [Co^{III}]^+ \longleftarrow ArS^{\bullet} + {}^{\bullet}CH_nPh_{3-n} + NR_3 + [Co^{III}]^+$$

Scheme 4

[Scheme 4, (*b*)] because these migrations occur in preference to methyl group migration in spite of greater steric hindrance. In accordance with the SET mechanism, the reactions proceed more efficiently in polar MeCN than in less polar $CHCl_3$ or protic MeOH.

Direct methyl transfer to a thiolate anion[8] *via* an S_N2 mechanism cannot explain the involvement of coenzyme-B_{12} in enzymatic processes. The present experimental findings account for assistance by a cobalt complex and suggest a possible scheme for the enzymatic process, in which N^5-protonated-N^5-methyltetrahydrofolic acid and homocysteinylthiolato–coenzyme B_{12} complex are reaction partners.

We thank Waseda University and the Ministry of Education, Sports, and Culture of Japan for financial support *via* the Annual Project Program (95A-252) and a Grant-in-aid for Scientific Research (09640649), respectively.

Footnotes and References

* E-mail: mtada@mn.waseda.ac.jp

† Reaction conditions were the same for all reactions of **3**. A mixture of **3** (0.2 mmol) and an ammonium salt (0.25 mmol) in MeCN (10 cm^3) was heated to 80 °C for 22 h and then concentrated to 1 cm^3. The concentrated mixture was subjected to Florisil chromatography (hexane–CH_2Cl_2) to remove polar non-volatile materials. The yields of **5** were obtained by GC analyses of the eluate using an internal standard, and those of **8**, **10**, **12** and **15** refer to the isolated products. In most cases the starting materials persisted but the reactions were stopped after 22 h to assess the relative reactivities.

‡ The direct attack of the arylthiyl radical on ammonium salts is ruled out by the lack of reactivity of the arylthiyl radical generated by PhSH–AIBN or photolysis of $(PhS)_2$.

1 R. G. Matthews and J. T. Drummond, *Chem. Rev.*, 1990 **90**, 1275.
2 A. A. DiMarco, T. A. Babik and S. S. Wolfe, *Annu. Rev. Biochem.*, 1990, **59**, 355; K. M. Noll, *Method in Enzymology*, ed, L. Lacker, Academic, San Diego, 1995, vol. 251, p. 470.
3 R. T. Tayor, B_{12}, ed D. Dolphin, Wiley, New York, 1982, vol. 2, p. 307; C. Temple, Jr. and J. A. Montogomery, *Folates and Pterins*, ed, R. L. Blackley and S. J. Benkovic, Wiley, New York, 1984, vol. 1, p. 62.
4 P. Van Beelen, A. P. M. Stassen, W. G. Bosch, G. D. Vogels, W. Guijt and C. A. G. Haasnoot, *Eur. J. Biochem.*, 1984, **138**, 563; J. T. Keltjens, P. C. Raemakers- Franken and G. D. Vogles, *Microbial Growth on C_1-Compounds*, ed, J. C. Murrell and D. P. Kelly, Intercept, Andover, 1993, p. 135.
5 R. G. Matthews, R. V. Banerjee and S. W. Ragsdale, *Bio Factors*, 1990, **3**, 147; B. Krautler, *FEMS Microbiol. Rev.*, 1990, **87**, 349.
6 S. M. Polsen, H. Hansen and L. G. Marzilli, *Inorg. Chem.*, 1997, **36**, 307.
7 H. P. C. Hogenkamp, G. T. Bratt and S.-Z. Sun, *Biochemistry*, 1985, **24**, 6428; G. N. Schrauzer and R. J. Windgassen, *J. Am. Chem. Soc.*, 1967, **89**, 3607.
8 E. Hilhorst. T. B. R. A. Chen, A. S. Iskander and U. K. Pandit, *Tetrahedron*, 1994, **50**, 7837.
9 R. G. Matthews, *Folates and Pterins*, ed, R. L. Blackley and S. J. Benkovic, Wiley, New York, 1984, vol. 1, p. 497.
10 C. D. Taylor and R. S. Wolfe, *J. Biol. Chem.*, 1974, **249**, 4879.
11 Y. Inouye, T. Kambe and M. Tada, unpublished work.
12 M. Tada and R. Shino, *J. Inorg. Biochem.*, 1991, **44**, 89; M. Tada, T. Yoshihara and K. Sugano, *J. Chem. Soc., Perkin Trans. 1*, 1995, 1941.

Received in Cambridge, UK, 22nd September 1997; 7/06823I

Chemoselective isomerization of amide-substituted oxetanes with Lewis acid to give oxazine derivatives or bicyclic amide acetals

Tomonari Nishimura,[a] Shigeyoshi Kanoh,*[a]† Hitoshi Senda,[a] Toshiyuki Tanaka,[b] Kohji Ando,[a] Hiroshi Ogawa[a] and Masatoshi Motoi*[a]

[a] *Department of Industrial Chemistry, Faculty of Engineering, Kanazawa University, Kodatsuno, Kanazawa 920-8667, Japan*
[b] *Department of Pharmacognosy, Gifu Pharmaceutical University, Mitahora-higashi, Gifu 502-8585, Japan*

The Lewis-acid catalyzed isomerization of secondary and tertiary amide-substituted oxetanes takes place chemoselectively, giving 5-hydroxymethyl-5,6-dihydro-4*H*-1,3-oxazines and reactive amide acetals consisting of a bicyclo[2.2.2]octane skeleton, respectively.

Oxetane and its various derivatives are well known to be polymerizable cationically *via* conventional ring-opening processes.[1,2] As an exception, certain oxetanes carrying a carbonyl-containing substituent, however, can undergo Lewis-acid catalyzed intramolecular nucleophilic attack of the unsaturated oxygen atom, for example, ester-substituted oxetanes **1** give the bridged orthoesters **2**,[3] and cyclic imide-substituted oxetanes **3** give bicyclic acetals with a lactam ring **4**[4] (Scheme 1). Here we report a novel chemoselective isomerization of oxetanes having an amide group at their 3-positions. The isomerization of the amide-substituted oxetanes **5** with Lewis acid gives two quite different types of products, depending on the structure of amide group. One type is 5-hydroxymethyl-5,6-dihydro-4*H*-1,3-oxazines **6** produced from the secondary amides of **5** by a new mode of rearrangement involving the oxetanyl group. The other type is bicyclic amide acetals, *i.e.* 2,6-dioxa-7-azabicyclo[2.2.2]octanes **7**, which are produced from the tertiary amides of **5** by a similar mode to those in the already reported cases of **1** and **3**.

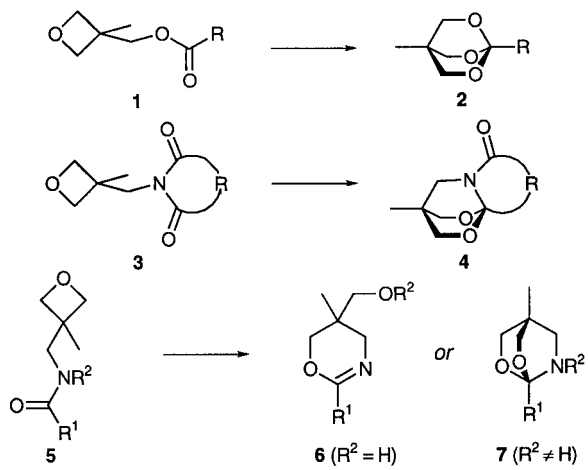

Scheme 1

Starting oxetane amides **5a**–**e** were prepared *via* acylation of oxetane amine **8** derived from **3** (phthalimide), and the resulting secondary amides were *N*-alkylated under phase-transfer catalyzed conditions[5] to give the tertiary amides **5f**–**k**.‡

The isomerization of **5** was successfully carried out in anhydrous chlorobenzene or CH_2Cl_2 using Lewis acids such as $BF_3{\cdot}OEt_2$ and $AlMe_3$ (Table 1).§ Like **1** and **3** cycloacetalization occurred in the reactions of **5f**–**k**. The products (**7f**–**k**) obtained are a new series of bicyclic amide acetals.¶ Analogous amide acetals of the bicyclo[*n*.3.0] type (*n* = 3 or 4) have already been synthesized by intermolecular cycloaddition or transacetalization, and they have been reported to possess high susceptibility to nucleophiles.[6] Similarly compounds **7** were so sensitive to moisture that hydrolytic fission proceeded rapidly under normal conditions.‖ When the above isomerization was run for 24 h at 100 °C and above, most of the **7** produced was consumed. The final products were oligomers having a polyether backbone.

In sharp contrast, the isomerization of **5a** unexpectedly afforded 5-hydroxymethyl-5-methyl-2-phenyl-5,6-dihydro-4*H*-1,3-oxazine **6a** instead of a bicyclic amide acetal, and no polymerization took place.¶ The molecular structure of **6a** was established by X-ray analysis (Fig. 1).** The isomerization of the other secondary amides (**5b**–**e**) always gave oxazine derivatives (**6b**–**e**) in good yields (Table 1).¶ Compounds **6** were stable during distillation or recrystallization, but chromatographic manipulation over alumina often caused hydrolysis to propanediols with amide groups.

Table 1 Lewis-acid catalyzed isomerization of oxetane amides **5**[a]

Amide		Lewis acid				Product	
	(R^1,R^2)		(mol%)	*T*/°C	*t*/h		Yield (%)[b]
5a[c]	(Ph, H)	$BF_3{\cdot}OEt_2$	(25)	35	96	**6a**	89
5b	(H, H)	$AlMe_3$	(50)	120	24	**6b**	50[d]
5c	(Me, H)	$AlMe_3$	(5)	120	24	**6c**	92
5d	(Pr^n, H)	$AlMe_3$	(5)	120	24	**6d**	89
5e	($PhCH_2$, H)	$AlMe_3$	(5)	120	24	**6e**	71
5f	(Ph, Et)	$BF_3{\cdot}OEt_2$	(5)	120	1	**7f**	59
5g	(Ph, $PhCH_2$)	$BF_3{\cdot}OEt_2$	(5)	130	1	**7g**	61
5h	(H, $PhCH_2$)	$BF_3{\cdot}OEt_2$	(35)	70	96	**7h**	63
5i	(Me, Et)	$BF_3{\cdot}OEt_2$	(5)	130	1	**7i**	55
5j	(Me, $PhCH_2$)	$BF_3{\cdot}OEt_2$	(5)	130	1	**7j**	65
5k	(Pr^i, Et)	$BF_3{\cdot}OEt_2$	(5)	130	1.5	**7k**	48

[a] In PhCl. [b] Isolated yield. [c] In CH_2Cl_2. [d] The reaction was quenched with Et_3N followed by MeOH containing a small amount of dilute NaOH.

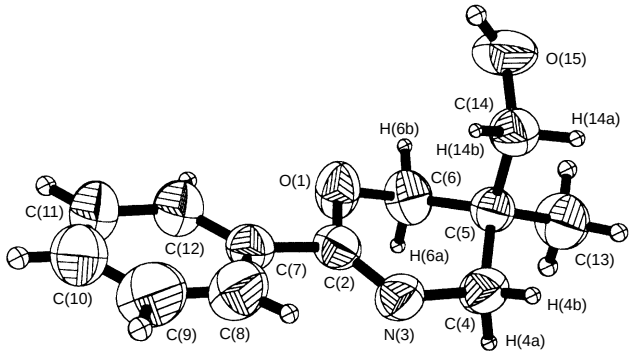

Fig. 1 ORTEP view of **6a** (30% probability thermal ellipsoids)

Although the secondary and tertiary amides of **5** are isomerized giving structurally different products, these reactions can be explained by the following mechanisms passing through a common intermediate **B** (Scheme 2). Both isomerizations begin with the coordination of Lewis acid E to oxetanyl oxygen atom of **5**, and then oxonium **A** undergoes intramolecular nucleophilic attack of the carbonyl oxygen atom by neighboring group participation. The fate of the resulting **B** determines the consequent chemoselection. For tertiary amides, subsequent ring closure of **B** gives an equilibrium mixture of **C** and **C′**. On the other hand, **B** is interconvertible to **B′** when R^2 is a hydrogen atom. The iminium and ammonium salts, **B′** and **C′**, are probably thermodynamically more stable than **B** and **C**, and the catalytic turnover of Lewis acid would decrease as the isomerization progresses. This was strongly supported by the observation that the isomerization rates of **5** steeply slowed down at increased yields of basic **6** and **7**. In order to force these reactions to completion, it was necessary to employ either high temperature or a very large amount of Lewis acid, or both (Table 1). Under such conditions, however, the yields of **7** began to decrease after reaching maxima at relatively early stages, because of inevitable polymerization as a competing reaction.

In the chemoselective isomerization of **5**, moderate to fairly good yields of **6** and **7** were obtained using simple operations. Like other bicyclic amide acetals,[6] compounds **7** are also interesting in a variety of chemical transformations not only as reactive amino ethers but also as ring-opening polymerizable monomers.[6,7] Numerous methods of preparing dihydro-1,3-oxazines appear in the literature.[8] The advantages (as well as differences) in the present reaction may be summarized as follows: (a) the preparation of dihydro-1,3-oxazines having a hydroxymethyl group, which is a useful functional group for further modification. (b) A general method for obtaining not only the phenyl- or alkyl-substituted oxzines at the 2-positions but also the unsubstituted oxazine.

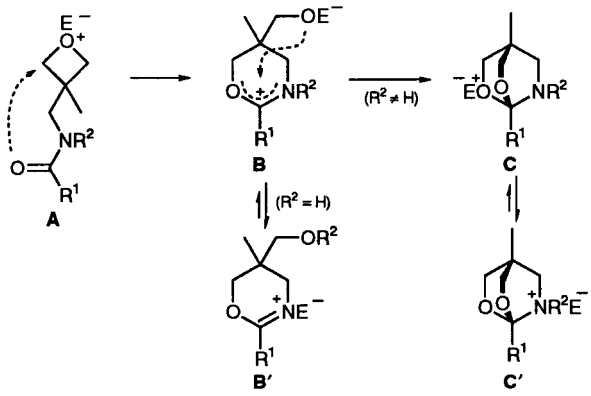

Scheme 2

Footnotes and References

† E-mail: kanoh@kenroku.ipc.kanazawa-u.ac.jp

‡

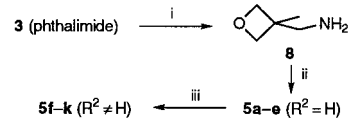

Reagents and conditions: i, 3-methyl-3-(phthalimidomethyl)oxetane[4] (1.0 equiv.), hydrazine hydrate (5 equiv.), in EtOH, 60 °C, 1.5 h, and then a catalytic amount of Raney Ni (*W*-2), vigorous reflux, 81% (GLPC purity 96%), bp 90–95 °C/100 mmHg; ii, acylating reagents: $(R^1CO)_2O$, HCO_2COMe, or R^1CO_2H (DCC coupling), 76–92%; iii, **5** (1.0 equiv.), R^2Br (1.1 equiv.), K_2CO_3 (1.0 equiv.), NaOH (2.5 equiv.), $Bu^n_4NHSO_4$ (0.10 equiv.), in benzene, 40 °C to reflux, 3–15 h, 55–78%.

§ *Typical experimental procedure*: To an anhydrous PhCl (1.0 ml) solution of **5c** (150 mg, 1.1 mmol) in a tube was added 1.0 mol l^{-1} $AlMe_3$ in hexane (0.05 mmol) under nitrogen. The resulting solution was allowed to react at 120 °C for 24 h. After the reaction was quenched by addition of Et_3N (0.1 ml) followed by MeOH (3.0 ml), the solvents were replaced by CH_2Cl_2 (10 ml). Distillation of the CH_2Cl_2-soluble part afforded **6c** in 92% yield, bp 100–110 °C/0.1 mmHg. Similarly, the isomerization of **5f** was carried out in a small distillation flask at 120 °C for 1 h. After the addition of anhydrous Et_3N (0.1 ml) followed by CaH_2 (*ca.* 50 mg), distillation of the resulting mixture afforded **7f** (0.12 g, 0.52 mmol) in 59% yield, bp 110–120 °C/0.1 mmHg. The product isolated was stable under nitrogen.

¶ All compounds were characterized by ^1H NMR and IR spectroscopy, although the IR spectra of **7** were always observed as a mixture of **7** and its hydrolysis product. *Selected data* for **6a**: mp 135–136 °C (CH_2Cl_2–hexane); ν_{max}(KBr)/cm^{-1} 3400 (OH), 1650 (C=N); the atomic numbering system refers to that used in Fig. 1; δ_H($CDCl_3$, *J*/Hz) 7.89 (dd-like, *J* 6.9, 1.5, 2 H, ArH_o), 7.44–7.33 (m, 3 H, $ArH_{m,p}$), 4.23 [dd, *J* 10.7, 2.4, 1 H, H(6b)], 3.92 [d-like, *J* 10.7, 1 H, H(6a)], 3.57, 3.47 [each d, *J* 10.7, 2 H, H (14a) and H (14b), 3.48 [dd, *J* 16.9, 2.2, 1 H, H (4b)], 3.27 [d-like, *J* 16.6, 1 H, H(4a)], 2.02 (br s, 1 H, OH), 1.02 [s, 3 H, C(13) H_3]; δ_C (100 MHz, $CDCl_3$) 155.0 [C(2)], 133.3 [C(7)], 130.5 [C(10)], 128.0 [C(9), C(11)], 127.0 [C(8), C(12)], 70.1 [C(6)], 65.8 [C(14)], 51.1 [C(4)], 32.7 [C(5)], 19.0 [C(13)]. HRMS: *m*/*z* 205.1115, calc. for $C_{12}H_{15}NO_2$: 205.1104. Analysis for $C_{12}H_{15}NO_2$, found (calc.): C, 69.96 (70.22); H, 7.33 (7.37); N, 6.76 (6.82%). For **7f**: δ_H(anhydrous $CDCl_3$ under nitrogen, *J*/Hz) 7.60 (dd, *J* 6.8, 3.2, 2 H, ArH_o), 7.38–7.29 (m, 3 H, $ArH_{m,p}$), 3.98 (s, 4 H, OCH_2), 2.99 (s, 2 H, NCH_2), 2.36 (q, *J* 7.2, 2 H, CH_2CH_3), 0.94 (t, *J* 7.3, 3 H, CH_2CH_3), 0.88 (s, 3 H, CCH_3). HRMS: *m*/*z* 233.1439, calc. for $C_{14}H_{19}NO_2$: 233.1417.

‖ The hydrolysis product is 2-ethylaminomethyl-2-hydroxymethylpropyl benzoate. The initially formed esters except for the benzoates and isobutyrate were spontaneously converted to the corresponding amide-substituted propanediols by acyl exchange.

** **6a**: Mp 135–136 °C (CH_2Cl_2–hexane). *Crystal data* for **6a**: space group $P2_1/c$, Z = 4, a = 11.044(1), b = 9.3865(8), c = 11.817(1) Å, β = 116.336(8)°, D_c = 1.242 g cm^{-3}. 2816 measured, 2685 independent reflections, of which 1813 were considered as observed [$I > 3.00\ \sigma(I)$]. R = 0.039, R_w = 0.035. CCDC 182/639.

1 M. P. Dreyfuss and P. Dreyfuss, in *Encyclopedia of Polymer Science and Engineering*, Wiley, New York, 1987, vol. 10, pp. 653–670.
2 H. Ogawa, T. Hosomi, T. Kosaka, S. Kanoh, A. Ueyama and M. Motoi, *Bull. Chem. Soc. Jpn.*, 1997, **70**, 175; M. Motoi, S. Sekizawa, K. Asakura and S. Kanoh, *Polym. J.*, 1993, **25**, 1283 and references cited therein.
3 E. J. Corey and N. Raju, *Tetrahedron Lett.*, 1983, **24**, 5571; P. Ducray, H. Lamotte and B. Rousseau, *Synthesis*, 1997, 404.
4 S. Kanoh, T. Hashiba, K. Ando, H. Ogawa and M. Motoi, *Synthesis*, 1997, in the press.
5 T. Gajda and A. Zwierzak, *Synthesis*, 1981, 1005.
6 R. Feinauer, *Synthesis*, 1971, 16.
7 C. Lu and G. Odian, *J. Polym. Sci., Part A: Polym. Chem.*, 1994, **32**, 2283.
8 W. Seeliger, E. Aufderhaar, W. Diepers, R. Feinauer, R. Nehring, W. Thier and H. Hellmann, *Angew. Chem., Int. Ed. Engl.*, 1966, **5**, 875 and references cited therein; Y. Ito, Y. Inubushi, M. Zenbayashi, S. Tomita and T. Saegusa, *J. Am. Chem. Soc.*, 1973, **95**, 4447.

Received in Cambridge, UK, 5th August 1997; 7/05679F

Supramolecular self-assembly of a toroidal inclusion complex, $[NH_4][Co_8(MeCO_2)_8(OMe)_{16}][PF_6]$

James K. Beattie, Trevor W. Hambley, John A. Klepetko, Anthony F. Masters* and Peter Turner

School of Chemistry, The University of Sydney, Sydney, NSW, 2006, Australia

Diamagnetic $[NH_4][Co_8(MeCO_2)_8(OMe)_{16}][PF_6]$, a compound with eight cobalt atoms bridged by methoxy and acetato ligands so as to form a planar ring with an ammonium ion at its centre, is isolated from the reaction between cobalt(III) acetate and methanol in the presence of NH_4PF_6.

We recently reported that slow recrystallisation of 'cobalt(III) acetate' in the presence of a halide source produced the mixed valence octanuclear compound $[Co_8O_4(MeCO_2)_6(OMe)_4Cl_4(OH_n)_4]\cdot 6H_2O$ (n = 1, 2).[1] Structural characterisation of this compound showed it to contain a central $[Co_8O_8]$ core consisting of a linear array of three face-sharing $[Co_4O_4]$ cubane fragments. A similar mixed valence Co_8 core had previously been reported in the compound $[Co_8O_4(MeCO_2)_6(OH)_4L_2][ClO_4]_2$ [L = tetradentate ligand, 1,2-bis(2,2′-bipyridyl-6-yl)ethane], prepared by H_2O_2 treatment of $Co(MeCO_2)_2\cdot 4H_2O$ (3 equiv.) in the presence of L (1 equiv.) and $LiClO_4$.[2] The isolation of $[Co_8O_4(MeCO_2)_6(OMe)_4Cl_4(OH_n)_4]$ suggests that supramolecular assembly of the Co_8 core (and possibly of other architectures) may occur even in the absence of polydentate ligands. Thus, another mixed valence octanuclear derivative, $[Co_8O_4(PhCO_2)_{12}L_4]$ [L_4 = $(MeCN)_3(H_2O)$], has been prepared by addition of aqueous H_2O_2 to a dmf solution of cobalt benzoate, followed by recrystallization from CH_2Cl_2–MeCN.[3,4] This material has a $[Co_8O_4]^{12+}$ framework in which trigonally bipyramidally coordinated Co^{II} atoms are bound to the oxygens of a central $[Co^{III}_4O_4]^{4+}$ cubane.

We report here the isolation and structural characterization of a second octanuclear material from 'cobalt(III) acetate', $[NH_4][Co_8(MeCO_2)_8(OMe)_{16}][PF_6]$ **1**. Reaction of 'cobalt(III) acetate' (0.5 g)[5] and NH_4PF_6 (0.61 mmol in 3 ml) in methanol over one week at ambient temperature gave an as yet unidentified green microcrystalline solid and large dark green, plate-like crystals of **1**. Pure **1** was obtained by decanting the remaining solution followed by rinsing and decanting diethyl ether suspensions of the microcrystalline solid. The initial yield of **1** was typically *ca*. 5% (0.03 mmol) based on NH_4PF_6. Although the yields have not been optimised, further, larger, crops of **1** and of the microcrystalline solid were obtained after leaving the filtrate for a period of several days to several weeks. Crystals suitable for single crystal X-ray diffraction analysis were obtained by leaving the reaction mixture undisturbed for several weeks. To prevent decomposition the crystals were kept under diethyl ether and subsequently used in single crystal X-ray diffraction measurements.† Single crystal X-ray diffraction‡ showed that **1** consists of a molecule of $[Co_8(MeCO_2)_8(OMe)_{16}]$ which functions as an inclusion host for an NH_4^+ cation. Charge balance is provided by a PF_6^- anion in the lattice. The $[Co_8(MeCO_2)_8(OMe)_{16}]$ molecule has a highly symmetric toroidal shape (Fig. 1), containing four $[Co_2(\mu\text{-}MeCO_2)(\mu\text{-}OMe)_2]$ units, forming eight edge-shared CoO_6 distorted octahedra. The cobalt atoms are situated at the vertices of a near regular planar octagon. Each pair of cobalt atoms is bridged by an acetate ligand and two stereochemically distinct methoxide ligands, one methoxide on either side of the Co_8 plane. The acetate ligands on adjacent pairs of cobalt atoms are alternatively above and below and at approximately 30° to the Co_8 plane. Of the eight methoxide ligands on each side of the Co_8 plane, four have O–C bonds perpendicular to the Co_8 plane, whereas the C–O bonds of the other four methoxide ligands are directed to the periphery of the molecule. This latter set of methoxide ligands eclipses the acetate ligands on the other side of the Co_8 plane. On each side of the Co_8 plane, then, the methoxide C–O bonds are alternatively perpendicular to (type A), and at approximately 30° to (type B) the Co_8 plane, similar to the orientation of the methoxide ligands in $[NBu_4]_2[V_8O_8(OMe)_{16}(C_2O_4)]$.[6] The NH_4^+ ion is situated at the centre of the $[Co_8(MeCO_2)_8(OMe)_{16}]$ molecule, with the nitrogen atom in the Co_8 plane. The NH_4^+ protons could not be located. Adjacent cobalt atoms are separated by an average of 2.863 Å, slightly longer than the hydroxy- and alkoxy-bridged Co···Co separations in the hydroxy-bridged dimers and most of the oxo-centred trimers.[7] The Co–O($MeCO_2$) distances are within the range 1.885(6)–1.916(6) Å, as observed in the dinuclear and trinuclear cobalt(III) complexes.[7] Bridging Co–O(OMe) dis-

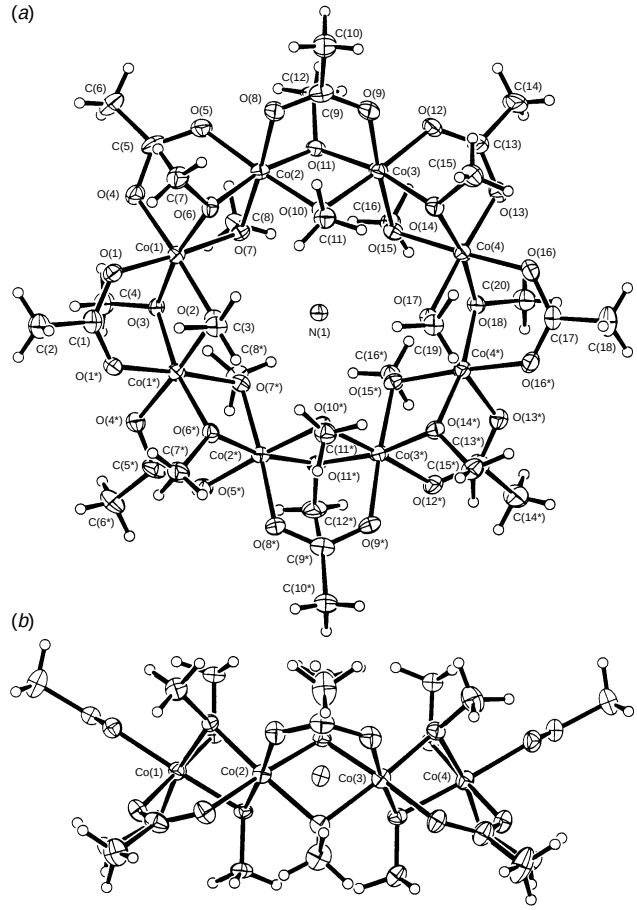

Fig. 1 ORTEP (25% probability)[17] representations of (*a*) the octanuclear $[Co_8(O_2CMe)_8(OMe)_{16}]$ host molecule and the guest NH_4^+ cation, showing the partial labelling scheme, viewed perpendicular to the Co_8 plane, and (*b*) the asymmetric unit viewed along the Co_8 plane

tances and angles are all similar and within the ranges 1.878(6)–1.918(5) Å and 97.7(4)–98.6(3)°, respectively. The Co_8 ring has a diameter of *ca*. 7.5 Å, the O_4 rings of the type A methoxides have diameters of *ca*. 5.3 Å.

The ^{1}H and ^{13}C NMR solution spectra are consistent with the solid state structure.§ Both spectra indicate a single acetate environment and equal populations of two methoxide environments. The ^{1}H NMR spectrum in CD_3OD includes a broad peak centred at δ 7.7 attributable to the protons of the NH_4^+ ion. This peak is shifted some 0.5 ppm downfield from that of NH_4PF_6 in CD_3OD (δ 7.2). The NMR spectra and the stoichiometry indicate that $[Co_8(MeCO_2)_8(OMe)_{16}]$ is diamagnetic.

Topological analogues of the $[Co_8(MeCO_2)_8(OMe)_{16}]$ structure have been reported in vanadium $\{[V_8O_8(OMe)_{16}(C_2O_4)]^{2+}$, $[MeCN(V_{12}O_{32})]^{4-}\}$,[6,8] chromium $\{[Cr_8F_8(Me_3CCO_2)_{16}]\}$,[9] molybdenum $\{[Mo_8O_{16}(OR)_8(C_2O_4)]^{2+}$; R = Me, Et$\}$,[6,10] iron $\{[Fe_8F_8(Me_3CCO_2)_{16}]\}$[11] and copper $\{[Cu_8L_8(OH)_8]$; L = 3,5-dimethylpyrazole$\}$[12] chemistries. The M_8 (M = V, Cr, Mo, Fe, Cu) rings of these compounds have diameters of some 7–9 Å.[6,9–12] The internal cavities of the similarly planar, cyclic, octameric $[Cu_8L_8(OH)_8]$ (L = 3,5-dimethylpyrazole) and $[M_8F_8(Me_3CCO_2)_{16}]$ (M = Cr, Fe) have diameters of *ca*. 6–7 Å.[9,11,12] The related $[Mo_8O_{16}(OMe)_8(PMe_3)_4]$ has a puckered Mo_8 ring with alternating five- and six-coordinated molybdenum atoms.[13] In some cases, solvent molecules are occluded in the structure, in others, oxalato ligands bridge four alternating metal atoms about the ring. The nitrogen atom of occluded Et_2NH is coplanar with the Fe_8 ring of $[Fe_8F_8(Me_3CCO_2)_{16}]$,[11] whereas occluded acetones are situated on either side of the Cr ring of $[Cr_8F_8(Me_3CCO_2)_{16}]$.[9] However, little precedent exists for this structural motif in cobalt chemistry (although compounds containing Co_6 rings are known[14–16]) and its association with the chemistry of 'cobalt(III) acetate' is completely unanticipated. It is not yet clear whether $[Co_8(MeCO_2)_8(OMe)_{16}]$ self assembles (possibly about a cationic template) as a result of a reaction between one or more constituents of 'cobalt(III) acetate' and methanol, or whether a species such as $[Co_8(MeCO_2)_8(OH)_{16}]$ self assembles in 'cobalt(III) acetate' and reacts with alcohols analogously to other species derived from 'cobalt(III) acetate'. What is clear is that the deceptively simple 'cobalt(III) acetate' can form a wide variety of ionic and neutral species and that the driving force for self assembly in these systems must be considerable, even in the presence of only the ubiquitous acetate ligand. A detailed study of related inclusion complexes will be published later.

We thank the Australian Research Council and the School of Chemistry, University of Sydney (scholarship to J. A. K.) for support.

Footnotes and References

* E-mail: masters@chem.usyd.edu.au

† Elemental analysis: calc. for $C_{32}H_{76}Co_8F_6NO_{32}P\cdot0.5C_4H_{10}O$: C, 24.9; H, 5.0; N, 0.9. Found: C, 25.0; H, 4.9; N, 0.9%.

‡ *Crystal data* for $Co_8(MeCO_2)_8(OMe)_{16}\cdot NH_4\cdot PF_6\cdot1.4C_4H_{10}O$, $C_{37.60}Co_8H_{86}F_6NO_{33.40}P$: M = 1703.11, monoclinic, space group $P2_1/m$ (no. 11), a = 8.621(1), b = 25.345(6), c = 16.368(3) Å, β = 104.81(1)°, U = 3457(1) Å^3, $F(000)$ = 1733.60, Z = 2, D_c = 1.632 g cm^{-3}, Mo-Kα radiation, λ = 0.710 69 Å, μ(Mo-Kα) = 19.90 cm^{-1}; R value 0.048 (R_w 0.042) for 3022 absorption-corrected reflections with $I > 3\sigma(I)$. CCDC 182/664.

§ ^{1}H NMR (200 MHz, CD_3OD, TMS reference) δ 7.74 (1 H, br s, NH_4), 2.45 (6 H, s, μ-O_2CMe), 2.23 (6 H, s, μ-OMe), 2.16 (6 H, s, μ-OMe); ^{13}C NMR (200 MHz, CD_3OD, TMS reference) δ 192.31 (μ-O_2CMe), 52.89 (μ-OMe), 51.67 (μ-OMe), 24.02 (μ-O_2CCH_3); ESIMS (90 V) *m/z* 1458.1 ($[M - PF_6]^+$).

1 J. K. Beattie, T. W. Hambley, J. A. Klepetko, A. F. Masters and P. Turner, *Polyhedron*, 1997, **16**, 2109.
2 V. A. Grillo, Z. Sun, K. Folting, D. N. Hendrickson and G. Christou, *Chem. Commun.*, 1996, 2233.
3 K. Dimitrou, K. Folting, W. E. Streib and G. Christou, *J. Chem. Soc., Chem. Commun.*, 1994, 1385.
4 K. Dimitrou, J.-S. Sun, K. Folting and G. Christou, *Inorg. Chem.*, 1995, **34**, 4160.
5 S. Uemura, A. Spencer and G. Wilkinson, *J. Chem. Soc., Dalton Trans.*, 1973, 2565.
6 Q. Chen, S. Liu and J. Zubieta, *Inorg. Chem.*, 1989, **28**, 4433.
7 J. K. Beattie, T. W. Hambley, J. A. Klepetko, A. F. Masters and P. Turner, *Polyhedron*, 1996, **15**, 2141.
8 V. W. Day, W. G. Klemperer and O. M. Yaghi, *J. Am. Chem. Soc.*, 1989, **111**, 5959.
9 N. V. Gerbeleu, Y. T. Struchkov, G. A. Timko, A. S. Batsanov, K. M. Indrichan and D. A. Popovich, *Dokl. Acad. Nauk SSSR*, 1990, **313**, 1459.
10 Q. Chen, S. Liu and J. Zubieta, *Angew. Chem., Int. Ed. Engl.*, 1988, **27**, 1724.
11 N. V. Gerbeleu, Y. T. Struchkov, D. S. Manole, G. A. Timko and A. S. Batsanov, *Dokl. Akad. Nauk SSSR*, 1993, **331**, 184.
12 G. A. Ardizzoia, M. A. Angaroni, G. L. Monica, F. Cariati, M. Moret and N. Masciocchi, *J. Chem. Soc., Chem. Commun.*, 1990, 1021.
13 D. J. Darensbourg, R. L. Gray and T. DeLord, *Inorg. Chim. Acta*, 1985, **98**, L39.
14 G. E. Lewis and C. S. Kraihanzel, *Inorg. Chem.*, 1983, **22**, 2895.
15 R. Schmid, J. Beck and J. Strahle, *Z. Naturforsch., Teil B*, 1987, **42**, 911.
16 B. Cornils, I. Forster, C. Kruger and Y.-H. Tsay, *Transition Met. Chem.*, 1976, **1**, 151.
17 C. K. Johnson, ORTEP, a Thermal Ellipsoid Plotting Program, Report ORNL-5138, Oak Ridge National Laboratories, TN, 1976.

Received in Cambridge, UK, 7th October 1997; 7/07228G

Nickel(0) complex-catalysed detelluration of diorganyl tellurides and ditellurides with phosphines

Li-Biao Han and Masato Tanaka*

National Institute of Materials and Chemical Research, Tsukuba, Ibaraki 305, Japan

Nickel(0) complexes efficiently catalyse detelluration of diaryl tellurides and diaryl ditellurides in the presence of phosphines to afford biaryls in high yields.

Organotellurium compounds are becoming increasingly important in organic synthesis.[1] As reported by Bergman *et al.* more than two decades ago,[2] aryltelluriums undergo detelluration upon treatment with degassed Raney nickel to afford biaryls. The high accessibility of the aryltelluriums[1,2] has made the detelluration a convenient method for the synthesis of biaryls. However, attempted transition metal-catalysed detelluration has been unsuccessful to data.[2,3] Hence, although the reaction is interesting and synthetically useful, the necessity of more than a stoichiometric amount of the metal is still a serious drawback. Herein reported are (*i*) highly successful nickel-catalysed detelluration of diaryl tellurides with phosphines affording biaryls and (*ii*) its mechanism involving an unexpected disproportionation of the complexes formed by oxidative addition of C–Te bonds to $Ni(PEt_3)_4$.[4]

Heating a mixture of dianisyl telluride (**1a**, 684 mg, 2 mmol) and $Ni(PEt_3)_4$ (106 mg, 10 mol% relative to **1a**) in benzene (4 ml) at 80 °C slowly formed black precipitates to give the detelluration product 4,4′-bianisyl **2a** in 13% GC yield after 20 h.† Prolonged heating did not improve the yield, indicating a very poor turnover of the complex catalyst. However, a higher turnover was achieved when a free phosphine was added to the reaction system [eqn. (1)]. Thus, the yield of **2a** increased to

$$\underset{\mathbf{1a}}{Te(C_6H_4OMe\text{-}4)_2} + PR_3 \xrightarrow[80\ ^\circ C,\ 20\ h]{Ni(PEt_3)_4\ (10\ mol\%)} \underset{\mathbf{2a}}{(4\text{-}MeOC_6H_4)_2} + Te{=}PR_3 \quad (1)$$

30% and further to 65% when the reaction was conducted under the same conditions in the presence of 1.2 and 3.0 equiv. (relative to **1a**) of free PEt_3, respectively (Table 1). Although reactions in acetonitrile gave slightly higher yields than those in benzene, the difference was marginal. The effect of the concentration of **1a** on the yield was not significant either at concentrations ranging from 0.8 to 2 mmol of **1a** in 4 ml of the solvent. However, the nature of the phosphine employed exerted a decisive effect. PBu_3 was as effective as PEt_3, but the use of more sterically demanding or less electron-donating phosphines such as PPr^i_3 and $PMePh_2$ reduced the yield. As compared to these triorganophosphines, however, aminophosphines proved much more efficient to achieve significant improvement in the product yield. In the presence of 1.2 equiv. of $P(pyrro)_3$ (pyrro = pyrrolidinyl), for example, starting telluride **1a** disappeared completely after 20 h (80 °C) to afford **2a** quantitatively. Note that a yield as high as 95% was obtained even when the amount of the nickel catalyst was reduced to 3 mol%. Obviously, the yield of **2a** increases in the order $PMePh_2$ < PEt_3 ≈ PBu_3 < $P(NEt_2)_3$ < $P(pip)_3$ (pip = piperidinyl) < $P(pyrro)_3$. The trend is in good agreement with the reactivity of phosphines toward tellurium to form phosphine tellurides ($Te{=}PR_3$), $P(pyrro)_3$ being most reactive.[5]‡

The Ni-catalysed detelluration could be readily applied to other diaryl tellurides affording the corresponding biaryls in good yields (Scheme 1).§ Besides methoxy group, the amino functionality was also tolerant towards the reaction, and a good yield of the corresponding product was obtained. Moreover, the new procedure could be successfully applied to diaryl ditellurides. Thus, the reactions of $(PhTe)_2$ and $(4\text{-}MeOC_6H_4Te)_2$ with 2.5 equiv. of $P(pyrro)_3$ catalysed by $Ni(PEt_3)_4$ (10 mol%) in acetonitrile under similar conditions readily afforded high yields of the corresponding biaryls in both cases. The reaction of $(4\text{-}ClC_6H_4Te)_2$ was particularly noticeable; 4,4′-dichlorobiphenyl was selectively formed in 79% yield despite the potential reactivity of chloroarenes toward Ni^0 species. Since diaryl ditellurides are more readily synthesized then tellurides, successful application of the procedure to ditellurides significantly expands the scope of the reaction.

Table 1 Detelluration of dianisyl telluride **1a** catalysed by $Ni(PEt_3)_4$[a]

Run	Solvent/quantity of **1a** (mmol)/ additive (equiv. relative to **1a**)	GC yield of **2a** (%)
1	C_6H_6/2/none	13
2	C_6H_6/2/PEt_3 (1.2)	30
3	C_6H_6/2/PEt_3 (3.0)	65
4	MeCN/2/PEt_3 (1.2)	41
5	MeCN/0.8/PEt_3 (1.2)	42
6	MeCN/2/PEt_3 (3.0)	73
7	MeCN/1.2/PEt_3 (5.0)	93
8	MeCN/2/PBu_3 (1.2)	40
9	MeCN/0.8/Pi-Pr_3 (1.2)	29
10	MeCN/0.8/$PMePh_2$ (1.2)	20
11	MeCN/0.8/$P(NEt_2)_3$ (1.2)	41
12	MeCN/0.8/$P(pip)_3$ (1.2)[b]	56
13	MeCN/0.8/$P(pyrro)_3$ (1.2)[b]	*ca.* 100
14	MeCN/0.8/$P(pyrro)_3$ (0.5)[b]	70
15	MeCN/0.8/$P(pyrro)_3$ (1.2)[b]	95[c]
16	MeCN/0.8/$P(pyrro)_3$ (1.2)[b]	61[d]

[a] All reactions were run in a Schlenk flask under argon atmosphere at 80 °C for 20 h, using 10 mol% of $Ni(PEt_3)_4$ and 4 ml of a solvent. Yields of **2a** were determined by GC using biphenyl as an internal standard. [b] pip = Piperidinyl; pyrro = pyrrolidinyl. [c] 3 mol% $Ni(PEt_3)_4$ was used. [d] 3 mol% $Ni(PPh_3)_4$ was used as the catalyst.

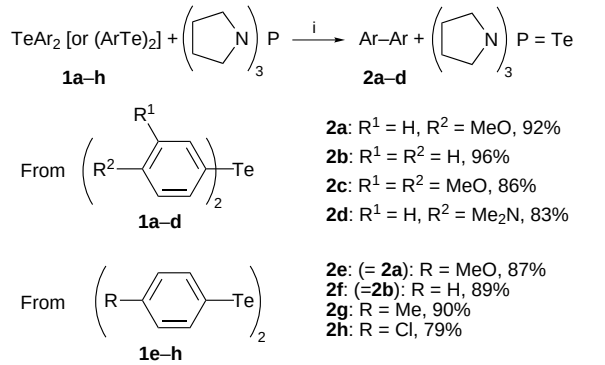

Scheme 1 *Reagents and conditions*: i, telluride or ditelluride (2.0 mmol), $Ni(PEt_3)_4$ (10 mol%), $P(pyrro)_3$ (2.4 or 5.0 mmol for telluride or ditelluride respectively), MeCN, 80 °C, overnight

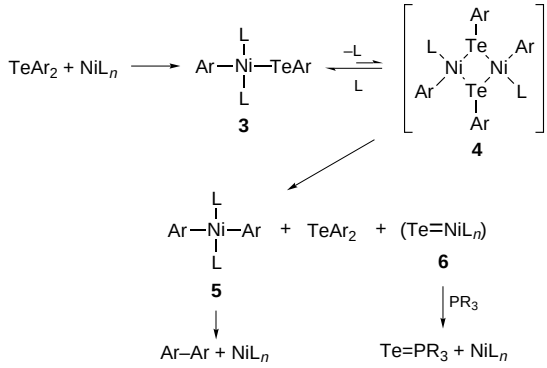

Scheme 2

The detelluration of tellurides is likely to proceed, as depicted in Scheme 2, *via* oxidative addition of a telluride to the nickel complex, disproportionation of the resulting complex **3** to generate diarylnickel species **5**, and its reductive elimination. The mechanism is substantiated by the following observations. As previously reported,[4] treatment of $TePh_2$ (340 mg, 1.206 mmol) with $Ni(PEt_3)_4$ (427 mg, 0.804 mmol) in C_6D_6 at room temp. gave complex **3b** in 10 min, which displayed a singlet at δ 10.3 in its ^{31}P NMR spectrum [eqn. (2)]. Complex **3b** was

a, Ar = C_6H_4OMe-4; **b**, Ar = Ph; **c**, Ar = $C_6H_3(OMe)_2$-3,4

liquid and rather unstable so prohibiting further purification. Telluride **1a** also reacted similarly to form oily complex **3a**. However, oxidative addition of $Te[C_6H_3(OMe)_2\text{-}3,4]_2$ **1c** with the nickel complex gave analytically pure complex **3c** (87% yield) as a black solid.¶

These nickel complexes **3** gradually decomposed even at room temp. For example, NMR spectroscopy revealed that the spontaneous decomposition of **3b** in C_6D_6 resulted in precipitation of a black solid (presumably a nickel telluride like **6**) to generate *trans*-$NiPh_2(PEt_3)_2$ **5b**[6] and $TePh_2$ (approximately 1 : 1 ratio; the conversion of **3b** was *ca.* 50% after 2 d) in solution. A very similar decomposition process was observed with complex **3c**, where the diarylnickel complex **5c** and the telluride **1c** were found by ^1H and ^{31}P NMR spectroscopy to be formed in addition to the black precipitates. As expected, the decomposition was faster at elevated temperatures. Thus, while only *ca.* 50% of complex **3c** decomposed at room temp. over 10 h, it disappeared completely within 3 h at 50 °C to afford **5c** and **1c** in *ca.* 1 : 1 ratio, which accounted for over 93% of the total aryl groups as estimated by ^1H NMR spectroscopy. Heating to even higher temperatures induced a secondary decomposition (reductive elimination); diarylnickel complex **5c** generated *in situ* through the decomposition of **3c** at 50 °C in a sealed NMR tube disappeared after overnight heating at 100 °C and the corresponding biaryl was obtained in 91% NMR yield (based on the quantity of **1c**). This reductive elimination process obviously results in regeneration of Ni^0 species, which carries the catalysis. Interaction of **6** with a phosphine molecule forming a phosphine telluride presumably is another route to the Ni^0 species. Further mechanistic detail of the decomposition of **3** leading to the generation of **5** is ambiguous at the moment. It may involve a dimeric intermediate such as **4** (Scheme 2), palladium analogues of which have been proposed.[7] A supportive observation was made in a catalytic reaction [1.2 equiv. $P(pyrro)_3$, 3 mol% $Ni(PEt_3)_4$, acetonitrile, 80 °C, 10 h] of an unsymmetrical telluride, $TeAr^1Ar^2$ (Ar^1 = $C_6H_4NMe_2$-4, Ar^2 = C_6H_4OMe-4), which gave not only Ar^1–Ar^2 but also cross-over products, Ar^1–Ar^1 and Ar^2–Ar^2 (Ar^1–Ar^1 : Ar^1–Ar^2 : Ar^2–Ar^2 = 1 : 3 : 1) in 73% total yield. The telluride recovered in *ca.* 10% was also a mixture of $TeAr^1{}_2$, $TeAr^1Ar^2$ and $TeAr^2{}_2$.

Further synthetic application of the facile oxidative addition of C–Te bonds to Ni, Pd and Pt complexes[4] is now under extensive study.

Financial support from the Japan Science and Technology Corporation (JST) through the CREST (Core Research for Evolution Science and Technology) program is gratefully acknowledged.

Footnotes and References

* E-mail: mtanaka@ccmail.nimc.go.jp

† Most of **1a** (83% based on GC) remained unreacted. In the absence of the nickel catalyst, no coupling product was formed under similar conditions, indicating that the nickel catalyst was essential for the reaction.

‡ Formation of $Te{=}P(pyrro)_3$ in the detelluration reaction with $P(pyrro)_3$ was confirmed by ^{31}P NMR. See ref. 5.

§ *Typical experimental procedure:* A mixture of telluride **1a** (684 mg, 2 mmol), $P(pyrro)_3$ (579 mg, 2.4 mmol) and $Ni(PEt_3)_4$ (106 mg, 0.2 mmol) in acetonitrile (5 ml) was heated at 80 °C overnight (20 h). The reaction mixture was poured into 10 ml of 1M HCl to liberate metallic tellurium instantly. Extraction using CH_2Cl_2, drying over $MgSO_4$ and concentration afforded crude **2a**, which was subsequently passed through a short silica gel column (ethyl acetate–chloroform–hexane = 0.5 : 1 : 8) to give pure product **2a** as a white solid (394 mg, 1.84 mmol, 92%).

¶ A mixture of **1c** (371 mg, 0.923 mmol) and $Ni(PEt_3)_4$ (500 mg, 0.941 mmol) in benzene (6 ml) was stirred at room temp. for 15 min. Concentration of the reaction mixture to *ca.* 0.5 ml resulted in the precipitation of analytically pure complex **3c** as a black solid in 87% yield (560 mg, 0.803 mmol). *Selected data* for **3c**: ^1H NMR (300 MHz, C_6D_6) δ 7.78 (d, 1 H, *J* 8.0 Hz), 7.67 (s, 1 H), 7.11 (s, 1 H), 6.89 (d, 1 H, *J* 7.8 Hz), 6.66 (d, 1 H, *J* 7.8 Hz), 6.41 (d, 1 H, *J* 8.0 Hz), 3.67 (s, 3 H), 3.52 (s, 3 H), 3.50 (s, 3 H), 3.40 (s, 3 H), 1.34–1.42 (m, 12 H), 0.90–1.09 (m, 18 H); ^{31}P (121.5 MHz, C_6D_6) δ 11.3. Anal. Calc. for $C_{28}H_{48}NiO_4P_2Te$: C, 48.26; H, 6.94. Found: C, 48.21; H, 7.07%.

1 K. Y. Irgolic, *The Organic Chemistry of Tellurium*, Gordon and Breach, New York, 1974; *The Chemistry of Organic Selenium and Tellurium Compounds*, ed. S. Patai and Z. Rapport, John Wiley & Sons, New York, 1986, vol. 1 and 1987, vol. 2; *Comprehensive Organometallic Chemistry II*, ed. E. W. Abel, F. G. A. Stone and G. Wilkinson, Pergamon, Oxford, 1995, vol. 11, pp. 571–601; N. Petragnani, *Tellurium in Organic Synthesis*, Academic Press, London, 1994.

2 J. Bergman, R. Carlsson and B. Sjöberg, *Org. Synth.*, 1977, **57**, 18; J. Bergman, *Tetrahedron*, 1972, **28**, 3323; J. Bergman and L. Engman, *Tetrahedron*, 1980, **36**, 1275.

3 S. Uemura, H. Takahashi and K. Ohe, *J. Organomet. Chem.*, 1992, **423**, C9; Y. Nishibayashi, C. S. Cho, K. Ohe and S. Uemura, *J. Organomet. Chem.*, 1996, **526**, 335; D. H. R. Barton, N. Ozbalik and M. Ramesh, *Tetrahedron Lett.*, 1988, **29**, 3533.

4 L.-B. Han, N. Choi and M. Tanaka, *J. Am. Chem. Soc.*, 1997, **119**, 1795.

5 C. Rømming, A. J. Iversen and J. Songstad, *Acta Chem. Scand., Part A*, 1980, **34**, 333; R. A. Zingaro, B. H. Steeves and K. Irgolic, *J. Organomet. Chem.*, 1965, **4**, 320.

6 The formation of **5b** was confirmed spectroscopically by comparing with an authentic sample synthesized by an established method. J. Chatt and B. L. Shaw, *J. Chem. Soc.*, 1960, 1718.

7 L. Y. Chia and W. R. McWhinnie, *J. Organomet. Chem.*, 1978, **148**, 165.

Received in Cambridge, UK, 29th September 1997; 7/06985E

Chemoselective platinum(0)-catalysed hydrophosphination of ethyl acrylate

Emiliana Costa, Paul G. Pringle* and Kerry Worboys

School of Chemistry, University of Bristol, Cantocks Close, Bristol, UK BS8 1TS

Platinum(0) complexes of $P(CH_2CH_2CO_2Et)_3$ are efficient and selective catalysts for the addition of PH_3 to CH_2=$CHCO_2Et$.

Homogeneous catalysis of the addition of Si–H,[1] B–H[2] or P–H[3–5] to C=C bonds by transition-metal complexes is a field of academic interest and industrial potential. We are interested in the additions of P^{III}–H to C=C bonds catalysed by metal–phosphine complexes and have shown that platinum(0) complexes of tris(cyanoethyl)phosphine catalyse the hydrophosphination of acrylonitrile.[3] We report here that the synthesis of the triester phosphine **1** by the addition of PH_3 to CH_2=$CHCO_2Et$ [eqn. (1)] is catalysed by platinum(0) com-

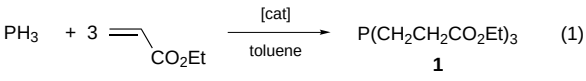

plexes of **1** and the efficiency and selectivity of this catalysis is superior to the alternative radical-initiated process. Phosphine **1** is of interest as a flame retardant intermediate[6] and as a phosphine ligand amenable to further functionalisation.[7]

Rauhut *et al.*[8] reported that at 70 °C and *ca*. 25 atm of PH_3, hydrophosphination of ethyl acrylate [eqn. (2)] is promoted by

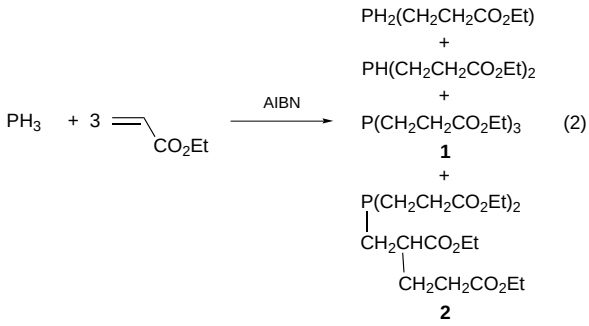

AIBN to give a mixture of primary, secondary and tertiary phosphines in the ratio of *ca*. 1 : 1 : 1. The conversion based on ethyl acrylate was 83% and the tertiary phosphine component was a *ca*. 1 : 1 mixture of phosphine **1** and the telomer **2**. Thus the overall selectivity of this radical reaction to the desired phosphine **1** is *ca*. 15%. We investigated the efficacy of platinum(0) complexes as catalysts for the hydrophosphination of ethyl acrylate in the hope that they would be more selective than the radical initiated process.

Treatment of [Pt(norbornene)$_3$] with 2 or 3 equiv. of **1** in toluene gave platinum(0) complexes assigned structures **3** and **4** on the basis of the characteristic ^{31}P NMR data and the multiplicity of the ^{195}Pt NMR signals.† Addition of further ligand **1** to solutions of **4** led to broad ^{31}P NMR signals for both **1** and **4** showing that ligand exchange takes place on the NMR timescale at ambient temperatures but there was no evidence for a stable [Pt$(PR_3)_4$] species. Addition of 1 equiv. of ethyl acrylate to a solution of **3** in toluene gave a species assigned structure **5** on the basis of the AB pattern observed in the ^{31}P NMR

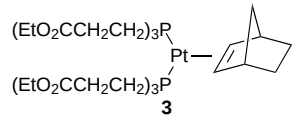

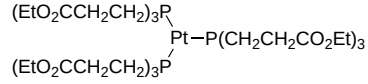

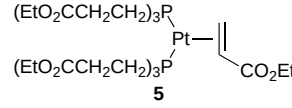

spectrum and the doublet of doublets in the ^{195}Pt NMR spectrum. Interestingly the same species **5** is obtained upon addition of 1 equiv. of ethyl acrylate to **4** but in this case the ^{31}P NMR signals are broad for both **5** and displaced **1** indicating that phosphine exchange is taking place; addition of 5 equiv. of phosphine **1** to solutions of **5** broadened the signals further but there was no evidence for reformation of **4**. It was therefore inferred that the equilibrium shown in eqn. (3) lies to the right

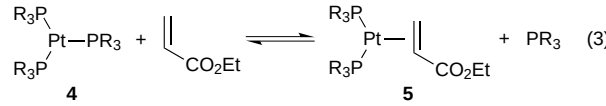

and K was estimated to be > 100. This suggests that complex **5** will be the predominant form of the platinum(0) during the course of the catalysis described below particularly in the initial stages when the ethyl acrylate is in abundance. Complexes **3**–**5** are very reactive and attempts to isolate them in pure form were unsuccessful; thus they have been generated *in situ* for the catalysis.

When PH_3 is bubbled through a warmed solution of ethyl acrylate, no reaction is apparent after 3 h but under similar conditions‡ in the presence of 0.002 equiv. of platinum(0), the reaction proceeded smoothly and after 8 h essentially all of the ethyl acrylate had been consumed. According to ^{31}P NMR spectroscopy, a *ca*. 10 : 1 mixture of the tertiary phosphines **1** and **2** was the product and therefore the selectivity of the platinum(0) process for **1** is > 90%. The addition of PH_3 to ethyl acrylate involves three consecutive hydrophosphinations and the preference for tertiary phosphine in the product implies that the rate of the P–H additions increases in the order PH_3 < RPH_2 < R_2PH. From the proportion of **1** obtained in the product, the average selectivity of each step is apparently *ca*. 97%.

The final step in the hydrophosphination [eqn. (4)] has been

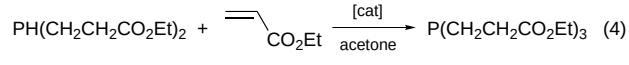

monitored by ^{31}P NMR spectroscopy in the presence and absence of platinum(0) complex **3**. Under the conditions used,§

the P–H addition [eqn. (4)] proceeded 30% after 24 h in the absence of platinum(0) while in the presence of **3** (0.1 equiv.) the hydrophosphination had proceeded 50% after 15 min and was complete in less than 90 min with the desired phosphine **1** constituting >95% of the product according to ^{31}P NMR spectroscopy.

Platinum(0) complexes are catalysts for the hydrophosphination of CH_2=CHZ (Z = CN or CO_2Et).[3,4] Both of these Z substituents withdraw electron density from the C=C bond by virtue of their electronegativity (−I) and resonance (−R) effects. Since no catalysis was detected when PH_3 was passed through a toluene solution of CH_2=$CHCF_3$ in the presence of [Pt{$P(CH_2CH_2CF_3)_3$}$_2$(norbornene)], it is the resonance (or Michael) activation of the alkene that appears to be critical.

While the coordination chemistry of the commercially available $P(CH_2CH_2CN)_3$ has been well studied,[9] to our knowledge, the reported metal complex chemistry of **1** is restricted to one iridium cluster.[7] A study of the precious metal chemistry of **1** is in progress.

We should like to thank Albright and Wilson and EPSRC for support and Johnson-Matthey for the loan of platinum compounds.

Footnotes and References

* E-mail: paul.pringle@bristol.ac.uk

† *NMR data* for compounds **1**–**5**: Phosphine **1**: ^{1}H NMR ($CDCl_3$, 270 MHz) δ 1.27 [t, ^3J(HH) 7.2 Hz, 3 H], 1.75 [t, ^3J(HH) 8.3, ^2J(HP) 8.3 Hz, 2 H], 2.45 [dt, ^3J(HH) 8.3, ^3J(HP) 8.1 Hz, 2 H], 4.15 [q, ^3J(HH) 7.2 Hz, 2 H]; ^{13}C NMR ($C_6D_5CD_3$, 100 MHz, assigned with the aid of DEPT) δ 14.2 (s, CH_3), 21.9 [d, ^1J(CP) 14.7 Hz, CH_2], 30.7 [d, ^2J(CP) 16.5 Hz, CH_2], 60.2 (s, CH_2), 172.5 [d, ^3J(CP) 11.0 Hz, C=O]; ^{31}P{^{1}H} NMR ($C_6D_5CD_3$, 162 MHz) δ −25.9. Phosphine **2** characterised in solution by subtracting the peaks for **1** from the spectra of mixtures of **1** and **2**: ^{13}C NMR ($C_6D_5CD_3$, 100 MHz, assigned with the aid of DEPT) δ 14.3 (s, CH_3), 22.3 [d, ^1J(CP) 14.7 Hz, CH_2], 22.4 [d, ^1J(CP) 14.7 Hz, CH_2] 27.8 (s, CH_2), 30.7 [d, ^1J(CP) 16.5 Hz, CH_2], 31.9 (s, CH_2), 44.6 [d, ^2J(CP) 14.7 Hz, CH], 60.6 (s, CH_2), 60.4 (s, CH_2), 60.3 (s, CH_2), 172.1 (s, C=O), 172.5 [d, ^3J(CP) 11.0 Hz, C=O], 174.5 [d, ^3J(CP) 3.0 Hz, C=O]; ^{31}P{^{1}H} NMR ($C_6D_5CD_3$, 162 MHz) δ −30.1. Complex **3**: ^{31}P{^{1}H} NMR (C_6D_6, 162 MHz) δ −19.7 [^1J(PtP) 3390 Hz]; ^{195}Pt{^{1}H} NMR [C_6D_6, 85.6 MHz, δ relative to Ξ(Pt) 21.4 MHz] δ −574.6 [t, ^1J(PtP) 3390 Hz]. Complex **4**: ^{31}P{^{1}H} NMR (C_6D_6, 162 MHz) δ −40.5 [^1J(PtP) 4202 Hz]; ^{195}Pt{^{1}H} NMR (C_6D_6, 85.6 MHz) δ −0.6 [q, ^1J(PtP) 4202 Hz]. Complex **5**: ^{31}P{^{1}H} NMR (C_6D_6, 162 MHz) δ 15.9 [d, ^2J(PP) 46, ^1J(PtP) 3410 Hz], 17.4 [d, ^2J(PP) 46, ^1J(PtP) 3854 Hz]; ^{195}Pt{^{1}H} NMR (C_6D_6, 64.2 MHz) δ −604.0 [dd, ^1J(PtP) 3405, 3865 Hz].

‡ **CAUTION**: Phosphine gas is extremely toxic and should only be handled in a well ventilated fume cupboard; the exit gases were passed through a solution of commercial bleach to oxidise unreacted PH_3. Toluene (50 cm^3) was carefully deaerated by passing nitrogen through it for 1.5 h and then [Pt(norbornene)$_3$] (0.123 g, 0.257 mmol), the phosphine **1** (1.034 g, 3.093 mmol) and ethyl acrylate (13.1 cm^3, 121 mmol) were added sequentially. PH_3 gas was bubbled through the solution for 8 h maintaining the temperature at 55 °C. The solution was stirred for a further 3 h at 55 °C and the reaction was monitored throughout by ^{31}P NMR spectroscopy.

§ Oxygen was rigorously excluded from the reaction mixture. In an 5 mm NMR tube, to a solution of [Pt(norbornene)$_3$] (5 mg, 0.010 mmol) in $C_6D_5CD_3$ (0.10 cm^3), phosphine **1** (7.0 μl, 0.020 mmol) and then ethyl acrylate (35.0 μl, 0.32 mmol) were added. To this mixture a solution of $PH(CH_2CH_2CO_2Et)_3$ (50 μl, 0.21 mmol) in $C_6D_5CD_3$ (0.30 cm^3) was added in one portion and the reaction monitored by ^{31}P NMR spectroscopy.

1 T. Ishiyama, N. Matsuda, M. Murata, F. Ozawa, A. Suzuki and N. Miyaura, *Organometallics*, 1996, **15**, 713 and references 8(*a*)–(*p*) within; B. Marciniec and J. Gulinski, *J. Organomet. Chem.*, 1993, **446**, 15 and references therein.

2 K. Burgess, W. A. van der Donk, S. A. Westcott, T. B. Marder, R. T. Baker and J. C. Calabrese, *J. Am. Chem. Soc.*, 1992, **114**, 9350 and references therein; K. Burgess and M. J. Ohlmeyer, *Chem. Rev.*, 1991, **91**, 1179 and references therein.

3 P. G. Pringle and M. B. Smith, *J. Chem. Soc., Chem. Commun.*, 1990, 1701; E. Costa, P. G. Pringle, M. B. Smith and K. Worboys, *J. Chem. Soc., Dalton Trans.*, 1997, 4277.

4 D. K. Wicht, I. V. Kourkine, B. M. Lew, J. M. Nthenge and D. S. Glueck, *J. Am. Chem. Soc.*, 1997, **119**, 5039.

5 L.-B. Han and M. Tanaka, *J. Am. Chem. Soc.*, 1996, **118**, 1571; N. Choi, L.-B. Han and M. Tanaka, *Organometallics*, 1996, **15**, 3259.

6 R. K. Valetdinov, A. N. Zuikova and R. D. Murtazina, *USSR Pat.* 819 115, 1981; *Chem. Abstr.*, 1981, **95**, 62 414.

7 J. Werner, *Z. Naturforsch., Teil B*, 1989, **44**, 79.

8 M. M. Rauhut, H. A. Currier, A. M. Semsel and V. P. Wystrach, *J. Org. Chem.*, 1961, **26**, 5138.

9 A. G. Orpen, P. G. Pringle, M. B. Smith and K. Worboys, *J. Organomet. Chem.*, 1997, in press, and references therein.

Received in Cambridge, UK, 16th September 1997; 7/06718F

Stereoselective formation of (*Z*)-γ-substituted allylsilanes by the titanocene(II)-promoted reaction of thioacetals with trialkyl(allyl)silanes

Tooru Fujiwara, Mayumi Takamori and Takeshi Takeda*

Department of Applied Chemistry, Tokyo University of Agriculture and Technology, Koganei, Tokyo 184, Japan

The reaction of organotitanium species prepared by the desulfurizative titanation of thioacetals with $(C_5H_5)_2Ti[P(OEt)_3]_2$ in the presence of trialkyl(allyl)silanes gives γ-substituted allylsilanes with *Z* stereoselectivity.

Since allylsilanes are useful synthetic intermediates in organic synthesis, a number of procedures for their preparation have been reported. Among them, the methods utilizing an olefination process are attractive because they enable us to prepare regioisomeric pure allylsilanes. Two types of olefination have been investigated; (i) Wittig olefination of carbonyl compounds using $Ph_3P{=}CHCH_2SiMe_3$,[1] and (ii) metal alkylidene catalysed olefin cross metathesis using trialkyl(allyl)silane. Crowe *et al.* showed that the cross metathesis of allyltrimethylsilane with terminal olefins using Schrock's molybdenum catalyst $PhMe_2CCH{=}Mo{=}N(2,6\text{-}Pr^iC_6H_3)[OCMe(CF_3)_2]_2$ gave (*E*)-γ-substituted allylsilanes predominantly.[2] On the other hand, the stereochemistry of Grubb's ruthenium $\{Cl_2[c\text{-}C_6H_{11})_3P]_2Ru{=}CHPh\}$ catalysed ring opening metathesis of strained cyclic olefins with allyltrimethylsilane is reported to be unpredictable.[3]

Recently we reported the titanocene(II)-promoted reactions of thioacetals with organic compounds having a multiple bond such as carbonyls,[4] alkenes[5] and alkynes.[6] It was suggested that these reactions proceeded through the carbene complexes of titanium **1** formed by the desulfurization of thioacetals with low valent titanium species. Since the intermediate of olefin metathesis is assumed to be a metal alkylidene species, we expected that substituted allylsilanes would be formed by the titanocene(II)-promoted reaction of thioacetals **2** with allylsilanes **3** through the metathesis process.

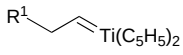

1

As would be expected, 1-triisopropylsilyl-5-phenylpent-2-ene **4b** was produced in 50% yield along with a small amount of the homoallylsilane **5b** (7%) when the thioacetal **2a** was treated with the titanocene(II) species $(C_5H_5)_2Ti[P(OEt)_3]_2$ **6** in the presence of a two-fold excess allyltriisopropylsilane **3b** at room temperature for 48 h (Scheme 1). The starting material disappeared within a short period of time (3 h), and **4b** was obtained in a comparable yield when the reaction was carried out in refluxing THF. The yield of **4b** was increased by increasing the molar ratio of **3b** (Table 1, entry 2).†

In a similar manner, the reactions of several thioacetals **2** with trialkyl(allyl)silanes **3** were performed, and the mixtures of the corresponding substituted allylsilanes **4** and the homoallylsilanes **5** were produced in a ratio of 7.1 : 1 to 1.9 : 1 depending on the alkyl substituents on silicon atom of **3** and the structure of thioacetal **2**. For example, the reaction using allyltriisopropylsilane gave substituted allylsilanes preferentially. On the other hand, in the case of the reaction using allyltrimethylsilane or allyldimethyl(phenyl)silane, a substantial amount of **5** was produced. What is striking is that

Table 1 Reaction of thioacetals **2** with trialkyl(allyl)silanes **3**[a]

			Products (% yield; *E* : *Z*)	
Entry	**2**	**3**	**4**	**5**[b]
1	**2a**	**3a**	**4a** (64; 13 : 87)	**5a** (13)
2	**2a**	**3b**	**4b** (64; 12 : 88)	**5b** (9)
3	**2b**	**3a**	**4c** (55; 16 : 84)	**5c** (29)
4	**2b**	**3b**	**4d** (85; 23 : 77)	**5d** (12)
5	**2b**	**3c**	**4e** (45; 14 : 86)	**5e** (23)
6	**2c**	**3b**	**4f** (78; 11 : 89)	**5f** (16)
7	**2c**	**3c**	**4g** (48; 10 : 90)	**5g** (20)
8	**2d**	**3a**	**4h** (44; 14 : 86)	**5h** (20)
9	**2d**	**3b**	**4i** (44; 14 : 86)	**5i** (18)

[a] Carried out with 5 equiv. of **3**. [b] The stereochemistry was not determined.

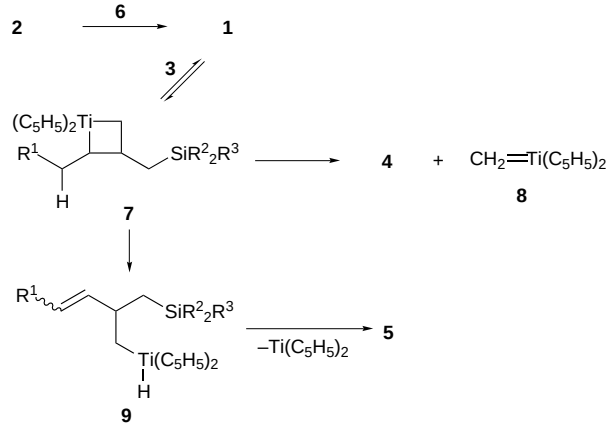

Scheme 2

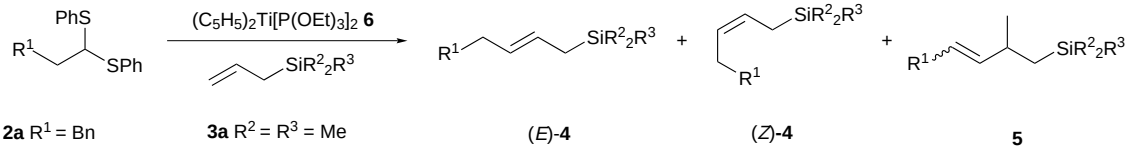

2a R^1 = Bn
b $R^1 = C_6H_{13}$
c $R^1 = Pr^i$
d $R^1 = PhO(CH_2)_3$

3a $R^2 = R^3$ = Me
b $R^2 = R^3 = Pr^i$
c R^2 = Me, R^3 = Ph

(*E*)-**4**

(*Z*)-**4**

5

Scheme 1

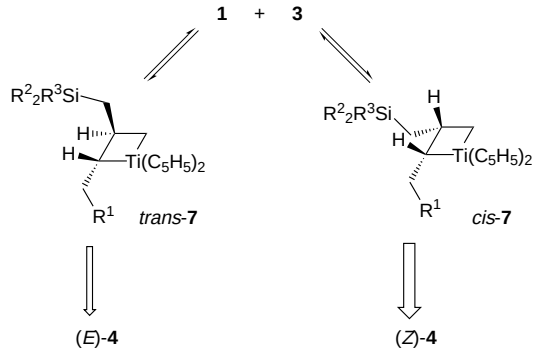

Scheme 3

(*Z*)-allylsilanes (*Z*)-**4** were selectively produced by the present reaction regardless of the substituents on the thioacetals or allylsilanes.‡

The formation of organosilyl compounds **4** and **5** is explained by the following reaction pathway (Scheme 2), which involves the initial formation of α,β-disubstituted titanacyclobutane intermediate **7**.[7] The metallacycle intermediate then cleaves to form a γ-substituted allylsilane **4** and titanocene methylidene complex **8**. The homoallylsilane **5** is produced by elimination of the β-hydride from **7**, followed by elimination of the titanocene(II) species from the homoallyltitanium **9**. A similar process was observed in the reaction of carbene complexes with alkynes.[6]

As for the cleavage of α,β-disubstituted titanacyclobutane leading to the formation of a carbene complex and an olefin, it was shown that the configuration of the metallacycle derived from Tebbe's reagent, 3,3-dimethylcyclopropene and a norbornene diester was retained during the process.[8] Since the *cis*-α,β-disubstituted metallacycle is much less stable than the corresponding *trans*-isomer,[9] the preferential formation of (*Z*)-allylsilanes by the present reaction is explicable in terms of much faster cleavage of *cis*-titanacyclobutane *cis*-**7** than of *trans*-**7** (Scheme 3).

In conclusion, we have found that the reaction of titanium carbene complexes with allylsilanes affords (*Z*)-allylsilanes regio- and stereo-selectively. It should be noted that the present study first revealed the stereochemistry of the cross metathesis between an alkylidenetitanocene and an acyclic olefin. Further study on the reactions of carbene complexes formed from thioacetals with various olefins is now in progress.

This work was supported by a Grant-in-aid for Scientific Research on Priority Area No. 09231213 from the Ministry of Education, Science, Sports and Culture, Japan.

Footnotes and References

* E-mail: takeda-t@cc.tuat.ac.jp

† *Typical experimental procedure*: To a flask charged with finely powdered molecular sieves 4A (150 mg), magnesium turnings (3 mmol) and titanocene dichloride (1.5 mmol) was added THF (3 ml), triethyl phosphite (3 mmol) and trialkyl(allyl)silane (2.5 mmol) successively with stirring. After 2 h, a THF (1 ml) solution of **2** (0.5 mmol) was added and the reaction mixture was refluxed for 6 h. After being cooled to room temperature, the reaction mixture was diluted with pentane (30 ml). The insoluble materials were filtered off through Celite and the filtrate was concentrated. Purification was accomplished by preparative TLC providing a mixture of **4** and **5** as a clear, colourless oil; the excess trialkyl(allyl)silane was removed by distillation prior to purification when necessary. The yields of **4** and **5** were determined by NMR analysis.

‡ The configurations of **4a**–**d** were determined by comparison with authentic samples of the *E*- and *Z*-isomers. The *Z*-isomers (*Z*)-**4** were prepared by the stereoselective reduction of the corresponding prop-2-ynylsilanes with DIBAL-H reported by Rajagopalan and Zweifel,[10] and *E*-isomers (*E*)-**4** were obtained by their diphenyl disulfide mediated photoisomerization[11] [**4a** (*E*:*Z* = 74:26), **4b** (*E*:*Z* = 83:17), **4c** (*E*:*Z* = 79:21), **4d** (*E*:*Z* = 82:18)]. The configurations of other allylsilanes were assigned on the basis of the coupling constant of their vinyl protons.

1 D. Seyferth, K. R. Wursthorn and R. E. Mammarella, *J. Org. Chem.*, 1977, **42**, 3104; D. Seyferth, K. R. Wursthorn and T. F. O. Lim, *J. Organomet. Chem.*, 1979, **181**, 293; I. Fleming and I. Paterson, *Synthesis*, 1979, 446; J. G. Smith, S. E. Drozda, S. P. Petraglia, N. R. Quinn, E. M. Rice, B. S. Taylor and M. Viswanathan, *J. Org. Chem.*, 1984, **49**, 4112.

2 W. E. Crowe, D. R. Goldberg and Z. J. Zhang, *Tetrahedron Lett.*, 1996, **37**, 2117. The molybdenum-catalysed cross metathesis of terminal olefins with allylstannanes has also been reported; J. Feng, M. Schuster and S. Blechert, *Synlett*, 1997, 129.

3 M. F. Schneider, N. Lucas, J. Velder and S. Belchert, *Angew. Chem., Int. Ed. Engl.*, 1997, **36**, 257.

4 Y. Horikawa, M. Watanabe, T. Fujiwara and T. Takeda, *J. Am. Chem. Soc.*, 1997, **11**9, 1127.

5 Y. Horikawa, T. Nomura, M. Watanabe, T. Fujiwara and T. Takeda, *J. Org. Chem.*, 1997, **62**, 3678.

6 T. Takeda, H. Shimokawa, Y. Miyachi and T. Fujiwara, *Chem. Commun.*, 1997, 1055.

7 The regio- and stereo-selective formation of *trans*-α,β-disubstituted titanacyclobutanes by the reaction of trimethylsilylmethylene complex $(C_5Me_5)_2Ti{=}CHSiMe_3$ with terminal olefins was reported; J. L. Polse, R. A. Andersen and R. G. Bergman, *J. Am. Chem. Soc.*, 1996, **118**, 8737.

8 J. R. Stille, B. D. Santarsiero and R. H. Grubbs, *J. Org. Chem.*, 1990, **55**, 843.

9 D. A. Straus and R. H. Grubbs, *J. Mol. Catal.*, 1985, **28**, 9.

10 S. Rajagopalan and G. Zweifel, *Synthesis*, 1984, 113.

11 A. Thalman, K. Oertle and H. Gerlach, *Org. Synth.*, 1990, **Coll. Vol. VII**, 470.

Received in Cambridge, UK, 6th October 1997; 7/07177I

Segregation of mixed micelles in the presence of polymers

Peter Griffiths,*[a] Richard Abbott,[a] Peter Stilbs[b] and Andrew Howe[c]

[a] *Department of Chemistry, University of Wales Cardiff, PO Box 912, Cardiff, UK CF1 3TB*
[b] *Department of Physical Chemistry, Royal Institute of Technology, Stockholm, Sweden S-100 44*
[c] *Kodak European Research, Headstone Drive, Harrow, Middlesex, UK HA1 4TY*

The diffusion behaviour of an aqueous mixture of the sugar-based non-ionic surfactant dodecylmalono-bis-*N*-methylglucamide DBNMG and the anionic surfactant of similar tail length, sodium dodecyl sulfate SDS, are examined in the presence of 5 mass% gelatin; the results clearly show that there are two types of mixed micelle present in the system arising through competition between gelatin and the non-ionic micelle for the anionic surfactant.

The interactions between common synthetic polymers, *e.g.* homopolymers,[1,2] hydrophobically modified polymers[3–5] and polyelectrolytes,[6,7] and selected surfactants have been studied extensively. Generally, the polymer/surfactant complex consists of spherical, monodisperse micelles adsorbed onto the polymer chain in a 'bead and necklace' manner.[8] The presence of the polymer stabilises the formation of the adsorbed micelles and these form at lower concentrations [denoted c.a.c. or c.m.c. (1)], compared with the polymer-free critical micelle concentration (c.m.c.). Recent theoretical modelling[9,10] of these systems is based on the fact that the polymer segments bind in the micelle palisade layer thereby partially shielding some of the hydrophobic core from contact with the continuous aqueous phase. This results in a decrease in the interfacial free energy of the system and hence, provides the driving force for the interaction.

In commercial polymer/surfactant systems, a single surfactant is rarely employed. Most often, a mixture of surfactants is present and synergistic or antagonistic effects are used to mediate and control the overall polymer/surfactant behaviour. The molecular basis for these effects is poorly understood but very important for the improvement of product formulations. It is possible however, to build up a picture of the structure of the polymer/mixed surfactant complex from a knowledge of the diffusion behaviour of the various components. Here, we present as far as we are aware, the first such attempt to do this.

The simultaneous measurement of the (self)-diffusion coefficient of each component present in a multi-component mixture can be achieved using pulsed-gradient spin-echo nuclear magnetic resonance, PGSE NMR. The normal procedure for measuring the self-diffusion coefficient of a species in a multi-component solution is to isolate a resolvable peak, extract the peak integral (intensity) or height for a series of spectra separated in time and fit the resultant exponential time decay. In many useful polymer/surfactant mixtures, resolvable peaks are not present and one must resort to the fitting of multi-exponential decays. For example, consider the data shown in Fig. 1(*a*). The most intense peak (at δ 1.45) corresponds to CH_2 groups present in both surfactants as well as the gelatin. A new data analysis has been developed however, to overcome this problem, called component resolved (CORE) PGSE NMR.[11] The fit to the data is given in Fig. 1(*b*). This approach significantly enhances the accuracy of the diffusion coefficients obtained. A further advantage of CORE PGSE NMR, is that the T_2 weighted 1D spectrum for each component is extracted from the component bandshape. Unequivocal assignment of the diffusion coefficient to each component is then possible.

Gelatin interacts strongly with SDS but not DBNMG, whilst SDS and DBNMG form mixed micelles in the absence of gelatin.[10,12–14] The self-diffusion coefficients of the three components SDS, DBNMG and 5 mass% gelatin are presented in Fig. 2 for a series of 5 mass% aqueous gelatin solutions containing 20 mM SDS and a range of DBNMG concentrations. The broken line corresponds to the diffusion behaviour of DBNMG in the presence of 5 mass% gelatin. This diffusion is slower by a factor of approximately two-thirds than that in the absence of gelatin owing to the obstructing effects of the polymer: the micelle has to diffuse around the gelatin, thereby increasing its diffusion pathlength. The diffusion of DBNMG is further retarded when SDS is present in the system indicative of binding to the much more slowly diffusing gelatin. The gelatin diffusion is an order of magnitude slower than that measured in the simple gelatin and gelatin/DBNMG solutions, again indicative of binding of surfactant micelles to the gelatin.

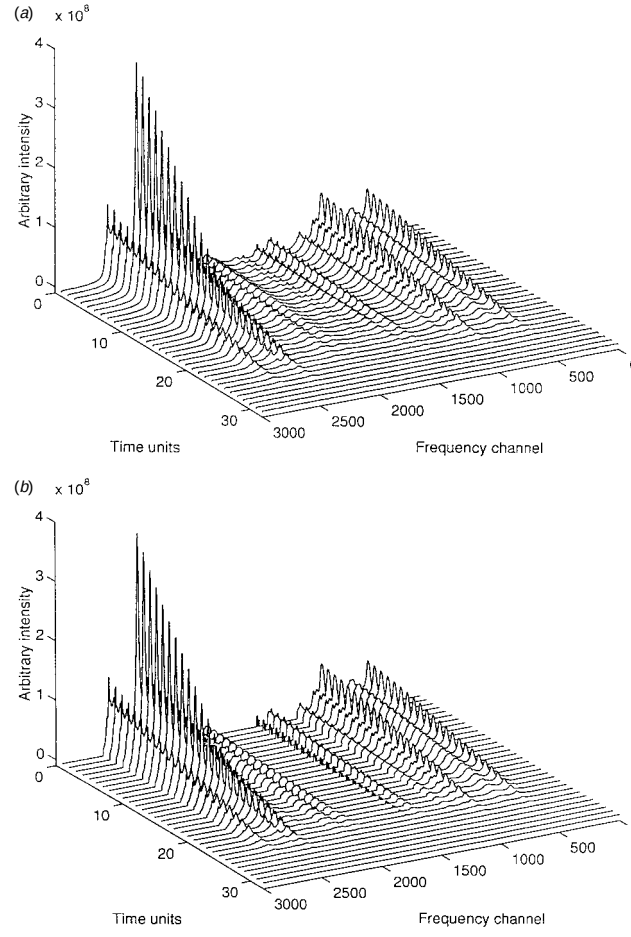

Fig. 1 (*a*) Experimental data for a 5 mass% gelatin solution containing 40 mM SDS and 5 mM DBNMG; (*b*) the CORE processed simulation

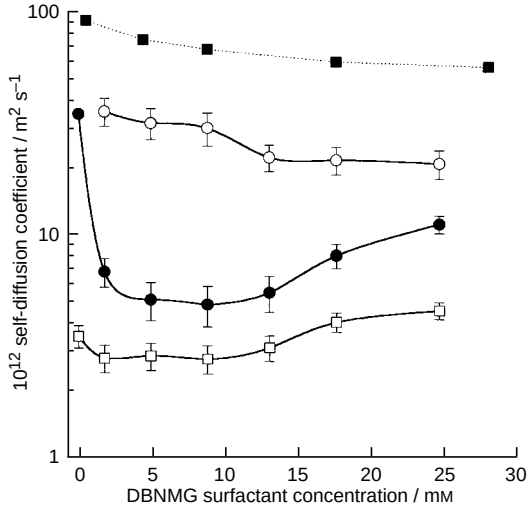

Fig. 2 Diffusion in 5 mass% aqueous gelatin/DBNMG/SDS solutions; gelatin (□), DBNMG (○), and SDS (●). The diffusion of DBNMG in the presence of 5 mass% gelatin only (■) is also shown.

The most striking conclusion however, comes from the behaviour of the SDS. If only one type of micelle is present in the system, and assuming that the unimer concentrations are low, the two surfactants should diffuse at the same rate. This is not observed. Since c.m.c.(1) for gelatin/SDS is higher than $c.m.c._{DBNMG}$, the concentration of unimeric SDS in the system should be greater than that of the DBNMG and hence, the self-diffusion coefficient of SDS should be greater than that of the DBNMG. This too is not observed. The highly unexpected, yet obvious conclusion is that two mixed micellar environments must be present, SDS-rich micelles bound to the gelatin and DBNMG-rich micelles present in solution.

At higher DBNMG concentrations, both the SDS and gelatin self-diffusion coefficients increase, the faster diffusing DBNMG-rich micelles in solution are 'pulling' SDS from the slower diffusing micelles bound to the gelatin. The SDS concentration bound to the gelatin therefore decreases, causing the diffusion of gelatin to increase.

Footnote and References

* E-mail: griffithspc@cardiff.ac.uk

1 K. Chari, B. Antalek, M. Y. Lin and S. K. Sinha, *J. Chem. Phys.*, 1994, **100**, 5294.
2 E. D. Goddard, *J. Am. Oil Chem. Soc.*, 1994, **71**, 1.
3 J. Francois, J. Dayantis and J. Sabbadin, *Eur. Polym. J*, 1985, **21**, 165.
4 R. A. Gelman and H. G. Barth, *Polym. Mater. Sci. Eng.*, 1984, **51**, 556.
5 K. Loyen, I. Iliopoulos, U. Olsson and R. Audebert, *Prog. Colloid Polym. Sci.*, 1995, **98**, 42.
6 Y. J. Li, P. L. Dubin, H. A. Havel, S. L. Edwards and H. Dautzenberg, *Macromolecules*, 1995, **28**, 3098.
7 F. Guillemet and L. Piculell, *J. Phys. Chem.*, 1995, **99**, 9201.
8 B. Cabane and R. Duplessix, *J. Phys.*, 1987, **48**, 651.
9 Y. J. Nikas and D. Blankschtein, *Langmuir*, 1994, **10**, 3512.
10 T. H. Whitesides and D. D. Miller, *Langmuir*, 1994, **10**, 2899.
11 P. Stilbs, K. Paulsen and P. C. Griffiths, *J. Phys. Chem.*, 1996, **100**, 8180.
12 P. C. Griffiths, P. Stilbs, T. Cosgrove and A. M. Howe, *Langmuir*, 1996, **12**, 2884.
13 P. C. Griffiths, P. Stilbs, A. M. Howe and T. H. Whitesides, *Langmuir*, 1996, **12**, 5302.
14 P. C. Griffiths, P. Stilbs, K. Paulsen, A. M. Howe and A. R. Pitt, *J. Phys. Chem. B*, 1997, **101**, 915.

Received in Cambridge, UK, 29th September 1997; 7/07003I

Chiral and somewhat hydrophilic hemicarceplexes

Bong Ser Park, Carolyn B. Knobler, Clark N. Eid, Jr., Ralf Warmuth and Donald J. Cram*

Department of Chemistry and Biochemistry, University of California, Los Angeles, CA 90095-1569, USA

Five new hemicarceplexes involving chiral hosts 1 and 2 have been synthesized and characterized, two by crystal structure determinations; chiral recognition by one host in complexing butan-2-ol is described.

This research had two objectives: to prepare chiral hemicarcerands for chiral recognition of guests in complexation studies, and to obtain hemicarcerands soluble in hydroxylic solvents for examination of solvent effects on complexation. Previously, we found that diastereomers of **3**⊙EtCHBrCH$_2$Br decomplexed at rates that differed by a factor of 9 in $CDCl_3$ at 23 °C.[1] In the present work we report the syntheses and characterizations of complexes of **1** and **2** from tetrol **5** and (*S*,*S*)-(−)-1,4-di-*O*-tosyl-2,3-isopropylidene-L-threitol.[2] The shell closures were conducted in Me_2SO to give 16% of **1**⊙Me_2SO,† in Me_2NCOMe to give 22% of **1**⊙Me_2NCOMe† and in Me_2NCHO to provide 20% of **1**⊙Me_2NCHO.† Products were separated chromatographically from substantial amounts of diol containing only three bridges, which suggests the rates of introducing the fourth bridge were substantially slower than for the first three bridges, probably for steric reasons. Complex **1**⊙Me_2SO required heating at 230 °C in Ph_2O for two days to decomplex, but considerable host decomposition accompanied decomplexation. Clean decomplexation occurred with **1**⊙Me_2NCOMe in Ph_2O or 1,2,4-$Cl_3C_6H_3$ (214 °C, 8 h) or **1**⊙Me_2NCHO in either solvent (150–160 °C, 3 d) to give empty **1**† (80–90%). The acetonide protecting groups were removed (80–90%) from **1**⊙Me_2NCOMe without decomplexation by heating its solution at reflux in $(CH_2)_4O$ containing 10 drops of concentrated aqueous HCl for 2 h to provide **2**⊙Me_2NCOMe (80%).†‡ Similar treatment of **1**⊙Me_2SO and **1**⊙Me_2NCHO gave **2**⊙$(CH_2)_4O$.† Thus decomplexation accompanied deprotection. We suggest that **1**⊙Me_2SOH^+ and **1**⊙Me_2NCHOH^+ are respective intermediates in these decomplexations, and that these cations decomplex much more rapidly than does the neutral starting material. In a different host, host⊙$Et_2NH_2^+$ decomplexed instantaneously under conditions such that host⊙Et_2NH was stable.[3]

In $CDCl_2CDCl_2$ as solvent at 150 °C the appearance of free guest ^{1}H NMR signals showed half lives for decomplexation of **1**⊙Me_2NCOMe and **2**⊙Me_2NCOMe to be ~113 and ~4.5 h, respectively. The rigidity of the acetonide bridges of **1** appears to inhibit the loss of Me_2NCOMe from the inner phase of **1** more than does the more flexible acyclic bridge system of **2**. The decomplexation half-life of **1**⊙Me_2NCHO at 138 °C in $CDCl_2CDCl_2$ was ~1.5 h, reflecting the smaller size of Me_2NCHO compared to Me_2NCOMe.

Crystal structures of **1**⊙Me_2SO and **2**⊙Me_2NCOMe show the disposition of the chiral bridges.§ Side and top stereoviews are portrayed in Fig. 1, the latter including only the guest and bridges connecting the two hemispheres, whose four oxygens are each joined by lines to form two near squares. Notice the unshared electron pairs of the bridge oxygens invariably face inward toward the cavity, which orients the other atoms outward away from the cavity. The two squares are within 1–2° of occupying parallel planes, and are rotated with respect to each other about their long normal axis by 15° in **1**⊙Me_2SO and by 13° in **2**⊙Me_2NCOMe. The average distances between oxygen planes are 3.27 and 3.67 Å, respectively. The crystals are

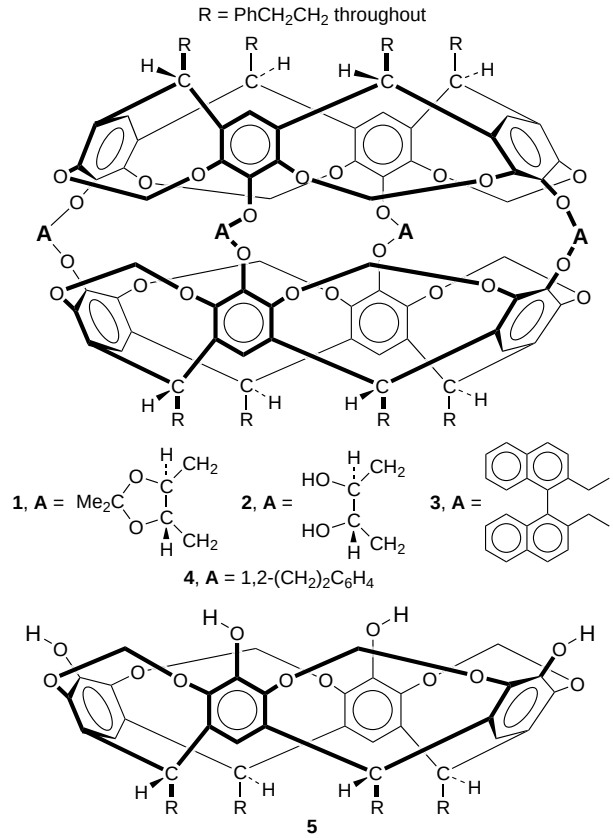

somewhat disordered in the regions of the feet and solvent and with respect to the guests' locations relative to their hosts. In the disorder model for **1**⊙Me_2SO, two Me_2SO guest locations are equally likely, either with one Me in the upper bowl (as in the drawing) or with one Me in the lower bowl of **1**. This model is in agreement with ^{1}H NMR evidence and with crystal structures of similar complexes. The plane of the Me_2NCOMe guest in either of its orientations in **2**⊙Me_2NCOMe lies nearly along one of the diagonals of the O_4 squares, and its long MeNCMe axis is essentially aligned with the host's long axis. The twisting of the two hemispheres of the hosts with respect to one another is less than the 24° observed in the crystal structure of **4**⊙Me_2NCOMe.[4]

The 500 MHz ^{1}H NMR spectrum of **1**⊙Me_2SO in $CDCl_3$ gave two CH_3 singlets at δ −0.91 and −1.03 and thus $\Delta\delta$ = 0.12 ppm. Variable-temperature ^{1}H NMR spectra of **1**⊙Me_2SO in $CDCl_2CDCl_2$ from −80 to 180 °C showed no sign of either splitting or coalescence of these signals, and the whole spectrum showed little temperature dependence. Thus the two guest methyl signals reflect their enantiotopic character in the asymmetric environment of the chiral host. Separately, **1** was heated in 4:1 (v/v) Pr^iOH–Ph_2O to 80 °C for 4 d to form **1**⊙Pr^iOH,¶ which in $CDCl_3$ similarly exhibited 500 MHz ^{1}H NMR signals (two sets) for two enantiotopically related Me groups at δ −2.03 and −2.18 to give a $\Delta\delta$ = 0.15 ppm.

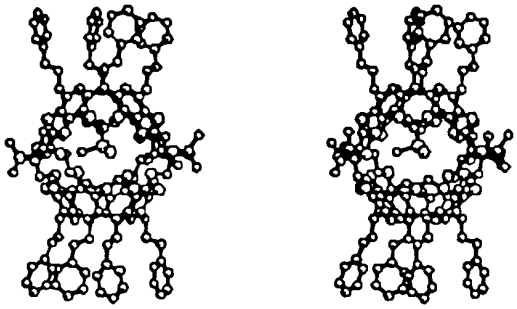

1⊙Me_2SO side stereoview of crystal structure

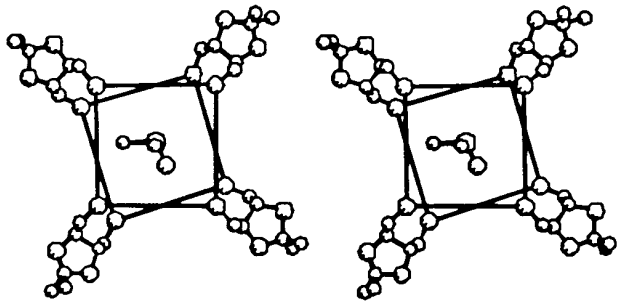

1⊙Me_2SO partial top stereoview of crystal structure

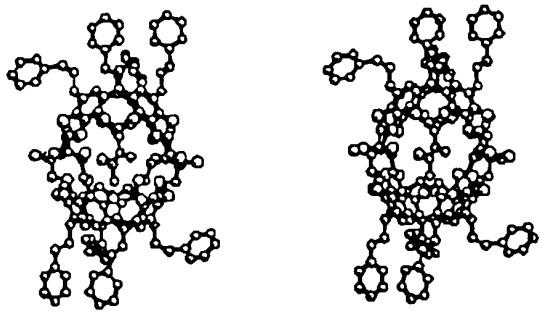

2⊙Me_2NCOMe side stereoview of crystal structure

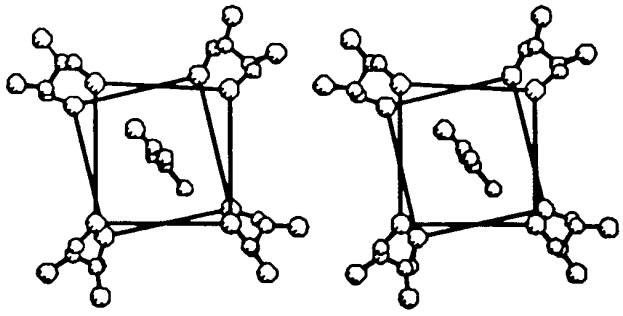

2⊙Me_2NCOMe partial top stereoview of crystal structure

Fig. 1

In an exploratory chiral recognition experiment, (*S,S*)-**1** was heated in a mixture of 1 : 4 (v/v) Ph_2O–Bu^sOH (racemic) for three days at 95–100 °C, and the complex was precipitated with MeOH and submitted to TLC on silica gel plates with 20 : 1 (v/v) $CHCl_3$–EtOAc to provide a 2 : 1 ratio of diastereomeric complexes¶ (^{1}H NMR guest measurements), R_f = 0.8 major product, and R_f = 0.5 minor product. This result shows a surprisingly large sensitivity of the surface-absorption properties of the (*S,S*)-**1** host to the *configuration* of an incarcerated and largely inner-phase-mobile guest separated from the surface of the complex by the host's multi-Ångstrom-thick shell. Further chiral recognition studies involving **1** and **2** should provide interesting results. The fact that **2**⊙guests are soluble in EtOH and higher alkanols suggests that if the eight $PhCH_2CH_2$ groups of **2** are replaced by Me groups, the host might be water soluble. We are investigating this possibility.

Footnotes and References

* E-mail: maverick@chem.ucla.edu

† Elemental analyses including N and S of guests were within 0.30 of theory, FAB MS gave host⊙guest signals as the parent ion, and the expected ^{1}H NMR spectra were found in $CDCl_3$.

‡ The following experiments are illustrative. To a stirred suspension under argon of Rb_2CO_3 (2.5 g) in dry Me_2NCHO (50 ml) at 70 °C was added tetrol **5** (0.50 g, 0.50 mmol) and (*S,S*)-(−)-1,4-ditosyl-2,3-isopropylidene-L-threitol (1.16 g, 2.50 mmol) dissolved in Me_2NCHO (50 ml) over a period of 12 h. The mixture was stirred 1 d at 70 °C, 1.16 g of additional ditosylate was added, and the mixture stirred at 70 °C for 2 d and at 100 °C for 1 d. The mixture was filtered, and the filtrate was evaporated under vacuum to a solid, which was extracted with $CHCl_3$ and filtered. The solvent was evaporated and the product chromatographed on silica gel with 20 : 1 $CHCl_3$–EtOAc (v/v) to give 0.128 g (20%) of **1**⊙Me_2NCHO.† Deprotection of **1**⊙Me_2NCOMe was accomplished by heating 31 mg of the acetonide in 5 ml of $(CH_2)_4O$ and 10 drops of concentrated aqueous HCl at reflux for 2 h. The organic layer was dried ($MgSO_4$) and evaporated, and the resulting solid was chromatographed [silica gel, 10% MeOH in CH_2Cl_2 (v/v)] to give 27 mg (87%) of **2**⊙Me_2NCOMe.† Decomplexation of **1**⊙Me_2NCHO was accomplished by heating 30 mg of the complex in 2 ml of Ph_2O at 150 °C for 3 d. The product was precipitated with MeOH to give 25 mg of **1**.† Complexation of **1** with racemic Bu^sOH involved heating 20 mg of **1** in a mixture of 1 ml of Ph_2O and 4 ml of Bu^sOH for 3 d under argon at 95 °C. The solution was cooled and **1**⊙Bu^sOH was precipitated with excess MeOH and purified by preparative silica gel TLC [20 : 1 $CHCl_3$: EtOAc (v/v)] to give 15 mg of **1**⊙Bu^sOH.†

§ *Crystal data*: the crystal structures of **1**⊙Me_2SO and **2**⊙Me_2NCOMe were each determined at 25 °C from cut colorless crystals in capillaries mounted on a Syntex $P\bar{1}$ diffractometer with Cu-Kα radiation, maximum 2θ = 100°. The structure of **1**⊙Me_2SO (crystallized from CH_2Cl_2–EtOH–EtOAc) belongs to the monoclinic space group $P2_1$, a = 17.7483(7), b = 19.5425(7), c = 26.231(1) Å, β = 107.200(1)°, V = 8691 Å^3, Z = 2, 10 080 unique reflections, 5081 > 4$\sigma(F)$, was solved by direct methods (SHELXS90)[5a] and was refined to R = 0.14. Disordered or low-occupancy solvent molecules, some EtOAc and some unidentified fragments, were found in 12 regions of the unit cell.

The structure of **2**⊙Me_2NCOMe (crystallized from $CHCl_3$–Pr^nOH) belongs to the triclinic space group $P1$, a = 13.811(7), b = 16.239(9), c = 20.785(11) Å, α = 111.38(1), β = 95.13(1), γ = 110.90(1)°, V = 3924 Å^3, Z = 1, 8059 unique reflections, 4566 > 4$\sigma(F)$, was solved by direct methods (SHELX86)[5a] and was refined to R = 0.14. The solvent content is uncertain; the final model includes 2 $CHCl_3$, 1 Pr^nOH and 3 other solvent fragments. For both structures, final refinements were performed with SHELXL93[5b] with isotropic displacement parameters and hydrogen atoms in calculated positions. CCDC 182/647.

¶ FAB MS gave host⊙guest or host signals as parent ion and the expected ^{1}H NMR spectra were found in $CDCl_3$.

1 J. K. Judice and D. J. Cram, *J. Am. Chem. Soc.*, 1991, **113**, 2790.
2 E. A. Mash, K. A. Nelson, S. van Deusen and S. B. Hemperly, *Org. Synth.*, 1993, **Coll. Vol. VIII**, 155.
3 D. J. Cram, M. E. Tanner and C. B. Knobler, *J. Am. Chem. Soc.*, 1991, **113**, 7717.
4 D. J. Cram, M. T. Blanda, K. Paek and C. B.Knobler, *J. Am. Chem. Soc.*, 1992, **114**, 7765.
5 (*a*) G. M. Sheldrick, *Acta Crystallogr., Sect. A*, 1990, **46**, 467; (*b*) G. M. Sheldrick, SHELXL93, 1993, University of Göttingen, Germany.

Received in Columbia, MO, USA, 4th September 1997; 7/06482I

Surface plasmon excitation of a porphyrin covalently linked to a gold surface

Akito Ishida,* Yoshiteru Sakata and Tetsuro Majima*

The Institute of Scientific and Industrial Research, Osaka University, Mihogaoka 8-1, Ibaraki 567, Japan

Fluorescence of a porphyrin covalently linked to a gold surface is observed with surface plasmon excitation using p-polarized light to show higher excitation efficiency for the Q-bands than the Soret band.

Surface plasmon resonance (SPR) is a near-field phenomenon, in which the plasma oscillation of a metal is coupled with the incident light at the resonance angle resulting in strong polarization on the metal surface.[1] SPR has been mainly used as an excellent sensing method for biological purposes.[2,3] Since surface plasmon (SP) has field enhancement effects,[1] photochemical reactions at the surface are expected to be assisted by SPR similar to the surface enhanced spectroscopy. Here, we have studied electronic excitation of a porphyrin chromophore covalently linked to a gold surface by SPR.

SPs were generated on a gold surface with an attenuated total reflection (ATR) method using a Kretschmann–Raether configuration[4] [Fig. 1(*a*)]. The reflectivity was recorded as a function of the incident angle (θ). At the ATR minimum denoted as a SPR angle (θ_R), SPs were created on the opposite side of the gold film. A disulfide derivative of porphyrin **1** was used as a modification reagent to effectively introduce porphyrin chromophores {–S(CH_2)$_{10}$CONH–Por, Por = *p*-[tris(*p*-tolyl)porphyrinyl]phenyl} on the gold surface. The Au–S covalent bond has been confirmed by X-ray photoelectron spectroscopy by one of us (Y. S.).[5] All the measurements were performed at room temperature.

A 15 × 15 × 15 mm BK-7 right-angle prism was rigorously cleaned by ultrapure water, spectroscopic grade methanol, acetone and 1,2-dichloroethane. A 50 nm gold film was evaporated on the hypotenuse face from a 99.9995% Au source at a pressure $< 6 \times 10^{-4}$ Pa, rinsed with spectroscopic grade 1,2-dichloroethane, dried in class-100 air, and used as a control bare film. The θ_R was measured with p-polarized 632.8 nm light

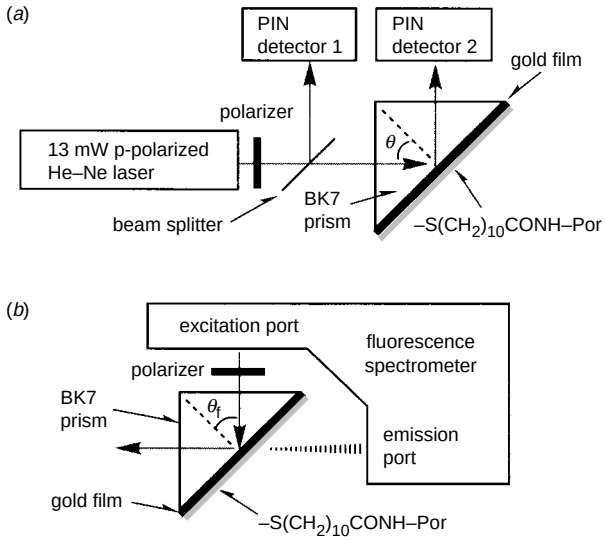

Fig. 1 Experimental configurations of ATR minimum (*a*) and fluorescence (*b*) measurements

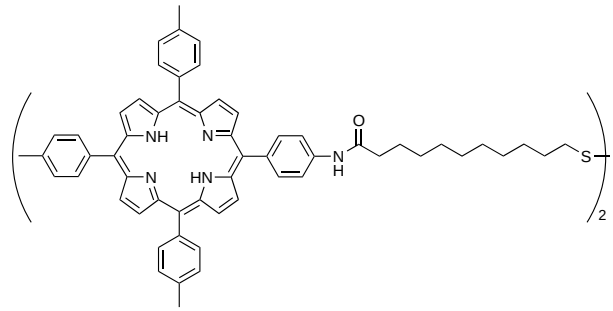

1

from a He–Ne laser. The bare film showed θ_R of 43.6° (Fig. 2) which is consistent with the reported values.[6]

Modification of the gold surface by **1** was performed as follows. The bare film was immersed in a 0.5 mmol dm^{-3} 1,2-dichloroethane solution of **1** for 2 min, washed with a sufficient amount of 1,2-dichloroethane 10 times, and dried in air. After modification, the θ_R shifted to 43.9° (Fig. 2). The shift is attributable to the change in the refractive index for the gold surface covered with –S(CH_2)$_{10}$CONH–Por. The shift required immersion for 2 min for saturation. Therefore, the gold surface was virtually covered with the porphyrin layer after 2 min immersion.

A transmission absorption spectrum of –S(CH_2)$_{10}$CONH–Por was measured using two gold films prepared on BK-7 flat plates as the sample and reference films. The sample film was modified by –S(CH_2)$_{10}$CONH–Por similarly to the prism. As shown in Fig. 3, the difference absorption spectrum showed the characteristic bands of tetraarylporphyrin and is quite similar to that of the film of tetraphenylporphyrin evaporated under vacuum on a glass.[7] Assuming the refractive index of –S(CH_2)$_{10}$CONH–Por film as 1.5, similar to those of usual organic thin films such as protein[6] and poly(methyl methacrylate),[8] the thickness was estimated to be *ca*. 2 nm. This suggests that the –S(CH_2)$_{10}$CONH–Por moiety adopts a linear conformation perpendicular to the gold surface.[9] In other words, the gold

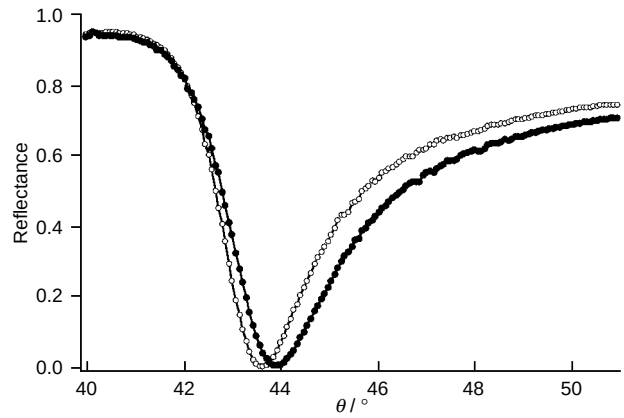

Fig. 2 SPR reflectivity curves for the gold film on a BK-7 right-angle prism (○) and that modified by –S(CH_2)$_{10}$CONH–Por (●)

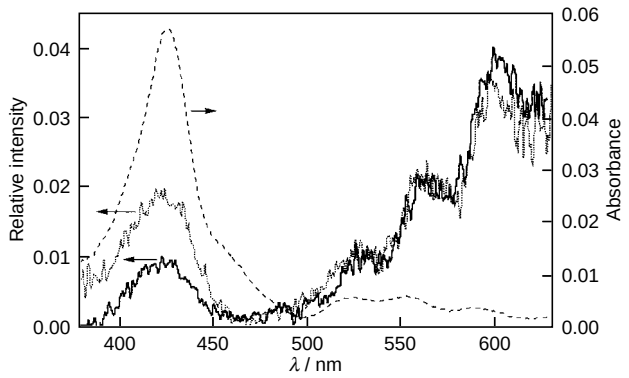

Fig. 3 The excitation spectra of the 655 nm fluorescence band in $-S(CH_2)_{10}CONH-$Por film on a gold surface with the SPR excitation at the incident angles of θ = 45° (—) and 75° (···), and a transmission absorption spectrum of the film (---)

surface is covered with the monolayer of linearly ordered $-S(CH_2)_{10}CONH-$Por.

The electromagnetic field of SP shows a maximum on the surface and decays exponentially into the space along the axis perpendicular to the surface.[8] Since the porphyrin chromophore is bonded to the gold surface at the distance < 2 nm, it can obtain effectively the energy of SP for the electronic excitation. The emission from the gold surface covered with $-S(CH_2)_{10}CONH-$Por was measured using a fluorescence spectrometer, in which the p-polarized visible light illuminated the gold film through a prism at the incident angle (θ_f) of 45° [Fig. 1(*b*)]. The characteristic fluorescence spectrum of tetraarylporphyrin was observed with maxima at 655 and 720 nm, while the fluorescence excitation spectrum using SPR was different from the absorption spectrum (Fig. 3). The intensity ratio between the $Q_x(1,0)$-band and Soret band, I_Q/I_S = 4.0 was significantly larger than that of the absorption spectrum (0.06).†

Because of the dispersion of SP, θ_R varies depending on the wavelength of the incident light. Therefore, we should consider an appropriate θ for the excitation wavelength. The excitation spectrum was measured at θ_f of 75° in order to confirm the θ dependence on the excitation wavelength. The Soret band at θ_f = 75° was certainly increased compared to that at θ_f = 45°, while the I_Q/I_S was still large, 1.8 (Fig. 3).

Since the amplitude of the electromagnetic field of SP exceeds that of the incident field, the evanescent field of SP is expected to enhance inelastic emission such as fluorescence and Raman scattering from molecules adjacent to the metal film.[10] The field enhancement effect of SP is larger in the longer wavelength region. For example, the electric field of SP on the gold surface created by 650 nm light is approximately 50 times larger than that of the incident light.[8] This is consistent with the preferable excitation at the longer wavelength light in the SPR excitation of the $-S(CH_2)_{10}CONH-$Por film.

The fluorescence lifetime with the SPR excitation was measured by a single photon counting method. The obtained decay profile was analysed by two components with 500 ps (65%) and 3.5 ns (35%),‡ both of which were longer than that (310 ps) of a film of tetraphenylporphyrin evaporated under vacuum on Pt surface with the direct photoirradiation.[7] The long lifetimes seem to be due to weak electronic interaction between the porphyrin chromophore and the gold surface through the $-S(CH_2)_{10}CONH-$ group. Recently, a $-S(CH_2)_{10}-$ spacer between a fluorophore and a gold surface has been reported to suppress energy transfer quenching by the gold surface giving high fluorescence yield.[11] Similarly, it is suggested that the $-S(CH_2)_{10}CONH-$ group interrupts the energy transfer from the porphyrin excited state to the gold surface.

The present study demonstrates that SP is an effective and specific excitation source of a porphyrin covalently linked to a gold surface. We are currently studying the effects of the spacer length and the nature of metals upon the fluorescence properties.

Dr Hiroshi Imahori and Tsuyoshi Akiyama are acknowledged for their synthetic advice. This work is partly supported by a Grant-in Aid for Scientific Research (No. 08650979 and 09279224 to A. I.; No. 09238234, 09226223 and 09875209 to T. M.) from the Ministry of Education, Science, Sports and Culture of Japan, and by Research Area of 'Fields and Reactions', Precursory Research for Embryonic Science and Technology, Japan Science and Technology Corporation, and NEDO (A. I.).

Footnotes and References

* E-mail: ishida@sanken.osaka-u.ac.jp

† The characteristic fluorescence spectrum was also observed in the direct photoirradiation of the $-S(CH_2)_{10}CONH-$Por film, while the value I_Q/I_S was smaller (0.44) than that in the SPR excitation and larger than that of the absorption spectrum.

‡ Although the fluorescence decay profile showed multi-exponential components, it was analysed by the sum of two components with χ^2 = 1.40. This suggests that the porphyrin chromophores are in different structural and electronic environments.

1 H. Raether, *Surface Plasmons on Smooth and Rough Surfaces and on Gratings*, ed. G. Höhler, Springer-Verlag, Berlin, 1988, pp. 4–39.
2 X. Sun, S. Shiokawa and Y. Masui, *Jpn. J. Appl. Phys.*, 1989, **28**, 1725.
3 B. Cunningham and J. A. Wells, *J. Mol. Biol.*, 1993, **234**, 554.
4 E. Kretschmann, *Z. Phys.*, 1971, **241**, 313.
5 T. Akiyama, H. Imahori and Y. Sakata, *Chem. Lett.*, 1994, 1447.
6 C. E. Jordan, B. L. Frey, S. Kornguth and R. M. Corn, *Langmuir*, 1994, **10**, 3642.
7 K. Tanimura, T. Kawai and T. Sakata, *J. Phys. Chem.*, 1980, **84**, 751.
8 H. Kano and S. Kawata, *Opt. Lett.*, 1996, **21**, 1848.
9 J. Zak, H. Yuan, M. Ho, L. K. Woo and M. D. Porter, *Langmuir*, 1993, **9**, 2772.
10 R. E. Benner, R. Dornhaus and R. K. Chang, *Opt. Commun.*, 1979, **30**, 145.
11 K. Motesharei and D. C. Myles, *J. Am. Chem. Soc.*, 1994, **116**, 7413.

Received in Exeter, UK, 11th September 1997; 7/06623F

First innermolecular Diels–Alder reaction of *o*-benzyne inside a molecular container compound

Ralf Warmuth*

Department of Chemistry and Biochemistry, University of California, Los Angeles, CA 90095-1569 USA

1,2-Didehydrobenzene 1, incarcerated in the inner phase of a hemicarcerand 2, undergoes an innermolecular Diels–Alder reaction with its surrounding host, which is a new type of reaction at the borderline between intra- and intermolecular reactions.

Previously, we reported the successful generation of the highly reactive *o*-benzyne **1** in the inner phase of a molecular container compound.[1] The synthesis and application of molecular container compounds was developed by D. J. Cram.[2] They are particularly suitable for the generation and study of highly reactive species, which cannot be isolated under usual conditions in solution.[3] *o*-Benzyne was generated inside hemicarcerand **2**[4] by UV illumination of incarcerated benzocyclopropenone **3** at 77 K in [$^2H_8$]THF. It was stable enough in solution to determine and fully interpret for the first time its solution ^{1}H and ^{13}C NMR spectra.[1] However, the high reactivity of **1**, even at low temperature, led to the inner phase reaction of the incarcerated *o*-benzyne with hemicarcerand **2**. This reaction is the first reported reaction[2c,5] where the guest reacts with the surrounding host shell. Now we report the results of a detailed investigation of this reaction.

Incarcerated *o*-benzyne **2**⊙**1** was prepared photochemically from a solution of **2**⊙**3** in [$^2H_8$]THF at 77 K as described previously.[1] During the warming of the sample to room temperature the incarcerated **1** reacts with the host to form the addition product **4** (> 90%) (Scheme 1).† This new compound **4** was isolated and analysed. The elemental analysis, FT-IR spectrum and the FAB-MS, which shows only a single peak at the expected mass of the benzyne hemicarceplex [M + 1] = 2327, are all consistent with a reaction product of *o*-benzyne with the host **2**. In the ^{1}H NMR spectrum of **4** (Fig. 1) the outward pointing hydrogens H^a of the eight methylene spanners, which are equivalent in **2**⊙**3**,[1] are split into four doublets. Each integrates for two protons. The same is true for the inward pointing methylene protons H^i and the eight methine protons, which give four triplets. The proton signals originating from *o*-benzyne were identified at δ 6.14 (d, 1 H, H^1), 5.21 (t, 1 H, H^2), 4.58 (t, 1 H, H^3) and 3.12 (d, 1 H, H^4). Their relationship was identified by ^{1}H homonuclear shift correlation experiments. The only reaction that is consistent with the observed ^{1}H NMR spectrum is the [4 + 2] Diels–Alder reaction illustrated in Scheme 1.

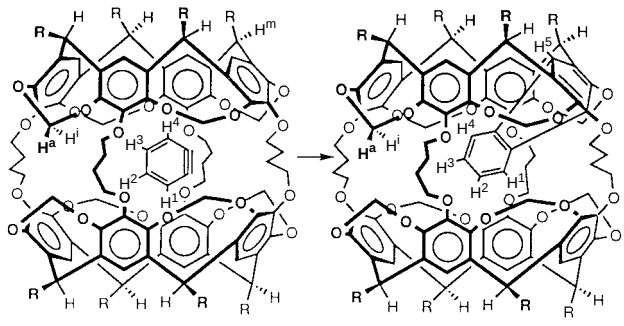

Scheme 1

o-Benzyne (ene component) adds to one of the aryl ether units of **2** (diene component) to give the geminal *para* adduct **4**. In the ^{13}C NMR spectrum of the $^{13}C_6$ labelled Diels–Alder product, obtained from the addition of ^{13}C labelled *o*-benzyne **5** to **2**,[1] the signals for the six carbons originating from **5** appear at δ 149.20, 142.98, 122.38 (*C*-H^2), 120.85 (*C*-H^3), 119.34 (*C*-H^4) and 117.04 (*C*-H^1). The chemical shifts agree well with the corresponding chemical shifts of benzocyclooctatriene model compounds.[6]

We studied *o*-benzyne and its reactivity in the inner phase of **2** by ^{1}H NMR spectroscopy in the temperature range between −75 and −108 °C in [$^2H_8$]THF. In this temperature range, we noticed an upfield shift of the signal assigned to the protons H^1 and H^4 and a downfield shift of the signal of the protons H^2 and H^3 with increasing temperature [Fig. 2(*a*)]. These shift differences seem to be too large to be just a temperature effect, since the downfield shift of the guest protons of **2**⊙benzene ($\Delta\delta$ 0.033 ppm) is only 8% of the shift of H^1 and H^4. We believe that upon lowering the temperature the two cavitands of **2** are squeezed together more tightly to increase the number of van der Waals contacts. As a consequence, the shape of the inner cavity, which is characterized by the ratio of the length of the polar axis l_{pa} and the equatorial axis l_{ea}, will change, leading to a smaller l_{pa}/l_{ea} ratio at lower temperature [Fig. 2(*b*)].

Due to its shape, *o*-benzyne **1** will be more likely located inside **2** with its C_2 axis parallel to the polar axis of **2** at low temperature [orientation **I** in Fig. 2(*b*)]. This leads to a stronger shielding of H^2 and H^3, which would be located in the polar region of **2**. Upon increasing the temperature, orientation **II** in Fig. 2(*b*) will be more populated, resulting in an enhanced shielding of H^1 and H^4 and a deshielding of H^2 and H^3. Orientation **I** would explain the high tendency of **1** to undergo a reaction with **2** even at very low temperatures, since in this orientation the reactive triple bond of **1** is facing into one of the polar regions of **2**. It would also explain why incarcerated *o*-benzyne does not react with water in the bulk solvent even though H_2O is small enough to pass through the equatorial portals of **2**.

The course of the Diels–Alder reaction was followed by the decrease of the signal assigned to the *o*-benzyne protons H^1 and H^4.[1] At all temperatures we observed first-order kinetics for the reaction of **1** with **2**.

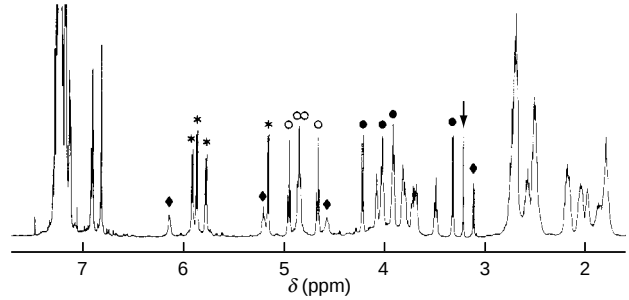

Fig. 1 ^{1}H NMR spectrum (500.113 MHz; $CDCl_3$; 25 °C) of **4**: (*) outward pointing methylene bridge protons, (●) inward pointing methylene bridge protons, (○) methine protons, and (◇) protons originating from *o*-benzyne. Arrow indicates the proton H5.

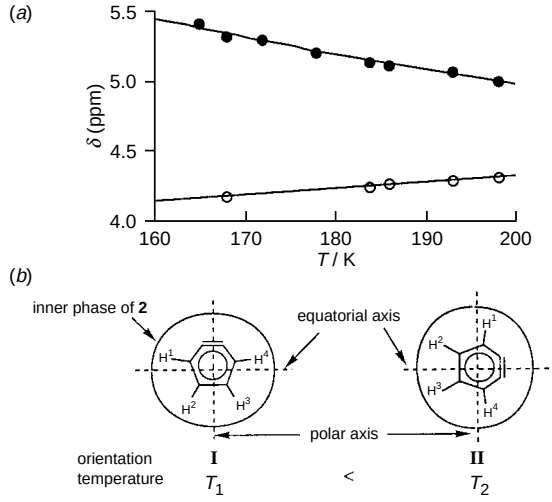

Fig. 2 (*a*) ^{1}H NMR chemical shifts of the *o*-benzyne protons (●) H^1 and H^4 and (○) H^2 and H^3 in [$^2H_8$]THF as function of the temperature. (*b*) Simplified representation of the orientation of **1** in the inner phase of **2** at different temperatures.

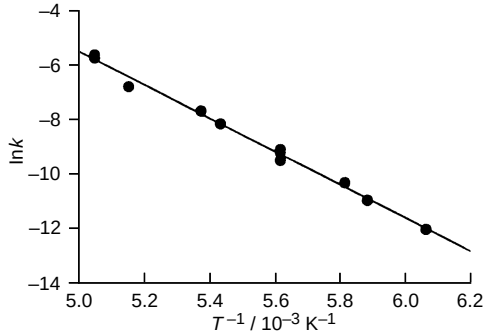

Fig. 3 Arrhenius plot for the reaction of **1** inside **2**

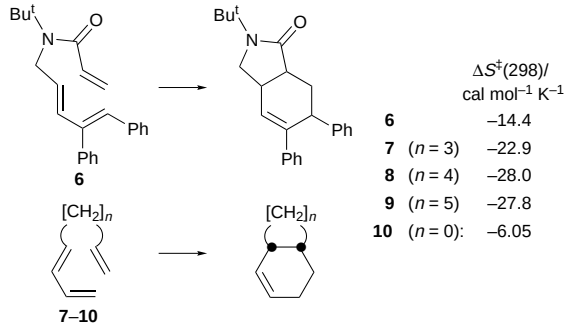

		ΔS‡(298)/ cal mol^{-1} K^{-1}
6		–14.4
7	(*n* = 3)	–22.9
8	(*n* = 4)	–28.0
9	(*n* = 5)	–27.8
10	(*n* = 0):	–6.05

Scheme 2

From an Arrhenius plot (Fig. 3) we determined the activation parameters of this reaction: $\Delta G^{\ddagger}$(298 K) = 14.7 kcal mol^{-1}; $\Delta S^{\ddagger}$(298 K) = −10.7 cal mol^{-1} K^{-1} and $\Delta H^{\ddagger}$(298 K) = 11.6 kcal mol^{-1}, which gives excellent agreement with the calculated $\Delta H^{\ddagger}$ (298 K) = 10.7 kcal mol^{-1} for the addition of *o*-benzyne to benzene.[7] The enthropy of activation $\Delta S^{\ddagger}$(298 K) is a good measure of the degree of preorganization of this reaction. The measured value is much smaller than the $\Delta S^{\ddagger}$(298 K) values of intermolecular Diels–Alder reactions [$\Delta S^{\ddagger}$(298 K) ≈ −40 cal mol^{-1} K^{-1}][8] and of the intramolecular Diels–Alder reactions of trienes **6**–**9**,[9,10] but much larger than the $\Delta S^{\ddagger}$(298 K) value of the Cope rearrangement of hexatriene **10** (Scheme 2).[11]

In the present case *o*-benzyne has the possibility of reacting in two different orientations, of which both differ by a 180° rotation of **1** around its C_2 axis, with eight equivalent aryl ether units of **2** to form **4**. This would favour $\Delta S^{\ddagger}$ by $\Delta\Delta S^{\ddagger}$ = Rln 16 = 5.51 cal mol^{-1} K^{-1}. Subtracting $\Delta\Delta S^{\ddagger}$ from the measured $\Delta S^{\ddagger}$ gives −16.2 cal mol^{-1} K^{-1}, which is between the $\Delta S^{\ddagger}$ values of the intramolecular Diels–Alder reactions of **6** and **7**.

According to the kinetic parameters, we place the Diels–Alder reaction of **1** with **2** in the category of intramolecular Diels–Alder reactions. Like intramolecular reactions, the reaction of **1** and **2** shows first-order reaction behaviour. However, both reaction partners, **1** and **2**, are not covalently connected but are held together by incarceration. They are separate, individual species, free to rotate in all dimensions. Hence, in this specific case we observed for the first time a bimolecular reaction which, contrary to bimolecular reactions in solution or in the gas phase, obeys first order kinetics. Reactions of this type are only possible if one reactant A is completely encapsulated inside the closed surface of inner phase[3,12] of the second reaction component B and is retained inside B by constrictive binding.[13] Therefore, we would like to introduce the name *innermolecular* reaction for this new type of reaction, which is an intermolecular reaction with a rate law of an intramolecular reaction and which is limited to the *inner phase* of molecular container compounds.[14] Since the inner phase of reactant B is the reaction medium, the course of an innermolecular reaction is expected to be independent of the bulk phase, which might be the solid, the liquid or the gas phase.[3]

The author extends special thanks to Professor D. J. Cram in whose research group this work was conducted. We are very grateful for his many helpful, critical and stimulating discussions. Furthermore, we thank Professor K. N. Houk, Dr R. C. Helgeson and Dr C. Sheu for helpful discussions and the Alexander von Humboldt Foundation for a Feodor-Lynen fellowship. We warmly thank the U.S. Public Health Service for supporting grant GM-12640 (D. J. Cram, principal investigator).

Footnotes and References

* E-mail: warmuth@ksu.edu

† All new compounds gave C and H elemental analyses within 0.5% of theory, M$^+$ *m/z* signals of substantial intensity in their FAB-MS, and ^{1}H and ^{13}C NMR spectra consistent with their structure.

1 R. Warmuth, *Angew. Chem., Int. Ed. Engl.*, 1997, **36**, 1347.
2 (*a*) D. J. Cram, *Science*, 1983, **219**, 1177; (*b*) D. J. Cram, S. Karbach, Y. H. Kim, L. Baczynskyj and G. W. Kalleymeyn, *J. Am. Chem. Soc.*, 1985, **107**, 2575; (*c*) D. J. Cram and J. M. Cram, *Container Molecules and Their Guests*, ed. J. F. Stoddart, Royal Society of Chemistry, Cambridge, 1994, vol. 4.
3 D. J. Cram, M. E. Tanner and R. Thomas, *Angew. Chem.*, 1991, **103**, 1048; *Angew. Chem., Int. Ed. Engl.*, 1991, **30**, 1024.
4 T. Robbins, C. B. Knobler, D. Bellew and D. J. Cram, *J. Am. Chem. Soc.*, 1994, **116**, 111.
5 D. J. Cram, M. E. Tanner and C. B. Knobler, *J. Am. Chem. Soc.*, 1991, **113**, 7717; T. A. Robbins and D. J. Cram, *J. Am. Chem. Soc.*, 1993, **115**, 12 199; S. K. Kurdistani, R. Helgeson and D. J. Cram, *J. Am. Chem. Soc.*, 1995, **117**, 1659.
6 C. V. Kumar, B. A. R. C. Murty, S. Lahiri, E. Chackachery, J. C. Scaiano and M. V. George, *J. Org. Chem.*, 1984, **49**, 4923.
7 B. R. Beno, C. Sheu, K. N. Houk, R. Warmuth and D. J. Cram, unpublished results.
8 A. Wassermann, *Diels–Alder Reactions*, Elsevier, Amsterdam, 1965, p. 44.
9 M. K. Diedrich, Dissertation, University GH Essen, Germany, 1995.
10 H. W. Gschwend, A. O. Lee and H. P. Meier, *J. Org. Chem.*, 1973, **38**, 2169.
11 J. W. Moore and R. G. Pearson, *Kinetics and Mechanism*, 3rd edn., Wiley, New York, 1981, p. 214.
12 D. J. Cram, *Nature*, 1992, **356**, 29.
13 D. J. Cram, M. T. Blanda, K. Paek and C. B. Knobler, *J. Am. Chem. Soc.*, 1992, **114**, 7765.
14 For similar reactions of carbenes in the open cavity of cyclodextrins, see S. R. McAlpine and M. A. Garcia-Garibay, *J. Am. Chem. Soc.*, 1995, **118**, 2750; U. Brinker, R. Buchkremer, M. Rosenberg, M. D. Polkis, M. Orlando and M. L. Gross, *Angew. Chem., Int. Ed. Engl.*, 1993, **32**, 1344.

Received in Columbia, MO, USA, 6th May 1997; 7/03099A

New hydrogenation and isomerization reactions involving thiaplatinacycles derived from benzothiophene

Alexei Iretskii,[a] Harry Adams,[a] Juventino J. Garcia,[b] Graciela Picazo[b] and Peter M. Maitlis[a]

[a] *Department of Chemistry, The University of Sheffield, Sheffield, UK S3 7HF*
[b] *Facultad de Química, Universidad Nacional Autónoma de México, 04510 México D.F.*

Hydrogenation of the thiaplatinacycle [Pt{*C*,*S*-(CH=CHC$_6$H$_4$S)}(dppe)] 2 (dppe = Ph$_2$PCH$_2$CH$_2$PPh$_2$) derived from benzothiophene, leads to [Pt{*C*,*S*-(CHMeC$_6$H$_4$S)}(dppe)] 3 in which 2H have added and a H-shift has occurred; the X-ray structures of 2 and 3 are reported.

Thiophenes (T), benzothiophenes (BT), dibenzothiophenes (DBT), and their alkyl derivatives pose particular problems for hydrodesulfurization (HDS) as they occur in substantial amounts, notably in the heavier crude oils, and are rather resistant to normal HDS catalysts such as Co–Mo–S on alumina.[1] Quite recently platinum has emerged as a viable catalyst for second stage industrial hydrotreating;[2] this has allowed the production of the so-called city diesel fuel, with a very low sulfur content (⩽30 ppm).

In our researches to model such HDS reactions we have found that the platinum(0) complex [Pt(PEt$_3$)$_3$] can reversibly oxidatively insert into the C–S bonds of T, BT or DBT, giving six-membered thiaplatinacycles.[3–5] These thiaplatinacycles extrude S and Pt on reaction with sources of hydride to give hydrocarbons, thus demonstrating a full HDS sequence mediated by platinum.

Related thiametallacycles are formed by the oxidative insertion of other metals (*e.g.* Rh and Ir[6]) into the thiophene; those derived from BT generally react with hydrogen to give 2-ethylthiophenol (or a salt thereof)[7] or 2,3-dihydrobenzothiophene,[8] though ethylbenzene can be obtained under forcing conditions.[9] We have now isolated and characterised a novel isomerisation product from partial hydrogenation of a thiaplatinacycle derived from BT, which indicates that the HDS cycle may be more complex than previously proposed.

The trimethylphosphine complex **1**† was synthesised either from reaction of BT with pure [Pt(PMe$_3$)$_4$] in refluxing toluene [eqn. (1); 83%] or, more conveniently [eqn. (2); 69%] by a one-pot reaction of K$_2$PtCl$_4$, NaOH, and trimethylphosphine, forming [Pt(PMe$_3$)$_4$] *in situ*, to which BT was then added. Reaction of **1** with a small excess of dppe (Ph$_2$PCH$_2$CH$_2$PPh$_2$) gave complex **2** [eqn. (3); 89%].

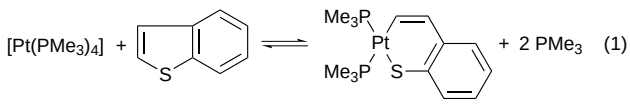

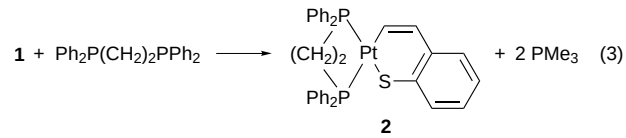

The complexes were characterised by microanalysis, NMR spectra and an X-ray structure determination for **2**.‡ This showed the expected arrangement (Fig. 1) and was very similar to the structure already determined for [Pt{*C*,*S*-(CH=CHC$_6$H$_4$S)}(PEt$_3$)$_2$].[3] Complex **2** was hydrodesulfurised by reaction with LiAlH$_4$ in toluene–thf to give ethylbenzene (42%). Similar results but poorer yields were obtained for complex **1** and for [Pt{*C*,*S*-(CH=CHC$_6$H$_4$S)}(dppp)].

Complex **2** could also be hydrogenated (toluene solution, 120 °C, 20 atm H$_2$) directly to give a mixture of ethylbenzene (6%) and free BT (12%). The low yield of HDS product under these conditions is explained by the additional formation of a new platinum complex (in 74% yield). FABMS showed it to have a molecular ion at *m*/*z* 730 corresponding to [Pt(C$_8$H$_8$S(dppe)], indicating that 2 H have added to **2**. The new complex was identified as **3**§ by an X-ray determination which showed that the S-ligand did not have the expected saturated six-membered thiaplatinacycle structure; instead a ring contraction had occurred and the product had a methyl attached to CH in a five-membered thiaplatinacycle (Fig. 2).

The structure for **3** indicates that a hydrogen shift has occurred in addition to the hydrogenation so that the benzylic carbon is now attached to the metal. This also has structural consequences: the benzothiaplatinacycle in complex **2** is very nearly planar with a dihedral angle of only 3.2° between the plane C(1)–Pt–S and the best plane through S–C(8)···C(2)–C(1). By contrast, and as a consequence of the presence of the sp^3 carbon at C(1) the thiaplatinacycle in complex **3** is much more bent, with a dihedral angle of 27.8° between the planes C(1)–Pt–S and C(1)–C(2)–C(3).

The difference in the structures is also manifested in their reactions with HCl. Complex **3** was degraded to give

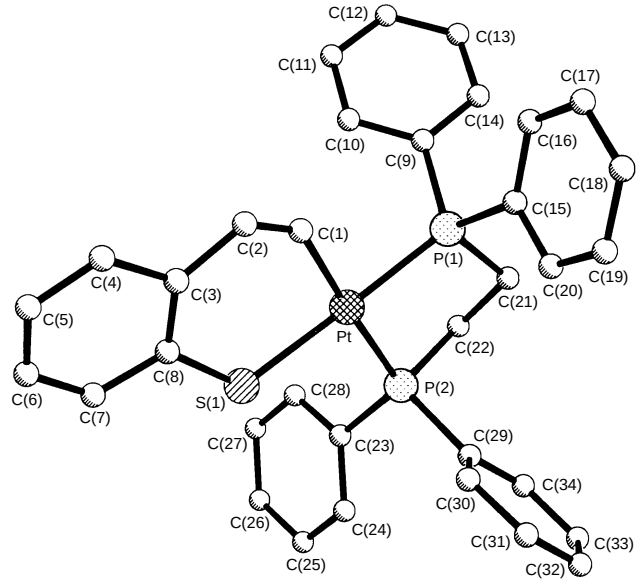

Fig. 1 The molecular structure determined for **2**. Bond lengths (Å) and angles (°): Pt–P(1) 2.2474(13), Pt–P(2) 2.2969(14), Pt–S 2.260(2), Pt–C(1) 2.054(4); C(1)–Pt–P(1) 93.1(2), P(1)–Pt–P(2) 85.20(5), C(1)–Pt–S 88.4(2), P(2)–Pt–S 93.40(5)°.

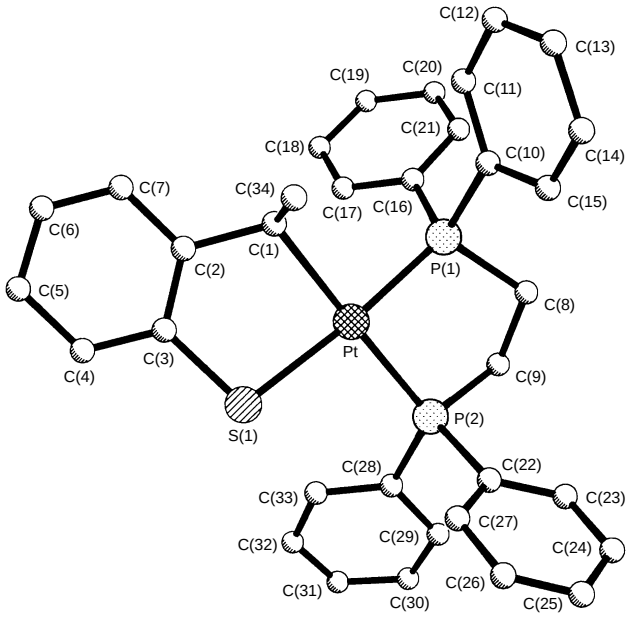

Fig. 2 The molecular structure determined for **3**. Bond lengths (Å) and angles (°): Pt–P(1) 2.232(4), Pt–P(2) 2.313(4), Pt–S 2.328(4), Pt–C(1) 2.202(14), Pt–C(34) 3.05 Å; C(1)–Pt–P(1) 93.3(4), P(1)–Pt–P(2) 85.49(13), C(1)–Pt–S, 82.7(4), P(2)–Pt–S 98.60(13)°.

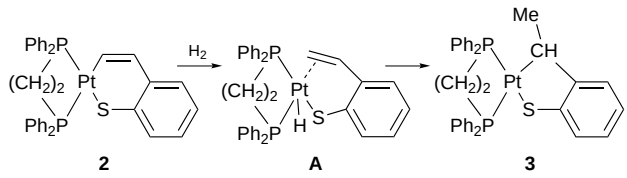

Scheme 1

2-ethylthiophenol, while the six-membered thiaplatinacycles [Pt{*C*,*S*-(CH=CHC$_6$H$_4$S)}(PEt$_3$)$_2$] and **2** gave 2-vinylthiophenol.[4]

One attractive mechanism by which the reaction **2** → **3** can occur is *via* a σ-*S* bonded π-alkene (η^3) intermediate (**A**), as shown in Scheme 1. Such species have been previously invoked in the reactions of various thiophenes with metal hydrides; a related iridium complex derived from thiophene itself has been isolated and characterised as [(triphos)Ir(η^3-S(Me)CH=CHCH=CH$_2$)]$^+$ [triphos = MeC(CH$_2$PPh$_2$)$_3$], and this shows equivalent bonding of the iridium to both the CH [2.19(3) Å] and to the CH$_2$ [2.12(3) Å].[10] That complex **3** does not have a type **A** structure is shown by the Pt···Me distance [Pt···C(34)] of 3.05 Å, which is well outside bonding; by contrast the distance Pt–C(1) is 2.202(14) Å.

Complex **3** can be hydrodesulfurised to ethylbenzene (*ca.* 80%) with LiAlH$_4$ (thf, 20 °C); this demonstrates a new HDS pathway, BT → **2** → **3** → PhEt.

We thank the EPSRC, the Royal Society, EERO, the European Community (Contract CL1*CT94-0062) and CONACYT for support and Professor W. Clegg for collecting the data for complex **2**.

Footnotes and References

* E-mail: P.Maitlis@Sheffield.ac.uk

† [Pt(*C*,*S*-SC$_8$H$_6$)(PMe$_3$)$_2$] **1**. Anal. Calc. for C$_{14}$H$_{24}$P$_2$PtS: C, 34.9; H, 5.0; S, 6.65. Found: C, 35.0; H, 4.95; S, 6.7%. NMR (CDCl$_3$): ^{1}H: δ 1.2–2.0 (m, 18 H, CH$_3$), 7.0–7.1 (m, 1 H, CH), 7.1–7.2 (m, 1 H, CH), 7.2–7.4 (m, 2 H, CH), 7.4–7.6 (m, 1 H, CH), 7.9 (m, 1 H, CH). ^{31}P: δ −22.6 [d, ^{1}*J*(PPt) 3065 Hz], −29.3 [d, ^{1}*J*(PPt) 1708 Hz]. ^{13}C{^{1}H}: δ 138.6 [t, CH, ^{2}*J*(PtC) 85 Hz], 131.4 (s, 2CH), 129.8 (s, C), 129.8 (s, CH), 129.7 [dd, CH, ^{2}*J*(*trans*-PC) 100.6, ^{2}*J*(*cis*-PC) 8.6 Hz], 125.3 (s, C), 121.7 (s, CH).

‡ [Pt(*C*,*S*-SC$_8$H$_6$)(dppe)] **2**. Anal. Calc. for C$_{34}$H$_{30}$P$_2$PtS·CH$_2$Cl$_2$: C, 51.7; H, 4.0. Found: C, 52.2; H, 3.8%. NMR (CDCl$_3$), ^{1}H δ 2.25–2.6 (m, CH$_2$, 4 H), 7.0–8.0 (m, CH + Ar, 26 H). ^{31}P: δ 41.5 [d, ^{1}*J*(PtP) 1743 Hz, ^{2}*J*(PP) 6 Hz], 46.3 [d, ^{1}*J*(PtP) 3122 Hz]. FABMS: *m*/*z* 728.

Crystal data for C$_{35}$H$_{32}$Cl$_2$P$_2$PtS: *M* = 812.60, crystallised from CH$_2$Cl$_2$–hexane as yellow blocks and containing one molecule of CH$_2$Cl$_2$; crystal dimensions 0.48 × 0.38 × 0.27 mm. Monoclinic, space group $P2_1/n$ (a non-standard setting of $P2_1/c$,C^5_{2h}, no. 14), *a* = 9.5594(7), *b* = 19.5003(14), *c* = 17.4993(12) Å, β = 91.683(2), *U* = 3260.7(4) Å^3, *Z* = 4, D_c = 1.655 Mg m^{-3}, Mo-Kα radiation (λ = 0.710 73 Å), μ(Mo-Kα) = 4.653 mm^{-1}, *F*(000) = 1600.

Refinement converged at a final *R* = 0.0318 (*wR*$_2$ = 0.0863, for all 5728 unique data, 372 parameters, mean and maximum δ/σ 0.000, 0.000), with allowance for the thermal anisotropy of all non-hydrogen atoms. Minimum and maximum final electron density −1.087 and 1.308 e A^{-3}.

§ [Pt(*C*,*S*-SC$_8$H$_8$)(dppe)], **3**. Anal. Calc. for C$_{34}$H$_{32}$P$_2$PtS·0.5CHCl$_3$: C, 52.5; H, 4.2; Found: C, 53.1; H, 4.4%. NMR spectra in CDCl$_3$, ^{1}H: δ 1.1–1.4 (m, 3 H, CH$_3$), 1.9–2.7 (m, 4 H, CH$_2$), 3.1–3.5 (m, 1 H, CH), 6.7 (t, 1 H, Ar), 6.8 (t, 1 H, Ar), 6.9 (d, 1 H, Ar), 7.4–8.0 (m, 21 H, Ar). ^{31}P: δ 43.0 [^{1}*J*(PtP) 1594, ^{2}*J*(PP) 4 Hz], 45.9 [^{1}*J*(PtP) 3190 Hz]. FABMS: *m*/*z* 730.

Crystal data for **3**: C$_{34}$H$_{32}$P$_2$PtS; *M* = 729.69, crystallised from CH$_2$Cl$_2$–hexane as yellow blocks; crystal dimensions 0.43 × 0.26 × 0.12 mm. Monoclinic, space group $P2_1/c$ (C^5_{2h}, No. 14), *a* = 9.266(4), *b* = 15.142(7), *c* = 21.303(9) Å, β = 98.51(3), *U* = 2956(2) Å^3, *Z* = 4, D_c = 1.640 Mg m^{-3}, Mo-Kα radiation (λ = 0.710 73 Å), μ(Mo-Kα) = 4.948 mm^{-1}, *F*(000) = 1440.

Refinement converged at a final *R* = 0.0665 (*wR*$_2$ = 0.1506, for all 5188 unique data 344 parameters, mean and maximum δ/σ 0.000, 0.000), with allowance for the thermal anisotropy of all non-hydrogen atoms. Minimum and maximum final electron density −0.892 and 1.150 e A^{-3}. CCDC 182/670.

1 H. Topsoe, B. S. Clausen and F. Massoth, *Hydrotreating Catalysis*, Springer, Berlin, p. 114; A. N. Startsev, *Catal. Rev. Sci. Eng.*, 1995, **37**, 353; B. C. Weygand and C. Friend, *Chem. Rev.*, 1992, **92**, 491; C. M. Friend and D. A. Chen, *Polyhedron*, 1997, **16**, 3165; B. Delmon, *Catal. Lett.*, 1993, **1**–**2**, 1; O. Weisser and S. Landa, *Sulphide Catalysts, their Properties and Applications*, Pergamon, Oxford, 1973.

2 J. P. van den Berg, J. P. Lucien, G. Germaine and G. L. B. Thielemans, *Fuel Process. Technol.*, 1993, **35**, 119; B. H. Cooper, A. Stanislaus and P. N. Hannerup, *Hydrocarbon Process.*, 1993, 83; I. E. Maxwell, J. E. Naber and K. P. de Jong, *Appl. Catal., A: Gen.*, 1994, **113**, 153; S. Mignard, N. Marchal and S. Kasztelan, *Bull. Soc. Chim. Belg.*, 1995, **104**, 259; M. Sugioka, F. Sado, Y. Matsumoto and N. Maesaki, *Catal. Today*, 1996, **29**, 255.

3 J. J. Garcia, B. E. Mann, H. Adams, N. A. Bailey and P. M. Maitlis, *J. Am. Chem. Soc.*, 1995, **117**, 2179; see also: J. J. Garcia and P. M. Maitlis, *J. Am. Chem. Soc.*, 1993, **115**, 12 200.

4 J. J. Garcia, A. Arevalo, V. Montiel, F. Del Rio, B. Quiroz, H. Adams and P. M. Maitlis, *Organometallics*, 1997, **16**, 3216.

5 J. J. Garcia, A. Arevalo, S. Capella, A. Chehata, M. Hernandez, V. Montiel, G. Picazo, F. Del Rio, R. Toscano, H. Adams and P. M. Maitlis, *Polyhedron*, 1997, **16**, 3185.

6 R. J. Angelici, *Polyhedron*, 1997, **16**, 3073 and following articles in *Polyhedron Symposium in Print on Hydrotreating*; see also: C. Bianchini and A. Meli, *J. Chem. Soc., Dalton Trans.*, 1996, 801.

7 C. Bianchini, A. Meli, M. Peruzzini, F. Vizza, P. Frediani, V. Herrera and R. A. Sanchez-Delgado, *J. Am. Chem. Soc.*, 1993, **115**, 7505; C. Bianchini, A. Meli, M. Peruzzini, F. Vizza, S. Moneti, V. Herrera and R. A. Sanchez-Delgado, *J. Am. Chem. Soc.*, 1994, **116**, 4370; C. Bianchini, A. Meli, V. Patinec, V. Sernau and F. Vizza, *J. Am. Chem. Soc.*, 1997, **119**, 4945.

8 V. Herrera, A. Fuentes, M. Rosales, R. A. Sanchez-Delgado, C. Bianchini, A. Meli and F. Vizza, *Organometallics*, 1997, **16**, 2465.

9 D. A. Vicic and W. D. Jones, *Organometallics*, 1997, **16**, 1912.

10 C. Bianchini, A. Meli, M. Peruzzini, F. Vizza, P. Frediani, V. Herrera and R. A. Sanchez-Delgado, *J. Am. Chem. Soc.*, 1993, **115**, 2731.

11 G. M. Sheldrick, SHELXL93, An integrated system for solving and refining crystal structures from diffraction data, University of Gottingen, Germany 1993.

Received in Cambridge, UK, 15th September 1997; 7/06707K

Self-assembling tetranuclear copper(II) complex of a bis-bidentate Schiff base: double-helical structure induced by aromatic π··π and CH··π interactions

Noboru Yoshida,*[a] Hiroki Oshio[b] and Tasuku Ito[b]

[a] *Laboratory of Molecular Functional Chemistry, Division of Material Science, Graduate School of Environmental Earth Science, Hokkaido University, Sapporo 060, Japan*
[b] *Department of Chemistry, Graduate School of Science, Tohoku University, Sendai 980-77, Japan*

The synthesis and structure of a tetranuclear copper(II) complex of a bis-N,O-bidentate Schiff base is reported; two types of copper(II) centers and the preference for two conformational degrees of freedom in the ligand lead to the unique formation of a novel supramolecular architecture not requiring a preorganized synthetic approach.

Self-assembly and molecular recognition appear to be essential factors for the construction of supramolecular architectures utilizing the formation of non-covalent bonds in solution.[1] The use of metal ions with specific preferences for particular coordination geometries has been developed rapidly in order to produce non-covalently organized structures, resulting in self-assembly of target ligands.[2] Many types of oligopyridines have been used because of their preorganized characteristics in self-assembling processes.[3]

Recently, new ligand systems have been exploited to construct unprecedented structures formed by self-assembling processes in solution and in the solid phase.[4,5] The requirement of the supramolecular structure is principally controlled by the appropriate combination of various types of weak non-covalent interactions and the geometrical preference of the metal ion. Our recent investigation using bis-bidentate Schiff base ligands (Scheme 1) allows for the synthesis of a variety of metal-assisted supramolecular structures. A dinuclear triple-helical Zn^{II} complex of L^{17},[5] a dinuclear double-helical Cu^{II} complex of L^{16},[6] and polynuclear Zn^{II} complexes of L^{16},[5] have been synthesized.

Here we describe a novel and general strategy for the construction of metal-assisted supramolecular architectures using ligand L^8. This architecture is prepared readily utilizing the weak aromatic π··π and CH··π interactions operating between the bridging groups of the bis-bidentate Schiff bases (Scheme 2).

The Schiff base ligand L^8 contains two N,O-bidentate chelating moieties linked *via* the azomethine groups with bis(3-aminophenyl)sulfone (Scheme 1). Reaction of L^8 with $Cu(MeCO_2)_2 \cdot H_2O$ in a 1 : 1 molar ratio in hot ethanol (*ca.* 60–70 °C) afforded a light-green solid **1**.† Elemental analysis suggests the formation of a Cu^{II} : L^8 2 : 2 complex and fast-atom bombardment mass spectroscopy (FABMS) also indicated a 2 : 2 complex for **1**.‡ However, positive-ion electrospray MS (*m*/*z* 2073.5) suggested the existence of a 4 : 4 complex for **1**. The electronic absorption spectrum of **1** shows a π–π* band at 379.5

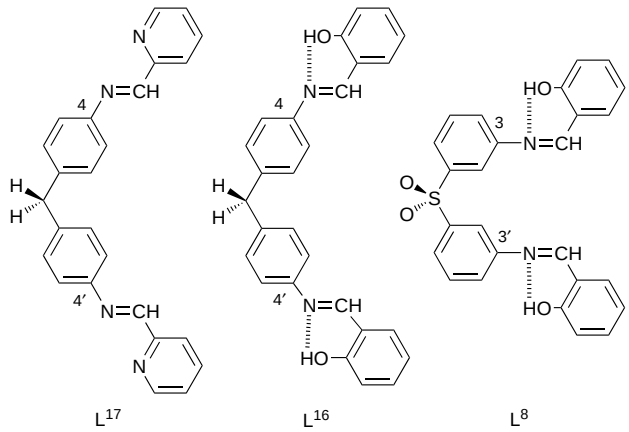

Scheme 1

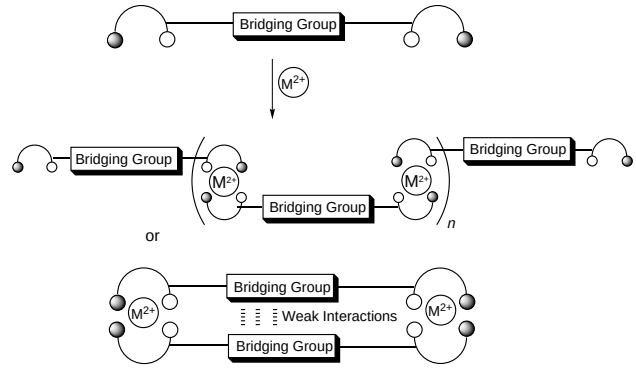

Scheme 2

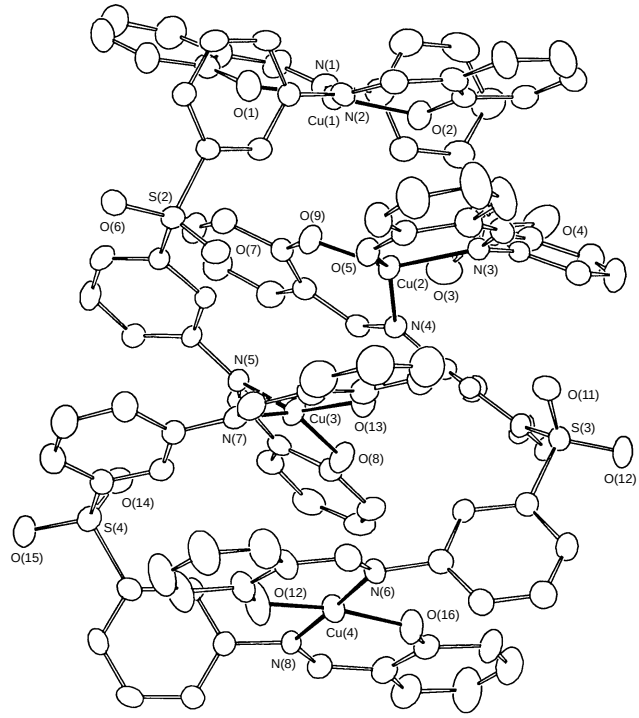

Fig. 1 Crystal structure of $[Cu(H_{-1}L^8)]_4$ **1**

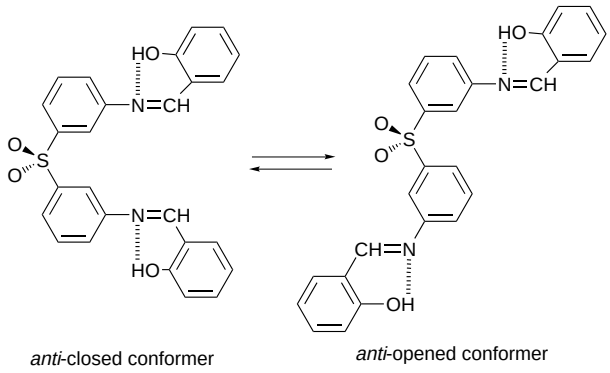

Fig. 2 Two main conformers of L^8

nm in the visible region which indicates deprotonation of the OH groups and N,O-coordination of Cu^{II}.[7]

Single crystals were obtained from chloroform–diethyl ether. An X-ray diffraction study confirms the formation of the $Cu^{II}:L^8$ 4:4 structure as shown in Fig. 1.§ The tetranuclear double helical structure appears to be stabilized by CH–π and π–π aromatic interactions (3.2–3.9 Å) between the bridging groups ($–C_6H_4SO_2C_6H_4–$). Complex **1** contains four Cu^{II} ions and four ligands. Two Cu^{II} ions at the top [Cu(1)] and bottom [Cu(4)] of the tetranuclear $(CuL^8)_4$ core adopt a square-planar (*SP*) coordination geometry, whereas the two remaining Cu^{II} ions [Cu(2), Cu(3)] in the middle adopt a tetrahedral (T_d) coordination geometry. Each Cu^{II} ion is coordinated by N,O-bidentate sites originating from two different ligands. Each ligand interacts with two Cu^{II} ions with a different coordination geometry. Furthermore, two types of conformations of L^8 are observed in this tetranuclear core (Fig. 2). The conformations of $L^8(1)$ and $L^8(4)$ are *anti*-closed (E_{steric} = −27.58 kcal mol^{-1}, 1 cal = 4.184 J) (Fig. 2), whereas the conformations of $L^8(2)$ and $L^8(3)$ are similar and *anti*-opened (E_{steric} = −27.16 kcal mol^{-1}).¶

Fig. 3 shows selected bond lengths and angles around the four Cu^{II} centers of the tetranuclear core of **1**. The Cu–N distances lie between 1.968(6)–2.024(6) Å and Cu–O is in the range 1.858(6)–1.903(5) Å. Angles O–Cu(1)–O, N–Cu(1)–N N–Cu(1)–O [O–Cu(4)–O, N–Cu(4)–N, N–Cu(4)–O] are in the range 174.9(2), 171.4(2), 88.1(2)–91.4(2)° [170.4(3), 177.6(2), 88.6(2)–91.8°], respectively. Thus, the coordination geometries around Cu(1) and Cu(4) are almost square-planar. On the other hand, O–Cu(2)–O, N–Cu(2)–N, N–Cu(2)–O [O–Cu(3)–O, N–Cu(3)–N, N–Cu(3)–O] angles are 89.6(2), 99.2(2), 147.2(2)–148.8(2)° [89.2(2), 100.1(2), 144.6(2)–148.7(2)°] which show a distorted tetrahedral geometry around Cu(2) and Cu(3). Four Cu^{II} ions having different coordination spheres lie almost in one plane and in a rhombus arrangement with Cu···Cu

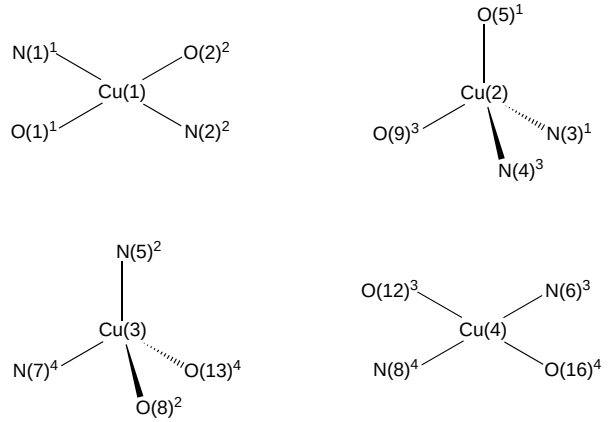

Fig. 3 Coordination geometries around the four Cu^{II} ions of **1**

distances between 4.043 and 7.659 Å. The sum of the interior angles is 353.26°. Other metal complexes with Zn^{II}, Ni^{II} and Co^{II} which are insoluble in most organic solvents appear to form $(1:1)_n$ polymeric structures (Scheme 2).

Flexible geometry of Cu^{II} (*SP* or T_d) and the flexible conformational freedom in the ligand lead to CH–π and π–π aromatic interactions between the bridging groups and the tetranulear double-helical structure. These conformational preferences in the ligand and metal-coordination geometry are an unusual example in metallosupramolecular chemistry. The subtle change in the bridging group leads to an unprecedented organized structure in the absence of a preorganized synthetic approach. The development of new ligand systems using Schiff base series is now in progress.

Footnotes and References

* E-mail: nyoshida@high.hokudai.ac.jp

† 3,3′-Diaminosulfone (0.5 mol) was added gradually to an EtOH solution (100 ml) of salicylaldehyde (1 mol) and the solution was stirred for 30 min at 60 °C and the orange solid precipitate was collected by filtration. Elemental analysis was in accord for L^8. A mixture of L^8 (0.78 g, 1.72 mmol) and $Cu^{II}(MeCO_2)_2·H_2O$ (0.34 g, 1.7 mmol) was dissolved in EtOH (100 ml) and heated and the resulting green powder was collected by filtration and washed with hot EtOH. This powder dissolves readily in DMF and $CHCl_3$. X-Ray quality crystals were grown by slow diffusion of Et_2O into a $CHCl_3$ solution of **1**. Satisfactory elemental analysis was obtained.

‡ MM2 force-field calculations also suggested the possibility for the existence of $Cu^{II}:L^8$ 2:2 complexes, the minimum-energy self-assembling structures, **2** (SP–SP for two Cu^{II}) and **3** (T_d–T_d coordination geometry). The force-field structure **3** (E_{steric} = −32.212 kcal mol^{-1}) is considerably more stable than that of **2** (E_{steric} = 8.662 kcal mol^{-1}); Tektronix CAChe System, (Version 3.7).

§ *Crystal data* for **1**: $C_{104}H_{72}Cu_4N_8O_{16}S_4$, 0.50 × 0.30 × 0.25 mm, M = 2072.18, brown prismatic crystal, monoclinic, space group $P2_1/c$, a = 18.026(2), b = 23.450(3), c = 22.743(2) Å, β = 90.299(9)°, U = 9613(1) Å^3, Z = 4, D_c = 1.432 g cm^{-3}, μ(Mo-Kα) = 9.64 cm^{-1}, $F(000)$ = 4240. 17 487 data collected at −100 °C on a Rigaku AFC 7S four circle diffractometer equipped with graphite monochromated Mo-Kα radiation (λ = 0.710 73 Å). The structure was solved by direct methods with SHELX-86 (G. M. Sheldrick, University of Göttingen, 1986) and Fourier techniques, and refined by full-matrix least-squares on F^2 data using SHELXL-93 (G. M. Sheldrick, University of Göttingen, 1993). and converged at R_1 = 0.0667, wR_2 = 0.1652. CCDC 182/663.

¶ Although L^8 can adopt many conformations, molecular mechanics (MM2) calculations revealed the four minimum-energy structures as *anti*-closed and *anti*-opened conformers. These two isomers have almost the same energy. Other minimum-energy structures, *syn*-opened (E_{steric} = −27.4973 kcal mol^{-1}) and *syn*-closed (E_{steric} = −28.820 kcal mol^{-1}) conformers have similar energy.

1 J.-M. Lehn, *Supramolecular Chemistry, Concepts and Perspectives*, VCH, Weinheim, 1995; D. Philips and J. F. Stoddart, *Angew. Chem., Int. Ed. Engl.*, 1996, **35**, 1154 and references therein.
2 C. Piguet, G. Bernardinelli, A. E. Williams and B. Bocquet, *Angew. Chem., Int. Ed. Engl.*, 1995, **34**, 582.
3 E. C. Constable, A. J. Edwards, P. R. Raithby, D. R. Smith, J. V. Walker and L. Whall, *Chem. Commun.*, 1996, 2551 and references therein.
4 J. C. Jeffery, P. L. Jones, K. L. N. Mann, E. P. Psillakis, J. A. McCleverty, M. D. Ward and C. M. White, *Chem. Commun.*, 1997, 175; C. M. Hartshorn and Peter J. Steel, *ibid.*, 1997, 541; D. M. L. Goodgame, S. Menzer, A. M. Smith and D. J. Williams, *ibid.*, 1997, 339; M. J. Hannon, C. L. Painting and W. Errington, *ibid.*, 1997, 307; P. N. W. Baxter, G. S. Hanan and J-.M. Lehn, *ibid.*, 1996, 2019; R. Bhalla, M. Helliwell and C. D. Garner, *ibid.*, 1996, 921; P. C. M. Duncan, D. M. L. Goodgame, S. Menzer and D. J. Williams, *ibid.*, 1996, 2127; M. Albrecht and S. Kotila, *ibid.*, 1996, 2309; T.Beissel, R. E. Powers and K. N. Raymond, *Angew. Chem., Int. Ed. Engl.*, 1996, **35**, 1084; R. W. Saalfrank, N. Loew, F. Hampel and H.-D. Stachel, *ibid.*, 1996, **35**, 2209; A. J. Amoroso, J. C. Jeffery, P. L. Jones, J. A. McCleverty, P. Thornton and M. D. Ward, *ibid.*, 1995, **34**, 1443; E. J. Enemark and T. D. P. Stack, *ibid.*, 1995, **34**, 996.
5 N. Yoshida and K. Ichikawa, *Chem. Commun.*, 1997, 1091.
6 N. Yoshida and H. Kuma, unpublished work.
7 N. Yoshida and M. Fujimoto, *Bull. Chem. Soc. Jpn.*, 1976, **49**, 1557.

Received in Cambridge, UK 28th August 1997; 7/06284B

Three step syntheses of naphthofurans and phenanthrofurans related to (−)-morphine from *ortho*-benzoquinone monoketals by Diels–Alder and Cope reactions

Rina Carlini, Kerianne Higgs, Russell Rodrigo* and Nicholas Taylor

Guelph-Waterloo Centre for Graduate Work in Chemistry, Department of Chemistry, University of Waterloo, Waterloo, Ontario, Canada N2L 3G1

Adducts of the intramolecular Diels–Alder reaction of *o*-benzoquinone monoketals are rapidly converted to oxygen heterocycles *via* Cope rearrangements.

The considerable synthetic potential of *ortho*-benzoquinonoid monoketals remains largely unexploited despite a few noteworthy applications[1] in natural product synthesis. Our laboratory has recently embarked on a program to study the inter-[2] and intra-molecular Diels–Alder (IMDA) reactions[3] of such intermediates and to evaluate the synthetic utility of the resulting adducts. We recently reported[3] the Cope rearrangement of one adduct and its use in a brief and efficient synthesis of the pentacyclic marine sponge metabolite (±)-Xestoquinone. The success of this two step IMDA–Cope sequence has prompted us to explore the Cope rearrangements of several additional bridged IMDA adducts to demonstrate their generality and illustrate their value with a convergent three-step route to a 3-hydroxy-9c-allylphenanthro[4,5-*bcd*]furan **14b** constituting rings A, B, C and E of morphine.[4]

Each of four substituted guaiacols **1a**–**d** were treated with a minimum of 5 equiv. of (*E*)-penta-2,4-dienol in the presence of bis(trifluoroacetoxy)iodobenzene (BTIB), to provide the mixed monoketals **2** that reacted *in situ* to generate the IMDA adducts **3** and **4** in combined yields of 53–88% (Table 1 and Scheme 1). After separation of the adducts, thermal Cope rearrangements of the bridged compounds **3a**–**f** were effected (Table 2).[5] Several naphtho[1,8-*bc*]furan tricycles **4a**, **b**, **e**, **f**, all *endo*† isomers and bearing a carbon substituent (R^3) at a ring junction, are thus obtainable in two steps from simple starting materials. Bridged adduct **3e** generated the naphthofuran **7e** upon heating in aromatic hydrocarbon solvents (entries 8 and 9). This is presumably the result of a facile dienone–phenol rearrangement of intermediate **5e**. We have observed that thiol esters like **5e** are particularly prone to such migrations. Acid-catalysed elimination of MeOH (using TFA) from **4f**, and subsequent alkaline hydrolysis of the ester, produced the phenol **7** (R^1 = R^3 = H) after spontaneous decarboxylation (90%).‡

The tetracyclic phenanthrofuran system is also readily accessible by application of the same chemistry. The reaction of methyl vanillate **1f** with 3 equiv. of 3-vinylcyclohex-2-enol[6] **9a** produced a mixture of *exo* (**10a**) and *endo* (**11a**) IMDA adducts, together with a small amount of the bridged adduct **12a** (Scheme 2). X-Ray crystal structures§ of **10a** and **11a** were obtained to establish their structure and relative configurations.

Table 1 Diels–Alder reactions of guaiacols **1** with (*E*)-penta-2,4-dienol

Substituted guaiacol[a]	Products (% yield)
1a	**3a** (72), **4a** (16)
1b	**3b** (65), **4b** (13)
1c	**3c** (65), **4c** (7)
1d	**3d** (52), **4d** (1)

[a] For three more examples, see ref. 3.

The *endo* isomer (**11a**) was easily aromatized in two steps: brief treatment with TFA to eliminate MeOH produced the dienone **13a** (92%), and saponification of the ester resulted in spontaneous decarboxylation and aromatization to **14a** (90%). The ketal moiety of the *exo* isomer (**10a**) was remarkably stable to prolonged acid treatment at room temperature.

It is generally acknowledged that acid hydrolysis of an acetal is promoted by the presence of at least one non-bonded electron pair on the endocyclic oxygen atom in an antiperiplanar relationship with the exocyclic carbon–oxygen bond that is being cleaved in the reaction.[7] Furthermore, the relationship between C–O bond lengths and O–C–O angles of acetals in the ground state and the ease of acid-catalysed hydrolysis has been convincingly demonstrated.[8,9] The relevant bond lengths and angles of **10a** and **11a** are shown in Table 3, together with projections along the O(4)–C(3a) bond derived from the X-ray structures (Fig. 1), with the non-bonding sp^3 orbitals of O(4) added in approximately tetrahedral orientations. These projections clearly show that the stereoelectronic requirements for the acid-catalysed elimination of MeOH can only be met in the *endo*-adduct **11a**, and this is reflected in the corresponding changes in bond lengths of C(3a)–OMe (longer) and C(3a)–O(4) (shorter), exactly opposite to the situation in the *exo*-

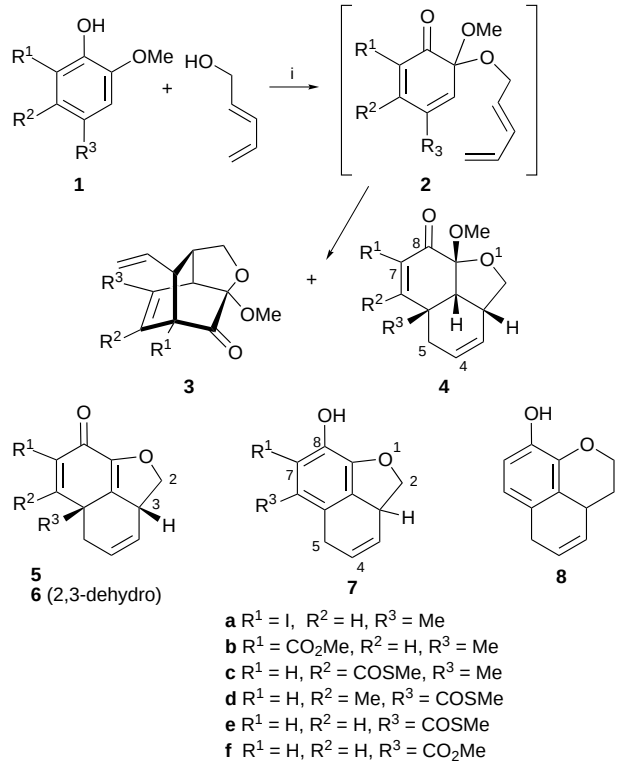

Scheme 1 *Reagents and conditions*: i, BTIB, THF, 0 °C

Table 2 Thermal Cope rearrangements of bridged IMDA adducts **3** in various solvents

Entry	Reactant	Solvent[a] (% conversion)	Products (% yield)
1	**3a**	TMB[a] (100)	**4a** (38)[b]
2	**3a**	Decane[c] (100)	**6a** (50)
3	**3a**	TCE[a] (61)	**6a** (70)
4	**3b**	TCE[c] (100)	**4b** (10), **6b** (32)
5	**3c**	Decane[c] (72)	**6c** (25)
6	**3d**	Decane	Decomposition product
7	**3e**[d]	Decane (84)	**4e** (81)
8	**3e**[d]	*p*-Xylene (100)	**4e** (6), **7e** (28)
9	**3e**[d]	TMB (100)	**7e** (42)
10	**3f**[d]	TMB (100)	**4f** (46), **5f** (20)
11	**3f**[d]	*p*-Xylene (93)	**4f** (21), **5f** (44)

[a] TMB = 1,2,4-trimethylbenzene; TCE = 1,1,2,2-tetrachloroethane. [b] Iodine was also produced. [c] Some thermal rearrangements performed in decane and TCE resulted in significant decomposition. [d] For the preparation of **3e** and **3f**, see ref. 3.

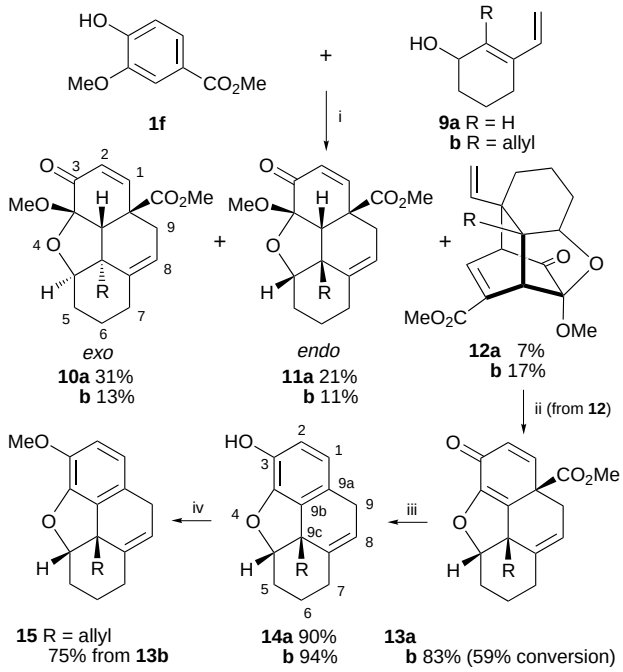

Scheme 2 *Reagents and conditions*: i, BTIB; ii, $Cl_2CHCHCl_2$, heat; iii, NaOH, MeOH; iv, K_2CO_3, Me_2SO_4, acetone

Table 3 Bond lengths and angles at the C(3a) ketal carbon atom of **10a** and **11a**

	Bond length/Å		
	C(3a)–O(4)	C(3a)–OMe	Bond angle (°) O(4)–C(3a)–OMe
10a (*exo*)	1.422	1.401	109.1
11a (*endo*)	1.407	1.416	111.6

adduct **10a**. The reluctance of the latter adduct to undergo the elimination can thus be understood.

The 2-allylcyclohexenol **9b**, prepared from 2-allylcyclohexane-1,3-dione[10] in a similar manner to **9a**, reacted with methyl vanillate **1f** to provide a mixture of three adducts **10b**, **11b** and **12b** (Scheme 2). Again, the *exo*-adduct **10b** was stable to acid while the *endo*-isomer **11b** was converted to dienone **13b** by brief exposure to TFA. When the bridged adduct **12b** was subjected to the thermal Cope rearrangement in refluxing 1,1,2,2-tetrachloroethane, elimination of MeOH also occurred

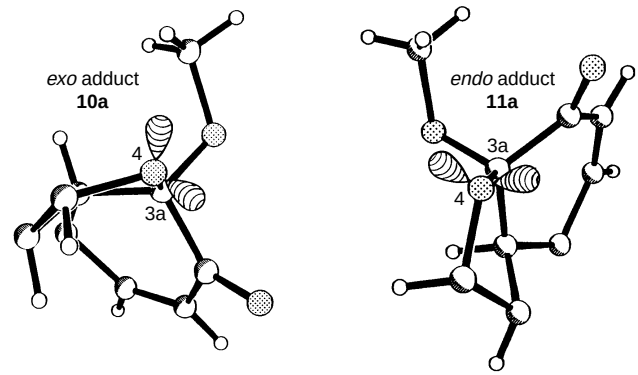

Fig. 1 Projections along the C(3a)–O(4) bonds adapted from X-ray structures of **10a** and **11a**

to produce **13b** (83% yield, 59% conversion), which was saponified as before to produce **14b** (94%).

Reduction of 2-allyl-3-vinylcyclohex-2-enone with borane and 20 mol% of the (*R*)-oxazaborolidine[11] provided the (*S*)-(−)-cyclohexenol **9b** in 84% yield and 88% ee.¶ Repetition of the same sequence of reactions with (−)-**9b** afforded **15**, the methyl ether of phenol **14b** in 75% yield (88% ee) from **13b**. Further progress in the conversion of **14b** or **15** to a morphinan[12] will be reported in due course.‖

We thank the Natural Sciences and Engineering Research Council of Canada for support of this work.

Footnotes and References

* E-mail: rrodrigo@mach1.wlu.ca

† The terms *exo* and *endo* are used with respect to the *o*- quinonoid ring.

‡ The same sequence of reactions was also used to generate the naphtho[1,8-*bc*]pyran system **8** from methyl vanillate and hexa-3,5-dienol.

§ *Crystal Data* for **10a**: Colourless plate of $C_{17}H_{20}O_5$, triclinic, space group $P\bar{1}$, M = 304.3, a = 7.8603(8), b = 7.9599(8), c = 12.6351(11) Å, α = 103.516(5), β = 104.685(5), γ = 100.226(7)°, V = 719.6(2) Å^3, Z = 2, T = 160 K, $w^{-1} = \sigma^2(F) + 0.00007F^2$, wR (all data) = 5.02%, wR (obs. data) = 4.97%. For **11a**: Colourless needle prism fragment of $C_{17}H_{20}O_5$, orthorhombic, space group *Pbca*, M = 304.3, a = 23.109(3), b = 10.525(1), c = 12.005(2) Å, V = 2919.9(8) Å^3, Z = 8, T = 160 K, $w^{-1} = \sigma^2(F)$, wR (all data) = 3.80%, wR (obs. data) = 3.74%. CCDC 182/672.

¶ The enantiomeric excesses of **9b** and **15** were determined in each instance by HPLC separation on a Chiralcel OD column using hexane–isopropanol.

‖ All new compounds prepared in this study provided satisfactory spectroscopic data. Full details will be published later.

1 P. Deslongchamps, *Pure Appl. Chem.*, 1977, **49**, 1329; S. Yamamura, Y. Shizumi, H. Shigemori, Y. Okuno and M. Okhubo, *Tetrahedron*, 1991, **47**, 635; T. H. Lee, C.-C. Liao and N. C. Liu, *Tetrahedron Lett.*, 1996, **37**, 5897.
2 R. Carlini, C.-L. Fang, D. Herrington, K. Higgs, R. Rodrigo and N. Taylor, *Aust. J. Chem.*, 1997, **50**, 271.
3 R. Carlini, K. Higgs, C. Older, S. Randhawa and R. Rodrigo, *J. Org. Chem.*, 1997, **62**, 2330.
4 For recent syntheses of morphinans, see J. Mulzer, J.W. Bats, B. List, T. Opatz and D. Trauner, *Synlett*, 1997, 441 and references cited therein.
5 A Cope rearrangement of an intermolecular adduct of cyclopentadiene with an *o*-benzoquinone has been reported; M. F. Ansell, A. F. Gosden, V. J. Leslie and R. A. Murray, *J. Chem. Soc.* (*C*), 1971, 1041.
6 E. J. Corey and A. G. Meyers, *Tetrahedron Lett.*, 1984, **25**, 3559.
7 P. Deslongchamps, in *Stereoelectronic Effects in Organic Chemistry*, Pergamon Oxford, 1983.
8 P. G. Jones and A. J. Kirby, *J. Chem. Soc., Chem. Commun.*, 1979, 288.
9 H. B. Bürgi, J. D. Dunitz and E. Shefter, *Acta Crystallogr.*, 1974, **B30**, 1517; P. G. Jones, O. Kennard, S. Chandrasekhar and A. J. Kirby, *Acta Crystallogr.*, 1978, **B34,** 3835.
10 H. Stetter and W. Dierichs, *Chem. Ber.*, 1952, **85**, 1061.
11 E. J. Corey, P. Da Silva Jardine and T. Mohri, *Tetrahedron Lett.*, 1988, **29**, 6409.
12 T. Hudlicky, C. H. Boros and E. E. Boros, *Synthesis*, 1992, 174.

Received in Corvallis, OR, USA, 11th August 1997; 7/05848I

Strategies of fungal pathogens: detoxification of a cruciferous phytoalexin by mimicry

M. Soledade C. Pedras* and Francis I. Okanga

Department of Chemistry, University of Saskatchewan, 110 Science Place, Saskatoon SK, Canada S7N 5C9

Two different isolates of the phytopathogen *Phoma lingam* metabolized and phytoalexin cyclobrassinin 3 to the phytoalexins dioxibrassinin 5 and brassilexin 9; both 5 and 9 were further metabolized and detoxified by each fungal isolate.

Phytoalexins[1] are part of the induced chemical defenses produced by plants in response to several forms of stress, including fungal attack. In spite of the enormous interest in phytoalexins, cruciferous[2] phytoalexins may have further significance due to their unique chemical structures and additional biological activity.[3] Brassinin **1**, methoxybrassinin **2**

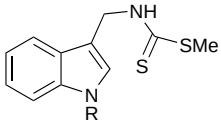

1 R = H
2 R = OMe

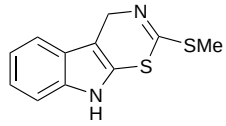

3

and cyclobrassinin **3** were the first reported[4] sulfur-containing phytoalexins produced by crucifers, a plant family with high sulfur requirements.[5] In general, the timing, rate of accumulation and relative amounts of phytoalexins synthesized in leaf tissues play crucial roles in plant resistance to pathogen invasion.[6] However, when pathogenic fungi can effectively disarm the plant by detoxifying phytoalexins, the outcome of the interaction can favour the pathogen and be detrimental to the plant. Although to date only a few examples demonstrate that brassica pathogens can detoxify phytoalexins efficiently,[2] multiple examples exist in other plant species.[7] We have demonstrated previously that the blackleg fungus [*Phoma lingam* (Tode ex Fr.) Desm., perfect stage *Leptosphaeria maculans* (Desm.) Ces. et de Not.], one of the most destructive pathogens of rapeseed (*Brassica napus, B. rapa*) can overcome the plant's chemical defenses by promptly transforming brassinin **1** into non-toxic indole-3-carboxylic acid.[8] Here we describe the unprecedented biotransformation of the brassica phytoalexin cyclobrassinin **3** to the phytoalexins dioxibrassinin **5** and brassilexin **9**, by the 'virulent' and 'avirulent' isolates of *P. lingam*,[9] respectively.

In initial experiments, cyclobrassinin **3**[10] was incubated with the so-called 'avirulent' isolate Unity† to establish a time-course transformation profile.[11] Analysis of organic extracts of culture samples by HPLC‡ indicated a rapid decrease in the concentration of **3** (HPLC retention time, t_r = 24.5 min) and the concurrent appearance of two additional constituents (t_r = 7.2 and 12.1 min) over a 12 h period. Subsequently, to obtain sufficient quantities of each constituent, larger-scale fungal cultures incubated with cyclobrassinin **3** were extracted with Et_2O, the extract fractionated by chromatography§ and each fraction analysed by HPLC. The fractions containing the aforementioned new constituents were analysed by standard spectroscopic methods (NMR, HRMS, FTIR, UV) for structural elucidation. Based on these results the constituent of t_r = 12.1 min was established to be the known phytoalexin brassilexin **9**,¶ whose structure we confirmed by synthesis.[2] The structure of the constituent of t_r = 7.2 min, a relatively less-stable metabolite, was assigned as a mixture of the related tautomers

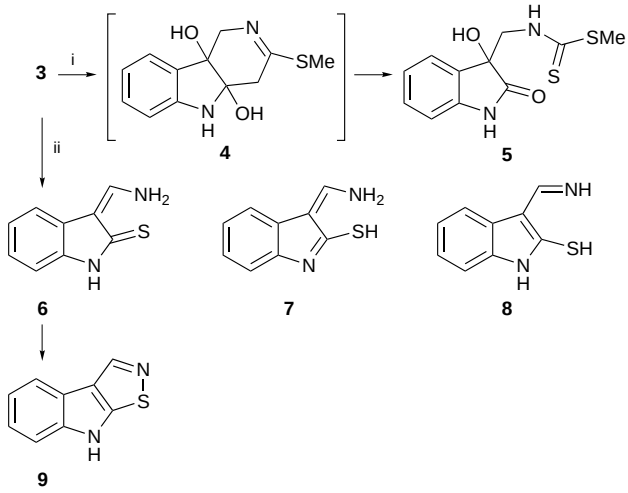

Scheme 1

3-methylenaminoindole-2-thione **6**, 3-methylenaminoindole-2-thiol **7** and 3-(methylimino)indole-2-thiol **8**, based on spectroscopic data‖ and derivatization. Two days after incubation of the isolate Unity with cyclobrassinin, no brassilexin or other phytoalexins or putative metabolites were detected in any of the cultures or their extracts. The mycelial mass of cultures incubated with cyclobrassinin **3** was similar to that of control cultures. Similar experiments carried out with the 'virulent' isolate BJ-125† incubated with cyclobrassinin **3** for 12 h afforded yet another known phytoalexin, dioxibrassinin **5**[12] (t_r = 7.5 min), whose chemical structure we confirmed by synthesis. Two days after incubation of the virulent isolate BJ-125 with cyclobrassinin **3**, no phytoalexins or derivatives were detected in any of the cultures or their extracts. In addition, the mycelial mass of cultures incubated with cyclobrassinin **3** was similar to that of control cultures. These remarkable results indicate that cyclobrassinin **3** is detoxified *via* the phytoalexins brassilexin **9** or dioxibrassinin **5**, depending on the particular fungal species, as shown in Scheme 1. The reactive intermediate **4**, similar to that proposed for the biosynthesis of a brassica phytoalexin,[12] could explain the formation of **5** through enzymatic dioxygenation of **3**. Additional experiments with other fungal isolates incubated with cyclobrassinin indicated similar results within the same species. It is worthy to note that cyclobrassinin **3** has been proposed as an *in planta* biosynthetic precursor of both brassilexin **9**[13] and brassicanal A **10**.[14]

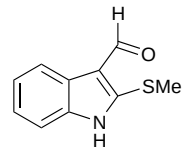

10

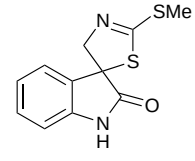

11

However, *in planta*, biosynthetic relationships have only been established between brassinin **1** and cyclobrassinin **3** and brassinin **1** and spirobrassinin **11**.[12,15]

Our results suggest that two different fungal species, the so-called 'virulent' and 'avirulent' groups,† can metabolize the phytoalexin cyclobrassinin **3** 'mimicking' pathways that may operate in the plant (*i.e.* **3** to **5** and **3** to **9**, respectively).** Considering that fungal pathogens have been coevolving with plants for multiple generations, the detoxification of phytoalexins by 'mimicry' appears quite plausible. Nonetheless, because *in planta* only a part of the biosynthetic pathway of cruciferous phytoalexins has been established, such a hypothesis remains to be demonstrated. A clearer picture will eventually unfold upon tracing a complete map of phytoalexin transformation in both cruciferous plants and their pathogenic fungi.

We gratefully acknowledge the financial support of the Natural Sciences and Engineering Research Council of Canada and the University of Saskatchewan.

Footnotes and References

* E-mail: pedras@sask.usask.ca

† The fungal species *Phoma lingam* is subdivided in various groups (see for example ref. 9); the so-called 'avirulent' group (*e.g.* isolate Unity) is now considered a species different from that of the 'virulent' group (*e.g.* BJ-125), although no formal reclassification has been done. General procedures for fungal culturing and analyses were carried out as described in ref. 11.

‡ HPLC analysis was performed with a liquid chromatograph equipped with quaternary pump, automatic injector, photodiode array detector, degasser and a Hypersil ODS column (5 μm particle size silica, 4.6 × 200 mm) equipped with an in-line filter. Mobile phase: 75% H_2O–25% MeCN to 100% MeCN, 35 min (linear gradient), flow rate = 1.0 ml min^{-1}.

§ A clean separation of the constituents could only be achieved on C-18 reversed-phase silica gel; normal silica gel chromatography lead to decomposition of the product with t_r = 7.2 min.

¶ Brassilexin **9** was first isolated from *B. juncea* (*cf.* M. Devys, M. Barbier, I. Loiselet, T. Rouxel, A. Sarniguet, A. Kollmann and J. Bousquet, *Tetrahedron Lett.*, 1988, **29**, 6447) and later synthesized (*cf.* M. Devys and M. Barbier, *Org. Prep. Proced. Int.*, 1993, **25**, 344).

‖ The ^{1}H NMR spectrum obtained (CD_3CN or CD_2Cl_2) for the tautomeric mixture of **6** and **8** displayed a doublet of doublets (dd) at δ 8.15 attributed to (=C)–*H*(NH_2); this assignment was corroborated by proton decoupling of *H*$_2$N (δ 11.15 and 6.24). Selected *spectroscopic data* for tautomeric mixture (HPLC t_r = 7.2 min): δ_H (500 mHz, CD_2Cl_2) 11.15 (br s, side-chain NH*H*), 8.98 (br s, indolic NH), 8.15 (dd, *J* 14.8, 8.2, H-1′) 7.41 (d, *J* 7.5, H-4), 7.15–7.07 (m, H-5 to H-7, 3 H), 6.24 (br s, side-chain NH*H*); δ_C (125.8 MHz, CD_2Cl_2) 179.0, 148.9, 138.0, 128.3, 124.1, 122.2, 115.3, 109.7, 108.4; δ_C (125.77 MHz, CD_3OD) (multiple signals attributable to tautomeric mixture) 177.6, 153.7, 151.7, 148.7, 140.4, 139.5, 129.9, 126.9, 125.0, 124.9, 124.1, 123.4, 122.5, 121.6, 120.9, 119.6, 115.8, 112.9, 111.7, 110.8, 110.5, 108.6; EIMS: *m/z* 176 (M^+, 100%), 149 (46), 117 (11). CIMS: *m/z* 177 (M^+ + 1, 100%), 164 (11), 145 (13).

** It is worthy to note a few examples in which fungal pathogens produce metabolites similar or identical to those of higher plants, such as some gibberellins produced by *Gibberella fukjukuroi* and a *Phaeosphaeria* sp., and abscisic acid produced by *Cercospora rosicola*. For a recent review see, for example, P. M. Dewick, *Nat. Prod. Re.*, 1995, **12**, 507.

1 C. J. W. Brooks and D. G. Watson, *Nat. Prod. Rep.*, 1985, 427; C. J. W. Brooks and D. G. Watson, *Nat. Prod. Rep.*, 1991, 367.
2 For a recent review on cruciferous phytoalexins, see M. S. C. Pedras, A. Q. Khan and J. L. Taylor, in *Phytochemicals for Pest Control*, ed. P. A. Hedin, R. M. Hollingworth, E. P. Masler, J. Miyamoto and D. G. Thompson, *ACS Symp. Ser.*, 658, 1997, pp. 155–166 and references cited therein.
3 R. G. Meheta, J. Liu, A. Constantinou, M. Hawthorn, J. M. Pezzuto, R. C. Moon and R. Moriarty, *Anticancer Res.*, 1994, **14**, 1209. Recent studies attributed a cancer preventive role to the phytoalexins brassinin, cyclobrassinin and spirobrassinin.
4 M. Takasugi, N. Matsui and A. Shirata, *J. Chem. Soc., Chem. Commun.*, 1986, 1077.
5 R. Marquard, K. C. Walker, in *Brassica Oilseeds*, ed. D. Kimber and D. I. McGregor, CAB International, Wallingford, UK, 1995, pp. 195–213.
6 C. J. Smith, *New Phytol.*, 1996, **132**, 1; W. Barz, W. Bless, G. Börger-Papendorf, W. Gunia, V. Mackenblock, D. Meier, C. Otto and E. Süpei, in *Bioactive Compounds from Plants*, Ciba Foundation Symposium, Wiley, Chichester, England, 1990, pp. 140–156.
7 *Handbook of Phytoalexin Metabolism and Action*, ed. M. Daniel and R. P. Purkayastha, Marcel Dekker Inc., New York, 1995, p. 650; H. D. VanEtten, D. E. Mathews and P. S. Mathews, *Annu. Rev. Phytopathol.*, 1989, **27**, 143.
8 M. S. C. Pedras and J. L. Taylor, *J. Org. Chem.*, 1991, **56**, 2619; M. S. C. Pedras, I. Borgmann and J. L. Taylor, *Phytochem.* (*Life Sci. Adv.*), 1992, **11**, 1; M. S. C. Pedras and J. L. Taylor, *J. Nat. Prod.*, 1993, **56**, 731.
9 M. S. C. Pedras, J. L. Taylor and V. M. Morales, *Phytochemistry*, 1995, **38**, 1215; J. L. Taylor, M. S. C. Pedras and V. M. Morales, *Trends Microbiol.*, 1995, **3**, 202.
10 M. Takasugi, K. Monde, N. Katsui and A. Shirata, *Bull. Chem. Soc. Jpn.*, 1988, **61**, 285.
11 M. S. C. Pedras and A. Q. Khan, *J. Agric. Food Chem.*, 1996, **44**, 3403.
12 First isolation: K. Monde, K. Sasaki, A. Shirata and M. Takasugi, *Phytochemistry*, 1991, **30**, 2915. For synthesis, see K. Monde, M. Takasugi and T. Ohnishi, *J. Am. Chem. Soc.*, 1994, **116**, 6650.
13 M. Devys and M. Barbier, *Z. Naturforsch., Teil C*, 1992, **47**, 318.
14 K. Monde, A. Tanaka and M. Takasugi, *J. Org. Chem.*, 1996, **61**, 9053.
15 K. Monde and M. Takasugi, *J. Chem. Soc., Chem. Commun.*, 1991, 1582.

Received in Corvallis, OR, USA, 19th September 1997; 7/06819K

Alkyl succinimidyl carbonates undergo Lossen rearrangement in basic buffers

Samuel Zalipsky*

SEQUUS Pharmaceuticals, Inc., 960 Hamilton Court, Menlo Park, CA 94025, USA

A side reaction producing β-alanine and derivatives through Lossen rearrangement was found to accompany hydrolysis of alkyl succinimidyl carbonates in basic aqueous buffers.

Alkyl succinimidyl† carbonate (SC) derivatives are useful alkoxycarbonylating reagents. In particular, their reactivity with primary amines has found a wide use for the introduction of urethane protecting groups,[1] protein modification,[2–5] and covalent attachment of ligands to matrices for solid-phase synthesis[6] and affinity chromatography.[7] Often these carbamoylation reactions are carried out in aqueous or aqueous–organic medium at mildly basic pH. Such conditions are dictated by the solubility properties of the amino reactants, amino acids, aminosugars, proteins, *etc.* In recent years, we have used SC derivatives of poly(ethylene glycol) (SC-PEG) for attachment of the polymer residues to amino groups of proteins, lipids and various biologically-relevant ligands.[3–5,8,9] In the course of these studies it was noticed that occasionally upon completion of a protein modification reaction using an excess of SC-PEG, there were larger amounts of primary amino group-containing compounds in solution than originally present on the protein. Accurate determinations of the extent of protein modification were only realized following removal of low molecular weight amines by extensive diafiltration.[4] These observations lead to the belief that the low molecular weight amine originated from the SC reagent itself. In order to verify this hypothesis, several ^{1}H NMR experiments were performed with bis-SC-PEG-2000[3,9] and benzyl succinimidyl carbonate (Bn-SC) under conditions often used for protein modification. Herein I present the results of these experiments and their corroboration by amino acid analysis (AAA), all of which indicate that SC derivatives undergo Lossen-type rearrangement producing β-Ala and its derivatives.

Table 1 Quantities of β-Ala formed after dissolution of bis-SC-PEG (10 mg, 8.4×10^{-4} equiv. SC per g) in tetraborate or carbonate buffers (0.1 M, pH 9.3, 0.65 ml) and incubation at 23 °C for 24 h. Aliquots taken from the reaction solutions were subjected to AAA, both directly and after hydrolysis (6 M HCl, 24 h, 110 °C). Amino groups were determined by the 2,4,6-trinitrobenzene sulfonate assay[17] using β-Ala for calibration

	β-Ala/10^{-5} mol g^{-1} [% of SC group]		
Buffer type	Total (HCl hydrolysis)	Free amino acid	Amino groups/ 10^{-5} mol g^{-1}
Tetraborate	15.8 [19]	4.6 [5.5]	8.6
Carbonate	20.6 [24]	6.6 [7.8]	10.3

Hydrolysis of bis-SC-PEG in D_2O [δ 2.96 (s, Su of SC, 8H), 3.71 (s, PEG, 180H), 4.58 (m, CH_2-O$_2$COSu, 4H)] proceeded slowly over 24 h without any side reactions, yielding *N*-hydroxysuccinimide [HOSu, δ 2.77 (s)] quantitatively. Next, the degradation of SC-PEG was examined in D_2O-based potassium tetraborate buffer and monitored by ^{1}H NMR

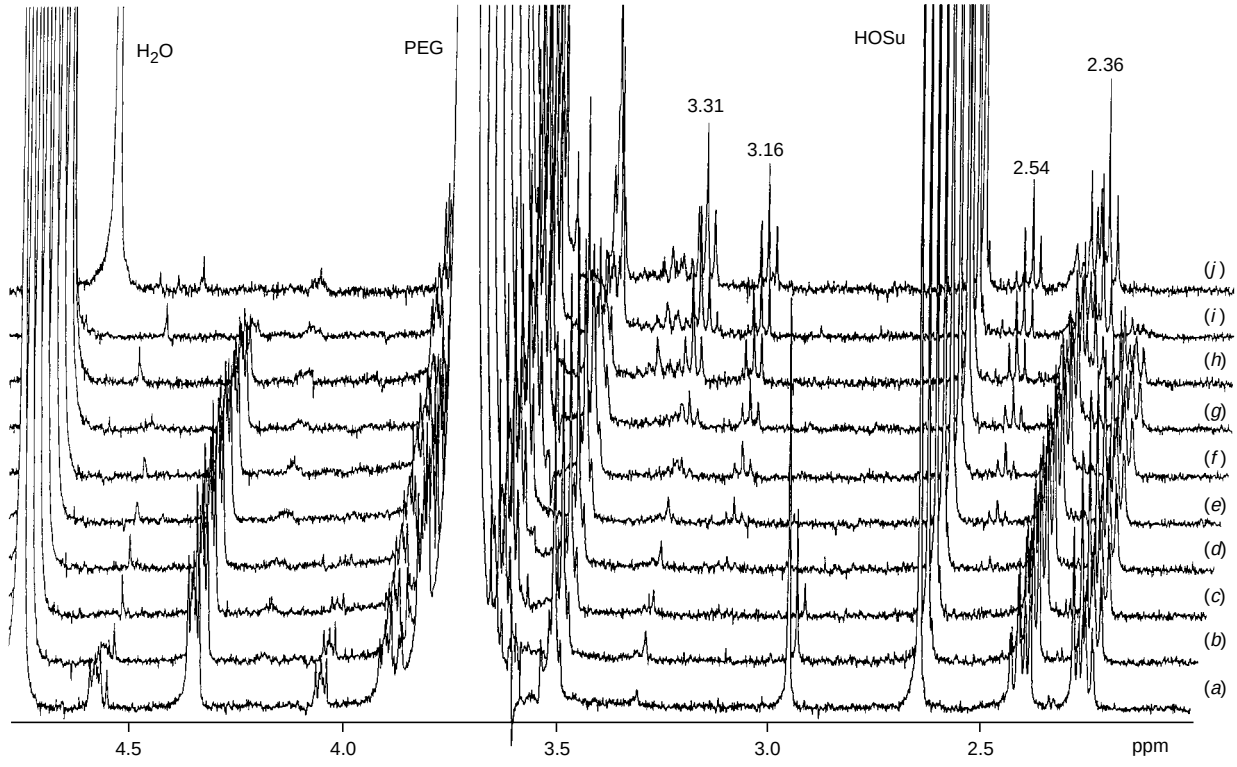

Fig. 1 Progress of the bis-SC-PEG (10 mg) decomposition monitored by 360 MHz ^{1}H NMR spectroscopy in D_2O–tetraborate buffer (0.1 M, pH 9.3, 0.65 ml). Spectra were acquired at (*a*) 3 min, (*b*) 5 min, (*c*) 8 min, (*d*) 11 min, (*e*) 16 min, (*f*) 30 min, (*g*) 45 min, (*h*) 2 h, (*i*) 4 h and (*j*) 20 h.

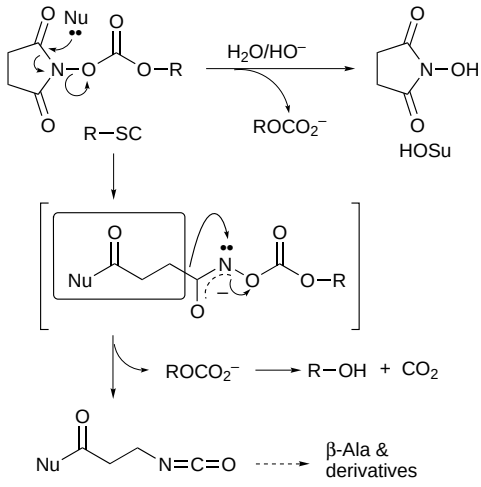

R = $–CH_2CH_2O(CH_2CH_2O)_{43}CH_2CH_2–$, $–CH_2C_6H_5$
Nu = ^-OH, ^-OSu

Scheme 1 Reaction pathways of alkyl-SC degradation through hydrolysis and through Lossen rearrangement

spectroscopy (Fig. 1). Although the disappearance of SC groups [δ 2.96 (s), 4.58 (m)] was complete within 10 min, and most of the SC was hydrolyzed to −OSu [δ 2.65 (s)], additional reactions have also taken place. Appearance of a new signal [δ 4.35 (m)] of the terminal methylene group of PEG and two symmetrical sets of peaks of type X–CH_2–CH_2–Y at δ 2.3 and 2.4 suggest that a substantial amount of the starting SC-PEG has been converted into a new derivative resulting from the succinimide (Su) ring opening. Within 16 min two triplets at δ 2.54 and 3.16, representing free β-Ala, have appeared and increased in size for the next few hours. At the end of the experiment, in addition to the β-Ala peaks, signals clustering around δ 2.3–2.5 and 3.2–3.4 with two major triplets at δ 2.36 and 3.31 were apparent. These chemical shifts are in the areas where various acylated derivatives of β-Ala yield NMR peaks.[10,11] Similar observations in the ^{1}H NMR spectra were made by following the decomposition of SC-PEG in a D_2O–carbonate buffer.

Quantitation of β-Ala in both buffer solutions by AAA (Table 1), either directly or after extensive hydrolysis, revealed that 20–25% of the original SC groups underwent conversion into β-Ala. Approximately one third of the total β-Ala was found in the free amino acid form. Amounts of primary amine somewhat higher than of free β-Ala were detected, suggesting that some of the amines were present in the form of β-Ala derivatives, *e.g.* β-Ala-β-Ala. Due to its low water solubility, Bn-SC was first dissolved in CD_3CN and then diluted ten-fold with D_2O–tetraborate buffer. ^{1}H NMR spectra again showed decomposition of the SC groups proceeded as in the case of SC-PEG yielding β-Ala and derivatives. This experiment confirmed that the observed reaction is more general, and is not exclusive to SC-PEG. The reaction pathways shown in Scheme 1 are consistent with the above observations. Opening of the succinimide ring by a nucleophile, Nu, leads to a Lossen-type hydroxamic acid intermediate, which rearranges into isocyanate *via* a scission of the N–O bond with the concomitant departure of the alkoxycarboxylate, and 1,2-migration of the outlined residue.[12] The isocyanate is expected either to hydrolyze, or to react with various nucleophilic groups (amino, carboxylate, hydroxy), yielding free β-Ala as well as its urea, amide and urethane derivatives. Specifically, β-isocyanatopropionate (Nu = OH) is known to produce 3,3′-ureylenedipropionic acid and oligo(β-Ala), among other β-Ala acylates.[10] This explains why most of the β-Ala was found in the form of acylated derivatives as revealed by AAA after hydrolysis (Table 1).

The tendency of Su-OX derivatives, where OX constitutes a good leaving group, to undergo Lossen rearrangement initiated by a nucleophilic attack on the succinimide ring by either −OH, −OSu, or even amine, is known.[12–16] Although alkoxycarboxylates are recognized as very effective leaving groups, this is the first time that alkyl-SC (Su-OCO_2R) derivatives are implicated in this process. It is pertinent to note that nucleophilic attack by an amino group on the exocyclic carbonyl of SC-derivatives, occurring during carbamoylation reactions, is a lot faster than the side reactions described here. However, the reactions described here can potentially be a source of undesirable by-products, particularly in protein modifications with an excess of alkyl-SC. Preliminary observations in our laboratory suggest that this rearrangement can be measurably suppressed by lowering the pH or the temperature of the solution.

Footnotes and References

* E-mail: SamuelZ@SEQUUS.com
† IUPAC: succinimido.

1 M. Frankel, D. Ladkany, C. Gilon and Y. Wolman, *Tetrahedron Lett.*, 1966, 4765; H. Gross and L. Bilk, *Angew. Chem., Int. Ed. Engl.*, 1967, **6**, 570; A. Paquet, *Can. J. Chem.*, 1981, **60**, 976; A. K. Mallams, J. B. Morton and P. Reichert, *J. Chem. Soc., Perkin Trans. 1*, 1981, 2186; L. Lapatsanis, G. Milias, K. Froussios and M. Kolovos, *Synthesis*, 1983, 671.
2 G. I. Tesser, R. A. de Hoog-Declerck and L. W. Westerhuis, *Z. Physiol. Chem.*, 1975, **356**, 1625; T. Miron and M. Wilchek, *Bioconjugate Chem.*, 1993, **4**, 568.
3 S. Zalipsky, R. Seltzer and K. Nho, in *Polymeric Drugs and Drug Delivery Systems*, ed. R. L. Dunn and R. M. Ottenbrite, ACS Symposium Series, Washimgton, DC, 1991, p. 91.
4 S. Zalipsky, R. Seltzer and S. Menon-Rudolph, *Biotechnol. Appl. Biochem.*, 1992, **15**, 100.
5 H.-C. Chiu, S. Zalipsky, P. Kopeckova and J. Kopecek, *Bioconjugate Chem.*, 1993, **4**, 290.
6 J. Alsina, F. Rabanal, E. Giralt and F. Albericio, *Tetrahedron Lett.*, 1994, **35**, 9633.
7 T. Miron and M. Wilchek, *Methods Enzymol.*, 1987, **135**, 84, and references cited therein.
8 S. Zalipsky, *Bioconjugate Chem.*, 1993, **4**, 296; S. Zalipsky, E. Brandeis, M. S. Newman and M. C. Woodle, *FEBS Lett.*, 1994, **353**, 71; T. M. Allen, E. Brandeis, C. B. Hansen, G. Y. Kao and S. Zalipsky, *Biochim. Biophys. Acta*, 1995, **1237**, 99.
9 A. Nathan, D. Bolikal, N. Vyavahare, S. Zalipsky and J. Kohn, *Macromolecules*, 1992, **25**, 4476; A. Nathan, S. Zalipsky, S. I. Erthel, S. N. Agathos, M. L. Yarmush and J. Kohn, *Bioconjugate Chem.*, 1993, **4**, 54.
10 H. R. Kricheldorf and R. Mülhaupt, *Makromol. Chem.*, 1979, **180**, 1419; H. R. Kricheldorf and R. Mülhaupt, *J. Macromol. Sci. Chem.*, 1980, **14**, 349.
11 D. D. Mueller, T. D. Morgan, J. D. Wassenberg, T. L. Hopkins and K. J. Kramer, *Bioconjugate Chem.*, 1993, **4**, 47.
12 L. Bauer and O. Exner, *Angew. Chem., Int. Ed. Engl.*, 1974, **13**, 376 and references cited therein.
13 M. E. Van Verst, C. L. Bell and L. Bauer, *J. Heterocycl. Chem.*, 1979, **16**, 1329.
14 H. Gross and L. Bilk, *Tetrahedron*, 1968, **24**, 6935.
15 T. M. Chapman and E. A. Freedman, *J. Org. Chem.*, 1973, **38**, 3908.
16 M. Wilchek and T. Miron, *Biochemistry*, 1987, **26**, 2155.
17 S. L. Snyder and P. Z. Sobocinski, *Anal. Biochem.*, 1975, **64**, 284.

Received in Corvallis, OR, USA, 10th September 1997; 7/06713E

Asymmetric aldol reaction of 2-cyanopropionates catalysed by *trans*-chelating chiral diphosphine ligand TRAP–rhodium(I) complex

Ryoichi Kuwano,† Hiroshi Miyazaki and Yoshihiko Ito*

Division of Synthetic Chemistry and Biological Chemistry, Graduate School of Engineering, Kyoto University, Sakyo-ku, Kyoto 606-01, Japan

***trans*-Chelating chiral diphosphine TRAP ligands bearing *P*-aromatic groups are effective for Rh^{I}-catalysed asymmetric aldol reaction of 2-cyanopropionates with an aldehyde to give the corresponding aldol adduct with up to 93% ee.**

The asymmetric aldol reaction provides a most useful tool for stereoselective construction of α-substituted β-hydroxy carbonyl units with vicinal chiral centres, and is widely used in the synthesis of complex organic molecules.[1] Recently, it was found that some low-valent transition metal complexes catalyse aldol and Michael reactions with cyano compounds having active α-methylene groups,[2] and we developed a highly enantioselective Michael reaction of 2-cyanopropionates catalysed by a rhodium(I) complex coordinated with *trans*-chelating chiral diphosphine TRAP (**1**).[3–6] The transition metal

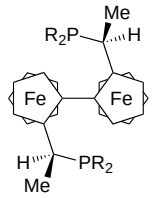

(*S*,*S*)-(*R*,*R*)-TRAP

1a R = Ph (PhTRAP)
b R = *p*-MeO-C_6H_4
c R = *p*-Cl-C_6H_4
d R = Pr^{i}
e R = Pr

catalysed reactions involve enolate intermediates of 2-cyanopropionates coordinating to the metal atom through the cyano nitrogen, which then react directly with electrophiles.[2] Herein, we report the catalytic asymmetric aldol reaction of 2-cyanopropionates **2** using a TRAP–Rh^{I} complex.

Asymmetric aldol reactions of **2** with paraformaldehyde (10 wt% in water) were carried out with a rhodium(I) catalyst generated *in situ* from Rh(acac)$(CO)_2$ and (*S*,*S*)-(*R*,*R*)-PhTRAP **1a** (Table 1).‡ The enantioselectivity of the asymmetric aldol reaction was heavily dependant upon reaction solvent. Bu_2O was the solvent of choice.§ Bulky ester groups of **2** are essential to attain high enantioselectivities for the aldol reactions (entries 1–5). 2-Cyanopropionates **2d** and **2e** bearing bulky secondary alkyl ester group gave aldol adducts (*S*)-**3d** and (*S*)-**3e** in 91 and 93% ee, respectively. Surprisingly, use of formalin hardly affected the enantiopurity of **3d** (93% ee). The enantioselectivity of the aldol reaction of **2d** was slightly increased by using **1b**, which has electron-donating aromatic groups attached to the phosphorus atoms (entry 6), while electron-withdrawing substituents on the *P*-aromatics group gave lower enantioselectivity and reactivity (entry 7). Conceivably, the *P*-aromatic substituents of TRAP play an important role in the enantioface selection of enolate of **2** coordinated to the rhodium atom, because ligands **1d** and **1e** with *P*-aliphatic substituents showed lower enantioselectivities (entries 8 and 9).

Other aldehydes **4a**–**d** were subjected to asymmetric aldol reaction with (*S*,*S*)-(*R*,*R*)-PhTRAP–Rh^{I} catalyst (Table 2). The aldol reactions of ethyl ester **2b** and isopropyl ester **2c** with acetaldehyde **4a** resulted in not only low enantioselectivities but also low diastereoselectivities (entries 1 and 2). However, the use of **2d** gave *anti*-(2*S*,3*S*)-**7a** (86% ee) with good *anti*-selectivity (*anti* : *syn* = 81 : 19) (entry 3). The aldol reaction of **2d** with **4b** proceeded, but with lower stereoselectivity (entry 4). Benzaldehyde **4c** did not react at all (entry 5). However, aldehyde **4d** smoothly reacted with **2d** giving a mixture of *anti*-(2*S*,3*R*)-**7d** (91% ee) and *syn*-(2*S*,3*S*)-**7d** (63% ee) in a ratio of 68 : 32 (entry 6).

The observed stereochemistry at the 2-position of the aldol products suggests that (*S*,*S*)-(*R*,*R*)-PhTRAP on the catalyst can differentiate between the steric bulkiness of the α-Me and ester substituents of **2**, with one of the *P*-phenyl substituents blocking the approach of the aldehyde to the *si*-face of the enolate coordinated to the rhodium atom.[4] The preferential formation of *anti*-**7** in the aldol reactions of **2d** with **4** may suggest that this reaction proceeded through antiperiplanar transition state **TS1**, which avoids the steric repulsion between the aldehyde substituent (R) and the bulky $CHPr^{i}_2$ ester (Fig. 1). The lack of diasereoselectivity in the reactions with **2b** and **2c** may be due to the lesser steric repulsion between the R and ester groups, which does not produce any enantioface selection by the aldehyde. Synclinal transition state **TS2** giving an *anti*-aldol would be sterically unfavourable due to the steric interaction between R and one of *P*-phenyl groups of **1a**.

In conclusion, we have accomplished the highly enantioselective aldol reaction of **2** with some aldehydes. Further studies are currently in progress to improve the catalyst's efficiency and to widen its applicability to a variety of aldehydes.

Table 1 Asymmetric aldol reaction of **2** with formaldehyde catalysed by **1**–Rh^{I} complex[a]

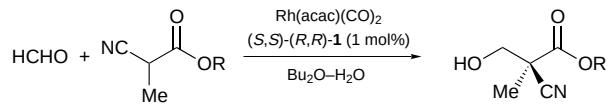

2a R = Me
b R = Et
c R = Pr^{i}
d R = $CHPr^{i}_2$
e R = $CHBu^{t}_2$

3a R = Me
b R = Et
c R = Pr^{i}
d R = $CHPr^{i}_2$
e R = $CHBu^{t}_2$

					Products **3**	
Entry	**2**	TRAP (**1**)[b]	*T*/°C	*t*/h	Yield (%)[c]	Ee (%)[d,e]
1	**2a**	**1a**	−30	100	67	35
2	**2b**	**1a**	−30	42	85	74 (−)
3	**2c**	**1a**	−30	90	86	78 (−)
4	**2d**	**1a**	−10	24	82	91 (−)
5	**2e**	**1a**	−10	24	86	93 (−)
6	**2d**	**1b**	−10	24	87	92 (−)
7	**2d**	**1c**	−10	24	44	74 (−)
8	**2d**	**1d**	−10	24	58	3 (−)
9	**2d**	**1e**	−10	24	86	22 (−)

[a] All reactions were carried out in Bu_2O. **2** (0.50 M)–formaldehyde–Rh(acac)$(CO)_2$–**1** = 1 : 1.3 : 0.010 : 0.011. [b] (*S*,*S*)-(*R*,*R*)-**1** was used. [c] Isolated yield. [d] Determined by HPLC analysis. [e] The sign of the specific rotation of **3** in $CHCl_3$ is given in parentheses.

Table 2 Asymmetric aldol reaction of **2** with **4** catalysed by (*S*,*S*)-(*R*,*R*)-**1a**–Rh[I] complex[a]

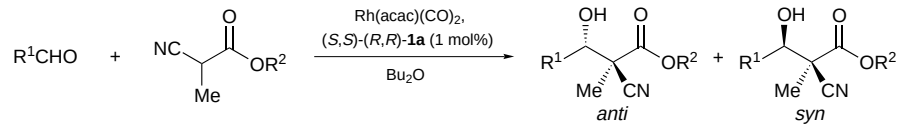

4a R^1 = Me **2b** R = Et
b R^1 = Et **c** R = Pr^i
c R^1 = Ph **d** R = $CHPr^i_2$
d R^1 = CO_2Et

5 R^1 = Me, R^2 = Et
6 R^1 = Me, R^2 = Pr^i
7a–d R^1 = Me, Et, Ph, CO_2Et, R^2 = $CHPr^i_2$

								Ee (%)[d] (config.)	
Entry	**4**	**2**	*T*/°C	*t*/h	Product	Yield (%)[b]	*anti* : *syn*[c]	*anti*	*syn*
1	**4a**	**2b**	0	24	**5**	63	45/55	31	23
2	**4a**	**2c**	0	24	**6**	61	47/53	55	50
3	**4a**	**2d**	0	24	**7a**	67	81/19	86 (2*S*,3*S*)	33
4	**4b**[e]	**2d**	0	48	**7b**	76	75/25	57 (2*S*,3*S*)	10
5	**4c**	**2d**	20	72	No reaction		—	—	—
6	**4d**[f]	**2d**	0	40	**7d**	88	68/32	91 (2*S*,3*R*)	63 (2*S*,3*S*)

[a] All reactions were carried out in Bu_2O. **2** (0.25 M)–**4**–Rh(acac)$(CO)_2$–**1a** = 1 : 7.5 : 0.010 : 0.011 unless otherwise noted. [b] Isolated yield of a mixture of *anti*- and *syn*-aldols. [c] Determined by ^{1}H NMR analysis. [d] Determined by HPLC analysis. [e] 10 equiv. of **4b** was used. [f] 2.0 equiv. of **4d** was used.

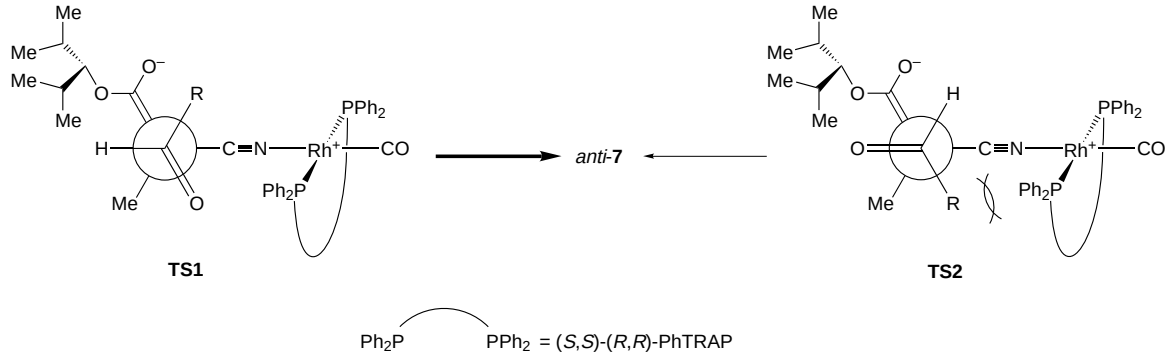

Fig. 1

Footnotes and References

† E-mail: kuwano@sbchem.kyoto-u.ac.jp
‡ *Typical procedure*: A suspension of paraformaldehyde (100 mg) in H_2O (1.0 ml) was heated under reflux for 1 h, giving a clear aqueous solution of paraformaldehyde. A solution of Rh(acac)$(CO)_2$ (5.0 μmol) and (*S*,*S*)-(*R*,*R*)-**1a** (5.4 μmol) in 2.0 ml of Bu_2O was stirred at room temperature for 10 min. To the solution was successively added **2** (0.50 mmol) and the freshly prepared solution of paraformaldehyde in water (0.67 mmol) at −10 °C. The mixture was stirred at −10 °C. After completion of the reaction, the mixture was diluted with brine, and extracted with EtOAc. The organic layer was washed with brine, dried over Na_2SO_4 and evaporated. After passing through a short silica gel column (EtOAc), the residue was purified *via* medium-pressure liquid chromatography MPLC.
§ The enantioselectivities of the aldol reactions of **2b** at 0 °C in various solvents were as follows: MeOH: 0; CH_2Cl_2: 11; toluene: 1; THF: 47; Et_2O: 54; Bu_2O: 60% ee.

1 For a review of catalytic asymmetric aldol reactions, see M. Sawamura and Y. Ito, in *Catalytic Asymmetric Synthesis*, ed. I. Ojima, VCH, New York, 1993, p. 367.
2 T. Naota, H. Taki, M. Mizuno and S.-I. Murahashi, *J. Am. Chem. Soc.*, 1989, **111**, 5954; S.-I. Murahashi, T. Naota, H. Taki, M. Mizuno, H. Takaya, S. Komiya, Y. Mizuho, N. Oyasato, M. Hiraoka, M. Hirano and A. Fukuoka, *J. Am. Chem. Soc.*, 1995, **117**, 12 436; S. Paganelli, A. Schionato and C. Botteghi, *Tetrahedron Lett.*, 1991, **32**, 2807; H. Nemoto, Y. Kubota and Y. Yamamoto, *J. Chem. Soc., Chem. Commun.*, 1994, 1665.
3 TRAP = (*R*,*R*)-2,2″-Bis[(*S*)-1-(dialkylphosphino)ethyl]-1,1″-biferrocene: M. Sawamura, H. Hamashima and Y. Ito, *Tetrahedron: Asymmetry*, 1991, **2**, 593; M. Sawamura, H. Hamashima, M. Sugawara, R. Kuwano and Y. Ito, *Organometallics*, 1995, **14**, 4549.
4 M. Sawamura, H. Hahashima and Y.Ito, *J. Am. Chem. Soc.*, 1992, **114**, 8295; *Tetrahedron*, 1994, **50**, 4439; M. Sawamura, H. Hamashima, H. Shinoto and Y. Ito, *Tetrahedron Lett.*, 1995, **36**, 6479.
5 K. Inagaki, K. Nozaki and H. Takaya, *Synlett*, 1997, 119.
6 Asymmetric allylic alkylation with TRAP–Rh–Pd catalyst system, see M. Sawamura, M. Sudoh and Y. Ito, *J. Am. Chem. Soc.*, 1996, **118**, 3309.

Received in Cambridge, UK, 15th September 1997; 7/06662G

Selective oxidation of substituted xylenes to toluic acids by hypochlorite–Ru system under phase transfer conditions

Yoel Sasson,* Abed El-Aziz Al Quntar and Ami Zoran

Casali Institute of Applied Chemistry, The Hebrew University of Jerusalem, Jerusalem 91904, Israel

Instantaneous aqueous extraction of toluic acid salts is the basis for a novel selective process for the oxidation of a single methyl group of various xylenes; aqueous hypochlorite is inert towards methylbenzenes at pH higher than 9.0, however, in the presence of an organic solvent, a Ru catalyst and a phase transfer agent, rapid oxidation to benzoic acids is observed at 25 °C.

The combination of ruthenium tetroxide as catalyst with sodium hypochlorite as primary oxidant was shown to be effective in the oxidation of olefins, alkynes and aromatic rings. The system could be improved by the addition of a phase transfer catalyst (PTC).[1] We have shown that methylbenzenes can readily be transformed into benzoic acids at room temperature upon exposure to aqueous sodium hypochlorite at pH 9–10 in the presence of $RuCl_3$ and tetra-*n*-butylammonium bromide (TBAB) catalysts in a two phase system [eqn. (1)].[2]

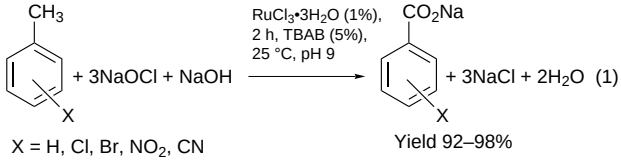

In a recent study we subsequently observed that this system is also capable of converting alkanes and cycloalkanes into ketones accompanied by some chlorinated products,[3] similar to other ruthenium catalyzed oxidations.[4]

A major feature of the Ru–NaOCl–PTC system in the oxidation of methylbenzenes is the instantaneous transport of the benzoic acid product as it forms into the basic aqueous phase thus allowing the facile separation of the product from the catalysts which abide in the organic phase ready for reuse in a succeeding reaction batch. This unique characteristic can also be the foundation for the design of a continuous catalytic liquid–liquid oxidation process.

The instantaneous extraction of benzoic acids (as sodium salts) into the aqueous phase can also be utilized for a selective oxidation of one methyl group in polymethylbenzenes such as xylenes or trimethylbenzenes. This is the subject of this communication. We have found that when xylenes are reacted under the above conditions complete conversion is achieved after two hours with only one methyl group selectively oxidized to the corresponding carboxylic acid.

Toluic acids are obtained in the autoxidation of xylenes in the presence of a cobalt(II) catalyst in acetic acid solvent but high selectivity to the desired products is obtained only at relatively low conversions.[5,6] At higher conversions the major product is the dicarboxylic acid. Thus alternative methods were proposed for the preparation of substituted toluic acids. Typical examples are the hydrolysis of toluonitriles[7,8] (obtained by diazotization of anilines in presence of CuCN) and the oxidation of methylacetophenones *via* the haloform reaction.[9,10]

Our new oxidation system is demonstrated with the following typical procedure. 4-Chloro-*o*-xylene (4.6 g, 33 mmol), tetra-*n*-butylammonium hydrogen sulfate[11] (TBHS, 0.47 g, 1.6 mmol) and ruthenium chloride trihydrate (70 mg, 0.33 mmol) were dissolved in 1,2-dichloroethane (25 ml) in a 300 ml flask equipped with a mechanical stirrer, a thermometer, a pH meter and a dual dropping funnel, one filled with commercial aqueous hypochlorite and the other with 20% aqueous NaOH. Aqueous hypochlorite (200 ml) was added into the flask with stirring at a rate of 1.5 ml min^{-1} while keeping the system at 25 °C. The pH was maintained throughout the process at 9.0 by manual gradual addition of 20% aqueous NaOH (28 ml in total was added). After two hours the aqueous phase was separated, acidified with 20% aqueous sulfuric acid to pH 3 and the precipitate was filtered and dried to give 4-chloro-2-methylbenzoic acid (5.50 g, 98%), mp 170 °C, were obtained. The structure of the product was confirmed by comparison with an authentic sample.

Interestingly, when 4-nitro-*o*-xylene was reacted under an identical procedure, the *meta* methyl group was oxidised to yield 2-methyl-5-nitrobenzoic acid (mp 176 °C) in 90% yield. This is shown in eqns. (2) and (3).

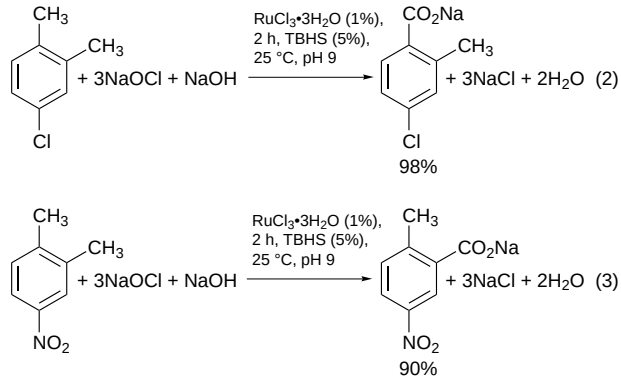

The reaction was found to be of a general nature with numerous substituted xylenes. These experiments have revealed the following observations. (a) When unsubstituted xylenes or xylenes bearing electron donating groups (such as methoxy-xylenes) are reacted under the above conditions, the major reaction taking place is ring chlorination accompanied with some side chain chlorination. The ring chlorinated xylenes were further oxidized to the corresponding toluic acids resulting in a mixture of toluic acids and side-chain chlorinated xylenes. (b) In oxidizing xylenes bearing an electron withdrawing substituent which also has a lone pair of electrons available to stabilize the carbonium ion, such as bromine or chlorine, the methyl group *para* or *ortho* to the substituent is oxidized. (c) In reactions of xylenes with electron withdrawing substituents not containing an unshared pair of electrons such as nitro, sulfonate or carboxylate, the methyl group *meta* to the substituent is selectively oxidized. (d) The oxidation rate is slower when substituents with stronger −I effect are present. (e) No oxidation reaction is taking place in the aqueous phase thus once the toluic acid product is extracted into the water no further oxidation is observed. (f) Non-selective oxidation was realized when 4-nitro-*m*-xylene was reacted with formation of both possible toluic acids.

These observations support our originally proposed mechanism for the Ru–NaOCl–PTC system.[2] The key step is a hydride abstraction from the substrate by RuO_4 to form a carbonium ion which is promptly hydrolyzed.

With chlorine in the 4-position the carbonium ion is more stable on the *para* methyl group due to existence of canonical structures with the positive charge on the chlorine atom. Such forms are not possible when the ion is on the *meta* methyl group [eqn. (4)]. With 4-nitro substituted xylene the −I effect of the

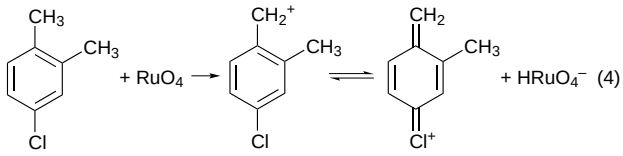

(4)

substituent destabilizing the carbonium ion, is more pronounced for the *para* methyl group resulting in activation of the *meta* methyl group.

Upon attempts to recycle the catalytic system for consecutive runs we have found some deactivation of the catalytic activity. This could be corrected by modifying the solvent with addition of a nitrile. When using a solvent mixture of 1 : 1 (w/w) 1,2-dichloroethane and benzonitrile (which is known to stabilize RuO_4 in the organic phase[12]) the catalysts could be recycled in the same solvent for seven consecutive runs without any apparent loss in activity.

Footnote and References

* E-mail: ysasson@vms.huji.ac.il

1 J. Skarzewski and R. Siedlecka, *Org. Prep. Proced. Int.*, 1992, 624.
2 Y. Sasson, G. D. Zappi and R. Neumann, *J. Org. Chem.*, 1986, **51**, 2880.
3 Y. Sasson, T. Gelbaum, G. Rothenberg and A. Zoran, unpublished work.
4 S. I. Murahashi, *Angew. Chem., Int. Ed. Engl.*, 1995, **34**, 2443.
5 A. S. Hay, J. W. Eustance and H. S. Blanchard, *J. Org. Chem.*, 1960, **25**, 616.
6 J. Dakka, A. Zoran and Y. Sasson, *US Pat.*, 1991, 4 990 659.
7 F. Delos, F. De Tar and D. I. Relyea, *J. Am. Chem. Soc.*, 1956, **78**, 4304.
8 J. F. Bunnett and M. M. Rauhut, *Org. Synth.*, 1963, **Coll. Vol. IV**, 114.
9 G. Grethe, H. L. Lee, M. Uskokovic and A. Brossi, *J. Org. Chem.*, 1968, **33**, 496.
10 G. M. Hoop, *J. Am. Chem. Soc.*, 1962, 4859.
11 This catalyst was found to function better than the bromide counterpart.
12 P. H. J. Carlsen, T. Katsuki, V. S. Martin and K. B. Sharpless, *J. Org. Chem.*, 1981, **46**, 3936.

Received in Cambridge, UK, 23rd October 1997; 7/07676B

Efficient synthesis of β- and γ-amino acid derivatives using new functionalised zinc reagents: enhanced stability and reactivity of β-amido zinc reagents in dimethylformamide

Charles S. Dexter and Richard F. W. Jackson*

Department of Chemistry, Bedson Building, The University of Newcastle, Newcastle upon Tyne, UK NE1 7RU

The new zinc reagents 3 and 4 are not sufficiently stable to be prepared efficiently in THF, but they can be prepared in DMF under mild and convenient conditions; subsequent palladium- catalysed coupling with aromatic iodides gives protected β- and γ-amino acids 11 and 12 in generally good yields.

There has been increasing interest in the development of new synthetic routes to β-amino acids, due to their importance as components of natural products and modified peptides.[1] The asymmetric synthesis of β-amino acids has most often relied on use of the chiral pool. For example, homologation of α-amino acids,[2] ring-opening of aziridine carboxylates[3] and modification of aspartic acid[4–6] and asparagine[7] have each been explored. γ-Amino acids have also been prepared using similar strategies, for example by modification of glutamic acid[4] and by homologation of α-amino acids.[8] A direct asymmetric synthesis of aryl β- and γ-amino acids has also been recently reported.[9]

In view of our development of other amino acid-derived zinc reagents, such as the nucleophilic alanine equivalent **1** prepared from protected iodoalanine **2**,[10] we have explored the potential of the related reagents **3** and **4** for the synthesis of enantiomerically pure β- and γ-amino acids. The necessary iodide precursors for the two reagents, **9** and **10**, were prepared from the protected aspartic and glutamic acid derivatives **5** and **6** by standard methods.†

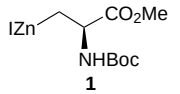

1

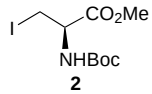

2

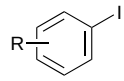

8a R = H
b R = 2,3-(C=C)$_2$
c R = 4-Me
d R = 2-MeO
e R = 4-MeO
f R = 2-NH$_2$
g R = 4-Br
h R = 2-F
i R = 4-F
j R = 2-NO$_2$
k R = 3-NO$_2$
l R = 4-NO$_2$

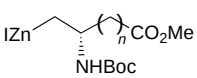

3 *n* = 1
4 *n* = 2

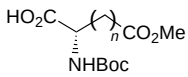

5 *n* = 1
6 *n* = 2

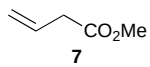

7

Our initial efforts to prepare the zinc reagents **3** and **4**, by using zinc dust activated using the Knochel procedure in THF as solvent,[11] were disappointing. For example, formation and coupling of the zinc reagent **3** with *p*-iodonitrobenzene **8l**, under the conditions previously developed for the zinc reagent **1**, gave the β-homophenylalanine derivative **11l** in disappointing yield (25%). Similar results were obtained using the zinc reagent **4**.

^{1}H NMR spectroscopy of the zinc reagent **3** prepared in [$^2H_8$]THF indicated clearly that the main problem was β-elimination of the urethane group to give the alkene **7**. Examination of the ^{13}C NMR spectrum of the reagent **3** in [$^2H_8$]THF indicated that there was significant coordination of the urethane carbonyl group to zinc (implied by the downfield shift of the urethane carbon atom upon formation of the zinc reagent), whilst coordination of the ester carbonyl was much less pronounced (Table 1). We suggest that this lack of ester coordination results in a relatively facile β-elimination of the urethane group (promoted by the internal Lewis acid), since the conformation required for elimination can be easily attained. This stands in sharp contrast to the ^{13}C NMR spectrum of the serine-derived reagent **1** in [$^2H_8$]THF, which indicates that both ester and urethane carbonyl groups are coordinated to zinc, which in turn, we believe, is responsible for the significantly greater stability of this reagent than the reagent **3** in THF. In contrast to the situation in [$^2H_8$]THF, the ^{13}C NMR spectrum of **3** in [$^2H_7$]DMF showed no significant changes in the shifts of the two carbonyl carbon atoms on conversion of iodide **9** into zinc reagent **3**, which we interpret as indicating that there is no coordination of either carbonyl group to zinc in this solvent. It is interesting to note that in [$^2H_7$]DMF, the serine-derived zinc reagent **1** preserves ester coordination (Table 1), indicating that intramolecular co-ordination of an ester group which results in a 5-membered ring is especially favourable. We therefore explored the preparation of the zinc reagent **3** in dipolar aprotic solvents, and were pleased that all solvents employed (DMF, DMA, NMP and DMSO) were effective.[12] In all the solvents, preparation of the zinc reagent **3** and its subsequent coupling with iodobenzene, to give **11a**,‡ occurred at room temperature in good yield. Given the convenience of using DMF,[13] subsequent reactions were all carried out with this solvent, and are summarised in Table 2 and Scheme 1. The only disappoint-

Table 1 ^{13}C NMR chemical shifts (δ) of zinc reagents **1** and **3**

	THF		DMF	
	Ester	Carbamate	Ester	Carbamate
2	171.93	157.20	169.57	155.10
1	177.28	159.91	175.35	154.24
9	172.68	157.04	170.50	154.88
3	174.14	160.79	171.38	154.34

Table 2 Preparation of β-amino acids

Aryl iodide	Product	Ar	Yield (%)[a]
8a Iodobenzene	**11a**	Ph	73
8b 1-Iodonaphthalene	**11b**	1-Naphthyl	61
8c 4-Iodotoluene	**11c**	4-MeC_6H_4	73
8d 2-Iodoanisole	**11d**	2-MeOC_6H_4	56
8e 4-Iodoanisole	**11e**	4-MeOC_6H_4	68
8f 2-Iodoaniline	**11f**	2-$H_2NC_6H_4$	33
8g 4-Bromoiodobenzene	**11g**	4-BrC_6H_4	58
8h 2-Fluoroiodobenzene	**11h**	2-FC_6H_4	46
8i 4-Fluoroiodobenzene	**11i**	4-FC_6H_4	65
8j 2-Iodonitrobenzene	**11j**	2-$O_2NC_6H_4$	20
8k 3-Iodonitrobenzene	**11k**	3-$O_2NC_6H_4$	47
8l 4-Iodonitrobenzene	**11l**	4-$O_2NC_6H_4$	89

[a] All yields are based on iodide **9**.

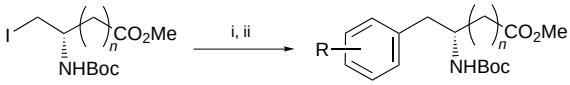

9 $n = 1$ **11** $n = 1$
10 $n = 2$ **12** $n = 2$

Scheme 1 *Reagents and conditions:* i, Zn* (prepared from Zn dust using 1,2-dibromoethane, followed by Me_3SiCl, in DMF), 15 min, room temp.; ii, **8** (1.33 equiv.), $Pd_2(dba)_3$ (2.5 mol%), P(*o*-$MeC_6H_4)_3$ (10 mol%), room temp., 3 h

Table 3 Preparation of γ-amino acids

Aryl iodide	Product	Ar	Yield (%)[a]
8a Iodobenzene	**12a**	Ph	68
8c 4-Iodotoluene	**12c**	4-MeC_6H_4	68
8d 2-Iosoanisole	**12d**	2-$MeOC_6H_4$	69
8e 4-Iodoanisole	**12e**	4-$MeOC_6H_4$	68
8f 2-Iodoaniline	**12f**	2-$H_2NC_6H_4$	56
8h 2-Fluoroiodobenzene	**12h**	2-FC_6H_4	34
8l 4-Iodonitrobenzene	**12l**	4-$O_2NC_6H_4$	80

[a] All yields are based on iodide **10**.

ing yields occur with the use of *ortho* substituents, which appear to be caused by steric problems, rather than by electronic ones. The reasonable result obtained with 2-fluoroiodobenzene is in sharp contrast to our previous complete failure to promote coupling with this substrate.[10]

In an analogous way, the iodide **10** can be converted into the zinc reagent **4**, which then undergoes coupling with a range of aromatic iodides in good yield to give a series of γ-amino acids **12**. These results are summarised in Table 3.

These results indicate that it is possible to prepare both β- and γ-amino acids using organozinc chemistry at room temperature in a straightforward manner. Further applications of zinc reagents **3** and **4**, and of related zinc/copper reagents, to the synthesis of other classes of β- and γ-amino acid derivatives will be reported in a future full paper.

We thank the EPSRC for a CASE award (C. S. D.) and for an equipment grant (NMR spectrometer), Dr N. H. Rees for NMR spectra, Merck Sharpe and Dohme, Terlings Park, for support, the EU TMR programme (ERB-FMRX-CT96-0011), Dr J. Elliott (MSD) for helpful discussions, L. Hitzel (MSD) for chiral phase capillary electrophoresis and Dr S. Connolly, Astra Charnwood, for experimental details of the preparation of iodides **9** and **10**. R. F. W. J. also thanks the Nuffield Foundation for a One Year Science Research Fellowship.

Footnotes and References

* E-mail: r.f.w.jackson@newcastle.ac.uk

† The aspartic and glutamic acid derivatives **5** and **6** were converted into the corresponding *N*-hydroxysuccinimide esters (*N*-hydroxysuccinimide, *N*,*N*′-dicyclohexylcarbodiimide) (ref. 14), reduced to the alcohols ($NaBH_4$, H_2O–THF), and then converted into the iodides **9** and **10**, respectively (PPh_3, I_2 imidazole, CH_2Cl_2) (ref. 15).

‡ The enantiomeric purity of **11a** was determined by comparison of its specific rotation, [$[\alpha]_D$ +20.8 (*c* 1.28, MeOH)] with the literature value [+19.9 (*c* 1.29, MeOH] (ref. 16). As an additional check, the ee of this compound was determined as >98% (by comparison with a racemic sample) by capillary electrophoresis using α-cyclodextrin as chiral selector.

1 For recent reviews, *Enantioselective Synthesis of β-Amino Acids*, ed. E. Juaristi, Wiley-VCH, New York, 1996; D. C. Cole, *Tetrahedron*, 1994, 9517; G. Cardillo and C. Tomasini, *Chem. Soc. Rev.*, 1996, 117.
2 For a recent example, see C. Guibourdenche, D. Seebach and F. Natt, *Helv. Chim. Acta*, 1997, **80**, 1.
3 J. E. Baldwin, R. M. Adlington, I. A. O'Neil, C. Schofield, A. C. Spivey and J. Sweeney, *J. Chem. Soc., Chem. Commun.*, 1989, 1852.
4 A. El Marini, M. L. Roumestant, P. Viallefont, D. Razafindramboa, M. Bonato and M. Follet, *Synthesis*, 1992, 1104.
5 C. W. Jefford and J. Wang, *Tetrahedron Lett.*, 1993, **34**, 1111.
6 J. M. Bland, *Synth. Commun.*, 1995, **25**, 467.
7 P. Gmeiner, *Tetrahedron Lett.*, 1990, **31**, 5717.
8 For example, see S. Hanessian and R. Schaum, *Tetrahedron Lett.*, 1997, **38**, 163.
9 Y. S. Park and P. Beak, *J. Org. Chem.*, 1997, **62**, 1574.
10 R. F. W. Jackson, N. Wishart, A. Wood, K. James and M. J. Wythes, *J. Org. Chem.*, 1992, **57**, 3397; M. J. Dunn, R. F. W. Jackson, J. Pietruszka and D. Turner, *J. Org. Chem.*, 1995, **60**, 2210.
11 P. Knochel and R. D. Singer, *Chem. Rev.*, 1993, **93**, 2117 and references cited therein.
12 For previous work on the preparation of simple β-amido zinc reagents, including an example in which a DMSO–THF mixture was found to be preferable to THF alone, see R. Duddu, M. Eckhardt, M. Furlong, H. P. Knoess, S. Berger and P. Knochel, *Tetrahedron*, 1994, **50**, 2415.
13 For earlier examples of the use of DMF for palladium-catalysed cross-coupling reactions of zinc reagents, see E.-i. Negishi, Z. R. Owczarczyk and D. R. Swanson, *Tetrahedron Lett.*, 1991, **32**, 4453. For examples of the use of dipolar aprotic solvents for the preparation of organozinc reagents, see T. N. Majid and P. Knochel, *Tetrahedron Lett.*, 1990, **31**, 4413; C. Jubert and P. Knochel, *J. Org. Chem.*, 1992, **57**, 5425, and references therein.
14 K. Shimamoto, M. Ishida, H. Shinozaki and Y. Ohfune, *J. Org. Chem.*, 1991, **56**, 4167.
15 G. L. Lange and C. Gottardo, *Synth. Commun.*, 1990, **20**, 1473.
16 E. M. Gordon, J. D. Godfrey, N. G. Delaney, M. M. Assad, D. Von Langen and D. W. Cushman, *J. Med. Chem.*, 1988, **31**, 2199.

Received in Liverpool, UK, 30th September 1997; 7/07062D

Novel heterocyclic betaines relevant to the mechanism of *tyrosinase*-catalysed oxidation of phenols

John Clews,[a] Christopher J. Cooksey,[b] Peter J. Garratt,[b] Edward J. Land,[c] Christopher A. Ramsden*[a] and Patrick A. Riley[d]

[a] *Department of Chemistry, Keele University, Keele, Staffordshire, UK ST5 5BG*
[b] *Department of Chemistry, Christopher Ingold Laboratories, UCL, 20 Gordon Street, London, UK WC1H 0AJ*
[c] *CRC Department of Biophysical Chemistry, Paterson Institute for Cancer Research, Christie Hospital NHS Trust, Wilmslow Road, Manchester, UK M20 9BX*
[d] *Windeyer Institute, UCL Medical School, 46 Cleveland Street, London, UK W1P 6DB*

Betaines formed by dianisyltellurium oxide oxidation of *N*,*N*-dialkyldopamines are identical to the products formed by *tyrosinase* oxidation of *N*,*N*-dialkyltyramines or *N*,*N*-dialkyldopamines and provide evidence that *tyrosinase* does not act as a *tyrosine hydroxylase*; oxidations of higher homologues of *N*,*N*-diethyldopamine are also described.

Tyrosinase [EC 1.14.18.1] catalyses the formation of *ortho*-quinones **3** from both phenolic (**1**) and catecholic (**2**) substrates (Scheme 1):[1] the mechanism of the phenol oxidation (**1** → **3**) has been the subject of disagreement.[2] There is a lag phase during initial *tyrosinase*-catalysed oxidation of monohydric phenols **1** because the enzyme requires activation by a catechol: this process is believed to involve reduction of Cu^{II} ions in the active site. Once formed, initially by largely unactivated enzyme, quinone derivatives of primary amines, such as dopaquinone **3a**, undergo rapid cyclisation and subsequent disproportionation with a second molecule of quinone to give a catechol amine (*e.g.* **2a**) (eqn. 1) which then activates more enzyme. The catechol **2** is not, therefore, formed directly by the

2 dopaquinone (**3a**) → dopa (**2a**) + dopachrome (1)

enzyme acting as a *tyrosine hydroxylase*, as is widely claimed,[2] but by a subsequent sequence of non-enzymic reactions. We have recently reported oximetry studies that firmly support the exclusive operation of this indirect mechanism of auto-activation of *tyrosinase*.[3] We now report novel chemical studies relevant to these conclusions.

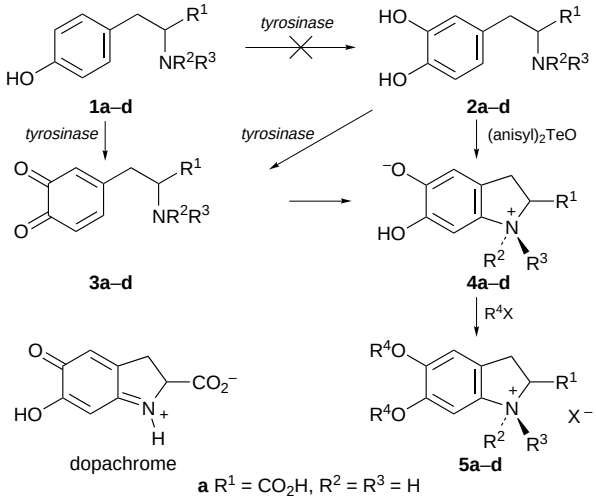

a $R^1 = CO_2H$, $R^2 = R^3 = H$
b $R^1 = H$, $R^2 = R^3 = Me$
c $R^1 = H$, $R^2 = R^3 = Pr$
d $R^1 = H$, $R^2–R^3 = (CH_2)_5$

Scheme 1

A priori it is not clear whether the *ortho*-quinone of a tertiary amine **3** (R^2 and $R^3 \neq H$) will cyclise. Other workers,[4] in a study of protein binding of oxidised catechols, have recently expressed the view that formation of 2,3-dihydroindole derivatives (*e.g.* **3** → **4**) *via* *N*,*N*-dialkylquinones **3** is unlikely. However, a close examination of the literature reveals that this type of cyclisation was encountered by Robinson and Sugasawa[5] during studies of chloranil oxidation of laudanosaline but, as far as we are aware, this remains the only example. In this context, we have observed[3] that *tyrosinase* oxidises *N*,*N*-di-*n*-propyldopamine **2c** with an oxygen stoichiometry of 0.5 to give a stable product that is not an *ortho*-quinone. Similar oxidation of *N*,*N*-dimethyltyramine **1b** by pre-activated *tyrosinase* gives a similar product with an oxygen stoichiometry of 1.0: no enzymic oxidation of this phenolic precursor **1b** occurred without pre-activation by a trace of dopa **2a**. Spectroscopic evidence suggested that these enzymic products are the betaines **4b** and **4c** formed by rapid cyclisation and aromatisation of the initially formed *ortho*-quinones **3** (Scheme 1). Significantly, oxidative cyclisation of the tertiary amines **1** does not lead to catecholic products that can function as *tyrosinase* activators. Since there is no autocatalysis using the tyramine precursor **1b** we have concluded that direct formation of catechols by *tyrosinase* acting as a hydroxylase (*e.g.* **1b** → **2b**) does not occur. We now describe the chemical synthesis and characterisation of the indol-1-ium-5-olates **4b**–**d** and products obtained by oxidation of the higher homologues **6** and **7**.

Our recent interest in hypervalent oxidising agents[6] led us to investigate the use of dianisyltellurium oxide (DAT), which has been shown to be particularly mild and selective for quinone formation.[7] Oxidations were monitored in deuterated solvents *via* ^1H NMR spectroscopy. Amine **2c** was rapidly and quantitatively transformed to the betaine **4c** upon treatment with 1 equiv. of DAT in CH_2Cl_2–MeOH (9 : 1) solution. The water soluble betaine **4c**, obtained as a crystalline solid, mp 115–120°C (90%), was easily separated from the accompanying dianisyltelluride by $CHCl_3$–water partitioning and the proposed structure is fully supported by its spectroscopic properties. The ^1H NMR (D_2O) spectrum exhibits two aromatic protons (singlets at δ 6.42 and 6.46) indicating formation of the second ring at C-5 of the catechol ring. Further evidence of ring formation is provided by the non-equivalence of each pair of methylene protons (CH_aH_b) of the *N*-*n*-propyl substituents (NCH_2CH_2Me) which, as a result of the quaternary nitrogen atom, are also significantly shifted downfield and appear as pairs of multiplets at δ 3.16 and 3.35 and at δ 1.19 and 1.40. A COSY spectrum confirmed the expected proton coupling. A high resolution mass spectrum of compound **4c** confirmed the constitution of the molecular ion (*m*/*z* 235). The UV spectrum of the betaine **4c** in 0.1 M phosphate buffer was pH dependent [pH 7.4: λ_{max} 290 (ε 4122) and 312(sh) nm (1453); pH 6.5: λ_{max} 290

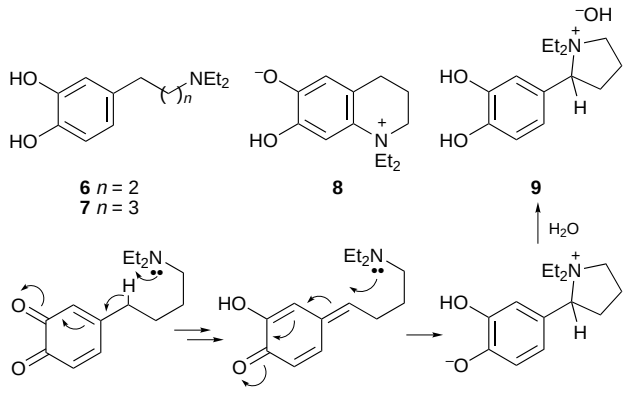

Scheme 2

nm (ε 3923)] and this change is attributed to the formation of the salt **5c** (R^4 = H) at low pH.

Attempts to monomethylate the betaine **4c** using MeI were unsuccessful and gave mixtures. However, use of MeI and solid K_2CO_3 in acetone gave exclusively the dimethoxy iodide **5c** (R^4 = Me, X = I), mp 172–173 °C (95%).† Significantly, the UV spectrum of this salt **5c** was pH independent [λ_{max} 284 nm (ε 4115)] and showed no shoulder at higher wavelength. In a similar manner the betaines **4b**,**d** were prepared, characterised and converted to their dimethoxy iodides **5b**,**d** (R^4 = Me, X = I). The synthetic products **4b**,**c** were found to be identical in all respects to the material produced by *tyrosinase* oxidation of amines **1b** and **2c**.[3]

Oxidation of the higher homologue **6** resulted in a similar quantitative cyclisation giving the tetrahydroquinolin-1-ium-6-olate **8** which was obtained as a crystalline solid, mp 95–100 °C (84%). The ^{1}H NMR [δ_H(D_2O) 6.42 and 6.63 (s, 2 × arom H), 3.4–3.8 (m, 3 × CH_2N$^+$), 2.57 (t, CH_2Ar), 2.0 (m, $CH_2CH_2CH_2$) and 1.09 (t, 2 × CH_3)] and UV [pH 7.4: λ_{max} 286 nm (ε 2831)] spectra are analogous to those of the betaines **4** and fully consistent with structure **8**. Evidence of spirocyclisation was not detected by NMR spectroscopy. Methylation (MeI–K_2CO_3) gave the expected 6,7-dimethoxy iodide as a crystalline solid mp 230–231 °C (90%).

A different mode of reaction occurred when the 4-alkylamine chain was extended by an additional methylene unit. Again, clean formation of a single product was observed by ^{1}H NMR spectroscopy when the amine **7** was treated with 1 equiv. of DAT and after isolation this was identified as the quaternary salt **9**, mp 118–120 °C (86%) [*m/z* 236.1642 ($C_{14}H_{22}N_1O_2$), M − OH$^-$]. In particular the ^{1}H NMR spectrum (D_2O) showed non-equivalent ethyl groups [δ_H 0.99 and 1.25 (t, 2 × CH_2CH_3)] and a low field pseudo-triplet at δ_H 4.60 corresponding to the methine proton. There was no evidence of cyclisation to a seven-membered betaine. We rationalise the formation of the product **9** by an isomerisation of the initially formed *ortho*-quinone **10** to the quinomethane **11**, assisted by intramolecular deprotonation (Scheme 2). The quinomethane **11** then undergoes a 5-*exo*-*trig* cyclisation giving the observed product **9** *via* the betaine **12**. This cyclisation (**11** → **12**) is analogous to that proposed for the formation of the tetrahydrofuran ring in the biosynthesis of lignans (*e.g.* pinoresinol and olivil)[8] and for the epimerisation of profisetinidins.[9] The formation of a quinomethane intermediate *via* an *ortho*-quinone (**10** → **11**) is also relevant to the role of *quinone isomerase* in the sclerotization of insect cuticles.[10]

We thank the EPSRC National Mass Spectrometry Service Centre, Swansea, for high resolution mass spectra.

Footnotes and References

* E-mail: cha33@cc.keele.ac.uk

† New compounds were characterised by spectroscopy and elemental analysis.

1 H. S. Raper, *Physiol. Rev.*, 1928, **8**, 245; H. S. Mason, W. L. Fowlks and E. Paterson, *J. Am. Chem. Soc.*, 1955, **77**, 2914; J. M. Nelson and C. R. Dawson, *Adv. Enzymol.*, 1944, **4**, 99; A. B. Lerner, T. B. Fitzpatrick, E. Calkins and W. H. Summerson, *J. Biol. Chem.*, 1950, **187**, 793; H. S. Mason, *Nature*, 1956, **177**, 79; K. Lerch, in *Metal Ions in Biological Systems*, ed. H. Sigel, Marcel Dekker, New York, vol. 13, pp. 143–186; E. I. Solomon and M. D. Lowery, *Science*, 1993, **259**, 1575.

2 A. Sánchez-Ferrer, J. N. Rodríguez-López, F. García-Cánovas and F. García-Carmona, *Biochim. Biophys. Acta*, 1995, **1247**, 1.

3 C. J. Cooksey, P. J. Garratt, E. J. Land, S. Pavel, C. A. Ramsden, P. A. Riley and N. Smit, *J. Biol. Chem.*, 1997, **272**, 26 226.

4 C. T. Jagoe, S. E. Kreifels and J. Li, *Bioorg. Med. Chem. Lett.*, 1997, **7**, 113.

5 R. Robinson and S. Sugasawa, *J. Chem. Soc.*, 1932, 789.

6 C. A. Ramsden and H. L. Rose, *J. Chem. Soc., Perkin Trans. 1*, 1997, 2319; M. Bodajla, G. R. Jones and C. A. Ramsden, *Tetrahedron Lett.*, 1997, **38**, 2573; C. A. Ramsden and H. L. Rose, *Synlett*, 1997, 27; P. Nongkunsarn and C. A. Ramsden, *J. Chem. Soc., Perkin Trans. 1*, 1996, 121; A. P. Lothian and C. A. Ramsden, *Synlett*, 1993, 753.

7 S. V. Ley, C. A. Meerholz and D. H. R. Barton, *Tetrahedron*, 1981, **37**, 213.

8 K. Freudenberg, *Pure Appl. Chem.*, 1962, **5**, 9; D. C. Ayers and J. D. Loike, in *Lignans: Chemical, Biological and Clinical Properties*, Cambridge University Press, Cambridge, 1990.

9 P. J. Steynberg, J. P. Steynberg, E. V. Brandt, D. Ferreira and R. W. Hemingway, *J. Chem. Soc., Perkin Trans. 1*, 1997, 1943.

10 M. Sugumaran, V. Semensi, B. Kalyanaraman, J. M. Bruce and E. J. Land, *J. Biol. Chem.*, 1992, **267**, 10 355.

Received in Liverpool, UK, 27th August 1997; 7/06281H

Total synthesis of rutamycin B *via* Suzuki macrocyclization

James D. White,* Thomas Tiller, Yoshihiro Ohba, Warren J. Porter, Randy W. Jackson, Shan Wang, and Roger Hanselmann

Department of Chemistry, Oregon State University, Corvallis, OR 97331-4003, USA

The macrolide rutamycin B containing 17 stereogenic centres and a 26-membered ring was synthesized by a route which features a chelate-controlled, double differentiating aldol reaction and ring closure by means of a vinyl–vinyl coupling.

Rutamycins A and B are structurally complex macrolide antibiotics isolated from *Streptomyces* species.[1] A total synthesis of rutamycin B (**1**) by Evans[2] confirmed the structural assignment,[3] and the absolute configuration of **1** was deduced from synthesis of the spiroketal segment obtained by degradation of the rutamycins.[4] Herein, we report a convergent synthesis of rutamycin B in which the 26-membered ring is closed by means of a Suzuki macrocyclization.

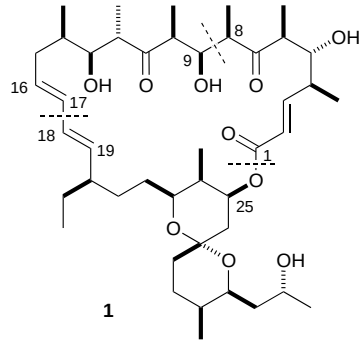

1

Selective silylation of triol **2**[5] took advantage of the different steric environments of the three hydroxy groups in this structure and was accomplished by reaction with Bu^tMe_2SiCl, which gave **3**, and then by treatment with $Bu^tMe_2SiOSO_2CF_3$ to yield **4** (Scheme 1). The remaining secondary alcohol was converted to its benzoate **5**, and the primary silyl ether was selectively removed by treatment with HF·pyridine complex. The resultant primary alcohol **6** was oxidized to aldehyde **7**, which was subjected to a Takai reaction[6] with CHI_3 in the presence of $CrCl_2$ to yield *trans* iodo alkene **8**. After saponification of the benzoate, the liberated alcohol **9** was reacted with diethoxyphosphorylacetyl chloride to give **10**. Horner–Emmons condensation of the lithio anion of **10** with keto aldehyde **11**, previously prepared from methyl (2*R*)-3-hydroxy-2-methylpropionate,[7] afforded α,β-unsaturated ester **12**.

Synthesis of the C9–C16 segment **26** of **1** was initiated by asymmetric crotylation of (*R*)-**13** with (*E*)-crotylboronate **14** derived from (*S*,*S*)-tartrate (Scheme 2).[8] The alcohol **15** resulting from *re* face addition to the aldehyde was converted to the bis(silyl ether) **16**, and the primary ether was selectively cleaved to give **17**. The tosylate **18** of this alcohol was displaced with cyanide and the resultant nitrile **19** was reduced to **20** and then to alcohol **21**. The latter was converted to its bis(silyl ether) **22** before ozonolysis to **23**. The reaction of **23** with (*E*)-crotylboronate **24** derived from (*R*,*R*)-tartrate[8] afforded alcohol **25** with good stereoselectivity (> 95 : 5) in this matched (Felkin) addition to the *si* face of the aldehyde. Alcohol **25** was protected as its *p*-methoxybenzyl (PMB) ether **26** and the latter upon ozonolysis yielded **27**.

Coupling of the (*Z*)-chlorotitanium enolate[9] of **12** and **17** gave the *syn*,*syn* (Felkin) aldol product **28** as the sole stereoisomer (Scheme 3).[10] A rationale for this high stereoselectivity invoking secondary complexation of the aldehyde carbonyl with the PMB ether has been suggested previously,[7] and it is noteworthy that the aldol reaction of **12** with **27** is completely nonstereoselective when the PMB group of **12** is replaced by a Et_3Si ether. Thus, it appears that the PMB ether not only obstructs the anti-Felkin pathway in this coupling, but

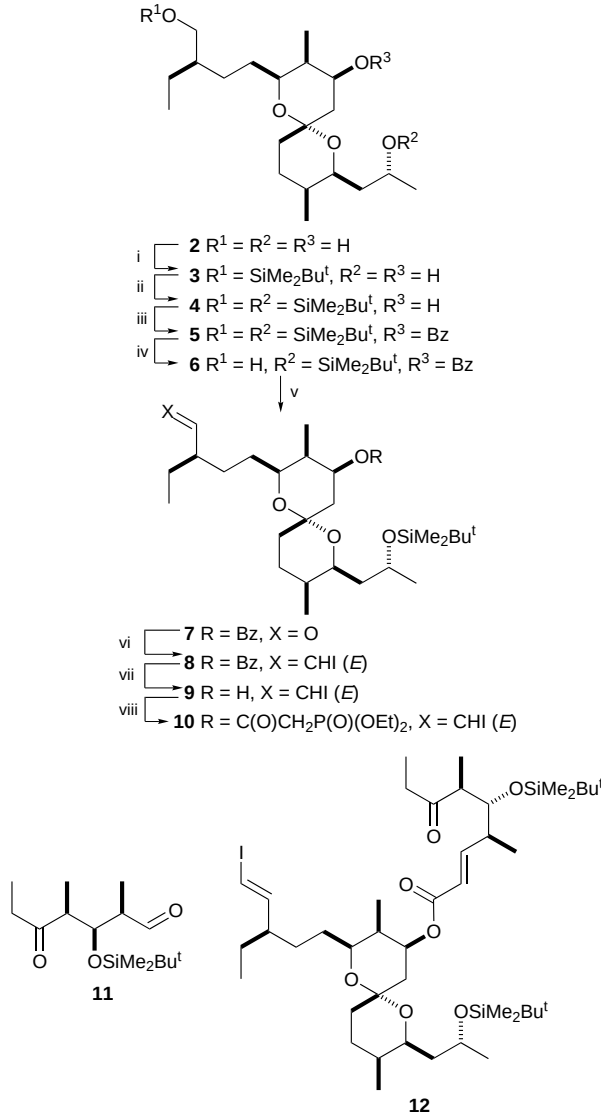

11

12

Scheme 1 *Reagents and conditions*: i, Bu^tMe_2SiCl, pyridine, $AgNO_3$, THF; ii, $Bu^tMe_2SiOSO_2CF_3$, 2,6-lutidine, CH_2Cl_2, −78 °C, 66%; iii, BzCl, Et_3N, DMAP, CH_2Cl_2, 90%; iv, HF·pyridine, pyridine, 61%; v, $(COCl)_2$, DMSO, Et_3N; CH_2Cl_2, −78 °C, 96%; vi, CHI_3, $CrCl_2$, THF, 0 °C, 76%; vii, LiOH, MeOH–H_2O–THF, ~100%; viii, $(EtO)_2(O)PCH_2COCl$, pyridine, DMAP, 82%; ix, LDA, THF, then **11**, −78 → 0 °C, 88%

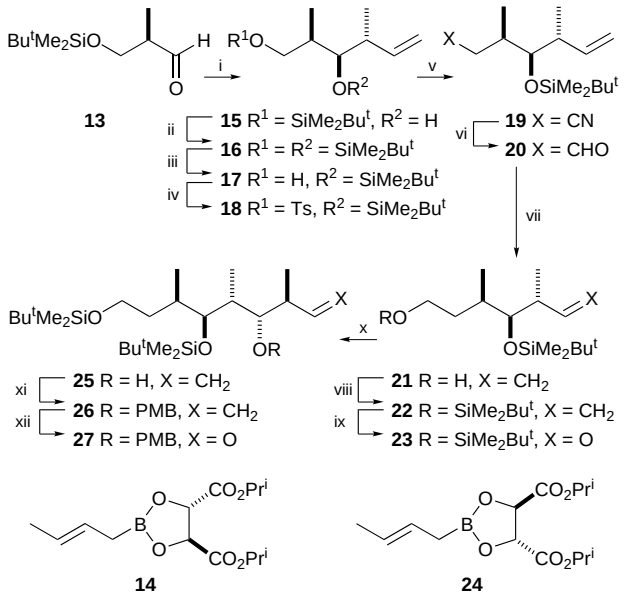

Scheme 2 *Reagents and conditions*: i, **14**, 4 Å MS (powder), toluene, −78 °C, 86% (78% de); ii, $Bu^tMe_2SiOSO_2CF_3$, Et_3N, CH_2Cl_2, 99%; iii, NH_4F, MeOH, heat, 85%; iv, TsCl, pyridine, 92%; v, NaCN, DMSO, 94%; vi, DIBAL-H, toluene, −78 °C, 75%; vii, $NaBH_4$, Pr^iOH, 0 °C, 87%; viii, Bu^tMe_2SiCl, imidazole, DMF, 96%; ix, O_3, CH_2Cl_2–MeOH, −78 °C, Me_2S, 94%; x, **24**, 4 Å MS (powder), toluene, −78 °C, 78% (> 98% de); xi, $PMBOC(=NH)CCl_3$, CF_3SO_3H, −10 °C, 68%; xii, O_3, MeOH–CH_2Cl_2, 79%

plays a positive role by favouring attack at the *re* face of the aldehyde carbonyl by the *si* face of the titanium enolate.

β-Hydroxy ketone **28** was converted to its silyl ether **29**, and the PMB ether was cleaved to give **30**, which was immediately oxidized to **31** (Scheme 4). The primary silyl ether was selectively removed from **31** and the resultant alcohol **32** was oxidized to **33**. Condensation of **33** with the dichloromethylboronic ester **34**[11] of pinacol in the presence of $CrCl_2$ and LiI afforded (*E*)-vinyl boronate **35**[12] which was subjected to palladium-catalysed intramolecular coupling[13] in the presence of Ag_2O[14] and $AsPh_3$. The ensuing macrocyclization proceeded in good yield and furnished the tetrasilyl ether **36** of rutamycin B, identical in all respects with a sample prepared from the natural material by exhaustive silylation with Bu^tMe_2SiO-SO_2CF_3. Final cleavage of the four Bu^tMe_2Si ethers from **36** by sequential addition of aq. HF in pyridine gave **1**, identical with natural rutamycin B.

We thank Dr Herbert Kirst and Ms Margaret Niedenthal, Eli Lilly Co., Indianapolis (USA) for a sample of natural rutamycin B, and Professor David Evans (Harvard University) for a generous quantity of a derivative of **2**. This research was supported by grants from the U.S. National Institutes of Health (GM50574 and AI10964). Postdoctoral fellowships are gratefully acknowledged by T. T. (Fonds der Chemischen Industrie, Germany) and R. W. J. (US NIH GM16472).

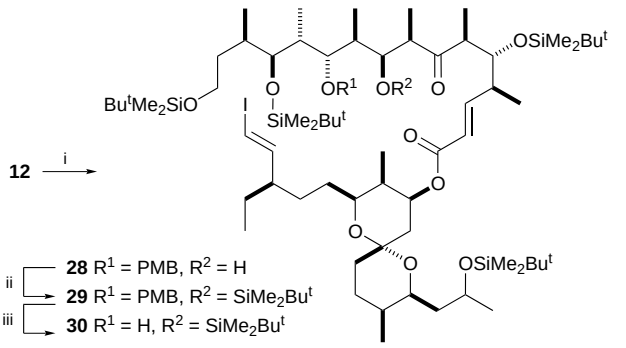

Scheme 3 *Reagents and conditions*: i, $TiCl_4$, Pr^i_2NEt, CH_2Cl_2, −78 °C, then **27**, 52% (> 98% de); ii, $Bu^tMe_2SiOSO_2CF_3$, Et_3N, CH_2Cl_2, 0 °C, 86%; iii, DDQ, H_2O–CH_2Cl_2

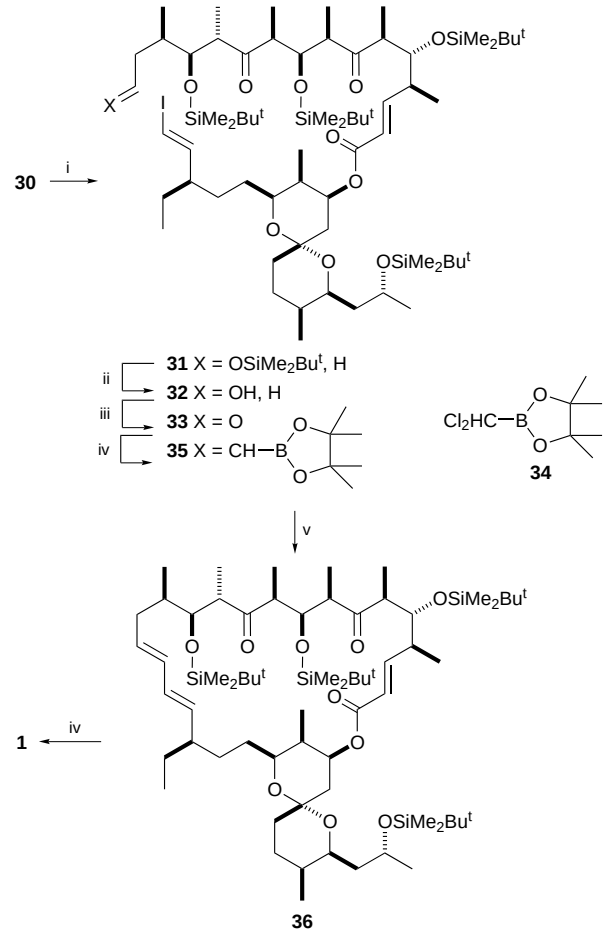

Scheme 4 *Reagents and conditions*: i, Dess–Martin periodinane, 93% from **29**; ii, HF·pyridine, MeCN–H_2O–$CHCl_3$, 79%; iii, Dess–Martin periodinane, 95%; iv, **34**, $CrCl_2$, LiI, THF, 76%; v, $Pd(MeCN)_2Cl_2$, $AsPh_3$, Ag_2O, THF, 70%; vi, aq. HF, pyridine, 4 d, 70%

Footnote and References

* E-mail: whitej@ccmail.orst.edu

1 S. Omura, in *Macrolide Antibiotics: Chemistry, Biology, and Practise*, ed. S. Omura, Academic Press, Orlando, Florida, 1984, p. 511.
2 D. A. Evans, H. P. Ng and D. L. Rieger, *J. Am. Chem. Soc.*, 1993, **115**, 11 446.
3 D. Wulthier, W. Keller-Schierlein and B. Wahl, *Helv. Chim. Acta*, 1984, **67**, 1208.
4 D. A. Evans, D. L. Rieger, T. K. Jones and S. W. Kaldor, *J. Org. Chem.*, 1990, **55**, 6260.
5 J. D. White, Y. Ohba, W. J. Porter and S. Wang, *Tetrahedron Lett.*, 1997, **38**, 3167.
6 K. Takai, K. Nitta and K. Utimoto, *J. Am. Chem. Soc.*, 1986, **108**, 7408.
7 J. D. White, W. J. Porter and T. Tiller, *Synlett*, 1993, 535.
8 W. R. Roush, A. D. Palkowitz and K. Ando, *J. Am. Chem. Soc.*, 1990, **112**, 6348.
9 D. A. Evans, D. L. Rieger, M. T. Bilodeau and F. Urpi, *J. Am. Chem. Soc.*, 1991, **113**, 1047.
10 For a similar result in a closely related aldol reaction, see D. A. Evans and H. P. Ng, *Tetrahedron Lett.*, 1993, **34**, 2229.
11 P. M. G. Wuts and P. A. Thompson, *J. Organomet. Chem.*, 1982, **234**, 137.
12 K. Takai, N. Shinomiya, H. Kaihara, N. Yoshida and T. Moriwake, *Synlett*, 1995, 963.
13 A. Suzuki, *Pure Appl. Chem.*, 1994, **66**, 213.
14 T. Gillmann and T. Weeber, *Synlett*, 1994, 649.

Received in Cambridge, UK, 7th October 1997; 7/07251A

Directed conjugate addition of organolithium reagents to α,β-unsaturated carboxylic acids

Barbara Plunian, Michel Vaultier and Jacques Mortier*

Université Rennes-I, Synthèse et électrosynthèse organiques, UMR 6510 associée au CNRS, campus de Beaulieu, 35042 Rennes Cedex, France

α,β-Unsaturated carboxylic acids undergo predominantly conjugate addition with organolithium reagents at low temperature (−78 °C) in THF and lead to various substituted alkanoic acids after quenching with electrophiles; with (*E*)-3-phenylpropenoic acid, this tandem alkylation sequence also affords significant amounts of isomeric 1,3-addition products.

1,4-Additions of organolithium reagents to α,β-unsaturated carbonyl compounds are usually promoted by steric interference of the 1,2-addition process.[1] Literature furnishes little information regarding the conjugate addition of *unprotected* α,β-unsaturated acids to organolithiums[2,3] and the data, scarce as they are, even appear to be inconsistent at first sight. Majewski and Snieckus described in 1984 the reaction in THF at 0 °C between senecioic acid [(*E*)-3-methylbut-2-enoic acid] and 2-lithiodithiane which afforded the 1,4-addition product in 65% yield.[4] Reaction of (*E*)-3-trimethylsilylpropenoic acid with *n*-butyllithium in THF–hexane at −70 °C was reported to give a mixture of 1,2-(55%) and 1,4-(45%) addition products.[5] The conjugate addition of α-silylated α,β-unsaturated acids to organolithiums appears to be a particular case.[6] Indeed the 1,2-addition is suppressed by the placement of a unit of negative charge adjacent to the carbonyl group. Furthermore the enolate dianions resulting from such additions are not efficiently intercepted with alkylating agents.

We have recently described the efficient addition of organolithium reagents to naphthalene-1- and -2-carboxylic acids followed by electrophilic trapping.[7] The diastereoisomeric ratios of 1,1,2- and 1,2,2-trisubstituted-1,2-dihydronaphthalenes were found to contain only *trans* addition products. The *trans* addition was verified in each system by single X-ray determination. Thus, in either case, the electrophile approached the naphthalene nucleus from the side opposite to the organolithium. We now describe results which demonstrate that the process can be expanded to simple α,β-unsaturated carboxylic acids.

Typical unsaturated carboxylic acids **1**–**3** underwent 1,4-addition reactions with lithium reagents in THF at low temperature (−78 °C) over the course of several minutes

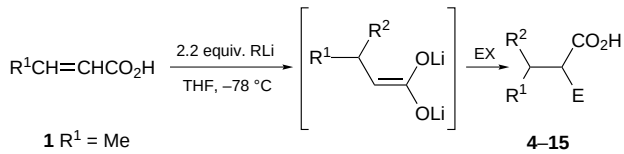

1 R^1 = Me
2 R^1 = Ph
3 R^1 = H

4–15

giving carboxylic acid dilithium enolates which, when quenched with a proton source (CF_3CO_2H) or an alkyl halide (MeI),[8] gave moderate to good yields of substituted alkanoic acids **4**–**15**. These reactions almost certainly involve deprotonation of the acid first, which reduces but does not suppress the reactivity of the carbonyl towards 1,2-addition.[9] At −78 °C, *n*-butyllithium and *sec*-butyllithium added efficiently to the carboxylic acid derivatives **1**–**3**. The use of phenyllithium, however, proceeded very sluggishly to **1** and **2** and after trapping with trifluoroacetic acid gave only **6** and **11** in 40 and 20% purified yields, respectively (Table 1, entries 3 and 7). Methyllithium failed to react (entries 5 and 9) and gave mainly products resulting from carbonyl addition at higher temperatures.

Reaction of *n*-butyllithium with (*E*)-3-methylpropenoic acid **1**, followed by quenching with trifluoroacetic acid, provided the 1,4-adduct **4** in good yield (entry 1). A 1:1 mixture of the diastereoisomers **5′** and **5″** was obtained when the enolate was trapped with methyl iodide (entry 2). When **1** was treated with *sec*-butyllithium, proton quench with trifluoroacetic acid afforded the conjugate 1,4-addition product in moderate yield as a mixture of diastereoisomers (**7′** and **7″**) differing in their configuration at C-3 and C-4 (7:3 ratio, entry 4). Reactions of (*E*)-3-phenylpropenoic acid **2** with *n*-butyllithium and *sec*-butyllithium gave mixtures of the conjugate 1,4-addition products **9** and **12′**, **12″** as well as the isomeric products **10** and **13′**, **13″**, respectively. Structures of types **9**, **10** and **12**, **13** were easily distinguished by their ^{13}C NMR spectra by the multiplicity and the order of the chemical shift of the carbon in α-position of the carboxylic acid. 1,3-Addition reactions of Grignard and organolithium reagents to cinnamate derivatives, involving the addition of a free radical produced by a single electron transfer from the organometallic reagent to the alkene, are precedented.[2a,5,10] Turning to acrylic acid **3**, it was found that *n*-butyllithium with **3** in THF at −78 °C followed by hydrolysis, gave **14** and **15** (5:3) which were isolated in 50% yield (entry 10). Compound **15** resulted presumably from the double conjugate addition of the organolithium reagent to the lithium acrylate.

The following procedure for the synthesis of 3-methylheptanoic acid **4** is representative. In a 250 ml flask maintained under argon, were placed 40 ml of dry THF and 20 ml of *n*-butyllithium (1.6 M in hexanes, 33 mmol). The mixture was then cooled to −78 °C and (*E*)-methylpropenoic acid **1** (1.29 g, 15 mmol) in THF (40 ml) was slowly added. After the mixture was stirred for 1 h at −78 °C, a THF solution (20 ml) of an excess of trifluoroacetic acid (4.62 ml, 60 mmol) was added. The solution was allowed to warm slowly to room temperature with stirring, then treated with water, washed with diethyl ether, and shaken. The aqueous layer was acidified with 2 M HCl, diluted with diethyl ether, and the organic layer was separated, washed with aq. $NaHCO_3$ and water, and dried with $MgSO_4$. Filtration and concentration *in vacuo* afforded **4** which was purified by distillation (bp 75–80 °C/1 mmHg, 1.72 g, 80%).

Table 1 Additions of organolithium reagents to acyclic α,β-unsaturated carboxylic acids[a]

Entry	Acceptor	R^3Li[b]	Product(s)	Ratio[c]	Yield (%)[d]
1	**1**	Bu^nLi	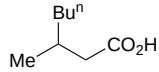 **4**	—	80 (90)
2	**1**	Bu^nLi	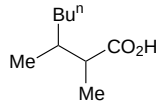 **5′**,**5″**	1 : 1	76 (85)
3	**1**	PhLi	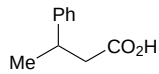 **6**	—	40 (70)
4	**1**	Bu^sLi	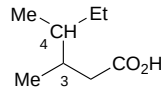 **7′**,**7″**	7 : 3	46 (62)
5	**1**	MeLi	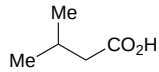 **8**	—	0
6	**2**	Bu^nLi	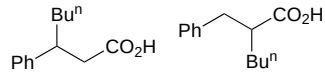 **9** **10**	7 : 3	60 (73)
7	**2**	PhLi	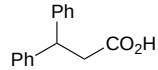 **11**	—	20 (32)
8	**2**	Bu^sLi	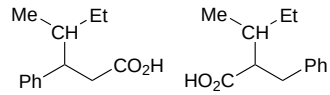 **12′**,**12″** **13′**,**13″**	42 : 22 : 23 : 13	70 (78)
9	**2**	MeLi	**6**	—	0
10	**3**	Bu^nLi	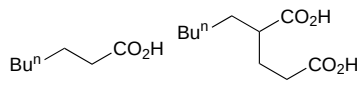 **14** **15**	5 : 3	50 (64)

[a] All structures are supported by spectral and analytical data. [b] Bu^nLi in hexane; Bu^sLi in cyclohexane–hexane; MeLi and PhLi in diethyl ether; 2.2 equiv. of RLi is used. [c] Determined by ^1H NMR spectroscopy. [d] Yields refer to purified isolated compounds. Yields in parenthesis are based on the consumed starting material.

We acknowledge the staff of the Analytical Sciences in our university for spectral measurements.

Footnote and References

* E-mail: jacques.mortier@univ-rennes1.fr

1 Reviews: D. A. Hunt, *Org. Prep. Proced. Int.*, 1989, **21**, 705; P. Perlmutter, in *Conjugate Addition Reactions in Organic Synthesis*, Tetrahedron Organic Chemistry Series, Pergamon Press, Oxford, 1992, vol. 9.
2 Reviews on the reactions of carboxylic acids with organolithium reagents: (*a*) M. J. Jorgenson, *Org. React.*, 1970, **18**, 1; (*b*) N. Petragnani and M. Yonashiro, *Synthesis*, 1982, 521.
3 Reactions of simple α,β-unsaturated acids with Grignard reagents give low yields of 1,4-adducts: J. H. Wotiz, J. S. Matthews and H. Greenfield, *J. Am. Chem. Soc.*, 1953, **75**, 6342; J. Klein, *Tetrahedron*, 1964, **20** 465; J. Klein and R. M. Turkel, *J. Am. Chem. Soc.*, 1969, **91**, 6186; J. Klein and N. Aminadav, *J. Chem. Soc.*, 1970, 1380; J. Klein and S. Zitrin, *J. Org. Chem.*, 1970, **35**, 666; conjugate additions to α,β-unsaturated acids using modified organocopper reagents ($RCu{\cdot}BF_3$): Y. Yamamoto and K. Maruyama, *J. Am. Chem. Soc.*, 1978, **100**, 3240; Y. Yamamoto, S. Yamamoto, H. Yatagai, Y. Ishihara and K. Maruyama, *J. Org. Chem.*, 1982, **47**, 119.
4 M. Majewski and V. Snieckus, *J. Org. Chem.*, 1984, **49**, 2682.
5 K. Kruithof, A. Mateboer, M. Schakel and G. Klumpp, *Recl. Trav. Chim. Pays-Bas*, 1986, **105**, 62.
6 M. P. Cooke, Jr., *J. Org. Chem.*, 1987, **52**, 5729.
7 B. Plunian, J. Mortier, M. Vaultier and L. Toupet, *J. Org. Chem.*, 1996, **61**, 5206.
8 Other electrophiles such as PhSSPh, $ClCO_2Me$, CO_2 were also effective.
9 In either case 1,2-addition products were obtained as by-products (3–10%).
10 T. Holm, I. Crossland and J. Ø. Madsen, *Acta Chem. Scand., Ser. B*, 1978, **32**, 754.

Received in Cambridge, UK, 30th September 1997; 7/07028D

Catalytic *C*-amidoalkylations: synthesis of β-amido aldehydes by three-component condensations

Charles M. Marson*† and Asad Fallah

Department of Chemistry, University of Sheffield, Sheffield, UK S3 7HF

Primary amides condense with aliphatic aldehydes (2 equiv.) in the presence of trifluoromethanesulfonic acid to give β-amido aldehydes.

The condensation of aldehydes with primary and secondary amides can lead to valuable products by means of amidoalkylation.[1,2] However, amidoalkylation at carbon has been generally limited to the condensation of an active methylene compound *other than* an aldehyde with an imine substrate usually containing an aromatic substituent.[1,2] In most cases, the amidoalkylating agent must be separately prepared and isolated prior to reaction with the active methylene compound. Whereas amidoalkylation is well-established for cases where either the aldehyde or the amide is aromatic[1,2] (or both are), condensations involving only aliphatic reactants are rare, and appear confined to one example of a cyclic amide [eqn. (1)].[3] Such

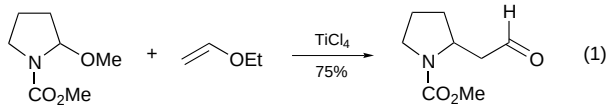

(1)

aliphatic amidoalkyations could significantly extend the scope of aliphatic and heterocyclic N–C bond formation, with particular importance for alkaloids and related pharmaceutical products. In this area, the nature of the acid catalyst is known to be crucial; for aromatic reactants, polyphosphoric acid[4] or polyphosphate ester[5] have been shown to effect amidoalkylation followed by cyclization. However, the harshness of these reagents led to decomposition when applied to aliphatic reactants. Accordingly, trifluoromethanesulfonic acid was investigated, since its mildness, and ease of control of reagent concentration result in good yields in acid-catalyzed condensations,[6] notably in the cyclization of β,γ-unsaturated amides to lactams.[7]

Multiple component condensations offer powerful strategies in combinatorial chemistry[8a] and general synthesis.[8b] A new three-component amidoalkylation is here reported that is to the best of our knowledge the first amidoalkylation to deliver acyclic aliphatic aldehydes [eqn. (2)]. Unique features include:

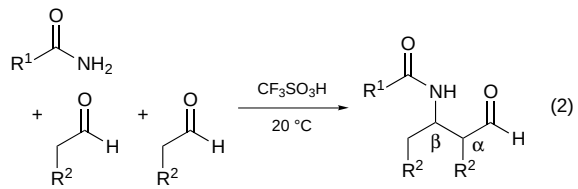

(2)

(a) *in situ* formation[2] of the presumed imine substrate (from an amide and an aldehyde), (b) subsequent amidoalkylation by an aldehyde, in an overall one-pot process to give (c) an isolable β-amido aldehyde as the product, under mild conditions of acid catalysis at 20 °C. β-Amido aldehydes are protected, relatively stable forms of β-amino aldehydes which are generally only isolable with difficulty[9] or accessible *via* indirect synthetic protocol.[10] β-Acetylamino aldehydes are key intermediates in the synthesis of amino cyclitols.[11] Table 1 shows that β-amido aldehydes‡ of the form $R^1CONHCHR^2CHR^2CHO$ can be prepared from an amide R^1CONH_2 and an aldehyde R^2CH_2CHO (2 equiv.). For entries 1 and 5, the *syn* : *anti* diastereoisomer ratio is respectively 1 : 2 and 1 : 5,[12] whereas for entries 2 and 3 a 1 : 1 ratio was observed. The diastereoselection found in entries 1 and 5 can be accounted for on the basis of a Zimmerman–Traxler model, leading to preponderance of the *anti*-diastereoisomer.[13]

Notable is the variety of amides (some functionalized) and sensitive aliphatic aldehydes (or their equivalent) that participate under the mild conditions. Attempts to obtain β-amido aldehydes using polyphosphoric acid or polyphosphate ester were unsuccessful in all cases studied, and we have generally observed that simple aliphatic aldehydes and ketals are rapidly decomposed by reagents other than dilute trifluoromethanesulfonic acid. The β,γ-unsaturated amides used in entries 2, 3 and 4 have been shown to cyclize either as the sole reactant[7] or in the presence of an aromatic aldehyde;[4,5] it is noteworthy that in the present reactions the double bond does not participate in a cyclization, but remains intact.

The reaction of amides with aldehydes can give a number of products, depending on the reagent and conditions. Thus, amides have been shown to add reversibly to aldehydes,

Table 1 Condensation of amides with aldehydes in the presence of 2% v/v trifluoromethanesulfonic acid in dichloromethane at 20 °C

Entry	Amide	Aldehyde or acetal	*t*/h	β-Amido aldehyde	Yield (%)
1		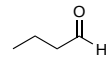	16	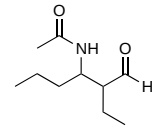	60
2	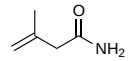	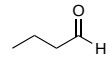	12	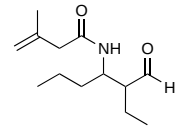	50
3	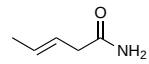	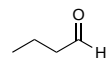	24	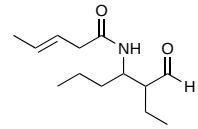	54
4	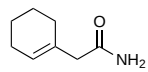	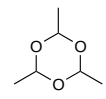	16	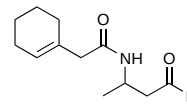	51
5			48	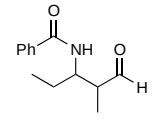	69
6	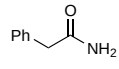	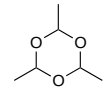	48	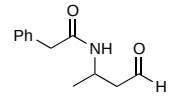	66

particularly formaldehyde, to give *N*-hydroxymethylamides.[2,14] For the latter, basic conditions are usually employed because acidic catalysis is usually either ineffective or affords mixtures. In general (and depending on the stoichiometry), *N*,*N*′-alkylidenebis(amides), $R^1CH(NHCOR^2)_2$, can be prepared by condensing R^1CHO with R^2CONH_2.[15]

Preliminary experiments with α,β-unsaturated aldehydes and amides in the presence of CF_3SO_3H did not lead to β-amido aldehydes, and would appear to exclude an initial aldol condensation with dehydration, followed by conjugate addition. More probable is an initial condensation of the amide with one equivalent of aldehyde to give an acyl imine or acyl iminium intermediate which then undergoes attack by an enolic form of a second equivalent of the aldehyde, either in its enolic form, or possibly as an enamide derivative.

In conclusion, a new three-component condensation[8] is disclosed which provides a flexible route to β-amido aldehydes that have been hitherto largely inaccessible. The β-amido aldehydes are of synthetic value in themselves, being relatively stable derivatives of the difficulty isolable β-amino aldehydes.[9] These condensations of amides with aldehydes proceed at 20 °C with acid catalysis, and without the need for protection or derivatisation of the aldehyde function. The new condensation is clearly distinguishable from other related amide–carbonyl condensations; synthetic applications and mechanistic aspects are under investigation.

We thank the EPSRC for a postdoctoral fellowship to A. F.

Footnotes and References

* E-mail: c.m.marson@qmw.ac.uk
† *Current address*: Department of Chemistry, Queen Mary and Westfield College, University of London, London, UK E1 4NS.

‡ All compounds gave satisfactory spectral data (NMR, IR, mass), and all new compounds gave satisfactory elemental analyses or HRMS. The procedure is described for entry 4 (Table 1). To a solution of cyclohex-1-enylacetamide (1.49 g, 0.01 mol) and paraldehyde (1.32 g, 0.01 mol) in dichloromethane (50 ml) was added trifluoromethanesulfonic acid (1.0 ml). After stirring at 20 °C for 16 h the mixture was poured over ice (50 g), made alkaline with aqueous sodium hydroxide (5%), and extracted with dichloromethane (3 × 50 ml). The combined extracts were dried, evaporated, and the residue purified by column chromatography [silica, 1 : 1 ethyl acetate–light petroleum (40–60 °C)] to give *N*-(4-oxopropan-2-yl)cyclohex-1-enylacetamide (1.1 g, 51%) as an oil; δ_H 9.77 (1 H, s, C*H*O), 6.00 (1 H, brd s, N*H*), 5.63 (1 H, brd s, =C*H*), 4.42 (1 H, m, NC*H*), 2.86 (2 H, s, CH_2CO, 2.65 (2 H, dd, *J* 7 and 2 Hz, CH_2CHO), 2.10 (2 H, brd s, allylic *H*), 1.95 (2 H, brd s, allylic *H*), 1.65 (4 H, m, CH_2CH_2), 1.25 (3 H, d, *J* 7 Hz, CH_3); δ_C 201.0, 170.6, 132.6, 127.0, 49.7, 46.3, 40.9, 28.3, 25.3, 22.7, 21.9, 20.4. Found: HRMS, M^+, 209.1416. $C_{12}H_{19}NO_2$ requires M^+, 209.1416.

1 H. E. Zaugg, *Synthesis*, 1984, 85; 1984, 181.
2 H. E. Zaugg and W. B. Martin, *Org. React.*, 1965, **14**, 52.
3 T. Shono, Y. Matsumura and K. Tsubata, *J. Am. Chem. Soc.*, 1981, **103**, 1172.
4 C. M. Marson, U. Grabowska, T. Walsgrove, D. S. Eggleston and P. W. Baures, *J. Org. Chem.*, 1991, **56**, 2603; 1994, **59**, 284.
5 C. M. Marson, U. Grabowska and T. Walsgrove, *J. Org. Chem.*, 1992, **57**, 5045; C. M. Marson, U. Grabowska, A. Fallah, T. Walsgrove, D. S. Eggleston and P. W. Baures, *J. Org. Chem.*, 1994, **59**, 291.
6 P. J. Stang and M. R. White, *Aldrichim. Acta*, 1983, **16**, 15.
7 C. M. Marson and A. Fallah, *Tetrahedron Lett.*, 1994, **35**, 293.
8 (*a*) P. A. Tempest, S. D. Brown and R. W. Armstrong, *Angew. Chem., Int. Ed. Engl.*, 1996, **35**, 640; (*b*) G. H. Posner, *Chem. Rev.*, 1986, **86**, 831.
9 S. G. Davies and T. D. McCarthy, *Synlett*, 1995, 700; I. E. Markó and A. Chesney, *Synlett*, 1992, 275.
10 B. F. Bonini, M. Comes-Franchini, G. Mazzanti, A. Ricci and M. Sala, *J. Org. Chem.*, 1996, **61**, 7242.
11 T. Suami, K. Tadano and S. Horiuchi, *Bull. Chem. Soc. Jpn.*, 1975, **48**, 2895.
12 ^{1}H NMR spectra of the separated diastereoisomeric acids obtained by aerial oxidation of the aldehydes in entry 1 exhibit couplings for the vicinal methine hydrogen atoms of 10 and 5 Hz (isolated as the minor diastereoisomer), and 3 and 5 Hz (major diastereoisomer). The former values are consistent with the *syn*-isomer in a preferred conformation in which the amido and aldehyde groups are antiperiplanar, and the methine hydrogen atoms are disposed *trans* (J = 10 Hz). ('*syn*' refers to relation of α-alkyl and β-amido groups, the aldehyde being drawn as part of the 'backbone' of the product.) Such assignments are consistent with those for other β-amido carbonyl compounds: H. Estermann and D. Seebach, *Helv. Chim. Acta*, 1988, **71**, 1824.
13 H. Zimmerman and M. Traxler, *J. Am. Chem. Soc.*, 1957, **79**, 1920.
14 J. F. Walker, *Formaldehyde*, Reinhold, New York, NY, 3rd edn., 1964, pp. 359–414.
15 E. E. Gilbert, *Synthesis*, 1972, 30; W. A. Noyes and D. B. Forman, *J. Am. Chem. Soc.*, 1933, **55**, 3493.

Received in Liverpool, UK, 16th October 1997; 7/07484K

A bridged pyrrolic *ansa*-ferrocene. A new type of anion receptor

Markus Scherer, Jonathan L. Sessler,* Andreas Gebauer and Vincent Lynch

Department of Chemistry and Biochemistry, The University of Texas at Austin, Austin, TX 78712, USA

Reaction of an activated bis(pyrrolyl)ferrocene with 2,2′-(ethylenedioxy)bis(ethylamine) under standard amide-forming conditions gives rise to a novel *ansa*-ferrocene system that acts as a redox-based sensor for F^- and $H_2PO_4^-$ anions.

The construction of metallocene-based anion sensors constitutes an area of active research.[1] In general, successful systems reported in the literature have consisted of a redox active metallocene 'marker' covalently linked to an anion recognition subunit and in this context a wide range of anion binding agents have been employed. One set of anion chelating agents that appears attractive in terms of anion sensor development, but which, apparently, has yet to be explored, is polypyrroles.[2] Pyrrole-containing species, both cyclic and acyclic, often possess H-bond donating characteristics that, depending on the details of structure, can make them effective and selective as anion binding agents both in solution and in the solid state. We thus thought that combining a suitable pyrrolic anion binding entity with a ferrocene marker group could give rise to a new type of anion sensing device. Here, we report the first successful test of this hypothesis. Specifically, we describe the synthesis, solid state characterization, and solution phase anion binding behavior of the *ansa*-ferrocene system **1**; this system acts as an effective redox-based sensor for F^- and $H_2PO_4^-$.

The synthesis of **1** and its acyclic control **2**, is summarized in Scheme 1. Here, the key precursor **4** was obtained starting from an isomeric mixture of cyclopentadienyl functionalized pyrroles **3**.[3,†] Deesterification of **4** under reductive conditions led to the corresponding diacid **5**. Reaction with 2,2′-(ethylenedioxy)bis(ethylamine) under standard amide-forming conditions then gave the desired *ansa*-ferrocene system **1**, with the acyclic analog **2** being prepared from 2-methoxyethylamine in a similar way.

The *ansa*-ferrocene **1** was characterized *inter alia* by X-ray diffraction analyses. Diffraction-grade single crystals of **1** were obtained by slow diffusion of a CH_2Cl_2 solution of **1** into hexanes in the case of the solvent-free structure (Fig. 1), and by slow evaporation of a CH_2Cl_2–hexanes solution at −10 °C in the case of the water-containing structure (Fig. 2). The resulting structures revealed a *trans*-type arrangement about the ferrocene subunit and the presence of an internal 'pocket' that, depending on the anion size, might be expected to accommodate either one or two negatively charged substrates.‡ In the absence of a bound guest, this suggested propensity towards substrate binding is accommodated in the solid state *via* a dimerization process, wherein amide and oxygen atoms from one macrocyclic subunit are bound, *via* H-bonding interactions, to the pyrrolic and amido NH portions of another macrocycle (Fig. 1).§

Interestingly, the second structure alluded to above (Fig. 2) actually provided a more concrete 'hint' that receptor **1** can accommodate a substrate in its binding pocket. In this case a single water molecule is found to be bound within the macrocyclic cavity.‡ A second water molecule, not constrained within the cavity, is found H-bonded to the encapsulated water and to an amide oxygen of an adjacent macrocycle.

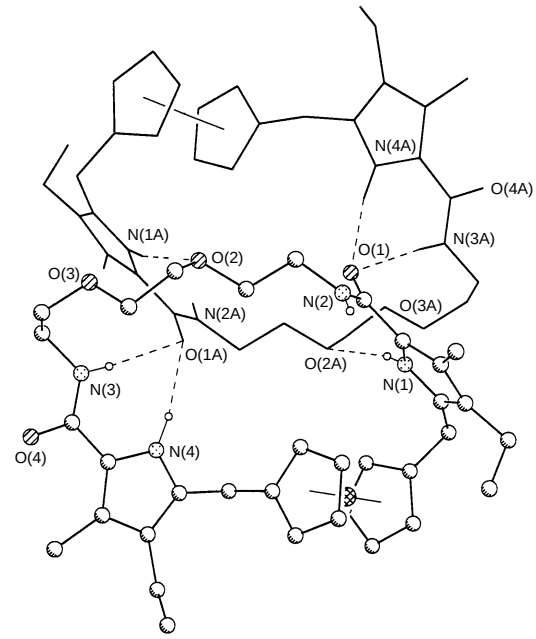

Fig. 1 View of the H-bound dimer of **1** obtained in the solid state. One molecule is shown in ball-and-stick form while a second related by $1 - x$, $1 - y$, $-z$ is shown in wireframe form. Dashed lines are indicative of a H-bonding interaction. With the exception of the amide- and amino-H all other H atoms are omitted for clarity.

The solution phase anion-binding properties of **1** and **2** were studied by carrying out ^1H NMR spectroscopic titrations. Stability constants were then calculated using the EQNMR

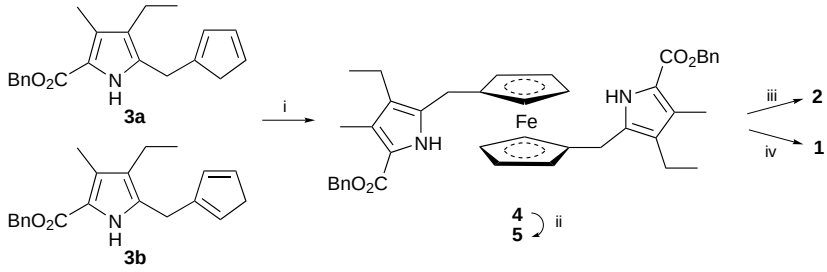

Scheme 1 Syntheses of the receptor systems **1** and **2**. *Reagents*: i, TlOEt, THF then $FeCl_2$; ii, Pd/C–H_2, THF; iii, BOP, NEt_3, DMF, $H_2NCH_2CH_2OMe$; iv, BOP, NEt_3, DMF, $H_2NCH_2CH_2OCH_2CH_2OCH_2CH_2NH_2$.

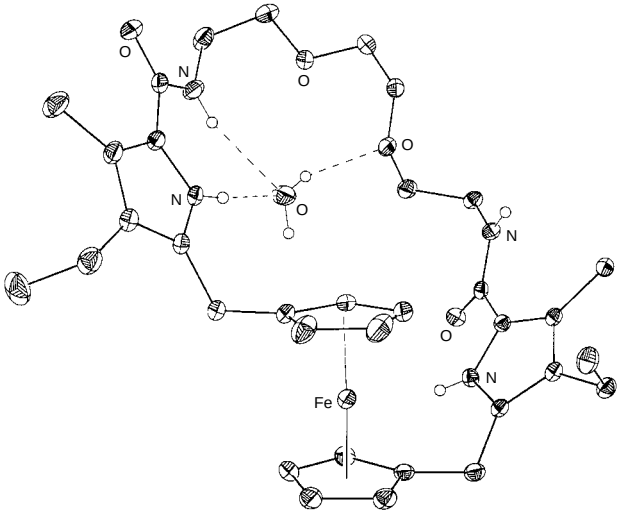

Fig. 2 Solid state structure of **1**·2H_2O (the second water molecule, not contained in the cavity, has been omitted for clarity). Thermal ellipsoids are scaled to the 30% probability level. H atoms shown are drawn at an arbitrary scale. With the exception of the amide and amino hydrogens all other H atoms are omitted for clarity.

computer program.[4] As summarized in Table 1, it was determined that **1** and **2** bind both $H_2PO_4^-$ and Cl^- anions with high affinity in acetonitrile. Although the relevant interactions are clearly weaker, effective anion binding was also observed when Br^- and HSO_4^- anions were tested as substrates. The reduced affinities observed for Br^- and HSO_4^- are ascribed to the lower basicity of these anions and a set of correspondingly weaker H-bond interactions.[1]

Not surprisingly, **2** displays overall affinity constants that are weaker for all of the anions tested. Given the fact that identical functionality is present in both **1** and **2**, this disparity in anion affinity is easily interpreted in terms of the greater preorganization (and lower flexibility) presumed to pertain in receptor **1**.

Table 1 Relevant electrochemical data and stability constants for anion complexes formed from receptors **1** and **2**

	Receptor 1				Receptor 2			
Anion[a]	K_a[b]/dm^3 mol^{-1}	$E_{1/2}$[c]/ mV	ΔE[d]/ mV	BEF[e]	K_a[b]/dm^3 mol^{-1}	$E_{1/2}$[c]/ mV	ΔE[d]/ mV	BEF[e]
None	N/A	396	—	N/A	—	424	—	N/A
F^-	$>10^5$	316	80	—[f]	$>10^5$	368	56	—[f]
Cl^-	9031	372	24	2.5	1260	388	36	4.1
Br^-	857	388	8	1.4	66	404	20	2.2
HSO_4^-	889	380	16	1.9	258	392	32	8.8
$H_2PO_4^-$	11305	260	136	199.0	4181	280	144	271.7

[a] $NBu^n_4^+$ salts. [b] Association constants for anion binding; recorded in CD_3CN; errors < 15%; determined from $\Delta(\delta)$/ppm NH(amide). [c] Determined in acetonitrile containing 0.1 M $NBu^n_4PF_6$ as the supporting electrolyte. Solutions of **1**/**2** were 5×10^{-4} M and potentials were determined with reference to Ag/AgCl, 10 Hz frequency in square wave voltammetry. [d] Cathodic shift observed after the addition of 5 molar equiv. of added anion. [e] Enhancement factor (BEF) for anion coordination after oxidation. [f] Since a 2 : 1 binding mode pertains the BEF could not be defined.

As was revealed by Job plots, different binding stoichiometries are observed (for both **1** and **2**) depending on the size of the anion. In particular, F^- was determined to bind in a 2 : 1 ratio while all other anions tested were found to be bound in a 1 : 1 fashion.

The above findings led us to consider whether systems **1** and **2** could be used to detect the presence of various anions electrochemically through the species specific perturbation of the ferrocene–ferrocenium (Fc/Fc^+) redox couple. As reflected by the data summarized in Table 1, it was found that this could in fact be done. Specifically, the addition of an added, non-electrolyte anion was found to induce a cathodic shift in the reversible Fc/Fc^+ couple seen in both **1** and **2**. These studies, carried out in acetonitrile to allow the calculation of binding enhancement factors,[5] also served to highlight the facts that (*i*) among the five test anions studied, the response factor for both **1** and **2** is greatest for $H_2PO_4^-$ anion followed by F^- and Cl^- and (*ii*) the purely electrochemical sensitivity (*i.e.* $\Delta E_{1/2}$) of these two systems is similar.

In conclusion, the employment of a 1,1′-dipyrrole substituted ferrocene as a building block in an *ansa*-ferrocene type anion system leads to the generation of receptors that not only display unusually high affinities for the 1 : 1 binding of Cl^- and $H_2PO_4^-$ relative to other systems in literature[1] but also allows the detection of these species *via* electrochemical means.

This research was supported by the National Science Foundation (grant CHE 9725399 to J. L. S.). M. S. thanks the Alexander von Humboldt-Stiftung for a post-doctoral research fellowship (Feodor-Lynen stipend). We are grateful to Dr P. A. Gale for numerous helpful discussions, and for providing a copy of ref. 5 prior to publication.

Footnotes and References

* E-mail: sessler@mail.utexas.edu

† All compounds gave spectroscopic and analytical data consistent with the proposed structures.

‡ *Crystal data*: for $C_{34}H_{44}N_4O_4Fe$: yellow crystals, triclinic, $P\bar{1}$, a = 9.248(2), b = 11.622(2), c = 15.681(3) Å, α = 70.168(13), β = 74.160(14), γ = 89.070(13)°, U = 1519.7(6) Å^3, Z = 2, μ = 5.42 cm^{-1}, D_c = 1.37 g cm^{-3}. For $C_{68}H_{88}FeN_8O_8{\cdot}2H_2O$. Yellow clusters, crystal size = 0.17 × 0.36 × 0.99 mm, triclinic, $P\bar{1}$, Z = 2, a = 9.8278(7), b = 13.015(1), c = 14.049(1) Å, α = 79.044(6), β = 73.254(4), γ = 76.547(6), U = 1658.9(3) Å^3, D_c = 1.33 g cm^{-3}, $F(000)$ = 708. CCDC 182/675.

§ The solution and gas phase behavior of **1** was studied by vapor pressure osmometry (VPO) and electrospray mass spectrometry (ESMS), respectively. In solution only weak dimerization could be detected (calc. for $C_{34}H_{44}FeN_4O_4$ 628.6, found: 831). Similarly, only a weak peak of the dimer (2% compared to 100% for the monomer) was observed in ESMS.

1 P. D. Beer and J. K. Smith, *Prog. Inorg. Chem.*, 1997, **46**, 1, and references therein.
2 P. A. Gale, J. L. Sessler, V. Král and V. Lynch, *J. Am. Chem. Soc.*, 1996, **118**, 5140; J. L. Sessler, A. Andrievsky, P. A. Gale and V. Lynch, *Angew. Chem.*, 1996, **108**, 2954; *Angew. Chem., Int. Ed. Engl.*, 1996, **35**, 2782; J. L. Sessler and S. J. Weghorn, *Expanded, Contracted and Isomeric Porphyrins*, Elsevier, NY, 1997, p. 453, and references therein.
3 The syntheses of the pyrrole substituted cyclopentadienes **1** (and also of dipyrrole functionalized cyclopentadienes) is described in: M. Scherer, J. L. Sessler, A. Gebauer and V. Lynch, *J. Org. Chem.*, in press.
4 M. J. Hynes, *J. Chem. Soc., Dalton Trans.*, 1993, 311.
5 P. D. Beer, P. A. Gale and Z. Chen, *Adv. Phys. Org. Chem.*, 1997, in press.

Received in Columbia, MO, USA, 26th August, 1997; 7/06168D

Incorporation of vanadium species in a dealuminated β zeolite

S. Dzwigaj,[a]† M. J. Peltre,[a] P. Massiani,[a]* A. Davidson,[a]* M. Che,[a] T. Sen[b] and S. Sivasanker[b]

[a] *Laboratoire de Réactivité de Surface, URA 1106-CNRS, Université P. et M. Curie, 4 Place Jussieu, 75252 Paris Cedex 05, France*

[b] *National Chemical Laboratory, Pune 411008, India*

V-loaded β zeolites can be prepared by a two-step post-synthesis method which consists of first creating vacant T-sites by dealumination of the β zeolite with nitric acid, then contacting them with an ammonium metavanadate solution; the SiOH consumption and the nature of the incorporated V species are characterized by IR, UV–VIS and ^{29}Si MAS NMR spectroscopies.

Transition metal cations can be efficiently dispersed in molecular sieves by using a two-step post-synthesis method.[1–3] The zeolite is first dealuminated with a strong acid (HCl, HNO_3, *etc.*) to generate vacant T-sites associated with silanol functional groups, which are then reacted with a highly reactive metallic precursor such as $TiCl_4$.[1,2] The procedures are often highly demanding, requiring both a perfectly anhydrous atmosphere and a high temperature (typically 673–773 K). The present work shows that a similar two-step method can be used to disperse vanadium species in a β zeolite even at room temp. using an aqueous solution as a V precursor.

A tetraethylammonium β zeolite (TEAβ) provided by RIPP (China) was separated into two fractions. The first fraction was calcined (12 h, 823 K) to obtain the non-dealuminated organic-free Hβ (Si/Al = 11). The second fraction was treated in a 13 M HNO_3 solution (4 h, 353 K) to give the dealuminated organic-free Siβ (Si/Al > 1300) used without further calcination. As already reported,[4] the dealumination does not affect the zeolite crystallinity of the β zeolite. The IR vibrations of the hydroxyls in these two solids are compared in Fig. 1(*a*). The three bands attributed to OH in Al–OH groups (3780, 3662, 3609 cm^{-1})[4,5] disappear after dealumination, confirming elimination of the Al atoms. Simultaneously, the intensity of several bands related to Si–OH groups increases (narrow bands of isolated silanol groups within the range 3700–3740 cm^{-1}, and a broad band of H-bonded SiOH groups centered near 3520 cm^{-1}).[6] Furthermore, a new IR peak is detected at *ca.* 960 cm^{-1} (not shown) which is assigned to uncoupled (Si–O) oscillators belonging to defective Si–OH groups.[7,8] ^{29}Si NMR spectroscopy confirms that stable silanol groups are generated by the dealumination. In all the spectra presented in Fig. 1(*b*) (MAS) and (*c*) (CP MAS), two main broad peaks, located at high field (δ −110 to −115) and downfield (δ −100 to −104) are observed. The high-field peak is due to framework Si atoms in a $Si(SiO)_4$ environment, located in different crystallographic sites.[9] For the non-dealuminated Hβ sample, the downfield peak is associated with Si atoms in $Si(OSi)_3(OAl)$ and $Si(OH)(OSi)_3$ environments.[4] The contribution from Si atoms associated with hydroxyl groups is revealed by the intense band which is detected at δ −102 when cross-polarization is applied. For the dealuminated Siβ sample, the downfield peak only corresponds to Si atoms in a $Si(OH)(OSi)_3$ environment. A small proportion of Si atoms in a $Si(OH)_2(OSi)_2$ environment is also evident (weak signal at *ca.* δ −91 in the cross-polarized spectrum of Siβ).[10]

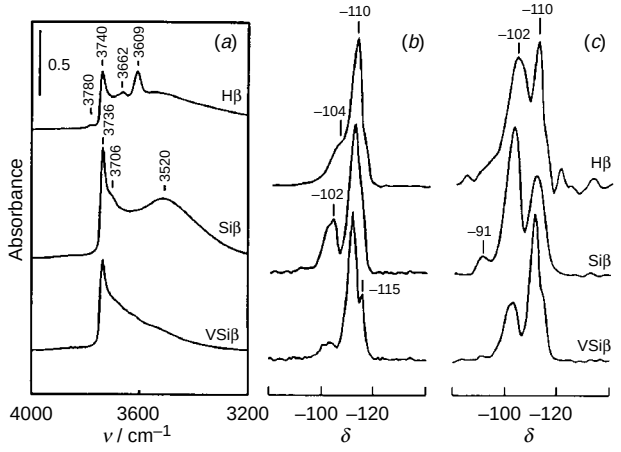

Fig. 1 (*a*) FTIR, (*b*) ^{29}Si MAS NMR and (*c*) ^{1}H–^{29}Si CP MAS NMR spectra of Hβ, Siβ and VSiβ samples (V/Si atomic ratio 0.007). The FTIR spectra were recorded on a Bruker IFS 66V FTIR spectrometer after calcination at 573 K (8 h, 120 ml min^{-1} O_2) and evacuation (10^{-5} Torr, 6 h) at the same temperature. The ^{29}Si NMR spectra were recorded on a Bruker MSL 400 at 79.5 MHz. The pulse length and recycle delay were 2.5 μs and 10 s respectively (MAS spectra). The proton π/2 pulse length, contact time, and recycle delay were 6.5 μs, 5 ms and 5 s, respectively (CP MAS).

Each sample (Hβ and Siβ) was contacted with an aqueous solution of NH_4VO_3 at 298 K (V/Si atomic ratio in the suspension within the range 0.007–0.021). Fig. 2(*a*) shows, as a function of time, the absorbance of the more diluted solution, measured at a constant wavelength of 380 nm, where the $O^{2-} \rightarrow V^{V}$ charge-transfer transitions are detected. With the Siβ zeolite, the absorbance decreases rapidly and disappears within a few hours indicating that the V ions initially present in the solution have reacted with the zeolite. With the Hβ sample, the absorbance rapidly reaches a non-zero constant value, showing that a non-negligible proportion of the V species

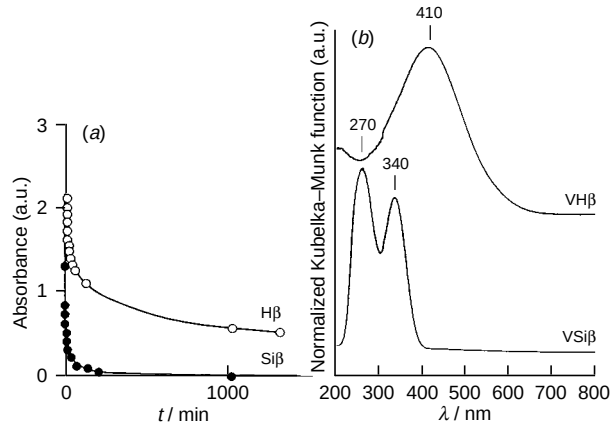

Fig. 2 (*a*) Evolution as a function of time of the UV–VIS absorbance measured at 380 nm on a 258 Ciba-Corning spectrometer, of an ammonium metavanadate solution (298 K, 7×10^{-4} mol l^{-1}) contacted with the Hβ and dealuminated Siβ samples (130 mg zeolite in 3 ml solution); (*b*) UV–VIS diffuse reflectance spectra of the VHβ and VSiβ zeolites (V/Si atomic ratios 0.013, 0.021 respectively), measured on a Cary spectrometer, using the parent V-free β zeolites as references.

remains in the solution, even after several days of contact with the non-dealuminated solid. The same trends have been observed using V solutions three times more concentrated.

After 3 days of contact with the solutions, the solids were recovered by centrifugation and dried overnight at 353 K. By chemical analysis, all the V species present in the initial solutions were detected inside the dealuminated VSiβ samples. By contrast, < 60% of the V species present in the initial solutions were found in the non-dealuminated VHβ solids. The VHβ samples were pale yellow whereas the VSiβ samples were white and their colour did not change even after several months in moist air. As indicated by Newsam *et al.*,[11] X-ray diffractograms of β materials are complex due to the intergrowth of a monoclinic and a quadratic polytype which makes unit-cell measurements difficult. For simplification, the *d*-spacings of single peaks indexed in a purely quadratic geometry are generally used to evidence lattice contraction and/or expansion.[12] On the non-dealuminated samples, no significant change in the d_{302} spacing was observed upon V incorporation (< 0.1%). In contrast, the d_{302} spacing which has decreased from 3.960 (Hβ) to 3.920 Å (Siβ) upon dealumination, increases with increasing V loading in Siβ to reach a maximum value of 3.940 Å when the atomic V/Si ratio is 0.021. Because of the relative values of the Al–O, Si–O and V–O bond distances (1.790, 1.660 and 1.755 Å, respectively),[13] these variations strongly suggest that the vanadium species have been incorporated into the zeolite framework.

To obtain more information on the microstructure of the V sites, we have compared the diffuse reflectance UV–VIS spectra of V-loaded solids [Fig. 2(*b*)]. The absence of d–d transitions within the range 600–800 nm clearly indicates that no reduced V^{IV} species is formed, oxidized V^{V} species being mainly present.[14] For the VHβ sample, the major absorption located near 410 nm is due to a low-energy charge transfer transition occurring between octahedral oxygen ligands and a central V^{V} atom.[14,15] The spectrum of the VSiβ sample is different and exhibits two bands at 270 and 340 nm. associated with pseudotetrahedral $O_{3/2}V{=}O$ species, anchored to the zeolitic walls by three Si–O–V bridges and possessing a V=O double bond.[14–16]

Chemical analysis indicates that the octahedral V^{V} species detected in the VHβ samples are almost completely leached out by washing (12 h, 298 K) in a 1 M ammonium acetate solution. By contrast, the pseudotetrahedral species present in the VSiβ samples are strongly anchored to the zeolitic walls, < 10% of them being extracted by a similar washing. Furthermore, after incorporation of V on Siβ, the intensities of the broad IR band near 3520 cm^{-1} [Fig. 1(*a*)] and the downfield ^{29}Si MAS NMR peak at δ −102 [Fig. 1(*b*)] are significantly reduced, which confirms that a specific reaction takes place between the vanadium precursor and the silanol groups. Moreover, the aspect of the IR peak near 960 cm^{-1} is strongly modified with appearance of two maxima at 950 and 978 cm^{-1} as will be described elsewhere.

The catalytic behaviour of the VSiβ materials was tested in the oxidation of toluene in aqueous solution using H_2O_2 as an oxidant (molar ratio toluene/H_2O_2 = 3; 0.1 g of catalyst for 1 g of toluene).[17] After 9 h of reaction at 80 °C, toluene conversion was *ca.* 5% and the products distribution was 5–10% cresols, 85–90% benzaldehyde, 5% benzyl alcohol and benzoic acid.

In conclusion, catalytically active vanadium species can be easily dispersed within the porosity of a β zeolite using a two-step method. Because of its stacking faults, the β zeolite accepts a high density of silanols and depletion sites generated upon elimination of Al species. The silanol groups generated upon strong dealumination react with NH_4VO_3 aqueous solution, even at room temp., thus obviating the need for a highly reactive metallic precursor such as $VOCl_3$. Pseudotetrahedral and stable V^{V} species attached to the zeolitic walls are formed with the silanol-rich dealuminated sample, whereas loosely bonded octahedral V^{V} species are mostly generated when the non-dealuminated β is used instead. This clearly illustrates the role of the vacant T-sites and their associated silanol groups in the incorporation of vanadium species. To the best of our knowledge, this is the first time that vanadium species have been incorporated into a dealuminated β zeolite, which may be of importance in mild oxidation reactions that must be performed in the absence of strong acidity, as described by Corma and coworkers for Ti-β.[29]

The Indo–French Center for the Promotion of Advanced Research (IFCPAR) is gratefully acknowledged for financial support under award IFC 1006-1. The authors thank RIPP (China) for providing the parent TEAβ zeolite.

Footnotes and References

* E-mail: massiani@ccr.jussieu.fr; davidson@ccr.jussieu.fr
† On leave from the Institute of Catalysis and Surface Chemistry, Polish Academy of Sciences, ul. Niezapominajek, 30-239 Krakow, Poland.

1 B. Kraushaar and J. H. C. Van Hoof, *Catal. Lett.*, 1988, **1**, 81.
2 R. J. Saxton, W. Chester, J. G. Zajacek and G. L. Crocco, *US Pat.*, 5 374 747, 1994.
3 G.-J. Kim, D.-S. Cho, K.-H. Kim, W.-S. Ko, J.-H. Kim and H. Shoji, *Catal. Lett.*, 1995, **31**, 91.
4 E. Bourgeat-Lami, F. Fajula, D. Anglerot and T. des Courières, *Microporous Mater.*, 1993, **1**, 237.
5 A. Janin, M. Maache, J. C. Lavalley, J. F. Joly, F. Raatz and N. Szydlowski, *Zeolites*, 1991, **11**, 391.
6 A. Zecchina, S. Bordiga, G. Spoto, L. Marchese, G. Petrini, G. Leofanti and M. Padovan, *J. Phys. Chem.*, 1992, **96**, 4991.
7 M. Decottigues, J. Phalippou and Z. Zarzycki, *J. Mater. Sci.*, 1978, **13**, 2605.
8 M. A. Camblor, A. Corma, A. Martinez and J. Perez-Pariente, *J. Chem. Soc., Chem. Commun.*, 1995, 589.
9 C. A. Fyfe, H. Strobl, G. T. Kokotailo, C. T. Pasztor, G. E. Barlow and S. Bradley, *Zeolites*, 1988, **8**, 132.
10 G. L. Woolery, L. B. Alemany, R. M. Dessau and A. W. Chester, *Zeolites*, 1986, **6**, 14.
11 J. M. Newsam, M. M. J. Treacy, W. T. Koetsier and C. B. Gruyter, *Proc. R. Soc. London Ser. A*, 1988, **420**, 375.
12 M. A. Camblor, A. Corma and J. Perez-Pariente, *Zeolites*, 1993, **13**, 82.
13 R. D. Shannon and C. T. Prewitt, *Acta Crystallogr., Sect. B*, 1969, **25**, 925.
14 G. Centi, S. Perathoner, F. Trifîro, A. Aboukais, C. F. Aissi and M. Guelton, *J. Phys. Chem.*, 1992, **96**, 2617.
15 T. Sen, P. R. Rajamohanan, S. Ganapathy and S. Sivasanker, *J. Catal.*, 1996, **354**, 163.
16 N. Das, H. Eckert, H. Huo, I. E. Wachs, J. F. Wolzer and J. G. Feher, *J. Phys. Chem.*, 1989, **93**, 6786.
17 S. Dzwigaj, M. J. Peltre, P. Massiani, T. Sen, S. Sivasanker, A. Davidson and M. Che, unpublished work.
18 M. A. Camblor, M. Costantini, A. Corma, L. Gilbert, P. Esteve, A. Martinez and S. Valencia, *Chem. Commun.*, 1996, 1339.

Received in Bath, UK, 30th June 1997; 7/04556E

Regioselective solvation in a polymeric lithium amide: remarkable twisted ladder structure of $[\{[PhCH_2N(H)Li]_2{\cdot}H_2NCH_2Ph\}_\infty]$

Alan R. Kennedy, Robert E. Mulvey* and Alan Robertson

Department of Pure and Applied Chemistry, University of Strathclyde, Glasgow, UK G1 1XL

The hemi-benzylamine complex of lithium benzylamide exists in the crystal as an infinite, twisted-ladder structure of fused $(NLi)_2$ rings; curiously, one edge of the ladder is solvated by benzylamine molecules, while the other is solvent-free.

Lithium amide molecules can self-assemble by the process known as 'ring-laddering' to generate ladder structures, as most recently demonstrated by the cyclic octameric ladder structure of $[\{Bu^tN(H)Li\}_8]$.[1] This primary amide represents a special case in being oligomeric, on account of the bulky steric nature of its alkyl group. Generally, the absence of solvating ligands is thought to encourage continuous ladder growth rendering many lithium amide compounds polymeric. These infinite ladder structures can be broken down to smaller, partially solvated, ladders of a finite length, when exposed to certain solvating ligands. As a rule, this partial solvation takes place at the ladder ends (outer rungs), *e.g.* as found in the pyrrolidide $[\{[H_2C(CH_2)_3NLi]_2{\cdot}tmeda\}_2]$;[2] inner-rung solvation,[3] as studied theoretically by *ab initio* MO calculations on the model ladder tetramers $[(H_2NLi)_4{\cdot}nH_2O]$ (n = 0, 2 or 4),[2] has a destabilising influence. To the best of our knowledge, the possibility of donor molecules selectively ligating the ladder framework, along one edge only, has never been considered previously. In this paper we present experimental proof of such in the remarkable twisted-ladder structure of $[\{[PhCH_2N(H)Li]_2{\cdot}H_2NCH_2Ph\}_\infty]$ **1**. What is more, the selective solvation is achieved without interrupting the infinite nature of the ladder arrangement, so providing a rare example of a crystallographically characterised polymeric lithium amide (a lithium thiolate with an infinite ladder structure of Li–S rungs has been reported[4]). This study represents the first structural investigation of a lithium (mono) benzylamide species, and it is apt that it should provide such an important finding since it follows over a decade of activity in dibenzylamido systems[5] which has contributed significantly to our basic understanding of alkali metal amide structural chemistry.

Solubility problems necessitated the deliberate use of excess benzylamine in the reaction sequence producing **1**. Pure solvent-free, lithium benzylamide, prepared by treating freshly distilled benzylamine (10 mmol) with Bu^nLi (10 mmol) under standard inert-atmosphere conditions, precipitated as a pink slurry from hexane, and could not be dissolved on addition of toluene. However, dissolution was achieved by introducing a second equivalent of benzylamine (10 mmol) dropwise and strongly heating the mixture. Pink delicate platelets of **1** crystallised on cooling the resulting solution to *ca.* −30 °C for 1 d (yield of first batch, 40%). On isolation from solution, the crystals collapse to a melt in a matter of hours. While the synthesis proved reproducible, different batches of **1** were found to contain various amounts of benzylamine and occasionally toluene, suggesting that the loss of crystallinity is due to the product losing these solvents with time.†

An X-ray diffraction study‡ revealed that **1** adopts an infinite ladder structure of fused $(NLi)_2$ rings, only one Li centre of which is solvated by a benzylamine molecule [Fig. 1(*a*)]. Therefore one ladder edge has unsolvated, three-coordinate, pyramidal Li centres [Li(3), Li(4)], while the other has solvated, four-coordinate, distorted-tetrahedral ones [Li(1), Li(2)]. The pattern of N–Li bond lengths reflects this coordinative inequality. Rungs involving Li(3), Li(4) are distinctly shorter than those involving Li(1), Li(2) (respective mean values; 1.996, 2.102 Å); edge lengths are also generally shorter for the former atoms (mean value, 2.055 Å; *cf.* 2.116 Å for the latter atoms), the exception being N(3)–Li(3) which is longer than its opposite edge [N(4)–Li(1)] although the difference [0.012(7)Å] is not statistically significant. Alternating above and below the ladder framework along one edge, the benzylamine molecules form relatively long bonds to Li (mean length, 2.130 Å). By failing to

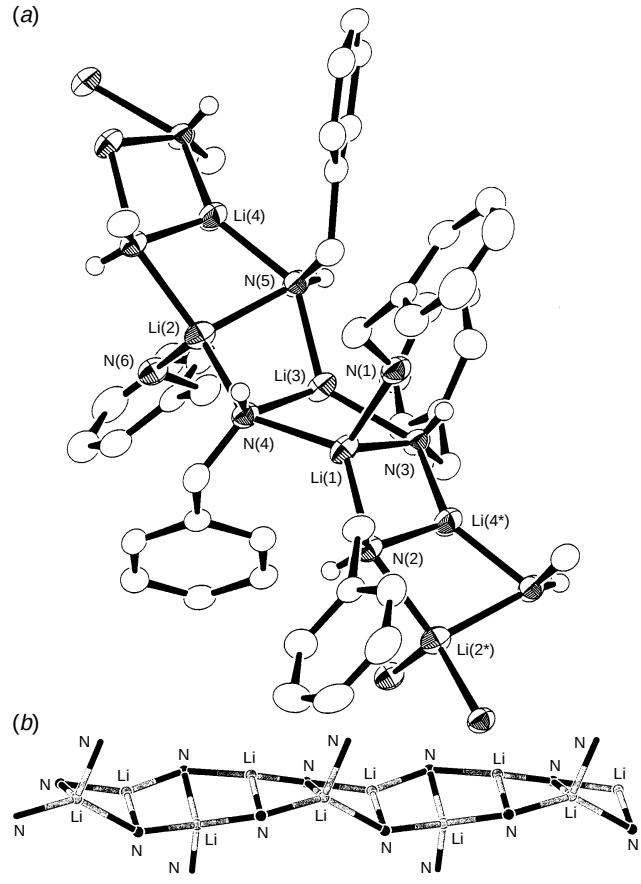

Fig. 1 (*a*) Section of the polymeric structure of **1** including the atom labelling scheme. Hydrogen atoms, apart from N–H ones, have been omitted for clarity. Selected bond lengths (Å) and angles (°): N(1)–Li(1) 2.135(5), N(2)–Li(1) 2.134(5), N(2)–Li(2*) 2.136(5), N(2)–Li(4*) 1.998(6), N(3) –Li(1) 2.102, N(3)–Li(3) 2.091(5), N(3*)–Li(4) 2.053(5), N(4)–Li(1) 2.079(5), N(4)–Li(2) 2.115(5), N(4)–Li(3) 1.993(5), N(5)–Li(2) 2.102(5), N(5)–Li(3) 2.060(5), N(5)–Li(4) 2.015(5) N(6)–Li(2) 2.125(5), N(2)–Li(1)–N(3) 104.4 (2), N(3)–Li(1)–N(4) 105.6(2), Li(1)–N(3)–Li(3) 69.7 (2), N(3)–Li(3)–N(4) 109.3 (2), N(4)–Li(3)–N(5) 104.0 (2), Li(1)–N(4)–Li(3) 72.0 (2), Li(2)–N(4)–Li(3) 73.5 (2), N(4)-Li(2)–N(5) 98.5 (2), N(5)–Li(2)–N(2*) 99.6 (2), Li(2)–N(5)–Li(3) 72.5 (2), Li(2)–N(5)–Li(4) 71.5 (2), N(5)–Li(4)–N(2*) 107.5 (2), N(2*)–Li(4)–N(3*) 111.4 (2), Li(2)–N(2*)–Li(4) 71.1 (2). (*b*) Stick drawing of a longer section of **1** emphasising the severe twisting within the ladder framework.

interrupt the laddering process and simply attaching itself to the ladder framework, this primary amine exhibits contrasting behaviour to that of the tertiary, chelating amines tmeda and pmdeta, which have been reported to break down (suspected) long ladders to finite ladders of limited length, *e.g.* as in $[\{[H_2C(CH_2)_3NLi]_2{\cdot}tmeda\}_2]$ and $[\{[H_2C(CH_2)_3NLi]_3{\cdot}pmdeta\}_2]$, respectively.[2] The four crystallographically distinct $(NLi)_2$ rings repeated throughout the ladder structure of **1** are non-planar. Two of them, Li(3)N(4)Li(2)N(5) and Li(2)N(5)-Li(4)N(2*), are much more distorted from planarity than the other pair, Li(1)N(2)Li(4*)N(3) and Li(1)N(3)Li(3)N(4) (respective summed bond angles: 348.5, 349.7, 356.6, 356.6°; respective mean rms deviations: 0.227, 0.212, 0.124, 0.123 Å); this factor contributes to the severe twisting within the ladder framework (symmetry code: * = $x + 1, y, z$). The twist is most pronounced at the solvated Li(2) centre [Fig. 1(*b*)]: considering only ladder framework N atoms, it is the most pyramidal of the Li centres [summed bond angle, 333.2°; *cf.* 337.9, 348.7 and 359.9° for Li(1), Li(3) and Li(4), respectively]; it also displays the smallest endocyclic N–Li–N bond angles (*i.e.* mean value, 99.1°; *cf.* range of others, 104.0–111.4°). Endocyclic angles at the N atoms cover a narrower range (69.7–73.5°) These five-coordinate N atoms have severely distorted trigonal bipyramidal geometries with the axial bonds positioned along the Li–N–Li ladder edges (range of axial bond angles, 137.0–143.3°). The benzylamine N atoms have distorted tetrahedral coordination geometries.

There is another unique feature to the ladder structure of **1**. The conformation of the bridging amido substituents ($PhCH_2$, H) with respect to the four-membered $(NLi)_2$ rings, alternates between *cisoid* and *transoid*. In the octamer $[\{Bu^tN(H)Li\}_8]$[1] the conformation is exclusively *cisoid* (the bulky alkyl substituents all project *exo* from the N_8Li_8 framework), and it is this feature which dictates that the ladder turns in on itself and cyclises. However, most discrete lithium amide ring dimers exhibit *transoid* set-ups. In the laddering principle,[6] it is reasoned that ladder structures have their origin in the lateral association of two or more dimeric rings of formula $(R^1R^2NLi)_2$, but the possible ring conformations involved were not considered. The next goal is therefore to establish a correlation between the *cisoid/transoid* nature of the constituent $(NLi)_2$ rings and the final shape and size of the ladder.

We thank the EPSRC (studentship to A. R.) for sponsoring this research.

Footnotes and References

* E-mail: r.e.mulvey@strath.ac.uk

† Satisfactory C, H, Li, N analyses. ^{1}H NMR (25 °C, 400 MHz, C_6D_6) δ −1.09 (t, NH), 0.30 (s, NH_2), 2.11 (s, CH_3, toluene) 3.67 (s, CH_2 amine), 4.18 (d, CH_2), 7.13 (br m, Ph).

‡ *Crystal data*: **1** $[C_{42}H_{50}Li_4N_6]_n$, monoclinic, space group $P2_1$, a = 7.638(3), b = 23.841(7), c = 10.532(4) Å, β = 92.78(3)°, U = 1915.6(10) Å^3, 7644 collected reflections, 6735 unique (R_{merge} = 0.039). Data collected at −150 °C on a Rigaku AFC7S diffractometer, λ = 0.710 69 Å, $2\theta_{max}$ = 50°. All reflections were collected with their Friedel mates. The absolute configuration could not be determined. Data was corrected for L_p effects only and then equivalent reflections were merged. Solution was by direct methods and Fourier techniques.[7] The H atoms bonded to N were refined isotropically but all other H atoms were placed in calculated positions. Final full-matrix least-squares refinement on F converged at R = 0.0514, R_w = 0.0586, S = 1.80 based on 5957 observations [$I > 2\sigma(I)$] and 485 parameters. All calculations were performed using the teXsan package. TeXsan, Crystal Structure Analysis Package, Molecular Structure Corp., 1993. CCDC 182/668.

1 N. D. R. Barnett, W. Clegg, L. Horsburgh, D. M. Lindsay, Q.-Y. Liu, F. M. Mackenzie, R. E. Mulvey and P. G. Williard, *Chem. Commun*., 1996, 2321.
2 D. R. Armstrong, D. Barr, W. Clegg, S. M. Hodgson, R. E. Mulvey, D. Reed, R. Snaith and D. S. Wright, *J. Am. Chem. Soc.*, 1989, **111**, 4719.
3 However, inner-solvation has been observed in the special case of the mixed-anion, four-rung, ladder structure of $[\{Pr^i_2N\text{-}Li{\cdot}[(Me_2NCH_2)_2CHOLi]\}_2]$: K. W. Henderson, D. S. Walther and P. G. Williard, *J. Am. Chem. Soc.*, 1995, **117**, 8680.
4 A. J. Banister, W. Clegg and W. R. Gill, *J. Chem. Soc., Chem. Commun.*, 1987, 850.
5 P. C. Andrews, D. R. Armstrong, D. R. Baker, R. E. Mulvey, W. Clegg, L. Horsburgh, P. A. O'Neil and D. Reed, *Organometallics*, 1995, **14**, 427.
6 D. R. Armstrong, D. Barr, W. Clegg, R. E. Mulvey, D. Reed, R. Snaith and K. Wade, *J. Chem. Soc., Chem. Commun.*, 1986, 869.
7 M. C. Burla, M. Camalli, G. Cascarano, C. Giacovazzo, G. Polidori, R. Spagna and D. Viterbo, *J. Appl. Crystallogr.*, 1989, **22**, 389.

Received in Cambridge, UK, 11th September 1997; 7/06615E

Sorbate–framework interactions as an aid to vibrational mode assignment: FT-Raman studies of ETS-10

Sunil Ashtekar,[a] A. M. Prakash,[b] Larry Kevan[b] and Lynn F. Gladden[a]

[a] *Department of Chemical Engineering, University of Cambridge, Pembroke Street, Cambridge, UK CB2 3RA*
[b] *Department of Chemistry, University of Houston, Houston, Texas 77204, USA*

***p*-Xylene–framework interactions enable identification of Ti–O stretch and three-membered ring structures in the FT-Raman spectrum of ETS-10.**

In recent years there has been increasing interest in the application of Raman spectroscopy and, in particular, FT-Raman techniques to the study of the structure of molecular sieve materials and adsorption processes within them.[1–3] However, the characterisation of aluminosilicate frameworks using FT-Raman spectroscopy remains limited by the intrinsically weak Raman effect associated with these materials. Further, there exists controversy as to the ability of the technique to identify specific structural units such as three-membered rings (3MR) within aluminosilicate and related frameworks. In this study we exploit the effect of sorbate–framework interactions on the frequency of the Raman bands characteristic of the framework structure to assign bands to specific stretches and structural units. In so doing we identify specific bands associated with 3MR structures. The framework structure considered here is the microporous titanosilicate ETS-10 which consists of corner-sharing tetrahedrally coordinated silicon and octahedrally coordinated titanium linked through bridging oxygens. The structure consists of 12-, 7-, 5- and 3-membered rings.[4,5] The main pore system is a three-dimensional 12-membered ring channel network and displays a considerable degree of disorder. Every titanium atom is connected to four silicon and two titanium atoms. Each TiO_6 unit carries a -2 charge that is balanced by extraframework cations such as Na^+ and K^+. $[TiO_6]^{2-}$ units are part of the 7- and 3-membered ring channels.

The ETS-10 sample used in the present work was synthesized using the procedure reported by Anderson *et al.*[4] Phase purity was checked by powder X-ray diffraction, which confirmed the absence of any TiO_2 impurity. Contamination of the sample with ETS-4 and AM-1 phase impurities was below that reported for the sample studied by Anderson *et al.*[5] Electron microprobe analysis performed on a JEOL JXA-8600 spectrometer showed that the Si/Ti ratio was 5 : 1, consistent with the previously reported composition of ETS-10.[5] The pure ETS-10 sample was calcined overnight at 500 °C in air prior to the FT-Raman experiment. A further sample containing 0.5 mmol *p*-xylene (g dry ETS-10)$^{-1}$ was also prepared; *p*-xylene was chosen because it demonstrates significant changes in polarisability during interaction with the ETS-10 framework whilst still being small enough to move easily within the micropore structure. The *p*-xylene/ETS-10 sample was prepared by evacuating the calcined ETS-10 material at 10^{-6} Torr at 200 °C for 12 h, the required sorbate loading was then introduced using a gravimetric technique. The sample was then equilibrated at 65 °C and held at this temperature for 12 h to ensure that the adsorbate was evenly distributed within the ETS-10 framework. Raman measurements were performed at room temperature on a Nicolet-Magna-IR 750 spectrometer equipped with a Raman module and an InGaAs detector. A Nd : YAG laser was used operating at a power of 200 mW at an excitation wavelength of 1064 nm. The resolution was 4 cm^{-1}. For each spectrum, 4000 scans were co-added giving a data acquisition time of *ca*. 2 h.

Fig. 1 shows the FT-Raman spectrum of ETS-10. A very high signal-to-noise ratio, consistent with the absence of a high fluorescence background, is observed indicative of the absence of any organic impurity as expected given that ETS-10 does not require an organic template for its synthesis and is synthesised in an environment totally free of organic species. Reviews of previously published Raman studies of aluminosilicate frameworks show the most prominent band to occur in the region between 300 and 550 cm^{-1} followed by weaker bands in the 700–900 and 1000–1200 cm^{-1} regions.[6] Bands in the 300–550 cm^{-1} region have been assigned to the motion of an oxygen atom in a plane perpendicular to the T–O–T (T=Si, Al) bonds.[1,2,7] The spectrum of ETS-10 exhibits a very strong peak at 726 cm^{-1} along with a small peak to its low frequency side at 639 cm^{-1}. Given that silicates have a relatively low Raman scattering cross-section, we assign the strong band at 726 cm^{-1} to the Ti–O stretch of the $[TiO_6]^{2-}$ rod structure present in the framework. This band was not observed in the FT-Raman spectrum of Ti-silicalite-1 (TS-1); we also note that the bands seen in the present study are not characteristic of the anatase or rutile phases of titania.[8] The spectrum also contains bands of low intensity at 987 and 1104 cm^{-1}, generally ascribed to the asymmetric stretching vibration of the Si–O bond.[3] Bands at 307, 427 and 539 cm^{-1} are assigned to the various T–O–T, O–T–O bending and skeletal deformation modes of the framework. The band at 539 cm^{-1} lies to higher frequency of the bands in the 470–510 cm^{-1} region characteristic of framework structures containing rings with four or more T atoms (T = Si, Al). Previous literature suggests that this band,

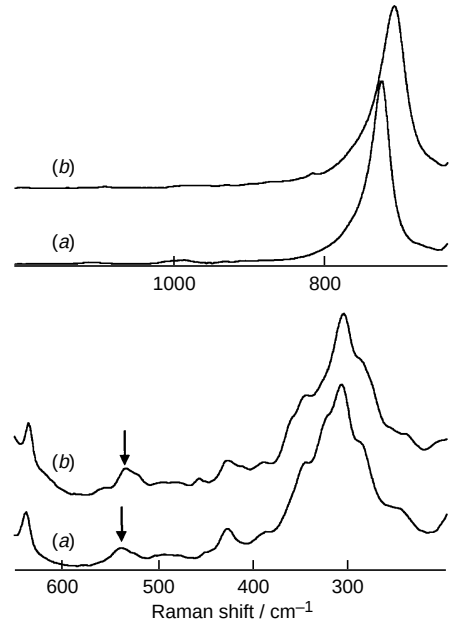

Fig. 1 FT-Raman spectra of (*a*) ETS-10 and (*b*) ETS-10 with a loading of *p*-xylene of 0.5 mmol (g dry ETS-10)$^{-1}$. The arrow indicates the band at 539 cm^{-1} in the pure ETS-10 spectrum.

as well as the band at 726 cm^{-1}, might be associated with 3MR structures. Assuming the correlation between average T–O–T (T=Si, Al) angle and Raman frequency to be valid,[2] and further that the same correlation applies to the case of the T atom being Si or Ti, a band at a frequency of 539 cm^{-1} would be consistent with a T–O–T bond angle of less than 138.1° and therefore consistent with the bond angle expected for a 3MR structure. An EXAFS analysis of ETS-10 has previously suggested a Ti–O–Si bond angle in ETS-10 of 130°.[9] Further, Annen and Davis[10] have suggested that if a band associated with a 3MR structure is observable it should occur in the frequency region of 550–800 cm^{-1}, the particular frequency being dependent upon the type of T-atoms that are contained within the ring. However, in their work no common vibrational bands assignable to 3MR structures were observed in the range of materials studied.

Assignment of the bands at 726 and 539 cm^{-1} to 3MR structures is obtained by consideration of the FT-Raman spectrum of *p*-xylene sorbed within the ETS-10 framework. Consider first the band at 726 cm^{-1} assigned to the Ti–O stretch; the Ti–O bond being part of a 3MR structure. The sorbed aromatic is expected to associate itself with the charged species within the ETS-10 framework, and this is reflected in a shift of 16 cm^{-1} in the Ti–O stretch to lower frequency upon *p*-xylene sorption. The observed shift can be interpreted as follows. The *p*-xylene must reside within the 12-membered ring channels, and will interact through the π-electrons with the Na^+/K^+ cations which are present in order to balance the −2 negative charge associated with each Ti atom.[9] The presence of sorbed *p*-xylene modifies the electrostatic interaction between the oxygens in the framework and the cations, thus causing the shift in Ti–O stretching frequency. We also note that there is a significant shift of the *p*-xylene C–H ring deformation mode from 1184 cm^{-1} in the pure liquid to 1193 cm^{-1} in the sorbed state, consistent with a strong sorbate–sorbent interaction.[11] A smaller shift in the 539 cm^{-1} band is observed again consistent with the 3MR structure, of which Ti is a constituent atom, being in close proximity to the sorbed *p*-xylene molecule; shifts in other bands are negligible.

Dr S. Ashtekar thanks BNFL for financial support. Drs A. M. Prakash and L. Kevan thank the US National Foundation and the Robert A. Welch Foundation for support. We also wish to thank Dr D. W. Lewis and Dr P. J. Barrie for their help in the preparation of this manuscript.

Footnote and References

* E-mail: Gladden@cheng.cam.ac.uk

1 P. K. Dutta, D. C. Shieh and M. Puri, *Zeolites*, 1988, **8**, 306.
2 P. K. Dutta, K. M. Rao and J. Y. Park, *J. Phys. Chem.*, 1991, **95**, 6654.
3 P. Knops-Gerrits, D. E. deVos, E. J. P. Feijen and P. A. Jacobs, *Microporous Mater.*, 1997, **8**, 3.
4 M. W. Anderson, O. Terasaki, T. Ohsuna, A. Philippou, S. P. MacKay, A. Ferreira, J. Rocha and S. Lidin, *Nature*, 1994, **367**, 347.
5 M. W. Anderson, O. Terasaki, T. Ohsuna, P. J. O. Malley, A. Philippou, S. P. MacKay, A. Ferreira, J. Rocha and S. Lidin, *Philos. Mag. B*, 1995, **71**, 813.
6 C. Bremard and D. Bougeard, *Adv. Mater.*, 1995, **7**, 10.
7 W. Pilz, *Z. Phys. Chem.* (*Leipzig*), 1990, **271**, 219.
8 *The Handbook of Infrared and Raman Spectra of Inorganic Salts*, ed. R. A. Nyquist, C. L. Putzig and A. A. Leugers, Academic Press, San Diego, 1996, vol. 2, pp. 102–103.
9 G. Sankar, R. G. Bell, J. M. Thomas, M. W. Anderson, P. A. Wright and J. Rodia, *J. Phys. Chem.*, 1996, **100**, 449.
10 M. J. Annen and M. E. Davis, *Microporous Mater.*, 1993, **1**, 57.
11 J.-L. Guth, P. Jaques, F. Stoessel and R. Wey, *J. Colloid Interface Sci.*, 1980, **76**, 298.

Received in Cambridge, UK, 9th September 1997; 7/06563I

Insertion of manganese into a C–S bond of dibenzothiophene: a model for homogeneous hydrodesulfurization

Xiao Zhang,[a] Conor A. Dullaghan,[a] Gene B. Carpenter,[a] Dwight A. Sweigart*[a] and Qingjin Meng[b]

[a] *Department of Chemistry, Brown University, Providence, Rhode Island 02912, USA*
[b] *Coordination Chemistry Institute, State Key Laboratory of Coordination Chemistry, Nanjing University, Nanjing 210093, PR China*

Coordination of $Mn(CO)_3^+$ to a carbocyclic ring of dibenzothiophene activates a C–S bond to reductive cleavage, affording a novel tetramanganese metallathiacycle 5 that reacts with H_2 to form a dimanganese complex 9 containing bridging hydride and thiolate ligands; methylation of 5 followed by hydrogenation results in desulfurization of the dibenzothiophene and formation of $[Mn(CO)_5(SMe)]$.

Much of the research in the field of catalytic hydrodesulfurization (HDS) has focused on the problem of sulfur removal from thiophenic molecules.[1] Benzothiophene (BT) and dibenzothiophene (DBT) are of particular interest in this regard because their substituted derivatives are difficult to desulfurize and, as a consequence, are relatively abundant in fossil fuels.[2] A key step in HDS is cleavage of the C–S bonds by insertion of a metal. A recent study indicates that the energy barrier to metal insertion is considerably greater for DBT than for BT, or for thiophene itself.[3] This higher barrier to C–S cleavage in DBT (which is probably steric in origin) most likely accounts for the relatively small number of published reports of metal insertion into DBT to give metallathiacycle **1**. Nevertheless, there are reports of metal-promoted scission of the C–S bonds in DBT to give characterizable organometallic products with systems based on Rh, Ir, Pt and Co.[3,4] We recently showed[5,6] that precoordination of a $Mn(CO)_3^+$ fragment to the carbocyclic ring in BT or the η^5 π-system of thiophene activates the C–S bonds to facile electron-transfer induced cleavage, affording the bimetallic metallathiacycles **2** and **3**, respectively. Here, we show that a C–S bond in the dibenzothiophene complex $[(\eta^6\text{-DBT})Mn(CO)_3]^+$ **4** is also activated and that chemical reduction leads (in part) to the novel metallathiacycle **5**, the multimetallic nature of which may be relevant to hydrogenolysis and desulfurization reactions occurring with industrial heterogeneous HDS catalysts (Mo/Co, *etc.*).[7] The reactions of **5** with H_2 and electrophilic reagents were investigated and are described below.

Reduction of **4**$[BF_4]$[8] with cobaltocene or Na/Hg produced as the major product an isomeric mixture of the yellow bis(cyclohexadienyl) complexes $[(\eta^5\text{-DBT})Mn(CO)_3]_2$, an example of which is shown as structure **6**.† Isomers of **6** occur because the dienyl rings can couple at various sites. Analogous ring-coupled dimeric cyclohexadienyl complexes are known to result from the reduction of $[(arene)Mn(CO)_3]^+$ (arene = benzene, mesitylene).[9] Far more interesting is a dark red minor product that was isolated† and shown by X-ray crystallography to be **5**.‡ The yield of **5** was only *ca.* 10%, but this improved to > 20% when $[Mn_2(CO)_{10}]$ was added to the reaction mixture. The structure of **5**, illustrated in Fig. 1, shows that precoordination of $Mn(CO)_3^+$ to a carbocyclic ring of DBT provides sufficient activation so that manganese can insert into the adjacent C–S bond. The transformation **4** → **5** is initiated by electron transfer, probably by a mechanistic pathway that depends on the known[10] ease with which ring slippage and arene ligand displacement occur with conjugated polyarene complexes of $Mn(CO)_3^+$.

A novel feature of **5** is the coordination of the sulfur to three metal atoms. The sulfur atom in the metallathiacyclic ring acts as a bridging ligand to $Mn_2(CO)_8$, in analogy to the bridging sulfur in $[Mn_2(CO)_8\{S(CH_2)_4\}]$, which is obtained by the reaction of tetrahydrothiophene and $[Mn_2(CO)_{10}]$.[11] Thus, the sulfur atom in **5** has significantly enhanced donor properties in comparison to the sulfur in free DBT. An attempt was made to remove the $Mn_2(CO)_8$ fragment from **5** by ligand substitution with CO at room temp., but this was unsuccessful. However, treatment of **5** in CH_2Cl_2 with HBF_4 in CH_2Cl_2 led to a change from red to yellow; after chromatography on neutral alumina, a low yield (17%) of a thermally unstable red complex was obtained that is assigned structure **7** based on comparison of spectroscopic data to that of **2** (R = H). It is likely that the initial yellow product in this reaction contained a protonated sulfur, which converted to **7** during the chromatographic procedure. In a similar vein, the reaction of **5** with methyl triflate afforded a good yield of the methylated complex **8**.§ An X-ray structural study of **8**$[CF_3SO_3]$ was plagued by disorder in the triflate anion, but the data were sufficient to establish the structure unequivocally.¶ Complex **5** has a highly non-planar metallathiacyclic ring. The twist angle between the arene rings in **5**, as measured by the C(2)–C(3)–C(9)–C(8) torsion angle, is

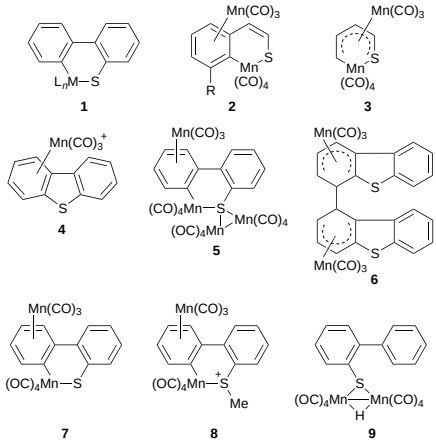

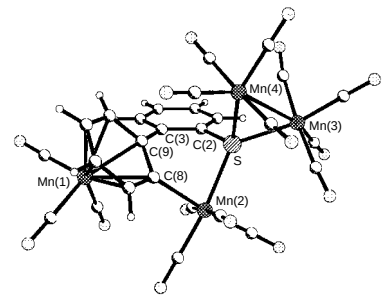

Fig. 1 Crystal structure of **5**. Selected bond distances (Å) and angles (°): Mn(2)–S 2.408(1), Mn(2)–C(8), 2.095(4), Mn(3)–S 2.301(1), Mn(4)–S 2.320(1), Mn(3)–Mn(4), 2.773(1), C(2)–S 1.804(4), C(2)–C(3) 1.394(6), C(3)–C(9) 1.499(6), C(8)–C(9) 1.447(6), S–Mn(3)–Mn(4) 53.43(3), Mn(3)–S–Mn(4) 73.76(4), S–Mn(4)–Mn(3) 52.81(3), S–Mn(2)–C(8) 80.82(11).

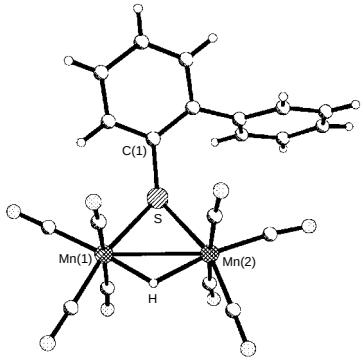

Fig. 2 Crystal structure of **9**. Selected bond distances (Å) and angles (°): Mn(1)–S 2.315(14), Mn(2)–S 2.346(2), Mn(1)–H 1.66(4), Mn(2)–H 1.75(4), Mn(1)–Mn(2) 2.883(1), S–C(1) 1.801(5), Mn(1)–S–Mn(2) 75.71(4), Mn(1)–H–Mn(2) 115(2). The twist angle between the arene rings in the thiolate ligand is 54°.

47.1(6)° and is somewhat larger than the 30–40° range found by Myers *et al.*[4j] for a series of dibenzothiophenes having the (η-C_5Me_5)Rh(PMe_3) fragment inserted into a C–S bond.

Reaction of **5** with H_2 at 500 psi and 97 °C for 3 h led to clean hydrogenolysis of the Mn–C σ-bond to afford complex **9**, which features bridging hydride and biphenyl thiolate ligands, and a Mn–Mn bond.‖ The structure and relevant intramolecular parameters for **9** are given in Fig. 2.** Interestingly, the bimetallic structural unit Mn_2(H)(SR) found in **9** also forms when the manganese thiophene and benzothiophene bimetallics **2** and **3** are hydrogenated.[5b,12] Analogous bridging species containing the fragment Ir_2(H)(SR) and RhW(H)(SR) have very recently been reported in model HDS studies of thiophene and benzothiophene complexes.[7c,13] The structural unit M_2(H)(SR) is significant because of a possible relationship to species occurring on the surface of heterogeneous HDS catalysts.[7,13] Preliminary hydrogenation experiments with **8** under conditions similar to those used with **5** gave [$Mn(CO)_5$(SMe)] rather than **9** as the major organometallic product.†† This shows that complete desulfurization of DBT can be achieved by alkylation of the multimetallic intermediate **5** (or **7**).

In conclusion, we have demonstrated that coordination of $Mn(CO)_3^+$ to a carbocyclic ring of dibenzothiophene activates a C–S bond to reductive cleavage, affording the tetrametallic species **5**. Hydrogenation of **5** produces the bridging hydride **9**, while methylation of **5** followed by hydrogenation results in desulfurization of the DBT with the concomitant formation of [$Mn(CO)_5$(SMe)].

This work was supported by grants from the National Science Foundation (CHE-9400800 and 9705121) and the Petroleum Research Fund, administered by the American Chemical Society.

Footnotes and References

* E-mail: Dwight_Sweigart@Brown.edu

† Cobaltocene (47 mg, 0.249 mmol) was added to a suspension of **4**[BF_4] (105 mg, 0.256 mmol) in CH_2Cl_2 (5 ml) and the mixture stirred under N_2 for 30 min at room temp. The solvent was then stripped and the residue chromatographed on deactivated neutral alumina with pentane to elute [$Mn_2(CO)_{10}$], free DBT and unidentified trace products, then with Et_2O to elute **6** (and its isomers, collectively labeled '**6**'), and finally with CH_2Cl_2 to elute **5**. The isolated yields of **6** and **5** were 45 and 5 mg, respectively. When [$Mn_2(CO)_{10}$] was added to the reaction mixture (215 mg, 0.551 mmol), the yield of **5** increased to 20 mg. The presence of an atmosphere of CO had no discernable effect on the product distribution. IR, NMR, MS and elemental analysis data for **5**–**9** and [$Mn(CO)_5$(SMe)] are available upon request from the authors.

‡ Crystal dimensions 0.11 × 0.20 × 0.34 mm, crystal system triclinic, space group $P\bar{1}$, a = 10.0482(3), b = 10.1494(3), c = 16.3738(5) Å, α = 73.532(1), β = 78.792(1), γ = 78.268(1)°, U = 1551.19(8) Å^3, Z = 2, D_c = 1.765 g cm^{-3}, μ = 1.730 mm^{-1}, θ range 2.09–26.45°, 424 variables refined with 6139 independent reflections to final R indices [$I > 2\sigma(I)$] of R = 0.0587 and wR_2 = 0.1160 and GOF = 1.113. CCDC 182/678.

§ Methyl triflate (100 μl, 0.883 mmol) was added to **5** (22 mg, 0.027 mmol) in CH_2Cl_2 (5 ml) and the solution was stirred for 18 h at room temp. under N_2, during which time it changed from red to yellow. The solution was then filtered through cotton wool and concentrated. Diethyl ether was added to precipitate the product as a yellow powder in a yield of 86% (15 mg, 0.023 mmol).

¶ The crystal structure of **8**[CF_3SO_3] was determined as described in footnote ‡. However, owing to low intensities and disorder in the triflate anion, the structure refined only to R = 0.140. Nevertheless, the atom connectivity indicated in structure **8** is unequivocal.

‖ Complex **5** (25 mg, 0.030 mmol) in dry CH_2Cl_2 (2 ml) was placed in a Parr bomb and treated with H_2 at 500 psi and 97 °C for 3 h. (A gas mixture consisting of 95% H_2 and 5% CO gave the same results.) After cooling to room temp., the product was purified by TLC on silica gel with pentane eluent. A bright yellow band separated cleanly, from which **9** was isolated in 87% yield (13.8 mg, 0.0265 mmol) as a yellow oil.

** Crystal dimensions 0.22 × 0.14 × 0.09 mm, crystal system triclinic, space group $P\bar{1}$, a = 7.1767(1), b = 15.3254(1), c = 19.6549(1), α = 90.363(1), β = 93.210(1), γ = 95.236(1)°, U = 2149.21(3) Å^3, Z = 4, D_c = 1.608 g cm^{-3}, μ = 1.316 mm^{-1}, θ range 1.68 to 24.83°, 567 variables refined with 7224 independent reflections to final R indices [$I > 2\sigma(I)$] of R = 0.0549 and wR_2 = 0.0889, and GOF = 1.005.

†† Complex **8** in CH_2Cl_2 was pressurized to 550 psi with H_2–CO (95 : 5) at 97 °C for 9 h. After solvent removal, the product, [$Mn(CO)_5$(SMe)], was extracted into hexanes.

1 R. A. Sanchez-Delgado, *J. Mol. Catal.*, 1994, **86**, 287; R. J. Angelici, *Bull. Soc. Chim. Belg.*, 1995, **104**, 265; A. N. Startsev, *Catal. Rev. Sci. Eng.*, 1995, **37**, 353; C. Bianchini and A. Meli, *J. Chem. Soc., Dalton Trans.*, 1996, 801.
2 C. Willey, M. Iwao, R. N. Castle and M. L. Lee, *Anal. Chem.*, 1981, **53**, 400; T. Kabe, A. Ishihara and H. Tajima, *Ind. Eng. Chem. Res.*, 1992, **31**, 1577.
3 C. Bianchini, D. Fabbri, S. Gladiali, A. Meli, W. Pohl and F. Vizza, *Organometallics*, 1996, **15**, 4604.
4 (*a*) K. M. Rao, C. L. Day, R. A. Jacobson and R. J. Angelici, *Inorg. Chem.*, 1991, **30**, 5046; (*b*) W. D. Jones and L. Dong, *J. Am. Chem. Soc.*, 1991, **113**, 559; (*c*) J. Chen, Y. Su, R. A. Jacobson and R. J. Angelici, *J Organomet. Chem.*, 1992, **428**, 415; (*d*) W. D. Jones and R. M. Chin, *J. Organomet. Chem.*, 1994, **472**, 311; (*e*) J. J. Garcia, B. E. Mann, H. Adams, N. A. Bailey and P. M. Maitlis, *J. Am. Chem. Soc.*, 1995, **117**, 2179; (*f*) C. Bianchini, M. V. Jimenez, A. Meli, S. Moneti, F. Vizza, V. Herrera and R. A. Sanchez-Delgado, *Organometallics*, 1995, **14**, 2342; (*g*) C. Bianchini, M. V. Jimenez, A. Meli, S. Moneti and F. Vizza, *J. Organomet. Chem.*, 1995, **504**, 27; (*h*) C. Bianchini, J. A. Casares, M. V. Jimenez, A. Meli, S. Moneti, F. Vizza, V. Herrera and R. Sanchez-Delgado, *Organometallics*, 1995, **14**, 4850; (*i*) C. Bianchini and A. Meli, *J. Chem. Soc., Dalton Trans.*, 1996, 801; (*j*) A. W. Myers and W. D. Jones, *Organometallics*, 1996, **15**, 2905.
5 (*a*) C. A. Dullaghan, S. Sun, G. B. Carpenter, B. Weldon and D. A. Sweigart, *Angew. Chem., Int. Ed. Engl.*, 1996, **35**, 212; (*b*) S. Sun, C. A. Dullaghan and D. A. Sweigart, *J. Chem. Soc., Dalton Trans.*, 1996, 4493.
6 C. A. Dullaghan, X. Zhang, Q. Meng, D. Walther, G. B. Carpenter and D. A. Sweigart, *Organometallics*, in press.
7 (*a*) J. Chen, L. M. Daniels and R. J. Angelici, *J. Am. Chem. Soc.*, 1991, **113**, 2544; (*b*) K. M. K. Dailey, T. B. Rauchfuss, A. L. Rheingold and G. P. A. Yap, *J. Am. Chem. Soc.*, 1995, **117**, 6396; (*c*) C. Bianchini, M. V. Jimenez, C. Mealli, A. Meli, S. Moneti, V. Patinec and F. Vizza, *Angew. Chem., Int. Ed. Engl.*, 1996, **35**, 1706.
8 J. D. Jackson, S. J. Villa, D. S. Bacon, R. D. Pike and G. B. Carpenter, *Organometallics*, 1994, **13**, 3972.
9 M. V. Gaudet, A. W. Hanson, P. S. White and M. J. Zaworotko, *Organometallics*, 1989, **8**, 286; R. L. Thompson, S. J. Geib and N. J. Cooper, *J. Am. Chem. Soc.*, 1991, **113**, 8961; S. Lee, S. R. Lovelace, D. J. Arford, S. J. Geib, S. G. Weber and N. J. Cooper, *J. Am. Chem. Soc.*, 1996, **118**, 4190.
10 S. Sun, L. K. Yeung, D. A. Sweigart, T.-Y. Lee, S. S. Lee, Y. K. Chung, S. R. Switzer and R. D. Pike, *Organometallics*, 1995, **14**, 2613; S. Sun, C. A. Dullaghan, G. B. Carpenter, A. L. Rieger, P. H. Rieger and D. A. Sweigart, *Angew. Chem., Int. Ed. Engl.*, 1995, **34**, 2540.
11 E. Guggolz, K. Layer, F. Oberdorfer and M. Z. Ziegler, *Z. Naturforsch., Teil B*, 1985, **40**, 77.
12 C. A. Dullaghan, G. B. Carpenter, D. A. Sweigart, D. S. Choi, S. S. Lee and Y. K. Chung, *Organometallics*, in press; X. Zhang, C. A. Dullaghan, G. B. Carpenter and D. A. Sweigart, unpublished work.
13 D. A. Vicic and W. D. Jones, *Organometallics*, 1997, **16**, 1912.

Received in Bloomington, IN, USA, 19th August 1997; 7/06096C

The first sandwich silver cluster of a trinuclear cyclic gold(I) complex

Alfredo Burini,*[a] John P. Fackler, Jr.,*[b] Rossana Galassi,[a] Bianca R. Pietroni[a] and Richard J. Staples[c]

[a] *Dipartimento di Scienze Chimiche dell'Universita, via S. Agostino 1, I-62032 Camerino, Italy*
[b] *Department of Chemistry and Laboratory for Molecular Structure and Bonding, Texas A & M University, College Station, Texas 77843-3255, USA*
[c] *Department of Chemistry and Chemical Biology, Harvard University, 12 Oxford Street, Cambridge, MA 02138, USA*

A new type of metal sandwich structure [Ag{[Au(μ-N^3,C^2-bzim)]$_3$}$_2$]BF_4·CH_2Cl_2 1, is formed by reacting the neutral, triangular cluster [Au(μ-N^3,C^2-bzim)]$_3$ with Ag^+; these units stack with two short intermolecular Au···Au distances of *ca.* 3.2 Å.

In 1970 Vaughan[1] reported the synthesis of organogold derivatives of the 2-pyridyl ligands that were thought to be trinuclear cyclic gold(I) species, based upon the coordination requirements of the gold(I) atoms. In the following years analogous compounds were isolated and depending upon the types of 1,2 bridging ligands, N–Au–C^2 or N–Au–N^3 arrangements were described. Some of these were structurally characterized.[4] The structures all have nine-atom rings where the intramolecular Au···Au distances range between 3.224(1) and 3.368(1) Å. Only weak metal–metal interactions are present, hence these compounds are classified as polynuclear non-cluster species.

Reactivity investigations of these trimeric gold(I) complexes indicate that the bridging ligand plays an important role. While the carbeniato gold(I) derivatives undergo stepwise oxidative halogen addition to form three distinct complexes, [AuC(O-Me)=NMe]$_3X_n$ (n = 2,4, 6; X = Br, I),[5] the pyrazolato trimers [Au(μ-3.5-R_2pz)$_3$} (R = alky1, aryl) only oxidized at one center yielding mixed valence $Au^I_2Au^{III}$ complexes: [Au(μ-3,5-R_2pz)]$_3I_2$;[6] [Au(μ-3,5-Ph_2-4-Cl-pz)]$_3Cl_2$.[7] Additionally, [Au(μ-N^3,C^2-bzim)]$_3$ (N^3,C^2-bzim = 1-benzylimidazolate) also undergoes oxidation by only 1 equiv. of I_2 yielding the mixed-valence complex [Au(μ-N^3,C^2-Bzim)]$_3I_2$.[8] However, this complex can be oxidized completely to a Au^{III} derivative [Au(μ-N^3,C^2-bzim)]$_3C1_6$[9] by $SOCl_2$.

While reactions of metal ions such as $AuPPh_3^+$, $Ag(PPh_3)_2^+$ or Ag^+ with transition metal clusters represent a well known method for cluster expansion synthesis,[10] few examples of the addition of metal ions to dinuclear gold(I) complexes have been reported.[11] An addition strategy has not been reported at all for cyclic trimer gold(I) compounds. Here we describe the results of the reaction of [Au(μ-N^3,C^2-bzim)]$_3$ with Ag^+ to produce a novel[12] silver sandwich cluster [Ag{[Au(μ-N^3,C^2-bzim)]$_3$}$_2$]$^+$. By layering a solution of $AgBF_4$ in MeCN over a CH_2Cl_2 solution of [Au(μ-N^3,C^2-bzim)]$_3$, a yellow luminescent† precipitate was formed immediately in almost quantitative yield. After several months, the precipitate, standing in contact with the solvent was completely transformed into small yellow crystals of the cluster [Ag{[Au(μ-N^3,C^2-bzim)]$_3$}$_2$]BF_4·CH_2Cl_2 **1**. The compound is stable in the solid state‡ but dissolution in a coordinating solvent like Me_2SO yields the starting materials as determined by NMR spectroscopy.

The molecular structure§ of the cation **1** is shown in Fig. 1 while Fig. 2 presents the stacking arrangement observed. The naked silver ion center is bonded to six gold atoms to form a distorted, Ag^I centered trigonal prism of Au^I atoms with Ag–Au distances ranging from 2.731(2) to 2.922(2) Å, indicative of appreciable metal–metal bonding. These distances are close to distances observed in other gold–silver derivatives[11] wherein the silver atoms bridging two gold centers are always supported by other ancillary ligands.

The gold–silver bonds may be regarded as arising from a nucleophilic or Lewis base interaction of the gold atoms with the silver ion, which acts as a Lewis acid. The d^{10}–d^{10} closed shell Au^I–Ag^I bonds probably also relate to the weak Au···Au bonds, estimated to be 6–8 kcal mol^{-1} (1 cal = 4.184 J), which arise from correlation and relativistic effects.[13] The average Au···Au intramolecular distance in the cyclic trimer moiety

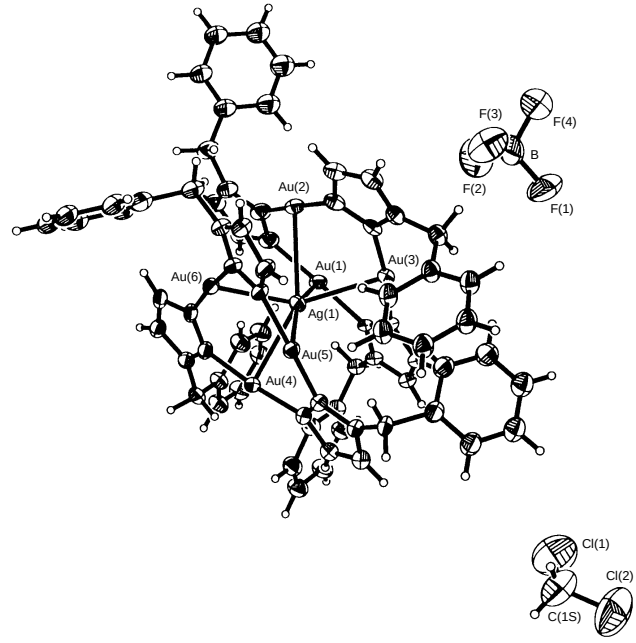

Fig. 1 Thermal ellipsoid drawing (50% probability) of the structure of [Ag{[Au(μ-N^3,C^2-bzim)]$_3$}$_2$]BF_4·CH_2Cl_2 **1**. The Ag–Au distances range from 2.731(2) to 2.922(2) Å.

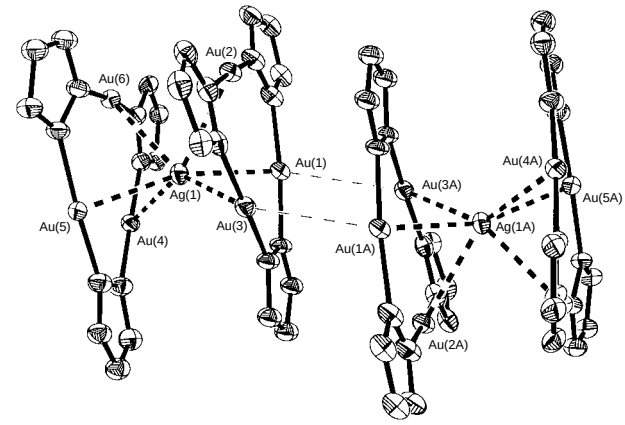

Fig. 2 Stacked sandwich structure of the cation of [Ag{[Au(μ-N^3,C^2-bzim)]$_3$}$_2$]BF_4·CH_2Cl_2 **1**. The intermolecular Au(1)···Au(3A) distance is 3.268(2) Å.

forming the sandwich unit is 3.19 Å. This is shorter than the distance observed for $Au^{I}\cdots Au^{I}$ in $[Au(\mu\text{-}N^3,C^2\text{-Bzim})]_3I_2$.[8]

In Fig. 2, the interactions between two close sandwich units can be seen. The short distances Au(3)···Au(1A) 3.268 Å and Au(4)···Au(5A) 3.116 Å, are indicative of weak intermolecular bonds between gold atoms. Considering also the atoms Au(2) and Au(2A) which are widely separated, a characteristic Au_6 cycle is formed in a chair conformation. This arrangement also was observed in the carbeniato trimer $[AuC(OEt)=NC_6H_4Me]_3$ structure.[4] The inter- and intra-molecular interactions present in **1** result in the formation of an infinite chain of gold–silver atoms which are expected to show interesting properties as observed for molecular chain compounds such as $[Rh_6(MeCN)_4]^{9+}$.[14]

In cluster **1** the bridging imidazole rings show C–Au and N–Au distances of *ca.* 2.0 Å, similar to distances found in $[Au(\mu\text{-}N^3,C^2\text{-bzim})]_3I_2$.[8] Three of the N–Au–C angles show significant distortions from linearity, namely N(1)–Au(1)–C(9) [173.9(8)], N(3)–Au(3)–C(5) [172.9(7)] and N(6)–Au(6)–C(17) [172.9(7)]. This distortion could be a result of the interaction of the silver atom with the gold atoms. Further investigations into the reactivity of other trinuclear cyclic gold(I) complex with electrophilic metal ions are underway.

The studies at the University of Camerino have been supported by MURST while those at Texas A&M University have been supported by the Robert A. Welch Foundation.

Footnotes and References

* E-mail: fackler@chemxx.TAMU.edu

† Luminescence studies will be reported elsewhere.

‡ Anal. Found; C, 30.83; H.2.61; N, 6.65. Calc. for $C_{61}H_{56}AgAu_6BC1_2F_4N_{12}$; C, 30.47; H, 2.35; N, 6.99%.

§ *Crystal data* for 1; $C_{61}H_{56}AgAu_6BC1_2F_4N_{12}$, M = 2404.57; triclinic, space group $P\bar{1}$, a = 14.4505(1), b = 15,098(2), c = 15.9571(1) Å, α = 106.189(3), β = 103.551(5), γ = 101.310(5)°, U = 3120.3(5) Å^3, Z = 2, D_c = 2.547 g cm^{-3}, F(000) 2192, λ = 0.710 73 Å , T = 213(2) K, crystal size = 0.15 × 0.10 × 0.05 mm.

Data were collected using a Siemens SMART CCD (charge coupled device) based diffractometer equipped with an LT-2 low temperature apparatus operating at 213 K. A total of 13 371 reflections were collected using ω scans with 1.40 < 2θ < 22.50°. Of these 8077 were unique (R_{int} = 0.0503 after absorption correction applied, based on ψ scans, $T_{min,max}$ 0.9361, 0.6366). The structure was solved by the direct method using the SHELXS-97 program and refined by least squares methods on F^2. SHELXL-97[16] incorporated in SHELXTL-PC V 5.03.[17] All non-hydrogen atoms were refined anisotropically. Hydrogens were calculated by geometrical methods and refined as a riding model. The crystal used for the diffraction study showed no decomposition during data collection. The refinement converged at R_1 = 0.0583 [$I > 2\sigma(I)$] and wR_2 = 0.1217 (all data). The final difference map showed no peak greater than + 0.639 e Å^{-3} and no hole larger than −0.454 e Å^{-3}. CCDC 182/688.

1 L. G. Vaughan, *J. Am. Chem. Soc.*, 1970, **11**, 730.
2 G. Minghetti and F. Bonati, *Angew. Chem., Int. Ed. Engl*., 1972, **11**, 429; F. Bonati, A. Burini, B. R. Pietroni and B. Bovio, *J. Organomet. Chem*., 1989, **375**, 147.
3 F. Bonati, G. Minghetti and G. Banditelli, *J. Chem. Soc., Chem. Commun.*, 1974, 88.
4 A. Tiripicchio, M. Tiripicchio Camellini and G. Minghetti, *J. Organomet. Chem*., 1979, **171**, 399 ([AuC(OEt)=NC$_6$H$_4$Me-*p*]$_3$ structure); H. H. Murray, R. G. Raptis and J. P. Fackler, Jr., *Inorg. Chem*., 1988, **27**, 26; B. Bovio, F. Bonati and G. Banditelli, *Inorg. Chim. Acta*, 1984, **87**, 25.
5 A. L. Balch and D. J. Doonan, *J. Organomet. Chem*., 1977, **131**, 137
6 G. Minghetti, G. Banditelli and F. Bonati, *Inorg. Chem*., 1979, **18**, 658.
7 R. G. Raptis and J. P. Fackler, Jr., *Inorg. Chem.*, 1990, **21**, 5003.
8 B. Bovio, S. Calogero, F. E. Wagner, A. Burini and B. R. Pietroni, *J. Organomet. Chem*., 1994, **470**, 275.
9 F. Bonati, A. Burini, B. R. Pietroni and B. Bovio, *J. Organomet. Chem*., 1991, **408**, 271.
10 D. M. P. Mingos and M. J. Watson, *Adv. Inorg. Chem.*, 1992, **39**, 327; D. V. Toronto and A. L. Balch, *Inorg. Chem*., 1994, **33**, 6132; L. Hao, J. Vittal and R. J. Puddephatt, *Inorg. Chem.*, 1996, **35**, 269; A. D. Burrows, A. A. Gosden, C. M. Hill and D. M. P. Mingos, *J. Organomet, Chem*., 1993, **452**, 251; C. W. Liu, C. J. McNeal and J. P. Fackler, Jr., *J. Cluster Sci.*, 1996, **7**, 385.
11 R. Uson, A. Laguna and M. Laguna, *J. Chem. Soc., Chem. Commun*., 1981, 1097; J. Vincente, M. T. Chicote and M. C. Lagunas, *Inorg. Chem.*, 1993, **32**, 3748; M. Cantel, J. Garrido, M. C. Gimeno, J. Jimenez, P. G. Jones, A. Laguna and M. Laguna, *Inorg. Chim. Acta*, 1997, **254**, 157.
12 M. F. Hallam, D. M. P. Mingos, T. Adatia and M. McPartin, *J. Chem. Soc., Dalton Trans.*, 1988, 335. This paper describes some related Cu, Ag and Hg metal sandwich compounds of trinuclear Pt clusters.
13 H. Schmidbaur, *Gold Bull*., 1990, **23**, 11.
14 G. M. Finniss, E. Canadell, C. Campana and K. R. Dunbar, *Angew. Chem., Int. Ed. Engl*., 1996, **35**, 2772.
15 G. M. Sheldrick, SHELXS-90, Program for the Solution of Crystal Structures, University of Göttingen, Germany, 1993.
16 G. M. Sheldrick, SHELXL-97, Program for the Refinement of Crystal Structure, University of Göttingen, Germany, 1997.
18 SHELTXTL 5.03 (PC-Version), Program library for Structure Solution and Molecular Graphics, Siemens Analytical Instrument Division, Madison, WI, 1995.

Received in Bloomington, IN, USA, 18th September 1997; 7/06795J

Catalytic hydroxylation of alkanes by immobilized mononuclear iron carboxylate

Keiji Miki* and Takeshi Furuya

National Institute for Resources and Environment, 16-3 Onogawa, Tsukuba, Ibaraki 305, Japan

Mononuclear iron carboxylate complex immobilized and isolated on a modified silica surface (1) catalyzes oxidation of hexane to a mixture of hexan-1-ol, -2-ol and -3-ol without ketone formation in the presence of mercaptan, acetic acid, triphenylphosphine and O_2 at ambient conditions.

Biomimetic oxidation studies on non-heme iron enzymes have been extensively reported for the direct hydroxylation of saturated hydrocarbons at ambient conditions.[1,2] Most of the efforts have been focused on the modeling of dinuclear iron complexes, because of the structural correspondence to the active site of methane monooxygenase (MMO). In this report we describe a novel catalytic oxidation yielding only alcohols from alkanes by mononuclear iron carboxylate complex immobilized and isolated on a modified silica surface (**1**) in the presence of mercaptan (propane-1,3-dithiol, PDT), acetic acid (AcOH), triphenylphosphine (PPh_3) and O_2.

For the effective catalytic turnover, it was necessary to protect the complex against decomposition. Immobilization and isolation on an amorphous silica powder (Aerosil 200, specific surface area = 200 $m^2\ g^{-1}$) was employed for this purpose. A dilute solution of masked ligand, isopropylidene ketal and *tert*-butyl ester of 3-[*N*-(2,3-dihydroxypropyl)-*N*-carboxymethyl]-aminopropylmethylsilyl group,† was first anchored on the surface and the remnant silanols were subsequently blocked by diethoxydodecylmethylsilane. Removal of the protecting groups resulted in the attachment of highly dispersed ligands at a concentration of 4.8×10^{-2} mmol g^{-1} (3.2% of total silanols) as quantified by the measurement of nitrogen content. Loaded dodecylmethylsilyl groups, 3.75×10^{-1} mmol g^{-1} based on carbon content, were estimated to cover 25.3% of total silanols. The high coverage implies that long alkylsilyl groups are tightly packed in the cylindroid arrangement on the surface.[3]

Complexation in 2.5 mM $Fe(NO_3)_3$–methanol, followed by thorough washing with methanol yielded immobilization of 4.3×10^{-2} mmol g^{-1} iron (determined colorimetrically) which occupied 90% of the ligands previously anchored. The formation of complex was confirmed by the appearance of asymmetric CO vibration at 1570 cm^{-1} and a decrease in the signal representing free carboxyl groups at 1715 cm^{-1} with FTIR. Taking into account the remainder of a trace amount of ester (1740 cm^{-1}), the complexation seemed to be accomplished in almost quantitative yield. In addition treatment of the white powder in 200 mM HCl–dioxane gave three methanol molecules per iron, while the elemental analysis did not show the presence of nitrogen derived from NO_3. The EPR spectrum revealed a broad signal at $g = 4.2$ which was assigned to a high spin mononuclear iron(III). We thus propose the structure shown in Scheme 1 for synthesized complex **1**.

Oxidation of alkanes was carried out in an acetonitrile solution as described in Table 1. No oxidation took place if either O_2 or PDT was omitted. In the presence of PDT alone or AcOH/PDT without PPh_3, hexane was not oxidized, but cyclohexane yielded a trace of cyclohexanol. By contrast, assay containing PPh_3 remarkably improved the reaction. Without AcOH, conversion was low, but in the complete system, hexane was selectively oxidized to hexanols with a total turnover number of 59 in the ratio of 1-ol (14%), 2-ol (44%) and 3-ol (42%). Similarly cyclohexane was converted to cyclohexanol alone with a turnover of 109. Catalyst recovered by acetonitrile washing after the assay showed a slight decrease in iron content,‡ but there was no change in the hydroxylation activity. The catalytic turnover is evidently due to the immobilized mononuclear iron carboxylate. Recovered catalyst, however, showed an iron : methanol molar ratio of 1 : 1 which differed from the original 1 : 3. Since this phenomenon was not observed in the catalyst recovered from an anaerobic assay, the change in the iron environment can be accounted for through the

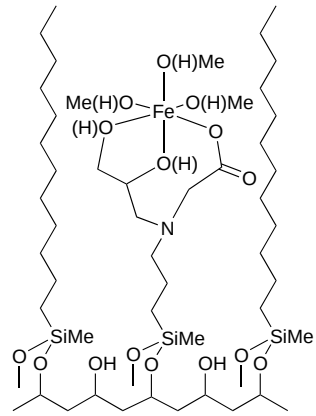

1

Scheme 1 Proposed structure for immobilized iron carboxylate

Table 1 Hydroxylation of alkanes by immobilized mononuclear iron carboxylate (**1**)[a]

Run	Substrate	Additives	Products (yield)[b]	Total yield
1	Hexane	PDT, PPh_3	1-ol (1.0), 2-ol (1.7), 3-ol (1.4)	4.1
2	Hexane	AcOH, PDT, PPh_3	1-ol (8.1), 2-ol (26.0), 3-ol (25.3)	59.4
3[c]	Hexane	AcOH, PDT, PPh_3	1-ol (8.3), 2-ol (25.5), 3-ol (24.8)	58.6
4	Cyclohexane	PDT, PPh_3	Cyclohexanol (10.0)	10.0
5	Cyclohexane	AcOH, PDT, PPh_3	Cyclohexanol (109.2)	109.2

[a] Catalyst (0.5 μmol iron), substrate (3.5 mmol), AcOH (0.25 mmol), PDT (0.25 mmol), PPh_3 (0.25 mmol) were placed into a 20 ml vial containing acetonitrile (2.6 ml) and sealed with a Teflon septum. After replacing the gas phase by O_2, the vial was shaken at 180 strokes min^{-1} and 25 °C for 4 h using a Bioshaker. [b] Moles of product per mole of iron. [c] Catalyst recovered from the assay scaled up tenfold was used.

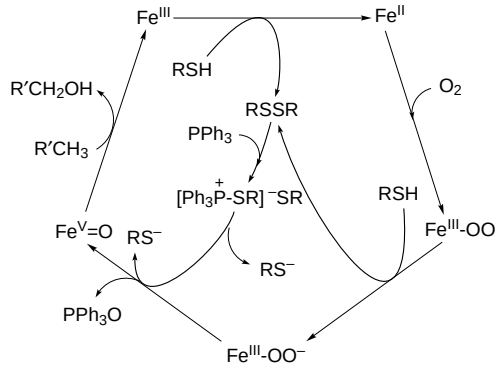

Scheme 2 Hypothetical catalytic cycle of immobilized mononuclear iron carboxylate (**1**) for alkane hydroxylation

participation of oxygen during the catalytic cycle. After release of oxygen, acetonitrile may serve as alternative ligands.

When oxidation was carried out without substrate, PPh_3 was converted to PPh_3O with a turnover number of 136. Also we can not rule out unavoidable oxidation of the alkane chains adjacent to the active center in **1**, considering the strong oxidative capability toward primary C–H. Such competitive oxidation explains the rapid consumption of PPh_3 causing unexpected termination of the catalytic turnover as well as the requirement of high concentration of substrate for effective hydroxylation in our system.

A hypothetical mechanism for this notable catalytic hydroxylation is illustrated in Scheme 2. The reduction of Fe^{III} to Fe^{II} by mercaptan initiates the reaction. Mercaptan consumed at this stage is converted to alkyl disulfide which is subsequently attacked by the PPh_3 nucleophile to form thioalkoxyphosphonium cation intermediate.[4] Since the intermediate is known to be readily trapped by a carboxylic acid in refluxing acetonitrile to yield mercaptan, thioester and PPh_3O,[5] a similar reaction could be possible in the presence of AcOH. On the other hand, the assay using $^{18}O_2$ demonstrated almost quantitative ^{18}O incorporation into both PPh_3O and hexanols regardless of the AcOH addition. Accordingly the intermediate is directly attacked by a dioxygen– metal adduct, presumably a peroxoiron species, to release PPh_3O. The resulting O–O bond scission is thought to allow the generation of an iron–oxo species from which oxygen is transferred to the substrate. The role of AcOH is therefore assumed to protonate the thiolate anion and promote its dissociation from the intermediate ion pair.

The participation of PPh_3 in the O–O bond cleavage is similar to that of acylating reagents in cytochrome P450 model studies.[6] In fact we could detect the same hexanols in the hydroxylation of hexane using **1**, KO_2–18-crown-6 and acetic anhydride in benzene although the yield was low (total turnover number = 0.12). Furthermore [tetrakis(pentafluorophenyl)porphyrinate] iron(III) hydroxide instead of **1** oxidized hexane to only hexanols in comparable product yield and distribution in our system. The results again support the formation of a high-valent iron–oxo species being responsible for the hydroxylation of alkanes by **1**.

Interestingly a hydroperoxoiron(III) species was identified by EPR spectroscopy at 77 K (g = 2.27, 2.20, 1.97)[7] when the porphyrin iron complex was reduced with an equivalent of PDT and then exposed to O_2. Addition of H_2O_2 gave an identical EPR signal. The same intermediate has been reported in the model studies of bleomycin with mononuclear iron coordinating nitrogen ligands.[8] By contrast this phenomenon was not found in the investigation using **1**, and there was no effect of the intermediate on the hydroxylation of alkanes even with the addition of PPh_3 or AcOH–PPh_3. The fact may reflect a characteristic nature of the iron complex with oxygen-rich ligands involving carboxylate different from those bearing a porphyrin or nitrogen ligands.

It now appears that mononuclear iron carboxylate can catalyze highly selective hydroxylation of alkanes by reductive dioxygen activation. The key reaction is assumed to be the efficient heterolytic scission of the O–O bond by the PPh_3 participated deoxygenation. However, regarding the generation of putatively unstable Fe^{V}=O species in a mononuclear iron core, there is an argument against delocalization of the oxidizing equivalents.[2] This point contrasts to a Fe^{IV}=O dinuclear cluster which has been reported recently as the critical intermediate of MMO.[9] The results obtained in this work could be attributed to unique properties of the complex with predominantly oxygen ligation in a hydrophobic microenvironment analogous to the active site of an enzyme buried in a protein matrix.

Footnotes and References

* E-mail: miki@nire.go.jp

† Ligand was prepared from 3-aminopropyldiethoxymethylsilane *via* 2 steps: (a) condensation with 2,2-dimethyl-4-chloromethyl-1,3-dioxolan at 220 °C; (b) treatment with chloroacetic acid *tert*-butyl ester in acetonitrile at 50 °C in the presence of triethylamine, followed by extraction with hexane and purification using an activated carbon column. Purity was checked by GC, GCMS and NMR spectroscopy.

‡ Iron content of the recovered catalyst after hexane oxidation was 3.7×10^{-2} mmol g^{-1} (86% of the initial catalyst).

1 J. B. Vincent, J. C. Huffman, G. Christou, Q. Li, M. A. Nancy, D. N. Hendrickson, R. H. Fong and R. H. Fish, *J. Am. Chem. Soc.*, 1988, **110**, 6898; R. M. Buchanan, S. Chen, J. F. Richardson, M. Bressan, L. Forti, A. Morvillo and R. H. Fish, *Inorg. Chem.*, 1994, **33**, 3208; A. L. Feig and S. J. Lippard, *Chem. Rev.*, 1994, **94**, 759; A. L. Nivorozhkin and J.-J. Girerd, *Angew. Chem., Int. Ed. Engl.*, 1996, **35**, 609; B. J. Wallar and J. D. Lipscomb, *Chem. Rev.*, 1996, **96**, 2625.
2 L. Que, Jr. and R. Y. N. Ho, *Chem. Rev.*, 1996, **96**, 2607.
3 D. W. Sindorf and G. E. Maciel, *J. Phys. Chem.*, 1982, **86**, 5208; K. Miki and Y. Sato, *Bull. Chem. Soc. Jpn.*, 1993, **66**, 2385.
4 L. E. Overman and E. M. O'Connor, *J. Am. Chem. Soc.*, 1976, **98**, 771.
5 T. Mukaiyama, *Angew. Chem.*, 1976, **88**, 111.
6 J. T. Groves, Y. Watanabe and T. J. McMurry, *J. Am. Chem. Soc.*, 1983, **105**, 4489; A. M. Khenkin and A. A. Shteinman, *J. Chem. Soc., Chem. Commun.*, 1984, 1219.
7 K. Tajima, M. Shigematsu, J. Jinno, K. Ishizu and H. Ohya-Nishiguchi, *J. Chem. Soc., Chem. Commun.*, 1990, 144.
8 R. J. Guajardo and P. K. Mascharak, *Inorg. Chem.*, 1995, **34**, 802; M. Lubben, A. Meetsma, E. C. Wilkinson, B. Feringa and L. Que, Jr., *Angew. Chem., Int. Ed. Engl.*, 1995, **34**, 1512.
9 L. Shu, J. C. Nesheim, K. Kauffmann, E. Münck, J. D. Lipscomb and L. Que, Jr., *Science*, 1997, **275**, 515.

Received in Cambridge, UK, 26th August, 1997; 7/06178A

Control of ligand–metal interaction at the lower rim of *p-tert*-butylcalix[5]arene

Maomian Fan, Hongming Zhang and Michael Lattman*

Department of Chemistry, Southern Methodist University, Dallas, Texas 75275-0314, USA

The lower rim of *p-tert*-butylcalix[5]arene is able to accommodate both a ligand and metal in close proximity allowing subtle electronic changes to dramatically affect ligand–metal interaction.

The ability to constrain the mobility of a ligand relative to a metal can have far-reaching applications from catalysis to molecular devices. This is particularly true when such systems can stabilize relatively weak ligand–metal interactions. Herein we report the synthesis of such a system based on a calix[5]arene and demonstrate the control of ligand–metal bonding *via* small electronic changes at the metal.

Treatment of *p-tert*-butylcalix[5]arene[1] with tris(dimethylamino)phosphine[2] inserts a Me_2NP moiety into the calixarene.† The ^{1}H NMR spectrum of **1** is consistent with the symmetry of the proposed structure: three singlets in the *tert*-butyl region in a 2 : 1 : 2 ratio and six doublets in the methylene region owing to the fact that the two hydrogens on each methylene carbon are non-equivalent. Also, the ^{31}P NMR signal at δ 131 is in the region for a three-coordinate phosphorus with two phenolic groups and a dialkylamino group.[3] If the cavity of the calix[5]arene is large enough, the three remaining hydroxyls should be able to bind a metal. In fact, insertion of tungsten proceeds smoothly by the reaction of **1** with $(Bu^tN)_2W(NHBu^t)_2$[4] *via* elimination of 2 moles of *tert*-butylamine (Scheme 1).‡ As expected, the ^{1}H NMR spectrum of **2** is similar to **1** in the *tert*-butyl and methylene regions. In addition, two new Bu^t singlets are present due to the tungsten-bound *tert*-butyl-amido and -imido ligands. The ^{31}P NMR signal at δ 116 is only 15 ppm upfield of **1**. More importantly, this signal shows a small coupling to W of 43 Hz, significantly smaller than usual $^1J_{PW}$ values.[5] This suggests a weak (through-space?) P–W interaction. Amido and imido ligands are known to be excellent π donors to high-oxidation-state metals.[6] If one of these ligands could be replaced with another that puts less electron density at the metal, this might increase the P–W interaction. This is exactly what occurs when triflate replaces *tert*-butylamido *via* the reaction of **2** with an excess of trifluoromethanesulfonic acid in refluxing toluene to give **3**.§ The $^1J_{PW}$ value in **3** of 352 Hz is in the usual range of P–W bonds which is indicative of a significantly stronger P–W interaction.

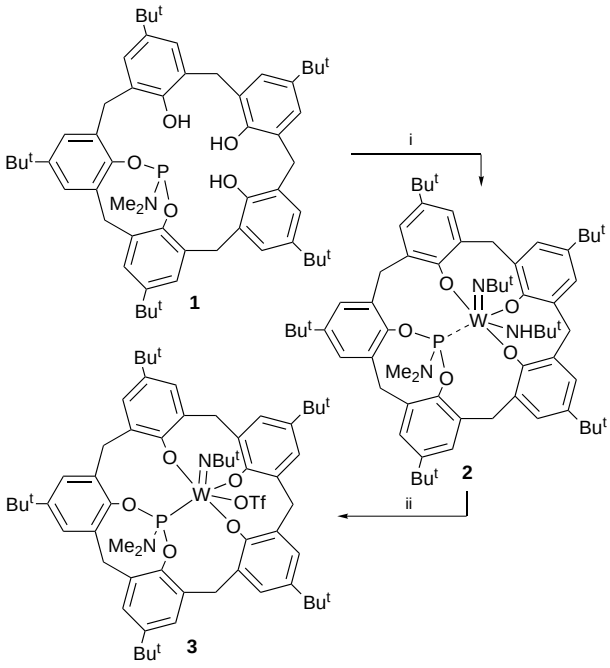

Scheme 1 *Reagents and conditions:* i, $+(Bu^tN)_2W(NHBu^t)_2$, -2 H_2NBu^t; ii, excess HOTf, reflux, $-H_2NBu^t$

The X-ray crystal structures¶ of **2** and **3** substantiate the above spectral interpretations and provide detail on the structural changes associated with increasing the P–W interaction. The structures of **2** and **3** are illustrated in Figs. 1 and 2, respectively. Selected bond lengths and angles are given in the captions. In **2**, the calix[5]arene backbone adopts a somewhat flattened conformation. The phosphorus has a distorted pyramidal geometry, while the tungsten adopts a distorted square-pyramidal geometry. The phosphorus lone pair is oriented towards the vacant sixth coordination site at the tungsten with a P···W distance of 3.15 Å, well outside the longest bond lengths reported for P–W bonds;[7] however, it is close enough to exhibit a small through-space PW coupling in the NMR spectrum. After

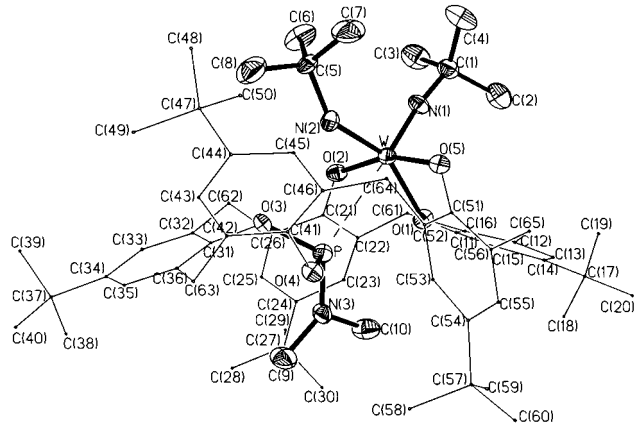

Fig. 1 Molecular structure and atom numbering scheme for **2**. Selected distances (Å) and angles (°): W–P 3.148(3), W–N(1) 1.714(8), W–N(2) 1.924(8), W–O(1) 1.961(7), W–O(2) 1.976(6), W–O(5) 1.972(7), P–N(3) 1.631(9), P–O(3) 1.645(7), P–O(4) 1.644(7), N(1)–C(1) 1.448(14), N(2)–C(5) 1.503(13), N(3)–C(9) 1.454(14), N(3)–C(10) 1.447(14); N(1)–W–P 178.0(3), N(2)–W–P 75.9(3), O(1)–W–P 76.0(2), O(5)–W–P 84.8(2), O(2)–W–P 79.5(2), N(1)–W–N(2) 102.7(4), N(1)–W–O(1) 105.3(4), N(2)–W–O(1) 151.8(3), N(1)–W–O(5) 96.7(3), N(2)–W–O(5) 95.4(3), O(1)–W–O(5) 83.9(3), N(1)–W–O(2) 99.2(3), N(2)–W–O(2) 90.4(3), O(1)–W–O(2) 82.7(3), O(5)–W–O(2) 161.4(3), W–P–O(3) 93.1(2), W–P–O(4) 129.4(3), W–P–N(3) 123.8(3), N(3)–P–O(4) 98.9(4), N(3)–P–O(3) 109.9(4), O(4)–P–O(3) 96.8(4), C(1)–N(1)–W 169.6(8), C(5)–N(2)–W 140.3(7), C(10)–N(3)–C(9), 112.6(9), C(10)–N(3)–P 120.1(7), C(9)–N(3)–P 127.0(7), C(11)–O(1)–W 139.6(6), C(21)–O(2)–W 136.2(6), C(51)–O(5)–W 125.8(6).

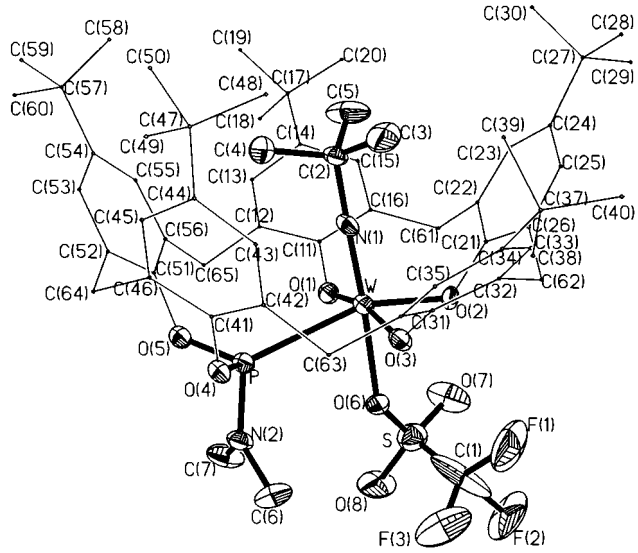

Fig. 2 Molecular structure and atom numbering scheme for **3**. Label for C(36) [carbon attached to C(31) and C(35)] omitted for clarity. Selected distances (Å) and angles (°): W–N(1) 1.725(7), W–O(2) 1.907(5), W–O(1) 1.936(6), W–O(3) 1.943(5), W–O(6) 2.188(6), W–P 2.743(2), P–O(5) 1.598(6), P–O(4) 1.616(6), P–N(2) 1.633(7), N(1)–C(2) 1.464(11), N(2)–C(6) 1.456(11), N(2)–C(7) 1.471(12); N(1)–W—O(2) 102.3(3), N(1)–W–O(1) 96.1(3), O(2)–W–O(1) 90.8(2), N(1)–W–O(3) 97.1(3), O(2)–W–O(3) 89.5(2), O(1)–W–O(3) 166.4(2), N(1)–W–O(6) 177.0(3), O(2)–W–O(6) 80.5(2), O(1)–W–O(6) 82.8(2), O(3)–W–O(6) 83.9(2), N(1)–W–P 99.5(2), O(2)–W–P 158.2(2), O(1)–W–P 86.9(2), O(3)–W–P 87.7(2), O(6)–W–P 77.7(2), O(5)–P–O(4) 106.6(3), O(5)–P–N(2) 97.6(3), O(4)–P–N(2) 99.9(3), O(5)–P–W 118.2(2), O(4)–P–W 118.0(2), N(2)–P–W 113.3(3), C(2)–N(1)–W 178.9(5), C(6)–N(2)–C(7) 113.6(8), C(6)–N(2)–P 121.6(7), C(7)–N(2)–P 121.8(6), C(11)–O(1)–W 133.2(5), C(21)–O(2)–W 123.4(5), C(31)–O(3)–W 134.0(5), S–O(6)–W 138.9(4).

ligand exchange, the calix[5]arene backbone in **3** adopts the cone conformation with the phosphorus bound to the tungsten at the 'lower' rim. The P–W distance is 2.74 Å which is long but still within reported ranges for P–W bonds. The triflate lies outside the cavity of the calixarene, while the imido is within the cavity. As expected, the W–O(6) (triflate) distance is longer than the other W–O distances, indicative of a more weakly bound group.

The structures of **2** and **3** also account for certain anomalies in their ^{1}H NMR spectra. The dimethylamino group resonance in **2** at δ 1.53 is about 1.5 ppm upfield of its usual position, and the (imido) *tert*-butyl group resonance in **3** at δ − 1.03 is about 2 ppm upfield of its usual position. Figs. 1 and 2 show that the protons of these groups lie above and inside the aromatic rings of the calix[5]arene resulting in upfield ring current shifts for these signals.

We have demonstrated that a calix[5]arene is large enough to bind both a ligand and metal at the lower rim. Moreover, the macrocycle appears to orient the ligand and metal toward one another. This constraint supports both a weak and strong ligand–metal interaction, depending on the electron density at the metal. It may also be useful to view the tri-deprotonated form of **1** as a tetradentate ligand with three hard (oxygen) binding sites and one soft (phosphorus) binding site. Work is currently under way to determine how general this chemistry is by incorporating other metals and ligands.

Acknowledgement is made to the National Science Foundation (CHE-9522606), Robert A. Welch Foundation, and the donors of the Petroleum Research Fund, administered by the American Chemical Society, for financial support.

Footnotes and References

* E-mail: mlattman@mail.smu.edu

† In an inert atmosphere, a stirred solution of *p-tert*-butylcalix[5]arene (0.765 g, 0.943 mmol) in toluene (30 ml) was treated dropwise with tris(dimethylamino)phosphine (0.154 g, 0.944 mmol). The mixture was stirred for 1 d. The volatiles were then pumped off and the resulting solid washed with hexane (3 × 2 ml) and pumped dry to yield **1** as a white, air- and moisture-stable solid (0.72 g, 86%). Analytically pure samples can be obtained by recrystallization from toluene to give **1**·C_6H_5Me. Mp 148–150 °C. Anal. Calc. for $C_{57}H_{74}NO_5P\cdot C_7H_8$: C, 78.73; H, 8.47. Found: C, 78.80; H, 8.39%. ^{1}H NMR ($CDCl_3$): δ 1.20 (s, 18 H, Bu^t), 1.21 (s, 9 H, Bu^t), 1.29 (s, 18 H, Bu^t), 2.35 (s, 3 H, CH_3 of toluene), 2.96 (d, 6 H, NCH_3, $^3J_{PH}$ 10.2 Hz), 3.39 (d, 2 H, CH_2, $^2J_{HH}$ 14.9 Hz), 3.46 (d, 1 H, CH_2, $^2J_{HH}$ 13.6 Hz), 3.51 (d, 2 H, CH_2, $^2J_{HH}$ 14.2 Hz), 4.13 (d, 2 H, CH_2, $^2J_{HH}$ 14.1 Hz), 4.48 (d, 2 H, CH_2, $^2J_{HH}$ 14.8 Hz), 4.49 (br d, 1 H, CH_2, $^2J_{HH}$ *ca*. 14 Hz), 7.10–7.36 (m, 15 H, aromatic calix and toluene). ^{31}P NMR ($CDCl_3$): δ 131.

‡ In an inert atmosphere, a stirred solution of (Bu^{t}N)$_2$W(NHBu^t)$_2$ (0.396 g, 0.839 mmol) in toluene (20 ml) was treated dropwise with a solution of **1** (0.744 g, 0.841 mmol) in toluene (20 ml). The mixture was stirred for 3 d. The mixture was then filtered to remove a small amount of solid, and the volume of the filtrate was reduced to *ca*. 5 ml. A solid precipitated over a few days. This product was filtered and dried to yield **2**·C_6H_5Me as a yellow, crystalline, air-sensitive solid (0.649 g, 77%). Mp 270 °C (decomp.). Anal. Calc. for $C_{65}H_{90}N_3O_5PW\cdot C_7H_8$: C, 66.50; H, 7.60. Found: C, 66.14; H, 7.64%. ^{1}H NMR ($CDCl_3$): δ 1.12 (s, 18 H, Bu^t), 1.18 (s, 9 H, Bu^t), 1.33 (s, 18 H, Bu^t), 1.34 (s, 9 H, Bu^t), 1.36 (s, 9 H, Bu^t), 1.53 (d, 6 H, NCH_3, $^3J_{PH}$ 9.4 Hz), 2.34 (s, 3 H, CH_3 of toluene), 3.29 (d, 2 H, CH_2, $^2J_{HH}$ 13.9 Hz), 3.44 (d, 2 H, CH_2, $^2J_{HH}$ 15.8 Hz), 3.51 (d, 1 H, CH_2, $^2J_{HH}$ 15.5 Hz), 4.38 (d, 2 H, CH_2, $^2J_{HH}$ 13.8 Hz), 4.44 (d, 1 H, CH_2, $^2J_{HH}$ 15.3 Hz), 4.58 (d, 2 H, CH_2, $^2J_{HH}$ 15.7 Hz), 6.99–7.62 (m, 15 H, aromatic calix and toluene). ^{31}P NMR ($CDCl_3$): δ 116 ($^1J_{PW}$ 43 Hz). The toluene of crystallization can be removed by extended pumping.

§ In an inert atmosphere, a stirred solution of **2** (0.960 g, 0.795 mmol) in toluene (40 ml) was treated dropwise with trifluoromethanesulfonic acid (0.361 g, 2.41 mmol). The mixture was refluxed for 3 d. The mixture was then filtered to remove a small amount of solid, and the filtrate was pumped to dryness. The residue was recrystallized from toluene yielding **3**·0.5-C_6H_5Me as a red, air- and moisture-stable solid (0.65 g, 61%). Mp 343–345 (decomp.). Anal. Calc. for $C_{62}H_{80}F_3N_3O_8PSW\cdot 0.5C_7H_8$: C, 59.10; H, 6.36. Found: C, 58.97; H, 6.63%. ^{1}H NMR ($CDCl_3$): δ −1.03 (s, 9 H, Bu^t), 1.16 (s, 18 H, Bu^t), 1.24 (s, 9 H, Bu^t), 1.30 (s, 18 H, Bu^t), 2.34 (s, 1.5 H, CH_3 of toluene), 3.28 (d, 6 H,NCH_3, $^3J_{PH}$ 9.7 Hz), 3.30 (d, 2 H, CH_2, $^2J_{HH}$ 13.1 Hz), 3.35 (d, 2 H, CH_2, $^2J_{HH}$ 13.7 Hz), 3.51 (d, 1 H, CH_2, $^2J_{HH}$ 13.4 Hz), 4.36 (dd, 1 H, CH_2, $^2J_{HH}$ 13.3, $^5J_{PH}$ 2.4 Hz), 4.52 (d, 2 H, CH_2, $^2J_{HH}$ 13.6 Hz), 4.70 (d, 2 H, CH_2, $^2J_{HH}$ 13.1 Hz), 7.11–7.50 (m, 12.5 H, aromatic calix and toluene). ^{31}P NMR ($CDCl_3$): δ 125 ($^1J_{PW}$ 352 Hz).

¶ *Crystal data*: **2**: $C_{65}H_{90}N_3O_5PW\cdot 2C_7H_8$, M = 1392.49, triclinic, space group $P\bar{1}$, a = 14.073(2), b = 16.615(1), c = 17.880(1) Å, α = 95.67(1), β = 110.23(1), γ = 105.49(1)°, U = 3694.9(6) Å^3, Z = 2, T = 228(2) K, λ = 0.71073 Å, D_c = 1.252 g cm^{-3}, μ = 1.635 mm^{-1}, for 7561 observed reflections [$I > 2\sigma(I)$], R_1 = 0.0484, wR_2 = 0.1245.

3: $2(C_{62}H_{80}F_3N_2O_8PSW)\cdot 2C_7H_8\cdot 0.5C_6H_6$, M = 2793.64, triclinic, space group $P\bar{1}$, a = 13.282(3), b = 23.909(3), c = 25.770(3) Å, α = 115.844(7), β = 101.995(12), γ = 94.853(12)°, U = 7060(2) Å^3, Z = 2, T = 228(2) K, λ = 0.71073 Å, D_c = 1.314 g cm^{-3}, μ = 1.748 mm^{-1}, for 12 959 observed reflections [$I > 2\sigma(I)$], R_1 = 0.0460, wR_2 = 0.1072.

Both structures were refined on F^2 (SHELX93, G. M. Sheldrick, 1993, University of Göttingen, Germany). CCDC 182/656.

1 D. R. Stewart and C. D. Gutsche, *Org. Prep. Proced. Int.*, 1993, **25**, 137.
2 A. B. Burg and P. J. Slota, *J. Chem. Soc.*, 1958, 1107.
3 *Top. Phosphorus Chem.*, 1969, **5**, 227.
4 W. A. Nugent and R. L. Harlow, *Inorg. Chem.*, 1980, **19**, 777.
5 J. G. Verkade and J. A. Mosbo, in *Phosphorus-31 NMR Spectroscopy in Stereochemical Analysis*, ed. J. G. Verkade and L. D. Quin, VCH, Deerfield Beach, FL, 1987.
6 M. F. Lappert, *Metal and Metalloid Amides: Syntheses, Structures, and Physical and Chemical Properties*, Halsted Press, New York, 1980.
7 F. H. Allen and O. Kennard, *Chem. Des. Automat. News*, 1993, **8**, 1; 31.

Received in Columbia, MO, USA, 25th September 1997; 7/06951K

Subvalent germanium and tin complexes supported by a dianionic calixarene ligand: structural characterization of *exo* and *endo* isomers of [Bu^{t}calix$^{(TMS)2}$]Ge

Tony Hascall,[a] Arnold L. Rheingold,[b] Ilia Guzei[b] and Gerard Parkin*[a]

[a] *Department of Chemistry, Columbia University, New York, New York 10027, USA*
[b] *Department of Chemistry and Biochemistry, Univesity of Delaware, Newark, Delaware 19716, USA*

The 1,3-bis(trimethylsilyl) ether of *p-tert*-butylcalix[4]arene, [Bu^{t}calix$^{(TMS)2}$]H$_2$, has been synthesized and used as a dianionic ligand for Ge and Sn; notably, the Ge complex [Bu^{t}calix$^{(TMS)2}$]Ge exhibits *exo*/*endo* isomerism, and provides the first calixarene system for which both isomers have been structurally characterized.

The calix[*n*]arenes are a class of 'chalice-like' macrocyclic molecules that have recently attracted widespread attention.[1] In particular, these molecules have been extensively studied as receptors for small organic molecules and simple cations.[1] By comparison, however, calix[*n*]arenes have been infrequently used as ancilliary ligands for studying the chemistry of transition and main group metals.[2,3] Moreover, for those situations where calix[*n*]arenes have been employed as supporting ligands, their application has been mainly restricted to the use of *p-tert*-butylcalix[4]arene in its tetraanionic form.† 1,3-Dialkyl ethers of calix[4]arenes, [calix^{R2}]H$_2$, on the other hand, offer the potential for providing dianionic macrocyclic ligands which may be considered as oxygen relatives of well known N-containing macrocycles, such as porphyrins, phthalocyanines and tetraazaannulenes. Despite such analogies, the application of 1,3-diethers of calix[4]arenes as ligands for main group metals has been limited to recent reports concerned with the 1,3-dimethyl ether of *p-tert*-butylcalix[4]arene.[3*a*–*c*] Here, we report the synthesis of a more sterically demanding, 1,3-disubstituted calix[4]arene, namely bis(trimethylsilyl)-*p-tert*-butylcalix[4]arene, its use as a ligand for divalent Ge and Sn, and the first structural characterization of a pair of *exo* and *endo* isomers of a calix[*n*]arene derivative.

Our particular interest in the use of 1,3-dialkylcalix[4]arenes as O-donor macrocyclic ligands derives from recent studies concerned with Ge and Sn complexes supported by the octamethyldibenzotetraaza[14]annulene dianion, *e.g.* the subvalent and terminal chalcogenido complexes [η^4-Me$_8$taa]M and [η^4-Me$_8$taa]ME (M = Ge, Sn; E = S, Se, Te).[4–6] In order to extend this chemistry, we sought to synthesize analogous complexes derived from related macrocycles which contain O (rather than N) donor functionalities. For this purpose, 1,3-dialkyl ether calix[4]arene derivatives incorporating bulky substituents (*e.g.* SiMe$_3$) appeared ideal. Although 1,3-diethers of *p-tert*-butylcalix[4]arene incorporating primary alkyl substituents have been synthesized previously by the reaction of the calix[4]arene with 2 equiv. of alkyl halides in the presence of a weak base,[1*c*] the bis(trimethylsilyl) derivative [Bu^{t}calix$^{(TMS)2}$]H$_2$ could not be isolated using such procedures.‡[8] Nevertheless, we have found that the reaction of *p-tert*-butylcalix[4]arene with Me$_3$SiI (2 equiv.) in the presence of pyridine (2 equiv.) affords a useful synthesis of [Bu^{t}calix$^{(TMS)2}$]H$_2$ (Scheme 1).

Divalent Ge and Sn complexes [Bu^{t}calix$^{(TMS)2}$]M are readily obtained by the reaction of [Bu^{t}calix$^{(TMS)2}$]H$_2$ with M[N(SiMe$_3$)$_2$]$_2$ (M = Ge, Sn) as illustrated in Scheme 1. Each of the products has been structurally characterized by X-ray diffraction, as shown in Fig. 1 and 2.§ Interestingly, for the Ge

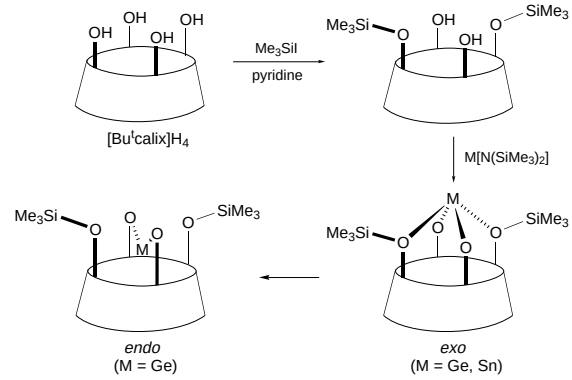

Scheme 1

system, the reaction yields sequentially two isomers, namely *exo*- and *endo*-[Bu^{t}calix$^{(TMS)2}$]Ge, which differ in the location of the Ge atom with respect to the calixarene cavity (Figs. 1 and 2).¶ *Exo* and *endo* isomerism of this type has previously been suggested for the aluminium hydride complex [Bu^{t}calix^{Me2}]-AlH, for which the Al–H moiety may be directed into, or away from, the calixarene cavity.[3*b*] However, only the structure of *exo*-[Bu^{t}calix^{Me2}]AlH has been determined by X-ray diffraction, with the nature of the *endo* isomer having been inferred by NMR spectroscopy. The Ge complexes described here, therefore, constitute the first pair of *exo* and *endo* isomers to be structurally characterized.

The coordination geometries about Ge in *exo*- and *endo*-[Bu^{t}calix$^{(TMS)2}$]Ge are summarized in Table 1, from which it is evident that both complexes exhibit Ge–O bond lengths to the phenoxide moieties which are comparable to, but slightly shorter than, the sum of their covalent radii (1.96 Å).‖ For the *endo* isomer, the Ge center is located *ca.* 3.5 Å from the O atoms of the trimethylsilylether groups, so that it is appropriately

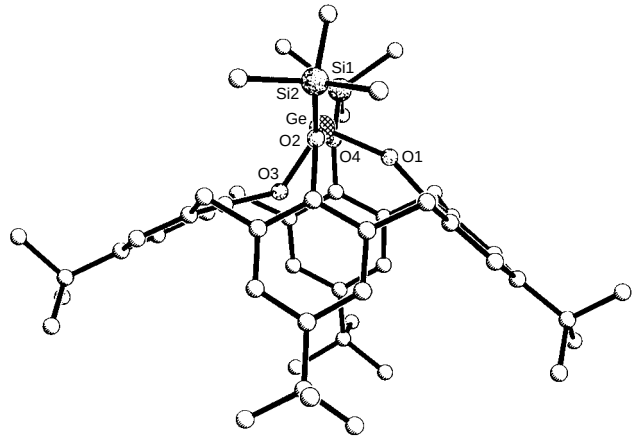

Fig. 1 The molecular structure of *exo*-[Bu^{t}calix$^{(TMS)2}$]Ge (the Sn analogue is similar)

Table 1 Metrical data for [Bu^{t}calix$^{(TMS)_2}$]M (M = Ge, Sn)

	d(M–O^1)/Å	d(M–O^3)/Å	d(M···O^2)/Å	d(M···O^4)/Å	O–M–O/°
exo-[Bu^{t}calix$^{(TMS)_2}$]Ge	1.765(6)	1.842(6)	2.421(5)	2.486(5)	100.2(3)
endo-[Bu^{t}calix$^{(TMS)_2}$]Ge	1.841(5)	1.853(5)	3.460(5)	3.565(6)	92.81(22)
	1.840(5)	1.849(5)	3.454(6)	2.458(5)	92.02(23)
exo-[Bu^{t}calix$^{(TMS)_2}$]Sn	1.956(7)	2.011(9)	2.521(6)	2.532(6)	96.3(4)

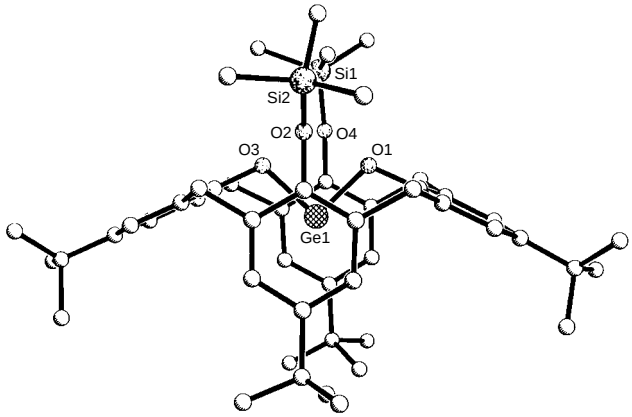

Fig. 2 The molecular structure of *endo*-[Bu^{t}calix$^{(TMS)_2}$]Ge (only one of the crystallographically independent molecules is shown)

considered to be two-coordinate, with the dianionic calixarene acting as a bidentate, rather than tetradentate, ligand. As such, the coordination environment offered by the dianionic calixarene provides a contrast with the tetracoordination provided by related macrocyclic derivatives, *e.g.* [η^4-Me$_8$taa]Ge.[4] The ability of the calixarene to sustain monomeric two-coordinate Ge^{II} centers is of interest since complexes with such coordination environments are uncommon; for example, only two two-coordinate Ge^{II} alkoxide complexes are listed in the Cambridge Structural Database (Version 5.13), namely (ArO)$_2$Ge (Ar = C$_6$H$_2$MeBu$^t_2$) and (Bu$^t_3$CO)$_2$Ge.‖ In contrast to the two-coordinate *endo* isomer, the *exo* isomer does exhibit interactions with the O atoms of the trimethylsilylether groups (*ca.* 2.45 Å) that are shorter than the sum of their van der Waals radii (3.40 Å).‖

It is interesting to note that, despite the observation that the dative interaction between Ge and the trimethylsilyl ether groups is shorter for the *exo* isomer, the *endo* isomer is evidently the more thermodynamically stable, as judged by the observed *exo* to *endo* isomerization.**,†† Thus, the [O→Ge] dative interactions in the *exo* isomer are presumably weak and insufficient to compensate for other structural changes which accompany the isomerization. For example, one factor which favors the *endo* isomer being the more stable is concerned with the possibility that the calixarene conformation is such that it furnishes a more appropriate bite angle for Ge in the *endo* position than for Ge in the *exo* position (compare Figs. 1 and 2). Supporting this notion, the O–Ge–O bond angle for the *exo* isomer [100.2(3)°] is notably larger than is observed for simple (RO)$_2$Ge complexes (*ca.* 86–92°)‖ which are not subject to the constraints of the macrocyclic configuration. In contrast, the *endo* isomer does exhibit a O–Ge–O bond angle (*ca.* 92.4°) that is comparable to the values for (RO)$_2$Ge derivatives, thereby suggesting that there is less strain for the *endo* isomer, so that it may be more thermodynamically favored.‡‡

We thank the National Science Foundation (CHE 96-10497) for support of this research. G. P. is the recipient of a Presidential Faculty Fellowship Award (1992–1997).

Footnotes and References

* E-mail: parkin@chem.columbia.edu

† For the use of neutral calixarene ligands, see ref. 3(*f*).

‡ Specifically, only recovered *p-tert*-butylcalix[4]arene was obtained from the reaction of (*i*) *p-tert*-butylcalix[4]arene with Me$_3$SiCl and (Me$_3$Si)$_2$NH, and (*ii*) *p-tert*-butylcalix[4]arene with Me$_3$SiCl and Li$_2$S. The latter reaction, however, did provide evidence for formation of the bis-(trimethylsilyl) ether derivative, but the product could not be isolated.[7a] Tetrakis(trimethylsilyl)-*p-tert*-butylcalix[4]arene has, however, been obtained by the reaction of the calix[4]arene with N,O-tris(trimethylsilyl)-acetamide.[7b]

§ *Crystallography. exo*-[Bu^{t}calix$^{(TMS)_2}$]Ge·C$_6$H$_5$Me is monoclinic, $P2_1/c$ (no. 14), a = 23.275(3), b = 18.829(2), c = 13.245(1) Å, β = 105.059(7)°, U = 5605(1) Å^3, Z = 4, R [$I > 2\sigma(I)$] = 0.0738. *endo*-[Bu^{t}calix$^{(TMS)_2}$]Ge is monoclinic, $P2_1/c$ (no. 14), a = 28.2718(3), b = 18.4591(1), c = 20.5583(1) Å, β = 111.245(1)°, U = 9999.7(1) Å^3, Z = 8, R [$I > 2\sigma(I)$] = 0.1027. *exo*-[Bu^{t}calix$^{(TMS)_2}$]Sn·C$_6$H$_6$ is monoclinic, $P2_1/c$ (no. 14), a = 23.339(7), b = 18.684(4), c = 13.204(3) Å, β = 105.98(1)°, U = 5535(1) Å^3, Z = 4, R [$I > 2\sigma(I)$] = 0.0744. CCDC 182/655.

¶ In contrast, for the Sn system, only the *exo* isomer has been isolated so far.

‖ For comparison, the following metrical data have been reported for two-coordinate Ge and Sn alkoxide and aryloxide complexes: (*i*) (ArO)$_2$Ge (Ar = C$_6$H$_2$MeBu$^t_2$): (Ge–O) 1.802(8), 1.812(7) Å; O–Ge–O 92.0(4)°;[9–a] (*ii*) (ArO)$_2$Sn (Ar = C$_6$H$_2$MeBu$^t_2$): (Sn–O) 1.995(4), 2.022(4) Å; O–Sn–O 88.8(2)°;[9a] (*iii*) (Bu$^t_3$CO)$_2$Ge: (Ge–O) 1.896(6), 1.832(11) Å; O–Ge–O 85.9(4)°.[9b]

** The conversion of *exo*-[Bu^{t}calix$^{(TMS)_2}$]Ge to its *endo* isomer (*ca.* 95%) has been observed to occur over a 1 h at *ca.* 80 °C, as monitored by ^{1}H NMR spectroscopy.

†† The *endo* isomer of [Bu^{t}calix^{Me_2}]AlH has also been reported to be more stable than its *exo* isomer. See ref. (3*b*).

‡‡ Other factors, such as the small conformational differences of the calixarene ligand, may also influence the stability of the *endo* with respect to *exo* isomer.

1 (*a*) G. D. Gutsche, *Calixarenes*, Royal Society of Chemistry, Cambridge, 1989; (*b*) *Calixarenes: A Versatile Class of Macrocyclic Compounds*, ed. J. Vincens and V. Böhmer, Kluwer, Dordrecht, 1991; (*c*) V. Böhmer, *Angew. Chem., Int. Ed. Engl.*, 1995, **34**, 713.
2 D. M. Roundhill, *Prog. Inorg. Chem.*, 1995, **43**, 533.
3 For recent examples of the use of calix[*n*]arenes as ligands in main group metal chemistry, see: (*a*) M. G. Gardiner, S. M. Lawrence, C. L. Raston, B. W. Skelton and A. H. White, *Chem. Commun.*, 1996, 2491; (*b*) M. G. Gardiner, G. A. Koutsantonis, S. M. Lawrence, P. J. Nichols and C. L. Raston, *Chem. Commun.*, 1996, 2035; (*c*) J. L. Atwood, M. G. Gardiner, C. Jones, C. L. Raston, B. W. Skelton and A. H. White, *Chem. Commun.*, 1996, 2487; (*d*) J. L. Atwood, P. C. Junk, S. M. Lawrence and C. L. Raston, *Supramol. Chem.*, 1996, **7**, 15; (*e*) J. M. Smith and S. G. Bott, *Chem. Commun.*, 1996, 377; (*f*) S. G. Bott, A. W. Coleman and J. L. Atwood, *J. Incl. Phenom.*, 1987, **5**, 747.
4 M. C. Kuchta and G. Parkin, *J. Chem. Soc., Chem. Commun.*, 1994, 1351.
5 M. C. Kuchta and G. Parkin, *J. Am. Chem. Soc.*, 1994, **116** 8372.
6 M. C. Kuchta and G. Parkin, *Chem. Commun.*, 1996, 1669.
7 (*a*) C. D. Gutsche, B. Dhawan, K. H. No and R. Muthukrishnan, *J. Am. Chem. Soc.*, 1981, **103**, 3782; (*b*) C. D. Gutsche, B. Dhawan, J. A. Levine, K. H. No and L. J. Bauer, *Tetrahedron*, 1983, **39**, 409.
8 For some other examples of O-silylated calixarenes see: (*a*) M. M. Olmstead, G. Sigel, H. Hope, X. Xu and P. P. Power, *J. Am. Chem. Soc.*, 1985, **107**, 8087; (*b*) X. Delaigue, M. W. Hosseini, A. De Cian, J. Fischer, E. Leize, S. Kieffer and A. Van Dorsselaer, *Tetrahedron Lett.*, 1993, **34**, 3285; (*c*) S. Shang, D. V. Khasnis, J. M. Burton, C. J. Santini, M. Fan, A. C. Small and M. Lattman, *Organometallics*, 1994, **13**, 5157; (*d*) M. Fan, H. Zhang and M. Lattman, *Organometallics*, 1996, **15**, 5216.
9 (*a*) B. Cetinkaya, I. Gümrükcü, M. F. Lappert, J. L. Atwood, R. D. Rogers and M. J. Zaworotko, *J. Am. Chem. Soc.*, 1980, **102**, 2088; (*b*) T. Fjeldberg, P. B. Hitchcock, M. F. Lappert, S. J. Smith and A. J. Thorne, *J. Chem. Soc., Chem. Commun.*, 1985, 939.

Received in Bloomington, IN, USA, 13th August 1997; 7/05937J

A coordination network based on d^0 transition-metal centers: synthesis and structure of the [2,4]-connected layered compound $[(TiCl_4)_2Si(C_6H_4CN\text{-}p)_4]\cdot 1.5C_7H_8$

Feng-Quan Liu and T. Don Tilley*

Department of Chemistry, University of California, Berkeley, Berkeley, CA 94720-1460, USA
Chemical Sciences Division, Lawrence Berkeley Laboratory, 1 Cyclotron Road, Berkeley, CA 94720, USA

The tetrafunctional silane $Si(C_6H_4CN\text{-}p)_4$ forms a coordination network with $TiCl_4$ consisting of 4,2-connected layers containing large (56 atom) rings.

There has been considerable recent interest in the construction and study of coordination networks based on coordinate bonds between polyfunctional ligands and various metal centers.[1–8] These materials often possess well defined (crystalline) structures which are related to those for more condensed mineral phases such as diamond,[1] $SrSi_2$,[9] α-$ThSi_2$,[10] rutile[11] and PtS.[12] Since coordination networks may possess large pores or channels,[12,13] which in principle might contain strategically located transition metal centers, there is interest in developing such systems as selective, heterogeneous catalysts.[14] A few reports have appeared on the use of tetrahedral ligands, in combination with Cu and Ag, as building blocks for construction of coordination networks.[1,2] Our work in this area is based on the tetrafunctional silane $Si(C_6H_4CN\text{-}p)_4$ **1**, which has been used to prepare Ag-containing networks.[15]

To our knowledge, there have been no reports on three-dimensional coordination networks based on early transition metal d^0 centers. Such materials might be expected to function as catalysts for a variety of reactions, including alkene polymerization.[16] Here we report initial efforts in this area, involving the synthesis and characterization of the titanium-containing network solid $[(TiCl_4)_2Si(C_6H_4CN\text{-}p)_4]\cdot 1.5C_7H_8$, which has a layered structure related to that of α-HgI_2.

Layering a solution of $TiCl_4$ (2 equiv.) in benzene over a solution of **1** in dichloromethane resulted in the slow precipitation of a yellow solid, which was isolated by filtration after 5 d and dried under vacuum for 4 h. By combustion and ^1H NMR analysis, this material is formulated as $(TiCl_4)_2Si(C_6H_4CN\text{-}p)_4\cdot 0.6C_6H_6$ **2a**.† Light-yellow crystals of **2b** were obtained in 55% yield by heating a sealed tube containing **2a** and toluene to 140 °C for 10 h, followed by slow cooling over 6 h to room temp.‡ The IR spectrum of **2b** exhibits bands for the nitrile groups which are blue shifted to 2231 and 2271 cm^{-1} with respect to the band for the tetrahedral ligand **1** (ν_{CN} 2229 cm^{-1}).[17]

The structure of **2b** consists of [4,2]-connected infinite layers formed by the linking of molecules of **1** by $TiCl_4$ units (Fig. 1).§ Each molecule of **1** is coordinated to four Ti centers, each of which links two units of **1** *via cis*-coordination of nitrile groups in the roughly octahedral titanium coordination sphere. There are two independent Ti centers in the unit cell, which possess slightly different bond distances and angles. The octahedral coordination geometries for the independent titanium centers are significantly distorted such that the '*trans*' chloride ligands form Cl–Ti–Cl angles of 162.31(3) and 160.67(7)°. These chloride ligands are associated with Ti–Cl distances [2.253(2)–2.310(2) Å] which are longer than those for chloride ligands *trans* to the nitrile groups [2.209(2)–2.241(2) Å]. The silicon centers are in distorted tetrahedral environments, such that the C–Si–C bond angles range from 103.2(2)–113.7(2)°. The N–Ti–N angles for the two pseudo-octahedra are 78.0(2) and 81.4(2)°. For comparison, Zaworotko has previously reported two-dimensional frameworks based on tetrahedral building blocks.[6]

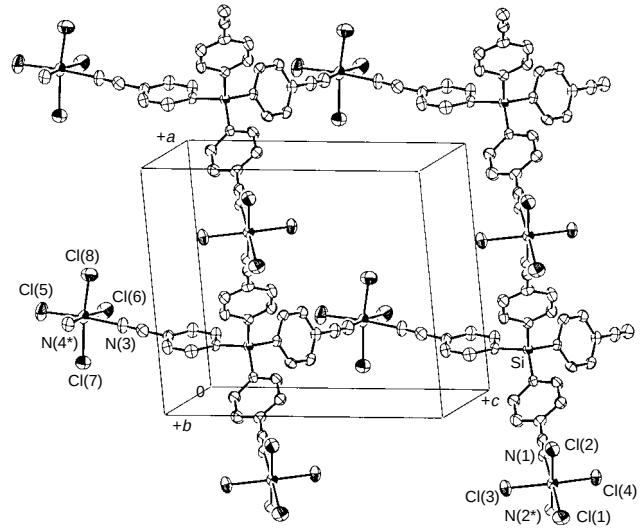

Fig. 1 ORTEP diagram illustrating part of a net in the structure of **2b**

The layers in the structure lie in the *ac* plane, and there are two such layers in each repeat along the *b*-axis, which are overlapping and related by centers of inversion in the structure. The tetrahedral ligands **1** form a square network in each net, with $TiCl_4$ groups protruding above and below the planes. A simplified drawing of two overlapping nets, illustrating their 'buckled' character, is given in Fig. 2. All of the 'upward' $TiCl_4$ groups pack in a rough column along the *b*-axis, as do all the 'downward' $TiCl_4$ groups. Disordered toluene molecules are packed between the layers, to fill voids in the structure. The two-dimensional framework of **2b** may therefore be described as a [4,2]-connected net, with tetraconnected silicon centers and biconnected titanium centers in a 1:2 ratio.[18] Thus, this

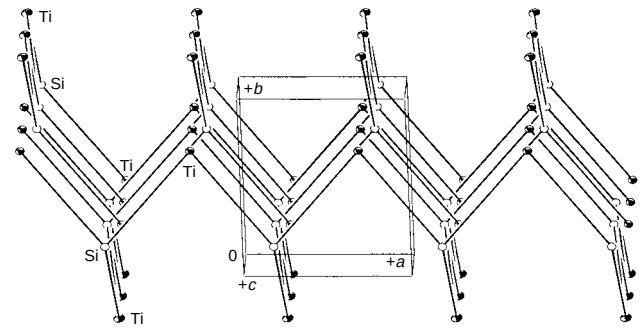

Fig. 2 A view of two overlapping nets in the structure of **2b**. The $-NCC_6H_4-$ linkages are depicted as long 'bonds', the titanium centers are shown as shaded ellipsoids, and the silicon atoms appear as unshaded ellipsoids.

structure is related to those adopted by some binary compounds with the AX_2 formula. Since the titanium centers link the tetrahedral building blocks **1** *via cis*-bonding of nitrile groups, the structure of **2b** is similar to that of α-HgI_2 in which the tetrahedral Hg centers lie in a plane.[19]

Thermogravimetry (TG) of **2a** and **2b** indicate that these networks are somewhat thermally unstable. Thus, the TG traces for these materials exhibit significant mass losses (*ca*. 32 and 35%, respectively) over the temperature range 25–280 °C, but **2a** loses mass much faster than **2b** during this step, which corresponds to loss of solvent as well as some decomposition of the framework. Both **2a** and **2b** exhibited the same decomposition step over the temperature range 340–500 °C.

A preliminary test of **2b** as a catalyst for the polymerization of propylene in the presence of triethylaluminium as cocatalyst (heptane solvent, 1 atm propylene) produced only 0.400 g of polypropylene from 0.190 g of **2b**.[20,21] The heptane-soluble fraction (atactic, M_n = 24 400; PDI = 3.3, by gel permeation chromatography using polystyrene standards) represented 75% of the sample by mass and the remaining (presumably isotactic) heptane-insoluble fraction (M_n = 93 000; PDI = 2.1) was slightly soluble in THF.

This work was supported by the Director, Office of Energy Research, Office of Basic Energy Sciences, Chemical Sciences Division, of the U.S. Department of Energy under Contract No. DE-AC03-76SF00098.

Footnotes and References

* E-mail: tdtilley@socrates.berkeley.edu

† The ^{1}H NMR spectrum of **2a** in [$^2H_6$]acetone revealed a 5 : 3 ratio of **1**[15] to benzene. Anal. Found: C, 44.87; H, 2.57; N, 6.37. Calc. for $C_{31.60}H_{19.60}Cl_8N_4SiTi_2$: C, 43.99; H, 2.29; N, 6.49%).

‡ The ^{1}H NMR spectrum of **2b** in [$^2H_6$]acetone revealed a 2 : 3 ratio of **1**[15] to toluene. Anal. Found: C, 47.87; H, 2.56; N, 5.82. Calc. for $C_{38.50}H_{28}Cl_8N_4SiTi_2$: C, 48.46; H, 2.96; N, 5.87%.

§ *Crystal data*: $C_{38.5}H_{28}Cl_8N_4SiTi_2$, M = 954.18, triclinic, space group $P\bar{1}$ (no. 2), a = 12.4273(5), b = 13.4378(5), c = 14.1035(5) Å, α = 110.423(1), β = 96.468(1), γ = 90.752(1)°, U = 2189.6(1) Å^3, Z = 2, D_c = 1.447 g cm^{-3}, μ(Mo-Kα) = 9.12 cm^{-1}, F(000) = 962. The data collection was performed at −86 °C with Mo-Kα radiation (λ = 0.710 69 Å) using a Siemens SMART diffractometer with a CCD area detector, by the ω–2θ scan method within the limits 3.00 < 2θ < 45.00°. The data were corrected for Lorentz and polarization effects. The structure was solved by direct methods (SIR 92) and refined by full-matrix least-squares analysis based on 4580 observed reflections [$I > 3.00\sigma(I)$] and 437 variable parameters and converged with unweighted and weighted agreement factors of R = 0.049, R_w = 0.062. All non-hydrogen atoms except those in the disordered solvent regions were refined anisotropically. CCDC 182/669.

1 B. F. Hoskins and R. Robson, *J. Am. Chem. Soc.*, 1990, **112**, 1546.
2 D. Venkataraman, S. Lee, J. S. Moore, P. Zhang, K. A. Hirsch, G. B. Gardner, A. C. Covey and C. L. Prentice, *Chem. Mater.*, 1996, **8**, 2030.
3 K. R. Dunbar, *Angew. Chem., Int. Ed. Engl.*, 1996, **35**, 1659.
4 O. M. Yaghi, C. E. Davis, G. Li and H. Li, *J. Am. Chem. Soc.*, 1997, **119**, 2861.
5 D. Venkataraman, G. B. Gardner, S. Lee and J. S. Moore, *J. Am. Chem. Soc.*, 1995, **117**, 11 600.
6 M. J. Zaworotko, *Chem. Soc. Rev.*, 1994, 283; S. B. Copp, S. Subramanian and M. J. Zaworotko, *Angew. Chem., Int. Ed. Engl.*, 1993, **32**, 706; C. Davies, R. F. Langler, C. V. K. Sharma and M. J. Zaworotko, *Chem. Commun.*, 1997, 567.
7 S. R. Batten, B. F. Hoskins and R. Robson, *J. Am. Chem. Soc.*, 1995, **117**, 5385.
8 L. Carlucci, G. Ciani, D. M. Proserpio and A. Sironi, *Angew. Chem., Int. Ed. Engl.*, 1996, **35**, 1088.
9 L. Carlucci, G. Ciani, D. M. Proserpio and A. Sironi, *J. Am. Chem. Soc.*, 1995, **117**, 12 861.
10 G. B. Gardner, D. Venkataraman, J. S. Moore and S. Lee, *Nature*, 1995, **374**, 792.
11 S. R. Batten, B. F. Hoskins and R. Robson, *J. Chem. Soc., Chem. Commun.*, 1991, 445.
12 B. F. Abrahams, B. F. Hoskins, D. M. Michall and R. Robson, *Nature*, 1994, **369**, 727.
13 G. B. Gardner, Y.-H. Kiang, S. Lee, A. Asgaonkar and D. Venkataraman, *J. Am. Chem. Soc.*, 1996, **118**, 6946.
14 M. Fujita, Y. J. Kwon, S. Washizu and K. Ogura, *J. Am. Chem. Soc.*, 1994, **116**, 1151.
15 F.-Q. Liu and T. D. Tilley, *Inorg. Chem.*, 1997, **36**, 5090.
16 J. Boor, Jr., *Ziegler-Natta Catalysts and Polymerizations*, Academic Press, New York, 1979.
17 B. N. Storhoff, *Coord. Chem. Rev.*, 1977, **23**, 1.
18 A. F. Wells, *Structural Inorganic Chemistry*, Clarendon Press, Oxford, 5th edn., 1984, p. 118.
19 A. F. Wells, *Structural Inorganic Chemistry*, Clarendon Press, Oxford, 5th edn., 1984, p. 196.
20 K. K. Kang, T. Shiono and T. Ikeda, *Macromolecules*, 1997, **30**, 1231.
21 Y. Doi, E. Suzuki and T. Keii, *Makromol. Chem., Rapid Commun.*, 1981, **2**, 293.

Received in Columbia, MO, USA; 18th August 1997; 7/06020C

Binuclear cyclopalladated cyclophanes: towards a new family of metallomesogens

Bernhard Neumann,[a] Torsten Hegmann,[a] Raik Wolf[b] and Carsten Tschierske*[a]

[a] *Martin-Luther-Universität Halle-Wittenberg, Institut für Organische Chemie, Kurt-Mothes-Straße 2, D-06120 Halle, Germany*
[b] *Martin-Luther-Universität Halle-Wittenberg, Institut für Pharmazeutische Technologie und Biopharmazie, Wolfgang-Langenbeck-Straße 4, D-06120 Halle, Germany*

Macrocyclic liquid crystals consisting of a biphenyl rigid core and a 2-phenylpyrimidine unit are fused by cyclopalladation giving a novel type of metallomesogens with nematic and smectic mesophases.

The continuing development of liquid-crystal-based technologies requires novel mesomorphic materials with special physical properties and much research has been carried out to prepare new types of liquid crystalline materials. In recent years metal containing liquid crystals have been developed and intensively investigated.[1] These metallomesogens allow the creation of quite unusual molecular geometries, which are difficult to achieve with purely organic materials. Additionally, interesting electronic and magnetic properties have been reported. Recently, another type of unconventional liquid crystals has been described. These are macrocyclic compounds incorporating conformationally flexible[2] or rigid[3] rod-like groups connected by appropriate flexible spacer units. It was found that they exhibit mesophases that are more stable than those of the corresponding low and high molecular mass open chain liquid crystals. Based on this observation we decided to synthesise macrocycles incorporating two different units. One of them is mainly responsible for the liquid crystalline properties whereas the other one should introduce a certain functionality, such as electron acceptor/donor properties,[4] photosensitivity or molecular recognition ability. Using the macrocycle approach these functional units can be connected with the mesogenic groups in a side specific manner, which should allow the tailoring of specific properties hopefully without losing the liquid crystalline properties.

Here, we describe the synthesis and the liquid crystalline behaviour of novel macrocyclic compounds which combine a 4,4′-substituted biphenyl core with a 2-phenylpyrimidine unit connected by polyether chains. The 2-phenylpyrimidine units can serve as ligands for the formation of liquid crystalline organometallics by orthopalladation.[5,6] In this way it should be possible to fuse two macrocyclic liquid crystals side by side. This novel molecular architecture combines a flat metallomesogenic heart with two additional calamitic mesogens.

The synthesis of the macrocycles **1** and **2** was carried out as outlined in Scheme 1 by cyclisation of 4,4′-bis[13-(toluenesulfonyloxy)-2,5,8,11-tetraoxatridecyl]biphenyl[7] or 4,4′-bis[12-(toluenesulfonyloxy)-4,7,10-trioxadodecyloxy]biphenyl† with 2-(hydroxyphenyl)-5-hydroxypyrimidine under high dilution conditions in the presence of potassium toluene-*p*-sulfonate (K^+OTs^-) as a template resulting in a yield of 21 and 35%, respectively. Correct spectral data which support the cyclic structure were obtained for both compounds.‡ The $[M + H]^+$, $[M + Na]^+$ and $[M + K]^+$ peaks in the electrospray MS§ correspond to the cyclic structures. No additional peaks could be detected in the scanned range up to $m/z = 2000$. Therefore other macrocycles with larger sizes should be absent.

The phase behaviour of the macrocycles was investigated by polarising microscopy. Compound **1** shows a monotropic nematic phase with a clearing temperature at 142 °C. The isotropic melt of compound **2** in which the polyether chains are connected *via* flexible methylene units with the biphenyl core can easily be supercooled to room temp. without transition to a liquid crystalline phase.

The orthopalladation reaction was carried out by reaction of the macrocyclic ligands **1** and **2** with $Pd(PhCN)_2Cl_2$[8] which leads in moderate yields (63 and 42%, respectively) to the corresponding metallomesogens **Pd1** and **Pd2** (Scheme 1). The ^1H NMR spectra of the complexes show a substitution pattern expected for palladium attack at C-2′ and one of the nitrogen atom of the phenylpyrimidine core. In negative ionization ESMS several peaks with typical isotopic pattern corresponding

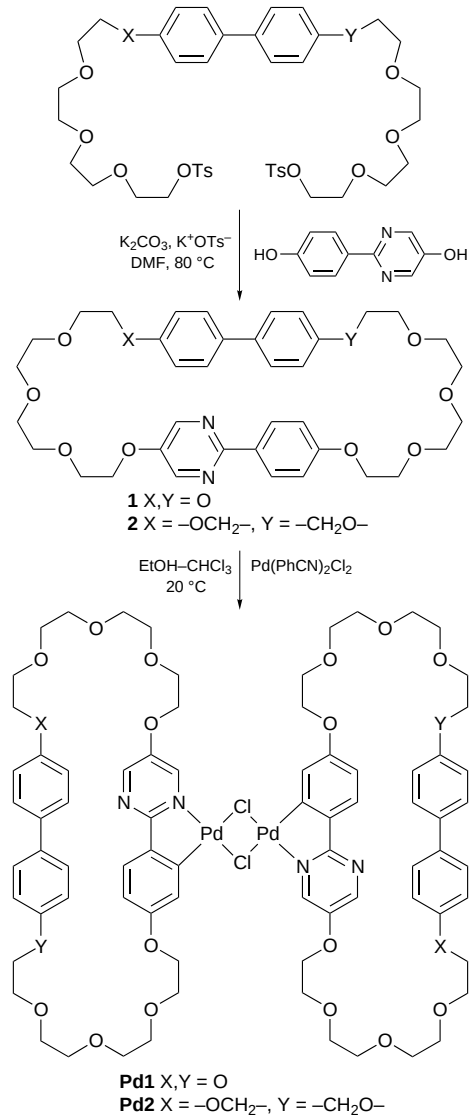

Scheme 1

Table 1 Phase transition temperatures (*T*/°C)

Compound	X	Y	cr		S_A		N		is
1	O	O	•	172	—	—	(•	142)	•
Pd1	O	O	•	168	•	208	•	226[a]	•
2	OCH_2	CH_2O	•	87	—	—	—	—	•
Pd2	OCH_2	CH_2O	•	118	—	—	(•	91)	•

[a] Decomposition.

to $[Pd_2(Cl)_2L_2 + Cl]^-$ occur.¶ From these results and from the structures of related 2-phenylpyrimidine-Pd^{II} complexes[5] we assume the complexes contain a dimetallic core in which each Pd^{II} atom is in a square geometry.

The phase transition temperatures of **Pd1** and **Pd2** are shown and compared with the free ligands in Table 1. Compound **Pd1** exhibits an enantiotropic nematic phase indicated by the typical *schlieren* texture and marbelled textures observable between crossed polarizers. The clearing temperature of the nematic phase is significantly enhanced in comparison to the parent macrocycle **1**. On cooling below 208 °C the transition to another enantiotropic phase takes place which is indicated by the occurrence of a focal conic fan texture. This can easily be homeotropically aligned and thus clearly indicates a smectic A phase.

The metallomesogen **Pd2** obtained from the non-mesomorphic cyclophane **2** shows exclusively a monotropic nematic phase with a clearing temperature at 91 °C.

The higher clearing temperatures of the complexes in comparison with the ligands, the formation of an S_A layer structure in the phase sequence of compound **Pd1**, and the induction of a liquid crystalline nematic phase in the metallomesogen **Pd2** indicate a significant mesophase stabilisation caused by the orthopalladation with formation of a fused macrocyclic ring system. The amount of mesophase stabilisation corresponds to that observed for the orthopalladation of conventional 2-phenylpyrimidines[5] and should result from the better intermolecular interaction due to the $Pd(\mu\text{-}X)_2Pd$ core as well as from their rigid molecular structure.

The unusual molecular shape of compounds **Pd1** and **Pd2** imposes the question concerning the type of the observed nematic phases. One can assume that they represent uniaxial nematic phases made up by the individual rod-shaped rigid building blocks. On the other hand the molecules as a whole can probably adapt a disc- or a board-like shape. Thus, the nematic phases could also be made up by disc-shaped molecules. However, the occurrence of a smectic layer structure as a low temperature mesophase in the phase sequence of compound **Pd1** and the complete miscibility of the nematic phases of **Pd1** and **Pd2** with those of calamitic compounds are in line with a nematic phase made up of rod like molecules.

Interestingly, a biaxial nematic phase was recently proposed for a macrocyclic liquid crystal.[9] However, no hint of the presence of a biaxial nematic phase‖ has been found for the macrocyclic metallomesogens **Pd1** and **Pd2**.

In summary, the macrocyclic 2-phenylpyrimidine derivatives **1** and **2** are able to form dinuclear metallomesogens. The orthopalladated compounds **Pd1** and **Pd2** represent a novel type of metallomesogens and form more stable liquid crystalline phases than the parent macrocyclic ligands.

This work was supported by the Deutsche Forschungsgemeinschaft and the Fonds der Chemischen Industrie.

Footnotes and References

* E-mail: coqfx@mlucom.urz.uni-halle.de

† Synthesised from 4,4′-bis[2-(2-(2-(2-hydroxyethoxy)ethoxy)ethoxy)-ethoxy]biphenyl].[7]

‡ *E.g.* **1**: ^{1}H NMR (400 MHz, $CDCl_3$, $SiMe_4$) 3.70–3.76 (m, 16 H, OCH_2), 3.86–3.93 (m, 8 H, OCH_2), 4.01 (t, ^3J 4.7 Hz, 2 H, OCH_2), 4.07–4.11 (m, 6 H, OCH_2), 6.77 (d, ^3J 8.8 Hz, 2 H, H-3′, 5′ Ph), 6.84 (d, ^3J 8.6 Hz, 2 H, H-3, 5 Ph), 6.89 (d, ^3J 9.0 Hz, 2 H, H-3, 5 *Ph*py), 7.25 (d, ^3J 8.8 Hz, 2 H, H-2′, 6′ Ph), 7.30 (d, ^3J 8.6 Hz, 2 H, H-2, 6 Ph), 8.17 (d, ^3J 9.0 Hz, 2 H, H-2, 6 *Ph*py) 8.32 (s, 2 H, H-4, 6 py); ESMS: *m/z* 691 $[M + H]^+$ (100), 713 $[M + Na]^+$ (35), 729 $[M + K]^+$ (8).

§ A solution of the compound in $CHCl_3$–MeOH–H_2O with a concentration of *ca.* 10 μg ml^{-1} was used for the ESMS investigations with a Finnigan MAT LCQ spectrometer.

¶ *E.g.*: **Pd1**: ^{1}H NMR (400 MHz, $CDCl_3$, $SiMe_4$) 3.70–3.73 (m, 32 H, OCH_2), 3.81–3.94 (m, 16 H, OCH_2), 4.08–4.12 (m, 16 H, OCH_2), 6.58 (d, ^3J 8.4 Hz, 2 H, H-5′ *Ph*py), 6.75 (d, ^3J 8.4 Hz, 4 H, H-3′, 5′ Ph), 6.84 (d, ^3J 8.4 Hz, 4 H, H-3, 5 Ph), 6.92 (s, 2 H, H-3′ *Ph*py), 7.26 (d, ^3J 8.4 Hz, 4 H, H-2′, 6′ Ph)), 7.32 (d, ^3J 8.4 Hz, 2 H, H-6′ *Ph*py) 7.36 (d, ^3J 8.4 Hz, 4 H, H-2, 6 Ph) 8.24 (s, br, 2 H, H-4 py) 8.32 (s, br, 2 H, H-6 py). ESMS (negative ionisation), *m/z* (relative intensity): 1704 (30), 1703 (49), 1702 (52), 1701 (78),1700 (98), 1699 (90), 1698 (100), 1697 (80), 1696 (60), 1695 (46), 1694 (34), 1693 (21) $[Pd_2(Cl)_2L_2 + Cl]^-$, 1727 (28), 1726 (33), 1725 (35), 1724 (47), 1723 (40), 1722 (54), 1721 (52), 1720 (51), 1719 (43), 1718 (35), 1717 (25) $[Pd_2(Cl)_2L_2 + AcO]^-$; ESMS/MS (parent ion 1662 ± 5, 29%) daughter ion *m/z*: 1628, 1627, 1626, 1625 $[Pd_2ClL_2 + H]^+$; ESIMS^n n = 3 (parent ion 1626 ± 5, 31%) daughter ion *m/z*: 799, 798, 797, 796, 795, 794, 793 $([PdL + H]^+)$.

‖ The absence of four-brush disclinations in the nematic *schlieren* textures was suggested as a hint on the biaxiality of nematic phases.[10] However, not only two-brush but also four-brush disclinations were found in the textures of the nematic phases of **Pd1** and **Pd2**.

1 *Metallomesogens*, ed. J. L. Serrano, VCH, Weinheim, 1996.
2 V. Percec and M. Kawasumi, *Adv. Mater.*, 1992, **4**, 573; V. Percec, A. D. Asandei and P. Chu, *Macromolecules*, 1996, **29**, 3736; V. Percec, P. J. Turkaly and A. D. Assandei, *Macromolecules*, 1997, **30**, 943, and references therein.
3 P. R. Ashton, D. Joachimi, N. Spencer, J. F. Stoddart, C. Tschierske, A. P. White, D. J. Williams and K. Zab, *Angew. Chem., Int. Ed. Engl.*, 1994, **33**, 1503; D. Joachimi, P. R. Ashton, C. Sauer, N. Spencer, C. Tschierske and K. Zab, *Liq. Cryst.*, 1996, **20**, 337.
4 B. Neumann, D. Joachimi and C. Tschierske, *Adv. Mater.*, 1997, **9**, 241.
5 M. Ghedini, D. Pucci, G. de Munno, D. Viterbo, F. Neve and S. Armentano, *Chem. Mater.*, 1991, **3**, 65; M. Ghedini, D. Pucci, R. Bartolino and O. Francescangeli, *Liq. Cryst.*, 1993, **13**, 255.
6 M. Ghedini, M. Longeri and R. Bartolino, *Mol. Cryst. Liq. Cryst.*, 1982, **84**, 207; M. Ghedini, S. Armentano and F. Neve, *Inorg. Chim. Acta*, 1987, **134**, 23; M. Ghedini, D. Pucci, G. D. Munno, D. Viterbo, F. Neve and S. Armentano, *Chem. Mater.*, 1991, **3**, 65; M. Marcos, M. B. Ros and J. L. Serrano, *Liq. Cryst.*, 1988, **3**, 1129; K. Praefcke, D. Singer and B. Gündogan, *Mol. Cryst. Liq. Cryst.*, 1992, **223**, 181; B. Gründogan and K. Praefcke, *Chem. Ber.*, 1993, **126**, 1253.
7 D. Armspach, P. R. Ashton, R. Ballardini, V. Balzani, A. Godi, C. P. Moore, L. Prodi, N. Spencer, J. F. Fraser, M. S. Tolley, T. J. Wear and D. J. Williams, *Chem. Eur. J.*, 1995, **1**, 33.
8 M. Ghedini and D. Pucci, *J. Organomet. Chem.*, 1990, **359**, 105.
9 J.-F. Li, V. Percec, C. Rosenblatt and O. D. Lavrentovich, *Europhys. Lett.*, 1994, **25**, 199.
10 S. Chandrasekhar, G. G. Nair, K. Praefcke and D. Singer, *Mol. Cryst. Liq. Cryst.*, 1996, **288**, 7 and references therein.

Received in Bath, UK, 22nd August 1997; 7/06485C

Mechanism of low thermal expansion in the cation-ordered Nasicon structure

David A. Woodcock,[a] Philip Lightfoot*[a] and Clemens Ritter[b]

[a] *School of Chemistry, University of St. Andrews, St. Andrews, Fife, UK KY16 9ST*
[b] *Institut Laue Langevin BP 156, 38042, Grenoble Cedex 9, France*

Variable temperature neutron powder diffraction data are used to pinpoint the mechanism of low thermal expansivity in the Nasicon-related material $Sr_{0.5}Ti_2(PO_4)_3$; this behaviour is contrasted with that of the parent phase $NaTi_2(PO_4)_3$.

There has recently been considerable interest in materials displaying the remarkable property of negative, or very low, thermal expansivity. New materials displaying this property include $ZrP_{2-x}V_xO_7$[1] and ZrW_2O_8,[2] but by far the most widely studied types have been the Nasicon or NZP family, based on the $NaZr_2(PO_4)_3$ structure.[3–5] The NZP structure is a three-dimensional lattice consisting of vertex-linked TiO_6 and PO_4 polyhedra, with the large Na cation occupying interstitial trigonal prismatic (MI) sites spaced at intervals along the *c*-axis (Fig. 1). $NaZr_2(PO_4)_3$ itself crystallises in space group $R\bar{3}c$, having only one crystallographically distinct Na site. A wide variety of adaptations may be made to the basic NZP stoichiometry by substitutions at all three non-oxygen sites. One such series is $M_{0.5}Ti_2(PO_4)_3$, where M is a divalent cation (Ca, Sr, Ba). The Ca and Sr compounds adopt the lower symmetry $R\bar{3}$ space group owing to alternate ordering of M and vacancy along the *c*-axis, leading to crystallographically distinct MIa and MIb sites. Measurements of lattice parameter evolution *vs.* temperature, by X-ray powder diffraction, have shown that, in general, the thermal expansivity behaviour of the $R\bar{3}c$ and $R\bar{3}$ families is different, with the former showing a positive coefficient of the *c*-axis expansivity (α_c) and a negative coefficient of the *a*-axis expansivity (α_a), while the situation for the $R\bar{3}$ family is reversed.[5,6] Although a very elegant general model has been proposed to describe the thermal behaviour of these materials, in terms of cooperative rotations of linked polyhedra,[7,8] the specific issue of the contrasting behaviour of the $R\bar{3}c$ and $R\bar{3}$ series has not been satisfactorily addressed. Here, we show that this behaviour is directly related to the cation-vacancy ordering, and is due to the compressibility of the vacant site along the *c*-axis.

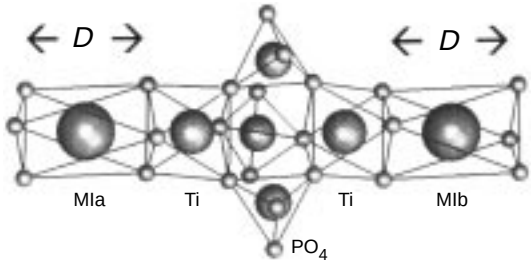

Fig. 1 Portion of the ideal NZP structure showing packing of polyhedral units along the *c*-axis. In $Sr_{0.5}Ti_2(PO_4)_3$ the MIa site (0,0,0) is fully occupied while the MIb site (0,0,1/2) is vacant. The parameter *D* refers to the O···O distance along the *c*-axis.

Samples were prepared from stoichiometric quantities of TiO_2, $(NH_4)_2HPO_4$ and Na_2CO_3 or $SrCO_3$. Thoroughly ground mixtures were preheated at 200 °C, followed by subsequent heat treatments at 600, 900 and 1000 °C with intermediate regrinding. For the Sr sample a final treatment at 1200 °C was required. Neutron diffraction data were collected on the high flux diffractometer D1B at the ILL, Grenoble, using a wavelength of 2.522 Å and a fixed detector bank covering 80° in 2θ. In order to determine the thermal evolution of the lattice parameters, a series of 123 short (*ca.* 10 min) scans was collected over the range $25 < T < 835$ °C. These scans were refined with the cyclic version of the refinement program FULLPROF[9] using the result for a run at a given temperature as input file for the following run with slightly higher temperature. Runs at selected temperatures were then chosen for detailed structural analysis. Rietveld refinement was carried out using the GSAS package.[10] The starting model for the refinement of the $Sr_{0.5}Ti_2(PO_4)_3$ structure was taken from Senbhagaraman *et al.*[11] A typical refinement consisted of 17 structural para-

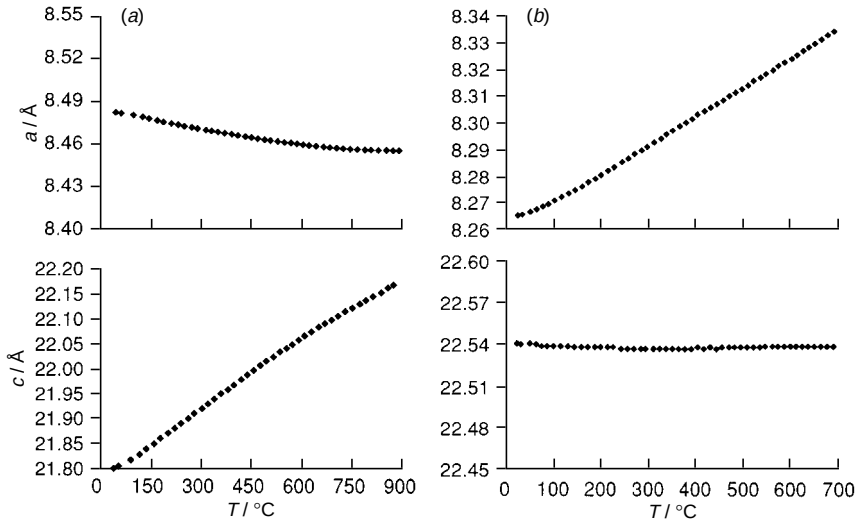

Fig. 2 Thermal evolution of lattice parameters for (*a*) $NaTi_2(PO_4)_3$ and (*b*) $Sr_{0.5}Ti_2(PO_4)_3$

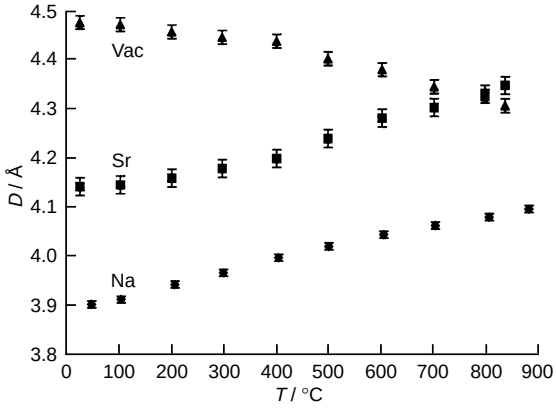

Fig. 3 Thermal evolution of the trigonal prismatic MI sites (*i.e.* O···O distance, *D*, along the *c*-axis). In $NaTi_2(PO_4)_3$ the *c*-axis expansivity is governed by $2 \times D$(Na), in $Sr_{0.5}Ti_2(PO_4)_3$ by *D*(Sr) + *D*(vac).

meters, with 400 data points and 80 contributing reflections over the range $18 < 2\theta < 98°$.

Plots of the thermal evolution of the lattice parameters for both compounds are shown in Fig. 2. Values of α_a and α_c are -5.3 and 20.8×10^{-6} °C^{-1} for $NaTi_2(PO_4)_3$ in the range 25–500 °C and 13.2 and -0.02×10^{-6} °C^{-1} for $Sr_{0.5}Ti_2(PO_4)_3$ in the range 25–800 °C, which are in good agreement with those reported by earlier studies.[5,6,12] Although thermal evolution of lattice parameters by X-ray powder diffraction has been carried out for both these samples, the present study provides, for the first time, precise structural details by neutron diffraction, which allows us to pinpoint the mechanism of their behaviour. One of the most significant trends is the near-zero expansivity of the *c*-axis for the Sr compound. It has previously been suggested that the largest contribution to the expansivity in NZP materials is the expansion of the Na–O bond itself. This governs the 'size' of the trigonal prismatic site along the *c*-axis (*i.e.* the O–O contact), which is plotted in Fig. 3. In the case of the Sr compound in $R\bar{3}$ there are two such sites to consider, the Sr site and the vacancy site, which are confirmed to be completely ordered from the refinements. It can be seen that, in the Na compound this site expands, by *ca*. 0.20 Å over the full temperature range, accounting completely for the overall expansivity α_c (two per unit cell), whereas in the Sr compound there is an expansion of the Sr site but a contraction of the vacancy site. These two almost exactly cancel out, resulting in the observed near-zero expansion coefficient, α_c. These parameters in turn result in the cooperative polyhedral rotations described by earlier workers, and lead to the expansivities along the *a*-axis. A full analysis of these effects will be the subject of a later paper, but the fundamental explanation of the *c*-axis expansivity lies simply in the relative expansion/contraction of the occupied and vacant MI sites. The anomaly previously observed in the case of $Ca_{0.5}Zr_2(PO_4)_3$, which shows the behaviour of an $R\bar{3}c$ structure rather than an $R\bar{3}$ structure[13] lies in the fact that in that case both the Ca site and the vacancy site expand with temperature, resulting in a net expansion of the *c*-axis. Apparently the smaller vacancy site in that case (*ca*. 4.1 Å at 25 °C) is not as compressible as the vacancy site in the present phase. A diffraction experiment cannot differentiate whether the unusual behaviour of the Sr phase is due to cation-ordering *per se* or merely the presence of equal numbers of filled and vacant MI sites. However, it is interesting to note that a larger value of $\alpha_c = 1.37 \times 10^{-6}$ °C^{-1} has been reported for $Ba_{0.5}Ti_2(PO_4)_3$, which crystallises in the disordered $R\bar{3}c$ structure type.[6] A comparative, detailed neutron diffraction study of the Sr and Ba materials is therefore currently in progress.

We would like to thank the EPSRC for the provision of a studentship to D. A. W., and Mr C. J. Milne for help in collecting the neutron diffraction data.

Footnote and References

* E-mail: pl@st-and.ac.uk

1 V. Korthuis, N. Khosrovani, A. W. Sleight, N. Roberts, R. Dupree and W. R. Warren, *Chem. Mater.*, 1995, **7**, 412.
2 T. A. Mary, J. S. O. Evans, T. Vogt and A. W. Sleight, *Science*, 1996, **277**, 90.
3 T.Oota and I. Yamai, *J. Am. Ceram. Soc.*, 1986, **69**, 1.
4 J. Alamo and R. Roy, *J. Am. Ceram. Soc.*, 1984, **67**, C78.
5 E. Breval and D. K. Agrawal, *Br. Ceram. Trans.*, 1995, **94**, 27.
6 C.-Y. Huang, D. K. Agrawal and H. A. McKinstry, *J. Mater. Sci.*, 1995, **30**, 3509.
7 G. E. Lenain, H. A. McKinstry, J. Alamo and D. K. Agrawal, *J. Mater. Sci.*, 1987, **22**, 17.
8 J. Alamo, *Solid State Ionics*, 1993, **63**–**65**, 547.
9 J. Rodriguez-Carvajal, *Physica B*, 1993, **192**, 55.
10 A. C. Larson and R. B. Von Dreele, Los Alamos National Laboratory Report No. LA-UR-86-748, 1987.
11 S. Senbhagaraman, T. N. Guru Row and A. M. Umarji, *J. Mater. Chem.*, 1993, **3**, 309.
12 J. L. Rodrigo, P. Carrasco and J. Alamo, *Mater. Res. Bull.*, 1989, **24**, 611.
13 J. Alamo and J. L. Rodrigo, *Solid State Ionics*, 1993, **63**–**65**, 678.

Received in Bath, UK, 19th September 1997; 7/06928F

Synthesis and optical sensing properties of a boronic acid appended rhenium(I) complex for sugar

Vivian Wing-Wah Yam* and Alex Sze-Fai Kai

Department of Chemistry, The University of Hong Kong, Pokfulam Road, Hong Kong, PR China

A rhenium(I) complex with boronic acid pendant is synthesized and characterized; the complex is shown to exhibit pH dependent electronic absorption characteristics; the photophysical properties and sugar sensing behaviour are also investigated.

Boronic acids, which have been known to form covalently bonded complexes with diols in aqueous system, have attracted a great deal of attention as an interactive tool for sugar recognition.[1,2] Much attention has been focused on the application of boronic acids with organic backbones as fluorescent chemosensors for sugars.[2] Although there were reports on the synthesis of iron(II) complexes with boronic acid-containing ligands, they were mainly confined to those of electrochemical[3] and circular dichroism (CD) spectroscopic studies.[4] There has been, to the best of our knowledge, no report of transition metal coordination/organometallic compounds of this kind employed as absorbance or luminescence probes. With our recent interest in the utilization of metal-to-ligand charge transfer (MLCT) excited states as spectrochemical and luminescence probes as well as in the study of host–guest interactions,[5] an attempt to extend our attention to sugar recognition was pursued. Herein are reported the synthesis and luminescence behaviour of a rhenium(I) complex **1** with boronic acid pendant. The changes in the electronic absorption and luminescence properties induced by the presence of various types of mono- and di-saccharides have been investigated and the binding constants determined using spectrochemical methods. Complexes **2** and **3** have also been synthesized for comparative spectrochemical studies. All complexes **1**–**3** have been characterized by ^{1}H NMR, IR spectroscopy and positive FAB mass spectrometry, and gave satisfactory elemental analyses.†

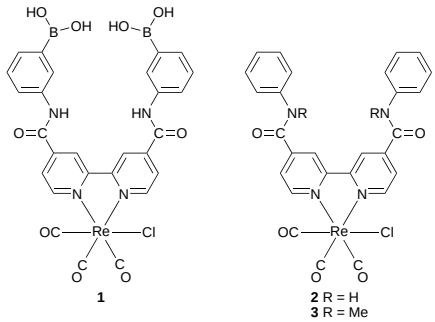

The UV–VIS spectrum of complex **1** shows a low energy absorption band at *ca*. 370 nm, typical of the MLCT transition of rhenium(I) diimines.[6] Excitation of an aqueous solution of **1** at λ = 430 nm showed an intense luminescence at *ca.* 620 nm, which is typical of the phosphorescence derived from the triplet rhenium-to-diimine metal-to-ligand charge transfer (^{3}MLCT) excited state.[6] Both the MLCT absorption and emission bands in Me_2SO–H_2O (1 : 1 v/v) were found to show a blue shift in energy as the pH[7] was increased. Besides the blue shift from *ca.* 670 nm in acidic medium to *ca.* 620 nm in alkaline medium was observed in the emission maxima, a rise in emission intensity was found to occur as the pH increased. The pK_a of **1** was found to be 5.9, which we attributed to hydroxide capture by the boronic acid group. A typical pK_a of *ca.* 9 was reported for phenylboronic acid in aqueous solution,[8] quite different from the medium used in the present system. It is believed that coordination of the ligand to the metal centre would stabilize the boronate pendant and hence lowered its pK_a value. A similar pK_a has been obtained in a separate experiment using a universal phosphate–citrate buffer with constant ionic strength.[9] In order to choose an optimum working pH for the sugar binding studies, the absorption spectra of **1** at pH 5.5–10.5 both in the absence and in the presence of 0.2 mol dm^{-3} D-fructose were measured. D-Fructose was chosen as it has previously been reported to show the largest spectral change among the various types of saccharides studied.[1,2,8] The largest spectral change induced by D-fructose was observed at pH 8.3 for **1**, which was thus employed for our subsequent measurements.

The UV–VIS spectral traces of **1** in glycine–NaOH buffer[10] at pH 8.3 in the presence of various amounts of added D-fructose showed an isosbestic point at *ca*. 350 nm. Fig. 1 depicts the titration curve of **1** with different sugar substrates. D-Fructose was found to induce the largest spectral change of **1**. By applying the equation $A_0/(A_0 - A) = (\varepsilon_0/\varepsilon_0 - \varepsilon)[(1/K[S]) + 1]$[11] and a plot of $A_0/(A_0 - A)$ *vs.* $[S]^{-1}$, the stability constants K could be obtained from the ratio slope/*y*-intercept, where A_0 and A are the respective absorbances at 376 nm in the absence and in the presence of saccharide S with concentration [S], and ε_0 and ε are the absorption coefficients for the free and sugar-bound rhenium(I) complex, respectively. The stability constants for 1 : 1 complexation in glycine–NaOH buffer : Me_2SO (1 : 1 v/v) are: D-fructose (log K = 2.40); L-arabinose (log K = 1.56); D-galactose (log K = 1.54); D-mannose (log K = 1.29); D-glucose (log K = 1.18); maltose (log K = 0.91); lactose (log K = −0.37). It was found that D-fructose gives the largest log K value. Similar trends have also been observed in the related organic systems.[1,2]

The selective preference of **1** for mono- over di-saccharides has been attributed to the covalent bonding interaction of the hydroxyl groups on the saccharides to the boronate ions; the

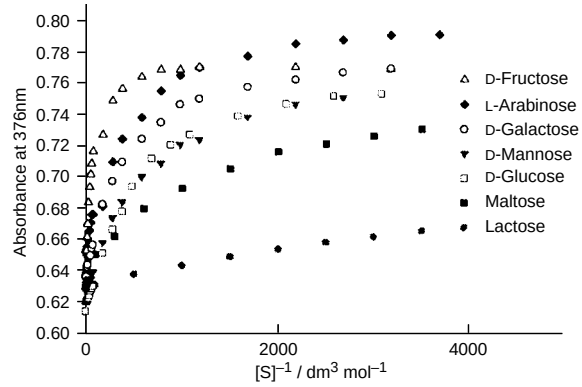

Fig. 1 Plot of absorbance of **1** (0.1 mM) at 376 nm in glycine–NaOH buffer : Me_2SO (1 : 1 v/v) at pH 8.3 as a function of sugar concentration for selected sugars

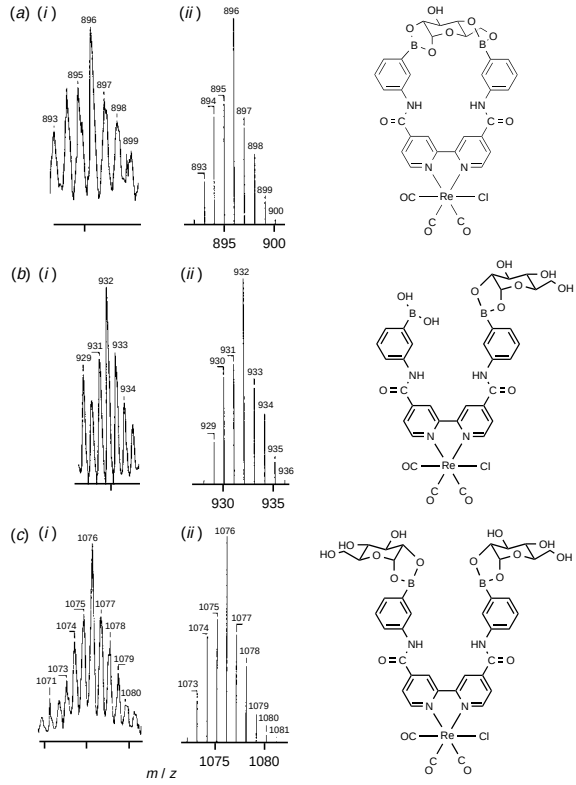

Fig. 2 Expanded ion cluster from the negative FAB mass spectrum of a buffered solution containing **1** and D-glucose. (*a*) (*i*) *m*/*z* 896, (*ii*) simulated isotope pattern for $ReB_2C_{33}ClH_{24}N_4O_{11}$; (*b*) (*i*) *m*/*z* 932, (*ii*) simulated isotope pattern for $ReB_2C_{33}ClH_{28}N_4O_{13}$; (*c*) (*i*) *m*/*z* 1076, (*ii*) simulated isotope pattern for $ReB_2C_{39}ClH_{36}N_4O_{17}$.

selectivity of which is controlled by the size of cavity as governed by the two boronate groups. The existence of the 1:1 complex of **1** with D-glucose was established by negative FAB mass spectrometry. Fig. 2 shows the expanded ion clusters observed in the mass spectrum of a mixture of **1** and D-glucose. The binding of monosaccharides, like D-glucose, to **1** gave both 1 : 1 cyclic and 1 : 1 non-cyclic bound species at low saccharide concentrations. At high concentration of saccharides, apart from the 1 : 1 complexes, the 1 : 2 complex also exists. The site of binding has also been confirmed by related studies using the analogous complex **2** in which the boronic acid groups were absent as a control. Unlike **1**, addition of D-fructose to **2** at pH 8.3 induces no spectral change, indicative of the importance of the boronic acid pendants in the binding action. However, as the pH is increased to 12.1, both **1** and **2** showed a similar increase in the absorbance upon addition of D-fructose with the absence of isosbestic points in the electronic absorption spectral traces. It is likely that under such high pH conditions, deprotonation of the amide group would occur to bind the saccharides. Deprotonation of the amido proton has been reported to occur at high pH. Organic amides such as benzanilide and *p*-bromobenzanilide showed pK_a values of 16.53 and 15.73, respectively;[12] the pK_a values are dependent on the electronic factors with electron withdrawing substituents stabilizing the imide anion, and lowering the pK_a value. The emissive behaviour of **1** and **2** is similar, each showing an emission maximum at *ca*. 620 nm, the intensity of which increased significantly upon addition of sugars. Similar changes in the emission behaviour were not observed for **1** and **2** at pH 8.3. In order to investigate the behaviour of complex **2** under high pH condition, complex **3** was prepared in which the amido protons were replaced by methyl substituents. Unlike complexes **1** and **2**, the addition of D-fructose to **3** at pH 12.1 induces no spectral change. It is worth noting that the role played by the amido group in sugar binding at high pH values should not be overlooked. Work is in progress to explore the potential of such binding properties.

V. W.-W. Y. acknowledges financial support from the Croucher Foundation. A. S.-F. K. acknowledges the receipt of the Croucher Studentship and the Croucher Scholarship, both administered by the Croucher Foundation.

Footnotes and References

* E-mail: wwyam@hkucc.hku.hk

† **1**: ^{1}H NMR [300 MHz, $(CD_3)_2SO$, 298 K, relative to TMS]: δ 7.40 (q, 2 H, aryl), 7.63 (d, 2 H, aryl), 7.93 (d, 2 H, aryl), 8.07 (s, 2 H, aryl), 8.13 (s, 4 H, OH), 8.21 (dd, 2 H, bipyridyl), 9.24 (dd, 2 H, bipyridyl), 9.26 (s, 2 H, bipyridyl), 10.83 (s, 2 H, amido). **2**: ^{1}H NMR [300 MHz, $(CD_3)_2SO$, 298 K, relative to TMS]: δ 7.20 (t, 2 H, aryl), 7.43 (t, 4 H, aryl), 7.79 (d, 4 H, aryl), 8.18 (dd, 2 H, bipyridyl), 9.25 (dd, 2 H, bipyridyl), 9.26 (s, 2 H, bipyridyl), 10.87 (s, 2 H, amido). **3**: ^{1}H NMR [300 MHz, $(CD_3)_2SO$, 298 K, relative to TMS): δ 3.33 (s, 6 H, Me), 7.17 (m, 10 H, aryl), 7.32 (dd, 2 H, bipyridyl), 8.32 (s, 2 H, bipyridyl), 8.74 (dd, 2 H, bipyridyl). Positive FABMS: ion cluster at *m*/*z* 725 [M^+].

1 J. P. Lorand and J. D. Edwards, *J. Org. Chem*., 1959, **24**, 769.
2 *Fluorescent Chemosensors for Ion and Molecular Recognition*, ed. A. W. Czarnik, ACS, Washington, 1993; *Chemosensors of Ion and Molecular Recognition*, ed. J. P. Desvergne and A. W. Czarnik, NATO ASI Series C, Kluwer Academic Press, Dordrecht, 1997, vol. 492; T. D. James, K. R. A. S. Sandanayake and S. Shinkai, *Chem. Commun*., 1996, **3**, 281; J. Y. Yoon and A. W. Czarnik, *J. Am. Chem. Soc.*, 1992, **114**, 5874.
3 A. Ori and S. Shinkai, *J. Chem. Soc., Chem. Commun*., 1995, **15**, 1771; H. Yamamoto, A. Ori, K. Ueda, C. Dusemund and S. Shinkai, *Chem. Commun*., 1996, **3**, 407.
4 K. Nakashima and S. Shinkai, *Chem. Lett*., 1994, 1267.
5 V. W. W. Yam, K. M. C. Wong, V. W. M. Lee, K. K. W. Lo and K. K. Cheung, *Organometallics*, 1995, **14**, 4034; V. W. W. Yam, K. K. W. Lo and K. K. Cheung, *Inorg. Chem*., 1995, **34**, 4013; V. W. W. Yam, K. K. W. Lo, K. K. Cheung and R. Y. C. Kong, *J. Chem. Soc., Dalton Trans.*, 1997, 2067; V. W. W. Yam, V. W. M. Lee, F. Ke and K. W. M. Siu, *Inorg. Chem*., 1997, **36**, 2124; V. W. W. Yam and V. W. M. Lee, *J. Chem. Soc., Dalton Trans.*, 1997, 3005.
6 M. S. Wrighton and K. L. Morse, *J. Am. Chem. Soc*., 1974, **96**, 998; A. J. Lees, *Comments Inorg. Chem*., 1995, **17**, 319, K. Kalyanasundaram, *Photochemistry of Polypyridine and Porphyrin Complexes*, Academic Press, London, 1992; O. Horváth and K. L. Stevenson, *Charge Transfer Photochemistry of Coordination Compounds*, VCH, New York, 1993; J. V. Caspar, B. P. Sullivan and T. J. Meyer, *Inorg. Chem*., 1984, **23**, 2104.
7 All pH values quoted in H_2O–Me_2SO (1 : 1 v/v) are apparent pH* values, with pH* = pH − δ, where δ is taken to be 0.45 (from R. G. Bates, M. Paabo and R. A. Robinson, *J. Phys. Chem*., 1963, **67**, 1833 and G. Douheret, *Bull. Soc. Chim. Fr*., 1968, 513).
8 H. Nakatani, T. Morita and K. Hiromi, *Biochim. Biophys. Acta*, 1978, **525**, 423; J. Juillard and N. C. R. Geugue, *Acad. Paris C*, 1967, **264**, 259.
9 P. J. Elving, J. M. Markowitz and I. Rosenthal, *Anal. Chem*., 1956, **28**, 1179.
10 D. D. Perrin and B. Dempsey, *Buffers for pH and Metal Ion Control*, Chapman and Hall, London, 1974.
11 S. Fery-Forgues, M. T. Le Bris, J. P. Ginette and B. Valeur, *J. Phys. Chem*., 1988, **92**, 6233; J. Bourson and B. Valeur, *J. Phys. Chem*., 1989, **93**, 3871.
12 K. Bowden, *Chem. Rev*., 1996, **66**, 119.

Received in Cambridge, UK, 15th September 1997; 7/06656B

Novel channel-type inclusion compounds of 3-epiursodeoxycholic acid

Yasuhito Miyake, Junji Hirose, Yasuhiro Hasegawa, Kazuki Sada and Mikiji Miyata*

Material and Life Science, Graduate School of Engineering, Osaka University, Yamadaoka, Suita, Osaka 565, Japan

A new host, 3-epiursodeoxycholic acid, forms inclusion crystals with naphthalene derivatives with 1 : 1 stoichiometry.

Ursodeoxycholic acid (3α,7β-dihydroxy-5β-cholan-24-oic acid **1**), one of the bile acids, is well-known as a medicine,[1] originally isolated from the gall of bears.[2] Compound **1** and its 3β-isomer, 3-epiursodeoxycholic acid **2**, were believed to yield only guest-free crystals in the presence of organic substances,[3,4] although other bile acids, such as deoxycholic acid and cholic acid, tend to form inclusion crystals.[5] In contrast, our recent research has revealed that **2** includes a wide range of organic compounds. Here we report that **2** forms a layered assembly with large channels where naphthalene derivatives are included in a 1 : 1 host-to-guest ratio.

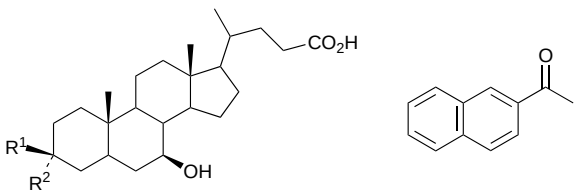

1 R^1 = H, R^2 = OH
2 R^1 = OH, R^2 = H

3

Compound **2** was prepared from commercially available **1** as described in the literature.[6] The acid was recrystallized from neat organic liquids, or from alcoholic solvents dissolving the third solid components.[7] The resulting crystals were characterized by thermogravimetric analysis, and solid state IR and ^{1}H NMR spectroscopy. A wide variety of organic compounds, such as aromatic and aliphatic alcohols, ketones, ethers, esters and so on, were included by **2** as a host, whereas they were not included by **1**. Table 1 shows a number of the inclusion compounds. It is noteworthy that **2** includes both small ketones such as pentan-3-one and naphthalene derivatives such as 2′-acetonaphthone **3** in a 1 : 1 molar ratio of host to guest. We did not observe such an inclusion in the case of other bile acids and their derivatives. For example, deoxycholic acid formed inclusion compounds with **3** in a 3 : 1 molar ratio of host to guest.

Table 1 Inclusion ability of **2** with various organic compounds

Guest	Host–guest ratio
4-Methylpentan-2-ol	1 : 1 [a,b]
2-Methylpentan-1-ol	1 : 1 [a,b]
Isobutyl acetate	1 : 1 [a,b]
Propyl propionate	1 : 1 [a,b]
Ethyl benzoate	1 : 1 [a,b]
Pentan-2-one	1 : 1 [a,b]
Pentan-3-one	1 : 1 [a,b]
4-Methylcyclohexanone	1 : 1 [a,b]
Acetophenone	1 : 1 [a,b]
Anisole	1 : 1 [a,b]
Ethylbenzene	1 : 1 [a,b]
n-Propylbenzene	1 : 1 [a,b]
Styrene	1 : 1 [a,b]
o-Xylene	1 : 1 [a,b]
2′-Acetonaphthone	1 : 1 [b]
1′-Hydroxy-2′-acetonaphthone	1 : 1 [b]
2-Methylnaphthalene	1 : 1 [b]
1-Methoxynaphthalene	1 : 1 [b]

[a] Determined by thermogravimetric analysis–differential scanning calorimetry. [b] Determined by ^{1}H NMR spectroscopy.

X-Ray powder diffraction studies showed that the inclusion compounds have very similar structures, indicating that the inclusion crystals have similar molecular assembly modes. This was confirmed by single crystal X-ray structural analysis. Single crystals suitable for analysis were obtained by recrystallization of **2** with **3**.† Fig. 1 depicts the crystal packing of the inclusion compound viewed along the crystallographic *c* axis. It can be seen that the host molecules are arranged in a 'chicken-wire' network with large channel-type inclusion spaces. The molecular assembly mode is quite unique, as inclusion crystals of other bile acids tend to form bilayered structures.[5] All the host molecules are connected by hydrogen bonds. The helical network has the sequence O(3)H··O(7)H··O(24a)=C–O(24b)H··O(3)H, where the hydrogen bonding distances are 2.744(5), 2.894(5) and 2.595(4) Å, respectively.

The channel was analysed as a space filling model, which showed that the channel could be described as a straight pillar with a rectangular cross-section of approximate dimensions 7.4 × 11.5 Å. The guest molecules are accommodated in the channels with only van der Waals contacts. It is interesting that **3** arranges perpendicular to the channel and forms a column along the crystallographic *c* axis. In the column, **3** stacks with a distance of 3.51 Å, which corresponds to half of the crystal *c* dimension (7.020 Å). The space filling model of one column is depicted in Fig. 2.

In addition, we obtained single crystals *via* recrystallization of **2** from pentan-3-one. The X-ray measurement at 193 K indicated that the guest molecules were disordered in the channels. This indicates that the guest molecules are too small in size to provide thermally stable inclusion compounds.

In conclusion, this study demonstrates that **2** forms inclusion compounds with a wide range of organic compounds. These form a new channel-type large inclusion space as compared with any other bile acids, enabling the inclusion naphthalene derivatives with 1 : 1 stoichiometry.

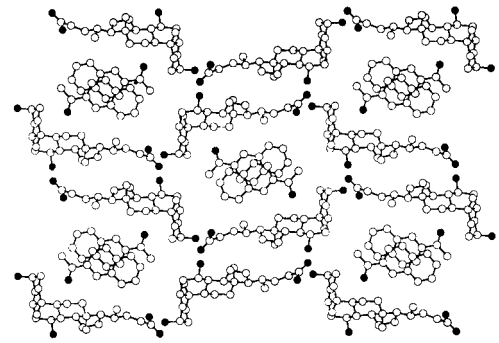

Fig. 1 The crystal structure of a 1 : 1 complex between **2** and **3** viewed down the crystallographic *c* axis. Carbon and oxygen atoms are represented by empty and filled circles, respectively. Hydrogen atoms are omitted for clarity.

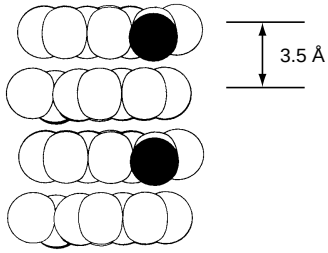

Fig. 2 Schematic drawing of one column of **3** in the inclusion space. Carbon and oxygen atoms are represented by empty and filled circles, respectively.

This work was supported by a Grant-in-Aid for Scientific Research from the Ministry of Education, Science, Sports and Culture, Japan.

Footnotes and References

* E-mail: miyata@ap.chem.eng.osaka-u.ac.jp

† *Crystal data* for **2·3**: $C_{24}H_{40}O_4{\cdot}C_{12}H_{10}O_1$, M = 562.79, orthorhombic, space group $P2_12_12_1$, a = 15.81(1), b = 28.106(3), c = 7.0207(8) Å, V = 3120(1) Å^3, Z = 4, D_c = 1.198 g cm^{-3}. Intensity data were collected on Rigaku RAXIS-IV diffractometer with graphite-monochromated Mo-Kα radiation. 2683 Reflections were unique, and 1583 observed reflection with $|F_o| > 3\sigma(|F_o|)$ were used for further calculations after Lorentz and polarization corrections. The structure was solved by direct methods (SIR92) and refined against the F_o data by full-matrix least-squares methods. All non-hydrogen atoms were refined anisotropically. Hydrogen atoms attached to carbon were placed in calculated positions, while O–H positions were obtained from difference Fourier synthesis. A total of 370 parameters were refined to final residuals R = 0.037 and Rw = 0.040. All calculations were performed using the TEXSAN crystallographic software package of the Molecular Structure Corporation. CCDC 182/665.

1 A. Ward, R. N. Brodgen, R. C. Heel, T. M. Speight and G. S. Avery, *Drugs*, 1984, **27**, 95.
2 M. Shoda, *J. Biochem.* (*Tokyo*), 1927, **7**, 505.
3 T. Higuchi, S. Kamitori, K. Hirotsu and H. Takeda, *Yakugaku Zasshi*, 1985, **105**, 1115; P. F. Lindley and M. C. Carey, *J. Crystallogr. Spectrosc. Res.*, 1987, **17**, 231.
4 T. Higuchi, N. Yabe and H. Takeda, *Yakugaku Zasshi*, 1992, **112**, 563.
5 M. Miyata and K. Sada, in *Comprehensive Supramolecular Chemistry*, ed. D. D. MacNicol, F. Toda and R. Bishop, Pergamon, Oxford, 1996, vol. 6, p. 147.
6 A. K. Bose, B. Lal, W. A. Hoffmann, III and M. S. Manhas, *Tetrahedron Lett.*, 1973, **18**, 1619.
7 K. Nakano, K. Sada and M. Miyata, *Chem. Lett.*, 1994, 137.

Received in Cambridge, UK, 21st July 1997; 7/05184K

Novel synthesis of calamitic and discotic liquid crystalline derivatives of tetrathiafulvalene (TTF)

Richard A. Bissell,[a] Neville Boden,[a] Richard J. Bushby,*[a] Colin W. G. Fishwick,[a] Edward Holland,[a] Bijan Movaghar[a] and Goran Ungar[b]

[a] *Centre for Self-Organising Molecular Systems (SOMS), University of Leeds, Leeds, UK LS2 9JT*
[b] *Department of Engineering Materials, University of Sheffield, Sheffield, UK S1 3JD*

A synthesis has been developed for both calamitic and discotic mesogens based on the bis(phenylenedithio-TTF) (BPhDT-TTF) nucleus.

Only recently has attention been given to the charge transport properties of liquid crystals and the new applications that could stem from them.[1] Well defined hole transits have been obtained from the columnar phases of discotic liquid crystals[2] and it has been shown that quasi-one-dimensional electronic conduction can be induced in these systems either by n-doping[3] or by p-doping.[4] More recently it has been shown that phenylbenzothiazole-based calamitic smectic A phases (quasi-two-dimensional) give both electron and ion transits.[5] The highly efficient, anisotropic charge transport obtained suggests applications in photosensors, light-emitting diodes,[6] electrophotography and many other areas. There is, however, a need for new molecular systems. Although the success of crystalline TTF conductors[7] makes liquid crystalline derivatives of TTF an obvious synthetic target little progress has been made in this area.[8]

Our synthesis, which is shown in Scheme 1, enables us to make both calamitic and discotic mesogens based on the bis(phenylenedithio-TTF) (BPhDT-TTF) nucleus. The novel step involves a cycloaddition between 2,3-bis(methoxycarbonyl)benzoquinone **2** and 1,3-dithiole-2,4,5-trithione [depolymerised oligo(1,3-dithiole-2,4,5-trithione)] **1**.[9] Addition of simple four π electron components to 2,3-disubstituted quinones normally yields adducts of the 2,3-double bond[10] (in this case the 'wrong' regioisomer) but, fortunately, the sole product obtained was the desired hydroquinone **3**. The remainder of the synthesis, shown in Scheme 1, uses well-established reactions and procedures. Compounds **4a**, **4b** and **4c** were non-liquid crystalline (**4a**, mp 48 °C; **4b**, mp 129–130 °C and **4c**, mp 182–184 °C) but the bis(anhydride) **5** and the bis(imide) **6** both displayed enantiotropic liquid crystalline behaviour.

Force field (MM2) calculations on the BPhDT-TTF nucleus and crystal structures of related compounds suggest that it adopts the elongated shallow 'chair' conformation shown in Fig. 1 making it, perhaps, a more obvious choice for creating calamitic than discotic liquid crystals.

Compound **5** gives a smectic A phase between 91.5 and 107.3 °C, with a layer repeat distance of 24.3 Å, comparable to the length of the molecules. More surprisingly, compound **6** behaves as a discogen, giving a D_r columnar phase between room temperature and 64.7 °C. This is unusual, but not unprecedented, for a molecule with such a non-planar, elongated core.[11] When viewed between cross polarisers, thin films of compound **6** obtained by slow cooling from the isotropic phase showed the characteristic dendritic structures of a columnar mesophase and the X-ray analysis of this phase is detailed in Table 1. Compounds **4a**, **5** and **6** are soluble in common organic solvents and solutions display two reversible one electron oxidation waves in the anodic window showing the formation of stable radical cations. The dc and ac conductivity response of thin films (12 μm) of compounds **5** and **6** has been investigated using a variety of electrode types (indium tin oxide, gold and aluminium).[12] The liquid crystalline phase of compound **5** did not align under these conditions but compound **6** aligned homeotropically when annealed at 55 °C. Dc studies showed that both materials gave a linear (Ohmic) response up to an applied voltage of 1 V.[12] As expected, the ac conductivities (10^1–10^6 Hz, 1 V) were very low (10^{-12}–10^{-7} S cm^{-1}) and

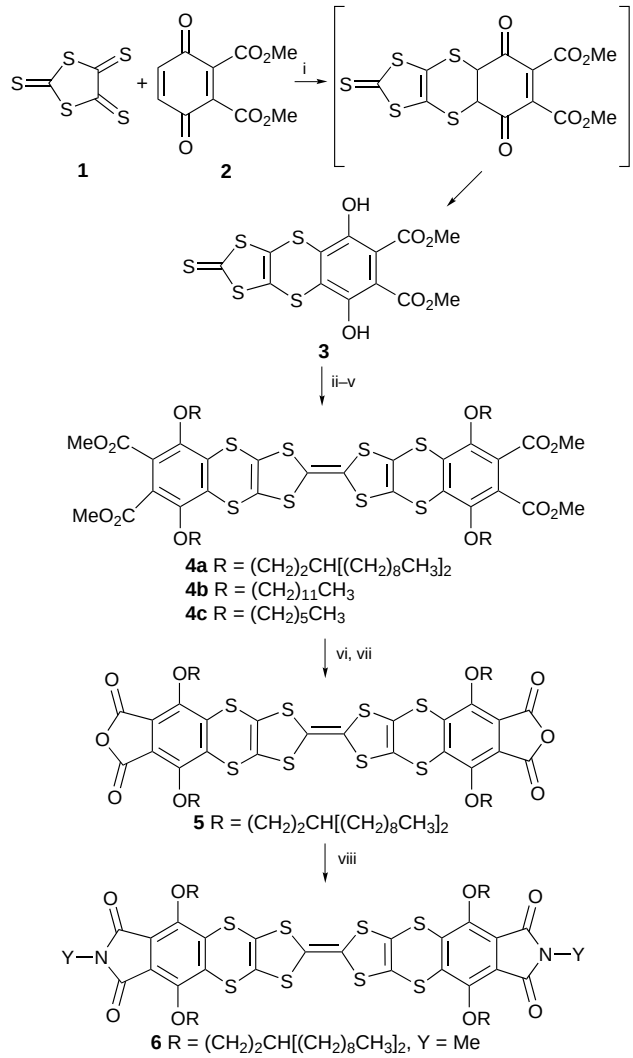

Scheme 1 *Reagents and conditions*: i, THF, reflux, 8 h, 24%; ii, Ac_2O, DMAP, CH_2Cl_2, 2 h, 94%; iii, $Hg(OAc)_2$, AcOH, CH_2Cl_2, 4 h, 94%; iv, $P(OMe)_3$, C_6H_6, reflux, 5 h, 60%; v, RX, K_2CO_3, DMF, heat, 74–94%; vi, KOH, THF, MeOH, reflux, 5 h, 78%; vii, 90 °C, vacuum, 5 h, 88%; viii, $MeNH_2$·HCl, K_2CO_3, DMAP, DMF, $CHCl_3$, 3 Å molecular sieves, 80 °C, 3 days, 60%. All new compounds gave satisfactory combustion analyses and spectroscopic data.

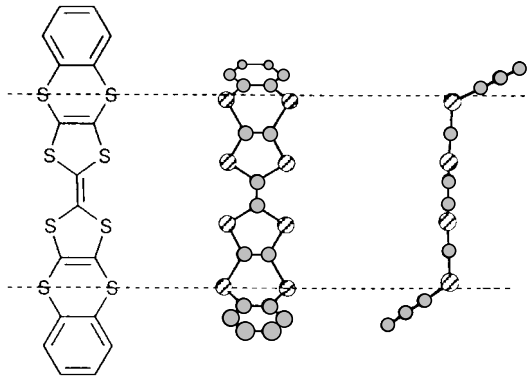

Fig. 1 Optimised geometry of BPhDT-TTF obtained using the MM2 force field method

Table 1 Powder X-ray diffraction data for the D_r phase of the diimide **6**. The calculated data is that expected for a two-dimensional cell, a = 27.3, b = 22.9 Å. Additionally there is a rather broad reflection at 4.00 Å corresponding to the separation between the rings within the stacks. It is greater than that found in crystalline TTF derivatives (ref. 13)

Reflection	Calculated/Å	Observed/Å
10	27.3	27.3
01	22.9	absent
11	17.5	17.8
20	13.7	13.7
02	11.4	11.4
21	11.7	11.4
12	10.6	10.8
30	9.1	9.7

dominated by trace ionic impurities. More surprising was the finding that, when a sample of compound **6** was p-doped with 2 mol% of antimony pentachloride, giving a radical cation concentration ~ 10^{20} cm^{-3} (EPR), the ac conductivity (10^{1}–10^{6} Hz, 1 V) only increased to 10^{-11}–10^{-6} S cm^{-1}. This is very much lower than that normally found in doped discotics[2,3] and the reasons for this are not immediately apparent. It may imply that the radical cations formed are highly localised (small polarons) and/or pinned by the counterions. Alternatively it may be that there is a major difference in geometry between the neutral molecule and the radical cation resulting in large local lattice distortions (a structural polaron). Experiments aimed at resolving this problem and at producing related TTF derivatives with higher conductivities are in progress.

We thank the EPSRC and Leeds University for financial support and the Royal Society for a fellowship to R. A. B.

Footnote and References

* E-mail: richardb@chem.leeds.ac.uk

1 N. Boden, R. A. Bissell, J. Clements and B. Movaghar, *Curr. Sci.*, 1996, **71**, 599.
2 D. Adam, F. Closs, T. Frey, D. Funhoff, D. Haarer, H. Ringsdorf, P. Schuhmacher and K. Siemensmeyer, *Phys. Rev. Lett.*, 1993, **70**, 457.
3 N. Boden, R. C. Borner, R. J. Bushby and J. C. Clements, *J. Am. Chem. Soc.*, 1994, **116**, 10 807.
4 N. Boden, R. J. Bushby, J. Clements, M. V. Jesudason, P. F. Knowles and G. Williams, *Chem. Phys. Lett.*, 1988, **152**, 94; N. Boden, R. J. Bushby and J. Clements, *J. Chem. Phys.*, 1993, **98**, 5920; N. Boden, R. J. Bushby, J. Clements, B. Movaghar, K. J. Donovan and T. Kreouzis, *Phys. Rev. B*, 1995, **52**, 13274.
5 M. Funahashi and J. Hanna, *Jpn. J. Appl. Phys.*, 1996, **35**, L703; *Appl. Phys. Lett.*, 1997, **71**, 602; *Phys. Rev. Lett.*, 1997, **78**, 2184.
6 T. Christ, B. Glusen, A. Greiner, A. Kettner, R. Sander, V. Stumpflen, V. Tsukruk and J. H. Wendorff, *Adv. Mater.*, 1997, **9**, 48.
7 U. T. Mueller-Westerhoff, A. Nazzal, R. J. Cox and A.-M. Giroud, *J. Chem. Soc., Chem. Commun.*, 1980, 497; C. Polycarpe, E. Torreilles, L. Giral, A. Babeau, N. H. Tinh and H. Gasparoux, *J. Heterocycl. Chem.*, 1984, **21**, 1741; M. R.Bryce, *J. Mater. Chem.*, 1995, **5**, 1481; J. M. Williams, A. J. Schultz, U. Geiser, K. D. Carlson, A. M. Kini, H. H. Wang, W.-K. Kwok, M.-H. Whangbo and J. E. Schirber, *Science*, 1991, **252**, 1501; P. Day, *Chem. Soc. Rev.*, 1993, 51.
8 G. Saito, *Pure Appl. Chem.*, 1987, **59**, 999; M. A. Fox and H. Pan, *J. Org. Chem.*, 1994, **59**, 6519; S. Frenzel, S. Arndt, R. Ma, G. Mullen and K. Mullen, *J. Mater. Chem.*, 1995, **5**, 1529; M. J. Cook, G. Cooke and A. Jafari.-Fini, *Chem. Commun.*, 1996, 1925; R. Andreu, J. Barbera, J. Garin, J. Orduna, J. L. Serrano, T. Sierra, P. Leriche, M. Salle, A. Riou, M. Jubault and A. Gorguess, *Synth. Met.*, 1997, **86**, 1869.
9 N. Svenstrup and J. Becher, *Synthesis*, 1995, 215.
10 M. F. Ansell, B. W. Nash and D. A. Wilson, *J. Chem. Soc.*, 1963, 3012.
11 R. J. Bushby and A. Cammidge, *Discotic Liquid Crystals—Synthesis and Structural Features*, in *Handbook of Liquid Crystals*, ed. D. Demus, J. W. Goodby, G. W. Gray, H. W. Spiess and V. Vill, VCH, Weinheim, 1997, in the press.
12 N. Boden, R. J. Bushby, J. Clements and B. Movaghar, *J. Appl. Phys.*, in the press.
13 C. Nakano, K. Imaeda, T. Mori, Y. Maruyama, H. Inokuchi, N. Iwasawa and G. Saito, *J. Mater. Chem.*, 1991, **1**, 37.

Received in Cambridge, UK, 18th September 1997; 7/06797F

Observation and quantification of a chiral medium induced difference in rate of enantiomerization

Kai Rossen,* Jess Sager and Yongkui Sun

Process Research and Development, Merck Research Laboratories, PO Box 2000, Rahway, NJ 07065, USA

A chiral stationary phase HPLC column has been used both to separate the enantiomers of a γ-lactol and also to observe the rate of enantiomerization of the individual enantiomers; the rate of enantiomerization differed for both enantiomers in the presence of the chiral stationary phase.

A chiral medium interacting with a pair of enantiomers results in energetically differentiated, diastereomeric complexes and this differential stabilization of the enantiomers will contribute to the different reaction rates of the enantiomers in the chiral medium.[1] Chiral stationary phases (CSPs) have developed into very useful and reliable tools for the determination of the enantiomeric composition of mixtures. One of the most successful types of chiral stationary phases for HPLC and SFC (supercritical fluid chromatography) is prepared from crystalline carbamoylated or acylated cellulose or amylose deposited on SiO_2 (commercially available as Chiralcel and Chiralpak columns).[2]

The combination of these columns with the use of supercritical CO_2 as eluent is a particularly powerful tool for enantiomer separation.[3] The chromatographic separation of the enantiomers results from the formation of energetically different diastereomeric complexes between the enantiomers and the CSP and it would therefore appear reasonable to expect that enantiomers react at different rates in the presence of a chiral stationary phase.[4] We have examined this premise using the enantiomerization of γ-lactol **1** as a model reaction (Scheme 1) where (*R*)-**1** and (*S*)-**1** are chiral but the reaction intermediate hydroxy aldehyde **2** is not.†

Examination of **1** by ^{1}H NMR spectroscopy shows that it is exclusively present in the closed form, as would be expected from a *gem*-dimethyl substituted five-membered lactol. The enantiomers of **1** are separated on a Chiralpak AD column [25 cm length, supercritical CO_2 at 300 bar with 8% modifier (Pr^iOH–H_2O 95 : 5), flow 1 ml min^{-1}, 40 °C, retention time

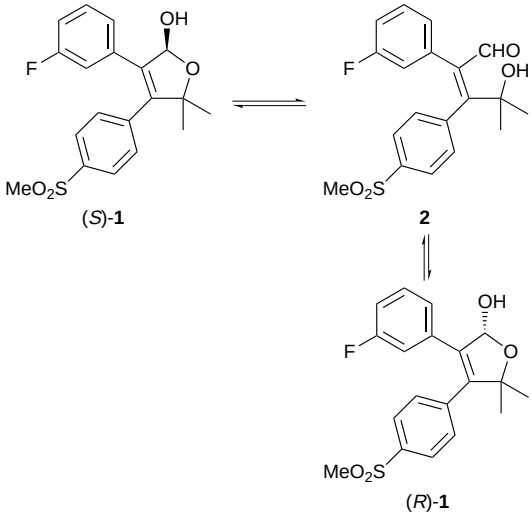

Scheme 1

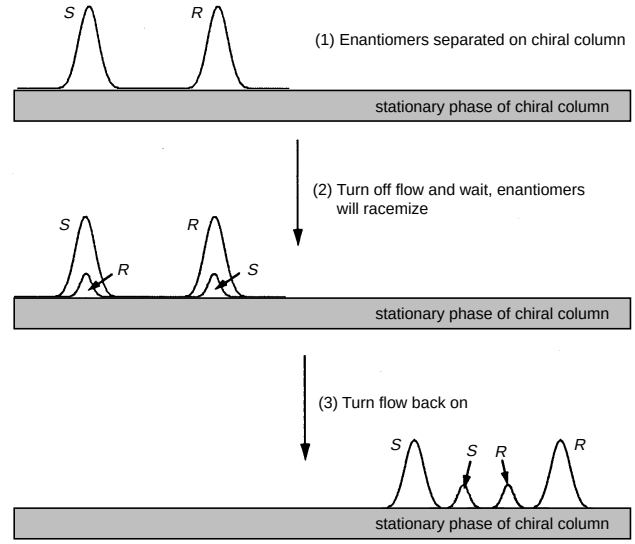

Fig. 1

t_R = 21.0 min, t_S = 29.8 min, dead volume time t_0 = 3.3 min, assignment of first peak as the *R*-isomer is arbitrary].‡ The procedure for measuring the rates of enantiomerization is described in Fig. 1. The flow of the mobile phase is turned off at a fraction of the regular run time when the enantiomers are already spatially separated on the column (*e.g.* at t_X = 0.33 t_R). The enantiomers are then allowed to partially enantiomerize in the presence of the chiral medium for a period of time *t* before the flow resumes.[5] A four-peak pattern is obtained, with the inside peaks resulting from the enantiomerization of the previously separated peaks.§

By varying the time *t* for which the flow is turned off, the rate of enantiomerization of each enantiomer in the presence of the chiral stationary phase can be determined. A plot of conversion R/R_0 and S/S_0 *vs. t* (Fig. 2) shows that the enantiomers react at

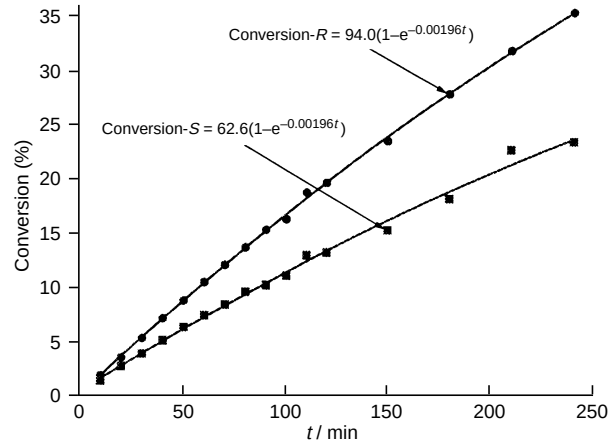

Fig. 2

different rates! Least square fit of the data to the kinetic equations of a reversible first-order system gives $k_R = 1.19 \times 10^{-3}$ min^{-1} and $k_S = 7.75 \times 10^{-4}$ min^{-1}.¶ This rate difference can be used to calculate the difference in Gibbs energy of activation for the enantiomerization of (*R*)- and (*S*)-**1** in the presence of the chiral medium at 40 °C: $\Delta G^{\ddagger} = \Delta G_R^{\ddagger} - \Delta G_S^{\ddagger} = -RT\ln k_R/k_S = -1.10$ kJ mol^{-1}. However, the differential binding energy of the two enantiomers on the CSP is responsible for the separation of the enantiomers on the column. It can be calculated from the observed chromatogaphic separation factor $\alpha = (t_S - t_0)/(t_R - t_0) = 1.50$ according to $\Delta G = -RT\ln \alpha$ and gives $\Delta G = -1.06$ kJ mol^{-1} (40 °C). As the intermediate hydroxy aldehyde **2** is achiral, the difference in Gibbs energy of activation $\Delta G^{\ddagger}$ obtained from the kinetic measurements will result from the differential binding strength of the two enantiomers of **1** on the chiral column as long the influence of the chiral medium on the energy of the transition states leading to the achiral intermediate **2** is negligible. Indeed, the value obtained from the kinetic measurement ($\Delta G^{\ddagger} = 1.10$ kJ mol^{-1}) is in good agreement with the number obtained from the chromatographic separation factor ($\Delta G = 1.06$ kJ mol^{-1}). Thus, the different rates of enantiomerization are caused by the differential binding of the enantiomers of the lactol **1** with the chiral medium and the transition states leading from **2** to the enantiomers of **1** are of nearly identical energy in the presence of the chiral medium.

In summary, we have demonstrated that the enantiomers of a chiral compound react at different rates in the presence of a CSP and that this rate difference is caused by the differential energetic stabilization of the individual enantiomers of the γ-lactol by the chiral medium. This example adds to the list of examples[6] where enantiodifferentiating reactivity is achieved by performing a reaction in the chiral environment provided by a chiral host.

Footnotes and References

* E-mail: kai_rossen@merck.com

† An alternative mechanism would involve the oxonium ion, which is also achiral.

‡ All experiments were performed with the Hewlett Packard SFC (HP 1205) system with a HP 1050 diode array detector and instrument control and data analysis with the HP Chemstation Software. The Chiralpak AD column was obtained from Chiral Technologies, Exton, PA 19341. The lactol **1** was prepared by DIBAL-H reduction of the corresponding lactone.

§ The retention times of the middle peaks can be calculated as $t_R + (t_R - t_X)(t_S - t_R)/t_R$ and $t_R + t_X(t_S - t_R)/t_R$, where the retention times of the outer peaks are t_R and t_S, and the flow is stopped at time t_X. The timespan t during which the flow is stopped is obviously subtracted from the observed times and the issues involved with regaining equilibrium when the flow of the column is resumed are ignored. This is reasonable as the Hewlett Packard SFC instrument controls the pressure at the end of the column.

¶ The data were fitted to the equations of a reversible first-order reaction [eqns. (1) and (2)]

$$\text{conversion-}S = k_R/(k_R + k_S)\,[1 - e^{-(k_R + k_S)t}]$$

$$\text{conversion-}R = k_S/(k_R + k_S)\,[1 - e^{-(k_R + k_S)t}]$$

to give $k_R + k_S = 1.96 \times 10^{-3}$ min^{-1} and $k_R/k_S = 1.53$.

1 E. L. Eliel, S. H. Wilen and L. N. Mander, *Stereochemistry of Organic Compounds*, Wiley, New York, 1994, ch. 6.
2 S. G. Allenmark, *Chromatographic Enantiosepartion: Methods and Applications*, Ellis Horwood, Chichester, 2nd edn., 1991; J. Dingenen, in *A Practical Approach to Chiral Separations by Liquid Chromatography*, ed. G. Subramanian, VCH, Weinheim, 1994, ch. 6; W. Lindner, in *Methods of Organic Synthesis (Houben-Weyl), Stereoselective Synthesis*, ed. G. Helmchen, R. W. Hoffmann, J. Mulzer and E. Schaumann, Thieme Verlag, Stuttgart, 1996, ch. 3.1.6.
3 P. Petersson and K. E. Markides, *J. Chromatogr., A*, 1994, **666**, 381; M. Schleimer and V. Schurig, *Anal. Supercrit. Fluids: Extr. Chromatogr.*, 1992, 134.
4 W. Bürkle, H. Karfunkel and V. Schurig, *J. Chromatogr.*, 1984, **288**, 1; G. Weseloh, C. Wolf and W. A. König, *Chirality*, 1996, **8**, 441.
5 G. Weseloh, C. Wolf and W. A. König, *Angew. Chem., Int. Ed. Engl.*, 1995, **34**, 1635; M. Jung and V. Schurig, *J. Am. Chem. Soc.*, 1992, **114**, 529; V. Schurig, A. Glausch and M. Fluck, *Tetrahedron: Asymmetry*, 1995, **6**, 2161; V. Schurig, M. Jung, M. Schleimer and F. Klärner, *Chem. Ber.*, 1992, **125**, 1301.
6 R. Gerdil, G. Barchietto and C. W. Jefford, *J. Am. Chem. Soc.*, 1984, **106**, 8004; M. Sakamoto, *Chem. Eur. J.*, 1997, **3**, 684.

Received in Corvallis, OR, USA, 25th September 1997; 7/06959F

Structure of templated microcrystalline DAF-5† ($Co_{0.28}Al_{0.72}PO_4C_{10}H_{20}N_2$) determined by synchrotron-based diffraction methods

Gopinathan Sankar,[a] Joanna K. Wyles,[a] Richard H. Jones,[b] John Meurig Thomas,*[a] C. Richard A. Catlow,[a] Dewi W. Lewis,[a,c] William Clegg,*[d,e] Simon J. Coles[a,d] and Simon J. Teat[d,e]

[a] *Davy Faraday Research Laboratory, The Royal Institution of GB, 21 Albemarle Street, London, UK W1X 4BS*
[b] *Department of Chemistry, University of Keele, Keele, Staffordshire, UK ST5 5BG*
[c] *Department of Materials, University of Cambridge, Cambridge, UK CB2 1EW*
[d] *CCLRC, Daresbury Laboratory, Daresbury, Warrington, Cheshire, UK WA4 4AD*
[e] *Department of Chemistry, University of Newcastle upon Tyne, Newcastle, UK NE1 7RU*

Micro-single crystal diffraction techniques employing synchrotron radiation are used to determine the structures of the disordered template (4-piperidinopiperidine) within the recently synthesised, chabazite-related cobalt aluminium phosphate known as DAF-5; the structural details revealed are inaccessible by high-resolution powder diffraction.

In the search for microporous solids possessing unusual catalytic and other properties[1] accurate knowledge of template–host interaction is of crucial importance. Computational techniques[2,3] are indeed able to design templates for the synthesis of specific microporous architectures. Experimental determination of the location, orientation and disorder of templates within the microporous host is however, necessary for improving our ability to predict and optimise the appropriate templates. Recently[4] the *de novo* design code ZEBEDEE led to the choice of 4-piperidinopiperidine ($C_{10}H_{20}N_2$) as the template for producing a chabazitic cavity which is more symmetrical than that achieved in the open-structured cobalt phosphate known as DAF-4, a solid-acid catalyst (closely related in structure to the zeolitic mineral levyne) that shape-selectively converts methanol preferentially to ethene and propene.[5] Here, microcrystalline diffraction techniques, feasible only with synchrotron radiation, are used to establish the structural properties of the template within this new chabazitic aluminophosphate.

DAF-5 was crystallised from a gel of composition 0.4 CoO : 0.8 Al_2O_3 : 1.5 P_2O_5 : 30 H_2O : 2.5 $C_{10}H_{20}N_2$ which was heated under hydrothermal pressure at 160 °C for 3–6 h. A phase-pure material was produced which gave a unique X-ray powder diffractogram collected on station 2.3 of the Daresbury Synchrotron radiation source (which operates at 2 GeV with a typical current between 120 and 250 mA) in capillary mode using a wavelength of 1.399 94 Å. Unit cell parameters were obtained using the auto-indexing program TREOR.[6] Structure factor amplitudes were extracted using a Le Bail decomposition.[7] These data were used to solve the structure by direct methods using the program SIRPOW,[8] the starting model so obtained being utilized for subsequent Rietveld refinement.[9,10] This clearly established the nature of the framework [the best fit is shown in Fig. 1 and the framework structure, as subsequently determined together with the template, in Fig. 2(*a*)]. Difference Fourier maps indicated that the organic molecule experiences extensive disorder; but detailed structural information could not be derived from the powder diffraction data.

To determine the nature of the disorder of this template and find its possible orientations we employed single-crystal diffraction methods on a microcrystal of DAF-5 having dimensions close to 30 × 30 × 30 μm.‡ Collection of accurate data on such small crystals can be best performed using synchrotron sources,[11–13] such as the facility recently commissioned at station 9.8 of the Daresbury SRS,[14] where focusing optics ensures high photon flux on the sample. Data were collected on a Siemens SMART CCD Area detector at a wavelength of 0.6889 Å. The structure was again solved by direct methods.[15] The location of the template molecule could

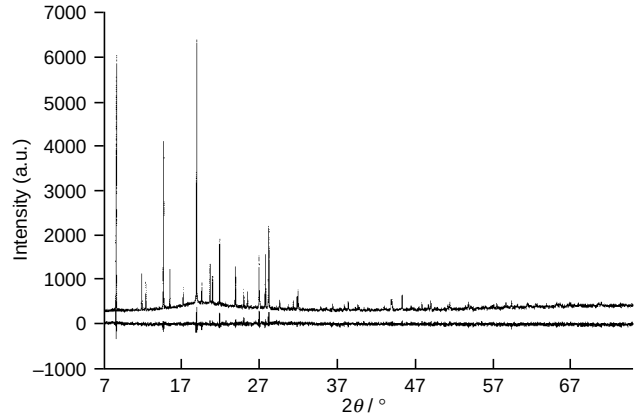

Fig. 1 High-resolution X-ray powder diffraction pattern (solid line) recorded at station 2.3 of the Daresbury Synchrotron radiation source employing a wavelength of 1.3999 Å. The dashed curve shows the best fit to the experimental data generated using the Rietveld analysis program GSAS. The difference profile is shown in the bottom of the figure.

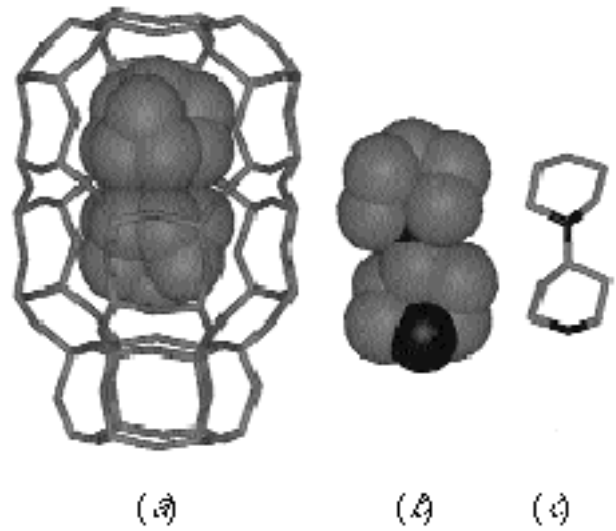

Fig. 2 Graphical representation of the structures of DAF-5 derived from the single crystal experiment is shown in (*a*). For clarity only one of the cages is given which contains all possible conformations of the occluded template molecule 4-piperidinopiperidine. One of the possible conformations of the template molecule is also shown using ball (*b*) and stick (*c*) representations where carbon atoms are shown in grey and nitrogen in black.

be ascertained from a careful interpretation of the difference Fourier map in terms of the possible conformers. This approach yielded plausible template orientations shown in the location inside the cage in Fig. 2, which also depicts one of the orientations of the single template molecule. The calculated position of the template[5] has six equivalent, statically disordered positions. Furthermore, molecular dynamics simulations (using Discover[16]) indicate independent rotation around the C–N bridge in the molecule as well as a precessional motion. However, the symmetry of the molecule is such that the extremes of the molecule and bridging atoms show small amplitudes of thermal motion. These findings are consistent with the atomic positions found in the diffraction study.

Our study demonstrates the power of microcrystalline diffraction techniques together with computer modelling in revealing complex structural features of templated microporous solids.

The authors thank EPSRC for financial support and CCLRC for the provision of beam time. D. W. L. thanks the Oppenheimer Trust of the University of Cambridge for an Oppenheimer Fellowship.

Footnotes and References

† Davy Faraday Number 5. For DAF-4 see ref. 5.

‡ *Crystal data*: $Co_{0.28}Al_{0.72}PO_4C_{1.67}N_{0.33}H_{3.33}$, M_r = 158.96, trigonal space group $R\bar{3}$, a = 13.537(5), c = 15.480(6) Å, U = 2457 Å^3, Z = 18, D_c = 1.934 g cm^{-3}, μ = 1.361 mm^{-1}, $F(000)$ = 1433. Crystal of size 0.03 × 0.03 × 0.03 mm. Data were collected at 295 K employing a wavelength of 0.6889 Å, on a Siemens SMART CCD area detector diffractometer, equipped with a silicon (111) crystal monochromator and a palladium coated focusing mirror on the single crystal diffraction station (no. 9.8) at the Daresbury Laboratory Synchrotron Radiation Source. Coverage of a hemisphere of reciprocal space was achieved by 0.2° frame increments in ω, with θ_{min} = 2.11° and θ_{max} = 26.47° (index ranges $-5 \leqslant h \leqslant 16$, $-16 \leqslant k \leqslant 4$, $-15 \leqslant l \leqslant 19$). Corrections were applied to account for incident beam decay and absorption effects. A solution was provided *via* direct methods and refined by full-matrix least-squares on F^2. 2188 reflections were measured, producing 969 unique data with R_{int} = 0.0455. 100 parameters and 264 restraints (imposed in order to model the disordered template molecule; these consisted of restraints on geometry, to impose approximate non-crystallographic molecular symmetry and similarity of groups of bond lengths and angles as well as equivalence of crystallographically independent disorder components, and on atomic displacement parameters, to approximate a rigid bond model and similarity of displacements for disorder sites) refined to R_1 = 0.0633 and wR_2 = 0.1785 [$I > 2\sigma(I)$] with s = 0.971 and a residual electron density of 0.58, −0.71 e Å^{-3}.

1 I. E. Maxwell and P. W. Lednor, *Curr. Op. Solid State Mater. Chem.*, 1996, **1**, 57.
2 D. W. Lewis, D. J. Willock, C. R. A. Catlow, J. M. Thomas and G. J. Hutchings, *Nature*, 1996, **382**, 604.
3 D. J. Willock, D. W. Lewis, C. R. A. Catlow, J. M. Thomas and G. J. Hutchings, *J. Mol. Catal. A*, in press.
4 D. W. Lewis, G. Sankar, J. K. Wyles, J. M. Thomas, C. R. A. Catlow and D. J. Willock, *Angew. Chem., Int. Ed. Engl.*, 1997, in press.
5 P. A. Barrett, R. H. Jones, J. M. Thomas, C. Saukar, I. J. Shannon and C. R. A. Catlow, *Chem. Commun.*, 1996, 2001.
6 P. E. Werner, L. Eriksson and M. Westdahl, *J. Appl. Crystallogr.*, 1985, **18**, 367.
7 A. LeBail, H. Duroy and J. L. Fourquet, *Mater. Res. Bull.*, 1988, **23**, 447.
8 C. Giacovazzo, *Acta. Crystallogr., Sect. A*, 1996, **52**, 331.
9 H. M. Rietveld, *J. Appl. Crystallogr.*, 1969, **2**, 65.
10 A. C. Larson and R. B. von Dreele, GSAS, Report no. LA-UR-86-748, Los Alamos National Library, NM, 1987.
11 H. E. King, L. A. Mundi, K. G. Strohmaier and R. C. Haushalter, *J. Solid State Chem.*, 1991, **92**, 1.
12 G. W. Noble, P. A. Wright, P. Lightfoot, R. E. Morris, K. J. Hudson, A. Kvick and H. Graafsma, *Angew. Chem., Int. Ed. Engl.*, 1997, **36**, 81.
13 G. Cheetham and M. M. Harding, *Zeolites*, 1996, **16**, 245.
14 R. J. Cernik, W. Clegg, C. R. A. Catlow, G. Bushell-Wye, J. V. Flaherty, G. N. Greaves, I. D. Burrows, D. J. Taylor, S. J. Teat and M. Hamichi, *J. Synchrotron Rad.*, 1997, in press.
15 G. M. Sheldrick, SHELXS86 User guide, University of Göttingen, 1986.
16 Discover v95.0, Molecular Simulations Inc., San Diego, CA, 1996.

Received in Bath, UK, 25th September 1997; 7/06950B

Synthesis of iminopolyols *via* Henry reaction: a short route to the α-mannosidase inhibitor 1,4-dideoxy-1,4-imino-D-mannitol and to amino analogues†,[1]

Frank-Michael Kieß,[a] Philip Poggendorf,[a] Sylviane Picasso[b] and Volker Jäger*[a]

[a] *Institut für Organische Chemie der Universität Stuttgart, Pfaffenwaldring 55, D-70569 Stuttgart, Germany*
[b] *Institut de Chemie Organique, Université de Lausanne, CH-1015, Lausanne-Dorigny, Switzerland*

The α-mannosidase inhibitor 1,4-dideoxy-1,4-imino-D-mannitol (DIM) as well as amino analogues of DIM and of deoxy-*manno*-nojirimycin, respectively, have been prepared using a diastereoselective nitroaldol addition as the key step.

Many polyhydroxy-pyrrolidines and -piperidines (iminoglycitols) act as strong and specific inhibitors of glycosidases,[2–4] *e.g.* 1,4-dideoxy-1,4-imino-D-mannitol **1**[3] or deoxy-*manno*-nojirimycin **2**.[4] Due to their potential as anti-diabetic, anti-viral or anti-tumour agents,[2c] many efforts have been directed towards syntheses of this class of compounds, usually based on modification of carbohydrate precursors or cycloaddition methods.[5]

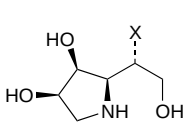

1 X = OH
3 X = NH_2

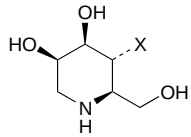

2 X = OH
4 X = NH_2

For some time, we have been studying the diastereoselectivity of the nitroaldol addition (Henry reaction),[6] with a view to efficient construction of nitro- and amino-polyols and further uses in the preparation of various amino- and imino-polyols.[7] We now report a simple synthesis of DIM **1**, and of new amino analogues **3**, **4** of DIM and of **2**, respectively, based on diastereoselective nitroaldol additions catalyzed by tetrabutylammonium fluoride trihydrate.[7,8] (C_3 + C_3)-Assembly of nitro compounds, bearing an α-oxy or α-amino function, and the glyceraldehydes **7** leads to nitrohexitols (see Scheme 2), which can be reduced to the corresponding amino compounds. Cyclization would then give access to iminopolyols. Thus, the question should be replaced by an amino function, to retain or alter inhibition of glycosidases.

The optically active nitro compounds **5**, **6** were prepared from the corresponding aldehydes[9,10] by oximation,[9d,10c] followed by oxidation with trifluoroperacetic acid[11] (Scheme 1).

For the aldehyde part, 2-*O*-benzylglyceraldehyde **7** was chosen, readily available in both enantiomeric forms from

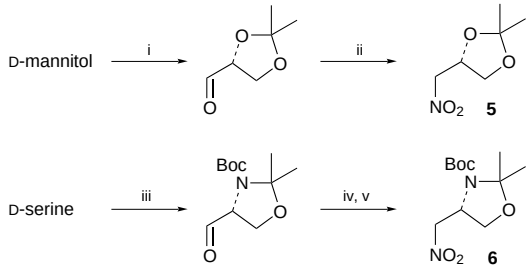

Scheme 1 *Reagents and conditions*: i, ref. 9(*a*), (*b*), 53%; ii, ref. 9(*d*), 11, 67%; iii, ref. 10(*a*), (*b*), 84%; iv, NH_2OH·HCl, K_2CO_3, MeOH, H_2O, 0 °C, 2 h; [ref. 10(*c*)]; v, H_2O_2 (85%), $(CF_3CO)_2O$, Na_2HPO_4, MeCN, 0 °C, 2 h, 76% (iv, v)

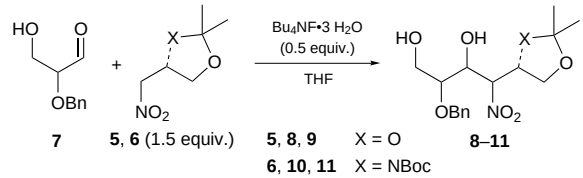

7 **5**, **6** (1.5 equiv.) **5**, **8**, **9** X = O **8–11**
6, **10**, **11** X = NBoc

Scheme 2

Table 1 Nitroaldol addition of **5** and **6** to **7**

Reactants	Conditions	Products	Yield[a] (%)	Dr[b]	Major isomer
D-**7** + **5**	−20 °C, 6 d	**8a,8b,8c**	90	67 : 22 : 11	D-*manno*
L-**7** + **5**	−20 °C, 6 d	**9a,9b,9c**	92	69 : 18 : 13	D-*gulo*
D-**7** + **6**	0 °C, 7 d	**10a,10b**	88	90 : 10	D-*manno*
L-**7** + **6**	0 °C, 7 d	**11a,11b**	81	90 : 10	D-*gulo*

[a] Pure material after flash chromatography on silica. [b] From ^{13}C NMR and/or HPLC analyses of crude mixture; other diastereomers < 5%.

tartrates,[12] which had given the best diastereomer ratios in related cases.[7] The addition of **5** to D- or L-**7** afforded the nitro alcohols **8** and **9** in high yields as mixtures of diastereomers,[7c] from which the major isomers **8a** (D-*manno*) and **9a** (D-*gulo*) were separated by chromatography (Scheme 2, Table 1). As seen earlier,[7] 1,2-induction from the aldehyde stereocentre strongly favoured 2,3-*erythro* formation, and the non-induced stereoselection concerning C3/C4 preferentially led to a *threo* relationship. Double stereodifferentiation, as observed in related cases,[1,7b,c] was not operative here.

The nitroaldol **8a** was converted into the amine **12** by catalytic hydrogenation.[13] Cyclization of **12** with the Appel reagent (Ph_3P, CCl_4, Et_3N),[14] followed by ion exchange chromatography and hydrochloric acid treatment, afforded the D-iminomannitol **1** in 74% yield after conversion into the hydrochloride (Scheme 3); the overall yield from D-mannitol was 10% (seven steps). Starting from **9a**, the D-*gulo* isomer[15] was accessible likewise, as confirmed by crystal structure analysis.[16]

Addition of the nitro compound **6** to D-**7** occurred with a considerably higher diastereomer ratio: the 5-amino-4-nitrohexitol **10** was preferred by 90 : 10 (D-*manno* : D-*talo*; from L-**7**: **11a** and **11b**, D-*gulo* and D-*allo* were formed; Table 1). The nitro alcohol mixture **10** was converted to the corresponding amines

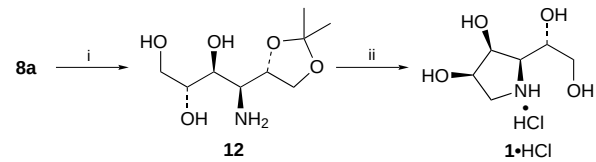

Scheme 3 *Reagents and conditions*: i, H_2 (4 bar), Pd–C, MeOH (*cf.* ref. 13), 25 °C, 21 h, 84%; ii, Ph_3P, CCl_4, Et_3N, pyridine, 25 °C, 2 d; Lewatit S 100 (H^+ form); 1 M HCl; 74% **1**·HCl, mp 147–148 °C, $[\alpha]_D^{20}$ −15.8 (*c* 0.97, H_2O) {lit.[3] mp 148–149 °C, $[\alpha]_D^{20}$ −16.3 (*c* 1.00, H_2O)}

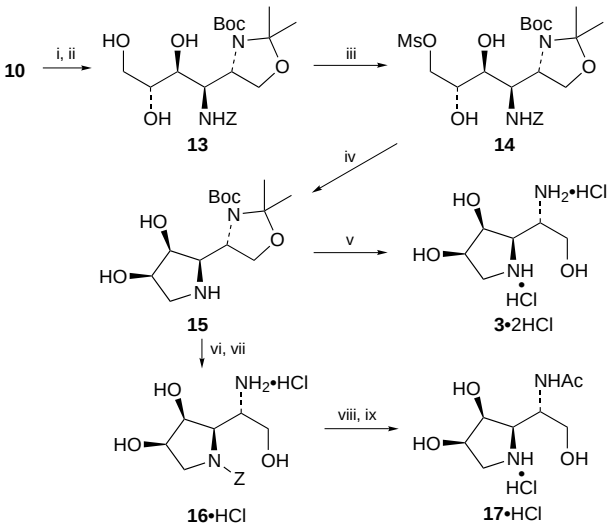

Scheme 4 *Reagents and conditions*: i, H_2 (4 bar), Pd–C, MeOH, 25 °C, 22 h; ii, ZCl, $NaHCO_3$, dioxane, H_2O, 0 to 25 °C, 24 h, then crystallization (hexanes–EtOAc), 61% (**10**→**13**); iii, MsCl, NEt_3, CH_2Cl_2, −10 to 25 °C, 22 h, 84%; iv, H_2 (4 bar), Pd–C, MeOH, 25 °C, 18 h, 96%; v, 5 M HCl, 0 °C, 2 h, 90%; vi, ZCl, $NaHCO_3$, dioxane, H_2O, 0 to 25 °C, 20 h, 91%; vii, 3 M HCl, MeOH, 0 to 25 °C, 3 h, 98%; viii, Ac_2O, $KHCO_3$, dioxane, H_2O, 0 to 25 °C, 3 h, 87%; ix, H_2, Pd–C, 0.1 M HCl, MeOH, 18 h, 96%

by hydrogenation, followed by *N*-protection with benzyl chloroformate (ZCl) (Scheme 4). The major diastereomer **13** (D-*manno*) was separated by crystallization. Regioselective mesylation of the primary hydroxy group then led to the methanesulfonate **14**. Hydrogenolysis of the Z group was accompanied by *N*-cyclization[7] to afford the pyrrolidine **15**. On treatment of **15** with hydrochloric acid, the amino analogue of DIM **3** was obtained as the bis(hydrochloride). The configuration of **3** was again secured by X-ray crystallography.[7c] Due to orthogonal protection, the two amino groups of **14** could be functionalized individually, as is shown by the syntheses of the 5-acetylaminopyrrolidine **17** and the 4-aminopiperidine **4**. After Z protection of the ring nitrogen in **15**, the 5-amino function was liberated with aqueous acid to yield **16**. *N*-Acetylation and finally removal of Z furnished the 5-acetamido target compound **17** in the form of its hydrochloride (Scheme 4).

Next, the isomeric structure of the piperidine **4** was sought from the methanesulfonate **14**, by changing the order of steps. After removal of both the Boc and the acetonide protecting groups with acid, cyclization to the piperidine **18** took place on treatment with base. Catalytic hydrogenation under acidic conditions, followed by ion exchange chromatography, and subsequent reaction with hydrobromic acid led to the piperidine **4** in form of the bis(hydrobromide) (Scheme 5). The L-*manno* enantiomers of **3** and **4** were prepared according to the same protocol, starting with D-**6**, readily accessible from L-serine.

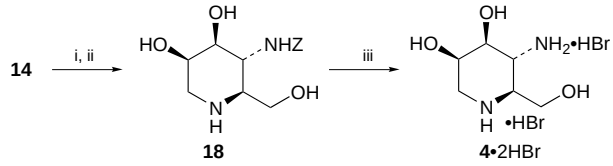

Scheme 5 *Reagents and conditions*: i, 3 M HCl, MeOH, 0 to 25 °C, 6 h, quant.; ii, $KHCO_3$, H_2O, 25 °C, 18 h, 92%; iii, H_2, Pd–C, 1 M HCl, MeOH, 25 °C; 2.5 h; Dowex 50 W (H^+ form); 1 N HBr; 94%

The iminopolyols were tested concerning their inhibitory activity on 24 glycosidases.[17] While DIM **1**, in accord with the literature,[3] showed strong and very selective inhibition of α-mannosidases [jack bean, IC_{50}/μM 3, K_i /μM 1.6; almond, IC_{50} 6, K_i 1.6], the 5-amino analogues **3** and **17** were inactive; this emphasizes the crucial role of the 5-hydroxy function in **1**.[18] The piperidines **4** and **18** showed no activity either, nor did the L-enantiomers of **3**, **4** and **18**. In contrast, the *N*-protected intermediates **16**, **18** proved moderately active towards β-galactosidases [**16**: bovine liver, IC_{50}/μM 460, K_i/μM 228; *Aspergillus orizae*, IC_{50} 540, K_i 705; **18**: bovine liver, 31% inhibition at 1 mM].

In summary, short and efficient syntheses of 1,4-imino-D-mannitol and -D-gulitol as well as of new amino analogues of DIM and of deoxy-*manno*-nojirimycin are presented, demonstrating the potential of the Henry reaction for the diastereoselective assembly of iminopolyols.

Financial support by the Landesgraduiertenförderung Baden-Württemberg (doctoral fellowship to F.-M. K.) and by the Fonds der Chemischen Industrie is gratefully acknowledged.

Footnotes and References

* E-mail: jager.ioc@po.uni-stuttgart.de

† Nitro compounds, Part 6. Part 5: V. Jäger and P. Poggendorf, *Org. Synth.*, 1996, **74**, 130.

1 F.-M. Kieß, S. Picasso and V. Jäger, presented in part at the 15th International Symposium, *Synthesis in Organic Chemistry*, Oxford, July 22–24, 1997, A21.

2 *E.g.* see (*a*) H. Paulsen and K. Todt, *Adv. Carbohydr. Chem.*, 1968, **23**, 115; (*b*) G. Legler, *Adv. Carbohydr. Chem. Biochem.*, 1990, **48**, 319; (*c*) B. Winchester and G. W. J. Fleet, *Glycobiology*, 1992, **2**, 199; (*d*) M. L. Sinnott, *Chem. Rev.*, 1990, **90**, 1171.

3 G. W. J. Fleet, P. W. Smith, S. V. Evans and L. E. Fellows, *J. Chem. Soc., Chem. Commun.*, 1984, 1240.

4 L. E. Fellows, E. A. Bell, D. G. Lynn, F. Pilkiewicz, I. Miura and K. Nakanishi, *J. Chem. Soc., Chem. Commun.*, 1979, 977.

5 For reviews see *e.g.* G. Casiraghi, F. Zanardi, G. Rassu and P. Spanu, *Chem. Rev.*, 1995, **95**, 1677; T. Hudlicky, D. A. Entwistle, K. K. Pitzer and A. J. Thorpe, *Chem. Rev.*, 1996, **96**, 1195; V. Jäger, R. Müller, T. Leibold, M. Hein, M. Schwarz, M. Fengler, L. Jaroskova, M. Pätzel and P.-Y. LeRoy, *Bull. Soc. Chim. Belg.*, 1994, **103**, 491.

6 L. Henry, *C. R. Hebd. Seances Acad. Sci.*, 1895, **120**, 1265; G. Rosini, in *Comprehensive Organic Synthesis*, ed. B. M. Trost, Pergamon, New York, 1991, vol. 2, p. 321; M. Shibasaki, H. Sasai and T. Arai, *Angew. Chem., Int. Ed. Engl.*, 1997, **36**, 1236.

7 (*a*) V. Jäger and V. Wehner, *Angew. Chem., Int. Ed. Engl.*, 1990, **29**, 1169; (*b*) J. Raczko, V. Jäger, K. Peters, V. Wehner, R. Öhrlein, B. Steuer and P. Poggendorf, *Abstr. Pap. XVIth Int. Carbohydr. Symp.*, Paris, July 5–10, 1992, A 227; (*c*) F.-M. Kieß, Dissertation, Universität Stuttgart, planned; (*d*) A. Menzel, H. Griesser, R. Öhrlein, V. Wehner and V. Jäger, unpublished work.

8 R. Öhrlein and V. Jäger, *Tetrahedron Lett.*, 1988, **29**, 6083; B. Aebischer, J. H. Bieri, R. Prewo and A. Vasella, *Helv. Chim. Acta*, 1982, **65**, 2251; *cf.* use of 'anhydrous' Bu_4NF for silyl nitronate additions: D. Seebach, A. K. Beck, T. Mukhopadhyay and E. Thomas, *Helv. Chim. Acta*, 1982, **65**, 1101.

9 (*a*) G. J. F. Chittenden, *Carbohydr. Res.*, 1980, **84**, 350; (*b*) B. Häfele and V. Jäger, *Liebigs Ann. Chem.*, 1987, 85; (*c*) J. Jurzak, S. Pikul and T. Bauer, *Tetrahedron*, 1986, **42**, 447; (*d*) R. W. Hoffmann, G. Eichler and A. Endesfelder, *Liebigs Ann. Chem.*, 1983, 2000.

10 (*a*) S. Guttmann and R. A. Boissonnas, *Helv. Chim. Acta*, 1958, **41**, 1852; (*b*) P. Garner, *Tetrahedron Lett.*, 1984, **25**, 5855; (*c*) A. J. Blake, E. C. Boyd, R. O. Gould and R. M. Paton, *J. Chem. Soc., Perkin Trans 1*, 1994, 2841.

11 W. D. Emmons and A. S. Pagano, *J. Am. Chem. Soc.*, 1955, **77**, 4557; T. M. Williams and H. S. Mosher, *Tetrahedron Lett.*, 1985, **26**, 6269.

12 V. Jäger and V. Wehner, *Angew. Chem., Int. Ed. Engl.*, 1989, **28**, 469; B. Steuer, V. Wehner, A. Lieberknecht and V. Jäger, *Org. Synth.*, 1996, **74**, 1.

13 F. W. Lichtenthaler and H. P. Albrecht, *Chem. Ber.*, 1969, **102**, 964.

14 R. Appel and R. Kleinstück, *Chem. Ber.*, 1974, **107**, 5; for application to cyclizations see, *e.g.* Y. Chen and P. Vogel, *Tetrahedron Lett.*, 1992, **33**, 4917; U. Veith, O. Schwardt and V. Jäger, *Synlett*, 1996, 1181; see also ref. 5.

15 J. G. Buchanan, K. W. Lumbard, R. J. Sturgeon and D. K. Thompson, *J. Chem. Soc., Perkin Trans. 1*, 1990, 699.

16 **1**: S. Henkel, F.-M. Kieß and V. Jäger, *Z. Kristallogr.*, 1997, **212**, 213; D-*gulo* isomer: S. Henkel, F.-M. Kieß and V. Jäger, *ibid.*, 217.

17 A. Brandi, S. Cicchi, F. M. Cordero, R. Frignoli, A. Goti, S. Picasso and P. Vogel, *J. Org. Chem.*, 1995, **60**, 6806.

18 D. A. Winkler and G. Holan, *J. Med. Chem.*, 1989, **32**, 2084; B. Winchester, S. Al Daher, N. Carpenter, I. Cenci di Bello, S. S. Choi, A. J. Fairbanks and G. W. J. Fleet, *Biochem. J.*, 1993, **290**, 743.

Received in Liverpool, UK, 23rd September 1997; 7/06915D

Synthesis, X-ray structure and binding properties of molecular clips based on dimethylpropanediurea

Rob J. Jansen,[a] Alan E. Rowan,[a] René de Gelder,[b] Hans W. Scheeren*[a] and Roeland J. M. Nolte*[a]†

[a] *Department of Organic Chemistry, NSR Center, University of Nijmegen, Toernooiveld, 6525 ED Nijmegen, The Netherlands*
[b] *Crystallography Laboratory, NSR Center, University of Nijmegen, Toernooiveld, 6525 ED Nijmegen, The Netherlands*

New concave host molecules show strong noncovalent binding of hydroxybenzene derivatives by an induced fit mechanism (K_a up to 3.4 × 10^6 dm^3 mol^{-1}).

The design and synthesis of host molecules for neutral guests continues to be an area of great interest in supramolecular chemistry.[1] In recent years a series of receptors derived from the concave molecule glycoluril (see **1**) have been developed in our

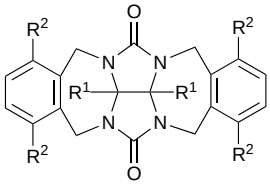

1a R^1 = Ph, R^2 = H
b R^1 = Ph, R^2 = OMe
c R^1 = Me, R^2 = H

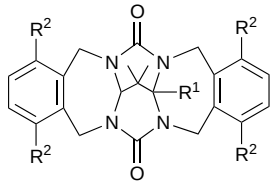

2a R^1 = H, R^2 = H
b R^1 = Me, R^2 = H
c R^1 = H, R^2 = OMe

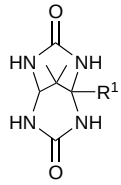

3a R^1 = H
b R^1 = Me

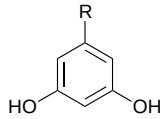

4a R = Me
b R = H
c R = OMe
d R = $CO_2C_6H_{13}$
e R = Cl
f R = CN

laboratory.[2] These receptors, which are U-shaped, bind dihydroxybenzenes by hydrogen bonding interactions between the hydroxy groups of the guest and the urea carbonyl groups of the host and by π–π stacking interactions between the guest and the host side-walls. Although the supramolecular chemistry of glycoluril-based clips has been widely explored, and their sidewalls extensively varied,[2] relatively little attention has been given to variations in the diphenylglycoluril part of the clip molecules. Here we describe the synthesis, X-ray structures and binding properties of a new type of related molecular clips derived from 2,4,6,8-tetraazabicyclo[3.3.1]nonane-3,7-dione (propanediurea, see **2**). Molecular modelling studies suggested that the *o*-xylylene side walls of these new clips would be more parallel than the walls of glycoluril derived clips, which would result in better π–π stacking interactions with an aromatic guest molecule sandwiched between the side walls of the clip and hence lead to increased binding affinities for aromatic molecules. Here we show that compound **2** indeed binds aromatic guest molecules with very high association constants (K_a > 10^6 dm^3 mol^{-1}).

Clip molecules **2a**,**b** were prepared in *ca*. 20% yield by reacting the respective propanediurea derivatives **3a**,**b** with α,α′-dibromo-*o*-xylene in DMSO in the presence of NaH. Compound **3a** was accessible following a literature procedure,[3] and compound **3b** was synthesized in 90% yield by refluxing 2,2-dimethyl-3-oxobutanal with urea in toluene in the presence of TFA with azeotropic removal of water. Clip molecule **2c** could be obtained in 20% yield by reacting **3a** with 2,3-bis-(bromomethyl)-1,4-dimethoxybenzene in DMSO in the presence of NaH. The latter compound was prepared from 3,6-dimethoxyphthalic anhydride[4] by reduction with $LiAlH_4$ followed by reaction with PBr_3. Full experimental details will be reported in a forthcoming paper.‡

Single crystals of **2a** were obtained by vapour diffusion using $CHCl_3$ as the solvent and hexane as the precipitant and of **2c** by vapour diffusion using CH_2Cl_2 as the solvent and Et_2O as the precipitant. The crystal structure of **2a** revealed that this clip molecule has a U-shaped cavity similar to that of diphenylglycoluril derived clips.[2a] In contrast to previous clip molecules of type **1** the crystal structure of **2c**§ shows an asymmetric geometry with respect to the side walls (Fig. 1), which is attributed to its greater flexibility. The clip molecule dimerizes to give a 'head-to-head' packing, with the wall of one clip molecule being buried in the cavity of another clip. This dimerization was not observed in $CDCl_3$ solution.

The binding properties of hosts **2** and, for comparison, hosts **1** with a number of hydroxybenzene derivatives (**4a**–**f**, **5**–**7**), were measured by NMR titration experiments in $CDCl_3$ using the outer wall protons of the host and the aromatic protons of the guest as probes.¶ The results are summarized in Table 1. The new clip molecules bind resorcinol derivatives significantly more strongly than diphenylglycoluril molecular clips. The binding constant is a factor of three higher for hosts **2a**,**b** when compared to host **1a**.‖ In the case of **2c** the increase in binding constant strongly depended on the type of guest used (see Table 1). For guests **4a**–**c** the binding was increased by a factor of three, five and twelve respectively when compared to host **1b**. For guests **4d**–**f** the binding constants were so large that they could not be measured by standard NMR titrations.[5] We therefore determined the binding constants of **4d**,**e** by competition experiments with **4c**, and of **4f** by a competition experiment with **4e**.[6] A plot of the binding free energies of guests **4a**–**f** as a function of the Hammett parameter [σ_m (R)] of the guest's substituent (Fig. 2) reveals a linear correlation which has been previously observed for clip **1b**.[2b] From the gradients of the

Fig. 1 X-Ray structure showing a dimer of clip **2c**

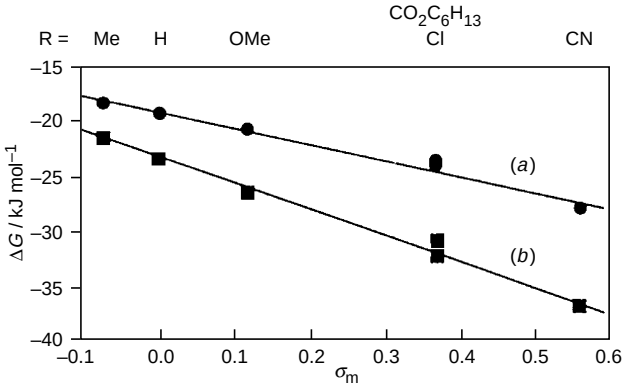

Fig. 2 Binding free energies of guests **4a**–**f** in clips (*a*) **1b** and (*b*) **2c** as a function of the Hammett parameter [σ_m(R)] of the guest's substituent

plots it is clear that binding of guests in clip **2c** is more sensitive to the substituent on the guest than binding in clip **1b**. Previous analysis of the binding properties of clips of type **1** showed that the steeper the gradient the greater the hydrogen bonding contribution is to the overall binding.[2b] One of the reasons for the stronger binding of **2c** is the fact that the carbonyl oxygens atoms are situated slightly higher with respect to the cavity walls than the carbonyl oxygens atoms in clip **1b**, as is clear from the X-ray structures. Previously it has been shown that the optimal distance for π–π interaction of a guest in clips **1** is at a position further out of the cavity than that for optimal hydrogen bonding.[2b] This means that in clip **2c** the complexation geometry is more ideal for optimum π–π interactions than in clip **1b**. Furthermore, the carbonyl–carbonyl distance in clip **2c** (5.2 Å) is closer to the ideal value for resorcinol binding (3.9 Å)** than this distance in clip **1b** (5.5 Å). Although the difference is small, it is significant since **1b** is shown to be better suited for binding of guest molecules with relatively large OH–OH distances such as 2,7-dihydroxynaphthalene **5** than **2c** (Table 1); this guest prefers a carbonyl–carbonyl distance of 6.3 Å.** The enhanced binding of catechol **6** in **2c** can be explained by the smaller carbonyl–carbonyl distance.‖ Other factors, apart from the position of the carbonyl groups, also contribute to the difference in binding properties of the clips. The binding of 4-nitrophenol **7**, which has only one hydroxy group and hence forms one strong optimum hydrogen bond, is stronger in clip **2c** than in clip **1b** (Table 1), suggesting that additional factors, *e.g.* the possibility of a guest to adopt a more parallel orientation with respect to the cavity walls, play a role in the enhanced binding.††

The NMR data suggest that the binding of a guest in clips of type **2** takes place *via* an induced fit mechanism, which is in agreement with the increased flexibility predicted by molecular modelling and suggested in the asymmetry observed in the X-ray crystal structures. The signals due to the benzylic protons of clip **2c** were found to shift considerably upon binding of a guest (**4d**: up to +0.44 ppm for the upfield benzylic proton signals and −0.29 ppm for the downfield benzylic proton signals), in contrast to those of clips **1**, for which virtually no shifts were observed. These shifts indicate that the conformation of the clip's side walls changes upon binding of a guest and are consistent with a tightening of the cavity upon binding of an aromatic guest.

In conclusion, a new type of molecular clips is presented which show enhanced binding of aromatic guest molecules. Applications of these receptor molecules in the construction of new supramolecular architectures are under investigation.

Table 1 Association constants of complexes between various host and guest molecules in $CDCl_3$, T = 25 °C

	Host	
Guest	**2c**	**1b**
4a	5500[a]	1900[b]
4b	14000[a]	2600[c]
4c	53000[a]	4400[b]
4d	$2.7\cdot10^5$[d]	16500[b]
4e	$4.2\cdot10^5$[d]	16000[b]
4f	$3.4\cdot10^6$[e]	$1\cdot10^5$[b]
5	2300[a]	7100[b]
6	130[d]	60[c]
7	4400[a]	1200[c]

[a] Estimated error, 20%. [b] Values taken from ref. 2(*a*). [c] Values taken from ref. 2(*b*). [d] Estimated error, 30%. [e] Estimated error, 40%.

Footnotes and References

† E-mail: tijdink@sci.kun.nl

‡ All new compounds were fully characterized by ^{1}H and ^{13}C NMR and mass spectroscopy and elemental analysis. *Selected data* for **2c**: δ_H (300 MHz) 6.74 (s, 4 H), 5.43 (d, 2 H, ^2J 15.1), 4.32 (s, 2 H), 3.90 (d, 4 H, ^2J 15.2), 3.78 (s, 12 H), 1.35 (s, 6 H).

§ *Crystal data and data collection parameters* for **2c**: $C_{27}H_{32}N_4O_6$, M = 508.57, monoclinic, a = 11.760(2), b = 15.300(3), c = 14.574(7) Å, β = 106.849(12)°, V = 2509.7(14) Å^3, T = 293(2) K, space group $P2_1/a$, λ = 1.54184 Å, Z = 4, D_c = 1.346 Mg m^{-3}, F(000) = 1080, colourless crystal with dimensions 0.29 × 0.19 × 0.16 mm, μ(Cu-Kα) = 0.791 mm^{-1}, Enraf-Nonius CAD4 diffractometer, θ–2θ scans, 3.17 < θ < 62.19°, +h, +k, ±l, maximum drift 14.526%, 4186 reflections measured, 3967 unique (R_{int} = 0.0098). The structure was solved using the program CRUNCH (ref. 8), and refined anisotropically, by full-matrix least squares on F^2 [program SHELXL (ref. 9)]. The final $wR(F^2)$ was 0.1991, with conventional $R(F)$ 0.0549.

¶ NMR titration experiments were performed as described in ref. 2(*a*). The chloroform used was standard NMR grade and predried on molecular sieves (4 Å) before use. The NMR spectra used for the determination of the binding constants showed only a small water peak.

‖ For example: for **4d**: K_a = 2000 M^{-1} with clip **2a** and 600 M^{-1} with clip **1c**; for **4b**: K_a = 550 M^{-1} with clip **2b** and 165 M^{-1} with clip **1c**.

** Assuming that the hydrogen bonds are linear and that the O–H–O distance is 2.7 Å (ref. 7).

†† Since clip molecules **1a** and **1c** have different groups at their convex sides, we compared the binding affinities of **1a** and **1c** with guests **4b**, **4d** and **4f**. The binding constants were the same within the experimental error (*e.g.* K_a = 165 and 175 M^{-1}, respectively, for **1a** and **1c** with guest **4b** and K_a = 3600 and 3500 M^{-1}, respectively, with guest **4f**), which indicates that the groups at the convex side of clips **1** do not contribute significantly to the binding. Clip molecule **1c** was prepared in 60% yield from dimethylglycoluril and α,α′-dibromo-*o*-xylene in DMF at room temperature in the presence of NaH.

1 For an overview, see R. M. Izatt, J. S. Bradshaw, K. Pawlak, R. L. Bruening and B. J. Tarbet, *Chem. Rev.*, 1992, **92**, 1261.
2 (*a*) R. P. Sijbesma, A. P. M. Kentgens, E. T. G. Lutz, J. H. van der Maas and R. J. M. Nolte, *J. Am. Chem. Soc.*, 1993, **115**, 8999; (*b*) J. N. H. Reek, A. H. Priem, H. Engelkamp, A. E. Rowan, J. A. A. W. Elemans and R. J. M. Nolte, *J. Am. Chem. Soc.*, 1997, **119**, 9956; (*c*) J. N. H. Reek, J. A. A. W. Elemans and R. J. M. Nolte, *J. Org. Chem.*, 1997, **62**, 2234.
3 B. N. Khasapov, T. S. Novikova, O. V. Lebedev, L. I. Khmel'nitskii and S. S. Novikov, *Zh. Org. Khim.*, 1973, **9**, 23.
4 C. Cardani and F. Piozzi, *Lincei-Rend. Sc. Fis. Mat. Nat.*, 1952, **12**, 719.
5 B. J. Whitlock and H. W. Whitlock, *J. Am. Chem. Soc.*, 1990, **112**, 3910.
6 J. S. Alper, R. I. Gelb, D. A. Laufer and L. M. Schwartz, *Anal. Chim. Acta*, 1989, **220**, 171.
7 I. Olovsson and P.-G. Jönsson, in *The Hydrogen Bond*, ed. P. Schuster, G. Zundel and C. Sandorfy, North Holland Publishing Company, Amsterdam, New York, Oxford, 1976, vol. II, pp. 393–456.
8 R. de Gelder, R. A. G. de Graaff and H. Schenk, *Acta Crystallogr., Sect. A*, 1993, **49**, 287.
9 G. M. Sheldrick, SHELXL-97, Program for the refinement of crystal structures, University of Göttingen, Germany, 1997.

Received in Cambridge, UK, 15th August 1997; 7/06012B

Highly enantioselective chiral base mediated [2,3]-Wittig rearrangement

Susan E. Gibson (née Thomas),*[a] Peter Ham[b] and Gary R. Jefferson[a]

[a] *Department of Chemistry, Imperial College of Science, Technology and Medicine, South Kensington, London, UK SW7 2AY*
[b] *SmithKline Beecham Pharmaceuticals, Discovery Research, New Frontiers Science Park, Third Avenue, Harlow, Essex, UK CM19 5AW*

A chiral non-racemic base promoted [2,3]-Wittig rearrangement of a series of (allyloxymethylbenzene)tricarbonylchromium(0) complexes proceeds with remarkably high enantioselectivity.

The [2,3]-Wittig (sigmatropic) rearrangement is a useful carbon–carbon bond-forming reaction.[1] As such, asymmetric versions of it are a desirable goal and research in recent years has produced several approaches to such systems.[2] The greatest success has been achieved using chiral auxiliaries.[3] For example, rearrangement of a range of α-allyloxy ketone hydrazones derived from a non-racemic chiral hydrazine proceeded in excellent yield (89–100%), with very good *syn*/*anti* selectivity (80–94% de) and good enantioselectivity (63–90% ee).[3a] Enantioselective versions of the [2,3]-Wittig rearrangement involving an achiral substrate and a chiral non-racemic base are synthetically more attractive but this approach has been much less successful, providing very moderate yields, diastereoselectivities and enantioselectivities.[4] The best results to date for a linear† system were obtained very recently using diprop-2-ynyl ethers as substrates.[4a] These rearranged in modest yield (29–57%) and with moderate enantioselectivity (46–62% ee) on treatment with a base derived from norpseudoephedrine. In view of the moderate success achieved so far for the chiral non-racemic base mediated [2,3]-Wittig rearrangement, we reveal herein a rearrangement that proceeds with relatively high enantioselectivity (84–96% ee) and, with appropriate substitution, very good yield (80–82%).

Our recent observation that the benzylic methylene group in tricarbonylchromium(0) complexes of alkyl benzyl ethers **1** may be functionalised asymmetrically in high yield and enantiomeric excess by treatment with the chiral non-racemic base **2** and an external electrophile,[6] together with earlier reports that tricarbonylchromium(0) complexes of allyl benzyl ethers undergo [2,3]-Wittig rearrangements,[7] suggested to us that the action of base **2** on allyl benzyl ether complexes may lead to a highly enantioselective [2,3]-Wittig rearrangement. Accordingly a series of allyl benzyl ether complexes were synthesised using standard procedures‡ and the outcome of their reactions with base **2** determined (Scheme 1).

Initially the reaction of parent complex **3** with base **2** was examined. Complex **3** was added dropwise to a mixture of 1.1 equiv. of base **2**[8] and 1 equiv. of LiCl in THF at −78 °C. The reaction mixture was allowed to warm to −50 °C over 2 h and then stirred at −50 °C for a further 5 h. Addition of methanol and work-up gave a yellow oil that was identified as the [2,3]-Wittig rearrangement product **4** by comparison of its spectroscopic data with literature values.[7d] The enantiomeric purity of **4** was readily assessed by chiral HPLC (Chiralpak AD) and, to our delight, was found to be 96%. In order to determine the absolute configuration of product **4**, the tricarbonylchromium(0) unit was removed (*hν*, 83% yield) and the $[\alpha]_D$ of the resulting alcohol compared with literature values.[9] This revealed that the absolute configuration of **4** was *R*, a result consistent with the sense of asymmetric induction observed for the functionalisation of complexes **1** with external electrophiles.[6]

The effect of substituents on the chemical yields and enantioselectivity of the [2,3]-Wittig rearrangement were examined next starting with substituent patterns that would lead to products containing just one chiral centre. Complexes **5**, **7** and **9** rearranged to give the novel§ alcohol complexes **6**, **8** and **10** with very good enantioselectivity (84–94%).¶ Although the chemical yield of **6** was good (82%), the yields of **8** and **10** were relatively poor (25 and 33% respectively) probably reflecting, for **8**, the hindered trajectory presented to the base by **7** and, for **10**, the extra electron donating substituent on an already electron-rich centre[10] in the transition state leading to **10**.

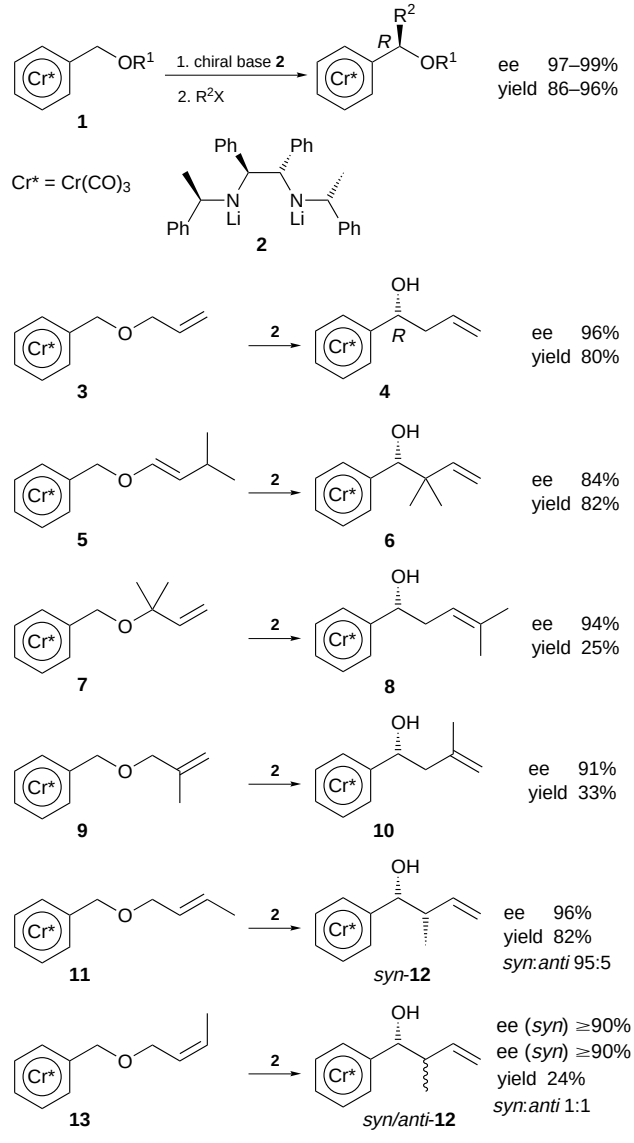

Scheme 1

Finally complexes **11** and **13** were reacted with base **2** in order to determine the level of stereochemical control this asymmetric [2,3]-Wittig rearrangement would exert over the generation of two adjacent chiral centres. The (*E*)-but-2-enyl complex **11** rearranged smoothly to give a good yield (82%) of alcohol **12**. The diastereomeric ratio of the product complex was found to be 95 : 5 and the relative stereochemistry of the major isomer was identified as *syn* by comparison of the ^{1}H NMR spectroscopic data of **12** and its decomplexation product with literature values obtained from a racemic sample.[7c] Chiral HPLC analysis revealed that the ee of **12** was 96%. In contrast the (*Z*)-but-2-enyl complex **13** rearranged to give a relatively poor yield of a 1 : 1 mixture of diastereomers,‖ although it was noted that the ee of each of the diastereomers was ⩾90%.

The authors thank Nichola C. Stevens of SmithKline Beecham Pharmaceuticals for several chiral HPLC analyses. G. R. J. also gratefully acknowledges a CASE award from SmithKline Beecham Pharmaceuticals.

Footnotes and References

* E-mail: s.gibson@ic.ac.uk

† The best result recorded to date for a *cyclic* system is the conversion of a 13-membered prop-2-ynylic ether into a 10-membered prop-2-ynylic alcohol in 69% ee and 82% yield using lithium bis[(*S*)-1-phenylethyl]amide.[5] This success was attributed to special conformational effects as the same base gave a poorer result with a 17-membered homologue (30% ee, 78% yield), and racemic products when applied to acyclic α-(allyloxy)acetic acids and amides.[5]

‡ The novel complexes **5** and **7**, and the known complexes **11** and **13**[7c] were synthesised by heating $Cr(CO)_6$ with the appropriate allyl benzyl ether (62–78%), whilst the uncharacterised complex **3**[7d] and the novel complex **9** were made by reacting (hydroxymethylbenzene)tricarbonylchromium(0) with NaH–allyl bromide (86%) and $ZnCl_2$–2-methylprop-2-en-1-ol (54%) respectively.

§ The novel complexes **3**, **5**–**10** and **12** all gave satisfactory microanalytical and spectroscopic (IR, ^{1}H NMR, ^{13}C NMR, *m/z*) data.

¶ The absolute stereochemistry of products **6**, **8**, **10** and **12** has been assigned by analogy with the rearrangement of complex **3** to **4** under the influence of base **2**.

‖ The clean rearrangement of the (*E*)-but-2-enyl complex **11** to a *syn* product and the uncontrolled rearrangement of the (*Z*)-but-2-enyl complex **12** is consistent with results obtained with racemic complexes[7] and contrasts with the (*Z*)-*syn* selectivity normally observed for the [2,3]-Wittig rearrangement of but-2-enyl systems.[1,7,10]

1 T. Nakai and K. Mikami, *Org. React.*, 1994, **46**, 105; J. A. Marshall, in *Comprehensive Organic Synthesis*, ed. B. M. Trost and I. Fleming, Pergamon, Oxford, 1991, vol. 3, pp. 975–1014; R. Brückner, in *Comprehensive Organic Synthesis*, ed. B. M. Trost and I. Fleming, Pergamon, Oxford, 1991, vol. 6, pp. 873–908.
2 For a recent review, see T. Nakai and K. Tomooka, *Pure Appl. Chem.*, 1997, **69**, 595.
3 For example, see (*a*) D. Enders and D. Backhaus, *Synlett*, 1995, 631; (*b*) O. Takahashi, K. Mikami and T. Nakai, *Chem. Lett.*, 1987, 69.
4 S. Minabe, *Chem. Commun.*, 1997, 737; J. A. Marshall and X. Wang, *J. Org. Chem.*, 1992, **57**, 2747; J. Kang, W. O. Cho, H. G. Cho and H. J. Oh, *Bull. Korean Chem. Soc.*, 1994, **15**, 732.
5 J. A. Marshall and J. Lebreton, *J. Am. Chem. Soc.*, 1988, **110**, 2925.
6 E. L. M. Cowton, S. E. Gibson (née Thomas), M. J. Schneider and M. H. Smith, *Chem. Commun.*, 1996, 839.
7 (*a*) M. Uemura, H. Nishimura and Y. Hayashi, *J. Organomet. Chem.*, 1989, **376**, C3; (*b*) J. Brocard, M. Mahmoudi, L. Pelinski and L. Maciejewski, *Tetrahedron Lett.*, 1989, **30**, 2549; (*c*) M. Uemura, H. Nishimura, T. Minami and Y. Hayashi, *J. Am. Chem. Soc.*, 1991, **113**, 5402; (*d*) M. Mahmoudi, L. Pelinski, L. Maciejewski and J. Brocard, *J. Organomet. Chem.*, 1991, **405**, 93.
8 K. Bambridge, M. J. Begley and N. S. Simpkins, *Tetrahedron Lett.*, 1994, **35**, 3391.
9 E. J. Corey and S. S. Kim, *Tetrahedron Lett.*, 1990, **31**, 3715.
10 Y.-D. Wu, K. N. Houk and J. A. Marshall, *J. Org. Chem.*, 1990, **55**, 1421.

Received in Liverpool, UK, 7th October 1997; 7/07232E

Synthesis of a mordenite/ZSM-5/chabazite hydrophilic membrane on a tubular support. Application to the separation of a water–propanol mixture

Miguel A. Salomón, Joaquín Coronas, Miguel Menéndez and Jesús Santamaría*

Department of Chemical and Environmental Engineering, University of Zaragoza, 50009, Zaragoza, Spain

A selectivity of 71 is achieved in the separation of a gas phase water–propanol mixture, using a mordenite/ZSM-5/chabazite membrane that is hydrothermally synthesized onto the inner surface of a porous α-alumina tubular support.

In recent years, the synthesis of zeolite membranes on porous inorganic substrates (disks or tubes) has received much attention. To prepare such a membrane, the crystals must form a continuous, defect-free two-dimensional layer, so that only transport through the zeolite pores takes place. Several methods have been proposed for the preparation of zeolite membranes. For ZSM-5 membranes, it was demonstrated that permeation and separation properties depend strongly on the preparation procedure used.[1] The most usual liquid-phase preparation method involves immersing the porous support into the zeolite precursor gel. With this method MFI-type zeolite,[1,2] zeolite A[3] and zeolite Y[4] tubular or flat membranes have been prepared. It is noticed that, although tubular supports are more interesting from an industrial point of view, there are still very few examples of zeolite membranes synthesized on them. This is due to the development of mechanical tensions during the drying/calcination steps, that often result in the formation of defects such as cracks and pinholes. The vapour phase method has been used to prepare ZSM-5 and ZSM-35,[5] ferrierite[6] and mordenite[7] flat membranes, where vapors containing amines and water were employed to zeolitize silica and/or alumina layers previously deposited onto the support.

Most of these zeolite membranes have been used for separations of organic–organic,[1] water–organic[3,4,8] and permanent gas–organic[2] mixtures. When there are significant differences in polarity between the components of a mixture (*e.g.* water–alcohol mixtures), the organophilic or hydrophilic character of the zeolite can play an important role. For instance, water permeated faster than ethanol through membranes of zeolites A and Y (both of them hydrophilic),[3,4] while through silicalite membranes the permeation of ethanol was faster.[8] Here we present the synthesis and some permeation properties of a mordenite/ZSM-5/chabazite membrane on a tubular α-alumina support. To our knowledge this is the first report on the preparation of such a tubular membrane. The constituting zeolites differ in their physical properties: ZSM-5 is a high-silica zeolite (Si/Al ratios between 2.5 and 100), with a structure consisting of straight channels of 0.54 × 0.56 nm, intersecting with sinusoidal channels of 0.53 × 0.55 nm; with mordenite, the Si/Al ratio is around 5, and there are large channels of 0.67 × 0.7 nm, and small channels of 0.26 × 0.57 nm; finally, chabazite is a smaller pore size zeolite (its larger channels are 0.38 × 0.38 nm), but in this case the Al content is higher, with a Si/Al ratio between 1.6 and 3. Since the hydrophilicity of a zeolite increases with its Al content, it can be expected that the presence of mordenite and chabazite increase the selectivity for the separation of water, with respect to what could be achieved on a pure ZSM-5 membrane.

The synthesis method employed 0.65 mm id asymmetric porous α-alumina microfiltration tubes with a 200 nm pore diameter separation layer (US Filter, SCT). An aluminosilicate gel was prepared using Aerosil 300 (Degussa) and sodium aluminate (Carlo Erba) as silica and alumina sources, respectively, tetraethylammonium hydroxide (TEAOH) solution 35 mass% in water (Aldrich) as template, NaOH and distilled water. A gel was prepared with a molar composition 80 SiO_2 : 2080 H_2O : 32 NaOH : 40 TEAOH : 1 $Na_2Al_2O_4$. The starting solution consisted of Aerosil 300 and approximately two thirds of the above amount of deionized water. This solution was kept under vigorous stirring for 5 h. Then, a solution containing the other substances was added, one fifth every 30 min, to the first solution. The resulting gel was aged under stirring for 3 days. The gel was cloudy but not thick, and had a pH of *ca*. 12.1. The gel was not completely stable, and two different phases appeared a few hours after stirring was stopped. Before synthesis, the outer surface of the dry alumina tube was wrapped with Teflon tape to avoid penetration of the gel from this side, and the tube was then immersed in the synthesis gel filling a Teflon-lined autoclave. The tube was fixed axially, and the autoclave was placed horizontally in a convection stove at 443 K for 21–23 h. The synthesis was repeated four times, with the tube–autoclave ensemble rotated 90° in each step. After the last synthesis, the tube was tested for permeability to N_2, at room temp. and pressure differences of up to 3 bar. Strict impermeability was required, which sometimes required a fifth synthesis. Finally, to remove the template, the membrane was calcined, at 753 K for 8 h using 1 K min^{-1} heating and cooling rates. The composition of the gel used for the synthesis is optimized to obtain mordenite. However, during the synthesis of the membrane on an Al_2O_3 support, it can be expected that part of the support is dissolved and incorporated into the synthesis gel, and thus other compositions such as ZSM-5 and chabazite are possible.

The zeolite mass gain and the N_2 permeance were measured for several membranes, samples M1–M3 (Table 1) to characterize initially the membrane and assess the reproducibility of the synthesis method. After the hydrothermal synthesis, crystals not attached to the support were recovered from the autoclave. These crystals which should have a composition similar to the material deposited as a continuous layer on the alumina support, were characterized by XRD analysis (Rigaku/Max System, Cu-Kα radiation, graphite monochromator). XRD patterns of the composite membrane and of zeolite crystals prepared by homogeneous synthesis (*i.e.* in the absence of a porous alumina support) using the same gel were also obtained. Fig. 1(*a*) shows the XRD pattern of zeolite crystals prepared by homogeneous synthesis. By comparison with XRD data in the literature[9] it can be seen that the pattern is practically coincident with that of a pure mordenite zeolite. On the other hand, Fig. 1(*b*) indicates that the XRD pattern of the crystals collected in the remaining liquid after the synthesis of the membrane in the presence of α-Al_2O_3 contains a significant amount of other zeolites (ZSM-5 and chabazite), in addition to mordenite. Finally, the pattern shown in Fig. 1(*c*) corresponds to composite membrane M3 (see Table 1), and is a combination of α-alumina (marked with an asterisk), and the ZSM-5, chabazite and mordenite crystals already shown in Fig. 1(*b*). The zeolite peaks in the XRD diagram corresponding to the composite membrane are smaller than those shown in Fig. 1(*b*), because the zeolite contributed only 7% to the total membrane mass, the rest being α-Al_2O_3. A closer examination of the XRD pattern of the composite

Table 1 Some characteristics of the composite zeolite membranes

Membrane	Mass gain/ mg zeolite (g support)$^{-1}$	N_2 single gas permeance/ mol (s m^2 Pa)$^{-1}$	Water–propanol–air mixture[a]		
			H_2O permeance/ mol (s m^2 Pa)$^{-1}$	Water/ propanol selectivity	Water/O_2 selectivity
M1	67	3.0×10^{-7}	2.0×10^{-7}	50	5.3
M2	79	2.5×10^{-7}	2.7×10^{-7}	71	10
M3	69	Not measured	2.8×10^{-7}	16	13

[a] Partial pressure (kPa): water = 2.4; propanol = 0.36.

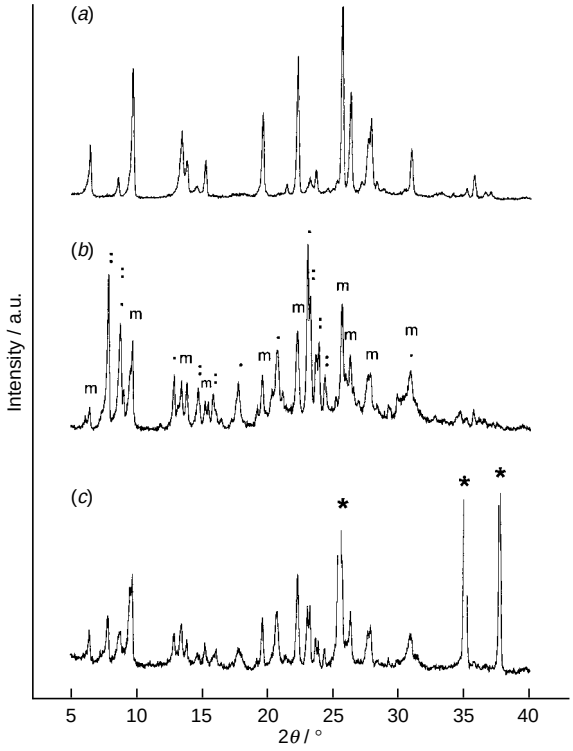

Fig. 1 X-Ray diffraction patterns of (*a*) mordenite powder; (*b*) powder collected in the remaining liquid after the synthesis of the composite zeolite membrane, ● = chabazite, ●● = silicalite, m = mordenite; (*c*) composite zeolite membrane, * = Al_2O_3 support. For clarity, zeolite peaks have not been marked.

membrane shows some additional interesting features: first, the orientation of the zeolite crystals does not change from Fig. 1(*a*) to Fig. 1(*b*) and (*c*). Second, a comparison of the intensities of the main characteristic bands in the XRD diagram gives a rough estimation of the relative proportions of the different zeolites as mordenite : ZSM-5 : chabazite = 2 : 1 : 1, *i.e.* mordenite is the preponderant species, but there are very significant amounts of ZSM-5 and chabazite.

SEM (JEOL JSM-6400) observations of cross-sections of the composite membranes (not shown) indicated that the zeolite crystals formed a continuous layer 10 μm thick, on top of the inner surface of the alumina support. Further SEM observations showed that zeolite crystals also dispersed among the large α-alumina particles of the support, indicating that the hydrothermal synthesis took place not only on the support but also inside its pores. The thickness of the mordenite layer estimated by SEM agrees well with the Si/Al profile across the membrane measured by EPMA (not shown). The Si/Al ratio in the zeolite film was lower than in the gel, as noted in other case of hydrothermal synthesis of zeolite membranes on alumina supports.[1] This indicates that a part of the alumina support was leached during the synthesis procedure, being incorporated into the composite membrane, and is consistent with the appearance of high alumina zeolites such as chabazite. The preparation procedure (in which the tube was placed horizontally and rotated 90° after every synthesis) was successful in dealing with the instability of the synthesis gel, and allowed deep penetration of the gel into the alumina support, as the 67–79 mg mass gain per g of support indicates (Table 1).

In the water–propanol separation experiments, the membrane was sealed with silicon o-rings in a stainless steel module. A gaseous mixture containing a predetermined proportion of water and propanol was obtained by mixing two air streams after passing them through two saturator trains containing liquid water and propanol respectively. This mixture was fed into the tube side of the membrane, and permeated through the membrane wall. The shell side was swept with a N_2 stream. Both the air and the N_2 streams were mass-flow controlled at approximately 34 cm^3(STP) min^{-1}. The total pressure (*ca.* 1 atm) and the pressure differential between both sides of the membrane (close to zero) were accurately maintained by means of an automated control system. When the steady state was reached, as indicated by GC analysis of both exit streams (usually after keeping the membrane under the mixture stream for around 2 h), the separation selectivities were calculated as the ratios of permeances for water and propanol, using the log(mean partial pressure) difference in the calculations. Table 1 shows the results of the water–propanol separation experiments performed with membranes M1–M3. The highest water–propanol selectivity was 71 at room temp. for membrane M2. The high selectivity of the composite membrane in the water–propanol separation may be attributed to the selective sorption of water in this hydrophilic membrane.

Footnote and References

* E-mail: iqcatal@posta.unizar.es; Fax: +34 76 762142

1 J. Coronas, J. L. Falconer and R. Noble, *AIChE J.*, 1997, **43**, 1797.
2 M. D. Jia, B. Chen, R. D. Noble and J. L. Falconer, *J. Membr. Sci.*, 1994, **90**, 1.
3 H. Kita, K. Horii, Y. Ohtoshi and K. Okamoto, *J. Mater. Sci. Lett.*, 1995, **14**, 206.
4 H. Kita, T. Inoue, H. Asamura, K. Tanaka and K. Okamoto, *Chem. Commun.*, 1997, 45.
5 J. Dong, T. Dou, X. Zhao and L. Gao, *J. Chem. Soc., Chem. Commun.*, 1992, 1056.
6 N. Nishiyama, K. Ueyama and M. Matsukata, *Stud. Surf. Sci. Catal.*, 1997, **105**, 2195.
7 N. Nishiyama, K. Ueyama and M. Matsukata, *Microporous Mater.*, 1996, **7**, 299.
8 Q. Liu, R. D. Noble, J. L. Falconer and H. H. Funke, *J. Membr. Sci.*, 1996, **117**, 163.
9 D. W. Breck, *Zeolite Molecular Sieves*, Krieger Publishing Company, Malabar, 1984.

Received in Bath, UK, 22nd October 1997; 7/07626F

Zwitterionic alkene polymerization catalyst derived from $Cp_2Zr(\eta^2\text{-}C_2H_4)PPh_2Me$ and $B(C_6F_5)_3$

Yimin Sun,[a] Warren E. Piers*[a] and Steven J. Rettig[b]

[a] *Department of Chemistry, University of Calgary, 2500 University Dr. NW, Calgary, Alberta, Canada T2N 1N4*
[b] *Department of Chemistry, University of British Columbia, 2036 Main Mall, Vancouver, British Columbia, Canada V6T 1Y6*

The phosphine stabilized ethylene complex of zirconocene, Cp_2Zr, reacts with 1 equiv. of $B(C_6F_5)_3$ to form the girdle-type zwitterion $Cp_2Zr^+(PPh_3Me)CH_2CH_2B^-(C_6F_5)_3$ 2, which serves as an ethene polymerization catalyst either with or without added $B(C_6F_5)_3$.

Bent metallocenes[1] are highly active for the polymerization of alkenic monomers to important commodity plastics.[2] Two principal factors contribute to this molecular fragment's ability to circumvent the barrier associated with the exothermic alkene enchainment process: the high electrophilicity of the formally 14 electron $[Cp_2M–R]^{n+}$ species and the ideally configured frontier orbital structure of the bent metallocene unit.[3] Since the former attribute is enhanced when $n = 1$, most commercially viable catalysts are based on group 4 metal cations; use of sufficiently weakly ccordinating counter-anions is necessary in order to attain high activities.

Zwitterionic analogs of cationic metallocenes, in which the counter-anion and the active cation are covalently linked in some fashion, have been touted as a way to modulate ion pairing in these catalysts, thus increasing activity.[4] Two classes of zwitterionic metallocenes have been reported: ring-type zwitterions in which the anion is affixed to one of the Cp donors,[5] and girdle-type betaines, where the counter-anion is located on the alkyl group occupying the reactive wedge of the metallocene.[6] In the latter type, the zwitterionic nature of the catalysts lasts only until the first termination step, while in the former, the charge separated structure is maintained throughout the polymerization process.

Girdle-type zwitterionic compounds have been accessed mainly through electrophilic attack by $B(C_6F_5)_3$[7] on suitable hydrocarbyl ligands of neutral group 4 bent metallocenes. Herein we report the reaction of the phosphine stabilized zirconocene ethylene complex, $Cp_2Zr(\eta^2\text{-}C_2H_4)PPh_2Me$[8] **1**, with this borane; the product may be considered to be the 'parent' girdle-type zwitterionic zirconocene.

When **1** is treated with one equivalent of $B(C_6F_5)_3$ in toluene, the zwitterionic product **2** is isolated as an orange solid in 92% yield (Scheme 1).† Although the phosphine ligand in the starting material is labile,‡ the electrophile preferentially attacks the coordinated alkene; no formation of $Ph_2MeP{\cdot}B(C_6F_5)_3$ was observed. The ^{11}B chemical shift of δ −10.8 for **2** is diagnostic for anionic, four-coordinate boron,[9] supporting the formulation of **2** as a zwitterionic species with a high degree of charge separation. For comparison, a ^{11}B NMR chemical shift of δ 2.0, more closely associated with neutral four-coordinate boron, was found for the product formed from reaction of **1** with $HB(C_6F_5)_2$,[10] which features a strong borate–zirconium cation interaction.[11]

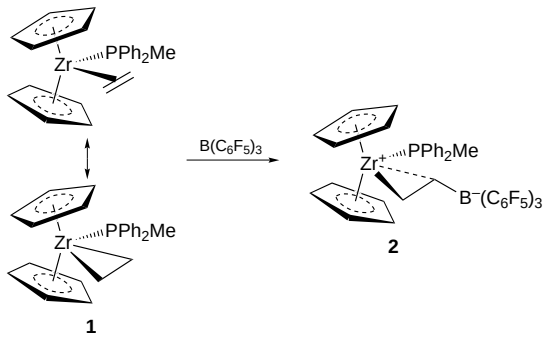

1 **2**

Scheme 1

Although the ^{11}B NMR chemical shift of **2** is suggestive of significant charge separation, several spectral criteria are met which are suggestive of a strong β-CH agostic interaction[12] which electronically compensates the cationic zirconium center. Signals for the β-CH_2 protons and carbon atom appear upfield of the resonances for the α-methylene atoms in the ^1H and ^{13}C NMR spectra. At room temp., the averaged J_{CH_β} coupling constant is 105 Hz, indicative of weakened C–H bonds at this position.[13] The coupling constant of 145 Hz for the α-C–H bonds is characteristic of an acute $Zr–C_\alpha–C_\beta$ bond angle, expected in the event of a β-agostic interaction.[12,14] Furthermore, when the ^1H NMR spectrum is monitored as the temperature is lowered, the signals for the $ZrCH_2CH_2B$ unit undergo decoalescence behavior until at −90 °C four signals reappear at δ 2.24 and 0.75 for the Zr–CH_2 pair and δ −0.05 and −1.55 for the two CH_2B hydrogens. From the NMR data, the rate of exchange at coalescence (−67 °C) was determined[15] to be 1.46×10^3 s^{-1} and a $\Delta G^‡$ of 9.0(5) kcal mol^{-1} (1 cal = 4.184 J) was calculated for this exchange using the Eyring equation. This is a relatively high barrier for interchange of β-agostic protons in zirconocene cations, which is typically faster than the NMR timescale.[12,16]

The solid state structure of **2** also features this agostic motif. Suitable crystals of the compound were obtained from toluene; protons associated with the $ZrCH_2CH_2B$ moiety were located and refined isotropically.§ An ORTEP diagram of the compound is shown in Fig. 1 and pertinent metrical parameters are summarized in Table 1, along with analogous data for two related, non-zwitterionic compounds reported previously by Jordan and coworkers. Compound **2** is a zwitterionic analog of Jordan's ethyl cation[12] but is structurally more similar to the trimethylsilyl substituted derivative[16] in that the β-agostic alkyl group adopts an *endo* coordination geometry rather than the *exo* structure seen in the ethyl complex. Since the Me_3Si group was essentially coplanar with Zr, C_α and C_β, Jordan proposed an organometallic γ silicon effect, in which the back lobe of the Si–C_β bond donates to the zirconium center, as the basis for this observation. In **2**, the borate boron is tilted *ca.* 17° out of the Zr–C(12)–C(11) plane and the C_β–H bond is clearly involved in an agostic interaction with the deficient zirconium center. It is, however, feasible that the back lobe of the B–C_β carbon may also be involved in the Zr–C_β contact. At any rate, the observed strength of the β-agostic interaction in **2** suggests that the negative charge of the borate group is substantially localized on C_β, rendering it a more effective donor than the C_β–$SiMe_3$ group in Jordan's compound.

Although it could be argued that attack by $B(C_6F_5)_3$ at the *exo* carbon of the coordinated ethylene in **1** should be preferred on steric and electronic grounds,¶ the *endo* isomer of **2** appears to

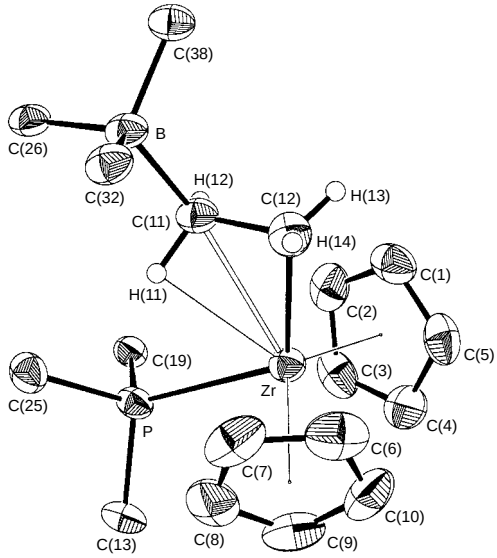

Fig. 1 ORTEP diagram of girdle zwitterion **2**. Phenyl and pentafluorophenyl groups have been omitted for clarity. Key metrical parameters are given in Table 1.

Table 1 Metrical parameters for **2** and related compounds

	2	$Cp_2Zr^+(PMe_3)(H)(H)$	$Cp_2Zr^+(thf)(H)(H)(SiMe_3)$
Zr–C_α/Å	2.260(4)	2.290(9)	2.26(2)
Zr–C_β/Å	2.607(4)	2.629(2)	2.57(2)
Zr–H_β/Å	2.39(3)	2.16	—
Zr–P,O/Å	2.828(1)	2.691(3)	2.320(11)
Zr–C_α–C_β/°	85.3(2)	84.7(5)	84(1)
P,O–Zr–C_α/°	119.0(1)	73.6(3)	115.9(5)
Zr–C_β–B,Si/°	164.9	—	174.1

be the kinetic as well as the thermodynamic product. Thus, when the reaction was monitored at −90 °C by ^{1}H or ^{31}P NMR spectroscopy, no intermediates were observed and only *endo*-**2** was formed. If attack at the *exo* carbon is preferred, rearrangement to *endo*-**2** must be very fast.

The zwitterion **2** polymerizes ethylene under ambient conditions,[17] although for optimal activity, an additional equivalent of $B(C_6F_5)_3$ is required. Activities of $3.2(4) \times 10^4$ g polymer (mol Zr atm h)$^{-1}$ (M_w = 26 100, M_w/M_n = 2.2) were observed in the absence of added $B(C_6F_5)_3$, while productivities more in line with expected values [$9.4(4) \times 10^5$; M_w = 133 700; M_w/M_n = 2.0] were found when **2** was treated with borane in the presence of ethene. Presumably, the added $B(C_6F_5)_3$ serves to sequester the phosphine ligand blocking the coordination site necessary for optimal polymerization rates. In the absence of ethene, a complex mixture of products results when **2** is treated with $B(C_6F_5)_3$, indicating that the 'naked' zwitterion is not stable in solution under these conditions.

Financial support for this work was provided by the Novacor Research and Technology Corporation of Calgary, Alberta and by the Natural Sciences and Engineering Council of Canada's Research Partnerships program. W. E. P. thanks the Alfred P. Sloan Foundation for a Research Fellowship (1996–98).

Footnotes and References

* E-mail: wpiers@chem.ucalgary.ca

† *Synthesis* of **2**. Toluene (20 ml) was condensed into an evacuated flask cooled to −196 °C containing **1** (609 mg, 1.35 mmol) and $B(C_6F_5)_3$ (693 mg, 1.35 mmol). The mixture was warmed to −78 °C, stirred for 30 min and then warmed to room temp. The yellow slurry was concentrated and filtered. The solid was washed with hexane (15 ml) and **2** (1.2 g, 92%) was obtained as yellow powder. Partial ^{1}H NMR (C_6D_6, 23 °C): δ 1.50 (t, J_{HH} 6.5 Hz, 2 H, $ZrCH_2CH_2B$), −0.74 (br, 2 H, $ZrCH_2CH_2B$). Partial $^{13}C\{^1H\}$ NMR (C_6D_6, 23 °C): δ 41.6 (s, J_{CH} 145 Hz, $ZrCH_2CH_2B$), −14.0 (br m, J_{CH} 105 Hz, $ZrCH_2CH_2B$).

‡ For example, the reaction of PPh_2Me stabilized **1** with the more basic phosphine PMe_3 gave the trimethyl phosphine adduct $Cp_2Zr(\eta^2\text{-}C_2H_4)PMe_3$ essentially upon mixing.

§ *Crystal data* for **2**: $C_{43}H_{27}BF_{15}PZr$, M = 961.67, orthorhombic, *Pbca*, a = 18.782(1), b = 22.5024(9), c = 18.740(2) Å, U = 7920.3(9) Å^3, D_c = 1.613 Mg m^{-3} for Z = 8. $F(000)$ = 3840.00, μ(Cu-Kα) = 36.71 cm^{-1}, λ = 1.541 78 Å, T = 294 K. A total of 8944 reflections were collected using the ω–2θ scan technique to a maximum 2θ value of 155°. The data were corrected for Lorentz and polarisation effects and the structure solved by heavy-atom Patterson methods and expanded using Fourier techniques. The non-hydrogen atoms were refined anisotropically. The hydrogen atoms associated with the β-ethyl moiety were refined isotropically, the rest were fixed in idealized positions with C–H = 0.98 Å. The final cycle of full-matrix least-squares refinement was based on 4690 observed reflections [$I > 3\sigma(I)$] and 567 variable parameters and converged (largest parameter shift was 0.003 times its esd) with R = 0.034, R_w = 0.034, GOF = 1.88. CCDC 182/687.

¶ A MacSpartan Plus *ab initio* calculation on $Cp_2Zr(PH_3)(\eta^2\text{-}C_2H_4)$ at the 3-21G* level showed that the HOMO is roughly equally distributed on the *exo* and *endo* carbons; a slightly higher charge density exists on the *exo* carbon, which is also sterically much more accessible.

1 H. H. Brintzinger, D. Fischer, R. Mülhaupt, B. Rieger and R. M. Waymouth, *Angew. Chem., Int. Ed. Engl.*, 1995, **34**, 1143; M. Bochmann, *J. Chem. Soc., Dalton Trans.*, 1996, 255; T. J. Marks, *Acc. Chem. Res.*, 1992, **25**, 57; R. F. Jordan, *Adv. Organomet. Chem.*, 1991, **32**, 325.
2 A. M. Thayer, *Chem. Eng. News*, 1995, **73**, 15; R. G. Harvan, *Chem. Ind.*, 1997, 212.
3 J. W. Lauher and R. Hoffmann, *J. Am. Chem. Soc.*, 1976, **98**, 1729.
4 W. E. Piers, *Chem. Eur. J.*, 1998, in press.
5 (*a*) R. E. v H. Spence and W. E. Piers, *Organometallics*, 1995, **14**, 4617; (*b*) Y. Sun, R. E. v H. Spence, W. E. Piers, M. Parvez and G. P. A. Yap, *J. Am. Chem. Soc.*, 1997, **119**, 5132; (*c*) M. Bochmann, S. J. Lancaster and O. B. Robinson, *J. Chem. Soc., Chem. Commun.*, 1995, 2081; (*d*) J. Ruwwe, G. Erker and R. Fröhlich, *Angew. Chem., Int. Ed. Engl.*, 1996, **35**, 80.
6 B. Temme, G. Erker, J. Karl, H. Luftmann, R. Fröhlich and S. Kotila, *Angew. Chem., Int. Ed. Engl.*, 1995, **34**, 1755; B. Temme, J. Karl and G. Erker, *Chem. Eur. J.*, 1996, **2**, 919; B. Temme, G. Erker, R. Fröhlich and M. Grehl, *Angew. Chem., Int. Ed. Engl.*, 1994, **33**, 1480; W. Ahlers, B. Temme, G. Erker, R. Fröhlich and T. Fox, *J. Organomet. Chem.*, 1997, **527**, 191; B. Temme, G. Erker, R. Fröhlich and M. Grehl, *J. Chem. Soc., Chem. Commun.*, 1994, 1713; G. G. Hlatky, H. W. Turner and R. R. Eckman, *J. Am. Chem. Soc.*, 1989, **111**, 2728.
7 A. G. Massey and A. J. Park, *J. Organomet. Chem.*, 1964, **2**, 245; W. E. Piers and T. Chivers, *Chem. Soc. Rev.*, 1997, in press.
8 T. Takahashi, M. Murakami, M. Kunishige, M. Saburi, Y. Uchida, K. Kozawa, T. Uchida, D. R. Swanson and E. Negishi, *Chem. Lett.*, 1989, 761.
9 R. G. Kidd, in *NMR of Newly Accessible Nuclei*, ed. P. Laszlo, Academic Press, New York, 1983, vol. 2.
10 D. J. Parks, R. E. v H. Spence and W. E. Piers, *Angew. Chem., Int. Ed. Engl.*, 1995, **34**, 809.
11 Y. Sun, W. E. Piers and S. J. Rettig, *Organometallics*, 1996, **15**, 4110.
12 R. F. Jordan, P. K. Bradley, N. C. Baenziger and R. E. LaPointe, *J. Am. Chem. Soc.*, 1990, **112**, 1289; Y. W. Alelyunas, Z. Guo, R. E. LaPointe and R. F. Jordan, *Organometallics*, 1993, **12**, 544.
13 M. Brookhart, M. L. H. Green and L. Wong, *Prog. Inorg. Chem.*, 1988, **36**, 1.
14 T. Yonezawa, I. Moreshima, M. Fujii and K. Fuki, *Bull. Chem. Soc. Jpn.*, 1965, **38**, 1226; R. Aydin and H. Gunther, *J. Am. Chem. Soc.*, 1981, **103**, 1301.
15 Using the equation $k_c = \pi\Delta\nu_c/\sqrt{2}$, where $\Delta\nu_c$ = the peak separation in Hz at coalescence (estimated from the peak separation in the low temperature limit). See: J. Sandstrom, *Dynamic NMR Spectroscopy*, Academic Press, New York, 1982, pp. 77–92.
16 Y. W. Alelyunas, N. C. Baenziger, P. K. Bradley and R. F. Jordan, *Organometallics*, 1994, **13**, 148.
17 See ref. 5(*b*) for experimental conditions used in our laboratory.

Received in Bloomington, IN, USA, 7th August 1997; 7/05782B

Alkali metal cation cooperative iodide anion recognition by new heteroditopic bis(calix[4]arene) rhenium(I) bipyridyl receptor molecules

Paul D. Beer* and James B. Cooper

Inorganic Chemistry Laboratory, University of Oxford, South Parks Road, Oxford, UK OX1 3QR

New heteroditopic bis(calix[4]arene) rhenium(I) bipyridyl receptors are synthesised and shown to simultaneously bind alkali metal cations and iodide anion with positive cooperativity.

The design of new ditopic[1] ligands for the simultaneous complexation of anionic and cationic guest species is a new exciting area of coordination chemistry of significant relevance to the selective extraction and/or transportation of metal salts across lipophilic membranes. Rare examples of receptors containing appropriate covalently linked binding sites for anions and cations include Lewis-acidic boron,[2] uranyl,[3] polyammonium[4] centres combined with crown ether moieties and crown ether or urea functionalised calix[4]arene ionophores[5,6] which are capable of solubilising alkali metal salts into organic solvent media. We have shown that charged or neutral transition metal organometallic and coordination amide containing receptor systems can selectively bind and sense anions.[7] Lower rim ester functionalised calix[4]arenes are known to coordinate alkali metal cations.[8] Incorporating these two types of recognition sites on to the calix[4]arene building block will create potential heteroditopic receptors capable of binding anions and cations. We report here the syntheses of new heteroditopic bis(calix[4]arene) rhenium(I) bipyridyl receptors which display positive cooperative upper rim binding of the iodide anion *via* lower rim complexation of alkali metal cations.

The new upper rim mono-amine–lower rim ester substituted calix[4]arene derivatives **1** and **2** were prepared according to Scheme 1. Condensation reactions of 2 equiv. of **1** and **2** with 4,4′-bis(chlorocarbonyl)-2,2′-bipyridine **3**[9] followed by complexation with $Re(CO)_5Cl$ gave the new receptors L^1 and L^2 in good yields (Scheme 2).

The cation and anion coordination properties of both receptors were investigated by ^1H NMR titration experiments in CD_3CN solution. The addition of $LiClO_4$, $NaClO_4$ and KPF_6 salts typically caused the ester methylene receptors' protons to initially broaden and sharpen again after 2 equiv. suggesting complexes of $2M^+:L$ stoichiometry are being formed in

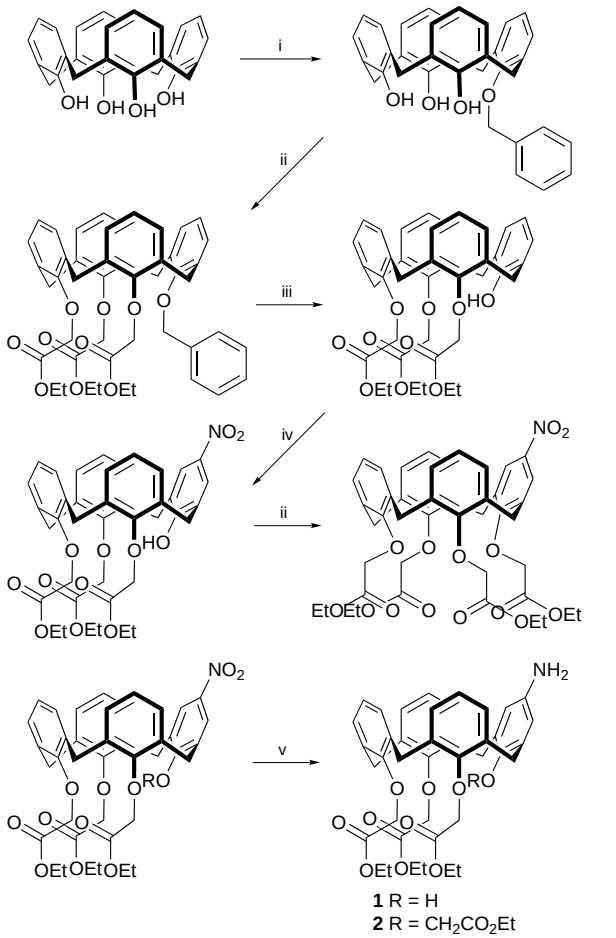

Scheme 1 *Reagents and conditions* i, 1 equiv. $PhCH_2Br$, 0.5 equiv. K_2CO_3, MeCN reflux, 24 h; ii, $BrCH_2CO_2Et$ (excess), K_2CO_3 (excess), MeCN reflux 48 h; iii, Pd/C, HCO_2NH_4, EtOH reflux; iv, NH_4NO_3, HCl, H_2O, acetic anhydride, CH_2Cl_2; v, Zn (excess), HCl (excess), reflux EtOH, 24 h

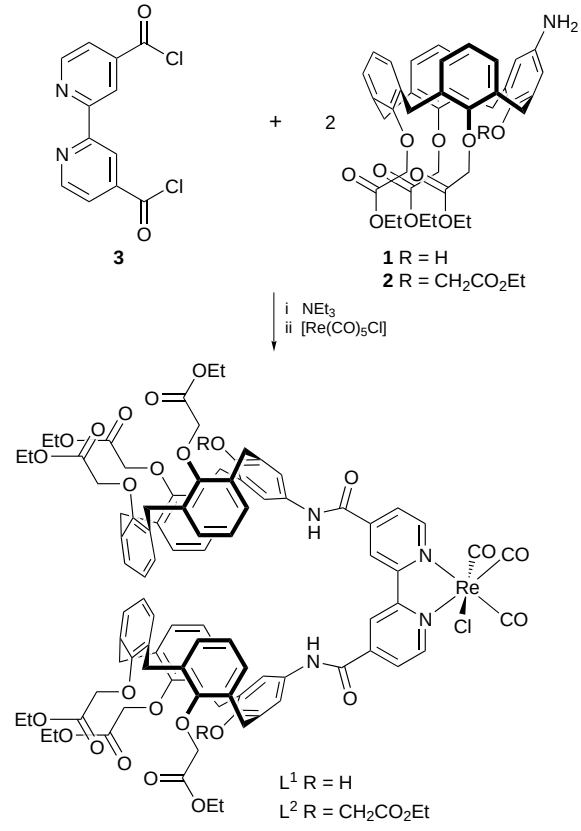

Scheme 2

Table 1 Stability constants for iodide binding in the presence and absence of alkali metal cations in CD_3CN

Receptor	Metal cation[b]	K[a]/dm^3 mol^{-1}
L^1	None	67
L^1	Li^+	294
L^1	Na^+	202
L^1	K^+	100
L^2	None	40
L^2	Li^+	305
L^2	Na^+	322
L^2	K^+	209

[a] Errors estimated to be ⩽5%. [b] Titration carried out in the presence of 2 equiv. of alkali metal cation salt, perchlorates for lithium, sodium and hexafluorophosphate for potassium.

solution, with the alkali metal cations coordinated at the lower rim ester recognition sites. The addition of tetrabutylammonium chloride, iodide and benzoate salts caused substantial downfield perturbations of the respective receptor's amide, H_3bipyridyl and aryl calix[4]arene protons indicating anion binding is taking place at the upper-rim bis(calix[4]arene) vicinity of the receptor. In all cases the resulting titration curves indicated 1 : 1 complex stoichiometry. Stability constants were calculated from the titration data using EQNMR[10] for complexation with iodide (Table 1). Unfortunately the anion complexes with Cl^- and $PhCO_2^-$ are so strong in CD_3CN that only a semi-quantitative estimate of the value of $K > 10^4$ dm^3 mol^{-1} could be made. The ^{1}H NMR iodide titration experiments were repeated in the presence of 2 equiv. of alkali metal salt and the stability constant values are presented in Table 1. Clearly with both receptors there is a significant increase in the strength of iodide binding when the alkali metal cations are co-bound by nearly an order of magnitude in the case of L^2 and sodium cations. This positive cooperative binding of the iodide anion may be attributed to each lower rim ester complexed metal cation rigidifying the calix[4]arene structure in such a way as to preorganise the upper rim for anion binding.[11] Also through bond electrostatic effects of the complexed metal cation may enhance the relative acidity of the receptors' amide protons and lead to stronger hydrogen bonding with the iodide guest anion. Interestingly Table 1 shows that receptor L^2 exhibits the largest positive cooperative iodide anion binding effect with the sodium cation, which is known to form highly selective complexes with lower rim tetrasubstituted ethyl ester calix[4]arenes.[8]

In conclusion these new heteroditopic bis(calix[4]arene) rhenium(I) bipyridyl receptors are capable of simultaneously binding alkali metal cations and iodide anion with positive cooperativity.

We thank the EPSRC for a studentship and for use of the mass spectrometry service at University College, Swansea.

Footnote and References

* E-mail: paul.beer@icl.ox.ac.uk

1 J.-M. Lehn, *Angew. Chem., Int. Ed. Engl.*, 1988, **27**, 89.
2 M. T. Reetz, C. M. Niemeyer and K. Harris, *Angew. Chem., Int. Ed. Engl.*, 1991, **30**, 1472.
3 D. M. Rudkevich, Z. Brzozka, M. Palys, H. C. Visser, W. Verboom and D. N. Reinhoudt, *Angew. Chem., Int. Ed. Engl.*, 1994, **33**, 467.
4 K. I. Kinnear, D. P. Mousley, E. Arafar and J. C. Lockhart, *J. Chem. Soc., Dalton Trans.*, 1994, 3637.
5 P. D. Beer, M. G. B. Drew, R. J. Knubley and M. I. Ogden, *J. Chem. Soc., Dalton Trans.*, 1995, 3117.
6 J. Scheerder, J. P. M. van Duynhoven, J. F. J. Engbersen and D. N. Reinhoudt, *Angew. Chem., Int. Ed. Engl.*, 1996, **35**, 1090.
7 P. D. Beer, *Chem. Commun.*, 1996, 689 and references therein.
8 F. Arnaud-Neu, E. M. Collins, M. Deasy, G. Ferguson, S. J. Harris, B. Kaitner, A. J. Lough, M. A. McKervey, E. Marques, B. L. Ruhl, M. J. Schwing-Weill and E. M. Seward, *J. Am. Chem. Soc.*, 1989, **111**, 8681.
9 C. P. Whittle, *J. Heterocycl. Chem.*, 1977, **14**, 191.
10 M. J. Hynes, *J. Chem. Soc., Dalton Trans.*, 1993, 311.
11 In ref. 6, lower rim complexation of alkali metal cations is essential for upper rim halide anion complexation.

Received in Cambridge, UK, 10th October 1997; 7/07324K

Synthesis of spherical particulate polysiloxane resins as catalyst supports

Katherine I. Alder and David C. Sherrington*

University of Strathclyde, Department of Pure and Applied Chemistry, 295 Cathedral Street, Glasgow, UK G1 1XL

Spherical particulate polysiloxanes are synthesised for the first time, chemically derivatised and employed as a support in molybdenum(VI) catalysed alkene epoxidation.

The use of polymer supports in organic synthesis is escalating.[1,2] Currently a particularly active area of research is polymer-supported metal complex catalysts,[3] including asymmetric catalysts.[4] In the case of oxygenation reactions thermo-oxidatively stable supports such as polybenzimidazoles[5,6] and polyimides[7,8] are very attractive.

Polysiloxanes also offer potential in this context, and although these species have been used in a membrane form as metal complex catalyst supports[9–13] and some largely silica-based precipitates have been so described,[14] as far as we are aware these materials have never been produced in a spherical particulate form of dimensions suitable for direct and independent use as heterogeneous supports. This work describes our recent synthesis and characterisation of such spherical particulate polysiloxanes.

The synthetic strategy (Scheme 1) involves the suspension polycondensation of a dispersion of a pre-formed silanol S10 or S5 with tetraethoxysilane (TEOS) catalysed by tin(II) octanoate in an immiscible continuous phase, such as liquid paraffin, ethylene glycol, or water. The product is essentially a spherical particulate crosslinked polydimethylsiloxane elastomer. The reaction is carried out in a thermostatted 250 ml flanged glass parallel-sided reactor with efficient overhead stirring.[5] Typical reaction conditions are summarised in Table 1 using *e.g.* 25 g of S10. Fig. 1 shows an optical micrograph of resin 8. Aggregation of the product and fouling of the stirrer and reactor can be a problem in small-scale suspension polymerisations. None of the stabilisers we examined to minimise this showed any significant effect [*e.g.* resin 3, Akcros Chem. Monolan E80, polyethylene oxide-polypropylene oxide diblock; resins 7 and 8, Dow Corning Siloxane 2-2502, C_{18} trimethoxysilane], and in our standard procedure (*e.g.* resins 1 and 4) we use no stabilising additives in the continuous phase. Yields of beaded product vary typically from 30 to 70%, average particle diameters were *ca.* 50–200 μm and C, H analysis confirmed the organic content to be close to theoretical.

In all cases the resins formed are elastomeric since the glass transition temperature, T_g, of the polydimethylsiloxane constituting the network is −125 °C. Resins 1 and 4 were prepared with mole ratios of silanols (S10 and S5) and TEOS, such that on average a highly uniform network would result with one S10 or S5 residue between each TEOS derived crosslink. Resins 2 and 3 were prepared with higher levels of TEOS in an attempt to produce some degree of homo-polycondensation of the latter, and hence generate some more rigid silica-like domains in the networks. In practice there is little physical difference between resins 1–4 and this may be due to loss of some TEOS into the continuous phase (liquid paraffin) in which it has some solubility. Resins 5 and 6 were prepared using a slightly different strategy involving dimethyldimethoxysilane (DMDMS) condensed with TEOS under hydrolysing conditions (Scheme 2). Water proved to be a convenient continuous phase in this case and the mole ratio for DMDMS/TEOS was chosen in an attempt to achieve a single dimethylsilanoxy residue between all crosslinks. These products proved to be very

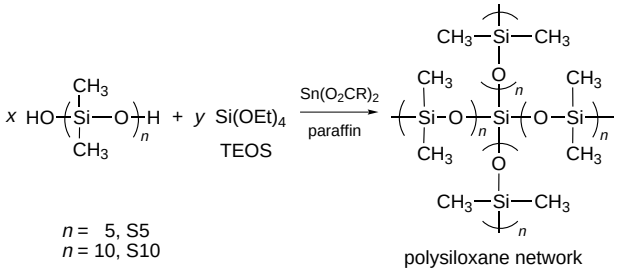

Scheme 1

Table 1 Synthesis of spherical particulate polysiloxane resins—Reaction conditions

Resin	Polymerisation mixture (mol ratio reactive end groups)	Continuous phase (vol. ratio disp. : cont.)[a]	Stirrer speed/ rpm	Reaction time/h	Reaction temp./ °C
1	S10/TEOS (2 : 1)	P (1 : 7)	700	24	70
2	S10/TEOS (1 : 2)	EG (1 : 5)	600	48	80
3	S10/TEOS (1 : 5)	EG (1 : 6)	300	18	80
4	S5/TEOS (2 : 1)	P (1 : 7)	700	24	70
5	DMDMS/TEOS (2 : 1)	H_2O (1 : 7)	600	20	70
6	DMDMS/TEOS (2 : 1)	H_2O (1 : 7)	400	22	r.t.[b]
7	S5/CMPTMS (1.5 : 1)	P (1 : 7)	600	48	70
8	S10/TEOS/TMOSEP (3.6 : 1 : 1)	P (1 : 7)	700	24	70

[a] P = Liquid paraffin, EG = ethylene glycol. [b] r.t. = Room temperature.

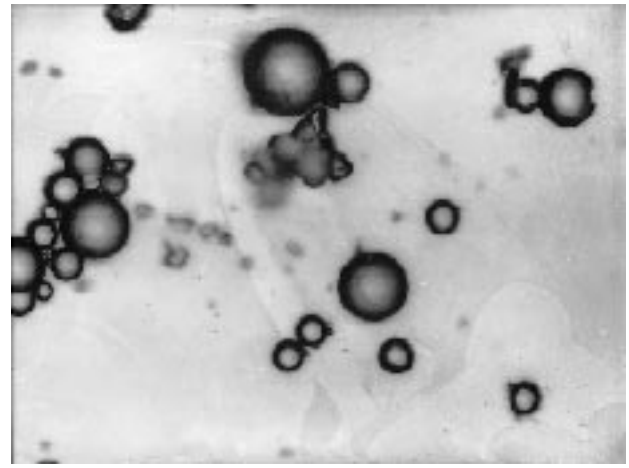

Fig. 1 Spherical particulate polysiloxane, resin 4, × 100

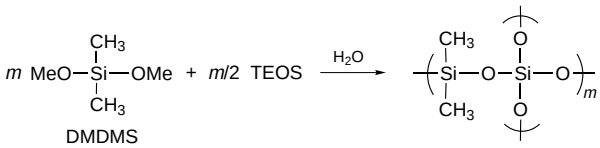

Scheme 2

emulsion-like owing to the very small particle sizes. The latter approach is related to the procedure described by Yacoub-George *et al.*[15] which yields essentially a silica-based species with a very low level of organic functionality.

Resin 7 was prepared from silanol S5 but with the TEOS crosslinker replaced by chloromethylphenyltrimethoxysilane (CMPTMS) (with adjustment to the molar ratio) in order to generate functionality in the product. The polycondensation was as before and the content of chloromethyl groups was found to be close to the theoretical value (Calc. from Cl: 1.44 mmol CH_2Cl g^{-1}. Found: 1.55 mmol CH_2Cl g^{-1}), the functionality being located on the crosslinks. Resin 8 was prepared from silanol S10 and TEOS but with half of the latter replaced by trimethoxysilyl-2-ethylpyridine (TMOSEP). Again the polycondensation proceeded as before yielding a content of 0.69 mmol of pyridine per g of resin 8 calculated from N% (theoretical content 0.36 mmol g^{-1}). This higher than expected incorporation of TMOSEP may reflect loss of some of the main components S5/TEOS to the continuous phase. In all cases the resins were found to absorb significant levels (typically *ca.* 4 ml g^{-1} resin) of non-polar solvents (toluene, dichloromethane, light petroleum) but very low levels of ethanol and, of course, water. Thermogravimetry (TG) indicates that all the resins are stable in O_2 to well above 200 °C, with 10% mass loss not occurring typically until *ca.* > 400 °C. All the resins were unaffected by 2 M H_2SO_4 but in common with the susceptibility of SiO_2 to dissolve in aqueous alkali, these resins also digested readily in 2 M NaOH.

Amination of resin 7 with an excess of trimethylamine in ethanol at room temp. appears to proceed essentially quantitatively (%Cl, theoretical 5.0; found 4.8: %N, theoretical 2.0, found 2.1), whereas the alkylation of resin 8 with excess MeI in toluene was less efficient (%I theoretical 4.3; found 0.9: %N theoretical 0.5, found 0.65). This was a little surprising since toluene swells the resins better than ethanol. However, the content of chloromethylphenyl groups in resin 7 is substantially higher than the pyridine contents in resins 8, and so overall accessibility may be more impaired in the latter case.

Resin 8 was also treated with a 2 molar excess (relative to pyridine residues) of $[MoO_2(acac)_2]$ in refluxing toluene. Following exhaustive extraction with toluene and vacuum drying, dark blue (typical of mixed Mo^{VI}–Mo^{VI} species) somewhat aggregated elastomeric beads were recovered. Through we have not been able to demonstrate unambiguously coordination of resin-bound pyridine to Mo, non-functional supports have previously been shown to be unable to retain such complexes on extraction in a Soxhlet.

Alkaline alcoholic digestion of the resin supported Mo complex and analysis of ICP-AAS yielded a Mo content of 0.43 mmol g^{-1}, corresponding to a pyridine ligand : Mo ratio of 1.5 : 1. This particulate polysiloxane-supported Mo complex turned bright yellow (characteristic of Mo^{VI}) on contact with *tert*-butyl hydroperoxide (*t*-BHP) and showed very high activity and selectivity as a catalyst in the epoxidation of cyclohexene by *t*-BHP, under conditions very similar to those we have used before. Furthermore, the activity was superior to that of soluble $[MoO_2(acac)_2]$ used at the same molar level. Very surprisingly, however, the supported catalyst was also more active than our previously reported polybenzimidazole-supported Mo system since it was used at a much lower level (Mo : *t*-BHP 1 : 450) than we have used previously (Mo : *t*-BHP 1 : 80).[16] Mo analysis of the supernatant solution from the epoxidation indicated that < 0.02% of the Mo was leached from the support and there is little doubt that the major catalytic component is Mo heterogenised on the polysiloxane.

Further details on the synthesis, characterisation and exploitation as catalyst supports of these spherical particulate polysiloxanes will be reported in due course.

K. A. is grateful to the EPSRC for a research assistantship under the ROPA scheme supported by ICI. We are also grateful to Dr Robert Drake of Dow Corning for the supply of precursors S5 and S10 and for useful discussions.

Footnote and References

* E-mail: m.p.a.smith@strath.ac.uk

1 *Syntheses and Separations Using Functional Polymers*, ed. D. C. Sherrington and P. Hodge, Wiley, Chichester, UK, 1988.
2 *Combinatorial Peptide and Non-peptide Libraries*, ed. G. Jung, VCH, Weinheim, Germany, 1996.
3 F. R. Hartley, *Supported Metal Complexes*, Reidel, Dordrecht, Germany, 1985.
4 D. Pini, A. Petri, A. Mastantuono and P. Salvadori, in *Chiral Reactions in Heterogeneous Catalysis*, ed. G. Jannes and V. Dubois, Plenum, New York, 1995, p. 155.
5 T. Brock and D. C. Sherrington, *Polymer*, 1992, **33**, 1773.
6 M. M. Miller and D. C. Sherrington, *J. Chem. Soc., Perkin Trans. 2*, 1994, 2091.
7 T. Brock, D. C. Sherrington and J. Swindell, *J. Mater. Chem.*, 1994, **4**, 229.
8 J. H. Ahn and D. C. Sherrington, *Chem. Commun.*, 1996, 643.
9 E. N. Eijke, R. V. Parish and A. Jideonwo, *J. Appl. Polym. Sci.*, 1989, **38**, 171.
10 E. Lindner, R. Schreiber, T. Schneller, P. Wegner and H. A. Mayer, *Inorg. Chem.*, 1996, **35**, 514.
11 K. Soga, T. Arai, B. T. Hoang and T. Uozumi, *Macromol. Rapid Commun.*, 1995, **16**, 905.
12 I. F. J. Vankelecom, D. Tas, R. F. Parton, V. Vande Vyver and P. A. Jacobs, *Angew. Chem., Int. Ed. Engl.*, 1996, **35**, 1346.
13 Dr B. J. Brisdon, Department of Chemistry, University of Bath, UK, personal communication.
14 Z. C. Brezezinska, W. R. Cullen and G. Strukul, *Can. J. Chem.*, 1980, **58**, 750.
15 G. Yacoub-George, E. Bratz and H. Tiltscher, *J. Non-Cryst. Solids*, 1994, **167**, 9.
16 M. Miller and D. C. Sherrington, *J. Catal.*, 1995, **152**, 377.

Received in Cambridge, UK, 18th September 1997; 7/06777A

Active catalysts prepared using a vanadium-containing oligosilsesquioxane for selective photo-assisted oxidation of methane into methanal

K. Wada, M. Nakashita, A. Yamamoto and T. Mitsudo*

Department of Energy and Hydrocarbon Chemistry, Graduate School of Engineering, Kyoto University, Sakyo-ku, Kyoto 606-01, Japan

Catalysts of characteristic pore structure derived from silica-supported vanadium-containing silsesquioxane show excellent activity towards the selective photo-assisted catalytic oxidation of methane into methanal (at 493 K, 139 μmol h^{-1}, TON *ca.* 9 h^{-1}, selectivity 81%), indicating its potent abilities as an excellent precursor for porous oxide catalysts.

Supported vanadium oxide catalysts are very important in the chemical industry, especially for the selective oxidation of hydrocarbons.[1] We have reported the excellent activities of silica-supported vanadium oxide catalysts towards the selective photo-assisted catalytic oxidation of methane, ethane and propane at relatively high temperature into the corresponding aldehydes.[2] Only highly dispersed, isolated tetrahedral VO_4 species were considered to be active species, and the reactions were quite sensitive to the state of the surface. However, strict control of the surface structure is generally quite difficult.[3] Thus the development of novel methods for the preparation of catalysts which have well ordered surface species is desirable.

On the other hand, oligometallasilsesquioxanes such as compound **1a** have attracted attention from the viewpoint of

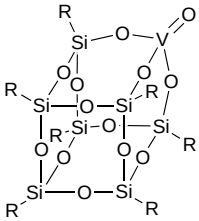

1a (R = c-C_6H_{11})
b (R = c-C_5H_9)

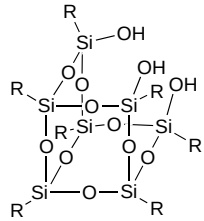

2b (R = c-C_5H_9)

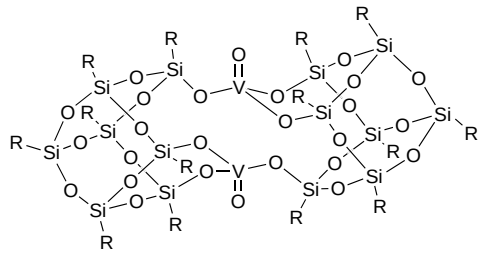

3b (R = c-C_5H_9)

well defined, homogeneous models for surface active sites of supported catalysts or metal-containing zeolites.[4] The catalytic activities of these oligometallasilsesquioxanes, however, have been mainly focused on alkene polymerization and metathesis. Their activities for other reactions were not well investigated.[5] It should be noted that the activity of a titanium-containing silsesquioxane towards the epoxidation of alkenes was recently reported.[6]

From the background described above, we have reported the fair to excellent activity of a vanadium-containing silsesquioxane **1b**, a cyclopentyl derivative of **1a**, for the photooxidation of benzene and cyclohexane, indicating its ability as a homogeneous analog of silica-supported catalysts.[7] Here, in order to investigate the possibility of **1b** as a precursor for heterogeneous catalysts, we prepared supported **1b**-based catalysts, and found that thermal treatment of the catalysts induces high activities towards the selective photo-assisted catalytic oxidation of methane into methanal.

Preparation of a vanadium-containing silsesquioxane **1b** was based on the procedure reported by Feher *et al.*[5a] The reaction of vanadyl triisopropoxide with incompletely condensed silsesquioxane **2b**, which was prepared by the hydrolytic condensation of cyclopentyltrichlorosilane, gave a white powder of dimer **3b** in 44% yield.[5a,7] The resultant product exists as a monomer **1b** in organic solutions at above room temperature. **1b** shows an absorption at *ca.* 252 nm in cyclohexane solution (ε = 4840 dm^3 mol^{-1} cm^{-1}). The silica-supported catalysts were prepared by incipient wetness impregnation from a pentane solution of **1b** using silica (Alfa, evacuated at 423 K for 2 h, mass ratio **1b**:silica = 1:3, V 1.9 mol%). The vacuum dried catalyst was designated **A**. We also prepared catalysts **B** and **C** by air-flow treatment (20 cm^3 min^{-1}) for 2 h at 523 and 723 K, respectively. It should be noted that heat treatment of **3b** without silica support often produced non-porous glassy materials.

The reaction was performed by using an upstream flow fixed-bed reactor made of silica glass. The catalyst was mounted in a flat cell (10 × 20 mm, inner thickness 1.5 mm), and covered by another silica glass tube. UV irradiation was performed from the outer side of the reactor using a 200 W high-pressure mercury lamp with a water filter. Details of the reaction apparatus were described elsewhere.[2] Chemical actinometry using iron(III) ammonium oxalate revealed that the number of photons irradiated into the catalyst bed is 6.6×10^{-7} einstein s^{-1} (250–500 nm, 1.6×10^{-7} einstein s^{-1} for 250–300 nm).

Liquid and gaseous products were collected in cold traps and gas sampling bags, respectively, followed by analysis using gas chromatography, GC–MS and ^{1}H NMR spectroscopy.

Silica-supported vanadium-containing silsesquioxane-based catalysts showed fair to excellent activities for photooxidation of methane into methanal [eqn. (1); see Table 1] and results are shown in Table 1. Preliminary experiments showed that catalyst

Table 1 Photo-assisted catalytic oxidation of methane[a]

$$CH_4 + O_2 \xrightarrow[493\ K,\ [cat.]]{h\nu} HCHO + H_2O \qquad (1)$$

Run	Catalyst	Yield/μmol h^{-1}		
		HCHO	CO	CO_2
1	None	0	0	0
2	**B**	7.2	9	18
3	**C**	139	26	6
4	V_2O_5/SiO_2[b]	61	13	7

[a] Typical reaction conditions: amount of catalyst 50 mg, molar ratio methane:O_2:He = 12:1:11, total gas flow rate 20 cm^3 min^{-1}, reaction temperature 493 K, reaction time 1 h.

A afforded very small amounts of the products. The result without catalyst shown in run 1 exhibits the absence of the photo-chemical reaction of methane. Control experiments without alkanes afforded none of the products, eliminating the contribution by the oxidation of organic groups of the silsesquioxane moiety. Reaction using silica support also did not afford the products.

The reaction using catalyst **C**, calcined in air at 723 K, produced methanal in a yield of 139 μmol h^{-1} (0.56% of fed methane) with the selectivity of > 80%. Turnover frequency for the formation of methanal was *ca*. 9 h^{-1}. Only a trace amount of methanal was formed by the reaction at *ca.* 300 K, indicating the necessity of a reaction temperature as high as 493 K. Reaction without UV irradiation did not proceed at all. For comparison, we examined the performance of a silica-supported vanadium oxide catalyst prepared by evaporation-to-dryness impregnation using ammonium metavanadate, which showed the highest activity in the previous study.[2] However, it gave only 61 μmol h^{-1} of methanal under the same reaction conditions, indicating the excellence of catalyst **C**. It should be noted that catalyst **B** including organic substituents (*vide infra*) also produced methanal, but the yield and the selectivity were low. This probably indicates the difference of the activity between the surface vanadium species on silica and that on the silsesquioxane moiety.

Then we investigated various properties of the supported catalysts. The XPS spectra of the catalysts **A** and **B** showed almost the same ratio of C 1s, corresponding to organic substituents of the silsesquioxane moiety, to Si 2p, indicating the absence of oxidation of organic substituents by treatment at 523 K in air. On the other hand, catalyst **C** was found to consist of oxides, since only trace amounts of carbonaceous materials were detected on the surface of catalyst **C**. While the BET surface area of original silica support was 259 m^2 g^{-1}, those of catalyst **A** (180 m^2 g^{-1}) and **B** (171 m^2 g^{-1}) were smaller. On the other hand, catalyst **C** had a larger surface area (349 m^2 g^{-1}). Fig. 1 shows the pore size distribution of the catalysts estimated from the desorption isotherm of nitrogen at 77 K by Dollimore–Heal method. It should be noted that the catalyst **C** was more rich in mesopores around 30 Å than the parent silica support. These characteristic features indicate the possibility of oligometalla-silsesquioxanes as novel precursors for porous oxide materials.

In conclusion, we have shown fair to excellent activities of the heterogeneous catalysts prepared using a vanadium-containing silsesquioxane **1b** for the selective photo-assisted oxidation of methane into methanal. The present results indicate the possibility of oligometallasilsesquioxanes as excellent precursors for porous oxide catalysts. We are now investigating not only the detailed structure, but also the shape selectivity of the supported catalysts.

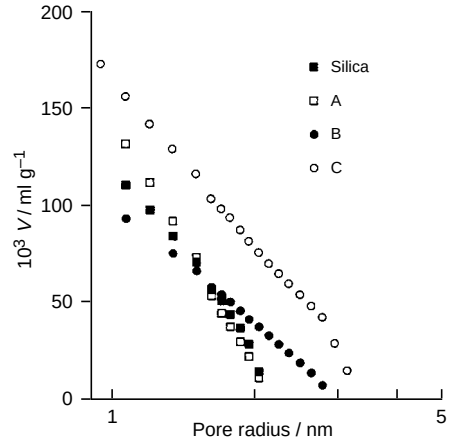

Fig. 1 Pore size distribution of silica and supported catalysts estimated by the Dollimore–Heal method (desorption, integral data)

Footnote and References

* E-mail: mitsudo@scl.kyoto-u.ac.jp

1 G. I. Golodets, *Heterogeneous Catalytic Reactions Involving Molecular Oxygen*, Elsevier, New York, 1983.
2 K. Wada and Y. Watanabe, in *Methane and Alkane Conversion Chemistry*, ed. M. M. Bhasin and D. W. Slocum, Plenum, New York, 1995, p. 179 and references therein.
3 *Preparation of Catalysts III*, ed. G. Poncelet, P. Grange and P. A. Jacobs, Elsevier, Amsterdam, 1983.
4 J. F. Brown, Jr. and L. H. Vogt, *J. Am. Chem. Soc.*, 1965, **87**, 4313; F. J. Feher and T. A. Budzichowski, *Polyhedron*, 1995, **14**, 3239; R. Murugavel, A. Voigt, M. G. Walawalker and H. W. Roesky, *Chem. Rev.*, 1996, **26**, 2205.
5 (a) F. J. Feher and J. F. Walker, *Inorg. Chem.*, 1991, **30**, 689; (b) F. J. Feher, J. F. Walzer and R. L. Blanski, *J. Am. Chem. Soc.*, 1991, **113**, 3618; (c) W. A. Herrmann, R. Anwander, V. Dufaud and W. Scherer, *Angew. Chem., Int. Ed. Engl.*, 1994, **33**, 1285.
6 H. Abbenhuis, S. Krijnen and R. van Santen, *Chem. Commun.*, 1997, 331.
7 K. Wada, M. Nakashita, A. Yamamoto, H. Wada and T. Mitsudo, *Chem. Lett.*, in press.

Received in Cambridge, UK, 6th October 1997; 7/07173F

Synthesis and structure of a novel binuclear rhenium(I) complex containing an unusual bridging ligand derived from coordinated acetonitrile. Unusual reactivity of $[Re(CO)_3(bpy)(MeCN)]^+$

Vivian Wing-Wah Yam,* Keith Man-Chung Wong and Kung-Kai Cheung

Department of Chemistry, The University of Hong Kong, Pokfulam Road, Hong Kong, PR China

$[Re(CO)_3(bpy)(MeCN)]^+$ forms a novel binuclear rhenium(I) complex containing a N≡CCH=C(CH_3)NH bridge derived from the reaction of the coordinated acetonitrile with NaH; the crystal structure of which has been determined.

There has always been considerable interest in transition metal nitriles which are extensively used as starting materials for a large variety of coordination and organometallic complexes, as well as in the activation of organonitriles in organic transformation reactions, which result from changes in the electrophilicity or nucleophilicity of the nitrile upon coordination to the metal center.[1,2] The coordination chemistry of coordinated nitriles at rhenium(I) centers has recently been reviewed,[1f,2] in which the coordinated nitrile carbon has been observed to be prone to attack by electrophiles such as H^+. Although there have been reports on the nucleophilic attack on nitriles coordinated to electron-deficient metal centers such as those of Co^{III},[3] to the best of our knowledge, there has been no report on reactions involving nucleophilic attack on the nitriles coordinated to rhenium(I) metal centers, which are normally accepted as being electron rich. Complexes such as $[ReCl(NCR)(dppe)_2]$ have been reported to undergo protonation at the nitrile carbon, due to the strong π electron releasing ability of the Re^I center to the NC π* orbitals of the coordinated nitrile,[1f,2] to yield azavinylidene derivatives. Herein we report the unusual reactivity of $[Re(CO)_3(bpy)(MeCN)]^+$ and the first example of a nucleophilic attack at the nitrile coordinated to the rhenium(I) center. The crystal structure of the novel binuclear rhenium(I) product, $[\{Re(CO)_3(bpy)\}_2\{NHC(CH_3)CHCN\}]^+$ **1** has also been determined.

Reaction of $[Re(CO)_3(bpy)(MeCN)]OTf$ (0.5 mmol) with NaH (0.3 mmol) in thf (20 ml) at room temp. for 2 min under nitrogen afforded a reddish brown solution, which was then purified by column chromatography on silica gel using dichloromethane–acetone (1 : 1 v/v) as eluent to yield $[\{Re(CO)_3(bpy)\}_2\{NHC(Me)CHCN\}]^+$ as dark red crystals; the identity of which has been confirmed by characterization with ^1H NMR, ^{13}C NMR, IR, FABMS, elemental analyses,† and X-ray crystallography.‡

The perspective drawing of the complex cation of **1** is depicted in Fig. 1. The structure of the complex consists of two rhenium diimine moieties bridged by an enamino–nitrile ligand. The coordination geometry at each Re atom is distorted octahedral with the three carbonyl ligands arranged in a *fac* fashion.[4] Bond distances worthy of special comment are N(4)–C(16) [1.29(1) Å], which is indicative of a C–N bond intermediate between those of single and double bond character, C(14)–C(15) [1.40(1) Å] and C(15)–C(16) [1.41(2) Å] which are intermediate between those expected for single and double bonds and are closer to that expected for alkenes. Although the bond distance N(3)–C(14) [1.13(1) Å] is quite short, the IR stretching frequency for the C≡N bond is 2194 cm^{-1}, which is at lower frequency than that found in $[Re(CO)_3(bpy)(MeCN]^+$ (2315 cm^{-1}),§ and may be suggestive of a bond weaker than that for a true triple bond character. These data strongly suggest that the π bonding or electron is extensively delocalized over the NCCCN moiety of the bridging ligand (Scheme 1). Such delocalization has also been observed in other systems.[5] The enamino–nitrile ligand containing N(3), C(14), C(15), C(16) and N(4) shows a coplanar arrangement with a mean deviation of 0.0114 Å from the least-squares plane, which is in accordance with the π bonding being delocalized over the NCCCN moiety.

The room temp. ^1H NMR spectrum shows two sets of chemical shifts for each resonance signal of CH_3, NH and CH groups. This has been attributed to the presence of two conformers existing in equilibrium in solution. The two

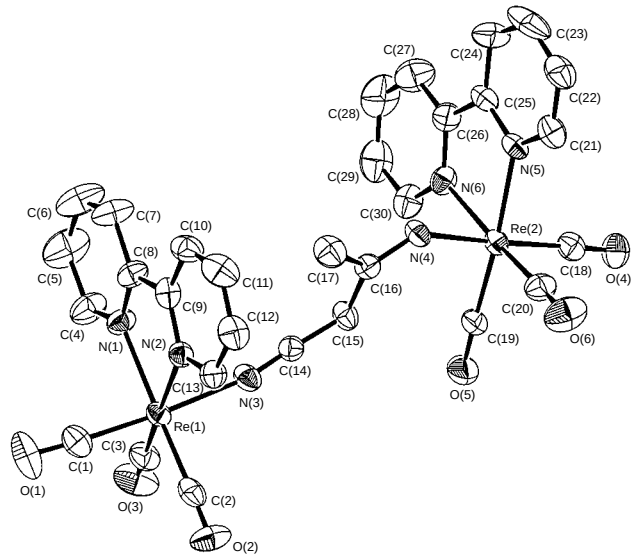

Fig. 1 Perspective drawing of the complex cation of **1** with atomic numbering scheme. Thermal ellipsoids are shown at the 40% probability levels.

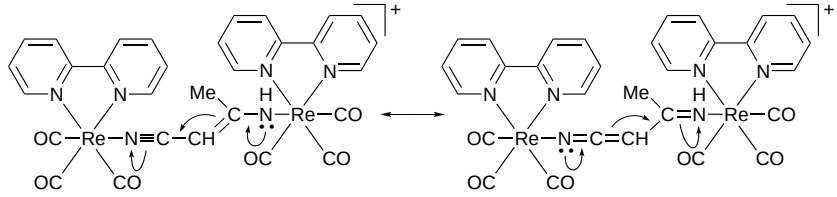

Scheme 1

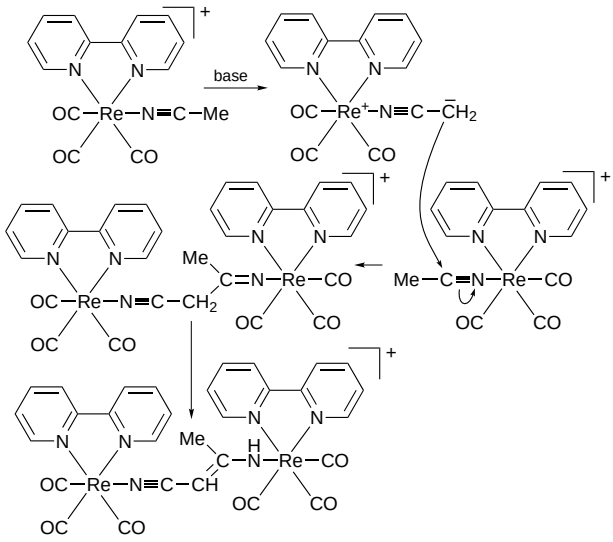

Scheme 2

conformers or rotamers are the *cis*- and *trans*-isomers owing to the restricted rotation about the C=C bond in the N≡CC=CN system. The two isomers are in equilibrium, resulting from the mesomerism, and the relative populations of the isomers change with different solvent polarities, which are common in organic compounds with the O=CC=CN moiety.[6] The relative populations of the *cis*- and *trans*-isomers are *ca*. 7 : 1 in acetonitrile and *ca*. 5 : 1 in acetone. The ^{13}C NMR spectrum also shows two distinct resonances for CH_3 and CH groups which are in accord with results obtained from ^{1}H NMR spectroscopy; the identities of the CH_3 and CH signals have also been confirmed by DEPT-135 NMR spectroscopy.

A mechanism involving the initial deprotonation of the α-methylene proton in the coordinated acetonitrile in the presence of a strong base to give the carbanion $[Re(CO)_3(bpy)(N{\equiv}CCH_2)]$, followed by its attack on the electrophilic nitrile carbon of a second molecule of $[Re(CO)_3(bpy)(MeCN)]^+$, is proposed. The imine group in the bridging ligand finally tautomerizes to the enamine, despite the fact that imine is commonly more stable than enamine (Scheme 2). It is likely that the presence of delocalization of electron over the bridging ligand in this enamino–nitrile form favors the tautomerism. The deprotonation step has also been proposed to occur in other electron-deficient transition metal nitrile complexes.[3] It is likely that the Re$^{\text{I}}$ center in $[Re(CO)_3(bpy)(MeCN)]^+$ which carries a positive charge and contains strong π-accepting CO groups, unlike the neutral $[ReCl(RCN)(dppe)_2]$, is fairly electron deficient, and is thus capable of activating the coordinated acetonitrile towards deprotonation. The electrophilic nature of Re$^{\text{I}}$ has been reflected by the higher ν(C≡N) stretching frequencies observed in $[Re(CO)_3(bpy)(MeCN)]^+$ than in free acetonitrile.[7] Similar frequency shifts have been reported for the cobalt(III) complexes which have been proposed to undergo base hydrolysis *via* an initial deprotonation step.[3] Preliminary studies show that $[\{Re(CO)_3(bpy)\}_2\{NHC(Me)CHCN\}]^+$ is strongly luminescent, typical of triplet MLCT emission in related rhenium(I) diimine systems.[5,8]

The detailed photophysical and reactivity studies of this complex, as well as the preparation of related complexes containing different bridging ligands by employing coordinated nitriles other than acetonitrile, are in progress.

V. W.-W. Y. acknowledges financial support from the Research Grants Council and The University of Hong Kong. K. M.-C. W. acknowledges the receipt of a Croucher Studentship (1995–97) and a postgraduate studentship (1997–98), administered by The Croucher Foundation and The University of Hong Kong, respectively.

Footnotes and References

* E-mail: wwyam@hkucc.hku.hk

† *Characterization of* **1**. ^{1}H NMR [300 MHz, $(CD_3)_2CO$, 298 K, relative to TMS]: δ 1.20, 1.54 (s, 3 H, CH_3), 3.10, 3.82 (s, 1 H, CH), 5.12, 5.68 (s, 1 H, NH), 7.78 (t, 2 H, bpy), 7.90 (t, 2 H, bpy), 8.34 (t, 2 H, bpy), 8.42 (t, 2 H, bpy), 8.74 (d, 2 H, bpy), 8.80 (d, 2 H, bpy), 9.00 (d, 2 H, bpy), 9.20 (d, 2 H, bpy). ^{13}C{^{1}H} NMR [67.9 MHz, $(CD_3)_2CO$, 298 K, relative to TMS]: δ 24 (CH_3), 52 (CH), 126 (bpy), 129 (bpy), 137 (C≡N), 142 (bpy), 155 (bpy), 157 (NH*C*MeCHCN), 177 (C≡O), 199 (C≡O). IR (Nujol, cm^{-1}): ν(NH) 3302; ν(C≡N) 2172; ν(C≡O) 2027, 2014, 1936, 1903. Positive ESIMS: ion clusters at *m/z* 933 {M}$^+$, 905 {M − CO}$^+$, 509 {M − [Re(bpy)(CO)$_3$]}$^+$. UV–VIS [λ/nm (ε_{max}/dm^3 mol^{-1} cm^{-1})] (MeCN) 246 (41 460), 314 (42 360), 338 (27 280), 450 (1280). Found: C, 34.25; H, 1.88; N, 7.79. Calc. for **1**·H_2O: C, 34.82; H, 2.15; N, 7.86%.

‡ *Crystal data* for **1**: $\{[Re_2O_6N_6C_{30}H_{21}]^+CF_3SO_3^-\}$; M = 1083.01, monoclinic, space group $P2_1/c$ (no. 14), a = 10.632(2), b = 16.607(2), c = 20.611(3) Å, β = 103.83(2)°, U = 3533.7(10) Å^3, Z = 4, D_c = 2.036 g cm^{-3}, μ(Mo-Kα) = 69.83 cm^{-1}, F(000) = 2056, T = 301 K. Convergence for 448 variable parameters by least squares refinement on F with $w = 4F_o^2/\sigma^2(F_o^2)$ where $\sigma^2(F_o^2) = [\sigma^2(I) + (0.020F_o^2)^2]$ for 3915 reflections with $I > 3\sigma(I)$ was reached at R = 0.034 and wR = 0.043 with a goodness-of-fit of 2.18. CCDC 182/680.

§ Assignment of ν(C≡N) for $[Re(CO)_3(bpy)(MeCN)]^+$ is confirmed by comparison with $[Re(CO)_3(bpy)(CD_3CN)]^+$.

1 (*a*) R. A. Walton, *Q. Rev. Chem. Soc.*, 1965, **19**, 126; (*b*) B. N. Storhoff and H. C. Lewis, *Coord. Chem. Rev.*, 1997, **23**, 1; (*c*) Yu. N. Kukushkin, *Koord. Khim.*, 1981, **7**, 323; (*d*) *Comprehensive Coordination Chemistry*, ed. H. Endres, G. Wilkinson, R. D. Gillard and J. A. McCleverty, Pergamon, Oxford, 1987, vol. 2, p. 261; (*e*) K. R. Dunbar, *Comments Inorg. Chem.*, 1992, **13**, 313; (*f*) R. A. Michelin, M. Mozzon and R. Bertani, *Coord. Chem. Rev.*, 1996, **147**, 299; (*g*) M. Goto, Y. Ishikawa, T. Ishihara, C. Nakatake, T. Higuchi, H. Kurosaki and V. L. Goedken, *Chem. Commun.*, 1997, 539.

2 A. J. L. Pombeiro, D. L. Hughes and R. L. Richards, *J. Chem. Soc., Chem. Commun.*, 1988, 1052; A. J. L. Pombeiro, M. C. G. Silva, D. L. Hughes and R. Richards, *Polyhedron*, 1989, **8**, 1872; A. J. L. Pombeiro, *Inorg. Chim. Acta*, 1992, **198**–**200**, 179; *New J. Chem.*, 1994, **18**, 163.

3 D. A. Buckingham, F. R. Keene and A. M. Sargeson, *J. Am. Chem. Soc.*, 1973, **95**, 5649; I. I. Creaser and A. M. Sargeson, *J. Chem. Soc., Chem. Commun.*, 1975, 324.

4 E. Horn and M. R. Snow, *Aust. J. Chem.*, 1980, **33**, 2369; W. Tikkanen, W. C. Kaska, S. Moya, T. Layman and R. Kane, *Inorg. Chim. Acta*, 1983, **76**, L29; J. C. Calabrese and W. Tam, *Chem. Phys. Lett.*, 1987, **133**, 244; V. W.-W. Yam, V. C.-Y. Lau and K.-K. Cheung, *J. Chem. Soc., Chem. Commun.*, 1995, 259; *Organometallics*, 1995, **14**, 2749; 1996, **15**, 1740; V. W.-W. Yam, K. M.-C. Wong and K.-K. Cheung, 1997, **16**, 1729.

5 N. E. Dixon, D. P. Fairlie, W. G. Jackson and A. M. Sargeson, *Inorg. Chem.*, 1983, **22**, 4038; D. P. Fairlie and W. G. Jackson, *Inorg. Chem.*, 1990, **29**, 140; S. G. Feng, P. S. White and J. L. Templeton, *Organometallics*, 1994, **13**, 1214; R. Cini, P. A. Caputo, F. P. Intini and G. Natile, *Inorg. Chem.*, 1995, **34**, 1130.

6 J. Dabrowski and L. Kozerski, *Chem. Commun.*, 1968, 568; *J. Chem. Soc. B*, 1971, 345.

7 M. W. Skinner and H. W. Thompson, *J. Chem. Soc.*, 1955, 487.

8 M. S. Wrighton and D. L. Morse, *J. Am. Chem. Soc.*, 1974, **96**, 998; M. S. Wrighton, *J. Am. Chem. Soc.*, 1974, **74**, 4801; S. M. Fredericks, J. C. Luong and M. S. Wrighton, *J. Am. Chem. Soc.*, 1979, **101**, 7415; J. V. Caspar and T. J. Meyer, *J. Phys. Chem.*, 1983, **87**, 952; G. T. Tapolsky, R. Duesing and T. J. Meyer, *J. Phys. Chem.*, 1989, **93**, 3885; *Inorg. Chem.*, 1990, **29**, 2285; B. P. Sullivan and T. J. Meyer, *J. Chem. Soc., Chem. Commun.*, 1984, 1244; B. P. Sullivan, C. M. Bolinger, D. Conrad, W. J. Vining and T. J. Meyer, *J. Chem. Soc., Chem. Commun.*, 1985, 1414; B. P. Sullivan, *J. Phys. Chem.*, 1989, **93**, 24; A. J. Lees, *Chem. Rev.*, 1987, **87**, 711; *Comments Inorg. Chem.*, 1995, **17**, 319; D. J. Stufkens, *Comments Inorg. Chem.*, 1992, **13**, 359; K. S. Schanze, D. B. MacQueen, T. A. Perkins and L. A. Cabana, *Coord. Chem. Rev.*, 1993, **122**, 63.

Received in Cambridge, UK, 20th October 1997; 7/07514F

Racemisation behaviour of trinuclear helicates formed from ethylene-bridged tris(catechol) ligands and titanium(IV) ions

Markus Albrecht* and Matthias Schneider

Institut für Organische Chemie, Universität Karlsruhe, Richard-Willstätter-Allee, D-76131 Karlsruhe, Germany

Trinuclear helicates are self-assembled from ligand H_6L^1 and Ti^{IV} ions in the presence of sodium or potassium carbonate and they racemise by consecutive inversion of the three complex units.

Movement, flexibility and dynamic behaviour are important features of chemical compounds. Although we tend to rationalise and visualise molecules as rigid structures, their behaviour very often is dominated by their ability to move or to undergo conformational changes. A very simple dynamic process of a supramolecular aggregate which is formed in a metal-directed self-assembly process is the racemisation of helicates.[1–3] In some special cases this process can be followed by NMR spectroscopy using diastereotopic protons as a stereochemical probe.[1,2] Just recently Raymond and coworkers showed that the racemisation of dinuclear gallium helicates with bis(catecholate) ligands proceeds by stepwise inversion of the two chiral metal complex units. The energy barrier for a simultaneous inversion of the two moieties should be twice as high as those of analogous mononuclear compounds. However, very similar barriers are observed for the mono- and di-nuclear complexes.[1] Additionally we could show that the racemisation barrier of dinuclear triple-stranded cryptand-type alkyl-bridged titanium(IV) helicates depends on the length of the spacer as well as the counter-ion which is present.[2]

Herein, we present the first self-assembly of a trinuclear triple-stranded helicate, which is formed from oxygen-donor ligands.[4] Analogous trinuclear double- or triple-stranded systems which contain nitrogen donor ligands have already been described in the literature.[5] Additionally we investigated the racemisation behaviour of the coordination compounds and we can show that the racemisation of the triple-stranded helicate occurs by a stepwise inversion of the complex units.

Preparation of the coordination compounds $M_6(L^1{}_3Ti_3)$ (M = Na, K) is done by simple mixing of ligand H_6L^1 (1 equiv.), $TiO(acac)_2$ (1 equiv., acac = acetyl acetonate) and alkali-metal carbonate (1 equiv.) in methanol. Red solutions are formed

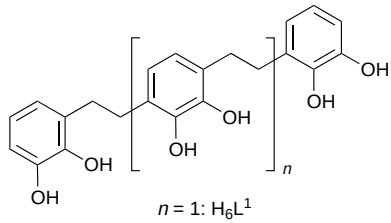

$n = 1$: H_6L^1
$n = 0$: H_4L^2

overnight and solvent is evaporated *in vacuo*. The residue is purified by chromatography (Sephadex LH 20, methanol) to obtain red complexes $M_6(L^1{}_3Ti_3)$ [M = Na (20%), K (33%)].† Owing to the high charge of the complex salts, it is difficult to obtain satisfactory mass spectra. However, for $K_6(L^1{}_3Ti_3)$ a positive FAB MS spectrum could be obtained with glycerine as matrix showing at high molar masses only characteristic peaks at *m/z* = 1430 $[K_4(L^1{}_3Ti_3H_3)^+]$, 1469 $[K_5(L^1{}_3Ti_3H_2)^+]$ and 1507 $[K_6(L^1{}_3Ti_3H)^+]$.

The ^{1}H NMR spectra (CD_3OD, 500 MHz) of the sodium *cf.* the potassium salt possess different features. NMR signals of the sodium salt $Na_6(L^1{}_3Ti_3)$ are observed at δ = 6.42 (dd, *J* 7.6, 1.6 Hz, 6 H), 6.36 (s, 6 H), 6.36 (t, *J* 7.6 Hz, 6 H) and 6.25 (dd,

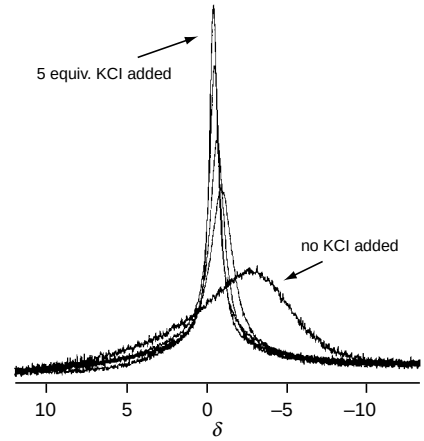

Fig. 1 Change of the ^{23}Na NMR signal of $Na_6(L^1{}_3Ti_3)$ in D_2O–H_2O upon addition of KCl

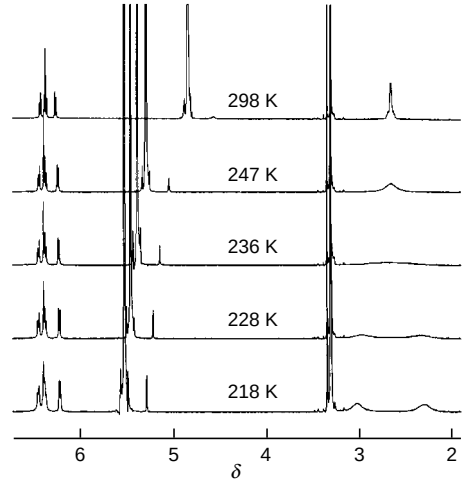

Fig. 2 ^{1}H NMR spectra of $Na_6(L^1{}_3Ti_3)$ at variable temperature (CD_3OD)

Table 1 Free energy barriers ($\Delta G^{\ddagger}$) for the racemisation of di- and trinuclear helicates $M_4(L^2{}_3Ti_2)$ and $M_6(L^1{}_3Ti_3)$ (M = Na, K

	$\Delta G^{\ddagger}$/kJ mol^{-1}	
	M = Na (CD_3OD)	M = K (D_2O)
$M_6(L^1{}_3Ti_3)$	43.9	70.7
$M_4(L^2{}_3Ti_2)^a$	45.2	64.4
$\Delta G^{\ddagger}_{tri}/\Delta G^{\ddagger}_{di}$	0.97	1.10

[a] Ref. 2.

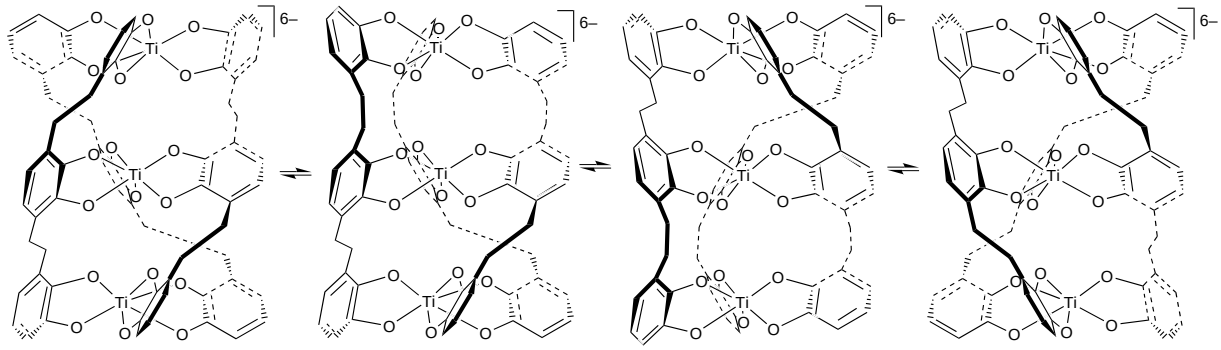

Scheme 1 Mechanism of the stepwise racemisation of ΔΔΔ-$[L^1{}_3Ti_3]^{6-}$ to ΛΛΛ-$[L^1{}_3Ti_3]^{6-}$

J 7.6, 1.6 Hz, 6 H) for the aromatic protons. The spacer protons lead to a multiplet at δ 2.66 (24 H). In contrast, $K_6(L^1{}_3Ti_3)$ exhibits resonances at δ 6.52 (dd, *J* 7.6, 1.2 Hz, 6 H), 6.46 (s, 6 H), 6.44 (t, *J* 7.6 Hz, 6 H) and 6.25 (dd, *J* 7.6, 1.2 Hz, 6 H) for the ligand moieties and two multiplets at δ 2.90 (m, 12 H) and 2.33 (m, 12 H) for the spacer protons. The observed NMR spectroscopic results show that for the potassium salt $K_6(L^1{}_3Ti_3)$ the racemisation of the helicate at room temp. is slow with respect to the NMR timescale while the inversion of the corresponding sodium salt is fast. This is in agreement with results obtained for the analogous dinuclear complexes $M_4(L^2{}_3Ti_2)$ (M = Na, K).[2] As we showed previously, the difference in the dynamic behaviour of different alkali-metal salts of helicates is due to inclusion of the counter-ions in the cryptand-type interior.[6]

Inclusion of counter-ions in the cavities of the trinuclear helicate $[L^1{}_3Ti_3]^{6-}$ was indicated by titration of the sodium salt with potassium chloride. ^{23}Na NMR spectroscopy [D_2O–H_2O (1 : 1), 105.8 MHz, Fig. 1)] at room temp. shows that the initial broad signal at δ −2.4 ($\Delta\nu_{\frac{1}{2}}$ = 625 Hz) sharpens upon addition of KCl and is shifted towards the typical resonance for solvated sodium cations at δ −0.3. This observation is due to the binding of potassium cations in the interior of the cavities and removal of sodium.[6]

Fig. 2 presents the result of a low temperature NMR spectroscopic study of $Na_6(L^1{}_3Ti_3)$ in CD_3OD (500 MHz). While cooling the NMR sample, the signal of the protons of the spacer at δ 2.66 starts to broaden and at 236 K coalescence is observed. At lower temperatures (218 K) two multiplets can be detected at δ 3.02 and 2.31 for the diastereotopic spacer protons of the chiral helicate. From those NMR spectroscopic findings a free energy barrier of $\Delta G^{\ddagger}$ = 43.9 kJ mol^{-1} can be estimated for the racemisation of the hexaanionic helicate with sodium counter-ions, $Na_6(L^1{}_3Ti_3)$.

Upon heating of $K_6(L^1{}_3Ti_3)$ in CD_3OD (500 MHz) coalescence can not be reached. However, if the same experiment is performed in D_2O, coalescence is observed at 364 K, indicating a racemisation barrier of $\Delta G^{\ddagger}$ = 70.7 kJ mol^{-1}.

As can be seen from Table 1, the observed $\Delta G^{\ddagger}$ values of the trinuclear complexes $M_6(L^1{}_3Ti_3)$ are very similar to those detected for the corresponding dinuclear compounds $M_4(L^2{}_3Ti_2)$. The largest deviation is found for the potassium salts with $\Delta G^{\ddagger}_{tri}/\Delta G^{\ddagger}_{di}$ = 1.1. If the racemisation proceeds by a simultaneous mechanism *via* an achiral coordination compound with three trigonal prismatic complex moieties, a ratio of $\Delta G^{\ddagger}_{tri}/\Delta G^{\ddagger}_{di}$ = 1.5 would be expected. The observed ratios of approximately 1.0 show that the racemisation takes place by a stepwise mechanism. This means that the helicate starts to invert at one terminus of the complex followed by inversion of the central complex unit and final racemisation of the second terminus (Scheme 1). (It is unlikely that the inversion starts at the central unit. This would lead to two *meso*-type relations of this unit to the two other complex moieties and would build up a high strain energy.[7])

To rule out a dissociative mechanism for the racemisation of the helicate,[1,3] NMR experiments were performed in the presence of an excess of ligand. No exchange of free and bound ligand could be observed.[6] Spin saturation transfer NMR experiments proved to be negative and thus supported our interpretations.

Using Raymond's strategy, we could show that the racemisation of flexible alkyl-bridged trinuclear tris(catecholato) titanium helicates proceeds similarly to the one of dinuclear gallium helicates with more rigid aryl amid linkages between the complex units.[1] However, in the case of $M_6(L^1{}_3Ti_3)$ the counter-ions are binding to the hexaanion and thus are influencing the racemisation barrier.

This work was supported by the Deutsche Forschungsgemeinschaft and the Fonds der Chemischen Industrie. We thank Dr Herbert Röttele for the measurement of the NMR spectra.

Footnotes and References

* E-mail: albrecht@ochhades.chemie.uni-karlsruhe.de

† $Na_6(L^1{}_3Ti_3)$: ^{13}C NMR (CD_3OD): δ 159.4 (C), 157.9 (C), 157.7 (C), 127.5 (C), 125.0 (C), 119.8 (CH), 118.7 (CH), 117.9 (CH), 110.5 (CH), 33.6 (CH_2), 33.5 (CH_2). Anal. Calc. for $C_{66}H_{48}Na_6O_{18}Ti_3\cdot 13\,H_2O$: C, 48.19; H, 4.53. Found: C, 48.33; H, 4.76%. $K_6(L^1{}_3Ti_3)$: ^{13}C NMR (CD_3OD): δ 159.0 (C), 157.5 (C, double intensity), 126.5 (C), 124.4 (C), 119.9 (CH), 119.4 (CH), 118.5 (CH), 110.1 (CH), 33.8 (CH_2), 32.5 (CH_2). Anal Calc. for $C_{66}H_{48}K_6O_{18}Ti_3\cdot 11\,H_2O$: C, 46.48; H 4.14. Found: C, 46.57; H, 4.80%.

1 B. Kersting, M. Meyer, R. E. Powers and K. N. Raymond, *J. Am. Chem. Soc.*, 1996, **118**, 7221.
2 M. Albrecht, M. Schneider and H. Röttele, *Chem. Ber./Recueil*, 1997, **130**, 615.
3 L. J. Charbonnière, A. F. Williams, U. Frey, A. E. Merbach, P. Kamalyprija and O. Schaad, *J. Am. Chem. Soc.*, 1997, **119**, 2488.
4 For examples of dinuclear oxygen-donor helicates, see: R. C. Scarrow, D. L. White and K. N. Raymond, *J. Am. Chem. Soc.*, 1985, **107**, 6540; E. J. Enemark and T. D. P. Stack, *Angew. Chem., Int. Ed. Engl.*, 1995, **34**, 996; M. Albrecht and S. Kotila, *Angew. Chem., Int. Ed. Engl.*, 1996, **35**, 1208.
5 Reviews: E. C. Constable, *Prog. Inorg. Chem.*, 1994, **42**, 67; A. F. Williams, *Chem. Eur. J.*, 1997, **3**, 15.
6 M. Albrecht, H. Röttele and P. Burger, *Chem. Eur. J.*, 1996, **2**, 1264.
7 M. Albrecht and C. Riether, *Chem. Ber.*, 1996, **129**, 829.

Received in Basel, Switzerland, 4th August 1997; 7/05663J

Syntheses and characterizations of two copolymers containing cone conformations of calix[4]arenes in the polymer backbone

Michael T. Blanda* and Eba Adou

Department of Chemistry, Southwest Texas State University, San Marcos, TX 78666, USA

Two new polymers containing calix[4]arenes in the cone conformation were synthesized *via* condensation reactions.

Calix[4]arenes are cyclic tetramers of *tert*-butylphenol and formaldehyde which can be synthetically manipulated to assume rigid, cone-like structures which possess an upper rim defined by the *para*-positions of the aromatic rings, and a lower rim defined by the oxygen atoms. This conformation of calix[4]arenes is highly preorganized and forms complexes with neutral molecules or metal ions.[1] In order to enhance the affinity of calix[4]arenes towards certain metal ions (in particular sodium) ionophoric groups containing carbonyl or ether functionality may be appended to the lower rim.[2]

We report a new application for the well established binding properties of calix[4]arenes that involves incorporating them into polymers. These new polymers may then be processed into materials suitable for chemical sensor devices such as ion-selective electrodes and filtration/extraction membranes. Previously reported sensor devices based on calixarenes have been fabricated by blending the calixarene molecules into polymer melts or other membrane composites.[3,4] Blending methods have several drawbacks including non-uniform ordering of the calixarene units, leaching, and difficulty in reproducing a given set of properties in the blend.

Calixarene-based polymers have just begun to receive attention, and of the few reported, the calixarene moieties have been appended to the polymer *via* the lower rim of the calixarene monomers.[5] A calixarene-based water soluble polymer has also been reported in which the upper rim of the calixarene was used as the site of attachment to the polymer.[6] Until very recently, no polymers have been reported in which the calixarenes were part of the polymer backbone. Dondoni *et al.* have successfully copolymerized a calixarene monomer in the 1,3-alternate conformation with Bisphenol A to yield a calixarene-based polymer which exhibited a higher binding affinity for silver ions than the individual calixarene monomer from which it was derived.[7] We report the syntheses of two calixarene-based copolymers with the following features: (1) the calixarene monomers are in the cone conformation, (2) the site of polymerization is located on the upper rim of the calixarene monomers and (3) the calixarene units are part of the polymer backbone.

The scarcity of calixarene-based polymers is in part due to the difficulty in synthesizing rationally designed monomers. The key intermediate to both monomers, 5,17-dichloromethyl-25,26,27,28-tetraethoxyethylcalix[4]arene† **1**, was derived from the principal starting material 5,11,17,23-tetra-*tert*-butyl-25,26,27,28-tetrahydroxycalix[4]arene.[8] The conformationally

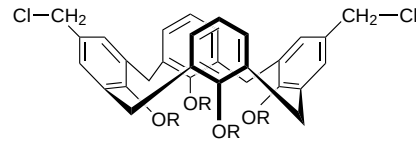

1
Cone conformation
R = CH_2CH_2OEt

mobile *tert*-butylcalixarene was first dealkylated at the upper rim using $AlCl_3$, then treated with 2-bromoethyl ethyl ether in the presence of sodium hydride to yield the tetraethoxyethyl calixarene which assumed the cone conformation.‡ The alkali metal binding properties of this ether-functionalized calix[4]-arene were investigated by Shinkai and showed high selectivity for the sodium ion, prompting us to elaborate on its structure so that it could be incorporated into different types of polymers.[9]

The tetraethoxyethylcalixarene was selectively formylated on the upper rim by treatment with dichloromethyl methyl ether in the presence of tin(IV) chloride followed by hydrolysis of the geminal dichloride.[10] The aldehyde groups were then reduced to alcohols and the corresponding diol was transformed into the dichloride **1** by treatment with thionyl chloride. The dichloride **1** was next transformed into the two penultimate monomer compounds by reacting it with either *p*-bromo- or *p*-cyanophenol in the presence of sodium hydride to yield the corresponding dibromo and dicyano compounds which were converted into the diol monomer **2** and diamine monomer **3**, respectively. The extension of the 'arms' at the upper rim proved to be critical in the subsequent condensation copolymerization reactions because initial attempts to copolymerize various calixarene monomers with shortened 'arms' did not yield high molecular weight polymers.

Both calixarene monomers **2** and **3** were condensed with equal molar amounts of terephthaloyl chloride in dimethylacetamide. The polyester reaction was heated at 60 °C while the polyamide reaction was run at room temperature. Both copolymerization condensation reactions were allowed to react for 36 h. After that time, the solvent volume was reduced and methanol was added to the reaction mixtures to precipitate the copolymers, **4** and **5**.§ The isolated yields of the two white amorphous copolymers were 66 and 50% for the polyester **4** and polyamide **5**, respectively. The glass transition temperatures (T_g) were measured using differential scanning calorimetry and the T_g for **4** was found to be 141 °C and that of **5** was determined to be 100 °C. Due to the amorphous structure of the copolymers, no melting transitions (T_m) were observed in the thermograms.

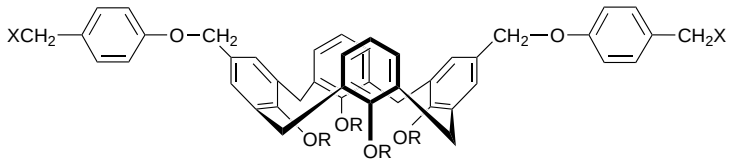

2 X = OH
3 X = NH_2

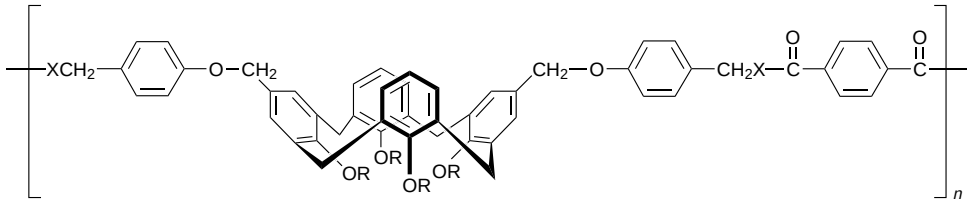

4 X = O
5 X = NH

The thermal stabilities of each copolymer were determined by thermal gravimetric analyses (TGA) in a nitrogen atmosphere. The temperatures at which 10% weight loss occurred were 352 and 380 °C, respectively, for **4** and **5**. The inherent viscosities for the copolymers were measured using an Ostwald viscometer with chloroform as the solvent at 25 °C and were found to be 0.12 dl g^{-1} for **4** and 0.14 dl g^{-1} for **5**.[11] The fact that both copolymers were completely soluble may provide additional evidence that the copolymers are amorphous.[11b] The molecular weights for each copolymer were determined by size exclusion chromatography (SEC) against polystyrene standards. The eluent used in the SEC analyses was THF and the samples were run at room temperature. The chromatograms for each polymer showed only one broad signal from which the number-average molecular weights (M_n) were determined to be 29 000 Da for the polyester **4** and 52 000 Da for the polyamide **5**. Qualitatively the broadness of the signals reflects a certain degree of polydispersity. However, since no experimental determination of the weight-average molecular weight (M_w) was made, a quantitative value of the polydispersity was not obtained. Based on the step-growth nature of the copolymers *via* the condensation reactions, the polydispersity is likely to be *ca*. 2.[11c] Even though the signals in the ^{1}H NMR spectrum for **4** and **5** were broadened at room temperature, it was possible to discern that the calixarene moieties were still in the cone conformation. We are currently investigating the alkali metal binding properties of each copolymer in comparison with the tetraethoxyethylcalixarene previously studied in order to determine if any cooperativity is displayed.[12]

M. T. B. thanks the Robert A. Welch Foundation, the Petroleum Research Fund and The Research Corporation for financial support. M. T. B. would also like to thank Drs John W. Fitch and Eric Fossum for helpful discussions.

Footnotes and References

* E-mail: mb29@swt.edu

† IUPAC name: 1^5,3^5,5^5,7^5-chloromethyl-1^2,3^2,5^2,7^2-(3-oxapentoxy)-1,3,5,7(1,3)-tetrabenzenacyclooctaphane.

‡ The cone conformation is identified in the ^{1}H NMR spectra of **1**–**5** by the presence of the AX quartet (doublet of doublets) typically at 4.4 and 3.4 ppm for the diastereotopic hydrogens of the methylene carbons connecting the aromatic rings in the calixarene moieties.

§ Compounds **2**–**5** gave elemental C and H analyses that were within 0.3% of theoretical and ^{1}H and ^{13}C NMR spectra consistent with their assigned structures.

1 For comprehensive reviews see: C. D. Gutsche, in *Calixarenes*, ed. J. F. Stoddart, Royal Society of Chemistry, Cambridge, 1989; *Calixarenes*, ed. J. Vicens and V. Bohmer, Kluwer Academic Press, Dordrecht, 1991; S. Shinkai, *Bioorg. Chem. Front.*, 1990, **1**, 161.
2 A. Arduini, A. Pochini, S. Reverberi and R. Ungaro, *Tetrahedron*, 1986, **42**, 2089; G. D. Andreeti, A. Pochini and R. Ungaro, *J. Inclusion Phenom.*, 1987, **5**, 123; S. K. Chang and I. Cho, *J. Chem. Soc., Perkin Trans. 1*, 1986, 211; M. A. McKervey, E. M. Seward, G. Ferguson, B. L. Ruhl and S. Harris, *J. Chem. Soc., Chem. Commun.*, 1985, 388; S. Shinkai, T. Otsuka, K. Fujimoto and T. Matsuda, *Chem. Lett.*, 1990, 835; T. Arimura, M. Kubota, T. Matsuda, O. Manabe and S. Shinkai, *Bull. Chem. Soc. Jpn.*, 1989, **62**, 1674; F. Arnald-Neu, E. M. Collins, M. Deasy, G. Ferguson, S. Harris, B. Kaitner, A. J. Lough, M. A. McKervey, E. Marques, B. L. Ruhl, M.J. Schwing-Weill and E. M. Seward, *J. Am. Chem. Soc.*, 1989, **111**, 8681.
3 K. Kimura, T. Miura, M. Matsuo and T. Shono, *Anal. Chem.*, 1990, **62**, 1510; W. H. Chan, K. K. Shiu and X. H. Gu, *Analyst*, 1993, **118**, 863; W. H. Chan, P. X. Cai, and X. H. Gu, *ibid.*, 1994, **119**, 1853.
4 K. Seiffarth, M. Shulz, G. Gormar and J. Bachmann, *Polymer Deg. Stab.*, 1989, **24**, 73.
5 D. W. M. Arrigan, G. Svehla, S. J. Harris and M. A. McKervey, *Analytical Proc.*, 1992, **29**, 27; H. Deligoz, M. Tavasli and M. Yilmaz, *J. Polym. Sci. Polym. Chem.*, 1994, **32**, 2961; S. J. Harris, G. Barrett and M. A. McKervey, *J. Chem. Soc., Chem. Commun.*, 1991, 1224; H. Kawabata, M. Aoki, K. Murata and S. Shinkai, *Supramolecular Chem.*, 1993, **2**, 33; M. T. Blanda and E. Adou, *Polymer*, in the press.
6 D. M. Gravett and J. E. Guillet, *Macromolecules*, 1996, **29**, 617.
7 A. Dondoni, C. Ghiglione, A. Marra and M. Scoponi, *Chem. Commun.*, 1997, 673.
8 C. D. Gutsche and P. F. Pagoria, *J. Org. Chem.*, 1985, **50**, 5795.
9 A. Ikeda and S. Shinkai, *J. Am. Chem. Soc.*, 1994, **116**, 3102.
10 A. Arduini, G. Manfredi, A. Pochini, A. R. Sicuri and R. Ungaro, *J. Chem. Soc., Chem. Commun.*, 1991, 936.
11 (*a*) H. R. Allcock and F. W. Lampe, in *Contemporary Polymer Chemistry*, Prentice Hall, Englewood Cliffs, NJ, 1981, pp. 378–404; (*b*) *ibid.*, pp. 332; (*c*) *ibid.*, pp. 25.
12 M. T. Blands, E. Adou and D. Farmer, unpublished results.

Received in Columbia, MO, USA, 12th June 1997; 7/04122E

Formation of an unusual tetralithium diplatinum complex $[Pt(C{\equiv}CBu^t)_2(PPh_2O)_2Li_2(\mu\text{-}H_2O)(Me_2CO)_2]_2$ containing $\mu_3\text{-}PPh_2O^-$ Ligands

Larry R. Falvello,[a] Juan Forniés,*[a] Elena Lalinde,*[b] Antonio Martín,[a] Teresa Moreno[b] and Jorge Sacristán[b]

[a] *Departamento de Química Inorgánica, Instituto de Ciencia de Materiales de Aragón, Universidad de Zaragoza-Consejo Superior de Investigaciones Científicas, 50009 Zaragoza, Spain*
[b] *Departamento de Química, Universidad de La Rioja, 26001, Logroño, Spain*

The very unusual complex $[Pt(C{\equiv}CBu^t)_2(PPh_2O)_2Li_2(\mu\text{-}H_2O)(Me_2CO)_2]_2$ 2 is obtained by the reaction of '$Li_2[Pt(C{\equiv}CBu^t)_4]$' with an excess of PPh_2H in acetone–ethanol and possesses an unusual linear chain of four Li atoms sandwiched between two square planar dianionic units *trans*-$^-OPPh_2\{Pt(C{\equiv}CBu^t)_2\}PPh_2O^-$, to which it is bound through $\mu_3\text{-}PPh_2O^-$ bridging ligands.

Platinum–alkynyl chemistry has long been the subject of intensive study[1] and recently there has been a growing interest in the synthesis of polymetallic species derived from dianionic (C_2^{2-}, $C_2RC_2^{2-}$, *etc.*) or substituted (pyridyl, bipyridyl, ruthenocenyl, ferrocenyl, *etc.*) building blocks due to their increasing importance in materials science.[1,2] The family of alkynyl Pt complexes, particularly that of mononuclear heteroleptic derivatives which are stabilised by tertiary phosphine ligands is now quite large.[1,2d,e,3] The chemistry of monomeric derivatives containing other types of ligands is comparatively less developed[1,3a,4] and analogous complexes containing secondary phosphines as additional ligands have not been explored. The presence of acidic protons in this type of ligand (PR_2H) probably prevents the use of the most general synthetic routes such as the reaction of halides with alk-1-ynes (base, CuI-catalysed)[1,2d,e,3b,4d] or with metal acetylide reagents.[1,4] Recently, we have reported the preparation of *trans*-$[Pt(C{\equiv}CBu^t)_2(PPh_3)_2]$[5] in high yield by partial displacement of the alkynyl groups with PPh_3 from the reactive species $Li_2[Pt(C{\equiv}CBu^t)_4]$, prepared '*in situ*'. We report here the application of this method to the diphenylphosphine ligand, which allows not only the preparation of the homologous complex *trans*-$[Pt(C{\equiv}CBu^t)_2(PPh_2H)_2]$ **1** but also the synthesis of an unexpected tetralithium diplatinum compound **2**, which contains lithium atoms in the form of an unusual linear chain of four Li atoms stabilised by $\mu_3\text{-}PPh_2O^-$ and $\mu\text{-}OH_2$ bridging ligands. Complex **2** represents the second alkynyl–platinum lithium complex crystallographically characterised,[6] and also the second example reported containing one small chain of four sandwiched Li ions.[7]

The tetraalkynylplatinatelithium species '$Li_2[Pt(C{\equiv}CBu^t)_4]$' was initially formed by addition of $LiC{\equiv}CBu^t$ to $[PtCl_2(tht)_2]$ (molar ratio 5.5 : 1) as previously reported.[5,8] Treatment of the colourless solution obtained by dissolving $Li_2[Pt(C{\equiv}CBu^t)_4]$ in acetone–ethanol with an excess of PPh_2H (1 : 3, N_2 atmosphere) causes the slow precipitatiion (7 h of stirring) of *trans*-$[Pt(C{\equiv}CBu^t)_2(PPh_2H)_2]$ **1** as a white microcrystalline solid (25% yield on the Pt starting material). Prolonged stirring (7 h) of the resulting filtrate under aerobic conditions produces the separation of a new white solid. Recrystallization of this solid from hot acetone yields the crystalline tetralithium diplatinum diphenylphosphinite complex **2** in *ca.* 45% yield. During our efforts to optimise the synthesis of complex **1** we observed that the relative yields of **1** and **2** vary with the presence of air in the reaction system (25–52% **1** to 45–11% **2**, on the Pt starting material). This fact clearly indicates that the presence of PPh_2O^- ligands in complex **2** stems from the partial oxidation of the PPh_2H ligand to PPh_2OH under the reaction conditions employed.[9] Complex **1** was characterised analytically and spectroscopically.

The identity of complex **2** has been established by X-ray structure analysis† which revealed the unexpected tetralithiumdiplatinum species $[Pt(C{\equiv}CBu^t)_2(PPh_2O)_2Li_2(\mu\text{-}H_2O)(Me_2CO)_2]_2$.‡ Molecule A (Fig. 1) is formed by two identical dianionic fragments '*trans*-$^-OPPh_2\{Pt(C{\equiv}CBu^t)_2\}PPh_2O^-$' which act as didentate ligands, bridging the four Li centers pairwise through the oxygen atoms. Each PPh_2O^- ligand is Pt–P bonded [Pt(1)–P(1,2) 2.301(2), 2.306(2) Å] and as mentioned bridges two Li centres [Li–O range 1.907(10)–1.969(10) Å], giving two planar Li_2O_2 rings, Li(1,2)O(1,2′) and Li(1′,2′)O(1′,2), which are rigorously coplanar. The central atoms are connected by two H_2O molecules [O(5), O(5′)]. All this results in a final linear disposition of four non-bonded Li atoms [Li(2)···Li(1,2) 2.610(13), 2.848(19) Å], Li(1)–Li(2)–Li(2′) 176.7(6)°], which is very similar to the Li disposition in the compound recently described by Roesky and coworkers,[7] $Li_4[(MeGa)_6(\mu_3\text{-}O)_2(Bu^tPO_3)_6]\cdot 4thf$. This structural feature contrasts with the most prevalent structural motif, cubane-like, found in other tetralithium derivatives[10] which has been rationalised using ring-stacking ideas.[11] The Li atoms in

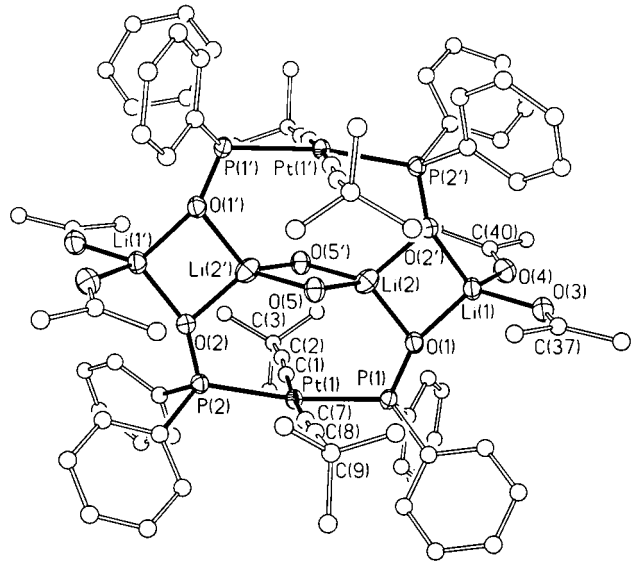

Fig. 1 Molecular structure of **2**. Ellipsoids depicted at their 50% probability level. Important molecular geometry parameters include: interatomic distances (Å): Li(1)–O(1) 1.907(10), Li(1)–O(2′) 1.927(10), Li(2)–O(2′) 1.957(11), Li(2)–O(1) 1.969(10), Li(2)–O(5) 2.0481(10), Li(2)–O(5′) 2.048(10), Pt(1)–C(1) 2.001(6), Pt(1)–C(7) 2.006(6), C(1)–C(2) 1.207(8), C(7)–C(8) 1.203(8). Bond angles (°): O(3)–Li(1)–O(4) 99.0(4), O(1)–Li(1)–O(2′) 96.9(4), Li(1)–O(1)–Li(2) 84.6(4), Li(1)–O(2′)–Li(2) 84.4(4), O(1)–Li(2)–O(2′) 93.9(4), O(5)–Li(2)–O(5′) 91.9(4), Li(2)–O(1)–P(1) 119.1(4), O(1)–P(1)–Pt(1) 111.65(15), O(2)–P(2)–Pt(1) 112.62(15), Pt(1)–C(1)–C(2) 175.8(5), C(1)–C(2)–C(3) 173.4(7), Pt(1)–C(7)–C(8) 177.0(5), C(7)–C(8)–C(9) 175.0(7). Primed atoms are related by inversion centre to unprimed ones.

each [Li(1,2)O_2] unit are chemically different. Thus the internal Li atoms [Li(2), Li(2′)] have tetrahedral coordination, being bonded to the O atoms [O(5), O(5′)] of the two bridging water ligands, while the external Li atoms [Li(1), Li(1′)] interact with two terminal acetone molecules [Li(1)–O(3),(4) 1.981(10), 1.997(10) Å]. Both the distortion from tetrahedral geometry at the Li centres and the Li–O bond lengths are in good agreement with those observed in other Li compounds containing similar LiO_4 tetrahedral coordination environments.[10–12] On the other hand, it is also remarkable that although a variety of metal coordination modes have been observed for diorganophosphinite ligands,[9a,12b,13] to our knowledge, complex **2** is the first example in which this ligand acts with a μ_3-κ^3:P,O,O′ bonding mode, bridging two hard Li atoms (μ-O) and also being P-bonded to a soft Pt centre. The P–O bond distances in **2** [1.537(4), 1.539(4) Å] are comparable to those observed for structurally characterised $[PPh_2–O]^-$ complexes displaying a μ-O,μ-P metal bridging mode.[13] The square-planar coordination at Pt is unexceptional, exhibiting, as expected, essentially linear acetylenic fragments (see Fig. 1).

In accord with the solid structure, the IR spectrum of **2** shows, in addition to a medium ν(C≡C) band at 2092 cm^{-1}, the presence of water (3646, 3402, 1611 cm^{-1}) and typical absorptions for ν(P=O) (996, 1006, 1030 cm^{-1}), characteristic of phosphinito-bridged complexes.[13] In the ^{31}P NMR spectrum a singlet shifted far downfield (δ 67.37, $^1J_{PtP}$ 2510 Hz) is observed,indicative of P oxidation to P^V.[13] The ^1H NMR spectrum of **2** in CD_3COCD_3 exhibits a singlet at δ 0.46 due to equivalent alkynyl groups (C_2Bu^t); however, the difficulty in assigning OH bands, even after addition of D_2O, does not allow us to determine with certainty whether the H_2O molecules remain coordinated in solution.

The Li-ionic conductivity of the Li derivative **2** has also been measured using the well known complex impedance method,[14] but it is near zero. This fact is in agreement with previous results obtained for other tetrahedral LiO_4 derivatives.[15]

We thank the Dirección General de Enseñanza Superior (Spain, Projects PB95-0003C02-01 02 and PB95-0792) and the University of LaRioja (API-97/B13) for financial support.

Footnotes and References

* E-mail: juan.fornies@posta.unizar.es

† *Crystal data* for **2**·0.5Me_2CO: $C_{43.50}H_{53}Li_2O_{5.50}Pt$, M = 934.77, triclinic, space group $P\bar{1}$ (no. 2), a = 13.858(3), b = 13.858(3), c = 24.693(7) Å, α = 83.79(3), β = 87.53(2), γ = 65.02(2)°, U = 4590(2) $Å^3$, Z = 2, T = 173 K, μ = 3.166 mm^{-1}, graphite monochromated Mo-Kα radiation, λ = 0.710 73 Å, colourless prism with dimensions 0.56 × 0.46 × 0.30 mm, Siemens AED2/STOE diffractometer with Oxford Cryogenics low-temperature attachement, ω–θ scans, data collection range $4 < 2\theta < 48°$, semiempirical absorption correction based on ψ scans, transmission factors 0.889–0.577, 1001 refined parameters with 13 628 unique (R_{int} = 0.026) reflections (15 247 measured). Full-matrix least-squares refinement of this model against F^2 (program SHELXL 93[16]) converged to final residual indices R_1 = 0.033, wR_2 = 0.070. (R factors defined in ref. 16), GOF 1.05. Final difference electron density maps showed four peaks > 1 e $Å^{-3}$ (1.98, 1.43, 1.31, 1.03; largest diff. hole −1.21) lying closer than 1.12 Å from the Pt atoms. CCDC 182/698.

‡ The crystal structure determination† reveals that there are two independent, but very similar, half-molecules per asymmetric unit. For simplicity, we will discuss here only the molecule denoted by **A**.

1 R. Nast, *Coord. Chem. Rev.*, 1982, **47**, 89.
2 (*a*) *Inorganic Materials*, ed. D. W. Bruce and D. O'Hare, Wiley, 2nd edn., 1996, p. 460; (*b*) W. Beck, B. Niemer and M. Weiser, *Angew. Chem., Int. Ed. Engl.*, 1993, **32**, 923; (*c*) N. J. Long, *Angew. Chem., Int., Ed. Engl.*, 1995, **34**, 21; (*d*) R. Faust, F. Diederich, V. Gramlich and P. Seiler, *Chem. Eur. J.*, 1995, **1**, 111; (*e*) A. Harriman, M. Hissler, R. Ziessel, A. D. Cian and J. Fisher, *J. Chem. Soc., Dalton Trans.*, 1995, 4067 and references therein.
3 (*a*) J. Manna, K. D. John and M. D. Hopkins, *Adv. Organomet. Chem.*, 1995, **38**, 79; (*b*) M. I. Bruce, M. Ke and P. J. Low, *Chem. Commun.*, 1996, 2405; (*c*) J. Manna, J. A. Whiteford and P. J. Stang, *J. Am. Chem. Soc.*, 1996, **118**, 8731.
4 (*a*) J. Forniés and E. Lalinde, *J. Chem. Soc., Dalton Trans.*, 1996, 2587; (*b*) I. Ara, J. R. Berenguer, J. Forniés, E. Lalinde and M. T. Moreno, *Organometallics*, 1996, **15**, 1820; (*c*) R. J. Cross and M. F. Davidson, *J. Chem. Soc., Dalton Trans.*, 1986, 1987; (*d*) S. Tanaka, T. Yoshida, T. Adachi, T. Yoshida, K. Onitsuka and K. Sonogashira, *Chem. Lett.*, 1994, 877; (*e*) S. L. James, G. Verspui, A. L. Spek and G. van Koten, *Chem. Commun.*, 1996, 1309.
5 J. R. Berenguer, J. Forniés, F. Martínez, J. C. Cubero, E. Lalinde, M. T. Moreno and A. J. Welch, *Polyhedron*, 1993, **12**, 1797.
6 $[Pt_2(C{\equiv}CPh)_4(PEt_3)_2(Bu^n)_2(\mu\text{-}Li)_2]$: A. Sebald, B. Wrackmeyer, Ch. R. Theocharis and W. Jones, *J. Chem. Soc., Dalton Trans.*, 1984, 747.
7 M. G. Walawalkar, R. Murugaval, A. Voigt, H. W. Roesky and H. G. Schmidt, *J. Am. Chem. Soc.*, 1997, **119**, 4656.
8 P. Espinet, J. Forniés, F. Martínez, M. Tomás, E. Lalinde, M. T. Moreno, A. Ruiz and A. J. Welch, *J. Chem. Soc., Dalton Trans.*, 1990, 791.
9 The formation of phosphinito complexes starting from PPh_2H has been previously observed: J. Vicente, M. T. Chicote and P. G. Jones, *Inorg. Chem.*, 1993, **32** 4960.
10 M. A. Beswick and D. S. Wright, *Comprehensive Organometallic Chemistry II*, ed. E. W. Abel, F. G. A. Stone and G. Wilkinson, Elsevier, 1995, vol. 1, pp. 1–34; E. Weiss, *Angew. Chem., Int. Ed. Engl.*, 1993, **32**, 1501; K. Gregory, P. v. R. Schleyer and R. Snaith, *Adv. Inorg. Chem.*, 1994, **37**, 47; D. Seebach, *Angew. Chem., Int. Ed. Engl.*, 1988, **27**, 1624.
11 R. E. Mulvey, *Chem. Soc. Rev.*, 1991, **20**, 167.
12 (*a*) *Lithium Chemistry—A Theoretical and Experimental Overview*, ed. A.-M. Sapse and P. v. R. Schleyer, Wiley, New York, 1995, ch. 9 and references therein; (*b*) M. A. Beswick, N. L. Cromhout, C. N. Harmer, J. S. Palmer, P. R. Raithby, A. Steiner, K. L. Verhorevoort and D. S. Wright, *Chem. Commun.*, 1997, 583.
13 Homonuclear examples, see: D. E. Fogg, N. J. Taylor, A. Meyer and A. J. Carty, *Organometallics*, 1987, **6** 2252; N. W. Alcock, P. Bergamini, T. M. Gomes-Carniero, R. D. Jackson, J. Nicholls, A. G. Orpen, P. G. Pringle, S. Sostero and O. Traverso, *J. Chem. Soc., Chem. Commun.*, 1990, 980; V. Riera, M. A. Ruiz, F. Villafane, C. Bois and Y. Jeannin, *Organometallics*, 1993, **12**, 124. Heteronuclear examples, see: P. M. Veitch, J. R. Allen, A. J. Blake and M. Schroder, *J. Chem. Soc., Dalton Trans.*, 1987, 2853; D. M. Roundhill, R. P. Sperline and W. B. Beaulieu, *Coord. Chem. Rev.*, 1978, **26**, 263.
14 B. V. R. Chowdari, K. Radhakrishnan, K. A. Thomas and G. V. Subba Rao, *Mater. Res. Bull.*, 1989, **24**, 221.
15 H. Aono, N. Imanaka and G.-Y. Adachi, *Acc. Chem. Res.*, 1994, **27**, 265.
16 G. M. Sheldrick, SHELXL-93, a Program for Crystal Structure Refinement, University of Göttingen, Germany, 1993.

Received in Basel, Switzerland, 30th July 1997; 7/05522F

New dianionic ligands η^5-$\bar{C}_5H_4Si(Me)_2\bar{C}(H)SiMe_3$ and η^5-$\bar{C}_5H_4SiMe_2\{NC(Bu^t)C(H)SiMe_3\}^-$; syntheses, structures and reactivity of their lithium and zirconium derivatives†

Peter B. Hitchcock, Jin Hu and Michael F. Lappert*

The Chemistry Laboratory, University of Sussex, Brighton, UK BN1 9QJ

Lithium and zirconium complexes $[Li_2(B)(tmen)]_2$ 4, $[Li_4(C)_2(tmen)]$ 5, $[Zr(B)_2]$ 7 and $[Zr(C)_2]$ of the new ligands η^5-$\bar{C}_5H_4Si(Me)_2\bar{C}(H)SiMe_3$ ($\equiv$[B]$^{2-}$) and η^5-$\bar{C}_5H_4Si(Me)_2\{NC(Bu^t)C(H)SiMe_3\}^-$ ($\equiv$[C]$^{2-}$) are reported, as well as the X-ray structures of the centrosymmetric dimer 4 and of 5 (having each of the four Li atoms in a different environment) and the catalytic activity of 7 for α-alkene polymerisation.

Examples of cyclopentadienyl ligands bearing a neutral Lewis base substitutent include those containing an amine,[1a] ether,[1b] pyridyl,[1c] phosphine,[1d] or vinyl[1e] side chain. Analogues having an anionic substituent are rare. The earliest examples are the 'tucked-in' metal complexes, such as $[\bar{W}(\eta^5\text{-}C_5Me_4\bar{C}H_2)(\eta^5\text{-}C_5Me_5)H_2]$,[2] but the cyclopentadienyl amide [**A**]$^{2-}$ is noteworthy,[3] because its derived Ti^{IV} complex [Ti(**A**)Cl_2] is the Dow catalyst for the production of ethylene–styrene copolymer.[4] A cyclopentadienyl(iminoacyl) ligand has been found in a number of Ti^{IV} and Zr^{IV} complexes.[5]

We now draw attention to two new dianionic cyclopentadienyl ligands [**B**]$^{2-}$ and [**C**]$^{2-}$, having an alkyl and a

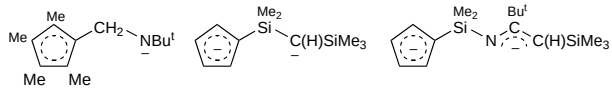

[**A**]$^{2-}$ [**B**]$^{2-}$ [**C**]$^{2-}$

1-azaallylsilyl side-chain, respectively, which may well find a useful role in organometallic chemistry.

Treatment of Cl_2SiMe_2 with $LiCH_2SiMe_3$ gave $ClSi(Me)_2CH_2SiMe_3$,[6] which with NaC_5H_5 gave **1** (Scheme 1, step i). From **1** and $LiBu^n$ (even when used in excess) in tetrahydrofuran (thf), only the monodeprotonated complex $LiC_5H_4Si(Me)_2C(H)_2SiMe_3$ **2** was obtained (step ii), derivatised (step iii) as the 1 : 1tmen adduct **3** [tmen = $(Me_2NCH_2)_2$]. However, from **1**, 2 $LiBu^n$ and 2 tmen, the dimeric complex $[Li_2(\mathbf{B})(tmen)]_2$ **4** was isolated (step iv). Reacting **4** with Bu^tCN led (step v) to the tetranuclear complex $[Li_4(\mathbf{C})_2(tmen)]$ **5**. The reaction between $ZrCl_4$ and each of the lithium compounds **2**, **4** and **5** gave (steps vi–viii, respectively) **6**–**8**, respectively. Complexes **6** and **7** (but not **8**) with methylaluminoxane (MAO) were shown to be effective catalysts for the polymerisation of C_2H_4, and **7** also for $MeCH{=}CH_2$ and $PhCH{=}CH_2$.

Since treatment of $Li\{CH(SiMe_3)_2\}$ with Bu^tCN readily gave the 1-azaallyllithium compound $[\bar{L}i\{N(SiMe_3)C(Bu^t)\bar{C}(H)SiMe_3\}]_2$,[7] in which a 1,3-$SiMe_3$ migration from C → N had taken place, there appeared to be two possible pathways upon reacting **4** with Bu^tCN, *a* and *b* in eqn. (1). In the event, Scheme 1, step v, as ultimately the X-ray structure of **5** revealed (*vide infra*) migration of the η^5-$C_5H_4SiMe_2$ group (pathway *a*) was preferred over $SiMe_3$.

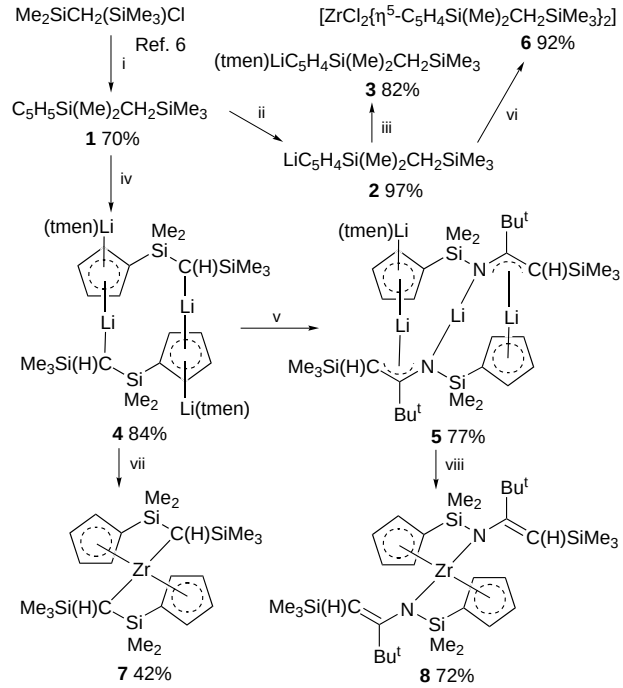

Scheme 1 *Reagents and conditions*: i, NaCp, thf, 24 h, 0 °C; ii, $LiBu^n$, C_6H_{14}, 24 h, 0 °C; iii, tmen, C_6H_{14}, 3 h, 25 °C; iv, 2 tmen, 2 $LiBu^n$, C_6H_{14}, 24 h, 0 °C; v, Bu^tCN, Et_2O, 24 h, 25 °C; vi, 1/2 $ZrCl_4$, C_6H_{14}, 48 h, 25 °C; vii, or viii, $ZrCl_4$, C_6H_{14}, 48 h, 25 °C

Each of the compounds **1** and **3**–**8** gave satisfactory microanalysis, as well as multinuclear NMR spectra. For **1** [bp 93–98 °C (13 mmHg)], GCMS confirmed its purity and EI mass spectra showed the parent molecular ion to be the highest *m/z* peak for each of the zirconium compounds **6**–**8**. Compounds **3**–**8** were isolated as crystals and X-ray diffraction data‡ on **4** (Fig. 1) and **5** (Fig. 2) established their molecular structures; such data for **6** and **8** will be presented in a full paper.

Crystalline **4** is a centrosymmetric dimer. Each cyclopentadienyl group bridges two Li one of which Li(2)/Li(2′) has its coordination environment completed by a chelating tmen ligand, while the other Li(1)/Li(1′) has the carbanionic carbon C(1)/C(1′). Atoms Li(1)/Li(1′) are arranged in an almost linear fashion with respect to C(1)/C(1′) and the centroid M(1′)/M(1) of the cyclopentadienyl ring, C(1)–Li(1)–M(1′) 178.5. The Li(1)–C(1) bond of 2.075(8) Å is longer than the Li(1)–M(1′) distance of 1.93 Å. The former may be compared with the Li–C

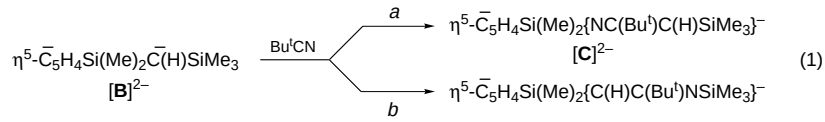

(1)

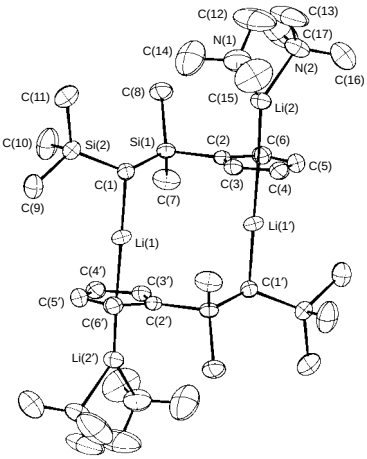

Fig. 1 The molecular structure of **4**. Selected bond lengths (Å) and angles (°) (also see text): Li(2)–M(1) 1.96, Li(2)–N(2) 2.092(8), Li(2)–N(1) 2.108(9); M(1) is the centroid of the C(2)–C(6) ring.

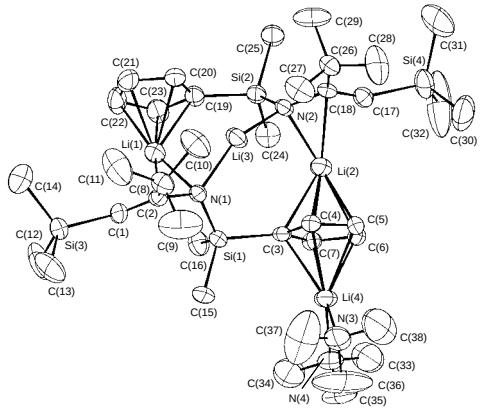

Fig. 2 The molecular structure of **5**. Selected bond lengths (Å) and angles (°) (see also **5a** and **5b**, and text): Li(4)–M(1) 2.004, Li(4)–N(3) 2.104(10), Li(4)–N(4) 2.093(10); M(1) is the centroid of the C(3)–C(7) ring, M(2) of the C(19)–C(23) ring.

bond lengths in $[Li\{CH(SiMe_3)_2\}]_\infty$ [av. 2.19(5) Å][8] and $Li\{CH(SiMe_3)_2\}\{N(Me)(CH_2CH_2NMe_2)_2\}$, 2.13(5) Å.[9] The Li(1)–M(1′) distance is similar to that in $Li(\eta^5\text{-}C_5H_4SiMe_3)$-(tmen), 1.928 Å;[10] the latter has average Li–N bond lengths of 2.13(1) Å, compared with 2.100(9) Å in **4**.

Crystalline **5** is a tetranuclear complex in which each of the four Li atoms is in a different environment. Li(1) and Li(2) are somewhat similar (see **5a** and **5b**), except that the cyclopentadienyl having the centroid M(1) bridges Li(2) and Li(4), whereas the cyclopentadienyl having the centroid M(2) acts as a terminal ligand with respect to Li(1). The coordination environment around Li(4) is completed by a chelating tmen. The situation regarding Li(3) is the most unusual: it is two-coordinate, being the bridge between N(1) and N(2) of the two 1-azaallyl moieties, N(1) and N(2) being four-coordinate and N(1)–Li(3)–N(2) 145.2(5)°. The azaallyl–lithium environment around L(1) and Li(2) is similar to that in $[Li\{N(SiMe_3)C(Bu^t)C(H)SiMe_3\}]_2$.[7]

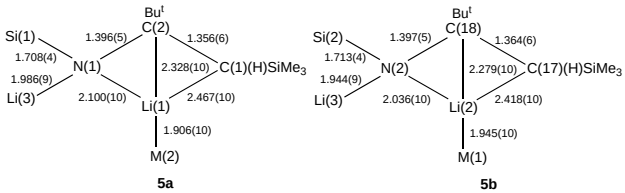

The catalytic activity of the zirconocene(IV) chloride **6** (with MAO) for polymerisation of ethylene was comparable to that of $[Zr(\eta^5\text{-}C_5H_5)Cl_2]$.§ While this is not surprising, the activity of **7** (with MAO) for C_2H_4 (mp of polymer: 138 °C by DSC), C_3H_6 (atactic oligomer of low average molecular mass) and PhCH=CH_2§ (atactic polymer of high average molecular mass) was unexpected. The high activity combined with the relatively low chain lengths for the latter two suggests that chain transfer is frequent, consistent with the high polydispersity. As far as we are aware, a zirconium(IV) bis(chelate) catalyst has not previously been reported.

Ligands related to $[\mathbf{B}]^{2-}$ and $[\mathbf{C}]^{2-}$, including $\eta^5\text{-}\overline{C}_5H_4Si(Me)_2\overline{C}(SiMe_3)_2$ are being explored, as are extensions to their role in titanium chemistry.

We thank EPSRC for providing a fellowship for J. H., and Mr D. Whiteman and Dr N. C. Billingham and RAPRA for the characterisation§ of the polymers.

Footnotes and References

* E-mail: M.F.Lappert@sussex.ac.uk

† No reprints available.

‡ *Crystal data*: **4**, $C_{34}H_{72}Li_4N_4Si_4$, M = 677.1, monoclinic, space group $P2_1/n$, a = 10.730(2), b = 10.126(2), c = 22.125(4) Å, β = 103.73(2)°, U = 2335.2(8) Å^3, $F(000)$ = 744, Z = 2, D_c = 0.96 g cm^{-3}, μ(Mo-Kα) = 0.15 mm^{-1}, specimen 0.35 × 0.20 × 0.20 mm, 4088 unique reflections for $2 < \theta < 25°$, R_1 = 0.068 for 2170 reflections with $I > 2\sigma(I)$, wR_2 = 0.191 (all data), S = 1.012, the dimer lies on a crystallographic inversion centre. **5**, $C_{38}H_{74}Li_4N_4Si_4$, M = 727.13, triclinic, space group $P\overline{1}$ (no. 2), a = 13.811(3), b = 13.848(3), c = 14.683(3) Å, α = 88.65(2), β = 89.32(2), γ = 60.51(2)°, U = 2443.7(9) Å^3, $F(000)$ = 796, Z = 2, D_c = 0.99 g cm^{-3}, μ(Mo-Kα) = 0.15 mm^{-1}, specimen 0.5 × 0.3 × 0.1 mm, 8596 unique reflections for $2 < \theta < 25°$, R_1 = 0.080 for 3824 reflections with $I > 2\sigma(I)$, wR_2 = 0.211 (all data), S = 1.018. T = 273 K, Enraf-Nonius CAD-4 diffractometer, λ(Mo-Kα) = 0.710 73 Å, no absorption corrections, solution by direct method, full-matrix least-squares refinement on all F^2. CCDC 182/681.

§ Catalytic properties of **7** for α-alkene polymerisation [25 °C in toluene (*ca*. 200 cm^3)]. C_2H_4: **7** (0.064 mM), MAO (12.7 mM), 1.4 bar; activity, 1.41 × 10^5 g PE (mol Zr)$^{-1}$ h^{-1} (bar)$^{-1}$; $\overline{M}_w$, 7.4 × 10^5 (using polystyrene as calibrant for PE); $\overline{M}_w/M_n$, 4.4; mp 138 °C. C_3H_6: **7** (0.048 mM), MAO (15 mM); activity, 1.86 × 10^5 g PP (mol Zr)$^{-1}$ h^{-1} (bar)$^{-1}$; $\overline{M}_w$, 710; M_w/M_n, 1.4; oil. $PhCHCH_2$: **7** (0.050 mM), MAO (40 mM); activity, 1.16 × 10^6 g PS (mol Zr)$^{-1}$ h^{-1} (bar)$^{-1}$; $\overline{M}_w$, 22.3 × 10^3; M_w/M_n, 3.2.

1 (*a*) P. J. Shapiro, W. D. Cotter, W. P. Schaefer, J. A. Labinger and J. E. Bercaw, *J. Am. Chem. Soc.*, 1994, **116**, 4623; (*b*) P. van de Weghe, C. Bied, J. Collin, J. Marçalo and I. Santos, *J. Organomet. Chem.*, 1994, **475**, 121; (*c*) J. R. van den Hende, P. B. Hitchcock, M. F. Lappert and T. A. Nile, *ibid.*, 1994, **472**, 79; (*d*) R. T. Kettenbach and H. Buternschön, *New J. Chem.*, 1990, **14**, 599; (*e*) C. P. Gibson, D. S. Bern, S. B. Falloon, T. K. Hichens and J. E. Cortopassi, *Organometallics*, 1992, **11**, 1742, and references therein.

2 F. G. N. Cloke, J. C. Green, M. L. H. Green and C. P. Morley, *J. Chem. Soc., Chem. Commun.*, 1985, 945.

3 P. J. Shapiro, E. Bunel, W. P. Schaefer and J. E. Bercaw, *Organometallics*, 1990, **9**, 867.

4 *Cf.* A. D. Horton, *Trends Poly. Sci.*, 1994, **2**, 153.

5 R. Fandos, A. Meetsma and J. H. Teuben, *Organometallics*, 1991, **10**, 2665.

6 R. West and G. A. Gornowich, *J. Organomet. Chem.*, 1971, **28**, 25.

7 P. B. Hitchcock, M. F. Lappert and D.-S. Liu, *J. Chem. Soc., Chem. Commun.*, 1994, 2637.

8 M. F. Lappert, L. M. Engelhardt, C. L. Raston and A. H. White, *J. Chem. Soc., Chem. Commun.*, 1982, 1323.

9 J. L. Atwood, T. Fjeldberg, M. F. Lappert, N. T. Luong-Thi, R. Shakir and A. J. Thorne, *J. Chem. Soc., Chem. Commun.*, 1984, 1163.

10 M. F. Lappert, A. Singh, L. M. Engelhardt and A. H. White, *J. Organomet. Chem.*, 1984, **262**, 271.

Received in Basel, Switzerland, 28th July 1997; 7/05424F

Engineering layers in molecular solids with the cyclic dipeptide of (*S*)-aspartic acid

G. Tayhas R. Palmore* and Mary T. McBride

Department of Chemistry, University of California, Davis, CA 95616, USA

Hydrogen-bonded tapes formed by the cyclic dipeptide of (*S*)-aspartic acid 1 are used as a scaffold on which to build two-dimensonal layers that vary in size, shape and chemical composition.

Numerous research groups have demonstrated considerable success at using non-covalent interactions to build supramolecular structures in crystalline solids.[1] The most common interaction in these structures is the hydrogen bond, which occurs between functional groups strategically located on the constituent molecules.[2–5] Several molecules have been investigated, including a few that form robust supramolecular structures that can be modified in terms of their size and shape (*i.e.* modular). The advantage of a supramolecular structure that is both robust and modular is that it provides a scaffold with which to engineer the structure (and possibly the function) of molecular solids.

We have initiated a program of research aimed at understanding the influence of molecular structure on the kinetics of crystal growth using atomic force microscopy. To simplify these studies, we require molecular solids with a common supramolecular structure whose dimensions can be modified systematically. Our approach to preparing a series of related solids is to use the strength and directional character of hydrogen bonds to build the supramolecular structure, and exploit the selectivity of hydrogen bonds for different hydrogen-bond donors and acceptors to modify the supramolecular structure. We have focused our efforts on the cyclic dipeptide of (*S*)-aspartic acid **1** based on the following rationale.[6] First, **1** is representative of a family of molecules known to form hydrogen-bonded tapes in their crystalline solids [Fig. 1(*a*)].[1,7] Tapes are one-dimensional aggregates that typically pack with their long axes parallel. Second, **1** contains two types of functional groups (*cis*-amide and carboxylic acid) that contain both a hydrogen bond donor and a hydrogen bond acceptor.

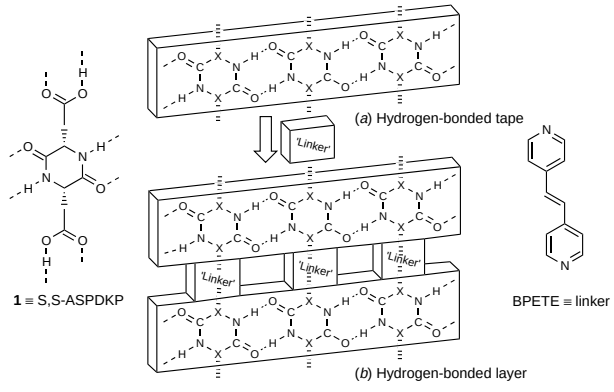

Fig. 1 (*a*) Tape that results when the *cis*-amides of (*S,S*)-ASPDKP (**1**) form a pair of hydrogen bonds (dashed lines) with the *cis*-amides of two adjacent molecules. X represents a substituted carbon atom. (*b*) Layer that forms when parallel tapes are cross-linked either directly through functional groups on X or indirectly through cocrystallization with 'linker' molecules (*e.g.* BPETE).

Functional groups such as *cis*-amides and carboxylic acids are known to form an $R_2^2(8)$ pattern of hydrogen bonds—a two-point interaction that is stronger and orientationally more restrictive than chains of hydrogen bonds.[8–10] Third, the hydrogen-bonding functional groups in **1** are positioned to preorganize the direction of their hydrogen bonds mutually orthogonal, which will promote the formation of hydrogen-bonded layers through the cross-linking of tapes [Fig. 1(*b*)]. Layers are two-dimensional aggregates that should pack with their planes parallel. Fourth, *cis*-amides and carboxylic acids have different selectivities for hydrogen-bond donors and acceptors.[10] With cocrystallization techniques, this difference in selectivity can be exploited to modify the interdigitation of tapes or the shape of the hydrogen-bonded layers.

Our first objective was to demonstrate that the two *cis*-amide functional groups in **1** form a symmetric $R_2^2(8)$ pattern of hydrogen bonds with adjacent molecules to generate the tape motif in the solid state. Based on Etter's rules for hydrogen-bonds, where the strongest hydrogen bond donor (acid hydroxy) preferentially interacts with the strongest hydrogen bond acceptor (amide carbonyl), carboxylic acids crystallized in the presence of amides should form an asymmetric $R_2^2(8)$ pattern of hydrogen bonds.[10,11] Further evidence that supports the preferential formation of an asymmetric $R_2^2(8)$ pattern of hydrogen bonds is the packing modes of monocarboxamide derivatives of dicarboxylic acids.[8] Due in part to restrictions in the conformation of **1** imposed by its stereochemistry, the crystalline solid of **1** contains the tape motif generated from a *symmetric* $R_2^2(8)$ pattern of hydrogen bonds between the *cis*-amide functional groups. The asymmetric unit cell contains two crystallographically distinct molecules of **1** that generate two distinct tapes, labelled A and B (Fig. 2).† Tapes pack with their long axes parallel. The hydrogen bond distances and angles between the *cis*-amides depend on the tape to which **1** belongs: N–H···O = 2.860 Å, 166° and 2.868 Å, 167° for tape A; 2.864 Å, 163° and 2.871 Å, 163° for tape B. Although a C_2-axis of symmetry is present in a two-dimensional drawing of **1**, this symmetry element is absent in the solid state due to the different conformations adopted by the two side-chains. Consequently, a

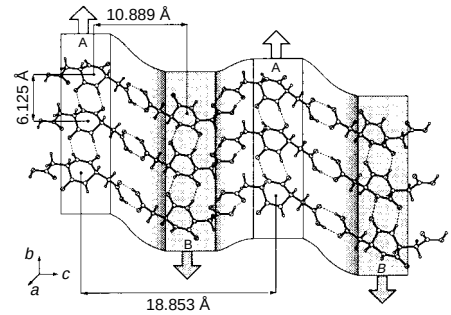

Fig. 2. Layer in crystal structure of **1**. The asymmetric unit cell contains two molecules of **1**, each of which generate a distinct tape (A and B), which alternate in their direction of propagation (arrows). Each tape is cross-linked to adjacent tapes through an $R_2^2(8)$ pattern of hydrogen bonds between the carboxylic acid groups to form a *non-planar* layer.

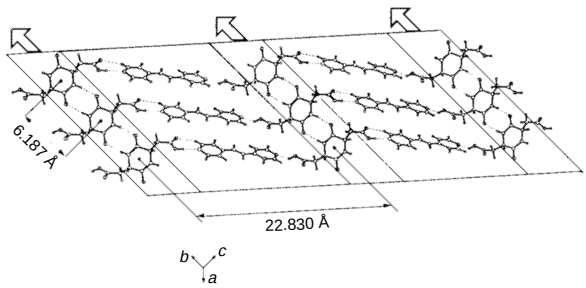

Fig. 3 Layer in crystal structure of **1**–**BPETE**. A symmetric $R_2^2(8)$ pattern of hydrogen bonds between the *cis*-amides of **1** form tapes, which are cross-linked into planar layers through an $R_2^2(7)$ pattern of hydrogen bonds between the carboxylic acid functional groups on **1** and the nitrogen atom and *ortho* carbon atom on BPETE. All tapes propagate in the same direction relative to tapes in the same layer and in adjacent layers (arrows).

non-planar layer results when each tape is cross-linked to adjacent tapes through a symmetric $R_2^2(8)$ pattern of hydrogen bonds between carboxylic acid functional groups (O–H···O interactions: 2.665 Å, 176°; 2.633 Å, 161°; 2.753 Å, 174°; and 2.740 Å, 175°). Layers pack with a slippage of 3.737 Å along the *c* axis while maintaining a periodicity of 4.985 Å between layers. Close contacts between layers include: O9–H16···O4, 2.886 Å and C15–H15···O2, 3.088 Å.

For the purpose of engineering related solids, the formation of a symmetric $R_2^2(8)$ pattern of hydrogen bonds in the crystalline solid of **1** is significant in that it suggests the tape motif can be used as a scaffold on which to build layers with different repeat distances between tapes. For example, a guest molecule can be inserted within the layer of **1** by cocrystallization techniques, which allows for systematic modification of the periodicity of tapes within the layer. We illustrate this point in Fig. 3, which shows the crystal structure of **1** cocrystallized with (*E*)-1,2-bis(4-pyridyl)ethene (BPETE).‡ In this example, parallel tapes are cross-linked into a planar layer through hydrogen bonding interactions between the carboxylic acid functional groups on **1** and the nitrogen and *ortho* carbon atoms of BPETE (O–H··N = 2.893 Å, 162°; and 2.633 Å, 143°; C–H··O = 3.103 Å, 126°; and 3.511 Å, 116°). The carboxylic acid functional groups do not form an $R_2^2(8)$ pattern of hydrogen bonds in the presence of BPETE because the pyridyl nitrogen atom is a stronger hydrogen-bond acceptor than the carbonyl oxygen atom of carboxylic acids.§ Moreover, the interaction is not ionic; proton transfer from the carboxylic acid to BPETE does not occur. We base this assertion on the similar C–N–C bond angles of BPETE in the presence (115.8°) or absence (115.4°) of **1**.[12] In a manner similar to the crystalline solid of **1**, the crystalline solid of **1**–**BPETE** contains an $R_2^2(8)$ pattern of hydrogen bonds between *cis*-amides of adjacent molecules to give tapes (N1–H1··O2 = 2.857 Å, 166°, N2–H2··O1 = 2.829 Å, 167°). Tapes lie with their long axes parallel. Layers pack with slippage of 4.511 Å along the *c*-axis and a periodicity of 4.211 Å between adjacent layers. The closest contact between layers is 3.203 Å (C20–H20··O5).

Several research groups have demonstrated that hydrogen-bonded layers can be assembled in crystalline solids from molecules that are designed to form hydrogen bonds in two directions. Compound **1** is a new addition to this type of molecule. An important feature of **1** is that the presence of competing hydrogen-bonding functional groups, either as part of (carboxylic acid) or external (pyridyl) to the molecular structure of **1**, does not preclude the formation of tapes defined by an $R_2^2(8)$ pattern of hydrogen bonds between *cis*-amide functional groups. Consequently, these tapes can be modified in terms of their interdigitation or used as scaffolds on which to build layers (or three-dimensional structures) that systematically differ in their size, shape and chemical composition. We demonstrate the use of tapes as scaffolds with the two examples shown, which are representative of the tremendous potential that molecules such as **1** have in engineering layers in the solid state. Studies of other layered solids built with **1** are currently in progress and will be the subject of future reports.

We thank Dr Marilyn M. Olmstead for helpful discussions and the PRF for financial support.

Footnotes and References

* E-mail: palmore@chem.ucdavis.edu

†All data were collected at 130 K on a Siemens P4/RA diffractometer with graphite-monochromated Cu-Kα radiation (λ = 1.541 78 Å) using 2θ scans over the range 2–57°. Lattice parameters were determined from least-squares analysis of 30–35 reflections. Two standard reflections were measured every 198 reflections. Structures were solved by direct methods and refined by full-matrix least-squares on F^2 using SHELXTL, Version 5.03. All non-hydrogen atoms were refined anisotropically. All hydrogen-bonded hydrogen atoms were refined after location on a difference map with isotropic temperature factors. Other hydrogen atoms were placed in idealized positions with assigned isotropic thermal parameters. *Crystal data* for **1**: $C_8H_{10}N_2O_6$, M = 230.18 g mol^{-1}, triclinic $P\bar{1}$, colorless needle measuring 0.18 × 0.06 × 0.04 mm, a = 4.985(1), b = 5.039(1), c = 18.853(4) Å, α = 82.50(3), β = 88.47(3), γ = 75.33(3)°, V = 454.2(2) Å^3, Z = 2, D_c = 1.683 Mg m^{-3}, μ = 1.275 mm^{-1}; T_{max} = 0.96, T_{min} = 0.93, GOF on F^2 = 1.083; R_1 = 0.0344, R_{all} = 0.0346 for 1215 independent observed reflections, based on $I > 2.0\sigma(I)$.

‡ Cocrystals of **1** and BPETE were obtained by slow evaporation from a methanol solution containing an equimolar mixture of **1** and BPETE. *Crystal data* for cocrystal of **1**–**BPETE**: $C_{20}H_{20}N_4O_6$; M = 412.40 g mol^{-1}, triclinic $P\bar{1}$, yellow needles measuring 0.52 × 0.14 × 0.08 mm, a = 6.1779(13), b = 6.187(2), c = 13.404(3) Å, α = 82.63(2), β = 83.92(2), γ = 68.23(2)°, V = 471.0(2) Å^3, Z = 1, D_c = 1.454 Mg m^{-3}, μ = 0.919 mm^{-1}; T_{max} = 0.94, T_{min} = 0.89, GOF on F^2 = 1.043; R_1 = 0.0860, R_{all} = 0.0982 for 1240 independent observed reflections, based on $I > 2.0\sigma(I)$.

§ Based on β-values for pyridine (0.64) and ethyl acetate (0.41).

1 J. C. MacDonald and G. M. Whitesides, *Chem. Rev.*, 1994, **94**, 2383.
2 R. E. Melendez, C. V. Krishnamohan Sharma, M. J. Zaworotko, C. Bauer and R. D. Rogers, *Angew. Chem., Int. Ed. Engl.*, 1996, **35**, 2213.
3 M. D. Hollingsworth, M. E. Brown, B. D. Santarsiero, J. C. Huffman and C. R. Goss, *Chem. Mater.*, 1994, **6**, 1227.
4 V. A. Russell and M. D. Ward, *Chem. Mater.*, 1996, **8**, 1654.
5 X. Wang, M. Simard and J. D. Wuest, *J. Am. Chem. Soc.*, 1994, **116**, 12 119.
6 R. J. Bergeron, O. Phanstiel, G. W. Yao, S. Milstein and W. R. Weimar, *J. Am. Chem. Soc.*, 1994, **116**, 8479.
7 S. Palacin, D. Chin, E. E. Simanek, J. C. MacDonald, G. M. Whitesides, M. T. McBride and G. T. R. Palmore, unpublished work.
8 L. Leiserowitz, *Acta Crystallogr., Sect. B*, 1976, **32**, 775.
9 G. C. Pimentel and A. L. McClellan, *The Hydrogen Bond*, Freeman, San Francisco, 1960.
10 M. C. Etter, *Acc. Chem. Res.*, 1990, **23**, 120; *J. Phys. Chem.*, 1991, **95**, 4601.
11 J. Bernstein, R. E. Davis, L. Shimoni and N.-L. Chang, *Angew. Chem., Int. Ed. Engl.*, 1995, **34**, 1555.
12 J. Vansant and G. Smets, *J. Org. Chem.*, 1980, **45**, 1557.

Received in Columbia, MO, USA, 1st July 1997; 7/04598K

Hydrolysis of an RNA dinucleoside monophosphate by neomycin B

Sarah R. Kirk and Yitzhak Tor*

Department of Chemistry and Biochemistry, University of California, San Diego, La Jolla, CA 92093-0358, USA

Neomycin B is shown to accelerate the phosphodiester hydrolysis of adenylyl(3′–5′)adenosine (ApA) more effectively than a simple unstructured diamine.

Current approaches to site-directed RNA hydrolysis involve the conjugation of a reactive moiety capable of cleaving phosphodiester bonds to a recognition element capable of sequence-specifically hybridizing to RNA.[1] In most cases, a metal complex is covalently attached to a DNA strand which forms a stable heteroduplex. Upon hybridization, a Lewis acid is placed in close proximity to the RNA backbone to effect hydrolysis.[2] In a similar fashion, DNA–polyamine conjugates have been demonstrated to induce site-directed RNA strand scission.[3] While these high molecular-weight conjugates are promising sequence-specific RNA cleavers, combining recognition and catalysis in a single small organic molecule has remained a challenging problem.[4]

The discovery that aminoglycoside antibiotics interact specifically with diverse RNA molecules such as group I introns,[5] hammerhead ribozymes[6] and the HIV-1's TAR[7] and RRE[8] sites has attracted considerable interest and stimulated studies attempting to identify the elements involved in these recognition phenomena.[9–11] As highly functionalized polycationic oligosaccharides, interactions between the aminoglycosides' polar residues (*i.e.* amino and hydroxy groups) and the RNA backbone and/or heterocyclic bases are likely to occur. Since simple unstructured polyamines[12,13] as well as basic polypeptides[14] have been shown to catalyze RNA hydrolysis, we hypothesized that aminoglycoside antibiotics may exhibit similar effects. As a first step toward developing small molecules capable of both recognizing RNA and cleaving it, we demonstrate that neomycin B is able to accelerate the hydrolysis of a ribodinucleoside monophosphate.

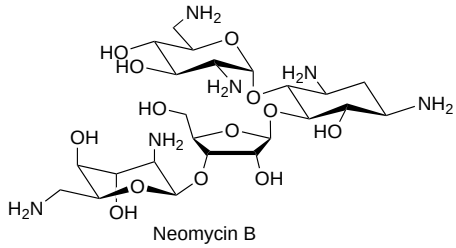

Neomycin B

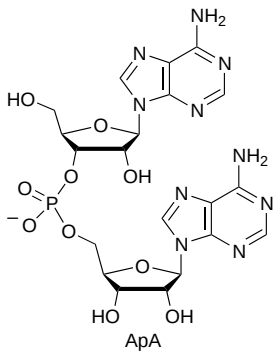

ApA

The hydrolysis rate of adenylyl(3′–5′)adenosine (ApA) in the presence of 0.3 M neomycin B, 1,3-diaminopropane and 3-aminopropan-1-ol was investigated at pH 8.0 and 50 °C.† Reversed-phase HPLC was employed to measure the rate of appearance of adenosine (A) against the loss of ApA.‡ Neomycin B hydrolyzes ApA with a pseudo-first-order rate constant of $1.6 \pm 0.1 \times 10^{-5}$ min^{-1}, approximately three times faster than 1,3-diaminopropane ($5 \pm 1 \times 10^{-6}$ min^{-1}) and more than 50 times faster than Tris buffer alone or 3-aminopropan-1-ol ($3–4 \pm 2 \times 10^{-7}$ min^{-1}) (Fig. 1).§ The observed hydrolysis rates were not significantly altered when 2 mM EDTA was added, excluding metal ion-mediated hydrolysis. Furthermore, the observed formation of adenosine 2′,3′-cyclic monophosphate (A > p) and its subsequent degradation to adenosine 2′-phosphate (A′2p) and 3′-phosphate (A′3p) rules out the possibility of nuclease-mediated hydrolysis that would generate A′3p exclusively.[15] These observations clearly show that an aminoglycoside antibiotic is capable of significantly accelerating the hydrolysis of a ribodinucleoside phosphate.

The rate of ApA hydrolysis by neomycin B is pH dependent. When the pH of the buffered 0.3 M neomycin B was lowered from 8.0 to 7.0, the rate of hydrolysis was slowed down by a factor of three. As demonstrated earlier for simple diamines, the hydrolysis rate acceleration is dependent on the relative abundance of the neutral, monoprotonated and diprotonated forms.[13] While the uncharged form has the highest hydrolytic activity and the dicationic form is essentially inactive, the monocationic form—which is the most populated form at pH 7—is the major contributor to the observed catalysis. Neomycin B contains six amino groups with pK_a values between 5.7 and 8.8.[16] As the pH is lowered and neomycin B becomes highly protonated, the rate of ApA hydrolysis is expected to decrease, which indeed is observed.

Neomycin B has three times as many amines as 1,3-diaminopropane, yet the three-fold rate enhancement observed for ApA hydrolysis may be coincidental. *A priori*, several factors may contribute to the observed rate acceleration: the number of amino groups, their stereochemical relationships, as well as

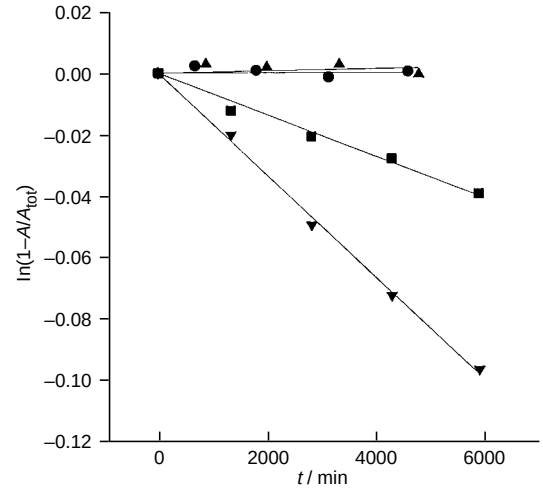

Fig. 1 Kinetic analysis of ApA hydrolysis by (▼) 0.3 M neomycin B, (■) 0.3 M 1,3-diaminopropane, (▲) 0.3 M 3-aminopropan-1-ol and (●) 50 mM Tris·HCl at pH 8.0 and 50 °C (see footnotes † and §)

their individual pK_a values. As reported earlier,[13] simple oligoamines such as diethylenetriamine and triethylenetetramine are essentially as effective as 1,3-diaminopropane in hydrolyzing ApA. This suggests that the number of amino groups may not be the major factor distinguishing neomycin B from 1,3-diaminopropane. Since the observed rate is a combination of individual hydrolysis rates mediated by various pairs of amino groups, it is likely that some pairs are much more active than others. This may be due to their spatial positioning and individual pK_a values, as well as the lower conformational freedom of neomycin B when compared to simple unstructured diamines. Since cyclohexane-1,3-diamine has been found to be as effective as 1,3-diaminopropane in hydrolyzing ApA,[13] we favor the modulation of individual pK_a values as the likely source for the rate enhancement observed with neomycin B. While the amines in 1,3-diaminopropane are rather basic, (pK_a 8.1 and 9.8),[13] certain pairs in neomycin B are less basic and display a wider difference in their pK_a. For example, the pK_a values reported for N^1 and N^3 are 8.04 and 5.74, respectively.[16] This may lead to a higher population of a monocationic form at a given pH compared to 1,3-diaminopropane, and therefore to a faster hydrolysis.

Neomycin B has been shown to bind to various RNA sequences[5–8] and now to hydrolyze an RNA dinucleoside phosphate. These observations provide new leads for the design of small molecules that combine RNA recognition with hydrolysis. Such molecules may become useful chemical probes for RNA structure and folding.[17] We are currently exploring these possibilities with larger and well-defined RNA structures.

This work was supported by the Universitywide AIDS Research Program, University of California, grant No. R96-SD-067, and by the Hellman Faculty Fellowship (Y. T.).

Footnotes and References

* E-mail: ytor@ucsd.edu

† All samples contained 50 mM Tris and 0.1 mM ApA. The pH was adjusted to 8.0 at room temperature (21 °C) with highly pure HCl (low trace metals: iron < 1 ppb, lead < 0.01 ppb, lutetium < 0.005 ppb, zinc < 0.02 ppb). At 50 °C, there is a drop of approximately 0.5 pH unit.

‡ HPLC analysis was performed using a C18 reversed-phase column with 25 mM sodium phosphate buffer, pH 3.5, containing 2% MeCN as the initial eluent, at a flow-rate of 1 ml min^{-1}. Gradient elution up to 50% MeCN was used to optimize separation.

§ The chromatograms were monitored at 260 nm and the resolved peaks were integrated and corrected for any volume changes against a peak of 2′-deoxyadenosine used as an internal standard. Plotting $\ln(1 - A/A_{tot})$ *vs.* t (min), where A = integration for adenosine, and A_{tot} = sum of integrals for all species, gives a straight line with a slope of $-k$. The linear correlation coefficient was > 0.99 for samples with substantial hydrolysis (*e.g.* neomycin B and 1,3-diaminopropane) and somewhat lower for control samples with very little hydrolysis, as expected. The rate constants reported for the neomycin B and 1,3-diaminopropane samples are the average of four independent runs.

1 For general references discussing RNA hydrolysis, see J. Chin, *Acc. Chem. Res.*, 1991, **24**, 145; R. Breslow, E. Anslyn and D.-L. Huang, *Tetrahedron*, 1991, **47**, 2365; J. Vincent, M. Crowder and B. Averill, *TIBS*, 1992, **17**, 105; E. Anslyn and D. Perreult, *Angew. Chem., Int. Ed. Engl*., 1997, **36**, 430 and references cited therein.

2 D. Magda, R. A. Miller, J. L. Sessler and B. L. Iverson, *J. Am. Chem. Soc.*, 1994, **116**, 7439; K. Matsumura, M. Endo and M. Komiyama, *J. Chem. Soc., Chem. Commun.*, 1994, 2019; J. Hall, D. Hüsken, U. Pieles, H. E. Moser and R. Häner, *Chem. Biol.*, 1994, **1**, 185; J. K. Bashkin, E. I. Frolova and U. Sampath, *J. Am. Chem. Soc*., 1994, **116**, 5981; J. Hall, D. Hüsken and R. Häner, *Nucleic Acids Res*., 1996, **24**, 3522; D. Magda, S. Crofts, A. Lin, D. Miles, M. Wright and J. L. Sessler, *J. Am. Chem. Soc.*, 1997, **119**, 2293; D. Magda, M. Wright, S. Crofts, A. Lin and J. L. Sessler, *J. Am. Chem. Soc.*, 1997, **119**, 6947.

3 M. Endo, Y. Azuma, Y. Saga, A. Kuzuya, G. Kawai and M. Komiyama, *J. Org. Chem.*, 1997, **62**, 846.

4 For the hydrolytic cleavage of $tRNA^{Phe}$ by metal-free bleomycin, see M. V. Keck and S. M. Hecht, *Biochemistry*, 1995, **34**, 12 029.

5 U. von Ahsen, J. Davies and R. Schroeder, *Nature*, 1991, **353**, 368; U. von Ahsen, J. Davies and R. Schroeder, *J. Mol. Biol.*, 1992, **226**, 935; J. Davies, U. von Ahsen and R. Schroeder, *The RNA World*, ed. R. F. Gesteland and J. F. Atkins, Cold Spring Harbor Laboratory Press, New York, 1993, pp. 185–204.

6 T. K. Stage, K. J. Hertel and O. C. Uhlenbeck, *RNA*, 1995, **1**, 95.

7 H.-Y. Mei, A. A. Galan, N. S. Halim, D. P. Mack, D. W. Moreland, K. B. Sanders, H. N. Troung and A. W. Czarnik, *Bioorg. Med. Chem. Lett*., 1995, **5**, 2755.

8 M. L. Zapp, S. Stern and M. R. Green, *Cell*, 1993, **74**, 969; G. Werstuck, M. L. Zapp and M. R. Green, *Chem. Biol.*, 1996, **3**, 129.

9 M. Hendrix, P. B. Alper, E. S. Priestley and C.-H. Wong, *Angew. Chem., Int. Ed. Engl.*, 1997, **36**, 95.

10 H. Wang and Y. Tor, *J. Am. Chem. Soc.*, 1997, **119**, 8734; H. Wang and Y. Tor, *Bioorg. Med. Chem. Lett.*, 1997, **7**, 1951; H. Wang and Y. Tor, *Angew. Chem.*, in the press.

11 T. Hermann and E. Westhof, *J. Mol. Biol.*, in the press.

12 K. Yoshinari, K. Yamazaki and M. Komiyama, *J. Am. Chem. Soc.*, 1991, **113**, 5899. See also: K. N. Dalby, A. J. Kirby and F. Hollfelder, *Pure Appl. Chem.*, 1994, **66**, 687.

13 M. Komiyama and K. Yoshinari, *J. Org. Chem.*, 1997, **62**, 2155.

14 B. Barbier and A. Brack, *J. Am. Chem. Soc.*, 1992, **114**, 3511.

15 H. Dugas, *Bioorganic Chemistry, A Chemical Approach to Enzyme Action*, 2nd edn., Springer Verlag, New York, 1989, pp. 123–137.

16 R. E. Botto and B. Coxon, *J. Am. Chem. Soc.*, 1983, **105**, 1021. See also: D. E. Dorman, J. W. Paschal and K. E. Merkel, *J. Am. Chem. Soc.*, 1976, **98**, 6885; L. Szilágyi, Z. Sz. Pusztahelyi, S. Jakab and I. Kovács, *Carbohydr. Res*., 1993, **247**, 99.

17 C. P. H. Vary and J. N. Vournakis, *Proc. Natl. Acad. Sci. USA*, 1984, **81**, 6978; J. M. Kean, S. A. White and D. E. Draper, *Biochemistry* 1985, **24**, 5062; C. Ehresmann, F. Baudin, M. Mougel, P. Romby, J.-P. Ebel and B. Ehresmann, *Nucleic Acids Res.*, 1987, **15**, 9109; G. Knapp, *Methods Enzymol.*, 1989, **180**, 192; D. S. Sigman and C.-H. Chen, *Annu. Rev. Biochem.*, 1990, **59**, 207; D. S. Sigman, A. Mazumder and D. M. Perrin, *Chem. Rev*., 1993, **93**, 2295.

Received in Corvallis, OR, USA, 15th August 1997; 7/06023H

A novel synthesis of unsymmetrical tertiary phosphines: selective nucleophilic substitution on phosphorus(III)

Sumita Singh and Kenneth M. Nicholas*

Department of Chemistry and Biochemistry, University of Oklahoma, Norman, OK, 73019, USA

A new synthesis of unsymmetrical tertiary phosphines has been developed employing selective, sequential alkylation of chloroaminophosphines by Grignard and organolithium reagents.

Phosphines constitute the most important class of ligands used in transition metal catalysed reactions.[1] The activity and selectivity of such catalysts are often acutely sensitive to the structure of the phosphine, necessitating the synthesis and testing of a variety of ligands to optimize the catalyst. Hence, the development of efficient and selective preparative routes to structurally diverse phosphine libraries, both in solution and on solid supports, is an important objective. Initial approaches to high throughput parallel syntheses of peptide-derived chiral phosphines[2] and of other ligands[3] and catalysts[4] for asymmetric synthesis have been reported recently.

We sought to develop a general and efficient preparation of tertiary phosphines which ultimately would be adaptable for solid phase parallel synthesis. Solution phase preparation of phosphines usually involves displacement of halide or alkoxide using organometallic reagents[5] (Scheme 1) but access to unsymmetrical tertiary phosphines **1** is complicated by polysubstitution. Selective displacement of chloride in the presence of alkoxide is sometimes possible using a combination of organocadmium and Grignard reagents,[6] organozinc and organolithium reagents,[7] and *via* other approaches[8] but these methods often employ inconvenient organometallics, require multiple steps, and/or lack selectivity or generality. We describe herein a new approach (Scheme 2) which exploits the vastly different leaving group abilities of chloride *vs.* amide and the differential reactivity of organolithium *vs.* organomagnesium reagents.

To first establish the leaving group ability of the dialkylamino unit, the interaction of **4a**–**c**[9] with representative RLi, RMgX, and R_3Al reagents was investigated. Dialkylaminophosphines **4a**,**b** proved unreactive even when these organometallics were employed in excess at elevated temperature.† *N*-Methyl-*N*-phenylaminodiphenylphosphine **4c**[9] possessing an expectedly better leaving group, however, reacted extremely slowly with excess MeMgCl at high temperature but rapidly

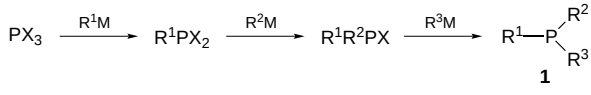

Scheme 1

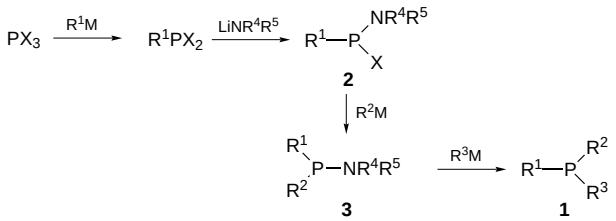

Scheme 2

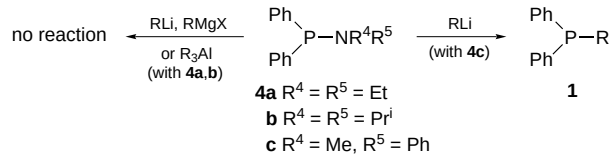

Scheme 3

with MeLi at room temperature, yielding the desired phosphine (Scheme 3).

The key chloroaminophosphines **2** (**a** R = Ph; **b** R = Et) are efficiently prepared (*ca.* 75%) by reaction of readily available organodichlorophosphines‡§ with LiNMePh[9] (THF, 20 °C, Scheme 2).¶ These, in turn undergo selective reaction with Grignard reagents (1.5 equiv, THF, 20 °C) producing aminophosphines **3a**–**j** in excellent yields following aqueous workup (Table 1).‖ A variety of substituents, including alkyl, vinyl and aryl groups, are efficiently incorporated.

Organolithium reagents readily react with the aminophosphines **3** (THF, 20 °C) giving unsymmetrical tertiary phosphines **1a**–**j** (Scheme 2, Table 1).** Although isolated yields of volatile dialkylaryl phosphines were only fair, diarylalkyl derivatives, including sterically hindered ones (*e.g.* **1e**–**g**), could be obtained in high yield.

Finally, we note that the complete sequence from PR^1Cl_2 to $PR^1R^2R^3$ can be conveniently accomplished without the isolation of intermediates. In this way phosphine **1f** was obtained in 59% yield by sequential treatment of $PhPCl_2$ with LiNMePh, *o*-tolMgBr and then MeLi.††

Application of this methodology for the solid-phase synthesis of phosphine libraries is under investigation.

We thank the National Science Foundation (in part) and the University of Oklahoma Research Council for financial support of this work.

Table 1 Preparation of unsymmetrical tertiary phosphines

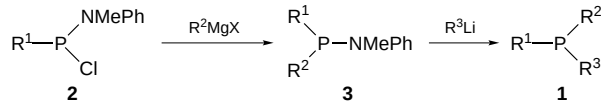

2	R^1	R^2	X	**3**	Yield[a] (%)	R^3	**1**	Yield[a] (%)
2a	Ph	Pr^i	Cl	**3a**	86	Me	**1a**	16
2a	Ph	Me	Cl	**3b**	83	Bu^t	**1b**	44
2a	Ph	Vinyl	Br	**3c**	95	Me	**1c**	54
2a	Ph	*p*-tol	Br	**3d**	94	Me	**1d**	95
2a	Ph	*p*-tol	Br	**3e**	94	Bu^t	**1e**	76
2a	Ph	*o*-tol	Br	**3f**	96	Me	**1f**	93
2a	Ph	2,6-$Me_2C_6H_3$	Br	**3g**	89	Me	**1g**	70
2a	Ph	Me_3SiCH_2	Cl	**3h**	87	Me	**1h**	98[b]
2b	Et	*p*-tol	Br	**3i**	90	Ph	**1i**	99
2b	Et	Bn	Cl	**3j**	77	Ph	**1j**	78

[a] Isolated yield. [b] Mixture of phosphine and PhNHMe (3 : 1) by ^{1}H NMR spectroscopy. Yield calculated *via* integration.

Footnotes and References

* E-mail: knicholas@ou.edu

† Synthesis of tertiary phosphines *via* reaction of Grignard reagents with aminoarylphosphines bearing a coordinating heteroatomic group at the *ortho* position on the phenyl ring has been previously reported (ref. 10). Based on the non-reactivity of unsubstituted aryldialkylaminophosphines observed by us, the ligating *ortho* substituent seems to be a prerequisite.

‡ Some organodichlorophosphines are commercially available; they also can be obtained *via* reaction of phosphorus trichloride with organometallic reagents (ref. 5).

§ Reactions and transfers for the preparation of **1**–**3** were conducted under N_2. All compounds exhibited satisfactory ^{1}H and ^{31}P NMR spectra.

¶ *Preparation* of **2**: Bu^{n}Li (35 mmol in hexane) was added slowly to PhNHMe (30 mmol) in THF (5 ml) at 0 °C and the resulting white suspension was stirred at room temp. for 45 min. The solvent was evaporated, the white solid was dissolved in THF (150 ml), and the solution was added dropwise to $RPCl_2$ in THF (1.25 M, R = Et, Ph) at 0 °C. After stirring at room temp. for 2 h, the solvent was evaporated, CH_2Cl_2 (40 ml) was added, the mixture filtered, and the solvent evaporated to provide crude **2a**,**b** which could be purified by vacuum distillation.

‖ *Preparation* of **3**: To a stirred solution of **2a** or **b** in THF (1 M) at 0 °C was added 1.5 equiv. of Grignard reagent. The mixture was stirred at room temp. until all of **2** had reacted (by ^{1}H and ^{31}P NMR spectroscopy). The mixture was then cooled in ice and 1 M NH_4Cl was added slowly for complete neutralization. The organic layer was separated, dried over Na_2SO_4, and the solvent evaporated to give the aminophosphines **3a**–**j** as pale yellow liquids which could be used in the next step without further purification.

** *Preparation* of **1**: To a solution of **3** in THF (1 M) at 0 °C was added 1.5 equiv. of RLi. After warming to room temp., the mixture was stirred until reaction completion was indicated (by ^{1}H and ^{31}P NMR spectroscopy). The solvent was evaporated and hexane (30–40 ml) was added. After stirring for a few minutes, the mixture was filtered, and the solvent was evaporated to yield the phosphines.

†† *'No isolation' preparation* of **1**: PhMeNLi was prepared and added to $PhPCl_2$ in THF as described for the preparation of **2**. When the starting material was consumed (2 h, by NMR spectroscopy), *o*-tolylMgBr (1.5 equiv.) was added at 0 °C and the reaction mixture was then warmed to room temperature. Once the formation of aminophosphine was complete (1.5 h), the solvent was evaporated and the residue was triturated with 50 ml benzene. The combined extracts were evaporated and the residue was dissolved in 10 ml THF, treated with MeLi (5.5 equiv.) at 0 °C, and then stirred at room temperature for 3 h. Phosphine **1f** was isolated as described for the preparation of **1** above.

1 W. Keim, A. Behr and M. Roper, *Comprehensive Organometallic Chemistry*, ed. G. Wilkinson and J. Abels, Elsevier, London, 1982, vol. 8, pp. 372–462; J. P. Collman, L. S. Hegedus, J. R. Norton and R. G. Finke, *Principles and Applications of Organo-transition Metal Chemistry*, 2nd edn., University Science Books, Mill Valey, CA., 1987, pp. 621–632; K. E. Koenig, *Asymmetric Synthesis*, ed. J. D. Morrison, Academic Press, New York, 1985, vol. 5, pp. 71–101; R. Noyori, *Asymmetric Catalysis in Organic Synthesis*, Wiley, New York, 1994, pp. 95–121; S. A. Godleski, *Comprehensive Organic Synthesis*, ed. B. M. Trost, Pergamon, Oxford, 1991, vol. 4, p. 585; B. M. Trost, *Acc. Chem. Res.*, 1980, **13**, 385.

2 S. R. Gilbertson and X. Wang, *Tetrahedron Lett.*, 1996, **37**, 6475.

3 J. Ellman and G. Liu, *J. Org. Chem.*, 1995, **60**, 7712.

4 A. Hoveyda and M. L. Snapper, *Angew. Chem., Int. Ed. Engl.*, 1996, **35**, 1668; M. B. Francis, N. S. Finney and E. A. Jacobsen, *J. Am. Chem. Soc.*, 1996, **118**, 8983; K. Burgess, H.-J. Lim, A. M. Porte and G. A. Sulikoski, *Angew. Chem., Int. Ed. Engl.*, 1996, **35**, 220.

5 D. G. Gilheany and C. M. Mitchel, *The Chemistry of Organophosphorus Compounds*, ed. F. R. Hartley, Wiley, 1990, vol. 1, 151–191 and the references cited therein.

6 M. Pankowski, W. Chodkiewicz and M.-P. Simonnin, *Inorg. Chem.*, 1985, **24**, 533; C. Jore, D. Guillerm and W. Chodkiewicz, *J. Organomet. Chem.*, 1978, **149**, C7; W. Chodkiewicz, D. Guillerm, D. Jore, E. Mathieu and W. Wodzki, *J. Organomet. Chem.*, 1984, **269**, 107.

7 G. Wittig, H. Braun and H.-J Cristau, *Liebigs. Ann. Chem.*, 1971, **751**, 17.

8 W. E. McEwen, K. F. Kumli, M. Zanger and C. A. VanderWerf, *J. Am. Chem. Soc.*, 1964, **86**, 2378; M. Sander, *Chem. Ber.*, 1960, **93**, 1220; L. Horner, F. Schedlbauer and P. Beck, *Tetrahedron Lett.*, 1964, 1421; A. M. Aguiar, J. R. S. Irelan, C. J. Morrow, J. P. John and G. W. Prejean, *J. Org. Chem.*, 1969, **34**, 2684.

9 H.-J. Cristau, A. Chene and H. Christol, *Synthesis*, 1980, 551.

10 L. Horner and G. Simons, *Phosphorus Sulfur Relat. Elem.*, 1984, **19**, 65.

Received in Corvallis, OR, USA, 29th August 1997; 7/06428D

Unambiguous synthesis of stromal cell-derived factor-1 by regioselective disulfide bond formation using a DMSO–aqueous HCl system

Hirokazu Tamamura,* Fumihiro Matsumoto, Kyoko Sakano, Akira Otaka, Toshiro Ibuka and Nobutaka Fujii*†

Graduate School of Pharmaceutical Sciences, Kyoto University, Sakyo-ku, Kyoto 606-01, Japan

Total synthesis of human and murine stromal cell-derived factor-1s (SDF-1s) (residues 1–67) containing two disulfide bonds and an oxidation-sensitive Trp residue was achieved unequivocally by stepwise disulfide-forming reactions: A silver trifluoromethanesulfonate (AgOTf)–(DMSO)–aqueous HCl system was used in combination with air oxidation to form regioselectively each disulfide bond.

SDF-1,[1] a lymphocyte chemoattractant, belongs to the CXC-chemokines between two subfamilies, the CXC- and CC-chemokines.[2] Recently, it was reported that the CXC-chemokine receptor, CXCR4/fusin, and the CC-chemokine receptor, CCR5, serve as coreceptors in association with CD4 for the entry of T-cell line-tropic (T-tropic) and macrophage-tropic (M-tropic) strains of HIV-1, respectively,[3] and that SDF-1 blocks infection of T-cells by T-tropic HIV-1.[4] Thus, SDF-1 and its derivatives have the potential to become attractive candidates for the chemotherapy and prophylaxis of HIV-1 infection. The human SDF-1 (residues 1–67), having two intramolecular disulfide bonds and Trp (the sequence shown in Scheme 1), was synthesized by Springer and co-workers, and was identical in activity to the purified natural murine SDF-1.[4a] For the synthesis of human SDF-1, the researchers employed random disulfide bond formation of the fully reduced SDF-1 ([Cys(SH)^{9,11,34,50}]-SDF-1) by air oxidation. However, it is desirable that each disulfide bond be formed regioselectively in order to suppress the formation of disulfide isomers, particularly since Cys^{9} and Cys^{11} are present in close proximity in human SDF-1. The natural SDF-1 contains two disulfide bonds between Cys^{9} and Cys^{34} and between Cys^{11} and Cys^{50}.[5] It would be valuable to define the activity of this peptide whose disulfide bridges are correctly formed. Thus, we attempted to synthesize SDF-1(1–67) by regioselective disulfide bond formation. The differential *S*-protection of four Cys residues and the following stepwise disulfide bond formation must be carried out regioselectively. Several disulfide bond-forming reactions, *i.e.* iodine,[6] thallium(III) trifluoroacetate,[7] DMSO[8] and sulfoxide-silylating reagents,[9] have been found to convert some *S*-protected Cys into cystine by us and others. The regioselective syntheses using these reactions in combination with a conventional air oxidation method have been reported; however, one potential limitation to the use of these reactions is the oxidative decomposition of Trp.

We have recently developed a new procedure for disulfide bond formation in *S*-Acm-containing‡ peptides[10] using an AgOTf– DMSO–aq. HCl system.[11] In this protocol, *S*-Acm groups are removed from Cys(Acm) residues by AgOTf[12] and subsequent DMSO–aq. HCl treatment effects two reactions: the conversion of Cys(Ag) residues into Cys(SH) residues besides precipitation of AgCl by the action of HCl, and the disulfide bond formation of Cys(SH) residues by the action of DMSO in aqueous media.[13] Under these reaction conditions, no significant side reactions are observed with oxidation-sensitive amino acids such as Met, Tyr and Trp. Thus, in the present study, we synthesized human and murine SDF-1s(1–67) by the regioselective disulfide bond formation using a combination of the AgOTf–DMSO–aq. HCl system with air oxidation in order to investigate the feasibility of practical applications of this strategy to relatively large and complicated peptides.

SDF-1(1-67) has a single substitution of Ile to Val at a position 18 between mouse and human. The peptidyl resins of human and murine SDF-1s were constructed by Fmoc-based† solid-phase synthesis on *p*-alkoxybenzyl alcohol resins[14] (Scheme 1). To form regioselectively two disulfide bridges, two different protecting groups were employed with suitable pairs for the protection of four SH groups of the Cys residues: Trt‡ groups for Cys^{9} and Cys^{34}, and Acm groups for Cys^{11} and Cys^{50}. *S*-Trt groups are removable *via* Me_3SiBr treatment,[15]

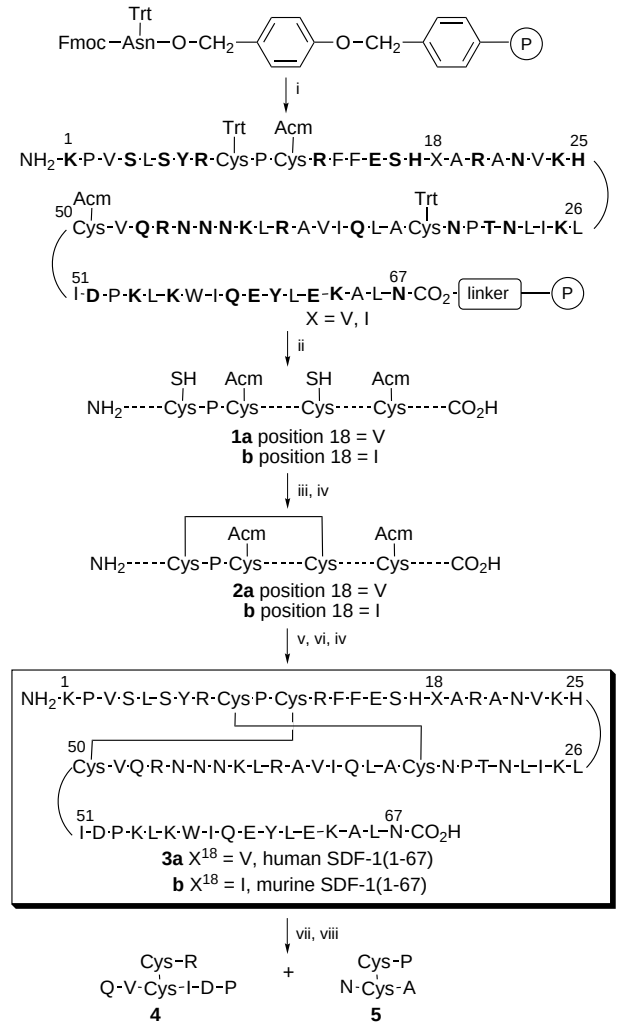

Scheme 1 *Reagents and conditions*: i, Fmoc-based solid phase synthesis; ii, Me_3SiBr–thioanisole–TFA; iii, air oxidation; iv, HPLC purification; v, AgOTf–TFA; vi, DMSO–aq. HCl; vii, trypsin; viii, prolyl endopeptidase. Bold letters indicate protected amino acids.

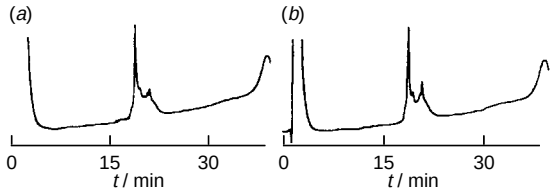

Fig. 1 Analytical HPLC of the crude (*a*) human and (*b*) murine SDF-1s. HPLC conditions: a μBondasphere 5 μC18-100 Å (3.9 × 150 mm) column, a linear gradient of MeCN (25–55%, for 30 min) in 0.1% aq. TFA at a flow rate of 1 cm^3 min^{-1}, a Waters LC module 1 equipped with a Waters 741 Data Module, UV absorption measurement at 220 nm.

whereas *S*-Acm groups are stable during to Me_3SiBr treatment, but can be removed *via* AgOTf treatment. For the side-chain protection of the other amino acid residues, the following groups were used: Trt groups for Asn and Gln, Boc groups for Lys and His, Bu^t groups for Glu, Tyr, Asp, Thr and Ser, and Pmc‡ groups for Arg. The protected resins were treated with 1 mol dm^{-3} Me_3SiBr–thioanisole–TFA to cleave peptides from the resins and remove all the protecting groups except for the *S*-Acm groups.[15] The resulting crude dihydropeptides, [Cys(SH)^{9,34}, Cys(Acm)^{11,50}]-SDF-1s (Scheme 1, **1a**,**b**), were air-oxidized to establish the first disulfide bond. After HPLC purification, monocyclic products, [Cys(Acm)^{11,50}]-SDF-1s (**2a**,**b**), were subjected to sequential treatment with AgOTf–TFA and 50% DMSO–1 mol dm^{-3} aq. HCl (v/v) to establish the second disulfide bond. Each crude bicyclic product exhibited a sharp main peak on analytical HPLC (Fig. 1) without significant side products. HPLC purification gave human and murine SDF-1s (**3a**,**b**) in satisfactory yields.§ The effective concentrations (EC_{50}) of the synthetic human and murine SDF-1s for 50% protection in an assay of HIV-induced cytopathogenicity were 463 and 201 μmol m^{-3}, respectively, and for 50% inhibition of HIV-1 p24 antigen production were 630 and 750 μmol m^{-3}, respectively. Furthermore, these peptides have the ability to induce an increase in intracellular Ca^{2+} through CXCR4/fusin (data not shown). These activities are comparable with those reported by Springer and co-workers.

In conclusion, total synthesis of human and murine SDF-1s (1-67) has been accomplished by stepwise and regioselective disulfide bond formation using air oxidation and the AgOTf–DMSO–aq. HCl system. This combination protocol has proven to be useful for preparation of relatively large and complicated bis(disulfide) peptides, particularly when Trp residues are present.

We are grateful to Professor N. Yamamoto and Dr T. Murakami, Tokyo Medical and Dental University, Tokyo, Japan, and Professor H. Nakashima and Dr R. Arakaki, Kagoshima University Dental School, Kagoshima, Japan, for the anti-HIV assay.

Footnotes and References

† E-mail: nfujii@pharmsun.pharm.kyoto-u.ac.jp

‡ *Abbreviations*: Acm = acetamidomethyl, Fmoc = fluoren-9-ylmethoxycarbonyl, Trt = triphenylmethyl, Pmc = 2,2,5,7,8-pentamethylchroman-6-ylsulfonyl.

‡ Human SDF-1(1-67) **3a** was prepared by the following procedure: The protected human SDF-1(1–67) resin (203 mg, 13.5 μmol) was treated with 1 mol dm^{-3} Me_3SiBr–thioanisole–TFA (20 cm^3) in the presence of *m*-cresol (1 cm^3, 860 equiv.) and ethane-1,2-dithiol (0.4 cm^3, 520 equiv.) at 4 °C for 2 h. After removal of the resin by filtration, the filtrate was concentrated *in vacuo*. Ice-cold dry Et_2O (30 cm^3) was then added, and the resulting powder was collected by centrifugation. After washing three times with ice- cold dry Et_2O (3 × 20 cm^3), the product **1a** was dissolved in 50% AcOH (2 cm^3). Subsequently, the total solution volume was adjusted to 400 cm^3 with H_2O and the pH was then adjusted to 8 with conc. NH_4OH. After 1 day of air oxidation, the pH of the solution was adjusted to 5 with AcOH. The crude product was purified by preparative HPLC [Waters Delta Prep 4000 on a Cosmosil packed column (5 μC18-100 Å, 20 × 250 mm) using a linear gradient of MeCN (31–33%, for 30 min) in 0.1% aq. TFA at a flow rate of 7 cm^3 min^{-1}]. The solvent was removed by lyophilisation to give [Cys(Acm)^{11,50}]-human SDF-1 **2a** as a fluffy white powder: (17.4 mg, 1.80 μmol). [Cys(Acm)^{11,50}]-human SDF-1 (17.2 mg, 1.78 μmol) was treated with AgOTf (45.6 mg, 100 equiv.) in TFA (2 cm^3) in the presence of anisole (0.02 cm^3) at 4 °C. After 2 h, ice-cold dry Et_2O (30 cm^3) was then added. The resulting product was washed three times with ice-cold dry Et_2O (3 × 20 cm^3), and then treated with 50% DMSO–1 mol dm^{-3} aq. HCl (v/v, 17 cm^3) at room temperature for 7 h. After removal of the AgCl precipitate by filtration, the filtrate was diluted with H_2O (150 cm^3). The crude peptide was purified by preparative HPLC [a linear gradient of MeCN (30–32%, for 30 min)] to give human SDF-1 **3a** as a fluffy white powder [2.1 mg, 0.245 μmol, 13.8% (calculated from **2a**)]: [IS-MS (reconstructed): Found, 7827.5. Calc. for $C_{350}H_{566}N_{104}O_{92}S_4$, 7826.5]. Its disulfide pairings proved to be identical with those of the natural peptide based on ion spray mass analysis of peptide fragments (**4** and **5** in Scheme 1) derived from the successive digestion treatment of the synthetic peptide by trypsin (TRCK-treated type XIII from bovine pancreas) and prolyl endopeptidase (from Flavobacterium). $[\alpha]_D^{28}$ −92.3 (*c* 0.1, H_2O).

Murine SDF-1(1-67) **3b** was prepared by the same procedure as described above, [16.4% (calculated from (**2b**)]: [IS-MS (reconstructed): Found, 7841.0. Calc. for $C_{351}H_{568}N_{104}O_{92}S_4$, 7840.6]. Its disulfide pairings proved to be identical with those of the natural peptide. $[\alpha]_D^{28}$ −84.8 (*c* 0.1, H_2O).

1 T. Nagasawa, H. Kikutani and T. Kishimoto, *Proc. Natl. Acad. Sci. USA*, 1994, **91**, 2305; C. C. Bleul, R. C. Fuhlbrigge, J. M. Casasnovas, A. Aiuti and T. A. Springer, *J. Exp. Med.*, 1996, **184**, 1101.
2 H. Iizasa and K. Matsushima, *Clinical Immunology*, 1996, **28**, 733 and references cited therein).
3 M. P. D'Souza and V. A. Harden, *Nat. Med. (NY)*, 1996, **2**, 1293 and references cited therein.
4 (*a*) C. C. Bleul, M. Farzan, H. Choe, C. Parolin, L. Clark-Lewis, J. Sodroski and T. A. Springer, *Nature*, 1996, **382**, 829; (*b*) E. Oberlin, A. Amara, F. Bachelerie, C. Bessia, J.-L. Virelizier, F. Arenzana-Seisdedos, O. Schwartz, J.-M. Heard, L. Clark-Lewis, D. F. Legler, M. Loetscher, M. Baggiolini and B. Moser, *Nature*, 1996, **382**, 833.
5 The disulfide array of natural SDF-1 was deduced from that of human Interleukin 8 which belongs to the same CXC-chemokine superfamily: G. M. Clore, E. Appella, M. Yamada, K. Matsushima and A. M. Gronenborn, *Biochemistry*, 1990, **29**, 1689.
6 B. Kamber, A. Hartmann, K. Eidler, B. Riniker, H. Rink, P. Sieber and W. Rittel, *Helv. Chim. Acta*, 1980, **63**, 899.
7 N. Fujii, A. Otaka, S. Funakoshi, K. Bessho and H. Yajima, *J. Chem. Soc., Chem. Commun.*, 1987, 163.
8 A. Otaka, T. Koide, A. Shide and N. Fujii, *Tetrahedron Lett.*, 1991, **32**, 1223.
9 K. Akaji, T. Tatsumi, M. Yoshida, T. Kimura, Y. Fujiwara and Y. Kiso, *J. Am. Chem. Soc.*, 1992, **114**, 4137; T. Koide, A. Otaka, H. Suzuki and N. Fujii, *Synlett*, 1991, 345.
10 D. F. Veber, D. Milkowski, Jr., S. L. Varga, R. G. Denkewalter and R. Hirschmann, *J. Am. Chem. Soc.*, 1972, **94**, 5456.
11 H. Tamamura, A. Otaka, J. Nakamura, K. Okubo, T. Koide, K. Ikeda and N. Fujii, *Tetrahedron Lett.*, 1993, **34**, 4931.
12 N. Fujii, A. Otaka, T. Watanabe, A. Okamachi, H. Tamamura, H. Yajima, Y. Inagaki, M. Nomizu and K. Asano, *J. Chem. Soc., Chem. Commun.*, 1989, 283.
13 N. Fujii, A. Otaka, A. Okamachi, T. Watanabe, H. Arai, H. Tamamura, S. Funakoshi and H. Yajima, in *Peptides 1988*, ed. G. Jung and E. Bayer, Walter de Gruyter, Berlin, 1989, vol. 1988, p. 58; J. P. Tam, C.-R. Wu, W. Liu and J.-W. Zhang, *J. Am. Chem. Soc.*, 1991, **113**, 6657.
14 S. S. Wang, *J. Am. Chem. Soc.*, 1973, **95**, 1328.
15 N. Fujii, A. Otaka, N. Sugiyama, M. Hatano and H. Yajima, *Chem. Pharm. Bull.*, 1987, **35**, 3880.

Received in Cambridge, UK, 18th September 1997; 7/06774G

Electrochemical syntheses and doping properties of poly(3,3′-dialkylsulfanyl-2,2′-bithiophene)s: novel materials which exhibit facile n- and p-dopability

Siu-Choon Ng,* Ping Miao and Hardy S. O. Chan

Department of Chemistry, National University of Singapore, Singapore 119260

Novel and stable electroactive polymer films which can undergo facile electrochemical p- and n-doping are successfully prepared for the first time from the electrochemical polymerization of symmetrical 3,3′-dialkylsulfanyl-2,2′-bithiophenes with long pendant chains.

In the course of our ongoing investigations into novel electrically conducting polymers, it was found that, in striking contrast to 3-alkylsulfanylthiophenes,[1–8] 3,3′-dialkylsulfanyl-2,2′-bithiophenes (DSABT) can be successfully polymerized by both chemical (using $FeCl_3$ as oxidant) and electrochemical approaches. Apart from the formation of stable films, the electrochemically derived polymers demonstrated reversible electrochemical p- and n-dopability. For most polymers, although p-doping activity has been well researched, n-type doping studies are comparatively rare due to the poor stability of the polymers at extreme negative potentials. However, from an application viewpoint, materials which are both p- and n-dopable are important, for example as light-emitting diode materials,[9] electrochemical cells[10] or in the construction of type III capacitors,[11] wherein one electrode is p-doped and the other is n-doped when the capacitor is charged. Studies on polythiophenes and polybithiophenes[12,13] have shown that p-doping generally occurs at high positive potentials whilst n-doping occurs at large negative potentials. Although introduction of pendant alkoxy groups at the 3-position of thiophene significantly reduced the oxidation potential, the n-doping process was found to be irreversible with a very small anodic current.[14] To the best of our knowledge, the electrochemical n-doping properties of alkylsulfanyl functionalized polythiophenes have not been studied.

The synthesis of monomers was accomplished starting from 3,3′-dibromo- 2,2′-bithiophene as reported previously.[15] Electrochemical polymerization of DSABTs was performed either by *via* cyclic voltammetry (CV), with the sweep potential varied from 0 to 1.1 V [*versus* a saturated calomel electrode (SCE)] at a scan rate of 20 mV s^{-1}, or by the galvanostatic method at a current density of 100 μA cm^{-2}. The monomers and electrolyte (Bu_4NBF_4 in MeCN) concentrations were 0.002 and 0.1 M, respectively. The resulting polymer films were rinsed carefully with absolute ethanol and acetone and then dried in an argon steam prior to the cyclic voltammetry studies and spectrophotometric analyses.

In contrast to 3-alkylsulfanylthiophenes, symmetrical 3,3′-dialkylsulfanyl-2,2’-bithiophenes with long pendant chains can undergo a facile oxidative polymerization *via* both the CV and galvanostatic methods, with the resulting polymers exhibiting excellent film formation behaviour. The monomer oxidation potential in $Bu^n_4N^+BF_4^-$ (0.1 M) at a scan rate of 20 mV s^{-1} was *ca*. 1.10 V. In the CV polymerization approach, a cathodic peak (*ca*. 0.75 V) was observed during the first scan, which increased in intensity with increasing number of scans. One main anodic peak at approximately 0.80 V with two shoulder peaks at 0.75 and 0.85 V were evident after the second scan. The increase in peak currents observable with the number of scans, is indicative of progressive polymer growth on the surface of the electrode. Polymer film prepared *via* galvanostatic polymerization methods exhibited a monomer oxidation potential at *ca*. 1.0 V at a current density of 100 μA cm^{-2}. The film quality was found to be dependent on the alkylsulfanyl chain lengths. Hence, monomers with lengthy alkylsulfanyl moieties (*e.g.* DSDeBT) can be electrochemically polymerized to afford excellent films with good stability on both platinum foil and ITO glass. These electrochemically generated films are completely soluble in $CHCl_3$, partially soluble in acetone, but insoluble in MeCN, MeOH and EtOH. On the other hand, electrochemical polymerization of DSABTs with short pendant chains (*e.g.* DSBuBT), results only in oligomers which are soluble in MeCN and alcohol. In this instance, even though a film can be obtained, it is not stable for long periods of time in the electrolyte solution. The p-doping mechanism for all four polymer films is highly reversibly with strong electrochromistic behaviour, being dark blue in the doped oxidised state and lilac in the neutral undoped state. The peak anodic potentials (E_{pa}) of the polymers range from 0.66 to 0.82 V and the peak cathodic potentials (E_{pc}) from 0.62 to 0.72 V. Long pendant groups resulted in a slightly increased oxidation potential of polymers, due presumably to accentuated steric effects exerted *via* the head-to-head linkages. The values of E_{pa} and E_{pc} increased slightly, whilst both the anodic and cathodic peak currents were found to scale linearly with increasing scan rate, which is characteristic of an electroactive polymer film grafted on to a electrode where the current is not diffusion controlled.[15]

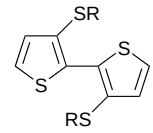

DSBuBT R = C_4H_9
DSOcBT R = C_8H_{17}
DSDeBT R = $C_{10}H_{21}$
DSDoBT R = $C_{12}H_{25}$

Fig. 1 depicts the cyclic voltammograms of thin films of poly(DSOcBT), poly(DSDeBT) and poly(DSDoBT) deposited on the platinum in the potential range −2.3 to + 1.1 V at a scan rate of 100 mV s^{-1}. Both p- and n-type redox cycles exhibit characteristic wave shapes between sharp reduction peaks and the corresponding sharp oxidation peaks. The stability of p- and n-doping is related to the quality of the films. As discussed above, electrochemical polymerization of DSOcBT, DSDeBT and DSDoBT afforded high quality films. Thus, both p-doping and n-doping are stable and highly reversibly with strong electrochromism, from dark blue (p-doped) → lilac (neutral state) → dark blue (n-doped) → transparent (neutral state). On the other hand, only p-doping is observable for poly(DSBuBT), as the film is unstable in MeCN. The electrochemical oxidation potentials (E_p) of poly(DSOcBT), poly(DSDeBT) and poly(DSDoBT) are 0.75, 0.75 and 0.82 V. These three polymers have the same onset potential (E_{on}) value (0.49 V) and consequently the same ionisation potential (IP) (4.89 eV),

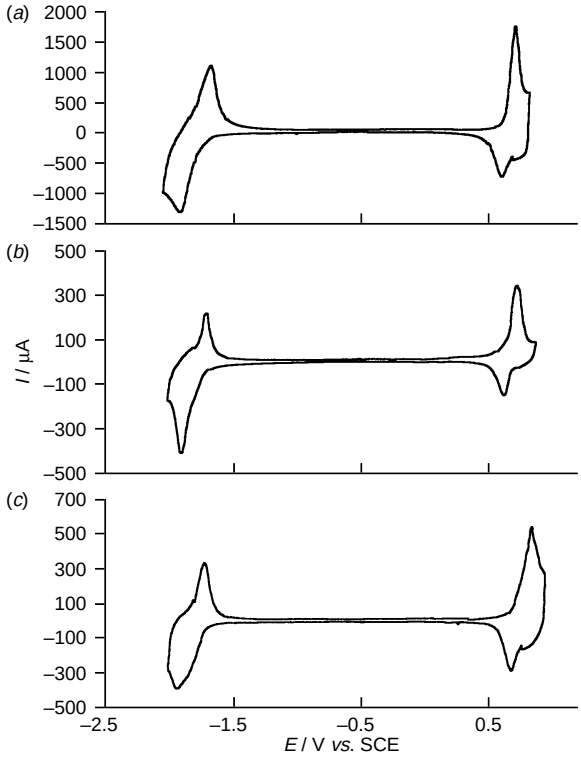

Fig. 1 CVs of (*a*) poly(DSOcBT), (*b*) poly(DSDeBT) and (*c*) poly(DSDoBT)

suggesting that the IP of DSABTs is independent of the pendant chain lengths. The peak potentials for the electrochemical reduction of the above polymers are −1.94, −1.89 and −1.98 V, with onset potentials of −1.41, −1.41 and −1.46 V, respectively. The corresponding electron affinities (EA) of these polymers are therefore 2.99, 2.99 and 2.94 eV. The observed electrochemical band gaps (the difference between the IP and the EA) are 1.90 eV for poly(DSOcBT) and poly(DSDeBT) and 1.95 eV for poly(DSDoBT). In addition, at sweep rates of 50 to 100 mV s^{-1}, both cathodic and anodic peak currents of the n-type redox cycle were found to scale linearly with respect to the sweep rate, suggesting that kinetic limitation of the electrochemical reduction of these two polymers is not significant.[16]

Fig. 2 depicts the optical absorption spectra of a typical poly(DSDeBT) film. All neutral polymer films exhibited absorption maxima at *ca*. 480, 520 and 570 nm with bandgap values between 1.77 and 1.82 eV, as derived from extrapolation of the low-energy absorption edges,[17] which agree well with the electrochemically-determined bandgap values. The high degree of conjugation in these head-to-head polymers might be ascribable to a relatively low energy barrier between their most stable configuration and the coplanar conformation.[18] Consequently, a coplanar conformation is readily attainable for poly[DSABT]s in their condensed film state. The polymer films were found to be soluble in $CHCl_3$ with solution UV absorption maxima in the range 408–450 nm depending on the length of

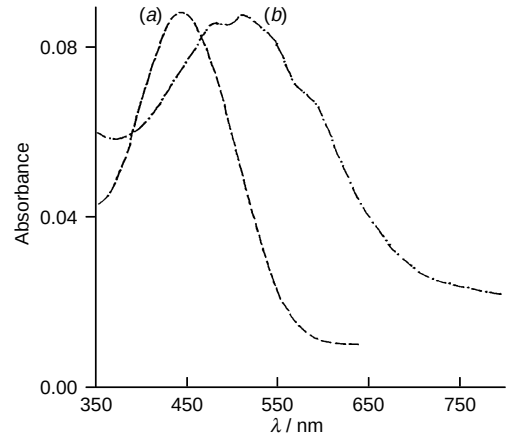

Fig. 2 UV–Visible spectra of poly(DSDeBT) in (*a*) $CHCl_3$ (λ_{max} = 441 nm) and (*b*) film state (λ_{max} at 482, 514 and 584 nm)

alkylsulfanyl moiety. Thus, these pendant groups affect the conformation of polymer both in solution and the solid state.

The authors thank the National University of Singapore for financial support through research grant RP960613. P. M. is grateful to NUS for the award of a research scholarship.

Footnote and References

* E-mail: chmngsc@leonis.nus.sg

1 R. L. Elsenbaumer, K. Y. Jen and R. Oboodi, *Synth. Met*., 1986, **15**, 169.
2 S. Tanaka, M. Sato and K. Kaeriyama, *Synth. Met.*, 1988, **25,** 277.
3 J. R. Reynolds, J. P. Ruiz, F. Wang, C. A. Jolly, K. Nayak and D. S. Marynick, *Synth. Met.*, 1989, **28**, C621.
4 J. P. Ruiz, M. B. Gieselman, K. Nayak, D. S. Marynick and J. R. Reynolds, *Synth. Met*., 1989, **28**, C481.
5 P. Bauerle, G. Gotz, A. Synowczyk and J. Heinze, *Liebigs Ann*., 1996, 279.
6 J. P. Ruiz, K. Nayak, D. S. Marynick and J. R. Reynolds, *Macromolecules*, 1989, **22**, 1231.
7 E. W. Tsai, S. Basak, J. P. Ruiz, J. R. Reynold and K. Rajeshwar, *J. Electrochem. Soc*., 1989, **136**, 3683.
8 X. Wu, T.-A. Chen and R. D. Rieke, *Macromolecules*, 1995, **28**, 2101; X. Wu, T.-A. Chen and R. D. Rieke, *Macromolecules*, 1996, **29**, 7671.
9 Q. Pei, G. Yu, C. Zhang, Y. Yang and A. J. Heeger, *Science*, 1995, **269**, 1086.
10 M. Onoda, H. Nakayama, S. Morita and K. Yoshino, *J. Appl. Phys*., 1993, **73**, 2859.
11 K. Gerff and J. H. Simon, *J. Mater. Chem*., 1995, **5**, 447.
12 M. Mastragostino and L. Soddu, *Electrochim. Acta*, 1990, **35**, 463.
13 W.-C. Chen and S. A. Jenekhe, *Macromolecules*, 1995, **28**, 465.
14 Y. Miyazaki, T. Kanbara, K. Osakada and T. Yamamoto, *Chem. Lett*., 1993, 415.
15 S. C. Ng, H. S. O. Chan, H. H. Huang and R. S. H. Seow, *J. Chem. Res*., 1996, (*S*) 232; (*M*) 1285.
16 E. M. Genies, G. Bidan and A. F. Diaz, *J. Electroanal. Chem*., 1983, **149**, 101.
17 H. Eckardt, L. W. Shacklette, K.-Y. Jen and R. L. Elsenbaumer, *J. Chem. Phys*., 1989, **91**, 1303.
18 N. D. Lesare, M. Belletete, G. Durocher and M. Leclerc, *Chem. Phys. Lett.*, 1997, **275**, 533.

Received in Cambridge, UK, 8th September 1997; 7/06551E

Stereoselective synthesis of highly functionalized *cis*-decalins from masked *o*-benzoquinones

Polisetti Dharma Rao, Chien-Hsing Chen and Chun-Chen Liao*

Department of Chemistry, National Tsing Hua University, Hsinchu, Taiwan 30043

Highly functionalized *cis*-decalins are prepared from commercially available 2-methoxyphenols and acyclic 1,3-dienes.

The decalin skeleton features in a large variety of natural products with interesting biological properties, *e.g.* kaurenes, aphidicolanes, quassinoids and azadirachtins.[1,2] A functionalized decalin has often been the starting point for the synthesis of the above mentioned classes of terpenoids. Owing to this, there is continued interest in the stereoselective synthesis of decalins, as is amply evidenced by the recent flurry of reports by various groups including ours.[3,4] Herein we report a novel method for the preparation of highly functionalized decalins from commercially available 2-methoxyphenols and acyclic 1,3-dienes.

Masked *o*-benzoquinones, *i.e.*, 6,6-dialkoxycyclohexa-2,4-dienones **1**, when compared to their counterparts derived from *p*-benzoquinones,[5] are a relatively underutilized class of compounds. Prior to our studies, there have been only sporadic reports on their chemistry.[6,7] The main reason for this could be their high propensity to dimerize. In most cases, they were isolated in poor yields as dimers. For the last ten years we have been interested in exploiting the synthetic potential of this neglected class of compounds. We have already shown that the masked *o*-benzoquinones **1**, generated *in situ* by the oxidation of 2-methoxyphenols **2** with (diacetoxy)iodobenzene (DAIB) or [bis(trifluoroacetoxy)]iodobenzene (BTIB) in presence of a dienophile in MeOH, an allyl alcohol in CH_2Cl_2 or a 2,4-dienol in THF, undergo Diels–Alder reactions to provide compounds of the types **3**, **4**, and **5** and **6**, respectively (Scheme 1).[4,8]

Masked *o*-benzoquinones, or cyclohexa-2,4-dienones in general, are commonly used as dienes.[7,9] We and others have recently found that they can also act as dienophiles in an intramolecular sense when forced by their structures.[4,10] We now report that masked *o*-benzoquinones **11**–**14**, generated *in situ* from phenols **7**–**10**, exhibit sufficient dienophilicity to react even with unactivated acyclic dienes such as 2,3-dimethylbutadiene **15**, *trans*-piperylene **16** and 1-acetoxybutadiene **17** to provide highly substituted *cis*-decalins with very high regio- and stereo-selectivity (Scheme 2). To the best of our knowledge, these findings are unprecedented.

Phenols **7**–**10** were oxidized by slow addition of a solution of DAIB in MeOH in presence of an excess of a diene in MeOH at

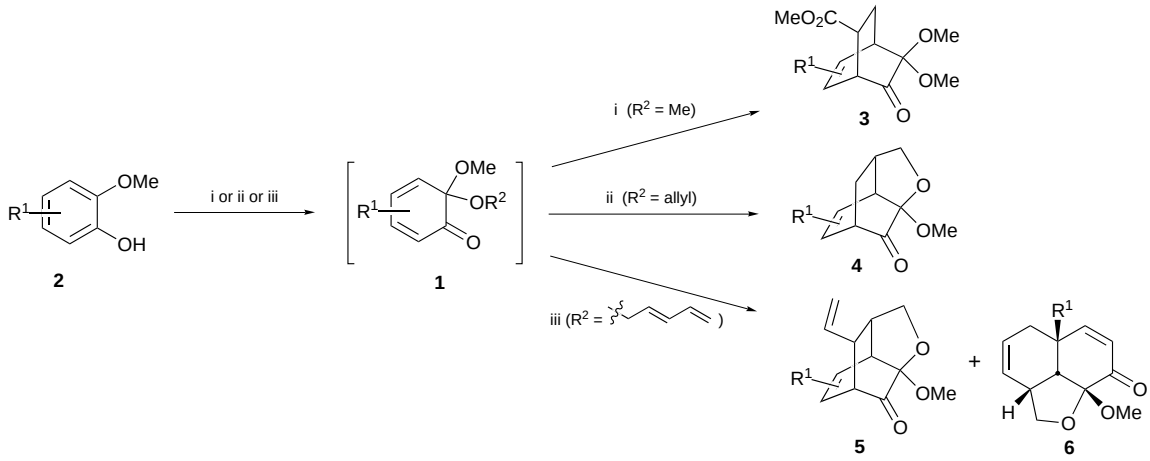

Scheme 1 *Reagents and conditions*: i, DAIB, methyl acrylate, MeOH; ii, DAIB, allyl alcohol, CH_2Cl_2; iii, BTIB, 2,4-dienol, THF

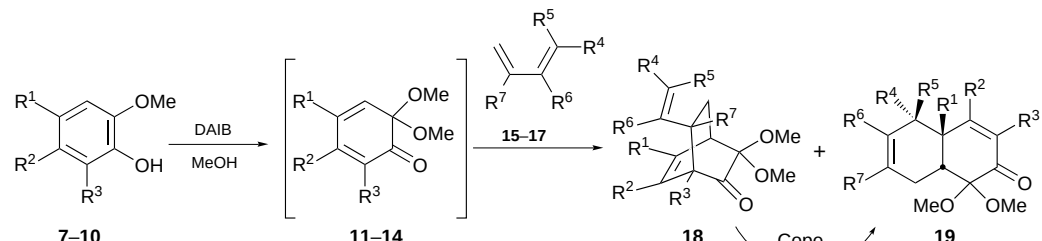

7–**10** **11**–**14** **18** **19**

7,**11** $R^1 = CO_2Me$, $R^2 = R^3 = H$
8,**12** $R^1 = CO_2Me$, $R^2 = H$, $R^3 = OMe$
9,**13** $R^1 = R^3 = H$, $R^2 = CO_2Me$
10,**14** $R^1 = Me$, $R^2 = R^3 = H$

15 $R^4 = R^5 = H$, $R^6 = R^7 = Me$
16 $R^4 = Me$, $R^5 = R^6 = R^7 = H$
17 $R^4 = OAc$, $R^5 = R^6 = R^7 = H$ (*cis* + *trans*)

Scheme 2

Table 1 Stereoselective synthesis of *cis*-decalins **19**

			Diels–Alder reaction					Cope rearrangement of **18**[d]			
Entry	Phenol	Diene	*T*/°C[a]	*t*/h[b]	Ratio **18** : **19**	Yield of **18**[c] (%)	Yield of **19**[c] (%)	*T*/°C	*t*/h	Yield of **19**[c] (%)	Total yield of **19**[c] (%)
a	**7**	**15**	80	3	1 : 2	29	53	220	24	95	91
b	**7**	**16**	50	3	2 : 1	55	25	200	50	91[e]	—
c	**7**	**17**	80	0.1	2 : 1	62	34	200	40	87	88
d	**8**	**15**	80	3	0 : 1	—	81	—	—	—	81
e	**8**	**16**	50	3	6 : 1	64	11	200	24	85[e]	—
f	**8**	**17**	80	0.5	4 : 1	61	16	200	40	91	71
g	**9**	**15**	80	3	4 : 1	56	14	220	24	86	62
h	**9**	**16**	50	3	1 : 0	81	—	200	50	87[e]	—
i	**9**	**17**	80	0.5	5 : 1	64	14	180	40	89	71
j	**10**	**15**	80	6	3 : 1	34	12	220	24	98	45
k	**10**	**16**	50	6	—	40[f]	—				
l	**10**	**17**	50	6	—	60[f]	—				

[a] Oil bath. [b] During which DAIB is added. [c] Yields are of isolated products and unoptimized. [d] Reaction conditions: **18** + $HC(OMe)_3$ (1 equiv.), mesitylene, heat. [e] Based on consumed starting material. [f] An inseparable mixture of bicyclo[2.2.2]octenones is obtained.

appropriate temperature to obtain compounds **18** and **19**.† In all the cases, the bicyclo[2.2.2]octenone derivatives **18a**–**j** underwent Cope rearrangement, smoothly providing *cis*-decalins **19** in very high yields.† The total yields of decalins are quite high and hence a new efficient method for the stereoselective preparation of *cis*-decalins has been developed. Although many isomers are possible, we generally isolate only two products, except in case of phenol **10**, showing that these reactions are highly regio- and stereo-selective and obey the ground rules of the Diels–Alder reaction.

The *cis*-decalins **19** could result from either direct Diels–Alder reactions, in which masked *o*-benzoquinones behave as dienophiles, or from tandem processes involving Diels–Alder reactions, in which masked *o*-benzoquinones act as dienes and the resultant vinylbicyclo[2.2.2]octenones **18** then undergo Cope rearrangement. In order to ascertain the actual pathway, the bicyclo[2.2.2]octenones **18e** and **18g** were subjected to heating in MeOH containing AcOH and the corresponding diene in the appropriate proportions for 3 h. In the case of **18e**, the crude reaction mixture was found to contain compounds **18e** and **19e** in a 97 : 3 ratio *via* ^{1}H NMR spectroscopy. On the other hand, compound **18g** remained unchanged. We therefore believe that the decalins **19** are generally primary products. Nevertheless the aforementioned tandem process can not be completely ruled out.

All the compounds were characterized by ^{1}H and ^{13}C NMR, IR and mass spectral analysis. The structural assignments of bicyclo[2.2.2]octenones **18** are based on the fact that they isomerize to *cis*-decalins **19** smoothly. The stereochemical assignments of the decalins are based on NOE studies and coupling constants. Closely related compounds can be obtained *via* the reaction of *o*-benzoquinones with acyclic dienes, but the senstive α-dicarbonyl moiety makes these compounds less attractive. Moreover, they aromatize to naphthalene derivatives very easily.[11]

It is quite clear from Table 1 that the masked *o*-benzoquinones can be good dienophiles. Apparently, it is difficult to predict whether a masked *o*-benzoquinone would behave as a diene or a dienophile in its reactions with added dienes. It is obviously linked to the structure of added diene and the nature and/or the position of the substituents present on the masked *o*-benzoquinone. For example, the methoxycarbonyl group on masked *o*-benzoquinone **13** diminishes the dienophilicity due to cross conjugation, which reinforces the diene character. Similarly, the methyl group on masked *o*-benzoquinone **14** increases the diene character, possibly *via* hyperconjugation.

Masked *o*-benzoquinone **11** is undoubtedly the best, exhibiting optimum reactivity and very high selectivity in all respects. On the other hand, **14** showed very poor selectivity, providing mixtures of bicyclo[2.2.2]octenones under various conditions except with 2,3-dimethylbutadiene.

In conclusion, our studies throw light on the nature of masked *o*-benzoquinones and have resulted in the development of a simple method for the synthesis of highly functionalized *cis*-decalins. More detailed studies on the nature of masked *o*-benzoquinones and the transformation of decalin **19f** into (±)-vernolepin are in progress in our laboratory.

We thank the National Science Council (NSC) of Taiwan, R.O.C., for financial support. P. D. R. thanks the NSC for a post-doctoral fellowship.

Footnotes and References

* E-mail: ccliao@faculty.nthu.edu.tw

† *General procedure* for the Diels–Alder reaction: In a preheated oil bath was placed a flask containing phenol (2 mmol) and diene (20 mmol) in MeOH (8 ml) was immersed. DAIB (2.4 mmol) in MeOH (6 ml) was added over the period given in the Table 1. The reaction was stirred for 10 min, and then MeOH and excess diene were removed and the residue was dissolved in CH_2Cl_2 (20 ml). The solution was washed with saturated aq. $NaHCO_3$ and brine, and dried ($MgSO_4$). Removal of the solvent followed by column chromatography yielded compounds **18** and **19**. The ratio of **18** and **19** was determined by ^{1}H NMR analysis of the crude reaction mixture.

1 J. R. Hanson, *Nat. Prod. Rep.*, 1997, **14**, 245 and references cited therein.
2 S. V. Ley, A. A. Denholm and A. Wood, *Nat. Prod. Rep.*, 1993, **10**, 110.
3 W. P. Jackson and S. V. Ley, *J. Chem. Soc., Perkin Trans. 1*, 1981, 1516.
4 P.-Y. Hsiu and C.-C. Liao, *Chem. Commun.*, 1997, 1085 and references cited therein.
5 J. S. Swenton, in *The Chemistry of Quinonoid Compounds*, ed. S. Patai and Z. Rappoport, Wiley, New York, 1988, vol. **2**, p. 899.
6 G. Andersson, *Acta Chem. Scand.*, 1976, **B30**, 403 and references cited therein.
7 C.-C. Liao, in *Modern Methodology in Organic Synthesis*, ed. T. Shono, Kodansha, Tokyo, 1992, p. 409.
8 C.-S. Chu, T.-H. Lee and C.-C. Liao, *Synlett*, 1994, 635.
9 F. Fringuelli and A. Taticchi, *Dienes in the Diels-Alder Reaction*, Wiley, New York, 1990.
10 R. Carlini, K. Higgs, C. Older, S. Randhawa and R. Rodrigo, *J. Org. Chem.*, 1997, **62**, 2330.
11 M. F. Ansell, A. J. Bignold, A. F. Gosden, V. J. Leslie and R. A. Murray, *J. Chem. Soc. C*, 1971, 1414.

Received in Cambridge, UK, 18th August 1997; 7/06058K

An oligooxamacrocycle containing a π-donor tetrathiafulvalene and a π-acceptor quinone. Molecular and supramolecular structure

Robert M. Moriarty,*[a] Anping Tao,[a] Richard Gilardi,[b] Zhengzhe Song[a] and Sudersan M. Tuladhar[a]

[a] *Department of Chemistry, University of Illinois at Chicago, Chicago, Illinois 60608, USA*
[b] *Naval Research Laboratory, 4555 Overlook Ave, Washington, DC 20375, USA*

Tetrathiafulvalenedicarbonyl chloride reacts with 2,5-bis[(2-hydroxyethoxy)ethyl]-1,4-benzoquinone to afford a novel charge-transfer oligooxamacrocycle whose molecular and supramolecular structure are reported.

The π-donor charge transfer role of tetrathiafulvalene (TTF) (**2a**) as a molecular redox component is a key feature of organo-electrochemical devices such as conducting and super-conducting materials, sensors, molecular shuttles, NLO materials, organic ferromagnets and C_{60}-complexes.[1] An important structural feature in these materials is the spatial arrangement of the TTF with respect to the π-acceptor unit, either a non-covalent self-assembled array, or a covalently bonded system in which the position of the interacting (charge transfer groups) is fixed by synthetic design. Structures of increasingly evolved synthetic design have been reported, notably, the synthesis of tetrathiafulvalenoparacyclophanes and tetrathiafulvalenophanes by Staab *et al*.,[2] the joining of TTF-thiols by Hg^{2+} or Ni^{2+},[3] the incorporation of TTF into crown ethers,[4] cages[5] and [3]-pseudocatenanes,[6] the coupling of TTF to a ferrocenyl unit,[7] and the incorporation of TTF into a dimacrocycle with a catenated cyclobis(paraquat-*p*-phenylene).[8] Incorporation of TCNQ into a [2.2]paracyclophane has been accomplished; however, the π-donor was not TTF but the essentially irrelevant phenyl[9] and 1,4-dimethoxyphenyl groups.[10]

These molecules and others[11] represent only partial solution to the synthetic problem of fixing both the π-donor TTF and π-acceptor within the same molecule. We now report the synthesis of such a molecule as embodied in the oligooxamacrocycle **6** (Scheme 1).

Macrocycle **5** is a yellow crystalline material which could not be oxidized to **6** using ceric ammonium nitrate (CAN) or AgO. Charge transfer complex **6** is a black crystalline material.† The UV-VIS spectrum of **6** in chloroform shows absorptions at 252, 285, 302, 314 and 424 nm. There is no difference in the UV-VIS spectrum of **6** when measured as a film made by spin-coating from chloroform solution. In the VIS-NIR range no absorption appears between 600–2500 nm. The position of the ^{1}H NMR chemical shift for the TTF portion in **6** is at 7.44 ppm compared with 7.35 ppm for **2b**. Likewise, the quinone hydrogen is at 6.65 ppm in **4** and 6.79 ppm in **6**. The conductivity of a film of **6** (0.1 mm thick, 4 probe method) is $\sigma = 2.1\times 10^{-5}$ S cm^{-1}, which reveals the material to be a semiconductor.

The X-ray structure‡ of **6** may be discussed in terms of the unit molecule **6** (Fig. 1), an arbitrary dimer and its stacking (Fig. 2), and the supramolecular crystalline architecture (Fig. 3). Fig. 1 shows the unit molecular structure. In agreement to expectation, the quinone and TTF do not lie directly above and below each other, although they do lie in parallel planes. The distance between the centres of the non-overlapping quinone and TTF is 6.869 Å. The quinone occupies a plane about 3.6 Å above the extended parallel plane of the TTF. Fig. 2 shows a stack of three pairs of 'dimers.' Each pair is composed of two almost parallel planes of quinone and TTF. Going from the left to the right of Fig. 2, the first two molecules of **6** nestle together to afford partial overlap of TTF and quinone. These two are related by a crystal inversion center [1.0 − *x*, 1.0 − *y*, *z*] in the cell. However, the relationship between the second and the third molecule is such that there are certain close atom contacts, but the quinone and TTF of adjacent molecules do not overlap. They are related by a different inversion centre [1.0 − *x*, 1.0 − *y*, 1.0 − *z*]. Repeats of these operations produce an oblique stack of pairs (dimers that possess quinone–TTF overlaps) culminating in the depicted array of six stacks (including solvent $CHCl_3$) as shown in Fig. 3.

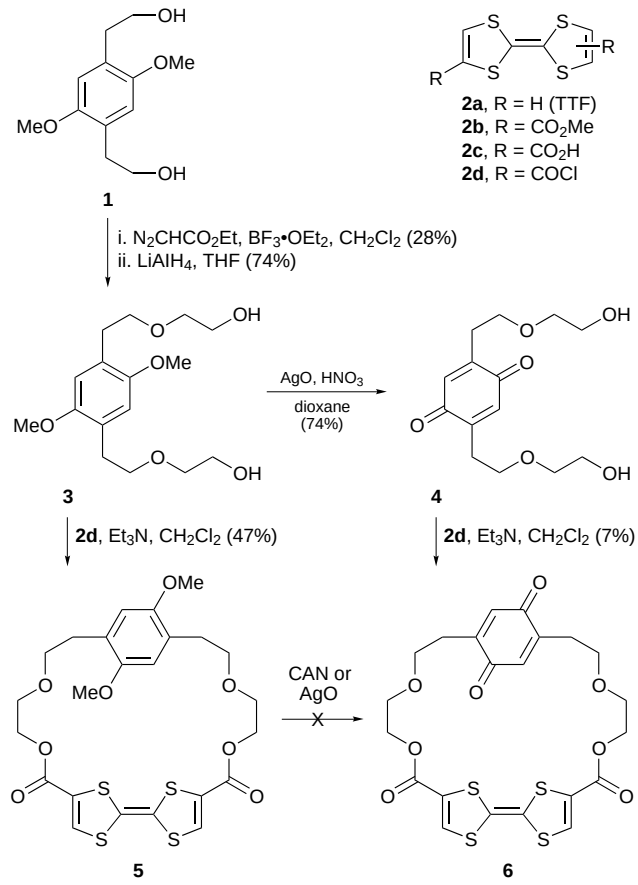

Scheme 1

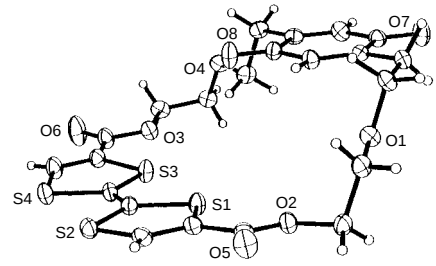

Fig. 1 X-Ray structure of the unit molecule **6**

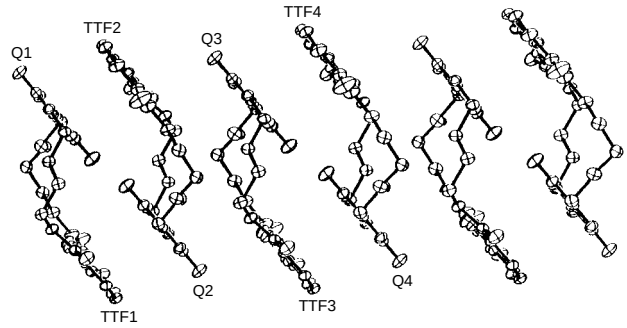

Fig. 2 Stack of three dimers. Hydrogens and solvent ($CHCl_3$) are removed for clarity

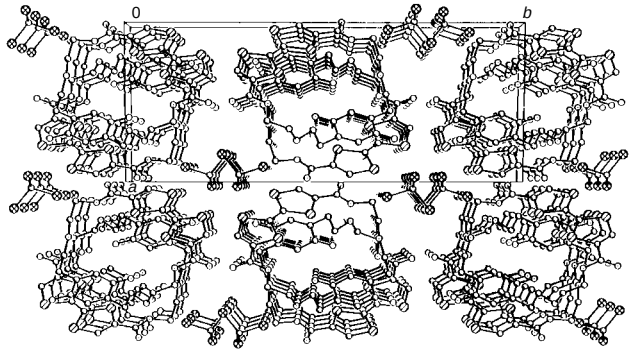

Fig. 3 Six stacks viewed down the *c* axis of the unit cell. Solvent chloroform is included in channels.

The basic molecule **6** and higher oligooxa homologue tethers of increasing $–OCH_2CH_2O–$ units available by modification of the synthetic route offer the interesting possibility of complexation of alkali metal ions. Finally, the design of **6** owes much to the pioneering work of Staab and coworkers on oligooxaparacyclophane charge-transfer quinhydrones.[12]

Generous support of this work by the National Science Foundation under grant CHE-9520157 is gratefully acknowledged. We thank Nicholas Castellucci of Northrop Grumman Co. for important advice and suggestions. We also thank Dr Larry L. Miller and Yoshihito Kunugi for measuring the electrical conductivity and UV-VIS spectra.

Footnotes and References

* E-mail: Moriarty@uic.edu

† The starting material **1** was prepared from 2,5-dihydroxy-benzene-1,4-diacetic acid (J. H. Wood and R. E. Gibson, *J. Am. Chem. Soc*., 1949, **71**, 393). **2d** was prepared from carbon disulfide and methyl propiolate *via* three steps (L. R. Melby, H. D. Hartzler and W. A. Sheppard, *J. Org. Chem*., 1974, **39**, 2456). Compound **6** was isolated from the reaction mixture by filtration and purified by column chromatography.

‡ The crystalline compound **6** is monoclinic with space group $P2_1/c$. Parameters of the unit cell at 294 K: a = 10.8785, b = 26.237, c = 10.5339 Å, $\alpha = \gamma = 90$, β = 108.530°, V = 2850.7 Å^3, Z = 4. Refinement method: full-matrix least-squares on F^2. Final R indices [$I > 2\sigma(I)$]: R = 0.0491, wR = 0.1080; R indices for all data: R = 0.1023, wR = 0.1284. CCDC 182/671.

1 T. K. Hansen and J. Becher, *Adv. Mater*., 1993, **5**, 288.
2 H. A. Staab, J. Ippen, C. Tao-pen, C. Krieger and B. Starker, *Angew. Chem. Int. Ed. Engl*., 1980, **19**, 66; J. Ippen, C. Tao-pen, B. Starker, D. Schweitzer and H. A. Staab, *Angew. Chem., Int. Ed. Engl*., 1980, **19**, 67.
3 N. Le Narvor, N. Robertson, E. Wallace, J. D. Kilburn, A. E. Underhill, P. N. Bartlett and M. Webster, *J. Chem. Soc., Dalton Trans*., 1996, 823.
4 T. K. Hansen, T. Jørgensen, P. C. Stein and J. Becher, *J. Org. Chem*., 1992, **57**, 6403.
5 F. Bertho-Thoroval, A. Robert, A. Souizi, K. Boubekeur and P. Batail, *J. Chem. Soc., Chem. Commun*., 1991, 843.
6 Z.-T. Li, P. Stein, N. Svenstrup, K. H. Lund and J. Becher, *Angew. Chem., Int. Ed. Engl.*, 1995, **34**, 2524.
7 A. J. Moore, P. J. Skabara, M. R. Bryce, A. S. Batsanov, J. A. K. Howard and S. T. A. K Daley, *J. Chem. Soc., Chem. Commun*., 1993, 417.
8 D. Philp, A. M. Z. Slawin, N. Spencer, J. F. Stoddart and D. J. Williams, *J. Chem. Soc., Chem. Commun*., 1991, 1584.
9 M. Yoshida, H. Tatemistu, Y. Sakata and S. Misumi, *Tetrahedron Lett*., 1976, 3821.
10 H. A. Staab and H.-E. Henke, *Tetrahedron Lett*., 1978, 1955.
11 K. Matsuo, K. Takimiya, Y. Aso, T. Otsubo and F. Ogura, *Chem. Lett*. 1995, 523; K. Takimiya, Y. Shibata, K. Imamura, A. Kashibara, Y. Aso and T. Otsubo, *Tetrahedron Lett*., 1995, **36**, 5045.
12 H. A. Staab and W. Rebafka, *Chem. Ber*., 1977, **110**, 3333; H. A. Staab, C. P. Herz, C. Krieger and M. Rentzea, *Chem. Ber*., 1983, **116**, 3813; H. Bauer, V. Matz, M. Lang, C. Krieger and H. A. Staab, *Chem. Ber*., 1994, **127**, 1993.

Received in Corvallis, OR, USA, 13th August 1997; 7/05917E

ChemComm
FEATURE ARTICLE

Counterattack reagents in organic synthesis: versatility and efficiency

Jih Ru Hwu*[a,b] and Shwu-Chen Tsay[c]

[a] *Organosilicon and Synthesis Laboratory, Institute of Chemistry, Academia Sinica, Nankang, Taipei, Taiwan 11529, Republic of China*
[b] *Department of Chemistry, National Tsing Hua University, Hsinchu, Taiwan 30043, Republic of China*
[c] *Development Center for Biotechnology, Taipei, Taiwan 10671, Republic of China*

The concept of 'counterattack reagents' has been applied in the development of various chemical transformations. The use of counterattack reagents allows complicated reactions to be accomplished in a single flask without the isolation of intermediates. Thus multistep transformations can be simplified to 'one-step' operations. Representative examples of applications illustrated herein include oxidation, reduction, C–C single and double bond formation, cyclization, C–Si bond formation, *O*- and *N*-silylations and allylsilylation, as well as dealkylation. Comparisons are made between the results from traditional and 'counterattack' methods. Examples also include the utilization of 'pseudo-counterattack' and 'intramolecular counterattack' strategies in organic synthesis. The 'counterattack reagents' involved in those reactions are often, but not limited to, silicon-containing compounds.

Synthetic chemists are always seeking processes that lead from starting materials to target molecules with efficiency and a minimum number of operations. Here we describe the application of the concept of 'counterattack reagents' which provides a method to improve the efficiency of organic syntheses.

A synthetic sequence involving two steps often requires two individual reactions by traditional approaches. Method 1 in Scheme 1 shows an example in which a nucleophile Nu is treated with the reagent RX to give X and NuR in the first reaction. After isolation, the intermediate NuR is allowed to react with nucleophile L (from another source ML) to give the desired product in the second reaction. For certain synthetic sequences, one may combine these two reactions into one by using the 'counterattack strategy', as shown in Method 2.[1] The reagent RL is chosen with care; it is first attacked by Nu to give NuR and L. The leaving group L then counterattacks the intermediate NuR *in situ* to afford the final product. The reagent RL is thus referred to as a 'counterattack reagent'.[1]

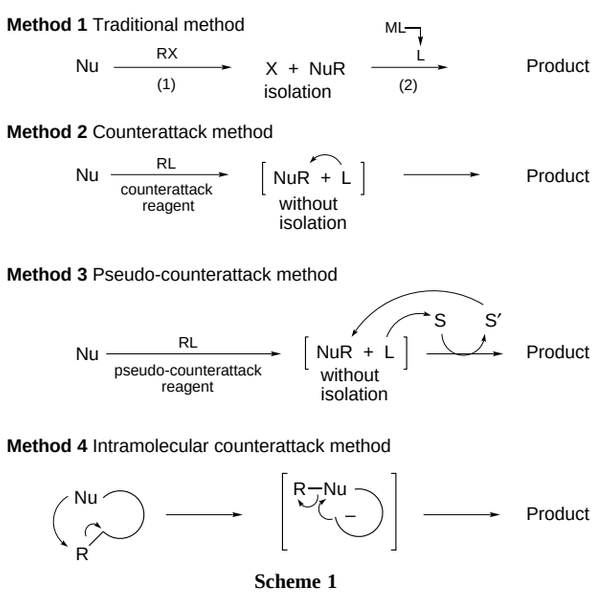

Scheme 1

Method 3 in Scheme 1 shows another efficient way that sequential reactions can be combined into a 'one-flask' process.[2] The first step, analogous to that in Method 2, involves the reaction between Nu and RL to give NuR and the leaving group L. This leaving group then reacts with compound S to generate an active species S′, which subsequently attacks the intermediate NuR *in situ*. Because L does not counterattack NuR directly as in Method 2, we refer to the compound RL as a 'pseudo-counterattack reagent'.[2] Furthermore, Method 4 in Scheme 1 represents an 'intramolecular counterattack process'.[3] It involves attacking and subsequent counterattacking processes occurring in one molecule.

In the past fifteen years, our research group has applied the concept of 'counterattack reagents' to organic reactions of various types. Here, twelve novel and efficient chemical transformations will be illustrated which involve the use of various organic compounds in a counterattack, pseudo-counterattack or intramolecular counterattack process.[2–15]

Counterattack *versus* traditional methods

Given the potential advantages associated with counterattack reagents, we will first make a direct comparison of their results with those from traditional methods.

Direct synthesis of ketene dithioacetals and 2-trimethylsilyl-1,3-dithiane derivatives from 1,3-dithiane[4]

Ketene dithioacetals **6** are useful synthetic intermediates.[16] Traditionally, the preparation of ketene dithioacetals involves two steps. The first step involves generation and isolation of 2-trimethylsilyl-1,3-dithiane **3** (71% yield) from 1,3-dithiane **1**.[17] The second step involves reaction of its corresponding lithium salt **5** with various carbonyl compounds to give the desired ketene dithioacetals **6** in 62–80% yield.[18–20] The overall yields are in the range 40–57%. In comparison, use of the 'counterattack strategy', as shown in Scheme 2, allows a 'one-flask' synthesis of **6** in 65–92% yield from 1,3-dithiane **1**.

Scheme 2 depicts the mechanism, which includes an intriguing role for $Me_3SiSiMe_3$. Bu^nLi is used to remove a C-2 proton from 1,3-dithiane **1** to give anion **2**, which attacks $Me_3SiSiMe_3$ to produce 2-trimethylsilyl-1,3-dithiane **3** and Me_3Si^- **4**. This anionic silyl leaving group then counterattacks compound **3** to generate the Me_3Si-stabilized anion **5**. Thus $Me_3SiSiMe_3$ can be regarded as a 'counterattack reagent'.

Using this 'one-flask' synthetic strategy, α,β-unsaturated ketones can act as Michael acceptors for **5** to give ketones **7** in 94% yield. Furthermore, alkyl, allyl and benzyl bromides undergo substitution to produce Me_3Si-containing 1,3-dithianes **8** in 54–98% yields.

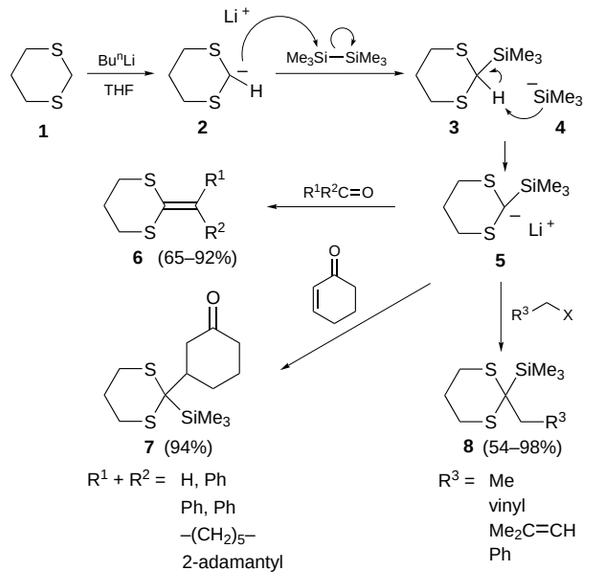

Scheme 2

Preparation of N-*methyl*-N,O-*bis(trimethylsilyl)-hydroxylamine from hydroxylamine*[5]

N-Methyl-*N*,*O*-bis(trimethylsilyl)hydroxylamine **14**, which is widely used in organic synthesis,[21] is the trimethylsilylated equivalent of *N*-methylhydroxylamine **10**. Silylated hydroxylamine **14** can be prepared from anhydrous *N*-methylhydroxylamine **10**.[22] Nevertheless, the route used to obtain **10** is tedious. Alternatively, hydroxylamine **14** can also be synthesized *via* use of hexamethyldisilazane; however, the yield is only 18%.[23,24] A way to solve these problems is to apply the concept of 'counterattack reagents'.

Thus, MeNHOH·HCl **9** is treated with KH and then $Me_3SiSiMe_3$ in a mixture of Et_2O and HMPA to give the desired hydroxylamine **14** in 41% yield. The mechanism is depicted in Scheme 3. After removal of the acid (*i.e.* HCl) in salt **9** and the OH proton in **10** using KH, the resultant oxide **11** attacks $Me_3SiSiMe_3$ to generate monosilylated hydroxylamine **12** and $^-SiMe_3$ **4**. This silyl anion **4**, acting as a base, counterattacks compound **12** to give amide **13**. Reaction of **13** with a second equivalent of $Me_3SiSiMe_3$ affords the desired product **14** and $^-SiMe_3$ **4**, which could substitute for KH to convert **10** to **11** by proton abstraction. Therefore **14** can be obtained from a mixture of **10** and $Me_3SiSiMe_3$ by use of a catalytic amount of KH.

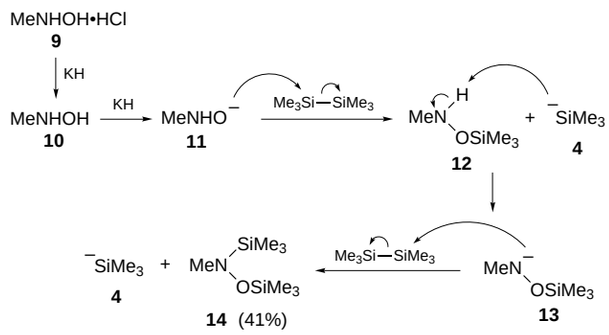

Scheme 3

Direct preparation of polysilylated hydrazines from hydrazines:[6] *a consecutive triple-counterattack process*

Polysilylated hydrazines are ideal starting materials for the generation of various organic species.[25,26] Nevertheless, it is tedious to prepare these compounds by classic means.[27] A typical way to prepare $(Me_3Si)_2NN(SiMe_3)_2$ **16** from H_2NNH_2 **15** includes three separate silylations, utilizes two different bases (pyridine and Bu^{n}Li), requires strong silylating agents (Me_3SiCl and Me_3SiBr) and gives only a *ca.* 8% overall yield (see Scheme 4). Use of hexamethyldisilane as a 'counterattack reagent', however, allows the hydrazines to be polysilylated in one reaction without isolation of any of the intermediates, and provides the target **16** in an excellent yield (91%).

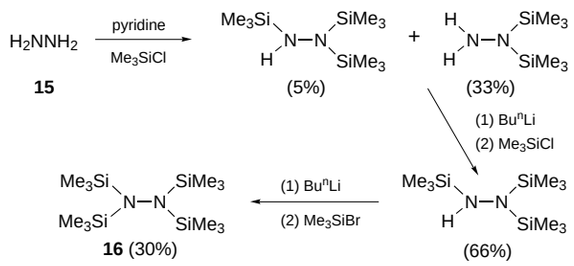

Scheme 4

Scheme 5 illustrates this 'one-flask' preparation of tetrakis(trimethylsilyl)hydrazine **16** from hydrazine **15** and Me_3Si-$SiMe_3$ under alkaline conditions. The disilane, $Me_3SiSiMe_3$, plays a dual role in this reaction: silylating agent and source of base. In the overall process, proton abstraction alternates with silylation. This alternation is repeated four times and thus allows H_2NNH_2 **15** to be converted to $(Me_3Si)_2NN(SiMe_3)_2$ **16** in an efficient way.

With regard to both the manipulation and the yield (91 *versus* 8%), the counterattack method shown in Scheme 5 is much more efficient than the classic procedure shown in Scheme 4. It also represents an example of a 'consecutive triple-counterattack process.'

New counterattack methods

The concept of 'counterattack reagents' has also been applied to new methods for the generation of molecules with synthetically valuable functionalities or biological significance. Scheme 6 shows an example in which various starting materials are converted to an important class of products. Scheme 8 shows examples of how a simple starting materials can be transformed into products of various kinds.

Direct conversion of aldehydes, ketones and allyl alcohols to allyltrimethylsilanes[7]

The allyltrimethylsilane moiety possesses umpolung character and is regarded as a synthon for allyl cations and anions.[28,29] Use of the counterattack method facilitates the preparation of allyltrimethylsilanes from allyl alcohols, enals, enones, aldehydes or ketones, as shown in Scheme 6. Treatment of allyl alcohols (*i.e.* **17** and **18**) with MeLi and $Me_3SiSiMe_3$ in a mixture of HMPA and Et_2O gives the desired allylsilanes **21** (Method 1). The substrates include primary allyl alcohols **17** [*e.g.* geraniol, (−)-myrtenol], secondary allyl alcohols **18** (*e.g.* linalool), benzyl alcohol and homobenzylic alcohol (*e.g.* phenylethyl alcohol). Method 2 in Scheme 6 shows a new method for the preparation of allylsilanes **21** from enals and enones (*i.e.* **19**) by use of alkyllithium and $Me_3SiSiMe_3$. Acrolein and methyl vinyl ketone are converted to allylsilanes by use of Bu^{n}Li and $Me_3SiSiMe_3$. Moreover, reactions of saturated aldehydes and ketones (*i.e.* **20**) with vinyllithium and $Me_3SiSiMe_3$ generate allylsilanes **21** as indicated in Method 3. The starting materials include hexanal, heptan-2-one, and cyclohexanone.

For the preparation of allyltrimethylsilanes by Methods 1–3, the first step is to generate an allyl alkoxide: removal of a proton from an allyl alcohol with MeLi in Method 1; 1,2-addition of RLi to an α,β-unsaturated aldehyde or ketone in Method 2; or addition of vinyllithium to a saturated carbonyl compound in

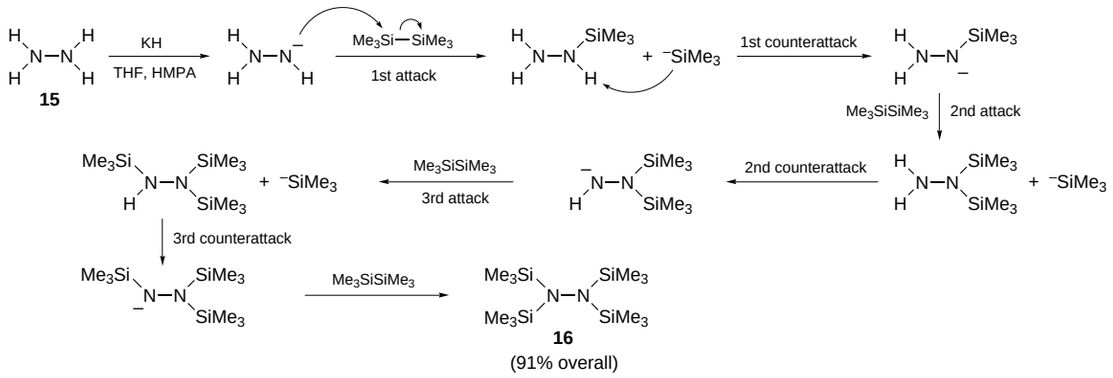

Scheme 5

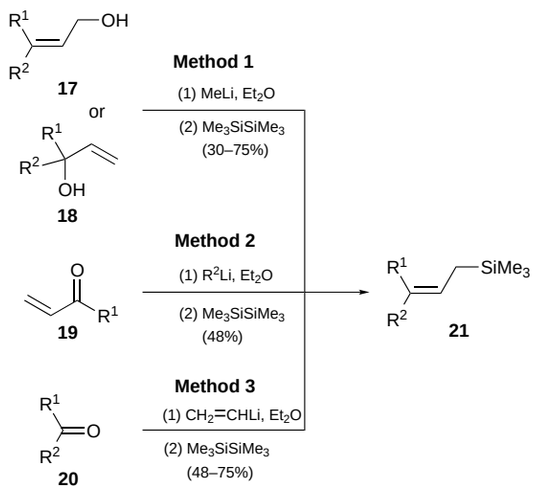

Scheme 6

Method 3. The allyl alkoxides then react with $Me_3SiSiMe_3$ by a novel pathway to give allyltrimethylsilanes *in situ*, as represented in Scheme 7. Hexamethyldisilane is attacked by allyl alkoxides **23**, generated by addition of vinyllithium to ketone **22**, to give allyl trimethylsilyl ether **24** and Me_3Si^- **4**. An *in situ* substitution reaction subsequently occurs between **24** and **4** to produce allyltrimethylsilanes **25** in 75% yield. Hexamethyldisilane acts as an 'electrophilic counterattack reagent' in these one-flask reactions.

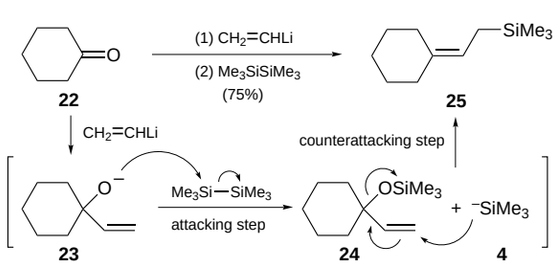

Scheme 7

Formation of thiohydroxamic acids, thiohydroximates, nitriles and oximes from nitro compounds[8,9]

Thiohydroxamic acids [RC(=S)NHOH] and thiohydroximates [RC(SR′)=NOH] contain a moiety with three adjacent nucleophilic atoms (*i.e.* N, O and S). Thiohydroxamic acids play various roles in analytical and biological chemistry. Phenylacetothiohydroximate exists in *Tropaeolum majus*;[33,34] it is also an intermediate in the biosynthesis of benzyl glucosinolate, a mustard oil glucoside.[33] Thiohydroximates are also used as starting materials for the synthesis of the carbamate derivatives $R^1C(SR^2)=NOC(=O)NR^3R^4$.[35] Some carbamates are utilized as pesticides.

The counterattack strategy has been applied in the syntheses of thiohydroxamic acids from readily available nitro compounds (Scheme 8). Thus reaction of various primary nitro compounds **26** with KH and hexamethyldisilathiane in THF gives thiohydroxamic acids **27** in 56–92% yield. The substrates, including esters, acetals, arenes and thiols, are all stable to the reaction conditions. By the same strategy, a thiohydroxamic acid is obtained in 50% yield after treatment of *trans*-β-nitrostyrene with Pr^iSLi and $Me_3SiSSiMe_3$ in THF.

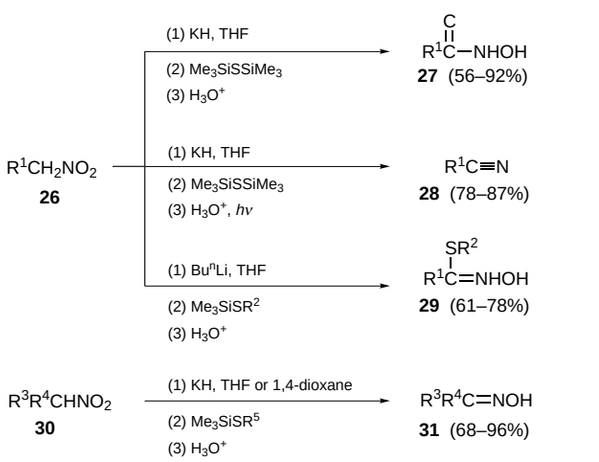

R^1 = Me, C_5H_{11}, $MeO_2C(CH_2)_2$, $THPOCH_2$, Bn, PhMeCH, $Ph(Pr^iS)CH$
R^2 = Me, Ph
$R^3 + R^4$ = Me + Me, Me + C_5H_{11}, Me + Ph, Me + $Ph(CH_2)_2$, $-(CH_2)_5-$, $-(CH_2)_4CHMe-$, 1,7,7-trimethylbicyclo[2.2.1]heptan-2-yl
R^5 = $SiMe_3$, Me

THP =

Scheme 8

Moreover, primary nitro compounds **26** can be converted to nitriles **28** under UV irradiation. The first step is to generate potassium thiohydroxamates in the dark as previously described. These salts are then neutralized with an acid and desulfurized by light to afford nitriles **28** in 78–87% yield (Scheme 8).[9] On the other hand, treatment of primary nitro compounds **26** with Bu^nLi and thiosilanes (*i.e.* $MeSSiMe_3$ or $PhSSiMe_3$) in THF generates the corresponding thiohydroximates **29** in 61–78% yield. Secondary nitro compounds **30** are converted to oximes **31** in 68–96% yields by reaction with KH and $Me_3SiSSiMe_3$ or $MeSSiMe_3$ in THF or 1,4-dioxane.

The role of $Me_3SiSSiMe_3$ is depicted in Scheme 9 for the 'one-flask' conversion of primary nitro compounds **32** into thiohydroxamic acids **35**. The entire transformation involves multiple steps and the formation of several intermediates, of which isolation is unnecessary. Scheme 10 illustrates a mechanism for the conversion of secondary nitro compounds **36** into oximes **39** *via* reaction with $Me_3SiSSiMe_3$. In this transformation, a 1,1-elimination occurs in the intermediate $R^1R^2C(N{=}O)S^-$ **38** to give sulfur and an oxime.

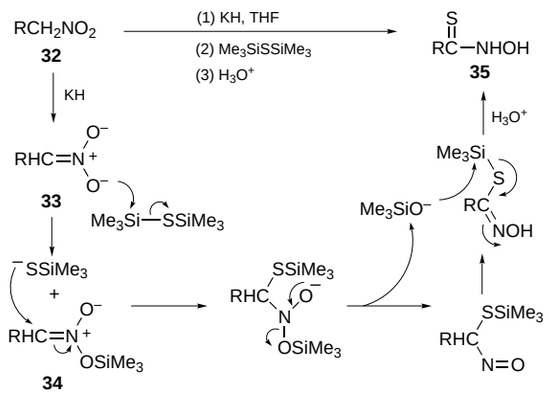

Scheme 9

A common feature of the reactions shown in Scheme 8 is the generation of a nitronate intermediate (*cf.* **33** in Scheme 9 and **37** in Scheme 10). Reagents $Me_3SiSSiMe_3$, $MeSSiMe_3$ and $PhSSiMe_3$ are first attacked by nitronates (*i.e.* **33** and **37**) at a silicon centre. The leaving group, Me_3SiS^-, MeS^- or PhS^-, then counterattacks the silylated nitronate intermediates (*e.g.* **34**). Thus $Me_3SiSSiMe_3$, $MeSSiMe_3$ and $PhSSiMe_3$ can be regarded as 'counterattack reagents'.

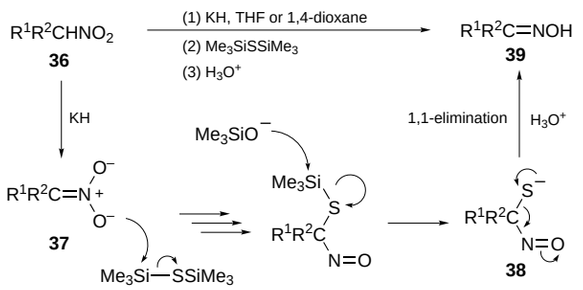

Scheme 10

Protection and deprotection of hydroxy groups

The protection and deprotection of hydroxy groups are common synthetic processes. Traditional methods for the disilylative protection of diols and bis-*O*-demethylation of protected aromatic diols are performed stepwise. The disadvantages include low yields and tedious transformations. The concept of counterattack reagents can be applied to perform the protection and deprotection in an efficient manner.

Disilylation of diols by use of MeC(OSiMe₃)=NSiMe₃:[10] *a tandem double-counterattack process*

Trimethylsilylation is useful in the protection of functional groups bearing labile protons. Silylation of alcohols, especially diols, polyols and carbohydrates, can increase their volatility and thermal stability. Consequently, the silylated species are more suitable than the parent alcohols for analysis by GC and mass spectrometry.[36]

Reaction of various diols with bis(trimethylsilyl)acetamide **40** in THF under alkaline conditions gives the corresponding bis(trimethylsilyl) ethers in good to excellent yields (60–95%). The diols may contain other functionalities, such as amides, amines, ethers and thioethers.[10]

Stepwise silylations of resorcinol with hexamethyldisilathiane give the corresponding disiloxylbenzene in 55% overall yield;[37] however, the counterattack method leads to an 80% yield. Use of chlorotrimethylsilane and pyridine to silylate the diols in a carbohydrate gives the corresponding bis(trimethylsilyl) ether in 41% yield;[38] the counterattack method results in a 65% yield. These results clearly indicate the efficiency of the counterattack method.

In the disilylation, $MeC(OSiMe_3){=}NSiMe_3$ **40** acts as a counterattack reagent and exhibits multiple functions (see Scheme 11). In addition to transferring both Me_3Si groups onto the diol, reagent **40** provides amide anions **41** and **42**. These anions deprotonate the intermediates and the starting diols. Therefore, only a catalytic amount of base (*i.e.* KH) is needed for initiation of the disilylation. This 'one-flask' disilylation involves sequential deprotonation–silylation–deprotonation–silylation. This double trimethylsilylation also represents an example of a 'tandem double-counterattack process', in which bis(trimethylsilyl)acetamide offers three reacting centres (*i.e.* two electrophilic silicon atoms and one nucleophilic nitrogen atom).

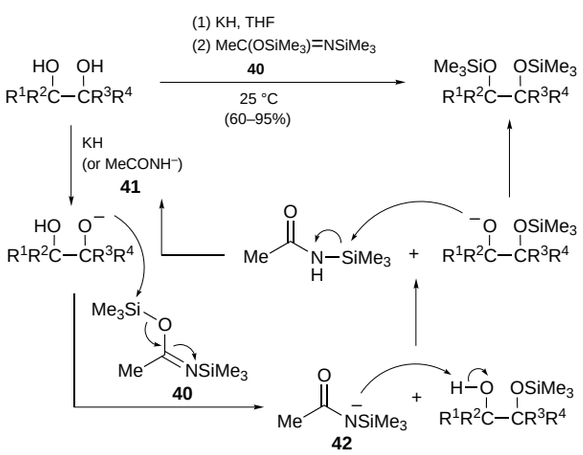

Scheme 11

Deprotection of aryl methyl ethers by sodium trimethylsilanethiolate and hexamethyldisilathiane[11]

Commonly used reagents for demethylation of aryl methyl ethers give mono-*O*-demethylated products; a few of them can bis-*O*-demethylate substrates.[39] Sequential demethylation of dimethoxybenzenes in one flask is difficult using nucleophilic reagents, as shown in Scheme 12. The first demethylation involves attack of a nucleophilic reagent on a methyl group of dimethoxybenzenes **43** to give methoxyphenolates **44**. It is unlikely that nucleofuge **44** could be demethylated by another nucleophile in an efficient manner (*i.e.* **44** → **45**) because the resultant species **45** would bear two negative charges.

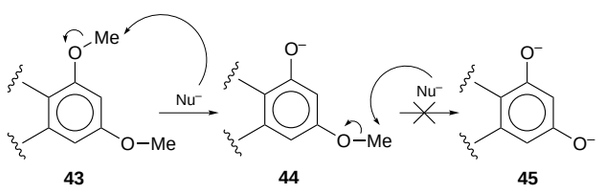

Scheme 12

This problem can be circumvented by utilization of the 'counterattack reagent' concept. Use of Me_3SiSNa and Me_3-

$SiSSiMe_3$ as counterattack reagents causes aryl methyl ethers to bis-*O*-demethylate efficiently under alkaline conditions. Treatment of an aryl methyl ether containing two methoxy units with *ca*. 2.5 equiv. of Me_3SiSNa in 1,3-dimethyl-2-imidazolidinone at 185 °C in a sealed tube gives the corresponding aryl diols in 78–96% yield after aqueous workup. The starting materials also include an aryl alcohol containing a biphenyl or naphthalene unit.

Moreover, $Me_3SiSSiMe_3$ is used to bis-*O*-demethylate aromatic compounds containing one free hydroxy group and two methoxy units, which react with 1.5 equiv. of NaH and then with 1.5 equiv. of $Me_3SiSSiMe_3$ at 185 °C in a sealed tube to afford the corresponding triols in 78–83% yield. Sodium trimethylsilanethiolate and hexamethyldisilathiane can be used to remove two methyl groups *in situ* from an aryl methyl ether. In these bis-*O*-demethylations, Me_3SiSNa and $Me_3SiSSiMe_3$ act as 'counterattack reagents'.

Scheme 13 shows the mechanism for the bis-*O*-demethylation of 1,3-dimethoxybenzene **46**, in which Me_3SiSNa acts as a 'nucleophilic counterattack reagent'. This reagent contains both a nucleophilic centre (*i.e.* S) and an electrophilic centre (*i.e.* Si), which react with the intermediates at different points in the reaction. Furthermore, Scheme 14 depicts an example involving $Me_3SiSSiMe_3$ as an 'electrophilic counterattack reagent', which is used for the bis-*O*-demethylation of dimethoxyphenol **47**. The reactions shown in Schemes 13 and 14 share common features—the design is complicated and the manipulation is simple.

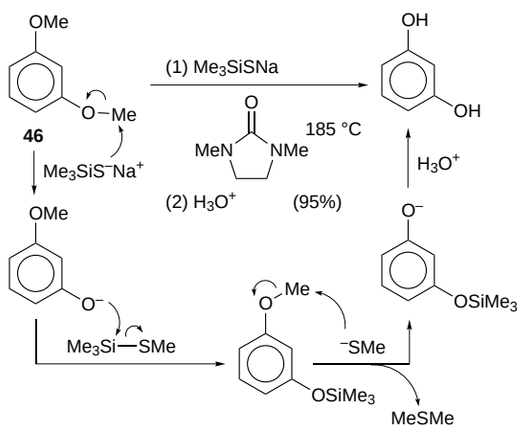

Scheme 13

Similarly, this demethylation procedure is also applicable to pyridines with two methoxy groups, using Me_3SiSNa.[40] Furthermore, chlorotrimethylsilane, in combination with sodium sulfide, can be used as the equivalent of sodium trimethylsilanethiolate in the demethylation of dimethoxybenzenes.[41]

Oxidation reactions involving counterattack strategy

Counterattack strategy can also be applied to oxidation reactions. Examples include the oxidative desulfonylation of sulfones to aldehydes or ketones, oxidation of hydrazines to 2-tetrazenes, and conversion of benzyl alcohols to phenones or benzaldehydes. In these transformations, silicon reagents are utilized both as an oxidant and as a 'counterattack reagent'.

Oxidative desulfonylation of sulfones to aldehydes or ketones by use of $Me_3SiOOSiMe_3$[12]

The sulfone group is commonly used in organic synthesis. This group generally has to be removed after the desired transformations have been accomplished. An efficient method for the oxidative desulfonylation of sulfones to aldehydes or ketones is reported, which uses $Me_3SiOOSiMe_3$ under alkaline conditions. As shown in Scheme 15, removal of a proton in sulfone **48** with Bu^nLi in THF at −78 °C generates the corresponding carbanion **49**. $Me_3SiOOSiMe_3$ is then attacked by the sulfonyl carbanion **49** to generate siloxy sulfone **50** and Me_3SiO^- **51**. Without isolation, the siloxy sulfone **50** is counterattacked by Me_3SiO^- to give the desired carbonyl product **52**.

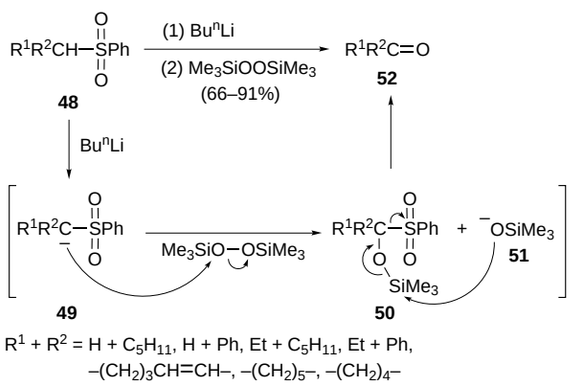

Scheme 15

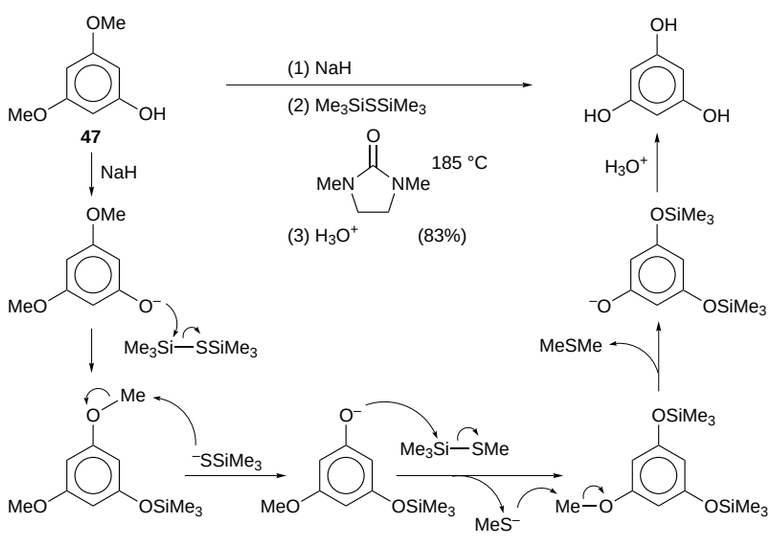

Scheme 14

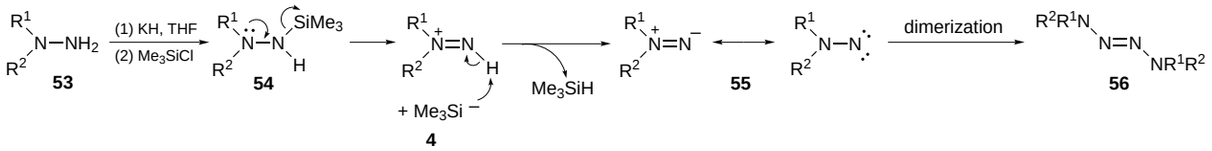

$R^1 + R^2$ = Ph + Me, $–(CH_2)_5–$, $–CHMe(CH_2)_3CHMe–$, $–CH_2CH_2OCH_2CH_2–$, $–(CH_2)_6–$

Scheme 16

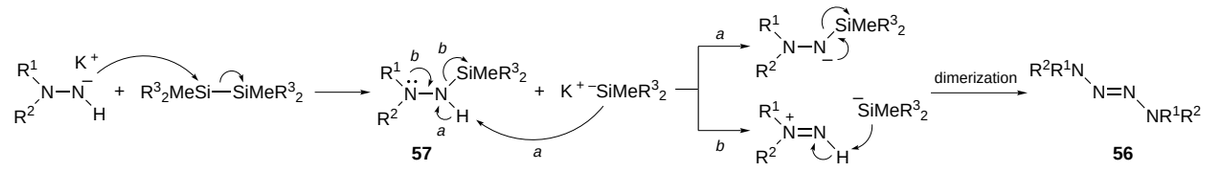

$R^1 + R^2$ = Ph + Me, $–(CH_2)_5–$, $–CHMe(CH_2)_3CHMe–$, $–CH_2CH_2OCH_2CH_2–$, $–(CH_2)_6–$

R^3 = Me, Ph

Scheme 17

This 'one-flask' method can be used to convert alkyl, allylic, benzylic and cycloalkyl sulfones to aldehydes or ketones in 66–91% yield. In the attacking step (**49** → **50**) as shown in Scheme 15, the trimethylsiloxy moiety in $Me_3SiOOSiMe_3$ behaves like a leaving group. In the counterattacking step (**50** → **52**), Me_3SiO^- **51** acts as a nucleophile. Therefore $Me_3SiOOSiMe_3$ is an 'electrophilic counterattack reagent' in this oxidative desulfonylation.

Conversion of hydrazines to 2-tetrazenes by use of Me_3SiCl, $Me_3SiSiMe_3$ and $Ph_2MeSiSiMePh_2$ as oxidizing agents[13]

Silicon compounds Me_3SiCl, $Me_3SiSiMe_3$ and $Ph_2MeSiSiMePh_2$ are commonly used as silylating or reducing agents. By use of a 'counterattack procedure', these silicon reagents can be utilized as oxidants. Reaction of 1,1-disubstituted hydrazines **53** with Me_3SiCl, $Me_3SiSiMe_3$ or $Ph_2MeSiSiMePh_2$ in the presence of KH gives the corresponding 2-tetrazenes **56** in fair to good yields (Schemes 16 and 17). In these reactions, Me_3SiCl, $Me_3SiSiMe_3$ and $Ph_2MeSiSiMePh_2$ behave as oxidizing agents.

These new methods for the formation of 2-tetrazenes **56** involve several transformations: silylation of hydrazines **53** to give monosilylhydrazines **54**, decomposition of monosilylhydrazines **54** to generate amino nitrenes **55**, and dimerization of amino nitrenes **55** to afford 2-tetrazenes **56**. The characteristic feature of these reactions is that the R_3Si^- species can depart from the $NSiR_3$ moiety in **54** and **57**. Schemes 16 and 17 depict the 'counterattack processes' for the oxidation of hydrazines to 2-tetrazenes by Me_3SiCl and disilanes, respectively.

Oxidation of benzyl alcohols to phenones[14] *or benzaldehydes*[15] *by use of $Me_3SiSiMe_3$: a tandem double-counterattack process*

Hexamethyldisilane can also act as an oxidant in the conversion of benzyl alcohols to carbonyl compounds. Under basic conditions, reaction of α-cyclopropylbenzyl alcohol **58** or 3-methoxybenzyl alcohol **63** with $Me_3SiSiMe_3$ generates γ-trimethylsilylbutyrophenone **62** or 3-methoxybenzaldehyde **65**, respectively.

The mechanism for the one-flask oxidation and cyclopropyl ring opening procedure is depicted in Scheme 18.[14] Disilane $Me_3SiSiMe_3$ is attacked by alkoxide **59** to produce silyl ether **60** and Me_3Si^- **4**. Subsequently, Me_3Si^- counterattacks the benzylic proton in **60** to give cyclopropyl phenyl ketone **61** and regenerates Me_3Si^-. Me_3Si^- then re-counterattacks intermediate **61** to give γ-silylphenone **62** as the major product. The entire mechanism includes two counterattack processes. The first is to convert **59** to **61** using $Me_3SiSiMe_3$; the trimethylsilyl moiety serves as a leaving group in $Me_3SiSiMe_3$ and as a counterattack species for intermediate **60**. The second is to transform **60** to **62** using Me_3Si^- **4**; the trimethylsilyl moiety behaves as a leaving group in **60** and as a counterattack species for intermediate **61**. This sequence provides an example of a 'tandem double-counterattack process'.

Similarly, the oxidation of 3-methoxybenzyl alcohol **63** to 3-methoxybenzaldehyde **65** by use of $Me_3SiSiMe_3$ under basic conditions occurs *via* the mechanism shown in Scheme 19.[15] In these transformations, the Me_3Si^- species is utilized as a catalyst, which can also oxidize trimethylsilyl ethers (*i.e.* **60** in Scheme 18 and **64** in Scheme 19) possessing acidic protons at the position α to the corresponding carbonyl compounds (*i.e.* **62**

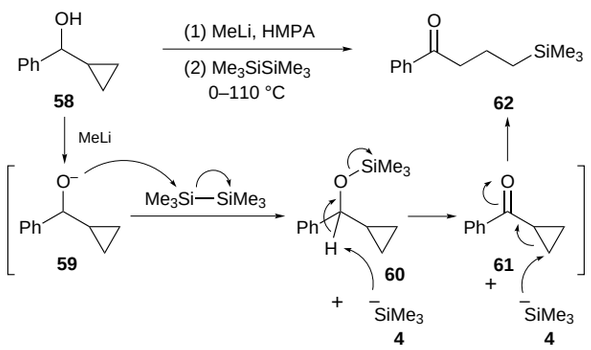

Scheme 18

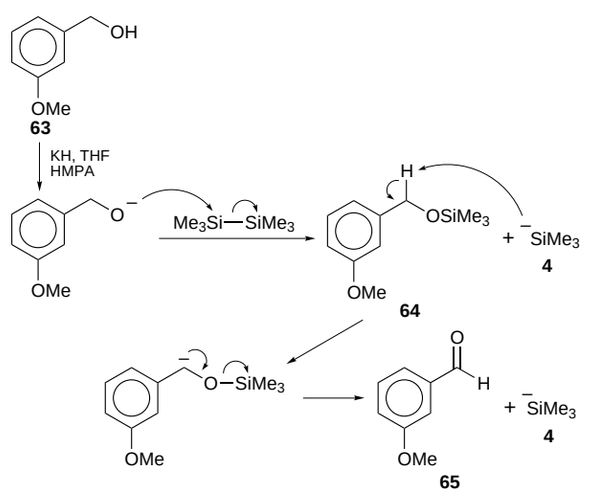

Scheme 19

and **65**). Thus the interconversions can constitute a novel cycle among α-silylalkoxides **66**, α-siloxy carbanions **67** and carbonyl compounds **68** accompanied by R_3Si^-, as shown in Scheme 20.[15] This newly established cycle involves Brook rearrangement, the silyl-Wittig rearrangement, a β-elimination and a 1,2-addition.

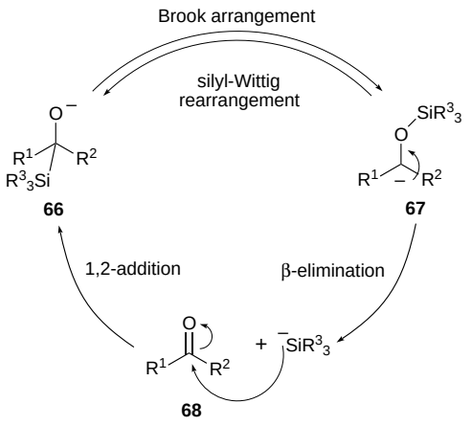

Scheme 20

Preparation of prop-2-ynylic alcohols by use of organic amides as pseudo-counterattack reagents[2]

Prop-2-ynylic alcohols can be used in the synthesis of pheromone components[42] and the ω-chain in prostaglandins.[43] For the preparation of prop-2-ynylic alcohols, a one-flask method has been established by use of a 'pseudo-counterattack process'. Reaction of an organolithium reagent, an organic amide and phenylacetylene generates prop-2-ynylic alcohols in 71–93% yield. The amides, including *N*,*N*-dimethyl-, *N*,*N*-diethyl- and *N*,*N*-diisopropyl-formamide, 1-formylpyrrolidine, 1-formylpiperidine, *N*,*N*-dimethylacetamide and *N*,*N*-diethyldodecanamide, behave as pseudo-counterattack reagents in this transformation.

The mechanism is illustrated in Scheme 21 for the reaction involving Bu^nLi, *N*,*N*-diisopropylformamide **69** and phenylacetylene **71**. In the first step, *N*,*N*-diisopropylformamide **69** is attacked by Bu^nLi to give the stable intermediate valeraldehyde **70**. The $Pr^i_2N^-$ anion formed from the amide reacts with phenylacetylene **71** to generate lithium phenylacetylide **72**. This nucleophilic species attacks the intermediate valeraldehyde **70** *in situ* to afford the desired prop-2-ynylic alcohol **73** in 87% yield. Thus, *N*,*N*-diisopropylformamide serves both as a substrate for the organolithium reagent and as the solvent. In the entire transformation, the organic amide can be considered as a 'pseudo-counterattack reagent'.

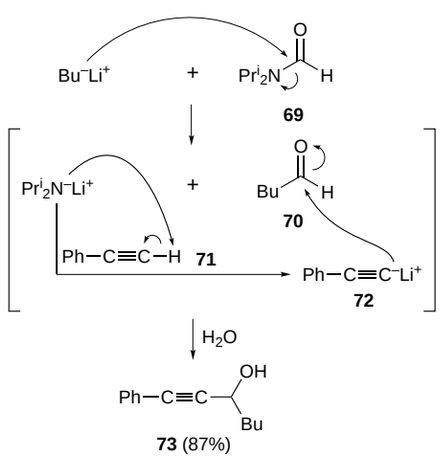

Scheme 21

Intramolecular counterattack strategy in the synthesis of biologically active isopenams[3]

The concept of counterattack reagents can be extended to the performance of chemical transformations in one molecule. Use of this method allows the synthesis of isopenams having important biological activities in high yields.

The synthesis of isopenams, involving an 'intramolecular counterattack process', is illustrated in Scheme 22. Formation of the thiazolidine ring in isopenams **80** and **81** from the corresponding thioesters **74** and **75**, respectively, is accomplished under basic conditions. Accordingly, the sulfides **76** and **77** are generated by deacetylation of thioesters **74** and **75**, respectively, with piperidine. The α-chloro ester moiety in **76** and **77** is first attacked intramolecularly by the sulfide moiety. The resultant carbanions **78** and **79** then counterattack the S–Cl unit to form the thiazolidine ring in **80** and **81**. Thus the thioesters **74** and **75** act as 'intramolecular counterattack reagents'.

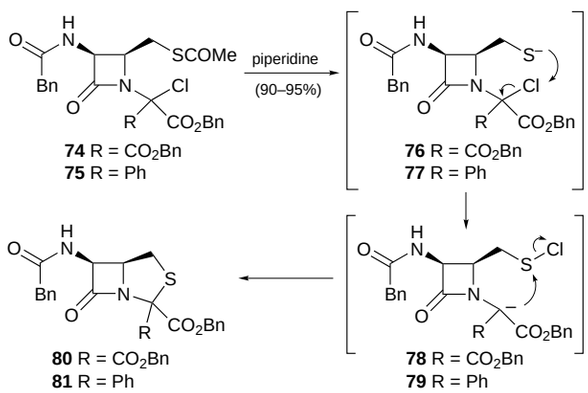

Scheme 22

A similar mechanism, shown in Scheme 23, is responsible for the transformation of sulfone malonate **82** to isopenam **80** *via* sulfide **83** and malonate anion **84**. The key steps involve the sulfone moiety in **83** being attacked by the sulfide unit, and the resultant carbanion **84** counterattacking the S–SO_2Me unit to form the thiazolidine ring in **80**. Thus sulfone **82** also functions as an 'intramolecular counterattack reagent'. Using this intramolecular counterattack mechanism, we can efficiently construct a heterocyclic ring fused to a β-lactam nucleus.

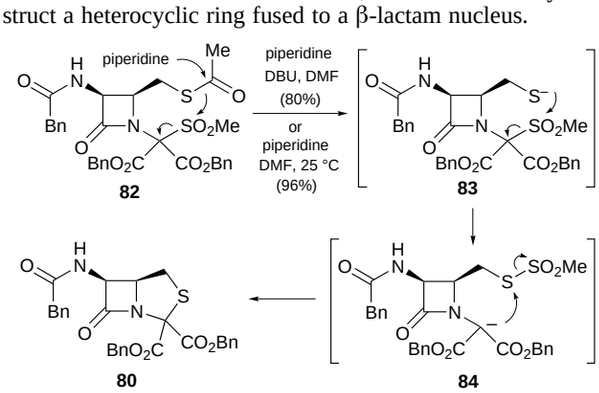

Scheme 23

Conclusions

Twelve examples have been given which demonstrate the efficient ways counterattack reagents can be used in organic synthesis. These reagents function either as electrophilic or nucleophilic 'counterattack reagents'. Their structures can be symmetric or non-symmetric. In addition to being attacked by substrates and then counterattacking the intermediates *in situ*, some counterattack reagents can follow very complicated

reaction pathways, such as the 'tandem double-counterattack process' and the 'consecutive triple-counterattack process'. This new concept has also been extended to the 'intramolecular counterattack strategy' and the 'pseudo-counterattack process' in the synthesis of valuable organic targets.

A multistep chemical transformation can be simplified into a 'one-flask' reaction using a counterattack reagent. In comparison with established classic methods, this new approach often gives higher yields with less manipulation. There is a bright future for the application of counterattack reagents to transformations of various types. An extreme example might involve hundreds or thousands of consecutive attacking and counter-attacking processes in polymer syntheses. The deliberate design of the reagent applied in each transformation is the key to the creation of new 'counterattack reagents'.

Acknowledgment

We thank the National Science Council of Republic of China and Academia Sinica for financial support.

Professor Jih Ru Hwu was born in Taipei, Taiwan, in 1954. He received his BS degree from the National Taiwan University (1972–1976) and PhD degree from Stanford University (1978–1982), during which time he worked under the guidance of Professor Eugene E. van Tamelen. Upon graduation, he joined the faculty at The Johns Hopkins University (1982–1991). He moved to the National Tsing Hua University as a professor in 1990 and has held a joint appointment as Research Fellow at Academia Sinica since then. Professor Hwu has been awarded an Alfred P. Sloan Research Fellowship for 1986–1990, the 1992/1993 Distinguished Young Chemist Award by the Federation of Asian Chemical Societies, a Ten Outstanding Young Persons of the Republic of China award (1993), two Distinguished Research Awards (1992–94, 1995–97) from the National Science Council, The Outstanding Young Persons of the World award for 1994 in the category of scientific and technological development by Junior Chamber International and the 1997 Third World Academy of Sciences Award in Chemistry. He was elected as the president of the Chinese American Chemical Society, USA (1991, 1992) and as an Associate Member of the IUPAC Commission on Nomenclature of Organic Chemistry (1989–97). He has also served as a Regional Advisory Editor for *Chemical Communications* (1994–1997). His research interests include silicon chemistry, organic synthesis, polymer science and genetic engineering.

Dr Shwu-Chen Tsay was born in Taipei, Taiwan, in 1962. She received her BS degree from the National Taiwan University (1981–1985) and PhD degree from The Johns Hopkins University (1986–1990, with Professor J. R. Hwu). Upon graduation, she joined the research group of Professor K. C. Nicolaou at The Scripps Research Institute as a Research Associate (1991–1992). Currently she is a Research Fellow at the Development Center for Biotechnology and an Associate Professor at Fu Jen Catholic University. In 1996 she was awarded a Ten Outstanding Young Women of the Republic of China award. Currently, she is an Associate Member of the IUPAC Commission on Nomenclature of Organic Chemistry. Her research interests include organic synthesis, bioorganic chemistry, medicinal chemistry and biotechnology.

Footnote and References

* E-mail: jrHwu@chem.nthu.edu.tw

1 J. R. Hwu and B. A. Gilbert, *Tetrahedron*, 1989, **45**, 1233.
2 J. R. Hwu, G. H. Hakimelahi, F. F. Wong and C. C. Lin, *Angew. Chem., Int. Ed. Engl.*, 1993, **32**, 608.
3 J. R. Hwu, S.-C. Tsay, A. A. Moosavi-Movahedi and G. H. Hakimelahi, unpublished work.
4 J. R. Hwu, T. Lee and B. A. Gilbert, *J. Chem. Soc., Perkin Trans. 1*, 1992, 3219.
5 J. R. Hwu, J. A. Robl, N. Wang, D. A. Anderson, J. Ku and E. Chen, *J. Chem. Soc., Perkin Trans. 1*, 1989, 1823.
6 J. R. Hwu and N. Wang, *Tetrahedron*, 1988, **44**, 4181.
7 J. R. Hwu, L. C. Lin and B. R. Liaw, *J. Am. Chem. Soc.*, 1988, **110**, 7252.
8 J. R. Hwu and S.-C. Tsay, *Tetrahedron*, 1990, **46**, 7413.
9 S.-C. Tsay, P. Gani and J. R. Hwu, *J. Chem. Soc., Perkin Trans. 1*, 1991, 1493.
10 J. R. Hwu, D. A. Anderson, N. Wang, M. M. Buchner, P. Gani and S.-C. Tsay, *Chem. Ber.*, 1990, **123**, 1667.
11 J. R. Hwu and S.-C. Tsay, *J. Org. Chem.*, 1990, **55**, 5987.
12 J. R. Hwu, *J. Org. Chem.*, 1983, **48**, 4432.
13 J. R. Hwu, N. Wang and R. T. Yung, *J. Org. Chem.*, 1989, **54**, 1070.
14 J. R. Hwu, *J. Chem. Soc., Chem. Commun.*, 1985, 452.
15 J. R. Hwu, S.-C. Tsay, N. Wang and G. H. Hakimelahi, *Organometallics*, 1994, **13**, 2461.
16 W. Carruthers, *Some Modern Methods of Organic Synthesis*, Cambridge University Press, 3rd edn., 1986, p. 45.
17 E. J. Corey, D. Seebach and R. Freedman, *J. Am. Chem. Soc.*, 1967, **89**, 434.
18 P. F. Jones, M. F. Lappert and A. C. Szary, *J. Chem. Soc., Perkin Trans. 1*, 1973, 2272.
19 F. Carey and A. S. Court, *J. Org. Chem.*, 1972, **37**, 1926.
20 C. A. Brown and A. Yamaichi, *J. Chem. Soc., Chem. Commun.*, 1979, 100.
21 J. R. Hwu and S.-C. Tsay, in *Encyclopedia of Reagents for Organic Synthesis*, ed. L. A. Paquette, Wiley, New York, 1995, vol. 5, pp. 3436–3437.
22 O. Smrekar and U. Wannagat, *Monatsh. Chem.*, 1969, **100**, 760.
23 R. West and P. Boudjouk, *J. Am. Chem. Soc.*, 1973, **95**, 3987.
24 Y. H. Chang, F.-T. Chiu and G. Zon, *J. Org. Chem.*, 1981, **46**, 342.
25 H.-P. Malach, R. Bussas and G. Kresze, *Liebigs Ann. Chem.*, 1982, **7**, 1384 and references cited therein.
26 J. R. Dilworth, S. J. Harrison, R. A. Henderson and D. R. M. Walton, *J. Chem. Soc., Chem. Commun.*, 1984, 176 and references cited therein.
27 K. Seppelt and W. Sundermeyer, *Chem. Ber.*, 1969, **102**, 1247.
28 W. P. Weber, *Silicon Reagents for Organic Synthesis*, Springer-Verlag, Berlag, 1983, ch. 11.
29 E. Colvin, *Silicon in Organic Synthesis*, Butterworths, Boston, 1981, ch. 9.
30 A. J. Mitchell, K. S. Murray, P. J. Newman and P. E. Clark, *Aust. J. Chem.*, 1977, **30**, 2439.
31 W. Walter and E. Schaumann, *Synthesis*, 1971, 111 and references cited therein.
32 M. H. Benn and M. G. Ettlinger, *J. Chem. Soc., Chem. Commun.*, 1965, 445.
33 M. Matsuo and E. W. Underhill, *Biochem. Biophys. Res. Commun.*, 1969, **36**, 18.
34 M. Matsuo and E. W. Underhill, *Phytochemistry*, 1971, **10**, 2279.
35 Shell Internationale Research Maatschappij, N. V. Neth. Appl. 6 615 725/1967 (*Chem. Abstr.*, 1968, **69**, 35430s).
36 J. Myerson, W. F. Haddon and E. L. Soderstorm, *Tetrahedron Lett.*, 1982, **23**, 2757.
37 E. P. Lebedev, V. A. Baburina and V. O. Reikhsfel'd, *J. Gen. Chem. USSR* (*Engl. Transl.*), 1975, **45**, 337.
38 E. J. Hedgley and W. G. Overend, *Chem. Ind.* (*London*), 1960, 378.
39 M. V. Bhatt and S. U. Kulkarni, *Synthesis*, 1983, 249.
40 M.-J. Shiao, W.-S. Ku and J. R. Hwu, *Heterocycles*, 1993, **36**, 323.
41 M.-J. Shiao, L.-L. Lai, W.-S. Ku, P.-Y. Lin and J. R. Hwu, *J. Org. Chem.*, 1993, **58**, 4742.
42 R. G. Vogt, in *Pheromone Biochemistry*, ed. G. D. Prestwich and G. J. Blomquist, Academic Press, New York, 1987.
43 J. Rokach and J. Adams, *Acc. Chem. Res.*, 1985, **18**, 87.

7/05054B

Biosynthesis of (−)-β-barbatene from ^{13}C- and ^{2}H-labelled acetate, mevalonate and glycerol†

Kensuke Nabeta,*[a] Kaori Komuro,[a] Tomoaki Utoh,[a] Hiroyuki Tazaki[a] and Hiroyuki Koshino[b]

[a] *Department of Bioresource Science, Obihiro University of Agriculture and Veterinary Medicine, Obihiro, 080 Japan*
[b] *The Institute of Physical and Chemical Research, (Riken) Wako, 351-01 Japan*

The ^{2}H and ^{13}C enrichment, ^{13}C–^{13}C coupling patterns and β-^{2}H isotope shifts observed in β-barbatanol prepared from (−)-β-barbatene incorporating variously ^{2}H- and ^{13}C-labelled mevalonates, acetates and glycerol verifies a 1,4-hydrogen shift and a double 1,2-methyl migration in the formation of β-barbatene in cultured cells of *Heteroscyphus planus*, and also indicates the diversity of regulation and the sole operation of the mevalonate pathway in extrachloroplastidic sesquiterpene biosynthesis.

The irregular sesquiterpene, β-barbatene **6**, has been proposed to be related biogenetically to the trichothecanes and cuparanes, the biosynthesis of which apparently involves a usual 1,4-hydride shift.[1] β-Barbatene is formed by further methyl migration by two routes, one involving a double 1,2-methyl migration [route (*a*) in Scheme 1], while the other features 1,3-methyl migration [route (*b*)]. Further cyclization and deprotonation of **5** affords β-barbatene. We fed deuteriated mevalonates (MVA) ([2,2-$^{2}H_2$] and [4,4-$^{2}H_2$]), ^{13}C- and ^{2}H-labelled acetates ([2-^{13}C], [1,2-$^{13}C_2$] and [2,2,2-$^{2}H_3$, 1-^{13}C]), [2-^{13}C]glycerol and [6,6-$^{2}H_2$]glucose to cultured cells of *Heteroscyphus planus* to elucidate the details of these steps and to determine whether extrachloroplastidic terpenoids are produced *via* a non-mevalonate-utilizing pathway.[2]

Cell cultures of *H. planus* were grown in MSK-4 medium[3] (75 ml), and fed 1.0 mmol of the potassium deuteriated MVAs (isotopic purity 99 atom%), 0.5 mmol of labelled acetate (isotopic purity 99 atom%), 0.5 mmol of [2-^{13}C]glycerol (60 atom%) and 11.1 mmol of [6,6-$^{2}H_2$]glucose (20 atom%) under continuous light at 25 °C. After extraction with methanol, the labelled β-barbatene was partitioned with pentane and separated by silica gel chromatography. The partially purified β-barbatene was then converted to β-barbatanol **7**, by reaction with borane–methyl sulfide, to avoid loss of volatile β-barbatene during further purification. β-Barbatanol was finally purified by repeated HPLC. Full assignment of the natural abundance ^{1}H and $^{13}C\{^{1}H\}$ NMR spectra of β-barbatanol and its acetate **8** was achieved by ^{1}H–^{1}H 2D COSY, ^{1}H–^{13}C 2D COSY, DEPT, differential NOE, DQF-COSY, PFG- HMQC and PFG-HMBC NMR studies.

$^{2}H\{^{1}H\}$ NMR spectra of β-barbatanyl [4,4-$^{2}H_2$]mevalonate indicated that ^{2}H-6 and ^{2}H-10 retained in farnesyl diphosphate **1** were incorporated into the C-5 position of β-barbatanol [δ_D 1.05 and 2.05 ($CDCl_3$), see Scheme 1] *via* the 1,4-hydride shift from cation **2** to **3** and ^{2}H-2 was incorporated into the C-7 (δ_D 1.61) position, while deuterium atoms of [2,2-$^{2}H_2$]MVA were incorporated into C-3 , C-9 and C-14 positions of β-barbatanol. ^{2}H enrichment of β-barbatanol (10.3 atom% excess) incorporating deuteriated MVA was determined by GC–MS analysis.[4] These labelling patterns indicated the 1,4-hydride shift and migration of the methyl group originating from the C-3 methyl of MVA. $^{13}C\{^{1}H\}$ NMR examination of the β-^{2}H isotope shifts[5] in β-barbatanyl [1-^{13}C, 2,2,2-$^{2}H_3$]acetate indicated the retention of two ^{2}H atoms at C-5 (ratio of $C^{2}H_2 : C^{2}H^{1}H : C^{1}H_2$ of C-4 = *ca.* 1 : 2 : 5, $\Delta\delta$ −0.22 and −0.11 ppm, Table 1) which supports the 1,4-hydride shift. No apparent ^{13}C signals due to a β-isotope shift of the C-2 carbon by $^{13}C^{2}H_3$ were observed.

The $^{13}C\{^{1}H\}$ NMR spectrum of β-barbatanyl [1,2-$^{13}C_2$]acetate showed three ^{13}C enriched peaks with doublets due to ^{13}C–^{13}C coupling (C-1–C-12, C-2–C-13 and C-8–C-15, see footnote of Table 1). The relative peak intensity of doublet to the central ^{13}C peak of C-13 (0.17) was much lower than that of C-15 (0.77) or that estimated on the basis of average ^{13}C enrichment (0.76 atom% excess), indicating that [1,2-$^{13}C_2$]acetate was not incorporated into the C-2 and C-13 positions. Intense ^{13}C–^{13}C couplings between C-1–C-10, C-4–C-5,

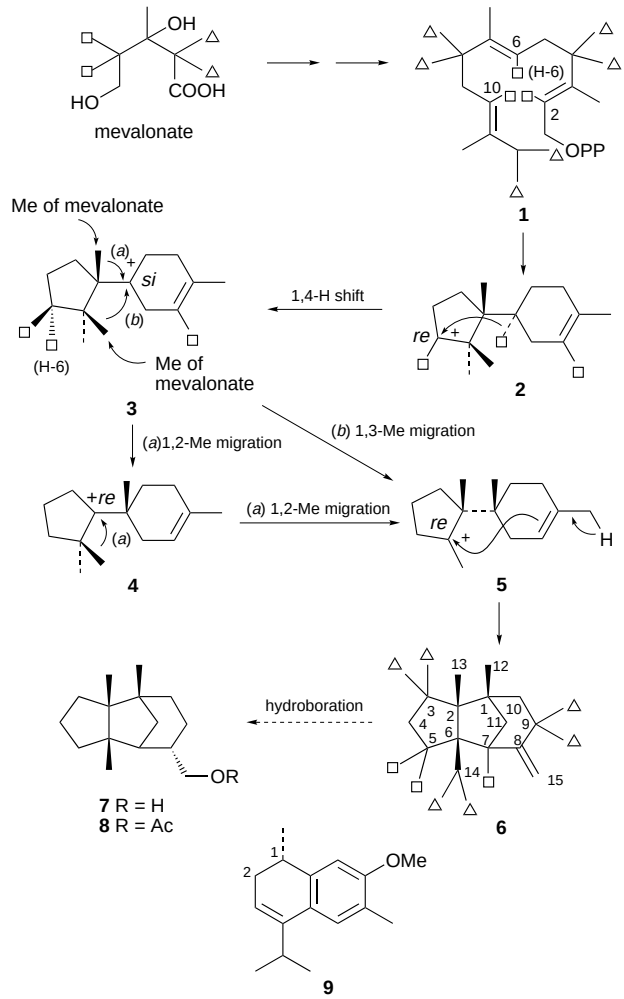

Scheme 1 Biosynthetic pathway of (−)-β-barbatene from deuteriated mevalonate in cultured cells of *H. planus*. Relative peak intensity of ^{2}H peaks at δ_D 1.73, 1.52 and 0.96 = 1 : 2 : 3 and that at δ_D 2.05, 1.61 and 1.05 = 1 : 1 : 1. H-6 in the carbocation **3** corresponds to H-6 in farnesyl diphosphate **1**.

Table 1 ^{13}C enrichment of carbons in β-barbatanol acetates incorporating ^{13}C- and ^{2}H-labelled acetates. Figures in parentheses show ^{13}C enrichment (atom% excess). Figures in square brackets show ^{13}C chemical shift of β-barbatanol

	δ_C					[1-^{13}C,$^{2}H_3$]Acetate incorporation	
Carbon	Non-labelled β-barbatanol	[2-^{13}C]	[1,2-$^{13}C_2$]	^{13}C–^{13}C Coupling observed[a]	[1-^{13}C,$^{2}H_3$]	$^{2}H:{}^{1}H$[b]	$\Delta\delta$[c] (ppm)
1	43.3 [43.4]	43.3 (0.8)[d]	43.3 (−0.1)	C-10, C-12 and C-11			
2	54.7 [54.7]		54.7 (0.4)	Unresolved	54.7 (2.7)		
3	34.2 [34.1]	34.2 (1.8)	34.1 (0.6)	C-2 and C-4			
4	27.9 [27.9]		27.9 (1.3)	C-5 and C-3	27.9 (0.8)	19 : 40 : 100[e]	−0.22, −0.11
5	36.7 [36.7]	36.7 (1.8)	36.7 (0.5)	C-4 and C-6			
6	54.8 [54.9]		54.8 (0.2)	Unresolved	54.8 (0.7)		
7	46.5 [46.3]	46.5 (0.8)	46.5 (0.7)	C-11, C-6 and C-8			
8	42.8 [46.8]		42.5 (0.7)	C-15, C-7 and C-9	42.5 (0.8)	30 : 32 : 100[e]	−0.18, −0.09
9	23.5 [23.4]	23.5 (1.0)	23.5 (1.2)	C-8 and C-10			
10	37.7 [37.9]		37.7 (1.3)	C-1 and C-9	37.7 (1.6)		
11	48.6 [48.7]		48.5 (0.6)	C-7 and C-1	48.5 (0.3)	31 : 100	−0.13
12	24.6 [24.7]	24.6 (0.4)[d]	24.6 (0.8)	C-1			
13	23.0 [23.0]	23.0 (1.1)	23.0 (1.2)	C-2			
14	29.0 [29.0]	29.0 (1.8)	29.0 (1.3)	C-6			
15	68.6 [67.2]	68.6 (1.8)	68.6 (0.8)	C-8			
Acetyl Me	21.1						
Acetyl C=O	171.3						
Average		1.24	0.76	1.14			

[a] Coupling constant in β-barbatanol incorporating [1,2-^{13}C]acetate, $J_{C,C}$/Hz, C-2–C-3 33.0, C-3–C-4 33.0, C-4–C-5 32.3, C-5–C-6 34.0, C-7–C-8 36.0, C-8–C-9 30.5, C-9–C-10 33.2, C-10–C-1 34.1, C-11–C-1 31.7, C-11–C-7 31.7, C-12–C-1 37.9, C-13–C-2 31.8, C-14–C-6 29.3, C-15–C-8 37.9. $J_{C\text{-}1,\,C\text{-}2}$, $J_{C\text{-}2,\,C\text{-}6}$ and $J_{C\text{-}6,\,C\text{-}7}$ were not determined, because of the low intensity of quaternary carbon atoms. [b] Ratio of carbon peak intensities for β-isotope shifted signals. [c] β-Isotope shifts due to ^{2}H. [d] Coupling constant in β-barbatanol incorporating [2-^{13}C]acetate, $J_{C,C}$/Hz, C-1–C-12 31.4. [e] $CD_2:CDH:CH_2$.

C-7–C-11 and C-8–C-15 were confirmed by a PFG-INADEQUATE experiment.[6]

Despite the low level of incorporation, the results of feeding cultured cells with [1,2-$^{13}C_2$]acetate demonstrated that all the carbon atoms in β-barbatanol were coupled with every adjacent carbon atoms. Couplings were observed between carbon atoms of different acetate units or those of different isoprene units, C-2–C-13, C-3–C-4 and C-9–C-10 (see footnote of Table 1). This suggests that β-barbatene biosynthesis is compartmentalized and occurs rapidly, *e.g.* within organelles.[7] However, in the formation of labelled (1*S*)-7-methoxy-1,2-dihydrocadalene[3] (cadinane **9**, 0.80 atom% excess) incorporating [1,2-$^{13}C_2$]acetate, which was isolated together with labelled β-barbatanol from the pentane extract of cultured cells fed with [1,2-$^{13}C_2$]acetate, no coupling was observed between the carbons of the different isoprene units. Contrasting results for β-barbatene and the cadinane suggest that their biosynthesis is regulated differently. These findings suggest a diversity of regulation in sesquiterpene biosynthesis. Although cultured cells of *H. planus* accumulate both cadinanes and bisabolanes,[3] only cadinane synthases have been detected in the 40 000 g supernatants.[8] This observation supported the suggestion that the cyclases which form bisabolanes including β-barbatene are associated with organelles, while cadinane synthases are localized in cytosol.

Labels were detected as intense singlets at C-2, C-4, C-6, C-8, C-10 and C-11 of β-barbatanol incorporating [2-^{13}C]glycerol, all of which were observed as intense singlet peaks. No deuterium atoms from [6,6-$^{2}H_2$]glucose were incorporated into β-barbatanol.

The labelling pattern supported the sole operation of the mevalonate pathway in biosynthesis of the extrachloroplastidic sesquiterpenes. In contrast the simultaneous operation of two distinct pathways, a mevalonate- and a non-mevalonate-mediated pathway, has been identified in the formation of the phytyl side-chain within chloroplasts.[9]

These obsevations are consistent with the occurrence of a 1,4-hydride shift and double 1,2-methyl migration during formation of β-barbatene and exclude the possibility of 1,3-methyl migration. They also suggested that the diversity of regulation and the sole operation of the mevalonate-utilizing pathway in the extrachloroplastidic biosynthesis of sesquiterpenes.

We are grateful to Professor H. Seto (Tokyo University) and Professor K. Kakinuma (Tokyo Institute of Technology) for the generous gift of [6,6-$^{2}H_2$]glucose. These investigations were supported by Grants-in-aid for Scientific Research (A. No. 08306021) and (C. No. 08660125), from the Ministry of Education, Science and Culture, Japan.

Footnotes and References

* E-mail: knabeta@obihiro.ac.jp

† This ChemComm is also available in expanded format *via* the World Wide Web: http://www.rsc.org/ccenhanced

1 D. E. Cane, in *Biosynthesis of Isoprenoid Compounds*, ed. J. W. Porter and S. L. Spurgeon, Wiley, New York 1981, vol. 1, p. 283.
2 H. Rohmer, M. Knani, P. Simonin, R. Sutter and H. Sahm, *Biochem. J.*, 1993, **295**, 517.
3 K. Nabeta, K. Katayama, S. Nakagawara and K. Katoh, *Phytochemistry*, 1993, **32**, 117.
4 K. Nabeta, *Dev. Food. Sci.*, 1995, **37**, 951.
5 J. C. Vederas, *Nat. Prod. Rep.*, 1987, **4**, 277 and references cited therein.
6 H. Koshino and J. Uzawa, *Bull. Magn. Reson.*, 1995, **17**, 260.
7 C. A. West, A. F. Louis, K. A. Wickham and Y.-Y. Ren, *Recent Adv. Phytochem.*, 1990, **24**, 219.
8 K. Nabeta, K. Kigure, M. Fujita, T. Nagoya, T. Takasawa, H. Okuyama and T. Takasawa, *J. Chem. Soc., Perkin Trans. 1*, 1995, 1935; K. Nabeta, M. Fujita, K. Komuro, K. Katayama and T. Takasawa, *J. Chem. Soc., Perkin Trans 1*, 1997, 2065.
9 S. Saitoh, K. Adachi, K. Komuro and K. Nabeta, Proceedings of the 41st Symposium on the Chemistry of Terpenes, Essential Oils and Aromatics, Morioka, 1997, p. 426.

Received in Cambridge, UK, 8th August 1997; revised M/S received, 17th October 1997; 7/07506E

Very long C–H···O contacts can be weak hydrogen bonds: experimental evidence from crystalline [Cr(CO)$_3${η^6-[7-*exo*-(C≡CH)C$_7$H$_7$]}]

Thomas Steiner,*[a] Bert Lutz,[b] John van der Maas,[b] Antoine M. M. Schreurs,[c] Jan Kroon[c] and Matthias Tamm*[d]

[a] *Institut für Kristallographie, Freie Universität Berlin, Takustraße 6, D-14195 Berlin, Germany*
[b] *Department of Analytical Molecular Spectrometry, Faculty of Chemistry, Utrecht University, Sorbonnelaan 16, 3584 CA Utrecht, The Netherlands*
[c] *Bijvoet Center for Biomolecular Research, Department of Crystal and Structural Chemistry, Utrecht University, Padualaan 8, 3584 CH Utrecht, The Netherlands*
[d] *Institut für Anorganische und Analytische Chemie, Freie Universität Berlin, Fabeckstraße 34-36, D-14195 Berlin, Germany*

The crystal structure of the title compound contains a very long C–H···O contact from the ethynyl group to a carbonyl ligand with a H···O separation of 2.92 Å; weakly hydrogen bonding character of this contact is inferred from the Raman and the IR absorption spectra, showing the long range nature of the C–H···O hydrogen bond.

Terminal alkynes are among the best studied donors of C–H···X hydrogen bonds.[1,2] This is because of two reasons: one is the high acidity and hence the strong donor potential, and one is the good and robust suitability for vibrational spectroscopic experiments.[3] In C–H···O hydrogen bonds donated by terminal alkynes, H···O separations are typically in the range 2.1–2.6 Å, with the mean value 2.37(4) Å.[1,4] If particularly strong acceptors like P=O are involved, H···O distances can be as short as 2.0 Å.[5] Whereas no conceptual problems arise for strong acceptors and short C≡C–H···O contacts, very little is known about long C–H···O (and more generally on long D–H···A) contacts. The open question is very simple: to which distances can C–H···O interactions be elongated before losing their hydrogen bond character? Currently, there seems to be consensus that no clear distance limits can be given, and that for increasing H···O and C···O separations, there is a gradual transition from hydrogen bond interactions to 'nothing'.[1] Still, the question remains: to which distances can physical effects of C–H···O interactions be detected, and when do the effects become more or less undetectable? In this contribution, we report structural and spectroscopic data on the longest alkynyl C–H···O contact discussed so far, which can still be reasonably regarded as a weak 'hydrogen bond'.

As part of our studies on ligands containing cycloheptatrienylium rings,[6] we prepared compound **1**.†

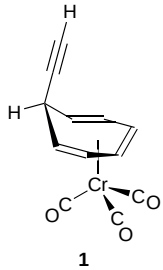

1

In terms of hydrogen bond potentials, the strongest donor in **1** is the ethynyl group and as hydrogen bond partners, there are the weak C≡C,[7] C=C[8] and CO[9] acceptors available. In this situation, it is impossible to predict which of the potentially resulting hydrogen bond types would eventually be formed in the solid state (if one is formed at all). In the crystal structure,‡ **1** is found in the expected conformation, Fig. 1(*a*). The shortest intermolecular contact of the ethynyl group is with a CO ligand of a neighboring molecule, Fig. 1(*b*). This contact is very long with H···O 2.92 Å (for C–H 1.08 Å) and C···O 3.71 Å, and the C–H···O angle is bent far from linearity, 130°.§ When looking only at the geometry, it is questionable how to interpret this contact: the distance is very long, much longer than van der Waals separation, the angle is strongly bent, and the CO ligand is one of the weakest O-acceptors known. No C–H···O contact of such a geometry has ever been clearly identified as a hydrogen bond. On the other hand, weak hydrogen bond nature has been shown for similarly long C≡C–H··π contacts,[7,8] suggesting this matter should be followed in further depth.

In vibrational spectroscopic experiments,¶ the alkynyl C–H stretching frequency $\nu_{\equiv C-H}$ was determined under a variety of sampling conditions in the crystalline state and in apolar solvents. This is to exclude possible matrix or solvent effects on $\nu_{\equiv C-H}$. Most important is the data on matrix-free polycrystalline **1** (determined by FT-Raman spectroscopy), which was obtained from small crystals taken without further sample treatment from

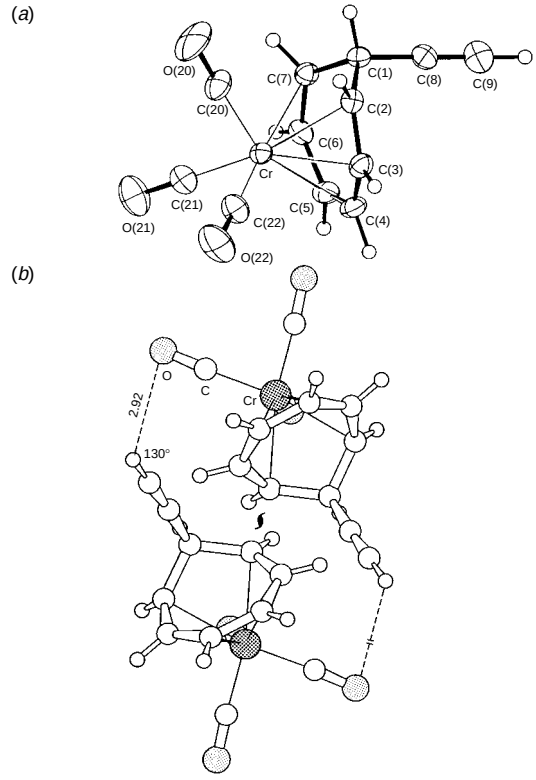

Fig. 1 (*a*) Molecular structure and atomic numbering scheme of **1**. (*b*) The very long C–H···O contact in crystalline **1**, numerical data is given for C–H 1.08 Å. The projection is along the screw axis of the space group; the apparently cyclic motif is therefore in fact a screw.

Table 1 IR alkynyl C–H stretching frequencies (cm^{-1}) of **1** in different environments

Sample of **1**	Spectrum	$\nu_{\equiv C-H}$
Polycrystalline matrix-free	FT-Raman	3293
Polycrystalline in poflu-oil[a]	FTIR	3293
Polycrystalline in KBr	FTIR	3293
Solution in *n*-hexane	FTIR	3315
Solution in CCl_4	FTIR	3310

[a] Poly(chlorotrifluoroethylene).

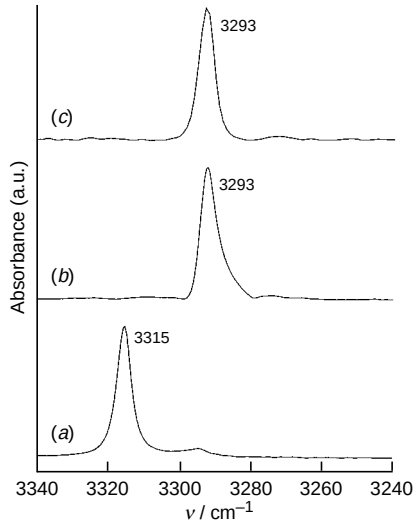

Fig. 2 Alkynyl C–H stretching region of the vibrational spectrum. (*a*) FT-Raman spectrum of a matrix-free polycrystalline sample. (*b*) FTIR spectrum of a polycrystalline sample in a poly(chlorotrifluoroethylene) mull. (*c*) FTIR spectrum of a dilute solution in *n*-hexane.

the same batch as the crystal used for X-ray data collection. FTIR spectra of polycrystalline samples in an inert mull and in KBr were also determined. All three $\nu_{\equiv C-H}$ values are identical at 3293 cm^{-1} (Table 1 and Fig. 2), which is slightly but significantly reduced compared to the *ca.* 3315 cm^{-1} which are typical for 'free' alkynyl $\nu_{\equiv C-H}$.[3] The identity of the three values under different sampling conditions makes matrix and sample preparation artifacts unlikely. Since $\nu_{\equiv C-H}$ of 'free' molecules R–C≡C–H can slightly depend on the nature of R and also on the experimental conditions, IR absorption spectra were determined of dilute solutions in the apolar solvents *n*-hexane and CCl_4. The $\nu_{\equiv C-H}$ values of 3315 and 3310 cm^{-1}, respectively, correspond to alkynyl groups which experience only very small (but necessarily non-zero) intermolecular interactions with 'inert' solvent molecules. The reduction of $\nu_{\equiv C-H}$ in the crystalline state of *ca.* 20 cm^{-1} shows that in crystals, the alkynyl covalent C–H bond is slightly but detectably weakened owing to its intermolecular interactions. This bond weakening is an appropriate (and normally used[3]) indicator of C–H···X hydrogen bonding. A red-shift of 20 cm^{-1} is only a small effect. In 'normal' alkynyl C–H···O interactions, the corresponding red-shifts are in the range 40–100 cm^{-1}, and for strong C≡C–H···O=P hydrogen bonds, they can be 145 cm^{-1} and more.[3,5] This means that the intermolecular interactions in **1** do have an effect on the vibrational spectum, but this effect is small. We see no other interactions that the C–H···O contact that might be responsible, and therefore call it a 'weak hydrogen bond' (the terminologic classification, though, is of minor importance here).

The discussed contact with H···O 2.92 Å, is, to our knowledge, the longest C–H···O interaction for which effects on vibrational spectra have been experimentally shown. This is strong support for the long-range nature of C–H···O interactions, and clearly disfavours views that hydrogen bond character stops at the distance of the sum of van der Waals radii. On the other hand, one must consider that the red-shift of IR wavenumbers is only *ca.* 20 cm^{-1}, which is much smaller than for C–H···O interactions in optimal geometry: the strength of C–H···O hydrogen bonds at such distances is already very small. Since the donor studied here, C≡C–H, is stronger than most other C–H groups,[1] C–H···O contacts of similar geometries with less acidic C–H groups will be correspondingly weaker. We explicitly do not conclude that 'every C–H···O contact with H···O 2.9 Å is a hydrogen bond', but we state (based on experimental evidence) that such a contact can be a hydrogen bond.

T. S. thanks Professor W. Saenger for giving him the opportunity to carry out part of this work in his laboratory, and the Research Network of the European Union 'Molecular Recognition Phenomena' for supporting a stay in Utrecht. M. T. thanks the Deutsche Forschungsgemeinschaft (Ta 189/1-4,5) and the Fonds der Chemischen Industrie for financial support.

Footnotes and References

* E-mail: steiner@chemie.fu-berlin.de

† Complex **1**, tricarbonyl[η⁶-(7-*exo*-ethynyl-1,3,5-cycloheptatriene)]-chromium(0), $[Cr(CO)_3\{\eta^6\text{-}[7\text{-}exo\text{-}(C{\equiv}CH)C_7H_7]\}]$, was prepared in 86% yield from $[Cr(CO)_3(C_7H_7)]BF_4$ and lithiated (trimethylsilyl)acetylene followed by desilylation in methanolic KOH. ^1H NMR ($CDCl_3$): δ 6.08 (m, 2 H), 5.91 (m, 2 H), 3.84 (t, 1 H, *endo*-H), 3.68 (m, 2 H), 2.09 (s, 1 H, C≡H). ^{13}C NMR ($CDCl_3$): δ 231.0 (CO), 98.9, 98.2 (C_7 CH), 83.8 (C≡CH), 71.2 (C≡CH), 60.3 (C_7 CH), 26.3 (C_7 C-7). Satisfactory C, H and N analyses were obtained.

‡ *Crystallography*: crystallisation from diethyl ether–hexane yields brown, block-shaped crystals. $C_{12}H_8CrO_3$, M = 252.2, monoclinic, space group $P2_1/c$ (no. 14), a = 10.367(1), b = 8.291(2), c = 13.135(2) Å, β = 95.93(1)°, U = 1120.1(3) Å^3, Z = 4, D_c = 1.495 g cm^{-3}, μ = 1.007 mm^{-1}. Enraf-Nonius FAST area detector, Mo-Kα radiation with λ = 0.710 73 Å, crystal dimensions 0.4 × 0.3 × 0.3 mm, room temp., 7779 reflections measured, 2569 independent (R_{int} = 0.062), 2025 with $I > 2\sigma(I)$, no absorption correction. Standard crystallographic computations[10,11] (refinement on F^2 of all reflections, H-atoms treated in the riding model with isotropic displacement parameter refined, 154 parameters vaired). Final R = 0.054 (for observed reflections), wR_2 = 0.119 (for all reflections). CCDC 182/689.

§ The second shortest contact of C≡C–H is to a CO ligand of a different neighbour with H···O 3.12 Å and C–H···O 109°.

¶ FT-NIR-Raman spectra were recorded of a matrix-free polycrystalline sample at room temp. (Perkin Elmer 2000 system, Nd/YAG laser, λ = 1064 nm, InGaAs detector, resolution 4 cm^{-1}, 128 scans). IR absorption spectra were recorded of polycrystalline **1** in a poly(chlorotrifluoroethylene) mull and in a KBr pellet, and of dilute solutions in *n*-hexane and in CCl_4 at room temp. (Perkin Elmer Model 2000 FTIR system, DTGS detector, optical resolution: 2 cm^{-1}; 8 scans, medium apodization, 0.5 mm KBr cells at concentrations < 0.5 mg ml^{-1}).

1 Th. Steiner, *Chem. Commun.*, 1997, 727.
2 G. R. Desiraju, *Acc. Chem. Res.*, 1996, **29**, 441.
3 E. Steinwender, E. T. G. Lutz, J. H. van der Maas and J. A. Kanters, *Vib. Spectrosc.*, 1993, **4**, 217; B. Lutz, J. van der Maas and J. A. Kanters, *J. Mol. Struct.*, 1994, **325**, 203.
4 G. R. Desiraju, *J. Chem. Soc., Chem. Commun.*, 1990, 454.
5 Th. Steiner, J. van der Maas and B. Lutz, *J. Chem. Soc., Perkin Trans. 2*, 1997, 1287.
6 M. Tamm, A. Grzegorzewski and I. Brüdgam, *J. Organomet. Chem.*, 1996, **519**, 217; M. Tamm, A. Grzegorzewski, Th. Steiner, W. Werncke and T. Jentzsch, *Organometallics*, 1996, **15**, 4984; M. Tamm, W. Werncke and T. Jentzsch, *ibid.*, 1997, **16**, 1418; M. Tamm, A. Grzegorzewski and Th. Steiner, *Chem. Ber./Recueil*, 1997, **130**, 225.
7 Th. Steiner, M. Tamm, A. Grzegorzewski, N. Schulte, N. Veldman, A. M. M. Schreurs, J. A. Kanters, J. Kroon, J. van der Maas and B. Lutz, *J. Chem. Soc., Perkin Trans. 2*, 1996, 2441.
8 B. Lutz, J. A. Kanters, J. van der Maas, J. Kroon and Th. Steiner, *J. Mol. Struct.*, in press.
9 D. Braga and F. Grepioni, *Acc. Chem. Res.*, 1997, **30**, 81.
10 G. M. Sheldrick, SHELXS86, in *Crystallographic Computing 3*, ed. G. M. Sheldrick, C. Krüger and R. Goddard, Oxford University Press, pp. 175–189.
11 G. M. Sheldrick, SHELXL-93, Program for the Refinement of Crystal Structures, University of Göttingen, Germany, 1993.

Received in Cambridge, UK, 26th September 1997; 7/06980D

A novel and direct α-azidation of cyclic sulfides using a hypervalent iodine(III) reagent

Hirofumi Tohma, Masahiro Egi, Makoto Ohtsubo, Hiroaki Watanabe, Shinobu Takizawa and Yasuyuki Kita*

Faculty of Pharmaceutical Sciences, Osaka University, 1-6, Yamada oka, Suita, Osaka 565, Japan

A novel and direct α-azidation of cyclic sulfides using a hypervalent iodine(III) reagent in the presence of Me_3SiN_3 is described; the present method is applicable to substrates which are easily aromatized under oxidative conditions.

α-Azido sulfides have attracted much attention because of their interesting reactivities under various conditions (*e.g.* photochemical, thermal, and other conditions[1]) and their utility as amino cation equivalents.[2] Furthermore, α-azido sulfides have potential for the synthesis of various *N*,*S*-acetals, since the azido moiety can be changed to other aza substituents *via* PPh_3 and catalytic hydrogenation.[3] Generally, *N*,*S*-acetals[4] are difficult to synthesize because of their instability. However, several methods have appeared for the syntheses of *N*,*S*-acetals, *e.g.* addition of thionucleophiles to imine intermediates[5] and addition of aza nucleophiles to thionium intermediates.[6] However, most of the methods have problems in terms of yield and vigorous reaction conditions. Hence, subsequent to the first report[7] by Böhme and Morf, acyclic α-azido sulfides have usually been synthesized stepwise,[1,8] *via* halogenation followed by azidation of sulfides, or *via* thioketals.[9]

On the other hand, α-azidation of cyclic sulfides, especially dihydrobenzothiophenes, has never been reported, probably due to readily occuring side reactions such as aromatization, sulfoxide formation, benzylic oxidation and α-oxidation of the sulfur atom under oxidative conditions. In particular, α-azidohydrobenzothiophene is thought to be a suitable precursor for the total synthesis of the recently isolated marine anti-cancer alkaloids, discorhabdin A,[10] B,[11] D[12] and makaluvamine F,[13]

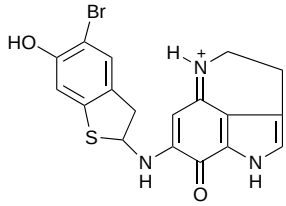

Makaluvamine F

whose total syntheses have yet to be accomplished owing to difficulties in constructing their *N*,*S*-acetal skeletons. This prompted us to develop an efficient and general α-azidation method for cyclic sulfides. First, we examined the known stepwise methods to obtain α-azidohydrobenzothiophene. The initial chlorination of **1a** by *N*-chlorosuccinimide (NCS) or SO_2Cl_2,[7,8] however, exclusively gave 5-methoxybenzothiophene **3a**, and oxidation of **1a** to the sulfoxide followed by Pummerer-type azidation gave predominantly **3a** and not **2a**. As part of our continuing studies of hypervalent iodine(III) oxidation,[14] we report here a novel and direct α-azidation method for cyclic sulfides using a combination of PhI=O and Me_3SiN_3 (Scheme 1).

A typical experimental procedure is as follows. To a stirred solution of **1a** in MeCN, Me_3SiN_3 (4.0 equiv.) was added dropwise at −40 °C under nitrogen atmosphere. Iodosylbenzene (2.0 equiv.) was added to the reaction mixture, which was then slowly warmed to −25 °C with stirring for 1–2 h.

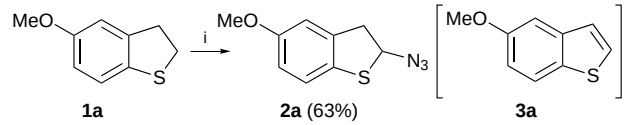

1a **2a** (63%) **3a**

Scheme 1 *Reagents and conditions*: i, PhI=O (2 equiv.), Me_3SiN_3 (4 equiv.), MeCN, −40 to −25 °C

Evaporation of solvent followed by preparative TLC or column chromatography gave **2a** in 63% yield. Of the combination of reagents investigated, PhI=O with Me_3SiN_3 was the best since using $PhI(OCOCF_3)_2$–Me_3SiN_3 or other combined reagents† gave **3a** as the main product. Although the reaction of dihydrobenzothiophene bearing alkoxy substituents with hypervalent iodine(III) reagents has various possibility for (i) α-azidation, (ii) aromatic azidation,[15] (iii) benzylic azidation,[16] (iv) sulfoxide formation,[17] and (v) aromatization to benzothiophene, the present method makes the α-azidation of cyclic sulfides possible predominantly by the use of the combined reagent, PhI=O–Me_3SiN_3. The structure of **2a** was unambiguously established by ^1H NMR, IR and mass spectral and elemental analysis.‡

Table 1 shows that the present method is also applicable to mono- and bi-cyclic sulfides **1b**–**i** including dihydrobenzothiophene to give the corresponding α-azido sulfides **2b**–**i** in moderate to good yields. Among the substrates bearing an alkoxy group at the *para* position of the alkyl side chain, benzylic azidation products have also been obtained. In such cases, α-azidation proceeded after protection of the phenolic OH group with an acetyl group (runs 2 and 4).

A plausible reaction mechanism is proposed in Scheme 2. Iodosulfonium cation **4** initially formed from the reaction of

Table 1 α-Azidation of cyclic sulfides using PhI=O–Me_3SiN_3

Entry	Substrate **1**	*n*	R^1	R^2	R^3	Product **2**	Yield (%)
	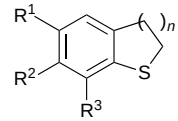					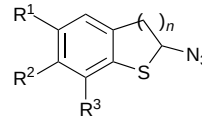	
1	**1a**	1	OMe	H	H	**2a**	63
2	**1b**	1	H	OAc	H	**2b**	70[a]
3	**1c**	1	OMe	OMe	OMe	**2c**	42
4	**1d**	1	OAc	OAc	H	**2d**	25[a] (67)[b]
5	**1e**	1	H	H	H	**2e**	69
6	**1f**	2	OMe	H	H	**2f**	70
7	**1g**	2	OMe	H	H	**2g**	63
						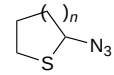	
8	**1h**	1	—	—	—	**2h**	48
9	**1i**	2	—	—	—	**2i**	62

[a] PhI=O (5.0 equiv.) and Me_3SiN_3 (10.0 equiv.) were used. [b] Yield based on reacted substrate.

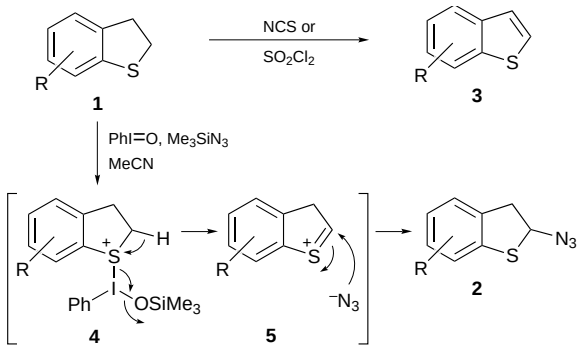

Scheme 2

sulfide **1** with PhI=O–Me_3SiN_3, a mechanism well studied by Magnus and co-workers,[18] is then deprotonated to give cation intermediate **5**. Azido anion attack on the α-position of **5** gives the α-azido sulfide **2**. On the other hand, NCS or SO_2Cl_2 causes β-proton abstraction of **5** to give benzothiophene **3** exclusively rather than a nucleophilic attack on the α-carbon. This is probably because the chloride anion is more basic than the Me_3SiO^- anion, generated in the azidation step, and also because Me_3SiO^- is readily neutralized to the siloxane under the reaction conditions used.

In conclusion, a novel and direct α-azidation of cyclic sulfides has been accomplished. This work opens the way to effective syntheses of biologically active natural products carrying *N*,*S*-acetal structures, and provides a direct and efficient method for the synthesis of cyclic α-azido sulfides.

Footnotes and References

* E-mail: kita@phs.osaka-u.ac.jp

† Other combinations [*e.g.* $PhI(OAc)_2$–NaN_3, *o*-iodobenzoic acid–Me_3SiN_3) were also examined, but only low yields of **2** were obtained.

‡ *Selected data* for **2a**: ν(KBr)/cm^{-1} 2936, 2108, 1597, 1578 and 1473; δ_H (270 MHz, $CDCl_3$) 3.25 (d, 1 H, *J* 16), 3.48 (dd, 1 H, *J* 6, 16), 3.78 (s, 3 H), 5.38 (d, 1 H, *J* 6), 6.78 (d, 1 H, *J* 9), 6.85 (s, 1 H), 7.16 (d, 1 H, *J* 9); δ_C ($CDCl_3$) 44.1, 55.5, 71.0, 111.4, 113.7, 122.9, 128.8, 138.5, 158.1 (Calc. for $C_9H_9N_3OS$: C, 52.16; H, 4.38; N, 20.27; S, 15.47%. Found: C, 52.23; H, 4.43; N, 20.21; S, 15.23%). All newly formed compounds gave satisfactory spectroscopic data.

1 I. W. J. Still, W. L. Brown, R. J. Colville and G. W. Kutney, *Can. J. Chem.*, 1984, **62**, 586 and references cited therein.

2 B. M. Trost and W. H. Pearson, *J. Am. Chem. Soc.*, 1981, **103**, 2483; A. Hassner, P. Munger and B. A. Belinka Jr., *Tetrahedron Lett.*, 1982, **23**, 699.

3 E. M. Suh and Y. Kishi, *J. Am. Chem. Soc.*, 1994, **116**, 11 205; J. Zaloom, M. Calandra and D. C. Roberts, *J. Org. Chem.*, 1985, **50**, 2601; J. Garcia, F. Urpi and J. Vilarrasa, *Tetrahedron Lett.*, 1984, **25**, 4841; Review: E. F. V. Scriven and K. Turnbull, *Chem. Rev.*, 1988, **88**, 297.

4 G. C. Barrett, in *Comprehensive Organic Chemistry*, ed. D. Barton and W. D. Ollis, Pergamon, Oxford, 1979, vol. 3, p. 55.

5 C. Z. Ding and R. B. Silverman, *Synth. Commun.*, 1993, **23**, 1467; G. Apitz and W. Steglich, *Tetrahedron Lett.*, 1991, **32**, 3163; A. R. Katritzky, M. Szajda and S. Bayyuk, *Synthesis*, 1986, 804; H. Sakai, K. Ito and M. Sekiya, *Chem. Pharm. Bull.*, 1973, **21**, 2257.

6 A. F. Janzen, G. N. Lypka and R. E. Wasylishen, *J. Heterocycl. Chem.*, 1979, **16**, 415; S. Rakhit, M. Georges and J. F. Bagli, *Can. J. Chem.*, 1979, **57**, 1153; U. Lerch and J. G. Moffatt, *J. Org. Chem.*, 1971, **36**, 3391.

7 H. Böhme and D. Morf, *Chem. Ber.*, 1957, **90**, 446.

8 H. Böhme and F. Ziegler, *Liebigs Ann. Chem.*, 1974, 734.

9 B. M. Trost, M. Vaultier and M. L. Santiago, *J. Am. Chem. Soc.*, 1980, **102**, 7929.

10 N. B. Perry, J. W. Blunt and M. H. G. Munro, *Tetrahedron*, 1988, **44**, 1727.

11 N. B. Perry, J. W. Blunt, M. H. G. Munro, T. Higa and R. Sakai, *J. Org. Chem.*, 1988, **53**, 4127; J. W. Blunt, M. H. G. Munro, C. N. Battershill, B. R. Copp, J. D. McCombs, N. B. Perry, M. R. Prinsep and A. M. Thompson, *New J. Chem.*, 1990, **14**, 761.

12 J.-F. Cheng, Y. Ohizumi, M. R. Wälchli, H. Nakamura, Y. Hirata, T. Sasaki and J. Kobayashi, *J. Org. Chem.*, 1988, **53**, 4621 and references cited therein.

13 D. C. Radisky, E. S. Radisky, L. R. Barrows, B. R. Copp, R. A. Kramer and C. M. Ireland, *J. Am. Chem. Soc.*, 1993, **115**, 1632.

14 Y. Tamura, T. Yakura, J. Haruta and Y. Kita, *Tetrahedron Lett.*, 1985, **26**, 3837; *J. Org. Chem.*, 1987, **52**, 3927; Y. Kita, H. Tohma, K. Kikuchi, M. Inagaki and T. Yakura, *J. Org. Chem.*, 1991, **56**, 435; Y. Kita, H. Tohma, M. Inagaki, K. Hatanaka and T. Yakura, *J. Am. Chem. Soc.*, 1992, **114**, 2175; Y. Kita, R. Okunaka, M. Kondo, H. Tohma, M. Inagaki and K. Hatanaka, *J. Chem. Soc., Chem. Commun.*, 1992, 429; Y. Kita, T. Takada, S. Mihara, B. A. Whelan and H. Tohma, *J. Org. Chem.*, 1995, **60**, 7144; Y. Kita, M. Gyoten, M. Ohtsubo, H. Tohma and T. Takada, *Chem. Commun.*, 1996, 1481; Y. Kita, M. Egi, A. Okajima, M. Ohtsubo, T. Takada and H. Tohma, *Chem. Commun.*, 1996, 1491; Y. Kita, M. Egi, M. Ohtsubo, T. Saiki, T. Takada and H. Tohma, *Chem. Commun.*, 1996, 2225.

15 Y. Kita, H. Tohma, M. Inagaki, K. Hatanaka and T. Yakura, *Tetrahedron Lett.*, 1991, **32**, 4321; Y. Kita, H. Tohma, K. Hatanaka, T. Takada, S. Fujita, S. Mitoh, H. Sakurai and S. Oka, *J. Am. Chem. Soc.*, 1994, **116**, 3684.

16 Y. Kita, H. Tohma, T. Takada, S. Mitoh, S. Fujita and M. Gyoten, *Synlett*, 1994, 427.

17 The reaction of **1a** with $PhI(OCOCF_3)_2$ in MeOH gave the corresponding sulfoxide in 89% yield. For previously reported examples: see J. P. A. Castrillón and H. H. Szmant, *J. Org. Chem.*, 1967, **32**, 976; A. W. Czarnik, *J. Org. Chem.*, 1984, **49**, 924; G. F. Koser, P. B. Kokil and M. Shah, *Tetrahedron Lett.*, 1987, **28**, 5431; D. G. Ray III and G. F. Koser, *J. Am. Chem. Soc.*, 1990, **112**, 5672 and references cited therein.

18 The formation of hypervalent azido iodine(III) reagents by the reaction of Me_3SiN_3 with PhI=O at −40 °C has been reported; Magnus and Lacour, *J. Am. Chem. Soc.*, 1992, **114**, 767; 1992, **114**, 3993; P. Magnus, C. Hulme and W. Weber, *J. Am. Chem. Soc.*, 1994, **116**, 4501; P. Magnus, J. Lacour, P. A. Evans, M. B. Roe and C. Hulme, *J. Am. Chem. Soc.*, 1996, **118**, 3406.

Received in Cambridge, UK, 27th October 1997; 7/07727K

^{71}Ga and ^{31}P solid state NMR: a powerful tool for the characterization of the first gallium phosphonates

Florence Fredoueil,[a] Dominique Massiot,[b] Damodara Poojary,[c] Martine Bujoli-Doeuff,[d] Abraham Clearfield[c] and Bruno Bujoli*[a]

[a] *Laboratoire de Synthèse Organique, UMR CNRS 6513 BP 92208, 2 Rue de la Houssinière, 44322 Nantes Cedex 03, France*
[b] *Centre de Recherches sur la Physique des Hautes Températures, UPR CNRS 4212, 1D Avenue de la Recherche Scientifique, 45071 Orléans Cedex 02, France*
[c] *Department of Chemistry, Texas A & M University, College Station, TX 77843, USA*
[d] *Institut des Matériaux de Nantes, UMR CNRS 6502, BP 92208, 2 Rue de la Houssinière, 44322 Nantes Cedex 03, France*

Two new gallium phosphonates $Ga(OH)(O_3PC_2H_4CO_2H)\cdot H_2O$ 1 and $Ga_3(OH)_3(O_3PC_2H_4CO_2)_2\cdot 2H_2O$ 2 are prepared and characterized, using ^{31}P MAS and ^{71}Ga static NMR spectroscopy, showing a good correspondence between the fitted NMR parameters and the crystallographic data.

In recent papers, we have demonstrated that catalytic complexes (*i.e.* manganese porphyrins)[1] could be efficiently heterogenised as divalent metal phosphonates, in which significant shape selectivity effects imposed by the inorganic framework were observed. The key feature of this approach is to functionalize the catalytic complex by phosphonic acid PO_3H_2 moieties, that are then 'polymerised' by reaction with a metal (M) salt in solution, to build up a $M(RPO_3)_x$ network.[2] Taking into account that the resulting immobilised catalysts are usually poorly crystalline, our interest was to find a good method for the characterisation of such materials (*i.e.* get information about both the metal and the PO_3 group environments). One attractive solution to achieve that goal should be to use solid state NMR, provided that the metal atom reacted with the PO_3 groups can be observed by this technique, with the potential advantage (in comparison with EXAFS) to be able to determine the number of metallic sites and their relative amounts, as well as their coordination. In this paper, we describe our attempts in this field, by studying gallium phosphonate systems, the preparation of which seemed possible by analogy with gallium phosphates.[3] As a matter of fact, the stabilities of these materials towards acidic and basic media are higher than the divalent metal analogues and this can be of interest, as far as catalytic applications are concerned. Thus, by reaction of (2-carboxymethyl)phosphonic acid with gallium(III) nitrate in water in an autoclave, two novel gallium hydroxyphosphonates were prepared: $Ga(OH)(O_3PC_2H_4CO_2H)\cdot H_2O$ **1** and $Ga_3(OH)_3(O_3PC_2H_4CO_2)_2\cdot 2H_2O$ **2**. It is worth noting that the presence of hydroxide groups in phosphonates is unusual, except for recent examples described by us in the copper(II) system.[4]

Solid state NMR study of gallium is rendered difficult as it undergoes strong quadrupolar couplings, which give rise to severe second order broadening of the powder spectrum of its central $<1/2>$ transition. Gallium has two NMR active isotopes, ^{69}Ga and ^{71}Ga, both having $I = 3/2$ spins with higher gyromagnetic ratio and lower quadrupolar momentum for ^{71}Ga, which is thus the easiest to observe. At the principal magnetic field of 9.4 T (122 MHz Larmor frequency for ^{71}Ga), the width of the ^{71}Ga spectra of these two new gallium phosphonates (400 **1**, 600 **2** kHz) exceeds the bandwidth accessible with a single experiment (typically 300 kHz). The spectra have thus been acquired in static conditions as a sum of nine full echo signals obtained by varying the offset of the carrier frequency (with a 100 kHz step), according to the VOCS protocol that we have recently described in a study of ^{69,71}Ga in β-Ga_2O_3.[5] The second order quadrupolar broadening is so high in these compounds that MAS experiments cannot give resolution (unlike aluminophosphonates, for which MQ ^{27}Al MAS has proved to be efficient),[6] while the possible DAS[7] or newly described QPASS[8] experiments remain ineffective.

Owing to these intrinsic experimental difficulties, there is little known on Ga solid state NMR, even though there is a well established and confirmed correlation that links gallium and aluminium chemical shifts for four- and six-fold coordination in silicate, phosphates, zeolites and organic complexes.[5,9,10] The results obtained from the simulation of the two observed ^{71}Ga spectra (Fig. 1) are summarized in Table 1, showing two different Ga sites for **1** in a 1 : 1 ratio and one single site for **2**. The chemical shifts of these signals can be unambiguously

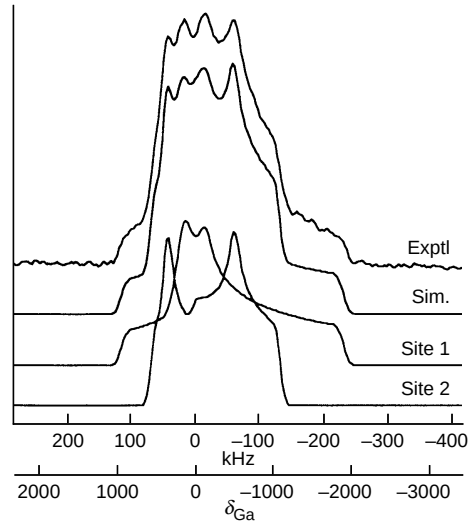

Fig. 1 Experimental ^{71}Ga static NMR spectrum of **1**, and simulated spectrum with second order quadrupolar broadened shape, according to parameters described in Table 1

Table 1 Experimental values for chemical shift and electric field gradient for compounds **1** and **2**

	δ_{iso}[a]	C_Q[b]/MHz	ηQ[c]
1	−6 (site 1: 50%)	13.5	0.85
	2 (site 2: 50%)	12.0	0.35
2	−3	17.0	0.9

[a] Chemical shifts are referenced to ^{71}Ga resonance in a 1 M gallium nitrate solution; error in the measured value: ±10 ppm. [b] Quadrupolar coupling constant ($C_Q = e^2qQ/h$); error in the measured value: ±0.25 MHz. [c] Asymmetry factor.

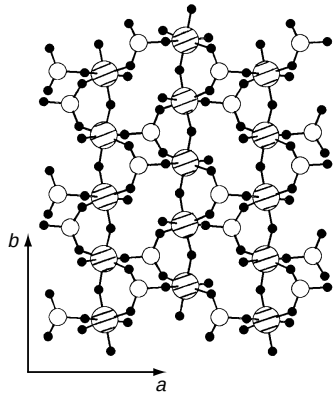

Fig. 2 Schematic representation of a $Ga(OH)(O_3P(CH_2)_2CO_2H)\cdot H_2O$ layer as seen perpendicular to the *c*-axis; Ga (hatched), P (white), O (black) and carbon atoms omitted for clarity. Selected interatomic distances (Å): Ga(1)–O 1.889(7), 1.906(6) (OH), 1.926(7) (OH), 1.978(8), 2.019(7), 2.061(7) (H_2O); Ga(2)–O 1.913(7) (OH), 1.922(6) (OH), 1.949(7), 1.965(7), 2.018(7), 2.060(7) (H_2O).

assigned to sixfold coordination, while their respective electric field gradient tensors characterize the asymmetry of their local environments. In the case of **1**, the presence of the two GaO_6 sites was confirmed by a structure determination from its powder X-ray diffraction pattern (Fig. 2).† On the other hand, even if six-coordinate gallium centres were clearly evidenced from the XANES–EXAFS spectra of this compound, it was however not possible to detect the two different independent metal atoms in this layered compound. Moreover, it is reasonable to think that in compound **1**, the most distorted gallium site Ga(1) [Ga–O bond lengths ranging from 1.889(7) to 2.061(7) Å; see Fig. 2] corresponds to the highest value measured for C_Q (13.5 MHz, site 1 in Table 1). For compound **2**, the observed value for C_Q (17 MHz) is significantly higher, thus giving evidence of a probably more distorted GaO_6 environment present in this latter phase. The structure of **1** consists of GaO_6 octahedra (composed of three phosphonate oxygens, two hydroxide groups and one water molecule) sharing two opposite vertices, thus forming chains parallel to the *b*-axis. These chains are connected by O–P–O bridges in the *a*-direction, to build a two-dimensional network. The organic chains are oriented roughly perpendicular to the layers, and the CO_2H groups are not coordinated, in contrast with **2** [ν(CO) 1590 cm^{-1}], for which a pillared layered structure is likely to be present, resulting from **1** by a probable coordination of the carboxylic acid moieties with gallium atoms. These two layered structures are in contrast to the only other reported gallium phosphonate, $Li_4[(MeGa)_6(\mu_3\text{-}O)_2(Bu^tPO_3)_6]\cdot 4thf$, an anionic molecular cage containing sandwiched lithium ions.[11]

Finally, from the simulation of the static and MAS ^{31}P spectra of gallium phosphonates **1** and **2**, the number of independent PO_3 groups was extracted together with their relative amounts and their respective chemical shift anisotropy parameters[12] [δ_{iso}, Ω (span), κ (skew)]. In a recent paper devoted to zinc phosphonates,[13] we have demonstrated that the κ parameter (chemical shift asymmetry) gave a good signature of the connectivity of the PO_3 groups (*i.e.* the number of zinc atoms connected to each of the three oxygen atoms bound to phosphorus). The value of κ is directly related to the range of variation of the bond strength at the phosphonate oxygens (Δ_pO^{2-}),[14] that in this case, was different for the various types of connectivity, that were thus easily determined: (111) connectivity [$\kappa = -0.6$ to -0.5; $\Delta_pO^{2-} \approx 0.05$ to 0.1], (112) [$\kappa = -0.2$; $\Delta_pO^{2-} \approx 0.2$] and (122) [$\kappa = 0.05$–0.1; $\Delta_pO^{2-} \approx 0.3$]. Similarly in compound **1**, the highest value of the κ parameter is probably found for the highest Δ_pO^{2-} (0.29). As the two PO_3 sites exhibit the same (111) coordination mode, we can see, for a given connectivity, that the range of variation of

Table 2 ^{31}P chemical shift tensor data for gallium phosphonates **1** and **2**

	δ_{iso}	Ω^b	κ^c	Δ_pO^{2-} (v.u.)^d
1	14.9 (site 1: 50%)	76.5	−0.3	0.29
	12.0 (site 2: 50%)	74.5	−0.5	0.15
2	25.3 (site 1: 50%)	53.1	0.0	—
	23.9 (site 2: 50%)	52.6	−0.2	—

[a] Chemical shifts are referenced to ^{31}P resonance in 85% H_3PO_4. [b] Chemical shift span defined as $\delta_{11} - \delta_{33}$ with $\delta_{11} \geqslant \delta_{22} \geqslant \delta_{33}$, see ref. 12(*b*). [c] Chemical shift skew defined as $3(\delta_{22} - \delta_{iso})/\Omega$. [d] Bond strength range at oxygens, see ref. 14(*b*).

Δ_pO^{2-} is far larger than it was in the case of zinc phosphonates. It would be very helpful to know if the differentiation of the various connectivities from the κ parameter is still possible in gallium phosphonates, but additional crystallographic references are necessary, and work is in progress for this purpose. Nevertheless, if we look at the κ values measured for compound **2** (Table 2), it is reasonable to think that the site at δ 25.3 ($\kappa = 0.0$) denotes a PO_3 group with a connectivity higher than (111).

In summary, the work reported here illustrates that original gallium phosphonates can be obtained and efficiently characterized using ^{31}P MAS and ^{71}Ga static NMR spectroscopy.

Footnotes and References

* E-mail: bujoli@chimie.univ-nantes.fr

† *Structure* of **1**: $GaPO_7C_3H_8$, orthorhombic, space group $Pca2_1$, $a = 9.5111(2)$, $b = 7.2829(1)$, $c = 20.3977(5)$ Å. The structure was refined using the full X-ray powder pattern in GSAS, with final *R*-factors: $R_{wp} = 0.106$, $R_p = 0.083$, $R_F = 0.053$ for 1674 reflections (statistically expected $R_{wp} = 0.039$). CCDC 182/701.

1 D. Deniaud, B. Schöllhorn, D. Mansuy, J. Rouxel, P. Battioni and B. Bujoli, *Chem. Mater.*, 1995, **7**, 995.
2 For recent articles about the chemistry of phosphonates, see for example: G. Cao, H. Hong and T. E. Mallouk, *Acc. Chem. Res.*, 1992, **25**, 420; M. E. Thompson, *Chem. Mater.*, 1994, **6**, 1168; H. E. Katz, *Chem. Mater.*, 1994, **6**, 2227; A. Clearfield, *Curr. Opin. Solid State Mater. Sci.*, 1996, **1**, 268; G. Alberti, in *Comprehensive Supramolecular Chemistry*, ed. G. Alberti and T. Bein, Pergamon, New York, 1996, vol. 7, p. 151.
3 See for example: W. Tieli, Y. Guandji, F. Shouhua, S. Changjiang and X. Ruren, *J. Chem. Soc., Chem. Commun.*, 1989, 948; M. Estermann, L. B. McCusker, C. Baerlocher, A. Merrouche and H. Kessler, *Nature*, 1991, **352**, 320; R. H. Jones, J. M. Thomas, Q. Huo, R. Xu, M. B. Hursthouse and J. Chen, *J. Chem. Soc., Chem. Commun.*, 1991, 1520.
4 S. Drumel, P. Janvier, M. Bujoli-Doeuff and B. Bujoli, *Inorg. Chem.*, 1996, **35**, 5786.
5 D. Massiot, I. Farnan, N. Gautier, D. Trumeau, A. Trokiner and J. P. Coutures, *Solid State NMR*, 1995, **4**, 241.
6 J. Rocha, Z. Lin, C. Fernandez and J. P. Amoureux, *Chem. Commun.*, 1996, 2513.
7 N. Gautier, D. Massiot, I. Farnan and J. P. Coutures, *J. Chim. Phys.*, 1995, **92**, 1843.
8 D. Massiot, V. Montouillout, F. Fayon, P. Florian and C. Bessada, *Chem. Phys. Lett.*, 1997, **272**, 295.
9 S. M. Bradley, R. F. Howe and R. A. Kydd, *Magn. Reson. Chem.*, 1993, **31**, 883.
10 T. Vosegaard, D. Massiot, N. Gautier and H. J. Jakobsen, *Inorg. Chem.*, 1997, **36**, 2446.
11 M. G. Walawalkar, R. Murugavel, A. Voigt, H. W. Roesky and H. Schmidt, *J. Am. Chem. Soc.*, 1997, **119**, 4656.
12 (*a*) D. Massiot, H. Thiele and A. Germanus, *Bruker Rep.*, 1994, **140**, 1762; (*b*) J. Mason, *Solid State Nucl. Magn. Reson.*, 1993, **2**, 285; (*c*) J. Herzfeld and A. E. Berger, *J. Chem. Phys.*, 1980, **73**, 6021.
13 D. Massiot, S. Drumel, P. Janvier, M. Bujoli-Doeuff and B. Bujoli, *Chem. Mater.*, 1997, **9**, 6.
14 (*a*) A. K. Cheetam, N. J. Clayden, C. M. Dobson and R. J. B. Jakeman, *J. Chem. Soc., Chem. Commun.*, 1986, 195; (*b*) I. D. Brown and D. Altermatt, *Acta Crystallogr., Sect. B*, 1985, **41**, 244.

Received in Basel, Switzerland, 22nd July, 1997; 7/05270G

Enzymatic epoxidation of polybutadiene

Ann W. P. Jarvie,* Nigel Overton and Christopher B. St Pourçain†

Division of Chemical Engineering and Applied Chemistry, Aston University, Aston Triangle, Birmingham, UK B4 7ET

An immobilised lipase isolated from *Candida antarctica* (Novozym 435) catalyses the selective epoxidation of polybutadiene.

The use of enzymes in organic synthesis is becoming increasingly widespread. There are previous reports of the use of lipases in polytransesterification reactions, but their application to the modification of the backbone of synthetic polymers has not been explored.[1] We now report the enzyme catalysed epoxidation of a monophenyl terminated polybutadiene ($M_n \simeq$ 1300; 45% 1,2-vinyl, 35% 1,4-*trans*, 20% 1,4-*cis*) in a three phase system, under very mild conditions. The polybutadiene was treated with a 27.5 wt% aq. solution of hydrogen peroxide, catalytic quantities of acetic acid, and an immobilised lipase isolated from *Candida antarctica* (Novozym 435), in CH_2Cl_2 at room temperature.‡ The reaction proceeded rapidly over 24 h. Little further epoxidation and no opening of the epoxide rings (absence of OH absorptions in the infrared spectra) occurred over an additional 72 h. Reactions carried out in the absence of enzyme showed no evidence of epoxidation. The molecular weight of the polymer, determined by GPC, did not alter significantly during the epoxidation procedure, indicating the absence of chain scission and coupling reactions. The degree of epoxidation was readily calculated from the ^{1}H NMR spectrum and the elemental analysis of the polymer. The results from both techniques were in close agreement. It was found that 29% of the double bonds had been oxidised over 24 h. The ^{1}H NMR spectra also allowed the relative numbers of 1,4-*cis*, 1,4-*trans* and 1,2-vinyl double bonds to be calculated. The signals arising from the phenyl end group were vital to this procedure. It was apparent that the reaction was highly selective, and under all conditions studied the 1,4-*cis* and 1,4-*trans* double bonds of the backbone were epoxidised whilst the 1,2-vinyl groups remained untouched. Thus the epoxidation of 29% of all the double bonds in the polymer after 24 h corresponds to 52% of the backbone double bonds being epoxidised.

Some selective preference for epoxidation of the double bonds of the backbone (1,4-*cis* > 1,4-*trans* ⩾ 1,2-vinyl) has been observed in previous attempts to epoxidise polybutadiene.[2–4] In these systems the vinyl groups began to react before all of the backbone double bonds had reacted and some of the backbone double bonds remained unreacted. Small amounts of ring opened products were also observed in the epoxidation of polybutadiene with a 1 : 2 mixture of acetic acid and 60 wt% hydrogen peroxide.[2] The mild conditions of the enzymatic epoxidation procedure allowed the selective epoxidation of the backbone double bonds without opening the epoxide rings. Only one approach, using a molybdenum catalyst, has shown both high selectivity and complete conversion.[5] With this catalyst the backbone double bonds were completely epoxidised within 3 h at room temperature and there was no further change in the next 70 h. No epoxidation of the 1,2-vinyl groups was observed.

The conditions of the reaction were varied in the hope that the selective epoxidation of all the backbone double bonds would be achieved. It has been reported that for monomeric systems the dropwise addition of the hydrogen peroxide over the course of the reaction gives better yields of epoxides than the addition of the oxidant in one portion at the beginning of the reaction.[6] We found that the percentage of epoxidised double bonds was reduced from 29 to 18% using this procedure. Changing the solvent from CH_2Cl_2 to toluene, while using the same dropwise addition procedure, increased the percentage of epoxidation from 18 to 30%. In contrast, using hexane gave only 2% epoxidation. The poor yield of epoxide obtained with hexane as solvent was surprising as hexane had been reported to be amongst the best solvents for the epoxidation of monomeric systems with this enzyme.[6] It is known that the enzyme is deactivated during the course of the reaction.[6] It was anticipated that increasing the amount of enzyme would increase the reaction rate, and more double bonds would be epoxidised in the time taken for the enzyme to become inactive. In fact, doubling the amount of enzyme had no effect and the yield of epoxide was virtually unchanged.

It has been established that the role of the enzyme in this system is to catalyse the synthesis of peracid, the actual species which attacks the double bond.[6] The enzyme plays no part in the actual epoxidation step. The generation of peracid *in situ* removes the need for handling these potentially hazardous compounds. Medium chain alkanoic acids (C_8 to C_{16}) were used with this enzyme in previous epoxidation reactions of monomeric systems.[6] With polymeric systems we found that very stable emulsions were formed, making the work up procedure extremely difficult. The use of acetic acid, instead of medium chain alkanoic acids, allowed the reaction to proceed efficiently and greatly simplified the work up procedure. Confirmation that the enzyme plays no part in the epoxidation of alkene by peracetic acid was obtained by epoxidising the polymer in CH_2Cl_2 with a 32% solution of peracetic acid in acetic acid with and without enzyme present. In both cases, over 96 h polybutadiene was completely epoxidised and the majority of the epoxide rings opened and esterified [ν_{max} (thin film) 1736 cm^{-1}]. There was no evidence of residual acid being retained by the polymer. Interestingly, the epoxide groups of polyepoxide polymers derived from polybutadiene have been reported to be relatively inert to ring opening reactions with carboxylic acids, requiring forcing conditions.[7]

Table 1 Enzymatic epoxidation of polybutadiene

Run	*t*/h	Solvent	Hydrogen peroxide addition[a]	Enzyme/ wt%	Yield of epoxide (%)[b]	Yield of 1,4-*cis* and 1,4-*trans* epoxide (%)[b]
1	2	CH_2Cl_2	A	10	~0	~0
2	6	CH_2Cl_2	A	10	12	21
3	24	CH_2Cl_2	A	10	29	52
4	96	CH_2Cl_2	A	10	31	57
5	24	CH_2Cl_2	B	10	18	33
6	24	Hexane	B	10	2	4
7	24	Toluene	B	10	30	55
8	24	CH_2Cl_2	B	20	21	39

[a] A: Oxidant added in one portion at the start of the reaction. B: Oxidant added dropwise over the course of the reaction. [b] Determined *via* ^{1}H NMR spectroscopy.

Further investigation of this intriguing approach to polymer modification and its potential for modifying polymers for speciality materials applications, such as biomaterials, and polymer degradation are currently underway.

We thank the EPSRC for a studentship (to N. O.) and Novo Nordisk for the gift of Novozym 435.

Footnotes and References

† E-mail: stpourcb@aston.ac.uk

‡ A typical procedure is as follows: Polybutadiene (5.0 g, 92 mmol of double bonds) was dissolved in CH_2Cl_2 (100 cm^3). AcOH (0.23 cm^3, 9 mmol), a 27.5 wt% aq. solution of H_2O_2 (17.0 cm^3, 0.14 mol) and Novozym 435 (0.5 g) were added and the mixture stirred for 24 h in the dark. The mixture was then filtered, extracted with saturated aq. $NaHCO_3$ and sodium metabisulfite, and dried ($MgSO_4$). The solvent was removed and the polymer dried in a vacuum oven at 55 °C and 1 mmHg.

1 A. W. P. Jarvie, B. K. Samra and A. J. Wiggett, *J. Chem. Res.* (*S*), 1996, 129.
2 D. Zuchowska, *Polymer*, 1980, **21**, 514.
3 R. V. Gemmer and M. A. Golub, *J. Polym. Sci.*, 1978, **16**, 2985.
4 M. Aguiar, S. Cabral de Menzezes and L. Akcelrud, *Macromol. Chem. Phys.*, 1994, **195**, 3937.
5 M. Gahagan, A. Iraqui, D. C. Cupertino, R. K. Mackie and D. J. Cole-Hamilton, *J. Chem. Soc., Chem. Commun.*, 1989, 1689.
6 F. Björkling, S. E. Godtfredsen and O. Kirk, *J. Chem. Soc., Chem. Commun.*, 1990, 1301.
7 A. Iraqui and D. J. Cole-Hamilton, *J. Mater. Chem.*, 1992, **2**, 183.

Received in Liverpool, UK, 3rd October 1997; 7/07168J

Theoretical and experimental studies of the unprecedented spin-dependent structures of $[Cp_2Fe_2(CO)_2]$, the double-CO-loss product of $[Cp_2Fe_2(CO)_4]$

Marcello Vitale, Marsi E. Archer and Bruce E. Bursten*

Department of Chemistry, The Ohio State University, Columbus, OH 43210, USA

Photochemically generated $[(\eta\text{-}C_5R_5)_2Fe_2(CO)_2]$, which is a triplet molecule with terminal CO ligands, undergoes thermal relaxation to the singlet ground state of the molecule, which has bridging CO ligands.

Dinuclear organometallic complexes (DOCs) demonstrate remarkably rich and diverse photochemistry.[1] This paper focuses on new aspects of the photochemistry of one of the best studied DOCs, namely the diiron complex $[Cp_2Fe_2(CO)_4]$ (**1**, Cp = η^5-C_5H_5), and its half-methylated and permethylated derivatives $[Cp(Cp^*)Fe_2(CO)_4]$ (**1′**, Cp* = η^5-C_5Me_5) and $[Cp^*_2Fe_2(CO)_4]$ **1***.[2] We report evidence here for a remarkable and unprecedented spin-dependent structural change in an organometallic photoproduct.

In 1983, Rest and coworkers[3] and Wrighton and coworkers[4] demonstrated that irradiation of **1** in frozen hydrocarbon matrices leads to CO loss and the formation of $[Cp_2Fe_2(\mu\text{-}CO)_3]$ **2**, which has a formal Fe–Fe double bond and three symmetrically bridging CO ligands (ν_{CO} = 1812 cm^{-1}). Complex **2** is unusual inasmuch as it has a triplet ground state owing to its high, pseudo-D_{3h} symmetry.[5] We demonstrated that irradiation of **1** in softer hydrocarbon matrices leads to subsequent loss of CO from **2**, yielding the double-CO-loss product $[Cp_2Fe_2(CO)_2]$ **3**:[6]

$$\underset{\mathbf{1}}{[\{CpFe(CO)\}_2(\mu\text{-}CO)_2]} \xrightarrow{h\nu,\,-CO} \underset{\mathbf{2}}{[(CpFe)_2(\mu\text{-}CO)_3]} \xrightarrow{h\nu,\,-CO} \underset{\mathbf{3}}{[\{CpFe(CO)\}_2]} \quad (1)$$

Based on the positions and near-equal intensities of its IR bands in the CO-stretching region (1904, 1958 cm^{-1}), we proposed that **3** has a C_2 structure in which two equivalent CpFe(CO) fragments are bonded together *via* an unsupported Fe–Fe triple bond, with a dihedral angle of *ca*. 90° between the two CO ligands.[6] Compounds **1′** and **1*** exhibit wholly analogous matrix photochemistry, with methylation of the Cp ligands leading to the expected red-shift of the CO-stretching bands in the IR.†

The presence of terminal CO ligands in **3**, **3′** and **3*** is highly unusual. Other $[\{CpM(EO)\}_2]$ complexes of first-row transition elements, such as $[\{CpCo(CO)\}_2]$, contain bridging EO ligands.[7] $[\{CpPt(CO)\}_2]$ does have terminal CO ligands, but it seems likely that the Pt–Pt single bond in the latter is too long to support bridging CO ligands.[8]

In order to add insight into the unusual structure of **3**, we have performed electronic structure calculations of **3** using density functional theory.‡ We and others have used this methodology to predict the structures of metal carbonyl complexes with good success.[9] The calculated lowest-energy structure of **3** has C_{2v} symmetry with two symmetric bridging CO ligands [Fig. 1(*a*)], corresponding to a $^1A_1$ closed-shell electron configuration. The calculated dihedral angle between the two Fe–C(O)–Fe planes is 125°; it can therefore be viewed as structurally analogous to **2** with the removal of one of the μ-CO ligands.

We were initially puzzled by the apparent disagreement between this calculated structure of **3** and the one indicated by experiment. However, **3** is produced by a triplet precursor (**2**), and **3** readily back-reacts to form **2**, even in frozen matrices at < 90 K. These observations suggest that the conversion **3** + CO → **2** is a spin-allowed reaction, which would require that **3** be a triplet molecule. Our calculations on excited triplet states of **3** indicate that a low-lying ^3B state has a C_2 structure in perfect accord with that proposed from the matrix experiments, *viz.* terminal CO ligands and a dihedral angle of 86° [Fig. 1(*b*)].§ These calculations provide support for the notion that the double-CO-loss products **3**, **3′** and **3*** are produced as excited triplet molecules.

Our calculated Fe–Fe bond lengths for *trans*-**1** (2.548 Å) and **2** (2.274 Å)[10] are in good agreement with the crystallographic Fe–Fe bond lengths in *trans*-**1** (2.534 Å)[11] and **2** (2.265 Å).[5] These results give us confidence in the reliability of our calculated Fe–Fe bond lengths in the singlet and triplet forms of **3**, which are 2.116 Å and 2.189 Å, respectively. Both of these are significantly shorter than the Fe–Fe bond length in **2**, consistent with an increase in the formal Fe–Fe bond order from two in **2** to three in **3**.

The gross structural change predicted between the ground-state bridging-CO singlet form of **3** (denoted ^{1}**3**) and the terminal-CO triplet form of **3** (^{3}**3**) is unprecedented and suggests that ^{3}**3** is the kinetically favored product of the irradiation of **2**.

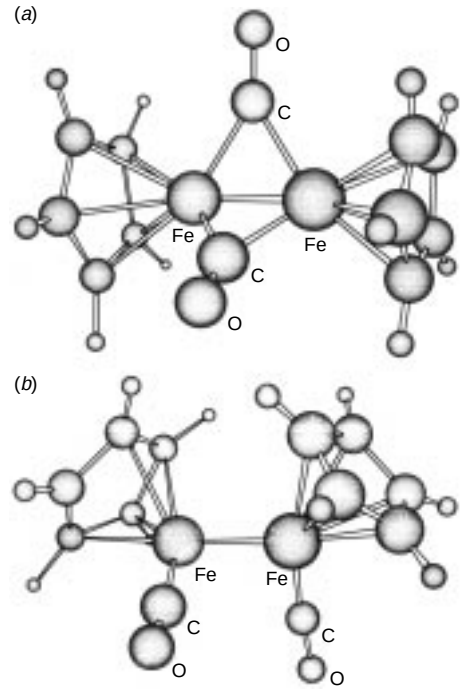

Fig. 1 (*a*) Calculated structure of the singlet ground-state structure of $[Cp_2Fe_2(CO)_2]$ **3**. Selected calculated metric parameters: Fe–Fe 2.116 Å, Fe–C(CO) 1.926 Å, Fe–(Cp centroid) 1.773 Å, Fe–Fe–(Cp centroid) 174°, dihedral angle between Fe–C(CO)–Fe planes 125°. (*b*) Calculated structure of the unbridged ^{3}B excited state of **3**. Selected calculated metric parameters: Fe–Fe 2.189 Å, Fe–C(CO) 1.778 A, Fe–(Cp centroid) = 1.850 A, Fe–Fe–(Cp centroid) 141°, dihedral angle between Fe–Fe–C(CO) planes 86°.

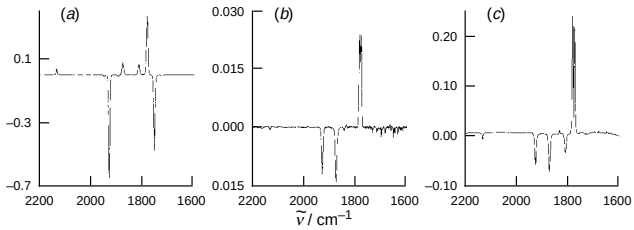

Fig. 2 Difference IR spectra of the CO-stretching region of a frozen solution of **1*** in 3-methylpentane at 98 K. (*a*) Difference spectrum obtained by subtracting the initial spectrum prior to irradiation from the spectrum obtained after 150 min irradiation. (*b*) Difference spectrum obtained by subtracting the spectrum immediately following 150 min irradiation from the spectrum obtained after 150 min irradiation followed by 5 min of thermal (dark) reaction at 98 K. (*c*) Difference spectrum obtained by subtracting the spectrum immediately following 150 min irradiation from the spectrum obtained after 150 min irradiation followed by dark warming of the matrix to 163 K and cooling back to 98 K.

It also suggests that, under appropriate conditions, ^{3}**3** should relax to form ground-state ^{1}**3**. We now believe that we have observed ^{1}**3*** in new matrix photochemical experiments.

When a frozen solution of **1*** (1 mM) in neat 3-methylpentane is irradiated for 150 min, we observe IR bands for free CO (2132 cm^{-1}), **2*** (1785 cm^{-1}), and ^{3}**3*** (1876 cm^{-1}; the 1929 cm^{-1} band of ^{3}**3*** is obscured by a band of **1***). We also observe a new bridging-CO band at 1812 cm^{-1} [Fig. 2(*a*)]. Observation at short irradiation times (< 5 min) indicates that the species that causes the band at 1812 cm^{-1} is formed only after ^{3}**3*** is formed. If the irradiation is discontinued and the matrix maintained at 98 K, we observe, *via* difference IR spectroscopy, only the thermal back-reaction ^{3}**3*** + CO → **2***, as was the case in the original report of **3** [Fig. 2(*b*)].[6] The band at 1812 cm^{-1} does not disappear on standing at 98 K. However, if the dark matrix is warmed to 163 K, we observe that free CO, ^{3}**3***, and the species at 1812 cm^{-1} are consumed as **2*** is produced [Fig. 2(*c*)]. We see analogous results upon prolonged irradiation of a matrix of **1′**, with the new band blue-shifted to 1833 cm^{-1}.

These new experimental data are consistent with the slow thermal or photochemical formation of ^{1}**3*** and ^{1}**3′** from ^{3}**3*** and ^{3}**3′**, respectively, and the slower (higher activation energy) back-reactions of ^{1}**3*** and ^{1}**3′** with CO to reform **2*** and **2′**. The slowness of these conversions is expected given that they are spin-forbidden. If our calculated structure of ^{1}**3** is correct, then the 1812 and 1833 cm^{-1} bands are likely the antisymmetric (B_1 under C_{2v} symmetry) stretching mode of the bridging CO ligands in ^{1}**3*** and ^{1}**3′**, respectively. The symmetric A_1 mode for each molecule should be at higher energy and, assuming the dipole moment changes are similar, will be only about half as intense as the B_1 mode. We have not yet observed the A_1 band for either ^{1}**3*** or ^{1}**3**. Our proposed series of transformations in the matrix photochemistry of **1*** is summarized in Scheme 1.

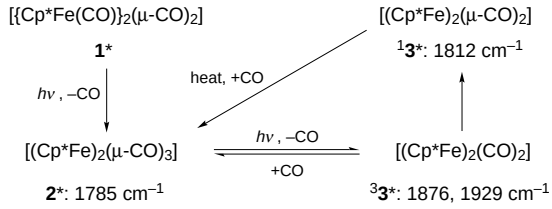

Scheme 1 Summary of proposed matrix photochemistry of **1*** in frozen 3-methylpentane

Direct kinetic access to the triplet double-CO-loss photoproducts such as **3** is a consequence of the symmetry-driven triplet ground state of the single-CO-loss photoproduct **2**. Lowering the symmetry of the initial precursor should favor the formation of singlet rather than triplet products. We believe that we have observed such an effect in the photochemistry of the lower-symmetry precursor [{Cp*Fe(CO)}$_2$(μ-CO)(μ-CH$_2$)], which forms a double-CO-loss product with a bridging or semi-bridging CO ligand.[12] We will continue to explore this interplay between spin state and structure in the photochemistry of other DOCs.

We thank Timothy Barckholtz for helpful discussions. We gratefully acknowledge the National Science Foundation (Grant CHE-9528568) and the Ohio Supercomputer Center for support of this research. M. E. A. is thankful for support as a GAANN Fellow, granted by the US Department of Education and administered by The Ohio State University.

Footnotes and References

* E-mail: bursten.1@osu.edu

† IR data in the CO-stretching region for relevant species in frozen 3-methylpentane at 90–100 K: **2′**, 1797 cm^{-1}; **2***, 1785 cm^{-1}; **3′**, 1886, 1942 cm^{-1}; **3***, 1876, 1929 cm^{-1}.

‡ *Computational details*: density functional calculations were carried out using the Amsterdam Density Functional (ADF) package, Version 2.1 (Theoretical Chemistry, Vrije Universiteit, Amsterdam, The Netherlands). The calculations employed the local density functional of Vosko, Wilk, and Nusair (S. H. Vosko, L. Wilk and M. Nusair, *Can. J. Phys.*, 1980, **58**, 1200). Non-local corrections to the exchange and correlation used the methods of Becke (A. D. Becke, *Phys. Rev. A*, 1988, **38**, 3098) and Perdew (J. P. Perdew, *Phys. Rev. B*, 1986, **33**, 8822), respectively. The atomic basis sets used were triple-ζ for the Fe atoms, double-ζ plus polarization for the CO ligands, and double-ζ for the Cp ligands. Geometries were fully optimized using gradient techniques under the constraint of C_2 symmetry.

§ The ^{3}B state is not the lowest energy triplet state of **3**. The lowest-energy triplet state, $^3B_1$, which we calculate to be *ca*. 20 kcal mol^{-1} (1 cal = 4.184 J) lower than the ^{3}B state, corresponds to a doubly bridged C_{2v} structure, like the ground state. We propose that the irradiation of **2*** produces both ^{3}B unbridged and $^3B_1$ bridged **3***. We further propose that the latter state, which we do not observe experimentally, undergoes a rapid, essentially barrier-free back-reaction with CO to reform **2***. A complete analysis of the excited states will be provided in a separate publication.

1 T. J. Meyer and J. V. Caspar, *Chem. Rev.*, 1985, **85**, 187.
2 Representative examples: T. J. Meyer and J. V. Caspar, *J. Am. Chem. Soc.*, 1980, **102**, 7794; B. D. Moore, M. Poliakoff and J. J. Turner, *J. Am. Chem. Soc.*, 1986, **108**, 1819; P. E. Bloyce, A. K. Campen, R. H. Hooker, A. J. Rest, N. R. Thomas, T. E. Bitterwolf and J. E. Shade, *J. Chem. Soc., Dalton Trans.*, 1990, 2833; A. J. Dixon, M. W. George, C. Hughes, M. Poliakoff and J. J. Turner, *J. Am. Chem. Soc.*, 1992, **114**, 1719; S. Zhang and T. L. Brown, *J. Am. Chem. Soc.*, 1993, **115**, 1779.
3 R. H. Hooker, K. A. Mahmoud and A. J. Rest, *J. Chem. Soc., Chem. Commun.*, 1983, 1022.
4 A. F. Hepp, J. P. Blaha, C. Lewis and M. S. Wrighton, *Organometallics*, 1984, **3**, 174.
5 J. P. Blaha, B. E. Bursten, J. C. Dewan, R. B. Frankel, C. L. Randolph, B. A. Wilson and M. S. Wrighton, *J. Am. Chem. Soc.*, 1985, **107**, 4561.
6 F. A. Kvietok and B. E. Bursten, *J. Am. Chem. Soc.*, 1994, **116**, 9807.
7 [(CpFe)]$_2$(μ-NO)$_2$]: J. L. Calderón, S. Fontana, E. Frauendorfer, V. W. Day and S. D. A. Iske, *J. Organomet. Chem.*, 1974, **64**, C16; [(Cp*Co)$_2$(μ-CO)$_2$]: W. I. Bailey, Jr., D. M. Collins, F. A. Cotton, J. C. Baldwin and W. C. Kaska, *J. Organomet. Chem.*, 1979, **165**, 373; L. M. Cirjak, R. E. Ginsburg and L. F. Dahl, *Inorg. Chem.*, 1982, **21**, 940; [(CpNi)$_2$(μ-CO)$_2$]: L. R. Byers and L. F. Dahl, *Inorg. Chem.*, 1980, **19**, 680; M. J. Winter, *Adv. Organomet. Chem.*, 1989, **29**, 101.
8 [(Cp*PtCO)$_2$]: N. M. Boag, *Organometallics*, 1988, **7**, 1446.
9 Representative examples: T. Ziegler, *Chem. Rev.*, 1991, **91**, 651; B. Delley, M. Wrinn and H. P. Lüthi, *J. Chem. Phys.*, 1994, **100**, 5785; T. A. Barckholtz, H. B. Lavender, F. A. Kvietok and B. E. Bursten, *Abstracts of Papers*, 209th ACS National Meeting, Anaheim, CA, 1995, Abstract INOR 128; A. Rosa, G. Ricciardi, E. J. Baerends and D. J. Stufkens, *Inorg. Chem.*, 1995, **34**, 3425.
10 M. Vitale, and B. E. Bursten, unpublished work.
11 P. T. Greene and R. F. Bryan, *J. Chem. Soc. A*, 1970, 3064.
12 Y. H. Spooner, E. M. Mitchell and B. E. Bursten, *Organometallics*, 1995, **14**, 5251.

Received in Bloomington, IN, USA, 28th August 1997; 7/06303B

One-step synthesis of a quaternary tetrapyridinium macrocycle as a new specific receptor of tricarboxylate anions

Satoshi Shinoda,*[a] Makoto Tadokoro,[a] Hiroshi Tsukube[a] and Ryuichi Arakawa[b]

[a] *Department of Chemistry, Faculty of Science, Osaka City University, Sugimoto, Sumiyoshi-ku, Osaka 558, Japan*
[b] *Department of Applied Chemistry, Kansai University, Yamate-cho, Suita 564-80, Japan*

A new type of quaternary tetrapyridinium macrocycle has been readily prepared *via* a one-step reaction, which showed characteristic selectivity for certain tricarboxylate anions upon 1 : 1 complexation.

Because anion recognition plays an important role in many biological processes, much effort has been devoted to designing specific anion receptors in molecular recognition chemistry.[1,2] In most of the reported receptors, positively charged groups such as ammonium and guanidinium units have been commonly introduced as binding sites, with electrostatic attraction between ion pairs predominantly contributing to the stability of the complexes.[3] Structural complementarity also affects both the selectivity and stability of the anion complexation. Kimura and Hosseini and Lehn demonstrated[4] that some protonated polyazamacrocycles bound carboxylates and phosphates, and exhibited interesting anion selectivity. Since the number of synthetic receptors specific for anions is still limited, a new class of macrocycles having well-defined geometrical and binding features should be developed, especially for specific recognition of biologically important organic polyanions.

Here, we present the one-step synthesis, crystal structure and anion binding property of a new macrocyclic receptor **1**.† Although polyammonium macrocycles have been presented as effective anion receptors, macrocycle **1** is remarkable for the following reasons. (1) Macrocycle **1** was directly derived from 3-bromomethylpyridine and its synthetic procedure was extremely simple. (2) The macro-ring is composed of four pyridinium rings having structurally and electrostatically well-defined features. (3) The positive charge of **1** is permanent and active even under neutral or weakly alkali conditions, while corresponding aliphatic polyammoniums are not fully protonated under such conditions.

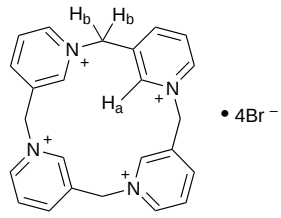

1

An aqueous solution of 3-bromomethylpyridinium bromide (4.5 g, 18 mmol) was neutralized with $NaHCO_3$ and the resulting 3-bromomethylpyridine was immediately extracted in CH_2Cl_2 (40 ml). When the solvent was evaporated at room temperature, *N*-alkylation vigorously occurred to yield a mixture of quaternary pyridinium salts. Hydrated single crystals of the tetrapyridinium bromide **1**, $C_{24}H_{24}N_4Br_4{\cdot}2H_2O$,‡ were isolated by recrystallization from water (230 mg, 0.32 mmol). A mixture of linear oligomeric pyridinium salts was obtained as major products, but product analysis by capillary electrophoresis revealed that cyclic compounds having different ring sizes were not formed under the employed conditions. *N*-Alkylation also occurred in refluxing CH_2Cl_2, which gradually yielded cyclic tetramer and linear polymer.

The crystal structure§ of **1**·$2H_2O$, determined by an X-ray diffraction study, indicates that the 16-membered ring containing four pyridine nitrogen atoms with positive charges is almost in one plane (Fig. 1). Of the four counter bromide anions, two are located inside the macrocycle, while the others are located outside the macrocycle. The distances between these bromide anions and the H_a protons of the pyridine rings are in the range 2.65–2.79 Å, which are shorter than the sum of the van der Waals radius of a hydrogen atom and the ionic radius of a bromide anion (3.17 Å).[5]

The binding property¶ of **1** for tricarboxylate anions was investigated by ^1H NMR titration experiments in D_2O in which the pH value was initially adjusted to be 7–8 with $NaHCO_3$ to make guest anions in the trivalent forms. Five tricarboxylic acids were employed: acyclic tricarboxylic acids **2**–**4** and cyclohexane tricarboxylic acids **5** and **6**. When **3** was employed as a guest, large downfield shifts ($\Delta\delta$ = 0.83 ppm, 1 equiv.) were observed for the H_a proton signal†† while the signals for other aryl protons shifted slightly upfield ($\Delta\delta$ = 0.13 ppm, 1 equiv.). Other tricarboxylates **2**, **4** and **5** gave similar ^1H NMR spectral changes and the observed titration curves showed saturation and were well fitted by the 1 : 1 complexation, although **6** provided too small changes in the ^1H NMR spectra to precisely analyze. The binding constants *K* were calculated

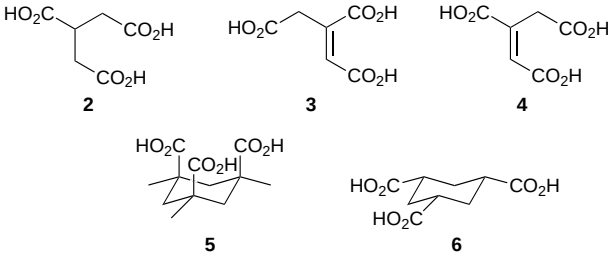

2

3

4

5

6

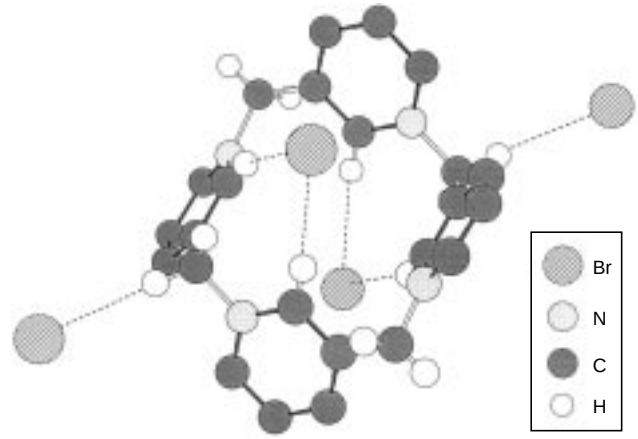

Fig. 1 Crystal structure of **1**·$2H_2O$. Hydrogen atoms other than H_a and H_b are omitted for clarification.

from the computer analysis,[6] indicating that **1** offered interesting anion selectivity for the four tricarboxylates; **3** (log K = 5.1) > **4** (4.5) ≈ **2** (4.4) > **5** (4.1). Among the acyclic tricarboxylates **2**–**4**, **3**, having two carboxylates fixed at the *cis*-1,2 positions, offered the largest K value. Because the employed tricarboxylates have the same net charges, the geometry of the three carboxyl groups should be an important factor for determining the stability and selectivity.[7] The order of the log K values parallels that of the chemical shift changes ($\Delta\delta$) of the H_a protons.‖

We have successfully prepared a new type of macrocyclic receptor *via* a one-step synthesis. Because of the pre-organized macrocyclic structure and highly positive charge, it specifically binds tricarboxylate anions at pH 7. Since its anion recognition behavior varied considerably from those observed with common protonated macrocyclic polyamines,[4,7] this study presents a new aspect of anion recognition chemistry with wide applications in related fields.

We thank Ms. S. Takeda of the Osaka National Research Institute, AIST, and Professor Akio Ichimura of Osaka City University for their helpful discussions. This research was supported by a Grant-in-Aid for Scientific Research (No. 08454205) from the Ministry of Education, Science, Sports and Culture, Japan.

Footnotes and References

* E-mail: shinodas@sci.osaka-cu.ac.jp

† R. E. Cramer and co-workers (ref. 8) prepared cyclic tetramers containing positive charge from vitamin B_1. Although they formed crystalline complexes with inorganic anions such as chloride, nitrate and $[Hg_2I_7]^{3-}$, their receptor functions have not been characterized in aqueous solutions.

‡ *Selected data* for **1**: mp 290 °C (decomp.) (Calc. for $C_{24}H_{24}N_4Br_4{\cdot}2H_2O$: C, 39.81; H, 3.90; N, 7.74. Found: C, 39.88; H, 3.81; N, 7.73%.) $\delta_H(D_2O)$ 9.43 (s, 4 H), 9.27 (d, 4 H), 8.91 (d, 4 H), 8.30 (t, 4 H) and 6.21 (s, 8 H); $\delta_C(D_2O)$ 151.02, 149.20, 147.21, 137.05, 132.98 and 63.25; λ_{max} (H_2O)/nm 263. With 3-chloromethylpyridine as a starting material, cyclic products were also found to be formed from the ^{1}H NMR spectrum of the reaction mixture. Unlike the bromide salt, they did not crystallize from the reaction mixture.

§ *Crystallographic data* for **1**·$2H_2O$: $C_{24}H_{28}O_2N_4Br_4$, triclinic, space group $P\bar{1}$ (#2), a = 9.664(6), b = 10.955(5), c = 7.115(2) Å, α = 108.11(3), β = 104.60(3), γ = 67.17(3)°, V = 652.3(5) Å^3, Z = 1; 3004 independent reflections measured at 296 K using a Rigaku AFC7S diffractometer; Mo-Kα; 2185 reflections with $I > 3\sigma(I)$ and 155 variables yields R = 0.045, R_w = 0.066. CCDC 182/692.

¶ The complexation between **1** and **5** was confirmed by ESI-MS spectroscopy in H_2O–MeOH (pH 7); $[(\mathbf{1}–4Br^-)^{4+} + (\mathbf{5}–3\ H^+)^{3-}]^+$ was found at 623, $[(\mathbf{1}–3\ Br^-)^{3+} + (\mathbf{5}–2\ H^+)^{2-}]^+$ at 703 and $[(\mathbf{1}–4\ Br^-)^{4+} + (\mathbf{5}–2\ H^+)^{2-}]^{2+}$ at 312.

‖ Similar NMR spectral changes were reported in non-cyclic pyridinium molecule systems and some contributions from the hydrogen bonding between anion guests and protons of the pyridinium ring were suggested. See K.-S. Jeong and Y. L. Cho, *Tetrahedron Lett.*, 1997, **38**, 3279.

1 C. Seel and J. de Menzoza, in *Comprehensive Supramolecular Chemistry*, ed. J. L. Atwood, J. E. D. Davis, D. D. Macnicol, F. Vögtle and J. M. Lehn, Elsevier, 1996, vol. 2, pp. 519; B. Dietrich, *Pure Appl. Chem.*, 1993, **65**, 1457.

2 P. D. Beer, A. R. Graydon, A. O. M. Johnson and D. K. Smith, *Inorg. Chem.*, 1997, **36**, 2112; M. Staffilani, K. S. B. Hancock, J. W. Steed, K. T. Holman, J. L. Atwood, R. K. Juneja and R. S. Burkhalter, *J. Am. Chem. Soc.*, 1997, **119**, 6324; B. Dietrich, B. Dilworth, J.-M. Lehn, J.-P. Souchez, M. Cesario, J. Guilhem and C. Pascard, *Helv. Chim. Acta*, 1996, **79**, 569; D. A. Nation, J. Reibenspies and A. E. Martell, *Inorg. Chem.*, 1996, **35**, 4597; A. Bencini, A. Bianchi, C. Giorgi, P. Paoletti, B. Valtancoli, V. Fusi, E. García-España, J. M. Llinares and J. A. Ramírez, *Inorg. Chem.*, 1996, **35**, 1114; M. Fernandez-Saiz, H.-J. Schneider, J. Satorius and W. D. Wilson, *J. Am. Chem. Soc.*, 1996, **118**, 4739.

3 H.-J. Schneider, T. Blatter, A. Eliseev, V. Rüdiger and O. A. Raevsky, *Pure Appl. Chem.*, 1993, **65**, 2329.

4 E. Kimura, *Top. Curr. Chem.*, 1985, **128**, 113; M. W. Hosseini and J. M. Lehn, *Helv. Chim. Acta*, 1986, **69**, 587.

5 F. A. Cotton, G. Wilkinson and P. L. Gaus, *Basic Inorganic Chemistry*, Wiley, 3rd edn., 1995.

6 H. Tsukube, H. Furuta, A. Odani, Y. Takeda, Y. Kudo, Y. Inoue, Y. Liu, H. Sakamoto and K. Kimura, in *Comprehensive Supramolecular Chemistry*, ed. J. L. Atwood, J. E. D. Davis, D. D. Macnicol, F. Vögtle and J. M. Lehn, Elsevier, 1996, vol. 8, pp. 425.

7 Complexation between polyamine [21]laneN$_7$ with seven carboxylate anions including **5**: A. Bencini, A. Bianchi, M. I. Burguete, P. Dapporto, A. Doménech, E. García-España, S. V. Luis, P. Paoli and J. A. Ramírez, *J. Chem. Soc., Perkin Trans. 2*, 1994, 569.

8 R. E. Cramer, C. A. Waddling, C. H. Fujimoto, D. W. Smith and E. Kim, *J. Chem. Soc., Dalton Trans.*, 1997, 1675; R. E. Cramer, V. Fermin, E. Kuwabara, R. Kirkup and M. Selman, *J. Am. Chem. Soc.*, 1991, **113**, 7033.

Received in Cambridge, UK, 13th October 1997; 7/07358E

The facile loss of formic acid from an anion system in which the charged and reacting centres cannot interact

Suresh Dua,[a] John H. Bowie,[a] Blas A. Cerda[b] and Chrys Wesdemiotis[b]

[a] *Department of Chemistry, The University of Adelaide, Adelaide, South Australia, 5005, Australia*
[b] *Department of Chemistry, The University of Akron, Akron, Ohio, 44325-3610, USA*

Both the 3-[2-(2-formyloxy-1,3-[$^2H_6$]propyl)]adamantane carboxyate anion and cation undergo loss of HCO_2D from the 3 substituent by processes which occur remote from and uninfluenced by the carboxylate charged centre.

It has been proposed that reactions which occur remote from and uninfluenced by the charged centre (charge-remote reactions) can occur following collisional activation of even electron organic anions in the gas phase.[1,2] In support of this, charge-remote loss of a radical from an $(M - H)^-$ ion is sometimes observed when the product formed is a stable radical anion.[3] The evidence in favour of the loss of (even electron) neutrals commonly occurring by charge-remote processes from even electron anions is not strong however.[4] One such process which has been substantiated is the Gross reaction:[1,2,5,6] the particular example shown in eqn. (1) is energetically unfavourable (calculations indicate that $\Delta H = +209$ kJ mol^{-1} while the activation barrier is some 370 kJ mol^{-1}), and occurs following extensive hydrogen exchange along the carbon skeleton.[6] It appears that charge-remote reactions may occur when anion directed fragmentations are energetically unfavourable in comparison.

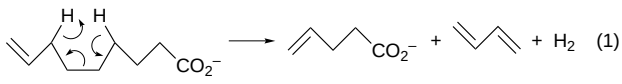

(1)

We have continued our search for charge-remote reactions utilising a system in which the anion site is unable to approach the reacting centre. Certain 1,3-disubstituted adamantanes fulfil this prerequisite, and we have chosen the carboxylate group as the anion site.

When cyclohexyl acetate is heated to 160 °C in solution, cyclohexene and acetic acid are formed in almost quantitative yield.[7] The reaction is slightly endothermic [$\Delta G = +18$ kJ mol^{-1} (ref. 8)] and the barrier is calculated [at MP4 (SDTQ)/6-31G* level for the model system ethyl formate] to be near 220 kJ mol^{-1}.[9] We have synthesised **1**† as an anion model for this reaction. The two substituents in **1** can neither interact through bonds, nor approach through space. The parent $(M - H)^-$ ion fragments by exclusive loss of HCO_2D (Fig. 1): this charge-remote reaction (which shows similarities to both the McLafferty rearrangement of a radical cation, and the Norrish 2 rearrangement of a diradical) is summarised in eqn. (2).

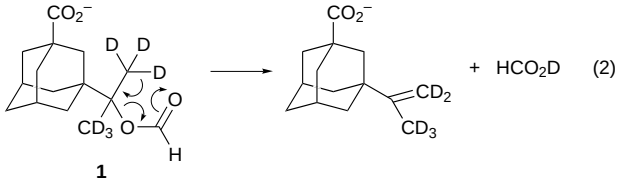

(2)

1

The neutrals formed following collisional activation of the unlabelled analogue corresponding to **1** have also been studied: the $^-N_fR^+$ spectrum (the compositive positive ion spectrum produced by ionisation of all neutrals formed following collisional activation of the parent negative ion)[5,6] of these shows a small peak on the side of the $CO_2^{\cdot+}$ peak which corresponds to *m/z* 46 ($HCO_2H^{\cdot+}$), establishing that formic acid is amongst the neutrals formed during fragmentation of unlabelled parent anion corresponding to **1**.

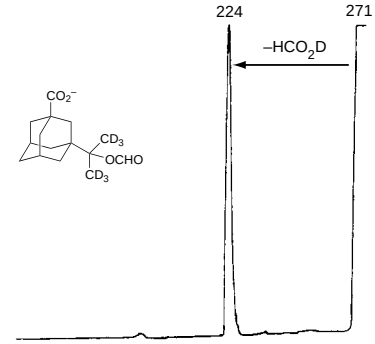

Fig. 1 Collisional activation mass analysed ion kinetic energy spectrum of **1**. VG ZAB 2HF mass spectrometer operating in negative chemical ionisation mode. The carboxylic acid precursor is deprotonated by HO^- (from H_2O), source pressure *ca.* 10^{-1} Torr (1 Torr = 133.322 Pa), collision gas Ar (pressure 5×10^{-7} Torr), for full experimental details see ref. 6.

Finally, if this reaction is uninfluenced by the charged centre, then it should also operate for the cognate species containing a carboxylate cation centre, provided of course that there is no low energy positive ion fragmentation which occurs in preference to the charge-remote reaction. A carboxylate cation cannot be formed by conventional positive ion mass spectrometry, but it is accessible by charge reversal[11] of anion **1**. The charge reversal spectrum of **1** (Fig. 2) [a charge reversal spectrum is the positive ion spectrum resulting from the energised $(M - H)^+$ species formed following collision induced charge stripping of the $(M - H)^-$ ion] shows small peaks due to $(M - H)^+$, $[(M - H)^+ - CO_2]$ and $[(M - H)^+ - HCO_2D]$

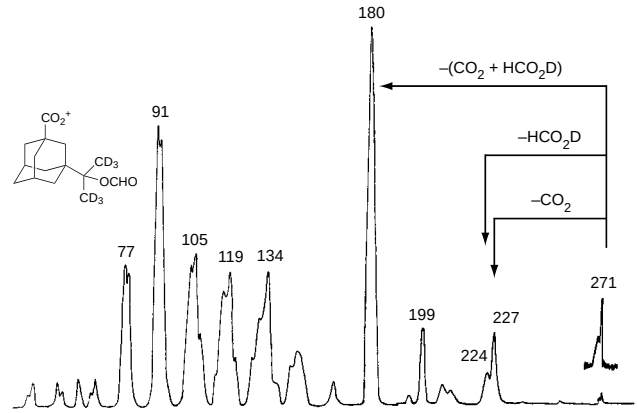

Fig. 2 Charge reversal (positive ion) mass spectrum of anion **1**. VG ZAB 2HF spectrometer. Experimental conditions as for Fig. 1 except that the voltage of the electric sector is reversed to allow the transmission of positive ions.

ions. The base peak is produced by the overall process [$(M - H)^+ - (CO_2 + HCO_2D)$] but it is not known whether loss of HCO_2D in this instance occurs from the $(M - H)^+$ and/or the [$(M - H)^+ - CO_2$] ions.

It is thus established experimentally that charge-remote loss of HCO_2D occurs from anion **1**, and also *via* the corresponding carboxylate cation.

We acknowledge funding from the Australian Research Council (J. H. B. and S. D.) and the National Institutes of Health, USA (C. W.).

Footnotes and References

* E-mail: jbowie@chemistry.adelaide.edu.au

† Dimethyl-1,3-adamantane dicarboxylate was reacted with 2.1 mol equiv. of CD_3Li to form methyl 3-[2-(2-hydroxy-1,3-[$^2H_6$]propyl)]adamantane carboxylate, which was hydrolysed under base catalysed conditions to the corresponding carboxylic acid, which was formylated using acetic–formic anhydride[10] to yield 3-[2-(2-formyloxy-1,3-[$^2H_6$]propyl)]adamantane carboxylic acid (the neutral precursor of **1**) in 60% overall yield.

1 J. Adams and M. L. Gross, *J. Am. Chem. Soc.*, 1989, **111**, 435 and references therein; M. L. Gross, *Int. J. Mass Spectrom. Ion Process.*, 1992, **118**/**119**, 137.
2 J. Adams, *Mass Spectrom. Rev.*, 1990, **9**, 141.
3 P. C. H. Eichinger and J. H. Bowie, *Int. J. Mass Spectrom. Ion Process.*, 1991, **110**, 123.
4 V. H. Wysocki, M. H. Bier and R. G. Cooks, *Org. Mass Spectrom.*, 1988, **23**, 627; V. H. Wysocki, M. M. Ross, S. R. Horning and R. G. Cooks, *Rapid Commun. Mass Spectrom.*, 1988, **2**, 214; V. H. Wysocki and M. M. Ross, *Int. J. Mass Spectrom. Ion Process.*, 1991, **104**, 179.
5 M. M. Cordero and C. Wesdemiotis, *Anal. Chem.*, 1994, **66**, 861.
6 S. Dua, J. H. Bowie, B. A. Cerda, C. Wesdemiotis, M. J. Raftery, J. F. Kelly, M. S. Taylor, S. J. Blanksby and M. A. Buntine, *J. Chem. Soc., Perkin Trans. 2*, 1997, 695.
7 C. H. DePuy and R. W. King, *Chem. Rev.*, 1960, **60**, 431.
8 Data from G. Aylward and T. Findlay, *S. I. Chemical Data*, Wiley, New York, 3rd edn., 1994.
9 S. A. Boehm and P. N. Skauche, *Int. J. Quantum Chem.*, 1991, **40**, 491.
10 W. Stevens and A. Van, *Rec. Trav. Chim. Pays-Bas.*, 1964, **83**, 1287; 1294.
11 J. H. Bowie and T.Blumenthal, *J. Am. Chem. Soc.*, 1975, **97**, 2959; J. E. Szulejko, J.H. Bowie, I. Howe and J. H. Beynon, *Int. J. Mass Spectrom. Ion Phys.*, 1980, **13**, 76.

Received in Cambridge, UK, 9th September 1997; 7/06571J

Tandem Michael-aldol induced ring closure of dimethyl 2-phenylselenofumarate: a diastereoselective entry to novel 4-phenylseleno butano-4-lactone derivatives, versatile precursors of naturally occurring compounds

Franco D'Onofrio,*[b] Roberto Margarita,[a,b] Luca Parlanti,*[a,b] Giovanni Piancatelli[a] and Maurizio Sbraga[a]

[a] Dipartimento di Chimica and [b] Centro CNR di Studio per la Chimica delle Sostanze Organiche Naturali (Istituto Nazionale di Coordinamento 'Chimica dei Sistemi Biologici'), Università 'La Sapienza' P.le A. Moro 5, 00185 Roma, Italy

Tandem Michael-aldol induced ring closure of dimethyl 2-phenylsenofumarate gives, with good yields and diastereoselectivities, highly substituted 4-phenylselenobutano-4-lactones, which can be further transformed into naturally occurring substances.

The synthesis of trisubstituted butenolides and butano-4-lactones, in particular of their 4-carboxy-derivatives (paraconic acids), has attracted considerable attention in recent years, because of the wide range of biological activities exhibited by this class of compounds,[1] which includes substances such as lichesterinic, protolichesterinic, dihydroprotolichesterinic,[1b,2h,i] roccellaric,[2j] nephromopsinic,[2f] pertusarinic[2k] and phaseolinic[2l] acids. Many synthetic approaches to these molecules have been developed by a number of research groups over the past decades.[2,3]

In connection with our previous studies on the reactivity of dimethyl 2-phenylselenofumarate **1** as a Michael acceptor,[4b,c] we describe here a simple method for the diastereocontrolled synthesis of the novel highly functionalized 4-phenylselenobutano-4-lactones **2a–d**, **3a–d**, which involves a tandem Michael-Aldol induced ring closure [reaction (1), Table 1]. We

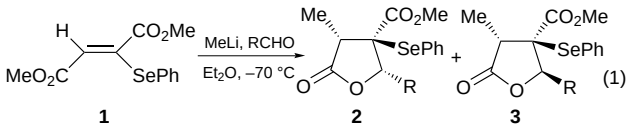

1 **2** **3**

also show the synthetic utility of the new molecules, which can be easily transformed into naturally occurring products, such as saturated and unsaturated paraconic acids.

As we described in a previous paper, the diester **1**, which is easily available from dimethyl maleate,[4a] reacts with MeLi in a Michael reaction, with no trace of the 1,2 addition products.[4b]

The anion resulting from this Michael addition can be easily trapped by adding an aldehyde to the reaction mixture; the resulting aldol adduct then instantaneously undergoes lactonization affording 4-phenylselenobutano-4-lactones **2a–d**, **3a–d** with good overall process yields [reaction (1), Table 1].†

As summarized in Table 1, the reaction proceeds with excellent diastereoselectivities when R = *n*-alkyl, aryl or 2-furyl; a lower diastereoselectivity is observed when an α,β-unsaturated aldehyde is used. The stereochemistry of the process could be rationalised assuming the formation of the chelated intermediate **A** resulting from the attack of MeLi and the subsequent approach of the aldehyde from the favoured *si*-face (Scheme 1).[5] However, the assignment of the relative stereochemistries of diastereoisomers **2** and **3** is based upon the following chemical evidence arising from further transformations of these compounds.

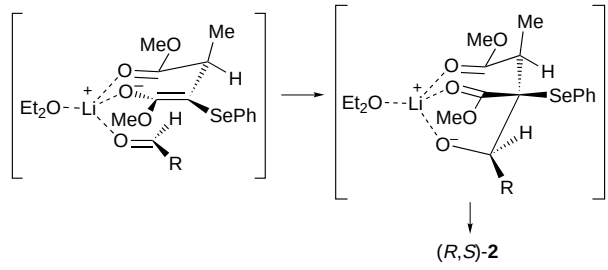

Scheme 1

First, **2** and **3** gave butenolides **4** *via* selenoxide *syn*-elimination when treated with $NaIO_4$,[6] [reaction (2), Table 2],

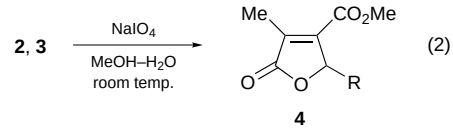

4

indicating that the phenylselenenyl and methyl groups in **2** and **3** must be in a *trans* relative configuration. Using **2a** and **3a** as starting compounds in this reaction allowed the synthesis of (*R*,*S*)-lichesterinic acid methyl ester **4a**; (*R*,*S*)-lichesterinic acid has been isolated from Icelandic moss *Cetraria islandica*.[7] This paraconic acid shows antibacterial activity towards Gram positive organisms,[7c] and various syntheses have already been reported in the literature.[3d,7c,8]

Secondly, in order to determine the relative configurations at C-5 in lactones **2** and **3**, hydrogenolysis of the C–Se bond of **2a**,**b** was carried out.[9] The resulting products were identified as

Table 1 Synthesis of γ-lactones **2a–d**, **3a–d**

R	**2** + **3**	Yield (%)	**2** : **3**
n-$C_{13}H_{27}$	**a**	71	93 : 7
Ph	**b**	58	89 : 11
2-Furyl	**c**	55	91 : 9
CH_3CH=CH	**d**	66	71 : 29

Table 2 Transformation of γ-lactones **2a–d**, **3a–d** to butenolides **4a–d**

R	**4**	Yield (%)
n-$C_{13}H_{27}$	**a**	92
Ph	**b**	73
2-Furyl	**c**	81
CH_3CH=CH	**d**	82

5a,**b**, **6a**,**b** by comparison with the literature data [reaction (3)];[2k] this outcome was interpreted in terms of a structure for

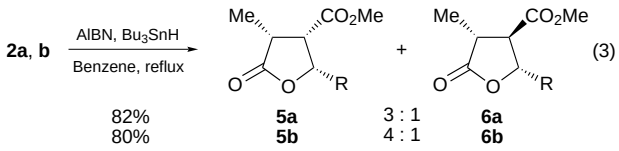

(3)

82% **5a** 3 : 1 **6a**
80% **5b** 4 : 1 **6b**

compound **2** in which the substituent at C-5 and the methyl group at C-3 are in a *cis* relative configuration. Consequently, the lactone **3** must have the same groups in a *trans* configuration.

In addition, as the predominant isomer **5a** can be easily epimerized to **6a**,[2k] this transformation also has synthetic relevance, as **6a** is the methyl ester of the naturally occurring roccellaric acid, isolated from the chilenic lichen species *Roccellaria mollis*.[2b]

In conclusion, we have described a facile diastereoselective synthesis of novel highly functionalized 4-phenylselenobutano-4-lactones and their application in the synthesis from **1** of racemic paraconic acids esters *e.g.* **4a** and **6a**, with good overall yields (65 and 58%, respectively). Furthermore, this strategy allows good flexibility with respect to the substituent at C-5, which is characteristic of paraconic acids.

Development of a stereocontrolled methodology to prepare enantiomerically pure compounds[2] *via* this sequential process and extension of the methodology are underway in our laboratory.

Footnotes and References

* E-mail: piancatelli@axrma.uniromal.it

† Typical experimental procedure: MeLi (1.1 mmol) was added to a stirred solution of **1** (1 mmol, 300 mg) at −70 °C in 10 ml of dry Et_2O, under argon atmosphere; the reaction mixture was allowed to react for 10 min and then the aldehyde (1.2 mmol), dissolved in 2 ml of dry Et_2O, was added. The resulting mixture was stirred at −70 °C for 1 h after which the temperature was raised to 0 °C and water was added. The solution was then extracted with ethyl acetate and the combined organic extracts were washed with aqueous $NaHCO_3$ and brine, dried over anhydrous Na_2SO_4 and concentrated under reduced pressure. Column chromatography on SiO_2 (hexane–ethyl acetate 9 : 1) afforded pure products **2** and **3**. Representative ^1H NMR; spectra δ($CDCl_3$); **2a**: 0.86 (3 H, m), 1.23 (3 H, d, *J* 7.0 Hz), 1.2–1.5 (22 H, m), 1.8–2.1 (2 H, m), 2.34 (1 H, q, *J* 7.0 Hz), 3.77 (3 H, s), 4.10 (1 H, dd, *J* 2.3 Hz, J_2 9.9 Hz); 7.3–7.5 (3 H, m), 7.5–7.6 (2 H, m). **2b**: 1.31 (3 H, d, *J* 7.0 Hz), 2.52 (1 H, q, *J* 7.0 Hz), 3.38 (3 H, s), 5.38 (1 H, s), 7.3–7.8 (10 H, m). Representative IR spectra; ν($CDCl_3$)/cm^{-1}. **2a**: 1773 (C=O, br), 1728 (C=O, br). **2b**: 1781 (C=O, br), 1731 (C=O, br).

1 (*a*) B. K. Park, M. Nakagawa, A. Hirota and M. Nakayama, *J. Antibiot.*, 1988, **41**, 751; (*b*) M. M. Murta, M. B. M. de Azevedo and A. E. Greene, *J. Org. Chem.*, 1993, **58**, 7537, and references cited therein.

2 (*a*) M. Pohmakotr, V. Reutrakul, T. Phongpradit and A. Chansri, *Chem. Lett.*, 1982, 687; (*b*) C. H. Bruckner and H. U. Reissig, *J. Org. Chem.*, 1988, **53**, 2440; (*c*) J. W. Lawlor and M. B. MgNamee, *Tetrahedron Lett.*, 1983, **24**, 2211; (*d*) J. Mulzer, P. de Lassalle, A. Chucholowski, U. Blascheck and G. Bruntrupp, *Tetrahedron*, **1984**, 40, 2211; (*e*) J. Mulzer and L. Kattner, *Angew. Chem., Int. Ed. Engl.*, 1990, **29**, 679; (*f*) J. Mulzer, L. Kattner, A. Stracker, C. Schroder, J. Buschmann and P. Luger, *J. Am. Chem. Soc.*, 1991, **113**, 4218; (*g*) M. B. M. de Azevedo, M. M. Murta and A. E. Greene, *J. Org. Chem.*, 1992, **57**, 4567; (*h*) J. Mulzer, N. Saliml and H. Hartl, *Tetrahedron: Asymmetry*, 1993, **4**, 457; (*i*) M. R. Banks, I. M. Dawson, I. Gosney, P. K. G. Hodgson and P. Thorburn, *Tetrahedron Lett.*, 1995, **36**, 3567; (*j*) M. P. Sibi and J. Ji, *Angew. Chem., Int. Ed. Engl.*, 1997, **36**, 274; (*k*) S. Shimada, H. Hashimoto and K. Saigo, *J. Org. Chem.*, 1993, **58**, 5226; (*l*) P. A. Jacobi and P. Herradura, *Tetrahedron Lett.*, 1996, **37**, 8297 and references cited therein.

3 (*a*) Y. S. Rao, *Chem. Rev.*, 1964, **64**, 353; 1976, **76**, 625; (*b*) M. Franck-Neumann and C. Berger, *Bull. Soc. Chim. Fr.*, 1968, 4067; (*c*) W. Haefliger and T. Petrzilka, *Helv. Chim. Acta*, 1966, **49**, 1937; (*d*) I. P. Soppo, *Heterocycles*, 1978, **9**, 1047; (*e*) I. Beltaief, R. Besbes, H. Amri and J. Villiéras, *Tetrahedron Lett.*, 1997, **38**, 813.

4 (*a*) F. D'Onefrio, L. Parlanti and G. Piancatelli, *Tetrahedron Lett.*, 1955, **36**, 1929; (*b*) F. D'Onofrio, L. Parlanti and G. Piancatelli, *Synlett*, 1966, 63; (*c*) M. Bella, F. D'Onofrio, R. Margarita, L. Parlanti, G. Piancatelli and A. Mangoni, *Tetrahedron Lett.*, 1997, **38**, 7917.

5 J. E. Dubois and J. F. Fort, *Tetrahedron*, 1972, **28**, 1665; D. A. Evans, *Asymmetric Synthesis*, ed. J. D. Morrison, Academic Press, New York, 1984, vol. 3, p. 2.

6 H. J. Reich, J. M. Renga and I. L. Reich, *J. Am. Chem. Soc.*, 1975, **97**, 5434.

7 (*a*) W. Zopf, *Liebigs Ann. Chem.*, 1902, **324**, 39; 1904, **336**, 46; (*b*) M. Asano and T. Kanematsu, *Chem. Ber.*, 1932, **65B**, 1175; (*c*) C. J. Cavallito and D. M. Fruehauf, *J. Am. Chem. Soc.*, 1948, **70**, 3724.

8 J. L. Bloomer, W. R. Eder and W. F. Hoffman, *J. Chem. Soc. (C)*, 1970, 1848.

9 C. Paulmier, *Selenium Reagnets and Intermediates in Organic Chemistry*, Pergamon Press, Oxford, 1986, p. 107 and references cited therein.

Received in Liverpool, UK, 1st October 1997; 7/07148E

Synthesis, structure and properties of $[Cr_2(PS_4)_4]^{6-}$; the first discrete transition metal cluster from thiophosphate flux reactions

Volkmar Derstroff, Vadim Ksenofontov, Philipp Gütlich and Wolfgang Tremel*

Institut für Anorganische Chemie und Analytische Chemie, Universität Mainz, Becherweg 24, D-55099 Mainz, Germany

The molecular cluster compound $[Cr_2(PS_4)_4]^{6-}$ forms by the reaction of Cr metal with thiophosphate fluxes.

Understanding the structural and reactivity relationships between molecules and extended solids of comparable compositions is a major challenge of synthetic inorganic chemistry. Many molecular cage and cluster compounds whose structural, and sometimes reactivity, features are comparable to those of metal oxide/chalcogenide/halide solids have been reported.[1–3] The well known behavior of metal alkoxides to oligomerize both in solution and in the solid state[4] has triggered studies on systems where a facile conversion of molecules to solids under mild conditions is possible, *e.g.* by using the sol–gel process[5] or by pyrolysis[6] of suitable precursors to achieve the desired solid product. The reverse process, an excision[7] of discrete metal clusters from extended solids, has received less attention so far.[8] Pioneering work has been done by the groups of Corbett[9] and Holm[10] who used solid state compounds containing discrete clusters as precursors for the synthesis of soluble species that are not accessible by solution methods. In contrast to tetrathiometalate complexes[11] metal coordination compounds with group 15 tetrathio anions as ligands (so-called Zintl-type ligands) are extremely difficult to stabilize in solution[12] because of their high negative charge and the lack of charge delocalization. The first representatives of this class of compounds are, however, easily accessible through solid state reactions† using polythiophosphate fluxes.[13]

The facile syntheses of the one-dimensional chain compounds $A_3[Cr_2(PS_4)_3]$ (A = K, Tl) whose structures contain the polymeric $^1_\infty[(Cr_2(PS_4)_3]^{3-}$ species[14] indicated that discrete $[Cr_2(PS_4)_4]^{6-}$ units might form from reaction systems containing a higher tetrathiophosphate content. In one Cr–P_2S_5–K_2S system containing the reactants in a 1 : 2 : 3 ratio at 600 °C the title compound formed in 85% yield after one week. The structure‡ of the title compound contains binuclear $[Cr_2(PS_4)_4]^{6-}$ clusters which are well separated from each other by K^+ cations. The anion portion of the clusters is shown in Fig. 1. The centrosymmetric $[Cr_2(PS_4)_4]^{6-}$ cluster consists of a $Cr_2(PS_4)_2$ core which is terminated on each side by two $[PS_4]^{3-}$ thiophosphate ligands in a bidentate fashion. In the core two $[PS_4]^{3-}$ ligands bridge two octahedrally coordinated Cr atoms employing three S atoms each. The remaining S atom is nonbonding. Relative to the idealized T_d anion symmetry, metal coordination decreases the S–P–S angle while the angle unbridged by Cr is considerably expanded. The Cr atoms are coordinated by three $[PS_4]^{3-}$ ligands where each thiophosphate group furnishes two S atoms to complete the octahedral S coordination of the metal. The Cr···Cr distance within the dimer is 3.523(1) Å. The unique Cr–S distance is comparable to that in CrP_3S_{9+x}[15] the individual Cr–S distances ranging from 2.387(1) to 2.485(1) Å.

Magnetic susceptibility measurements in the temperature range 4–300 K show that the Cr^{3+} centers within the binuclear units are antiferromagnetically coupled. This can be ascribed to a small antiferromagnetic exchange coupling between the Cr atoms in the dimeric units. The magnetic behavior can be modeled with the use of an isotropic Heisenberg–Dirac–Van Vleck dimer model for an $S_1 = S_2 = 3/2$ and an exchange coupling constant $J = -4$ cm^{-1}. The corresponding room temp. moment corrected for diamagnetism, $\mu_{eff} = 3.78\ \mu_B$, is slightly smaller than the spin-only value of 3.87 μ_B for Cr^{III} with $S = 3/2$. The optical spectrum of $K_6[Cr_2(PS_4)_4]$ exhibits a sharp optical gap consistent with semiconducting behavior. The experimentally determined value is $E_g = 1.36$ eV. Thermal analysis shows that $K_6[Cr_2(PS_4)_4]$ melts without decomposition at 433.8 °C.

$K_6[Cr_2(PS_4)_4]$ easily dissolves in DMF or acetonitrile upon addition of 2,2,2-cryptand, although so far we were unable to obtain precipitates with large cations in single-crystalline form. This behavior indicates the potential of $[Cr_2(PS_4)_4]^{6-}$ as a precursor for the synthesis of Zintl anion complexes in solution. The solutions of $K_6[Cr_2(PS_4)_4]$ in DMF are stable according to UV–VIS for 1–2 days. In DMF solution the $[Cr_2(PS_4)_4]^{6-}$ chromophore shows one strong absorption at 615 nm.

$K_6[Cr_2(PS_4)_4]$, the first transition metal thiophosphate with PS_4^{3-} ligands has been synthesized from molten polythiophosphate fluxes. Its structure contains the $[Cr_2(PS_4)_4]^{6-}$ cluster as a molecular analogue of the $[Cr_2(PS_4)_3]^{3-}$ units observed in the one-dimensional chain compound $K_6[Cr_2(PS_4)_4]$.[14] The $[Cr_2(PS_4)_4]^{6-}$ cluster is one of the few known complexes with a complete Zintl anion coordination sphere; it is stable in solution and may be useful as a synthon for 'wet' chemistry.

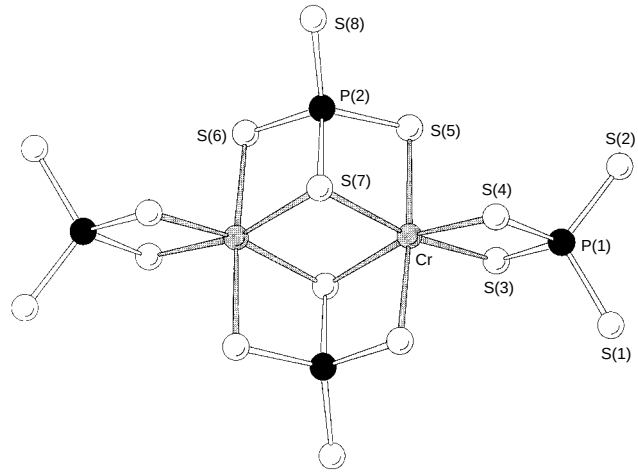

Fig. 1 Structure of the $[Cr_2(PS_4)_4]^{6-}$ anion with atomic labeling scheme. Selected bond lengths (Å) and angles (°): Cr–S(3) 2.387(1), Cr–S(4) 2.391(1), Cr–S(5) 2.416(1), Cr–S(6) 2.399(1), Cr–S(7) 2.451(1), Cr–S(7a) 2.485(1), P(1)–S(1) 2.003(2), P(1)–S(2) 2.004(2), P(1)–S(3) 2.090(2), P(1)–S(4) 2.073(2), P(2)–S(5) 2.048(2), P(2)–S(6) 2.045(2), P(2)–S(7) 2.114(2), P(2)–S(8) 1.967(2), S(3)–Cr–S(4) 84.05(4), S(3)–Cr–S(5) 85.94(5), S(3)–Cr–S(6) 99.37(5), S(3)–Cr–S(7) 167.52(5), S(3)–Cr–S(7a) 92.36(4), S(4)–Cr–S(5) 96.59(4), S(4)–Cr–S(6) 84.59(4), S(4)–Cr–S(7) 97.68(4), S(4)–Cr–S(7a) 165.09(4), S(5)–Cr–S(6) 174.66(5), S(5)–Cr–S(7) 81.58(4), S(5)–Cr–S(7a) 97.59(4), S(6)–Cr–S(7) 93.10(4), S(6)–Cr–S(7a) 81.72(4), S(1)–P(1)–S(2) 113.68(7), S(1)–P(1)–S(3) 198.73(7), S(1)–P(1)–S(4) 112.29(7), S(2)–P(1)–S(3) 111.13(7), S(2)–P(1)–S(4) 109.84(7), S(3)–P(1)–S(4) 100.39(6), S(5)–P(2)–S(6) 109.89(7), S(5)–P(2)–S(7) 99.61(6), S(5)–P(2)–S(8) 115.94(8), S(6)–P(2)–S(7) 100.39(6), S(6)–P(2)–S(8) 113.28(7), S(7)–P(2)–S(8) 115.93(7).

This work was supported by the Deutsche Forschungsgemeinschaft and the Fonds der Chemischen Industrie. We are indebted to Heraeus Quarzschmelze Hanau (Dr Höfer) for a generous gift of silica tubes.

Footnotes and References

* E-mail: tremel@indigotrem1.chemie.uni.mainz.de

† A mixture of Cr powder (0.104 g, 2 mmol), P_2S_5 (0.221 g, 2 mmol), K_2S (0.331 g, 3 mmol) and S (0.096 g, 3 mmol) was loaded into a silica tube in a glovebox. The tube was sealed under vacuum, heated to 600 °C for 4 d and then cooled slowly to room temp. at 4 °C h^{-1}. $K_6[Cr_2(PS_4)_4]$ can be isolated in high yields (> 85%) in the form of dark green platelets. The air-sensitive crystals are soluble in aprotic polar solvents upon addition of 2,2,2-cryptand.

‡ *Crystal data* for $K_6[Cr_2(PS_4)_4]$ at 25 °C: orthorhombic, space group *Pbca* (no. 61), a = 13.110(3), b = 12.050(2), c = 18.720(4) Å, U = 2957.3(8) $Å^3$, Z = 4, λ = 0.710 73 Å, D_c = 2.191 g cm^{-3}, μ(Mo-Kα) = 2.92 mm^{-1}, crystal platelike, dimensions 0.1 × 0.2 × 0.2 mm, θ_{max} = 54°, data collected at 25 °C on a Nicolet $P2_1$ four circle diffractometer, 6456; unique data, 3.226; data with $F_o^2 > 4\sigma(F_o^2)$, 2449; number of variables, 129. Structure solved and refined using SHELXS86 and SHELXL93, An empirical absorption correction based on ψ scans was applied to the data. Final R, R_w = 0.038, 0.094 (0.062, 0.094 for all data). CCDC 182/673.

1 Oxometalates: M. T. Pope, *Heteropoly and Isopoly Oxometalates*, Springer Verlag, New York, 1983; M. T. Pope and A. Müller, *Angew. Chem.*, 1991, **103**, 56; *Angew. Chem., Int. Ed. Engl.*, 1991, **30**, 34.

2 Metal thiolates: I. G. Dance, *Polyhedron*, 1986, **5**, 1037; B. Krebs and G. Henkel, *Angew. Chem.*, 1991, **103**, 785; *Angew. Chem., Int. Ed. Engl.*, 1991, 769.

3 Metal chalcogenides and halides: H. Schäfer and H. G. von Schnering, *Angew. Chem.*, 1964, **76**, 833; A. Simon, *Angew. Chem.*, 1981, **93**, 23, *Angew. Chem., Int. Ed. Engl.*, 1981, **20**, 1; F. A. Cotton, T. Hughbanks, C. E. Runyan and W. A. Wojtczak, *Early Transition Metal Clusters with π-Donor Ligands*, ed. M. H. Chisholm, VCH, New York, 1995, p. 1.

4 R. C. Haushalter, L. M. Meyer and J. Zubieta, *Early Transition Metal Clusters with π-Donor Ligands*, ed. M. H. Chisholm, VCH, New York, 1995, p. 217.

5 J. Livage, *Proceedings: Soft Chemistry Routes to the New Materials*, Trans Tech Publications, Aedermannsdorf, Switzerland, 1994, p. 43.

6 J. G. Brennan, T. Siegrist, S. M. Stuczynski and M. L. Steigerwald, *J. Am. Chem. Soc.*, 1989, **111**, 9240; 1990, **112**, 9233; D. C. Bradley, *Chem. Rev.*, 1989, **89**, 1317.

7 S. C. Lee and R. H. Holm, *Angew. Chem.*, 1990, **102**, 868; *Angew. Chem., Int. Ed. Engl.*, 1990, **29**, 840.

8 See, for example: F. Stollmaier and A. Simon, *Inorg. Chem.*, 1985, **24**, 168; M. R. Bond and T. Hughbanks, *Inorg. Chem.*, 1992, **31**, 5015; V. P. Fedin, M. N. Sokolov, O. A. Geras'ko, B. A. Kolesov, V. Ye Fedorov, A. V. Mironov, D. S. Yufit, Y. L. Slovokhtov and Y. T. Strutchkov, *Inorg. Chim. Acta*, 1990, **175**, 217.

9 F. Rogel and J. D. Corbett, *J. Am. Chem. Soc.*, 1990, **112**, 8198; F. Rogel, J. Zhang, M. W. Payne and J. D. Corbett, in *Electron Transfer in Biology and the Solid State*, ed. M. K. Johnson, R. B. King, D. M. Kurtz, Jr., C. Kutal, M. L. Norton and R. A. Scott, American Chemical Society, Washington, DC, 1990.

10 O. M. Yaghi, M. J. Scott and R. H. Holm, *Inorg. Chem.*, 1992, **31**, 840; J. C. Gabriel, K. Boubekeur and P. Batail, *Inorg. Chem.*, 1993, **32**, 2894; J. Long and R. H. Holm, *J. Am. Chem. Soc.*, 1995, **117**, 8139.

11 A. Müller, E. Diemann, R. Jostes and H. Bögge, *Angew. Chem.*, 1981, **93**, 957; *Angew. Chem., Int. Ed. Engl.*, 1981, **20**, 934.

12 B. Krebs, *Angew. Chem.*, 1983, **95**, 113; *Angew. Chem., Int. Ed. Engl.*, 1983, **22**, 113; H. J. Korte, Diploma Thesis, University of Münster, 1978; H. F. Klein, M. Gaß, U. Koch, B. Eisenmann and H. Schäfer, *Z. Naturforsch., Teil B*, 1988, **43**, 830; U. Bolle, Diploma Thesis, University of Münster, 1988; U. Bolle, Ph.D. Dissertation, University of Münster, 1991.

13 V. Derstroff and W. Tremel, *25. GDCh Hauptversammlung*, Münster, 1995, Abstr. p. 243; V. Derstroff and W. Tremel, submitted for publication; K. Chondrouris and M. G. Kanatzidis, *Chem. Commun.*, 1996, 1371; 1997, 401.

14 V. Derstroff, V. Ksenofontov, J. Ensling, P. Gütlich and W. Tremel, *Inorg. Chem.*, submitted for publication.

15 P. Fragnaud, M. Evain, E. Prouzet and R. Brec, *J. Solid State Chem.*, 1993, **102**, 390.

16 J. D. Corbett, *Chem. Rev.*, 1985, **85**, 383; U. Bolle and W. Tremel, *J. Chem. Soc., Chem. Commun.*, 1992, 93; 1994, 217.

Received in Cambridge, UK, 7th October 1997; 7/07240F

Steric acceleration in the reaction of aryl bromides with tributylstannyl radicals

David Crich* and Francesco Recupero

Department of Chemistry, University of Illinois at Chicago, 845 West Taylor Street, Chicago, IL 60607-7061, USA

Approximate absolute rate constants for the abstraction of bromine from a series of aryl bromides by stannyl radicals have been determined: 2,4,6-tri-*tert*-butylbromobenzene and 2,4,6-triphenylbromobenzene are found to be unusually reactive, most likely owing to steric acceleration.

Like many radical reactions,[1–5] the abstraction of a halogen atom from an aryl or vinyl halide by a stannyl radical is subject to polar effects. This much was demonstrated by Curran who showed that aryl halides carrying electron-withdrawing groups in the *ortho* or *para* positions react more rapidly with tin hydrides than do their unsubstituted congeners.[6] This is readily understood in terms of a polar transition state [eqn. (1)] with a partial negative charge on the sigma framework of the developing aryl radical.[6] We had therefore anticipated that 2,4,6-tri-*tert*-butylbromobenzene, with its sterically bulky, electron-donating alkyl groups, would be considerably less reactive than bromobenzene itself toward stannyl radicals. In the event, as we report here, the opposite was found to be the case: the abstraction of bromine from 2,4,6-tri-*tert*-butylbromobenzene by $Bu_3Sn\cdot$ is subject to a considerable acceleration due to the relief of steric strain.

In the course of an ongoing investigation, we had occasion to prepare 2,4,6-tri-*tert*-butyl- and 2,4,5-tri-iso-propylbromobenzene and to compare their reactivity toward tributyltin hydride with that of bromobenzene itself. Crude competition experiments revealed that, contrary to expectation, both were consumed somewhat more rapidly than the parent compound. We therefore undertook a more thorough investigation, comprising a series of competition experiments for a limited quantity of stannane. The initial and final ratios of both substrates in a given competition were determined by capillary GC or ^{1}H NMR spectroscopy, as appropriate, and the relative rates (k_{Rel}) computed using eqn. (2).[6,7]

$$k_1/k_2 = \{\ln[[Ar^1Br]_i/([Ar^1Br]_i - [Ar^1H])]\}/ \{\ln[[Ar^2Br]_i/([Ar^2Br]_i - [Ar^2H])\} \quad (2)$$

In this manner the relative rates set out in Table 1 were obtained.† The approximate absolute rate constants were then obtained using the known bimolecular rate constant for reaction of $Bu_3Sn\cdot$ with 1-bromodecane.[6] As is clear from Table 1, 2,4,6-tri-*tert*-butylbromobenzene is indeed considerably more reactive toward bromine abstraction by the stannyl radical than is 2,4,6-tri-iso-propylbromobenzene, being only slightly less reactive than 1-bromodecane. 2,4,6-Tri-iso-propylbromobenzene has comparable reactivity to 2-phenylbromobenzene and is some 2.6 times less reactive than 2-acetylbromobenzene. As this latter was found to be 6.7 times more reactive than 4-*tert*-butylbromobenzene, considered to be a model for bromobenzene itself, by Curran,[6] we conclude that 2,4,6-tri-iso-propylbromobenzene is some 2.6 times more reactive than bromobenzene. 2,4,6-Triphenylbromobenzene[8,9] was found to have identical reactivity to 1-bromodecane. We also studied pentafluorobromobenzene and found that it was so reactive toward the stannyl radical that we were unable to determine accurate ratios in competition experiments with 2-acetylbromobenzene; consequently we report a only minimum relative rate. With the likely exception of the perfluoroalkyl bromides,[10] pentafluorobromobenzene is the most reactive aryl or alkyl bromide toward stannyl radicals studied to date.

The reactivities of 2-phenyl- and 2-acetyl-bromobenzene are fully in accord with the polarized transition state [eqn. (1)] proposed by Curran. That of pentafluorobromobenzene likewise fits this model, although we cannot rule out an electron transfer chain mechanism in this case. The enhanced reactivity of 2,4,6-tri-iso-propylbromobenzene and especially that of 2,4,6-tri-*tert*-butylbromobenzene we attribute to acceleration due to relief of steric strain.‡ Such examples of steric acceleration of bimolecular radical reactions are much less common[1,11] than their unimolecular counterparts.[12] The reactivity of 2,4,6-triphenylbromobenzene can be ascribed to the symbiosis of three effects: (i) the stabilization of the polar transition state by the three phenyl groups phenyl substituents, (ii) relief of steric strain and (iii) relief of steric inhibition of resonance. However, as with pentafluorobromobenzene, we cannot rule out a single electron transfer mechanism in this case.

In conclusion, we have provided evidence that the abstraction of bromine from aryl bromides by stannyl radicals is accelerated when it leads to a relief of steric strain with bulky *ortho* substituents. Moreover, this acceleration is sufficient to overcome unfavourable polar effects in the transition state.

We thank the NSF (CHE 9625256) for partial support of this work. F. R. thanks the Politecnico di Milano for study leave and support.

Table 1 Relative reactivity of aryl bromides toward tributyltin radicals

Entry	Bromide	k_{Rel}	k/M^{-1} s^{-1}
1	Pentafluorobromobenzene	> 50	$> 1 \times 10^8$
2	1-Bromodecane	15.2	5.8×10^7
3	2,4,6-Triphenylbromobenzene	15.2	5.8×10^7
4	2,4,6-Tri-*tert*-butylbromobenzene	9.5	2.9×10^7
5[a]	2-Acetylbromobenzene	6.7	1.6×10^7
6	2-Phenylbromobenzene	2.6	6.2×10^6
7	2,4,6-Tri-iso-propylbromobenzene	2.6	6.2×10^6
8[a]	4-*tert*-Butylbromobenzene	1	2.4×10^6

[a] Taken from ref. 6.

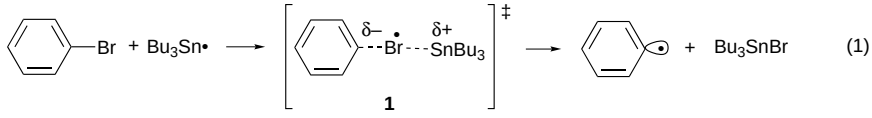

Footnotes and References

* E-mail: DCRICH@uic.edu

† All experiments were conducted a minimum of two times with good reproducibility.

‡ Space filling molecular models (CHEM3D) show that while the bromine atom in both 2,4,6-tri-*tert*-butylbromobenzene and 2,4,6-triphenylbromobenzene is in a very congested environment, it is sufficiently well-exposed to permit abstraction by $Bu_3Sn\cdot$ through a linear transition state.

1 G. A. Russell, in *Free Radicals*, ed. J. K. Kochi, Wiley, New York, 1973, vol. 1, pp. 275–331.
2 B. Giese, *Angew, Chem., Int. Ed. Engl.*, 1983, **22**, 753.
3 J. M. Tedder and J. C. Walton, *Tetrahedron*, 1980, **36**, 701.
4 J. M. Tedder, *Angew. Chem., Int. Ed. Engl.*, 1982, **21**, 401.
5 R. P. Allen, B. P. Roberts and C. R. Willis, *J. Chem. Soc., Chem. Commun.*, 1989, 1387.
6 D. P. Curran, C. P. Jasperse and M. J. Totleben, *J. Org. Chem.*, 1991, **56**, 7169.
7 M. Newcomb, *Tetrahedron*, 1993, **49**, 1151.
8 J. Graham and J. R. Quayle, *J. Chem. Soc.*, 1955, 3814.
9 A. Haaland, K. Rypdal, H. P. Verne, W. Scherer and W. R. Thiel, *Angew. Chem., Int. Ed. Engl.*, 1994, **33**, 2443.
10 W. R. Dolbier, *Chem. Rev.*, 1996, **96**, 1557.
11 P. A. Brady and J. Carnduff, *J. Chem. Soc., Chem. Commun.*, 1974, 816.
12 C. H. Ruchardt, *Top. Curr. Chem.*, 1980, **88**, 1.

Received in Corvallis, OR, USA, 16th September 1997; 7/06753D

Cobaltabis(dicarbollide) derivatives as extractants for europium from nuclear wastes

Clara Viñas,[a] Sílvia Gomez,[a] Josep Bertran,[a] Francesc Teixidor,*[a]† Jean-François Dozol*[b]‡ and Hélène Rouquette[b]

[a] *Institut de Ciència de Materials de Barcelona, Campus de la U.A.B., 08193 Bellaterra, Spain*
[b] *D.C.C./D.E.S.D./S.E.P., C.E.A. Cadarache, 13108 Saint Paul lez Durance, France*

Carbon substituted derivatives of [3,3′-Co(1-Me-2-R-1,2-$C_2B_9H_9)_2$]$^-$ incorporating lipophilic chains [R = $(CH_2)_3O(CH_2)_2OMe$ 1, $(CH_2)_3OCH_2CHMe_2$ 2, $(CH_2)_6O(CH_2)_3Me$ 3, $(CH_2)_3Me$ 4], are synthesized for the first time and tested for extraction of ^{152}Eu; compound 3 showed the best performance, and it proved to have higher efficiency in transport at low acidity than the well known calixarene derivatives.

Up to now, a large variety of metallacarboranes have been prepared using the [7,8-$C_2B_9H_{11}$]$^{2-}$ (dicarbollide) ligand.[1,2] Of them, [3,3′-Co(1,2-$C_2B_9H_{11})_2$]$^-$ [cobaltabis(dicarbollide)] has attracted the most attention, as it is very robust, withstanding strong acid, moderate base, high temperatures and intense radiation.[3] The stability of this ion makes it interesting in nuclear waste remediation.[3,4]

Cobaltabis(dicarbollide) is capable of removing caesium ions (and with much less efficiency strontium and trivalent lanthanides and actinides) with high selectivity from acidic fission product solution.[3,4]

The problem of removing caesium and strontium from nuclear wastes has been widely treated previously.[3–7] However, the extraction of trivalent actinides has still to be investigated. Since the properties of lanthanides and trivalent actinides are very similar, and handling of lanthanides is easier, the transplutonium elements were simulated by the γ emitter ^{152}Eu. We report here on some C-substituted derivatives of [3,3'-Co(1,2-$C_2B_9H_{11})_2$]$^-$, which in addition to maintaining the extracting properties of ^{137}Cs and ^{90}Sr, have proven to be very efficient in the extraction of ^{152}Eu.

Following a synthetic procedure developed previously in our group,[8] the reaction of [7-Me-8-R-7,8-$C_2B_9H_{10}$]$^-$ [R = $(CH_2)_3O(CH_2)_2OMe$, $(CH_2)_3OCH_2CHMe_2$, $(CH_2)_6O(CH_2)_3Me$, or $(CH_2)_3Me$],[9] with KOBu^t and $CoCl_2$ in dimethoxyethane at reflux for 30 h leads, after precipitation with aqueous CsCl, to a set of new products which are purified by TLC [ethyl acetate–acetonitrile (10 : 2)]; R_f (**1**) = 0.38, R_f (**2**) = 0.62, R_f (**3**) = 0.65, R_f (**4**) = 0.65 (Fig. 1).

A mixture of two geometric isomers were produced in this synthesis, which we were not able to separate (racemic mixture and *meso* form), owing to their extremely similar physical properties, however, chemical analyses establish their stoichiometric formulae. The shape of the NMR resonances clearly suggests the existence of more than one isomer.§

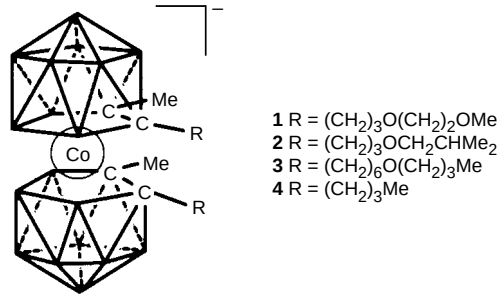

1 R = $(CH_2)_3O(CH_2)_2OMe$
2 R = $(CH_2)_3OCH_2CHMe_2$
3 R = $(CH_2)_6O(CH_2)_3Me$
4 R = $(CH_2)_3Me$

Fig. 1 Cobaltabis(dicarbollide) derivatives

Table 1 lists the distribution coefficient of europium, D_{Eu}, defined as the equilibrium ratio of europium between the organic and the aqueous phases. These were determined as previously described,[12] with the feed phase being an aqueous HNO_3 solution containing the radionuclides and the organic receiving phase being nitrophenyl hexyl ether.

At pH 3, compound **4** shows a very low D_{Eu}. The values of D_{Eu} are much better for compounds **2** and **3** which have only one oxygen atom in the alkylic chain. When a second oxygen atom is incorporated, as for compound **1**, D_{Eu} decreases. The results of the tests also show that the larger the exocluster chain the better the performance of the extracting agent. Compound **3** gives the best extraction coefficient. Attempts to synthesize cobaltabis(dicarbollide) derivatives with longer exocluster chains led to products which were difficult to isolate.

The distribution coefficient of the cation strongly decreases as acidity increases in the feeding solution.[4b] Despite this decrease of extracting ability in acidic medium, compounds **2** and **3** display good efficiency for the extraction of ^{152}Eu at pH 3.

The excellent results obtained for compound **3** prompted us to use it in transport tests at pH 3 using a reported method.[12] The transport of ^{152}Eu from aqueous HNO_3 solutions was followed by regular measurement of the decrease of radioactivity in the feed solution by γ spectrometry analysis. This allowed determination of the permeability constants P (cm h^{-1}) of ^{152}Eu permeation through the supported liquid membrane (SLM) for 3.5 h, as is described in the model of mass transfer proposed by Danesi[10]

$$\ln(C/C^0) = -\varepsilon\frac{S}{V}Pt$$

where C^0 and C are the concentrations of the cation in the feed solution at time t = 0 and t (mol dm^{-3}); ε is volumic porosity of the SLM (%); S is membrane surface area (cm^2); V is volume of feed and stripping solutions (cm^3); and t is time (h).

Transport experiments were carried out with addition of a linear polyether, nonylphenylnonaethylene glycol (Slovafol 909) to the organic phase (0.003 M) and using aqueous 1 M methylene diphosphonic acid (MDPA) as complexing agent in the stripping phase, to improve the transport of Eu.

Table 1 Distribution coefficients of ^{152}Eu (D_{Eu}) in aqueous HNO_3–nitrophenyl hexyl ether

	D_{Eu}		
Compound	pH = 3	pH = 2	pH = 1
1	16	9	0.06
2	> 1000[a]	> 1000[a]	0.05
3	> 1000	—	0.15
4	3.5	0.09	0.05

[a] A precipitate appears, which leads to a lack of precision in the determination of the distribution coefficient D.

It is found that transport is very rapid at pH 3. Under these conditions, compound **3** shows a permeability P of 8.9 cm h^{-1}, *i.e.* an extraction of 31.2% after 1 h or 91.3% after 3.5 h. Calixarene derivatives, which are known as excellent extractants for this type of radionuclides, show a value of 7.0 cm h^{-1} for ^{239}Pu (feeding phase: aqueous 1 M HNO_3),[11] *i.e.* lower than the value obtained with compound **3**. Furthermore, with other carriers such as diphosphine dioxides under similar conditions, transport is much slower: a permeability of 1.4 cm h^{-1} for ^{237}Np and 3.4 cm h^{-1} for ^{239}Pu were reported (feeding phase: aqueous 1 M HNO_3).[12]

This report shows that the efficient ^{137}Cs extractants, $[3,3'\text{-Co}(1,2\text{-}C_2B_9H_{11})_2]^-$, can be adequately tuned by appropriate cluster C-substitution to enhance ^{152}Eu and hopefully transplutonides. By this monoxygen C-substitution, the ^{152}Eu affinity of the $[3,3'\text{-Co}(1,2\text{-}C_2B_9H_{11})_2]^-$ derivatives has been extraordinarily enhanced with respect to the non-substituted parent compound, and its affinity towards ^{137}Cs and ^{90}Sr has not been decreased. For instance, **3** displays $D_{Cs} > 1000$ and $D_{Sr} = 8$ at pH 3, with $P = 15.8$ and 22.3 cm h^{-1}, respectively. Owing to the existence of more specific ^{137}Cs extracting agents such as calixarene or $[3,3'\text{-Co}(1,2\text{-}C_2B_9H_{11})_2]^-$, it should be possible to separate the elements. However, many questions arise in terms of the coordinating mode of these ligands towards ^{152}Eu that require further work, such as the position of the oxygen in the organic chain, or why the membrane transport is accelerated when polyethyleneglycols are incorporated in it.

This work was supported by EU project CIPA-CT93-0133. J. B. also thanks the Generalitat de Catalunya for a Predoctoral Grant (FIAP/96-98.469).

Footnotes and References

† E-mail: teixidor@icmab.es
‡ E-mail: DOZOLjf@DESDCAD.cea.fr

§ Compound **1**: ^{11}B NMR: δ {−13.97 [d, ^1J(BH) 192.6 Hz], −10.01 (m), −8.58 [d, ^1J(BH) 160.5 Hz], −4.78 [d, ^1J(BH) 128.4 Hz], −3.54 [d, ^1J(BH) 128.4 Hz], −1.22 [d, ^1J(BH) 128.4 Hz], 16B}, 7.31 [d, ^1J(BH) 96.3 Hz, 2B]. ^{11}B NMR data for the other compounds are analogous to that of **1**.

1 M. F. Hawthorne, D. C. Young and P. A. Wegner, *J. Am. Chem. Soc*., 1965, **87**, 1818.
2 Some leading references: A. K. Saxena and N. S. Hosmane, *Chem. Rev*., 1993, **93**, 1081; W. S. Rees Jr., D. M. Schubert, C. B. Knobler and M. F. Hawthorne, *J. Am. Chem. Soc*., 1986, **108**, 5367; J. C. Jeffery, P. A. Jelliss and F. G. A. Stone, *J. Chem. Soc., Dalton Trans*., 1993, 1073; G. C. Bazan, W. P. Schaefer and J. E. Bercaw, *Organometallics*, 1993, **12**, 2126.
3 J. Rais and P. Selucky, *Nucleon*, 1992, **1**, 17.
4 (*a*) J. Plesek, *Chem. Rev*., 1992, **92**, 269; (*b*) S. D. Reilly, C. F. V. Mason and P. H. Smith, *Cobalt (III) Dicarbollide: A Potential* ^{137}Cs *and* ^{90}Sr *Waste Extraction Agent*, Report LA-11695, Los Alamos National Laboratory, Los Alamos, NM, 1990.
5 P. K. Hurlburt, R. L. Miller, K. D. Abney, T. M. Foreman, R. J. Butcher and S. A. Kinkead, *Inorg. Chem*., 1995, **34**, 5215.
6 *Radioactive Waste Management and Disposal*, ed. L. Cecille, Elsevier, London, 1991.
7 R. Ungaro, A. Casnati, F. Ugozzoli, A. Pochini, J. F. Dozol, C. Hill and H. Rouquette, *Angew. Chem., Int. Ed. Engl*., 1994, **33**, 1506.
8 C. Viñas, J. Pedrajas, J. Bertran, F. Teixidor, R. Kivekäs and R. Sillanpää, *Inorg. Chem*., 1997, **36**, 2482.
9 F. Teixidor, S. Gomez, J. Bertran and C. Viñas, unpublished work.
10 P. R. Danesi, *Sep. Sci. Technol*., 1983–1985, **19**, 857.
11 F. Arnaud-Neu, V. Böhmer, J. F. Dozol, C. Grüttner, R. A. Jakobi, D. Kraft, O. Mauprivez, H. Rouquette, M. J. Schwing-Weill, N. Simon and W. Vogt, *J. Chem. Soc., Perkin Trans. 2*, 1996, 1175.
12 H. J. Cristau, P. Mouchet, J. F. Dozol and H. Rouquette, *Heteroatom Chem*., 1995, **6**, 533.

Received in Basel, Switzerland, 6th August 1997; Revised Manuscript received 22nd October 1997; 7/07835H

Homogeneous catalysis. Mechanisms of the catalysed Mukaiyama cross-aldol reaction

William W. Ellis and B. Bosnich*

Department of Chemistry, The University of Chicago, 5735 South Ellis Avenue, Chicago, Illinois 60637, USA

It is shown that [2 + 2] addition intermediates can form reversibly in the catalysed Mukaiyama reaction; these serve to prevent formation of the catalyst Me_3Si^+ and the reactivities of the [2 + 2] intermediates can affect the enantioselectivity of the reaction.

The Mukaiyama cross-aldol reaction is a versatile carbon–carbon bond-forming reaction which is catalysed by a variety of Lewis acids.[1] It is generally assumed to proceed by way of a cyclic intermediate **1** which allows for transfer of the silyl group (Scheme 1). For certain Lewis acids, however, intramolecular silicon transfer does not occur, rather the trimethylsilyl group is captured by the carbonyl substrate[2,3] and catalysis occurs by means of the powerful Me_3Si^+ catalyst.[2] Despite the possible widespread intervention of the (achiral) Me_3Si^+ catalytic path, there are a number of reports of chiral Lewis acid catalysts which give excellent enantiomeric excesses (ees),[4] indicating that for these catalysts, the unwanted Me_3Si^+ path is suppressed. The question then arises as to which type of Lewis acids will allow for one or other of the possible catalytic paths. It is probable that if the Lewis acid–oxygen bond of the aldolate **1** is weak and the bound oxygen atom is a good nucleophile, the rate of the silyl transfer step will be enhanced and consequently the capture of the Me_3Si^+ group by external nucleophiles will be suppressed. The direct silyl transfer path as illustrated in Scheme 1, however, may not be the only component of the mechanism because it is possible that an oxetane could form by capture of the carbenium ion of the intermediate. It is known that oxetanes are formed by Lewis acid-catalysed coupling of aldehydes and dialkyl ketene acetals.[5] The formation of the oxetane would be the equivalent of the Mukaiyama reaction, as an acidic workup would provide the desired aldol product. We report here on the detection of oxetanes in the Mukaiyama reaction using lanthanide and zinc complexes, both of which were expected to form aldolate intermediates with weak metal–oxygen bonds.

In benzene solution at 20 °C, the catalyst [Eu(hfc)$_3$] **2** (4 mol%) promotes the reaction between benzaldehyde and the ketene acetal **3** to give initially the two oxetane isomers **4** and **5** (Scheme 2). We have not been able to isolate these oxetanes in pure form but they have been characterized by their ^{1}H and ^{13}C NMR spectra, although the identity of the isomers **4** and **5** was not established.† The initial (kinetic) ratio of the isomers is 48 : 52 which slowly reaches an equilibrium ratio of 38 : 62. At 1 M concentration of each of the substrates, a maximum yield of 56% for the two oxetanes is obtained after 1 h in benzene solution at 20 °C using 4 mol% catalyst. Isomer equilibrium occurs over 2 h. The maximum yield of oxetanes (**4** and **5**) decreases upon dilution of the reaction solution, indicating that

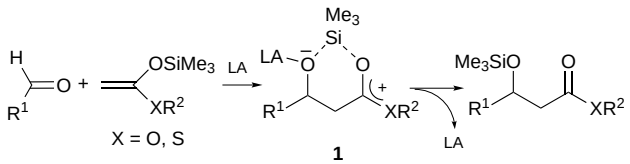

Scheme 1

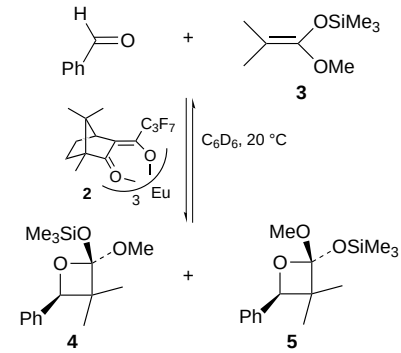

Scheme 2

the equilibrium illustrated in Scheme 2 obtains ($K \approx 3$ at 20 °C). Addition of 1 M pyridine quenches catalysis, but the addition of the hindered base, 2,6-di-*tert*-butyl-4-methylpyridine, does not affect the rate of catalysis. This latter observation indicates that the reaction in Scheme 2 is neither proton-initiated nor proton-catalysed. Under these conditions—4 mol% catalyst, 1 M each of substrates, benzene solution, 20 °C—the Mukaiyama product begins to appear after several hours and, after seven days, all of the substrates and intermediates are converted to this product. The Mukaiyama product is irreversibly formed because a 15% ee (*S*)[6] was found using the (+)-hfc catalyst, and the ee of the product did not change in the presence of the catalyst after two weeks. It was found that, after equilibration of the two oxetanes, their hydrolysed product had 0% ee using the (+)-hfc catalyst but a 5% ee (*S*) was observed for the hydrolysed products derived from the kinetically formed oxetanes (*ca.* 10% conversion to oxetanes).‡ This observation also supports the view that equilibration between substrates and oxetanes exists (Scheme 2).

The results are consistent with the mechanism outlined in Scheme 3 (Ln = **2**). In this case, the rate of production of the oxetanes by carbenium ion capture and the reverse reaction are faster than silyl transfer to produce the Mukaiyama product **7**. As might be expected, these relative rates vary according to the nature of the substrates and the catalyst. This is illustrated by a

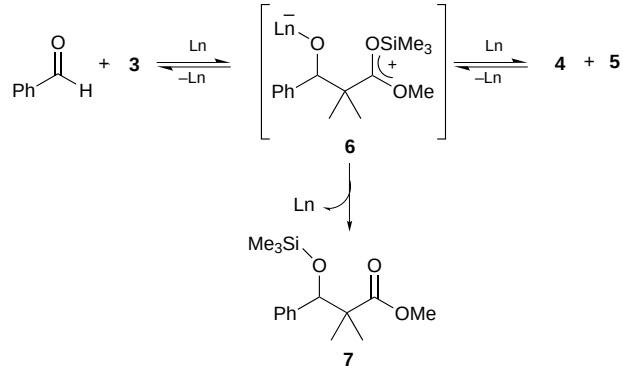

Scheme 3

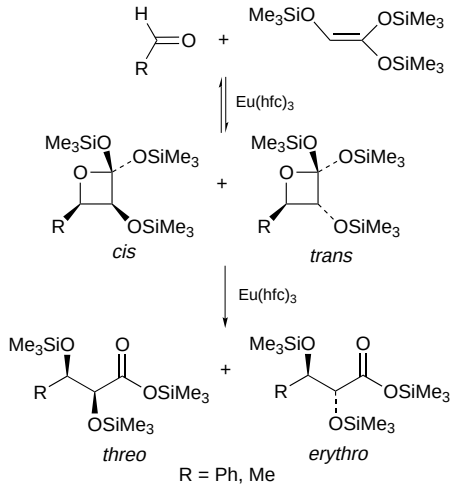

Scheme 4

comparison of the reactions shown in Scheme 4, where it is found that in catalysis of benzaldehyde, a *cis*:*trans* ratio of 80:20 is observed for the Mukaiyama product. For 1 mol% catalyst at 20 °C in benzene solution, the benzaldehyde reaction gives a *cis*:*trans* ratio of 75:25 at 40% conversion to the two oxetanes and 55:45 after 60% conversion.§ This change in isomer ratio occurs before significant amounts of the Mukaiyama products are formed, indicating that equilibration between the substrates and oxetanes occurs. Final equilibrium may not be established under these conditions, however, because a constant *cis*:*trans* ratio was not observed before the Mukaiyama product began to appear. For the analogous reaction with acetaldehyde (Scheme 4), under the same conditions, the rates of formation of the oxetanes and the Mukaiyama product are comparable. Similarly, the [Zn(facac)$_2$·2H$_2$O] (facac = hexafluoroacetylacetonate) complex catalyses the coupling between benzaldehyde and **3** but the equilibrium **4** ⇌ **5** is not established before significant amounts of the Mukaiyama product is formed (Scheme 2). With this zinc catalyst, no [2 + 2] addition products are observed in the coupling of benzaldehyde and CH$_2$=C(OSiMe$_3$)SBu^t indicating that catalysis proceeds either wholly by direct silyl transfer or, if [2 + 2] products are formed, their concentrations are very low. We note that neither the Eu nor the Zn catalysts lead to coupling of ketones with silyl ketene acetals nor coupling of silyl enol ethers with aldehydes or ketones.

The discovery of the [2 + 2] addition path for the catalysed Mukaiyama is significant in a number of respects. For cases where silyl transfer is slow in the intermediate **6** (Scheme 3), the more rapid oxetane formation will reduce the life-time of this intermediate. Consequently, the probability of Me_3Si^+ capture in **6** by external nucleophiles will be reduced. The Me_3Si^+ group is stable in the oxetanes. As was noted earlier, the mechanism illustrated in Scheme 3 is more likely to occur when the Lewis acid–alkoxide bond of the intermediate **6** is weak. Intermediates having strong alkoxide–Lewis acid bonds are unlikely to lead to oxetane formation or to silyl transfer. This appears to be the case for many catalysts which only serve as initiators for the production of Me_3Si^+ catalyst.[2]

These results suggest that identification of the enantioselective step can be a complicated problem because the ee will depend on the relative rates of formation of the various species. If equilibration between the substrates and oxetanes is much faster than formation of the Mukaiyama product, the ee will depend on the relative rates of silyl transfer which lead to the formation of the two enantiomers of the product. If, however, the rates of equilibration and product formation are comparable, the ee will depend on a complex mix of rates associated with all of the diastereomeric species in the mechanism. Under these circumstances, there would not be a single chirality-controlling step. The observations presented here may help in the design of effective enantioselective catalysts for the Mukaiyama reaction.

This work was supported by grants from the NIH.

Footnotes and References

* E-mail: bos5@midway.uchicago.edu

† *Selected spectroscopic data* for the major and minor oxetanes (at equilibrium): δ_H (400 MHz, C_6D_6) (major isomer) 7.3–7.1 (m, 5 H), 4.95 (s, 1 H), 3.26 (s, 3 H), 1.27 (s, 3 H), 0.76 (s, 3 H), 0.29 (s, 9 H); (minor isomer) 7.3–7.1 (m, 5 H), 4.99 (s, 1 H), 3.34 (s, 3 H), 1.25 (s, 3 H), 0.76 (s, 3 H), 0.23 (s, 9 H); δ_C (125 MHz, $CDCl_3$) (major isomer) 139.0 (s), 127.7 (d), 127.2 (d), 125.1 (d), 116.2 (s), 82.6 (d), 49.4 (s), 48.8 (q), 23.5 (q), 21.1 (q), 1.05 (q); (minor isomer) 138.5 (s), 127.7 (d), 127.0, 125.6 (d), 115.7 (s), 81.8 (q), 50.7 (s), 49.0 (q), 19.0 (q), 18.1 (q), 1.06 (q).

‡ Mild acid hydrolysis of the mixture of oxetanes leads to the formation of the β-hydroxy ester. Enantiomeric excesses of the hydrooxy ester were determined using Eu(tfc)$_3$ as a chiral shift reagent.

§ The *cis* and *trans* oxetanes where R = Ph and Me were identified by conversion of mixtures of these compounds to mixtures of their respective *threo* and *erythro* 2,3-dihydroxyalkanoic acids according to the reported procedure (ref. 7). In both cases, where R = Ph or Me, it is noted that hydrolysis of the *cis* and *trans* oxetanes leads to formation of the *threo* and *erythro* products, respectively, which were identified by comparison with spectroscopic data from the literature (ref. 8).

Selected spectroscopic data for the oxetanes: δ_H (400 MHz, C_6D_6) (R = Ph, *threo*) 7.47 (m, 2 H), 7.2–7.0 (m, 3 H), 5.18 (d, *J* 6.2, 1 H), 4.69 (d, *J* 6.2, 1 H), 0.29 (s, 9 H), 0.27 (s, 9 H), −0.22 (s, 9 H); (R = Ph, *erythro*) 7.43 (m, 2 H), 7.2–7.0 (m, 3 H), 4.98 (d, *J* 4.9, 1 H), 4.35 (d, *J* 4.8, 1 H), 0.35 (s, 9 H), 0.26 (s, 9 H), 0.01 (s, 9 H); (R = Me, *threo*) 4.42 (d, *J* 6.3, 1 H), 4.28 (m, 1 H), 1.25 (d, *J* 6.4, 3 H); (R = Me, *erythro*) 4.10 (m, 1 H), 4.02 (d, *J* 4.8, 1 H), 1.21 (d, *J* 6.2, 3 H). The OSi(CH_3)$_3$ resonances for R = Me were left unassigned due to the complexity of this region in the ^{1}H NMR spectrum of the reaction mixture.

1 S. Murata, M. Suzuki and R. Noyori, *J. Am. Chem. Soc.*, 1980, **102**, 3248; C. Mukai, S. Hashizome, K. Nagami and M. Hanaoka, *Chem. Pharm. Bull.*, 1990, **38**, 1509; H. Sukurai, K. Sasaki and A. Hosami, *Bull. Chem. Soc. Jpn.*, 1983, **56**, 3195; N. Iwasawa and T. Mukaiyama, *Chem. Lett.*, 1987, 463; T. Mukaiyama, S. Kobayashi, M. Tamura and Y. Sagawa, *Chem. Lett.*, 1987, 491; T. Mukaiyama, S. Kobayashi and M. Murakami, *Chem. Lett.*, 1985, 447; T. Mukaiyama, S. Kobayashi and M. Murakami, *Chem. Lett.*, 1984, 1759; S. Kobayashi, M. Murakami and T. Mukaiyama, *Chem. Lett.*, 1985, 1535; M. T. Reetz and A. E. Vougioukas, *Tetrahedron Lett.*, 1987, **28**, 793; S. Sato, I. Matsuda and Y. Izumi, *Tetrahedron Lett.*, 1987, **28**, 6657; S. Sato, I. Matsuda and Y. Izumi, *Tetrahedron Lett.*, 1986, **27**, 5517; T. Mukaiyama, T. Soga and H. Takenoshita, *Chem. Lett.*, 1989, 1273; S. Kobayashi, I. Hachiya and T. Takahori, *Synthesis*, 1993, 371; S. Kobayashi and I. Hachiya, *Tetrahedron Lett.*, 1992, **33**, 1625; S. Kobayahi, *Chem. Lett.*, 1991, 2187; S. Kobayashi, I. Hachiya, H. Ishitani and M. Araki, *Synlett*, 1993, 472; T. Bach, D. N. A. Fox and M. T. Reetz, *J. Chem. Soc., Chem. Commun.*, 1992, 1634; R. Hara and T. Mukaiyama, *Chem. Lett.*, 1989, 1909; T. Mukaiyama and R. Hara, *Chem. Lett.*, 1989, 1171.

2 T. K. Hollis and B. Bosnich, *J. Am. Chem. Soc.*, 1995, **117**, 4570.

3 E. M. Carreira and R. A. Singer, *Tetrahedron Lett.*, 1994, **35**, 4323.

4 E. M. Carreira, R. A. Singer and W. Lee, *J. Am. Chem. Soc.*, 1994, **116**, 8837; R. A. Singer and E. M. Carreira, *J. Am. Chem. Soc.*, 1995, **117**, 12 360; E. R. Parmee, O. Tempkin and S. Masamune, *J. Am. Chem. Soc.*, 1991, **113**, 9365.

5 J. W. Scheeren, *Recl. Trav. Chim. Pays-Bas*, 1986, **105**, 71; R. W. Aben and J. W. Scheeren, *Synthesis*, 1978, 400; H. Sugimura and K. Osumi, *Tetrahedron Lett.*, 1989, **30**, 1571; S. Vasudevan, C. P. Brock, D. S. Watt and H. Morita, *J. Org. Chem.*, 1994, **59**, 4677; T. Bach, *Tetrahedron Lett.*, 1994, **35**, 5845.

6 M. Guette, J. Capillon and J.-P. Guette, *Tetrahedron*, 1973, **29**, 3659.

7 A. Wissner, *Synth. Comm.*, 1979, 27.

8 T. Oesterle and G. Simchen, *Liebigs Ann. Chem.*, 1987, 693; T. Sakai, T. Nakamura, K. Fukuda, E. Amano, M. Utaka and A. Takeda, *Bull. Chem. Soc. Jpn.*, 1986, **59**, 3185.

Received in Corvallis, OR, USA, 7th August 1997; 7/05801B

New metallomesogens core. New copper complexes with calamitic mesophases using tropolone based ligands. Crystal structure of bis(5-octyloxytropolonato)copper

John R. Chipperfield, Steve Clark, James Elliott and Ekkehard Sinn*

Department of Chemistry, University of Hull, Hull, UK HU6 7RX

A new class of metallomesogens based on 5-substituted tropolones with both enantiotropic and monotropic mesophase behaviour are prepared, the mesogenic properties are in line with the rod-like, calamitic nature of bis(5-octyloxytropolonato)copper shown in its crystal structure.

Most metallomesogens[1–4] have made use of benzene rings as integral parts of the rigid core. Seven-membered ring cores in metallomesogens are reported here for the first time. Tropolone-based organic liquid crystals have been reported by Uemura *et al.*,[5] and Mori *et al.*[6–9] Tropolone forms complexes with many metals in a manner analogous to acetylacetone,[10] but none were reported to be metallomesogens. We report here the first syntheses and studies of mesogenic complexes **1** based on tropolone.

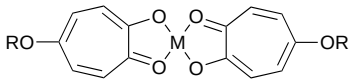

1 R = C_nH_{2n+1} (n = 8, 10, 12, 14, 16); M = Cu, Ni, VO

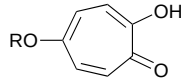

2a R = H,
b R = alkyl

We have modified the literature method[8] to make 5-substituted tropolones, **2b**, from 5-hydroxytropolone, **2a**, by using dimethylimidazolidinone (DMI) as solvent for alkylation of the 5-position to replace the carcinogenic HMPA.[8] DMI has in the past been reported as replacement for HMPA,[11–14] but we believe that this is the first reported use for tropolone derivatives Scheme 1.

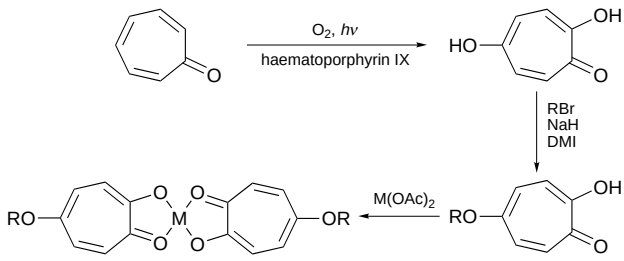

Scheme 1

The copper complexes of these 5-substituted tropolones (**1**, M = Cu) have been synthesised in the usual way† and their mesomorphic nature has been studied using polarised optical microscopy and differential scanning calorimetry. Variable temperature X-ray powder studies are in progress.

The decyl substituted copper complex displays a monotropic S_B phase. Both the dodecyl and tetradecyl copper complexes exhibit a short range S_C mesophase (which despite the high temperatures are stable) as well as S_B and crystal G phases. The hexadecyl substituted copper complex exhibits a S_B phase and an anisotropic plastic crystal phase which cannot be pinpointed. The mesogenic data are summarized in Table 1.

Long chain alkoxy derivatives are very difficult to crystallise in forms suitable for X-ray structure determination. Generally very fine needles are obtained. Crystallisation of bis(5-octyloxytropolonato)copper from 1,4-dioxan containing 10% acetic acid in a similar way to that used for bis(tropolonato)-copper(II)[15] yielded a suitable crystal for an X-ray diffraction study.‡ The CuO_4 centre is required by crystallographic symmetry to be precisely planar, and the entire molecule is planar within 7%. The ligand plane O(1)C(1)C(7)O(2) attached to the Cu makes an angle of 2° with the tropolone ring. The molecular structure shown in Fig. 1 confirms the calamitic nature of the tropolone derivatives, while the packing in the crystal shows a similar arrangement to that in the smectic C phase. No solvent molecules are incorporated into the structure and there is no Cu–Cu interaction, the closest Cu···Cu approach being along the *c*-axis at 6.413(4) Å. The alkyl chain thermal parameters are interesting in that they exhibit partial melting at room temperature.

NMR analysis of 5-alkoxy tropolones confirmed their structure. Satisfactory analyses were obtained for the complexes. Over a period of time, the copper complexes are prone to hydrate, making them difficult to dry. However, because of the high transition temperatures, all water will have evaporated from the copper complex and have no effect on the mesophase behaviour. This is confirmed by uniform phase identification (and transition temperatures) of the copper complexes when dry and hydrated. IR data for bis[5-(decyloxy)tropolonato]-copper(II) (KBr disc): 2918s, 2850s, 1516s, 1432vs, 1350s, 1241s, 1204s, 789w.

Table 1 Phase transition temperatures and corresponding enthalpies (kJ mol^{-1}) of copper tropolonate complexes

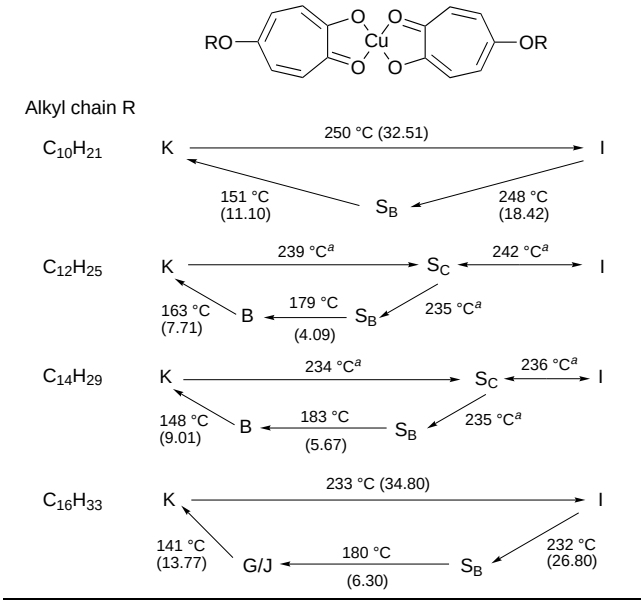

[a] Overlapping peaks, enthalpies could not be resolved.

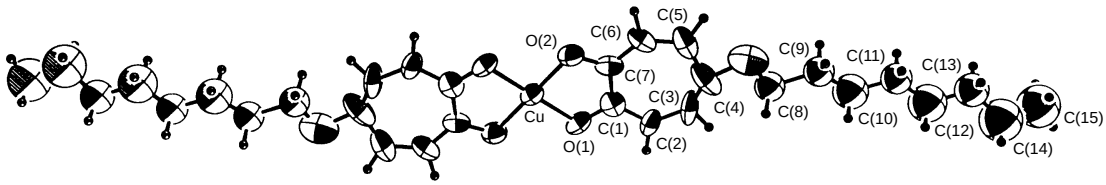

Fig. 1 View of bis(5-octyloxytropolonato)copper(II) from X-ray data

Nickel and oxovanadium(IV) complexes of the 5-substituted tropolone ligands have been prepared. However, despite having melting points which are 50 and 90 °C lower respectively than their copper complex counterparts, none have displayed any mesophases. For the nickel complexes, IR spectra suggest octahedral nickel.

While mesophases are still at high temperatures, appropriate substitution on the tropolone rings enables the length-to-breadth ratio to be adjusted, and initial work gives the promise of metallotropolonates with much lower mesophase transition temperatures. The use of tropolone derivatives in medicine (colchicine is a valuable anti-tumour agent while hinokitiol has strong biocidal properties), indicates potential uses for metal tropolonate derivatives outside the field of display devices.

The authors would like to thank EPSRC for financial support, and Professor J. Goodby and Dr P. Styring for help with phase identification.

Footnotes and References

* E-mail: e.sinn@chemistry.hull.ac.uk

† *Example*: bis[5-(decycloxy)tropolonato]copper(II): 5-decyloxytropolone (0.18 g, 0.71 mmol), sodium acetate (0.1 g, 1.4 mmol) and copper acetate (0.072 g, 0.359 mmol) were dissolved in methanol (15 cm^3). The mixture was refluxed for 3 h before cooling and filtration of the copper complex as a green powder. Recrystallisation in dichloromethane yielded bis[5-(decycloxy)tropolonato]copper(II) as green needles.

‡ *Crystal data*: $C_{80}H_{42}CuO_6$, triclinic, space group $P\bar{1}$, a = 7.607(4), b = 15.871(8), c = 6.413(4) Å, α = 96.32(4), β = 105.46(3), γ = 97.449(3)°, U = 731(1) $Å^3$, Z = 1, T = 24 °C, μ(Mo-Kα) = 7.84 cm^{-1}, R, R_w = 0.055 for 990 independent reflections collected on a Rigaku AFC6S diffractometer. The small crystal size led to a relatively small data set. The copper, oxygen and ring carbons were refined with anisotropic thermal parameters. Cu lies on a special position (origin): Cu–O(1) 1.916(2) Å, Cu–O(2) 1.902(9) Å; O(1)–Cu–O(2) 85.0(4)°. CCDC 182/694.

1 A.-M. Giroud-Godquin and P. M. Maitlis, *Angew. Chem., Int. Ed. Engl.*, 1991, **30**, 375.
2 P. Espinet, M. A. Esteruelas, L. A. Oro, J. L. Serrano and E. Sola, *Coord. Chem. Rev.*, 1992, **117**, 215.
3 D. W. Bruce, *J. Chem. Soc., Dalton Trans.*, 1993, 2983.
4 S. A. Hudson and P. M. Maitlis, *Chem. Rev.*, 1993, **93**, 861.
5 T. Uemura, S. Takenaka, S. Kusabayashi and S. Seto, *Mol. Cryst. Liq. Cryst.*, 1983, **95**, 287.
6 A. Mori, K. Katahira, K. Kida and H. Takeshita, *Chem. Lett.*, 1992, 1767.
7 A. Mori, H. Takeshita, K. Kida and M. Uchida, *J. Am. Chem. Soc.*, 1990, **112**, 8635.
8 A. Mori, N. Kato, H. Takeshita, M. Uchida, H. Taya and R. Nimura, *J. Mater. Chem.*, 1991, **1**, 799.
9 A. Mori, H. Taya and H. Takeshita, *Chem. Lett.*, 1991, 579.
10 *Comprehensive Coordination Chemistry*, ed. G. Wilkinson, R. D. Gillard and J. McCleverty, Pergamon, 1987, vol. 2, p. 397.
11 B. J. Barker, J. Rosenfarb and J. A. Caruso, *Angew. Chem., Int. Ed. Engl.*, 1979, **18**, 503.
12 D. D. MacNicol, P. R. Mallinson, A. Murphy and G. J. Sym, *Tetrahedron Lett.*, 1982, **23**, 4131.
13 D. Seebach, R. Henning and T. Mukhopadhyay, *Chem. Ber.*, 1982, **115**, 1705.
14 D. Seebach, *Chem. Br.*, 1985, **21**, 632.
15 J.-E. Berg, A.-M. Pilotti, A.-C. Soederholm and B. Karlsson, *Acta Crystallogr., Sect. B*, 1978, **34**, 3071.

Received in Cambridge, UK, 7th October 1997; 7/07255D

The chalcogeno-Baylis–Hillman reaction: the first examples catalysed by chalcogenides in the presence of Lewis acids

Tadashi Kataoka,* Tetsuo Iwama and Shin-ichiro Tsujiyama

Gifu Pharmaceutical University, 6-1, Mitahora-higashi 5-Chome, Gifu 502, Japan

The chalcogeno-Baylis–Hillman reaction catalysed by sulfides and selenides, the group 16 element compounds, in the presence of Lewis acids gave coupling products in moderate to good yield even after only 1 h at room temperature.

The coupling of activated alkenes with aldehydes or ketones is referred to as the Baylis–Hillman reaction (Scheme 1).[1] The reaction requires a compound containing a tertiary group 15 element as a catalyst. Generally tertiary amines are utilised as catalysts, and 1,4-diazabicyclo[2.2.2]octane (DABCO) is the most popular. There are some known examples which utilise tertiary phosphine catalysts.[2] Although the Baylis–Hillman reaction provides useful building blocks for organic synthesis,[1] it has a number of disadvantages. The main drawback is the slow reaction rate, and much attention has been paid to accelerating such reactions.[2c,3–8] Recently, Aggarwal *et al.* reported that lanthanides and group 3 metal triflates accelerate the Baylis–Hillman reaction, and that standard Lewis acids such as $TiCl_4$ and $BF_3{\cdot}Et_2O$ decelerate the reaction due to formation of an amine–Lewis acid complex.[6] Imagawa *et al.* described the Baylis–Hillman reaction promoted by a phosphine catalyst and Et_2AlCl due to activation of the aldehyde by coordination with the Lewis acid.[9] Therefore, we aimed to develop new catalysts other than those containing group 15 elements. We report here a preliminary study on the first chalcogeno-Baylis–Hillman reaction catalysed by sulfides and selenides, compounds containing group 16 elements, in the presence of Lewis acids.

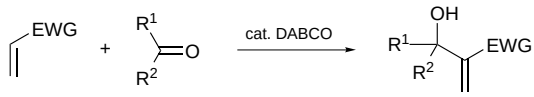

Scheme 1

We examined the reaction of *p*-nitrobenzaldehyde **1** and 3 equiv. of cyclohex-2-en-1-one **2** in the presence of chalcogenides **4**, **5**,[10] **6**,[11] **7**, **8**,[12] **9**,[13] **10**,[14] **11**,† **12**,[15] **13**[14] and **14**‡ in CH_2Cl_2 at room temperature for 1 h (Scheme 2, Table 1).§ First, **4** was used in order to confirm the possibility of sulfide catalysts for the Baylis–Hillman reaction. A mixture of compounds **1** and **2** was treated with 1 equiv. of the sulfide **4** at room temperature for 4 days, and no coupling product **3** was obtained (entry 1). For the purpose of enhancing the reactivity of the enone towards the Michael addition of the sulfide, 0.1 equiv. of $TiCl_4$ was used and the Baylis–Hillman product **3** was produced in 17% yield (entry 2). Therefore, we examined the reaction with a catalytic amount of **4** (0.1 equiv.) in the presence of 1 equiv. of $TiCl_4$ and obtained the adduct **3** in 60% yield (entry 3). The reaction time was reduced to 10 min in refluxing CH_2Cl_2 (entry 4). It is significant that the reaction rate was dramatically accelerated in comparison to reactions utilising amine catalysts. Generally, it takes a few days or more to complete reactions catalysed by tertiary amines.[1] In addition it is also noteworthy that 1 equiv. of $TiCl_4$ is necessary for smooth reaction even though deceleration of the reaction has been observed when using an amine catalyst and $TiCl_4$ because of the formation of a deactivated amine–Lewis acid complex.[6]

A plausible mechanism is shown in Scheme 3. Activation of enone **2** by coordination with $TiCl_4$ allows addition of methyl sulfide **4** to complex **I** to generate an enolate intermediate **II**. The aldol reaction of the enolate **II** and aldehyde **1** gives an adduct **III**, which provides a Baylis–Hillman product–$TiCl_4$ complex **3′** *via* β-elimination and regeneration of methyl sulfide **4**. Formation of the complex **3′** requires a stoichiometric amount of $TiCl_4$ for a smooth reaction. Next, we examined several Lewis acids under standard conditions. The use of $BF_3{\cdot}Et_2O$ and $SnCl_4$ gave no coupling product (entries 5 and 6). The yields of the adduct **3** increased with increasing Lewis acidity in the cases

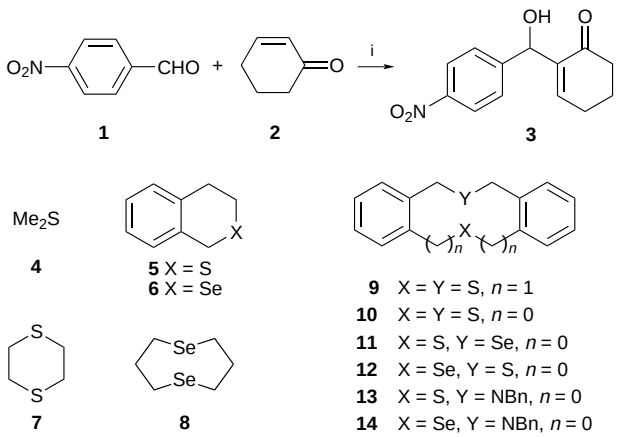

Scheme 2 *Reagents and conditions*: i, **1** (1 equiv.), **2** (3 equiv.), chalcogenide, Lewis acid, CH_2Cl_2, room temp., 1 h

Table 1 Chalcogeno-Baylis–Hillman reaction in the presence of Lewis acids[a]

Entry	Chalcogenide (equiv.)	Lewis acid (equiv.)	**3** (% yield)[b]
1[c]	**4** (1)	—	—
2	**4** (1)	$TiCl_4$ (0.1)	17
3	**4** (0.1)	$TiCl_4$ (1)	60
4[d]	**4** (0.1)	$TiCl_4$ (1)	58
5	**4** (0.1)	$BF_3{\cdot}Et_2O$ (1)	—
6	**4** (0.1)	$SnCl_4$ (1)	—
7	**4** (0.1)	$AlCl_3$ (1)	30
8	**4** (0.1)	$EtAlCl_2$ (1)	13
9	**4** (0.1)	Et_2AlCl (1)	11
10	**5** (0.1)	$TiCl_4$ (1)	71
11	**6** (0.1)	$TiCl_4$ (1)	70
12	**7** (0.1)	$TiCl_4$ (1)	69
13	**8** (0.1)	$TiCl_4$ (1)	85
14	**9** (0.1)	$TiCl_4$ (1)	71
15	**10** (0.1)	$TiCl_4$ (1)	74
16	**11** (0.1)	$TiCl_4$ (1)	78
17	**12** (0.1)	$TiCl_4$ (1)	71
18	**13** (0.1)	$TiCl_4$ (1)	76
19	**14** (0.1)	$TiCl_4$ (1)	69

[a] 3 equiv. of enone **2** was used against aldehyde **1**. Reactions were carried out in CH_2Cl_2 at room temperature for 1 h. [b] Isolated yield based on aldehyde **1**. [c] The reaction was carried out at room temperature for 4 d. [d] The reaction was carried out in refluxing CH_2Cl_2 for 10 min.

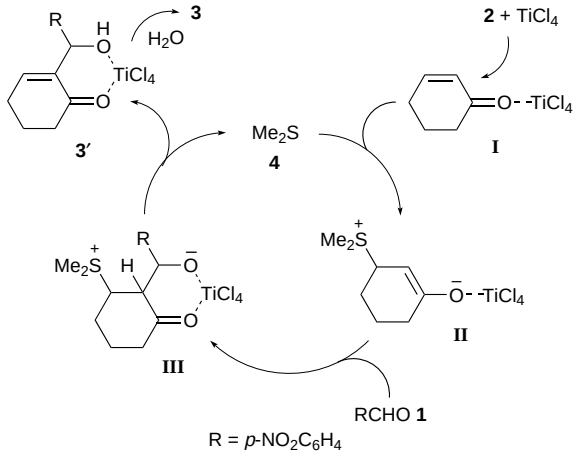

Scheme 3

Table 2 Reactions of some enones and aldehydes catalysed by Me_2S–$TiCl_4$[a]

Entry	Aldehyde	Enone	Product (% yield)[b]
1	PhCHO	**2**	**17** (25)
2	*p*-ClC_6H_4CHO	**2**	**18** (43)
3	*p*-MeC_6H_4CHO	**2**	**19** (13)
4	*p*-$NO_2C_6H_4CHO$	**15**	**20** (68)
5	*p*-$NO_2C_6H_4CHO$	**16**	**21** (63)

[a] Conditions: 1 equiv. of aldehyde, 3 equiv. of enone, 0.1 equiv. of Me_2S, 1 equiv. of $TiCl_4$, CH_2Cl_2, room temp., 1 h. [b] Isolated yield based on the aldehyde.

of aluminium Lewis acids (entries 7–9). The best result was obtained when using $TiCl_4$. Chalcogenide catalysts **5**–**14** were examined in the presence of 1 equiv. of $TiCl_4$. Cyclic monochalcogenides **5** and **6** catalysed the chalcogeno-Baylis–Hillman reaction to provide the adduct **3** in 71 and 70% yield, respectively. We considered that the electron-releasing ability of the chalcogenide might promote the Michael addition step, and selected bis-chalcogenides **7**–**12** and related chalcogenides **13** and **14** are expected to donate electrons to a cationic species by transannular interaction of a chalcogen and a heteroatom.[16] Some (**8**, **10**, **11** and **13**) gave better results than monochalcogenides **5** and **6**, and others (**7**, **9**, **12** and **14**) gave similar results. The best result was obtained using bis-selenide **8**, probably due to transannular interaction (entry 13). In the cases of aromatic chalcogenides **9**–**14** steric interaction, for example between *peri*-hydrogens of the aromatic rings and the enone, may prevent the Michael addition step.

Various aldehydes and enones were applied to the chalcogeno-Baylis–Hillman reaction under standard conditions (Table 2).§ The yields of the adducts **4**, **18**, **17** and **19** decreased with the decreasing electrophilicity of the aldehydes (entry 3 in Table 1, entries 2, 1 and 3 in Table 2, respectively). Reactions of *p*-nitrobenzaldehyde **1** with enones **15** and **16** gave coupling products **20** and **21**, respectively, in moderate yields.

Reactions of other substrates such as acrylonitrile and an aliphatic aldehyde using the Me_2S–$TiCl_4$ system resulted in low (< 24%) yields. Further examination of different combinations of chalcogenides and Lewis acids, and extension of the chalcogeno-Baylis–Hillman reaction to various substrates, is now under investigation.

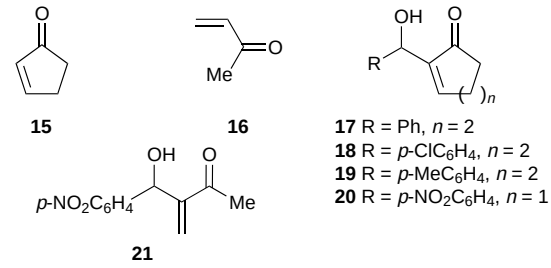

Footnotes and References

* E-mail: kataoka@gifu-pu.ac.jp

† Chalcogenide **11** was prepared by the reaction of bis(2-bromomethylphenyl) sulfide and Na_2Se (prepared from Se and $NaBH_4$ in EtOH) in EtOH by a procedure similar to that for compound **10** (ref. 14).

‡ Selenide **14** was prepared from bis(2-bromomethylphenyl) selenide (ref. 15) and benzylamine by the same procedure as for sulfide **13** (ref. 14). The *N*-methyl derivative of selenide **14** has been synthesised: H. Fujihara, H. Mima, T. Erata and N. Furukawa, *J. Chem. Soc., Chem. Commun.*, 1991, 98.

§ *Typical procedure* for the chalcogeno-Baylis–Hillman reaction: To a stirred solution of *p*-nitrobenzaldehyde (151 mg, 1 mmol), cyclohex-2-en-1-one (0.29 ml, 3 mmol) and methyl sulfide (7 μl, 0.1 mmol) in CH_2Cl_2 (2 cm^3) was added a 1 M solution of $TiCl_4$ in CH_2Cl_2 (1 ml, 1 mmol) at room temperature. The mixture was stirred for 1 h at ambient temperature, and the reaction was quenched by addition of water (5 cm^3). The precipitate of inorganic material was removed by filtration through Celite, and the filtrate was extracted with CH_2Cl_2 (20 ml × 2). The extracts were dried ($MgSO_4$) and the solvent was evaporated under reduced pressure. The residue was purified by preparative TLC on silica gel eluting with ethyl acetate–hexane (1 : 1, v/v) to give 148 mg (60%) of an adduct **3**.

1 D. Basavaiah, P. D. Rao and R. S. Hyma, *Tetrahedron*, 1996, **52**, 8001; S. E. Drewes and G. H. P. Roos, *Tetrahedron*, 1988, **44**, 4653.
2 (*a*) T. Miyakoshi, H. Omichi and S. Saito, *Nippon Kagaku Kaishi*, 1979, 748; (*b*) K.Morita, Z. Suzuki and H. Hirose, *Bull. Chem. Soc. Jpn.*, 1968, **41**, 2815; (*c*) S. Rafel and J. W. Leahy, *J. Org. Chem.*, 1997, **62**, 1521.
3 J. S. Hill and N. S. Isaacs, *J. Chem. Res.*, 1988, (*S*) 330; (*M*) 2641.
4 G. H. P. Roos and P. Rampersadh, *Synth. Commun.*, 1993, **23**, 1261.
5 M. K.Kundu, S. B. Mukherjee, N. Balu, R. Padmakumar and S. V. Bhat, *Synlett*, 1994, 444.
6 V. K. Aggarwal, G. J. Tarver and R. McCague, *Chem. Commun.*, 1996, 2713.
7 J. Auge, N. Lubin and A. Lubineau, *Tetrahedron Lett.*, 1994, **35**, 7947.
8 E. P. Kündig, L. H. Xu, P. Romanens and G. Bernardinelli, *Tetrahedron Lett.*, 1993, **34**, 7049; E. P. Kündig, L. H. Xu and B. Schnell, *Synlett*, 1994, 413.
9 T. Imagawa, K. Uemura, Z. Nagai and M. Kawanisi, *Synth. Commun.*, 1984, **14**, 1267.
10 F. G. Hollimann and F. G. Mann, *J. Chem. Soc.*, 1945, 37.
11 M. Hori, T. Kataoka, H. Shimizu, K. Tsutsumi, Y.-Z. Hu and M. Nishigiri, *J. Chem. Soc., Perkin Trans. 1*, 1990, 39.
12 H. Fujihara, R. Akaishi, T. Erata and N. Furukawa, *J. Chem. Soc., Chem. Commun.*, 1989, 1789; I.Cordova-Reyes, H. Hu, J.-H. Gu, E. Vanden-Hoven, A. Mohammed, S. Holdcroft and B. M. Pinto, *Can. J. Chem.*, 1996, **74**, 533.
13 M.-K. Au, T. C. W. Mak and T.-L. Chan, *J. Chem. Soc., Perkin Trans. 1*, 1979, 1475.
14 R. P. Gellatly, W. D. Ollis and I. O. Sutherland, *J. Chem. Soc., Perkin Trans. 1*, 1976, 913.
15 H. Fujihara, H. Mima, J.-J. Chiu and N. Furukawa, *Tetrahedron Lett.*, 1990, **31**, 2307.
16 K. Akiba, K. Takee and K. Ohkata, *J. Am. Chem. Soc.*, 1983, **105**, 6965; H. Fujihara and N. Furukawa, *Rev. Heteroatom Chem.*, 1992, **6**, 263.

Received in Cambridge, UK, 22nd September 1997; 7/06821B

Synthesis of group 4 complexes that contain the tridentate diamido ligands $[(ArNCH_2CH_2)_2O]^{2-}$ (Ar = C_6H_3-Me_2-2,6 or $C_6H_3Pr^i_2$-2,6)

Richard R. Schrock,* Florian Schattenmann, Michael Aizenberg and William M. Davis

Department of Chemistry 6-331, Massachusetts Institute of Technology, 77 Massachusetts Avenue, Cambridge, MA 02139, USA

Complexes of Zr and Hf of the type $[(2,6\text{-}R_2C_6H_3NCH_2CH_2)_2O]ZrMe_2$ (R = Me or Pr^i) can be activated by $[PhNMe_2H][B(C_6F_5)_4]$ or $[Ph_3C][B(C_6F_5)_4]$ in chlorobenzene or bromobenzene to yield catalysts for the polymerization of hex-1-ene, but analogous titanium catalysts are relatively poorly behaved.

Significant advances have been made in the synthesis of 'well defined' alkene polymerization catalysts of the early metals (largely group 4) in the last 15 years, the vast majority of which contain two cyclopentadienyl-like rings.[1–3] (See, however, ref. 4, and references therein.) Recently group 4 complexes that contain chelating diamido ligand systems have received increased attention as potential alkene polymerization catalysts.[5–13] The most successful so far appear to be dialkyl complexes of Ti that contain diamido ligands such as $[ArNCH_2CH_2CH_2NAr]^{2-}$ (Ar = $C_6H_3Pr^i_2$-2,6),[5,6] and dialkyl complexes of Zr that contain the 'diamido/donor' ligand, $[(o\text{-}[^2H_6]Bu^tNC_6H_4)_2O]^{2-}$ ($[NON]^{2-}$).[10] Both types can be activated to yield (presumably) cationic catalysts for the living polymerization of hex-1-ene. We report here Ti, Zr and Hf complexes that contain potentially interesting 'diamido/donor' variations of the $[NON]^{2-}$ ligand, $[(2,6\text{-}R_2C_6H_3NCH_2CH_2)_2O]^{2-}$ (R = Me, Pr^i), and preliminary experiments concerning their use as catalysts for the polymerization of hex-1-ene.

The diamines, $(2,6\text{-}Me_2C_6H_3NHCH_2CH_2)_2O$ (H_2L^{1a}) and $(2,6\text{-}Pr^i_2C_6H_3NHCH_2CH_2)_2O$ (H_2L^{1b}), can be prepared readily from $(TsOCH_2CH_2)_2O$ (TsO = tosylate) and 2 equiv. of $LiNH(C_6H_3Me_2$-2,6) or $LiNH(C_6H_3Pr^i_2$-2,6), respectively, in thf.† Compound H_2L^{1a} can be obtained in 60% yield as colorless crystals upon crystallization from pentane.‡,§ Compound H_2L^{1b} is obtained in 80% yield as an oil that has crystallized in some instances upon standing for several days, and that can be crystallized from pentane in low yield at −30 °C.†,‡ Crude H_2L^{1b} can be used in subsequent reactions.

The reaction between H_2L^{1a} or H_2L^{1b} and $Zr(NMe_2)_4$ in pentane at room temp. yields crystalline $ZrL^{1a}(NMe_2)_2$‡ or $ZrL^{1b}(NMe_2)_2$‡ readily. The dimethylamido compounds react with excess $SiMe_3Cl$ in ether overnight at room temp. to yield $ZrL^{1a}Cl_2$‡ and $ZrL^{1b}Cl_2$‡ as colorless, relatively insoluble crystals. NMR spectra of $ZrL^{1b}(NMe_2)_2$ and $ZrL^{1b}Cl_2$ show two sets of isopropyl methyl groups, but only one methine resonance, consistent with restricted rotation of the aryl ring about the N–C_{ipso} bond, a phenomenon that was also noted by McConville and co-workers[5–8,14] in complexes containing the $[ArNCH_2CH_2CH_2NAr]^{2-}$ and related ligands. Only a single amido methyl resonance is observed in all dimethylamido compounds at room temp. in C_6D_6.

Alkylation of $ZrL^{1a}Cl_2$ with MeMgBr in ether gives $ZrL^{1a}Me_2$ **1a**‡ in good yield, while alkylation of $ZrL^{1b}Cl_2$ with Me or Bu^i Grignard reagents in ether yields $ZrL^{1b}Me_2$ **1b**‡ or $ZrL^{1b}(CH_2CHMe_2)_2$ **2b**,‡ respectively, in good yields as colorless cubes. NMR spectra are again consistent with slow rotation around the N–C_{ipso} bond on the NMR timescale. In all dialkyl compounds the alkyl groups are equivalent, consistent either with a pseudotrigonal bipyramidal structure of type **A** or a pseudotrigonal bipyramid of type **B** in which the alkyl groups become equivalent on the NMR timescale *via* a rapid 'flipping' of the ligand backbone through an intermediate with structure **A**.

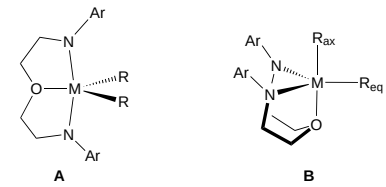

An X-ray study of $ZrL^{1a}Me_2$ (Fig. 1)¶ showed it to have structure **A** with 'axial' Zr–N bond distances of 2.084(3) Å and a Zr–O(2) bond length of 2.336(3) Å. The compound has a crystallographic mirror plane defined by Zr, O(2), C(5) and C(6). The planes of the aryl rings are perpendicular to the ZrO(2)N(3)N(4) pseudo-plane. The structure is closely related to that of $[(2,6\text{-}Et_2C_6H_3NCH_2)_2NC_5H_3]ZrMe_2$ [N–Zr–N 139.6(2)° and C–Zr–C 102.4(3)°][8] and contrasts markedly with that of $\{[(o\text{-}[^2H_6]Bu^tNC_6H_4)_2O]ZrMe\}\{MeB(C_6F_5)_3\}$,[10] in which $B(C_6F_5)_3$ has partially removed Me_{ax}. The two Me groups are technically inequivalent in the solid state structure of $ZrL^{1a}Me_2$ [C(8)–O(2)–C(18) 113.7(4)°] as a consequence of C(18) and C(8) not lying in the ZrN_2 plane.

Reactions similar to those employed to prepare Zr compounds can be employed to prepare $HfL^{1a}(NMe_2)_2$,‡ $HfL^{1a}Cl_2$,‡ and $HfL^{1a}Me_2$ **3a**.‡ The Hf compounds are virtually identical to the Zr compounds in physical properties and NMR characteristics.

Addition of Li_2L^{1a} to $TiCl_4(thf)_2$ in diethyl ether at −30 °C led to formation of a deep red precipitate, which could be recrystallized from CH_2Cl_2 to yield $TiL^{1a}Cl_2$ in 57% yield. Alkylation of $TiL^{1a}Cl_2$ in ether with MeMgCl in thf at −30 °C gave $TiL^{1a}Me_2$ **4a** in 53% yield as a yellow powder from pentane. Red, crystalline $TiL^{1a}(CH_2Ph)_2$ **5a** was prepared in low yield (*ca*. 15%) *via* the reaction between $Ti(CH_2Ph)_4$ (2 mmol)

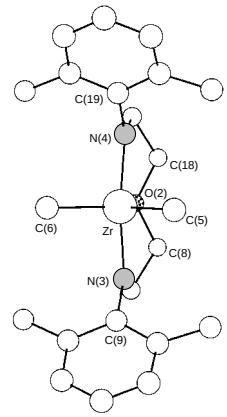

Fig. 1 A view of the structure of $ZrL^{1a}Me_2$ nearly opposite the Zr–O bond in the ZrC_2 plane. Bond lengths (Å) and angles (°): Zr–C(5) 2.253(6); N(4)–Zr–N(3) 139.1(2), C(8)–O(2)–C(18) 113.7(4), Zr–N(3)–C(9) 120.2(2), C(5)–Zr–C(6) 100.0(2)°.

Table 1 GPC and yield data for poly(hex-1-ene)[a]

Complex	Activator	M_n(theory)	M_n[b]	M_w[b]	M_w/M_n[b]	Yield (%)
$ZrL^{1b}Me_2$	$[NHMe_2Ph]^+$	13 440	2 670	3 560	1.33	96
$ZrL^{1b}Me_2$	$[CPh_3]^+$	16 800	2 460	4 220	1.72	96
$ZrL^{1b}(CH_2CHMe_2)_2$	$[NHMe_2Ph]^+$	16 800	2 650	8 550	3.23	94
$ZrL^{1b}Me_2$	$[CPh_3]^+$	16 800	11 700	18 000	1.55	100

[a] Dialkyl complex (44 μmol), activator (40 μmol), 200 equiv. hex-1-ene (except first entry = 160 equiv.), 10 ml chlorobenzene. [b] Determined by GPC coupled with on-line light scattering (Wyatt Technology).

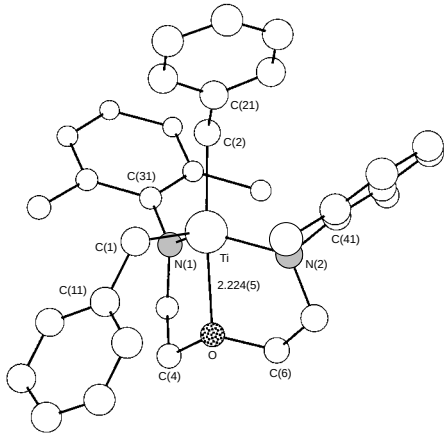

Fig. 2 A view of the structure of $TiL^{1a}(CH_2Ph)_2$. Bond lengths (Å) and angles (°): Ti–C(1) 2.129(10), Ti–N(1) 1.962(6), C(2)–Ti–O 169.3(3).

and H_2L^{1a} (2 mmol) in pentane (*ca*. 15 ml) in 40 h. In **4a** and **5a** the alkyl groups are equivalent on the NMR timescale at room temp., although several proton and carbon resonances in **5a** are broad at 22 °C. The structure of $TiL^{1a}(CH_2Ph)_2$ (Fig. 2)¶ is best described as type **B** in which O and C(2) are in the apical position and N(1), N(2), and C(1) are in the equatorial positions of a pseudotrigonal bipyramid. Surprisingly, the benzyl groups are bound only in an η^1 fashion; if two Ti–N π bonds can form, the metal should be viewed as having a 14 electron count, an electron deficiency that has led in many situations to η^2 or η^3 binding of benzyl ligands.[15]

Activation of alkyl complexes **1a**,**b**, **2b** and **3a** by either $[PhNMe_2H][B(C_6F_5)_4]$ or $[Ph_3C][B(C_6F_5)_4]$ yields initiators for the polymerization of hex-1-ene in chlorobenzene at 0 °C.‖ Polymerization yields are high, but the molecular masses of the polymers were found to be significantly smaller than expected when $ZrL^{1b}Me_2$ and $ZrL^{1b}(CH_2CHMe_2)_2$ were employed (Table 1). These results suggest that chain termination competes with propagation, but that the catalyst remains active thereafter and polymerization of a new chain is initiated. The $[PhNMe_2H]^+$ and $[Ph_3C]^+$ activators seem to be equally efficient. The number average molecular mass of poly(hex-1-ene) prepared using $ZrL^{1a}Me_2$ is approximately that expected if no significant chain termination is taking place. In all cases polymerization activity ceases when 2,4-dimethylpyridine is added to the catalyst mixture, consistent with competitive binding of the nitrogen base to a cationic metal center. Analogous experiments employing $HfL^{1a}Me_2$ yielded results similar to those employing $ZrL^{1a}Me_2$, but use of $TiL^{1a}Me_2$ (activated by $[PhNMe_2H][B(C_6F_5)_4]$ in $[^2H_5]$bromobenzene) led to only *ca*. 75% consumption of 25 equiv. of hex-1-ene to give poly(hex-1-ene).

We conclude that $[(2,6\text{-}R_2C_6H_3NCH_2CH_2)_2O]^{2-}$ ligands produce stable five-coordinate dialkyl complexes of Ti, Zr and Hf, and that 'cations' formed by protonation or oxidative cleavage of an alkyl group from Zr or Hf are initiators for the polymerization of hex-1-ene. These results should be contrasted with results obtained by McConville and co-workers[5,6] where Ti is the most successful when the diamido ligand does not contain an additional donor.

R. R. S. thanks the Department of Energy (DEFG02-86ER13564) and Exxon for supporting this research, and M. A. is grateful for a Rueff-Wormser Postdoctoral Fellowship.

Footnotes and References

† Solid $(TsOCH_2CH_2)_2O$ (5 g, 12.0 mmol) was added to a chilled (−30 °C) solution of 2,6-$Pr^i_2C_6H_3NHLi$ (4.53 g, 24.8 mmol) in thf (30 ml). After 24 h all solvents were removed *in vacuo* and the residue was extracted with pentane. The pentane was removed *in vacuo* to yield an orange oil (4.2 g, 82%). An analytically pure sample was obtained by recrystallization from a concentrated pentane solution at −30 °C: ^{1}H NMR (C_6D_6) δ 7.18–7.14 (m, 6, H_{aryl}), 3.60 (t, 2, NH), 3.48 (spt, 4, C*H*Me_2), 3.35 (t, 4, OCH_2), 3.07 (q, 4, CH_2N), 1.06 (d, 24, CH*Me*$_2$); ($CDCl_3$) δ 7.18–7.05 (m, 6, H_{aryl}), 3.70 (t, 4, OCH_2), 3.57 (br, 2, NH), 3.36 (spt, 4, C*H*Me_2), 3.14 (br t, 4, CH_2N), 1.27 (d, 24, CH*Me*$_2$).

‡ Satisfactory elemental analyses have been obtained (C, H, N).

§ ^{1}H NMR (C_6D_6) δ 3.15 (t, 4, OCH_2), 2.95 (dt, 4, CH_2N), 2.24 (s, 12, Ar*Me*).

¶ *Crystallographic data*: $ZrL^{1a}Me_2$: Siemens SMART/CCD, orthorhombic, space group *Pnma*, a = 12.741(3), b = 22.663(5), c = 7.518(2) Å, U = 2170.9(8) Å^3, Z = 4, D_c = 1.321 g cm^{-3}, R = 0.0368, R_w = 0.1009, GOF = 1.179. For $TiL^{1a}(CH_2Ph)_2$: Siemens SMART/CCD, orthorhombic, space group *Fdd*2, a = 32.803(8), b = 42.342(13), c = 8.547(4) Å, U = 11872(7) Å^3, Z = 16, D_c = 1.210 g cm^{-3}, R = 0.0609, R_w = 0.1269, GOF = 1.095. CCDC 182/679.

‖ In a typical experiment a chilled (−30 °C) solution of **1b** (19 mg, 44 μmol) in chlorobenzene (3 ml) was added to a suspension of $[PhNMe_2H][B(C_6F_5)_4]$ (32 mg, 40 μmol) in chlorobenzene (6 ml) at −30 °C. The reaction mixture was allowed to warm to room temp. and was stirred for 15 min. The reaction mixture was cooled to 0 °C and hex-1-ene (1.0 ml, 8.0 mmol) was added all at once. After stirring for 1 h at 0 °C the reaction was quenched with HCl (1.0 M in ether, 4 ml). In a typical experiment employing $[Ph_3C][B(C_6F_5)_4]$ the reaction mixture was stirred for 2 min at −30 °C and allowed to equilibrate at 0 °C before hex-1-ene (1.0 ml, 8.0 mmol) was added all at once.

1 H. H. Brintzinger, D. Fischer, R. Mulhaupt, B. Rieger and R. M. Waymouth, *Angew. Chem., Int. Ed. Engl.*, 1995, **34**, 1143.
2 W. Kaminsky and M. Ardnt, *Adv. Polym. Sci.*, 1997, **127**, 144.
3 M. Bochmann, *J. Chem. Soc., Dalton Trans.*, 1996, 255.
4 Y.-X. Chen and T. J. Marks, *Organometallics*, 1997, **16**, 3649.
5 J. D. Scollard and D. H. McConville, *J. Am. Chem. Soc.*, 1996, **118**, 10 008.
6 J. D. Scollard, D. H. McConville, N. C. Payne and J. J. Vittal, *Macromolecules*, 1996, **29**, 5241.
7 J. D. Scollard, D. H. McConville and J. J. Vittal, *Organometallics*, 1995, **14**, 5478.
8 F. Guérin, D. H. McConville and J. J. Vittal, *Organometallics*, 1996, **15**, 5586.
9 K. Aoyagi, P. K. Gantzel, K. Kalai and T. D. Tilley, *Organometallics*, 1996, **15**, 923.
10 R. Baumann, W. M. Davis and R. R. Schrock, *J. Am. Chem. Soc.*, 1997, **119**, 3830.
11 A. D. Horton, J. de With, A. J. van der Linden and H. van de Weg, *Organometallics*, 1996, **15**, 2672.
12 F. G. N. Cloke, T. J. Geldbach, P. B. Hitchcock and J. B. Love, *J. Organomet. Chem.*, 1996, **506**, 343.
13 T. H. Warren, R. R. Schrock and W. M. Davis, *Organometallics*, 1996, **15**, 562.
14 F. Guérin, D. H. McConville and J. J. Vittal, *Organometallics*, 1995, **14**, 3154.
15 J. P. Collman, L. S. Hegedus, J. R. Norton and R. G. Finke, *Principles and Applications of Organotransition Metal Chemistry*, University Science Books, Mill Valley, CA, 2nd edn., 1987.

Received in Bloomington, IN, USA, 3rd September 1997; 7/06452G

Lithium enamides, β-diketiminates and 1,3-diazaallyls from the 1 : 1 insertion of an isonitrile into the Li–C bond of $LiCH(SiMe_3)_2$†‡

Peter B. Hitchcock, Michael F. Lappert* and Marcus Layh

The Chemistry Laboratory, University of Sussex, Brighton, UK BN1 9QJ

The diverse behaviour of $LiCHR_2$ A towards an isonitrile R′NC is unravelled; depending on reaction conditions and choice of R′, the product was an enamide Li[N(R′)C(R)=C(H)R](tmen), a β-diketiminate Li[N(R′)C(R)C(H)C(R)N(R′)], a 1,3-diazaallyl (with additionally PhCN) Li[N(Ph)C(R)NC(Ph)=C(H)R](tmen) or a 1 : 1 adduct of A and Li[N(R′)C(R)C(H)C(R)N(R′)](CNR′) (R′ = Bu^t), (R = $SiMe_3$, tmen = $Me_2NCH_2CH_2NMe_2$ and R′ = Bu^t, Ph or $C_6H_3Me_2$-2,6).

We have previously noted that the reaction between bis(trimethylsilyl)methyllithium $LiCHR_2$ **A** and the α-H-free nitrile PhCN or Bu^{t}CN gave under ambient conditions and irrespective of stoichiometry the 1 : 2 or 1 : 1 adduct, the lithium β-diketiminate $[LiN(R)C(Ph)C(H)C(Ph)N(R)]_2$ **B**[1] or 1-azaallyl $[LiN(R)C(Bu^t)C(H)R]_2$[2] (R = $SiMe_3$). We now report new findings on the $LiCHR_2$–PhCN system and on the variety of reactions between $LiCHR_2$ and the isonitrile R′NC (R′ = Ph, Bu^t or $C_6H_3Me_2$-2,6).

Treatment of a lithium alkyl LiR[1] and an isonitrile R^2NC was shown by Walborsky *et al.* to give the lithioaldimine $LiC(R^1)=NR^2$, which was not isolated, but used *in situ* as a source of an aldehyde, ketone, α-keto acid, β-hydroxyketone or a heterocycle.[3]

We now report (*i*) the synthesis of three diverse adducts **1**, **2** and **3** formed from $LiCHR_2$ **A** and R′NC (R′ = Bu^t or $C_6H_3Me_2$-2,6); (*ii*) that the previously examined $LiCHR_2$–PhCN system[1] is modified in the presence of $(Me_2NCH_2)_2$ (= tmen) to yield the 1 : 1 adduct **4**; (*iii*) that the enamide **1** with PhCN or **4** with PhNC yields the lithium β-diketiminate **5** or 1,3-diazaallyl **6**, respectively; (*iv*) that the β-diketiminate **B**[1] with $LiCHR_2$ and 1 equiv. of Et_2O or thf (OC_4H_8) gives the dilithium [bis(trimethylsilyl)methyl-β-diketiminate] donor (Et_2O or thf) adduct **7a** or **7b** (similar in type to the *tert*-butyl isonitrile adduct **3**); and (*v*) the characterisation of each of **1**–**7**,§ including the X-ray structures of **6** (to be published in the full paper) and **7b**.¶ The reactions leading to compounds **1**–**7** are summarised in Scheme 1.

It is noteworthy (Scheme 1) that the nature of the product, a lithium enamide **1** or β-diketiminate **2**, or (irrespective of stoichiometry) an isonitrile adduct of a dilithium [bis(trimethylsilyl)methyl-β-diketiminate] **3**, obtained from $LiCHR_2$ **A** and the isonitrile R′NC, in good yield under ambient conditions in Et_2O, was dependent on one or more of the variables: the nature of R′, the stoichiometry and the presence or absence of tmen. A transient lithium β-diketiminate may well have been an intermediate along the pathway to **3**, as evident from the isolation of the related dilithium compounds **7a** and **7b** from **A** and **B**.

The formation of the stable compound **4** (from $LiCHR_2$–PhCN–tmen) lends credence to the suggestion that the previously reported $LiCHR_2$–PhCN reaction (which gave the lithium β-diketiminate **B**)[1] proceeded *via* a transient η^3-1-azaallyl (an isomer of the tmen-free **4**). The function of the tmen may have been to have promoted the $\eta^3 \rightarrow \eta^1$ isomerisation. This is also consistent with the present observation that **4** + PhNC gave the Li(tmen) 1,3-diazaallyl compound **6** rather than the isomer 0.5 **B** (tmen) (*cf.*, the reaction of the Li enamide **1** + 2,6-$Me_2C_6H_3NC \rightarrow$ Li β-diketiminate **2**). The possibility (*cf.*, ref. 5) that in this reaction PhNC was initially isomerised into PhCN is discounted because **4** + PhCN gave an isomer of **6**, in which the Ph and Me_3Si groups at N(1) and C(2) were exchanged.

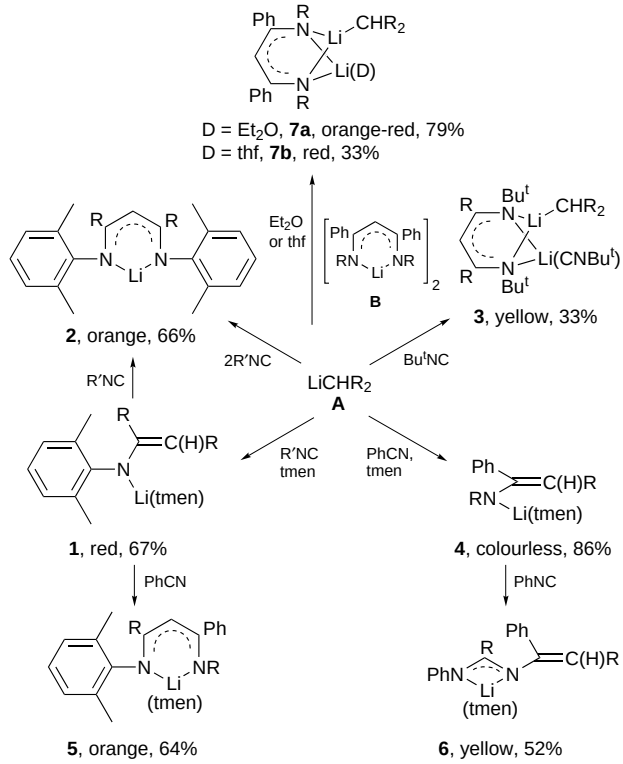

Scheme 1 Synthesis of the crystalline compounds **1**–**7** from $LiCH(SiMe_3)_2$. Reactions carried out in C_5H_{12} or Et_2O (**2**–**4**) at −78 °C to *ca.* 25 °C; yields refer to recrystallised complexes; R′ = $C_6H_3Me_2$-2,6.

The multifarious reaction products observed in the $LiCHR_2$–R′NC system (Scheme 1) may be accommodated by the pathways shown in Scheme 2. Thus, we propose that (i) an initial 1 : 1 complex **8** is (ii) transformed into the lithioaldimine **9**, which (iii) induces a C(1) → C(2) shift of an Me_3Si (= R) group yielding the lithium 1-azaallyl **10** ⇌ **11**, this (iv)

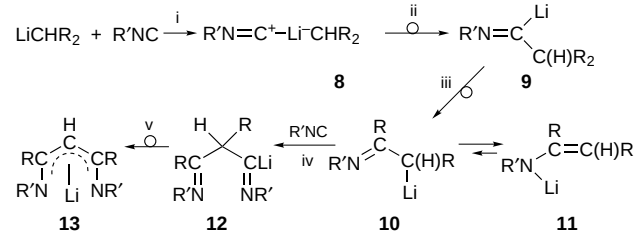

Scheme 2 Reaction pathways in the $LiCHR_2$–R′NC systems

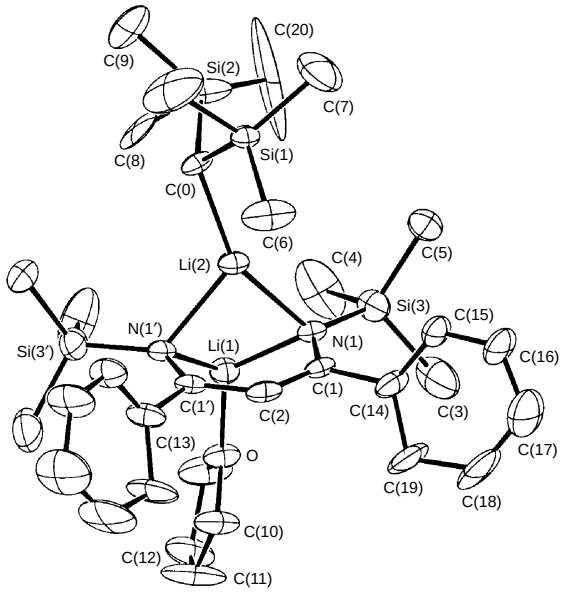

Fig. 1 Molecular structure of **7b** with selected bond distances (Å): N(1)–Li(1) 2.00(2), N(1)–Li(2) 2.13(2), C(0)–Li(2) 2.07(3), N(1)–C(1) 1.32(1), C(1)–C(2) 1.41(1), O–Li(1) 1.86(3).

behaving as a C-centred nucleophile adds to R′NC giving the lithiodiimine **12**, which (v), by a process similar to (*iii*), yields the lithium β-diketiminate **13**.

Although isonitrile complexes of certain transition metals are established, isonitrile adducts of a main group metal are rare {see, *e.g.*, [6a] $Ph_2CNCLi[(-)$-sparteine$](thf)_2$ and [6b] $AlPh_3(CNC_6H_{11}$-*c*$)$}, complex **3** may serve as a model for **8**. The propensity for an Me_3Si group to undergo a 1,2- or 1,3-shift in an anionic complex is well documented[4] [*e.g.*,[1,2] 1,3-C → N in the $LiCHR_2$–R′CN systems], and this provides support for propositions (iii) and (v) of Scheme 2. The isolated complexes **1**, **2** and **3** correspond to a tmen adduct of **11**, **13** and a composite of **8** and **13**, respectively.

The nature of the donor adducts **3**, **7a** and **7b**, of a dilithium [bis(trimethylsilyl)methyl-β-diketiminate] requires comment. In principle, each may be regarded as being either a 1 : 1 cocrystal of $LiCHR_2$(donor) and Li(β-diketiminate) or a discrete compound. We favour the latter for the following reasons. First, repeated recrystallisation of **3** from different solvents led in each case to a product of precise 1 : 1 composition. Second, their colours (Scheme 1) are distinct from those of their possible factors (**B** is pale yellow). Third, the X-ray structure of **7b** (Fig. 1) shows each lithium atom to be closely bound to the two nitrogen atoms of the β-diketiminate moiety [as, indeed, appears to be the case for **3**, but the quality of the crystals was such that an accurate structure was not established, R_1 {$I > 2\sigma(I) \approx 0.20$}]. Finally, the $^7Li\{^1H\}$ NMR spectrum of **7a** in $C_6D_5CD_3$ showed a single signal at δ 2.30 at 293 K, but three separate signals at δ 2.36, 1.44 and 1.37 at 193 K; this is attributed to there being an equilibrium between **7a** and its factors **A** and **B**. Variable temperature NMR spectra of **3** and **7b** are under investigation.

Crystalline **7b** has a mirror plane containing the atoms O and C(13) of the thf molecule, the two lithium, the two silicon atoms and the methyl group C(6), as well as C(2) [corresponding to the C(H) of the β-diketiminate moiety]. The methine carbon, C(0) of the CHR_2 group, and the remaining atoms C(10), C(11) and C(12) of the thf molecule are disordered across the mirror plane. The nitrogen atoms N(1) and N(1′) are bridged by Li(1) (bonded to thf) and Li(2), one above and the other below the nearly planar and completely delocalised diketiminato skeleton, with Li(1)–N(1) 2.00(2) and Li(2)–N(1) 2.13(2) Å. This contrasts with the situation in the dimeric lithium β-diketiminate **B**, which has only one of the two nitrogen atoms of each boat-shaped, incompletely delocalised lithiated ligand in a bridging mode with Li–N 1.952(9) and 2.095(9) Å, for the four- and three-coordinate nitrogens, respectively.[1] The Li(2)–C(0) distance of 2.07(3) Å may be compared with 2.14(3)–2.27(2) Å in crystalline $[LiCHR_2]_\infty$.[7]

The lithium compounds **1**–**7** are available as ligand transfer agents to provide a variety of new s-, p-, d- and f-block metal coordination compounds. We also conclude that isonitriles have an as yet unexplored potential for main group metal chemistry.

We thank ESPRC for a fellowship for M. L. and for other support.

Footnotes and References

* E-mail: m.f.lappert@sussex.ac.uk

† No reprints available.

‡ Dedicated to Professor Dr Manfred Weidenbruch, as a mark of friendship and respect, on the occasion of his 60th birthday.

§ *Selected spectroscopic data* [^1H at 300.1, $^7Li\{^1H\}$ at 116.6 and $^{13}C\{^1H\}$ at 75.5 MHz in C_7D_8 **1**, **2**–**7** in C_6D_6]. **1**: ^1H (values for major rotamer only) δ 0.03 (CHSi*Me*$_3$), δ 0.20 ($SiMe_3$, s), 3.80 (CH, s); $^7Li\{^1H\}$ δ 0.51; $^{13}C\{^1H\}$ δ 84.7 (CH, s), 172.2 (CN, s). **2**: ^1H δ 0.05 ($SiMe_3$, s), 5.48 (CH, 1); $^7Li\{^1H\}$ δ −0.83; $^{13}C\{^1H\}$ δ 104.6 (CH, s), 172.3 (CN, s). **3**: ^1H δ −1.69 ($CHSi_2$, s), 5.40 (CH, s); $^7Li\{^1H\}$ δ 0.83 (s); $^{13}C\{^1H\}$ δ 3.3 ($CHSi_2$, s), 108.5 (CH, s), 179.9 (CN, s). **4**: ^1H δ 0.11 ($SiMe_3$, s), 0.22 ($SiMe_3$, s), 3.67 (CH, s); $^7Li\{^1H\}$ δ 0.88; $^{13}C\{^1H\}$ δ 83.1 (CH, s), 175.9 (CN, s). **5**: ^1H δ 0.07 ($SiMe_3$, s), 0.11 ($SiMe_3$, s), 5.57 (CH, s); $^7Li\{^1H\}$ δ 1.45; $^{13}C\{^1H\}$ δ 105.1 (CH), 169.0, 177.9 (CN, s). **6**: ^1H δ 0.24 ($SiMe_3$, s), 0.45 ($SiMe_3$, s), 4.79 (CH, s); $^7Li\{^1H\}$ δ 1.54; $^{13}C\{^1H\}$ δ 96.7 (CH, s), 154.1 (C=CH, s), 165.7 (CN_2, s). **7a**: ^1H δ −1.94 ($CHSi_2$, s), 5.51 (CH, s); $^7Li\{^1H\}$ δ 2.30(s); $^{13}C\{^1H\}$ δ 1.8 ($CHSi_2$, s), 105.4 (CH, s), 177.2 (CN, s). **7b**: ^1H δ −1.90 ($CHSi_2$, s), 5.09 (CH, s); $^7Li\{^1H\}$ δ 2.30 (s); $^{13}C\{^1H\}$ δ 1.4 ($CHSi_2$, s), 105.4 (CH, s), 176.8 (CN, s).

¶ *Crystal data for* **7b**: $C_{32}H_{56}Li_2N_2OSi_4$, M = 611.0, orthorhombic, space group $P2_1nm$ (non-standard no. 31), a = 9.043(4), b = 11.943(5), c = 18.406(10) Å, U = 1980(2) Å^3, Z = 2, D_c = 1.02 Mg m^{-3}, $F(000)$ = 664, λ(Mo-Kα) 0.710 73 Å, μ = 0.173 mm^{-1}. Data were collected at 173(2) K on a Enraf Nonius CAD4 diffractometer in the ω–2θ mode for the range $2 < \theta < 25°$. The structure was solved by direct methods (SHELXS86) and refined with full matrix least squares on all F^2 (SHELXL93). The molecule is disordered across the crystallographic mirror plane with ordered sites for the Li, Si, O, C(6), C(7) and C(13) atoms and the [(R)NC(Ph)C(H)C(Ph)N(R)] ligand. Distances from Si(2) to C(8), C(9) and C(20) were fixed at 1.88 Å. Two reflections badly affected by extinction were omitted. All non-hydrogen atoms were anisotropic, and hydrogen atoms were included in the riding mode with U_{iso}(H) = 1.2 U_{eq}(C) or 1.5 U_{eq} for Me groups, except for the disordered thf group for which H atoms were omitted. Final residuals for 1921 independent reflections were R_1 = 0.162, wR_2 = 0.272 and for the 1009 with $I > 2\sigma(I)$, R_1 = 0.092, wR_2 = 0.220. CCDC 182/683.

1 P. B. Hitchcock, M. F. Lappert and D.-S. Liu, *J. Chem. Soc., Chem. Commun.*, 1994, 1699.
2 P. B. Hitchcock, M. F. Lappert and D.-S. Liu, *J. Chem. Soc., Chem. Commun.*, 1994, 2637.
3 H. M. Walborsky, W. H. Morrison and G. E. Niznik, *J. Am. Chem. Soc.*, 1970, **92**, 6675; H. M. Walborsky and P. Ronman, *J. Org. Chem.*, 1978, **43**, 731.
4 R. West, *Adv. Organomet. Chem.*, 1977, **16**, 1.
5 H. M. Walborsky, G. E. Niznik and M. P. Periasamy, *Tetrahedron*, 1971, **52**, 4965; M. P. Periasamy and H. M. Walborsky, *J. Org. Chem.*, 1974, **74**, 611.
6 (*a*) B. Ledig, M. Marsch, K. Harms and G. Boche, *Angew. Chem., Int. Ed. Engl.*, 1992, **31**, 79; (*b*) J. D. Fischer, M.-Y. Wei, R. Willett and P. J. Shapiro, *Organometallics*, 1994, **13**, 3324.
7 J. L. Atwood, T. Fjeldberg, M. F. Lappert, N. T. Luong-Thi, R. Shakir and A. J. Thorne, *J. Chem. Soc., Chem. Commun.*, 1984, 1163.

Received in Cambridge, UK, 15th September 1997; 7/06709G

A chiroptically enhanced fluorescent chemosensor

Jesus M. Castagnetto and James W. Canary*

Department of Chemistry, New York University, New York, NY 10003, USA

One sensor molecule gives both fluorescence and exciton-coupled circular dichroism signals upon metal ion complexation, suggesting a novel strategy for detection, identification and quantification of multiple analytes.

One important strategy for the design of efficient sensors for the determination of metal ion concentrations in solution utilizes fluorescent chemosensors in which a metal ion binding event is coupled to a change in the luminescence behavior of the ligand upon forming a complex.[1–4] The classic approach to selective metal ion sensor design involves the engineering of selectivity through control of ligand stereoelectronic features including donor atoms and geometry. Sensor arrays with multivariate calibration offer especially exciting potential in this field.[5] Recently, multiple wavelength excitation[6] and ratiometric detection[7] schemes have offered sophisticated analysis of two metal ions with a single ligand. Here, we wish to report a strategy wherein both isotropic and anisotropic absorption signals from the optical response of a single sensory molecule provide not only detection but also differentiation of multiple analytes.

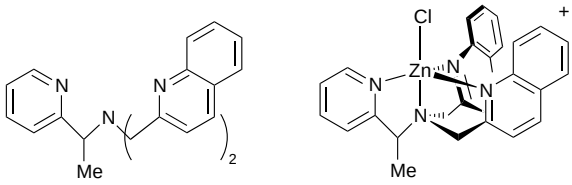

1 α-MeBQPA **2** [Zn(α-MeBQPA)Cl]$^+$

The ligand **1** {α-MeBQPA, bis[(2-quinolyl)methyl][1-(2-pyridyl)ethyl]amine} generates strong signals in exciton-coupled circular dichroism spectra (ECCD) upon formation of complexes with trigonal bipyramidal metal ions (Zn^{II}, Cu^{II}) as shown in Fig. 1.[8] Contrastingly, complexes with octahedral metal ions (Cd^{II}, Fe^{II}) do not give strong CD signals. The physical basis for tripodal ligand ECCD response to metal ion geometry has been discussed.[8,9]

Since quinoline ligands were employed in the development of practical fluorescent sensors for ions such as Ca^{II}, Mg^{II} and Mn^{II},[10,11] we envisioned that **1** might also display useful fluorometric sensory properties. Fig. 1 shows fluorescence spectra of the free ligand and four coordination complexes in aqueous solution at pH = 7.1; the fluorescence intensities of diamagnetic complexes increase relative to the free ligand,[12] with observed enhancements (378 nm, H_2O, pH = 7) of 30 : 1 (Zn^{II}) and 6 : 1 (Cd^{II}). The fluorescence enhancement derives from an N-heterocycle characteristic change from an n–π* electronic transition (leading to phosphorescence)[10,13] to a π–π* transition upon metal ion complexation, resulting in fluorescence.[10,13] The observed binding of Zn^{II} and Cd^{II} to the α-MeBQPA is strong ($K_a > 10^6$ dm^3 mol^{-1}) as expected,[14] which was evidenced by the linear response of the fluorescence enhancement at micromolar concentrations [*e.g.* Fig. 2(*b*)].

The fluorescence and ECCD properties of the complexes result in the interesting situation that the ligand can not only signal the presence of a metal ion, but evaluation of both properties can allow identification of the metal. Detection of both fluorescence enhancement and anisotropic absorption distinguish, for example, Zn^{II} (strong fluorescence and ECCD response), Cu^{II} (strong ECCD but no fluorescence), Cd^{II} (strong fluorescence but no ECCD) and Fe^{II} (neither fluorescence nor ECCD). These results illustrate for the first time the principle that both isotropic and anisotropic detection may be utilized to maximize the information transmitted by a single sensor molecule.

The optical behavior of the ligand upon presentation of Zn^{II} and Cd^{II} mixtures serves to illustrate the approach. The overall ratio of fluorescence signals of the Zn^{II} and Cd^{II} ions at micromolar concentrations is 5 : 1 at 378 nm. However, the circular dichroic responses are more highly differentiated; at 242 nm (H_2O, pH = 7) the ratio of $\Delta\varepsilon(ZnL) : \Delta\varepsilon(CdL)$ is 12 : 1. The relative fluorescence measured follows eqn. (1)

$$I = \chi_{Zn} I_0^{ZnL} + (1 - \chi_{Zn}) I_0^{CdL} \quad (1)$$

$$\theta = A[Zn^{2+}] + B \quad (2)$$

where I_0^{ZnL} and I_0^{CdL} are the intensities for the 1 : 1 M : L complex, and χ_{Zn} the mole fraction of Zn^{II} in the mixture. The CD signal is mainly sensitive to [Zn^{II}]; assumption that Cd^{II}

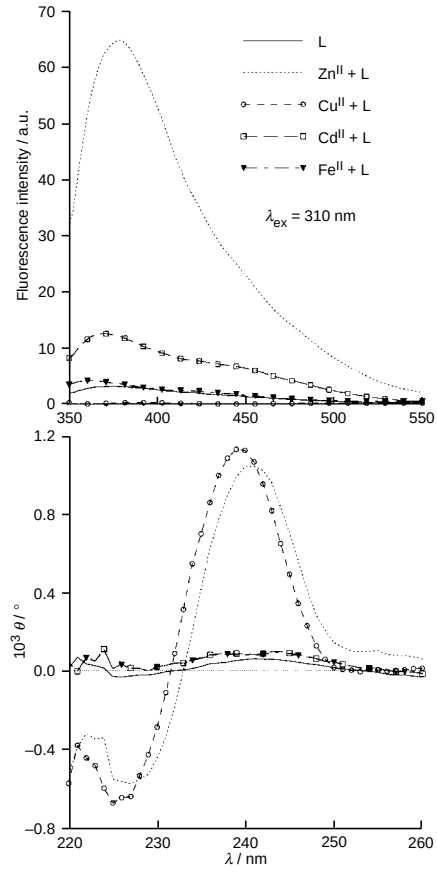

Fig. 1 Fluorescence and circular dichroism spectra of (*R*)-α-MeBQPA (5.1 μM) and complexes with $Zn(ClO_4)_2$ (5.1 μM), $Cd(NO_3)_2$ (5.1 μM), $Cu(ClO)_4)_2$ (5.2 μM) and $FeCl_2$ (5.0 μM) in aqueous HEPES buffer (0.1 M), pH = 7.09, 25 °C (λ_{ex} = 310 nm)

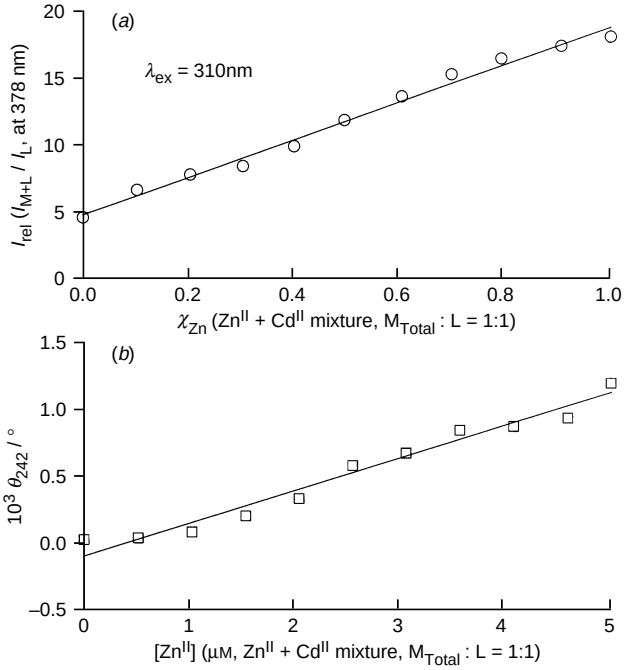

Fig. 2 Change in fluorescence intensity (378 nm, r = 0.995) and CD signal (242 nm, r = 0.984) of a 5 μM solution of (*R*)-α-MeBQPA in water (0.1 M HEPES, pH = 7.09)

does not contribute gives eqn. (2). Rearranging eqn. (1) into linear form and combining with eqn. (2) we obtained eqn. (3) which will give the [Cd^{II}] as a function of the two observables.

$$[Cd^{2+}] = \left(\frac{I_0^{ZnL} - I}{I - I_0^{CdL}}\right)\left(\frac{\theta - B}{A}\right) \quad (3)$$

Based on this chemistry, a device measuring both isotopic and anisotropic absorbance would permit the calculation of the concentrations of two species. This may be done by measurement of light absorption (UV–VIS and CD) or emission (*e.g.*, fluorescence and fluorescence-detected CD) since all four responses are proportional to absorption of the light.

We thank the National Institutes of Health (GM49170), for support of this work. Some mass spectra were obtained at the Michigan State University Mass Spectrometry Facility (supported in part by grant DRR-00480, from the Biotechnology Research Technology Program, NCRS, NIH).

Footnote and References

* E-mail: James.Canary@nyu.edu

1 A. W. Czarnik, *Chem. Biol.*, 1995, **2**, 423 and references therein.
2 L. Fabbrizzi and A. Poggi, *Chem. Soc. Rev.*, 1995, 197.
3 A. P. de Silva and C. McCoy, *Chem. Ind.*, 1994, 992.
4 P. Ghosh, P. K. Bharadwaj, S. Mandal and S. Ghosh, *J. Am. Chem. Soc.*, 1996, **118**, 1553.
5 D. G. Buerk, *Biosensors. Theory and Applications*, Technomic Publishing Co., Inc., Lancaster, 1993; T. Kuriyama and J. Kimura, in *Applied Biosensors*, ed. D. L. Wise, Butterworth Publishers, Boston, 1989, pp. 93–114.
6 M. D. Prat, J. Guiteras and J. L. Beltrán, *J. Fluoresc.*, 1991, **1**, 267.
7 M. E. Huston, C. Engleman and A. W. Czarnik, *J. Am. Chem. Soc.*, 1990, **112**, 7054.
8 J. W. Canary, C. S. Allen, J. M. Castagnetto and Y. Wang, *J. Am. Chem. Soc.*, 1995, **117**, 8484.
9 J. M. Castagnetto, X. Xu, N. D. Berova and J. W. Canary, *Chirality*, 1997, **9**, 616.
10 E. L. Wehry, in *Practical Fluorescence*, ed. G. G. Guilbault, M. Dekker, New York, 2nd edn., 1990, pp. 75–125; G. G. Guilbault, *ibid.*, pp. 185–230.
11 R. Y. Tsien and T. Pozzan, *Methods Enzymol.*, 1989, **172**, 230.
12 B. Valeur, in *Topics in Fluorescence Spectroscopy*, ed. J. R. Lakowicz, Plenum, New York, 1994, vol. 4, pp. 21–50.
13 N. Mataga, Y. Kaifu and M. Koizumi, *Bull. Chem. Soc. Jpn.*, 1956, **29**, 373; M. A. El-Sayed and M. Kasha, *Spectrochim. Acta*, 1959, **15**, 758; M. Yagi, T. Kaneshima, Y. Wada, K. Takemura and Y. Yokoyama, *J. Photochem. Photobiol. A: Chem.*, 1994, **84**, 27.
14 G. Anderegg and F. Wenk, *Helv. Chim. Acta*, 1971, **54**, 216.

Received in Columbia, MO, USA, 28th July 1997; 7/05443B

Stereoselective preparation and reactions of configurationally-defined mixed acyclic dialkylzincs

Christophe Darcel, Felix Flachsmann and Paul Knochel*

Fachbereich Chemie der Philipps-Universität Marburg, Hans-Meerwein-Strasse, D-35032 Marburg, Germany

Mixed acyclic dialkylzincs are stereoselectively prepared from *E*- and *Z*-trisubstituted alkenes.

The preparation of configurationally defined reactive organometallics is of great interest,[1] since it offers the potential of transferring the stereochemical information at the α-carbon of the metal to a variety of organic compounds *via* reaction with various electrophiles. Recently,[2] we have shown that organoboranes **1** can be converted by an exchange reaction[3] with Pr^i_2Zn to configurationally stable[4] mixed diorganozincs **2**. These zinc reagents can be reacted with electrophiles like D_2O or allylic halides, providing products of type **3** (Scheme 1).

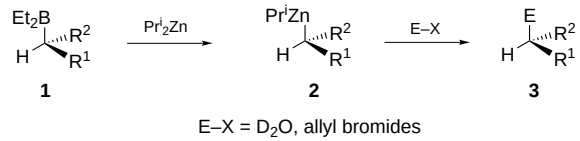

Scheme 1

In all these experiments, *trans*-cycloalkylborane derivatives **4** were used and converted to *trans*-cycloalkylzinc compounds **5**. To demonstrate the stereoselectivity of the boron–zinc exchange, the use of *cis*-cycloalkylboranes **6** would have been necessary. Since these molecules are not available by hydroboration with Et_2BH, we examined the hydroboration of open-chain trisubstituted *E*- and *Z*-olefins **7**. Herein, we report the stereoselective preparation of open-chain secondary dialkylzincs and their stereoselective deuterolysis and allylation.

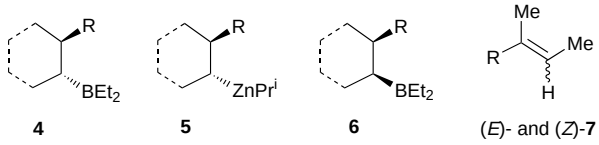

Thus, the hydroboration of *E*- and *Z*-styrene derivatives **8** with Et_2BH was complete after 14 h at 25 °C; the intermediate diethylorganoboranes were treated with Pr^i_2Zn, furnishing the mixed diorganozincs **9** and **10**, which were quenched with D_2O resulting in the formation of the deuterated product **11** (Scheme 2). The presence of the *o*-methoxy group was found to accelerate significantly the rate of the boron–zinc exchange reaction, allowing the completion of this exchange starting from (*Z*)- or (*E*)-**8** within 3 h at 0 °C. Under these conditions, the deuterolysis of **9** provides mainly the *anti*-deuterated product **11** (*syn* : *anti* < 1 : 99) whereas the deuterolysis of **10** furnishes the product **11** as a *syn* : *anti* mixture of 77 : 23. The *syn* : *anti* ratio of the deuterated products was determined by ^2H NMR spectroscopy. These experiments demonstrate for the first time the stereoselectivity of the boron–zinc exchange reaction for open-chain systems. It is interesting to note that performing the boron–zinc exchange at 25 °C instead of 0 °C leads to lower stereoselectivities, *i.e.* a *syn* : *anti* ratio of 22 : 78 starting from (*Z*)-**8** and 73 : 27 starting from (*E*)-**8**.

The mixed dialkylzincs **9** and **10** could also be transmetalated to copper–zinc compounds *via* reaction with CuCN·2LiCl, leading after treatment with allyl bromide to the desired allylated products **12** with a *syn* : *anti* ratio of 24 : 76 starting from the zinc intermediate **9** and 81 : 19 starting from the zinc reagent **10**. The lower stereoselectivity of the allylation of **9** compared to the deuterolysis may be due to a slow isomerization of **9** during the allylation reaction.†

Whilst the presence of the *o*-methoxy group of **8** facilitates the subsequent boron–zinc exchange, it is possible to extend the reaction to (*E*)- and (*Z*)-styrenes **13** with similar selectivities. This proves that the configurational stability of the organozinc intermediates does not depend on the presence of a heteroatom in close proximity. In this case, the deuterium signals after quenching of the intermediate zinc reagent **14** were not separated, so that the selectivity could not be determined. However, after transmetalation with CuCN·2LiCl and allylation the desired allylated product **15** was obtained stereoselectively. The *Z*-olefin **13** gave allylation product **15** with a *syn* : *anti* ratio of 19 : 81, whereas the *E*-olefin **13** gave a *syn* : *anti* ratio of 78 : 22 for **15** (Scheme 3).

The relative stereochemistry of the product **15** (*syn* : *anti* ratio of 78 : 22) was determined by converting it to 3,4-dimethyl-1-tetralone **18** by ozonolysis followed by oxidation of the

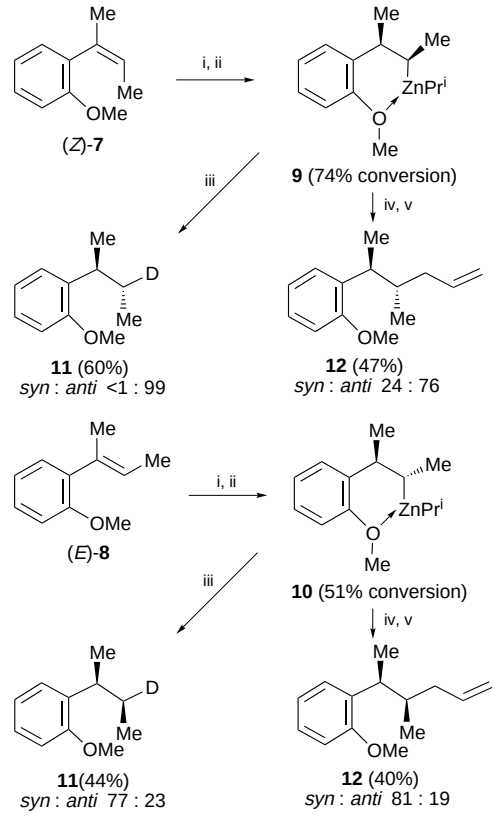

Scheme 2 *Reagents and conditions*: i, $HBEt_2$ (3 equiv.), 25 °C, 14.5 h; ii, Pr^i_2Zn (2 equiv.), 0 °C, 3 h; iii, D_2O, THF, −78 °C; iv, CuCN·2LiCl; v, allyl bromide, −78 to 25 °C

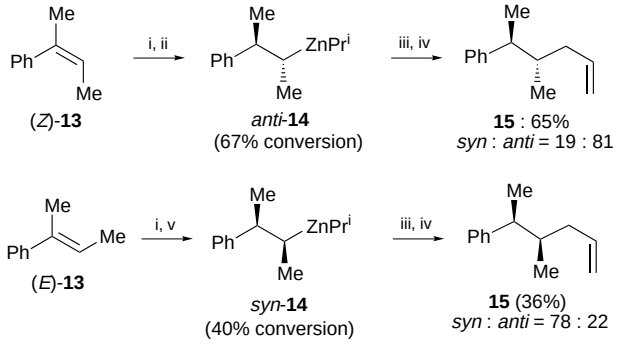

Scheme 3 *Reagents and conditions*: i, $BHEt_2$ (3 equiv.), 25 °C, 13 h; ii, Pr^i_2Zn (2 equiv.), 25 °C, 3 h; iii, CuCN·2LiCl, −78 °C; iv, allyl bromide, −78 to 25 °C; v, Pr^i_2Zn (2 equiv.), 25 °C, 4 h

resulting aldehyde **16** to the acid **17**. Friedel–Crafts cyclization of the corresponding acid chloride furnishes the *cis*- and *trans*-ketones **18** (*cis*:*trans* = 22:78). Both the major *trans* isomer and the minor *cis* isomer could be unequivocally identified by NMR spectroscopy (Scheme 4).

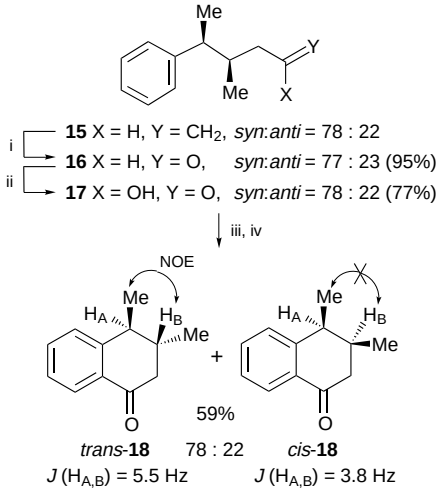

Scheme 4 *Reagents and conditions*: i, O_3, then Me_2S; ii, $NaClO_2$, $Me_2C{=}CHMe$, NaH_2PO_4, Bu^tOH, 25 °C, 1 h; iii, $SOCl_2$, 60 °C, 1 h; iv, $AlCl_3$ (1.25 equiv.), $ClCH_2CH_2Cl$, 25 °C, 4 h

In conclusion, we have shown that the boron–zinc exchange performed with Pr^i_2Zn on open-chain secondary zinc reagents proceeds stereoselectively. Although the relative stereochemistry of the zinc reagents could not be directly determined, we assume that this exchange reaction proceeds with retention of configuration as well as the allylation (and deuterolysis),‡ since an overall retention of configuration is observed. Current work in order to improve the level of stereoselectivity and to extend the number of electrophiles that can quench stereoselectively the intermediate organozinc reagents is underway.

The authors thank the Deutsche Forschungsgemeinschaft (SFB 260 and Leibniz program) and the Fonds der Chemischen Industrie for generous support of this research. We thank the A. von Humboldt-Stiftung for a fellowship to C. D., and BASF (Ludwigshafen), Witco (Bergkamen), Chemetall (Frankfurt) and Sipsy (Avrillé) for generous gifts of chemicals.

Footnotes and References

* E-mail: knochel@ps151S.chemie.uni-marburg.de

† We have observed in separate experiments that secondary copper–zinc reagents are more prone to epimerization than the organozinc precursors. Treatment of *trans*-1-methylindanyl)(isopropyl)zinc **19** (see ref. 2) with D_2O affords the corresponding *trans*-deuterated indane **20** with a *cis*:*trans*

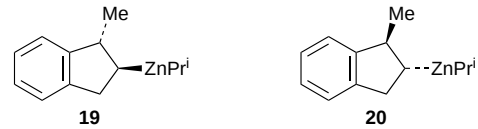

ratio of 1:99. Treatment of this zinc reagent with stoichiometric amounts of CuCN·2LiCl provides a copper–zinc reagent which was slowly warmed to 0 °C. After deuterolysis a *cis*:*trans* ratio of 11:89 was obtained. However, keeping this copper–zinc reagent at −78 °C and treating it with another equivalent of $ZnBr_2$ provides a *cis*:*trans* ratio of 1:99, showing that the zinc–copper reagent has good configurational stability at −78 °C and that, at this temperature, the zinc salts produced during the allylation reaction are not responsible for the epimerization reaction.

‡ The relative configuration between the methyl group and the deuterium atom in **20** was proven to be *trans* by comparison of NOE measurements for dihydro-1-methylindane and **20**.

1 W. C. Still and C. Sreekumar, *J. Am. Chem. Soc.*, 1980, **102**, 1201; J. M. Cong and E. K. Mar, *Tetrahedron*, 1989, **45**, 7709; D. S. Matteson, P. B. Tripathy, A. Sarkar and K. M. Sadhu, *J. Am. Chem. Soc.*, 1989, **111**, 4399; J. M. Chong and E. K. Mar, *Tetrahedron Lett.*, 1990, **31**, 1981; J. M. Chong and S. B. Park, *J. Org. Chem.*, 1992, **57**, 2220; W. H. Pearson and A. C. Lindbeck, *J. Am. Chem. Soc.*, 1991, **113**, 8546; H. J. Reich, M. A. Medina and M. D. Bowe, *J. Am. Chem. Soc.*, 1992, **114**, 11 003; O. Zschage and D. Hoppe, *Tetrahedron*, 1992, **48**, 5647; D. Hoppe, F. Hintze, P. Tebben, M. Paetow, H. Ahrens, J. Schwerdtfeger, P. Sommerfeld, J. Haller, W. Guarnieri, S. Kolczewski, T. Hense and I. Hoppe, *Pure Appl. Chem.*, 1994, **66**, 1479; S. T. Kerrick and P. Beak, *J. Am. Chem. Soc.*, 1991, **113**, 9708; S. Thayumanavan, S. Lee, C. Lui and P. Beak, *J. Am. Chem. Soc.*, 1994, **116**, 9755; R. W. Hoffmann and W. Klute, *Chem. Eur. J.*, 1996, **2**, 694.

2 L. Micouin, M. Oestreich and P. Knochel, *Angew. Chem.*, 1997, **109**, 274; *Angew. Chem., Int. Ed. Engl.*, 1997, **36**, 245.

3 F. Langer, L. Schwink, A. Devasagayaraj, P.-Y. Chavant and P. Knochel, *J. Org. Chem.*, 1996, **61**, 8229; W. Oppolzer and R. N. Radinov, *J. Am. Chem. Soc.*, 1993, **115**, 1593; M. Srebnik, *Tetrahedron Lett.*, 1991, **32**, 2449.

4 R. Duddu, M. Eckhardt, M. Furlong, P. Knoess, S. Berger and P. Knochel, *Tetrahedron*, 1994, **50**, 2415; S. Klein, I. Marek and J.-F. Normant, *J. Org. Chem.*, 1994, **59**, 2925; S. Sakami, T. Houkawa, M. Asaoka and H. Takei, *J. Chem. Soc., Perkin Trans. 1*, 1995, 285; T. Houkawa, T. Ueda, S. Sakami, M. Asaoka and H. Takei, *Tetrahedron Lett.*, 1996, **37**, 1045.

Received in Liverpool, UK, 20th October 1997; 7/07570G

$Cp^*TaCl_2B_4H_8$: synthesis, crystal structure and spectroscopic characterization of an air-stable, electronically unsaturated, chiral tantalaborane

Simon Aldridge, Hisako Hashimoto, Maoyu Shang and Thomas P. Fehlner*

Department of Chemistry and Biochemistry, University of Notre Dame, Notre Dame, Indiana, 46556, USA

Reaction between Cp^*TaCl_4 ($Cp^* = \eta^5$-C_5H_5) and BH_3·thf at 40 °C yields the pale red electronically unsaturated cluster $Cp^*TaCl_2B_4H_8$ 1 which despite having two electrons fewer than the seven pairs required for the observed square pyramidal geometry is stable in air; viewed as a cluster, 1 is the first example of an unsaturated cluster containing a single metal atom; viewed as a chiral 16-electron organometallic complex it is isoelectronic with $Cp(C_2B_9H_{11})TaCl_2$ and $Cp[(Me_3Si)_2C_2B_4H_4]TaCl_2$.

The rôle of unsaturated species in catalyzing or mediating industrially important transformations has long been acknowledged,[1] although examples of such species in transition metal cluster chemistry are rare.[2] Within the realms of metallaborane chemistry unsaturated species, that is those which are formally electron deficient with respect to the number of skeletal pairs required to sustain the observed molecular geometry, are limited to the sensitive group 6 metallaboranes $(Cp^*Cr)_2B_4H_8$[3] and $(Cp^*MoCl)_2B_3H_7$[4] both of which, having five skeletal electron pairs are formally two electrons deficient in terms of Wade's rules.[5] We now report the synthesis of the six-electron pair cluster $(Cp^*TaCl_2)B_4H_8$ **1** which has a *nido* structure formally derived from B_5H_9 by replacement of a basal BH fragment by Cp^*TaCl_2. Although **1** has two fewer electrons than the seven pairs expected for such a geometry, it is remarkably stable in air and sufficiently thermodynamically robust that it can be sublimed *in vacuo* at 230 °C.

Reaction of Cp^*TaCl_4 with 3.5 equiv. of BH_3·thf at 40 °C leads initially (4 h reaction time) to an extremely air- and moisture-sensitive deep blue intermediate thought to be a BH_3 adduct of the known dimeric tantalum hydride $(Cp^*TaCl_2H)_2$.[6] Longer reaction times lead to the isolation of the pale red air-stable cluster $Cp^*TaCl_2B_4H_8$ **1**.† **1** has been characterized by ^1H and ^{11}B NMR, IR spectroscopy and high-resolution mass spectrometry and by single crystal X-ray diffraction.‡ Consumption of BH_3·thf during the reaction is accompanied by evolution of BH_2Cl; the effective use of BH_3·thf as a dual reagent to build up a metallaborane cluster and to remove Cl as BH_2Cl has been demonstrated previously for cobalt[7] and molybdenum[4] metallaboranes. In addition, the reaction of Cp^*TaCl_4 with BH_3·thf contrasts with the analogous reaction with the more strongly reducing BH_4^-, which we find to give the known compound $(Cp^*TaB_2H_6)_2$.[8] The differing reactivities of BH_3·L and BH_4^- towards Cp^*MX_n species have been demonstrated previously for M = Cr, Mo and Co.[3,4,7]

The crystal structure of **1** is illustrated in Fig. 1 and can be interpreted as a *nido* cluster formally derived from B_5H_9 by replacement of a basal BH group by Cp^*TaCl_2. The skeletal electron count for such a molecule is six pairs, one pair short of the seven required for a square pyramidal geometry.[5] That the molecule is indeed square pyramidal, rather than trigonal bipyramidal (as would be expected for six pairs) is reflected by Ta–B(4) and B(1)–B(3) distances [3.338(12), 2.59(2) Å, respectively] which are sufficiently long to preclude any significant bonding interaction. Cluster **1** is therefore electronically unsaturated and is the first example of an unsaturated cluster containing a single metal atom.

The square pyramidal geometry of **1** is further confirmed by similarities with the only other crystallographically characterized 2-metallapentaborane, 2-$CpCoB_4H_8$.[9] The two clusters display similar B–B distances and B–B–B angles. Although the metal–apical boron distances are consistent with the differences in the covalent radii of the metals, the metal–basal boron distance for **1** is longer than expected from the structure of the cobalt compound. However, as M–B distances for hydrogen-bridged interactions exhibit large variations for the same metal, this difference is difficult to interpret.

A comparison of the molecular orbital schemes for **1** and 2-$CpCoB_4H_8$ calculated by Fenske–Hall methods[10] offers some insight into the nature of the unsaturated tantalaborane.§ For 2-$CpCoB_4H_8$ the SHOMO is an antibonding combination consisting mainly of a metal-based d orbital along with a minor contribution from a borane-based fragment orbital which is symmetric with respect to the molecular mirror plane and has a high percentage of apical boron 2p character. In the tantalum case the corresponding MO has similar character but is shifted to much higher energy (+0.41 for **1** *vs.* −12.47 eV) principally because the participating metal-based orbital is itself at much higher energy (−5.99 for **1** *vs.* −13.09 eV). In essence the significantly higher energy of the early transition metal d orbitals shifts a predominantly metal-based MO to much higher energy such that it is unoccupied, and **1** is stable despite one skeletal electron pair fewer than 2-$CpCoB_4H_8$. Although **1** is unique in being an unsaturated cluster featuring a single metal atom, the electronic factors underlying its apparent stability, the high-lying nature of the metal d orbitals and their ability to overlap well with borane-based orbitals, have much in common

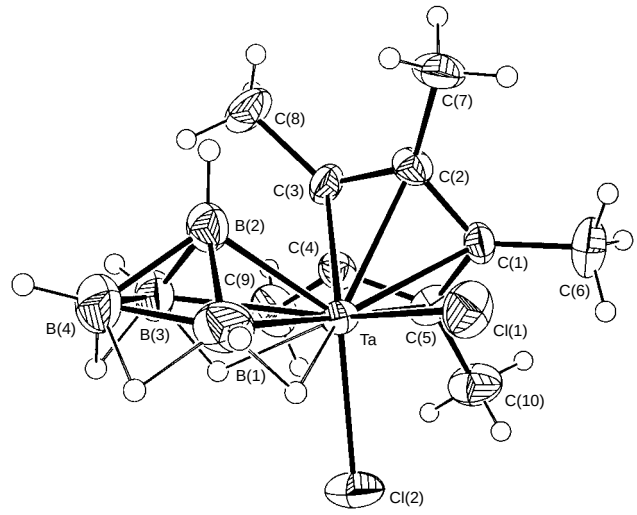

Fig. 1 The molecular structure of **1**. Relevant bond lengths (Å) and angles (°): Ta–Cl(1) 2.341(2), Ta–Cl(2) 2.370(2), Ta–Cp*(centroid) 2.123(9), Ta–B(1) 2.495(12), Ta–B(2) 2.249(12), Ta–B(3) 2.495(14), B(1)–B(2) 1.70(2), B(1)–B(4) 1.77(2), B(2)–B(4) 1.71(2), B(1)–H(11) 1.33(4), B(1)–H(12) 1.34(5), B(1)–H(13) 0.98(6), Ta–H(11) 1.88(5); Cl(1)–Ta–Cl(2) 99.20(10), H(11)–Ta–H(31) 79(3), B(1)–Ta–B(3) 62.4(5), B(1)–B(2)–B(3) 99.9(10), B(1)–B(4)–B(3) 94.0(9).

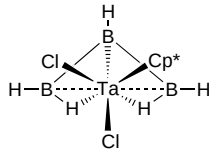

Fig. 2 Structure of **1** viewed along the Ta–B(4) axis showing the non-symmetrical distribution of ligands about the tantalum centre

with the factors stabilizing other unsaturated early transition metal metallaboranes featuring two metal centres *i.e.* $(Cp^*Cr)_2B_4H_8$[3] and $(Cp^*MoCl)_2B_3H_7$.[4]

Cluster **1** represents a rare example of a structurally characterized molecule containing a Ta–B bond[8,11–14] and comparison with $(Cp^*TaBr)_2B_2H_6$[8] (which contains both Ta–B and Ta–H–B linkages) shows similar hydrogen-bridged Ta···B distances [2.495 Å for **1**; 2.41 Å for $(Cp^*TaBr)_2B_2H_6$][8] but a significantly shorter direct Ta–B linkage (2.249 *vs*. 2.37 Å). The Ta–B bond is also decidedly shorter than those found in η^5 bound tantalum carborane complexes (which are typically in the range 2.4–2.5 Å),[11,13,14] but of similar length to that found in both isomers of the η^1 complex $Cp_2Ta(H)_2(BO_2C_6H_4)$ (2.263, 2.295 Å[12]).

An alternative view of **1** is as a 16-electron organometallic complex containing either a d^0 Ta^V centre coordinated to a six-electron $B_4H_8^{2-}$ ligand or a Ta^{III} centre and a four-electron neutral B_4H_8 ligand. The $B_4H_8^{2-}$ ligand is comparable to the six-electron units $C_2B_9H_{11}^{2-}$ or $(Me_3Si)_2C_2B_4H_4^{2-}$ in the analogous molecules $Cp(R)TaCl_2$ [R = $C_2B_9H_{11}$[13] or $(Me_3Si)_2C_2B_4H_4$[14]]. In contrast to these carborane complexes, however, **1** is chiral with the plane of mirror symmetry present in other 2-metallapentaboranes such as 2-$CpCoB_4H_8$[9] being eliminated by the non-symmetrical distribution of ligands about the tantalum centre (see Fig. 2). This results in non-equivalence of borons B(1) and B(3) which consequently give rise to two distinct ^{11}B NMR signals (at δ_B −2.9, 0.5). A similar situation arises in the osmapentaborane *nido*-$[(OC)(Ph_3P)_2OsB_4H_8]$ which also gives rise to four distinct ^{11}B signals;[15] in the case of **1** the barrier to rotation is sufficiently high that no hint of coalescence is observed even at 90 °C.

Although reactions of monocyclopentadienylmetal halides, $CpMX_n$, with nucleophiles have been extensively investigated,[16] reactions with electrophiles have received comparatively little attention to date. Reaction of one such transition metal complex, Cp^*TaCl_4 with the electrophile BH_3·thf yields the highly unusual cluster $(Cp^*TaCl_2)B_4H_8$ **1**. Cluster **1** is remarkable enough in being an electronically unsaturated mono-metallated borane cluster, but its thermodynamic stability, together with its stability in air, make it unique. The synthesis and on-going investigation of the chemistry of **1** [with particular emphasis on the synthesis of chiral tantalum(v) alkyl derivatives] represents an exciting development in the little investigated area of early transition metal metallaboranes.

The support of the National Science Foundation is gratefully acknowledged. S. A. also thanks the J. William Fulbright Scholarship Board for the award of a research scholarship. We thank Professor R. N. Grimes (University of Virginia) for providing fractional atomic coordinates for 2-$CpCoB_4H_8$.

Footnotes and References

* E-mail: thomas.p.fehlner.1@nd.edu

† Reaction of Cp^*TaCl_4 (300 mg, 0.66 mmol) with 3.5 equiv. of BH_3·thf in toluene at 40 °C for 96 h, followed by removal of volatiles (including BH_2Cl) *in vacuo* and extraction with hexane gives an orange–red solution from which pale red crystals of $Cp^*TaCl_2B_4H_8$ **1** can be grown by controlled cooling; **1** can also be isolated from the reaction of $Cp^*TaCl_2(CO)_2$(thf) with a fivefold excess of BH_3·thf in toluene at 40–50 °C over a period of 24 h. **1** is stable to air in both solid and solution phases (toluene or hexane), is obtained in yields of up to 45% (based on boron) and can be sublimed under continuous vacuum at *ca*. 230 °C without significant decomposition. **1** has been characterized by ^{1}H and ^{11}B NMR (including selective decoupling experiments), IR, high-resolution mass spectrometry and single crystal X-ray diffraction. *Spectroscopic data* for **1**: MS (EI), M^+ = 438, 1 Ta, 4 B, 2 Cl atoms, calc. *m/z* 438.1029, obs. 438.1041. ^{11}B NMR (toluene 21 °C), [J(^{11}B–^{1}H) in parentheses] δ 6.3 [d, 1B, B(2) (150 Hz)], 4.8 [d, 1B, B(4) (160 Hz)], δ 0.5 [d, 1B, B(1) or B(3) (160 Hz)], −2.9 [d, 1B, B(1) or B(3) (140 Hz)]. ^{1}H NMR ([$^2H_6$]benzene, 21 °C), δ −1.24 [partially collapsed quartet (pcq), 2 H, accidental overlap of both TaHB signals (80 Hz)], −0.67 (br, 2 H, overlap of both BHB signals), 1.85 (s, 15 H, Cp*) δ 2.81 [q, 1 H, terminal H attached to B(2) (150 Hz)], 4.52 [overlapping pcq, 3 H, overlap of terminal H attached to B(1), B(3) and B(4) (*ca*. 150 Hz)]. IR (KBr, cm^{-1}) 2996w (sh), 2965m, 2912m, 2863w (sh), ν(CH); 2567s, 2544s, 2530m (sh), ν(B–H$_t$); 2076w (sh), 2057m (br), 1646m (br), ν(B–H$_b$); 1443m (br); 1378s, δ(CH$_3$); 700m, 614w, ρ(CH$_3$). (ν = stretching mode, δ = deformation mode, ρ = rocking mode).

‡ *Crystallographic data* for **1**: monoclinic, space group $P2_1/c$, a = 14.149(2), b = 8.6357(12), c = 14.328(2) Å, β = 116.981(13)°, U = 1560.1(4) Å^3, Z = 4, D_c = 1.866 g cm^{-3}. Of the 2744 reflections collected [CAD4 diffractometer, Mo-Kα radiation (λ = 0.710 73 Å, 293 K)], all were independent and 2430 were observed [$I > 2\sigma(I)$]. All non-hydrogen atoms were anisotropically refined and difference Fourier synthesis located all hydrogen atoms. Both methyl and borane hydrogens were included in the final refinement, the former as idealized riding atoms [r(C–H) = 0.96 Å, U_{iso}(H) = 1.5 U_{eq}(C)], the latter isotropically with three free-variables to restrain B–H(terminal) B–H(bridging) and Ta–H bond lengths. R_1 = 0.0433, wR_2 = 0.1118 for observed unique reflections [$I > 2\sigma(I)$] and R_1 = 0.0494, wR_2 = 0.1199 for all 2744 unique reflections including those with negative intensities. The max., min. residual electron densities on the final difference Fourier map were 2.037 and −1.750 e Å^{-3}, respectively. The first five peaks were all within 1.4 Å of the heavy Ta atom and might have been caused by satellite diffraction and/or imperfection in the empirical absorption correction. Since no observable abnormality of the structure details was found, no further effort was made to improve the index for residual electron density. CCDC 182/705.

§ Fenske–Hall calculations were carried out on the 2-$CpTaCl_2B_4H_8$ and 2-$CpCoB_4H_8$ molecules, with coordinates taken from the results of single crystal X-ray diffraction studies. In the tantalum case the simplification was made that the Cp* (η^5-C_5Me_5) ligand was replaced by Cp (η^5-C_5H_5).

1 See, for example: G. Lavigne and H. D. Kaesz, *Metal Clusters in Catalysis*, ed. B. C. Gates, L. Guczi and H. Knözinger, Elsevier, Amsterdam, 1986, pp. 43–120.
2 R. D. Adams and S. Wang, *Organometallics*, 1986, **5**, 1272; 1987, **6**, 739; D. A. McCarthy, D. A. Krause and S. G. Shore, *J. Am. Chem. Soc.*, 1990, **112**, 8587.
3 J. Ho, K. J. Deck, Y. Nishihara, M. Shang and T. P. Fehlner, *J. Am. Chem. Soc.*, 1995, **117**, 10 292.
4 S. Aldridge, M. Shang and T. P. Fehlner, *J. Am. Chem. Soc.*, 1997, **119**, 1120.
5 K. Wade, *New Sci.*, 1974, **62**, 615.
6 P. A. Belmonte, R. R. Schrock and C. S. Day, *J. Am. Chem. Soc.*, 1982, **104**, 3082.
7 Y. Nishihara, K. J. Deck, M. Shang, T. P. Rehlner, B. S. Haggerty and A. L. Rheingold, *Organometallics*, 1994, **13**, 4510.
8 C. Ting and L. Messerle, *J. Am. Chem. Soc.*, 1989, **111**, 3449.
9 L. G. Sneddon and D. Voet, *J. Chem. Soc., Chem. Commun.*, 1976, 118.
10 M. B. Hall and R. F. Fenske, *Inorg. Chem.*, 1972, **11**, 768.
11 See, for example: R. Uhrhammer, Y.-X. Su, D. C. Swenson and R. F. Jordan, *Inorg. Chem.*, 1994, **33**, 4398; G. C. Bazan, S. J. Donnelly and G. Rodriguez, *J. Am. Chem. Soc.*, 1995, **117**, 2671.
12 D. R. Lantero, D. H. Motry, D. L. Ward and M. R. Smith, III, *J. Am. Chem. Soc.*, 1994, **116**, 10 811.
13 R. Uhrhammer, D. J. Crowther, J. D. Olson, D. C. Swenson and R. F. Jordan, *Organometallics*, 1992, **11**, 3098.
14 K. E. Stockman, K. L. Houseknacht, E. A. Boring, M. Sabat, M. G. Finn and R. N. Grimes, *Organometallics*, 1995, **14**, 3014.
15 J. Bould, N. N. Greenwood and J. D. Kennedy, *J. Organomet. Chem.*, 1983, **249**, 11.
16 R. Poli, *Chem. Rev.*, 1991, **91**, 509.

Received in Bloomington, IN, USA, 4th September 1997; 7/06483G

Electron transfer-induced sequential transformations of malonates by the ferrocenium ion

Ullrich Jahn* and Philip Hartmann

Institut für Organische Chemie, Technische Universität Braunschweig, Hagenring 30, D-38106 Braunschweig, Germany

Malonate enolates undergo single electron oxidation with the ferrocenium ion followed by radical cyclisation and radical or cationic termination of the reaction sequence.

In the course of investigations towards the incorporation of oxidative electron transfer in tandem reactions, we became interested in the development of general strategies for the use of enolates as precursors for the generation of radicals, with the choice of subsequent oxidation of the latter to carbocations in 'heterointermediate reaction sequences' [eqn. (1)].

$$\text{Educt} \rightarrow (R^1)^- \rightarrow (R^2)^- \xrightarrow{-e^-} (R^3)^{\cdot} \rightarrow (R^4)^{\cdot} \xrightarrow{-e^-} (R^5)^+ \rightarrow (R^6)^+ \rightarrow \text{Product} \quad (1)$$

Enolates have been used in oxidative dimerisations involving various metal salts.[1] Cyclisations of highly acidic β-dicarbonyl compounds onto phenolates with alkaline $K_3[Fe(CN)_6]$ were reported by Kende.[2] The electrochemical oxidation of enolates is known, but these reactions are often limited by low yields and competing reaction pathways.[3] For the generation of α-carbonyl radicals from neutral carbonyl compounds, $Mn(OAc)_3$[4] or cerium ammonium nitrate (CAN)[5] were employed, but these reagents are not applicable to enolates.

Here we introduce ferrocenium hexafluorophosphate **1** as an efficient and selective single electron oxidant for enolates and certain radical types in reaction sequences.† In addition to its mildness, **1** is easily recovered and recycled and is thus more economical than other heavy metal oxidants.

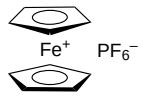

1

The starting point of our studies was the 5-*exo* cyclisations of the substituted malonates **2a**–**e** (Scheme 1). After deprotonation with $(Me_3Si)_2NLi$ or LDA at −78 °C in DME (50 mM), the enolate solutions were treated with portions of **1** at 0 °C.‡ The course of the reactions was easily monitored by the colour change of the mixtures. The reactions were finished when the colour of the solution remained green.

Depending on the structure of the acceptor double bonds in **2**, different products were obtained (Scheme 1, Table 1). Malonate **2a** gave a single bicyclic lactone **3a**§ in 64% yield (entries 1 and 2). The dimethyl derivative **2b** yielded the lactone **3b** and the elimination product **4b** together with a small amount of the disproportionation product **5b**. $(Me_3Si)_2NLi$ was the more efficient base for the bicyclisation to lactone **3b** (entries 3 and 4). Oxidative cyclisation of the phenyl compounds **2c** or **2d** afforded a partly separable mixture of the diastereoisomerically pure lactone **3c** and the dimer **6c** (entries 5 and 6). The

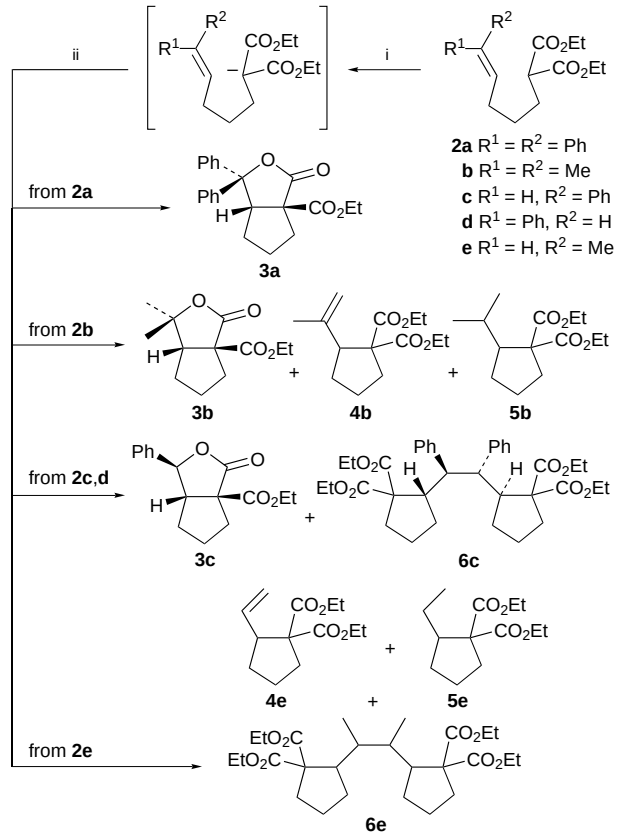

Scheme 1 *Reagents and conditions:* i, LDA or $(Me_3Si)_2NLi$, −78 °C, DME; ii, **1**, 0 °C

Table 1 Cyclisation products of the malonates **2** with **1** and product ratio of cationic or radical termination of the sequence

			Products (%)				
Entry	Educt	Base (equiv.)	**3**	**4**	**5**	**6**[a]	Cationic : radical
1	**2a**	LDA (2.5)	64	—	—	—	100 : 0
2	**2a**	$(Me_3Si)_2NLi$ (1.75)	54	—	—	—	100 : 0
3	**2b**	$(Me_3Si)_2NLi$ (1.75)	52	26	6	—	6 : 1
4	**2b**	LDA (3)	27	28	2	—	13 : 1
5	**2c**	$(Me_3Si)_2NLi$ (2.5)	7	—	—	24	1 : 3.4
6	**2d**	LDA (1.75)	28	—	—	48	1 : 1.7
7	**2e**	$(Me_3Si)_2NLi$ (2)	—	25	25	34[b]	0 : 100

[a] Yield based on **2**. [b] Diastereoisomeric mixture, stereochemistry not assigned.

Table 2 Termination of the oxidative cyclisations of the malonates **2** with TEMPO **10**

Entry	Educt	Base (equiv.)	Equiv. TEMPO	Product (%) **3**	**11**	**12** (dr)[a]	Cyclic : acyclic
1	**2a**	$(Me_3Si)_2NLi$ (1.75)	2	26	33	—	1 : 1.3
2	**2a**	LDA (1.75)	2	25	47	—	1 : 1.9
3	**2b**	$(Me_3Si)_2NLi$ (1.75)	2	—	—	87	100 : 0
4	**2c**,**d**	$(Me_3Si)_2NLi$ (1.75)	2	—	—	72 (100 : 0)	100 : 0
5	**2e**	$(Me_3Si)_2NLi$ (1)[b]	1	—	—	69 (1.8 : 1[c])	100 : 0
6	**2e**	$(Me_3Si)_2NLi$ (2)	2	—	41	42 (2 : 1[c])	1 : 1

[a] Diastereoisomeric ratio. [b] 6% Educt recovered. [c] Stereochemistry could not be assigned.

stereochemical assignment is based on spectral data and is in agreement with the stereochemistry of the TEMPO-trapping product (*vide infra*). The (*E*)-Hex-4-enylmalonate **2e** provided the disproportionation products **4e** and **5e** and a diastereomeric mixture of the dimer **6e** in a ratio of 1.5 : 1.5 : 1 (entry 7).

Clear trends emerge from these results. Enolates **2** are efficiently oxidised to radicals **7** by **1** (Scheme 2). The 5-*exo* cyclisation provides the rearranged radicals **8**. The structure of **8** determines their stabilisation. Radicals **8a,b** are oxidised to carbocations **9a,b**, which undergo intramolecular nucleophilic trapping to lactones **3a,b** or elimination to **4b**, respectively. The endergonic oxidation of the benzylic radical **8c** occurs,[6] but is slower than radical dimerisation and yields a mixture of **3c** and **6c**. Secondary alkyl radicals are not oxidised and undergo typical radical processes to products **4e**, **5e** and **6e**.

Trapping experiments with TEMPO **10** confirm these hypotheses and give rise to an efficient oxidative radical cyclisation/termination process with remote oxy-functionalisation (Scheme 3, Table 2). Addition of **1** to the reaction mixtures in the presence of 1–2 equiv. of **10**, as described above, gave the following results. Malonate **2a** yielded a mixture of the acyclic TEMPO adduct **11a** and lactone **3a** (entry 1). Substrates **2b**–**e** provided the cyclised TEMPO adducts **12** with moderate to excellent stereoselectivity (entries 2–5). The acyclic compounds **11** were detected in traces if at all, but by using a larger excess of **10** their amount increased (entry 6). The structure and stereochemistry of **12c** was proved by X-ray analysis.§ Thus on one hand, radical 5-*exo* cyclisation of **7** is (except in the case of **7a**) faster than their trapping by **10**. On the other hand, trapping of the cyclised radicals **8b**,**c** is strongly favoured over their oxidation and allows selective remote oxygenation.

Reductive N–O bond cleavage of **12b**,**e** with spontaneous lactonisation was achieved with Zn–AcOH and allows the preparation of **3b** and the otherwise not accessible lactone **3e** (*vide supra*) in a two-step procedure in 86 and 84% yield .

In conclusion, we have shown that enolates serve as a convenient source of radicals. Electron transfer-induced reaction sequences provide a simple access to bicyclic lactones with **1** as oxidant.

We thank the Fonds der Chemischen Industrie (Liebig-Stipendium for U. J.) for financial support and Professor Dr H. Hopf for ongoing support of this project.

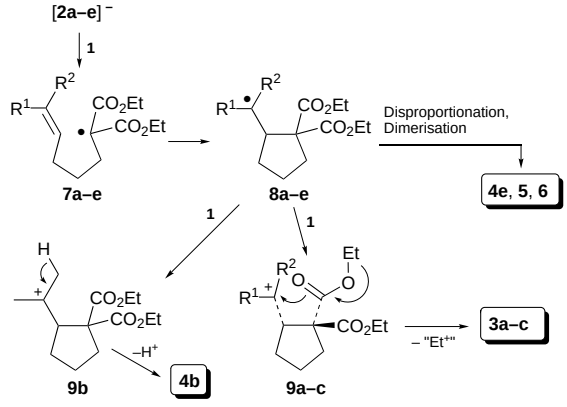

Scheme 2

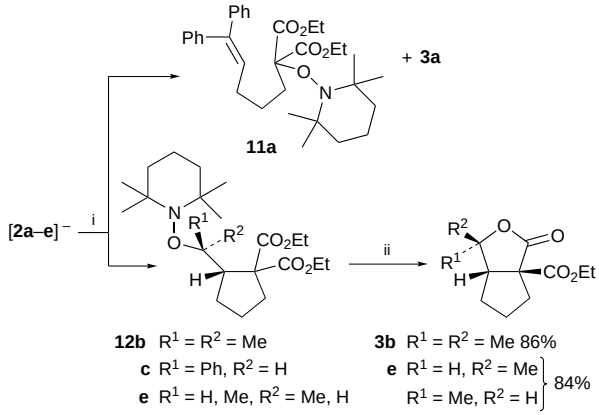

Scheme 3 *Reagents and conditions*: i, TEMPO, **1**, 0 °C, DME; ii, Zn, AcOH, THF, 70 °C

Footnotes and References

* E-mail: u.jahn@tu-bs.de

† Salt **1** has found widespread use in transition metal oxidation (ref. 7), although applications in organic chemistry are scarce (ref. 8). Ferrocenes have been employed as redox catalysts for enzymatic oxidations (ref. 9).

‡ The excess of base was applied to ensure complete deprotonation under dilution conditions. A control experiment showed that the free base was also oxidised with **1**. The outcome of the cyclisations was, however, only slightly influenced by the amount of base.

§ All new compounds exhibit satisfactory analytical data. X-Ray analyses of **3a** and **12c** proved their structures and will be published separately.

1 Reviews: P. I. Dalko, *Tetrahedron*, 1995, **51**, 7579; J. Iqbal, B. Bhatia and N. K. Nayyar, *Chem. Rev.*, 1994, **94**, 519.
2 A. S. Kende, K. Koch and C. A. Smith, *J. Am. Chem. Soc.*, 1988, **110**, 2210 and references cited therein.
3 Reviews: M. Schmittel, *Top. Curr. Chem.*, 1994, **169**, 183; H. J. Schäfer, *Angew. Chem., Int. Ed. Engl.*, 1981, **20**, 911.
4 Reviews: G. G. Melikyan, *Organic Reactions*, Wiley, New York, 1997, vol. 49, p. 427; B. B. Snider, *Chem. Rev.*, 1996, **96**, 339.
5 Review: V. Nair, J. Mathew and J. Prabhakaran, *Chem. Soc. Rev.*, 1997, **26**, 127.
6 D. D. M. Wayner and V. D. Parker, *Acc. Chem. Res.*, 1993, **26**, 287.
7 Review: N. G. Connelly and W. E. Geiger, *Chem. Rev.*, 1996, **96**, 877.
8 T. Langer, M. Illich and G. Helmchen, *Synlett*, 1996, 1137; H.-J. Knölker, F. Budei, J.-B. Pannek and G. Schlechtingen, *Synlett* 1996, 587; K. Narasaka and Y. Kohno, *Bull. Chem. Soc. Jpn.*, 1993, **66**, 3456; K. Narasaka, N. Arai and T. Okauchi, *Bull. Chem. Soc. Jpn.*, 1993, **66**, 2995; T. R. Kelly, S. K. Maity, P. Meghani and N. S. Chandrakumar, *Tetrahedron Lett.*, 1989, **30**, 1357; C. P. Casey, E. A. Austin and A. L. Rheingold, *Organometallics*, 1987, **6**, 2157; J. Lubach and W. Drenth, *Recl. Trav. Chim. Pays-Bas*, 1970, **89**, 144.
9 Review: W. A. Herrmann and B. Cornils, *Angew. Chem., Int. Ed. Engl.*, 1997, **36**, 1047.

Received in Cambridge, UK, 23rd September 1997; 7/06879D

First blue luminescent diborate compound: $B_2(\mu\text{-}O)Et_2(7\text{-azain})_2$ (7-azain = 7-azaindole anion)

Abdi Hassan and Suning Wang*

Department of Chemistry, Queen's University, Kingston, Ontario, Canada K7L 3N6

A novel blue luminescent diborate compound $B_2(\mu\text{-}O)Et_2(7\text{-azain})_2$ (7-azain = 7-azaindole anion) is synthesized and characterized structurally; it emits a blue color at λ_{max} = 422 nm in the solid and at λ_{max} = 419 nm in solution and is stable under air as a solid.

Blue luminescent compounds are among the most sought-after materials by scientists in both academia and industry because of their potential applications in electroluminescence displays.[1] Most of the previously reported blue luminescent compounds in electroluminescent displays are either aromatic organic molecules or organic polymers.[1] Blue luminescent inorganic and organometallic complexes are rather rare and have been limited to 8-quinoline or azomethine based complexes where either Al or Zn ions are involved.[2] During our investigation of alkylaluminium amido and imido chemistry, we have discovered two families of blue luminescent aluminium complexes based on either the deprotonated di-2-pyridyl amine ligand or 7-azaindole ligand.[3] Both di-2-pyridyl amine (Hdpa) and 7-azaindole (7-Hazain) have no visible blue luminescence under UV radiation at ambient temperature. Upon reaction with $AlMe_3$, these two ligands produce a variety of blue luminescent aluminium complexes.[4] One weakness associated with these aluminium compounds is their tendency to undergo hydrolysis upon exposure to air. Although we have found that the incorporation of alkoxo and oxo ligands into the complexes enhances their thermal and air stability without destroying the blue luminescence,[4] they are, however, still vulnerable, to some extent, to air and moisture. In contrast to organoaluminium compounds, organoboron compounds are in general more stable owing to the increased covalency of B–C and B–N bonds,[5] in comparison to those of Al–C and Al–N bonds. We therefore explored the synthesis of boron compounds containing either the di-2-pyridylamine or the 7-azaindole ligand. We report here the first example of a blue luminescent diborate compound, $B_2(\mu\text{-}O)Et_2(7\text{-azain})_2$ **1**.

The colorless diborate compound was isolated in *ca*. 30% yield from the reaction of BEt_3 with 7-azaindole and 1,1,1,3,3,3-hexafluoropropan-2-ol in a 2 : 2 : 1 ratio in toluene at 25 °C. This compound can also be obtained by the reaction of BEt_3 with 7-azaindole and water in a 2 : 2 : 1 ratio in *ca*. 10% yield. The role played by 1,1,1,3,3,3-hexafluoropropan-2-ol in the synthesis has not, as yet, been understood. ^{1}H NMR spectroscopy, single-crystal X-ray diffraction and elemental analyses† established the formula of this compound to be $B_2(\mu\text{-}O)Et_2(7\text{-azain})_2$ **1**. The crystal structure along with important bond lengths and angles are given in Fig. 1. Compound **1** contains two B atoms in a tetrahedral environment. The 7-azaindole ligand is bound to the B centers *via* both N atoms. Both 7-azaindole ligands are disordered with 50% occupancy for each of the disordered sites. Consequently, the B–N bond lengths are the average of B–N(indole) and B–N(pyridyl) bonds, ranging from 1.604(5) to 1.612(5) Å, which are consistent with the typical B–N bond lengths reported previously.[6,7] Each B is also bound by an ethyl group with a normal B–C bond length. The most interesting structural feature of this molecule is the bridging O atom which can be considered as the consequence of the reaction of two ethyl groups with one water molecule. A similar oxygen bridge has been observed in the compound $B_4(2,2'\text{-biimidazole})_2(O)Et_6$ reported by Niedenzu *et al.*[6a] The B–O bond lengths in compound **1** are typical[6,7] and similar to those found in Niedenzu's compound. The B–O–B angle [151(3)°] in Niedenzu's compound is, however, much larger than that in compound **1** [119.6(3)°] which can be attributed to the different steric strain imposed by the 2,2′-biimidazole and the 7-azaindole ligands. As a result of the bridging oxygen atom, compound **1** has a bicyclo[3.3.1]nonane-like structure. Similar B–O–B bridges have also been observed previously in heterocycles of boric or boronic acids or their acyloxy or acylamino derivatives based on the bicyclo-[3.3.1]nonane framework.[7] To our knowledge, compound **1** is the first example of biheterocycles involving 7-azaindole, boron and oxygen atoms.

The most exciting property of **1** is that it emits an intense blue color upon irradiation by UV light. The emission maximum in the solid is at λ = 422 nm. The free 7-azaindole does not have any observable blue luminescence in the solid state. The toluene solution of compound **1** emits at λ_{max} = 419 nm at 23 °C while the toluene solution of the free 7-azaindole ligand has an emission band at λ_{max} = 357 nm which is in the colorless UV region. In addition to the dramatic shift of the emission band, the relative emission intensity† of compound **1** in solution also appeared to be much greater than that of the free ligand (Fig. 2). The role of the boron atom in the blue luminescence of **1** was therefore considered to be perhaps twofold. First, the formation of covalent bonds between the B and N atoms *via* the donation of lone-pairs of the N atoms to the B atoms changes the emission energy from UV to blue, perhaps owing to the lowering of the energy gap between π^* and π. Second, the

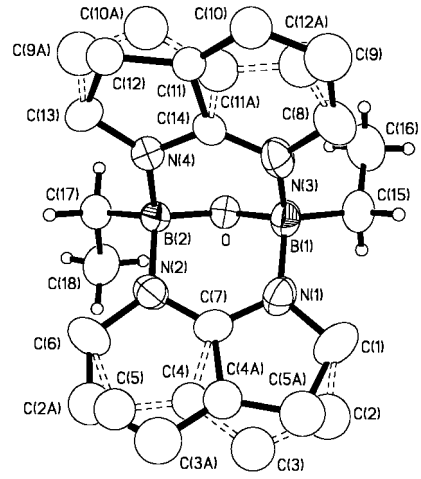

Fig. 1 The molecular structure of compound **1** with 50% thermal ellipsoids and labelling scheme. The second set of positions of the disordered 7-azaindole ligands are shown as dashed lines. Important bond lengths (Å) and angles (°): B(1)–O 1.430(5), B(1)–N(1) 1.604(5), B(1)–N(3) 1.609(5), B(1)–C(15) 1.595(6), B(2)–O 1.431(5), B(2)–N(2) 1.612(5), B(2)–N(4) 1.604(5), B(2)–C(17) 1.592(5); B(1)–O–B(2) 119.6(3), N(1)–B(1)–N(3) 104.6(3), O–B(1)–C(15) 115.9(4), N(2)–B(2)–N(4) 105.2(3), O–B(2)–C(17) 115.9(3)°.

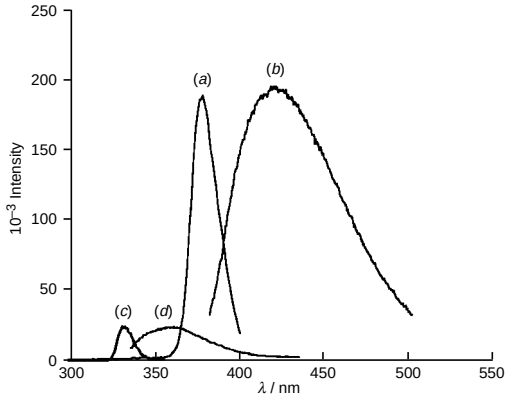

Fig. 2 Excitation and emission spectra of **1** and 7-azaindole in solution at 23 °C: (*a*) and (*b*) are the excitation and emission spectra of compound **1** (6.75×10^{-3} M in toluene); (*c*) and (*d*) are the excitation and emission spectra of 7-azaindole (3.67×10^{-2} M in toluene)

binding of the 7-azaindole ligand to two B atoms increases the rigidity of the ligand, thus reducing the loss of energy *via* vibrational motions and increasing the emission efficiency,[8a] a phenomenon well known to coordination compounds containing luminescent chelating ligands.[8b,c] However, our attempt to measure the quantum yields of the free ligand and the boron compound against a common reference compound was unsuccessful because they absorb at different regions. The emission quantum yield of compound **1** was determined to be 0.47, relative to that of 9,10-diphenylanthracene while the quantum yield of the free ligand was determined to be 0.92, relative to that of naphthalene. Efforts to gain a better understanding of the luminescent mechanism of **1** are being undertaken by our group.

As we anticipated, compound **1** is remarkably stable towards air in the solid state. In fact, it can be kept under air for days without decomposition. Compound **1** is also thermally stable. It melts at 290 °C without decomposition and can be sublimed at *ca*. 150 °C and 0.06 mmHg. The high stability of compound **1** can be attributed to both the presence of the bridging O atom and the covalency of B–C and B–N bonds, in comparison to the corresponding aluminium compounds. To our best knowledge, compound **1** is the first example of blue luminescent boron compounds. The high stability and volatility of **1** make it a good candidate as an emitter in electroluminescence display devices, which is being investigated in our laboratory.

We thank the Natural Science and Engineering Research Council of Canada for financial support, Dr Steven Brown and Samir Tabash for recording the excitation and emission spectra, as well as Drs Linda Johnston and Lorenzo Branealeon for assistance in quantum yield measurements.

Footnotes and References

* E-mail: wangs@chem.queensu.ca

† *Crystal data* for **1**: a = 12.865(4), b = 10.085(3), c = 13.476(4) Å, β = 103.81(2)°, U = 1698.0(8) Å^3, monoclinic, space group $P2_1/n$. Data were collected over the range 2θ 3–45° at 25 °C on a Siemens P4 diffractometer with Mo-Kα radiation (λ = 0, 710 73 Å), operated at 50 kV and 40 mA. Data were processed on a Pentium PC using Siemens SHELXTL software package. Convergence to the final R values of R_1 = 0.0678, wR_2 = 0.1840 for **1** were achieved by using 2193 reflections [$I > 2\sigma(I)$] and 218 parameters. Details of X-ray crystallographic analyses are given in supplementary material available from the authors. CCDC 182/707. Elemental analysis for $C_{18}H_{20}B_2N_4O$: calc. C, 65.51; H, 6.07; N, 16.98. Found: C, 65.35; H, 6.03; N, 16.80%. ^{1}H NMR ($CDCl_3$): δ 0.95 (t, 6 H, CH_3), 1.26 (q, 4 H, CH_2), 6.41 (d, 2 H, 7-azain), 7.04 (m, 2 H, 7-azain), 7.45 (d, 2 H, 7-azain), 7.97 (m, 2 H, 7-azain), 8.12 (m, 2 H, 7-azain). Excitation and emission spectra for compound **1** and the free ligand were recorded on a Photon Technologies International QM1 spectrometer. The solution spectra for both compounds were recorded under the same conditions except that the molar concentration of the free ligand was made 5.44 times higher than that of the boron compound owing to its low emission intensity.

1 P. D. Rack, A. Naman, P. H. Holloway, S. Sun and R. T. Tuenge, *Mater. Res. Bull.*, 1996, March, 49; H. J. Brouwer, V. V. Krasnikov, A. Hilberer and G. Hadziioannou, *Adv. Mater.*, 1996, **8**, 935; A. Edwards, S. Blumstengel, I. Sokolik, R. Dorsinville, H. Yun, K. Kwei and Y. Okamoto, *Appl. Phys. Lett.*, 1997, **70**, 298; Y. Ohmori, M. Uchida, K. Muro and K. Yoshino, *Jpn. J. Appl. Phys.*, 1991, **30**, L1941.

2 C. P. Moore, S. A. VanSlyke and H. J. Gysling, *US Pat.*, 5484922, 1996; T. Sano, M. Fujita, T. Fujii, Y. Nishio, Y. Hamada, K. Shibata and K. Kuroki, *US Pat.*, 5432014, 1995; Y. Hironaka, H. Nakamura and T. Kusumoto, *US Pat.*, 5466392, 1995; S. A. VanSlyke, P. S. Bryan and F. V. Lovecchio, *US Pat.*, 5150006, 1992; P. S. Bryan, F. V. Lovecchio and S. A. VanSlyke, *US Pat.*, 5141671, 1992.

3 S. Wang, W. Liu and A. Hassan, *US Pat.*, 1997, pending.

4 W. Liu, A. Hassan and S. Wang, *Organometallics*, 1997, **16**, 4257.

5 F. A. Cotton and G. Wilkinson, *Advanced Inorganic Chemistry*, Wiley, New York, 5th edn., 1988; C. E. Housecroft, in *Comprehensive Organometallic Chemistry, II*, ed. E. W. Abel, F. G. A. Stone and G. Wilkinson, volume editor C. E. Housecroft, Pergamon, Oxford, 1995, vol. 1, ch. 4, pp. 129–195.

6 (*a*) K. Niedenzu, H. Deng, D. Knoeppel, J. Krause and S. G. Shore, *Inorg. Chem.*, 1992, **31**, 3162; (*b*) L. Y. Hsu, J. F. Mariategui, K. Niedenzu and S. G. Shore, *Inorg. Chem.*, 1987, **26**, 143; (*c*) W. Kiegel, G. Lubkowitz, S. J. Rettig and J. Trotter, *Can. J. Chem.*, 1991, **69**, 234; 1217; 1227.

7 G. Heller, *Top. Curr. Chem.*, 1986, **131**, 39; A. Dal Negro, L. Ungaretti and A. Perotti, *J. Chem. Soc., Dalton Trans.*, 1972, 1639; H. Binder, W. Matheis, H.-J. Deiseroth and F.-S. Han, *Z. Naturforsch., Teil B*, 1984, **39**, 1717; W. Clegg, N. Noltemeyer, G. M. Shelderick, W. Maringgele and A. Meller, *Z. Naturforsch., Teil B*, 1980, **35**, 1499.

8 (*a*) *Fluorescence and Phosphorescence*, ed. D. Rendell, Wiley, New York, 1987; (*b*) *Photochemistry and Photophysics of Coordination Compounds*, ed. H. Yersin and A. Vogler, Springer-Verlag, Berlin, 1987; (*c*) *Concepts of Inorganic Photochemistry*, ed. A. W. Adamson and P. D. Fleischauer, Wiley, New York, 1975.

Received in Cambridge, UK, 10th July 1997; revised manuscript received 11th November 1997; 7/08312B

Synthesis of soluble conjugated metalloporphyrin polymers with tunable electronic properties

Biwang Jiang, Szu-Wei Yang, Denis C. Barbini and Wayne E. Jones Jr.*

Department of Chemistry and Institute for Materials Research, State University of New York at Binghamton, Binghamton, NY 13902-6016, USA

New linear conjugated porphyrin polymers are synthesized by a palladium-catalyzed cross-coupling reaction of [5,15-bis(ethynyl)-10,20-bis(mesityl)porphyrin]zinc and diiodobenzene derivatives; enhanced solubility of the conjugated porphyrin polymers is achieved by attachment of long alkyl ether or dialkyl amide groups to the aryl moiety, resulting in unambiguous characterization by ^{1}H NMR, IR, GPC, UV–VIS and fluorescence spectroscopy; in addition, the introduction of alkyl ether (electron donor) or dialkyl amide (electron acceptor) results in significant modulation of the electronic properties of the conjugated porphyrin polymers owing to strong electronic coupling.

Conjugated porphyrin polymers and oligomers are an attractive new class of materials with potential applications in the fields of electronics, optical devices, sensors and solar energy conversion.[1–7] Although the synthesis of a wide variety of porphyrin dimers or oligomers *via* the building block approach is well developed, relatively few soluble conjugated porphyrin polymers have been studied.[1] Anderson *et al*. have synthesized a soluble, linear conjugated *meso*-butadiyne-linked porphyrin polymer with long alkyl chains on the porphyrin periphery. The polymer exhibits an unusually high susceptibility $\chi^{(3)}$ and strong electronic communication as well as electronic absorption in the near IR.[1*a*] However, the electronic tuning of the *meso*-butadiyne-linked porphyrin polymers is synthetically challenging. Therien and DiMagno also reported the synthesis of poly(diethylnylaryl porphyrin) with limited characterization.[1*b*] Recently, we synthesized a series of soluble *meso*-phenylporphyrin-based polymers with tunable electronic and photophysical properties.[5,6] Unfortunately, the electronic communication along the polymer backbone was limited due to steric interactions between the phenyl *ortho* proton and the porphyrin β-hydrogen, resulting in a large dihedral angle between the porphyrin ring and the phenylenevinylene unit.[5–8] We present here a modified approach to soluble and fully conjugated porphyrin polymers with tunable electronic and optical properties that builds on previous efforts.

The design and synthesis of the new conjugated porphyrin polymers and their precursor porphyrin monomers are outlined in Scheme 1. The *meso*-(mesityl)dipyrromethane **1** was synthesized from pyrrole according to a literature procedure.[9] Condensation of **1** with (trimethylsilyl)propynal **2** gives trimethylsilyl-protected porphyrin **3a** in 30% yield.[10] Metallation of porphyrin **3a** with $Zn(OAc)_2$, followed by deprotection of the terminal acetylene with tetrabutylammonium fluoride leads to **3c**. Porphyrin polymers **5a** and **5b** were synthesized from palladium-catalyzed cross-coupling reaction of porphyrin monomer **3c** and the corresponding diiodoaryl compounds **4a** or **4b**[11] in 90% yields.† The high solubility of the polymers was achieved by attaching long pendant chains to the aryl units. The mesityl substituents on the porphyrin moiety also contribute to the solubility of the polymers.[12]

^{1}H NMR spectra of the polymers in $CDCl_3$ demonstrated the expected polymer structure (Scheme 1). For polymer **5b**, two broad peaks at δ 9.7 and 8.8 are observed and assigned to the β-pyrrole protons of the porphyrin subunits. The resonance of the two aromatic protons corresponding to aryl units appears at δ 8.1, much further downfield from δ 7.55 as seen in monomer **4b**. No signal was observed near δ 4.1 for an acetylenic proton, supporting the formation of the diethynylaryl-linked porphyrin polymer. Also no absorbance was observed at 2091 cm^{-1} in the IR spectrum due to acetylene end-groups, consistent with ^{1}H NMR results. The formation of the ethynyl link was further confirmed by absorbance at 2184 cm^{-1} in the IR spectrum. The NMR and IR data suggest a high degree of polymerization in these materials. The average molecular mass was determined by GPC to be M_w = 5.17 × 10^4, M_n = 2.45 × 10^4, using polystyrene standards. Attempts at using multi-angle light scattering to independently determine molecular mass were unsuccessful due to competitive absorption.

The insertion of a triple bond between the porphyrin and aryl subunits was expected to enhance electronic interaction in the main polymer chain as demonstrated previously for dimeric systems.[8] Fig. 1(*a*) shows the absorption spectra of polymers **5a** and **5b** compared with the monomer **3c**. In both cases, the porphyrin polymers exhibit dramatic red-shifts and broadening in both the B- and Q-type transition bands in comparison to porphyrin monomer **3c**. This would indicate strong electronic interactions along the conjugated porphyrin backbone.[1–3]

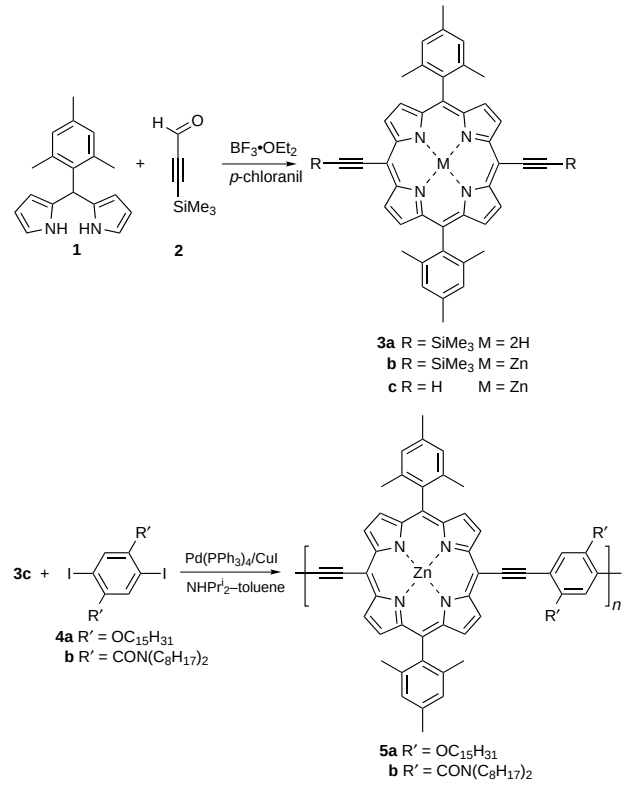

Scheme 1 Synthesis of conjugated porphyrin polymers and their precursors

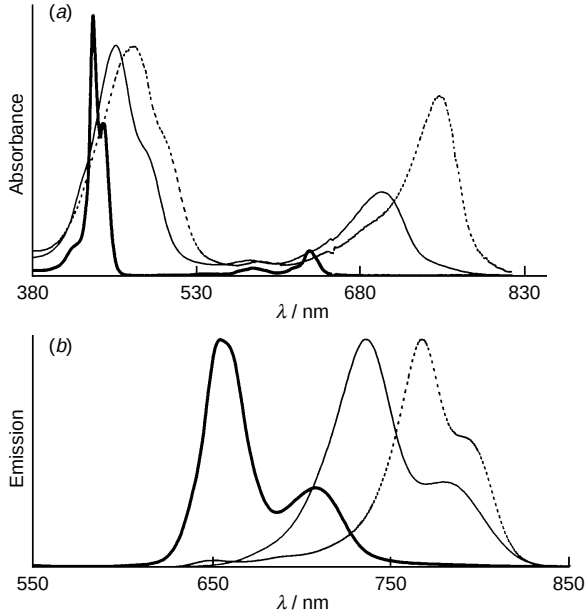

Fig. 1 (*a*) UV–VIS absorption spectra of monomer **3c** and polymers **5a** and **5b** in THF solution and (*b*) emission spectra of monomer **3c** and polymers **5a** and **5b** in THF solution (465 nm excitation); (—) monomer **3c**, (- - - -) polymer **5a**, (—) polymer **5b**

In the presence of strong electronic coupling, introduction of the aryl units into the porphyrin polymer main chain allows for facile modification of the electronic properties through the pendant aryl substituent. The observed decrease in absorption energy on going from polymer **5b** to **5a** is consistent with the electron donating character of the ether alkyl substituent and electron withdrawing character of the dialkyl amide substituent on the aryl 'bridge' units. Cyclic voltammetry measurements in 0.5 M tetrahydrofuran and dichloromethane solution show a shift in the oxidation potential from 0.94 to 0.75 V *vs.* SCE on going from polymer **5b** to **5a**. As compared to the monomer electrochemical oxidation at 0.95 V *vs.* SCE under similar conditions, substantial broadening in ΔE_p was observed. The observed modulation of ground-state electronic properties of the polymer suggests high electron coupling along the conjugation of the polymer backbone.

The emission spectra of the polymers and the monomer are shown in Fig. 1(*b*). Both polymers exhibit significant red-shifts in comparison to that of the monomer. Polymer **5a** displays a larger red shift than polymer **5b**, consistent with the electronic absorption spectra. The emission lifetimes of polymers **5a** and **5b** were 0.92 and 1.1 ns respectively, which is shorter than that of the porphyrin monomer (2.5 ns) measured in THF at room temp. The fluorescence quantum yields of the monomer and polymers **5a** and **5b** are 0.071, 0.028 and 0.069, respectively. The decrease in emission lifetime and the observed shifts in the emission spectra upon bridge substitution are also consistent with increased electronic delocalization in the polymer excited state relative to the *meso*-phenylene vinylene linked porphyrin polymers reported previously.[5] Enhanced exciton mobility in these soluble one-dimensional systems would also be consistent with these fluorescence data, but more information is necessary before this mechanism can be confirmed.

The electronic absorption and emission spectra of both polymers also display significant solvent dependence. The emission maximum shifts to lower energy on going from chloroform (704 nm) to *n*-butylamine (741 nm). This is related to the well known axial complexation ability of the central metal cation of the porphyrin toward different solvent ligands.[13] The electron-donating ability of the solvent ligand increases as the solvent basicity increases. Complexation of the solvent to the metal cation results in increased electron density on the porphyrin units. It is important to note that either an increase in the electron density of the diethynyl aryl unit through pendant groups or the porphyrin units through axial solvation leads to a red shift in the absorption and emission bands.

In summary, we have developed a modified approach to synthesizing a family of fully conjugated, soluble porphyrin polymers in which the porphyrin units are connected by the diethynylaryl group. The porphyrin monomers are easily synthesized, and the high solubility of the polymers in common organic solvents allows routine manipulation, chemical characterization and spectroscopic analysis. The ground and excited state electronic properties suggest enhanced delocalization which can be fine-tuned through the structural modification of the more synthetically accessible aryl bridge units, rather than by direct modification of the porphyrin moiety. The unique coordinating ability of the central metal cation, combined with the high electronic coupling and fluorescence in the polymers, may provide an opportunity to develop optical sensors based on this family of conjugated porphyrin polymers.[13]

We thank Dr Milissa Bolcar for helpful discussions. This research was funded by the Integrated Electronics and Engineering Center (IEEC) at the State University of New York at Binghamton. The IEEC receives funding from the NY State Science and Technology Foundation, the National Science Foundation and a consortium of industrial members.

Footnotes and References

* E-mail: wjones@binghamton.edu

† *Preparation of polymers (typical procedure)*: under an atmosphere of argon, diisopropylamine (1.5 ml) in THF (3 ml) was added to a 15 ml Schlenk flask containing porphyrin **3c** (0.05 g, 0.0076 mmol), diiodobenzene **4a** or **4b** (0.076 mmol), CuI (5 mg) and $Pd(PPh_3)_4$ (6.5 mg). This mixture was refluxed for 24 h and then subjected to $CHCl_3/H_2O$. The combined organic phase was washed with NH_4OH (50%), H_2O and dried over $MgSO_4$. Most of the solvent was evaporated in under vacuum and the concentrated solutions poured into MeOH. The polymer precipitated as a green solid in 90% yield.

1 (*a*) H. L. Anderson, S. J. Martin and D. D. C. Bradley, *Angew. Chem., Int. Ed. Engl.*, 1994, **33**, 655; (*b*) M. J. Therien and S. G. DiMagno, *US Pat.* 5 371 199.
2 H. L. Anderson, *Inorg. Chem.*, 1994, **33**, 972.
3 M. J. Crossley and P. L. Burn, *J. Chem. Soc., Chem. Commun.*, 1987, 39; *J. Chem. Soc., Chem. Commun.*, 1991, 1569.
4 V. S.-Y. Lin, S. DiMagno and M. J. Therien, *Science*, 1994, **264**, 1105.
5 B. Jiang, S. Yang and W. E. Jones Jr., *Chem. Mater.*, 1997, **9**, 2031.
6 B. Jiang, S. Yang and W. E. Jones Jr., *Synth. Met.*, submitted.
7 (*a*) P. J. Angiolilo, V. S.-Y. Lin, J. M. Vanderkooi and M. J. Therien, *J. Am. Chem. Soc.*, 1995, **117**, 12 514; (*b*) M. Chachisvilis, V. Chirony, A. M. Shulga, B. Kallebring, S. Lasson and V. Sundstrom, *J. Phys. Chem.*, 1996, **100**, 13 857; (*c*) V. S.-Y. Lin and M. J. Therien, *Chem. Eur. J.*, 1995, **1**, 645.
8 S. M. Lecours, S. G. DiMagno and M. J. Therien, *J. Am. Chem. Soc.*, 1996, **118**, 11 854; S. M. LeCours, H. Guan, S. G. DiMagno, C. H. Wang and M. J. Therien, *J. Am. Chem. Soc.*, 1996, **118**, 1497; S. Priyadarshi, M. J. Therien and D. N. Beratan, *J. Am. Chem. Soc.*, 1996, **118**, 1504; H. Imahori, H. Higuchi, Y. Matsuda, A. Itagaki, Y. Sakai, I. Ojima and Y. Sakata, *Bull. Chem. Soc. Jpn.*, 1994, **67**, 2500; (*e*) D. P. Arnold and D. A. James, *J. Org. Chem.*, 1997, **62**, 3460.
9 C. H. Lee and J. S. Lindsey, *Tetrahedron*, 1994, **50**, 11 427.
10 G. Scott and H. L. Anderson, *Synlett*, 1996, 1039.
11 (*a*) Q. Zhou and T. M. Swager, *J. Am. Chem. Soc.*, 1995, **117**, 12 593; (*b*) T. M. Swager, C. J. Gil and M. S. Wrighton, *J. Phys. Chem.*, 1995, 4886.
12 R. W. Wagner, T. E. Johnson and J. S. Lindsey, *J. Am. Chem. Soc.*, 1996, **118**, 11 166.
13 F. Bedioui and J. Devynck, *Acc. Chem. Res.*, 1995, **28**, 30.

Received in Columbia, MO, USA, 5th August 1997; revised manuscript received 5th November 1997; 7/08044A

Simple routes to supramolecular squares with ligand corners: 1 : 1 Ag^{I} : pyrimidine cationic tetranuclear assemblies

C. V. Krishnamohan Sharma, Scott T. Griffin and Robin D. Rogers*

Department of Chemistry, The University of Alabama, Tuscaloosa, AL 35487, USA

Simple, tetranuclear cationic supramolecular squares with ligands at the corners can be constructed using the geometry of the pyrimidine ligand and the directional tendencies of Ag^{I} coordination; the 1 : 1 Ag^{I} : pyrimidine squares have an open channel structure which facilitates selective ion exchange of pertechnetate over nitrate.

Discrete macrocyclic metal complexes and coordination polymers with open networks constitute a new family of inorganic host materials.[1,2] While inorganic macrocycles with their conformational rigidity provide an alternative to organic macrocycles such as, crown ethers, cyclophanes, and calixarenes, the open network coordination polymers represent zeolite-like materials with fine-tunable cavities and/or ion exchange properties.[1–3] The robustness of inorganic frameworks and their ability to selectively bind anionic species make them particularly suitable to extract a variety of anions.[3] Here, we report crystal engineering strategies for synthesizing novel supramolecular squares through tetranuclear self-assembly of Ag^{I} cations and pyrimidine ligands.[1] These supramolecular squares may be used to selectively remove the radioactive TcO_4^- anion from solution, currently a technological challenge in the clean-up of the Hanford radioactive waste tanks in the US.[4]

In general, formation of cyclamers, oligomers, or polymers in transition metal complexes depends on the coordination geometry of the metal, the metal to ligand ratio, the chemical structure of the organic ligands, and the donicity of counterion.[2,5] The 1 : 1 transition metal complexes of linear bifunctional ligands such as pyrazine and 4,4′-bipyridyl are known to form one-dimensional coordination polymers, but the possible network topologies for analogous metal complexes with simple angular bifunctional ligands, *e.g.* pyrimidine, are not well studied.[3,5b,6]† However, one can reasonably anticipate three different networks, or supramolecular isomers, for 1 : 1 pyrimidine metal complexes as delineated in Scheme 1.[7] Indeed, one type of isomer, discrete supramolecular squares [Scheme 1(*c*)], is of current interest owing to their potential host properties. Current synthetic strategies focus on using metal ions at the corners and linear ligands as the spacers, which often requires occupying several of the metal's coordination sites with chelating ligands to force discrete macrocycle formation.[1] We undertook the inverse, construction of such squares utilizing a ligand with angular geometry (pyrimidine) at the corners and a metal with a tendency for linear coordination (Ag^{I}) as the spacer.

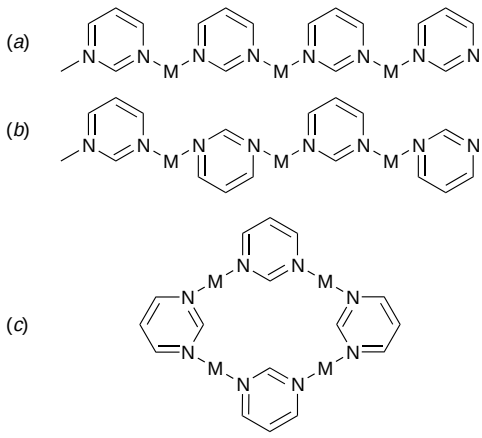

Scheme 1 M = Metal atom

Crystals of [Ag(pyrimidine)][NO_3] **1**, were obtained when methanolic solution (15 ml) of pyrimidine (0.08 g, 1 mmol) was reacted with $AgNO_3$ (0.169 g, 1 mmol) dissolved in acetonitrile (15 ml) through careful layering in a test tube at room temp. Complex **1** is an interesting cyclic self-assembly of pyrimidine and Ag^{I} forming a supramolecular square with H···H contacts within the cavity *ca.* 3.8 × 3.8 Å [Scheme 1(*c*), Fig. 1].‡ The squares exist in planar sheets with each square face-to-face stacked to six other squares (one edged stacked and two corner stacked each, in the sheets above and below the square plane, Fig. 2) at 3.45 Å. The planar sheets coincide every fifth sheet, thus the channels perpendicular to each plane of squares, are actually formed both by open squares and by an edge and two corners of three squares in the planes above and below. The NO_3^- anions are inside the channels and are weakly coordinated with the Ag^{I} cations (nine Ag···O interactions in the range 2.6–3.2 Å) and accept aromatic C–H···O hydrogen bonds. There are as many as 18 C–H···O hydrogen bonds with C···O

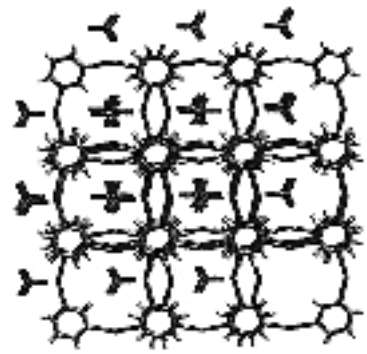

Fig. 1 Packing diagram of **1**. The channels depicted are formed from the supramolecular square in every fifth plane and by an edge and two corners of a total of three squares in all other planes. Additional channels through the centers of the squares exist at an angle to the square plane.

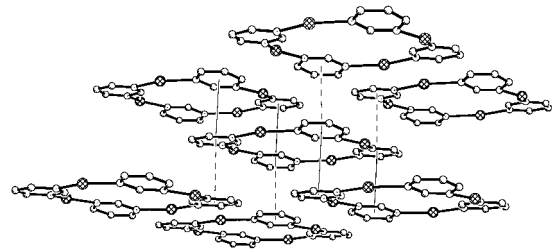

Fig. 2 The face-to-face stacking of a supramolecular square to six other squares is indicated with solid (square edges stacked) and dashed (square corners stacked) lines

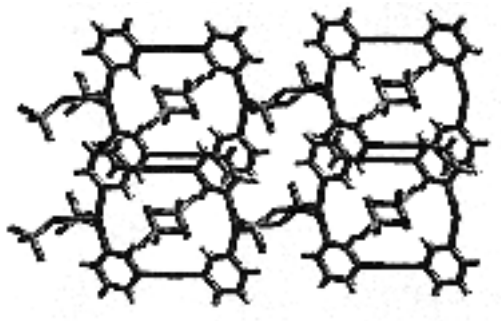

Fig. 3 The 1D coordination polymers of **2** are stacked to form open channel networks

distances and C–H···O angles in the range 3.0–3.5 Å and 110.7–150.4°.[8]

Because of the open and hydrophobic nature of the channels and the weak cation and anion interactions, we attempted to exchange the nitrate anions with larger softer anions such as ReO_4^- and TcO_4^-. 0.0158 g of complex **1** crystals were suspended in 1 ml of MeOH containing 0.114 μCi of $NH_4{}^{99}TcO_4$. After stirring for 2 h the activity of the solution was reduced by 12%. A significant reduction in the activity, *ca*. 40%, was observed after 24 h and the distribution ratio for TcO_4^- was calculated to be 95.§ We also examined the radioactivity of the above crystals after washing them thoroughly with fresh MeOH. A 0.008 g sample of the crystalline material used above showed an activity of 885 counts min^{-1} confirming the presence of TcO_4^-. Further, dissolution of complex **1** (0.062 g, 0.25 mmol) in 25 ml of MeOH–H_2O (3 : 1) containing $NaReO_4$ (0.068 g, 0.25 mmol) and recrystallization at room temp., yielded crystals of [Ag(pyrimidine)][ReO_4] **2**. Complex **2** also consists of supramolecular squares (internal cavity H···H separations*ca*. 3.3 × 4.3 Å) as observed in **1** with ReO_4^- both in the open channels and forming a 1D coordination polymer [Ag–O, 2.413(8), 2.480(10) Å] as shown in Fig. 3. The ReO_4^- anions in the channels form 15 C–H···O hydrogen bonds (C···O distances and C–H···O angles are within the ranges of 3.1–3.5 Å and 110.0–143.5°, respectively) in addition to long Ag···O contacts (four contacts found between 2.8 and 3.0 Å). The 3D structure of **2** is stabilized by face-to-face stacking of square edges (3.44 Å) such that each square stacks with only two other squares in a stair-step fashion (one above and one below the square plane, Fig. 3).

Our attempts to grow single crystals of the 1 : 1 complex of $AgClO_4$ (0.207 g, 1 mmol) and pyrimidine (0.08 g, 1 mmol) from MeOH (25 ml, room temp.) resulted in an unexpected 5 : 6 complex, $[Ag_{2.5}(pyrimidine)_3][ClO_4]_{2.5}$ **3**. The crystal structure of **3** is a 1D coordination polymer with supramolecular squares similar to **1** and **2** (internal cavity H···H separation,*ca*. 2.8 × 4.8 Å) but the squares are crosslinked by a dimeric pyrimidine unit vertically in a staircase fashion as shown in Fig. 4. Indeed, this is a combination of possible isomers outlined for 1 : 1 metal complexes in Scheme 1. One of the ClO_4^- anions is coordinated to Ag [Ag–O 2.496(7) Å] and one is found to be disordered. Further, the anions have eight Ag···O contacts between 2.7 and 3.2 Å and 20 C–H···O hydrogen bonds (C···O distances and C–H···O angles are within the ranges 3.1–3.5 Å and 113.0–172.5°, respectively). The 1D layers of **3** are face-to-face stacked on square edges in a stair-step fashion as observed for **2**, but at a longer 3.87 Å separation.

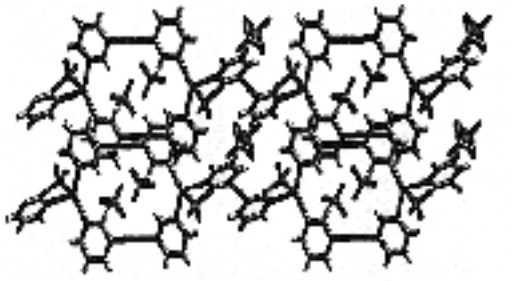

Fig. 4 The supramolecular squares of **3** are vertically crosslinked by dipyrimidine units in a staircase fashion to form 1D coordination polymers. The polymers are face-to-face stacked on edge in a stair-step fashion as observed in **2** albeit at a longer aromatic···aromatic separation. Note that one of the ClO_4^- anions is disordered.

In conclusion, the angular geometry of pyrimidine or of any other simple angular bifunctional ligands may be readily exploited to construct discrete inorganic macrocyclics and a variety of coordination polymers as well, by making subtle changes in the metal/ligand ratio (including the uncommon ratios as observed for complex **3**) or donicity of the anion. Currently, we are investigating the conditions required for preferential formation of the descrete supramolecular square *vs*. the 1D/2D coordination polymers in complexes of pyrimidine and its derivatives.

Footnotes and References

* E-mail: RDRogers@UA1VM.ua.edu

† A survey of the Cambridge Structural Database (April, 1997 release) for simple pyrimidine metal complexes resulted in five hits. Of these, only two complexes contain pyrimidine exclusively as a ligand, *i.e.*, with no other ligands additionally bonded to the metal (Refcodes: PMDPTA, PMDPTB). However, recently, pyrimidine has been used to generate an acentric 3D coordination polymer of Cu^I, S. W. Keller, *Angew. Chem., Int. Ed. Engl.*, 1997, **36**, 247.

‡ *Crystal data*: **1** [Ag(pyrimidine)][NO_3], M = 249.97, triclinic, space group $P\bar{1}$, a = 7.3996(3), b = 9.4356(3), c = 10.3679(4) Å, α = 90.046(1), β = 71.437(1), γ = 74.406(1)°, U = 658.00(4) Å^3, Z = 4, D_c = 2.523 Mg m^{-3}, F(000) = 480. R = 0.086, R_w = 0.215.

2: [Ag(pyrimidine)][ReO_4], M = 483.16, triclinic, $P\bar{1}$, a = 7.895(2), b = 8.095(3), c = 12.643(3) Å, α = 91.95(2), β = 96.11(1), γ = 98.51(1)°, U = 793.5(4) Å^3, Z = 4, D_c = 3.668 Mg m^{-3}, F(000) = 784. 3081 absorption corrected reflections out of 3611 unique reflections measured at 173 K for a crystal of dimensions, 0.04 × 0.10 × 0.18 mm, on convergence gave final values of R = 0.039, R_w = 0.090.

3: $[Ag_{2.5}(pyrimidine)_3][ClO_4]_{2.5}$, M = 758.58, triclinic, $P\bar{1}$, a = 7.2417(3), b = 8.1714(8), c = 19.187(2) Å, α = 81.274(2), β = 80.608(2), γ = 75.215(2)°, U = 1075.8(2) Å^3, Z = 2, D_c = 2.342 Mg m^{-3}, F(000) = 732. 2673 absorption corrected reflections out of 3171 unique reflections measured at 173 K for a crystal of dimensions, 0.20 × 0.30 × 0.38 mm, on convergence gave final values of R = 0.050, R_w = 0.111.

Data on **1**, **2** and **3** were collected with a Siemens CCD area detector (4 < θ < 56°). All non-H atoms were anisotropically refined and aromatic H atoms were calculated ($d_{C–H}$ = 0.95 Å) and fixed with the thermal parameters based upon the C atom to which they are bonded. CCDC 182/695.

§ The distribution ratio was calculated from [($A_i - A_f/A_f$)(volume of MeOH in ml/mass of complex **1** crystals, g)], where A_i = initial ^{99}Tc activity, A_f = final ^{99}Tc activity in the solution.

1 P. J. Stang, N. E. Persky and J. Manna, *J. Am. Chem. Soc.*, 1997, **119**, 4777 and references therein; M. Fujita, S. Nagao and K. Ogura, *J. Am. Chem. Soc.*, 1997, **117**, 1649.
2 M. J. Zaworotko, *Chem. Soc. Rev.*, 1994, 283; G. B. Gardner, D. Venkataraman, J. S. Moore and S. Lee, *Nature*, 1995, **374**, 792; O. M. Yaghi, G. Li and H. Li, *Nature*, 1995, **378**, 703; D. Hagrman, C. Zubieta, D. J. Rose, J. Zubieta and R. C. Haushalter, *Angew. Chem., Int. Ed. Engl.*, 1997, **36**, 873.
3 F. Robinson and M. J. Zaworotko, *J. Chem. Soc., Chem. Commun.*, 1995, 2413; O. M. Yaghi and H. Li, *J. Am. Chem. Soc.*, 1996, **118**, 295.
4 R. D. Rogers, J. Zhang and S. T. Griffin, *Sep. Sci. Technol.*, 1997, **32**, 699; R. D. Rogers, A. H. Bond, J. Zhang and C. B. Bauer, *Appl. Radiat. Isot.*, 1996, **47**, 497.
5 (*a*) B. F. Hoskins and R. Robson, *J. Am. Chem. Soc.*, 1990, **112**, 1546; (*b*) L. Carlucci, G. Ciani, D. M. Proserpio and A. Sironi, *J. Am. Chem. Soc.*, 1995, **117**, 4562.
6 R. G. Vranka and E. L. Amma, *Inorg. Chem.*, 1966, **5**, 1020.
7 T. L. Hennigar, D. C. MacQuarrie, P. Losier, R. D. Rogers and M. J. Zaworotko, *Angew. Chem., Int. Ed. Engl.*, 1997, **36**, 972.
8 G. R. Desiraju, *Acc. Chem. Res.*, 1991, **24**, 290.

Received in Columbia, MO, USA, 18th August 1997; 7/06021A

Regiocontrol in palladium-catalysed allylic alkylation by addition of lithium iodide

Motoi Kawatsura, Yasuhiro Uozumi and Tamio Hayashi*

Department of Chemistry, Faculty of Science, Kyoto University, Sakyo, Kyoto 606-01, Japan

Regioselectivity in the palladium-catalysed allylic alkylation of 1-arylprop-2-enyl acetates [ArCH(OAc)CH=CH_2] or (*E*)-3-phenylprop-2-enyl acetate (PhCH=$CHCH_2OAc$) with sodium enolates of soft carbon nucleophiles is controlled by addition of a catalytic amount of lithium iodide to give lienar products [(*E*)-ArCH=$CHCH_2$Nu] exclusively; their branch isomers [ArCH(Nu)CH=CH_2] were not detected.

In synthetic organic chemistry, palladium-catalysed allylic alkylation of allyl esters is a useful reaction for the formation of carbon–carbon bonds.[1] One of the challenging problems in catalytic allylic alkylation is control of the regiochemistry in the reaction that proceeds through unsymmetrically substituted π-allylpalladium intermediates. For example, the π-allylpalladium complex containing one substituent at the C-1 position usually produces both linear and branch isomers, the ratio being dependent on the substituents, nucleophiles and reaction conditions.[1–3] Here we report exclusive formation of the linear isomer in a palladium-catalysed allylic alkylation, which is realized by addition of a catalytic amount of lithium iodide.[4]

In the presence of 2 mol% of the palladium catalyst generated by mixing $[PdCl(\pi\text{-}C_3H_5)]_2$ with PPh_3 (2 equiv. to Pd), allyl acetates **1**–**4** were allowed to react with soft carbon nucleophiles in THF at 0 °C (Scheme 1). The regioselectivity of the reaction was found to be dramatically changed by the addition of lithium iodide. Thus, the reaction of 1-phenylprop-2-enyl acetate **1** with the sodium salt of dimethyl methylmalonate in the absence of lithium iodide gave a 96% yield of alkylation product; consisting of linear isomer (*E*)-**5a** and branch isomer **6a** in a ratio of 77 : 23 (entry 1, Table 1). On the other hand, the reaction carried out in the presence of 10 mol% of lithium iodide gave a quantitative yield of linear isomer **5a** with 100% regioselectivity (entry 2). The regioselectivity was not strongly affected by the addition of lithium fluoride, chloride or bromide, branch isomer **6a** being formed with about 20% regioselectivity (entries 3–5). High linear selectivity was also observed in the reaction in the presence of sodium iodide (entry 6), indicating that the iodide anion is important for control of the regioselectivity. The amount of lithium iodide additive can be decreased to 2 mol%, which is the same amount as that of the palladium catalyst (entry 7). Use of the palladium catalyst generated from $[PdI(\pi\text{-}C_3H_5)]_2$ instead of $[PdCl(\pi\text{-}C_3H_5)]_2$ showed the same linear selectivity in the absence of additional iodide anion (entry 8).

The selectivity in forming the linear isomer in the presence of lithium iodide was also observed in the reaction of 1-arylprop-2-enyl acetates **2** and **3** and 3-phenylprop-2-enyl acetate **4** with the sodium salt of dimethyl methylmalonate (entries 9–13) and

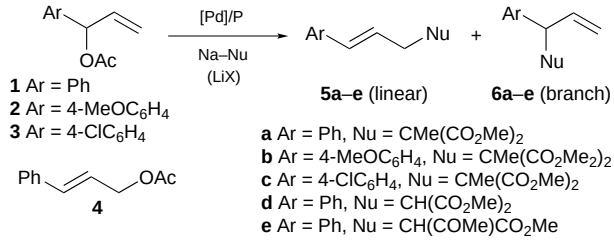

Scheme 1

Table 1 Effects of lithium salts on allylic alkylation of allyl acetates **1**–**4** catalysed by palladium–phosphine complexes[a]

Entry	Allyl ester	MX/equiv.	Phosphine ligand[b]	Nu	*t*/h	Yield (%)[c] **5** + **6**	Ratio[d] **5**:**6**
1	**1**	none	PPh_3	$CMe(CO_2Me)_2$	12	96	77 : 23
2	**1**	LiI (0.1)	PPh_3	$CMe(CO_2Me)_2$	24	99	100 : 0
3	**1**	LiF (0.1)	PPh_3	$CMe(CO_2Me)_2$	24	89	78 : 22
4	**1**	LiCl (0.1)	PPh_3	$CMe(CO_2Me)_2$	24	96	82 : 18
5	**1**	LiBr (0.1)	PPh_3	$CMe(CO_2Me)_2$	24	90	80 : 20
6	**1**	NaI (0.1)	PPh_3	$CMe(CO_2Me)_2$	24	93	98 : 2
7	**1**	LiI (0.02)	PPh_3	$CMe(CO_2Me)_2$	24	97	100 : 0
8[e]	**1**	none	PPh_3	$CMe(CO_2Me)_2$	24	96	100 : 0
9	**2**	none	PPh_3	$CMe(CO_2Me)_2$	12	98	72 : 28
10	**2**	LiI (0.1)	PPh_3	$CMe(CO_2Me)_2$	24	92	100 : 0
11	**3**	none	PPh_3	$CMe(CO_2Me)_2$	12	96	86 : 14
12	**3**	LiI (0.1)	PPh_3	$CMe(CO_2Me)_2$	24	89	100 : 0
13[f]	**4**	LiI (0.1)	PPh_3	$CMe(CO_2Me)_2$	24	99	100 : 0
14	**1**	none	PPh_3	$CH(CO_2Me)_2$	12	94	83 : 17
15	**1**	LiI (0.1)	PPh_3	$CH(CO_2Me)_2$	12	91	100 : 0
16	**1**	none	PPh_3	$CH(COMe)CO_2Me$	12	95	92 : 8
17	**1**	LiI (0.1)	PPh_3	$CH(COMe)CO_2Me$	12	89	100 : 0
18[f]	**1**	none	dppe	$CMe(CO_2Me)_2$	12	92	89 : 11
19[f]	**1**	LiI (0.1)	dppe	$CMe(CO_2Me)_2$	12	61	89 : 11

[a] All reactions were carried out in THF under nitrogen: THF (1.0 ml), allylic acetate (0.20 mmol), NaNu (0.40 mmol), $[PdCl(\pi\text{-}C_3H_5)]_2$ (0.002 mmol) and phosphine ligand at 0 °C. [b] The ratio of Pd : Phosphine = 1 : 2. [c] Isolated yield by silica gel column chromatography. [d] The ratio was determined by ^1H NMR analysis of the products. [e] $[PdI(\pi\text{-}C_3H_5)]_2$ was used. [f] Carried out at 20 °C.

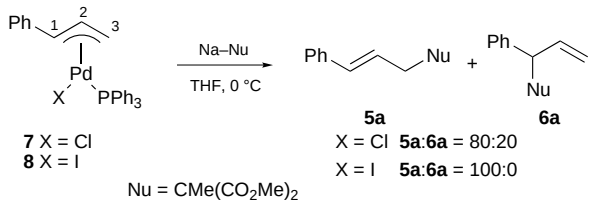

Scheme 2

in the reactions with dimethyl malonate and methyl acetoacetate (entries 14–17).

It is noteworthy that the addition of lithium iodide is not effective for the reaction catalysed by a palladium–bisphosphine complex. Thus, the reaction of **1** with dimethyl methylmalonate in the presence of a palladium catalyst prepared from $[PdCl(\pi\text{-}C_3H_5)]_2$ and 1,2-bis(diphenylphosphino)ethane (dppe) gave a mixture of **5a** and **5b** in a ratio of 89 : 11, irrespective of the addition of lithium iodide (entries 18 and 19). These results suggest that, in the reaction catalysed by triphenylphosphine–palladium, the iodide coordinates to the π-allylpalladium intermediate to form the intermediate $PdI(\pi\text{-allyl})(PPh_3)$, and that the iodide on the palladium controls the regioselectivity of the nucleophilic attack. Using the dppe ligand, the intermediate will be the cationic complex $[Pd(\pi\text{-allyl})(dppe)]^+X^-$, where iodide is not directly bonded to palladium.

Palladium complex $PdCl[\pi\text{-}(1\text{-phenyl})allyl](PPh_3)$ **7** and its iodide analogue **8** were prepared by mixing $[PdX[\pi\text{-}(1\text{-phenyl})allyl]]_2$ (X = Cl and I)[5] with PPh_3 (1 equiv. to Pd) and were characterized by ^{31}P, ^1H and ^{13}C NMR spectroscopy.† Both have the substituted carbon (C-1) of the π-allyl *trans* to the phosphorus atom of PPh_3 and the unsubstituted carbon (C-3) *cis* to phosphorus, as determined by the large coupling constants (J = 10.1 Hz in **7** and 10.5 Hz in **8**) between the C-1 proton and phosphorus, and no coupling between the C-3 protons and phosphorus. Stoichiometric reaction of chloride complex **7** with the sodium enolate of dimethyl methylmalonate in THF at 0 °C gave **5a** and **6a** in a ratio of 80 : 20, while the reaction of iodide complex **8** gave **5a** with 100% regioselectivity (Scheme 2). These selectivities are in good agreement with those observed in the catalytic reactions, demonstrating that the iodide ligand bonded to the π-allylpalladium intermediate controls the regioselectivity. Comparing the ^{13}C NMR spectra of **7** and **8**, the chemical shift for C-3 of the π-allyl group of **8** appears at lower field than that for **7** by 6.5 ppm and the chemical shift for C-1 of **8** appears at higher field than that for **7** by 3.1 ppm. The difference in the chemical shifts may support the idea that the C-3 carbon of the iodide complex **8** undergoes the nucleophilic attack giving linear isomer **5a** more selectively than that of **7**.[6]

This work was supported by the 'Research for the Future' Program, the Japan Society for the Promotion of Science.

Footnotes and References

* E-mail: thayashi@th1.orgchem.kychem.kyoto-u.ac.jp

† *Selected data* for **7**: $\delta_H(CDCl_3, -40\ °C)$ 2.88 (d, J 6.8, 1 H, *syn*-H on C-3), 2.97 (d, J 11.7, 1 H, *anti*-H on C-3), 5.37 (dd, J_{H-H} 13.2, J_{H-P} 10.1, 1 H, H on C-1), 6.08 (ddd, J 6.8, 11.7, 13.2, 1 H, H on C-2), 7.36–7.88 (m, 20 H); $\delta_P(CDCl_3, -40\ °C)$ 24.2 (s); $\delta_C(CDCl_3, -40\ °C)$ 58.2 (C-3), 99.6 (J_{C-P} 26.9, C-1), 111.4 (J_{C-P} 5.2, C-2). For **8**: $\delta_H(CDCl_3, -40\ °C)$ 3.47 (d, J 6.8, 1 H, *syn*-H on C-3), 3.14 (d, J 12.2, 1 H, *anti*-H on C-3), 5.21 (dd, J_{H-H} 13.0, J_{H-P} 10.5, 1 H, H on C-1), 6.08 (ddd, J 6.8, 12.2, 13.0, 1 H, H on C-2), 7.26–7.63 (m, 20 H); $\delta_P(CDCl_3, -40\ °C)$ 27.9 (s); $\delta_C(CDCl_3, -40\ °C)$ 64.7 (C-3), 96.5 (J_{C-P} 29.0, C-1), 111.0 (J_{C-P} 5.2, C-2).

1 For reviews on catalytic allylic substitutions: J. Tsuji, *Palladium Reagents and Catalyst*, Wiley, Chichester, 1995, pp. 290–340; J. A. Davies, in *Comprehensive Organometallic Chemistry II*, ed. E. W. Abel, F. G. A. Stone and G. Wilkinson, Pergamon, Oxford, 1955, vol. 9, ch. 6; S. A. Godleski, in *Comprehensive Organic Synthesis*, ed. B. M. Trost and I. Fleming, Pergamon, Oxford, 1991, vol. 4, p. 585; G. C. Frost, J. Holwarth and J. M. J. Williams, *Tetrahedron: Asymmetry*, 1992, **3**, 1089; G. Consiglio and M. Waymouth, *Chem. Rev.*, 1989, **89**, 257.

2 For examples: M. P. T. Sjogren, S. Hansson, B. Åkermark and A. Vitagliano, *Organometallics*, 1994, **13**, 1963; T. Hayashi, K. Kishi, A. Yamamoto and Y. Ito, *Tetrahedron Lett.*, 1990, **31**, 1743; B. M. Trost, M. J. Krische, R. Radinov and G. Zanoni, *J. Am. Chem. Soc.*, 1996, **118**, 6297.

3 T. Hayashi, M. Kawatsura and Y. Uozumi, *Chem. Commun.*, 1997, 561.

4 An anion effect on the enantioselectivity of palladium-catalysed asymmetric allylic amination has been reported: U. Burckhardt, M. Baumann and A. Togni, *Tetrahedron: Asymmetry*, 1997, **8**, 155.

5 P. R. Auburn, P. B. Mackenzie and B. Bosnich, *J. Am. Chem. Soc.*, 1985, **107**, 2033. $[PdI(\pi\text{-}C_3H_5)]_2$ was prepared by mixing $[PdCl(\pi\text{-}C_3H_5)]_2$ with LiI in THF.

6 B. Åkermark, B. Krakenberger, S. Hansson and A. Vitagliano, *Organometallics*, 1987, **6**, 620.

Received in Cambridge, UK. 23rd October 1997; 7/07652E

If Watson–Crick and Hoogsteen sites of guanine are blocked, hydrogen bonding with cytosine is *via* N^2 and N^3

Roland K. O. Sigel, Eva Freisinger and Bernhard Lippert*

Fachbereich Chemie, Universität Dortmund, D-44221 Dortmund, Germany

A novel hydrogen bonding scheme between cytosine and guanine nucleobases is observed if both N^1 and N^7 positions of the guanine are blocked by a metal entity and a methyl group, respectively.

Chemical modification of nucleobases can result in severely altered hydrogen bonding patterns as far as base selectivity and/or hydrogen bonding sites are concerned. When occurring in DNA, potentially dangerous consequences can be expected, as known in the case of guanine methylated at the 6-position.[1] Here we demonstrate, on a model nucleobase level, that the complementary nucleobases guanine (G) and cytosine (C) associate in a hitherto unknown fashion if both Watson–Crick, and Hoogsteen hydrogen bonding sites are blocked.

Base pairing between G and C is predominantly according to the Watson–Crick scheme (Scheme 1, **I**), and very rarely, *e.g.* between G_{15} and C_{48} in yeast $tRNA^{Phe}$, of the reversed Watson–Crick type (**II**).[2] With protonated cytosine, and possibly also with neutral cytosine in a rare tautomeric form,[3] pairing is of the Hoogsteen type (**III**). In addition to these principal hydrogen bonding patterns, there is also the possibility of association to quartet structures through dimerization of two Watson–Crick pairs *via* hydrogen bonds (**IV**).[4]

Metal binding at the N^7 site of G still permits types **I** and **IV** hydrogen bonding patterns.[5,6] Alternatively it can lead to a 'metal-modified' Hoogsteen pattern[5] or, upon guanine deprotonation at N^1, to either mispairing with free guanine[7] or formation of a quite unusual nucleobase quartet.[8] Additional blockage at N^1 leads to the pattern **V** hereafter.

7,9-Dimethylguanine (7,9-dmgua), a model of the rare nucleobase 7-methylguanosine, forms 2:1 complexes with *trans*-$Pt^{II}am_2$ (am = NH_3 or NH_2Me) of composition *trans*-$[Ptam_2(7,9\text{-dmgua-}N^1)_2]X_2{\cdot}nH_2O$. Recently we have published the X-ray structure analyses for the combination am = NH_2Me, X = NO_3^-, n = 0.[9] With am = NH_2Me, X = ClO_4^- cocrystallization with the model nucleobase 1-methylcytosine (mcyt) from water† gave crystals suitable for X-ray crystallography.‡

As can be seen in Fig. 1, each mcyt molecule forms two strong hydrogen bonds; one to a coplanar 7,9-dmgua ligand, N(3a′)···N(2) 2.881(8) Å, and the second one to the amine group of NH_2Me of another cation lying below the pyrimidine [O(2′)···N(10) 2.878(6) Å]. Furthermore the pyrimidine rings are stacking (3.4 Å) with the platinated purine ligands leading to an arrangement like tiles of a roof. These strong intermolecular interactions bring the exocyclic amino group of mcyt in relatively close proximity to N(3) of 7,9-dmgua [N(3)···N(4a′) 3.194(8) Å] leading to an arrangement as shown in Fig. 2. Although the latter distance is at the upper end of a hydrogen bond, the sum of the van der Waals radii of H and N (1.20 Å + 1.55 Å = 2.75 Å)[10] is still larger than the distance between the H and the acceptor N [2.340(8) Å], so it can still be considered as such,[11] especially in view of the near-coplanarity of the two bases [dihedral angle 2.3(3)°].

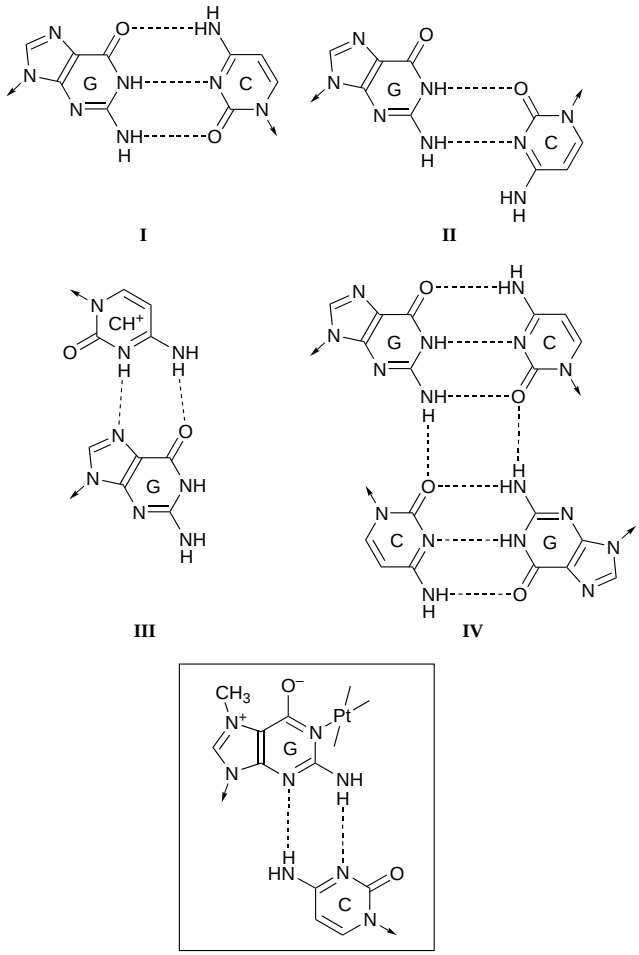

Scheme 1

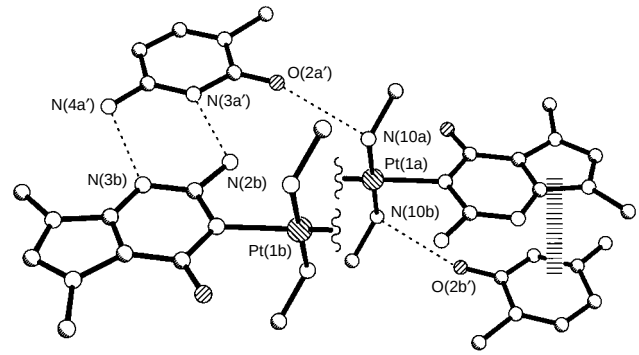

Fig. 1 Section of packing of cations and mcyt in the crystal lattice of *trans*-$[Pt(MeNH_2)_2(7,9\text{-dmgua-}N^1)_2][ClO_4]_2{\cdot}2$mcyt. There is stacking between 7,9-dmgua ligands and mcyt (distance 3.4 Å), one hydrogen bond of 2.878(6) Å between O(2a′) of the free mcyt and N(10a) of the NH_2Me group and another short hydrogen bond between N(3a′) and N(2b) [2.881(8) Å]. At each cation one 7,9-dmgua ligand is omitted for clarity.

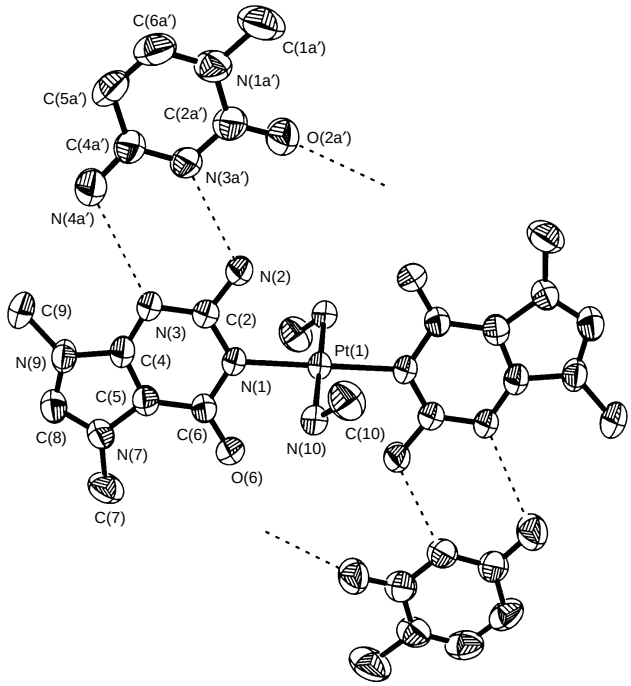

Fig. 2 Hydrogen bonding scheme between 7,9-dmgua and mcyt in *trans*-[Pt(MeNH$_2$)$_2$(7,9-dmgua-*N*^{1})$_2$][ClO$_4$]$_2$·2mcyt with two hydrogen bonds, N(2)···N(3′) 2.881(8) Å and N(3)···N(4′) 3.194(8) Å, between the two nucleobases. Hydrogen bond formation between O(2) sites and N(10) groups is schematically shown.

Involvement of guanine N^2 and N^3 sites in hydrogen bonding with another nucleobase has some precedence, although not with cytosine. In one of the four types of GA mispairs found in RNA,[12] as well as in a base quartet formed as a consequence of crystal packing, the guanine N^3 positions act as hydrogen bond acceptors.[13]

This work is dedicated to Professor H. Sigel, University of Basel, on the occasion of his 60th birthday. The authors acknowledge support of this research by the Swiss National Science Foundation and the Swiss Federal Office for Education and Science (TMR fellowship to R. K. O. S.; No. 83EU-046320) and the Deutsche Forschungsgemeinschaft.

Footnotes and References

* E-mail: Lippert@pop.uni-dortmund.de

† *trans*-[Pt(MeNH$_2$)$_2$(7,9-dmgua-*N*^{1})$_2$][ClO$_4$]$_2$·2mcyt was obtained from a 10 mM aqueous solution of *trans*-[Pt(MeNH$_2$)$_2$(7,9-dmgua-*N*^{1})$_2$[ClO$_4$]$_2$ with 2 equiv. of mcyt. After 5 d slightly yellow crystals, suitable for X-ray diffraction studies could be isolated in 38% yield. Anal. calc. for C$_{26}$H$_{42}$O$_{12}$N$_{18}$Cl$_2$Pt: C, 29.3; H, 4.0; N, 23.7. Found: C, 29.4; H, 4.1; N, 24.1%.

‡ *Crystal data for trans*-[Pt(MeNH$_2$)$_2$(7,9-dmgua-*N*^{1})$_2$][ClO$_4$]$_2$·2mcyt: C$_{26}$H$_{42}$N$_{18}$O$_{12}$Cl$_{12}$Pt, M = 1064.77, triclinic, space group $P\bar{1}$, a = 6.623(1), b = 9.819(2), c = 15.261(3) Å, α = 85.47(3), β = 82.85(3), γ = 79.73(3)°, U = 967.3(3) Å^3, Z = 2, D_c = 1.828 g cm^{-3}, μ(Mo-Kα) = 3.848 mm^{-1}, F(000) = 532, T = 293 K. The crystals were slightly yellow platelets with a size of 0.625 × 0.125 × 0.125 mm. Intensity data were collected on a Nonius KappaCCD with graphite-monochromated Mo-Kα radiation (λ = 0.710 69 Å). 3354 independent reflections were measured and 3012 reflections with $F_o > 4\sigma(F_o)$ were used in the refinement. Reflections which were partly measured on previous and following frames were used to scale these frames on each other. This procedure in part eliminates absorption effects and also considers crystal decay, if present. The structure was solved by Patterson method (SHELXS-86[14]) and refined on F_o^2 (SHELXS = 93[15]). Refinement and positional and anisotropic thermal parameters for all non-hydrogen atoms (276 parameters) converged to R_1 = 0.0365 and wR_2 = 0.0798. The final Fourier difference map showed residual electron density in the range of 2.612 to −0.752 e Å^{-3}. CCDC 182/676.

1 B. Singer and J. M. Essigmann, *Carcinogenesis*, 1991, **12**, 949.
2 W. Saenger, *Principles of Nucleic Acid Structure*, Springer, New York, 1984; *Nucleic Acids in Chemistry and Biology*, ed. G. M. Blackburn and M. J. Gait, Oxford University Press, Oxford, 1996.
3 J. Sponer, J. Leszczynski and P. Hobza, *J. Biomol. Struct. Dyn.*, 1996, **14**, 117; C. Colominas, F. J. Luque and M. Orozco, *J. Am. Chem. Soc.*, 1996, **118**, 6811.
4 M. C. Wahl and M. Sundaralingam, *Biopolymers*, 1997, **44**, 45; G. A. Leonard, S. Zhang, M. R. Peterson, S. J. Harrop, J. R. Helliwell, W. B. T. Cruse, B. Langelois d'Estaintot, O. Kennard, T. Brown and W. N. Hunter, *Structure*, 1995, **3**, 335.
5 I. Dieter-Wurm, M. Sabat and B. Lippert, *J. Am. Chem. Soc.*, 1992, **114**, 357.
6 G. Schröder, M. Sabat, I. Baxter, J. Kozelka and B. Lippert, *Inorg. Chem.*, 1997, **36**, 490.
7 G. Schröder, B. Lippert, M. Sabat, C. J. L. Lock, R. Faggiani, B. Song and H. Sigel, *J. Chem. Soc., Dalton Trans.*, 1995, 3767.
8 S. Metzger and B. Lippert, *J. Am. Chem. Soc.*, 1996, **118**, 12467.
9 S. Metzger, A. Erxleben and B. Lippert, *J. Biol. Inorg. Chem.*, 1997, **2**, 256.
10 R. Taylor and O. Kennard, *J. Am. Chem. Soc.*, 1982, **104**, 5063.
11 T. Steiner, *J. Chem. Soc., Chem. Commun.*, 1995, 1331.
12 Y. Li, G. Zon and W. D. Wilson, *Proc. Natl. Acad. Sci. USA*, 1991, **88**, 26; K. Maskos, B. M. Gunn, D. A. Le Blanc and K. M. Morden, *Biochemistry*, 1993, **32**, 3583.
13 B. Ramakrishnan and M. Sundaralingam, *J. Mol. Biol.*, 1993, **231**, 431.
14 G. M. Sheldrick, *Acta Crystallogr., Sect. A*, 1990, **46**, 467.
15 G. M. Sheldrick, SHELXL-93, Program for crystal structure refinement, University of Göttingen, 1993.

Received in Basel, Switzerland, 8th July 1997; 7/04837H

Differential incorporation of 1-deoxy-D-xylulose into monoterpenes and carotenoids in higher plants

Silvia Sagner,[a] Christoph Latzel,[a] Wolfgang Eisenreich,[b] Adelbert Bacher[b] and Meinhart H. Zenk*[a]

[a] *Lehrstuhl für Pharmazeutische Biologie, Universität München, Karlstrasse 29, D-80333 München, Germany*
[b] *Institut für Organische Chemie und Biochemie, Technische Universität München, Lichtenbergstr. 4, D-85747 Garching, Germany*

1-Deoxy-D-xylulose labelled with ^{13}C or ^{14}C is incorporated into the monoterpenoids menthone, menthol, menthofuran, eucalyptol, pulegone, geraniol and thymol by higher plants, however, the rate of incorporation was lower as compared with incorporation into carotene and phytol.

Recent evidence indicates that 1-deoxy-D-xylulose (DX) or a derivative such as the 5-phosphate is the committed precursor for the biosynthesis of isoprenoids in some bacteria.[1,2] The deoxyxylulose pathway is also operative in higher plants.[3–9] Thus, pigments of life, such as chlorophyll and carotenoids are formed in plants from the pentose derivative and not from mevalonate.[7,8] Recent incorporation experiments with ^{13}C-labelled glucose have also shown that essential oils in plants are formed *via* the alternative pathway.[9]

In order to study in more detail the involvement of DX in monoterpenoid biosynthesis, we prepared [1-^{13}C]- and [2-^{13}C]DX by condensation of D-glyceraldehyde with [3-^{13}C]- and [2-^{13}C]pyruvate, respectively, using pyruvate dehydrogenase as catalyst.[10,11] The spectral characteristics of the deoxypentulose obtained were identical to published values.[12] [1,2-$^{14}C_2$]DX was obtained similarly from [U-^{14}C]pyruvate (yield 75–83%; spec. act., 62.5 μCi μmol^{-1}).

Shoots of peppermint (*Mentha x piperita*) with a length of about 5 cm were cut and were allowed to form roots in hydroponic culture. A solution containing 27 μM [1,2-$^{14}C_2$]DX was applied to the rooted shoots for 48 h. The monoterpenes were obtained by steam distillation, and the metabolites were isolated as described earlier.[9] Relative specific activities of 0.1% for menthone, 0.2% for menthol, 0.3% for menthofuran and 0.3% for eucalyptol were observed. In similar experiments, *Mentha pulegium* showed incorporation into pulegon (0.2%), *Pelargonium graveolens* into geraniol (0.3%), and *Thymus vulgaris* into thymol (0.2%).

^{13}C-Labelled DX samples were supplied to *M. piperita* shoots at a concentration of 25 mM. Menthone was isolated[9] and was subjected to NMR analysis as described earlier.[7] Relative ^{13}C abundance of individual carbon atoms was calculated from the NMR signal integrals of biosynthetic samples by comparison with the natural abundance sample (% ^{13}C in Table 1). The values were referenced to 1.10% for the carbon with the lowest ^{13}C enrichment. In the experiment with [1-^{13}C]DX, the carbon atoms 7 and 9 of menthone were enriched with 1.49 and 1.41% ^{13}C abundance, respectively. The other atoms were virtually unlabelled with 1.16 ± 0.06% ^{13}C abundance. On the other hand, [2-^{13}C]DX labelled the carbon atoms 1 and 8 of menthone with 1.39 and 1.41% ^{13}C abundance, whereas the other atoms had a ^{13}C abundance of 1.20 ± 0.05% (Table 1). On the basis of the established isoprene dissection of the cyclic monoterpene it follows that [1-^{13}C]DX enriched C-5 of IPP/DMAPP and that [2-^{13}C]DX enriched C-3 of IPP/DMAPP, respectively (Fig. 1). This labelling pattern is in full accordance with terpenoid formation *via* the deoxyxylulose pathway.

It should be noted that the observed incorporation rates of DX into the monoterpenes under study are low. However, they exceed the rates achieved with labelled acetate or mevalonate by factors of at least 10 to 100 fold.[13] This indicates that the deoxyxylulose pathway is the dominant metabolic route for essential oil formation. Based on the incorporation of ^{13}C- and ^{14}C-labelled DX and on our previous [^{13}C]glucose feeding experiments using the same plants,[9] we conclude that the deoxyxylulose pathway leading to isopentenyl pyrophosphate (IPP) and dimethylallyl pyrophosphate (DMAPP) is operative in essential oil formation, which is at variance with previous reports.[14]

In experiments using *M. piperita* it was observed that [1,2-$^{14}C_2$]DX was incorporated with considerably higher rates into chlorophyll a and b (13%) and into β-carotine (10%) than into the monoterpenes. This is in accordance with incorporation rates of DX into chlorophylls and carotenoids in a cell culture of *Catharanthus roseus*.[7] The different incorporation rates of DX into monoterpenes and into chlorophylls/carotenoids could indicate that an enzyme involved in the utilization of exogenous DX (*e.g.* a kinase) is limiting in the plant glandular trichomes which have been recognized as sites of monoterpenoid biosynthesis,[14,15] but not in the chloroplasts where chlorophylls and carotenoids are synthesized. Limited transport of labelled DX into the plant glandular trichomes might also explain the discrepancy of incorporation rates.

Table 1 ^{13}C NMR analysis of menthone from *Mentha x piperita* supplied with ^{13}C labelled 1-deoxyxylulose (DX). Values indicative for IPP formation *via* the deoxyxylulose pathway are shown in bold type. The signal with lowest ^{13}C enrichment (marked by asterisk) was referenced to 1.1% ^{13}C abundance

		Proffered precursor	
Position	δ^b	[1-^{13}C]DX % ^{13}C	[2-^{13}C]DX % ^{13}C
1	35.3	1.10*	**1.39**
2	50.5	1.18	1.21
3	212.3	1.10	1.10*
4	55.5	1.12	1.15
5	27.4	1.18	1.19
6	33.5	1.16	1.20
7	21.9	**1.49**	1.25
8	25.4	1.12	**1.41**
9	18.3	**1.41**	1.23
10	20.9	1.29	1.27

[a] For signal assignments ref. 16. [b] Referenced to $CDCl_3$ solvent signal at 77.0 ppm.

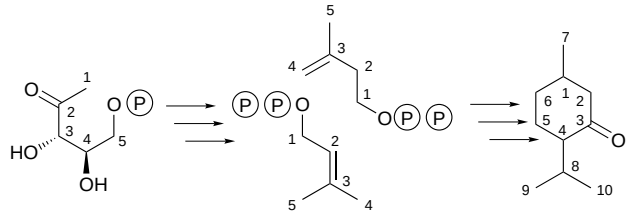

Fig. 1

We thank N. Hohenstein, Munich, for excellent technical assistance. This work was supported by the Deutsche Forschungsgemeinschaft (SFB 369), and by the Fonds der Chemischen Industrie.

Footnote and References

* E-mail: zenk@lrz.uni-muenchen.de

1 S. T. J. Broers, ETH Thesis (1994) No. 10978, Zürich.
2 M. Rohmer, M. Knani, P. Simonin, B. Sutter and H. Sahm, *Biochem. J.*, 1993, **295**, 517.
3 A. Cartayrade, M. Schwarz, B. Jaun and D. Arigoni, *Second Symposium of the European Network on Plant Terpenoids*, Strasbourg Bischenberg, France, Jan. 23–27, 1994, Abstr. PI.
4 M. K. Schwarz, ETH Thesis (1994) No. 10951, Zürich.
5 J. G. Zeidler, H. K. Lichtenthaler, H. U. May and F. W. Lichtenthaler, *Z. Naturforsch., C: Biosci.*, 1997, **52**, 15.
6 H. K. Lichtenthaler, J. Schwender, A. Disch and M. Rohmer, *FEBS Lett.*, 1997, **400**, 271.
7 D. Arigoni, S. Sagner, C. Latzel, W. Eisenreich, A. Bacher and M. H. Zenk, *Proc. Natl. Acad. Sci. USA*, 1997, **94**, 10 600.
8 J. Schwender, J. Zeidler, R. Gröner, C. Müller, M. Focke, S. Braun, F. W. Lichtenthaler and H. K. Lichtenthaler, *FEBS Lett.*, 1997, **414**, 129.
9 W. Eisenreich, S. Sagner, M. H. Zenk and A. Bacher, *Tetrahedron Lett.*, 1997, **38**, 3889.
10 A. Yokota and K. Sasajima, *Agric. Biol. Chem.*, 1984, **48**, 149.
11 A. Yokota and K. Sasajima, *Agric. Biol. Chem.*, 1986, **50**, 2517.
12 I. A. Kennedy, T. Hemscheidt, J. F. Britten and I. D. Spenser, *Can. J. Chem.*, 1995, **73**, 1329.
13 D. V. Banthorpe, B. V. Charlwood and M. J. O. Francis, *Chem. Rev.*, 1972, **72**, 115.
14 D. McCaskill and R. Croteau, *Planta*, 1995, **197**, 49.
15 J. Gershenzon, D. McCaskill, J. I. M. Rajaonarivony, C. Mihaliak, F. Karp and R. Croteau, *Anal. Biochem.*, 1992, **200**, 130.
16 F. Bohlmann, R. Zeisberg and E. Klein, *Org. Magn. Reson.*, 1975, **7**, 426.

Received in Glasgow, UK, 30th September 1997; 7/07083G

Oligomerisation of ethene by new palladium iminophosphine catalysts

Esther K. van den Beuken,[a] Wilberth J. J. Smeets,[b] Anthony L. Spek[b] and Ben L. Feringa*[a]

[a] *Department of Organic and Molecular Inorganic Chemistry, University of Groningen, Nijenborgh 4, 9747 AG Groningen, The Netherlands*

[b] *Bijvoet Center for Biomolecular Research, Department of Crystal and Structural Chemistry, Utrecht University, Padualaan 8, 3584 CH Utrecht, The Netherlands*

Oligomerisation of ethene in polar solvents at higher temperatures is achieved using new palladium iminophosphine catalysts and the oligomer selectivity can be controlled by the nature of the ligand substituents.

Oligomerisation and polymerisation of alkenes by early[1] and late transition metal catalysts[2] leads to important commercial products and currently much effort is devoted towards the development of more efficient and selective catalysts. Commonly, late transition metal complexes produce dimers of alkenes due to fast β-hydrogen abstraction.[3] Until now, only a limited number of oligomerisation or polymerisation reactions by late transition metal catalysts are known. An example is the ethene oligomerisation process with a nickel catalyst developed by Keim *et al.*,[4] well known as SHOP[1a] (Shell Higher Olefin Process). Recently, Brookhart and coworkers have reported on ethene polymerisation with bisimine Pd^{II} or Ni^{II} complexes in CH_2Cl_2 or toluene.[5] Furthermore, bisimine and bisphosphine Pd^{II} complexes are highly efficient in alkene/CO copolymerisation.[6] We report here new palladium catalysts based on iminophosphine ligands which result in the unexpected switch to oligomerisation of ethene in polar solvents.

Bidentate iminophosphine ligands are known to bind to Pd in a unique way: the soft P atom coordinates very strongly to Pd whereas the hard N donor is weakly bound.[7] We envisaged that these features might be exploited in tuning the reactivity of Pd complexes in alkene coupling reactions. For this purpose, we synthesised new iminophosphine ligands **3** from the corresponding amine and aldehyde[8] as shown in Scheme 1.

The catalysts were formed by the combination of the bidentate ligands **3**, $Pd(OAc)_2$ and a weakly or non-coordinating anion (X^-) for instance toluene-*p*-sulfonic acid (TsOH), *via* an anion exchange reaction. The oligomerisation reactions

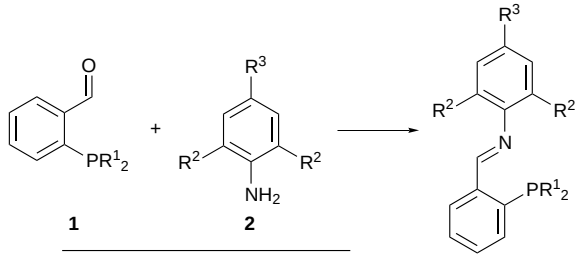

1 **2**

	R^1	R^2	R^3
3a	Ph	H	H
b	Ph	Me	H
c	Ph	Pr^i	H
d	C_6H_4OMe-*p*	Pr^i	H
e	C_6H_4OMe-*m*	Pr^i	H
f	C_6H_4OMe-*o*	H	Cl
g	C_6H_4OMe-*o*	H	H
h	C_6H_4OMe-*o*	H	OMe
i	C_6H_4OMe-*o*	Pr^i	H

Scheme 1 Synthesis of **3**

performed under 20 bar ethene with these complexes gave remarkable results: at a high temperature (100 °C) and in a polar solvent (MeOH) higher alkenes were obtained (Table 1). In sharp contrast with these results, diphosphines show higher conversion rates at these temperatures, but only dimers are obtained[3d] whereas Brookhart's diimine system[5] polymerises ethene at 25 °C. In the latter case, chain transfer took place only a few times (for 0.1 mmol Pd catalyst, 45.3 g polyethylene was obtained with $M_w = 11.2 \times 10^4$), while for the new ligand system this feature was observed many times (for **3i** *ca*. 250 times).

Table 1 shows the product ratios for various iminophosphine ligands.† Increasing the steric bulk at the nitrogen donor site, results in higher molecular masses (compare entries 1 and 2 with 3 and 7 with 9). Furthermore, when more steric bulk on the phosphorus site is introduced (in the case of *o*-OMe analog **3i**) the molecular mass is increased again (compare entries 3, 4, 5 and 9). This is in accordance with observations by Brookhart and coworkers, who found with bisimine ligands, that blocking of the axial positions led to polymers with higher molecular mass.[5]

To obtain more insight into the structure of the catalyst, an X-ray analysis was performed on [Pd(L)Me(Cl)] **4** (L = **3i**),‡ which was synthesised from **3i** and [Pd(cod)Me(Cl)] (cod = cycloocta-1,5-diene). In structure **4** (Fig. 1) Pd is coordinated by N, P, Cl and a Me group in a square planar mode. Examination of the space filling model of **4** showed that one axial position of Pd is blocked effectively by an Pr^i group and one *o*-OMe group (Fig. 2). The other axial position is partly blocked by the second *o*-OMe group.

Remarkably, the activity is increased dramatically (turnover number from 250 to 1100), by replacing the two Ph groups on P by *o*-OMePh groups (Table 1, entry 8). This is due to a steric effect because no higher activity was obtained for the *p*-methoxyphenyl analogue. The catalytic activity is furthermore influenced by electronic effects in the imino donor site; in particular electron releasing groups enhance the rate. For instance by changing R^3 from Cl **3f** to OMe **3h** an increase of turnover from 150 to 800 is observed.

Table 1 PN ligands in ethene oligomerisation and percentage of products[a]

Entry	Ligand	Time/h	T.O.[b]	C_6	C_8	C_{10}	C_{12}	C_{14}	C_{16}
1	**3a**	9	250	85	12	3			
2	**3b**	9	250	74	15	11			
3	**3c**	9	250	53	29	13	4	1	
4	**3d**	5	125	63	26	9	2		
5	**3e**	5	150	62	26	10	2		
6	**3f**	5	150	44	23	16	10	5	2
7	**3g**	5	500	34	26	19	12	6	3
8	**3h**	5	800	36	27	18	12	6	1
9	**3i**	5	1100	22	25	22	16	9	6

[a] 0.1 mmol $Pd(OAc)_2$, 0.11 mmol ligand, 0.21 mmol TsOH, 20 bar ethene, 50 ml MeOH, T = 100 °C (product ratio determined by GC). [b] T.O. = Turnover; mol consumed ethene/mol palladium.

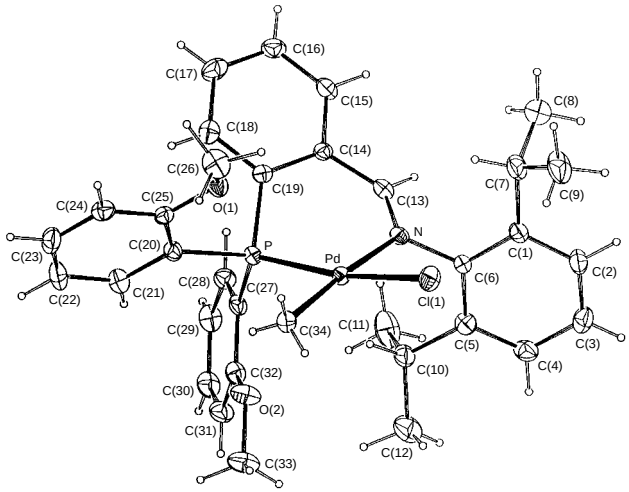

Fig. 1 Ellipsoid plot (drawn at 50% probability) of **4**, with adopted atom labelling (CH_2Cl_2 solvent not shown). Selected bond lengths (Å) and angles (°): Pd–P 2.2092(10), Pd–N 2.170(3), Pd–Cl 2.3734(11), Pd–C(34) 2.062(4); Cl–Pd–P 168.85(4), Cl–Pd–N 92.08(9), Cl–Pd–C(34) 88.29(10), P–Pd–N 89.72(9), P–Pd–C(34) 90.86(10), N–Pd–C(34) 175.08(12).

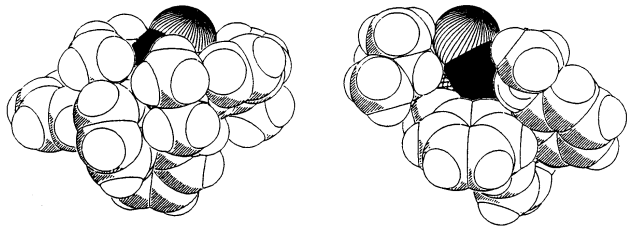

Fig. 2 CPK plots of **4** (top and bottom view, Pd = black)

A tremendous activity increase could be obtained by change of solvent. For instance, in ethylene glycol the activity increased to 1100 turnovers in 1.5 h by using ligand **3h**.

With all ligands, the molar growth factor K (moles C_{n+2}/mol C_n) is dependent on the chain length. When the chain length is higher, K decreases; for example **3i** gave $K(C_8/C_6) = 1.14$ while $K(C_{14}/C_{12}) = 0.6$ (Table 1). This suggests that chain migration takes place, giving branched alkyl fragments. This branching leads to a decreased propagation and increased termination owing to steric hindrance. This is confirmed by the observation that for longer chains, more branched products were found (Table 2). Furthermore, the isomerisation increased (K decreased) at higher temperatures [*e.g.* **3i** gave $K(C_8/C_6) = 1.46$ at 70 °C and 0.88 at 120 °C, Table 3] as well as the amount of branched products (Table 2). Decrease of the steric hindrance in the ligand, resulted also in more branched products (compare **3c** and **3i**).

Table 2 Percentage linearity of C_6–C_{12}

Entry	Ligand	T/°C	Linear C_6 (%)	Linear C_8 (%)	Linear C_{10} (%)	Linear C_{12} (%)
1	**3c**	100	92	88	83	77
2	**3i**	100	94	92	89	83
3	**3i**	120	94	89	77	76

Table 3 Product ratio (%) dependence on temperature for **3i**

Entry	T/°C	Time/h	T.O.	C_6	C_8	C_{10}	C_{12}	C_{14}	C_{16}
1	70	16	650	17	24	22	17	12	8
2	100	5	1100	22	25	22	16	9	6
3	120	5	1650	32	28	20	11	6	3

In conclusion, a new palladium based catalyst system for ethene oligomerisation has been developed. Remarkable features are the excellent stability in polar solvents at high temperatures, the formation of C_6–C_{16} oligomers at these temperatures and the possibility to tune the oligomer selectivity by the iminophosphine ligands.

This work was financially supported by Shell Research B.V. The assistance of and valuable discussions with Dr E. Drent are gratefully acknowledged.

Footnotes and References

* E-mail: feringa@chem.rug.nl

† The amount of butenes was not measured due to the volatility. Therefore, the combined C_6–C_{16} fractions are set at 100%; the relative mol percentages for the alkenes in this range are given. However, it should be noted that in case the amount of octenes is larger than the amount of hexenes, the amount of butenes is expected to be lower than the amount of hexenes.

‡ *Crystal data* for **4**: $C_{34}H_{39}ClNO_2PPd{\cdot}CH_2Cl_2$, M_r = 751.47, yellowish block shaped crystal (0.13 × 0.20 × 0.50 mm), monoclinic, space group $C2/c$, a = 38.074(5), b = 10.851(1), c = 17.661(1) Å, β = 111.10(1), U = 6807.2(1) Å^3, Z = 8, D_c = 1.467 g cm^{-3}, $F(000)$ = 3088, μ(Mo-Kα) = 8.6 cm^{-1}; 8340 reflections ($1.15 < \theta < 27.50°$; ω scan; T = 150 K) were measured on an Enraf-Nonius CAD-4T diffractometer (rotating anode, graphite-monochromated Mo-Kα radiation [λ = 0.71073 Å]). Data were corrected for L_p effects, for the linear decay (0.4%) of the intensity control reflections during 19 h of X-ray exposure and merged into a dataset of 7671 unique reflections. The structure was solved with standard Patterson methods (DIRDIF 96) and difference Fourier techniques. Hydrogen atoms were introduced at calculated positions and refined riding on their carrier atoms. All non-H atoms were refined on F^2 (SHELXL-96) using all 7671 unique reflections, with anisotropic thermal parameters. Convergence was reached at R_1 = 0.0460 for 5757 reflections with $I > 2.0\sigma(I)$ and 421 parameters; wR_2 = 0.1065, S = 1.011 for all 7671 reflections, $w = 1/\sigma^2(F_o^2) + (0.0488P)^2 + 5.42P$. A final difference Fourier map shows residual densities between −1.11 and +0.70 e Å^{-3}. CCDC 182/690.

1 For leading references, see: G. W. Parshall and S. D. Ittel, *Homogenous Catalysis*, 2nd edn., Wiley, New York, 1992, ch. 4; H.-H. Brintzinger, D. Fischer, R. Mülhaupt, B. Rieger and R. Waymouth, *Angew. Chem., Int. Ed. Engl.*, 1995, **34**, 1143; W. Kaminsky and K. Külper, *Angew. Chem., Int. Ed. Engl.*, 1985, **24**, 507; P. C. Möhring and N. J. Coville, *J. Organomet. Chem.*, 1994, **479**, 1; G. W. Coates and R. M. Waymouth, *Science*, 1995, **267**, 217; X. Yang, C. L. Stern and T. J. Marks, *J. Am. Chem. Soc.*, 1994, **116**, 10 015.

2 G. Wilke, *Angew. Chem., Int. Ed. Engl.*, 1988, **27**, 185; V. M. Möhring and G. Fink, *Angew. Chem., Int. Ed. Engl.*, 1985, **24**, 1001; A. S. Abu-Surrah and B. Rieger, *Angew. Chem., Int. Ed. Engl.*, 1996, **35**, 2475; A. Sen and T. W. Lai, *J. Am. Chem. Soc.*, 1981, **103**, 4627.

3 (*a*) E. Drent, *Pure Appl. Chem.*, 1990, **62**, 661; (*b*) F. Rix and M. Brookhart, *J. Am. Chem. Soc.*, 1995, **117**, 1137; (*c*) G. M. DiRenzom, P. S. White and M. Brookhart, *J. Am. Chem. Soc.*, 1996, **118**, 6225; (*d*) F. C. Rix, M. Brookhart and P. S. White, *J. Am. Chem. Soc.*, 1996, **118**, 4746; E. Drent and O. Aalbers, *Eur. Pat.*, 85201048.7, 1989.

4 M. Peuckert and W. Keim, *Organometallics*, 1983, **2**, 594; W. Keim, R. Appel, A. Storeck, C. Krüger and R. Goddard, *Angew. Chem., Int. Ed. Engl.*, 1981, **20**, 116.

5 L. K. Johnson, C. M. Killian and M. Brookhart, *J. Am. Chem. Soc.*, 1995, **117**, 6414; C. M. Killian, D. J. Tempel, L. K. Johnson and M. Brookhart, *J. Am. Chem. Soc.*, 1996, **118**, 11664.

6 E. Drent and P. H. M. Budzelaar, *Chem. Rev.*, 1996, **96**, 663; E. Drent, J. A. M. van Broekhoven and M. J. Doyle, *J. Organomet. Chem.*, 1991, **417**, 235; F. C. Rix, M. Brookhart and P. S. White, *J. Am. Chem. Soc.*, 1996, **118**, 4746.

7 E. Drent, P. Arnoldy and P. H. M. Budzelaar, *J. Organomet. Chem.*, 1993, **455**, 247; G. P. C. M. Dekker, A. Buijs, J. Elsevier, P. W. N. M. van Leeuwen, W. J. J. Smeets, A. L. Spek, Y. F. Wang and C. H. Stam, *Organometallics*, 1992, **11**, 1937.

8 T. L. Marxen, B. J. Johnson, P. V. Nilson and L. H. Pignolet, *Inorg. Chem.*, 1984, **23**, 4663.

Received in Cambridge, UK, 17th October 1997; 7/07495F

NMR spectroscopic evidence for chromium(VI) alkoxides with α-hydrogen atoms

Christian Limberg,* Sven Cunskis and Axel Frick

Universität Heidelberg, Anorganisch-Chemisches Institut, Im Neuenheimer Feld 270, D-69120 Heidelberg, Germany

Selective insertion of epoxides into one Cr–Cl bond of chromyl chloride at −50 °C enabled, for the first time, the spectroscopic identification of Cr^{VI} alkoxides with α-hydrogen atoms.

For quite some time alkene oxidation with chromyl chloride seemed to proceed completely unspecifically and uncontrollably.[1] In 1977 Sharpless *et al.* made an attempt to explain the occurrence of the various products and the stereochemistry involved *via* several intermediates[2] which subsequently aggregate to the Etard complex and none of which have ever been characterised.

Recently, with the aid of matrix isolation an alkene oxidation by chromyl chloride could be stopped before aggregation and the species $O{=}CrCl_2\cdots O{=}CHCH_3$ [eqn. (1)] was identified.[3]

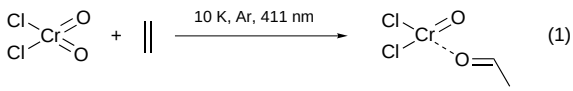

(1)

This finding could provide an explanation for the isolation of carbonyl compounds after such reactions, which had previously been understood as a result of the rearrangement of chlorohydrins and epoxides in solution.[1]

Formation of this complex could be considered *via* photolysis of the intermediate $O{=}CrCl_2\cdots\overline{OCH_2CH_2}$ stimulating an investigation concerning the behaviour of ethylene oxide in the presence of Lewis acids at low temperatures. Since $O{=}CrCl_2$ is not available on a preparative scale, in search of an appropriate reagent which could model some of the properties of $O{=}CrCl_2$, the initial starting material, CrO_2Cl_2, was studied. After co-condensation of this reagent with 1 equiv. of ethylene oxide and CD_2Cl_2 in an NMR tube and flame-sealing the sample was investigated at −80 °C. ^{1}H NMR spectra (Fig. 1) showed that ethylene oxide co-ordinates to CrO_2Cl_2, as indicated by a broad resonance at δ 3.29 for the ethylene oxide protons.† This signal remains at this position if a second equiv. of ethylene oxide is added meaning that CrO_2Cl_2 is capable of co-ordinating up to two epoxide molecules. Consequently the complex shown in eqn. (2) must be in equilibrium not only with free CrO_2Cl_2 but

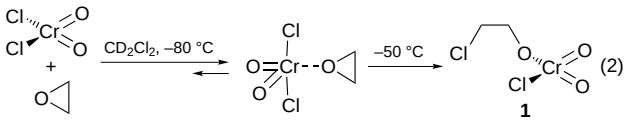

(2)

1

also with $CrO_2Cl_2{\cdot}2OC_2H_4$. Correspondingly, if 4 equiv. of ethylene oxide are reacted with CrO_2Cl_2 a signal at δ 3.01, intermediate between free and co-ordinated oxirane, is observed. Photolysis at this stage resulted in C–H activation and formation of paramagnetic compounds. However, warming of a 1 : 1 sample to −50 °C triggered a cleavage reaction of the three-membered ring[4] by one Cl ligand of CrO_2Cl_2 producing the species $O_2Cr(OCH_2CH_2Cl)Cl$ **1**. After 60 min the yield of **1** amounts to 75%, however, at this stage the decomposition rate of **1** becomes faster than its formation.

Dark red **1** has been characterised by ^{1}H, ^{13}C (135° DEPT), ^{1}H/^{13}C-HMQC and ^{1}H/^{1}H-COSY NMR spectra showing two coupling CH_2 groups‡ both of which appear in the characteristic regions for the proposed connectivity. In addition ^{17}O NMR data of concentrated samples were recorded: the initial signal of the CrO_2 group of the CrO_2Cl_2–oxirane complex (one broad resonance at δ 1476) decreased at −50 °C in favour of a new signal for the terminal oxygens in **1** at δ 1429 indicating that the CrO_2 group has been preserved. Signals for the oxirane and alkoxide oxygens could not be detected in accordance with the results of investigations concerning molybdate esters.[5] Concentration dependent experiments in the presence of a standard (CH_2Cl_2) confirmed that only 1 equiv. of ethylene oxide per Cr centre is consumed during the formation of **1** and that accordingly ethylene oxide inserts into only one Cr–Cl bond excluding the formation of the bis(2-chloroethyl) chromate ester. Instead, increasing the initial concentration of the oxirane decreases the lifetime of **1**, which decomposes to paramagnetic dark brown compounds, so terminating the NMR experiments. These species, small amounts of which are constantly generated at −50 °C at any ethylene oxide concentration, can explain the continuous broadening of the signal of ethylene oxide and its shifting to higher field (Fig. 1): ethylene oxide equilibrating rapidly between its free state and complexation to CrO_2Cl_2 and **1** also binds reversibly to the paramagnetic compounds and therefore the averaged signal observed in the experiment is increasingly broadened with time. In $CFCl_3$ the paramagnetic complexes precipitate as brown solids and accordingly the ethylene oxide signal does not shift or broaden significantly. The positive results after replacement of CD_2Cl_2 additionally rule out its participation in the reaction sequence leading to **1**.

1 is contaminated by only one other compound, **2** (*ca*. 8% in the experiment shown in Fig. 1), whose identification proved difficult because of its low concentration, limited stability and

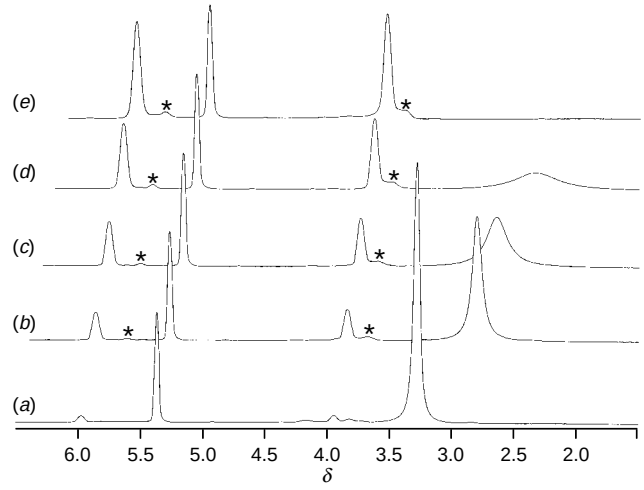

Fig. 1 ^{1}H NMR spectra of a mixture of 0.8 mmol CrO_2Cl_2 and 0.8 mmol of ethylene oxide in CD_2Cl_2 (*a*) at −80 °C and after annealing to −50 °C for (*b*) 10 min, (*c*) 20 min, (*d*) 40 min and (*e*) 60 min. The signals marked with an asterisk belong to **2**.

considerable linewidths of its signals thwarting all attempts to record COSY spectra. Its ^{1}H and ^{13}C NMR data may be interpreted in terms of the compound $O_2Cr(Cl)OCH_2CH_2OCH_2CH_2Cl$ being formed by insertion of two ethylene oxide molecules into one Cr–Cl bond. This is supported by the fact that $FeCl_3$ has been found to react with ethylene oxide to give uncharacterised chloroferric alkoxides producing chloroethanol and 2-(2-chloroethoxy)ethanol upon hydrolysis.[6] However, due to the insufficient spectroscopic data the assignment of **2** is speculative.

Scheme 1

Compound **1** is remarkable because it is the first Cr^{VI} alkoxide with α-hydrogens whose existence has been proved spectroscopically.§ It is well known that Cr^{VI} compounds oxidise primary and secondary alcohols to carbonyl compounds[8] and recent DFT calculations by Deng and Ziegler[10] have shown that the key step in CrO_2Cl_2 oxidations is probably that shown in Scheme 1. While chromate esters of tertiary alcohols[11] are protected against this decomposition route the activation of α-hydrogens by terminal Cr=O groups is possible for **1** so that its thermal sensitivity (decomp. within 15 min at −30 °C) is not a surprise. However, the smooth synthesis presented above which can be performed at low temperatures without simultaneous formation of by-products allows its NMR spectroscopic characterisation. Attempts to isolate **1** and **2** at −50 °C by removal of all volatiles led to a brown glass, whose hydrolysis yielded, as expected, 2-chloroethanol and chloroacetaldehyde contaminated by small amounts of compounds of unknown composition, some of which were identical with the chromyl chloride oxidation products of 2-(2-chloroethoxy)ethanol, supporting the assignment of **2**. When the brown glass is annealed to room temp. in the absence of any reactant a heterogeneous decomposition product is obtained in which the organic oxidation products remain coordinated to the chromium centres as they do in the Etard complex.[12] Accordingly its IR spectrum is dominated by strong bands at 3301 [ν(OH)], 1640/1570/1430 [ν(C=O)] and 1066 cm^{-1} [ν(C–O)].

Surprisingly, when propylene oxide was reacted with CrO_2Cl_2 at −50 °C both possible regioisomers[12] were found in a close to 1 : 1 ratio [eqn. (3)]. A similar lack of selectivity has

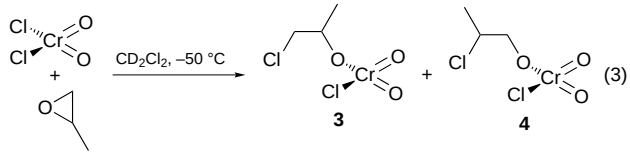

(3)

been found *e.g.* in epoxide cleavages using VCl_3·3thf.[13] The reaction mechanism and the stereochemistry involved in epoxide opening by CrO_2Cl_2 are under current investigation. Further research also concerns the expansion of this novel route yielding oxochromium(VI) alkoxides to the syntheses of stable candidates of this class of compounds, *i.e.* those eluding α-hydrogens, which find application as useful oxidation reagents.[10]

C. L. thanks the Deutsche Forschungsgemeinschaft for a scholarship as well as funding and Professor Dr G. Huttner for his generous support.

Footnotes and References

* E-mail: Limberg@sun0.urz.uni-heidelberg.de

† Free ethylene oxide shows a singlet at δ 2.58.

‡ Owing to the linewidths of the signals no coupling information could be deduced from the COSY experiments. In Fig. 1 no coupling is resolved, in other experiments, however, a triplet structure for the two signals became obvious. ^{1}H NMR (200 MHz, CD_2Cl_2, −50 °C, $SiMe_4$): δ_H 5.96 [2 H, br t, ^3J(HH) 4.8 Hz, OCH_2], 3.95 [2 H, br t, ^3J(HH) 4.8 Hz, $ClCH_2$]; ^{13}C NMR (200 MHz, CD_2Cl_2, −50 °C, $SiMe_4$): δ_C 94.22 (OCH_2), 46.06 ($ClCH_2$).

§ Chada *et al.*[7] claim to have prepared oligomers of $O_2Cr(OCH_2CH_2Cl)_2$ (said to show just one singlet by ^{1}H NMR) by refluxing CrO_2Cl_2 with the corresponding alcohol in CCl_4 and **1** (neither analytical nor spectroscopic data are given) by treatment of CrO_2Cl_2 with $Li(OCH_2CH_2Cl)$ in CCl_4. Since primary and secondary alcohols are oxidised by Cr^{VI} compounds at room temp.[8] it did not surprise us that these rather drastic conditions in our hands did not yield the compounds mentioned above rather than green solids with strong ν(C=O) bands in the IR spectra. An NMR spectroscopic investigation showed that $HOCH_2CH_2Cl$ reacts with CrO_2Cl_2 already at temperatures below −80 °C producing paramagnetic species. Westheimer *et al.*[9] reported the *in situ* preparation of bisisopropyl chromate from CrO_3 and Pr^iOH which was characterised by elemental analyses of its decomposition products.

¶ **3**: δ_H 6.14 (1 H, br m, OCH), 3.82 (2 H, br m), $ClCH_2$), 1.68 [3 H, d, ^3J(HH) 5.20 Hz, CH_3]; δ_C 99.38 (OCH), 49.43 ($ClCH_2$), 21.41 (CH_3). **4**: δ_H 5.83 [2 H, d, ^3J(HH) 4.8 Hz, OCH_2], 4.37 (1 H, m, ClCH), 1.57 [3 H, d, ^3J(HH) 5.20 Hz, CH_3]; δ_C 98.14 (OCH_2), 57.69 (ClCH), 21.35 (CH_3).

1 M. A. Etard and H. M. Moissan, *Compt. Rend.*, 1893, **116**, 434; S. J. Cristol and K. R. Eilar, *J. Am. Chem. Soc.*, 1950, **72**, 4353; R. A. Stairs, D. G. M. Diaper and A. L. Gatzke, *Can. J. Chem.*, 1963, **41**, 1059; F. Freeman, P. J. Cameran and R. H. Dubois, *J. Org. Chem.*, 1968, **33**, 3970; F. Freeman, R. H. Dubois and N. J. Yamachika, *Tetrahedron*, 1969, **25**, 3441; F. Freeman and K. W. Arledge, *J. Org. Chem.*, 1972, **37**, 2656; K. B. Sharpless and A. Y. Teranishi, *J. Org. Chem.*, 1973, **38**, 185; F. Freeman, P. J. Cameran and R. H. Dubois, *J. Org. Chem.*, 1986, **33**, 3970.

2 K. B. Sharpless, A. Y. Teranishi and J.-E. Bäckvall, *J. Am. Chem. Soc.*, 1977, **99**, 3120.

3 C. Limberg, R. Köppe and H. Schnöckel, *Angew. Chem.*, 1998, in press.

4 For Cr-catalysed epoxide cleavage reactions, *cf.*: J. F. Larrow, S. E. Schaus and E. N. Jacobsen, *J. Am. Chem. Soc.*, 1996, **118**, 7420; W.-H. Leung, M.-C. Wu, J. L. C. Chim, M.-T. Yu, H.-W. Hou, W.-T. Wong and Y. Wang, *J. Chem. Soc., Dalton Trans.*, 1997, 3525.

5 M. H. Chisholm, K. Folting, J. C. Huffman and C. C. Kirkpatrick, *Inorg. Chem.*, 1984, **23**, 1021.

6 A. B. Borkovec, *J. Org. Chem.*, 1958, **23**, 826.

7 S. L. Chadha, V. Sharma and A. Sharma, *J. Chem. Soc., Dalton Trans.*, 1987, 1253.

8 G. W. Parshall and S. D. Ittel, *Homogeneous Catalysis*, 2nd edn., Wiley-Interscience, New York, 1992; *Comprehensive Organic Synthesis*, ed. B. M. Trost, Pergamon, New York, 1991, vol. 7 (*Oxidation*); W. A. Nugent and J. M. Mayer, *Metal–Ligand Multiple Bonds*, Wiley, New York, 1988; *Organic Syntheses by Oxidation with Metal Compounds*, ed. W. J. Mijs and C. R. H. I. de Jonge, Plenum, New York, 1986.

9 F. H. Westheimer and A. Leo, *J. Am. Chem. Soc.*, 1952, **74**, 4383.

10 L. Deng and T. Ziegler, *Organometallics*, 1997, **16**, 716.

11 M. Dobler, J. D. Dunitz, B. Gubler, H. B. Weber, G. Buchi and J. O. Padilla, *Proc. R. Chem. Soc., London Ser. A*, 1963, 383; K. B. Sharpless and K. Akashi, *J. Am. Chem. Soc.*, 1975, **97**, 5927; V. Amirthalingam, D. F. Grant and A. Senol, *Acta Crystallogr., Sect. B*, 1972, **28**, 1340; E. J. Corey, E.-P. Barrette and P. A. Magriotis, *Tetrahedron Lett.*, 1985, **48**, 5855; P. Stavropoulos, N. Bryson, M.-T. Youinou and J. A. Osborn, *Inorg. Chem.*, 1990, **29**, 1807.

12 G. K. Cook and J. M. Mayer, *J. Am. Chem. Soc.*, 1994, **116**, 1855.

13 T. Inokuchi, H. Kawafuchi and S. Torii, *Synlett*, 1992, 511.

Received in Cambridge, UK, 29th September 1997; 7/06987A

Highly diastereoselective synthesis of β-hydroxy carbonyl compounds using π-allyltricarbonyliron lactone complexes: a formal 1,7-asymmetric induction of chirality in a Mukaiyama aldol reaction

Steven V. Ley* and Liam R. Cox

Department of Chemistry, University of Cambridge, Lensfield Road, Cambridge, UK CB2 1EW

The reaction of π-allyltricarbonyliron lactone complex 2 with a variety of achiral aldehydes affords the corresponding aldol products in good yields and with good to excellent levels of stereocontrol.

The aldol reaction remains one of the most important C–C bond constructing processes in modern organic synthesis. While many methods towards the preparation of diastereoisomerically pure aldol products have been developed,[1] the direct synthesis of isomerically pure β-hydroxy ketones lacking an α-substituent has proved to be much more difficult, since the α-substituent is often a key stereocontrolling requirement in the addition event.[2]

We now report that a trimethylsilyl enol ether **2** appended to the side-chain of a π-allyltricarbonyliron lactone complex undergoes a Mukaiyama aldol reaction[3] with a range of achiral aldehydes, affording β-hydroxy ketone products in good yield and with good to excellent levels of stereocontrol. The reaction constitutes what is formally a 1,7-asymmetric induction of chirality[4] and as such is quite unprecedented in aldol chemistry.[5]

π-Allyltricarbonyliron lactone complexes bearing ketone functionality in the side-chain are readily prepared *via* a four-step sequence starting from an allylic alcohol.[6] The ketone group positioned in the side-chain of the allyl ligand preferentially adopts an s-*cis* conformation.[6] This, combined with the steric bulk of the tricarbonyliron moiety, ensures that nucleophiles add to the ketone to afford a single diastereoisomeric product.[6,7] Starting from (*E*)-oct-2-en-1-ol, the model methyl ketone complex **1** was prepared and treated with $Me_3SiOSO_2CF_3$ and Et_3N in CH_2Cl_2 at 0 °C to afford the remarkably stable trimethylsilyl enol ether **2** in excellent yield (Scheme 1). We envisaged that this silyl enol ether functionality would also adopt a preferred conformation and therefore might react with aldehydes producing the corresponding aldol products with some degree of stereocontrol.

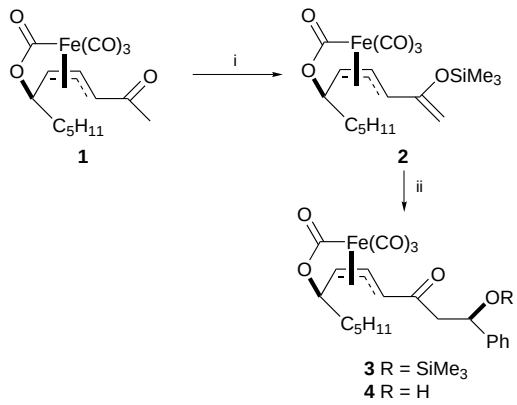

Scheme 1 *Reagents and conditions*: $Me_3SiOSO_2CF_3$ (1.2 equiv.), Et_3N (1.4 equiv.), CH_2Cl_2, 0 °C, 1 h, 89%; ii, PhCHO (1.5 equiv.), $BF_3{\cdot}OEt_2$ (1.4 equiv.), Et_2O–CH_2Cl_2 (5 : 1), −78 °C, 5 h, then Et_3N (1.4 equiv.), −78 °C, 61% (**3**), 20% (**4**)

Addition of an ethereal solution of benzaldehyde and $BF_3{\cdot}OEt_2$ to a solution of silyl enol ether **2** at −78 °C afforded the aldol products **3** and **4** in good yield and, in both cases, mainly as one diastereoisomer (Scheme 1). Treatment of the crude reaction mixture with HF·pyridine allowed quantitative conversion of the silyl aldol product **3** to the free alcohol **4**† and subsequent determination of the overall diastereoselectivity of the aldol reaction by high field ^{1}H NMR analysis.‡

Encouraged by this result, we applied the same reaction conditions to a range of achiral aldehydes and the results are outlined in Table 1.§ Aldehydes with α-branching (entries 3–5) showed the best levels of diastereocontrol, with the sterically encumbered pivalaldehyde affording only one diastereoisomer as evidenced by ^{1}H NMR analysis on the crude reaction mixture. α,β-Unsaturated aldehydes reacted in high yield but showed decreased levels of diastereocontrol.

The relative stereochemical outcome of the aldol addition was determined as follows: reduction of the ketone group in **3** with $AlPr^n_3$ proceeded stereoselectively, in accord with earlier results, producing one diastereoisomer **5**.[6] Protection of the 1,3-diol unit as the acetonide **6** revealed a *syn* relationship between the alcohol functionalities as determined by characteristic shifts for the acetal carbon at δ 99.7[8] and the acetal methyl groups at δ 19.9 and 29.6 (Scheme 2).[9] By induction the relative configuration of the stereogenic centre formed in the aldol reaction to that at the lactone tether was determined.

In summary, the lactone tether imparts, *via* the tricarbonyliron moiety, a high degree of 1,7-induction of chirality in the Lewis acid-mediated reaction between silyl enol ether **2** and a wide range of achiral aldehydes. In general, the more sterically bulky the aldehyde, the greater the diastereoselectivity of the reaction. Such remote induction in an acyclic system is very unusual. The generated β-hydroxy carbonyl or *syn* 1,3-diol units are ubiquitous motifs in many biologically important molecules and since π-allyltricarbonyliron lactones are easily prepared in

Table 1 Mukaiyama aldol reaction of achiral aldehydes with π-allyltricarbonyliron lactone complex **2**

Entry	Aldehyde	Overall yield (%)[a]	Ratio of **3** : **4**[b]	De (%)[c]
1	PhCHO	81	75 : 25	86
2	$CH_3(CH_2)_4CHO$	74	23 : 77	82
3	$CH_3CH(CH_3)CHO$	66	39 : 61	94
4	$CH_3C(CH_3)_2CHO$	57	26 : 74	> 95[d]
5	cyclohexyl–CHO	75	57 : 43	91
6	$CH_3(CH_2)_3CH{=}CHCHO$	65[e]	72 : 28	79
7	$CH_3(CH_2)_4C{=}CCHO$	78	79 : 21	47

[a] Isolated yield after chromatography. [b] Determined from isolated yields of **3** and **4**. [c] De determined from the crude reaction mixture by 600 MHz ^{1}H NMR analysis after silyl deprotection. [d] Only one diastereoisomer was observable in the crude reaction mixture by 600 MHz ^{1}H NMR analysis. [e] Up to *ca.* 8% dehydration product was also isolated.

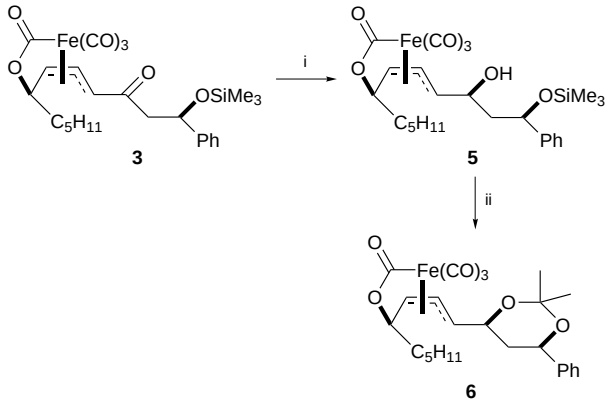

Scheme 2 *Reagents and conditions*: i, $AlPr^n_3$ (2.4 equiv.), CH_2Cl_2, −78 → 0 °C, 1 h 75%; ii, HF·pyridine (3 equiv., *ca.* 2.25 mol dm^{-3} solution), THF, 25 °C, then pyridinium *para*-toluenesulfonate (PPTS) (0.05 equiv.), 2,2-dimethoxypropane (20 equiv.), DMF, 25 °C, 12 h, 71%

enantiomerically enriched form (> 95%),[7] and can be decomplexed to β-, γ- and δ-lactones,[10] (*E*,*E*)-dienes,[10] or alkenols,[10,11] we envisage that this addition to their chemistry will yet further extend their utility in natural product synthesis. Work exploring the scope of this reaction and possible reaction mechanisms is presently underway within our laboratory.

We thank the EPSRC (L. R. C.), the Isaac Newton Trust Bursary Scheme (L. R. C.), Zeneca Pharmaceuticals (L. R. C.), the B.P. Endowment (S. V. L.) and the Novartis Research Fellowship (S. V. L.) for supporting this work.

Footnotes and References

* E-mail: sv11000@cus.cam.ac.uk

† *General procedure* for the aldol reaction: synthesis of **4**. A solution of PhCHO (0.035 cm^3, 0.35 mmol) and BF_3·OEt_2 (0.047 cm^3, 0.34 mmol) in Et_2O (1.0 cm^3) was added dropwise to a cooled (−78 °C) solution of silyl enol ether **2** (0.099 g, 0.23 mmol) in Et_2O–CH_2Cl_2 (1.5 cm^3, 2 : 1). After 5 h, Et_3N (0.047 cm^3, 0.34 mmol) was added dropwise with vigorous stirring. After 2 min, the solution was filtered through a pad of Celite, washing the residue with Et_2O–CH_2Cl_2 (50 cm^3, 4 : 1). Concentration of the filtrate *in vacuo* followed by treatment of the residue with a solution of HF·pyridine (0.69 mmol, 0.300 cm^3 of a *ca*. 2.25 mol dm^{-3} solution in THF) for 30 min afforded, after standard aqueous work-up and purification by flash column chromatography (silica, eluent: Et_2O–light petroleum, 7 : 3), aldol product **4** as a yellow oil (0.087 g, 81%); ν_{max}(film)/cm^{-1} 3458 (OH), 3031, 2928, 2858, 2088 (CO), 2016 (CO), 1667 (C=O), 1496, 1454, 1417, 1363, 1323, 1233, 1204, 1027, 760, 701, 654; δ_H(500 MHz) 0.88 (3 H, t, *J* 6.2, 12-H × 3), 1.23–1.62 (8 H, m, 8-H × 2, 9-H × 2, 10-H × 2, 11-H × 2), 2.96–3.19 (3 H, m, 2-H × 2, OH), 3.83 (1 H, d, *J* 11.3, 4-H), 4.34 (1 H, app q, *J* 5.6, 7-H), 5.03 (1 H, dd, *J* 8.3, 4.5, 6-H), 5.26–5.28 (1 H, m, 1-H), 5.59 (1 H, dd, *J* 11.3, 8.3, 5-H), 7.28-7.39 (5 H, m, Ph-*H*); δ_C(100 MHz) 13.9 (CH_3, 12-C), 22.4 (CH_2), 26.5 (CH_2), 31.5 (CH_2), 36.6 (CH_2), 51.7 (CH_2, 2-C), 65.5 (CH), 70.1 (CH), 77.0 (CH), 84.9 (CH), 92.0 (CH), 125.7 (CH), 127.9 (CH), 128.7 (CH), 142.5 (quat. C), 199.6 (CO), 202.4 (CO), 203.6 (CO), 204.4 (CO), 207.8 (CO); *m*/*z* (FAB) 457 (MH^+, 25%), 442 (17), 429 (6, MH − CO), 411 (15, MH − CO − H_2O), 399 (20, M − H − 2CO), 383 (13, M − H − 2CO − O), 373 (5), 353 (18), 345 (38, MH − 4CO), 327 (61, MH − 4CO − H_2O), 239 (33), 223 (37), 179 (48), 151 (50), 136 (100) [Found (MH^+): 457.0984. $C_{22}H_{25}FeO_7$ requires *M*H, 457.0950].

‡ Diastereoisomeric excess of the aldol products was determined by ^1H NMR analysis using a Bruker DRX-600 spectrometer.

§ All new compounds exhibited satisfactory spectral and mass data. Yields refer to chromatographically and spectroscopically homogeneous materials.

1 For general reviews on the aldol reaction: C. H. Heathcock, B. Moon Kim, S. F. Williams, S. Masamune, I. Paterson and C. Gennari, in *Comprehensive Organic Synthesis*, ed. B. M. Trost and I. Fleming, Pergamon, Oxford, 1991, vol. 2 and references cited therein; A. S. Franklin and I. Paterson, *Contemp. Org. Synth.*, 1994, **1**, 317 and references cited therein.

2 For approaches to the asymmetric synthesis of α-unsubstituted β-hydroxy ketones: M. Braun, *Angew. Chem., Int. Ed. Engl.*, 1987, **26**, 24; M. Braun, in *Advances in Carbanion Chemistry*, ed. V. Snieckus, JAI, Greenwich, 1992, p. 216; M. Franck-Neumann, P.-J. Colson, P. Geoffroy and K. M. Taba, *Tetrahedron Lett.*, 1992, **33**, 1903; M. Franck-Neumann, P. Bissinger and P. Geoffroy, *Tetrahedron Lett.*, 1997, **38**, 4469; 1997, **38**, 4473; 1997, **38**, 4477; M. Sodeoka, R. Tokunoh, F. Miyazaki, E. Hagiwara and M. Shibasaki, *Synlett*, 1997, 463; K. Mikami, S. Matsukawa, M. Nagashima, H. Funabashi and H. Morishima, *Tetrahedron Lett*., 1997, **38**, 579; Y.-M. Li, X.-J. Yao, X. Feng, X.-M. Wang and J.-T. Wang, *J. Organomet. Chem*., 1996, **509**, 221; E. M. Carreira, W. Lee and R. A. Singer, *J. Am. Chem. Soc*., 1995, **117**, 3649; K. Ishihara, T. Maruyama, M. Mouri, Q. Gao, K. Faruta and H. Yamamoto, *Bull. Chem. Soc. Jpn*., 1993, **66**, 3483; E. J. Corey, C. L. Cywin and T. D. Roper, *Tetrahedron Lett*., 1992, **33**, 6907; I. Paterson and J. M. Goodman, *Tetrahedron Lett*., 1989, **30**, 997; M. Muraoka, H. Kawasaki and K. Koga, *Tetrahedron Lett*., 1988, **29**, 337; M. T. Reetz, F. Kunisch and P. Heitmann, *Tetrahedron Lett*., 1986, **27**, 4721.

3 For a general review on the Mukaiyama reaction: T. Mukaiyama, *Org. React*., 1982, **28**, 203.

4 For other examples of 1,7-asymmetric induction in organic synthesis: J. S. Carey and E. J. Thomas, *J. Chem. Soc., Chem. Commun*., 1994, 283; G. A. Molander and K. L. Bobbitt, *J. Am. Chem. Soc*., 1993, **115**, 7517.

5 Examples of remote asymmetric induction in aldol reactions of methyl ketones. 1,4-Asymmetric induction: B. R. Lagu and D. C. Liotta, *Tetrahedron Lett*., 1994, **35**, 4485; B. R. Lagu, H. M. Crane and D. C. Liotta, *J. Org. Chem*., 1993, **58**, 4191; B. M. Trost and H. Urabe, *J. Org. Chem*., 1990, **55**, 3982; I. Paterson, J. M. Goodman and M. Isaka, *Tetrahedron Lett*., 1989, **30**, 7121. 1,5-Asymmetric induction: D. A. Evans, P. J. Coleman and B. Côté, *J. Org. Chem*., 1997, **62**, 788; I. Paterson, K. Gibson and R. M. Oballa, *Tetrahedron Lett*., 1996, **37**, 8585.

6 S. V. Ley, G. Meek, K.-H. Metten and C. Piqué, *J. Chem. Soc., Chem. Commun*., 1994, 1931; S. V. Ley, L. R. Cox, G. Meek, K.-H. Metten, C. Piqué and J. M. Worrall, *J. Chem. Soc., Perkin Trans. 1*, 1997, 3299.

7 S. V. Ley and L. R. Cox, *Chem. Commun*., 1996, 657; *J. Chem. Soc., Perkin Trans. 1*, 1997, 3315.

8 D. A. Evans, D. L. Reiger and J. R. Cage, *Tetrahedron Lett*., 1990, **31**, 7099.

9 S. D. Rychnovsky and D. J. Skalitzky, *Tetrahedron Lett*., 1990, **31**, 945; S. D. Rychnovsky, B. Rogers and G. Yang, *J. Org. Chem*., 1993, **58**, 3511.

10 For a general review on the synthetic utility of π-allyltricarbonyliron lactone complexes: S. V. Ley, L. R. Cox and G. Meek, *Chem. Rev*., 1996, **96**, 423 and references cited therein.

11 S. V. Ley, S. Burckhardt, L. R. Cox and J. M. Worrall, *Chem. Commun*., 1997, 229.

Received in Cambridge, UK, 3rd October 1997; 7/07153A

A novel decomplexation of π-allyltricarbonyliron lactone complexes using borohydride reagents: a new route to stereodefined acyclic 1,5-diols and 1,5,7-triols

Steven V. Ley,* Svenja Burckhardt, Liam R. Cox and Julia M. Worrall

Department of Chemistry, University of Cambridge, Lensfield Road, Cambridge, UK CB2 1EW

π-Allyltricarbonyliron lactone complexes undergo a highly stereoselective decomplexation reaction on treatment with sodium triacetoxyborohydride to afford acyclic alcohols in excellent yields.

Remote asymmetric induction in acyclic systems remains a challenging problem in contemporary organic synthesis. The use of a complexed transition metal as a temporary structural feature is a strategy which is finding increasing utility in addressing this problem.[1] The higher level of organisation and rigidity in such an organometallic system can allow the transfer of stereochemical information across distances of several atoms, for a variety of different bond forming reactions and functional group transformations.

We have previously shown that the use of a π-allyltricarbonyliron lactone complex as a scaffold affords excellent diastereoselectivity in the manipulation of a ketone group appended to the allyl unit (Scheme 1). Thus a 1,5 stereochemical relationship of oxygen functionalities may be established in a controlled manner by the addition of organoaluminium reagents[2] or allylstannanes[3] into the side-chain ketone. We have now also demonstrated high diastereocontrol in Mukaiyama aldol reactions of aldehydes with π-allyltricarbonyliron lactone complexes bearing a silyl enol ether functionality in the side-chain.[4] The products of these reactions have a 1,7 stereochemical relationship between the new chiral centre and the lactone tether.

Existing methods for the removal of the iron carbonyl moiety are limited in scope.[5] Treatment with ceric ammonium nitrate leads to the stereoselective formation of β-lactones,[6] while δ-lactones can be accessed under exhaustive carbonylation conditions.[7,8] Treatment with barium hydroxide affords (η⁴-diene)tricarbonyliron complexes.[2b,7] We now report a new decomplexation reaction which effectively unwraps the carbon chain from the iron centre to reveal a linear molecule, with the chiral centre at the lactone tether preserved as a free alcohol and the side-chain functionality intact.

Our interest in hydride donors as potential decomplexing agents was initially aroused by the reaction between ketone **1** and sodium borohydride in 50% MeOH–CH_2Cl_2 at −78 °C.[9] After 1 h the ketone group was completely reduced to afford a single diastereoisomer of the corresponding secondary alcohol **2** in 88% yield. Over longer reaction times, however, the product began to react further and small quantities of chromatographically inseparable decomplexation products, tentatively assigned as **3** and **4**, could be isolated (Scheme 2).

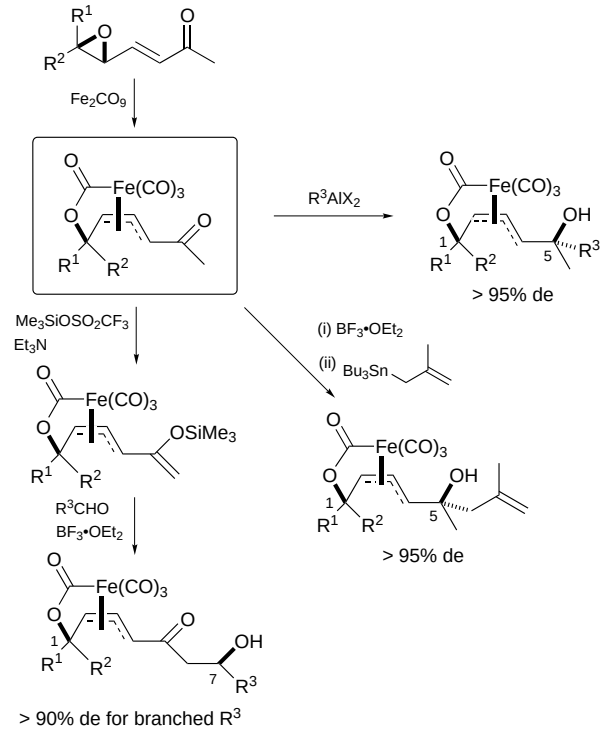

Scheme 1

In order to drive the decomplexation reaction to completion it was necessary to use a large excess of sodium borohydride, added portionwise to a methanolic solution of the diastereomerically pure secondary alcohol complex at room temperature. Under these conditions a further, saturated product **5** could be detected in the diol mixture (Scheme 2). Hydrogenation of the mixture afforded exclusively saturated diol, but with a diastereomeric excess of only 56%. These results indicate

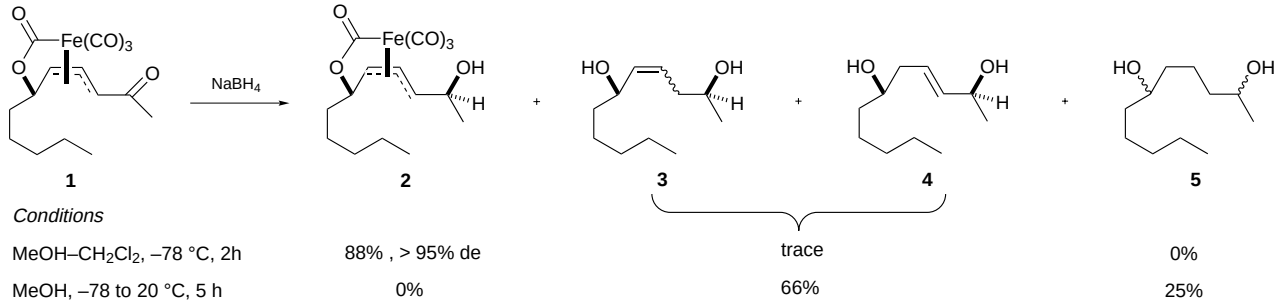

Scheme 2

Table 1 Decomplexation of a range of functionalised π-allyltricarbonyliron lactone complexes using $NaBH(OAc)_3$

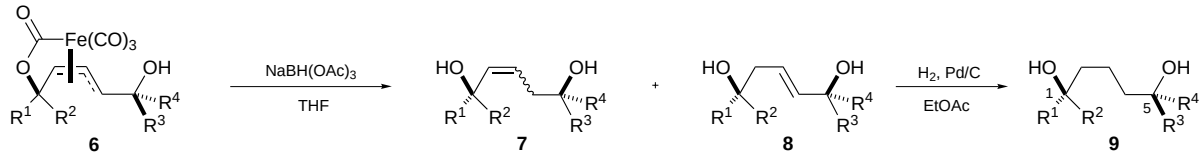

Complex	R^1	R^2	R^3	R^4	Yield of **9** (%)[a]	De (%)[b]
6a	C_5H_{11}	H	H	H	59	—
6b	C_5H_{11}	H	Ph	H	71	96
6c	Me	H	$(CH_2)_4OBn$	H	63	> 96
6d	H	C_5H_{11}	Me	H	82 (97)[c]	> 96
6e	H	C_5H_{11}	Me	Pr^n	52 (67)[c]	> 96
6f	H	C_5H_{11}	$CH_2CH(OH)Ph$	H	65[d] (87)[c]	> 96

[a] Isolated yield of **9** over two steps from **6**. [b] Diastereomeric excess of **9** determined by comparison of integrals in the 600 MHz ^1H NMR spectra. [c] Yield based on recovered starting material. [d] The OH at C-7 was lost during hydrogenation; see text.

that positional isomerisation of the double bonds in products **3** and **4** had taken place during decomplexation. Formation of the saturated product **5** could then be explained by initial iron carbonyl catalysed double bond isomerisation to form an enol,[10] followed by decomplexation and non-stereospecific borohydride reduction of the tautomeric ketone.

Extensive screening of different reducing systems revealed that decomplexation could be achieved without isomerisation using sodium triacetoxyborohydride in dry THF. A variety of different lactone complexes were exposed to these conditions and the results are shown in Table 1. In each case, the major component of the product mixture was *cis*-**7** which could generally be isolated by careful flash chromatography; the proportion of *cis*-**7** : (*trans*-**7** + **8**) was typically around 2 : 1. The products were combined and hydrogenated in order to facilitate characterisation and determination of the diastereomeric excesses.

In the case of the *syn* 5,7-diol complex **6f**, prepared by a Mukaiyama aldol reaction followed by stereoselective reduction of the C-5 ketone group,[4] the 1,5,7-triol decomplexation product *cis*-**7f** was isolated in 55% yield. After recombination with the other ene triol products and hydrogenation according to the standard procedure, however, a fully saturated 1,5-diol was obtained, which was formed by elimination of the C-7 hydroxy group during hydrogenation. This problem should be avoidable by variation of the hydrogenation conditions.

In summary, a new decomplexation reaction has been developed which allows removal of the iron carbonyl moiety from functionalised π-allyltricarbonyliron lactone complexes and conversion into functionalised alcohols without loss of stereochemical integrity. Application of this procedure to the nucleophilic adducts of ketone complexes constitutes an expedient route to stereodefined 1,5-diols, while application to the products of Mukaiyama aldol reactions allows access to stereodefined 1,5,7-triols. Studies on the mechanism of the decomplexation reaction and its utility in natural product synthesis will be published in due course.

We gratefully acknowledge financial support from the EPSRC (to L. R. C. and J. M. W.), the Isaac Newton Trust (to L. R. C.), Zeneca Pharmaceuticals (to L. R. C.), the Dr Carl-Duisberg Stiftung (to S. B.), the BP Endowment and the Novartis Research Fellowship (to S. V. L.).

Footnote and References

* E-mail: sv11000@cus.cam.ac.uk

1 For some recent examples of remote asymmetric induction using transition metal complexes, see: W. R. Roush and C. K. Wada, *J. Am. Chem. Soc*., 1994, **116**, 2151; D. Enders, U. Frank, P. Fey, B. Jandeleit and B. Bhushan Lohray, *J. Organomet. Chem*., 1996, **519**, 147; M. Franck-Neumann, P. Bissinger and P. Geoffroy, *Tetrahedron Lett*., 1997, **38**, 4477; E. J. Thomas, *Chem. Commun*., 1997, 411 and references cited therein.

2 (*a*) S. V. Ley, G. Meek, K-H. Metten and C. Piqué, *J. Chem. Soc., Chem. Commun*., 1994, 1931; (*b*) S. V. Ley, L. R. Cox, G. Meek, K- H. Metten, C. Piqué and J. M. Worrall, *J. Chem. Soc., Perkin Trans. 1*, 1997, 3299.

3 S. V. Ley and L. R. Cox, *Chem. Commun*., 1996, 657; *J. Chem. Soc., Perkin Trans. 1*, 1997, 3315.

4 S. V. Ley and L. R. Cox, *Chem. Commun.*, 1997, 227.

5 For a general review on the synthetic utility of π-allyltricarbonyliron lactone complexes, see S. V. Ley, L. R. Cox and G. Meek, *Chem. Rev*., 1996, **96**, 423 and references cited therein.

6 S. V. Ley, G. D. Annis and R. Sivaramakrishnan, *J. Chem. Soc., Perkin Trans. 1*, 1981, 270.

7 R. Aumann, H. Ring, C. Krüger and R. Goddard, *Chem. Ber*., 1979, **112**, 3644.

8 A. M. Horton, Ph.D. Thesis, University of London, 1984.

9 This mild reducing system is known to selectively reduce ketones in the presence of enones; D. E. Ward, C. K. Rhee and W. M. Zoghaib, *Tetrahedron Lett*., 1988, **29**, 517.

10 For a review on the isomerisation of olefins by iron carbonyl derivatives, see J. Rodriguez, P. Brun and B. Waegell, *Bull. Soc. Chim. Fr*., 1989, **126**, 799.

Received in Cambridge, UK, 3rd October 1997; 7/07155H

Cooperative binding of potassium cation and chloride anion by novel rhenium(I) bipyridyl amide crown ether receptors

James E. Redman,[a] Paul D. Beer,*[a] Simon W. Dent[a] and Michael G. B. Drew[b]

[a] *Inorganic Chemistry Laboratory, University of Oxford, South Parks Road, Oxford, UK OX1 3QR*
[b] *Department of Chemistry, University of Reading, Reading, UK RG6 6AD*

New rhenium(I) bipyridyl amide crown ether receptors are prepared and shown to complex K^+Cl^- ion pairs in which crown ether complexation of the potassium cation co-operates in the binding of chloride anion.

Ion pair recognition, the simultaneous binding of cationic and anionic guest species by ditopic receptors is a new emerging field of coordination chemistry.[1–5] These multisite ligand systems as well as being potential selective extraction/membrane transportation reagents for metal salts can also be designed to exhibit allosteric and cooperative behaviour whereby the binding of one charged guest can influence the subsequent coordination of the pairing ion. We have recently shown that charged or neutral transition metal organometallic and coordination amide containing receptors can selectively bind and sense anionic guest species.[6] The covalent attachment of benzo crown ether metal cation recognition sites to these anion receptors will create novel ion pair binding reagents. We report here the synthesis and preliminary coordination chemistry of new neutral rhenium(I) bipyridyl amide crown ether receptors that complex potassium cations and simultaneously bind chloride anions with positive cooperativity which is a first step towards the design of ion pair recognition systems.

The bipyridyl amide functionalised benzo-18-crown-6 and 3,4-dimethoxyphenyl ligands were prepared in good yields according to Scheme 1. Reaction of each of these bipyridyl ligands with $[Re(CO)_5Br]$ in THF produced the target receptors L^1–L^5 as yellow solids (Scheme 2). The potassium cation and chloride anion coordination properties of the receptors were investigated by ^1H NMR titration experiments in $(CD_3)_2SO$ solution. The addition of KPF_6 to ^1H NMR solutions of L^2, L^3 and L^5 caused the crown ether methylene protons to significantly shift to lower field. Analysis of the resulting titration curves with the computer program EQNMR[7] suggested the respective crown ether recognition site of each receptor to form a 1 : 1 complex with the potassium cation, with stability constant values of *ca.* 500 $dm^3\ mol^{-1}$ for L^3 and L^5. Negligible shifts were observed with L^1 and L^4 suggesting K^+ complexation only takes place at the crown ether binding sites. The addition of tetrabutylammonium chloride to $(CD_3)_2SO$ solutions of L^1–L^5 caused significant downfield perturbations of the respective receptor's amide and H^3-bipyridyl protons by up to $\Delta\delta = 0.55$ ppm, indicating anion binding is taking place exclusively in the amide-bipyridyl vicinity of the receptor. In all cases the titration curves suggested 1 : 1 complex stoichiometry. The titrations with chloride were repeated in the presence of 2 equiv. of KPF_6 and EQNMR[7] determined stability constant values for both titration experiments are presented in Table 1. Table 1 clearly shows the addition of KPF_6 to the crown ether containing receptors L^2, L^3 and L^5 leads to a substantial increase in the magnitude of stability constant, by nearly threefold for L^2, for the respective chloride anion receptor-complex. It is noteworthy that receptors L^1, L^4, lacking crown ether moieties, do not exhibit such an increase in stability constant in the presence of KPF_6 which suggests the origin of positive co-operativity is an intramolecular electrostatic attraction between a simultaneously crown ether bound potassium cation and bipyridyl amide complexed chloride anion.

Receptor L^3 was co-crystallized with KCl and the X-ray crystal structure of the ion-pair complex $[L^3KCl]_2 \cdot 2H_2O$ which has a crystallographic centre of symmetry is shown in Fig. 1 and 2.†‡

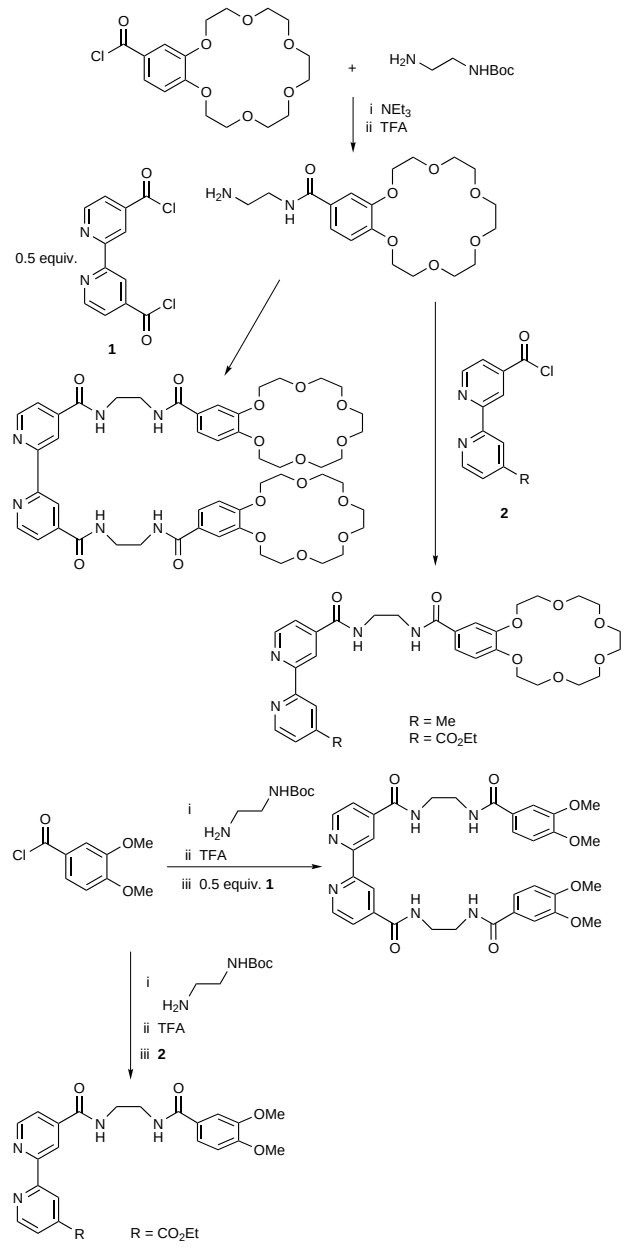

Scheme 1

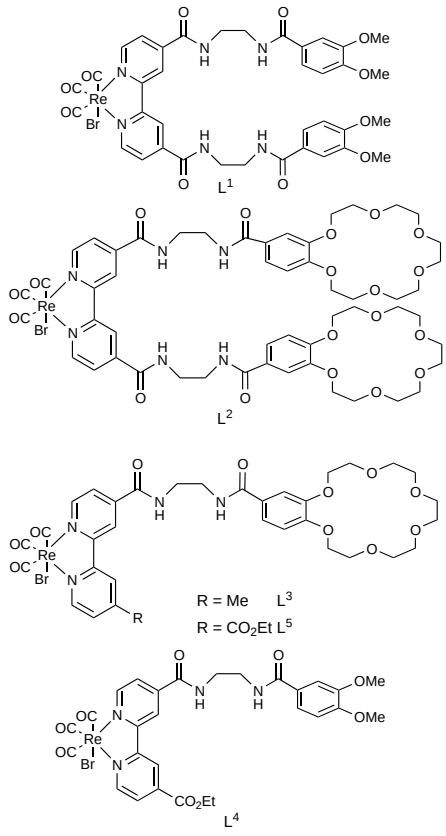

Scheme 2

Table 1 Stability constants for chloride anion binding in the presence and absence of potassium cations in $(CD_3)_2SO$

Receptor	K^a/dm^3 mol^{-1}
L^1	44
$L^1 + KPF_6$ (2 equiv.)	46
L^2	48
$L^2 + KPF_6$ (2 equiv.)	120
L^3	24
$L^3 + KPF_6$ (2 equiv.)	57
L^4	15
$L^4 + KPF_6$ (2 equiv.)	15
L^5	—[b]
$L^5 + KPF_6$ (2 equiv.)	35

[a] Errors estimated to be ⩽5%. [b] Very weak binding, a stability constant could not be determined.

In the $Re(CO)_3$(bipy) moieties, the environment of the metal is octahedral with dimensions in the expected range. Each bipy is linked *via* an amide group to a benzo-18-crown-6 in which is encapsulated a potassium ion. The benzo crown has a planar conformation with the six oxygens coplanar to within 0.10 Å with the potassium 0.24 Å from the plane. The hexagonal bipyramidal potassium coordination is completed by two axial bonds to a water molecule and to an amide oxygen atom from another substituted $Re(CO)_3$(bipy) moiety, thus forming the centrosymmetric dimer. The chloride anion is disordered over two positions 1.07 Å apart with relative occupancies 56 and 44%, but each anion is hydrogen bonded to both amide nitrogen atoms, Cl(21) to N(63) at 3.25 and N(66) at 3.41 Å and Cl(22) to N(63) 3.12 and N(66) at 3.29 Å.

In summary, these new rhenium(I) bipyridyl amide crown ether receptors are capable of binding K^+Cl^- ion pairs in which crown ether complexation of the potassium cation co-operates in the complexation of chloride anion.

We thank Kodak Ltd for a studentship (S. W. D.) and the EPSRC for use of the mass spectrometry service at University College Swansea. The University of Reading and EPSRC are gratefully acknowledged for funding towards the crystallographic image-plate system.

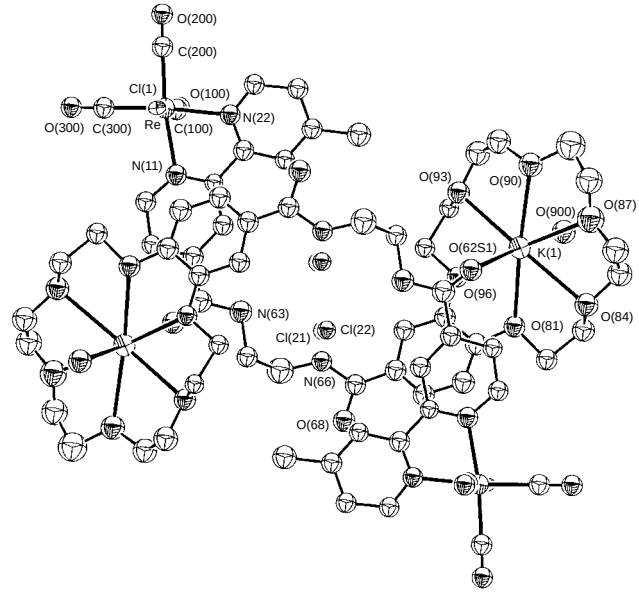

Fig. 1 The centrosymmetric dimer $[L^3KCl]_2 \cdot 2H_2O$ with ellipsoids shown at 20% probability together with the atomic numbering scheme. Bond lengths from the potassium to crown oxygens are to O(81) 2.752(13), O(84) 2.913(15), O(87) 2.76(2), O(90) 2.801(16), O(93) 2.881(13), O(96) 2.722(14) Å and to the amide oxygen O(62S1) 2.654(17) and to the water molecule O(900) 2.753(17) Å.

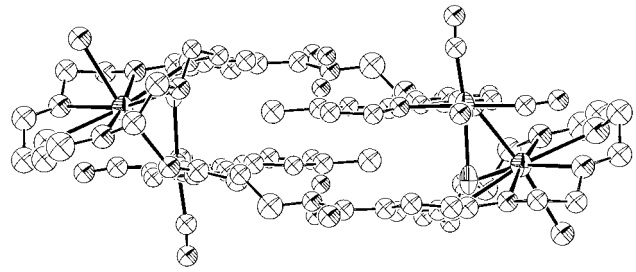

Fig. 2 The centrosymmetric dimer $[L^3KCl]_2 \cdot 2H_2O$ with ellipsoids shown at 20% probability

Footnotes and References

* E-mail: paul.beer@icl.ox.ac.uk

† *Crystal data*: $C_{68}H_{76}Cl_4K_2N_8O_{24}Re_2$, M = 1981.76, triclinic, space group $P\bar{1}$, Z = 1, a = 11.445(12), b = 14.668(17), c = 16.328(17) Å, α = 115.27(1), β = 90.02(1), γ = 112.34(1)°, U = 2249 Å^3, D_c = 1.463 Mg m^{-3}, μ = 29.69 mm^{-1}, $F(000)$ = 988, 7037 independent reflections, 1191 with $I > 2\sigma(I)$ refined on F^2 to R of 0.0808 for data with $I > 2\sigma(I)$. CCDC 182/697.

‡ A substitution of Br for Cl has occurred at the Re^I centre. During the NMR titrations no evidence of this reaction was ever seen over the course of the experiment for *ca*. 2 h.

1 M. T. Reetz, C. M. Niemeyer and K. Harris, *Angew. Chem., Int. Ed. Engl.*, 1991, **30**, 1472.
2 D. M. Rudkevich, Z. Brzozka, M. Palys, H. C. Visser, W. Verboom and D. N. Reinhoudt, *Angew. Chem., Int. Ed. Engl.*, 1994, **33**, 467.
3 K. I. Kinnear, D. P. Mousley, E. Arafar and J. C. Lockhart, *J. Chem. Soc., Dalton Trans.*, 1994, 3637.
4 P. D. Beer, M. G. B. Drew, R. J. Knubley and M. I. Ogden, *J. Chem. Soc., Dalton Trans.*, 1995, 3117.
5 J. Scheerder, J. P. M. van Duynhoven, J. F. J. Engbersen and D. N. Reinhoudt, *Angew. Chem., Int. Ed. Engl.*, 1996, **35**, 1090.
6 P. D. Beer, *Chem. Commun.*, 1996, 689 and references therein.
7 M. J. Hynes, *J. Chem. Soc., Dalton Trans.*, 1993, 311.

Received in Cambridge, UK, 24th October 1997; 7/07680K

Isomeric clusters $[Ru_4(\mu_4\text{-}PPh)(\mu_4\text{-}C_4H_3N)(CO)_{11}]$ containing diagonal C,C and parallel C,N bonded pyrrolyne ligands

Alejandro J. Arce,[b] Antony J. Deeming,*[a] Ysaura De Sanctis,[b] Sharnjit K. Johal,[a] Caroline M. Martin,[a] Mukesh Shinhmar,[a] Despo M. Speel[a] and Alexander Vassos[a]

[a] *Department of Chemistry, University College London, 20 Gordon Street, London, UK WC1H 0AJ*
[b] *Centro de Quimíca, Instituto Venezolano de Investigaciones Científicas (IVIC), Apartado 21827, Caracas 1020-A, Venezuela*

The three isomeric tertiary phosphines, diphenyl-*n*-pyrrolylphosphine (*n* = 1, 2 or 3) lead to two isomeric tetranuclear clusters $[Ru_4(\mu_4\text{-}PPh)(\mu_4\text{-}C_4H_3N)(CO)_{11}]$ which contain the diagonal C,C bonded and parallel C,N bonded pyrrolyne ligands.

The organometallic chemistry of pyrrole is important from the point of view of the hydrodenitrogenation (HDN) process.[1] There are few examples of mononuclear pyrrole complexes but it coordinates as pyrrolyl in complexes related to cyclopentadienyl compounds.[2] However, in clusters there are both aromatic and non-aromatic, doubly and triply bridging ligands derived from pyrrole, mostly by C–H bond activation and hydrogen atom transfer.[3] Up to now it has been unknown as a μ_4 ligand. This paper describes the synthesis and structure of two isomeric pyrrolyne ligands that bridge square faces of tetranuclear ruthenium complexes.

Treatment of $[Ru_3(CO)_{12}]$ with equimolar amounts of any of the three isomeric pyrrolyl phosphines, $Ph_2P(n\text{-}C_4H_4N)$ (L^1, n = 1; L^2, n = 2; L^3 n = 3),[4] leads firstly to simple substitution products $[Ru_3(CO)_{11}L^n]$ with L^n coordinated through phosphorus, closely related to known tertiary phosphine clusters.[5] The clusters $[Ru_3(CO)_{11}L^n]$ were only formed in small quantities because they readily lose CO to allow metallation at the pyrrolyl rings, in preference to the phenyl rings, to give products **1**–**3** (Scheme 1). For **2** and **3** pure samples were isolated and in the case of **3** the crystal structure has been determined (to be reported elsewhere). Compound **1** was not detected, however, and its intermediacy can only be reasoned from the isolation and full characterisation, including X-ray structure, of the corresponding osmium complex formed from L^1 and $[Os_3(CO)_{12}]$.[6] Compounds **1** to **3** react further with $[Ru_3(CO)_{12}]$ under the reaction conditions to give isomers of $[Ru_4(\mu_4\text{-}PPh)(\mu_4\text{-}C_4H_3N)(CO)_{11}]$, C,N-bonded **4** or C,C-bonded **5** as shown in Scheme 1. Clusters **4** and **5** gave similar but different IR ν(CO) spectra, both showing bridging CO bands.† Whereas **4** showed three sharp ^{1}H NMR signals for the pyrrolyne ligand at δ 7.43, 6.19 and 7.07 consistent with these all being CH groups, **5** gave signals at δ 6.62, 5.90 and 7.90. The broad signal at δ 7.90 for **5** is assigned to NH, while the other two signals are much sharper.

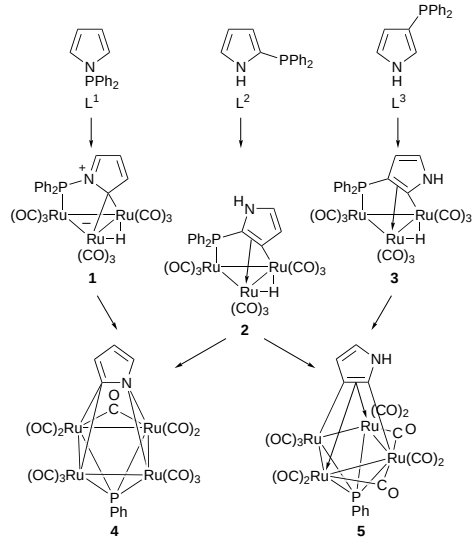

Scheme 1 Formation of clusters **4** and **5** from L^n and $[Ru_3(CO)_{12}]$

The X-ray structures of two red crystalline modifications of **4** have been determined: a triclinic crystal deposited from heptane on cooling and a monoclinic crystal formed by evaporation of a hexane–CH_2Cl_2 mixture.‡ Their molecular structures are very similar and only one is shown (Fig. 1). The molecular structure of **5** is shown in Fig. 2.

Fig. 3 shows the cores of these molecules to emphasize the clearly different ways that the C_4H_3N ligands coordinate in clusters **4** and **5**. In the C,C-bonded form **5** [Fig. 2 and 3(*b*)] the geometry is closely related to known structures of the type $[Ru_4(\mu_4\text{-}PR)(\mu_4\text{-}X)(CO)_{11}]$, where X = alkyne,[7] thiophyne,[8] *etc.*, with the diagonal vertical arrangement with the ligand vertical. Like other diagonally coordinated complexes of the type, there are two bridging CO ligands along the shorter Ru–Ru edges. The angle between the C_4H_2NH plane and the Ru_4 plane is 90.3°. Benzyne analogues $[Ru_4(\mu_4\text{-}PR)(\mu_4\text{-}C_6H_4)(CO)_{11}]$ **6** have been synthesised from $[Ru_3(CO)_{12}]$ and arylphosphines[9] and are also formed as a minor byproduct from $[Ru_3(CO)_{12}]$ and L^2. The μ_4-C_6H_4 ligand behaves as a six-electron donor and adopts a parallel tilted orientation; the

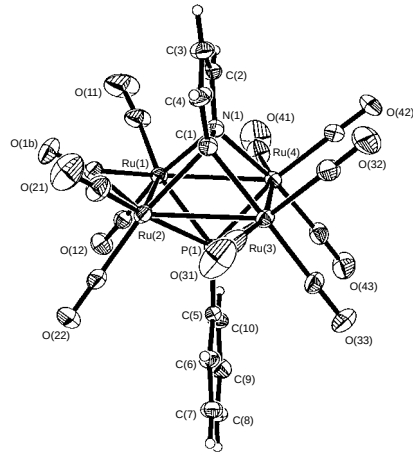

Fig. 1 Molecular structure of **4**. The monoclinic form is shown; the triclinic form is similar. Selected bond lengths (Å) are given for the monoclinic crystal with those for the triclinic crystal in square brackets: Ru(1)–Ru(2) 2.8316(7) [2.8035(9)], Ru(2)-Ru(3) 2.8752(8) [2.8318(7)], Ru(3)–Ru(4) 2.9069(7) [2.8637(9)], Ru(4)–Ru(1) 2.8720(8) [2.8522(8)], Ru(1)–N(1) 2.211(4) [2.177(5)], Ru(2)–C(1) 2.217(4) [2.188(5)], Ru(3)–C(1) 2.193(4) [2.178(5)], Ru(4)–N(1) 2.194(4) [2.170(5)], C(1)–N(1) 1.462(6) [1.441(7)], C(1)–C(4) 1.400(7) [1.374(8)], C(2)–C(3) 1.388(9) [1.381(10)], C(3)–C(4) 1.385(8) [1.400(9)], C(2)–N(1) 1.407(7) [1.373(8)].

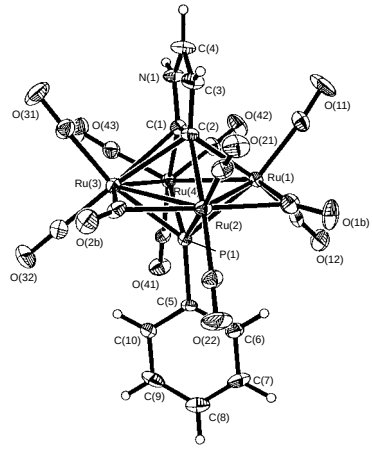

Fig. 2 Molecular structure of **5**. Selected bond lengths (Å) and angles (°): Ru(1)–Ru(2) 2.7553(13), Ru(2)–Ru(3) 2.7533(11), Ru(3)–Ru(4) 2.9035(13), Ru(1)–Ru(4), 2.8730(11), Ru(1)–C(1) 2.456(8), Ru(1)–C(2) 2.372(7), Ru(2)–C(2) 2.182(7), Ru(3)–C(1) 2.468(8), Ru(3)–C(2) 2.366(8), Ru(4)–C(1) 2.081(8), C(1)–C(2) 1.418(11), C(1)–N(1) 1.383(11), C(2)–C(3) 1.450(10), C(3)–C(4) 1.350(12), C(4)–N(1) 1.367(11).

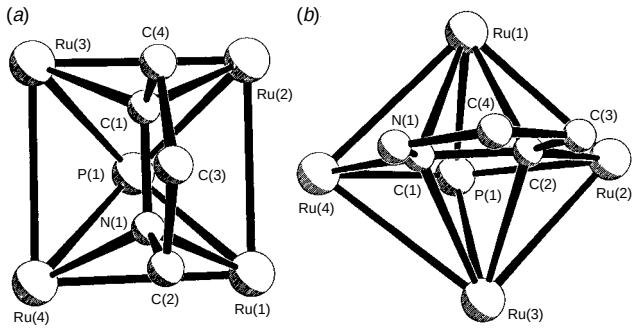

Fig. 3 A comparison of (*a*) the C,N bonded **4** and (*b*) the C,C bonded **5**

coordinated C–C bond is parallel to a Ru–Ru edge and the C_6H_4 plane is 49.7 and 54.7° to the Ru_4 plane (two independent molecules) when R = Ph. A related 1,2-naphthyne cluster is also known.[10] In C,N-bonded pyrrolyne cluster **4** [Fig. 1 and 3(*a*)] a parallel arrangement is found with the C(1)–N(1) bond parallel to the Ru(1)–Ru(2) and Ru(3)–Ru(4) edges of the Ru_4 square. However, in this case the organic ring is essentially vertical with a dihedral angle to the metal plane of 84.2° (monoclinic form) and 85.2° (triclinic form). In many ways the isomers **4** and **5** correspond to the C,N-bonded (ligand vertical) and the C,C-bonded (ligand tilted) forms of pyrrolyne in trisomium clusters $[Os_3(\mu\text{-}H)(\mu\text{-}C_4H_3N)(CO)_9]$ **7**[3c] and $[Os_3(\mu\text{-}H)(\mu\text{-}C_4H_2NMe)(CO)_9]$ **8**.[3b] The existence of these different isomers at both triangular and square metal faces in trinuclear and tetranuclear clusters respectively strongly points to the possibility of having similar isomeric forms for pyrrolyne at metal surfaces.

We thank the EPSRC, the British Council and CONICIT (Venezuela) for support for this work

Footnotes and References

* E-mail: a.j.deeming@ucl.ac.uk

† *Syntheses*: Reaction of L^1 with $[Ru_3(CO)_{12}]$: a solution of L^1 [4a] (0.057 g) and $[Ru_3(CO)_{12}]$ (0.145 g) in refluxing octane gave after TLC separation three products: $[Ru_3(CO)_{11}(Ph_2PC_4H_4N)]$ as an orange solid (0.025 g, 17%), $[Ru_3(CO)_9(Ph_2PC_4H_4N)_3]$ as a dark red solid (0.041 g, 28%) and **4** as red crystals (0.016 g, 11%).

Reaction of L^2 with $[Ru_3(CO)_{12}]$: a solution of L^2 [4b] (0.059 g) and $[Ru_3(CO)_{12}]$ (0.150 g) in refluxing toluene gave after TLC separation **2** as a yellow oil (10%), $[Ru_3(\mu\text{-}H)(\mu_3\text{-}Ph_2PC_4H_2NH)(CO)_8(Ph_2PC_4H_3NH)]$ as a yellow oil (10%), **4** as red crystals (7%) and **6** as an orange oil (3%).

Reaction of L^3 with $[Ru_3(CO)_{12}]$: a solution of L^3 [4b] (0.0903 g) and $[Ru_3(CO)_{12}]$ (0.22 g) in refluxing toluene gave after TLC separation **3** as orange crystals (20%), $[Ru_3(\mu\text{-}H)(\mu_3\text{-}Ph_2PC_4H_2NH)(CO)_8(Ph_2PC_4H_3NH)]$ as dark orange crystals (25%) and **5** as a brown solid (5%).

‡ *Crystal data*: cluster **4**, $C_{21}H_8NO_{11}PRu_4$, M = 885.53, monoclinic, space group $P2_1/n$, a = 9.241(2), b = 17.182(3), c = 17.891(4) Å, β = 90.51(3)°, U = 2840.6(10) Å^3, Z = 4, D_c = 2.071 Mg m^{-3}, $F(000)$ = 1680, red plate, 0.70 × 0.50 × 0.01 mm, μ(Mo-Kα) = 21.96 cm^{-1}. 5900 unique data collected in the range $5 \leqslant 2\theta \leqslant 53°$, final R = 0.0373 [$I > 2\sigma(I)$], wR_2 = 0.1008 (all data), GOF = 1.005, maximum Δ/σ = 0.001, max. peak, hole in final difference Fourier = 0.846, −1.380 e Å^{-3}. Cluster **4**, triclinic, space group $P\bar{1}$, a = 9.4707(13), b = 9.621(2), c = 15.855(4) Å, α = 92.41(2), β = 95.65(2), γ = 110.990(12)°, U = 1337.7(4) Å^3, Z = 2, D_c = 2.199 Mg m^{-3}, $F(000)$ = 840, red plate, 0.40 × 0.38 × 0.03 mm, μ(Mo-Kα) = 23.31 cm^{-1}. 4642 unique data collected in the range $5 \leqslant 2\theta \leqslant 50°$, final R = 0.0375 [$I > 2\sigma(I)$], wR_2 = 0.1109 (all data), GOF = 1.059, max. Δ/σ = 0.001, max. peak, hole in final difference Fourier = 0.63, −1.11 e Å^{-3}. Cluster **5**, $C_{21}H_8NO_{11}PRu_4$, M = 885.53, triclinic, space group $P\bar{1}$, a = 9.110(2), b = 9.577(3), c = 16.298(4) Å, α = 89.93(2), β = 105.11(2), γ = 107.89(2)°, U = 1301.6(6) Å^3, Z = 2, D_c = 2.260 Mg m^{-3}, $F(000)$ = 840, red plate, 0.22 × 0.18 × 0.03 mm, μ(Mo-Kα) = 23.96 cm^{-1}. 4519 unique data collected in the range $5 \leqslant 2\theta \leqslant 50°$, final R = 0.0421 [$I > 2\sigma(I)$], wR_2 = 0.1271 (all data), GOF = 1.089, maximum Δ/σ = 0.001, max. peak, hole in final difference Fourier = 0.74, −0.89 e Å^{-3}. For each structure, data were collected at 273(2) K on a Nicolet R3v/m diffractometer in the ω–2θ scan mode, absorption corrections (ψ-scans) were applied, relative transmission factors: 0.924–0.189 (**4**, monoclinic), 1.000–0.661 (**4**, triclinic), 0.961–0.699 (**5**). Structures were solved by direct methods (SHELXTL PLUS)[11] and full-matrix least-squares refinement on F^2 (SHELXL 93).[12] All non-hydrogen atoms were refined anisotropically except the coordinated C and N atoms of the pyrrolyne in **4** (both forms) which were refined isotropically. In the two modifications of **4** a model was refined with disorder involving two enantiomeric orientations of the pyrrolyne ligand. The orientation shown in Fig. 1 is the major one in each case with C(1) and N(1) reversed in the other. CCDC 182/682.

1 R. M. Laine, *Ann. N. Y. Acad. Sci.*, 1983, **415**, 271; R. H. Fish, *ibid.*, 1983, **415**, 292; A. Eisenstadt, C. M. Giandomenico, M. F. Frederick and R. M. Laine, *Organometallics*, 1985, **4**, 2033 and references therein; see also various articles in Polyhedron Symposium-in-Print, Number 19, *Polyhedron*, 1997, **16**, 3071.

2 K. K. Joshi, P. L. Pauson, A. R. Qazi and W. H. Stubbs, *J. Organomet. Chem.*, 1964, **1**, 471.

3 (*a*) A. J. Arce, Y. De Sanctis and A. J. Deeming, *J. Organomet. Chem.*, 1986, **311**, 371; (*b*) A. J. Deeming, A. J. Arce, Y. De Sanctis, M. W. Day and K. I. Hardcastle, *Organometallics*, 1989, **8**, 1408; (*c*) M. W. Day, K. I. Hardcastle, A. J. Deeming, A. J. Arce and Y. De Sanctis, *ibid.*, 1990, **9**, 6; (*d*) A. J. Arce, J. Manzur, M. Marquez, Y. De Sanctis and A. J. Deeming, *J. Organomet. Chem.*, 1991, **412**, 177; (*e*) A. J. Arce, Y. De Sanctis, L. Hernandez, M. Marquez and A. J. Deeming, *ibid.*, 1992, **436**, 351; (*f*) A. J. Arce, R. Machado, M. V. Capparelli, Y. De Sanctis, R. Atencio, J. Manzur and A. J. Deeming, *Organometallics*, 1997, **16**, 1735.

4 (*a*) K. G. Moloy and J. L. Peterson, *J. Am. Chem. Soc.*, 1995, **117**, 7696; (*b*) D. W. Allen, J. R. Charlton and B. G. Huntley, *Phosphorus*, 1976, **6**, 191.

5 A. J. Deeming, *Comprehensive Organometallic Chemistry II*, ed. E. W. Abel, F. G. A. Stone and G. Wilkinson, Pergamon, 1994, vol. 7, p. 711.

6 A. J. Deeming and S. K. Johal, unpublished work.

7 J. Lunnis, S. A. MacLaughlin, N. J. Taylor, A. J. Carty and E. Sappa, *Organometallics*, 1985, **4**, 2066; J. F. Corrigan, S. Doherty, N. J. Taylor and A. J. Carty, *ibid.*, 1993, **12**, 1365.

8 A. J. Deeming, S. N. Jayasuriya, A. J. Arce and Y. De Sanctis, *Organometallics*, 1996, **15**, 786.

9 S. A. R. Knox, B. R. Lloyd, A. G. Orpen, J. M. Vinas and M. Weber, *J. Chem. Soc., Chem. Commun.*, 1987, 1498; J. P. H. Charmont, H. A. A. Dickson, N. J. Grist, J. Keister, S. A. R. Knox, D. A. V. Morton, A. G. Orpen and J. M. Vinas, *J. Chem. Soc., Chem. Commun*., 1991, 1393; T. C. Zheng, W. R. Cullen and S. J. Rettig, *Organometallics*, 1994, **13**, 3594.

10 W. R. Cullen, S. J. Rettig and T. C. Zheng, *Organometallics*, 1995, **14**, 1466.

11 G. M. Sheldrick, SHELXTL PLUS, program for crystal structure solution, released by Nicolet, 1986.

12 G. M. Sheldrick, SHELXL 93, program for crystal structure refinement, University of Göttingen, 1993.

Received in Cambridge, UK, 7th October 1997; 7/07249J

Conformational effects and cyclodimer formation in intramolecular [2 + 2] photocycloadditions

Sylvie Piva-Le Blanc, Jean-Pierre Pete and Olivier Piva*

Unité mixte de recherche CNRS, Université de Reims Champagne Ardenne, BP 1039, 51687 Reims Cedex 2, France

Cyclodimer formation competes with intramolecular [2 + 2] photocycloaddition during the photolysis of ω-alkenyl 3-carboxylatocyclohexenones.

Intramolecular [2 + 2] photocycloadditions are very useful reactions for multistep syntheses of polycyclic molecules.[1] The efficiency of the process depends mainly on the length of the chain between the enone and the alkene moiety and on the strain involved during the cycloaddition process. Intramolecular photocycloadditions can be disfavoured when medium ring cycles would otherwise be formed simultaneously to the formation of cyclobutane. In these cases, hydrogen abstraction[2] or polymerization[3] predominate when conformational restrictions decrease the rate of the intramolecular cycloaddition process. Since they should be good candidates for asymmetric [2 + 2] photocycloadditions,[4] we have studied the reactivity of unsaturated esters of 3-carboxylatocyclohex-2-enone and we now report the unusual effect of the ester linkage on the photocycloaddition process. (Scheme 1).

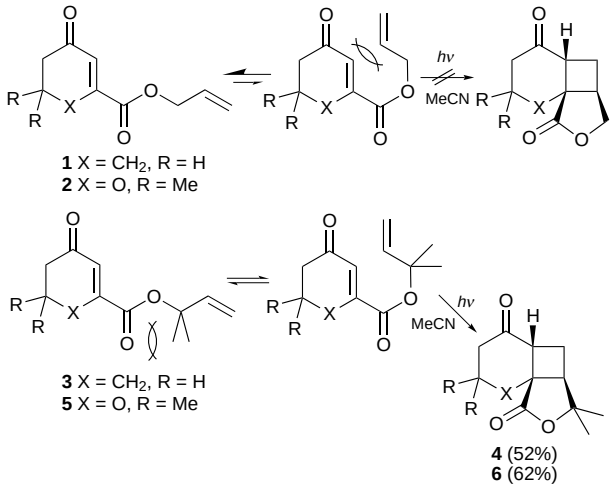

Scheme 1

Intermolecular photocycloadducts could not be isolated from allyl esters **1** or **2** and photodimerization of the enone chromophore (< 5%) was the main reaction observed. The absence of intramolecular photocycloaddition might result from conformational effects as already pointed out by Pirrung and Thomson with other types of carboxylic derivatives.[5] Due to the large preference for an s-*trans* conformation around the CO–O bond of the ester group,[6] the ethylenic bond would be situated too far from the excited enone to allow an intramolecular photocycloaddition process to occur. The conformational origin of the absence of cycloadducts from **1** and **2** was verified by using the *gem*-dimethyl effect.[7] Introduction of two Me groups into the chain of 1,1-dimethylallyl esters **3** and **5** restores its conformational mobility and, as expected, adducts **4** and **6** were isolated in good yields. Use of butenyl esters should minimize the conformational restrictions associated with an ester group and indeed, irradiation at room temperature of butenyl ester **7** (10^{-2} mol l^{-1}) in MeCN or CH_2Cl_2, led to the expected cycloadduct **8** [reaction (1)].[8]

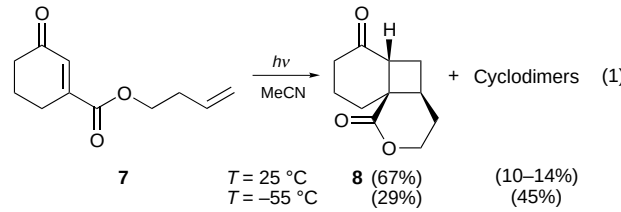

Interestingly, the chemical yield of **8** decreased at low temperatures and a mixture of cyclodimers (up to 45%) was obtained at −55 °C. Analysis of the crude reaction mixture by NMR spectroscopy, at high conversion yields, showed no ethylenic bonds.† Methanolysis of the mixture of oligomers afforded **10** and **11** which were prepared independently by an intermolecular photocycloaddition of oxo ester **9** with but-3-en-1-ol [reaction (2)].

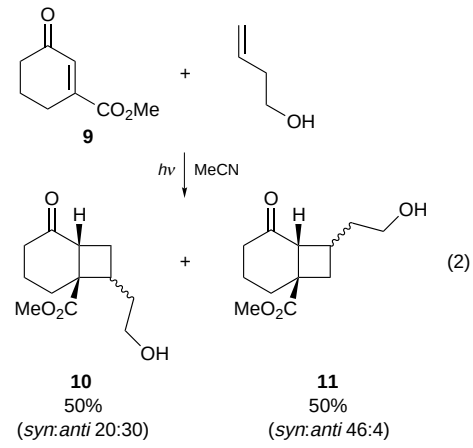

ESMS confirmed the dimeric nature of the isolated oligomers and detected some trimers of the starting material in the reaction mixture. By successive chromatography, crystallization and NMR studies, seven cyclodimers **12**–**18** were isolated‡ and characterized§ (Scheme 2). Formation of these adducts can be rationalised by a succession of intermolecular and intramolecular photocycloadditions, none of which appeared to be regio- or stereo-selective.[9] In order to increase the yield of macrocyclic structures, we performed the reaction at higher concentration (10^{-1} mol l^{-1}). Unfortunately, photodimerization between the two cyclohexenone moieties was preferred.

To the best of our knowledge, formation of cyclic photodimers has not yet been reported for cycloalkenone derivatives. That an intermolecular process competes with the expected intramolecular cycloaddition probably results from a relatively unfavourable conformation of the substrate. The observed temperature effect might indicate that the reactive conformer for an intramolecular process is more easily accessible at higher temperatures. The unexpected formation of 12-membered ring

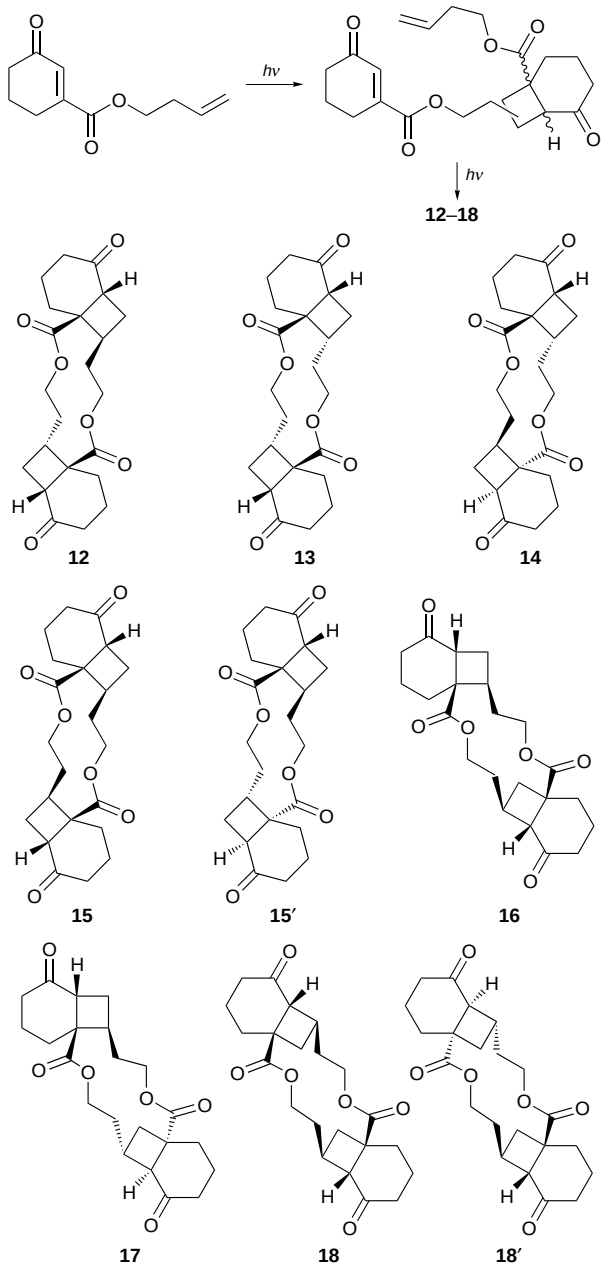

Scheme 2

bis-lactones in cyclodimers rather than linear oligomers, in the second photocycloaddition process, indicates that due to steric restrictions, the two reactive entities of the same molecule should be very close in the opened dimer favouring a further intramolecular process.

S. P. L. B. thanks 'Région Champagne-Ardenne' for financial support. We are indebted to Dr T. G. C. Bird (Zeneca Pharma, Reims) for his help with preparing the text of the manuscript.

Footnotes and References

* E-mail: olivier.piva@univ-reims.fr

† Even at conversion yields of about 50% of the starting material, linear photodimers remained very minor compounds in the reaction mixture.

‡ The solvent was first concentrated and the residue dissolved in MeOH. After partial evaporation, macrolide **12** readily crystallized. The MeOH was removed and the mixture chromatographed on silica (eluent: AcOEt–hexanes : 10–60 to 90–40) in order to separate the monomeric lactone **8** and an unseparable fraction of cyclodimers **13**–**18**. The macrocyclic compounds were totally or partially separated using HPLC with a Lichrosorb Si 60-7 column. By NMR analysis of each compound, and by comparison with spectra of the monomeric adduct and also those of compounds **10** and **11**, we were able to attribute the regiochemistry and relative stereochemistry.

§ *Selected data* for **4**: δ_H 1.35 (3 H, s), 1.40 (3 H, s), 1.70–1.90 (1 H, m), 2.00–2.55 (7 H, ma), 2.66 (1 H, td, 7.75, 1.0), 2.74 (1 H, t, 6.7). δ_C 22.35 (q), 22.5 (t), 23.0 (t), 28.7 (q), 28.84 (t), 40.5 (t), 44.0 (d), 46.2 (d), 54.7 (s), 84.2 (s), 179.9 (s), 210.8 (s); $\nu(CHCl_3)/cm^{-1}$ 1755, 1711; *m/z* 208 ($M^{\cdot+}$, 23), 165 (10), 164 (11), 149 (100), 135 (16), 121 (54), 107 (36) (Calc. for $C_{12}H_{16}O_3$: C 69.19; H 7.75. Found C 69.01, H 7.84%). For **8**: δ_H 1.75–1.90 (2 H, m), 1.95–2.27 (5 H, m), 2.32–2.46 (4 H, m), 3.17 (1 H, dd, 11.2, 6.7), 4.31 (1 H, ddd, 18.0, 9.0, 3.0), 4.50 (1 H, ddd, 18.0, 6.7, 3.0); δ_C 19.5 (t), 27.3 (t), 28.8 (t), 31.1 (t), 35.0 (d), 38.5 (t), 44.8 (d), 46.2 (t), 67.1 (t), 175.2 (q), 210.8 (q); $\nu(CHCl_3)/cm^{-1}$ 1720, 1710; *m/z* 176 ($M^{\cdot+}$, 49), 166 (10), 148 (35), 125 (55), 104 (56) (Calc. for $C_{11}H_{14}O_3$: C 68.03; H 7.27. Found C 68.11, H 7.58%). For **12**: δ_H 1.60–2.50 (21 H, m), 2.92 (1 H, dddd, 12.5, 10.3, 8.6, 4.6), 3.16 (1 H, t, 10.1), 3.20 (1 H, dd, 11.5, 5.3), 3.98 (1 H, td, 11.9, 1.1), 4.03–4.14 (3 H, m); δ_C 20.4 (t), 20.9 (t), 24.0 (t), 27.4 (t), 28.9 (t), 29.0 (t), 29.7 (t), 30.6 (t), 34.5 (d), 38.15 (t), 39.5 (t), 42.7 (d), 43.7 (d), 51.0 (s), 52.5 (s), 62.7 (t), 63.3 (t), 174.0 (s), 175.9 (s), 211.2 (s), 212.6 (s); *m/z* 411.96 ($M^{\cdot+}$ Na^+ + H).

1 D. De Keukeleire and S.-L. He, *Chem. Rev.*, 1993, **93**, 359; M. T. Crimmins, *Chem. Rev.*, 1988, **88**, 1453; T. L. Ho, *Carbocycle construction in terpene synthesis*, VCH, Weinheim, 1988.
2 A. Amougay, O. Letsch, J. P. Pete and O. Piva, *Tetrahedron*, 1996, **52**, 2405; C. Meyer, O. Piva and J. P. Pete, *Tetrahedron Lett.*, 1996, **37**, 5885; S. Le Blanc, J. P. Pete and O. Piva, *Tetrahedron Lett.*, 1992, **33**, 1993.
3 F. C. De Schryver, N. Boens and J. Put, *Advances in Photochemistry*, ed. J. N. Pitts, G. S. Hammond and K. Gollnick, Wiley, 1977, vol. 10, 379; B. A. Pearlman, *J. Am. Chem. Soc.*, 1979, **101**, 6398; W. L. Dilling, *Chem. Rev.*, 1983, **83**, 1.
4 J. P. Pete, *Advances in Photochemistry*, ed. D. C. Neckers, D. H. Volman and G. von Bünau, Wiley, 1996, vol. 21, 135.
5 M. C. Pirrung and S. A. Thomson, *Tetrahedron Lett.*, 1986, **27**, 2703.
6 E. L. Eliel, S. H. Wilen and L. N. Mander, *Stereochemistry of organic compounds*, Wiley, New York, 1994, 618.
7 P. G. Sammes and D. J. Weller, *Angew. Chem., Int. Ed. Engl.*, 1995, **34**, 1205. M. E. Jung and J. Gervay, *J. Am. Chem. Soc.*, 1991, **113**, 224; R. Keese and M. Meyer, *Tetrahedron*, 1993, **49**, 2055; A. L. Parrill and D. P. Dolata, *Tetrahedron Lett.*, 1994, **35**, 7319; M. E. Jung and M. Kiankarini, *J. Org. Chem.*, 1995, **60**, 7013.
8 S. Le Blanc, J. P. Pete and O. Piva, *Tetrahedron Lett.*, 1993, **34**, 635.
9 D. J. Maradyn and A. C. Weedon, *J. Am. Chem. Soc.*, 1995, **117**, 5359.

Received in Liverpool, UK, 29th September 1997; 7/07027F

First complexes with cuboidal-type M_4Te_4 (M = Mo, W) cluster cores: synthesis and structure of $K_7[Mo_4(\mu_3\text{-}Te)_4(CN)_{12}]\cdot 11H_2O$ and $K_6[W_4(\mu_3\text{-}Te)_4(CN)_{12}]\cdot 5H_2O$

Vladimir P. Fedin,*[a] Irina V. Kalinina,[a] Alexander V. Virovets,[a] Nina V. Podberezskaya[a] and A. Geoffrey Sykes*[b]

[a] *Institute of Inorganic Chemistry, Russian Academy of Sciences, pr. Lavrentjeva 3, Novosibirsk 630090, Russia*
[b] *Department of Chemistry, The University of Newcastle, Newcastle-upon-Tyne, UK NE1 7RU*

High-temperature reactions of $Mo_3Te_7I_4$ or WTe_2 with KCN at 450 °C produce M_4Te_4 cubane-type complexes, isolated here as $K_7[Mo_4(\mu_3\text{-}Te)_4(CN)_{12}]\cdot 11H_2O$ and $K_6[W_4(\mu_3\text{-}Te)_4(CN)_{12}]\cdot 5H_2O$ in high yields, and characterized by X-ray crystallography.

Homo- and heterometallic cuboidal cluster complexes with bridging chalcogenide ligands are known for a wide variety of transition metals, and appear to be one of the most important common basic structures of transition metal cluster complexes. Homometallic Mo_4S_4 cubane-type clusters have been known for some 20 years.[1–6] They have the general formula $[Mo_4Y_4L_{12}]$, where L denotes the ligating atoms, either neutral or anionic. Cubane-type molecular cluster complexes $[Mo_4Se_4(H_2O)_{12}]^{4+/5+/6+}$ have been reported.[7,8] Solid-state compounds $Mo_4S_4X_4$ (X = Cl, Br, I) and MMo_4Y_8 (M = Al, Ga, Y = S; M = Ga, Y = Se) containing Mo_4Y_4 clusters, with Mo atoms coordinated octahedrally by either three chalcogen and three halogen atoms or six chalcogen atoms have been isolated.[9–12]

Preparative routes to $[Mo_4Y_4(H_2O)_{12}]^{4+/5+/6+}$ (Y = S, Se) clusters by dimerization of chalcogenide Mo^V_2 complexes under reducing conditions, and from Mo_3Y_7 and Mo_3Y_4 cores, have been reported. Self-assembly routes have also been developed.[13] There are as yet no examples of cuboidal $[W_4Y_4(H_2O)_{12}]^{4+/5+/6+}$ clusters and the number of W_4 chalcogenide complexes is limited. Examples are (*i*) the raft-type complex $[W_4S_6(SH)_2(PMe_2Ph)_6]$,[14] (*ii*) the tetrahedral complex $[W_4S_6(PMe_2Ph)_4]$[14] having a $W_4(\mu_2\text{-}S)_6$ adamantane-like core, and (*iii*) $[W_4S_8(H_2NCH_2CH_2NH_2)_4]S$[15] which has a cuboidal $W_4S_4^{10+}$ core.

No Mo and W cubes, M_4Y_4 with Y = telluride, have as yet been prepared. Many of the traditional reagents used in the development of the sulfide/selenide chemistry, *e.g.* H_2Y or $[MY_4]^{2-}$ (M = Mo, W; Y = S, Se), are simply not known in the case of Y = Te.[16,17] Our recent research has therefore focused on the development of high-temperature techniques to synthesize solid-state molybdenum/tungsten tellurides as starting materials for the preparation of molecular telluride containing complexes.[18,19] The first complex having an M_3Te_7 core $Mo_3(\mu_3\text{-}Te)(\mu_2\text{-}Te_2)_3^{4+}$, was synthesized by extrusion of the polymeric solid-state product $Mo_3Te_7I_4$ from the high-temperature reaction of molybdenum, tellurium and iodine, with cyanide.[19]

Here we report the high-yield synthesis and crystal structure determination of the first complexes with Mo_4Te_4 and W_4Te_4 cluster cores. Cuboidal M_4Te_4 complexes are known for transition metals M = Mn, Re, Fe, Ru, Rh, Ir, Ni and Pt, but with the exception of Fe these do not have as highly developed M_4S_4 and M_4Se_4 chemistry as in the case of Mo.[20]

We have used a simple procedure starting from the elements for the synthesis of the title telluride cluster complexes of molybdenum and tungsten. Dark red–brown crystals of $K_7[Mo_4(\mu_3\text{-}Te)_4(CN)_{12}]\cdot 11H_2O$ **1** and $K_6[W_4(\mu_3\text{-}Te)_4(CN)_{12}]\cdot 5H_2O$ **2** were obtained in high yields by the high-temperature reaction of $Mo_3Te_7I_4$ or WTe_2 with KCN at 450 °C and further crystallization from aqueous solutions.† Complete X-ray structural determinations have revealed that the structures of **1** and **2** consist of discrete cluster anions of $[Mo_4(\mu_3\text{-}Te)_4(CN)_{12}]^{7-}$‡ or $[W_4(\mu_3\text{-}Te)_4(CN)_{12}]^{6-}$‡ and K^+ cations, and solvent water molecules. Fig. 1 and 2 show perspective views of the cluster units with important bond distances. The cluster anions display a cubane-like geometry, with the M_4Te_4 (M = Mo, W) cores constituted by two concentric interpenetrating tetrahedra of molybdenum/tungsten and tellurium. The tellurium atoms cap in a symmetrical manner the triangular faces of the molybdenum/tungsten tetrahedron [the mean Mo–Te distance is 2.674(1) Å; the mean W–Te distance is 2.686(2) Å]. The octahedral coordination of each molybdenum/tungsten center is completed by three cyanide ligands. For **1**, the distortion of the Mo_4 tetrahedron from ideal T_d symmetry is irregular, giving a relatively narrow range of Mo–Mo distances from 2.967(1) to 3.002(1) Å. Some notable differences, however, can be found for W–W bond distances: the W(1)–W(4) distance of 2.839(1) Å is significantly shorter than the W(2)–W(4) distance of 3.054(1) Å. The average oxidation state of the molybdenum atoms in **1** is 3.25 and the complex has one unpaired electron. The average oxidation state of the tungsten atoms in **2** is 3.5 and the complex is diamagnetic. The M_4Te_4 clusters of 5+ and 6+ charges, respectively, provide interesting comparisons with $[Mo_4Y_4]^{5+}$ and $[Mo_4Y_4]^{6+}$ (Y = S, Se) clusters.[8,13,21,22] The higher charge on the W_4Te_4

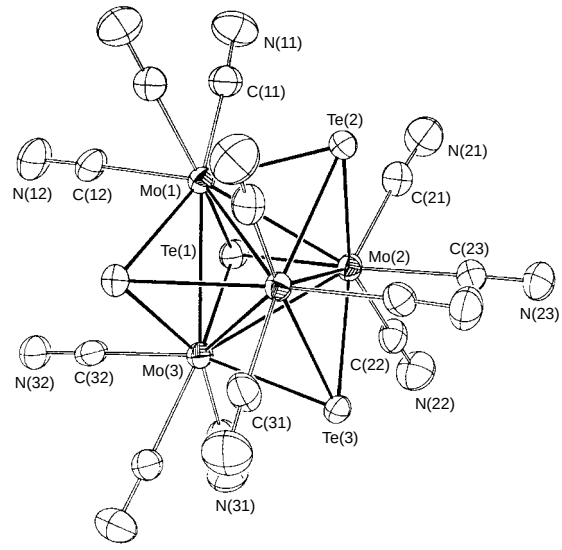

Fig. 1 Anion in **1** (thermal ellipsoids at 50% probability level). Some geometrical parameters (Å): Te–Mo 2.6663(8)–2.686(1), av. 2.674(1); Mo–Mo 2.967(1)–3.002(1), av. 2.993; Mo–C 2.14(1)–2.176(8), av. 2.162(9); C–N 1.13(1)–1.17(1), av. 1.15(1).

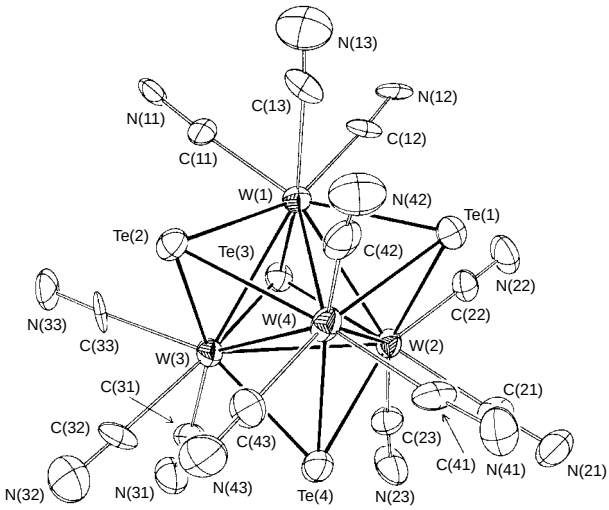

Fig. 2 Anion in **2** (thermal ellipsoids at 50% probability level). Some geometrical parameters (Å): W(1)–W(2) 2.957(1), W(1)–W(3) 2.923(1), W(1)–W(4) 2.839(1), W(2)–W(3) 3.054(1), W(2)–W(4) 3.008(1), W(3)–W(4) 2.991(2), W–Te 2.674(2)–2.704(2), av. 2.686(2); W–C 2.10(3)–2.20(3), av. 2.15(3); C–N 1.07(3)–1.20(3), av. 1.16(3).

cluster is consistent with the greater difficulty in reducing W to its lower oxidation states.

The cluster compounds **1** and **2** are stable indefinitely in air at 95 °C, and dissolve in aqueous solution, with no tendency to lose core atoms. Further studies on the reactivities of the telluride clusters, including an investigation of NMR and EPR spectra, and magnetic properties are in progress.

This work was supported by the Russian Foundation for Basic Research (research grant no. 96-03-33018), and an EU INTAS collaboration (research grant no. 96-1256).

Footnotes and References

† *General method* for preparation of $K_7[Mo_4(\mu_3\text{-}Te)_4(CN)_{12}]\cdot 11H_2O$ **1** and $K_6[W_4(\mu_3\text{-}Te)_4(CN)_{12}]\cdot 5H_2O$ **2**: a mixture of $Mo_3Te_7I_4$ (3.00 g) and KCN (3 g) or a mixture of WTe_2 (5.00 g) and KCN (5 g) was heated (450 °C; 2 days) in a sealed quartz tube. The product of the reaction was added to 50 ml of water and the mixture was refluxed for 3 h. After filtration, the solution was kept at 80 °C. During this time, the volume was decreased to 10 ml. After allowing to stand at 20 °C for 1 day, dark red–brown crystals were filtered off, washed with cold water and dried in air. Yield: 1.86 g of $K_7[Mo_4(\mu_3\text{-}Te)_4(CN)_{12}]\cdot 11H_2O$ (83%), 4.73 g of $K_6[W_4(\mu_3\text{-}Te)_4(CN)_{12}]\cdot 5H_2O$ (88%). Satisfactory elemental analyses (C, H, N, Mo, W and Te) were obtained. In order to ensure product homogeneity, the X-ray powder diffraction diagrams of **1** and **2** were obtained, and found to be identical with diagrams calculated from the single-crystal data. The UV–VIS absorption spectrum of **1** in H_2O gave peak positions [λ/nm (ε/M^{-1} cm^{-1} per M_4)] at 382 (6100), 535 (2080), 769 (420). The UV–VIS absorption spectrum of **2** in H_2O gave peak positions at 357 (8000), 382 (sh), 474 (3140), 869 (440). IR (KBr pellet): ν(CN) 2086 cm^{-1} (**1**); ν(CN) 2108, 2097 cm^{-1} (**2**). The magnetic susceptibility of **1** was measured at 77 K: μ = 2.03 μ_B. The magnetic susceptibility of **2** was measured at 300 K: $\chi_M = -360 \times 10^{-5}$ cm^3 mol^{-1}.

‡ *Crystallography*: **1**: single crystal (0.14 × 0.38 × 0.44 mm) obtained by recrystallisation from an aqueous solution of KCN. *Crystal data*: orthorhombic, space group *Pnma*, a = 12.112(1), b = 21.736(2), c = 16.109(1) Å, U = 4241.0(6) Å^3, Z = 4, D_c = 2.632 g cm^{-3}. Total 5874 reflections [in which 4707 $F_o > 4\sigma(F)$] were collected using standard techniques at room temperature on an Enraf-Nonius CAD4 diffractometer with Mo-Kα radiation (λ = 0.710 69 Å) up to $2\theta_{max}$ = 60°. The structure was solved by direct methods and refined in anisotropic approximation by full-matrix least-squares on F_o^2 using the SHELX-97[23] package. Absorption corrections were made using five azimuthal scan curves. Some hydrogen atoms of the solvent water molecules were found on Fourier map, but our attempts to refine these were unsuccessful. Final R values: $R(F)$ = 0.0473, $wR(F^2)$ = 0.1239 for 4707 $F_o > 4\sigma(F)$, $R(F)$ = 0.0612, $wR(F^2)$ = 0.1276, GOF = 1.153 for all data.

2: Single crystal (0.26 × 0.32 × 0.76 mm) obtained from recrystallisation from an aqueous solution of KCN. *Crystal data*: triclinic, space group $P\bar{1}$, a = 12.399(1), b = 13.187(1), c = 13.496(1) Å, α = 83.712(8), β = 66.575(8), γ = 63.223(9)°, U = 1801.1(2) Å^3, Z = 2, D_c = 3.471 g cm^{-3}. Total 8464 reflections (in which 8103 unique, R_{int} = 0.0594) were collected using standard techniques at room temperature on an Enraf-Nonius CAD4 diffractometer with Mo-Kα radiation (λ = 0.710 69 Å) up to $2\theta_{max}$ = 56°. The structure was solved by direct methods and refined in anisotropic approximation by full-matrix least-squares on F_o^2 using the SHELX-97[23] package. Absorption corrections were made using six azimuthal scan curves. Hydrogen atoms of solvate water molecules were not located. Final R values: $R(F)$ = 0.0696, $wR(F^2)$ = 0.2151 for 6752 $F_o > 4\sigma(F)$, $R(F)$ = 0.0796, $wR(F^2)$ = 0.2213, GOF = 1.143 for all unique data. CCDC 182/712.

1 T. Shibahara, *Adv. Inorg. Chem.*, 1991, **37**, 143.
2 T. Shibahara, *Coord. Chem. Rev.*, 1993, **123**, 73.
3 T. Saito, in *Early Transition Metal Clusters with π-Donor Ligands*, ed. M. H. Chisholm, VCH, New York, 1995, p. 63.
4 R. H. Holm, *Adv. Inorg. Chem.*, 1992, **38**, 1.
5 S. Harris, *Polyhedron*, 1989, **8**, 2843.
6 T. Saito, *Adv. Inorg. Chem.*, 1996, **44**, 45.
7 M. Nasreldin, G. Henkel, G. Kampmann, B. Krebs, G. J. Lamprecht, C. A. Routledge and A. G. Sykes, *J. Chem. Soc., Dalton Trans.*, 1993, 737.
8 W. McFarlane, M. Nasraldin, D. M. Saysell, Z.-S. Jia, W. Clegg, M. R. J. Elsegood, K. S. Murray, B. Moubaraki and A. G. Sykes, *J. Chem. Soc., Dalton Trans.*, 1996, 363 and references therein.
9 C. Perrin, R. Chevrel and M. Sergent, *Compt. Rend.*, 1975, **280**, 949.
10 J. M. Vandenberg and D. Brasen, *J. Solid State Chem.*, 1975, **14**, 203.
11 C. Perrin, R. Chevrel and M. Sergent, *Compt. Rend.*, 1975, **281**, 23.
12 A. Lebeuze, M. C. Zerrovski, H. Loirat and R. Lissillour, *J. Alloys Compd.*, 1992, **190**, 1.
13 T. Shibahara, H. Kyroya, H. Akashi, K. Matsumoto and S. Ooi, *Inorg. Chim. Acta*, 1993, **212**, 251 and references therein.
14 S. Kuwata, Y. Mizobe and M. Hidai, *J. Chem. Soc., Chem. Commun.*, 1995, 1057.
15 P. T. Wood, W. T. Pennington, J. W. Kolis, B. Wu and C. J. O'Connor, *Inorg. Chem.*, 1993, **32**, 129.
16 J. Beck, *Angew. Chem., Int. Ed. Engl.*, 1994, **33**, 163.
17 L. C. Roof and J. W. Kolis, *Chem. Rev.*, 1993, **93**, 1037.
18 V. P. Fedin, H. Imoto and T. Saito, *J. Chem. Soc., Chem. Commun.*, 1995, 1559.
19 V. P. Fedin, H. Imoto, T. Saito, W. McFarlane and A. G. Sykes, *Inorg. Chem.*, 1995, 5097.
20 Mn_4Te_4: H.-O. Stephan and G. Henkel, *Angew. Chem., Int. Ed. Engl.*, 1994, **33**, 2322; Re_4Te_4: Y. V. Mironov, T. E. Albrecht-Schmitt and J. A. Ibers, *Inorg. Chem.*, 1997, **36**, 944; Fe_4Te_4: H.-O. Stephan, Changneng Chen, G. Henkel, K. Griesar and W. Haase, *J. Chem. Soc., Chem. Commun.*, 1993, 886; P. Barbaro, A. Bencini, I. Bertini, F. Briganti and S. Midollini, *J. Am. Chem. Soc.*, 1990, **112**, 7238; M. L. Steigerwald, T. Siegrist, S. M. Stuczynski and Y. U. Kwon, *J. Am. Chem. Soc.*, 1992, **114**, 3155; M. L. Steigerwald, T. Siegrist, E. M. Gyorgy, B. Hessen, Y.-U. Kwon and S. M. Tanzler, *Inorg. Chem.*, 1994, **33**, 3389; H.-O. Stephan, Changneng Chen, G. Henkel, K. Griesar and W. Haase, *J. Chem. Soc., Chem. Comm.*, 1993, 886; Ru_4Te_4: E. J. Houser, T. B. Rauchfuss and S. R. Wilson, *Inorg. Chem.*, 1993, **32**, 4069; Rh_4Te_4: S. Schulz, M. Andruh, T. Pape, T. Heinze, H. W. Roesky, L. Haming, A. Kuhn and R. Herbst-Irmer, *Organometallics*, 1994, **13**, 4004; Ir_4Te_4: S. Schulz, M. Andruh, T. Pape, T. Heinze, H. W. Roesky, L. Haming, A. Kuhn and R. Herbst-Irmer, *Organometallics*, 1994, **13**, 4004; Ni_4Te_4: J. M. McConnachie, M. A. Ansari and J. A. Ibers, *Inorg. Chim. Acta*, 1992, **198**–**200**, 85; J. M. McConnachie, J. S. Bollinger and J. A. Ibers, *Inorg. Chem.*, 1993, **32**, 3923; Pt_4Te_4: J. M. McConnachie, J. C. Bollinger and J. A. Ibers, *Inorg. Chem.*, 1993, **32**, 3923.
21 F. A. Cotton, M. P. Diebold, Z. Dori, R. Llusar and W. Schwotzer, *J. Am. Chem. Soc.*, 1985, **107**, 6735.
22 A. Müller, W. Eltzner, W. Clegg and G. M. Sheldrick, *Angew. Chem., Int. Ed. Engl.*, 1982, **21**, 536.
23 G. M. Sheldrick, SHELX-93, Göttingen University, 1997.

Received in Cambridge, UK, 6th November 1997; 7/07995H

The first metal complexes of bicyclopropylidene, a unique tetrasubstituted alkene ligand

Jan Foerstner,[a] Sergej Kozhushkov,[b] Paul Binger,[c]† Petra Wedemann,[c] Mathias Noltemeyer,[d] Armin de Meijere*[b] and Holger Butenschön*[a]

[a] *Institut für Organische Chemie, Universität Hannover, Schneiderberg 1B, D-30167 Hannover, Germany*
[b] *Institut für Organische Chemie, Georg-August-Universität Göttingen, Tammannstrasse 2, D-37077 Göttingen, Germany*
[c] *Max-Planck-Institut für Kohlenforschung, Kaiser-Wilhelm-Platz 1, D-45470 Mülheim an der Ruhr, Germany*
[d] *Institut für Anorganische Chemie, Georg-August-Universität Göttingen, Tammannstrasse 4, D-37077 Göttingen, Germany*

The reactions of bicyclopropylidene 2 with bis(cyclopentadienyl)bis(trimethylphosphane)titanium(II) 1 and with the cobalt chelate 4 give the first known metal complexes of bicyclopropylidene 3 and 7, respectively, in good yields; the bicyclopropylidene cobalt complex 7 is characterized by an X-ray crystal structure analysis which shows a severe out-of-plane bending of the alkenic ligand, indicating considerable back-bonding which goes along with a release of strain in the ligand.

The organometallic chemistry of cyclopropane derivatives is dominated by ring opening reactions.[1,2] However, metal-mediated substitutions on vinylcyclopropane derivatives[3] and cycloadditions with methylenecyclopropane **5** and its derivatives[4–7] can also be achieved with retention of the ring. In view of their high-lying HOMOs,[8,9] methylenecyclopropane **5** and especially bicyclopropylidene **2** should be strong π-bases capable of efficiently donating electron density into the vacant orbitals of transition metals. In particular, strained alkenes have an increased ability to accept back-bonding and therefore are preferentially coordinated to transition metals,[10–13] and it is this feature which is frequently used to stabilize otherwise unstable alkenes and alkynes by complexation.[14,15] Indeed, some transition metal, including cobalt, complexes of methylenecyclopropane have been reported.[4,16]

Here, we report on the synthesis and the structural characterization of the first transition metal complexes of **2**,[17] which contains a more highly strained double bond[18] than methylenecyclopropane **5**.

A first attempt to bind an intact bicyclopropylidene unit to a metal was made by use of the titanocene fragment. (Alkene)-bis(cyclopentadienyl)titanium(II) complexes are known, and they are 16e complexes.[19] If there were a tendency towards ring opening of a bicyclopropylidene ligand by oxidative addition, it should happen with this complex fragment attached. One way to prepare titanium complexes with sensitive ligands starts from titanocene dichloride, which can easily be converted to $Cp_2Ti(PMe_3)$ **1**.[20,21] Treatment of **1** with 1.16 equiv. of **2** in pentane gave (η²-bicyclopropylidene)(bis-η⁵-cyclopentadienyl)titanium(II) **3** in 79% yield as a green solid (Scheme 1), which was characterized by its ^1H and ^{13}C NMR spectra‡ as well as by a correct elemental analysis. While signals for the CH_2 and cyclopentadienyl carbon atoms are clearly observed at δ 15.3 and 116.7 as a triplet and a doublet, respectively, the signal assigned to the coordinated quaternary carbon atoms of the bicyclopropylidene ligand appears as a singlet of only low intensity at δ93, a value which is in accord with those observed for related compounds.[22] A structural investigation of **3** has so far been precluded because suitable crystals for an X-ray structure analysis could not be obtained. Anyhow, **3** is the first example of an (alkene)bis(cyclopentadienyl)titanium(II) complex without a supporting PR_3 ligand or stabilizing methyl groups on the cyclopentadienyl ligands.[22]

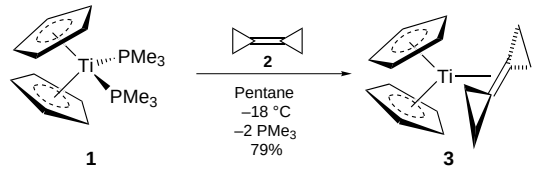

1 **3**

Scheme 1

Complexation of sensitive ligands without subsequent reactions is also possible with the {[2-(di-*tert*-butylphosphanyl)-*P*-ethyl]-η⁵-cyclopentadienyl}cobalt(I) fragment (CoCp#), with which the cyclopentadienyl ligand and the pending phosphane side arm coordinate at the metal to form a rather stable chelate.[23–25] For oligomerization reactions, frequently observed at normal cyclopentadienyl cobalt, to occur with this complex fragment, an advance decomplexation of the phosphane side arm would be necessary. In this case the phosphane side arm normally wins the competition with an external ligand for entropic reasons. A reliable method for the preparation of such complexes is the reductive complexation starting with the paramagnetic chloro complex **4** in the presence of sodium amalgam and the new ligand.[26] As a first test, **2** was treated with **4** at low temperature in this manner and gave a 72% yield of complex **6** (Scheme 2), which was identified by its spectral data. The NMR spectra show two signals for alkenic protons and two signals for non-alkenic cyclopropyl carbon atoms indicating an orientation of the methylenecyclopropane ligand as in formula **6**. In the mass spectrum the molecular ion peak is observed (*m*/*z* 350, 19%), the base peak resulting from decomplexation of **1**.

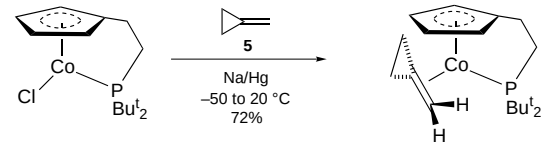

4 **6**

Scheme 2

Next, **2** was treated with **4** in the presence of sodium amalgam, and the corresponding cobalt complex **7** (Scheme 3) was obtained in even higher yield (83%) as large brown crystals of up to 7 mm edge length after crystallization from diethyl

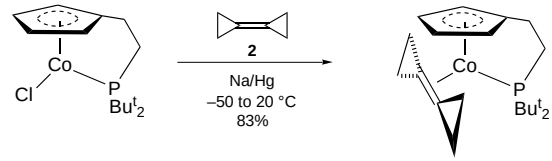

4 **7**

Scheme 3

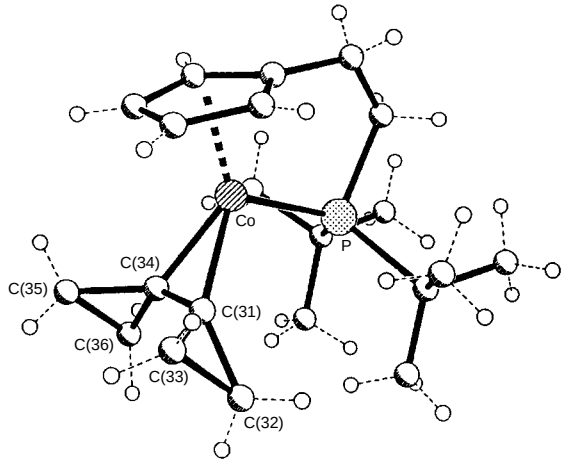

Fig. 1 Structure of the bicyclopropylidene cobalt complex **7** in the crystal.‡ Selected bond lengths (Å) and angles (°): Co–C(31) 1.956(4), Co–C(34) 1.965(3), C(31)–C(34) 1.401(5), C(31)–C(32) 1.482(5), C(32)–C(33) 1.499(12), C(33)–C(31)–C(32) 61.2(5), C(33)–C(31)–C(34) 129.5(5), C(32)–C(31)–C(34) 131.5(5), C(31)–C(34)–C(36) 133.8(3), C(31)–C(34)–C(35) 129.8(3).

ether. The NMR spectra indicate a plane of symmetry through the cobalt atom and the center of the double bond as in formula **7**. As for **6**, in the mass spectrum of **7** the molecular ion peak is observed (*m*/*z* 376, 27%), and the base peak also results from bicyclopropylidene decomplexation.

A suitable crystal of compound **7** was subjected to an X-ray structural analysis (Fig. 1). According to this the bicyclopropylidene ligand has undergone a remarkable out of plane bending by 40° at both termini of the double bond. This indicates a large back-bonding effect accepted by bicyclopropylidene, which is also documented by the long bond length of the coordinated double bond (1.401 Å) as compared to that in uncoordinated **2** (1.314 Å[27]). As a result of the complexation the double bond of bicyclopropylidene is expanded by *ca.* 6.6%. It is instructive to compare these numbers with those of ethene and the ethene complex corresponding to **7**. The bond length of ethene is 1.330 Å, in the ethene complex corresponding to **7** this value is 1.396 Å,[24] an increase of only 5.0%. The bonds in **2** and **7** adjacent to the double bond are of similar length, whereas the single bond opposite the double bond is significantly shortened from 1.544 Å in **2** to 1.499 Å in complex **7**. This is a consequence of the change in hybridization of the coordinated carbon atoms from sp^2 towards sp^3, causing a smaller endocyclic interorbital angle and thus shorter distal bonds in the ring.

A DTA–TG analysis revealed the remarkable thermal stability of **7**, as it can be heated up to 160 °C without decomposition. At 168 °C a strongly exothermic reaction takes place [$\Delta H = -52.1$ kcal mol^{-1} (1 cal = 4.184 J)]. A relative loss of mass of 11.5% is measured which, with a molecular mass of **7** of 376 g mol^{-1} corresponds to a loss of 40 g mol^{-1}, the molecular mass of cyclopropene. This suggests that the bicyclopropylidene ligand decomposes at elevated temperature. After the DTA–TG analysis the material was analyzed by FAB–MS indicating an M^+ peak at *m*/*z* 1304. This hints towards the formation of a $(CoCp\#)_4$ cluster with three cyclopropane rings.

In conclusion, bicyclopropylidene can be used as a ligand in transition metal complexes of early and late transition metals. The ligand displays a strong back-bonding effect as evidenced by the X-ray crystal structure analysis of the cobalt complex. We are currently investigating the chemistry of bicyclopropylidene complexes and related compounds with special emphasis of their thermochemical behaviour.

This work was supported by the Deutsche Forschungsgemeinschaft and the Fonds der Chemischen Industrie. We are grateful to Bayer AG, BASF AG, Chemetall GmbH, and Hüls AG for generous gifts of chemicals.

Footnotes and References

* E-mail: ameijer1@uni-goettingen.de and holger.butenschoen@m-box.oci.uni-hannover.de
† New address: Fachbereich Chemie, Organische Chemie, Universität Kaiserslautern, Erwin-Schrödinger-Strasse, D-67663 Kaiserslautern, Germany.
‡ Crystal structure analysis of **7**: $C_{21}H_{34}CoP$: crystal size 0.70 × 0.60 × 0.60 mm, crystal system triclinic, space group $P\bar{1}$ with three molecules in the asymmetric unit, a = 9.658(1), b = 14.731(2), c = 21.282(4) Å, α = 84.21(2), β = 80.64(1), γ = 88.46(1)°, U = 2972.1(8) Å^3, Z = 6, D_c = 1.262 g cm^{-3}, 3.51 < θ > 25.06°, Mo-Kα radiation, λ = 0.710 73 Å, T = 153(2) K, 17 372 measured reflections, 10 506 independent reflections, no absorption correction, structure solution with direct methods with SHELXS-86, refinement with SHELXL-93, 401 free parameters, hydrogen atoms in geometrically calculated positions, R_1 = 0.0544 [$I > 2\sigma(I)$], wR_2 = 0.1208 (all data), refinement to F^2, min., max. residual electron density −1.304, 1.304 e Å^{-3}. CCDC 182/686.

1 K. C. Bishop III, *Chem. Rev.*, 1976, **76**, 461.
2 P. Eilbracht, in *Houben-Weyl*, E 17c, ed. A. de Meijere, Thieme, Stuttgart, 1997, pp. 2677–2694.
3 A. Stolle, J. Ollivier, P. P. Piras, J. Salaün and A. de Meijere, *J. Am. Chem. Soc.*, 1992, **114**, 4051.
4 P. Binger and H. M. Büch, *Top. Curr. Chem.*, 1987, **135**, 77.
5 P. Binger and T. Schmidt in *Houben-Weyl*, E 17c, ed. A. de Meijere, Thieme, Stuttgart, 1997, pp. 2217–2294.
6 W. A. Donaldson, in *Advances in Metal-Organic Chemistry, Vol. 2*, ed. L. S. Liebeskind, JAI Press, Inc., Greenwich, 1991, pp. 269–293.
7 P. Eilbracht, in *Houben-Weyl*, E 17b, ed. A. de Meijere, Thieme, Stuttgart, 1997, pp. 1849–1903.
8 K. B. Wiberg, G. B. Ellison, J. J. Wendolosaki, C. R. Brundle and N. A. Kneber, *J. Am. Chem. Soc.*, 1976, **98**, 7179.
9 R. Gleiter, R. Haider, J.-M. Conia, J.-P. Barnier, A. de Meijere and W. Weber, *J. Chem. Soc., Chem. Commun.*, 1979, 130.
10 H. Butenschön and A. de Meijere, *Tetrahedron*, 1986, **42**, 1721.
11 H. Butenschön and A. de Meijere, *Angew. Chem.*, 1984, **96**, 722.
12 H. G. Wey and H. Butenschön, *Angew. Chem.*, 1990, **102**, 1469.
13 F.-W. Grevels and V. Skibbe, *J. Chem. Soc., Chem. Commun.*, 1984, 681.
14 E. Stamm, K. B. Becker, P. Engel, O. Ermer and R. Keese, *Angew. Chem.*, 1979, **91**, 746–747.
15 S. A. Godleski, K. B. Gundlach and R. S. Valpey, *Organometallics*, 1985, **4**, 296.
16 P. Binger, T. R. Martin, R. Benn, A. Rufinska and G. Schroth, *Z. Naturforsch., Teil B*, 1984, **39**, 993.
17 A. de Meijere, S. I. Kozhushkov, T. Spaeth and N. S. Zefirov, *J. Org. Chem.*, 1993, **58**, 502.
18 A. de Meijere, S. I. Kozhushkov and A. F. Khlebniktov, *Zh. Org. Khim.*, 1996, **32**, 1607.
19 M. Bochmann, in *Comprehensive Organometallic Chemistry II, Vol. 4*, ed. E. W. Abel, F. G. A. Stone and G. Wilkinson, Elsevier, Oxford, 1995, pp. 221–271.
20 L. B. Kool, M. D. Rausch, H. G. Alt, M. Herberhold, U. Thewalt and B. Wolf, *Angew. Chem.*, 1985, **97**, 425.
21 P. Binger, P. Müller, R. Benn, A. Rufinska, B. Gabor, C. Krüger and P. Betz, *Chem. Ber.*, 1989, **122**, 1035.
22 S. A. Cohen, P. R. Auburn and J. E. Bercaw, *J. Am. Chem. Soc.*, 1983, **105**, 1136.
23 R. T. Kettenbach, W. Bonrath and H. Butenschön, *Chem. Ber.*, 1993, **126**, 1657.
24 R. T. Kettenbach, C. Krüger and H. Butenschön, *Angew. Chem.*, 1992, **104**, 1052.
25 R. T. Kettenbach and H. Butenschön, *New J. Chem.*, 1990, **14**, 599.
26 J. Foerstner, R. Kettenbach, R. Goddard and H. Butenschön, *Chem. Ber.*, 1996, **129**, 319.
27 *Cf.* R. Boese, T. Haumann, E. D. Jemmis, B. Kiran, S. Kozhushkov and A. de Meijere, *Liebigs Ann.*, 1996, 913 and references therein.

Received in Cambridge, UK, 19th September 1997; 7/06805K

Synthesis of highly active tungsten-containing MCM-41 mesoporous molecular sieve catalyst

Zhaorong Zhang, Jishuan Suo, Xiaoming Zhang and Shuben Li*

State Key Laboratory for Oxo Synthesis and Selective Oxidation, Lanzhou Institute of Chemical Physics, Chinese Academy of Sciences, Lanzhou, 730000, P.R. China

A tungsten-containing MCM-41 mesoporous molecular sieve is synthesized by the hydrolysis of tetraethylorthosilicate and ammonium tungstate in the presence of cetylpyridinium bromide as template in acidic medium and found to be more active than the conventional WO_3 catalyst in the hydroxylation of cyclohexene using H_2O_2 as oxidant.

WO_3-based catalysts are important not only in hydrodesulfurization and alkene metathesis[1] but also in hydroxylation of unsaturated compounds.[2] Recently, the breakthrough discovery of silica-based mesoporous molecular sieves M41S, including the hexagonal MCM-41,[3,4] offered new opportunities for creating highly dispersed and more accessible catalytic sites by incorporating transition-metal ions into their silica-based frameworks.[5–9] Many of the mesoporous molecular sieve catalysts thus obtained therefore showed quite good catalytic properties in different reactions.[10,11] Here, we report the synthesis, characterization and catalytic performance of the tungsten-containing MCM-41 mesoporous molecular sieve catalyst (W-MCM-41) in the hydroxylation of cyclohexene with 30 mass% H_2O_2.

In a typical synthesis of the W-MCM-41, 5.67 g (20 mmol) of ammonium tungstate [Aldrich, 99.99% $(NH_4)_2WO_4$] was dissolved in 100 ml of water to prepare solution A; 6.2 g (15 mmol) of cetylpyridinium bromide (Aldrich, 98% $C_{16}H_{33}NC_5H_5Br{\cdot}H_2O$, CPBr) was combined with 60 ml of HCl (5 mol dm^{-3}) to form solution B. Then 11.4 g (50 mmol) of tetraethylorthosilicate [Aldrich, 98% $Si(OEt)_4$, TEOS] and a determined amount of solution A were simultaneously introduced into solution B under vigorous stirring to give the following composition: 1 TEOS : 0.3 CPBr : 0.02 W : 6 HCl : 60 H_2O. After allowing the resulting gel to age at 323 K under gentle stirring for 22 h, the solid product was centrifuged, washed with distilled water and air-dried. The calcination of the W-MCM-41 sample was carried out in air at *ca.* 533 K for 1.5 h, then at 873 K for 4 h.

The calcined W-MCM-41 sample was colorless, indicating the absence of colored crystalline WO_3 species outside the framework. This result was verified by Raman and UV–VIS spectroscopy.

An X-ray powder diffraction pattern (Rigaku, D/Max-2400, with Cu-Kα radiation; λ = 0.154 18 nm) of the calcined sample is depicted and indexed in Fig. 1 and corresponds to MCM-41 mesoporous silicas reported previously.[4,5]

Fig. 2 shows the Raman spectra (Nicolet, Raman 910) of W-MCM-41 and crystalline WO_3. Crystalline WO_3 is a very strong Raman scatterer, so the absence of intense peaks at *ca.* 804, 714, 327, 267 and 137 cm^{-1} (in WO_3) corresponding to octahedral WO_6 groups[13] in the spectrum of W-MCM-41 indicated that the W was highly dispersed in the silica-based framework structure. This result was also supported by the diffuse reflectance (DR) spectra of W-MCM-41 and WO_3 crystals in the UV–VIS region. In the DR UV–VIS spectrum of the calcined W-MCM-41 sample, there is no absorption band corresponding to crystalline WO_3.

The chemical analysis using ICP atomic emission spectroscopy (ARL 3520) showed the WO_3 content in the W-MCM-41 to be 7.1 mass% (SiO_2 : WO_3 *ca.* 50). The HK mean pore size and BET surface area of the as-synthesized W-MCM-41 calculated on the basis of nitrogen adsorption–desorption isotherms (Coulter, Omnisorp 360CX) were *ca.* 2.9 nm and 1059 $m^2\ g^{-1}$, respectively.

As mentioned above, different physicochemical characterizations confirmed that in the W-MCM-41 sample prepared, the W was highly dispersed in the silica-based framework structure, and it was found to be active for carrying out catalytic oxidations of unsaturated hydrocarbons using H_2O_2 as oxidant. Here the H_2O_2 hydroxylation of cyclohexene was carried out over W-MCM-41, Si-MCM-41 and conventional WO_3 catalysts suspended in acetic acid (HAc) media; where Si-MCM-41 was a pure silica sample synthesized by the method described above but leaving out the tungsten ion precursor. Since H_2O_2 in HAc alone is a hydroxylating agent,[2] a comparative experiment was also made in the absence of any catalyst. The results summarized in Table 1 clearly show that W-MCM-41 is a good catalyst for the test reaction, on which the hydroxylation rate of

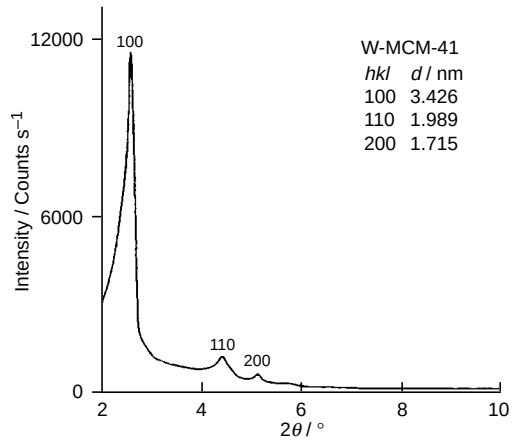

Fig. 1 PXRD pattern of the calcined W-MCM-41

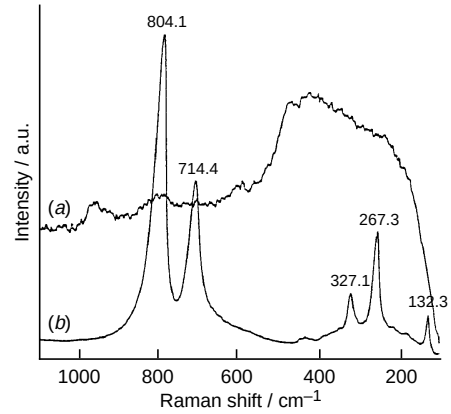

Fig. 2 Raman spectra of (*a*) W-MCM-41 and (*b*) crystalline WO_3

Table 1 Activity of W-MCM-41 and related materials for hydroxylation of cyclohexene with hydrogen peroxide[a]

					Conversion (%)		Selectivity (%)[b]	
Expt.	Catalyst	C_6H_{10}/mmol	H_2O_2/mmol	*t*/min	H_2O_2	C_6H_{10}	Glycol	Ester
1	W-MCM-41	50	50	80	*ca.* 100	84.6	80.3	12.0
2	W-MCM-41	50	65	60	97.1	*ca.* 100	78.1	10.4
3	WO_3	50	65	160	97.8	*ca.* 100	78.6	10.0
4	Si-MCM-41	50	65	240	94.5	*ca.* 100	72.4	7.4
5	None	50	65	240	94.1	*ca.* 100	74.0	6.7

[a] *Reaction conditions*: substrate/solvent: 1 : 20 (v/v), catalyst: 0.2 g, *T*: 353 K, H_2O_2: 30 mass% aqueous solution; C_6H_{10}: cyclohexene; *t*: time required for completing the reaction. [b] Calculated on alkene consumed; glycol: *trans*-cyclohexane-1,2-diol; ester: *trans*-cyclohexane-1,2-diol monoacetate.

cyclohexene could be increased significantly without decreasing the yields of *trans*-cyclohexane-1,2-diol. However, the Si-MCM-41 catalyst is equivalent to the blank H_2O_2–HAc system and inferior to the conventional WO_3 catalyst in activity. These data indicated that the highly dispersed W in silica-based molecular sieve might play a critical role in promoting the reaction. Systematic investigations toward understanding the mechanism for this catalytic reaction are still in progress.

Footnote and References

* E-mail: lasb@lzb.ac.cn

1 K. Weissermal and H. J. Arpe, *Industrial Organic Chemistry*, Verlag Chemie, New York, 1978.
2 M. Mugdan and D. P. Young, *J. Chem. Soc.*, 1949, 2988.
3 C. T. Kresge, M. E. Leonowicz, W. J. Roth, J. C. Vartuli and J. S. Beck, *Nature*, 1992, **359**, 710.
4 J. S. Beck, J. C. Vartuli, W. J. Roth, M. E. Leonowicz, C. T. Kresge, K. D. Schmitt, C. T.-W. Chu, D. H. Olson, E. W. Sheppard, S. B. McCullen, J. B. Higgins and J. L. Schlenker, *J. Am. Chem. Soc.*, 1992, **114**, 10834.
5 A. Coma, M. T. Navarro and J. Perez-Pariente, *J. Chem. Soc., Chem. Commun.*, 1994, 147.
6 P. T. Tanev, M. Chibwe and T. J. Pinnavaia, *Nature*, 1994, **368**, 321.
7 T. Blasco, A. Corma, M. T. Navarro and J. Perez-Pariente, *J. Catal.*, 1995, **156**, 65.
8 U. Junges, W. Jacobs, I. Voigt-Martin, B. Krutzsch and F. Schuth, *J. Chem. Soc., Chem. Commun.*, 1995, 2283.
9 W. Zhang, J. Wang, P. T. Tanev and T. J. Pinnavaia, *Chem. Commun.*, 1996, 979.
10 J. L. Casci, *Stud. Surf. Sci. Catal.*, 1994, **85**, 329.
11 A. Sayari, *Chem. Mater.*, 1996, **8**, 140.
12 M. D. Alba, Z. Luan and J. Klinowski, *J. Phys. Chem.*, 1996, **100**, 2178.
13 J. G. Graselli and B. J. Bulkin, *Analytical Raman Spectroscopy*, Wiley, New York, 1991, p. 352.

Received in Cambridge, UK, 16th September 1997; 7/06719D

Germylene and stannylene cleavage of Lawesson's reagent

Claire J. Carmalt, Jason A. C. Clyburne, Alan H. Cowley,* Viviana Lomeli and Brian G. McBurnett

Department of Chemistry and Biochemistry, The University of Texas at Austin, Austin, Texas, 78712, USA

Lawesson's reagent undergoes cleavage reactions with bis[bis(trimethylsilyl)amino]germanium(II) and bis[bis(trimethylsilyl)amino]tin(II) whilst with 1,3-di-*tert*-butyl-1,3,2-diazagermol-2-ylidene the product is a novel spirocyclic germanium derivative.

Lawesson's reagent **1** is one of the most versatile thiation reagents available and is highly effective, for example, for the conversion of aldehydes and ketones to the corresponding thio derivatives.[1] However, much less information is available regarding the interaction of **1** with transition metal[2] or main group reagents. Herein we describe the unusual reactions of **1** with some coordinatively unsaturated group 14 compounds.

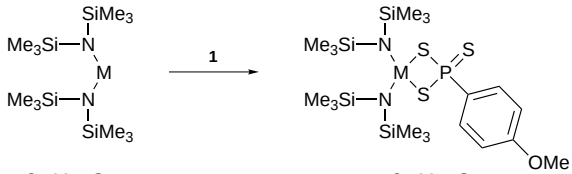

2a M = Ge
b M = Sn

3a M = Ge
b M = Sn

The reaction of **1** with stannylene **2b**[3] in THF solution resulted in a >90% isolated yield of **4b**.† Interestingly, the corresponding reaction of **1** with **2a**[3] produced a much smaller yield (*ca.* 10%) of the Ge analogue **3a**. ^{31}P NMR and HRMS(CI$^+$) data were consistent with the formulae proposed above for both compounds, and ^{1}H and ^{13}C NMR spectra indicated the presence of one *p*-MeOC$_6$H$_4$ and two (non-equivalent) N(SiMe$_3$)$_2$ groups.‡ However, in order to ascertain the atom connectivity, it was necessary to appeal to X-ray crystallography. Suitable single crystals of **3b** were obtained from CH_2Cl_2 solution. The central feature of the molecular structure of **3b**§ (Fig. 1) comprises a planar PS_2Sn ring [sum of angles = 360.00(3)°]. Such rings are rare as indicated by a search of the Cambridge Data Base which revealed only one previous example.[4] As expected, the average P–S$_{ring}$ bond distance [2.1125(9) Å] is longer than that of the external P–S bond [1.9315(9) Å]. Although the phosphorus and tin centres are four-coordinate, there is considerable deviation of the bond angles from the ideal tetrahedral value and the N–Sn–N angle in **3b** [116.07(7)°] is larger than that in **2b** [104.7(2)°].[5]

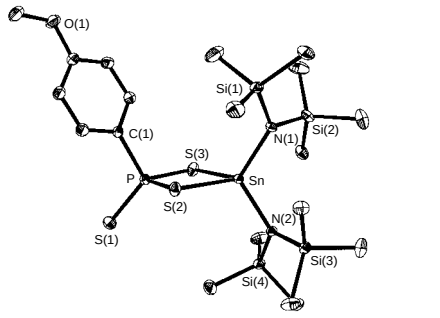

Fig. 1 Molecular structure of **3b** showing the atom numbering scheme. Selected distances (Å) and angles (°): P–C(1) 1.804(2), P–S(1) 1.9315(9), P–S(2) 2.1168(9), P–S(3) 2.1018(9), Sn–S(2) 2.4188(6), Sn–S(3) 2.4358(6), N(1)–Sn 2.015(2), N(2)–Sn 2.023(2), N–Si(1) 1.764(2), N–Si(2) 1.757(2), N(2)–Si(3) 1.757(2), N(2)–Si(4) 1.761(2); C(1)–P–S(1) 112.05(8), S(2)–P–S(3) 101.32(3), P–S(2)–Sn 87.17(3), P–S(3)–Sn 87.06(3), N(1)–Sn–N(2) 116.07(7), Sn–N(1)–Si(1) 122.83(10), Sn–N(1)–Si(2) 115.15(9), Sn–N(2)–Si(3) 116.33(9), Sn–N(2)–Si(4) 120.37(10), Si(1)–N(1)–Si(2) 120.73(10), Si(3)–N(2)–Si(4) 121.35(10).

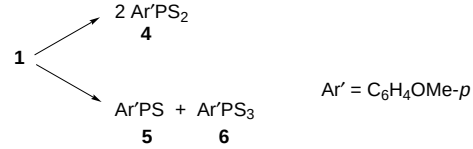

The mechanism of formation of **3a**,**b** is not clear, but plausible routes to these products include (*i*) oxidative addition of **2a**,**b** to **4**, which results from symmetrical cleavage of **1**, followed by addition of sulfur to phosphorus, (*ii*) addition of **2a**,**b** to an Ar′PS$_3$ (**6**) fragment resulting from unsymmetrical cleavage of **1**, and (*iii*) addition of sulfur to **2a**,**b** followed by reaction of the resulting germa- or stanna-thione with **4**. In an attempt to clarify this point, **7**,[6] which can be viewed as a cyclic dimer of the requisite stanna-thione **8**, was treated with an equimolar quantity of **1** in CD_2Cl_2 or C_6D_6 solution at 25 °C. NMR (^{31}P and ^{1}H) assay indicated quantitative conversion to **3b**. This observation is consistent with route (*iii*), and as such would represent a novel formal [2 + 2] cycloaddition involving P=S and Sn=S bonds.[7]

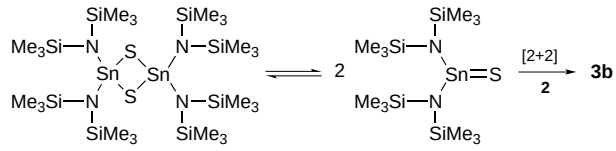

7 **8** **2**

In sharp contrast to the results obtained with **2a**, the cyclic germylene **9**[8] undergoes a completely different type of reaction with **1** and affords **10** as the major product. Whilst not appropriate as a mechanism, one way of thinking of this reaction is to consider that the cyclic germylene **9** serves as a source of Ge atoms for transfer to four Ar′PS (**5**) moieties. As pointed out above, **5** could arise *via* unsymmetrical cleavage of **1**.

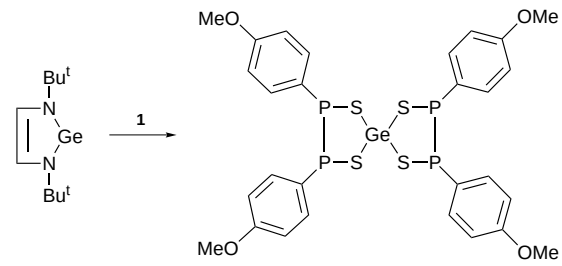

9 **10**

The X-ray crystal structure of **10** revealed an interesting spirocyclic geometry (Fig. 2). Individual molecules of **10** reside on a crystallographic twofold axis. The GeS_2P_2 rings are slightly puckered and the dihedral angle between the S–Ge–S planes is 81.7°. The geometry at Ge is essentially tetrahedral;

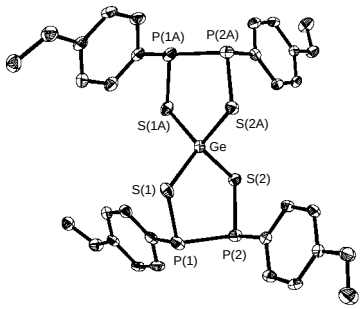

Fig. 2 Molecular structure of **10** showing the atom numbering scheme. Selected distances (Å) and angles (°): Ge–S(1) 2.222(1), Ge–S(2) 2.223(1), P(1)–S(1) 2.103(2), P(2)–S(2) 2.098(2), P(1)–P(2) 2.220(2); S(1)–Ge–S(2) 105.89(4), P(1)–S(1)–Ge 104.69(5), S(1)–P(1)–P(2) 104.46(6), S(2)–P(2)–P(1) 103.50(6), P(2)–S(2)–Ge 105.07(5).

however, the endocyclic S–Ge–S angles [105.89(4)°] are more acute than the exocyclic angles [117.10(6)°]. The average Ge–S [2.222(1) Å], P–S [2.100(2) Å] and P–P [2.220(2) Å] distances each correspond to a bond order of unity. Finally, the $R_2P_2S_2$ ligand does not appear to have been described previously; although a phosphorus–sulfur heterocycle is known[9] in which the $Ph_2P_2S_2$ ligand is associated with a PhP(S) moiety, *i.e.* $(PhPS)_3$.

We thank the National Science Foundation, and the Robert A. Welch Foundation for financial support.

Footnotes and References

* E-mail: cowley@mail.utexas.edu

† *Experimental procedure*: **3a**: compound **2a** (0.81 g, 2.1 mmol) in 50 cm³ of THF was added to a stirred slurry of **1** (0.80 g, 2.0 mmol) in 10 cm³ of THF. The solution was warmed to 60 °C for 20 min. The solvent was removed *in vacuo* and the resulting yellow residue was dissolved in 30 cm³ of CH_2Cl_2. After filtration through Celite the filtrate was concentrated and stored at −25 °C to afford a small quantity of yellow powder **3a** (0.09 g, 0.15 mmol, 8%), mp 132–136 °C.

3b: compound **2b** (1.25 g, 2.8 mmol) in 50 cm³ of THF was added to a stirred slurry of **1** (1.15 g, 2.8 mmol) in 10 cm³ of THF. The solution was warmed to 60 °C for 20 min. The solvent was removed *in vacuo* and the resulting pale yellow powder was dissolved in 30 cm³ of CH_2Cl_2. After filtration through Celite the filtrate was concentrated and stored at −25 °C to afford pale yellow crystals of **3b** (0.90 g, 1.3 mmol, 92% yield based on **1**), mp 140–143 °C.

10: compound **9** (0.67 g, 2.80 mmol) was dissolved in 30 cm³ of toluene and added to a stirred suspension of **1** (0.78 g, 1.94 mmol) in 40 cm³ of toluene at 25 °C. Over a 20 min period, the originally yellowish solution turned red as the solids dissolved. After 4 h a precipitate formed and the reaction mixture was allowed to stir for an additional 12 h. After filtration, the solvent and volatiles were removed from the filtrate and the residue was dissolved in CH_2Cl_2 and this solution was covered with a layer of hexane. Colourless crystals of **10** formed over a period of several days (0.15 g, 20% yield based on **1**), mp 200 °C (becomes opaque at 170 °C). HRMS: calculated for $C_{28}H_{28}GeO_4P_4S_4$ (M^+), 754.9111; found 754.9125.

‡ *Selected spectroscopic data*: **3a**: NMR (C_6D_6): $^{31}P\{^1H\}$ δ 42.0; ^1H δ 8.02–8.08 (m, 2 H, aryl), 6.80–6.82 (m, 2 H, aryl), 8.85 (s, 3 H, OCH_3), 0.47 [s, 18 H, $Si(CH_3)_3$], 0.34 [s, 18 H, $Si(CH_3)_3$]; ^{13}C δ 162.6 (s, *p*-C_{aryl}), 132.2 (d, $^3J_{PC}$ 14 Hz, *m*-C_{aryl}), 114.3 (d, $^2J_{PC}$ 16 Hz, *o*-C_{aryl}), 54.9 (s, OCH_3), 6.5 (s, $SiCH_3$), 5.5 (s, $SiCH_3$), *ipso*-C_{aryl} not observed. HRMS (CI^+): calc. for $C_{19}H_{43}GeN_2OPS_3Si_4$ (M^+), *m/z* 597.0826; found 597.0825.

3b: NMR (C_6D_6): $^{31}P\{^1H\}$ δ 56.5, satellites due to coupling with ^{119}Sn observed (75 Hz); $^{119}Sn\{^1H\}$ δ −240 (d, $^2J_{PSn}$ 76 Hz); ^1H δ 8.17–8.26 (m, 2 H, aryl), 7.02–7.06 (m, 2 H, aryl), 3.91 (s, 3 H, OCH_3), 0.49 [s, 18 H, $Si(CH_3)_3$], 0.31 [s, 18 H, $Si(CH_3)_3$]; ^{13}C δ 161.6 (s, *p*-C_{aryl}), 137.0 (d, $^1J_{PC}$ 94 Hz, *ipso*-C_{aryl}), 132.2 (d, $^3J_{PC}$ 15 Hz, *m*-C_{aryl}), 113.7 (d, $^2J_{PC}$ 17 Hz, *o*-C_{aryl}), 54.9 (s, OCH_3), 6.2 (s, $SiCH_3$), 5.7 (s, $SiCH_3$). HRMS (CI^+): calc. for $C_{19}H_{43}N_2OPS_3Si_4Sn$ (M^+), *m/z* 674.0374; found 674.0361.

10 NMR (C_6D_6): $^{31}P\{^1H\}$ δ 45.6; ^1H δ 7.47–7.50 (m, 2 H, aryl), 6.92–6.95 (m, 2 H, aryl), 3.79 (s, 3 H, OCH_3), 0.49 [s, 18 H, $Si(CH_3)_3$], 0.31 [s, 18 H, $Si(CH_3)_3$]; ^{13}C δ 161.6 (s, *p*-C_{aryl}), 133.4 (d, $^3J_{PC}$ 15 Hz, *m*-C_{aryl}), 114.6 (d, $^2J_{PC}$ 17 Hz, *o*-C_{aryl}), 54.0 (s, OCH_3), *ipso*-C_{aryl} not observed.

§ *Crystal data*: **3b**: $C_{19}H_{43}N_2OPS_3Si_4Sn$, M = 673.75, monoclinic, space group $I2/a$, a = 27.250(2), b = 11.542(1), c = 20.522(1) Å, β = 98.200(4)°, U = 6388.6(8) Å³, Z = 8, D_c = 1.401 g cm^{-3}, $F(000)$ = 2784, T = 183(2) K. 7313 independent reflections were collected on a Siemens P4 diffractometer using graphite-monochromated Mo-Kα radiation (λ = 0.710 73 Å, 2.01° < θ < 27.50°, μ = 4.35 cm^{-1}); an absorption correction was applied: wR_2 = 0.0578, R = 0.0261 for reflections with $I > 2\sigma(I)$.

10: $C_{28}H_{28}GeO_4P_4S_4$, M = 753.21, monoclinic, space group $C2/c$, a = 24.248(6), b = 7.931(1), c = 20.152(5) Å, β = 122.34(1)°, U = 3274.5(1) Å³, Z = 4, D_c = 1.528 g cm^{-3}, $F(000)$ = 1536, T = 293(2) K. 3721 independent reflections were collected on an Enraf Nonius CAD4 diffractometer using graphite-monochromated Mo-Kα radiation (λ = 0.710 73 Å, 2.39° < θ < 27.50°, μ = 14.19 cm^{-1}); an absorption correction was applied: wR_2 = 0.1243, R = 0.0499 for reflections with $I > 2\sigma(I)$. CCDC 182/691.

1 For a review, see: M. P. Cava and M. I. Levinson, *Tetrahedron*, 1985, **41**, 5061.
2 R. Jones, D. J. Williams, P. T. Wood and J. D. Woollins, *Polyhedron*, 1987, **6**, 539; G. A. Zank and T. B. Rauchfuss, *Organometallics*, 1984, **3**, 1191.
3 M. J. S. Gynane, D. H. Harris, M. F. Lappert, P. P. Power, P. Rivière and M. Rivière-Baudet, *J. Chem. Soc., Dalton Trans.*, 1977, 2004.
4 J. L. Lefferts, K. C. Molloy, M. B. Hossain, D. van der Helm and J. J. Zuckerman, *Inorg. Chem.*, 1982, **21**, 1410.
5 T. Fjeldberg, H. Hope, M. F. Lappert, P. P. Power and A. J. Thorne, *J. Chem. Soc., Chem. Commun.*, 1983, 639.
6 P. B. Hitchcock, E. Jang and M. F. Lappert, *J. Chem. Soc., Dalton Trans.*, 1995, 3179.
7 [2 + 2] reactions have also been suggested for a ferrocenyl analogue of Lawesson's reagent: M. R. StJ. Foreman, A. M. Z. Slawin and J. D. Woollins, *Chem. Commun.*, 1997, 1269.
8 W. A. Herrmann, M. Denk, J. Behm, W. Scherer, F. R. Klingan, H. Bock, B. Soluki and M. Wagner, *Angew. Chem., Int. Ed. Engl.*, 1992, **31**, 1485.
9 C. Lensch, W. Clegg and G. M. Sheldrick, *J. Chem. Soc., Dalton Trans.*, 1984, 723.

Received in Bloomington, IN, USA, 19th August 1997; 7/06097A

Taking advantage of the pH and pO_2 sensitivity of a luminescent macrocyclic terbium phenanthridyl complex

David Parker* and J. A. Gareth Williams

Department of Chemistry, University of Durham, South Road, Durham, UK DH1 3LE

Strong metal-based emission with [TbL^1] in aqueous media occurs in the absence of protons and oxygen; dissolved molecular oxygen quenches the phenanthridyl triplet ($1/K_{SV}$ = 58 Torr O_2) but back-energy transfer to the organic triplet occurs efficiently only with the excited protonated complex (pK_a'' = 5.7).

Responsive luminescent probes that signal the presence of molecules or ions in aqueous solution are of current interest because of their application to the analysis of biological or environmental samples.[1] There have been some recent reports of pH responsive luminescent lanthanide complexes[2] in which the delayed luminescence from the metal allows time-gating in monitoring the emission, so that problems such as autofluorescence and Rayleigh-scattering are obviated. As a consequence of the low absorption coefficients associated with lanthanide f–f transitions, a sensitising chromophore needs to be built in to such complexes, preferably one that can efficiently absorb incident light at wavelengths greater than 340 nm.[3] Several different aromatic chromophores can be used under ambient conditions, provided that they possess a triplet energy *ca.* 1500 cm^{-1} greater than that of the emissive lanthanide state. If this condition is not fulfilled, then competitive thermally activated back-energy transfer will occur and the metal-based luminescence will become sensitive to the presence of dissolved O_2.[3,4] Such a situation is depicted in Scheme 1, wherein molecular oxygen may quench the aromatic triplet excited state and similarly affect the lanthanide luminescence, depending on the relative magnitude of k_1, k_{-1}, $k_q[O_2]$ and k_2. Of course, sensors for molecular oxygen that operate on the quenching of an aromatic triplet excited state are well known and include polyaza ruthenium and palladium porphyrin complexes,[5] where values of k_q are typically of the order of 1.5×10^9 dm^3 mol^{-1} s^{-1}.[6]

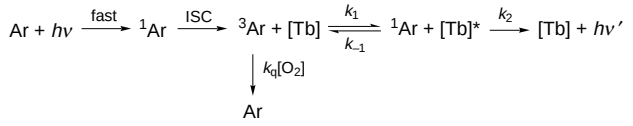

Scheme 1

The complex [TbL^1]† was prepared by reaction of the triphosphinate-phenanthridine ligand H_3L^1 reported previously[2a] with $Tb(OAc)_3$ in water, followed by purification by alumina chromatography. The fluorescent emission from the phenanthridine group at 403 nm was monitored together with the delayed luminescence from the terbium centre (λ_{em} = 547 nm) as a function of pH (Fig. 1), following excitation at the isosbestic wavelength (304 nm). The ligand-based fluorescence increases in intensity by a factor of 3 as the phenanthridyl nitrogen is protonated, consistent with the suppression of photoinduced electron transfer associated with protonation. The apparent pK_a was 4.2(1), in reasonable agreement with the value of 4.4(1) obtained with the analogous europium complex.[2a] The metal-based luminescence showed a luminescence enhancement of 125 but in the opposite sense. The neutral complex was highly emissive (φ_{H_2} = 0.025, τ_{H_2O} = 0.98 ms) and the protonated complex was not ($\varphi_{H_2O} = 9 \times 10^{-4}$, $\tau_{H_2O} < 0.1$ ms).

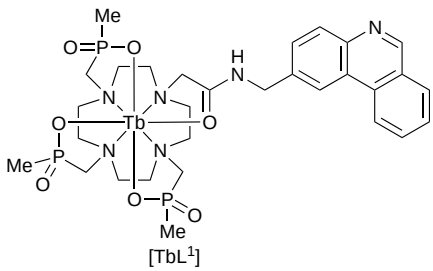

[TbL^1]

The phenanthridine triplet energies were estimated from the phosphorescence spectra of [GdL^1] at 77 K in an MeOH–EtOH glass and were found to be 22 000 cm^{-1} for the unprotonated form and 21 300 cm^{-1} for the protonated complex. These values are 1500 and 800 cm^{-1} higher than the energy of the Tb^{3+} emissive state ($^5D_4$, 20 500 cm^{-1}), respectively. Deactivation of the terbium complex by back-energy transfer to the organic triplet is thus much more significant for the protonated form. The excited-state pK_a of 5.75(10) for [TbL^1] is close to the pK_a reported for the triplet state of phenanthridine itself (5.7),[7] and is consistent with the establishment of an equilibrium between the triplet phenanthridyl excited state and the terbium $^5D_4$ excited state (Scheme 1). Further support for this hypothesis came from the effect of varying the partial pressure of O_2 in the sample. Removal of dissolved oxygen led to an increase in the overall quantum yield {φ = 0.12, pO_2 = 0, (H_2O)} and a concomitant increase in the terbium luminescent lifetime [τ_{H_2O} = 1.82 ms (pO_2 = 0)].† The triplet phenanthridyl excited state is quenched by O_2, and the extent of quenching is a function of dissolved [O_2] and is reported by changes in the terbium lifetime and emission intensity.‡ The N-methylated complex [TbL^2]$^+$ (prepared by alkylation in MeI–MeCN at 20 °C) also behaved as an oxygen sensor, with pO_2 ($S = \frac{1}{2}$) of 58 Torr, and an associated linear Stern–Volmer plot (Fig. 2).

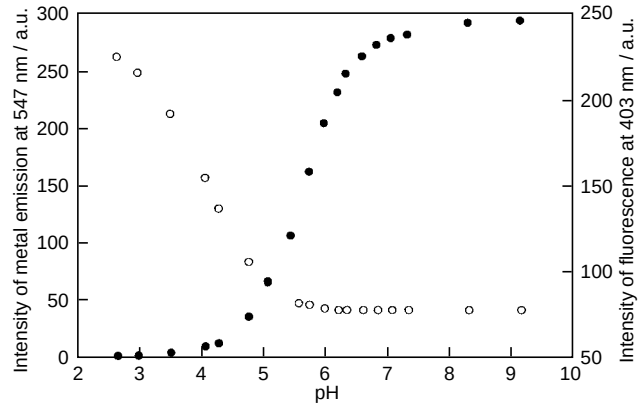

Fig. 1 Delayed luminescence emission intensity (●) and ligand-based fluroescence intensity (○) as a function of pH for [TbL^1], following pulsed excitation at 304 nm (isosbestic wavelength) and using a delay time of 0.1 ms [293 K, I = 0.1 (NMe_4ClO_4)]

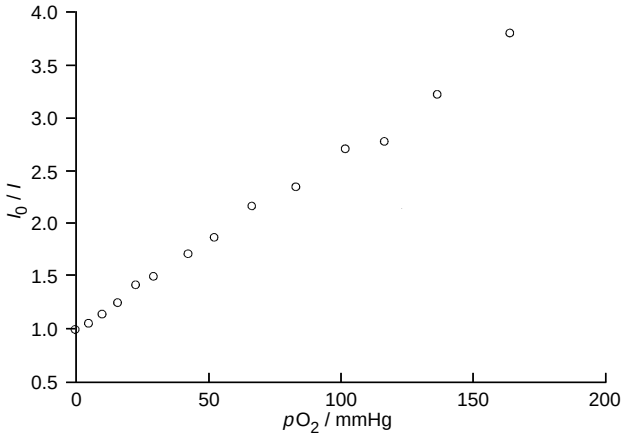

Fig. 2 Stern–Volmer plot of I_o/I *vs.* pO_2 for $[TbL^2]^+$ [293 K, I = 0.1 NMe_4ClO_4)]. Similar behaviour was exhibited by $[Tb(HL^1)]^+$.

The luminescence of this N-alkylated complex was independent of pH in the range 2–9.

The complex $[TbL^1]$ possesses several attractive sensory features. It exhibits a pH dependence in aqueous solution that embraces the range 3–7, because of the ability to examine either the ligand based fluorescence ($pK_a' = 4.2$) or the metal-based phosphorescence ($pK_a'' = 5.75$). Moreover, the luminescent enhancement factors for the former are at least 500, when an excitation wavelength of 375 nm is used, because the unprotonated complex does not absorb at this wavelength {*cf.* $\varepsilon_{375} = 3 \times 10^3$ dm^3 mol^{-1} cm^{-1} for $[Tb(HL^1)]^+$}, as was found for the analogous complex $[EuL^1]$.[2a]

The change in the lifetime of the terbium excited state upon protonation ($\Delta\tau_{H_2O}$ = 1 ms), means that lifetime measurements, rather than luminescence intensity measurements, may be used to characterise the pH dependence over the range 5–7, which may be usefully applied to biological systems. In addition, in the pH range 2–9 the sensitivity of the N-methylated salt to dissolved oxygen may be harnessed to determine pO_2 in aqueous solutions, measuring the lifetime or emission intensity from the Tb excited state. Finally, given that strong terbium luminescence (Table 1), occurs only when both acid and O_2 are not present, the complex $[TbL^1]$ could be construed as behaving as a molecular NAND logic gate[8] with H^+ and O_2 as the 'inputs' and delayed terbium luminescence as the signal 'output'.

Table 1 Lifetimes and quantum yields for lanthanide complexes (H_2O, 293 K, λ_{exc} 304 nm)[a]

Parameter	$[TbL^1]$	$[TbHL^1)]^+$	$[EuL^1]$[b,c]	$(Eu(HL^1)]^+$
φ_{aer}	2.5×10^{-2}	9.1×10^{-4}	0.011	0.03
$\varphi_{degassed}$	0.12	4.6×10^{-2}	0.011	0.03
$\tau_{H_2O_{aer}}$/ms	0.98	*ca.* 0.1	0.71	0.71
$\tau_{H_2O_{degassed}}$/ms	1.82	0.83	0.71	0.71

[a] Lifetimes were obtained using a Perkin-Elmer LS50B (gate time 0.1 ms); [b] Data from ref. 2(*a*); [c] In D_2O, τ = 1.92 ms for the free and 1.95 ms for the protonated complex.

We thank EPSRC for grant support.

Footnotes and References

* E-mail: david.parker@dur.ac.uk

† *Selected data* for $[TbL^1]$: *m*/*z* (ESMS, H_2O): 839.4 ($M^+ + 1$); δ_P(pD 5.9) 648, 621, 484. Found: C, 38.4; H, 5.99; N, 7.31. $C_{30}H_{44}N_5O_7P_3Tb \cdot 5H_2O$ requires: C, 38.8; H, 5.82; N, 7.54%.

‡ A laser flash photolysis study of several lanthanide complexes of a related enantiopure tetraamide ligand, incorporating the same pendant phenanthridine chromophore, has confirmed that in deoxygenated solution, the rate of decay of the phenanthridyl triplet matched the rate of growth of the Tb emission, *i.e.* in Scheme 1, $k_1 = 2 \times 10^5$ s^{-1}, $k_2 = 1060$ s^{-1} and $k_q = 0.7 \times 10^9$ dm^3 mol^{-1} s^{-1}. Full details will be reported elsewhere.

1 A. P. de Silva, H. Q. N. Gunaratne, T. Gunnlaugsson, A. J. M. Huxley, C. P. McCoy, J. T. Rademacher and T. R. Rice, *Chem. Rev.*, 1997, **97**, 1515.
2 (*a*) D. Parker, K. P. Senanayake and J. A. G. Williams, *Chem. Commun.*, 1997, 1777; (*b*) A. P. de Silva, H. Q. N. Gunaratne and T. E. Rice, *Angew. Chem., Int. Ed. Engl.*, 1996, **35**, 2116.
3 N. Sabbatini, M. Guardigli and J.-M. Lehn, *Coord. Chem. Rev.*, 1993, **123**, 201.
4 D. Parker and J. A. G. Williams, *J. Chem. Soc., Dalton Trans.*, 1996, 3613; A. Beeby, D. Parker and J. A. G. Williams, *J. Chem. Soc., Perkin Trans. 2*, 1996, 1565.
5 A. Mills, *Platinum Met. Rev.*, 1997, **41**, 115; A. Mills and A. Thomas, *Analyst*, 1997, **122**, 63; I. Klimant and O. S. Wolfbeis, *Anal. Chem.*, 1995, **67**, 3160; P. Hartmann and W. Trettnak, *Anal. Chem.*, 1996, **68**, 2615.
6 At amospheric pressure $[O_2] = 0.29 \times 10^{-3}$ mol dm^{-3} in water: S. L. Murov, I. Carmichael and G. L. Hug, *Handbook of Photochemistry*, Marcel Dekker, New York, 2nd edn., 1993.
7 E. Van der Donckt, R. Dramaix, J. Nasielski and C. Vogels, *Trans. Faraday Soc.*, 1969, **65**, 3258.
8 For examples of other fluorescent 'logic' gates see *inter alia*: A. P. de Silva, H. Q. N. Gunaratne and C. P. McCoy, *J. Am. Chem. Soc.*, 1997, **119**, 7891; A. Gedi, V. Balzani, S. J. Langford and J. F. Stoddart, *J. Am. Chem. Soc.*, 1997, **119**, 2679.

Received in Cambridge, UK, 28th October 1997; 7/07754H

First electrochemical synthesis of network silane and silane–germane copolymers: $(C_6H_{11}Si)_x(PhSi)_y$ and $(C_6H_{11}Si)_x(PhGe)_y$

Kui Huang and Lori A. Vermeulen*

Department of Chemistry and Biochemistry, Southern Illinois University at Carbondale, Carbondale, IL, 62901-4409, USA

An electrochemical technique is demonstrated for the synthesis of Si–Si and Si–Ge network copolymers poly(cyclohexylsilyne-*co*-phenylsilyne) and poly(cyclohexylsilyne-*co*-phenylgermyne); the molecular mass distributions of the electrochemically prepared polymers are more narrow in comparison to similar polymers prepared by the Wurtz coupling reaction.

Silicon-based polymers have attracted considerable attention owing to their interesting optical and electronic properties, which are strongly related to the dimensionality of the silicon backbone.[1] Polysilanes $(SiR^1R^2)_n$ which consist of a one-dimensional backbone structure exhibit intense near-UV absorption bands and sharp UV emission attributed to the Si backbone σ–σ* transition.[2] The network or crosslinked polysilynes $(SiR)_n$ in which each silicon atom is bonded to three other silicon atoms and one organic side group R are typically yellow materials that photoluminesce in the visible region of the spectrum.[3] It has been proposed that the structure of the network polysilynes consists of rings of different sizes and shapes that are fused together in a random arrangement. The optical features are attributed to the decrease in the Si σ–σ* bandgap compared to the linear polymers, which is caused by increasing the dimensionality of the silicon backbone from a 1D linear structure to a 2D cross-linked structure. Furthermore, it has been reported that Ge three-coordinate polymers (polygermynes)[4] as well as some silicon and germanium copolymers[5] can also be synthesized. The ability to tune the optical properties of these polymers by manipulation of the backbone architecture and composition is an intriguing challenge for the development of these polymers as optoelectronic materials.

The most general synthetic method for the preparation of these metallic backbone polymers is the Wurtz coupling reaction of organo-dichloro- or trichloro-silanes (or germanes) with a sodium dispersion in toluene at refluxing temperature.[2] However, there are several problems with the Wurtz coupling method, most notably the extreme difficulty in controlling the rate of the reaction and thereby obtaining polymers with reproducibly narrow molecular mass distributions. In particular, the network polysilynes that have been prepared by the Wurtz coupling reaction exhibit very broad electronic absorption and NMR spectra. These observations are attributed to the wide variety of macrostructures that are obtained in the Wurtz coupling reaction. Thus, alternative methods of synthesis are desirable for the preparation of materials with structural and optical properties that can be more precisely controlled. To this end, there have been several reports of employing electrochemical techniques for the synthesis of linear polysilanes and germane–silane copolymers.[6]

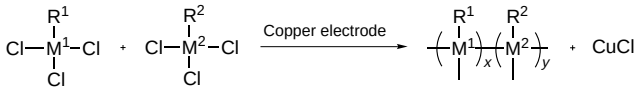

1 $M^1 = M^2 = Si$; $R^1 = Ph$, $R^2 = C_6H_{11}$
2 $M^1 = Si$, $M^2 = Ge$; $R^1 = C_6H_{11}$, $R^2 = Ph$

Scheme 1†

In the present study, we describe the synthesis and optical properties of two new network copolymers poly(cyclohexylsilyne-*co*-phenylsilyne) $(C_6H_{11}Si)_x(PhSi)_y$ **1** and poly(cyclohexylsilyne-*co*-phenylgermyne) $(C_6H_{11}Si)_x(PhGe)_y$ **2** by an electrochemical reduction utilizing copper electrodes and constant applied potential.† The network polymers were synthesized by the electrochemical reduction of 1,2-dimethoxyethane (DME) solution of a 1 : 1 mixture of the trifunctional monomers as depicted in Scheme 1.

Molecular mass, yield, NMR data, and optical properties of **1** and **2** are provided in Table 1. Notably, the ^{29}Si NMR spectrum

Table 1 Physical and optical properties of **1** and **2**

	x/y^a	Yield[b] (%)	M_n[c]	M_w/M_n	^{29}Si, δ	λ_{em}[d]/nm	λ_{ex}/nm
1	1.25	49	5839	1.4	−55, −65, −76(br)	470	350
2	1.04	23	3147	2.0	−50 to −80(br)	490	350

[a] Monomer ratio determined by ^1H NMR. [b] Isolated yield obtained by precipitation from toluene–methanol (1 : 8). [c] M_w determined by GPC *vs.* polystyrene. [d] Excitation λ = 300 nm.

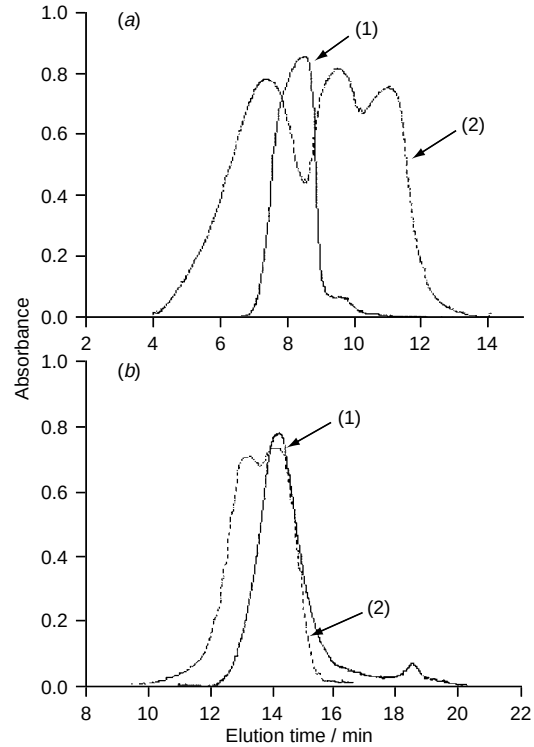

Fig. 1 GPC chromatogram for (*a*) poly(cyclohexylsilyne-*co*-phenylsilyne) (1) electrochemical product, (2) Wurtz product; (*b*) poly(cyclohexylsilyne-*co*-phenylgermyne) (1) electrochemical product, (2) Wurtz product. [Different columns were used for (*a*) and (*b*) and time scales are therefore different]

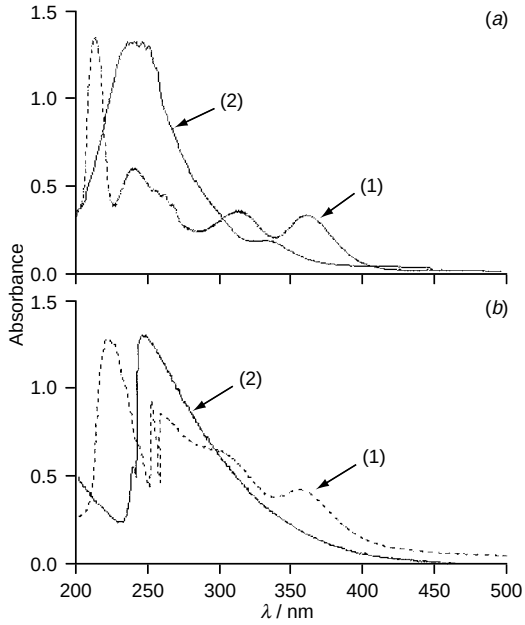

Fig. 2 Absorption spectra of (*a*) poly(cyclohexylsilyne-*co*-phenylsilyne) reaction mixture (1) immediately after quenching with methanol, (2) after ageing in the dark; (*b*) poly(cyclohexylsilyne-*co*-phenylgermyne) reaction mixture (1) immediately after quenching with methanol; (2) after ageing in the dark

of **1** exhibits three broad resolvable peaks in the region typical for tertiary Si atoms (Si bonded to three other Si atoms). Thermally prepared network polymers typically exhibit an extremely broad resonance in this region (δ −20 to −80, with no resolvable peaks).[3] The broad resonance typically observed is attributed to overlapping peaks corresponding to the wide variety of ways that the Si atoms can be bonded together in a random network arrangement. There are no resonances observed which would be typical for linear polysilylene segments.

For comparison, these two copolymers, which are not reported in the literature, were also prepared by the thermal reduction method under typical Wurtz conditions.[2]‡ The molecular mass distributions of all four polymers are shown in Fig. 1. As can be seen, the GPC for the same products obtained by the thermal Wurtz coupling reaction are broader and polymodal compared to those prepared electrochemically.

These network copolymers have optical properties which are typical for this class of materials, exhibiting both a broad absorption band edge that tails into the visible region and a broad emission band. The Ge–Si backbone polymer exhibits a broader emission which is slightly red-shifted compared to the Si backbone polymer, as expected.[4]

Because of the mild reaction conditions, we were able to observe precursors to the isolated products spectroscopically, which can not be observed from the Wurtz product mixture. Discrete peaks are observed in the absorption spectra of the two electrochemically prepared copolymers prior to work-up as shown in Fig. 2. Both samples were quenched with methanol and stored in the dark and the absorption spectrum was re-checked periodically. Over a period of two weeks, the discrete peaks gradually disappear and the spectrum begins to resemble that of the isolated polymer. The slow conversion to products provides an opportunity to more easily study the reaction mechanism, which is not readily accomplished with the thermal Wurtz reaction. The origin of the discrete peaks in the electronic spectra and a study of the reaction pathway are currently being investigated.

The authors gratefully acknowledge financial support from the National Science Foundation (NSF-CHE-9510481), an Oak Ridge Associated Universities Junior Faculty Award, and the Office of Research and Development Administration (ORDA) at SIU. We also acknowledge Dr. Bill Stevens for assistance with the NMR experiments.

Footnotes and References

* E-mail: vermeulen@chem.siu.edu

† *Conditions*: undivided electrolytic cell equipped with coiled copper wire 1 mm in diameter for both the cathode (14 cm^2) and anode (34 cm^2), constant applied potential (−3.0 V), ultrasound, TBAP supporting electrolyte (1.0 g), dry DME solvent (30 ml), cyclohexyltrichlorosilane (0.45 ml), phenyltrichlorosilane (0.40 ml). Reaction was continued until GPC no longer changed and then quenched with methanol. After removal of volatiles and electrolyte, product was purified by precipitation with methanol. Similar procedure was used for the preparation of **2**.

‡ A mixture of monomers in toluene was added slowly to a refluxing sodium dispersion under an atmosphere of Ar. The reaction was carried out at reflux for 5 h. The reaction was quenched by adding methanol and water. The organic layer was separated and washed with water and the isolated polymers were obtained by precipitation from the solution with methanol.

1 Y. Kanemitsu, K. Suzuki, K. S. Kyushin and H. Matsumoto, *Phys. Rev. B*, 1995, **51**, 13103.
2 D. Miller and J. Michl, *Chem. Rev.*, 1989, **89**, 1359.
3 A. Watanabe, H. Miike, Y. Tsutumi and M. Matsuda, *Macromolecules*, 1993, **26**, 2111; W. L. Wilson and T. W. Weidman, *J. Phys. Chem.*, 1991, **95**, 4568; K. Furukawa, M. Fujino and N. Matsumoto, *Macromolecules*, 1990, **23**, 3423; P. A. Bianconi, F. C. Schilling and T. W. Weidman, *Macromolecules*, 1989, **22**, 1697.
4 W. J. Szymanski, G. T. Visscher and P. A. Bianconi, *Macromolecules*, 1993, **26**, 869.
5 A. Watanabe, T. Komatsubara, M. Matsuda, Y. Yoshida and S. Tagawa, *Macromol. Chem. Phys.*, 1995, **196**, 1229; H. Kishida, H. Tachibana, M. Matsumoto and Y. Tokura, *Appl. Phys. Lett.*, 1994, **65**, 1358; T. Shono, S. Kashimura and H. Murase, *J. Chem. Soc., Chem. Commun.*, 1992, 896.
6 A. Kunai, E. Toyoda, T. Kawakami and M. Ishikawa, *Electrochim. Acta.*, 1994, **39**, 2089; M. Umezawa, M. Takeda, H. Ichikawa, T. Ishikawa, T. Koizumi and T. Nonaka, *Electrochim. Acta.*, 1991, **36**, 621; T. Shono, S. Kashimura, M. Ishifune and R. Nishida, *J. Chem. Soc., Chem. Commun.*, 1990, 1160; E. Hengge and G. Litscher, *Angew. Chem., Int. Ed. Engl.*, 1976, **15**, 370.

Received in Bloomington, IN, USA, 22nd July 1997; 7/05254E

Selective formation of HCO_2^- and $C_2O_4^{2-}$ in electrochemical reduction of CO_2 catalyzed by mono- and di-nuclear ruthenium complexes

Md. Meser Ali,[a] Hiroyasu Sato,[a] Tetsunori Mizukawa,[b] Kiyoshi Tsuge,[b] Masa-aki Haga[b] and Koji Tanaka*[b]

[a] *Department of Chemistry for Materials, Faculty of Engineering, Mie University, 1515 Kamihama Cho, Tsu 514, Japan*
[b] *Institute for Molecular Science, Department of Structural Molecular Science, Myodaiji, Okazaki 444, Japan*

Electrochemical reduction of carbon dioxide catalyzed by mono- and di-nuclear ruthenium complexes produced HCO_2H with trace amounts of CO and $C_2O_4^{2-}$ in the presence and absence of H_2O, respectively, in MeCN.

Reduction of CO_2 accompanied by carbon–carbon bond formation is highly desired because the electrochemical reduction of CO_2 catalyzed by metal complexes usually produces only CO and/or HCO_2H.[1–6] A key process for the activation of CO_2 on metals is how to create coordinately unsaturated low valent metal centers under mild conditions. We have found that $[(CpM)_3(\mu_3\text{-}S)_2]^{2+}$ (M = Co, Rh, Ir)[7] catalyzes electrochemical reduction of CO_2 to produce oxalate selectively, where the reaction sites for the first catalytic formation of $C_2O_4^{2-}$ are presumed to be created by an M–M bond cleavage upon the two-electron reduction of these M_3S_2 clusters. Metal complexes with unsymmetrical chelating rings may also provide sites for activation of CO_2 by dechelation in the electrochemical reduction of CO_2. We introduced 2,2′-bis(1-methylbenzimidazol-2-yl)-4,4′-bipyridine (dmbbbpy) as an unsymmetrical chelating ligand into a $Ru(bpy)_2$ moiety to aim not only to create reaction sites by opening the chelate ring but also to accumulate electrons into the ligand required in the reduction of CO_2. Here, we report almost selective HCO_2H and $C_2O_4^{2-}$ formation depending on the presence and the absence of H_2O in electrochemical reduction of CO_2 catalyzed by mono- and di-nuclear Ru complexes.

Scheme 1 shows the synthetic route for 2,2′-bis(1-methylbenzimidazol-2-yl)-4,4′-bipyridine (dmbbbpy) and the mono- and di-nuclear ruthenium complexes. Mono- (**1**) and di-nuclear Ru complexes (**2**) were synthesized by the reaction of $[Ru(bpy)_2Cl_2]$ with dmbbbpy with mol ratios of 1 : 1 and 2 : 1, respectively, in ethylene glycol. Both complexes were purified by column chromatography and characterized by electrospray MS and elemental analyses.

The cyclic voltammogram (CV) of **1** exhibited three reversible one electron redox couples at $E_{1/2}$ = −1.45, −1.75 and −1.99 V in MeCN resulting from dmbbbpy and two bpy based reductions, respectively. Complex **2** also showed three reversible redox couples with a small positive shift (0.2 V) of the dmbbbpy based redox wave. Introduction of CO_2 by bubbling into the solutions of **1** and **2** results in an increase in the cathodic currents at potentials more negative than −1.60 and −1.50 V, respectively, indicating that two-electron reduced forms of **1** and **2** have an ability to catalyze the reduction of CO_2 (Fig. 1).

Controlled potential electrolysis of **1** and **2** (0.2–0.3 mmol dm^{-3}) at −1.65 and −1.55 V (*vs.* Ag/AgCl) was conducted in CO_2 saturated MeCN (20 ml) in the presence of H_2O (0.5 ml). After 91 C was passed in the electrolysis of **1**,† HCO_2^- was produced with a current efficiency (η) of 89% together with a trace amount of CO (η = 2–3%). On the other hand, the similar electrochemical reduction of CO_2 in dry MeCN selectively produced oxalate‡ with an η of 64% without forming HCO_2^- and CO after 50 C was passed in the electrolysis. The electrochemical reduction of CO_2 catalyzed by **2** also generated almost selectively HCO_2^- (η = 90%) and $C_2O_4^{2-}$ (η = 70%) in the presence and the absence of H_2O, respectively, under similar conditions.

The reaction of CO_2 catalyzed by **1** was monitored in an IR cell with KBr windows equipped with a gold mesh for the working electrode, a platinum wire for a counter electrode and an Ag/AgCl reference electrode.[8] Reductive electrolysis at −1.65 V§ of **1** in CO_2-saturated CD_3CN solution resulted in the appearance of three bands at 1684, 1633 and 1603 cm^{-1} [Fig. 2(*b*)]. Reoxidation at −0.70 V causes the disappearance of the 1684 and 1603 cm^{-1} bands, while the 1633 cm^{-1} band assigned to $C_2O_4^{2-}$ remained unchanged. The three bands at 1684, 1633 and 1603 cm^{-1} shifted to 1638, 1600 and 1540 cm^{-1}, respectively, under similar electrolysis using $^{13}CO_2$

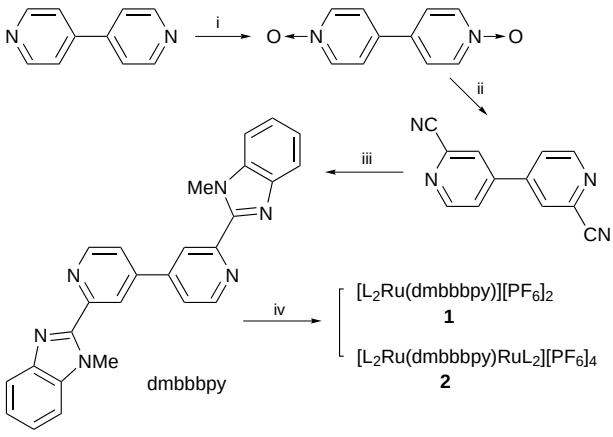

Scheme 1 Synthesis route for the bridging ligand, Ru mono- and di-nuclear complexes. *Reagents and conditions*: i, $MeCO_2H + H_2O_2$; ii, $(MeO)_2SO_2$, KCN; iii, *N*-methyl-1,2-phenylenediamine; iv, $[RuL_2Cl_2]$ (L = bpy).

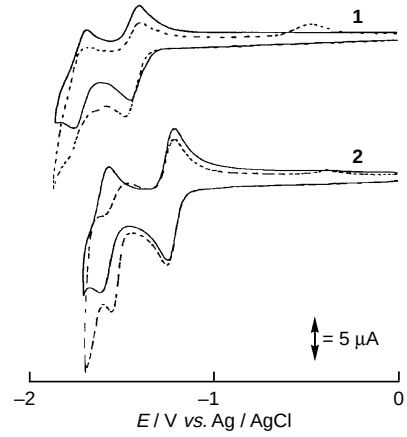

Fig. 1 Cyclic voltammograms of 0.3 mM **1** or **2** in 0.1 M NBu_4BF_4MeCN at glassy carbon electrode (id = 3.0 mm) under N_2 (——) and CO_2 (------) atmospheres. Scan rate = 50 mV s^{-1}.

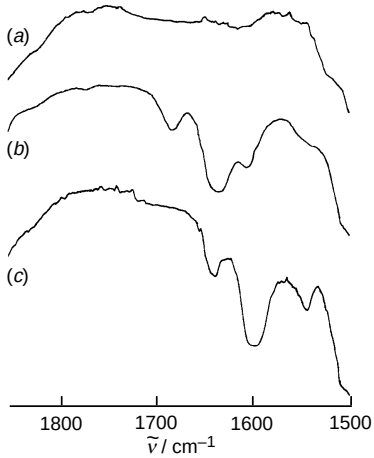

Fig. 2 IR spectra of **1** (0.8 mM) during a thin-cell bulk electrolysis in CD_3CN with $LiBF_4$. (*a*) Starting scan, (*b*) using $^{12}CO_2$, (*c*) using $^{13}CO_2$.

[Fig. 2(*c*)]. The bands at 1638 and 1540 cm^{-1} also disappeared upon reoxidation at −0.70 V suggesting that a CO_2 adduct probably formed by an attack of two molecules of CO_2 to the two-electron reduced form of **1** which acts as a precusor to oxalate in the electrochemical reduction of CO_2 in dry MeCN.

It is noteworthy that any interaction between reduced forms of $[Ru(bpy)_2L]^{2+}$ (L = bpy or 2-pyridyl-1-methylbenzimidazole¶) and CO_2 was not observed at all in the CV in MeCN. Indeed, these complexes have no ability to catalyze the electrochemical reduction of CO_2 under controlled potential electrolysis even at −1.80 V in the absence or presence of H_2O in MeCN. Moreover, $[Ru(bpy)_2(CO)X]^{n+}$ (*n* = 2, X = CO; *n* = 1, X = Cl)[9] works as an effective catalyst producing CO and/or HCO_2H in the electrochemical reduction of CO_2 under protic conditions, but the complex readily decomposes in the similar reduction of CO_2 in the absence of proton donor. Savéant and coworkers have shown that aromatic nitriles and esters with redox potentials more negative than −1.93 V mediate electrochemical reduction of CO_2 affording oxalate. The reaction is explained by an electrophilic attack of CO_2 to oxygen or nitrogen of the anion radicals followed by homolytic cleavage of the ArX–CO_2^- [X = OC(O)R, CN] bond and the subsequent coupling of free $CO_2^{\cdot -}$.[10] On the other hand, the IR spectra of **1** showed the two $\nu(CO_2)$ bands (1684, 1603 cm^{-1}) assignable to the precursor for oxalate under electrolysis at −1.65 V, suggesting that oxalate generation in the present study does not result from dimerization of free $CO_2^{\cdot -}$. If two-electron reduction of **1** and **2** causes dechelation of dmbbbpy, the resultant five-coordinate Ru and monodentate dmbbbpy$^-$ may provide two binding sites for an attack of CO_2, which would facilitate a coupling reaction of CO_2 affording oxalate. Thus, dmbbbpy of **1** and **2** greatly contributes to the first selective formation of $C_2O_4^{2-}$ and HCO_2^- depending upon the absence and the presence of H_2O, respectively, in the electrochemical reduction of CO_2.

This work was partly supported by Grant-in-Aid for Scientific Research on Priority Areas (No. 283, 'Innovative Synthetic Reactions') from Monbusho, and the authors also thank Monbusho for a scholarship (to M. M. A.).

Footnotes and References

* E-mail: ktanaka@ims.ac.jp

† HCO_2H was characterized using an isotachophoretic analyzer and ^{13}C NMR spectroscopy.

‡ Oxalate was characterized using an isotachophoretic analyzer [GC–MS (diester derivative, by esterification with diazomethane)] and ^{13}C NMR spectroscopy.

§ Electrolysis of **1** at potentials more negative than −1.75 V resulted in rapid growth of the 1633 cm^{-1} band so that electrolysis was conducted at −1.65 V to detect the emergence of the 1684 and 1603 cm^{-1} bands clearly.

¶ $[Ru(bpy)_2L]^{2+}$ (L = 2-pyridyl-1-methylbenzimidazole) was prepared and characterized by electrospray MS and elemental analyses.

1 F. Hutschka, A. Dedieu, M. Eichberger, R. Fornika and W. Leitner, *J. Am. Chem. Soc*., 1997, **119**, 4433.
2 P. G. Jessop, Y. Hsiao, T. Ikaiya and R. Noyori, *J. Am. Chem. Soc*., 1996, **118**, 352.
3 W. Leitner, *Angew. Chem., Int. Ed. Engl*., 1995, **34**, 2207; P. G. Jessop, T. Ikaiya and R. Noyori, *Chem. Rev*., 1995, **95**, 259.
4 K. M. Lam, K. Y. Wong, S. M. Yang and C. M. Che, *J. Chem. Soc*., *Dalton Trans*., 1995, 1103; H. Nakajima, T. Mizukawa, H. Nagao and K. Tanaka, *Chem. Lett*., 1995, 251.
5 A. M. Herring, B. D. Steffy, A. Miedaner, S. A. Wander and D. L. DuBois, *Inorg. Chem*., 1995, **34**, 1100; R. Fornica, B. Seemann and W. Leitner, *J. Chem. Soc*., *Chem. Commun*., 1995, 1479.
6 P. G. Jessop, T. Ikaiya and R. Noyori, *Nature*, 1994, **368**, 232; M. Collomb-Dunand-Saider, A. Deronizer and R. Ziessel, *J. Chem. Soc*., *Chem. Commun*., 1994, 189.
7 Y. Kushi, H. Nagao, T. Nishioka, K. Isobe and K. Tanaka, *J. Chem. Soc*., *Chem. Commun*., 1995, 1223; Y. Kushi, H. Nagao, T. Nishioka, K. Isobe and K. Tanaka, *Chem. Lett*., 1994, 2176.
8 H. Nakajima, Y. Kushi, H. Nagao and K. Tanaka, *Organometallics*, 1995, **14**, 181.
9 I. Ishida, K. Tanaka and T. Tanaka, *Organometallics*, 1987, **6**, 181.
10 A. Gennaro, A. A. Isse, J.-M. Saveant, M.-G. Severin and E. Vianello, *J. Am. Chem. Soc*., 1996, **118**, 7190.

Received in Cambridge, UK, 13th October 1997; 7/07363A

Interpenetrating three-dimensional rutile-like frameworks. Crystal structure and magnetic properties of $Mn^{II}[C(CN)_3]_2$

Jamie L. Manson,[a] Charles Campana[b] and Joel S. Miller*[a]

[a] *Department of Chemistry, University of Utah, 315 s. 1400 E. RM Dock, Salt Lake City, UT 84112-0850, USA*
[b] *Brucker Analytical X-ray Systems, Inc., 6300 Enterprise Lane, Madison, WI 53719-1173, USA*

The interpenetrating double-density rutile-like structure and magnetic properties of $Mn^{II}[C(CN)_3]_2$ are determined.

Molecule-based magnetic materials have been the focus of intense investigations since the ferromagnetic electron transfer salt $[FeCp^*_2]^{\cdot+}[TCNE]^{\cdot-}$[1,2] and the ferrimagnetic $Mn^{II}Cu^{II}$ chains[2,3] were discovered to magnetically order.[1,2] In the meantime, numerous one-, two-, and three-dimensional coordination polymers comprising paramagnetic transition metal cations and diamagnetic organic ligands exhibiting a wide variety of cooperative phenomena have been reported.[2,4] Furthermore, several diamagnetic examples of molecular materials that mimic three-dimensional inorganic network solids (*e.g.* α Po, diamond, α-$ThSi_2$, *etc.*) have also been described including systems in which interpenetration of two or more identical lattices occurs.[5] The majority of these polymeric frameworks are comprised of Ag^+ cations because of their propensity to afford multiple coordination geometries. Notable examples where Ag^+ possesses octahedral, tetrahedral, and trigonal planar geometries include $[Ag(pyz)_3]SbF_6$ (pyz = pyrazine),[6] $[Ag(DCPA)_2]ClO_4{\cdot}H_2O$ (DCPA = 3,3′-dicyanodiphenylacetylene),[7] and $[Ag_2(pyz)_3](BF_4)_2$,[8] respectively.

In order to construct new molecule-based magnetic materials it is important to assemble solid state structures analogous to those just described. To do this, appropriate paramagnetic transition metal ions and organic bridging ligands capable of significant spin coupling are required. Conjugated bridging ligands, such as cyanide and oxalato, have been shown to provide spin coupling between metals sites and extension to other classes of ligands are sought.[4] We selected tricyanomethanide, $[C(CN)_3]^-$, due to its ability to bind to three metal sites, and the aqueous reaction of $Mn^{II}(NO_3)_2$ and $[C(CN)_3]^-$ leads to the formation of $Mn[C(CN)_3]_2$.‡ The tricoordinate $[C(CN)_3]^-$ could lead to geometrical spin frustration.[10]

$Mn[C(CN)_3]_2$ has a complex interpenetrating network structure.‡ Each Mn^{II} bonds to six $[C(CN)_3]^-$ anions, Fig. 1, and each $[C(CN)_3]^-$ is μ_3-bonded to three Mn^{II} ions, Fig. 2, forming a rutile-like (TiO_2) lattice and is isomorphous to $Zn[C(CN)_3]_2$.[11] $[C(CN)_3]^-$ is planar with C(1)–C(3) and C(2)–C(3) bond distances of 1.404(2) and 1.412(2) Å (av. 1.408 Å), and C(1)–N(1) and C(2)–N(2) distances of 1.151(2) and 1.149(2) Å (av. 1.150 Å), respectively, as is typical of $[C(CN)_3]^-$.[11,12] The Mn^{II} cation occupies a 2/*m* special position while C(2) and N(2) reside on mirror planes, all on the crystallographic *a*-axis. Each Mn^{II} center is slightly elongated from octahedral symmetry with Mn–N(1) and Mn–N(2) bond distances of 2.222(1) and 2.272(2) Å, respectively, and averaging 2.247 Å. These Mn–N distances compare favorably to those found in related materials.[13] This distortion is significantly less than that observed for $Zn[C(CN)_3]_2$ with Zn–N(1) and Zn–N(2) distances of 2.120(2) and 2.211(2) Å,[11] respectively. Hence, the distortion is not a consequence of ligand-field effects, but is imposed by steric constraints. Likewise, owing to crystal packing forces the *cis*-N–M–N′ bond angles demonstrate a marked distortion from 90° and range from 88.9 to 96.7° for $Mn[C(CN)_3]_2$ and 84.4 to 95.6° for $Zn[C(CN)_3]_2$,[11] respectively. Additionally, the large $Mn\cdots C_{centroid}$ separations (*ca.* 4.8 Å) provide cavities of sufficient size for interpenetration of a second identical lattice, Fig. 2. Furthermore, the shortest intra- and inter-network Mn···Mn separations are 7.679 and 5.383 Å, respectively.

The rutile structure is a fundamental solid state structure-type and is one way to connect octahedral centers with trigonal planar ligands to form three-dimensional networks for spin coupling. Antiferromagnetic coupling between spin sites coupled *via* the D_{3h} μ_3-bridging $[C(CN)_3]^-$ ligand should lead to geometrical spin frustration akin to a Kagomé lattice.[10] Additionally, the interpenetrating rutile-like frameworks may lead to enhanced or unusual magnetic properties that may arise if communication between them is sufficient, thus leading to effective dipolar exchange.

The temperature dependence (2–300 K) of the magnetic susceptibility of $Mn[C(CN)_3]_2$ was measured and can be fit by the Curie–Weiss expression, $\chi \propto (T - \theta)^{-1}$, with $\theta = -5.1$ K indicative of finite antiferromagnetic coupling between the Mn^{II}

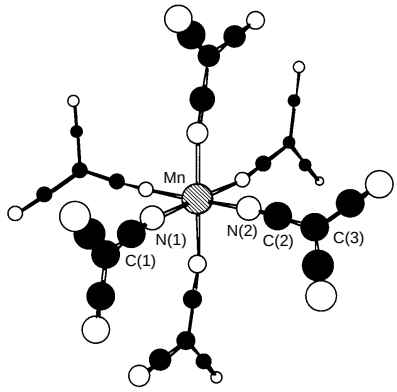

Fig. 1 Illustration showing only the first coordination sphere of the Mn^{II} cation (shaded). Filled and unfilled spheres represent C and N atoms, respectively. Bound nitriles do not coordinate linearly as can be seen clearly here in this view: Mn–N(1)–C(1) 170.03(10), Mn–N(2)–C(2) 166.4(2)°.

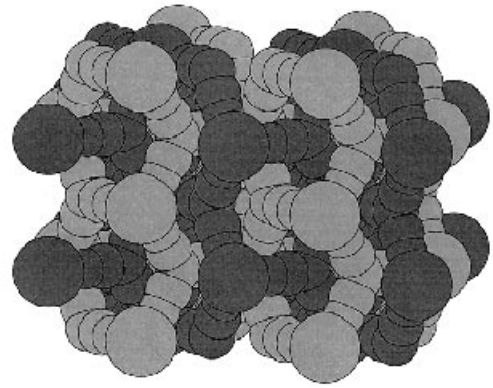

Fig. 2 Space filling model of $Mn^{II}[C(CN)_3]_2$ emphasizing the interpenetrating nature of the two identical rutile-like frameworks

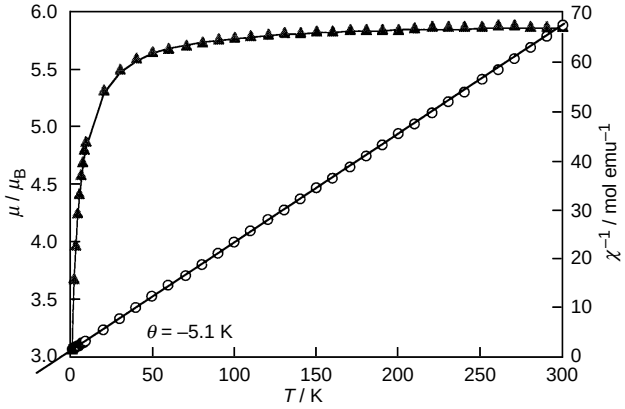

Fig. 3. Temperature dependence of the moment and the reciprocal molar magnetic susceptibility for $Mn^{II}[C(CN)_3]_2$. The data were fitted to the Curie–Weiss law (—) using the following parameters: S = 5/2, g = 2.00 and θ = −5.1 K.

metal centers, Fig. 3. At 300 K the effective moment is 5.86 μ_B, in good agreement with the expected value (5.92 μ_B) for isolated S = 5/2 Mn^{II} ions and decreases at lower temperatures owing to antiferromagnetic coupling. The −5.1 K θ-value is larger than expected for isolated Mn^{II} ions and suggests that (*a*) the diamagnetic $[C(CN)_3]^-$ ligand mediates a superexchange interaction between the Mn^{II} ions, and/or (*b*) owing to shorter internetwork Mn···Mn separation with respect to intranetwork separation, through-space (dipolar) antiferromagnetic coupling between the interpenetrating rutile networks may dominate and lead to bulk antiferromagnetic coupling. Both mechanisms are expected to contribute as the internetwork Mn···Mn separations leading to dipolar interactions are shorter than the intranetwork Mn···Mn separations leading to superexchange.

The authors gratefully acknowledge the ACS-PRF (Grant #30722-AC5) and the US Department of Energy (Grant #DE-FG03-93ER45504) for support of this work.

Footnotes and References

* E-mail: jsmiller@chemistry.utah.edu

† A 20 ml aqueous solution of $Mn(NO_3)_2{\cdot}4H_2O$ (0.1 mmol, 2.51 g) was mixed with an aqueous solution (20 ml) of $K[C(CN)_3]$ (0.2 mmol, 2.59 g). The final yellow solution was allowed to stand at room temp. for several months and small colorless crystals were obtained. ν_{CN} (Nujol): 2256w, 2195vs and 2152 (sh) cm^{-1}. The synthesis and room temp. effective moment of $Mn^{II}[C(CN)_3]_2{\cdot}0.25H_2O$ have been reported previously.[9]

‡ *Crystal data* for C_8MnN_6: M = 235.07, orthorhombic, space group *Pmna*, a = 7.6791(3), b = 5.3837(2), c = 10.6230(4) Å, U = 439.18(3) Å^3, Z = 2, D_c = 1.778 Mg m^{-3}, λ = 0.710 73 Å, T = 273 °C, $2\theta_{max}$ = 65.5°, R_1 = 0.0259, wR_2 = 0.0685, and a goodness of fit of 1.114, and the largest peak on the final difference map was 0.347 e$^-$ Å^{-3} are based upon the refinement of the *XYZ*-centroids of 2646 reflections above 20σ(I). The data was collected on a standard Siemens SMART™ CCD-based X-ray diffractometer system operated at 2000 W power. The detector was placed at a distance of 4.032 cm from the crystal and 1321 frames were collected with a scan width of 0.3° in ω and an exposure time of 30 s frame^{-1}. The frames were integrated with the Siemens SAINT© software package using a narrow-frame integration algorithm. The structure was solved and refined using the Siemens SHELXTL© (Version 5.0) Software Package. CCDC 182/703.

1 J. S. Miller, J. C. Calabrese, A. J. Epstein, R. W. Bigelow, J. H. Zhang and W. M. Reiff, *J. Chem. Soc., Chem. Commun.*, 1986, 1026; J. S. Miller, J. C. Calabrese, H. Rommelmann, S. R. Chittipeddi, J. H. Zhang, W. M. Reiff and A. J. Epstein, *J. Am. Chem. Soc*., 1987, **109**, 769.

2 D. Gatteschi, *Adv. Mater.*, 1994, **6**, 635; J. S. Miller and A. J. Epstein, *Angew. Chem., Int. Ed. Engl.*, 1994, **33**, 385; *Angew. Chem.*, 1994, **106**, 339; *Adv. Chem. Ser*., 1995, **245**, 161; O. Kahn, *Molecular Magnetism*, VCH, New York, 1993.

3 Y. Pei, M. Verdaguer and O. Kahn, *J. Am. Chem. Soc*., 1986, **108**, 428.

4 *e.g.* C. Mathonière, C. J. Nuttall, S. G. Carling and P, Day, *Inorg. Chem*., 1996, **35**, 1201; S. Ferlay, T. Mallah, R. Ouahes, P. Veillet and M. Verdaguer, *Nature*, 1995, **378**, 701; K. Inoue, T. Hayamizu, H. Iwamura, D. Hashizume and Y. Ohashi, *J. Am. Chem. Soc*., 1996, **118**, 1803; A. Böhm, C. Vazquez, R. S. McLean, J. C. Calabrese, S. E. Kalm, J. L. Manson, A. J. Epstein and J. S. Miller, *Inorg. Chem*., 1996, **35**, 3083; H. Stumpf, L. Ouahab, Y. Pei, D. Grandjean and O. Kahn, *Science*, 1993, **261**, 447; F. Lloret, M. Julve, R. Ruiz, Y. Journaux, K. Nakatani, O. Kahn and J. Sletten, *Inorg. Chem*., 1993, **32**, 27.

5 *e.g.* T. Soma, H. Yuge and T. Iwamoto, *Angew. Chem., Int. Ed. Engl.*, 1994, **33**, 1665; L. Carlucci, G. Ciani, D. M. Proserpio and A. Sironi, *Chem. Commun.*, 1996, 1393; T. Otieno, S. J. Rettig, R. C. Thompson and J. Trotter, *Inorg. Chem.*, 1993, **32**, 1607; K. A. Hirsch, D. Venkataraman, S. R. Wilson, J. S. Moore and S. Lee, *J. Chem. Soc., Chem. Commun.*, 1995, 2199; B. F. Hoskins and R. Robson, *J. Am. Chem. Soc*., 1990, **112**, 1546.

6 L. Carlucci, G. Ciani, D. M. Proserpio and A. Sironi *Angew. Chem., Int. Ed. Engl*., **1995**, **34**, 1895.

7 K. A. Hirsch, S. R. Wilson and J. S. Moore, *Inorg. Chem*., 1997, **36**, 2960.

8 L. Carlucci, G. Ciani, D. M. Proserpio and A. Sironi, *J. Am. Chem. Soc*., 1995, **117**, 4562.

9 J. H. Enemark and R. H. Holm, *Inorg. Chem.*, 1964, **3**, 1516.

10 A. P. Ramirez, *Annu. Rev. Mater. Sci*., 1994, **24**, 453; P. Schiffer and A. P. Ramirez, *Comments Condens. Mater. Phys.*, 1996, **18**, 21.

11 S. R. Batten, B. F. Hoskins and R. Robson, *J. Chem. Soc., Chem. Commun*., 1991, 445.

12 S. L. Schiavo, G. Bruno, P. Zanello, F. Laschi and P. Piraino, *Inorg. Chem*., 1997, **36**, 1004; D. A. Dixon, J. C. Calabrese and J. S. Miller, *J. Am. Chem. Soc*., 1986, **108**, 2582.

13 F. A. Mautner, R. Cortés, L. Lezama and T. Rojo, *Angew. Chem., Int. Ed. Engl*., 1996, **35**, 78; M. Ferigo, P. Bonhôte, W. Marty and H. Stoeckli-Evans, *J. Chem. Soc., Dalton Trans.*, 1994, 1549.

Received in Bloomington, IN, USA, 8th October 1997; 7/07289I

Cleavage of the Pt–S bond of thiolated terpyridine–platinum(II) complexes by copper(II) and zinc(II) ions in phosphate buffer

Chien-Chung Cheng* and Yen-Lin Lu

Institute of Chemistry, Academia Sinica, Taipei, Taiwan 11529, Republic of China

Using the chelation of a triamine moiety and an S-bridged heterodinuclear unit, cleavage of the Pt–S bond in the thiolate–platinum complexes, $[Pt(terpy)(BAT)]^{4+}$ and $[Pt(terpy)(AET)]^{+}$ is induced by adding transition metals such as Cu^{2+} or Zn^{2+} in phosphate buffer (pH 7–8) at room temp.

Many efforts in the development of platinum complexes as anticancer drugs have been contemplated in order to reduce the cytotoxicity and to improve the platin drug-resistance.[1] Since sulfur-containing compounds such as glutathione and metallothioneins are rich in cells, the formation of the S–Pt bond is generally believed to be one of the major mechanisms in the resistance to *cis*-platin drugs in biological processes.[2] In contrast, recent NMR studies by Sadler and coworkers reveal that S-bound L-methionine on Pt^{II} acts as a reversible binding ligand and is capable of undergoing intermolecular replacement by 5′-GMP in phosphate buffer (pH 7.2).[3] In fact, the concentration of glutathione (GSH) in intracellular cells is commonly high (> 1 mM). Therefore, in the reaction with platin drugs, the formation of thiolate–platinum adducts is inevitable.[4] The thiolate ion is capable of providing a stronger binding affinity owing to its better σ-donating ability.[5] Such a Pt–S bond is considered relatively inert, which may cause the inhibition of the anticancer activity of platin drugs. Thus, the great challenge is to break the Pt–S bond in the thiolate–platinum adducts.

To approach this goal, thiolated derivatives of terpy–platinum(II) complexes are used as a source to study the Pt–S bond owing to their characteristic electronic absorption and NMR spectra.[6–8] Here, we report that transition metals such as Cu^{II} or Zn^{II} are capable of inducing cleavage of the Pt–S bond of thiolated terpyridine platinum(II) complexes, $[Pt(terpy)(AET)]^{+}$ (AET = 2-aminoethanethiol) and $[Pt(terpy)(BAT)]^{4+}$ [BAT = *N*,*N*′-bis(aminoethyl)aminoethanethiol], particularly in phosphate buffer as shown in Fig. 1. The introduction of a triamine moiety to the complex structure increases the dissociation rate and the selectivity of the Pt–S bond cleavage in thiolate–platinum complexes. To our knowledge, this is the first reported example of Pt–S bond cleavage among thiolate–platinum(II) complexes in phosphate buffer.

$[Pt(terpy)(AET)]^{+}$ was prepared by published methods.[11] The synthesis of a triamine derivative, $[Pt(terpy)(BAT)]^{4+}$, was achieved by the coupling reaction of $[Pt(terpy)Cl]^{+}$ with the modified multistep synthesis[12–15] of triaminothiol, **1**, in water as illustrated in Scheme 1. The NMR spectrum of $[Pt(terpy)(BAT)]^{4+}$ in D_2O showed a new downfield peak at δ 8.82 and the UV–VIS spectrum displayed the absorbances at 486 nm (ε = 698 dm^3 mol^{-1} cm^{-1}), 342 (12 959), 329 (12 397) and 311 (11 903) in phosphate buffer (pH 8.0), which agreed with the characteristic features for establishing the formation of thiolate–platinum bonds in the previous report.[11] In addition, the integration ratio of protons of terpyridine and the triamine moiety in NMR spectra (D_2O) was approximately 0.93, suggesting no S-bridged diplatinum complex was generated.[14]

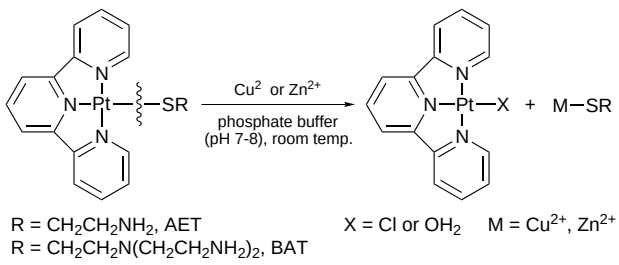

Fig. 1 General equation representing the cleavage of the Pt–S bond

In the presence of $CuCl_2 \cdot 6H_2O$ (42 μM), the solution of $[Pt(terpy)(BAT)]^{4+}$ (40 μM) exhibited a decreasing UV–VIS absorption at 342 nm accompanied by an increasing absorption at 329 nm in phosphate buffer (10 mM, pH 8.0). An isosbestic point was observed at 337 nm in the spectrum, suggesting no intermediate had been generated in the reaction with metal ions. Also, no significant alteration was observed in the absence of Cu^{II}. The cleavage of the Pt–S bond of $[Pt(terpy)(BAT)]^{4+}$ (40 μM) in the titration with Cu^{II} (10–84 μM) was found to require 1 equiv. of Cu^{II} to complete the reaction in 120 min. This dissociation of the Pt–S bond of $[Pt(terpy)(BAT)]^{4+}$ was revealed to be a pH dependent process in the range pH 4.8–10.0. The reactivity of the Pt–S bond cleavage was reduced with a decreasing pH and ceased at pH < 6, implying that the participation of the amino group plays a vital role in the cleavage. In fact, when a hydroxylthiol derivative of $[Pt(terpy)(SCH_2CH_2OH)]^{+}$, was used instead of an amino derivative, under the same conditions, no cleavage of the Pt–S bond was observed.

The isolation of the cleavage product was performed in MeOH in order to simplify the product analysis. After the addition of $CuCl_2 \cdot 6H_2O$, a red solution of $[Pt(terpy)(BAT)]^{4+}$ turned into a blue-green suspension containing orange solid. This orange solid was isolated in a yield of 75–80% with electronic absorptions at 382, 332 and 320 nm in phosphate buffer (pH 8) and NMR peaks in D_2O at δ 7.8 (m), 7.5 (m) and 7.2 (t), suggesting it lacked the Pt–S bond linkage. Furthermore, FAB mass and isotope abundance simulation studies disclosed that the molecular ion at 464 contained a chloride ion, suggesting that $[Pt(terpy)Cl]^{+}$ was one of the cleavage products.

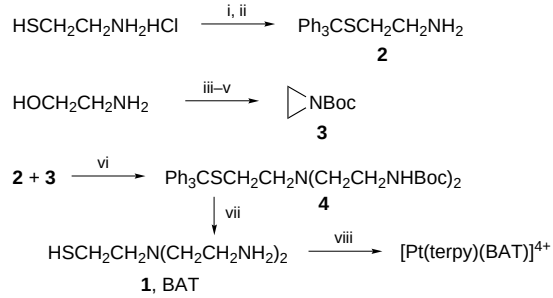

Scheme 1 *Reagents and conditions*: i, triphenylmethanol, neat TFA, 25 °C, 30 min, 89%; ii, NaOH(aq), 92%; iii, conc. H_2SO_4; vacuum (0.1 mmHg) at 80 °C, overnight, 62%; iv, KOH(aq), distillation; v, $(Boc)_2O$, dioxane–H_2O, 0 °C, warming to room temp. overnight; vi, MeCN, reflux, 3 days, 75–80%; vii, TFA, triethylsilane 84%; viii, deionized H_2O, $[Pt(terpy)Cl]Cl$, N_2, 25 °C, 5 h; recrystallization with MeOH–MeCN, 40%.

The chloride ion in the isolated product may be acquired from the use of metal chloride salt as the starting material. In addition, the residual Cu complex in the solution was determined to be a symmetric dimer of copper–triaminothiol complex by NMR and FAB MS analysis. The dimer adduct may be obtained by the coupling reaction with monomer of copper–triaminothiol once released from the platinum–thiolate complexes.

Furthermore, a comparison of the reactivity using different metals Ni^{II}, Cu^{II} and Zn^{II} in the Pt–S bond dissociation in $[Pt(terpy)(BAT)]^{4+}$ in phosphate buffer is also examined. Interestingly, the result shows that the dissociation induced by transition metals varied in a descending order: $Zn^{II} > Cu^{II} > Ni^{II}$, as illustrated in Fig. 2. The rate constant has been estimated under the first-order condition[15] to give a value of 7.9×10^{-3} s^{-1} for Zn^{II}, 5.3×10^{-4} s^{-1} for Cu^{II} and 1.9×10^{-4} s^{-1} for Ni^{II}. Moreover, the same cleavage product, $[Pt(terpy)Cl]^+$, also can be obtained from $[Pt(terpy)(BAT)]^{4+}$ using $ZnCl_2$ in phosphate buffer. Zn^{II} had the strongest preference for promoting Pt–S bond cleavage, and was about 15 times faster than $CuCl_2$. Besides, Zn^{II} also exhibited the highest selectivity in the cleavage of the Pt–S bond of the triaminothiol species, $[Pt(terpy)(BAT)]^{4+}$, but produced no reaction with the aminothiol species, $[Pt(terpy)(AET)]^+$.

In order to eliminate the possibility of the aggregation of polyaromatic compounds,[10] which may enhance the cleavage by neighboring complexes, the dissociation process was also examined at a low concentration (10–12 μM) of $[Pt(terpy)(BAT)]^{4+}$. The result showed no significant difference in the dissociation rate of the Pt–S bond at either a low or high concentration of polyaromatic compounds. Moreover, the preliminary cleavage mechanism has been studied using Cu^{II} in NMR. In phosphate buffer, one of the terpyridine peaks and all of the aliphatic protons are shifted from δ 8.88 and 2.2–2.7 to δ 9.06 and 2.7–3.1 respectively, indicating the S-bridged heterodinuclear moiety is generated while Cu^{II} is coordinating to the triamine moiety. As a result, it will weaken the Pt–S bond, resulting in Pt–S bond dissociation by the other nucleophiles such as Cl^-. Thus, the different coordination of triaminothiol to tetrahedral Zn^{II}, square-planar Cu^{II} and octahedral Ni^{II} in the transition state may be attributed to the different reactivity and selectivity of different metal ions in the Pt–S bond cleavage. The detailed mechanism is under current investigation.

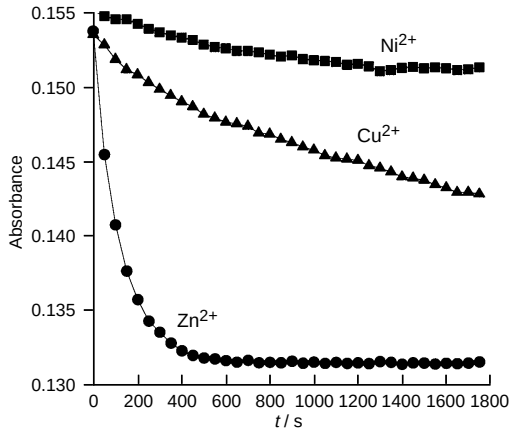

Fig. 2 Comparison of the reactivity in the cleavage of the Pt–S bond by Zn^{2+}, Cu^{2+} and Ni^{2+} ions. These data were collected at a fixed absorption wavelength of 342 nm at intervals of 50 s per cycle at a concentration of $[Pt(terpy)(BAT)]^{4+}$ (40 μM) and metal ion (40–42 μM) in 10 mM phosphate buffer (pH 8.0) at room temp. (●) Zn^{2+}, (▲) Cu^{2+}, (■) Ni^{2+}.

In summary, we have demonstrated that the cleavage of the Pt–S bond of $[Pt(terpy)(AET)]^+$ and $[Pt(terpy)(BAT)]^{4+}$ can be achieved by the addition of transition metal ions such as Zn^{II} or Cu^{II} in either phosphate buffer or MeOH. Importantly $[Pt(terpy)Cl]^+$ is isolated and identified as one of the major products in the dissociation of the Pt–S bond of $[Pt(terpy)(BAT)]^{4+}$ in the presence of $ZnCl_2$ or $CuCl_2$. In fact, the Cl ligand is very labile and readily replaced by other nucleophiles such as H_2O or imidazole.[6] Namely, in the biological system, the replacement of the labile Cl ligand may be achieved by surrounding guanine residues[2] resulting in the recovery of anticancer activity of platin drugs. Interestingly, the dissociation of the Pt–S bond and the formation of a labile chloro species can also be detected using $[Pt(dien)(BAT)]^{4+}$, (dien = diethylenetriamine) in phosphate buffer in the presence of Zn^{II} or Cu^{II} ions. Therefore, these results may provide an alternative pathway in the regeneration of the active Pt complexes from the platinum–thiolate adduct, which may relate to the restoration of the anticancer activity of platin drugs in biological systems.

C.-C. Cheng thanks Academia Sinica and the National Science Council, Taiwan, ROC, for financial support.

Footnote and References

* E-mail: ccheng@chem.sinica.edu.tw

1 S. B. Howell, *Platinum and Other Metal Coordination Compounds in Cancer Chemotherapy*, Plenum, New York, 1991.
2 S. L. Bruhn, J. H. Toney and S. J. Lippard, *Prog. Inorg. Chem.*, 1990, **38**, 477.
3 K. J. Barnham, M. I. Djuran, P. d. S. Murdoch and P. J. Salder, *J. Chem. Soc., Chem. Commun.*, 1994, 721; S. S. G. E. van Boom and J. Reedijk, *J. Chem. Soc., Chem. Commun.*, 1993, 1391.
4 J. D. Ranford, M. D. Rhodes and P. J. Sadler, *The Role of Thiolate Proteins and Metal-Thiolate Complexes, Metallodrugs*, ed. M. J. Stillman, C. F. Shaw III and K. T. Suzuki, VCH, New York, 1992, p. 408.
5 M. I. Djuran, E. L. M. Lempers and J. Reedijk, *Inorg. Chem.*, 1991, **30**, 2648.
6 H. M. Brothers and N. M. Kostic, *Inorg. Chem.*, 1988, **27**, 1761.
7 M. Howe-Grant and S. J. Lippard, *Inorg. Synth.*, 1980, **20**, 101.
8 T. K. Aldridge, E. M. Stacy and D. R. McMillin, *Inorg. Chem.*, 1994, **44**, 722; J. A. Bailey, V. W. Miskowski and H. B. Gray, *Inorg. Chem.*, 1993, **32**, 369; J. A. Bailey, M. G. Hill, R. E. Marsh, V. M. Miskowski, W. P. Schaefer and H. B. Gray, *Inorg. Chem.*, 1995, **34**, 4591.
9 K. W. Jennette, J. T. Gill, J. A. Sadownick and S. J. Lippard, *J. Am. Chem. Soc.*, 1976, **98**, 6159.
10 N. Bryson, J. C. Dewan, J. Lister-James, A. G. Jones and A. Davison, *Inorg. Chem.*, 1988, **27**, 2154.
11 C. S. Dewey and R. A. Bafford, *J. Org. Chem.*, 1965, **30**, 491.
12 M. Zinic, S. Alihodzic and V. Skaric, *J. Chem. Soc., Perkin Trans. 1*, 1993, 21.
13 M. Lipowska, L. Hansen, J. A. Taylor and L. G. Marzilli, *Inorg. Chem.*, 1996, **35**, 4484.
14 E. L. M. Lempers, K. Inagaki and J. Reedijk, *Inorg. Chim. Acta*, 1988, **152**, 201.
15 K. A. Connors, *Chemical Kinetics: The study of Reaction Rates in Solution*, VCH, New York, 1st edn., 1990, p. 34.

Received in Cambridge, UK, 12th November 1997; 7/08152I

Inclusion of symmetry for the enhanced determination of crystalline structures from powder diffraction data using simulated annealing

Luis Reinaudi,[a] Raúl E. Carbonio*[b] and Ezequiel P. M. Leiva[a]

[a] Unidad de Matemática y Física, and [b] Departamento de Fisicoquímica, INFIQ, Facultad de Ciencias Químicas, Universidad Nacional de Córdoba, Agencia Postal 4, C.C. 61, 5000 Córdoba, Argentina

Significant improvements compared with the results obtained by other authors are achieved when space symmetry information obtainable from powder diffraction data is applied to the calculation of the TiO_2(anatase) and TiO_2-(rutile) structure; imposing symmetry conditions increases the number of times that the correct structure is generated in a set of runs and leads to more accuracy in the atomic positions.

Simulated annealing techniques have been shown to be very efficient for calculating crystal structures with only knowledge of the unit cell dimensions and content.[1,2] However, the computational demand of the method does not allow it to be applied to very complex structures. As the complexity of the structure increases, not only the computing time increases but also the number of times the system gets trapped in local minima. To avoid this problem it is necessary to impose more constraints to the system to force convergence to the global minimum. Concerning this subject, Deem and Newsam successfully made use of the known symmetry in their study of zeolites;[3] but these prediction methods, which are based on empirical relationships, seem to be more appropriate for specific families of materials, such as zeolites, whose topologic characteristics are well known.

In the present work we propose to optimise the method by using symmetry information, which is easily obtainable from a powder diffraction experiment, in such a way that it can be applied to a wide range of systems for which less restrictive assumptions can be made. To this purpose we chose TiO_2 (anatase), and TiO_2 (rutile) which have been already calculated by Freeman *et al.*[1]

Calculations of the lattice energy (which was initially used as the cost function) were performed using a code developed by us, which uses an Ewald summation for the coulombic term and a real space evaluation of the short range terms. Formal charges were used (Ti^{4+} and O^{2-}). Parameters for short range potentials are listed in Table 1. The minimisation was carried out using the Metropolis importance sampling algorithm.[4,5] We used a cooling algorithm defined by $T_{n+1} = \alpha T_n$, ($\alpha = 0.90$) with a starting temperature $T_0 = 1.0 \times 10^6$ K.

For anatase and when no symmetry restriction was imposed, over a total amount of 50 runs, we obtained the real structure only four times, in agreement with Freeman *et al.*[1] By imposing symmetry restrictions the number of independent variables in the cost function significantly decreases. The reason for this is that during simulation only the coordinates of a group of atoms are randomly generated, the rest are determined through space symmetry operations and consequently, those configurations with atomic coordinates which are not correlated by these symmetry operations are excluded from the configurational space.

Table 1 Short range potential model for TiO_2 (taken from ref. 6); $V(r) = A \exp(r/\rho) - Cr^{-6}$

A(Ti–O)/eV	754.2
ρ(Ti–O)/Å	0.3879
A(O–O)/eV	22764.3
ρ(O–O)/Å	0.1490
C(O–O)/eV Å^{-6}	27.88

From all the space symmetry operations present in each space group, only centring (A, B, C, I, F), screw axes of the type X_1 and glide planes can be used, the rest of space symmetry operations and all the point symmetry operations may produce the overlapping of one atom with its image generated by the symmetry operation (Deem and Newsam overcome this by using a merging term in the cost function[3]). All these particular space symmetry operations are, in principle, obtainable from the extinctions in the powder diffractogram.

We have calculated the structure of TiO_2(anatase) imposing I centring or 4_1 screw axis. By doing this, over a total of 50 runs we obtained the correct structure 30 times with the I centring and 37 with the 4_1 screw axis; which is a significant improvement compared with the results obtained with no symmetry imposition (4 out of 50). Moreover, the atomic positions are more accurate, (as compared with the experimental ones) (Table 2) obtaining thus a better starting structural model for Rietveld refinement. Fig. 1 compares the structures predicted by the calculations with and without symmetry restrictions. The former is indistinguishable from the experimental one within the accuracy of the plot.

Space symmetry operations sometimes might not be so easily obtained from the extinctions in a powder diffractogram because in structures with low symmetry the overlapping of reflections might not allow to do this unambiguously. Besides, for a primitive structure without screw axes and glide planes, all atoms contained in the unit cell must be considered in the calculations. For these reasons we also propose an additional term for the cost function, which takes into account the minimum symmetry of the crystal system independently of the Bravais lattice or space group.

This term is based on the fact that, for a given crystal structure, the structure factors [$F(hkl)$] of most sets of equivalent reflections which have the same d spacing and belong to different crystal planes must all be the same (the fact that the structure factors of a given set of reflections are all the same or not, depends on the point group; however, for each crystal system, it is always possible to find such a set of reflections).[7] For example, in the orthorhombic crystal system, the reflections 123, $\bar{1}23$, $1\bar{2}3$, $12\bar{3}$, $\bar{1}\bar{2}3$, $\bar{1}23$, $1\bar{2}\bar{3}$, $\bar{1}\bar{2}\bar{3}$ all must have the same $F(hkl)$ values. This will be true only if the distribution of atoms in the unit cell is consistent with the crystal system, otherwise different values will be obtained. In order to obtain the same weight for the different atoms within the cell we defined an $F'(hkl)$ value in which all the atomic scattering factors (f) are set equal to one. The proposed term is:

$$E_{\text{sym}} = \sum_{i_{\text{ref}}} \sum_{i_{\text{at}}} W_{i_{\text{ref}} i_{\text{at}}} \quad (1)$$

where i_{ref} runs over each set of equivalent reflections and i_{at} runs

Table 2 Atomic coordinates: experimental and calculated by different means for TiO_2 (anatase) ($a = b = 3.785$, $c = 9.515$ Å). In the last two sets (centring and screw axis) the letters show atoms related by symmetry imposed to the system

	Experimental			Calculated without symmetry			Calculated with I centring			Calculated with screw axis 4_1		
	X/a	*Y/b*	*Z/c*	*X/a*	*Y/b*	*Z/c*	*X/a*	*Y/b*	*Z/c*	*X/a*	*Y/b*	*Z/c*
Ti(1)	0.000	0.000	0.000	0.000	0.000	0.000	0.000	0.000	0.000 a	0.000	0.000	0.000 a
Ti(2)	0.500	0.500	0.500	0.336	0.336	0.500	0.500	0.500	0.500 a	0.500	0.500	0.500 a
Ti(3)	0.000	0.500	0.250	−0.165	0.501	0.250	0.000	0.500	0.250 b	0.000	0.500	0.250 a
Ti(4)	0.500	0.000	0.750	0.502	−0.163	0.750	0.500	0.000	0.750 b	0.500	0.000	0.750 a
O(1)	0.000	0.000	0.208	−0.133	−0.022	0.195	0.000	0.000	0.197 c	0.000	0.000	0.197 b
O(2)	0.000	0.000	0.792	−0.021	−0.132	0.805	0.000	0.000	0.803 d	0.000	0.000	0.803 c
O(3)	0.000	0.500	0.042	−0.032	0.479	0.055	0.000	0.500	0.053 e	0.000	0.500	0.053 c
O(4)	0.000	0.500	0.458	−0.142	0.367	0.445	0.000	0.500	0.447 f	0.000	0.500	0.447 b
O(5)	0.500	0.000	0.542	0.369	0.141	0.555	0.500	0.000	0.553 e	0.500	0.000	0.553 c
O(6)	0.500	0.000	0.958	0.479	−0.031	0.946	0.500	0.000	0.947 f	0.500	0.000	0.947 b
O(7)	0.500	0.500	0.708	0.470	0.358	0.696	0.500	0.500	0.697 c	0.500	0.500	0.697 b
O(8)	0.500	0.500	0.292	0.358	0.470	0.305	0.500	0.500	0.303 d	0.500	0.500	0.303 c

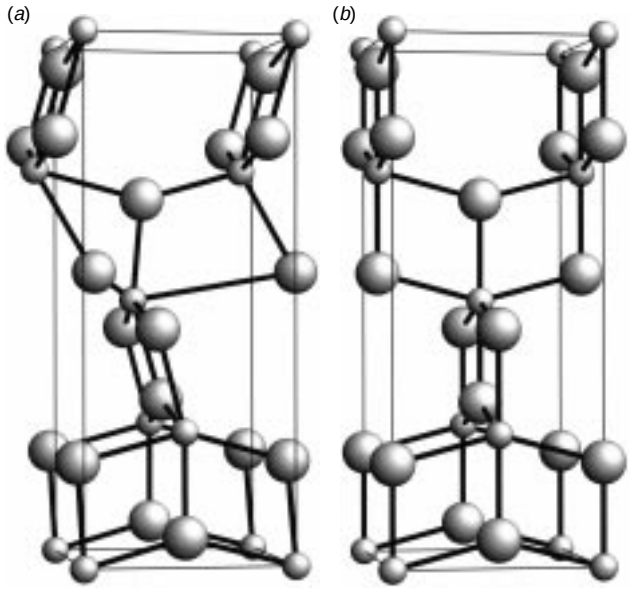

Fig. 1 Structures calculated without symmetry restrictions (*a*), and imposing I centring (*b*) for TiO_2 (anatase). Small spheres represent titanium atoms and large spheres, oxygen atoms.

over each kind of atom (in this case Ti^{4+} and O^{2-}). *W* is given by:

$$W = b\left(1 - \frac{1}{1 + a\sum_{j=1}^{K-1}\left|\left|F'_{j+1}\right| - \left|F'_j\right|\right|^n}\right) \qquad (2)$$

where *b*, *a* and *n* are adjustable parameters and F'_j is the modified structure factor corresponding to the *j*th reflection of a group of *K* equivalent reflections (reflections which should have the same structure factor for all the point group within this crystal system) and *K* is the multiplicity factor used in the powder method.[7] Each F'_j is then given by:

$$F'_j = \sum_{m=1}^{N} \exp\left[i2\pi(h_j x_m + k_j y_m + l_j z_m)\right] \qquad (3)$$

where *m* runs over the *N* atoms of a same kind and h_j, k_j, l_j are the Miller indexes of the *j*th reflection.

In eqn. (2) is observed that *W* tends to zero for distributions of atoms that are consistent with the crystal system symmetry and tends to *b* for distributions far from required symmetry.

For this particular case (tetragonal system) some of the {*hhl*} and {*h*0*l*} groups of equivalent reflections (which have a multiplicity of eight) were used[7] (use of the {*hkl*} reflections, with a multiplicity of 16, would imply a previous assumption about the point group).

For anatase, a new set of calculations was run adding an E_{sym} term corresponding to the reflections {112}, {304} and {221} and imposing I centring. The values used were $a = 1.0 \times 10^{-3}$, $b = 20.0$ eV, $n = 3$. These values were those, which led to the best minimisation of all *W* values for a set of 50 runs.

Over a total of 50 runs we obtained the correct structure 36 times. Atomic positions thus obtained are the same as those obtained with I centring only (Table 2).

For rutile, over a total of 50 runs and with no imposition of symmetry we obtained the correct structure 44 times; and when we added this symmetry term to the cost function we obtained the correct structure in all of the 50 runs, with atomic coordinates being the same as those obtained by Freeman *et al.*[1]

The predictions of crystal structures by simulated annealing based only on energetic considerations is impracticable for very complex structures, because of the large amount of local minima, which causes that incorrect structures are obtained in a large number of runs. The imposition of symmetry restrictions may decrease this number of local minima and in consequence may increase the number of times that the correct structure is obtained. Although these symmetry restrictions are expected to be more effective when dealing with a more symmetric structure, their application is general and, as these results suggest, may extend the use of simulated annealing to more complex systems.

Footnote and References

*E-mail: carbonio@fisquim.uncor.edu

1 C. M. Freeman, J. M. Newsam, S. M. Levine and C. R. A. Catlow, *J. Mater. Chem.*, 1993, **3**, 531.
2 J. Pannetier, J. Bassas-Alsina, J. Rodríguez-Carbajal and V. Caignaert, *Nature*, 1990, **346**, 242.
3 M. W. Deem and J. M. Newsam, *Nature*, 1989, **342**, 260.
4 M. P. Allen and D. J. Tildesley, *Computer Simulation of Liquids*, Oxford University Press, Oxford, 1987, p. 118.
5 *Numerical Recipes in FORTRAN*, Cambridge University Press, 1987.
6 C. R. A. Catlow, C. M. Freeman and R. L. Royle, *Physica B*, 1985, **131**, 1.
7 H. P. Klug and L. E. Alexander, *X-Ray Diffraction Procedures for Polycrystalline and Amorphous Materials*, Wiley, New York, 1974, p. 164.

Received in Cambridge, UK, 13th October 1997; 7/07351H

Is the calcium-ion catalysis of biological reoxidation of reduced PQQ purely electrostatic?†

Gudrun Schürer and Timothy Clark*

Computer-Chemie-Centrum, Institut für Organische Chemie, Friedrich-Alexander-Universität Erlangen-Nürnberg, Nägelsbachstraße 25, D-91052 Erlangen, Germany

Semiempirical (PM3) molecular orbital calculations on the mechanism of reoxidation of PQQ by triplet dioxygen suggest that the reaction can proceed purely by hydrogen-atom-transfer steps that are catalysed by the electrostatic effect of a coordinated calcium ion, rather than by an electron-transfer mechanism.

Pyrroloquinolinequinone (PQQ) **1** acts as the coenzyme in several bacterial oxidations.[1–3] It has been proposed[1–3] that the reoxidation of reduced PQQ ($PQQH_2$ **2**) is Ca-ion dependent.

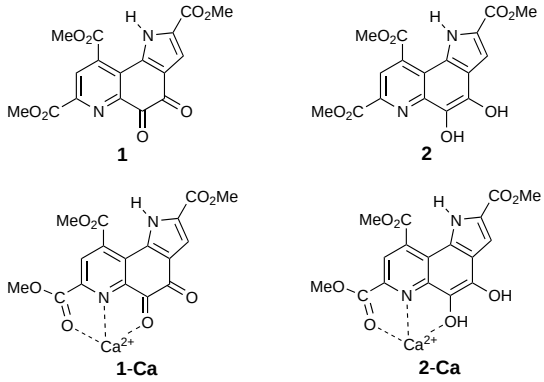

Itoh *et al.*[4] recently demonstrated the catalytic effect of Ca^{2+} on the oxidation of **2** in MeCN solution by triplet O_2. They proposed an electron-transfer mechanism on the basis of earlier suggestions[5,6] that the reaction of 1,5-dihydroflavin with $^3O_2$ must occur by a single electron-transfer (SET) mechanism. However, reaction of **2** with $^3O_2$ to give a triplet radical pair is a perfectly spin-allowed reaction and the electrostatic effect of an adjacent positive charge should be to bind electrons tighter than in the neutral compound. Furthermore, we have pointed out[7–9] that reactions of closed shell molecules with $^3O_2$ should be strongly favoured by complexation with metal cations. We now suggest that the role of Ca^{2+} in the biological reoxidation of reduced PQQ is that of an electrostatic catalyst,[9] and that the Ca-dependent enzymes that use PQQ as a coenzyme are possibly the best documented examples of this type of catalysis in biological systems.

The reaction system **2** + $^3O_2 \rightarrow$ **1** + H_2O_2 with and without complexation to Ca^{2+} was investigated using standard PM3 semiempirical MO theory[10] with VAMP6.5.[11] The unrestricted Hartree–Fock (UHF) formalism was used throughout (for both singlets and triplets) and relative energies of different spin states were also checked using configuration interaction (CI) calculations. The Ca PM3 parameters are those developed by Hehre *et al.*[12] and made available *via* the Wavefunction website. All stationary points were characterised by calculation of their normal vibrations and the reaction paths were checked by internal reaction coordinate (IRC) calculations.

The calculations were carried out with the conformations shown in the Schemes. Complexation with Ca^{2+} gives structures **1-Ca** and **2-Ca**, as found in X-ray structures of bacterial methanol dehydrogenase.[13,14] Abstraction of the OH hydrogen on C-5 in ^{1}**2** by $^3O_2$ occurs *via* transition state ^{3}**3** to give ^{3}**4** (Scheme 1; superscripts before structure numbers indicate the spin multiplicity) in the uncomplexed case with a calculated activation energy of 44.1 kcal mol^{-1} (1 cal = 4.184 J) in a reaction that is found to be endothermic by 12.1 kcal mol^{-1}, neither thermodynamically nor kinetically favourable enough to occur at room temperature in an enzymatic system.

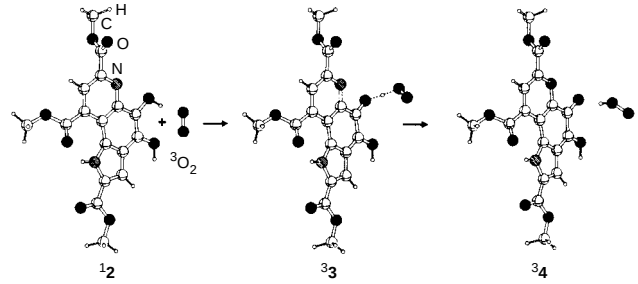

Scheme 1

The Ca-catalysed reaction **2-Ca** + $^3O_2 \rightarrow$ **4-Ca** *via* transition state **3-Ca** (Scheme 2), in contrast, requires an activation energy of only 3.9 kcal mol^{-1} and is exothermic by 33.2 kcal mol^{-1} and thus very favourable under biological conditions. Hence, both the kinetic stabilisation of the transition state arising from the charge effect on odd-electron bonds[15–18] and the thermodynamic effect of adding polar bonds to oxygen[7–9] are very effective in accelerating the reaction.

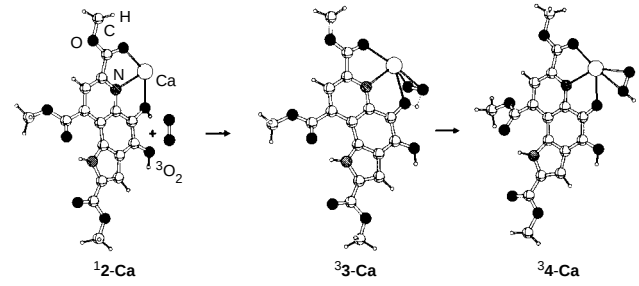

Scheme 2

Both single point CI calculations and UHF geometry optimisations of the singlet radical pairs corresponding to ^{3}**4** (^{1}**4** and ^{1}**4-Ca**) give energies that are almost degenerate with the triplet radical pairs. After geometry optimisation, ^{1}**4-Ca** is found to be 2.7 kcal mol^{-1} more stable than ^{3}**4-Ca**, so that intersystem crossing (ISC) to the singlet state should be fast, especially given the presence of the calcium ion and the oxygen centres.

After ISC, the system can transfer the second OH hydrogen to the hydroperoxy radical to give the product. In the uncomplexed system, however, this reaction occurs in two steps, as shown in Scheme 3 and Fig. 1.

In contrast, the Ca-catalysed reaction proceeds directly *via* transition state ^{1}**5-Ca** to the final product ^{1}**1-Ca** + $^3O_2$ in a

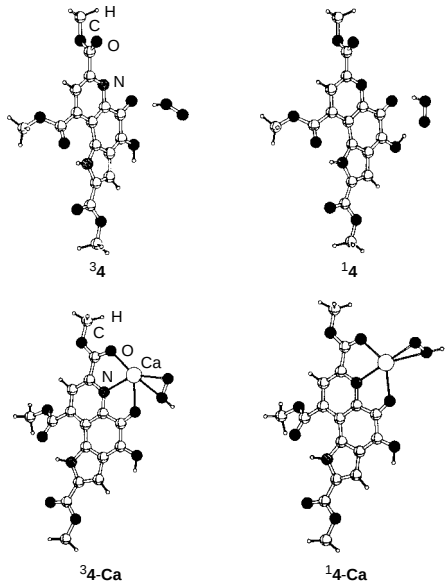

classical H-atom transfer step (Scheme 4). This reaction is calculated to have a barrier of 15.0 kcal mol^{-1}. The product is 55.2 and 19.3 kcal mol^{-1} more stable than ^{1}**4-Ca** and ^{1}**2-Ca** + $^3O_2$, respectively. The energy profiles for the two reaction paths are shown schematically in Fig. 1.

Although the SET mechanism has not been tested specifically, we believe that our calculations provide a strong indication that the role of the Ca ions in these systems is that of an electrostatic catalyst, as proposed in our model studies on

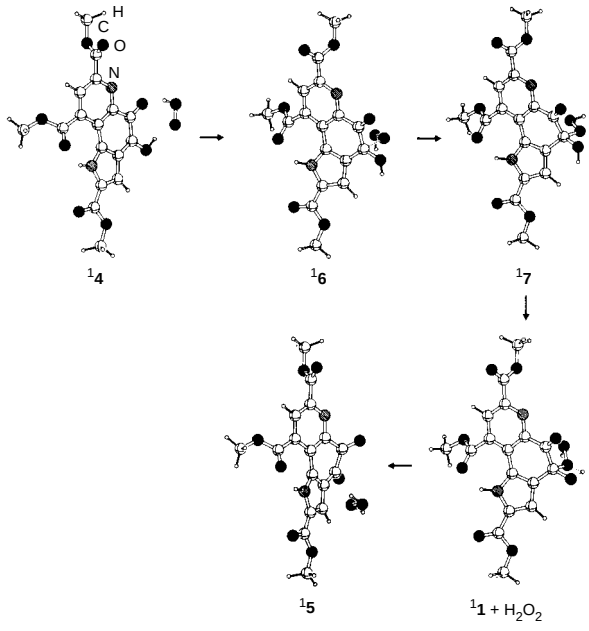

Scheme 3

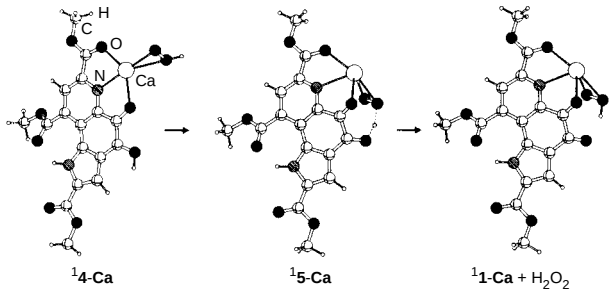

Scheme 4

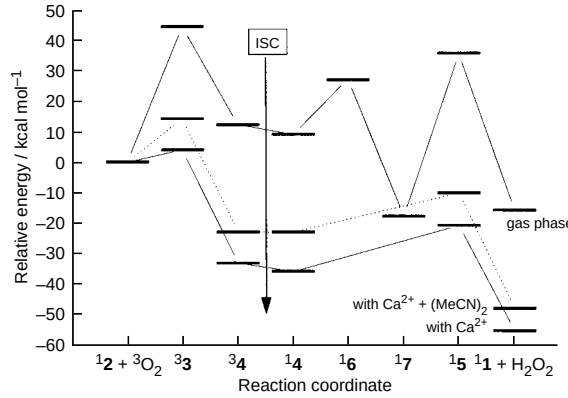

Fig. 1

methane oxidation and ethene epoxidation.[7–9] The PQQ-dependent systems therefore represent experimental examples of an effect first pointed out on the basis of model *ab initio* calculations.[7–9] We note especially that the direct formation of a covalent bond in such systems is not only spin-allowed, but is also a very facile process. There is no need to invoke an SET mechanism, especially in view of the likely fast ISC in **4-Ca**.

In order to investigate the effect of solvent, which would compete with oxygen for the complexation sites on the metal ion, we added two molecules of MeCN to the Ca-catalysed system. The energetic results are shown in Fig. 1. Although the effect of the metal is weakened somewhat, the total activation energy (14.1 kcal mol^{-1}) remains low enough for a very fast reaction at room temp.

This work was supported by the Fonds der Chemischen Industrie.

Footnotes and References

* E-mail: clark@organik.uni-erlangen.de

† This ChemComm is also available in enhanced multi-media format *via* the World Wide Web: http://www.rsc.org/ccenhanced

1 S. A. Salisbury, H. S. Forrest, W. B. T. Cruse and O. Kennard, *Nature*, 1979, **280**, 843.
2 C. Anthony, M. Ghosh and C. C. F. Blake, *Biochem. J.*, 1994, **304**, 665.
3 A. Mutzel and H. Görisch, *Agric. Biol. Chem.*, 1991, **55**, 1721; O. Geiger and H. Görisch, *Biochem. J.*, 1989, **261**, 415.
4 S. Itoh, H. Kawakami and S. Fukuzumi, *Chem. Commun.*, 1997, 29.
5 C. Kemal, T. W. Chan and T. C. Bruice, *J. Am. Chem. Soc.*, 1977, **99**, 7272; E. J. Nanni, Jr., D. T. Sawyer, S. S. Ball and T. C. Bruice, *J. Am. Chem. Soc.*, 1981, **103**, 2797; G. Eberlein and T. C. Bruice, *J. Am. Chem. Soc.*, 1982, **194**, 1449; 1983, **105**, 6685.
6 K. Maeda-Yorita and V. Massey, *J. Biol. Chem.*, 1993, **268**, 4134.
7 H. Hofmann and T. Clark, *Angew. Chem.*, 1990, **102**, 697; *Angew. Chem., Int. Ed. Engl.*, 1990, **29**, 648.
8 H. Hofmann and T. Clark, *J. Am. Chem. Soc.*, 1991, **113**, 2422.
9 T. Clark and H. Hofmann, *J. Phys. Chem.*, 1994, **98**, 13797.
10 J. J. P. Stewart, *J. Comput. Chem.*, 1989, **10**, 209; 221; 1191, **12**, 320.
11 G. Rauhut, A. Alex, J. Chandrasekhar, T. Steinke, W. Sauer, B. Beck, M. Hutter, P. Gedeck and T. Clark, VAMP 6.5, Oxford Molecular, Oxford, 1997.
12 J. Wu and W. J. Hehre, *J. Comput. Chem.*, to be submitted (implemented in SPARTAN from version 4.1 onwards).
13 S. A. White, G. D. Boyd, F. S. Mathews, Z.-X. Xia, W.-W. Dai, Y.-F. Zhang and V. L. Davidson, *Biochemistry*, 1993, **32**, 12 955; Z.-X. Xia, W.-W. Dai, Y.-F. Zhang, S. A. White, G. D. Boyd and F. S. Mathews, *J. Mol. Biol.*, 1996, **259**, 480.
14 C. C. F. Blake, M. Ghosh, K. Harlos, A. Avezoux and C. Anthony, *Nature Struct. Biol.*, 1994, **1**, 102; M. Ghosh, C. Anthony, K. Harlos, M. G. Goodwin and C. Blake, *Structure*, 1995, **3**, 177.
15 T. Clark, *J. Chem. Soc., Chem. Commun.*, 1986, 1774.
16 T. Clark, *J. Am. Chem. Soc.*, 1988, **110**, 1672.
17 A. von Onciul and T. Clark, *J. Chem. Soc., Chem. Commun.*, 1989, 1082.
18 T. Clark, *Top. Curr. Chem.*, 1995, **177**, 1.

Received in Cambridge, UK, 28th October 1997; 7/07780G

Synthesis of MCM-48 single crystals

Ji Man Kim, Seong Kyun Kim and Ryong Ryoo*

Materials Chemistry Laboratory, Department of Chemistry and Center for Molecular Science, Korea Advanced Institute of Science and Technology, Taeduk Science Town, Taejon, 305-701, Korea

Truncated rhombic dodecahedral crystals of the mesoporous molecular sieve MCM-48 are synthesised by a hydrothermal procedure using sodium silicate, hexadecyltrimethylammonium bromide and various kinds of alcohol.

The materials designated MCM-41 and MCM-48 are large-pore molecular sieves attracting much recent attention in catalysis and nanoscience.[1,2] The structure of MCM-48 consists of two independent and intricately interwoven networks of mesoporous channels,[2–5] while the structure of MCM-41 consists of hexagonal packing of one-dimensional channels. The three-dimensional channel network of MCM-48 is much more desirable than the one-dimensional channel of MCM-41 from a diffusional and catalytic point of view. However, surprisingly little research has been reported on MCM-48, compared with research on MCM-41.[6,7] We believe that this is due to the difficulty of the MCM-48 synthesis.

Here, we present a hydrothermal synthesis procedure to obtain MCM-48 readily using a sodium silicate solution as the silica source, hexadecyltrimethylammonium bromide (HTABr) as the structure-directing agent, and various kinds of alcohol such as methanol, ethanol and 2-methylpropan-2-ol as an additive for the mesophase control. The resultant MCM-48 material exhibits not only excellent structural order but also the unique crystalline morphology of a cube truncated by rhomb dodecahedron.

To prepare the silica source, colloidal silica, Ludox HS40 (39.5 mass% SiO_2, 0.4 mass% Na_2O and 60.1 mass% H_2O, Du Pont), was preheated to 343 K in a Erlenmeyer flask. An aqueous solution of 1.00 M NaOH was slowly added to the heated Ludox with vigorous magnetic stirring, to give a molar composition of 0.25 Na_2O : 1.0 SiO_2 : 12.5 H_2O for the resultant mixture. The resultant mixture became a clear sodium silicate solution after stirring continuously for *ca.* 1 h with heating to 343–353 K.[8] After further stirring for 1 h at the same temperature, the solution was cooled to room temp. and stored in a polypropylene bottle until used as the silica source.

In a typical synthesis batch, HTABr (Aldrich) was dissolved, by heating and magnetic stirring if necessary, in a mixture of doubly distilled water and ethanol to give the resulting molar composition of 1.0 HTABr : 5.0 EtOH : 120 H_2O. The above silica source was added to this surfactant solution at room temp., dropwise with vigorous magnetic stirring. The resulting gel mixture, with a molar composition of 1.4 SiO_2 : 1.0 HTABr : 0.35 Na_2O : 5.0 EtOH : 140 H_2O, was heated for 4 days at 373 K in an autoclave and subsequently cooled to 340 K. The supernatant liquid in the reaction mixture was quickly removed by decantation and filtration before further cooling. The solid product was washed quickly with hot distilled water before cooling. The product was then slurried in EtOH–HCl, filtered, washed with EtOH, dried in an oven, and calcined in air under static conditions, in the same way as described in our recent report.[9]

The product yield in a typical synthesis batch was *ca.* 50% on the basis of the silica recovery. About 50% of silica was dissolved in the supernatant liquid under the hydrothermal reaction condition. The dissolved silica had to be removed from the MCM-48 phase before cooling to below 340 K, because the cooling resulted in the formation of insoluble silicate gel and made it difficult to separate from the MCM-48 phase afterward.

Fig. 1 shows typical powder X-ray diffraction (XRD) patterns and field emission scanning electron micrographs (SEM) for MCM-48 samples obtained following the above procedure. The XRD patterns were obtained with a Cu-Kα X-ray source using a Rigaku D/MAX-III (3 kW) instrument. The field emission SEM images were obtained with a Hitachi S800 instrument. The XRD patterns in Fig. 1(*a*) indicate excellent structural order for the cubic crystallographic space group $Ia\bar{3}d$.[2–5] Fig. 1(*b*) shows a narrow distribution in the particle size around 0.3 μm for the present MCM-48 sample synthesised at 373 K. The SEM image in Fig. 1(*c*) was obtained from a MCM-48 sample after hydrothermal synthesis over 16 h at 413 K. The particle size increased markedly, compared with the sample synthesised at 373 K. It is very remarkable that the MCM-48 particles obtained at 413 K have the crystal shape of a cube truncated by rhomb dodecahedron. An activation energy of 14 kcal mol^{-1} (1 cal = 4.184 J) has been obtained from the Arrhenius plot between the crystallisation rate and the inverse of the synthesis temperature.[10] All these results show remark-

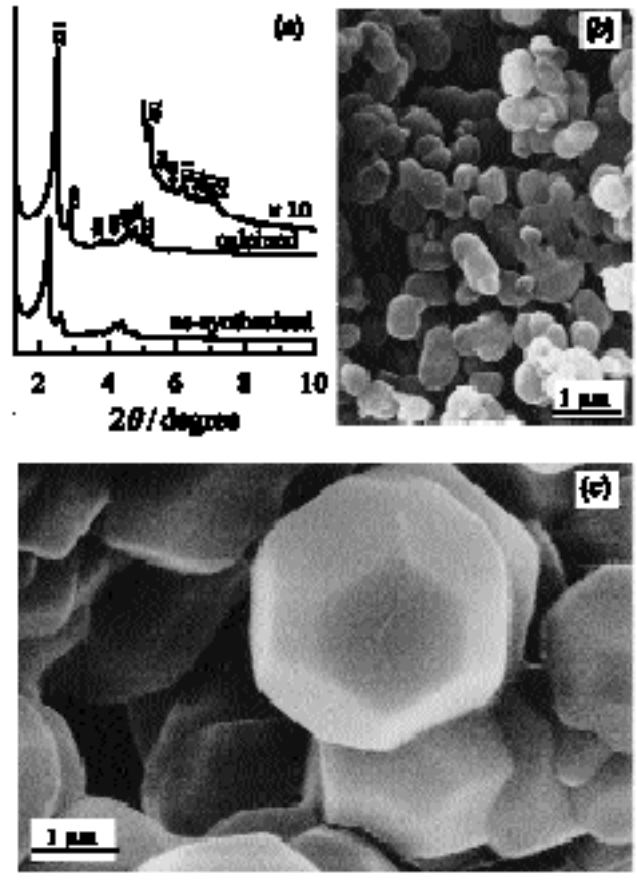

Fig. 1 (*a*) XRD patterns, (*b*) field emission SEM image for MCM-48 synthesised at 373 K and (*c*) at 413 K

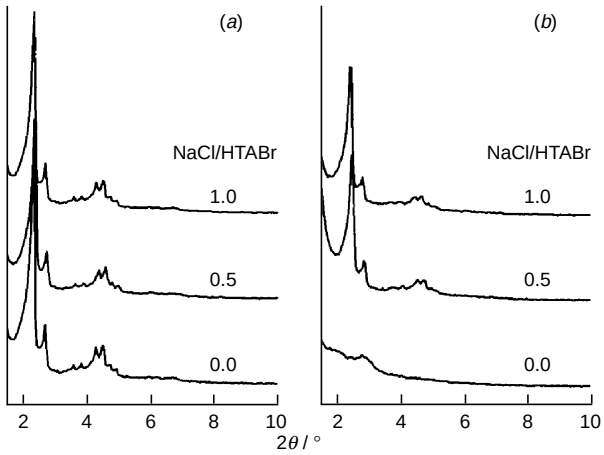

Fig. 2 XRD patterns for MCM-48 samples: (*a*) calcined and (*b*) after heating the calcined samples in distilled water at 373 K for 12 h. Numbers given to XRD patterns denote the NaCl/HTABr molar ratios used for the synthesis.

able similarities between the formation of MCM-48 particles under the present hydrothermal conditions and hydrothermal growth of other conventional zeolite crystals.

The MCM-48 phase was converted to a disordered phase when ethanol was allowed to evaporate under the present hydrothermal synthesis conditions. The role of the added ethanol in the formation of MCM-48 is the ability to cause a systematic rearrangement in the structure of the micelle by penetrating the micelle surface, just the same way as ethanol which is formed by the hydrolysis of tetraethylorthosilicate (TEOS) during the synthesis of MCM-48 with TEOS. The latter has been clarified recently by Huo *et al.*[11] using Cab-o-sil in place of TEOS as the silica source in the presence of other polar organic additives such as $Me_2NCH_2CH_2OH$ and $N(CH_2CH_2OH)_3$. The use of tetramethylorthosilicate instead of TEOS did not give MCM-48, and the result was attributed to the high polarity and hydrophilicity of the resulting methanol so that it could not penetrate the micelle surface. However, methanol is more effective for the formation of MCM-48 than ethanol. The substitution of 5.0 EtOH with 3.0 MeOH in our synthesis procedure described above gave just the same high-quality MCM-48 material. The EtOH could also be substituted by appropriate amounts of higher alcohol such as 1.5 Pr^iOH, 0.3 Bu^sOH and 0.3 Bu^tOH. All MCM-48 materials obtained with the alcohol showed similar BET surface areas in the range of 1000 ± 50 m^2 g^{-1}. However, the use of the higher alcohol resulted in a somewhat lower XRD peak resolution, compared with the use of EtOH and MeOH.

MCM-41 or a disordered mesoporous material[12] was obtained instead of MCM-48 when the amount of alcohol was insufficient. The use of excess alcohol resulted, on the other hand, in the formation of a lamellar phase. We have confirmed that MCM-48 can be obtained within a wide range of the gel composition, $x\ SiO_2 : 0.25x\ Na_2O : 1.0\ HTABr : 0.035y\ EtOH : y\ H_2O$ in a temperature range of 373–413 K, where x and y can be varied over 1.2–3.0 and 70–400, respectively. The formation of the MCM-48 phase followed a typical zeolite crystallisation curve, reaching a maximum in 4 d at 373 K. Subsequently, the MCM-48 phase was converted to a lamellar phase. At 413 K, the MCM-48 formation was accomplished in 16 h.[10]

After heating in boiling water for 12 h, our calcined samples gave no XRD patterns indicating the MCM-48 structure. This was due to the low hydrothermal stability of the MCM-48 samples.[13] The hydrothermal stability of the MCM-48 can be improved by using NaCl, similar to the salt effect for MCM-41.[14] To demonstrate this, the autoclave was cooled to room temp. after heating for 3.5 d at 373 K. The reaction mixture in the autoclave was then added to a conc. NaCl solution with magnetic stirring, to give NaCl/HTA = 0.1–1.0. The autoclave was closed and heated again for 1.5 d. The results are shown in Fig. 2.

This work was supported by Korea Science and Engineering Foundation. The authors thank Korea Material Analysis Co. for field emission SEM.

Footnote and References

* E-mail: rryoo@sorak.kaist.ac.kr

1 C. T. Kresge, M. E. Leonowicz, W. J. Roth, J. C. Vartuli and J. S. Beck, *Nature*, 1992, **359**, 710.
2 J. S. Beck, J. C. Vartuli, W. J. Roth, M. E. Leonowicz, C. T. Kresge, K. D. Schmitt, C. T.-W. Chu, D. H. Olson, E. W. Sheppard, S. B. McCullen, J. B. Higgins and J. L. Schlenker, *J. Am. Chem. Soc.*, 1992, **114**, 10 834.
3 A. Monnier, F. Schüth, Q. Huo, D. Kumar, D. Margolese, R. S. Maxwell, G. D. Stucky, M. Krishnamurty, P. Petroff, A. Firouzi, M. Janicke and B. F. Chmelka, *Science*, 1993, **261**, 1299.
4 V. Alfredsson and M. W. Anderson, *Chem. Mater.*, 1996, **8**, 1141.
5 R. Ryoo and C. H. Ko, *Chem. Commun.*, 1996, 2467.
6 A. Sayari, *Stud. Surf. Sci. Catal.*, 1996, **102**, 1.
7 X. S. Zhao, G. Q. Lu and G. J. Millar, *Ind. Eng. Chem. Res.*, 1996, **35**, 2075.
8 R. Ryoo and J. M. Kim, *J. Chem. Soc., Chem. Commun.*, 1995, 711.
9 R. Ryoo, S. Jun, J. M. Kim and M. J. Kim, *Chem. Commun.*, 1997, 2225.
10 J. S. Kim, S. K. Kim and R. Ryoo, manuscript in preparation.
11 Q. Huo, R. Leon, P. M. Petroff and G. D. Stucky, *Science*, 1995, **268**, 1324.
12 R. Ryoo, J. M. Kim, C. H. Ko and C. H. Shin, *J. Phys. Chem.*, 1996, **100**, 17718.
13 J. M. Kim and R. Ryoo, *Bull. Korean Chem. Soc.*, 1996, **17**, 66.
14 S. Jun and R. Ryoo, *J. Phys. Chem. B*, 1997, **101**, 317.

Received in Cambridge, UK, 23rd October 1997; 7/07677K

Synthesis and structure of [{$(Bu^tO)_2Sb_3(\mu\text{-}NCy)_3(\mu_3\text{-}NCy)$}K·$\eta^6$-$C_6H_5Me$]; a sandwich complex containing a unique Sb^{III} *nido* cage anion (Cy = cyclohexyl, C_6H_{11})

Michael A. Beswick,[a] Nick Choi,[b] Alexander D. Hopkins,[a] Mary McPartlin,[b] Michael A. Paver[a] and Dominic S. Wright*[a]

[a] *Chemical Laboratory, University of Cambridge, Lensfield Road, Cambridge, UK CB2 1EW*
[b] *School of Applied Chemistry, University of North London, Holloway Road, London, UK N7 8DB*

Reaction of the terminal NMe_2 groups of the *spiro* antimony(III) imido anion [{$(Me_2N)Sb(\mu\text{-}NCy)$}$_2$Sb]$^-$ with Bu^tOH results in major rearrangement in the Sb–N framework as witnessed in the structure of the sandwich complex [{$(Bu^tO)_2Sb_3(\mu\text{-}NCy)_3(\mu_3\text{-}NCy)$}K·$\eta^6$-$C_6H_5Me$] 1, containing the novel *nido* cage anion [$(Bu^tO)_2Sb_3(\mu\text{-}NCy)_3(\mu_3\text{-}NCy)$]$^-$.

We have recently investigated the structures and coordination chemistry of imido and phosphinidene anions of p block metals (group 13–15).[1–3] These species are readily prepared by the reactions of primary amido or phosphido lithium complexes, [REHLi] (E = N, P), with dimethylamido metal reagents or neutral metal imido cages and function as relatively robust ligands for a range of main group and transition metal ions.[4] For example, the transmetallation reaction of [{$Sb(NCy)_3$}$_2$$Li_6$] (Cy = cyclohexyl) with [$PbCp_2$] gives the cage [Pb_3{$Sb(NCy)_3$}$_2$], in which the [$Sb(NCy)_3$]$^{3-}$ trianions of the alkali metal precursor are transferred intact to Pb^{II}.[4a] Reactions of this type therefore provide a general strategy for the assembly of heterometallic cage compounds containing diverse mixed-metal stoichiometries. A current interest in this area concerns the factors controlling the formation and stability of these new ligand systems.[5] To this end we report here the investigation of the effects of ligand substitution on the SbN framework of one such anion arrangement, the *spiro* monoanion [{$(Me_2N)Sb(\mu\text{-}NR)_2$}$_2$Sb]$^-$.[3b]

The reaction of [{$(Me_2N)Sb(\mu\text{-}NR)_2$}$_2$Sb]K with [$Bu^tOH$] (1 : 2 equiv.) gives [{$(Bu^tO)_2Sb_3(\mu\text{-}NCy)_3(\mu_3\text{-}NCy)$}K·$\eta^6$-$C_6H_5Me$] **1**, for which spectroscopic and analytical analysis suggests that simple ligand exchange of the terminal NMe_2 groups of the precursor has occurred.† However, subsequent X-ray structural investigation of **1** reveals that ligand substitution is accompanied by isomerism of the initial *spiro* structure of the anion in to a *nido* cage arrangement (Scheme 1). It is interesting to note that the *spiro* structure of the precursor is preserved upon substitution with NHR groups.[4a] It therefore appears that this rearrangement is a consequence of the increased Lewis acidity of the O-attached Sb centres, with the *nido* structure of the anion of **1** maximising their coordination numbers. The same effect can also be seen to underlie the coordination of $NHMe_2$ to Sb^{III} in [$(Me_2NH)ClSb(\mu\text{-}NBu^t)$]$_2$ (during the reaction of [$(Me_2N)_2ClSb$] with NH_2Bu^t)[6] and the aggregation of [Cl_3SbNMe]$_4$ in to a cubane (as opposed to a dimer) structure.[7] However, the formation of **1** provides, to our knowledge, the first intramolecular example of the structure-directing influence of the electronegativity of substituents on cage geometry within such a p-block metal system.

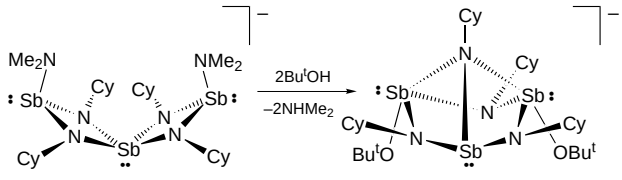

Scheme 1

The low-temperature X-ray structure of **1**‡ shows it to be the ion-contacted complex [{$(Bu^tO)_2Sb_3(\mu\text{-}NCy)_3(\mu_3\text{-}NCy)$}K·$\eta^6$-$C_6H_5Me$], in which the K^+ cation is coordinated at the open Sb_3N_3 face of the *nido* [$(Bu^tO)_2Sb_3(\mu\text{-}NCy)_3(\mu_3\text{-}NCy)$]$^-$ anion and by a π-bonded toluene molecule (Fig. 1). The [$(Bu^tO)_2Sb_3(\mu\text{-}NCy)_3(\mu_3\text{-}NCy)$]$^-$ anion of **1** is composed of three Sb^{III} centres which are linked together in the equator by three μ-NCy groups and capped by a μ_3-NCy group. In addition, Sb(1)

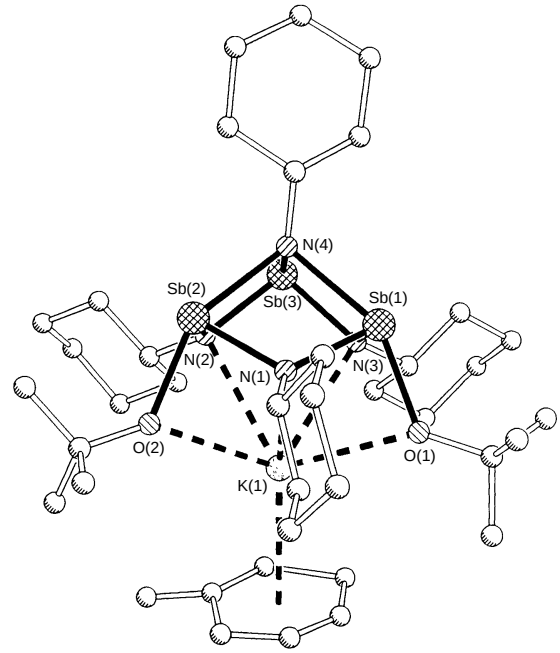

Fig. 1 Structure of **1**. H atoms have been omitted for clarity. Only major core components of the Bu^t group [on O(2)] and of the toluene molecule are shown. Key bond lengths (Å) and angles (°): Sb(1)–N(1) 2.064(5), Sb(1)–N(3) 2.090(5), Sb(1)–N(4) 2.335(5), Sb(1)–O(1) 2.113(4), Sb(2)–N(1) 2.061(5), Sb(2)–N(2) 2.077(5), Sb(2)–N(4) 2.311(4), Sb(2)–O(2) 2.122(4), Sb(3)–N(2) 2.027(5), Sb(3)–N(3) 2.025(5), Sb(3)–N(4) 2.033(5), K(1)–N(1) 2.718(5), K(1)–N(2) 2.991(5), K(1)–N(3) 2.953(5), K(1)–O(1) 2.942(4), K(1)–O(2) 2.865(4), K(1)···C 3.20–3.47, arene(centroid)···K 3.03; N(1)–Sb(1)–N(3) 98.9(2), N(1,3)–Sb(1)–N(4) av. 74.3, O(1)–Sb(1)–N(4) 147.6(2), N(1,3)–Sb(1)–O(1) av. 85.0, N(1)–Sb(2)–N(2) 100.5(2), N(1,2)–Sb(2)–N(4) av. 75.0, O(2)–Sb(2)–N(4) 146.0(2), N(1,2)–Sb(2)–O(2) 83.5(2), N(2)–Sb(2)–N(3) 92.5(2), N(2,3)–Sb(3)–N(4) av. 81.6, Sb(1)–N(4)–Sb(2) 95.3(2), Sb(1)–N(4)–Sb(3) 98.2(2), Sb(2)–N(4)–Sb(3) 97.9(2), N(1)–K(1)–N(2) 67.6(1), N(1)–K(1)–N(3) 67.5(1), N(1)–K(1)–O(1) 60.0(1), N(1)–K(1)–O(2) 59.8(1), O(1)–K(1)–N(3) 107.6(1), O(2)–K(1)–N(2) 107.9(1), O(1)–K(1)–O(2) 118.7(1).

and Sb(2) are bonded to terminal OBu^t groups [Sb(1,2)–O av. 2.12 Å], resulting in 10e pseudo-trigonal bipyramidal geometries for these centres and with Sb(3) adopting an 8e pyramidal geometry. Although the majority of the Sb–N bond lengths in **1** fall in a narrow range [2.027(5)–2.090(5) Å], longer Sb–N bonds occur between the μ_3-NCy group and the four-coordinate Sb centres [Sb(1)–N(4) 2.335(5), Sb(2)–N(4) 2.311(4) Å]. These correspond to the use of orbitals by Sb(1) and Sb(2) at an axial position of their pseudo-trigonal bipyramidal environments. The overall arrangement of the imido antimony(III) anion fragment of **1** is similar to that occurring in the neutral, isoelectronic complex $[Cl_2Sb_2Se(\mu\text{-}NBu^t)_3(\mu_3\text{-}NBu^t)]$, formed by the desilylation reaction of $[Se\{NBu^t(SiMe_3)\}_2]$ with $SeCl_2$.[8]

The bonding of the imido antimony(III) anion of **1** to the K^+ cation is very asymmetrical. The shortest contact between the imido antimony(III) anion and the K centre occurs with N(1) [2.718(5) Å] and is typical of those found in a range of amido potassium compounds.[9] However, far weaker interactions occur between the K^+ cation and the remaining N centres of the Sb_3N_3 face of the anion [N(2)–K(1) 2.991(5), N(3)–K(1) 2.953(5) Å]. In addition, the O atoms of the pendant OBu^t groups only weakly coordinate the K^+ cation {O(1)–K(1) 2.942(4), O(2)–K(1) 2.865(4) Å; *cf.* 2.788(8) Å for the thf O–K bonds in $[\{(RNH)Sb(\mu\text{-}NR)_2\}_2Sb]K\cdot 2thf$[10]}. This arrangement leaves the K^+ cation open to further coordination by the η^6-toluene ligand. Similar ion–dipole interactions of aromatic ligands with K^+ are well known in a variety of complexes, with typical centroid···K^+ distances lying in the range 3.18–3.59 Å.[11] The shortness of the arene···K interactions in **1** [centroid···K(1) 3.03 Å, K···C 3.20–3.47 Å] is a further reflection of the overall weakness of the interaction of the imido antimony(III) anion with the K^+ cation and of its sterically uncongested environment.

Clearly there are considerable differences between the electron-precise bonding present in the *nido* $[(Bu^tO)_2Sb_3(\mu\text{-}NCy)_3(\mu_3\text{-}NCy)]^-$ anion of **1** and structurally similar electron deficient borane ligands such as *nido*-2,3- and 2,4-$[R_2C_2B_4H_4]^{2-}$.[12] However, their geometric similarity and the fact that the $[Sb(\mu\text{-}NCy)]_3$ face (although localised) is isoelectronic with the open C_2B_3 face of the latter suggests that the *nido* $[(Bu^tO)_2Sb_3(\mu\text{-}NCy)_3(\mu_3\text{-}NCy)]^-$ anion may perform an analogous structural role as a building block in metal complexes.[13] In this regard, the structure of **1** which can be viewed as a mixed-ligand sandwich complex of K^+, provides an initial indication of this behaviour.

We gratefully acknowledge the EPSRC (M. A. B., A. D. H.), the Royal Society (D. S. W.) and Electron Tubes, Ruislip, UK (Case award for A. D. H.) for financial support.

Footnotes and References

* E-mail: DSW1000@cam.ac.uk

† *Synthesis* of **1**: to a solution of $[\{(Me_2N)Sb(\mu\text{-}NCy)_2\}_2Sb]Li$ (0.77 g, 0.91 mmol) in toluene (10 ml) was added Bu^{t}OK (0.10 g, 0.91 mmol). Stirring the solution at room temp. gave a change from yellow to orange. To this was added Bu^{t}OH (0.18 ml, 1.82 mmol) and the mixture was brought briefly to reflux and stirred at room temp. (24 h). The solvent was removed under vacuum and the colourless solid produced was dissolved in hexane (5 ml) and toluene (2 ml). Storage at −18 °C (48 h) gave colourless crystals of **1**. The low yield of crystalline **1** (0.22 g, 23%) is due to its high solubility; mp 130 °C; ^{1}H NMR (250 MHz, C_8D_6, 25 °C), δ 7.0 (m, 5 H, aryl C–H, toluene), 2.40 (m, 4 H, C$^\alpha$-H, μ-NCy), 2.11 (s, 3 H, Me, toluene), *ca.* 1.9–0.9 (overlapping m, 40 H, CH_2, Cy), 1.49 (s, 18 H, Bu^t). Found: C, 43.1; H, 6.6; N, 5.3. Calc. for $[C_{32}H_{62}KN_4O_2Sb_3.C_7H_8]_n$: C, 45.4; H, 6.8; N, 5.4%.

¶ *Crystal data* for **1**: $C_{39}H_{70}KN_4O_2Sb_3$, M = 1031.34, monoclinic, space group $P2_1/c$, a = 18.749(1), b = 13.113(1), c = 18.848(2) Å, β = 103.831(7)°, U = 4499.5(7) Å^3, Z = 4, D_c = 1.522 Mg m^{-3}, λ = 0.710 73 Å, T = 203(2) K, μ(Mo-Kα) = 1.915 mm^{-1}, $F(000)$ = 2080. Data were collected on a Siemens P4 diffractometer using an oil-coated rapidly cooled crystal[14] of dimensions 0.60 × 0.50 × 0.40 mm by the θ–2ω method (1.91 ≤ θ ≤ 25.00°). Of a total of 9158 collected reflections, 7727 were independent (R_{int} = 0.0512). The structure was solved by direct methods; all non-hydrogen atoms were refined with anisotropic displacement parameters and all hydrogen atoms were placed in idealised geometry riding on the relevant carbon atoms. The structure has a disordered Bu^t group [on O(2)] (*ca.* 60 : 40); the ring atoms of each disordered toluene component were fixed in a regular hexagonal geometry (C–C 1.39 Å). In the crystal the ion-contacted units of **1** are arranged in centrosymmetric pairs held together by π stacking interactions of the aryl rings with centroid offset distance of 1.27 Å (mean) and centroid···centroid distance 3.80 Å (mean). 421 parameters were refined on F^2 to final conventional R_1 = 0.043 [$F > 4\sigma(F)$] and wR_2 = 0.120 (all data) [$R_1 = \Sigma|F_o - F_c|/\Sigma F_o$ and $wR_2 = [\Sigma w(F_o^2 - F_c^2)^2/\Sigma w(F_o^2)^2]^{0.5}$, $w = 1/[\sigma^2(F_o^2) + (xP)^2 + yP]$, $P = F_o^2 + (2F_c^2/3)$], x = 0.0636, y = 5.28, $P = (F_o^2 + 2F_c^2)/3$;[15] largest peak and hole in the final difference map, 0.999 and −0.897 e Å^{-3}. CCDC 182/699.

1 R. E. Allan, M. A. Beswick, P. R. Raithby, A. Steiner and D. S. Wright, *J. Chem. Soc., Dalton Trans.*, 1996, 4135.
2 R. E. Allan, M. A. Beswick, N. L. Cromhout, M. A. Paver, P. R. Raithby, A. Steiner and D. S. Wright, *Chem. Commun.*, 1996, 1501; R. E. Allen, M. A. Beswick, N. Feeder, M. Kranz, M. E. L. G. Mosquera, P. R. Raithby and D. S. Wright, unpublished work.
3 (*a*) R. A. Alton, D. Barr, A. J. Edwards, M. A. Paver, M.-A. Rennie, C. A. Russell, P. R. Raithby and D. S. Wright, *J. Chem. Soc., Chem. Commun.*, 1994, 1481; (*b*) A. J. Edwards, M. A. Paver, M.-A. Rennie, C. A. Russell, P. R. Raithby and D. S. Wright, *Angew. Chem.*, 1994, **106**, 1334; *Angew. Chem., Int. Ed. Engl.*, 1994, **33**, 1277; (*c*) D. Barr, M. A. Beswick, A. J. Edwards, J. R. Galsworthy, M. A. Paver, M.-A. Rennie, C. A. Russell, P. R. Raithby, K. L. Verhorevoort and D. S. Wright, *Inorg. Chim. Acta*, 1996, **248**, 9; (*d*) M. A. Paver, C. A. Russell and D. S. Wright, *Angew. Chem.*, 1995, **107**, 1077; *Angew. Chem., Int. Ed. Engl.*, 1955, **34**, 1545; (*e*) M. A. Beswick, C. N. Harmer, A. D. Hopkins, M. A. Paver, P. R. Raithby, A. E. H. Wheatley and D. S. Wright, *Angew. Chem.*, submitted.
4 (*a*) M. A. Beswick, C. N. Harmer, M. A. Paver, P. R. Raithby, A. Steiner and D. S. Wright, *Inorg. Chem.*, 1997, **36**, 1740; (*b*) D. Barr, A. J. Edwards, S. Pullen, M. A. Paver, P. R. Raithby, M.-A. Rennie, C. A. Russell and D. S. Wright, *Angew. Chem.*, 1994, **106**, 1960; *Angew. Chem., Int. Ed. Engl.*, 1994, **33**, 1875; (*c*) A. J. Edwards, M. A. Paver, M.-A. Rennie, C. A. Russell, P. R. Raithby and D. S. Wright, *Angew. Chem.*, 1995, **107**, 1088; *Angew. Chem., Int. Ed. Engl.*, 1995, **34**, 1012.
5 N. D. R. Barnett, W. Clegg, L. Horsburgh, D. M. Linsay, Q.-Y. Liu, F. M. McKenzie, R. E. Mulvey and P. G. Williard, *Chem. Commun.*, 1996, 2321.
6 A. J. Edwards, N. E. Leadbeater, M. A. Paver, P. R. Raithby, C. A. Russell and D. S. Wright, *J. Chem. Soc., Dalton Trans.*, 1994, 1479; A. J. Edwards, M. A. Paver, M.-A. Rennie, P. R. Raithby, C. A. Russell and D. S. Wright, *J. Chem. Soc., Dalton Trans.*, 1994, 2963.
7 W. Neubert, H. Pritzkow and H. P. Latscha, *Angew. Chem.*, 1988, **100**, 298; *Angew. Chem., Int. Ed. Engl.*, 1988, **27**, 287.
8 M. Björgvinsson, H. W. Roesky, G. M. Sheldrick and F. Pauer, *Chem. Ber.*, 1992, **123**, 767.
9 See for example: K. Gregory, M. Bremer, P. v. R. Schleyer, P. A. A. Klusener and L. Brandsma, *Angew. Chem.*, 1989, **101**, 1261; *Angew. Chem., Int. Ed. Engl.*, 1989, **28**, 1224.
10 A. Bashall, M. A. Beswick, C. N. Harmer, A. D. Hopkins, M. E. G. Moquera, M. A. Paver, M. McPartlin and D. S. Wright, unpublished work.
11 See for example: C. J. Schavevien and J. B. van Mechelen, *Organometallics*, 1991, **10**, 1704; G. R. Fuentes, P. S. Coan, W. E. Streith and K. G. Caulton, *Polyhedron*, 1991, **10**, 2371; M. J. Geary, R. H. Cayton, K. Folting, J. C. Huffman and K. G. Caulton, *Polyhedron*, 1992, **11**, 1369; P. B. Hitchcock, M. F. Lappert, G. A. Lawless and B. Royo, *J. Chem. Soc., Chem. Commun.*, 1993, 554.
12 R. N. Grimes, *Comprehensive Organometallic Chemistry; Transition Metal Metallacarboranes*, ed. C. E. Housecroft, Pergamon, 1995, vol. 1, ch. 9, p. 373.
13 See for example: A. R. Oki, H. Zhang and N. S. Hosmane, *Angew. Chem.*, 1992, **104**, 441; *Angew. Chem., Int. Ed. Engl.*, 1992, **31**, 432; A. R. Oki, H. Zhang and N. S. Hosmane, H. Ro and W. E. Hatfield, *J. Am. Chem. Soc.*, 1991, **113**, 8531.
14 D. Stalke and T. Kottke, *J. Appl. Crystallogr.*, 1993, **26**, 615.
15 G. M. Sheldrick, SHELXL-93, structure refinement package, University of Göttingen, 1993.

Received in Cambridge, UK, 6th October 1997; 7/08083B

Two new nickel–dmit-based molecular conductors based on heteroleptic polymetallic complexes: synthesis, structures and electrical properties

Tianlu Sheng, Xintao Wu,* Wenjian Zhang, Quanming Wang, Xiancheng Gao and Ping Lin

State Key Laboratory of Structural Chemistry, Fujian Institute of Research on the Structure of Matter, The Chinese Academy of Sciences, Fuzhou, Fjuian, 350002, PR China

Two heteroleptic dmit complexes of polynuclear nickel(II), $[NEt_4]_2[Ni_5(edt)_4(dmit)_2]$ and $[AsPh_4]_2[Ni_3(pdt)_2(dmit)_2]\cdot 0.5MeOH$ (dmit = 2-thione-1,3-dithiole-4,5-dithiolate, H_2edt = ethane-1,2-dithiol, H_2pdt = propane-1,2-dithiol) are synthesized and characterized by X-ray crystallography and display room-temperature conductivities of 1.75×10^{-4} and 1.52×10^{-5} S cm^{-1}; this is the first report of semiconducting heteroleptic dmit complexes consisting of more than two nickel(II) centres.

During the search for new complexes with novel electric properties, metal complexes of the dmit ligand have received considerable attention[1,2] since some of them were reported to exhibit conductivities and even superconductivities.[3–7] Some non-planar metal–dmit complexes have also been reported to exhibit high conductivities.[8] Recently, it has been shown that intermolecular interactions in transition metal bis(dithiolate) complexes of this type are also important for the assembly of molecular ferromagnets.[9] A large number of metal–dmit complexes have been synthesized and structurally characterized but many of them are homoleptic. To our knowledge, heteroleptic polymetallic complexes of dmit in particular, are rare. These types of complexes reported in the literature are restricted to $[NBu_4]_2[Ni_2(C_2S_4)(dmit)_2]$,[10] $[Au_4(dmit)_2(Ph_2PCH_2PPh_2)_2]$ and $[Au_3(PPh_3)_3(dmit)]$.[11] We have now investigated whether dithiolate can be used as a bridging ligand to synthesize heteroleptic polymetallic complexes with dmit. As two examples, two heteroleptic nickel(II) derivatives $[NEt_4]_2[Ni_5(edt)_4(dmit)_2]$ **1** and $[AsPh_4]_2[Ni_3(pdt)_2(dmit)_2]\cdot 0.5MeOH$ **2**, were formed by using edt or pdt as bridging ligands; this is the first report of heteroleptic dmit complexes consisting of more than two nickel(II) centres.

4,5-Bis(benzoylthio)-1,3-dithiole-2-thione (prepared according to the detailed procedures described by Steimecke *et al.*[12]) (0.408 g, 1.0 mmol) was dissolved in a methanol solution (30 ml) containing sodium (0.046 g, 2.0 mmol). To the resulting purple–red solution of Na_2dmit was added H_2edt (0.06 ml, 1.4 mmol) and then $NiCl_2\cdot 6H_2O$ (0.24 g, 1.0 mmol) to give a purple solution. After stirring for 6 h at room temp. a methanol solution (10 ml) of NEt_4Br (0.2 g, 1.0 mmol) was added leading to the precipitation of a purple product. This was collected by filtration and redissolved in dmf (10 ml); then it was filtered after stirring for several minutes. This filtrate was diffused with Et_2O at room temp. for ten days, after which 0.12 g of black crystals of **1** were obtained. The preparation of complex **2** was similar to that of **1**, H_2edt and NEt_4Br being replaced by H_2pdt and $AsPh_4Cl$, respectively. The red precipitate was collected by filtration and redissolved in Me_2CO (10 ml) and then filtered after stirring for several min. The filtrate was diffused with Et_2O at room temp. for ten days after which 0.35 g of black crystals of **2** were obtained.†

The structures of **1** and **2** were established by single-crystal X-ray diffraction analysis‡ and reveal the edt or pdt ligands in bridging modes chelated to Ni atoms and dmit ligands coordinated to edge Ni atoms. The anions of **1** and **2** together with selected bond parameters are depicted in Figs. 1 and 2. In **1**, the anion occupies a crystallographic inversion center, the five Ni atoms are bridged by four edt ligands, Ni(1), Ni(2) and Ni(2′) are square-planar coordinated to four S atoms of edt ligands and both the edge Ni atoms are square-planar coordinated to two S atoms of edt ligands and to two S atoms from one dmit ligand. From the configuration of the five Ni atoms and two dmit ligands, the anion can be described as consisting of an $Ni_3(edt)_4^{2-}$ unit to which are *trans* attached two $Ni(dmit)_2$ fragments, the angle Ni(1)–Ni(2)–Ni(3) [Ni(1)–Ni(2′)–Ni(3′)] being 102.83°. The Ni···Ni bond distances are 2.852(1) and 2.817(1) Å and are slightly shorter than that in $[PPh_4]_2[Ni_2(edt)_3]$ **3**[17] [2.914(1) Å] and comparable to the distances in $[PPh_4]_2[Ni_3(edt)_4]$ **4**[18] [2.856(1) Å]. The Ni–S bond distances vary from 2.151(3) to 2.227(3) Å which are comparable to the Ni–S bond distances in **3**[17] [2.158(2)–2.221(2) Å] and **4**[18] [2.174(1)–2.210(1) Å] as well as

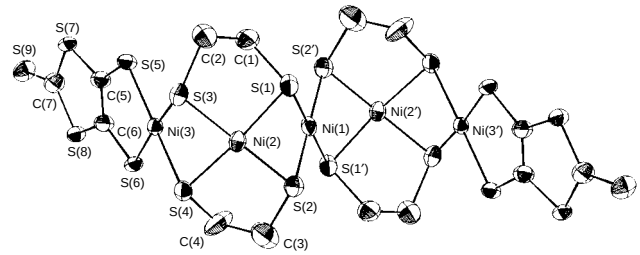

Fig. 1 ORTEP diagram of the anion of **1** (25% displacement ellipsoids). Selected bond lengths (Å) and angles (°): Ni(1)–Ni(2) 2.852(1), Ni(2)–Ni(3) 2.817(1), Ni(1)–S(1) 2.213(3), Ni(1)–S(2) 2.215(3), Ni(2)–S(1) 2.169(3), Ni(2)–S(2) 2.151(3), Ni(2)–S(3) 2.159(3), Ni(2)–S(4) 2.160(3), Ni(3)–S(3) 2.222(3), Ni(3)–S(4) 2.227(3), Ni(3)–S(5) 2.174(3), Ni(3)–S(6) 2.171(3); Ni(1)–Ni(2)–Ni(3) 102.83.

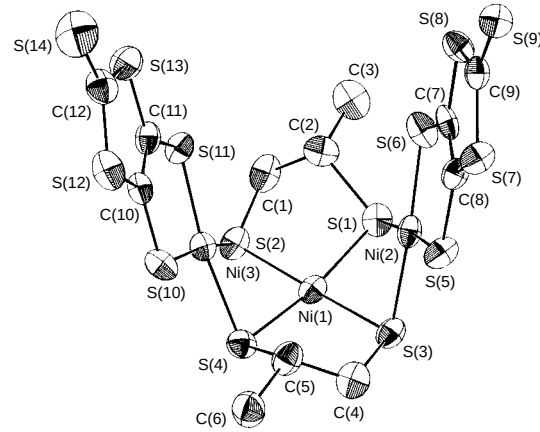

Fig. 2 ORTEP diagram of the anion of **2** (25% displacement ellipsoids). Selected bond lengths (Å) and angles (°): Ni(1)–Ni(3) 2.792(2), Ni(1)–Ni(2) 2.812(2). Ni(1)–S(1) 2.143(3), Ni(1)–S(2) 2.149(3), Ni(1)–S(3) 2.156(3), Ni(1)–S(4) 2.184(3), Ni(2)–S(5) 2.161(3), Ni(2)–S(6) 2.167(3), Ni(2)–S(1) 2.244(3), Ni(2)–S(3) 2.245(3), Ni(3)–S(11) 2.151(3), Ni(3)–S(10) 2.176(3), Ni(3)–S(2) 2.223(3), Ni(3)–S(4) 2.240(3); Ni(3)–Ni(1)–Ni(2) 102.47(5).

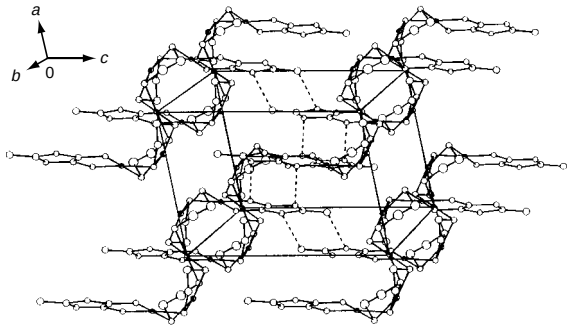

Fig. 3 The packing of **1** in the crystal. Dashed lines indicate non-bonded S···S contacts < 3.7 Å, the cations are omitted for clarity.

in $[AsPh_4]_2[Ni_2(S_2C_4)\{S_2C_2S_2C_2(CO_2Me)_2\}_2]$[19] and $[NBu_4]_2[Ni_2(C_2S_4)(dmit)_2]$.[10]

As shown in Fig. 2, the geometry around the Ni atoms in **2** is similar to those in **1**, the three Ni atoms adopt a V shape with the angle Ni(2)–Ni(1)–Ni(3) being 102.47°. In contrast to **1**, complex **2** can be achieved as an $Ni(pdt)^{2-}$ unit to which two $Ni(dmit)_2$ fragments are *cis* bonded. Compared to **1**, the Ni···Ni bond distances [Ni(1)–Ni(2) 2.812(2), Ni(1)–Ni(3) 2.792(2) Å] are slightly shorter, whereas the Ni–S bond lengths are almost the same as those in **1**.

In the crystal of complex **1** (as shown in Fig. 3), the anions interact with each other through S···S contacts of < 3.7 Å between the thiole and thione groups or the thiole and thiole groups of the dmit ligands on adjacent molecules to form a two-dimensional molecular interaction net. However, in the crystal of complex **2**, no S···S contacts < 3.7 Å are observed (the shortest intermolecular S···S distance is 3.92 Å); this may result from using the larger $AsPh_4^+$ ion.

The electrical conductivities of complexes **1** and **2** were measured with pressed pellets (two probe). Both complexes show semiconducting behaviour with room-temperature conductivities of 1.75×10^{-4} and 1.52×10^{-5} S cm^{-1}, respectively. The fact that the conductivity of **1** is higher than that of **2** may be the result of shorter intermolecular non-bonded S···S contacts.

This research was supported by State Key Laboratory of Structural Chemistry, Fujian Institute of Research on the Structure of Matter, the Chinese Academy of Sciences, and the Science Foundation of Nation and Fujian Province.

Footnotes and References

* E-mail: wxt@ms.fjirsm.ac.cn

† *Spectroscopic data*: for **1**: IR (KBr pellet: ν/cm^{-1}): ν(Ni–S) 338.2s, 316.7m, 472.1s, 514.6s; ν(C–S) and ν(C=S) 838.3s, 911.1s, 998s, 1024.2s, 1049s. UV–VIS (dmf solution): λ_{max}/nm (ε/dm^3 mol^{-1} cm^{-1}): 275 (4.2×10^4), 290 (4.62×10^4), 320 (4.09×10^4), 430 (1.12×10^4), 530 (2.2×10^4) (Found: C, 26.53; H, 4.18; N, 2.82; Ni, 22.20. Calc. for $C_{30}H_{56}N_2Ni_5S_{18}$: C, 27.39; H, 4.29; N, 2;13; Ni, 22.31%.)

For **2**: IR (KBr pellet: ν/cm^{-1}): ν(Ni–S) 364.4m, 465.9s, 476.0s, 515.8m; ν(C–S) and ν(C=S) 857.3w, 857.4m, 915.1s, 997.3s, 1023.6s, 1049.1s, 1079.7s. UV–VIS (dmf solution): λ_{max}/nm (ε/dm^3 mol^{-1} cm^{-1}): 293 (3.3×10^4), 310 (3.4×10^{-4}), 366 (1.4×10^4), 424 (2.2×10^3), 517 (1.7×10^4). (Found: C, 46.76; H, 3.62; Ni, 11.21. Calc. for $C_{60.5}H_{54}As_2Ni_3O_{0.5}S_{14}$: C, 46.47; H, 3.48; Ni, 11.26%).

‡ *Crystal data*: **1**: $C_{30}H_{56}N_2Ni_5S_{18}$, M_r = 1315.32, triclinic, space group $P\bar{1}$, a = 9.407(4), b = 11.665(3), c = 12.777(3), α = 106.45(2), β = 101.54(3), γ = 100.79(3)°, U = 1272(1) Å^3, Z = 1, D_c = 1.72 g cm^{-3}, T = 296 K, λ(Mo-Kα) = 0.710 73 Å, θ range 0–25°. Enraf-Nonius CAD4 diffractometer, ω–2θ scans. 4468 reflections are unique, 2821 reflections with $I > 3.0\sigma(I)$ were used in the refinement and used to calculate R and R_w. The last successful full-matrix least-squares refinement with anisotropic thermal parameters for all non-hydrogen atoms (250 variables) converged to R = 0.058, R_w = 0.062 $\{w = [\sigma^2(F_o)^2 + (0.020F_o)^2 + 1.000]^{-1}\}$, the final maximum residual electron density is 0.80 e Å^{-3}. The positions of hydrogen atoms were calculated in ideal positions and not used in the least-squares refinement. The structure was solved by direct methods, and the positions of Ni atoms were obtained from E maps. The remaining non-H atoms were located from successive difference Fourier maps. The refinement of the structure was performed by full-matrix least-squares techniques on F using MolEN.[13] Data were corrected for absorption with program DIFABS.[14]

2: $C_{60.5}H_{54}As_2Ni_3O_{0.5}S_{14}$, M_r = 1563.85, triclinic, space group $P\bar{1}$, a = 14.3284(2), b = 14.9487(3), c = 17.2496(3), α = 102.886(1), β = 101.898(1), γ = 102.687(1)°, U = 3385(2) Å^3, Z = 2, D_c = 1.534 g cm^{-3}, T = 293 K, λ(Mo-Kα) = 0.710 73 Å, θ range 1.90–23.2°. Siemens Smart CCD diffractometer, ω scans. 9438 unique reflections were used in the refinement and 6615 reflections with $I > 2.0\sigma(I)$ used to calculate R and R_w. The last successful full-matrix least-squares refinement with anisotropic thermal parameters for all non-hydrogen atoms except solution molecule (720 variables) converged to R = 0.0739, R_w = 0.2085 $\{w = [\sigma^2(F_o)^2 + (0.1355P)^2 + 4.7414P]^{-1}$, where $P = [(F_o)^2 + 2(F_c)^2]/3\}$. The solvent molecule is disordered. The final maximum residual electron density is 2.477 e Å^{-3}, lying 1.073 Å from Ni(1). The positions of hydrogen atoms were calculated in ideal positions and not used in the least-squares refinement. The structure was solved by direct methods, and the positions of three Ni atoms were obtained from E maps. The remaining non-H atoms were located from successive difference Fourier maps. The refinement of the structure was performed by full-matrix least-squares techniques on F^2 using SHELXL-93.[15] Data were corrected for absorption with SADABS.[16] CCDC 182/702.

1 P. Cassoux, L. Valade, H. Kobayashi, A. Kobayashi, R. A. Clark and A. E. Underhill, *Coord. Chem. Rev.*, 1991, **110**, 115.
2 R. M. Olk, B. Olk, W. Dietzsch, R. Kirmse and E. Hoyer, *Coord. Chem. Rev.*, 1992, **117**, 99.
3 M. Bousseau, L. Valade, J. P. Legros, P. Cassoux, M. Garbauskas and L. V. Interrante, *J. Am. Chem. Soc.*, 1986, **108**, 1908.
4 L. Brossard, M. Ribault, L. Valade and P. Cassoux, *Physica B*, 1986, **143**, 378.
5 L. Brossard, H. Hurdequint, M. Ribault, L. Valade, J.-P. Legros and P. Cassoux, *Synth. Met.*, 1988, **27**, 1315.
6 A. Kobayashi, H. Kobayashi, A. Miyamoto, R. Kato, R. A. Clark and A. E. Underhill, *Chem. Lett.*, 1991, 2163.
7 H. Tajima, A. Inokuchi, A. Kobayashi, T. Ohta, R. Kato, H. Kobayashi and H. Kuroda, *Chem. Lett.*, 1993, 1235.
8 T. Imakubo, H. Sawa and R. Kato, *J. Chem. Soc., Chem. Commun.*, 1995, 1097; W. E. Broderick, E. M. McGhee, M. R. Godfrey, B. M. Hoffman and J. A. Ibers, *Inorg. Chem.*, 1989, **28**, 2902; G. Matsubayashi, K. Akiba and T. Tanaka, *Inorg. Chem.*, 1988, **27**, 4744; J. D. Martin, E. Canadell and P. Batail, *Inorg. Chem.*, 1992, **31**, 3176.
9 A. T. Coomber, D. Beljonne, R. H. Friend, J. L. Bredas, A. Charlton, N. Robertson, A. E. Underhill, M. Kurmoo and P. Day, *Nature*, 1996, **380**, 144.
10 A. E. Pullen, R.-M. Olk, S. Zeltner, E. Hoyer, K. A. Abboud and J. R. Reynolds, *Inorg. Chem.*, 1997, **36**, 958.
11 E. Cerrada, A. Laguna, M. Laguna and P. G. Jones, *J. Chem. Soc., Dalton Trans.*, 1994, 1325.
12 G. Steimecke, H.-J. Sieler, R. Kirmse and E. Hoyer, *Phosphorus Sulfur*, 1979, **7**, 49.
13 MolEN, An Interactive Structure Solution Procedure, Enraf-Nonius, Delft, The Netherlands, 1990.
14 N. Walker and D. Stuart, DIFABS, *Acta Crystallogr., Sect. A*, 1983, **39**, 159.
15 G. M. Sheldrick, SHELXTL93, Program for the Refinement of Crystal Structure, University of Göttingen, 1993.
16 G. M. Sheldrick, SADABS, University of Göttingen, 1996.
17 B. S. Snyder, C. P. Rao and R. H. Holm, *Aust. J. Chem.*, 1986, **39**, 963.
18 W. Tremel, M. Kriege, B. Krebs and G. Henkel, *Inorg. Chem.*, 1988, **27**, 3886.
19 X. Yang, D. D. Doxsee, T. B. Rauchfuss and S. R. Wilson, *J. Chem. Soc., Chem. Commun.*, 1994, 821.

Received in Cambridge, UK, 23rd September 1997; 7/06685I

Synthesis and structural characterization of cyclic aryl ethers

Alaa S. Abd-El-Aziz,*[a] Christine R. de Denus,[a] Michael J. Zaworotko[b] and C. V. Krishnamohan Sharma[b]

[a] *Department of Chemistry, University of Winnipeg, Winnipeg, Manitoba, Canada, R3B 2E9*
[b] *Department of Chemistry, Saint Mary's University, Halifax, Nova Scotia, Canada, B3H 3C3*

The facile preparation of macrocyclic ethers is achieved using S_NAr reactions of (dichlorobenzene)$CpFe^+$ complexes with various dinucleophiles, followed by photolytic demetallation; X-ray crystallography gives unequivocal structural proof for one of these macrocycles.

Cyclic polyethers are important synthetic targets owing to their selective complexation and chiral recognition.[1–3] Interest in these materials originates from the size and nature of their cavity, which dictates whether or not such materials are capable of binding with other compounds.[2] Although a great deal of attention has been directed toward the encapsulation abilities of supramolecules, there is a growing interest in the synthesis of cyclic aryl ethers.[3–5] These compounds are appealing since the rigidity and stability of their structures greatly reduces conformational freedom which may allow chiral recognition or catalysis at high temperature or in hostile environments.[4a] Mullins *et al.* reported that cyclic aryl ethers may be subjected to ring-opening polymerization to produce linear polyethers without the release of side-products.[4b] Here, we report the synthesis of four new cyclic aryl ethers, and the crystal structure of **8** utilizing temporary complexation to the cyclopentadienyliron ($CpFe^+$) moiety.

The molecular design and controlled synthesis of aromatic polyethers with pendant $CpFe^+$ moieties has been a focus of our recent research. The complexation of chloroarenes to the $CpFe^+$ moiety has allowed nucleophilic aromatic substitution (S_NAr) reactions to take place with a large number of dinucleophiles.[6] This methodology has enabled us to prepare a number of oligomeric ethers, thioethers and amines under very mild experimental conditions. Owing to the paucity of existing methods for the preparation of cyclic aryl ethers, we have been exploring new routes for the synthesis of such materials. A drawback of the existing methods is the need for electron withdrawing substitutents on the haloarene ring to promote the substitution reactions.[5] The ease of complexation and decomplexation of the $CpFe^+$ to the arene systems shows the advantages of our methodology. The stepwise displacement of both chloro groups in [(η^6-1,2-dichlorobenzene)(η^5-cyclopentadienyl)]iron(II) hexafluorophosphate **10** or [(η^6-1,3-dichlorobenzene)(η^5-cyclopentadienyl]iron(II)hexafluorophosphate **1** with a variety of dinucleophiles has allowed for the facile preparation of macrocycles **8**, **9**, **17**, and **18**. To our knowledge there are few reports which outline the preparation of macrocyclic materials using S_NAr reactions of substituted chlorobenzenes activated by temporary complexation to a metal moiety.[7] The preparation of dibenzo crown ethers was achieved *via* the S_NAr reactions of (*o*-dichlorobenzene)-$Cr(CO)_3$ with diethylene glycol and bis(2-mercaptoethyl) ether.[7a] A disadvantage of this particular synthetic method is the implementation of harsh reaction conditions in order to obtain the desired products in rather modest yields.

Scheme 1 outlines the reaction sequence employed for the preparation of cyclic aryl ethers **8** and **9**. The initial reaction of complex **1** and dinucleophile **2** or **3** in a 2 : 1 molar ratio was carried out in order to obtain the bimetallic complex (**4** or **5**) in high yield. The reaction of **4** or **5** with **2** in an equimolar ratio led to the formation of complexed cyclic aryl ethers **6** and **7** in yields of 86 and 89%, respectively. The rigid nature of these complexed macrocycles introduces both *cis*- and *trans*-orientations of the $CpFe^+$ moieties attached to the arene ring.[8] The presence of two different cyclopentadienyl (Cp) resonances as well as a complex aromatic region in the ^1H NMR spectra indicated that there was a mixture of both *cis* and *trans* products present. Based on the integration of the respective Cp resonances, it was determined that for complex **6** the ratio was 3 : 1 while it was 1 : 1 for complex **7**. The major structure was predicted to be *trans* based on previous findings.[8]

Photolytic demetallation was implemented to allow for the recovery of the free organic macrocycles **8** or **9** in yields of 64 and 58%, respectively, which may be attributed to the poor solubility of these macrocyclic materials in most organic

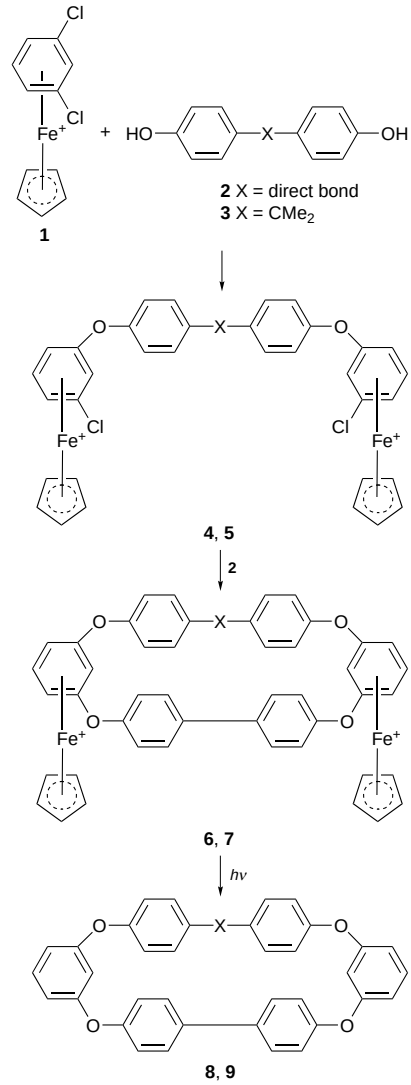

Scheme 1

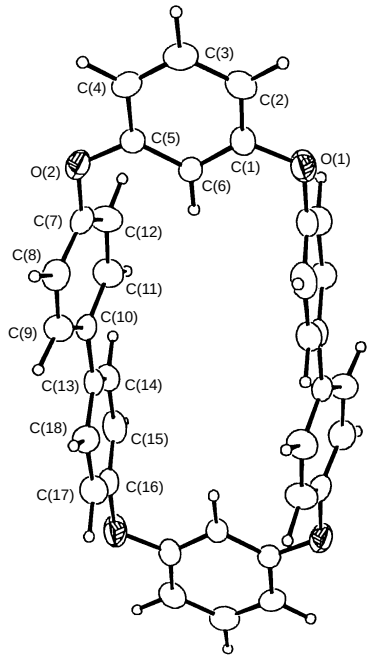

Fig. 1 ORTEP plot of cyclic aryl ether **8**. Selected bond lengths (Å) and angles (°): O(2)–C(5) 1.384(10), O(2)–C(7) 1.416(9), O(1)–C(1) 1.396(9), O(1)–C(16) 1.417(10), C(10)–C(13) 1.504(11); C(5)–O(1)–C(7) 117.7(5), C(1)–O(1)–C(16) 118.0(6), C(10)–C(13)–C(14) 121.0(7), C(10)–C(13)–C(18) 120.3(7).

solvents. The ^{1}H NMR spectra indicated the symmetric nature of these materials. It was noted that a triplet was present at a rather high field chemical shift of δ 5.6 (**8**) or 6.2 (**9**) which was attributed to the inner-ring protons of the benzene ring. This shift is explained by the large diamagnetic shielding caused by the two adjacent biphenyl rings on the inner-ring protons. Our observation is in accordance with similar cyclic aryl ether NMR shifts.[5] Unequivocal proof of the structure of **8** was obtained by an X-ray crystallographic study.† Single crystals suitable for X-ray analysis were obtained by slow evaporation of a chloroform solution of the cyclic aryl ether at room temp. Fig. 1 illustrates the rigidity imparted in the structure by the biphenyl and benzene rings, respectively. The biphenyl groups of the macrocycle are separated by 5.2 Å while the diagonal distance of oxygen atoms was found to be 10.9 Å.

Scheme 2 illustrates that an analogous sequence of reactions may be employed with the (*o*-dichlorobenzene)CpFe$^+$ complex (**10**) and dinucleophiles containing both aliphatic and aromatic bridges. In this fashion, macrocyclic compounds **17** and **18** with both oxygen and sulfur bridges were prepared. Once again NMR spectroscopy and elemental analyses were used to confirm the structure of all new materials. Unlike the rigid macrocycles prepared in Scheme 1, these structures have no inner ring protons and as a result no high field chemical shifts were observed.

This is the first example of iron cyclopentadienyl mediated cyclic aryl ether synthesis. The presented methodology will enable us to prepare a variety of these cyclic compounds under mild experimental conditions and in very high yields. An additional benefit of this process is the ability to isolate the intermediate bimetallic complex prior to ring closure. It has been demonstrated that it is possible to prepare both symmetric and asymmetric cyclic aryl ethers depending on the nucleophile used to close the macrocycle. Further investigations aimed at increasing the cavity size and varying the nature of the substituents are in progress and will be reported in due course.

Financial support provided by the Natural Sciences and Engineering Research Council of Canada (NSERC) and the University of Winnipeg is gratefully acknowledged. C. R. D. (graduate student, University of Manitoba) also thanks NSERC for a postgraduate scholarship.

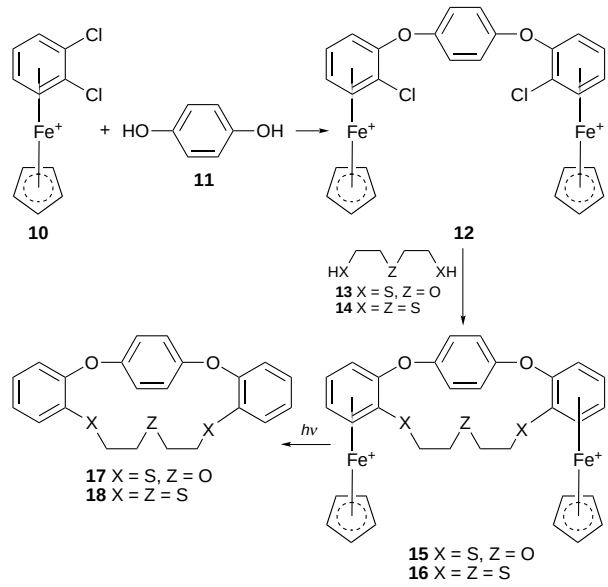

Scheme 2

Footnotes and References

* E-mail: abdelaziz@uwinnipeg.ca

† *Crystal data* for **8**. Colourless crystals from $CHCl_3$, crystal dimensions 0.40 × 0.20 × 0.20 mm, monoclinic, space group $P2_1/c$, a = 6.0546(16), b = 16.093(2), c = 13.514(4) Å, V = 1314.7(6) Å^3, Z = 4, μ = 0.07 mm^{-1}, 1814 reflections measured, 1736 unique, R = 0.058, R_w = 0.050. CCDC 182/696.

1 J. M. Lehn, *Angew. Chem., Int. Ed. Engl.*, 1988, **27**, 89; D. J. Cram, *Angew. Chem., Int. Ed. Engl.*, 1988, **27**, 1021; C. J. Pederson, *Angew. Chem., Int. Ed. Engl.*, 1988, **27**, 1021.

2 L. F. Lindoy, *The Chemistry of Macrocyclic Ligand Complexes*, Cambridge University Press, Cambridge, 1989; G. W. Gokel and S. H. Korzeniowski, *Macrocyclic Polyether Synthesis*, Springer-Verlag, New York, 1982; D. B. Amabilino, J. A. Preece and J. F. Stoddart, in *Macrocycle Synthesis: A Practical Approach*, ed. D. Parker, Oxford University Press, Oxford, 1996, pp. 71–91; E. Weber and F. Vogtle, *Top. Curr. Chem.*, 1981, **98**, 1.

3 H. An, J. S. Bradshaw, K. E. Krakowiak, B. J. Tarbet, N. K. Dalley, X. Kou, C. Zhu and R. M. Izatt, *J. Org. Chem.*, 1993, **58**, 7694; Y. Inoue, T. Hakushi and L.-H. Tong, *J. Org. Chem.*, 1993, **58**, 5411.

4 (*a*) M. J. Mullins, E. P. Woo, D. J. Murray, M. T. Bishop, *CHEMTECH*, August 1993, 25; (*b*) M. J. Mullins, E. P. Woo, C. C. Chen, D. J. Murray, M. T. Bishop and K. E. Balon, *Polym. Preprints* (*Am. Chem. Soc. Div. Polym. Chem.*), 1991, **32**, 174.

5 E. E. Boros, C. W. Andrews and A. O. Davis, *J. Org. Chem.*, 1996, **61**, 2553; B. B. Masek, B. D. Santarsiero and D. A. Dougherty, *J. Am. Chem. Soc.*, 1987, **109**, 4373; F. P. A. Lehmann, *Tetrahedron*, 1974, **30**, 727; G. Montaudo, F. Bottino and E. Trivellone, *J. Org. Chem.*, 1972, **37**, 504; P. A. Temussi, A. Segre and F. Bottino, *Chem. Commun.*, 1968, 1645; N. Sommner and H. A. Staab, *Tetrahedron Lett.*, 1966, 2837.

6 A. S. Abd-El-Aziz, C. R. de Denus, M. J. Zaworotko and L. R. MacGillvray, *J. Chem. Soc., Dalton Trans.*, 1995, 3375; A. S. Abd-El-Aziz, D. C. Schriemer and C. R. de Denus, *Organometallics*, 1994, **13**, 374; A. S. Abd-El-Aziz, K. M. Epp, C. R. de Denus and G. Fisher-Smith, *Organometallics*, 1994, **13**, 374.

7 (*a*) C. Baldoli, P. Del Buttero, S. Maiorana and A. Papagni, *J. Chem. Soc., Chem. Commun.*, 1985, 1181; (*b*) J. W. Janetka and D. H. Rich, *J. Am. Chem. Soc.*, 1995, **117**, 10585; (*c*) A. J. Pearson and K. Lee, *J. Org. Chem.*, 1995, **60**, 7153.

8 C. C. Lee, A. Piorko and R. G. Sutherland, *J. Organomet. Chem.*, 1983, **248**, 357; C. C. Lee, B. R. Steele and R. G. Sutherland, *J. Organomet. Chem.*, 1980, **186**, 265.

Received in Columbia, MO, USA, 20th June 1997; 7/04333C

Heterogeneous molybdate catalysts for the generation of singlet molecular oxygen ($^1\Delta_g$) from H_2O_2

F. van Laar,[a] D. De Vos,[a] D. Vanoppen,[a] B. Sels,[a] P. A. Jacobs,*[a] A. Del Guerzo,[b] F. Pierard[b] and A. Kirsch-De Mesmaeker[b]

[a] *Center for Surface Science and Catalysis, K.U. Leuven, Kardinaal Mercierlaan 92, B-3001 Heverlee, Belgium*
[b] *Physical Organic Chemistry, CP160/08, Université Libre de Bruxelles, 50 Av. F. D. Roosevelt, B-1050 Brussels, Belgium*

The immobilisation of molybdate on Mg,Al-LDH leads to an active, heterogeneous catalyst that generates singlet molecular oxygen from hydrogen peroxide in the absence of soluble base.

Molecular oxygen in the singlet state ($^1O_2$) is a unique reagent for oxyfunctionalisation, as its product distributions essentially differ from those of radical or electrophilic agents such as RO* radicals or (in)organic peracids.[1] Singlet O_2 can be generated from $^3O_2$ *via* visible excitation of dissolved or heterogenised photosensitisers (*e.g.* porphyrins or rose bengal), but the need for an efficient illumination and the photolability of many dyes are major drawbacks for scale-up of such systems.[2–5] An alternative pathway is the catalysed production of $^1O_2$ from alkaline H_2O_2.[6] Several metal ions can act as homogeneous catalysts for this reaction, in particular molybdate and calcium. This contribution presents a new solid catalyst for $^1O_2$ generation, consisting of active molybdate centers embedded in a layered double hydroxide (LDH) matrix. Such catalytic design eliminates the need for a soluble base. The production of $^1O_2$ is evidenced by spectral observations and by oxygenation of characteristic substrates.

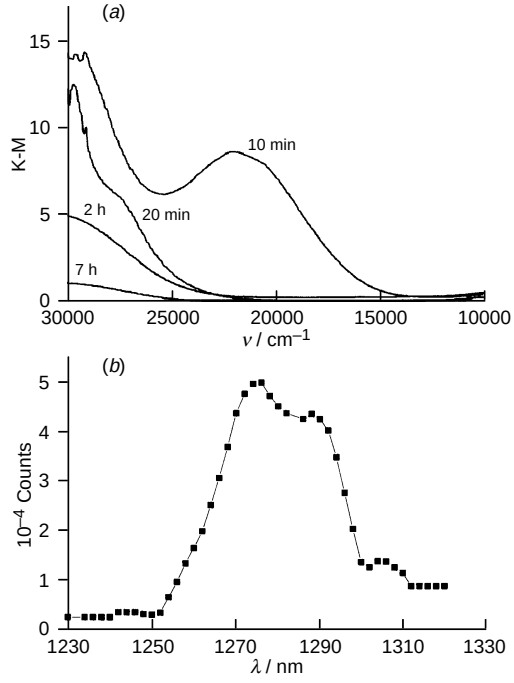

Fig. 1 Exposure of $Mg_{0.7}Al_{0.3}$-LDH-MoO_4 (37.5% AEC), suspended in 1,4-dioxane, to H_2O_2 (0.5 mmol, as 35% in water). (*a*) Diffuse reflectance UV–VIS spectrum recorded at different times after H_2O_2 addition (0.1 g LDH in 0.5 ml solvent; K–M = Kubelka–Munk). (*b*) IR luminescence spectrum, recorded with a liquid N_2 cooled Ge detector (0.025 g LDH in 1.75 ml solvent).

LDHs are analogues of the mineral hydrotalcite, and can be synthesised in a variety of elemental compositions, depending on the desired surface pH and anion exchange capacity.[7] For the present work, a $Mg_{0.7}Al_{0.3}$-LDH was precipitated in degassed water at pH 10, ion-exchanged with MoO_4^{2-} in the same conditions, and isolated by freeze-drying. A typical Mo loading of 5.5 mass% corresponds to occupation of 37.5% of the anion exchange capacity with divalent molybdate anions. When this catalyst is exposed to aqueous H_2O_2 in dioxane, the suspension turns brick-red. This colour change was studied with time-resolved diffuse reflectance spectroscopy [Fig. 1(*a*)]. Bands are observed at 330 and 450 nm. Especially the latter band is typical of polyperoxomolybdate species, *e.g.* $[MoO(O_2)_3]^{2-}$ and $[Mo(O_2)_4]^{2-}$. Such Mo species are formed in particular at high peroxide : Mo ratios and at high pH.[8] Monitoring the spectrum as a function of time shows a steady decrease of the intensity of the polyperoxo bands. This decay corresponds to the disproportionation of the peroxo groups into oxo groups and singlet oxygen, as is proved unequivocally by the near infrared luminescence spectrum. Simultaneously with the UV–VIS spectral change, an emission peak is observed at 1276 nm, which is in satisfactory agreement with the reported energy of the $^1\Delta_g \rightarrow {}^3\Sigma_g^-$ transition [Fig. 1(*b*)].[9] The smooth release of $^1O_2$ and the formation of the polyperoxomolybdates are in agreement with the basic nature of the LDH surface; in solution, the same processes would require addition of additional NaOH. When the $[MoO_4]^{2-}$ exchanged LDH is removed by filtration, the H_2O_2 decomposition stops completely. This proves that the Mo is really heterogeneous, even if the singlet oxygen may diffuse into the solution.

As the production of $^1O_2$ was firmly established from the physicochemical methods, we turned to the application of the material in $^1O_2$ mediated (per)oxidations (Scheme 1).† The 1,3-diene α-terpinene (**1**) was selected as a substrate for [2π + 4π] cycloaddition; the feasibility of $^1O_2$ 'ene' type reactions was tested with 1-methylcyclohexene **2** and 2,3-dimethyl-but-

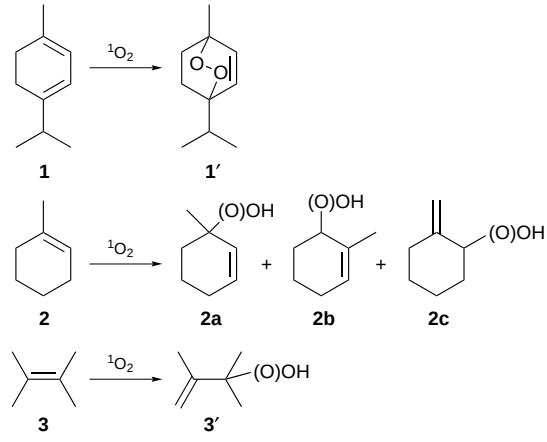

Scheme 1

Table 1 Yields for oxidations with $^1O_2$, generated from H_2O_2 by LDH-MoO_4 catalyst[a]

		Product yields (%)				
			$^1O_2$ products[d]			
Substrate	Catalyst[b]	Epoxide	**2a**	**2b**	**2c**	TON[c]
1-Methylcyclohex-1-ene	$Mg_{0.7}Al_{0.3}$-LDH-MoO_4[e]	0.6	11.7	2.3	5.0	17
	$Mg_{0.7}Al_{0.3}$-LDH-MoO_4[f]	0.6	12.4	2.9	5.4	29
	$Mg_{0.7}Al_{0.3}$-LDH-MoO_4	0.9	19.2	6.4	8.6	86
	$Mg_{0.8}Al_{0.2}$-LDH-MoO_4	0.6	23.5	4.3	11.6	98
	$Mg_{0.9}Al_{0.1}$-LDH-MoO_4	0.5	23.2 (53)[g]	7.1 (16)[g]	13.4 (31)[g]	109
	Rb[h]		(50[g]	(19)[g]	(31)[g]	
		Epoxide	$^1O_2$ products **3′**			
2,3-Dimethylbut-2-ene	$Mg_{0.7}Al_{0.3}$-LDH-MoO_4	4.7	19.6			49
	$Mg_{0.8}Al_{0.2}$-LDH-MoO_4	2.9	32.4			81
	$Mg_{0.9}Al_{0.1}$-LDH-MoO_4	2.3	47.9			120
		Endoperoxide **1′**				
α-Terpinene	$Mg_{0.7}Al_{0.3}$-LDH-MoO_4	14.4				36
	$Mg_{0.8}Al_{0.2}$-LDH-MoO_4	21.6				54
	$Mg_{0.9}Al_{0.1}$-LDH-MoO_4	24.5				61

[a] *Reaction conditions*: 2.5 mmol substrate, 5 mmol H_2O_2 35% in water, 0.05 g catalyst containing 10 μmol $[MoO_4]^{2-}$, 3 ml of 1,4-dioxane, 293 K. Product yields on substrate basis. [b] Subscripts for Mg and Al refer to molar fractions in LDH octahedral layer. [c] TON = moles of $^1O_2$ products per mol of Mo. [d] **2a** = 1-hydro(pero)xy-1-methylcyclohex-2-ene; **2b** = 1-hydro(pero)xy-2-methylcyclohex-2-ene; **2c** = 1-hydro(pero)xy-2-methylenylcyclohexane. [e] 28 μmol $[MoO_4]^{2-}$ on 0.05 g LDH, or 37.5% of the anion exchange capacity. [f] 18 μmol MoO_4^2 on 0.05 g LDH, or 25% of the anion exchange capacity. [g] Values between brackets: distribution of $^1O_2$ oxidation products (%). [h] Photosensitisation with rose bengal (3.10^{-5} M in ethanol), cold light source Schott KL 1500, 293 K.

2-ene **3** (Table 1). The endoperoxide ascaridole is obtained from **1** with a 98% selectivity. With **2** and **3**, hydroperoxide formation is accompanied by a double-bond shift, as expected for a non-free radical, $^1O_2$ mediated peroxidation. Characteristically, the double bond also shifts to the exocyclic position in the case of **2**; the product distribution is essentially the same as for a photosensitised reaction. While the recovered enols undoubtedly originate from the corresponding hydroperoxides, the only competing side reaction is a limited epoxidation. Such an epoxidation of double bonds by peroxo d^0 metals is well documented; however, in our reactions, epoxides in all cases amount to $< 20\%$ of the formed products.

A principal advantage of LDHs over other supports (*e.g.* polymers) is that the characteristics of the catalytic site's environment are easily modified. For instance, co-exchange of the LDH with $[MoO_4]^{2-}$ and an organic anion such as toluene-*p*-sulfonate (Ts) transforms the polar layered double hydroxide into a much more lipophilic material. With ($[MoO_4]^{2-}$,Ts)-LDH as a catalyst, the consumption of H_2O_2 is more gradual, which is undoubtedly due to a repulsion of the primary oxidant H_2O_2 by the apolar surface. While this catalyst modification increases the eventual conversion of *e.g.* 1-methylcyclohexene, this increase is almost totally accounted for by a fivefold multiplication of the epoxide yield. A more successful catalyst modification is the dilution of the $[MoO_4]^{2-}$ active centers over the hydrophilic support. When the occupancy of the anion exchange capacity by $[MoO_4]^{2-}$ is lowered from 37.5 to 12.5%, the yield of $^1O_2$ oxidation products almost doubles (Table 1). Apparently, a slow release of $^1O_2$ from well-dispersed active centers ensures an optimal capture of the $^1O_2$ by the organic substrate. A supplementary improvement of the catalyst is achieved by modification of the elemental composition of the LDH. Thus when the molar fraction of Al in the octahedral layer of the LDH is lowered to 10%, the epoxide formation becomes marginal, while the peroxidation yield further increases. Typically, up to 100 mol of $^1O_2$ product are formed per mol of Mo, proving that the process is truly catalytic in Mo.

Summarizing, this system is the first heterogeneous catalyst for $^1O_2$ generation from a peroxide for which the performance can be easily tuned by modification of the support. A soluble base, as required for the homogeneous molybdate system, becomes superfluous because of the basic characteristics of the LDH surface. The key to achieving high peroxidation yields is a gradual release of $^1O_2$ from a hydrophilic surface.

We thank the Belgian Government for supporting this work in the frame of an I.U.A.P.-P.A.I. project. We thank I.W.T. (F. v. L., D. V., B. S.), F.W.O. (D. D. V) and F.R.I.A. (F. P.) for fellowships, the Luxembourg Ministry of Education and Vocational Training (A. D. G.) for a research training grant and F.N.R.S. for a position of director of research (A. K. D. M.).

Footnotes and References

* E-mail: Jacobs.Pierre@agr.kuleuven.ac.be

† To a mixture of the catalyst, substrate and solvent, aqueous H_2O_2 was added in two portions with an interval of 8 h. For detailed reaction conditions, see footnotes of Table 1.

1 *Singlet* O_2, ed. A. A. Frimer, CRC Press, Boca Raton, FL, 1985, vol. 1–4.
2 R. J. Robbins and V. Ramamurthy, *Chem. Commun.*, 1997, 1071.
3 M. Nowakowska, E. Suster and J. E. Guillet, *Photochem. Photobiol. A: Chem.*, 1994, **80**, 369.
4 S. Tamagaki, C. E. Liesner and D. C. Neckers, *J. Org. Chem.*, 1980, **45**, 1573.
5 A. P. Schaap, A. L. Thayer, K. A. Zaklika and P. C. Valenti, *J. Am. Chem. Soc.*, 1979, **101**, 4016.
6 J. M. Aubry, *J. Am. Chem. Soc.*, 1985, **107**, 5844; J. M. Aubry and B. Cazin, *Inorg. Chem.*, 1988, **27**, 2013; J. M. Aubry, B. Cazin and F. Duprat, *J. Org. Chem.*, 1989, **54**, 726.
7 F. Cavani, F. Trifirò and A. Vaccari, *Catal. Today*, 1991, **11**, 173.
8 L. J. Csányi, I. Horváth and Z. M. Galbács, *Transition Met. Chem.*, 1989, **14**, 90; L. J. Csányi, *Transition Met. Chem.*, 1989, **14**, 298.
9 Q. J. Niu and C. S. Foote, *Inorg. Chem.*, 1992, **31**, 3472; K. Böhme and H.-D. Brauer, *Inorg. Chem.*, 1992, **31**, 3468.

Received in Cambridge, UK, 25th September 1997; 7/06936G

Detection of low levels of Brønsted acidity in Na^+Y and Na^+X zeolites

V. Jayathirtha Rao,[a] Deborah L. Perlstein,[a] Rebecca J. Robbins,[a] P. H. Lakshminarasimhan,[a] Hsien-Ming Kao,[b] Clare P. Grey[b] and V. Ramamurthy*[a]

[a] *Department of Chemistry, Tulane University, New Orleans, LA 70118, USA*
[b] *Department of Chemistry, State University of New York, Stony Brook, NY-11794, USA*

By using retinyl acetate, retinol and retinyl Schiff base as probes, zeolites NaY and NaX are demonstrated to possess a small number of Brønsted acidic sites; the color test employed here is potentially simple and may be universally applied.

Zeolites are finding increasing favor as supramolecular hosts for investigation of the photochemical and photophysical behavior of organic guests.[1] In this context, one would like to employ a reaction cavity that is 'passive'.[2] A set of zeolites that is commonly used as a reaction medium is M^+X and M^+Y.[3] The molecular formula as written for these X and Y zeolites, $M^+_x(AlO_2)_x(SiO_2)_y$, does not give any indication that they may possess reactive Brønsted acid sites.[4] However, it is becoming increasingly clear that the characteristics, especially Brønsted acidity, of commonly used monovalent cation exchanged zeolites can vary significantly from source to source. Even the presence of very small numbers of acidic sites may act in a catalytic manner and complicate the desired chemistry.[5] The characterization of the very small concentrations of Brønsted acid sites present in different samples of X and Y zeolites was, therefore, critical in order to rationalise the observed chemistry. Results of our investigation of Na^+X and Na^+Y zeolites are presented here.

One of our laboratories has recently developed new solid state double resonance NMR methods to probe the acidic sites present in zeolites.[6] Prompted by the success with H^+Y and $Ca^{2+}Y$ zeolites, we proceeded to investigate Na^+Y zeolites with solid state NMR. The basic probe molecules trimethylphosphine (TMP), dimethylamine and methylamine were used to test both Brønsted and Lewis acidity in these materials. Both room and low temperature studies were performed. Zeolite samples (obtained from Aldrich and Zeolyst International) were activated both in an oven at 500 °C in air or at *ca*. 300 °C under a vacuum, in order to mimic activation conditions used for the alkene reactions.[5] ^{1}H MAS NMR spectra of activated Na^+Y showed a resonance at δ 3.6 (both at −80 and −120 °C) possibly due to Brønsted acid sites.[7] The area underneath the peak was extremely small in comparison to the intensity of the residual water and the resonance due to the silanols. Hence it was very difficult to quantify the numbers of Brønsted acid sites per unit cell. A very weak signal was observed at $\delta -2$ in the ^{31}P MAS NMR spectrum (collected at −100 °C) of Na^+Y (from Aldrich) loaded with 26 molecules per unit cell of trimethylphosphine. This resonance was approximately 1/50 that of the main resonance at δ −60 from weakly bound/physisorbed TMP. Resonances from $TMPH^+$, formed by the protonation by the Brønsted acidic sites typically appear in the range δ 0 to −5.[6] Although the resonance at $\delta -2$ seen in the case of Na^+Y, cannot be definitely attributed to $TMPH^+$, it is clear that the number of acidic sites within Na^+Y is very small. From the intensity of this resonance, we estimate that there can be no more than *ca*. 0.5. Brønsted acid sites per unit cell in this sample. No resonances from $TMPH^+$ were observed in samples from Zeolyst (CBV-100) and Engelhardt (EZ-150). To check the presence of weakly acidic sites, stronger bases such as dimethylamine and methylamine were used as probes for Na^+Y. No Brønsted acid sites were detected in the ^{1}H MAS NMR with these probes. Based on these studies we conclude that the number of Brønsted acid sites in Na^+Y (CBV-100 and EZ-150) are small and beyond the detection limits of NMR when using these probe molecules (*i.e.* < *ca*. 0.5 acid sites per unit cell).

In spite of the above discouraging observations, we remained convinced that both Na^+Y and Na^+X contain acidic sites based on their influence on various alkenic substrates.[5] We, therefore, employed a different technique to detect the acidic sites within the zeolites. This involved detecting differences in electronic absorption characteristics between protonated and unprotonated forms of a probe molecule. Three probe molecules (**1a**, **1b** and **1c**) with different basicities were used (Scheme 1).

Both retinol (**1a**) and retinyl acetate (**1b**) in an acidic medium generate a blue color due to the formation of a short lived retinyl carbocation [Scheme 1, eqn. (1)].[8] We have adopted this color change to monitor the Brønsted acidity within zeolites. Four samples of Na^+Y (Aldrich, CBV-100, EZ-150 and LZY-52 from Union Carbide) and Na^+X (Aldrich) were tested for Brønsted acidity. The test consisted of monitoring the absorption changes upon addition of a small amount (50–200 mg) of an activated zeolite to a standard micromolar hexane solution (5 ml) of retinol or retinyl acetate. When activated Na^+Y was added to a standard solution of retinol or retinyl acetate, the zeolite immediately adopted a dark blue color. The color

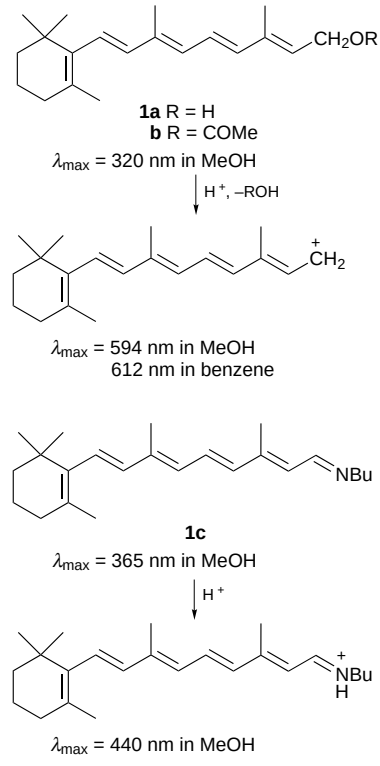

(1)

(2)

Scheme 1

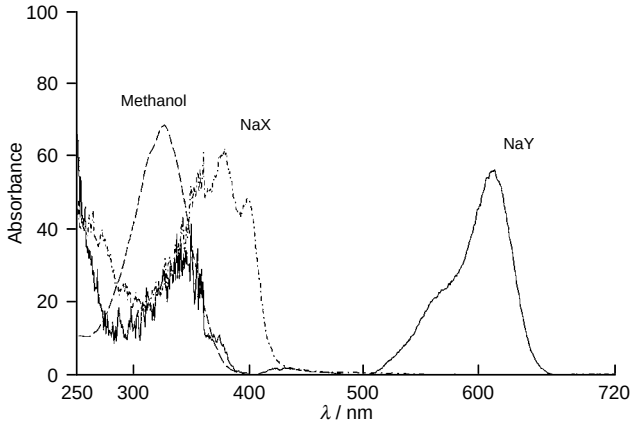

Fig. 1 The spectral change upon inclusion of retinyl acetate within NaY and NaX zeolites. A comparative spectrum in methanol solution is included. Absorption due to retinyl cation is observed in NaY. In NaX the absorption due to retinyl acetate is red shifted but no absorption due to retinyl cation is seen.

persisted for nearly an hour and the diffuse reflectance spectra of these samples are displayed in Fig. 1. The observed λ_{max} within zeolites is in the same range reported in solution.[8] The above observations can be interpreted to mean that Na^+Y contains Brønsted acidic sites that are strong enough to protonate **1a** and **1b**. Na^+X did not show a positive blue test with either **1a** or **1b**, indicating that Na^+X does not contain any protons that are sufficiently acidic to protonate **1a** and **1b**.

Another probe we employed to test the acidity is the more basic retinyl Schiff base **1c** [Scheme 1, eqn. (2)]. In methanol solution, the protonated Schiff base shows an absorption with a λ_{max} at 440 nm. Addition of the above four activated Na^+Y and Na^+X zeolites to a standard micromolar hexane solution of retinyl Schiff base resulted in a color change of the zeolite from white to light yellow orange. The orange colored species absorbs in the same region as the protonated retinyl Schiff base in CH_2Cl_2 solution (Fig. 2). The emission spectra recorded at 77 K are consistent with those reported for the protonated Schiff base.[9] As expected, addition of a large amount of *n*-butylamine displaced the Schiff base from the zeolite. Furthermore, while retinol and retinyl acetate did not indicate the presence of acidic sites within Na^+X, the more basic retinyl Schiff base showed that Na^+X zeolite is also acidic in nature. The difference is likely

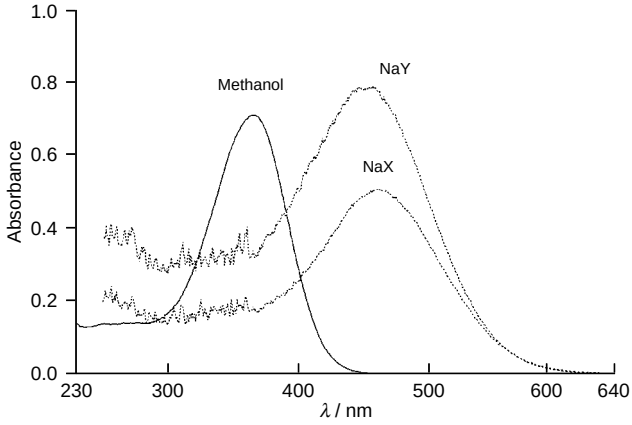

Fig. 2 The spectral change upon inclusion of retinyl Schiff base within NaY and NaX zeolites. A comparative spectrum of unprotonated Schiff base in methanol solution is included. Absorption due to protonated Schiff base is observed in NaY and NaX.

to result from the difference in strength of acidity of the sites present in these two structures.[10]

Diethylamine, a stronger base than **1a**, **1b** and **1c**, was added before the indicator, to react with the Brønsted acid sites, allowing us to estimate the number of acidic sites present in Na^+Y. Titration of the Brønsted acid sites was conducted with diethylamine as the base and **1a** and **1c** as the indicators.† Addition of 1 molecule of diethylamine per 12 supercages of Na^+Y completely quenched the protonation of the probe molecules **1a** and **1c**. This represents a maximum limit of acidic sites within NaY since the estimation assumes that all molecules of diethylamine are protonated under the experimental conditions.

Although extremely low levels of Brønsted acidity were detected, these levels were sufficient to alter the reaction pathways for a number of alkenic systems. We are in the process of characterizing the acidity distribution within different samples of Na^+Y and Na^+X with indicators of different basity. Our initial results suggest that these probes may serve to not only quantify the number of sites but to distinguish between sites of different acidity. Finally, because the method relies on the color changes of highly absorbent dye molecules, it extremely sensitive to low concentrations of acid sites.

Acknowledgement is made to the Donors of PRF-ACS for partial support of this research. The authors at Tulane thank the Division of Chemical Sciences, Office of Basic Energy Sciences, Office of Energy Research, US Department of Energy for support of this program. The solid state NMR spectrometer located at SUNY Stony Brook was purchased with a grant from the National Science Foundation.

Footnotes and References

* E-mail: murthy@mailhost.tcs.tulane.edu

† A known amount (1–10 μl) of diethylamine was added to the dried NaY (200 mg) in hexane and the mixture was stirred for 1 h; then 1 ml of a standard solution of **1a**, **1b** or **1c** was added to this slurry and stirred. The slurry was filtered and the diffuse reflectance spectrum of the solid was recorded. The intensity of the absorption due to the retinyl cation was dependent on the amount of the added diethylamine.

1 A few representative publications: N. J. Turro, N. Han, X. Lei, J. R. Fehlner and L. Abrams, *J. Am. Chem. Soc.*, 1995, **117**, 4881; I. K. Lednev, N. Mathivanan and L. J. Johnston, *J. Phys. Chem.*, 1994, **98**, 11 444; H. Frei, F. Blatter and H. Sun, *CHEMTECH*, 1996, **26**, 24; J. C. Scaiano, N. C. Lucas, J. Andraos and H. Garcia, *Chem. Phys. Lett.*, 1995, **233**, 5.

2 R. G. Weiss, V. Ramamurthy and G. S. Hammond, *Acc. Chem. Res.*, 1993, **26**, 530; V. Ramamurthy, R. G. Weiss and G. S. Hammond, *Adv. Photochem.*, 1993, **18**, 67.

3 D. W. Breck, *Zeolite Molecular Sieve*, Wiley, New York, 1974.

4 D. W. Breck, *Zeolite Molecular Sieve*, Wiley, New York, 1974, p. 461; J. W. Ward, in *Zeolite Chemistry and Catalysis*, American Chemical Society, Washington DC, 1976, p. 118.

5 R. Robbins and V. Ramamurthy, *Chem. Commun.*, 1997, 1071; X. Li and V. Ramamurthy, *J. Am. Chem. Soc.*, 1996, **118**, 10 666; R. Robbins, D. Perlstein and V. Ramamurthy, unpublished work.

6 H. M. Kao and C. P. Grey, *J. Phys. Chem.*, 1996, **100**, 5105; H. M. Kao and C. P. Grey, *Chem. Phys. Lett.*, 1996, **259**, 459; H. M. Kao and C. P. Grey, *J. Am. Chem. Soc.*, 1997, **119**, 627.

7 W. P. J. H. Jacobs, J. W. de Haan, L. J. M. van de Ven and R. A. van Santen, *J. Phys. Chem.*, 1993, **97**, 10 394.

8 P. E. Blatz and D. L. Pippert, *Tetrahedron Lett.*, 1966, 1117; P. E. Blataz and D. L. Pipert, *J. Am. Chem. Soc.*, 1968, **90**, 1296; T. Rosenfield, A. Alchalal and M. Ottolenghi, *Chem. Phys. Lett.*, 1973, **20**, 291; K. Bobrowski and P. K. Das, *J. Am. Chem. Soc.*, 1982, **104**, 1704.

9 R. S. Becker, *Photochem. Photobiol.*, 1988, **48**, 369.

10 H. G. Karge, V. Dondur and J. Weitkamp, *J. Phys. Chem.*, 1991, **95**, 283; H. G. Karge and V. Dondur, *J. Phys. Chem.*, 1990, **94**, 765.

Received in Columbia, MO, USA, 4th September 1997; 7/06480B

Coupling reaction of terminal allenes with themselves or acetylenes mediated by (η^2-propene)Ti(OPr^i)$_2$: some new selectivities and synthetic application

Daigaku Hideura, Hirokazu Urabe and Fumie Sato*

Department of Biomolecular Engineering, Tokyo Institute of Technology, 4259 Nagatsuta-cho, Midori-ku, Yokohama, Kanagawa 226, Japan

Treatment of an allene alone or with an acetylene with (η^2-propene)Ti(O-i-Pr)$_2$ generates a new titanacycle, which reacts with some electrophiles to give useful intermediates for organic synthesis.

Low-valent early transition metal complexes are well known to effect the coupling reactions of olefins and acetylenes to yield metallacycles *via* olefin– (or acetylene)–metal intermediates, which show wide application in organic synthesis.[1] Although some examples of allene coupling reactions based on (C_5H_5)$_2$Ti– or (C_5H_5)$_2$Zr–allene complexes have been documented,[2–4]† the small number of reactions utilizing just allenes as the starting material (rather than any other appropriate precursors) and, accordingly, the critical issues in organic synthesis of regio- and stereo-selectivity and the feasibility of the reaction with respect to various substrates, have not been sufficiently investigated. As some of the aforementioned cyclometallation reactions have recently been carried out with an inexpensive, readily available low-valent titanium species, (η^2-propene)Ti(OPr^i)$_2$ **1**,[5] we reinvestigated the coupling reaction of allenes themsleves and with other unsaturated compounds by taking advantage of this new method.

The homo-coupling reaction of 1,1-dimethylallene **2** with **1** proceeded at −50 °C for 2 h to give the symmetrically substituted **3** having two vinyl–metal bonds as a virtually single isomer (Scheme 1) as shown by the production of **4** (Table 1, entry 1) in accord with precedents of the (C_5H_5)$_2$Ti- or (C_5H_5)$_2$Zr-mediated reactions.[2,3a,4b] However, mono-substituted allene **5**[6] showed a completely different regioselectivity from **2** to give the titanabicycle **6**, which was identified by isolation of **7** as a mixture of *E*- and *Z*-olefinic isomers after aqueous workup (Table 1, entry 2). The latter regioselectivity is not seen in the homo-coupling reactions of representative types of allenes mediated by a low-valent titanium complex having cyclopentadienyl ligands.[2]

The *E*/*Z* ratio of the double bond in the above product could be controlled by the use of a silylallene.[7c] Thus, treatment of **8**[8]

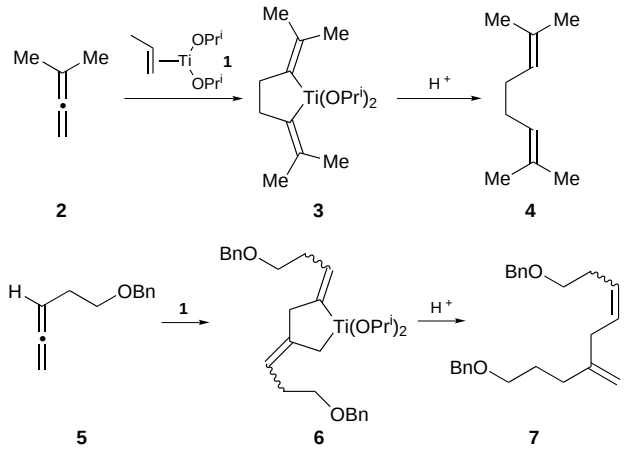

Scheme 1

Table 1 Coupling of allene mediated by **1**

Entry	Allene	Product	Yield (%)
1	**2**	**4**	75
2	**5**	**7**	65[a]
3	**8**	**10**	80[b]

[a] *E*:*Z* ratio = 24:76 (or *vice versa*). [b] *Z* isomer only.

with **1** under the same conditions as above initiated cyclization to afford the single product **10** after aqueous workup (Scheme 2 and entry 3, Table 1). The internal double bond of **10** had exclusively the *Z* configuration, as determined *via* examination of the coupling constants and an NOE study in the ^{1}H NMR spectrum. The titanacycle structure **9**‡ was verified by deuterolysis that gave the bis-deuterated product [$^2H_2$]-**10** (93 atom% at each position) as a single regioisomer.

More importantly, addition of **9** to aldehydes proceeded in a regioselective manner to give the adducts **11** and **12** as an approximately 3:1–4:1 mixture of diastereoisomers, which could be separated on silica gel. The addition of the vinyl–titanium bond in **9** to the aldehyde was not observed,[5b,9] although its presence was confirmed by the subsequent workup with deuteriochloric acid to give the product **12** having vinylic deuterium (93 atm%). Upon treatment with KH in THF,[10] the

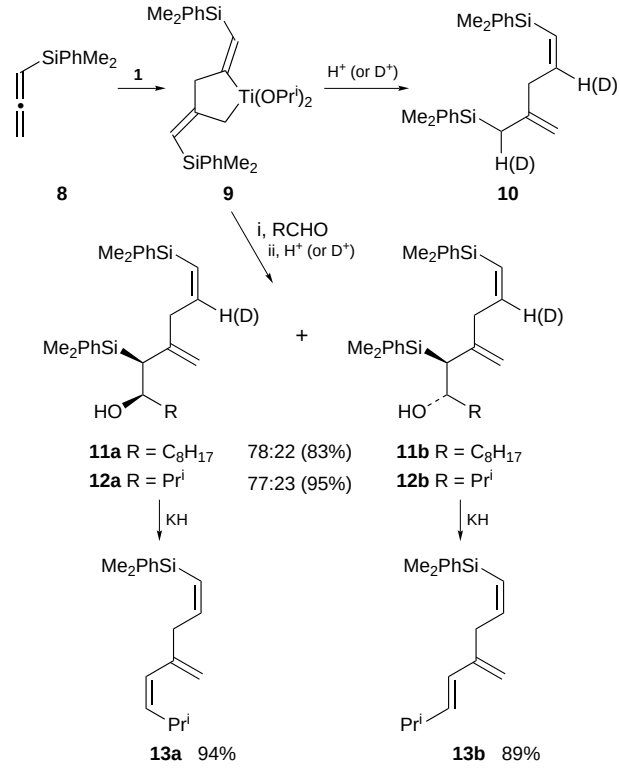

Scheme 2

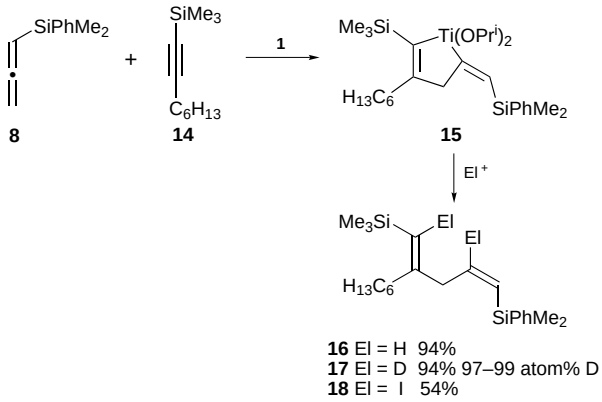

Scheme 3

major stereoisomer **12a** afforded the *Z,Z*-triene **13a**, while the minor **12b** gave *Z,E*-**13b**. These results not only established the orientation of the hydroxy group in **12** (and, hence, **11** by analogy) based on the well-precedented stereochemical course of the Peterson olefination,[10] but also demonstrated a synthetic application of the homo-coupling of the allene followed by aldehyde addition for the stereoselective preparation of trienes.

The hetero-coupling reaction between an allene and an acetylene is another important feature of the transformation involving allenes.[3a,4]† However, little information is available on the regio- and stereo-chemical aspects of the coupling reaction starting from unsymmetrical allenes and acetylenes.[4b] Thus, we first attempted the reaction of unsymmetrical substrates, a mono-substituted allene **8** and silylacetylene **14**, and found that the desired products **16** could be obtained in good yield and as an essentially single stereoisomer (Scheme 3). The stereochemistry of both double bonds in **16** was elucidated by ^{1}H NMR analysis. The high regioselectivity found for this unsymmetrical acetylene, as verified by the absence of another regioisomer, is also noteworthy. The presence of the intermediate titanacycle **15** was confirmed by the deuterolysis (1 M DCl) and iodinolysis (excess I_2) to give the bis-deuterated **17** and diiodide **18** in good yields.

This coupling reaction seems to be general for various substrates, as shown in Table 2. Alkylallene **5** preferentially affords the product **20** having an *E*-disubstituted double bond when reacted with di*alkyl*acetylene **19** (Table 2, entries 1 and 2), but gives **21** carrying a *Z*-disubstituted olefin with *silyl*acetylene **14** (entry 3), both in good yields. Alkoxyallene **22**[11] was able to participate in this coupling reaction as well. Although the yield of **23** is not particularly good due to partial decomposition of the allene in the presence of the titanium alkoxide, the exclusive *Z*-olefinic preference found in the product is somewhat amazing, provided that the stereoselectivity was simply controlled by the steric hindrance of the allenic substituent, which is usually less pronounced in the following order: trialkylsilyl > *n*-alkyl > *n*-alkyloxy (*cf.* entries 3–5). The resultant *cis*-vinyl ether moiety may be stereospecifically replaced by a carbon chain with a Grignard reagent under nickel catalysis[12] or hydrolyzed to aldehyde.

The coupling reaction based on allenes described herein, which enables the selective construction of a carbon framework and the facile introduction of an electrophile, is a synthetically useful entry to the metal-promoted coupling reactions of unsaturated compounds.

We thank the Ministry of Education, Science, Sports and Culture (Japan) for financial support.

Table 2 Coupling of allene and acetylene mediated by **1**[a]

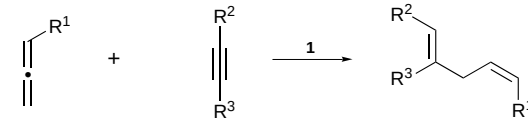

5 $R^1 = (CH_2)_2OBn$ **8** $R^1 = SiPhMe_2$ **22** $R^1 = OC_8H_{17}$

14 $R^2 = SiMe_2$, $R^3 = C_6H_{13}$

19 $R^2 = R^3 = Bu$

16, **20**, **21**, **23**

Entry	Allene	Acetylene	Product	*E* : *Z* ratio[b]	Yield (%)[c]
1	**5**	**19**	**20**	64 : 36	74
2	**5**	**19**[d]	**20**	64 : 36	70
3	**5**	**14**	**21**	25 : 75	72
4	**8**	**14**	**16**	*Z* only	94
5	**22**	**14**	**23**	*Z* only	45

[a] Allene (1.5 equiv.) and acetylene (1.0 equiv.), unless otherwise stated. [b] Refers to double bond substituted with R^1. [c] Isolated yields based on limiting substrate. [d] Allene (1.0 equiv.) and acetylene (1.5 equiv.).

Footnotes and References

* E-mail: fsato@bio.titech.ac.jp

† The *intra*molecular cyclization of allenes and acetylenes has also been documented (ref. 7).

‡ Two simple rules, namely that (i) the formation of the transient allene–titanium complex takes place from the less hindered side and (ii) the titanium atom is better located at the less crowded terminus of the allylic system (ref. 9), support the depicted structure of **9** (and also **6**) over the other possible isomeric formulations.

1 H. Yasuda, K. Tatsumi and A. Nakamura, *Acc. Chem. Res.*, 1985, **18**, 120; S. L. Buchwald and R. B. Nielsen, *Chem. Rev.*, 1988, **88**, 1047; E. Negishi, in *Comprehensive Organic Synthesis*, ed. B. M. Trost and I. Fleming, Pergamon, Oxford, 1991, vol. 5, p. 1163; E. Negishi and T. Takahashi, *Acc. Chem. Res.*, 1994, **27**, 124; F. Sato and H. Urabe, in *Handbook of Grignard Reagents*, ed. G. S. Silverman and P. E. Rakita, Marcel Dekker, New York, 1966, p. 23.

2 P. Binger, F. Langhauser, P. Wedemann, B. Gabor, R. Mynott and C. Krüger, *Chem. Ber.*, 1994, **127**, 39.

3 (*a*) J. Yin and W. M. Jones, *Tetrahedron*, 1995, **51**, 4395; (*b*) J. R. Schmidt and D. M. Duggan, *Inorg. Chem.*, 1981, **20**, 318; (*c*) D. M. Duggan, *Inorg. Chem.*, 1981, **20**, 1164.

4 (*a*) A. Maercker and A. Groos, *Angew. Chem., Int. Ed. Engl.*, 1996, **35**, 210; (*b*) K. M. Doxsee, J. J. J. Juliette, K. Zientara and G. Nieckarz, *J. Am. Chem. Soc.*, 1994, **116**, 2147; (*c*) J. Yin, K. A. Abboud and W. M. Jones, *J. Am. Chem. Soc.*, 1993, **115**, 3810.

5 (*a*) H. Urabe, T. Hata and F. Sato, *Tetrahedron Lett.*, 1995, **36**, 4261; (*b*) H. Urabe, T. Takeda and F. Sato, *Tetrahedron Lett.*, 1996, **37**, 1253; (*c*) H. Urabe and F. Sato, *J. Org. Chem.*, 1996, **61**, 6756; (*d*) K. Suzuki, H. Urabe and F. Sato, *J. Am. Chem. Soc.*, 1996, **118**, 8729.

6 P. Crabbé, B. Nassim and M.-T. Robert-Lopes, *Organic Syntheses*, ed. G. Saucy, Wiley, NY, 1985, vol. 63, p. 203.

7 (*a*) E. Negishi, S. J. Holmes, J. M. Tour, J. A. Miller, F. E. Cederbaum, D. R. Swanson and T. Takahashi, *J. Am. Chem. Soc.*, 1989, **111**, 3336; (*b*) F. A. Hicks, N. M. Kablaoui and S. L. Buchwald, *J. Am. Chem. Soc.*, 1996, **118**, 9450; (*c*) H. Urabe, T. Takeda, D. Hideura and F. Sato, *J. Am. Chem. Soc.*, 1997, **119**, 11 295.

8 A. G. Myers and B. Zheng, *J. Am. Chem. Soc.*, 1996, **118**, 4492.

9 M. T. Reetz, *Organotitanium Reagents in Organic Synthesis*, Springer-Verlag, Berlin, 1986; C. Ferreri, G. Palumbo and R. Caputo, in *Comprehensive Organic Synthesis*, ed. B. M. Trost and I. Fleming, Pergamon, Oxford, 1991, vol. 1, p. 139; M. T. Reetz, in *Organometallics in Synthesis*, ed. M. Schlosser, Wiley, Chichester, 1994, p. 195.

10 D. J. Ager, *Organic Reactions*, ed. L. A. Paquette, Wiley, New York, 1990, vol. 38, p. 1.

11 R. Zimmer, *Synthesis*, 1993, 165.

12 H. Urabe and F. Sato, in *Handbook of Grignard Reagents*, ed. G. S. Silverman and P. E. Rakita, Marcel Dekker, New York, 1996, p. 577.

Received in Cambridge, UK, 29th September 1997; 7/06998G

The biosynthesis of pramanicin: origin of the carbon skeleton

Paul H. M. Harrison,* Donald W. Hughes and R. William Riddoch

Department of Chemistry, McMaster University, 1280 Main Street West, Hamilton, Ontario, Canada L8S 4M1

Incorporation of labelled acetates and serine into pramanicin 1 in *Stagonospora* sp. ATCC 74235 shows that the carbon skeleton of 1 is derived from eight acetate units and a serine residue, implying that the biosynthesis of 1 proceeds *via* an acyl–tetramic acid intermediate 3.

Pramanicin **1** (Scheme 1), an inhibitor of *Cryptococcus neoformans*, and the closely related fatty acid epoxide **2** were isolated by Schwartz *et al.*[1] from a sterile fungus which has subsequently been identified as a species of *Stagonospora*. Our biomimetic template-directed synthesis of **2**[2] was based on a presumed biosynthetic pathway in which seven acetate units combine in a manner typical of fatty acids and polyketides[3] to give tetradeca-2,4-dienoyl-CoA; however, the biosynthetic origin of the pyrrolidone ring in **1** is not clear. Thus, this polar headgroup could be derived from a suitable five-carbon amino acid precursor such as proline or glutamate *via* pyroglutamate and a further Claisen-like condensation onto the CoA ester of fatty acid **2** [Scheme 1, path (*a*)]. On the other hand, **1** could also be viewed as being related to the tetramic acid family of natural products which contains the 3-acyl-Δ^3-pyrrolin-2-one moiety. Biosynthetic studies on erythroskyrine,[4] β-cyclopiazonic acid,[5] tenuazonic acid,[6] malonomicin,[7] streptolydigin,[8] ikarugamycin,[9] the cytochalasans,[10] and recently a preliminary report on aflastatin A[11] have shown that the five atoms of the pyrrolinone ring in these metabolites derive from C-1 and C-2 of one acetate unit and the carboxy- and α-carbon as well as the nitrogen of the appropriate amino acid (Val, Trp, Ile, 2,3-diaminopropanoate, β-methyl-Asp, ornithine, Trp and Ala, respectively). Tetramic acid intermediates have also been proposed in the biosynthesis of, for example, tenellin[12] and ilicicolin H.[13] Thus another potential pathway to **1** would involve the formation of a linear octaketide and cyclization with, presumably, serine as the amino acid [Scheme 1, path (*b*)]. Therefore we sought to determine which pathway was operational in formation of **1**, and describe herein the results of preliminary labelling experiments which establish the origin of the carbon skeleton of **1**.

Cultures of *Stagonospora* sp. ATCC 74235 were grown, and pramanicin was isolated with minor modifications† of the literature procedure.[1] When sodium [1-^{13}C]acetate was added to the cultures, enhanced signals in the {^{1}H}^{13}C NMR spectrum were observed in the resulting **1**, compared with an unlabelled control sample (Table 1). Labelling was observed at the unambiguously assigned sites 2, 7, 9, 11, 13 and 19, as well as at two other sites within the heavily overlapped region corresponding to C-14 to C-18. Therefore, eight acetate units are incorporated into **1**. When sodium [1,2-$^{13}C_2$]acetate was incorporated into **1**, the pulsed field gradient 2D INADEQUATE NMR spectrum of the resulting sample showed seven of the eight expected couplings within acetate-derived units (Table 1).†

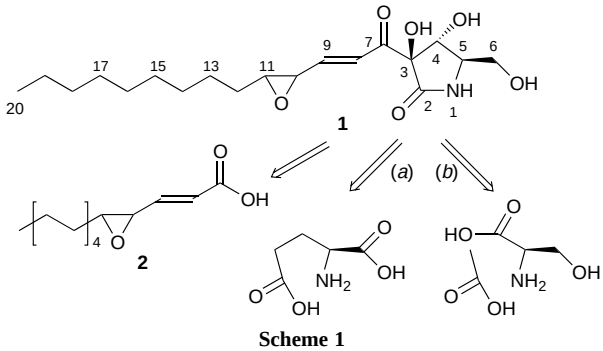

Scheme 1

These results show that the 4,5-epoxytetradec-2-enoyl hydrophobic tail of **1** is indeed derived from the expected 'head-to-tail' condensation of seven acetate units,‡ and at first sight imply a further cycle of chain extension on the fatty acid synthase to give a sixteen-carbon β-ketoacyl chain. However, acetate can enter the tricarboxylic acid cycle and can label glutamate and hence proline: [1-^{13}C]- and [1,2-$^{13}C_2$]-acetates give [5-^{13}C]- and [4,5-$^{13}C_2$]-glutamates, respectively, which are expected to label C-2 and C-2,3 of pramanicin if path (*a*) is operational. Hence, exactly the same labelling pattern is predicted for the direct chain extension pathway as is expected for indirect incorporation *via* glutamate, and these experiments cannot distinguish between the two proposed putative biogenetic pathways.

Incorporation of DL-[1-^{13}C]serine proceeded efficiently: only C-4 of **1** was labelled (Table 1). Although serine can be converted to glutamate or proline, the intermediacy of acetate is

Table 1

		Incorporation			Coupling	
Carbon[a]	δ_C[b]	[1-^{13}C]-NaOAc[c]	[1-^{13}C]-serine[c]	[1,2-$^{13}C_2$]-NaOAc[d]	*J*/Hz[e]	To[f]
7	197.91	0.81	−0.11	2.7	56	C-8
2	174.93	0.51	−0.11	3.1	52	C-3
9	145.13	0.69	−0.07	3.1	55	C-10
8	127.88	0.04	−0.07	2.5	56	C-7
3	88.10	0.06	0.04	2.6	52	C-2
4	78.99	0.02	5.24	—	—	
11	62.90	0.74	−0.10	2.6	43.7	C-12
6	62.12	0.06	0.00	—	—	
5	60.33	−0.02	0.11	—	—	
10	57.78	0.04	−0.08	2.9	55.4	C-9
12	33.02	−0.05[g]	−0.05[g]	2.5[g]	43.7	C-11
14–18	33.02				34.7	δ 30.5
14–18	30.61	0.30[g]	−0.01[g]	ND[h]	m[i]	ND[h]
14–18	30.61			ND[h]	m[i]	ND[h]
14–18	30.48	−0.03	0.03	ND[h]	m[i]	ND[h]
14–18	30.39	0.41	0.07	ND[h]	m[i]	ND[h]
13	26.92	0.60	−0.02	2.4	34.7	δ 30.5
19	23.69	0.43	0.10	2.6	34.7	C-20
20	14.38	−0.12	0.10	3.1	35	C-19

[a] The numbering system is based on ref. 1. [b] Determined in CD_3OD. [c] Expressed as number of fold increase in the height of the carbon-13 resonance relative to unlabelled **1**, with correction by standardizing the two samples using the mean peak height for all unlabelled carbons. [d] Determined by dividing the sum of the coupled peak heights by the height of the uncoupled, natural abundance peak. [e] Values which are stated to 0.1 Hz accuracy determined from a narrow-window high-resolution ^{13}C NMR experiment. [f] Coupled partner from 2D gradient INADEQUATE experiment. [g] Values averaged over two overlapping carbons. [h] ND = not determined. [i] Multiplet; coupling patterns could not be deduced in this region.

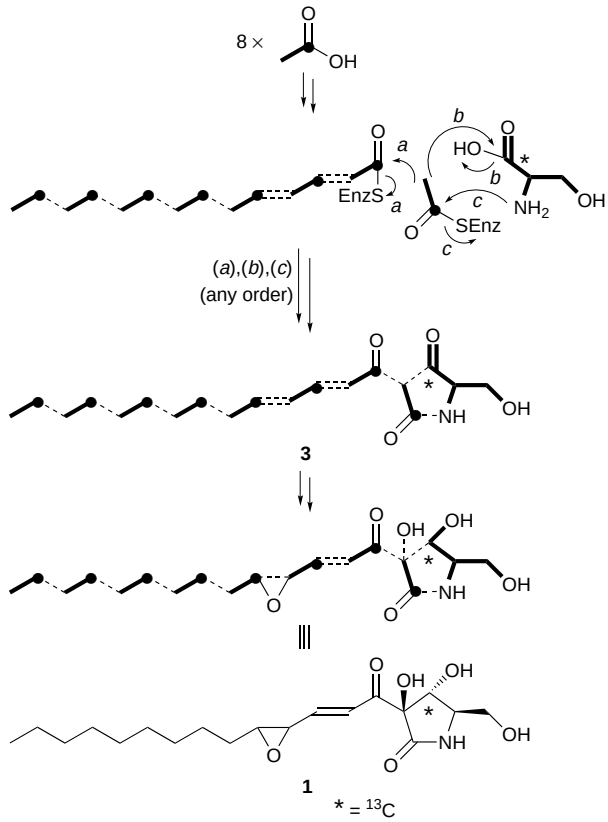

Scheme 2

required in this process, and label is expected to appear at C-5 of **1**. Since no incorporation into acetate-derived sites was observed in this experiment, glutamate and proline cannot be precursors of the pyrrolidone moiety in **1**. Rather, the results are consistent with formation of a linear octaketide; amide formation with the amino group of serine and cyclization by formal Claisen-like condensation of the β-ketoacyl enolate onto the presumably activated serine carboxy group would generate **3**, which contains the carbon skeleton and ring of **1** (Scheme 2). The order of these events [events (*a*), (*b*) and (*c*) in Scheme 2] remains to be established. Net addition of water across the C-3–C-4 bond, presumably by oxidative hydroxylation at C-3 and reduction at C-4 of intermediate **3**, and epoxidation gives **1**. Further investigation of this pathway is being undertaken, and will be reported in due course.

This work was financially supported by the Natural Sciences and Engineering Research Council of Canada and by McMaster University. Cambridge Isotopes Ltd. are gratefully acknowledged for a grant of isotopically labelled compounds.

Footnotes and References

* E-mail: pharriso@mcmail.cis.mcmaster.ca

† *Stagonospora* was cultured in liquid medium LCM,[1] with the glucose content reduced to 40 g l^{-1} (100 ml in each of twelve 500 ml Erlenmeyer flasks). Sodium [1-^{13}C]- and [1,2-$^{13}C_2$]-acetate (1 g each) or DL-[1-^{13}C]-serine (0.25 g) were added as sterile solutions in water at 24 h intervals over days 2–6. After seven days, the culture was worked up as previously described.[1] Final purification was by MPLC on a Merck LOBAR RP-8 column in MeOH–H_2O (70 : 30), giving 75 mg of **1**.

‡ The remaining correlation for the eighth unit corresponds to two carbon nuclei at *ca.* δ 30; these are strongly coupled and thus this correlation is not observed in the INADEQUATE spectrum. Careful examination of the 1D spectra shows that the two units C-17,18 and C-15,16 are each derived from an *intact* acetate unit; however, the *direction* of these units, implied in Scheme 2 in accord with biosynthetic convention,[3] is not unambiguously proven by these experiments.

1 R. E. Schwartz, G. L. Helms, E. A. Bolessa, K. E. Wilson, R. A. Giacobbe, J. S. Tkacz, G. F. Bills, J. M. Liesch, D. L. Zink, J. E. Curotto, B. Pramanik and J. C. Onishi, *Tetrahedron*, 1994, **50**, 1675.
2 C. Cow and P. Harrison, *Can. J. Chem.*, 1997, **75**, 884.
3 For recent reviews, see: C. W. Carreras, R. Pieper and C. Khosla, *Top. Curr. Chem.*, 1997, **188**, 85; D. O'Hagan, *Nat. Prod. Rep.*, 1995, **12**, 1.
4 S. Shibata, U. Sankawa, H. Taguchi and K. Yamasaki, *Chem. Pharm. Bull.*, 1966, **14**, 474.
5 C. W. Holzapfel and D. C. Wilkins, *Phytochemistry*, 1971, **10**, 351; R. M. McGrath, P. S. Steyn and N. P. Ferreira, *J. Chem. Soc., Chem. Commun.*, 1973, 812; R. M. McGrath, P. S. Steyn, N. P. Ferreira and D. C. Neethling, *Bioorg. Chem.*, 1976, **4**, 11; A. E. de Jesus, P. S. Steyn, R. Vleggaar, G. W. Kirby, M. J. Varley and N. P. Ferreira, *J. Chem. Soc., Perkin Trans. 1*, 1981, 3292; A. A. Chalmers, C. P. Gorst-Allman and P. S. Steyn, *J. Chem. Soc., Chem. Commun.*, 1982, 1367.
6 S. Gatenbeck and J. Sierankiewicz, *Acta Chem. Scand.*, 1973, **27**, 1825.
7 D. Schipper, J. L. van der Baan and F. Bickelhaupt, *J. Chem. Soc., Perkin Trans. 1*, 1979, 2017; D. Schipper, J. L. van der Baan, N. Harms and F. Bickelhaupt, *Tetrahedron Lett.*, 1982, **23**, 1293.
8 K. L. Rinehart, Jr., D. D. Weller and C. J. Pearce, *J. Nat. Prod.*, 1980, **43**, 1; C. J. Pearce, S. E. Ulrich and K. L. Rinehart, Jr., *J. Am. Chem. Soc.*, 1980, **102**, 2510; C. J. Pearce and K. L. Rinehart, Jr., *J. Antibiot.*, 1983, **36**, 1536.
9 H. Seto, H. Yonehara, S. Aizawa, H. Akutsu, J. Clardy, E. Arnold, M. Tanabe and S. Urano, *Koen Yoshishu - Tennen Yuki Kagobutsu Toronkai*, Kyushu University, 22nd Conference, 1979, 394 (*Chem. Abstr.*, 1980, **92**, 211459)
10 A. Probst and C. Tamm, *Helv. Chim. Acta*, 1981, **64**, 2065.
11 S. Sakuda, M. Ono, K. Furihata, J. Nakayama, A. Suzuki and A. Isogai, *J. Am. Chem. Soc.*, 1996, **118**, 7855.
12 A. G. McInnes, D. G. Smith, J. A. Walter, L. C. Vining and J. L. C. Wright, *J. Chem. Soc., Chem. Commun.*, 1974, 282; E. Leete, N. Kowanko, R. A. Newmark, L. C. Vining, A. G. McInnes and J. L. C. Wright, *Tetrahedron Lett.*, 1975, **47**, 4103; J. L. C. Wright, L. C. Vining, A. G. McInnes, D. G. Smith and J. A. Walter, *Can. J. Biochem.*, 1977, **55**, 678.
13 M. Tanabe and S. Urano, *Tetrahedron*, 1983, **39**, 3569.

Received in Corvallis, OR, USA, 17th September 1997; 7/06799B

Formation of bridged bicycloalkenes *via* ring closing metathesis

Andrew Morehead, Jr. and Robert Grubbs*

The Arnold and Mabel Beckman Laboratory of Chemical Synthesis, Division of Chemistry and Chemical Engineering, California Institute of Technology, Pasadena, California 91125, USA

Ring closing metathesis may be used in the formation of small ring bicycloalkenes from monocyclic diene precursors.

Ring closing metathesis (RCM), catalyzed by transition metal carbenes, has recently become an established method for the conversion of dienes to cyclic olefins.[1] While many applications of RCM have been reported,[2] only a few have involved the formation of bridged bicyclic compounds. The reported examples all involved macrocyclization (ring sizes > 12 atoms) except one, which involved the formation of a seven-membered ring leading to a bicyclo[9.5.1]alkene ring system.[3] Since small ring bridged bicycloalkanes and heterocycles are ubiquitous in natural products, the application of RCM in ring closures of this type would potentially lead to greatly broadened utility of this method.

A series of monocyclic diene substrates was synthesized† and the ring closure promoted by the well-defined ruthenium benzylidene complex[4] was examined [eqn. (1)].‡ The results of

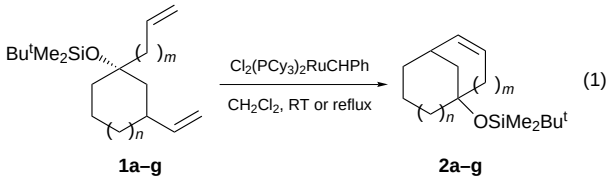

1a–g **2a–g** (1)

the cyclization reactions are summarized in Table 1.

The ring closure of five-, six- and seven-membered rings to form [3.*x*.1], [4.*x*.1] and [5.*x*.1] bicycloalkenes is a relatively facile process (entries 1, 2, 5, 6 and 8), while ring closure of eight-membered rings to give bicyclo[5.*x*.1]alkenes does not occur (entries 3, 9 and 10). Variation of the reaction temperature, concentration of the diene and catalyst type (Mo catalyst[5]) had no influence on the formation of the eight-membered rings, as starting material and oligomers were the only products isolated.

Formation of the bicyclo-[3.2.1]- and -[3.3.1]-alkenes when the six-membered ring is being closed is extremely facile (entries 1 and 6). In general, as the ring closure becomes slower, other processes such as dimerization may start to compete. Lower concentration disfavors the intermolecular coupling relative to the intramolecular ring closure, and allows clean formation of the products. Raising the temperature to that of refluxing CH_2Cl_2 was necessary only when the substrate was sterically hindered (entries 4 and 5) or the cyclization was very slow (entry 8).

The enthalpies of ring closure (including formation of ethylene) were calculated using the MM2 forcefield and are included in Table 1.[6] In general, if the calculated enthalpy is less than *ca.* 10 kcal mol^{-1}, the ring closure should be favorable due to the entropy gain from the generation of ethylene. An interesting comparision may be made between entry 5 and entry 3, both of which are calculated to have $\Delta H \approx 13$ kcal mol^{-1}. For substrate **1** (entry 5), the kinetic favorability of ring closure for five-membered rings, coupled with the loss of ethylene to the atmosphere, drives the reaction to completion. Note that at higher concentrations (entry 4), the yield is much lower, as a result of a significant amount of polymer being formed, suggesting that endothermic ring closures are possible if the concentration is kept below the critical concentration for polymerization. In the case of the eight-membered ring (entry 3), although the same loss of ethylene would occur, the ring closure is sufficently slow as to be non-competitive with polymerization. Linderman *et al.* have recently reported the use of removable Bu$^t_3$Sn groups to overcome the entropic barrier allowing formation of eight-membered rings,[7] a strategy that could potentially be applied here. The molecular mechanics also suggest that the silyl-protected alcohol plays a small role in the cyclization by decreasing the enthalpy of the ring flip to the bis-axial conformer needed for the ring closure by *ca.* 1 kcal mol^{-1} relative to the unprotected alcohol.

In conclusion, a number of small ring bridged bicycloalkenes have been synthesized from monocyclic dienes, demonstrating the power of ring closing metathesis to form carbocycles that contain a significant amount of strain.

A. T. M. acknowledges a postdoctoral fellowship from the National Institutes of Health (USA). We also thank Professor Dennis Dougherty for the use of the SGI Power Impact workstation and the software packages used for the calculations referred to in this paper.

Table 1 Conversion and ethalpies for ring closure of monocyclic dienes

Entry	Substrate	*n*	*m*	Conc./M	[Ru] (mol%)	*T*/°C	Yield (%)	ΔH^a/ kcal mol^{-1}
1	**1a**	0	1	0.050	5	RT	87	1.2
2	**1b**	0	2	0.005	5	RT	(> 95 Conv.)[b]	6.9
3	**1c**	0	3	0.005	10	Reflux	Oligo	13.1
4	**1d**	1	0	0.050	5	Reflux	41	13.3
5	**1d**	1	0	0.005	10	Reflux	84	13.3
6	**1e**	1	1	0.050	5	RT	95	1.7
7	**1f**	1	2	0.050	5	RT	Trace	10.0
8	**1f**	1	2	0.005	10	Reflux	96	10.0
9	**1g**	1	3	0.050	5	RT	Oligo	17.5
10	**1g**	1	3	0.005	10	Reflux	Oligo	17.5

[a] MM2 Calculations. [b] Conversion by NMR spectroscopy.

Footnotes and References

* E-mail: rhg@cco.caltech.edu

† The substrates were synthesized by addition of the appropriate Grignard reagent to 3-vinylcyclohexanone or cyclopentanone, and protection of the tertiary alcohol with the *tert*-butyldimethylsilyl group. The *cis* and *trans* isomers could be separated for the six- membered ring substrates, but not the five-membered ring substrates. The five-membered ring substrates were cyclized as mixtures and the product separated from the uncyclized *trans* diene by chromatography.

‡ *Typical experiment procedure* for **1**-(*tert*-butyldimethylsilyloxy)-bicyclo[3.3.1]non-6-ene (**2e**). The silyl ether protected diene **1e** (630 mg, 2.25 mmol) was dissolved in 45 ml CH_2Cl_2 and treated with [Cl_2(Cy-$_3$P)$_2$RuCHPh (ref. 5) 92.4 mg, 0.11 mmol, 0.05 equiv.]. The initial red solution rapidly turned light brown, was stirred for 4 h, and the solvent was removed. The brown oil was purified by filtration through silica gel using hexane as the eluent to give a clear oil (540 mg, 2.14 mmol, 95%): δ_H (300 MHz, $CDCl_3$) 0.08 (s, 6 H), 0.86 (s, 9 H), 1.34–1.38 (m, 2 H), 1.45–1.86 (m, 6 H), 2.13–2.32 (m, 2 H), 2.56–2.60 (m, 1 H), 5.52–5.57 (m, 1 H), 5.69–5.74 (m, 1 H); δ_C (75 MHz, $CDCl_3$) −1.7, 17.9, 19.7, 25.8, 28.1, 34.2, 41.0, 42.4, 42.7, 71.9, 127.8, 129.0; ν(film)/cm^{-1} 3023, 2930, 2855, 1472, 1253, 1112, 1013, 835.

1 For recent reviews of RCM see: R. H. Grubbs, S. J. Miller and G. C. Fu, *Acc. Chem. Res.*, 1995, **28**, 446; H.-G. Schmalz, *Angew. Chem., Int. Ed. Engl.*, 1995, **34**, 1833.

2 For selected examples see: S. F. Martin, Y. Liao, Y. Wong and T. Rein, *Tetrahedron Lett.*, 1994, **35**, 691; B. C. Borer, S. Deerenberg, H. Beiraugel and U. K. Pandit, *Tetrahedron Lett.*, 1994, **35**, 3191; A. F. Houri, Z. Xu, D. A. Cogan and A. H. Hoveyda, *J. Am. Chem. Soc.*, 1995, **117**, 2943; J. S. Clark and J. G. Kettle, *Tetrahedron Lett.*, 1997, **38**, 123 and 127; A. Fürstner and K. Langemann, *J. Org. Chem.*, 1996, **61**, 8746; A. Kinoshita and M. Mori, *J. Org. Chem.* 1996, **61**, 8356; K. C. Nicolaou, Y. He, D. Vourloumis, H. Valberg and Z. Yang, *Angew. Chem., Int. Ed. Engl.*, 1996, **35**, 2399.

3 M. D. E. Forbes, J. T. Patton, T. L. Myers, H. D. Maynard, D. W. Smith, Jr., G. R. Schulz and K. B. Wagener, *J. Am. Chem. Soc.*, 1992, **114**, 10 978.

4 P. Schwab, R. H. Grubbs and J. W. Ziller, *J. Am. Chem. Soc.*, 1996, **118**, 100.

5 R. R. Schrock, J. S. Murdzek, G. C. Bazan, J. Robbins, M. DiMare and M. O'Regan, *J. Am. Chem. Soc.*, 1990, **112**, 3875.

6 The molecular mechanics calculations were performed using the MM2 forcefield as implemented in the SPARTAN (ver. 4.1.1, Wavefunction, Inc., 18401 Von Karman Ave., #370, Irvine, CA, 92715 USA, © 1995 Wavefunction, Inc.) and MACROMODEL (F. Mohamadi, N. G. J. Richards, W. C. Guida, R. Liskamp, M. Lipton, C. Caufield, G. Chang, T. Hendrickson and W. C. Still, *J. Comput. Chem.*, 1990, **11**, 440, ver. 3.5a, Dept. of Chemistry, Columbia University, NY, 10027) software packages.

7 R. J. Linderman, J. Siedlecki, S. A. O'Neill and H. Sun, *J. Am. Chem. Soc.*, 1997, **119**, 6919.

Received in Corvallis, OR, USA, 25th August 1997; 7/06200A

Diastereoselective homogeneous hydrogenations without direction by substituents

Edward Farrington,[a] Mauro Comes Franchini[a,b] and John M. Brown*[a]

[a] *Dyson Perrins Laboratory, South Parks Road, Oxford, UK OX1 3QY*
[b] *Dipartimento di Chimica Organica 'A. Mangini', Università degli Studi di Bologna, 40136 Bologna, Italy*

The Rh complex catalysed hydrogenation of an α-(hydroxyalkyl)-*N*-methoxyacrylamide and the Ru complex catalysed hydrogenation of an α-(fluoroalkyl)acrylate both proceed with ⩾90% selectivity to give the *syn*-isomer.

In the directed hydrogenation of alkenes, coordination of a polar functionality to the catalyst leads to enhanced diastereoselectivity in the reduced product. Stereochemical control may arise by complexation of an alcohol, amide, ester or sulfoxide group.[1] The vast majority of substituent-directed diastereoselective reactions follow similar principles.[2] For the common case of an acyclic alkene with an allylic stereogenic centre, a simple model based on the constrained conformation of the complexed alkene **1a** suffices [Fig. 1(*a*)]. This model, for which the torsional angle H–C—**C**=C is 180°, is calculated to be 5 kJ mol^{-1} higher in enthalpy than the rotamer (H–C–C=C = 0°).[3] In the absence of complexation by a polar functional group, diastereoselectivity will be controlled by steric factors. An alternative mode of complexation, shown in Fig. 1(*b*), was required to test this prediction. In practice this was realised by synthesis of the corresponding *N*-methyl-*N*-methoxyamide according to Nahm and Weinreb.[4] In a related unsaturated amide, the preferred conformation of the amide side-chain has N–O *anti* to C=O, thus permitting the desired complexation.[5]

The synthetic route[6] from compound **1a** provides access to both alcohol **2a** and its Bu^{t}Me$_2$Si ether **2b**. Hydrogenation of **2a** was carried out with the Rh complex **3** as previously described[1] in either MeOH or ClCH$_2$CH$_2$Cl and gave a near-equal mixture of *syn*- and *anti*-diastereomers **4a** and **5a** (Scheme 1). This is in contrast to the results observed for hydrogenation of all other α-(hydroxyalkyl)acrylates under related conditions, where the *anti*-isomer predominates. The contrasting result obtained here suggests that there are two competing pathways in hydrogenation which operate in opposite senses, one involving N–O participation, the other O–H participation. Support for this proposal stems from hydrogenation of silyl ether **2b**, which gives 92% of the corresponding *syn*-product **4b**. In separate experiments it was verified that the α-silyloxyalkyl acrylates **1b**–**d** gave mixtures of both *syn*-**6b**–**d** and *anti*-**7b**–**d** on hydrogenation, confirming that the reduced basicity and increased bulk of the silyl ethers attenuates their complexation to rhodium relative to OH. Both the selectivity and the rate depend on the size of the siloxy group in the manner expected if the stereoselectivity is controlled by the relative steric bulk of the substituents at the α-stereogenic centre.

The hydrogenation of compound **2b** can be interpreted in accord with the model in Fig. 1(*b*). It is assumed that the side-chain can adopt its minimum energy conformation with α-C–H eclipsing C=C, and there are then two diastereomeric sets of intermediates which lead on to the diastereomeric products **4b** and **5b**. The proportions will be determined primarily by the perceived bulk of the two non-hydrogen substituents at the stereogenic centre. As would be expected on the basis of relative *A* values (1.79 for Et *vs.* 0.74 for OSiMe$_3$),[7] the ethyl group prefers to be remote from the metal complex (Scheme 2), leading to the observed preference for *syn* hydrogenation.

A further example of *syn*-directed hydrogenation was discovered adventitiously, in a search for fluorine participation in catalysis. There are precedents for C–F activation by several transition metal complexes, but none which demand C–F

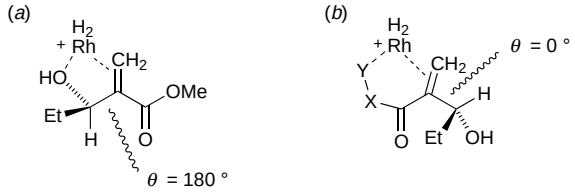

Fig. 1 Alternative reactant chelates in hydrogenation

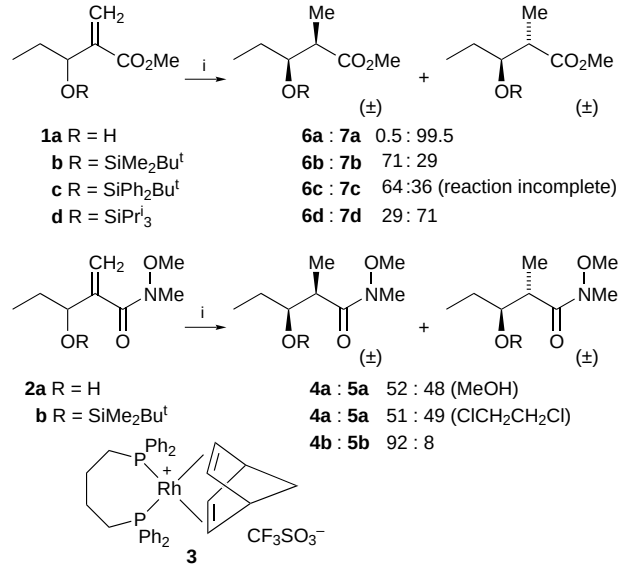

Scheme 1 *Reagents and conditions*: i, **3** (1–4 mol%), H_2 (1.5 atm)

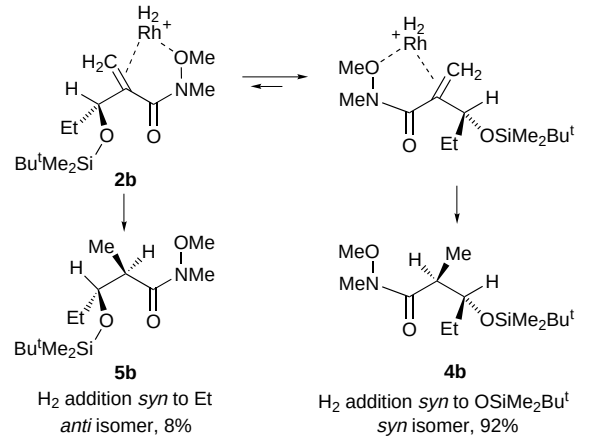

Scheme 2

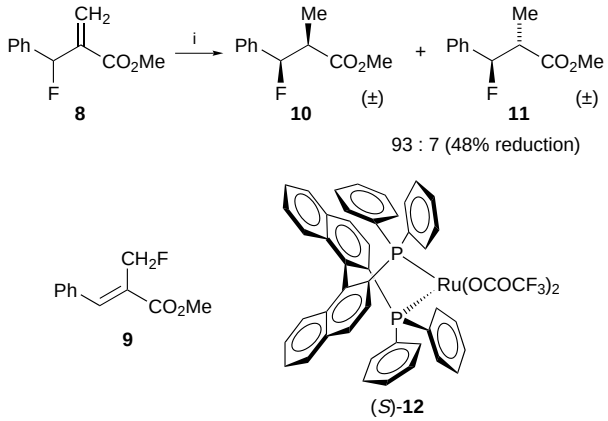

Scheme 3 *Reagents and conditions*: i, **12** (4 mol%), H_2 (3 atm), ClH_2CCH_2Cl, 40 h

participation to augment the selectivity of a catalytic process. Some examples of C–F···M interactions in organometallic crystal structures, and indeed the only two derived from late transition metals, involve Ru;[8] the Ru···F bond lengths are 2.366 and 2.489 Å, much longer than other bonds from Ru to second-row elements. These observations guided our approach.

The phenyl analogue of compound **1a** reacted with diethylaminosulfur trifluoride (DAST)[9] to produce the corresponding allyl fluoride **8** with *ca.* 5–10% competing allylic isomerisation to the primary fluoride (*Z*)-**9** (Scheme 3). In initial studies it was found that hydrogenation of compound **8** with Crabtree's catalyst[10] (25 °C, 2 atm, CH_2Cl_2) occurred cleanly with low diastereoselectivity. The diastereomers *syn*-**10** and *anti*-**11** were separately identified from independent synthesis of the *anti*-isomer **11** by DAST fluorodehydroxylation of its *anti*- alcohol precursor, which occurred with 75% retention of configuration,[11] verified by spectral comparison with literature assignments which are based on an X-ray analysis.[12] When hydrogenation of the allyl fluoride **8** was carried out with (*S*)- or *rac*-BINAP–Ru complexes **12**, the *syn*-diastereomer **10** was formed as 90% of the reduced product, but in a slow reaction sustained for up to 20 turnovers. The ee of recovered allyl fluoride was low when enantiomerically pure catalyst was employed. Since Ru and Rh give parallel stereoselectivity in directed hydrogenation,[13] this result cannot be the consequence of a fluorine-directed hydrogenation but rather reflects the preferred coordination of the reactant in the C=C–C–H = 0° conformation,[14] and the relative steric size of fluoro and phenyl substituents. The failure to observe clear-cut evidence for C–F participation at a potentially fluorophilic metal site has origins related to the reluctance of C–F to act as an hydrogen-bond acceptor.[15]

It has been a general rule that diastereoselectivity in organometallic catalysis requires substituent participation through complexation.[1,2] Although modest specificity has been obtained here, it is useful to realise that significant stereocontrol in homogeneous hydrogenation can arise from the intrinsic conformational preferences of the reactant.

We thank Dr Uma Sharma for NMR experiments and Johnson-Matthey for loans of precious metal salts. Dr D. J. Bayston made useful suggestions. A visit by M. C.-F. to Oxford was supported by the European Community HCM programme (CRTX-920067).

Footnote and References

* E-mail: john.brown@dpl.ox.ac.uk

1 J. M. Brown, *Angew. Chem., Int. Ed. Engl.*, 1987, **26**, 191.
2 A. H. Hoveyda, D. A. Evans and G. C. Fu, *Chem. Rev.*, 1993, **93**, 1307.
3 Through molecular mechanics calculations on constrained conformations of alcohol **1a**.
4 S. Nahm and S. M. Weinreb, *Tetrahedron Lett.*, 1981, **22**, 3815.
5 K. Schwarz, G. Neef, G. Kirsch, A. Muller-Fahrnow and A. Steinmeyer, *Tetrahedron*, 1995, **51**, 9543.
6 A. Wissner and C. V. Grudzinkas, *J. Org. Chem.*, 1978, **43**, 3972; the acid chloride derived from the bis(*tert*-butyldimethylsilyl) derivative of alcohol **1a** was reacted directly with MeONHMe·HCl and pyridine to give the desired amide **2b** in 66% yield.
7 E. L. Eliel and S. H. Wilen, *Stereochemistry of Organic Compounds*, Wiley-Interscience, New York, 1994, pp. 694–695.
8 J. L. Kiplinger, T. G. Richmond and C. E. Osterberg, *Chem. Rev.*, 1994, **94**, 373; J. Burdeniuc, B. Jedlicka and R. H. Crabtree, *Chem. Ber.*, 1997, **130**, 145.
9 M. Hudlicky, *Org. React.*, 1988, **35**, 513.
10 R. H. Crabtree and M. W. Davis, *J. Org. Chem.*, 1986, **51**, 2655.
11 For variation in the stereochemical course of DAST fluorinations of secondary alcohols, see D. F. Shellhamer, A. A. Briggs, B. M. Miller, J. M. Prince, D. H. Scott and V. L. Heasley, *J. Chem. Soc., Perkin Trans. 2*, 1996, 973; A. Focella, F. Bizzarro and C. Exon, *Synth. Commun.*, 1991, **21**, 2165; J. Leroy, E. Hebert and C. Wakselman, *J. Org. Chem.*, 1979, **44**, 3406.
12 K. Durkin, D. Liotta, J. Rancourt, J. F. Lavallee, L. Boisvert and Y. Guindon, *J. Am. Chem. Soc.*, 1992, **114**, 4912; C. Hassler, R. Batra and B. Giese, *Tetrahedron Lett.*, 1995, **36**, 7639.
13 J. M. Brown, M. Rose, F. I. Knight and A. Wienand, *Recl. Trav. Chim. Pays-Bas*, 1995, **114**, 242.
14 The two low energy conformations of allyl fluoride have allylic hydrogen and fluorine eclipsing the alkene respectively; J. R. Durig, M. J. Lee, H. M. Badawi, J. F. Sullivan and D. T. Durig, *J . Mol. Struct.*, 1992, **266**, 59. This was verified to apply to compound **8** through MM calculations.
15 J. D. Dunitz and R. Taylor, *Eur. J. Chem.*, 1997, **3**, 89.

Received in Liverpool, UK, 29th September 1997; 7/07025J

Organically templated layered uranium(VI) phosphates: hydrothermal syntheses and structures of $[NHEt_3][(UO_2)_2(PO_4)(HPO_4)]$ and $[NPr_4][(UO_2)_3(PO_4)(HPO_4)_2]$

Robin J. Francis,[a] Mark J. Drewitt,[a] P. Shiv Halasyamani,[a] Charusheela Ranganathachar,[a] Dermot O'Hare,*[a]† William Clegg[b] and Simon J. Teat[b]

[a] *Inorganic Chemistry Laboratory, South Parks Road, Oxford, UK OX1 3QR*
[b] *Department of Chemistry, University of Newcastle, Newcastle, UK NE1 7RU*

Two organically templated layered uranium(VI) phosphates have been prepared under hydrothermal conditions from U_3O_8 and H_3PO_4 using either NPr_4^+ or $NHEt_3^+$ ions as structure directing agents; both compounds have layered structures which contain infinite chains of edge-sharing $[UO_7]$ pentagonal bipyramids cross linked by bridging $[PO_4]$ tetrahedra to form two dimensional sheets of $[(UO_2)_n(HPO_4)_{n-1}(PO_4)]_m^{m-}$ anions.

Crystalline layered and microporous phosphates have attracted great attention owing to their rich chemistry based on the intercalation, ion-exchange, or absorption of guest molecules into the host framework.[1,2] This has led to interest in the synthesis of new metal phosphates with novel layered and open-framework structures. Recently a wide variety of new compounds have been synthesized in which metals such as Be,[3] Ga,[4] In,[5] Zn,[6] V,[7] Fe,[8] Co,[9] and Mo[10] have been incorporated into the phosphate framework. When the syntheses are performed under hydrothermal conditions in the presence of organic templates both layered and microporous phases are formed, which often display unusual framework topologies. To date, however, we are not aware of any organically templated hydrothermal syntheses of new phosphate materials incorporating actinide elements. It is expected that the incorporation of bulky organic templates in an actinide phosphate framework could result in new and unusual framework topologies. Clearfield and co-workers have synthesised a number of uranyl phosphonates in which the presence of the bulky organic substituents on the phosphonate groups leads to the formation of novel structure types.[11,12] We have been exploring the hydrothermal synthesis of uranium phosphate based materials in the presence of organic templates. We report here the synthesis and structural characterization of the first examples of organically templated layered uranium(VI) phosphates to be isolated, namely $[NHEt_3][(UO_2)_2(PO_4)(HPO_4)]$ **1** and $[NPr_4][(UO_2)_3(PO_4)(HPO_4)_2]$ **2**.

Single crystals of **1** were grown by heating mixtures of composition $U_3O_8 : 9H_3PO_4 : 3NEt_3 : 240H_2O$ under autogenous hydrothermal conditions in Teflon lined autoclaves at 180 °C for 3 d.‡ The crystals formed as flat plates together with a small amount of microcrystalline impurity. Single crystals of **2** were grown by heating mixtures of composition $U_3O_8 : 6H_3PO_4 : 3NPr_4OH : 240H_2O$ at 180 °C for 3 d.‡ The crystals formed as thin needles together with a small amount of a microcrystalline impurity.

Compound **1** adopts a layered structure§ in which the two unique U atoms are both coordinated in a slightly distorted pentagonal bipyramidal arrangement by seven O atoms, a common coordination environment for U. The axial O and the U atoms form almost linear [angles of 178.8(4)° and 169.1(3)°] uranyl UO_2^{2+} units with a mean U–O distance of 1.77 Å with the five equatorial O at a larger mean distance of 2.40 Å. These values are typical for U^{VI} in this coordination environment.[13] Valence sum calculations are consistent with this assignment.[14] Zigzag $PaCl_5$ type chains are formed along the (101) direction by UO_2O_5 pentagonal bipyramidal units sharing opposite edges. $(UO_2O_5)_n$ chains such as these are a common structural unit found in other uranium oxides and phosphates such as α-U_3O_8, UVO_5,[15] $U_2V_2O_{11}$,[15] and $U(UO_2)(PO_4)_2$.[16] Individual chains are cross-linked through O atoms of bridging tetrahedral phosphate units to form a corrugated layer structure in the [010] plane. Each phosphate group bonds to a U atom in one chain *via* two O atoms and also bonds to a second U atom in an adjacent chain *via* a third O atom (Fig. 1). The fourth O of the phosphate group does not bridge but instead projects above and below the phosphate layers. These layers are stacked along the (010) direction and are separated from adjacent layers by charge balancing $NHEt_3^+$ cations to form a structure consisting of alternating inorganic and organic layers. The separation between adjacent phosphate layers is 9.2 Å. To maintain charge balance, one of the phosphate groups must be protonated, giving the indicated formula $[NHEt_3][(UO_2)_2(PO_4)(HPO_4)]$. The IR spectrum of **1** also revealed broad weak bands at 2750 and 1620 cm^{-1} that are consistent with P–OH vibrations. The location of the OH proton could not be determined from the X-ray analysis, and a consideration of the P–O distances did not reveal any obviously longer bonds indicative of a P–OH group. The P–O distances range from 1.50(1) to 1.56(1) Å with an average of 1.54 Å. However, valence sum calculations indicate that the terminal O atoms projecting above and below the layers have unsatisfied valence and these calculations are consistent with the assumption that the proton is likely to be located on these atoms. However, it is not possible to determine which of the two unique phosphate groups contains the OH group. It seems likely that the H is disordered over both sites.

Compound **2** also forms as a layered structure.§ As in **1** the layers consist of $PaCl_5$ type $(UO_2O_5)_n$ chains formed from edge sharing pentagonal bipyramidal (UO_2O_5) units which are then further cross-linked by phosphate groups to form uranium

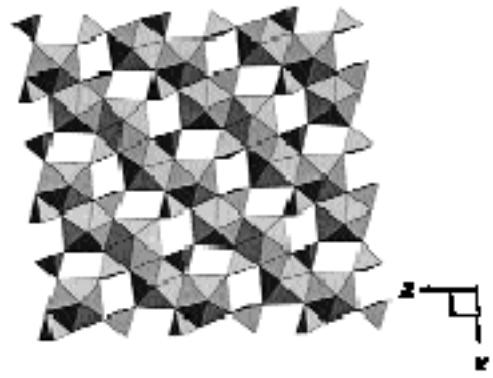

Fig. 1 A view of the structure of the layers in $[NHEt_3][(UO_2)_2(PO_4)(HPO_4)]$ **1** parallel to the *b* axis, showing the chains of edge-sharing $[UO_7]$ pentagonal bipyramids and bridging $[PO_4]$ tetrahedra

phosphate layers similar to those in **1** in the [01$\bar{1}$] plane. There are three unique U atoms in the asymmetric unit. The coordination around all three is again typical for a U^{VI} atom in this environment, with a mean uranyl U–O distance of 1.75 Å and a mean equatorial U–O distance of 2.40 Å. Valence sum calculations are consistent with this assignment.[14] Each tetrahedral phosphate group bonds to one U atom *via* two O atoms and another U atom in the next $(UO_2O_5)_n$ chain *via* a third O atom. The fourth O atom projects above and below the phosphate layers. Each phosphate layer is separated from the next by intercalated NPr_4^+ cations forming alternating inorganic–organic layers along the (01$\bar{1}$) direction. The separation between adjacent phosphate layers is 12.2 Å. As in **1**, to maintain charge balance the existence of protonated P–OH groups must be inferred.

Although the coordination of the uranium and phosphate species in both **1** and **2** are the same, subtle differences in the geometry of the bridging phosphate groups leads to differences in the structures of the layers. In **1** chains of bridging phosphate groups running along the (100) direction [*ca*. 45° to the $(UO_2O_5)_n$ chains] have terminal P–O bonds that either stick 'up' or 'down' from the layers in a strictly alternating [all-up : all-down : all-up] manner along the (001) direction. However, in **2** the same chains of bridging phosphates alternate in the sequence [all-up : both up and down : all-down] along (011). This has the effect that in **1** the layers are corrugated in an approximately sinusoidal manner, whereas in **2** the layers consist of approximately flat sections connected by 'steps' (Fig. 2).

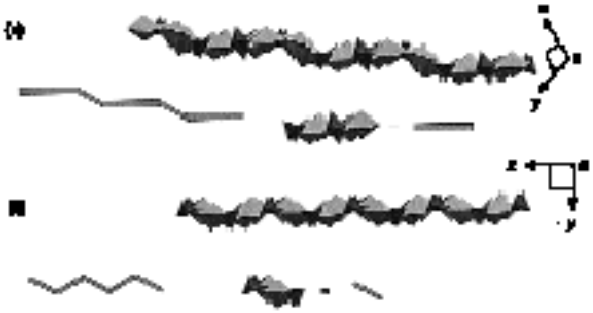

Fig. 2 View of a single layer of $[(UO_2)_n(HPO_4)_{n-1}(PO_4)]^-$ in **1** (*a*) and **2** (*b*) along the (100) direction; also shown is a schematic representation of the layer structure

The charged framework and large interlayer spacing found in these materials suggested that they may be capable of undergoing ion-exchange reactions with other charged species. Preliminary experiments indicate that the template molecules can indeed be exchanged for a variety of alkali metal, transition metal and other quaternary ammonium cations, such as Na^+, Co^{2+} and NMe_4^+, whilst still retaining the integrity of the uranium phosphate layers.

The isolation and characterization of **1** and **2** demonstrate that organic templates can be used to hydrothermally synthesize new hybrid inorganic–organic uranium phosphate materials in which the structure directing organic species is incorporated into the U/P/O framework. Furthermore, these materials show that the detailed structure of the inorganic layers can be influenced by the precise nature of the organic template used. Given the variety of coordination modes and framework topologies[13] displayed by uranium minerals and inorganic phases, there appears to be much scope for synthesizing new materials displaying novel structural features and properties using this methodology. We are currently investigating further the absorption, catalytic, and ion-exchange properties of **1** and **2**.

We would like to thank British Nuclear Fuels Limited for support, and the Leverhulme Fund (P. S. H.), the Commonwealth Scholarship Commission (C. R.) and EPSRC (R. J. F., M. J. D.) for financial support.

Footnotes and References

* E-mail: dermot.ohare@icl.ox.ac.uk
† D. O'Hare is the Royal Society of Chemistry Sir Edward Frankland Fellow.

‡ *Synthesis* **1**: a mixture of U_3O_8, H_3PO_4 NEt_3, and H_2O in mol ratio 1 : 9 : 3 : 240 was placed in a 23 ml capacity Teflon lined autoclave and heated to 180 °C at autogenous pressure for 3 d. After cooling to room temp., light green plates of **1** and a small amount of powder impurity were filtered, washed with water, and allowed to dry in air. The crystals could be easily separated by sieving. IR (Nujol mull, ν/cm^{-1}): 2750w (br), 1623m (br), 1096s, 1062s, 1030s, 959s, 919s, 850m, 800w, 721w, 612m, 538m.

2: a mixture of U_3O_8, H_3PO_4, NPr_4OH and H_2O in the mol ratio 1 : 6 : 3 : 240 was placed in a 23 ml capacity Teflon lined autoclave and heated to 180 °C at autogenous pressure for 3 d. After cooling to room temp., light green needles of **2** and a small amount of powder impurity were filtered, washed with water and allowed to dry in air. Due to the small size of the crystals it was difficult to obtain a sample suitable for analysis.

‡ *Crystal data*: $C_6H_{17}NO_{12}P_2U_2$ **1**: monoclinic, space group $P2_1/c$, a = 9.336(4), b = 18.325(5), c = 9.864(4) Å, β = 93.075(5)°, U = 1685.1(2) Å^3, Z = 4, D_c = 3.281 g cm^{-3}. 13 372 reflections collected (Enraf-Nonius DIP2000 diffractometer, Mo-Kα, 150 K), of which 3272 were independent and 2346 were observed [$I > 5\sigma(I)$]. Refinement converged with R = 0.0570, wR = 0.0650, S = 1.101.

$C_{12}H_{30}NO_{18}P_3U_3$ **2**: triclinic, space group $P\bar{1}$, a = 9.401(2), b = 13.048(3), c = 13.447(1) Å, α = 108.021(3), β = 103.164(2), γ = 100.978(4)°, U = 1465.4(3) Å^3, Z = 2, D_c = 2.904 g cm^{-3}. 10 394 reflections collected [Siemens SMART CCD diffractometer on the single-crystal diffraction station (9.8) at the Daresbury Laboratory Synchrotron Radiation Source, UK, λ = 0.6956 Å, 160 K], of which 8120 were independent and 5244 were observed [$I > 5\sigma(I)$]. Refinement converged with R = 0.0564, wR = 0.0661, S = 0.733. CCDC 182/660.

1 M. E. Davis and R. F. Lobo, *Chem. Mater.*, 1992, **4**, 756.
2 S. T. Wilson, B. M. Lok, C. A. Messina, T. R. Cannon and E. M. Flanigen, *ACS Symp. Ser.*, 1983, **218**, 79.
3 T. E. Gier and G. D. Stucky, *Nature*, 1991, **349**, 508.
4 M. Estermann, L. B. McCusker, C. Baerlocher, A. Merrouche and H. Kessler, *Nature*, 1991, **352**, 320.
5 A. M. Chippindale, S. J. Brech, A. R. Cowley and W. M. Simpson, *Chem. Mater.*, 1996, **8**, 2259.
6 W. T. A. Harrison, R. W. Broach, R. A. Bedard, T. E. Gier, X. Bu and G. D. Stucky, *Chem. Mater.*, 1996, **8**, 691.
7 M. I. Khan, L. M. Meyer, R. C. Haushalter, A. L. Schweitzer, J. Zubieta and J. L. Dye, *Chem. Mater.*, 1996, **8**, 43.
8 M. Cavellec, D. Riou and G. Ferey, *Acta Crystallogr., Sect. C*, 1995, **51**, 2242.
9 G. D. Stucky, *Nature*, 1997, **388**, 735.
10 R. C. Haushalter and L. A. Mundi, *Chem. Mater.*, 1992, **4**, 31.
11 D. M. Poojary, D. Grohol and A. Clearfield, *Angew. Chem., Int. Ed. Engl.*, 1995, **34**, 1508.
12 D. M. Poojary, A. Cabeza, M. A. G. Aranda, S. Bruque and A. Clearfield, *Inorg. Chem.*, 1996, **35**, 1468.
13 P. C. Burns, M. L. Miller and R. C. Ewing, *Can. Mineral.*, 1996, **34**, 845.
14 I. D. Brown and D. Altermatt, *Acta Crystallogr., Sect. B*, 1985, **41**, 244.
15 A. M. Chippindale, P. G. Dickens, G. J. Flynn and G. P. Studdard, *J. Mater. Chem.*, 1995, **5**, 141.
16 P. Benard, D. Louer, N. Dacheux, V. Brandel and M. Genet, *Chem. Mater.*, 1994, **6**, 1049.

Received in Cambridge, UK, 23rd September 1997; 7/06873E

Resolution and circular dichroism of an asymmetrically cage-opened [60]fullerene derivative

Jan C. Hummelen,*[a] Majid Keshavarz-K,[b] Joost L. J. van Dongen,[c] René A. J. Janssen,[c] E. W. Meijer[c] and Fred Wudl[b]

[a] *Department of Organic and Molecular Inorganic Chemistry, University of Groningen, Nijenborgh 4, 9747 AG Groningen, The Netherlands*
[b] *Institute for Polymers and Organic Solids, University of California at Santa Barbara, Santa Barbara, CA 93106, USA*
[c] *Laboratory of Organic Chemistry, Eindhoven University of Technology, 5600 MB Eindhoven, The Netherlands*

The enantiomers of the first cagewise *inherently* asymmetric C_{60} derivative, *i.e.* *N*-MEM (MEM = 2-methoxyethoxymethyl) keto lactam 1, have been separated by HPLC and their chiroptical properties compared with data obtained from C_{60} derivatives that are dissymmetric or asymmetric due to chiral addends.

N-MEM keto lactam **1** (Fig. 1) is the first example of a well-defined open-cage derivative of C_{60}.[1] It is obtained from C_{60} in two synthetic steps, and (±)-**1** serves as the key intermediate in the synthesis of azafullerenes, *e.g.* $(C_{59}N)_2$,[2] $C_{59}NH$[3] and $K_6C_{59}N$.[4] Stereochemically, **1** is an interesting molecule, because it can be regarded as a (highly symmetrical) sphere with a chiral orifice. A larger version could be envisioned as a chiral selector, operating by enantioselective endohedral complexation.

Various chiral C_{60} derivatives have been prepared thus far.[5,6] Chirality can be introduced into C_{60} derivatives *via* chiral addends, either asymmetric[7,8] or C_2-symmetric,[9] as well as *via* an inherently asymmetric addition or substitution pattern, such as in 2 : 1 adducts with C_2-symmetry.[10,11] Higher fullerenes and carbon nanotubes can be inherently chiral.[12] C_2 C_{76}, D_3 C_{78} and D_2 C_{80} have been obtained in enantiomerically pure form *via* kinetic resolution by asymmetric osmylation, providing optically active forms of carbon.[13] Since keto lactam **1** is the first open-cage C_{60} derivative with an inherently asymmetric cage functionalization pattern, it is of interest to determine a possible resemblance of the chiroptical properties of **1** with those of the chirally modified C_{60} compounds. Here we present the successful resolution of (±)-**1** and the chiroptical properties of the individual enantiomers.

Chromatography of racemic **1**[1] as a 0.3 mg ml^{-1} solution in toluene–1,2-dichlorobenzene (2 : 1 v/v) on an analytical chiral stationary phase HPLC column [Bakerbond Pirkle Type DNBPG 5 μm (4.6 × 250 mm)], using *n*-hexane–$CHCl_3$–Pr^{i}OH (70 : 30 : 1 v/v/v) as the eluent (flow rate 1 ml min^{-1}) and UV detection at λ = 328 nm, gave enough separation to yield the enantiomers in 80 and 92% ee (as inferred from a second HPLC experiment, Fig. 2), respectively. The two fractions were assigned to (+)-**1** and (−)-**1**, respectively, by determining their specific rotations at 589 nm.

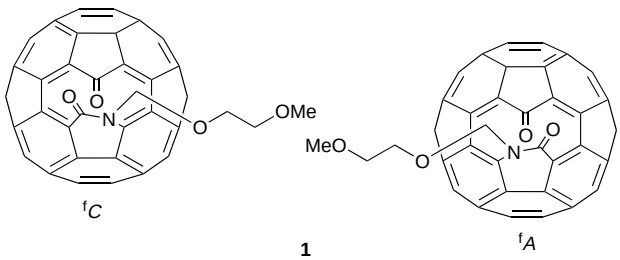

1

Fig. 1 Molecular structure of the two enantiomeric forms of **1** with configurational description ^fC and ^fA according to ref. 6

The UV–VIS spectrum of (±)-**1**, the circular dichroism (CD) spectrum and the resulting *g* value ($g = \Delta\varepsilon/\varepsilon \approx \Delta A/A$) of (+)-**1** are shown in Fig. 3. The CD spectrum of (−)-**1** was found to have a mirror image relation to that of (+)-**1**. Similar to the UV–VIS absorption, the CD spectrum of (+)-**1** extends throughout the 200–700 nm spectral range. The strongest Cotton effect is found at λ = 325 nm ($\Delta\varepsilon$ = +29 M^{-1} cm^{-1}), coinciding with the lowest energy dipole-allowed transition of **1** (λ = 328 nm). Comparison with, for example, (+)-hexahelicene, which has a *g* value of +7.0 × 10^{-3} at λ = 325 nm for the π–π* transition, shows however that the *g* value of (+)-**1** (g_{325} = +6.4 × 10^{-4}) is an order of magnitude lower and represents a typical value for a noninherently dissymmetric chromophore.[14] Various chirally modified [6,6]-dihydrofullerene derivatives show a diagnostic CD band at about λ = 430 nm, whose sign has been taken as an indicator for the absolute configuration.[8,15–17] For (+)-**1**, a local extreme in the CD spectrum is found at λ = 426 nm, where the Cotton effect is negative. Tentatively applying the sector rule of Wilson *et al.* to **1** suggests that (+)-**1** corresponds to the ^fA configuration (Fig. 1).[15] The largest *g* values of (+)-**1** are found in the wavelength range λ = 600–700 nm, with a maximum of $g = -1.7 \times 10^{-2}$ at 659 nm, a typical value for a magnetically-allowed dipole-forbidden transition.

In summary, we have separated the two enantiomers of the C_{60} derivative (±)-**1** using chiral HPLC, providing a first example of an open-cage fullerene with a chiral orifice. The inherently chiral functionalization of the eleven-membered ring causes a dissymmetric perturbation on the π system of the fullerene, resulting in optical activity extending over the entire

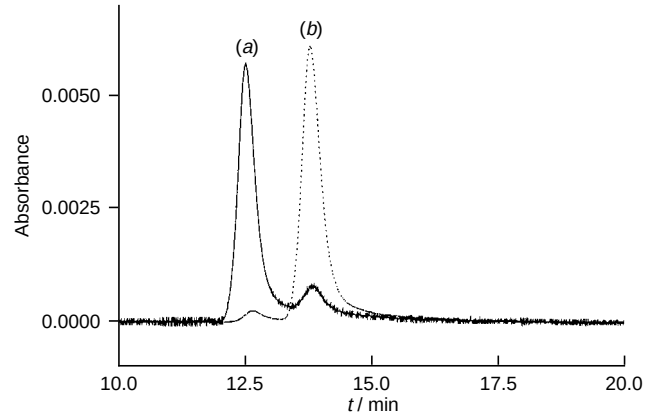

Fig. 2 Chiral HPLC chromatogram of separated samples of (*a*) (+)-**1** and (*b*) (−)-**1** (Bakerbond Pirkle Type DNBPG, eluent: *n*-hexane–$CHCl_3$–Pr^{i}OH (70 : 30 : 1 v/v/v), flow rate 1 ml min^{-1}, UV detection at λ = 328 nm)

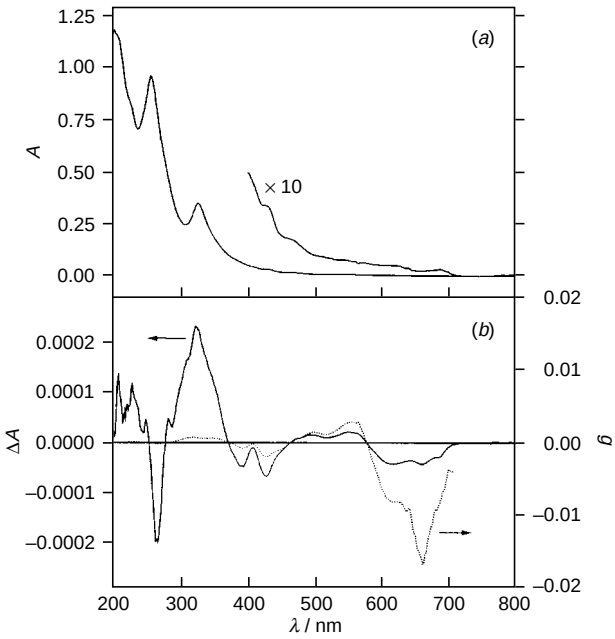

Fig. 3 (*a*) UV–VIS absorption spectrum of (±)-**1** ($c = 7.6 \times 10^{-6}$ M) [λ_{max}/nm = 204 ($\varepsilon = 1.5 \times 10^5$ M^{-1} cm^{-1}, *n*-hexane), 260 (1.2×10^5, $CHCl_3$), 328 (4.5×10^4, $CHCl_3$), 428 (4.7×10^3, $CHCl_3$) and 688 (4.2×10^2, $CHCl_3$)]. (*b*) CD spectra (left axis) and *g* value (right axis) of (+)-**1** ($c = 7.6 \times 10^{-6}$ M). The UV–VIS and CD spectra were recorded using a solution in *n*-hexane for the region $\lambda = 200$–248 nm and in $CHCl_3$ for the region $\lambda = 248$–800 nm. The $CHCl_3$ spectra were recorded at higher concentrations and mathematically scaled to the spectrum in *n*-hexane for representation.

absorption spectrum, with high *g* values in the low-energy region.

Dedicated to Professor Dr Hans Wynberg on the occasion of his 75th birthday on 28th November 1997.

Footnote and References

* E-mail: j.c.hummelen@chem.rug.nl

1 J. C. Hummelen, M. Prato and F. Wudl, *J. Am. Chem. Soc.*, 1995, **117**, 7003.
2 J. C. Hummelen, B. Knight, J. Pavlovich, R. González and F. Wudl, *Science*, 1995, **269**, 1554.
3 M. Keshavarz-K, R. González, R. G. Hicks, G. Srdanov, V. I. Srdanov, T. G. Collins, J. C. Hummelen, C. Bellavia-Lund, J. Pavlovich, F. Wudl and K. Holczer, *Nature*, 1996, **383**, 147.
4 K. Prassides, M. Keshavarz-K, J. C. Hummelen, W. Andreoni, P. Giannozzi, E. Beer, C. Bellavia, L. Cristofolini, R. González, A. Lappas, Y. Murata, M. Malecky, V. I. Srdanov and F. Wudl, *Science*, 1996, **271**, 1833.
5 F. Diederich, C. Thilgen and A. Herrmann, *Nachr. Chem. Tech. Lab.*, 1996, **44**, 9.
6 C. Thilgen, A. Herrmann and F. Diederich, *Helv. Chim. Acta*, 1997, **80**, 183.
7 A. Vasella, P. Uhlmann, C. A. A. Waldraff, F. Diederich and C. Thilgen, *Angew. Chem.*, 1992, **104**, 1388.
8 A. Bianco, M. Maggini, G. Scorrano, C. Toniolo, G. Marconi, C. Villani and M. Prato, *J. Am. Chem. Soc.*, 1996, **118**, 4072.
9 M. Maggini, G. Scorrano, A. Bianco, C. Toniolo and M. Prato, *Tetrahedron Lett.*, 1995, **36**, 2845.
10 J. M. Hawkins, A. Meyer and M. Nambu, *J. Am. Chem. Soc.*, 1993, **115**, 9844.
11 A. Hirsch, I. Lamparth and H. R. Karfunkel, *Angew. Chem.*, 1994, **106**, 453.
12 F. Diederich and R. L. Whetten, *Acc. Chem. Res.*, 1992, **25**, 119; S. Iijima, *Nature*, 1991, **354**, 56.
13 J. M. Hawkins and A. Meyer, *Science*, 1993, **260**, 1918; J. M. Hawkins, M. Nambu and A. Meyer, *J. Am. Chem. Soc.*, 1994, **116**, 7642.
14 M. S. Newman, R. S. Darlak and L. Tsai, *J. Am. Chem. Soc.*, 1967, **89**, 6191.
15 S. R. Wilson, Q. Lu, J. Cao, Y. Wu, C. J. Welch and D. I. Schuster, *Tetrahedron*, 1996, **52**, 5131.
16 M. Maggini, G. Scorrano, A. Bianco, C. Toniolo, R. P. Sijbesma, F. Wudl and M. Prato, *J. Chem. Soc., Chem. Commun.*, 1994, 305.
17 F. Novello, M. Prato, T. Da Ros, M. De Amici, A. Bianco, C. Toniolo and M. Maggini, *Chem. Commun.*, 1996, 903.

Received in Cambridge, UK, 8th October 1997; 7/07274K

Macrocyclic aromatic thioether sulfones

Ian Baxter,[a] Howard M. Colquhoun,[b]† Philip Hodge,[c]‡ Franz H. Kohnke,[c]§ and David J. Williams[a]

[a] *Department of Chemistry, Imperial College, South Kensington, London, UK SW7 2AY*
[b] *Science Research Institute and Department of Chemistry, University of Salford, Salford, UK M5 4WT*
[c] *Department of Chemistry, University of Manchester, Manchester, UK M13 9PL*

Reaction of 4,4′-sulfonylbis(thiophenol) with 4,4′-dichlorodiphenyl sulfone under pseudo-high-dilution conditions leads to a novel family of all-*para* macrocyclic thioether sulfones [-SϕSO$_2$ϕ-]$_n$ (ϕ = 1,4-phenylene); these include a highly strained [1 + 1] cyclodimer (*n* = 2), a cyclotrimer resulting from thioether exchange reactions, and a [2 + 2] cyclotetramer which can adopt two distinctly different conformations, one having molecular D_{2d} ('tennis-ball-seam') symmetry, in the crystalline state.

There is considerable and growing interest in the synthesis and ring-opening polymerisation chemistry of macrocyclic aromatic ethers[1] and thioethers.[2] The very low viscosities of such macrocycles, together with the absence of by-products during polymerisation, offer new possibilities for *in situ* fabrication of high-performance materials. We now report the discovery of a new class of potentially polymerisable macrocyclic aromatic thioethers, including an extremely strained cyclodimer, formed by polycondensation of 4,4′-sulfonylbis(thiophenol) **1**[3] with 4,4′-dichlorodiphenyl sulfone **2** under pseudo-high-dilution conditions.

A dimethylacetamide (DMA) solution containing equimolar quantities of **1** and **2** (0.13 M in each) was added *via* syringe-pump over 48 h to a refluxing suspension of K_2CO_3 in DMA–benzene (7.5 : 1, v/v). By-product water from the reaction was continuously removed by azeotropic distillation of benzene. After a further 2 h the reaction mixture was cooled and the products precipitated in water. Analysis by HPLC and FAB-mass spectrometry demonstrated the formation of a new family of macrocyclic oligomers [-SϕSO$_2$ϕ-]$_n$ (ϕ = 1,4-phenylene) in *ca*. 30% yield (Scheme 1), the remaining material being high molecular weight polymer. The principal macrocyclic product (*ca*. 15% yield) is the cyclic trimer, a result which indicates that cyclisation must be accompanied by extensive thioether exchange. Macrocycles where *n* is odd cannot be formed directly by condensation of **1** and **2**, and must therefore arise by redistribution or back-biting reactions (Scheme 2).

Extraction of the product mixture with $CHCl_3$ followed by gradient elution column chromatography on silica gel with CH_2Cl_2–EtOAc as eluent allowed several of the macrocyclic oligomers to be isolated as pure crystalline compounds, including the cyclodimer [-SϕSO$_2$ϕ-]$_2$ **3**, the cyclotrimer **4** and the cyclic tetramer **5**. Macrocycles were identified by ^{13}C and

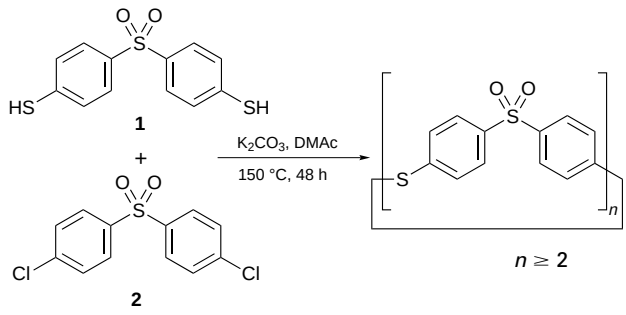

Scheme 1

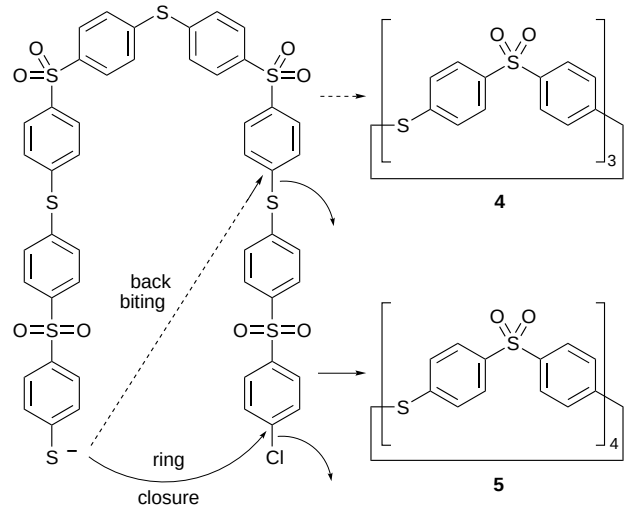

Scheme 2

^{1}H NMR spectroscopy and FAB-mass spectrometry. The cyclic trimer and tetramer give ^{1}H NMR spectra virtually identical to that of the linear polymer [-SϕSO$_2$ϕ-]$_n$, which shows a well-resolved AA′BB′ system at δ 7.85, 7.82, 7.44 and 7.41. In contrast, the ^{1}H NMR resonances for cyclic dimer **3**, where the effects of ring-closure are likely to be greatest, occur in a very much narrower range at δ 7.61, 7.58, 7.55, and 7.52.

The structures of **3**, **4** and **5** were investigated by single crystal X-ray methods.¶ The cyclic dimer **3** adopts a centrosymmetric, box-like conformation (Fig. 1) in which adjacent aromatic rings are orthogonal to within 1°. Although this 'open-book' type of conformation is well established in diaryl sulfones,[4] diaryl thioethers have up until now invariably displayed a 'skewed' conformation, even in the related cyclic oligomer [1,4-C$_6$H$_4$S]$_4$.[5] It thus appears to be the conformational preferences of the sulfone linkage which dominate the present structure.

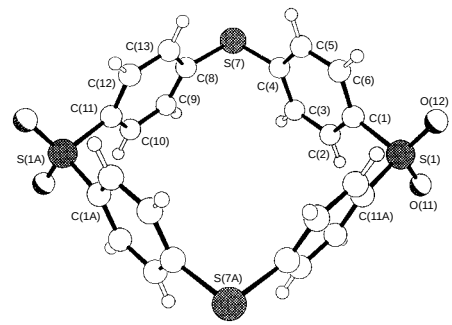

Fig. 1 Molecular structure of the cyclic dimer **3**: bond angles within the macrocycle at S(1) and S(7) are 101.4(2) and 96.4(2)°; the C(1)–C(6) and C(8)–C(13) rings are inclined by 88 and 81°, respectively, to the plane of the four sulfur atoms

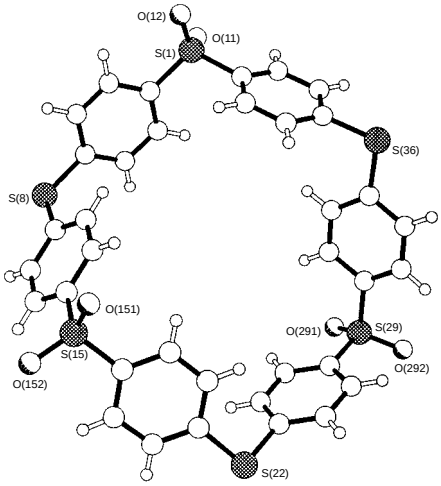

Fig. 2 Molecular structure of the cyclic trimer **4**: bond angles within the macrocycle at the sulfone sulfur atoms S(1), S(15) and S(29) are 105.7(4), 106.5(4) and 105.1(5)°, and those at the thioether sulfur atoms S(8), S(22) and S(36) are 101.5(4), 101.1(5) and 103.0(5)°

In the cyclic dimer **3**, C–S–C bond angles at thioether and sulfone are compressed by some 8 and 3°, respectively, from their normal open-chain values around 105°. Moreover, a distinct 'bowing' of the macrocycle is evident such that 1,4-related C–S bonds, which would normally be co-linear, here subtend an angle of *ca*. 171°. The very low yield of cyclodimer **3** (< 1%) thus clearly reflects the high strain-energy associated with formation of a cyclic thioether–sulfone oligomer containing only two repeat units.

The cyclotrimer **4** and cyclotetramer **5** were isolated in very much higher yields (*ca*. 15 and 10%, respectively), but despite the increased ring size, there is still evidence of some steric strain in the structure of **4**, all three independent thioether C–S–C bond angles being compressed by *ca*. 3° (Fig. 2).

The cyclic tetramer **5** adopts two entirely different conformations in the solid state, depending on the solvent of crystallisation. In the benzene solvate (**5a**) the oligomer displays a rather flattened conformation with the macrocyclic cavity being occupied by two of the five solvating benzene molecules. In another solvate (**5b**), however, the macrocycle adopts a 'tennis-ball-seam' conformation having non-crystallographic D_{2d} symmetry (Fig. 3). The solvent in **5b** is very substantially disordered and appears to comprise a mixture of both solvents used in its recrystallisation ($CHCl_3$ and CH_2Cl_2), limiting the overall precision of the structure. It is nevertheless evident from their bond and torsion angles that both **5a** and **5b** are virtually unstrained. In both conformers all diphenyl sulfone units have the conventional open-book geometry, so that interconversion between the two structures may be achieved simply by rotation about the thioether linkages.

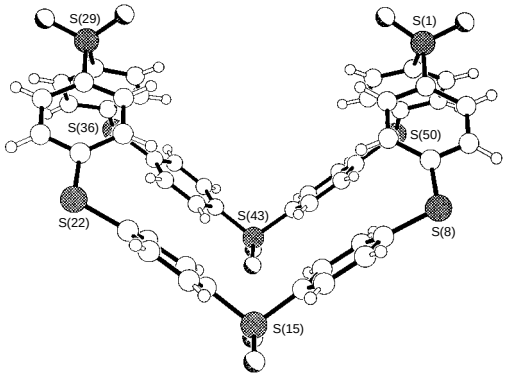

Fig. 3 The D_{2d} ('tennis-ball-seam') conformation adopted by the cyclic tetramer **5** in solvate **5b**: bond angles within the macrocycle at the sulfone sulfur atoms S(1), S(15), S(29) and S(43) are 103.7(4), 104.9(3), 103.9(3) and 104.6(3)°, and those at the thioether sulfur atoms S(8), S(22), S(36) and S(50) are 104.5(4), 104.3(4), 104.0(3), and 106.3(3)°

We have found that peroxide oxidation of the cyclic thioether sulfones $[\text{-S}\phi\text{SO}_2\phi\text{-}]_n$ affords a further series of macrocycles $[\text{-}\phi\text{SO}_2\text{-}]_{2n}$. These novel, cyclic oligomers of the highly crystalline and intractable polymer poly(1,4-phenylene sulfone)[6] will be described in a future communication.

We thank the Engineering and Physical Sciences Research Council for financial support of this research.

Footnotes and References

† E-mail: h.m.colquhoun@chemistry.salford.ac.uk
‡ E-mail: philip.hodge@man.ac.uk
§ On leave from the Department of Organic and Biological Chemistry, University of Messina, I-98166, Messina, Italy.

¶ *Crystal data* for **3**: $C_{24}H_{16}O_4S_4$, M = 496.61, monoclinic, space group $P2_1/c$, a = 9.912(1), b = 13.085(1), c = 10.007(1) Å, β = 117.67(1)°, Z = 2, U = 1149.7(2) Å^3, T = 203 K, D_c = 1.435 g cm^{-3}, μ(Cu-Kα) = 4.05 mm^{-1}, F(000) = 512. R_1 = 0.0398, wR_2 = 0.1003 for 1558 independent observed reflections [2θ < 126°, I > 2σ(I)]. For **4**: $C_{36}H_{24}O_6S_6\cdot 3CHCl_3$, M = 1103.02, monoclinic, space group *Ia*, a = 11.355(1), b = 32.209(2), c = 13.475(2) Å, β = 105.00(1)°, Z = 4, U = 4760.5(10) Å^3, T = 203 K, D_c = 1.529 g cm^{-3}, μ(Cu-Kα) = 7.67 mm^{-1}, F(000) = 2232. R_1 = 0.0693, wR_2 = 0.1833 for 3861 independent observed reflections [2θ < 126°, I > 2σ(I)]. For **5a**: $C_{48}H_{32}O_8S_8\cdot 5C_6H_6$, M = 1383.76, triclinic, space group $P\bar{1}$, a = 8.289(2), b = 13.049(1), c = 16.705(2) Å, α = 103.58(1), β = 101.88(1), γ = 90.85(1)°, Z = 1, U = 1714.9(5) Å^3, T = 203 K, D_c = 1.340 g cm^{-3}, μ(Cu-Kα) = 2.87 mm^{-1}, F(000) = 722. R_1 = 0.0579, wR_2 = 0.1360 for 4002 independent observed reflections [2θ < 126°, I > 2σ(I)]. For **5b**: $C_{48}H_{32}O_8S_8\cdot 5CHCl_3\cdot 0.5CH_2Cl_2$, M = 1632.52, triclinic, space group $P\bar{1}$, a = 15.147(1), b = 15.892(2), c = 16.591(2) Å, α = 72.68(1), β = 66.14(1), γ = 79.81(1)°, Z = 2, U = 3479.3(6) Å^3, T = 203 K, D_c = 1.558 g cm^{-3}, μ(Cu-Kα) = 8.44 mm^{-1}, F(000) = 1646. R_1 = 0.089, wR_2 = 0.214 for 5967 independent observed reflections [2θ < 120°, I > 2σ(I)]. Data for all four compounds were measured on a Siemens P4/RA diffractometer with graphite-monochromated Cu-Kα radiation using ω-scans. The data were absorption-corrected and the structures were solved by direct methods. Major-occupancy non-hydrogen atoms were refined anisotropically on F^2 data using the SHELXTL program package. CCDC 182/685.

1 J. A. Cella, J. J. Talley and J. M. Fukuyama, *Polym. Prepr. Am. Chem. Soc. Div. Polym. Chem.*, 1989, **30**(2), 581; H. M. Colquhoun, C. C. Dudman, M. Thomas, C. A. O'Mahoney and D. J. Williams, *J. Chem. Soc., Chem. Commun.*, 1990, 336; M. J. Mullins, E. P. Woo, D. J. Murray and M. T. Bishop, *Chemtech*, 1993 (August), 25; M. Chen, I. Guzei, A. L. Rheingold and H. W. Gibson, *Macromolecules*, 1997, **30**, 2516; Y.-F. Wang, M. Paventi and A. S. Hay, *Polymer*, 1997, **38**, 469.
2 Y. F. Wang and A. H. Hay, *Macromolecules*, 1997, **30**, 182; H. M. Colquhoun, D. F. Lewis, R. A. Fairman, I. Baxter and D. J. Williams, *J. Mater. Chem.*, 1997, 1; Y. E. Ovchinnikov, V. I. Nedel'kin, S. I. Ovsyannikova and Y. T. Struchkov, *Russ. Chem. Bull.*, 1994, **43**, 1384.
3 R. G. Feasey and J. B. Rose, *US Pat.*, 3 949 002/1976 (to ICI).
4 J. Kendrick, *J. Chem. Soc., Faraday Trans.*, 1990, **86**, 3995.
5 I. A. Zamaev, I. V. Razumovskaya, V. E. Schklover, Y. T. Struchkov, A. V. Astankov, V. I. Nedel'kin, V. A. Sergeev and Y. E. Ovchinnikov, *Acta Crystallogr., Sect. C*, 1989, **45**, 121.
6 D. R. Robello, A. Ulman and E. J. Urankar, *Macromolecules*, 1993, **26**, 6718; H. M. Colquhoun, *Polymer*, 1997, **38**, 991.

Received in Cambridge, UK, 1st October 1997; 7/07087J

α-Zincated phosphorus ylides

Matthias Steiner,[a] Hansjörg Grützmacher,*[a] Hans Prtizkow[b] and Laszlo Zsolnai[b]

[a] *ETH-Zürich, Laboratorium für Anorganische Chemie, Universitätsstrasse 6, CH-8092 Zürich, Switzerland*
[b] *Anorganisch Chemisches Institut der Universität, Im Neuenheimer Feld 270, D-69120 Heidelberg, Germany*

1,3-Dizincata-2,4-diphosphoniacyclobutane rearranges into a zincataphosphoniaindane which reacts with benzaldehyde to give 1,3-diphenylallene.

By reacting phosphorus ylides (R = aryl) with mercury bis(trimethylsilyamide) we found a simple synthesis of α-mercurated phosphorus ylides, $Ph_3P{=}CR[HgN(SiMe_3)_2]$, which react in a Wittig type alkenation reaction with aldehydes to give vinylmercury compounds.[1] We explored the possibility of synthesising comparable organozinc compounds in a similar way. These reagents seemed promising to us since they contain two oxophilic sites (P and low coordinated Zn) for the attack of a carbonyl oxygen centre. Like titanacycles **1**[2] or allenic diazophosphorus ylides **2**[3] they may serve as synthons for carbon atoms (Scheme 1). In the course of the studies, we observed an unprecedented cyclometallation reaction[4] involving, presumably, a low coordinated zinc centre.

When a toluene solution of ylides **3a**,**b** is added to zinc amide **4** at room temp. in toluene the expected adducts[1] **5a**,**b** are formed. They can be isolated as colourless precipitates after short reaction times (10 min) by concentrating the volume of the reaction mixture to 20% and adding *n*-hexane.†

While **5a** is thermally unstable, **5b** could be recrystallised from *n*-hexane and its structure determined by an X-ray analysis.‡ All bonds [av. Zn–N 1.956(3) Å, Zn–C 2.077(4) Å] to the slightly pyramidalised zinc centre (0.138 Å above the N(1)N(2)C(1) plane] are *ca.* 0.1 Å longer than comparable Zn–N (av. 1.857 Å) and Zn–C (av. 1.952 Å) bonds in other tricoordinated zinc compounds.[5] The P(1)–C(1) distance [1.738(3) Å] is slightly longer than corresponding distances in a lithium phosphorus ylide complex[6] (P–C 1.702 Å) or uncomplexed ylides themselves (*i.e.* **3a**: 1.693 Å).[7] Keeping solutions of **5a** at room temp. or adding pyridine causes loss of 1 equiv. of $HN(SiMe_3)_2$ and leads almost quantitatively to zincatacyclobutane **6** which precipitates as colourless crystals from the reaction mixture. Compound **6** can be recrystallised from THF–*n*-hexane (1 : 6 v/v). X-Ray analysis of **6**‡ reveals a four-membered planar centrosymmetric Zn_2C_2 heterocycle in which the Ph_3PCH units adopt bridging positions between the tricoordinated zinc centres. The Zn–N [1.931(3) Å] and Zn–C distances [2.068(4) Å] being again longer than in other low coordinated zinc compounds compare well with the ones in **5b**. The Zn–C–Zn angles [84.5(1)°] are smaller than the C–Zn–C angles [95.5(1)°]. In order to extrude 1 more equiv. of

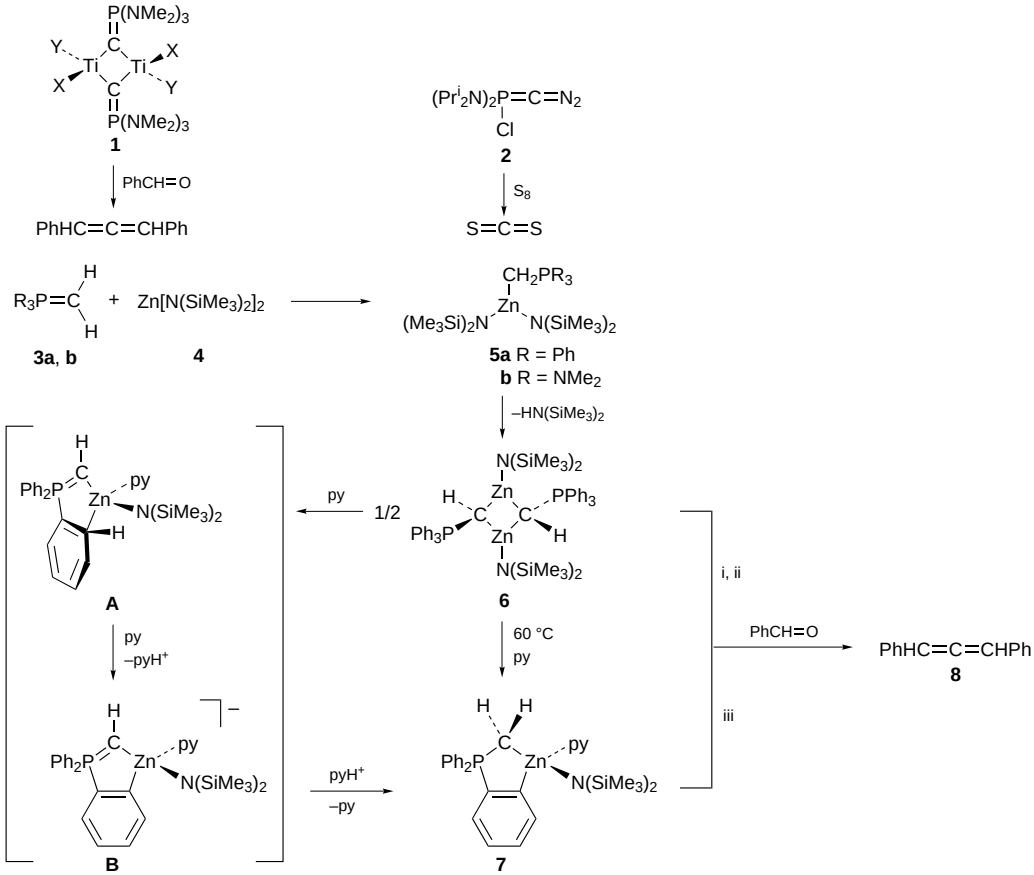

Scheme 1 *Reagents and conditions*: i, 60 °C, 24 h, no py, 7%; ii, 60 °C, 16 h, py, 12%; iii, 60 °C, 16 h, 31%

$HN(SiMe_3)_2$ we warmed **6** to 60 °C in presence of pyridine. A clean reaction was evidenced by one new ^{31}P resonance at δ 34.8 (**6**: δ 25.9). The new product **7** was purified by recrystallization from toluene–*n*-hexane and completely characterised including an X-ray analysis. In order to explain the formation of zincataphosphoniaindane **7**, we assume that pyridine cleaves the four-membered Zn_2C_2 heterocycle **6** to give intermediate **A** which corresponds to an η^1-arene complex to an electrophilic metal centre. Precedence for such a Zn–arene interaction is found in $ZnPh_2$ which forms a trapezoid dimer in the solid state with two *ipso*-carbon centres of the phenyl substituents adopting an unsymmetrical bridging binding mode (Zn–C 2.01, 2.40 Å).[8] Being an intramolecular organometallic σ-complex, **A** possesses a *ortho*-hydrogen centre which becomes sufficiently acidic to be abstracted by pyridine to give intermediate **B**. Reprotonation at the C(1) centre yields the thermodynamically more stable product **7**. Unfortunately, we could not isolate compound **B** by deprotonation of **7** with a strong base like $NaN(SiMe_3)_2$. Earlier work showed that **1a** may be lithiated by Bu^nLi either at the CH_2 group or at the *ortho*-position of one of the phenyl groups attached to the phosphorus centre.[9] Our results confirm that the first product may be obtained under kinetic control while the second one is thermodynamically more stable.

When zincatacyclobutane **6** is reacted with 4 equiv. of benzaldehyde in toluene at 60 °C, a pale yellow oil is obtained after hydrolysis from which *ca.* 7% diphenylallene **8** were isolated by column chromatography (*n*-pentane–Et_2O 7 : 1 v/v). Other products could not be identified. If the reaction is performed in presence of pyridine, the yield of allene **8** is augmented to 12%. Suspecting compound **7** may be involved in the formation of allene we reacted the zincataindane **7** with 2 equiv. of benzaldehyde. Indeed, the allene was formed in 31% yield. The mechanism of the seemingly simply Wittig alkenation is still not known with certainty[10] and our results show that reactions between metallated ylides and carbonyl compounds may be even more complex.

The structure of **7** is shown in Fig. 1. The five-membered heterocycle including a tetrahedrally distorted coordinated, chiral zinc centre (racemic mixture in the crystal) adopts an envelope conformation [angle between P(1)C(1)Zn and the ZnC(3)C(2)P plane = 30°].

The Zn–C(3) (aryl) bond length [2.049(3) Å] is normal while the Zn–C(1) (alkyl) bond [2.138(4) Å] is long. The Zn–$N(SiMe_3)_2$ bond [1.982(3) Å] is 0.1 Å shorter than the Zn–N_{py} bond. Owing to electrostatic interactions between the negatively charged carbon center C(1) (being bonded to the electropositive Zn centre) and the highly positively charged λ^5,σ^4-phosphorus centre, the P–C(1) (sp^3) bond [1.732(4) Å] is significantly shorter than the P–C(2) (sp^2) bond [1.803(3) Å].

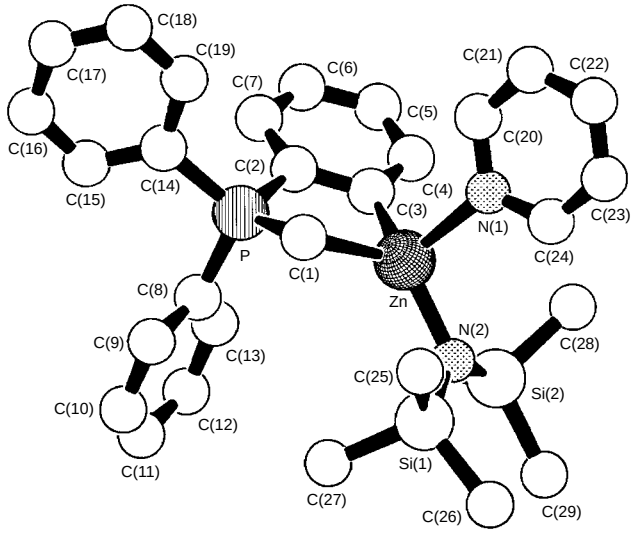

Fig. 1 Molecular structure of **7**: hydrogen atoms have been omitted for clarity. Selected bond lengths (Å) and angles (°): Zn–N(1) 2.174(3), Zn–N(2) 1.982(3), Zn–C(1) 2.137(4), Zn–C(3) 2.050(3), P–C(1) 1.733(4), P–C(2) 1.803(3), C(2)–C(3) 1.409(4); N(1)–Zn–N(2) 103.4(1), N(1)–Zn–C(1) 101.5(1), N(1)–Zn–C(3) 102.2(1), N(2)–Zn–C(1) 122.4(1), N(2)–Zn–C(3) 130.1(1), C(1)–Zn–C(3) 92.9(1), Zn–C(3)–C(2) 113.3(2), C(3)–C(2)–P 114.9(2), C(1)–P–C(2) 108.3(2), P–C(1)–Zn 100.8(2).

Footnotes and References

* E-mail: gruetz@inorg.chem.ethz.ch

† *Selected* ^1H (200 MHz), ^{13}C (50.232 MHz), ^{29}Si (17.75 MHz) and ^{31}P (36.19 MHz) *NMR data* for **5a**,**b** (C_6D_6), **6** ([$^2H_8$]THF) *and* **7** (C_6D_6): **5a**: Mp 187–189 °C. ^1H NMR: δ 0.37 (s, 36 H, $SiMe_3$), 1.30 (d, 2 H, $^2J_{HP}$ 16.8 Hz, CH_2), 6.95–7.16 (m, 9 H, *m, p*-H, PPh_3), 7.54–7.80 (m, 6 H, *o*-H, PPH_3). ^{13}C δ 3.7 (d, $^1J_{CP}$ 29.1 Hz, CH_2). ^{29}Si NMR: δ 6.6. ^{31}P NMR: δ 30.1. **5b**: 75 °C (decomp.). ^1H NMR: δ 0.48 (s, 36 H, $SiMe_3$), 1.53 (d, 2 H, $^2J_{HP}$ 17.0 Hz, CH_2), 2.08 (d, 18 H, $^3J_{HP}$ 9.3 Hz, NMe_2). ^{13}C: δ 2.8 (d, $^1J_{CP}$ 91.7 Hz, CH_2). ^{29}Si NMR: δ −7.0. ^{31}P NMR: δ 74.0. **6**: Mp 94–96 °C. ^1H NMR: δ −0.22 (s, 18 H, $SiMe_3$), 0.01 [A part of AA′XX′, 1 H, (J_{HP} + J_{HP}) 17.7 Hz, CH], 7.35–7.53 (m, 9 H, *m-, p*-H, PPh_3), 7.62–7.74 (m, 6 H, *o*-H, PPh_3). ^{13}C NMR: δ 6.1 (d, $^1J_{CP}$ 27.7 Hz, C_{ring}). ^{29}Si NMR: δ −7.3. ^{31}P NMR: δ 28.1. **7**: Mp 79 °C. ^1H NMR: δ 0.47 (s, $SiMe_3$, $^2J_{HSi}$ 6.2 Hz), 0.76 (d, $^2J_{CP}$ 9.5 Hz, CH_2), 6.55–6.64 (m, arom H), 6.80–740 (m, arom H). ^{13}C NMR (75.469 MHz, C_6D_6): δ 1.3 (d. $^1J_{CP}$ 47.5 Hz, CH_2), 126.4 (d, $^2J_{CP}$ 13 Hz, 6′-C, C_6H_4), 130.9 (d, $^4J_{CP}$ 4.0 Hz, 4′-C, C_6H_4), 131.5 (d, $^3J_{CP}$ 18.1 Hz, 5′-C, C_6H_4), 136.1 (d, $^1J_{CP}$ 105.7 Hz, 1′-C, C_6H_4), 139.4 (d, $^3J_{CP}$ 21 Hz, 3′-C, C_6H_4), 176.0 (d, $^2J_{CP}$ 45 Hz, 2′-C, C_6H_4). ^{29}Si NMR: δ −6.0 ^{31}P NMR: δ 34.2. All compounds gave satisfactorily elemental analyses.

‡ *Crystallography*: All data collected using Mo-Kα radiation, refinements by least-squares methods (full matrix) based on F_o^2 values (SHELXL-93). **5b**: monoclinic, $P2_1/n$, a = 16.065(12), b = 12.239(7), c = 17.191(11) Å, β = 109.81(5)°, U = 3180(4) Å^3, Z = 4, 3.0 < 2θ < 50.0°, 4568 reflections, 281 parameters, R_1 = 0.0357 (only observed reflections), wR_2 = 0.0604. **6**: monoclinic, $P2_1/n$, a = 12.352(14), b = 15.94(16), c = 14.999(16) Å, β = 114.37(8)°, U = 2690(5) Å^3, Z = 2, 3.62 < 2θ < 50.00°, 4290 reflections, 342 parameters, R_1 = 0.041 (only observed reflections), wR_2 = 0.1071. **7**: triclinic, $P\bar{1}$, a = 10.139(6), b = 14.245(8), c = 24.464(13) Å, α = 95.67(4), β = 99.39(4), γ = 96.09(4)°; U = 3442(3) Å^3, Z = 4, 4.1 < 2θ < 47.00°, 10 037 reflections, 719 parameters, R_1 = 0.039 (only observed reflections) wR_2 = 0.0961. CCDC 182/677.

1 M. Steiner, H. Pritzkow and H. Grützmacher, *Chem. Ber.*, 1994, **127**, 1177; reviews on metallated phosphorus ylides: H. Schmidbaur, *Angew. Chem.*, 1983, **95**, 980; *Angew. Chem., Int. Ed. Engl.*, 1983, **22**, 907; W. C. Kaska, *Coord. Chem. Rev.*, 1983, **48**, 1.

2 K. A. Hughes, P. G. Dopico, M. Sabat and M. G. Finn, *Angew. Chem.*, 1993, **105**, 603; *Angew. Chem., Int. Ed. Engl.*, 1993, **32**, 554.

3 J.-M. Sotiropoulos, A. Bacereido and G. Bertrand, *J. Am. Chem. Soc.*, 1987, **109**, 4711.

4 For a review on cyclometallations, see: G. R. Newkome, W. E. Pukett, V. K. Gupta and G. E. Kieffer, *Chem. Rev.*, 1986, **86**, 451.

5 Zn–N (av.) 1.857 Å, Zn–C (av.) 1.952 Å: H. Grützmacher, M. Steiner, H. Pritzkow, L. Zsolnai, G. Huttner and A. Sebald, *Chem. Ber.*, 1992, **125**, 2199 and references therein; M. M. Olmstead, P. P. Power and S. C. Shoner, *J. Am. Chem. Soc.*, 1991, **113**, 3379.

6 D. R. Armstrong, M. G. Davidson and D. Moncrieff, *Angew. Chem.*, 1955, **107**, 514; *Angew. Chem., Int. Ed. Engl.*, 1995, **34**, 478.

7 H. Schmidbaur, J. Jeong, A. Schier, W. Graf, D. L. Wilkinson, G. Müller and C. Krüger, *New J. Chem.*, 1989, **13**, 341.

8 P. R. Markies, G. Schat, O. S. Akkerman and F. Bickelhaupt, *Organometallics*, 1990, **9**, 2243.

9 E. J. Corey and J. Kang, *J. Am. Chem. Soc.*, 1982, **104**, 4724; E. J. Corey, J. Kang and K. Kyler, *Tetrahedron Lett.*, 1985, **26**, 555; B. Schaub, T. Jenny and M. Schlosser, *Tetrahedron Lett.*, 1984, **25**, 4097; B. Schaub and M. Schlosser, *Tetrahedron Lett.*, 1985, **26**, 1623.

10 E. Vedejs and M. J. Peterson, *Top. Stereochem.*, 1994, **21**, 1.

Received in Basel, Switzerland, 17th June 1997; 7/04248E

Typeset and printed by Black Bear Press Limited, Cambridge, England

ChemComm
FEATURE ARTICLE

Self-organization of small organic molecules in liquids, solutions and crystals: static and dynamic calculations

A. Gavezzotti[a]† and G. Filippini[b]

[a] *Dipartimento di Chimica Strutturale e Stereochimica Inorganica, University of Milano, via Venezian 21, 20133 Milano, Italy*
[b] *Centro CNR per lo Studio delle Relazioni tra Struttura e Reattività Chimica, University of Milano, via Golgi 19, 20133 Milano, Italy*

The phase behaviour of organic compounds is at the same time rich, appealing and complicated. From the properties of the pure liquid, to molecular recognition, aggregation and nucleation, both as a liquid and in solution, a number of different paths can be followed whose thermodynamics and kinetics are still to a large extent a mystery. Very little is known at a molecular level about the selective process that causes some nuclei to grow into crystals, while other aggregates are unproductive; similarly, the molecular details of the melting and dissolution processes are missing. Since the dimensions of objects and the timescale of events are scarcely or not at all accessible to experiment, computational simulation seems a viable alternative for the investigation of these phenomena.

Introduction

Modern chemistry has developed an extraordinary capability in the manipulation of molecular structures, and the synthesis of compounds of unusual or extreme chemical bonding (*e.g.* cubane), or stereochemical fine tuning (*e.g.* the total synthesis of taxol) are now within the range of possible, if not common, achievement. However, much less progress has been made in the control of molecular aggregation, and very little is known about the mechanisms of such commonplace events as melting, nucleation, growth and crystallization from the pure liquid or from solution. The main reason for this uneven development is that ordinary chemical bonding occurs in the range 10^2–10^3 kJ mol^{-1}, while molecular recognition and condensation lie in the range 10^0–10^1 kJ mol^{-1}; transformations among bonding patterns have therefore a much more predictable and reproducible course than intermolecular rearrangements, whose energetic landscape is but slightly undulated.

Of course, X-ray diffraction on single crystals has provided a tremendous amount of direct structural information on solids, and has fostered great advances also in our understanding of intermolecular interactions. Liquids and solutions are much less amenable to such detailed analysis, and, correspondingly, our knowledge of their intimate structure and properties is much less developed. It is perhaps obvious that studying intermolecular phenomena requires a knowledge of intermolecular potential energies and forces, out of which the fabric of macroscopic objects is woven. It is perhaps less frequently appreciated that thermal (*i.e.* kinetic) energy and entropy are also involved in determining the behaviour of matter. A 1985 textbook[1] appropriately stated: 'there is a big gap between knowing what the forces between two isolated molecules are and understanding how an assembly of such molecules will behave . . . even today there is no simple formula for deriving the properties of condensed phases from their intermolecular potentials . . .'. Much of this review will be devoted to the use of computer resources to bridge that gap and understand that derivation.

A first conceptual divide is the distinction between methods which explicitly include kinetic energy and account for thermal motion, and those which do not. For example, quantum chemical (QC) calculations can reproduce or predict structures, energies and activation barriers, but not the effects of thermal libration. The same applies to empirical calculations dealing, for example, with lattice energies of crystals and energy differences between polymorphs, using crystal structures frozen in the configuration derived from X-ray diffraction analyses or from some geometrical structure-guessing procedure. The effects of molecular librations may be somehow incorporated in the force field parameters, by calibrating them to reproduce specific volumes, but the description of libration itself is missing in the entirely static setup of both parametrization and modeling: all such calculations formally refer to a temperature of 0 K. Monte Carlo (MC)-type calculations include to some extent thermal energies, in that the Metropolis algorithm introduces a temperature-dependent Boltzmann factor for acceptance or rejection of phase space sampling steps. A full account of the dynamical evolution of a system under the action of potentials and including kinetic energies is given only by molecular dynamics (MD) calculations, which, at least in principle, allow a complete sampling of phase space and a *de novo* derivation of structural, thermodynamic and kinetic parameters.

The availability of accurate and easily applicable potential formulae and parameters is one of the key points in any theoretical treatment of condensed phases. In fact, one could contend that even in quantum chemical calculations the choice of the basis set and of the method for treating electron correlation are the equivalent of empirical parametrizations in classical force fields. However, the subject of potential formulation and optimization will not be considered here, since such a topic, even if schematically treated, would take up all the journal space allotted to this review. The problem of potentials will be addressed, in a cursory fashion, at some places, but the main emphasis will be on a perspective of what can or could be done to simulate, rationalize, predict or control molecular self-organization under the assumption that a suitable potential has indeed been made available. The reader should be conscious that this is not equivalent to saying that suitable potentials can always be derived, or, worse, that the power of MC, MD or quantum chemical algorithms is such that any potential formulation will do.

As is usual in these days of massive publication policies, the literature survey will be representative, rather than exhaustive.

Molecular recognition

Consider two molecules of different species, A and B, in the gas phase or in any condensed phase which allows substantial diffusional freedom. The most elementary definition of molecular recognition is the following aggregation step (1), neglecting the effects of the surrounding medium.

$$A + B \rightarrow AB \quad (1)$$

If this reaction describes hetero-recognition, self-recognition, relevant to condensation, nucleation and crystal growth in pure

substances, is given instead by step (2) where the expression [*n*A] denotes an aggregate of *n* identical molecules of species A.

$$A + A \rightarrow [2A] \qquad (2a)$$

$$[nA] + A \rightarrow [(n+1)A] \qquad (2b)$$

Processes (1) and (2*a*) can be studied quantum chemically, if the sizes of A and B are affordable (a base pair, but not a DNA strand and a ligand) given the required accuracy in the treatment of electron correlation. Process (2*b*) becomes quickly too expensive to be tackled by QC methods for molecular sizes (10–50 atoms) and *n*-values (10–100) of chemical significance.

High quality QC calculations on systems like (1) and (2*a*) can be used to derive cohesive energies and equilibrium distances which can then be exploited in the parametrization of empirical potentials. Typical results[2] indicate that, for example, the energies of C–H···C, C–H···S and S···S interactions are −2.9, −1.9 and −1.5 kJ mol^{-1}, respectively, an energy range which is consistent with that indicated in the opening statement of this review.

If a more realistic picture of the molecular recognition proceedings is desired, including solvation effects, one can use MC or MD calculations. Potentials here must be empirical, including usual intramolecular force field contributions plus intermolecular contributions, the latter being generally treated as a series of inverse powers of atom–atom distances, *i.e.* terms of the type CR^{-n} where *C*s are calibrating constants and the exponents are integers in the 1–12 range. Such events as solvation, dimerization and further aggregation can be simulated comfortably over systems consisting of a few thousand atoms. Using such techniques, for example, the optimized interaction energies of the benzene dimer in solution have been shown[3] to be within −7.1 and −9.6 kJ mol^{-1}, for widely different dimer structures; differences in stability between these aggregates are, again, in the range of a few to a few tenths of a kJ mol^{-1}.

A substantial drawback in this kind of calculation is that empirical potentials cannot account for molecular polarizability, at least for larger molecules with complex chemical features, since most force fields—at least the ones of more widespread applicability—are invariant with time and chemical environment. Indeed, describing steps (2*a*) and (2*b*) with the same force field for molecule A is unrealistic, and even less realistic is the use of an invariant field for molecule A when it is exposed to a strongly polarizing solvent, water to mention an obvious case.

A bonus of MD is that, besides thermodynamics, a picture of the interaction kinetics is obtained: this is vital if one considers molecular recognition as the preliminary step of condensation, ideally looking for liquid phase or solution precursors to crystal nucleation. Simulations of molecular aggregation by hydrogen-bonding in carboxylic acids and amides prove that in solution an equilibrium exists between cyclic and periodic chain arrangements.

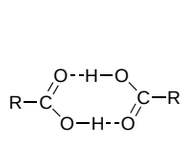

Cyclic dimer

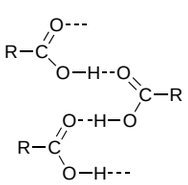

Chain ('catemer') motif

Thus, the relatively high abundance of the chain dimer for tetrolic acid in CCl_4 solution, predicted by MD,[4] is in agreement with the existence of two crystal polymorphs, one with the cyclic and one with the catemer motif. Understandably, such hydrogen-bonded aggregates survive in the apolar solvent, but break apart almost instantly in water. For 2-pyridone in CCl_4, the frequency of events in which one of the two hydrogen bonds of the cyclic dimer is cleaved,[5] most likely due to transfer of kinetic energy from solvent to solvate molecules, agrees with the significant dipole moment observed for the dimer in solution;[6] however, the high stability of the dimer is in contrast to the observed crystal structure, which exhibits the catemer motif. Fig. 1 shows typical time evolution graphs for the relevant hydrogen-bonding distances; such information is in principle very valuable for structural predictions, but clearly yields only a preliminary picture of the subsequent nucleation and growth processes.

Condensation; liquids

The notion that with an appropriate reduction in temperature and/or increase in overall pressure any vapor will condense into a liquid is trivial even in everyday words. Less widespread is the notion that even this familiar process requires a preliminary recognition leading to molecular clustering, a not so intuitive process for matter in the gas phase. Simulation studies of clustering from vapor have been presented,[7] but this topic will not be further pursued in this paper, which is mostly oriented towards molecular aggregation equilibria in condensed phases.

Organic compounds which are in the liquid state at around room temperature are made of small or apolar molecules. For these, the bulk liquid can be studied rather comfortably by MC or MD (*e.g.* ref. 3) with excellent results on the thermodynamics (heats of vaporization and C_p values) and on the structure (radial distribution curves). A recent MD study of liquid ethanol[8] afforded accurate estimates of thermodynamic and transport properties, of molecular conformations and orientational order,

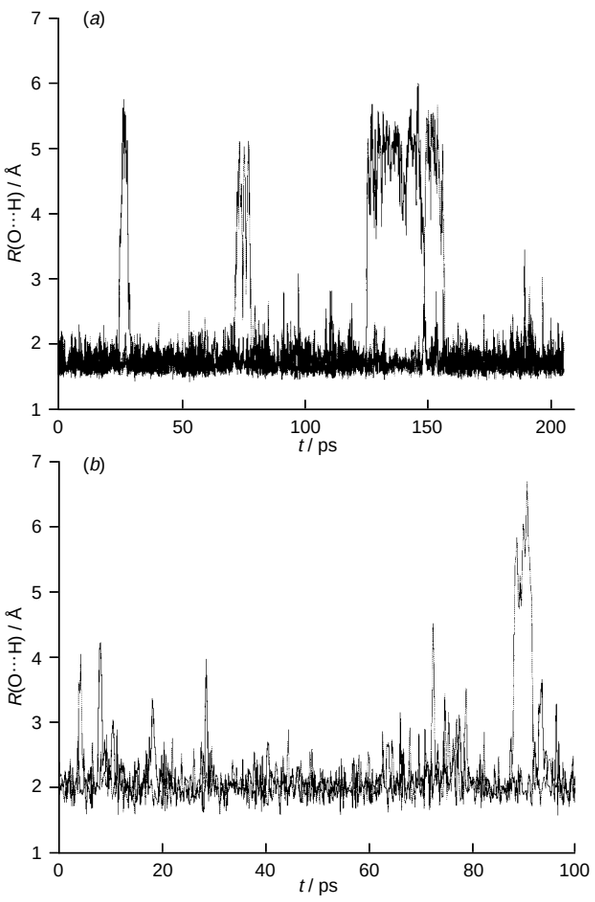

Fig. 1 Time evolution of the hydrogen-bonding O···H distances during MD simulations for cyclic dimers of (*a*) tetrolic acid (ref. 4) and (*b*) 2-pyridone (ref. 5)

as well as a description of the characteristics of hydrogen bonding states. Liquid phenol was studied[9] using an intermolecular potential derived from accurate QC calculations on the isolated molecule or dimers and trimers (remarkably, four dimers of widely different geometries span a cohesive energy range of just 4 kJ mol^{-1}, and the three most stable trimers of just 10 kJ mol^{-1}). MC simulations of the hydrogen bonding patterns in liquid formic acid[10] reveal that cyclic dimers occupy only 7% of the phase space, while in methanol clusters of 5 to 256 molecules,[11] small monocyclic aggregates were found to exhibit considerable persistency, presumably correlated with the high percentage of alcohol crystals with multimolecular asymmetric units composed of such cycles.[12]

The vast majority of organic compounds of molecular weight over 100 are solid at room temperature, and experimental measurements of the properties of their liquids can be awkward. Computer simulation can be very helpful here: test MD calculations[13] show that even simple 6–12 or 6–exponential atom–atom potentials, calibrated using static crystal structure data, can reliably estimate the density and heats of vaporization of comparatively large compounds, *e.g.* benzamide or coumarin. The complete calculation of specific volume as a function of temperature for liquid and crystal phases is also feasible (*e.g.* Fig. 2). Note that no timescale problem exists in the MD simulation of equilibrium bulk liquids, since experimental time constants for molecular diffusion span the 90 ps–20 fs range,[14] quite within the possibilities of today's MD. Presumably, the computational estimation of the thermochemical properties of small to medium-size organic molecules successfully competes, on the basis of cost : quality ratio, with experimental determinations.

Nucleation and the solid–liquid interface

A bulk liquid at a temperature much higher than its freezing point should ideally be completely disordered and hence perfectly homogeneous. Quite a different situation must arise when the temperature is lowered to the freezing point, and, even more, below it. An undercooled liquid must experience fluctuations towards the thermodynamically stable crystalline phase, and, if the size of nuclei formed during these fluctuations exceeds a certain critical threshold, evolution to the crystal is observed; otherwise, the subcritical nuclei merge back into the bulk fluid.[15] The theoretical study of these nucleation phenomena can proceed at an almost entirely macroscopic level, using comprehensive descriptors without regard to molecular structure,[15–17] or through several kinds of computational guinea pigs such as the Lennard–Jones system or other, similarly oversimplified (at least, with respect to ordinary organic chemistry) interaction sites.[18–20] Macroscopic theories of crystal growth have been developed mostly using cell models (like the Burton–Cabrera–Frank model), and models intermediate between the macroscopic and the molecular level exploit simple concepts such as the relationships between the growth speed of different crystal faces and the interplanar spacing (the Hartmann–Perdok model) or molecular attachment energies; however, these approaches lack resolution on the detail of molecular recognition, and hence are beyond our present scope. Heterogeneous nucleation, induced by interactions with random impurities, and hence orders of magnitude more complicated than homogeneous nucleation, will not be considered here for obvious reasons.

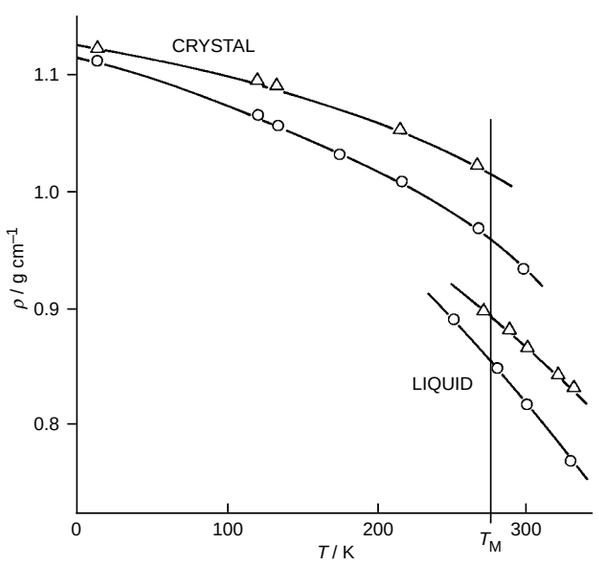

Fig. 2 Specific volume *versus* temperature for benzene from MD simulations of the liquid and crystal phases (from ref. 13). (○) calculated; (△) observed.

Progress on systems composed of real molecules has been made by joint experimental and theoretical studies of molecular clusters.[21] Clusters can be prepared in such conditions as to have nucleation rates as high as 10^{30} m^{-3} s^{-1}, perhaps 15 orders of magnitude larger than those in bulk liquids, and this is what makes them especially attractive targets for nucleation studies. For example, MD simulations on clusters including a few hundred molecules correctly reproduced solid–liquid transitions, and, even more significantly, an MD simulation on a cluster of 188 *tert*-butyl chloride molecules showed stability in the observed plastic crystalline tetragonal phase as well as spontaneous transformation to a low-temperature ordered, monoclinic crystalline phase, in agreement with electron and neutron diffraction data.[21] *tert*-Butyl compounds have a rich phase behaviour with several solid–solid and solid–liquid features, which have been studied by thermal analysis and theoretical dynamical methods (see ref. 22 for results and related literature).

While a complete phase diagram in the P–T plane can be obtained for a system of Lennard–Jones spheres,[23] solid–liquid equilibrium in molecular systems of moderate complexity is also almost within reach of present day computer capabilities. The nucleation and melting of linear C_n alkanes has been studied[24] by MD using an *n*-site Lennard–Jones representation of the molecules, in the NPT ensemble, *i.e.* at constant pressure, in a box with periodic boundary conditions resembling the bulk more than a cluster. The time evolution of thermodynamic and structural parameters could be monitored on line, in what can be considered an ideal computational experiment in nucleation. Similarly, encouraging results have been obtained for the liquid–solid phase transition of cyclohexane, with a six-site molecular model.[25] Using MD, the freezing of supercooled water, induced by an electric field, has been successfully simulated[26] over a period of a few hundred picoseconds, a quite affordable timescale for present-day computers.

Simulations of this kind, when extended to larger molecules, and analyzed for the identification of crystallization precursors, can be of extreme value in the progress of our understanding of nucleation from the melt.

Nucleation and crystallization from solvent

Nucleation of organic molecules within a solution is at present an essentially unaccessible phenomenon. The nuclei are too small to be seen by direct or scattered light, and their size distribution and dynamic growth properties cannot be determined experimentally. Computer experiments are therefore the only means to probe this elusive reality.

A first attempt to study the behaviour of elementary nuclei in solution was made[4] on dimers of tetrolic acid, as discussed previously in this paper. For a more comprehensive and significant test, an MD simulation was run on a computational box initially consisting of $9 \times 9 \times 9$ cells about 7 Å wide, 20 of which, picked at random, were occupied by (solute) acetic

acid molecules, the others being occupied by (solvent) CCl_4 molecules; no solute–solute distances below 15 Å were present in the starting configuration. Crystal potentials[27] were used for intermolecular interactions of the solute, and standard potentials[28] for the united-atom solvent molecules, applying the usual averaging rules for cross interactions and a 30 Å cutoff in intermolecular summations. The intramolecular geometry of the acetic acid molecules was frozen, except for the wagging motions of the acidic proton. Several runs were conducted at constant temperature between 200 and 300 K; the 200 K results are discussed, but the results did not change significantly with temperature. The GROMOS96 package[29] was employed.

The results are, if not conclusive, at least stimulating. Since no periodic boundaries were imposed, the starting box quickly relaxed into a pseudospherical shape [Fig. 3 and 4(*a*)], and at the same time a very fast condensation of solute molecules into small clusters made of 2–5 molecules was observed [Fig. 4(*b*) and 5], with geometries ranging from head-to-head dimers over the COOH function, to small hydrogen-bonded oligomers bound into cyclic structures. Not unexpectedly, no trace of intermolecular symmetry was found within these prototypical droplets, in which the molecular centers of mass stayed within cohesive distance during the simulation, while the detailed structure exhibited a highly fluxional behaviour. The solute potentials were of the 6–exp type,[27] transformed to 6–12 for compatibility with GROMOS; their well depth corresponds to a hydrogen-bonding energy (about 30 kJ mol^{-1}), but they fall off very quickly with distance. Therefore, to probe the efficiency of molecular attraction at long range, the computer experiment was then repeated supplementing the 6–exp potential with coulombic terms computed with the GROMOS96 charge distribution over the COOH group, thus increasing artificially, and even unrealistically, the intermolecular attractive forces. The stronger potentials bring molecules together more rapidly and hold them more tightly together within the droplets; although energies and trajectories differ somewhat, however, the final results in terms of structure and the total number of hydrogen bonds were essentially the same. One possible interpretation is that solute condensation is helped by solvent reorganization, besides solute–solute attractive interactions; in other words, some of the driving force for the segregation of solute molecules may come from the tendency of the solvent to squeeze out the disturbance to its own structure. If and how these conclusions can stand the trial of changes in the solute potential, in the length of the simulation, or in boundary conditions, remains to be seen; the example proves the feasibility, and hints to a possible usefulness, of this kind of simulation.

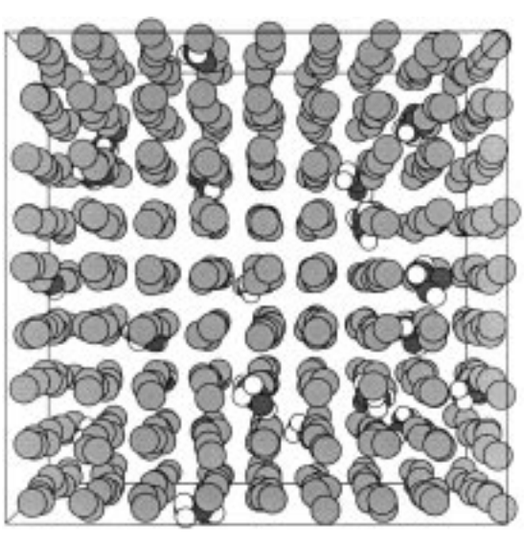

Fig. 3 Starting configuration within the computational box for 20 AcOH and 709 CCl_4 molecules; large circles are united-atom solvent molecules

The other relevant aspect of the solute–solvent equilibrium is the growth of macroscopic crystals once the nucleation stage has been overcome, and template crystal surface(s) are available within the solution. The timescale of events involved in crystal growth goes from (presumably) picoseconds for structural relaxation of molecules adsorbed on growing surfaces, to nanoseconds for molecular diffusion over the surface, to seconds for the growth of several monolayers; the first two steps are easily manageable by MD, but not the third. The so-called kinetic MC method can be employed, in which, roughly speaking, transition probabilities among configurations are weighted by estimated rates of the transition events, rather than by the Metropolis test as is the case in thermodynamic MC. Apparently, KMC simulations span formal times of the order of hundreds of seconds (see ref. 30 for further description and a review).

For chemical purposes, growth from solution is the method of choice. The concept of a relationship between a given crystal structure and the structure of precursor nuclei in solution has

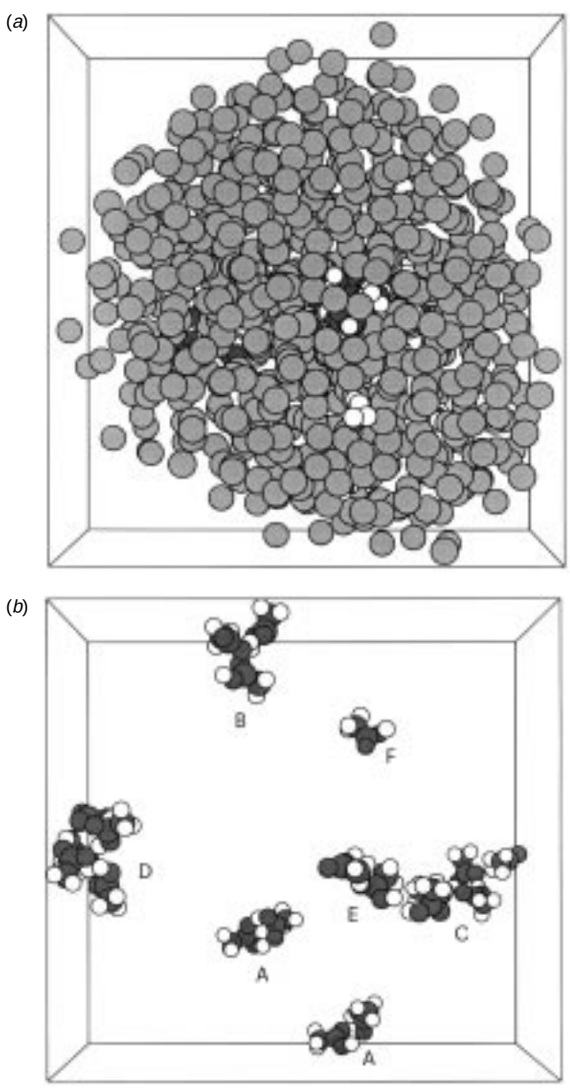

Fig. 4 (*a*) Overall view of the AcOH–CCl_4 system after 400 ps; 10 solvent molecules (not appearing) have departed from the drop, simulating evaporation. (*b*) Detail of the arrangement of AcOH molecules. A denotes cyclic dimers, B a chain trimer, C a four-molecule structure with bifurcated H-bonding and D a cyclic pentamer. In E, two molecules are close together but not H-bonded. F is an isolated molecule.

been introduced and exploited by the Weizmann school in a series of beautiful experiments, in which nucleation inhibitors were designed, on the basis of molecular structure, to bind stereospecifically at the surface of the stable polymorph, thus preventing its growth and enhancing the growth of metastable polymorphs (see ref. 31 for a recent account on the control of glycine polymorphism). At the other extreme, holistic analyses of the nucleation and growth kinetics produce phenomenological equations which lack molecular detail, but can be used[32] to study the rate-controlling processes in solvent-mediated phase transformations (Ostwald cycles).

Several experimental techniques are nowadays available for the *in situ* monitoring of crystal growth at atomic level; among others, atomic force microscopy[33] and laser interferometry.[34] The ideal computational experiment in crystal growth and dissolution involves the preparation of a computational box in which one or more crystal faces are exposed to either the pure solvent or a solution of the crystallizing substance, and the monitoring of the evolution in time of the system by MD. Problems of potentials (polarizability) and of timescale concur in making this experiment a very awkward one, *e.g.* given an elongation rate of 0.3 μm min^{-1} on a needle of the diameter of 10 μm,[35] a simple calculation shows that on a computational surface 100 × 100 Å wide, one should wait 3×10^8 ps to observe the attachment of a single molecule. This experimental result obviously incorporates an unknown time lag due to diffusional barriers within the solution; attachment and detachment events within the microscopic layer in intimate contact with the crystal surface may proceed at a much higher rate. In fact, MD simulations of the interface between a saturated urea solution and the urea crystal[36] revealed, at least, interesting preorganization details within the adsorbed layers. Well within the range of MD is instead the equilibration of water over crystal surfaces, or an essentially surface phenomenon, revealing details of the interaction with relevance to morphology[37] and wettability.[38]

Crystals

The final product of molecular recognition can be comfortably examined in the crystal structure, thanks to X-ray diffraction—at least in the majority of occurrences, but not always, since for yet unknown reasons a small but significant percentage of organic molecules refuse to organize into suitable single crystals. Present-day diffraction facilities, using stronger sources and two-dimensional detectors, have considerably reduced the number of inaccessible crystalline materials.

The dynamics of molecules in crystals far from transition temperatures is essentially harmonic, and hence rather uninspiring. Intermolecular librations can be successfully modeled by harmonic lattice dynamics, while extensive MD simulations are rather a tool for a more accurate calibration of potentials than for the discovery of new facts.[39]

Long before MD methods were devised, extensive computational work had been conducted on molecular crystals, dealing successfully with crystal packing analysis and crystal thermodynamics (see ref. 40 for a historical perspective). The background was thus laid for tackling more ambitious goals, like the enforcement of close-packing in translationally symmetrical molecular assemblies, and eventually, the computational prediction of crystal structures.

In the last five years or so, computational methods have been developed for guessing the crystal structure a compound will adopt, starting from the bare molecular constitution, and not without some success.[41–48] Such methods completely overlook all preliminary, dynamic molecular recognition stages, and rely on astute algorithms and shortcuts to assemble the crystal structure like a sort of molecular LEGO puzzle, the guiding concept being that the predicted crystal structure must be the one with the most stabilizing lattice energy. These procedures rely sometimes on random, Monte Carlo-type, or even brute force searches through the potential energy hypersurface, or on energy minimizing algorithms, and sometimes on symmetry considerations with an exploitation of close-packing principles; they are therefore essentially static in nature, although at some stages dynamic reshuffling in the form of simulated annealing may be applied, to facilitate the crossing of barriers and the unification of apparently different valleys. Typically, hundreds or thousands of plausibly close-packed structures are generated, and clustering of equivalent ones is problematic—consider, for example, just the problem of cell reduction in triclinic space groups. The basic result, common to all of these procedures, is a portrait of the potential energy landscape in the proximity of its minima, a picture that invariably reveals shallow regions among which the recognition of absolute stability is impossible. Fig. 6 and Tables 1–4 demonstrate this assertion.

Things could not be different, given the unavoidable physical nature of weak intermolecular interactions, and their energy range (see the introduction to this paper). The energetic resolution of empirical intermolecular potentials is presumably of the same order of magnitude as the energy differences they try to gauge; entropy differences are neglected. Besides, the starting molecular geometry is assumed *in vacuo*, and a reliable account of the interplay between the intra- and inter-molecular force field is awkward. Nevertheless, these structure prediction

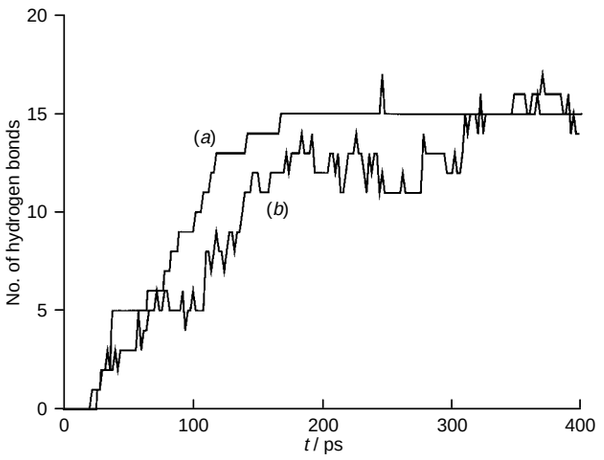

Fig. 5 AcOH in CCl_4: number of hydrogen bonds formed during the MD simulation, starting from the configuration in Fig. 3. Curve (*a*), with charges, curve (*b*), without charges (see text). T = 200 K.

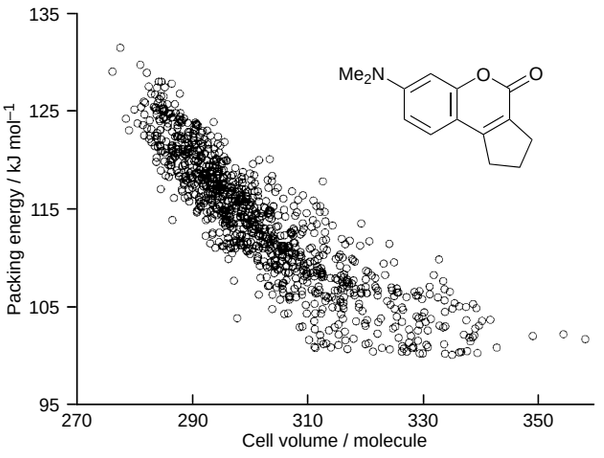

Fig. 6 Scatterplot of the cell volumes and packing energies of crystal structures generated in six different space-groups for the molecule shown in the inset (after ref. 48).

Table 1 Results of crystal structure prediction for isoiridomyrmecin (CSD refcode ISIRIN) (ref. 42)

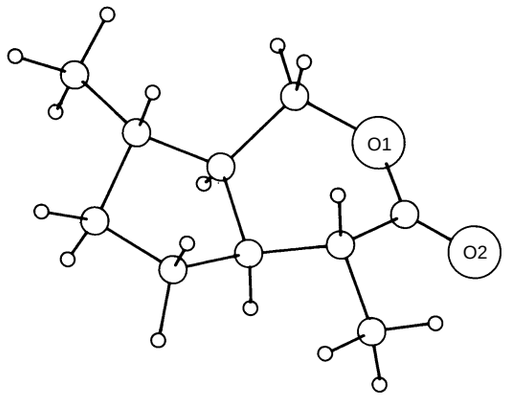

Space group	Z	E/kJ mol^{-1}	V_{cell}/Å^3	b axis
$P2_1$	2	103.0	473.8	6.42
		115.3	474.5	12.4
		111.3	471.9	9.02
		112.2	497.0	7.35
$P1$	1	103.5	241.1	—

Table 2 Predicted crystal structures for 1,8-dinitronaphthalene

Space group		(V/Z)/Å^3	E/kJ mol^{-1}	Ref.
$P2_12_12_1$	Exp	233.31	105.1	43
$P\bar{1}$		233.25	102.5	43
$P2_1$		237.04	103.4	43
$P2_1$/c		231.29	108.5	43
$P2_12_12_1$	Exp opt	219.5	123.8	49
$I2/a$		227.9	119.7	49
$P2_1/c$		221.4	123.4	49
$Pbca$		227.4	120.5	49

Table 3 First 10 structures predicted for durene (1,2,4,5-tetramethylbenzene, ref. 45)

Space group	E/kJ mol^{-1}	Z
$P\bar{1}$	89.64	1
$P\bar{1}$	83.74	1
$Pca2_1$	83.31	4
$Pbca$	82.81	4
$P2_1/a$	82.23	4
$P2_1/c$	81.68	4
$Pna2_1$	80.93	4
$P2_1$	80.64	2
$P2_1/a$	80.47	2
$P2_1/c$	79.76	2

Table 4 Crystal structure prediction for AcOH (ref. 47). For each space group N^o is the total number of structures generated, N' the number after clustering

	N^o	N'	Best E/kJ mol^{-1}
$P\bar{1}$	37 705	7	69.2
$P2_1$	2294	10	67.3
$P2_1/c$	60 683	113	69.7
$C2/c$	69 908	139	69.9
$P2_12_12_1$	7035	19	69.8
$Pna2_1$	3874	47	69.5
$Pbca$	9410	49	69.1
$Pnma$	15 100	40	63.5

algorithms are extremely valuable in that they usually can narrow down the choice to a few, typically 5–10 possible crystal structures, and this is an important result which should not be overlooked. Besides, when coupled with partial X-ray diffraction data (*e.g.* from faulty crystals or from powders) they lead to consistent structure prediction, the discrimination between computationally generated structures being taken care of by the reliable (often indisputable) experimental crystallographic information.[49,50] These facts are more than enough to foresee a wide impact of computational techniques, in the near future, on the design of novel molecular materials with desirable structure–property relationships. And, after all, with some luck and a modicum of chemical or crystallographic intuition, some of these methods can actually lead to a real *de novo* crystal structure prediction for some molecules; the trouble is, success or failure depends on still uncontrolled factors, and the success rate cannot be assessed in a systematic way, so that weak spots cannot be clearly identified and ameliorations cannot be rationally planned, at least thus far.

Phase behaviour of organic compounds

The study of organic molecules in the 100–1000 Da molecular weight range[51] is full of richness and fascination, although more so as regards their aggregation properties than the bare molecular structure, *i.e.* more in the inter- than in the intramolecular arena. The definition and modeling of weak recognition forces pose a great theoretical challenge, but also the applicative side is full of promise.

The *in vacuo* theoretical chemistry of small molecules includes a design step, done by sketching a molecular composition and connectivity on paper, and a structural exploration stage, in which quantum chemical or force field methods are used to define the conformation(s) and overall shape of the molecule in the absence of surrounding fields. If a high-quality wavefunction is available, the main features and even some detail of the molecular electrostatic field can be obtained for each conformation.

The study of the intermolecular theoretical chemistry of organic small molecules hits a big stumbling block in its very first stage, which is the polarization of the *in vacuo* molecular field by the environment. The study of condensed phases should start from the simplest one, a pure liquid; from there on, a wide range of possible paths can be envisaged in the modeling of the phase domain, using temperature/kinetic energy as a guideline. Several degrees and types of structuring and ordering set in as the temperature of the liquid decreases, from molecular clustering, to one- or two-dimensional translational ordering in liquid crystals (LC), to three-dimensional translational ordering with rotational disorder in plastic crystals; further on, or alternatively, a glassy state could be reached. All of these mesophases could be either thermodynamically stable or metastable with respect to the crystalline solid. At this stage the system assumes the status of a material with a macroscopic molecular assembly which can be used for specific purposes, since its texture interferes and specifically interacts with electromagnetic waves (LC display devices, non-linear optics), or with electric and magnetic fields (electrets and organic magnets).

In a conceptually final condensation stage, with further reduction of translational and rotational kinetic energies, the crystalline state is accessed, whose complete anisotropy of course enhances all possibilities for practical uses of the material. Even here, some flexibility is left in the consideration of possible polymorphism.

Binary solutions are just the two-component equivalent of the already immense one-component problem outlined above. Although neither pure liquids nor solutions can compete with solids for applicative purposes, the liquid state holds the premises for our comprehension of solidification. The basic dissolution–segregation process is in fact the key to an

understanding of the mechanisms of formation of the vast majority of organic solids.

Summary

Thus, the phase–mesophase behaviour of organic compounds is an inextricable tangle of kinetics and thermodynamics. We would like to conclude this article with some assessment of present or near-future computational approaches to its prediction and control. We assume that molecular structure and intermolecular potentials have been somehow established using the procedures and within the limitations outlined in the preceding sections.

Fairly accessible would be the prediction of the densities and cohesive energies of the liquid, liquid crystal, glassy and crystalline states of the substance. For the first three, dynamic calculations are necessary, but the corresponding computational boxes could be rather easily set up and equilibrated at any desired temperature. At least for the crystal, prediction could also go through static calculations, using one of the several algorithms described in a former section of this paper. Although the detailed geometrical structure of the crystal may not be accurately and reproducibly predicted, the available methods can usually produce 5–10 structures among which the possible polymorphs would almost certainly be included.

Quite a different problem would be the prediction of relative thermodynamic stabilities and of transition temperatures, for which an accurate evaluation of the enthalpies and entropies of all phases as a function of temperature would be needed. This is, so far, a prohibitive task. The dynamic simulation of the detailed transformation paths and of their kinetics is also so far extremely demanding, but steps are already being taken in this direction, and the promise for very quick development in the near future is high.

Control is a step beyond prediction. It would certainly be desirable to learn how to design the molecular architecture so as to engineer a certain property within the material, *e.g.* its propensity to form liquid crystal phases, or the presence or absence of a center of symmetry in the crystal, up to a fine tuning of molecular orientation in the solid to produce a certain electrooptical effect. A structural approach to crystal structure prediction and control makes use of the concept of crystal synthons, or basic recognition blocks which, when implanted in molecular objects, drive their spatial recognition to pre-established goals.[52] Its success depends on some systematization and much chemical intuition.

There is little that can be done directly, in terms of control of the properties of a material, by pure calculations; a computer computes properties, but cannot be confidently taught to appreciate the influence of molecular chemistry on them, a task which is more appropriate to the human than to the electronic mind (the crystal packing modes of primary amides had been codified and to some extent predicted[53] in times when computers were in their infancy). It is still for the human to line up all the computational information and to organize it towards comprehension. In this respect, what computers can easily do, besides brute force exploration of the phase space, is to gather at a fantastic speed, for the use of a human operator, information that would be too tedious or quite impossible to obtain by hand. Using computer-accessible collections of crystal information, like the Cambridge Structural Database,[54] one learns for instance[55] (after having programmed computers for decades to explore all the cell space) that molecular centers of mass must lie in special positions within the crystal cell, *i.e.* roughly halfway between inversion centers or between screw axes. Also, crystal structure prediction algorithms can be designed to learn from the structural or energetic properties of existing structures.[56] Together with the exponential increase in mere computing power, the near future should see a more and more widespread cooperation of human and electronic mindpower towards a more comprehensive understanding of the phase behaviour of organic compounds.

Angelo Gavezzotti graduated in Chemistry in 1968 at the University of Milano. He started his scientific career in X-ray crystallography and theoretical chemistry, under the supervision of Massimo Simonetta. His interests moved later to the simulation and prediction of organic crystal structures and properties, and, more recently, to computer techniques in the study of the physical chemistry of condensed phases of organic compounds.

Giuseppe Filippini received his degree in Chemistry from the University of Milano with a thesis in Crystallography (1968), under the supervision of Massimo Simonetta. He spent one postdoctoral year in Manchester with Professor D. W. J. Cruickshank. Currently, he is senior research scientist at the CNR Center for the Study of the Relationships between Structure and Chemical Reactivity. His active interests cover correlation and systematics of intermolecular interactions in organic crystals trough lattice dynamics and atom–atom potential calculations.

Notes and References

† E-mail: gave@stinch12.csmtbo.mi.cnr.it

1 J. N. Israelachvili, *Intermolecular and Surface Forces*, Academic Press, London, 1985, p. 9.
2 J. J. Novoa, M. Carme Rovira, C. Rovira, J. Veciana and J. Tarres, *Adv. Mater.*, 1995, **7**, 233.
3 W. L. Jorgensen, *Chemtracts: Org. Chem.*, 1991, **4**, 91.
4 A. Gavezzotti, G. Filippini, J. Kroon, B. P. van Eijck and P. Klewinghaus, *Chem. Eur. J.*, 1997, **3**, 893.
5 A. Gavezzotti, *Faraday Disc.*, 1997, **106**, 63.
6 K. DeSmet, P. Kedziora, J. Jadzyn and L. Hellemans, *J. Phys. Chem.*, 1996, **100**, 7662.
7 Z. Li and H. A. Scheraga, *J. Chem. Phys.*, 1990, **92**, 5499.
8 L. Saiz, J. A. Padrò and E. Guardia, *J. Phys. Chem.*, 1997, **101**, 78.
9 K. Sagarik and P. Asawakun, *Chem. Phys.*, 1997, **219**, 173.
10 P. Jedlovszky and L. Turi, *J. Phys. Chem.*, 1997, **101**, 5429.
11 D. Wright and M. S. El-Shall, *J. Chem. Phys.*, 1996, **105**, 11 199.
12 C. P. Brock and L. L. Duncan, *Chem. Mater.*, 1994, **6**, 1307.
13 A. Gavezzotti, G. Filippini and B. P. van Eijck, work in progress.
14 Y. J. Chang and E. W. Castner, *J. Phys. Chem.*, 1996, **100**, 3330.
15 C. K. Bagdassarian and D. W. Oxtoby, *J. Chem. Phys.*, 1994, **100**, 2139.
16 P. Harrowell and D. W. Oxtoby, *J. Chem. Phys.*, 1984, **80**, 1639.
17 H. Hettema and J. S. McFeaters, *J. Chem. Phys.*, 1996, **105**, 2816.
18 J. S. van Duijneveldt and D. Frenkel, *J. Chem. Phys.*, 1992, **96**, 4655.
19 V. Talanquer and D. W. Oxtoby, *J. Chem. Phys.*, 1995, **103**, 3686.
20 P. R. ten Wolde, M. J. Ruiz-Montero and D. Frenkel, *J. Chem. Phys.*, 1996, **104**, 9932.
21 L. S. Bartell, *J. Phys. Chem.*, 1995, **99**, 1080.
22 J. Reuter, D. Buesing, J. L. Tamarit and A. Wuerflinger, *J. Mater. Chem.*, 1997, **7**, 41.
23 R. Agrawal and D. A. Kofke, *Mol. Phys.*, 1995, **85**, 43.
24 K. Esselink, P. A. J. Hilbers and B. W. H. van Beest, *J. Chem. Phys.*, 1994, **101**, 9033.
25 A. Brodka and T. W. Zerda, *J. Chem. Phys.*, 1992, **97**, 5669.
26 I. N. Svihschev and P. G. Kusalik, *J. Am. Chem. Soc.*, 1996, **118**, 649.
27 A. Gavezzotti and G. Filippini, *J. Phys. Chem.*, 1994, **98**, 4831.
28 D. W. Rebertus and B. J. H. Berne, *J. Chem. Phys.*, 1979, **70**, 3395.
29 W. F. van Gunsteren, S. R. Billeter, A. A. Eising, P. H. Hunenberger, P. Kruger, A. E. Mark, W. R. P. Scott and I. G. Tironi, *Biomolecular Simulation: The GROMOS96 Manual and User Guide*, BIOMOS b.v., Zürich-Groningen, 1996.
30 M. Kotrla, *Comput. Phys. Commun.*, 1996, **97**, 82.
31 I. Weissbuch, L. Leiserowitz and M. Lahav, *Adv. Mater.*, 1994, **6**, 952.
32 R. J. Davey, P. T. Cardew, D. McEwan and D. E. Sadler, *J. Cryst. Growth*, 1986, **79**, 648.
33 A. J. Malkin, Y. G. Kutznetsov, W. Glantz and A. McPherson, *J. Phys. Chem.*, 1996, **100**, 11 736.
34 B. Y. Shekunov and R. J. Latham, *J. Phys. Chem.*, 1996, **100**, 5464.

35 R. J. Davey and J. Richards, *J. Cryst. Growth*, 1985, **71**, 597.
36 E. S. Boek, W. J. Briels and D. Feil, *J. Phys. Chem.*, 1994, **98**, 1674.
37 S. Khoshkoo and J. Anwar, *J. Chem. Soc., Faraday Trans.*, 1996, **92**, 1023.
38 J. Anwar and S. Khoshkoo, *Pharm. Res.*, 1996, **13**, 1006.
39 D. C. Sorescu, B. M. Rice and D. L. Thompson, *J. Phys. Chem.*, 1997, **101**, 798.
40 A. Gavezzotti and G. Filippini, in *Theoretical Aspects and Computer Modeling of the Molecular Solid State*, ed. A. Gavezzotti, Wiley, Chichester, 1997, ch. 3.
41 A. Gavezzotti, *J. Am. Chem. Soc.*, 1991, **113**, 4622.
42 H. R. Karfunkel and R. J. Gdanitz, *J. Comput. Chem.*, 1992, **13**, 1171.
43 J. R. Holden, Z. Du and H. L. Ammon, *J. Comput. Chem.*, 1993, **14**, 422.
44 B. P. van Eijck, W. T. M. Mooij and J.Kroon, *Acta Crystallogr., Sect. B*, 1995, **51**, 99.
45 A. M. Chaka, R. Zaniewski, W. Youngs, C. Tessier and G. Klopman, *Acta Crystallogr., Sect. B*, 1996, **52**, 165.
46 M. U. Schmidt and U. Englert, *J. Chem. Soc., Dalton Trans.*, 1996, 2077.
47 W. T. M. Mooij, B. P. van Eijck, S. Price, P. Verwer and J. Kroon, *J. Comput. Chem.*, 1997, **18**, in the press.
48 A. Gavezzotti, *Acta Crystallogr., Sect. B*, 1996, **52**, 201.
49 A. Gavezzotti and G. Filippini, *J. Am. Chem. Soc.*, 1996, **118**, 7153.
50 R.B. Hammond, K. J. Roberts, R. Docherty and M. Edmonson, *J. Phys. Chem.*, 1997, **101**, 6532.
51 A. Gavezzotti, submitted for publication in *Crystallogr. Rev.*
52 G. R. Desiraju, *Angew. Chem., Int. Ed. Engl.*, 1995, **34**, 2311.
53 L. Leiserowitz and A. T. Hagler, *Proc. R. Soc. Lond., Ser. A*, 1983, **388**, 133.
54 F. H. Allen and O. Kennard, *Chem. Des. Automat. News*, 1993, **8**, 31.
55 W. D. S. Motherwell, *Acta Crystallogr., Sect. B*, 1997, **53**, 726.
56 D. W. M. Hofmann and T. Lengauer, *Acta Crystallogr., Sect. B*, 1997, **53**, 225.

7/07818H

Hydrotalcite catalysis: heterogeneous epoxidation of olefins using hydrogen peroxide in the presence of nitriles

Shinji Ueno, Kazuya Yamaguchi, Kazushi Yoshida, Kohki Ebitani and Kiyotomi Kaneda*

Department of Chemical Science and Engineering, Graduate School of Engineering Science, Osaka University, 1–3 Machikaneyama, Toyonaka, Osaka 560, Japan

The layered hydrotalcite, $Mg_{10}Al_2(OH)_{24}CO_3$, acts as an efficient base catalyst for the epoxidation of various olefins using hydrogen peroxide in the presence of benzonitrile and with MeOH as solvent.

Hydrotalcites consist of Brucite-like layers having positive charge with anionic species in the interlayer, forming neutral materials.[1,2] Combination of different elements, changing the element ratios in the Brucite-like layer and selection of different anionic species can tune up the basicity of the hydrotalcites and the interlayer distance.[3] Recently, we found that hydrotalcites show high catalytic activities for the Baeyer–Villiger oxidation of various ketones using a combined oxidant of molecular oxygen and benzaldehyde or MCPBA; the surface hydroxy groups of the hydrotalcites acted as basic sites to promote the above oxidations.[4–7]Here, in relation to our studies on the base catalysis of hydrotalcites, we report that the heterogeneous epoxidation of various olefins using hydrogen peroxide is catalysed by hydrotalcites to give the corresponding epoxides [eqn. (1)].

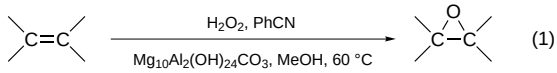

(1)

There are few reports concerning the oxidation of olefins by hydrotalcite catalysts using hydrogen peroxide.[8–11] Shape selective epoxidation was observed in the case of polyoxometalate-intercalated hydrotalcites. But diols and oxolanes were formed to some degree by successive cleavage of the epoxides. Notably, our oxidation system using hydrotalcites exculsively gives epoxides without other products.

Various hydrotalcites used in Table 1 were prepared by the literature procedures.[1,12,13] Elemental analyses for the hydrotalcites are in good agreement with literature values. After drying the hydrotalcites at 110 °C, they were stored in air and used without further pretreatment.†

Table 1 The epoxidation of cyclohexene catalysed by various hydrotalcites and NaOH using H_2O_2 and benzonitrile[a]

Catalyst	Conversion (%)	Yield (%)[b]	Heat of Adsorption[c]/ J g^{-1}
$Mg_{10}Al_2(OH)_{24}CO_3$	100	< 99	14.0
$Mg_5Al(OH)_{11}CO_3$	80	79	8.1
$Mg_6Al_2(OH)_{16}CO_3$	69	67	6.3
$Mg_6Al_2(OH)_{16}SO_4$	58	54	5.1
NaOH[d]	95	53[e]	—
Without catalyst	20	15	—

[a] Reaction conditions: cyclohexene (3.9 mmol), benzonitrile (10.5 mmol), hydrotalcite (0.05 g), MeOH 10 (ml), 30% aq. H_2O_2 (2.4 ml), 60 °C, 24 h. [b] Yields of epoxides were determined by GC analysis using internal standards, based on the olefins. [c] The basicity of the hydrotalcites was estimated by calorimetric heats of benzoic acid adsorption. [d] NaOH was equivalent to the amount of hydroxy functions in hydrotalcites (1.5 mmol). [e] Ring opening products of the epoxide, *e.g.* cyclohexane-1,2-diol and 2-methoxycyclohexan-1-ol, were formed.

In the presence of $Mg_{10}Al_2(OH)_{24}CO_3$, oxidations of cyclohexene using hydrogen peroxide with benzonitrile were carried out in various solvents such as methanol, benzene, toluene and 1,2-dichloroethane.‡ MeOH gave the highest yield of cyclohexene oxide. However, the oxidation hardly occurred in the absence of benzonitrile. Table 1 shows the catalytic effect of various hydrotalcites on the epoxidation of cyclohexene using benzonitrile in MeOH. Yields of cyclohexene oxide increased with increasing heat of benzoic acid adsorption on the hydrotalcites. The basicity of these hydrotalcites was estimated by a measurement of calorimetric heats of benzoic acid adsorption using microdifferential scanning calorimetry.[7] It is likely that the basic hydroxy groups of the hydrotalcites play an important role in the epoxidation. Bases such as NaOH and KOH catalyse the epoxidation of olefins using hydrogen peroxide in the presence of nitriles.[14,15] However, NaOH was not an effective base for our epoxidation.§

Table 2 shows results of the oxidation of olefins with benzonitrile in MeOH. Common linear and cyclic olefins such as oct-1-ene and cyclohexene gave the corresponding epoxides as sole products in excellent yield, respectively (entries 1–7). Norbornene gave only *exo*-norbornene oxide in quantitative yield (entry 8). Remarkably, styrene was oxidized to give styrene oxide in a high yield without formation of other oxidation products, *e.g.* acetophenone and benzaldehyde (entry 9). In the case of an α,β-unsaturated ketone, cyclohex-2-en-1-one, the epoxidation exclusively occurred without formation of the Baeyer–Villiger oxidation products (entry 10). This epoxidation proceeds stereospecifically with retention of configuration at the double bonds (entries 2 and 3).

Interestingly, we found that adding sodium dodecyl sulfate and sodium dodecylbenzene sulfate to the above oxidation system markedly increased the rates of the epoxidation; cyclooctene oxide was obtained quantitatively within 2 h.¶ This epoxidation consists of two phases; the olefin and nitrile are in the organic phase, while the hydrogen peroxide and hydrotalcite are in the aqueous phase. The above additives might act as a surfactant to form reverse micelles (aqueous phase in organic medium), which helps to increase contact area of the interface between the two phases. The detailed role of the additives in this epoxidation system is under investigation in our laboratory.

This epoxidation involves the following two steps; (i) formation of peroxycarboximidic acid by the reaction of a nitrile with hydrogen peroxide, and (ii) oxygen transfer from peroxycarboximidic acid to olefin, in which step (i) is promoted by bases.[14] It is likely that the hydrotalcite acts as a solid base and promotes the formation of peroxycarboximidic acid, leading to high yields of the epoxides.

In conclusion, we have developed an efficient heterogeneous catalyst system utilising hydrotalcites for epoxidation and using a combined oxidant of aqueous hydrogen peroxide and benzonitrile. The solid hydrotalcites are easily separated from the reaction mixture *via* filtration, which makes the work-up procedure simple. The hydrotalcite can be reused without an

Table 2 The epoxidation of various olefins catalysed by $Mg_{10}Al_2(OH)_{24}CO_3$ using H_2O_2 and benzonitrile[a]

Entry	Substrate	Product	Conversion (%)	Yield (%)[b]
1	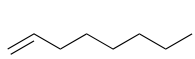	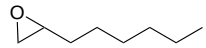	95	95
2[c]	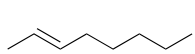	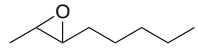	100	96
3[c]		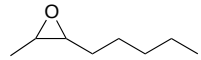	94	93
4[d]			100	95
5		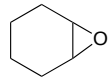	100	>99
6		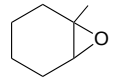	100	94
7		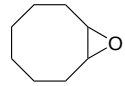	99	95
8	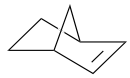		100	>99 (only *exo*)
9	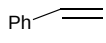	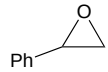	97	92
10	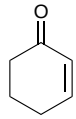	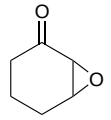	84	84
11	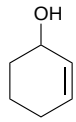	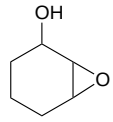	90	89 (*syn* : *anti* = 80 : 20)

[a] Reaction conditions: olefin (3.9 mmol), benzonitrile (10.5 mmol), $Mg_{10}Al_2(OH)_{24}CO_3$ (0.05 g), MeOH (10 ml), 30% aq. H_2O_2 (2.4 ml), 60 °C, 24 h. [b] Yields of epoxides were determined by GC analysis using internal standards, based on the olefins. [c] The relative epoxidation rate of *cis*- and *trans*-oct-2-ene was 1.5, which is similar to that of MCPBA. [d] 30 °C.

appreciable loss of catalytic activity. This system should prove useful for many base-catalysed selective oxidations.

Notes and References

* E-mail: kaneda@cheng.es.osaka-u.ac.jp

† *A typical procedure* for the epoxidation of cyclooctene: Into a reaction vessel with a reflux condenser were successively placed the hydrotalcite of $Mg_{10}Al_2(OH)_{24}CO_3$ (0.15 g), MeOH (40 ml), cyclooctene (14 mmol), benzonitrile (17 mmol) and 30% aq. H_2O_2 (7.5 ml). The resulting mixture was stirred at 60 °C for 24 h. The hydrotalcite was separated by filtration and the filtrate was treated with MnO_2 (0.03 g) to decompose the remaining H_2O_2. GC analysis of the filtrate showed a quantitative yield of cyclooctene oxide. The filtrate was diluted with deionized water (50 ml) and extracted with $CHCl_3$ (50 ml × 3). The extract was concentrated under reduced pressure and subjected to a silica gel chromatography using a mixture of *n*-hexane–Et_2O (40 : 1, v/v) as an eluent to give cyclooctene oxide (1.5 g, 87% yield). The isolated hydrotalcite can be reused without loosing its high catalytic activity.

‡ The order for yields of cyclohexene oxide using different nitrile compounds is as follows; benzonitrile > acetonitrile > propionitrile.

§ Under our reaction conditions, use of NaOH in place of the hydrotalcites resulted in a 53% yield of cyclohexene oxides, as shown in Table 1.

¶ Use of cationic surfactants, *e.g.* cetylpyridinium chloride monohydrate and tetra-*n*-propylammonium bromide, did not increase yields of cyclooctene oxide.

1 F. Cavani, F. Trifiro and A. Voccari, *Catal. Today*, 1991, **11**, 173.
2 K. A. Carrado and A. Kostapapas, *Solid State Ionics*, 1988, **26**, 77.
3 S. Miyata, *Clays. Clay Miner.*, 1983, **31**, 305.
4 K. Kaneda, S. Ueno and T. Imanaka, *J. Chem. Soc., Chem. Commun.*, 1994, 797.
5 K. Kaneda, S. Ueno and T. Imanaka, *J. Mol. Catal.*,1995, **102**, 135.
6 K. Kaneda and T. Yamashita, *Tetrahedron Lett.*, 1996, **37**, 4555.
7 S. Ueno, K. Ebitani, A. Ookubo and K. Kaneda, *Appl. Surf. Sci.*, 1997, **121**/**122**, 366.
8 T. Tatsumi, K. Yamamoto, H. Tajima and H. Tominaga, *Chem. Lett.*, 1992, 815.
9 B. F. Sels, D. E. D. Vos and P. A. Jacob, *Tetrahedron Lett.*, 1996, **37**, 8557.
10 C. Cativiela, F. Figueras, J. M. Fraile, J. I. García and J. A. Mayoral, *Tetrahedron Lett.*, 1995, **36**, 4125 .
11 J. M. Fraile, J. I. García, J. A. Mayoral and F. Figueras, *Tetrahedron Lett.*, 1996, **37**, 5995 .
12 W. T. Reichle, S. Y. Kang and D. S. Everhordt, *J. Catal.*, 1986, **101**, 352.
13 M. A. Drezdson, *Inorg. Chem.*, 1988, **27**, 4628.
14 G. B. Payne, P. H. Deming, and P. H. Williams, *J. Org. Chem.*, 1961, **26**, 651.
15 G. B. Payne, *Tetrahedron*, 1962, **18**, 763.

Received in Cambridge, UK, 23rd October 1997; 7/07655J

Anionic cyclisations of an *N*-benzyl naphthamide: a route to benzo[*e*]isoindolones

Anjum Ahmed,[a] Jonathan Clayden*[a] and Michael Rowley[b]

[a] *Department of Chemistry, University of Manchester, Oxford Road, Manchester, UK M13 9PL*
[b] *Merck Sharp and Dohme Neuroscience Research Centre, Terlings Park, Harlow, Essex, UK CM20 2QR*

On treatment with Bu^{t}Li and HMPA, *N*-*tert*-butyl-*N*-benzyl-1-naphthamide undergoes cyclisation to a tricyclic enolate which reacts diastereoselectively with electrophiles to give substituted 2,3,3a,9b-tetrahydro-1*H*-benzo[*e*]-isoindol-1-ones, the first example of an anionic cyclisation onto an aromatic ring.

When tertiary aromatic amides **1** are treated with organolithium bases, they are usually *ortho*-lithiated.[1–3] Amides bearing 2-alkyl groups may be laterally lithiated[4,5] and, in exceptional cases (for example if the 2 and 6 positions are blocked,[6–9] if the nitrogen bears an activating group such as benzyl[10] or with a lithium amide base[1,11]), lithiation may take place α to nitrogen.[12,13] Alkylation of these dipole-stabilised anions is well known,[13] and both *ortho*-lithiation[14] and lateral lithiation[15] followed by electrophilic quench have been made enantioselective by the addition of (−)-sparteine.[16]

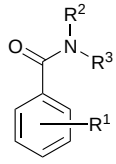

1

We have shown that both *ortho*-lithiated[17,18] and laterally lithiated[19] tertiary 1-naphthamides can react atroposelectively with electrophiles—frequently only one of two possible atropisomeric products (which arise from restricted rotation about the aryl–carbonyl bond) is formed.[19] For example, the 2-ethyl-*N*,*N*-diisopropylnaphthamide **2** reacts with Bu^{s}Li to give a single, configurationally stable (at both stereogenic axis and centre) organolithium[20] which reacts stereospecifically with many electrophiles to give a single atropisomer of the product **3** (Scheme 1).

In connection with this work, we lithiated *N*-*tert*-butyl-*N*-benzyl-1-naphthamide **4** with Bu^{t}Li and quenched the resulting red solution with MeI. We obtained two compounds, in a ratio of about 2 : 1: compound **7** results from methylation α to nitrogen, and **8** from methylation on the aromatic ring *ortho* to the amide group.† Lithiation of **4** therefore apparently gives a mixture of α- and *ortho*-lithiated compounds **5** and **6**.

When we treated this mixture of organolithiums with HMPA (6 equiv.), it underwent a remarkable cyclisation reaction.‡ After an aqueous quench, we isolated the tricyclic 2,3,3a,9b-tetrahydro-1*H*-benzo[*e*]isoindol-1-one **9** as a single diastereoisomer in 82% yield (Scheme 2). Nuclear Overhauser enhancement (NOE) experiments showed that the 6,5-ring junction was *cis*, with the phenyl group on the *exo* face. This is the more stable of the two ring-junction isomers: **9** was recovered as a single unchanged diastereoisomer after stirring overnight with Bu^{t}OK in Bu^{t}OH at 40 °C.§

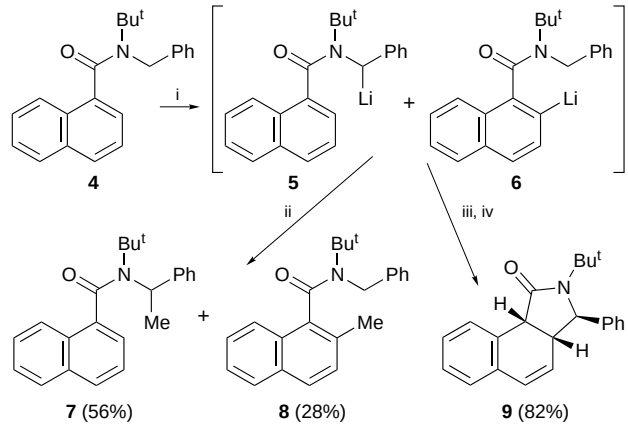

4 **5** **6** **7** (56%) **8** (28%) **9** (82%)

Scheme 2 *Reagents and conditions*: i, Bu^{t}Li (1.3 equiv.), THF, −78 °C, 2 h; ii, MeI, −78 °C; iii, HMPA (6 equiv.), −78 °C, 16 h; iv, NH_4Cl

The initial product of the cyclisation triggered by the HMPA is an enolate **10** which we could alkylate with MeI, Bu^{n}Br or BnBr, giving compounds **11** as shown in Scheme 3. Diastereoselectivity depended on the size of the electrophile, with BnBr being the most selective—**11** (R = Bn) was obtained as a single isomer **11a** (R = Bn) only. MeI gave a 3 : 1 ratio of **11a** and **11b**, and the same ratio of diastereoisomers is obtained by methylating the lithium enolate formed from **9** with LDA in the absence of HMPA: HMPA does not affect the diastereoselectivity of the

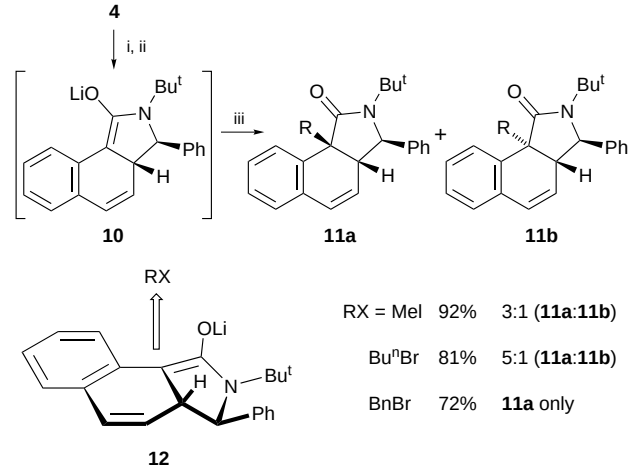

4 **10** **11a** **11b** **12**

Scheme 3 *Reagents and conditions*: i, Bu^{t}Li, −78 °C; ii, HMPA, −78 °C; iii, RX

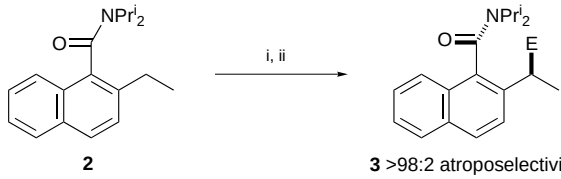

2 **3** >98:2 atroposelectivity

Scheme 1 *Reagents and conditions*: i, Bu^{s}Li, −78 °C; ii, E^+ (EtI or R_3SiCl)

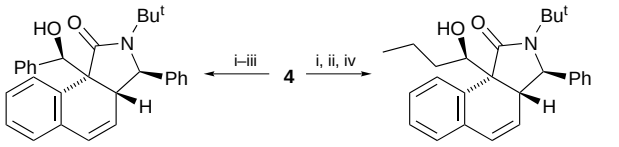

13 (81%)

14 (47%)
plus other diastereoisomers (37%)

Scheme 4 *Reagents and conditions*: i, Bu^{t}Li, −78 °C; ii, HMPA, −78 °C; iii, PhCHO; iv, Pr^{n}CHO

reaction. The identity of the diastereoisomers was determined by NOE experiments, and the major one in each case results from alkylation from the less hindered *exo* face of the enolate as shown (**12**), giving a *cis* 6,5-ring junction.

The cyclised enolate **10** also underwent clean aldol reactions (Scheme 4). A reaction with benzaldehyde gave the alcohol **13** as a single diastereoisomer in 81% yield. Tricycle **13** has four new adjacent chiral centres, and its relative stereochemistry was proved by X-ray crystallography (Fig. 1). An aldol reaction with *n*-butyraldehyde was somewhat less stereoselective, although NMR correlation indicated that again the major product **14** arose from attack of the aldehyde on the less hindered face of the enolate.

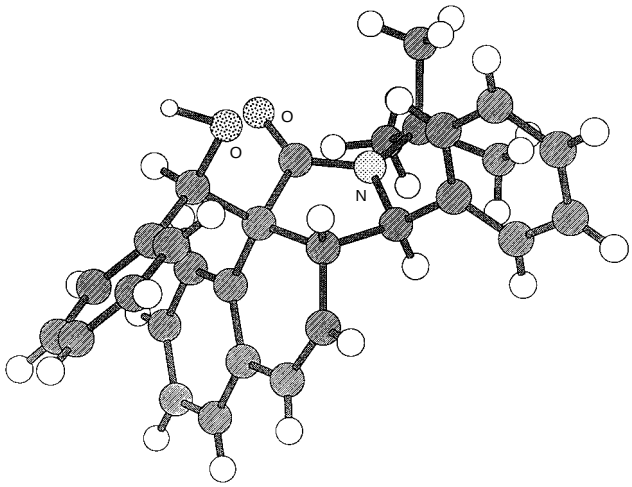

Fig. 1

While additions onto aromatic rings which result in loss of aromaticity are rare,[21] the addition of organometallic nucleophiles to electron-poor naphthalenes is precedented.[22] However, our cyclisation is, as far as we are aware, the first example of an *anionic cyclisation* onto an aromatic ring of any sort. Anionic cyclisation onto π systems is turning out to be a useful way of making rings, both carbocyclic[23,24] and heterocyclic,[25] but is invariably initiated by transmetallation and not deprotonation.[26] We are currently extending the scope and applicability of this new reaction as a promising method for the stereocontrolled synthesis of fused five-membered nitrogen heterocycles.[27]

We are grateful to the University of Manchester for a Research Support Grant, to the EPSRC for a CASE award (to A. A.) and to Dr Madeleine Helliwell for determining the X-ray crystal structure of **13**.

Notes and References

* E-mail: j.p.clayden@man.ac.uk

† Later, we found that this reaction also gives a small amount (*ca.* 10%) of **11** (R = Me).

‡ For an example of an anionic cyclisation triggered by $Me_2NCH_2CH_2NMe_2$, see ref. 24.

§ A kinetic protonation of the enolate with Bu^{t}Br likewise gave a single diastereoisomer of **9**.

1 P. Beak and V. Snieckus, *Acc. Chem. Res.*, 1982, **15**, 306.
2 P. Beak and R. A. Brown, *J. Org. Chem.*, 1982, **47**, 34.
3 V. Snieckus, *Chem. Rev.*, 1990, **90**, 879.
4 R. D. Clark and A. Jahangir, *Org. React.*, 1995, **47**, 1.
5 J. J. Court and D. J. Hlasta, *Tetrahedron Lett.*, 1996, **37**, 1335.
6 R. Schlecker, D. Seebach and W. Lubosch, *Helv. Chim. Acta*, 1978, **61**, 512.
7 D. Seebach, W. Wykypiel, W. Lubosch and H.-O. Kalinowski, *Helv. Chim. Acta*, 1978, **61**, 3100.
8 P. Beak, B. G. McKinnie and D. B. Reitz, *Tetrahedron Lett.*, 1977, 1839.
9 D. R. Hay, Z. Song, S. G. Smith and P. Beak, *J. Am. Chem. Soc.*, 1988, **110**, 8145.
10 R. R. Fraser, G. Boussard, I. D. Potescu, J. J. Whiting and Y. Y. Wigfield, *Can. J. Chem.*, 1973, **51**, 1109.
11 P. Beak, G. R. Brubaker and R. F. Farney, *J. Am. Chem. Soc.*, 1976, **98**, 3621.
12 N. G. Rondan, K. N. Houk, P. Beak, W. J. Zajdel, J. Chandrasekhar and P. v. R. Schleyer, *J. Org. Chem.*, 1981, **46**, 4108.
13 P. Beak and D. B. Reitz, *Chem. Rev.*, 1978, **78**, 275.
14 S. Thayumanavan, P. Beak and D. P. Curran, *Tetrahedron Lett.*, 1996, **37**, 2899.
15 S. Thayumanavan, A. Basu and P. Beak, *J. Am. Chem. Soc.*, 1997, **119**, 8209.
16 P. Beak, A. Basu, D. J. Gallagher, Y. S. Park and S. Thayumanavan, *Acc. Chem. Res.*, 1996, **29**, 552.
17 P. Bowles, J. Clayden and M. Tomkinson, *Tetrahedron Lett.*, 1995, **36**, 9219.
18 P. Bowles, J. Clayden, M. Helliwell, C. McCarthy, M. Tomkinson and N. Westlund, *J. Chem. Soc., Perkin Trans. 1*, 1997, 2607.
19 J. Clayden and J. H. Pink, *Tetrahedron Lett.*, 1997, **38**, 2561.
20 J. Clayden and J. H. Pink, *Tetrahedron Lett.*, 1997, **38**, 2565.
21 K. Maruoka, M. Ito and H. Yamamoto, *J. Am. Chem. Soc.*, 1995, **117**, 9091; T. Bach, *Angew. Chem., Int. Ed. Engl.*, 1996, **35**, 729; S. Saito, K. Shimada, H. Yamamoto, E. Martínez de Marigorta and I. Fleming, *Chem. Commun.*, 1997, 1299; D. W. Brown, M. Lindquist, M. F. Mahon, B. Malm, G. N. Nilsson, A. Ninan, M. Sainsbury and C. Westerlund, *J. Chem. Soc., Perkin Trans. 1*, 1997, 2337; J. Boivin, M. Yousfi and S. Z. Zard, *Tetrahedron Lett.*, 1997, **38**, 5985.
22 A. I. Meyers, G. P. Roth, D. Hoyer, B. A. Barner and D. Laucher, *J. Am. Chem. Soc.*, 1988, **110**, 4611; M. Shimano and A. I. Meyers, *J. Am. Chem. Soc.*, 1994, **116**, 6437; A. I. Meyers and A. N. Hulme, *J. Org. Chem.*, 1995, **60**, 1265; M. Shimano and A. I. Meyers, *J. Org. Chem.*, 1996, **61**, 5714; B. Plunian, J. Mortier, M. Vaultier and L. Toupet, *J. Org. Chem.*, 1996, **61**, 5206; K. Tomioka, M. Shindo and K. Koga, *Tetrahedron Lett.*, 1990, **31**, 1739; 1993, **34**, 681.
23 W. F. Bailey, A. D. Khanolkar, K. Gavaskar, T. V. Ovaska, K. Rossi, Y. Thiel and K. B. Wiberg, *J. Am. Chem. Soc.*, 1991, **113**, 5720; W. F. Bailey, A. D. Khanolkar and K. V. Gavaskar, *J. Am. Chem. Soc.*, 1992, **114**, 8053; W. F. Bailey and K. V. Gavaskar, *Tetrahedron*, 1994, **50**, 5957; A. Krief, B. Kenda, P. Barbeaux and E. Guittet, *Tetrahedron*, 1994, **50**, 7177; A. Krief and J. Bousbaa, *Tetrahedron Lett.*, 1997, **38**, 6291.
24 W. F. Bailey and Y. Tao, *Tetrahedron Lett.*, 1997, **38**, 6157.
25 C. A. Broka, W. J. Lee and T. Shen, *J. Org. Chem.*, 1988, **53**, 1336; C. A. Broka and T. Shen, *J. Am. Chem. Soc.*, 1989, **111**, 2981; I. Coldham, *J. Chem. Soc., Perkin Trans. 1*, 1993, 1275; I. Coldham and R. Hufton, *Tetrahedron Lett.*, 1995, **36**, 2157; I. Coldham, R. Hufton and D. J. Snowden, *J. Am. Chem. Soc.*, 1996, **118**, 5322; I. Coldham and R. Hufton, *Tetrahedron*, 1996, **52**, 12 541; I. Coldham, R. Hufton and R. E. Rathmell, *Tetrahedron Lett.*, 1997, **38**, 7617; I. Coldham, M. M. S. Lang-Anderson, R. E. Rathmell and D. J. Snowden, *Tetrahedron Lett.*, 1997, **38**, 7621; M. Lautens and S. Kumanovic, *J. Am. Chem. Soc.*, 1995, **117**, 1954; D. Zhang and L. S. Liebeskind, *J. Org. Chem.*, 1996, **61**, 2594; E. Piers and P. D. G. Coish, *Synthesis*, 1996, 502; D. L. Comins and Y.-m. Zhang, *J. Am. Chem. Soc.*, 1996, **118**, 12 248; W. F. Bailey and X.-L. Jiang, *J. Org. Chem.*, 1996, **61**, 2596; W. F. Bailey and M. W. Carson, *Tetrahedron Lett.*, 1997, **38**, 1329; J. Barluenga, R. Sanz and F. J. Fañanás, *Tetrahedron Lett.*, 1997, **38**, 2763.
26 See, however, I. Funaki, L. Thijs and B. Zwanenburg, *Tetrahedron*, 1996, **52**, 9909.
27 For a recently described approach to a similar ring system, see M. D. Andrews, A. G. Brewster, J. Chuhan, A. I. Ibbett, M. G. Moloney, K. Prout and D. Watkin, *Synthesis*, 1997, 305.

Received in Cambridge, UK, 24th October 1997; 7/07683E

Stereoselective intramolecular aldol reactions of (4*R*)-3-(3-oxobutanoyl)-1,3-thiazolidine-4-carboxylates believed to be directed by 'self-induced' axial chirality

Andrew G. Brewster,[a] Christopher S. Frampton,[b] Jay Jayatissa,[c] Mark B. Mitchell,[b] Richard J. Stoodley*[c]† and Shaheen Vohra[c]

[a] *Zeneca Pharmaceuticals, Mereside, Alderley Park, Macclesfield, Cheshire, UK SK10 4TG*
[b] *Roche Discovery Welwyn, Broadwater Road, Welwyn Garden City, Hertfordshire, UK AL7 3AY*
[c] *Department of Chemistry, UMIST, PO Box 88, Manchester, UK M60 1QD*

Essentially complete retention of configuration accompanies the base-induced aldol reaction of the thiazolidinecarboxylate 6c to give the fused heterocycles 7c and 8c and their retroaldol–acylation reactions to give the bicycle 9c.

Recently we showed[1] that the diazo esters **1a–c** underwent cyclisations under basic conditions to give the bicyclic compounds **2a–c** in a state of high enantiomeric purity (Scheme 1). We postulated that the reactions proceeded by way of planar ester enolate (or enol) intermediates that possessed axial chirality. For example, the species **3** (arbitrary enolate geometry) was considered to be involved in the **1a** → **2a** cyclisation. The marked kinetic preference for the diazo ester **1a** to undergo deprotonation to give the enolate **3** rather than its enantiomer was attributed to the greater ease in attaining the geometry **4** compared with the geometry **5** (in which a severe $A^{1,2}$ interaction exists between the *N*-acyl substituent and the CO_2Me group) required for the deprotonation reactions.

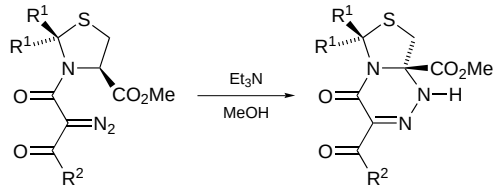

Scheme 1

Whilst the aforecited findings were of significant mechanistic interest in that they exemplified a new stereoinduction principle, they were of limited synthetic impact because a C–N bond had been generated at the expense of a C–H bond at the thiazolidine stereocentre. Obviously, the ability to develop a C–C bond would notably enhance the technology, particularly because of the high interest in enantiopure α-*C*-substituted α-amino acids.[2] We now report studies that have led to the achievement of this objective.

Seeking to prepare the bicycle **7a** and/or **8a**, the acetoacetyl thiazolidine **6a**[1] was treated with NEt_3 (300 mol%) in MeOH for 17 h. Subjection of the product to silica gel column chromatography led to the isolation of two fractions. The first fraction (10% yield), $[\alpha]_D$ −85 (*c* 0.34, CH_2Cl_2) was identified as a 75 : 25 mixture of the desired aldol products **7a** and **8a**.‡§ The second fraction was considered to be the triethylammonium salt **9a**;§ treatment of an ethereal solution of the material with potassium 2-ethylhexanoate (in BuOH–Et_2O) gave the potassium salt **9b**‡ (66% yield), mp 251–252 °C, $[\alpha]_D$ −116 (*c* 0.39, H_2O). When resubjected to the cyclisation conditions, the aldol products **7a** and **8a** were unaffected, establishing that the thiazolidine **6a** underwent two competing cyclisations by way of the enolates **10a** and **11a** (arbitrary enolate geometries).

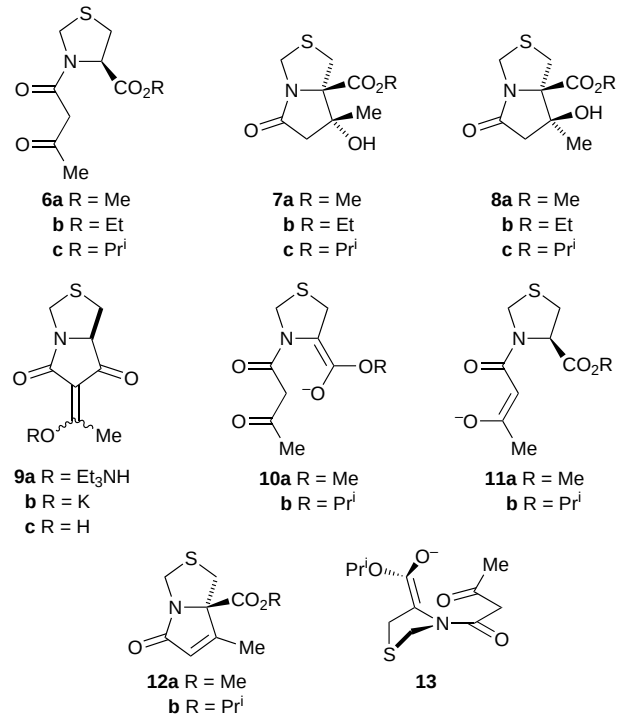

A study of the behaviour of the thiazolidine **6a** towards a variety of base/solvent combinations revealed that KCN (150 mol%) in MeOH was the most effective in promoting the desired cyclisation reactions, giving the results shown in Table 1. A simple work-up¶ provided a 76 : 24 mixture of the aldol products **7a** and **8a** in 32% yield {after chromatography, 29% yield; $[\alpha]_D$ −88 (*c* 0.25, CH_2Cl_2)}.

The slow step in the **6a** → **9b** transformation is likely to involve an intramolecular reaction of the intermediate **11a** in which the enolate adds to the ester carbonyl group. Hoping to dampen this reaction, the ethyl ester **6b**,‡‖ $[\alpha]_D$ −123 (*c* 0.41, CH_2Cl_2), and the isopropyl ester **6c**,‡‖ $[\alpha]_D$ −128 (*c* 0.59, CH_2Cl_2), were prepared. The outcomes of their cyclisation

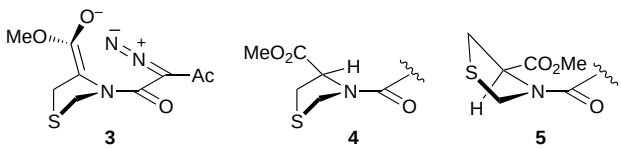

Table 1 Cyclisation reactions of thiazolidines of type **6**

Reactant	R	Conditions	*t*/h	Products	Ratio[a]
6a	Me	KCN–MeOH	2	**7a**,**8a**,**9b**	27 : 9 : 64
6b	Et	KCN–EtOH	4	**7b**,**8b**,**9b**	39 : 20 : 41
6c	Pr^i	KCN–MeOH	2	**7c**,**8c**,**9b**	69 : 23 : 8

[a] Determined by 300 MHz ^{1}H NMR spectroscopic analysis.

reactions are shown in Table 1. Work-ups provided a 72 : 28 mixture of the aldol products **7b** and **8b**‡ (47% yield after chromatography), mp 91–93 °C, $[\alpha]_D$ −98 (*c* 0.38, CH_2Cl_2), and a 72 : 28 mixture of the aldol products **7c** and **8c**‡ (68% yield after chromatography), mp 85–87 °C, $[\alpha]_D$ −95 (*c* 0.29, CH_2Cl_2). Clearly, the desired intramolecular aldol reactions became more favourable as the size of the ester group increased.

The similar optical rotations of the comparable mixtures of the aldol products **7a**/**8a**, **7b**/**8b** and **7c**/**8c** suggested common enantiomeric purities. This was substantiated by a chemical correlation involving the mixtures **7a**/**8a** and **7c**/**8c**. Thus, sequential treatment of the former mixture with Ac_2O–perchloric acid and DBU in CH_2Cl_2 gave the alkene **12a**,‡ mp 73–74 °C, $[\alpha]_D$ +228 (*c* 0.33, CH_2Cl_2). A similar sequence performed on the **7c**/**8c** mixture afforded the alkene **12b**,‡ mp 124–126 °C, $[\alpha]_D$ +215 (*c* 0.41, CH_2Cl_2), which was converted into the methyl ester **12a**, $[\alpha]_D$ +221 (*c* 0.27, CH_2Cl_2), under transesterification conditions (KCN in MeOH). On the basis of HPLC analysis,** compounds **7c** and **8c** were shown to have ees of 99%. It is concluded, therefore, that the aldol products **7a**–**c** and **8a**–**c** are essentially enantiopure.

It remained to establish that the intramolecular aldol reactions had occurred with retention of configuration at the thiazolidine stereocentre. Crystallisation of a 72 : 28 mixture of compounds **7c** and **8c** from hot water provided the major diastereomer, mp 104 °C, $[\alpha]_D$ −108 (*c* 0.33, CH_2Cl_2), which was shown to possess the absolute stereochemistry **7c** by X-ray crystallography†† (Fig. 1). Clearly, the C–H bond adjacent to the alkoxycarbonyl group had been replaced by a C–C bond with retention of configuration. Moreover, there was a kinetic preference to generate the aldol product **7c** over its diastereomer **8c** (and, similarly, of aldols **7a**,**b** over their diastereomers **8a**,**b**).

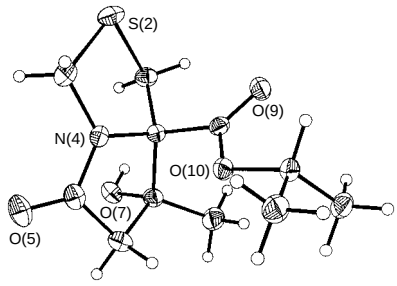

Fig. 1 Molecular structure of compound **7c**

Although stable to the cyclisation conditions, compounds **7c** and **8c** did react with KCN in refluxing MeOH to give mainly the potassium salt **9b**.‡‡ Acidification of an aqueous solution of the salt with Amberlite IR–120 (H^+) ion-exchange resin and subjection of the residue obtained after evaporation to silica gel column chromatography gave the enol **9c**‡ (82% yield), mp 142 °C, $[\alpha]_D$ −89 (*c* 0.51, CH_2Cl_2), as a 72 : 28 mixture of diastereomers, with an ee of 99%.** Evidently, under more forcing conditions, the aldol reaction can be reversed and the enolate intermediates **10a** and **10b** can be reprotonated with essentially complete retention of configuration to regenerate the thiazolidines **6a** and **6c**. Subsequent production of the enolates **11a** and **11b** then leads, by intramolecular acylation reactions, to the salt **9b** with no loss of stereochemical integrity.

As before,[1] we suggest that the stereochemical memory of the enolate **10b** can be accounted for by postulating its generation in an axially chiral form, *e.g.* **13**.

Recently, Fuji reported[3] examples of intermolecular alkylations of *N*-alkoxycarbonyl-*N*-methylphenylalanine esters that proceed with up to 82% ee. In reactions induced by lithium 2,2,6,6-tetramethylpiperidide in THF at −78 °C, they favoured the involvement of a *C*-lithiated intermediate formed with retention of configuration.

The aforecited results are of note in a number of respects. The finding that C–C bonds can be constructed stereoselectively considerably extends the scope of self-induced axial chirality as a stereocontrol element in synthesis.§§ Compounds **7a**–**c**, **8a**–**c** and **12a**,**b** are interesting classes of essentially enantiopure fused heterocycles; by appropriate manipulation they should be convertible into α-*C*-substituted 4-thiaprolines and 5-oxoprolines. Finally, the discovery that the kinetic cyclisation products **7c** and **8c** of the thiazolidine **6c** can be converted into the thermodynamic cyclisation product **9b** provides a striking illustration of stereoretentive protonation accompanying the retroaldol reaction.

We thank the Link Asymmetric Synthesis New Core Programme for a studentship (to J. J.) and the EPSRC/Zeneca Pharmaceuticals for a CASE studentship (to S. V.). We are also grateful to Dr C. M. Raynor (UMIST) and Mr J. A. Whatley (Roche) for the HPLC analyses.

Notes and References

† E-mail: richard.stoodley@umist.ac.uk

‡ The product displayed analytical and spectral properties that supported its assigned structure.

§ For analogous cyclisations on an oxazolidine framework, see ref. 4.

¶ After evaporation of the solvent, the product was partitioned between CH_2Cl_2 and brine; evaporation of the dried ($MgSO_4$) organic phase gave the aldol products **7a** and **8a** in a near-pure state.

‖ Compounds **6b** and **6c** were prepared from L-cysteine hydrochloride (in respective overall yields of 40 and 31%) by routes similar to that employed in the synthesis of compound **6a** (see ref. 1).

** The enantiomers were separated on a Chiralpak AD column, using hexanes–propan-2-ol (9 : 1) as eluent (flow rate: 0.5 cm^3 min^{-1}) in the cases of **7c**/*ent*-**7c** and **8c**/*ent*-**8c** and hexanes–ethanol (85 : 15) as eluent (flow rate: 0.7 cm^3 min^{-1}) in the case of **9c**/*ent*-**9c**.

†† *Crystal data* for **7c**: $C_{11}H_{17}NO_4S$, M = 259.32, orthorhombic, space group $P2_12_12_1$, a = 6.4154(15), b = 13.321(4), c = 14.961(5) Å, U = 1278.5(6) Å^3, Z = 4, D_c = 1.347 g cm^{-1}, μ = 0.256 mm^{-1} (Mo–Kα, λ = 0.71073 Å), F(000) = 552, T = 123(1) K. Siemens SMART CCD area-detector diffractometer, crystal size 0.18 × 0.20 × 0.60 mm, θ_{max} 29.15°, 14263 reflections measured, 3181 unique (R_{int} = 0.0419). Structure solution by direct methods, full-matrix least-squares refinement on F^2 with weighting $w^{-1} = \sigma^2(F_o^2) + (0.0676P)^2$, where $P = (F_o^2 + 2F_c^2)/3$, anisotropic displacement parameters, riding hydrogen atoms, no absorption correction, absolute structure parameter = −0.02(7). Final $Rw = \{\Sigma[w(F_o^2–F_c^2)^2]/\Sigma[w(F_o^2)^2]^{\frac{1}{2}}\}$ = 0.1002 for all data, conventional R = 0.0376 on F values of 2872 reflections with $I > 2\sigma(I)$, S = 1/073 for all data and 154 parameters. Final difference map between +0.31 and −0.44 e Å^{-3}, Programs: Siemens SMART and SAINT control and integration software, SHELXTL (G. M. Sheldrick, University of Gottingen, Germany). CCDC 182/717.

‡‡ Some transesterification, leading to compounds **7a** and **8a**, occurred during the course of this transformation.

§§ For a summary of asymmetric inductions directed by non-biaryl atropisomers, see ref. 5.

1 B. Beagley, M. J. Betts, R. G. Pritchard, A. Schofield, R. J. Stoodley and S. Vohra, *J. Chem. Soc., Perkin Trans. 1*, 1993, 1761.
2 T. Wirth, *Angew. Chem., Int. Ed. Engl.*, 1997, **36**, 225.
3 T. Kawabata, T. Wirth, K. Yahiro, H. Suzuki and K. Fuji, *J. Am. Chem. Soc.*, 1994, **116**, 10 809.
4 M. D. Andrews, A. G. Brewster and M. G. Moloney, *Synlett*, 1996, 612.
5 J. Clayden, *Angew. Chem., Int. Ed. Engl.*, 1997, **36**, 949.

Received in Liverpool, UK, 14th October 1997; 7/07388G

Cycloaddition of *o*-benzyne to benzene and the inner phase of a hemicarcerand

Brett R. Beno, Chimin Sheu, K. N. Houk,* Ralf Warmuth and D. J. Cram

Department of Chemistry and Biochemistry, University of California, Los Angeles, Los Angeles, CA 90095-1569, USA

Becke3LYP/6-31G* calculations predict a small energy of concert for the Diels–Alder reaction of *o*-benzyne with benzene, and force-field calculations indicate that steric interactions and transannular strain are responsible for the regiospecificity of the Diels–Alder reaction between *o*-benzyne and its host hemicarcerand.

In a previous communication, Warmuth reported the Diels–Alder (DA) reaction of an *o*-benzyne guest with an aromatic ring of its hemicarcerand host.[1] We have studied the DA reaction of *o*-benzyne with benzene,[2] and the hemicarcerand using computational methods.[2]

The narrow frontier orbital gap, and especially the low LUMO energy, of *o*-benzyne make it a good dienophile.[3] Owing to the poor overlap of the sp^2 orbitals which combine to form the in-plane π-bond, *o*-benzyne also has a significant amount of diradical character.[4] The *o*-, *m*-, and *p*-isomers of benzyne have been the subject of extensive high-level theoretical studies,[5] and the reactivity of *o*-benzyne as a DA dienophile is well known experimentally,[6] but no computational studies of DA reactions involving *o*-benzyne have been reported.

The benzene–*o*-benzyne DA reaction has been observed experimentally. Miller and Stiles isolated benzobicyclo-[2.2.2]octatriene **4**, biphenyl and benzocyclooctatetraene in a ratio of 1 : 3 : 4, respectively, from the thermal decomposition of benzenediazonium-2-carboxylate in benzene at 45 °C.[7a] The product ratio for the reaction is strongly influenced by Ag^+, a possible contaminant in the Miller and Stiles experiment.[7b,c] In its absence, **4** is the major product.

These results are remarkable, since the DA reactions of benzene are expected to strongly favor closed-shell concerted over stepwise diradical mechanisms.[8] The barrier for the concerted pathway of the benzene–ethene DA reaction is estimated to be 23 kcal mol^{-1} (1 cal = 4.184 J) below that of the stepwise diradical pathway.[8a] However, the diradical character of *o*-benzyne may allow a stepwise mechanism to compete more effectively with a concerted mechanism.

The concerted and stepwise DA reactions were studied using the Becke3LYP hybrid HF-DFT method[9] and 6-31G* basis set.[10] All DFT calculations were carried out using Gaussian 94.[11] RBecke3LYP and UBecke3LYP methods were used for closed- and open-shell species, respectively. Stationary points were characterized with vibrational frequency calculations and thermodynamic quantities were calculated from unscaled frequencies. The hemicarceplex and possible *o*-benzyne–hemicarcerand DA regioadducts were calculated with Macro-Model using the MM2*, MM3* and AMBER* force-fields.[12]

The Becke3LYP/6-31G* optimized geometries of benzene **1**, *o*-benzyne **2**, the concerted transition structure **3**, and cycloadduct **4** are shown in Fig. 1. The length of the partial triple bond in **2** is predicted to be 1.251 Å, in excellent agreement with the experimental value of 1.24 ± 0.02 Å .[13] The DFT structure of **1** is also in good agreement with experiment.[14]

Concerted transition structure **3** occurs early along the reaction coordinate. The forming C(1)–C(7) and C(4)–C(8) bonds are 2.383 Å in length. The benzene moiety is relatively undistorted in the transition structure: the C(2)–C(3) and C(5)–C(6) bonds have decreased in length by 0.024 Å, about 38% of the total difference of their lengths in benzene and cycloadduct **4**. The other four C–C bonds in the benzene moiety have increased in length by 0.025 Å in the transition structure, or 18% of the total change from reactants to products. The deviation of the benzene moiety from planarity is also small. These factors allow a substantial amount of the aromaticity of benzene to be conserved in the transition structure. The largest change in benzyne is a 0.037 Å elongation of the partial triple bond.

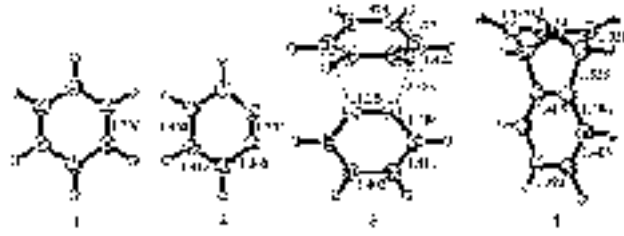

Fig. 1 RBecke3LYP/6-31G* optimized structures of the reactants (**1** and **2**), transition structure **3** and product **4** of the concerted Diels–Alder reaction of benzene with *o*-benzyne. All bond lengths are in Å.

The Becke3LYP/6-31G* $\Delta H^{\ddagger}$ and $\Delta S^{\ddagger}$ (298 K) are 10.7 kcal mol^{-1} and −36.2 cal mol^{-1} K^{-1} and the $\Delta H_{rxn.}$ is −48.7 kcal mol^{-1}. The $\Delta H^{\ddagger}$ for the concerted pathway of the butadiene–ethene DA reaction is 23.4 kcal mol^{-1} at the same level.[2a] Since benzene is not an especially good DA diene, the low barrier can be attributed to the high reactivity of *o*-benzyne as a dienophile.

The $\Delta H^{\ddagger}$ predicted for the benzene–*o*-benzyne DA reaction is coincidentally close to the 12 kcal mol^{-1} experimental value determined by Warmuth for the DA reaction of *o*-benzyne with the aromatic ring of the hemicarcerand (**5**).[1] The aromatic ring in **5** is highly substituted with electron donors, and should be electronically more reactive than benzene. However, steric effects and the difficulty of bending the aromatic ring toward the transition state should decrease its reactivity as a DA diene.

The predicted $\Delta S^{\ddagger}$ for the concerted benzene–*o*-benzyne DA reaction is 25.5 cal mol^{-1} K^{-1} more negative than the $\Delta S^{\ddagger}$ for the *o*-benzyne–hemicarcerand DA reaction.[1] This reflects the greater loss of mobility of the benzene in the intermolecular DA reaction, relative to the reaction within the hemicarcerand where the aryl moiety is already constrained within the framework of the host.

A diradical transition structure **6** and intermediate **7** for the stepwise addition of *o*-benzyne to benzene are shown in Fig. 2. In transition structure **6**, σ bond formation is more advanced than in concerted transition structure **3**, as shown by the relatively short C–C forming bond length of 1.976 Å. As with **3**, the benzyne moiety is relatively undistorted, except for a 0.06 Å lengthening of the partial triple bond.

The $\Delta H^{\ddagger}$ for formation of intermediate **7** is 13.1 kcal mol^{-1}; only 2.4 kcal mol^{-1} above the $\Delta H^{\ddagger}$ for the concerted addition of benzene to *o*-benzyne. The energy of concert is nearly zero. The energy of concert for the DA reaction of ethene with cyclobutadiene, which has significant diradical character, is also smaller.[15]

The $\Delta H_{rxn.}$ for formation of diradical intermediate **7** from **1** and **2** is predicted to be 2.3 kcal mol^{-1}, in good agreement with

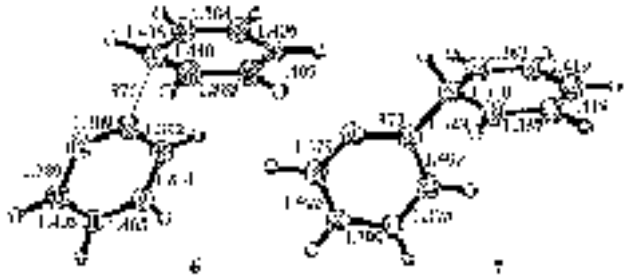

Fig. 2 UBecke3LYP/6-31G* diradical transition structure **6** and intermediate **7** in the stepwise diradical addition of *o*-benzyne to benzene. All bond lengths are in Å.

an estimate based on Benson equivalents[16] and the CASPT2 ΔH_f of benzyne.[5]

Intermediate **7** may lead to biphenyl by hydrogen atom abstraction from C(1) by the C(12) phenyl radical moiety, or [2 + 2] or [4 + 2] cycloadducts *via* rotation about the C(1)–C(7) bond followed by ring closure. These mechanistic pathways are currently being explored.

NMR evidence indicates that of the two possible regioisomeric *o*-benzyne–hemicarcerand DA adducts (Fig. 4), only **8** is formed experimentally.[1] The origin of this regiospecificity was probed using force-field methods. The minimum energy conformer of hemicarceplex **10** was located using molecular dynamics and simulated annealing techniques with the MM3* force-field (Fig. 3). This force-field was also used to obtain optimized geometries and steric energies of DA adducts **8** and **9** (Fig. 4). AMBER* and MM2* gave similar results.

In **10**, the orientation of benzyne is favorable for formation of **8**, *via* a concerted DA reaction (Fig. 3). However, both carbons of the benzyne partial triple bond are > 4 Å from the hemicarcerand atoms to which they are bound in **8**, and substantial motion is required to bring benzyne within bonding distance. Formation of **9** from **10** through a concerted pathway requires benzyne to rotate around its C_2 axis by *ca*. 120°. This should be sterically unfavorable. Either stepwise or concerted mechanisms should be possible.

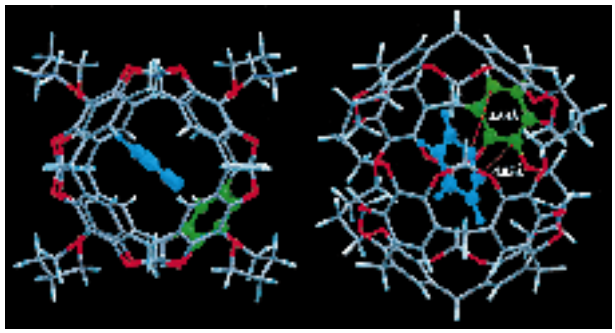

Fig. 3 MM3* minimum energy conformer of the *o*-benzyne hemicarceplex

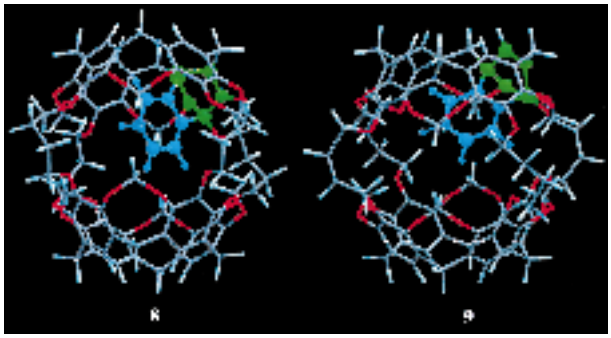

Fig. 4 MM3* optimized stuctures of *o*-benzyne–hemicarcerand Diels–Alder adducts **8** and **9**

Regioisomer **8** is predicted to be 20.0 kcal mol^{-1} more stable than **9**. It is likely that a significant fraction of this energy difference will be felt in the transition state, as well.

Unfavorable steric interactions and greater strain in **9** contribute to the thermodynamic preference for formation of **8**. The Ph group of the benzobicyclo[2.2.2]octatriene moiety is crowded into the top hemisphere of the hemicarcerand in **9**, and several unfavorable steric interactions result. In **8**, the Ph group of the benzobicyclo[2.2.2]octatriene moiety is in a less sterically hindered environment.

Calculations with MM3* on various DA adducts show that the greater transannular strain in **9** contributes significantly to the overall thermodynamic preference for formation of **8**.

We are grateful to the National Science Foundation for financial support of this research, and to the National Center for Supercomputing Applications (NCSA) and UCLA Office of Academic Computing for computer time and facilities.

Notes and References

* E-mail: houk@chem.ucla.edu

1 R. Warmuth, *Chem. Commun.*, 1998, 59.
2 Quantum mechanical calculations were performed with density-functional methods which have proven to give accurate potential energy surfaces for other Diels–Alder reactions: (*a*) E. Goldstein, B. Beno and K. N. Houk, *J. Am. Chem. Soc.*, 1996, **118**, 6036 and references therein; (*b*) K. N. Houk, B. R. Beno, M. Nendel, K. Black, H. Y. Yoo, S. Wilsey and J. K. Lee, *J. Mol. Struct.* (*THEOCHEM*), 1997, **398**–**399**, 169.
3 A. Rauk, *Orbital Interaction Theory of Organic Chemistry*, Wiley, New York, 1994, pp. 180–181.
4 G. Porter and J. I. Steinfield, *J. Chem. Soc. A*, 1968, 877.
5 For a recent CASPT2 study including references to many earlier high-level calculations, see: R. Lindh and M. Schütz, *Chem. Phys. Lett.*, 1996, **258**, 409.
6 R. W. Hoffmann, *Dehydrobenzene and Cycloalkynes*, Academic Press, New York, 1967, pp. 208–237.
7 (*a*) R. G. Miller and M. Stiles, *J. Am. Chem. Soc.*, 1963, **85**, 1798; (*b*) L. Friedman, *J. Am. Chem. Soc.*, 1967, **89**, 3071; (*c*) L. Friedman and D. F. Lindow, *J. Am. Chem. Soc.*, 1968, **90**, 2329.
8 (*a*) W. v. E. Doering, W. R. Roth, R. Breuckmann, L. Figge, H.-W. Lennartz, W. D. Fessner and H. Prinzbach, *Chem. Ber.*, 1988, **121**, 1 and references therein; (*b*) K. N. Houk, Y. Li and J. D. Evanseck, *Angew. Chem., Int. Ed. Engl.*, 1992, **31**, 682.
9 A. D. Becke, *J. Chem. Phys.*, 1993, **98**, 5648; C. Lee, W. Yang and R. G. Parr, *Phys. Rev. B*, 1988, **37**, 785.
10 W. J. Hehre, L. Radom, P. v. R. Schleyer and J. A. Pople, *Ab Initio Molecular Orbital Theory*, Wiley, New York, 1986.
11 GAUSSIAN 94, Revision D.2, M. J. Frisch, *et al*., Gaussian, Inc., Pittsburgh, PA, 1995.
12 MacroModel V5.0, F. Mohamadi, N. G. J. Richards, W. C. Guida, R. Liskamp, M. Lipton, C. Caufield, G. Chang, T. Hendrickson and W. C. Still, *J. Comput. Chem.*, 1990, **11**, 440. For a review of the force-fields used, see: A. K. Rappé and C. J. Casewit, *Molecular Mechanics across Chemistry*, University Science Books, Sausalito, 1997 and references therein.
13 A. M. Orendt, J. C. Facelli, J. G. Radziszewski, W. J. Horton, D. M. Grant and J. Michl, *J. Am. Chem. Soc.*, 1996, **118**, 846.
14 G. Herzberg, *Molecular Spectra and Molecular Structure III. Electronic Spectra and Electronic Structure of Polyatomic Molecules*, Van Nostrand, Princeton, 1967, p. 999.
15 B. Beno and K. N. Houk, unpublished work.
16 S. W. Benson, *Thermochemical Kinetics*, Wiley, New York, 1976.

Received in Columbia, MO, USA, 6th May 1997; revised manuscript received 17th October 1997; 7/07671A

Statistical analysis of C–H···N hydrogen bonds in the solid state: there*are* real precedents

Mark Mascal*

Department of Chemistry, University of Nottingham, Nottingham, UK NG7 2RD

A survey of the Cambridge Structural Database reveals hundreds of C–H··N contacts which are significantly shorter (< 2.45 Å) than the sum of the van der Waals radii (2.75 Å), effectively refuting recent claims to the contrary and supporting the description of this interaction as a hydrogen bond.

The nature of nonbonded C–H··N interactions has been called into question in the form of a recent publication which has appeared in this Journal.[1] Based on a self-declared 'superficial check of the literature', the authors of this work manage to discredit certain observations of C–H··N hydrogen bonds, while at the same time putting forward their own example of an apparently uncommon and authentic case of this phenomenon. A more thorough search however indicates that the published structure is not extraordinary, rather only one among nearly a thousand such cases.

We were first alerted to problems with the aforementioned paper by simple comparison with some of our own work. The authors make two major assertions, that: (i) 'in most, if not all, of the previously claimed examples of C–H··N "hydrogen bonds" the contact is little (or no) different from that expected for an ordinary, classic van der Waals contact,' and (ii) the C–H··N distance in $Co(dpa)_2$ 'is among the shortest of the C–H··Y, Y = N or O distances'. The $Co(dpa)_2$ complex has a C–H··N distance of 2.44 Å and C–H–N angle of 177°.[1] By way of comparison, the triazine–$2Br_2$ complex[2] has a C–H··N distance of 2.42 Å and a C–H–N angle of 180°, and, indeed, even this is not a particularly remarkable example of such nonbonded contact when the literature on the matter is properly consulted. A statistical analysis of the problem using the Cambridge Structural Database[3] currently indicates no less than 967 observations of intermolecular C–H··N contact with distances (r) less than 2.45 Å and C–H–N angles (α) between 120 and 180°, as identified using the query dialogue within QUEST3D[3] represented in Fig. 1. Histograms for both variables r and α are illustrated in Figs. 2 and 3. The mean C–H···N separation within the sample taken is 2.38 Å,[4] effectively disputing point (ii). Yet another claim, that 'the angles at the H atom are well below (often far below) 180°'[1] is also called into question by the data in Fig. 3, which show that over 100 entries have C–H–N angles between 170 and 180°. In fact, the mean α value of 155° is not far off that for classic N–H··O interactions, which is 161°.[5]

Another difficulty with such a sweeping statement as (i) above is that it entirely ignores the fact that C–H bonds can under some circumstances be as polar as a hydroxy group, whose capacity to participate in hydrogen bonding is not in question. A good example of an interaction involving an acidic C–H is seen in the crown ether **1**–nitromethane complex[6] (Fig. 4) with its C–H··N distance of 2.21 Å and C–H–N angle of 178°.

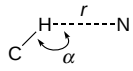

Fig. 1 The QUEST3D query, with conditions $r \leqslant 2.45$ Å and $120 \leqslant \alpha \leqslant 180°$

An entirely systematic study of this phenomenon would involve sampling the nearest neighbour contacts for every (C–)H atom in every structure containing C, H and N and demonstrating that the proportion of close approaches to nitrogen is statistically greater than the stoichiometric content of N in the database. In consideration of the number of structures involved this is clearly not practicable. However, in ground-breaking work, Taylor and Kennard,[7] using a small but representative subset of the databse (relevant neutron diffraction structures), were able to show that 'counterintuitive' C–H··C and C–H··H close contacts are comparatively rare,[8] and one could reason that the profusion of short C–H··N distances strongly implies a tendency for (C–)H to interact with nitrogen in preference to non-H-bond acceptors. Because such a strong case for C–H··O hydrogen bonding has already been made,[8,9] it is logically contentious to challenge the existence of C–H··N hydrogen bonds, since N is generally a more effective hydrogen acceptor than O.[10] Thus, although it is not possible to

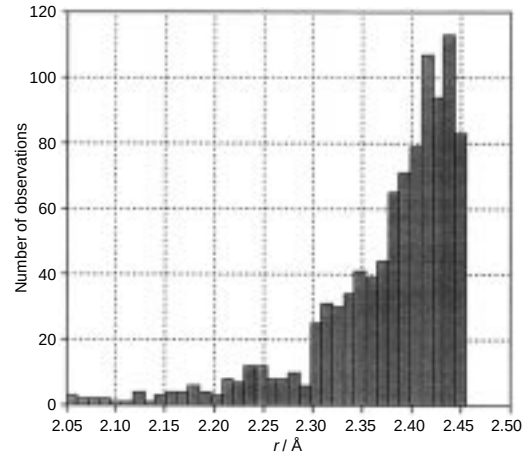

Fig. 2 Histogram for r (C–H···N)

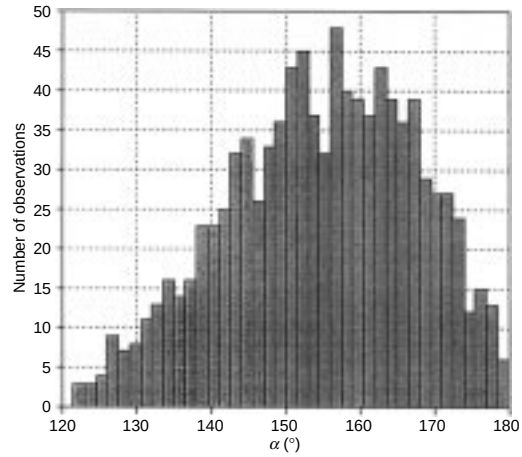

Fig. 3 Histogram for α (C–H–N)

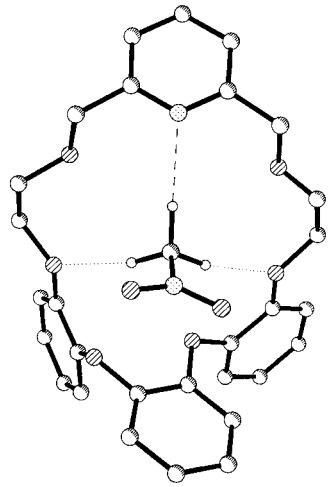

Fig. 4 Crystal structure of the **1**–$MeNO_2$ complex (ref. 6). The C–H··N distance (2.21 Å, dashed line) is actually shorter than the C–H··O distances (2.39 and 2.44 Å, dotted lines).

deliberate over the precise nature of these contacts without individually examining the many hundred occurrences of C–H··N relationships in the literature, the fact that such a large number are significantly shorter than the 2.75 Å sum of the van der Waals radii[11] indicates that the distinction between the classical van der Waals interaction and the hydrogen bond is not necessarily being 'blurred',[1] at least not when all of the available data are taken into consideration.

Dr A. J. Blake is thanked for helpful discussions, and the use of the EPSRC's Chemical Database Service[12] at Daresbury is gratefully acknowledged.

Notes and References

* E-mail: pczmm@vax.ccc.nottingham.ac.uk

1 F. A. Cotton, L. M. Daniels, G. T. Jordan IV and C. A. Murillo, *Chem. Commun.*, 1997, 1673.
2 M. Mascal, J. L. Richardson, A. J. Blake and W.-S. Li, *Tetrahedron Lett.*, 1996, **37**, 3505.
3 Version 5.13 (167 797 structures, April 1996 update): F. H. Allen and O. Kennard, *Chemical Design Automation News*, 1993, **8**, 31.
4 Twenty-one entries with r values between 1.47 and 1.99 Å were found dubious and therefore not used in the final analysis. If the range is increased to $r \leqslant 2.50$ Å with $120 \leqslant \alpha \leqslant 180°$, a total of 1841 observations are found with $r = 2.42$ and $\bar{\alpha} = 154°$. An identical search involving neutron diffraction structures (in which all protons are accurately located) produces 13 observations with $\bar{r} = 2.43$ Å (range 2.32–2.50 Å) and $\bar{\alpha} = 150°$ (range 139–166°).
5 R. Taylor and O. Kennard, *Acc. Chem. Res.*, 1984, **17**, 320.
6 E. Weber, S. Franken, H. Puff and J. Ahrendt, *J. Chem. Soc., Chem. Commun.*, 1986, 467.
7 R. Taylor and O. Kennard, *J. Am. Chem. Soc.*, 1982, **104**, 5063.
8 (C–)H atoms did however show a significant tendency to form close intermolecular contacts to oxygen (see also ref. 9). Due to the limited amount of data in this study, no real conclusions were drawn concerning C–H··N contact.
9 J. A. R. P. Sarma and G. R. Desiraju, *Acc. Chem. Res.*, 1986, **19**, 222; G. R. Desiraju, *Acc. Chem. Res.*, 1991, **24**, 290.
10 M. H. Abraham, *Chem. Soc. Rev.*, 1993, **22**, 73.
11 A. Bondi, *J. Phys. Chem.*, 1964, **68**, 441. A recent revision of the van der Waals radius of nitrogen to 1.60 Å would actually put the H to N contact distance at 2.80 Å (see S. C. Nyburg and C. H. Faerman, *Acta Crystallogr., Sect. B*, 1985, **41**, 274), while the Pauling radius of N (1.5 Å) gives a total of 2.7 Å (see L. Pauling, *The Nature of the Chemical Bond*, Cornell University Press, Ithica, 1942, p. 192).
12 The United Kingdom Chemical Database Service: D. A. Fletcher, R. F. McMeeking and D. Parkin, *J. Chem. Inf. Comput. Sci.*, 1996, **36**, 746.

Received in Liverpool, UK, 24th October 1997; 7/07702E

A new route towards deep desulfurization: selective charge transfer complex formation[1]

Valérie Meille,[ab] Emmanuelle Schulz,[a] Michel Vrinat[b] and Marc Lemaire*

[a] *Laboratoire de Catalyse et Synthèse Organique, IRC, UCBL, CPE, 43 Bd du 11 Novembre 1918, 69622 Villeurbanne Cedex, France*

[b] *Institut de Recherches sur la Catalyse, 2, Avenue A. Einstein, 69626 Villeurbanne Cedex, France*

An alternative to the classical hydrodesulfurization process is proposed, based on the formation and subsequent removal of insoluble charge-transfer complexes between suitable π-acceptors and alkylated dibenzothiophenes.

Due to more stringent environmental regulations to protect urban areas and new legislation in Europe, the sulfur level in diesel fuel is now limited to 0.05 wt%, and will certainly be lowered in the near future. However, present refinery diesel hydrodesulfurization (HDS) processes can only be achieved under severe conditions, leading to shorter catalyst life. It is now well established that the achievement of deep HDS is prevented by one type of sulfur compound, namely alkyldibenzothiophenes.[2,3] These molecules have been subject of numerous studies as models to improve the properties of HDS catalysts.[4–6] Recently, a new method has been proposed[7] where the hydrodesulfurized stream is treated with a solid material (activated carbon, alumina, zeolite *etc.*) capable of adsorbing substituted dibenzothiophenes (DBT) by 'form selectivity' and steric hindrance. However, this interesting method presents some limitations because the capacity of the described (weight percent DBT on adsorbent) does not exceed 12% and furthermore, the selectivity factor α [eqn. (1)] toward aromatic system models (1-methylnaphthalene, MN) is just 7.

$$\alpha = \frac{\mathrm{DBT}_{\mathrm{adsorbed}} \cdot \mathrm{MN}_{\mathrm{solution}}}{\mathrm{DBT}_{\mathrm{solution}} \cdot \mathrm{MN}_{\mathrm{adsorbed}}} \quad (1)$$

Considering the electron-rich structure of alkylated DBT, we have studied its ability for form charge-transfer complexes with π-acceptors in order to describe a new method for their specific removal from gas oil.

Electron donor–acceptor complexes are easily detected *via* UV–VIS spectroscopy because their formation is generally accompanied by the appearance of a new absorption band (Benesi–Hildebrand band). Following the method of Foster–Hammick–Wardley,[8] this phenomenon allows the calculation of the association constant (and hence the free enthalpy) characterizing the new complex.

DDQ was tested as a π-acceptor due to its easy availability and its known ability to form charge-transfer complexes. Indeed, a mixture of 4,6-dimethyldibenzothiophene (DMDBT)[9] and DDQ in $CHCl_3$ gave rise to a new absorption wave (λ_{max} 633 nm) corresponding to a ΔG of 15 kJ mol^{-1} (see Fig. 1). 1-Methylnaphtalene was chosen as a model to represent the aromatic compounds contained in the gas oil which are capable of complexing DDQ competitively with DMDBT to form charge-transfer complexes. Using the same procedure as for DMDBT, DDQ and MN formed a charge-transfer complex showing a maximum absorption at 654 nm (ΔG = 7.3 kJ mol^{-1}) (see Fig. 2). This result indicates stronger complexation of DDQ with the sulfur compound than with the aromatic one. Complexation thus appears to be selective toward alkyl–DBT species, although the π-acceptor's chosen structure had not been optimized.

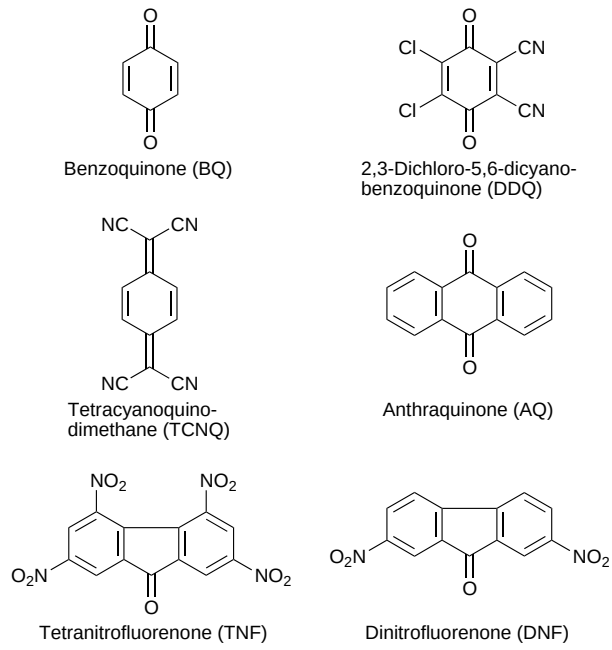

Having demonstrated the possibility of forming selectively a charge-transfer complex between DMDBT and DDQ, we have tested several other π-acceptors. The properties required are a high selectivity factor α for DMDBT toward the aromatics, and complete insolubility in alkanes in order to easily remove the complex formed from the gas oil.

The procedure used to test the different π-acceptors is as follows: an equimolar solution of DMDBT and MN in heptane (11 mmol l^{-1}) was stirred at room temperature in the presence of dodecane (1 equiv.) as the internal reference. The addition of the π-acceptor (1 equiv.) was followed by the immediate

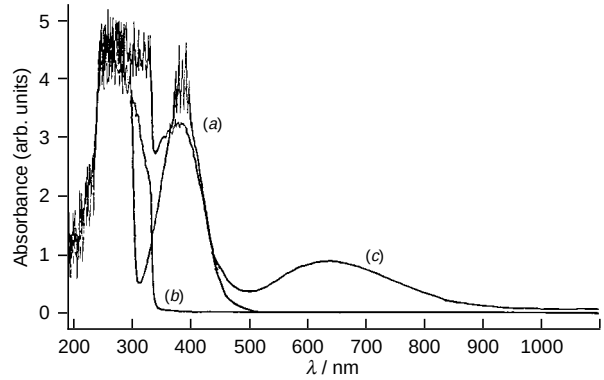

Fig. 1 UV–VIS spectrum from the donor–acceptor complex DMDBT–DDQ in $CHCl_3$; (*a*) DDQ, (*b*) 4,6-DMDBT and (*c*) complex

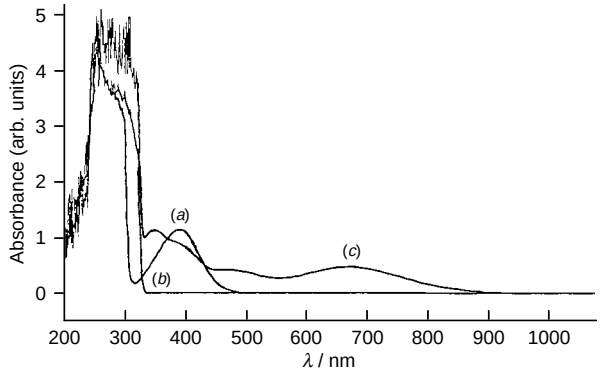

Fig. 2 UV–VIS spectrum from the donor–acceptor complex MN–DDQ in $CHCl_3$; (*a*) DDQ, (*b*) MN and (*c*) complex

formation of a coloured precipitate (except for *p*-benzoquinone). The samples were removed and the composition of the resulting solution analysed by gas chromatography to determine the amount of unreacted MN and DMDBT. The capacity value *C* [eqn. (2), where MW equals molecular weight] and the

$$C = \frac{\mathrm{MW_{DBT}}}{(\mathrm{MW_{DBT}} + \mathrm{MW_{acceptor}})} \times 100 \qquad (2)$$

separation factors α were calculated for each complexing material and are reported in Table 1 (for a direct comparison with results reported with solid materials as adsorbent, see ref. 7). Among all the π-acceptors tested, tetranitrofluorenone (TNF) seems to have the best characteristics, with a maximum factor of separation (rapidly reached) and a satisfactory capacity.

Fluorene was then used instead of MN to check the selectivity for DMDBT in the presence of a molecule rich in electrons with a similar geometry.[10] In this case, the selectivity factor was only 80 after 60 h stirring. Even if this value is lower than the previous one with MN, the selectivity remains higher than that obtained with adsorbent materials by shape selectivity.[7]

Following the results of this preliminary study on model molecules, the possible selective complexation of substituted DBT from a gas oil, already hydrodesulfurized (960 ppm) by classical methods, was examined. Firstly, the gas oil was diluted in heptane (15 g in 200 ml) and analysed by X-ray fluorescence spectroscopy, which showed a sulfur level of 214 ppm. Taking into account that this value is representative of the quantity of alkyldibenzothiophenes (and more precisely 4,6-DMDBT) present as refractory molecules, an equimolar quantity of TNF was added and the heterogeneous mixture was stirred at room temperature. After 74 h, the sulfur level of the solution obtained after filtration was only 120 ppm.

A similar experiment was conducted with pure gas oil (1920 ppm sulfur, at least 50% being 4,6-DMDBT) and the same π-acceptor, leading to 840 ppm sulfur after 92 h stirring. In these two examples, we have been able to remove 60 wt% of the initial sulfur containing compounds by formation of insoluble charge-transfer complexes. A detailed GC analysis would provide us with a precise distribution of the sulfur compounds contained in the residual gas oil. This work is in progress.

Table 1 Capacity and selectivity factor values for DMDBT and MN for different complexing materials depending on the stirring time

	α			
π-Acceptors	4 h 30 min	29 h	96 h	*C* (%)
BQ	Soluble	—	—	—
DNF	—	—	—	—
AQ	—	—	3	50
DDQ	28	35	> 1000	48
TNF	137	> 1000	> 1000	37
TCNQ	10	132	191	51

We have thus demonstrated that the sulfur compounds remaining in the gas oil after deep HDS (*i.e.* alkyldibenzothiophenes) are able to form stable electron donor–acceptor complexes with common π-acceptor compounds. These complexes are then easily separated from aliphatic/aromatic mixture by simple filtration. This behaviour is of major importance to the development of an analytical method for the determination of the exact composition and structure of the sulfur compounds contained in such mixtures. Work is in progress to create a polymer containing such a π-acceptor structure (and which is thus easily regenerated) and then a new process for limiting the sulfur level in the gas oil by formation and subsequent removal of charge–transfer complexes.

Notes and References

* E-mail: marc.lemaire@univ-lyon1.fr

1 M. Lemaire, E. Schulz, V. Meille, M. Vrinat and M. Breysse, *French Patent*, 97 07538, 1997.
2 M. Houalla, D. H. Broderick, A. V. Sapre, N. K. Nag, V. H. J. de Beer, B. C. Gates and H. Kwart, *J. Catal.*, 1980, **61**, 523.
3 T. Kabe, A. Ishihara and H. Tajima, *Ind. Eng. Chem. Res.*, 1992, **31**, 1577.
4 V. Lamure-Meille, E. Schulz, M. Lemaire and M. Vrinat, *Appl. Catal.*, 1995, **131**, 143.
5 V. Meille, E. Schulz, M. Lemaire and M. Vrinat, *J. Catal.*, 1997, **170**, 29.
6 M. Yumoto, K. Usui, K. Watanabe, K. Idei and H. Yamazaki, *Catal. Today*, 1997, **35**, 45.
7 D. W. Savage, B. K. Kaul, G. D. Dupre, J. T. O'Bara, W. E. Wales and T. C. Ho, *Deep desulfuriation of distillate fuels, US Pat.*, 5,454,933, 1995.
8 R. Foster, D. Ll. Hammick and A. A. Wardley, *J. Am. Chem. Soc.*, 1953, 3817.
9 V. Meille, E. Schulz, M. Lemaire, R. Faure and M. Vrinat, *Tetrahedron*, 1996, **52**, 3953.
10 T. K. Mukherjee, *J. Phys. Chem.*, 1969, **73**, 3442.

Received in Cambridge, UK, 23rd September 1997; 7/06877H

Novel formation of a phenylated isoquinolino[3′,4′ : 1,2][60]fullerene

Ala'a K. Abdul-Sada, Anthony G. Avent, Paul R. Birkett, Adam D. Darwish, Harold W. Kroto, Roger Taylor,* David R. M. Walton and Oliver B. Woodhouse

The Chemistry Laboratory, CPES School, University of Sussex, Brighton, UK BN1 9QJ

Reaction of $C_{60}Ph_5Cl$ with cyanogen bromide results in replacement of the chlorine by BrCN and ring closure between the addend and an adjacent phenyl ring, giving a 1-bromoisoquinoline derivative of [60]fullerene; this readily undergoes nucleophilic replacement of Br by OH to give the corresponding 1-isoquinolone derivative.

Recently we described a novel spontaneous oxidation of $C_{60}Ph_5X$ (X = H, Cl) into a benzo[*b*]furan derivative of [60]fullerene, whereby oxygen forms a bridge between the cage and one of the phenyl rings.[1] We now report a related ring closure whereby reaction of BrCN with the above chloro precursor results in chlorine loss, and formation of a bromine-substituted CN bridge between the cage and the *ortho* position of the adjacent phenyl ring. This product is a 1-bromoisoquinoline derivative of [60]fullerene **1**. The resulting product then undergoes nucleophilic substitution of the bromine by hydroxide followed by tautomerism to give the isoquinolone derivative **2**, the spectroscopic data for which further confirm the precursor structure.

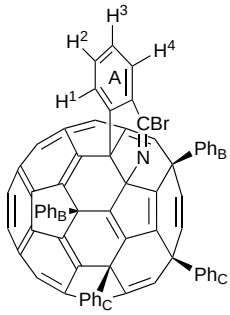

1

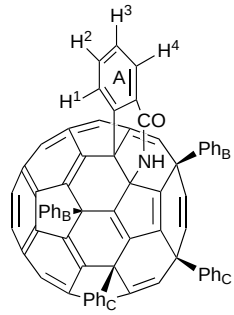

2

Cyanogen bromide (660 mg) and $FeCl_3$ (106 mg) were added to a solution of $C_{60}Ph_5Cl$ (52 mg) in dry benzene (50 cm^3). The mixture was heated under reflux for 4 h, during which time it was monitored by TLC. After *ca*. 45 min an orange microcrystalline solid began to form. The reaction mixture was cooled to room temperature, and the solvent removed under reduced pressure to give a dark residue which was washed with Et_2O to remove $FeCl_3$ and CNBr. The remaining orange–red solid was dissolved in CCl_4 (this can be helped by sonication) and then column chromatographed (SiO_2, CCl_4) to remove a small amount of $C_{60}Ph_5Cl$, giving a single orange fraction which, after solvent removal, produced an orange crystalline solid (80%). Washing the column with CH_2Cl_2 yielded a second orange fraction which, after solvent removal, was allowed to crystallise from benzene.

The FAB mass spectrum showed the parent ion at 1211 amu, which indicated overall replacement of Cl by CNBr. The IR spectrum showed a strong peak at 1646 cm^{-1} indicative of a C=N stretch and a band at 616 cm^{-1} attributable to a C–Br stretch (Fig. 1). This strongly suggests the presence of a C(Br)=N group in the molecule, and NMR spectroscopic analysis revealed the compound to be **1**.

The ^{13}C NMR spectrum shows **1** to have C_s symmetry, with four peaks in the sp^3 region for the cage carbons appearing at δ 74.84 (1 C), 59.77 (2 C), 57.77 (2 C) and 57.36 (1 C) [*cf.* 75.91 (1 C), 60.39 (2 C), 57.72 (2 C) and 62.98 (1 C) for the chloro precursor].[2] Previously we assigned the most downfield resonance to C-2 from a comparison of the resonance changes on replacing Cl by H (which causes an upfield shift of δ 17.5). The results suggest that the bromocyano group is likewise attached to C-2, and *via nitrogen*. For the cage the required 28 lines for sp^2 carbons (2 × 1 C, 26 × 2 C) appear (all 2 C except where indicated) at δ 161.10 154.21, 151.81, 148.65, 148.21, 148.16, 148.10, 148.04, 147.94, 147.76 (1 C), 147.64, 147.20, 146.86 (1 C), 146.82, 146.54, 146.42, 145.0, 144.74, 144.14 (4 C), 143.99, 143.67 (4 C), 143.48, 143.37, 143.26, 142.74 and 142.17. The spectrum also shows two *ortho* (4 C) peaks at δ 128.36/127.33, two *meta* (4 C) peaks at δ 127.81/127.24, two *para* (2 C) peaks at δ 127.33 (coincident)/126.87, four ipso peaks at δ 146.55 (1 C), 139.18 (2 C), 136.88 (2 C) and 132.07 (1 C) and five other peaks (all 1 C) at δ 131.49, 130.81, 127.04, 124.77 and 124.22 (one of this group being the carbon of the C(Br)N group). This shows that one phenyl ring has *two* substituents attached, namely the fullerene cage and the C(Br)N group.

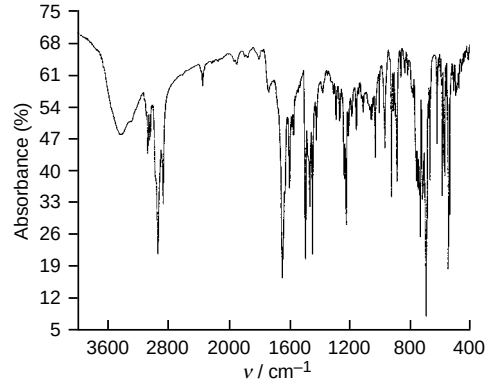

Fig. 1 IR spectrum (KBr) for $C_{91}H_{24}NBr$ (**1**)

The ^1H NMR spectrum is assigned as follows (aryl ring notation as in **1**): (i) rings B, δ 7.61–7.59 (4 H, dd, *o*-H), 7.34–7.31 (2 H, m, *p*-H), 7.26–7.22 (4 H, m, *m*-H); (ii) rings C, δ 7.21–7.19 (4 H, dd, *o*-H), 7.075–7.055 (2 H, m, *p*-H), 7.00–6.96 (4 H, m, *m*-H); (iii) ring A, δ 7.91 (1 H, dd, H^4), 7.79 (1 H dd H^1), 7.20 (1 H, dd, H^3), 7.17 (1 H dd, H^2); the couplings were approximately 7.5 and 1.5 Hz, but could not in some cases be accurately given because of peak coincidences.

The locations of the hydrogens in ring A were determined by 2D-COSY and NOE analysis, which showed interaction between H^1 and the *ortho* hydrogens of rings B. The downfield resonance for h^1 is consistent with our previous observation that resonances for hydrogens pointing towards the cage are shifted downfield,[3] whilst that for H^4 is attributable to the adjacent C–Br substituent.

The mechanism proposed (Scheme 1) is supported by the following: (i) reaction will not occur with the corresponding 4-fluoro derivative [$C_{60}(4\text{-}FC_6H_4)_5Cl$] and (ii) no reaction takes place in the absence of $FeCl_3$. If nucleophilic substitution by the nitrogen of the BrCN group were to take place on the aryl

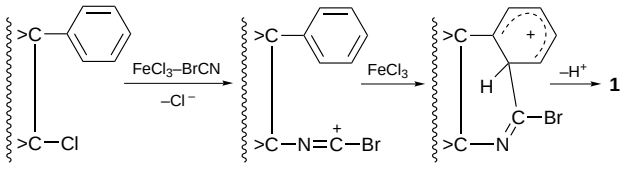

Scheme 1

addend (giving, ultimately, a quinoline derivative), this would be enhanced in the fluorophenyl compound and would occur *meta* to fluorine, *i.e. ortho* to the fullerene cage, which is the site required for the subsequent ring closure. Since reaction does not occur, electrophilic substitution by the carbon of the BrCN group into the aryl ring (giving an isoquinoline derivative) is indicated. However, this is unlikely to occur as a first step since substitution would in general take place at the more accessible position *para* to the cage. It is probable therefore that the initial step involves nucleophilic replacement of the cage-attached chlorine by BrCN, giving an intermediate fullerene–N=C$^+$–Br moiety, followed by electrophilic substitution by the imino carbocation of this group into the phenyl ring; $FeCl_3$ will aid polarisation of the cage–Cl bond just as it does in nucleophilic replacement of cage chlorines by phenyl groups.[2] Electrophilic substitution in aryl rings attached to fullerenes is normally difficult owing to the very strong electron withdrawal by the cage. However, the above intermediate will be strongly electrophilic, and the electrophilicity may be increased further through polarisation of the C–Br bond by $FeCl_3$. A related Lewis acid-catalysed intramolecular electrophilic aromatic substitution of isocyanide dihalides has also been described recently.[4] It is probable that the present reaction is synchronous and synergistic, since $C_{60}Cl_6$ itself does not react with cyanogen bromide–$FeCl_3$.

Confirmation of the structure comes from nucleophilic replacement of the bromine by hydroxide to give **2**, which has the low solubility typical of amides, obtained as orange–red plates from benzene. This occurs both on standing in air and was observed to result from reaction with either Zn–AcOH or HCl–AcOH. (Zinc accelerates the reaction, although the reason for this is unclear.) The mass spectrum of **2** gives the parent ion at the required 1148 amu. The IR spectrum (Fig. 2) shows a new C=O band at 1669 cm^{-1}, an N–H stretch at 3368 cm^{-1} and no C–Br stretch. The correct location of the carbon and nitrogen of the bridge with respect to the cage and phenylene group are confirmed by both the ^{13}C and ^{1}H NMR spectra.

The ^{13}C NMR spectrum shows the product to have C_s symmetry, the four peaks in the sp^3 region appearing at δ 65.56 (1 C), 60.74 (1 C), 60.57 (2 C) and 58.30 (2 C). Thus, whereas the ring carbons bearing the two pairs of phenyl rings have very similar shifts to those in the precursor, one of the two unique carbons has shifted markedly upfield whilst the other has shifted downfield (and to a smaller extent). This is entirely consistent with the proposed structure of **2** compared to that of **1**. The sp^2-hybridised nitrogen on the cage has changed to sp^3 hybridisation (thereby resulting in a marked upfield shift of the attached carbon), whereas the phenyl group now has an electron-withdrawing CO group attached, so that the fullerene carbon attached to this ring experiences a downfield shift. Since the electron withdrawing CO moiety is more remote than the electron-withdrawing –N= moiety, the downfield shift should be smaller than the upfield one, as observed.

For the cage, the required 28 lines for sp^2 carbons (2 × 1 C, 26 × 2 C) appear (all 2 C except where indicated) at δ 160.86, 154.22, 152.10, 148.62, 148.52 (4 C), 148.36, 148.22, 148.04 (1 C), 147.94, 147.84, 147.48, 147.35 (1 C), 147.01, 148.86, 146.77, 145.43, 144.79, 144.46, 144.38, 144.21, 143.99, 143.93, 143.90, 143.77, 143.17, 142.83 and 142.53; the resonance for the C=O group appears at δ 161.34. The ipso peaks appear at δ 133.78 (1 C), 139.42 (2 C), 136.99 (2 C) and 132.08 (1 C), and it can be seen that the last three values are

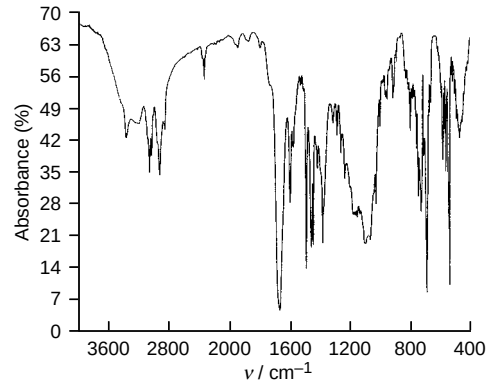

Fig. 2 IR spectrum (KBr) for $C_{91}H_{25}NO$ (**2**)

almost identical to those in the precursor **1**. The first value can be assigned to the aryl ring carbon which is adjacent to the C–Br group in **1** and the C=O group in **2**. The normally stronger electron withdrawing effect of the carbonyl group[5] is evidently moderated through resonance with the adjacent nitrogen lone pair.

The ^{1}H NMR spectrum is assigned as follows, the hydrogen locations being identified by 2D-COSY and NOE analysis. Ring notations are as in **2**; couplings are not given due to peak coincidences, and splitting could not be resolved for H^3 and H^2: (i) rings B, δ 7.66–7.64 (4 H, d, *o*-H), 7.36–7.33 (2 H, t, *p*-H), 7.29–7.25 (4 H, t, *m*-H); (ii) rings C, δ 7.27–7.25 (4 H, d, *o*-H), 7.09—7.06 (2 H, t, *p*-H), 7.01–6.98 (4 H, t, *m*-H); (iii) ring A, δ 8.12 (1 H, dd, H^4), 7.92 (1 H, dd, H^1), 7.28 (1 H, H^2), 7.23 (1 H, H^3); (iv) δ 7.03, (1 H, s, –CONH–).

This identification for H^1 was confirmed by NOE enhancement (4.1%) of the signal for the *ortho* hydrogens of ring B. The resonances for hydrogens in ring A are all shifted downfield relative to those in the precursor, which is consistent with CO being substituted on this ring, but not with –N= being attached originally to this ring and then converted to –NH– on hydrolysis. The relatively greater downfield shift in **2** compared to **1** of the resonance for H^1 relative to that of H^3 (both positions being *meta* to the substituent) is consistent with C–N bond lengthening in the quinolone relative to the quinoline, forcing H^1 slightly nearer to the cage. AM1 calculations indicate that the cage–H^1 distance is reduced from 2.634 Å in the bromoisoquinoline to 2.61 Å in the isoquinolone. Similarly, the greater downfield shift for H^4 (*ortho*) relative to H^2 (*para*) is consistent with the calculated H^4–O distance (2.49 Å) in **2** compared to the H^4–Br distance (2.63 Å) in **1**.

Notes and References

* E-mail: r.taylor@sussex.ac.uk

1 A. G. Avent, P. R. Birkett, A. D. Darwish, H. W. Kroto, R. Taylor and D. R. M. Walton, *Chem. Commun.*, 1997, 1579.
2 A. G. Avent, P. R. Birkett, J. D. Crane, A. D. Darwish, G. J. Langley, H. W. Kroto, R. Taylor and D. R. M. Walton, *J. Chem. Soc., Chem. Commun.*, 1994, 1463.
3 M. F. Meidine, R. Roers, G. J. Langley, A. G. Avent, A. D. Darwish, S. Firth, H. W. Kroto, R. Taylor and D. R. M. Walton, *J. Chem. Soc., Chem. Commun.*, 1993, 1342; M. F. Meidine, A. G. Avent, A. D. Darwish, H. W. Kroto, O. Ohashi, R. Taylor and D. R. M. Walton, *J. Chem. Soc., Perkin Trans. 2*, 1994, 1189.
4 K. S. Currie and G. Tennant, *J. Chem. Soc., Chem. Commun.*, 1995, 2295.
5 R. Taylor, *Electrophilic Aromatic Substitution*, Wiley, 1989, Table 11.1.

Received in Cambridge, UK, 15th October 1997; 7/07430A

Polymers and oligomers with transverse aromatic groups and tightly controlled chain conformations

Roger W. Alder,*† Kevin R. Anderson, Paul A. Benjes, Craig P. Butts, Panayiotis A. Koutentis and A. Guy Orpen

School of Chemistry, University of Bristol, Cantock's Close, Bristol, UK BS8 1TS

Anionic ring-opening polymerisation of spiro[cyclopropane-1,9′-fluorene] with fluorenyl anion as initiator yields polymers 1 with chains which are essentially all-*anti* and have transversely-oriented fluorenyl groups, as shown by strong upfield shifts for the mid-chain methylene and 1,8-fluorenyl protons; synthetic routes to some specific oligomers are also reported.

Controlling the secondary structure of acyclic molecules and polymers is important for many applications. We have shown that quaternary centres exert extensive conformational effects on adjacent chains.[1,2] Combining these effects with the rigid side groups provided by transversely-oriented fluorene rings should lead to a polymer **1** with a highly-constrained all-*anti* (extended chain) secondary structure; any *gauche* bonds in the chain create strong interactions between CH_2 groups in the chain and the 1,8-CH groups on the fluorene rings. Calculations on oligomers using the MM3 force field[3,4] predict that all-*anti* structures are 9–10 kJ mol^{-1} more stable than the next best conformation, which has one *gauche* bond in the terminal section of the chain. Introduction of *gauche* bonds in the interior parts of these oligomers costs 13.5–14 kJ mol^{-1}, corresponding to a > 200 : 1 preference for all-*anti* conformations at ambient temperature in these parts of the chain. In structures like **1**, *anti* conformations can be readily recognised from the upfield shifts in ^{1}H NMR spectra due to aromatic ring current effects. Thus the CH_2OH protons in diol **2** (n = 1, R = H), whose X-ray structure‡ is shown in Fig. 1, resonate at δ 2.85, whereas in acetal **3** the corresponding protons occur at δ 3.95.

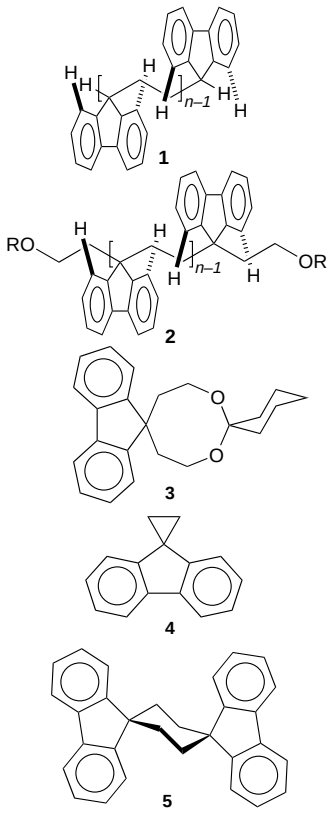

Anionic ring-opening polymerisation is a common process for heterocyclic monomers like epoxides, but it has barely been explored for hydrocarbon monomers like cyclopropanes. [1.1.1]Propellane[5] and some bicyclobutanes[6] (which have much higher strain energies) and a few vinylcyclopropanes[7] have been polymerised by this process. Simple 1,1-disubstituted cyclopropanes with two anion-stabilising groups appear good candidates, but the only example in the literature is with CO_2Me as the stabilising group.[8]

We find that polymerisation of spiro[cyclopropane-1,9′-fluorene][9] **4** can indeed be initiated by an S_N2 reaction with fluorenyllithium. Temperatures > 100 °C are required; we have used DMPU as solvent, but HMPA is also effective. During polymerisation reactions with monomer : initiator ratios > 3 : 1, a precipitate appears after about 10 min at 150 °C, raising concern that chain growth may be limited by the insolubility of the product. This insolubility precludes any simple determination of the degree of polymerisation (DP), but NMR data (see below) indicate that oligomers below the octamer **1** (n = 8) are almost absent in products from reactions with monomer : initiator ratios > 12 : 1, so polymerisation probably continues in spite of the precipitation. Further optimisation of this polymerisation will be undertaken and we intend making modified monomers with flexible chains on the periphery of the aromatic rings to improve solubility.

We found a much improved synthesis of **4** in > 90% yield from fluorene, BuLi and ethylene sulfate.[10] Ethylene sulfate is much more efficient in this reaction than 1,2-dibromoethane, which gives mixtures of dimer **1** (n = 2),[11] **4** and cyclohexane derivative **5**,§ even when fluorenyllithium is added slowly to excess dibromide. Ethane-1,2-diyl dimesylate only gives **4**, without **1** (n = 2) or **5**, but is relatively unreactive. We are investigating the reasons for the effectiveness of ethylene

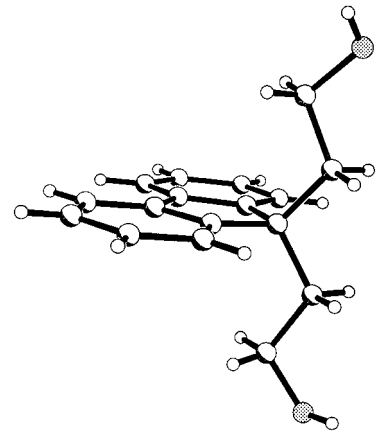

Fig. 1 X-Ray structure of diol **2** (n = 1, R = H) showing the all-*anti* aliphatic chain

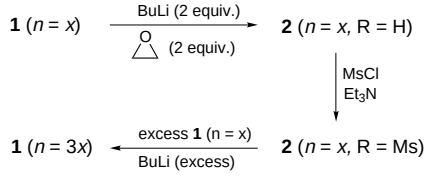

Scheme 1

sulfate in this cyclisation, and whether this observation has more general implications.

In order to examine the physical properties of the novel structure represented by **1**, we have prepared some specific oligomers by a general route. Thus reaction of an excess of the monoanion of dimer **1** (n = 2) (prepared using BuLi) with dimesylate **2** (n = 1, R = OMs) gives the pentamer **1** (n = 5), along with small amounts of the octamer from reaction of 3 equiv. of **1** (n = 2) with 2 equiv. of **2** (n = 1, R = OMs). Similarly, reaction of excess fluorenyl anion with dimesylate **2** (n = 2, R = OMs) gives the tetramer **1** (n = 4) and reaction of an excess of the monoanion of dimer **1** (n = 2) with dimesylate **2** (n = 2, R = OMs) gives the hexamer **1** (n = 6). Since mesylates **2** (R = OMs) are readily prepared from the hydrocarbons **1**, this route can potentially be used repetitively with a rapid growth in DP, as shown in Scheme 1, so long as starting oligomer can be separated from the product. Reaction of excess fluorenyl anion with dimesylate **2** (n = 1, R = OMs) only gives **5**, with no observable trimer formation, but trimer can be isolated by preparative TLC from polymerisation runs with 2 : 1 ratios of **4** : fluorenyllithium. These oligomers can be capped at both ends by double deprotonation with BuLi, and reaction with electrophiles [*e.g.* MeI, MEMCl, oxirane and $(PhS)_2$], and many of these derivatives show improved solubility.

Somewhat surprisingly, the best solvent for **1** is $CHCl_3$, the solubility of the tetramer, pentamer and hexamer are > 45, 31 and 26 mg ml^{-1} respectively; the heptamer is very insoluble. In the ^{1}H NMR spectra of oligomers **1** (n = 2–6) in $CDCl_3$, CH_2 groups and some aromatic protons are shifted upfield substantially, with shifts increasing towards the middle of the molecule and with increasing chain length. The shifts for CH_2 groups range from δ 1.75 for the dimer to δ 0.42 for the central CH_2CH_2 in the hexamer. As might be expected, the largest upfield shifts for the aromatic protons are observed for the 1,8-fluorenyl protons (Table 1), with progressively smaller shifts for the 2,7-, 3,6- and 4,5-protons.Upfield shifts for the 1,8-fluorenyl protons are predictable to within 0.02 ppm from a simple additivity scheme based on the number of fluorene units which are α (adjacent), $\Delta\delta$ −0.38, β (next to adjacent) $\Delta\delta$ −0.26, γ $\Delta\delta$ −0.11, δ $\Delta\delta$ −0.04, ε $\Delta\delta$ −0.02 and ϕ $\Delta\delta$ −0.01; this scheme allows us to identify the heptamer from polymerisation reactions and the octamer as a by-product of the preparation of the pentamer. It predicts that the 1,8-fluorenyl protons in the middle of the polymer should resonate at δ 6.04, and we believe that it provides excellent evidence for a strong preference for the all-*anti* conformation in solution. These polymers and oligomers therefore possess a novel architecture (flexible, but possessing many of the attributes of a rigid rod). They could be useful as molecular spacers, and the regular array of aligned aromatic rings is an intriguing feature. The distance between two aromatic rings on the same side of the polymer chain, calculated to be 7.71 Å, gives enough room to intercalate another aromatic ring between them. Furthermore, the intervening chains, while saturated, are perfectly aligned for maximum through-bond coupling,[12] and electron- and energy-transfer down these chains may well be rapid. Finally, we point out that anionic ring-opening polymerisation of 1,1-disubstituted cyclopropanes has now been observed for cases where the growing anion is a malonic ester derivative[8] (pK_a ~ 13) and where it is a fluorenyl anion (pK_a ~ 22). We are exploring the limits for this process, but we believe that many novel polymeric structures might be made this way.

Table 1 ^{1}H NMR chemical shifts in $CDCl_3$ for 1,8-fluorenyl protons in oligomers **1**

	δ_H(ppm)			
	Ar^1 (Terminal rings)	Ar^2	Ar^3	Ar^4
Dimer	7.28			
Trimer	7.01	6.89		
Tetramer	6.90	6.63		
Pentamer	6.86	6.53	6.39	
Hexamer	6.84	6.48	6.28	
Heptamer	6.83	6.46	6.24	6.18
Octamer	6.83	6.45	6.22	6.14

We thank EPSRC for support (grants GR/K15497 and GR/K76160) and for a studentship (K. R. A.).

Notes and References

† E-mail: Rog.Alder@bristol.ac.uk

‡ *Crystal data* for **2**: $C_{17}H_{18}O_2$, M = 254.31, monoclinic, space group $P2_1/c$, a = 7.391(1), b = 24.846(4), c = 7.898(1) Å, β = 103.50(1)°, V = 1410.3(3) Å^3, Z = 4, D_c = 1.198 g cm^{-3}, λ = 0.71073 Å, graphite monochromated Mo-Kα X-radiation, μ = 0.38 mm^{-1}, F(000) = 544, T = 293 K. Data were collected on a Siemens P4 four circle diffractometer for a quadrant of reciprocal space for 2.78 > 2θ > 40.00. The structure was solved by direct methods and refined by full-matrix least-squares methods (175 parameters) against all 1292 unique intensity data with I > 2σ(I) to final R1 = 0.0628 for the 723 reflections with I > 2σ(I). CCDC 182/714.

§ Dispiro[9*H*-fluorene-9,1′-cyclohexane-4′,9″-9*H*-fluorene] **5**, a new compound, shows a broadened absorption in its ^{1}H NMR spectrum for the methylene protons at room temperature; the variable temperature behaviour of this compound will be discussed elsewhere.

1 R. W. Alder, C. M. Maunder and A. G. Orpen, *Tetrahedron Lett.*, 1990, **46**, 6717.
2 R. W. Alder, P. R. Allen and E. Khosravi, *J. Chem. Soc., Chem. Commun.*, 1994, 1235.
3 N. L. Allinger, Y. H. Yuh and J.-H. Lii, *J. Am. Chem. Soc.*, 1989, **111**, 8551.
4 The MACROMODEL V5.5 implementation of MM3 (MM3*) was used: F.Mohamadi, N. G. J. Richards, W. C. Guida, R. Liskamp, M. Lipton, C. Caulfield, G. Chang, T. Hendrickson and W. C. Still, *J. Comput. Chem.*, 1990, **11**, 440.
5 A. D. Shlüter, *Macromolecules*, 1988, **21**, 1208; *Polymer Comm.*, 1989, **30**, 34.
6 H. K. Hall, E. P. Blanchard, S. C. Cherkofsky, J. B. Sieja and W. A. Sheppard, *J. Am. Chem. Soc.*, 1971, **93**, 110; H. K. Hall, C. D. Smith, E. P. Blanchard, S. C. Cherkofsky and J. B. Sieja, *ibid.*, 1971, **93**, 121; H. K. Hall, *Macromolecules*, 1971, **4**, 139.
7 I. Cho and K. D. Ahn, *J. Polym. Sci., Polym. Chem.*, 1979, **17**, 3183; I. Cho and J. B. Kim, *ibid.*, 1980, **18**, 3053; I. Cho and W. T. Kim, *J. Polym. Sci., Polym. Lett.*, 1986, **24**, 109; *J. Polym. Sci., Polym. Chem.*, 1987, **25**, 2791.
8 J. Penelle, G. Clarebout and I. Balikdjian, *Polym. Bull.*, 1994, **32**, 395; J. Penelle, H. Hérion, A. Sorée and P. Gorissen, *Polym. Prepr. Am. Chem. Soc., Div. Polym. Chem.*, 1996, **37**, 208.
9 R. Mechoulam and F. Sondheimer, *J. Am. Chem. Soc.*, 1958, **80**, 4386; R. Greenwald, M. Chaylovsky and E. J. Corey, *J. Org. Chem.*, 1963, **28**, 1128 and references cited therein; for a previous large scale preparation, see M. E. Jason, P. R. Kurzweil and C. C. Cahn, *Synth. Commun.*, 1981, **11**, 865.
10 G. Caron, G. W.-M. Tseng and R. J. Kazlauskas, *Tetrahedron: Asymmetry*, 1994, **5**, 83; Y. Gao and K. B. Sharpless, *J. Am. Chem. Soc.*, 1988, **110**, 7538.
11 W. Wislicenus and W. Mocker, *Chem. Ber.*, 1913, **46**, 2786; H. G. Alt, W. Milius and S. J. Palackal, *J. Organomet. Chem.*, 1994, **472**, 113.
12 R. Hoffmann, *Acc. Chem. Res.*, 1971, **4**, 1; K. D. Jordan and M. N. Paddon-Row, *Chem. Rev.*, 1992, **92**, 395; M. N. Paddon-Row and M. J. Shephard, *J. Am. Chem. Soc.*, 1997, **119**, 5355.

Received in Liverpool, UK, 13th October 1997; 7/07389E

A new approach to steroid ring construction based on a novel radical cascade sequence

Sandeep Handa, Gerald Pattenden*† and Wan-Sheung Li

Department of Chemistry, Nottingham University, Nottingham, UK NG7 2RD

A new approach to steroid ring construction based on sequential cascade 6-*endo-trig* cyclisation/macrocyclisation/ transannulation reactions and exemplified in the synthesis of the *cis, anti, cis, anti, cis* tetracycle 17 from 15, is presented.

Since their structures were firmly established some fifty years ago, there have been a wide range of imaginative approaches to the total synthesis of natural steroids and to steroidal ring systems. Perhaps paramount amongst the methods that have been developed are those based on either Diels–Alder reactions (inter- and intra-molecular, including transannular based)[1] or biomimetic-type electrophilic cyclisations of polyene precursor compounds.[2] In recent years our own research group has been examining the scope for a range of cascade radical processes in the synthesis of steroids, including those based on consecutive 6-*endo-trig* cyclisations from appropriate polyene acyl radical precursors,[3] and those based on radical macrocyclisations in tandem with radical transannulations.[4] Indeed, these approaches have led to some highly efficient routes to steroids, including aza-steroids[5] and some natural products.[6] We have now conceived a new approach to steroid constructions, based on these earlier studies, whereby the A/B ring system is elaborated by consecutive 6-*endo-trig* cyclisations (**1** → **2**), *in concert with* formation of the C/D ring system *via* a macrocyclisation/ transannulation sequence (**3** → **4** → **5**), from an appropriately functionalised cyclopropyl-based polyene precursor **1** (Scheme 1).

Thus we chose the cyclopropyl substituted trienone selenyl ester **7** as the starting point for our cyclisation studies. The selenyl ester group was chosen as the radical precursor because of the known propensity for hex-5-enoyl radicals to undergo 6-*endo* cyclisations,[3,7] and the conjugated enone group was incorporated in the substrate **7** to facilitate the 9-*endo-trig* cyclisation[8] following ring-opening of the cyclopropylcarbinyl radical intermediate (*cf.* **2** → **3** → **4**, Scheme 1). The synthesis of **7** was achieved in fifteen steps from the known bromo alcohol **6** (Scheme 2).[9,10] When a solution of the selenyl ester **7** in dry degassed benzene (4 mM), at reflux, was treated with Bu_3SnH (syringe pump addition over 4 h) in the presence of AIBN, one major product was isolated in *ca*. 40% yield. Analysis of the spectroscopic data for the compound showed that, instead of generating the steroid dione structure **9** resulting from the predicted cascade highlighted in Scheme 1, the acyl radical intermediate **8** had undergone a single 14-*endo-trig* cyclisation producing the macrocyclic 1,4-dione **10**.[11]

The efficient 14-*endo-trig* macrocyclisation of the nucleophilic acyl radical **8**, leading to **10**, over the competing 6-*endo-trig* cascade is no doubt a consequence of the electrophilicity of the terminal enone in **8**. In light of this we designed a new cyclisation precursor to avoid the competing pathway. The designed polyene selenyl ester **15** incorporates two carboxylate ester moieties, the first of which [at C(5)] was introduced in order to increase the rate of 6-*endo-trig* cyclisation of the acyl radical precursor and the second [at C(13)] was incorporated to lower the electrophilicity of the terminal olefin (with respect to **7**). The new precursor **15** was prepared as shown in Scheme 3. Thus formation of the Normant Grignard reagent from 3-chloro-

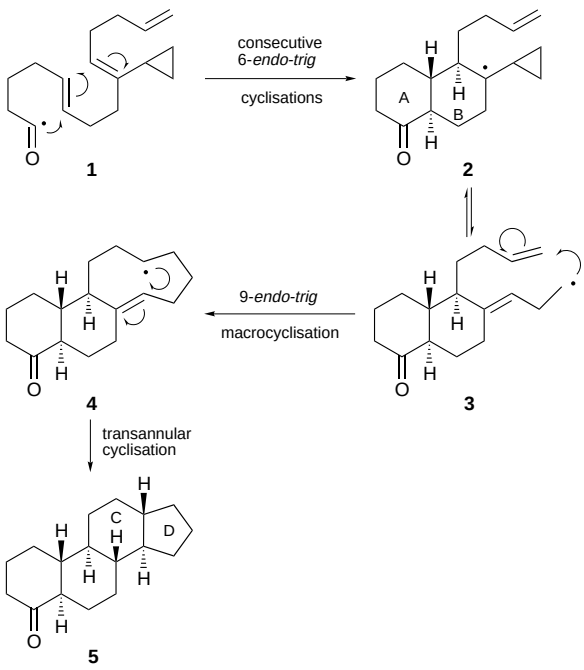

Scheme 1

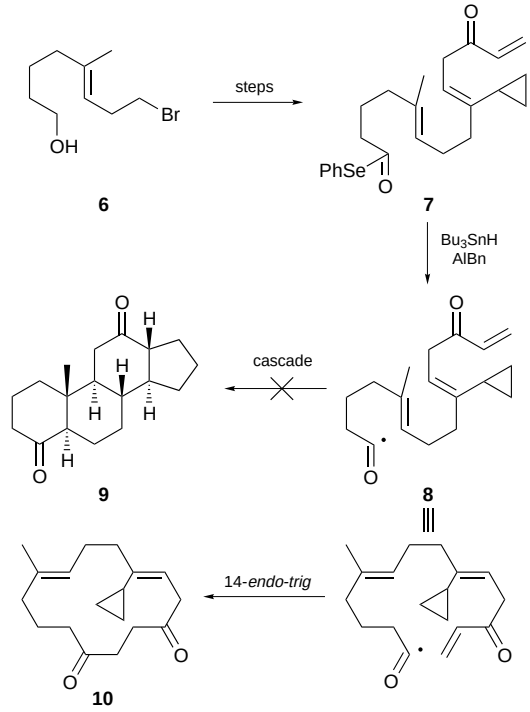

Scheme 2

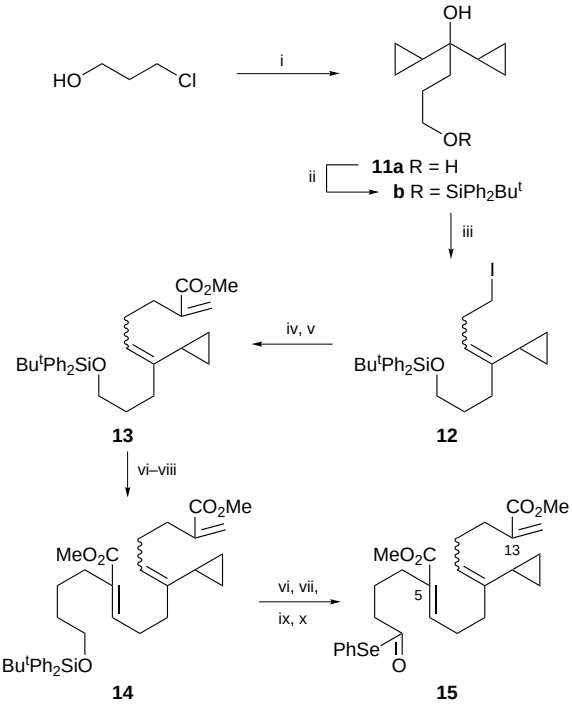

Scheme 3 *Reagents and conditions*: i, MeMgBr, THF, −30 °C, Mg, 70 °C, then dicyclopropyl ketone, 68%; ii, Bu^tPh_2SiCl, imidazole, 97%; iii, NIS, PPh_3, CH_2Cl_2 −30 °C, 64%; iv, NaH, trimethyl phosphonoacetate, DMSO, 73%; v, NaH, $(CH_2O)_3$, 85%; vi, TBAF, 91–95%; vii, Dess–Martin periodinane, 90–92%; viii, NaH, $Bu^tPh_2SiO(CH_2)_4CH(CO_2Me)PO(OMe)_2$ **16**, 0 °C, 87%; ix, KH_2PO_4, Bu^tOH, H_2O, $NaClO_2$, 2-methylbut-2-ene, 95%; x, *N*-(phenylseleno)phthalimide, PBu_3, −30 °C, 72%

propanol followed by reaction with dicyclopropyl ketone first gave the diol **11a** which was then protected selectively as its TBDPS ether **11b**. Selective ring opening of one of the cyclopropane rings in **11b** was achieved by treatment with *N*-iodosuccinimide (NIS)–PPh_3 to produce the vinyl cyclopropyl intermediate **12** as a 1 : 1 mixture of *E*- and *Z*-isomers. Nucleophilic displacement of the homoallylic iodide in **12** by the anion generated from trimethyl phosphonoacetate and subsequent Wadsworth–Emmons reaction with paraformaldehyde next installed the terminal methacrylate residue in the form of intermediate **13**. The silyl ether group in **13** was converted into the corresponding aldehyde which was then used in a further Wadsworth–Emmons olefination with the phosphate **16** giving the triene **14** as a mixture of separable isomers about the newly formed double bond. Finally, a series of functional group interconversions then led to the target selenyl ester **15**.

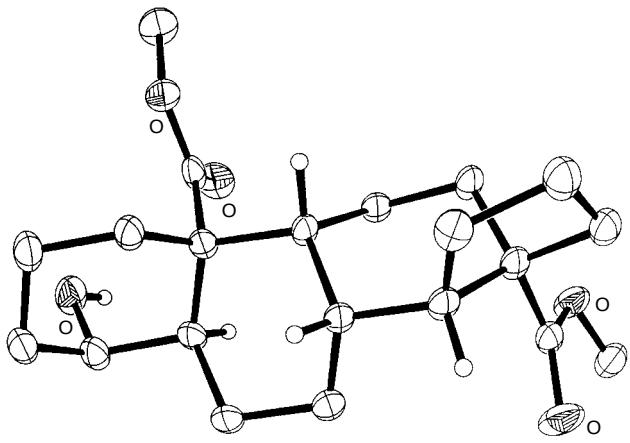

Fig. 1 X-Ray crystallographic structure of **18**

Treatment of the selenyl ester **15** with Bu_3SnH–AIBN under conditions similar to those which produced **10** from **7** led to the formation of one major product in *ca*. 45% yield, and some minor products. Detailed analysis of the NMR data for the separated major product indicated that the compound had the hoped-for tetracyclic (steroid) ring system, but the data could not define its stereochemistry unambiguously. Fortunately, the tetracyclic ketone product could be reduced selectively using $NaBH_4$ leading to the crystalline carbinol **18**, mp 126–128 °C (Et_2O–light petroleum). An X-ray crystallographic analysis of this tetracycle showed, surprisingly, that it had the very unusual *cis, anti, cis, anti, cis*-stereochemistry, *viz*. **17** and **18** (Fig. 1). Thus we had not only demonstrated the scope for the new strategy for steroid ring construction enunciated in Scheme 1, but we have also uncovered a route to the unusual all *cis*-stereochemistry for the steroid ring system produced when **15** undergoes a radical cascade cyclisation to **17**. Further studies are now in progress to develop this novel stratagem for polycycle construction in other fused ring systems.

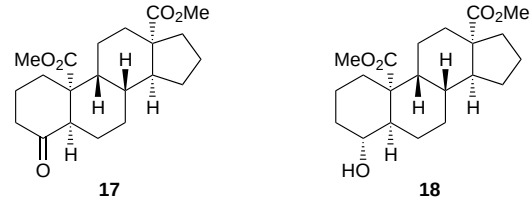

We thank the EPSRC for support of this work *via* a Postdoctoral Fellowships (to S. H. and W-S. L.) and purchase of the X-ray diffractometer.

Notes and References

† E-mail: gp@nottingham.ac.uk

‡ *Crystal data* for **18**: $C_{21}H_{32}O_5$, M = 364.47, triclinic, a = 7.499(6), b = 10.405(6), c = 12.297(7) Å, α = 82.70(4), β = 80.93(6), γ = 79.83(5)°, U = 927.7(11) Å^3, T = 150 K, space group $P\bar{1}$ (No. 2), Z = 2, D_c = 1.305 g cm^{-3}, μ(Mo-Kα) = 0.091 mm^{-1}, 5459 reflections measured, 3120 unique (R_{int} = 0.019), final R_1 [$F_o \geqslant 4\sigma(F_o)$] = 0.0628, wR_2 (all data) = 0.209 for 242 refined parameters. CCDC 182/715.

1 For specific examples of Diels–Alder approaches to steroidal systems, see L. Quellet, P. Langois and P. Deslongchamps, *Synlett*, 1997, 689; Y. Haruo, Y. Sakamoto and T. Takahashi, *Synlett*, 1995, 231; H. Pellissier and M. Santelli, *Tetrahedron*, 1996, **52**, 9093; T. Sugahara and K. Ogasawara, *Tetrahedron Lett.*, 1996, **37**, 7403; T. J. Grinsteiner and Y. Kishi, *Tetrahedron Lett.*, 1994, **35**, 8333 and references cited therein.

2 See: E. J. Corey and S. Lin, *J. Am. Chem. Soc.*, 1996, **118**, 8765; P. V. Fish, W. S. Johnson, G. S. Jones, F. S. Tham and R. K. Kullnig, *J. Org. Chem.*, 1994, **59**, 6150.

3 A. Batsanov, L. Chen, G. B. Gill and G. Pattenden, *J. Chem. Soc., Perkin Trans. 1*, 1996, 45 and references cited therein. For a specific example of a palladium-catalysed cascade approach to fused polycycles, see T. Sugihara, C. Copéret, D. Owczarczyk, L. S. Harring and E. Negishi, *J. Am. Chem. Soc.*, 1994, **116**, 7923.

4 G. Pattenden and P. Wiedenau, *Tetrahedron Lett.*, 1997, **38**, 3647 and references cited therein.

5 P. J. Double and G. Pattenden, unpublished work.

6 G. Pattenden and L. Roberts, *Tetrahedron Lett.*, 1996, **37**, 4191.

7 C. Chatgilialoglu, C. Ferreri, M. Lucarini, A. Venturini and A. A. Zavitsas, *Chem. Eur. J.*, 1997, **3**, 376; D. L. Boger and R. J. Mathvink, *J. Org. Chem.*, 1992, **57**, 1429; D. Batty and D. Crich, *J. Chem. Soc., Perkin Trans. 1*, 1992, 3205.

8 For a review of free-radical mediated macrocyclisations, see S. Handa and G. Pattenden, *Contemp. Org. Synth.*, 1997, **4**, 196.

9 S. Hatakeyama, H. Numata, K. Osanai and S. Takano, *J. Chem. Soc., Chem. Commun.*, 1989, 1893.

10 Details of the synthetic route to **7** will be reported in a full paper.

11 For examples of acyl radical mediated 14-*endo-trig* cyclisation over the competing 6-*endo-trig* pathway, see D. L. Boger and R. J. Mathvink, *J. Am. Chem. Soc.*, 1990, **112**, 4008; M. P. Astley and G. Pattenden, *Synthesis*, 1992, 101.

Received in Liverpool, UK, 9th October 1997; 7/07320H

High activity ethylene polymerisation catalysts based on chelating diamide ligands

Vernon C. Gibson,*[a] Brian S. Kimberley,[a] Andrew J. P. White,[a] David J. Williams[a] and Philip Howard[b]

[a] *Department of Chemistry, Imperial College, Exhibition Road, South Kensington, London, UK SW7 2AY*
[b] *BP Chemicals, Sunbury Research Centre, Chertsey Road, Sunbury on Thames, Middlesex, UK TW16 7LN*

Treatment of $Zr(NMe_2)_4$ with $RNH(SiPh_2)NHR$ and $RNH(Me_2SiCH_2CH_2SiMe_2)NHR$ (R = 2,6-$Me_2C_6H_3$) affords the four- and seven-membered chelate complexes $\{Zr[RN(SiPh_2)NR](NMe_2)_2(HNMe_2)\}$ and $\{Zr[RN(Me_2SiCH_2CH_2SiMe_2)NR](NMe_2)_2\}$ respectively; a dramatic effect of chelate ring size on ethylene polymerisation activity and kinetic profile is found.

There is considerable interest in the development of new generation 'non-metallocene' catalysts for the polymerisation of α-olefins. Chelating diamide complexes of the Group 4 metals have recently become the focus of much attention,[1–10] partly because of their close relationship to the commercially significant half-sandwich metal amido 'constrained geometry' catalyst system,[11,12] and more generally due to a relationship to metallocenes that may be traced through alkoxide relatives (Scheme 1).† A potential advantage of the bis(amido)metal system relative to the constrained geometry half-sandwich metal amide catalyst family is a lower formal electron count [$(R_2N)_2Zr$ is formally a $10e^-$ fragment, *cf.* $12e^-$ for $CpZr(NR_2)$] which is likely to result in a more electrophilic and therefore potentially more active catalyst fragment. However, it must be recognised that the bis(amido)metal system is sterically more open and may need steric tuning to minimise deactivation processes.

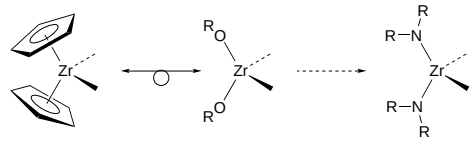

Scheme 1

We report a surprisingly active zirconium ethylene polymerisation catalyst system based on chelating diamide ligands. Of particular significance is the observation of dramatically enhanced activity and a more stable kinetic profile upon increase in the chelate ring size. Compounds **1** and **2** are readily synthesised in high yield *via* reaction of LiNHR (R = 2,6-$Me_2C_6H_3$) with the appropriate dichlorosilane (Scheme 2). Treatment of **1** and **2** with $Zr(NMe_2)_4$ in toluene at 90 °C leads to elimination of 2 equiv. of Me_2NH and formation of four- and seven-membered chelate complexes **3** and **4** in excellent yield.‡

The structures of **3** and **4** have been determined by X-ray crystallography.§ The structure of **3** reveals the formation of a distorted trigonal bipyramidal Zr complex (Fig. 1), the Zr being bonded to the bidentate chelating diamide **1**, two Me_2N groups and a molecule of Me_2NH. The equatorial plane is defined by N(2), N(6) and N(9), the axial positions being occupied by N(1) and N(3). The principal distortion in the coordination geometry is due to the small bite [71.3(1)°] of the chelating diamide, a consequence of which is 'reduced' steric congestion of the Zr centre allowing retention of three of the original four Me_2N ligands (rather than the expected two). The N_2SiZr chelate ring is planar to within 0.01 Å.

By contrast, the structure of **4** (Fig. 2) reveals a slightly distorted tetrahedral coordination at Zr, comprising the bidentate disilyldianilide [bite angle 109.2(1)°] and just two

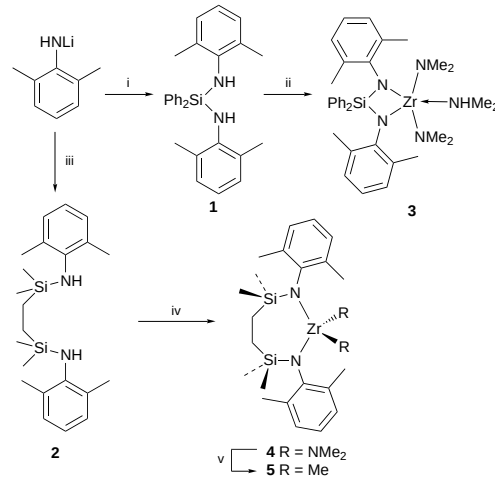

Scheme 2 *Reagents and conditions*: i, Cl_2SiPh_2 (0.5 equiv.), Et_2O, room temp., 12 h, 79%; ii, $Zr(NMe_2)_4$, toluene, 90 °C, 12 h, 98%; iii, $ClSi(Me)_2CH_2CH_2Si(Me)_2Cl$ (0.5 equiv.), Et_2O, room temp., 12 h, 74%; iv, $Zr(NMe_2)_4$, toluene, 90 °C, 12 h, 97%; $AlMe_3$ (5.0 equiv.), toluene, room temp., 30 min, 98%

Me_2N ligands. An important effect of increasing the size of the chelate ring in **4** (now seven-membered, *cf.* four-membered in **3**) is for the two aryl rings to partially envelop the Zr centre and one of the Me_2N ligands [N(10)]. The geometry of the seven-membered chelate ring appears to be somewhat strained, the internal angles at the N (131°) and C (117°) centres being significantly enlarged from normal trigonal and tetrahedral geometries, respectively. The reason(s) for these distortions are not immediately evident, although they are clearly a factor in the envelopment of the Zr centre described above. Complex **4** is readily converted to complex **5** upon reaction with excess $AlMe_3$.[13]

The results of preliminary studies on their activities for ethylene polymerisation are collected in Table 1. For the monosilyl bridged species **3**, pretreatment with Bu^nLi, to remove the bound Me_2NH, and prealkylation with excess $AlMe_3$, followed

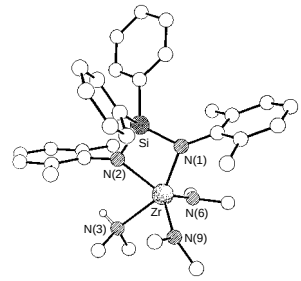

Fig. 1 Molecular structure of **3**. Selected bond lengths (Å) and angles (°): Zr–N(1) 2.158(2), Zr–N(2) 2.159(2), Zr–N(3) 2.426(2), Zr–N(6) 2.025(3), Zr–N(9) 2.057(3), Si–N(1) 1.709(2), Si–N(2) 1.725(2); N(6)–Zr–N(9) 108.5(1), N(6)–Zr–N(1) 106.1(1), N(9)–Zr–N(1) 105.2(1), N(6)–Zr–N(2) 128.1(1), N(9)–Zr–N(2) 122.4(1), N(1)–Zr–N(2) 71.3(1), N(6)–Zr–N(3) 91.8(1), N(9)–Zr–N(3) 89.2(1), N(1)–Zr–N(3) 151.6(1), N(2)–Zr–N(3) 80.3(1), N(1)–Si–N(2) 94.2(1), Si–N(1)–Zr 97.5(1), Si–N(2)–Zr 97.0(1).

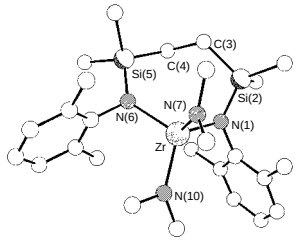

Fig. 2 Molecular structure of **4**. Selected bond lengths (Å) and angles (°): Zr–N(10) 2.024(4), Zr–N(7) 2.032(4), Zr–N(1) 2.084(4), Zr–N(6) 2.105(4), N(1)–Si(2) 1.735(4), Si(2)–C(3) 1.874(5), C(3)–C(4) 1.535(7), C(4)–Si(5) 1.869(5), Si(5)–N(6) 1.746(4); N(10)–Zr–N(7) 104.7(2), N(10)–Zr–N(1) 116.0(2), N(7)–Zr–N(1) 108.2(2), N(10)–Zr–N(6) 111.1(2), N(7)–Zr–N(6) 107.2(2), N(1)–Zr–N(6) 109.2(1), Si(2)–N(1)–Zr 129.0(2), N(1)–Si(2)–C(3) 107.8(2), C(4)–C(3)–Si(2) 116.8(4), C(3)–C(4)–Si(5) 116.6(4), N(6)–Si(5)–C(4) 110.8(2), Si(5)–N(6)–Zr 131.7(2).

by exposure to ethylene (10 atm) in the presence of MAO (750 equiv.) at 50 °C gave an active, although short-lived (< 15 min) catalyst; 450 mg of polyethylene was isolated, corresponding to an activity of 3 g $mmol^{-1}$ h^{-1} bar^{-1}. By contrast, under identical conditions of temperature, pressure and cocatalyst concentration (entry 2), complex **4** afforded a steady uptake of ethylene over the 60 min duration of the run at an activity of 490 g $mmol^{-1}$ h^{-1} bar^{-1}. Increasing the temperature (entries 2–4) gave a corresponding increase in activity, although a noticeable deactivation occurs over the course of the 60 min run at 50 °C, which becomes even more enhanced at 75 °C. The effect of MAO cocatalyst concentration can be seen from entries 3, 5 and 6, the more MAO the higher the activity and also the more stable the kinetic profile. If the procatalyst is not pre-alkylated with $AlMe_3$ (entry 7) reduced activity is found, consistent with the necessity for efficient alkylation of the Me_2N complex;[13] MAO on its own is known to be a relatively poor alkylating agent. The molecular weights of the polyethylenes generated using the most active catalysts are in the region of 10^5 (M_w) with relatively broad molecular weight distributions (PDIs 5–9). These will be discussed in more detail in a future publication.

Treatment of dimethylzirconium procatalyst **5** with trityltetrakis(pentafluorophenyl)borate at 50 °C initially gives a highly active catalyst that rapidly deactivates over 10 min. The same procatalyst in the presence of MAO gives a much more stable kinetic profile and an activity figure of merit comparable to prealkylated **4** (entry 3). This is consistent with the general stabilising effect found for MAO with metallocene catalyst systems.

The dramatically more favourable activity and kinetic profile characteristics found for **4** relative to **3** may be attributed to the steric protection of the zirconium centre by the bulky aryl substituents of the large ring chelate ligand. Not only do these prevent the binding of small base molecules such as Me_2NH, they also undoubtedly lend protection to the active catalyst site.

Table 1 Ethylene polymerisation characteristics[a] for **3**–**5**

Entry	Procatalyst	Cocatalyst (equiv.)	T/°C	Activity/ g $mmol^{-1}$ h^{-1} bar^{-1}
1	**3**	MAO (750)	50	3[b]
2	**4**	MAO (750)	25	250[c]
3	**4**	MAO (750)	50	490[d]
4	**4**	MAO (750)	75	680[e]
5	**4**	MAO (100)	50	140[b]
6	**4**	MAO (2000)	50	990[d]
7	**4**	MAO (750)[f]	50	70
8	**5**	$[Ph_3C][B(C_6F_5)_4]$	50	60[b]
9	**5**	MAO (750)	50	400[d]

[a] General conditions: procatalyst dissolved in toluene for runs 1–7 and 9, CH_2Cl_2 for run 8, pretreatment with excess $AlMe_3$ (10 equiv.) for runs 1–6, 1 litre autoclave, 10 atm ethylene pressure, isobutane solvent, $AlMe_3$ scavenger, runs carried out over 60 min. [b] Rapid deactivation. [c] Stable ethylene uptake over 1 h duration of run. [d] Slow deactivation over 1 h duration of run. [e] Deactivation more rapid than in footnote (*d*). [f] No prealkylation.

BP Chemicals Ltd and the EPSRC are thanked for a CASE studentship to B. S. K. BP Chemicals is also thanked for assistance with catalyst evaluation.

Notes and References

* E-mail: v.gibson@ic.ac.uk

† The similar 1σ,2π bonding characteristics of the cyclopentadienide and alkoxide ligands affords a direct isolobal relationship. It should be noted that, whilst closely related to the alkoxide moiety, the amide ligand is formally a 1σ,1π unit and therefore is not strictly isolobal; as a 1σ,1π ligand it also donates two fewer electrons to the metal centre.

‡ Satisfactory elemental analyses have been obtained. *Selected data* for **1**: $\delta_H(C_6D_6$, 298 K) 2.10 (s, 12 H, PhMe_2), 3.39 (br s, 2 H, NH), 6.80–6.91 (overlapping m, aryl H), 7.04–7.10 (overlapping m, aryl H), 7.66–7.84 (overlapping m, aryl H); $\delta_C(C_6D_6$, 298 K) 20.44, 122.13, 129.05, 130.10, 130.72, 134.81, 135.02, 136.82, 142.90. For **2**: $\delta_H(C_6D_6$, 298 K) 0.76 (s, 12 H, SiMe_2), 0.51 (s, 4 H, $(CH_2SiMe_2)_2$, 2.18 (s, 12 H, PhMe_2), 6.85 (t, 2 H, $^3J_{HH}$ 6.7, *p*-C_6H_3), 7.00 (d, 4 H, $^3J_{HH}$ 6.7, *m*-C_6H_3); $\delta_C(C_6D_6$, 298 K) −1.10, 9.75, 19.85, 122.01, 128.70, 131.45, 143.80. For **3**: $\delta_H(C_6D_6$, 298 K) 1.42 (br s, 1 H, *H*NMe_2), 1.68 (d, 6 H, $^3J_{HH}$ 5.9, HNMe_2), 2.26 (br s, 6 H, Ph*Me*), 2.42 (br s, 6 H, Ph*Me*), 2.79 (s, 12 H, NMe_2), 7.07–7.11 (overlapping m, aryl H), 7.61–7.64 (overlapping m, aryl H); $\delta_C(C_6D_6$, 298 K) 21.15, 39.43, 41.95, 120.99, 127.22, 128.65, 135.64, 142.83. For **4**: $\delta_H(C_6D_6$, 298 K) 0.13 (s, 12 H, SiMe_2), 1.21 (s, 4 H, Me_2SiCH_2), 2.39 (s, 12 H, PhMe_2), 2.48 (s, 12 H, NMe_2), 6.83 (t, 2 H, $^3J_{HH}$ 7.3, aryl H), 7.06 (d, 4 H, $^3J_{HH}$ 7.3, aryl H); $\delta_C(C_6D_6$, 298 K) 1.06, 10.72, 20.61, 42.42, 123.21, 128.95, 135.36, 146.13. For **5**: $\delta_H(C_6D_6$, 298 K) 0.12 (s, 12 H, SiMe_2), 0.23 (s, 6 H, ZrMe_2), 1.08 (s, 4 H, Me_2SiCH_2), 2.37 (s, 12 H, $C_6H_3Me_2$), 6.89–6.95 (m, 2 H, *p*-aryl H), 7.00–7.03 (m, 4 H, *m*-aryl H); $\delta_C(C_6D_6$, 298 K) 0.18 ($SiMe_2$), 9.38 ($C_6H_3Me_2$), 20.75 ($C_6H_3Me_2$), 43.07 ($ZrMe_2$), 125.48 (C_6H_3-C_m), 129.51 (C_6H_3-C_p), 137.00 (C_6H_3-C_o), 137.94 (C_6H_3-C_{ipso}).

§ *Crystal data* for **3**: $C_{34}H_{47}N_5SiZr$, M = 645.1, monoclinic, $P2_1/n$ (no. 14), a = 11.425(1), b = 19.501(1), c = 15.423(3) Å, β = 97.58(1)°, V = 3406.1(7) Å^3, Z = 4, D_c = 1.26 g cm^{-3}, μ(Cu-Kα) = 32.0 cm^{-1}, F(000) = 1360. A clear prism of dimensions 0.35 × 0.23 × 0.10 mm was used. For **4**: $C_{26}H_{46}N_4Si_2Zr$, M = 562.1, monoclinic, $P2_1/c$ (no. 14), a = 9.403(2), b = 33.301(6), c = 10.640(2) Å, β = 113.02(1)°, V = 3066(1) Å^3, Z = 4, D_c = 1.22 g cm^{-3}, μ(Mo-Kα) = 4.6 cm^{-1}, F(000) = 1192. A clear prism of dimensions 0.67 × 0.57 × 0.57 mm was used. For **3** (**4**), 5590 (4306) independent reflections were measured on a Siemens P4/PC diffractometer at 183 K (293 K) with graphite monochromated Cu-Kα—rotating anode source—(Mo-Kα) radiation using ω-scans. The structures were solved by direct methods and all the non-hydrogen atoms were refined anisotropically using full-matrix least-squares based on F^2 to give R_1 = 0.036 (0.046), wR_2 = 0.095 (0.099) for 5084 (3093) independent observed absorption corrected reflections [$|F_o| > 4\sigma(|F_o|)$, $2\theta \leqslant 128°$ (50°)] and 351 (299) parameters respectively. The N–H hydrogen atom in **3** was located from a ΔF map and refined isotropically subject to an N–H distance constraint (0.90 Å). CCDC 182/700.

1 J. D. Scollard, D. H. McConville, N. C. Payne and J. J. Vittal, *Macromolecules*, 1996, **29**, 5241.
2 F. G. N. Cloke, T. J. Geldbach, P. B. Hitchcock and J. B. Love, *J. Organomet. Chem.*, 1996, **506**, 343.
3 S. Tinkler, R. J. Deeth, D. J. Duncalf and A. McCamley, *Chem. Commun.*, 1996, 2623.
4 M. Oberthür, P. Arndt and R. Kempe, *Chem. Ber.*, 1996, **129**, 1087.
5 K. Aoyagi, P. K. Gantzel, K. Kalai and T. D. Tilley, *Organometallics*, 1996, **15**, 923.
6 R. Baumann, W. M. Davis and R. R. Schrock, *J. Am. Chem. Soc.*, 1997, **119**, 3830.
7 F. Jäger, H. W. Roesky, H. Dorn, S. Shah, M. Noltemeyer and H.-G. Schmidt, *Chem. Ber.*, 1997, **130**, 399.
8 D. R. Click, B. L. Scott and J. G. Watkin, Abstract 322, 213th ACS National meeting, San Francisco, April 13–17, 1997.
9 T. H. Warren, R. R. Schrock and W. M. Davis, *Organometallics*, 1996, **15**, 562.
10 N. A. H. Male, M. Thornton-Pett and M. Bochmann, *J. Chem. Soc., Dalton Trans.*, 1997, 2487.
11 J. C. Stevens, F. J. Timmers, D. R. Wilson, G. F. Schmidt, P. N. Nickias, R. K. Rosen, G. W. Knight and S.-Y. Lai, *Eur. Pat. Appl.*, 416-815-A2, 1990, Dow.
12 J. A. M. Cannich, *Eur. Pat. Appl.*, EP-420-436-A1, 1990, Exxon.
13 I. Kim and R. F. Jordan, *Macromolecules*, 1996, **29**, 489.

Received in Liverpool, UK, 28th August 1997; 7/06304K

Either γ-*syn*- or γ-*anti*-selective palladium-catalysed carbonyl allylation by mixed (*E*)- and (*Z*)-1,3-dichloropropene with tin(II) halides

Yoshiro Masuyama,* Akihiro Ito and Yasuhiko Kurusu

Department of Chemistry, Sophia University, 7-1 Kioicho, Chiyoda-ku, Tokyo 102, Japan

Palladium-catalysed carbonyl allylations by mixed (*E*)- and (*Z*)-1,3-dichloropropene with SnI_2–Bu_4NI and $SnCl_2$ diastereoselectively produce *syn* and *anti* 1-substituted 2-chlorobut-3-en-1-ols, respectively. These are transformed into *cis* and *trans* 1-substituted 2-vinyl epoxides.

Barbier-type carbonyl allylations by (*E*)-γ-substituted allylic metal reagents, derived from (*E*)-γ-substituted allylic halides with metals or metal halides, usually add *anti*-diastereoselectively at the γ-position of the allylic metal reagents to aldehydes; γ-*anti*-selective carbonyl allylation.[1] γ-*syn*-Selection is difficult for the Barbier-type carbonyl allylations by (*E*)-γ-substituted allylic metal reagents. We have found that halogens on the tin of but-2-enyltin reagents, prepared from (*E*)-rich 1-bromobut-2-ene and tin(II) halides, affect the diastereoselectivity in the γ-regioselective carbonyl allylation in THF–H_2O at room temperature; *anti*-selection with tin(II) chloride and *syn*-selection with tin(II) iodide–tetrabutylammonium bromide (or iodide).[2] We thus hoped that palladium-catalysed carbonyl allylation[3] by (*E*)-rich 3-chloroprop-2-enyltin reagents, derived from (*E*)- and (*Z*)-mixed 1,3-dichloropropene (**1**)† with $SnCl_2$ or SnI_2–Bu_4NI *via* the formation of 1-chloro-*syn*-π-allylpalladium complex, could lead to halogen-coordination controlled diastereoselectivity to produce diastereo-defined 1-substituted 2-chlorobut-3-en-1-ols, which could be transformed into the corresponding 1-substituted 2-vinyl epoxides (Scheme 1).[5]

Diastereoselectivity in the allylation of benzaldehyde by (*E*)- and (*Z*)-mixed 1,3-dichloropropene (**1**) in 1,3-dimethylimidazolidin-2-one (DMI)–H_2O‡ was investigated with tin(II) halides (SnX_2) and tetrabutylammonium halides (TBAX′). To a solution of SnX_2 (2.0 mmol) and TBAX′ (2.0 mmol) in DMI (3 ml)–H_2O (0.1 ml) in the presence or absence of a catalytic amount of $PdCl_2(PhCN)_2$ (0.02 mmol) was added **1** (2.0 mmol), and the solution was stirred at room temperature for 24 h. Benzaldehyde (1.0 mmol) was added to the solution, which was then stirred at room temperature. After the usual work-up, 2-chloro-1-phenylbut-3-en-1-ol (**2**, R=Ph) was obtained. The results are summarized in Table 1. The palladium-catalysed carbonyl allylation with $SnCl_2$ in DMI without H_2O led to usual *anti*-selectivity.[3] For addition of TBAX′, the carbonyl allylation with $SnBr_2$ or SnI_2 proceeded without any palladium catalyst. Use of either iodide (SnI_2 or TBAI) enhanced both the yield and the *syn*-selectivity. Addition of a catalytic amount of

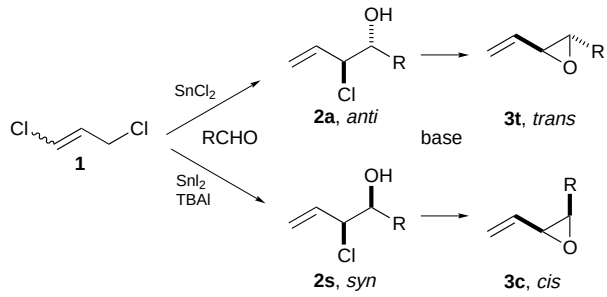

Scheme 1

Table 1 Allylation of benzaldehyde by 1,3-dichloropropene (**1**)

X	X′	*t*/h	Yield[a] of **2** (R = Ph) (%)	**2s**:**2a**[b]
Cl[c]	[d]	24	88	41:59
Cl[e]	[d]	65	70	22:78
Br	Br	130	22	46:54
Br	I	125	87	85:15
I	Br	121	66	90:10
I	I	122	63	92:8
I[c]	I	70	65	91:9
I[c]	I[f]	71	65	92:8

[a] Isolated yields. [b] The ratio was determined by ^1H NMR spectroscopy (JEOL GX-270).§ [c] $PdCl_2(PhCN)_2$ as a catalyst was added. [d] No TBAX′ was used. [e] The reaction was carried out without H_2O at 0 °C. [f] TBAI (0.2 mmol) and NaI (2.0 mmol) were used.

$PdCl_2(PhCN)_2$ accelerated the carbonyl allylation with SnI_2 and TBAI without lowering the *syn*-selectivity. The reaction with NaI accompanied by a catalytic amount of TBAI exhibited the same reactivity and selectivity as those of the reaction with an equimolar amount of TBAI to **1**.

Either *syn*- or *anti*-selective palladium-catalysed allylations of various aldehydes by **1** were carried out with SnI_2–TBAI–

Table 2 Diastereoselective carbonyl allylation by **1**[a]

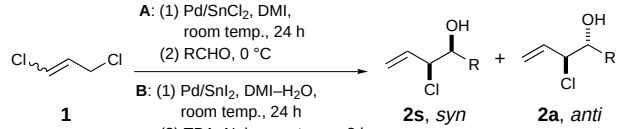

1 **2s**, *syn* **2a**, *anti*

R	Method	*t*/h	Yield[b] of **2** (%)	**2s**:**2a**[c]
4-ClC_6H_4	A	70	74	14:86
4-ClC_6H_4	B	71	80	93:7
4-NCC_6H_4	A	71	71	15:85
4-NCC_6H_4	B	68	72	91:9
4-$H_3CC_6H_4$	A	62	58	20:80
4-$H_3CC_6H_4$	B	72	49	91:9
3,4-$(CH_2O_2)C_6H_3$	A	78	56	24:76
3,4-$(CH_2O_2)C_6H_3$	B	97	24	93:7
(*E*)-$C_6H_5CH{=}CH$	A	72	78	15:85[a]
(*E*)-$C_6H_5CH{=}CH$	B	96	53	77:23[d]
$C_6H_5CH_2CH_2$	A	71	58	32:68
$C_6H_5CH_2CH_2$	B	96	64	76:24
$CH_3(CH_2)_5$	A	93	48	36:64
$CH_3(CH_2)_5$	B	95	48	84:16
$CH_2{=}CH(CH_2)_8$	A	70	62	26:74
$CH_2{=}CH(CH_2)_8$	B	94	63	78:22

[a] The allylation of aldehydes (1.0 mmol) by **1** (2.0 mmol) was carried out with $PdCl_2(PhCN)_2$ (0.02 mmol), SnX_2 (2.0 mmol), TBAI (0.2 mmol) and NaI (2.0 mmol) in DMI (3 ml) and H_2O (0.1 ml). [b] Isolated yields. [c] The ratio was determined by ^1H NMR spectroscopy (JEOL GX-270).§ [d] The ratios (*cis*:*trans*) refer to the corresponding vinyl epoxides.

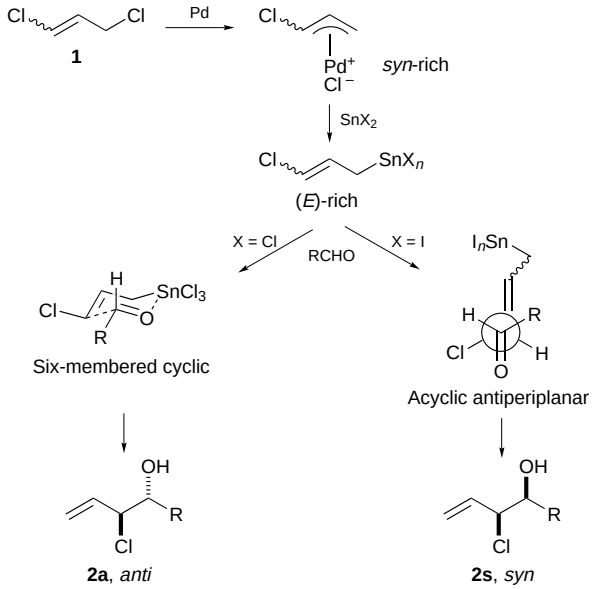

Scheme 2 Plausible mechanism in either γ-*syn*- or γ-*anti*-selective palladium-catalysed carbonyl allylation by mixed (*E*)- and (*Z*)-1,3-dichloropropene (**1**)

NaI and $SnCl_2$ in DMI–H_2O and DMI, respectively, as shown in Table 2. Any aldehyde, such as aromatic aldehydes bearing either an electron-donating group or an electron-withdrawing group, α,β-unsaturated aldehydes, and aliphatic aldehydes, can be used for the diastereo-defined carbonyl allylation. 1-Substituted 2-chlorobut-3-en-1-ols **2**, which are chlorohydrins, were transformed into the corresponding 1-substituted 2-vinyl epoxides **3** with aqueous $NaHCO_3$–THF solution in 70–90% yields [reaction (1)]. The *cis : trans* ratios of **3** were similar to the *syn : anti* ratios of **2**.§

The *anti*-selection with $SnCl_2$ probably occurs *via* the usual six-membered cyclic transition states (coordination) between (*E*)-rich 3-chloroprop-2-enyltrichlorotin, derived from *syn*-rich 1-chloro-π-allylpalladium chloride and tin(II) chloride, and aldehydes.[1] The coordination suggests high Lewis acidity of tin

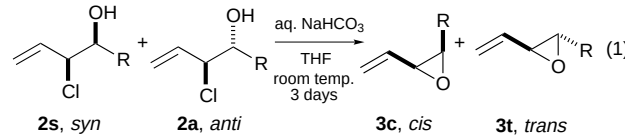

in (*E*)-3-chloroprop-2-enyltrichlorotin, as shown in Scheme 2. However, *syn*-selectivity with SnI_2–TBAI (–NaI) probably occurs *via* acyclic antiperiplanar transition states between pentacoordinate 3-chloroprop-2-enyltetraiodotin, in which the tin has no Lewis acidity, and aldehydes.[2] The *syn*-selection *via* the acyclic antiperiplanar transition state is independent of the olefinic geometry of 3-chloroprop-2-enyltin intermediate, in contrast to the *anti*-selection *via* the six-membered cyclic transition state.[1] Thus the *syn*-selectivity with SnI_2–TBAI is probably superior to the *anti*-selectivity with $SnCl_2$.

Notes and References

* E-mail: y-masuya@hoffman.cc.sophia.ac.jp

† 1,3-Dichloropropene (**1**, $E:Z$ = 48 : 52) was purchased from Tokyo Chemical Industry Co.

‡ DMI–H_2O is a most effective solvent in *syn*-selective carbonyl allylation by 1-chlorobut-2-ene with SnI_2–TBAI.

§ The *syn* (**2s**) and *anti* (**2a**) structures were determined by the ratios and structures of the *cis*- (**3c**) and *trans*-epoxides (**3t**). The *cis* (**3c**) and *trans* (**3t**) structures of the epoxides were determined from the coupling constants of vicinal protons of the epoxides in ^{1}H NMR spectra (JEOL GX-270); J_{cis} = 4.27–4.28 and J_{trans} = 2.03–2.45 Hz.[5]

1 For a review, see: Y. Yamamoto and N. Asao, *Chem. Rev.*, 1993, **93**, 2207.
2 Y. Masuyama, M. Kishida and Y. Kurusu, *Tetrahedron Lett.*, 1996, **37**, 7103.
3 For palladium-catalysed carbonyl allylation, see: Y. Masuyama, *J. Synth. Org. Chem. Jpn.*, 1992, **50**, 202; Y. Masuyama, in *Advances in Metal-Organic Chemistry*, ed. L. S. Liebeskind, JAI Press, Greenwich, 1994, vol. 3, p. 255.
4 For carbonyl allylation by (*Z*)-rich 1-chloro-3-iodoprop-1-ene with tin(II) chloride, see: J. Auge and S. David, *Tetrahedron Lett.*, 1983, **24**, 4009.
5 S. Hu, S. Jayaraman and A. C. Oehlschlager, *J. Org. Chem.*, 1996, **61**, 7513 and references cited therein.

Received in Cambridge, UK, 3rd November 1997; 7/07865J

Sulfonic acid functionalised ordered mesoporous materials as catalysts for condensation and esterification reactions

Wim M. Van Rhijn,* Dirk E. De Vos, Bert F. Sels, Wim D. Bossaert and Pierre A. Jacobs

Centre for Surface Science and Catalysis, KU Leuven, Kard. Mercierlaan 92, B-3001 Heverlee, Belgium

Mesoporous silicas were functionalised with sulfonic acid groups; the resulting materials are excellent catalysts for formation of bisfurylalkanes and polyol esters.

The discovery of mesoporous materials has raised the general expectation that the catalytic efficiency of microporous zeolites can be expanded to mesoporous dimensions.[1] It is necessary to introduce functionality into MCM or HMS structures, so surface modification techniques are enjoying a renewed interest, and it is clear that the pore walls of mesoporous materials are easily modified with either purely inorganic or with hybrid, semi-organic functional groups.[2,3] Reports on Ti–MCM-41 prove that this oxidation catalyst can indeed handle voluminous substrates such as alkylated phenols.[4] We recently illustrated the potential of a guanidine-functionalised MCM-41 in base-catalysed condensations.[5] Progress in acid catalysis is lagging behind, largely because of the low acid strength of Al-substituted mesoporous silicas such as Al–MCM-41.[6] As an alternative, we now propose the covalent attachment of alkylsulfonic acid groups to the surface of MCM and HMS molecular sieves, *via* secondary synthesis as well as *via* direct one-step synthesis. The resulting MCM–SO_3H and HMS–SO_3H materials perform well in typical strong-acid catalysed reactions. The hydrophobic nature of the active sites' environment can be exploited to perform reactions which are outside the reach of other inorganic solid acid catalysts.

The key precursor in the synthesis of alkylsulfonic acid functionalised mesoporous materials is 3-mercaptopropyltrimethoxysilane (MPTS). This molecule contains an SH group, a stable propyl spacer and a hydrolisable $Si(OMe)_3$ moiety. Hybrid mesoporous silicas were prepared either *via* silylation of preformed mesoporous silica, or *via* co-condensation of the primary building blocks.† First, MPTS and $Si(OEt)_4$ were hydrolysed together in the presence of an ionic or a non-ionic surfactant (*viz.* $C_{16}NMe_3Br$ and *n*-C_{12}-amine), leading to MCM or HMS type materials, respectively (Scheme 1, route 1). Alternatively, secondary modification comprised the silylation of a vacuum-dried pre-existing MCM support with MPTS in dry toluene, or the coating of a partially hydrated support with an MPTS layer (Scheme 1, routes 2*a* and *b*).[3] Both primary and secondary syntheses lead to materials functionalised with largely intact SH groups, as is evidenced by an IR ν_{S-H} vibration of medium intensity at 2575 cm^{-1}, and by the solid state ^{13}C NMR shifts [δ 11 (C_3), 27 (C_1, C_2)]. The MeO groups of the liquid MPTS spectrum are absent, while the CH_2(–Si) is slightly shifted downfield (from δ 8 to 11). These SH groups are easily converted into sulfonic acid groups by mild oxidation with neutralised H_2O_2, acidification and finally, thorough washing to remove all liquid acid. In view of the high loading of the material with functional groups, it is not surprising that some disulfide is observed in the final product (δ 41, 23). However, the major signals are observed at δ 54, 18 and 11. These are consistent with those calculated for *e.g.* propanesulfonic acid and give strong proof for the prevalence of $(CH_2)_3SO_3H$ surface groups.

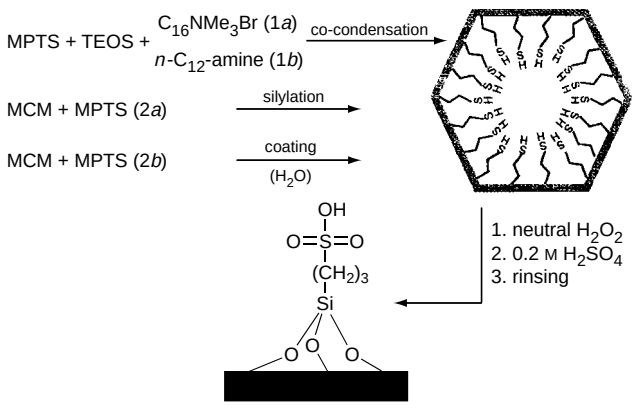

Scheme 1

In ambient conditions, the water affinity of the material is remarkably low, as proved by thermogravimetric analysis (less than 1 wt% H_2O) and by the weakness of the IR δ_{OH} vibration (1638 cm^{-1}). Typical loadings, as measured by thermogravimetry or *via* titration of the SO_3H groups, vary between 1.0 and 1.5 mequiv. g^{-1}. Sorption characteristics depend strongly on the preparation method. For instance, an MCM–SH material prepared *via* silylation (route 2*a*) displays a BET surface of 740 $m^2\ g^{-1}$ and a pore volume of 0.51 ml g^{-1} with a radius between 2 and 4 nm (from the Kelvin equation and the BJH method). These data evidence the mesoporous nature of the material, even if the specific surface and mesoporous volume are somewhat lower than for a typical MCM-41. However, coating of the material with an MPTS layer (route 2*b*) leads to a reduction of BET surface (510 $m^2\ g^{-1}$), average pore radius (< 2 nm) and pore volume (0.25 ml g^{-1}), as determined from T-plot analysis). Oxidation of the latter material to its sulfonic acid form leads to further minor changes of BET (399 $m^2\ g^{-1}$) and pore volume (0.19 ml g^{-1}). Isolated silanol groups, which reportedly absorb at 3740 cm^{-1},[7] were not detected in the IR spectra of MCM–SO_3H upon evacuation at 373 or 473 K. The absorption between 3500 and 2700 cm^{-1} may rather be assigned to hydrogen-bonded SO_3H groups. Summarising, the catalyst design leads to a hydrophobic mesoporous material, with uniform and well-characterized SO_3H groups.

The catalytic properties of the new materials were first tested in the synthesis of 2,2-bis(5-methylfuryl)propane (DMP). Bisfurylalkanes are relevant intermediates for macromolecular chemistry.[8] DMP is produced from 2-methylfuran (MF) and acetone in a strong acid catalysed condensation [reaction (1)].

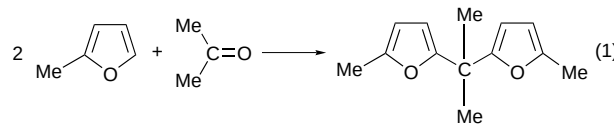

Zeolites may seem accomplished catalysts for such reactions. However, exposure of zeolites such as H-β or H-US-Y to furans leads to immediate formation of tarry oligomeric products, even for the substituted compounds such as MF.[9] Addition of acetone

Table 1 Solvent-free reaction of MF (1.8 g) with acetone (3.2 g) (molar ratio = 1 : 2.5) in the presence of 0.18 g acid catalyst (323 K, 24 h)

Entry	Catalyst	Conversion (%)[a]	Selectivity (%)[b]
1	—	0	—
2	H-β[c]	61	74
3	H-US-Y[d]	55	67
4	Al–MCM-41	5	95
5	MCM–SO_3H (coated)[e]	85	96
6	HMS–SO_3H (co-cond.; 10%)[f]	61	94
7	HMS–SO_3H (co-cond.; 20%)[g]	73	95
8	MCM–SO_3H (co-cond.; 20%)[g]	52	87
9	MCM–SO_3H (silylated)[c]	57	92

[a] Conversion of MF. [b] Selectivity for DMP, based on MF. [c] Si : Al = 12.5 (PQ). [d] Si : Al = 22.5. [e] Prepared *via* secondary modification with MPTS.† [f] Prepared *via* co-condensation of MPTS and TEOS (10 : 90). [g] As in *f*, with MPTS : TEOS = 20 : 80.

partially suppresses MF oligomerisation. As a result, catalyst deactivation is fast, and DMP selectivities are limited even at moderate conversions (Table 1, entries 2, 3). Moreover, the strong adsorption of DMP or other reaction intermediates in the relatively narrow zeolite pores leads to detectable secondary condensation products, which desorb with even greater difficulty than DMP itself. Such observations have led previous workers to use elevated catalyst concentrations;[10] in our reaction conditions, the side-reactions impose an upper limit of 45% on the overall DMP yield. While the DMP selectivity is better on Al–MCM-41, the low acid strength causes an unsatisfactory MF conversion. In contrast, the sulfonic acid MCMs combine a remarkable DMP selectivity (often up to 95%) with elevated MF conversions (entries 5–9). Apparently the hydrophobic surface prevents a too strong MF adsorption and oligomerisation, while the larger dimension of the pores facilitates product desorption. The highest DMP yield on MF basis, a remarkable 82%, is obtained with an MCM–SO_3H prepared *via* the surface coating procedure (entry 5). Thus, polarity, rather than the activity, makes the sulfonic MCMs superior to zeolites for this particularly demanding reaction.

Another application of the new materials may be found in polyol esterification. These reactions produce valuable products such as emulsifiers, detergents or low-calorific fats. The use of (preferably heterogeneous) catalysts may allow lower reaction temperatures, but the intrinsic immiscibility of the polyol and fatty acid phases is a major problem. Thus, in the esterification of *e.g.* D-sorbitol with lauric acid, zeolites such as H-β reside exclusively in the polyol layer. The only reaction is sorbitol degradation, and the fatty acid conversion is zero even after prolonged reaction times (Table 2, entry 2). In contrast, the much more hydrophobic MCM–SO_3H readily effects formation of a small amount of monoacylated products, and because of the detergency of the latter, homogenisation of the reaction medium. Main products are monolauroylisosorbide, which is an important detergent precursor,[11] or in a later stage, the isosorbide diester (entry 3).

In conclusion, sulfonic acid functionalised MCM or HMS materials are new and worthwhile materials for reactions in which zeolites fail.

This work is sponsored within a IUAP program of the Belgian Federal Government. W. V. R. and B. S. acknowledge IWT and D.D.V. FWO for fellowships. We thank B. Wouters for recording NMR spectra.

Table 2 Esterification of D-sorbitol (3.64 g) with lauric acid (24.0 g) (molar ratio = 1 : 6) catalysed by an acid zeolite or by a mesoporous sulfonic acid catalyst (0.36 g) (385 K, 24 h)[a]

Entry	Catalyst	Lauric acid conversion (%)	Product selectivity (%)[b]
1	—	0	—
2	H-β[c]	0	—
3	MCM–SO_3H (co-cond.; 20%)[d]	33	> 95

[a] Analysis with size-exclusion HPLC, ^1H–^{13}C NMR and COSY. [b] Selectivity, based on lauric acid, for dilaurylisosorbide. [c] Si : Al = 12.5 (PQ). [d] Prepared *via* co-condensation of MPTS and TEOS (20 : 80).

Notes and References

* E-mail: wim.vanrhijn@agr.kuleuven.ac.be

† Preparation of MCM–SO_3H and HMS–SO_3H *via* co-condensation (Scheme 1, route 1): MCM-41 type materials were synthesized from a mixture of MPTS (20 mol%) and $Si(OEt)_4$ (TEOS, 80 mol%). The molar gel composition was 0.12 $C_{16}NMe_3Br$: 0.5 NaOH : 1.0 total siloxane : 130H_2O (24 h, 293 K). An acid solvent extraction technique was used to remove the ionic surfactant. Mercaptopropyl-modified HMS was obtained from the following gel composition: 0.9 (or 0.8) TEOS : 0.1 (or 0.2) MPTS : 0.275 *n*-C_{12}-amine : 8.9 EtOH : 29.4 H_2O (24 h, 293 K). *n*-C_{12}-Amine was extracted with boiling EtOH (12 h, 3 times).

Silylation (Scheme 1, route 2*a*) was performed on a calcined and evacuated (393 K) MCM-41 (synthesised from Ludox), using excess MPTS in dry toluene (4 h, reflux), followed by Soxhlet extraction with Et_2O and CH_2Cl_2. For coating with an MPTS layer (route 2*b*), the MCM was refluxed in water (3 h), filtered and suspended in toluene. Part of the water was removed in an azeotropic distillation with a Dean–Stark trap. Further preparation followed route 2*a*.

Mercaptopropyl groups were oxidised with a three-fold excess of neutralised H_2O_2. After washing with H_2O and EtOH, and acidification in 0.2 M H_2SO_4, the powder was rinsed thoroughly with distilled H_2O and dried at 333 K.

1 J. S. Beck, J. C. Vartuli, W. J. Roth, M. E. Leonowicz, C. T. Kresge, K. D. Schmitt, C. T. Chu, D. H. Olson, E. W. Sheppard, S. B. McCullen, J. B. Higgins and Schlenker, *J. Am. Chem. Soc.*, 1992, **114**, 10 834; C. T. Kresge, M. E. Leonowicz, W. J. Roth, J. C. Vartuli and J. S. Beck, *Nature*, 1992, **359**, 710; P. T. Tanev and T. J. Pinnavaia, *Science*, 1995, **267**, 865; X. S. Zhao, G. Q. Lu and G. J. Millar, *Ind. Eng. Chem. Res.*, 1996, **35**, 2075.
2 S. L. Burkett, S. D. Sims and S. Mann, *Chem. Commun.*, 1996, 1367; D. J. Macquarrie, *Chem. Commun.*, 1996, 1961.
3 X. Feng, G. E. Fryxell, L.-Q. Wang, A. Y. Kim, J. Liu and K. M. Kemner, *Science*, 1997, **276**, 923; L. Mercier and T. J. Pinnavaia, *Adv. Mater.*, 1997, **9**, 500.
4 T. Maschmeyer, F. Rey, G. Sankar and J. M. Thomas, *Nature*, 1995, **378**, 159; P. T. Tanev, M. Chibwe and T. J. Pinnavaia, *Nature*, 1994, **368**, 321.
5 A. Cauvel, G. Renard and D. Brunel, *J. Org. Chem.*, 1997, **62**, 749; Y. V. S. Rao, D. E. De Vos and P. A. Jacobs, *Angew. Chem.*, 1997, in the press.
6 E. Armengol, M. L. Cano, A. Corma, H. Garcia and M. T. Navarro, *J. Chem. Soc., Chem. Commun.*, 1995, 519.
7 X. S. Zhao, G. Q. Lu, A. K. Whittaker, G. J. Millar and H. Y. Zhu, *J. Phys. Chem.*, 1997, **101**, 6525.
8 J. E. Hall, USP 4 429 090, 1984; A. Gandini, EPA 0 379 250, 1990.
9 A. Gandini and M. N. Belgacem, *Prog. Polym. Sci.*, 1997, in the press.
10 F. Algarra, A. Corma, H. Garcia and J. Primo, *Appl. Catal. A*, 1995, **128**, 119.
11 Y. Saheki, K. Negoro and T. Sasaki, *J. Am. Oil Chem. Soc.*, 1986, **63**, 927.

Received in Cambridge, UK, 16th October 1997; 7/07462J

Preparation and structure of *cis*-[Pt(BF$_2$)$_2$(PPh$_3$)$_2$]: the first crystallographically characterised complex containing the BF$_2$ ligand

Aidan Kerr,[a] Todd B. Marder,[b] Nicholas C. Norman,*[a] A. Guy Orpen,[a] Michael J. Quayle,[a] Craig R. Rice,[a] Peter L. Timms[a] and George R. Whittell[a]

[a] *The University of Bristol, School of Chemistry, Cantock's Close, Bristol, UK BS8 1TS*
[b] *The University of Durham, Department of Chemistry, Science Laboratories, South Road, Durham, UK DH1 3LE*

The platinum compound [Pt(PPh$_3$)$_2$(η-C$_2$H$_4$)] reacts with B$_2$F$_4$ affording the BF$_2$ complex *cis*-[Pt(BF$_2$)$_2$(PPh$_3$)$_2$] which is characterised by multinuclear NMR studies and X-ray crystallography.

A key step in many transition metal catalysed diboration reactions is oxidative addition of the B–B bond of a diborane(4) compound (R$_2$B–BR$_2$) to a low-valent transition metal centre affording a metal bis-boryl complex of the form L$_n$M(BR$_2$)$_2$.[1] Amongst the many studies which have been carried out,[1] one of the more thoroughly examined reactions, particularly in terms of this B–B bond oxidative addition step, has been the platinum catalysed diboration of alkynes described recently by the groups of Miyaura and Suzuki,[2] Smith[3] and Marder and Norman.[4] These and other studies[5,6] have resulted in a number of crystallographically characterised platinum bis-boryl species of the type *cis*-[Pt(BR$_2$)$_2$(PR′$_3$)$_2$]. In seeking to further explore the oxidative addition of B–B bonds to Pt^0, we examined the reaction between [Pt(PPh$_3$)$_2$(η-C$_2$H$_4$)] and diboron tetrafluoride, B$_2$F$_4$, and report herein the preparation and structural characterisation of the complex *cis*-[Pt(BF$_2$)$_2$(PPh$_3$)$_2$], the first example of a compound containing the BF$_2$ ligand.

The reaction between [Pt(PPh$_3$)$_2$(η-C$_2$H$_4$)][7] and a slight excess of B$_2$F$_4$[8] in toluene solution afforded, after work-up,† pale yellow crystals of the complex *cis*-[Pt(BF$_2$)$_2$(PPh$_3$)$_2$] **1**. The formula of **1** was evident from multinuclear NMR data‡ and the structure was confirmed by X-ray crystallography§ the results of which are shown in Fig. 1. The Pt centre in **1** adopts the expected square-planar coordination geometry (maximum atom deviation from the PtP$_2$B$_2$ mean plane is 0.025 Å) with the BF$_2$ groups in a *cis* configuration. Metric parameters of note are the Pt–B bond distances [Pt–B(1) 2.058(6) and Pt–B(2) 2.052(6) Å] together with the B–Pt–B [78.2(3)°] and P–Pt–P angles [99.4(1)°]. These values fall in or close to the range observed for other structurally characterised platinum(II) *cis* bis-boryl compounds[2–6] in which the boron atoms carry oxygen or sulfur substituents (Pt–B distances, B–Pt–B angles and non-chelate P–Pt–P anlges are in the range 2.03–2.076 Å, 73.0–81.0 and 100.38–107.14°, respectively).¶ There is no decisive crystallographic evidence for platinum-to-boron π-back-bonding in **1**.

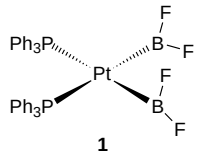

1

In **1**, the angles defined by the boron ligand planes and the mean platinum square plane are 81.1 and 87.4° for B(1) and B(2), respectively, therefore showing that the boryl ligands are essentially orthogonal to the platinum square plane [as observed for most platinum(II) *cis* bis-boryl complexes[2–6,9]]. Whether or not an electronic origin exists for the acute B–Pt–B angles (and large P–Pt–P angles) and/or the orientations of the boryl ligands is unclear at present, although we note that recent theoretical studies on model (PH$_3$)$_2$ platinum(II) *cis* bis-boryl complexes do reproduce the experimentally observed geometries.[10] Further insight into this matter, including the extent of any platinum-to-boron π-back-bonding, will have to await a more detailed theoretical analysis. The B···B distance in **1** [2.591(9) Å] is also typical (*cf.* the range 2.514–2.667 Å for the complexes described in refs. 2–6); for comparison and the B–B bond distance in crystalline B$_2$F$_4$ is 1.67 Å.[11]

It is noteworthy that **1** is isoelectronic with the product of double oxidation of the η^2-alkene complex [Pt(PPh$_3$)$_2$(η-C$_2$F$_4$)] {whose arsine analogue, [Pt(AsPh$_3$)$_2$(η-C$_2$F$_4$)],[12] has been structurally characterised; C–C 1.447(18) Å} implying that such a complex would be a bis-carbene species, [Pt(PPh$_3$)$_2$(CF$_2$)$_2$]$^{2+}$, with a significantly longer, non-bonding C···C interaction. The electronic requirements for this kind of alkene cleavage (as studied by Lappert and others; see ref. 13 and references therein) or its reverse, carbene coupling, have been examined by Hoffmann and coworkers.[13]

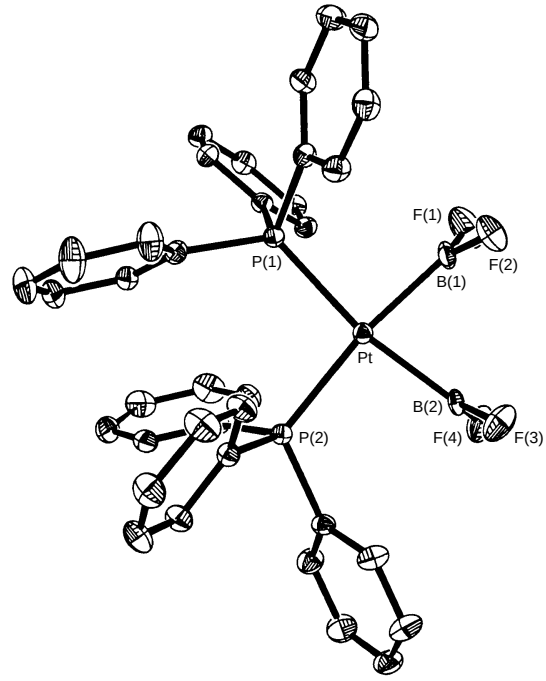

Fig. 1 A view of the molecular structure of **1** with key atoms labelled. Hydrogen atoms are omitted for clarity. Ellipsoids are drawn at the 50% level. Selected bond lengths (Å) and angles (°): Pt–B(1) 2.058(6), Pt–B(2) 2.052(6), B(1)–F(1) 1.324(7), B(1)–F(2) 1.342(7), B(2)–F(3) 1.327(6), B(2)–F(4) 1.330(7); B(1)–Pt–B(2) 78.2(3), P(1)–Pt–P(2) 99.35(5), F(1)–B(1)–F(2) 110.6(5), Pt–B(1)–F(1) 124.6(5), Pt–B(1)–F(2) 124.7(4), F(3)–B(2)–F(4) 110.8(5), Pt–B(2)–F(3) 125.7(4), Pt–B(2)–F(4) 123.5(4).

To the best of our knowledge, there are no previous reports of metal–BF_2 complexes although we note that a number of BCl_2 (and some BBr_2 and BI_2) complexes have been described, but not structurally characterised, by Nöth and coworkers.[14] Further studies are in progress to examine the reactivity of B_2F_4 towards a range of transition metal compounds with a view to preparing further examples of complexes containing BF_2 ligands; we have recently structurally characterised the complex *cis*-[$Pt(BF_2)_2$(dppb)] [dppb = 1,2-bis(diphenylphosphino)butane] full details of which will be described in a future full paper.[15]

T. B. M. thanks NSERC of Canada, N. C. N. thanks the EPSRC, Lapore plc and The Royal Society and A. G. O. thanks EPSRC for research support and a studentship (M. J. Q.). T. B. M. and N. C. N. also thank NSERC and The Royal Society for supporting this collaboration *via* a series of Bilateral Exchange Awards. Johnson Matthey Ltd. are thanked for generous supplies of platinum salts. We also thank one of the referees for helpful comments concerning the crystallographic aspects of this paper.

Notes and References

* E-mail: N.C.Norman@bristol.ac.uk

† A sample of [$Pt(PPh_3)_2(\eta$-$C_2H_4)$] (0.080 g, 0.011 mmol) was dissolved in toluene (5 cm^3) in a Young's tap tube after which the reaction flask was cooled in a liquid-nitrogen Dewar. A sample of B_2F_4 (*ca*. 0.03 mmol) was then condensed into the Young's tap tube and the contents allowed to warm to room temp. with stirring once the solvent had melted. A white precipitate formed at *ca*. −50 °C and once at room temp., stirring was continued for 30 min. After this time, the solvent volume was reduced slightly by vacuum and the reaction flask sealed under dinitrogen and cooled to −30 °C for *ca*. 24 h. The mother liquor was then removed by syringe and the remaining white solid dried under vacuum. Dissolution of this solid in CH_2Cl_2 (2 cm^3) afforded a cloudy pale yellow solution which was filtered affording a yellow filtrate to which a toluene overlayer (5 cm^3) was added. Solvent diffusion over a period of 7 days at −30 °C afforded pale yellow crystals of **1** (0.086 g, 97%) one of which was used for X-ray crystallography.

‡ *Spectroscopic data* for **1** (CD_2Cl_2): $^{31}P\{^1H\}$ NMR δ 24.3 (br t, $^1J_{PtP}$ 1607 Hz); $^{11}B\{^1H\}$ NMR δ 42.3; ^{19}F NMR δ −17.8 (br t, $^2J_{PtF}$ 1032 Hz); $^{13}C\{^1H\}$ NMR δ 134.4 (d, *o*-PPh_3, J_{PC} 12 Hz), 130.8 (s, *p*-PPh_3), 128.8 (d, *m*-PPh_3, J_{PC} 11 Hz), *ipso*-carbon not observed; ^1H NMR δ 7.32 (m, 18 H, PPh_3), 7.21 (m, 12 H, PPh_3). ^{31}P, ^{11}B and ^{19}F spectra were referenced to 85% H_3PO_4, $BF_3{\cdot}Et_2O$ and $BF_3{\cdot}Et_2O$ respectively. $C_{36}H_{30}B_2F_4P_2Pt$ requires C, 52.90; H, 3.70. Found C, 54.60; H, 3.90%. Mass spectrum (FAB), *m/z* 713 $[Pt(PPh_3)_2]^+$.

§ *Crystal data* for [$Pt(PPh_3)_2(BF_2)_2$]·0.5PhMe (**1**·0.5 PhMe): $C_{39.5}H_{34}B_2F_4P_2Pt$, M = 863.32, monoclinic, space group $P2_1/c$ (no. 14), a = 18.211(4), b = 9.5963(15), c = 20.422(3) Å, β = 90.617(14)°, U = 3568.7(11) Å^3, Z = 4, D_c = 1.607 Mg m^{-3}, λ = 0.71073 Å, μ = 4.070 mm^{-1}, F(000) = 1700, T = 173(2) K. Data were collected on a Siemens SMART diffractometer for 1.99 < θ < 27.57°. The structure was solved by direct methods and refined by least-squares methods against all 8156 F^2 values with $F^2 > -3\sigma(F^2)$ to wR_2 = 0.0701 [R_1 = 0.0373 for 5825 data with $F^2 > 2\sigma(F^2)$]. Other crystals inspected (which were isostructural with **1**) showed signs of compositional disorder consistent with partial hydrolysis having occurred during recrystallisation leading to replacement of some BF_2 ligands by some $B(OH)_2$ or B(OH)F. CCDC 182/713.

¶ A preliminary presentation of the structure of the complex [$Pt(PPh_3)_2\{B(OMe)_2\}_2$] reports Pt–B distances of 2.098(4) and 2.100(4) Å and B–Pt–B and P–Pt–P angles of 72.9(2) and 107.69(3)° respectively.[9]

1 M. J. G. Lesley, T. B. Marder, N. C. Norman, C. R. Rice, E. G. Robins, W. R. Roper and G. R. Whittell, manuscript in preparation.
2 T. Ishiyama, N. Matsuda, N. Miyaura and A. Suzuki, *J. Am. Chem. Soc.*, 1993, **115**, 11 018; F. Ozaura, A. Suzuki and N. Miyaura, *Organometallics*, 1996, **15**, 713.
3 C. N. Iverson and M. R. Smith, *J. Am. Chem. Soc.*, 1995, **117**, 4403; C. N. Iverson and M. R. Smith, *Organometallics*, 1996, **15**, 5155.
4 M. J. G. Lesley, P. Nguyen, N. J. Taylor, T. B. Marder, A. J. Scott, W. Clegg and N. C. Norman, *Organometallics*, 1996, **15**, 5137.
5 W. Clegg, F. J. Lawlor, G. Lesley, T. B. Marder, N. C. Norman, A. G. Orpen, M. J. Quayle, C. R. Rice, A. J. Scott and F. E. S. Souza, *J. Organomet. Chem.*, in press.
6 T. R. F. Johann, T. B. Marder, A. G. Orpen, T. M. Peakman, A. J. Scott, W. Clegg, N. C. Norman, M. J. Quayle and C. R. Rice, manuscript in preparation.
7 M. Camalli, F. Caruso, S. Chaloupka, E. M. Leber, H. Rimml and L. M. Venanzi, *Helv. Chim. Acta*, 1990, **73**, 2263.
8 P. L. Timms, *J. Am. Chem. Soc.*, 1967, **89**, 1629.
9 H. Nöth, IMEBORON Conference Abstracts, Heidelberg, 1996.
10 S. Sakaki and T. Kikuno, *Inorg. Chem.*, 1997, **36**, 226; Q. Cui, D. G. Musaev and K. Morokuma, *Organometallics*, 1997, **16**, 1355.
11 L. Trefonas and W. N. Lipscomb, *J. Chem. Phys.*, 1958, **28**, 54.
12 D. R. Russell and P. A. Tucker, *J. Chem. Soc., Dalton Trans.*, 1975, 1752.
13 C. N. Wilker, R. Hoffmann and O. Eisenstein, *Nouv. J. Chim.*, 1983, **7**, 535.
14 G. Schmid and H. Nöth, *J. Organomet. Chem.*, 1967, **7**, 129; G. Schmid, W. Petz, W. Arloth and H. Nöth, *Angew. Chem., Int. Ed. Engl.*, 1967, **6**, 696.
15 N. Lu, N. C. Norman, A. G. Orpen, M. J. Quayle, P. L. Timms and G. R. Whittell, unpublished work.

Received in Cambridge, UK, 9th October 1997; 7/07296A

Phase transition of ZnS nanocrystallites induced by surface modification at ambient temperature and pressure confirmed by electron diffraction

Kei Murakoshi,[a] Hiroji Hosokawa,[a] Naoko Tanaka,[a] Miwa Saito,[a] Yuji Wada,[a] Takao Sakata,[b] Hirotaro Mori[b] and Shozo Yanagida*[a]

[a] *Graduate School of Engineering, Osaka University, Suita, Osaka 565, Japan*
[b] *Research Center for Ultra-high Voltage Electron Microscopy, Osaka University, Ibaraki, Osaka 567, Japan*

Pentafluorothiophenol, thiophenol, 1-decanethiol, 1-hexanethiol, benzoic acid and cyanoacetic acid, which are confirmed to bind to the surface of ZnS nanocrystallites, induce phase transition of ZnS nanocrystallites from the hexagonal to the cubic phase, with retention of the crystalline size of 3 nm at ambient temperature and pressure.

The crystalline structure of quantum-confined semiconductor nanocrystallites is one of the important factors for determining their photophysical properties.[1] Generally, the difference in the crystalline structure of the solid leads to considerable change in the effective masses of electrons and holes in their electronic bands.[2] Although it is important to control the crystalline structure of semiconductor nanocrystallites with a definite size, phase transition whilst retaining their size has not been reported at ambient temperature and pressure. There are only a few reports concerning phase transitions at high pressure.[3] Generally, the surface of nanocrystallites plays a dominant role in determining the thermodynamics of the system because of their large surface-to-volume ratios. We recently revealed that coordination of solvent molecules, such as *N*,*N*′-dimethylformamide (DMF), to the surface of CdS[4] or ZnS[5] nanocrystallites also plays a crucial role in stabilizing nanocrystallites. In such systems, the crystalline structure as well as size of the CdS[6] or ZnS[7] nanocrystallites differs with the choice of solvent used for preparation. Here, we report the first control of the crystalline structure of size-controlled nanocrystallites at ambient temperature and pressure by surface modification.

As reported previously,[5] transparent colloidal ZnS nanocrystallites (ZnS–DMF) were prepared by introducing H_2S gas to a DMF solution (5 ml) of $Zn(MeCO_2)_2 \cdot 2H_2O$ (5 mM) with vigorous stirring on an ice bath. After purging ZnS–DMF with N_2 gas for 1.5 h to remove unreacted H_2S, a DMF solution (5 ml) of an organic molecule (2.5 mM), such as thiol, carboxylic acid, or phenol, was added into the 5 ml N_2-purged ZnS–DMF solution ([Zn] = 5 mM) with stirring on an ice bath for 30 min. Normalized absorption spectra of the ZnS–DMF solution after combination with the organic molecules were the same as those before the combination,[5] indicating that dissolution or growth of the ZnS nanocrystallites in DMF is negligibly small (the change of the size should be within a few Å) under the experimental conditions. The resulting transparent solution was placed on a copper grid covered with amorphous carbon, and dried carefully *in vacuo* at room temp. for transmission electron microscopy (TEM) and electron diffraction measurements (Hitachi H-9000, operating at 300 kV) to determine the size and crystalline structure of the resulting ZnS nanocrystallites, respectively. Their size and crystalline structure did not depend upon the choice of the observed areas, and were not changed by the irradiation by the electron beam in the TEM measurements. FTIR spectra of the ZnS powders dried *in vacuo* were obtained on a Perkin Elmer 2000 FTIR spectrophotometer using the KBr method.

Fig. 1 shows typical TEM images and the size distributions of ZnS–DMF and ZnS–DMF combined with C_6F_5SH. TEM observation revealed that both ZnS–DMF and ZnS–DMF combined with C_6F_5SH consisted of nanocrystallites with a mean diameter of *ca.* 3 nm. The size distribution and the mean diameter of the ZnS nanocrystallites (2.9 nm before combination) were not significantly changed after combination with the thiol (2.7 nm after combination). However, there lies a crucial difference in the crystalline structure between ZnS–DMF and ZnS–DMF combined with C_6F_5SH. In the electron diffraction pattern of ZnS–DMF [Fig. 2(*a*)], the apparent diffraction rings assigned to (100), (002), (101), (102), (110) and (103) of the hexagonal ZnS crystallites show that ZnS–DMF has a hexagonal crystalline structure. On the other hand, the diffraction rings assigned to (111), (200), (220) and (311) of cubic ZnS crystallites were observed, while the characteristic ring, (102), which was observed in the hexagonal ZnS crystallites, was not apparent for ZnS–DMF combined with C_6F_5SH [Fig. 2(*b*)]. The observation of the clear difference in the electron diffraction patterns indicates that the hexagonal structure of ZnS–DMF undergoes a phase transition when combined with C_6F_5SH, giving mainly (> 50%) the cubic phase at ambient temperature and pressure.[8]

It is seem that the crystalline structure of the resulting ZnS nanocrystallites depended on the choice of the added molecules (Table 1). All the thiols, *i.e.* pentafluorothiophenol, thiophenol, 1-decanethiol and 1-hexanethiol, induced the phase transition

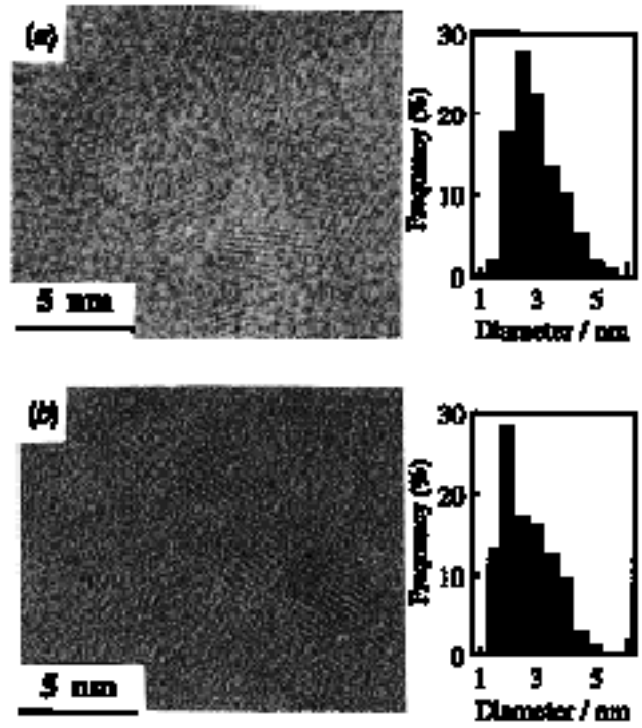

Fig. 1 TEM images and size distributions of (*a*) ZnS–DMF and (*b*) ZnS–DMF combined with C_6F_5SH

from the hexagonal to the cubic phase of the ZnS nanocrystallites without changing the crystallite size (3 nm). Additionally, the addition of carboxylic acid, *e.g.* benzoic acid and cyanoacetic acid, could also induce the phase transition. In contrast, combination with phenol, octanoic acid or acetic acid gave the same hexagonal phase as that of 'as-prepared' ZnS–DMF. The behavior of the phase transition depends on the pK_a value of the carboxylic acids and phenol. The carboxylic acids, *e.g.* benzoic acid (pK_a = 4.19) and cyanoacetic acid (pK_a = 2.45), which have lower pK_a values than acetic acid (pK_a = 4.76), were capable of inducing the phase transition, while neither acetic acid, octanoic acid (pK_a = 4.89), nor phenol (pK_a = 9.89) with higher pK_a values could induce the phase transition.[9] On the other hand, the phase transition did not depend on the pK_a value of the thiols.[10] These results suggest that the behavior of the phase transition is affected by interactions of the dissociated anions of the respective organic molecules with the surface of ZnS nanocrystallites.

The modified surface of the resulting ZnS nanocrystallites was characterized by FTIR spectroscopy. The surface zinc atoms of ZnS nanocrystallites in DMF are solvated by the oxygen atoms of DMF molecules, and interact with acetate anions derived from the starting zinc acetate;[5] FTIR analyses of powdered ZnS–DMF combined with carboxylic acid revealed that benzoate and cyanoacetate anions coordinated to the surface of ZnS nanocrystallites *via* the oxygen atoms since the peaks assigned to the C=O stretching vibration of the carboxylate (benzoate, 1536 cm^{-1}; cyanoacetate, 1623 cm^{-1}) were shifted to lower frequency than those of the free carboxylic acids (benzoic acid, 1688 cm^{-1}; cyanoacetic acid, 1736 cm^{-1}). In contrast, non-coordination of phenol, octanoic acid and acetic acid molecules was confirmed by FTIR spectra. These observations lead to the conclusion that the phase transition could be induced only when the added molecules react with the surface of ZnS nanocrystallites to form covalent or ionic bonds. For carboxylic acids with lower pK_a values than that of acetic acid, they must dissociate into the corresponding carboxylate anions in basic DMF to an appreciable extent; the carboxylate anions then coordinate to the ZnS nanocrystallite surface, resulting in the phase transition. On the other hand, since a thiolate anion has high nucleophilicity as a soft base, the thiolate anion readily binds to the surface zinc atom which is a soft acid, even when the concentration of the dissociated thiolate is low.[11] As a consequence, the phase transition of ZnS nanocrystallites was independent of the pK_a value of the thiol.

Generally, ZnS crystallizes to form the cubic structure at room temp. because the internal energy of the cubic phase is slightly lower than that of the hexagonal phase.[12] Thus, the hexagonal structure of ZnS–DMF must be formed due to the metastability caused by the effective coordination of DMF molecules to the ZnS nanocrystallite surface,[5] which should stabilize the phase during growth. The formation of nanocrystallites with metastable crystalline structure is often observed.[13] The formation of chemical bonds between the surface zinc atom of ZnS nanocrystallites and the added thiolate or carboxylate anion should lead to a change of the surface energy of ZnS nanocrystallites. This change of the surface energy could induce the phase transition from the metastable phase (hexagonal) to the stable phase (cubic) at ambient temperature and pressure, because the difference in the internal energy of ZnS between the hexagonal and the cubic phase is quite small (13.4 kJ mol^{-1}).[12] Further study is required for quantitative description of the surface energy to induce the phase transition.

In conclusion, control of crystalline structures of quantum-confined semiconductor nanocrystallites was achieved at ambient temperature and pressure through the phase transition from the hexagonal to the cubic structure by the chemical modification of the ZnS nanocrystalline surface with organic molecules for the first time.

This work was supported in part by the 'Research for the Future' Program of JSPS.

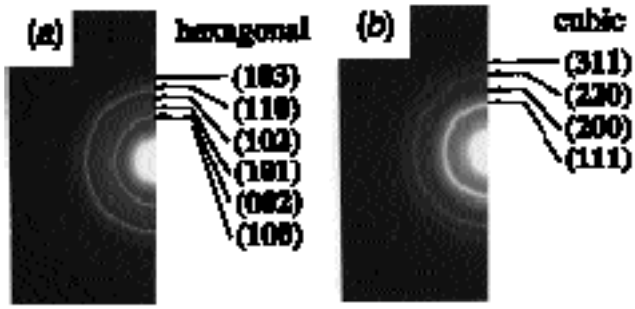

Fig. 2 Electron diffraction patterns of (*a*) ZnS–DMF and (*b*) ZnS–DMF combined with C_6F_5SH

Table 1 Dependence of crystalline structure of ZnS nanocrystallites on adding reagents

Added reagent	pK_a in water[a]	pK_a in DMF[b]	Crystalline structure
None			Hexagonal
C_6F_5SH	< 6.615[c]		Cubic
C_6F_5SH	6.615[d]		Cubic
$C_{10}H_{21}SH$	*ca.* 10[e]		Cubic
$C_6H_{13}SH$	10.3[d]		Cubic
$CH_2(CN)CO_2H$	2.45[f]		Cubic
$C_6H_5CO_2H$	4.19[f]	12.3	Cubic
CH_3CO_2H	4.76[f]	13.5	Hexagonal
$C_7H_{15}CO_2H$	4.89[f]		Hexagonal
C_6H_5OH	9.89[f]	> 16	Hexagonal

[a] Acidic dissociation constants in water at 25 °C. [b] Acidic dissociation constants in DMF at 25 °C. See ref. 14. [c] The value of pK_a of C_6F_5SH must be lower than that of C_6H_5SH because of the higher electronegativity of $C_6F_5S^-$. See ref. 15. [d] See ref. 10. [e] The value of pK_a of $C_{10}H_{21}SH$ must be the nearly same as that of $C_6H_{13}SH$. [f] See ref. 9.

Notes and References

* E-mail: yanagida@chem.eng.osaka-u.ac.jp

1 See reviews, for example: A. P. Alivisatos, *J. Phys. Chem.*, 1996, **100**, 13 226
2 M. V. Ramakrishna and R. A. Friesner, *J. Chem. Phys.*, 1991, **95**, 8309.
3 M. Haase and A. P. Alivisatos, *J. Phys. Chem.*, 1992, **96**, 6756; S. H. Tolbert and A. P. Alivisatos, *Science*, 1994, **265**, 373; *J. Chem. Phys.*, 1995, **102**, 4642.
4 H. Hosokawa, H. Fujiwara, K. Murakoshi, Y. Wada, S. Yanagida and M. Satoh, *J. Phys. Chem.*, 1996, **100**, 6649.
5 H. Hosokawa, K. Murakoshi, Y. Wada, S. Yanagida and M. Satoh, *Langmuir*, 1996, **12**, 3598.
6 M. Kanemoto, K. Ishihara, Y. Wada, T. Sakata, H. Mori and S. Yanagida, *Chem. Lett.*, 1992, 835.
7 M. Kanemoto, H. Hosokawa, Y. Wada, K. Murakoshi, S. Yanagida, T. Sakata, H. Mori, M. Ishikawa and H. Kobayashi, *J. Chem. Soc., Faraday Trans.*, 1996, **92**, 2401.
8 M. G. Bawendi, A. R. Kortan, M. L. Steigerwald and L. E. Brus, *J. Chem. Phys.*, 1989, **91**, 7282.
9 R. C. Weast, in *Handbook of Chemistry and Physics*, CRC Press, Cleveland, 52nd edn., 1972, p. D-120.
10 E. P. Serjeant and B. Dempsey, in *Ionization Constants of Organic Acids in Aqueous Solution*, Pergamon, Oxford, 1978.
11 T. L. Ho, in *Hard and Soft Acids and Bases Principle in Organic Chemistry*, Academic Press, New York, 1977.
12 D. R. Lide, in *CRC Handbook of Chemistry and Physics*, CRC Press, Boca Raton, FL, 75th edn., 1995, pp. 4–46.
13 M. L. Steigerwald, A. P. Alivisatos, J. M. Gibson, T. D. Harris, A. R. Kortan, A. J. Muller, A. M. Thayer, T. M. Duncan, D. C. Douglass and L. E. Brus, *J. Am. Chem. Soc.*, 1988, **110**, 3046.
14 K. Izutsu, in *Acid-Base Dissociation Constants in Dipolar Aprotic Solvents*, Blackwell Science, Oxford, 1990.
15 A. B. P. Lever, in *Inorganic Electronic Spectroscopy*, Elsevier, Amsterdam, 1984, p. 222.

Received in Cambridge, UK, 6th October 1997; 7/07176K

Amine and ester-substituted silsesquioxanes: synthesis, characterization and use as a core for starburst dendrimers

Frank J. Feher* and Kevin D. Wyndham

Department of Chemistry, University of California, Irvine, CA 92697-2025, USA

Practical procedures are reported for the syntheses of amine and ester-substituted silsesquioxane frameworks with the formula $R_8Si_8O_{12}$ with R = $CH_2CH_2CH_2NH_2$ (2), $[CH_2CH_2CH_2NH_3]Cl$ (3) and $CH_2CH_2CMe_2CH_2CO_2Me$ (4); the use of 2 as a core for starburst dendrimers with R = $CH_2CH_2CH_2N(CH_2CH_2CO_2Me)_2$ (5) and $CH_2CH_2CH_2N(CH_2CH_2C(O)NHCH_2CH_2NH_2)_2$ (6) is also described.

Polyhedral oligosilsesquioxanes (POSS) are an interesting class of clusters derived from the hydrolytic condensation of trifunctional organosilicon monomers.[1–3] Cube-octameric clusters (*e.g.* **1**) are most common, but a wide variety of other polyhedral frameworks have been identified. Interest in POSS has grown rapidly over the past several years, particularly for polymer-related applications, where several families of POSS monomers have been developed as precursors to hybrid inorganic–organic polymers.[4] Many other applications for POSS have emerged and developed rapidly as straightforward procedures have been devised for preparing frameworks with synthetically useful pendant groups.[5–9] Here, we report practical syntheses of several new silsesquioxanes that are attractive starting materials for more elaborate molecules, including amine- and ester-substituted frameworks that have excellent potential as cores for starburst dendrimers.

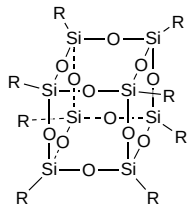

1 R = alkyl, vinyl or aryl
2 $CH_2CH_2CH_2NH_2$
3 $[CH_2CH_2CH_2NH_3]Cl$
4 $CH_2CH_2CMe_2CH_2CO_2Me$

Wacker-Chemie's 1991 US patent[10] claimed the preparation of **2**. This compound is ideally suited for many purposes, but no experimental details or characterization data were provided in the patent. We reinvestigated these claims and now confirm that the hydrolytic condensation of γ-aminopropyltriethoxysilane in MeOH–conc. HCl does indeed provide easy access to an amine-substituted framework,† but the product obtained under conditions reported by Wacker-Chemie is **3** rather than **2** (*i.e.* the free amine).[11] This hydrochloride is highly soluble in water (> 0.9 g ml^{-1}), poorly soluble or insoluble in most organic solvents and is somewhat hygroscopic. It is also surprisingly difficult to neutralize without destroying the Si/O framework, but neutralization of **3** to **2** can be accomplished by eluting solutions of **3** in methanol or 14 : 1 ethanol–water solutions across a column of Amberlite IRA-400 resin.‡ The resulting solution of **2** appears to be stable for 1–2 days at 25 °C, but decomposes to an ill-defined T-gel upon prolonged storage at 25 °C or when the solvent is removed.

It is interesting to note that a ^{29}Si NMR spectrum of the decomposition product is nearly identical to the published spectrum for products from the uncatalyzed hydrolysis γ-aminopropyltriethoxysilane in 14 : 1 EtOH–H_2O.[12] Both spectra exhibit several sharp resonances between δ −60 and −72, including a large resonance at δ −68.5 previously assigned[12] to **2**, but the characteristic resonance for pure **2** only appears as a minor resonance at δ −66.8. In light of the fact that MALDI-TOF mass spectra of both samples exhibit many peaks at $m/z < 3000$, but no large peaks attributable to $R_nSi_nO_{3n/2}$ (n = 6, 8, 10, 12), it appears that fully condensed frameworks containing free aminopropyl groups are not stable relative to incompletely condensed frameworks and/or T-gels.

Platinum-catalyzed hydrosilylation reactions of $H_8Si_8O_{12}$ provide convenient access to a wide variety of functionalized silsesquioxanes,[5,6,9,13,14] but in most cases the products are complicated mixtures of isomers because both α- and β-addition to the alkene are observed. Gentle and Bassindale[5] noted that β-addition and a number of side-reactions can be suppressed by increasing steric bulk on the γ-position and avoiding the use of vinyl silanes as alkenes. We have found that β-addition can be completely eliminated by using 3,3-disubstituted α-alkenes. In the case of $H_8Si_8O_{12}$[15] and readily available $H_2C{=}CHCMe_2CH_2CO_2Me$ (Aldrich), hydrosilylation with Speier's catalyst is complete within 48 h in refluxing hexanes to produce high yields of **4**, which spontaneously crystallizes from solution as large colorless crystals.§ We have not examined other hydridosilsesquioxanes (*e.g.* $H_{10}Si_{10}O_{15}$, $H_{12}Si_{12}O_{18}$, $H_{14}Si_{14}O_{21}$),[15,16] but these compounds should react similarly with $H_2C{=}CHCMe_2CH_2CO_2Me$ to produce isomerically pure derivatives containing ester-substituted pendant groups on each vertex. Ester-substituted frameworks should also be available from analogous Pt-catalyzed reactions of $H_2C{=}CHCMe_2CH_2CO_2Me$ with readily available hydride-substituted spherosilicates [*e.g.* $(HSiMe_2O)_8Si_8O_{12}$].[10]

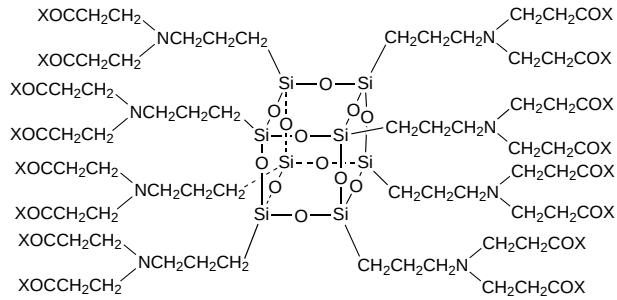

5 X = OMe
6 $NHCH_2CH_2NH_2$

An interesting ester-substituted framework can also be prepared *via* the reaction of **2** with methyl acrylate. When performed under conditions typically used to prepare PAMAM dendrimers from polyamine cores,[17,18] this reaction produces excellent yields of **5**; subsequent reaction of **5** with an excess of ethylenediamine produces **6**. Both **5** and **6** were identified on the basis of multinuclear NMR data and MALDI-TOF mass spectra.¶ Higher generation PAMAM dendrimers with a Si_8O_{12} core can presumably be synthesized by further synthetic iterations.

In summary, we have developed straightforward procedures for the synthesis of amine and ester-substituted silsesquioxane frameworks. We have also demonstrated that silsesquioxanes can be used as cores for the preparation of amine or ester-terminated starburst dendrimers. The use of silsesquioxanes as cores for dendrimers is particularly attractive[6] because their polyhedral structures should produce spherically symmetric dendrimers with smaller generation numbers then more conventional cores.[19] Our efforts to use amine and ester-substituted silsesquioxanes as building blocks for hybrid inorganic–organic materials[4,20] and as platforms for biologically active pendant groups will be reported separately.

These studies were supported by the National Science Foundation and Phillips Laboratory (Edwards AFB). We thank Dr Keith J. Weller (Witco/OSi Specialities) for a generous gift of silanes.

Notes and References

* E-mail: fjfeher@uci.edu

† The reaction of $H_2NCH_2CH_2CH_2Si(OEt)_3$ (150 ml, 0.627 mol) and conc. HCl (200 ml) in MeOH (3.6 l) produces **3** (30%) as a microcrystalline solid after 6 weeks at 25 °C. The crude product obtained after filtration, washing with MeOH and drying (0.001 Torr, 25 °C) is spectroscopically pure. Recrystallization from MeOH affords **3** as white microcrystalline powder. ^{1}H NMR [500.2 MHz, $(CD_3)_2SO$, room temp.] δ 8.25 (s, NH_3, 24 H), 2.75 (t, CH_2NH_3, 16 H), 1.71 (m, $SiCH_2CH_2$, 16 H), 0.71 (t, $SiCH_2$, 16 H). ^{13}C{^{1}H} NMR [125.8 MHz, $(CD_3)_2SO$, room temp.] δ 41.01 (s, CH_2NH_3), 20.61 (s, $SiCH_2CH_2$), 8.44 (s, $SiCH_2$). ^{29}Si NMR [99.4 MHz, $(CD_3)_2SO$, room temp.] δ −66.4 (s). IR (KBr): 3190, 3023, 2903, 1579, 1506, 1215, 1138, 1110, 994, 923, 808, 706 cm^{-1}. Anal. for $C_{24}H_{72}O_{12}Si_8N_8C_{18}$ (calc.): 24.69 (24.57), 6.40 (6.19), 9.40 (9.55%). Mass spectrum (MALDI-TOF, DHB matrix), *m/z* (relative intensity), 881.4 ([M + H − 8 HCl]$^+$, 100%), 863.4 ([M − NH_3]$^+$, 39%).

‡ Amberlite IRA-400 ion-exchange resin (37 g) is prepared by successive washing with H_2O (4 × 200 ml), 1 M NaOH (3 × 200 ml), H_2O (6 × 200 ml) and finally MeOH or 14 : 1 EtOH–H_2O (6 × 200 ml). Half of the beads are loaded onto a column (3.5 cm o.d.); the other half are used to dissolve a suspension of **3** (5 g) in a minimum amount of MeOH or EtOH–H_2O. Elution across the column produces a stock solution of **2** which tests negative for chloride. Small samples of **2** can be prepared by rapidly evaporating aliquots from the stock solution, but to avoid decomposition, the amine should be prepared immediately before use or stored in MeOH solutions at −35 °C. ^{1}H NMR (500.2 MHz, CD_3OD, room temp.) δ 4.4 (s, NH_2 and H_2O), 2.52 (t, CH_2N, 16 H), 1.46 (m, $SiCH_2CH_2$, 16 H), 0.56 (t, $SiCH_2$, 16 H). ^{13}C{^{1}H} NMR (125.8 MHz, CD_3OD, room temp.) δ 44.87 (s, CH_2N), 26.88 (s, $SiCH_2CH_2$), 9.57 (s, $SiCH_2$). ^{29}Si NMR (99.4 MHz, CD_3OD, room temp.) δ −66.4 (s). Mass spectrum (MALDI-TOF, DHB matrix), *m/z* (relative intensity), 881.5 ([M + H]$^+$, 100%), 863.5 ([M − NH_3]$^+$, 49%).

§ Methyl-3,3-dimethylpent-4-enoate (Aldrich) (11 ml, 0.068 mol) and $[HSiO_{3/2}]_8$ (3.30 g, 7.74 mmol) are reacted (48 h) in refluxing hexanes (8 ml) with a catalytic amount of Speier's catalyst as described in ref. 5; the yield is quantitative by ^{1}H, ^{13}C and ^{29}Si NMR spectroscopy. Upon cooling, ester **4** crystallizes as large colorless crystals (80%). ^{1}H NMR (500.1 MHz, $CDCl_3$, room temp.) δ 3.62 (s, OCH_3, 24 H), 2.179 (s, CH_2CO, 16 H), 1.401 (m, $SiCH_2CH_2$, 16 H), 0.959 (s, CH_3, 48 H), 0.567 (m, 16 H, $SiCH_2$). ^{13}C{^{1}H} NMR (127.8 MHz, $CDCl_3$, room temp.) δ 172.70 (s, CO), 51.02, 44.95, 35.31, 33.80 (s, $SiCH_2CH_2$), 26.48 (s, CH_3), 6.06 (s, $SiCH_2$). Anal. for $C_{64}H_{120}O_{28}Si_8$ (calc.): 49.59 (49.20), 7.72 (7.74%). Mass spectrum (EI, 70 eV, 200 °C), *m/z* (relative intensity), 1529.5 ([M − OCH_3]$^+$ 100%), 1417.3 ([M − $C_8H_{15}O_2$]$^+$, 40%).

¶ Ester **5** was prepared in 73% yield (204 mg) *via* the reaction (room temp., 24 h) of methyl acrylate (0.8 ml, 8.884 mmol) with freshly prepared **2** (65 mg, 0.029 mmol) in methanol (1 ml).[18] Subsequent reaction of **5** (48 mg 0.021 mmol) with an excess of $H_2NCH_2CH_2NH_2$ (220 equiv. ester, 4 °C, 4 d) afforded **6** in 100% yield (58 mg).[17] For **5**: ^{1}H NMR (500.2 MHz, CD_3OD, room temp.) δ 3.61 (s, CH_3, 48 H), 2.71 (t, CH_2CO, 32 H), 2.40 [m, $CH_2N(CH_2)_2$, 48 H] 1.51 (m, $SiCH_2CH_2$, 16 H), 0.593 (t, $SiCH_2$, 16 H). ^{13}C{^{1}H} NMR (125.8 MHz, CD_3OD, room temp.) δ 174.53 (s, CO), 57.23 [s, $CH_2N(CH_2)_2$], 52.13 (s, CH_2CO_2), 50.34 (s, CH_3), 33.27 [s, $CH_2N(CH_2)_2$], 21.48 (s, $SiCH_2CH_2$), 10.21 (s, $SiCH_2$). ^{29}Si NMR (99.4 MHz, CD_3OD, room temp.) δ −6.0(s). Mass spectrum (MALDI-TOF, DHB matrix), *m/z* (relative intensity); 2256.5 ([M]$^+$, 100%). For **6**: ^{1}H NMR (500.2 MHz, CD_3OD, room temp.) δ 3.18 (t, CH_2, 32 H), 2.70 (t, CH_2, 32 H), 2.66 (t, CH_2, 32 H), 2.43 (t, $SiCH_2CH_2$, 16 H), 2.31 (t, CH_2, 32 H), 1.50 (m, $SiCH_2CH_2$, 16 H), 0.58 (t, $SiCH_2$, 16 H). ^{13}C{^{1}H} NMR (125.8 MHz, CD_3OD, room temp.) δ 175.08 (s, CO), 57.13 [s, $CH_2N(CH_2)_2$], 50.81 (s, CH_2), 43.07 (s, CH_2), 42.11 (s, CH_2), 34.57 [s, $CH_2N(CH_2)_2$], 21.12 (s, $SiCH_2CH_2$), 10.57 (s, $SiCH_2$). ^{29}Si NMR (99.4 MHz, CD_3OD, room temp.) δ −66.2 (s). Mass spectrum (MALDI-TOF, DHB matrix), *m/z* (relative intensity); 2705.5 [M]$^+$.

1 M. G. Voronkov and V. Lavrent'ev, *Top. Curr. Chem.*, 1982, **102**, 199.
2 R. H. Baney, M. Itoh, A. Sakakibara and T. Suzuki, *Chem. Rev.*, 1995, **95**, 1409.
3 H. Bürgy, G. Calzaferri, D. Herren and A. Zhdanov, *Chimia*, 1991, **45**, 3.
4 J. D. Lichtenhan, *Comments Inorg. Chem.*, 1995, **17**, 115.
5 T. E. Gentle and A. R. Bassindale, *J. Inorg. Organomet. Pol.*, 1995, **5**, 281.
6 A. R. Bassindale and T. E. Gentle, *J. Mater. Chem.*, 1993, **3**, 1319.
7 F. J. Feher, D. Soulivong, A. G. Eklund and K. D. Wyndham, *Chem. Commun.*, 1997, 1185.
8 C. Zhang and R. M. Laine, *J. Organomet. Chem.*, 1996, **521**, 199.
9 U. Dittmar, B. J. Hendan, U. Flörke and H. C. Marsmann, *J. Organomet. Chem.*, 1995, **489**, 185.
10 R. Weidner, N. Zeller, B. Deubzer and V. Frey, *US Pat.*, 5,047,492, 1991.
11 (*a*) Similar results have been independently obtained by Gravel and Laine:[11b] (*b*) M.-C. Gravel and R. M. Laine, *ACS Polym. Prepr.*, 1997, **38**, 155.
12 P. M.-T. Olivera-Pastor, E. Rodriguez-Castellon, A. Jimenez-Lopez, T. Cassagneau, D. J. Jones and J. Roziere, *Chem. Mater.*, 1996, **8**, 1758.
13 J. V. Crivello and R. Malik, *J. Polym. Sci., Part A: Polym. Chem.*, 1997, **35**, 407.
14 A. Tsuchida, C. Bolln, F. G. Sernetz, H. Frey and R. Malhaupt, *Macromolecules*, 1997, **30**, 2818.
15 P. A. Agaskar, *Inorg. Chem.*, 1991, **30**, 2707.
16 P. A. Agaskar and W. G. Klemperer, *Inorg. Chim. Acta*, 1995, **229**, 355.
17 D. A. Tomalia, H. Baker, J. R. Dewald, M. Hall, G. Kallos, S. Martin, J. Roeck, J. Ryder and P. Smith, *Polym. J.*, 1985, **17**, 117.
18 A. D. Meltzer, D. A. Tirrell, A. A. Jones, P. T. Inglefield, D. M. Hedstrand and D. A. Tomalia, *Macromolecules*, 1992, **25**, 4541.
19 G. R. Newkome, C. N. Moorefield and F. Vogtle, in *Dendritic Molecules*, New York, 1996.
20 J. D. Lichtenhan, in *Silsesquioxane-Based Polymers*, ed. J. C. Salamone, New York, 1996.

Received in Bloomington, IN, USA, 2nd October 1997; 7/07140J

Remarkable activity enhancement by trimethylsilylation in oxidation of alkenes and alkanes with H_2O_2 catalyzed by titanium-containing mesoporous molecular sieves

Takashi Tatsumi,* Keiko A. Koyano and Naoko Igarashi

Engineering Research Institute, School of Engineering, The University of Tokyo, Yayoi, Tokyo 113, Japan

Titanium-containing mesoporous materials, Ti-MCM-41 and Ti-MCM-48, have been successfully modified by trimethylsilylation to exhibit enhanced catalytic activity in the oxidation of alkenes and alkanes with H_2O_2.

The recent discovery of a new family of mesoporous molecular sieves has received much attention.[1,2] Ti-substituted MCM-41[3] and MCM-48[4] and Ti-substituted hexagonal mesoporous silica (Ti-HMS[5]) have been synthesized, and pioneered the potential to oxidize bulky molecules which cannot enter into the micropores of zeolites such as TS-1, TS-2 and Ti-β. However, it has been reported that Ti-MCM-41 samples show a lower intrinsic activity and lower selectivity toward the use of H_2O_2 for alkene oxidation than either TS-1 or Ti-β owing to their high hydrophilicity.[6] It has been recently proposed that the hydrophilic/hydrophobic property of Ti zeolites plays an important role in their activity for liquid phase oxidations.[7] We have conducted trimethylsilylation of Ti-MCM-41 and Ti-MCM-48 in order to enhance activity in oxidation with dilute H_2O_2 through increasing their hydrophobicity. Here, we report that trimethylsilylation of Ti-containing mesoporous molecular sieves, Ti-MCM-41 and Ti-MCM-48, resulted in a remarkable enhancement of catalytic activity in oxidation of alkenes and alkanes with H_2O_2.

Ti-MCM-41 was synthesized as previously described.[8] Tetraethylorthosilicate, tetrabutylorthotitanate and cetyltrimethylammonium chloride (CTMACl) were used, and the molar composition of the gels subjected to hydrothermal synthesis was SiO_2 : 0.01 TiO_2 : 0.6 CTMA : 0.3 NMe_4OH : 60 H_2O. Ti-MCM-48 was similarly synthesized by using CTMACl/OH (Cl/OH = 70/30) as a template.[9] The molar composition of the gels was: SiO_2 : 0.02 TiO_2 : CTMA : 46.5 H_2O. Trimethylsilylation was conducted according to literature;[2] 0.5 g Ti-MCM-41 or -48, 10 g Me_3SiCl and 15 g $(Me_3Si)_2O$ were refluxed for 16 h under N_2. The HCl produced was stripped off and the dry powder obtained was thoroughly washed with dry acetone with centrifuging, and dried at 393 K for 3 h. The samples before and after trimethylsilylation are denoted Ti-MCM-41 or -48 (non-sil) and Ti-MCM-41 or -48 (sil), respectively. A typical oxidation run used 50 mg of a catalyst in 25 mmol of substrate in a round-bottom flask, to which was added 5 mmol of H_2O_2 (30% aqueous solution). The resulting mixture was stirred at various temperatures.

The X-ray diffraction patterns of Ti-MCM-41 and Ti-MCM-48 materials closely matched those of the pure silica isomorph.[1,2] Although the X-ray diffraction patterns and the *d* spacings were virtually unchanged after trimethylsilylation, the pore diameter determined by the Dolimore–Heal method, the BET surface area, and the pore volume decreased upon trimethylsilylation (Table 1). These observations could be accounted for by assuming that the silanol groups inside the pore were trimethylsilylated.

In the IR spectra of Ti-MCM-41 samples the band at 960 cm^{-1}, which is used as evidence for Ti incorporation into the framework in Ti-containing microporous molecular sieves such as TS-1 and Ti-β,[10,11] has significantly decreased upon trimethylsilylation. Similar phenomena were also observed with Ti-MCM-48. The band was also detected in the spectra of pure silica MCM-41 or -48 (non-sil) and completely disappeared upon trimethylsilylation. Moreover, the intensity of a broad peak in the range 3700–3500 cm^{-1} corresponding to silanol groups and adsorbed water in the spectra of both Ti-MCM-41 and Ti-MCM-48 decreased significantly upon trimethylsilylation. To determine the concentration of surface trimethylsilyl groups ^{29}Si MAS NMR measurements were carried out. Before trimethylsilylation, the ^{29}Si MAS NMR spectrum of Ti-MCM-41 (non-sil) exhibited two broad resonances, at δ −108.7 (73.7%) for the Q^4 silicate unit and at δ −100.5 (26.3%) for the Q^3 environment. After trimethylsilylation, a new peak ascribed to the silicon atoms of TMS appeared at δ 14.3 and the ratio of Q^3 silicate was significantly decreased. Deconvolution of the spectrum into three peaks (TMS, Q^3, Q^4) was made; the molar ratio of TMS : Q^3 : Q^4 was 17.2 : 11.7 : 71.1, indicating that the content of silanol groups after trimethylsilylation was 0.208 mol (mol Si)$^{-1}$ [mol Si for Ti-MCM-41 (non-sil)], while that of silanol groups before trimethylsilylation was 0.263 mol (mol Si)$^{-1}$. Thus a part of original silanol groups could not be trimethylsilylated and furthermore, the increase in Q^4 species was moderate compared to the expected increase resulting from the substitution of trimethylsilyl groups for silanol H atoms, suggesting that some silanol groups were newly formed during the trimethylsilylation. The incomplete trimethylsilylation is considered to be due to the bulkiness of the trimethylsilyl group (*ca*. 0.6 nm). Despite the incomplete modification of silanol groups, Ti-MCM-41 (sil) was highly hydrophobic; the amount of adsorbed water was measured by TG after exposure to moisture over saturated aqueous solution of NH_4Cl at room temperature for 24 h; Ti-MCM-41 (sil) adsorbed only 0.29 mass% H_2O, whereas Ti-MCM-41 (non-sil) adsorbed 55 mass% H_2O.

We performed oxidation of cyclohexene, hexane and pent-2-en-1-ol with H_2O_2 on Ti-MCM-41 and Ti-MCM-48 samples. The results are summarized in Table 2. Neither Ti-MCM-41 (non-sil) nor Ti-MCM-48 (non-sil) exhibited significant activity in the oxidation of cyclohexene. However, trimethylsilylation of these Ti-containing mesoporous solids resulted in a *ca*. 20-fold increase in the activity in the oxidation of cyclohexene. Furthermore, non-productive decomposition of H_2O_2 was inhibited by the trimethylsilylation. The turnover number

Table 1 Properties of Ti-containing mesoporous molecular sieves before and after trimethylsilylation

Catalyst	Si/Ti	BET surface area/m^2 g^{-1}	Pore diameter/nm	Pore volume/ml g^{-1}
Ti-MCM-41 (non-sil)	123	1015	2.32	0.88
Ti-MCM-48 (non-sil)	47	1048	2.32	0.91
Ti-MCM-41 (sil)	139	879	1.90	0.82
Ti-MCM-48 (sil)	51	839	1.90	0.71

Table 2 Effect of trimethylsilylation on catalytic activity of Ti-containing mesoporous molecular sieves

Catalyst	Conversion (mol% of max.)	TON/ mol (mol Ti)$^{-1}$	Selectivity (%)				H_2O_2 decomposition (%)
Cyclohexene oxidation			Alcohol	Ketone	Epoxide	Diol	
Ti-MCM-41 (non-sil)[a]	0.72	5.4	30.0	15.2	0	54.7	57.6
Ti-MCM-48 (non-sil)[b]	2.1	6.1	26.7	32.8	4.7	35.7	61.9
Ti-MCM-41 (sil)[a]	13.3	112.1	14.4	21.0	13.9	50.7	0
Ti-MCM-48 (sil)[a]	38.5	120.9	21.3	17.0	2.2	59.4	0
Hexane oxidation			2-ol	3-ol	2-one	3-one	
Ti-MCM-41 (non-sil)[b]	0	0	—	—	—	—	74.7
Ti-MCM-41 (sil)[b]	0.06	0.50	40.5	59.5	0.0	0.0	0.0
Ti-MCM-41 (sil)[c]	0.20	6.8	22.0	22.9	31.0	24.1	97.3
Ti-MCM-48 (non-sil)[b]	0	0	—	—	—	—	75.0
Ti-MCM-48 (sil)[b]	0.17	0.52	45.4	54.6	0.0	0.0	20.2
Pent-2-en-1-ol oxidation			Pent-2-enal		Epoxide		
Ti-MCM-41 (non-sil)[b]	32.4	242	81.0		19.0		0
Ti-MCM-48 (non-sil)[b]	32.0	92.9	78.9		21.1		3.0
Ti-MCM-41 (sil)[b]	14.7	124	81.6		18.4		0
Ti-MCM-48 (sil)[b]	20.7	59.3	73.4		26.5		0

[a] Catalyst 50 mg, substrate 25 mmol, H_2O_2 5 mmol, 323 K, 3 h. [b] Catalyst 50 mg, substrate 25 mmol, H_2O_2 5 mmol, 323 K, 2 h. [c] Catalyst 50 mg, substrate 100 mmol, H_2O_2 20 mmol, 353 K, 16 h.

(TON) per hour was even higher than that observed with Ti-β at 333 K.[12] The selectivity for epoxide/diol was increased at the expense of allylic oxidation. In the oxidation of hexane, no products were obtained with the non-trimethylsilylated samples, where H_2O_2 was mostly decomposed. On the other hand, hexane was oxidized on the trimethylsilylated samples with retarded decomposition of H_2O_2. The turnover number increased to 6.8 mol (mol Ti)$^{-1}$ with increasing reaction temperature, while the rate of H_2O_2 decomposition increased. The difference in the activity for cyclohexene and hexane oxidation between non-trimethylsilylated and trimethylsilylated samples may be explained in terms of hydrophobicity/hydrophilicity; excess water should prevent non-polar cyclohexene or hexane from adsorbing into the pores of the non-trimethylsilylated catalysts and/or approaching active sites inside the pores. It has been observed that trimethylsilylated catalysts exist in the organic phase because of their hydrophobicity, resulting in mitigation of the inhibition of oxidation caused by water. No leaching of Ti was observed during the oxidation.

As shown in Table 2, pent-2-en-1-ol was oxidized with H_2O_2 on both Ti-MCM-41 and -48 (non-sil) at a much higher rate than cyclohexene. The enhanced reactivity of this OH-containing alkenes may be due to the possible formation of a ring structure where alcoholic OH is bound to Ti as previously proposed.[13,14] It should be noted that the difference in the reactivity between alkenes and allylic alcohols on TS-1 was not so marked compared to this case.[15] Thus it is conceivable that, because of the presence of a considerable amount of silanol groups, pent-2-en-1-ol containing a polar hydroxyl group more easily migrates into the pores of non-trimethylsilylated catalysts than simple alkenes in competition with water, showing a much higher reactivity than cyclohexene. Trimethylsilylated samples Ti-MCM-41 (sil) and Ti-MCM-48 (sil) exhibited lower activity in the oxidation of pent-2-en-1-ol than the corresponding non-trimethylsilylated samples. Partial removal of silanol groups would reduce the capability to absorb the allylic alcohols through hydrogen bonding. The decreased activity might be also due to the difficulty in access to the active site caused by the introduction of rather bulky trimethylsilyl groups. Studies on the steric environment of the Ti site are in progress using a variety of reactants as probe molecules.

Trimethylsilylation leads to a further advantage: the mesoporous structure of Ti-containing samples is much less resistant to moisture than that of pure silica samples.[8] For example, the d_{100} peak height of Ti-MCM-41 (non-sil) decreased by 80% upon exposure to moisture over saturated aqueous solution of NH_4Cl for 3 days. In contrast the ordered structure of both Ti-MCM-41 (sil) and Ti-MCM-48 (sil) was found to be intact upon exposure to moisture for 30 days.

The authors are grateful to Dr S. Nakata and Mr Y. Tanaka (Chiyoda Corp.) for measuring ^{29}Si MAS NMR spectra. This work was supported in part by Grant-in-aid for Scientific Research on Priority Areas (No. 0742104) from the Ministry of Education, Science and Culture, Japan.

Notes and References

* E-mail: tatsumi@catal.t.u-tokyo.ac.jp

1 C. T. Kresge, M. E. Leonowicz, W. J. Roth, J. C. Vartuli and J. S. Beck, *Nature*, 1992, **359**, 710.
2 J. S. Beck, J. C. Vartuli, W. J. Roth, M. E. Leonowicz, C. T. Kresge, K. D. Schmitt, C. T.-U. Chu, D. H. Olson, E. W. Sheppard, S. B. McCullen, J. B. Higgins and J. L. Schlenker, *J. Am. Chem. Soc.*, 1992, **114**, 10 834.
3 A. Corma, M. T. Navarro and J. P. Pariente, *J. Chem. Soc., Chem. Commun.*, 1994, 147; M. D. Alba, Z. Luan and J. Klinowski, *J. Phys. Chem.*, 1996, **100**, 2178.
4 K. A. Koyano and T. Tatsumi, *Chem. Commun.*, 1996, 145; M. Morey, A. Davison and G. Stucky, *Microporous Mater.*, 1996, **6**, 99; W. Zhang and T. J. Pinnavaia, *Catal. Lett.*, 1996, **38**, 261.
5 P. T. Tanev, M. Chibwe and T. J. Pinnavaia, *Nature*, 1994, **368**, 321; S. Gontier and A. Tuel, *Zeolites*, 1995, **15**, 601.
6 T. Blasco, A. Corma, M. T. Navarro and J. P. Pariente, *J. Catal.*, 1995, **156**, 65.
7 A. Corma, P. Esteve and A. Martinez, *J. Catal.*, 1996, **161**, 11.
8 K. A. Koyano and T. Tatsumi, *Microporous Mater.*, 1997, **10**, 259.
9 K. A. Koyano and T. Tatsumi, *Stud. Surf. Sci. Catal.*, 1997, **105**, 93.
10 G. Deo, A. M. Turek and I. E. Wachs, *Zeolites*, 1993, **13**, 365.
11 M. A. Camblor, A. Corma and J. Perez-Pariente, *J. Chem. Soc., Chem. Commun.*, 1993, 557.
12 T. Tatsumi, Q. Xia and Nizamidin Jappar, *Chem. Lett.*, 1997, 677.
13 M. G. Clerici and P. Ingallina, *J. Catal.*, 1993, **140**, 71.
14 R. Kumar, G. C. G. Pais, B. Pandt and P. Kumar, *J. Chem. Soc., Chem. Commun.*, 1995, 1315.
15 T. Tatsumi, K. Yanagisawa, K. Asano, M. Nakamura and H. Tominaga, *Stud. Surf. Sci. Catal.*, 1994, **83**, 417.

Received in Cambridge, UK, 26th August, 1997; 7/06175G

Solution processible poly(1-alkyl-2,5-pyrrolenevinylenes): new low band gap conductive polymers

In Tae Kim and Ronald L. Elsenbaumer*

Department of Chemistry and Biochemistry, The University of Texas at Arlington, Arlington, Texas 76019, USA

Bis(phenylthiomethylene) derivatives of 1-alkylpyrroles afford conjugated polymers by base induced elimination of thiophenyl groups.

Electrochemically prepared polypyrrole is employed as an electrode in capacitors and batteries owing to its high conductivity (> 100 S cm^{-1}), relative stability to air and moisture in its oxidized form, ability to form strong coherent films and ease of synthesis.[1] Conductive properties are related to the nature of the counter anions in polypyrrole films.[2] Properties have also been modified by polymerizing pyrrole derivatives with 3-methyl and 3,4-dimethyl substituents. Conductivities of these polymers are 4 and 10 S cm^{-1}, respectively.[3,4] However, the room temperature conductivities of poly(1-alkyl-2,5-pyrrolylene) (alkyl = methyl, hexyl, dodecyl) prepared by chemical oxidation fall in the range 10^{-3} to 10^{-6} S cm^{-1}.[5,6] The large decrease in conductivity of doped poly(pyrrolylenes) with an *N*-alkyl substitutent and an increase in size of the alkyl substituent has been rationalized on a steric basis.[7]

Reduction of band gaps in conjugated polymers such as poly(*p*-phenylene) and poly(thienylene) has been achieved by the insertion of vinylene linkages between the aromatic rings in the polymer chain to give poly(phenylenevinylene) and poly(thienylenevinylene),[8–10] respectively. The backbone of these polymers is made of aromatic rings bridged by vinylene linkages wherein the vinylene linkage not only reduces steric hindrance between backbone rings attached to them, but also has a beneficial effect on electronic properties as evidenced by experimental and theoretical data on both poly(*p*-phenylenevinylene)[4] and poly(thienylenevinylene).[11]

Recently, we reported a new precursor and polymerization route for the preparation of high molecular mass poly(3,4-dialkoxy-2,5-thienylenevinylene)s as low band gap conductive polymers made by base/acid and thermally induced elimination of sulfoxide groups.[12] We now report a convenient synthesis of 1-alkyl-2,5-bis(phenylthiomethylene)pyrroles (**2a**–**c**) using the Mannich reaction.[13] These can be readily polymerized using 4 equiv. of Bu^{t}OK (Scheme 1). The present account is the first report of the use of phenylthio as a leaving group in forming poly(1-alkyl-2,5-pyrrolenevinylene)s (**1a**–**c**).

1-Alkylpyrroles (**5a**–**b**) were prepared as described in the literature.[14] Treatment of **5a**–**c** with aq. HCHO and $Me_2NH{\cdot}HCl$ at room temperature for 7 d, the Mannich reaction, gave 70–85% yields of 1-alkyl-2,5-bis[(dimethylamino)-methyl]pyrroles (**4a**–**c**) and these, in turn, were converted into bisquaternary ammonium salts (**3a**–**c**) (yield: 75–92%) after reaction with MeI in THF at room temperature. We chose 1-alkyl-2,5-bis[(trimethylammonio)methyl]pyrrole diiodide (**3a**–**c**) as initial target monomers because of their crystallinity and good stability. However, attempts to polymerize these monomers (**3a**–**c**) with 5–10% aq. NaOH in a temperature range from 0 °C to reflux have not been successful. Manipulation of the bisquaternary ammonium salt functional groups in **3a**–**c** into a phenylthio leaving group **2a**–**c** (yield: 55–70%) provided a facile approach to a new class of polymerizable monomers (Scheme 1).†

The bis(phenylthiomethylene) derivative **2b** of 1-alkylpyrrole was treated with Bu^{t}OK (4 mol) in THF at room temperature and then gradually warmed to reflux. This monomer polymerized to give poly(1-hexyl-2,5-pyrrolylenevinylene) (PHxPyV), **1b**. This polymer was purified by four reprecipitations from THF into MeOH and acetone and had a deep blue color with a gold luster. On exposure to air, the polymer became slightly doped reaching a limiting conductivity of 10^{-6} S cm^{-1}. On doping with $AuCl_3$, PHxPyV films (cast on quartz) exhibited conductivities of 2.5 S cm^{-1} (four-in-line probe) in air. The undoped conjugated polymer **1b** was soluble in many common organic solvents. Conversion from the bis-phenylthio monomer **2b** afforded PHxPyV in 72% yield, which is considerably higher than that typically obtained for poly(phenylenevinylene) prepared from bis-sulfonium salt precursors (20–40%).[15] As indicated by the UV–VIS–NIR spectrum shown in Fig. 1(*a*) on an undoped film of cast polymer **1b**,

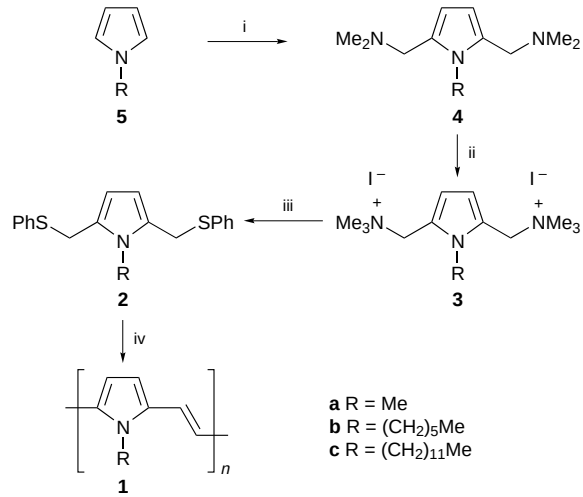

Scheme 1 *Reagents and conditions*: i, aq. CH_2O, $HClHN(CH_3)_2$, 0–25 °C; ii, MeI, THF, room temp.; iii, PhSNa, THF, reflux; iv, Bu^{t}OK, THF, reflux

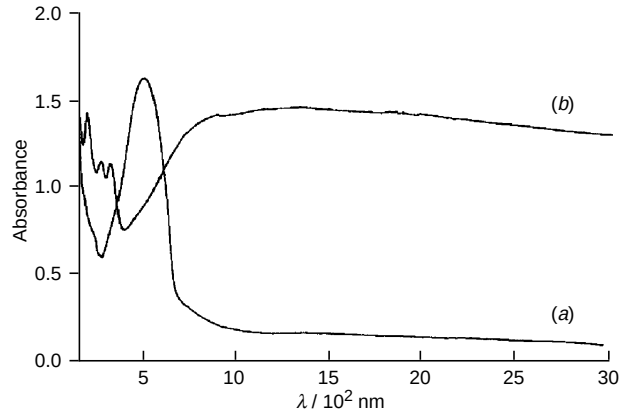

Fig. 1 UV–VIS–NIR absorption spectra of (*a*) undoped and (*b*) $FeCl_3$ doped PHxPyV (**1b**) (cast film on quartz)

Table 1 Properties of polymers **1a–c**

Polymer	λ_{max}/nm		Onset optical gap/eV	Solubility[a]	Doped conductivity/S cm^{-1} (dopant)
	THF	Film			
1a	500[b]	—	1.89	Insoluble	0.02 ($AuCl_3$), 0.001 ($FeCl_3$)[c]
1b	550	569	1.69	Very soluble	2.5 ($AuCl_3$), 0.15 ($FeCl_3$)[d]
1c	548	563	1.65	Very soluble	0.48 ($AuCl_3$), 0.11 ($FeCl_3$)[d]

[a] Solubility in moderately polar solvent such as $CHCl_3$, THF, CH_2Cl_2. [b] NMP. [c] Pressed powder pellet. [d] Cast film.

the onset band gap (low energy absorption edge) was determined to be 1.69 eV for PHxPyV. Poly(1-dodecyl-2,5-pyrrolylenevinylene) (PDoPyV), **1c**, was prepared from bis-phenylthio monomer **2c** as indicated in Scheme 1. This polymer had an onset band gap of 1.65 eV and had, by GPC using polystyrene standards, a number average weight (M_n) of 1.6×10^4 and a polydispersity (PD) of 1.16. This band gap is similar to that observed with PHxPyV. A comparison of the properties of **1a–c** made by the same route are summarized in Table 1.

The difference in conductivity between poly(1-alkyl-2,5-pyrrolylene) [$\sigma = 10^{-3}$ (methyl), 4.3×10^{-5} (hexyl) and 1.2×10^{-6} S cm^{-1} (dodecyl)] and **1a–c** suggests that the low conductivities of *N*-substituted polypyrroles as prepared by oxidative polymerization arise from a combination of steric interactions between adjacent rings[7] and from a mixture of α–α′, α–β′, and β–β′ coupled monomer.[16]

We have found the polymerization of bis-phenylthio monomers (**2a–c**) to be general for the electron rich 1-alkylpyrroles. Also, we fully expect that this polymerization process will be suitable for the preparation of other electron rich polymers, and we are presently in the process of attempting to prepare representative examples.

We thank the Robert A. Welch Foundation for support of this work. We also thank Professor Michael P. Cava, Professor Martin Pomerantz and Dr Haitao Cheng for helpful discussions.

Notes and References

* E-mail address: elsenbaumer@uta.edu

† Satisfactory spectroscopic and analytical data have been obtained for all new compounds.

1 Y. Kudoh, S. Tsuchiya, T. Kojima, M. Fukuyama and S. Yoshimura, *Synth. Met.*, 1991, **41/43**, 1133.
2 J. Ouyang and Y. Li, *Synth. Met.*, 1995, **75**, 1.
3 J. Bargon, S. Mohmand and R. J. Waltman, *IBM J. Res. Dev.*, 1983, **27**, 330.
4 A. Nazzal and G. B. Street, *J. Chem. Soc., Chem. Commun.*, 1983, 84.
5 P. Kovacic, I. Khoury and R. L. Elsenbaumer, *Synth. Met.*, 1983, **6**, 31.
6 I. T. Kim and R. L. Elsenbaumer, *Synth. Met.*, 1997, **84**, 157.
7 A. F. Diaz, J. Castillo, K. K. Kananzwa, A. Logan, M. Salmon and O. Fajardo, *J. Electroanal. Chem.*, 1982, **133**, 233.
8 H. Eckhart, L. W. Shacklette, K. Y. Jen and R. L. Elsenbaumer, *J. Chem. Phys.*, 1989, **91**, 1303.
9 K. Y. Jen, C. C. Han and R. L. Elsenbaumer, *Mol. Cryst. Liq. Cryst.*, 1990, **186**, 211.
10 K. Y. Jen, T. R. Jow and R. L. Elsenbaumer, *J. Chem. Soc., Chem. Commun.*, 1987, 1113.
11 K. Y. Jen, T. R. Jow, L. W. Shacklette, M. Maxfield, H. Eckhardt and R. L. Elsenbaumer, *Mol. Cryst. Liq. Cryst.*, 1988, **160**, 69.
12 H. Cheng and R. L. Elsenbaumer, *J. Chem. Soc., Chem. Commun.*, 1995, 1451.
13 G. B. Bachman and L. V. Heisey, *J. Am. Chem. Soc.*, 1946; W. Herz, K. Dittmer and S. J. Cristol, *J. Am. Chem. Soc.*, 1947, **69**, 1698.
14 D. J. Chadwick, *J. Chem. Soc., Perkin Trans. 1*, 1979, 2845.
15 R. W. Lenz, C. C. Han, J. Stenger-Smith and F. E. Karasz, *J. Polym. Sci., Part A: Polym. Chem.*, 1988, **26**, 3241.
16 I. T. Kim and R. L. Elsenbaumer, preliminary results.

Received in Corvallis, OR, USA, 17th September 1997; 7/06800J

The oxa-di-π-methane rearrangement of β,γ-unsaturated ketones induced by the external heavy atom cation effect within a zeolite

R. Sadeghpoor,[a] M. Ghandi,*[a] H. Mahmoudi Najafi[a] and F. Farzaneh[b]

[a] *Department of Chemistry, University of Tehran, Tehran, Iran*
[b] *Department of Chemistry, University of Az-Zahra, Tehran, Iran*

Photolyses of β,γ-unsaturated ketones 1 and 2 included in MY zeolites gave the oxa-di-π-methane products, which are believed to originate from the triplet state caused by heavy atom cations present within the supercage.

Recent application of zeolites in organic photochemistry,[1] and our interest in the chemistry of zeolites[2] and the photochemistry of β,γ-unsaturated ketones,[3] has prompted us to investigate the photochemistry of these compounds within the supercages of zeolite Y. We report here the observation of a 1,2-acyl shift, or oxa-di-π-methane (ODPM) rearrangement, of bicyclo-[2.2.1]hept-5-en-2-one (BHO) **1**† and bicyclo[2.2.2]oct-5-en-2-one (BOO) **2**[4] included in heavy cation-exchanged zeolite Y.

The chemistry of β,γ-unsaturated ketones is well-known and many publications on this subject have been published during the last two decades.[5] Upon direct irradiation, the majority of β,γ-unsaturated ketones undergo a singlet-mediated 1,3-acyl shift reaction to produce a rearranged β,γ-unsaturated ketone.[6] Triplet-sensitized photolysis of these compounds, on the other hand, leads to the well known and synthetically useful ODPM rearrangement.[7] Investigation of the extent of singlet–triplet interconversion of the excited guest molecule within a cage, channel or pore has been limited to the study of the photophysical processes of some aromatics and olefins,[8] and photochemical reactions like photodimerization of acenaphthylene [9] and photolysis of 2,3-diazabicyclo[2.2.2]oct-2-ene.[10] We felt that the heavy cations present within the Y-type faujasite supercage could provide interesting results for the photochemistry of β,γ-unsaturated ketones. Because LiY and NaY were not effective for ODPM rearrangement, and KY did not show more than 15% activity for this reaction,‡ we concentrated our experiments on CsY and TlY. It should be emphasized that the absence of triplet formation in LiY and NaY is consistent with their solution behaviour in which the intersystem crossing yields from singlet to triplet is reported to be near zero.[11] This led us to conclude that rearrangement in the supercages of LiY, NaY and mostly in KY is from the singlet excited state.‡

The Cs^+ and Tl^+ cations were exchanged into the NaY zeolite by mixing the powder with the appropriate 10% nitrate solution at 90 °C for 1 h. For each gram of zeolite, 10 ml of the cation nitrate solution was used. This cycle was repeated three times. The zeolite was filtered, washed thoroughly, and then held at 500 °C for 12 h. A typical procedure for the preparation of zeolite-guest complexes is provided below. Dry zeolite (2.1 g) and the ketone (30 mg)§ were stirred in dry hexane (30 ml) for about 2 h under a dry nitrogen atmosphere. The complex was filtered and washed several times with dry hexane to remove any surface adsorbed materials. GC analysis of the filtrates showed that most of the ketone had been introduced into the cavities. The dry solid inclusion complexes were then placed in a quartz tube and photolyzed at 253.7 nm in a Rayonet photoreactor with five lamps for 10–35 h.¶ The photolyses were carried out either in hexane slurry or in the solid state. The products were extracted by stirring the complex in 30 ml of dry Et_2O for *ca*. 12 h or dissolution of the zeolite framework with 1 M HCl. Mass balance in all cases was *ca*. 90%. Identification of products was made by GC (Perkin-Elmer 3920 gas chromatograph equipped with TCD detection and a packed column of 3% OV-17 on Chromosorb W) and comparison of retention times with those of authentic samples. The concentrations were determined by an internal standard procedure using cyclohexanone as the internal standard.‖ The results are shown in Tables 1 and 2.

Table 1 Photolyses results for BHO **1** under various conditions

	Solution[a]		Slurry[b]		Solid	
Medium	*t*/h	Yield (%)	*t*/h	Yield (%)	*t*/h	Yield (%)
Acetone	15	41				
CsY			10	21.4	25	39.2
CsY			15	24	30	40.4
CsY			20	27	35	41.9
TlY			10	33.6	25	55.5
TlY			15	34.3	30	57.8
TlY			20	35	35	61.1

[a] Yield based on photolysis at 253.7 nm (quartz). Photolysis with a low pressure merucury lamp led to 70.4% of **3**. [b] Increasing the photolysis time to more than 20 h did not improve the results.

Table 2 Photolyses results for BOO **2** under various conditions

	Solution[a]		Slurry[b]		Solid	
Medium	*t*/h	Yield (%)	*t*/h	Yield (%)	*t*/h	Yield (%)
Acetone	15	37.3				
CsY			10	12.2	25	29.1
CsY			15	18.6	30	30.6
CsY			20	20.5	35	32.1
TlY			10	24.1	25	38.6
TlY			15	25.6	30	40.5
TlY			20	26.1	35	44.7

[a] Yield based on photolysis at 253.7 nm (quartz). Photolysis with a low pressure mercury lamp led to 66.2% of **4**. [b] Increasing the photolysis time to more than 20 h did not improve the results.

Photolyses of either the hexane slurry or the solid complexes led to the ODPM ketones **3** and **4** as the sole products (Scheme 1). Only traces of 1,3-acyl shift ketones could be detected as byproducts.

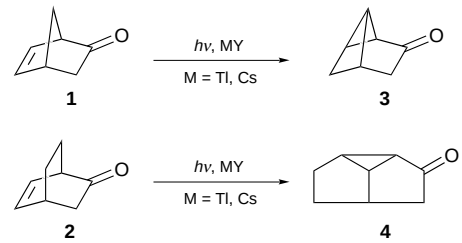

Scheme 1

Since intersystem crossing of β,γ-unsaturated ketones is usually slow following direct irradiation, population of the triplet excited state requires either to use of triplet energy sensitizers or the introduction of heavy atoms to decrease the barrier to the singlet–triplet transition (the heavy atom effect).[12] Because sensitization techniques have been difficult to apply in the crystalline state until now, the triplet state photochemistry of such compounds has not been studied in this medium, except for the remarkable work of Ramamurthy, who investigated the photolyses of Li^+, Na^+, K^+, Rb^+ and Cs^+ salts of a β,γ-unsaturated keto acid and found that there is a strong cation effect in the crystalline state but none in solution.[13]

The formation of the ODPM ketones under the effect of heavy cations within the Y zeolite in our system, particularly the 60% yield of the 1,2-acyl shift product in the presence of TlY, is strong support for the heavy atom cation effect in solid systems. The trends observed in the variation of the triplet yields with increasing mass, *i.e.* Li^+, $Na^+ < K^+ < Cs^+ < Tl^+$, is consistent with the expected spin-orbit coupling-induced triplet formation. The reason for the greater effect of heavy atom castions in the solid state than in the slurries might be attributed to the increased triplet lifetime of the ketone in the solid state, and the reduced diffusional mobility of the guest molecule toward the heavy cations when the channels are filled with solvent molecules. Such behaviour has been observed in the di-π-methane rearrangement of 11-hydroxymethyl-9,10-dihydro-9,10-ethanoanthracene within zeolite KY by the triplet–triplet energy transfer of several sensitizers to the guest molecule within the supercages.[14]

In conclusion, we believe that zeolite–guest complexes containing heavy cations can be considered as remarkable singlet–triplet transition matrices. Our results show it to be an efficient approach to energy transfer from a donor to an acceptor in the solid state. To the best of our knowledge, this is the first report of an ODPM rearrangement arising from an external heavy atom cation effect within a zeolite.

Acknowledgment is made to the Research Council of the University of Tehran for support of this research.

Notes and References

* E-mail: hymn74@khayam.ut.ac.ir

† This compound was prepared *via* oxidation of bicyclo[2.2.1]hept-5-en-2-ol using chromium oxide–pyridine in CH_2Cl_2.

‡ The main rearrangement within the LiY, NaY and KY was 1,3-acyl shift with the formation of rearranged ketone.

§ A ketone : zeolite ratio of 1 : 70 gave the best results.

¶ Photolyses of either the hexane slurries or the dry solids with a low pressure mercury lamp were not efficient.

‖ Ketones **3** and **4** were prepared according to the procedures mentioned in ref. 8(*a*) and were used after purification to establish the standard curves.

1 K. Pitchumani, M. Warrier and V. Ramamurthy, *J. Am. Chem. Soc.*, 1996, **118**, 9428; D. R. Corbin, D. F. Eaton and V. Ramamurthy, *J. Org. Chem.*, 1988, **53**, 5388; D. R. Corbin, D. F. Eaton and V. Ramamurthy, *J. Am. Chem. Soc.*, 1988, **110**, 4848; K. Prfchuman and V. Ramamurthy, *Tetrahedron Lett.*, 1996, **37**, 5297; V. Ramamurthy, D. R. Corbin, N. J. Turro and Y. Sato, *Tetrahedron Lett.*, 1989, **30**, 5829.

2 F. Farzaneh and F. Nikkhoo, *J. Sci. I.R. Iran*, 1995, **6**, 155; M. M. Akbarnejd, F. Farzaneh and M. Khatamian Oskooi, *Iran J. Chem. Chem. Eng.*, 1991, **10**, 14; F. Farzaneh, J. Soleimannejad and M. Ghandi, *J. Mol. Catal. A*, 1997, **118**, 223.

3 M. Ghandi and J. Ipaktschi, *J. Sci. I.R. Iran*, 1989, **1**, 29; 1990, **2**, 101.

4 D. A. Lightner and W. A. Beavers, *J. Am. Chem. Soc.*, 1971, **93**, 2677.

5 For a recent review on the photochemistry of β,γ-unsaturated ketones, see M. Demuth, *Organic Photochemistry*, ed. A. Padwa, Marcel Decker, New York, 1991, vol. 11, ch. 2.

6 L.-F.Hsu, C.-P. Chang, M.-C. Li and N.-C. Chang, *J. Org. Chem.*, 1993, **58**, 4756 and references cited therein.

7 T. J. Eckersley, S. D. Parker and N. A. J. Rogers, *Tetrahedron*, 1984, **40**, 3749; T. J. Eckersley and N. A. J. Rogers, *Tetrahedron*, 1984, **40**, 3759.

8 (*a*) V. Ramamurthy, J. V. Caspar, D. F. Eaton, E. Kuo and D. R. Corbin, *J. Am. Chem. Soc.*, 1992, **114**, 3882; (*b*) J. V. Caspar, V. Ramamurthy and D. R. Corbin, *Coord. Chem. Rev.*, 1990, **97**, 225.

9 V. Ramamurthy, D. R. Corbin, C. V. Kumar and N. J. Turro, *Tetrahedron Lett.*, 1990, **31**, 47.

10 M. A. Anderson and C. B. Grissom, *J. Am. Chem. Soc.*, 1996, **118**, 9552.

11 A. Samanta and R. W. Fessenden, *J. Phys. Chem.*, 1984, **93**, 5823.

12 For a review of the heavy atom effect in organic photochemistry, see J. C. Koziar and D. O. Cowan, *Acc. Chem. Res.*, 1978, **11**, 334.

13 B. Berecka, A. D. Gudmundsdottar, G. Olovsson, V. Ramamurthy, J. R. Scheffer and J. Trotter, *J. Am. Chem. Soc.*, 1994, **116**, 10 322.

14 K. Pitchumani, J. N. Gamlin, V. Ramamurthy and J. R. Scheffer, *Chem. Commun.*, 1996, 2049.

Received in Cambridge, UK, 24th September 1997; 7/06929D

Stereoselective preparation of quaternary benzylic centres using chiral imidazolines†

Peter I. Dalko and Yves Langlois*‡

Laboratoire de Synthèse des Substances Naturelles, associé au CNRS, ICMO, Bâtiment 410, Université de Paris-Sud, 91405 Orsay, France

Dianions derived from C_2 symmetric chiral imidazolines provide good to excellent stereocontrol in alkylation reactions affording fully substituted benzylic centres.

Stereoselective preparation of quaternary centres, particularly in benzylic positions, remains a challenge. Carbometallation followed by nucleophilic substitution is seemingly a simple method, however, difficulties arise in both the preparation of the organometallic intermediate and also in the control of the stereoselectivity of the carbometallation in an inherently crowded position. Reports of the asymmetric preparation of vicinal heteroatom-stabilized tertiary organolithium compounds[1,2] are still scarce, although it is being actively studied by a number of groups.[2] Furthermore, stereoselective formation of fully *C*-substituted carbons *via* deprotonative carbolithiation remains elusive.[3]

In the wake of other studies on five-membered heterocycles as chiral auxiliaries,[4] we were interested in testing imidazolines in asymmetric substitution reactions. We observed that dianions derived from C_2 symmetric chiral imidazoline **1**§ undergo diastereoselective alkylation in the presence of 1.1 equiv. of alkyl halides **2a**–**d** and afforded the corresponding fully *C*-substituted centres **3a**–**e** in good yield. The reaction was performed in THF and the dimetallated intermediate was formed without addition of supplementary complexing agents such as TMEDA or other additives.[5] Some representative examples are given in Table 1. Quaternary centres were obtained with good acyclic diastereoselectivity¶ and in good yield, as illustrated in entries 1–4. The presence of electron-donating substituents on the aryl side chain resulted in a drop in selectivity (entry 5).

Table 1 Alkylation of dianions derived from C_2 symmetric imidazolines using alkyl halides as electrophiles

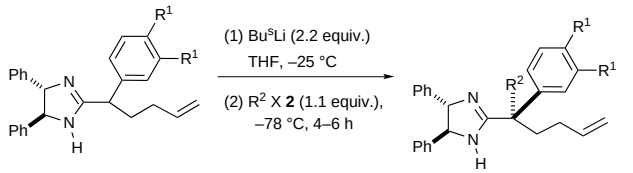

1a R^1 = H
b R^1 = OMe

3a R^1 = H, R^2 = Me
b R^1 = H, R^2 = $CH_2CH_2OBu^t$
c R^1 = H, R^2 = allyl
d R^1 = H, R^2 = Bn
e R^1 = OMe, R^2 = Me

Entry	1	2	Yield (%)	De (%)	3
1	**1a**	**2a** MeI	86	> 95	**3a**
2	**1a**	**2b** $Bu^tOCH_2CH_2I$	79	> 95	**3b**
3	**1a**	**2c** Allyl I	79	92	**3c**
4	**1a**	**2d** BnBr	75	> 95	**3d**
5	**1b**	**2a** MeI	85	80	**3e**

Alkylation of monoanions derived from *N*-alkylated imidazolines such as **4a** proceeded with slightly lower diastereoselectivity. However, good stereocontrol was observed using the conformationally restrained bicyclic imidazoline **4b** (Table 2). Surprisingly, the diastereoselectivity in these reactions was the opposite to the observed for non-substituted C_2 symmetric imidazolines **3a**–**e**, as was ascertained by chemical correlation between **3a** and **5a**: imidazoline **3a** was *N*-methylated using 1.1 equiv. of Bu^nLi and 1.1 equiv. of MeI at −78 °C, and the ^1H and ^{13}C MNR spectra of the resultant product were compared with that of **5a**.

Table 2 Alkylation of monoanions derived from *N*-substituted imidazolines using methyl iodide

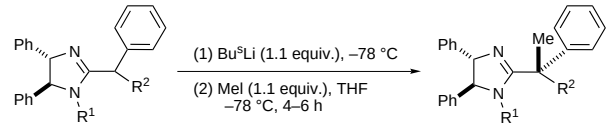

4a R^1 = Me, R^2 = CH_2allyl
b R^1–R^2 = CH_2CH_2

5a R^1 = Me, R^2 = CH_2allyl
b R^1–R^2 = CH_2CH_2

Entry	4	Yield (%)	De (%)	5
1	**4a**	86	72	**5a**
2	**4b**	21	> 95	**5b**

In order to provide a structural basis for the stereodifferentiation, the question of the *C-versus N*-lithiation dichotomy was addressed. A ^{13}C NMR study[6] of selected compounds **6** and **9** was undertaken (Scheme 1). The ^{13}C NMR spectrum at −69 °C of the monolithiated intermediate **7** shows in a single set of well-resolved signals which were in accord with the expected *N*-lithiated product [C_α δ 40.2 (t, $^1J_{C-H}$ 125 Hz)]. Dimetallation using the standard procedure afforded a single, unsymmetrical product whose ^{13}C NMR signals at −69 °C were in accord with those of the *N* and C_α bis-lithiated compound **8**. The lithiated carbon [C_α δ 64.2 (d)] was shown to be slightly pyramidalised ($^1J_{C-H}$ 157 Hz)[7] and thus is stereogenic. The two *ortho* carbons of the benzylic side chain were found to be magnetically non-equivalent at this temperature, which indicates restrained conformational freedom of the side chain.

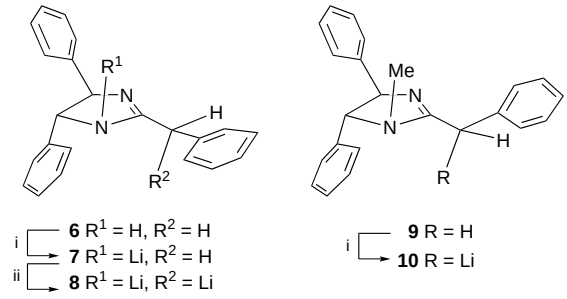

Scheme 1 *Reagents and conditions*: i, Bu^nLi (1.1 equiv.), −69 °C; ii, Bu^nLi (1.1 equiv.), −25 °C, 25 min, then −69 °C

Monolithiation of **9** under standard conditions afforded a single product whose ^{13}C NMR signals at −69 °C were in accord with those of the *C*-lithiated compound **10** [C_α δ66.4 (d, $^1J_{C–H}$ 158 Hz)], structurally similar to the dimetallated counterpart **8** (Scheme 1). These results suggest in both cases the presence of carbometallated species prior to alkylation rather than the formation of *N*-metallated aza-enolates. The stereoselectivity of the alkylation reaction is thus dependent to the stereochemistry of this carbolithiated species[1a,1b,8] and is currently being investigated in our laboratory.‖

In summary, the method described here allows the stereoselective preparation of either stereoisomeric quaternary benzylic centre independently of the stereochemistry of the inducting chiral auxiliary, using non-complexing alkyl halides.[8] Beyond the perspective of building fully *C*-substituted benzylic quaternary carbons[9] the method could also be useful in providing access to other, covalently linked stereodefined tertiary organometallic compounds useful in asymmetric synthesis.

Notes and References

† Dedicated to Professor Yoshito Kishi on the occasion of his 60th birthday.

‡ E-mail: langlois@icmo.u-psud.fr

§ Racemic imidazolines were used as starting materials for the alkylation reactions. Starting materials were prepared by classical condensation of the corresponding imino ether hydrochloride, itself obtained from arylacetonitrile, and *trans*-1,2-diphenylethylenediamine, see ref. 4(*c*).

¶ The diastereoselectivity of the reaction was measured by ^1H NMR analysis by integrating the α-methyl or other characteristic signals.

‖ The configuration of the newly formed stereocentre was established by chemical correlation. This synthesis will be presented in due course.

1 Recent reviews on stereoselective alkylation using organometallic intermediates and alkyl halides: (*a*) P. Beak, A. Basu, D. J. Gallagher, Y. S. Park and S. Thayumanavan, *Acc. Chem. Res.*, 1996, **29**, 552; (*b*) D. Seebach, A. R. Sting and M. Hoffmann, *Angew. Chem., Int. Ed. Engl.*, 1996, **35**, 2708; (*c*) *Stereoselective Synthesis*, in *Houben-Weyl-Methods of Organic Chemistry*, ed. G. Helmchen, R. W. Hoffmann, J. Mulzer and E. Schaumann, Thieme, Stuttgart, 1995, vol. E21a, pp. 762–881; (*d*) D. Hoppe, F. Hinze, P. Tebben, M. Paetow, H. Ahrens, J. Schwerdtfeger, P. Sommerfeld, J. Haller, W. Guarnieri, S. Kolczewski, T. Hense and I. Hoppe, *Pure Appl. Chem.*, 1994, **66**, 1479.

2 E. Lorthiois, I. Marek and J.-F. Normant, *Bull. Soc. Chim. Fr.*, 1997, **134**, 333; L. Micoulin, V. Jullian, J. C. Quirion and H. P. Husson, *Tetrahedron: Asymmetry*, 1996, **7**, 2839; T. L. Elworthy and A. I. Meyers, *Tetrahedron*, 1994, **50**, 6089; A. I. Meyers, *Tetrahedron*, 1992, **48**, 2589; D. Romo and A. I. Meyers, *Tetrahedron*, 1991, **47**, 9503; H.-J. Gais, G. Hellmann, H. Günther, F. Lopez, H. J. Lindner and S. Braun, *Angew. Chem., Int. Ed. Engl.*, 1989, **28**, 1025.

3 A. I. Meyers and G. P. Brengel, *Chem. Commun.*, 1997, 1; A. I. Meyers, M. A. Seefeld, B. A. Lefker and J. F. Blake, *J. Am. Chem. Soc.*, 1997, **119**, 4564; I. Hoppe, M. Marsch, K. Harms, G. Boche and D. Hoppe, *Angew. Chem., Int. Ed. Engl.*, 1995, **34**, 2158.

4 (*a*) C. Kouklovsky, A. Pouilhès and Y. Langlois, *J. Am. Chem. Soc.*, 1990, **112**, 6672; (*b*) T. Berranger and Y. Langlois, *J. Org. Chem.*, 1995, **60**, 1720; (*c*) P. I. Dalko and Y. Langlois, *Tetrahedron Lett.*, 1992, **33**, 5213.

5 A. G. Myers, J. L. Gleason, T. Yoon and D. W. Kung, *J. Am. Chem. Soc.*, 1997, **119**, 656 and references cited therein.

6 For use of ^{13}C NMR spectroscopy in investigating the structure of metalation products, see G. Fraenkel and F. Qiu, *J. Am. Chem. Soc.*, 1997, **119**, 3571; H. J. Reich and J. E. Holladay, *J. Am. Chem. Soc.*, 1995, **117**, 8470; G. Fraenkel and K. V. Martin, *J. Am. Chem. Soc.*, 1995, **117**, 10 336; D. Croisat, J. Seyden-Penne, T. Strzalko and L. Wartski, *J. Org. Chem.*, 1992, **57**, 6435.

7 $^1J_{C–H}$ couplings are diagnostic, and were used routinely to provide structural information. In particular, these couplings have been shown to be directly proportional to the fraction of s-character in the given C–H bonds, and this has been used to investigate the hybridization of molecules. See J. R. Abraham, J. Fisher and P. Loftus, *Introduction to NMR Spectroscopy*, Wiley, Chichester, 1988, pp. 51–53; E. Breitmaier and W. Voelter, *Carbon-13 NMR Spectroscopy*, 3rd edn. VCH, New York, 1987, pp. 134–140.

8 S. Thayumanavan, A. Basu and P. Beak, *J. Am. Chem. Soc.*, 1997, **119**, 8209.

9 For a review concerning the creation of asymmetric quaternary centres, see K. Fuji, *Chem. Rev.*, 1993, **93**, 2037.

Received in Liverpool, UK, 13th October 1997; 7/07387I

New synthetic methodology utilising 1,2-dioxines and stabilised phosphorus ylides: a highly diastereoselective cyclopropanation reaction

Thomas D. Avery,[a] Thomas D. Haselgrove,[a] Tanya J. Rathbone,[b] Dennis K. Taylor*[a] and Edward R. T. Tiekink[a]

[a] *Department of Chemistry, The University of Adelaide, Adelaide, Australia, 5005*
[b] *Department of Chemistry, Monash University, Clayton, Victoria, Australia, 3168*

A new method is described for the synthesis of diastereomerically pure cyclopropanes from substituted 1,2-dioxines 1a–c and stabilised phosphorus ylides 2a–e.

In 1994 the group of Adam and Treiber established for the first time that the peroxide bond of 1,2-dioxetanes is susceptible to nucleophilic 'attack' by simple diazoalkanes.[1] In this first report, 1,2-dioxetanes upon treatment with diazoalkanes afforded a mixture of products including 1,3-dioxolanes. More recently, the reactions between various methyl-substituted 1,2-dioxetanes and simple triphenylalkylidenephosphoranes were explored by the same group.[2] Initial nucleophilic 'attack' on the O–O linkage was proposed for the observed formation, at low temperature, of 2,2,2-triphenyl-1,4,2λ^5-dioxaphosphorinanes which, upon warming, ring-opened affording dipolar phosphonium alkoxides.

Herein we report that various 1,2-dioxines **1a**–**c** react under mild conditions with stabilised phosphorus ylides **2a**–**e** to afford novel diastereomerically pure cyclopropanes [reaction (1)]. To

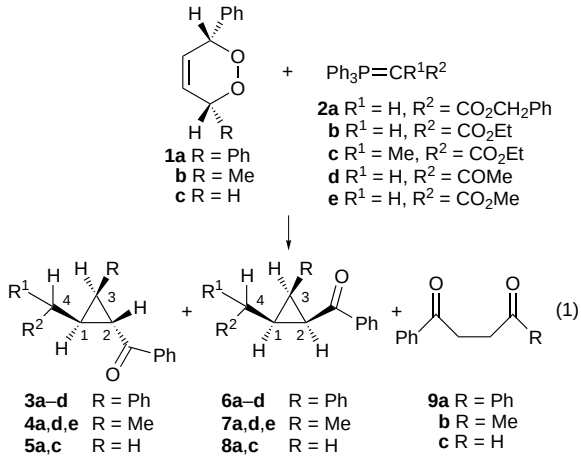

the best of our knowledge, the reactions of stabilised phosphorus ylides with 1,2-dioxines have not been reported until now. A typical reaction involved treatment of **1a**[3] with **2a** (1.1 equiv.) in an appropriate solvent (usually CH_2Cl_2) at ambient temperature. The major product formed was identified as the cyclopropane **3a** along with a trace of diketone **9a**[4]. Similar reactions afforded a variety of di- and tri-substituted cyclopropanes in excellent yields and are collated in Table 1. Compounds **1a** and **c** afforded essentially diastereomerically pure *trans*-cyclopropanes whilst **1b** afforded the *trans*-cyclopropane as the major diastereomer along with a minor amount of the *cis*-cyclopropane. Typically the isolated yields were within 10% of those quoted whilst the diastereomers were easily separated by column chromatography. The structure and relative stereochemistry of the cyclopropanes were unambiguously elucidated from a combination of ^{1}H, ^{13}C, DEPT, NOESY (^{1}H-COSY and HMQC with gradient coherence selection)

Table 1 Reaction of 1,2-dioxines **1a**–**c** with various stabilised phosphorus ylides **2a**–**e** at 25 °C[a]

1,2-Dioxine	Ylide	Yield of cyclopropane (%)		Yield of **9** (%)
1a	**2a**	**3a** (95)	**6a** (⩽2)	**9a** (3)
	2b	**3b** (96)	**6b** (⩽2)	**9a** (2)
	2c	**3c** (48)	**6c** (nd)	**9a** (52)
	2d	**3d** (nd)	**6d** (nd)	**9a** (100)
1b	**2a**	**4a** (84)	**7a** (15)	**9b** (⩽1)
	2d	**4d** (75)	**7d** (15)	**9b** (10)
	2e	**4e** (82)	**7e** (18)	**9b** (nd)
1c	**2a**	**5a** (100)	**8a** (nd)	**9c** (nd)
	2c	**5c** (80)	**8c** (nd)	**9c** (nd)[b]

[a] All reactions performed in CH_2Cl_2; yields were determined from the ^{1}H NMR spectra (600 MHz) of the crude reaction mixtures; nd denotes not detectable. [b] Another unidentified minor product present.

NMR techniques.† X-Ray analysis‡ of **4a** (Fig. 1) unambiguously confirmed the general structural and stereochemical assignments elucidated by NMR spectroscopy.

The effect of solvent and additives on the rate of reaction between **1a** and **2a** and the cyclopropane : diketone ratio **3a** : **9a** was evaluated. Our initial findings indicate that the overall rate of reaction increases only slightly with increasing solvent polarity. The small rate increase is inconsistent with a mechanism involving zwitterionic intermediates in the rate-determining step. The relative rate and product ratio was unaffected by the addition of TEMPO suggesting that free radicals are not involved. Additionally, the formation of 'free' carbenes can be excluded on the basis that addition of excess cyclohexene failed to compete in cyclopropane formation. This

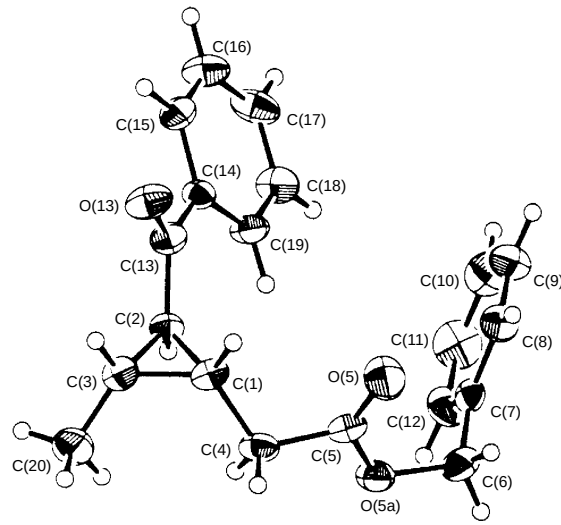

Fig. 1 Molecular structure of **4a** showing the crystallographic numbering scheme employed: O(5)–C(5)–C(4)–C(1) 34(1)°, C(5)–O(5a)–C(6)–C(7) −82.6(8)°, C(2)–C(13)–C(14)–C(15) 159.5(7)°

conclusion was further supported by the observation that only a trace of the carbene dimer (< 1%) could be detected by ^{1}H NMR analysis of the crude reaction mixtures. Finally, performing the reaction at 80 °C simply lead to an increased rate without a change in product outcome or ratio.

The reaction of equimolar amounts of **1a** and **2a** in C_6D_6 was monitored by ^{31}P NMR spectroscopy. At no time could any 'free' triphenylphosphine or zwitterionic intermediates be detected. Careful ^{1}H NMR analysis of the crude mixture after cessation of the reaction revealed the presence of **3a**, **9a**, Ph_3PO and unreacted **2a**. All **1a** had been consumed affording **3a** and **9a** in a 77 : 22 ratio. The remaining 1% constituted the *cis*-cyclopropane. Formation of Ph_3PO (75%) parallels the yield of the cyclopropane as expected. Most important was the observation that 22% unreacted **2a** remained and parallels **9a** formation (22%). This observation suggests that formation of **9a** is catalytic in ylide. Indeed, analysis of all crude reaction mixtures by ^{31}P and ^{1}H NMR spectroscopies showed the same trend. Blank reactions showed that formation of **9a**–**c** was not promoted by Ph_3PO. We have evidence that the rearrangement **1a** → **9a** is not promoted by 'free' Ph_3P liberated during the ylide reaction, *e.g.* addition of excess Ph_3P to the reaction mixture containing **1a** and **2a** failed to dramatically change product outcome. Based on these initial findings we suggest that formation of **9a** in the reaction of **1a** with **2a** is promoted by the ylide acting as a weak base[5] in a catalytic manner. Base catalysed rearrangement (Kornblum–De La Mare decomposition) of cyclic peroxides has been reported previously and is initiated by removal of a proton from the carbon adjacent to the O–O linkage.[6] Finally, the observation that the more sterically hindered **2c** affords less cyclopropane **3c** when compared to that for **2b** in identical solvents suggests that there is a steric component to the two competing processes.

A significant mechanistic finding was the observation of the *trans*-alcohol **10** intermediate during ^{1}H NMR monitoring of these reactions. Indeed, we were able to isolate a quantity of **10** from the reaction mixture and demonstrate that it lead to the observed cyclopropanes and no 1,2-diketone upon addition of ylid. Although the reaction manifold is complicated by many factors, Scheme 1 depicts a general mechanistic overview. Interaction of **1** and **2** leads in a rate-limiting step to the formation of the key intermediate **10**. Michael addition of the ylide to **10**, followed by cyclisation, proton transfer and extrusion of triphenylphosphine oxide from **11** affords the observed cyclopropanes. In competition with this process is the known cyclisation[6] of (*Z*)-**10** *via* the hemi-acetal and rearrangement leading to formation of **9**.

Synthetically, this novel reaction has several advantages over existing methods[7] for cyclopropane formation involving phosphorus ylides, as functionalised cyclopropanes are formed in a highly diastereoselective manner in excellent yields. We are currently evaluating the reactions of various 1,2-dioxines, alkyl hydroperoxides and disulfides with a variety of stabilised and non-stabilised ylides (phosphorus, sulfur *etc.*) and full mechanistic details will be presented in due course.

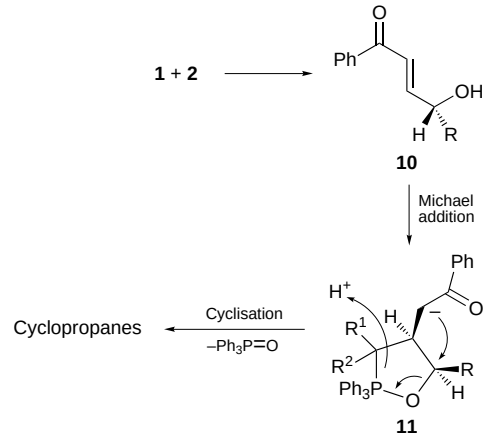

Scheme 1

Financial support in the form of set-up grants (Adelaide and Monash Universities, D. K. T.) and the ARC (E. R. T. T.) is greatly acknowledged. Assistance from Dr S. M. Pyke (Adelaide) in NMR spectral analysis is also acknowledged while Dr P. Perlmutter (Monash University) is thanked for co-supervision of T. J. R.

Notes and References

* E-mail: dtaylor@chemistry.adelaide.edu.au

† All new compounds have been fully characterised by elemental analysis, spectroscopy and mass spectrometry.

‡ *Crystal data*: $C_{20}H_{20}O_3$, triclinic, space group $P\bar{1}$ with a = 7.952(3), b = 18.417(4), c = 5.680(2) Å, α = 90.51(2), β = 92.28(3), γ = 85.25(3)°, U = 828.4(4) Å^3, Z = 2, D_c = 1.236 g cm^{-3} and μ = 0.82 cm^{-1}. Single-crystal X-ray diffraction data were collected at 293 K on a Rigaku AFC6R diffractometer (Mo-Kα radiation) with $\theta/2\omega$ scans, 3 < θ < 27.5°. The structure was solved with SIR92 and refined with the TEXSAN Structure Analysis Package (Molecular Structure Corporation, 1985) of crystallographic programs. A total of 937 reflections with $I \geqslant 3.0\sigma(I)$ were used in the refinement which converged with R = 0.063 and R_w = 0.050 $\{1/[\sigma^2(F) + 0.006F^2]\}$. CCDC 182/708.

1 W. Adam and A. Treiber, *J. Org. Chem.*, 1994, **59**, 840.
2 W. Adam, H. M. Harrer and A. Treiber, *J. Am. Chem. Soc.*, 1994, **116**, 7581.
3 M. Matsumoto, S. Dobashi, K. Kuroda and K. Kondo, *Tetrahedron*, 1985, **41**, 2147.
4 G. Rio and J. Berthelot, *Bull. Soc. Chim. Fr.*, 1969, **5**, 1664.
5 A. W. Johnson, in *Organic Chemistry*, (*Ylid Chemistry*), ed. A. T. Bloomquist, Academic Press, New York, 1966, vol. 7, pp. 64–70.
6 N. Kornblum and H. E. De La Mare, *J. Am. Chem. Soc.*, 1951, **73**, 881; M. G. Zabgorski and R. G. Salomon, *J. Am. Chem. Soc.*, 1980, **102**, 2501; M. E. Sengul, Z. Ceylan and M. Balci, *Tetrahedron*, 1997, **53**, 10 401.
7 D. B. Denny, J. J. Vill and M. J. Boskin, *J. Am. Chem. Soc.*, 1962, **84,** 3944; ref. 5, pp. 111–113 and 116–120 and references cited therein.

Received in Cambridge, UK, 13th, October 1997; 7/07360G

New route to organoaluminium sulfides: synthesis of $(Mes^*AlS)_2$ (Mes^* = -$C_6H_2Bu^t_3$-2,4,6) and its dimethyl sulfoxide adduct $[Mes^*AlS(OSMe_2)]_2$

Rudolf J. Wehmschulte and Philip P. Power*

Department of Chemistry, University of California, Davis, California 95616, USA

Treatment of the alane $(Mes^*AlH_2)_2$ (Mes^* = -$C_6H_2Bu^t_3$-2,4,6) with $S(SiMe_3)_2$ in refluxing toluene affords the novel organoaluminium sulfide $(Mes^*AlS)_2$ 1 which has a previously unobserved dimeric structure; treatment of 1 with 2 equiv. of Me_2SO furnishes the complex $[Mes^*AlS(OSMe_2)]_2$ 2 in which a dimeric configuration is retained, and which shows weak intermolecular interactions between neighboring dimers.

Group 13 organometallic chalcogenide species of formula $(RME)_n$ (R = alkyl, aryl; M = Al, Ga, In; E = O–Te) are usually synthesized with use of the organometallic precursors MR_3.[1] For the heavier chalcogenide derivatives, direct interaction of the elements themselves (*i.e.* S, Se, Te) with the metal trialkyls has afforded several new compounds which have three-dimensional cage structures.[2] For the lighter oxide derivatives, however, the reaction between water (or water complexed in metal salts)[3] remains the preferred method of synthesis of $(RMO)_n$ compounds.† Recently, it has been shown that aluminium hydride compounds are also useful precursors for the synthesis of organoalumoxanes.[4] Thus, the reaction of the hydride $(Mes^*AlH_2)_2$[5] (Mes^* = -$C_6H_2Bu^t_3$-2,4,6) with $(Me_2SiO)_3$ affords the unique tetramer $(Mes^*AlO)_4$ with elimination of SiH_2Me_2. We now report that the reaction of $(Mes^*AlH_2)_2$ with $S(SiMe_3)_2$‡ affords the unique, dimeric, heavier chalcogenide derivative $(Mes^*AlS)_2$ **1** and that treatment of **1** with Me_2SO does not effect dissociation of the dimeric structure but affords the adduct $[Mes^*AlS(OSMe_2)]_2$, **2**.

Compound **1**, which displays high thermal stability (mp > 200 °C), can be synthesized§ in almost quantitative yield by refluxing $(Mes^*AlH_2)_2$[5] with 2 equiv. of $S(SiMe_3)_2$ in either toluene or *n*-octane. X-Ray crystallographic data¶ for **1** show that it crystallizes as dimeric units (Fig. 1) which have a crystallographically required inversion center. The planar Al_2S_2 core is characterized by almost equal Al–S distances of 2.2083(9) and 2.2107(14) Å and internal ring angles of 78.09(3)° at S and 101.91(3)° at Al. The external S–Al–C angles, 127.94(7) and 130.14(7)°, are quite similar, so that the sum of the angles at Al is 359.99° indicating strictly planar coordination at Al. However, there are also short (2.26–2.33 Å) interactions between a number of *ortho*-Bu^t H atoms and Al. The angle between the normals to the $(AlS)_2$ and aromatic ring planes is 89.3°.

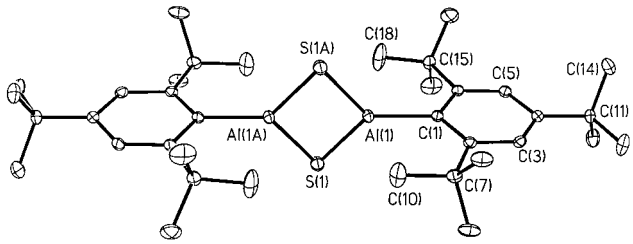

Fig. 1 Thermal ellipsoidal (30%) plot of **1** with H atoms not shown. Some important bond distances (Å) and angles (°): Al(1)–S(1) 2.2083(9), Al(1)–S(1A) 2.2107(14), Al–C(1) 1.956(2), Al(1)···Al(1A) 2.7835(13); Al(1)–S(1)–Al(1A) 78.09(3), S(1)–Al(1)–S(1A) 101.91(3), S(1)–Al(1)–C(1) 127.94(7), S(1A)–Al(1)–C(1) 130.14(7).

The dimeric structure of **1** may be contrasted with the tetrameric structure of the corresponding oxide species $(Mes^*AlO)_4$[4] which features an almost planar, eight-membered Al_4O_4 ring with wide (*ca.* 151°) Al–O–Al angles. The lower aggregation in **1** thus, may be a consequence of the reluctance of the S atoms to hybridize which imposes a narrower interbond angle. This leads to greater steric congestion in the molecule which results in the lower degree of aggregation observed for **1**. Apparently, **1** is only the second example of a mono-organoaluminium sulfide to be fully structurally characterized. The only previous example is the tetrameric species $[(Me_2EtC)AlS]_4$[2d] which has an Al_4S_4 cubane structure with Al–S distances in the range 2.295(8)–2.319(9) Å. The longer Al–S distances in that compound are due to the higher coordination numbers of both Al (four) and S (three). The short Al–S distances in **1** are similar to those observed in the low-coordinate compounds $Al(SMes^*)_3$[6] [Al–S 2.172(2)–2.191(2) Å], $S[Al\{CH(SiMe_3)_2\}]_2$[7] [Al–S 2.187(4) Å] and $Al_4I_4S_2(SMe)_4$[8] [Al–S (two-coordinate) 2.16(1)–2.20(1) Å].

The dimethyl sulfoxide adduct **2** was prepared by the addition of 2 equiv. of Me_2SO to **1** in benzene. Complex **2** was formed essentially instantaneously and it is precipitated from benzene at room temperature. Heating the solution to reflux temperature resulted in redissolution of the precipitate and cooling slowly resulted in crystals suitable for X-ray crystallography. The X-ray data for **2** show that the dimeric Al_2S_2 core structure (Fig. 2) remains intact and that the metals are each complexed by one dimethyl sulfoxide molecule which are disposed on opposite sides of the Al_2S_2 core. This results in an increase of *ca.* 0.05 Å in the Al–S bond lengths which span the narrow range 2.243(2)–2.259(2) Å. The Al–C distances are lengthened by about the same amount; from 1.956(2) Å in **1** to an average of 2.022(8) Å in **2**. The average Al–O distance is 1.86(1) Å, which is within the range found in related complexes.[9] Also, the Al_2S_2 core is folded slightly (fold angle 167.5°) along the S(1)···S(2) axis. Although each Al is complexed by one Me_2SO, it can be seen from Fig. 2 that the relative orientation of each donor molecule is different. Thus, the Me_2SO containing O(1) is oriented such that the SMe_2 moiety lies above the Al_2S_2 core whereas the O(2) containing Me_2SO is oriented away from the core. These different orientations are reflected in different Al–O–S angles of 114.2(2)° at O(1) and 130.0(2) at O(2). It seems that this unusual arrangement is a result of some weak intermolecular interactions involving the Me_2SO donor containing O(2). These interactions involve relatively short O···H distances [*e.g.* O(2)···H(40E) 2.89 Å, O(2)···H(39F) 2.63 Å], and S···H distances [*e.g.* S(1)···H(39C) 3.04 Å, S(2)···H(40E) 3.02 Å]. Another notable feature of the structure of **2** is the distorted geometry at the *ipso*-C atoms of the Mes* ligands. The averaged aromatic ring planes are bent by *ca.* 25° from the Al–C vector lines. Similar distortions have been observed in other Mes* group 13 derivatives.[10]

Finally, although no dissociation of the dimeric **1** was effected by the addition of Me_2SO, attempted redissolution of isolated **2** results in its partial decomposition and production of

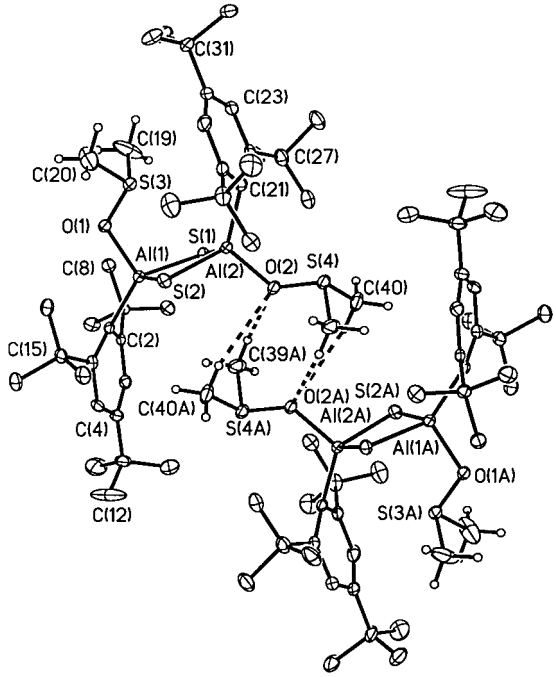

Fig. 2 Computer generated drawing of **2**. H atoms, except those involved in intermolecular interactions, are not shown. Some important bond distances (Å) and angles (°): Al(1)–S(1) 2.259(2), Al(1)–S(2) 2.243(2), Al(2)–S(1) 2.258(2), Al(2)–S(2) 2.247(2), Al(1)–O(1) 1.869(2), Al(2)–O(2) 1.847(3), Al(1)–C(1) 2.014(4), Al(2)–C(21) 2.029(4), S(3)–O(1) 1.553(3), S(4)–O(2) 1.548(3), Al(1)···Al(2) = 2.999(2), S–C(Me) av 1.766(8); S(1)–Al(1)–S(2) 95.91(6), S(1)–Al(2)–S(2) 95.84(6), Al(1)–S(1)–Al(2) 83.20(5), Al(1)–S(2)–Al(2) 83.83(5), S(1)–Al(1)–C(1) 118.79(12), S(2)–Al(1)–C(1) 118.25(12), O(1)–Al(1)–C(1) 115.30(14), O(2)–Al(2)–C(21) 115.16(14), S(3)–O(1)–Al(1) 114.2(2), S(4)–O(2)–Al(2) 130.0(2).

an orange–red solid. Attempts to identify the composition of this solid are currently underway.

We thank the National Science Foundation and the Donors of the Petroleum Research Fund administered by the American Chemical Society for financial support.

Notes and References

*E-mail: pppower@ucdavis.edu

† Alumoxanes of formula $R_2AlOAlR_2$ can be synthesized by the reaction of triorganoaluminium compounds with species containing reactive oxygen such as CO_2, $RC(O)NR_2$, $MeCO_2H$ and Me_2SO. See: H. Sinn and W. Kaminsky, *Adv. Organomet. Chem.*, 1980, **18**, 99; W. Uhl, M. Koch, W. Hiller and M. Heckel, *Angew. Chem., Int. Ed. Engl.*, 1995, **34**, 989.

‡ The compound $S(SiMe_3)_2$ has been extensively used recently in the synthesis of several transition metal sulfide cluster compounds. See: D. Fenske and S. Dehnen, *Chem. Eur. J.*, 1996, **2**, 1407.

§ All manipulations were carried out under anaerobic and anhydrous conditions. The compound $(Mes^*AlH_2)_2$[5] was synthesized as described in the literature and $S(SiMe_3)_2$ was purchased from Aldrich and used as received.

1 or **1**·PhMe: A solution of $(Mes^*AlH_2)_2$[5] (1.05 g, 1.91 mmol) in toluene (25 ml) was heated with $(Me_3Si)_2S$ (0.81 ml, 3.82 mmol, 0.68 g) at room temp. The clear, colorless solution was heated to 100–105 °C for *ca.* 21 h during which time large colorless plates of **1**·PhMe formed. Yield: 1.25 g, 93%. Mp: turns opaque at 120–140 °C (desolvation), melts at 305–310 °C. Crystals of unsolvated **1** suitable for X-ray diffraction studies were obtained *via* a similar procedure by the reaction of $(Mes^*AlH_2)_2$ with $(Me_3Si)_2S$ in *n*-octane at 115–120 °C for 38 h. Yield: 42%. Mp: turns slowly opaque at 250–280 °C, melts at 310–312 °C. ^{1}H NMR (C_6D_6, 85 °C): δ 7.51 (s, *m*-H, 4 H), 1.81 (s, *o*-CH_3, 36 H), 1.36 (s, *p*-CH_3, 18 H).

2: Dimethyl sulfoxide (0.06 ml, 0.8 mmol, 0.062 g) was added to a slurry of finely ground **1**·PhMe (0.16 g, 0.23 mmol) in benzene (25 ml) at room temp. to give an almost clear solution from which after a few seconds a fine, colorless solid precipitates. This was dissolved by heating to reflux for *ca.* 1 min to afford a clear colorless solution from which, after 3 days at room temp. *ca.* 0.04 g of colorless plates could be isolated. Yield: 23%. Mp: turns red at 235 °C, gradually darkens to almost black at 300 °C, does not melt below 300 °C.

It is noteworthy that **1** is practically insoluble in hydrocarbon solvents. It can be solubilized by the addition of Me_2SO or HMPA at elevated temperatures (the range 60–80 °C works best). From these solutions crystals are usually obtained upon cooling to room temp. These crystals do not redissolve without decomposition.

¶ Crystal data at T = 130 K with Mo-Kα, (λ = 0.710 73 Å) radiation for **1** and Cu-Kα, (λ = 1.541 78 Å) radiation for **2**: **1**, $C_{36}H_{58}Al_2S_2$, M = 608.9, monoclinic, space group $C2/c$, a = 26.924(5), b = 9.845(2), c = 16.780(3) Å, β = 125.86(3)°, U = 3064(1) Å^3, μ = 0.219 mm^{-1}, Z = 4 (8/2), wR_2 = 0.119 for all 4149 data, R_1 = 0.047 for 3164 [$I > 2\sigma(I)$] data; **2**, $C_{40}H_{70}Al_2O_2S_4$, M = 765.2 monoclinic, space group $P2_1/n$, a = 18.374(5), b = 9.883(2), c = 24.587(3) Å, β = 91.16(2)°, U = 4464(2) Å^3, μ = 2.560 mm^{-1}, Z = 4, wR_2 = 0.143 for all 5830 data, R_1 = 0.053 for 4550 [$I > 2\sigma(I)$] data. CCDC 182/706.

1 A. R. Barron, *Comments Inorg. Chem.*, 1993, **14**, 123.
2 (*a*) A. H. Cowley, R. A. Jones, P. R. Harris, D. A. Atwood, L. Contreras and C. J. Burek, *Angew. Chem., Int. Ed. Engl.*, 1991, **30**, 1143; (*b*) M. B. Power and A. R. Barron, *J. Chem. Soc., Chem. Commun.*, 1991, 1315; (*c*) M. B. Power, J. W. Ziller, A. N. Tyler and A. R. Barron, *Organometallics*, 1992, **11**, 1055; (*d*) C. J. Harlan, E. G. Gillan, S. G. Bott and A. R. Barron, *Organometallics*, 1996, **15**, 5479; (*e*) S. L. Stoll, S. G. Bott and A. R. Barron, *J. Chem. Soc., Dalton Trans.*, 1997, 1315.
3 M. K. Mason, J. M. Smith, S. G. Bott and A. R. Barron, *J. Am. Chem. Soc.*, 1993, **115**, 4971.
4 R. J. Wehmschulte and P. P. Power, *J. Am. Chem. Soc.*, 1997, **119**, 8387.
5 R. J. Wehmschulte and P. P. Power, *Inorg. Chem.*, 1994, **33**, 5611.
6 K. Ruhlandt-Senge and P. P. Power, *Inorg. Chem.*, 1991, **30**, 2633.
7 W. Uhl, A. Vester and W. Miller, *J. Organomet. Chem.*, 1993, **443**, 9.
8 A. Boardman, R. W. H. Small and I. J. Worrall, *Inorg. Chim. Acta*, 1986, **120**, L23.
9 M. B. Power, S. G. Bott, D. L. Clark, J. L. Atwood and A. R. Barron, *Organometallics*, 1990, **9**, 3086.
10 A. Meller, S. Pusch, E. Pohl, L. Häming and R. Herbst-Irmer, *Chem. Ber.*, 1993, **126**, 2255; H. Rahbarnoohi, M. Heeg and J. P. Oliver, *Organometallics*, 1994, **13**, 2123; (*c*) R. J. Wehmschulte, J. J. Ellison, K. Ruhlandt-Senge and P. P. Power, *Inorg. Chem.*, 1994, **33**, 6300.

Received in Bloomington, IN, USA, 2nd October 1997; 7/07142F

One-pot electrochemical formation of *meso,meso*-linked porphyrin arrays

Takuji Ogawa,*[a] Yoshihiro Nishimoto,[b] Naoya Yoshida,[c] Noboru Ono[b] and Atsuhiro Osukua*[c]

[a] *Institute for Fundamental Research of Organic Chemistry, Kyushu University, Hakozaki, Higashi-ku, Fukuoka 812-81, Japan*
[b] *Department of Chemistry, Faculty of Science, Ehime University, Matsuyama 790, Japan*
[c] *Department of Chemistry, Graduate School of Science, Kyoto University, Sakyo-ku, Kyoto 606-01, Japan*

Electrochemical oxidation of [5,15-bis(3,5-di-*tert*-butylphenyl)porphyrinato]zinc(II) 1, [5,15-bis(4-methoxycarbonylphenyl)porphyrinato]zinc(II), [5,15-bis(pentafluorophenyl)porphyrinato]zinc(II) or [10-bromo-5,15-diphenylporphyrinato]zinc(II) in benzonitrile using a platinum net as the working electrode afforded the corresponding *meso,meso*-linked oligomer porphyrin arrays, and up to the octamer porphyrin array could be isolated for 1.

Polynuclear porphyrins have been attracting considerable attention as biomimetic models of photosynthetic systems as well as photonic materials and functional molecular devices.[1–7]

In a previous communication we reported the oxidative coupling reaction of [5,15-bis(3,5-di-*tert*-butylphenyl)-porphyrinato]zinc(II) **1** with silver(I) salts to give the porphyrin dimer **2**, the porphyrin trimer **3** and the porphyrin tetramer **4**.[8] The possible mechanism proposed is an initial one-electron oxidation of zinc porphyrin with Ag^{I} followed by nucleophilic attack of a neutral zinc porphyrin. This mechanism suggests that electrochemical oxidation also may lead to the formation of the *meso,meso*-coupled porphyrin arrays. Here we report an electrochemical preparation of the porphyrin arrays, by which the usage of expensive silver salts is not required, the oxidizing potentials can be best tuned to the porphyrin used, and the long porphyrin arrays can be prepared in a one-step procedure through prolonged electrolysis.

Porphyrin **1** (n = 1) (219 mg, 0.293 mmol) was electrolyzed in dry benzonitrile (210 ml) in a single cell with NBu_4ClO_4 (0.1 M) as the electrolyte, a platinum net (1.8 × 2.4 cm) as the counter electrode, and a platinum net (3 × 4 cm) as the working electrode; the electricity used was 0.732 mF. The porphyrin products were purified by being passed through an alumina and then a silica gel chromatography column, and isolated by preparative scale HPLC using a gel permeation column (GPC–HPLC). The structures were identified through comparison with the authentic samples:[8] **1** (44.0%), **2** (n = 2) (20.7%), **3** (n = 3) (2.9%) and **4** (n = 4) (0.9%). When porphyrin **1** (211 mg, 0.282 mmol) was electrolyzed under similar conditions using electricity of 1.65 mF, the higher homologous pentamer **5** (n = 5), hexamer **6** (n = 6), heptamer **7** (n = 7) and octamer **8** (n = 8) could be isolated at yields of 0.5, 0.4, 0.2 and 0.05%, respectively, together with **1** (6.7%), **2** (10.2%), **3** (3.2%) and **4** (1.6%) by GPC–HPLC. The new product was characterized by ^{1}H NMR spectroscopy (500 or 600 MHz) and FAB mass spectrometry or MALDI-TOF mass spectrometry.†

Treatment of [5,15-bis(4-methoxycarbonylphenyl)porphyrinato]zinc(II) **9** at higher oxidation potential (+0.68 V *vs.* Ag/$AgNO_3$) than **1** (+0.54 V *vs.* Ag/$AgNO_3$) with $AgClO_4$ under the conditions reported previously[8] did not afford the corresponding *meso,meso*-linked porphyrin arrays, although an unidentified complex mixture together with *ca.* 60% of the recovered starting material were obtained. However, when **9** (51 mg, 79 μmol) was electrolyzed using electricity of 134 μF, it afforded the *meso,meso*-linked porphyrin dimer **10** (34.3%), porphyrin trimer **11** (6.9%) and the starting porphyrin **9** (47.4%). Similarly, [5,15-bis(pentafluorophenyl)porphyrinato]zinc(II) **12** (+0.77 V *vs.* Ag/$AgNO_3$) and (10-bromo-5,15-diphenylporphyrinato)zinc(II) **13** (+0.56 V *vs.* Ag/$AgNO_3$), which did not give the corresponding *meso,meso*-linked porphyrin arrays by the silver salt method, afforded the corresponding dimers **14** and **15** under similar conditions by electrolysis in isolated yields of 11.6 and 47.5%, respectively. Thus the electrochemical method has a wider scope for the substrates than the silver salt method.

These *meso,meso*-linked porphyrin arrays so far isolated were quite soluble in $CHCl_3$. Of particular note is the fact that even the arrays of porphyrin **9**, **12** and **13**, which have little sterical hindrance to prevent π–π stacking of the porphyrin planes, also had high solubility. This is probably because the porphyrin planes connect nearly perpendicular to each other due to their sterical requirement, and hence their intermolecular π–π stacking was largely prevented.

These results indicate that the present electrochemical method is a convenient way of preparing *meso,meso*-linked porphyrin arrays which should be good candidates for long 'molecular wires'[9,10] having a linear rigid structure and high solubility.

Work at Kyoto was partly supported by Grants-in Aid for Scientific Research (No. 08874074) from the Ministry of Education, Science, Sports and Culture of Japan and by the Tokuyama Science Foundation.

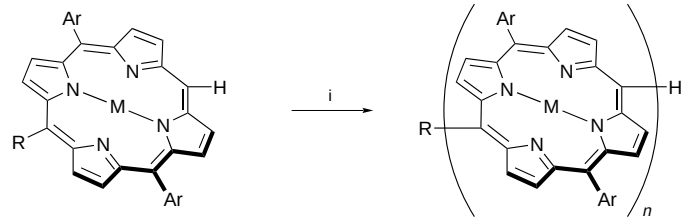

1; Ar = 3,5-di-*tert*-butylphenyl, R = H
9; Ar = 4-methoxycarbonylphenyl, R = H
12; Ar = pentafluorophenyl, R = H
13; Ar = phenyl, R = Br

2; n = 2 **3**; n = 3 **4**; n = 4 **5**; n = 5 **6**; n = 6 **7**; n = 7 **8**; n = 8
10; n = 2 **11**; n = 3
14; n = 2
15; n = 2

Scheme 1 *Reagents and conditions*: i, Anodic oxidation, Pt net as working electrode, Pt net as counter electrode, in benzonitrile, 0.1 M NBu_4ClO_4

Notes and References

* E-mail: ogawat@ms.ifoc.kyushu-u.ac.jp

† **5** (Ar = 3,5-di-*tert*-butylphenyl, R = H, *n* = 5): $\delta_H(CDCl_3)$ 1.37 (s, Bu^t), 1.40 (s, Bu^t), 1.50 (s, Bu^t), 7.62 (t, *J* 2.0, 4 H, Ar-4-H), 7.65 (t, *J* 1.5, 2 H, Ar-4-H), 7.76 (t, *J* 2.0, 4 H, Ar-4-H), 8.12 (d, *J* 2.0, 8 H, Ar-2,6-H), 8.15 (d, *J* 1.5, 4 H, Ar-2,6-H), 8.16 (d, *J* 2, 8 H, Ar-2,6-H) 8.19 (d, *J* 4.5, 4 H, β protons), 8.32 (d, *J* 4.5, 4 H, β protons), 8.35 (d, *J* 5.0, 4 H, β protons), 8.36 (d, *J* 5.0, 4 H, β protons), 8.75 (d, *J* 5.0, 4 H, β protons), 8.82 (d, *J* 4.5, 4 H, β protons), 8.84 (d, *J* 4.0, 4 H, β protons), 8.85 (d, *J* 4.5, 4 H, β protons), 9.22 (d, *J* 4.5, 4 H, β protons), 9.53 (d, *J* 4.5, 4 H, β protons) and 10.42 (s, 2 H); *m*/*z* (FAB) 3742.1 ($C_{240}H_{252}N_{20}Zn_5$ requires 3743.7). **6** (Ar = 3,5-di-*tert*-butylphenyl, R = H, *n* = 6): *m*/*z* (TOF) 4563 ($C_{288}H_{302}N_{24}Zn_6$ requires 4492). **7** (Ar = 3,5-di-*tert*-butylphenyl, R = H, *n* = 7): *m*/*z* (TOF) 5237 ($C_{336}H_{352}N_{28}Zn_7$ requires 5240). **8** (Ar = 3,5-di-*tert*-butylphenyl, R = H, *n* = 8): *m*/*z* (TOF) 6053 ($C_{384}H_{402}N_{32}Zn_8$ requires 5989). **10** (Ar = 4-methoxycarbonylphenyl, R = H, *n* = 2): $\delta_H(CDCl_3)$ 3.89 (s, 12 H), 8.03 (d, 4 H, *J* 5.0, β protons), 8.21 (d, 8 H, *J* 8.5, phenyl), 8.25 (d, 8 H, *J* 8.5, phenyl), 8.57 (d, 4 H, *J* 4.5, β protons), 9.03 (d, 4 H, *J* 4.5, β protons), 9.45 (d, 4 H, *J* 4.5, β protons) and 10.35 (s, 2 H, *meso* protons); *m*/*z* (FAB) 1281.1 ($C_{72}H_{46}N_8O_8Zn_2$ requires 1282.0). **11** (Ar = 4-methoxycarbonylphenyl, R = H, *n* = 3): $\delta_H[(CD_3)_2CO]$ 3.90 (s, 6 H, inner C*H*$_3$OCOC$_6$H$_4$), 4.04 (s, 12 H, outer C*H*$_3$OCOC$_6$H$_4$), 8.11 (d, 4 H, *J* 4.5, β protons), 8.23 (d, 4 H, *J* 4.5, β protons), 8.25–8.45 (m, 24 H, CH$_3$OCOC$_6$H$_4$), 8.57 (d, 4 H, *J* 5.0, β protons), 8.65 (d, 4 H, *J* 4.5, β protons), 9.05 (d, 4 H, *J* 4.5, β protons), 9.58 (d, 4 H, *J* 4.0, β protons) and 10.48 (s, 2 H, *meso* protons); *m*/*z* (FAB) 1921.7 ($C_{108}H_{68}N_{12}O_{12}Zn_3$ requires 1921.9). **14** (Ar = pentafluorophenyl, R = H, *n* = 2): $\delta_H(CDCl_3)$ 8.18 (d, 4 H, *J* 4.5, β protons), 8.65 (d, 4 H, *J* 5, β protons), 9.11 (d, 4 H, *J* 4.5, β protons), 9.61 (d, 4 H, *J* 5, β protons) and 10.50 (s, 2 H, *meso* protons); *m*/*z* (FAB) 1410 ($C_{64}H_{18}F_{20}N_8Zn_2$ requires 1410). **15** (Ar = Ph, R = Br, *n* = 2): $\delta_H(CDCl_3)$ 7.5–7.7 (m, 12 H, Ph), 8.06 (d, 4 H, *J* 5, β protons), 8.19 (dd, 8 H, *J* 8 and 2, Ph), 8.60 (d, 4 H, *J* 4.5, β protons), 9.04 (d, 4 H, *J* 5, protons) and 9.85 (d, 4 H, *J* 4.5, β protons); *m*/*z* (FAB) 1207.7 ($C_{64}H_{36}Br_2N_8Zn_2$ requires 1208.0).

1 M. O. Senge, W. W. Kalisch and K. Ruhlandt-Senge, *Chem. Commun.*, 1996, 2149.
2 L. Ruhlmann and A. Giraudeau, *Chem. Commun.*, 1996, 2007.
3 A. Giraudeau, L. Ruhlmann, L. E. Kahef and M. Gross, *J. Am. Chem. Soc.*, 1996, **118**, 2969.
4 A. Osuka, S. Marumo, N. Mataga, S. Taniguchi, T. Okada, I. Yamazaki, Y. Nishimura, T. Ohno and K. Nozaki, *J. Am. Chem. Soc.*, 1996, **118**, 155.
5 A. P. H. Schenning, F. B. G. Benneker, H. P. M. Geurts, X. Y. Liu and R. J. M. Nolte, *J. Am. Chem. Soc.*, 1996, **118**, 8549.
6 K. Susumu, T. Shimidzu, K. Tanaka and H. Segawa, *Tetrahedron Lett.*, 1996, **37**, 8399.
7 A. Osuka, S. Nakajima, T. Okada, S. Taniguchi, K. Nozaki, T. Ohno, I. Yamazaki, Y. Nishimura and N. Mataga, *Angew. Chem., Int. Ed. Engl.*, 1996, **35**, 92.
8 A. Osuka and H. Shimidzu, *Angew. Chem., Int. Ed. Engl.*, 1997, **36**, 135. Similar *meso*,*meso*-coupled porphyrin arrays have been prepared independently by different methods. Ref. 6 and R. G. Khoury, L. Jaquinod and K. M. Smith, *Chem. Commun.*, 1997, 1057.
9 J. S. Schumm, D. L. Pearson and J. M. Tour, *Angew. Chem., Int. Ed. Engl.*, 1994, **33**, 1360.
10 J. M. Tour, *Chem. Rev.*, 1996, **96**, 537.

Received in Cambridge, UK, 23rd October 1997; 7/07653C

Synthesis and characterization of $Ag_2C_2·2AgClO_4·2H_2O$: a novel layer-type structure with the acetylide dianion functioning in a μ_6-$\eta^1,\eta^1:\eta^2,\eta^2:\eta^2,\eta^2$ bonding mode inside an octahedral silver cage

Guo-Cong Guo, Qi-Guang Wang, Gong-Du Zhou and Thomas C. W. Mak*†

The Chinese University of Hong Kong, Shatin, New Territories, Hong Kong, PR China

In the novel double salt $Ag_2C_2·2AgClO_4·2H_2O$, the C_2^{2-} dianion [bond length 1.217(7) Å] is encapsulated inside an octahedral Ag_6 cage, and the resulting cationic $[C_2@Ag_6]$ units share corners to generate metallic layers between which the perchlorate anions and aqua ligands are accommodated.

The literature contains scant information on the ligand behaviour of C_2^{2-} (acetylide dianion), in contrast to the rich coordination chemistry of its isoelectronic analogues N_2 (dinitrogen) and CN^- (acting in either cyanide or isocyanide mode). The salt-like alkali and alkaline-earth metal acetylides are readily decomposed by water, the best known example being calcium carbide, CaC_2, which exists in at least four different crystalline modifications.[1] Of the group 11 metal acetylides, silver acetylide (Ag_2C_2, also known as silver carbide) was first prepared as an impure yellowish powder by Berthelot in 1866.[2] A linear polymeric structure for silver acetylide has been inferred from its chemical properties, which are consistent with those of a molecular compound; for example, it does not react with water and is highly explosive and sensitive to shock when completely dried.[3] However, the existence of the 'naked' acetylide dianion, C_2^{2-}, as a fully encapsulated species within rhombohedral Ag_8 and monocapped square-antiprismatic Ag_9 cages in the double salts $Ag_2C_2·6AgNO_3$[4,5] and $Ag_2C_2·8AgF$,[6] respectively, suggests that the coordination mode of the C_2^{2-} entity in silver acetylide is much more complex than hitherto imagined.

Recently we have initiated a research project to synthesize and elucidate the X-ray crystal structures of novel compounds containing silver acetylide as a component, so as to shed some light on the nature of the interaction between the acetylide dianion and silver(I) ions. We report here the synthesis and crystal structure of a new double salt of silver acetylide with silver perchlorate, in which the acetylide dianion acts in a μ_6-$\eta^1,\eta^1:\eta^2,\eta^2:\eta^2,\eta^2$ bonding mode that binds the silver cations into an unprecedented two-dimensional planar array.‡

In the crystal structure of $Ag_2C_2·2AgClO_4·2H_2O$, the atoms C(1), C(2), Ag(2) and Ag(3) all lie on the same crystallographic mirror plane. The measured C(1)–C(2) bond distance of 1.212(7) Å is comparable to that found in acetylene (1.205 Å), showing that the acetylide dianion retains its triple bond character inherited from the parent silver acetylide, as confirmed by its laser Raman stretching frequency. The C_2^{2-} dianion is σ-bonded to atoms Ag(2) and Ag(2^i) in the *c* direction, and π-bonded to Ag(3) and Ag(3^{ii}) in the *a* direction and to Ag(1) and Ag(1^{iii}) in the *b* direction (Fig. 1). Thus this dumbbell-like species is encapsulated inside an Ag_6 cage, and the resulting $[C_2@Ag_6]$ octahedra share vertices along the *a* and *c* directions to generate a layer structure. The distances of bridging atom Ag(2) to the C(1) and C(2^{iv}) atoms of its adjacent acetylide dianions are 2.087(3) and 2.108(6) Å, respectively, which are comparable to those (average 2.057 Å) of Ag atoms σ-bonded to the C≡CR groups in the alkynyl complexes $[Ph_3PAgC{\equiv}CPh]_4·3.5thf$ and $[Me_3PAgC{\equiv}CSiMe_3]_\infty$.[7] The C(2)–C(1)–Ag(2) and C(1)–Ag(2)–C(2^{iv}) bond angles are 179.9(3) and 178.5(2)°, respectively. Therefore the coordination mode of the acetylide dianion to two metal atom of type Ag(2) can be regarded as typical linear σ-bonding, as found in the discrete complexes $[\{Ru(CO)_2(Cp)\}_2(\mu\text{-}C{\equiv}C)]$,[8] $[\{Re(CO)_5\}_2(\mu\text{-}C{\equiv}C)]$[9] and $[Cu_4(\mu\text{-dppm})_4(C{\equiv}C)][BF_4]_2$.[10] However, to our knowledge the infinite linear chain resulting from an alternate arrangement of σ-bonded acetylide dianions and type Ag(2) silver atoms in the present compound is unprecedented.

The orthogonal pair of filled π orbitals of the acetylide dianion interact unsymmetrically with Ag(1) and Ag(3) and their symmetry equivalents, such that silver atoms of type Ag(3) serve as bridges to link adjacent infinite chains to form a metallic layer (Fig. 1). The distances of atom Ag(3) to C(1) and C(2) are 2.554(4) and 2.382(6) Å, and the C(1)–C(2)–Ag(3) and C(2)–C(1)–Ag(3) angles are 83.9(3) and 68.0(3)°, respectively. Thus the coordination mode of the acetylide dianion to silver atoms of type Ag(3) can be regarded as unsymmetrical π-bridging, which differs from the symmetrical acetylide–copper interaction observed in $[Cu_4(\mu\text{-dppm})_4(C{\equiv}C)][BF_4]_2$.[10] Similar unsymmetrical π-bonding also occurs between the acetylide dianion and silver atoms of type Ag(1), which are

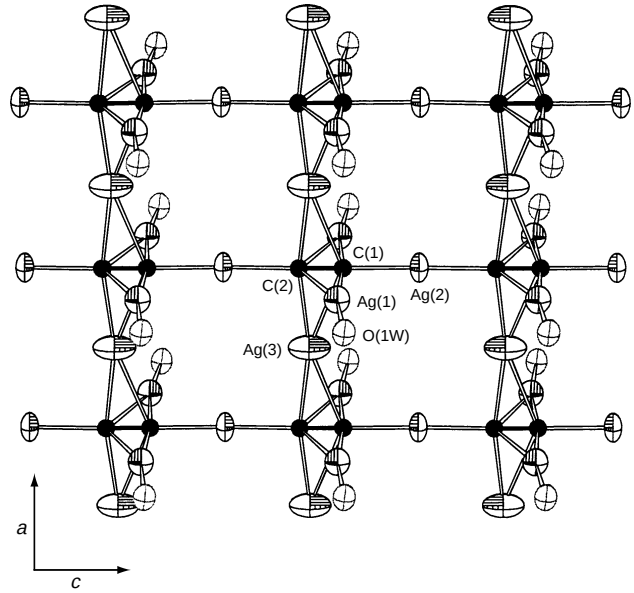

Fig. 1 Cationic layer composed of C_2^{2-} and Ag^+ ions in the crystal structure of $Ag_2C_2·2AgClO_4·2H_2O$ viewed along the *b* axis. The thermal ellipsoids are drawn at the 35% probability level. Selected bond lengths (Å) and angles (°): C(1)–C(2) 1.212(7), Ag(1)–C(1) 2.3448(4), Ag(1)–C(2) 2.579(2), Ag(2)–C(1) 2.087(3), Ag(2)–C(2^i) 2.108(6), Ag(3)–C(1) 2.554(1), Ag(3)–C(2) 2.382(6), Ag(3^{ii})–C(1) 2.596(4), Ag(3^{ii})–C(2) 2.448(6), Ag(1)–O(1W) 2.304(2); Ag(1)–C(1)–Ag(1^{iii}) 173.5(2), C(1)–Ag(1)–O(1W) 171.4(1), C(2)–C(1)–Ag(2) 179.9(3), C(1)–Ag(2)–C(2^{iv}) 178.5(2), C(2)–Ag(3)–C(2^v) 166.8(3), C(1)–C(2)–Ag(3) 83.0(3), C(2)–C(1)–Ag(3) 69.4(3). Symmetry codes: i, *x*, *y*, −1 + *z*, ii, 1 + *x*, *y*, *z*, iii, *x*, ½ − *y*, *z*, iv, *x*, *y*, 1 + *z*, v, −1 + *x*, *y*, *z*.

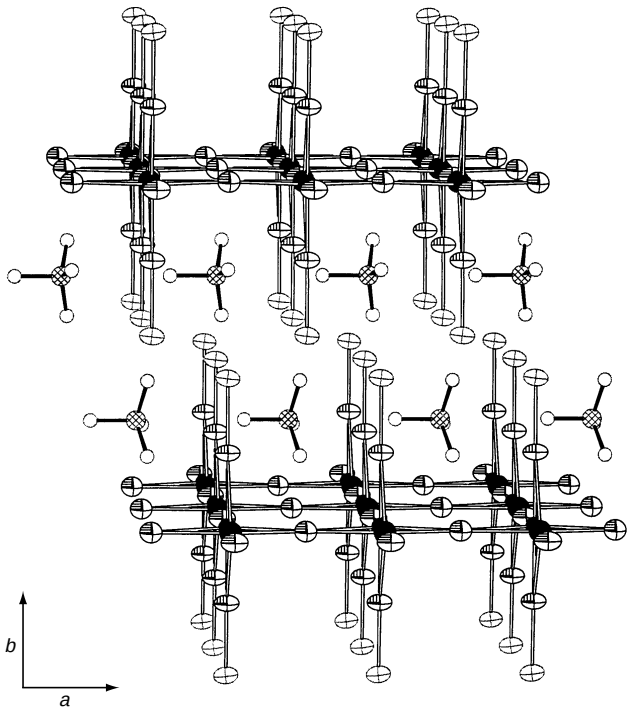

Fig. 2 Crystal structure of $Ag_2C_2·2AgClO_4·2H_2O$ viewed along the *c* axis. For clarity the disordered perchlorate ion is shown in only one of its two orientations, and the hydrogen bonds between the aqua ligands and the perchlorate ions have been omitted.

linked to C(1), C(2) and terminal aqua ligand O(1W) at distances of 2.3448(4), 2.579(2) and 2.304(2) Å, respectively. The dihedral angle between the planes defined by C(1)–C(2)–Ag(3) and C(1)–C(2)–Ag(1) is 90.7°.

The ClO_4^- ion exhibits twofold disorder with two equally populated, opposite orientations that share a common set of three basal oxygen atoms. The terminal aqua ligands that are coordinated to type Ag(1) silver atoms form donor hydrogen bonds to the ClO_4^- ions, thereby contributing to the stability of the structure. Fig. 2 shows that the cationic layers are completely separated by ClO_4^- anions, so that the crystal structure of the present compound may be considered as a stack of alternate conducting and insulating layers. This potential anisotropic conducting property of the metallic layer will be further studied.

This work is supported by Direct Grant No. 2060129 of The Chinese University of Hong Kong and Hong Kong Research Grants Council Earmarked Grant Ref. No. CUHK 456/95P.

Notes and References

* E-mail: tcwmak@cuhk.edu.hk

† *Synthesis of* $Ag_2C_2·2AgClO_4·2H_2O$: aqueous silver nitrate solution was stirred and a slow stream of acetylene gas was bubbled into it until saturation was reached at ambient temperature. The white precipitate of Ag_2C_2 was isolated by filtration, washed several times with deionized water, and stored in the dark in wet form. ***CAUTION***: Ag_2C_2 in the dry state detonates easily by mechanical shock, and only a small quantity should be prepared for immediate use in any chemical reaction. Moist Ag_2C_2 is added to 2 ml of a concentrated aqueous solution of $AgClO_4$ with stirring until saturation is reached. The excess amount of Ag_2C_2 was filtered off, and the solution was placed in a desiccator charged with P_2O_5. After several days a good crop of colorless crystals of $Ag_2C_2·2AgClO_4·2H_2O$ was obtained. The Raman spectrum (Renishaw Raman Image Microscope System 2000) of this product exhibits absorption peaks at 2103.9 and 2167.1 cm^{-1} in the $\Delta\nu$(C≡C) region, which originate from Fermi resonance between the stretching frequency of C_2^{2-} with the first overtone of the irradiating laser line at 1123.5 cm^{-1}.

§ *Crystal data*: $Ag_2C_2·2AgClO_4·2H_2O$, $C_2H_4Ag_3Cl_2O_{10}$, M = 690.43, monoclinic, space group $P2_1/m$ (no. 11), a = 4.798(1), b = 21.341(2), c = 5.406(1) Å, β = 90.01(1)°, U = 553.5(1) $Å^3$, Z = 2, μ(Mo-Kα) = 74.96 mm^{-1}; 767 observed data [$|F_o| > 4\sigma(F_o)$] out of 845 unique reflections converged to $R1 \equiv \Sigma(|F_o| - |F_c|)/\Sigma|F_o|$ = 0.053 and $wR2 \equiv [\{\Sigma w(F_o^2 - F_c^2)^2\}/\{\Sigma wF_o^4\}]^{\frac{1}{2}}$ = 0.157. CCDC reference 182/721.

1 U. Dehlinger and R. Glocker, *Z. Kristallogr.*, 1926, **64**, 296; N. C. Vanneberg, *Acta Chem. Scand.*, 1961, **15**, 769; 1962, **16**, 1212; T. C. W. Mak and G.-D. Zhou, *Crystallography in Modern Chemistry: A Resource Book of Crystal Structures*, Wiley-Interscience, New York, 1992, pp. 285–286.
2 M. P. Berthelot, *Ann.*, 1866, 245.
3 N. R. Thompson, in *Comprehensive Inorganic Chemistry*, ed. J. C. Bailar, Jr., H. J. Emeléus, R. Nyholm and A. F. Trotman-Dickenson, Pergamon, Oxford, 1973, vol. 3, p. 102; J. A. Shaw and E. Fisher, *J. Am. Chem. Soc.*, 1946, **68**, 2745; R. Vestin and E. Ralf, *Acta Chem. Scand.*, 1949, **3**, 101; A. D. Redhouse and P. Woodward, *Acta Crystallogr.*, 1964, **17**, 616.
4 J. Osterlof, *Acta Crystallogr.*, 1954, **7**, 637.
5 X.-L. Jin, G.-D. Zhou, N.-Z. Wu, Y.-Q. Tang and H.-C. Huang, *Acta Chem. Sinica*, 1990, **48**, 232 (in Chinese).
6 G.-C. Guo, G.-D. Zhou, Q.-G. Wang and T. C. W. Mak, *Angew. Chem., Int. Ed. Engl.*, in press.
7 C. Brasse, P. R. Raithby, M.-A. Rennie, C. A. Russell, A. Steiner and D. S. Wright, *Organometallics*, 1996, **15**, 639.
8 G. A. Koutsantonis and J. P. Selegue, *J. Am. Chem. Soc.*, 1991, **113**, 2316.
9 J. Heidrich, M. Steimann, M. Appel, W. Beck, J. R. Phillips and W. C. Trogler, *Organometallics*, 1990, **9**, 1296.
10 V. W.-W. Yam, W. K.-M. Fung and K.-K. Cheung, *Angew. Chem., Int. Ed. Engl.*, 1996, **35**, 1100.

Received in Cambridge, UK, 24th November 1997; 7508439K

Solution injection laser pyrolysis: a novel technique for gas phase pyrolysis of involatile compounds

Janet E. Everett, Noel D. Renner and Douglas K. Russell*

Department of Chemistry, University of Auckland, Private Bag 92019, Auckland, New Zealand

The gas phase pyrolysis of involatile species has been studied by injection of solutions in inert solvents into SF_6 gas heated by CO_2 laser radiation; the gas phase chemistry reflects the distribution of species present in solution, and may potentially be controlled through parameters such as solution pH.

IR laser powered homogeneous pyrolysis (LPHP) has been successfully exploited for over 20 years in the investigation of the mechanisms of thermal decomposition of volatile organic and organometallic compounds.[1,2] The advantages of the technique are well known; very small quantities of materials are needed, initiation of reaction is unambiguously homogeneous, and intermediates are readily trapped.[3,4] Among its shortcomings are difficulties in defining and measuring effective temperatures, although this may be overcome through the use of compounds of well known kinetic parameters. In addition, previous work has been restricted to compounds of at least moderate volatility (> 1 Pa). Here, we show that the latter limitation may be removed by a simple adaptation of the technique, and report some preliminary results.

The modification of IR LPHP described in this study is referred to as solution injection laser pyrolysis, SILP. Saturated solutions of target species in suitable solvents were introduced directly into the SF_6 gas heated by the CO_2 IR laser by means of a Hamilton syringe inserted through a rubber septum. In order to ensure rapid vaporisation of the solvent, the needle orifice was mechanically modified to produce a fine spray, and the needle tip heated to somewhat below red heat by positioning at the perimeter of the heated zone. Effective temperatures were not otherwise monitored in the present work although these are clearly needed in quantitative studies. Gaseous pyrolysis products were identified after injection by FTIR, and quantified with the aid of commercial software. For very soluble species, solution volumes of 10–50 μl yielded strong product IR spectra. In some experiments, additional gaseous reagents were introduced into the pyrolysis cell before solution injection in order to trap reactive intermediates, or the solution pH varied to modify the dominant solute species.

The volumes of solution injected are such that the vapour pressure of the solvent is usually exceeded in the pyrolysis cell; as a result, interpretation of observations might conceivably involve the partial dissolution of gaseous pyrolysis products in residual liquid solvent. In cases where evaluation of this complicating feature was possible, it proved to play no significant role, and has therefore been discounted. It is also possible that partial pyrolysis of solute might take place in solution within the heated needle tip before ejection. Again, investigations correlating product yield with needle tip location indicated that this was not the case; this conclusion is consistent with those from the early development of thermospray mass spectrometry, where orifice temperatures as high as 1000 °C were employed.[5]

The physical processes that occur as solution emerges from the needle tip into the heated gas zone are a matter of vigorous debate in the literature. In the most widely accepted model proposed by Iribarne and Thomson,[6] the majority of the solvent is vaporised into a fine spray as the solution leaves the capillary; the droplets that result may be charged, positively or negatively, in a statistical manner reflecting the distribution of ionic species in solution. As further solvent evaporates from the droplets, the charge density increases and eventually results in a series of 'Coulomb explosions' in which ions, either naked or solvated, are ejected into the gas phase. However, in contrast with electrospray or thermospray mass spectrometry, the principal focus of the present work is the subsequent thermal chemistry of solute species. This process also differs substantially from the suite of 'spray pyrolysis' methods developed for the generation of ceramic materials, where the major pyrolysis processes involve micro-aggregates of solute at heated surfaces.[7] The preliminary results described below confirm the viability of the technique, and illustrate its potential in mechanistic investigations.

Zinc oxoacetate and zinc acetate in toluene. The covalent zinc oxoacetate {hexakis[μ-(acetato-*O*:*O*′)]-μ_4-oxotetrazinc}, $Zn_4O(MeCO_2)_6$, provides a convenient reference point for the investigation of the gas phase pyrolysis chemistry of metal acetates; although little is known of the vapour of this compound, pyrolysis of the solid is known to produce largely CO_2 and acetone.[8] Its very slight volatility, and its stable tetrahedral Zn_4O unit, have also attracted interest in the parent compound as a potential precursor in the chemical vapour deposition of zinc oxide films.[9] In the present work, toluene was selected as the solvent, as it proved thermally inert at the temperatures employed. FTIR spectra (Fig. 1) of the gaseous products of SILP of saturated toluene solutions of $Zn_4O(MeCO_2)_6$ were dominated by solvent vapour and ketene, with smaller amounts of CO_2 and CH_4, and traces of CO, C_2H_4 and C_2H_2; no trace of acetone was detected. Clearly, pyrolysis pathways for isolated molecules in the vapour are very different from those in the bulk solid. Very similar results were found for the less soluble zinc acetate, although the yield of ketene was lower, and that of methane higher. In fully deuterated toluene, CH_3D was produced as well as CH_4, indicating the involvement of methyl radicals. These results concur with the known routes for decomposition of isolated acetate groups on oxide surfaces, and indicate that analogues of zinc oxoacetate may serve as molecular mimics for surface chemistry.[10]

Aqueous alkali metal acetates. There have been several reports on the dominant ionic species observed in the electro-

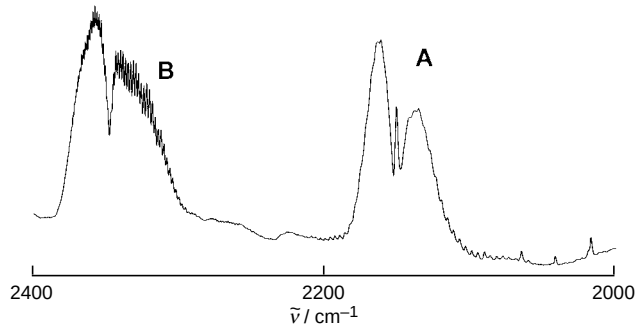

Fig. 1 Partial FTIR spectrum of the products of SILP of zinc oxoacetate in toluene, indicating the production of ketene (A) and CO_2 (B)

spray mass spectra of alkali metal acetates;[11] these include clusters of the form $[M_n(OAc)_{n\mp1}]^{\pm}$. In the SILP system, at high laser powers, the SF_6 photosensitiser was attacked, presumably by metal atoms or ions, resulting in the production of large quantities of SO_2 and extensive etching of the cell walls and windows. This reaction route was not explored in any detail; however, the observation of a blue chemiluminescence within the heated gas zone (presumably electronically excited SO_2) did provide clear visual confirmation of the homogeneous nature of reaction. At lower powers, all the alkali metal acetates behaved identically, and most experiments were conducted with saturated solutions of the potassium salt. In H_2O, the major products were CO_2 and CH_4, together with small amounts of CO and C_2H_2; no ketene was observed, in line with the known ready hydrolysis of ketenes.[12] In D_2O solution, extensive deuteration of C_2H_2 (as both C_2HD and C_2D_2) was observed, suggestive perhaps of ion–molecule reactions, but none of CH_4. Copyrolysis with H_2 resulted in almost complete suppression of CO_2 and CO, and a marked increase in CH_4 production; copyrolysis with D_2 resulted in some CH_3D, but no deuterated acetylenes. Conversely, copyrolysis with O_2 suppressed both hydrocarbons and increased the yield of oxides. Pyrolysis of a saturated solution of potassium acetate in 2 mol l^{-1} NaOH yielded no CO_2, and a marked increase in both CH_4 and C_2H_2.

Aqueous glycine. Many electrospray studies have focussed on systems of biological interest such as amino acids; in particular, the gas-phase chemistry of glycine-related anions and cations has been the subject of a number of experimental and theoretical investigations.[13] The IR-detectable gas phase products of SILP of aqueous solutions of glycine were CO_2, CO, NH_3, HCN, CH_4 and traces of C_2H_2. From 2 mol l^{-1} NaOH solution, no HCN was observed; from acidified solutions, no traces of CH_4, C_2H_2 or NH_3 were detected. With the ^{13}C-labelled $H_2N^{13}CH_2CO_2H$, only $H^{13}CN$ was observed, and both $^{13}CO_2$ and ^{13}CO were also detected at levels dependent on solution pH. From acidic solution, the ratio of $^{13}CO_2:{}^{12}CO_2$ was 1:5, and that of $^{13}CO:{}^{12}CO$ 1:1; from basic solutions, no labelled carbon oxides were generated. Unlike the alkali metal acetates, none of the solute species present in glycine solution are appreciably volatile, and we may conclude that these variations in pyrolysis products reflect changes in the major species appearing in the gas phase.

The above preliminary results indicate that the SILP technique provides the potential for the investigation of pyrolysis of isolated involatile species in the gas phase, most significantly of cations and anions, which are not readily produced by other methods.

We thank the University of Auckland for assistance with the purchase of equipment, the University of Auckland, Faculty of Science, for a Summer Studentship, and the New Zealand Federation of University Women for the Harriet Jenkins Award (to J. E. E.). We also are grateful to Professor Einar Uggerud (University of Oslo) for invaluable correspondence concerning the gas phase ion chemistry of glycine, and Leong Mar (University of New South Wales) for the sample of zinc oxoacetate.

Notes and References

* E-mail: d.russell@auckland.ac.nz

1 W. M. Shaub and S. H. Bauer, *Int. J. Chem. Kinet.*, 1975, **7**, 509.
2 D. K. Russell, *Chem. Soc. Rev.*, 1990, **19**, 407; *Chem. Vap. Deposition*, 1996, **2**, 223.
3 A. S. Grady, R. D. Markwell and D. K. Russell, *J. Chem. Soc., Chem. Commun.*, 1991, 929; R. E. Linney and D. K. Russell, *J. Mater. Chem.*, 1993, **3**, 587.
4 D. K. Russell, I. M. T. Davidson, A. M. Ellis, G. P. Mills, M. Pennington, I. M. Povey, J. B. Raynor, S. Saydam and A. D. Workman, *Organometallics*, 1995, **14**, 3717.
5 R. Blakley, J. J. Carmody and M. L. Vestal, *J. Am. Chem. Soc.*, 1980, **102**, 5931.
6 J. V. Iribarne and B. A. Thomson, *J. Chem. Phys.*, 1979, **71**, 4451.
7 T. T. Kodas and M. J. Hampden-Smith, in *The Chemistry of the Metal CVD*, ed. T. T. Kodas and M. J. Hampden-Smith, VCH, Weinheim, 1994, p. 463.
8 H. G. McAdie, *J. Inorg. Nucl. Chem.*, 1966, **28**, 2801.
9 P. Y. Timbrell, R. N. Lamb and G. L. Mar, *Springer Proc. Phys.*, 1993, **73**, 177.
10 M. A. Barteau, *Chem. Rev.*, 1996, **96**, 1413.
11 See, for example: Y. Cao and K. L. Busch, *Inorg. Chem.*, 1994, **33**, 3970 and references therein.
12 T. T. Tidwell, *Ketenes*, Wiley, New York, 1995.
13 Š. Beranová, J. Cai and C. Wesdemiotis, *J. Am. Chem. Soc.*, 1995, **117**, 9492.

Received in Exeter, UK, 15th October 1997; 7/07442E

Formation and co-coordination of lithium azide *via* lithium triazasulfite

Roland Fleischer and Dietmar Stalke*

Institut für Anorganische Chemie der Universität Würzburg, Am Hubland, D-97074 Würzburg, Germany

The triazasulfite $[Li_4\{(NBu^t)_3S\}_2]$ (the analogue of Li_2SO_3) provides the opportunity to complex *in situ* formed lithium azide and converts this inorganic solid into soluble monomeric residues.

Recently, we described the synthesis and structures of some nitrogen analogues of simple sulfur oxygen compounds. In these derivatives the oxygen atoms are substituted by isoelectronic NR groups to yield the dilithium triazasulfite dimer[1] $[(thf)Li_4\{(NBu^t)_3S\}_2]$ (the analogue of Li_2SO_3) and the dilithium tetraazasulfate monomer[2] $[(thf)_4Li_2(NBu^t)_4S]$ (analogue to Li_2SO_4). Polyimido polyanions containing p-block element bridgeheads like $[RSi(NSiMe_3)_3]_2^{3-}$,[3] $RE(E'R'_2NR'')_3^{3-}$ (R,R′ = H, alkyl; R″ = alkyl, aryl; E,E′ = C, Si),[4] $[Sb(NR)_3]^{3-}$,[5a] $[Sb_2(NR)_4]^{2-}$,[5b] and $[E(NBu^t)_3]^{2-}$ (E = Se, Te)[6] furnish a new family of ligand systems to construct macromolecular architectures of mixed metal cages and clusters.[7] While the alkali metal salts of these polyanions are mostly employed in metal metathesis reactions little is known of their anion solvation behaviour to metal salts. The flexible electronic structure of their alkali metal derivatives, *i.e.* the ability to localise or delocalise the charge in the anion core backbone, should provide the opportunity to complex neutral metal salts.

We report here the reaction of dilithium *N*,*N*′,*N*″-tris(*tert*-butyl)azasulfite $[(thf)Li_4\{(NBu^t)_3S\}_2]$ and trimethylsilyl azide to give the lithium azide adduct $[(thf)_2Li_3(\mu_4N_3)\{(NBu^t)_3S\}]_\infty$ **1**. Organo azides are mainly employed as oxidants in Staudinger type reactions.[8] In an attempt to obtain the aza analogue $Me_3SiNS(NBu^t)_3^{2-}$ of sulfate we added trimethylsilyl azide to a hexane solution of $[(thf)Li_4\{(NBu^t)_3S\}_2]$. During the reaction at room temperature a slight rise in temperature was detected, although no evolution of gas (N_2) was observed (Scheme 1). In addition, silicon could not be detected in the ^{29}Si NMR spectrum of the product and the ^7Li NMR spectrum displayed two different lithium sites in the ratio 1:2. To further investigate the actual composition of the product, an X-ray structure analysis of the air-sensitive crystals (the compound turned dark blue when exposed to oxygen) was performed which established the formation of a polymeric lithium azide adduct **1** of monomeric $[Li_2(NBu^t)_3S]$ (Scheme 2).

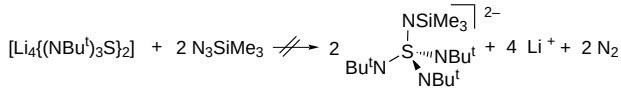

Scheme 1

Obviously the trimethylsilyl azide acts as an acid rather than an oxidant in this reaction. That the byproduct $Bu^tNS(Bu^tN\text{-}SiMe_3)_2$ could not be isolated is presumably owing to its instability with respect to decomposition to $S(NBu^t)_2$ and $Bu^tN(SiMe_3)_2$ which were isolated from the reaction mixture† and identified by ^1H and ^{13}C NMR spectroscopy.

Compound **1** crystallises from thf–hexane within a few hours storage at room temperature to give colourless needles.‡ Within the monomeric units (Fig. 1), three lithium atoms are coordinated by the dianionic $S(NBu^t)_3^{2-}$ ligand. The dianion shows almost ideal local C_3 symmetry at sulfur. The three S–N distances are identical within e.s.d.s and are of typical length (av. 163.7 pm).[1] Li(1) and Li(1a) are tetrahedrally coordinated by two nitrogen atoms of the dianionic $S(NBu^t)_3^{2-}$ ligand, one azide nitrogen atom, and a single thf donor molecule. In addition to the two nitrogen atoms of the $S(NBu^t)_3^{2-}$ ligand Li(2) is coordinated by two azide nitrogen atoms [N(5) and N(5a)] of different N_3^- anions completing the tetrahedral coordination sphere of Li(2). Each azide anion μ_4 bridges the three lithium atoms of one $Li_3(NBu^t)_3S$ unit [av. Li–N 220(1) pm] and one lithium atom of a neighbouring monomeric residue

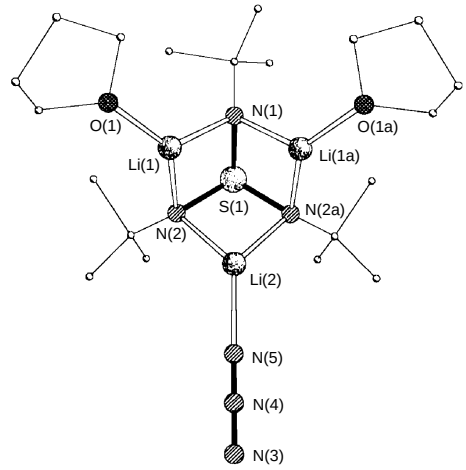

Fig. 1 Solid state structure of a monomeric unit of $[(thf)_2Li_3(\mu_4N_3)\{(NBu^t)_3S\}]_\infty$ **1**. Selected bond lengths (pm) and angles (°): S(1)–N(1) 163.3(5), S(1)–N(2) 164.2(4), Li(1)–N(1) 203.0(9), Li(1)–N(2) 200.3(8), Li(2)–N(2a) 203.3(8), Li(1)–N(5) 219.9(9), Li(2a)–N(5) 221.1(13), Li(2)–N(3) 195.9(12), Li(1)–O(1) 192.1(8), N(3)–N(4) 117.7(8), N(4)–N(5) 117.4(7); N(1)–S(1)–N(2) 100.5(2), N(2)–S(1)–N(2a) 100.8(3), N(3)–N(4)–N(5) 180.0(6), Li(2)–N(5)–N(4) 146.4(5).

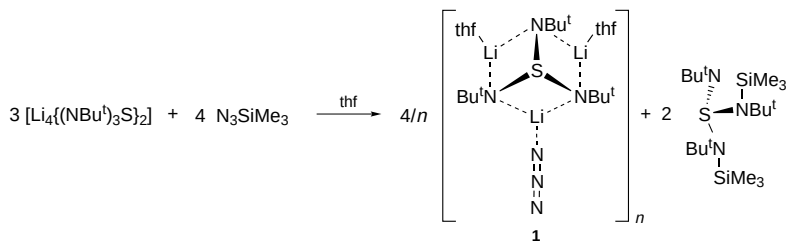

Scheme 2

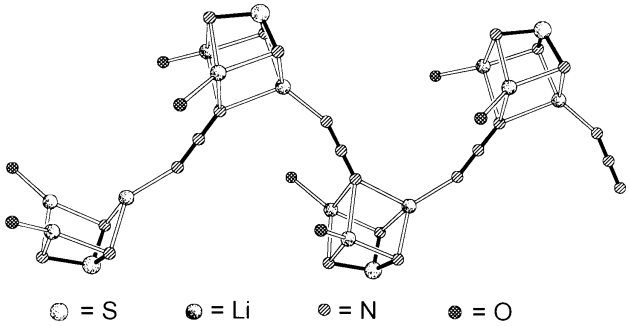

Fig. 2 Arrangement of monomeric **1** to give polymeric wave shaped ribbons; carbon atoms omitted for clarity

[N(5)–Li(2) 196(1) pm] with both terminal nitrogen atoms, such that a polymeric solid state structure is generated (Fig. 2).

In the solid state structure of LiN_3 every lithium atom is octahedrally coordinated by eight nitrogen atoms.[9] Every terminal nitrogen atom of an azide anion μ_3 bridges three lithium atoms with one short (221.4 pm) and two longer (228.9 pm) Li–N distances. In contrast, the Li–N distances of the terminal azide nitrogen atoms [N(3) and N(5)] in **1** are equal within e.s.d.s.

The *in situ* generated lithium azide is incorporated in a metal salt cocoordination complex owing to the capability of the $S(NBu^t)_3^{2-}$ triazasulfite anion to coordinate more than two metal centres.[10] Although balanced in terms of charge the Li_2N_3S framework can accommodate another lithium atom to form a LiN_3 monomer. The polyimido polyanions in general seem to provide access to soluble mixed metal aggregates[11] *via* incorporation of *in situ* generated inorganic solids into complex residues.

We are grateful to the Deutsche Forschungsgemeinschaft, the Stiftung Volkswagenwerk and the Fond der Chemischen Industrie. D. S. kindly acknowledges support of the Bruker axs-Analytical X-ray Systems, Karlsruhe.

Notes and References

* E-mail: dstalke@chemie.uni-wuerzburg.de

† *Preparation of* $[(thf)_2Li_3\{\mu_4N_3\}\{(NBu^t)_3S\}]$ **1**: a solution of trimethylsilyl azide (4 mmol, 0.46 g) in 5 ml hexane is added to a solution of $[Li_4\{(NBu^t)_3S\}_2]$ (2 mmol, 1.18 g) in 5 ml hexane and stirred for 1 h. All volatiles are removed *in vacuo*. Crystallisation from thf–hexane (2 : 3) solution gives colourless needles. M = 452.45 g mol^{-1}, yield 1.14 g (63%). Mp 113 °C. NMR: ^{1}H (200 MHz, C_6D_6) δ 1.37 (s, 18 H, Bu^t), 1.40 (m, 8 H, thf), 1.49 (s, 9 H, Bu^t), 3.63 (m, 8 H, thf). ^{13}C (100 MHz, C_6D_6) δ 25.65 (OCH_2CH_2, thf), 34.00, 34.35 [$C(CH_3)_3$], 52.92, 53.49 [$C(CH_3)_3$], 68.09 (OCH_2, thf). ^{7}Li (100 MHz, C_6D_6) δ 1.31 (s, 1Li), 2.88 (s, 2Li).

‡ *Crystal data* for $[(thf)_2Li_3\{\mu_4N_3\}\{(NBu^t)_3S\}]\cdot 0.5$ thf **1**: $C_{20}H_{43}Li_3N_6O_2S\cdot 0.5C_4H_8O$, M = 488.54, orthorhombic space group *Pnma*, a = 965.60(14), b = 1593.2(4), c = 2079.3(5) pm, U = 3.1988(12) nm^3, Z = 4, D_c = 1.014 Mg m^{-3}, $F(000)$ = 1064, λ = 71.073 pm, μ(Mo-Kα) = 0.128 mm^{-1}, T = 153(2) K, data were collected on a Stoe-Siemens AED. Intensities of a 0.5 × 0.2 × 0.2 mm rapidly cooled crystal in an oil drop[12] were collected by the 2θ–ω method in the range of $4.33 \leqslant \theta \leqslant 22.55°$. Of a total of 3931 reflections, 2179 were independent and together with 608 restraints, were used to refine 322 parameters, largest difference peak and hole: 509 and −255 e nm^{-3}, $R1[F > 4\sigma(F)]$ = 0.0760 and $wR2$ = 0.2369 (all data) with $R1 = \Sigma\|F_o| - |F_c\|/\Sigma|F_o|$ and $wR2 = \{\Sigma w(F_o^2 - F_c^2)^2/\Sigma w(F_o^2)^2\}^{\frac{1}{2}}$; $w = 1/\{\sigma^2(F_o^2) + (0.153P)^2 + 1.81P\}$; $P = (F_o^2 + 2F_c^2)/3$. The structure was solved by direct methods with SHELXS-96[13] and refined by full-matrix least squares on F^2.[14] The Bu^t moiety [C(21)–C(23)] exhibits a rotational disorder. It was refined to a split occupancy of 0.72/0.28. The twist disorder of the coordinated thf molecule [O(1), C(40)–C(43)] was modelled to a split occupancy of 0.61/0.39. Additionally, half an uncoordinated thf was found in the difference Fourier map. It is disordered over a special position and was refined to a split occupancy of 0.52/0.48. In the refinement of the Bu^t moiety [C(10)–C(13)], the symmetry (mirror plane) was suppressed. For the refinement of the disorder bond length and similarity restraints were applied. A riding model was applied in the refinement of the hydrogen atom positions. CCDC 182/720.

1 R. Fleischer, S. Freitag, F. Pauer and D. Stalke, *Angew. Chem.*, 1996, **108**, 208; *Angew. Chem., Int. Ed. Engl.*, 1996, **35**, 204.
2 R. Fleischer, A. Rothenberger and D. Stalke, *Angew. Chem.*, 1997, **109**, 1140; *Angew. Chem., Int. Ed. Engl.*, 1997, **36**, 1105.
3 D. J. Brauer, H. Bürger, G. R. Liewald and J. Wilke, *J. Organomet. Chem.*, 1986, **305**, 119; P. Kosse, E. Popowski, M. Veith and V. Huch, *Chem. Ber.*, 1994, **127**, 2103; I. Hemme, U. Klingebiel, S. Freitag and D. Stalke, *Z. Anorg. Allg. Chem.*, 1995, **621**, 2093.
4 H. Bürger, R. Meillies and K. Wiegel, *J. Organomet. Chem.*, 1977, **142**, 55; S. Friedrich, L. H. Gade, A. J. Edwards and M. McPartlin, *Chem. Ber.*, 1993, **126**, 1797; L. H. Gade and N. Mahr, *J. Chem. Soc., Dalton Trans.*, 1993, 489; K. W. Hellmann, L. H. Gade, A. Steiner, D. Stalke and F. Möller, *Angew. Chem.*, 1997, **109**, 99; *Angew. Chem., Int. Ed. Engl.*, 1997, **36**, 160; K. W. Hellmann, L. H. Gade, R. Fleischer and D. Stalke, *Chem. Commun.*, 1997, 527.
5 (*a*) R. A. Alton, D. Barr, A. J. Edwards, M. A. Paver, M.-A. Rennie, C. A. Russell, P. R. Raithby and D. S. Wright, *J. Chem. Soc., Chem. Commun.*, 1994, 1481; (*b*) A. J. Edwards, M. A. Paver, M.-A. Rennie C. A. Russell, P. R. Raithby and D. S. Wright, *Angew. Chem.*, 1994, **106**, 1334; *Angew. Chem., Int. Ed. Engl.*, 1994, **33**, 1277; (*c*) M. A. Paver, C. A. Russell and D. S. Wright, *Angew. Chem.*, 1995, **107**, 1077; *Angew. Chem., Int. Ed. Engl.*, 1995, **34**, 1545; (*d*) D. Barr, M. A. Beswick, A. J. Edwards, J. R. Galsworthy, M. A. Paver, M.-A. Rennie, C. A. Russell, P. R. Raithby, K. L. Verhorevoort and D. S. Wright, *Inorg. Chim. Acta*, 1996, **248**, 9.
6 N. J. Bremer, A. B. Cutcliffe, M. F. Farona and W. G. Kofron, *J. Chem. Soc.*, 1971, 3264; M. Björgvinsson, H. W. Roesky, F. Pauer and G. M. Sheldrick, *Chem. Ber.*, 1992, **125**, 767; T. Chivers, X. Gao and M. Parvez, *Angew. Chem.*, 1995, **107**, 2756; *Angew. Chem., Int. Ed. Engl.*, 1995, **34**, 2549; T. Chivers, M. Parvez and G. Schatte, *Inorg. Chem.*, 1996, **35**, 4094.
7 See, for example: K. W. Hellmann, L. H. Gade, R. Fleischer and T. Kottke, *Chem. Eur. J.*, 1997, **3**, 1801; J. K. Brask, T. Chivers, M. Parvez and G. Schatte, *Angew. Chem.*, 1997, **109**, 2075; *Angew. Chem., Int. Ed. Engl.*, 1997, **36**, 1986; M. A. Beswick, N. Choi, C. N. Harmer, A. D. Hopkins, M. McPartlin, M. A. Paver, P. R. Raithby, A. Steiner, M. Tombul and D. S. Wright, *Inorg. Chem.*, submitted.
8 H. Staudinger and J. Meyer, *Helv. Chim. Acta*, 1919, **2**, 635.
9 G. E. Pringle and D. E. Noakes, *Acta Crystallogr., Sect. B*, 1968, **24**, 262.
10 R. Fleischer and D. Stalke, *Organometallics*, in press; R. Fleischer, S. Freitag and D. Stalke, *J. Chem. Soc., Dalton Trans.*, in press.
11 F.-Q. Liu, D. Stalke and H. W. Roesky, *Angew. Chem.*, 1995, **107**, 2004; *Angew. Chem., Int. Ed. Engl.*, 1995, **34**, 1872; F.-Q. Liu, A. Künzel, A. Herzog, H. W. Roesky, M. Noltemeyer, R. Fleischer and D. Stalke, *Polyhedron*, 1997, **16**, 61.
12 H. Hope, *Acta Crystallogr., Sect. B*, 1988, **44**, 22; T. Kottke and D. Stalke, *J. Appl. Crystallogr.*, 1993, **26**, 615; T. Kottke, R. J. Lagow and D. Stalke, *J. Appl. Crystallogr.*, 1996, **29**, 465.
13 G. M. Sheldrick, *Acta Crystallogr., Sect. A*, 1990, **46**, 467.
14 G. M. Sheldrick, program for crystal structure refinement, Universität Göttingen, 1996.

Received in Basel, Switzerland, 14th October 1997; 7/07390I

Intermolecular hydrogen···metal interactions. The crystal structure of {*cis*-$[PdCl_2(TPA)_2]$}$_2$·H_2O, a water-soluble palladium(II) tertiary phosphine complex

Elmer C. Alyea,* George Ferguson and Shanmugaperumal Kannan

Department of Chemistry and Biochemistry, University of Guelph, Guelph, Ontario, Canada, N1G 2W1

The single-crystal X-ray structural determination of {*cis*-$[PdCl_2(TPA)_2]$}$_2$·H_2O (TPA = 1,3,5-triaza-7-phosphaadamantane) establishes that pairs of *cis*-$[PdCl_2(TPA)_2]$ molecules are linked about inversion centres by intermolecular Pd···H···C three-centre–four-electron interactions (2.86, 3.00 Å for the two independent dimers); the water molecule links these dimers *via* O–H···N hydrogen bonds to form infinite chains extending in the *c*-direction in the crystal lattice.

Attention has focused recently on complexes of the air-stable water-soluble phosphine 1,3,5-triaza-7-phosphaadamantane (TPA) with transition metal ions.[1,2] Darensbourg and co-workers have shown the high catalytic activity of certain ruthenium and rhodium complexes towards the hydrogenation of alkenes and the conversion of unsaturated aldehydes to saturated aldehydes or unsaturated alcohols.[1b,c,f] Given the potential for applications of water-soluble palladium and platinum complexes in catalysis, *e.g.* $[Pd(TPPTS)_4]$ [TPPTS = $P(m\text{-}C_6H_4SO_3Na)_3$] is used for the telomerization of dienes[3] and *cis*-$[PtCl_2(TPPTS)_2]$ for the functionalization of dienes,[4] we are currently extending our preliminary investigations of group 10 complexes of TPA.[2a,c] We report here our discovery that the crystal structure of the square-planar water-soluble palladium(II) complex of TPA, {*cis*-$[PdCl_2(TPA)_2]$}$_2$·H_2O **1** contains rare intermolecular C···H···Pd interactions; such C···H···M interactions, originally postulated in the literature as possible examples of agostic bonding, are best described as three-centre–four-electron (3c–4e) hydrogen bonds.[5]

The analytically pure compound was synthesized by the reaction of solid $PdCl_2$ with an excess of TPA in water.[6] The analytical, ^1H and ^{31}P NMR spectral data† of the isolated greenish–yellow product **1** show that the TPA ligand is bonded through its phosphorus atom to the metal ion in a 2 : 1 ratio. In contrast, a similar reaction employing $PtCl_2$ gave a product having the formula $[Pt(TPA)_3Cl]Cl$.[2c] Crystals of **1** suitable for X-ray diffraction analysis were obtained from a H_2O–MeCN–MeOH mixture by slow evaporation.‡ Our preliminary studies show that this complex is unstable in water, giving TPA oxide, but it is relatively stable in the presence of an excess of TPA. The mechanism of decomposition, which also occurs for the analogous Ni and Pt complexes, is under further investigation.[6]

Compound **1** crystallised in the triclinic space group $P\bar{1}$ and the asymmetric unit contains two molecules of *cis*-$[PdCl_2(TPA)_2]$ and a water molecule which links the two Pd complexes *via* O–H···N hydrogen bonds [O(1)–H(1)···N(13), O···N 2.916(6); O(1)–H(2)···N(33), O···N 2.914(6) Å]. A view of this hydrogen-bonded complex is in Fig. 1. The two independent Pd complexes have essentially identical stereochemistry and conformation; each palladium atom is surrounded by two chlorine and two TPA ligands, giving the expected square-planar geometry. It is well established that *cis*- and *trans*-isomerization in palladium(II) trialkylphosphine complexes of the type $[PdX_2L_2]$ (X = halogen, L = trialkylphosphine) is mainly determined by the phosphine size.[7–9] Thus, the PMe_3 (cone angle θ = 118°) complex is *cis*,[7] whereas larger phosphines such as PEt_3, PPr_3, PMe_2Ph, *etc.*, form isomeric mixtures[8] and the PCy_3 (θ = 170°) complex is *trans*.[9] Since the cone angle of TPA is only 102°,[1a] not surprisingly, in the present complex the two TPA ligands are arranged in a *cis*-orientation, and indeed the P–Pd–P bond angles [93.25(5), 93.58(5)°] are the smallest found for any *cis*-$[Pd(PR_3)_2X_2]$ complexes.[7–10] The P–Pd–P angle for the PMe_3 analogue is reported as 94.7(1) Å in the solid state.[7] Comparable values for *trans*-P–Pd–Cl bond angles also show that less distortion is present in the TPA complex, mean 176.8(4)° compared with a mean value of 172.5(1)° in the PMe_3 complex.[7] The observed Pd–P [2.2392(13)–2.2551(13) Å] and Pd–Cl bond distances [2.3467(14)–2.3777(13) Å] are similar to those in *cis*-$[Pd(PMe_3)_2Cl_2]$ [av. 2.257(2) and 2.368(3) Å respectively] and other analogous complexes.[7–10]

Although bridging hydrogen–palladium interactions are known for a few palladium–phosphine complexes,[5] {*e.g.* Pd···H 2.8 Å in $[Pd(PPhMe_2)_2I_2]$ and 2.92 Å in $[Pd(PEt_3)_2Cl(C_6H_4C\text{-}MeN_2HPh)]$} in most cases the interaction is purely an intramolecular one. Examination of the crystal structure of **1** with PLATON[11] shows that each Pd complex lies close to an

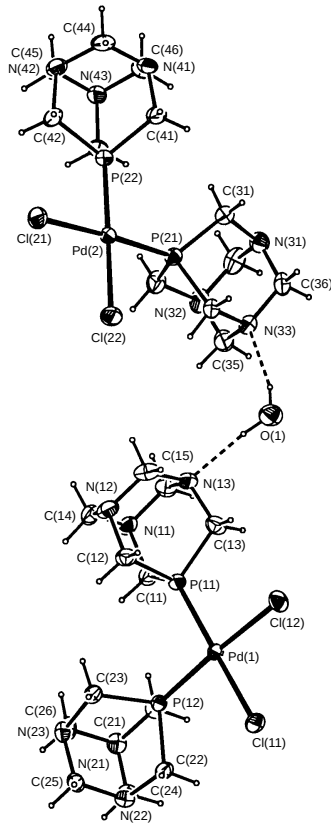

Fig. 1 A view of the asymmetric unit of **1** with our numbering scheme. Anisotropic displacement ellipsoids are drawn at the 40% probability level.

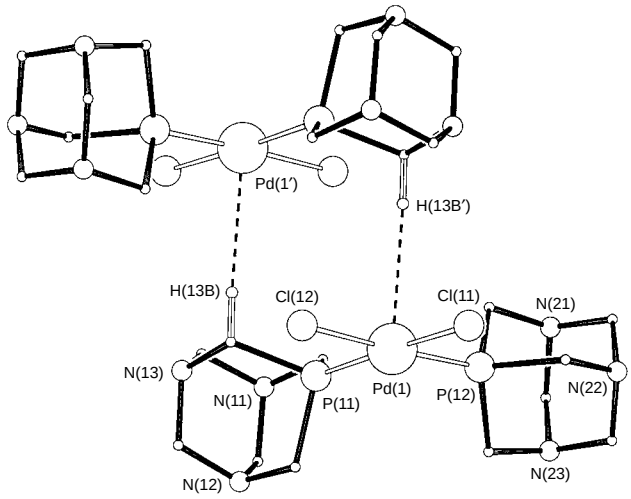

Fig. 2 A view of one of the 'hydrogen-bridged dimers' of *cis*-[$PdCl_2(TPA)_2$] [atom Pd(1′) is related to Pd(1) by the symmetry transformation $-x, -y, 1 - z$]

inversion centre and this leads to a short intermolecular Pd···H···C interaction with an H atom of a TPA ligand of a molecule related by the inversion centre. Each Pd complex forms essentially identical dimers in this way with Pd···H distances of 2.86 [Pd(1)···H(13B′) (at $-x, -y, -z$)] and 3.00 Å [Pd(2)···H(33B′) (at $-x, -y, 1 - z$)] some 0.5–0.6 Å less than the sum of the van der Waals radii. A view of the hydrogen-bridged dimer involving Pd(1) is in Fig. 2; a view of the dimer with Pd(2) is given in supplementary material available from the authors. The orientation of the bridging H atoms above the PdP_2Cl_2 planes is given by *e.g.* the angles P(12)–Pd(1)···H(13B′) (99°) and P(22)–Pd(2)···H(33B) (95°). In the crystal structure, the effect of these Pd···H···C interactions together with the O–H···N hydrogen bonds noted above is to generate infinite chains in the *c*-direction which have 'H-bridged dimers' linked *via* water molecules. These linear C–H···Pd interactions are best described as 3c–4e hydrogen bonds rather than 3c–2e agostic bonds (*i.e.* the out-of-plane Pd d orbital is filled), as has been well documented by Brammer.[5b]

E. C. A. and G. F. thank NSERC (Canada) for financial support.

Notes and References

* E-mail: alyea@chembio.uoguelph.ca

† *Selected analytical and spectroscopic data* for **1**: yield, 250 mg, 87%, mp. 235 °C (decomp.). Anal. Calc. for $2(C_{12}H_{24}Cl_2N_6P_2Pd)\cdot H_2O$: C, 28.79; H, 5.03; N, 16.79. Found: C, 28.8; H, 4.9; N, 16.7%. FT-Raman: 273, 302 cm^{-1}; $^{31}P\{^1H\}$ $[(CD_3)_2SO]$: δ −18.3. ^1H $[(CD_3)_2SO]$: δ 4.35–4.55 (m, PCH_2, NCH_2).

‡ *Crystal data* for **1**: $2(C_{12}H_{24}Cl_2N_6P_2Pd)\cdot H_2O$, M_r = 1001.2, space group $P\bar{1}$, a = 9.6132(6), b = 9.8611(5), c = 19.5682(8) Å, α = 98.902(4), β = 96.754(4), γ = 90.722(5)°, U = 1819.0(2) Å, Z = 2, D_c = 1.828 g cm^{-3}, $F(000)$ = 1012, $R(F_o)$ = 0.0360 for 4645 observed reflections with $I > 2\sigma(I)$, $wR_2(F^2)$ = 0.0822 for all 6381 unique reflections. Data were collected on an Enraf-Nonius CAD4 diffractometer and corrected for Lorentz, polarization and absorption (Gaussian) effects. The structure was solved using the Patterson heavy-atom method with NRCVAX[12] and refined using SHELXL97.[13] All non-H atoms were allowed anisotropic motion. All H atoms were visible in difference maps and were allowed for as riding atoms. CCDC 182/716.

1 (*a*) L. R. DeLerno, L. M. Trefonas, M. Y. Darensbourg and R. J. Majeste, *Inorg. Chem.*, 1976, **15**, 816; (*b*) D. J. Darensbourg, F. Joo, M. Kannisto, A. Katho and J. H. Reibenspies, *Organometallics*, 1992, **11**, 1990; (*c*) D. J. Darensbourg, F. Joo, M. Kannisto, A. Katho, J. H. Reibenspies and D. J. Daigle, *Inorg. Chem.*, 1994, **33**, 200; (*d*) J. P. Fackler, Jr., R. J. Staples and Z. Assefa, *J. Chem. Soc., Chem. Commun.*, 1994, 431; (*e*) Z. Assefa, B. G. McBurnett, R. J. Staples, J. P. Fackler, Jr., B. Assmann, K. Angermaier and H. Schmidbaur, *Inorg. Chem.*, 1995, **34**, 75; (*f*) D. J. Darensbourg, N. W. Stafford, F. Joo and J. H. Reibenspies, *J. Organomet. Chem.*, 1995, **488**, 99; (*g*) Note added in proof: subsequent to the submission of this paper, a brief description of the anhydrous *cis*-$PdCl_2(TPA)_2$ structure has appeared: D. J. Darensbourg, T. J. Decuir, N. W. Stafford, J. B. Robertson, J. D. Draper, J. H. Reibenspies, A. Katho and F. Joo, *Inorg. Chem.*, 1997, **36**, 4218.

2 (*a*) E. C. Alyea and K. J. Fisher, *Third Chemical Congress of North America, June 5–10, 1988*, Toronto, ON, *Inorg. Abstract*, 12, 420; (*b*) E. C. Alyea, K. J. Fisher and S. Johnson, *Can. J. Chem.*, 1989, **67**, 1319; (*c*) M. M. Muir, J. A. Muir, E. C Alyea and K. J. Fisher, *J. Cryst. Spect. Res.*, 1993, **23**, 745; (*d*) K. J. Fisher, E. C. Alyea and N. Shahnazarian, *Phosphorus, Sulfur, Silicon, Relat. Elem.*, 1990, **48**, 37; (*e*) E. C. Alyea, K. J. Fisher, S. Foo and B. Philip, *Polyhedron*, 1993, **12**, 484; (*f*) E. C. Alyea, G. Ferguson and S. Kannan, *Polyhedron*, 1997, **16**, in press; (*g*) E. C. Alyea, G. Ferguson and S. Kannan, *Polyhedron*, 1998, **17**, in press.

3 E. G. Kuntz, *Fr. Pat.*, 2 366 237, 1976.

4 W. A. Hermann, J. A. Kalpe, J. Kellner, H. Riepl, H. Bahrmann and W. Konkol, *Angew. Chem., Int. Ed. Engl.*, 1990, **29**, 391.

5 (*a*) M. Brookhart, M. L. H. Green and L. L. Wong, *Prog. Inorg. Chem.*, 1988, **36**, 1 and references therein; (*b*) L. Brammer, J. M. Charnock, P. L. Goggin, R. J. Goodfellow, A. G. Orpen and T. F. Koetzle, *J. Chem. Soc., Dalton Trans.*, 1991, 1789; (*c*) A. Albinati, P. S. Pregosin and F. Wombacher, *Inorg. Chem.*, 1990, **29**, 1812; (*d*) R. H. Crabtree, *Angew. Chem., Int. Ed. Engl.*, 1993, **32**, 789.

6 S. Kannan, E. C. Alyea and G. Ferguson, unpublished work.

7 G. Schultz, N. Yu. Subbotina, C. M. Jensen, J. A. Golen and J. Hagittai, *Inorg. Chim. Acta*, 1992, **85**, 191.

8 S. O. Grim and R. L. Keiter, *Inorg. Chim. Acta*, 1970, **4**, 56.

9 V. V. Grushin, C. Bensimon and H. Alper, *Inorg. Chem.*, 1994, **33**, 4804.

10 L. L. Martin and R. A. Jacobson, *Inorg. Chem.*, 1971, **10**, 1795; D. R. Powell and R. A. Jacobson, *Cryst. Struct. Commun.*, 1980, **9**, 1023; N. W. Alcock and J. H. Nelson, *Acta. Crystallogr., Sect. C*, 1985, **41**, 1748; J. J. MacDougall, J. H. Nelson, F. Mathey and J. J. Mayerle, *Inorg. Chem.*, 1980, **19**, 709; G. R. Newkome, D. W. Evans and F. R. Fronczek, *Inorg. Chem.*, 1987, **26**, 3500; T. Gebauer, G. Frenzen and K. Z. Dehnicke, *Z. Naturforsch., Teil B*, 1993, **48**, 1661; N. W. Alcock, T. J. Kemp and F. L. J. Wimmer, *J. Chem. Soc., Dalton Trans.*, 1981, 635.

11 A. L. Spek, PLATON Molecular Geometry Program, July 1997 version. University of Utrecht, Utrecht, Holland, 1997.

12 E. J. Gabe, Y. Le Page, J.-P. Charland, F. L. Lee and P. S. White, *J. Appl. Crystallogr.*, 1989, **22**, 384.

13 G. M. Sheldrick, SHELXL-97, Program for the Refinement of Crystal Structures, University of Göttingen, 1997.

Received in Bloomington, IN, USA, 27th August 1997; 7/06243E

The opening and filling of single walled carbon nanotubes (SWTs)

Jeremy Sloan,[a,b] Jens Hammer,[a] Marek Zwiefka-Sibley[a] and Malcolm L. H. Green*[a]

[a] *Inorganic Chemistry Laboratory, University of Oxford, South Parks Road, Oxford, UK OX1 3QR*
[b] *Department of Materials, University of Oxford, Parks Road, Oxford, UK OX1 3PH*

Single walled nanotubes (SWTs) can be selectively opened and filled using wet chemistry techniques; treatment of the carbon nanomaterials with concentrated HCl apparently leads to the selective opening of the SWTs at their tips; foreign materials can then be deposited inside the resulting cavities in a similar fashion to multi-walled carbon nanotubes (MWTs); the filling of SWTs with small spherical crystals and, additionally, preferentially orientated and elongated single crystals of Ru metal is described; the selective opening of SWTs was inferred from these observations.

Multi-walled carbon nanotubes (MWTs) have attracted much interest since their discovery owing to their high mechanical strength and electrical properties.[1,2] They have already proved to be valuable in their application as tips for scanning probe microscopy and also as field emission devices.[3,4] The discovery and large scale synthesis of single-walled nanotubes (SWTs)[5,6] has given further impetus to this research as they similarly exhibit useful physical and electronic properties. SWTs can be generated by co-evaporating carbon and certain metals in arc-evaporation[5–9] or laser-vaporisation of metal-doped graphite[10,11] although they have also been produced by thinning of MWTs using CO_2.[12] SWTs display a higher degree of uniformity with respect to their physical dimensions compared to MWTs as they consist only of a single cylindrical graphitic layer and exhibit both a smaller range of diameters and far fewer defects than their multi-walled counterparts. Similarly, therefore, a greater degree of uniformity may be anticipated from their physical properties. Theoretical studies suggest that the introduction of foreign material into the inner cavities of MWTs or SWTs may enhance or modify the properties of the resulting composite materials.[13–15] Therefore, following similar work with MWTs,[16,17] we have employed wet chemistry techniques to open and fill SWTs. Here, however, a milder process has been used to selectively open SWTs since the oxidation methodology employed for opening MWTs[16] (*i.e.* refluxing concentrated HNO_3) was found to be too harsh for SWTs and resulted in their destruction.

The SWTs used in these experiments were produced in a modified arc-discharge chamber also employed to make MWTs.[14] Cobalt doped graphite rods were evaporated under a dynamic vacuum with helium (500 Torr) using an electric arc generated from a potential of 30 V and a dc current of 200 A. The external environment of the electrodes was confined by a 10 cm id steel cylinder 20 cm in length. The SWTs were found in the highest yield (*ca.* 30%) in the web-like material deposited on the walls of the cylinder. The diameters of the SWTs were found by high-resolution transmission electron microscopy (HRTEM) to be in the range 1–3 nm. For the filling experiments, samples of SWTs were suspended in concentrated HCl and stirred for 8 h. After centrifuging for 5 min, a light blue solution containing $CoCl_2$ was removed and the specimen was dried at 70 °C for 8 h and then washed with deionised water. A saturated solution of $RuCl_3$ (*ca.* 5 ml) was then added to the SWT-containing specimen and the mixture stirred for 5 h at 35 °C after which the black residue was dried at 60 °C overnight. The sample was then heated in a stream of H_2 at a rate of 5 °C min^{-1} to 45 °C and kept at this temperature for 3 h. After washing with distilled water and drying at 60 °C the residue was prepared for HTREM.

Electron micrographs revealed that a small proportion (*ca.* 5%) of the opened SWT contained foreign material. Fig. 1(*a*) shows a group of three SWTs, two of which apparently are filled with Ru crystals (arrowed). By slightly altering the defocus of the microscope, these crystals were observed to stay at the same focus with the SWTs and therefore we conclude that they are encapsulated inside the SWTs. As with studies carried out with MWTs,[17] individual crystallites were observed to fill the entire width of the hollow core of the SWTs as is seen in Fig. 1(*a*). Energy dispersive X-ray (EDX) microanalyses, utilising a 3 nm probe, performed on clusters of encapsulated crystallites similar to those in Fig. 1(*a*), confirmed their chemical identity as Ru metal [Fig. 1(*b*)], although some slight oxidation is apparent. Encapsulated and elongated crystallites were also frequently observed and these were again identified by EDX to be Ru metal. Fig. 2(*a*) shows an elongated Ru crystallite encapsulated near the elbow of a bent or damaged SWT. Fig. 2(*b*) shows an elongated Ru crystallite growing along the bore of one SWT at

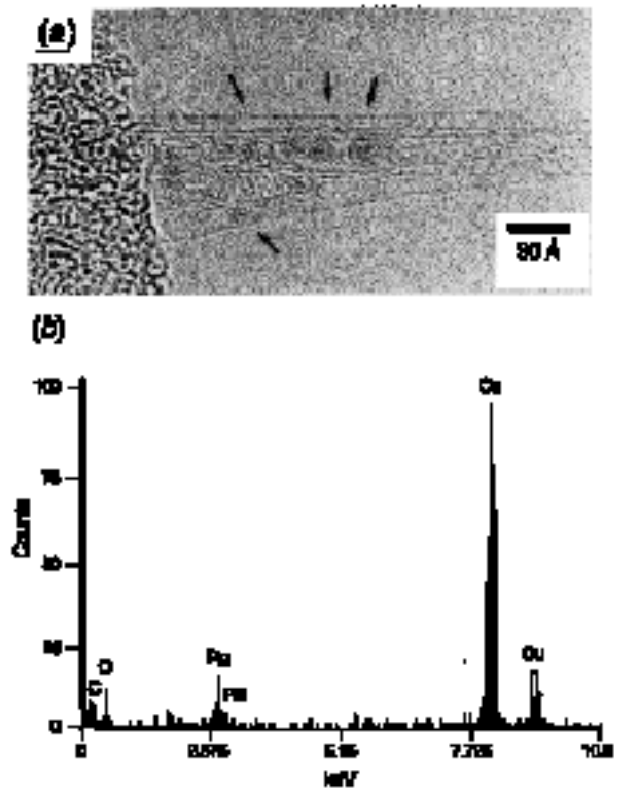

Fig. 1 (*a*) Individual Ru crystals encapsulated inside SWTs (arrowed). The diameter of the crystallites is apparently the same as that of the id of the SWT. (*b*) EDX microanalysis obtained from encapsulated Ru crystals similar to those observed in (*a*). O peak indicates that the crystallites are slightly oxidised. The Cu peak is from the copper TEM support grid.

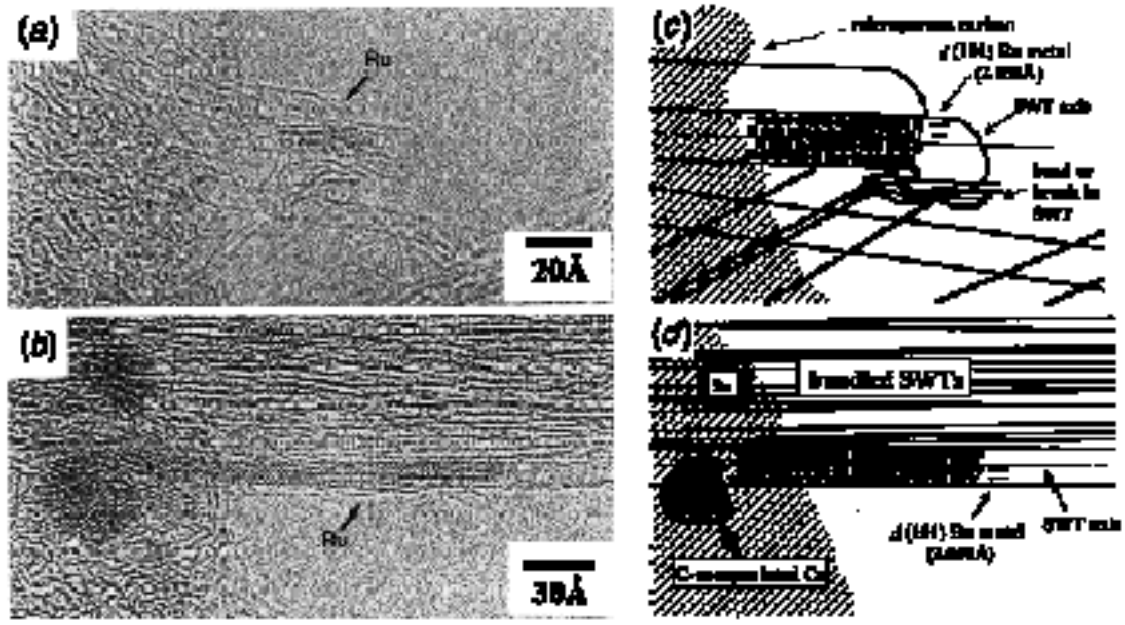

Fig. 2 (*a*) Elongated Ru crystallite encapsulated near the elbow of a bent or damaged SWT. The lattice fringes aligned parallel to the SWT axis corresponding to the *d*(101) lattice fringes of Ru metal. (*b*) Elongated Ru crystallite encapsulated inside a single SWT at the edge of a bundle of SWTs. As with the crystallite in Fig. 1(*a*), the *d*(101) Ru lattice fringes are orientated parallel to the SWT axis. (*c*) Schematic representation of (*a*). (*d*) Schematic representation of (*b*).

the edge of a bundle of SWTs (bundling of SWTs into 'ropes' is very common[10,11]). Both crystallites exhibit preferred orientations, with their *d*(101) lattice fringes[18] aligning parallel to the SWT axes. This phenomenon is represented schematically for Figs. 2(*a*) and (*b*) in Figs. 2(*c*) and (*d*), respectively. The phenomenon of preferred orientation inside SWTs is consistent with the observation of preferred crystallite orientation inside MWTs[19,20] and is most probably the result of the morphological influence of nanotube capillaries over crystallite growth during formation.[21] Other particles were also observed on the exterior of SWTs [Figs. 2(*b*) and (*d*)] and these were found by EDX to be either 'loose' Ru particles or carbon encapsulated Co particles which were presumably protected from acid attack by their carbon shells. It was not possible for us to conclusively image the opened tips of the SWTs by HRTEM because of their very low contrast compared to opened MWTs.[12] The selective opening of the SWTs was therefore inferred indirectly from the observation of their filling with Ru metal from solution which must have occurred in order for filling to occur. A further point is that we have not attempted to estimate the percentage of SWT opening in our experiments, partly for the above reason and also partly because the very high aspect ratio of SWTs would make this an extremely difficult proposition.

Experiments are currently under way in our laboratory to repeat this experiment with both ruthenium and other metals using a higher yield SWT method, similar to that recently reported by Journet *et al.*[22] We are also investigating methods for increasing the yield of the encapsulated product and are also trying to establish the mechanism by which opening occurs.

J. H. is grateful for a grant from the EC program TMR.

Notes and References

* E-mail: malcolm.green@chemistry.ox.ac.uk

1 M. M. J. Treacy, T. W. Ebbesen and J. M. Gibson, *Nature*, 1996, **381**, 678.
2 T. W. Ebbesen, H. J. Lezec, H. Hiura, J. W. Bennet, H. F. Ghaemi and T. Thio, *Nature*, 1996, **382**, 54.
3 H. J. Dai, J. H. Hafner, A. G. Rinzler, D. T. Colbert and R. E. Smalley, *Nature*, 1996, **384** 147.
4 W. A. Deheer, A. Chetelain and D. Ugarte, *Science*, 1996, **270**, 1179.
5 D. S. Bethune, C. H. Kiang, M. S. Devries, G. Gorman, R. Savoy, J. Vasquez and R. Beyers, *Nature*, 1993, **363**, 605.
6 P. M. Ajayan, J. M. Lambert, P. Bernier, L. Barbedette, C. Colliex and J. M. Planeix, *Chem. Phys. Lett.*, 1993, **215**, 509.
7 S. Iijima and T. Ichihashi, *Nature*, 1993, **363**, 603.
8 C. H. Kiang, W. A. Goddard, R. Beyeres, J. R. Salem and D. S. Bethune, *J. Phys. Chem.*, 1994, **98**, 6612.
9 S. Seraphim and Zhou, *Appl. Phys. Lett.*, 1994, **64**, 2087.
10 T. Guo, P. Nickolaev, A. Thess, D. T. Colbert and R. E. Smalley, *Chem. Phys. Lett.*, 1995, **243**, 49.
11 A. Thess, R. Lee, P. Nikolaev, H. Dai, P. Petit, J. Robert, C. Xu, Y. H. Lee, S. G. Kim, A. G. Rinzler, D. T. Colbert, G. E. Scuseria, D. Tomanek, J. E. Fischer and R. E. Smalley, *Science*, 1996, **273**, 483.
12 S. C. Tsang, P. J. F. Harris and M. L. H. Green, *Nature*, 1993, **362**, 520.
13 M. S. Dresselhaus, *Nature*, 1993, **358**, 195.
14 J. W. Mintmire, B. I. Dunlap and C. T. White, *Phys. Rev. Lett.*, 1992, **68**, 631.
15 R. Saito, M. Fujita, G. Dresselhaus and M. S. Dresselhaus, *Mater. Sci. Eng. B*, 1993, **19**, 185.
16 S. C. Tsang, Y. K. Chen, P. J. F. Harris and M. L. H. Green, *Nature*, 1994, **372**, 159.
17 Y. K. Chen, A. Chu, J. Cook, M. L. H. Green, P. J. F. Harris, R. Heesom, M. Humphries, J. Sloan, S. C. Tsang and J. C. F. Turner, *J. Mater. Chem.*, 1997, **7**, 545.
18 Powder Diffraction File card No. 6-663 (ASTM, Philadelphia, PA).
19 P. M. Ajayan, O. Stephan, P. Redlich and C. Colliex, *Nature*, 1995, **375**, 564.
20 J. Sloan, J. Cook, J. R. Heesom, M. L. H. Green and J. L. Hutchison, *J. Cryst. Growth*, 1997, **173**, 81.
21 J. Sloan, J. Cook, M. L. H. Green, J. L. Hutchison and R. Tenne, *J. Mater. Chem.*, 1997, **7**, 1089.
22 C. Journet, W. K. Maser, W. K., P. Bernier, A. Loiseau, M. L. Delachapelle, S. Lefrant, P. Deniard, R. Lee and J. E. Fischer, *Nature*, 1997, **388**, 756.

Received in Bath, UK, 18th October, 1997; 7/07632K

A novel 'build-bottle-around-ship' method to encapsulate metalloporphyrins in zeolite-Y. An efficient biomimetic catalyst

Bi-Zeng Zhan and Xiao-Yuan Li*

Department of Chemistry, The Hong Kong University of Science and Technology, Clear Water Bay, Kowloon, Hong Kong, PR China

Electrostatic interaction is introduced between the host and guest in the synthesis of faujasite-Y confined metallotetrakis(*N*,*N*,*N*-trimethylanilinium) porphyrin cations ($MTMAnP^{4+}$); the synthesized composites display high catalytic activity in the oxidation of cyclohexene.

One of the most attractive properties of zeolites are their well organized nanopores and nanochannels which serve readily as supporting hosts for various molecules. Encapsulation of catalytically active transition metal complexes inside the nanopores of zeolites, often referred to as 'ship-in-a-bottle' systems,[1] has been believed to be one of the most promising strategies in the development of viable industrial catalysts.[1–6] Extensive effort has been devoted to the synthesis and catalytic properties of zeolite entrapped metallocomplexes with such ligands as bipyridine, salen, polyamines and phthalocyanines.[1–6] In most of these syntheses, a so-called 'assemble-ship-inside-bottle' approach has usually been adopted in which the desired catalytic metallocomplex is synthesized inside the nanopores/channels of the zeolite in the presence of an excess of ligand or its synthetic precursors. As a consequence, what was usually obtained is a mixture of the desired complex with unreacted free ligand as well as side-products. For example, the synthesis of metalloporphyrin (MP) inside zeolites often leads to a significant portion of undesired polymerization product and the unmetallated free base porphyrin ligand.[7–9]

We report here a novel, efficient and quantitative method to synthesize high purity MPs incorporated in faujasite-Y at a controllable loading concentration. The novel aspect of this method is that an electrostatic interaction was introduced between the host (anionic aluminosilicate species) and the guest (cationic peripheral substituents on MPs) in a 'build-bottle-around-ship' approach, namely to synthesize the nanocages of zeolite around the high purity cationic MPs. The selected guest molecules have excellent solubility in aluminosilicate gel. In a typical synthesis, 240 mg of $MTMAnPCl_5$ was added into an aluminosilicate gel, freshly prepared by mixing silicate and aluminate solutions containing 4.6 g of silica, 6.2 g of NaOH, 3.2 g of $NaAlO_2$ and 80 ml of H_2O. The gel was then crystallized at 95 ± 2 °C under static and autogeneous conditions in a stainless steel bomb (250 ml) for 48 h. After cooling to room temp., a solid product was recovered by filtration. The complexes adsorbed on the exterior surfaces were removed by a thorough extraction with distilled water, methanol, pyridine (2%)–methanol, and methanol again, respectively. The removed complexes can be fully recovered for the next round of synthesis. The crystals were then dried at 60 °C for 24 h. Thermogravimetry (TG) of the composite indicates that 1.51 mass% is attributable to the confined guest, corresponding to *ca.* one MP complex for every forty supercages or a supercage occupancy of 2.5%.

The loading concentration of $MTMAnP^{4+}$ is adjustable by controlling its concentration in the aluminosilicate gel before crystallization. The largest loading of *ca.* 5 mass% of the guest molecule can be achieved if 800 mg of $MTMAnPCl_5$ is added to *ca.* 94 g of aluminosilicate gel. We speculate that the main driving force for the very successful nanoinclusion of $MTMAnP^{4+}$ cations in the zeolitic supercages in such a readily controllable manner is the electrostatic interaction between the anionic aluminosilicate species and the cationic peripheral substituents on the porphyrin macrocycle. The excellent aqueous solubility of the cationic MP may contribute to the enhanced loading concentration in the zeolite, but this factor alone does not guarantee successful encapsulation. This assertion is supported by the following experimental facts: (*a*) in addition to $MTMAnP^{4+}$, we have also successfully encapsulated other metalloporphyrins with cationic peripheral substituents into zeolitic cages such as metallo–tetrakis(*N*-methyl-4-pyridyl)porphyrins (M = transition metal ion); (*b*) metalloporphyrins with anionic peripheral substituents, such as metallo–tetra(4-sulfonatophenyl)porphyrin ($MTPPS^{4-}$), could not be entrapped into the supercages of zeolite by this method; and (*c*) metalloporphyrins with neutral peripheral substituents, such as metallo–tetraphenylporphyrin (MTPP), could only be incorporated into the zeolite in trace amounts independent of the initial concentration of the porphyrin in the gel. On the other hand, it is believed that the first step in the construction of the zeolitic framework is the formation of anionic aluminosilicate species.

X-Ray powder diffraction (XRD) patterns of the unloaded zeolite and zeolite entrapped $FeTMAnP^{4+}$ and $MnTMAnP^{4+}$ are in excellent agreement with the calculated simulation of the XRD pattern for faujasite zeolite.[10] The excellent signal to noise ratio in the XRD indicates that our synthesized faujasite crystals are of high quality. X-Ray induced fluorescence (XIF) analysis indicates that all the samples have a Si/Al ratio of *ca.* 1.6. This suggests that the framework around the guest molecule $MTMAnP^{4+}$ is faujasite-Y (denoted MTMAnP@NaY) (M = Fe^{III}, Mn^{III} *etc.*). The encapsulation of the cationic MP inside the zeolite nanopores is also supported by TG, UV–VIS DRS, surface area measurements, and resonance microRaman spectroscopy (μRR, *vide infra*). This observation suggests that the occluded $MTMAnP^{4+}$ cations fit well into the supercages of faujasite-Y. In view of the 13 Å diameter of supercage of faujasite, *ca.* 18 Å $MTMAnP^{4+}$ cation [across two opposite trimethylanilinium (TMAn) substituents assuming a planar macrocycle] must distort itself somewhat in order to fit into a supercage. The most plausible distortion is that each of the four peripheral TMAn groups swings toward one of the four channel windows (*ca.* 7 Å in diameter) tetrahedrally located in a supercage, leading to an overall ruffling of the macrocycle, a distortion commonly observed in the X-ray structures of similar MPs.[11]

Resonance Raman techniques are very powerful in the study of hemeproteins and zeolite confined molecules.[12,13] Here, we applied μRR to study the synthesized zeolite–porphyrin composites. Laser excitation at 632.8 nm, in close resonance with the Q_0 absorption band of $MTMAnPCl_5$, was used. Fig. 1 shows the μRR spectra of $MnTMAnPCl_5$ and its faujasite-Y confined composite MnTMAnP@NaY. The normal modes of $MnTMAnPCl_5$ and other similar compounds have been thoroughly studied and assigned.[13] Fig. 1 clearly shows that the basic RR features of $MnTMAnPCl_5$ are all retained in the spectrum of MnTMAnP@NaY, indicating that neither decom-

Table 1 Catalytic oxidation of cyclohexene with *t*-BHP over MnTMANP@NaY

No	Catalyst	Product distribution (%)				t^a/h	Conv. (%)	TOF^b/h^{-1}
		Oxide	Diol	Acid	Others			
1	MnTMAnP@NaY	18.9	77.4	1.4	2.3	24	5.0	2.1
2		15.7	75.7	5.8	2.8	48	28.6	6.1
3	MnTMAnP@NaY^c	12.4	87.6	Trace	Trace	24	24.5	10.2
4		12.4	69.5	18.1	Trace	48	45.1	10.3
5	H_2TMAnP@NaY^c	12.8	59.8	15.7	11.7	24	3.5	1.5

^{a} Reaction time. ^{b} Based on the efficiency of the inserted 'oxygen' into substrate. ^{c} 30 mg of pyridine was added into the reaction mixture (see text).

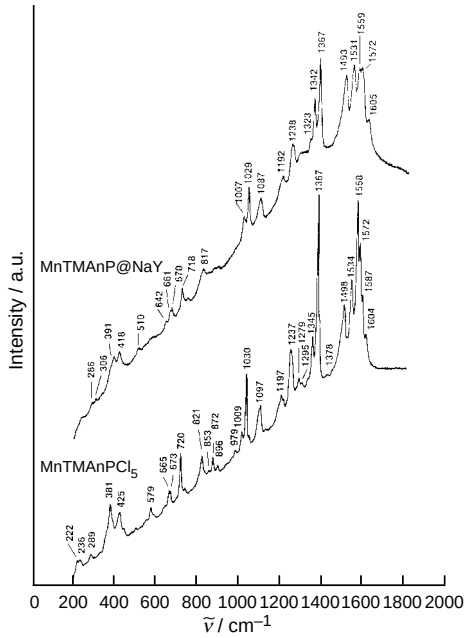

Fig. 1 Resonance microRaman spectra of $MnTMAnPCl_5$ (blank) and MnTMAnP@NaY; 632.8 nm excitation

position nor dimerization occurred during the process of hydrothermal crystallization. It is noticeable that (*a*) several structure sensitive bands located in the region 1300–1600 cm^{-1}, corresponding to the vibrations of $\nu(C_\alpha–N)$, $\nu(C_\alpha–C_\beta)$, $\nu(C_\beta–C_\beta)$, and $\nu(C_\alpha–C_m)$ of the MP macrocycle,[11–13] display some changes in their relative intensity but their frequencies remain more or less the same as that in the spectrum of $MnTMAnPCl_5$; (*b*) the anilinium distortion modes located at 810–900 cm^{-1} become broader and weaker in the spectrum of entrapped MP; and (*c*) the frequency of the Mn–N stretching mode at *ca.* 400 cm^{-1} shifted markedly by *ca.* 10 cm^{-1}. All these changes of vibrational signatures of the entrapped MP indicate that the entrapped complex is indeed distorted in the cavity of faujasite-Y.

The catalytic oxidation of cyclohexene over zeolite confined metalloporphyrins (MnAnP@NaY) with *tert*-butyl hydroperoxide (*t*-BHP) was performed in a glass tube with a stopper in a standard manner. At 50 °C, using a ratio of 1 : 1.5 for cyclohexene to *t*-BHP, and a mole ratio of 12 000 : 1000 : 1 for solvent : reactant : catalyst, we obtained a 28.6% conversion of cyclohexene with an average of 6.1 h^{-1} turnover frequency (TOF) in 48 h when MnTMAnP@NaY was used as the catalyst. Of particular interest is that the catalytic activity of MnTMAnP-@NaY is enhanced *ca.* fivefold in the presence of pyridine in the first 24 h (Table 1, entries 1 and 3). Everything else being the same as above, a blank experiment using H_2TMPyP@NaY gave a conversion of 3.5%, much lower than that of 24.5% for MnTMAnP@NaY (entries 3 and 5). This shows clearly that the encapsulated MP is indeed involved in the oxidation process. Longer reaction time leads to > 90% conversion of cyclohexene and gives adipic acid as the main product. To the best of our knowledge, this is the highest catalytic activity ever achieved in cyclohexene oxidation using a zeolite confined transition metallocomplex as catalyst. No significant loss of activity was detected in the reaction process. The mixture of the final products is colourless and no leaching of MPs into the reaction solution was detected according to atomic absorption spectroscopy. The catalytic activity of our catalyst was completely recovered by filtration of the reaction solution and washing of the catalyst with acetone at room temperature.

In conclusion, we have developed a novel, efficient and quantitative method to synthesize high purity metallo–tetrakis(*N*,*N*,*N*-trimethylanilinium) porphyrin encapsulated in the supercages of faujasite-Y. This method introduced an electrostatic interaction between the host (zeolite) and the guest (cationic MPs) in a 'built-bottle-around-ship' approach. The loading of the guest molecules can be adjusted easily by controlling the initial concentration of cationic MPs in aluminosilicate gel. In our preliminary study of the catalytic oxidation of cyclohexene by *t*-BHP, MnTMAnP@NaY gives very high activity and epoxidation selectivity. Its activity was enhanced *ca.* fivefold when pyridine was added to the reaction mixture.

This project was supported by the Research Grant Council (HK) and Hong Kong University of Science and Technology.

Notes and References

* E-mail: CHXYLI@usthk.ust.hk

1 V. Yu. Zakharov and B. V. Romanovsky, *Vestn. Mosk. Univ., Ser. 2: Khim.*, 1977, **18**, 142 (English Translation in *Sov. Moscow Univ. Bull.*, 1977, **32**, 16).
2 *Inclusion Chemistry with Zeolites*, ed. N. Herron and D. R. Corbin, Kluwer, Dordrecht, 1995.
3 P. P. Knops-Gerrits, D. E. De Vos, F. Thibault-Starzyk and P. A. Jacobs, *Nature*, 1994, **369**, 543 and references therein.
4 R. F. Parton, I. F. J. Vankelecom, M. J. A. Casselman, C. P. Bezoukhanova, J. B. Uytterhoeven and P. A. Jacobs, *Nature*, 1994, **370**, 541.
5 K. J. Balkus, Jr., M. Eissa and R. Levado, *J. Am. Chem. Soc.*, 1995, **117**, 10 753.
6 N. Herron, *Inorg. Chem.*, 1986, **25**, 4714.
7 M. Nakamura, T. Tatsumi and H. Tominaga, *Bull. Chem. Soc. Jpn.*, 1990, **63**, 3334.
8 G. Q. Li and R. Govind, *Inorg. Chim. Acta*, 1993, **217**, 135.
9 P. Battioni, R. Iwanejko, D. Mansuy, T. Mlodnicka, J. Poltowicz and F. Sanchez, *J. Mol. Catal. A: Chem.*, 1996, **109**, 91.
10 M. M. J. Treacy, J. B. Higgins and R. von Ballmoos, *Collection of Simulated XRD Powder Patterns for Zeolites*, Elsevier, 3rd edn., 1996.
11 W. R. Scheidt and Y. J. Lee, *Struct. Bonding*, 1987, **64**, 1.
12 B.-Z. Zhan and X.-Y. Li, *Stud. Surf. Sci. Catal.*, 1997, **105**, 615.
13 X.-Y. Li, R. S. Czernuszewicz, J. R. Kincaid, Y. O. Su and T. G. Spiro, *J. Phys. Chem.*, 1990, **94**, 31.

Received in Cambridge UK, 18th August 1997; 7/06030K

Novel nanostructures of gold–polypyrrole composites

S. Tamil Selvan*

Organic Chemistry III/Macromolecular Chemistry, University of Ulm, D-89069 Ulm, Germany

Different novel nanostructures of gold–polypyrrole composites are observed by the transmission electron microscopy, for the first time, with the advent of block copolymer micelles.

Nanoparticles of gold and other noble metals and semiconductor particles, in a more general sense, exhibit a variety of useful optical, electrical and catalytic properties. All these properties strongly depend on the careful choice of preparative strategies, which could provide long term stability and ease in processability.[1–4] Polymer nanocomposites is one such approach and one of the important objectives in recent research is to prepare monodisperse particles, regularly dispersed in a polymer matrix. The synthesis of noble metal sols in a polymerising nonconducting system such as poly(methyl methacrylate) has recently been documented in the literature.[5]. The first prerequisite for the formation of kinetically controlled monodisperse colloids is the availability of well defined dispersions. Block copolymer micelles provide an excellent means for such dispersions,[6] by which the particles of a definite size can be formed and stabilized within the core, yielding monodisperse colloids.

With the advent of block copolymer micelles, we have demonstrated very recently, a facile and versatile route to the fabrication of monodisperse, single gold (Au) nanocluster, *ca*. 7 nm, in diameter (core) surrounded by a shell of polypyrrole (PPY), both within the spherical microdomains.[7–9] In this report, the first observation of different, novel nanostructures of Au–PPY, is described.

In the first method, a micellar solution of polystyrene-block-poly(2-vinylpyridine) (0.5 mass%) in toluene was treated with tetrachloroauric acid (0.5 and 0.7 equiv. to 2VP units) which got selectively bound within the P2VP cores of the micelles. When this solution was treated with pyrrole (PY), polymerization occurred, yielding polypyrrole under concurrent formation of Au nanoparticles, as supported by FTIR and UV–VIS measurements. The bipolaron bands at 1210 and 925 cm^{-1} indicated the formation of PPY in its doped state.[7] The chemical conversion is depicted in Scheme 1.

TEM images were acquired with a Philips 400 microscope operating at 80 kV. The samples were prepared by placing a drop of the colloidal polymer solution onto a carbon-coated Cu grid on an underlying tissue paper, leaving behind a thin colloidal film. In a typical concentration, *i.e.* $[PY]/[HAuCl_4]$ = 4.0, uniform, monodisperse Au particles with a mean diameter of 7 and 9 nm, are vividly seen with a shell of PPY, respectively in Fig. 1(*a*) and (*b*), upon annealing the thin film at 130 °C for 1 h. When the above procedure is repeated, but with

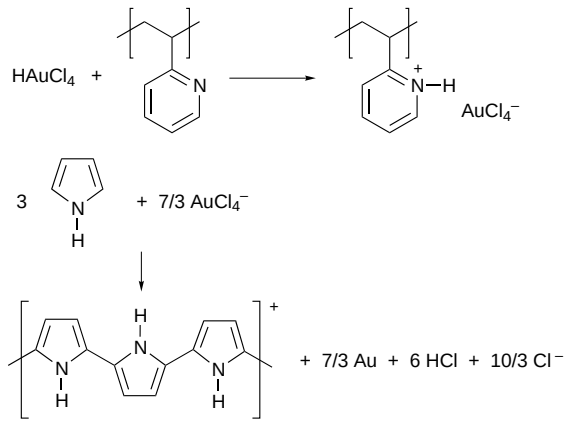

Scheme 1

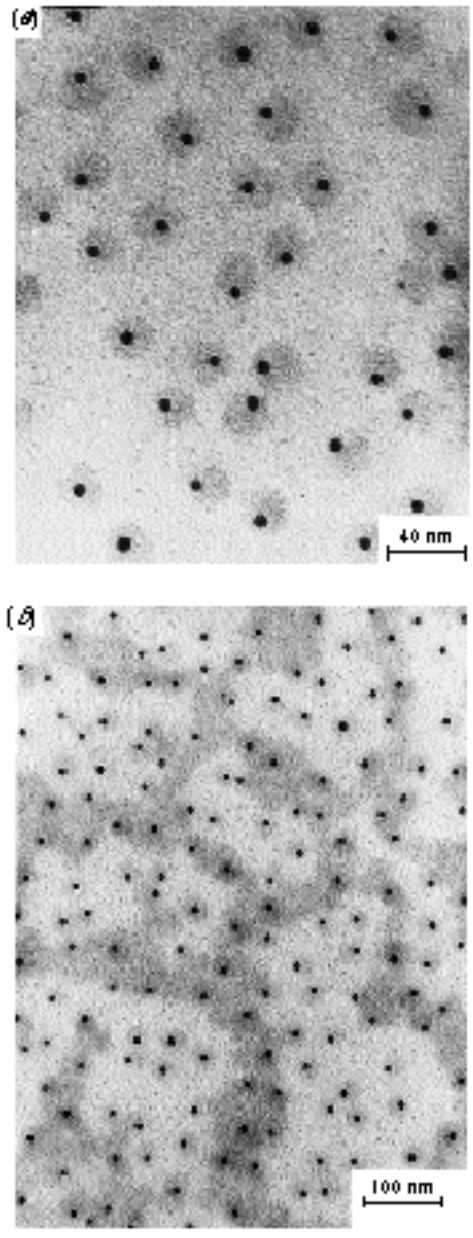

Fig. 1 Transmission electron micrographs of thin colloidal polymer films ($[PY]/[HAuCl_4]$ = 4.0) after annealing at 130 °C for 1 h. (*a*) 7 nm Au ($[HAuCl_4]/[2VP]$ = 0.5); (*b*) 9 nm Au ($[HAuCl_4]/[2VP]$ = 0.7) in each micelle. The grayish area represents PPY.

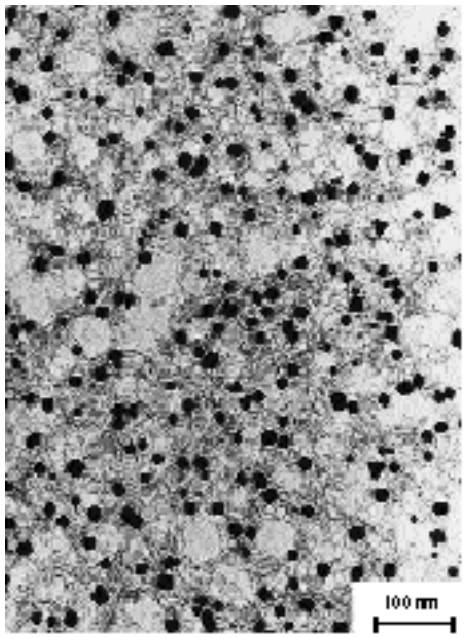

Fig. 2 Transmission electron micrograph of a thin film cast from a colloidal polymer solution (stirred heavily, but without annealing), exhibiting spherical, cubic, tetrahedral and octahedral Au particles

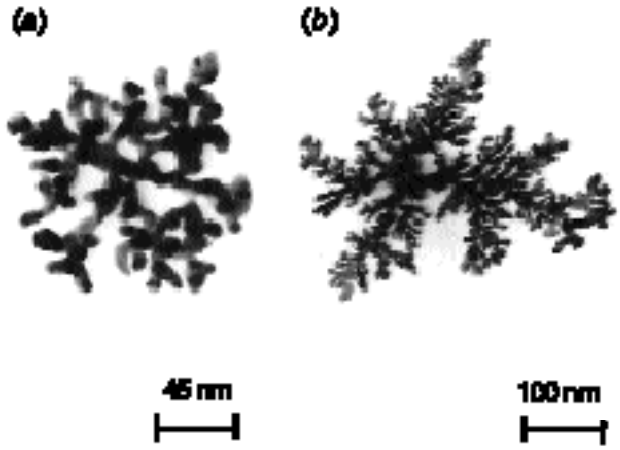

Fig. 3 TEM pictures depicting dendritic nanostructures of thin films cast from block copolymer ionomers, after vapour phase polymerization (VPP) of PY. (*a*) after 2 h of VPP; (*b*) after overnight VPP.

heavy stirring of the micellar solution and without heating, different shapes of Au particles, *viz*., spherical, cubic, tetrahedral and octahedral, are observed (Fig. 2). Here, the spherical domains cannot be seen owing to the fact that the spherical micelles coagulate with each other, yielding different shapes of Au, dispersed in a PPY matrix, marked by a grayish area. Most importantly, the nanoparticles of Au with different shapes resemble the shape-controlled synthesis of Pd nanoclusters.[10] It is obvious that an ordered aggregation produces uniform particles (Fig. 1), since a disordered aggregation would result in polydisperse particles of variable morphology (Fig. 2).

Interestingly, we have observed elegant 'dendritic' nanostructures (Au–PPY fractals?), in another different approach, by employing vapour phase polymerization of PY onto solution cast films of block copolymer ionomers (Fig. 3). Dendritic growth occurs even at a lesser polymerization time (⩽30 min). Thick branches radiated after 2 h of polymerisation. This large random supramolecular structure, known in short as DLA (diffusion-limited aggregate),[11] represents a very wide variety of growth (here, polymerization and coagulation), allowing building of one particle after the other and letting the particle diffuse and stick to the growing structure. The pioneering work of Kaufman *et al.* delineated PPY fractals obtained by the diffusion-limited electrochemical polymerization of PY.[12]

In conclusion, we have observed different elegant nanostructures of composites of Au, with a little nudge in the preparative strategies. Different (spheroids, cuboids) Au nanoparticles may have important implications in the field of catalysis. Importantly, the block copolymer architecture is useful for commercial applications of a processable form of PPY by providing colloidal stability to the suspension of PPY.[13] Furthermore, the new observation of 'dendritic' nanostructures, could open up new vistas in supramolecular structures. Over and above, conducting and semiconducting polymer/metal junctions could provide intriguing perspectives to develop novel electronic devices.[14]

The author gratefully acknowledges the Alexander von Humboldt (AvH) Foundation, Germany, for a Post-doctoral fellowship. Professor M. Moeller, is thanked for his invitation/facilities to work in his laboratory as a Humboldt Fellow.

Notes and References

* Present address: Department of Materials Science and Engineering, Nagoya Institute of Technology, Gokiso-cho, Showa-ku, Nagoya 466, Japan. E-mail: selvan@mse.nitech.ac.jp

1 G. Schmid, *Chem. Rev.*, 1992, **92**, 1709.
2 M. Brust, M. Walker, D. Bethel, D. J. Schiffrin and R. Whyman, *J. Chem. Soc., Chem. Commun.*, 1994, 801.
3 K. Vijaya Sarathy, G. U. Kulkarni and C. N. R. Rao, *Chem. Commun.*, 1997, 537.
4 J. P. Spatz, S. Moessmer and M. Moeller, *Chem. Eur. J.*, 1996, **2**, 1552.
5 Y. Nakao, *J. Colloid Interface Sci.*, 1995, **171**, 386.
6 A. Roescher and M. Moeller, *Adv. Mater.*, 1995, **7**, 151.
7 S. Tamil Selvan, J. P. Spatz, H.-A. Klok and M. Moeller, *Adv. Mater.*, in press.
8 S. Tamil Selvan, J. P. Spatz, H.-A. Klok and M. Moeller, in *Quantum Dot Materials for Nonlinear Optics Applications*, ed. R. F. Haglund, Kluwer Academic Press, 1997, in press.
9 M. Moeller, J. P. Spatz, A. Roescher, S. Moessmer, S. Tamil Selvan and H.-A. Klok, *Macromol. Symp.*, 1997, **117**, 207.
10 T. S. Ahmadi, Z. L. Wang, T. C. Green, A. Henglein and M. A. E. Sayed, *Science*, 1996, **272**, 1924.
11 O. Katzenelson, H. Z. H.-Or and D. Avnir, *Chem. Eur. J.*, 1996, **2**, 174.
12 J. H. Kaufman, C. K. Baker, A. I. Nazzal, M. Flickner and O. R. Melroy, *Phys. Rev. Lett.*, 1986, **56**, 1932.
13 E. Arca, T. Cao, S. E. Webber and P. Munk, *Polym. Prepr.* (*Am. Chem. Soc., Div. Polym. Chem.*), 1994, **35**, 334.
14 J. Unsworth, Z. Jin, B. A. Lunn and P. C. Innis, *Polym. Int.*, 1991, **26**, 245.

Received in Cambridge, UK, 10th November 1997; 7/08050F

Structural and magnetic properties of an asymmetric dicopper(II) anticancer drug analogue

Boujemaa Moubaraki,[a] Keith S. Murray,[a] John D. Ranford,*[b] Xiaobai Wang[b] and Yan Xu[c]

[a] *Chemistry Department, Monash University, Wellington Road, Clayton, Victoria 3168 Australia*
[b] *Department of Chemistry, National University of Singapore, Kent Ridge Crescent, Singapore 119260*
[c] *Department of Chemistry, National Institute of Education, 469 Bukit Timah Road, Singapore 259756*

The single-crystal X-ray structure and variable temperature magnetic properties of the novel dicopper(II) anticancer drug analogue $[\{Cu_2(HL)(H_2PO_4)_2\}_2][NO_3]_2{\cdot}2H_2O$ [H_2L = bis(pyridine-2-aldehyde) thiocarbohydrazone] is determined; the complex shows a dimer of dimeric $\{Cu_2(HL)\}^{3+}$ units with dihydrogenphosphato and sulfur bridges between the inequivalent Cu^{II} centres, resulting in three antiferromagnetic exchange interactions: a dominant intradimer J of -109 to -116 cm^{-1}, and two weaker interdimer interactions.

Thiosemicarbazones have been extensively studied because of their biological properties. Cu^{II} is necessary for activity for kethoxal bis(thiosemicarbazone),[1] with the mode of action proposed to involve inhibition of DNA synthesis and oxidative phosphorylation,[2] and *N*-methylisatin-β-thiosemicarbazone can inactivate tumour viruses.[3] Attention has however focused on pyridine-2-aldehyde thiosemicarbazone (Hpt) and derivatives as the Cu^{II} complexes are more bioactive than the metal free ligands.[2,4] The metal-free 5-OH analogue underwent clinical trials as an anticancer drug but side effects such as disruption of iron metabolism prevented clinical use.[5] However, administration of a preformed metal complex may alleviate this. Adducts of $[Cu(pt)]^+$ with sulfur and nitrogen donors have been detected in biological fluids[6] with stable model thiolato complexes isolated from aqueous solution.[7] Crystallographic studies have revealed ternary nitrogen adduct formation,[7,8] complexation of dihydrogen phosphate[9] and pyrophosphate[10] and the system's remarkable ability to form complexes of both the anionic and neutral ligand.[11] The H_2L ligand may be considered as an extension of Hpt, now with a possible extra metal binding domain. Antiviral activity has been reported for 2-acetylpyridine thiocarbohydrazones[12] and H_2L is antifungal[13] and cytotoxic[14] but little chemical and no structural work has been carried out on the Cu–H_2L system. On the human leukemia cell line MOLT4 (at 10 μM), H_2L is more cytotoxic than Hpt, $Cu_2(HL)^{3+}$ and $Cu(pt)^+$ show equal activity whereas, surprisingly $Cu(HL)^+$ is the most cytotoxic.[14] Here we report the first crystallographic study of H_2L with Cu^{II}, $[\{Cu_2(HL)(H_2PO_4)_2\}_2][NO_3]_2{\cdot}2H_2O$, giving a dimer of dicopper(II) moieties with $H_2PO_4^-$ and weak sulfur bridges. Variable temperature magnetic studies reveal three antiferromagnetic exchange interactions involving superexchange pathways across the planar ligand, a three-atom $H_2PO_4^-$ bridge and direct $Cu^{II}\cdots Cu^{I}$ and/or out-of-plane (*via* S) interactions.

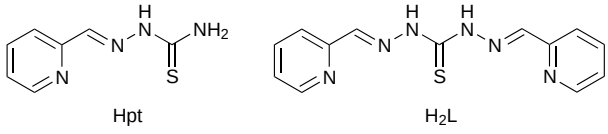

The starting nitrate complex, $[Cu_2L(NO_3)_2]{\cdot}3H_2O$ **1**, used in subsequent metathetical reactions with phosphate was prepared by addition of H_2L (0.616 g, 2.16 mmol) in hot ethanol (150 ml) to $Cu(NO_3)_2{\cdot}3H_2O$ (1.05 g, 4.34 mmol) in the same solvent (10 ml). After stirring for 1 h the product was filtered, washed with ethanol then dried *in vacuo* (913 mg, 72%). $[\{Cu_2(HL)(H_2PO_4)_2\}_2][NO_3]_2{\cdot}2H_2O$ **2** was prepared by dissolving **1** (157 mg, 0.267 mmol) and $NaH_2PO_4{\cdot}H_2O$ (37 mg, 0.268 mmol) in H_3PO_4 (2 ml, 2 M). Dark green crystals suitable for X-ray analysis were collected after 20 days (82 mg, 45%).

X-Ray analysis of **2**† shows the structure (Fig. 1) to be best described as a centrosymmetric dimer of dicopper(II) moieties with dihydrogenphosphato and weak sulfur bridges. Cu(1) has a square-pyramidal geometry with the monoanionic HL bound through pyridyl and imine nitrogens and sulfur. The coordination sphere is completed by phosphato oxygens O(11) and O(21). Cu(2) adopts a tetragonal '4 + 2' geometry with pyridyl, imine and deprotonated amide nitrogens from HL and phosphato oxygen in the plane. Much weaker axial interactions to O(11) and S(1A) 3.24 Å] are from symmetry related molecules. The dimeric $Cu_2(HL)^{3+}$ units are linked *via* three-atom phosphato [Cu(1)–O(21)–P(2)–O(1A)–Cu(2)] and one-atom sulfur bridges with adjacent dimers connected by the weak Cu(2)–O(11) interaction and a hydrogen-bonding network involving phosphato, water and nitrate oxygens and protonated amide [N(3)] nitrogen. Other metric parameters may be considered normal.[7–12] The two phosphate ions adopt different coordination modes, with P(2) chelating and P(1) being monodentate and P(2) binds through the keto oxygen [P(2)–O(1) 1.468(4) Å].

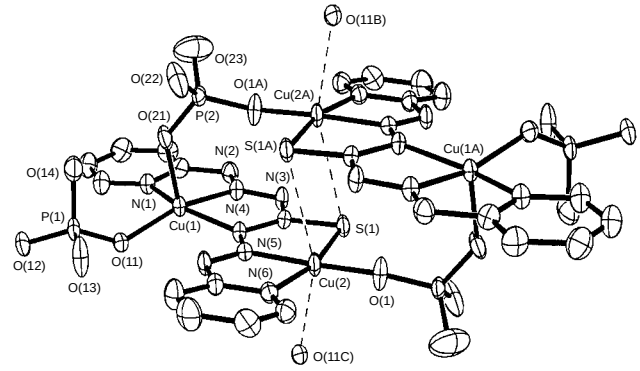

Fig. 1 Molecular structure of the dimeric dicopper(II) ion $[\{Cu_2(HL)(H_2PO_4)_2\}_2]^{2+}$ of **2**. Hydrogen atoms are omitted for clarity. Selected bond distances (Å) and angles (°): Cu(1)–N(1) 2.053(4), Cu(1)–N(2) 1.954(4), Cu(1)–N(4) 2.076(4), Cu(1)–O(11) 1.933(3), Cu(1)–O(21) 2.159(3), Cu(2)–N(5) 1.966(3), Cu(2)–N(6) 2.004(4), Cu(2)–O(1) 1.890(3), Cu(2)–S(1) 2.263(2), Cu(2)–O(11C) 2.860(4), Cu(2)–S(1A) 3.242(2), Cu(1)···Cu(2) 4.996, Cu(1)···Cu(2A) 5.076, Cu(2)···Cu(2A) 3.905, Cu(2)···Cu(2C) 3.797, Cu(1)···Cu(1A) 9.326; O(11)–Cu(1)–N(1) 95.4(2), N(4)–Cu(1)–O(11) 140.5(1), O(21)–Cu(1)–N(1) 97.4(2), O(21)–Cu(1)–O(11) 95.0(1), N(1)–Cu(1)–N(4) 155.1(1), N(2)–Cu(1)–O(11) 160.5(2), O(1)–Cu(2)–N(6) 92.8(2), S(1)–Cu(2)–O(1) 100.7(1), S(1)–Cu(2)–N(6) 165.4(1), S(1)–Cu(2)–N(5) 84.9(1), O(1)–Cu(2)–N(5) 171.9(2), O(11)–Cu(2)–S(1) 86.6(1), O(11)–Cu(2)–O(1) 107.4(1), O(11)–Cu(2)–N(5) 78.6(1), O(11)–Cu(2)–S(1A) 159.2(2), S(1A)–Cu(2)–S(1) 94.7(1), S(1A)–Cu(2)–O(1) 92.8(1).

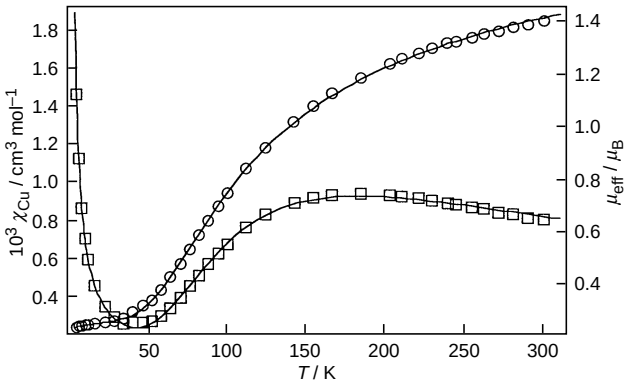

Fig. 2 Temperature dependence of χ_{Cu} and μ_{Cu} *vs.* T for [{Cu_2(HL)(H_2PO_4)$_2$}$_2$](NO_3)$_2$·2H_2O **2**. Solid lines represent the best fit calculated values.

The temperature dependence of magnetic susceptibility and moment, per Cu^{II}, for **2** is shown in Fig. 2. A maximum in χ at *ca*. 180 K is clearly indicative of medium strength antiferromagnetic exchange occurring. The rapid increase in χ at low temperature is due to monomer impurity. Use of a simple dinuclear Bleaney–Bowers model[15] ($-2\,JS_1S_2$ Hamiltonian) did not precisely reproduce the shape of the susceptibility in the region of χ_{max} but did yield an approximate J_{12} value of *ca*. -105 cm^{-1}, albeit with a low g value of 1.98 and a large interdimer θ parameter (in T–θ) of -25 K. Excellent fits could be obtained when the tetranuclear model of Hatfield[16] was employed. The rhomboidal framework of the dimer of dimers is shown in Fig. 3 together with the J labels. The value of the long Cu(1)···Cu(1A) parameter $J_{1,1A}$ was set at zero and the other parameters were varied widely for best-fit. It was found that two parameter sets gave equally excellent fits *i.e.* set A: $g = 2.00 \pm 0.02$, $N_\alpha = (60 \pm 3) \times 10^{-6}$ cm^3 mol^{-1}, $J_{2,2A} = -75.4 \pm 0.2$ cm^{-1}, $J_{1,2} = -116.6 \pm 0.2$ cm^{-1}, $J_{1,2A} = -16.8 \pm 0.2$ cm^{-1}, % monomer 1.7 ± 0.1. This fit is shown in Fig. 2. Set B: $g = 2.00 \pm 0.02$, $J_{2,2A} = -46.0 \pm 0.5$ cm^{-1}, $J_{1,2} = -109.5 \pm 0.2$ cm^{-1}, $J_{1,2A} = -47.9 \pm 0.2$ cm^{-1}, % monomer 1.7 ± 0.1. Thus the dominant coupling, $J_{1,2}$, remains virtually constant in both fits and occurs across the planar thiocarbohydrazonato moiety. It involves superexchange pathways in the *x*–*y* plane such as a two-atom *trans*-Cu–N–N–Cu pathway and three- or four-atom pathways Cu–S–C–N–Cu or Cu–S–C–N–N–Cu. The value of $J_{1,2}$ is similar to that of a structurally related carbohydrazonato dinuclear analogue, reported recently[17] having $J = -106.6$ cm^{-1} (there is a factor of two error in J in ref. 17). The size of the 'edge' and 'short-diagonal' parameters $J_{1,2A}$ and $J_{2,2A}$ could not be identified unambiguously. When using set B, but with $J_{2,2A}$ set at zero or slightly positive, {as anticipated from a previous study[18] on a related S-bridged complex [CuCl(S_2CNEt)]$_4$} much poorer fits were obtained, with the calculated and observed curves crossing each other in the region of χ_{max}. Thus it appears that the Cu(2)S(1)-Cu(2A)S(1A) pathways yield stronger antiferromagnetic coupling (minimum of -46 cm^{-1}) than do related Cu(SR)CuCl or Cu(SR)Cu(SR) pathways[18] in [CuCl(S_2CNEt)]$_4$ and [Cu(S_2CNEt)$_2$]$_2$. The antiferromagnetic coupling across the three-atom $H_2PO_4^-$ bridge, with J of at least -16.8 cm^{-1}, is weak as anticipated and involves axial–equatorial d-orbital overlap, respectively on Cu(1) and Cu(2A). The uncertainties and correlation in the $J_{1,2A}$ parameters may also be influenced by the weak axial interaction Cu(2)–O(11) and Cu(2)–S occurring between teramers, although these are expected to be very weak. In this regard, the visible spectra of solid and H_3PO_4 solutions of **2** are nearly identical.

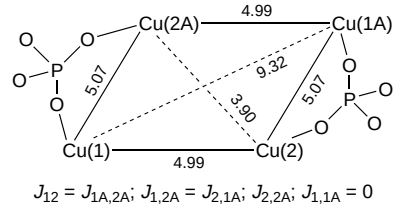

$J_{12} = J_{1A,2A}$; $J_{1,2A} = J_{2,1A}$; $J_{2,2A}$; $J_{1,1A} = 0$

Fig. 3 Rhomboidal framework for the Cu^{II} centres of **2** showing distances (Å) together with the J labels.

The X-band ESR spectrum of a neat powder of **2** at 298 K shows a broad, symmetrical signal at $g = 2.1$. At 77 K this signal is resolved into a typical axial lineshape ($g_\parallel = 2.19$, $A_\parallel = 184.6$ gauss, $g_\perp = 2.00$) probably due to the monomer impurity (*vide supra*). Triplet state lines due to $Cu^{II}\cdots Cu^{I}$ interactions[19] are evident as weak broad lines at 'half-field' (1500 G) and 3700 G. The same spectrum is observed in frozen 2 M H_3PO_4 solution, with evidence for a weaker monomer lineshape ($g_\parallel = 2.33$, $A_\parallel = 175$ G, $g_\perp = 2.06$) superimposed.

This work was supported by grants from the National University of Singapore (RP 3950651) and the Australian Research Council (Large Grants) and Dr J. J. Vittal's help with the crystallography is acknowledged.

Notes and References

* E-mail: chmjdr@nus.edu.sg

† *Crystal data*: $C_{13}H_{17}Cu_2N_7O_{12}P_2S$, $M = 684.4$, dark green crystal, 0.15 × 0.1 × 0.1 mm, triclinic, space group $P\bar{1}$, $a = 8.604(2)$, $b = 10.719(2)$, $c = 14.268(3)$ Å, $\alpha = 109.57(3)$, $\beta = 90.11(3)$, $\gamma = 110.62(3)°$, $U = 1149.6(4)$ Å^3, $D_c = 1.977$ g cm^{-3}, $Z = 2$, $F(000) = 688$, μ(Mo-Kα) = 2.157 mm^{-1}; $R = 0.041$, $R_w = 0.122$ using 3150 unique reflections with $I > 4\sigma(I)$. CCDC 182/711.

1 *Inorganic and Nutritional Aspects of Cancer*, ed. G. N. Schrauzer, Plenum, New York, 1978.
2 J. R. Sorenson and W. M. Willingham, *Trace Elements Med.*, 1986, **3**, 139.
3 W. C. Kaska, C. Carrano, J. Michalowski, J. Jackson and W. Levinson, *Bioinorg. Chem.*, 1978, **8**, 225; W. Rohde, R. Shafer, J. Idriss and W. Levinson, *J. Inorg. Biochem.*, 1979, **10**, 183.
4 W. E. Antholine, P. Gunn and L. E. Hopwood, *Int. J. Radiat. Oncology Biol. Phys.*, 1981, **7**, 491; L. A. Saryan and E. A. Petering, *J. Med. Chem.*, 1979, **22**, 1218; E. W. Ainscough, A. M. Brodie, R. Cresswell, J. D. Ranford and J. M. Waters, submitted.
5 R. C. DeConti, B. R. Toftness, K. C. Agrawal, R. Tomchick, J. A. Mead, J. R. Bertino, A. C. Sartorelli and W. A. Creasey, *Cancer Res.*, 1972, **32**, 1455.
6 W. E. Antholine and F. Taketa, *J. Inorg. Biochem.*, 1982, **16**, 145.
7 E. W. Ainscough, A. M. Brodie, J. D. Ranford and J. M. Waters, *J. Chem. Soc., Dalton Trans.*, 1991, 1737.
8 E. W. Ainscough, E. N. Baker, A. M. Brodie, R. J. Cresswell, J. D. Ranford and J. M. Waters, *Inorg. Chim. Acta*, 1990, **172**, 185.
9 E. W. Ainscough, A. M. Brodie, J. D. Ranford and J. M. Waters, *J. Chem. Soc., Dalton Trans.*, 1997, 1251.
10 E. W. Ainscough, A. M. Brodie, J. D. Ranford, J. M. Waters and K. S. Murray, *Inorg. Chim. Acta*, 1992, **197**, 107.
11 E. W. Ainscough, A. M. Brodie, J. D. Ranford and J. M. Waters, *J. Chem. Soc., Dalton Trans.*, 1991, 2125; A. G. Bingham, H. Bögge, A. Müller, E. W. Ainscough and A. M. Brodie, *J. Chem. Soc., Dalton Trans.*, 1987, 493; C. F. Bell and C. R. Theocharis, *Acta Crystallogr., Sect. C*, 1987, **43**, 26; J. Garcia-Tojal, M. K. Urtiaga, R. Cortés, L. Lezama, M. I. Arriortua and T. Rojo, *J. Chem. Soc., Dalton Trans.*, 1994, 2233.
12 T. A. Blumenkopf, J. A. Harrington, C. S. Koble, D. D. Bankston, R. W. Morrison, Jr., E. C. Bigham, V. L. Styles and T. Spector, *J. Med. Chem.*, 1992, **35**, 2306.
13 B. G. Choi, *Yakhak Hoechi*, 1986, **30**, 79.
14 K. O. Lian, Y. C. Long, J. D. Ranford and X. Wang, unpublished work.
15 B. Bleaney and K. D. Bowers, *Proc. R. Soc. London, Ser. A*, 1952, **214**, 451.
16 W. E. Hatfield and G. W. Inman, Jr., *Inorg. Chem.*, 1969, **8**, 1376.
17 A. Bacchi, A. Bonini, M. Carcelli, F. Ferraro, E. Leporati, C. Pelizzi and G. Pelizzi, *J. Chem. Soc., Dalton Trans.*, 1996, 2699.
18 P. D. W. Boyd and R. C. Martin, *J. Chem. Soc., Dalton Trans.*, 1977, 105.
19 T. D. Smith and J. R. Pilbrow, *Coord. Chem. Rev.*, 1974, **13**, 173.

Received in Cambridge, UK, 22nd September 1997; 7/08414E

Design, synthesis and metal binding properties of a mixed-donor macrobicycle

Mark Mascal,* Jens Hansen, Alexander J. Blake and Wan-Sheung Li

Department of Chemistry, University of Nottingham, Nottingham, UK NG7 2RD

A cryptand is resolved into its three independent macrocyclic components leading to novel, dynamic metal ion complexation.

Chelating agents which operate with the benefit of the macrocyclic effect possess an exceptional complexation potential which has facilitated the study of metals in unusual circumstances, *e.g.* uncommon coordination numbers, coordination geometries, donor atoms and/or oxidation states.[1] We describe below a case where, through innovative ligand design, Cu^{I} and Ag^{I} ions are guests in a novel and dynamic environment.

Macrobicycle L^1 was conceptualised as a logical extension of an earlier study on the conformational preferences of [*n.n*]cyclophanes.[2] The molecule lies in a potential energy minimum where the aromatic rings are face to face and the three heteroatoms are in fixed equatorial positions.[3] An important design consideration of this ligand system is that sandwich-type complexation involving η^6-bonding to the benzene rings is disfavoured by the large Ar···Ar separation (*ca.* 5.0 Å), and no assistance from the nitrogens can be expected owing to the distance between these atoms and the centre of the trigonal plane (*ca.* 3.0 Å) which they define. This means that L^1, formally a cryptand, is reduced conceptually to three independent, 16-membered azamacrocycles (Fig. 1) each capable of complexing a metal, especially if some contribution from the aromatic systems was forthcoming. Since only one of these three equivalent 'facets' can be occupied at any one time, it should be possible to promote spontaneous migration of the guest from nitrogen to nitrogen within the perimeter of the benzene rings above a characteristic temperature, effectively constituting 'dynamic' sandwich complexation with the centre of gravity of the metal coinciding with the molecular C_3 axis.

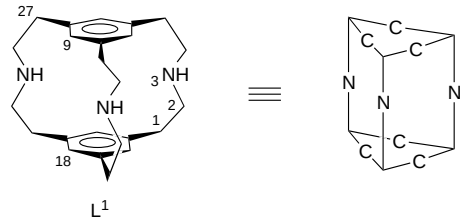

Fig. 1 Structure of L^1 and representation in terms of ligand sets

Compound L^1 can be conveniently synthesised by the cyclotrimerisation method shown in Scheme 1.[4] Thus benzene 1,3,5-triacetic acid **1**, available by Willgerodt–Kindler reaction on commercial triacetylbenzene, is condensed with 4-aminobut-1-yne to give triyne **2** in 94% yield. Reaction of **2** with catalytic $[CoCp(CO)_2]$ provides the bicyclic amide **3** as an inseparable mixture of 1,2,4- and 1,3,5-isomers (1.3 : 1, ratio) in 54% overall yield. The mixture is finally reduced with borane, whereupon L^1 can be isolated by column chromatography.

A stable complex is formed between L^1 and Cu^{I} by simply adding a solution of $[Cu(MeCN)_4]BF_4$ in acetonitrile to an equimolar quantity of the macrocycle in dichloromethane at room temp. The ^1H and ^{13}C NMR spectra of this material show a desymmetrisation of the ligand resonances consistent with the expected mode of inclusion. In particular, the aromatic CH

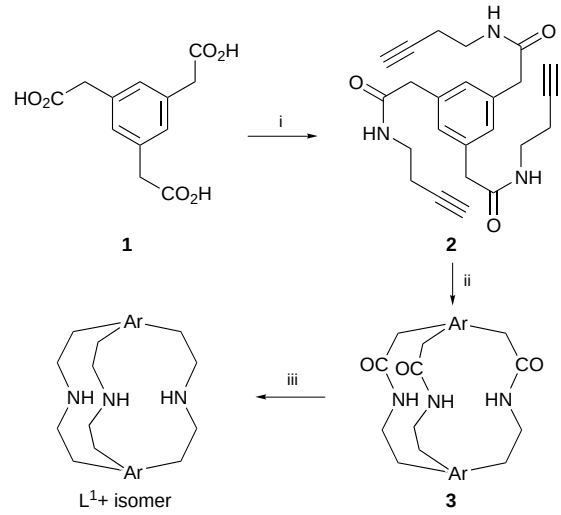

Scheme 1 *Reagents and conditions*: i, carbonyldiimidazole, 4-aminobut-1-yne, THF; ii, $[CoCp(CO)_2]$, *o*-xylene, heat; iii, $BH_3{\cdot}SMe_2$, THF, heat then MeOH, heat

signal associated with the Cu is shifted 0.59 ppm downfield of the other two protons, indicative of electron withdrawal to the metal bond. Mass spectral data are also consistent with the formation of a 1 : 1 complex. Colourless crystals of $[CuL^1]BF_4{\cdot}H_2O$ suitable for X-ray diffraction were obtained from dichloromethane/ether solution, and determination of the structure† (Fig. 2) served to confirm our model. The Cu sits in a general position with Cu–N bond lengths of 2.01 Å. The closing of the N···N distance in L^1 in order to achieve these bond lengths is made possible by a puckering inwards of the chains

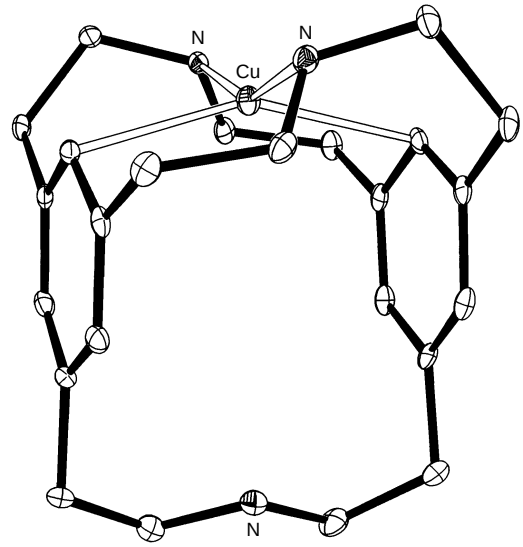

Fig. 2 Crystal structure of $[CuL^1]BF_4{\cdot}H_2O$. Displacement ellipsoids are represented at the 30% probability level. The H-atoms, counter-ion and water of crystallization are omitted for clarity.

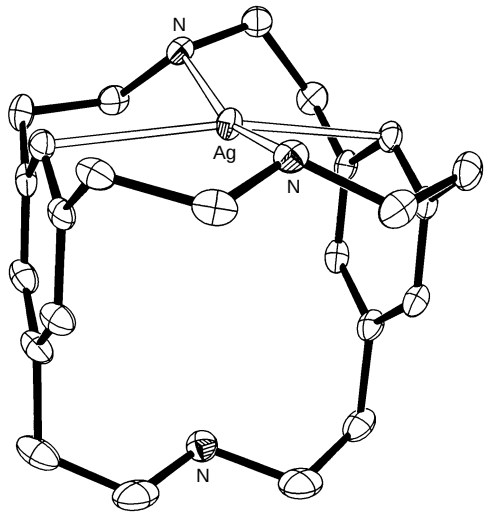

Fig. 3 Crystal structure of [AgL¹]OTf. Displacement ellipsoids are represented at the 20% probability level and the H-atoms and counter-ion are omitted for clarity. Only the major component of disorder affecting the free nitrogen [N3] is shown.

between which the metal is located. An interesting feature of this structure is the relationship of Cu to the benzene rings. This may involve either the metal acting as an electron acceptor in η^1 bonds to C,[5] or three-centre, two-electron σ complexation to the aromatic C–H bonds.[6] The Cu···C distances are 2.38 and 2.40 Å, and the 0.57 Å displacement of the metal away from C(9)–C(18) axis puts the contacts to the midpoint of the C–H bonds at 2.37 and 2.39 Å. The downfield shift in the NMR of the protons involved argues in favour of this type of interaction and against agostic bonding to the H, which would normally result in an upfield shift.[7] It is noted that interactions between copper(I) and aryl rings are somewhat of a novelty in any case, with only five other structurally characterised examples appearing in the literature.[8] All of these show exclusively η interactions to carbon, most with the Cu located over a π bond in an η^2 fashion.[9]

We then examined the dynamics of ligand exchange in [CuL¹]. The ^{1}H NMR spectrum ($CDCl_2CDCl_2$) shows temperature dependent fluxional behaviour, with collapse of the two aromatic signals to a single, broad peak occurring around 95 °C. Migration of the copper nominally involves breaking away from one of the nitrogens and both carbons [or C–H(σ) → Cu bonds] of a C_2N_2 ligand set before regaining the same from another set, although progression from site to site would take place under the continuous influence of the π system.

Reaction of the macrobicycle with AgOTf in THF gave the corresponding complex [AgL¹]OTf. Unlike [CuL¹]BF_4, the proton NMR (CD_2Cl_2) of this material showed a single resonance in the aromatic region at room temperature, and only on cooling below −50 °C did the signal split analogously to the copper(I) system into two sharp peaks (1 : 2), separated in this case by 0.27 ppm. This indicated a much greater degree of mobility for the silver ion than for Cu^I. The X-ray crystal structure of [AgL¹]OTf† (Fig. 3) was comparable to that of [CuL¹]BF_4, the major difference being that only one of the two CCNCC chains needed to distort from the ideal all-*trans* conformation to accommodate the larger silver ion (Ag–N 2.32 Å). The outward displacement of the silver from the C9–C18 axis (0.40 Å) is slightly less than that for copper(I), but the same general NMR and structural arguments apply and either η^1 complexation or two electron donation from the C–H bonds can be invoked. A longer range contact to one of the oxygens of the triflate ion (2.92 Å) is also observed normal to the (approximate) C_2N_2 plane.

Future work in this area will address the behaviour of other metal ions in the presence of L¹, as well as structural modifications to the macrocycle (O, S analogues) which should further expand its scope as a novel ligand.

This research was supported by a grant from the European Commission (to J. H.), and we would like to thank Martin Schröder for helpful discussions.

Notes and References

* E-mail pczmm@vax.ccc.nottingham.ac.uk

† *Single crystal structure determinations*: [CuL¹]BF_4·H_2O: $C_{24}H_{33}BCuF_4N_3$]·H_2O, M_r = 531.90, colourless irregular plate 0.39 × 0.39 × 0.10 mm, triclinic, space group $P\bar{1}$ (no. 2), a = 9.937(12), b = 10.094(6), c = 13.656(15) Å, α = 83.23(7), β = 81.19(12), γ = 61.24(6)°, U = 1185.0(17) Å^3, Z = 2, D_c = 1.491 g cm^{-3}, μ(Mo-Kα) = 0.976 mm^{-1}, T = 150 K. Stoe Stadi-4 four-circle diffractometer, Mo-Kα radiation (λ = 0.710 73 Å) $2\theta_{max}$ = 50°. Numerical absorption corrections (T = 0.756–0.908). The structure was solved by automatic direct methods (G. M. Sheldrick, SHELXS-96. *Acta Crystallogr., Sect. A*, 1990, **46**, 467) and refined by full-matrix least squares on F^2 (G. M. Sheldrick, SHELXL-96. University of Göttingen, Germany, 1996) with all non-H atoms assigned anisotropic displacement parameters. Methylene H atoms were placed geometrically, others being located from ΔF syntheses; thereafter those of H_2O were refined freely with others constrained to ride on their parent atoms. Final R_1 [$F_o > 4\sigma(F_o)$] = 0.0551, wR_2 (all data) = 0.1264 for 4150 unique reflections and 328 refined parameters.

[AgL¹]OTf: $C_{25}H_{33}AgF_3N_3O_3S$, M_r = 620.5, colourless plate 0.53 × 0.48 × 0.11 mm, monoclinic, space group $P2_1/c$ (no. 14), a = 13.152(5), b = 10.655(5), c = 19.306(4) Å, β = 106.50(2)°, U = 2594.0(9) Å^3, Z = 4, D_c = 1.589 g cm^{-3}, μ(Mo-Kα) = 0.911 mm^{-1}, T = 220 K. Data were collected as for [CuL¹]BF_4·H_2O and absorption corrections (T = 0.582–0.775) based on azimuthal scans were applied. The structure was solved and refined as for [CuL¹]BF_4·H_2O. Static disorder was modelled in the region of the non-coordinating N, with major (0.76) and minor (0.24) components and with restraints applied to C–C and C–N distances. The H atom on the minor component was omitted, that on the major was restrained during refinement and all others were riding on their parent atoms. Final R_1 [$F_o > 4\sigma(F_o)$] = 0.0414, wR_2 (all data) = 0.1071 for 4561 unique reflections and 328 refined parameters. CCDC 182/710.

1 L. F. Lindoy, *The Chemistry of Macrocyclic Ligand Complexes*, Cambridge University Press, Cambridge, 1989; A. J. Blake and M. Schröder, *Adv. Inorg. Chem.*, 1990, **35**, 1.
2 M. Mascal, J.-L. Kerdelhué, A. S. Batsanov and M. J. Begley, *J. Chem. Soc., Perkin Trans. 1*, 1996, 1141.
3 Modelling of L¹ was carried out using MACROMODEL, version 4.0, with the MM3 force field: F. Mohamadi, N. G. J. Richards, W. C. Guida, R. Liskamp, M. Lipton, C. Caufield, G. Chang, T. Hendrickson and W. C. Still, *J. Comput. Chem.*, 1990, **11**, 440. An X-ray crystal structure of L¹ which confirms structural predictions has been obtained and will be presented when the work is published in full.
4 Adaptation of the classic method of: A. J. Hubert, *J. Chem. Soc. C*, 1967, 6, who described an all-hydrocarbon analog of L¹.
5 For a description of η^1 coordination of benzene to silver(I) see: K. Shelly, D. C. Finster, Y. J. Lee, W. R. Scheidt and C. A. Reed, *J. Am. Chem. Soc.*, 1985, **107**, 5955.
6 R. H. Crabtree, *Angew. Chem., Int. Ed. Engl.*, 1993, **32**, 789.
7 M. Brookhart, M. L. H. Green and L.-L. Wong, *Prog. Inorg. Chem.*, 1988, **36**, 1.
8 Cambridge Structural Database: F. H. Allen and O. Kennard, *Chemical Design Automation News*, 1993, **8**, 31.
9 R. W. Turner and E. L. Amma, *J. Am. Chem. Soc.*, 1966, **88**, 1877; G. B. Ansell, M. A. Modrick and J. S. Bradley, *Acta Crystallogr., Sect. C*, 1984, **40**, 365; H. Schmidbaur, W. Bublak, B. Huber, G. Reber and G. Müller, *Angew. Chem., Int. Ed. Engl.*, 1986, **25**, 1089; C. J. Brown, P. J. McCarthy, I. D. Salter, K. P. Armstrong, M. McPartlin and H. R. Powell, *J. Organomet. Chem.*, 1990, **394**, 711; D. Ohlmann, H. Pritzkow, H. Grützmacher, M. Anthamatten and R. Glasser, *J. Chem. Soc., Chem. Commun.*, 1995, 1011.

Received in Cambridge, UK, 13th October 1997; 7/07354B

Cu_2O as a photocatalyst for overall water splitting under visible light irradiation

Michikazu Hara,[a] Takeshi Kondo,[a] Mutsuko Komoda,[a] Sigeru Ikeda,[a] Kiyoaki Shinohara,[b] Akira Tanaka,[b] Junko N. Kondo[a] and Kazunari Domen*[a]

[a] *Research Laboratory of Resources Utilization, Tokyo Institute of Technology, 4259 Nagatsuta, Midori-ku, Yokohama 226, Japan*
[b] *Nikon Corp., 1-10-1 Azamizodai, Sagamihara 228, Japan*

Photocatalytic decomposition of water into H_2 and O_2 on Cu_2O under visible light irradiation is investigated; the photocatalytic water splitting on Cu_2O powder proceeds without any noticeable decrease in the activity for more than 1900 h.

So far, many photocatalysts have been reported to decompose water into H_2 and O_2 under UV light irradiation.[1–5] From the view point of solar energy conversion, however, a photocatalyst which works under visible light irradiation (>400 nm) is indispensable, but such a photocatalyst has not yet been found. In this report, we introduce Cu_2O, a well-known p-type semiconductor, which acts as a photocatalyst for overall water splitting under visible light irradiation ($\leqslant$600 nm).

The solid state physics of Cu_2O, which abundantly exists as cuprite in nature, has been extensively investigated for a long time since Cu_2O is a simple metal oxide semiconductor with a small band gap energy. As shown in an energy correlation between the band gap model of Cu_2O and the redox potentials of relevant electrode reactions in an aqueous solution at pH 7,[6] the conduction and valence band edges of Cu_2O, which are separated by a band gap energy of 2.0–2.2 eV,[7,8,9] seem to be available for reduction and oxidation of water, respectively. Therefore, Cu_2O is, in principle, capable of decomposing water into H_2 and O_2 under visible light excitation. However, as yet, such a photochemical reaction has not been accomplished on any Cu_2O electrode since they undergo photodegradation in aqueous solution.[9] In fact, visible light irradiation (470 nm) of a cathode-polarized Cu_2O single crystal electrode in aqueous solution resulted in reduction of Cu_2O to metallic Cu.[10] For this reason, overall water splitting on Cu_2O photocatalysts has not been investigated despite the band structure available for the reaction. In this study, we confirmed the photocatalytic overall water splitting on Cu_2O powder under visible light irradiation.

Cu_2O powder prepared by the hydrolysis of CuCl was used in this study. CuCl was hydrolyzed by adding 1 M aqueous Na_3PO_4 (40 cm^3) to a 5 M aqueous NaCl solution containing 0.04 mol of CuCl (400 cm^3) with vigorous stirring under an Ar flow. A yellow precipitate was produced by the hydrolysis which was washed with distilled water (200 cm^3) 5–7 times followed by decantation under vacuum and drying *in vacuo*. Cu_2O powder was obtained by heating the yellow precipitate at 673 K for 24 h *in vacuo*, followed by boiling in water under an Ar atmosphere to remove unreacted CuCl from Cu_2O. The particle size and surface area of Cu_2O were estimated to be 0.3–0.5 μm and 6 $m^2\ g^{-1}$, respectively. Only the XRD pattern due to Cu_2O was seen with no evidence for other diffraction patterns such as for CuO, metallic Cu or other impurities. The XP spectra of Cu 2p and the Cu LMM Auger spectra indicated that the surface of Cu_2O was composed of Cu^{I}.[11,12] The band gap energy of Cu_2O was estimated at *ca.* 2.0 eV (λ *ca.* 620 nm) by UV–VIS spectroscopy.

The photodecomposition of water was carried out in a Pyrex cell with 0.5 g of Cu_2O and 200 cm^3 of distilled water, which was vigorously magnetically stirred. The cell was irradiated at room temperature from one side with visible light ($\lambda > 460$ nm) from a 300 W Xe lamp with a cut-off filter. A closed gas circulation and evacuation system (300 cm^3) made of Pyrex glass was connected to the reaction cell, and evolved gases were directly transferred to a gas chromatograph to avoid any contamination from air.

Fig. 1 shows several typical time courses of H_2 and O_2 evolution from Cu_2O under visible light irradiation (>460 nm). The reaction system was evacuated after each run. As shown in run 1, only O_2 evolved for 10 h after the beginning of the reaction, and then the evolution of H_2 was observed as the reaction proceeded. The rate of H_2 evolution increased gradually in the subsequent runs. The ratio of the amount of evolved H_2 to O_2 (H_2/O_2) was 0.8 in run 1 and increased to 1.8 in run 4. After run 4, the ratio was between 2.0 and 2.5. The reaction proceeds without any noticeable decrease in the activity for more than 30 runs as shown in Fig. 1. The total amounts of evolved H_2 and O_2 for 1900 h reached 3.8 and 1.9 mmol, respectively, and are comparable to the amount of Cu_2O used (0.5 g, 3.5 mmol). Furthermore, there was no noticeable difference in pH of the suspension before reaction (pH 7.3) and after run 31 (pH 7.1). In order to elucidate the origin of the evolved O_2, an experiment using $H_2{}^{18}O$ was carried out. In another small Pyrex cell (50 cm^3), 0.1 g of Cu_2O (after reaction for 400 h) suspended in a mixture of $H_2{}^{16}O$ (5 cm^3) and $H_2{}^{18}O$ (1 cm^3) was irradiated with visible light (>460 nm). H_2 and O_2 were stoichiometrically evolved after light irradiation and it was confirmed by mass spectral analysis that the ratio, $^{16}O_2 : {}^{16}O{}^{18}O : {}^{18}O_2$, in the evolved O_2 species for 24 h was 254 : 94 : 13. The result indicates that the atomic ratio, $^{16}O : {}^{18}O$, in the total amount of evolved O_2 is 5.0 corresponding to that in the mixed water. As a result, the evolved O_2 is attributed to the water cleavage on Cu_2O. The photoresponse on Cu_2O was observed for visible light through a cut-off filter of 600 nm, while there was no photoresponse at $\lambda > 650$ nm.

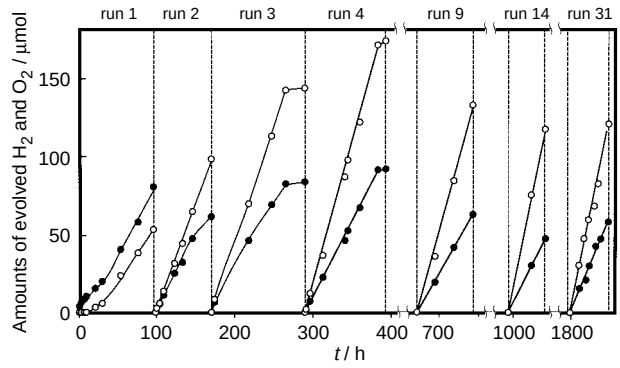

Fig. 1 Time courses of H_2 (open circles) and O_2 (filled circles) evolution in Cu_2O under visible light ($\lambda \geqslant 460$ nm) irradiation. Catalyst: 0.5 g, H_2O: 200 cm^3. The reaction system was evacuated with light irradiation after each run. Time courses in runs 5–8, 10–13 and 15–30 are omitted.

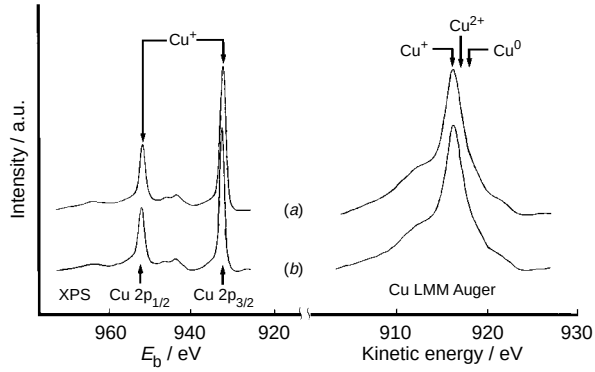

Fig. 2 X-Ray photoelectron spectra of Cu 2p and Cu LMM Auger spectra of Cu_2O before (*a*) and after (*b*) reaction for 400 h. The binding and kinetic energies were referenced to the Au $4f_{7/2}$ level at 83.8 eV.

Fig. 2 shows the XP spectra of Cu 2p and Cu LMM Auger peaks of Cu_2O before and after reaction for 400 h. There was no noticeable difference in the XP spectra of Cu_2O, indicating that Cu_2O powder was neither reduced nor oxidized after photocatalytic reaction. These results are in total contrast to the observation on Cu_2O electrodes and strongly suggest that Cu_2O powder catalytically decomposes water into H_2 and O_2 under visible light irradiation. To the best of our knowledge, such a reaction on Cu_2O photocatalysts has not yet been reported. The reaction mechanism as well as the reason for the difference between the electrode and the powder systems are still not clear. Nevertheless it is inferred that the photocatalytic reaction on a Cu_2O particle in distilled water is clearly different from the photoelectrochemical reaction on polarized Cu_2O electrodes in an aqueous electrolyte. The quantum efficiency of the photocatalytic reaction was estimated at *ca*. 0.3% between 550 and 600 nm.

One of the characteristic features of the Cu_2O photocatalyst is the excess evolution of O_2 above the stoichiometry at the early stage of the reaction (runs 1 and 2). Cu_2O is known to absorb a relatively large amount of oxygen in bulk as well as adsorbing oxygen as O^- or O_2^- on the surface.[13,14] The excess oxygen on the surface or in the bulk leads to p-type semiconducting behaviour and unique oxidation catalysis of Cu_2O. The release of these excess oxygen species from Cu_2O by visible light irradiation may cause the excess evolution of O_2 above the stoichiometry at the early stage of the reaction. Another feature to be noted is the O_2 pressure dependence of the reaction.

As shown in runs 3 and 4 of Fig. 1, the evolution rates of H_2 and O_2 became slow or stopped when the amount of evolved O_2 exceeded *ca.* 80 μmol which corresponded to 500 Pa of O_2 in our system. In all runs after run 5, H_2 and O_2 evolved without any significant decrease in the activity so long as the evolved gas was evacuated before the pressure of O_2 reached 500 Pa. These results suggest that O_2 at more than a certain pressure (500 Pa) in the reaction system inhibits the overall water splitting on Cu_2O. Such an inhibition might be attributed to the photoadsorption of oxygen on the Cu_2O surface. p-Type semiconductors are known to photoadsorb O_2 under light irradiation when O_2 in gas phase exceeds a certain pressure.[15] The photoadsorption largely depends on the O_2 pressure as well as on the wavelength and intensity of incident light, temperature, *etc.* Although the dependence of photoadsorption on O_2 pressure in a Cu_2O–H_2O–O_2/H_2 system as in the present case has not yet been investigated, it is probable that preferential O_2 photoadsorption inhibits the overall water splitting on the Cu_2O surface.

Although Cu_2O has been regarded as an unstable material for water decomposition under light irradiation from the results of photoelectrochemistry, the present study has revealed Cu_2O to be a photocatalyst able to decompose water into H_2 and O_2 under visible light irradiation. The reaction mechanism on Cu_2O is under investigation.

Recently, we have also found that $CuFeO_2$ evolves H_2 and O_2 under visible light irradiation, and detailed results will be reported soon. $CuFeO_2$ has a delafossite type layered structure where the iron oxide layers are connected to each other through linear –O–Cu^I–O– bonds.[16–18] The Cu_2O lattice consists of chains of linear bonds. This suggests that Cu^I containing materials with linear –O–Cu^I–O– bonds are available for the overall water splitting under visible light irradiation. Such Cu^I containing materials may become potential candidates for converting solar energy into H_2 energy.

Notes and References

* E-mail: kdomen@res.titech.ac.jp

1 D. Duonghong, E. Borgarello and M. Graetzel, *J. Am. Chem. Soc.*, 1981, **103**, 4685.
2 K. Domen, S. Naito, T. Onishi, K. Tamaru and M. Soma, *J. Phys. Chem.*, 1982, **86**, 3657.
3 K. Domen, A. Kudo, A. Shinozaki, A. Tanaka, K. Maruya and T. Onishi, *J. Chem. Soc., Chem. Commun.*, 1986, 356.
4 Y. Inoue, T. Kubokawa and K. Sato, *J. Chem. Soc., Chem. Commun.*, 1990, 1298.
5 K. Sayama and H. Arakawa, *J. Chem. Soc., Chem. Commun.*, 1992, 150.
6 H. Gerischer, *J. Electroanal. Chem.*, 1977, **82**, 133.
7 C. Kittel, in *Introduction to Solid State Physics*, 5th edn., Wiley, New York, 1976, p. 341.
8 P. W. Baumeister, *Phys. Rev.*, 1961, **121**, 359.
9 G. Nagasubramanian, A. S. Gioda and A. J. Bard, *J. Electrochemcal Soc.*, 1981, **128**, 2158.
10 H. Gerischer, *Ber. Bunsenges Phys. Chem.*, 1971, **75**, 1237.
11 R. V. Siriwardane and J. A. Poston, *Appl. Surf. Sci.*, 1993, **68**, 65.
12 K. Domen, S. Naito, M. Soma, T. Onishi and K. Tamaru, *J. Chem. Soc., Faraday Trans. 1*, 1982, **78**, 845.
13 H. Dünwald and C. Wagner, *Z. Phys. Chem. B*, 1933, **40**, 197.
14 B. J. Wood, H. Wise and R. S. Yolles, *J. Catal.*, 1969, **15**, 355.
15 Th. Wokenstein and IV. Karpenko, *J. Appl. Phys.*, 1962, **33**, 460.
16 A. Pabst, *Am. Mineral.*, 1946, **31**, 539.
17 R. D. Shannon, D. B. Rogers and C. T. Prewitt, *Inorg. Chem.*, 1971 **10**, 713.
18 C. Prewitt, R. D. Shanonn and D. B. Rogers, *Inorg. Chem.*, 1971, **10**, 719.

Received in Cambridge, UK, 15th October 1997; 7/07440I

Friedel–Crafts alkylation in supercritical fluids: continuous, selective and clean

Martin G. Hitzler,[a] Fiona R. Smail,[a] Stephen K. Ross[b] and Martyn Poliakoff[a]*†

[a] *Department of Chemistry, University of Nottingham, Nottingham, UK NG7 2RD*
[b] *Thomas Swan & Co. Ltd, Crookhall, Consett, Co. Durham, UK DH8 7ND*

Continuous Friedel–Crafts alkylation of mesitylene, $C_6H_3Me_3$, and anisole, C_6H_5OMe, with propene or propan-2-ol has been carried out in supercritical propene or CO_2 using a heterogeneous polysiloxane-supported solid acid Deloxan® catalyst in a small fixed bed reactor (10 ml volume); 100% selectivity for mono-alkylated products with 50% conversion could be obtained by adjusting the reaction parameters, *e.g.* temperature, pressure, flow rates, *etc.*

Numerous chemical syntheses involve Friedel–Crafts or Friedel–Crafts-type alkylation reactions, both on laboratory and industrial scales. Friedel–Crafts chemistry is therefore of major importance and research in this field is of continuing chemical interest.[1–5] Frequently, the reaction is used to add only a *single* alkyl group to the substrate, but addition of the first alkyl group activates the substrate so that subsequent alkylation is made easier. Thus, conditions have to be controlled precisely, often with long reaction times and low temperatures, to minimise the formation of poly-alkylated by-products.

Friedel–Crafts reactions are usually carried out batch-wise in a large excess of the substrate or in an organic solvent. Generally, the reaction is carried out in the presence of Lewis acid catalysts (*e.g.* $AlCl_3$, BF_3, $TiCl_4$) or strong protic acids (*e.g.* HF, H_2SO_4). Relatively high concentrations of catalyst are needed; often the amounts are near stoichiometric, especially when H_2O is generated. These problems make most Friedel–Crafts processes inherently dirty. Therefore, the development of environmetally more benign Friedel–Crafts processes is a high priority. Solid acid catalysts based on clays, zeolites or even graphite[6] could be the answer to *cleaner* Friedel–Crafts chemistry, but until recently rapid catalyst deactivation has prevented the development of a commercial process.[7] Not only can solid catalysts be easily separated from liquid products, they also offer the possibility of carrying out Friedel–Crafts reactions in continuous rather than batch reactors.[8] Continuous flow reactors can be smaller than the batch reactors needed to generate comparable amounts of product.[9] A reactor of smaller size usually increases safety and reduces capital cost.

Very recently, we described[10] how the supercritical hydrogenation of a wide a range of organic compounds can be carried out extremely efficiently in small-scale *continuous* flow reactors (5 or 10 ml) using Pd and Pt heterogeneous catalysts supported on polysiloxane (Deloxan®, Degussa AG). Here we show how the *same* reactor can be used to carry out continuous Friedel–Crafts alkylation using a commercially available solid acid catalyst based on the *same* Deloxan® support.‡ In our process,§ the organic solvent is replaced by a supercritical fluid, *e.g.* $scCO_2$. The separation of the product occurs simply by expanding the fluid to atmospheric pressure, so the crude product can be analysed without further work-up. Although reaction temperatures are high, because of short residence times, our process maintains high product selectivity.

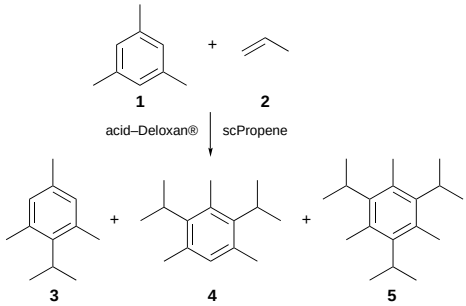

Scheme 1

Our initial reactions involved mesitylene **1** ($C_6H_3Me_3$) with propene **2**, which acts both as alkylating agent and as supercritical solvent [scPropene, T_c = 91.9 °C, p_c = 46.0 bar (10 bar = 1 MPa)]. This reaction was chosen because the mono- **3**, di- **4** and tri-alkylated product **5** each have only *one* possible isomer (Scheme 1), which simplifies product analysis.¶

Table 1 shows that Friedel–Crafts chemistry can indeed be carried out *continuously* under these conditions. The selectivity is reasonable for 1-isopropyl-2,4,6-trimethylbenzene **3** but significant amounts of **4** and dimers of propene **2** are formed. Table 1 also shows that the yield of **3** cannot easily be improved by varying the reaction conditions.

By contrast, selectivity for the formation of **3** is much higher in the alkylation of **1** with propan-2-ol, **6**, in supercritical CO_2 ($scCO_2$, T_c = 31.1 °C, p_c = 73.8 bar) using the same solid acid Deloxan® catalyst. The reaction forms water but this is not a serious problem; the organic and water layers are easily separated after the $scCO_2$ has been vented. Initially, the reaction was carried out with a three-fold excess of **6** over **1** (total flow rate of **1** + **6**: 0.50 ml min^{-1}) at 220 bar and T_{cat} = 200 °C with a gaseous CO_2 flow rate of 0.43 l min^{-1}. Analysis of the organic layer showed that the conversion of **1** was 46% with **3** as the major product (40% yield). As side-products, **4** was found in 5% yield along with traces of diisopropyl ether (1%). Table 2 summarises the results obtained by varying the reaction conditions. The yield of **3** can be improved by optimising the temperature and raising the pressure. When **1** is in excess, **3** *is the only detectable organic product.*

Previous attempts to run *continuous* Friedel–Crafts alkylation have frequently been thwarted by poor catalyst lifetimes but the lifetime of the Deloxan® catalyst is relatively long. In fact, when the reaction was started using a *fresh* sample of ASP I/7 acid Deloxan® catalyst, the activity actually increased after an induction period of *ca.* 100 min and was maintained for at least a further 15 h operation. We initially attributed this induction to some activating effect of the H_2O formed in the reaction. However, the yields of **3** were dramatically lower

Table 1 Alkylation of mesitylene **1** with propene **2** at 200 bar pressure[a]

			Yield (%)					
T_{cat}/°C	Flow rate of **1**/ ml min^{-1}	Flow rate[b] of propene	**1**	**3**	**4**	**5**	Dimers of **2**	Trimers of **2**
160	0.30	0.65	57	25	6	0	12	0
160	0.30	0.43	47	25	10	0	14	4
180	0.30	0.43	32	27	14	2	16	9

[a] The reaction was carried out in a heated reactor of 10 ml volume containing 9 ml of the solid acid Deloxan® catalyst (ASP I/7, particle size: 0.1–0.4 mm). No reaction was observed when the catalyst was replaced by Nafion as the solid acid. [b] Flow rate of propene in 1 min^{-1} measured at 1 atm and 20 °C, as determined by bubble flow meter.

Table 2 Investigation[a] of (I) temperature, (II) pressure and (III) molar ratio on yield of **3**

	Molar ratio of **1** : **6**	Flow rate of **1** + **6**/ g min^{-1}	T_{cat}/°C	p CO_2/bar	Found[b] **3** (%)	Yield[c] of **3** (%)	Production rate of **3**/g min^{-1}
I	2.0 : 1.0	0.60	200	200	15.0	30.0	0.09
	2.0 : 1.0	0.60	230	200	21.0	42.0	0.13
	2.0 : 1.0	0.60	250	200	21.0	42.0	0.13
	2.0 : 1.0	0.60	270	200	15.0	30.0	0.09
	2.0 : 1.0	0.60	300	200	7.5	15.0	0.05
II	2.0 : 1.0	0.60	250	200	21.0	42.0	0.13
	2.0 : 1.0	0.60	250	150	18.5	37.0	0.11
	2.0 : 1.0	0.60	250	100	16.0	32.0	0.10
III	1.0 : 5.0	1.51	250	150	19.0[d]	19.0[d]	0.29
	2.0 : 1.0	0.60	250	150	18.5	37.0	0.11
	5.0 : 1.0	0.52	250	150	10.0	50.0	0.05

[a] All reactions carried out in $scCO_2$ (0.65 l min^{-1}) with **3** as the only detectable product. [b] Product analysis was by ^{1}H NMR spectroscopy ($CDCl_3$). [c] Based on the amount of **6** in the initial reaction mixture. [d] Yield based on **1**. In addition, 3% of **4** and traces of side-products were found.

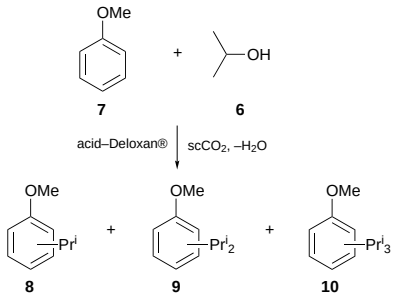

Scheme 2

when the catalyst was conditioned with water for 30 min prior to use. When operated for maximum flow of **3** (see Table 2) the catalyst can produce twice its volume of **3** per hour.

The supercritical reactor can also be applied sucessfully to the continous alkylation of anisole **7** by scPropene **2** or by propan-2-ol **6** in $scCO_2$ (Scheme 2). As with the alkylation of **1**, there is significant selectivity in favour of the mono-alkylated product. Thus, **6** reacted with **7** at a molar ratio of 1.0 : 3.0 to form isomers of **8** (30% yield) and **9** (*only* 6% yield).‖ No further products could be detected by GC–MS. When **7** was alkylated at a flow rate of 0.2 ml min^{-1} with scPropene (flow rate of gaseous propene: 0.43 l min^{-1}) under the same conditions, the yield of **8** was 38% with the same isomer ratio as was found with propan-2-ol.‖ However, the yield of **9** increased to 18% (three isomers at a ratio of 5 : 2 : 1). In addition, **10** was found in 5% yield (peak ratio 5 : 2 at a mass of 234) as well as trace amounts (3%) of propene di- and tri-mers.

The supercritical fluid probably plays several roles in these reactions. Compared to liquid phase reactions, the fluid reduces mass transport restrictions at the surface of the catalyst. Compared to a gas phase reaction, it increases the density of the reaction medium and hence increases the residence time of the substrate in a given size of reactor. This allows continuous alkylation to be caried out on a reasonable scale in a small reactor. Finally, it may reduce coking of the catalyst preventing premature deactivation of the catalytic sites.

This investigation has shown that aromatic substrates can undergo *continuous and sustainable* Friedel–Crafts alkylation in supercritical fluid solution over solid acid heterogeneous catalysts. The reactions can be carried out in a flow reactor, which differs only in the peripheral pipework from that used for the supercritical hydrogenation of organic compounds.[10] The method of alkylation has features of potential importance for the manufacture of fine chemicals. It is selective, organic solvents are eliminated and a *clean* heterogeneous catalyst replaces a liquid–based system. Thus, supercritical alkylation is a step closer to ennvironmentally acceptable Friedel–Crafts chemistry.

We thank Thomas Swan & Co Ltd for fully funding this work and D. Campbell, S. K. Ross and J. C. Toler for their assistance. We are grateful to Degussa AG for donating the catalysts. We thank M. W. George, M. Guyler, S. M. Howdle, K.-H. Pickel, K. Stanley, T. Tacke and S. Wieland for their help. M. P. thanks the EPSRC/Royal Academy of Engineering for a Fellowship.

Notes and References

† Web page: http://www.nottingham.ac.uk/supercritical/

‡ Deloxan® ASP catalysts (ref. 11) are specially designed polysiloxane based solid acids, formed by sol-gel condensation of alkyl sulfonic acid functionalized organosilane monomers, *e.g.* $HO_3SCH_2CH_2CH_2Si(OH)_3$, which overcome the drawbacks of organic polymers by virtue of their inert matrix material and excellent compatability with almost all organic solvents. The sol-gel process yields products with a relatively narrow particle size distribution, high porosity, large pore diameters (> 20 nm) and high BET surface areas (300–600 m^2 g^{-1}).

§ The substrate, reactant and supercritical fluid are brought together in a heated mixer, passed through the hot reactor (10 ml volume; 9 mm i.d., length 152 mm) containing the catalyst, and then expanded to separate the product from the fluid. The reactor is assembled from commercially available units: $scCO_2$ and scPropene pump PM 101 and Expansion Module PE 103 (all from NWA GmbH, Lörrach, Germany), a high pressure mixer (Medimix) and Gilson pumps 303, 305 (for substrate and reactant). ***SAFETY NOTE:*** *Reactions in supercritical fluids involve high pressures and should only be carried out with appropriate equipment.*

¶ Product analysis by GC–MS or ^{1}H NMR spectroscopy.

‖ Pressure, 220 bar; catalyst temperature, 200 °C, flow rate of gaseous CO_2 of 0.2 l min^{-1}; total flow rate of **6** + **7**, 1.0 ml min^{-1}. The product analysis is more complicated for the reactions of **7** than for those of **1** becasue the products (**8**, **9** and **10**) all have more than one possible isomer. Thus, GC–MS gave *three* peaks for **8** (*m*/*z* 150) in the ratio of 13 : 12 : 1, corresponding to the *ortho*, *para* and *meta* isomers. Similarly, *two* peaks (*m*/*z* 192) were found in the ratio 4 : 1 for the isomers of **9**.

1 G. A. Olah, *Friedel–Crafts and Related Reactions*, Wiley Interscience, New York and London, 1963–1964, vol. I–IV; G. A. Olah, R. Krishnamuri and G. K. Surya Prakash, in *Comprehensive Organic Synthesis*, ed. B. M. Trost, Pergamon, Oxford, 1991, vol. 3, ch. 1.8.
2 J. H. Clark and D. J. Macquarrie, *Org. Proc. Res. Develop.*, 1997, **1**, 149.
3 R. Streekumar and R. Padmakumar, *Synth. Commun.*, 1997, **27**, 781.
4 M. Y. Croft, E. J. Murphy and R. J. Wells, *Anal. Chem.*, 1994, **66**, 4459.
5 Y. Gao, Z. N. Zhu and W. K. Yuan, *Prog. Nat. Sci.*, 1996, **6**, 625.
6 M. Kodomari, Y. Suzuki and K. Yoshida, *Chem. Commun.*, 1997, 1567.
7 L. Fan, I. Nakamura, S. Ishida and K. Fujimoto, *Ind. Eng. Chem. Res.*, 1997, **36**, 1458 and references cited therein.
8 J. S. Beck and W. O. Haag, *Handbook of Heterogeneous Catalysis*, ed. G. Ertl, H. Knözinger and J. Weitmap, Wiley-VCH, Weinheim, 1997, vol. 5, p. 2123.
9 P. Tundo, *Continuous Flow Methods in Organic Synthesis*, Ellis Horwood, 1991.
10 M. G. Hitzler and M. Poliakoff, *Chem. Commun.*, 1997, 1667; M. G. Hitzler, F. R. Smail, S. K. Ross and M. Poliakoff, *Org. Proc. Res. Develop.*, 1998, in the press.
11 S. Wieland, E. Auer, A. Freund, H. Lansink Rotgerink and P. Panster, in *Catalysis of Organic Reactions*, ed. R. E. Malz, Jr., Marcel Dekker, New York, 1996, pp. 277–286.

Received in Liverpool, UK, 1st October 1997; 7/07149C

A new promising π-donor of the tetrathiafulvalene series: bis(2,3-dithiabutane-1,4-diyl)tetrathiafulvalene, the symmetrical outer S-position isomer of BEDT-TTF

C. Durand,[a,b] P. Hudhomme,*[a]† G. Duguay,[a] M. Jubault[b] and A. Gorgues*[b]‡

[a] *Laboratoire de Synthèse Organique, Université de Nantes, UMR-CNRS 6513, 2 rue de la Houssinière, F-44322 Nantes Cedex 3, France*

[b] *Laboratoire d'Ingénierie Moléculaire et Matériaux Organiques, Université d'Angers, UMR-CNRS 6501, 2 Bd Lavoisier, F-49045 Angers Cedex, France*

New functionalities are introduced into the 2-(thi)oxo-1,3-dithiole system and applied to the synthesis of the title compound.

Among the organic donors of the tetrathiafulvalene (TTF) family,[1] bis(ethylenedithio)tetrathiafulvalene **1** (BEDT-TTF or ET) is still regarded as the best precursor for superconducting organic metals[2] endowed with the highest T_c in that series.[3] In their solid state structure, the related radical cation salts exhibit bidimensional character mainly originating from strong peripheral S···S intermolecular interactions. Therefore, modifications of ET are of interest to establish relationships between the solid state structure and the transport properties of the corresponding salts, particularly by varying the position and the nature (S, Se, Te) of the chalcogen.[2b,4]

In this context, we have become interested in the unsymmetrical and symmetrical S-position isomers of ET, **2** and **3** respectively, with the aim of understanding the possible role of the position of the peripheral sulfur atoms on the dimensionality of the related materials.[5] After our previous study devoted to the unsymmetrical ET isomer **2** and some of its charge transfer salts,[6] we have extended this work to the symmetrical ET isomer **3**. We report here on the synthesis of the latter, based on the introduction of new functionalities on the 2-(thi)oxo-1,3-dithiolic precursors,[7] and also describe some preliminary electrochemical results emphasizing its promising π-donor ability for molecular conductors.

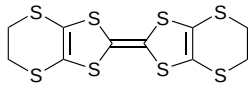

1 (BEDT-TTF or ET)

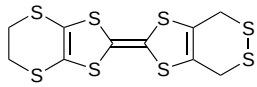

2

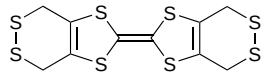

3

In our synthetic approach, we first studied a pathway involving the standard symmetrical or cross-coupling of the corresponding 2-(thi)oxo-1,3-dithioles **4a** and **4b**. These were synthesized according to Scheme 1 *via* two possible routes, A and B.

In route A, we used our standard procedure[6] allowing the conversion of the 4,5-bis(hydroxymethyl)-2-(thi)oxo-1,3-dithiole **5a**[8] or **5b** to **6a** or **6b** with thioacetic acid, either *via* the Mitsunobu reaction[9] (32% yield for **6a**) or after activation of the alcoholic groups with *N*,*N*-dimethylformamide diethyl acetal[10] (52% yield for **6b**). In route B, diol **5a** was easily dibrominated with PBr_3 in 94% yield,[11] similar results being also obtained for **5b**. Upon treatment of **7a** and **7b**[12] with thioacetic acid and pyridine or its potassium salt, the corresponding thioesters were formed in good yield (*ca*. 90%), even on a large scale. To achieve the S–S intramolecular closure, best results were

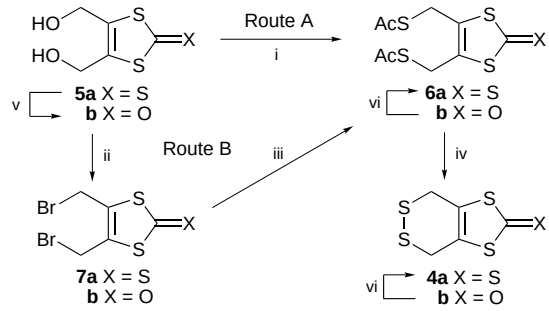

Scheme 1 *Reagents and conditions*: i, (for **6a**) DEAD, PPh_3, AcSH, THF (32%); (for **6b**) $Me_2NCH(OEt)_2$, CH_2Cl_2, 40 °C (52%); ii, PBr_3, THF–CCl_4 (1 : 2, v/v) (**7a** = 94%, **7b** = 62%); iii, AcSH, THF, Py or ACS^-K^+, THF (**6a** = 94%, **6b** = 89%); iv, CsOH, MeOH, then I_2, Et_2O (**4a** = 85%, **4b** = 46%); v, $Hg(OAc)_2$, AcOH–$CHCl_3$ (44%); vi, P_4S_{10}, toluene, 100 °C (**6a** = 28%, **4a** = 37%)

obtained by cleaving[13] the thioester groups with CsOH in MeOH and by oxidizing the corresponding generated dithiolate with iodine in Et_2O. Note that the $NaBH_4$–LiCl mediated cleavage successfully used in the corresponding TTF series[6] affords **4a** or **4b** in poorer yields.§

Whereas the trialkyl phosphite induced self- or cross-coupling reaction of 2-(thi)oxo-1,3-dithioles is a classical method for TTF core building,[14] all attempts from **4a** and **4b** were inefficient, as they were when using octacarbonyl dicobalt.[15] A similar failure was observed of **6a** and $P(OMe)_3$, the expected derivative **11** being formed only as a side product (5% yield), besides the main product, the oxo derivative **6b** (70% yield).[16]

Given these results, we investigated the other pathway depicted in Scheme 2. Methylation of **6a** with MeOTf in dry

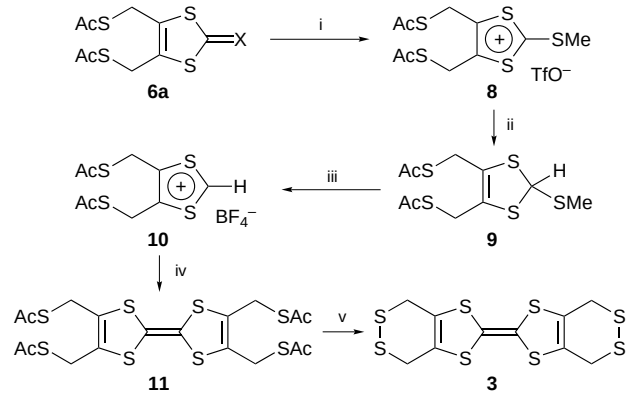

Scheme 2 *Reagents and conditions*: i, MeOTf, CH_2Cl_2 (98%); ii, $NaBH_4$, Pr^iOH–MeCN (1 : 8, v/v) (82%); iii, HBF_4, Ac_2O (83%); iv, Et_3N, MeCN (61%); v, MeO^-Na^+, MeOH–DMF (10 : 1, v/v) (63%)

Table 1 Oxidation peak potentials[a] $E\text{pa}_1$ and $E\text{pa}_2$

Compound	E/V *vs.* SCE[b]		
	$E\text{pa}_1$	$E\text{pa}_2$	$\Delta E\text{p}$
BEDT-TTF **1**	0.51	0.92	0.41
2	0.49	0.93	0.44
3	0.54	0.99	0.45

[a] Pt electrode, 20 °C, under nitrogen atmosphere, $Bu_4N^+PF_6^-$ 0.1 M in CH_2Cl_2, scan rate 0.1 V s^{-1}, [compound] ≈ 10^{-3} M. [b] Saturated calomel electrode.

CH_2Cl_2 afforded the corresponding salt **8** quantitatively. Reduction of the latter with $NaBH_4$ in Pr^iOH–MeCN at 0 °C produced **9** in 82% yield. Subsequent conversion to the 1,3-dithiolium tetrafluoroborate **10** was performed under classical conditions (HBF_4–Ac_2O) (83% yield).[17] Upon immediate treatment of **10** with an excess of Et_3N in MeCN, the TTF derivative **11** was obtained in fairly good yield (61%). Finally, transformation of **11** to the required target compound **3** could also be carried out as indicated above for the analogous conversion of **6** to **4**, but the yields were improved (63%) by treatment of **11** with MeO^- in MeOH–DMF, without isolation of the dithiolate intermediate.¶

The cyclovoltammogram of **3** resembles that of TTF derivatives, with two reversible oxidation peaks indicative of the successive generation of stable radical cation $\mathbf{3}^{\bullet+}$ and dication $\mathbf{3}^{2+}$, at potential values ($E\text{pa}_1$ and $E\text{pa}_2$) close to those of their isomeric counterparts **1** (ET) and **2** (Table 1). This π-donor behaviour is also confirmed by the ready formation of black charge transfer salts upon oxidation with Br_2, I_2 and TCNQ, and also upon electrooxidations in the presence of various anions, structural studies of the resulting materials being currently underway.

Notes and References

† E-mail: hudhomme@chimie.univ-nantes.fr
‡ E-mail: gorgues@univ-angers.fr

§ Transformations of **5a** into the corresponding 2-oxo-1,3-dithiole **5b** using $Hg(OAc)_2$ in AcOH–$CHCl_3$, and **4b** and **6b** into 2-thioxo-1,3-dithioles **4a** and **6a** using P_4S_{10} in toluene at reflux, were carried out but yields were not as good as expected.

¶ All new compounds gave satisfactory analytical and spectral data. *Selected data* for **3**: pink powder, mp 220 °C (decomp.); δ_H (CS_2 + $CDCl_3$) 3.45 (s, SCH_2CH_2S); *m/z* 384 ($M^{\bullet+}$, 39%), 320 (67), 256 (100), 172 (25), 128 (18); Raman/cm^{-1} 511 (S–S), 1542 (C=C); Calc. for $C_{10}H_8S_8$ (384.655): C, 31.22; H, 2.10; S, 66.68. Found: C, 31.25; H, 2.06; S, 66.59%.

1 G. Schukat and E. Fanghänel, *Sulfur Rep.*, 1993, **14**, 245; J. Garin, *Adv. Heterocycl. Chem.*, 1995, **62**, 249 and references cited therein.
2 (*a*) J. M. Williams, J. R. Ferraro, R. J. Thorn, K. D. Carlson, U. Geiser, H. H. Wang, A. M. Kini and M. H. Whangbo, *Organic Superconductors* (*including fullerenes*), Prentice Hall, Englewood Cliffs, New Jersey, 1992; (*b*) J. P. Farges, *Organic conductors. Fundamentals and applications*, Marcel Dekker, New York, 1994.
3 κ-(BEDT-TTF)$_2$Cu[N(CN)$_2$]X (T_c = 11.6 K at ambient pressure for X = Br and 12.8 K at 0.3 kbar for X = Cl): A. M. Kini, U. Geiser, H. H. Wang, K. D. Carlson, J. M. Williams, W. K. Kwok, K. G. Vandervoort, J. E. Thompson, D. L. Stupka, D. Jung and M. H. Whangbo, *Inorg. Chem.*, 1990, **29**, 2555; J. M. Williams, A. M. Kini, H. H. Wang, K. D. Carlson, U. Geiser, L. K. Montgomery, G. J. Pyrka, D. M. Watkins, J. M. Kommers, S. J. Boryschuk, A. V. Strieby Crouch, W. K. Kwok and M. H. Whangbo, *Inorg. Chem.*, 1990, **29**, 3272.
4 J. M. Williams, *Prog. Inorg. Chem.*, 1985, **33**, 183; L. Binet, J. M. Fabre and J. Becher, *Synthesis*, 1997, 26.
5 J. J. Novoa, M. C. Rovira, C. Rovira, J. Veciana and J. Tarrés, *Adv. Mater.*, 1995, **7**, 233; M. C. Rovira, J. J. Novoa, J. Tarrés, C. Rovira, J. Veciana, S. Yang, D. O. Cowan and E. Canadell, *Adv. Mater.*, 1995, **7**, 1023.
6 P. Hudhomme, P. Blanchard, M. Sallé, S. Le Moustarder, A. Riou, M. Jubault, A. Gorgues and G. Duguay, *Angew. Chem., Int. Ed. Engl.*, 1997, **36**, 878.
7 H. Gotthardt, *Comprehensive Heterocyclic Chemistry*, ed. A. R. Katritzky, Pergamon, Oxford, 1984, vol. 6, p. 813.
8 M. A. Fox and H. Pan, *J. Org. Chem.*, 1994, **59**, 6519.
9 R. P. Volante, *Tetrahedron Lett.*, 1981, **22**, 3119; K. C. Nicolaou and A. L. Smith, *Phosphorus Sulfur Silicon Relat. Elem.*, 1993, **74**, 47.
10 R. F. Abdulla and R. S. Brinkmeyer, *Tetrahedron*, 1979, **35**, 1675.
11 This result has to be compared with a similar reaction (CBr_4, PPh_3) very recently described for **7a** (70% yield); P. J. Skabara and K. Müllen, *Synth. Met.*, 1997, **84**, 345.
12 R. M. Renner and G. R. Burns, *Tetrahedron Lett.*, 1994, **35**, 269.
13 R. Gasiorowski, T. Jorgensen, J. Moller, T. K. Hansen, M. Pietraszkiewicz and J. Becher, *Adv. Mater.*, 1992, **4**, 568.
14 M. Narita and C. U. Pittman, *Synthesis*, 1976, 489; A. Krief, *Tetrahedron*, 1986, **42**, 1209 and references cited therein.
15 G. Le Coustumer and Y. Mollier, *J. Chem. Soc., Chem. Commun.*, 1980, 38.
16 An analogous desulfurization with $P(OMe)_3$ was observed for thionolactone to afford corresponding lactone: S. Ayral-Kaloustian and W. C. Agosta, *Synth. Commun.*, 1981, **11**, 1011.
17 We are investigating the possibility of accessing the unsymmetrical TTF from the phosphonate, easily obtained in 75% yield by classical reaction of **10** with NaI and $P(OMe)_3$: A. J. Moore and M. R. Bryce, *Synthesis*, 1991, 26.

Received in Liverpool, UK, 16th October 1997; 7/07486G

Incorporation of hydrophobic helix-bundle peptides into lipid bilayer membranes facilitated by a peptide-umbrella structure

Hiroki Ueda,[a] Shunsaku Kimura*[a] and Yukio Imanishi[b]

[a] *Department of Material Chemistry, Graduate School of Engineering, Kyoto University, Yoshida Honmachi, Sakyo-ku, Kyoto, Japan 606-01*

[b] *Graduate School of Material Science, Nara Institute of Science and Technology, 8916-5 Takayama-cho, Ikoma, Nara, Japan 630-01*

Hydrophobic helical peptides, which are covered by hydrophilic peptides, are transferred into a phospholipid bilayer to form helix-bundle structures as a consequence of their peptide-umbrella structure.

The hydrophobic helix-bundle structure is one of the common structures for membrane proteins found in nature, for example, in receptors of peptide hormones[1] and ion channels.[2] Therefore, phospholipid bilayer membranes embedded with helix-bundle peptides are of research interest for developing information-processing systems. However, a difficulty in the preparation of the molecular system exists in the insolubility of hydrophobic peptides in water, which restricts distribution of peptides in water to a phospholipid bilayer membrane. For this reason, water-soluble amphiphilic helical peptides have been synthesized[3] which form helix-bundle structures by association in water, and which have their hydrophilic surface facing outward and the hydrophobic surface facing inward. Generally, however, transfer of charged amino acid residues from the aqueous phase to the hydrophobic core region of the membrane is energetically unfavourable,[4] and most of amphiphilic peptides tend to stay at the membrane surface.[5] To realize a transmembrane helix-bundle in high yield, hydrophobic helices may be more favourable than amphiphilic helices,[6] and thus the design of hydrophobic helices able to be solubilized in water is presented here.

We have conceived a novel class of peptide molecules that mimic the structure of umbrellas, *i.e.* peptide molecules that are composed of hydrophobic helices in a 'handle' structure with hydrophilic segments shielding the helices. Upon binding to phospholipid bilayer membranes, the hydrophobic helices are inserted into the membrane vertically, with the hydrophilic segments staying at the membrane surface or in the aqueous phase just like an open umbrella. Regen[7] also presented a 'molecular umbrella' concept, but their molecules are designed for drug delivery and not for a functional membrane peptide.

In the present study, hydrophobic helix-bundle peptides were designed and synthesized with an umbrella structure, and their interaction with a phospholipid bilayer membrane was investigated. The molecular structures of the peptides are shown in Fig. 1. Two or three hydrophobic helices were connected together through pentaoxyethylenebis(amine) or tris(3-aminopropyl)amine in a parallel arrangement of helices. The hexadecapeptide –(Ala-Aib)$_8$– was chosen as the hydrophobic helix peptide because Boc–(Ala-Aib)$_8$–OMe has been found to have an α-helix conformation by X-ray diffraction[8] and to form a bundle structure for a voltage-dependent ion channel in a lipid membrane.[9] A naphthyl group was connected as a fluorescent probe. Oligosarcosine chains were connected to the hydrophobic peptides (**2αZ** and **3αZ**) to make them soluble in water (**2αS** and **3αS**). Nap–(Ala-Aib)$_8$–OBz **1α** (Nap represents a β-naphthaleneacetic group) was used as a reference hydrophobic helix peptide. The peptides were synthesized *via* conventional liquid phase methods.

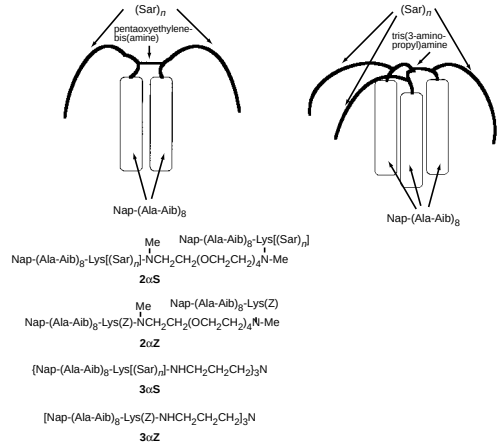

Fig. 1 Molecular structures of the hydrophobic helical peptides and peptide umbrellas. The average degree of polymerization of Sar is 11 for **2αS** and 9 for **3αS**.

The conformations of the peptides were investigated by circular dichroism (CD) spectroscopy. The CD spectra of the peptides showed a double-minimum pattern, indicating formation of an α-helical conformation in MeOH solution (Fig. 2). The helix content increases in the order **1α** < **2αZ** ≈ **2αS** < **3αZ** ≈ **3αS**. It is considered that the presence of helix chains in close proximity favours the formation of a helical conformation due to Van der Waals interactions. On the other hand, the introduction of oligosarcosine chains does not influence the conformation of the peptides in MeOH (**2αZ** ≈ **2αS** and **3αZ** ≈ **3αS**), suggesting the absence of any interactions between the oligosarcosine chains and the helix chains. However, in water

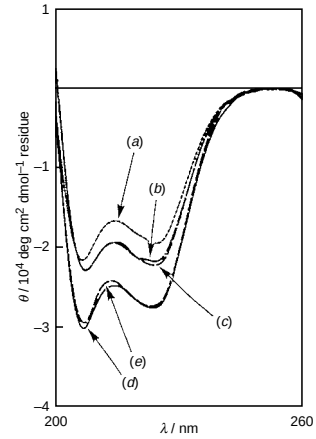

Fig. 2 CD spectra of the peptides in MeOH (**3αZ** and **3αS**) or MeOH–EtOH [2 : 1 (v/v), **1α**, **2αZ** and **2αS**]: (*a*) **1α**, (*b*) **2αS**, (*c*) **2αZ**, (*d*) **3αS** and (*e*) **3αZ**. Total concentration of Ala and Aib residues = 0.5 mM. The molar ellipticity stems from the amino acid residues of the helix segments.

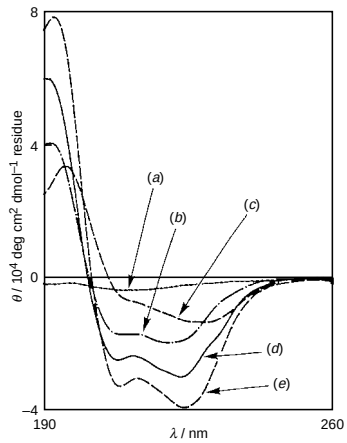

Fig. 3 CD spectra of the peptides in water: (*a*) **1α**, (*b*) **2αS**, (*c*) **2αZ**, (*d*) **3αS** and (*e*) **3αZ**. Total concentration of Ala and Aib residues = 0.5 mM.

the peptides show different CD spectra (Fig. 3). Compound **1α** showed very weak ellipticity due to low solubility in water. Compound **2αZ** showed a shoulder at 208 nm and a broad peak centred at 228 nm, suggesting the occurrence of severely distorted helices by strong aggregation in water. On the other hand, **2αS** shows the double-minimum pattern with increasing negative intensity at 222 nm, suggesting a weak association of helix chains in water.[10] It is evident in these CD patterns that the oligosarcosine chains of **2αS** suppresses the strong aggregation seen for **2αZ** by increasing water solubility. Compounds **3αZ** and **3αS** showed increasing negative intensity at 224 nm and their CD patterns are similar to those of **2αS** and **2αZ**. The oligosarcosine chains of **3αS** should stabilize the helical conformation of the peptide in water by avoiding strong aggregation. Unexpectedly, **3αZ** showed evidence of stable helix-bundle structures in water. It is considered that the tertiary amino group of the peptide increases the hydrophilicity of the molecule to form a micelle structure *via* self-assembly, which remains to be investigated.

The interactions of the peptides with DMPC liposomes was investigated by CD spectroscopy (Fig. 4). Compound **1α** showed a double-minimum-type CD spectrum with increasing negative intensity at 225 nm, indicating spontaneous distribution of the peptides to the membrane and formation of a helix-bundle structure. On the other hand, CD spectra of **2αZ** and **3αZ** showed a weak Cotton effect in the presence of DMPC liposomes. The liposome suspension became turbid upon addition of the peptides, indicating aggregation of liposomes triggered by enhanced hydrophobic contact of liposomes and/or

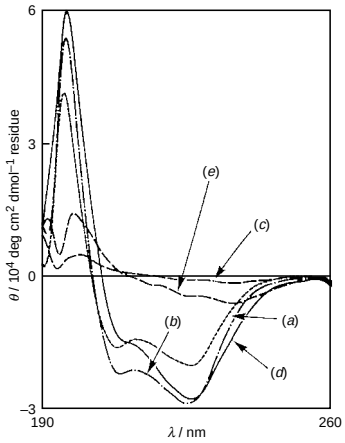

Fig. 4 CD spectra of the peptides in the presence of DMPC liposomes: (*a*) **1α**, (*b*) **2αS**, (*c*) **2αZ**, (*d*) **3αS** and (*e*) **3αZ**. [DMPC] = 1.0 mM. DMPC liposomes were prepared by the sonication method using Tris buffer (0.01 M, pH 7.4) containing NaCl (0.1 M) and EDTA (0.1 mM). Total concentration of Ala and Aib residues = 0.5 mM.

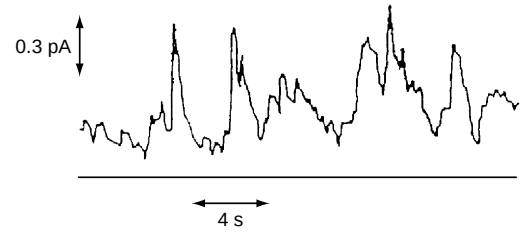

Fig. 5 Current fluctuation of the bilayer lipid membrane (BLM) in the presence of **3αS**. The membrane is made of soybean lectin and formed on an aperture of 0.2 mm diameter. Aqueous solution contains 1 M KCl. A membrane potential of 190 mV was applied using a salt bridge. [**3αS**] = 0.026 μM.

membrane disorder caused by the hydrophobic peptides. Notably, aggregation of liposomes was not induced by the addition of **2αS** or **3αS**, and the peptides were taken in spontaneously by the phospholipid membrane. Oligosarcosine chains should suppress liposomal aggregation by making the liposome surface hydrophilic. With **2αS** and **3αS**, the relative molar ellipticity at 208 nm to that at 225 nm was smaller in the presence of DMPC liposomes than in pure water, suggesting a stronger aggregation of the helix chains in the lipid membrane than in water.[10]

Distribution of the peptides into the phospholipid membrane was also investigated by fluorescence quenching of the naphthyl group with acrylmaide, which is a water-soluble quencher. The Stern–Volmer constants[11] for the collisional quenching process K_{SV} (mM^{-1}) were 8.3 for **2αS** in buffer, 1.8 for **2αS** with liposome, 6.5 for **3αS** in buffer and 2.1 for **3**α**S** with liposome. The lower K_{SV} values in the presence of liposomes indicate that the naphthyl groups are buried in the hydrophobic core region of the membrane due to vertical insertion of the helices.

It is considered that the helix-bundle structure, in which the peptide chains take a parallel arrangement, should function as ion channels in the lipid membrane. Compound **3αS** (0.026 μM) was added to the bilayer lipid membrane (BLM) to measure the current–voltage response. Current fluctuation at an applied voltage of 190 mV was observed (Fig. 5). Current peaks of the same level were observed frequently, but were not detected with **1α** at the same concentraton. This indicates an important contribution from the umbrella-like structure of **3αS** in the formation of the ion channel under a transmembrane electric potential. An unusual observation was that the current fluctuation was not a stepwise response typical of ion channels. Probably, a part of the current response may be due to disorder of the membrane produced by the peptide insertion.

This work is partly supported by Japan Securities Scholarship Foundation.

Notes and References

* E-mail: h54519@sakura.kudpc.kyoto-u.ac.jp

1 B. L. Kieffer, *Cell. Mol. Neurobiol.*, 1995, **15**, 615.
2 N. Unwin, *J. Mol. Biol.*, 1993, **229**, 1101; U. Ludewig, M. Pusch and T. J. Jentsch, *Nature*, 1996, **383**, 340.
3 A. Grove, M. Mutter, J. E. Rivier and M. Montal, *J. Am. Chem. Soc.*, 1993, **115**, 5919.
4 G. Von Heijne and C. Blomberg, *Eur. J. Biochem.*, 1979, **97**, 175.
5 S. Kimura, J. Zhao, Y. Imanishi, E. Okamura and J. Umemura, *Peptide Chem.*, 1994, 133.
6 Y. Imanishi and S. Kimura, *The Handbook of Nonmedical Applications of Liposomes Vol. II, Models for Biological Phenomena*, ed. Y. Barenholz and D. D. Lasic, Boca Raton, 1996, pp. 189–200.
7 V. Janout, M. Lanier and S. L. Regen, *J. Am. Chem. Soc.*, 1997, **119**, 640.
8 K. Otoda, Y. Kitagawa, S. Kimura and Y. Imanishi, *Biopolymers*, 1993, **33**, 1337.
9 K. Otoda, S. Kimura and Y. Imanishi, *Biochim. Biophys. Acta*, 1993, **1150**, 1.
10 N. J. Gibson and J. Y. Cassim, *Biochemistry*, 1988, **28**, 2134.
11 M. R. Eftink and C. A. Ghiron, *Anal. Biochem.*, 1981, **114**, 199.

Received in Cambridge, UK, 6th November 1997; 7/07988E

Efficient synthesis of a new, highly versatile chiral derivatizing agent, α-cyano-α-fluoro-*p*-tolylacetic acid (CFTA)

Yoshio Takeuchi,*[a] Miyuki Konishi,[a] Hitoshi Hori,[a] Tamiko Takahashi,[a] Tadashi Kometani[b] and Kenneth L. Kirk[c]

[a] *Toyama Medical and Pharmaceutical University, Sugitani 2630, Toyama 930-01, Japan*
[b] *Toyama National College of Technology, Hongo 13, Toyama 939, Japan*
[c] *Laboratory of Bioorganic Chemistry NIDDK, National Institutes of Health, Bethesda, MD, 20892, USA*

The new and versatile chiral derivatizing agent, α-cyano-α-fluoro-*p*-tolylacetic acid (CFTA), has been efficiently synthesized in optically pure form by *Candida rugosa* lipase-mediated kinetic resolution of racemic CFTA ethyl ester, the latter being readily prepared by fluorination of ethyl α-cyano-*p*-tolylacetate with $FClO_3$.

Rapid progress has been made in the development of techniques for determination of ees of chiral molecules. However, despite many advances, there are few agents that can be applied to a broad spectrum of molecules encountered in modern synthetic and analytical chemistry.[1] We recently developed one such agent, α-cyano-α-fluorophenylacetic acid (CFPA), which far surpassed the capabilities of existing chiral derivatizing agents (CDAs) with respect both to reactivity[2] and resolution efficiency.[3] However, the involved synthesis of this agent has precluded its general use. We now report a related CDA, α-cyano-α-fluoro-*p*-tolylacetic acid (CFTA), that retains the merits of CFPA but, through effective use of enzymatic resolution, is readily available in its optically pure state.

Treatment of *p*-xylyl cyanide with $CO(OEt)_2$ produced ethyl α-cyano-*p*-tolylacetate which, in turn, was treated with $FClO_3$† to give CFTA ethyl ester **1** in excellent overall yield. Among twenty commercial hydrolytic enzymes that were screened for the enantioselective hydrolysis of **1**, *Candida rugosa* lipase (CRL)‡ gave the best results with respect to reactivity, although the enantioselectivity (*E* value[5] of *ca.* 3) was clearly insufficient for our purposes. Fortunately, after much investigation, we found that pre-treatment of CRL with Pr^{i}OH improved the enantioselectivity more than ten-fold, consistent with the previous results obtained by Kazlauskas for the resolution of 2-aryl- and 2-aryloxy-propionic esters.[6] Thus, hydrolysis of racemic ester **1**, catalysed by pre-treated commercial CRL [50% (v/v) Pr^{i}OH in 2-(*N*-morpholino)ethanesulfonate buffer solution (pH 6.0), according to the procedure of Kazlauskas], gave, at 56% conversion, (*R*)-**1** with an ee of 99% and (*S*)-CFTA [(*S*)-**2**] with an ee of 78%, corresponding to an *E* value of 40 (Scheme 1). This dramatic increase in enantioselectivity can be attributed to a change in stereostructure of CRL caused by Pr^{i}OH treatment, as demonstrated earlier by Kazlauskas (see below).[6]

The *R* configuration of the remaining ester **1** was determined by X-ray crystallographic analysis§ of the (*S*)-α-phenethylamide **3** prepared from **1**. Therefore, the more readily hydrolysed ester has the *S*-configuration and (*S*)-**2** is enriched in the product. Kazlauskas proposed an empirical rule¶ to predict the stereochemical outcome of ester hydrolysis catalysed by Pr^{i}OH-treated CRL, as shown in Fig. 1.[7] The active site of the CRL apparently accepts F as a replacement for H, with CN corresponding to the medium-sized substituent.

(*R*)-CFTA [(*R*)-**2**] was obtained by LiOH hydrolysis of the remaining ester (*R*)-**1**. The (*S*)-α-phenethylamine salt of (*R*)-**2** and the (*R*)-α-phenethylamine salts of the (*S*)-**2**-enriched hydrolysis product were each recrystallized from $CHCl_3$–hexane to afford optically pure enantiomers, the (*R*)-α-phenethylamine salt of (*S*)-CFTA {mp 135–137 °C, $[\alpha]_D^{25}$ −3.3 (*c* 0.99, MeOH)} and the (*S*)-α-phenethylamine salt of (*R*)-CFTA {mp 135–137 °C, $[\alpha]_D^{25}$ +3.3 (*c* 0.99, MeOH)}. These enantiomeric salts were treated with acid to afford (*R*)-CFTA {$[\alpha]_D^{25}$ +36.8 (*c* 1.21, $CHCl_3$)} and (*S*)-CFTA {$[\alpha]_D^{25}$ −36.3 (*c* 1.05, $CHCl_3$)} as colourless oils in isolated overall yields of 38 and 19%, respectively, from racemic CFTA ethyl ester.‖

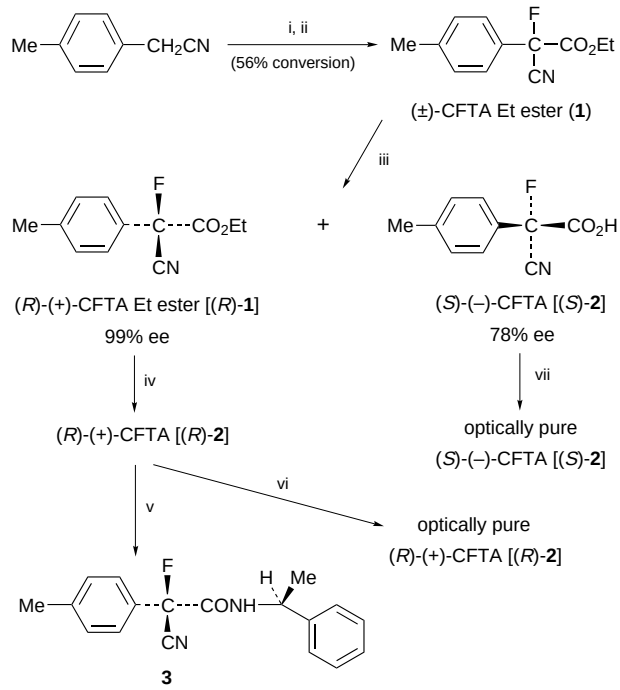

Scheme 1 *Reagents and conditions*: i, NaH, $CO(OEt)_2$, THF, reflux, 2 h, 98%; ii, NaH, THF, room temp., 1 h, then $FClO_3$, room temp., 40 min, 90%; iii, Pr^{i}OH-treated CRL, isooctane, 1 M phosphate buffer (pH 7.0), 25 °C, 41% for (*R*)-**1** (99% ee), 46% for (*S*)-**2** (78% ee); iv, 1 M LiOH, THF–H_2O (1 : 1), room temp., 5 min, 100%; v, (*S*)-α-phenethylamine, DCC, CH_2Cl_2, room temp., 6 h, 95%; vi, (*S*)-α-phenethylamine, recrystallization, then 1 M HCl, 78%; vii, (*R*)-α-phenethylamine, recrystallization, then 1 M HCl, 41%

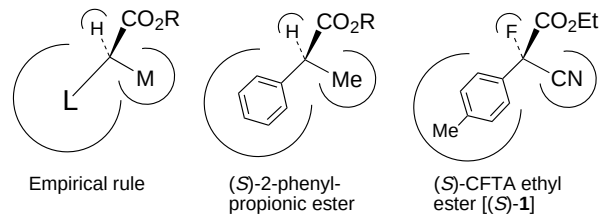

Fig. 1 Enantiopreference of Pr^{i}OH-treated CRL-mediated kinetic hydrolysis

Table 1 ^{19}F NMR Chemical shift differences ($\Delta\delta_F$ values in ppm) for diastereomeric CFTA and MTPA esters

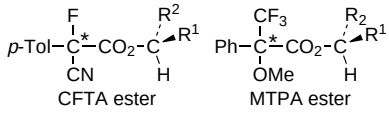

		$\Delta\delta_F = \delta_{SR} - \delta_{RR}$	
R^1	R^2	CFTA ester	MTPA ester
Me	Et	+0.09	0.00[a]
Me	Pr^i	+0.51	−0.18[a]
Me	C_6H_{11}	+0.32	−0.05[a]
Me	Ph	+0.88	−0.20[a]
Bornyl		+0.71	+0.10[b]
Menthyl		+0.58	−0.12[a]

[a] Ref. 8. [b] Ref. 9.

Table 2 ^{1}H NMR Chemical shift differences ($\Delta\delta_H$ values in ppm) for diastereomeric CFTA and MTPA esters

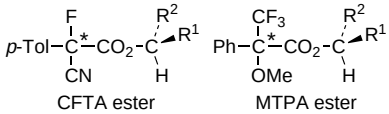

		$\Delta\delta_H = \delta_{SR} - \delta_{RR}$			
		CFTA ester		MTPA ester	
R^1	R^2	Me of R^1	Me of R^2	Me of R^1	Me of R^2
Me	Et	+0.14	−0.22	+0.13[a]	−0.10[a]
Me	Pr^i	+0.16	−0.19	+0.08[a]	−0.08[a]
Me	C_6H_{11}	+0.14	−0.03	+0.08[a]	—
Me	Ph	+0.10	—	+0.06[a]	—
Bornyl		—	−0.22[c]	—	−0.08[b,c]
Menthyl		+0.03[d]	−0.26[e]	+0.03[b,d]	−0.12[b,e]
			−0.19[e]		−0.10[b,e]

[a] Ref. 10. [b] Ref. 9. [c] C1-Me. [d] C5-Me. [e] Me of Pr^i.

The chemical shift differences between the two diastereomers ($\Delta\delta$ values)** in both the ^{19}F and ^{1}H NMR spectra for several CFTA and MTPA esters are shown in Tables 1 and 2, respectively.†† The greater efficiency of CFTA compared to MTPA in ee determinations is apparent from the much greater $\Delta\delta$ values consistently obtained for the CFTA derivatives.[8–10] Furthermore, in addition to the greater magnitude of the $\Delta\delta$ values, the consistency of the sign of these shifts suggests that the CFTA procedure is more reliable[11] than the Mosher method in assigning absolute configurations of secondary alcohols based on ^{19}F NMR[8,9] and ^{1}H NMR[9,10] spectroscopy. We are currently investigating in greater detail the relationship between stereostructure and chemical shift value, especially in the ^{19}F NMR spectra.

We thank Ms H. Kakuda for the X-ray crystallographic analysis of **3**. This work was supported by a Grant-in-Aid from the Ministry of Education, Science, Sports and Culture, Japan and a grant from the Ciba-Geigy Foundation (Japan).

Notes and References

* E-mail: takeuchi@ms.toyama-mpu.ac.jp

† $FClO_3$ gas diluted with N_2 is safely and conveniently generated in ordinary glassware by reaction of $KClO_4$ with FSO_3H (ref. 4).

‡ Lipase OF (CRL) was purchased from Meito Sangyo Co., Ltd.

§ *Crystal data* for **3**: $C_{18}H_{17}FN_2O$, M = 296.34, monoclinic, a = 9.647(2), b = 17.686(3), c = 9.915(2) Å, β = 109.64(1)°, U = 1593.3(5) Å^3, T = 203 K, space group $P2_1$ (no. 4), Z = 4, μ(Cu-Kα) = 0.698 mm^{-1}, 2626 reflections measured, 2469 reflections unique, 1322 reflections observed [$I > 3\sigma(I)$]. Two aryl groups (phenyl and *p*-tolyl) were disordered over two positions with occupancies 0.5 for all disorder components. For this reason, the R value was relatively high. The final cycle of full-matrix least-squares refinement (for 218 parameters) was converged with R_w = 0.111, R = 0.116. CCDC 182/709.

¶ The rule was derived from the results of enantioselective hydrolysis of 16 esters, where L is a large substituent such as Ar or OAr, and M is a medium-sized substituent such as Me or OH (refs. 6 and 7).

‖ The enantiomeric purity of both (*R*)- and (*S*)-CFTA was determined to be > 99.5% by comparison of the ^{1}H and ^{19}F NMR spectra of their cholesteryl esters with those of the cholesteryl ester of recemic CFTA.

** The $\Delta\delta$ value is defined as the difference in the ^{19}F (F or CF_3 signal for CFTA or MTPA ester, respectively) or ^{1}H (Me signal of R^1 and R^2) NMR chemical shifts for the (*S*)-agent/(*R*)-alcohol diastereomer (δ_{SR}) and the (*R*)-agent/(*R*)-alcohol diastereomer (δ_{RR}) for each CFTA or MTPA ester (ref. 9).

†† The preparation of CFTA chloride and condensation of CFTA chloride with chiral alcohols were carried out according to procedures described for derivatization of CFPA (ref. 3).

1 S. Hamman, *J. Fluorine Chem.*, 1993, **60**, 225; Y. Takeuchi and T. Takahashi, in *Enantiocontrolled Synthesis of Fluoro-organic Compounds. Stereochemical Challenges and Biomedical Targets*, ed. V. Soloshonok, Wiley, Chichester, 1998 and references cited therein.
2 Y. Takeuchi, N. Itoh and T. Koizumi, *J. Chem. Soc., Chem. Commun.*, 1992, 1514; *Chem. Ind.*, 1992, 874.
3 Y. Takeuchi, N. Itoh, H. Note, T. Koizumi and K. Yamaguchi, *J. Am. Chem. Soc.*, 1991, **113**, 6318; Y. Takeuchi, N. Itoh, T. Satoh, T. Koizumi and K. Yamaguchi, *J. Org. Chem.*, 1993, **58**, 1812.
4 Y. Takeuchi, K. Nagata and T. Koizumi, *J. Org. Chem.*, 1989, **54**, 5453.
5 C. Chen, Y. Fujimoto, G. Girdaukas and C. J. Sih, *J. Am. Chem. Soc.*, 1982, **104**, 7294.
6 I. J. Colton, S. N. Ahmed and R. J. Kazlauskas, *J. Org. Chem.*, 1995, **60**, 212.
7 S. N. Ahmed, R. J. Kazlauskas, A. H. Morinville, P. Grochulski, J. D. Schrag and M. Cygler, *Biocatalysis*, 1994, **9**, 209.
8 G. R. Sullivan, J. A. Dale and H. S. Mosher, *J. Org. Chem.*, 1973, **38**, 2143.
9 I. Ohtani, T. Kusumi, Y. Kashman and H. Kakisawa, *J. Am. Chem. Soc.*, 1991, **113**, 4092.
10 J. A. Dale and H. S. Mosher, *J. Am. Chem. Soc.*, 1973, **95**, 512.
11 T. Kusumi, *J. Synth. Org. Chem.*, 1993, **51**, 462 and references cited therein.

Received in Cambridge, UK, 28th October 1997; 7/07755F

A metallacyclic λ⁵-phosphaalkenyl complex of ruthenium(II): X-ray structure of [Ru{κ²-P(=O)CBu^{t}C(=O)}(CNBu^t)$_2$(PPh$_3$)$_2$]

Anthony F. Hill,*†[a] Cameron Jones,*‡[b] Andrew J. P. White,[a] David J. Williams[a] and James D. E. T. Wilton-Ely[a]

[a] *Department of Chemistry, Imperial College of Science Technology and Medicine, South Kensington, London, UK SW7 2AY*
[b] *Department of Chemistry, University of Wales, Swansea, Singleton Park, Swansea, UK SA2 8PP*

The reaction of [Ru(P=CHBu^t)Cl(CO)(PPh$_3$)$_2$] 1 or [Ru(P=CHBu^t)Cl(CNBu^t)(CO)(PPh$_3$)$_2$] 2b with excess pivalo isonitrile under aerobic conditions provides the novel metallacyclic λ⁵-phosphaalkenyl-*P* complex [Ru{κ²-P(=O)CBu^{t}C(=O)}(CNBu^t)$_2$(PPh$_3$)$_2$], which has been crystallographically characterised.

The λ³-phosphaalkenyl-*P* complex [Ru(P=CHBu^t)Cl(CO)(PPh$_3$)$_2$] **1**[1] is intriguing in that despite effective atomic number considerations for ruthenium, both the spectroscopic features and the emerging reactivity profile[2–4] point to a nucleophilic phosphorus centre (**A**). The RuCl(CO)(PPh$_3$)$_2$ fragment, possessing 15 valence electrons might be expected to commandeer three electrons from the phosphaalkenyl ligand **B** and thereby enforce linearity and attendant electrophilic character at phosphorus. This is, however, not the case. We have interpreted this counter-intuitive behaviour with reference to a similar dichotomy which prevails for nitrosyl ligands bound to metal centres with high d-occupancies.[1] One aspect of the 'semi-bent' nature of the phosphaalkenyl ligand in **1** is that the ruthenium centre readily, though reversibly, accepts two-electron ligands, resulting in a metal centre which requires bent (one-electron) phosphaalkenyl coordination. The resulting nucleophilic nature of the phosphorus centre has been demonstrated by its reduction to a complex of the unusual fluorophosphine Bu^{t}CH$_2$PHF ligand *via* the reaction of the isonitrile adduct [Ru(P=CHBu^t)Cl(CNC$_6$H$_3$Me$_2$-2,6)(CO)(PPh$_3$)$_2$] **2a** with HBF$_4$.[2] Herein we wish to report a curious transformation of **1** into a metallacyclic phosphaalkenyl complex **3**. This is accompanied by oxidation of the phosphorus from λ³ to λ⁵ (**C**), resulting in a rare example of a trigonal phosphorus centre surrounded by three π-interactive substituents. A notable feature of **3** is that it is, we believe, the first example of a λ⁵-phosphaalkenyl-*P* complex.

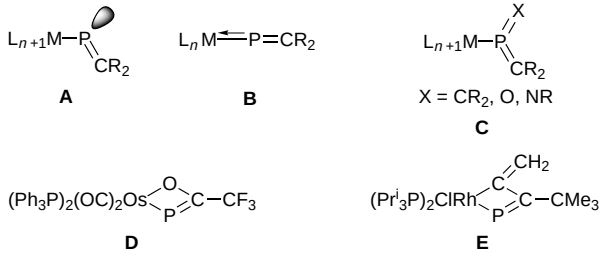

Whilst complex **1** readily forms a 1:1 adduct **2a** with CNC$_6$H$_3$Me$_2$-2,6, the same reaction with pivalo isonitrile (CNBu^t) is somewhat more complex. Under strict control of reagent stoichiometry and reaction conditions it is possible to prepare the adduct [Ru(P=CHBu^t)Cl(CNBu^t)(CO)(PPh$_3$)$_2$] **2b**, spectroscopic data for which are comparable to those for **2a**.§ On occasion however, complex **2b** is contaminated with a second product, which is also formed in low yield from **2b** on standing in solution. This second compound is the exclusive product if an excess of CNBu^t is used, under aerobic conditions. Spectroscopic data§ and a crystallographic study (Fig. 1)¶ confirm the identity of the new compound as the novel metallacyclic λ⁵-phosphaalkenyl-*P* complex [Ru{κ²-P(=O)CBu^{t}C(=O)}(CNBu^t)$_2$(PPh$_3$)$_2$] **3**. Of note amongst the spectroscopic data for **3**, is the ^{31}P{^{1}H} NMR resonance for the phosphaalkenyl centre which appears as a triplet [δ 47.0 ^2J(P$_2$P) 25.2 Hz], to substantially higher field of those observed for **2b** [δ 389.8 ^2J(P$_2$P) 11.7 Hz] or **1** [δ 450.4 ^2J(P$_2$P) 10.0 Hz]. The phosphoryl group contributes to a strong absorption in the infrared spectrum at 1198 cm^{-1}(Nujol), whilst the acyl group is apparent at 1644 cm^{-1}. All other spectroscopic data are as expected and unremarkable.

The geometry at ruthenium is essentially octahedral with *cis*-interligand angles in the range 85.2(2)–96.1(3)°, the exception being P(1)–Ru–C(2) which is contracted to 66.5(2)° by virtue of the constraints of chelation. The two ruthenium isonitrile distances are 1.988(10) and 2.037(10) Å suggesting that the *trans* influence of the phosphaalkenyl ligand is comparable to that of the acyl component of the metallacycle. The principle structural feature of interest is the metallacycle, the unsaturation of which is reflected in the coplanarity to within 0.03 Å of the atoms C(5), C(1), P(1) O(3), C(2), O(4) and Ru, a planarity which extends to include the CN groups of the isonitriles. Owing to the novelty of **3**, very little directly comparable structural data exists. Two metallacyclic λ³-phosphaalkenyl complexes have been structurally characterised (**D**[5] and **E**),[6]

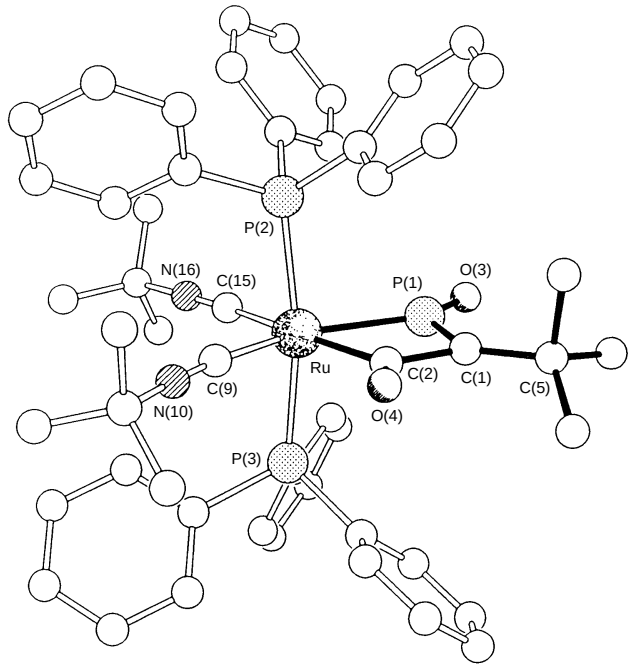

Fig. 1 Crystal structure of **3**

though perhaps more relevant here are the structural features of the phosphaalkene complexes [Ru{P(AuPPh$_3$)=CHBu^t}Cl$_2$(CO)(PPh$_3$)$_2$] **4**[3] and [Ru(PMe=CHBu^t)ClI(CO)(PPh$_3$)$_2$] **5**[4] where the Ru–P separations are 2.296(2) and 2.280(2) Å, respectively. The Ru–P(1) bond length of 2.350(2) Å in **3** thus indicates a substantially reduced degree of Ru–P multiple bond character, consistent with a perhaps surprising decrease in apparent π-acidity for the λ^5-phosphorus centre, notwithstanding the perturbations associated with chelation. This counter-intuitive result is possibly due to the co-ordination of a competitive π-acceptor *trans* to P(1), whilst the phosphaalkene ligands in **4** and **5** are *trans* to π-donor ligands. The P(1)–C(1) separation of 1.713(11) Å is marginally longer than the P=C bond lengths of 1.664(9) and 1.657(8) Å, found for **4** and **5**, respectively but falls within the range 1.68–1.72 Å found for free phosphaalkenes,[7] indicating substantial double bond character. In contrast the C(1)–C(2) bond at 1.54(1) Å is long for a single C_{sp^2}–C_{sp^2} bond length.

It remains for the mechanism to be established whereby **3** forms from **1** or **2b**, however we would make the following points which taken together support the route proposed in Scheme 1. The reaction proceeds in polar solvent mixtures suggesting ruthenium–chloride ionisation occurs. This is supported by the formation and isolation of the salt *cis*,*cis*,*trans*-[Ru(P=CHBu^t)(CO)(CNBu^t)$_2$(PPh$_3$)$_2$]Cl **4**§ when **1** is treated with 2 equiv. of pivaloisonitrile and isolated immediately. The β-position of vinyl ligands is typically nucleophilic in nature, in particular for later transition metals, and it seems reasonable to expect a similar property for phosphavinyl ligands. The carbonyl ligand will be activated towards nucleophilic attack as a result of the complex being cationic. Ring closure could provide the saturated metallacycle shown, and the proton which is α to both phosphorus and a carbonyl group would be expected to be acidic. Deprotonation then leads to unsaturation of the metallacycle. The aerial oxidation of the phosphorus centre is, in contrast to **1**, an endearing feature of which is its remarkable aerobic stability. Nevertheless, the Ru(CNBu^t)$_2$(PPh$_3$)$_2$ fragment would be expected to be particularly π-basic, activating the π-acid phosphorus centre towards oxidation. Notably the conversion of **4** to **3** is accelerated by addition of a non-nucleophilic base (DBU). We have so far been unsuccessful in isolating the intermediates between **4** and **3**, however the alternative route of deprotonation prior to cyclisation seems less favourable, given that it would produce a 20-valence electron phosphaalkyne complex of zerovalent ruthenium.[8]

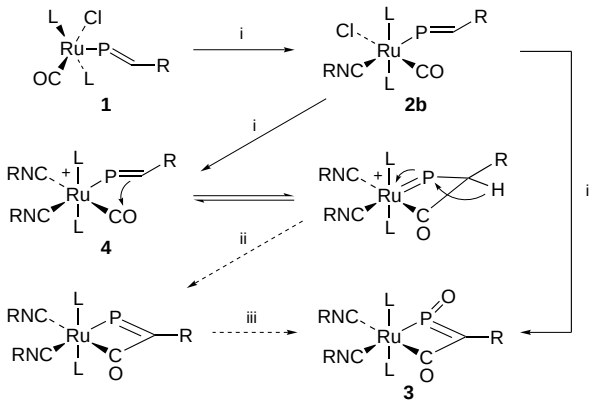

Scheme 1 L = PPh$_3$, R = Bu^t. *Reagents*: i, CNR; ii, −HCl; iii, O$_2$.

The chemistry of λ^3 phosphaalkenyl ligands has seen substantial growth in recent times.[1–6,9] With the advent of a λ^5 example, it will be interesting to see how their respective coordination chemistries compare.

This work was supported by the EPSRC in the form of a studentship (to J. D. E. T. W.-E.) and a diffractometer and by the Nuffield Foundation (to C. J.). A. F. H. gratefully acknowledges the Leverhulme Trust and the Royal Society for the award of a Senior Research Fellowship.

Notes and References

† E-mail: a.hill@ic.ac.uk
‡ E-mail: c.a.jones@swansea.ac.uk

§ Selected data for new complexes [25 °C, IR Nujol(CH$_2$Cl$_2$), NMR (CDCl$_3$), satisfactory microanalytical data obtained]. **2b**: IR: 2148 (2148) [ν(CN)], 1930 (1961) [ν(CO)] cm^{-1}. NMR: ^{1}H δ 0.79 (s, 9 H, PCCCH$_3$), 0.97 (s, 9 H, NCCH$_3$), 7.24–7.95 (m, 31 H, C$_6$H$_5$ + P=CH) ^{31}P{^{1}H} δ 389.8 [t, ^2J(P$_2$P) 11.7 Hz], 24.6 [d, ^2J(P$_2$P) 11.7 Hz]. FABMS: *m/z* 874 [MH]$^+$, 772 [MH − HP=CHBu^t]$^+$, 744 [MH − HP=CHBu^t − CO]$^+$, 709 [MH − HP=CHBu^t − Cl − CO]$^+$. **3**: IR: 2169, 2028 (2171, 2038) [ν(CN)], 1644 (1606) [ν(CO)] cm^{-1}. NMR ^{1}H δ 0.61 (s, 9 H, PCCCH$_3$), 0.86 (s, 9 H, NCCH$_3$), 1.27 (s, 9 H, NCCH$_3$) 7.27–8.09 (m, 30 H, C$_6$H$_5$). ^{31}P{^{1}H} δ 47.0 [t, ^2J(P$_2$C) 25.2 Hz], 31.2 [dd, ^2J(P$_2$P) 25.2, 8.4 Hz]. FABMS: *m/z* 856 [M − CNBu^t]$^+$, 602 [M − CNBu^t − PPh$_3$]$^+$. **4**: IR: 2184(sh), 2163 (2179, 2156) [ν(CN)], 2003, 1980(sh) (2021) [ν(CO)] cm^{-1}. NMR: ^{1}H δ 0.66 (s, 9 H, PCCCH$_3$), 0.96 (s, 9 H, NCCH$_3$), 1.18 (s, 9 H, NCCH$_3$), 7.32–7.76 (m, 31 H, C$_6$H$_5$ + P=CHBu^t). ^{31}P{^{1}H} δ 336.9(s), 33.5(s). FABMS: *m/z* 921 [M]$^+$, 838 [M − CNBu^t]$^+$, 810 [M − CNBu^t] − CO]$^+$, 530 [M − CNBu^t − PPh$_3$]$^+$.

¶ *Crystal data* for **3**: $C_{52}H_{57}N_2O_2P_3Ru\cdot CH_2Cl_2$, M = 1020.9, triclinic, space group $P\bar{1}$ (no. 2), a = 13.616(1), b = 14.629(2), c = 15.473(3) Å, α = 89.93(1), β = 89.39(1), γ = 66.72(1)°, U = 2830.9(7) Å^3, Z = 2, D_c = 1.198 g cm^{-3}, μ(Cu-Kα) = 42.0 cm^{-1}, λ = 1.54178 Å, F(000) = 1060. A colourless prism of dimensions 0.27 × 0.20 × 0.05 mm was used. Data were measured on a Siemens P4/PC diffractometer with graphite monochromated Cu-Kα radiation (ω-scans). 7804 Independent reflections were measured ($2\theta \leqslant 116°$) of which 5605 had $|F_o| > 4\sigma(|F_o|)$ and were considered to be observed. The structure was solved by direct methods and all the major occupancy non-hydrogen atoms of the complex were refined anisotropically by full-matrix least squares based on F^2 using absorption-corrected data to give R_1 = 0.082, wR_2 = 0.205 for the observed data and 530 parameters. The somewhat high R factors are a consequence of disorder in the Bu^t substituents and the included solvent molecule. CCDC 182/727.

1 R. B. Bedord, A. F. Hill and C. Jones, *Angew. Chem., Int. Ed. Engl.*, 1996, **35**, 547.
2 R. B. Bedford, D. E. Hibbs, A. F. Hill, M. B. Hursthouse, K. M. A. Malik and C. Jones, *Chem. Commun.*, 1996, 1895.
3 R. B. Bedford, A. F. Hill, C. Jones, J. D. E. T. WIlton-Ely, A. J. P. White and D. J. Williams, *Chem. Commun.*, 1997, 179.
4 R. B. Bedford, A. F. Hill, C. Jones, J. D. E. T. Wilton-Ely, A. J. P. White and D. J. Williams, *J. Chem. Soc., Dalton Trans.*, 1997, 139; 1113.
5 D. S. Bohle, G. R. Clark, C. E. F. Rickard and W. R. Roper, *J. Organomet. Chem.*, 1988, **353**, 355.
6 P. Binger, J. Haas, A. T. Herrmann, F. Langhauser and C. Krüger, *Angew. Chem., Int. Ed. Engl.*, 1991, **30**, 310.
7 R. Appel, F. Knoll and I. Ruppert, *Angew. Chem., Int. Ed. Engl.*, 1981, **20**, 731; A. H. Cowley, R. A. Jones, J. G. Lasch, N. C. Norman, C. A. Stewart, A. L. Stuart, J. L. Atwood, W. E. Hunter and H.-M. Zhang, *J. Am. Chem. Soc.*, 1984, **106**, 7015.
8 The complex [Ru(P≡CC$_6$H$_2$Bu$^t_3$)(CO)$_2$(PPh$_3$)$_2$] has however been described recently: R. B. Bedford, A. F. Hill, M. D. Francis, C. Jones and J. D. E. T. Wilton-Ely, *Inorg. Chem.*, 1997, **36**, 5142.
9 For a recent review, see: L. Weber, *Angew. Chem., Int. Ed. Engl.*, 1996, **35**, 271.

Received in Cambridge, UK, 6th November 1997; 7/07987G

New route to monoorganotin oxides and alkoxides from trialkynylorganotins

Pascale Jaumier,[a] Bernard Jousscaume,*[a] Mohammed Lahcini,[b] François Ribot[c] and Clément Sanchez[c]

[a] *Laboratoire de Chimie Organique et Organométallique, URA 35 CNRS, Université Bordeaux I, 351, cours de la Libération, 33504-Talence-Cedex, France*
[b] *Laboratoire de Chimie, Université Cadi Ayyad, Avenue A. Khattabi, BP 618, Marrakech, Morocco*
[c] *Laboratoire de Chimie de la Matière Condensée, URA 1466 CNRS, Université P. et M. Curie, T54-E5, 4, place Jussieu, 75252-Paris Cedex 05, France*

Functional monoorganotin oxides and alkoxides are synthesised in high yield by hydrolysis or alcoholysis of the corresponding trialkynylorganotins; the hydrolytic behaviour of trialkynylorganotins is the same as for trialkoxyorganotins.

Most metallic oxides can be prepared by the sol–gel process, the starting materials being usually metallo-organic compounds such as alkoxides.[1] Hydrolysis and condensation reactions of these precursors lead to the formation of a metal–oxo based macromolecular network. Generally, these sol–gel derived materials are subject to shrinkage and cracking upon solvent removal. Incorporation of organic phases, linked to the metal either by metal–oxygen–carbon or metal–carbon bonds, allows a strong improvement of the mechanical properties of the resulting hybrid materials.[2,3] These types of materials have been extensively studied with silicon,[3,4] which forms hydrolytically stable metal–carbon bonds. As tin affords such stable bonds, and changes its coordination number and oxidation state more readily than Si, organotin oxide derived hybrid materials should show interesting properties. So far, few tin based hybrids have been developed using functional organotin trialkoxides as precursors.[5] However, these precursors offer only a limited number of polymerizable or reactive organic functionalities.[5,6] Indeed, alkene-type double bonds could be introduced in the precursors but ester groups were found to be incompatible with both available methods of preparation of organotrialkoxytins. Reaction of ω-(alkoxycarbonylalkyl)trichlorotins with *tert*-amyl alcohol in the presence of diethylamine[7] did not lead to completion because the coordination of the metal by the functional group decreases its electrophilic properties. On the other hand, with sodium *tert*-amylate, intractable compounds were only obtained.[8]

Thus, other precursors, filling several requirements were sought for: they should be cleaved by water, prepared from conveniently obtained trichlorides and, finally, they should be as tolerant as possible towards functional groups. As alkynyltins are moisture sensitive compounds, alkynyl groups were thought to be good replacements for alkoxy groups. Actually, the hydrolysis of the tin–alkynyl bond is the reverse reaction of the useful access to alkynyltins by reaction of stannoxanes or alkoxyorganotins with terminal alkynes.[9]

Treatment[10] of functional trichloroorganotins[6] with 3 equiv. of hex-1-ynyllithium (Scheme 1) led to the corresponding alkyltrialkynyltins in good yields. They were stable enough to be manipulated in the air for short periods of time and to be purified by column chromatography on Florisil. Main results are presented in Table 1.

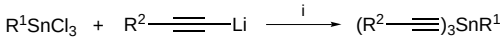

1

Scheme 1 *Reagents and conditions*: i, toluene, −78 °C to room temp., 5 h; purification by chromatography on Florisil

Table 1 Preparation of trialkynylorganotins

R^1	R^2	Yield (%)[a]
Me	Ph	71[b]
Bu	Me	83[b]
Bu	Bu	79[b]
Ph	Bu	75[b]
4-$(CH_2{=}CH)C_6H_4(CH_2)_4$	Bu	60[c]
$MeO_2C(CH_2)_2$	Bu	36
$AcO(CH_2)_3$	Bu	45
$AcO(CH_2)_5$	Bu	42
$MeCH{=}CHCO_2(CH_2)_5$	Bu	46

[a] Compounds **1** were isolated and fully characterised by ^{1}H, ^{13}C, ^{119}Sn NMR spectroscopy and mass spectrometry. [b] Chromatography was not necessary. [c] This compound was obtained by direct alkylation of a tetraalkynyltin.[11]

Upon hydrolysis (Scheme 2), either in chloroform with aqueous THF or in aqueous alcohols, tin–alkynyl bonds were cleaved and Sn–O–Sn bonds were formed. For alkyltrialkynyltins, $R^1Sn(C{\equiv}CR^2)_3$, solution ^{119}Sn NMR spectroscopy of the hydrolysed product showed two equally intense sharp signals at δ *ca.* −280 and −450, accompanied by two sets of satellites corresponding to ^2J(Sn–Sn) coupling constants of *ca.* 200 and 380 Hz.† These peaks are characteristic of the *closo* cluster $[(R^1Sn)_{12}(\mu_3O)_{14}(\mu_2OH)_6](OH)_2$,[12,13] where six tins are five-coordinate and six are six-coordinate. This compound was previously obtained from the hydrolysis of tris(isopropoxy)-butyltin.[13] Thus, as these trialkynylorganotins behave similarly to the corresponding trialkoxides, alkynyl groups appear to be the viable substitutes for alkoxy groups. Moreover, substitution of the alkynyl moiety by alkyl or aryl groups has no influence on the reaction as tris(phenylethynyl)-, tri(hex-1-ynyl)- and tri-(prop-1-ynyl)-butyltins were hydrolyzed at about the same rate.

With 3-acetoxypropyl as substituent at the metal, a soluble oxo-polymer‡ in which all tin atoms are six-coordinate, a precursor of the corresponding organostannoic acid, was formed. The strong coordinating effect[14] of the functional group disfavors five-coordinate tin and formation of the corresponding *closo* cluster.

Reaction of trialkynylorganotins with alcohols was also studied (Scheme 3). To our knowledge, cleavage of [4-(ethenyloxy)but-1-ynyl]triethyltin with butanol giving butoxytriethyltin

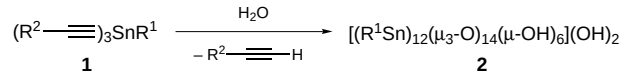

1 **2**

a R^1 = Bu
b R^1 = 4-$(CH_2{=}CH)C_6H_4(CH_2)_4$
c R^1 = $AcO(CH_2)_5$
d R^1 = $MeCH{=}CHCO_2(CH_2)_5$

Scheme 2 *Reagents and conditions*: aqueous THF, 20 °C, 12 h

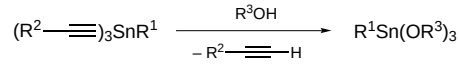

Scheme 3 *Reagents and conditions*: cyclohexane, 60 °C, 16 h; the compounds were purified by distillation

Table 2 Preparation of trialkoxyorganotins

R^1	R^2	R^3	Yield (%)[a]
Bu	Me	Bu^s	55
Bu	Me	Bu^i	76
Bu	Me	CH_2Ph	80
Me	Ph	Bu^s	50
Bu	Ph	Pr^i	59

was the only previous example of this reaction.[15] When primary or secondary alcohols were used, cleavage of alkynyl groups occurred readily upon moderate heating. Tertiary alcohols were not acidic enough to be useful. In this way, trialkoxymethyl- and trialkoxybutyl-tins[16] were prepared in good yields and results are presented in Table 2. The results show the higher reactivity of trialkynylorganotins compared to organosilanes. Indeed, Si–alkynyl bonds can be cleaved by alcohol molecules, but only at 80 °C and in the presence of F^- as catalyst.[17]

These results show that alkynyl derivatives of tin can be used instead of the corresponding alkoxides in sol–gel process and that these alkynyl derivatives are also good precursors of alkoxides. Moreover, these new precursors offer wide scope of opportunities for the introduction of a variety of organic functionalities inside tin oxide based hybrid materials.

Notes and References

* E-mail: b.jousseaume@lcoo.u-bordeaux.fr

† ^{119}Sn NMR [74.6 MHz, $CDCl_3$, ^2J (^{119,117}Sn–^{119}Sn)/Hz] **2a** δ −282.2 (*J* 380, 177), −449.0 (*J* 380, 205); **2b** δ −280.0, −470.4 (unresolved satellites); **2c** δ −280.7 (*J* 373, 178), −443.7 (*J* 373, 207); **2d** δ −282.2, −449.0 (unresolved satellites).

‡ ^{1}H NMR (250 MHz, $CDCl_3$) δ 1.0 (2 H, br). 1.9 (2 H, br), 2.0 (3 H, br), 4.1 (2 H, br); ^{13}C NMR (62.9 MHz, $CDCl_3$) δ 20.3, 21.6, 25.1, 67.8, 171.1; ^{119}Sn NMR (74.6 MHz, $CDCl_3$) δ −465 (0.5 Sn), −490 (0.5 Sn).

1 C. J. Brinker and G. W. Scherer, *Sol–Gel Science*, Academic Press, London, 1990.
2 H. I. J. Wuang, B. Orler and G. L. Wilkes, *Macromolecules*, 1987, **20**, 1322.
3 B. M. Novak, *Adv. Mater*., 1993, **5**, 422.
4 H. Schmidt and B. Seiferling, *Mater. Res. Soc. Symp. Proc.*, 1986, **73**, 739; C. Sanchez and F. Ribot, *New J. Chem.*, 1994, **18**, 1007; U. Schubert, N. Hüsing and A. Lorenz, *Chem. Mater*., 1995, **7**, 2010; D. A. Loy and K. J. Shea, *Chem. Rev.*, 1995, **95**, 1431.
5 F. Ribot, F. Banse, C. Sanchez, M. Lahcini and B. Jousseaume, *J. Sol–Gel Sci. Technol.*, 1997, **8**, 529; F. Ribot, F. Banse and C. Sanchez, *Mater. Res. Soc. Symp. Proc.*, 1994, **346**, 121.
6 B. Jousseaume, M. Lahcini, M.-C. Rascle, F. Ribot and C. Sanchez, *Organometallics*, 1995, **14**, 685.
7 I. M. Thomas, *US Pat.*, 3946056, 1976.
8 A. G. Davies, L. Smith and P. J. Smith, *J. Organomet. Chem.*, 1972, **39**, 279; D. P. Gaur, G. Sivastrata and R. C. Mehrotra, *J. Organomet. Chem.*, 1973, **63**, 221.
9 W. Neumann and F. G. Kleiner, *Tetrahedron Lett.*, 1964, **5**, 3779; M. W. Logue, *J. Org. Chem.*, 1982, **47**, 2549; B. Jousseaume and P. Villeneuve, *Tetrahedron*, 1989, **45**, 1145.
10 B. Wrackmeyer, G. Kehr, D. Wettinger and W. Milius, *Main Group Met. Chem.*, 1993, **16**, 445.
11 P. Jaumier, PhD Thesis, University Bordeaux 1, 1997.
12 H. Puff and H. Reuter, *J. Organomet. Chem.*, 1989, **373**, 173; D. Dakternieks, H. Zhu, E. R. T. Tiekink and R. Colton, *J. Organomet. Chem.*, 1994, **476**, 33.
13 F. Banse, F. Ribot, P. Tolédano, J. Maquet and C. Sanchez, *Inorg. Chem.*, 1995, **34**, 6371.
14 M. Biesemans, R. Willem, S. Damoun, P. Geerlings, M. Lahcini, P. Jaumier and B. Jousseaume, *Organometallics*, 1996, **15**, 2237.
15 V. S. Zavgorodnii, B. I. Ionin and A. A. Petrov, *J. Gen. Chem. USSR*, 1967, **37**, 898.
16 J. D. Kennedy, W. McFarlane, P. J. Smith, R. F. M. White and L. Smith, *J. Chem. Soc., Perkin Trans. 2*, 1973, 1785.
17 R. J. P. Corriu, J. J. E. Moreau, P. Thepot and M. Wong Chi Man, *Chem. Mater.*, 1996, **8**, 100.

Received in Cambridge, UK, 9th October 1997; 7/07298H

Isonitrile gold(I) nitrates as precursors for iron oxide-supported gold catalysts for CO oxidation

Trevor J. Mathieson,[a] Alan G. Langdon,[a] Neil B. Milestone[b] and Brian K. Nicholson*[a]

[a] *Department of Chemistry, University of Waikato, Private Bag 3105, Hamilton, New Zealand*
[b] *Industrial Research Limited, Box 31-310, Lower Hutt, New Zealand*

The synthesis and X-ray crystal structure of [Au(NO_3)(CNBu^t)] are reported, a first for a C- and O-bonded gold(I) species; it is an effective precursor for chemical deposition of gold on iron oxide to give catalysts which efficiently oxidise CO in air at low temperatures.

Haruta *et al.* have shown that finely-divided metallic gold on iron oxide catalyses the oxidation of CO to CO_2 in air at ambient pressures and at temperatures as low as −70 °C, a process of technological importance for the removal of CO.[1,2] Originally, preparations involved co-precipitation from solutions of Au^{III} and Fe^{III} followed by heating to generate gold particles on the iron oxide surface.[1] This process requires careful control of the rates of addition and pH to ensure active catalysts, and thorough washing to remove chloride ions which poison the catalyst. More recently a new approach involving vapour deposition of [$AuMe_2$(acac)] onto TiO_2 has given active catalysts for CO oxidation.[3]

We are exploring an alternative method of catalyst preparation, using organometallic gold compounds as substrates for deposition. The ideal precursor should be readily prepared, should be adsorbed efficiently onto the metal oxide/hydroxide surface, and preferably should not contain elements such as Cl, S or P which may act as catalyst poisons. Iwasawa and coworkers[4] have prepared active catalysts by adsorption of [Au(NO_3)(PPh_3)] onto iron hydroxide followed by calcination, which suggests that phosphorus can be tolerated. Here, we report our parallel studies on the use of the novel gold(I) complex [Au(NO_3)(CNBu^t)] **1**, for this purpose.

Complex **1** is prepared from $AgNO_3$ and [AuCl(CNBu^t)] in CH_2Cl_2–MeOH at −45 °C.† After removal of AgCl from the mixture, **1** can be isolated in reasonable yield (65%) as colourless crystals. The compound is thermally- and light-sensitive but can be readily handled as a solid at room temperature with suitable precautions, and can be stored indefinitely in the dark at −20 °C. Solutions of **1** in CH_2Cl_2 show signs of decomposition after *ca.* 15 min at room temperature, while MeOH solutions deteriorate much more rapidly. Characterisation of **1** included a single-crystal X-ray structure analysis,‡ which confirms it as the first example of a gold(I) complex with both Au–O and Au–C bonds, incorporating a normal Bu^{t}NC ligand and an η^1-NO_3 ligand about an essentially linearly coordinated gold atom. The only previous example of a gold(I) nitrate complex to be structurally characterised is [Au(NO_3)(PPh_3)];[5] the Au–ONO_2 fragments of the two are very similar.

The major structural interest is in the cell packing and intermolecular association which is clearly controlled by secondary Au···Au interactions, as expected from the recent structural and theoretical work on 'auriophilicity' from the groups of Schmidbaur,[6] Pyykkö[7] and others.[8] As shown in Fig. 1, compound **1** adopts a puckered chain arrangement with adjacent parallel monomers packing head-to-tail with alternating Bu^{t}NC and NO_3^- ligands. The alternating Au···Au interactions are 3.296(1) and 3.324(1) Å, which are the shortest yet reported for a chain structure involving Au(CNR)X species, distances less than this having been found mainly for compounds which pack as dimers or tetramers.[6] For **1** the short distances are presumably encouraged by the small ligands with low electron-donating tendencies. For comparison the Au···Au distances in the chains found for [Au(CN)(CNBu^t)] are 3.568 Å and those in [AuCl(CNBu^t)] are 3.695 Å.[9,10]

The corresponding [Au(NO_3)(CNEt)] complex was isolated similarly, but so far we have only been able to isolate the [Au($CNC_6H_3Me_2$-2,6)$_2$]NO_3 compound from analogous reaction mixtures; these structures will be reported separately.

Preparation of a catalyst for CO oxidation from **1** was straightforward.§ A sample of **1** was added to a slurry of freshly precipitated[4] $Fe(OH)_3$ in acetone to give a *ca.* 3% Au : Fe_2O_3 ratio by mass in the final product. The gold complex appears to be completely adsorbed onto the solid phase. The suspension was dried by evaporation under vacuum and heated at 400 °C in air for 2 h to convert the adsorbed gold to the metallic state, giving a brown powder. The presence of gold in the sample was confirmed by bulk EDAX analysis, but individual particles of gold were not visible under the scanning electron microscope, suggesting that they were smaller than *ca.* 4 nm, the maximum resolving power available to us. Haruta has shown that highest activity is associated with small gold particle size.[1]

To test the catalytic activity a 10 mg sample was placed in a micro-reactor and a stream of CO (1%) in air was passed through it at 2 ml min^{-1}. The effluent stream was monitored by a fuel-cell based detector which showed complete conversion of CO was achieved down to −5 °C, the lowest temperature so far examined. Catalytic activity continued without diminution for many hours.

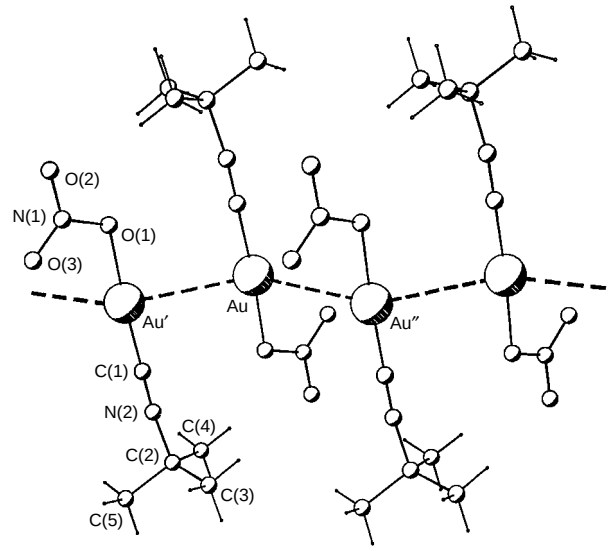

Fig. 1 The packing of [Au(NO_3)(CNBu^t)] **1** along one chain. Selected bond parameters: Au–C(1) 1.92(1), Au–O(1) 2.062(9), C(1)–N(2) 1.13(2), Au···Au′ 3.2955(8) Au···Au″ 3.3243(8) Å; C(1)–Au–O(1) 176.3(4), Au′···Au···Au″ 142.27(3)°. Symmetry operations: Au′ $-x, 1-y, 1-z$; Au″ $1-x, 1-y, 1-z$.

It is worth noting that a catalyst prepared in the same way from [AuCl(CNBu^t)] displayed no catalytic activity towards CO oxidation, even at 100 °C.

In conclusion, we have shown that isonitrile gold nitrates are stable enough for characterisation, that **1** packs with short Au···Au distances, and that chemical deposition of **1** on iron hydroxide provides a simple route to a highly active oxidation catalyst for CO.

We thank Associate Professor Cliff Rickard and Allen Oliver, University of Auckland, for collection of X-ray intensity data.

Notes and References

* E-mail: b.nicholson@waikato.ac.nz

† *Synthesis* of [Au(NO_3)(CNBu^t)]. An argon-flushed Schlenk flask containing $AgNO_3$ (0.30 g, 1.8 mmol) in MeOH (30 ml) was covered in foil to exclude light, and cooled to −45 °C. To this stirred solution was added [AuCl(CNBu^t)] (0.45 g, 1.4 mmol) in CH_2Cl_2 (10 ml) with the temperature maintained at −45 °C. The mixture was stirred for 30 min. The solvent was evaporated under vacuum and the residue extracted with cold CH_2Cl_2 (5 ml). The filtered extract was treated with light petroleum (60–80 °C fraction) to precipitate [Au(NO_3)(CNBu^t)] (0.32 g, 65%) as a colourless, microcrystalline powder after drying under vacuum. Found: C, 17.76; H, 2.47; N, 8.30%. Calc. for $C_5H_9AuN_2O_3$: C, 17.55; H 2.65; N, 8.19%. IR (KBr disk, cm^{-1}): 2258 [ν(C≡N)], 1512, 1272, 977 (monodentate NO_3^- ligand[11]). NMR ($CDCl_3$): ^{1}H δ 1.60 (s, Bu^t); ^{13}C δ 29.7 [s, (*C*H$_3$)$_3$CNC], 60.1 [s, (CH$_3$)$_3$*C*NC], 122.2 [t, $^1J_{C\equiv N}$ 24 Hz, (CH$_3$)$_3$CN*C*]. **WARNING**: The crystals decompose violently without melting at *ca.* 118 °C. X-Ray quality crystals were obtained by slow diffusion of light petroleum into a CH_2Cl_2 solution of the complex.

‡ *Structure* of [Au(NO_3)CNBu^t]. $C_5H_9AuN_2O_3$, M = 342.11, monoclinic, space group $P2_1/n$, a = 6.2642(1), b = 13.5595(3), c = 10.6118(1) Å, β = 102.18(1)°, U = 881.07(3) Å^3, Z = 4, D_c = 2.579 g cm^{-3}, λ = 0.710 73 Å. T = 203(2) K, μ(Mo-Kα) = 16.661 mm^{-1}, F(000) = 624. Data were collected on a Siemens SMART diffractometer using a crystal of dimensions 0.43 × 0.34 × 0.23 mm. A total of 4203 reflections were collected to 2θ = 56°, 1921 unique (R_{int} = 0.0552), and were corrected for absorption using SADABS ($T_{max, min}$ 0.102, 0.023). The structure was solved by Patterson methods and refined on F^2 to R_1 = 0.0574 [1645 data with $F > 4\sigma(F)$], wR_2 = 0.1543, GoF = 1.002 (all data). Largest final features were +4.1, −3.9 e Å^{-3}, adjacent to the gold atom. All calculations were with the SHELX-96 suite of programs.[12] CCDC 182/738.

§ *Preparation of the catalyst.* Iron(III) hydroxide was freshly prepared by adding a solution of sodium carbonate to a solution of iron(III) nitrate.[4] The precipitate was thoroughly washed and then suspended in acetone. Sufficient solid [Au(NO_3)(CNBu^t)] was added to give an Au/Fe_2O_3 ratio of 3% by mass and the slurry was stirred for 10 h. The acetone was pumped away under vacuum and the residue was heated in air for 2 h at 400 °C to convert the adsorbed gold complex to metallic gold particles, and the $Fe(OH)_3$ to Fe_2O_3.

1 M. Haruta, N. Yamada, T. Kobayashi and S. Iijima, *J. Catal.*, 1989, **115**, 301; M. Haruta, S. Tsubota, T. Kobayashi, H. Kageyama, M. J. Genet and B. Delmon, *J. Catal.*, 1993, **144**, 175

2 See for example: D. Risser and B. Schneider, *J. Forensic Sci.*, 1995, **40**, 368; R.-S. Koskela, *Scand. J. Work Environ. Health*, 1994, **20**, 286.

3 M. Okumura, K. Tanaka, A. Ueda and M. Haruta, *Solid State Ionics*, 1997, **95**, 143.

4 Y. Yuan, A. P. Kozlova, K. Asakura, H. Wan, K Tsai and Y. Iwasawa, *J. Catal.*, 1997, **170**, 191; Y. Yuan, K. Asakura. H. Wan, K Tsai and Y. Iwasawa, *Chem. Lett*., 1996, 129; 755.

5 J. C. Wang, M. N. I. Khan and J. P. Fackler, *Acta Crystallogr., Sect. C*, 1989, **45**, 1008; P. F. Barron, L. M. Engelhardt, P. C. Healy, J. Oddy and A. H. White, *Aust. J. Chem.*, 1987, **40**, 1545.

6 H. Schmidbaur, *Chem. Soc. Rev*., 1995, **24**, 383; W. Schneider, K. Angermaier, A. Sladek and H. Schmidbaur, *Z. Naturforsch., Teil B*, 1996, **51**, 790; K. Angermaier, E. Zeller and H. Schmidbaur, *J. Organomet. Chem*., 1994, **472**, 371; H. Schmidbaur, W. Graf and G. Müller, *Angew. Chem., Int. Ed. Engl*., 1988, **27**, 1544; J. Vicente, M-T. Chicote, M-D. Abrisqueta, R. Guerrero and P. G. Jones, *Angew. Chem., Int. Ed. Engl*., 1997, **36**, 1203.

7 P. Pyykkö, J. Li and N. Runeberg, *J. Chem. Soc., Chem. Commun.*, 1993, 1812; P. Pyykkö and Y. F. Zhao, *Angew. Chem., Int. Ed. Engl.*, 1991, **30**, 604.

8 S. S. Pathaneni and G. R. Desiraju, *J. Chem. Soc., Dalton Trans*., 1993, 319; M. J. Calhorda and L. F. Veiros, *J. Organomet. Chem.*, 1994, **478**, 37; L. F. Veiros and M. J. Calhorda, *J. Organomet. Chem*., 1996, **510**, 71; D. M. P. Mingos, *J. Chem. Soc., Dalton Trans.*, 1996, 561.

9 C. M. Che, H. K. Yip, W. T. Wong and T. F. Lai, *Inorg. Chim. Acta*, 1992, **197**, 177

10 D. S. Eggleton, D. F. Chodosh, R. L. Webb and L. L. Davis, *Acta Crystallogr., Sect. C*, 1986, **42**, 36.

11 K. Nakamoto, *Infrared and Raman spectra of inorganic and coordination compounds*, John Wiley and Sons, New York, 3rd edn., 1977, p. 244–246.

12 G. M. Sheldrick, SHELX-96, Programs for X-ray Crystallography, University of Göttingen, 1996.

Received in Cambridge, UK, 20th October 1997; 7/07522G

High solubility of $UO_2(NO_3)_2$·2TBP complex in supercritical CO_2

Mike J. Carrott,[a] Brenda E. Waller,[a] Neil G. Smart[b] and Chien M. Wai*[a]

[a] *Department of Chemistry, University of Idaho, Moscow, ID 83844, USA*
[b] *Research and Technology, BNFL, Sellafield, Cumbria, UK CA20 1PG*

$UO_2(NO_3)_2$·2TBP is highly soluble in supercritical CO_2, with concentrations of 0.0025–0.4981 M attainable at modest temperatures and pressures, demonstrating that supercritical CO_2 can provide a viable substitute for organic solvents used in nuclear fuel processing.

Recently there has been growing interest in the use of supercritical CO_2 for extracting metals and radioisotopes from waste materials. This technology is particularly attractive to the nuclear industry, where the replacement of organic solvents with supercritical CO_2 has the potential to minimize or eliminate the secondary waste produced by conventional extraction techniques, such as the PUREX process. Metal ions in solid and liquid matrices can be extracted by supercritical CO_2 using the *in situ* chelation method originally reported by Wai and coworkers.[1] This method neutralizes the charge on the metal using organic ligands dissolved in supercritical CO_2, to produce soluble metal chelates. A recent review reported the solubility data available to date for 49 metal chelates in CO_2,[2] however, the low solubility of many metal chelates in supercritical CO_2 is a major limitation of this method for practical metal processing. This problem has been partially overcome by the use of fluorinated ligands which have been shown to enhance the solubility of the resulting metal chelate by over two orders of magnitude.[3] Supercritical CO_2 has already been successfully applied to the extraction of U, Th and lanthanides from liquid and solid matrices using fluorinated β-diketone ligands.[4,5] Recent work has shown that UO_2^{2+} and Th^{4+} can be effectively extracted from nitric acid solution using CO_2 modified with tributylphosphate (TBP).[6,7] The uranyl species extracted by supercritical CO_2 is a neutral uranyl nitrate–TBP complex, $UO_2(NO_3)_2$·2TBP, which is identical to the species extracted in the PUREX process using 20% TBP in kerosene.

SFE offers several advantages over conventional solvents employed in the PUREX process, the most important of which is the potential to minimize the amount of secondary waste generated by reprocessing spent fuel. Since the solvating power of supercritical CO_2 is density dependent, extracted species are easily recovered by expanding the fluid to atmospheric pressure, thus precipitating the solutes and allowing the CO_2 to be recycled. In addition CO_2 is inexpensive, non-toxic and stable under high radiation.

In order to develop models for the extraction process and assess the feasibility of using CO_2 to replace organic solvents in the PUREX process, solubility data for the complex in supercritical CO_2 is essential. Here we report the first solubility measurements for $UO_2(NO_3)_2$·2TBP in supercritical CO_2.

$UO_2(NO_3)_2$·2TBP was prepared using a similar method reported for the synthesis of the triphenylphosphine analog.[8] Approximately 2 g of $UO_2(NO_3)_2$·$6H_2O$ were placed in a 200 ml round bottomed flask, 2 mol equiv. of TBP in 100 ml hexane were added and the mixture stirred for *ca.* 2 h at room temperature. When the uranyl nitrate had dissolved, the organic phase was separated from the water of hydration displaced by TBP, and the solvent evaporated to yield the product as a viscous yellow oil. The product was further purified by dissolving in *ca.* 15 ml hexane, freezing to −50 °C to crystallize the complex and cold filtering. This process was repeated three times to remove excess TBP. Thin film IR spectra of the liquid phase were obtained using NaCl plates; cm^{-1}: 2962s, 2878s, 1526s, 1355w, 1281m, 1192s, 939m, and the absorption bands are in good agreement with those reported by Auwer *et al.*[9]

The solubility of $UO_2(NO_3)_2$·2TBP in supercritical CO_2 was determined by UV–VIS spectroscopy,† over a pressure range of 100–300 atm and at temperatures of 40, 50 and 60 °C. Prior to the solubility measurements the molar absorptivity of the complex at 411 nm was determined using standards of $UO_2(NO_3)_2$·2TBP in hexane,‡ and found to be 8.77 l mol^{-1} cm^{-1} at 411 nm. Using Beer–Lambert's law the concentration of the complex in supercritical CO_2 was calculated from subsequent spectroscopic measurements. A typical UV–VIS spectrum of $UO_2(NO_3)_2$·2TBP in supercritical CO_2 is shown in Fig. 1. The solubility curves for $UO_2(NO_3)_2$·2TBP under the conditions investigated are presented in Fig. 2. It can clearly be seen that the solubility of the complex increases dramatically with pressure, particularly at low temperatures. At 40 °C the concentration of $UO_2(NO_3)_2$·2TBP in CO_2 increases from 0.0025 M at 100 atm to 0.4291 M at 225 atm, corresponding to 2.31 and 397.3 g l^{-1} respectively, and represents an increase in

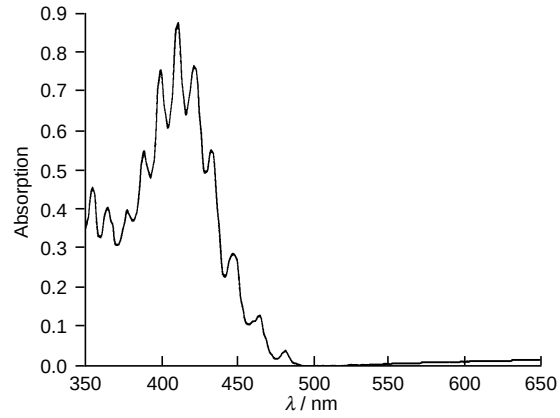

Fig. 1 UV–VIS spectrum of $UO_2(NO_3)_2$·2TBP in supercritical CO_2

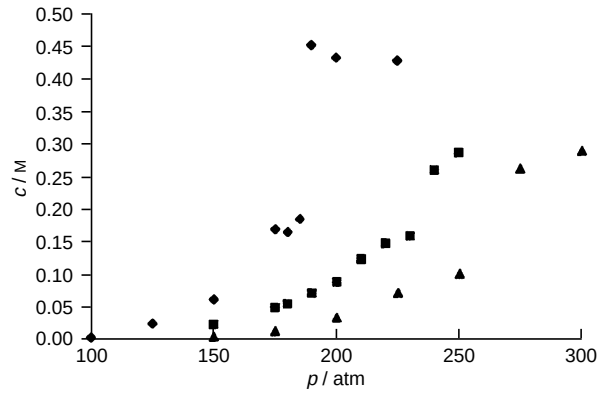

Fig. 2 Solubility of $UO_2(NO_3)_2$·2TBP in supercritical CO_2 at 40 °C (◆), 50 °C (■) and 60 °C (▲)

solubility over two orders of magnitude. Similar curves were obtained at 50 and 60 °C, although the solubility was observed to decrease with increasing temperature. This effect is due to the lower density and hence decreased solvating power of the fluid at higher temperatures. At 50 and 60 °C no appreciable solubility (< 0.001 M) was observed below 125 atm, but the concentration of $UO_2(NO_3)_2 \cdot 2TBP$ increased rapidly in excess of 0.2 M at 240 and 275 atm, respectively. The use of a high pressure view cell as a saturation vessel enabled the phase behaviour of the complex to be observed during the spectroscopic measurements. Initially two distinct phases were present, an intense yellow liquid (lower) phase due to the complex and a pale yellow supercritical (upper) phase due to the CO_2 saturated with $UO_2(NO_3)_2 \cdot 2TBP$. With increasing pressure the yellow colour of the supercritical phase became progressively more intense due to the increasing solubility of the complex, also the liquid phase became darker in colour until it appeared almost black, possibly due to CO_2 being dissolved in the liquid phase. Further increases in pressure produced a very turbid, opaque (almost black) phase in which the meniscus had virtually disappeared, and eventually resulted in an intense yellow single phase. This transition to a single phase occurred very rapidly, over a small pressure range, and is apparent from the sharp increases in concentration observed at 190, 240 and 275 atm for the solubility curves at 40, 50 and 60 °C, respectively. Upon formation of a single phase the concentration remained constant with further increases in pressure, and the solubility curve reached a plateau due to complete dissolution of the complex. Valid solubility data cannot be obtained after this point as the CO_2 was no longer saturated with the complex. Since uranyl nitrate itself is insoluble in pure CO_2 the high solubility of the complex can be attributed to the shielding of the central metal ion by the TBP ligands and increased solute–solvent interactions between the butyl groups and CO_2.

In conclusion, this study has shown that it is possible to obtain extremely high concentrations of $UO_2(NO_3)_2 \cdot 2TBP$ in supercritical CO_2, which surpasses the solubility of any metal chelate previously reported in the literature.§ Most significantly, the concentrations of $UO_2(NO_3)_2 \cdot 2TBP$ in supercritical CO_2 are comparable to those encountered in the waste streams of the PUREX process, typically 0.13–0.47 M in the organic phase.[10] In conjunction with previous extraction work,[6,7] this clearly demonstrates CO_2 can offer a viable alternative to the organic solvents currently employed in nuclear fuel processing.

The authors wish to express their gratitude to British Nuclear Fuels Ltd. (BNFL), and Idaho NSF-EPSCoR for financial support. We also thank Varian for the loan of the fibre optic interface for the Cary 1E UV–VIS spectrometer.

Notes and References

* E-mail: cwai@uidaho.edu

† Measurements were performed using high pressure fibre optic cells constructed in-house. The cells are connected in series and have path lengths of 1 cm, 733 μm and 38 μm, enabling measurements to be made over a wide concentration range. CO_2 was saturated with the complex using a high pressure view cell,[3] with a volume of 15 ml, as an equilibration vessel. Approximately 5–7 ml of $UO_2(NO_3)_2 \cdot 2TBP$ were loaded into the view cell, and, after a period of equilibration, the saturated CO_2 was introduced into the fibre optic cells and UV spectra recorded.

‡ Hexane has a similar polarity to CO_2, and UV–VIS spectra have been shown to exhibit similar absorption coefficients and negligible shifts in the positions of absorption maxima.[11] Our work has also shown that the molar absorptivity of the complex is not affected by changes in the density of the fluid. A high pressure view cell, with a path length of 5 cm and a volume of 15 ml[3], was employed to determine the effect of temperature and pressure on the spectrum of the complex. An aliquot of $UO_2(NO_3)_2 \cdot 2TBP$ was placed in the cell, such that complete dissolution of the complex was achieved under supercritical conditions. Spectra were recorded over a temperature range of 40–60 °C and at pressures of 150–300 atm. No change was observed in the absorption spectrum, thus confirming the molar absorptivity is unaffected by the temperatures and pressures employed in this work.

§ The highest solubility previously reported for a metal chelate in supercritical CO_2, was chromium(III) dipivaloylmethane, $Cr(thd)_3$, with a concentration of 0.126 M at 40 °C and 310 atm.[12]

1 K. E. Laintz, C. M. Wai, C. R. Yonker and R. D. Smith, *Anal. Chem.*, 1992, **64**, 2875.
2 N. G. Smart, T. Carleson, T. Kast, A. A. Clifford, M. D. Burford and C. M. Wai, *Talanta*, 1997, **44**, 137.
3 K. E. Laintz, C. M. Wai, C. R. Yonker and R. D. Smith, *J. Supercrit. Fluids*, 1991, **4**, 194.
4 Y. Lin, R. D. Brauer, K. E. Laintz and C. M. Wai, *Anal. Chem.*, 1993, **65**, 2549.
5 Y. Lin, C. M. Wai, F. M. Jean and R. D. Brauer, *Environ. Sci. Technol.*, 1994, **28**, 1190.
6 Y. Lin, N. G. Smart and C. M. Wai, *Environ. Sci. Technol.*, 1995, **29**, 2706.
7 Y. Meguro, S. Iso, H. Takeishi and Z. Yoshida, *Radiochim. Acta*, 1996, **75**, 185.
8 N. W. Alcock, M. M. Roberts and D. Brown, *J. Chem. Soc., Dalton Trans.*, 1982, 25.
9 C. D. Auwer, C. Lecouteux, M. C. Charbonnel, C. Madic and R. Guillaumont, *Polyhedron*, 1997, **16**, 2233.
10 M. Benedict, T. H. Pigford and H. W. Levi, *Nuclear Chemical Engineering*, McGraw-Hill Book Co., New York, 2nd edn., 1981, pp. 508.
11 K. D. Bartle, A. A. Clifford, S. A. Jafar and G. F. Shilstone, *J. Phys. Chem. Ref. Data*, 1991, **20**, 713.
12 A. F. Laglante, B. N. Hansen, T. J. Bruno and R. E. Sievers, *Inorg. Chem.*, 1995, **34**, 5781.

Received in Cambridge, UK, 11th November 1997; 7/08113H

N-Hydroxypyrazinone-bearing homotrioxacalix[3]arene: its cooperative molecular recognition by metal complexation

Junko Ohkanda, Hiroyuki Shibui and Akira Katoh*

Department of Industrial Chemistry, Faculty of Engineering, Seikei University, Musashino, Tokyo 180, Japan

Artificial receptors in which three bidentate hydroxypyrazinones are linked to homotrioxacalix[3]arene through an α,ω-diamine as a spacer exhibited cooperative molecular recognition with gallium ion toward ammonium cations.

Recently, artificial allosteric receptors have been widely investigated from the viewpoint of the application of regulated functions controlled by cooperativity in natural proteins to biomimetic molecular recognition systems.[1] Previously we have demonstrated that *N*-hydroxyamide-containing diazines such as *N*-hydroxypyrazinones acted as a bidentate ligand to Fe^{III} and Ga^{III}.[2] Homotrioxacalix[3]arene[3] is flexible compared to calix[4]arene due to its ethereal linkages, and has a C_3 symmetrical structure which is expected to be particularly useful in receptors of primary ammonium cations.[4] We focused our interest on this compound as a platform for the construction of a flexible host molecule. In the course of our studies on the application of diazines to multifunctional receptors, new host molecules **1a**,**b**, in which three *N*-hydroxypyrazinones were linked to homotrioxacalix[3]arene by an alkyl spacer group, were synthesized. The hosts would be expected to control their cavity size and rigidity upon transition metal chelation, which enables them to exhibit cooperative molecular recognition toward primary ammonium cations. We describe herein the synthesis of the receptors **1a**,**b** and their ammonium cation extraction abilities.

Receptors **1a**,**b** were synthesized by coupling *N*-3-(1-benzyloxy-5,6-dimethyl-2-oxo-1,2-dihydropyraz-3-yl)propanoyldiaminoalkane hydrochloride (n = 4, 6)[2b] with the cone-type tricarboxylic acid[5] derived from homotrioxacalix[3]arene by using WSC·HCl and HOBt† and subsequent hydrogenation according to Scheme 1. Compounds **1a**,**b** were characterised by IR and ^{1}H NMR spectroscopy and elemental analysis, respectively.‡

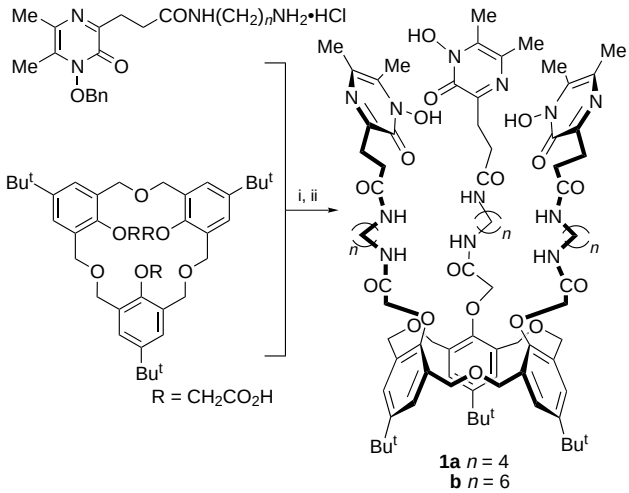

Scheme 1 *Reagents and conditions*: i, WSC·HCl, HOBt, Et_3N, CH_2Cl_2, room temp., 72 h, 52%; ii, H_2, 10% Pd–C, MeOH, 70%

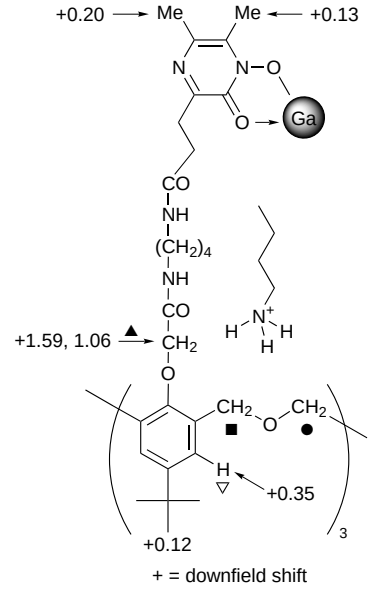

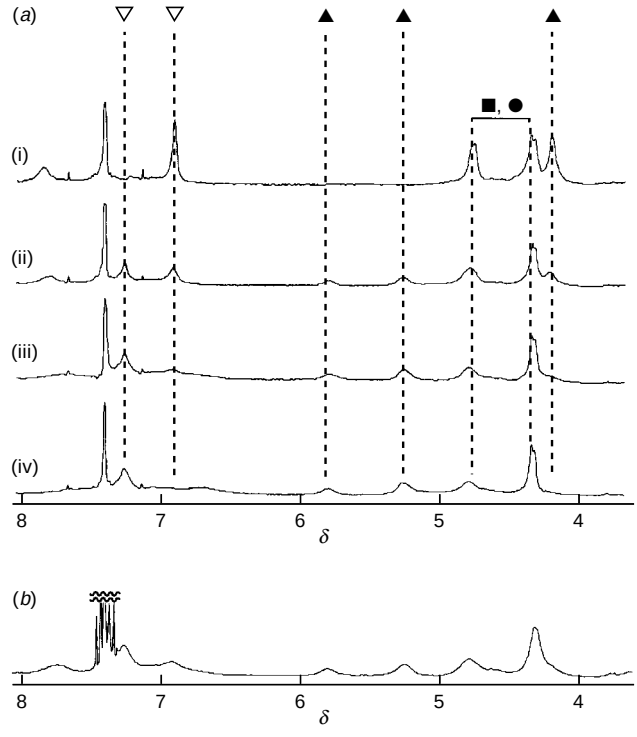

Fig. 1 (*a*) ^{1}H NMR spectra (400 MHz) of **1a** at [$BuNH_3ClO_4$] = (i) 0, (ii) 0.51, (iii) 1.02 and (iv) 1.53 mM; T = 23 °C, [**1a**] = 0.7 mM, [$Ga(acac)_3$] = 0.84 mM. (*b*) ^{1}H NMR spectrum of **1a** in the presence of $C_6H_{11}NH_3^+$; [**1a**] = 0.54 mM, [$C_6H_{11}NH_3ClO_4$] = 0.79 mM.

The 1 : 1 gallium complexation was ascertained by a mole ratio plot. In the ^{1}H NMR spectrum of **1a** with 1.2 equiv. of $Ga(acac)_3$ in 25% CD_3CN in $CDCl_3$, only the two singlets of the 5- and 6-methyl groups of the pyrazinone ring showed downfield shifts ($\Delta\delta$ +0.20 for 5-methyl, +0.13 for 6-methyl), whereas titration with $BuNH_3ClO_4$ induced large downfield shifts of the OCH_2CO (▲) and ArH (▽) protons, as shown in Fig. 1(*a*). The formation of 1 : 1 complex of **1a** with $BuNH_3^+$ was confirmed by a Job plot. It has been reported that the triester derivative of homotrioxacalix[3]arene is bound to an ammonium cation *via* the interaction of three phenolic oxygens and three carbonyl oxygens with the cation.[6] As for **1a**, the singlet for the OCH_2CO protons (▲) changed to two broad singlets when the ammonium salt was added, but no apparent downfield shifts were observed for the signals from the ethereal methylene protons (■, ●). Thus, it is likely that **1a** binds to $BuNH_3^+$ through C=O···HN‡ and ArO···HN‡ interactions similar to those previously reported.

By using a CH_2Cl_2 solution of **1** or a mixture of **1** and an equimolar amount of $Ga(acac)_3$, extraction of primary ammonium picrate from an aqueous phase was carried out. The amounts of ammonium picrates extracted into the organic phase are shown in Fig. 2.§ $Bu^tNH_3^+$ was not extracted efficiently when compared to $BuNH_3^+$ and $HexNH_3^+$, suggesting that the bulky substituent disturbs inclusion of the guest into the cavity. This result also indicates that the extracted amounts of $BuNH_3^+$ and $Bu^tNH_3^+$ increased in the presence of Ga^{3+}, indicating a cooperative molecular recognition of **1** and Ga^{3+} toward the primary ammonium cation. Furthermore, it was noted that the amount of $HexNH_3^+$ extracted by **1a** decreased in the presence of Ga^{3+}. This result was consistent with the difference in the association constants of **1a**–$HexNH_3^+$ in the absence [K_a 4375, Fig. 1(*b*)] and in the presence of Ga^{3+} (K_a 2833).¶ On the basis of molecular modelling, this observation might be attributed to the regulation of the cavity size by metal complexation; the Ga–**1** complex thus provides a rigid cavity that is suitable for selective recognition of ammonium cations.

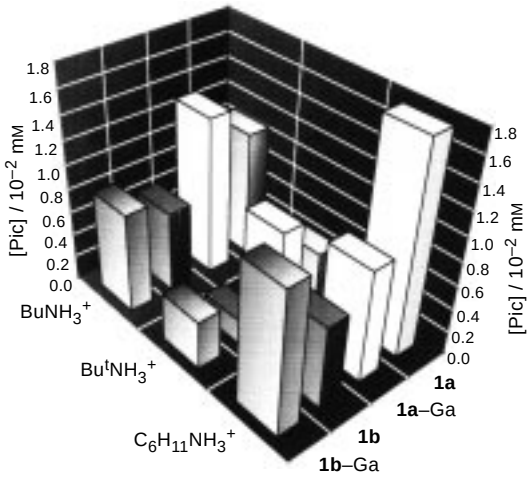

Fig. 2 Two phase solvent extraction of primary ammonium cations

This work was partially supported by a Grant-in-Aid for Scientific Research from the Ministry of Education, Science, Sports and Culture, Japan.

Notes and References

* E-mail: katoh@chgw.ch.seikei.ac.jp

† *Abbreviations*: WSC·HCl = 1-[3-(dimethylamino)propyl]- 3-ethylcarbodiimide hydrochloride (water soluble carbodiimide); HOBt = 1-hydroxybenzotriazole.

‡ *Selected data* for **1a**: ν_{max}(KBr)/cm^{-1} 3310, 1651; δ_H [$(CD_3)_2SO$, 23 °C] 1.03 (s, 27 H), 1.45 (m, 12 H), 2.09, 2.20, 2.45 (each s, 18 H), 2.43 (m, 6 H), 2.84 (m, 6 H), 3.06 (m, 6 H), 3.19 (m, 6 H), 4.12 (s, 6 H), 4.42 (d, *J* 12, 6 H), 4.64 (d, *J* 12, 6 H), 6.89 (s, 6 H), 7.95 (br s, 3 H), 8.01 (br s, 3 H); Calc. for $C_{81}H_{102}N_{12}O_{18}\cdot 4H_2O$: C, 60.65; H, 6.9; N, 10.4. Found: C, 60.6; H, 7.2; N, 10.1%.

§ A CH_2Cl_2 solution (2 ml) containing **1** (0.045 mM) was shaken with an aqueous solution (2 ml) containing ammonium picrate (0.12 mM) and the corresponding hydrochloride salt (0.1 M) at 23 °C for 9 h. The amount of each ammonium cation extracted into the CH_2Cl_2 phase was estimated from $[Pic]_c - [Pic]_f$, $[Pic]_f$ and $[Pic]_c$ being the picrate concentrations in the aqueous phase after the extraction and in the corresponding control sample, respectively.

¶ The association constant (K_a) of the 1 : 1 complex of **1a** with $HexNH_3ClO_4$ was directly estimated from the ^{1}H NMR spectra. Error estimated to be < 15%.

1 J. Rebek, Jr., *Acc. Chem. Res.*, 1984, **17**, 258; T. Nabeshima, T. Inaba and N. Furukawa, *Tetrahedron Lett.*, 1987, **28** 6211; Y. Kobuke and Y. Satoh, *J. Am. Chem. Soc.*, 1992, **114**, 789; M. Inouye, T. Konishi and K. Isagawa, *J. Am. Chem. Soc.*, 1993, **115**, 8091.
2 (*a*) J. Ohkanda and A. Katoh, *J. Org. Chem.*, 1995, **60**, 1583; (*b*) J. Ohkanda and A. Katoh, *Tetrahedron*, 1995, **51**, 12 995.
3 B. Dhawan and C. D. Gutsche, *J. Org. Chem.*, 1983, **48**, 1536; P. Zerr, M. Mussrabi and J. Vicens, *Tetrahedron Lett.*, 1991, **32**, 1879.
4 H. Matsumoto, S. Nishio, M. Takeshita and S. Shinkai, *Tetrahedron*, 1995, **51**, 4647.
5 M. Takeshita and S. Shinkai, *Chem. Lett.*, 1994, 125.
6 K. Araki, N. Hashimoto, H. Otsuka and S. Shinkai, *J. Org. Chem.*, 1993, **58**, 5958.

Received in Cambridge, UK, 23rd September 1997; 7/06869G

Carboxylate-derived calixarenes with high selectivity for actinium-225

Xiaoyuan Chen,[a] Min Ji,[a] Darrell R. Fisher[b] and Chien M. Wai[a]

[a] *Department of Chemistry, University of Idaho, Moscow, Idaho 83844, USA*
[b] *Molecular Biosciences Department, PNNL, Richland, Washington 99352, USA*

The binding properties of two ligands, 5,11,17,23-tetra-*tert*-butyl-25,26,27,28-tetrakis(carboxymethoxy)calix[4]arene 1 and 5,11,17,23,29,35-hexa-*tert*-butyl-37,38,39,40,41,42-hexakiscarboxymethoxy)calix[6]arene 2, which show high selectivity for $^{225}Ac^{3+}$ (an α-emitter with $t_{1/2}$ = 10 days) over Na^+, K^+, Mg^{2+}, Ca^{2+} and Zn^{2+} are described.

In recent years there has been an increased interest in the development of monoclonal antibodies that may be linked with a radioisotope as targeting agents in radioimmunodiagnosis and radioimmunotherapy of cancer tumors.[1] The success of such approaches depends on the development of bifunctional complexing agents that can bind a specific radioisotope tightly and selectively and can be linked to antibodies. Chelators that can hold the desired radioisotope with high stability under physiological conditions are essential to deliver the radioisotope to the antigen binding site on tumor cells.[2] Linkage of β-emitters such as ^{90}Y and ^{67}Cu to the moab part of monoclonal antibodies *via* bifunctional aza- and peraza-crown ether macrocycles has shown good results for the treatment of a number of cancer patients.[3] For radioimmunotherapy, α-emitters are much better cytotoxic agents than β-emitters since they dissipate a large amount of energy along straight particle tracks of 40–70 μm (*ca*. 8 cell diameters).[4] Among the α-emitters having an appropriate physical half-life for such an application is actinium-225 ($t_{1/2}$ = 10.0 d).[5] ^{225}Ac decays through a chain of daughter products to stable ^{209}Bi with the emission of a total of four α and two β particles, releasing about 28 MeV of radiation energy to the absorbing medium.[6]

Solvent extraction experiments performed recently in our laboratory indicate that 5,11,17,23-tetra-*tert*-butyl-25,26,27,28-tetrakis(carboxymethoxy)calix[4]arene **1** and 5,11,17,23,29,35-hexa-*tert*-butyl-37,38,39,40,41,42-hexakis-(carboxymethoxy)calix[6]arene **2** (Fig. 1) exhibit high Ac^{3+} selectivity over alkali, alkaline earth, and zinc metal ions under neutral and weak acidic conditions. These calixarene derivatives were synthesized in our laboratory according to the known procedures in the literature.[7,8] The two-phase solvent extraction experiments were carried out between water (1.5 ml, [^{225}Ac] = 10^{-3} mM) and chloroform (1.5 ml, [ionophore] = 2 mM). The pH of the aqueous phase was adjusted with HCl for pH 1–3, succinic acid–NH_4OH for pH 4–6, and Tris–HCl for pH 7–8. The mixture was shaken at 25 °C for 30 min, which was long enough to reach equilibrium based on our time variation studies. The distribution ratio *D* ([Ac^{3+}] in the organic phase/[Ac^{3+}] in the aqueous phase) was determined by measuring the ^{225}Ac activity in each phase using a Ge(Li) detector. Percentage extraction of Ac^{3+} (Ex%) was calculated by $D/(1 + D)$. Fig. 2 shows Ex% of Ac^{3+} with ligands **1** and **2** plotted *vs*. pH of the aqueous phase. For **1**, Ex% becomes appreciable at pH 2.0 and reaches nearly 100% around pH 4.0. Ex% decreases rapidly at pH > 7.3 reaching only 40% at pH 8.0. Ex% for **2** shows a similar pH dependence. The Ex% increases from pH 1.5, reaching saturation at pH around 3.0 and decreasing sharply above pH 7.5.

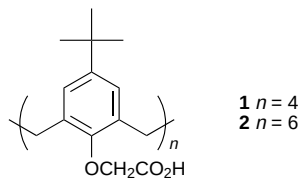

1 *n* = 4
2 *n* = 6

Fig. 1 Structures of the carboxylate-derived calixarenes which show high selectivity for Ac^{3+}

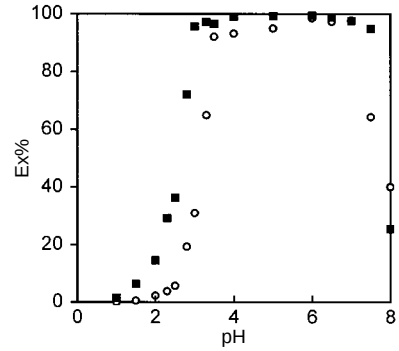

Fig. 2 pH dependence of extraction of actinium-225 with ligands **1** and **2**. The pH of the aqueous phase was adjusted with HCl for pH 1–3, succinic acid–NH_4OH for pH 4–6 and Tris–HCl for pH 7–8; (○) **1** (*n* = 4), (■) **2** (*n* = 6).

Fig. 3 shows plots of log *D vs*. −log[L] for the extraction of Ac^{3+} by ligands **1** and **2** at pH = 6.0, where [L] is the concentration of the ionophore in the organic phase. A linear relationship between log *D* and −log[L] is observed with the slope of both lines roughly equal to −1 suggesting that both **1** and **2** form a 1 : 1 complex with Ac^{3+}.

Owing to its short half-life and high radioactivity, it was not possible for us to obtain the stability constants of the ^{225}Ac complexes using common spectroscopic or potentiometric titration methods. We used a competition extraction method to obtain the relative extraction constants of Ac^{3+} by ligands **1** and **2** with respect to EDTA. To obtain the relative stability constants of the Ac complexes, the following competition experiments were performed. The Ac^{3+} in water at pH 7 was

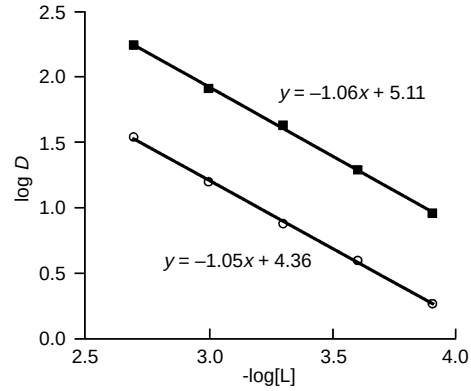

Fig. 3 Plot of log *D vs.* −log[L] for the extraction of Ac^{3+} by ligands **1** and **2**. The slopes were 1.05 and 1.06, respectively; (○) **1**, (■) **2**.

first extracted into the chloroform phase containing **1** or **2**. The organic phase was then back-extracted with an aqueous phase containing EDTA at pH = 7.0. No data for Ac^{3+} hydrolysis is available. We estimated the hydrolysis of Ac^{3+} based on the known values of Am^{3+} ($\log \beta_1 = -6.4 \pm 0.7$, $\log \beta_2 = -14.1 \pm 0.6$, $\log \beta_3 = -25.7 \pm 0.5$ at $I = 0$ and 25 °C), which fall in the range of the hydrolysis constants reported for the trivalent lanthanides.[9] According to these values, the distribution of Ac^{3+}, $Ac(OH)^{2+}$ and $Ac(OH)_2^{+}$ should be 71, 28 and 1%, respectively, at pH 6 and 17, 68 and 15%, respectively, at pH 7. Thus, ^{225}Ac could also be extracted as the Ac(OH)–calixarene complexes in near neutral solutions.

The following equilibrium relations were obtained based on the assumptions that neither $EDTA^{3-}$ nor $Ac(OH)(EDTA)^{-}$ was soluble in chloroform and the solubility of the H_2L^{2-} and $Ac(OH)(H_2L)$ in the aqueous phase was negligible. The new distribution ratio D' was taken as $[Ac(OH)(H_2L)]_{org}/[Ac(OH)(EDTA)^{-}]_{aq}$, where $Ac(OH)(H_2L)$ represented the Ac–calixarene complex.

$$EDTA^{3-} + Ac(OH)^{2+} = Ac(OH)(EDTA)^{-}$$

$$K_1 = [Ac(OH)(EDTA)^{-}]/[EDTA^{3-}][Ac(OH)^{2+}]$$

$$H_2L^{2-} + Ac(OH)^{2+} = Ac(OH)(H_2L)$$

$$K_2 = [Ac(OH)(H_2L)]/[H_2L^{2-}][Ac(OH)^{2+}]$$

$$K_2/K_1 = [Ac(OH)(H_2L)][EDTA^{3-}]/[Ac(OH)(EDTA)^{-}][H_2L^{2-}]$$

$$\log(K_2/K_1) = \log D' + \log[EDTA^{3-}]/[H_2L^{2-}]$$

A linear relationship is observed between log D' and log[EDTA]/[L] for both ligands (Fig. 4) with slope close to unity suggesting that the assumptions are reasonable. From the intercept, we obtain the extraction constants of the Ac–calixarene complexes relative to that of EDTA. Ligand **1** has $K_2 = 1.11\,K_1$ and **2** has $K_2 = 5.75\,K_1$, where K_1 is the extraction constant of Ac with H_4EDTA at pH 7.

We also investigated whether the actinium complexes could tolerate high concentrations of alkali, alkaline earth and zinc metal ions. We took aliquots of the organic phase containing the ^{225}Ac complexes and back-extracted with an aqueous solution

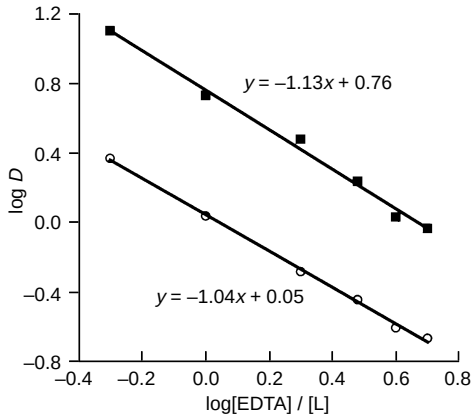

Fig. 4 Plot of log D *vs.* log[EDTA]/[L] at pH = 7.0 shows a straight line for both ligands; (○) **1**, (■) **2**

containing a mixture of 10 mM each of Ca^{2+}, Mg^{2+}, Na^{+}, K^{+} and Zn^{2+} at pH 7.0. After shaking for 5 h, ligand **1** showed no measurable loss of Ac^{3+} from the organic phase to the aqueous phase. For ligand **2**, about 5% of the Ac originally present in the organic phase was extracted to the aqueous phase. The high selectivity of the calixarene carboxylate ligands for Ac^{3+} may be related to the high charge density of the Ac^{3+} ion favoring electrostatic interactions with the anionic ligands.[10] Ligand **2** shows a slightly lower selectivity for Ac^{3+} than **1** which may be due to the structural difference between the two ligands. Because **2** has a larger and more flexible cavity, it probably can accommodate the competing cations better than **1**. Also **2** is more acidic than **1**, thus it can coordinate with the alkaline earth metal ions at lower pH values.

In conclusion, this study shows that both **1** and **2** have an ionophore cavity capable for selective complexation with Ac^{3+} in weak acid and neutral solutions. They appear to be suitable candidates as ^{225}Ac carriers. The next step in our research is to selectively functionalize the upper rim of the calixarene ring with amine, bromine, aldehyde or acid chloride forming bifunctional ligands that may be attached to the desired monoclonal antibodies.

This work was supported by the Pacific Northwest National Laboratory (PNNL).

Notes and References

* E-mail: cwai@uidaho.edu

1 S. J. DeNardo, J. S. Peng, G. L. DeNardo, S. L. Mills and A. L. Epstein, *Nucl. Med. Biol.*, 1986, **13**, 303; C. F. Meares and T. G. Wensel, *Acc. Chem. Res.*, 1984, **17**, 202; L. Yuanfang and W. Chuanchu, *Pure Appl. Chem.*, 1991, **63**, 427; D. Parker, *Chem. Soc. Rev.*, 1990, **19**, 271.

2 J. L. Klein, P. K. Leichner, K. M. Callahan, K. A. Kopher and S. E. Order, *Antibody, Immunoconjugates, Radiopharm.*, 1988, **1**, 55; S. V. Desphande, S. J. DeNardo, C. F. Meares, M. J. McCall, G. P. Adams, M. K. Moi and G. L. DeNardo, *J. Nucl. Med.*, 1988, **29**, 217; J. P. L. Cox, J. R. Morphy, K. J. Jankowski and D. Parker, *Pure Appl. Chem.*, 1989, **61**, 1637.

3 M. K. Moi and C. F. Meares, *J. Am. Chem. Soc.*, 1988, **110**, 6266; J. P. L. Cox, K. J. Jankowski, R. Kataky, D. Parker, M. A. W. Eaton, N. R. A. Beeley, A. T. M. Millican, A. Harrison and C. Walker, *J. Chem. Soc., Chem. Commun.*, 1989, 797; M. K. Moi, C. F. Meares, M. J. McCall, W. C. Cole and S. J. DeNardo, *Anal. Biochem.*, 1984, **148**, 249; J. R. Morphy, D. Parker, R. Alexander, A. Bains, M. A. W. Eaton, A. Harrison, A. Millican, R. Timas and D. Weatherby, *J. Chem. Soc., Chem. Commun.*, 1988, 156; C. J. Anderson, J. M. Connett, S. W. Schwarz, P. A. Rocque, L. W. Guo, G. W. Phillott, K. R. Zinn, C. F. Meares and M. J. Welch, *J. Nucl. Med.*, 1992, **33**, 2006.

4 D. S. Wilbur, *Antibody, Immunoconjugates, Radiopharm.*, 1991, **4**, 85.

5 M. W. Geerlings and R. Van der Hout, *Nucl. Med. Commun.*, 1993, **14**, 121.

6 M. W. Geelings, *Int. J. Biol. Markers*, 1993, **8**, 180; M. W. Geelings, F. M. Kaspersen, C. Apostolidis and R. Van der Hout, *Nucl. Med. Commun.*, 1993, **14**, 121.

7 S. Shinkai, H. Horeishi, K. Ueda and O. Manabe, *J. Chem. Soc., Chem. Commun.*, 1986, 733.

8 S. Shinkai, H. Horeishi, K. Ueda, T. Arimura and O. Manabe, *J. Am. Chem. Soc.*, 1987, **109**, 6371.

9 R. J. Silva, G. Bidoglio, M. H. Rand, P. B. Robouch, H. Wanner and I. Puigdomenech, in *Chemical Thermodynamics, Vol. 2: Chemical Thermodynamics of Americium*, Elsevier, 1995; C. F. Baes and R. E. Mesmer, in *The Hydrolysis of Cations*, Wiley, New York, 1976.

10 F. Arnaud-Neu, S. Cremin, S. Harris, M. A. McKervey, M.-J. Schwing-Weill, P. Schwinté and A. Walker, *J. Chem. Soc., Dalton Trans.*, 1997, 329.

Received in Cambridge, UK, 18th September 1997; 7/06776C

Preparation and characterization of the kinetic and thermodynamic isomers of dinuclear molybdenum and tungsten complexes with metal–metal triple bonds supported by *p-tert*-butylcalix[4]arene anions†

Malcolm H. Chisholm,* Kirsten Folting, William E. Streib and De-Dong Wu

Department of Chemistry and Molecular Center, Indiana University, Bloomington, IN 47405, USA

The reaction between $M_2(NMe_2)_6$ and < 2 equiv. of *p-tert*-butylcalix[4]arene (H_4L) in hydrocarbon solvents leads to $(H_2NMe_2)_2[M_2(\mu,\eta^2,\eta^2\text{-}L)_2]$ 1 (M = Mo, W), which isomerizes to the unbridged isomers $(H_2NMe_2)_2[M_2(\eta^4\text{-}L)_2]$ 2 upon heating in refluxing pyridine (L = quadruply deprotonated calix[4]arene); related complexes $M_2(\eta^4\text{-}HL)_2$ 3 (M = Mo, W) are prepared from reactions involving $M_2(OBu^t)_6$ and H_4L, and these react with $HNMe_2$ to give 2 (M = Mo and W) while $[NH_2Me_2][W_2(\eta^4\text{-}L)(\eta^4\text{-}HL)]$ 4 can be obtained by the reaction between 2 and 3 (M = W) in a 1 : 1 ratio.

The recent communication of the elegant synthesis of W–W bonded complexes supported by the *p-tert*-butylcalix[4]arene tetraanion, L, namely $Na_2W_2(\eta^4\text{-}L)_2(\mu\text{-}Cl)_2$ (M=M) and $Na_2W_2(\eta^4\text{-}L)_2$ (M≡M),[1] leads us to report on our related findings concerning $(M{\equiv}M)^{6+}$ centers.

The reaction between $M_2(NMe_2)_6$ and *p-tert*-butylcalix-[4]arene, H_4L (1.7 equiv.) in a hydrocarbon solvent leads to the formation of green compounds **1** (M = Mo, W).‡ The ^1H NMR spectrum reveals one type of Bu^t group and two CH_2 groups, each being diastereotopic, consistent with the structure found for M = Mo in the solid-state shown in Fig. 1.§ The μ,η^2,η^2-L bridging of the calix[4]arene ligand is similar to that reported for the Mo–Mo quadruple bonded complex $Mo_2(OAc)_2(\mu,\eta^2,\eta^2\text{-}H_2L)$[2] but the Mo–Mo distance in the M–M triple bonded complex is larger by *ca*. 0.07 Å as is commonly seen in comparing Mo–Mo bonded complexes of bond order 4 and 3.[3] Also the Mo–O distances are somewhat shorter in the present structure consistent with the Mo_2^{6+} center. The W complex is isomorphous.§

We recently have prepared a number of complexes of the type $Mo_2(NMe_2)_2(\mu\text{-diolate})_2$ and noted that bridged diolates are often formed kinetically. The addition of pyridine and heat causes isomerization to the chelate isomers, $Mo_2(NMe_2)_2(\eta\text{-diolate})_2$, which represent the thermodynamic products.[4] We thus reasoned that the dumb-bell-like isomer $Mo_2(\eta^4\text{-}HL)_2$ might be thermodynamically favored and, indeed, upon refluxing in pyridine the green solutions of $(H_2NMe_2)_2[Mo_2(\mu,\eta^2,\eta^2\text{-}L)_2]$ **1** turn amber.‡ The ^1H NMR spectrum becomes simpler revealing again one type of Bu^t group and one CH_aH_b group with a large chemical shift difference (δ 5.3 and 3.3 ppm) as might be expected if one CH bond were proximal and the other distal to the Mo–Mo triple bond.[5] Amber crystals of $[NH_2Me_2]_2[Mo_2(\eta^4\text{-}L)_2]$ **2** were obtained that were suitable for an X-ray study and the molecular structure is shown in Fig. 2.§

It is interesting to note that in both structural determinations the calix[4]arene ligands encapsulate or attract molecules of dimethylamine, as $[NH_2Me_2]^+$ cations, and solvent molecules. However, upon heating crystalline samples of the kinetic and thermodynamic isomers in a dynamic vacuum, **1**·4thf (M = Mo) loses only thf molecules whereas **2**·4py (M = Mo) loses

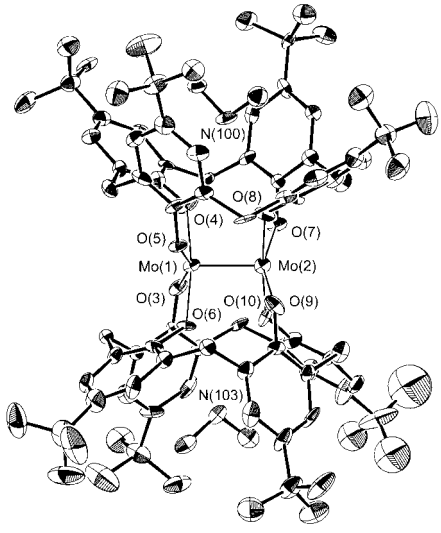

Fig. 1 An ORTEP drawing of **1** (M = Mo) showing the atom numbering scheme. Selected bond lengths (Å) and bond angles (°): Mo(1)–Mo(2) 2.194(2), Mo(1)–O(3) 2.033(7), Mo(1)–O(4) 1.959(8), Mo(1)–O(5) 2.009(7), Mo(1)–O(6), 1.968(7), Mo(2)–O(7) 2.035(7), Mo(2)–O(8) 1.989(7), Mo(2)–O(9) 2.025(7), Mo(2)–O(10) 1.954(8); Mo(2)–Mo(1)–O(3) 101.6(2), Mo(2)–Mo(1)–O(4) 94.1(3), Mo(2)–Mo(1)–O(5) 101.9(2), Mo(2)–Mo(1)–O(6) 94.5(2), Mo(1)–Mo(2)–O(7) 102.2(2), Mo(1)–Mo(2)–O(8) 92.1(2), Mo(1)–Mo(2)–O(9) 100.7(2), Mo(1)–Mo(2)–O(10) 92.8(2).

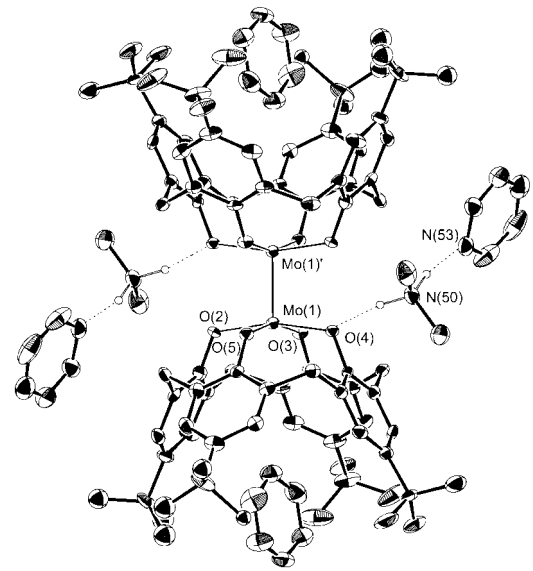

Fig. 2 An ORTEP drawing of **2**·4py (M = Mo) showing the atom numbering scheme. Selected bond lengths (Å) and bond angles (°): Mo(1)–Mo(1′) 2.226(1), Mo(1)–O(2) 2.009(4), Mo(1)–O(3) 1.975(4), Mo(1)–O(4) 2.028(4), Mo(1)–O(5) 1.973(4); Mo(1′)–Mo(1)–O(2) 97.9(1), Mo(1′)–Mo(1)–O(3) 98.8(1), Mo(1′)–Mo(1)–O(4) 97.1(1), Mo(1′)–Mo(1)–O(5) 100.1(1). The molecule has a crystallographically imposed inversion center.

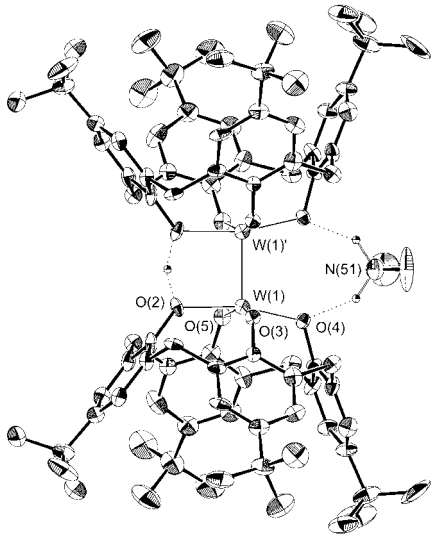

Fig. 3 An ORTEP drawing of **4** (M = W) showing the atom numbering scheme. Selected bond lengths (Å) and bond angles (°): W(1)–W(1′) 2.3039(8), W(1)–O(2) 2.066(6), W(1)–O(3) 1.947(6), W(1)–O(4) 1.973(6), W(1)–O(5) 1.959(6); W(1′)–W(1)–O(2) 90.5(2), W(1′)–W(1)–O(3) 99.6(2), W(1′)–W(1)–O(4) 102.8(2), W(1′)–W(1)–O(5) 98.8(2). The molecule has a crystallographically imposed mirror plane.

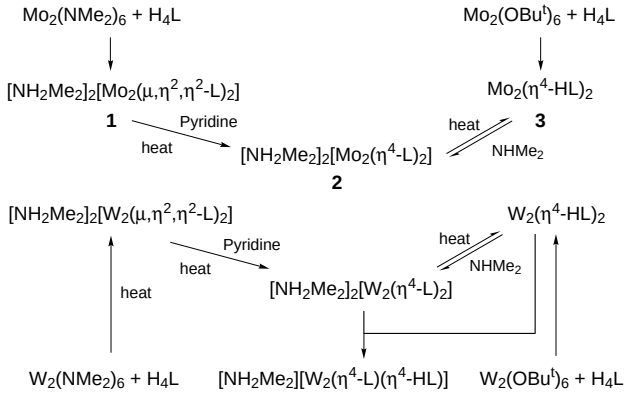

Scheme 1

pyridine as well as $NHMe_2$ leaving behind the complex $M_2(\eta^4\text{-}HL)_2$ **3** (M = Mo) as evidenced by NMR spectroscopy. Complex **3**, as well as its tungsten analogue $W_2(\eta^4\text{-}HL)_2$, can also be prepared from the reaction of $M_2(OBu^t)_6$ (M = Mo, W) with H_4L.‡

The addition of $NHMe_2$ to **3** (M = Mo, W) in benzene leads to **2** (M = Mo, W).‡ In the case of M = W, the reaction between **2** and **3** in a 1:1 ratio gives the pale green compound $[NH_2Me_2][W_2(\eta^4\text{-}L)(\eta^4\text{-}HL)]$ **4**, which has the structure shown in Fig. 3.§ These reactions are summarized in Scheme 1 and reveal the fascinating substitution chemistry resulting from reactions involving $(M{\equiv}M)^{6+}$ complexes (M = Mo, W) and the *p- tert*-butylcalix[4]arene ligand.

We thank the National Science Foundation for support of the work.

Notes and References

* E-mail: chisholm@indiana.edu

† This ChemComm is also available in enhanced multi-media format *via* the World Wide Web: http://www.rsc.org/ccenhanced

‡ *Syntheses and spectroscopic data*: **1** (M = Mo): the reaction mixture of $Mo_2(NMe_2)_6$ (280 mg, 0.60 mmol) and H_4L (650 mg, 1.00 mmol) in 15 ml of benzene was stirred at room temp. overnight. The volatile components were removed *in vacuo* and the residue was suspended in hexanes to give a green precipitate **1**, which was collected and dried *in vacuo* (685 mg, yield: 90%). Crystals of **1**·4thf (M = Mo) suitable for X-ray analysis were obtained by slow evaporation of a thf solution. Selected ^{1}H NMR data (300 MHz, C_6D_6): δ 7.29 (br, 8 H), 6.93 (br, 8 H), 6.46 (d, 4 H), 3.59 (d, 4 H), 3.27 (d, 4 H), 2.89 (d, 4 H), 1.22 (br, 72 H), 0.79 (t, 12 H).

1 (M = W): the same procedure as **1** (M = Mo) except stirring the mixture with refluxing (yield: 63%). Selected ^{1}H NMR data (300 MHz, C_6D_6): δ 7.30 (d, 8 H), 6.96 (d, 8 H), 6.51 (d, 4 H), 3.61 (d, 4 H), 3.57 (d, 4 H), 3.03 (d, 4 H), 1.22 (br, 72 H), 0.67 (t, 12 H).

2 (M = Mo): a green solution of **1** (M = Mo) (260 mg, 0.17 mmol) in 8 ml of pyridine was refluxed for 0.5 h, the resulting amber solution was cooled and allowed to stand at room temp. overnight to yield amber crystals of **2**·4py (M = Mo) (203 mg, yield: 65%), which were suitable for X-ray analysis. Selected ^{1}H NMR data (300 MHz, C_6D_6): δ 7.24 (s, 16 H), 5.29 (d, 8 H), 3.34 (d, 8 H), 1.58 (s, 12 H), 1.23 (s, 72 H). Yellow solid **2** (M = Mo) can be also prepared by addition of an excess of $NHMe_2$ to **3** (M = Mo).

3 (M = Mo): a reaction mixture of $Mo_2(OBu^t)_6$ (202 mg, 0.32 mmol) and H_4L (326 mg, 0.50 mmol) in 10 ml of toluene was stirred at room temp. for 2 days. The volatile components were removed *in vacuo* and the residue was suspended in hexanes to give a pale brown precipitate **3** (M = Mo), which was collected and dried *in vacuo* (336 mg, yield: 91%). Selected ^{1}H NMR data (300 MHz, C_6D_6): δ 7.09 (s, 16 H), 5.17 (d, 8 H), 3.39 (d, 8 H), 1.12 (s, 72 H).

3 (M = W): the same procedure as **3** (M = Mo), (yield: 86%). Selected ^{1}H NMR data (300 MHz, C_6D_6): δ 7.10 (s, 16 H), 5.14 (d, 8 H), 3.39 (d, 8 H), 1.12 (s, 72 H).

2 (M = W): $NHMe_2$ (2.4 mmol) was added to the frozen reddish brown solution of **3** (M = W) (480 mg, 0.29 mmol) at −196 °C employing a calibrated gas manifold. After the solution was warmed to room temp., the green precipitate **2** (M = W) was collected and dried *in vacuo* (482 mg, yield: 95%).

4 (M = W): a reaction mixture of **2** (M = W) (105 mg, 0.060 mmol) and **3** (M = W) (100 mg, 0.060 mmol) in 10 ml of benzene was stirred at room temp. The green solid was gradually dissolved in solution, and the brown solution turned green. After 3 h, the volatile components were removed *in vacuo* and the residue was suspended in hexanes to give a pale green precipitate **4** (M = W), which was collected and dried *in vacuo* (186 mg, yield: 89%). Recrystallization in benzene afforded green crystals of **4**·7C_6H_6 (M = W) suitable for X-ray analysis. Selected ^{1}H NMR data (300 MHz, C_6D_6): δ 7.20 (s, 16 H), 5.18 (d, 8 H), 3.42 (d, 8 H), 1.45 (br, 6 H), 1.20 (s, 72 H).

§ *Crystal data*: for **1**·4thf (M = Mo): T = −170 °C monoclinic, space group $P2_1$, a = 13.105(4), b = 18.631(6), c = 20.543(6) Å, β = 94.04(2)°, Z = 2. Final residuals are $R(F)$ = 0.067 and $R_w(F)$ = 0.066 using 7500 observed data.

For **1**·*x*thf (M = W): T = −170 °C: a = 13.08(2), b = 18.61(3), c = 20.60(3) Å, β = 94.03(3)°. Collection of diffraction data was not processed because of the poor quality of the crystal.

For **2**·4py (M = Mo): T = −170 °C, monoclinic, space group $P2_1/n$, a = 12.384(2), b = 22.130(3), c = 18.621(3) Å, β = 100.26(1)°, Z = 2. Final residuals are $R(F)$ = 0.059 and $R_w(F)$ = 0.058 using 4799 observed data.

For **4**·7C_6H_6 (M = W): T = −168 °C, orthorhombic, space group *Pnma*, a = 25.421(3), b = 34.611(3), c = 13.113(1) Å, Z = 4. Final residuals are $R(F)$ = 0.058 and $R_w(F)$ = 0.052 using 6231 observed data. CCDC 182/704.

Full crystallographic data are also available from the Reciprocal Data Base *via* Internet at URL http://www.iumsc.indiana.edu. Request data and files for 97055 for **1**·4thf (M = Mo), 97056 for **2**·4py (M = Mo) and 97064 for **4**·7C_6H_6 (M = W).

1 L. Giannini, E. Solari, A. Zanotti-Gerosa, C. Floriani, A. Chiesi-Villa and C. Rizzoli, *Angew. Chem., Int. Ed. Engl.*, 1997, **36**, 753.
2 J. A. Acho and S. J. Lippard, *Inorg. Chim. Acta*, 1995, **229**, 5; J. A. Acho, T. Ren, J. W. Yun and S. J. Lippard, *Inorg. Chem.*, 1995, **34**, 5226.
3 F. A. Cotton and R. A. Walton, *Multiple Bonds Between Metal Atoms*, Oxford University Press, New York, 2nd edn., 1993.
4 M. H. Chisholm, J.-H. Huang, J. C. Huffman and I. P. Parkin, *Inorg. Chem.*, 1997, **36**, 1642; M. H. Chisholm, K. Folting, W. E. Streib and D.-D. Wu, *Inorg. Chem.*, 1998, in press.
5 *Cf.* proximal and distal NMe group in $Mo_2(NMe_2)_6$: M. H. Chisholm, F. A. Cotton, B. A. Frenz, W. W. Reichert, L. W. Strive and R. R. Stultz, *J. Am. Chem. Soc.*, 1976, **98**, 4469.

Received in Cambridge, UK, 29th July 1997; revised manuscript received 17th November 1997; 7/08268A

Molecular structure of the unusual tris(tribromoindate)methane anion, $[HC(InBr_3)_3]^{3-}$

José Arimateia Nobrega,[a] Clovis Peppe,[a] Martyn A. Brown[b] and Dennis G. Tuck[b]

[a] *Departamento de Química-CCEN, Universidade Federal da Paraiba, 58.059-900, Joaõ Pessoa-PB, Brazil*
[b] *Department of Chemistry and Biochemistry, University of Windsor, Windsor, Ontario, Canada N9B 3P4*

The title molecule, which is obtained as the tetraphenylphosphonium salt following the reaction of InBr and $HCBr_3$, is shown to involve pseudo-tetrahedral carbon and indium(III) sites; it is a member of a series of related $[H_{4-n}C(InBr_3)_n]^{n-}$ anions.

There is increasing interest in the synthesis and structural investigation of complexes in which metal atoms cluster around a centre which may be metallic or non-metallic. Schmidbaur[1] has reviewed his extensive work on molecules in which $[(R_3P)Au]^+$ and similar gold(I) cations are bonded to a large variety of such centres, and has emphasized the important isolobal relationship between LAu^+ and the H^+ and R^+ cations.[2]

In earlier papers, the reactions of indium(I) halides (InX, X = Cl, Br, I) with halogenomethanes were shown to proceed *via* oxidative addition to give neutral derivatives of X_2InCH_2X and $X_2InCH_2InX_2$ and the anionic complexes $[X_3InCH_2X]^-$ and $[H_2C(InX_3)_2]^{2-}$ have also been reported, although not for all X.[3,4] We have now prepared the salt $[PPh_4]_3[HC(InBr_3)_3]$, and established its structure. The room temperature reaction between InBr and $CHBr_3$ (1 : 3 mole ratio, mmol quantities) in 1,4-dioxane (diox) gave, on work-up, a colourless solid, shown to be the 1 : 1 adduct $Br_2InCHBr_2$·diox. (Calc. for $C_5H_9O_2Br_4In$, In 21.4. Found: In 21.2%) ^{1}H NMR [$(CD_3)_2SO$] δ 5.36 (s, 1 H, CH), 3.60 (m, 8 H, diox). ^{13}C NMR [$(CD_3)_2SO$] δ 37.31 (CH), 67.77 (diox). This was redissolved in dioxane and treated with 2 equiv. of InBr, to give an oil, which was dissolved in acetonitrile; addition of PPh_4Br, concentration and crystallization from MeCN–ethanol gave $[PPh_4]_3[HC(InBr_3)_3]$ **1** in 84% yield.† It seems very probable that the reaction proceeds by successive oxidative additions, with the related $Br_2InCHBr_2$ and $(Br_2In)_2CHBr$ species as intermediates.

The structure of the anion of **1** is shown in Fig. 1.‡ The In–Br bond distances are similar to those for other inorganic and organometallic compounds of indium(III) [*e.g.* $InBr_4^-$, r = 2.479(2);[5] $Br_3InCH_2PPh_3$, r = 2.512(2);[3] Br_3InCH_2(tmtu), r = 2.517(6) Å (tmtu = 1,1,3,3-tetramethyl-2-thiourea)[6]], as are the In–C distances; the lengthening of the In–Br bonds relative to those in the neutral ylide adducts is ascribed to the repulsive effect of the triple negative charge on this molecule. The sum of the angles in a tetrahedral MX_4 molecule is 657°, and in the present case the corresponding sums at the three indium atoms are 655.1, 655.5 and 654.4°, respectively, so that these are pseudo-tetrahedral sites, as in the molecules previously noted. The In–C–In angles lead to a similar conclusion for the carbon atom of this molecule.

This anion can be regarded as a member of the series $[H_{4-n}C(InBr_3)_n]^{n-}$. The salts of $H_3CInX_3^-$ have been known for some time,[7] and crystallographic studies of $[H_3CInCl_3]^-$ and $[C_2H_5InI_3]^-$ have confirmed the pseudo-tetrahedral symmetry at metal and carbon atoms in such anions.[8,9] As noted above, the anions $[H_2C(InX_3)_2]^{2-}$ have also been prepared; the structure of the neutral adducts such as (tmen)$Cl_2InCH_2InCl_2$(tmen) (tmen = *N*,*N*,*N*′,*N*′-tetramethylethanediamine) demonstrates the presence of the central $H_2C(InX_2)_2$ group.[10] The series is therefore complete except for n = 4; work on this is proceeding.

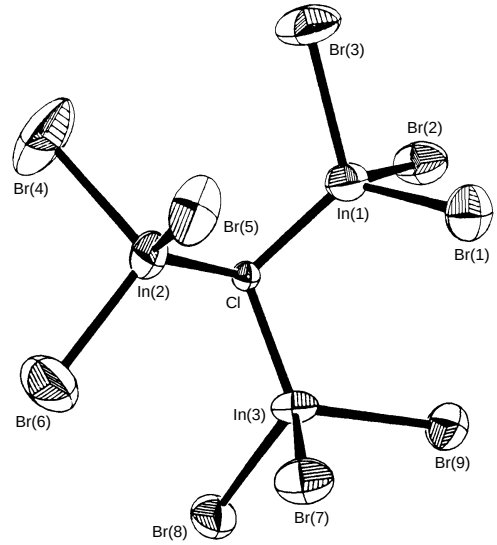

Fig. 1 Molecular structure of the $[HC(InBr_3)_3]^{3-}$ anion, showing 30% probability ellipsoids. Selected bond distances (Å) and bond angles (°): In(1)–Br (av.) 2.545, In(2)–Br (av.) 2.526, In(3)–Br(av.) 2.546, overall In–Br range 2.518(6)–2.560(5), In–C 2.11(3), 2.13(3), 2.17(3); Br–In(1)–Br (av.) 103.0, Br–In(2)–Br (av.) 104.0, Br–In(3)–Br 102.1, overall range 98.9 (2)–106.92(2), In–C–In 115(2), 112(1), 113(1).

It seems probable that similar series can be prepared with other metallo-ligands of main group elements. In particular, some members of the series of tin compounds $H_{4-n}C(SnMe_3)_n$ are already known, and analogous sets of related compounds are easily formulated, at least on paper. We also note the existence of complexes such as $[Pt(SnCl_3)_5]^{3-}$, in which the trichlorostannate group acts as an anionic ligand, and it could well be that analogous species with InX_3^- ligands will be accessible.

This work was supported in part by operating grants (to C. P.) for the Conselho Nacional de Desenvolvimento Cientifico e Tecnologico do Brasil, and by Research Grants (to D. G. T.) from the Natural Sciences and Engineering Research Council of Canada. J. A. Nobrega thanks CAPES (Brazil) for the award of a scholarship.

Notes and References

* E-mail: dgtuck@uwindsor.ca

† *Elemental analysis*. Calc. for $C_{73}H_{61}Br_9In_3P_3$: C 41.9; H, 2.93; Br, 34.3; In, 16.4. Found C, 41.8; H, 3.07; Br, 34.0; In, 16.0%. ^{1}H NMR [$(CD_3)_2SO$] δ 8.01–7.71 (m, 60 H, C_6H_5), 0.20 (s, 1 H, In_3CH). ^{13}C NMR (CD_3CN) δ 135.27 [d, J(PC_p) 2.68 Hz], 134.41 [d, J(PC_o) 10.56 Hz], 130.38 [d, J(PC_m) 12.82 Hz], 117.57 [d, J(PC_i) 88.90 Hz]. No ^{13}C resonance was detected for the In_3CH atom, and this is ascribed to the immediate presence of high-spin indium atoms (^{115}In, I = 9/2); similar problems have been reported for related organoindium compounds.[3,6]

‡ The diffraction experiment at 23 °C on a Rigaku AFC6S instrument, using graphite monochromated Mo-Kα radiation, (λ = 0.710 69 Å), $2\theta_{max}$ = 45°, structure solution by Patterson method, refinement against F^2 of data with redundants removed. *Crystal data*: $C_{73}H_{61}Br_9In_3P_3$, M = 2094.8, triclinic, space group $P\bar{1}$ (no. 2), a = 14.609(6), b = 22.468(12), c = 12.109(7) Å, α = 101.91(4), β = 108.59(4), γ = 90.11(4)°, U = 4004(3) Å^3, Z = 2. D_c = 1.74 g cm^{-3}, T = 32.38 cm^{-1}, crystal size 0.5 × 0.4 × 0.5 mm., 9207 reflections total, 8708 unique, 2849 observed, R = 0.063, 429 variables, R_w = 0.058, goodness of fit 2.15, max., min. peaks on final difference map = 1.65, −0.85 e Å^{-3}. CCDC 182/733.

1 H. Schmidbaur, *Chem. Soc. Rev*., 1995, **24**, 391.
2 R. Hoffmann, *Angew. Chem., Intl. Ed. Engl*., 1982, **21**, 711.
3 T. A. Annan, D. G. Tuck, M. A. Khan and C. Peppe, *Organometallics*, 1991, **10**, 2159.
4 M. A. M. A. Maurera, C. Peppe and D. G. Tuck, unpublished work.
5 M. A. Khan and D. G. Tuck, *Acta Crystallogr., Sect. B*, 1982, **38**, 803.
6 A. C. de Souza, C. Peppe, Z. Tian and D. G. Tuck, *Organometallics*, 1993, **12**, 3354.
7 D. G. Tuck, *Comprehensive Organometallic Chemistry*, ed. G. Wilkinson, Pergamon, Oxford, 1983, vol. 1, p. 683.
8 H. J. Guder, W. Schwartz, J. Weidlein, H. J. Widler and H. D. Hausen, *Z. Naturforsch., Teil B*, 1976, **31**, 1185.
9 M. A. Khan, C. Peppe and D. G. Tuck, *J. Organomet. Chem*., 1985, **280**, 17.
10 M. A. Khan, C. Peppe and D. G. Tuck, *Organometallics*, 1986, **5**, 525.

Received in Bloomington, IN, USA, 7th August 1997, revised manuscript received 17th November 1997; 7/08869H

New synthesis of Fischer-type hydrazino(alkyl) complexes. First X-ray characterisation of a chelate hydrazino derivative

Emanuela Licandro,*[a] Stefano Maiorana,[a]† Raffaella Manzotti,[a] Antonio Papagni,[a] Dario Perdicchia,[a] Mary Pryce,[b] Antonio Tiripicchio*[c] and Maurizio Lanfranchi[c]

[a] *Dipartimento di Chimica Organica e Industriale, Università degli Studi di Milano, via C. Golgi, 19, I-20133 Milan, Italy*
[b] *School of Chemical Sciences, Dublin City University, Dublin 9, Ireland*
[c] *Dipartimento di Chimica Generale ed Inorganica, Chimica Analitica, Chimica Fisica, Università di Parma, Centro di Studio per la Strutturistica Diffrattometrica del CNR, viale delle Science, I-43100 Parma, Italy*

The first Fischer-type hydrazino(methyl)carbene complex has been synthesized from the appropriate acetylhydrazine and $Na_2Cr(CO)_5$; the new complex has some peculiar features in comparison with aminocarbene complexes: (i) the *E* rotamer can be completely transformed into the *Z* rotamer through the formation of its anion, and (ii) as a result of a thermal reaction, the *Z* isomer affords a new unusual chelate hydrazino(methyl)carbene complex that can be mono- or di-alkylated.

Only a few hydrazinocarbene complexes have so far been reported in the literature.[1] This is certainly due to the very limited applicability of the hydrazinolysis reaction of alkoxycarbenes,[2] which seems to be partially successful only in the case of alkynyl carbene complexes.[1b]

Alkyl(hydrazino)carbene complexes are unknown and could in principle have some unique features due to the potential of the β-nitrogen of the hydrazine moiety as a coordinating group to the metal, and the influence of this coordination on the stereodynamic properties of the complex and the reactivity of the α-carbanions.

We here report the synthesis of the first hydrazino(methyl)carbene complex **1**, its thermally promoted transformation, and the reaction of its anion with electrophiles. The

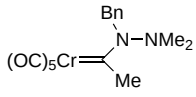

1

apparently simple but long-standing problem associated with the controlled synthesis of alkyl (hydrazino)carbene complexes has been solved by extending the known Hegedus method[3] for preparing amino carbene complexes from amides to hydrazide derivatives. The hydrazide **2** was reacted with disodium pentacarbonylchromate,[3] affording complex **1** as a 1 : 1.3 *E* : *Z* rotameric mixture (Scheme 1).‡ The (*E*)-**1** and (*Z*)-**1** rotamers were fully characterized after chromatographic separation over silica gel. Rotamer (*E*)-**1** proved to be thermally stable, remaining unchanged after heating in hexane at 50 °C for 2 h whereas, after heating at 39 °C in CH_2Cl_2 for 3.5 h, (*Z*)-**1** was transformed into a new, red–orange solid complex, **3**‡ with the

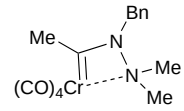

3

displacement of a CO ligand. As far as we know, only one example of an *N*-chelate complex with a four-membered ring has been previously reported.[4] The structure of **3** was supported by the X-ray analysis of the structure of the homologue **5a**§ whose formation is described below (Scheme 2). The pure rotamers (*E*)-**1** and (*Z*)-**1** were treated with Bu^nLi at −70 °C and quenched with a saturated aq. NH_4Cl; rotamer (*E*)-**1** was completely transformed into rotamer (*Z*)-**1**, whereas the latter proved to be configurationally stable. The complete conversion of (*E*)-**1** into (*Z*)-**1** is rather surprising since this transformation is usually incomplete in aminocarbene complexes and generally leads to a mixture of the two rotamers. The treatment of the anion generated from the pure (*E*)-**1** or (*Z*)-**1** rotamers with alkylating reagents such as iodomethane and allyl bromide gave the expected ethyl(hydrazino)carbene complexes (*Z*)-**4a** and (*Z*)-**4b**, together with the tetracarbonyl *N*-chelate derivatives **5a** and **5b** (Scheme 2).‡ It can be seen that the formation of the coordinated derivatives **3**, **5a** and **5b** is easier as the bulk of the α- substituent increases (Me < Et < allyl). Column chromatography over silica gel gave pure samples of the complexes **5a** and **5b**, whereas complexes **4a** and **4b** were always recovered in the form of mixtures with **5a** and **5b** respectively.‡ Unlike an amino(ethyl)carbene complex, the ethyl(hydrazino)carbene **5a** can easily be further alkylated with MeI to give complex **6** (Scheme 3).‡ Compound **5a** is the first structurally characterized chelate hydrazinocarbene complex (see Fig. 1). The coordination around Cr is distorted octahedrally, with the organic moiety acting as a chelating ligand through N(1) and C(5). The four-membered ring is planar, and the chelation N(1)–Cr–C(5) angle is very narrow at 62.9(2)°. Although the Cr–N bond length of 2.211(4) Å is comparable with the average

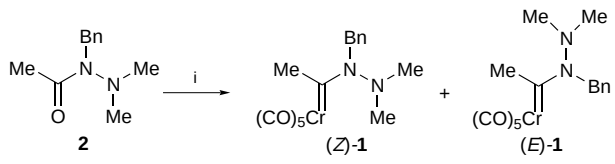

Scheme 1 *Reagents and conditions*: i, $Na_2Cr(CO)_5$ (2 equiv.), anhydrous THF, N_2, −78 °C, 40 min, allowed to warm to 0 °C, 4 h, then cooled to −78 °C, Me_3SiCl (3 equiv.), −78 °C, 30 min, then Al_2O_3 (45 g on a base of 0.61 g of **2**), 45 min, then chromatographic separation on silica gel to give (*E*)-**1** (0.32 g) and (*Z*)-**1** (0.36 g), eluent light petroleum–CH_2Cl_2 8 : 2 (overall yield 59%)

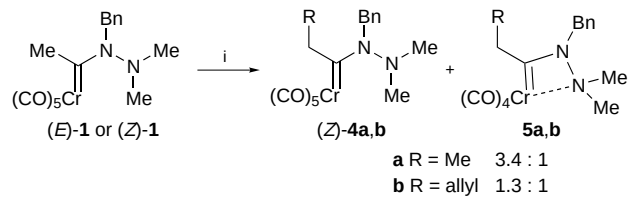

Scheme 2 *Reagents and conditions*: Bu^nLi (1 equiv.), THF, N_2, −78 °C, 30 min, then RX, −78 °C, 10 min, 0 °C, 30 min

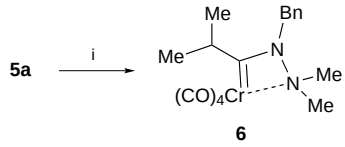

Scheme 3 *Reagents and conditions*: Bu^{n}Li (1 equiv.), THF, N_2, −78 °C, 30 min, then MeI, −78 °C, 10 min then 0 °C, 20 min, then room temp., 10 min

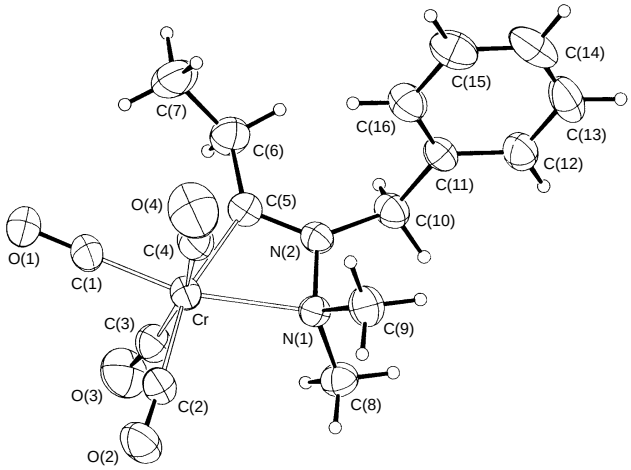

Fig. 1 View of the molecular structure of complex **5a** together with the atomic numbering system. Selected bond distances (Å) and angles (°): Cr–C(5) 2.028(4), Cr–N(1) 2.221(4), C(5)–N(2) 1.308(7), N(1)–N(2) 1.451(5), N(2)–C(10) 1.481(6), C(5)–C(6) 1.494(7); N(1)–Cr–C(5) 62.9(2), Cr–C(5)–N(2) 101.3(3), Cr–N(1)–N(2) 88.5(2), N(1)–N(2)–C(5) 107.3(3), N(1)–N(2)–C(10) 120.8(3), C(5)–N(2)–C(10) 131.8(4).

value found in complexes of Cr^0 with tertiary amines (2.21 Å), the 2.028(4) Å Cr–C(5) bond length is much shorter than those found in aminocarbene complexes of Cr^0 (in the range of 2.123–2.156 Å).[5] This means that the Cr–C(5) bond has a more noticeably double bond character than the other aminocarbene complexes. It is also worth noting that the 1.813(6) Å Cr–C(1) bond involving the carbonyl *trans* to the aminic N(1) atom is shorter than other Cr–C(carbonyl) bonds [in the range 1.871(5)–1.882(5) Å].

We thank the M.U.R.S.T. and the C.N.R. of Rome, and the European community (HCM Programme, contract ERBCHRXCT940501), for their financial support.

Notes and References

† E-mail: maior@icil64.cilea.it

‡ *Selected data* for (*E*)-**1**: mp 57 °C (decomp.); δ_H (300 MHz, $CDCl_3$) 2.45 [s, 6 H, $N(CH_3)_2$], 3.05 (s, 3 H, CH_3), 5.55 (s, 2 H, CH_2Ph), 7.40–7.20 (m, 5 H, arom); δ_C (300 MHz, $CDCl_3$) 39.6 (q, CH_3), 44.3 [q, $N(CH_3)_2$], 56.2 (t, CH_2), 126.6, 128.0, 128.8 (arom), 135.6 (s, arom), 217.6 (s, CO *cis*), 223.4 (s, CO *trans*), 277.5 (s, C=Cr); *m/z* (EI) 368 [M^+]. For (*Z*)-**1**: mp 85 °C; δ_H (300 MHz, $CDCl_3$) 2.65 [s, 6 H, $N(CH_3)_2$], 2.70 (s, 3 H, CH_3), 4.95 (s, 2 H, CH_2Ph), 7.40–7.20 (m, 5 H, arom); δ_C (300 MHz, $CDCl_3$) 39.1 (q, CH_3), 44.2 [q, $N(CH_3)_2$], 48.9 (t, CH_2), 125.2, 127.8, 129.3 (arom), 133.5 (s, arom), 218.4 (s, CO *cis*), 225.2 (s, CO *trans*), 280.6 (s, C=Cr); *m/z* (EI) 368 [M^+]. For **3**: mp 123–6 °C; *ν* (Nujol)/cm^{-1} 1997, 1888–1830 (CO); δ_H (80 MHz, $CDCl_3$) 2.73 (s, 3 H, CH_3), 2.78 [s, 6 H, $N(CH_3)_2$], 4.65 (s, 2 H, CH_2Ph), 7.05–7.55 (m, 5 H, arom); *m/z* (FAB+) 340 [M^+]. For **5a**: mp 120 °C (decomp.); *ν* (Nujol)/cm^{-1} 1998 (CO *trans*), 1917–1803 (CO *cis*); δ_H (80 MHz, $CDCl_3$) 1.50 (t, 3 H, CH_2CH_3), 2.65 (q, 2 H, CH_2CH_3), 2.80 [s, 6 H, $N(CH_3)_2$], 4.65 (s, 2 H, CH_2Ph), 7.10–7.45 (m, 5 H, arom); δ_C (300 MHz, $CDCl_3$) 13.0 (q, CH_3), 34.7 (q, CH_3), 49.1 (t, CH_2), 52.3 [q, $N(CH_3)_2$], 126.1, 128.5, 129.5 (arom), 133.5 (s, arom), 218.5 (s, 2CO *cis*), 230.1 (s, CO *cis*), 232.2 (s, CO *trans*), 294.7 (s, C=Cr); *m/z* (FAB+) 354 [M^+]. Spectroscopic and analytical data for complexes **4a**, **4b**, **5b** and **6** are in line with the reported structure.

§ *Crystal data* for **5a**: $C_{16}H_{18}CrN_2O_4$, M_r = 354.32, monoclinic, space group *C*2/*c*, *a* = 21.346(6), *b* = 12.782(4), *c* = 14.136(4) Å, *β* = 113.70(2)°, *V* = 3532(2) Å^3, *Z* = 8, ρ_{calc} = 1.333 Mg m^{-3}, *F*(000) = 1472, *λ* = 1.54184 Å, *μ*(Cu-Kα) = 5.507 mm^{-1}. Crystal dimensions: 0.15 × 0.21 × 0.33 mm. The intensity data were collected by means of a Siemens AED diffractometer using the *θ*–2*θ* scan technique at room temperature. 3494 reflections were measured (with *θ* in the range 3–70°) of which 3357 were independent and included in the structural refinement. Correction for absorption was applied (maximum and minimum values for the transmission coefficient were 1.000 and 0.637). The structure was solved by means of direct and Fourier methods, and refined using full-matrix least-squares procedures (based on F_o^2), with anisotropic thermal parameters in the last cycles of refinement for all of the non-hydrogen atoms. The hydrogen atoms were introduced into the geometrically calculated positions and refined riding on the parent atoms. The refinement converged at wR_2 = 0.1579 for all data, and 209 variables [R_1 = 0.0506 for 1603 reflections with $I > 2\sigma(I)$]; min/max residual electron density: −0.356/0.408 e Å^{-3}. The SHELXS-86 and SHELXL-93 computer programs were used (ref. 6). CCDC 182/726.

1 (*a*) H. Fischer and G. Roth, *J. Organomet. Chem.*, 1995, **490**, 229; (*b*) R. Aumann, B. Jasper and R. Fröhlich, *Organometallics*, 1995, **14**, 2447.
2 E. O. Fischer and R. Aumann, *Chem. Ber.*, 1968, **101**, 963.
3 R. Imwinkelried and L. S. Hegedus, *Organometallics*, 1988, **7**, 702.
4 K. H. Dötz and C. G. Kreiter, *Chem. Ber.* , 1976, **109**, 2026.
5 J. A. Connor and O. S. Mills, *J. Chem. Soc. A*, 1969, 334; H. Rudler, A. Parlier, R. Yefsah, B. Denise, J.-C. Daran, J. Vaissermann and C. Knobler, *J. Organomet. Chem.*, 1988, **358**, 245; R. Aumann, S. Althaus, C. Kruger and P. Betz, *Chem. Ber.*, 1989, **122**, 357; A. Parlier, N. Rudler, H. Rudler, R. Goumont, J.-C. Daran and J. Vaissermann, *Organometallics*, 1995, **134**, 2760.
6 G. M. Sheldrick, SHELXS-86 Program for the solution of crystal structures, University of Göttingen, 1986; SHELXL-93 Program for crystal structure refinement, University of Göttingen, 1993.

Received in Liverpool, UK, 6th November 1997; 7/08018B

On the origin of the *endo*/*exo* selectivity in Diels–Alder reactions

D. Suárez and J. A. Sordo*

Departamento de Química Física y Analítica, Facultad de Química, Universidad de Oviedo, Julián Clavería 8, 33006 Oviedo, Principado de Asturias, Spain

The *endo*/*exo* selectivity in Diels–Alder reactions is analyzed in terms of the pre-reactive van der Waals complexes located on the potential energy surface.

The Diels–Alder reaction has been the subject of a wide variety of both experimental and theoretical studies.[1] Of particular relevance from the mechanistic viewpoint is the explanation of the observed *endo*/*exo* selectivity. As established from the very beginning, there is usually a preference for the *endo* adducts (*endo* Alder rule[2]). Such an *endo* preference has been ascribed to quite different factors.[3] On the other hand, the first documented example of regiospecifity of Diels–Alder reactions being primarily controlled by the dispersion (attractive van der Waals) interactions has been recently reported by Cioslowski *et al.*[4] Additional work in this direction was announced by Gillies *et al.*[5b]

The above explanations have in common that they all focus on the transition structures. The impressive advances in the last two decades leading to the development of rather sophisticated spectroscopic techniques, including Raman, microwave and infrared spectrocopies,[5c] have made it possible to gain a deeper insight into the nature of van der Waals interactions, and it has been recently recognized[5b] that the formation of van der Waals systems in the very early (pre-reactive) stages of certain cycloaddition reactions can exert a significant influence upon the stereochemical outcome. Gillies *et al.* concluded[5b] that it is possible to relate the geometry of van der Waals intermediates to the geometry of the transition structure and the product of certain cycloaddition reactions. Recent findings using intermolecular perturbation theory[6] seem to provide further support to this point. Here, theoretical evidence is presented showing the important role that pre-reactive van der Waals complexes, present in the potential energy surface, might play in determining the stereochemical outcome of Diels–Alder reactions. The prototype reaction between cyclopentadiene and maleic anhydride has been investigated.

The geometries of the significant structures located at the MP2/6-31G* level on the potential energy surface of the Diels–Alder reaction between cyclopentadiene and maleic anhydride: three van der Waals intermediates (**vdW1** and **vdW2**, leading to the *endo* and *exo* transition structures, respectively, and **vdW3**, showing a T-shaped structure intermediate between **vdW1** and **vdW2**), two van der Waals transition structures connecting **vdW1** and **vdW3** (**vdW1** → **3**) and **vdW2** and **vdW3** (**vdW2** → **3**), and two transition structures leading to the *endo* (**TS1**) and *exo* (**TS2**) products (**P1** and **P2**), are not presented because of space limitations but are available upon request. All these structures were characterized by computing the Hessian matrix (at the HF level) and checking the sign of the corresponding eigenvalues. Table 1 collects the energy results, which include single-point calculations at the MP4SDQ/6-31G* level and an estimate of the solvent effects. In cycloaddition reactions between ethylene and ozone, occurring both in the gas phase and in condensed media, a van der Waals (pre-reactive) intermediate was experimentally detected in the gas phase[5] (where rather sophisticated spectroscopic techniques are available). It is difficult to make *a priori* predictions about the role played by different solvents on the stabilization/destabilization[7a] (a detailed discussion on this point for a reaction involving a *zwitterionic* intermediate can be found elsewhere[7b]) of these van der Waals intermediates (exploratory calculations using a model where the solvent is represented by a dielectric continuum characterized by its static dielectric permittivity[7c] ε_0, suggest that the energy changes introduced by the solvent are not too drastic, see Table 1, but there is experimental evidence for the important role played by van der Waals interactions in Diels–Alder reactions in solution.[4]

In Fig. 1 a simplified scheme of the potential energy surface is presented. Examination of this figure suggests that the van der Waals structures might play a decisive role in determining the stereochemical outcome of Diels–Alder reactions. Indeed, the *endo*/*exo* ratio is related to the barrier $\Delta\Delta E^{\neq}$(**vdW**) = [E(**TS2**) − E(**vdW2**)] − [E(**TS1**) − E(**vdW1**)]. If the van der Waals structures were not present in the potential energy surface the *endo*/*exo* ratio should be computed as $\Delta\Delta E^{\neq}$(**R**) = [E(**TS2**) − E(**R**)] − [E(**TS1**) − E(**R**)] (R = reactants). In the present case (at the MP4SDQ/6-31G*//MP2/6-31G* level of theory), $\Delta\Delta E^{\neq}$(**R**) = 2.1 kcal mol^{-1} (97.1% *endo* at 298 K) and $\Delta\Delta E^{\neq}$(**vdW**) = 2.6 kcal mol^{-1} (98.8% *endo* at 298 K); the greater stability of **vdW2** leading to the *exo* transition structure **TS2** enhances the *endo* preference. The experimental *endo* preference is[8] 2.5 kcal mol^{-1} (98.5% *endo* at 298 K). It is important to remark that, while $\Delta\Delta E^{\neq}$(**R**) is affected by the basis set superposition error (BSSE)[9] [consideration of the BSSE by means of the *counterpoise* procedure,[9] including fragment relaxation terms,[10] gives $\Delta\Delta E^{\neq}$(**R**) = 2.0 kcal mol^{-1} (96.5% *endo* at 298 K), moving away from the experimental

Table 1 Relative Energies (including zero point energy correction from HF/6-31G* frequencies) of van der Waals intermediates, transition structures and products with respect to reactants for the [4 + 2] cycloaddition reaction between cyclopentadiene and maleic anhydride. Geometries were optimized at the MP2/6-31G* theory level (single-point SCRF = self-consistent-reaction field calculations to estimate electrostatic solvent effects). Relative energies of the Diels–Alder transition structures with respect to the corresponding van der Waals intermediates are shown in parentheses

	Relative energy/kcal mol^{-1}		
	MP2/6-31G*	MP2/6-31G* (SCRF[a] ε_0 = 2.24[b])	MP4SDQ/6-31G*
vdW1 *endo*	−7.4	−7.0	−3.8
TS **vdW1** → **3**	−3.2	−2.9	−2.1
vdW3	−4.2	−3.8	−3.2
TS **vdW2** → **3**	−4.1	−3.7	−3.1
vdW2 *exo*	−6.6	−5.9	−4.3
[4 + 2] **TS1** *endo*	−0.4 (7.0)	−0.8 (6.2)	14.1 (17.9)
[4 + 2] **TS2** *exo*	1.9 (8.5)	1.8 (7.7)	16.2 (20.5)
[4 + 2] *endo* Adduct **P1**	−34.1	−33.8	−29.0
[4 + 2] *exo* Adduct **P2**	−34.5	−34.0	−29.6

[a] See ref. 7(*d*) for an excellent example of how the estimate of barriers in solution by means of single-point SCRF calculations are approximate but useful indicators of energetic trends. [b] A relative permittivity of 2.24 was used to simulate benzene, which has been used as solvent in this reaction (see ref. 8).

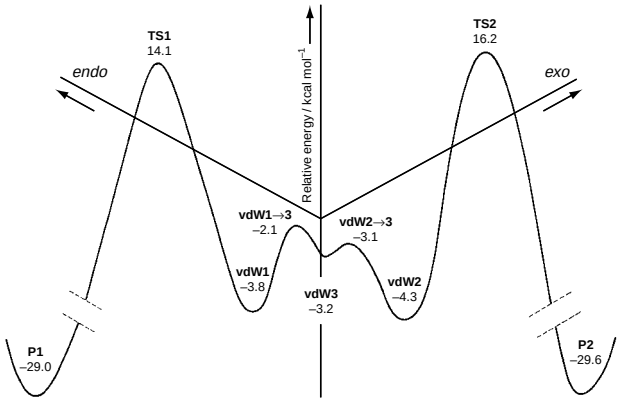

Fig. 1 Simplified scheme of the potential energy surface corresponding to the Diels–Alder reaction between cyclopentadiene and maleic anhydride

value], $\Delta\Delta E^{\neq}$(**vdW**) is BSSE free.[11]. It is important to stress at this point that the above results are consistent with the so-called Curtin–Hammett principle,[12] which states that when the barriers involving the **vdW** systems in Fig. 1 are much lower than the reaction barriers **TS1** and **TS2**, then the (*endo*/*exo*) product ratio depends only upon the difference in energy of the transition structures **TS1** and **TS2**. In the present case, the Curtin–Hammett principle should apply (see Fig. 1) and the *endo*/*exo* ratio could be estimated from $\Delta\Delta E^{\neq}$(**R**), in agreement with the above results [*i.e.* $\Delta\Delta E^{\neq}$(**vdW**) $\approx$ $\Delta\Delta E^{\neq}$(**R**)].

Although the difference between $\Delta\Delta E^{\neq}$(**R**) and $\Delta\Delta E^{\neq}$(**vdW**) is not (quantitatively) drastic in the present case, it must be stressed that a detailed inspection of the potential energy surface shows that consideration of the van der Waals structures is strictly needed to avoid serious topological inconsistencies in the computed potential energy surface. Indeed, at the MP2/6-31G* level, where optimizations were carried out, the **TS1** and **TS2** structures (without taking into account the zero-point energy correction) are energetically lower than reactants and higher than products (the energies relative to reactants are −2.3 and −0.1 kcal mol^{-1} for **TS1** and **TS2**, respectively). Therefore, if the van der Waals intermediates were not considered, **TS1** and **TS2** would not be maximums along the reaction paths and, consequently, they could not be real transition structures (saddle points separating two energy minima) in clear contradiction with the information provided by the Hessian matrix (see above). Of course, consideration of the van der Waals structures reported in this work indicates that **TS1** and **TS2** are saddle points connecting two minima (*i.e.* transition structures): **vdW1** and **P1**, and **vdW2** and **P2**, respectively (the energies of **TS1** relative to **vdW1**, and of **TS2** relative to **vdW2**, without considering the zero-point energy correction, are both positive: +7.4 and +9.1 kcal mol^{-1}, respectively).

Finally, we would like to make a short comment on the nature of the interaction in the van der Waals intermediates and transition structures. The application of a configurational analysis on the corresponding wave functions[13] shows that for **TS1** and **TS2** the most significant contributions, apart from the zero configuration AB (A = cyclopentadiene, B = maleic anhydride) come from the HOMO(cyclopentadiene) $\rightarrow$ LUMO(maleic anhydride) ($w \approx 0.35$)† A^+B^- and HOMO-(maleic anhydride) $\rightarrow$ LUMO(cyclopentadiene) ($w \approx 0.15$) A^-B^+ (back donation[14]) monotransferred configurations. The same kind of interactions, with smaller weights ($w \approx 0.10$, A^+B^-, and $w \approx 0.02$, A^-B^+) are already present in the van der Waals intermediates **vdW1** and **vdW2**. Therefore, in agreement with previous suggestions,[5] the present calculations show that the (pre-reactive) van der Waals intermediates are located at the entrance of the cycloaddition reaction (*endo*/*exo*) channels, thus being precursors to the actual Diels–Alder products.

Notes and References

* E-mail: jasg@dwarfl.quimica.uniovi.es

† w_i is the weight of the i-th fragment electronic configuration when the wave function, Ψ, of a complex system formed by two fragments (A, B) is written as:

$$\Psi = w_0\Psi(AB) + w_1\Psi(A^+B^-) + w_2\Psi(A^-B^+) + \cdots + w_k\Psi(A^*B) + \cdots (A = \text{diene, B = dienophile})$$

where A^+B^- or A^-B^+ represent monotransferred configurations (one electron in an occupied MO in any of the two fragments is transferred to an unoccupied MO of a different fragment), A*B monoexcited configurations (one electron in an occupied MO of any of the two fragments is transferred to an unoccupied MO of the same fragment), *etc.*

1 W. Carruthers, *Cycloaddition Reactions in Organic Synthesis*, Pergamon NY, 1990; K. N. Houk, Y. Li and J. D. Evanseck, *Angew. Chem., Int. Ed. Engl.*, 1992, **31**, 682; K. N. Houk, J. González and Y. Li, *Acc. Chem. Res.*, 1995, **28**, 81.

2 K. Alder and G. Stein, *Angew. Chem.*, 1937, **50**, 514.

3 See for example: J. Sauer and R. Sustmann, *Angew. Chem., Int. Ed. Engl.*, 1980, **19**, 779; M. F. Ruiz-López, X. Assfeld, J. I. García, J. A. Mayoral and L. Salvatella, *J. Am. Chem. Soc.*, 1993, **115**, 8780; D. Suárez, X. Assfeld, J. González, M. F. Ruiz-López, T. L. Sordo and J. A. Sordo, *J. Chem. Soc., Chem. Commun.*, 1994, 1183; D. Suárez, T. L., Sordo and J. A. Sordo, *J. Am. Chem. Soc.*, 1994, **116**, 763; D. Suárez, J. González, T. L. Sordo and J. A. Sordo, *J. Org. Chem.*, 1994, **59**, 8058; D. Suárez, R. López, J. Gonzalez, T. L. Sordo and J. A. Sordo, *Int. J. Quantum Chem.*, 1996, **57**, 493; M. Sodupe, R. Rios, V. Branchadell, T. Nicholas, A. Oliva and J. J. Dannenberg, *J. Am. Chem. Soc.*, 1997, **119**, 4232 and references cited therein.

4 J. Cioslowski, J. Sauer, J. Hetzenegger, T. Karacher and J. Hierstetter, *J. Am. Chem. Soc.*, 1993, **115**, 1353.

5 (*a*) J. Z. Gillies, C. W. Gillies, R. D. Suenram, F. J. Lovas and W. Stahal, *J. Am. Chem. Soc.*, 1991, **113**, 2421; (*b*) C. W. Gillies, J. Z. Gillies, R. D. Suenram, F. J. Lovas, E. Kraka and D. Cramer, *J. Am. Chem. Soc.*, 1991, **113**, 2412; (*c*) K. R. Leopold, G. T. Fraser, S. E. Novick and W. Klemperer, *Chem. Rev.*, 1994, **94**, 1807.

6 S. L. Craig and A. J. Stone, *J. Chem. Soc., Faraday Trans.*, 1994, **90**, 1663.

7 (*a*) For major reviews, see V. D. Kiselev and A. I. Konovalov, *Russ. Chem. Rev.*, 1989, **58**, 230; C. Cativiela, J. I. García, J. A. Mayoral and L. Salvatella, *Chem. Soc. Rev.*, 1996, **25**, 209; (*b*) R. López, M. F. Ruiz-López, D. Rinaldi, J. A. Sordo and T. L. Sordo, *J. Phys. Chem.*, 1996, **100**, 10 600; (*c*) K. B. Wiberg, T. A. Keith, M. J. Frisch and M. Murcko, *J. Phys. Chem.*, 1995, **99**, 9072; (*d*) R. D. Bach, J. E. Winter and J. J. W. McDovall, *J. Am. Chem. Soc.*, 1995, **117**, 8586.

8 L. M. Stephenson, D. E. Smith and S. P. Current, *J. Org. Chem.*, 1982, **47**, 4170.

9 S. F. Boys and F. Bernardi, *Mol. Phys.*, 1970, **19**, 553.

10 S. S. Xantheas, *J. Chem. Phys.*, 1996, **104**, 8821.

11 J. A. Sordo, *J. Chem. Phys.*, 1997, **106**, 6204; V. M. Rayón and J. A. Sordo, *J. Phys. Chem.*, 1997, **101**, 7414; V. M. Rayón and J. A. Sordo, *J. Chem. Phys.*, 1997, **107**, 7912; V. M. Rayón and J. A. Sordo, *Theor. Chem. Acc.*, in the press.

12 D. Y. Curtin, *Rec. Chem. Progr.*, 1954, **15**, 111; For an excellent review, see J. I. Seeman, *Chem. Rev.*, 1983, **83**, 83.

13 See for example: M. I. Menéndez, J. A. Sordo and T. L. Sordo, *J. Phys. Chem.*, 1992, **96**, 1185; R. López, M. I. Menéndez, D. Suárez, T. L. Sordo and J. A. Sordo, *Comput. Phys. Commun.*, 1993, **76**, 235; D. Suárez, J. A. Sordo and T. L. Sordo, *J. Phys. Chem.*, 1996, **100**, 13 462.

14 D. Suárez, T. L. Sordo and J. A. Sordo, *J. Org. Chem.*, 1995, **60**, 2848.

Received in Exeter, UK, 1st October 1997; 7/07086A

First structurally defined catalyst for the asymmetric addition of trimethylsilyl cyanide to benzaldehyde

Vitali I. Tararov,[b] David E. Hibbs,[c] Michael B. Hursthouse,[c] Nicolai S. Ikonnikov,[b] K. M. Abdul Malik,[c] Michael North,*[a]† Charles Orizu[a] and Yuri N. Belokon*[b]

[a] *Department of Chemistry, University of Wales, Bangor, Gwynedd, UK LL57 2UW*
[b] *A.N. Nesmeyanov Institute of Organoelement Compounds, Russian Academy of Sciences, 117813 Vavilov 28, Moscow, Russia*
[c] *Department of Chemistry, University of Wales, Cardiff, PO Box 912, Park Place, Cardiff, UK CF1 3TB*

Titanium complex $TiCl_2L$ [H_2L = (*R*,*R*)-*N*,*N*′-bis(3,5-di-*tert*-butylsalicylidene)hexane-1,2-diamine] 2 has been prepared, characterised by X-ray crystallography and shown to be an active catalyst for the asymmetric addition of Me_3SiCN to benzaldehyde, producing (*S*)-2-phenyl-2-trimethylsilyloxyacetonitrile in 86% ee at room temperature.

Enantiomerically pure cyanohydrins are important synthetic intermediates in the synthesis of other chiral compounds and hence are of significant industrial importance.[1] A number of catalytic methods have been reported for the asymmetric synthesis of cyanohydrins, including the use of enzymes, peptides and transition metal complexes.[2] Recently, we reported the use of chiral Ti^{IV} (salen)$(OPr^i)_2$ complexes as chiral catalysts for the asymmetric addition of Me_3SiCN to aldehydes,[3] and related work has been reported by other workers.[4] Whilst some of these catalysts have given cyanohydrin silyl ethers with > 90% ee, the structures of the catalysts have never been determined and this has restricted mechanistic investigations aimed at further improving the enantiomeric excesses and substrate tolerance. The catalysts have generally been prepared *in situ* by mixing a chiral ligand and titanium(IV) species. In the case of ligand **1**–$Ti(OPr^i)_4$ we have shown that at least three species can subsequently be detected by NMR spectroscopy.[5] Here we describe the synthesis of the first isolable and characterisable catalyst for the asymmetric addition of Me_3SiCN to benzaldehyde.

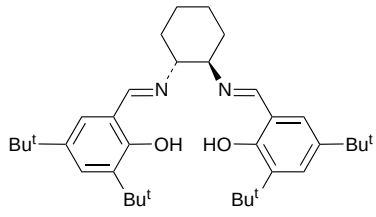

1

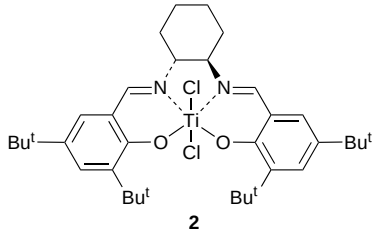

2

Reaction of ligand **1**[6] with titanium(IV) chloride in CH_2Cl_2 at room temperature for 2 h followed by evaporation of the solvent *in vacuo* and washing of the solid with Et_2O and Et_2O–hexane (1 : 1) gave a brown solid of structure **2** which could be recrystallised from $CHCl_3$. The spectral (^1H and ^{13}C NMR, IR) properties of compound **2** {$[\alpha]_D^{22}$ +736 (*c* 0.0125, $CHCl_3$), mp 330 °C (decomp.)} were entirely consistent with a single species of the proposed structure, and the monomeric nature and geometry of compound **2** were proven by X-ray structure analysis‡ (Fig. 1). Compound **2** has two independent molecules in the crystals, both with the *R*,*R* configuration and comparable geometry parameters. Each molecule adopts a slightly distorted octahedral geometry in which the two chlorine atoms are repelled by the *tert*-butyl groups (Cl–Ti–Cl bond angle ≈ 169°). Although X-ray structures of similar achiral titanium complexes have been reported,[7] only one other example of the X-ray structure of a monomeric, chiral (salen) titanium complex has been reported,[8] and in that case the salen ligand did not adopt four equatorial positions around the titanium.[9]

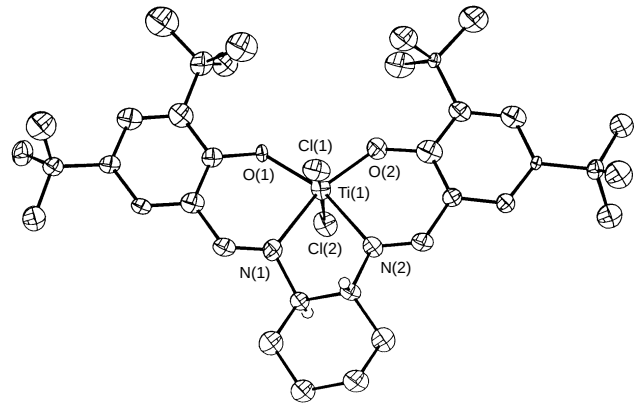

Fig. 1 Solid state structure of one independent molecule of **2**. Thermal ellipsoids are drawn at 50% probability. The structure of the other molecule is closely similar.

Compound **2** was active as a catalyst for the asymmetric addition of Me_3SiCN to benzaldehyde (Scheme 1). Thus treatment of a CH_2Cl_2 solution of benzaldehyde and Me_3SiCN (2.3 equiv.) with complex **2** (0.1 mol%) at room temperature resulted after 24 h in complete conversion of the benzaldehyde to (*S*)-2-phenyl-2-trimethylsilyloxyacetonitrile **3** in 86% ee, as determined by chiral gas chromatography. It is notable that catalyst **2** is active at room temperature and at very high substrate to catalyst ratios, results which contrast with previously reported catalysts for this reactions.[2–4]

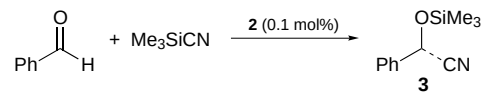

3

Scheme 1

Further work on the mechanism and synthetic applications of this chemistry is underway and will be reported in due course. The authors thank the EPSRC, INTAS, the EU (INCO-COPERNICUS) and the Russian Fund for Fundamental Research (grant No. 95-03-08046) for financial support.

Notes and References

† E-mail: m.north@bangor.ac.uk

‡ *Crystallographic data* for **2**: $C_{36}H_{52}Cl_2N_2O_2Ti.CHCl_3$ (FW 782.96), triclinic, space group *P*1 (No. 1); a = 12.032(3), b = 13.376(5), c = 14.938(5) Å, α = 63.42(3), β = 75.75(3), γ = 72.92(3)°, V = 2036.6(11) Å^3; Z = 2; D_c = 1.277 Mg m^{-3}, λ(Mo-Kα) = 0.71069 Å, F(000) = 824. The structure was solved by direct methods (SHELXS86) (ref. 10) using previously described procedures (ref. 11) and refined on F^2 by full-matrix least-squares (SHELXL93) (ref. 12) using all 6227 unique data corrected for Lorentz and polarisation factors but not for absorption. The structure was finally refined (823 parameters) to R [on F,$F_0 > 4\sigma(F_0)$] and wR [on F^2, all data)] values of 0.0524 and 0.1013, respectively. CCDC 182/732.

1 C. G. Kruse, in *Chirality in Industry*, ed. A. N. Collins, G. N. Sheldrake and J. Crosby, Wiley, Chichester, 1992, ch. 14.

2 M. North, *Synlett*, 1993, 807; F. Effenberger, *Angew. Chem., Int. Ed. Engl*., 1994, **33**, 1555; M. North, in *Comprehensive Organic Functional Group Transformations*, ed. A. R. Katritzky, O. Meth-Cohn, C. W. Rees and G. Pattenden, Pergamon, Oxford, 1995, vol. 3, ch. 18.

3 Y. Belokon', N. Ikonnikov, M. Moscalenko, M. North, S. Orlova, V. Tararov and L. Yashkina, *Tetrahedron: Asymmetry*, 1996, **7**, 851; Y. Belokon', M. Flego, N. Ikonnikov, M. Moscalenko, M. North, C. Orizu, V. Tararov and M. Tasinazzo, *J. Chem. Soc., Perkin Trans. 1*, 1997, 1293.

4 A. Abiko and G.-q. Wang, *J. Org. Chem*., 1996, **61**, 2264. See also the references cited in refs. 2 and 3.

5 Y. Belokon', N. Ikonnikov, M. North, C. Orizu and V. Tararov, unpublished results.

6 J. F. Larrow, E. N. Jacobsen, Y. Gao, Y. Hong, X. Nie and C. Zepp, *J. Org. Chem*., 1994, **59**, 1939 and references cited therein.

7 G. Gilli, D. W. J. Cruickshank, R. L. Beddoes and O. S. Mills, *Acta. Crystallogr., Sect. B*, 1972, **28**, 1889; M. Pasquali, F. Marchetti, A. Landi and C. Floriani, *J. Chem. Soc., Dalton Trans*., 1978, 545; C. Floriani, E. Solari, F. Corazza, A. Chiesi-Villa and C. Guastini, *Angew. Chem., Int. Ed. Engl*., 1989, **28**, 64; E. Solari, C. Floriani, A. Chiesi-Villa and C. Rizzoli, *J. Chem. Soc. Dalton Trans*., 1992, 367; F. Franceschi, E. Gallo, E. Solari, C. Floriani, A. Chiesi-Villa, C. Rizzoli, N. Re and A. Sgamell, *Chem. Eur. J*., 1996, **2**, 1466; T. Repo, M. Klinga, M. Leskela, P. Pietikainen and G. Brunow, *Acta. Crystallgr., Sect. C*., 1996, **52**, 2742; E. Gallo, E. Solari, F. Franceschi, C. Floriani, A. Chiesi-Villa and C. Rizzoli, *Inorg. Chem*., 1995, **34**, 2495.

8 K. M. Carroll, J. Schwartz and D. M. Ho, *Inorg. Chem*., 1994, **33**, 2707.

9 For dimeric and polymeric chiral (salen)titanium complexes, see K. Nakajima, C. Sasaki, M. Kojima, T. Aoyama, S. Ohba, Y. Saito and J. Fujita, *Chem. Lett*., 1987, 2189; T. Aoyama, S. Ohba, Y. Saito, C. Sasaki, M. Kojima, J. Fujita and K. Nakajima, *Acta. Crystallogr., Sect. C*, 1988, **44**, 1309; A. Kless, C. Lefeber, A. Spannenberg, R. Kempe, W. Baumann, J. Holz and A. Börner, *Tetrahedron*, 1996, **52**, 14 599.

10 G. M. Sheldrick, *Acta. Crystallogr*., 1990, **A46**, 467.

11 J. A. Darr, S. R. Drake, M. B. Hursthouse and K. M. A. Malik, *Inorg. Chem*., 1993, **32**, 5704.

12 G. M. Sheldrick, 'SHELXL93: Program for Crystal Structure Refinement', University of Gottingen, Germany, 1993.

Received in Liverpool, UK, 18th August 1997; 7/06121H

Two versatile new routes to dinuclear molybdenum dithiolene complexes

Andrew Abbott,[a] Matthew N. Bancroft,[a] Michael J. Morris,*[a] Graeme Hogarth[b] and Simon P. Redmond[b]

[a] *Department of Chemistry, University of Sheffield, Sheffield, UK S3 7HF*
[b] *Department of Chemistry, University College London, 20 Gordon Street, London, UK WC1H 0AJ*

Two routes to the dithiolene complexes [$Mo_2S(\mu\text{-}S)_2(SCR^1{=}CR^2S)(\eta\text{-}C_5H_5)_2$] starting from the complexes [$Mo_2(\mu\text{-alkyne})(CO)_4(\eta\text{-}C_5H_5)_2$] are described; in one case the dithiolene ligand is derived from the alkyne, and in the other from a 1,3-dithiole-2-thione reagent.

A combination of techniques have indicated that the molybdenum atom in the molybdenum cofactor (Moco) common to a range of oxotransferase enzymes is coordinated by a pterin ligand which is bonded through a dithiolene linkage.[1] Recent protein crystallographic studies, however, have shown that in some of these enzymes the metal atom is ligated by one dithiolene ligand whereas in other cases, unexpectedly, two such ligands were present.[2] Molybdenum (and tungsten) dithiolene complexes have been known for many years,[3] and are of continuing interest as model systems for the metal site in the cofactor.

Here, we describe two versatile routes to dimolybdenum complexes containing terminal dithiolene or tetrathiooxalate ligands, both of which start with the alkyne complexes [$Mo_2(\mu\text{-}R^1C{\equiv}CR^2)(CO)_4(\eta\text{-}C_5H_5)_2$] **1a–e**. We have recently shown that reactions of these compounds with thiols often proceed with C–S bond cleavage to give sulfido-bridged species.[4] In contrast, it is notable that the reactions discussed here involve the formation of C–S bonds as well as their scission.

In the first approach we found that heating a toluene solution of **1** with elemental sulfur for 5 h provided the green dithiolene complexes [$Mo_2S(SCR^1{=}CR^2S)(\mu\text{-}S)_2(\eta\text{-}C_5H_5)_2$] **2a–e** in yields of up to 80% after isolation by column chromatography (Scheme 1). Five representative examples are given but the reaction works equally well with other complexes of type **1**. Complex **2c** and the corresponding oxo species [$Mo_2O(SCH{=}CPhS)(\mu\text{-}S)_2(\eta\text{-}C_5H_5)_2$] **3** have been prepared previously by a different route,[5] but in contrast to this report we find that complexes of type **2** are not particularly air sensitive even in solution, and only slowly convert into the oxo complexes analogous to **3**; small amounts of these were isolated from some reactions.

The dithiolene compounds were characterised spectroscopically (and by comparison with the published values for **2c**, for which our data agree exactly).† In the ^1H NMR spectrum each complex displays two rather widely separated signals for the C_5H_5 rings and appropriate resonances for the substituents R^1 and R^2. In the complexes derived from terminal alkynes, the signal for the CH group appears shifted downfield at δ 8–9. This is a characteristic feature of terminal dithiolene complexes and can be regarded as arising either from the contribution of a dithioglyoxal canonical form[6,7] or the presence of a ring current in the pseudo-aromatic metalladithiolene unit.[8] Interestingly the products all gave high intensity molecular ions in their electron impact mass spectra, but most evidently disintegrated completely when subjected to fast atom bombardment (FAB).

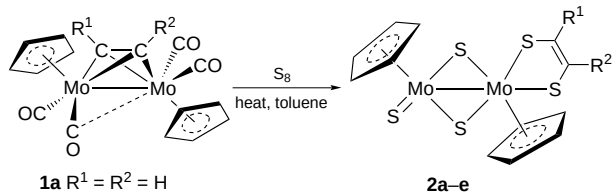

1a $R^1 = R^2 = H$
b $R^1 = H$, $R^2 = Me$
c $R^1 = H$, $R^2 = Ph$
d $R^1 = R^2 = Et$
e $R^1 = R^2 = CO_2Me$

2a–e

Scheme 1

The result of an X-ray crystal structure determination of **2a** is shown in Fig. 1.‡ The molecule is based on a dimolybdenum centre with a metal–metal distance of 2.984(1) Å, which is similar to that of 2.927(1) Å observed in [$Mo_2O(SCH{=}CPhS)(\mu\text{-}S)_2(\eta\text{-}C_5H_5)_2$] **3**.[5] The coordination geometry in the two complexes is also very similar. Thus Mo(1) has a pseudo-tetrahedral coordination (if the C_5H_5 ligand is regarded as occupying one site) whereas Mo(2) is in a square pyramidal environment. The $Mo_2(\mu\text{-}S)_2$ core is not planar: the dihedral angle between the two intersecting Mo_2S planes is 161.3°, whereas in **3** the corresponding angle is 144.6°. This contrasts with related Mo^V dimers with imido ligands, *e.g.* [$Mo_2(NPh)_2(\mu\text{-}NPh)_2(\eta\text{-}C_5H_4Me)_2$] which all contain strictly planar cores.[9]

The bond lengths between Mo(2) and the bridging sulfur atoms are significantly longer than the distances from Mo(1) to the same sulfurs. Together with the rather short S(4)–C(11) and S(5)–C(12) bonds within the dithiolene ligand itself, this could be regarded as evidence for some contribution of the dithioglyoxal canonical form: if the dithiolene ligand is dianionic, each Mo atom is formally Mo^V, but if it is bonded in the dithioglyoxal form, Mo(2) would be formally Mo^{III}. Again an alternative interpretation is that the dithiolene ligand acts as a delocalised 6π pseudo-aromatic system which is a better π-donor than the sulfide ligand on Mo(1).

Our second approach is shown in Scheme 2. We recently reported that alkyne complex **1e** reacted with 1,3-dithiole-2-thiones by cleavage of the C=S bond, ring opening of the resulting carbene and coupling with the alkyne ligand to

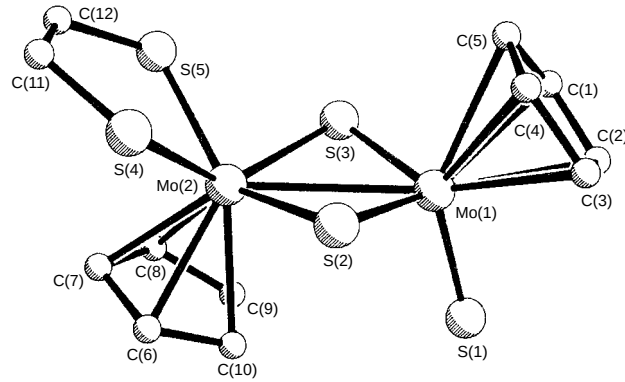

Fig. 1 Molecular structure of complex **2a** in the crystal. Selected bond lengths (Å): Mo(1)–Mo(2) 2.984(1), Mo(1)–S(1) 2.154(1), Mo(1)–S(2) 2.263(1), Mo(1)–S(3) 2.263(1), Mo(2)–S(2) 2.406(1), Mo(2)–S(3) 2.398(1), Mo(2)–S(4) 2.387(1), Mo(2)–S(5) 2.384(1), S(4)–C(11) 1.708(5), S(5)–C(12) 1.705(4), C(11)–C(12) 1.348(7).

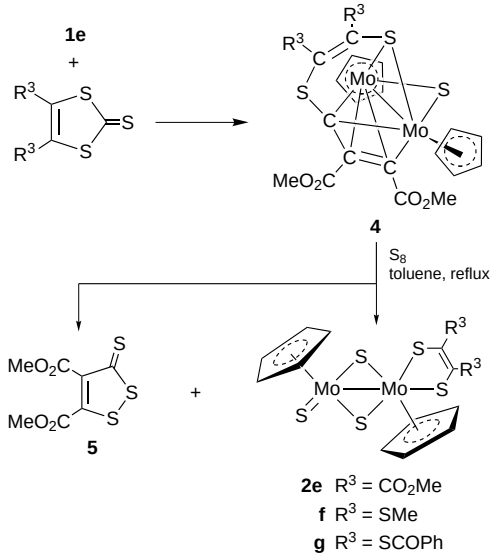

Scheme 2

produce complexes of type **4** (R^3 = CO_2Me, SMe, SCOPh).[10] Remarkably, we have now discovered that these compounds also react rapidly (2 h) with elemental sulfur in boiling toluene to give dithiolene complexes **2e**–**g**, in which the dithiolene ligand originates from the backbone of the original thione rather than the alkyne. Compounds **2f** and **2g** are rare examples of dialkyl- and diacyl-tetrathiooxalate (or ethenetetrathiolate) complexes respectively.

The alkyne ligand is recovered in the form of the interesting new sulfur heterocycle **5**, a hitherto inaccessible derivative of the important 1,2-dithiole-3-thione ring system.[11] Indeed, in the case of R^3 = CO_2Me, the reaction represents an elaborate isomerisation of the 1,3-dithiole-2-thione ring. The mechanism presumably involves insertion of three sulfur atoms into the Mo–C bonds of the bridging ligand of **4**, cleavage of the μ-C–S bond to afford the dithiolene ligand, and reductive elimination of the organic by-product **5**. It is notable that this process reforms the thione unit which is cleaved during the formation of **4**.

In summary, the two synthetic routes described here are complementary: simple dithiolene ligands are easily accessed from the appropriate alkyne by the first method, whereas in the second case the availability of convenient synthetic procedures for a large number of requisite thiones, which are readily made by alkylation or acylation of $[NEt_4]_2[Zn(C_3S_5)_2]$, should enable the introduction of a wide variety of more complex substituents including functionalised derivatives such as crown ethers, macrocycles, *etc*. Moreover, compounds containing the 1,2-dithiole-3-thione ring system have been studied for their pharmaceutical properties, particularly as anticancer agents. We are currently exploiting this methodology to synthesize a representative range of dithiolene complexes and heterocycles for further investigation.

We thank the EPSRC for the award of a studentship (M. N. B.).

Notes and References

* E-mail: M.Morris@sheffield.ac.uk

† *Selected spectroscopic data*: (NMR in $CDCl_3$, all signals are singlets unless otherwise stated). Satisfactory elemental analyses were obtained for all new compounds.

2a: yield 64%. mp 196–198 °C. ^{1}H NMR δ 8.37 (2 H, CH), 6.00 (5 H, C_5H_5), 5.38 (5 H, C_5H_5); ^{13}C NMR δ 149.5 (CH), 103.7 (C_5H_5), 100.1 (C_5H_5); MS *m*/*z* 508 (M^+), 482 ($M - C_2H_2^+$). The dithiolene complexes **2a**–**f** all show peaks at *m*/*z* 450, 418, 386, 353 and 323 ($Mo_2S_{4-n}Cp_2^+$, n = 0–4) in the EI mass spectrum.

2b: yield 54%. mp 234 °C (decomp.). ^{1}H NMR δ 8.00 (1 H, CH), 6.00 (s, 5 H, C_5H_5), 5.40 (5 H, C_5H_5), 2.80 (3 H, Me); ^{13}C NMR δ 163.0 (CMe), 145.6 (CH), 103.6 (C_5H_5), 100.1 (C_5H_5), 23.4 (Me). MS *m*/*z* 522 (M^+), 482 ($M - HC_2Me^+$).

2d: yield 70%. mp 232–233 °C. ^{1}H NMR δ 6.00 (5 H, C_5H_5), 5.35 (5 H, C_5H_5), 3.10 (dq, *J* 7 Hz, 2 H, 1 H of CH_2), 2.85 (dq, *J* 7 Hz, 2 H, 1 H of CH_2), 1.55 (t, *J* 7 Hz, 6 H, Me); ^{13}C NMR δ 163.2 (CEt), 103.6 (C_5H_5), 100.0 (C_5H_5), 29.8 (CH_2), 16.6 (Me); MS *m*/*z* 564 (M^+), 532 ($M - S^+$), 482 ($M - C_2Et_2^+$).

2e: yield 80%. mp > 250 °C. ^{1}H NMR δ 6.00 (5 H, C_5H_5), 5.50 (5 H, C_5H_5), 3.87 (s, 6 H, Me); ^{13}C NMR δ 165.1 (CO_2Me), 154.7 (CCO_2Me), 103.8 (C_5H_5), 100.9 (C_5H_5), 53.0 (Me); MS *m*/*z* 624 (M^+), 592 ($M - S^+$), 482 [$M - C_2(CO_2Me)_2^+$].

2f: yield 66%. mp 230 °C (decomp.). ^{1}H NMR δ 6.02 (5 H, C_5H_5), 5.40 (5 H, C_5H_5), 2.70 (6 H, Me); ^{13}C NMR δ 153.6 (*C*SMe), 103.7 (C_5H_5), 100.2 (C_5H_5), 19.3 (Me); MS *m*/*z* 600 (M^+).

2g: yield 58%. mp 214 °C. ^{1}H NMR δ 8.03–7.43 (m, 10 H, Ph), 6.03 (5 H, C_5H_5), 5.84 (5 H, C_5H_5); ^{13}C NMR 189.4 (COPh), 151.4 (*C*SCOPh), 136.4 (C_{ipso}), 133.8–127.7 (m, Ph), 103.7 (C_5H_5), 101.4 (C_5H_5); FAB MS *m*/*z* 780 (M^+).

5: Yield 70%. mp 93–94 °C. ^{1}H NMR δ 3.97 (3 H, Me), 3.95 (3 H, Me); ^{13}C NMR δ 210.4 (C=S), 162.7, 159.4 (both CO_2Me), 156.1, 146.2 (both CCO_2Me), 54.4, 53.7 (both Me); MS *m*/*z* 250 (M^+).

‡ *Crystal data* for **2a**: $C_{12}H_{12}Mo_2S_5$, M = 508.40, monoclinic, space group *C*2/*c* (no. 15), a = 22.2528(29), b = 11.0848(21), c = 12.9379(26) Å, β = 105.933(15)°, U = 3068.7(9) Å^3, F(000) = 1984, Mo-Kα radiation (λ = 0.710 73 Å), μ(Mo-Kα) = 22.34 cm^{-1}, Z = 8, D_c = 2.20 g cm^{-3}.

Room temperature X-ray data were collected on a Nicolet R3mV diffractometer. A total of 3937 reflections (3779 unique) were measured in the range $5 < 2\theta < 50°$ by the ω–2θ scan technique, all of which were corrected for Lorentz and polarisation effects and for absorption by analysis of ψ-scans (minimum and maximum transmission coefficients 0.806 and 0.913); 2634 data with $I \geqslant 3.0\sigma(I)$ were used in the refinement. The structure was solved by direct methods and developed by alternating cycles of least squares refinement and difference Fourier synthesis. All non-hydrogen atoms were refined anisotropically while hydrogen atoms were placed in idealised positions (C–H 0.96 Å) and assigned a common isotropic thermal parameter (U = 0.08 Å^2). The last cycle of least squares refinement included 172 parameters for 2497 variables. The final R values were R = 0.035 and R_w = 0.042 and the final difference Fourier map contained no peaks > 1.00 e Å^{-3}. The structure was solved using the SHELXTL PLUS program package[12] on a Micro Vax II computer. CCDC 182/722.

1 D. Collison, C. D. Garner and J. A. Joule, *Chem. Soc. Rev.*, 1996, **25**, 25.
2 M. J. Romao, M. Archer, I. Moura, J. J. G. Moura, J. LeGall, R. Engh, M. Schneider, P. Hof and R. Huber, *Science*, 1995, **270**, 1170; H. Schindelin, C. Kisker, J. Hilton, K. V. Rajagopalan and D. C. Rees, *Science*, 1996, **272**, 1615; M. K. Chan, S. Mukund, A. Kletzin, M. W. W. Adams and D. C. Rees, *Science*, 1995, **267**, 1463.
3 J. A. McCleverty, *Prog. Inorg. Chem.*, 1969, **10**, 49; R. Eisenberg, *Prog. Inorg. Chem.*, 1970, **12**, 295; R. P. Burns and C. A. McAuliffe, *Adv. Inorg. Chem. Radiochem.*, 1979, **22**, 303; U. T. Mueller-Westerhoff and B. Vance, in *Comprehensive Coordination Chemistry*, ed. G. Wilkinson, R. D. Gillard and J. A. McCleverty, Pergamon, Oxford, 1987, vol. 2, ch. 16.5.
4 H. Adams, N. A. Bailey, S. R. Gay, T. Hamilton and M. J. Morris, *J. Organomet. Chem.*, 1995, **493**, C25; H. Adams, N. A. Bailey, S. R. Gay, L. J. Gill, T. Hamilton and M. J. Morris, *J. Chem. Soc., Dalton Trans.*, 1996, 2403; 3341.
5 L. D. Tanner, R. C. Haltiwanger, J. Noordik and M. Rakowski DuBois, *Inorg. Chem.*, 1988, **27**, 1736; L. D. Tanner, R. C. Haltiwanger and M. Rakowski DuBois, *Inorg. Chem.*, 1988, **27**, 1741.
6 R. B. King and C. A. Eggers, *Inorg. Chem.*, 1968, **7**, 340.
7 G. N. Schrauzer and V. P. Mayweg, *J. Am. Chem. Soc.*, 1965, **87**, 3585.
8 S. Boyde, C. D. Garner, J. A. Joule and D. J. Rowe, *J. Chem. Soc., Chem. Commun.*, 1987, 800.
9 J. Fletcher, G. Hogarth and D. A. Tocher, *J. Organomet. Chem.*, 1991, **403**, 345; **405**, 207; M. L. H. Green, G. Hogarth, P. C. Konidaris and P. Mountford, *J. Chem. Soc., Dalton Trans.*, 1990, 3781.
10 H. Adams, M. N. Bancroft and M. J. Morris, *Chem. Commun.*, 1997, 1445.
11 C. T. Pedersen, *Adv. Heterocycl. Chem.*, 1982, **31**, 63; *Sulfur Rep.*, 1995, **16**, 173.
12 G. M. Sheldrick, SHELXTL PLUS program package for structure solution and refinement, version 4.2, Siemens Analytical Instruments Inc., Madison WI, 1990.

Received in Cambridge, UK, 5th November 1997; 7/07958C

$HAlCl_4$ in the gas phase is stronger than $HTaF_6$

André H. Otto,*[a] Thomas Steiger[b] and Sigurd Schrader[c]

[a] *Johanna-Tesch-Strasse 28, 12439 Berlin, Germany*
[b] *Federal Institute of Materials Research and Testing, Rudower Chaussee 5, 12484 Berlin, Germany*
[c] *University of Potsdam, Institute of Solid State Physics, Am Neuen Palais 10, 14469 Potsdam, Germany*

***Ab initio* MO calculations at the {MP2(fc)/6-311++G(d,p)//3-21G(*)+ZPVE[3-21G(*)]} and {MP2(fc)/D95++G(d,p)//3-21G(*)+ZPVE[3-21G(*)]} levels of sophistication and also an analogous DFT/DNP study reveal that $HAlCl_4$ has a gas phase deprotonation energy of *ca.* 264 kcal mol^{-1} (1 cal = 4.184 J) being lower than the value predicted for $HTaF_6$ (269 kcal mol^{-1}).**

Superacids are a very intriguing tool in applied experimental[1–6] and theoretical[7–9] chemistry. It was previously shown[7] by applying the density functional theory (DFT) to calculating deprotonation energies (DEs) that in the gas phase $HSbF_6$ ($HF{\cdot}SbF_5$) is the strongest acid known (DE = 258 kcal mol^{-1}), in full agreement with various investigations of the corresponding Hammett acidity function in condensed media.[4] Further, $HTaF_6$ ($HF{\cdot}TaF_5$) has been predicted to be clearly weaker[7] possessing a DE of 269 kcal mol^{-1}.

On the other hand, the place of Friedel–Crafts acid of the $HX{\cdot}AlX_3$ (X = Cl, Br) type in the acidity scale is unknown thus far. Moreover, there was a controversy more than 10 years ago[4,10,11] concerning the relative strengths of $HAlBr_4$ ($HBr{\cdot}AlBr_3$). Farcasiu *et al.*[10] argued that the latter should exhibit an acidity comparable to $HSbF_6$ since it is capable of protonating benzene at 0 °C. Kramer proposed the same ranking based on his selectivity parameter.[11] However, it was claimed[4] that $HAlBr_4$ is very unlikely comparable to $HSbF_6$ as it is incapable of protonating weak bases or ionising precursors. Although the order of acidic strength might change in solution[12] it is of principal significance to determine the DEs of $HAlCl_4$ and $HAlBr_4$. Here, quantum chemical calculations on $HAlCl_4$, $AlCl_4^-$, $AlCl_3$, HCl and Cl^- are presented, which have been used to determine the energies of the following processes. (i) The DE of the superacid, $HAlCl_4 \rightarrow H^+ + AlCl_4^-$ (1); (ii) the decomposition energy of the superacid, $HAlCl_4 \rightarrow HCl + AlCl_3$ (2); (iii) the decomposition energy of the conjugated base, $AlCl_4^- \rightarrow AlCl_3 + Cl^-$ (3) and (iv) the DE of hydrogen chloride, $HCl \rightarrow H^+ + Cl^-$ (4).

The last process is considered to obtain information of the performance of the methods used.

In order to obtain reliable results we used a suggestion of Koppel *et al.*[13] that MP2(fc)/6-311++G(d,p) perform rather well already at 3-21G [or 3-21G(*) in the cases of molecules containing second row elements] fully optimised geometries. Very recently we reported[8] on the gas phase DEs of some superacids ($HClO_4$, FSO_3H, $ClSO_3H$) applying the 6-31+G(d) basis set for calculating structures. Nevertheless, we are of the opinion now that the smaller valence basis sets also attain this objective, providing deviations from experiment of < 3 kcal mol mol^{-1};[13] at this point evidence is given of the reliability of the level of sophistication mentioned above for calculating DEs of HPF_6 ($HF{\cdot}PF_5$).[9]

The geometries for two conformations of $HAlCl_4$, *cis* and *trans*, the conjugated base $AlCl_4^-$ and also for the Lewis acid $AlCl_3$ have been fully optimised (Table 1) by using the 3-21G(*) basis set followed by vibrational analyses at the same level. All stationary points were found to be minima. Then the energies were improved by carrying out MP2(fc)/6-311++G(d,p) calculations. Since for calculating the DE the energy of the low lying conformation of $HAlCl_4$ had to be used depending on the level of investigation, the corresponding values of either *cis* or *trans* geometry have been employed. Nevertheless, both conformations are almost equal in stability and, therefore, DE is practically unaffected by the energy chosen for the acid.

Details on current *ab initio* MO theory and common standard procedures are given elsewhere.[14] Furthermore, single point energy calculations have been also performed with Dunnings split valence basis set D95.[15] All *ab initio* MO calculations were performed using Hyperchem software[16] and run on a Pentium PC.

All *ab initio* DFT computations were performed with the DMol program[17] on an Indigo-2 workstation. The Becke 1988 exchange functional[18] was used in combination with the Lee–Yang–Parr correlation (LYP).[19] All electrons were taken into account and the DNP (double numeric augmented by polarization functions at both hydrogen and non-hydrogen atoms) basis set was used together with a high number of mesh points that is almost to the saturation point of the mesh grid. Completely optimised geometries as well as the corresponding energies have been calculated with this basis which is[17] comparable to 6-31G(d,p) followed by vibrational analyses. All stationary points were found to be minima. It has been shown[7] that DNP reproduces the DE of strong acids and superacids quite well.

Table 1 Calculated total energies ($-E_h$) and ZPVEs (kcal mol^{-1})

Compound	Point group	ZPVE 3-21G(*)	ZPVE B-LYP/DNP	3-21G(*)[a]	6-31+G(d)[a]	6-31+G(d,p)	D95++G(d,p)	6-311++G(d,p)	MP2/6-31+G(d,p)	MP2/D95++G(d,p)	MP2/6-311++G(d,p)	B-LYP/DNP
$HAlCl_4$, *cis*	C_s	8.78	7.78	2071.08345	2080.64470	2080.65075	2080.62684	2080.77494	2081.28968	2081.66018	2081.72054 (2081.72000)[b]	2084.14452
$HAlCl_4$, *trans*	C_s	8.84	7.64	2071.08350	2080.64438	2080.65085	2080.63852	2080.77496	2081.28998	2081.67213	2081.72075 (2081.71482)[b]	2084.14448
$AlCl_4^-$	T_d	3.91	3.37	2070.67394	2080.23457	2080.23455	2080.22098	2080.35608	2080.86515	2081.23394	2081.29120 (2081.29098)[b]	2083.71675
$AlCl_3$	D_{3h}	3.19	2.87	1613.09168	1620.57802	1620.57802	1620.55913	1620.67310	1621.05833	1621.36398	1621.40989	1623.31904
HCl	$D_{\infty v}$	4.56	3.94	457.98139	460.06100	460.06734	460.06191	460.09621	460.21834	460.28323	460.29680	460.82018
Cl^-	$^1S_0$	0.00	0.00	457.44410	459.53964	459.53964	459.53440	459.56562	459.68144	459.74856	459.75418	460.28427

[a] Fully optimised geometries. [b] Energies at 6-31+G(d) geometries.

Table 2 Processes considered in this investigation[a] (kcal mol^{-1})

Reaction	3-21G(*)[b]	6-31+ G(d)[b]	6-31+ G(d,p)	D95++ G(d,p)	6-311++ G(d,p)	MP2/6-31+ G(d,p)	MP2/D95++ G(d,p)	MP2/6-311++ G(d,p)	B-LYP/ DNP
(1) $HAlCl_4 \rightarrow H^+ + AlCl_4^-$	252.6	253.0	256.8	257.6	258.5	262.1	263.1	265.0 (264.8)[c]	264.1
(2) $HAlCl_4 \rightarrow HCl + AlCl_3$	5.61	2.63	2.45	10.00	2.59	7.40	14.69	7.87	2.37
(3) $AlCl_4^- \rightarrow AlCl_3 + Cl^-$	86.0	72.7	72.7	79.3	73.0	78.0	75.6	79.1	70.7
(4) $HCl \rightarrow H^+ + Cl^-$	333.0[d]	323.0	327.0	326.9	328.8	332.8	331.4	333.5	332.3

[a] The ZPVE corrections are scaled by 0.9 for the 3-21G(*) calculations and they are unscaled when the DFT values were used. [b] Fully optimised geometries. [c] The DE when the 6-31+G(d) geometry is used. [d] Experimental values (enthalpies at 298 K) are[26] 333.4 ± 0.3 and 333.7 ± 2.2 kcal mol^{-1}.

Detailed information on the current state and performance of modern DFT theory is given in the user manual[17] and in some recent comprehensive books and papers.[20]

In order to turn out an incidental failure of the chosen procedure, the geometries have also been fully optimised employing the medium size 6-31+G(d) basis set. The gradients of the 6-311++G(d,p) energies (not given in the text) are smaller when the 3-21G(*) geometries are used and the corresponding energies (Table 1) are lower. Thus, the 3-21G(*) structures are closer to the 6-311++G(d,p) ones and they are applied throughout in this study. The DE values are practically unaffected by this difference in the geometries used. The values calculated (Table 2) are 265.0 kcal mol^{-1} (3-21G(*)) and 264.8 kcal mol^{-1} (6-31+G(d)).

It is noteworthy that the results for DE from all MO calculations rigorously depend on the size of the basis sets applied (Table 2). It was found that the MP2(fc)/6-31+(d,p) level of investigation provides a good estimate for predicting the acidity of $HAlCl_4$. On the other hand, it is remarkable that both remaining MP2 calculations provide almost identical values of DE (263.1 and 265.0 kcal mol^{-1}). Moreover, the DFT gives a value (264.1 kcal mol^{-1}) lying between the two latter ones. Thus, the mean DE of $HAlCl_4$ amounts to *ca.* 264 kcal mol^{-1}. This is less than the corresponding value for $HTaF_6$ (269 kcal mol^{-1})[7] which was obtained applying the same DFT procedure as in the present work. The order of acidity is, therefore, $HSbF_6$ > $HAlCl_4$ > $HTaF_6$ since there is a complete agreement between the experimental and DFT results of DEs on one hand[7] and the same was found for the DFT and MP2(fc)/6-311++G(d,p) sets of values, on the other hand.[8]

Beside the acidity the decomposition of the acid toward HCl and $AlCl_3$ is of interest. The positive energies for reaction (2) collected in Table 2 reveal that generation of $HAlCl_4$ is favoured, however, the values are small and indicate a weak van der Waals (vdW) interaction. Indeed, all attempts of Brown and Pearsall[21] failed to detect any complexation of $AlCl_3$ with HCl even at temperatures as low as 150 K. Many years later, however, aggregates were found[22] with a composition corresponding to $2HAlCl_4 \cdot 3Et_2O$ indicating the necessity of an auxiliary 'complexation generator'.

Finally, the stability of the anion $AlCl_4^-$ towards chloride ion detachment has been investigated (Table 2). Previously it was found[23] that the MP2/6-31+G(d) energy required to dissociate $AlCl_4^-$ in agreement with reaction (3) is 51.57 kcal mol^{-1}. The latter value is, however, erroneous. We calculated from the total energies reported[23] the correct one (77.6 kcal mol^{-1}). This result was confirmed by our calculations (Table 2).

Thus, $AlCl_4^-$ is, for example, comparable in stability to the conjugated base PF_6^- for which a fluoride ion detachment of 85 ± 10 kcal mol^{-1} was determined experimentally,[24] in complete agreement with quantum chemical calculations.[9,25]

The following significant concluding remarks can to be made. (*a*) $HAlCl_4$ belongs to the strongest superacids since its gas phase acidity is between those of $HSbF_6$ and $HTabF_6$. (*b*) The acid itself exhibits a weakly bonded vdW complex between HCl and $AlCl_3$ which is rather unstable *in vacuo* even at low temperatures. (*c*) The conjugated base ($AlCl_4^-$) is a stable species with respect to chloride ion abstraction possessing a detachment energy which is comparable to those of usual ordinary chemical bonds.

All optimised geometries are available from the authors by request. Furthermore, they will be published in a subsequent paper.

Notes and References

* E-mail: schrader@aca.fta-berlin.de

1 G. A. Olah, *Angew. Chem.*, 1973, **85**, 183.
2 G. A. Olah., G. K. S. Prakash and J. Sommer, *Science*, 1979, **206**, 13.
3 G. A. Olah and J. Sommer, *Recherche*, 1979, **10**, 624.
4 G. A. Olah, G. K. S. Prakash and J. Sommer, *Superacids*, Wiley, New York, 1985.
5 R. Jost and J. Sommer, *Rev. Chem. Intermed.*, 1988, **9**, 171.
6 R. Okuda, *Admits Giro*, 1996, **39**, 405 (Japan); *Chem. Abstr.*, 1996, **125**, 274878a.
7 A. H. Otto, Th. Steiger and S. Schrader, *J. Am. Chem. Soc.*, in press.
8 A. H. Otto, S. Schrader, Th. Steiger and M. Schneider, *J. Chem. Soc., Faraday Trans.*, 1997, **93**, 3927.
9 A. H. Otto, Th. Steiger and S. Schrader, *Nouv. J. Chim.*, submitted.
10 D. Farcasiu, S. L. Fisk, M. T. Melchior and K. D. Rose, *J. Org. Chem.*, 1982, **47**, 453.
11 G. M. Kramer, *J. Org. Chem.*, 1975, **40**, 298, 302.
12 J. F. King, in *Chemistry of Sulphonic Acids, Esters and Their Derivatives*, ed. S. Patai and Z. Rappoport, Wiley, New York, 1991, p. 249.
13 I. A. Koppel, R. W. Taft, F. Anvia, Sh.-Zh. Zhu, L.-Q. Hu, K. S. Sung, D. D. DesMarteau, L. M. Yagupolskii, Yu. L. Yagupolskii, N. V. Ignatév, N. V. Kondratenko, A. Yu. Volkonskii, V. M. Vlasov, R. Notario and P. Ch. Maria, *J. Am. Chem. Soc.*, 1994, **116**, 3047.
14 W. J. Hehre, L. Radom, P. v. R. Schleyer and J. A. Pople, *Ab Initio Molecular Orbital Theory*, Wiley, New York, 1986.
15 T. H. Dunning and P. J. Hay, in *Modern Theoretical Chemistry*, ed. W. H. Miller and H. F. Schaefer, Plenum , New York, 1976.
16 HyperChem, release 5.01 for Windows, 1996, publication HC5-00-02-00: Hypercube, Science and Technology Park, 1115 NW-Gainesville, 4th street, FL 32601, USA.
17 DMol 96.0, User Guide, version 4.0.0, Biosym Technologies, San Diego, 1996.
18 A. D. Becke, *Phys. Rev. A*, 1988, **38**, 3098.
19 C. Lee, W. Yang and R. G. Parr, *Phys. Rev. A*, 1988, **37**, 785.
20 See for example J. M. Seminario and P. Politzer, *Modern Density Functional Theory: A Tool for Chemistry*, Elsevier, Amsterdam, 1995.
21 H. C. Brown and H. W. Pearsall, *J. Am. Chem. Soc.*, 1951, **73**, 4681.
22 R. J. H. Clark, B. Crociani and A. Wassermann, *J. Chem. Soc. A*, 1970, 2458.
23 Ch. W. Bock, M. Trachtman and G. J. Mains, *J. Phys. Chem.*, 1994, **98**, 478.
24 J. W. Larson and T. B. McMahon, *J. Am. Chem. Soc.*, 1985, **107**, 766.
25 G. S. Tschumper, J. T. Fermann and H. F. Schaefer, III, *J. Chem. Phys.*, 1996, **104**, 3676.
26 S. G. Lias, J. E. Bartmess, J. F. Liebmann, J. L. Holmes, R. D. Levin and W. G. Mallard, *J. Phys. Chem. Ref. Data, Suppl. No.1*, 1988, **17**, 1.

Received in Exeter, UK, 17th October 1997; 7/07493J

The importance of nitrogen substituents in chiral amino thiol ligands for the asymmetric addition of diethylzinc to aromatic aldehydes

James C. Anderson*† and Michael Harding

Department of Chemistry, University of Sheffield, Sheffield, UK S3 7HF

A new series of *N*,*S*-chelate ligands derived from (*S*)-valine, which possess the capability of a stereogenic nitrogen donor atom, are catalysts for the addition of diethylzinc to aromatic aldehydes and gave the product secondary alcohols in up to 82% ee.

The successful use of metal complexes for enantioselective catalysis is largely dependant upon the structure and electronic properties of chiral ligands. We set out to develop a series of new chiral *N*,*S*-chelates, derived from amino acids, that would help us understand the origins of chirality in a variety of asymmetric catalytic processes. Very recently enantiomerically pure amino thiols have been shown to catalyse the addition of diethylzinc to benzaldehyde in high enantiomeric excess. Most noteworthy are systems derived from ephedrine,[1,2] (1*R*,2*S*)-(−)-1,2-diphenyl-2-aminoethanol[3] and van Koten's *N*,*S*-chelated bis{2-[(*R*)-1-)dimethylamino)ethyl]phenylthiolato}-zinc complex.[4] All of these ligands possess a symmetrical nitrogen donor atom and we anticipated that a potentially stereogenic nitrogen donor atom could have positive effects in this reaction system and other metal catalysed processes. In the design of our ligands careful attention was paid to the notion that the chirality inherent to the backbone of the amino acid could be transmitted closer towards the reaction centre by the correct choice of substituents on nitrogen. Upon chelation, the nitrogen atom could become stereogenic and reinforce the stereoinducing power of the ligand. We have tackled this idea by preparing ligands **1**–**5** that all possess a ligating sulfur atom in place of the hydroxy group from the derived amino acid. We hoped we could get good catalytic activity as sulfur would have a high affinity towards most metals useful in catalytic reactions, and has less tendency to diminish the Lewis acidity of the metal compared to metal alcoholates.‡ For instance, when ligand **1**

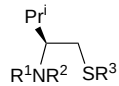

1 $R^1 = R^2 = Ph$, $R^3 = H$
2 $R^1 = R^2 = Bn$, $R^3 = H$
3 R^1–$R^2 = -(CH_2)_5-$, $R^3 = H$
4 $R^1 = Ph$, $R^2 = Me$, $R^3 = H$
5 $R^1 = R^3 = Ph$, $R^2 = H$

chelates to a metal atom the nitrogen donor with two phenyl substituents will possess different orientations of its atomatic rings [Fig. 1(*a*)]. The rotational freedom of the β-phenyl ring will be restricted by the proximity of the chiral centre. The

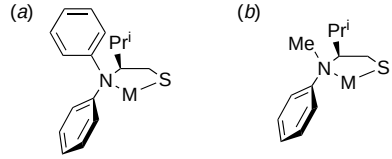

Fig. 1

orientation of this phenyl ring will affect that of the α-phenyl ring and render the nitrogen atom stereogenic.§ In ligands of type **4** the nitrogen atom is substituted with a large and small group. Upon coordination to a metal atom the *N*-methyl substituent should occupy the same face as the chiral centre on the backbone of the chelate, forcing the larger phenyl substituent to the underface [Fig. 1(*b*)], thus again rendering the nitrogen atom stereogenic.¶ Here we report our initial studies concerning these ligands in the 1,2-addition of diethylzinc to aromatic aldehydes, in order to assay their enantioselectivity and catalytic reactivity.

The syntheses of our desired ligands were accomplished in high yield starting from either (*S*)-valine methyl ester or (*S*)-valinol derived from the reduction of (*S*)-valine (Scheme 1).[5] Diphenylation of (*S*)-valine methyl ester or (*S*)-valine was not possible using palladium catalysed methods recently reported.[6] Instead monophenylation using triphenylbismuth diacetate, promoted or catalysed by copper diacetate,[7] gave **7** in 85% yield. This material could then be phenylated again, under similar conditions, to give **8** in 69% yield. Reduction of the diphenylamine **8** with LAH was followed by substitution of the hydroxy function with sulfur under Mitsunobu-type conditions and gave ligand **1** in 75% yield. Formation of the *N*-phenylformamide by warming **7** with acetic formic anhydride[8] in 96% yield was followed by treatment with LAH to effect simultaneous reduction to the *N*-methyl substituent and

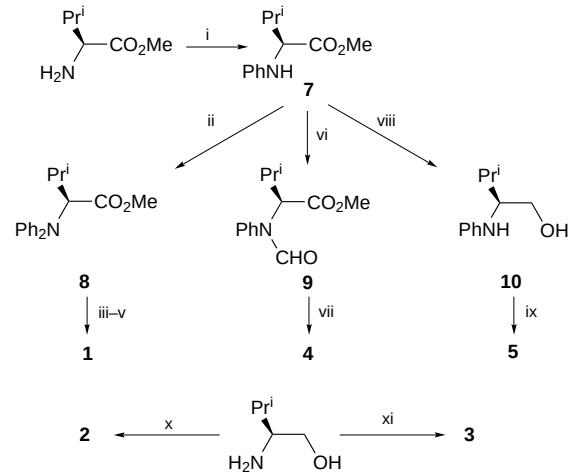

Scheme 1 *Reagents and conditions*: i, $Ph_3Bi(OAc)_2$ (1.2 equiv.), $Cu(OAc)_2$ (10 mol%), CH_2Cl_2, room temp., 24 h, 85%; ii, $Ph_3Bi(OAc)_2$ (1.5 equiv.) $Cu(OAc)_2$ (1 equiv.), CH_2Cl_2, room temp., 14 d, 69%; iii, LAH (4 equiv.), Et_2O–THF, room temp., 1 h; iv, diisopropyl azodicarboxylate (2 equiv.), Ph_3P (2 equiv.), AcSH (2 equiv.), room temp., 77% over two steps; v, LAH (4 equiv.) Et_2O–THF, 0 °C, 5 min, 98%; vi, AcOCHO (2.6 equiv.) HCO_2H (3.2 equiv.), THF, 70 °C, 2.5 h, 96%; vii, LAH (5 equiv.) Et_2O, 60 °C, 0.5 h, then (iv) followed by (v), 84% over three steps; viii, LAH (2 equiv.), Et_2O–THF, room temp., 0.5 h, 93%; ix, PhSSPh (3 equiv.), Bu_3P (4 equiv.), THF, 80 °C, sealed tube, 24 h, 75%; x, BnBr (2.2 equiv.), K_2CO_3 (2.5 equiv.), EtOH, room temp. 24 h, 91%, then (iv) followed by (v), 81% over two steps; xi, $Br(CH_2)_5Br$ (2 equiv.), K_2CO_3 (5 equiv.), EtOH, 60 °C, 48 h, 78%, then (iv) followed by (v), 72% over two steps

hydroxy function. Substitution by sulfur as before gave ligand **4** in 84% yield over three steps. Treatment of **7** with LAH gave alcohol **10** in 93% yield which was converted to the phenylthiol ligand **5** by heating in a sealed tube with diphenyl disulfide and tri-*n*-butylphosphine in 75% yield.[9]

Dibenzylation of (*S*)-valinol was achieved by treatment with benzyl bromide and potassium carbonate in 91% yield. Dialkylation of the amine function of (*S*)-valinol with 1,5-dibromopentane, under similar conditions, proceeded in 78% yield to form a piperidine. Substitution of the hydroxy function in each of these compounds by the aforementioned method gave ligands **2** and **3** in 81 and 72% yield, respectively (Scheme 1). The enantiohomogeneity of these ligands has been verified by racemic synthesis followed by NMR and HPLC comparison of their Mosher derivatives with the enantiomerically pure materials.

With these ligands in hand we screened their effectiveness as enantioselective catalysts in the addition of diethylzinc to aromatic aldehydes. Our initial experiments in this area are promising, as summarised in Table 1, and show good levels of enantioinduction in the presence of catalytic amounts (10 mol%) of the ligands **1**–**5**. Reactions were performed in toluene, at room temperature, for 3–20 h using 2.2 equiv. of diethylzinc.

These preliminary studies indicate that giving the nitrogen atom the potential to become stereogenic leads to a better system for enantioselection, as evidenced by the superior enantioselection of ligands **1** and **4** over **2** and **3** respectively. The best enantioselection (82% ee, entries 8 and 9) found with ligand **4** suggests that the donating ability of the nitrogen lone pair could be a factor in the efficiency of these ligands. This necessitates the need for further studies to try and separate the steric and electronic factors that are responsible for enhanced enantioselection. Ligands having a labile proton on nitrogen perform very poorly as catalysts in this particular reaction and along with the desired addition product, benzyl alcohol (38%) was formed from reduction of benzaldehyde.[10] These results show that non-symmetrical phenyl-substituted nitrogen donor atoms have a positive effect on the efficiency of these particular ligand systems. We believe we have a system with which we can probe the origins of chiral induction by further manipulation of the steric and electronic properties of these ligands. Further systematic modifications, studies designed to describe a transition state model and investigation of other metal catalysed systems will be reported in due course.

Table 1 Diethylzinc additions to aromatic aldehydes catalysed by chelate ligands **1**–**5**

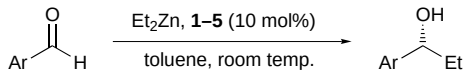

Entry	Ligand	Ar	Yield (%)[a]	Ee (%)[b]
1	**1**	Ph	85	74
2	**1**	*o*-$MeOC_6H_4$	88	52
3	**1**	*p*-$MeOC_6H_4$	91	62
4	**2**	Ph	91	58
5	**3**	Ph	78	66
6	**3**	*o*-$MeOC_6H_4$	92	65
7	**3**	*p*-$MeOC_6H_4$	100	62
8	**4**	Ph	80	82
9	**4**	*o*-$MeOC_6H_4$	83	82
10	**4**	*p*-$MeOC_6H_4$	90	78
11	**5**	Ph	35[c]	0

[a] Isolated yield. [b] Determined by chiral GLC using a Chrompack™ CP-Cyclodex B column or optical rotation (see note ‖). [c] Reaction time 3 days.

We thank the EPSRC (M. H.), the University of Sheffield, Pfizer and Zeneca for financial support. The loan of GC equipment from Dr Varinder K. Aggarwal and the help of Dr Elfyn Jones with GC is gratefully acknowledged.

Notes and References

† E-mail: j.anderson@sheffield.ac.uk

‡ These original assumptions have been supported by other workers (ref. 11).

§ A similar transmission of chirality occurs in the successful chiral diphosphine ligand chiraphos in various asymmetric palladium catalysed reactions (ref. 12).

¶ A similar conformational analysis has been invoked to explain the excellent enantioselectivities obtained in Diels–Alder reactions using an enantiomerically pure [N,*N*′-bis(trifluoromethylsulfonyl)-1,2-diphenylethane-1,2-diamine]aluminium complex as catalyst (ref. 13).

‖ In each case a positive rotation was obtained, indicating the (*R*)-enantiomer (ref. 14).

1 R. P. Hof, M. A. Poelert, N. C. M. W. Peper and R. M. Kellog, *Tetrahedron: Asymmetry*, 1994, **5**, 31.
2 J. Kang, J. W. Lee and J. I. Kim, *J. Chem. Soc., Chem. Commun.*, 1994, 2009.
3 J. Kang, D. S. Kim and J. I. Kim, *Synlett*, 1994, 842.
4 E. Rijnberg, J. T. B. H. Jastrzebski, M. D. Janssen, J. Boersma and G. van Koten, *Tetrahedron Lett.*, 1994, **35**, 6521.
5 M. J. McKennon, A. I. Meyers, K. Drauz and M. Schwarm, *J. Org. Chem.*, 1993, **58**, 3568.
6 A. S. Guram, R. A. Rennels and S. L. Buchwald, *Angew. Chem., Int. Ed. Engl.*, 1995, **34**, 1348; J. Louie and J. F. Hartwig, *Tetrahedron Lett.*, 1995, **36**, 3609; D.Ma and J. Yao, *Tetrahedron: Asymmetry*, 1996, **7**, 3075.
7 D. H. R. Barton, J.-P. Finet and J. Khamsi, *Tetrahedron Lett.*, 1989, **30**, 937.
8 S. Krishnamurthy, *Tetrahedron Lett.*, 1982, **23**, 3315.
9 R. Siedlecka and J. Swarzewski, *Synlett*, 1996, 757.
10 B. Marx, E. Henry-Basch and P. Freon, *C. R. Acad. Sci., Ser.*, 1967, 264.
11 J. Kang, J. B. Kim, J. W. Kim and D. Lee, *J. Chem. Soc., Perkin Trans. 2*, 1997, 189.
12 B. Bosnich and M. D. Fryzuch, in *Topics in Stereochemistry*, ed. G. L. Geoffroy, Wiley, 1981, vol. 12, p. 119 (see pp. 121–125).
13 E. J. Corey, R. Imwinkelried, S. Pikul and Y. B. Xiang, *J. Am. Chem. Soc.*, 1989, **111**, 5493.
14 R. H. Pickard and J. Kenyon, *J. Chem. Soc.*, 1914, 1115.

Received in Cambridge, UK, 4th November 1997; 7/07937K

Radical cyclization of α-iodo enones by photoinduced electron transfer reaction

Chin-Kang Sha,*† K. C. Santhosh, Chen-Tso Tseng and Chien-Ting Lin

Department of Chemistry, National Tsing Hua University, Hsinchu 300, Taiwan, ROC

A facile intramolecular radical cyclization of α-iodo enones effected by triethylamine-mediated photoinduced electron transfer (PET) reactions is described.

Photoinduced electron transfer (PET) reactions have been widely used for one electron reduction and cyclization reactions.[1] Recently, Cossy has employed a triethylamine-promoted PET reaction for the generation of alkyl radicals[2] and for various cyclization reactions.[3] Mattay has described the radical cyclization reactions of cyclopropyl and epoxy ketones effected by triethylamine-mediated PET reactions.[4] Triethylamine-induced carbocyclization of β-bromoprop-2-ynyl ethers in pyrimidenedione has also been reported.[5] As part of our investigation directed toward the total synthesis of natural products based on α-ketone[6] and α-enone[7] radical cyclizations, we were in search of an efficient and mild alternative route to the tributyltin hydride method. In this context we examined the triethylamine-mediated PET reactions of α-iodo ketones, α-iodo enones and vinyl iodides. Herein we report the preliminary results of our investigation.

We initiated our study with α-iodo ketones.[1] α-Iodo ketone **1** or **4** with triethylamine (10 equiv.) in MeCN (0.02 M) was irradiated in a Rayonet photoreactor with low pressure mercury lamp for 15 min (Scheme 1). The reaction mixture was purified by silica-gel column chromatography to afford the cyclized product **2** or **5** in low yield (35 and 40%, respectively). The other compounds isolated were the reduction products **3** and **6**. Attempts to improve the yields of this reaction under various conditions were futile. We then examined the PET radical cyclization of α-iodo enones. The α-iodo enones were synthesized from the corresponding enones[8] *via* a literature procedure.[9] A solution of α-iodo enone **8** or **11** in MeCN (0.02 M) with triethylamine (10 equiv.) was irradiated for 45 min. Upon workup, we obtained the cyclized product **9** ($E:Z$ = 3 : 1) or **12** ($E:Z$ = 1 : 1) in 74 and 61% yield, respectively. The generality of this PET radical cyclization of α-iodo enones was then investigated. The results are summarized in Table 1.

α-Iodo vinylogous esters **14** and **20** with a terminal acetylenic moiety and **17** and **23** with trimethylsilyl acetylenic groups underwent cyclization readily. While α-iodo enones and α-iodo vinylogous esters underwent smooth cyclization, the corresponding unprotected α-iodo vinylogous amide **26** failed to cyclize under these photolysis conditions. However, *N*-protected α-iodo vinylogous amide **29** underwent clean cyclization and afforded the double bond isomerized compound **30** upon silica-gel column chromatography. In order to test the limitations of this method, we also tried a similar procedure with vinyl iodides. The required iodo compounds **31** and **33** were prepared by standard procedures.[10] Compound **31** was photolyzed with triethylamine for 2 h, but the expected cyclization did not occur. Instead **31** underwent simple reduction to give compound **32**. Similarly, iodo compound **33** failed to cyclize upon irradiation and led only to the formation of reduction product **34** (Scheme 2).

Table 1 Irradiation of iodo enones, vinylogous esters and amides in the presence of triethylamine

Entry	Enones	α-Iodo enones	Cyclized products	Yield (%)[a,b] $E:Z$
1	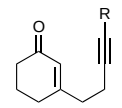	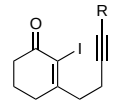	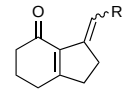	
	7 R = TMS	**8** R = TMS	**9** R = TMS	74 3:1[c]
	10 R = Et	**11** R = Et	**12** R = Et	61 1:1[c]
2	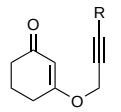	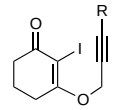	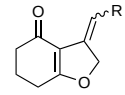	
	13 R = H	**14** R = H	**15** R = H	72 —
	16 R = TMS	**17** R = TMS	**18** R = TMS	68 5:3[c]
3	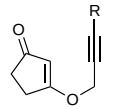	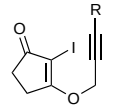	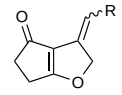	
	19 R = H	**20** R = H	**21** R = H	64 —
	22 R = TMS	**23** R = TMS	**24** R = TMS	64 3:1[c]
4	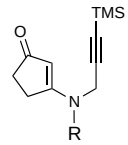	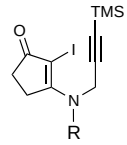	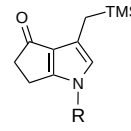	
	25 R = H	**26** R = H	**27** R = H	— —
	28 R = Boc	**29** R = Boc	**30** R = Boc	51[d] —

[a] Isolated yield. [b] The uncyclized reduction products were 10–25% for entries 1–3. [c] The *Z* and *E* isomers were characterized by NOE experiments. [d] The exocyclic double bond was isomerized to form the pyrrole ring during silica-gel column chromatography.

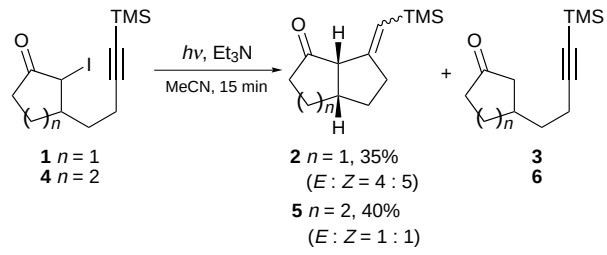

1 *n* = 1
4 *n* = 2

2 *n* = 1, 35% (*E* : *Z* = 4 : 5)
5 *n* = 2, 40% (*E* : *Z* = 1 : 1)

3
6

Scheme 1

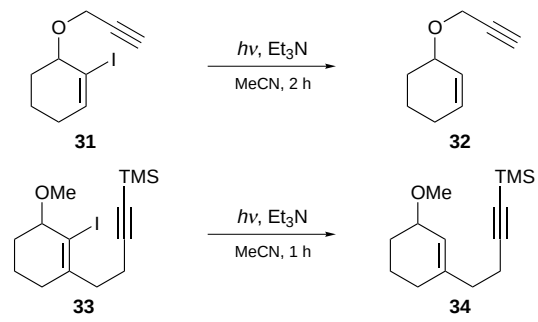

31 **32** **33** **34**

Scheme 2

In conclusion, we have achieved the efficient radical cyclization of α-iodo enones *via* triethylamine-mediated PET reactions, whereas the radical cyclization of α-iodo ketones using PET conditions afforded the cyclized product only in moderate yield. Presumably α-enone radicals, having the radical orbital orthogonal to the π-system of the enone, is more reactive and hence undergoes cyclization more effectively. Mild reaction conditions and easy product isolation make this route an attractive alternative to the tributyltin hydride method. This method eliminates the tedious separation of the tin compounds and would permit large scale preparations. The application of this method toward the total synthesis of natural products is being investigated in our laboratories.

We gratefully acknowledge a grant (NSC87-2113-M-007-043) from the National Science Council of the Republic of China.

Notes and References

† E-mail: cksha@chem.nthu.edu.tw

1 *Photoinduced Electron Transfer Reaction Part C*, eds. M. A. Fox and M. Chanon, Elsevier, New York, 1988; *Advances in Electron Transfer Chemistry*, ed. P. S. Mariano, JAI Press, Greenwich, CT, 1994, vol. 4; T. Kirschberg and J. Mattay, *Photochemical Key Steps in Organic Synthesis*, ed. J. Mattay and A. G. Griesbeck, Verlag Chemie, Weinheim, 1994; U. C. Yoon and P. S. Mariano, *Acc. Chem. Res.*, 1992, **25**, 233; S.-K. Khim, E. Cederstrom, D. C. Ferri and P. S. Mariano, *Tetrahedron*, 1996, **52**, 3195; D. Belotti, J. Cossy, J. P. Pete and C. Portella, *J. Org. Chem*., 1986, **51**, 4196 and references cited therein; E. Hasegawa, K. Ishiyama, T. Fujita, T. Kato and T. Abe, *J. Org. Chem*., 1997, **62**, 2396.

2 J. Cossy, J.-L. Ranaivosata and V. Bellosta, *Tetrahedron Lett*., 1994, **35**, 8161.

3 J. Cossy, A. Bouzide, S. Ibhi and P. Aclinou, *Tetrahedron*, 1991, **47**, 7775; J. Cossy and M. Guha, *Tetrahedron Lett*., 1994, **35**, 1715; J. Cossy, N. Furet and S. Bouzbouz, *Tetrahedron*, 1995, **51**, 11 751; J. Cossy and S. Bouabouz, *Tetrahedron Lett*., 1996, **37**, 5091.

4 T. Kirschberg and J. Mattay, *J. Org. Chem*., 1996, **61**, 8885.

5 J.-P. Dulcere, N. Baret, J. Rodriguez and R. Faure, *Synlett*, 1995, 705.

6 C.-K. Sha, R.-T. Chiu, C.-F. Yang, N.-T.Yao and W.-H. Tseng, *J. Am. Chem. Soc*., 1997, **119**, 4130; C.-K. Sha, T.-S. Jean and D.-C. Wang, *Tetrahedron Lett*., 1990, **31**, 3745.

7 C.-K. Sha, C.-Y. Shen, T.-S. Jean, R.-T.Chiu and W.-H. Tseng, *Tetrahedron Lett*., 1993, **34**, 7641.

8 Enones **7** and **10** were synthesized by the reaction of 3-ethoxycyclohex-2-en-1-one with 4-trimethylsilylbut-3-ynylmagnesium bromide or hex-3-ynylmagnesium bromide followed by acid hydrolysis: D. Becker, Z. Harel, M. Nagler and A. Gillon, *J. Org. Chem*., 1982, **47**, 449. Compounds **13**, **16**, **19**, **22** and **25** were prepared by condensation of 3-trimethylsilylprop-2-yn-1-ol or prop-2-yn-1-ol or 3-trimethylsilyl-prop-2-ynylamine with cyclohexane-1,3-dione or cyclopentane-1,3-dione.

9 C.-K. Sha and S.-J. Huang, *Tetrahedron Lett*., 1995, **36**, 6927; C. R. Johnson, J. P. Braun, C. B. W. Senanayake, P. M. Wovkulich and M. R. Uskokovic, *Tetrahedron Lett*., 1992, **33**, 917.

10 Compound **31** was prepared from 2-iodocyclohex-2-enone by reduction with sodium borohydride–cerium chloride followed by treatment with sodium hydride and prop-2-ynyl bromide. Compound **33** was obtained by reduction of **8** using sodium borohydride–cerium chloride followed by treatment with sodium hydride and iodomethane.

Received in Cambridge, UK, 24th November 1997; 7/08441B

Excited state properties of the (tropylium)molybdenum tricarbonyl cation

H. Kunkely and A. Vogler*

Institut für Anorganische Chemie, Universität Regensburg, 93040 Regensburg, Germany

The electronic spectrum of $[(\eta\text{-}C_7H_7)Mo^0(CO)_3]^+$ shows its longest-wavelength absorption at λ_{max} = 379 nm which is assigned to a $Mo^0 \rightarrow \eta\text{-}C_7H_7^+$ MLCT transition; the ^{3}MLCT excited state is luminescent at room temperature; solid $[(\eta\text{-}C_7H_7)Mo^0(CO)_3]PF_6$ as well as solutions of the complex in MeCN display this emission at λ_{max} *ca.* 580 nm; the MLCT state is also reactive; in EtOH solutions $[(\eta\text{-}C_7H_7)Mo^0(CO)_3]^+$ is reduced to $[(\eta\text{-}C_7H_8)Mo^0(CO)_3]$ with ϕ = 0.18 at λ_{irr} = 366 nm.

An important family of luminescent transition metal compounds comprises polypyridyl complexes such as $[Ru^{II}(bipy)_3]^{2+}$ [1,2] and $[Re^{I}(bipy)(CO)_3Cl]$.[3–5] These emitters are characterized by a reducing d^6 metal ion of the second or third transition series and heteroaromatic ligands which provide low-energy empty π^* orbitals. The emission originates from the lowest energy metal-to-ligand charge transfer (MLCT) triplet excited state. An analogous behavior may be observed for organometallic complexes which contain aromatic molecules or ions such as benzene or cyclopentadienyl anion as 6π-electron ligands. Unfortunately, the metal $\rightarrow \pi^*$ (aromatic hydrocarbon) MLCT states of such complexes are apparently located above the lowest energy ligand-field (LF) excited states. Accordingly, these compounds do not emit under ambient conditions, but undergo photosubstitution.[3] However, an emission could occur, if by a suitable choice of the aromatic ligand, the MLCT state is pushed below the LF states. In contrast to $C_5H_5^-$ and C_6H_6, the tropylium cation is a strong acceptor.[6,7] The electronic spectra of ion pairs consisting of $C_7H_7^+$ and donor anions such as I^- show characteristic long-wavelength outer sphere CT absorptions.[7–9] It follows that the tropylium cation should be an appropriate acceptor ligand in order to observe a low-energy and hence emitting MLCT state. We explored this possibility and selected the cation $[(\eta\text{-}C_7H_7)Mo^0(CO)_3]^+$[10–13] for the present study. This complex is easily accessible from $[(\eta\text{-}C_7H_8)Mo^0(CO)_3]$[11,14] which is commercially available (Aldrich).

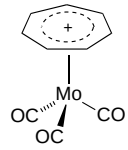

The electronic spectrum of $[(\eta\text{-}C_7H_7)Mo(CO)_3]^+$ in EtOH (Fig. 1) shows absorptions at λ_{max} = 379 nm (ε/dm^3 mol^{-1} cm^{-1} 1200), 298 (23 800), 236 (sh, 15 800). The energy of the long-wavelength bands is scarcely dependent on the solvent polarity. Solid $[(\eta\text{-}C_7H_7)Mo(CO)_3]PF_6$ shows a yellow emission at λ_{max} = 580 nm at room temperature. In solution this luminescence is slightly shifted (Fig. 1) and appears at λ_{max} = 578 nm. The excitation spectrum of $[(\eta\text{-}C_7H_7)Mo(CO)_3]^+$ matches essentially the absorption spectrum. This emission intensity is rather low in solution (ϕ *ca.* 10^{-5}). In EtOH the complex is light sensitive. The photolysis is accompanied by spectral changes (Fig. 2) which indicate the formation of $[(\eta\text{-}C_7H_8)Mo(CO)_3]$. At the isosbestic point (λ = 317 nm) $[(\eta\text{-}C_7H_7)Mo(CO)_3]^+$ and $[(\eta\text{-}C_7H_8)Mo(CO)_3]$ have the same

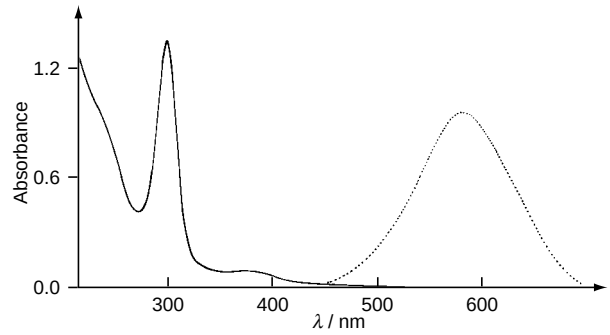

Fig. 1 Electronic absorption (—) and emission (---) spectra of $[(\eta\text{-}C_7H_7)Mo(CO)_3]PF_6$ at room temperature under argon. Absorption: 5.63 $\times$ 10^{-5} M in EtOH, 1 cm cell. Emission: in MeCN, λ_{exc} = 380 nm, intensity in arbitrary units.

absorption coefficient (4100). In a qualitative analysis protons and acetaldehyde are detected as further photoproducts. The progress of the photolysis was monitored by measuring the decrease of the optical absorption at 298 nm where the absorption coefficients of $[(\eta\text{-}C_7H_7)Mo(CO)_3]^+$ and $[(\eta\text{-}C_7H_8)Mo(CO)_3]$ are 23 800 and 3700, respectively. The quantum yield of this photoreaction is ϕ = 0.18 at λ_{irr} = 366 nm.

Complexes of the type $[(arene)M^0(CO)_3]$ can be viewed as pseudo-octahedral d^6 complexes in which the arene occupies three coordination sites at the central metal. The electronic spectra and photochemistry of a variety of such complexes have been studied in the past.[3] These compounds display $M^0 \rightarrow \pi^*$ arene MLCT absorptions near 300 nm. However, LF excited states are apparently located below these MLCT states as indicated by the emission behavior and photochemical properties. While related complexes such as $[Re^{I}(bipy)(CO)_3Cl]$ are characterized by lowest energy MLCT states which are luminescent under ambient conditions,[3–5] $[(arene)M^0(CO)_3]$

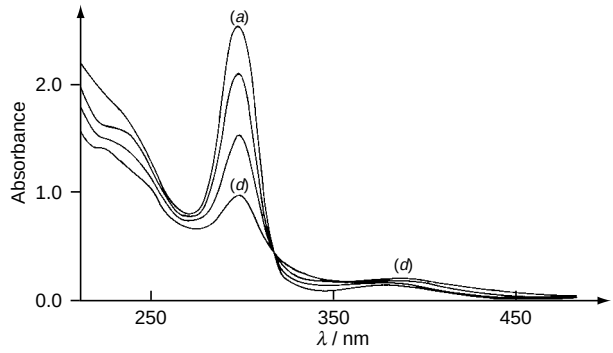

Fig. 2 Spectral changes during the photolysis of 1.06 $\times$ 10^{-4} M $[(\eta\text{-}C_7H_7)Mo(CO)_3]PF_6$ in EtOH under argon at room temp. after 0 (*a*), 5 (*b*), 10 (*c*) and 20 s (*d*) irradiation time, λ_{irr} = 313 nm (1 kW Xe/Hg 977 B-1 lamp), 0.1 cm cell

complexes are not emissive at room temperature and in solution.[3,4] The presence of lowest energy LF excited states is also consistent with the observation that these complexes undergo efficient photosubstitution reactions.[3]

If arenes in [(arene)$M(CO)_3$] are replaced by the isoelectronic aromatic tropylium cation which is a strong electron acceptor[6,7] MLCT states should be shifted to lower energies and might now occur below the photoactive LF states. The results of the present study are in agreement with this expectation.

The rather intense absorption of $[(\eta\text{-}C_7H_7)Mo(CO)_3]^+$ at λ_{max} = 379 nm (Fig. 1) is assigned to the $M^0 \rightarrow \pi^*$ $C_7H_7^+$ MLCT transition. This band is scarcely solvent dependent. However, the strong interaction of the tropylium ligand with Mo[10,13,15] is certainly associated with a considerable mixing of ligand and metal orbitals. Accordingly, the CT character should be reduced and the change of dipole moment during MLCT excitation might be quite small. On the other hand, the appearance of a room temperature emission is consistent with a MLCT assignment. It is assumed that the emitting state is a triplet in analogy to many other luminescing d^6 complexes with metals of the second and third transition row.[1–5]

In ethanol $[(\eta\text{-}C_7H_7)Mo(CO)_3]^+$ undergoes a photoreduction according to eqn. (1).

$$[(\eta\text{-}C_7H_7)Mo^0(CO)_3]^+ + EtOH \rightarrow [(\eta\text{-}C_7H_8)Mo^0(CO)_3] + H^+ + MeCHO \quad (1)$$

This reaction consists of a hydride transfer from ethanol to the $C_7H_7^+$ ligand yielding the cycloheptatriene complex and acetaldehyde. In the ground state only the reaction of $[(\eta\text{-}C_7H_7)Mo(CO)_3]^+$ with strong H^- donors such as BH_4^- generates the trialkene complex.[12,13] Although the mechanism of the photoreduction of coordinated $C_7H_7^+$ to C_7H_8 is unknown, it should be related to the nature of the reactive excited state. In the MLCT state the complex may be regarded as a Mo^I complex which contains a C_7H_7 radical as a ligand. The C_7H_7 radical should be able to abstract a hydrogen atom from ethanol [eqn. (3)].

$$[(C_7H_7^+)Mo^0(Co)_3]^+ \xrightarrow{MLCT} [(\cdot C_7H_7)Mo^I(CO)_3]^+ \quad (2)$$

$$[(\cdot C_7H_7)Mo^I(CO)_3]^+ + EtOH \rightarrow [(C_7H_8)Mo^I(CO)_3]^+ + Me\dot{C}HOH \quad (3)$$

The $Me\dot{C}HOH$ radical is a strong reductant and transfers an electron to the oxidizing Mo^I complex yielding the final products.

In conclusion, it has been shown that $[(\eta\text{-}C_7H_7)Mo(CO)_3]^+$ is characterized by a lowest energy MLCT state which is luminescent and, in the presence of suitable substrates, also reactive.

This work was supported by the Deutsche Forschungsgemeinschaft.

Notes and References

1 K. Kalyanasundaram, *Photochemistry of Polypyridine and Porphyrin Complexes*, Academic Press, London, 1992.
2 K. Kalyanasundaram, *Coord. Chem. Rev*., 1982, **46**, 159.
3 G. L. Geoffroy and M. S. Wrighton, *Organometallic Photochemistry*, Academic Press, New York, 1979.
4 A. J. Lees, *Chem. Rev*., 1987, **87**, 711.
5 D. J. Stufkens, *Comments Inorg. Chem*., 1992, **13**, 359.
6 A. Roberts and M. W. Whiteley, *J. Organomet. Chem*., 1993, **458**, 131.
7 K. B. Yoon and J. K. Kochi, *J. Phys. Chem*., 1991, **95**, 1348.
8 E. M. Kosover and P. E. Klinedinst, *J. Am. Chem. Soc*., 1956, **78**, 3493.
9 T. G. Beaumont and K. M. C. Davis, *J. Chem. Soc. B*, 1968, 1010.
10 G. R. Clark and G. J. Palenik, *J. Organomet. Chem*., 1973, **50**, 185.
11 R. B. King, *Organomet. Synth*., 1965, **1**, 141.
12 G. Deganello, *Transition Metal Complexes of Cyclic Polyolefins*, Academic Press, London, 1979, ch. 1.
13 R. Davis and L. A. P. Kane-Maguire, in *Comprehensive Organometallic Chemistry*, ed. G. Wilkinson, F. G. A. Stone and E. W. Abel, Pergamon, Oxford, 1982, vol. 3, ch. 27.2.
14 H. J. Dauben and L. R. Honnen, *J. Am. Chem. Soc*., 1958, **80**, 5570.
15 G. R. Clark and G. J. Palenik, *Chem. Commun*., 1969, 667.

Received in Cambridge, UK, 17th September 1997; 7/06767D

Controlled cleavage of $R_8Si_8O_{12}$ frameworks: a revolutionary new method for manufacturing precursors to hybrid inorganic–organic materials

Frank J. Feher,* Daravong Soulivong and Andrew G. Eklund

Department of Chemistry, University of California, Irvine, CA 92697-2025, USA

Cube-octameric polyhedral silsesquioxanes ($R_8Si_8O_{12}$) react with strong acids (HX) to produce $R_8Si_8O_{11}X_2$ frameworks resulting from selective cleavage of one Si–O–Si linkage; subsequent hydrolysis affords $R_8Si_8O_{11}(OH)_2$ frameworks derived from the net hydrolysis of one Si–O–Si linkage in $R_8Si_8O_{12}$; these results demonstrate for the first time that readily available $R_8Si_8O_{12}$ frameworks can be used as precursors to incompletely condensed Si/O frameworks and have important implications for the manufacture of hybrid inorganic–organic materials based on discrete polyhedral clusters of silicon and oxygen.

Discrete polyhedral clusters containing silicon and oxygen have recently emerged as precursors to new families of network solids[1] and hybrid inorganic–organic materials.[2] Two broad families of polyhedral Si/O clusters exist: (*i*) spherosilicates (*e.g.* **1**),[1a] which are most often prepared by silylation of silicate solutions;[3] and (*ii*) polyhedral silsesquioxanes[4a] (*e.g.* **2**, **3**),

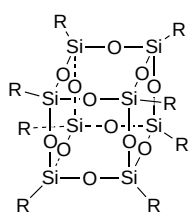

1 R = $OSiR^1R^2R^3$
2 alkyl or aryl
3 c-C_6H_{11}
4 c-C_6H_5

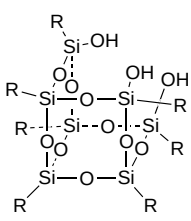

5 R = Cy
6 c-C_5H_9

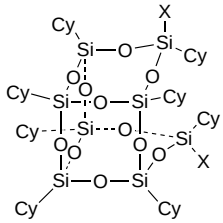

7 X = F
8 $OSnMe_3$
9 OH
10 OTf

which are usually obtained from hydrolytic condensation reactions of trifunctional organosilicon monomers ($RSiX_3$),[3b,4] hydrosilylation of hydridosilsesquioxanes[2c,f,5] or 'corner-capping' reactions of trisilanols **5** and **6**.[6a,b] Both families have enormous potential as building blocks for advanced materials if cost-effective methods can be devised to produce appropriately functionalized Si/O frameworks on a large scale.

Here, we outline a new strategy for preparing functionalized silsesquioxanes from fully condensed [$R_8Si_8O_{12}$] frameworks (*e.g.* **3**). The salient feature of our approach is a general and remarkably selective method for effecting cleavage of a single framework siloxane linkage. Products from this reaction are versatile precursors to a wide range of functionalized Si/O frameworks, including several that could be manufactured on a large scale from readily available organosilicon monomers.

The addition of an excess of $HBF_4{\cdot}OMe_2$ (4.6 equiv.) and $BF_3{\cdot}OEt_2$ (6 equiv.) to a solution of **3** in $CDCl_3$ or C_6D_6 does not produce an immediate reaction at 25 °C, but upon standing for several hours or brief refluxing, NMR resonances for a new fluoride-substituted silsesquioxane appear at the expense of resonances for **3**. On the basis of multinuclear NMR data (^1H, ^{13}C, ^{29}Si, ^{19}F), a high-resolution mass spectrum, and the strong preference for stereochemical inversion at Si in related reactions,[6c,d] this product was identified as **7**, a C_{2v}-symmetric framework derived from cleavage of a single Si–O–Si linkage.† Difluoride **7** is the only Si-containing product formed by the reaction, but the reaction consistently stops at 70–85% conversion because water produced during the reaction lowers the activity of HBF_4 to a point where protonation and subsequent cleavage of Si–O–Si linkages are no longer favorable.

Like other fluoride-substituted silsesquioxanes, **7** is stable to air and water, but it can be hydrolyzed with retention of stereochemistry at Si in two steps by sequential treatment with Me_3SnOH and aqueous HCl.[6c,d] The reaction of **7** with Me_3SnOH (reflux, 46 h, $CHCl_3$) proceeds with complete retention of stereochemistry at Si to afford **8**, which reacts rapidly with dilute aqueous HCl to produce **9**. Yields for both reactions are quantitative by NMR spectroscopy, so the three-step synthesis of **9** from **3** can be accomplished easily on a laboratory scale with good overall yield.

It is tempting to conclude that cleavage of Si–O–Si bonds by HBF_4/BF_3 is driven by the formation of strong Si–F bonds, but it is clear from reactions of **3** with other strong acids that the acidity of HBF_4 is more important for Si–O–Si cleavage than the availability of fluoride. In fact, a source of fluoride is not required to induce framework cleavage. We have examined a number of strong acids, but our preliminary results with triflic acid (CF_3SO_3H, TfOH) are particularly promising.

Triflic acid is one of the strongest organic acids available, and under normal conditions it is not a source of fluoride. The reaction of **3** with an excess of TfOH (5 equiv., 25 °C, C_6H_6) occurs quickly upon mixing and within 30 min produces a quantitative yield of a new C_{2v}-symmetric ditriflate derived from cleavage of a single Si–O–Si linkage. Ditriflate **10** is the product expected if framework cleavage by TfOH is mechanistically analogous to the reaction of **3** with HBF_4/BF_3, but structure **11** is equally consistent with all of our spectroscopic data and should not be dismissed until the stereochemical consequences of silsesquioxane–triflic acid reactions (*vide infra*) are independently corroborated by X-ray diffraction studies.‡ Regardless of its structure, the ditriflate is surprisingly resistant to further framework cleavage under conditions where **3** is completely consumed. It is not obvious why this is the case because most crystallographic data suggest that $R_8Si_8O_{12}$ frameworks adopt structures with strain-free Si–O–Si linkages,[4a] but it is clear from our results that **3** is at least two orders of magnitude more susceptible to cleavage by TfOH than the ditriflate derived from cleavage of a single Si–O–Si linkage.

In stark contrast to difluoride **7**, which does not react with water (even at 80 °C in the presence of pyridine), the ditriflate obtained from **3** is very difficult to handle without producing hydrolysis products. In fact, hydrolysis of both Si–OTf groups occurs immediately upon exposure to water to produce disilanol **12** and variable amounts of **3**, which presumably forms *via* intramolecular cyclization of the intermediate monosilanol/monotriflate. When hydrolysis is performed by adding Et_2O solutions of the ditriflate and excess NEt_3 to water-saturated Et_2O, **12** and **3** are produced in a 97 : 3 ratio.

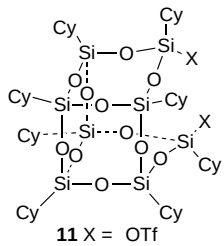

11 X = OTf
12 OH

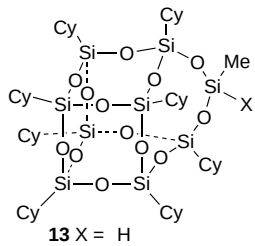

13 X = H
14 $CH_2CH_2CMe_2CH_2CO_2Me$

Structural assignment of **12** was made on the basis of multinuclear NMR spectroscopy, a high-resolution mass spectrum and combustion analysis. The *endo* orientation of both Si–OH groups is evident from the ^{1}H NMR spectrum, which exhibits a broad resonance at δ 4.44 for the two H-bonded SiOH groups. This is within the chemical shift range observed for other intramolecularly H-bonded SiOH groups[6a,e] and nearly 2.5 ppm downfield from the ^{1}H NMR resonance for the isolated SiOH groups in **9** (δ 2.00). Final confirmation of our assignment is provided by the reaction of **12** with $MeHSiCl_2$ (25 °C, NEt_3–Et_2O) which produces quantitative yields of **13**. Subsequent hydrosilylation (Kardstedt's catalyst, C_6D_6, 25 °C, 1.5 h)[5a] of **13** with $H_2C{=}CHCMe_2CH_2CO_2Me$ affords **14** as the sole Si-containing product.

The two-step synthesis of **12** from **3** requires both the reaction of **3** with TfOH and hydrolysis of the resulting ditriflate to occur with the same stereochemical consequences at silicon. Both reactions must proceed with complete inversion at Si or both must proceed with complete retention. Inversion at silicon during nucleophilic displacement reactions is usually observed when good leaving groups are replaced by poor (*i.e.* soft) nucleophiles.[7] Retention at silicon is usually favored when poor leaving groups are replaced by strong (*i.e.* hard) nucleophiles.[7] Water is a much poorer nucleophile than MeLi or hydroxide, and triflate (*i.e.* $CF_3SO_3^-$) is a much better leaving group than fluoride. Both factors should favor stereochemical inversion during hydrolysis of Si–OTf. It is therefore highly probable that both the reaction of **3** with excess TfOH (to produce **10**) and the subsequent formation of **12** proceed with complete inversion of stereochemistry at Si.

Most $R_8Si_8O_{12}$ frameworks are thermally very stable and surprisingly unreactive toward reagents that normally attack cyclic siloxanes.[4a] When framework cleavage was observed in the past, it normally produced complicated product mixtures or occurred under conditions where extensive framework degradation was followed by equilibration to other thermodynamically stable clusters ($R_{10}Si_{10}O_{15}$, $R_{12}Si_{12}O_{18}$, *etc.*).[8] The work presented here describes a revolutionary advance in the chemistry of silsesquioxanes because it demonstrates for the first time that a readily available $R_8Si_8O_{12}$ framework can be used as a precursor to incompletely condensed Si/O frameworks. In fact, the net monohydrolysis of $Cy_8Si_8O_{12}$ **3** can be accomplished selectivity with either of two useful stereochemical outcomes (*i.e.* **9** or **12**). In light of the fact that **3** can be prepared in high yield *via* the catalytic hydrogenation of $Ph_8Si_8O_{12}$ **4**,[4c] which in turn can be prepared in nearly quantitative yield from relatively inexpensive $PhSiX_3$ monomers,[4d] the transformations described here present the very real possibility that functionalized Si/O frameworks can be manufactured on a truly large scale for production of advanced inorganic–organic hybrid materials. The results from our work to expand the scope of these powerful new synthetic methods, as well as our efforts to use ditriflate **10** as a precursor to new Si/O and Si/O/M frameworks will be reported in due course.

These studies were supported by the National Science Foundation and Phillips Laboratory (Edwards AFB).

Notes and References

* E-mail: fjfeher@uci.edu

† *Selected spectroscopic data*: **7**: ^{13}C{^{1}H} NMR (125 MHz, $CDCl_3$, 25 °C) δ 27.41–26.04 (CH_2), 23.47, 22.85, 21.86 (d, *J* 23.2 Hz) (2 : 1 : 2 for CH). ^{29}Si{^{1}H} NMR (99 MHz, $CDCl_3$, 25 °C) δ −63.69 (d, *J* 274 Hz), −67.44, −68.26 (2 : 4 : 2). EIMS (70 eV, 200 °C, relative intensity): *m/z* 1019 ([M − Cy]$^+$, 100%). **9**: ^{1}H NMR (500 MHz, $CDCl_3$, 25 °C) δ 2.00 (br s, SiOH, 2 H), 1.74 (br m, 40 H), 1.24 (br m, 40 H), 0.82 (br m, 2 H), 0.76 (br m, 6 H). ^{13}C{^{1}H} NMR (125 MHz, $CDCl_3$, 25 °C) δ 27.54–27.33 (CH_2), 26.83–26.54 (CH_2), 23.83, 23.27, 23.02 (2 : 1 : 1 for CH). ^{29}Si{^{1}H} NMR (99 MHz, $CDCl_3$, 25 °C) δ −56.88, −67.31, −68.45 (1 : 1 : 2). MS (70 eV, 200 °C, relative intensity): *m/z* 1015 ([M − Cy]$^+$, 100%). **10**: ^{1}H NMR (500 MHz, C_6D_6, 25 °C) δ 2.10 (br m), 1.75 (br m), 1.57 (br m), 1.24 (br m). ^{13}C{^{1}H} NMR (125 MHz, C_6D_6, 25 °C) δ 119.20 (CF_3, *J* 317 Hz), 27.67, 27.61, 27.31, 27.02, 26.90, 26.40, 26.01 (s for CH_2), 24.04, 23.51, 23.33 (s, 4 : 2 : 2 for CH). ^{29}Si{^{1}H} NMR (99 MHz, C_6D_6, 25 °C) δ −63.55, −66.32, −67.60 (s, 2 : 2 : 4 for CH). **12**: ^{1}H NMR (500 MHz, $CDCl_3$, 25 °C) δ 4.45 (br s, SiOH), 1.77 (br s, 40 H), 1.24 (br s, 40 H), 0.75 (br s, 8 H) ^{13}C{^{1}H} NMR (125 MHz, $CDCl_3$, 25 °C) δ 27.54, 27.47, 26.87, 26.77, 26.53, 26.51 (s for CH_2), 23.77, 23.65, 23.05 (s, 4 : 2 : 2 for CH). ^{29}Si{^{1}H} NMR (99 MHz, $CDCl_3$, 25 °C) δ −59.84, −67.58, −69.82 (s, 2 : 2 : 4). MS (70 eV, 200 °C, relative intensity): *m/z* 1015 ([M − Cy]$^+$, 100%). **13**: ^{1}H NMR (500 MHz, $CDCl_3$, 25 °C) δ 4.64 (d, 1 H, SiH, $^3J_{HH}$ 1.6, J_{HSi} 246.5 Hz), 1.75 (br s, 40 H), 1.24 (br s, 40 H), 0.76 (br s, 8 H), 0.20 (d, 3 H, CH_3, $^3J_{HH}$ 1.6 Hz). ^{13}C{^{1}H} NMR (125 MHz, $CDCl_3$, 25 °C) δ 27.60, 27.57, 27.52, 26.92, 26.78, 26.58 (s for CH_2), 23.90, 23.75, 23.13 (s, 2 : 4 : 2 for CH), 0.57 (CH_3). ^{29}Si{^{1}H} NMR (99 MHz, $CDCl_3$, 25 °C) δ −35.68 [Si(H)Me], −67.80, −69.26, −70.24, −70.34 (s, 2 : 2 : 2 : 2). MS (70 eV, 200 °C, relative intensity): *m/z* 1139 ([M − H]$^+$, 3%), 1125 ([M − Me]$^+$, 5%), 1057 ([M − Cy]$^+$, 100%). **14**: ^{1}H NMR (500 MHz, $CDCl_3$, 25 °C) δ 3.65 (s, 3 H, OCH_3), 2.18 (s, 2 H, CH_2CO), 1.74 (br s, 40 H), 1.34 (m, 2 H, CH_2), 1.23 (br s, 40 H), 0.97 (s, 6 H, CMe_2), 0.74 (br s, 6 H), 0.68 (br s, 2 H), 0.50 (m, 2 H, $SiCH_2$), 0.10 (s, 3 H, $SiCH_3$). ^{13}C{^{1}H} NMR (125 MHz, $CDCl_3$, 25 °C) δ 172.98 (C=O), 50.99 (OCH_3), 45.23 (CH_2CO), 35.67 ($SiCH_2CH_2$), 33.86 (*C*Me_2), 27.58, 27.55, 27.50, 26.91, 26.86, 26.73, 26.71, 26.55 (s, for CH_2), 26.49 (C*Me*$_2$), 24.08, 23.76, 23.72, 23.10 (s, 2 : 2 : 2 : 2 for CH), 10.61 ($SiCH_2$), −1.49 ($SiCH_3$). ^{29}Si{^{1}H} NMR (99 MHz, $CDCl_3$, 25 °C) δ −20.69 [Si(Me)CH_2], −67.88, −70.38, −70.42, −70.44 (s, 2 : 2 : 2 : 2). MS (MALDI-TOF, dithranol, relative intensity): *m/z* 1199 ([M − Cy]$^+$, 20), 1139 ([M − $C_8H_{15}O_2$]$^+$, 100%).

‡ We hope to establish the structure of the ditriflate by a single-crystal X-ray diffraction study, but the compound is extremely water-sensitive, highly soluble in all solvents with which it does not react, and prone to precipitate as poorly diffracting microcrystals.

1 (*a*) P. A. Agaskar, *Colloids Surf.*, 1992, **63**, 131; (*b*) H. C. L. Abbenhuis, H. W. G. van Herwijnen and R. A. van Santen, *Chem. Commun.*, 1996, 1941.

2 (*a*) J. D. Lichtenhan, in *Silsesquioxane-Based Polymers*, ed. J. C. Salamone, New York, 1996; (*b*) J. D. Lichtenhan, *Comments Inorg. Chem.*, 1995, **17**, 115; (*c*) A. Tsuchida, C. Bolln, F. G. Sernetz, H. Frey and R. Mulhaupt, *Macromolecules*, 1997, **30**, 2818; (*d*) A. Sellinger and R. M. Laine, *Chem. Mater.*, 1996, **8**, 1592; (*e*) I. Hasegawa, *J. Sol-Gel Sci. Technol.*, 1995, **5**, 93; (*f*) J. V. Crivello and R. Malik, *J. Polym. Sci., Part A: Polym. Chem.*, 1997, **35**, 407.

3 (*a*) D. Hoebbel, I. Pitsch, T. Reiher, W. Hiller, H. Jancke and D. Muller, *Z. Anorg. Allg. Chem.*, 1989, **576**, 160; (*b*) R. Weidner, N. Zeller, B. Deubzer and V. Frey, *US Pat.*, 5 047 492, 1991.

4 (*a*) M. G. Voronkov and V. Lavrent'ev, *Top. Curr. Chem.*, 1982, **102**, 199; (*b*) U. Dittmar, B. J. Hendan, U. Flörke and H. C. Marsmann, *J. Organomet. Chem.*, 1995, **489**, 185; (*c*) F. J. Feher and T. A. Budzichowski, *J. Organomet. Chem.*, 1989, **373**, 153; (*d*) J. F. Brown, *J. Am. Chem. Soc.*, 1965, **87**, 4317.

5 A. R. Bassindale and T. E. Gentle, *J. Mater. Chem.*, 1993, **3**, 1319; (*b*) D. Herren, H. Bürgy and G. Calzaferri, *Helv. Chim. Acta*, 1991, **74**, 24.

6 (*a*) F. J. Feher, D. A. Newman and J. F. Walzer, *J. Am. Chem. Soc.*, 1989, **111**, 1741; (*b*) F. J. Feher, T. A. Budzichowski, R. L. Blanski, K. J. Weller and J. W. Ziller, *Organometallics*, 1991, **10**, 2526; (*c*) F. J. Feher, D. Soulivong and G. T. Lewis, *J. Am. Chem. Soc.*, 1997, **119**, 11 323; (*d*) F. J. Feher, S. H. Phillips and J. W. Ziller, *J. Am. Chem. Soc.*, 1997, **119**, 3397; (*e*) F. J. Feher and D. A. Newman, *J. Am. Chem. Soc.*, 1990, **112**, 1931.

7 R. J. P. Corriu and C. Guerin, *J. Organomet. Chem.*, 1980, **198**, 231.

8 (*a*) E. Rikowski and H. C. Marsmann, *Polyhedron*, 1997, **16**, 3357; (*b*) J. F. Brown, L. H. Vogt and P. I. Prescott, *J. Am. Chem. Soc.*, 1964, **86**, 1120.

Received in Bloomington, IN, USA, 30th September 1997; 7/07061F

Catalytic conversions in water. Part 9. High activity of the Pd/dpppr-s/Brønsted acid system in the alternating copolymerization of ethene and carbon monoxide {dpppr-s = C_3H_6-1,3-[P(C_6H_4-*m*-$SO_3Na)_2]_2$}

GöranVerspui, Georgios Papadogianakis and Roger A. Sheldon*†

Laboratory for Organic Chemistry and Catalysis, Delft University of Technology, Julianalaan 136, NL-2826 BL Delft, The Netherlands

The formation of alternating copolymers of ethene and carbon monoxide proceeds rapidly in the aqueous phase in the presence of a water-soluble palladium catalyst and a Brønsted acid; activities of >4 kg of polymer per g palladium per hour were observed.

Currently there is a growing interest in organometallic catalysis in water.[1] The replacement of organic solvents by water is advantageous for environmental, safety and economical reasons and the use of biphasic systems facilitates catalyst recycling. Nevertheless, there are few examples of (biphasic) aqueous systems with acceptable catalytic activities.

The palladium catalyzed alternating copolymerization of α-olefins and carbon monoxide affords polyketones with commercially interesting properties.[2] The most active catalysts are palladium(II) complexes with bidentate phosphines, *e.g.* 1,3-bis(diphenylphosphino)propane (dpppr).[3] Jiang and Sen[4] attempted to perform the alternating copolymerization in pure water but, unfortunately, their system suffered from low catalytic activity (470 g polymer per gram Pd in 22 h).

We recently found high activities for the water-soluble palladium catalyst [Pd(tppts)$_3$] [tppts = P(C_6H_4-*m*-$SO_3Na)_3$] in the biphasic hydrocarboxylation of propene.[5] We now report on the facile formation of alternating copolymers of ethene and carbon monoxide in the presence of the bidentate water-soluble phosphine C_3H_6-1,3-[P(C_6H_4-*m*-$SO_3Na)_2]_2$ (dpppr-s) and a Brønsted acid cocatalyst (*vide infra*). Indeed, under mild and only partly optimized reaction conditions, the catalyst exhibits activities (*ca.* 4 kg polymer per gram Pd per hour, ±7600 mol ethene per mol Pd per hour) comparable to those observed with Pd/dpppr systems in organic solvents, *e.g.* MeOH which is quite extraordinary for a water-soluble catalyst.

We applied a recently developed sulfonation procedure for the synthesis of the water-soluble analogue of dpppr;[6] dpppr-s‡ was obtained in high yield (90%) and purity (98%) and its structure was confirmed by ^{1}H, ^{13}C and ^{31}P NMR and elemental analysis.

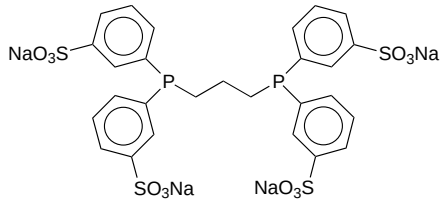

The catalyst was prepared *in situ* by addition of dpppr-s dissolved in water to an aqueous solution of [Pd{OTs}$_2${NCMe}$_2$]. Analogous to non-aqueous systems, the use of a bidentate ligand has a dramatic effect on the outcome of the reaction (Scheme 1). Whereas tppts affords predominantly propionic acid, the water-soluble bidentate dpppr-s results in the formation of the alternating copolymer. The reaction conditions§ are rather mild and only extremely low concentrations of palladium (< 0.14 mmol l^{-1}) are needed for a rapid conversion. Under these conditions no low molecular weight compounds (n = 1–6) are formed, as determined by HPLC analysis.

The optimum dpppr-s : Pd ratio is 1 : 1 (see Table 1). Without ligand metallic palladium is formed, while an excess of ligand (dpppr-s : Pd = 2 : 1) inhibits the reaction. The addition of a Brønsted acid is important for the stability of the catalyst. At low Brønsted acid concentration a lower catalyst activity is observed and large amounts of metallic palladium are formed during the reaction. The optimum results were obtained with 50 equiv. of Brønsted acid per palladium (1.0 mmol, run 7).

The anion of the Brønsted acid should be weakly- or non-coordinating, *e.g.* $CF_3CO_2^-$ or TsO^-. With the strongly coordinating iodide anion no catalytic activity was observed (run 6). These results are consistent with those observed in the Pd/tppts-catalyzed hydrocarboxylation of α-olefins.[5]

The copolymers are white solids that precipitate during the reaction, which implies that the reaction can proceed heterogeneously in aqueous media. The average molecular weights (Table 1) are lower than for copolymers obtained in the Pd/dpppr system in MeOH (6.6 *vs.* 8.5 kg mol^{-1}).[3a]

We assume that the aqueous phase copolymerization proceeds *via* a similar reaction pathway to that proposed by Drent *et al.*[3a] for the organic soluble system (Scheme 2). Initiation takes place by ethene insertion in a palladium–hydride bond. The palladium hydride [PdH{dpppr-s} {L}]$^+$ (L = H_2O,

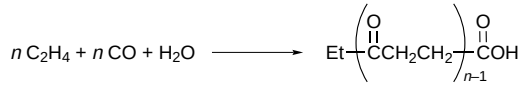

Scheme 1

Table 1 The alternating copolymerization of ethene and carbon monoxide catalyzed by the aqueous Pd/dpppr-s system[a]

Run	Ligand	Ligand : Pd	Brønsted acid	(mmol)	Activity[b]	Molecular weight/kg mol^{-1}[c]
1[d,e]	—	0.0	TsOH	(30.0)	0	—
2	dpppr-s	1.0	TsOH	(10.0)	3.58	6.1
3	dpppr-s	1.5	TsOH	(10.0)	1.56	6.5
4	dpppr-s	2.0	TsOH	(10.0)	0.56	6.1
5	dpppr-s	1.0	TFA	(10.0)	3.87	6.9
6	dpppr-s	1.0	HI	(10.0)	0	—
7	dpppr-s	1.0	TsOH	(1.0)	4.03	6.6
8[d]	dpprs-s	1.0	TsOH	(0.2)	3.44	7.7
9[d]	dpprs-s	1.0	—	(0.0)	2.83	6.5
10[f]	dpprs-s	1.0	TsOH	(10.0)	2.04	10.9

[a] Reaction conditions: 0.020 mmol [Pd{OTs}$_2${NCMe}$_2$], ligand and Brønsted acid in water, 141.9 g of total reaction mixture, 0.20 mol ethene, 40 bar constant total pressure, 90 °C, 60 min, stirring speed: 1000 rpm. [b] In kg polymer per gram Pd per hour. [c] Determined by quantitative ^{13}C NMR analysis. [d] Formation of metallic palladium during reaction. [e] Reaction time: 120 min. [f] Reaction temperature: 70 °C, reaction time: 65 min.

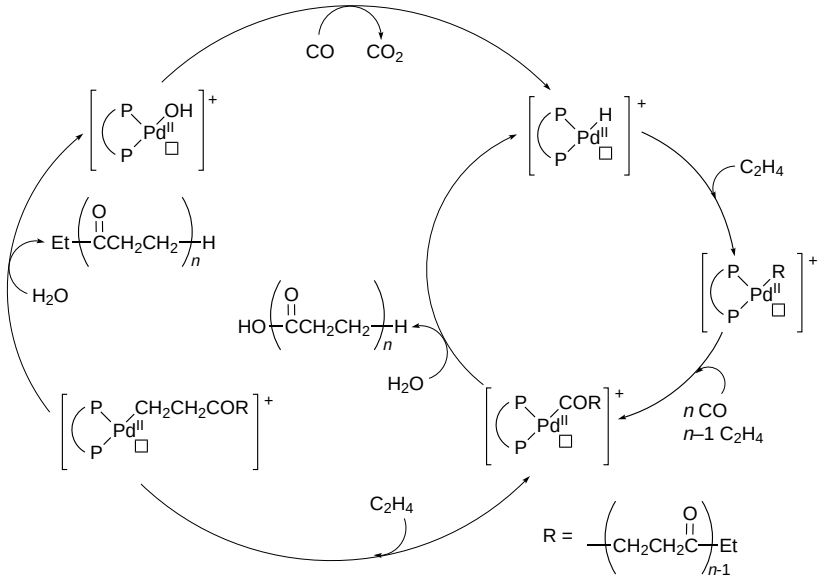

Scheme 2

NCMe, anion or monomer) can for instance be formed *in situ* by successive reduction of [Pd{dpppr-s} {L}]$_2$]$^{2+}$ by CO and water to a Pd^0 complex[7] and oxidative addition of the Brønsted acid. The initiation is followed by alternating insertion of carbon monoxide into a palladium–alkyl bond and ethene insertion in a palladium–acyl bond. The strictly alternating fashion of chain growth is terminated by hydrolysis of either a palladium–acyl or a palladium–alkyl bond, resulting in the formation of a carboxylic or a keto end group, respectively. In the latter case a palladium(II) hydroxo species is formed which can be reduced by carbon monoxide to regenerate the original hydride.

The much higher activity of our system compared to that previously reported[4] can be explained by the addition of a Brønsted acid cocatalyst and the high purity of the ligand. The addition of a Brønsted acid prevents decomposition of the catalyst and thus enhances its productivity. Moreover, impurities, such as partly oxidized ligand [Ar_2PO–$(CH_2)_3$–PAr_2] and inorganic salts can inhibit the reaction by occupying free coordination sites on the palladium.

We conclude that the alternating copolymerization of olefins and carbon monoxide in water constitute an alternative, environmentally friendly method for the preparation of new low-cost polymers with interesting properties. Studies are underway aimed at further optimization of this system and confirming the molecular weights of the polymers by alternative techniques.

Financial support by the Foundation for Chemical Research in the Netherlands (SON/NWO) is greatly acknowledged.

Notes and References

† E-mail: r.a.sheldon@stm.tudelft.nl

‡ *Ligand synthesis*: 4.95 g of dpppr (12.0 mmol) was dissolved in a solution of 4.00 g of orthoboric acid (64.7 mmol) in 37.5 ml of H_2SO_4 (98%). After *ca.* 90 min 67.5 ml oleum (65%) was added at 0–5 °C under vigorous stirring. After the addition the solution was stirred at room temperature for 48 h. The mixture was hydrolyzed at 0–5 °C with 800 ml of H_2O. The product was extracted from the water phase with tri-isooctylamine in toluene. The organic layer was washed repeatedly with water. By addition of 5% aq. NaOH, the pH was increased and the fraction of pH 4.6–12.5 was collected, washed with pentane and evaporated to dryness. Yield: 90%, purity: 98% (based on ^{31}P-NMR analysis). *Selected data*: δ_H (300.2 MHz, 25 °C, D_2O) δ: 7.70 (m, 4 H), 7.65 (m, 4 H), 7.35 (m, 8 H), 2.19 (t, *J* 8 Hz, 4 H), 1.39 (m, 2 H); δ_C (100.6 MHz, 25 °C, D_2O) 144.4 (d, *J* 6 Hz), 140.0 (d, *J* 12 Hz), 136.8 (d, *J* 17 Hz), 131.0 (s), 130.8 (d, *J* 15 Hz), 121.6 (s), 29.1 and 29.0 (dd, *J* 9 Hz), 22.7 (t, *J* 16 Hz); δ_P (121.5 MHz, 25 °C, D_2O) −16.3 (s). Calc. for $C_{27}H_{22}O_{12}P_2S_4Na_4{\cdot}4H_2O$: P, 6.67, S, 13.81. Found: P, 6.52, S, 13.6% (S/P = 2.0).

§ *Copolymerization reactions*. Under an argon atmosphere an aqueous solution of [Pd{OTs}$_2${NCMe}$_2$] (0.020 mmol), dpppr-s and Brønsted acid was transferred to a 300 ml Hasteloy C autoclave and diluted to give 141.9 g of reaction mixture ([Pd] = 0.14 mmol l^{-1}). The argon was replaced by carbon monoxide after five pressurizing–depressurizing cycles. The reaction mixture was stirred (1000 rpm) and the autoclave was pressurized with carbon monoxide *via* a stainless steel cylinder that contained 0.20 mol of ethene and heated to the reaction temperature. The pressure was kept constant by addition of carbon monoxide. After the reaction the autoclave was cooled to room temperature immediately. The reactant gasses were vented and the product was filtered, washed with water (50 ml) and EtOH (2 × 50 ml) and dried *in vacuo*. The average molecular weights of the copolymer samples were determined by quantitative ^{13}C NMR analysis in a mixture of 1,1,1,3,3,3-hexafluoropropan-2-ol and $CDCl_3$ (9 : 1).

1 F. Joó and A. Kathó, *J. Mol. Cat. A.*, 1997, **116**, 3; G. Papadogianakis and R. A. Sheldon, *New J. Chem.*, 1996, **20**, 175; I. T. Horváth and F. Joó, *NATO ASI Ser., Ser. 3*, 1995, 5 (*Aqueous Organometallic Chemistry and Catalysis*); W. A. Herrmann and C. W. Kohlpaintner, *Angew. Chem.*, 1993, **105**, 1588; *Angew. Chem., Int. Ed. Engl.*, 1993, **32**, 1524.

2 E. Drent and P. H. M. Budzelaar, *Chem. Rev.*, 1996, **96**, 663; A. Sen, *Acc. Chem. Res.*, 1993, **26**, 303.

3 (*a*) E. Drent, J. A. M. van Broekhoven and M. J. Doyle, *J. Organomet. Chem.*, 1991, **417**, 235; (*b*) E. Drent, *Pat. Appl.*, EP 121 965 (1984) (to Shell).

4 Z. Jiang and A. Sen, *Macromolecules*, 1994, **27**, 7215.

5 G. Papadogianakis, G. Verspui, L. Maat and R. A. Sheldon, *Catal. Lett.*, 1997, **47**, 43; see also F. Bertoux, S. Tilloy, E,. Monflier, Y. Castanet and A. Mortreux, *New. J. Chem.*, 1997, **21**, 529.

6 W. A. Herrmann, G. P. Albanese, R. B. Manetsberger, P. Lappe and H. Bahrmann, *Angew. Chem.*, 1995, **107**, 893; *Angew. Chem., Int. Ed. Engl.*, 1995, **34**, 811; G. P. Albanese, R. B. Manetsberger and W. A. Herrmann, *Pat. Appl.* DE 4435189 (1994) (to Hoechst).

7 [PdCl{tppts}$_3$]$^+$ is reduced to [Pd{tppts}$_3$] within 5 min under 2 bar CO pressure: G. Papadogianakis, J. A. Peters, L. Maat and R. A. Sheldon, *J. Chem. Soc., Chem. Commun.*, 1995, 1105.

Received in Liverpool, UK, 20th October 1997; 7/07572C

Metal-directed assembly of a box-like structure

Edwin C. Constable* and Emma Schofield

Institut für Anorganische Chemie, Spitalstrasse 51, CH-4056 Basel, Switzerland

A dinuclear octacationic box is assembled by the reaction of a dicationic bis(2,2′:6′,2″-terpyridine) ligand with iron(II); an {FeL_2} unit [L = 4′-(4-pyridyl)-2,2′:6′,2″-terpyridine] acts as an analogue of 4,4′-bipyridine.

Metal-directed self-assembly is a widely used methodology in supramolecular chemistry.[1] In the synthesis of new systems such as helicates, cyclohelicates, boxes, cylinders and grids, *inter alia*, conventional organic substructures are conceptually replaced by metal-containing units. This strategy has been successfully used by Stang and Olenyuk[2] and Lehn and coworkers[3] amongst others[4] for the synthesis of box-like structures. Here, we report the use of the $[FeL_2^{2+}$ unit [L = 4′-(4-pyridyl)-2,2′:6′,2″-terpyridine] as an analogue of 4,4′-bipyridine.

Stoddart and coworkers have reported a range of topologicaly complex structures based upon the molecular box $\mathbf{1}^{4+}$ (Scheme 1).[5] Paradoxically, the key compound $\mathbf{1}^{4+}$ remains elusive and is only obtained in low yield under forcing conditions in the absence of a template,[6] although improved yields are obtained in templated syntheses.[7] We considered the synthesis of $\mathbf{2}^{8+}$ in which the key cyclisation step involved the formation of the 4,4′-bipyridine analogue in a step involving the formation of twelve Fe–N bonds.

Our initial approach to the synthesis of $\mathbf{2}^{8+}$ was a direct analogy to the preparation of $\mathbf{1}^{4+}$ and involved the reaction in acetonitrile of 4,4′-bis(bromomethyl)biphenyl with $[FeL_2][PF_6]_2$,[8] the metallogue of 4,4′-bipyridine. The iron salt was added over 6 h to a boiling solution and heating continued for 72 h to give a dark blue solution which TLC indicated to contain one major blue component. This compound was isolated by chromatography [Kieselgel 60, gradient starting with MeCN:sat. KNO_3 (aq):H_2O (7:1:0.5) and gradually increasing the H_2O content] and identified as $\mathbf{3}[PF6]_6$ (25%).† None of the numerous minor fractions appeared to contain the desired $\mathbf{2}^{8+}$ species. Attempts to prepare $\mathbf{2}^{8+}$ by the reaction of

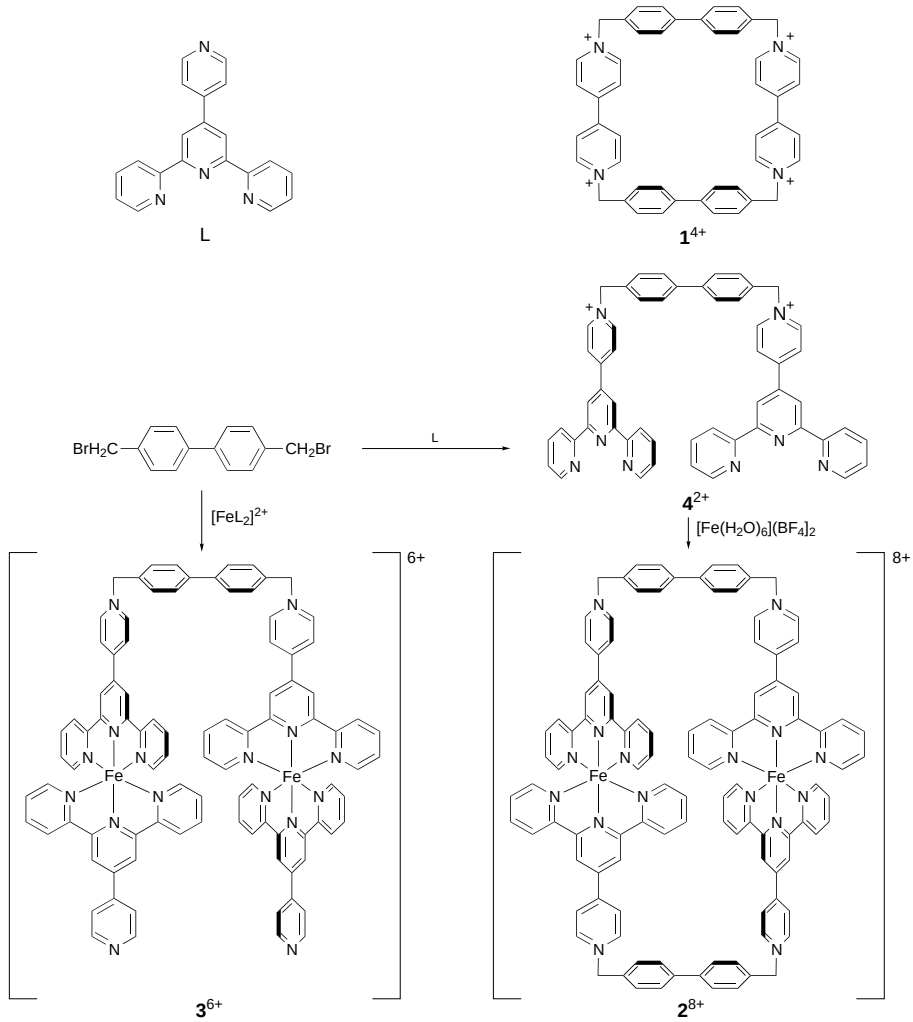

Scheme 1

$\mathbf{3}^{6+}$ with a second equivalent of 4,4′-bis(bromomethyl)biphenyl in acetonitrile were also unsuccessful.

Accordingly, we adopted an alternative strategy in which the iron is incorporated into the metallocycle in the final step. The reaction of L with 4,4′-bis(bromomethyl)biphenyl proceeded smoothly in acetonitrile to give $\mathbf{4}^{2+}$ which was isolated as its hexafluorophosphate salt in 62% yield (Scheme 1).‡ The subsequent cyclisation was performed under high dilution conditions (6×10^{-5} mol dm^{-3} in each component) by the addition of 1 equiv. of iron(II) tetrafluoroborate to 1 equiv. of $\mathbf{3}[PF_6]_2$ in 1 : 1 methanol–acetonitrile solution (Scheme 1). Finally, the deep blue solution was treated with an excess of NH_4PF_6 and the blue solid collected by filtration. Fractional recrystallisation yielded $\mathbf{2}[PF_6]_8$ as deep blue microcrystals in 35% yield.§ Chromatographic analysis and separation indicated that a series of higher oligomers with varying metal : ligand stoichiometries were formed.

The ^{1}H NMR spectrum of a solution of $\mathbf{2}[PF_6]_8$ in CD_3CN is surprisingly simple§ and fully confirms the structural proposal with a single chemical and magnetic 2,2′ : 6′,2″-terpyridine environment and a single AB pattern for the biphenylene unit. The primary characterisation relied upon electrospray mass spectrometry which exhibited a series of ions corresponding to the species $\{\mathbf{2}(PF_6)_n\}^{(8-n)+}$ indicating the formation of the dinuclear species rather than a higher oligomer. This was further confirmed by the preparation of the tetraphenylborate analogue by metathesis with $NaBPh_4$; the electrospray mass spectrum revealed the expected peaks assigned to $\{\mathbf{2}(BPh_4)_n\}^{(8-n)+}$. Attempts to obtain X-ray quality crystals have failed and even the very small crystals that we have obtained are extremely prone to solvent loss.

To date we have been unable to obtain NMR evidence for the inclusion of electron rich aromatic guest molecules into the cavity of $\mathbf{2}^{8+}$ although modelling studies indicate that such interactions are reasonable. We note that the compound is obtained in a highly solvated form containing significant numbers of acetone, methanol or water molecules which may be removed under high vacuum to yield material with somewhat different solubility characteristics. We are currently studying the introduction of such guest molecules.

We should like to thank the Schweizerischer Nationalfonds zur Föderung der wissenschaftlichen Forschung and the University of Basel for support.

Notes and References

* E-mail: constable@ubaclu.unibas.ch

† $\mathbf{3}[PF_6]_6$: ^{1}H NMR (250 MHz, CD_3CN): δ 9.32 (4 H, s, H^{3b}), 9.26 (4 H, s, H^{3D}), 9.20 (4 H, d, J 6.8 Hz, H^{3M}), 9.03 (4 H, d, J 6.4 Hz, H^{3N}), 8.91 (4 H, d, J 6.8 Hz, H^{2M}), 8.65 (8 H, m, H^{3A}), 8.24 (4 H, d, J 5.9 Hz, H^{2N}, 7.94 (8 H, m, H^{4A}), 7.93, 7.77 (4 H, d, J 8.3 Hz, H^{Y}), 7.15 (16 H, m, $H^{5A,6A}$), 6.00 (4 H, s, CH_2). ESMS (calc.): *m/z* 255.9 (255.4, $[M - 6PF_6]^{6+}$); 455.5 (455.6, $[M - 4PF_6]^{4+}$).

‡ $\mathbf{4}[PF_6]_2$: ^{1}H NMR (250 MHz, CD_3CN): δ 8.91 (4 H, d, J 6.8 Hz, H^{6A}), 8.88 (4 H, s, H^{3B}), 8.73 (8 H, m, $H^{3M,2M/3A}$), 8.50 (8 H, d, J 6.8 Hz, $H^{2M/3A}$), 8.01 (4 H, ddd, J 7.8, 2 Hz, H^{4A}, 7.80 (4 H, d, J 8.8 Hz, H^{Y}), 7.59 (4 H, d, J 8.3 Hz, H^{Y}), 7.55 (4 H, m, H^{5A}), 5.83 (4 H, s, CH_2). LD TOF-MS (calc.): *m/z* 947 (945, $[M - PF_6]^+$), 799 (800, $[M - 2PF_6]^+$). Mp 195–196 °C.

§ $\mathbf{2}[PF_6]_8$: ^{1}H NMR (250 MHz, CD_3CN): δ 9.22 (8 H, s, H^{3B}), 9.17 (4 H, d, J 6.9 Hz, H^{3M}), 9.81 (8 H, d, J 6.4 Hz, H^{2M}), 8.55 (8 H, d, J 8.3 Hz, H^{3A}), 7.78 (24 H, m, $H4_{A,Y}$), 7.00 (16 H, m, $H^{5A,6A}$), 5.97 (8 H, s, CH_2). ESMS (calc.): *m/z* 265.6 (265.5, $[M - 7PF_6]^{7+}$), 334.0 (333.9, $[M - 6PF_6]^{6+}$), 429.6 (429.7, $[M - 5PF_6]^{5+}$), 573.3 (573.4 $[M - 4PF_6]^{4+}$), 812.5 (812.8, $[M - 3PF_6]^{3+}$), 1291.9 (1291.7, $[M - 2PF_6]^{2+}$). $\mathbf{2}[BPh_4]_8$: *m/z* 1175.5 (1176.0, $[M - 6PF_6]^{2+}$), 1334.9 (1335.7, $[M - 5PF_6]^{2+}$), 1494.7 (1495.3, $[M - 4PF_6]^{2+}$), 1656.0 (1654.9, $[M - 3PF_6]^{2+}$), 1814.0 (1814.5, $[M - 2PF_6]^{2+}$).

Throughout, the notation used is: A, terminal tpy ring; B, central tpy ring with free 4-pyridyl; D, central tpy ring with quaternised 4-pyridyl; M, quaternised 4-pyridyl ring; N, free 4-pyridyl ring; Y, biphenyl spacer.

1 See, for example: *Comprehensive Supramolecular Chemistry*, ed. J. L. Atwood, J. E. D. Davies, D. D. MacNicol and F. Vögtle, Pergamon, Oxford, 1996, vol. 9, ch. 1–8.
2 P. J. Stang and B. Olenyuk, *Angew. Chem., Int. Ed. Engl.*, 1996, **35**, 732 and references therein.
3 P. N. W. Baxter, J.-M. Lehn, B. O. Kneisel and D. Fenske, *Chem. Commun.*, 1997, 2231 and references therein.
4 See, for example: M. Fujita, J. Yazaki and K. Ogura, *J. Am. Chem. Soc.*, 1990, **112**, 5645; M. J. Hannon, C. L. Painting and W. Errington, *Chem. Commun.*, 1997, 307; 1805.
5 D. Philp and J. F. Stoddart, *Angew. Chem.*, 1996, **108**, 1242; *Angew. Chem., Int. Ed. Engl.*, 1996, **35**, 1155.
6 D. B. Amabilino, P. R. Ashton, C. L. Brown, E. Cordova, L. A. Godinez, T. T. Goodnow, A. E. Kaifer, S. P. Newton, M. Pietraszkiewicz, D. Philp, F. M. Raymo, A. S. Reder, M. T. Rutland, A. M. Z. Slawin, N. Spencer, J. F. Stoddart and D. J. Williams, *J. Am. Chem. Soc.*, 1995, **117**, 1271.
7 P. R. Ashton, S. Menzer, F. M. Raymo, G. K. H. Shimizu, J. F. Stoddart and D. J. Williams, *Chem. Commun.*, 1996, 487; M. Asakawa, P. R. Ashton, S. Menzer, F. M. Raymo, J. F. Stoddart, A. J. P. White and D. J. Williams, *Chem. Eur. J.*, 1996, **2**, 877; F. M. Raymo and J. F. Stoddart, *Pure Appl. Chem.*, 1996, **68**, 313.
8 E. C. Constable and A. M. W. Cargill Thomson, *J. Chem. Soc., Dalton Trans.*, 1994, 1409.

Received in Cambridge, UK, 25th November 1997; 7/08488I

Facile synthesis of arylated heterofullerenes $ArC_{59}N$

Berthold Nuber and Andreas Hirsch*

Institut für Organische Chemie, Henkestasse 42, D-91054 Erlangen, Germany

The thermal treatment of the heterofullerene dimer $(C_{59}N)_2$ with anisole, toluene and 1-chloronaphthalene in the presence of toluene-*p*-sulfonic acid and air leads to the formation monoarylated azafullerenes $ArC_{59}N$ in very good yields.

The simplest nitrogen heterofullerene $C_{59}N$ is a reactive radical intermediate and stabilizes after its formation upon dimerization to the closed shell system **1**.[1–3] So far, only a limited number of monomeric closed shell derivatives, namely the parent hydroazafullerene $HC_{59}N$ and $RC_{59}N$ (R = Ph_2CH) described by Wudl and co-workers,[4,5] as well the alkoxides $ROC_{59}N$ and $ROC_{69}N$ (R = CH_2CH_2OMe) reported by our group,[2] are known. These compounds are formed either during the synthesis of the heterofullerenes themselves as by-products or starting from the dimer **1** by trapping the homolysis product $C_{59}N$, for example, with Ph_2CH_2 in a radical substitution sequence. Here we report on an easy method for the synthesis of arylated mono adducts of $C_{59}N$ in high yields by the thermal treatment of the dimer $(C_{59}N)_2$ **1** with aromatics in the presence of acid and oxygen.

Refluxing a solution of 25 mg of **1** in 30 ml of a 5 : 3 mixture of 1,2-dichlorobenzene (ODCB) and the corresponding aromatic with 50 equivs. of toluene-*p*-sulfonic acid in the presence of air for about 2–5 h results in almost quantitative conversion to the heterofullerene derivatives **2**–**4** (Scheme 1). After chromatographic purification (silica gel; toluene) the monoadducts **2**–**4** were obtained in 78–90% isolated yield. Compounds **2** and **3** are the *para*-substitution products of anisole and toluene, whereas **4** is a mixture of different substitution products of 1-chloronaphthalene. We did not observe arylations with

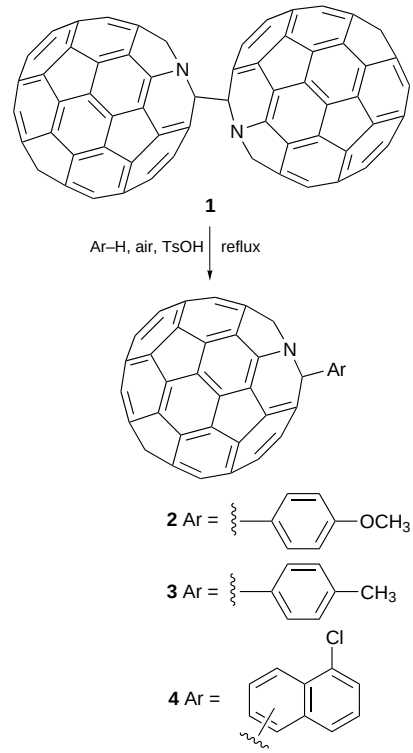

Scheme 1

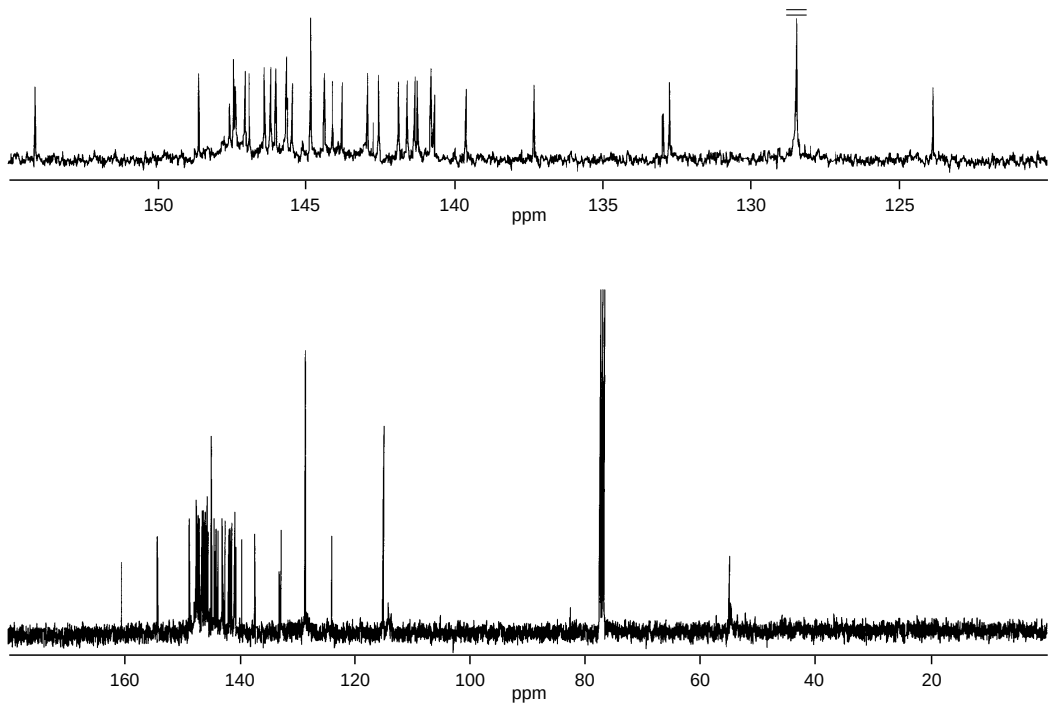

Fig. 1 ^{13}C NMR (100.5 MHz, CS_2, 20% $CDCl_3$) spectrum for **2**, (top: expanded 120–155 ppm region)

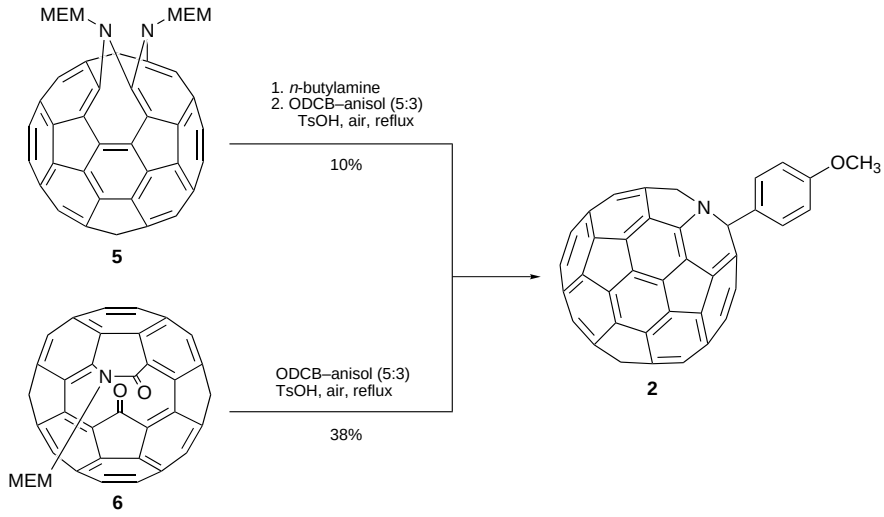

Scheme 2

deactivated aromatics, which allows use of ODCB as solvent. In the absence of an acid or oxygen these derivatizations do not take place. The arylation with *N*,*N*-dimethylaniline failed. This is presumably due to the protonation of the Me_2N group causing deactivation towards electrophilic substitution.

The monoadducts **2**–**4** were characterized by ^{1}H NMR, ^{13}C NMR, UV–VIS and FTIR spectroscopy as well as by mass spectrometry.† The ^{1}H NMR spectrum of **2**, for example, shows the expected ddd-pattern of an AA′BB′-spin system for a *para*-substituted aromatic ring. The protons of the methoxy group resonate at δ 4.03. The ^{13}C NMR spectrum of **2** (Fig. 1) clearly proves C_s symmetry showing the 30 expected fullerene resonances in the sp^2 region between δ 155 and 123. The five different C-atoms of the anisyl addend resonate at δ 160.36, 132.94, 128.47, 115.01 and 54.93. The peak at δ 82.33 is due to the resonance of the sp^3 carbon of the fullerene skeleton, which is a typical value for a corresponding C atom in $RC_{59}N$.[6] The UV–VIS spectra of **2**–**4** displaying the most intensive absorptions† at *ca*. 260, 320 and 440 nm are basically identical to that of **1**. All three compounds are green in solution. The FTIR spectra† of **2**–**4** show the typical characteristics for fullerene derivatives (monoadducts), especially the absorptions in the fingerprint region between 480 and 590 cm^{-1} with the strongest peak at about 523 cm^{-1}. MALDI-TOF mass spectrometry shows the M^+ peak of each compound together with a strong fragmentation peak at *m*/*z* 722 for $C_{59}N^+$.

We assume that the mechanism of this reaction is an electrophilic aromatic substitution (S_EAr). The electrophile is presumably $C_{59}N^+$, which might be formed *via* thermal homolysis of **1** and subsequent oxidation with O_2. The reaction times depend on the nature of the aromatic reagent used. For example, the reaction of **1** with toluene took almost 5 h, whereas quantitative conversion with anisole was achieved within 2 h, which is in line with the lower S_EAr activity of toluene. The role of the acid is not clear. It is possible that it is needed to trap the reduced oxygen species.

It is important to mention that arylated adducts like **2** can also be obtained starting directly from the precursor molecules **5** and **6**, which are usually used for the synthesis of the heterofullerene dimer **1** (Scheme 2). Although the yields are considerably lower than those of the corresponding conversions using isolated **1**, one separation step can be avoided. However, the yields can be increased upon raising the reaction temperature. The direct treatment of **5** in 1-chloronaphthalene at 220 °C leads to the formation of **4** in 46% isolated yield.

Investigations on the chemical behaviour as well as on the electronic and photophysical properties of the stable arylated heterofullerene derivates like **2**–**4** are currently underway.

We thank the DFG for financial support.

Notes and References

* E-mail: hirsch@organik.uni-erlangen.de

† *Selected spectroscopic data* of the newly synthesised compounds **2**–**4**. **2**: FTIR: ν(KBr)/cm^{-1} 2995, 2945, 2924, 2900, 2828, 1507, 1421, 1250, 1175, 1032, 966, 899, 840, 822, 718, 638, 587, 555, 523 and 482; UV–VIS λ_{max}(cyclohexane)/nm 257, 323, 444, 591, 723 and 789; δ_H(400 MHz, CS_2–20% $CDCl_3$) 8.72 (ddd, J_{AB} 9.02, $J_{AB'}$ 3.10, $J_{AA'}$ 2.75, 1 H), 7.35 (ddd, J_{AB} 9.02, $J_{AB'}$ 3.10, $J_{AA'}$ 2.75, 1 H) and 4.03 (s, 3 H); δ_C(100.5 MHz, CS_2–20% $CDCl_3$) 160.36 (C–OMe, 1C), 154.10 (2C), 148.61 (2C), 147.58 (1C), 147.44 (2C), 147.38 (2C), 147.06 (2C), 146.91 (2C), 146.41 (2C), 146.19 (2C), 146.02 (2C), 145.66 (2C), 145.63 (1C), 145.46 (2C), 144.83 (4C), 144.37 (2C), 144.11 (2C), 143.79 (2C), 142.93 (2C), 142.55 (2C), 141.89 (2C), 141.60 (2C), 141.34 (2C), 141.24 (2C), 140.80 (2C), 140.68 (2C), 139.60 (2C), 137.31 (2C), 132.94 [C-$(CH)_2$COMe, 1C], 132.72 (2C), 128.47 (C–CHCOMe, 2C), 123.89 (2C), 115.01 (C–COMe, 2C), 82.33 (1C) and 54.93 (Me); MALDI-MS *m*/*z* 828 (M^+), 814 (M^+ − Me) and 722 ($C_{59}N^+$). **3**: FTIR: ν(KBr)/cm^{-1} 2919, 2845, 1736, 1629, 1509, 1422, 1374, 1344, 1316, 1262, 1236, 1186, 1095, 1020, 968, 901, 844, 803, 774, 719, 707, 679, 554, 525, 495, 483, 438, 428 and 409; UV–VIS λ_{max}(cyclohexane)/nm 263, 323, 440, 588, 722 and 790; δ_H(400 MHz, CS_2–20% $CDCl_3$) 8.70 (ddd, not completely resolved, J_{AB} 7.77, 1 H), 7.67 (ddd, not completely resolved, J_{AB} 7.77, 1 H) and 2.66 (s, 3 H); δ_C(100.5 MHz, CS_2–20% $CDCl_3$) 154.19 (2C), 148.69 (2C), 147.59 (1C), 147.42 (2C), 147.39 (2C), 147.08 (2C), 147.01 (2C), 146.41 (2C), 146.21 (2C), 146.03 (2C), 145.67 (2C), 145.65 (1C), 145.46 (2C), 144.84 (4C), 144.39 (2C), 144.11 (2C), 143.80 (2C), 142.95 (2C), 142.56 (2C), 141.90 (2C), 141.62 (2C), 141.34 (2C), 141.25 (2C), 140.80 (2C), 140.69 (2C), 139.61 (2C), 139.22 (q, 1C), 138.02 (q, 1C), 137.34 (2C), 132.75 (2C), 130.42 (C–CMe, 2C), 127.07 (C–CHCMe, 2C), 123.94 (2C), 82.60 (1C) and 21.48 (Me); MALDI-MS *m*/*z* 813 (M^+) and 722 ($C_{59}N^+$). **4**: FTIR: ν(KBr)/cm^{-1} 2962, 2923, 2854, 1635, 1508, 1420, 1375, 1318, 1261, 1092, 1028, 800, 747, 722, 524 and 472; UV–VIS λ_{max}(cyclohexane)/nm 256, 320, 436, 580, 711 and 793; δ_H(400 MHz, CS_2–20% $CDCl_3$) several multiplets between δ 7.0 and 10.5; δ_C(100.5 MHz, CS_2–20% $CDCl_3$) 154.23, 148.34, 147.66, 147.53, 147.41, 147.27, 147.15, 146.73, 146.48, 146.38, 146.27, 146.24, 146.14, 145.74, 145.54, 144.96, 144.43, 144.34, 144.22, 143.79, 143.07, 142.81, 142.08, 141.86, 141.32, 140.96, 140.80, 139.80, 137.39, 137.38, 136.99, 133.34, 133.00, 129.20, 128.76, 128.05, 127.61, 127.45, 126.97, 126.50, 126.30, 125.75, 125.25, 124.82, 124.02 and 122.82; MALDI-MS *m*/*z* 884 (M^+) and 722 ($C_{59}N^+$).

1 J. C. Hummelen, B. Knight, J. Pavlovich, R. Gonzalez and F. Wudl, *Science*, 1995, **269**, 1554.
2 B. Nuber and A. Hirsch, *Chem. Commun.*, 1996, 1421.
3 Gruss, K.-P. Dinse, A. Hirsch, B. Nuber and U. Reuther, *J. Am. Chem. Soc.*, 1997, **19**, 8728.
4 M. Keshavarz-K., R. Gonzalez, R. G. Hicks, G. Srdanov, V. I. Srdanov, T. G. Collins, J. C. Hummelen, C. Bellavia Lund, J. Pavlovich, F. Wudl and K. Holczer, *Nature*, 1996, **383**, 147.
5 C. Bellavia-Lund, R. Gonzalez, J. C. Hummelen, R. G. Hicks, A. Sastre and F. Wudl, *J. Am. Chem. Soc.*, 1997, **119**, 2946.
6 C. Bellavia-Lund, M. Keshavarz-K., T. Collins and F. Wudl, *J. Am. Chem. Soc.*, 1997, **119**, 8101.

Received in Cambridge UK, 27th October 1997; 7/07704A

Self-assembly of carcerand-like dimers of calix[4]resorcinarene facilitated by hydrogen bonded solvent bridges

Kristie N. Rose, Leonard J. Barbour, G. William Orr and Jerry L. Atwood*†

Department of Chemistry, University of Missouri-Columbia, Columbia, Missouri 65211, USA

In the presence of solvent molecules which can act simultaneously as hydrogen bond donors and acceptors, the calix[4] resorcinarene 1 can self-assemble into a dimeric carcerand-like complex utilizing an intricate array of hydrogen bonds with the solvent such that pairs of concave molecules associate indirectly in a rim-to-rim fashion to form a relatively large supramolecular cavity.

One of the main goals of supramolecular chemistry[1] is to use cleft-containing molecules to 'recognize' a substrate on the basis of size, shape, functionality and electrostatic profile. This concept was borrowed from Nature where the process of molecular recognition is central to the chemistry of life.[2] Although bowl-shaped molecules such as the calixarenes[3] and cyclodextrins[4] have been studied extensively over the last two decades, their molecular cavities are relatively small. An increasing trend towards the design of systems with larger voids has resulted in the development of systems which utilize multiple bowl-shaped molecules as building blocks. In this context, the pioneering work of Cram[5] and Collet[6] introduced the carcerands and cryptophanes—covalent cavities with the ability to confine guest molecules. Although these systems are of great conceptual importance, the guest cannot usually be removed without the rupture of at least one covalent bond of the host. Consequently, there has been much interest in the utilization of hydrogen bonded interactions to assemble concave building blocks in order to produce large cavities. In general, such cage systems are attractive because the molecular association is reversible under relatively mild conditions. Rebek and co-workers[7] have elegantly demonstrated these principles using self-complementary molecules that contain hydrogen bond donor and acceptor moieties positioned about the rims of their cavities. Moreover, one of us recently reported[8] a solid-state supramolecular assembly composed of six calix[4]resorcinarene molecules which are linked by solvent water molecules, thus forming a large cavity approximately 1375 Å^3 in volume. We are keenly interested in the supramolecular complexation of fullerenes,[9] and have been investigating the possibility of encapsulating C_{60} within a calix[4]resorcinarene hexamer. Since a solitary C_{60} molecule is too small to fill the void efficiently, the complex would also require encapsulation of a significant amount of solvent in order to stabilize the structure. During the course of our attempts at assembling such a system, we have instead produced a dimeric carcerand-like complex in which two concave calix[4]resorcinarene molecules are linked indirectly by hydrogen bond bridges involving eight propan-2-ol solvent molecules. Crystallographic characterization of a dimeric system of this nature is unprecedented and is an important extension of the work initiated by Rebek.

Single crystals suitable for X-ray diffraction analysis‡ were grown by slow diffusion of propan-2-ol into a solution of **1**[10] and C_{60} (5:1 molar ratio) in *o*-dichlorobenzene. The most striking feature of the structure is that pairs of concave calix[4]resorcinarene molecules are arranged in a rim-to-rim fashion to form dimers, as shown in Fig. 1. The eight hydroxy groups of one calix[4]resorcinarene form hydrogen bonds with eight oxygen atoms belonging to propan-2-ol solvent molecules. The latter, in turn, form hydrogen bonds to a second

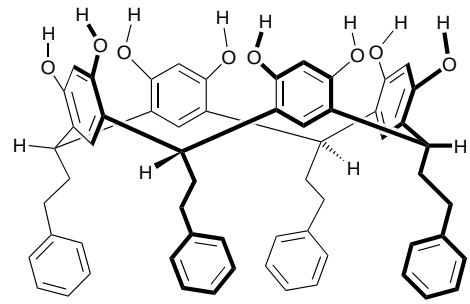

1

claix[4]resorcinarene molecule, thus completing the dimer. No hydroxy group hydrogen atoms were located and hydrogen bonds are inferred from short O··O contacts. The proximate hydroxy O··O contacts within each calixresorcinarene are 2.771(7) Å, implying that these oxygen atoms are also hydrogen bonded to one another. The unique calix[4]resorcinarene-to-solvent O··O distances are 2.660(9) and 2.743(9) Å. The two calix[4]resorcinarene molecules each have C_{4v} symmetry and are related to one another by a mirror plane at *x*,*y*,0 which passes through all of the propan-2-ol oxygen atoms. The assembly of the dimer is thus facilitated by the formation of sixteen intermolecular hydrogen bonds, while a further eight intramolecular hydrogen bonds impart structural rigidity of the calix[4]resorcinarene molecules. The symmetry relationship between the constituents of the dimer requires all of the hydrogen atoms involved in hydrogen bonding to be disordered.

The effective van der Waals volume of the cavity was calculated[11] to be 230 Å^3 and its cross section, measured at *x*,*y*,0, is approximately equal in dimensions to a molecule of *o*-dichlorobenzene. In order to maintain structural stability, it is probable that the cavity contains several solvent molecules, perhaps of both *o*-dichlorobenzene and propan-2-ol. Relatively

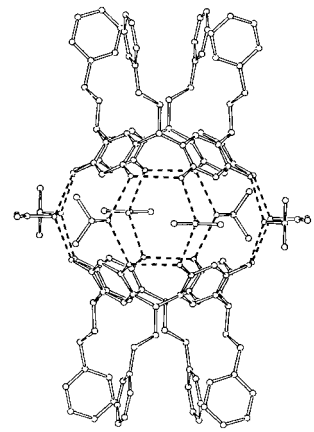

Fig. 1 Projection showing the calix[4]resorcinarene dimer. Hydrogen atoms are omitted for clarity and hydrogen bonded interactions are shown as broken bars.

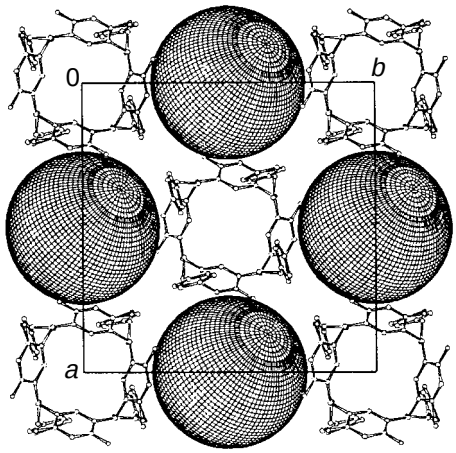

Fig. 2 Packing diagram (only calix[4]resorcinarene and C_{60} molecules are shown) viewed along [001], parallel to the molecular columns

large peaks of electron density within the cavity appear to indicate the presence of chlorine atoms, but crystallographically imposed symmetry precludes the use of a cogent model for included solvent molecules. As shown in Fig. 2, the calix[4]resorcinarene dimers are stacked in columns along 0,0,*z* and $\frac{1}{2},\frac{1}{2},z$ while the C_{60} molecules are similarly arranged along $0,\frac{1}{2},z$ and $\frac{1}{2},0,z$. The calix[4]resorcinarene columns involve alternating head-to-head and tail-to-tail associations of the molecules. The latter result in the formation of lattice voids bounded by phenethyl moieties belonging to the host and also appear to contain disordered *o*-dichlorobenzene solvent.

We have shown that the solvent-assisted hexameric assembly of calix[4]resorcinarenes to form carcerand-like complexes has a dimeric analogue. Characterization of such systems is a significant step towards understanding the principles involved in the design of supramolecular cavities of diverse shapes and sizes, and assemblies of this nature are important because, like their biological counterparts, the contents of large molecular voids are often considered[12] to represent an additional phase of matter.

We are grateful for funding from the National Science Foundation.

Notes and References

† E-mail: chemja@showme.missouri.edu

‡ *Crystal data* for $C_{60}H_{56}O_8{\cdot}4(C_3H_8O){\cdot}C_{60}$: M = 1866.14; dark red orthorhomboid, 0.30 × 0.25 × 0.20 mm, tetragonal, *I*4/*m*; $a = b$ = 18.9296(7), c 27.2702(13) Å; Z = 4; V = 9771.7(7) Å^3, D_c = 1.216 g cm^{-3}, Siemens SMART CCD diffractometer, Mo-Kα radiation, λ = 0.7107 Å; T = −100 °C; $2\theta_{max}$ = 54.4°, 27652 reflections collected, 5531 unique (R_{int} = 0.0388). final GoF = 1.045, $R1$ = 0.1193, $wR2$ = 0.3393, R indices based on 5531 reflections with $F > 4\sigma(F)$, Lp and absorption corrections applied, μ = 0.077 mm^{-1}, min transition factor = 0.743. All calculations were performed using the Siemens SHELX-TL software suite. All non-hydrogen atoms of the claix[4]resorcinarene molecule were refined anisotropically and, with the exception of the hydroxy group hydrogen atoms which are disordered, hydrogens were placed in calculated positions. The C_{60} molecule is disordered over two orientations and was modeled accordingly. The final model also included propan-2-ol and disordered *o*-dichlorobenzene solvent molecules. CCDC 182/731.

1 *Comprehensive Supramolecular Chemistry*, ed. J. L. Atwood, J. E. D. Davies, D. D. MacNicol and F. Vögtle, Elsevier Science, Oxford, 1996.
2 J.-M. Lehn, *Supramolecular Chemistry: Concepts and Perspectives*, VCH, Weinheim, 1995.
3 C. D. Gutsche, *Calixarenes, Monographs in Supramolecular Chemistry*, Royal Society of Chemistry, London, 1989; *Calixarenes: A versatile Class of Macrocyclic Compounds*, ed. J. Vicens and V. Böhmer, Kluwer, Holland, 1990.
4 J. Szejtli, *Cyclodextrin Technology*, Kluwer, Dordrecht, 1988.
5 D. J. Cram, H.-J. Choi, J. A. Bryant and C. B. Knobler, *J. Am. Chem. Soc.*, 1992, **114**, 7748; D. J. Cram, M. T. Blanda, K. Paek and C. B. Knobler, *J. Am. Chem. Soc.*, 1992, **114**, 7765.
6 A. Collet, *Tetrahedron*, 1987, **43**, 5725.
7 R. Wyler, J. de Mendoza and J. Rebek, *Angew. Chem., Int. Ed. Engl.*, 1993, **32**, 1699; K. D. Shimizu and J. Rebek, *Proc. Natl. Acad. Sci., USA*, 1995, **92**, 12 403; R. S. Meissner, J. Rebek and J. de Mendoza, *Science*, 1995, **270**, 1485; B. C. Hamann, K. D. Shimizu and J. Rebek, *Angew. Chem., Int. Ed. Engl.*, 1996, **35**, 1326; J. Rebek, *Chem. Soc. Rev.*, 1996, 255; R. M. Grotzfeld, N. Branda and J. Rebek, *Science*, 1996, **271**, 487.
8 L. R. MacGillivray and J. L. Atwood, *Nature*, 1997, **389**, 469.
9 J. L. Atwood, G. A. Koustantonis and C. L. Raston, *Nature*, 1994, **368**, 229; J. L. Atwood, M. J. Barnes, M. G. Gardiner and C. L. Raston, *Chem. Commun.*, 1996, 1449; C. L. Raston, J. L. Atwood, P. J. Nichols and I. B. N. Sudria, *Chem. Commun.*, 1996, 2615; J. L. Barbour, G. W. Orr and J. L. Atwood, *Chem. Commun.*, 1997, 1439.
10 L. M. Tunstad, J. A. Tucker, E. Dalcanale, J. Weiser, J. A. Bryant, J. C. Sherman, R. C. Helgeson, C. B. Knobler and D. J. Cram, *J. Org. Chem.*, 1989, **54**, 1305.
11 L. J. Barbour, CAVITY—unpublished computer program. A program to compute the volume available to a sphere of given radius within a molecular cavity. The program requires the van der Waals radii and Cartesian coordinates of all the atoms surrounding the cavity. A cube of length j is systematically stepped through the Euclidean space containing all the atoms. If the cube can reside within any sphere of radius r, which can in turn reside completely within the cavity, the volume (initially set to zero) is incremented by i^3. Values of j = 0.2 Å and r = 1.52 Å were used. Van der Waals radii were obtained from A. Bondi, *J. Phys. Chem.*, 1964, **68**, 441.
12 P. Jacopozzi and E. Dalcanale, *Angew. Chem., Int. Ed. Engl.*, 1997, **36**, 613.

Received in Cambridge, UK, 29th October 1997; 7/07802A

Sulfinyl *versus* allylic stereocontrol in Diels–Alder cycloadditions of hydroxy 2-sulfinyl butadienes

Roberto Fernández de la Pradilla,*[a]† Carlos Montero[a] and Alma Viso[b]

[a] *Instituto de Química Orgánica, CSIC, Juan de la Cierva, 3, E-28006 Madrid, Spain*
[b] *Departamento de Química Orgánica I, Facultad de Química, Universidad Complutense, E-28040 Madrid, Spain*

Enantiopure hydroxy 2-sulfinyl butadienes undergo a highly face selective Diels–Alder cycloaddition with *N*-phenylmaleimide and phenyltriazolinedione controlled by the chiral sulfur atom; the related enantiopure sulfonyl dienes display complimentary π-facial selectivity.

The asymmetric Diels–Alder reaction is a fundamental process in contemporary organic synthesis since up to four enantio- and diastereo-merically pure stereogenic centres are created in a single step.[1] Within this field, the use of enantiopure dienes is comparatively less developed and the clarification of issues concerning stereocontrol for these protocols is a current challenge.[2] In most studies involving enantiopure dienes, the chiral auxiliary is only utilized to induce asymmetry in the Diels–Alder process, and further asymmetric transformations are not readily envisaged. In contrast, simple 2-sulfinyl dienes are especially appealing substrates since, after a highly selective Diels–Alder cycloaddition,[3,4] a vinyl sulfoxide, which may undergo subsequent chirality transfer operations,[5] is generated. Here we report the first examples of highly diastereoselective sulfur directed Diels–Alder cycloadditions of enantiopure hydroxy 2-sulfinyl dienes which display a non-reinforcing relationship of stereocontrolling elements.[6]

We have recently described a short and completely stereocontrolled route to enantiopure dienes **1** (Scheme 1).[7] At the onset of this research we envisioned that dienes **1** would provide a unique opportunity to assess the relative π-facial stereodirecting abilities of two powerful elements of stereocontrol in a Diels–Alder process,[4,8,9] and lead to enantiopure cycloadducts **A** or **B**. It should be noted that for dienes **1**, the allylic hydroxy-bearing stereocentre and the sulfinyl auxiliary are expected to direct the approach of the dienophile with maximum efficiency due to mutual 1,3-allylic strain,[10] and to *opposite* faces of the diene moiety.[11]

To gain insight into the stereochemical outcome of a basic intermolecular Diels–Alder process, we selected *N*-phenylmaleimide (NPM) and diene **1a**[7] for our initial studies, and the results obtained are shown in Scheme 2. In this fashion, cycloadduct **2a** was produced as a single isomer (300 MHz ^{1}H NMR analysis of the crude reaction mixture) and isolated in good yield after recrystallization. Treatment of a solution of **2a** with silica gel resulted in spontaneous lactonization and partial epimerization to produce a separable 25 : 75 mixture of amides **3a** (β-amide) and **4a** (α-amide) which displayed significant NOE enhancements between H_a and H_b (11.5 and 10.4% respectively).‡

To extend the scope of our methodology, and seeking additional support for the stereochemical assignments, we prepared enantiopure hydroxy sulfonyl diene **7a** from sulfoxide **1a** by a simple oxidation with magnesium monoperoxyphthalate (MMPP).[12] Diene **7a** underwent smooth cycloaddition

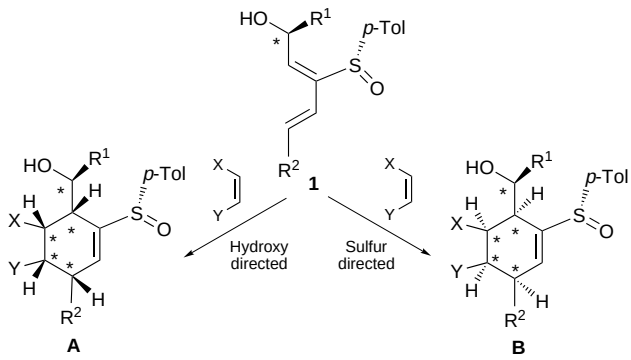

Scheme 1

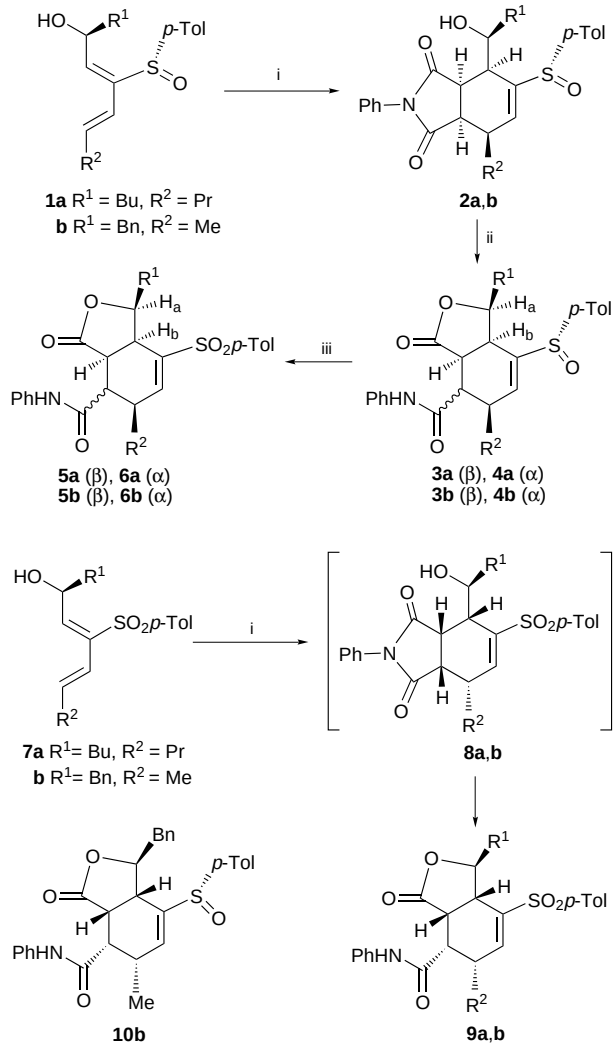

Scheme 2 *Reagents and conditions*: i, NPM (1–1.5 equiv.), toluene, room temp., 2–5 d, 70% for **2a**, 69% for **2b**, 86% for **9a** and 82% for **9b**; ii, SiO_2, CH_2Cl_2, room temp., 4 d, 91% for **3a**/**4a** and 95% for **4b**; iii, MCPBA, (1.5 equiv.), CH_2Cl_2, −78 °C to room temp., 2–5 h, 80% for **5a**, 83% for **6a** and 75% for **6b**

with NPM affording the very unstable cycloadduct **8a**§ as a single isomer which lactonized spontaneously in the reaction medium to give **9a**. This result shows that the allylic hydroxy group is a powerful element of stereocontrol in these cases.[9] The diastereomeric relationship found between amides **9a** and **5a**/**6a** (prepared by oxidation of pure samples of **3a** and **4a**), along with the NOE enhancements observed for **3a** and **4a**, conclusively establish that the π-facial selectivity of the cycloaddition between **1a** and NPM is exclusively controlled by the chiral sulfur atom.

Encouraged by these results we sought to test the generality of this sulfoxide directed cycloaddition by studying the reaction of diene **1b**,[7] with a bulkier R^1 substituent, and NPM which afforded a 95 : 5 mixture of cycloadduct **2b** and sulfinyl amide **10b**,¶ respectively, as judged by ^{1}H NMR analysis of the crude reaction mixture. Treatment of **2b**, isolated by recrystallization, with SiO_2 resulted in smooth cyclization and epimerization affording amide **4b** along with trace amounts of **3b**. Oxidation of **4b** afforded sulfone **6b** while the cycloaddition between sulfonyl diene **7b** and NPM produced diastereomeric sulfonyl amide **9b**. We believe that lactones **3a** and **3b** undergo a facile epimerization at the amide-bearing carbon due to the location of the R^1 substituent in the sterically demanding concave region of the molecule, while for lactones **9**, R^1 is placed in the convex face. The enhanced degree of epimerization found for R^1 = Bn *versus* Bu is likely to be related to the different steric requirements of these substituents.

Scheme 3 gathers our results for the cycloaddition between sulfinyl diene **1a**, sulfonyl diene **7a** and phenyltriazolinedione (PTAD). These cycloadditions took place with complete facial selectivity and in high yield to produce adducts **11a** and **13a** respectively. Standard oxidation of **11a** afforded **12a** whose spectral features clearly indicated a diastereomeric relationship to **13a**. These observations establish a sulfur-directed π-facial selectivity for hydroxy sulfoxide **1a**, and an allylic-directed π-facial selectivity for hydroxy sulfone **7a**.

In summary, readily available enantiopure acyclic hydroxy 2-sulfinyl butadienes,[7] which display a nonreinforcing relationship of stereocontrolling elements,[6] undergo a highly face-selective Diels–Alder cycloaddition with *N*-phenylmaleimide and phenyltriazolinedione to generate densely functionalized cycloadducts. To the best of our knowledge, the complete reversal of facial selectivity found for sulfoxides **1**, relative to related sulfonyl dienes **7**, is unprecedented and demonstrates that the sulfinyl functionality is not just synthetically useful but also an extremely powerful element of stereocontrol for intermolecular Diels–Alder cycloadditions, Further studies on the scope and limitations of this methodology, including its intramolecular variant as well as applications toward natural products syntheses, will be reported in due course.

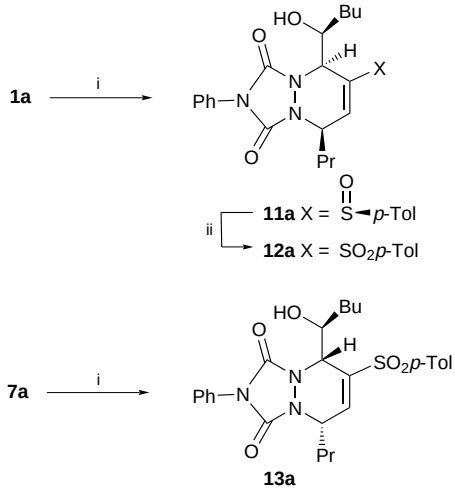

Scheme 3 *Reagents and conditions*: i, PTAD (1.5–2.0 equiv.), CH_2Cl_2, −78 °C to room temp., 1 h, 87% for **11a** and 79% for **13a**; ii, MCPBA (1.5 equiv.), CH_2Cl_2, −78 °C to room temp., 4 h, 88%

We thank DGICYT (PB94-0104 and PB96-0822) for support of this research and the CAM for a doctoral fellowship to C. M.

Notes and References

† E-mail: rif@cc.csic.es

‡ Pure amide **3a** also yielded a 25 : 75 mixture of **3a** and **3b** upon treatment with SiO_2.

§ Careful examination of the crude reaction mixture by 300 MHz ^{1}H NMR spectroscopy at intermediate reaction times showed mixtures of diene **7a**, cycloadduct **8a** and lactone **9a**.

¶ Pure **10b**, isolated by chromatography of the mother liquors of **2b**, afforded sulfonyl amide **9b** upon oxidation with MCPBA.

1 J. Jurczac, T. Bauer and C. Chapuis, in *Methoden Org. Chem. Houven-Weyl*, Thieme, Stuttgart, 1995, vol. E21, p. 2735; W. Oppolzer, in *Comprehensive Organic Synthesis*, ed. B. M. Trost and I. Fleming, Pergamon, New York, 1991, vol. 5, p. 315; H. B. Kagan and O. Rian, *Chem. Rev*., 1992, **92**, 1007.

2 For a review, see: E. Winterfeldt, *Chem. Rev*., 1993, **93**, 827. For leading references on enantiopure dienes bearing a chiral group at C-1, see: C. Burnouf, J. C. López, F. García Calvo-Flores, M. A. Laborde, A. Olesker and G. Lukacs, *J. Chem. Soc., Chem. Commun*., 1990, 823; R. M. Giuliano, A. D. Jordan, Jr., A. D. Gauthier and K. Hoogsteen, *J. Org. Chem*., 1993, **58**, 4979; S. A. Kozmin and V. H. Rawal, *J. Am. Chem. Soc*., 1997, **119**, 7165; M. Virgili, A. Moyano, M. A. Pericàs and A. Riera, *Tetrahedron Lett*., 1997, **38**, 6921. For enantiopure dienes bearing a chiral group at C-2, see: R. H. Schlessinger and C. P. Bergstrom, *Tetrahedron Lett*., 1996, **37**, 2133; J. Barluenga, M. Tomás, L. A. López and A. Suárez-Sobrino, *Synthesis*, 1997, 967; J. Barluenga, F. Aznar, C. Ribas and C. Valdés, *J. Org. Chem*., 1997, **62**, 6746.

3 For a review on sulfinyl dienes see: M. C. Aversa, A. Barattucci, P. Bonaccorsi and P. Giannetto, *Tetrahedron: Asymmetry*, 1997, **8**, 1339; For a leading reference, see: R. S. Paley, A. de Dios, L. A. Estroff, J. A. Lafontaine, C. Montero, D. J. McCulley, M. B. Rubio, M. P. Ventura, H. L. Weers, R. Fernández de la Pradilla, S. Castro, R. Dorado and M. Morente, *J. Org. Chem*., 1997, **62**, 6326.

4 T.-K. Yang, H.-Y. Chu, D.-S. Lee and T.-S. Chou, *Tetrahedron Lett*., 1996, **37**, 4537; P. Gosselin, E. Bonfand and C. Maignan, *J. Org. Chem*., 1996, **61**, 9049; M. C. Aversa, A. Barattucci, P. Bonaccorsi, P. Giannetto and D. N. Jones, *J. Org. Chem*., 1997, **62**, 4376.

5 For reviews, see: M. C. Carreño, *Chem. Rev*., 1995, **95**, 1717; C. M. Rayner, *Contemp. Org. Synth*., 1996, **3**, 499. For leading references, see: R. Fernández de la Pradilla, S. Castro, P. Manzano, J. Priego and A. Viso, *J. Org. Chem*., 1996, **61**, 3586; H. Künzer, M. Thiel and B. Peschke, *Tetrahedron Lett*., 1996, **37**, 1771; C. Louis and C. Hootelé, *Tetrahedron: Asymmetry*, 1997, **8**, 109.

6 D. A. Evans, M. J. Dart, J. L. Duffy and M. G. Yang, *J. Am. Chem. Soc*., 1996, **118**, 4322.

7 R. Fernández de la Pradilla, M. V. Martínez, C. Montero and A. Viso, *Tetrahedron Lett*., 1997, **38**, 7773.

8 For an early study on the cycloaddition between *meso* and C_2-symmetric butadienyl 1,4-bis(allylic) ethers and tetracyanoethylene, see: R. Grée, J. Kessabi, P. Mosset, J. Martelli and R. Carrié, *Tetrahedron Lett*., 1984, **25**, 3697.

9 W. Adam, J. Glässer, K. Peters and M. Prein, *J. Am. Chem. Soc*., 1995, **117**, 9190 and references cited therein.

10 For a review, see: R. W. Hoffman, *Chem. Rev*., 1989, **89**, 1841. The *Z* geometry of the C_1–C_2 bond for dienes **1** is expected to favour the s-*trans* conformation about the C–S bond. See: T. Koizumi, Y. Arai, H. Takayama, K. Kuriyama and M. Shiro, *Tetrahedron Lett*., 1987, **28**, 2689.

11 For the expected π-facial selectivities of dienols and dienyl sulfoxides, see refs 4 and 9.

12 To the best of our knowledge, our methodology is the first general route to enantiopure acyclic 2-sulfonyl dienes. For a leading reference see: J. S. Xiang, A. Mahadevan and P. L. Fuchs, *J. Am. Chem. Soc*., 1996, **118**, 4284.

Received in Liverpool, UK, 17th November 1997; 7/08272J

Structural evidence for resonance-assisted O–H···S hydrogen bonding

Thomas Steiner*

Institut für Kristallographie, Freie Universität Berlin, Takustraße 6, D-14195 Berlin, Germany

By far the shortest hydrogen bonds of the O–H···S type occur in monothio-ß-diketones and related substances (H···S distances 1.9–2.0 Å); it is shown with crystal correlation techniques that this very short hydrogen bonding is facilitated by resonance assistance similar to that occurring in the oxygen analogues.

Although O–H···S hydrogen bonds occur in many chemical and biological systems, they have been little investigated until today. The first comprehensive statistical analysis of intermolecular O–H···S hydrogen bond geometries was only recently published by Allen *et al.*[1] It is observed that in intermolecular hydrogen bonds, H···S distances are restricted to values > 2.2 Å. In this present work, the database analysis of Allen *et al.* was followed, but intramolecular hydrogen bonds were also included.[2]† The distribution of H···S separations is clearly bimodal (Fig. 1). The large peak centred in the range 2.3–2.4 Å represents intermolecular hydrogen bonds, mostly of the type O–H···S=C < .[1] The small peak centred in the range 1.9–2.0 Å was not evident in the previous study and represents exclusively intramolecular hydrogen bonds, which are apparently unusually strong. To discover what kind of interactions cause this prominent peak, the examples with H···S < 2.1 Å were inspected individually. It was found that they are all structurally very similar and are formed in the structural fragments shown in Fig. 2 (numerical data given in Table 1).

The largest fraction of the data sample in Fig. 2 is composed of monothio-β-diketones in the enol tautomeric form [Fig. 2(*a*)]. As an archetypal example, the structure of 3-mercapto-1,3-diphenylprop-2-en-1-one, which has been determined by neutron diffraction,[3] is show in Fig. 3. Note that the covalent O–H bond length of 1.024(8) Å is appreciably elongated from the *ca.* 0.98 Å which is typically observed in moderate O–H···O hydrogen bonds,[4,5] indicating an interaction of considerable strength. For fragment (*b*) [2-hydroxybenzene-1-carbothioamides], IR spectroscopy shows redshifts of O–H stretching frequencies of around 450 cm^{-1} compared to free phenolic O–H, which are similar values as in the oxygen analogues.[6]

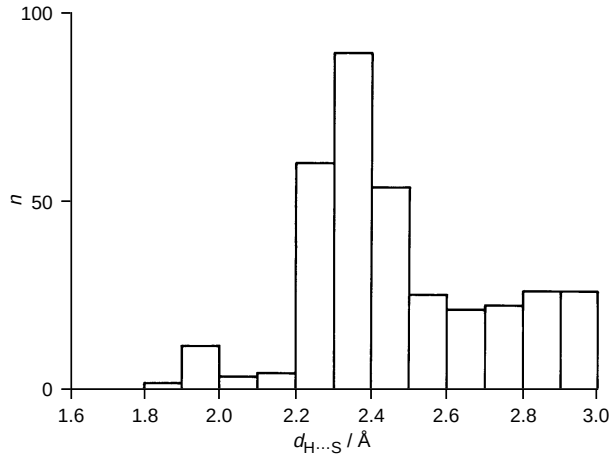

Fig. 1 Distribution of H···S distances in inter- and intra-molecular O–H···S hydrogen bonds (for normalised H-atom position). The large peak centred at 2.3–2.4 Å is derived mainly from intermolecular hydrogen bonds and the small peak centred at 1.9–2.0 Å arises exclusively from intramolecular hydrogen bonds.

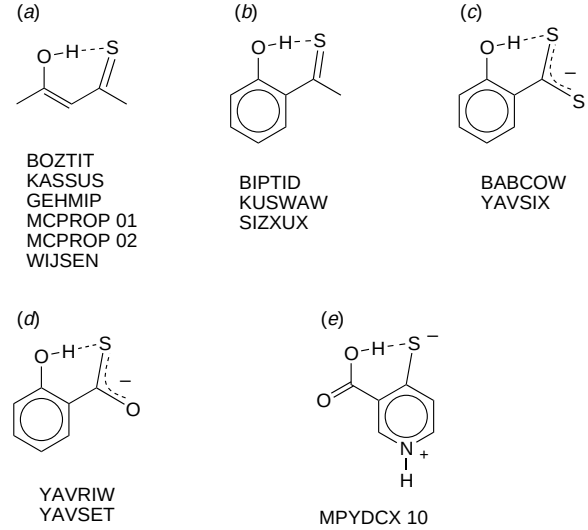

Fig. 2 The crystal structures exhibiting intramolecular O–H···S hydrogen bonds with H···S < 2.1 Å; (*a*) and (*b*) represent molecular fragments, (*c*)–(*e*) are drawn as they occur in the crystal

The short intramolecular hydrogen bonds in monothio-β-diketones lead directly to the concept of resonance assisted hydrogen bonding (RAHB), which has been introduced by Gilli *et al.* to explain the observed strong hydrogen bonding in the oxygen analogue,[7] and was later put into a wider conceptual frame.[5,8] In this model, strong hydrogen bonding is possible if a suitably polarizable system of π-bonds allows charge flow through covalent bonds from the donor to the acceptor. Such systems are provided, for example, by conjugated double bonds. This cooperativity mechanism is well established for cyclic and

Table 1 Crystal structures containing O–H···S hydrogen bonds with H···S distances < 2.1 Å. All are intramolecular and resonance assisted (for X-ray structures based on normalised H-atom positions)

Compound	$d_{H\cdots S}$/Å	$d_{O\cdots S}$/Å	O–H···S (°)
BABCOW	1.92	2.848	156
BIPTID	1.95	2.886	159
BOZTIT	1.96	2.884	155
GEHMIP	2.04	2.979	159
KASSUS	1.98	2.898	155
KUSWAW	2.06	2.937	148
MCPROP 01 (neutron diffr.)	1.90	2.865	155
MCPROP 02	1.93	2.865	157
MPYDCX 10	1.94	2.868	157
SICXUX	1.94	2.904	167
SICXUX	2.00	2.919	154
WIJSEN	1.97	2.874	153
YAVSIX	2.01	2.891	149
YAVRIW	1.88	2.847	165
YAVSET	1.97	2.882	153

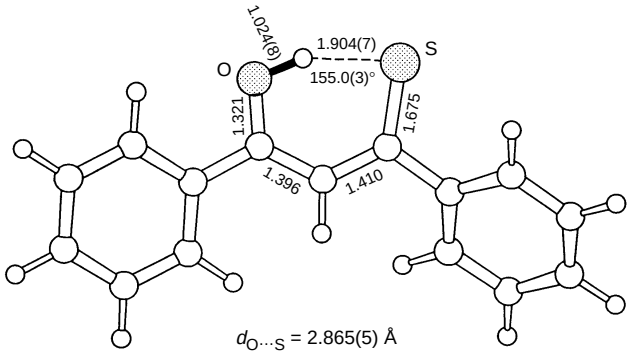

Fig. 3 Molecular structure of a monothio-β-diketone determined by neutron diffraction: mercapto-1,3-diphenylprop-2-en-1-one[3]

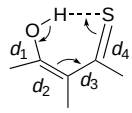

1

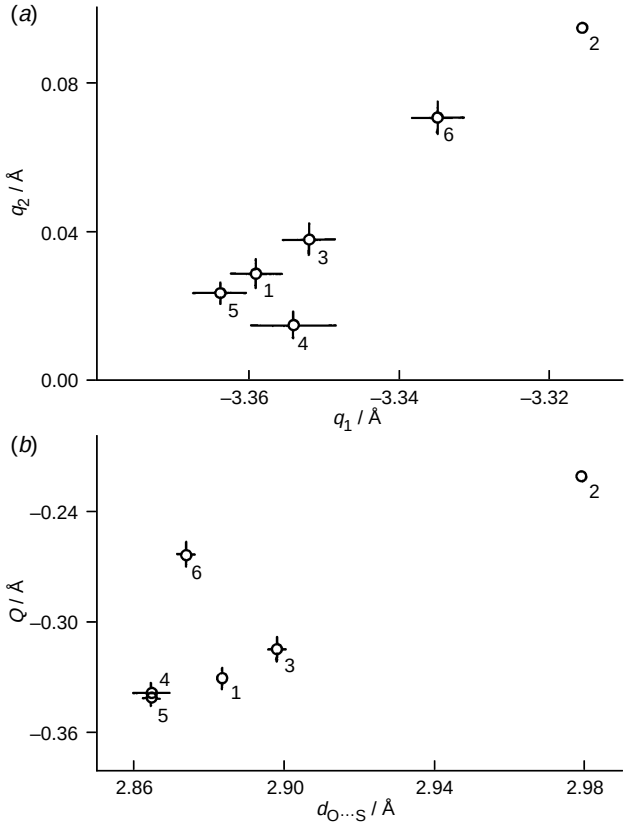

Fig. 4 (*a*) Correlation of the parameter q_1 (= $d_1 - d_4$) and q_2 (= $d_3 - d_2$). (*b*) Correlation of $Q = q_1 + q_2$ with the hydrogen bond distance O···S. The observed correlations imply that the arrangement in **1** is in fact a resonant cycle.[6] Note that a value of $q_2 = 0$ corresponds to complete π-delocalisation of C=C–C. Error bars are included where standard errors of bond lengths were given in the original publication. Data are identified as **1**: BOZTIT. **2**: GEHMIP. **3**: KASSUS. **4**: MCPROP01. **5**: MCPROP02. **6**: WIJSEN.

non-cyclic O=C–C=C–O–H systems and for related heteronuclear cases with N–H donors,[9] and has even been postulated for C–H donors.[10] Since it has not been investigated as yet for sulfur acceptors, the mechanism is looked at more closely here.

If the RAHB model is applicable to the monothio-β-diketones **1**, the situation should exactly parallel the oxygen analogue, as is shown below. Because of the hydrogen bond, the O–C and the C–C bonds gain some double bond character and are shortened, whereas the C=C and C=S bonds loose part of their double bond character and are lengthened. To see if this is more than a suggestion, and if the hydrogen bond arrangement in fact represents a resonant cycle, it is necessary to perform geometrical tests. There are several ways to quantify π-system delocalisation; to make comparison easy, the formalism used by Gilli *et al.*[6] is also used here. It is obvious that in RAHB of increasing strengths, the bond length d_1 reduces and d_4 increases; since C=S is longer than O–C, this means that the difference $q_1 = d_1 - d_4$ is negative and becomes more negative with increasing hydrogen bond strength. The difference in the C–C and the C=C bond lengths, $q_2 = d_3 - d_2$, is positive and decreases with increasing hydrogen bond strength. In the case of total π-delocalisation at C=C–C, q_2 becomes zero. If the arrangement as a whole is a resonant cycle, there must be a correlation between the parameters q_1 and q_2. Furthermore, the π-delocalisation must increase with reducing hydrogen bond distance, so that q_1, q_2 and their sum $Q = q_1 + q_2$ must correlate with O···S (or H···S). The corresponding correlation plots for the monothio-β-diketones are shown in Fig. 4. Despite the limited amount of data the correlations are sufficiently clear to show the anticipated trends [the single outlier in Fig. 4(*b*) is unexplained upon inspection]. This is conclusive evidence that the mechanism of resonance assisted hydrogen bonding is operative in this fragment.

The amount of data for the arrangements in Fig. 2(*b*)–(*e*) is insufficient for statistical analysis, but the structural and electronic similarities immediately suggest that they also represent decent RAHBs, which for arrangements (*c*)–(*e*) even contain a contribution of charge assistance.[5]

The arrangements in Fig. 2 represent by far the shortest O–H···S hydrogen bonds known, about 0.4 Å shorter than typical intermolecular hydrogen bonds. This circumstance is readily explained by the operation of resonance effects within the cyclic fragments, *i.e.* by resonance assisted hydrogen bonding which is analogous to that in β-diketones.[7] The general importance of this concept[5,7] is thereby further emphasised and its applicability for heteronuclear hydrogen bonds is confirmed. The other mechanisms that can produce strong hydrogen bonds, in particular charge assistance,[8] are not apparent in the pure form in the currently available structural data for O–H···S hydrogen bonding.

The author thanks Professor W. Saenger for giving him the opportunity to carry out this work in his laboratory.

Notes and References

* E-mail: steiner@chemie.fu-berlin.de

† Database analysis: Cambridge Structural Database,[2] June 1997 update with 167 797 entries, ordered and error-free organic crystal structures with R values < 0.08 and H-atom positions normalised. The examples in Fig. 2 were individually inspected using the original publications.

1 F. H. Allen, C. M. Bird, R. S. Rowland and P. R. Raithby, *Acta Crystallogr., Sect. B*, 1997, **53**, 680; 1997, **53**, 596.
2 F. H. Allen and O. Kennard, *Chem. Des. Autom. News*, 1993, **8**, 1.
3 L. F. Power, K. E. Turner and F. H. Moore, *J. Chem. Soc., Perkin Trans. 2*, 1976, 249.
4 T. Steiner and W. Saenger, *Acta Crystallogr., Sect. B*, 1994, **50**, 348.
5 V. Bertolasi, P. Gilli, V. Ferretti and G. Gilli, *Chem. Eur. J.*, 1996, **2**, 925.
6 E. Steinwender and W. Mikenda, *Montash. Chem.*, 1990, **121**, 809.
7 G. Gilli, F. Bellucci, V. Ferretti and P. Gilli, *J. Am. Chem. Soc.*, 1989, **111**, 1023.
8 P. Gilli, V. Bertolasi, V. Ferretti and G. Gilli, *J. Am. Chem. Soc.*, 1994, **116**, 909.
9 V. Bertolasi, P. Gilli, V. Ferretti and G. Gilli, *Acta Crystallogr., Sect. B*, 1994, **50**, 617.
10 T. Steiner, *Chem. Commun.*, 1997, 727.

Received in Cambridge, UK, 15th October 1997; 7/07434D

Modeling the active sites of bacteriophage T7 lysozyme, bovine 5-aminolevulinate dehydratase, and peptide deformylase: synthesis and structural characterization of a bis(pyrazolyl)(thioalkoxy)hydroborato zinc complex, $[(Ph_2CHS)Bp^{Bu^t,Pr^i}]ZnI$

Prasenjit Ghosh and Gerard Parkin*

Department of Chemistry, Columbia University, New York, New York 10027, USA

Insertion of thiobenzophenone into a B–H bond of $[Bp^{Bu^t,Pr^i}]ZnI$ achieves the synthesis of $[(Ph_2CHS)Bp^{Bu^t,Pr^i}]ZnI$, a complex in which the *in situ* generated [NNS] donor ligand models the binding of the histidine and cysteine residues at the active sites of bacteriophage T7 lysozyme, bovine 5-aminolevulinate dehydratase and peptide deformylase.

Zinc is essential to all forms of life.[1,2] Of the trace metals, its abundance in biological systems is second only to iron, with an average human containing *ca.* 3 g of zinc. Correspondingly, there are many biological functions of zinc and a large number of zinc enzymes are known. Interestingly, the active sites of many of these enzymes exhibit a common structural motif which comprises a pseudo-tetrahedral zinc center to which a single water molecule is attached, with the three remaining sites being occupied by a combination of nitrogen, oxygen and sulfur donors provided by histidine, glutamate, aspartate and cysteine residues of the protein backbone.[3] Despite the overall similarity in the structure of the active sites of these enzymes, however, each performs a different function. It is, therefore, important to understand the manner in which a $[N_xO_yS_z]$ donor array modifies the chemistry of a tetrahedral zinc center. A first step to achieve such an objective involves the synthesis and structural characterization of well defined complexes with a series of appropriate $[N_xO_yS_z]$ donor ligands. For this reason, we are actively studying synthetic analogues of zinc enzymes which differ in the ligand complement, *e.g.* carbonic anhydrase [NNN],[4–6] thermolysin [NNO],[7] and liver alcohol dehydrogenase [NSS].[8] In this paper, we describe the construction of a [NNS] ligand which provides a model of the groups that bind zinc at the active sites of bacteriophage T7 lysozyme, bovine 5-aminolevulinate dehydratase and peptide deformylase.

Bacteriophage T7 lysozyme is a zinc enzyme which destroys bacteria by cleaving polysaccharide components within their cell walls.[9,10] X-Ray diffraction studies of a mutant lysozyme (AK6) reveal that the active site is located in a cleft within the protein which is *ca.* 22–26 Å long and 10–11 Å deep. The tetrahedral zinc center of the active site is bound to the protein backbone *via* one sulfur and two nitrogen donors of cysteine (Cys-130) and histidine (His-17 and His-122) residues; the fourth site is occupied by a water molecule.[10] Bovine 5-aminolevulinate dehydratase[11] and peptide deformylase[12] are enzymes that are related to T7 lysozyme by virtue of the common coordination of one cysteine and two histidine donors to the zinc center of the active site. In order to mimic the tetrahedral binding of zinc to the protein backbone of these enzymes, a [NNS] ligand which presents the nitrogen and sulfur donors as a facial, rather than T-shaped, array is required. For this purpose, we have focused attention on the construction of ligands in which the donor groups are linked to a common tetrahedral center, since we have previously noted that such attachment serves to enforce facial binding to zinc.[7,8] Significantly, a monomeric zinc complex containing a facially tridentate [NNS] donor ligand, namely $[(Ph_2CHS)Bp^{Bu^t,Pr^i}]ZnI$, may indeed be constructed by insertion of thiobenzophenone into a B–H of $[Bp^{Bu^t,Pr^i}]ZnI$[13] (Scheme 1).

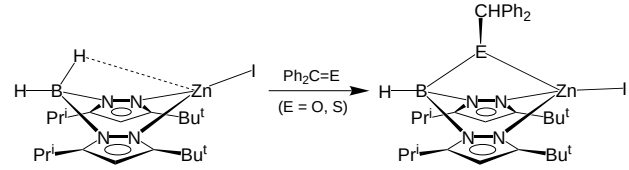

Scheme 1

The molecular structure of $[(Ph_2CHS)Bp^{Bu^t,Pr^i}]ZnI$ (Fig. 1) has been determined by X-ray diffraction.[14] Of most importance, the diffraction study demonstrates that (*i*) $[(Ph_2CHS)Bp^{Bu^t,Pr^i}]ZnI$ exists as a well defined monomeric complex, and (*ii*) the [NNS] ligand supports a pseudo-tetrahedral zinc center that is structurally related to the active sites of T7 lysozyme,[15] 5-aminolevulinate dehydratase,[16] and peptide deformylase.[12]

The significance of isolating $[(Ph_2CHS)Bp^{Bu^t,Pr^i}]ZnI$ is further underscored by noting that other attempts to use tridentate [NNS] ligands to support monomeric tetrahedral zinc complexes of the type [NNS]ZnX have not been very successful. For example, Vahrenkamp has used *N*-(2-mercaptoethyl)picolylamine (MEPAH) in an attempt to provide a [NNS] environment pertinent to zinc enzymes.[17] Unfortunately, however, the zinc chemistry derived from MEPAH was found to be very complex, with polymeric

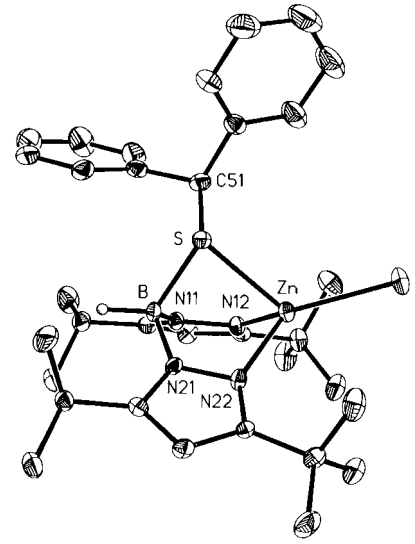

Fig. 1 Molecular structure of $[(Ph_2CHS)Bp^{Bu^t,Pr^i}]ZnI$. Selected bond lengths (Å) and angles (°): Z–N(12) 2.031(5), Zn–N(22) 2.040(5), Zn–S 2.460(2), Zn–I 2.4869(8); N(12)–Zn–N(22) 94.6(2), N(12)–Zn–S 88.61(14), N(22)–Zn–S 84.00(14), N(12)–Zn–I 125.63(13), N(22)–Zn–I 129.34(13), S–Zn–I 121.71(5).

$[(MEPA)ZnX]_n$ (X = Cl, Br), trinuclear $[(MEPA)_4Zn_3]X_2$ (X = BF_4, ClO_4, NO_3), dinuclear $[(MEPA)Zn(OAc)]_2$, and other complexes being isolated; in no instance was a monomeric tetrahedral [NNS]ZnX complex strucurally characterized.[18] Undoubtedly, one of the principal reasons for the difficulty in isolating mononuclear [NNS]ZnX complexes is associated with the propensity of sulfur to act as a bridge between metal centers.[19] In view of the difficulty associated with isolating such complexes, the *in situ* construction of a [NNS] donor ligand by elaboration of a [NN] donor ligand at a metal center therefore provides a useful method of synthesis of other [NNS]ZnX derivatives.[20]

In addition to $[(Ph_2CHS)Bp^{Bu^t,Pr^i}]ZnI$, the alkoxide analogue $[(Ph_2CHO)Bp^{Bu^t,Pr^i}]ZnI$ has also been synthesized (Scheme 1) and structurally characterized by X-ray diffraction.[21] Other than the difference in Zn–O *vs.* Zn–S bond lengths, the coordination environment about zinc is similar for $[(Ph_2CHS)Bp^{Bu^t,Pr^i}]ZnI$ and $[(Ph_2CHO)Bp^{Bu^t,Pr^i}]ZnI$. The geometry at the chalcogen in each case is distinctly pyramidal, with the $[Ph_2CH]$ alkyl substituent being displaced from the B–E–Zn plane, so that both molecules are chiral. The barriers to enantiomer interconversion are, however, considerably different for the two derivatives. For example, whereas the thioalkoxide complex $[(Ph_2CHS)Bp^{Bu^t,Pr^i}]ZnI$ exhibits two sets of resonances in the 500 MHz ^1H NMR spectrum at −50 °C for the two diasterotopic pyrazolyl groups, the corresponding ^1H NMR spectrum of the alkoxide analogue $[(Ph_2CHO)Bp^{Bu^t,Pr^i}]ZnI$ shows only a single set due to chemical exchange as a result of isomerization. The barrier for enantiomer interconversion, is, therefore, considerably lower for the alkoxide complex than for the thioalkoxide derivative.[22] Enantiomer interconversion for $[(Ph_2CHS)Bp^{Bu^t,Pr^i}]ZnI$ is, however, observed to occur rapidly on the NMR timescale at ambient temperature,[23] with an activation barrier ($\Delta G^{\ddagger}$) of 14.5(3) kcal mol^{-1} (1 cal = 4.184 J) at 25 °C.[24,25] Two possible mechanisms for enantiomer interconversion include (*i*) cleavage of the E → Zn dative bond, rotation about the B–E bond, followed by re-coordination, and (*ii*) pyramidal inversion at E. Although we have no evidence to distinguish between these mechanisms, if enantiomer interconversion were to proceed *via* a common mechanism, the observation that the exchange is more facile for the alkoxide than for the thioalkoxide suggests that the mechanism may involve direct inversion at the chalcogen, since barriers to inversion are typically lower for second row (*i.e.* O), as opposed to third row (*i.e.* S), elements.[22,26] Some support for this notion is provided by the observation that the $[Ph_2CH]$ substituent is much closer to planarity with the B–E–Zn plane in the alkoxide than in the thioalkoxide derivative, as judged by the respective sum of bond angles at O (336°) and S (288°). In contrast, however, if enantiomer interconversion were to require dissociation of the E → Zn dative bond, then the exchange would be expected to be more facile for the complex with the weaker bond, *i.e.* the thioalkoxide derivative.

In summary, the insertion of thiobenzophenone into a B–H bond of $[Bp^{Bu^t,Pr^i}]ZnI$ results in the synthesis of $[(Ph_2CHS)Bp^{Bu^t,Pr^i}]ZnI$. Importantly, the [NNS] ligand so obtained is capable of sustaining a monomeric tetrahedral geometry about zinc and resembles the histidine and cysteine residues that bind zinc at the active sites of T7 lysozyme, 5-aminolevulinate dehydratase and peptide deformylase.

We thank the National Institutes of Health (Grant GM46502) and Kanagawa Academy of Science and Technology for support of this research. G. P. is the recipient of a Presidential Faculty Fellowship Award (1992–1997).

Notes and References

*E-mail: parkin@chem.columbia.edu

1 B. L. Vallee and D. S. Auld, in *Matrix Metalloprotinases and Inhibitors*, ed. H. Birkedal-Hansen, Z. Werb, H. G. Welgus and H. E. van Wart, Gustav Fischer Verlag, New York, 1992, pp. 5–19; B. L. Vallee and D. S. Auld, *Biochemistry*, 1990, **29**, 5647; 1993, **32**, 6493.
2 J. E. Coleman, *Annu. Rev. Biochem.*, 1992, **61**, 897.
3 B. L. Vallee and D. B. Auld, *Acc. Chem. Res.*, 1993, **26**, 543; W. N. Lipscomb and N. Sträter, *Chem. Rev.*, 1996, **96**, 2375; R. H. Holm, P. Kennepohl and E. I. Solomon, *Chem. Rev.*, 1996, **96**, 2239.
4 R. Alsfasser, S. Trofimenko, A. Looney, G. Parkin and H. Vahrenkamp, *Inorg. Chem.*, 1991, **30**, 4098; A. Looney, R. Han, K. McNeill and G. Parkin, *J. Am. Chem. Soc.*, 1993, **115**, 4690.
5 Bis(pyrazolyl)hydroborato ligands are represented by the abbreviations $[Bp^{R,R}]$ with the 3- and 5-alkyl substituents listed respectively as superscripts. See: G. Parkin, *Adv. Inorg. Chem.*, 1995, **42**, 291.
6 C. Kimblin, W. E. Allen and G. Parkin, *J. Chem. Soc., Chem. Commun.*, 1995, 1813.
7 C. Dowling and G. Parkin, *Polyhedron*, 1996, **15**, 2463.
8 C. Kimblin, T. Hascall and G. Parkin, *Inorg. Chem.*, 1997, **36**, 5680.
9 Specifically, T7 lysozyme cleaves the amide bond between L-alanine and *N*-acetylmuramate moieties. See: M. Inouye, N. Arnheim and R. Sternglanz, *J. Biol. Chem.*, 1973, **248**, 7247.
10 In addition to its lyase activity, T7 lysozyme also inhibits transcription by binding to T7 RNA polymerase. However, zinc is not required for such action. See: X. Cheng, X. Zhang, J. W. Pflugrath and F. W. Studier, *Proc. Natl. Acad. Sci. USA*, 1994, **91**, 4034.
11 A. J. Dent, D. Beyersmann, C. Block and S. S. Hasnain, *Biochemistry*, 1990, **29**, 7822.
12 T. Meinnel, C. Lazennec and S. Blanquet, *J. Mol. Biol.*, 1995, **254**, 175; T. Meinnel, S. Blanquet and F. Dardel, *J. Mol. Biol.*, 1996, **262**, 375; T. Meinnel, C. Lazennec, S. Villoing and S. Blanquet, *J. Mol. Biol.*, 1997, **267**, 749.
13 $[Bp^{Bu^t,Pr^i}]ZnI$ is obtained by reaction of ZnI_2 with $Tl[Bp^{Bu^t,Pr^i}]$ (C. Dowling, P. Ghosh and G. Parkin, *Polyhedron*, 1997, **16**, 3469).
14 $[(Ph_2CHS)Bp^{Bu^t,Pr^i}]ZnI{\cdot}0.5C_7H_8$ is monoclinic, $P2_1/c$ (no. 14), a = 20.474(2), b = 9.228(1), c = 20.785(2) Å, β = 90.767(6)°, U = 3926.4(7) Å^3, and Z = 4. CCDC 182/718.
15 Selected bond lengths in T7 lysozyme: 2.52 Å [Zn–N(His-17)], 2.67 Å [Zn–N(His-122)] and 2.15 Å [Zn–S(Cys-130)]. See ref. 10.
16 Selected bond lengths (EXAFS) in bovine 5-aminolevulinate dehydratase: 2.05 Å [Zn–N(His)], 2.05 Å [Zn–N(His)] and 2.32 Å [Zn–S(Cys)]. See ref. 11.
17 U. Brand and H. Vahrenkamp, *Inorg. Chem.*, 1995, **34**, 3285.
18 Likewise, *N*-(2-mercaptophenyl)picolylamine has not yielded monomeric [NNS]ZnX complexes that have been structurally characterized. See: U. Brand and H. Vahrenkamp, *Chem. Ber.*, 1996, **129**, 435.
19 I. G. Dance, *Polyhedron*, 1986, **5**, 1037; P. J. Blower and J. R. Dilworth, *Coord. Chem. Rev.*, 1987, **76**, 121; R. H. Prince, in *Comprehensive Coordination Chemistry*, ed. G. Wilkinson, R. D. Gillard and J. McCleverty, Pergamon, Oxford, 1987, vol. 5, pp. 925–1045.
20 Copper and tungsten derivatives of related $[(RS)Bp^{RR'}]$ ligands, namely $[(p\text{-}TolS)Bp^{Me_2}]CuSR$[20a] and $[(p\text{-}TolCH_2S)Bp]Mo(CO)_2(\eta^2\text{-}S_2CR)$,[20b] have also been reported, although they have not been structurally characterized. (*a*) J. S. Thompson, J. L. Zitmann, T. J. Marks and J. A. Ibers, *Inorg. Chim. Acta*, 1980, **46**, L101; (*b*) A. F. Hill and J. M. Malget, *J. Chem. Soc., Dalton Trans.*, 1997, 2003.
21 $[(Ph_2CHO)Bp^{Bu^t,Pr^i}]ZnI$ is orthorhombic, $Pca2_1$ (no. 36), a = 10.826(2), b = 16.378(3), c = 19.729(4) Å, U = 3498(1) Å^3 and Z = 4. CCDC 182/718.
22 It is also worth noting that barriers to rotation follow a similar trend. For example, rotation about the B–O bond in R_2BOR' complexes is more facile than rotation about the B–S bond in R_2BSR'. See: M. T. Ashby and N. A. Sheshtawy, *Organometallics*, 1994, **13**, 236.
23 For a brief review on dynamic NMR spectroscopy, see: G. Binsch and H. Kessler, *Angew. Chem., Int. Ed. Engl.*, 1980, **19**, 411.
24 The enthalpy and entropy of activation are: $\Delta H^{\ddagger}$ = 9(1) kcal mol^{-1} and $\Delta S^{\ddagger}$ = −19(5) cal K^{-1} mol^{-1}.
25 For other examples of inversion that have been studied by dynamic NMR spectroscopy, see: E. W. Abel, S. K. Bhargava and K. G. Orrell, *Prog. Inorg. Chem.*, 1984, **32**, 1.
26 For example, it is well documented that the inversion barrier of NH_3 is considerably lower than that of PH_3 owing to the reduced tendency of phosphorus to hybridize and obtain a planar transition state. Related effects are also observed with the chalcogens which indicate that oxygen has a greater tendency to participate in hybridization than do its heavier congeners (*e.g.* the bond angle in H_2O is considerably greater than the almost 90° bond angles in H_2S, H_2Se and H_2Te). See: W. Kutzelnigg, *Angew. Chem., Int. Ed. Engl.*, 1984, **23**, 272; W. Cherry and N. Epiotis, *J. Am. Chem. Soc.*, 1976, **98**, 1135; J. Lambert, *Top. Stereochem.*, 1971, **6**, 19.

Received in Bloomington, IN, USA, 15th October 1997; 7/07444A

Oxidation of organic cyclic sulfites to sulfates: a new reaction catalyzed by cyclohexanone monooxygenase

Stefano Colonna,*[a]† Nicoletta Gaggero,[a] Giacomo Carrea[b] and Piero Pasta[b]

[a] *Istituto di Chimica Organica, Facoltà di Farmacia, Università di Milano, Via Venezian 21, I 20133 Milano, Italy*
[b] *Istituto di Chimica degli Ormoni, CNR, Via Mario Bianco 9, I 20131, Milano, Italy*

Cyclohexanone monooxygenase from *Acinetobacter* catalyzes the enantioselective oxidation of organic cyclic sulfites to sulfates.

Cyclohexanone monooxygenase (CHMO) (EC 1.14.13.22) from *Acinetobacter* NCIB 9871 is a flavoenzyme of about 60 000 Daltons, active as a monomer which contains one firmly but non-covalently bound FAD unit per enzyme molecule.[1] It has wide potential for application in the manufacture of fine chemicals and in organic synthesis based on the Baeyer–Villiger reaction.[2] The only reagents consumed are dioxygen, NADPH and the substrate ketone, which are transformed enantioselectively into the corresponding ester and water.

Walsh showed that CHMO can oxygenate heteroatoms, due to the high reactivity of the 4a-hydroperoxyflavin intermediate which acts as an electrophile to trimethyl phosphite and iodide ions, and as a nucleophile to boronic acids.[1] Walsh[3] and our group[4] have also shown that this enzyme catalyzes the asymmetric sulfoxidation of numerous alkyl aryl sulfides with high enantioselectivity. The versatility of CHMO in promoting enantioselective sulfoxidation was recently exploited also with 1,3-dithioacetals[5] and dialkyl sulfides.[6]

We were interested in exploring whether CHMO was able to oxidize organic cyclic sulfites to the corresponding sulfates, a reaction that, to the best of our knowledge, has not been described previously in the literature. Furthermore, this enzymatic procedure could also serve as an alternative route to the only chemical sysnthesis of sulfates of practical interest described so far. This method, developed by Sharpless and Gao, employs sodium metaperiodate as the stoichiometric reoxidant for a ruthenium tetroxide catalyst.[7] Cyclic sulfites and sulfates can be considered synthetic equivalents of epoxides, capable of reacting with a large variety of nucleophiles.[8] In many instances cyclic sulfates are more reactive than oxiranes and, unlike the latter, can lead to disubstitution products.[8]

The diastereoisomeric cyclic sulfites **1**, **3**, **4** and **6**, prepared in racemic form according to the literature,[7] were separated by flash chromatography into their *cis* and *trans* components. The enzymatic oxidation of sulfites (reactions 1–4, Scheme 1) was coupled to a second enzymatic reaction to regenerate NADPH; therefore only a catalytic quantity of NADPH was required. The regenerating system was glucose-6-phosphate and glucose-6-phosphate dehydrogenase (G6PDH) (reaction 5, Scheme 1).[3]

The time-course of reactions (1) and (2) (see Scheme 1) was monitored by HPLC both for conversion and ee. The absolute configurations of the remaining substrates **1b** and **3b** were assigned by comparison of their elution order in chiral HPLC with that of *cis*-(2*R*,4*S*)-**1b** and *trans*-(2*S*,4*R*)-**3b** prepared according to the literature.[9]

The results of the oxidation of 4-benzyloxymethyl-1,3,2-dioxathiolane 2-oxides, *cis*-**1a**, and -**1b** and *trans*-**3a** and -**3b**, reported in Table 1, show that indeed cyclohexanone mono-

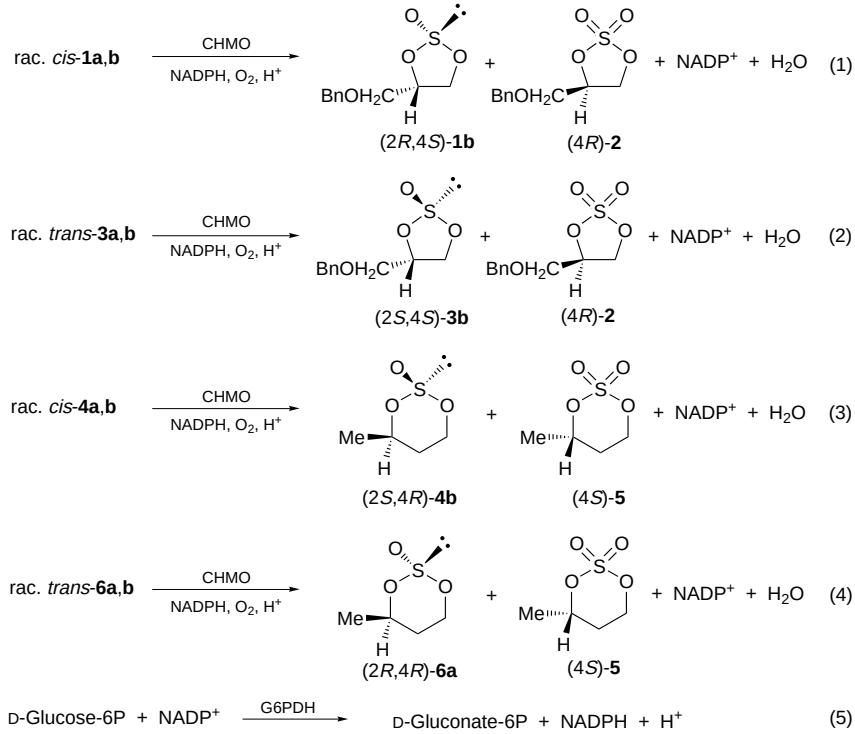

Scheme 1

oxygenase in the presence of dioxygen is able to transfer an oxygen atom to the cyclic sulfite in satisfactory chemical yield. The enzymatic reaction is a 'clean' alternative to the chemical oxidation that needs a mixture of CCl_4 and MeCN as solvent. The stereoselective formation of the (4*R*)-sulfate **2** is the result of a kinetic resolution of the starting racemic substrates. The *cis* diastereoisomers (**1a** and **1b**) were more reactive than the *trans* (**3a** and **3b**), as shown by their higher conversion at the same reaction times. The enantioselectivity in the kinetic resolution was also more pronunced for the *cis* sulfite; indeed **1b** was obtained in 94% ee after 60 min, the ee of **3b** being 21%. The stereochemical course of the oxidation is dictated by the absolute configuration of the carbon atom (and not by that of sulfur) since both diastereoisomers afforded the (*R*)-sulfate **2**. The same behaviour was also shown by 4-benzylmethyl- and 4-(benzyl)-1,3,2-dioxathiolane 2-oxide, the *cis* diastereoisomers being more reactive than the *trans*. The kinetic resolution was also more satisfactory for the *cis* sulfites, the ees being in the range 15–70 and 35–50% for the starting material and the reaction products, respectively.

Interestingly, the order of reactivity and the enantioselectivity were reversed in the oxidation of 4-methyl-1,3,2-dioxathiane 2-oxides **4** and **6**. As shown in Table 1, the *trans* sulfites **6a** and **6b** reacted faster than the *cis* sulfites **4a** and **4b** and showed higher stereoselectivity. We do not know whether this behaviour is due to the more flexible nature of the five-membered ring than the six-membered ring,[10] which may affect their interactions with the active site of CHMO or, more generally, to a dramatic influence of the substrate structure on the stereochemical course of the oxidation at sulfur, as we previously found with biosulfoxidation reactions.[4]

Table 1 CHMO catalyzed oxidation of sulfites to sulfates[a]

Substrate	*t*/min	Conversion (%)	Ee (%)	
			Sulfite	Sulfate
1a, **1b**	15	22	26	93
	30	34	44	84
	60	62	94	58
	90	74	⩾99	47
	120	80	⩾99	36
3a, **3b**	15	8	6	66
	30	17	11	56
	60	31	21	47
	90	63	60	35
	120	79	79	25
4a, **4b**	15	7	5	68
	30	17	12	58
	45	27	18	47
	60	32	23	44
	90	60	50	31
	120	69	60	21
6a, **6b**	15	19	20	85
	30	34	32	61
	45	50	54	45
	60	68	71	22
	90	77	80	12
	120	85	93	5

[a] The oxidation of sulfites to sulfates was carried out as follows: the sulfite (10 mM) was reacted at 25 °C, under stirring, in 5 ml of 50 mM Tris–HCl buffer, pH 8.6, containing NADP (1 mM), glucose- 6-phosphate (50 mM), 10 units CHMO [purified as described by Latham and Walsh (ref. 17)] and 100 units of glucose-6-phosphate dehydrogenase. At scheduled times, the reaction mixture was extracted with ethyl acetate (3 × 5 ml), dried and analyzed by chiral HPLC or GLC to determine the degree of conversion and ee. HPLC was carried out in a Chiralpak AS column (Daicel) using *n*-hexane–propan-2-ol (9 : 1) as the mobile phase. The column separated the enantiomers of sulfites *cis*-**1** and *trans*-**3** and of sulfate **2**. The retention times were: **1a**, 9.0; **1b**, 9.9; **3a**, 12.8; **3b**, 17.3; (*R*)-**2**, 30.2; (*S*)-**2**, 31.8 min. GLC was carried out on a CP-cyclodextrin-β-2,3,6-M19 column (Chrompack) under the following conditions: oven temperature 100 to 150 °C; heating rate 1 °C min^{-1}; H_2 as carrier gas. The column separated the enantiomers of sulfites *cis*-**4** and *trans*-**6** and of sulfate **5**. Retention times were: **4a**, 17.8; **4b**, 17.1; **6a**, 10.1; **6b**, 10.6; (*R*)-**5**, 40.2; (*S*)-**5**, 40.8 min.

The absolute configurations of dioxathianes **4** and **6** were assigned by GLC comparison with authentic samples prepared according to the literature.[11]

In conclusion, this new oxidation reaction catalyzed by cyclohexanone monooxygenase, likely *via* 4a-hydroperoxyflavin as intermediate, expands the synthetic importance of this enzyme. The oxygen transfer at sulfur is enantioselective, thus allowing the obtainment of cyclic sulfites and sulfates with high ee under appropriate conditions. We are now investigating the oxidation by CHMO of other sulfites. Since the high electrophilic reactivity of 4a-hydroperoxyflavin is reminescent of that of dioxiranes we are also examining the behaviour of these oxidants in the oxidation of some substrates in organic solvents. It is worth mentioning that, so far, the only reported example of enzymatic oxidation of an organic sulfite is that of dimethyl sulfite, catalyzed by chicken liver sulfite oxidase.[12]

Concerning the scale-up of CHMO catalyzed reactions, we are assessing the possibility of using membrane reactors and macromolecular NADPH, as already done with other coenzyme dependent oxidoreductases.[13,14] However, there are some drawbacks that need to be overcome. One is represented by the stability of the enzyme, which is not very high especially in the presence of bubbling oxygen, which is an essential reagent. Considerable stability improvements have been described recently by feeding oxygen through a thin-walled silicone tube.[15] Another limitation is represented by the low water solubility of substrates. The solution to this problem could be the use of integrated extractive procedures[14] or of hydrophobic resins that act as reservoirs for both substrates and products.[16]

Financial support from CNR and MURST is gratefully acknowledged.

Notes and References

† E-mail: colonna@imiucca.csiunimi.it

1 C. T. Walsh and Y. C. J. Chen, *Angew. Chem., Int. Ed. Engl.*, 1988, **27**, 333; *Angew. Chem.*,1988, **100**, 342.
2 S. Petit and R. Furstoss, *Tetrahedron: Asymmetry*, 1993, **4**, 1341; R. Gagnon, G. Grogan, M. S. Levitt, S. M. Roberts, P. W. Wan and A. J. Willetts, *J. Chem. Soc., Perkin Trans. 1*, 1994, 2537.
3 D. R. Light, D. J. Waxman and C. T. Walsh, *Biochemistry*, 1982, **21**, 2490.
4 S. Colonna, N. Gaggero, P. Pasta and G. Ottolina, *Chem. Commun.*, 1996, 2300; G. Carrea, B. Redigolo, S. Riva, S. Colonna, N. Gaggero, E. Battistel and D. Bianchi, *Tetrahedron: Asymmetry*, 1992, **3**, 1063.
5 S. Colonna, N. Gaggero, A. Bertinotti, G. Carrea and P. Pasta, *J. Chem. Soc., Chem. Commun.*, 1995, 1123; S. Colonna, N. Gaggero, G. Carrea, P. Pasta and A. Bernardi, *Tetrahedron: Asymmetry*, 1996, **7**, 565.
6 S. Colonna, N. Gaggero, G. Carrea and P. Pasta, *Chem. Commun.*, 1997, 439.
7 Y. Gao and K. B. Sharpless, *J. Am. Chem. Soc.*, 1988, **110**, 7538.
8 H. C. Kolb, M. S. Van Nieuwenhze and K. B. Sharpless, *Chem. Rev.*, 1994, **94**, 2483; M. Pilkington and J. D. Wallis, *J. Chem. Soc., Chem. Commun.*, 1993, 1857; B. B. Lohray, *Synthesis*, 1992, 1035; R. Oi and K. B. Sharpless, *Tetrahedron Lett.*, 1991, **32**, 999.
9 H. J. Carlsen and K. Aase, *Acta Chem. Scand.*, 1993, **47**, 737.
10 D. G. Hellier and H. G. Liddy, *Magn. Reson. Chem.*, 1988, **26**, 671.
11 G. Lowe and M. J. Parrat, *Bioorg. Chem.*, 1988, **16**, 283.
12 M. S. Brody and R. Hille, *Biochim. Biophys. Acta*, 1995, **1253**, 133.
13 G. Carrea, P. Pasta, N. Gaggero, G. Grogan and A. J. Willetts, *Biotechnol. Lett.*, 1996, **18**, 1123.
14 U. Kragl, W. Kruse, W. Hummel and C. Wandrey, *Biotechnol. Bioeng.*, 1996, **52**, 309.
15 S. Rissom, U. Schwarz-Linek, M. Vogel, V.I. Tishkov and U. Kragl, *Tetrahedron: Asymmetry*, 1997, **8**, 2523.
16 J. T. Vincenzi, M. J. Zmjiewski, M. R. Reinhard, B. E. Landen and P. G. Marler, *Enzyme Microb. Technol.*, 1997, **20**, 494.
17 J. A. Latham and C. T. Walsh, *J. Am. Chem. Soc.*, 1987, **109**, 3421.

Received in Liverpool, UK, 28th October 1997; 7/07749A

Synthesis of a cobalt complex of a pyrano[2,3-*b*]quinoxaline-3,4-dithiolate related to molybdopterin

Ben Bradshaw, Andrew Dinsmore, C. David Garner and John A. Joule*†

Chemistry Department, The University of Manchester, Manchester, UK M13 9PL

Cobalt complex 2 has been synthesised in which the key features of molybdopterin—a dithiolene ligand on a tetrahydropyrano[2,3-*b*]pyrazine—are modelled.

The pioneering analytical studies on representatives of the oxomolybdoenzymes by Rajagopalan[1] showed the presence of a pteridine (molybdopterin) carrying a C-6 side-chain having two sulfur atoms which ligate molybdenum. X-Ray crystallographic determinations on the oxomolybdoenzymes aldehyde oxidase from *Desulfovibrio gigas*,[2] DMSO reductase from *Rhodobacter sphaeroides* and *R. capsulatus*[3] and formate dehydrogenase from *Escherichia coli*[4] and on the hyperthermophilic tungsten enzyme ferredoxin aldehyde oxidoreductase from *Pyrococcus furiosus*,[5] clearly define the nature of molybdopterin and its mode of ligation to Mo and W **1**. Thus,

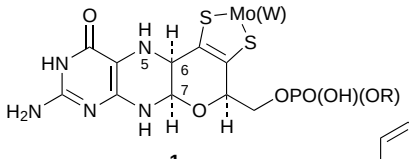

1

(R = H or nucleoside)
(other ligands on metal not shown)

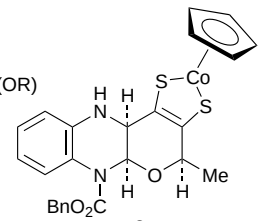

2

the metals are chelated by an ene-1,2-dithiolate (dithiolene) which is attached at C-6 to a reduced pteridine ring, as originally proposed by Rajagopalan.[1] However, unsuspected from the degradative and spectroscopic studies of Rajagopalan,[1] all of the protein crystallographic studies observe a tetrahydropyran ring, which can be viewed as resulting from cyclisation of a side-chain hydroxy group to C-7 of a 5,6-dihydropteridine.

Given the results of these protein crystallographic studies, we have modified our earlier synthetic strategies[6–7] to take account of the presence of the tetrahydropyran ring and herein describe the synthesis of cobalt complex **2** which involves ligation of the metal by a dithiolene moiety linked to pyran and pyrazine rings as identified for molybdopterin.[2–5]

2-Chloroquinoxaline[9] was coupled with but-3-yn-2-ol, without protection of the alcohol, using Pd^0 catalysis, and the product **3a** was oxidised to **3b** following Taylor (Scheme 1).[10] Following precedents,[11] heating the ketone in 4-phenyl-1,3-dithiolane-3-thione[12] at 150 °C gave the 1,3-dithiole-2-thione **4a** in 75% yield. This short route to masked, unsymmetrically substituted dithiolenes has considerable advantages over those we have used earlier.[7,13]

Selective reduction of the ketone functionality with $NaBH_4$ gave alcohol **4b**; conversion to 1,3-dithiol-2-one **4c** was then achieved in high yield with mercury(II) acetate in AcOH at room temperature.

We had shown earlier[14] that treatment of 2-substituted quinoxalines with $NaBH_4$ in the presence of benzyl chloroformate leads to 2-substituted 4-benzyloxycarbonyl-1,2,3,4-tetrahydroquinoxalines, *via* initial *N*-4-acylation then trapping of the resulting quinoxalinium salt by hydride addition at C-7 and finally reduction of the remaining 5,6-imine unit. Therefore, it seemed possible that alcohols such as **4b** and **4c** might react with a chloroformate, in the absence of reductant, to form products in which a first-formed *N*-4-acylquinoxalinium salt has been trapped by an intramolecular nucleophilic attack at C-7 by the side-chain hydroxy group resulting in a cyclisation and giving a pyran ring oriented, with respect to the pyrazine, just as in molybdopterin. We were aware that simple *O*-acylation could compete with these aspirations and indeed, under most of the conditions examined in an extended study of **4b**, *O*-acylation was the only or the predominant reaction observed.

After considerable experimentation it was found that treatment of **4c** with benzyl chloroformate, in the absence of solvent or added base at room temperature, produced the desired cyclisation with no *O*-acylation. Even more rewarding was the finding that one diastereoisomer was formed almost exclusively and that the relative stereochemistry in this tricycle mirrors that in molybdopterin. Thus, **4c** was converted into tetracycle **5** in 90% yield, the relative stereochemistry in **5** being established by the observation of an NOE between the two methine hydrogen signals at δ 6.02 (s) and 4.92 (q, J 6.6) for the BnO_2CN-C*H*OCHMe and MeC*H*OCHNCO_2Bn protons, respectively. Reduction of the remaining imine unit with sodium cyanoborohydride in the presence of AcOH produced only one

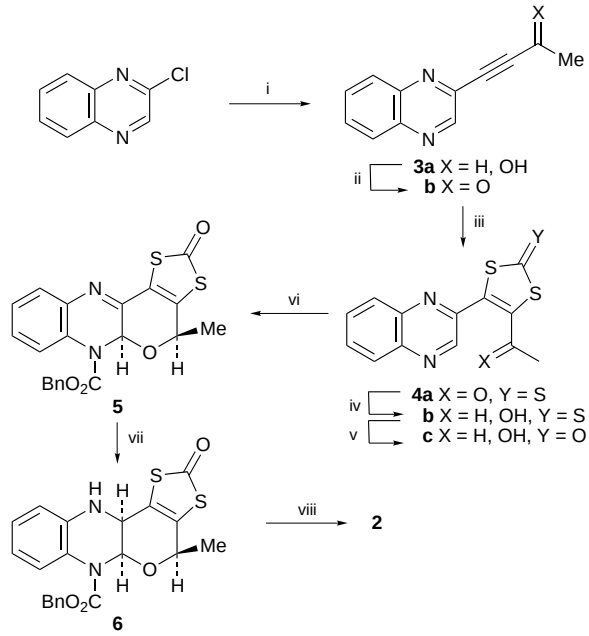

Scheme 1 *Reagents and conditions*: i, HC≡CCH(OH)Me, $Pd(OAc)_2$, CuI, Ph_3P, Et_3N (88%); ii, CrO_3, H_2SO_4, Me_2CO, 0 °C (76%); iii, 4-phenyl-1,3-dithiolane-2-thione, 150 °C, N_2 (75%); iv, $NaBH_4$, THF, Pr^iOH, H_2O (69%); v, $Hg(OAc)_2$, Me_2CO, AcOH, room temp. (98%); vi, $ClCO_2Bn$, room temp., N_2 (90%); vii, $NaB(CN)H_3$, AcOH, CH_2Cl_2, MeOH, room temp. (95%); viii, CsOH, MeOH, CH_2Cl_2, room temp., then $Co(Cp)I_2$ (77%).

stereoisomer of the dihydro derivative, shown to have structure **6**, the predicted *cis* relationship of hydrogen atoms at the ring junction being confirmed by an NOE between the protons resonating at δ 5.95 (d, *J* 2.19) ($BnO_2CNCHOCHMe$) and 4.45 (d, *J* 2.19) (NCHCHOCHMe). Thus, this proligand, and the cobalt complex **2** formed from it, possess the same relative stereochemistry at the three chiral centres as in the natural cofactor. Hydrolysis of **6** with aq. CsOH at room temperature produced a solution to which was added cyclopentadienyl (diiodo)cobalt resulting in the formation of purple crystals of **2** in 77% yield, having ^{1}H NMR signals which verified that the organic ligand has been incorporated intact into the metal-containing complex.

We are currently pursuing the application of the methodology described above for the synthesis of molybdopterin, especially to ascertain the chemistry of this biologicaly important ligand. For example, it is not yet established whether the form of molybdopterin identified by protein crystallography represents the catalytically active form. Simple proton-catalysed processes would lead from the structure shown in **1** to forms in which the N–C–O unit has been cleaved, introducing a double bond into the pyrazine ring and allowing electronic communication (*i.e.* conjugation) between the metallocycle and the pteridine unit, and we have speculated on the possible involvement of such interactions in the biological mode of action of these cofactors.[15]

We thank the EPSRC for post-doctoral (A. D.) and student (B. B.) support of this work.

Notes and References

† E-mail: j.a.joule@man.ac.uk

1 For a leading reference, see R. M. Garrett and K. V. Rajagopalan, *J. Biol. Chem*., 1996, **271**, 7387.
2 M. J. Romão, M. Archer, I. Moura, J. J. G. Moura, J. LeGall, E. Engh, M. Schneider, P. Hof and R. Huber, *Science*, 1995, **270**, 1170.
3 H. Schindelin, C. Kisker, J. Hilton, K. V. Rajagopalan and D. C. Rees, *Science*, 1996, **272**, 1615; F. Schneider, J. Löwe, R. Huber, H. Schindelin, C. Kisker and J. Knäblein, *J. Mol. Biol*., 1996, **263**, 53; A. S. McAlpine, A. G. McEwan, A. G. Shaw and S. Bailey, *J. Biol. Inorg. Chem*., 1997, **2**, 680.
4 J. C. Boyington, V. Sladishev, S. V. Khangulov, T. C. Stadtman and P. D. Sun, *Science*, 1997, **275**, 1305.
5 M. K. Chan, S. Mukund, A. Kletzin, M. W. W. Adams and D. C. Rees, *Science*, 1995, **267**, 1463.
6 D. Collison, C. D. Garner and J. A. Joule, *Chem. Soc. Rev*., 1996, 25 and references cited therein.
7 A. Dinsmore, J. H. Birks, C. D. Garner and J. A. Joule, *J. Chem. Soc., Perkin Trans. 1*, 1997, 801.
8 E. S. Davies, R. L. Beddoes, D. Collison, A. Dinsmore, A. Docrat, J. A. Joule, C. R. Wilson and C. D. Garner, *J. Chem. Soc., Dalton Trans*., 1997, 3985.
9 A. H. Gowenlock, G. T. Newbold and F. S. Spring, *J. Chem. Soc*., 1945, 622.
10 E. C. Taylor and R. Dötzer, *J. Org. Chem*., 1991, **56**, 1816.
11 B. R. O'Connor and F. N. Jones, *J. Org. Chem*., 1970, **35**, 2002; A. Gorgues, P. Batail and A. Le Coq, *J. Chem. Soc., Chem. Commun*., 1983, 405.
12 C. C. J. Culvenor, *J. Chem. Soc*., 1946, 1050.
13 D. J. Rowe, C. D. Garner and J. A. Joule, *J. Chem. Soc., Perkin Trans. 1*, 1985, 1907; L. Larsen, C. D. Garner and J. A. Joule, *J. Chem. Soc., Perkin Trans 1*, 1989, 2311 L. Larsen, D. J. Rowe, C. D. Garner and J. A. Joule, *J. Chem. Soc., Perkin Trans. 1*, 1989, 2317.
14 J. R. Russell, C. D. Garner and J. A. Joule, *J. Chem. Soc., Perkin Trans. 1*, 1992, 1245.
15 E. M. Armstrong, M. S. Austerberry, J. H. Birks, C. D. Garner, M. Helliwell, J. A. Joule and J. R. Russell, *J. Inorg. Biochem*., 1991, **43**, 588; E. M. Armstrong, M. S. Austerberry, J. H. Birks, R. L. Beddoes, M. Helliwell, J. A. Joule and C. D. Garner, *Heterocycles*, 1993, **35**, 563; S. P. Greatbanks, I. H. Hillier, C. D. Garner and J. A. Joule, *J. Chem. Soc., Perkin Trans. 2*, 1997, 1529.

Received in Liverpool, UK, 19th November 1997; 7/08366A

Calix[4]arenes with a novel proton-ionizable group: synthesis and metal ion separations

Galina G. Talanova, Hong-Sik Hwang, Vladimir S. Talanov and Richard A. Bartsch*†

Department of Chemistry and Biochemistry, Texas Tech University, Lubbock, Texas 79409-1061, USA

New calix[4]arenes with two *N*-(X)sulfonyl carboxamide groups of 'tunable' acidity are synthesized from the corresponding calixarene dicarboxylic acid and exhibit good to excellent extraction selectivity for Pb^{2+} over most alkali, alkaline earth and transition metal ions.

Calixarenes are an important class of macrocyclic host molecules that efficiently and selectively bind a variety of ionic and neutral guest species.[1–4] They find applications in separation processes involving organic and inorganic substances, phase transfer catalysis, chromatography, ion-selective electrodes, *etc*.[2] Calixarenes functionalized with pendent proton-ionizable groups (carboxylic acid, hydroxamic acid, phosphonic acid and phosphonic acid monoalkyl ester) are of special interest as potential agents for separations of polyvalent metal ions by liquid extraction and membrane transport[5–10] or sorption when immobilized on polymer matrices.[11–14] The ligation properties of such compounds are controlled by the nature of the ionizable groups, in particular their acidity. For example, calixarene carboxylic acids[5] were found to be much more efficient interphase carriers for alkaline earth cations than related nonfunctionalized calixarenes which contain phenolic groups on the lower rim. Developing new types of calixarenes with a wider variety of proton-ionizable functions may lead to additional applications of these compounds in metal ion separation processes.

In recent work, we have introduced the *N*-(X)sulfonyl carboxamide moiety as a novel pendent proton-ionizable group in lariat ethers **1** to obtain macrocyclic ligands with 'tunable' acidity that exhibit high Na^+ selectivity in competitive solvent extraction of alkali metal cations.[15] We now report the synthesis and application in metal ion extraction of a new type of calixarenes, the calix[4]arene bis[*N*-(X)sulfonyl carboxamides] **2**–**5**. It was anticipated that these new ligands would exhibit appreciable acidity and effectiveness in extracting divalent metal ions from aqueous solutions.

Calix[4]arenes **2**–**5**‡ were prepared in two steps from the calixarene dicarboxylic acid **6**.[16]§ The positions and shapes of the signals in the ^1H NMR spectra of **2**–**5** were found to vary with the identity of the solvent and concentration, which demonstrates that the calixarenes exist in solution as mixtures of conformers and also associate by NH··O=C hydrogen bonding. The conformational and associative behavior is especially pronounced for **5**. Solution and solid-state structures of the new ligands are under continued investigation.

The new di-ionizable calixarenes **2**–**5** efficiently extract Pb^{2+} from acidic (HNO_3) solutions into $CHCl_3$¶ (Fig. 1). The acidities of the new calixarene ligands are expected to be strongly influenced by the electron-withdrawing ability of X in the *N*-(X)sulfonyl group. Values of the pH for half-extraction ($pH_{1/2}$) in the extraction profiles are found to vary with X in the order: CF_3 (2.0) > Ph (5.2) > 4-$O_2NC_6H_4$ (5.3) > Me (5.5). Although the $pH_{1/2}$ values for **2**–**4** fall in the anticipated ordering for the electron-withdrawing ability of X,[15] that for **5** with X = 4-nitrophenyl is considerably less acidic than expected. It is suggested that the reduced acidity of **5** in $CHCl_3$ arises from inter- or intra-molecular NH··O=C hydrogen bonding or by conformational peculiarities of the compound that hinder metal ion complexation.

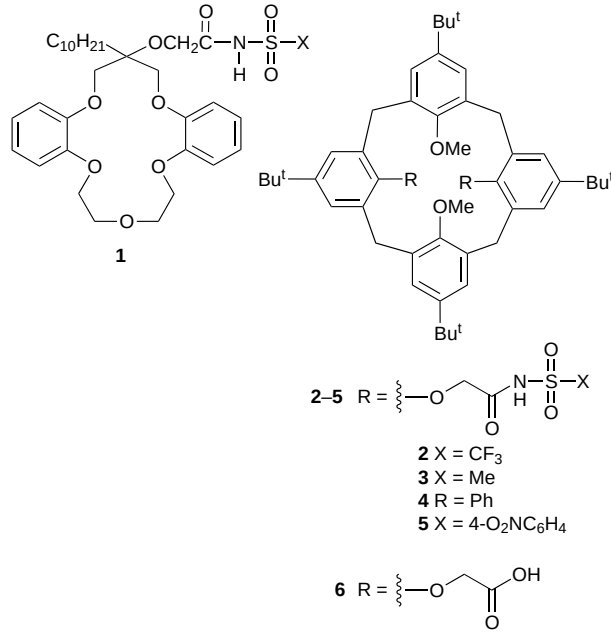

The extraction selectivity of **2** at pH 2.5 was examined for equimolar binary mixtures of Pb–M,‖ where M is Na^+, K^+, Cs^+, Sr^{2+}, Cu^{2+}, Ni^{2+}, Co^{2+}, Zn^{2+}, Cd^{2+} or Hg^{2+} (Fig. 2). High selectivity is observed for Pb^{2+} over K^+, Cs^+ and all of the transition metal ions examined except Hg^{2+}. Good extraction selectivity for Pb^{2+} over Na^+ and Sr^{2+} is also evident. Interference to Pb^{2+} extraction by the presence of Hg^{2+} was significantly reduced by the addition of chloride ions to the aqueous solution.

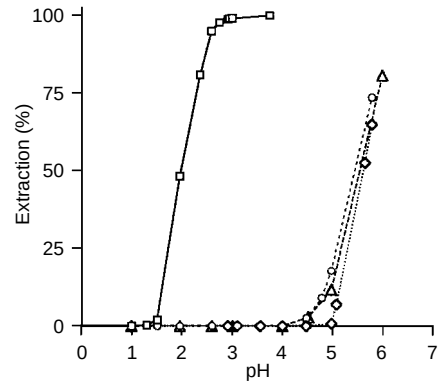

Fig. 1 pH profiles for Pb^{2+} extraction from 0.50 mM aq. $Pb(NO_3)_2$ into $CHCl_3$ with 1.00 mM calix[4]arene *N*-(X)sulfonyl carboxamides (□ **2**, (◇) **3**, (○) **4** and (△) **5**

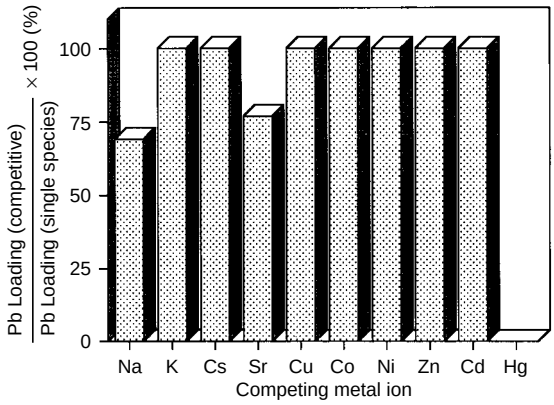

Fig. 2 Pb^{2+} loading of **2** in competitive extraction of 0.50 mM Pb^{2+} and 0.50 mM competing metal ion from an aqueous nitrate solution at pH 2.5 relative to the Pb^{2+} loading for extraction of Pb^{2+} under the same conditions, but in the absence of the competing metal ion

Further investigations of the metal ion separation properties of these novel proton-ionizable calixarenes are in progress.

This research was supported by the Division of Chemical Sciences of the Office of Basic Energy Sciences of the US Department of Energy (Grant DE-FGO3-94ER14416).

Notes and References

† E-mail: rabartsch@ttu.edu

‡ *Selected data* for **2**: mp 233–234 °C (Calc. for $C_{52}H_{64}F_6N_2O_{10}S_2$: C, 59.19; H, 6.11; N, 2.65. Found: C, 59.39; H, 6.19; N, 2.65%); ν_{max}(deposit from CH_2Cl_2 solution onto a NaCl plate)/cm^{-1} 3324, 3240, 1758, 1300, 1131, 1205, 1057; δ_H (300 MHz, [$^2H_6$]DMSO) 0.93 (br s, 18 H), 1.30 (s, 18 H), 3.68 (br m, 18 H), 6.80 (br m, 8 H), 10.31 (br s, 2 H). For **3**: mp 268–270 °C (Calc. for $C_{52}H_{70}N_2O_{10}S_2$: C, 65.93; H, 7.45; N, 2.96. Found: C, 65.56; H, 7.66; N, 2.95%) ν_{max} (deposit from CH_2Cl_2 solution onto a NaCl plate)/cm^{-1} 3355, 3241, 1731, 1347, 1151, 1199, 1122; δ_H(300 MHz, [$^2H_6$]DMSO) 0.99 (s, 18 H), 1.30 (s, 18 H), 3.74 (br m, 24 H), 6.55 (br m, 4 H), 7.15 (br s, 4 H), 11.80 (br s, 2 H). For **4**: mp 233–235 °C (Calc. for $C_{62}H_{74}N_2O_{10}S_2$: C, 69.50; H, 6.96. N, 2.61. Found: C, 69.77; H, 6.90; N, 2.55%); ν_{max}(deposit from CH_2Cl_2 solution onto a NaCl plate)/cm^{-1} 3352, 3248, 1732, 1361, 1163, 1196, 1089; δ_H(300 MHz, [$^2H_6$]DMSO) 0.96 (br s, 18 H), 1.22 (br s, 18 H), 3.63 (br m, 18 H), 6.47 (br m, 4 H), 7.10 (s, 4 H), 7.65 (m, 6 H), 8.00 (br s, 4 H), 12.39 (br s, 2 H). For **5**: mp 238–240 °C (Calc. for $C_{62}H_{72}N_4O_{14}S_2$: C, 64.12; H, 6.25; N, 4.82. Found: C, 63.74; H, 6.51; N, 4.48%); ν_{max}(deposit from CH_2Cl_2 solution onto a NaCl plate)/cm^{-1} 3346, 1719, 1350, 1162, 1197, 1089, 1532, 1350; δ_H(300 MHz, [$^2H_6$]DMSO 0.95 (br s, 18 H), 1.20 (br s, 18 H), 3.56 (br m, 18 H), 6.73 (br m, 8 H), 8.26 (s, 4 H), 8.46 (m, 4 H), 12.78 (br s, 2 H).

§ *Typical procedure* for conversion of **6** into the corresponding bis(*N*-trifluoromethanesulfonyl carboxamide) **2**: To a solution of **6** (2.50 g, 3.15 mmol) in dry benzene (50 ml) was added oxalyl chloride (3.25 ml, 37.4 mmol). The reaction mixture was refluxed for 4 h under nitrogen and evaporated *in vacuo*. The resultant acid chloride was dissolved in dry THF (50 ml) and added to a mixture of pentane-washed KH (35% in mineral oil, 3.63 g, 31.7 mmol) and trifluoromethanesulfonamide (1.38 g, 9.3 mmol) in dry THF (25 ml). The mixture was stirred at room temperature for 10 h (1 h for **5**) under nitrogen, then water (15 ml) was carefully added to destroy the residual KH. The THF layer was separated and diluted with EtOAc (100 ml). The organic solution was washed with a 10% aq. K_2CO_3 (3 × 50 ml) and evaporated *in vacuo*. Column chromatography on alumina with CH_2Cl_2 and then MeOH–CH_2Cl_2 (1 : 9) as eluents gave a white solid which was dissolved in CH_2Cl_2 (50 ml) and washed with 1 M HCl (50 ml). The CH_2Cl_2 solution was dried over $MgSO_4$ and evaporated *in vacuo* to give a white solid which was recrystallized from Et_2O–hexanes to give **2** (2.35 g, 71%). Calixarenes **3**–**5** were prepared similarly in 60, 80 and 70% yields, respectively.

¶ A 1.0 mM solution of the calixarene in $CHCl_3$ (5.0 ml) and 5.0 ml of 0.50 mM aq. $Pb(NO_3)_2$ (pH adjusted with dil. HNO_3) in a 15 ml, metal-free capped plastic centrifuge tube was shaken on a vortex mixer for 5 min, allowed to stand for 5 min, and shaken for another 5 min. The mixture was centrifuged for 5 min and an aliquot of the aqueous phase was removed and diluted with deionized water for Pb^{2+} analysis by atomic absorption spectrophotometry.

‖ A 5.0 mM solution of **2** in $CHCl_3$ (5.0 ml) and 5.0 ml of an aqueous mixture (pH 2.5, HNO_3) which was 0.50 mM (each) in Pb^{2+} and the other metal nitrate was shaken on a vortex mixer for 5 min, allowed to stand for 5 min, and shaken again for 5 min. The mixture was centrifuged for 5 min and an aliquot was removed and diluted with deionized water. The Pb^{2+} concentration in the diluted aqueous phase was determined by atomic absorption spectrophotometry and compared with the result of Pb^{2+} extraction from the aqueous solution of 'pure' $Pb(NO_3)_2$ under the same conditions.

1 C. D. Gutsche, *Calixarenes*, The Royal Society of Chemistry, Cambridge, 1989.
2 *Calixarenes: A Versatile Class of Macrocyclic Compounds*, ed. J. Vicens and V. Bohmer, Kluwer, Boston, 1991.
3 D. M. Roundhill, in *Progress in Inorganic Chemistry*, ed. K. D. Karlin, Wiley, New York, 1995, vol. 43, pp. 533–591.
4 A. Ikeda and S. Shinkai, *Chem. Rev*., 1997, **97**, 1713.
5 R. Ungaro, A. Pochini and G. D. Andretti, *J. Inclusion Phenom*., 1984, **2**, 199.
6 K. Ohto, M. Yano, K. Inoue, T. Yamamoto, M. Goto, F. Nakashio, S. Shinkai and T. Nagasaki, *Anal. Sci*., 1995, **11**, 893.
7 S. Shinkai, Y. Shirahama, H. Satoh, O. Manabe, T. Arimura, K. Fujimoto and T. Matsuda, *J. Chem. Soc., Perkin Trans. 2*, 1989, 1167.
8 T. Nagasaki, S. Shinkai and T. Matsuda, *J. Chem. Soc., Perkin Trans. 1*, 1990, 2617.
9 T. Nagasaki, T. Arimura and S. Shinkai, *Bull. Chem. Soc. Jpn*., 1991, **64**, 2575.
10 K. Araki, N. Hashimoto, H. Otsuka, T. Nagasaki and S. Shinkai, *Chem. Lett*., 1993, 829.
11 S. Shinkai, H. Kawaguchi and O. Manabe, *J. Polym. Sci., Polym. Lett*., 1988, **26**, 391.
12 S. Hutchinson, G. A. Kearney, E. Horne, B. Lynch, J. D. Glennon, M. A. McKervey and S. J. Harris, *Anal. Chim. Acta*, 1994, **291**, 269.
13 R. Brindle, K. Albert, S. J. Harris, C. Treltzsch, E. Horne and J. D. Glennon, *J. Chromatogr. A*, 1996, **731**, 41.
14 K. Ohto, Y. Tanaka and K. Inoue, *Chem. Lett*., 1997, 647.
15 V. J. Huber, S. N. Ivy, J. Lu and R. A. Bartsch, *Chem. Commun*., 1997, **16**, 1499.
16 R. Ostaszewski, T. W. Stevens, W. Verboom and D. N. Reinhoudt, *Recl. Trav. Chim. Pays-Bas*, 1991, **110**, 294.

Received in Corvallis, OR, USA, 12th November 1997; 7/08150B

Transition metal complex-templated asymmetric free radical polymerisation

Brodyck J. L. Royles and David C. Sherrington*

Department of Pure and Applied Chemistry, University of Strathclyde, 295 Cathedral Street, Glasgow, UK G1 1XL

For the first time an amino acid Schiff base copper complex has been used as a chiral template—auxiliary for the induction of configurational asymmetry into the backbone of 4-vinylpyridine-*co*-indene polymers, yielding main chain optically active macromolecules *via* free radical polymerisation.

The synthesis of vinyl polymers whose optical activity arises solely as a result of the configuration of stereogenic carbon centres in the main chain is of increasing importance because of their unique properties and potential applications in (second order) nonlinear optics, liquid crystals, ferroelectrics and asymmetric catalysis.[1] Whereas main chain optically active (co)polymers employing non-alkene comonomers (*e.g.* CO, epoxides) have been prepared using optically active metal complex initiators, the synthesis of main chain optically active vinyl (co)polymers *via* a simple free radical mechanism remains problematical. To date, a number of ingenious strategies[1–3] have been reported which circumvent the inherent complex symmetry properties (*e.g.* glide reflection and mirror planes) associated with stereoregular macromolecular systems (*note* isotactic and syndiotactic vinyl polymers are *not* optically active), and therefore lead to main chain optically active polymers. Unfortunately, however, the majority[1,2] suffer from various disadvantages (such as multistep syntheses of monomers, expensive reagents/starting materials or products that are not readily amenable to functionalisation) that render them unsuitable for commercial exploitation. Thus for 'asymmetric synthesis polymerisation' (whereby a chiral auxiliary, or template, is attached to an achiral monomer prior to polymerisation and then removed afterwards to leave optically active polymer)[2] to achieve viability in a commercial process or as a routine laboratory procedure, the auxiliary must be of low cost, readily attached to everyday monomers and easily removed from the newly formed polymer.

We now adumbrate a novel and highly expedient strategy for preparing main chain optically active polymers in which the chiral auxiliary is a transition metal salicylidene–amino acid Schiff base complex. A vinyl monomer containing a suitable donor group (*e.g.* a vinylpyridine) will coordinate to the metal centre, thus forming a chiral monomer unit. Upon completion of the polymerisation the template complex, being attached only through relatively weak dative bonds, should be easily removed, thus liberating the vinyl polymer (Scheme 1).

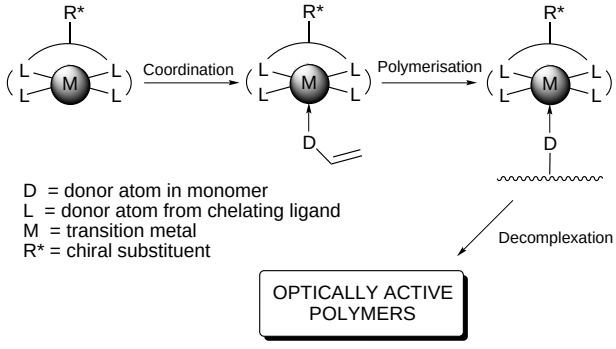

Scheme 1

If a chiral monomer complex of this type were copolymerised with achiral monosubstituted or cyclic 1,1-disubstituted vinyl (or related) compounds, we realised that there would be a strong likelihood that nonsymmetric Wulff-type[1] triads (**1**) or related diads (**2**), respectively, would be formed along at least some sections of the polymer backbone. Should this in fact be the case, any such polymers would display optical activity as a result of the main chain configuration.

1 **2**

Accordingly, we have now synthesised the copper(II) amino acid Schiff base complex **3** from (*S*,*S*)-(+)-isoleucine, salicylaldehyde and copper(II) acetate in aqueous solution (see Table 1).[4] The amino acid was chosen because of its non-functionalised alkyl side chain, which provides steric bulk on the 'upper' face of the complex without the possibility of any undesirable side reactions occurring. Copper Schiff base complexes have long been known[5] and generally possess square planar geometry about the metal. Furthermore, such complexes have a high affinity for, and are readily coordinated by, one or two pyridine molecules to form five- or six-coordinate species.[5] Precedent exists for the free-radical polymerisation of transition metal complexes without any adverse interactions with the metal (*e.g.* electron transfer from a radical centre): copper[6,7] and cobalt[8] Schiff base complexes have been used to prepare imprinted polymer networks containing enzyme mimetic or chiral binding cavities, respectively.

Polymerisations were performed, under an inert atmosphere, in (deoxygenated) MeOH solutions of **3**, 4-vinylpyridine (4-VPy) **4** and indene (IN) **5** with AIBN (1 wt%) as the radical souce (Scheme 2). Evaporation of the solvent gave dark green Schiff base–polymer adducts **6**; these were not characterised except for measurement of the specific rotation in one case (see Table 2, entry 4). These adducts were broken down through acid hydrolysis before the free polymers were precipitated from the acidic aqueous solution by basifiying with aqueous ammonia. Further reprecipitation from MeOH solutions into aqueous ammonia produced the polymers **7** as off-white powders. Attempts to measure the molecular weights of **7**, using gel permeation chromatography, have so far failed because the copolymers appear to be absorbed onto the poly(styrene–divinylbenzene) column packings. This is a recognised problem

Table 1 Data for the copper(II) amino acid Schiff base complex **3** and (*S*,*S*)-(+)-isoleucine

	$[\alpha]^{25}/10^{-1}$ deg cm^2 g^{-1}	
λ/nm	(*S*,*S*)-(+)-Ile	Complex **3**
365	+6.4[a]	—[b]
436	+13.6[a]	−1014[c]
589	+27.1[a]	+128.6[c]

[a] $c = 0.14 \times 10^{-2}$ g cm^{-3} in MeOH. [b] $c = 0.07 \times 10^{-2}$ and 0.035×10^{-2} g cm^{-3} in MeOH. The sample absorbed too much light at these concentrations for a reading to be obtained. [c] $c = 0.07 \times 10^{-2}$ g cm^{-3}.

Table 2 Data for poly(4-vinylpyridine-*co*-indene) copolymer **7**

Entry	Reactants/mmol			T/°C	t/h	Polymer composition[a]	$[\alpha]^{25}/10^{-1}$ deg cm^2 g^{-1}			$c/10^{-2}$ g cm^{-3}	Solvent	Yield/g (%)
	3	**4**	**5**			4-Vpy : IN	365 nm	436 nm	589 nm			
1	5	5	5	65	18	3 : 1	—[b]	−4.0	−1.2	0.57	MeOH	0.59 (53)
2	7.5	7.5	7.5	65	18	4 : 1	−6.3	—[c]	−2.0	0.32	MeOH	0.85 (49)
3	7.5	7.5	7.5	65	16	4 : 1	−6.5	—[c]	−2.1	0.30	MeOH	0.79 (46)
4	5.2	5.2	5.2	65	18	3 : 1	−5.8	−4.2[d]	−2.3[d]	0.31	MeOH	0.58 (51)
5	0	10	10	65	16	7 : 2	0	0	0	0.52	$CHCl_3$	1.21 (54)

[a] Determined using ^{1}H NMR spectroscopy. [b] The sample absorbed too much light at this concentration for a reading to be obtained. [c] No readings taken. [d] Specific rotation of adduct **6** was −688.2 at 436 nm and +76.5 at 589 nm (*c* 0.017, MeOH).

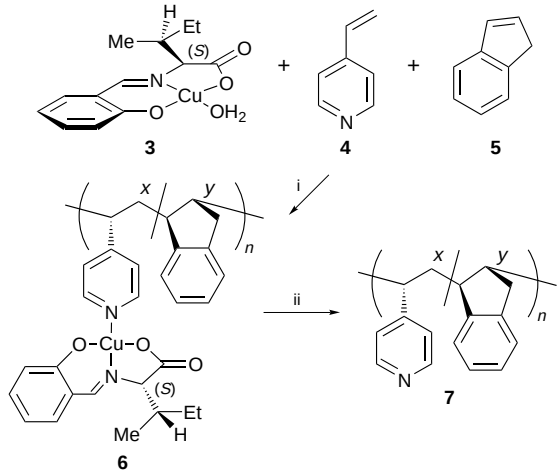

Scheme 2 *Reagents and conditions:* i, AIBN, MeOH, reflux N_2; ii, 2 M HCl then NH_3 (aq)

with poly(4-vinylpyridine) systems[9] which we are currently addressing. However, the materials **7** do show all the characteristics of macromolecular systems, including broad NMR resonances and initially becoming gel-like before slowly dispersing to form isotropic solutions in organic solvents.

Each of the polymers **7a**–**d** which were prepared using the chiral auxiliary template displayed *negative* optical rotations at 365, 436 and 589 nm (see Table 2). The polymer **7e** which resulted from a blank control experiment (without template) was, as expected, optically inactive. Obviously, the asymmetric induction which has taken place during the polymerisation process is due to the stereogenic centre in complex **3**. In order to be absolutely certain that the optical activity observed arose from the main chain configuration of the polymers **7** we carried out a detailed study of the optical rotary properties of the complex **3** and the Schiff base-polymer adduct **6**, as well as (*S*,*S*)-(+)-isoleucine itself: at 589 nm all these have *positive* optical rotations of varying magnitude.

Thus we can unequivocally conclude that polymers possessing main chain optical activity have been obtained. It is important to appreciate that for a chemical process to achieve this, not only must a significant number of stereogenic centres be generated enantioselectively but it is also essential for some higher order asymmetry to be generated simultaneously. At the moment we are not able to specify precisely the configurations of the stereogenic carbon centres along the backbone although free-radical propagation of cyclic alkenes does generally proceed *via* a *trans* reaction. The overall configurations giving rise to the observed optical activity are therefore not clear cut, but there must be an excess of the diads, **2**, in the backbone.

We have described a simple, low cost and effective method for the synthesis of main chain optically active polymers. To the best of our knowledge this is the first example where a chiral transition metal complex has been employed as a template for asymmetric induction during a polymerisation reaction. It is also the first instance where non-covalent interactions have been utilised to attach the chiral auxiliary. We are currently expanding the range of copolymers produced in this way, and of course considerable scope exists for exploiting chiral Schiff base (or other) metal complexes involving other amino acids and indeed other chiral molecules.

We acknowledge the EPSRC for the award of a post doctoral fellowship to B. J. L. R. and RAPRA Technology Ltd. for help with GPC molecular weight determinations.

Notes and References

* E-mail: m.p.a.smith@strath.ac.uk

† Since free radical attack on cyclic alkenes usually occurs as a trans process **2** is more clearly represented as:

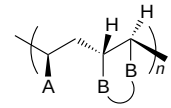

1 G. Wulff, *Angew. Chem., Int. Ed. Engl.*, 1989, **28**, 21.
2 Y. Okamoto and T. Nakano, *Chem. Rev.*, 1994, **94**, 349.
3 I. H. Donnelly, P. Kambouris, D. C. Nonhebel, T. Rohr and D. C. Sherrington, *J. Chem. Soc., Perkin Trans. 2*, 1996, 1821.
4 The synthetic procedure was based on the work of L. G. Macdonald, D. H. Brown, J. H. Morris and W. E. Smith, *Inorg. Chim. Acta*, 1982, **67**, 7. Good quality crystals of **3** were grown which allowed the single crystal X-ray structure to be determined.
5 S. Yamada, *Coord. Chem. Rev.*, 1966, **1**, 415.
6 Y. N. Belokon, V. I. Tararov, T. F. Savel'eva and V. M. Belikov, *Makromol. Chem.*, 1980, **181**, 2183.
7 Y. N. Belokon, V. I. Tararov, T. F. Savel'eva, O. L. Lependina, G. I. Timofeyeva and V. M. Belikov, *Makromol. Chem.*, 1982, **183**, 1921.
8 Y. Fujii, K. Matsutani and K. Kikuchi, *J. Chem. Soc., Chem. Commun.*, 1985, 415.
9 L. Ortez, K. Smitherman, L. Pratt and I. Khan, *Am. Chem. Soc., Polym. Prepr.*, 1997, **38**, 255.

Received in Cambridge, UK, 10th November 1997; 7/08059J

A tetraphenylporphyrin–peptide hybrid with high affinity for single-stranded DNA

Rishi K. Jain, David A. Sarracino and Clemens Richert*†

Department of Chemistry, Tufts University, Medford, MA 02155, USA

A tetraphenylporphyrin bearing four peptide chains, synthesized in two steps from *meso*-tetrakis(*p*-aminophenyl)porphyrin and the peptide CGKWK, binds single-stranded DNA oligomers with high affinity and inhibits degradation by nuclease S1.

Small ligands that bind single-stranded DNA (ssDNA) with high affinity are scarce. Non-protein ligands, such as cationic peptides with an intercalating residue,[1,2] cationic tetraarylporphyrins and sapphyrins[3] and naphthalene diimide intercalators,[4] give dissociation constants at or above the micromolar level. Lower dissociation constants are found for ssDNA binding proteins, but their crystal structures[5] do not suggest a simple way of designing small ligands with similar affinity. Further, increasing the length of a peptidic binder does not necessarily increase its affinity for ssDNA, as enthalpy gains are usually matched by entropic cost.[6] Since recent studies have shown that binding to ssDNA can inhibit polymerases, including HIV reverse transcriptase,[7,8] the search for tight ssDNA binders poses not only an intellectual challenge, but also promises to lead to drug candidates.

Presented here is the lead compound in our search for ssDNA binders. This is a tetraphenylporphyrin core molecule bearing short peptide chains. The design of this compound was based on the notions that (i) single stranded nucleic acids are highly flexible, favoring large rigid ligands to reduce the entropic penalty for complex formation, and (ii) ssDNA presents more lipophilic surface area than double-stranded DNA, where the nucleobases are buried, and its complexes may therefore gain substantial stabilization from hydrophobic interactions. Tetraphenylporphyrins are not only large, rigid and lipophilic macrocycles, they are also chromophores, allowing for sensitive monitoring of binding events. Further, tetraphenylporphyrins are straightforward to synthesize and easily detected by quantitative laser desorption mass spectrometry, a technique that has allowed us to perform monitored *in vitro* selection experiments.[9] The peptide sequence Lys-Trp-Lys (KWK), a known ssDNA-binder,[1] was chosen as substituent to provide additional binding affinity and solubility in aqueous media. A cysteinyl-glycine linker was designed to span the distance between KWK and the 'termini' of the phenylporphyrin and to provide a reactive thiol group.

Assembly of the peptide–porphyrin hybrid started from *meso*-tetrakis(*p*-aminophenyl)porphyrin **1**,[10] which was converted to the chloroacetamido derivative **2** under the conditions reported by Collman *et al.*[11] The subsequent coupling of **2** with CGKWK‡ was monitored by MALDI-TOF mass spectrometry. Thioether formation to the desired tetrapeptide **3** proceeded slowly under conditions optimized for peptide–DNA hybrids[12] (aqueous buffer, pH 7.0, 40 °C) and DMF as a co-solvent. Even with a 150-fold excess of the peptide and several days reaction time, less than 20% tetrasubstituted porphyrin **3** was found. Rigorous exclusion of air to prevent disulfide formation and stepwise addition of the peptide did not improve the yield. Further, purification of **3** from the crude product was complicated by the presence of many side products of similar molecular weight. Interestingly, coupling in dry DMF with Cs_2CO_3 as base,[13] conditions less typical for bioconjugations, proceeded smoothly with 2 equiv. peptide per chloroacetamide group.§ Despite the limited solubility of both the caesium salt and the highly charged peptide in the organic solvent, the reaction was more than 90% complete after 20 min at room temperature. Tetrasubstituted porphyrin hybrid **3** made up more than 65% of the crude product and could be obtained in satisfactory purity in a single HPLC step.¶

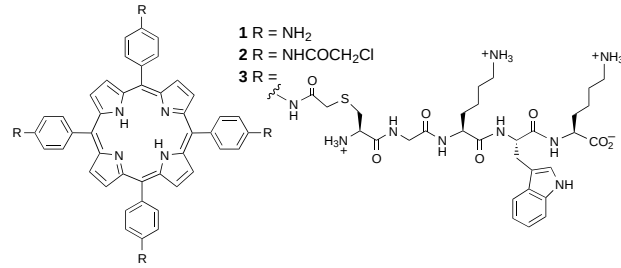

Addition of DNA octamers 5′-TGGTTGAC-3′ **4** and $(dC)_8$ **5** to solutions of **3** led to > 50% hypochromicity of the Sôret band but little shift of the maximum. Comparable hypochromicity has been found for a macrocyclic porphyrin-containing cryptand bound to poly(dT).[14] Unlike this single-strand specific cryptand, which is too bulky for intercalation, and cationic tetraarylporphyrins that intercalate, or, more probably, hemi-intercalate[15] into double-stranded DNA, **3** appeared to bind quite tightly to the short, single-stranded oligomers. Unconjugated KWK (2 equiv.) in the solution did not influence the binding curve measurably. Further evidence for tight binding came from the observation that the complex **3·4** did not show hyperchromicity when the NaCl concentration was raised to 3 M. In the plot of the titration data (Fig. 1) hypochromicity levels off at 1 equiv. of DNA, both at 900 and 400 nM **3**. This suggests that a 1 : 1 complex between **3** and the DNA strands is preferred when a molar excess of DNA is available, and that above 1 equiv. DNA very little unbound **3** exists at these concentrations. The latter makes it difficult to determine the dissociation constant accurately‖ but allows an estimation of $K_d \leqslant 5$ nM. This

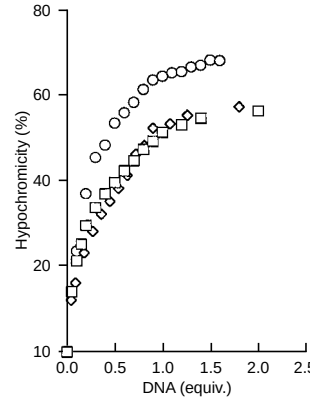

Fig. 1 Hypochromicity of the Sôret and absorption of **3** (415 nm) upon addition of DNA octamers **4** and **5**, 10 mM ammonium acetate solution, pH 6.0: (□) **3** (900 mM) + **5**, (◇) **3** (900 mM) + **4** and (○) **3** (400 nM) + **4**

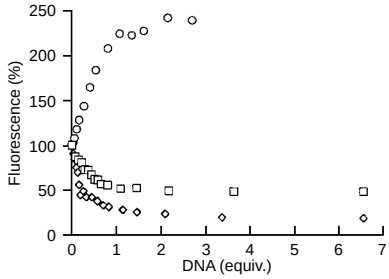

Fig. 2 Changes in fluorescence intensity (λ_{ex} = 415 nm, λ_{det} = 660 nm) upon addition of DNA octamer **4** to a solution of **3** (55 ± 10 nM) at (□) pH 6.0, (◇) 4.6 and (○) 2.5 (10 mM ammonium acetate buffers)

estimate was corroborated by fluorescence titrations performed at 55 nM **3** and increasing amounts of **4**, **5**, $(dA)_8$ **6** and 5′-GTCAAA-3′ **7** (Figs. 2 and 3). The fluorescence of **3** changed with the concentration when up to 1 equiv. DNA was added, but remained mostly unchanged at higher DNA : hybrid ratios. Only for the oligopyrimidine **5**, and the shorter oligomer **7** was a fraction of unbound porphyrin detected at 1 equiv.

When titrations with **4** were performed at pH 2.5, where the porphyrin core is at least partially protonated,[16] a fluorescence increase rather than decrease accompanied addition of DNA (Fig. 2). Apparently, **3** can reverse its fluorescence reporter properties. At a pH where the porphyrin ring is uncharged, DNA induces quenching, just like in other neutral chromophors. At low pH, however, DNA induces the fluorescence enhancement typical for cationic aromatic intercalators, such as the ethidium, acridine orange and proflavin ions. In both states, tight 1 : 1 complexes appear to form with the DNA octamer.

Exploratory experiments show that 2 equiv. of **3** inhibit the degradation of **4** by nuclease S1 by more than 50% at 37 °C [28 μM **4** in 83 mM $(NH_4)_2SO_4$–5 μM ZnSO4, pH 5.6, 0.8 u μl^{-1} nuclease, monitored by quantitative MALDI-TOF MS[17]]. Footprinting analysis[17] indicates that nuclease cleavage after the third, fourth and fifth nucleotide is similarly inhibited in the presence of **3**, with a slightly decreased protection at the latter site (not shown). This suggests that hybrid **3** covers more than a small fraction of DNA octamer **4**.

In conclusion, we report a facile synthesis of a porphyrin-peptide hybrid. The synthetic methodology requires only unmodified deprotected peptides, which are accessible *via* standard automated peptide synthesis and biotechnological processes. Hybrids prepared *via* the route presented here may become valuable bioorganic model compounds, *e.g.* as heme protein analogs[18] or photosynthetic reaction centre maquettes.[19] Further, the finding that porphyrin–tetrapeptide hybrid **3** binds ssDNA corroborates assumptions (i) and (ii) about the nature of tight ssDNA binders (*vide supra*). Initial results from a study on the binding of **3** and related compounds to double-stranded DNA, presently under way in these laboratories, shows that such hybrids can bind to short ssDNA oligomers without preventing duplex formation. Therefore, **3** may also be a lead compound for the development of protective 'coats' for antisense oligonucleotides, as, unlike complementary oligonucleotide strands, the only other known high affinity ligands to ssDNA, **3** does not seem to block Watson–Crick base pairing.

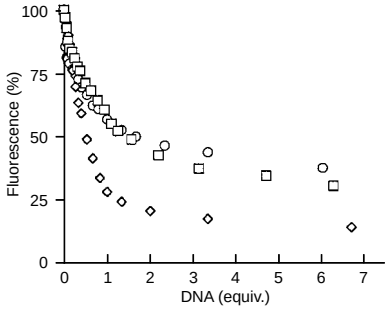

Fig. 3 Fluorescence quenching upon addition of DNA oligomers (□) $(dC)_8$ **5**, (◇) $(dA)_8$ **6** and (○) GTCAAA **7** to a solution of **3** at pH 4.6; experimental conditions are the same as in Fig. 2

The authors thank M. Simon for the preparation of synthetic intermediates and C. Tetzlaff for the acquisition of NMR spectra. Support by the NIH (grant GM54783 to C. R.) is gratefully acknowledged.

Notes and References

† E-mail: crichert@emerald.tufts.edu

‡ Synthesized *via* a standard Fmoc/Bu^t protocol. Homogeneous by RP_{18}-HPLC and single peak in MALDI-TOF MS.

§ All steps were performed under exclusion of light to prevent photosensitized oxidation. Typically, a mixture of porphyrin **3** (0.15 mg, 0.15 μmol) CGKWK (0.74 mg, 1.2 μmol), and Cs_2CO_3 (3.9 mg, 12 μmol) was dried *in vacuo*, and stirred under argon for 15 min, followed by addition of dry DMF (120 μl). The reaction was monitored by MALDI-TOF MS, and quenched after 0.7–20 h by addition of 0.2% TFA. Extended coupling (> 20 h) led to noticeable cleavage of the linking acetamide, most likely *via* transamidation to the free *N*-terminus of the peptide. Experiments with acetoxy-linked hybrids show that acyl transfer cleavage can be suppressed by acetylation of the *N*-terminus.

¶ HPLC: Vydac RP_{18} column, A = 0.1% TFA, B = MeCN, linear gradient of 0–33% B in 90 min, elution after 71 min. UV–VIS (10 mM ammonium acetate, pH 6.0) λ_{max}/nm 657, 598 (sh), 569, 527, 414, 282; δ_H([$^2H_6$]DMSO, 300 MHz, selected resonances) 8.86 (s, 8 H, pyrrole H), 8.73 (br s, 4 H, amide NH), 8.33 (br s, 4 H, amide NH), 8.19–8.03 (m, 20 H, phenyl H and amide NH), 7.83 (br s, 4 H, amide NH), 7.55, 7.31, 7.02, 6.94 (4 m, 4 × 4 H, six-membered ring H Trp), 7.14 (s, 4 H, H^{δ} Trp), −2.92 (br s, 2 H, porphyrin NH); MALDI-TOF MS (α-cyano-4-hydroxycinnamic acid matrix, positive mode, delayed extraction): calc. for $C_{164}H_{211}N_{40}O_{28}S_4$ [M + H]$^+$, 3316.5; found 3315.6. Hybrid **3** does adsorb onto glass surfaces and extensive handling and repetitive lyophilizations should be avoided. Titrations were performed from MS-checked HPLC fractions in H_2SO_4- or HNO_3-cleaned cuvettes.

‖ Compare *e.g.* footnote 8 in: Y. Kuroda, A. Kawashima, Y. Hayashi and H. Ogoshi, *J. Am. Chem. Soc.*, 1997, **119**, 4929.

1 J.-J. Toulme and C. Hélène, *J. Mol. Biol.*, 1977, **252**, 244; C. Hélène and J.-L. Dimicoli, *FEBS Lett.*, 1972, **26**, 6.
2 D. P. Mascotti and T. M. Lohman, *Biochemistry*, 1997, **36**, 7272.
3 R. F. Pasternack, R. A. Brigandi, M. J. Abrams, A. P. Williams and E. J. Gibbs, *Inorg. Chem.*, 1990, **29**, 4483; B. L. Iverson, K. Shreder, V. Kral, P. Samson, V. Lynch and J. L. Sessler, *J. Am. Chem. Soc.*, 1996, **118**, 1608.
4 S. Takenaka, M. Manabe, M. Yokoyama, M. Nishi, J. Tanaka and H. Kondo, *Chem. Comm.*, 1996, 379.
5 A. Bochkarev, R. A. Pfuetzner, A. M. Edwards and L. Frappier, *Nature*, 1997, **385**, 176.
6 D. P. Mascotti and T. M. Lohman, *Biochemistry*, 1993, **32**, 10 568.
7 R. L. Rill and K. H. Hecker, *Biochemistry*, 1996, **35**, 3525.
8 R. M. Wadkins, E. A. Jares-Erijman, R. Klement, A. Rüdiger and T. M. Jovin, *J. Mol. Biol.*, 1996, **262**, 53.
9 K. Berlin, R. K. Jain, C. Tetzlaff, C. Steinbeck and C. Richert, *Chem. Biol.*, 1997, **4**, 63.
10 A. Bettelheim, B. A. White, S. A. Raybuck and R. W. Murray, *Inorg. Chem.* , 1987, **26**, 1009; B. C. Bookser and T. C. Bruice, *J. Am. Chem. Soc.*, 1991, 113, 4208.
11 J. P. Collman, B. Boitrel, L. Fu, J. Galanter, A. Strautmanis and M. Rapta, *J. Org. Chem.*, 1997, **62**, 2308.
12 K. Arar, A.-M. Aubertin, A.-C. Roche, M. Monsigny and R. Mayer, *Bioconjugate Chem.*, 1995, **6**, 573.
13 J. Buter and R. M. Kellogg, *J. Chem. Soc., Chem. Commun.*, 1980, 466; J. Buter and R. M. Kellogg, *J. Org. Chem.*, 1981, **46**, 4481.
14 A. Slama-Schwok and J.-M. Lehn, *Biochemistry*, 1990, **29**, 7895.
15 L. A. Lipscomb, F. X. Zhou, S. R. Presnell, R. J. Woo, M. E. Peek, R. R. Plaskon and L. D. Williams, *Biochemistry*, 1996, **35**, 2818.
16 R. Pottier and J. C. Kennedy, *J. Photochem. Photobiol. B: Biol.*, 1990, **8**, 1.
17 D. Sarracino and C. Richert, *Bioorg. Med. Chem. Lett.*, 1996, **6**, 2543.
18 J. P. Collman, L. Fu, P. C. Herrmann and X. Zhang, *Science*, 1997, **275**, 949.
19 F. Rabanal, W. F. DeGrado and P. L. Dutton, *J. Am. Chem. Soc.*, 1996, **118**, 473.

Received in Corvallis, OR, USA, 28th October 1997; 7/07803J

Dopamine recognition in templated silicate films

Rajendra Makote and Maryanne M. Collinson*

Department of Chemistry, Kansas State University, Manhattan, KS 66506-3701, USA

Dopamine templated nanoporous silica gel films prepared *via* the hydrolysis and cocondensation of tetramethoxysilane with phenyltrimethoxysilane show an enhanced affinity for dopamine and its related structures relative to non-templated films.

Considerable attention has recently been given to the design and development of new materials with improved molecular recognition capabilities.[1] Materials with tailor-made porosity, morphology, and chemical functionality are particularly important in the development of highly selective chemical sensors, stationary phases for HPLC, binding assays, polymeric membranes, and catalytic supports. One of the most promising technologies for the creation of recognition sites within a host structure involves molecular templating.[2,3] In this approach, a polymeric network is assembled around a suitable template molecule. Upon removal of the template, microcavities with a distinct pore size, shape and/or chemical functionality remain in the host.

Sol–gel technology provides a valuable approach for the creation of nanostructured silicate materials through the hydrolysis and condensation of silicon alkoxides.[4] The inherent processing flexibility enables thin films to be readily fabricated whereas the mild polymerization conditions enable specific reagents to be readily introduced within the highly cross-linked, porous host structure without the problems of thermal or chemical decomposition.[5] In previous work it has been demonstrated that nanostructured silica with enhanced porosity can be prepared *via* template-based sol polymerization.[3] In one method, surfactant molecules are used as templates to prepare periodic mesoporous silicate materials.[3,6] In the second method, molecular sized voids are created in a silicate matrix *via* the pyrolysis of the organic functional groups[3,7] covalently bound to the silicate framework.[8] While the pore size and connectivity of the host structure can be designed at the molecular level *via* careful control of the template concentration and sol–gel process conditions,[3] improvements in chemical selectivity need to be made.

In this report, we describe a unique template based method for the fabrication of thin porous chemically selective films, that can be used to fabricate materials with improved properties. This procedure involves the blending of organosilicon precursors with the inorganic reagents to produce a composite material[8] that shows an increased affinity for a specific class of molecules once the template has been extracted from the gel. The inorganic silicon precursor acts as the cross-linking agent whereas the organosilicon precursor introduces a specific functionality in the matrix which improves chemical specificity *via* an increase in porosity, polarity and/or intermolecular interactions. The feasibility of this approach is demonstrated in this work *via* the development of a material that shows an affinity toward dopamine and its related structures. The catechol amines were selected because of the important role they play in neurotransmission and the necessity of developing methodologies that allow their differentiation in the presence of numerous interferents including ascorbic acid (AA).[9]

In these experiments, a sol stock solution was prepared by combining tetramethoxysilane (TMOS), phenyltrimethoxysilane (PTMOS), ethoxy ethanol (EE), water and 0.1 M hydrochloric acid. PTMOS was selected as the functionalized monomer because it is a trifunctional silane containing a bulky, aromatic constituent whereas EE was utilized as the solvent owing to its both polar and non-polar solvating properties. After stirring for 1 h, dopamine was added to the sol followed by the addition of potassium hydroxide to raise the pH of the sol to *ca.* 7. The molar ratio of monomers to template was 1 : 0.1 : 0.04 (TMOS : PTMOS : DA). After 30 min, a 50 μl aliquot of the sol was cast on a polished glassy carbon electrode (5 mm diameter) using an in-house built rotator (*ca.* 7000 rpm, 60 s) and the resulting films allowed to dry for 2 days in a desiccator at ambient temperature. The average film thickness as measured *via* surface profilometry was *ca.* 450 nm. The template (*e.g.*, dopamine) was leached out of the matrix by placing the film in pH 7 phosphate buffer for 2 h. Under these conditions, approximately 90% of the dopamine was leached out of the film as evident from a cyclic voltammogram (CV) of gel-encapsulated dopamine acquired before and after leaching. In control experiments, non-templated films were prepared in a similar manner with the exception that dopamine was not added to the sol.

To characterize the affinity of the templated and non-templated films for dopamine and its structurally related compounds, cyclic voltammetry was used. Fig. 1(*a*) shows a CV at a non-templated film prepared from an undoped PTMOS–TMOS sol in a solution of 0.1 mM dopamine. The lack of significant faradaic current indicates the film is compact and dopamine is unable to reach the underlying electrode surface. In distinct contrast, the films prepared from a doped PTMOS–TMOS sol show a distinguishable affinity for dopamine as evidenced from the quasi-reversible voltammogram obtained at the templated film, Fig. 1(*b*). The peak current for the oxidation of dopamine achieves a constant value within 3–4 min indicative of the relatively fast response of the templated films toward dopamine. The response of the templated film toward dopamine is *ca.* 70% of that observed for an identical solution concentration at a bare glassy carbon electrode.

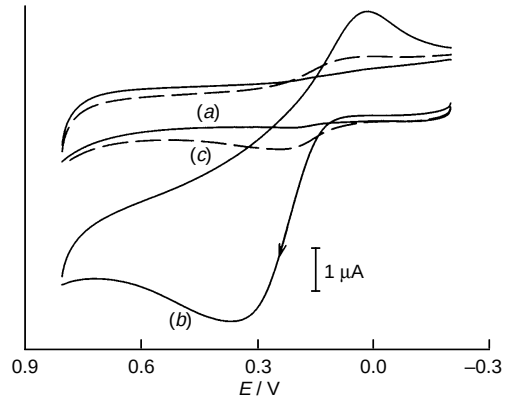

Fig. 1 Cyclic voltammograms (CVs) of 0.1 mM dopamine at (*a*) a non-templated PTMOS–TMOS film, (*b*) a templated PTMOS–TMOS film and (*c*) a templated film prepared from TMOS. The CVs were acquired after the silicate films had been in solution for 4–5 min. Solution conditions: 0.1 M, pH 7.0 phosphate buffer. Scan rate = 100 mV s^{-1}. Electrode potentials are *vs.* Ag/AgCl (1.0 M KCl).

To establish the importance of the phenyl functionality in the recognition properties of the material, templated films were prepared only from TMOS. The CV response of the templated TMOS film toward dopamine is slight as shown in Fig. 1(*c*), but significantly less than that observed at the templated PTMOS–TMOS silicate film. These results attest to the importance of the organosilicon precursor in enhancing the response of the film toward dopamine.

The dopamine templated PTMOS–TMOS films were also exposed to solutions of structurally related or biologically significant compounds including epinephrine, norepinephrine and ascorbic acid. These results showed that the templated films were not selective solely for dopamine but have an affinity for other catechol amines as well. This is expected since the host matrix is sufficiently porous and lacks specific binding sites as commonly observed for molecularly imprinted polymers.[2] The templated films, however, are able to discriminate against ascorbic acid as shown in Fig. 2. The lack of a noticeable voltammetric signal at the templated PTMOS–TMOS film and the non-templated PTMOS–TMOS film indicates that these materials have little affinity for ascorbic acid. The basis of this discrimination is likely due to electrostatics as the silicate matrix (pK_a of the silanol groups[10] is *ca*. 2) and ascorbic acid are both negatively charged at neutral pH. Alternatively, polarity may also be another factor as ascorbic acid is a relatively polar molecule whereas the phenyl-modified silicate films are more nonpolar.

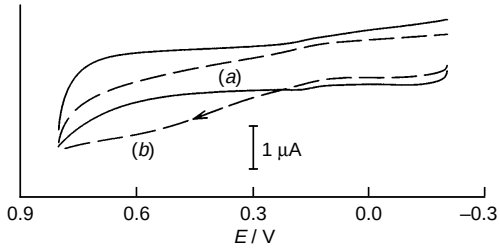

Fig. 2 Cyclic voltammograms of 0.1 mM ascorbic acid at (*a*) a nontemplated PTMOS–TMOS film and (*b*) a templated PTMOS–TMOS film. The CVs were acquired after the silicate films had been in solution for 4–5 min. Solution conditions: 0.1 M, pH 7.0 phosphate buffer. Scan rate = 100 mV s^{-1}. Electrode potentials are *vs.* Ag/AgCl (1.0 M KCl).

In summary, this study has demonstrated the feasibility of utilizing aqueous based inorganic polymerization techniques to fabricate nanoporous templated films with short response times that exhibit chemical selectivity. It is anticipated that this work will lead to promising developments in the design of improved molecular recognition materials.

We gratefully acknowledge support of this work through the National Science Foundation through CHE-9624813.

Notes and References

* E-mail: mmc@ksu.edu

1 J.-M. Lehn, *Angew. Chem., Int. Ed. Engl.*, 1990, **29**, 1304.
2 D. Kriz, O. Ramstrom and K. Mosbach, *Anal. Chem. A*, 1997, 345.
3 N. K. Raman, M. T. Anderson and C. J. Brinker, *Chem. Mater.*, 1996, **8**, 1682.
4 J. Brinker and G. Scherer, *Sol–Gel Science*, Academic Press, New York, 1989.
5 D. Avnir, *Acc. Chem. Res.*, 1995, **28**, 328.
6 H. Yang, N. Coombs, I. Sokolov and G. Ozin, *Nature*, 1996, **381**, 589; H. Yang, N. Coombs and G. Ozin, *Nature*, 1997, **386**, 692.
7 N. K. Raman and C. J. Brinker, *J. Membr. Sci.*, 1995, **105**, 273.
8 J. Wen and G. L. Wilkes, *Chem. Mater.*, 1996, **8**, 1667.
9 R. M. Wightman, L. J. May and A. C. Michael, *Anal. Chem. A*, 1988, **60**, 769.
10 R. K. Iler, *The Chemistry of Silica*, Wiley, New York, 1979.

Received in Columbia, MO, USA, 31st July 1997; 7/05536F

Highly efficient synthesis of phosphorodithioates derived from 3′-thiothymidine by anhydro-ring opening of 2,3′-anhydro-5′-*O*-tritylthymidine with *O,O*-disubstituted phosphorodithioic acids

Wojciech Dąbkowski,[a]† Maria Michalska[b] and Izabela Tworowska[a]

[a] *Centre of Molecular and Macromolecular Studies, Polish Academy of Sciences, 90-363 Łódź, Sienkiewicza 112, Poland*
[b] *Laboratory of Organic Chemistry, Institute of Chemistry, Medical University, 90-151 Łódź, Muszyńskiego 1, Poland*

Thymidine 3′-*S*-phosphorodithioate 4 and dithymidine-3′-*S*-phosphorodithioate 7 derived from 3′-thiothymidine are synthesized in excellent yield under mild conditions by the nucleophilic ring opening of 2,3′-anhydrothymidine with phosphorodithioic acids.

The rapid development of antisense chemotherapy[1] and studies to elucidate the mechanism of rybozyme action[2] have encouraged organic chemists to undertake the synthesis of oligonucleotide analogues in which the sugar residues and internucleotide linkages are modified. Interest in oligonucleotides containing 3′-*S*- or 5′-*S*-phosphorothioate linkages has recently increased, but methods presented to date, although elegant, are laborious and rather difficult to carry out.[3–9]

5′-Deoxy-5′-*S*-nucleosidyl phosphates have been prepared from 5′-iodo-2′-deoxynucleosides by condensation with trisodium phosphorothioate.[3] 2′-Deoxy-5′-*O*-thymidyl-5′-*S*-thymidyl phosphorothioate has been obtained by allowing thymidine 5′-phosphorothioate to react with 5′-iodothymidine.[4] A variation of this approach is the use of 5′-*O*-tosyl nucleoside for condensation with mono- or di-esters of phosphorothioic acid.[5] Cosstick has synthesized dithymidine phosphate analogues containing 3′-thiothymidine by phosphitylation of 5′-*O*-monomethoxytrityl-3′-thiothymidine.[6] The resulting dinucleosidyl phosphorothioite has been oxidized to the corresponding 3′-phosphorothioate. Dithymidine-3′-*S*-phosphorodithioate has been prepared, in an analogous fashion, as a mixture of diastereoisomers and separated after deprotection.[7]

More recently Cosstick has devised a synthesis of internucleoside 3′-phosphorothiolate linkages *via* electrophilic 3′-*S*-thymidinethiol derivatives, specifically, mixed disulfides with one strongly electronegative substituent, which were allowed to react with 3′-*O*-(*tert*-butyldimethylsilyl)thymidin-5′-yl trimethylsilyl phosphite.[8] A similar strategy has been used by Liu and Reese[9] in investigating the chemistry of RNA. Okruszek *et al.* have found that 3′-*O*-phosphorodithioates react in DMF solution with 5′-bromo-5′-deoxythymidine to give corresponding dinucleoside-5′-*S*-phosphorodithioate.[10] In spite of the elegance of Cosstick's, Reese's and Okruszek's approaches, formation of phosphorothiolate linkages requires laborious operations and depends on access to 3′-*S*- or 5′-*S*-thionucleosides and 5′-bromonucleoside which are not readily available. For this reason we have sought an alternative strategy avoiding 3′-*S*- or 5′-*S*-thionucleosides. Our long-standing interest in the chemistry of sugar thiophosphates[11] and modified nucleotides[12] also stimulated this work.

It is known that 2,3′-anhydrothymidine reacts with a variety of nucleophiles, usually under harsh conditions.[13] We discovered that 2,3′-anhydrothymidine reacts rapidly with phosphorus dithioacids [RR′P(S)SH] at ambient temperature in almost quantitative yield, and the ring opening proceeds with inversion of configuration at the 3′-carbon. Protonation of the anhydro-ring oxygen and the high nucleophilicity of phosphorus dithioacids make this procedure efficient and mild. Phosphorus dithioacids, including those derived from nucleosides,[14] are readily available.

Our methodology is exemplified by reactions of 5′-*O*-trityl-2,3′-anhydrothymidine[15] **1** with *O,O*-dimethyl phosphorodithioate[16] **2**‡ and with *O*-(5′-*O*-tritylthymidin-3′-yl) *O*-(2-cyanoethyl) phosphorodithioate **5**§ (Scheme 1). The dithioic acid **5** was prepared *in situ* by treating its DBU salt **5a** with excess of toluene-*p*-sulfonic acid monohydrate. Water introduced with

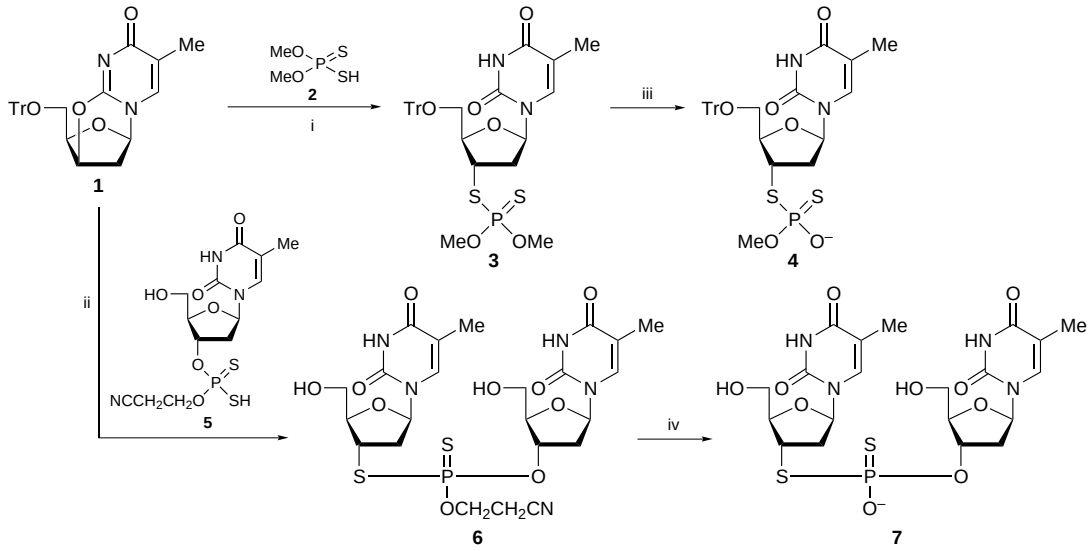

Scheme 1 *Reagents and conditions*: i, THF, 2 h, 20 °C; ii, MeCN, TsOH, 2 h, 20 °C; iii, *tert*-butylamine, 8 h, 20 °C; iv, THF–DBU (9 : 1), 1 h, 20 °C

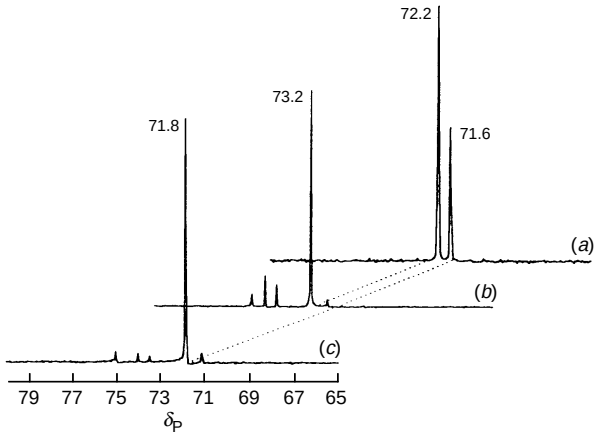

Fig. 1 The ^{31}P NMR spectra of (*a*) **4**, (*b*) **4b** (slow diastereoisomer) and (*c*) **4a** (fast diastereoisomer)

toluene-*p*-sulfonic acid does not interfere with the ring opening reaction but effects the removal of the trityl group. The analogous reaction with the DBU salt of **5a** requires severe conditions.

Both reactions proceed in THF or MeCN solution at 20 °C and are completed within 2 h yielding phosphorodithioates **3** and **6** in almost quantitative yield.

The demethylation of phosphorodithioate **3** by *tert*-butylamine and removal of the 2-cyanoethyl group of phosphorodithioate **6** leads to the corresponding salts **4a**, **b** and **7a**, **b**, respectively. These stable compounds contain a chiral phosphorus centre and are formed as a mixture of diastereoisomers. The 1 : 1 mixture of diastereoisomers **4** was separated into the 'fast' **4a** and 'slow' **4b** diastereoisomers by silica gel chromatography. ^{31}P NMR spectra of phosphorodithioates **4**, **4a** and **4b** are shown in Fig. 1.

We are currently exploring the use of nucleoside anhydrides to construct analogues of oligonucleotides containing 3′-*S*- or 5′-*S*-phosphorothiolate linkages by this methodology.

These studies were supported by grants No 3T09A 146 08 (M. M.) and No 3T09A 155 10 (W. D. and I. T.) of the Committee of Scientific Research, Poland.

Notes and References

† E-mail: wdabkow@free.polbox.pl

‡ *Experimental procedure*: to a solution of 2,3′-anhydro-5′-*O*-tritylthymidine **1** (0.1 mmol) in 10 ml of dry THF was added a solution of *O*,*O*-dimethyl phosphorodithioate **2** (0.1 mmol) in 10 ml of dry THF and the mixture was kept for 2 h at 20 °C. The reaction mixture was concentrated under reduced pressure. The residue was purified by column chromatography on silica gel (230–400 mesh, Merck 9835) using CH_2Cl_2–Me_2CO (10 : 2 v/v) as eluent to give **3** (80%); $\delta_P(C_6D_6)$ 96.55. Compound **3** was dissolved in *tert*-butylamine, the reaction mixture was stirred for 8 h at room temperature and was solvent evaporated *in vacuo*. The product **4** was isolated by silica gel chromatography [CH_2Cl_2–Me_2CO–Et_3N, 10 : 2 : 0.5 (v/v/v)] as a mixture of diastereoisomers (1 : 1) of the *tert*-butylammonium salt of **4** (95%); $\delta_P(C_6D_6)$ 72.2, 71.6. The diastereoisomers were resolved by column chromatography using CH_2Cl_2–Me_2CO–Et_3N [10 : 2 : 0.5 (v/v/v)] as eluent and collecting small fractions. Fast diastereoisomer **4a**: $\delta_P(C_6D_6)$ 71.7. Slow diastereoisomer **4b**: $\delta_P(C_6D_6)$ 73.2.

§ A solution of 2,3′-anhydro-5′-*O*-tritylthymidine **1** (0.1 mmol) and *O*-[(5′-*O*-trityl)-thymidin-3′-yl] *O*-(β-cyanoethyl) phosphorodithioate **5** (0.1 mmol) in 10 ml of MeCN was acidified with toulene-*p*-sulfonic acid monohydrate (0.25 mmol). After 2 h at 20 °C the reaction mixture was concentrated *in vacuo* and the residue was purified by column chromatography on silica gel (230–400 mesh, Merck 9835) using CH_2Cl_2–Me_2CO [10 : 2 (v/v)] as eluent to give **6** as a mixture of diastereoisomers (95%); $\delta_P(C_6D_6)$ 92.401, 91.751 (3 : 4). A solution of **6** (0.1 mmol) in THF–DBU (9 : 1, 10 ml) was left at room temperature for 1 h. The product **7** was a mixture of diastereoisomers (3 : 2) (90%); $\delta_P(C_6D_6)$ 67.53, 67.27 (3 : 2).

1 *Oligonucleotides: Antisense Inhibitors of Gene Expression*, ed. J. S. Cohen, Macmillan, London, 1989.
2 W. A. Picken, D. B. Olsen, F. Benseler and F. Eckstein, *Science*, 1991, **253**, 314.
3 A. Hampton, L. W. Brox and M. Bayer, *Biochemistry*, 1969, **8**, 2303; E. F. Rossomando, G. A. Cordis and G. D. Markham, *Arch. Biochem. Biophys.*, 1983, **220**, 71.
4 A. F. Cook, *J. Am. Chem. Soc.*, 1970, **92**, 190.
5 A. F. Cook, *J. Am. Chem. Soc.*, 1970, **92**, 190; J. Nagyvary, S. Chladek and J. Roe, *Biochem. Biophys. Res. Commun.*, 1970, **39**, 878; S. Chladek and J. Nagyvary, *J. Am. Chem. Soc.*, 1972, **94**, 2079; J. Kresse, K. L. Nagpal, J. Nagyvary and J. T. Uchlic, *Nucleic Acids Res.*, 1975, **2**, 1.
6 J. S. Vyle, X. Li and R. Cosstick, *Tetrahedron Lett.*, 1992, **33**, 3017.
7 R. Costick and J. S. Vyle, *Nucleic Acids Res.*, 1990, **4**, 829.
8 X. Li, G. K. Scott, A. D. Baxter, R. J. Taylor, J. S. Vyle and R. Cosstick, *J. Chem. Soc., Perkin. Trans. 1*, 1994, 2123; L. B. Weinstein, D. J. Earnshaw, R. Cosstick and T. R. Cech, *J. Am. Chem. Soc.*, 1996, **118**, 10 341; A. P.Higson, G. K. Scott, D. J. Earnshaw, A. D. Baxter, R. A. Taylor and R. Cosstick, *Tetrahedron*, 1996, **52**, 1027.
9 X. Liu and C. B. Reese, *Tetrahedron Lett.*, 1996, **37**, 925.
10 A. Okruszek, M. Olesiak and W. J. Stec, *Phosphorus Sulfur Silicon Relat. Elem.*, 1996, **111**, 81.
11 W. Kudelska and M. Michalska, *Tetrahedron*, 1986, **42**, 629 and references cited therein; M. Michalska, E. Brzezinska and P. Lipka, *J. Am. Chem. Soc.*, 1991, **113**, 7945; H. Bielawska and M. Michalska, *J. Carbohydr. Chem.*, 1991, **10**, 107; W. Kudelska and M. Michalska, *Synthesis*, 1995, 1539.
12 W. Dąbkowski, J. Michalski and Q. Wang, *Angew. Chem., Int. Ed. Engl.*, 1990, **29**, 522; J.Heliński, W. Dąbkowski and J. Michalski, *Nucleosides Nucleotides*, 1993, **12**, 597; W. Dąbkowski, I. Tworowska and R. Saiakhov, *Tetrahedron Lett.*, 1995, **36**, 9223.
13 S. Czernecki and J.-M. Valéry, *Synthesis*, 1991, 239; G. V. Zaitseva, E. I. Kvasyuk, E. V. Vaaks, V. N. Barai, S. B. Bokut, A. I. Zinchenko and I. A. Mikhailopulo, *Nucleosides Nucleotides*, 1994, **13**, 819; B.-Ch. Chen, S. L. Quinlan and J. G. Reid, *Tetrahedron Lett.*, 1995, **36**, 7961.
14 A. Okruszek, A. Sierzchala, M. Sochacki and W. J. Stec, *Tetrahedron Lett.*, 1992, **33**, 7585; A. Okruszek, M. Olesiak, D. Krajewska and W. J. Stec, *J. Org. Chem.*, 1997, **62**, 2269.
15 B. Bennua-Skalmowski and H. Vorbrüggen, *Nucleosides Nucleotides*, 1996, **15**, 739.
16 J. L. Lefferts, K. C. Molloy, J. J. Zuckerman, I. Haiduc, C. Guta and D. Ruse, *Inorg. Chem.*, 1980, **19**, 1662.

Received in Glasgow, UK, 26th August 1997; 7/06211G

5-Hydroperoxycarbonylphthalimide: a new reagent for epoxidation

Alun P. James,[a] Robert A. W. Johnstone,*[b]† Moya McCarron,[b] J. Phillip Sankey[a] and Brian Trenbirth[c]

[a] *Solvay Research and Development Laboratories, Widnes, UK WA8 0FE*
[b] *Department of Chemistry, University of Liverpool, Liverpool, UK L69 3BX*
[c] *Contract Chemicals, Knowsley Industrial Park South, Prescot, UK L34 9HY*

Peroxycarboxylic acids, widely used for epoxidation in industry and general research, have various drawbacks, such as difficulty of preparation in a pure state, cost and the possibly ring-opening of the product epoxides due to acid-catalysed reactions; a new reagent, 5-hydroperoxycarbonylphthalimide, overcomes these problems.

The formation of epoxides (oxiranes) from alkenes is a widely used reaction, either for the product epoxides themselves or for their preparation as intermediates in further synthesis.[1] The manufacture of epoxides ranges in scale from the small requirements of a research reaction to the huge tonnages of industrial epoxides and bis-epoxides. Hydrogen peroxide, a clean oxidant producing only water as a by-product, would be ideal if it could be used to produce epoxides directly. Although epoxidation can be effected with hydrogen peroxide through use of metal catalysts such as those of tungsten[2] or molybdenum,[3] titanium silicalites[4] and porphyrins,[5] these catalysts are not universally applicable for various reasons, including cost, lack of specificity, inability to selectively epoxidise without formation of serious quantities of by-products and lack of reactivity towards alkenes having electron-deficient double bonds. Such catalysts have not found general favour, except in some specialised instances. There is widespread use of hydrogen peroxide by first converting it into a suitably reactive form, such as *tert*-butyl peroxide and the popular peroxycarboxylic acids. Of the latter, although many are known, only a few are in general use.[6] Thus, peroxyformic, peroxyacetic, peroxybenzoic, peroxyphthalic (also as its magnesium salt), peroxytrifluoroacetic and *m*-chloroperoxybenzoic acids are the ones most frequently employed. Generally, the relatively cheap, lower molecular mass, liquid peroxyformic and peroxyacetic acids are used for large-scale industrial epoxidation and the higher molecular mass, solid *m*-chloroperoxybenzoic acid is widely employed for research or very small scale purposes. There are serious disadvantages to the use of peroxyformic and peroxyacetic acids, including their difficulty of synthesis in high concentration, their lack of stability, the need for buffering of a reaction medium to lessen acid-induced side reactions and the difficulty of recycling the parent acid. *m*-Chloroperoxybenzoic acid is not available commercially in large quantities or in pure form because of its easy thermal decomposition and sensitivity to mechanical shock;[7] the peroxyacid is also expensive because of the cost of the starting acid and the need to use methanesulfonic acid to catalyse its formation from hydrogen peroxide. Nevertheless, *m*-chloroperoxybenzoic acid does have desirable properties, in being capable of effecting many kinds of epoxidation and in giving a product acid that is relatively insoluble in non-polar solvents. The present research has shown that 5-hydroperoxycarbonylphthalimide **1** (5-PCP; 1,3-dioxo-1,3-dihydroisoindole-5-peroxycarboxylic acid; Scheme 1)[8] is an excellent, cheaper reagent for effecting epoxidation, ameliorating or overcoming many of the disadvantages listed above. Its preparation is described in a footnote to Table 1.

The alkenes shown in Table 1 were epoxidised at temperatures between 0 and 60 °C in various solvents (Scheme 1). The

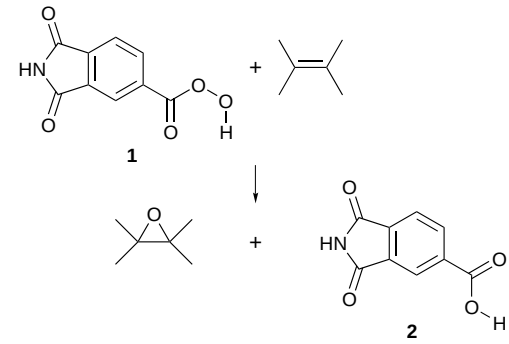

Scheme 1

Table 1 Alkenes epoxidised with 5-hydroperoxycarbonylphthalimide **1** (5-PCP)[a]

Alkene	*T*/°C[b]	Solvent	*t*/h[c]
2,3-Dimethylbut-2-ene	20	CH_2Cl_2	2
Cyclohexene	20	CH_2Cl_2	6
1-Methylcyclohexene	20	CH_2Cl_2	2
	20	Toluene	3
Cyclooctene	20	CH_2Cl_2	2
α-Pinene	20	CH_2Cl_2	2
β-Pinene	20	CH_2Cl_2	2.5
Limonene	20	CH_2Cl_2	2 + 4[d]
Oct-1-ene	35	CH_2Cl_2	24
cis-Stilbene	35	CH_2Cl_2	24
trans-Stilbene	35	CH_2Cl_2	24
Allyl phenyl ether	60	$ClCH_2CH_2Cl$	113
Styrene	35	CH_2Cl_2	24
Diallyl maleate	60	$ClCH_2CH_2Cl$	150
6-Methylhept-5-en-2-one	0	CH_2Cl_2	7
1,2-Diallyloxyethane	55	EtOAc	70

[a] To conc. H_2SO_4 (29.4 g; 98% w/w) was added water (1.7 g; demineralised), with stirring and cooling, followed by hydrogen peroxide (3.66 g; 85% w/w; 0.0915 mol), maintaining the reaction temperature below 15 °C. After addition had been completed, the mixture was warmed to 40 °C, at which stage 1,3-dihydro-1,3-dioxoisoindole-5-carboxylic acid (ref. 10) (5-carboxyphthalimide **2**; 5 g) was added. The mixture was stirred at 40 °C for 45 min, after which it was cooled and quenched by addition of ice–water. 5-Hydroperoxycarbonylphthalimide **1** (5-PCP) crystallised out. The product was filtered off, washed normally with water to pH 3 and air-dried to give the pure compound in > 90% yield, mp 175 °C. [b] In a typical reaction (Scheme 1), 1-methylcyclohexene (48 mg; 0.5 mmol) in CH_2Cl_2 (2 ml) was stirred with 5-PCP (0.12 g; 0.6 mmol) at room temperature for 2 h. The course of the reaction was monitored by GC and by GC–MS. At the end of reaction, the precipitated 5-carboxyphthalimide **2** was filtered off, the solvent was evaporated and the product was weighed and examined by ^1H NMR spectroscopy. All the epoxides are known and authentic materials were used for comparison with the epoxides produced with 5-PCP. Yields were between 98–100%. [c] Approximate time to complete reaction, as revealed by the disappearance of the starting alkene. [d] With 1 equiv. of 5-PCP, only the 1,2-*mono*(epoxide) was isolated after 2 h. Addition of a further 1 equiv. of 5-PCP at this stage gave the 1,2 : 9,10 *bis*(epoxide) after a further 4 h.

alkenes were chosen to explore the general suitability of 5-PCP for epoxidation. Thus, the reactivity of the alkenes towards electrophilic oxygen ranged from the electron-rich 2,3-dimethylbut-2-ene (containing a tetraalkyl-substituted double bond) to the electron-deficient allyl phenyl ether (containing a monosubstituted, oxygen-deactivated double bond). Other alkenes were chosen to demonstrate the stability of the resulting epoxide under the reaction conditions (styrene, α-pinene, 1,2-diallyloxyethane), the stereo integrity of reaction (*cis*- and *trans*-stilbene) or the selectivity of reaction (limonene, having two different double bonds).

In each case, epoxidation proceeded to give virtually a 100% yield of very pure product epoxide. Reaction rates were as expected from the known mechanism of epoxidation with peroxyacids.[1,6] Thus, at room temperature, reaction of 2,3-dimethylbut-2-ene, 1-methylcyclohexene, cyclohexene, cyclooctene and α- and β-pinene with 5-PCP was fast in CH_2Cl_2. For the less reactive alkenes, such as oct-1-ene, allyl phenyl ether, 1,2-diallyloxyethane and diallyl maleate, higher temperatures were needed to achieve reaction in a reasonable time. Such reactions could be carried out in CH_2Cl_2 under reflux (35 °C), 1,2-dichloroethane (at 50 °C), EtOAc (at 55 °C) and toluene (at 50 °C). When the epoxidation was carried out at higher temperatures than these, reaction was faster and a clean product was still obtained, but there was some small loss of active oxygen over long periods of time. In these cases, somewhat more than a 1 equiv. of peroxyacid to each double bond was needed. Thus, after a period of about 100 h at 60 °C with 2 equiv. of 5-PCP, epoxidation of the two allylic bonds in diallylmaleate ceased at about 60–70% because of depletion of the peroxyacid; addition of a further 1 equiv. (0.5 equiv. for each bond) caused the reaction to proceed to completion and to give a very pure product.

In all of the reactions, the product acid (5-carboxyphthalimide **2**) was almost totally insoluble in the solvent. This behaviour is highly advantageous in two ways. First, the product acid can be filtered off easily from the reaction medium and re-used; this potentially low-cost acid can be recycled with hydrogen peroxide to give little or no environmentally disadvantageous by-product. Second, the insolubility of the acid, due to extensive strong intermolecular hydrogen-bonding,[9] means that the hydrogen ion concentration in solution is extremely low. In turn, this means that acid-catalysed changes in the epoxide, when formed, are reduced to a very low level, enabling the isolation of even acid-sensitive epoxides in high yield and purity. 5-PCP itself is partly soluble in the solvents described here. This implies it has all of the kinetic advantages of a homogeneous reaction but, being a very weak acid, does not produce a significant hydrogen ion concentration in the reaction medium. Thus, there is little or no effect from acid-catalysed decomposition of the product epoxide. In the most sensitive epoxides prepared in this work (*e.g.* styrene oxide), reaction proceeded to virtually 100% yield with no evidence for acid-catalysed rearrangement products (phenylacetaldehyde in the case of styrene oxide). Until full hazard information is available, 5-PCP should be treated with caution, as with any peroxy compound.

Notes and References

† E-mail: rj05@liv.ac.uk

1 See for example, M. Hudlicky, *Oxidations in Organic Chemistry*, ACS Monograph 186, American Chemical Society, Washington DC, 1990, pp. 60–65; J. March, *Advanced Organic Chemistry*, Wiley, New York, 1985, pp. 733–735.
2 C. Venturello, M. Abneri and M. Ricci, *J. Org. Chem.*, 1983, **48**, 3831.
3 R. Landau, G. Sullivan and D. Brown, *Chem. Technol.*, 1979, **9**, 602.
4 A. Tuel and Y. B. Taarit, *J. Chem. Soc., Chem. Commun.*, 1994, 1667.
5 A. M. d'A Rocha Gonsalves, R. A. W. Johnstone, M. M. Pereira and J. Shaw, *J. Chem. Soc., Perkin Trans. 1*, 1991, 645.
6 D. Swern, in *Organic Peroxides*, ed. D. Swern, Wiley-Interscience, New York, 1970, vol. 1, pp. 313–374 and see ref. 1 above.
7 M. Hirano, S. Yakabe, A. Satoh, J. H. Clark and T. Morimoto, *Synth. Commun.*, 1996, **26**, 4591; T. Mino, S. Masuda, M. Nishio and M. Yamashita, *J. Org. Chem.*, 1997, **62**, 2633.
8 J. P. Sankey and A. P. James, (Interox Chemicals), *PCT Int. Appl.*, WO 91 09,843, 11th July, 1991; *Chem. Abstr.*, 1991, **115**, 282510h.
9 N. Feeder and W. Jones, *Acta Crystallogr., Sect. C*, 1994, **50**, 824.
10 W. H. Perkin and J. F. S. Stone, *J. Chem. Soc.*, 1925, **127**, 2295.

Received in Cambridge, UK, 13th November 1997; 7/08179K

Fluorescence sensing due to allosteric switching of pyrene functionalized *cis*-cyclohexane-1,3-dicarboxylate

Carol Monahan, Jeffrey T. Bien and Bradley D. Smith*†

Department of Chemistry and Biochemistry, University of Notre Dame, Notre Dame, IN 46556, USA

The excimer/monomer fluorescence ratio for a pyrene functionalized *cis*-cyclohexane-1,3-dicarboxylate decreases upon titration with divalent and monovalent metal cations, as well as strong and weak acids.

Molecules that can be chemically switched between different conformations have been used as allosteric receptors, catalysts, transport carriers, liquid crystalline materials and sensors.[1] The main approach with allosteric sensors has been to change the proximity between two interacting fluorophores,[2] or to alter the solvent polarity surrounding a fluorophore.[3] Here we describe the allosteric properties of *cis*-1,3-disubstituted cyclohexane-1,3-dicarboxylic acids **1** and in particular how the **cis**-1,3-bispyrenyl derivative **1b** acts as a fluorescent cations sensor.[4]

Initially, the *cis*-1,3-dimethyl analogue **1a** was prepared,† and shown by ^{1}H NMR spectroscopy to adopt a chair conformation with both carboxyl groups in axial positions (Scheme 1).§ This conformational preference is in agreement with the higher steric *A* value for a methyl group compared to a carboxy group. Conversion to the dianion results in a switch to the alternate chair structure **2a** with diequatorial carboxylate groups.§ The driving force for this conformational change is the electrostatic repulsion of the proximal anionic carboxylates. In agreement with an earlier report by Menger *et al*., titration of a 1 : 1 MeOH–H_2O solution of **2a** with Mg^{2+} induces a conformational flip to **3a**.[6] Addition of Na^+, however, has a negligible effect on conformation in such a polar solvent. Two factors drive the conformational change induced by Mg^{2+}: (i) partial neutralization of the anionic carboxylates by the Mg^{2+} ion, and (ii) release of steric strain as the methyl groups transfer from diaxial to more accommodating diequatorial positions.

Based on this knowledge it was hypothesized that compound **1b** would show substantial changes in fluorescence upon conformational switching. The two pyrenyl groups in structure **2b** are in close proximity to each other and are able to exhibit intramolecular excimer fluorescence. With structures **1b**, **3b** and **4b**, the pyrenyl groups are separated and the favorability of excimer formation is decreased.[2] This was found to be the case in MeCN solution where titration of the bis(tetrabutylammonium) salt of **2b** with strong acid resulted in a stoichiometric decrease in the excimer/monomer fluorescence ratio. The titration curve (Fig. 1) indicates that only 1 equiv. of nitric acid is needed to completely switch the excimer/monomer ratio. Thus, protonation of one of the carboxylates relieves the strain due to dianionic repulsion and causes a flip to the alternate chair conformation **4b**. In contrast, alkali metal cations induce much gentler decreases in excimer/monomer ratio suggesting a gradual formation of **3b**, where M is one or two M^+ ions.§ Titration with ammonium chloride or ammonium nitrate generated plots that were identical to the nitric acid curve (Figs. 1 and 2). It appears that the ammonium also transfers a proton to **2b** and forms **4b**. Although carboxylic acids are more acidic than ammonium salts in aqueous solution, the reverse order is observed in aprotic solvents such as MeCN. For example, ammonium (pK_a 16.5) is more acidic than glutaric acid (pK_{a_1} 19.2, pK_{a_2} 29.9), a dicarboxylic acid that is structurally related to **1**.[7–9]

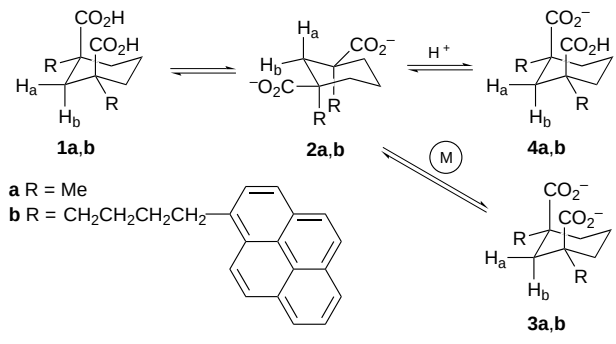

Scheme 1

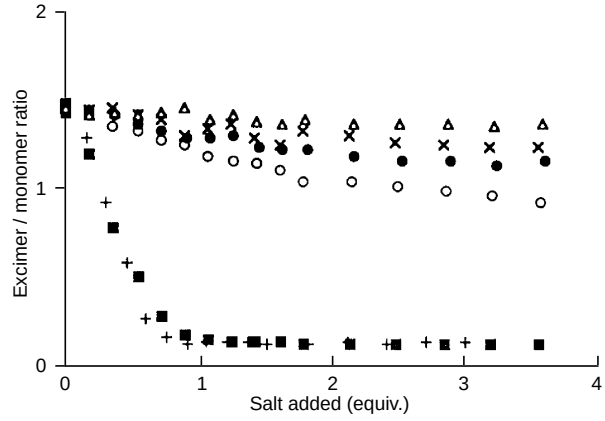

Fig. 1 Change in excimer/monomer ratio for **2b** (3 μM) in MeCN upon titration with (Δ) $CsNO_3$, (x) $RbNO_3$, (●) KNO_3, (○) $NaNO_3$, (■) NH_4NO_3 and (+) HNO_3. Excitation at 346 nm, monomer emission at 397 nm, excimer emission at 470 nm, T = 298 K.

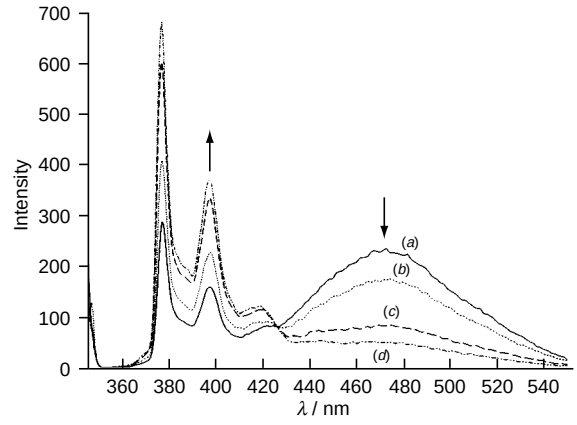

Fig. 2 Fluorescence emission for **2b** in MeCN (3 μM, excitation at 346 nm) in the presence of (*a*) 0, (*b*) 1.0, (*c*) 2.2 and (*d*) 10.6 μM of NH_4NO_3

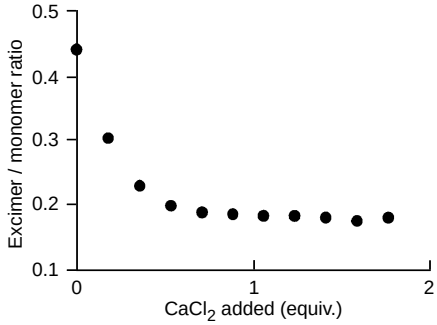

Fig. 3 Change in excimer/monomer ratio for **2b** (3 μM in MeOH upon titration with $CaCl_2$. Excitation at 346 nm, monomer emission at 397 nm, excimer emission at 470 nm, T = 298 K.

Strong evidence that the change in fluorescence is due to a conformational change was obtained from the following control experiments. (i) All of the fluorescence titrations were repeated using tetrabutylammonium pyrene-1-butyrate as a replacement fluorophore. In all cases, negligible changes in fluorescence were observed, indicating that the excimer/monomer switching is not due to due to intermolecular or environmental factors. (ii) Treatment of a CD_3CN solution of **1a** with 2 equiv. of tetramethylammonium hydroxide changes the difference in ^1H NMR chemical shifts for H_a and H_b $\Delta\delta$ = 1.36 to 0.50 ppm, which is consistent with a change from **1a** to **2a**.§ A subsequent titration of this solution with ammonium thiocyanate results in smooth migration back to $\Delta\delta$ = 1.61 ppm, suggesting that **2a** becomes protonated and converts to **4a**. The fluorescence switching effects of ammonium and alkali metal cations are essentially negligible in polar, competitive solvents such as MeOH. However, moderate descreases in excimer/monomer ratio are induced by titrating **2**b with alkaline metal dichlorides to produce **3b** (Fig. 3).

In summary, a simple but sensitive allosteric system is described that can undergo large changes in molecular shape. Depending on the experimental conditions, the conformational switching can be induced by divalent and monovalent metal cations, as well as strong and weak acids. Analogue **1b** exhibits large changes in fluorescence and is thus sensor for Lewis and Brønsted acids. Future efforts will attempt to incorporate this conformational switch into the structures of other molecular devices.

This work was supported by the National Science Foundation (USA).

Notes and References

† E-mail: smith.115@nd.edu

‡ Compound **1a** was synthesized by treating dimethyl cyclohexane-1,3-dicarboxylate with LDA (2 equiv). followed by Me_2SO_4 (2 equiv.). Saponification gave **1a** in 40% overall yield. Similarly, compound **1b** was prepared by treating the di-*tert*-butyl cyclohexane-1,3-dicarboxylate with LDA (2 equiv.) followed by 4-(pyren-1-yl)butyl trifluoromethylsulfonate (2 equiv.). Acid hydrolysis gave **1b** in 15% overall yield.

§ The conformational assignments are based on the close homology of the NMR data with Kemp *et al*. (ref. 5) and Menger *et al*. (ref. 6), who examined the conformational switching of *cis,cis*-1,3,5-trimethylcyclohexane-1,3,5-tricarboxylic acid (Kemp's triacid). In particular, the non-equivalent methylene protons between the two carboxy group in **1a** (H_a and H_b) resonate at δ 2.63 and 1.13, respectively, in 1 : 1 MeOH–H_2O ($\Delta\delta$ = 1.50 ppm). The chemical shift for H_a is strongly deshielded due to the anisotropy of the neighbouring carbonyl groups. In the case of dianion **2a**, the resonances for H_a and H_b are much closer together ($\Delta\delta$ = 0.35 ppm) indicating that they are nearly equidistant from the carboxylates, which can only occur if the carboxylates have assumed equatorial positions. Structure **3** is drawn as a classical chair with the carboxylates in diaxial positions, however, another possibility is a flattened half-chair which provides the carboxylates with slightly more spacious psuedo-axial environments. (ref. 6).

1 H.-J. Schneider and A. K. Mohammad-Ali, in *Comprehensive Supramolecular Chemistry*, ed. J. L. Atwood, J. E. D. Davies, D. D. MacNicol and F. Vögtle, Pergamon, New York, 1996, vol. 2, pp. 81–86.
2 G. L. Arnold and S. A. van Arman, *Tetrahedron Lett*., 1997, **38**, 4745; G. E. Collins and L.-S. Choi, *Chem. Commun*., 1997, 1135; H. Matsumoto and S. Shinkai, *Tetrahedron Lett*., 1996, **37**, 77; M. Takeshita and S. Shinkai, *Chem. Lett*., 1994, 125; I. Aoki, T. Harada, T. Sakaki, Y. Kawahara and S. Shinkai, *J. Chem. Soc., Chem. Commun*., 1992, 1341.
3 G. K. Walkup and B. Imperiali, *J. Am. Chem. Soc*., 1996, **118**, 3053; H. Ikeda, M. Nakamura, N. Ise, N. Oguma, A. Nakamura, T. Ikeda, F. Toda and A. Ueno, *J. Am. Chem. Soc*., 1996, **118**, 10 980.
4 Other switchable cyclohexane-based systems include the following: V. V. Samoshin, V. A. Chertkov, L. P. Vatlina, E. K. Dobretsova, N. A. Simonov, L. P. Kastorsky, D. E. Gremyachinsky and H.-J. Schneider, *Tetrahedron Lett*., 1996, **37**, 3981; M. Goodall, P. M. Kelly, D. Parker, K. Gloe and H. Stephan, *J. Chem. Soc., Perkin Trans. 2*, 1997, 59; S. M. Shirdkar and G. R. Weisman, *J. Chem. Soc., Chem. Commun*., 1989, 236.
5 D. S. Kemp and K. S. Petrakis, *J. Org. Chem*., 1981, **46**, 5140.
6 F. M. Menger, P. A. Chicklo and M. J. Sherrod, *Tetrahedron Lett*., 1989, **30**, 6943.
7 K. Izutsu, *Dissociation Constants in Dipolar Aprotic Solvents*, Blackwell Scientific Publications, Oxford, 1990.
8 I. M. Kolthoff, M. K. Chantooni and S. Bhowmik, *J. Am. Chem. Soc*., 1968, **90**, 23.
9 I. M. Kolthoff and M. K. Chantooni, *J. Am. Chem. Soc*., 1975, **97**, 1376.

Received in Columbia, MO, USA, 28th July 1997; 7/05445I

A fullerene-modified protein

Arnd Kurz,[a] Catherine M. Halliwell,[a] Jason J. Davis,[a] H. Allen O. Hill*[a]† and Gerard W. Canters[b]

[a]*Inorganic Chemistry Laboratory, University of Oxford, Oxford, UK*
[b] *Leiden Institute of Chemistry, Leiden University, Gorlaeus Laboratories, Leiden, The Netherlands*

A surface cysteine-containing redox protein (azurin mutant S118C) has been labelled with a C_{60}-based thiol-selective reagent leading to electrochemical interactions between the fullerene and protein redox centre.

In recent years much interest has been drawn to the biological activities of fullerenes, such as cytotoxic activity,[1] selective DNA cleavage[2] and antiviral activity against HIV.[3] However, biological studies have been hindered because of the hydrophobic nature of fullerenes. In an effort to overcome problems associated with their insolubility in aqueous solution, several strategies have been developed such as the formation of complexes with cyclodextrin,[4] liposomes,[5] poly(vinylpyrrolidone)[6] and derivatization with water-solubilising moieties.[7] The C_{60} cage is able to reversibly accept up to six electrons under suitable conditions,[8] so C_{60}, that is covalently attached to biomolecules, can be sensed electrochemically. As C_{60} is insoluble in water little is known about its electrochemical behaviour in aqueous media, although the electrochemistry of films[9] and γ-cyclodextrin inclusion complexes[10] has been studied. The C_{60} radical monoanion has recently[11] been reported to be stable in water and monoanion containing salts have been isolated from aqueous solutions. We report herein the modification of a redox protein (azurin mutant S118C) with buckminsterfullerene and the electrochemical behaviour of the adduct so formed.

Azurin is a small blue copper redox protein which acts as an electron transfer agent in the denitrification chains of a number of bacteria. It has a molecular weight of about 14 000 kDa. As wild type azurin does not contain any surface cysteines (and hence free thiols), a mutant‡ containing just one surface cysteine was created by polymerase chain reaction (PCR) mutagenesis methods[12] and expressed according to published methods.[13] Serine 118 was genetically replaced by a cysteine, this being a conservative mutation to ensure the mutant closely resembled the wild type azurin. The position was chosen to allow labelling close to the redox centre, a copper ion in the case of azurin, in order to investigate the possibility of electrochemical communication between copper and fullerene. The previously described *N*-(triphenylmethyl)-3,4-fulleropyrrolidine[14] was reacted with 3-maleimidopropionyl chloride in the synthesis (Scheme 1) of a thiol selective fullerenomaleimide.§

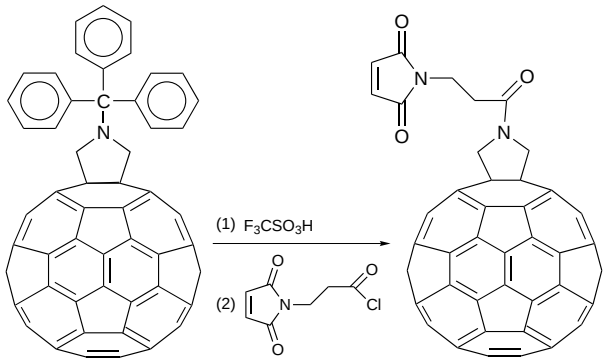

Scheme 1

This label is not soluble in water and only sparingly soluble in polar organic solvents, but is reactive enough as a suspension to couple to the protein. For the labelling reaction, the fullerenomaleimide (in 100-fold molar excess) was suspended in a 60 μM solution of azurin S118C in 20 mM HEPES buffer at pH 7. The suspension was then stirred for 72 h at 4 °C. The originally blue solution turned green after 24 h. Over the same time period the characteristic electronic absorption band of C_{60} at 330 nm appeared (Fig 1). Unreacted fullerene was removed by size exclusion chromatography (PD-10, Pharmacia). A SDS-PAGE gel (15% polyacrylamide) indicated the presence of a new band at higher mass. The mass increase was estimated to be 5%, consistent with the addition of one fullerene moiety per protein. The reaction appeared to go to completion as no native protein could be detected by SDS-PAGE or by cyclic voltammetry. The cyclic voltammogram of the product shows the presence of a new redox couple at −302 mV assigned to the first electron reduction and reoxidation of C_{60} (Fig 2). The potential lies between that reported[11] for a solution of C_{60} in DMF (−250 mV) and a γ-cyclodextrin inclusion complex of C_{60} in water (−570 mV).[10] The redox couple of the protein copper appears at −42 mV. It is shifted by 41 mV to a more negative potential

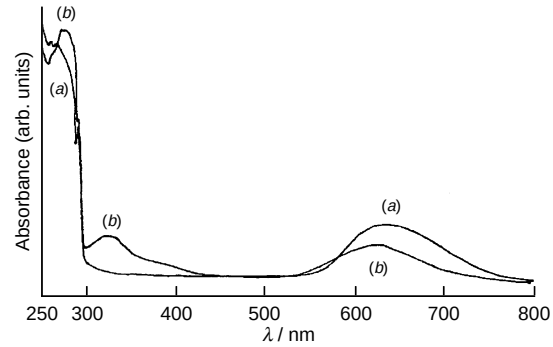

Fig. 1 UV–VIS spectrum (H_2O) of (*a*) azurin S118C and (*b*) fullerene-modifed S118C

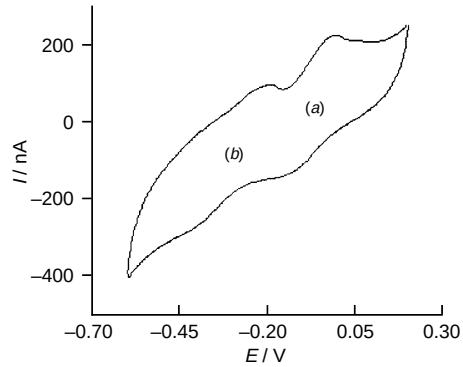

Fig. 2 Cyclic voltammogram at an edge plane graphite electrode of 65 μM fullerene modified S118C in 20 mM HEPES buffer (pH 7.0) containing 5% THF and 5% DMSO at 50 mV s^{-1} and 25 °C. The solutions were purged with argon for 60 min before measurement. (*a*) Copper redox couple Cu^{+2}/Cu^{+1} and (*b*) fullerene redox couple $C_{60}°/C_{60}^{-1}$.

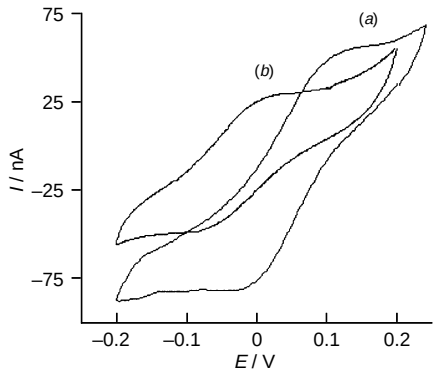

Fig. 3 Cyclic voltammogramm of (*a*) wild type azurin and (*b*) fullerene modified S118C under the same conditions as in Fig 2

compared to the unmodifed protein (−1 mV) under the same experimental conditions (Fig 3). As the fullerene is attached next to histidine 117, which is a copper ligand, modification-induced changes in the redox potential are likely. If the potential range is restricted to that of the azurin copper, a reversible couple is observed with reduction and re-oxidation peak areas of equal magnitude. If scans are continued to more negative potentials (at which the fullerene is reduced) the anodic peak of the Cu couple changes, as does the ratio of anodic to cathodic current. This behaviour suggests communication between copper centre and fullerene. Spectroscopic (UV–VIS) and electrochemical data prove that the fullerene modification did not lead to the denaturation of the protein.

The covalent modification of protein with buckminsterfullerene opens up the possibility of extensive investigations into the aqueous and biological chemistry of these 'fulleryl proteins'.

The support of the Dutch Science Foundation (C. M. H.), MediSense (A. K.) and the BBSRC (A. K., C. M. H., J. J. D.) is gratefully acknowleged. We thank Professor M. L. H. Green for access to arc vaporisation equipment and Drs P. D. Barker, M. J. Rosseinsky and G. Sanghera for helpful discussions.

Notes and References

† E-mail: allen.hill@chemistry.ox.ac.uk

‡ Preparation of S118C: Mutagenesis of azurin *Pseudomonas aeruginosa* was performed by PCR with the primers: 5′GCACCTTCCCGGGC-CAC*TGC*GCGCTGATG-3′ (5′-primer) and 5′-AAACGACGGCCAGT-3′ (3′-primer). The azurin mutant S118C was expressed and stored as the apoform. Dithiothreitol (DTT) was added to the buffers to give a final DTT concentration of 3 mM in order to prevent dimerisation. Prior to labelling the DTT was removed through the use of desalting columns (PD-10, Pharmacia). The protein was reconstituted by addition of an equimolar amount of a 10 mM solution of $Cu(NO_3)_2$.

§ Preparation of *N*-(3-maleimidopropionyl)-3,4-fulleropyrrolidine: *N*-(triphenylmethyl)-3,4-fulleropyrrolidine (30 mmol) (ref. 14) in dry CH_2Cl_2 (10 ml) was treated with trifluoromethanesulfonic acid (100 μl) for 1 h. The precipitate was washed with Et_2O–H_2O and dried. The amine was suspended in dry CH_2Cl_2 (10 ml) and dry pyridine (1 ml). A 30 molar excess of *N*-maleoylpropionyl chloride was added. After stirring for 3 h at room temperature the mixture was purified on silica gel (CH_2Cl_2): δ_H (500 MHz, CS_2–[$^2H_6$]benzene 4 : 1) 6.78 (s 2 H), 5.47 (s 2 H), 5.37 (s 2 H), 3.84 (t 2 H), 3.19 (t 2 H); *m*/*z* (MS-FAB) 913 (M-1, 50%), 720 (C_{60}, 100); λ_{max} (CH_2Cl_2)/nm 232, 260, 332, 406.

1 H. Tokuyama, S. Yamago and E. Nakamura, *J. Am. Chem. Soc.*, 1993, **115**, 7918.
2 A. S. Boutorine, H. Tokuyama, M. Takasugi, H. Isobe, E. Nakamura and C. Hélène, *Angew. Chem., Int. Ed. Engl.*, 1994, **33**, 2462.
3 S. H. Friedman, D. L. DeCaamp, R. P. Sijbesma, G. Srdanov, F. Wudl and G. L. Kenyon, *J. Am. Chem. Soc.*, 1993, **115**, 6506; P. Rajagopalan, F. Wudl, R. F. Schinazi and F. D. Boudinot, *Antimicrob. Agents Chemother.*, 1996, **40**, 2262.
4 T. Andersson, K. Nilsson, M. Sundahl, G.Westman and O. Wennerström, *J. Chem. Soc., Chem. Commun.*, 1992, 604.
5 H. Hungerbühler, D. M. Guldi and K.-D. Asmus, *J. Am. Chem. Soc.*, 1993, **115**, 3386.
6 Y. N. Yamakoshi, T. Yagami, K. Fuhuhara, S. Sueyoshi and N. Miyata, *J. Chem. Soc., Chem. Commun.*, 1994, 517.
7 R. Sijbesma, G. Srdanov, F. Wudl, J. A. Castoro, C. Wilkins, S. H. Friedman, D. L. DeCamp and G. L. Kenyon, *J. Am. Chem. Soc.*,1993, **115**, 6510.
8 Y. Ohsawa and T. Saji, *J. Chem. Soc., Chem. Commun.*, 1992, 781.
9 A. Szücs, A. Loix, J. B. Nagy and L. Lamberts, *J. Electroanal. Chem.*, 1995, **397**, 191; J. J. Davis, H. A. O. Hill, A. Kurz, A. D. Leighton and A. Y. Safronov, *J. Electroanal. Chem.*, 1997, **429**, 7.
10 P. Boulas, W. Kutner, M. T. Jones and K. M. Kadish, *J. Phys. Chem.*, 1994, **98**, 1282.
11 X. Wei, M. Wu, L. Qi and Z. Xu, *J. Chem. Soc., Perkin. Trans. 2*, 1997, 1389.
12 T. J. White, N. Arnheim and H. A. Ehrlich, *Trends Genet.*, 1989, **15**, 185.
13 M. van de Kamp, F. C. Hali, N. Rosato, A Finazzi-Agrò and G. W. Canters, *Biochim. Biophys. Acta*, 1990, **1019**, 283.
14 M. Prato, M. Maggini, C. Giacometti, G. Scorrano, G. Sandonà and G. Farnia, *Tetrahedron*, 1996, **52**, 5221.

Received in Cambridge, UK, 7th November 1997; 7/08026C

Separation of carbon nanotubes by size exclusion chromatography

G. S. Duesberg,* M. Burghard, J. Muster, G. Philipp and S. Roth

Max-Planck-Institut für Festkörperforschung, Heisenbergstr. 1, D-70569 Stuttgart and EU TMR network Namitech, Germany and University of Dublin, Trinity College, Physics Department, Dublin 2, Ireland

Size exclusion chromatography has been performed on micellar aqueous dispersions of soot from an arc discharge experiment to yield chemically unmodified, almost impurity free and size separated multiwall nanotubes.

Several large-scale synthesis routes for carbon nanotubes (NTs) have been reported,[1–3] however, they lead to by-products of other carbon species. In addition to multiwall NTs the soot of a conventional arc discharge experiment contains fullerenes, carbon polyhedra, and amorphous carbon, which are interconnected in a dense network. For a number of proposed applications of NTs, which include field emission[4] and electronic devices,[5,6] their purification and size separation is of great importance.

In destructive methods, like oxidation, the soot material is purified by decomposition of the small particles while some tubes remain. However, the caps of the tubes are opened and chemical functionalities are introduced on the tube surface.[7,8] In addition, no size separation of the tubes can be accomplished by these methods.

Non-destructive methods like filtering or flocculation have been reported but their efficiency is limited,[9,10] and especially in filtration techniques blocking of pores is a severe problem.

Here, we report the purification and size separation of multiwall NTs by size exclusion chromatography (SEC), which is a multistep process using a stationary phase with defined pore sizes. SEC is a powerful tool for the separation of large molecules, *e.g.* biological macromolecules or virus particles.[11]

A dispersion of multiwall NTs in water was prepared with the aid of sodium dodecyl sulfate (SDS). Through the action of the surfactant the carbon particles were incorporated into micelles.[10] 10 mg of the raw soot from a conventional arc discharge experiment was added to 2 ml of a 1 mass% aqueous SDS solution and sonicated for 5 min with an ultrasonic tip. After a settling time of 15 min a black supernatant was obtained, leaving a sediment of some undispersed aggregates. The colloidal dispersion was stable for days and was used directly for chromatography.

Two successive columns were used for the fractionation. The purpose of the first column was to remove the gross of small particles and fullerenes. The packing (7 × 2 cm) consisted of controlled pore glass (CPG) with an average pore size of 140 nm (CPG 1400 Å, Fluka). This material is characterized by a narrow pore size distribution and is chemically inert. The column was loaded with 1.5 ml of the supernatant and eluted with a 0.25 mass% aqueous SDS solution buffered at pH 7. The flow rate was adjusted to 9 ml h^{-1}. After a void volume of 16 ml, two fractions of 6 ml were collected. The first fraction was concentrated to 1.5 ml by addition of 100 mg of polyacrylamide adsorbent gel (Fluka) followed by continuous shaking for 30 min. No darkening of the gel was observed, indicating that this technique allows the concentration of aqueous NT dispersions without an apparent loss of material.

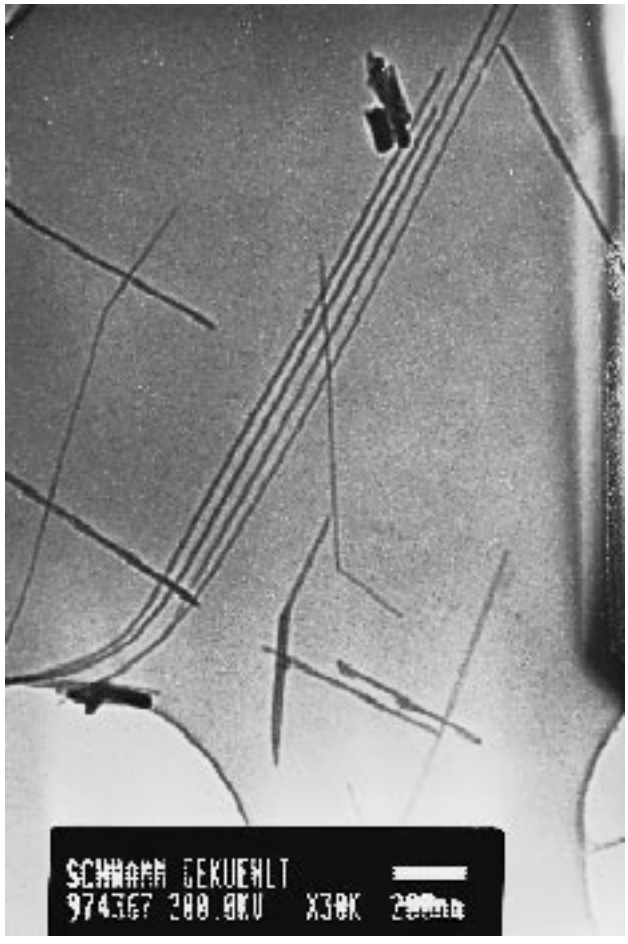

Fig. 1 Transmission electron micrograph of fraction 3: multiwall nanotubes purified by size exclusion chromatography

Fig. 2 Scanning electron micrograph of purified carbon nanotubes adsorbed on a chemically modified Si wafer

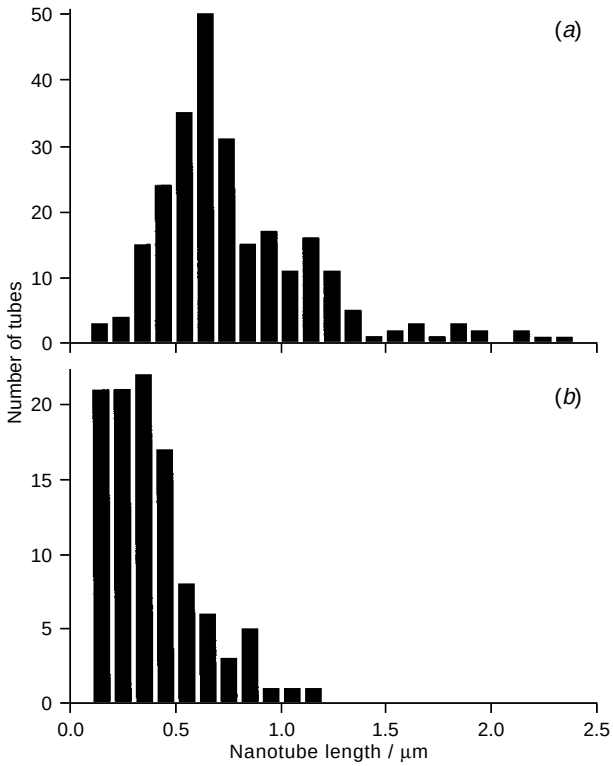

Fig. 3 Histograms of nanotube lengths in the third fraction (*a*) and sixth fraction (*b*)

The concentrated first fraction was loaded into the second column (33 × 1 cm) filled with CPG with an average pore size of 300 nm (CPG 3000 Å, Fluka). The same eluent as before was used with a flow rate of 5 ml h^{-1}. After a void volume of 16 ml, eight fractions of 1.5 ml were collected.

The fractions were characterised by transmission and scanning electron microscopy (TEM/SEM) as well as atomic force microscopy (AFM). For the TEM investigations, the carbon grids were treated with a fraction for 15 min and then rinsed briefly with water. Fig. 1 shows a typical TEM micrograph of the third fraction. Individual NTs are clearly recognized, demonstrating that the network of the soot was successfully disintegrated by the surfactant. Furthermore, scarcely any small spherical particles were observed in this fraction, revealing successful purification of the NTs.

For the determination of NT sizes in the different fractions, the NTs were adsorbed onto chemically modified Si wafers. The wafers were silanized for 30 min in an aqueous solution of 3-aminopropyltriethoxylsilane (2.5 mM), and then treated with the NT dispersion for 30 min. After drying, they were immersed in water for 1 min to remove the surfactant. The adsorbed NTs were investigated by SEM and AFM, which revealed that the surfactant was removed from the surface by the washing step.

In the first fraction from the second column (fraction 1), aggregates of NTs and other carbon species were found while fractions 7 and 8 contained mainly spherical particles and a few short tubes, both < 0.1 μm. Fractions 2–6 consisted of individual nanotubes and, for the later fractions, a low content of spherical particles. Fig. 2 presents a representative SEM image of the third fraction. It shows individual NTs, mainly with a length of *ca.* 1 μm.

A statistical evaluation of the size distribution was performed using the NT lengths determined from a number of SEM and AFM images. The histograms of fraction 3 and 6 are shown in Fig. 3(*a*) and (*b*), respectively. There is a significant difference in the length distribution of the NTs: the average NT length in fraction 3 was calculated to be 0.8 μm and in fraction 6 to be 0.4 μm.

In conclusion, the chromatographic technique presented is an effective, non-destructive method for purification and size separation of carbon NTs. This type of chromatography should also be applicable to micellar dispersions of single wall NTs. This work is now in progress. In addition, the method can easily be scaled up and by the use of more sophisticated chromatographic systems, *e.g.* HPLC, the size separation could be improved.

Supported by EU TMR network Namitech.

Notes and References

* E-mail: duesberg@klizix.mpi-stuttgart.mpg.de

1 T. W. Ebbesen and P. M. Ajayan, *Nature*, 1992, **358**, 220.
2 A. Thess, H. Dai and R. Smalley, *Science*, 1996, **273**, 483.
3 K. Hernadi, A. Fonseca, J. B. Nagy, D. Bernaerts, J. Riga and A. Lucas, *Synth. Met.*, 1996, **77**, 31.
4 W. A. de Heer, J.-M. Bonard, K. Fauth, A. Chatelain, L. Forro and D. Ugarte, *Adv. Mater.*, 1997, **9**, 87.
5 L. Chico, V. H. Crespi, L. X. Benedict, S. G. Louie and M. L. Cohen, *Phys. Rev. Lett.*, 1996, **76**, 971.
6 S. Saito, *Science*, 1997, **278**, 77.
7 H. Hiuara, T. W. Ebbesen and K. Tanigaki, *Adv. Mater.*, 1995, **7**, 275.
8 T. W. Ebbesen, P. M. Ajayan, H. Hiura and T. Tanigaki, *Nature*, 1994, **367**, 519.
9 W. A. de Heer, W. S. Bacsa, A. Chatelain, T. Gerfin, R. Humphrey-Baker, L. Forro and D. Ugarte, *Science*, 1995, **268**, 845.
10 J.-M. Bonard, T. Stora, J.-P. Salvetat, F. Maier, T. Stöckli, C. Duschl, L. Forro, W. A. de Heer and A. Chatelain, *Adv. Mater.*, 1997, **9**, 827.
11 *Handbook of Size Exclusion Chromatography*, ed. C.-S. Wu, Marcel Dekker, 1995.

Received in Cambridge, UK, 16th October 1997; 7/07465D

The structures of premithramycinone and demethylpremithramycinone, plausible early intermediates of the aureolic acid group antibiotic mithramycin

Jürgen Rohr,*[a]†‡ Ulrike Weißbach,[a] Claus Beninga,[a] Eva Künzel,[a] Karsten Siems,[b] Kai U. Bindseil,[b] Felipe Lombó,[c] Laura Prado,[c] Alfredo F. Braña,[c] Carmen Méndez[c] and Jose A. Salas[c]

[a] *Institut für Organische Chemie der Universität, Tammannstr. 2, D-37077 Göttingen, Germany*
[b] *AnalytiCon AG, Bereich Wirkstoffe, Hermannswerder Haus 17, D-14473 Potsdam, Germany*
[c] *Departamento de Biología Funcional e Instituto Universitario de Biotecnología de Asturias, Universidad de Oviedo, Julian Claveria S/N, E-33006 Oviedo, Spain*

The structures of premithramycinone and its demethyl analogue suggest that the aureolic acid antibiotics are biosynthetically formed *via* a tetracycline-type, and not a tetracenomycin-type, folded decaketide.

Mithramycin[1] **1** (aureolic acid, plicamycin, mithracin, LA-7017 *etc*.[2]) and related aureolic acid group antibiotics, such as the chromomycins, olivomycins and UCH9, are important anticancer agents, effective against various experimental and human tumours.[1–6] Mithramycin in particular has been clinically used for the treatment of certain tumours as well as for Paget's bone disease.[7,8] For its mechanism of action, a Mg^{2+} dimer complex binding to GC-rich DNA regions has been investigated.[9]

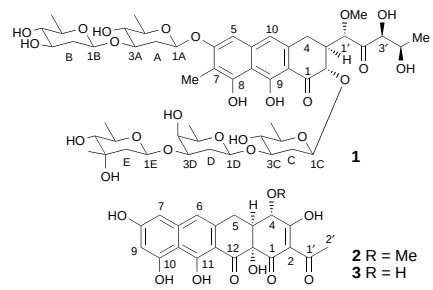

Incorporation experiments on chromomycin A_3 with various single and double ^{13}C labelled acetates by Montanari and Rosazza revealed that all carbon atoms of the aglycon moiety of the aureolic acid group antibiotics are acetate, *i.e.* polyketide, derived.[10] Because of the unexpected incorporation pattern, hypotheses were raised in which two or three independent acetate chains are condensed to form the aglycon.[10] Recent molecular biology experiments[11,12] confirmed our earlier hypothesis[13] that the entire aglycon backbone of such compounds derives from a single decaketide chain. To explain Rosazza's acetate incorporation pattern, a tetracenomycin-type intermediate was suggested.[11–13] Therefore, the aureolic acid group was proposed to be biosynthetically closely related to the tetracenomycins. The tetracenomycins, produced by *Streptomyces glaucescens*, are unique among the polycyclic aromatic polyketides insofar as the formation of their tetracyclic ring skeleton requires a folding of the hypothetical decaketide intermediate leading to a first cyclization between carbons 9/14, instead of the more typical first cyclization between carbons 7/12 which is found, *e.g.* for anthracyclines, angucyclines and tetracyclines.[13–15]

Premithramycinone **2** and its demethyl analogue **3** (in smaller amounts) are accumulated by the disrupted M7D1 mutant of *Streptomyces argillaceus* ATCC 12956, which is a mithramycin producer. In the mutant M7D1 the *mtmD* gene encoding a glucose-1-phosphate : thymidylyl transferase[16,17] was inactivated through the insertion of an apramycin resistance cassette into a unique *Bam*Hl site of this gene and through gene replacement of the wild type region of the chromosome by the *in vitro* mutated one.[16] Glucose-1-phosphate : TTP thymidylyl transferase is a key enzyme of the deoxysugar biosynthesis. As a consequence, no sugar substrates for the glycosyl transfer steps in the mithramycin biosynthesis can be provided, and an aglycon substrate can be expected to be accumulated in such a mutant strain, as was discussed previously.[16] However, a wrong structure was initially suggested for premithramycinone.

The (revised) structures of **2** and **3** were determined on various physicochemical data, in particular on one- and two-dimensional ^1H and ^{13}C NMR spectra (Tables 1 and 2, Fig. 1).[18] Fig. 1 shows the $^nJ_{C,H}$ couplings (n = 2,3; HMBC) found for **2** (for **3** analogously), including the key couplings supporting these structures *vs*. the formerly suggested premithramycinone structure which can be observed between 2′-CH_3/1′-C=O and 2′-CH_3/C-2. The stereochemistry shown in **2** and **3** is suggested taking into consideration the observed H,H and C,H couplings

Table 1 ^1H NMR data (MeOH) for **2** and **3**

	δ (multiplicity, *J*/Hz)	
Proton	**2**[a]	**3**[b]
4-H	4.00 (br d, 11)	4.00 (br d, 11)
4-OCH_3	3.54 (br s)	—
4a-H	2.68 (ddd, 11, 4.5, 3)	2.50 (m)
5-H_a	3.48 (ddd, 16.5, 4.5, 1.5)	3.46 (br d, 16)
5-H_e	3.10 (dd, 16.5, 3)	3.19 (br d, 16)
6-H	6.93 (dd, 1.5, 0.5)	6.89 (s)
7-H	6.54 (dd, 2.5, 0.5)	6.52 (d, 2)
8-H	6.36 (d, 2.5)	6.33 (d, 2)
2′-H_3	2.63 (s)	2.65 (s)

[a] 300 MHz. [b] 400 MHz.

Table 2 ^{13}C NMR data (MeOH) **2** and **3**, multiplicities from APT and C,H COSY experiments

	δ (multiplicity)			δ (multiplicity)	
Carbon	**2**[a]	**3**[b]	Carbon	**2**[a]	**3**[b]
C-1	196.4 (s)[c]	196.7 (s)[c]	C-9	102.9 (d)	102.8 (d)
C-2	112.2 (s)	111.6 (s)	C-10	161.2 (s)	161.0 (s)
C-3	167.8 (s)[c]	167.4 (s)[c]	C-10a	108.1 (s)	108.1 (s)
C-4	78.7 (d)	70.0 (d)	C-11	164.0 (s)[c]	163.8 (s)[c]
C-4a	45.5 (d)	46.6 (d)	C-11a	108.1 (s)	107.9 (s)
C-5	27.0 (t)	26.7 (t)	C-12	197.4 (s)[c]	197.6 (s)[c]
C-5a	135.7 (s)	135.5 (s)	C-12a	80.0 (s)	78.9 (s)
C-6	118.8 (d)	119.0 (d)	C-1′	202.0 (s)	203.6 (s)
C-6a	143.4 (s)	143.3 (s)	C-2′	30.7 (q)	30.7 (q)
C-7	103.7 (d)	103.6 (d)	OCH_3	61.6 (q)	—
C-8	164.0 (s)	163.9 (s)			

[a] 125.7 MHz. [b] 100.6 MHz. [c] Interchangeable due to tautomerisation.

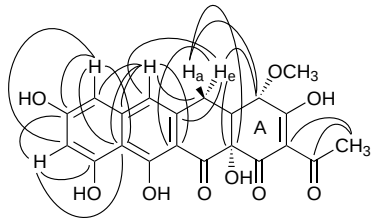

Fig. 1 $^{2,3}J_{C,H}$ Couplings observed in the HMBC spectra of **2** and **3**. Several theoretical couplings in ring A are not detectable due to tautomerisation

(Table 1, Fig. 1) and the given stereochemistry of **1** along with the conversion mechanism involving a Baeyer–Villiger type oxidation (Scheme 1). The structures **2** and **3** resemble certain tetracyclines, *e.g.* the aglycon moiety of chromocyclomycin,[19] BMS-192548 and others.[20]

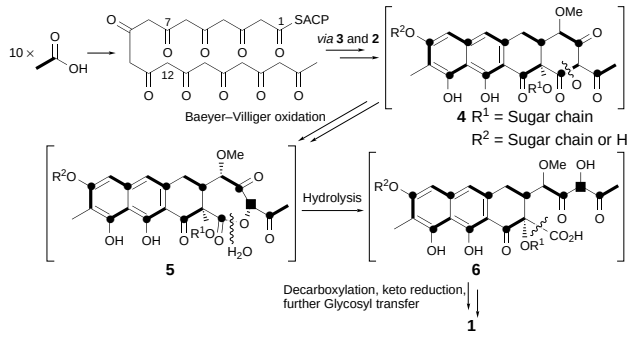

Scheme 1

Thus, **2** is plausibly the substrate for the first glycosyl transfer reaction, and its glycosylated derivative[21] is likely to be the substrate for an enzyme responsible for a C–C bond scission leading to the typical tricyclic aureolic acid chromophore. For this cleavage reaction, we suggest here also[22] a Baeyer–Villiger type oxidation of **4** leading to the ε-lactone containing intermediate **5**. Its subsequent hydrolysis to **6** along with a decarboxylation reaction and eventual further glycosylation reaction leads to **1**. As an alternative, a retro-aldol-type cleavage and a subsequent oxidation of the resulting side chain (Scheme 2) may also be taken into consideration.[23] Both mechanistic sequences (Schemes 1 and 2) are also in agreement with Rosazza's and our own ^{13}C labelled acetate incorporation pattern.[10,24]

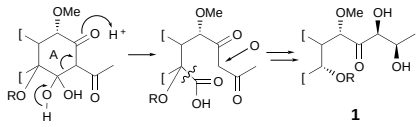

Scheme 2

The studies described here show the (presumably oxidative) C–C bond cleavage of a tetracyclic compound to be the biosynthetic key step leading to the aglycon skeleton of the aureolic acid group antibiotics, as was suggested earlier.[11–13] However, the tetracyclic compounds **2** and **3**, which are presumably biosynthetic intermediates of mithramycin, are structurally related to the tetracyclines, and not to the tetracenomycins. Thus, a tetracycline-type folding (Scheme 1) rather than a tetracenomycin-type folding and a standard first cyclase reaction between carbons 7/12 of the hypothetical decaketide intermediate (Scheme 1) is also true in the biosynthetic formation of the aureolic acid antibiotics, and all former hypotheses involving a tetracenomycin-type intermediate[12–15] have to be corrected, including the previously suggested wrong structure for premithramycinone.[16]

The authors thank the European Community (BIO4-CT96-0068), the Fonds der Chemischen Industrie, the Deutsche Forschungsgemeinschaft (SFB 416), the Deutsche Akademische Austauschdienst (314-Al-e-dr) and Plan Nacional en Biotecnología (BIO94-0037) for generous financial support of this cooperation project on antitumour agents, and R. Machinek, Institut für Organische Chemie, Universität Göttingen, Germany, for excellent NMR spectra. Both referees are acknowledged for their constructive suggestions.

Notes and References

† E-mail: rohrj@musc.edu

‡ *Current address:* Medical University of South Carolina, Department of Pharmaceutical Sciences, 171 Ashley Avenue, Charleston, SC 29425-2303, USA.

1 The structure elucidation on mithramycin by Thiem *et al*. (ref. 4), lead to a different sequence of the sugar moieties. We reinvestigated the structure of the mithramycin, produced by *S. argillaceus* ATCC 12956, because of contradictions to the compounds found in our glycosyltransferase inhibition studies (ref. 21). The structure of mithramycin, produced by *S. argillaceus*, is definitely **1**: E. Künzel, S.-E. Wohlert, R. Machinek, C. Méndez, J. A. Salas and J. Rohr, *J. Org. Chem.*, submitted.

2 *The Merck Index*, ed. S. Budavari, M. J. O'Neil, A. Smith, P. E. Heckelman and J. F. Kinneary, Merck & Co., Whitehouse Station, NJ, 12th edn., number 7696, 1996, pp. 1298–1299.

3 J. D. Skarbek and M. K. Speedie, in *Antitumor Compounds of Natural Origin*, ed. A. Aszalos, CRC Press, Boca Raton, FL, 1981, vol. 1, pp. 191–235.

4 J. Thiem, G. Schneider and V. Sinnwell, *Liebigs Ann. Chem.*, 1986, 814 and references cited therein.

5 W. A. Remers, in *The Chemistry of Antitumor Antibiotics*, Wiley-Interscience, New York, 1979, vol. 1, pp. 133–175.

6 H. Nakano, H. Ogawa, Y. Yamashita, R. Katahira, S. Chiba, T. Iwasaki and T. Ashizawa, WO 95 06054, *JP Appl.* 93/211572, 2.5. 1995 (*Chem. Abstr.*, 1995, 123, 8030p).

7 B. J. Kennedy, J. W. Yarbo, V. Kickertz and M. Sandberg Wollheim, *Cancer Res.*, 1968, **28**, 91.

8 E. G. Elias and J. T. Evans, *J. Bone Jt. Surg., Am. Vol.*, 1972, **54-A**, 1730.

9 M. Sastry and D. J. Patel, *Biochemistry*, 1993, **32**, 6588.

10 A. Montanari and J. P. N. Rosazza, *J. Antibiot.*, 1990, **43**, 883.

11 G. Blanco, H. Fu, C. Mendez, C. Khosla and J. A. Salax, *Chem. Biol.*, 1996, **3**, 193.

12 E. Künzel, S.-E. Wohlert, C. Beninga, S. Haag, H. Decker, C. R. Hutchinson, G. Blanco, C. Mendez, J. A. Salas and J. Rohr, *Chem. Eur. J.*, 1997, **3**, 1675.

13 J. Rohr, *J. Org. Chem.*, 1992, **57**, 5217.

14 B. Shen, R. G. Summers, E. Wendt-Pienkowski and C. R. Hutchinson, *J. Am. Chem. Soc.*, 1995, **117**, 6811.

15 P. J. Kramer, R. J. X. Zawada, R. McDaniel, C. R. Hutchinson, D. A. Hopwood and C. Khosla, *J. Am. Chem. Soc.*, 1997, **119**, 635.

16 F. Lombó, K. Siems, A. F. Brana, C. Méndez, K. Bindseil and J. A. Salas, *J. Bacteriol.*, 1997, **179**, 3354.

17 F. Lombó, G. Blanco, E. Fernández, C. Mendez and J. A. Salas, *Gene*, 1996, **172**, 87.

18 *Selected data* for **2**: *m/z* (EI-MS) 414 (M^+, 64%), 258 (100), 241 (25), 229 (22), 216 (20), 156 (72); λ(MeOH)/nm (ε) 230 (27 400), 276 (49 700), 323 (7700), 411 (13 100); λ_{extr}(MeOH)/nm (θ) 232 (−15 400), 284 (158 000), 412 (−23 800); ν_{max}(KBr)/cm^{-1} 3408, 2923, 1672, 1636, 1449, 1401, 1343, 1161, 1096, 1013, 996, 873, 743, 609. For **3**: *m/z* (EI-MS) 400 (M^+, 8%), 259 (61), 241 (48), 230 (100), 133 (90).

19 Yu. A. Berlin, M. N. Kolosov, I. V. Vasina and I. V. Yartseva, *J. Chem. Soc., Chem. Commun.*, 1968, 762.

20 Y.-Z. Shu, J. Q. Cutrone, S. E. Klohr and S. Huang, *J. Antibiot.*, 1995, **48**, 1060.

21 Inactivation of a mithramycin-glycosyltransferase gene in the mithramycin producer *S. argillaceus* resulted in four different glycosylated compounds containing one, two or all three sugars of the mithramycin trisaccharide chain, and premithramycinone (for one monosaccharide) and its 9-methyl analogue (for the other mono-, di- and tri-saccharide), respectively, as aglycon moiety: E. Fernández, A. F. Braña, C. Méndez, J. A. Salas, U. Weißbach and J. Rohr, unpublished results.

22 M. Gerlitz, G. Udvarnoki and J. Rohr, *Angew. Chem., Int. Ed. Engl.*, 1995, **34**, 1617.

23 This mechanistically interesting alternative to the Baeyer–Villiger oxidation was suggested by one of the referees.

24 Routine feeding experiments on *S. argillaceus* using [1-^{13}C]- and [2-^{13}C]-acetate resulted in an incorporation pattern in mithramycin identical to that found earlier in chromomycin A_3 (ref. 10).

Received in Glasgow, UK, 15th October 1997; 7/07446H

Structure and molecular magnetism of the rutile-related compounds $M(dca)_2$, M = Co^{II}, Ni^{II}, Cu^{II}, dca = dicyanamide, $N(CN)_2^-$

Stuart R. Batten,[a,b] Paul Jensen,[b] Boujemaa Moubaraki,[b] Keith S. Murray*[b] and Richard Robson*[a]

[a] *School of Chemistry, University of Melbourne, Parkville, Victoria 3052, Australia*
[b] *Department of Chemistry, Monash University, Clayton, Victoria 3168, Australia*

The isomorphous rutile-related network structures of $Co(dca)_2$, $Ni(dca)_2$ and $Cu(dca)_2$, dca = dicyanamide, $N(CN)_2^-$, are shown to behave as ferromagnets (T_c = 9 and 20 K) and a near-paramagnet, respectively.

The deliberate design and construction of coordination polymers with predetermined topology is an area of much current interest.[1–3] A number of new compounds with interesting properties such as high porosity and catalytic activity has been made following these principles. Here, we describe a series of such compounds which display unusual magnetic properties, including long-range ferromagnetic ordering. A number of existing coordination polymers are already known to display unusual magnetic properties. For instance, $(rad)_2Mn_2[Cu(opba)]_3(Me_2SO)_2{\cdot}2H_2O$, opba = *o*-phenylenebis(oxamato), rad^+ = 2-(4-*N*-methylpyridinium)-4,4,5,5-tetramethylimidazoline-1-oxyl-3-oxide consists of two sets of 2D hexagonal sheets of $Mn_2[Cu(opba)]_3^{2-}$ which interpenetrate each other at an angle of 72.7°.[4] Rad^+ cations connect the sheets, and the solid behaves as a magnet below 22.5 K. The magnetic properties of a large number of bimetallic oxalate structures, $AMM'(ox)_3$ ($A^+ = NR_4^+$), which have a hexagonal sheet structure, have also been studied recently.[5] There is a great need to explore bridging groups other than these N,O-bonded oxamides and O-bonded oxalates.

The results described herein form part of a study we are undertaking on the binary structures of metal–pseudohalide compounds. The structures of $M(tcm)_2$, tcm = tricyanomethanide, $C(CN)_3^-$, M = Cr^{II}, Mn^{II}, Fe^{II}, Co^{II}, Ni^{II}, Cu^{II}, Zn^{II}, Cd^{II}, Hg^{II}, consist of two interpenetrating rutile nets,[6] and have been found to display weak antiferromagnetic coupling.[7] The structures and novel magnetochemistry of the binary metal complexes of dicyanamide, dca, $N(CN)_2^-$, are now described.

dca =

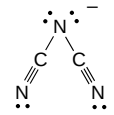

Following the method of Köhler,[8] combination of aqueous solutions of cobalt nitrate, nickel nitrate or copper nitrate with aqueous solutions of sodium dicyanamide results in small pink rods of $Co(dca)_2$, a blue microcrystalline powder of $Ni(dca)_2$, and green rods of $Cu(dca)_2$, respectively. As in Köhler's original work, there is evidence from IR and microanalytical data† for a small amount of water in $Ni(dca)_2$ even when we prepared it from $Ni(NO_3)_2{\cdot}6H_2O$ in MeCN using $[N(PPh_3)_2](dca)$.

The structure of $Cu(dca)_2$ was determined by single crystal X-ray crystallography.‡ It was found to consist of a single rutile-related network (Fig. 1). Each dca is coordinated to three metal atoms *via* the two nitrile nitrogens and the central amido nitrogen. Each copper in turn is coordinated to six dca ligands, four *via* the nitrile nitrogens and two *via* the amido nitrogens. The copper shows considerable Jahn–Teller distortion, with the two axial amido nitrogens considerably further from the copper [2.478(2) Å] than the four equatorial nitrile nitrogens [1.975(1) Å]. There is evidence of π–π interactions between pairs of dca ligands across the square channels seen in Fig. 1, with the closest interactions being N_{amido}–N_{amido} 3.463 Å, C–C 3.513 Å and N_{amido}–C 3.603 Å. The distortions in the framework seen in Fig. 1 may maximise these interactions. The structures of polycrystalline $Co(dca)_2$ and $Ni(dca)_2$ have been shown by X-ray powder diffraction to be isomorphous with $Cu(dca)_2$,§ but with a few very small peaks not indexing and not present in the XRD of $Cu(dca)_2$.

It is interesting to compare the structures of $M(dca)_2$ and $M(tcm)_2$. In both cases the networks have a rutile-like topology with six-connected metal centres and three-connected ligands. In $M(tcm)_2$, all three connections between the trigonal centres and the octahedral centres of the rutile networks are C–CN–M (*ca.* 4.50–4.99 Å), and the structures are composed of two interpenetrating networks. The interpenetration produces a tightly packed structure in which each of the nets is considerably distorted to accommodate the other. In $M(dca)_2$, two of these connections are N–CN–M (4.368 Å), which are comparable with those in $M(tcm)_2$. The third connection between trigonal and octahedral nodes, however, is a direct N–M bond [2.478(2) Å], and there is no longer enough room within the structure for a second rutile-related net to be accommodated. Indeed, the packing efficiency of $Cu(dca)_2$ is very similar to that of $Cu(tcm)_2$ (D_c = 2.01 and 1.918 g cm^{-3}, volume/atom = 14.7 and 14.1 $Å^3$, respectively.)

While Hvastijova *et al.*[9] have made many studies of the magnetism of chain-like compounds of type $M(tcm)_2L_2$ and $M(dca)_2L_2$, where L = pyridine, imidazole, pyrazole, there have been no detailed studies until now on the parent

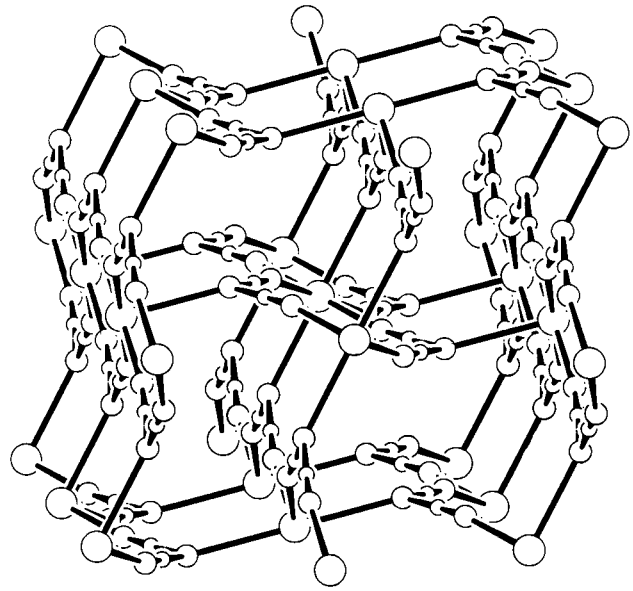

Fig. 1 The rutile-related structure of $Cu(dca)_2$. The circles represent in order of decreasing size Cu, N and C.

compounds. We find that $Cu(dca)_2$ shows near-Curie behaviour in a field of 1 T (C = 0.438 cm^3 K mol^{-1}, θ = −1.8 K) indicative of extremely weak antiferromagnetic coupling. The μ_{eff} values decrease a little from 1.87 μ_B at 300 K to 1.77 μ_B at 4.2 K. Magnetization studies in a field of 5 Oe show that long-range ordering is not occurring above 2 K. Chain-like $Cu^{II}(dca)_2L_2$ adducts also display very weak coupling and long-range ordering at low temperautres has occasionally been claimed but without proof.[9]

In contrast, the $Co(dca)_2$ and $Ni(dca)_2$ samples both display well behaved long-range ferromagnetic ordering with T_c values, respectively, of 9 and 20 K. The first evidence of ferromagnetism is given in the Curie–Weiss susceptibility plots obtained in fields of 1 T. Positive Weiss constants are noted with best-fit parameters of C = 2.074, θ = +6.1 K (Co) and C = 1.086, θ = +21.4 K (Ni). In small applied fields of 5 Oe, the χT values increase sharply at T_c reaching values much higher than anticipated for short-range order. Plots of field-cooled (FCM), zero-field cooled (ZFCM) and remanent magnetization (RM), shown in Fig. 2 for $Ni(dca)_2$, are typical of those expected for a magnetically ordered system.[10] The very sharp increase in the magnetization isotherms at small field values, followed by a gradual increase towards a saturation magnetization value of $2N\mu_B$ [for $Ni(dca)_2$] in high fields (Fig. 2), lends further support for a ferromagnetic phase transition. Hysteresis loops are observed with the value of the coercive field for $Ni(dca)_2$ being 191 Oe.

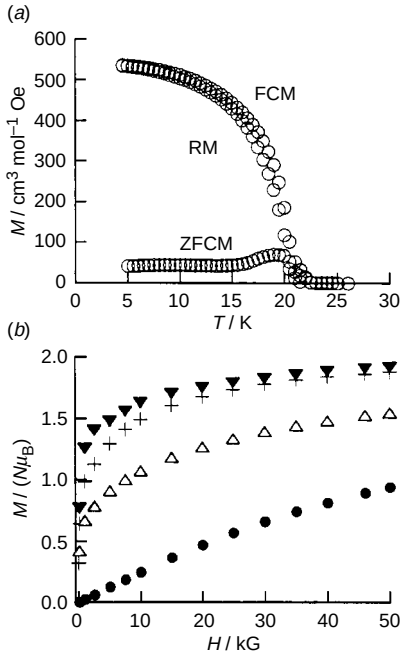

Fig. 2 (*a*) Plots of field-cooled (FCM), zero field-cooled (ZFCM) and remanent magnetization (RM) *vs.* temperature for $Ni(dca)_2{\cdot}xH_2O$ and (*b*) plots of magnetization, M (in units $N\mu_B$) *vs.* applied field at various temperatures for $Ni(dca)_2{\cdot}xH_2O$: (●) 30 K, (△) 20 K, (+) 10 K, (▼) 5 K

The origin of ferromagnetic ordering in the Co^{II} and Ni^{II} dca compounds and the lack thereof in the structurally characterized Cu^{II} species is intriguing and is being vigorously pursued. If we assume that the majority *Pnnm* phase in all three samples (*vide supra*) is responsible for the magnetic behaviour then Jahn–Teller distortions in $Cu(dca)_2$, along the Cu–N(amido) links, may prevent magnetic interactions between $Cu(dca)_2$ chains in the crystal, while such interchain interactions can occur in the Co and Ni derivatives. This contrasts with the situation in one of the few know homometallic ferromagnetic systems $(NH_3R)_2[MX_4]$, (Mn^{II} = Cu, Cr; X = Cl, Br), in which Jahn–Teller elongated M–X bonds within metal–halide layers are orthogonal from one MX_6 octahedron to the next,[10,11] thus giving the required orthogonality of neighbouring magnetic orbitals. Orthogonality relationships are not obvious from Fig. 1 but presumably must involve the M–N≡C–N–M pathways otherwise $Cu(dca)_2$ should behave likewise. In conclusion, it is clear that some of these d-blocks pseudohalide species provide new and fascinating examples of molecular magnets.

This work was supported by grants (to K. S. M. and R. R.) from the Australian Research Council.

Notes and References

* E-mail: Keith.S.Murray@sci.monash.edu.au

† Analyses: $Cu(dca)_2$. Found: C, 24.9; H, 0; N, 43.1. Calc. C, 24.6; H, 0; N,43.0%. $Ni(dca)_2{\cdot}0.5H_2O$. Found: C, 24.1; H < 0.2; N, 41.9. Calc C, 24.0; H, 0.5; N, 42.0%. ν(OH) 3400 cm^{-1} (br), δ(OH) 1636 cm^{-1}. $Co(dca)_2$. Found: C, 25.2; H, 0; N, 44.2. Calc. C, 25.1; H, 0; N, 44.0%.

‡ *Crystal data* for $Cu(dca)_2$: C_4CuN_6, M = 195.63, orthorhombic, space group *Pnnm* (no. 58), a = 7.340(1), b = 6.1218(8), c = 7.1815(6) Å, U = 322.69(7) Å^3, T = 293 K, Z = 2, F(000) = 190, D_c = 2.013 g cm^{-3}, μ(Mo-Kα) = 3.312 mm^{-1}, $2\theta_{max}$ = 37.5°. A green rod (0.09 × 0.09 × 0.4 mm). Absorption corrections applied (T_{min} 0.9639, T_{max} 0.9817). 1426 total reflections, 905 independent reflections (R_{int} = 0.0579), of which 765 were observed [$I > 2\sigma(I)$]. At final convergence R_1 [$I > 2\sigma(I)$] = 0.0260, wR_2 (all data) = 0.0802 for 29 parameters, S = 1.162. CCDC 182/723.

§ Common space group *Pnnm*: $Co(dca)_2$: a = 7.301(7), b = 6.014(4), c = 7.073(5) Å; $Ni(dca)_2$: a = 7.294(2), b = 6.024(4), c = 7.023(2) Å; $Cu(dca)_2$: a = 7.352(2), b = 6.126(1), c = 7.180(1) Å.

1 R. Robson, B. F. Abrahams, S. R. Batten, R. W. Gable, B. F. Hoskins and J. Liu, *Supramolecular Architecture*, ed. T. Bein, *ACS Symp. Ser. 499*, Washington, DC, 1992, ch. 19.
2 B. F. Abrahams, S. R. Batten, H. Hamit, B. F. Hoskins and R. Robson, *Angew. Chem., Int. Ed. Engl.*, 1996, **35**, 1691; B. F. Hoskins, R. Robson and D. A. Slizys, *J. Am. Chem. Soc.*, 1997, **119**, 2952; B. F. Abrahams, S. J. Egan, B. F. Hoskins and R. Robson, *Chem. Commun.*, 1996, 1099.
3 C. L. Bowes and G. A. Ozin, *Adv. Mater.*, 1996, **8**, 13; M. J. Zaworotko, *Coord. Chem. Rev.*, 1994, 283; M. Bertelli, L. Carlucci, G. Ciani, D. M. Proserpio and A. Sironi, *J. Mater. Chem.*, 1997, **7**, 1271; K. A. Hirsch, S. R. Wilson and J. S. Moore, *Inorg. Chem.*, 1997, **36**, 2960; O. M. Yaghi, C. E. Davis, G. Li and H. Li, *J. Am. Chem. Soc.*, 1997, **119**, 2861.
4 H. O. Stumpf, L. Ouahab, Y. Pei, D. Grandjean and O. Kahn, *Science*, 1993, **261**, 447; H. O. Stumpf, L. Ouahab, Y. Pei, P. Bergerat and O. Kahn, *J. Am. Chem. Soc.*, 1994, **116**, 3866.
5 P. Day, *J. Chem. Soc., Dalton Trans.*, 1997, 701; H. Tamaki, Z. J. Zhong, N. Matsumoto, S. Kida, M. Koikawa, N. Achiwa, Y. Hashimoto and H. Okawa, *J. Am. Chem. Soc.*, 1992, **114**, 6974; S. Decurtins, H. W. Schmalle, H. R. Oswald, A. Linden, J. Ensling, P. Gutlich and A. Hauser, *Inorg. Chim. Acta*, 1994, **216**, 65; L. O. Atovmyan, G. V. Shilov, N. S. Ovanesyan, A. A. Pyalling, R. N. Lyubovskaya, E. I. Zhilyaeva and Y. G. Morozov, *Synth. Met.*, 1995, **71**, 1809.
6 S. R. Batten, B. F. Hoskins and R. Robson, *J. Chem. Soc., Chem. Commun.*, 1991, 445; S. R. Batten, B. F. Hoskins and R. Robson, unpublished work.
7 S. R. Batten, B. Moubaraki, K. S. Murray and R. Robson, unpublished work.
8 H. Köhler, *Z. Anorg. Allg. Chem.*, 1964, **331**, 237.
9 M. Hvastijova, J. Kozisek, J. Kohout, L. Jäger and H. Fuess, *Transition Met. Chem.*, 1995, **20**, 276; M. Hvastijova, J. Kohout, J. Mrozinski and L. Jäger, *Pol. J. Chem.*, 1995, **69**, 852.
10 O. Kahn, *Molecular Magnetism*, VCH, New York, 1994, ch. 12, p. 287; *Adv. Inorg. Chem.*, 1995, **43**, 179.
11 P. Day, *Chem. Soc. Rev.*, 1993, 51 and references therein.

Received in Columbia, MO, USA, 7th October 1997; 7/07264C

ChemComm
FEATURE ARTICLE

Neutral anion receptors: design and application

Martijn M. G. Antonisse and David N. Reinhoudt*†

Department of Supramolecular Chemistry and Technology, MESA Research Institute, University of Twente, PO Box 217, 7500 AE Enschede, Netherlands

After the development of synthetic cation receptors in the late 1960s, only in the past decade has work started on the development of synthetic neutral anion receptors. Combination and preorganization of different anion binding groups, like amides, urea moieties, or Lewis acidic metal centers lead to receptor molecules that strongly bind inorganic anions with high selectivity. Combined with neutral cation ligands, ditopic receptors were obtained for the complexation of inorganic salts. The molecular complexation properties of anion receptors has been transduced into macroscopic properties in membrane separation processes and in sensors for selective anion detection.

Introduction

Host–guest systems for ionic species have played an important role in the development of the field of supramolecular chemistry, the chemistry of the non-covalent interactions. The research of Pedersen in 1967 on the complexation of alkali metal ions by crown ethers initiated the development of many other neutral host species for metal ions.[1,2] Compared with the cation receptors, anion receptors were developed much later, although already in 1968 the first synthetic receptor for inorganic anions was reported[3] (size selective binding of Cl^- anions was described with diprotonated 1,11-diazabicyclo-[9.9.9]nonacosane **1**). The field started to develop in 1976 when Graf and Lehn reported that *protonated* cryptate **2** encapsulates F^-, Br^- and Cl^- anions.[4] Since then several other *positively charged* anion receptors have been developed that have protonated nitrogen atoms or metal ions.[5] In these receptors mainly coulomb interactions contribute to the attractive force.

In Nature, the transport of sulfate or phosphate anions through cell membranes is regulated by *neutral* anion binding proteins.[6] The high specificity is due to a recognition site in which the anion is completely desolvated and bound exclusively *via* hydrogen bonds. Furthermore, a so-called macrodipole effect, caused by orientation of the amino terminus of the protein backbones towards the negative guest, contributes to the stability of the complex.[7] This article will focus on the recent developments in the design of synthetic *neutral* receptors for inorganic anions. The individual interactions in these receptors are weaker than coulomb interactions and strongly depend on the directionality of the interaction and on the electron density of the anion. Nevertheless, combination and preorganization of several binding sites can lead to selective neutral receptors for anions.

The neutral anion binding receptors can be divided into two classes: receptors that bind anions exclusively by hydrogen bonding or ion–dipole interactions, and receptors that coordinate anions at the Lewis acidic centers of a neutral organometallic ligand. The corresponding ditopic receptors that are formed by the combination of neutral anion and cation receptor sites are included in the second part of this review. Finally some applications of anion receptors in anion transport and sensing will be discussed.

Anion recognition by hydrogen bonding

In an attempt to mimic nature in its high binding selectivity, several anion receptors have been developed with three-dimensional arrangements of hydrogen bond donating moieties, like amides, sulfonamides, and (thio)ureas. Receptor **3**, which has three amido substituents connected *via* a tris(aminoethyl)amine spacer, binds $H_2PO_4^-$ with an association constant of 6100 M^{-1} in MeCN.[8] The increased electrophilicity of the sulfonamide NH moieties in **4**, in combination with preorganization of the binding site by Π-stacking, enhances the $H_2PO_4^-$ binding with **4** ($K_a = 1.4 \times 10^4$ M^{-1}) and results in an almost 400-fold selectivity over HSO_4^-. The tris(aminoethyl)amine spacer was also used to preorganize urea moieties (receptor **5**).[9] This receptor strongly binds PO_4^{3-} ($K_a = 1.4 \times 10^4$ M^{-1} in [$^2H_6$]DMSO) and SO_4^{2-} ($K_a = 3 \times 10^3$ M^{-1}). Reduction of the rotational freedom of the urea substituents with the *cis*-1,3,5-tris(aminomethyl)cyclohexane spacer lowers the PO_4^{3-} association to 1100 M^{-1}. Recently Umezawa and coworkers reported bis(*N*′-phenylthioureylene)xanthene **6**.[10] The rigid spacer prevents the self-association of the urea substituents

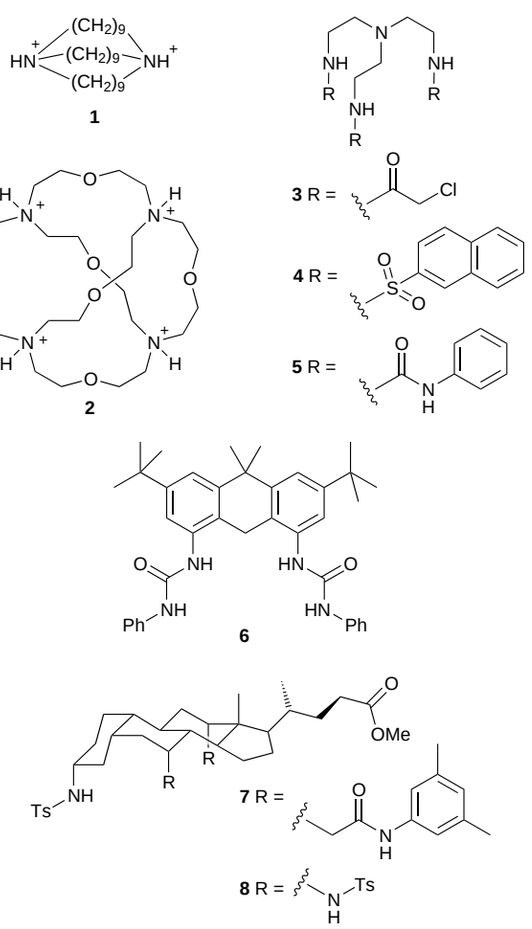

and consequently the association constant for $H_2PO_4^-$ is very high. The value of 1.95×10^5 M^{-1} in [$^2H_6$]DMSO was obtained from an NMR titration experiment in competition with 10 equiv. of Cl^- (K_a = 1000 M^{-1}). Davis and co-workers have utilized cholic acid as a building block for neutral anion receptors.[11] Bis-carbamate **7** preferentially binds F^- over other halides, but does not discriminate between chloride or bromide. Functionalization of cholic acid with sulfonamido moieties (**8**) yields a receptor that binds the more basic chloride more strongly than bromide (K_a = 92 000 and 9200 M^{-1}, respectively, in $CDCl_3$).

Calixarenes are versatile building blocks that have been used in the design of many cation receptors.[12] Hydrogen bond donating substituents at either the *upper* or *lower* rim yield receptor molecules suitable for anion binding. Functionalization of a calix[4]arene with upper rim sulfonamido substituents leads to a three-dimensional cavity (receptor **9**) which complexes

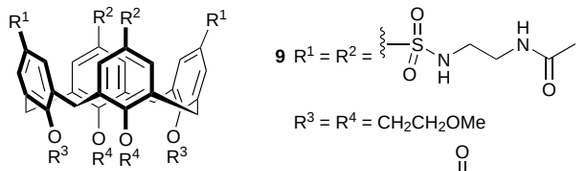

9 $R^1 = R^2 =$

$R^3 = R^4 = CH_2CH_2OMe$

10 R^1 = H, $R^2 =$

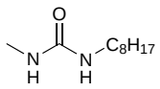

$R^3 = R^4 = CH_2CO_2Et$

11 $R^1 = R^2 = Bu^t$,
$R^3 = R^4 = (CH_2)_4NHC(O)NHPh$

12 $R^1 = R^2 = Bu^t$,
R^3 = Pr, $R^4 = (CH_2)_4NHC(O)NHPh$

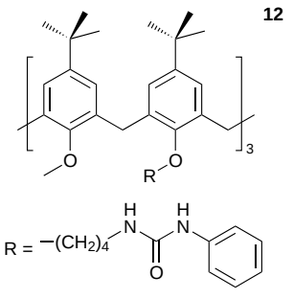

13

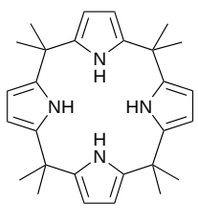

14

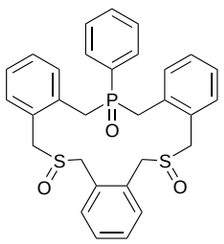

15

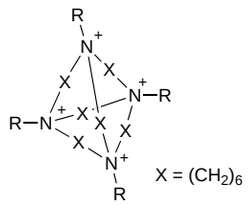

16 $R = BH_3^-$

17 R =

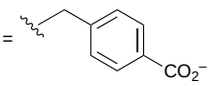

tetrahedral HSO_4^- better than spherical Cl^- or planar NO_3^-.[13] We also introduced octylurea moieties at the upper rim of a calix[4]arene tetra(ethyl ester) yielding calix[4]arene **10**. However, upon addition of Bu_4NCl or Bu_4NBr in $CDCl_3$ no complexation of halide anions was observed.[14] This is due to the strong intramolecular hydrogen bonding between the diametrically positioned urea moieties, stabilizing **10** in a pinched cone conformation.[15] This conformation is stable up to at least 120 °C in $C_2D_2Cl_4$. In contrast to the upper rim functionalized derivatives, calix[4]arenes functionalized at the lower rim with urea substituents bind specifically halide anions. The tetrakis(phenylurea) derivative **11** binds Cl^- and Br^- ions in $CDCl_3$ with association constants of 2015 and 1225 M^{-1}, respectively.[16] The very strong hydrogen bond acceptors F^- and $H_2PO_4^-$ are not bound by **11**. Although bidentate phenylurea derivative **12** has only four hydrogen bond donor sites, the association constants are significantly higher than with **11** and the selectivity for Cl^- over Br^- is enhanced (K_a = 7105 and 2555 M^{-1}, respectively). The extent of inter- and intramolecular hydrogen bond formation is much lower in **12** than in the tetrakis(phenylurea) derivative **11**, favouring the complexation of anions. The larger binding cavity in tris(phenylurea) calix[6]arene derivative **13** reverses the selectivity and Br^- binding is favoured over Cl^-.[17] Beer *et al.* covalently linked the upper and lower rim of two calix[4]arenes with hydrogen bond donating amide bonds.[18] The resulting cavity is too small for encapsulation of $H_2PO_4^-$ or HSO_4^-, but Cl^- and F^- are bound, favouring F^- with one order of magnitude.

Recently, Sessler and co-workers reported the anion binding ability of calixpyrroles.[19] These *meso*-substituted porphyrinogens are, unlike porphyrinogens with *meso*-hydrogen atoms, stable towards auto-oxidation, and can adopt cone and 1,3-alternate conformations like calix[4]arenes. Crystal structures show that calix[4]pyrrole **14** is fixed in a cone conformation upon Cl^- or F^- binding. The receptor preferentially binds F^- (K_a = 1.7 $\times 10^4$ M^{-1} in CD_2Cl_2) over Cl^- (K_a = 350 M^{-1}) or Br^- (K_a = 10 M^{-1}). Substitution of **14** with electron-withdrawing bromine atoms increases the anion binding (K_a = 2.7 $\times 10^4$ M^{-1} and 4.3 $\times 10^3$ M^{-1} for F^- and Cl^-, respectively).

Phosphine oxide disulfoxide **15** binds halide ions ($Cl^- \approx Br^- > I^- > F^-$) *via* ion–dipole interactions.[20] The association with Cl^-, Br^- (both K_a = 65 M^{-1}) and I^- (K_a = 40 M^{-1}) was investigated by NMR titration in 2 vol% CD_3OD in $CDCl_3$. A similar experiment with F^- induced only small shifts. Also the macrotricyclic borane–amine adduct **16** encapsulates anions driven by ion–dipole interactions.[21] All four borane–amine bonds are in a fixed orientation with the positive ends pointing to the center of the cavity. The small Cl^- and CN^- anions can easily enter the cavity with only a little conformational adaptation of the host. Optimal association was observed for Br^-. Zwitterionic macrotricycle **17** is able to recognize anions in water.[21b] Halides are complexed in a 1 : 1 stoichiometry with association constants from 270 M^{-1} for Cl^- to 6480 M^{-1} for I^-.

Anion recognition with organometallic ligands

Several Lewis acidic atoms have been investigated for binding of anions. In particular, group 14 metals have been used extensively in macrocyclic organometallic anion receptors. 12-Silacrown-3 **18** preferentially binds Cl^- over all other halides in bulk liquid membrane transport experiments.[22] Takeuchi and co-workers investigated several organogermanium macrocycles (receptor **19**) as carrier in bulk liquid membranes.[23] The Lewis acidity of bis-methyl or bis-phenyl substituted germanium was too low for anion transport. The enhanced acidity of methyl(chloro)germanium results in effective Cl^- binding, and transports Cl^- with selectivity over Br^-. Methyl(bromo)-bis(chloro)- and bis(bromo)-germanium are unsuitable due to easy decomposition by hydrolysis. The halide substituted tin centers at the bridgehead position of macrobicycle **20** coordinate with encapsulated Cl^- or Br^-.[24] Optimal selectivity in the case of Cl^- is obtained with eight methylene units between the tin centers; for Br^- a larger cavity is necessary (10 methylene units).

Mercury has also been used for the design of Cl^- receptors. Two phenylene-1,2-dimercury dichloride molecules coordinate with an additional Cl^- anion in the electrophilic cavity that is formed by the four C–Hg–Cl arms.[25] Hawthorne and Zheng studied the anion recognition of carborane-supported multidentate mercury hosts.[26] Cl^- can coordinate with the four mercury atoms in the preorganized cavity of mercuracarborand **21**. Iodide anions are bound in a 1 : 2 host–guest stoichiometry with the I^- ions slightly above and below the plane formed by the mercury atoms.

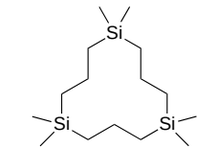

18

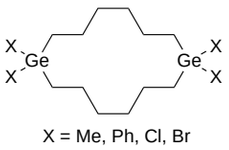

X = Me, Ph, Cl, Br

19

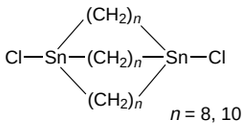

n = 8, 10

20

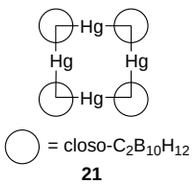

= closo-$C_2B_{10}H_{12}$

21

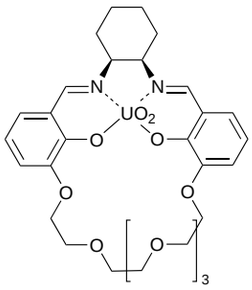

22

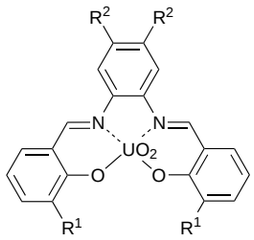

23 $R^1 = R^2 = H$
24 $R^1 = OMe$, $R^2 = H$
25 $R^1 = H$, $R^2 = OC_{12}H_{25}$
26 $R^1 = OMe$, $R^2 = OC_{12}H_{25}$

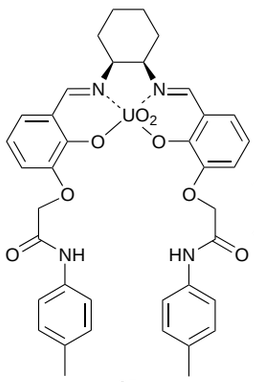

27

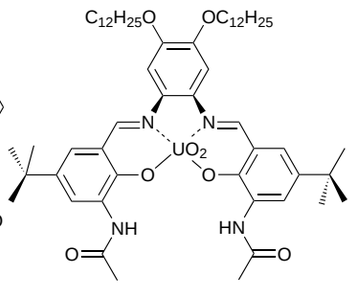

28

Katz developed F^- receptors with Lewis acidic boron centers.[27] Both naphthalene-1,8-diylbis(dimethylborane) and (8-trimethylsilyl)-1-naphthyl(dimethylborane) coordinate the anion between the two electron accepting atoms. The boron atom of ferroceneboronic acid binds F^- with an association constant of 1000 M^{-1} (in MeOH–H_2O 1 : 9).[28] The association is reflected in a strong decay in the absorbance at 665 nm. Other ions, like Cl^- or Br^-, hardly affect the absorbance.

In our group we have developed neutral anion receptors based on an immobilized uranyl cation. Complexed in a salophen unit the uranyl cation prefers a pentagonal bipyramidal coordination, with the two oxygen atoms at the apical positions and four of the equatorial positions occupied by the salophen ligand. The fifth equatorial position can coordinate to nucleophilic guest species. This can either be a nucleophilic moiety (*e.g.* C=O or S=O) of a neutral molecule,[29] as we illustrated with the transport of urea with carrier **22** through supported liquid membranes,[30] or anionic species.[31,32] Uranyl salophen **23** binds $H_2PO_4^-$ more strongly than Cl^- (K_a = 1.5 × 10^4 and 4.0 × 10^2 M^{-1} in MeCN–DMSO 99 : 1), which is in accordance with the principle that the hard Lewis acidic uranyl cation favours interactions with hard Lewis basic anions. The advantage of our system is that additional hydrogen bond binding sites can be introduced close to the uranyl center and this makes it possible to improve or change the selectivity in anion binding. Hydrogen bond accepting methoxy substituents (**24**) enhance the $H_2PO_4^-$ over Cl^- selectivity. The crystal structure of the $H_2PO_4^-$ complex of **24** (Fig. 1) clearly shows the additional hydrogen bond between the anion and the methoxy oxygen atom. Salophen **27**, with *N*-(4-methylphenyl)acetamide moieties, has both hydrogen bond accepting ether oxygens and hydrogen bond donating amide functions. This salophen binds $H_2PO_4^-$ by coordination at the uranyl center and three hydrogen bonds. These additional interactions are reflected in the increased association constant for $H_2PO_4^-$ (K_a > 5 × 10^5 M^{-1}). Recently we have synthesized uranyl salophen **28** with hydrogen bond *donating* acetamido moieties close to the uranyl coordination site. The resulting F^- binding is reflected in the selectivity of sensors based on this receptor. According to ^1H NMR titrations in $CDCl_3$ a 2 : 1 host–guest complex is formed in which the fluoride anion is hydrogen bonded to the amide moieties and coordinated to the uranyl centers.

Ditopic receptors, combined recognition of anions and cations

The new neutral anion receptors opened the way for neutral *ditopic* receptors that complex *both* anions and cations. Anion binding, based on hydrogen bonds or coordination to Lewis acids, has been combined with cation binding, *e.g.* crown ethers or calix[4]arene derivatives. We combined the anion binding uranyl salophen building block with several cation ligands. Ditopic receptor **29** binds K^+ between the crown ether substituents, while the uranyl center can coordinate with phosphate.[33] The binding was investigated by ^1H NMR spectroscopy, cyclic voltammetry and fast atom bombardment mass spectroscopy (FAB-MS). The spectra of the latter technique show intense peaks for [**29** + K^+]$^+$ and [**29** + $H_2PO_4^-$]$^-$, while the signal of [**29** + K^+ + $H_2PO_4^-$]$^-$ is also present, which clearly proves the complexation of the salt. In the ditopic receptor **30** a Cs^+ selective 1,3-alternate calix[4]arene crown-6 is combined with a uranyl salophen and this receptor complexes CsCl.[34] Furthermore, the Na^+ selective calix[4]arene tetra(ethyl ester) was linked at the upper rim *via* amide bonds to a uranyl salophen unit.[35] FAB-MS spectra of the NaH_2PO_4 complex of this receptor show intense signals for the receptor + Na^+ and for the receptor + $H_2PO_4^-$.

Also Reetz and co-workers combined Lewis acidic centers with a cation binding crown ether. Boronic acid crown ether derivative **31** forms a ditopic complex with KF when the receptor is added to a suspension of the salt in CH_2Cl_2.[36] Other potassium salts (KBr or KCl) do not exhibit either monotopic or hetrotopic interactions. This selectivity is also observed in

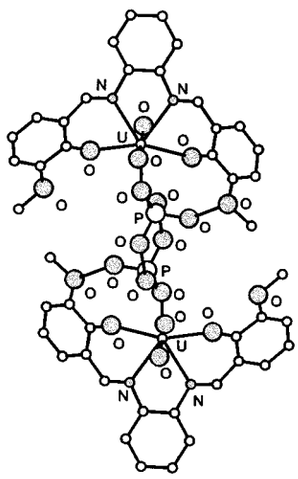

Fig. 1 Crystal structure of the complex **24**·H_2PO_4. Hydrogen atoms are omitted for clarity.

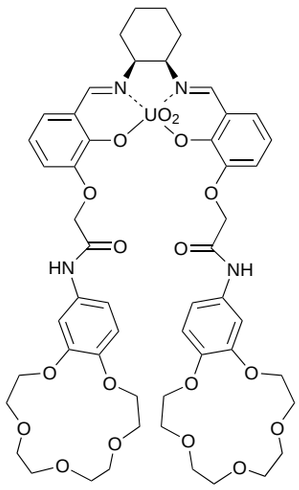

29

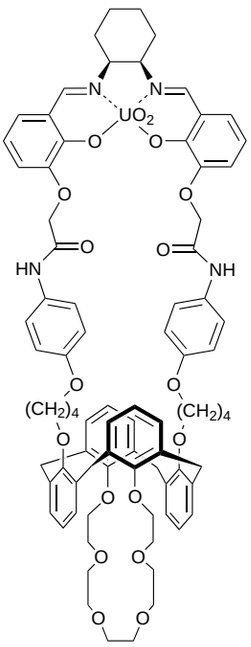

30

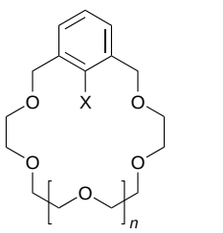

31 n = 2, X = 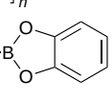

32 n = 1, X = $OAlMe_2$

competition experiments, as in a mixture of KF, KCl, KBr and KI, the KF adduct of **31** is exclusively formed. With aluminium phenolate as the Lewis acid (receptor **32**) the selectivity is reversed. With the Li^+ or K^+ salts of F^- no binding is observed, whereas Cl^-, Br^-, or I^- salts all show ditopic binding. Shinkai and co-workers combined a calix[4]arene with a neutral anion binding porphyrin–Zn^{2+} complex (receptor **33**).[37] The two building blocks are covalently linked *via* lower rim amido substituents. The cation (*e.g.* Na^+ or K^+) is coordinated by the four $OCH_2C(O)NH$ linkages and a cavity is formed between the two metal ions. In the case of the K^+ complex strong I^- complexation is observed. For the Na^+ complex the association constant for encapsulation of I^- is lower. This is due to the different electron accepting character of Na^+ and the larger distance between the Zn^{2+} and Na^+ ion. Anion binding porphyrin **34** and cation binding calix[4]arene **35** form a bifunctional receptor by self-assembly.[38] The hydrogen bonds between the diaminopyridine and thymine moieties brings the two recognition sites into close proximity. When no cation is bound in the cavity formed by the ethyl ester moieties, the diaminopyridine fragment interacts with these substituents *via* hydrogen bonding and cannot form the aggregate with the thymine units. Sodium complexation of **35** initiates the self-assembly as it coordinates with the ethyl ester carbonyl oxygen atoms. The self-assembly of the bifunctional receptor enhances the binding of the investigated anion (SCN^-) to the porphyrin. The association constant of the self-assembled complex (**34**·SCN^-)(**35**·Na^+) is 2.5×10^4 M^{-1} in toluene, and is very different from that for free **34** which binds SCN^- only weakly (K_a = 10 M^{-1}).

When we investigated anion binding *via* hydrogen bonds with the above mentioned urea-functionalized calix[4]arene **10** it was observed that cation complexation is essential for anion complexation (positive heterotropic allostery). The tetra ester functionalized lower rim of **10** is a ligand that is highly selective

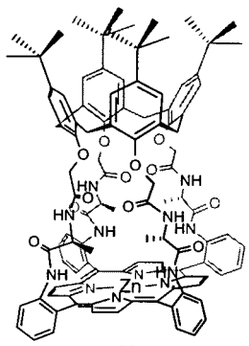

33

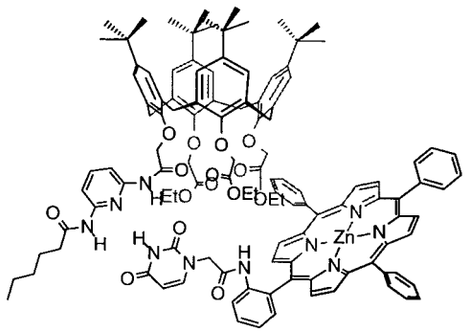

34•35

for Na^+.[39] Upon complexation of Na^+, the conformation of the calix[4]arene is converted from a pinched cone to a symmetrical cone.[14] In this conformation intramolecular hydrogen bonding is not possible and the urea moieties become available for hydrogen bonding to anions. The Na^+ complex of **10** prefers Cl^- binding over the 'softer' Br^- anion. Calix[4]arene **10** is capable of solubilizing simple alkali salts in $CHCl_3$. The selectivity of the cation binding part of the receptor is expressed by the relative amount of Cl^- alkali salt complex that is transferred in liquid–solid extractions. NaCl results in 100% of [Na^+·Cl^-·**10**] complex, but with KCl only partial complexation is observed (29%). No complexation of CsCl is observed, apparently because Cs^+ is too large to fit in the cavity. Beer *et al.* reported NMR studies with the K^+ or NH_4^+ complex of calix[4]arene **36**.[40] K^+ or NH_4^+ form a sandwich complex with the bis(crown ether), rigidifying the hydrogen-bonding arrangement of the two amides and the two phenolic protons in a pseudo-tetrahedral cavity in which Cl^- or HSO_4^- is bound.

Anion transport and sensing

Supramolecular chemistry has always been associated with possible applications. As in the case of cation receptors, anion receptors are now applied as the selector element in separation membranes[41] and in ion-selective electrodes.[42] Recently we have studied anion transport through supported liquid membranes (SLMs). The pores of a microporous film are filled with a solution of anion receptor in *o*-nitrophenyl octyl ether and the film is placed between two aqueous phases: a source phase with the anion to be transported and a receiving phase. The transport of KH_2PO_4 is facilitated by a 1 : 1 mixture of anion receptor **36** and the K^+ selective calix[4]arene crown-5.[43] Salt transport solely by the cation receptor is very low (0.6×10^{-8} mol m^{-2} s^{-1}) due to the low partition of $H_2PO_4^-$. Transport of KH_2PO_4 by **37** alone increases the transport (5.1×10^{-8} mol m^{-2} s^{-1}), but the flux is much larger using a mixture of cation and anion receptor (12.5×10^{-8} mol m^{-2} s^{-1}). A transport selectivity for $H_2PO_4^-$ over Cl^- of 143 for the combination of the cation carrier and **36** is observed. Bifunctional receptor **29** transports CsCl and the flux has been compared with the transport of $CsNO_3$.[34] The interactions of *both* the anion and the cation of CsCl with **29** is reflected in a higher transport rate for CsCl than

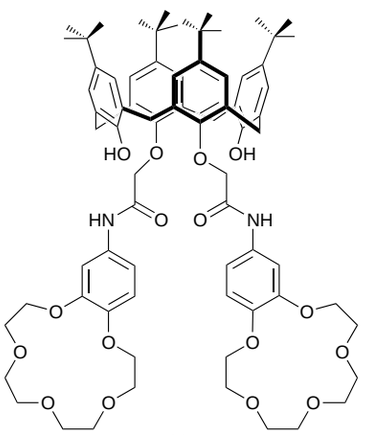

36

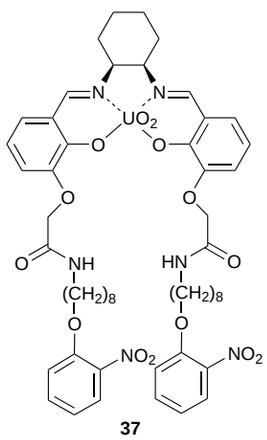

37

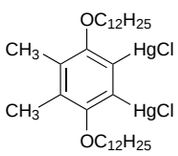

38

for $CsNO_3$. Tsukube *et al.* applied neutral tris(β-ketonate) lanthanide complexes as anion carriers in bulk liquid membrane transport experiments.[44] The transport of Cl^- is more efficient than that of the more lipophilic Br^- I^- or ClO_4^-.

In potentiometric sensors, *e.g.* ion-selective electrodes (ISEs) or chemically modified field effect transistors (CHEMFETs[45]), the molecular interaction between the receptor and the ionic species can be converted into an electronic signal. Most anion receptors applied in potentiometric sensors are organometallic molecules, but recently Umezawa and co-workers reported the application of **6** as a sensor selector.[46] Remarkably, $H_2PO_4^-$ could not be detected as would be expected based on the association constants; instead a moderate Cl^- sensor was obtained. The potentiometric selectivity coefficient *vs.* Br^- ($\log K^{Pot}_{Cl,Br} = 0.4$) reflects almost equal sensitivity for Cl^- and Br^-. Simon and co-workers developed chloride selective electrodes with organometallic trialkyltin derivatives as the neutral anion receptor.[47] With di- or tetra-dentate organotin derivatives the selectivity favours the binding of $H_2PO_4^-$.[48] The sensors show selectivity over the very lipophilic anions, *e.g.* SCN^- and ClO_4^-. Sensors with a high chloride selectivity are based on lipophilic *ortho*-dimercury aromatic compounds like **38**.[49] Chloride is preferred over other halides, as expressed by the potentiometric selectivity coefficients *vs.* I^-, Br^- and F^- of respectively −1.7, −1.4 and −6.6 ($\log K^{Pot}_{Cl,j}$).

Recently in our group we investigated uranyl salophen derivatives as anion receptors in CHEMFETs that are selective for hydrophilic anions.[32,50] For this purpose novel derivatives were synthesized with lipophilic substituents to enhance the solubility in the membrane matrix. The high association constants of uranyl salophen derivatives for $H_2PO_4^-$ could be transduced into sensors with high sensitivity and selectivity for this anion. Application of uranyl salophen **25**, the lipophilic equivalent of **23**, results in sensors that start to respond to $H_2PO_4^-$ at activities $\geqslant 6 \times 10^{-4}$ M. Even in the presence of the more lipophilic NO_3^- anion the sensor is twenty times more sensitive for $H_2PO_4^-$ ($\log K^{Pot}_{H_2PO_4,NO_3} = -1.3$). The introduction of hydrogen bond donating methoxy substituents (receptor **26**) increases the $H_2PO_4^-$ binding and consequently an improved detection limit of 1.6×10^{-4} M is obtained. Also the selectivity in the presence of halides and SO_4^{2-} is further enhanced by a factor 3 to 10. Incorporation of salophen derivative **28** in the CHEMFET membrane gives excellent F^- sensitivity and selectivity. The strong binding of the hydrophilic F^- anion in the small cleft is reflected by the hundred-fold or higher selectivity ($\log K^{Pot}_{F,j} \leqslant -2.0$) for fluoride over other halides, nitrate and sulfate. As shown in Fig. 2, even in the presence of a large excess of the very lipophilic ClO_4^- anion (0.1 M) it is possible to detect F^- at the (sub)millimolar level ($\log K^{Pot}_{F,ClO_4} = -1.7$).

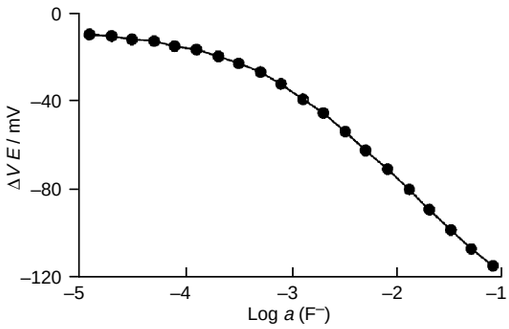

Fig. 2 Fluoride response of CHEMFET with receptor **28** in the presence of 0.1 M ClO_4^- (in 0.01 M MES buffer, pH 6.0)

Conclusions

This article illustrates that neutral anion receptors with high binding selectivity can be synthesized. The organometallic ligands show the highest association constants, but three-dimensional arrangements of hydrogen bond donating ligands are promising recent developments. The combination of anion receptors with cation receptors revealed interesting events like synergistic effects and (positive) heterotropic allostery.

Acknowledgments

We thank all our colleagues and co-workers, several of whose names appear in the references, for their valuable contributions to this work. The Netherlands Organization for Scientific Research (NWO) and the Technology Foundation (STW), Technical Science Branch of NWO are gratefully acknowledged for financial support.

David N. Reinhoudt was born in Wolfaartsdijk, The Netherlands. He received his MSc (1966) and PhD (1969) from Delft University of Technology. In 1970 he joined the Koninklijke/Shell Laboratories in Amsterdam as a research chemist in the Department of Organic Chemistry. In 1975 he was appointed as a part-time Professor (extraordinarius) in Organic Chemistry (now Supramolecular Chemistry and Technology) at the University of Twente, followed by a full-time appointment in 1978. His research deals with supramolecular chemistry, *e.g.* the synthesis of supramolecular building blocks such as crown ethers, calixarenes and (hemi)spherands, complexation studies with neutral and charged guests, and the technological application of the molecules in membrane transport, electronic or optical sensors, catalysis and molecular (NLO) materials.

Martijn M. G. Antonisse was born in Boskoop, The Netherlands. He received his MSc (1994) from the University of Twente and is currently a PhD student in the Department of Supramolecular Chemistry and Technology at the University of Twente. He is involved in the development of novel anion

receptors and their application in durable potentiometric sensors (CHEMFETs).

Notes and References

† E-mail: d.n. reinhoudt@ct.utwente.nl

1 C. J. Pedersen, *J. Am. Chem. Soc.*, 1967, **89**, 7017.
2 *Comprehensive Supramolecular Chemistry*, ed. J. L. Atwood, J. E. D. Davies, D. D. MacNicol, F. Vögtle, J.-M. Lehn and G. W. Gokel, Elevier Science, Oxford, 1996, vol. 1.
3 C. H. Park and H. E. Simmons, *J. Am. Chem. Soc.*, 1968, **90**, 2431.
4 E. Graf and J.-M. Lehn, *J. Am. Chem. Soc.*, 1976, **98**, 6403.
5 For recent reviews also dealing with charged anion receptors, see F. P. Schmidtchen and M. Berger, *Chem. Rev.*, 1997, **97**, 1609; J. L. Atwood, K. T. Holman and J. W. Steed, *Chem. Commun.*, 1996, 1401; J. Scheerder, J. F. J. Engbersen and D. N. Reinhoudt, *Recl. Trav. Chim. Pays-Bas*, 1996, **115**, 307; P. D. Beer, *Chem. Commun.*, 1996, 689; B. Dietrich, *Pure Appl. Chem.*, 1993, **65**, 1457.
6 J. J. He and F. A. Quiocho, *Science*, 1991, **251**, 1479; Z. F. Kanyo and D,. W. Christianson, *J. Biol. Chem.*, 1991, **266**, 4246; H. Luecke and F. A. Quiocho, *Nature*, 1990, **347**, 402.
7 J. W. Pflugrath and F. A. Quiocho, *J. Biol. Chem.*, 1988, **200**, 163.
8 S. Valiyaveettil, J. F. J. Engbersen, W. Verboom, and D. N. Reinhoudt, *Angew. Chem., Int. Ed. Engl.*, 1993, **32**, 900.
9 C. Raposo, M. Almaraz, M. Martin, V. Weinrich, L. Mussons, V. Alcazar, C. Caballero and J. R. Mosan, *Chem. Lett.*, 1995, 759.
10 P. Bühlmann, S. Nishizawa, K. P. Xiao and Y. Umezawa, *Tetrahedron*, 1997, **53**, 1647.
11 A. P. Davis, J. F. Gilmer and J. J. Perry, *Angew. Chem., Int. Ed. Engl.*, 1996, **35**, 1312; A. P. Davis, J. J. Perry and R. P. Williams, *J. Am. Chem. Soc.*, 1997, **119**, 1793
12 A. Ikeda and S. Shinkai, *Chem. Rev.*, 1997, **97**, 1713; V. Böhmer, *Angew. Chem., Int. Ed. Engl.*, 1995, **34**, 713; M. A. McKervey, M.-J. Schwing-Weill and F. Arnaud-Neu, *Cation Binding by Calixarenes*, in *Comprehensive Supramolecular Chemistry*, ed. J. L. Atwood, J. E. D. Davies, D. D. MacNicol, F. Vögtle, J.-M. Lehn and G. W. Gokel, Elevier Science, Oxford, 1996, vol. 1, ch. 15, pp. 537–603.
13 Y. Morzherin, D. M. Rudkevich, W. Verboom and D. N. Reinhoudt, *J. Org. Chem.*, 1993, **58**, 7602.
14 J. Scheerder, J. P. M. van Duynhoven, J. F. J. Engbersen and D. N. Reinhoudt, *Angew. Chem., Int. Ed. Engl.*, 1996, **35**, 1090.
15 J. Scheerder, R. H. Vreekamp, J. F. J. Engbersen, W. Verboom, J. P. M. van Duynhoven and D. N. Reinhoudt, *J. Org. Chem.*, 1996, **61**, 3476.
16 J. Scheerder, M. Fochi, J. F. J. Engbersen and D. N. Reinhoudt, *J. Org. Chem.*, 1994, **59**, 7815.
17 J. Scheerder, J. F. J. Engbersen, A. Casnati, R. Ungaro and D. N. Reinhoudt, *J. Org. Chem.*, 1995, **60**, 6448.
18 P. D. Beer, P. A. Gale and D. Hesek, *Tetrahedron Lett.*, 1995, **36**, 767.
19 P. A. Gale, J. L. Sessler, V. Král and V. Lynch, *J. Am. Chem. Soc.*, 1996, **118**, 5141; P. A. Gale, J. L. Sessler, W. E. Allen, N. A. Tvermoes and V. Lynch, *Chem. Commun.*, 1997, 665.
20 P. B. Savage, S. K. Holmgren and S. H. Gellman, *J. Am. Chem. Soc.*, 1994, **116**, 4069.
21 (*a*) K. Worm, F. D. Schmidtchen, A. Schier, A. Schäfer and M. Hesse, *Angew. Chem., Int. Ed. Engl.*, 1994, **33**, 327; (*b*) K. Worm and F. D. Schmidtchen, *Angew. Chem., Int. Ed. Engl.*, 1995, **34**, 65.
22 M. E. Jung and H. Xia, *Tetrahedron Lett.*, 1988, **29**, 297.
23 S. Aoyagi, K. Tanaka and Y. Takeachi, *J. Chem. Soc., Perkin Trans. 2*, 1994, 1549.
24 M. T. Blanda, J. H. Horner and M. Newcomb, *J. Org. Chem.*, 1989, **54**, 4626; M. Newcomb, J. H. Horner, M. T. Blanda and P. J. Squattrito, *J. Am. Chem. Soc.*, 1989, **111**, 6294.
25 A. L. Beauchamp, M. J. Olivier, J. D. Wuest and B. Zacharie, *J. Am. Chem. Soc.*, 1986, **108**, 73.
26 M. F. Hawthorne and Z. Zheng, *Acc. Chem. Res.*, 1997, **30**, 267 and references cited herein.
27 H. E. Katz, *J. Org. Chem.*, 1985, **50**, 5027; *J. Am. Chem. Soc.*, 1986, **108**, 7640.
28 C. Dusemund, K. R. A. Samankumara Sandanayake and S. Shinkai, *J. Chem. Soc., Chem. Commun.*, 1995, 333; H. Yamamoto, A. Ori, K. Ueda, C. Dusemund and S. Shinkai, *Chem. Commun.*, 1996, 407.
29 D. N. Reinhoudt, A. R. van Doorn and W. Verboom, *J. Coord. Chem.*, 1992, **27**, 91; C. J. van Staveren, D. E. Fenton, D. N. Reinhoudt, J. van Eerden and S. Harkema, *J. Am. Chem. Soc.*, 1987, **109**, 3456.
30 W. F. van Straaten-Nijenhuis, A. R. van Doorn, A. M. Reichwein, F. de Jong and D. N. Reinhoudt, *J. Org. Chem.*, 1993, **58**, 2265; W. F. Nijenhuis, A. R. van Doorn, A. M. Reichwein, F. de Jong and D. N. Reinhoudt, *J. Am. Chem. Soc.*, 1991, **113**, 3607.
31 D. M. Rudkevich, W. Verboom, Z. Brzozka, M. J. Palys, W. P. R. V. Stauthamer, G. J. van Hummel, S. M. Franken, S. Harkema, J. F. J. Engbersen and D. N. Reinhoudt, *J. Am. Chem. Soc.*, 1994, **116**, 4341.
32 M. M. G. Antonisse, B. H. M. Snellink-Ruël, I. Yigit, J. F. J. Engbersen and D. N. Reinhoudt, *J. Org. Chem.*, 1997, **62**, 9034.
33 D. M. Rudkevich, Z. Brzozka, M. Palys, H. C. Visser, W. Verboom and D. N. Reinhoudt, *Angew. Chem., Int. Ed. Engl.*, 1994, **33**, 467.
34 D. M. Rudkevich, J. D. Mercer-Chalmers, W. Verboom, R. Ungaro, F. De Jong and D. N. Reinhoudt, *J. Am. Chem. Soc.*, 1995, **117**, 6124.
35 D. M. Rudkevich, W. Verboom and D. N. Reinhoudt, *J. Org. Chem.*, 1994, **59**, 3683.
36 M. T. Reetz, C. M. Niemeyer and K. Harms, *Angew. Chem., Int. Ed. Engl.*, 1991, **30**, 1472; M. T. Reetz, B. M. Johnson and K. Harms, *Tetrahedron Lett.*, 1994, **35**, 2525.
37 T. Nagasaki, H. Fujishima, M. Takeuchi and S. Shinkai, *J. Chem. Soc., Perkin Trans. 1*, 1995, 1883.
38 D. M. Rudkevich, A. N. Shivanyuk, Z. Brzozka, W. Verboom and D. N. Reinhoudt, *Angew. Chem., Int. Ed. Engl.*, 1995, **34**, 2124.
39 F. Arnaud-Neu, E. M. Collins, M. Deasy, G. Ferguson, S. J. Harris, B. Kaitner, A. J. Lough, M. A. McKervey, E. Marques, B. L. Ruhl, M. J. Schwing-Weill and E. M. Seward, *J. Am. Chem. Soc.*, 1989, **111**, 8681.
40 P. D. Beer, M. G. B. Drew, R. J. Knubley and M. I. Ogden, *J. Chem. Soc. Dalton Trans.*, 1995, 3117.
41 H. C. Visser, D. N. Reinhoudt and F. De Jong, *Chem. Soc. Rev.*, 1994, 75.
42 D. N. Reinhoudt, *Recl. Trav. Chim. Pays-Bas*, 1996, **115**, 109.
43 H. C. Visser, D. M. Rudkevich, W. Verboom, F. De Jong and D. N. Reinhoudt, *J. Am. Chem. Soc.*, 1994, **116**, 11554.
44 H. Tsukube, J. Uenishi, H. Shiba and O. Yonemitsu, *J. Membrane Sci.*, 1996, **114**, 187.
45 CHEMFETs are silicon-based microsensors that can transduce the membrane potential of an ion selective membrane deposited on top of the semiconductor into an electronic signal.
46 K. P. Xiao, P. Buhlmann, S. Nishizawa, S. Amemiya and Y. Umezawa, *Anal. Chem.*, 1997, **69**, 1038.
47 U. Wuthier, H. V. Pham, E. Pretsch, D. Ammann, A. K. Beck, D. Seebach and W. Simon, *Helv. Chim. Acta*, 1985, **68**, 1822; U. Wuthier, H. V. Pham, R. Zünd, D. Welti, R. J. J. Funck, A. Bezegh, D. Ammann, E. Pretsch and W. Simon, *Anal. Chem.*, 1994, **56**, 535.
48 J. K. Tsagatakis, N. A. Chaniotakis and K. Jurkschat, *Helv. Chim. Acta*, 1994, **77**, 2191; N. A. Chaniotakis, K. Jurkschat and A. Ruhleman, *Anal. Chim. Acta*, 1993, **282**, 345.
49 M. Rothmaier, U. Schaller, W. E. Morf and E. Pretsch, *Anal. Chim. Acta*, 1996, **327**, 17; M. Rothmaier and W. Simon, *Anal. Chim. Acta*, 1993, **271**, 135.
50 M. M. G. Antonisse, B. H. M. Snellink-Ruël, J. F. J. Engbersen and D. N. Reinhoudt, submitted for publication.

7/07529D

Indium-mediated highly diastereoselective allenylation in aqueous medium: total synthesis of (+)-goniofufurone

Xiang-Hui Yi, Yue Meng and Chao-Jun Li*

Department of Chemistry, Tulane University, New Orleans, Louisiana 70118, USA

(+)-Goniofufurone was synthesized from D-glucurono-6,3-lactone *via* an indium-mediated highly regio- and diastereo-selective allenylation of carbonyl compounds in aqueous medium.

The Asian trees of the genus *Goniothalamus* have long been recognized as a potential source of chemotherapeutical agents. The extracts and leaves of *Goniothalamus* have traditionally been used for the treatment of edema and rheumatism,[1] a pain killer and a mosquito repellent,[2] as well as used as an abortifacient.[3] Recently, from the constituents of these plants, McLaughlin discovered a number of novel styryl lactones which were found to possess moderate to significant cytotoxicities against several human tumors. These findings have attracted considerable biological and synthetic attention to these styryl compounds. Among the key components in the extracts are (+)-goniofufurone **1**[4] and (+)-7-*epi*-goniofufurone **2**.[5] The

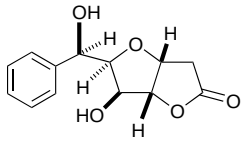

1 (+)-Goniofufurone

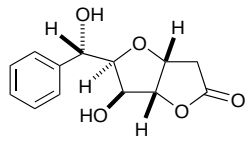

2 (+)-7-*epi*-Goniofufurone

absolute stereochemistry of (+)-goniofufurone was established by Shing through the total synthesis of *ent*-(−)-**1**.[6] Subsequently, several synthetic studies have been carried out on the synthesis of **1**.[7–13]

The recent advances in Barbier–Grignard type carbon–carbon bond formations in aqueous medium[14] offer opportunities to synthesize various heavily oxygenated biologically important agents in a concise manner. Out continued interest in metal mediated carbon–carbon bond formation in aqueous media, particularly the synthetic application of these reactions, drew our attention to these styryl compounds. Here we report a highly regio- and diastereo-selective indium-mediated allenylation[15,16] of carbonyl compounds in aqeuous medium, which leads to a concise total synthesis of (+)-goniofufurone from a readily available starting material. The retrosynthetic analysis of (+)-goniofufurone is illustrated in Scheme 1.

Initially, the coupling between 1-phenyl-3-bromopropyne and several carbohydrate substrates mediated by indium were investigated in aqueous EtOH (Table 1). In each case, the corresponding allenylation product was obtained with high diastereoselectivity, favoring the *syn* diastereomer. The high diastereoselectivity of this indium-mediated allenylation reaction could be attributed to chelation control.[17]

The results of the allenylation study confirmed the key step for the outlined synthesis. Thus, the commercially available D-glucurono-6,3-lactone **5** was readily converted into the corresponding bromo compound **6** based on the modification of a literature procedure for synthesizing a related chloro derivative.[18] Then allenylation of the compound with prop-2-ynyl bromide **4**, mediated by indium in aqueous EtOH, generated a mixture of allenylation products (56%) in which the allene **7** is the major component, together with debromination and re-

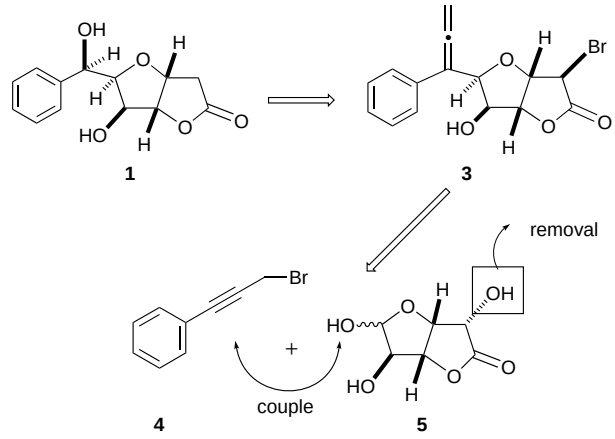

Scheme 1

Table 1 Diastereoselective allenylation of carbonyl compounds

Entry	Carbonyl compound	Product	Diastereo-selectivity	Yield (%)[a]
1	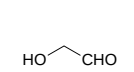	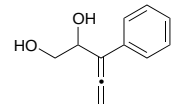	—	57
2	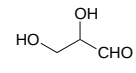	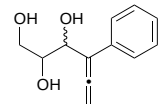	(10:1)	63[b]
3	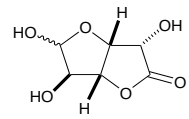	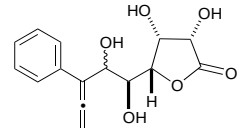	(>10:1)	63[b]
4	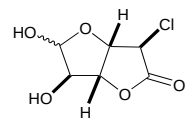	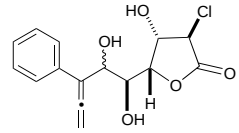	(9:1)	72
5	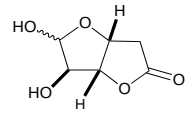	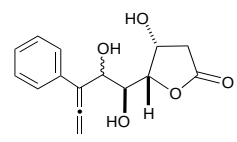	(8:1)	49[b]

[a] The yields were those of the isolated major isomers after column chromatograph on silica gel and were not optimized. [b] Determined after peracetylation. Conditions: stirred in 0.1 M aq. HCl–EtOH (1 : 9) overnight at room temperature.

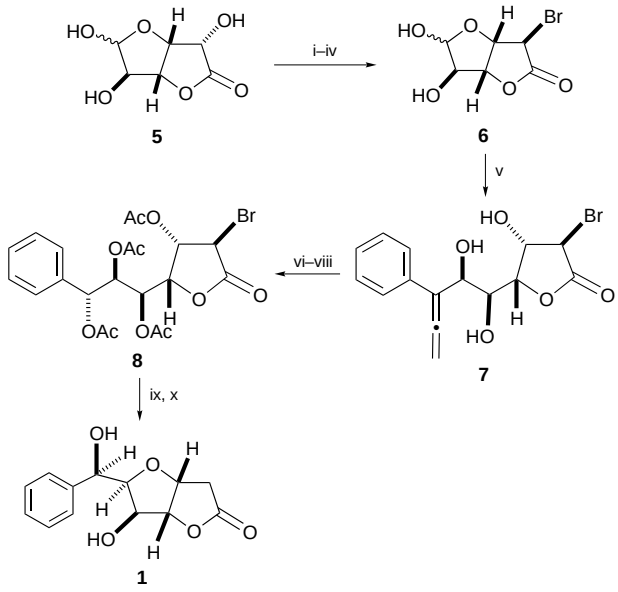

Scheme 2 *Reagents and conditions*: i, acetone, H_2SO_4, room temp., 5 h, 86%; ii, Tf_2O, Py, CH_2Cl_2, −40 °C, 94%; iii, LiBr, acetone, room temp., 1 h, 97%; iv, TFA–H_2O (3 : 1), room temp., 4.5 h, 98%; v, **4**, In, 0.1 M HCl–EtOH (1 : 9), room temp., 14 h; vi, O_3, MeOH, −78 °C, then DMS; vii, $NaBH_4$, MeOH, −10 °C, 30 min, then AcOH quench; viii, H_2SO_4, Ac_2O, room temp., 75% from **7**; ix, Na_2HSO_3, Na_2SO_3, MeOH–H_2O, room temp., 3 h, quant.; x, HCl (g), MeOH, room temp., 2 d, 44% from **8**

ductive elimination products. The allene **7** again shows a high (> 10 : 1) *syn* diastereoselectivity (the desired isomer). Standard ozonolysis of the allene compound in MeOH, followed by a diastereoselective reduction with $NaBH_4$, provided the corresponding alcohol as the predominant product (de = 3 : 1). The initial assignment of the stereochemistry for the reduction was confirmed after completion of the total synthesis. Subsequent reaction of the polyol with conc. H_2SO_4 in Ac_2O generated the peracetylation product **8** (*ca.* 75% from **7**) which decomposed on silica gel. Direct treatment of the peracetylation product with Na_2HSO_3 and Na_2SO_3 in MeOH–H_2O generated an α,β-unsaturated γ-lactone, as shown by ^{1}H NMR analysis of the crude material. In order to remove the acetyl protecting groups, the crude product was treated with HCl in MeOH resulting in the deprotected product which cyclized *in situ* giving the target natural product in 44% yield over two steps. The spectroscopic data and melting point of the target molecule synthesized by this method are consistent with previous literature reports.[7]

In conclusion, (+)-goniofufurone has been synthesized in a short sequence from D-glucurono-6,3-lactone using an indium-mediated, highly regio- and diastereo-selective allene formation in aqueous medium. The scope and application of the current indium-mediated method to the syntheses of other carbohydrates is presently under investigation.

Notes and References

† E-mail: CJLi@Mailhost.Tcs.Tulane.Edu

1 Y. C. Wu, C. Y. Duh, F. R. Chang, G. Y. Chang, S. K. Wang, J. J. Chang, D. R. McPhail, A. T. McPhail and K. H. Lee, *J. Nat. Prod.*, 1991, **54**, 1077.
2 S. K. Talapatra, D. Basu, T. Deb, S. Goswami and B. Talapatra, *Indian J. Chem., Sect. B*, 1985, **24**, 29.
3 T. W. Sam, C. S. Yeu, S. Matsjeh, E. K. Gan, D. Razak and A. L. Mohamed, *Tetrahedron Lett.*, 1987, **28**, 2541.
4 X. P. Fang, J. E. Anderson, C. J. Chang, P. E. Fanwick and J. L. McLaughlin, *J. Chem. Soc., Perkin Trans. 1*, 1990, 1655.
5 X. P. Fang, J. E. Anderson, C. J. Chang, J. L. McLaughlin and P. E. Fanwick, *J. Nat. Prod.*, 1991, **54**, 1034.
6 T. K. M. Shing and H. C. Tsui *J. Chem. Soc., Chem. Commun.*, 1992, 432.
7 T. K. M. Shing, H. C. Tsui and Z. H. Zhou, *J. Org. Chem.*, 1995, **60**, 3121 and references cited therein.
8 T. K. M. Shing, H. C. Tsui and Z. H. Zhou, *J. Chem. Soc., Chem. Commun.*, 1992, 810.
9 P. J. Murphy and S. T. Dennison, *Tetrahedron*, 1993, **49**, 6695.
10 K. R. C. Prakash and S. P. Rao, *Tetrahedron*, 1993, **49**, 1505.
11 M. Tsubuki, K. Kanai and T. Honda, *Synlett*, 1993, 653.
12 C. Mukai, I. J. Kim and M. Hanaoka, *Tetrahedron Lett.*, 1993, **34**, 6081.
13 J. Ye, R. K. Bhatt and J. R. Falck, *Tetrahedron Lett.*, 1993, **34**, 8007.
14 C. J. Li, *Tetrahedron*, 1996, **52**, 5643.
15 M. B. Isaac and T. H. Chan, *J. Chem. Soc., Chem. Commun.*, 1995, 1003.
16 E. Kim, D. M. Gordon, W. Schmid and G. M. Whiteside, *J. Org.. Chem.*, 1995, **58**, 5500.
17 L. A. Paquette and T. M. Mitzel, *J. Am. Chem. Soc.*, 1996, **118**, 1931.
18 H. Parolis, *Carbohydr. Res.*, 1983, **114**, 21.

Received in Corvallis, OR, USA, 31st October 1997; 7/07881A

An E_4O_4 heterocubane structure with a trivalent element of group 13 realized in $In_4O_4[C(SiMe_3)_3]_4$

Werner Uhl* and Michael Pohlmann

Fachbereich Chemie, Universität, Postfach 2503, D-26111 Oldenburg, Germany

The tetrahedral indium(I) compound $In_4[C(SiMe_3)_3]_4$ 1 reacts with the oxygen donor *o*-nitrosotoluene to form the extremely hygroscopic $In_4O_4[C(SiMe_3)_3]_4$ 2 in moderate yield, which exhibits a distorted In_4O_4 molecular center with normal In–O bond lengths, but short intracage In···In and O···O distances.

Although heterocubane type compounds $X_4(ER)_4$ with E a group 13 element, X a chalcogen atom and R an alkyl or aryl group have been known for several years with a continually increasing number of X = S, Se or Te,[1–4] no information concerning the properties or structure of the oxygen analogues is available from literature. Recently, a new method for the synthesis of such derivatives was developed by the treatment of tetrahedral element(I) clusters like $In_4[C(SiMe_3)_3]_4$ **1**[3,5] with elemental sulfur, selenium or tellurium, which gave the heterocubane compounds in high yields.[3,4] Their formation and structure can be described by the occupation of all tetrahedral faces of the cluster by chalcogen atoms. Dry oxygen and **1** gave no isolable products and, as previously reported,[5] moist air yielded the compound $In_4O(OH)_6[C(SiMe_3)_3]_4$[6] upon partial hydrolysis. Therefore, we searched for a suitable oxygen donor to oxidize **1** under mild conditions and to synthesize the up to now unknown In_4O_4 derivative.

Phosphane oxides or trimethylamine *N*-oxide did not react with **1**, and mixtures of unknown products resulted with bis(trimethylsilyl)peroxide. *p*-Nitrotoluene gave the In_4O_4 product **2** in a low yield, but the reaction was not well reproducible. The best result was obtained with *o*-nitrosotoluene (Scheme 1),† which formed, upon transfer of its oxygen atom to **1**, the corresponding dark red diazobenzene derivative identified by IR, NMR and UV–VIS spectroscopy. Mixed crystals of both products were isolated from hexane, in which the diazo compound was so strongly disordered that the structure could not be refined satisfactorily. Treatment with toluene to dissolve the more readily soluble diazo compound and recrystallization from hexane gave the colorless In_4O_4 derivative **2** in a yield of 24%. Compound **2** is hygroscopic and forms $In_4O(OH)_6[C(SiMe_3)_3]_4$[6] upon hydrolysis, which can be separated from the less soluble **2** by recrystallization. Crystalline **2** decomposes at 390 °C and is thermally more stable than its analogues with heavier chalcogens, for which decomposition points gradually decrease (330 °C for X = Te).[3,4] The molecule does not dissociate in benzene, as shown by the cryoscopically determined molar mass.

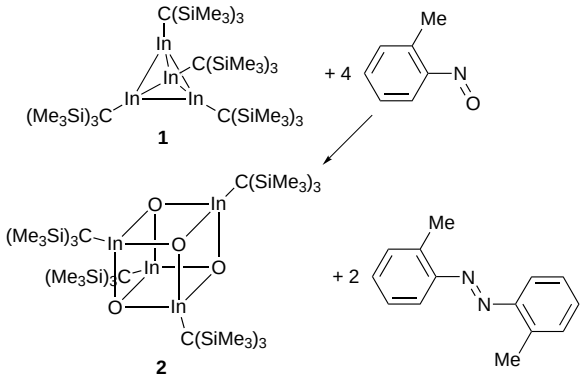

Scheme 1

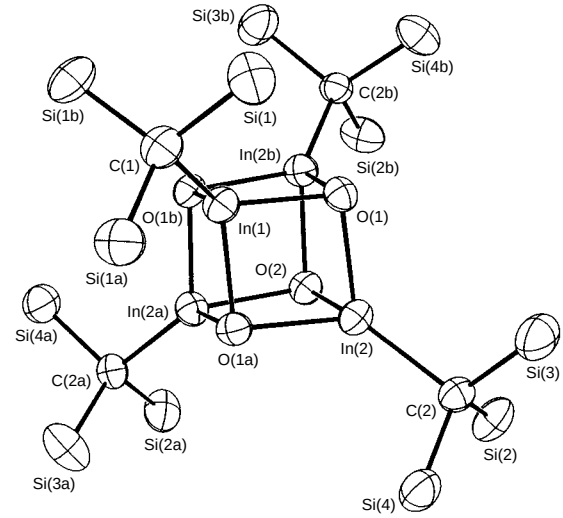

Fig. 1 Molecular structure of **2**. Selected bond lengths (pm) and angles (°): In(1)–O(1) 214.3(5), In(2)–O(1) 213.3(5), In(2)–O(1a) 214.0(5), In(2)–O(2) 213.8(5), In(1)–C(1) 222(1), In(2)–C(2) 216.5(7); O–In–O 84.4(2)–84.8(2), In–O–In 95.0(3)–95.3(2).

The structure of **2** (Fig. 1) shows a distorted In_4O_4 heterocubane in the molecular center with normal In–O bond lengths [213.3(5)–214.3(5) pm] and each In atom bound to a terminal alkyl group.‡ To the best of our knowledge, similar structures have not been observed before. The compounds $[MeIn(OH)(O_2PPh_2)]_4 \cdot 4py$ (py = pyridine) and $Ga_8(pz)_{12}O_4Cl_4$ (pz = pyrazolate) exhibit an $In_4(OH)_4$ or a Ga_4O_4 cube,[7] but due to the coordination number of four at the oxygen atoms and the bridging of faces or edges of the cages they are not comparable to the $E_4X_4R_4$ compounds discussed here. Also, the thallium(I) alcoholates with $Tl_4(OR)_4$ heterocubanes,[8] μ_3-OR groups and no alkyl substituents at the Tl atoms belong to another class of compounds. The series of the tetrachalcogen derivatives of **1** is completed with the synthesis of **2**. Comparison of important structure parameters in Table 1 shows that, with the exception of the oxygen compound **2**, the sum of

Table 1 Comparison of important structure parameters of the heterocubane molecules $In_4X_4R_4$ [X = chalcogen, R = $C(SiMe_3)_3$, Σr(X) = sum of the van der Waals radii of the chalcogen atoms,[9] Σr(In) = 380 pm]

	In–X/ pm	In–X–In/°	X–In–X/°	In···In/ pm	X···X/ pm	Σr(X)/ pm
$In_4O_4R_4$	214.0	95.1	84.6	315.7	287.9	300
$In_4S_4R_4$	254.9	86.8	93.1	350.4	370.0	360
$In_4Se_4R_4$	267.1	85.4	94.4	362.1	392.1	380
$In_4Te_4R_4$	286.4	83.7	95.6	382.9	425.2	420

the van der Waals radii[9] is exceeded between the chalcogen atoms, which may be caused by the charge distribution in the cage and a strong electrostatic repulsion between the more electronegative atoms. In contrast, the In–In distances are equal to (X = Te) or smaller (X = S, Se) than the sum of the van der Waals radii (380 pm). The difference between the intramolecular In···In and X···X distances increases from 20 pm for X = S to 42 pm for X = Te with the smallest distance always between the In atoms. The situation changes with the oxygen derivative **2**, where the In···In distance (315.7 pm) is larger than the O···O distance (287.9 pm). Both are smaller than the sum of the van der Waals radii, and the In···In distance approaches the bond length in the indium(I) compound **1** (300.2 pm)[3] indicating a considerable steric stress in the molecule. The inverse ratio of the homoatomic intracage distances leads to quite different bond angles. The most acute angles (< 90°) of **2** are observed at the In atoms, while with X = S, Se and Te they occur at the chalcogen atoms. The largest distortion of the cube is observed for the Te derivative, it decreases gradually to X = S and is reversed between X = S and O. The bond angles in **2** are in good agreement with values predicted by Barron and coworkers from a relation between intracage bond angles in known E_4X_4 cubane molecules and the ratio of the covalent radii of the elements.[2]

We are grateful to the Deutsche Forschungsgemeinschaft and the Fonds der Chemischen Industrie for generous financial support.

Notes and References

* E-mail: Uhl@chemie.uni-oldenburg.de

† Compound **1** (200 mg, 0.145 mmol) was treated under argon with 20 ml (0.579 mmol) of a solution of sublimed *o*-nitrosotoluene in *n*-hexane (stored over molecular sieve, c = 3.5 mg l^{-1}), the mixture was warmed to 50 °C for 36 h, during which it changed from violet to brown–red. After concentration and cooling to −50 °C, red crystals were isolated which were washed with toluene and recrystallized from hexane. Yield: 56 mg (24%); decomp. 390 °C. ^{1}H NMR (300 MHz, C_6D_6): δ 0.49. ^{13}C NMR (75.5 MHz, C_6D_6): δ 29.7 (InC), 6.3 ($SiMe_3$). IR (paraffin, cm^{-1}): 1260m, 1250m (δCH_3); 1169vw, 1154vw, 1017vw; 858vs, 766s, 721m (ρCH_3); 671m, 654w, 615w (νSiC); 520w, 496w, 466w, 426w, 399w (νInC), (νInO); 362 (δSiC). FD-MS: m/z 1448.9 (M^+). Molar mass (cryoscopically in benzene): obs. 1375, calc. 1449.6 g mol^{-1}.

‡ *Crystal data*: single crystals from *n*-hexane; two solvent molecules included; $C_{40}H_{108}In_4O_4Si_{12}\cdot 2C_6H_{14}$, cubic, space group $Pa\bar{3}$ (no. 205), a = 25.536(2) pm, U = 16 652(2) Å^3; Z = 8; D_c = 1.271 g cm^{-3}; crystal dimensions 0.5 × 0.4 × 0.4 mm, T = 293 K; μ(Mo-Kα) = 1.299 mm^{-1}; ω–2θ scan, range $3 < 2\theta < 50°$, $0 \leqslant h \leqslant 20$, $0 \leqslant k \leqslant 21$, $2 \leqslant l \leqslant 30$; STOE STADI4 diffractometer; 4774 independent reflections; 2555 reflections with $F > 4\sigma(F)$; structure solved by direct methods and refined with all independent structure factors based on F^2;[10] 239 parameters; $R1$ = 0.079, $wR2$ = 0.113; max., min. residual electron density 0.548, −0.394. The molecule is located on a crystallographic threefold rotation axis across the atoms C(1), In(1) and O(2). The hexane molecules are disordered; their carbon atoms were refined isotropically; hydrogen atoms were not considered. CCDC 182/728.

1 Very recent publications: U. App and K. Merzweiler, *Z. Anorg. Allg. Chem*., 1997, **623**, 478; S. L. Stoll, S. G. Bott and A. R. Barron, *J. Chem. Soc., Dalton Trans*., 1997, 1315.
2 C. J. Harlan, E. G. Gillan, S. G. Bott and A. R. Barron, *Organometallics*, 1996, **15**, 5479.
3 W. Uhl, R. Graupner, M. Layh and U. Schüz, *J. Organomet. Chem*., 1995, **493**, C1.
4 W. Uhl, R. Graupner, M. Pohlmann, S. Pohl and W. Saak, *Chem. Ber*., 1996, **129**, 143; $Al_4Cp^*_4$: S. Schulz, H. W. Roesky, H. J. Koch, G. M. Sheldrick, D. Stalke and A. Kuhn, *Angew. Chem., Int. Ed. Engl*., 1993, **32**, 1729.
5 R. D. Schluter, A. H. Cowley, D. A. Atwood, R. A. Jones and J. L. Atwood, *J. Coord. Chem*., 1993, **30**, 25.
6 S. S. Al-Juaid, N. H. Buttrus, C. Eaborn, P. B. Hitchcock, A. T. L. Roberts, J. D. Smith and A. C. Sullivan, *J. Chem. Soc., Chem. Commun*., 1986, 908.
7 A. M. Arif and A. R. Barron, *Polyhedron*, 1988, **7**, 2091. M. V. Capparelli, P. Hodge and B. Piggott, *Chem. Commun*., 1997, 937.
8 S. Harvey, M. F. Lappert, C. L. Raston, B. W. Skelton, G. Srivastava and A. H. White, *J. Chem. Soc., Chem. Commun*., 1988, 1216; H. Rothfuss, K. Folting and K. G. Caulton, *Inorg. Chim. Acta*, 1993, **212**, 165; H. Kunkely and A. Vogler, *Inorg. Chim. Acta*., 1991, **186**, 155.
9 J. E. Huheey, E. A. Keiter and R. L. Keiter, *Inorganic Chemistry*, Harper Collins, 1993.
10 SHELXTL-Plus REL. 4.1, Siemens Analytical X-RAY Instruments Inc., Madison, WI, 1990; G. M. Sheldrick SHELXL-93, Program for the Refinement of Structures, Universität Göttingen, 1993.

Received in Basel, Switzerland, 19th September 1997; 7/06810G

Tertiary amine–S_2Cl_2 chemistry: interception of reaction intermediates

Carlos F. Marcos,[a] Oleg A. Rakitin,[b] Charles W. Rees,[c] Ljudmila I. Souvorova,[b] Tomás Torroba,[a] Andrew J. P. White[c] and David J. Williams[c]

[a] *Departamento de Química Orgánica, Facultad de Veterinaria, Universidad de Extremadura, 10071 Cáceres, Spain*
[b] *N. D. Zelinsky Institute of Organic Chemistry, Academy of Sciences, Leninsky Prospect, 47, 117913 Moscow, Russia*
[c] *Department of Chemistry, Imperial College of Science, Technology and Medicine, London, UK SW7 2AY*

The reaction of *N*-(2-chloroethyl)diisopropylamine 1a with S_2Cl_2 allows the selective one-pot preparation of the tricyclic 4-(2-chloroethyl)bisdithiolothiazines 8 and 9 or, by addition of phosphorus pentasulfide at a late stage of the reaction, of the dithiolothiazine 6b characterised by X-ray crystallography; the chloroethyl derivative 8 is also obtained from (2-diisopropylamino)ethanethiol 1b and its disulfide 1c and S_2Cl_2, in a rare conversion of a thiol or disulfide into the corresponding chloro compound.

We have shown that Hünig's base, a simple saturated tertiary amine, is converted in a one-pot reaction by disulfur dichloride S_2Cl_2 into the fully unsaturated tricyclic bis[1,2]dithiolo[3,4-*b*:4′,3′-*e*][1,4]thiazine ring system[1] or, at a higher temperature, into the bis[1,2]dithiolo[4,3-*b*:3′,4′-*d*]pyrrole system[2] by selective sulfur extrusion from the thiazine.

Only the isopropyl groups of Hünig's base reacted with S_2Cl_2, the ethyl group being untouched. This led us to consider the reactivity of functionalised ethyl groups, both to broaden the reaction scope and hopefully to intercept proposed intermediates on the long reaction pathway, by cyclisations involving the ethyl group substituents. The key intermediates in our earlier proposals[6] were considered to be **2**, **3** and **4** (Scheme 1) when X = H, with **4** finally reacting with sulfur and oxygen nucleophiles to give the observed products. If X is a sufficiently nucleophilic group such as SH, the intermediates **2** and **3** could be diverted (arrows in **5**), to give the bicyclic compounds **6a**, or **6b** (Scheme 2). If X is a leaving group such as Cl then, at a later stage in the reaction when the dithiolium salt has been converted into the thione **7**, nucleophilic displacement could lead to the same bicyclic intermediates **6** (Scheme 2).

We therefore selected the commercially available *N*-(2-chloroethyl)diisopropylamine **1a**, which was readily converted into the thiol **1b** and its disulfide **1c**.[3] These compounds (1 equiv.) were each treated with S_2Cl_2 (10 equiv.) and DABCO (10 equiv.) in 1,2-dichloroethane for 3 d at room temperature.

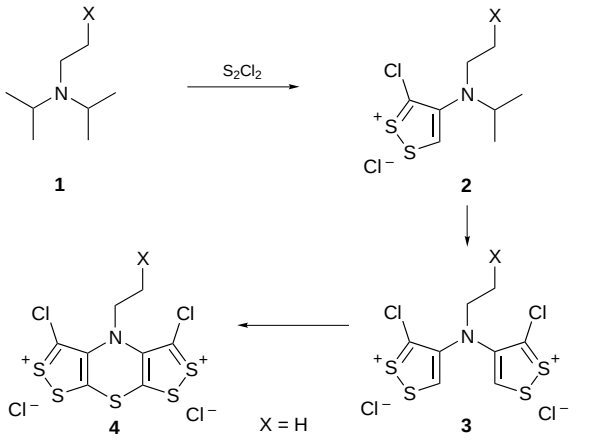

Scheme 1

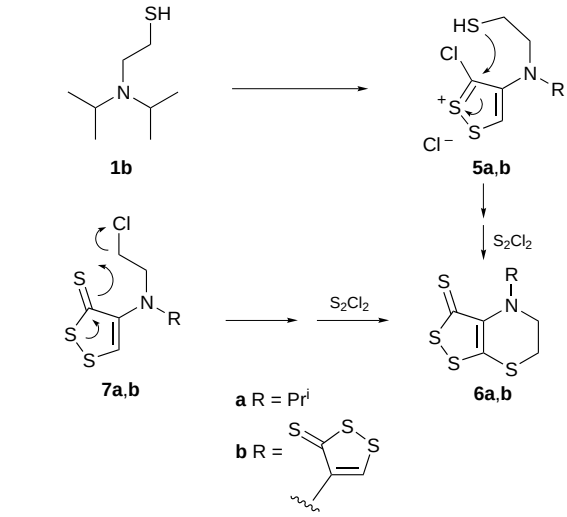

Scheme 2

Formic acid (20 equiv.) was then added and the mixture heated under reflux for 1 h, since we find that this treatment gives clean reactions by converting the 3-chlorodithiolium salts into dithiol-3-ones. To our surprise all three starting materials **1a–c** gave exactly the same product **8** as a yellow solid, mp 175–177 °C (16–25%) after chromatography (Scheme 3). When the reaction of **1a** (1 equiv.) with S_2Cl_2 (1 equiv.) was performed in THF without addition of DABCO or formic acid, the oxo thione **9** was obtained as an orange solid, mp 256–258 °C (10%),† together with **8** (30%)† (Scheme 3). The structures of **8** and **9** were fully supported by all their spectroscopic properties.

In these reactions the chloroethylamine **1a**, the mercaptoethylamine **1b** and the disulfide **1c** reacted with S_2Cl_2 in the same way as Hünig's base itself, without detectable diversion of

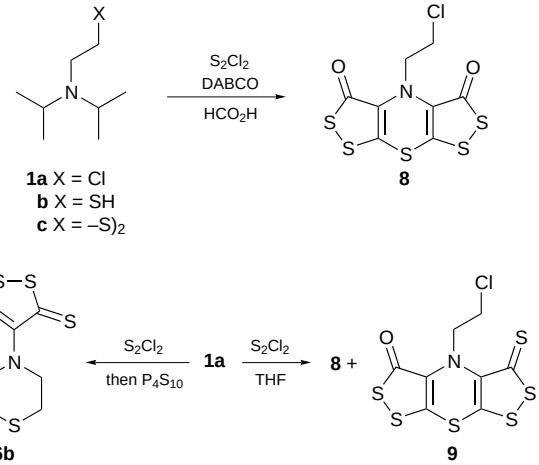

Scheme 3

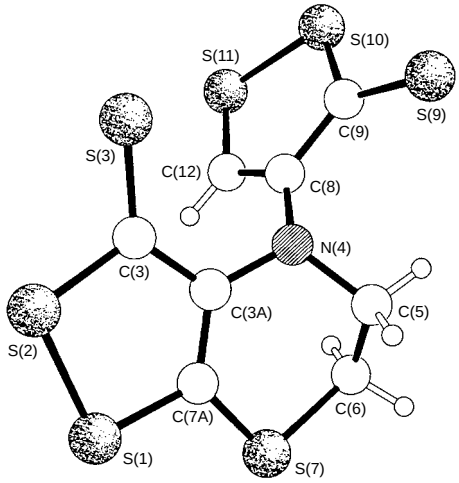

Fig. 1 The molecular structure of **6b**. Selected bond lengths (Å), S(1)–S(2) 2.057(1), S(2)–C(3) 1.731(3), C(3)–C(3A) 1.431(3), C(3A)–C(7A) 1.371(4), C(7A)–S(1) 1.729(3). C(3A)–N(4) 1.410(3), N(4)–C(8) 1.418(4), C(8)–C(9) 1.437(4), C(9)–S(10) 1.729(3), S(10)–S(11) 2.055(1), S(11)–C(12) 1.705(3) and C(12)–C(8) 1.348(4).

the reaction pathway, but with the additional conversion at some stage of the thiol and disulfide into the corresponding chloro compound. This last transformation is surprisingly rare, but has been achieved with sulfuryl chloride, followed by treatment with triphenylphosphine.[4]

These results suggest that S_2Cl_2 reacted with the sulfur groups faster than with the isopropyl groups; we therefore decided to try to regenerate a thiol derivative from the chloro compound by addition of a sulfur nucleophile at a late stage in the reaction. Treatment of the 2-chloroethylamine **1a** (1 equiv.) and S_2Cl_2 (1 equiv.) in THF for 3 d at room temperature was followed by addition of phosphorus pentasulfide (P_4S_{10}, 0.3 mol) and heating under reflux for 5.5 h. Chromatography gave new compound **6b** ($C_8H_5NS_7$) as shining orange needles, mp 240–241 °C (40%)† (Scheme 3). This did not contain chlorine (mass spectrum), although two different methylene groups were still present, together with an aromatic methyne group (^{1}H and ^{13}C NMR spectra) and a thiocarbonyl but not a carbonyl group (IR). The presence of an aromatic proton indicated that the fully fused tricyclic system of **8** and **9** had not been reached, and suggested the presence of a 1,2-dithiole with one ring hydrogen; structure **6b** was confirmed by X-ray crystallography (Fig. 1).‡ The partially saturated 1,4-thiazine ring has an 'envelope' conformation with C(5) lying 0.7 Å out of the plane of the remaining five atoms (which are co-planar to within 0.07 Å). There is a noticeable pyramidalization at N(4), the nitrogen atom lying 0.28 Å out of the plane of its substituents. The two dithiole rings are oriented approximately orthogonally (*ca*. 80°) thereby minimising interactions between them.

Taken in conjunction with our previous work on the conversion of Hünig's base with S_2Cl_2 into the *N*-ethyl analogues of compounds **8** and **9**,[1] the present results can be explained by the overall mechanism outlined in Scheme 4. The basic '*N*-ethyl' reaction does extend to other *N*-substituents and an appropriate functional group can divert the proposed reaction intermediates to form, in the present case, the new [1,2]dithiolo[3,4-*b*][1,4]thiazine ring system of **6b**. These complex 1,2-dithioles, now readily available from commercial materials in one-pot reactions, may be useful in the chemistry of new materials[5] and in pharmaceutical research.[6]

We gratefully acknowledge financial support from the Dirección General de Enseñanza Superior of Spain (DGDES Project ref. PB96-0101), the Consejería de Educación de la Junta de Extremadura y Fondo Social Europeo (ref. PRI97C123) and the NATO Linkage Grant 970596, and we thank the Wolfson Foundation for establishing the Wolfson Centre for Organic Chemistry in Medical Science at Imperial College.

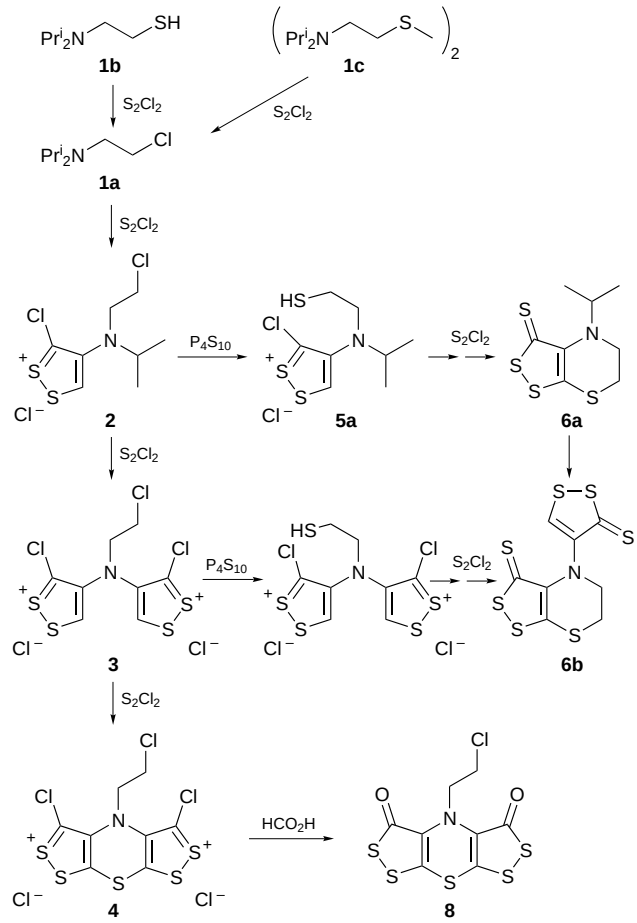

Scheme 4

Notes and References

† In the absence of DABCO, yields are calculated on the basis of 15 mol of amine **1** giving 1 mol of product and 14 mol of amine **1** hydrochloride.

‡ *Crystal data* for **6b**: $C_8H_5NS_7$, M = 339.6, orthorhombic, space group *Pbca* (no. 61), a = 14.672(1), b = 8.757(2), c = 19.626(2) Å, V = 2521.7(6) Å^3, Z = 8, D_c = 1.789 g cm^{-3}, μ(Cu-Kα) = 113.2 cm^{-1}, λ = 1.54178 Å, F(000) = 1376. An orange platy needle of dimensions 0.67 × 0.22 × 0.02 mm was used. Data were measured on a Siemens P4/PC diffractometer with Cu-Kα radiation (graphite monochromator) using ω-scans. 2089 Independent reflections were measured ($2\theta \leqslant 128°$) of which 1855 had $|F_o| > 4\sigma(|F_o|)$ and were considered to be observed. The structure was solved by direct methods and the non-hydrogen atoms were refined anisotropically by full-matrix least-squares based on F^2 using absorption corrected data (face-indexed numerical, maximum and minimum transmission factors 0.80 and 0.16, respectively) to give R_1 = 0.036, wR_2 = 0.096 for the observed data and 146 parameters. CCDC 182/736.

1 C. F. Marcos, C. Polo, O. A. Rakitin, C. W. Rees and T. Torroba, *Angew. Chem.*, 1997, **109**, 283; *Angew. Chem., Int. Ed. Engl.*, 1997, **36**, 281.
2 C. F. Marcos, C. Polo, O. A. Rakitin, C. W. Rees and T. Torroba, *Chem. Commun.*, 1997, 879.
3 F. A. Davis, J. K. Ray, S. Kasperowicz, R. M. Przeslawski and H. D. Durst, *J. Org. Chem.*, 1992, **57**, 2594.
4 I. W. J. Still, G. W. Kutney and D. McLean, *J. Org. Chem.*, 1982, **47**, 560.
5 A. Terzis, E. I. Kamitsos, V. Psycharis, J. S. Zambounis, J. Swiatek and G. C. Papavassiliou, *Synth. Met.*, 1987, **19**, 481; E. Fanghänel, A. M. Richter, B. Kordts and N. Beye, *Phosphorus Sulfur*, 1989, **43**, 165.
6 M. L. Aimar and R. H. Rossi, *Tetrahedron Lett.*, 1996, **37**, 2137 and references cited therein.

Received in Liverpool, UK, 20th November 1997; 7/08396C

LNA (locked nucleic acids): synthesis and high-affinity nucleic acid recognition

Sanjay K. Singh,[a] Poul Nielsen,[b] Alexei A. Koshkin[a] and Jesper Wengel*[a]

[a] *Department of Chemistry, University of Copenhagen, Universitetsparken 5, DK-2100 Copenhagen, Denmark*
[b] *Department of Chemistry, Odense University, Campusvej 55, DK-5230 Odense M, Denmark*

A novel class of nucleic acid analogues, termed LNA (locked nucleic acids), is introduced. Following the Watson–Crick base pairing rules, LNA forms duplexes with complementary DNA and RNA with remarkably increased thermal stabilities and generally improved selectivities.

During the last decade a plethora of DNA and RNA analogues have been chemically synthesized,[1–6] *e.g.* with the aim of improving nucleic acid recognition. We[7] and others[8] have reported promising, but not satisfactory, properties of oligonucleotides containing conformationally restricted monomers. We report here the synthesis of a novel conformationally restricted nucleic acid mimic, LNA (see Scheme 1). Molecular modelling† and simple model building suggested to us that the LNA monomers would be favourably preorganized in an N-type conformation thus enabling the formation of entropically favoured duplexes with complementary DNA and RNA. As an attractive feature, the structural change from DNA (or RNA) to LNA is limited from a chemical perspective, namely the introduction of an additional 2′-*C*,4′-*C*-oxymethylene link.

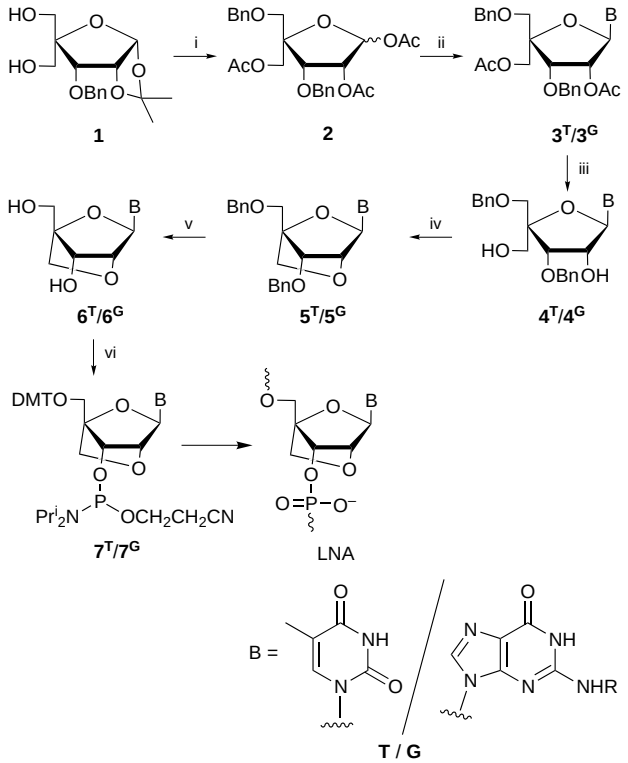

Scheme 1 *Reagents and conditions* (for **7T**): i, (*a*) NaH, BnBr, DMF, (*b*) Ac_2O, Py (64%, two steps), (*c*) 80% AcOH, (*d*) Ac_2O, Py (86%, two steps); ii, thymine, *N*,*O*-bis(trimethylsilyl)acetamide, TMS triflate, acetonitrile (76%) [for **3G**: 2-*N*-isobutyrylguanine, *N*,*O*-bis(trimethylsilyl)acetamide, TMS triflate, dichloroethane]; iii, NaOMe, MeOH (97%); iv, (*a*) TsCl, Py (47%), (*b*) NaH, DMF (89%); v, 20% $Pd(OH)_2$/C, EtOH, H_2 (98%); vi, (*a*) DMTCI, Py (93%), (*b*) *N*,*N*-diisopropylethylamine, 2-cyanoethyl *N*,*N*-diisopropylphosphoramidochloridite, CH_2Cl_2 (70%)

For synthesis of the LNA monomers we chose a strategy starting from the known 4′-*C*-hydroxymethyl pentofuranose derivative **1**[9] (Scheme 1). Regioselective 5-*O*-benzylation, acetylation and acetolysis, followed by another acetylation, afforded furanose **2**, a key intermediate for coupling with silylated nucleobases. Stereoselective reaction with silylated thymine[10] yielded nucleoside **3T** which was deacetylated to give nucleoside diol **4T**. Tosylation followed by base-induced ring closure afforded the 2′-*O*,4′-*C*-linked bicyclic nucleoside derivative **5T**. Debenzylation yielded the unprotected analogue **6T** as the first example of a nucleoside diol with the (1*S*,3*R*,4*R*,7*S*)-7-hydroxy-1-hydroxymethyl-2,5-dioxabicyclo-[2.2.1]heptane structure. The assigned structure of **6T** was verified by NMR spectroscopy, including NOE experiments.‡ The absence of a coupling constant between 1′-H and 2′-H, and the unusual and strong mutual NOE effects (9%/8%) between 3′-H and 6-H (thymine base), strongly indicate structural preorganization of the pentofuranose ring of the LNA monomer into an N-type conformation.[5,11] Similar synthetic procedures were applied to synthesize the guanine derivatives **3G**–**6G** *via* coupling of **2** and 2-*N*-isobutyrylguanine. Transformation of nucleosides **6** into the 5′-*O*-4,4′-dimethoxytrityl (5′-*O*-DMT) protected analogues and subsequently into the phosphoramidite derivatives **7**§ yielded the desired monomeric building blocks for automated oligonucleotide synthesis.

LNAs¶ and unmodified reference strands (Tables 1 and 2) were effectively synthesized using the phosphoramidite approach.[12] Stability against 3′-exonucleolytic degradation is a prerequisite for most *in vivo* applications of oligonucleotide analogues The LNA 5′-$\mathbf{T^L}_{13}$T displayed complete 3′-exonucleolytic stability when measured by a procedure described earlier using snake venom phosphodiesterase.[13] The thermal stabilities (melting temperatures, T_m) of duplexes involving LNA oligonucleotides towards both DNA and RNA complements were determined and compared to their unmodified references (Tables 1 and 2). In all experiments, sharp monophasic transitions were observed with hyperchromicities of 1.2–1.4. No transitions were observed when running LNAs without complements in control experiments.

Table 1 Hybridization data of oligothymidylates

		DNA Complement dA_{14}		RNA Complement A_{14}	
Entry	Sequence[a] 5′ → 3′	T_m/°C	($\Delta T_m/\mathbf{T^L}$)/°C	T_m/°C	($\Delta T_m/\mathbf{T^L}$)/°C
1	T_{14}	35.5	Ref.	32.0	Ref.
2	$T_7\mathbf{T^L}T_6$	35.5	0.0	36.0	+4.0
3	$T_3(\mathbf{T^L}T)_4T_3$	47.0	+2.9	52.5	+5.1
4	$T_5\mathbf{T^L}_4T_5$	42.0	+1.6	51.5	+4.9
5	$\mathbf{T^L}_{13}$T	> 90.0	> +4.2	87.5	+4.3
6	T_{10}	24.0	Ref.	18.0	Ref.
7	$\mathbf{T^L}_9$T	80.0	+4.9	70.5	+4.3
8	T_6	< 10.0	Ref.	< 10.0	Ref.
9	$\mathbf{T^L}_5$T	32.0	> +4.4	40.0	> +6.0

[a] See footnote to Table 2.

Table 2 Hybridization data of mixed sequences

Entry	Sequence[a] 5′ → 3′		T_m/°C	[ΔT_m/ $\mathbf{T^L}$($\mathbf{G^L}$)]/ °C
1	d(GTGATATGC)	d(GCATATCAC)	28.0	Ref.
2	d(G$\mathbf{T^L}$GA$\mathbf{T^L}$A$\mathbf{T^L}$GC)	d(GCATATCAC)	44.0	+5.3
3	d(G$\mathbf{T^L}$GA$\mathbf{T^L}$A$\mathbf{T^L}$GC)	d(——— T ———)	27.0	—
4	d(G$\mathbf{T^L}$GA$\mathbf{T^L}$A$\mathbf{T^L}$GC)	d(——— G ———)	30.0	—
5	d(G$\mathbf{T^L}$GA$\mathbf{T^L}$A$\mathbf{T^L}$GC)	d(——— C ———)	23.0	—
6	d(GTGAGATGC)	d(GCATCTCAC)	33.0	Ref.
7	d(G$\mathbf{T^L}$GA$\mathbf{G^L}$A$\mathbf{T^L}$GC)	d(GCATCTCAC)	49.0	+5.3
8	d(GTGATATGC)	GCAUAUCAC	28.0	Ref.
9	d(G$\mathbf{T^L}$GA$\mathbf{T^L}$A$\mathbf{T^L}$GC)	GCAUAUCAC	50.0	+7.3
10	d(GTGAGATGC)	GCAUCUCAC	33.0	Ref.
11	d(G$\mathbf{T^L}$GA$\mathbf{G^L}$A$\mathbf{T^L}$GC)	GCAUCUCAC	58.0	+8.3

[a] A = adenosine monomer, C = cytidine monomer, G = guanosine monomer, U = uridine monomer, T = thymidine monomer, $\mathbf{T^L}$/$\mathbf{G^L}$ = LNA monomers. Oligodeoxynucleotide sequences are depicted as d(sequence). 'Ref' indicates reference duplex. Hybridization mixtures of 1 ml were prepared using a buffer solution (10 mM Na_2HPO_4, pH 7.0, 100 mM NaCl, 0.1 mM EDTA) and equimolar (1.0 or 1.5 μM) amounts of the oligonucleotides. The absorbance at 260 nm was recorded while the temperature was raised linearly from 10 to 93 °C (1 °C min^{-1}). The melting temperatures (T_m values) were obtained as the maxima of the first derivatives of the melting curves.

The results for oligothymidylates are depicted in Table 1. Generally, significant increases in T_m values were obtained. Against complementary DNA (dA_{14}), the results ranged from no effect (incorporation of one LNA monomer, entry 2) to an increase in T_m of 4.9 °C per $\mathbf{T^L}$ incorporated for the LNA $\mathbf{T^L}_9$T (entry 7). The effect on the thermal stabilities of duplexes towards RNA (A_{14}) was significant (and additive) in all experiments (entries 2–9, increases in T_m of 4.0–6.0 °C per $\mathbf{T^L}$ incorporated).

The remarkable nucleic acid recognition potential of oligothymidylate LNAs was extended to mixed sequences containing the pyrimidine LNA monomer $\mathbf{T^L}$ and/or the purine LNA monomer $\mathbf{G^L}$ (Table 2). Thus, convincing stabilizing effects were observed when hybridizing nonamer LNAs towards DNA (ΔT_m = +5.3 °C per LNA monomer incorporated), whereas unprecedented increases in thermal stability (ΔT_m = +7.3 and +8.3 °C per LNA monomer incorporated) of the corresponding LNA:RNA duplexes were observed. The selectivity of the mixed sequence LNAs is, if anything, improved compared to the corresponding DNA references. This can be extracted from experiments where mis-matched nucleotides were in turn introduced in the position opposite to the middle $\mathbf{T^L}$/$\mathbf{G^L}$ monomers (and T/G monomers). The decreases in thermal stabilities obtained were slightly more pronounced for the LNAs compared to the reference DNAs (representative results are shown in entries 3–5; similar results were obtained when evaluating the binding selectivity of $\mathbf{G^L}$ and the binding selectivity against complementary RNA). These results indicate that LNA obeys the standard Watson–Crick pairing rules and that the complexes are bimolecular duplexes.**

In this report it has been demonstrated that preorganized LNAs display 3′-exonucleolytic stability and excellent ability to recognize complementary DNA and RNA. These results should make LNA a prime candidate for development of oligonucleotide-based therapeutics and diagnostic probes, and LNA-mediated nucleic acid recognition a novel concept of general applicability.

We thank The Danish Natural Science Research Council, The Danish International Development Agency, and Exiqon A/S, Denmark for financial support.

Footnotes and References

* E-mail: wengel@kiki.dk

† Molecular modelling was performed using HYPERCHEM™ version 4.0; MM+ force field; Polak-Ribiere conjugate gradient geometry optimization.

‡ *NMR data* for $\mathbf{6^T}$ (conventional nucleoside numbering is used): δ_H [$(CD_3)_2SO$] 11.33 (1 H, br s, NH), 7.62 (1 H, d, *J* 1.1, 6-H), 5.65 (1 H, d, *J* 4.4, 3′-OH), 5.41 (1 H, s, 1′-H), 5.19 (1 H, t, *J* 5.6 Hz, 5′-OH), 4.11 (1 H, s, 2′-H), 3.91 (1 H, d, *J* 4.2, 3′-H), 3.82 (1 H, d, *J* 7.7, 5″-H_a), 3.76 (2 H, d, *J* 5.7, 5′-H), 3.63 (1 H, d, *J* 7.7, 5″-H_b), 1.78 (3 H, d, *J* 0.7, CH_3); key NOE contacts, signifying close interatom distances, were identified between: 5″-H_b and 1′-H, 6-H and 3′-H, 5′-OH and 5′-H, 5′-OH and 3′-H, and 5′-OH and 6-H.

§ *NMR data* for: $\mathbf{7^T}$ δ_P($CDCl_3$) 149.06, 148.74. For $\mathbf{7^G}$ δ_P ($CDCl_3$) 148.17, 146.07.

¶ The term LNA describes oligonucleotides containing one or more LNA monomer(s). For synthetic convenience, the LNAs of this first study were synthesized (0.2 μmol scale) on commercial supports carrying a natural 2′-deoxynucleoside. Step-wise coupling yields: $\mathbf{7^T}$ > 98% (12 min coupling), $\mathbf{7^G}$ > 95% (12 min coupling), deoxynucleoside phosphoramidites > 98% (2 min coupling). After standard cleavage and deprotection, capillary gel electrophoresis or reversed-phase HPLC was used to verify the purity (> 90%) of the synthesized oligonucleotides. Selected MALDI-MS experiments: 5′-$T_5\mathbf{T^L}_4T_5$ [M − H]$^-$ 4307.0 (calc. 4307.8); 5′-$\mathbf{T^L}_{13}$T [M − H]$^-$ 4557.8 (calc. 4559.7); 5′-d(G$\mathbf{T^L}$GA$\mathbf{G^L}$A$\mathbf{T^L}$GC) [M − H]$^-$ 2862.2 (calc. 2861.9).

** At pH 7.0, cytosine nucleobases are non-protonated and thus unable to form triple-helical structures. Triple-helical complexation for the oligothymidylate LNAs of Table 1 is theoretically possible, but no biphasic transitions were detected, even for the lower melting complexes. As further evidence, strikingly similar CD curves for LNA complexes and the corresponding reference duplexes were obtained.

1 E. Uhlmann and A. Peyman, *Chem. Rev.*, 1990, **90**, 544.
2 S. L. Beaucage and R. P. Iyer, *Tetrahedron*, 1993, **49**, 6123.
3 P. Herdewijn, *Liebigs Ann.*, 1996, 1337.
4 B. Hyrup and P. E. Nielsen, *Bioorg. Med. Chem.*, 1996, **4**, 5; P. E. Nielsen and G. Haaima, *Chem. Soc. Rev.*, 1997, 73.
5 D. G. Schultz and S. M. Gryaznov, *Nucleic Acids Res.*, 1996, **24**, 2966.
6 A. Van Aerschot, I. Verheggen, C. Hendrix and P. Herdewijn, *Angew. Chem., Int. Ed. Engl.*, 1995, **34**, 1338; C. Hendrix, H. Rosemeyer, I. Verheggen, F. Seela, A. Van Aerschot and P. Herdewijn, *Chem. Eur. J.*, 1997, **3**, 110.
7 P. Nielsen, H. M. Pfundheller and J. Wengel, *Chem. Commun.*, 1997, 825; P. Nielsen, H. M. Pfundheller, C. E. Olsen and J. Wengel, *J. Chem. Soc., Perkin Trans. 1*, 1997, 3423.
8 See, *e.g.* M. Bolli, J. C. Litten, R. Schütz and C. J. Leumann, *Chem. Biol.*, 1996, **3**, 197; V. E. Marquez, M. A. Siddiqui, A. Ezzitouni, P. Russ, J. Wang, R. W. Wagner and M. D. Matteucci, *J. Med. Chem.*, 1996, 39, 3739.
9 R. D. Youssefyeh, J. P. H. Verheyden and J. G. Moffatt, *J. Org. Chem.*, 1979, **44**, 1301.
10 H. Vorbrüggen, K. Krolikiewicz and B. Bennua, *Chem. Ber.*, 1981, **114**, 1234; H. Vorbrüggen and G. Höfle, *Chem. Ber.*, 1981, **114**, 1256.
11 C. Altona and M. Sundaralingam, *J. Am. Chem. Soc.*, 1973, **95**, 2333; S. Obika, K Morio, D. Nanbu and T. Imanishi, *Chem. Commun.*, 1997, 1643.
12 M. H. Caruthers, *Acc. Chem. Res.*, 1991, **24**, 278.
13 P. Nielsen, F. Kirpekar and J. Wengel, *Nucleic Acids Res.*, 1994, **22**, 703.

Received in Glasgow, UK, 28th November 1997; 7/08608C

Intramolecular [4 + 2] cycloadditions involving transient phosphaalkene intermediates as dienophiles: a useful entry to phosphabicyclo[4.3.0]non-4-ene derivatives

Jean-François Pilard, Annie-Claude Gaumont, Céline Friot and Jean-Marc Denis*†

Synthèse et électrosynthèse organiques, UMR 6510, Université de Rennes 1, Campus de Beaulieu, F-35042, Rennes, France

Three representative phosphabicyclo[4.3.0]non-4-ene derivatives are formed in high yields and various diastereomeric forms by [4 + 2] intramolecular cycloadditions involving transient phosphaalkenes as dienophiles; complete diastereoselectivity is observed with the P-substituted derivative.

Free cyclic phosphines and their metal coordination complexes are valuable intermediates in organophosphorus chemistry.[1] They are prepared by many different approaches, among them, cycloaddition reactions involving C=P double bonds with dienes and dipoles appear to be of synthetic value.[1,2] the main problem encountered by using this methodology is keeping the reactivity of the P=C double bond under control. Self-condensations are usually avoided by steric or electronic effects and by complexation with a transition metal. Some cycloadditions lacking stabilisation of the P^{III} intermediate occur in high yield,[3] especially when the cycloadducts spontaneously aromatize, thus giving a useful entry to functionalised phosphinines;[4] in most cases however the desired cycloadducts are accompanied of various amounts of self-condensed products.[2d] In order to circumvent this problem we thought to trap the transient species by internal cycloaddition. Under these conditions, the rates of the reactions are expected to be strongly enhanced by entropic assistance, hopefully making the self-condensation reactions of transient species negligible. Intermolecular reactions between conjugated dienes and phosphaalkenes have been recently reviewed.[2a] It is now well established that, with the exception of some derivatives bearing electronegative substituents, the reaction takes place with retention of the phosphaalkene stereochemistry. Furthermore, at least with cyclopentadiene derivatives, the *endo* preference is respected with substituents on phosphorus. Thus, the potential versatility of intramolecular cycloadditions involving low coordinated phosphorus derivatives as dienophiles should afford a useful entry to tailored and hopefully stereocontrolled polycyclic systems. As a first evaluation of this methodology, we present here the synthesis of three differently substituted 2-phosphabicyclo[4.3.0]non-4-ene phosphines **5a**–**c** by intramolecular [4 + 2] cycloadditions involving the corresponding terminal phosphaalkenes **4a**–**c** as dienophiles. Conditions for controlling the stereochemistry are described.

We have recently developed a general route to non-stabilized phosphaalkenes which involves as a key step the dehydrohalogenation of α-chloroalkylphosphines with a Lewis base[2d,5] (Scheme 1). This procedure is attractive for the following reasons: (i) the α-chlorophosphonate and phosphinate precursors **A** are readily available by conventional anionic routes,[6,7] allowing introduction of the desired substituents both on phosphorus and carbon, (ii) the reduction of esters **A** into phosphines **B** with dichloroalane is chemoselective,[8] and (iii) HCl elimination occurs under mild conditions at a temperature which depends both on the strength of the base and the P–H acidity of the phosphine, allowing us to determine the best conditions for the trapping of the transient phosphaalkene **C**. We decided to adopt this strategy for the synthesis of the phosphabicyclononenes **5a**–**c** (Scheme 2).

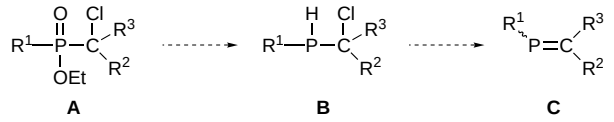

Scheme 1

Chlorophosphonate **2a** was prepared by halogen–metal exchange of trichloromethylphosphonate $[Cl_3CP(O)(OEt)_2]$[6] with BuLi (2 equiv.) followed by selective monosilylation [Me_3SiCl (1 equiv.)], alkylation [(*E*)-1-bromohepta-4,6-diene **1** (1 equiv.)][9] of the resulting lithiated intermediates and subsequent hydrolysis in basic media.[10] The phosphonate **2b** and phosphinate **2c** were prepared by halogen–metal exchange of trichloromethylphosphonate $[Cl_3CP(O)(OEt)_2]$ and trichloromethylphenylphosphinate[6] $[Cl_3CP(O)(OEt)Ph]$[7] respectively with BuLi (1 equiv.) followed by alkylation of the resulting intermediates with **1** (Scheme 2). The yields of **2a** and **2b** were greater than 85% after purification by chromatography on silica. The yield for **2c** is lower (57%), a small amount of the starting material **1** being recovered at the end of the reaction. Chemoselective reduction of esters **2a**–**c** with dichloroalane[5,8] in THF afforded the free phosphines **3a**–**c**. The low volatility of the latter prevents purification by the general procedure involving successive vacuum transfers.[5] The following protocol was used: after hydrolysis of the crude mixture at −10 °C with deoxygenated water, the organic solution was filtered off under a slight pressure of neutral gas, washed again and then dried.

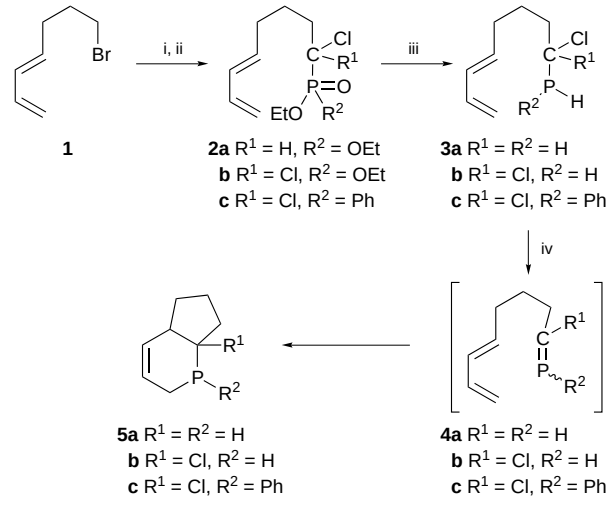

Scheme 2 *Reagents and conditions*: i, THF, BuLi (2 equiv. for **2a**, 1 equiv. for **2b,c**), −85 °C, then $Cl_3CP(O)(OEt)_2$; ii (for **2a**), −85 °C, Me_3SiCl (1 equiv.), then −85 °C, $Br(CH_2)_3CH{=}CHCH{=}CH_2$, then 20 °C, aq. LiOH; (for **2b,c**), −85 °C, $Br(CH_2)_3CH{=}CHCH{=}CH_2$; iii, '$AlHCl_2$', THF, −80 to 20 °C, then deoxygenated H_2O, −10 °C, then $MgSO_4$; iv (for **5a,b**), −60 °C, Py (3 equiv.), then −60 to 20 °C; (for **5c**) −30 °C, Et_3N (2.5 equiv.), then −30 to 20 °C

Solutions were used without further purification, and the chlorophosphines **3a–c** were stable in the absence of oxygen. Yields determinated by NMR spectroscopy with an internal reference were greater than 70% (purity > 90%). The characterisation was supported by HRMS and ^{31}P, ^{1}H and ^{13}C NMR data, all of which were consistent with the assigned structure.‡

We have shown in our previous work that (i) transient phosphaalkenes are detectable by ^{31}P NMR spectroscopy in the dehydrochlorination of primary and secondary α-chloroalkylphosphines[2d,5] under controlled temperature conditions (from −80 to 20 °C) and (ii) polymerisation of the chlorophosphaalkene intermediates was observed in the elimination of HCl from α,α′-dichlorophosphines by a weak Lewis base (pyridine) in the absence of a trapping agent.[11,12] Whatever the nature of the Lewis base, we never detected in this work the expected phosphaalkene intermediates **4a–c** starting from **3a–c**. The only observed products were the cycloadducts **5a–c** characterized by new signals in the ^{31}P NMR spectra and the corresponding J_{PH} couplings: cyclic phosphines **5a** and **5b** were observed when the temperature rose to −60 °C in the presented pyridine (3 equiv.). Due to the lower P–H acidity[5] of secondary phosphines, elimination of HCl from α,α′-chlorophosphine **3c** occurred at −30 °C with a stronger base [NEt_3 (2.5 equiv.)]. Intramolecular [4 + 2] cycloaddition of **4a–c** with the diene counterpart is consequently a fast step. Self-condensations are strongly inhibited, as was confirmed by the high yield of cycloadducts (*i.e.* yield for **5c** > 80%, determined by ^{31}P NMR spectroscopy with an internal reference). All these results are consistent with entropic activation.

Since cycloaddition reactions take place with retention of stereochemistry at the P^{III} centre,[2a] both (*Z*)- and (*E*)-phosphaalkene intermediates are expected from elimination of HCl from α-chlorophosphines **3**, giving four isomeric cycloadducts. The observed stereochemical course differs strongly with the structure of the dienophile. We observed a weak selectivity starting from **4a** [four isomers, at δ −91.5 (d, $^{1}J_{PH}$ = 187 Hz), −88.4 (d, $^{1}J_{PH}$ = 191 Hz), −85 (d, $^{1}J_{PH}$ = 182 Hz) and −68.7 (d, $^{1}J_{PH}$ = 178 Hz); ratio = 57 : 20 : 14 : 9, respectively]. A higher selectivity is encountered for **4b** [two isomers at δ −76 ($^{1}J_{1PH}$ = 186 Hz) and −65 ($^{1}J_{PH}$ = 195 Hz); ratio = 81 : 19, respectively]. These results are consistent with the presence of the two (*Z*)- and (*E*)-phosphaalkene intermediates for **4a** and **4b**. On the other hand, intramolecular cycloaddition of **4c** is highly selective, and only one isomer is observed. The stereochemistry of the P(1), C(8) and C(9) centres is controlled (Scheme 3). (i) The relative configuration at P and C(8) of **5c** was established on the basis of the $^{2}J_{PC(7)}$ coupling constant: the observed value (15 Hz) favours a *trans* relationship between the lone pair and C(7).[3,13,14]§ (ii) The *cis*-fused cycloadduct is proposed to take into account the preference of the P-substituent for the *endo* postions.[2a,15,16] The phenyl and chloride substituents in **4c** are consequently in a *trans* relationship. The ^{1}H, ^{31}P and ^{13}C NMR data and mass spectra (HRMS) of **5a–c** are fully consistent with their assigned structures.

4c **5c**

Scheme 3

In summary, we have shown that intramolecular [4 + 2] cycloadditions involving phosphaalkenes can be considered as a potentially useful route for the construction of stereocontrolled polycyclic structures bearing a phosphorus atom, with the entropic effect suppressing the polymerisation of the transient intermediate. A more detailed mechanistic study of this reaction is under active investigation.

Footnotes and References

† E-mail: Jean-Marc Denis@univ-rennes1.fr

‡ All new products were characterized by ^{31}P, ^{1}H and ^{13}C NMR spectroscopy and mass spectrometry (HRMS).

§ The so called '*cis* rule' (ref. 15) is applied. For tetrahydrophosphinines: *cis*-geometry, $^{2}J_{PC}$ = 20–22 Hz; *trans*-geometry, $^{2}J_{PC}$ = 15–16 Hz (refs. 13, 14).

1 L. D. Quin and A. N. Hughes, *The chemistry of organophosphorus compounds*, ed. F. R. Hartley, Wiley, Chichester, 1990, vol. 1.
2 (*a*) F. Mathey, *Acc. Chem. Res.*, 1992, **25**, 90; (*b*) M. Regitz and P. Binger, *Angew. Chem., Int. Ed. Engl.*, 1988, **27**, 1484; (*c*) R. Appel and F. Knoll, *Adv. Org. Chem.*, 1989, **33**, 258; (*d*) A. C. Gaumont and J. M. Denis, *Chem. Rev.*, 1994, **94**, 1413.
3 L. D. Quin, A. N. Hughes and B. Pete, *Tetrahedron Lett.*, 1987, **28**, 5783.
4 P. Pellon, Y. Y. Yeung Lam Ko, P. Cosquer, J. Hamelin and R. Carrié, *Tetrahedron Lett.*, 1986, **27**, 5611; P. Le Floch and F. Mathey, *Tetrahedron Lett.*, 1989, **30**, 817.
5 A. C. Gaumont, B. Pellerin, J. L. Cabioch, X. Morise, M. Lesvier, P. Savignac, P. Guenot and J. M. Denis, *Inorg. Chem.*, 1996, **35**, 6667 and references cited therein.
6 P. Coutrot, C. Laurenco, J. F. Normant, P. Perriot, P. Savignac and J. Villieras, *Synthesis*, 1977, 615.
7 X. Morise, P. Savignac and J. M. Denis, *J. Chem. Soc., Perkin Trans. 1*, 1996, 2179.
8 J. L. Cabioch and J. M. Denis, *J. Organomet. Chem.*, 1989, **377**, 227.
9 J. A. Marshall, J. Grote and J. E. Audia, *J. Am. Chem. Soc.*, 1987, **108**, 1186.
10 For a general procedure see M. P. Teulade and P. Savignac, *J. Organomet. Chem.*, 1988, **338**, 295.
11 J. C. Guillemin, M. Le Guennec and J. M. Denis, *J. Chem. Soc., Chem. Commun.*, 1989, 988.
12 C. Grandin, E. Abbout-Joudet, N. Collignon, J. M. Denis and P. Savignac, *Heteroatom Chem.*, 1992, **3**, 337.
13 M. Abbadi, P. Cosquer, F. Tonnard, Y. Y. Yeung Lam Ko and R. Carrié, *Tetrahedron*, 1991, **47**, 71.
14 L. D. Quin and M. J. Gallagher, in *Phosphorus-31 NMR Spectroscopy in Stereochemical Analysis*, ed. J. G. Verkade and L. D. Quin, VCH, Weinheim, 1987.
15 R. Appel, J. Menzel and F. Knoch, *Chem. Ber.*, 1985, **118**, 4068.
16 R. de Vaumas, A. Marinetti, L. Ricard and F. Mathey, *J. Am. Chem. Soc.*, 1992, **114**, 261.

Received in Liverpool, UK, 6th November 1997; 7/08020D

Asymmetric tandem reactions based on nitroalkenes: a one-pot construction of functionalized chiral bicycles by a three-component reaction

Martín Avalos,*† Reyes Babiano, Pedro Cintas, José L. Jiménez, Juan C. Palacios and María A. Silva

Departamento de Química Orgánica, Facultad de Ciencias, Universidad de Extremadura, E-06071 Badajoz, Spain

Asymmetric tandem cycloaddition of a chiral carbohydrate nitroalkene with ethyl vinyl ether in the presence of electron-withdrawing alkenes produces a facile assembly of bicyclic systems, which can further be selectively cleaved to give homologated carbohydrates.

The construction of complex organic molecules by sequential transformations is one of the most important and efficient synthetic strategies. The advantages of these so-called tandem or domino reactions are many and have been thoroughly discussed.[1] Sequential [4 + 2]/[3 + 2] cycloadditions relying on nitroalkenes have been developed by Denmark and his group over the last decade, exploiting the use of a homochiral auxiliary on the dienophile and demonstrating the versatility of this methodology in alkaloid synthesis.[2]

Recently we have also demonstrated the efficiency of the tandem nitroalkene cycloaddition as a viable approach to densely functionalized molecules, but the heterodiene now imparts chirality by using a readily available carbohydrate-appended nitroalkene (Scheme 1).[3] These processes occur through the intermediacy of nitronate species such as **2**.

Given the distinctive electronic character of nitroalkenes and nitronates, it would be possible to perform a multicomponent reaction combining electron-rich and electron-withdrawing alkenes without them interfering with each other. Thus when the heterodiene **1** was reacted with excesses of ethyl vinyl ether (EVE) and an electron-withdrawing alkene such as methyl vinyl ketone (MVK), methyl acrylate (MA), acrylonitrile (AN) and dimethyl maleate (DMM) in ethanolic solution at room temperature for 5–7 days, the corresponding nitrosoacetals **4**–**7** were obtained as crystalline solids (Scheme 2 and Table 1).‡ The initial inverse electronic demand [4 + 2] cycloaddition occurs with ethyl vinyl ether, whereas the resulting nitronate will react exclusively in a [3 + 2] fashion with the electron-deficient alkene.

Analyses of crude samples by ^{1}H NMR spectroscopy ($CDCl_3$, 400 MHz) reveal that the reactions are regiospecific and exhibit a pronounced facial diastereoselectivity. Only two diastereoisomers were detected, one of which was always prevalent. Remarkably, the mixtures could be purified by flash chromatography (ethyl acetate–hexane eluent system) and the major isomers were obtained as diastereoisomerically pure samples by crystallization from EtOH. In the cases of the MA and AN reactions, the minor isomers could also be obtained in crystalline form in 4 and 10% yields, respectively.

We have confirmed by X-ray diffractometry that the initial [4 + 2] cycloaddition occurs with a complete *endo* selectivity to the *re* face of the heterodiene, whereas the [3 + 2] cyclization follows in the *exo* sense, which is sterically more favorable than the competitive *endo* approach.[3] This type of *exo–endo* facial selectivity has been observed before with related 5,5-fused systems.[4] Based on such results and with the information provided by proton coupling constants, suggesting that both substituents of five- and six-membered fused rings are located at α-equatorial positions, we have tentatively assigned the absolute stereochemistry of the major isomers **4**–**7**. Because similar coupling constants have also been found for the isolated minor isomers, their formation must have taken place with the opposite *endo* orientation in the [3 + 2] cyclization.

The usefulness of these functionalized polyhydroxyalkyl heterocycles was further illustrated through their selective six-membered ring opening under mild conditions. Cleavage of nitrosoacetals may be induced by acidic treatment with dilute AcOH in ethanolic solution, but reaction mixtures were difficult to purify owing to the presence of unidentified side products. However, when cycloadducts were heated at reflux in a 1 : 1 EtOH–H_2O mixture, homologated sugar aldehydes[5,6] such as **10** and **11** were cleanly obtained in quantitative yield (Scheme 3).‡ These substances were further characterized by preparing their hydrazone derivatives **12** and **13**, respectively. Compounds **10**–**13** also bear an attractive isoxazoline ring that could

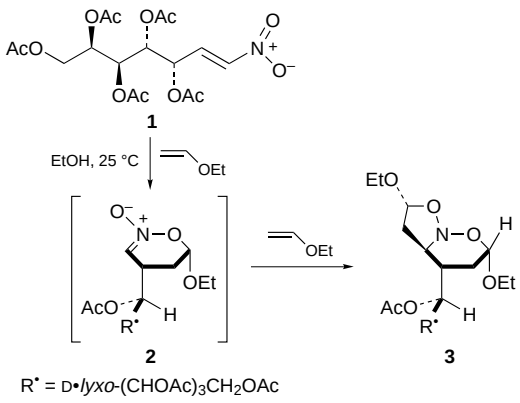

Scheme 1

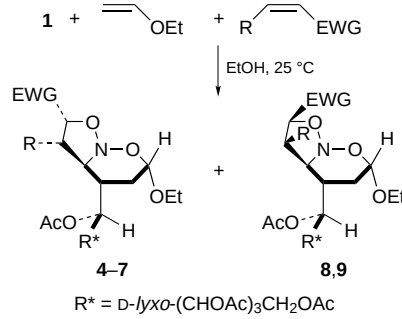

Scheme 2

Table 1 Reaction of **1** with EVE and electron deficient alkenes

		Product (% yield[a])	
R	EWG	Major	Minor
H	COMe	**4** (70)	—[b]
H	CO_2Me	**5** (75)	**8** (4)
H	CN	**6** (60)	**9** (10)
CO_2Me	CO_2Me	**7** (50)	—[b]

[a] Isolated yields after crystallization. [b] Not isolated.

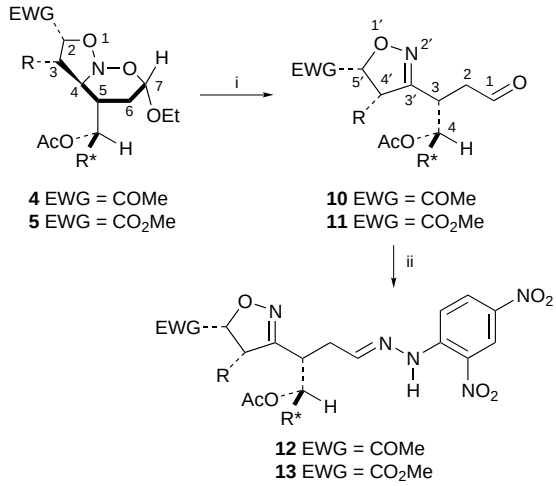

Scheme 3 *Reagents and conditions*: i, EtOH–H_2O, reflux, 12 h, 100%; ii, 2,4-$(O_2N)_2C_6H_3NHNH_2$, MeOH, room temp., 12 h

be further manipulated to afford vicinal amino alcohols and crossed aldol products.[7,8]

In conclusion, we have successfully explored a tandem cycloaddition which involves *in situ* formation of a chiral nitronate having a sugar moiety and its subsequent diastereofacial selective dipolar cycloaddition with a series of electron-deficient alkenes. Variations in the system undergoing cyclization allows subsets of richly functionalized nitrogen-containing polycycles to be produced from an acyclic precursor. The formation of homologated carbohydrates in a few steps is also notable. With the understanding of transition state preferences, this methodology will become a useful element in synthetic design and further investigations are currently under way in our laboratories.

This work was supported by grants from the Spanish Ministerio de Educación y Cultura (D.G.I.C.Y.T., Project PB95-0259-CO2-01) and the Junta de Extremadura-Fondo Social Europeo (PRI97-C175). We also thank the Junta de Extremadura for a fellowship to M. A. S.

Notes and References

† E-mail: mavalos@unex.es

‡ Satisfactory spectroscopic (IR, ^{1}H, ^{13}C, ^{1}H-COSY, and ^{1}H-^{13}C-HETCOR NMR) and analytical data were obtained for all new compounds. *Selected data for* **3**: (the numbering system used for NMR assignments is in agreement with the literature data, see ref. 9): mp 188 °C (EtOH); $[\alpha]_D$ +7.5 (*c* 1, $CHCl_3$); ν_{max} (KBr)/cm^{-1} 2970, 1730, 1360, 1225, 1100, 1050, 1020; δ_H ($CDCl_3$, 400 MHz) 5.32 (dd, $J_{1',2'}$ 1.2, $J_{2',3'}$ 9.9, 1 H, H-2′), 5.27–5.21 (m, 2 H, H-1′, H-4′), 5.18 (dd, $J_{2',3'}$ = 9.9, $J_{3',4'}$ = 1.8, 1 H, H-3′), 4.90 (dd, $J_{2,3a}$ 9.8, $J_{2,3b}$ = 4.6, 1 H, H-2), 4.75 (t, $J_{6a,7}$ $J_{6b,7}$ 7.0, 1 H, H-7), 4.32 (dd, $J_{4',5a'}$ 4.5, $J_{5a',5b'}$ = 11.8, 1 H, H-5a′), 3.95 (m, 1 H, CH_3CH_2O–C-7), 3.78 (dd, $J_{4',5b'}$ 7.6, $J_{5a',5b'}$ 11.8, 1 H, H-5b′), 3.51 (m, 1 H, CH_3CH_2O–C-7), 3.30 (m, 1 H, H-4), 2.32 (m, 1 H, H-3a), 2.26–2.16 (m, 2 H, H-3b, H-6a), 2.21 (s, 3 H, CH_3CO–C-2), 2.14 (s, 3 H, OAc), 2.12 (s, 3 H, OAc), 2.11 (s, 3 H, OAc), 2.09 (s, 3 H, OAc), 2.02 (s, 3 H, OAc), 1.83–1.70 (m, 2 H, H-5, H-6b), 1.27 (t, 3 H, CH_3CH_2O– C-7); δ_C ($CDCl_3$, 100 MHz) 206.2 (CH_3CO), 170.5 (2C, OAc), 170.3 (OAc), 170.1 (OAc), 169.9 (OAc), 99.7 (C-7), 87.9 (C-2), 71.8 (C-4′), 69.7 (C-4), 67.7, 67.6, 67.5 (3C, C-1′, C-2′, C-3′), 63.6 (CH_3CH_2O–C-7), 62.4 (C-5′), 38.7 (C-5), 34.3 (C-3), 28.0 (C-6), 26.7 (CH_3CO), 20.7 (OAc), 20.7 (OAc), 20.6 (3C, OAc), 15.0 (CH_3CH_2O–C-7). Calc. for $C_{25}H_{37}NO_{14}$: C, 52.17; H, 6.48; N, 2.43. Found: C, 52.02; H, 6.51; N, 2.43%). *For* **8** (note that the longest sugar chain is cited first with the lowest number to the aldehyde group; primed numbers are located on the hererocycle): δ_H ($CDCl_3$, 400 MHz) 9.65 (s, 1 H, CHO), 5.37 (dd, $J_{4,5}$ 1.4, $J_{5,6}$ 11.0, 1 H, H-5), 5.25–5.19 (m, 3 H, H-4, H-6, H-7), 4.79 (dd, $J_{5',4a'}$ 5.6, $J_{5',4b'}$ 11.5, 1 H, H-5′), 4.28 (dd, $J_{8a,7}$ 4.7, $J_{8a,8b}$ 11.7, 1 H, H-8a), 3.78 (dd, $J_{8b,7}$ 7.5, $J_{8a,8b}$ 11.7, 1 H, H-8b) 3.29–3.18 (m, 2 H, H-3, H- 4a′), 3.12 (dd, $J_{4b',5'}$ 5.6, $J_{4a',4b'}$ 17.4, 1 H, H-4b′), 2.96 (dd, $J_{2a,3}$ 5.0, $J_{2a,2b}$ 18.3, 1 H, H-2a), 2.82 (dd, $J_{2b,3}$ 2.3, $J_{2a,2b}$ 18.3, 1 H, H-2b), 2.27 (s, 3 H, CH_3CO–C-5′), 2.10 (s, 9 H, 3 OAc), 2.07 (s, 3 H, OAc), 2.02 (s, 3 H, OAc); δ_C($CDCl_3$, 100 MHz) 207.8 (CH_3CO), 198.1 (CHO), 170.5 (OAc), 170.3 (2C, OAc), 170.0 (OAc), 169.8 (OAc), 158.1 (C-3′), 83.5 (C-5′), 69.7 (C-5), 67.9, 67.7, 67.4 (C-4, C-6, C-7), 62.2 (C-8), 43.3 (C-2), 38.4 (C-4′), 33.5 (C-3), 26.4 (CH_3CO), 20.7 (OAc), 20.6 (4C, OAc).

1 For reviews on tandem reactions: T.-L. Ho, *Tandem Organic Reactions*, Wiley, New York, 1992; L. F. Tietze, and U. Beifuss, *Angew. Chem., Int. Ed. Engl.*, 1993, **32**, 131; R. A. Bunce, *Tetrahedron*, 1995, **51**, 13 103; J. D. Winkler, *Chem. Rev.*, 1996, **96**, 167.

2 For a review on tandem cycloadditions of nitroalkenes: S. E. Denmark and A. Thorarensen, *Chem. Rev.*, 1996, **96**, 137.

3 M. Avalos, R. Babiano, P. Cintas, F. J. Higes, J. L. Jiménez, J. C. Palacios and M. A. Silva, *J. Org. Chem.*, 1996, **61**, 1880.

4 R. N. Butler, D. Cunningham, E. G. Marren, P. McArdle and D. F. O'Shea, *J. Chem. Res. (S)*, 1992, 256.

5 For reviews on branched and higher carbon sugars: J. Yoshimura, *Adv. Carbohydr. Chem. Biochem.*, 1984, **42**, 69; A. Zamojski and S. Jarosz, *Pol. J. Chem.*, 1992, **66**, 525.

6 A general route for the homologation-amination of aldehydes by addition of sugar nitrones to metalated thiazoles has been recently devised: A. Dondoni, S. Franco, F. Junquera, F. L. Merchán, P. Merino, T. Tejero and V. Bertolasi, *Chem. Eur. J.*, 1995, **1**, 505 and references cited therein; A. Dondoni, F. Junquera, F. L. Merchán, P. Merino, M.-C. Scherrmann and T. Tejero, *J. Org. Chem.*, 1997, **62**, 5484.

7 For reviews on syntheses of isoxazolines by inter- and intramolecular 1,3-dipolar cycloadditions, see A. Padwa, in *Comprehensive Organic Synthesis*, ed. B. M. Trost, I. Fleming and M. F. Semmelhack, Pergamon, Oxford, 1991, vol. 4, pp. 1069–1109; P. A. Wade, *ibid*, vol. 4, pp. 1111–1168; For a review on chiral isoxazolines: B. H. Kim and D. P. Curran, *Tetrahedron*, 1993, **49**, 293; For the formation of aldol-type products by ring-cleavage of isoxazolines: W. Carruthers, *Cycloaddition Reactions in Organic Synthesis*, Pergamon, Oxford, 1990, p. 293.

8 The reduced chiral systems, optically active isoxazolidines, can also be utilized in organic synthesis: M. Frederickson, *Tetrahedron*, 1997, **53**, 403.

9 K. Undheim, in *Comprehensive Heterocyclic Chemistry*, ed. A. R. Katritzky and C. W. Rees, Pergamon, Oxford, 1984, vol. 6, pp. 632–633.

Received in Liverpool, UK, 14th November 1997; 7/08222C

Direct versatile route to conformationally constrained glutamate analogues

James Dyer,[a] Steve Keeling[b] and Mark G. Moloney*[a]

[a] *The Department of Chemistry, Dyson Perrins Laboratory, University of Oxford, South Parks Road, Oxford, UK OX1 3QY*
[b] *GlaxoWellcome, Medicines Research Centre, Gunnels Wood Road, Stevenage, Hertfordshire, UK SG1 2NY*

Novel conformationally constrained glutamate analogues are readily available from (*S*)-pyroglutamic acid; using a bicyclic lactam template, diastereocontrolled and sequential modification of the pyrrolidine ring is possible, allowing a versatile access to several glutamate and kainoid analogues; variations in the C(2)H–C(3)H coupling constants were observed depending upon the nature of remote substituents on the heterocyclic ring, consistent with modification of the ring conformation.

Nitrogen heterocycles occur widely in nature, in isolation and as structural subunits in many families of alkaloids, and possess wide ranging biological and pharmacological activities.[1–3] Of particular current interest are conformationally constrained glutamines,[4] which have been shown to possess potent activity at both the ionotropic and metabotropic receptors.[5,6] These receptors are selectively activated by excitatory amino acids, and are known to play an important role in various physiological processes, such as memory and learning, neuroendocrine regulation, and acute and chronic neuronal disfunction.[7] Excessive activation of these receptors can in some cases lead to cell death.[8] The search for selective agonists and antagonists offers the potential for both the structural and physiological characterisation of the receptors, and treatment of a range of physiological disorders, in particular Alzheimer's and Parkinson's diseases. Highly functionalised pyrrolidines have been found to have activity at these receptors,[9] and there has therefore been considerable recent interest in the development of practical and versatile methodology for the preparation of this important class of compound;[10,11] particularly elegant protocols have been developed by Shirahama[12,13] and by Baldwin[14–16] which use 4-hydroxyproline as a chiral starting material, and which offer considerable simplicity and generality for the introduction of the ring substituents. We report here an alternative but equally versatile and simple approach to functionalised pyroglutamates which uses a sequential conjugate addition/alkylation or arylation strategy to a $\Delta^{3,4}$ pyrrolidinone derivative. This method has been applied to the synthesis of a novel class of conformationally restricted glutamates, which possess a similar ring substitution pattern to the kainoid group of amino acids.

We used the recently described and readily available lactam **1** as a template for manipulation to a variety of functionalised pyrrolidinones.[17,18] Thus, conjugate addition of the Reformatsky reagent derived from *tert*-butyl bromoacetate generated in THF and DMPU with ultrasonic irradiation gave the diester **2**, in 77% yield as a mixture of diastereomers at the C(7) position, using our previously reported method;[19] conjugate additions to a related enone have been reported previously, although not with Reformatsky reagents.[19,20] This compound was readily functionalised at C(7) by direct arylation using several aryllead triacetates [$ArPb(OAc)_3$, $CHCl_3$, Py, reflux, 72 h][21,22] to give the aryl derivatives **3a**–**d** in good yield as mixtures of diastereomers at C(7) (Table 1) which could be separated only with some difficulty.[23] In the case of **3a**,**b**, the stereochemistry of the C(7)–Ar *exo*- diasteromer was assigned by a series of NOE experiments. Alternatively, alkylation with benzyl bromide under previously reported conditions (NaH, THF, reflux)[24] gave the derivative **3e** as a separable mixture of diastereomers in very good yield. In all arylations, a diastereomeric mixture was obtained, in which preferential addition of the aryl substituent to the *exo* face of **2** was predominant, although for the alkylation with benzyl bromide, a slight preference for *endo* addition was observed.

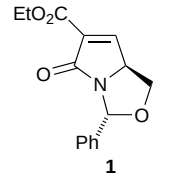

1

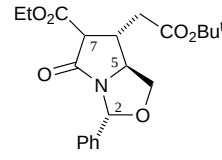

2

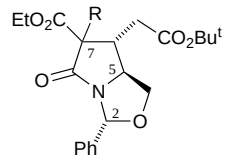

3a R = Ph
b R = *p*-BrC_6H_4
c R = *p*-$MeOC_6H_4$
d R = *o*-$MeOC_6H_4$
e R = Bn

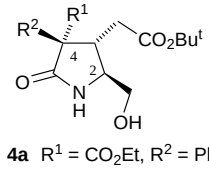

4a R^1 = CO_2Et, R^2 = Ph
b R^1 = Ph, R^2 = CO_2Et
c R^1 = Ph, R^2 = H
d R^1 = H, R^2 = Ph
e R^1 = Ph, R^2 = CO_2H
f R^1 = Bn, R^2 = CO_2Et
g R^1 = CO_2Et, R^2 = Bn
h R^1 = Bn, R^2 = CO_2H
i R^1 = R^2 = H

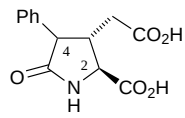

5

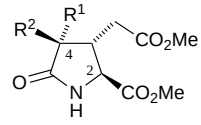

6a R^1 = Ph, R^2 = H
b R^1 = H, R^2 = Ph
c R^1 = Bn, R^2 = H
d R^1 = H, R^2 = Bn
e R^1 = CO_2Et, R^2 = Bn
f R^1 = CO_2Me, R^2 = Bn
h R^1 = R^2 = H

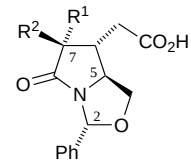

7a R^1 = Ph, R^2 = H
7b R^1 = H, R^2 = Ph

Table 1 Yields of C(7) functionalised products of **3**

Compound	R	Isolated yield (%)	Diastereomer ratio[a] *exo*:*endo*
3a	Ph	86	2.4:1
3b	*p*-BrC_6H_4	76	2.25:1
3c	*p*-$MeOC_6H_4$	38[b]	2.3:1
3d	*o*-$MeOC_6H_4$	72	1.7:1
3e	Bn	75	1:1.2

[a] Determined by ^1H NMR analysis of the crude reaction mixture. [b] Contains starting material, in the ratio **2**:**3c** = 1:1.3.

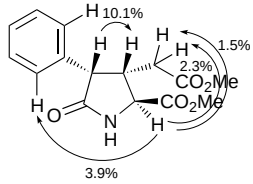

6a

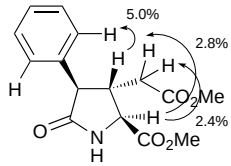

6b

Fig. 1 NOE enhancements for **6a** and **6b**

In the case of the arylated derivative **3a**, acidic deprotection of the hemiaminal ether function gave the separable diastereomeric alcohols **4a**,**b** in 28 and 52% yield, respectively. Treatment of **4b** with 1 M NaOH in EtOH gave the hydrolysed and decarboxylated products **4c**,**d** on extraction of the basic mixture with EtOAc, and a mixture of the acid **4e** and product **4c**,**d** on extraction of the aqueous mixture after acidification with 2 M HCl. Heating of this mixture at 135 °C at 0.8 mBar for 30 min gave the product **4c**,**d** as a 1 : 1 mixture of diastereomers, in a combined yield of 82%. Acidic deprotection (TFA–CH_2Cl_2) of the *tert*-butyl ester function of **4c**,**d** and then oxidation (RuO_2, $NaIO_4$, MeCN, CCl_4, H_2O) afforded the acid **5** [as a mixture of diastereomers at C(4)] which was partially purified using base wash and then treated with MeOH–H_2SO_4 (catalytic) giving the diesters **6a** and **6b** each in 33% yield (from **4c**,**d**), whose relative stereochemistry was determined by NOE experiments (Fig. 1). An alternative route to **6a**,**b**, which involved treatment of **3a** with 2 M NaOH–EtOH at 50 °C for 5 h to give concomitant ethyl ester hydrolysis, decarboxylation and *tert*-butyl ester hydrolysis, was limited by incomplete and variable hydrolysis of the ester functions, leading to impure **7a**,**b**.

The benzyl derivative **3e** was also amenable to similar manipulation. Thus, hemiaminal ether cleavage of each of the benzyl diastereomers of **3e** (TFA in CH_2Cl_2) afforded the products **4f**,**g**. Hydrolysis (NaOH–EtOH) of **4f** gave **4h** in 99% crude yield, which after heating to effect decarboxylation, and then *tert*-butyl ester removal, oxidation (RuO_2, $NaIO_4$, MeCN, CCl_4, H_2O) and esterification (CH_2N_2) provided the separable diastereomeric benzyl derivatives **6c**,**d** in a ratio of 1 : 4.4 and 38% overall yield. An alternative path, involving hydrolysis of **4g**, followed by direct *tert*-butyl ester removal, oxidation, and esterification using the above conditions gave a 1 : 1 mixture of products **6e**,**f**, indicating that the initial hydrolyis was incomplete.

Pyrrolidinones which were unfunctionalised at C(4) were also available by this route. Thus, direct decarboxylation of the starting lactam **2**, by treatment with ethanolic NaOH followed by thermolysis and deprotection with TFA, afforded **4i** in 33% yield, a compound which has been previously reported in the literature.[25] Conversion to lactam **6h** was achieved by *tert*-butyl ester removal, oxidation as before and esterification (CH_2N_2) in 53% yield over the three steps.

Noteworthy was variation of the C(2)–H/C(3)–H vicinal proton coupling constants for each of the substituted pyroglutamates **6** (Table 2); molecular modelling studies of each of these compounds[27] indicated that the dihedral angle of the energy minimised structures also varied with the nature of the C(4) substituent, particularly for the more sterically congested C(4)–aryl series of compounds **6a**,**b**. Thus, it would appear that analogues of well-defined glutamate conformers could be available by variation in the C(4) substituent of compounds of type **6**.

Table 2 Proton–proton C(2)–H/C(3)–H coupling constant data and corresponding dihedral angles

Compound	*J*/Hz[a]	Dihedral angle (°)[b]
6h	5.5 (5.5)	117
6a	6.5 (6.5)	121
6b	8.0 (8.0)	153
6c	2.5 (2.5)	125
6d	6.0 (6.5)	118

[a] In $CDCl_3$ (in C_6D_6). [b] Ref. 27.

This route represents a novel and simple, but potentially generalisable, approach to highly functionalised pyrrolidinones, and is complementary to existing literature protocols. It in particular provides access to novel pyroglutamate analogues of the kainoid group of amino acids possessing substituents with π-electron density at C(4).

We thank the EPSRC and GlaxoWellcome for funding of a studentship to J. D., and we gratefully acknowledge the use of the EPSRC Chemical Database Service at Daresbury[28] and the EPSRC National Mass Spectrometric Service Centre at Swansea.

Note and References

† E-mail: mark.moloney@chem.ox.ac.uk

1 A. O. Plunkett, *Nat. Prod. Rep.*, 1994, **11**, 581.
2 M. S. Chorghade and C. Csehe, *Pure Appl. Chem.*, 1994, 2211.
3 G. Massiot and C. Delaude, *The Alkaloids*, 1986, **27**, 300.
4 J. S. Sabol, G. A. Flynn, D. Friedrich and E. W. Huber, *Tetrahedron Lett.*, 1997, **38**, 3687.
5 D. T. Monaghan and R. J. Wenthold, *Ionotropic Glutamate Receptors*, Humana, Totowa (New Jersey), 1997.
6 B. S. Meldrum, *Excitatory Amino Acid Antagonists*, Blackwell Scientific, Oxford, 1991.
7 D. Lodge, *Excitatory Amino Acids in Health and Disease*, Wiley-Interscience, Chichester, 1988.
8 A. Guidotti, *Neurotoxicity of Excitatory Amino Acids*, Raven Press, New York, 1990.
9 M. G. Moloney, *Nat. Prod. Rep.*, 1998, in the press.
10 A. F. Parsons, *Tetrahedron*, 1996, **52**, 4149.
11 T. Harrison, *Contemp. Org. Synth.*, 1996, 259.
12 M. Horikawa, Y. Shima, K. Hashimoto and H. Shirahama, *Heterocycles*, 1995, **40**, 1009.
13 M. Horikawa and H. Shirahama, *Synlett.*, 1996, 95.
14 J. E. Baldwin, A. M. Fryer, M. R. Spyvee, R. C. Whitehead and M. E. Wood, *Tetrahedron Lett.*, 1996, 6923.
15 J. E. Baldwin, S. J. Bamford, A. M. Fryer and M. E. Wood, *Tetrahedron Lett.*, 1995, **36**, 4869.
16 J. E. Baldwin and M. Rudolph, *Tetrahedron Lett.*, 1994, **35**, 6163.
17 M. Bamford, M. Beard, D. T. Cherry and M. G. Moloney, *Tetrahedron: Asymmetry*, 1995, **6**, 337.
18 J. H. Bailey, D. T. Cherry, K. M. Crapnell, M. G. Moloney, S. B. Shim, M. Bamford and R. B. Lamont, *Tetrahedron*, 1997, 11 731.
19 J. Dyer, S. Keeling and M. G. Moloney, *Tetrahedron Lett.*, 1996, **37**, 4573.
20 A. Diaz, J. G. Siro, J. L. Garcia-Navio, J. J. Vaquero and J. Alvarez-Builla, *Synthesis*, 1997, 559.
21 J. T. Pinhey, in *Comprehensive Organometallic Chemistry II*, ed. A. McKillop, Pergamon, Oxford, 1995, vol. 11.
22 J. T. Pinhey, *Aust. J. Chem.*, 1991, **44**, 1353.
23 All new compounds gave satisfactory spectroscopic and/or high resolution mass spectrometric or analytical data.
24 M. J. Beard, J. H. Bailey, D. T. Cherry, M. G. Moloney, S. B. Shim, K. Statham, M. Bamford and R. B. Lamont, *Tetrahedron*, 1996, **52**, 3719.
25 T. Sato, K. Matsubayashi, K. Yamamoto, H. Ishikawa, H. Ishibashi and M. Ikeda, *Heterocycles*, 1995, **40**, 261.
26 Structures optimised with CACHE Scientific Worksystem Version 3.9, available from Oxford Molecular Group (Medawar Centre, Oxford Science Centre, Oxford, UK) (Augmented MM2 Parameters using Conjugate Gradient Optimisation Method).
27 D. A. Fletcher, R. F. McMeeking and D. Parkin, *J. Chem. Inf. Comput. Sci.*, 1996, **36**, 746.

Received in Liverpool, UK, 21st November 1997; 7/08429C

Highly efficient and regioselective cyclization catalyzed by titanium silicate-1

Asim Bhaumik† and Takashi Tatsumi

Engineering Research Institute, The University of Tokyo, Yayoi, Tokyo 113, Japan

Highly regioselective cyclization of 3,4, 4,5 and 5,6 unsaturated alcohols to tetrahydrofuranols and tetrahydropyranols is reported using the TS-1–H_2O_2 system for the first time.

Since the discovery of the titanium silicate molecular sieve, TS-1,[1] and its use in liquid phase heterogeneous oxidation catalysis[2] in the presence of dilute hydrogen peroxide, it has been the subject of tremendous research activity to establish its applicability to various organic transformations.[3–7]

Substituted tetrahydrofuran and tetrahydropyran rings are common in many natural products, and thus play an important role as building blocks for the synthesis of various biologically active organic target molecules.[8] Hence, new methods for the synthesis of these oxacyclic compounds have long been sought. A strategy involving electrophilic activation of the double bond[9,10] in pent-4-en-1-ol or hex-5-en-1-ol followed by intramolecular nucleophilic attack of the oxygen atom of the hydroxy group offers a convenient route for the stereoselective synthesis of these compounds. Ring closure of substituted pent-4-en-1-yloxy and hex-5-en-1-yloxy radicals[11,12] is also of notable synthetic utility. Here, we report a highly efficient regioselective cyclization of such olefinic alcohols over TS-1, under mild reaction conditions using dilute hydrogen peroxide as oxidant. A similar oxidative cyclization (bifunctional behavior, epoxidation followed by acid catalyzed cyclization) was observed in the oxidation of linalool[13] over Al-Ti-Beta and Al-Ti-MCM-41, where the acidity at the Al sites was responsible for the cyclization.

TS-1 used in the present study was synthesized by the standard literature procedure[1] and thoroughly characterized *via* X-ray diffraction and FT-IR and UV-VIS spectroscopy. The liquid phase reaction was carried out in a two-necked glass reactor fitted with a water condenser under an N_2 atmosphere at the required temperature (298 and 333 K) with vigorous stirring. In a typical reaction the following constituents were employed: substrate (0.02 mol), aq. H_2O_2 (0.02 mol, 30 wt%), catalyst (TS-1, Si/Ti = 27, 20 wt% with respect to the substrate), acetone (10 g), butan-2-ol or H_2O (in a three phase system). At various reaction times products were analyzed *via* capillary gas chromatography (Shimatzu 14 A, OV-1 and Chiraldex G-TA with Flame Ionization Detector). Products were identified *via* GC retention times and GC–MS using authentic reference samples. When authentic samples were unavailable identification was performed *via* ^{1}H NMR spectroscopy.

Cyclization of the simplest molecule in this series, but-3-en-1-ol, occurs at room temperature using the TS-1–H_2O_2 system. In butan-2-ol the reaction rate is slow and it takes 18 h to reach a yield of 82%, 3-hydroxytetrahydrofuran **1** being the sole product (Scheme 1). However, in the presence of water as the dispersion medium (solid catalyst, aq. H_2O_2 and organic substrate initially forms three distinct phases) reaction proceeds at a faster rate (93.6% conversion after 6 h). Selectivity towards **1** decreases to 75.5%. In this case oxirane ring opening *via* attack of external H_2O molecules from the medium competes with intramolecular cyclization, leading to dihydroxylation (butane-1,2,4-triol, selectivity 24.5%). Interestingly, increasing the reaction temperature to 333 K in the latter case decreases the yield of **1** to 2.5% with selective dihydroxylation.[14] Unlike the benzenesulfenyl chloride system,[10] the cyclization of but-3-en-1-ol is relatively efficient in the present TS-1–H_2O_2 system. Another important aspect of the TS-1 catalyzed cyclization is that, unlike the radical addition reaction, the products are hydroxy-substituted oxacyclic compounds.

The tetrahydrofuran derivative 2-methyl-4-hydroxytetrahydrofuran **2** (*trans* : *cis* ratio 70 : 30) was formed from (±)-pent-4-en-2-ol in acetone (80% yield at room temperature after 18 h). In water at room temperature, the selectivity for **2** drops to 70%, with a *trans* : *cis* ratio of 67 : 33 after 12 h. At higher temperature in a water dispersion medium the dihydroxylation product predominates in a manner similar to that for but-3-en-1-ol. Interestingly, here also the intermediate epoxide is highly reactive and undergoes very rapid oxirane ring opening *via* either intramolecular cyclization or hydrolysis. However, using butan-2-ol as solvent **2** forms as the sole product in 84% yield (*trans* : *cis* ratio 72 : 28). The high *trans* selectivity among the diastereomers of **2** may be due to the higher stability of the transition state at the active site.

The cyclization of pent-4-en-1-ol occurred regioselectively to the 5-*exo* product tetrahydrofuran-2-methanol **3**. Attack of the hydroxy nucleophile definitely does not take place at the other carbon atom of the intermediate oxirane ring. Irrespective of the reaction medium (butan-2-ol, acetone or water), **3** was exclusively obtained in 98–99% yield. This is interesting, since 2,4,6,6-tetrabromocyclohexa-2,4-dienone-induced[9] cyclization leads to a mixture of tetrahydopyran to tetrahydrofuran in the ratio 3 : 1. In water at high temperature (333 K) no dihydroxylation product is formed. Although theoretical calculations on the transition state energies for the pent-4-en-1-yloxyl radical[11] indicates that the 5-*exo* product is strongly favored, and in the TS-1–H_2O_2 system oxidation is believed to occur *via* titanium hydroperoxo species **4**[15] (Scheme 2) and is thus essentially ionic in nature. Restricted geometry inside the TS-1 channel (MFI topology with intersecting 10-membered rings of 5.3 × 5.6 and 5.1 × 5.5 Å pore diameters and 0.10 $cm^3\ g^{-1}$ internal void volume helps in bending the chain) might play a crucial role in the regioselectivity of the cyclization. The decreasing trend for the ratio of tetrahydropyran to tetrahydrofuran from mesoporous MCM-41 to large pore Beta[13] followed by exclusive formation of tetrahydrofuran rings over medium pore TS-1 supports the above proposition.

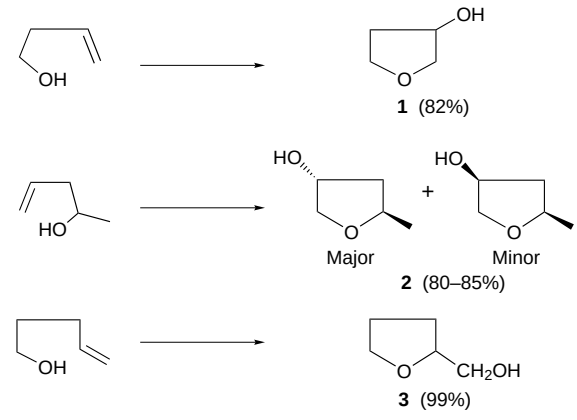

Scheme 1

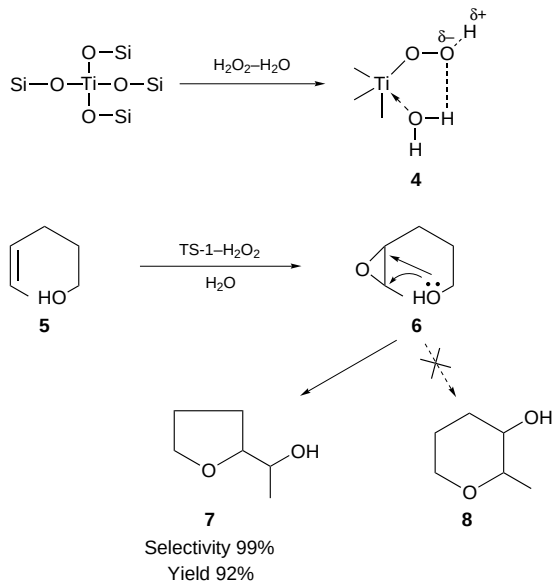

Scheme 2

One might suggest that the 5-*exo* product formation from **3** could be accounted for by the acidic nature of TS-1; if the reaction follows an S_N1 pathway, the hydroxy group would attack preferentially at the more substituted carbon atom due to the higher stability of the corresponding carbocation. On the contrary, alkyl group substitution at C_5 does not cause any change in the regioselectivity of cyclization as observed for *cis*-hex-4-en-1-ol **5** (Scheme 2). Between the two possibilities for the ring-opening of the intermediate oxirane **6**, the 5-*exo* product, 1-(tetrahydro-2-furyl)ethanol **7**, forms exclusively in 92% yield in acetone at 333 K. The 6-*endo* product, 2-methyl-3-hydroxytetrahydropyran **8**, is not formed. The titanium hydroperoxo species 4 protonates the oxirane **6** and thus activates[13] it for the nucleophilic attack of the hydroxy groups at C_1.

For the cyclization of hex-5-en-1-ol, where two products are possible, tetrahydropyran-2-methanol **9** only is formed in 90% yield in acetone at 333 K (Scheme 3). Interestingly, no intermediate epoxide was detected while studying the kinetics of various constituents of the reaction mixture by GC, indicating that TS-1 catalyzed the present cyclization process at a very fast rate and that ring closure takes place inside the cages of the zeolite immediately after the epoxidation.

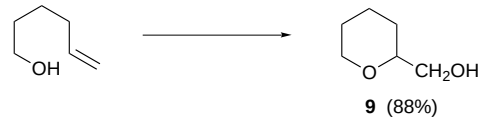

Scheme 3

In conclusion, we can say that, in the presence of aq. H_2O_2, TS-1 generates titanium hydroperoxo species **4**, which not only efficiently epoxidizes the double bond of the olefinic alcohols, but catalyzes epoxy ring-opening *via* intramolecular attack of the hydroxy nucleophile leading to oxacyclic ring formation. This reaction not only has enormous potential for the regioselective synthesis of substituted tetrahydrofuran and tetrahydropyran derivatives, but also opens up a new area involving the use of titanium silicates in cyclization reactions.

A. B. thanks the Japan Society for the Promotion of Science for a Post Doctoral Fellowship.

Note and References

† E-mail: asim@catal.t.u-tokyo.ac.jp

1 M. Taramaso, G. Perego and B. Notari, *US Pat.* 4410501, 1983; B. Notari, *Stud. Surf. Sci. Catal.*, 1987, **37**, 413.
2 T. Tatsumi, M. Nakamura, S. Negishi and H. Tominaga, *J. Chem. Soc., Chem. Commun.*, 1990, 476.
3 D. R. C. Huybrechts, L. DeBruycker and P. A. Jacobs, *Nature*, 1990, **345**, 240.
4 M. G. Clerici and P. Ingallina, *J. Catal.*, 1993, **140**, 71.
5 A. Thangaraj, S. Sivasanker and P. Ratnasamy, *J. Catal.*, 1991, **131**, 394; T. Tatsumi and N. Jappar, *J. Catal.*, 1996, **161**, 570.
6 J. S. Reddy and P. A. Jacobs, *J. Chem. Soc., Perkin Trans. 1*, 1993, 2665.
7 R. Reddy, J. S. Reddy, R. Kumar and P. Kumar, *J. Chem. Soc., Chem. Commun.*, 1992, 84.
8 M. D. Lord, J. T. Negri and L. A. Paquette, *J. Org. Chem.*, 1995, **60**, 191.
9 P. C. Ting and P. A. Bartlett, *J. Am. Chem. Soc.*, 1984, **106**, 2668.
10 S. M. Tuladhar and A. G. Fallis, *Tetrahedron Lett.*, 1987, **28**, 523.
11 J. Hartung, R. Stowasser, D. Vitt and G. Bringmann, *Angew. Chem., Int. Ed. Engl.*, 1996, **35**, 2820.
12 B. M. Trost and C. J. Li, *J. Am. Chem. Soc.*, 1994, **116**, 10 819.
13 A. Corma, M. Iglesias and F. Sanchez, *J. Chem. Soc., Chem. Commun.*, 1995, 1635.
14 A. Bhaumik and T. Tatsumi, unpublished work.
15 G. Bellussi, A. Carati, M. G. Clerici, G. Maddinelli and R. Millini, *J. Catal*., 1992, **133**, 220.

Received in Cambridge, UK, 26th November 1997; 7/08528A

Hydrogen bonding and cooperativity effects on the assembly of carbohydrates

Manuela López de la Paz, Jesús Jiménez-Barbero and Cristina Vicent*†

Departamento de Química Orgánica Biológica, Institut de Química Orgánica, CSIC, Juan de la Cierva 3, E-28006 Madrid, Spain

The effect of intramolecular hydrogen bonds on the cooperative assembly of carbohydrate derivatives has been evaluated; the 1,3-diaxial OH··OH intramolecular hydrogen bond is at the origin of the dimerization of diol 1; and one intermolecular OH··OH bond accounts for 2.5 kcal mol^{-1} in $CDCl_3$ and 3 kcal mol^{-1} in $CDCl_3$–CCl_4.

Hydrophobic interactions, hydrogen bonding and cation binding are at the origin of the recognition processes in which carbohydrates are involved. The study of carbohydrate OH··OH hydrogen bond energetics is of fundamental interest for understanding these recognition processes.

One particular characteristic of hydrogen bonding is cooperativity, considered as the enhancement of the first hydrogen bond (HB) between a donor and an acceptor when a second HB is formed between one of these two species and a third partner.[1] A quantitative treatment of HB cooperativity was described initially by Huyskens.[2] Theoretical[3] and experimental[4] methods have also allowed the quantification of this effect. Evidence of intramolecular σ-cooperativity in carbohydrates has arisen from neutron diffraction data of crystalline structures of mono- and di-saccharides.[5] In solution, intramolecular cooperativity has been studied by NMR spectroscopy in polar solvents[6] and by FTIR.[7] In contrast, evidence of intermolecular cooperativity in carbohydrates has only come from neutron diffraction data of carbohydrates[8] and protein–carbohydrate complexes.[9]

This report represents a contribution within a project to design self-assembled structures based on carbohydrate intermolecular OH··OH hydrogen bonds.[10] Here we have evaluated the energetic advantage of establishing cooperative intermolecular HBs for assembling simple carbohydrates. In addition, we have also studied the relative stereochemistry of OH groups that favour this process.

The possibility of self-assembly of diols of 1,6-anhydro-β-D-glycopyranosides of different relative configuration and position with respect to the anomeric centre [2,4 (*a*,*a*) *cis*-diol **1**, 3,4 (*a*,*e*) *cis*-diol **4**, 2,3 (*e*,*a*) *cis*-diol **5** and 3,4 (*e*,*e*) *trans*-diol **6**] has been explored.‡ The only diol that showed significant aggregation behaviour in $CHCl_3$ was the glucose 1,3-diaxial diol **1**.

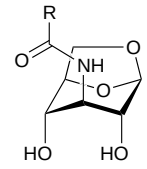

1 R = $C_{15}H_{31}$

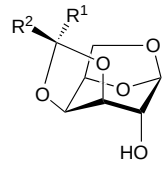

2a R^1 = R^2 = Me
b R^1 = Ph, R^2 = H

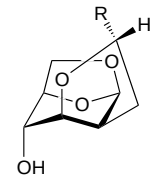

3a R = C_6H_4OMe
b R = Ph

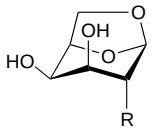

4 R = OAc

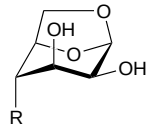

5 R = OBn

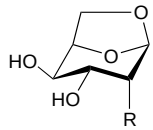

6 R = OBz

A detailed study of the intramolecular HB network for the monomer of **1** was carried out in dilute $CDCl_3$ solution by ^{1}H NMR spectroscopy. Additionally, the axial monoalcohols, 1,6-anhydro-β-D-glycopyranosides **2a** and **3a**, were used as models to study the influence of a second hydroxy group with a 1,3-diaxial orientation, as present in diol **1**, on intermolecular cooperativity.

Monoalcohols **2a** and **3a** in $CDCl_3$ at low concentration show high $^3J_{CH,OH}$ values (9 Hz), consistent with a fixed conformation of the CHOH angle (larger than 150°), which can be attributed to an hydrogen bonded OH.[6c] For the 1,3-diaxial diol **1**, the OH(2) resonance follows the same trend [as expected for hydrogen bonding to OH(4) or O(5)] but, in contrast, the OH(4) resonance now has a medium size $^3J_{CH,OH}$ value, indicating that it is not hydrogen bonded. Neither of the OH(2) or OH(4) resonances achieve exchange decoupling at any accessible concentration, a characteristic feature of fixed OHs.[6c]

Partial deuteration of **1** in $CDCl_3$ at low concentration shows that the OH(2) resonance has a negative isotopic effect (−0.0165 ppm), consistent with OH(2) being a donor.[6b] Therefore, these results show that both monoalcohols **2a** and **3a** have their hydroxy groups intramolecularly fixed by a HB to O(5). In contrast, for **1** the 1,3-diaxial orientation of both hydroxy groups favour OH(2) to be hydrogen bonded, as a donor, to OH(4). These HBs must affect the self-assembly characteristics of the different compounds.

The characterization of the aggregates in solution was performed using different methods. ^{1}H NMR dilution experiments in $CDCl_3$ at 299 K of **1**–**6** allowed us to calculate the stability constants of the dimerization process.§ Neither of the monoalcohols **2a** or **3a** dimerize.¶ In contrast, diol **1** [2,4(*a*,*a*)] presents a dimerization constant of 70 M^{-1} at 299 K ($\Delta G°$ = −2.5 ± 0.1 kcal mol^{-1}).

Vapour pressure osmometry measurements (VPO)[11] in $CHCl_3$ suggested that, for a concentration range between 0.05–0.01 M, the monoalcohols **2a** and **3a** are monomers. On the other hand, **1** presents a molecular weight which corresponds to 1.6 times that of the monomer. This value is in agreement with the percentage of dimer which is present in solution according to the NMR-derived stability constant (80%).

Chemical shifts, ^3J values and temperature coefficients also indicate that the assembly is mediated by OH··OH hydrogen bonds. Table 1 shows that the coefficients of OH(2) for **2a** and OH(4) for **3a** are not concentration dependent, in contrast with the observations made for **1**.[12] The $^3J_{CH,OH}$ values of **1**–**3** at high concentration indicate their involvement in HBs, with the exception of OH(4) of **1** which shows a *J* value of 5.4 Hz at all concentrations. The NH of **1** does not show any concentration dependence for the NMR parameters. This experimental evidence is consistent with the amide not being involved in the self-association process.‖

The clear difference in the solution self-assembly behaviour of **1** with respect to monoalcohols **2a** and **3a** indicates that the addition of the extra OH in a pyranoid ring having a 1,3-*syn* diaxial orientation accounts for an extra stabilization of the dimer of 2.5 kcal mol^{-1} in $CDCl_3$ compared to the monoalcohols. As a test for a non-intramolecular hydrogen bonded OH, ethanol under the same conditions measured for **1**–**6** did not show any measurable dimerization constant.

Thermodynamic parameters for the dimerization of **1** in $CDCl_3$–CCl_4 (1–1.3) were obtained from a Van't Hoff plot (from 296–318 K). Values of $\Delta H°$ = −6.5 kcal mol^{-1} and $\Delta S°$

Table 1 ^{1}H NMR chemical shifts coupling constants and temperature coefficients of OH resonances of **1**, **2a** and **3a** at two different concentrations

Compound	Concentration/ mM	δ (ppm)	OH(2) $^3J^a$/Hz	$\Delta\delta_{OH(2)}/\Delta T^b$ (ppm K^{-1})	δ (ppm)	OH(4) $^3J^a$/Hz	$\Delta\delta_{OH(1)/\Delta T}{}^b$ (ppm K^{-1})
1	110	4.00	9.0	-1.0×10^{-2}	4.68	5.4	-1.6×10^{-2}
	0.05	2.82	10.2	-2.3×10^{-3}	2.73	5.4	-4.0×10^{-3}
2a	110	2.21	8.4	-5.5×10^{-3}	—	—	—
	0.05	1.95	8.7	-2.2×10^{-3}	—	—	—
3a	110	—	—	—	2.534	8.7	-5.2×10^{-3}
	0.05	—	—	—	2.304	9.3	-2.4×10^{-3}

[a] Data at 298 K. [b] Measured between 297 and 313 K.

= +11.8 kcal mol^{-1} K^{-1} were estimated. The stability constant of the dimer at 299 K was 150 M^{-1} ($\Delta G° = -3.0 \pm 0.1$ kcal mol^{-1}). Ethanol under the same conditions showed a dimerization constant of 0.1 M^{-1}.

To quantify the effect of cooperativity on the dimerization process, it is important to know the structure of the dimer. In principle, the structure of the dimer present in solution could be of two types: an open dimer with one cooperative intermolecular HB stabilizing the dimer [Fig. 1(*a*)], and a closed dimer with two intermolecular HBs established in a cyclic and cooperative way [Fig. 1(*b*)]. The implication of O(5) in the network cannot be excluded.

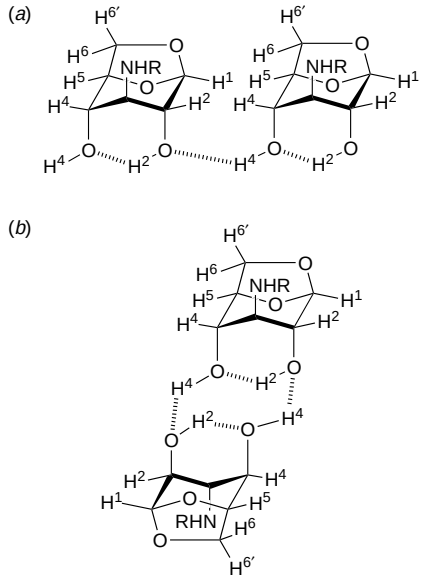

Fig. 1 Schematic representation of two possible dimeric structures for **1**: (*a*) open dimer and (*b*) closed dimer

NOESY experiments of a concentrated solution of **1** (0.1 M) were performed in order to obtain structural information about the dimer. Since two free OH groups are present in the molecule, regular experiments as well as MINSY-type spectra[13] were recorded in order to exclude chemical exchange-mediated cross peaks. Thus, besides the regular NOESY spectrum, additional experiments saturating OH(2) and OH(4) hydroxy groups were recorded. The obtained results unambiguously indicate the presence of intermolecular NOEs. In particular, H(1)/H(6*exo*), H(1)/H(6*endo*), H(1)/H(5), H(2)/H(4), H(5)/H(2) and H(1)/H(4) cross-peaks were detected. These NOEs are not seen when the experiments are carried out at low concentration and are only compatible with the existence of an open dimer structure. This open structure is also supported by the measured $^3J_{CH,OH}$ values. MM2* calculations** of this structure show that it is stable and account for the observed NOEs. This structure shows that the carbonyl group cannot be hydrogen bonded to any donor moiety.

Thus, a single cooperative intermolecular OH··OH bond accounts for 2.5 kcal mol^{-1} in $CDCl_3$ and 3 kcal mol^{-1} in $CDCl_3$–CCl_4.

The difference in the self-assembly behaviour of **1** with respect to diols **4**, **5** and **6** has to be related to the difference in strength and directionality of the intramolecular HBs.[7c,14]

We are now extending this study to diols involving other positions in the pyranoid ring in order to evaluate the energetic advantage of intermolecular HB cooperativity.

Financial support by DGICYT (Grant PB96-0833) is gratefully acknowledged. M. L. P. thanks Comunidad de Madrid for a fellowship. C. V. thanks Dr Soledad Penadés for introducing her to the field of carbohydrate recognition. We thank Dr Jose García de la Campa for helpful discussions.

Notes and References

† E-mail: cristina@csic.es

‡ All new compounds gave satisfactory elemental analyses and spectroscopic data. ^3J analysis shows that all compounds adopt a chair conformation in $CDCl_3$ solution.

§ All dilution experiments were carried out three times and the $\Delta G°$ values were reproducible within ±0.1 kcal mol^{-1}. Dilution data were fitted to a dimerization process using an infinite non-cooperative model. We thank Dr C. A. Hunter (University of Sheffield) for kindly providing the fitting program.

¶ Diols **4** and **5** showed small dimerization constants (1.8 and 1.4 M^{-1}, respectively).

‖ Additionally, a concentration dependent FTIR experiment shows no evidence for intermolecular hydrogen bonded species involving the NH or C=O of the amide (ν_{NH} 4335 and ν_{CO} 1772 cm^{-1} at high and low concentration).

** Molecular Mechanics Calculations were carried out using MM2* with the GB/SA solvent model for $CHCl_3$.

1 H. S. Frank and W. Y. Wen, *Discuss. Faraday Soc.*, 1957, **24**, 133.
2 P. L. Huyskens, *J. Am. Chem. Soc.*, 1977, **99**, 2578.
3 H. Guo and M. Karplus, *J. Phys. Chem.*, 1994, **98**, 7104; R. P. Sear and G. Jackson, *J. Chem. Phys.*, 1996, **105**, 1113.
4 H. Kleeberg, D. Klein and W. A. Luck, *J. Phys. Chem.*, 1987, **91**, 3200; B. Frange, J.-L. M. Abboud, C. Benamou and L. Bellon, *J. Org. Chem.*, 1982, **47**, 4553; G. Maes and J. Smets, *J. Phys. Chem.*, 1993, **97**, 1818.
5 *Hydrogen Bonding in Biological Structures*, ed. G. A. Jeffrey and W. Saenger, Springer-Verlag, 1991, p. 569.
6 (*a*) J. C. Christofides and D. B. Davies, *J. Chem. Soc., Perkin Trans. 2*, 1987, 97; (*b*) B. N. Craig, M. U. Janssen, B. M. Wickersham, D. M. Rabb, P. S. Chang and D. J. O'Leary, *J. Org. Chem.*, 1996, **61**, 9610; (*c*) C. M. Pearce and J. K. M. Sanders, *J. Chem. Soc., Perkin Trans. 1*, 1994, 1119.
7 P. Uhlman and A. Vasella, *Helv. Chim. Acta*, 1992, **75**, 1979; R. G. Zhbankov, *J. Mol. Struct.*, 1992, **270**, 523.
8 M. Notelmeyer and W. Saenger, *J. Am. Chem. Soc.*, 1980, **102**, 2710.
9 N. K. Vyas, *Curr. Opin. Struct. Biol.*, 1991, **1**, 732.
10 M. López de la Paz, G. Ellis, S. Penadés and C. Vicent, *Tetrahedron Lett.*, 1997, **38**, 1659.
11 X. Li, D. N. Chin and G. M. Whitesides, *J. Org. Chem.*, 1996, **61**, 1779.
12 H. Kessler, *Angew. Chem., Int. Ed. Engl.*, 1982, **21**, 512.
13 W. M. Jr. and A. G. Redfield, *J. Magn. Reson.*, 1988, **78**, 150.
14 L. P. Kuhn, *J. Am. Chem. Soc.*, 1952, **74**, 2492; P. v. R. Schleyer, *J. Am. Chem. Soc.*, 1961, **83**, 1368.

Received in Cambridge, UK, 20th November 1997; 7/08386F

Anion coordination by aminoglycosides: structural and charge effects

Tsuyoshi Ohyama, Dongqing Wang and James A. Cowan*†

Evans Laboratory of Chemistry, The Ohio State University, 100 West 18th Avenue, Columbus, Ohio 43210, USA

Aminoglycosides provide new approaches to the recognition and specific binding of anionic species, and show promise for development as anion sensors in biological and separation science.

Aminoglycoside antibiotics constitute a large family of molecules that find extensive clinical use in the treatment of gram-negative infections.[1] Recent reports have also demonstrated specific and high affinity (μM) binding of aminoglycosides to RNA structural motifs.[2–6] Aminoglycoside complexes of metal ions have previously been reported,[7–10] however, the large positive charge density of the drug in neutral solution suggested to us that such molecules might prove to be efficient anion complexing agents. This work contrasts with earlier studies of anion binding that have focused on polyamine macrocycles including hexaaza ligands and porphyrin derivatives,[11–14] Novel advances in this chemistry should afford significant opportunities for the development of anion sensors,[15–17] and in separation science.[18–20] Here, we communicate our initial findings on the coordination chemistry of neomycin B **1** with a variety of negatively charged species. Binding thermodynamics have been evaluated by isothermal titration calorimetry (Fig. 1), and structural insight obtained by ^{1}H, ^{13}C, ^{15}N and ^{31}P NMR spectroscopy.‡ These studies complement recent work on ferrocenyl receptors of anions.[16] In contrast to the classic inner-sphere coordination chemistry of metal ions, anion binding more typically involves outer-sphere binding of multi-atomic species; although outer-sphere interactions of cationic complexes are also well established in biological chemistry.[21–24]

Neomycin B, **1**, possesses six ionizable amino functional groups, with pK_as > 6.5, and it was expected that such a highly charged molecule might complex anionic species with moderate to high affinity. Fig. 1 establishes this fact with K_a varying from 332 dm^3 mol^{-1} for CrO_4^{2-} to 1.3 × 10^5 dm^3 mol^{-1} for

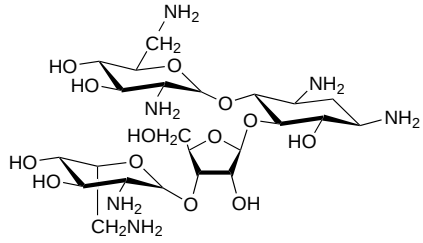

1

$Fe(CN)_6^{4-}$. The coordination chemistry of neomycin B has been explored with two classes of anionic species, differing in their distribution of charge density and described as spherical [$Fe(CN)_6^{3-}$, $Fe(CN)_6^{4-}$, $Cr(C_2O_4)_3^{3-}$, CrO_4^{2-}], where the charge is confined in a spherical array, and linear [AMPH$^-$, ADPH^{2-}, ATPH^{3-}, and adenosine tetraphosphate (AtetraPH^{4-})], where the charge is spread along a chain of atoms. Distinct thermodynamic data (Fig. 1) were obtained for the spherical and linear charged species. Also the binding affinity is found to increase with increasing charge on both the aminoglycoside and bound anion, although different factors control the experimental K_as for each class of anion. The linear adenosine phosphate series demonstrates an approximately constant binding enthalpy [ΔH *ca.* −6.6 kcal mol^{-1} (1 cal = 4.184 J), Fig. 1], with the charge dependence of the binding affinity arising through variation of the entropy term, presumably as a result of more extensive disruption of the solvation state for the longer phosphate chain. In contrast, the spherical charged species show a marked variation for both the entropy and enthalpy terms; although for both spherical and linear charged species the magnitude of the ΔH term demonstrates that binding is enthalpically controlled. This contrasts with binding to oligo- or poly-nucleotides where ligand binding is typically entropically driven.

Our attention was drawn to the mode of binding of the anions to the aminoglycosides. None of the anion–aminoglycoside complexes demonstrate the direct inner-sphere binding mode typical of classical metal ion coordination to a basic ligand. Rather, outer-sphere binding must be mediated either through hydrogen bonding and/or electrostatic interactions. The similarity in binding affinity for ATPH^{3-}, $Fe(CN)_6^{3-}$ and $Cr(C_2O_4)_3^{3-}$, and their very different hydrogen-bond accepting abilities (decreasing across the series), suggest the dominance of electrostatic attraction in defining K_a. Further support for this conclusion came from the salt dependence of K_a. In the Debye concentration range, the linear dependence of ln K_a with [NaCl]$^{1/2}$, where NaCl is the background electrolyte, is consistent with outer-sphere complex formation and long-range electrostatic interactions.[25] Plots of ln K_a *vs.* [NaCl]$^{1/2}$ for $Fe(CN)_6^{4-}$, ATPH^{3-} and CrO_4^{2-} binding to neomycin B were fitted to the equation, $\ln K_a = \ln\{(4\pi N_L a^3)/3000\} + b - ab\{(2Z^2e^2)/(\varepsilon\varepsilon_0 kT)\}^{1/2}[\mathrm{NaCl}]^{1/2}$, where symbols are defined in ref. 25. In each case linearity was maintained in the Debye range, and gradients of −5.7, −11.9 and −9.4, were obtained, respectively.

Structural aspects of anion binding to neomycin B have been evaluated by heteronuclear 1D and 2D NMR methods.

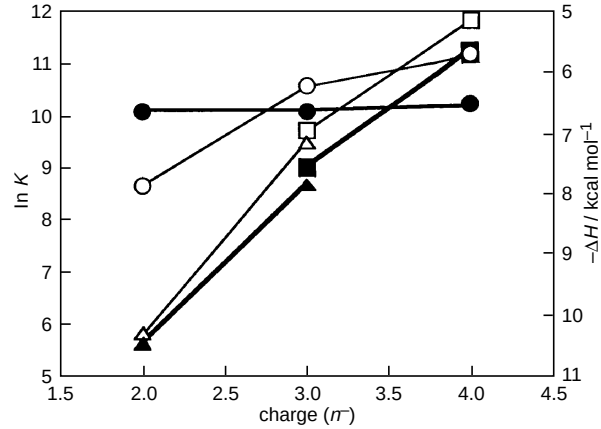

Fig. 1 Variation of thermodynamic binding parameters with the total charge of the anionic species (*n*). ADPH^{2-}, ATPH^{3-}, AtetraPH^{4-} (circles); $Fe(CN)_6^{3-/4-}$ (squares); CrO_4^{2-}, $Cr(C_2O_4)_3^{3-}$ (triangles), where open and closed symbols refer to ln *K* and ΔH data, respectively. Data were collected on a Microcal OMEGA isothermal titration calorimeter at pH 5.5 in 10 mM sodium acetate. No evidence for irreversible or covalent interactions was noted with these complexation reactions. Errors are within the radius of the symbols.

Assignments for ^{1}H, ^{13}C and ^{15}N resonances of neomycin have been previously reported.[26,27] Neither ^{1}H, ^{13}C, nor ^{15}N resonances or crosspeaks in 1D or 2D NMR experiments, respectively, demonstrated a significant change after binding of any of the anionic species to neomycin B, and so complex formation does not involve significant structural perturbation of the sugar rings. Fast exchange is indicated by the occurrence of only sharp exchange-averaged resonances for bound and free forms. ^{31}P NMR spectra of $ADPH^{2-}$, $ATPH^{3-}$ and $AtetraPH^{4-}$ show significant changes in the shift value of only the terminal phosphate upon binding to neomycin B. Also double protonation of the terminal phosphate at ATP at reduced pH (= 5) resulted in loss of binding, even though the overall charges of $ADPH^{2-}$ and $ATPH_2^{2-}$ are identical. These results support an end-on binding mode rather than a parallel mode (below). Such a hypothesis is also consistent with the approximately constant ΔH for binding of the adenosine phosphates (Fig. 1) to neomycin B, since only the terminal phosphate serves as an hydrogen-bond acceptor.

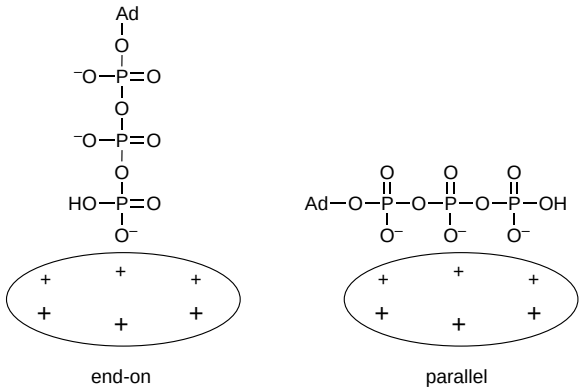

In conclusion, aminoglycosides have been shown to bind a variety of negatively charged species with moderate to high affinities, and structural differentiation of charge arrays (spherical and linear) has been demonstrated. The critical need for such molecules as biological sensors[10,17] and in separation science,[18–20] will fuel further efforts in our laboratory.

Notes and References

* E-mail: cowan@chemistry.ohio-state.edu

† J. A. C. is a Camille Dreyfus Teacher-Scholar (1994–99). Supported by grants from the donors of the Petroleum Research Fund (administered by the American Chemical Society) and the National Science Foundation (CHE-9706904).

‡ ^{1}H, ^{13}C, ^{31}P and ^{15}N NMR spectra were recorded on a Bruker 300 MHz spectrometer. ^{15}N measurements were made in 10 mm sample tubes with 200 mM solutions of neomycin. Other experiments were performed in 5 mm tubes with 100 mM neomycin solutions. A 200 mM sodium acetate buffer solution (pH 5) was used with 10% D_2O for spin lock. Buffer concentrations were higher than for calorimetry experiments to accommodate the increased neomycin concentration. 2D C–H correlation spectra were recorded with a phase-sensitive DEPT polarization transfer pulse sequence.

1 D. Moazed and H. H. Noller, *Nature*, 1987, **327**, 389.
2 M. L. Zapp, S. Stern and M. R. Green, *Cell*, 1993, **74**, 969.
3 Y. Wang and R. R. Rando, *Chem. Biol*., 1995, **2**, 281.
4 D. Fourmy, M. I. Recht, S. C. Blanchard and J. D. Puglisi, *Science*, 1996, **274**, 1367.
5 T. K. Stage K. J. Hertel and O. C. Uhlenbeck, *RNA*, 1995, **1**, 95.
6 U. von Ahsen, J. Davies and R. Schroeder, *J. Mol. Biol*., 1992, **226**, 935.
7 S. Hanessian and G. Patil, *Tetrahedron Lett*., 1978, **12**, 1031.
8 H. A. Kirst, B. A. Trudell and J. E. Toth, *Tetrahedron Lett*., 1981, **22**, 295.
9 A. Mashaly, *Polyhedron*, 1993, **12**, 745.
10 A. W. Czarnik, *Trends Org. Chem*., 1993, **4**, 123.
11 P. A. S. Gale, L. Jonathan, V. Kral and V. Lynch, *J. Am. Chem. Soc*., 1996, **118**, 5140.
12 P. S. Y. Ledvina, C. Nanhua, Q. Abha and A. Florante, *Proc. Natl. Acad. Sci. USA*, 1996, **93**, 6786.
13 D. A. R. Nation, J. Martell and E. Arthur, *Inorg. Chem*., 1996, **35**, 4597.
14 D. M. V. Rudkevich, W. Brzozka, P. Zbigniew, J. Marcin, W. P. R. V. Stauthamer, G. J. van Hummel, S. M. Franken, S. Harkema, J. F. J. Engbersen and D. N. Reinhoudt, *J. Am. Chem. Soc*., 1994, **116**, 4341.
15 P. D. Beer and D. K. Smith, *Prog. Inorg. Chem*., 1997, **46**, 1.
16 P. D. Beer, K. R. Graydon, A. O. M. Johnson and D. K. Smith, *Inorg. Chem*., 1997, **36**, 2112.
17 A. W. Czarnik, *Chem. Biol*., 1995, **2**, 423.
18 R. D. Rogers and J. Zhang, *Ion Exch. Solvent Extr*., 1997, **13**, 141.
19 K. M. Rohal, D. M. Van Seggen, J. F. Clark, M. K. McClure, C. K. Chambliss and S. H. Strauss, *Solvent Extr. Ion. Exch*., 1996, **14**, 401.
20 C. F. Baes and B. A. Moyer, *J. Phys. Chem. B*, 1997, **101**, 6566.
21 J. A. Cowan, *Inorganic Biochemistry: An Introduction*., Wiley–VCH, New York, 1997, pp. 20–23 and 242–247.
22 J. A. Cowan, *J. Inorg. Biochem*., 1993, **49**, 171.
23 C. B. Black and J. A. Cowan, *J. Am. Chem. Soc*., 1994, **116**, 1174.
24 C. B. Black, M. Foster and J. A. Cowan, *J. Biol. Inorg. Chem.*, 1996, **1**, 500.
25 S. Petrucci, in *Ionic Interactions*, ed. S. Petrucci, Academic Press, New York, 1971, vol. 1, pp. 117–177.
26 R. Botto and B. Coxon, *J. Am. Chem. Soc*., 1983, **105**, 1021.
27 D. G. Reid and K. Gajjar, *J. Biol. Chem*., 1987, **262**, 7967.

Received in Bloomington, IN, USA, 19th August 1997, revised manuscript received 2nd December 1997; 7/08868J

Highly dissymmetric chelate coordination of 3,4,7,8-tetramethyl-1,10-phenanthroline to Cu^{I}(SR)

Andreas F. Stange, Torsten Sixt and Wolfgang Kaim*

Institut für Anorganische Chemie, Universität Stuttgart, Pfaffenwaldring 55, D-70550 Stuttgart, Germany

Not only Au^{I} and Hg^{II} species but also Cu^{I}(SR) fragments can bind in a highly dissymmetrical fashion to symmetrical diimine chelate ligands; the 2 + 1 coordination arrangement observed for the metal in two complexes (tmphen)Cu(SR) (tmphen = 3,4,7,8-tetramethyl-1,10-phenanthroline) is characterised by obtuse angles *α*[N(1)–Cu–S] > 159° and by two very different distances Cu–N(1) and Cu–N(2).

The copper(I) state is characterised by the lack of a clear preference for specific coordination numbers (CN) or coordination geometries, the most common arrangements being close to tetrahedral (CN 4) or trigonal planar (CN 3).[1,2] Higher and lower coordination numbers, in particular CN 2, have also been documented.[2]

In probing copper–thiolate–N-chelate ligand chemistry to mimic the Cu_A dinuclear electron transfer center of enzymes[3] we reacted the α-diimine ligand 3,4,7,8-tetramethyl-1,10-phenanthroline (tmphen)[4] with electrolytically[5] obtained 2,4,6-trimethyl- and 2,6-diphenyl-thiophenolatocopper(I), Cu(SMes) and Cu(SDpp). The result† was not a di- or tetra-nuclear arrangement[3c,d] but mononuclear copper(I) complexes which could be crystallised for structural characterisation (Figs. 1 and 2).‡

Copper(I) does not normally display the same strong preference for a coordination number of two with linear coordination geometry as do gold(I) or mercury(II) centres, yet the list in Table 1 illustrates that the complexes (tmphen)Cu(SR) exhibit unusually distorted geometries as evident from very obtuse angles α and large differences between the distances Cu–N(1) and Cu–N(2), despite the formal equivalence of both nitrogen donor sites and the symmetry of the aryl groups, R (Table 1).

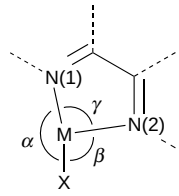

Gold(I) or mercury(II) centres which strongly prefer the linear geometry can be forced to accept a third donor atom *via* chelate coordination. Structurally characterised examples related to the neutral species (tmphen)Cu(SR) include the ionic systems [(bpy)Au(PPh_3)]PF_6[6a] and [(bpy)HgMe]NO_3 (Table 1; bpy = 2,2′-bipyridine).[6b] Ligands, especially thiolates, with steric bulk may cause a similar distortion from the trigonal geometry of d^{10} metal centres as has been realized in the T-shaped $(Et_2O)Zn^{II}(SC_6H_2Bu^t_3\text{-}2,4,6)_2$[7b] and, in attenuated form, with the compound (phen)Cu[$SSi(OBu^t)_3$] (phen = 1,10-phenanthroline).[7b]

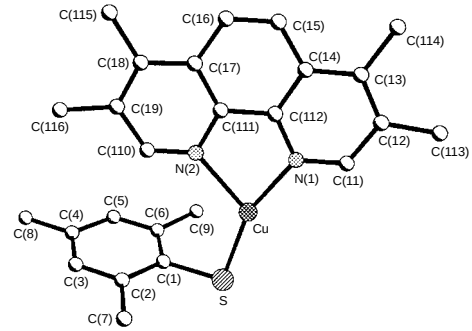

Fig. 1 Molecular structure of the metal complex in (tmphen)Cu(SMes)·0.5C_3H_6O with atom numbering. Selected bond lengths (Å) and angles (°): Cu–N(1) 1.976(2), Cu–N(2) 2.159(2), Cu–S 2.1470(8), S–C(1) 1.787(3); N(1)–Cu–N(2) 80.4(1), N(1)–Cu–S 159.13(8), S–Cu–N(2) 120.48(7), C(1)–S–Cu 98.7(1). Cu lies in the S–N(1)–N(2) plane; torsional angles (°): N(1)–Cu–S–C(1) −166.96(2), N(2)–Cu–S–C(1) 13.1(1).

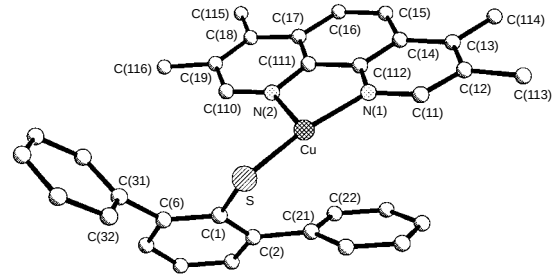

Fig. 2 Molecular structure of (tmphen)Cu(SDpp) with atom numbering. Selected bond lengths (Å) and angles (°): Cu–N(1) 1.972(4), Cu–N(2) 2.172(4), Cu–S 2.1687(14), S–C(1) 1.775(5), C(21)–C(22) 1.388(7); N(1)–Cu–N(2) 79.9(2), N(1)–Cu–S 164.37(12), S–Cu–N(2) 115.68(12), C(1)–S–Cu 97.8(2). Cu lies 0.026(2) Å over the S–N(1)–N(2) plane; torsional angles (°): N(1)–Cu–S–C(1) −136.1(5), N(2)–Cu–S–C(1) 50.2(2).

Table 1 Geometrical parameters for complexes with 2 + 1 coordination arrangement

Complex	α/°	β/°	γ/°	M–N(1)/Å	M–N(2)/Å	Ref.
(tmphen)Cu(SDpp)	164.4	115.7	79.9	1.972	2.172	This work
(tmphen)Cu(SMes)	159.1	120.5	80.4	1.976	2.158	This work
(phen)Cu[$SSi(OBu^t)_3$]	144.6	133.5	80.9	2.031	2.108	7(*b*)
[(bpy)Au(PPh_3)]$^+$	157.4	130.4	71.4	2.166	2.406	6(*a*)
[(bpy)HgMe]$^+$	164.0	126.0	69.4	2.236	2.421	6(*b*)
$(Et_2O)Zn(SC_6H_2Bu^t_3)_2$	159.6[a]	—	—	—	—	7(*a*)

[a] Angle S(1)–Zn–S(2).

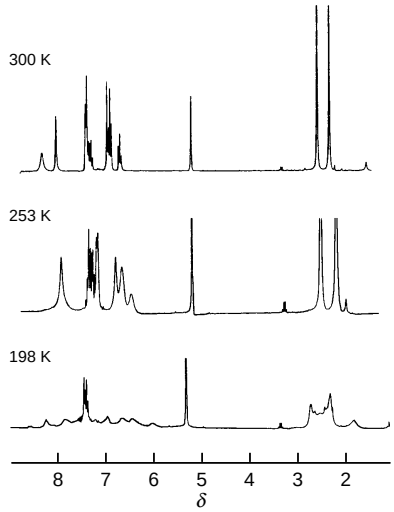

Fig. 3 Temperature-dependent ^{1}H NMR spectra of (tmphen)Cu(SDpp) in CD_2Cl_2 (300, 253 and 198 K, from top to bottom; 250 MHz)

The unsymmetrical coordination of the chelate ligand to the Cu^I center as observed in the solid state is probably responsible for the selective broadening in the ^{1}H NMR spectrum of (tmphen)Cu(SDpp) (Fig. 3).

These observations suggest a low but non-negligible barrier for the 'movement' of Cu between two equivalent energy minimum sites, separated by *ca*. 0.28 Å. No intermolecular interactions were recognised in the crystal structures which can be made responsible for this unusual copper(I)–thiolate[3c,d,8] coordination arrangement. To rationalise the observed dissymmetry we thus invoke the strong σ and π donor effect of thiolate groups SR and the donor substitution of the α-diimine tmphen.[4] There appears to be no need then for full coordination of a third donor atom to the electron-rich copper(I) centres, leaving the inevitably close second nitrogen atom N(2) of the chelate ligand as a lesser coordinated donor centre to result in the observed coordination number 2 + 1.

Notes and References

* E-mail: kaim@iac.uni-stuttgart.de

† *Synthesis*: Arylcopper(I) precursors were obtained by electrolysing[5] solutions of the thiophenols[9,10] in acetonitrile–2 mmol dm^{-3} NBu_4ClO_4 in a cell containing a copper anode.

(2,4,6-Trimethylthiophenolato)(3,4,7,8-tetramethyl-1,10-phenanthroline)copper(I) was prepared by adding 250 mg (1.18 mmol) of the thiolatocopper precursor to a suspension of 278 mg (1.18 mmol) tmphen in 20 ml toluene. After reflux for 2.5 h the clear brownish solution was filtered hot, cooling produced 352 mg (62%) of (tmphen)Cu(SMes)·C_7H_8. Single crystals suitable for X-ray diffraction were obtained from acetone as (tmphen)Cu(SMes)·0.5C_3H_6O (correct C, H, N elemental analysis). ^{1}H NMR (CD_2Cl_2, 300 K): δ 2.16 (s, 6 H, Mes-4-CH_3), 2.41 (s, 24 H, tmphen-3,8-CH_3 and Mes-2,5-CH_3), 2.65 (s, 6 H, tmphen-4,7-CH_3), 6.66 (s, 4 H, Mes-3,5-H), 8.03 (s, 4 H, tmphen-5,6-H), 8.34 (s, 4 H, tmphen-2,9-H).

(2,6-Diphenylthiophenolato)(3,4,7,8-tetramethyl-1,10-phenanthroline)copper(I) was prepared by adding 120 mg (0.37 mmol) of the thiolatocopper precursor to a solution of 87 mg (0.37 mmol) tmphen in 25 ml toluene. After reflux for 1 h the clear brownish solution was filtered hot, and careful cooling produced 50 mg (24%) of the compound, partially as single crystals suitable for X-ray diffraction. Correct elemental analysis (C, H, N). ^{1}H NMR (CD_2Cl_2, 300 K): δ 2.45 (s, 6 H, 3,8-CH_3), 2.70 (s, 6 H, 4,7-CH_3), 6.79 (t, *J* 7.4 Hz, 2 H, aryl-H), 6.96–7.05 (m, 5 H, aryl-H), 7.35–7.50 (m, 6 H, aryl-H), 8.11 (s, 2 H, 5,6-H), 8.40 (br s, 2 H, 2,9-H). Selective broadening of the resonances was observed upon cooling to 198 K (Fig. 3).

‡ *Crystallography*: (tmphen)Cu(SMes)·0.5C_3H_6O: $C_{25}H_{27}CuN_2S$·0.5C_3H_6O, M = 480.16, crystal size 0.4 × 0.4 × 0.4 mm, monoclinic, space group $P2_1/n$ (no. 14), a = 8.1319(7), b = 14.8164(12), c = 19.6605(12) Å, β = 98.388(8)°, U = 2343.5(3) Å^3, D_c = 1.351 g cm^{-3}, μ(Mo-Kα) = 1.039 mm^{-1}, F(000) = 994, Wyckoff scans, 6561 measured reflections, 6156 independent reflections, 5830 reflections used for refinement, Lorentz polarisation, R = 0.0501 for 4244 reflections with $I > 2\sigma(I)$; 183 K, Siemens P4 diffractometer with graphite monochromator and Mo-Kα radiation (λ = 0.710 73 Å). The structure was solved by direct methods (Siemens SHELXTL-PC) and refined (SHELXL-93) by full-matrix least squares on F^2 (362 parameters). One half equivalent of a solvent molecule had to be included. Hydrogen atoms were introduced at calculated positions and refined freely; (tmphen)Cu(SDpp): $C_{34}H_{29}CuN_2S$, M = 561.19, crystal dimensions 0.4 × 0.4 × 0.3 mm, monoclinic, space group $P2_1/n$ (no. 14), a = 11.949(2), b = 13.284(2), c = 17.636(2) Å, β = 104.56(1)°, U = 2709.5(6) Å^3, D_c = 1.376 g cm^{-3}, μ(Mo-Kα) = 0.909 mm^{-1}, F(000) = 1168, Wyckoff scans, 6188 measured reflections, 5971 independent reflections, 5499 reflections used for refinement, Lorentz polarisation, R = 0.0687 for 3490 reflections with $I > 2\sigma(I)$; 183 K, Siemens P4 diffractometer with graphite monochromator and Mo-Kα radiation (λ = 0.710 73 Å). The structure was solved by direct methods (Siemens SHELXTL-PC) and refined (SHELXL-93) by full-matrix least squares on F^2 (430 parameters). Hydrogen atoms were introduced at calculated positions and refined freely. CCDC 182/737.

1 H. tom Dieck and L. Stamp, *Z. Naturforsch., Teil B*, 1990, **45**, 1369; M. J. Begley, P. Hubberstey, C. E. Russell and P. H. Walton, *J. Chem. Soc., Dalton Trans.*, 1994, 2483; A. Müller, H. Bögge and U. Schimanski, *Inorg. Chim. Acta*, 1980, **45**, L249.
2 C. E. Holloway and M. Melnik, *Rev. Inorg. Chem.*, 1995, **15**, 147.
3 (*a*) H. Bertagnolli and W. Kaim, *Angew. Chem.*, 1995, **107**, 847; *Angew. Chem., Int. Ed. Engl.*, 1995, **34**, 771; (*b*) W. Kaim and J. Rall, *Angew. Chem.*, 1996, **108**, 47; *Angew. Chem., Int. Ed. Engl.*, 1996, **35**, 43; (*c*) A. F. Stange, E. Waldhör, M. Moscherosch and W. Kaim, *Z. Naturforsch., Teil B*, 1995, **50**, 115; (*d*) A. F. Stange, K.-W. Klinkhammer and W. Kaim, *Inorg. Chem.*, 1996, **35**, 4087.
4 A. Klein, W. Kaim, E. Waldhör and H.-D.Hausen, *J. Chem. Soc., Perkin Trans. 2*, 1995, 2121.
5 M. C. Chakravorti and G.V. B. Subrahmanyan, *Coord. Chem. Rev.*, 1994, **135**/**136**, 65.
6 (*a*) W. Clegg, *Acta Crystallogr., Sect. B*, 1976, **32**, 2712; (*b*) A. J. Canty, A. Marker and B. M. Gatehouse, *J. Organomet. Chem.*, 1975, **88**, C31; A. J. Canty and A. Marker, *Inorg. Chem.*, 1976, **15**, 425.
7 (*a*) P. P. Power and S. C. Shoner, *Angew. Chem.*, 1990, **102**, 1484; *Angew. Chem., Int. Ed. Engl.*, 1990, **29**, 1403; (*b*) B. Becker, W. Wojnowski, K. Peters, E.-M. Peters and H. G. von Schnering, *Polyhedron*, 1992, **11**, 613.
8 M. D. Janssen, D. M. Grove and G. van Koten, *Prog. Inorg. Chem.*, 1997, **46**, 97.
9 P. J. Blower, J. R. Dilworth, J. P. Hutchinson and J. A. Zubieta, *J. Chem. Soc., Dalton Trans.*, 1985, 1533.
10 P. T. Bishop, J. R. Dilworth, T. Nicholson and J. Zubieta, *J. Chem. Soc., Dalton Trans.*, 1991, 385.

Received in Basel, Switzerland, 12th June 1997; revised manuscript received 2nd December 1997; 7/08867A

Enzyme assay using ultra-low volume surface micromachined sensors

Craig D. T. Bratten,[a,b] Peter H. Cobbold[b] and Jonathan M. Cooper*[a]

[a] *Bioelectronics Group, Department of Electronics and Electrical Engineering, University of Glasgow, UK G12 8QQ*
[b] *Department of Human Anatomy and Cell Biology, University of Liverpool, Liverpool, UK L69 3BX*

We demonstrate an amperometric enzyme-linked assay within an ultra-low volume (600 pl) micromachined device for the rapid determination of (hypo)xanthine *via* a catalytically generated hydrogen peroxide intermediate, thereby illustrating the potential of this technology in a variety of bioanalytical measurements involving the oxidases.

Techniques used in planar microfabrication have shown considerable promise in analytical biotechnology by enabling miniaturised metallic sensing electrodes to be made routinely, with precise control over their two-dimensional geometry.[1–5] More recently, however, micromachining has provided a complementary technology (to microfabrication), allowing for a greater degree of flexibility in structural design, by defining the geometry of a device in all three dimensions.

In general, the analytical benefits of miniaturisation of such devices become apparent through the scaling laws (which dictate that, for example, within a diffusion limited system, as the dimension of the structure is reduced, so transport of analyte becomes more efficient, with an improvement in both response times and signal to noise).[5,6] As a consequence, within the last two years, the potential for performing biological analyses within micromachined structures has been demonstrated, including examples of novel device configurations, capable of electrophoretic separation of high molecular mass analytes,[6] 'on-chip' PCR[7] and electrophoretic manipulations of cells.[8]

Many of the devices which have been machined have been generated by the annealing of glasses and/or silicon to form three-dimensional channels and chambers.[6–8] However, there are still technical problems in introducing functional sensors or actuators within a micromachined volume. For example, although Clark *et al.*,[9] have embossed very low volume polystyrene vials for electrochemical analysis, the electrodes must be introduced into the device as 'probes' from above. Recently, in order to overcome this problem, we described the use of a photoactive polyimide (Probimide 7020), which can be used in combination with two-dimensional (planar) microfabrication procedures to produce low volume (sub-nl) titre chambers with integrated electrochemical microelectrodes. We have previously characterised these devices by investigating the electrochemistry of the inorganic redox mediator, ferrocene monocarboxylic acid.[10]

The method by which we fabricated this surface micromachined device was adapted from procedures which have previously been described,[10] and involved using photolithography, metal evaporation and lift-off to produce a planar two-electrode array, consisting of gold micro-ring electrodes, adhered on a glass slide using a Ti/Pd underlayer (Ti/Pd/Au 10 : 10 : 100 nm). Importantly, in order to prevent subsequent fouling of the gold electrochemical surface during microchamber processing, the gold was coated with a 10 nm sacrificial layer of NiCr (60% : 40%, also known as 'nichrome'). The volume above the microelectrode (600 pl) was defined by photopolymerisation of the light sensitive polyimide (λ = 436 nm) through an appropriate chrome on quartz mask, followed by exposure to the OCG™ developer. The diameter of the chamber was 200 μm, and the depth of the chamber, as defined by the thickness of the polymer was 20 μm.[10]

After producing the chamber, residual polyimide was removed from the electrochemical surface by wet etching the 'sacrificial' nichrome in 0.6 M acetic acid and 0.37 M ammonium cerium(IV) nitrate, followed by ultrasonication (undercutting the polymer, and thus freeing it from the metal). Fig. 1(*a*) shows the electroanalytical device, coated with the nichrome layer and the contaminating polymer, prior to the wet etching process. Subsequently, Fig. 1(*b*) and (*c*) show the sequential 'cleaning' of the gold by nichrome etching, leaving the electrochemical surface available for further functionalisation (see below).

In order to produce a stable electrochemical surface, platinum was electrodeposited galvanostatically onto both the working and counter gold electrodes from a solution containing 24 mM platinum(IV) chloride and 2.1 mM lead acetate, maintaining a constant current of 1 μA for 1 min.[11,12] Bioelectrochemical measurements were made in a two-electrode configuration, with an outer (larger) micro-ring (inner diameter 120 μm, width 20 μm) acting as the platinum pseudo-reference counter (+270 mV *vs.* Ag/AgCl), and a smaller inner ring electrode (inner diameter 100 μm, width 10 μm) as the (platinum coated) working electrode, see Fig. 1(*a*). The ratio of the respective geometric areas of the counter and the working electrode was > 2 : 1.

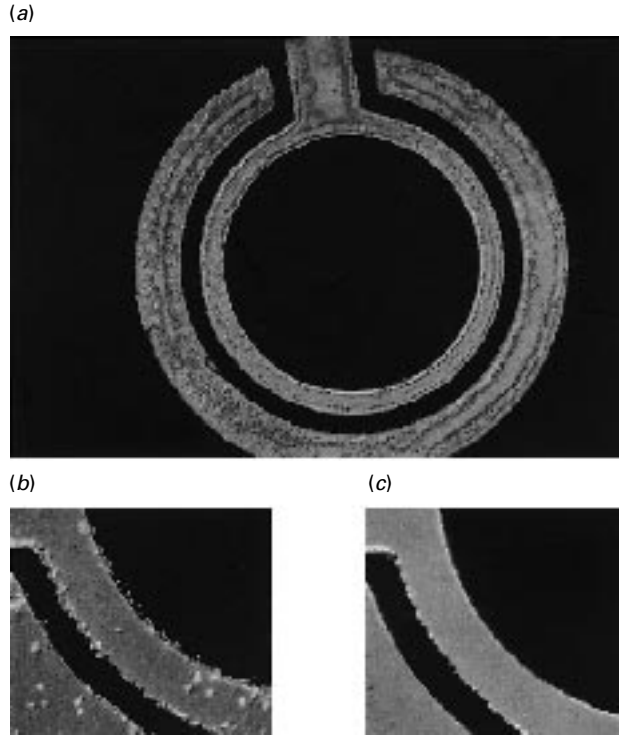

Fig. 1 A method for producing polyimide free electrodes, within the μ-electrochemical chamber: (*a*, above) shows the nichrome layer (with contaminating polymer); (*b*, below, left) and (*c*, below, right) show the sequential etching of the 'sacrificial' nichrome to remove the polymer residue. The opaque polymer surrounding the microelectrode is the photocured polyimide, which defines the three dimensional structure.

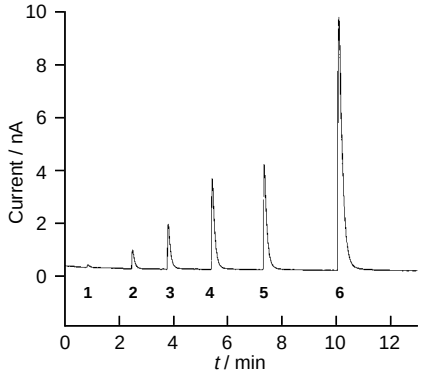

Fig. 2 *i–t* responses for successive additions of 8 pl buffer (1) and subsequently 1 pl (2), 8 pl (3), 30 pl (4), 66 pl (5) and 220 pl (7) of hydrogen peroxide to 600 pl μ-electroanalytical chamber containing a platinised micro-ring working electrode (geometric area = 3.3×10^3 μm²), poised at a potential equivalent to +420 mV *vs.* Ag/AgCl

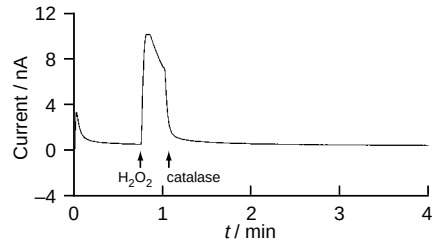

Fig. 3 Corroborative evidence that the responses in Fig. 2 are due to the electro-oxidation of hydrogen peroxide, shown by the addition of 2.5 nmol of catalase (equivalent to 25 units of enzyme), thereby acting as an effective catalytic scavenger. Responses were measured at a potential equivalent to +420 mV *vs.* Ag/AgCl.

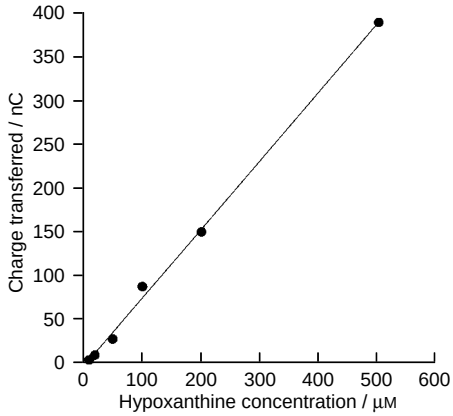

Fig. 4 Calibration curve for hypoxanthine in the concentration range between 10 μM (60 fmol) and 500 μM (3 pmol), (r = 0.99). Substrate additions were made to stock solutions of Ringers buffer containing 1.75×10^{-5} units of XOD in a volume of 600 pl.

In the first instance, hydrogen peroxide was ultramicropipetted into the μ-electroanalytical chamber through a layer of mineral oil (to prevent solvent evaporation),[10] and *i–t* measurements were made using a BAS CV 37 potentiostat (Bioanalytical Systems, UK) at a potential equivalent to +420 mV *vs.* Ag/AgCl.[11,12] Responses to successive additions of hydrogen peroxide are shown in Fig. 2, which are very fast, owing to the short electrode diffusion lengths. Measurements were integrated, as the total oxidation charge for hydrogen peroxide, giving a linear calibration curve over a range of analyte concentrations between 8.3 μM (5 fmol) and 1.83 mM (1.10 pmol), *i.e.* $y = 0.1\,x + 6.1$ nC (r = 0.99, n = 3). That the observed signals were generated by the electro-oxidation of hydrogen peroxide was corroborated by the addition of catalase during one such experiment (Fig. 3), which scavenged the analyte efficiently, as expected.

In order to further demonstrate the potential application of this device to bioanalytical measurements, a series of experiments involving the measurement of hypoxanthine were performed, using the oxidase enzyme, xanthine oxidase (XOD). The quantification of hypoxanthine is of interest in biomedicine, not least as it is produced during purine catabolism, and therefore has relevance in assessing the nucleotide pool in tissue. In the XOD catalysed reaction, under study here, two hydrogen peroxide equivalents are generated as a consequence of the oxidation of hypoxanthine, Eqn. (1) and (2), and these are subsequently measured through their electrochemical oxidation at the working electrode, according to Eqn. (3).

$$\text{Hypoxanthine} \xrightarrow[\text{XOD, pH 7.4}]{} \text{Xanthine} + H_2O_2 \quad (1)$$

$$\text{Xanthine} \xrightarrow[\text{XOD, pH 7.4}]{} \text{Uric acid} + H_2O_2 \quad (2)$$

$$H_2O_2 \xrightarrow[+420\text{ mV } \textit{vs.}\text{ Ag/AgCl}]{} O_2 + 2H^+ + 2e^- \quad (3)$$

The calibration curve for the electrochemical measurement of hypoxanthine is shown in Fig. 4. Measurements are the integral of the total (*i–t*) response, as before, after the addition of substrate within the range 10 μM (60 fmol) to 500 μM (3 pmol), $y = 0.79\,x - 5.04$ nC (n = 1, r = 0.99).

Although in both cases (for the generalised measurement of H_2O_2 and for the specific measurement of hypoxanthine) the responses do not correspond exactly to theoretical values, calculated on the assumption that all analyte is consumed, the results do demonstrate the general principle of bio-electrochemical detection within a confined ultra-low volume.

At present, routine *in situ* single cell measurements are limited to determinations of ions and ATP. The technique that we have developed has potential implications for the rapid, low volume detection of a wide range of new analytes, *e.g.* for determinations from single cells using oxidase enzymes to catalytically generate an electroactive coproduct, including glucose (*cf.* glucose oxidase) or lactate (*cf.* lactate oxidase).

The authors wish to thank the Wellcome Trust and Glaxo-Wellcome for their support.

Notes and References

* E-mail: jmcooper@elec.gla.ac.uk

1 M. Lambrechts and W. Sansen, in *Biosensors: Microelectrochemical Devices*, New York, Institute of Physics, 1992, pp. 98–155.
2 V. Cammarata, D. R. Talham, R. M. Crooks and M. S. Wrighton, *J. Phys. Chem.*, 1990, **95**, 2680.
3 V. V. Cosofret, M. Erdosy, T. A. Johnson, R. P. Buck, R. B. Ash and M. R. Neuman, *Anal. Chem.*, 1995, **67**, 1647.
4 R. J. Elliott-Martin, T. T. Mottram, J. W. Gardner, P. J. Hobbs, and P. N. Bartlett, *J. Agric. Eng. Res.*, 1997, **67**, 267.
5 E. Dempsey, D. Diamond, M.R. Smyth, G. Urban, G. Jobst, I. Moser, E. M. J. Verpoorte, A. Manz, H. M. Widmer, K. Rabenstein and R. Freaney, *Anal. Chim. Acta*, 1997, **346**, 341.
6 D. E. Raymond, A. Manz and H. M. Widmer, *Anal. Chem.*, 1996, **68**, 2515.
7 A. T. Woolley, D. Hadley, P. Landre, A. J. Demello, R. A. Mathies and M. A. Northrup, *Anal. Chem.*, 1996, **68**, 4081.
8 P. C. H. Li and J. D. Harrison, *Anal. Chem.*, 1997, **69**, 1564.
9 R. A. Clark, P. B. Hietpas and A. G. Ewing, *Anal. Chem.*, 1997, **69**, 259.
10 C. D. T. Bratten, P. H. Cobbold and J. M. Cooper, *Anal. Chem.*, 1997, **69**, 253.
11 J. Wang and L. Angnes, *Anal. Chem.*, 1992, **64**, 456.
12 S. F. White, A. P. F. Turner, R. D. Schmid, U. Bilitewski and J. Bradley, *Electroanalysis*, 1994, **6**, 625.

Received in Cambridge, UK, 17th November 1997; 7/08233I

Self-assembling chiral monolayers of helical peptides bound to gold *via* side-chain thioethers

Andrew E. Strong and Barry D. Moore*

Department of Pure and Applied Chemistry, University of Strathclyde, Thomas Graham Building, 295 Cathedral Street, Glasgow, UK G1 1XL

A helical oligopeptide containing three methionine residues, positioned so their side-chains align along one side of the helix, forms self-assembled monolayers on gold as characterised by cyclic voltammetry and reflection–absorption IR spectroscopy.

Self-assembling monolayers (SAMs) of sulfur-containing molecules on gold are attractive systems for tailoring surface properties and the study of interfacial phenomena.[1] Our aim is to develop this technology so that ordered surfaces can be prepared featuring different functional groups positioned at relative predetermined positions on the nanometer scale. To this end we are investigating the formation and structure of self-assembling monolayers of helical oligopeptides. A few examples of self-assembled monolayers of peptides have recently appeared.[2,3] In all of these cases the peptides had only one strong attachment point to the gold surface, either through the side-chain of an N-terminal Cys residue[2] or *via* a thioalkyl carboxylic acid coupled to the N-terminal.[3] In order to obtain a defined alignment parallel to the surface we investigated binding a helical peptide to gold *via* multiple weaker interactions arising from methionine (Met) thioether side-chains. Peptides bound in this way provide maximum scope for organisation of other amino acids at the outer face to produce functionalised chiral surfaces.

Peptide **1**, Fcb-Ala-Aib-Ala-Met-Aib-Ala-Ala-Met-Ala-Aib-Met-Ala-Ala-NH_2, was designed so that in an α-helical conformation the thioether-containing side-chains of the three Met residues would align along the same side of the helix, able to bind to a gold surface. The remaining amino acids used, Ala and Aib (α-aminoisobutyric acid), are known strong helix formers in organic solvents[4] and have small methyl side-chains to minimise unfavourable steric interactions with the surface. The N-terminus was acylated with ferrocene butyric acid (Fcb) to provide a convenient electrochemical label. Peptide **2**, Fcp-Ala-Aib-Ala-Ala-Leu-Aib-Ala-Ala-Ala-Aib-Leu-Ala-NH_2, available from previous studies provided a convenient, non-sulfur-containing control of similar length, composition and secondary structure to **1**.

The peptides were prepared by conventional solid-phase peptide synthesis on a modified Rink-type resin using Fmoc chemistry and PyBOP® coupling protocols.† N-Acylation with the ferrocene carboxylic acids was carried out on the resin. Analysis of the cleaved precipitated products by reversed-phase HPLC and electrospray mass spectrometry‡ showed that in each case they were > 90% the desired peptide. Attempts to further purify peptide **1** invariably led instead to introduction of other impurities due to autooxidation of the methionine groups and hence the peptide was used freshly cleaved.

The CD spectra of peptide **1** in methanol and acetonitrile are shown in Fig. 1. The double minima at 208 and 222 nm are characteristic of a predominantly α-helical structure.[5] Analysis of the spectra[6] indicated that **1** was > 65% α-helical in methanol and 50% α-helical in acetonitrile. Other contributions can be assigned to 3_{10}-helix or random coil caused by fraying of the helix ends. Formation of the observed α-helix preorganises the three thioether side-chains to favour multipoint binding to a metal surface.

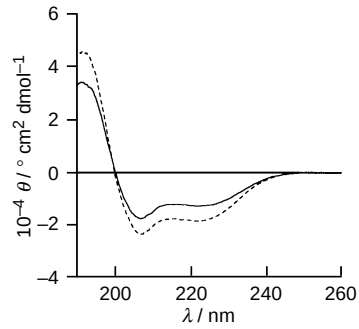

Fig. 1 CD spectra of oligopeptide **1** in MeCN (continuous line) and in MeOH (dashed line) at room temperature

Cyclic voltammetry was used as a convenient tool for monitoring the formation and relative stability of self-assembled monolayers of sulfur-containing peptide **1** compared to sulfur-free **2**. Ethanolic solutions of each peptide (*ca*. 1 mM) were contacted with a polished gold disk electrode for 20–26 h.§ Following rinsing with pure solvent, cyclic voltammograms were measured in ethanol (Fig. 2). Peaks characteristic of reversible electrochemistry of the covalently attached ferrocene were observed for both peptides. However the wave for peptide **2** was typically < 15% of peptide **1**.¶ Monolayers formed by peptide **1** were found to be remarkably stable to repetitive cycling. In fact, cycling appeared to condition the film so that the background current and peak to peak separation reduced while the Faradaic current remained constant [Fig. 2(*a*)]. In contrast the wave associated with the monolayer of peptide **2**

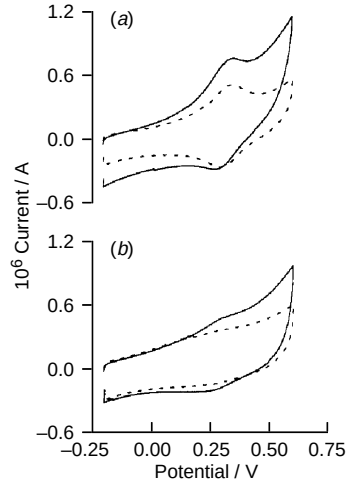

Fig. 2 (*a*) Cyclic voltammograms of films of peptide **1** adsorbed at a gold electrode, continuous line: recorded on immersion, dashed line: after sweeping for 30 min. (*b*) As above but for peptide **2**. The CVs were recorded at 0.5 V s^{-1} in 10 mM $NBu^n_4BF_4$ in EtOH *vs*. Ag/AgCl.

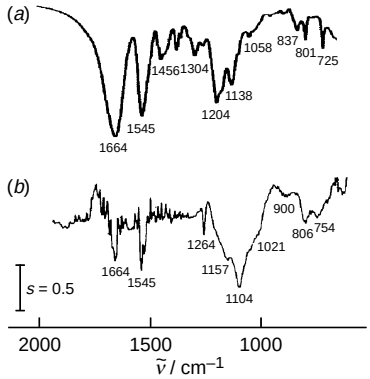

Fig. 3 IR spectra of oligopeptide **1**. (*a*) KBr spectrum and (*b*) reflection–absorption spectrum of the self-assembled film [scale bar applies to (*b*) only]

rapidly decreased during cycling under the same conditions [Fig. 2(*b*)]. The high stability of monolayers of **1** in ethanol, where hydrophobic interactions are absent, is consistent with the proposed mode of self-assembly *via* binding of the thioether side-chains to the gold surface.

The conformation and orientation of the adsorbed peptides were investigated by reflection–absorption IR spectroscopy (RAIRS).‖ The spectra of peptide **1** in a KBr pellet and self-assembled at gold** are shown in Fig. 3. The main indication of peptide secondary structure is the frequency of the amide I band (1600–1700 cm^{-1}).[7] Bands at 1620–1640 and above 1680 indicate β-structures while those at 1650–1658 are typical of α-helices. Interestingly the amide I band of peptide **1** appears at 1664 cm^{-1} close to that previously observed for 3_{10}-helices of Aib-containing peptides.[8]

The RAIRS technique also allows the orientation of the peptides at the surface to be inferred using the surface selection rule, because only vibrations with a component normal to the surface are enhanced.[9] The main component of the amide I band is stretching of the carbonyl groups and in a helical peptide these will be aligned along the helix axis. The main contributions to the amide II and III bands are in-plane bending of N–H and C=O, and C–C and C–N stretching.[10] For each of these vibrations the transition dipole moment subtends a range of angles to the helical axis. In the self-assembled peptide monolayers, binding *via* the methionine side-chains is expected to align the helical axis parallel to surface. This is expected to lead to a dramatic reduction in the intensity of the RAIRS amide I band relative to the amide II and III bands, as compared to the powder spectra. It can be seen in Fig. 3 that this is exactly what is found. The amide I band at 1664 cm^{-1} is significantly weaker in the reflectance spectra relative to the respective amide II and III bands at 1545 and 1264 cm^{-1}. RAIRS of peptide **2**, which lacks the thioether groups, showed weak bands consistent with a helical conformation at 1660, 1540 and 1300 cm^{-1} in the reflectance spectra. However their relative ratios were similar to those in the powder spectrum suggesting no particular orientation of the peptide at the surface.

We have shown peptide **1** adopts a helical secondary structure resulting in preorganisation of three surface binding thioether groups along one side of the helix. The peptide forms stable monolayers on gold with the helix aligned parallel to the surface. Future work will involve introduction of other amino acids into the sequence to produce functionalised chiral surfaces.

We thank EPSRC, Sharon Kelly and the BBSRC CD facility at Stirling University, Ras Raval and Elaine Cooper at University of Liverpool and Novabiochem.

Notes and References

* E-mail: b.d.moore@strath.ac.uk

† The oligopeptides were synthesised using a Novasyn Crystal solid-phase peptide synthesiser, Novasyn PR500 resin, Fmoc protected amino acids and PyBOP coupling chemistry. Each residue was double coupled using a threefold excess (for **1**) or a twofold excess (for **2**) of amino acid. Cleavage was with 10% TFA in CH_2Cl_2 for 2 × 45 min.

‡ Analytical HPLC was *via* reversed-phase HPLC on a C_8 column using an MeOH–H_2O gradient. ESMS data: peptide **1**, *m/z* 1417.6, found at *m/z* 1418.4 ($M + H^+$), 1400.7 ($M + H^+ - NH_3$), 740.9 ($M + Na^+ + K^+$), 732.6 ($M + 2Na^+$), 700.9 ($M + 2H^+ - NH_3$), 665.4 ($M + 2H^+ - Ala - NH_3$). Peptide **2**, *m/z* 1236.3, found at *m/z* 1274.8 ($M + K^+$), 1258.8 ($M + Na^+$), 1236.8 ($M + H^+$), 1219.8 ($M + H^+ - NH_3$), 638.1 ($M + K^+ + H^+$), 629.9 ($M + Na^+ + H^+$), 619.1 ($M + 2H^+$), 610.3 ($M + 2H^+ - NH_3$), 585.6 ($M + 2H^+ - Ala$).

§ The gold disk electrode (2 mm in diameter, purchased from Oxford Electrodes) was manually polished with alumina paste, rinsed with H_2O and immersed in 4 : 3 : 1 H_2O–conc. HCl–conc. HNO_3 for 60 s, rinsed with H_2O for 10 s and immersed in the peptide solution.

¶ A surface coverage of 17% was calculated modelling the helices as 27 × 12 Å rectangles and using a surface roughness of 2.

‖ RAIRS spectra were accumulated over 200 scans at 4 cm^{-1} resolution using a Unicam Galaxy Series FTIR 7000 spectrometer equipped with a Hg–Cd–Te detector and FT85 specular reflector from SpectraTech Inc. The sample compartment was purged with dry air.

** Peptide monolayers were assembled by evaporating 5 nm Cr and 50 nm Au onto a glass slide. The wafers were placed in 0.4 mmol dm^{-3} solutions of peptide **1** (in MeCN) for 16 h or peptide **2** (in CH_2Cl_2) for 4 h, rinsed with solvent and dried gently in a stream of He.

1 L. H. Dubois and R. G. Nuzzo, *Annu. Rev. Phys. Chem.*, 1992, **43**, 437 and references therein.
2 C. Duschl, M. Liley, G. Corradin and H. Vogel, *Biophys. J.*, 1994, **67**, 1229; M. Knichel, P. Heiduschka, W. Beck, G. Jung and W. Gopel, *Sensors Actuators B*, 1995, **28**, 85; C. Duschl, A. F. Sevinlandais and H. Vogel, *Biophys. J.*, 1996, **70**, 1985.
3 R. P. H. Kooyman, D. J. van den Heuvel, J. W. Drijfhout and G. W. Welling, *Thin Solid Films*, 1994, **244**, 913; J. K. Whitesell and H. K. Chang, *Science*, 1993, **261**, 73; S. Sakamoto, H. Aoyagi, N. Nakashima and H. Mihara, *J. Chem. Soc., Perkin Trans. 2*, 1996, 2319; R. Naumann, A. Jonczyk, R. Kopp, J. van Esch, H. Ringsdorf, W. Knoll and P. Graber, *Angew. Chem., Int. Ed. Engl.*, 1995, **34**, 2056.
4 I. L. Karle and P. Balaram, *Biochemistry*, 1990, **29**, 6747; C. Toniolo and E. Benedetti, *Trends Biochem. Sci.*, 1991, **16**, 350.
5 R. W. Woody, in *The Peptides*, ed. S. Udenfriend and J. Meienhofer, Academic Press, 1995, vol. 7, p. 15.
6 S. W. Provencher and J. Glöckner, *Biochemistry*, 1981, **20**, 33.
7 P. I. Haris and D. Chapman, *Biopolymers*, 1995, **37**, 251.
8 D. F. Kennedy, M. Crisma, C. Toniolo and D. Chapman, *Biochemistry*, 1991, **30**, 6451.
9 R. J. Greenler, *J. Chem. Phys.*, 1966, **44**, 310.
10 S. Krimm and J. Bandekar, *Adv. Protein Chem.*, 1986, **38**, 181.

Received in Bath, UK, 2nd December 1997; 7/08663F

‘Self-complexing’ tetrathiafulvalene macrocycles; a tetrathiafulvalene switch

Mogens Brøndsted Nielsen, Steen Brøndsted Nielsen and Jan Becher*

Department of Chemistry, Odense University, DK-5230 Odense M, Denmark

Two ‘self-complexing’ macrocycles based on the electron donor TTF and a cyclic bipyridinium acceptor are prepared.

The construction of molecular devices which can operate as machines upon external energy transfer has been of high interest recently, as such systems may be able to store and process information at the molecular level.[1,2] A recent example is provided by a pseudorotaxane system in which a naphthalene or hydroquinone π-donor and the π-acceptor cyclobis(paraquat-*p*-phenylene) are covalently linked.[3]

We have prepared a number of donor–acceptor catenanes by incorporating the π-donor tetrathiafulvalene (TTF) into macrocyclic systems,[4] as well as systems in which the TTF unit and the bipyridinium unit are linked, either in a rigid conformation, *e.g.* as a donor–acceptor cyclophane, or in a noncyclic system.[5] Here we have extended these concepts by incorporating TTF into macrocycles which may self-complex in order to investigate their switching properties. For synthetic reasons we attached the TTF unit to the unsymmetrical *m*-*p* linked cyclophane of cyclobis(paraquat-*p*-phenylene).[6] The corresponding symmetric *m*-*m* linked cyclophane was discarded due to its poor ability to act as a host, as reported by Stoddart.[7]

First, **2** and **3** were prepared by *O*-alkylations of dimethyl 5-hydroxyisophthalate **1** (Scheme 1). The TTF derivative **4** was deprotected with CsOH (1 equiv.) (Scheme 2),[8] and the resulting monothiolate was treated *in situ* with **2** or **3** affording **5** and **6**, respectively. The two ester groups were reduced with $LiAlH_4$ followed by mesylation in the presence of DBU. The mesylated compounds were converted directly to the corresponding chloro compounds by reaction with an excess of LiCl, giving fair yields of **9** and **10**. Subsequent Finkelstein reactions with LiBr gave the TTF-linked *m*-xylene dibromides **11** and **12**.†

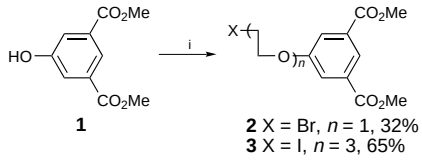

1

2 X = Br, *n* = 1, 32%
3 X = I, *n* = 3, 65%

Scheme 1 *Reagents and conditions*: i, K_2CO_3, $BrCH_2CH_2Br$ (*n* = 1) or $I(CH_2CH_2O)_2CH_2CH_2I$ (*n* = 3), acetone, reflux, 16 h

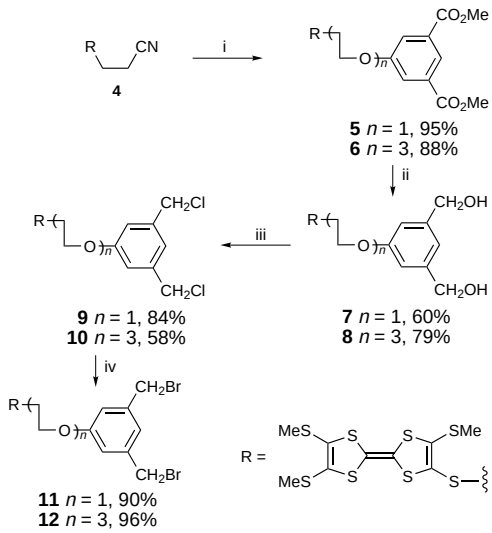

5 *n* = 1, 95%
6 *n* = 3, 88%

7 *n* = 1, 60%
8 *n* = 3, 79%

9 *n* = 1, 84%
10 *n* = 3, 58%

11 *n* = 1, 90%
12 *n* = 3, 96%

Scheme 2 *Reagents and conditions*: i, $CsOH·H_2O$ (1 equiv.), **2** or **3**, DMF, room temp., 3 h; ii, $LiAlH_4$, THF, reflux, 2 h; iii, MsCl, DBU, LiCl, CH_2Cl_2, room temp., 24 h; iv, LiBr, acetone, reflux, 24 h

The new anchimeric-complexed‡ macrocycles **14a** and **15a** were obtained by treating **11** and **12**, respectively, with the dipyridinium dication of **13** under ultra-high pressure (10 kbar) for 6 days (Scheme 3). The crude green products were subjected to column chromatography and ion exchange.[4] During work-up of **15a**, partial isomerisation ‘decomplexation’ to the orange coloured form **15b** was observed. Repeated fractional crystallization *via* slow evaporation of Pr^i_2O into MeCN solutions of **14a** and **15a** resulted in removal of small amounts of impurities. In this way it was possible to obtain **14b** and **15b** as orange microcrystalline compounds, *e.g.* in the completely ‘decomplexed’ forms. Redissolution of **15b** in MeCN initially gave an orange solution which slowly turned greener on standing due to partial anchimeric complexation. However, an MeCN solution of ‘decomplexed’ **14** did not change colour, and according to UV–VIS spectroscopy only a very small charge-transfer (CT) absorption could be detected after several days. Thus, when first ‘decomplexed’, the short linker of **14b** more or less prevents the TTF unit from intramolecularly slipping back into the cyclic acceptor. Besides, the persistent orange colour indicates the absence of intermolecular complexation.

The UV–VIS absorption of the initially orange crystals of **15b** dissolved in MeCN was followed over time [Fig. 1(*a*)]. After about 20 h the equilibrium between **15a** and **15b** was established, as seen from the constant CT absorption (λ_{max} ~785 nm). The relatively weak CT absorption indicates that only a small degree of anchimeric complexation occurs, which was confirmed by ^1H NMR spectroscopy (estimated ratio **15a** : **15b**: 1 : 10). The anchimeric complexation results in a complicated set of bipyridinium proton resonances and a downfield shift of the SMe protons in agreement with observations for comparable TTF-based catenanes.[4d] The question is whether the complexation is truly of the auchimeric

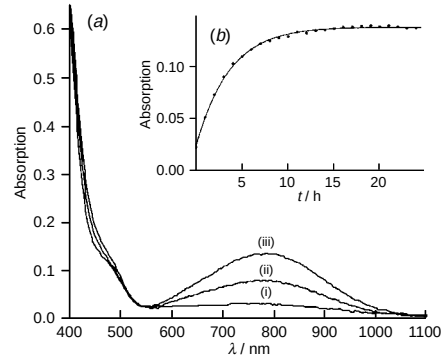

Fig. 1 (*a*) The UV–VIS absorption spectrum of the initially decomplexed **15b** in MeCN at (i) 0, (ii) 3 and (iii) 19 h. (*b*) The time variation of the maximum absorbance (λ_{max} ~785 nm) of initially decomplexed **15b**. A first-order fit matches the points very well. Concentration of compound = 0.26 mmol dm^{-3}.

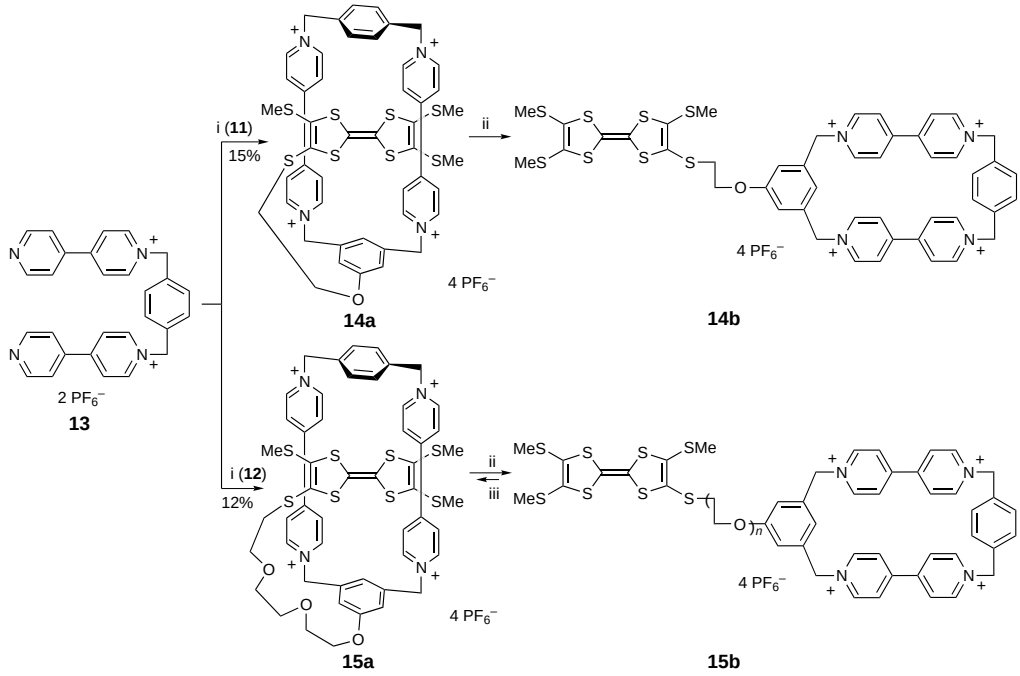

Scheme 3 *Reagents and conditions*: i, DMF, 10 kbar, room temp., 6 d; ii, fractional crystallization; iii, equilibrium in MeCN

type. The formation of an intramolecular 'complex' by anchimeric complexation would be expected to follow a first-order rate equation. In Fig. 1(*b*) the observed absorption maxima are plotted against time, and a curve fitted using eqn. (1)§ confirms that the data are in good agreement with first-order conditions. Of course this is not a final proof for exclusive anchimeric complexation. Nevertheless, since **14b** did not readily undergo intermolecular slipping in dilute solution, we would not expect this to be likely for **15b** either.

Refluxing the equilibrium solution of **15a,b** in MeCN for 45 min caused almost complete conversion to **15b**. However, the next day a CT absorption close to the starting equilibrium absorption at room temperature was reestablished. This anchimeric decomplexation/recomplexation could be repeated.¶ Thus, **15** behaves as a thermal molecular switch, the state of which is determined by both thermodynamics and kinetics. The solution of **15a,b** was subjected to 10 kbars of pressure (room temp., 4 days); however, this caused no significant change in absorption, *i.e.* in no displacement of the equilibrium.

Compounds **14** and **15** were characterized by electrospray mass spectrometry (ESMS) showing peaks assignable to $[M - nPF_6]^{n+}$ (n = 1–4), $[M - nPF_6]^{(n+1)+}$ (n = 1–3) and $[M - nPF_6]^{(n-1)+}$ (**14**, n = 3,4). Furthermore, a $[2M - 3PF_6]^{3+}$ ion was observed in the gas phase, but whether this is a real dimer or a dimeric cluster ion cannot be concluded. Collisional activation (MS/MS) of the mass selected $[M - 4PF_6]^{4+}$ ions caused similar fragmentations of the cyclic acceptor, as already observed for related TTF based catenanes.[4d]

Notes and References

* E-mail: jbe@chem.ou.dk

† According to plasma desorption mass spectrometry (PDMS), **11** and **12** could not be separated by chromatography from a small amount of the monobrominated compounds (Cl, Br). All other compounds were obtained pure and gave satisfactory elemental analyses. *Selected data* for **5**: $\delta_H(CDCl_3)$ 2.41–2.43 (3 s, 9 H, SCH_3), 3.21 (t, *J* 6.4, 2 H, SCH_2), 3.95 (s, 6 H, CO_2CH_3), 4.26 (t, *J* 6.4, 2 H, OCH_2), 7.77 (d, *J* 1.4, 2 H, Ar.), 8.30 (t, *J* 1.4, 1 H, Ar.); PDMS: *m/z* 610.1 (M^+). For **7**: $\delta_H(CDCl_3)$ 2.40–2.44 (3 s, 9 H, SCH_3), 3.18 (t, *J* 6.5, 2 H, SCH_2), 4.21 (t, *J* 6.7, 2 H, OCH_2), 4.68 (d, *J* 5.2, 4 H, CH_2OH), 6.85 (s, 2H, Ar), 6.97 (s, 1 H, Ar); PDMS: *m/z* 554.2 (M^+). For **9**: $\delta_H(CDCl_3)$ 2.39–2.45 (3 s, 9 H, SCH_3), 3.17 (t, *J* 4.9, 2 H, SCH_2), 4.21 (m, 2 H, OCH_2), 4.55 (s, 4 H, $ClCH_2$), 6.89 (d, *J* 1.2, 2 H, Ar), 7.02 (s, 1 H, Ar); PDMS: *m/z* 590.4 (M^+). For **11**: $\delta_H(CDCl_3)$ 2.39–2.44 (3 s, 9 H, SCH_3), 3.17 (t, *J* 6.5, 2 H, SCH_2), 4.20 (t, *J* 6.5, 2 H, OCH_2), 4.43 (s, 4 H, $BrCH_2$), 6.86 (d, *J* 1.1, 2 H, Ar), 7.02 (s, 1 H, Ar); PDMS: *m/z* 680.2 (M^+). For **14b**: $\delta_H(CD_3CN)$ 2.40–2.41 (2 s, 9 H, SCH_3), 3.28 (t, *J* 5.9, 2 H, SCH_2), 4.34 (t, *J* 6.0, 2 H, OCH_2), 5.69 (s, 4 H, NCH_2), 5.76 (s, 4 H, NCH_2), 6.89 (s, 1 H, Ar), 7.30 (d, *J* 1.3, 2 H, Ar), 7.60 (s, 4 H, Ar), 8.05 (d, *J* 6.8, 4 H, β-H), 8.07 (d, *J* 6.9, 4 H, β-H), 8.74 (d, *J* 6.9, 4 H, α-H), 8.85 (d, *J* 7.1, 4 H, α-H).

‡ Anchimeric assistance is normally used to describe neighbouring group participation in a reaction. The expression 'complexation' is incorrect when used to describe an intramolecular reaction. We suggest using the expression 'anchimeric complexation' to describe the present type of isomerisation ('self-complexation') taking place between two covalently linked groups.

§ The time-dependence of the absorbance (A) for first-order recomplexations with rate constant k_+ is shown by eqn. (1),

$$A = A_0 \exp[-(k_+ + k_-)t] + \text{constant}\cdot\{1 - \exp[-(k_+ + k_-)t] \qquad (1)$$

where k_- is the rate constant for the decomplexation reaction.

¶ A small decrease of the equilibrium CT absorption (*ca*. 5%) was observed after each experiment, which may be due to a chemical decomposition upon refluxing.

1 J.-M. Lehn, *Angew. Chem., Int. Ed. Engl.*, 1988, **27**, 89; 1990, **29**, 1304.
2 R. Ballardini, V. Balzani, A. Credi, M. T. Gandolfi, S. J. Langford, S. Menzer, L. Prodi, J. F. Stoddart, M. Venturi and D. J. Williams, *Angew. Chem., Int. Ed. Engl.*, 1996, **35**, 978 and references therein.
3 P. R. Ashton, R. Ballardini, V. Balzani, S. E. Boyd, A. Credi, M. T. Gandolfi, M. Gómez-López, S. Iqbal, D. Philp, J. A. Preece, L. Prodi, H. G. Ricketts, J. F. Stoddart, M. S. Tolley, M. Venturi, A. J. P. White and D. J. Williams, *Chem. Eur. J.*, 1997, **3**, 152.
4 (*a*) Z.-T. Li, P. C. Stein, N. Svenstrup, K. H. Lund and J. Becher, *Angew. Chem., Int. Ed. Engl.*, 1995, **34**, 2524; (*b*) Z.-T. Li, P. C. Stein, J. Becher, D. Jensen, P. Mørk and N. Svenstrup, *Chem. Eur. J.*, 1996, **2**, 624; (*c*) Z.-T. Li and J. Becher, *Chem. Commun.*, 1996, 639; (*d*) M. B. Nielsen, Z.-T. Li and J. Becher, *J. Mater. Chem.*, 1997, **7**, 1175.
5 K. B. Simonsen, K. Zong, R. D. Rogers, M. P. Cava and J. Becher, *J. Org. Chem.*, 1997, **62**, 679.
6 D. Philp, A. M. Z. Slawin, N. Spencer, J. F. Stoddart and D. J. Williams, *J. Chem. Soc., Chem. Commun.*, 1991, 1584; P. R. Ashton, R. A. Bissel, R. A. Spencer, J. F. Stoddart and M. S. Tolley, *Synlett*, 1992, 923; W. Devonport, M. A. Blower, M. R. Bryce and L. M. Goldenberg, *J. Org. Chem.*, 1997, **62**, 885; P.-L. Anelli, M. Asakawa, P. R. Ashton, R. A. Bissel, G. Clavier, R. Górski, A. E. Kaifer, S. J. Langford, G. Mattersteig, S. Menzer, D. Philp, A. M. Z. Slawin, N. Spencer, J. F. Stoddart, M. S. Tolley and D. J. Williams, *Chem. Eur. J.*, 1997, **3**, 1113.
7 D. B. Amabilino, P. R. Ashton, M. S. Tolley, J. F. Stoddart and D. J. Williams, *Angew. Chem., Int. Ed. Engl.*, 1993, **32**, 1297.
8 J. Becher, Z.-T. Li, P. Blanchard, N. Svenstrup, J. Lau, M. B. Nielsen and P. Leriche, *Pure Appl. Chem.*, 1997, **69**, 465 and references therein.

Received in Liverpool, UK, 29th September 1997; 7/07026H

Electrochemical immobilization of a pH sensitive fluorescein derivative: synthesis and characterization of a fluorescein-derivatised polythiophene

David Millar, Mahesh Uttamlal,*† Ross Henderson and Alexis Keeper

Department of Physical Sciences, Glasgow Caledonian University, City Campus, Cowcaddens Road, Glasgow, Scotland, UK G4 0BA

The electrochemical immobilization of a pH sensitive fluorescein derivative was achieved by preparing a fluorescein-substituted thiophene species, followed by its electropolymerization on a Pt electrode.

Immobilization of fluorescein[1] for the preparation of fibre-optic pH sensors has been achieved using several techniques.[2] Simple entrapment in sol-gel matrices has been reported by several workers.[3] Fluorescein derivatives have also been used to create a covalent link between the indicator and the optical fibre surface.[2] The photochemical covalent immobilization of fluoresceinamine has been reported for the preparation of fibre-optic chemical sensors (FOCSs) for pH measurement.[4] Here we report the first example of the electrochemical immobilization of a pH sensitive fluorescein derivative.

Electropolymerization is a simple and attractive approach for the immobilization of fluorophores in the form of a polymer on a substrate surface. The process of electropolymerization can be controlled by electrode potential and allows accurate control of the amount of fluorophore immobilized. In this work the electrochemical immobilization of fluoresceinamine is being undertaken in order to prepare a FOCS for pH and to study the effect of electrode potential on the fluorescence properties of the new polymer.

Scheme 1 shows the reaction for the preparation of fluorescein-derivatised polythiophene. The new monomer for electropolymerization was prepared using thiophene-3-acetic acid (TAA), a well characterized compound for preparing conducting polymers.[5] From TAA, thiophene-3-acetyl chloride (TAC) **1** was prepared *via* reaction with thionyl chloride.[6]‡ TAC was then reacted with fluoresceinamine, to yield **2**.§

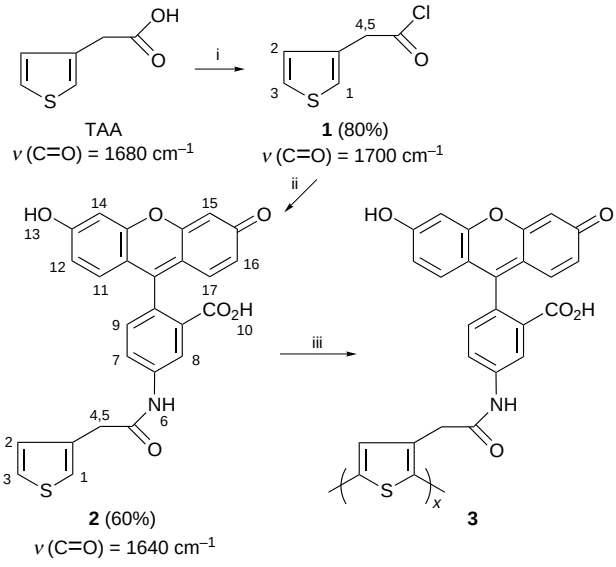

Scheme 1 *Reagents and conditions:* i, excess $SOCl_2$, 60 °C, 2 h (ref. 6); ii, fluoresceinamine, acetone, reflux, then $CHCl_3$–H_2O extraction; iii, electrochemical polymerisation (ref. 7)

Polymer **3** was prepared *via* the electrochemical polymerization on Pt coated glass in MeCN using the method reported for the preparation of poly-TAA.[7]¶ Polymer **3** was produced as a golden film. Under the experimental conditions used, the polymer film produced is probably over-oxidised and consequently non-conducting. However, the electrical properties of the polymer are not of interest here and will not be discussed further.

Fluorescein itself in aqueous solution occurs in cationic, neutral and anionic forms, making its absorption and fluorescence properties strongly pH dependent.[1] It has been shown to be electrochemically active in non-aqueous media.[8] At neutral and high pHs in aqueous media the equilibrium shown in Fig. 1 dominates.

The fluorescence intensity ratio *vs.* pH curves for sodium fluorescein (NaFlu) and for **2** in aqueous solution are given in Fig. 2. The emission wavelength for **2** was identical to that of NaFlu and had a value of 515 nm. The two titration curves have very similar characteristics and indicate that the modification of fluorescein with thiophene has little effect on the pH sensitivity of the fluorescein moiety. The solid lines are theoretical plots generated by fitting Eqn. (1) to the data. This model yields approximations for the pK_a of the indicators. For NaFlu the pK_a is 6.3 and that for **2** it is 6.2. The reported value for fluorescein is in the range 6.2–6.9.[1]

Fig. 2 also shows the pH titration curve for **3**. Polymer **3** shows a well-defined titration with a lower pH sensitivity compared to NaFlu and **2** in solution. The decrease in sensitivity is attributed to small changes in the fluorescence properties of the fluorescein moiety in its new environment. This phenomenon is also observed for photochemically immobilized fluorescein in hydrogel films.[4]

This work has for the first time reported an electrochemical immobilization method for a pH sensitive fluorescein derivative. We have shown that the pH sensitive polymer has similar response characteristics to that of fluorescein in solution. Current investigations are concerned with the effect of electrode potential on the fluorescence properties of the polymer and the preparation of copolymers with TAA. Indole and pyrrole derivatives as alternative monomer units are also being investigated.

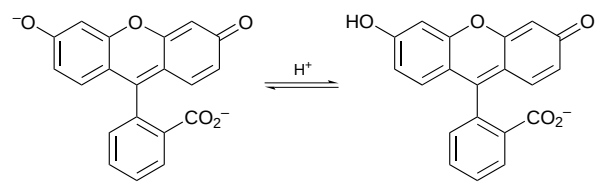

Fig. 1 Dominant equilibrium of fluorescein at neutral and high pH. Fluorescein has a high molar absorbitivity at 488 nm, a large fluorescence quantum yield and high photostability. An attractive feature of this indicator is that it has an excitation maximum at 488 nm, and a pH insensitive shoulder at 430 nm making it suitable for use in the 'ratiometric' mode which overcomes problems in measurement associated with photobleaching, light intensity fluctuation in the excitation source, ionic strength and indicator concentration (ref. 9).

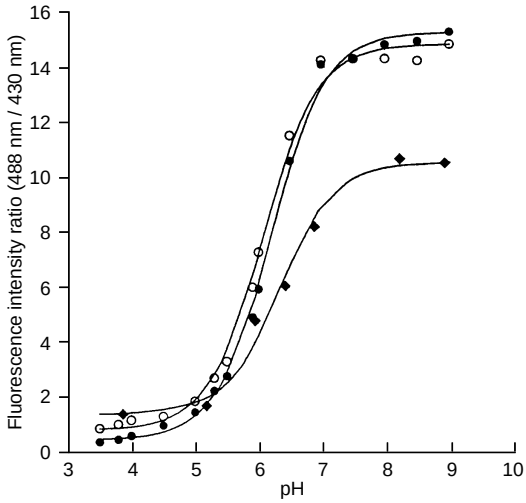

Fig 2 pH Titration curve for (○) **2** (pK_a = 6.1), (◆) **3** (pK_a = 6.3) and (●) NaFlu (pK_a = 6.2). The overall equilibrium can be written. HIn ⇌ H^+ + In^-, where HIn (not fluorescent) and In^- (fluorescent) are the protonated and deprotonated forms of the indicator respectively. The pH is related to the fluorescent intensity by pH = pK_a + log[I/(I_o − I)] (ref. 2) where the fluorescence intensity (or intensity ratio) I = [In^-] and I_o = [In^-]$_o$ where I_o is the maximum fluorescence intensity. This equation can be re-written in terms of I to give eqn. (1):

$$I = \frac{I_o}{1 + (10^{\mathrm{pH} - \mathrm{p}K_a})^{-1}} + B$$

An additional term B is introduced where B is the fluorescence intensity when [In^-] = 0. The solid lines are theoretical fits using eqn. (1).

The authors thank Miss Katrina Rae and (the late) Mr Joe Gillick for technical assistance, Mr Jim Gall (Department of Chemistry, Glasgow University) for NMR analysis and Drs P. A. Bather and J. MacLachlan for helpful discussion. This work was funded by a grant from The Nuffield Foundation (NUF-URB97). This communication is dedicated to Mr Joe Gillick, Senior Chemistry Technician, who died suddenly on 25th May 1997. Mr Gillick gave 22 years service to chemistry education at the institution.

Notes and References

† E-mail: m.uttamlal@gcal.ac.uk

‡ *Experimental procedure* for **1**:[6] The reaction of TAA (1.00 g, Acros, 98%) with $SOCl_2$ (0.8 cm³) at 60 °C for 2 h in dry conditions gave an orange–brown liquid **1** (the excess $SOCl_2$ was evaporated *in vacuo* at 35 °C) with a yield of *ca*. 80%. δ_H (360 MHz, [$^2H_6$]acetone) 7.24 (d, H1), 7.21 (d, H3), 7.05 (s, H2), 4.25 (s, H4, H5).

§ *Experimental procedure* for **2**: Compound **1** (0.74 g) was reacted with fluoresceinamine (4.00 g) in boiling acetone (125 cm³) and cooled. Chloroform (100 cm³) and de-ionised water (100 cm³) were added to the reaction mixture, which was transferred to a separation funnel with 25 cm³ of 5% NaOH. The aqueous layer containing the product was removed and 100 cm³ of 5% HCl was added. Vacuum filtration and recrystalisation from EtOH–H_2O (1 : 1) gave orange crystals of **2** with a yield of *ca.* 60%. δ_H(360 MHz, [$^2H_6$]acetone 9.82 (s, H10), 8.94 (s, H13), 8.42 (s, H15), 7.96 (s, H14), 7.48 (d, H9), 7.33 (d, H7), 7.18–7.16 (2d, H2, H3), 6.82–6.76 (2d, H11, H12), 6.7–6.68 (2d, H8, H1), 6.62–6.59 (2d, H16, H17), 3.79 (s, H4, H5), 2.83 (s, H6).

¶ *Experimental procedure* for polymer **3**: Electrochemical cell consisted of a Pt coated glass working electrode, Ag/Ag^+ reference electrode and Pt gauze counter electrode. The electrolyte solution was 0.10 mol dm^{-3} tetrabutylammonium perchlorate (TBAP) and 0.021 mol dm^{-3} **2** in MeCN. Compound **2** was deposited using cyclic voltammetry. The potential was applied *via* an Oxford Electrodes potentiostat at 100 mV s^{-1} between −0.2 and 2.6 V *vs.* Ag/Ag^+ reference electrode for 20 cycles. A golden film was produced on the electrode surface.

Fluorescence emission intensities were measured on a Perkin-Elmer LS50B luminescence spectrophotometer. The fluorescence intensity ratio was measured using excitation at 430 and 488 nm The emission wavelength was 515 nm.

Platinum deposition on glass was achieved using thermal vapour deposition.

1 R. Sjoback, J. Nygren and M. Kubista, *Spectrochim. Acta: Part A*, 1995, **51**, L-7 and references cited therein.
2 T. E. Edmonds, *Chemical Sensors*, Blackie, Glasgow, 1988; S. A. Momin and R. Narayanaswamy, *Optical Fibre Chemical Sensors: Current State Reviews*, UMIST, 1993; T. E. Edmonds, N. J. Flatters, C. F. Jones and J. N. Miller, *Talanta*, 1988, **35**, 103 and references cited therein.
3 B. D. MacCraith, *Sens. Actuators B*, 1993, **11**, 29; B. D. MacCraith, C. M. McDonagh, G. O'Keeffe, A. K. McEvoy, T. Butler and F. R. Sheridan, *Sens. Actuators B*, 1995, **29**, 51; L. M. Shamansky, M. Yang, M. Olteanu and E. L. Chronister, *Mater. Lett.*, 1997, **26**, 113.
4 S. M. Barnard and D. R. Walt, *Nature*, 1991, **353**, 338; K. S. Bronk, K. L. Michael, P. Pantano and D. R. Walt, *Anal. Chem.*, 1995, **67**, 2750; W. D. Sloan and M. Uttamlal, *Sensors and their Applications VIII*, ed. A. T. Augousti and N. M. White, Institute of Physics, Bristol, 1997, 275.
5 W. J. Albery, F. B. Li and A. Mount, *J. Electroanal. Chem.*, 1991, **310**, 239; F. B. Li and W. J. Albery, *Electrochim. Acta*, 1991, **37**, 293; F. B. Li and W. J. Albery, *Langmuir*, 1993, **8**, 1645; H. P. Welzel, G. Kossmehl, H. J. Stein, J. Schneider and W. Plieth, *Electrochim. Acta*, 1995, **40**, 577.
6 E. Lee-Ruff and F. J. Ablenas, *Can. J. Chem.*, 1987, **65**, 1663.
7 P. N. Bartlett and D. H. Dawson, *J. Mat. Chem.*, 1994, **4**, 810.
8 J. C. Eklund, D. N. Waller, T. O. Rebbitt and R. G. Compton, *J. Chem. Soc. Perkin-Trans 2*,1995, 1981; R. G. Compton, J. C. Eklund, F. Marken, *Electroanalysis*, 1997, **9**, 509 and references therein.
9 J. E. Jones and R. C. Spooncer, *J. Phys. E.*, 1983, **16**, 1124.

Received in Liverpool, UK, 12th November 1997; 7/08160J

Synthesis and reactivity of α-allenylhydroxylamines: a new efficient access to 3,6-dihydro-1,2-oxazines

Estelle Dumez and Jean-Pierre Dulcère

RéSo, Réactivité en Synthèse organique, UMR 6516, Faculté des Sciences et Techniques de St. Jérôme, Boîte D 12, Av. Esc. Normandie-Niemen, F-13397 Marseille Cedex 20, France

SmI_2-promoted reduction of α-allenyl nitro derivatives 2a–f using controlled conditions provides either 3-amino-4-vinylidenetetrahydrofuran 3a or 3-hydroxylamino-4-vinylidenetetrahydrofurans 4b–f, which undergo intramolecular cyclization consistent with a reverse Cope elimination to afford 3,6-dihydro-1,2-oxazines 5b–f.

The *C*-nitroso group (R–N=O) acts as a heterodienophile in hetero-Diels–Alder reactions with 1,3-dienes to afford regioselectively 3,6-dihydro-1,2-oxazines.[1] The intramolecular variant Diels–Alder reaction has received some attention since resulting 3,6-dihydro-1,2-oxazines are involved in strategies for the synthesis of indolizidine alkaloids.[2] The most useful synthetic application of these cycloadditions is the easy cleavage of the N–O bond in the adduct to generate 1,4-bifunctional groups.[3]

Despite their synthetic potential, 3,6-dihydro-1,2-oxazines have exclusively been prepared by [4 + 2] cycloaddition.[4] Nevertheless, the well documented electrophilic-catalyzed intramolecular cyclizations of β-allenyl alcohols into dihydropyrans[5] suggest that cyclic derivatives of hydroxylamines, namely 3,6-dihydro-1,2-oxazines, should alternatively be provided by related cyclization of α-allenylhydroxylamines.

Although a number of methods are available for the synthesis of allenic amines,[6] to the best of our knowledge, among nitrogen related derivatives with higher oxidation state, allenylhydroxylamines have never been described. Nevertheless, addition of alkylhydroxylamines to allenyl carbonyl compounds provides allenyl nitrones which have been postulated as intermediates[7] in 1,3-dipolar cycloadditions leading to bicyclic isoxazolidines. Moreover, a diastereoselective synthesis of nitroallenes has recently been reported.[8]

We disclose here the efficient reduction of nitroallenes **2b**–**f** upon treatment with SmI_2 to the corresponding hydroxylamines **4b**–**f**, which are subsequently converted into 3,6-dihydro-1,2-oxazines **5b**–**f** by remarkably facile cyclization (Scheme 1).

3-Nitro-4-vinylidenetetrahydrofurans **2a**–**e** were prepared[8] by tandem oxa-Michael addition–S_N2' substitution of 4-chlorobut-2-yn-1-ol with nitroalkenes **1a**–**e**, while the same sequence with **1f** afforded 3-nitro-4-vinylidenetetrahydropyran **2f** when 5-chloropent-3-yn-1-ol was used as nucleophile. Reduction of nitro compounds has been used for a long time as a routine method for the preparation of various nitrogen derivatives such as amines and hydroxylamines;[9] however, in many cases over reduction occurs and further reduction to amines is difficult to avoid. Since the previous work of Kagan and co-workers on the reactivity of SmI_2 with nitrogen compounds,[10] alkylhydroxylamines and alkylamines have been prepared selectively from nitroalkanes and SmI_2 under mild conditions.[11]

According to this procedure, allenyl amine **3a**† was obtained by treatment of **2a** with 6 equiv. of SmI_2 in THF–Bu^{t}OH, while reaction of **2b**–**f** with 4 equiv. of SmI_2 allowed the isolation of the corresponding hydroxylamines **4b**–**f** in 60–65% yield.‡§

Upon standing at room temperature without catalyst, **4b**,**c**,**e**,**f** (6 h) or **4d** (15 d) were converted into **5b**–**f**¶ in 62–92% yield. This non-catalyzed intramolecular cyclization of hydroxylamines is in contrast to the well-known electrophilic catalysis required for the cyclization of functionalized allenic derivatives.[5,12] Although intramolecular cyclization of α-allenyl amines proceeds according to a 5-*endo-trig* mode to afford pyrroline derivatives[13] the chemo- and regio-selectivities of the cyclization of **4b**–**f** allow the formation of **5b**–**f** *via* apparently exclusive intramolecular *O*-alkylation. Nevertheless, while it is premature to propose a definitive mechanism, the fact that the cyclizations proceed uncatalyzed at ambient temperature strongly suggests a pathway which features a reverse Cope elimination [eqn. (1)].[14]‖ Moreover, this pathway proceeds according to the usual reactivity of hydroxylamines, which undergo alkylation on nitrogen rather than on oxygen by addition to the activated double bond.[15]

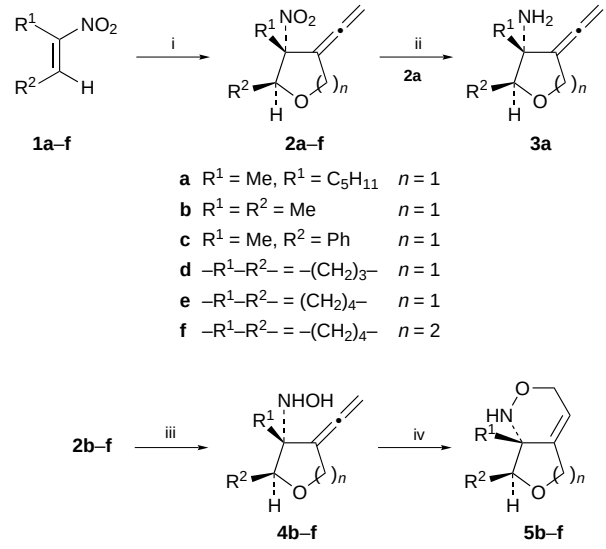

Scheme 1 *Reagents and conditions*: i, **1** (1 equiv.), THF, Bu^{t}OK (1.5 equiv.), $ClCH_2C{\equiv}C(CH_2)_nOH$ (1.5 equiv.), 0 °C, 10 min, then room temp., 15–30 min, n = 1 (ref. 8), n = 2 (74%); ii, SmI_2 (6 equiv.), THF, Bu^{t}OH, 15 min, 42%; iii, SmI_2 (4 equiv.), THF, Bu^{t}OH, 15 min, 60–65%; iv, room temp., 6 h to 15 d, 62–92%

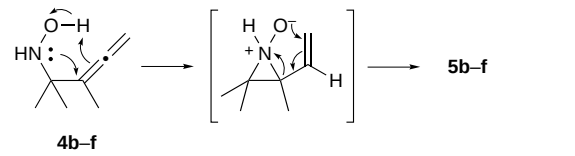

In conclusion, the SmI_2-controlled mild reduction of **2b**–**f** constitutes a new access to allenyl hydroxylamines **4b**–**f** which are precursors of 3,6-dihydro-1,2-oxazines **5b**–**f**, probably by reverse Cope elimination.

Notes and References

* E-mail: jean-pierre.dulcere@reso.u-3mrs.fr

† *Selected data* for **3a**: ν_{max}(neat)/cm^{-1} 3367, 2964, 1965, 1092, 1021; δ_H(400 MHz, $CDCl_3$) 0.90 (m, 3 H), 1.14 (s, 3 H), 1.19–1.81 (m, 8 H), 3.90

[t, *J* 1.8, 1 H ($C_5H_{11}CHO$–)], 4.35 [dt, *J* 12.3, 4.7, 1 H (OCH_AH_B)], 4.46 [dt, *J* 12.3, 4.2, 1 H (OCH_AH_B)], 4.73 [dt, *J* 9.8, 4.5, 1 H (=CH_AH_B)], 4.80 [dt, *J* 9.8, 4.5, 1 H (=CH_AH_B)]; δ_C(100.61 MHz, $CDCl_3$) 14.2, 22.6, 22.7, 26.7, 29.2, 32.1, 66.6 (OCH_2), 71.1 (C–N), 81.3 (=CH_2), 88.1 (C_5H_{11}–C–O), 103.9, 197.6; *m/z* (12 eV) 196 (M + 1), 194, 178, 123, 99, 95, 82 (100%).

‡ Bicyclic adducts **2d**–**f** are *cis* ring fused (refs. 8 and 16), and this stereochemistry is recovered in **4**, **5d**–**f**.

§ *Selected data* for **4c**: ν_{max}(neat)/cm^{-1} 3555, 3257, 3033, 2859, 2969, 1966, 1058; δ_H(400 MHz, C_6D_6) 0.79 (s, 3 H), 4.52 [dt, *J* 11.9, 5.0, 1 H (OCH_AH_B)], 4.60 [dt, *J* 11.9, 3.5, 1 H (OCH_AH_B)], 4.70 [ddd, *J* 10.3, 4.9, 3.4, 1 H (C=CH_AH_B)], 4.76 (ddd, *J* 10.3, 5.2, 3.6, 1 H), 5.20 [s, 1 H (PhCHO)], 7.12 (tt, *J* 7.4, 1.2, 1 H), 7.21 (t, *J* 7.4, 2 H), 7.50 (d, *J* 7.5, 2 H); δ_C(100.61 MHz, $CDCl_3$) 20.4, 68.6 (OCH_2), 71.4 (C–N), 81.2, 84.3 (PhCHO–), 106.9, 126.8, 127.6, 128.2, 139.8, 199.2.

¶ *Selected data* for **5e**: ν_{max}(neat)/cm^{-1} 3387, 3265, 3218, 2930, 1657, 1011; δ_H(400 MHz, $CDCl_3$) 1.33–1.61 (m, 6 H), 1.95–2.07 (m, 2 H), 3.44 [m, 1 H (C_6 ring CHO–)], 4.14 [ddd, *J* 16, 5.6, 3, 1 H (OCH_AH_B–C_6ring)], 4.21 [ddt, *J* 16, 3.1, 2.1, 1 H (OCH_AH_B–C_6ring)], 4.34 [ddd, *J* 12.6, 4.1, 2.3, 1 H (OCH_AH_B–C_5ring)], 4.53 [ddd, *J* 12.6, 5.4, 3.1, 1 H (OCH_AH_B–C_5ring)], 5.55 [tt, *J* 3.1, 2.0, 1 H (=CH)]; δ_C (100.61 MHz, $CDCl_3$) 20.0, 21.1, 27.0, 27.1, 60.3 (C–N), 66.2 (OCH_2, C_6ring), 68.2 (OCH_2, C_5ring), 79.1 (O–CH–), 114.9, 142.9; *m/z* (12 eV) 182, 181 (100%, M^+), 150, 149, 111, 96, 83.

‖ This pathway has been suggested by referees.

1 G. W. Kirby, *Chem. Soc. Rev.*, 1997, **6**, 1; G. E. Keck, *Tetrahedron Lett.*, 1978, **48**, 4767; J. Streith, G. Augelmann, H. Fritz and H. Strub, *Tetrahedron Lett.*, 1982, **23**, 1909.

2 G. E. Keck and D. G. Nickell, *J. Am. Chem. Soc.*, 1980, **102**, 3632; H. Iida, Y. Watanabe and C. Kibayashi, *J. Am. Chem. Soc.*, 1985, **107**, 5534; T. P. Burkholder and P. L. Fuchs, *J. Am. Chem. Soc.*, 1988, **110**, 2341; Y. Watanabe, H. Iida and C. Kibayashi, *J. Org. Chem.*, 1989, **54**, 4088; Y. Shishido and C. Kibayashi, *J. Org. Chem.*, 1992, **57**, 2876.

3 N. J. Leonard, A. J. Playtis, F. Skoog and R. Y. Schmitz, *J. Am. Chem. Soc.*, 1971, **93**, 3056; G. E. Keck, S. Fleming, D. Nickell and P. Weider, *Synth. Commun.*, 1979, **9**, 281; D. L. Boger and M. Patel, *J. Org. Chem.*, 1984, **49**, 4098; H. Iida, Y. Watanabe and C. Kibayashi, *Tetrahedron Lett.*, 1984, **25**, 5091; M. Sabuni, G. Kresze and H. Braun, *Tetrahedron Lett.*, 1984, **25**, 5377.

4 C.-T. Lin and W.-J. Hsu, *Can. J. Chem.*, 1989, **67**, 2153; H. Felber, G. Kresze, R. Prewo and A. Vasella, *Helv. Chem. Acta*, 1986, **69**, 1137; H. Nitsch and G. Kresze, *Angew. Chem., Int. Ed. Engl.*, 1976, **15**, 760; H. Felber, G. Kresze, H. Braun and A. Vasella, *Tetrahedron Lett.*, 1984, **25**, 5381.

5 L. I. Olsson and A. Claesson, *Synthesis*, 1979, 743; J. Grimaldi and A. Cormons, *C. R. Acad. Sci. C*, 1979, **289**, 373; J. J. Chilot, A. Doutheau and J. Goré, *Tetrahedron Lett.*, 1982, **23**, 4693; J. J. Chilot, A. Doutheau and J. Goré, *Bull. Soc. Chim. Fr.*, 1984, II, 307.

6 S. R. Landor, *The Chemistry of The Allenes*, Academic Press, 1982, vol. 1, p. 165.

7 R. L. Funk, G. L. Bolton, J. U. Daggett, M. M. Hansen and L. H. M. Horcher, *Tetrahedron*, 1985, **41**, 3479; N. A. LeBel and E. Banucci, *J. Am. Chem. Soc.*, 1970, **92**, 5278; A. Padwa, M. Meske and Z. Ni, *Tetrahedron*, 1995, **51**, 89.

8 J.-P. Dulcère and E. Dumez, *Chem. Commun.*, 1997, 971.

9 J. March, *Advanced Organic Chemistry*, Wiley, New York, 3rd edn., 1985, p. 1103; G. W. Kabalka and R. S. Varma, *Comprehensive Organic Synthesis*, ed. B. M. Trost, Pergamon Press, 1991, vol. 8, p. 373.

10 J. Souppe, L. Danon, J. L. Namy and H. B. Kagan, *J. Organomet. Chem.*, 1983, **250**, 227.

11 A. S. Kende and J. S. Mendoza, *Tetrahedron Lett.*, 1991, **32**, 1699.

12 S. R. Landor, *The Chemistry of The Allenes*, Academic Press, 1982, vol. 2, p. 369; G. M. Coppola and H. F. Schuster, *Allenes in Organic Synthesis*, Wiley, New York, 1984; J. Grimaldi, J. Hatem, C. Henriet-Bernard and R. Maurin, *J. Chem. Res.* (*S*), 1994, 36; J. Grimaldi and A. Cormons, *Tetrahedron Lett.*, 1986, **27**, 5089; J. Grimaldi and A. Cormons, *Tetrahedron Lett.*, 1987, **28**, 3487; J. Grimaldi and A. Cormons, *Tetrahedron Lett.*, 1985, **26**, 825; J. Grimaldi and A. Cormons, *C. R. Acad. Sci., II*, 1989, 1753; J. Grimaldi and A. Cormons, *Tetrahedron Lett.*, 1988, **29**, 6609; J. J. Chilot, A. Doutheau, J. Goré and A. Saroli, *Tetrahedron Lett.*, 1986, **27**, 849; P. Audin, A. Doutheau and J. Goré, *Bull. Soc. Chim. Fr.*, 1984, II, 297.

13 A. Claesson, C. Sahlberg and K. Luthman, *Acta Chem. Scand., Ser. B*, 1979, 309.

14 E. Ciganek, *J. Org. Chem.*, 1990, **55**, 3007; E. Ciganek, J. M. Read and J. C. Calabrese, *J. Org. Chem.*, 1995, **60**, 5795; E. Ciganek, *J. Org. Chem.*, 1995, **60**, 5803; W. Oppolzer, A. C. Spivey and C. G. Bochet, *J. Am. Chem. Soc.*, 1994, **116**, 3139; M. P. Coogan and D. W. Knight, *Tetrahedron Lett.*, 1996, **37**, 6417; M. B. Gravestock, D. W. Knight and S. R. Thornton, *J. Chem. Soc., Chem. Commun.*, 1993, 169.

15 F. Becke and G. Mutz, *Chem. Ber.*, 1965, **98**, 1322; J. Thesing, A. Müller and G. Michel, *Chem. Ber.*, 1955, **88**, 1027; J. E. Baldwin, L. M. Harwood and M. J. Lombard, *Tetrahedron*, 1984, **40**, 4363; S. Maciejewski, I. Panfil, C. Belzecki and M. Chmielewski, *Tetrahedron*, 1992, **48**, 10 363; M. Jurczak, D. Socha and M. Chmielewski, *Tetrahedron*, 1996, **52**, 1411; Y. Xiang, H.-J. Gi, D. Niu, R. F. Schinazi and Z. Zhao, *J. Org. Chem.*, 1997, **62**, 7430.

16 T. Yakura, T. Tsuda, Y. Matsumura, S. Yamada and M. Ikeda, *Synlett*, 1996, 985.

Received in Liverpool, UK, 31st October 1997; 7/07840D

LiOH promoted allomerization of pyropheophorbide *a*. A convenient synthesis of 13²-oxopyropheophorbide *a* and its unusual enolization

Andrei N. Kozyrev, Thomas J. Dougherty and Ravindra K. Pandey*†

Chemistry Section, Department of Radiation Biology, Division of Radiation Medicine, Roswell Park Cancer Institute, Buffalo, NY 14263, USA

Treatment of pyropheophorbide *a* with aqueous LiOH–THF gave the corresponding enolate, which on *in situ* oxidation produced the corresponding 13²-oxo derivative in 79% yield; prolonged autoxidation gave purpurin-18 and purpurin-5 as major products and a mechanism for the formation of 12-formyl derivative from 13²-oxopyropheophorbide *a* under unusual enolization is discussed; the electronic absorption spectroscopy data of the enolic intermediates showed a considerable perturbation in the π-systems of the macrocycle.

The term 'allomerization' was first introduced to chlorophyll chemistry by Willstatter,[1] who used it to describe then unknown modification reactions of chlorophylls occurring on standing in alcohol solution in contact with air. Thus, allomerization is identical with the term 'autoxidation', which implies oxidation by triplex oxygen ($^3O_2$). In chlorophyll chemistry, besides allomerization, the enolization of the isocyclic ring has been studied extensively and it is now well established that allomerization takes place after the formation of chlorophyll enolates.[2] The isocyclic ring of all chlorophylls (except the chlorobium Chls) is a substituted β-keto ester and therefore has a tendency to enolize. Due to the activation by the two carbonyl functions, the 13²-hydrogen atom is abnormally acidic. On the basis of oxidation potentials, Wasielewski *et al.*[3] have proposed an enolate ion of chlorophyll *a* as the possible primary electron donor in Photosystem I of plant photosynthesis.

We recently reported the formation of a formyl analog as a minor product in the synthesis of purpurin-18 imides.[4] In our investigation on the mechanism for the formation of such formyl derivatives, we used a variety of chlorins including 13²-oxopyropheophobide *a* as substrates. Here we report a simple and efficient method for the preparation of diketone **3**, its 'alomerization' behavior, spectroscopic studies and a possible mechanism for the formation of the corresponding 12-formyl analog.

In contrast to natural chlorophylls and their free bases, pyropheophorbide *a* **1** which lacks an acidic hydrogen at 13²-position was believed not to undergo enolization. This was further confirmed by Conant and Hyde[5] on the basis of a negative Molisch 'phase test'. We reinvestigated this reaction under milder basic conditions, and observed that pyropheophorbide *a* on treatment with LiOH indeed produced stable enolate derivative **2** (Scheme 1), which was detected spectroscopically. It exhibited a characteristic UV–VIS spectrum with the split and red shifted Soret band at λ_{max} = 449 nm. Stronger bases, such as KOH and NaOH, did not produce any spectroscopic changes. This phenomenon could be explained due to the well-known property of lithium salts to form partially covalent bonds.[2] As a result of enolization, methyl pyropheophorbide *a* **1** was completely autoxidized on stirring in THF at room temperature for extended time (12 h) to produce 13²-oxo derivative **3** in 79% yield. Prolonged oxidation (72 h) gave the products of further degradation, which after standard work-up and CH_2N_2 treatment were separated by preparative chromatography. The faster moving band was identified as purpurin-18 methyl ester **4** (32%).[6] The slower moving band was characterized as purpurin-5 dimethyl ester **5** (a key product inWoodward's 'purpurin reaction') and was isolated in 38% yield.[7] The formation of chlorin **5** is obviously due to the basic hydrolysis of the dicarbonyl C–C bond of the diketocyclopentane ring. The other two gray–green porphyrins were isolated in small amounts (*ca*. 2%) and were identified as 13²-oxophylloerythrin methyl ester **6** and 15-*meso*-formylrhodoporphyrin XV dimethyl ester **7**. Both porphyrins showed unique 'reverse-rhodo' visible absorption spectra (Fig. 1) which were found to be different from those generally reported in porphyrin chemistry.[8] These newly discovered green porphyrins can be compared to those related to verdins, or recently reported emeraldins containing fused anhydride or imide ring systems.[9]

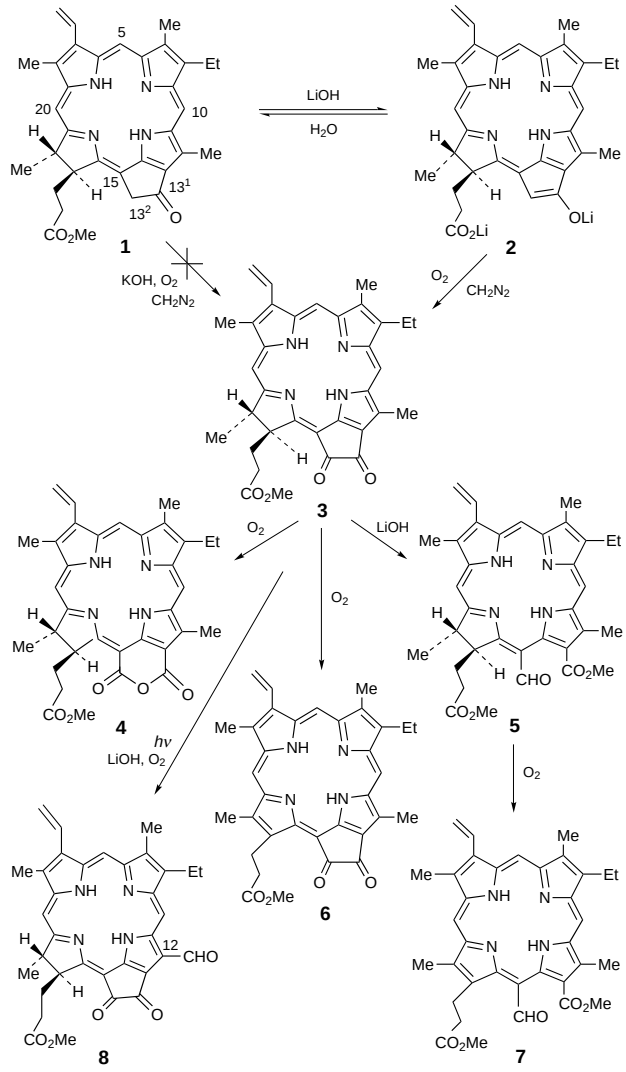

Scheme 1

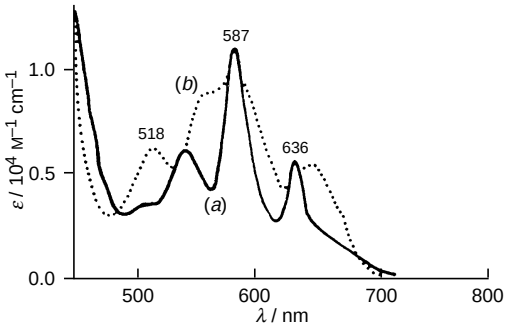

Fig. 1 Electronic absorption spectra (in CH_2Cl_2) of (*a*) dioxoporphyrin **6** and (*b*) porphyrin **7**

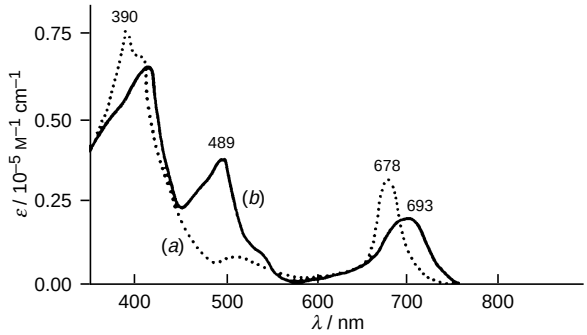

Fig. 2 Electronic absorption spectra (in CH_2Cl_2) of (*a*) chlorin **3** and (*b*) its enolate **3a**

Further purification of this complex mixture also gave a novel chlorin (5% yield) with a significantly red shifted absorption Q_y-band at 710 nm and a Soret band at 440 nm. Compared to 13²-oxopyropheophorbide *a*, the ^{1}H NMR spectrum of this chlorin showed the presence of a distinctive singlet for a formyl group at δ 11.08 and disappearance of the resonances for the 12-methyl protons. The mass spectrum of this product gave a molecular ion peak at *m/z* 576, confirming the replacement one of the methyl group by a formyl substituent. The ^{1}H NMR and 2D ROESY data supported the structure as 12-demethyl-12-formyl-13²-oxopyropheophorbide *a* methyl ester **8**. The formation of chlorin **8** from 13²-oxopyropheophorbide *a* **3**, which lacks protons at 13²-position, possibly proceeds *via* a vinylogous enolization involving the methyl protons attached to the adjacent pyrrolic ring (ring C). This process would certainly be facilitated by the presence of strong electron-withdrawing carbonyl functions at the adjacent cyclopentane ring. A proposed mechanism for the formation of chlorin **8** is shown in Scheme 2. The key step in this reaction is the formation of a reactive intermediate species **3a**. Reaction of enolate **3a** with singlet oxygen, *via* [4 + 2] cycloaddition and subsequent rearrangement, would generate the 12-formyl analog **8**. Chlorins in general are known to convert molecular oxygen to singlet oxygen ($^1O_2$) on irradiating with light. In order to further confirm the [4 + 2] cycloaddition mechanism with singlet oxygen, we used purpurin-18 imide,[4] as a more stable substrate, which could also undergo vinylogous enolization similar to **3a**. Photooxidation of purpurin-18 imide in aqueous LiOH–THF on exposing to sunlight produced the corresponding 12-formyl derivative in high yield (up to 60%). When the reaction was performed in the dark, the 12-formyl analog was not detected.[10]

Despite intensive studies in chlorophyll chemistry, this is the first example in which this type of enolization is observed. The

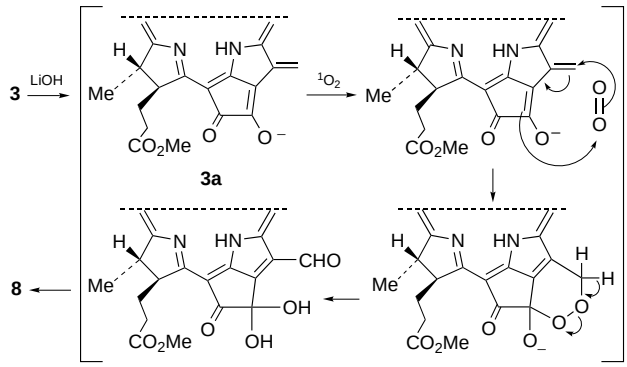

Scheme 2

evidence of enolization in 13²-oxopyropheophorbide *a* **3** was also confirmed by its specific UV–VIS spectrum (splitting of the Soret band), a characteristic property of enolates in pheophorbide system (Fig. 2). The enolic form **3a** produced under other basic conditions (KOH, NaOH) was found to be stable in non-polar solvents. However, traces of alcohol or water completely destroyed the potassium and sodium enolates, while the lithium salt appeared to be quite stable.

The chemistry discussed here might explain the origin of deoxophylloerythrioetioporphyrin (12-demethyl-DPEP), a minor petroporphyrin structure isolated by Callot.[11]

The newly discovered LiOH promoted enolization of pyropheophorbide *a* has opened a simple and effective way for the preparation of 13²-oxopyropheophorbide *a* **3** which had previously been isolated as a by-product in minor quantities.[6] Further studies are underway to explore the reactivity of the cyclopentanedione ring system for the preparation of novel chlorins with linear conjugation as photosensitizers for photodynamic therapy and models for photosynthetic reaction centers.

This work was supported by grants from Mallinckrodt Medical Inc., St. Louis, the National Institutes of Health (CA 55791) and the Oncologic Foundation of Buffalo.

Notes and References

† E-mail: pdtctr@sc3101.buffalo.edu

1 R. Willstatter and A. Stoll, *Untersuchungen uber Chlorophyll*, Springer, Berlin, 1913.
2 P. H. Hynninen, in *Chlorophylls*, ed. H. Scheer, CRC Press, Ann Arbor, 1991, p. 145.
3 M. R. Wasielewski, J. R. Norris, L. L. Shipman, C. P. Lin and W. A. Svec, *Proc. Natl. Acad. Sci. USA*, 1981, **78**, 2957.
4 A. N. Kozyrev, G. Zheng, C. Zhu, T. J. Dougherty, K. M. Smith and R. K. Pandey, *Tetrahedron Lett.*, 1996, **37**, 6431.
5 J. K. Conant and J. F. Hyde, *J. Am. Chem. Soc.*, 1929, **51**, 3668.
6 L. Ma and D. Dolphin, *J. Org. Chem.*, 1996, **61**, 2501.
7 R. B. Woodward, W. A. Ayer, J. M. Beaton, F. Bickelhaupt, R. Bonnett, P. Buchschacher, G. L. Closs, H. Dutler, J. Hannan, F. P. Hauck, S. Ito, A. Langemann, E. Le Goff, W. Leimgruber, W. Lwowski, J. Sauer, Z. Valenta and H. Volz, *Tetrahedron*, 1990, **46**, 7599.
8 K. M. Smith, *General features of the structure and chemistry of porphyrin compounds*, in *Porphyrins and Metalloporphyrins*, ed. K. M. Smith, Elsevier, Amsterdam, 1975.
9 A. N. Kozyrev, G. Zheng, E. Lazarou, T. J. Dougherty, K. M. Smith and R. K. Pandey, *Tetrahedron Lett.*, 1997, **38**, 3335.
10 A. N. Kozyrev and R. K. Pandey, unpublished results.
11 J. Verne-Mismer, R. Ocampo, C. Bauder, H. L. Callot and P. Albrecht, *Energy Fuels*, 1990, **4**, 639.

Received in Corvallis, OR, USA, 27th October 1997; 7/07805F

Cyclic enediynes: relationship between ring size, alkyne carbon distance, and cyclization barrier

Peter R. Schreiner

Institut für Organische Chemie der Georg-August Universität Göttingen, Tammannstr. 2, D-37077 Göttingen, Germany

This work presents the first detailed study on a series of cyclic hydrocarbon enediynes showing that the cyclization barrier depends upon the ground state energy differences of the biradical products, and that pure density functional methods can be used reliably to estimate the activation enthalpies of the Bergman reaction.

While the Bergman-3-enecyclization[1] of (*Z*)-hex-1,5-diynes (**1**, enediynes) is driven thermodynamically by subsequent formation of two C–H bonds, the pharmacological activity[2] of cyclic enediynes (**3**)[3] is also related to changes in ring strain upon cyclization.[4,5] Ring closure in enediyne carrying drugs complexed to the minor grove of DNA is triggered by subtle structural perturbations.[4] Hence, enediynes are highly promising pharmacophors, but reactivity control is still a problem.

It has been suggested that if the distance *d* of the acetylene carbons forming the new bond is in the critical range of 3.31–3.20 Å, cyclization should occur at room temperature.[6] Based on experimental activation enthalpies, X-ray structures of C_9–C_{12} cyclic enediynes and empirical computations, it was proposed that differential molecular strain in the educts and transition states is most important.[7–10] There have been several studies attempting to clarify the relationship between *d* and cyclic enediyne cyclization as well as the ground state energy differences, but transition structures for other than the smallest enediynes were never computed.[9–14] The modeling of larger enediynes is currently only possible with molecular mechanics,[13] semiempirical[10,14] or lowest-level *ab initio* methods,[11] but these cannot be used to compute accurate enediyne transition structures and activation energies; much higher level treatments are needed,[12,15,16] Density functional theory (DFT) offers a suitable compromise for multi-reference cases, as it is the electron density instead of the wavefunction which is the decisive quantity.[17] While hybrid Hartree-Fock DFT methods like B3LYP do not perform well for computing the heat of formation of *p*-benzyne **2a**,[16] 'pure' (*i.e.* non-hybrid DFT treatments give acceptable accuracy (Table 1).[18] We have therefore used the BLYP/6-311+G**//BLYP/6-31G* level throughout, unless noted otherwise.[19]

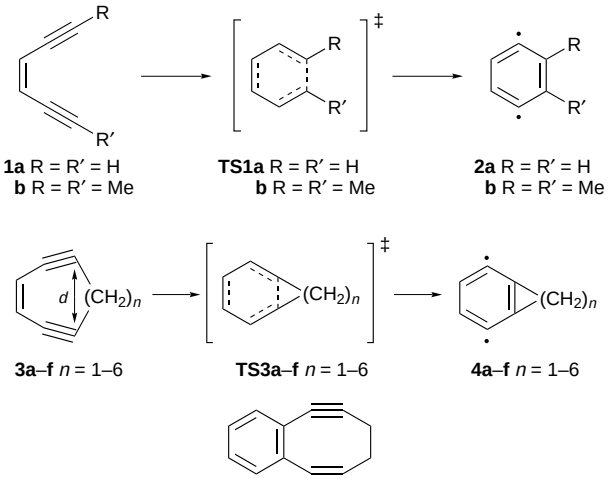

Scheme 1

The experimental activation enthalpies are well reproduced at our reference level: (theory *vs.* expt.) 28.4 *vs.* 28.2 kcal mol^{-1} for **TS1a**;[20] 25.0 *vs.* 23.8[6] and 24.0 kcal mol^{-1} for **TS3d**.[21] Enediynes **1a** and **1b** have almost the same *d* value but the difference in $\Delta H^{\ddagger}$ values is 7 kcal mol^{-1}. This is primarily due to the fact that methyl groups stabilize (by *ca.* 10 kcal mol^{-1}) acetylenic (**1b**) much more than olefinic bonds (partially developed in **TS1b**). Thus, dialkyl substitution increases both the activation barriers and the reaction endothermicities of the Bergman reaction for acyclic enediynes.

As expected, both **3a** and **3b** do not cyclize, despite small *d* values; **5** was found experimentally not to cyclize either.[22] The cyclization products would contain highly strained [olefin strain (OS) = 54.4 kcal mol^{-1}, Table 1][23] cyclopropene (in **3a**) and cyclobutene moieties (in **3b** and **5**; OS = 30.6 kcal mol^{-1}).[23] Nine-membered **3c** was suggested to cyclize spontaneously at room temperature,[4,6] and the relatively low activation barrier of 16.3 kcal mol^{-1} for **TS3c** supports this finding. While **3d** with *d* = 3.413 Å[21] cyclizes spontaneously at room temp., **3e** does not, despite *d* being only slightly larger (3.588 Å).[4] Part of the activation enthalpy difference (7 kcal mol^{-1}) is due to olefin strain (OS) energy differences[23] between the cyclohexene (OS = 2.5 kcal mol^{-1}) and cycloheptene (OS = 6.7 kcal mol^{-1}) moieties in the products. Thus, there is no linear relationship between the alkyne carbon distance *d* and $\Delta H^{\ddagger}$ for Bergman-cyclization of monocyclic enediynes.

The reaction enthalpy ($\Delta_r H_{OK}$, Table 1) of the Bergman reaction is more difficult to compute than the activation enthalpies due to the pronounced multi-reference-character of

Table 1 Parameter *d* (in Å), activation enthalpy ($\Delta H^{\ddagger}$/kcal mol^{-1}), reaction enthalpy ($\Delta_r H_{OK}$/kcal mol^{-1}) for the Bergman reaction of **3a–f**; olefin ring strain (OS) of non-benzenoid product ring and stability of enediyne at room temperature. Level of theory: BLYP/6-311+G**//BLYP/6-31G*, unless noted otherwise

Ring size	Species (PG)[a]	*d*	$\Delta H^{\ddagger}$	$\Delta_r H_{OK}$	Corrected[b] $\Delta_{cr} H_{OK}$	OS[c]	Stable at 25 °C
—	**1a** (C_{2v})	4.548	28.4	17.6	8.5	—	yes[d]
—	**1b** (C_{2v})	4.571	35.6	29.9	20.8	—	yes[d]
7	**3a** (C_{2v})	2.512		—[e]		54.4	n.a.
8	**3b** (C_{2v})	2.636		—[e]		30.6	yes[f]
9	**3c** (C_s)	2.924	16.3	11.4	2.3	6.8	no[g]
10	**3d** (C_2)	3.413[h]	25.0[i]	18.3	9.2	2.5	no[g]
11	**3e** (C_2)	3.588[j]	31.9	25.4	16.3	6.7	yes[g]
12	**3f** (C_2)[k]	4.353	40.3	36.3	27.2	7.4	yes[g]

[a] PG = point group. [b] Corrected for the computational error in $\Delta_r H_{OK}$ of **2a** at 0 K (correction = −9.1 kcal mol^{-1}). [c] Ref. 23. [d] Ref. 24. [e] No ring closure, see text. [f] Ref. 22. [g] Ref. 6. [h] Experimentally estimated distance *ca.* 3.4 Å (refs. 24 and 21). [i] Experimental activation barrier = 23.8 (ref. 6) and 24.0 kcal mol^{-1} (refs. 14 and 21). [j] Experimental distance (X-ray) = 3.661(5) Å (ref. 6). [k] Using a 6-311G** basis set for the energy single point. Despite extensive efforts, the wavefunction did not converge with added diffuse ('+') functions on the heavy atoms.

2a. It is therefore sensible to correct $\Delta_r H_{OK}$ for the error (9.1 kcal mol^{-1}) in evaluating the enthalpy of the parent reaction. This correction seems reasonable based on the fact that nine- and ten-membered enediynes cyclize reversibly.[4,24] Larger enediyne cyclizations are much more endothermic and the corresponding transition structures are product-like.[12,15] This is confirmed by the increase in the activation enthalpy of the parent (**1a** → **TS1a**: $\Delta H^{\ddagger}$ = 28.4 kcal mol^{-1}) *vs*. the dimethyl enediyne system (**1b** → **TS1b**; $\Delta H^{\ddagger}$ = 35.6 kcal mol^{-1}): **TS1b** already experiences part of the higher relative energy of the product, where the methyl groups at olefinic carbons are less stabilizing.

The relationship between $\Delta H^{\ddagger}$ for Bergman cyclization of monocyclic enediynes can thus roughly be estimated from the endothermicity of eqn. (1).

$$\Delta H^{\ddagger} = \Delta_{cr} H_{OK} + 14 \pm 2 \text{ kcal mol}^{-1} \quad (1)$$

In conclusion, there is excellent agreement between the experimental and pure DFT-computed $\Delta H^{\ddagger}$ values for Bergman cyclization of monocyclic enediynes. There is no predictive linear relationship between *d* and $\Delta H^{\ddagger}$, but the 'critical range' for 3.31–3.2 Å for spontaneous cyclization may be extended to 3.4–2.9 Å. However, cyclization may be inhibited by large olefin strain in the products. Although dialkyl substitution increases the endothermicity of the Bergman reaction, ring strain effects can dominate.

The author thanks the Fonds der Chemischen Industrie (Liebig-Fellowship), the Deutsche Forschungsgemeinschaft, the RRZ Niedersachsen and Professor de Meijere for support. Discussions with Professors R. R. Squires and C. J. Cramer are highly appreciated.

Notes and References

* E-mail: pschrei@gwdg.de Coordinates of all optimized structures are available through the author by e-mail request.

1 R. R. Jones and R. G. Bergman, *J. Am. Chem. Soc.*, 1972, **94**, 660.
2 L. G. Paloma, J. A. Smith, W. J. Chazin and K. C. Nicolaou, *J. Am. Chem. Soc.*, 1994, **116**, 3697.
3 M. D. Lee, T. S. Dunne, M. M. Siegel, C. C. Chang, G. O. Morton and D. B. Borders, *J. Am. Chem. Soc.*, 1989, **109**, 3464.
4 K. C. Nicolaou and W.-M. Dai, *Angew. Chem.*, 1991, **103**, 1453.
5 R. Glcitcr and D. Kratz, *Angew. Chem.*, 1993, **105**, 884.
6 K. C. Nicolaou, G. Zuccarello, Y. Ogawa, E. J. Schweiger and T. Kumazawa, *J. Am. Chem. Soc.*, 1988, **110**, 4866.
7 P. Magnus, R. T. Kewis and J. C. Huffman, *J. Am. Chem. Soc.*, 1988, **110**, 6921.
8 P. A. Carter and P. Magnus, *J. Am. Chem. Soc.*, 1988, **110**, 1626.
9 J. P. Snyder, *J. Am. Chem. Soc.*, 1989, **111**, 7630.
10 J. P. Snyder, *J. Am. Chem. Soc.*, 1990, **112**, 5367.
11 K. C. Nicolaou, W.-M. Dai, Y. P. Hog, S.-C. Tsay, K. K. Baldridge and J. S. Siegel, *J. Am. Chem. Soc.*, 1993, **115**, 7944.
12 E. Kraka and D. Cremer, *J. Am. Chem. Soc.*, 1994, **116**, 4929.
13 M. F. Semmelhack, J. Gallagher and D. Cohen, *Tetrahedron Lett.*, 1990, **31**, 1521.
14 P. Magnus, S. Fortt, T. Pitterna and J. P. Snyder, *J. Am. Chem. Soc.*, 1990, **112**, 4986.
15 N. Koga and K. Morokuma, *J. Am. Chem. Soc.*, 1991, **113**, 1907.
16 R. Lindh and M. Schütz, *Chem. Phys. Lett.*, 1996, **258**, 409.
17 H. F. Bettinger, P. R. Schreiner, P. v. R. Schleyer and H. F. Schaefer, in *Carbenes—A Test Ground for Electronic Structure Methods*, in *The Encyclopedia of Computational Chemistry*, ed. P. v. R. Schleyer, N. L. Allinger, T. Clark, J. Gasteiger, P. A. Kollman, H. F. Schaefer and P. R. Schreiner, Wiley, Chichester, 1998, in the press.
18 C. J. Cramer, J. J. Nash and R. R. Squires, *Chem. Phys. Lett.*, 1998, **277**, 311.
19 All computations were carried out with GAUSSIAN 94: M. J. Frisch, G. W. Trucks, H. B. Schlegel, P. W. M. Gill, B. G. Johnson, M. A. Robb, J. R. Cheeseman, T. Keith, G. A. Petersson, J. A. Montgomery, K. Raghavachari, M. A. Al-Laham, V. G. Zakrzewski, J. V. Ortiz, J. B. Foresman, C. Y. Peng, P. Y. Ayala, W. Chen, M. W. Wong, J. L. Andres, E. S. Replogle, R. Gomperts, R. L. Martin, D. J. Fox, J. S. Binkley, D. J. Defrees, J. Baker, J. J. P. Stewart, M. Head-Gordon, C. Gonzalez and J. A. Pople, Pittsburgh, 1995. The computed transition structures of the parent system were characterized by second derivative calculations. This is, however, computationally not feasible for the larger structures. In this case, the updated Hessian matrix was used to characterize stationary points as ground or transition states. Although solvent effects are not overly important for uncharged species, these could be computed with reaction field models. However, these methods are of limited applicability for non-dynamic DFT-work and were thus not utilized.
20 W. R. Roth, H. Hopf and C. Horn, *Chem. Ber.*, 1994, **127**, 1765.
21 P. Magnus and R. A. Fairhurst, *J. Chem. Soc., Chem. Commun.*, 1994, 1541.
22 H. Hopf, P. G. Jones, P. Bubenitschek and C. Werner, *Angew. Chem.*, 1995, **107**, 2592; W. R. Roth, H. Hopf, T. Wasser, H. Zimmerman and C. Werner, *Liebigs Ann*, 1996, 1691.
23 P. v. R. Schleyer, J. E. Williams and K. R. Blanchard, *J. Am. Chem. Soc.*, 1970, **92**, 2377.
24 R. G. Bergman, *Acc. Chem. Res.*, 1973, **6**, 25.

Received in Liverpool, UK, 31st October 1997; 7/07836F

First X-ray crystal structure and NMR spectroscopic analysis of a lithiated 1,2-diazapentadiene

Arndt Krol, Roland Fröhlich and Ernst-Ulrich Würthwein*†

Institute of Organic Chemistry, Westfälische Wilhelms-Universität, Corrensstr. 40, D-48149 Münster, Germany

Deprotonation of 1,2-diazapentadienes in Et_2O leads to the respective lithium compounds which, in the case of $[(\eta^1\text{-PhNLiNCHCMeCHPh})\cdot Et_2O]_3$, consists of an almost planar $(Li–N)_3$ hexagon resulting in a tunnel-like arrangement of the W-shaped 1,2-diazapentadienyl chains; the X-ray structure, solution NMR spectra and reactions with electrophiles are reported.

Nitrogen containing organolithium compounds[1] play a major role in synthetic organic chemistry. Therefore, much effort has been focused on the elucidation of the coordination chemistry of lithium bases,[2,3] lithium hydrazides[4] or azapolyenyl metal compounds.[5] In spite of their widespread use in organic chemistry only rarely has evidence for solution or solid state structures of lithiated hydrazone intermediates been published.[2,6,7]

We became interested in the theoretical, synthetic and structural aspects of aza- and diaza-polyenyl metal compounds. Our studies involve the dependence of the electronic and structural behaviour of the intermediates on the positions and nature of the heteroatoms within the conjugated lithiated polyenyl chain.[5] Here we report on the single crystal X-ray structure and NMR spectroscopic analysis of the hitherto unknown 4-methyl-1,5-diphenyl-1,2-diazapentadienyllithium.

4-Methyl-1,5-diphenyl-1,2-diazapentadiene **1** was obtained by condensation of phenylhydrazine and 2-methylcinnamaldehyde following the method of Schantl and Hebeisen.[8] Subsequent deprotonation with LDA or Bu^nLi in Et_2O or THF at −78 °C yielded a dark red solution of the respective lithium hydrazide **2** (Scheme 1).

^1H and ^{13}C NMR spectra of **2** in [$^2H_8$]THF were recorded in the temperature range −80 to 50 °C.‡ The spectra show two sets of signals which have been assigned to the W-shaped conformers **2a** and **2b** (Scheme 2) in a ratio 65 : 35 (**2a** : **2b**), which remains constant over the whole temperature range.

The equilibrium between the two isomers (Scheme 2) could not be frozen out. At 50 °C the spectra resulting from NOE experiments surprisingly show a negative NOE of one isomer upon saturation of the other. Although coalescence could not be achieved this NOE must be due to a transfer of saturation from **2a** to **2b** which can be observed beneath the coalescence temperature when the equilibration occurs faster than the relaxation of the spin system.[9]

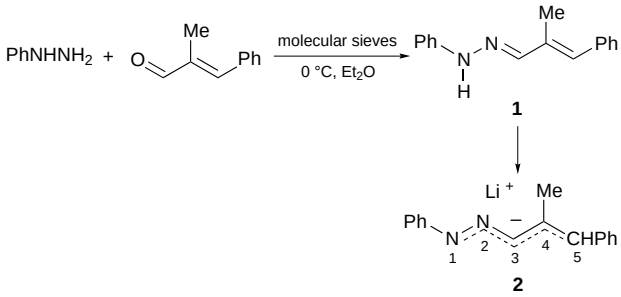

Scheme 1

In the ^{13}C NMR spectra of **2** the resonance frequencies of C(5) and C(3) are shifted by about 11 ppm to higher field, while for C(4) a downfield shift of about 5 ppm relative to the resonances of **1** can be observed. This can be explained by delocalization of the negative charge in the diazapentadienyl unit producing large HOMO coefficients on atoms 1, 3 and 5 and approximately nodal positions on atoms 2 and 4. So, C(3) and C(5) are positioned on centres of high electron density while C(4) is deshielded. As indicated by the ^{13}C NMR shifts, the phenyl substituents are also involved in the charge delocalization, which is additionally confirmed by the deep red colour of the reaction solution. The exact position of the lithium cation will be determined using Li NMR techniques in further experiments.

Crystallization from Et_2O–*n*-hexane leads to yellow single crystals of the trimeric compound **2a**§ whose molecular structure is shown in Fig. 1.

The X-ray diffraction analysis¶ reveals the trimeric structure $[(PhNLiNCHCMeCHPh)\cdot Et_2O]_3$ of **2a** (containing one hexane molecule per unit cell) in which the lithium cations are η^1-coordinated to the nitrogen atoms N(1) of two W-shaped diazapentadienyl moieties and to one Et_2O molecule. Each metal cation is involved in one shorter Li···N link of 1.995(7) Å [2.022(6) and 2.020(6) Å, respectively] and one longer metal–nitrogen contact of 2.066(7) Å [2.085(6) and 2.051(6) Å, respectively]. Such values are typical for end-on bound lithium hydrazides.[10] The resulting $(Li–N)_3$ hexagon with a diameter of 4.05 Å shows a slight boat-shaped distortion. The average Li···Li distance of 3.35 Å implicates a weaker intermetal contact than reported by Nöth *et al.*[10] which can be explained by the steric hindrance caused by the ligands. The lithium centres exhibit a trigonal planar coordination formed by two N(1) nitrogen atoms and one Et_2O molecule.

The nitrogen atoms N(1) in the $(Li–N)_3$ hexagon show a trigonal pyramidalically distorted tetrahedral geometry. The average N–N–Li angle of 109.3 Å and the Ph–N–N angle of 111.5 Å indicate sp^3 hybridization of the hydrazide nitrogen atom N(1). The short N–N distance of 1.38 Å is in remarkable contrast to the N(1)–N(2) distances of 1.55 Å reported for bis-silylhydrazides by Klingebiel[11] or 1.47 Å of Nöth *et al.*[10] in Li–diethylhydrazides and corresponds to non-negotiable double bond character. The N(2)–C(3) bond length of 1.29 Å correlates with the value of 1.305(5) Å found by Collum[12] in the dimeric lithiated 2-methoxycarbonylcyclohexanone dimethylhydrazone for which they postulate the contribution of C–N single and C=N double bond character. The C–C bond distances implicate a localized bond structure containing alternating single and double bonds with delocalization to a small extent. The solid

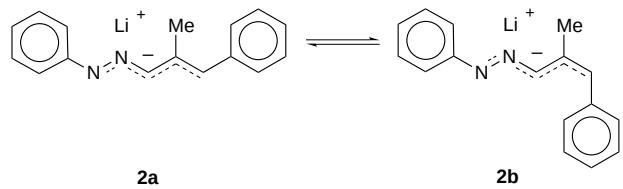

Scheme 2

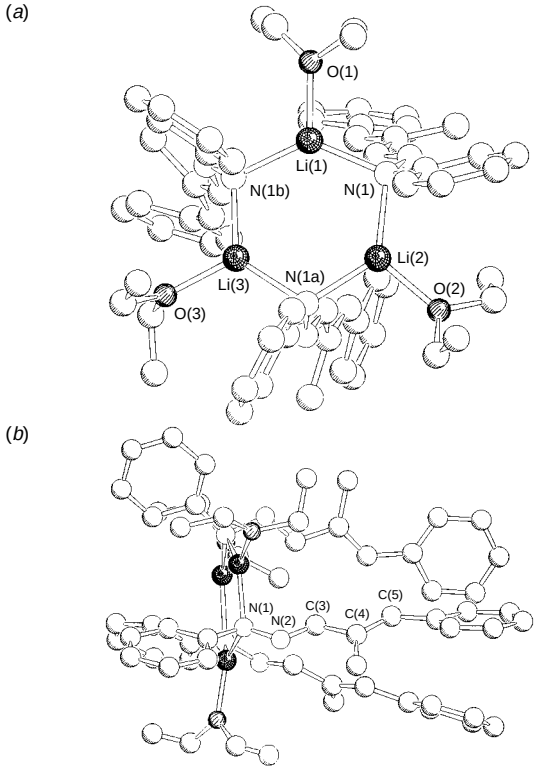

Fig. 1 Molecular structure of **2a**: (*a*) top view and (*b*) side view (hydrogen atoms omitted for clarity)

state structure can best be described as an end-on lithiated hydrazide with some contribution of a 1,2-diazaallyllithium resonance structure.

According to semiempirical calculations using PM3[13] the trimer of **2a** corresponds to a minimum on the potential energy hyperface in the gas phase, which indicates that the tunnel-like structure of the diazapentadienyl chains is not due to crystal packing forces. The W-shaped geometry of the unsubstituted 1,2-diazapentadienyl anion has also been obtained as the energetically most favoured conformer in *ab initio* calculations using the MP2/6-31+G*//RHF/6-31+G*[14] basis set.[15]

Reaction of the intermediate **2** with several alkyl or acyl electrophiles leads regioselectively to the N(1)-substituted *E,E*-hydrazones. *Ab initio* calculations indicate that the 1,2-diazapentadienyl anion bears the highest electron density on N(1)—as expected—and so, structure **2** implicates an electrophilic attack on N(1) which may also be the result of thermodynamic control. Regarding the solid state structure of **2a** the regioselectivity can be explained by a metal controlled nucleophilic substitution at the attacking electrophile.

The authors thank Mr L. Terfloth for valuable help in NMR analysis. We gratefully acknowledge financial support by the Deutsche Forschungsgemeinschaft, by the Graduiertenkolleg 'Hochreaktive Mehrfachbindungssysteme' (DFG) at the University of Münster and by the Fonds der Chemischen Industrie.

Notes and References

† E-mail: wurthwe@uni-muenster.de

‡ *Synthesis and ^1H and ^{13}C NMR analysis* of **2**. The lithium compound **2** was prepared by use of the syringe technique directly in the NMR tube. To a white slurry of LDA (0.5 mmol; from 0.3 ml Bu^{n}Li in *n*-hexane and 0.075 ml Pr$^i_2$NH) in 0.3 ml [$^2H_8$]THF was added a solution of **1** (85 mg, 0.36 mmol) in 0.3 ml [$^2H_8$]THF at −78 °C with shaking. The NMR tube was sealed with Parafilm and analysed *via* NMR spectroscopy. δ_H(599.77 MHz, 223 K, [$^2H_8$]THF): **2a** 2.34 (s, 3 H, 10-H), 6.02 (s, 1 H, 5-H), 6.20 (dd, ^3J 7.7, 7.1, 1 H, H_{arom}), 6.85 (t, ^3J 7.3, 2 H, H_{arom}), 6.98 (t, ^3J 7.2, 2 H, H_{arom}), 7.22 (m, 3 H, H_{arom}), 7.29 (d, ^3J 8.2, 2 H, 7′-H), 7.47 (s, 1 H, 3-H); **2b** 2.17 (s, 3 H, 10-H), 5.94 (s, 1 H, 5-H), 6.21 (t, ^3J 7.3, 1 H, H_{arom}), 6.85 (t, ^3J 7.3, 2 H, 7-H), 7.00 (t, ^3J 7.2, 2 H, H_{arom}), 7.19 (m, 3 H, H_{arom}), 7.26 (d, ^3J 8.2, 2 H, 7′-H), 8.02 (s, 1 H, 3-H). δ_C(150.85 MHz, 223 K, [$^2H_8$]THF): **2a** 14.9 (C-10), 113.2 (C_{arom}), 115.2 (C_{arom}), 121.2 (C-5), 124.5 (C_{arom}), 128.5 (C_{arom}), 128.7 (C_{arom}), 128.9 (C-3), 129.7 (C_{arom}), 140.8 (C-4), 140.8 (C-6′), 160.8 (C-6); **2b** 14.2 (C-10), 113.7 (C_{arom}), 115.2 (C_{arom}), 118.0 (C-5), 124.8 (C_{arom}), 128.4 (C_{arom}), 128.8 (C_{arom}), 129.4 (C_{arom}), 135.1 (C-3), 139.4 (C-4), 140.9 (C-6′), 160.7 (C-6).

§ *Synthesis* of [(PhNLiNCHCMeCHPh)·Et$_2$O]$_3$ **2a**. To a solution of Bu^{n}Li (2.8 ml, 4.5 mmol in *n*-hexane) in 15 ml Et$_2$O was added dropwise a solution of **1** (0.74 g, 3.1 mmol) in 25 ml Et$_2$O at −78 °C. After stirring the red solution for 30 min, the mixture was warmed to −20 °C. Recrystallization of the yellow precipitate from Et$_2$O–*n*-hexane yielded yellow crystals.

¶ *Crystal data* for [(PhNLiNCHCMeCHPh)·Et$_2$O]$_3$, monoclinic, space group $P2_1/c$ (No. 14), with unit cell parameters a = 12.013(1), b = 17.608(3), c = 28.633(2) Å, β = 97.69° (1), V = 6002.1(12) Å^3, ρ_{calc} = 1.098 g cm^{-3}. The crystals were analyzed using an Enraf Nonius automatic CAD4 Diffractometer with Cu-Kα radiation (λ = 1.54178 Å) utilizing a graphite monochromator. The yellow single crystal of $(C_{20}H_{25}N_2OLi\cdot 1/6C_6H_{14})_3$ (M = 992.16, crystal size: 0.50 × 0.30 × 0.30 mm^3) was measured at −50 °C. 10391 reflections were collected ($\pm h$, $+k$, $+l$) leading to 10 170 independent and 6106 observed [$(\sin\theta)/\lambda]_{max}$ = 0.59 Å^{-1}. An empirical absorption correction *via* ψ-scan data (0.914 ⩽ C ⩽ 0.999) was carried out, absorption coefficient μ = 5.12 cm^{-1}. 672 refined parameters. R = 0.085, R_w^2 = 0.259, max. residual electron density ρ = 0.53 (−0.35) e Å^{-3}. The structure was solved and refined using SHELXS-86 and SHELXL-93 with hydrogens calculated and refined as riding model, graphics SCHAKAL92. The unit cell contains one totally disordered hexane molecule which has been refined isotropically. CCDC 182/774.

1 A. Krol, Diploma Thesis, University of Münster, 1996.
2 A.-M. Sapse and P. v. R. Schleyer, *Lithium Chemistry: A Theoretical and Experimental Overview*, Wiley, 1995, pp. 125–172; G. Boche, *Angew. Chem.*, 1989, **101**, 286; *Angew. Chem., Int. Ed. Engl*, 1989, **28**, 277.
3 R. E. Mulvey, *Chem. Soc. Rev.*, 1991, **20**, 167.
4 I. Hemme, B. Tecklenburg, M. Noltemeyer and U. Klingebiel, *Chem. Ber.*, 1995, **128**, 351.
5 S. Klötgen and E.-U. Würthwein, *Tetrahedron Lett.*, 1995, **36**, 7065; S. Klötgen, R. Fröhlich and E.-U. Würthwein, *Tetrahedron*, 1996, **52**, 14 801; G. Wolf and E.-U. Würthwein, *Chem. Ber.*, 1991, **124**, 655; G. Wolf and E.-U. Würthwein, *Chem. Ber.*, 1991, **124**, 889.
6 H. Kloosterziel, *Recl. Trav. Chim. Pays-Bas*, 1973, **92**, 1167.
7 D. Enders, G. Bachstädter, K. A. M. Kremer, M. Marsch, K. Harms and G. Boche, *Angew. Chem.*, 1988, **100**, 1580; *Angew. Chem., Int. Ed. Engl.*, 1988, **27**, 1522.
8 J. G. Schantl and P. Hebeisen, *Tetrahedron*, 1990, **46**, 395.
9 D. Neuhaus and M. P. Williamson, *The Nuclear Overhauser Effect in Structural and Conformational Analysis*, VCH, Weinheim, 1989, p. 141.
10 H. Nöth, H. Sachdev, M. Schmidt and H. Schwenk, *Chem. Ber.*, 1995, **128**, 845.
11 K. Bode, C. Drost, C.Jäger, U. Klingebiel, M. Noltemeyer and Z. Zak, *J. Organomet. Chem.*, 1994, **482**, 285.
12 R. A. Wanat, D. B. Collum, G. van Duyne, J. Clardy and R. T. DePue, *J. Am. Chem. Soc.*, 1986, **108**, 3415.
13 J. J. P. Stewart, *J. Comput. Chem.*, 1989, **10**, 209; E. Anders, R. Koch and P. Freunscht, *J. Comput. Chem.*, 1993, **14**, 1301.
14 M. J. Frisch, G. W. Trucks, H. B. Schlegel, P. M. W. Gill, B. G. Johnson, M. A. Robb, J. R. Cheeseman, T. Keith, G. A. Petersson, J. A. Montgomery, K. Raghavachari, M. A. Al-Laham, V. G. Zakrzewski, J. V. Ortiz, J. B. Foresman, J. Cioslowski, B. B. Stefanov, A. Nanayakkara, M. Challacombe, C. Y. Peng, P. Y. Ayala, W. Chen, M. W. Wong, J. L. Andres, E. S. Replogle, R. Gomperts, R. L. Martin, D. J. Fox, J. S. Binkley, D. J. Defrees, J. Baker, J. P. Stewart, M. Head-Gordon, C. Gonzalez and J. A. Pople, GAUSSIAN 94, Revision B.2, Gaussian, Inc., Pittsburgh PA, 1995.
15 N. C. Aust, *ab initio* calculations, unpublished results.

Received in Liverpool, UK, 12th November 1997; 7/08151K

Optically active 'adjacent' type non-centrosymmetrically substituted phthalocyanines

Nagao Kobayashi†

Department of Chemistry, Graduate School of Science, Tohoku University, Sendai 980-8578, Japan

Optically active 'adjacent' type non-centrosymmetrically substituted phthalocyanines (Pcs) and benzo-substituted Pcs having π-systems with C_{2v} symmetry have been synthesized in high yields in a mixed condensation using bisphthalonitriles (which do not racemize under general Pc formation conditions) and a second phthalonitrile, and characterized by UV–VIS, natural and magnetic circular dichroism spectroscopy.

Control of the molecular symmetry of Pcs is not always easy. Here we describe a convenient route leading to *adjacent* and non-centrosymmetrically substituted *optically active* Pcs.

Our key starting materials are compounds **1** which can be obtained *via* a single step high yielding reaction (more than 90%) from commercially available (*S*)-(−)- or (*R*)-(+)-2,2′-dihydroxy-1,1′-binaphthyl and 3-nitrophthalonitrile without optical loss.[1,2] The most important property of compounds **1** is that they do not racemize under general Pc synthesis conditions because of the large steric hindrance due to the two bulky dicyanophenoxy groups, and of course no opposite isomer is produced. In addition, since the distance between the two phenoxy groups is close to the minimum to link two adjacent benzene rings of Pc, the formation of oligomeric Pcs is suppressed. Compounds (*S*)-**1** and (*R*)-**1** were converted to isoindoline derivatives by bubbling ammonia gas in dry MeOH[3] followed by reaction with 2 equiv. of 4,5-dimethoxyisoindoline[4] in refluxing *N*,*N*-dimethylaminoethanol for 3 h.[3] After evaporation of the solvent, the residue was separated on a basic alumina column (Act III) using CH_2Cl_2–MeOH (9 : 1 v/v) and then CH_2Cl_2–pyridine (1 : 1 v/v). The blue–green fraction was collected and separation was attempted by gel-permeation chromatography using Bio-beads SX-2 (Bio-rad) and CH_2Cl_2–MeOH (9 : 1 v/v). Three blue–green bands appeared, but the separation between the first and second bands was too small to effect separation. The third band (blue) was identified as (*S*)-**$H_2$2** and (*R*)-**$H_2$2** with two binaphthyl units *via* FAB mass spectroscopy (5–7%).[2,5,6] The first and second bands were accordingly mixed together and then separated on a column of Bio-beads SX-8 using THF as eluent. The first band was collected and recrystallized from CH_2Cl_2–EtOAc and then THF–EtOAc to give the optically active non-centrosymmetric (*S*)-**$H_2$3** and (*R*)-**$H_2$3** as a blue–green powder in 21–26% yield. Similarly, (*S*)-**$H_2$4** was prepared from the diiminoisoindoline derivatives of (*S*)-**1** and 6-*tert*-butyl-2,3-dicyanonaphthalene in 9% yield. Interestingly, the NMR signal of the pyrrole protons of (*S*)-**$H_2$4** appeared at two separate positions, one at δ −2.40 and the other at −4.05 (one proton each).[2] Judging from the fact that the ring current in naphthalocyanine (Nc) is smaller than that in Pc,[7] the signal from the former may be attributed to a pyrrole proton at the naphthalene ring site. The zinc and cobalt derivatives [*i.e.* (*S*)-**Zn3**, (*R*)-**Zn3**, (*S*)-**Co3**, (*R*)-**Co3** and (*S*)-**Co4**] were prepared by refluxing (*S*)-**$H_2$3** and (*R*)-**$H_2$3** with $Zn(OAc)_2$ and $CoCl_2$, and (*S*)-**$H_2$4** with $CoCl_2$, as previously described.[1]

Fig. 1 shows the electronic absorption, magnetic circular dichroism (MCD) and circular dichroism (CD) spectra of (*S*)-**$H_2$2** and (*R*)-**$H_2$2** in two solvents. In the absorption spectra, the four component Q band, characteristic of metal-free Pc, is seen and the spectra on the shorter wavelength side of the Soret band are to some extent deformed by the superimposition of the absorption due to the ^1L_a transition of naphthalene.[8] In the 220–250 nm region, a strong absorption attributable to the ^1B_b transition of the naphthalene moiety is observed. The MCD

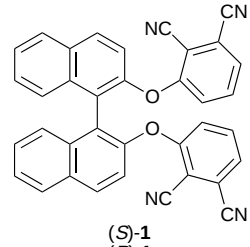

(*S*)-**1**
(*R*)-**1**

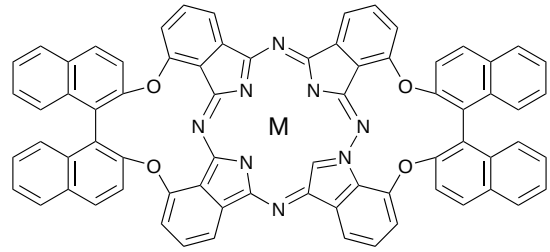

(*S*)-**$H_2$2**, (*R*)-**$H_2$2** M = H_2
(*S*)-**Zn2**, (*R*)-**Zn2** M = Zn
(*S*)-**Co2**, (*R*)-**Co2** M = Co

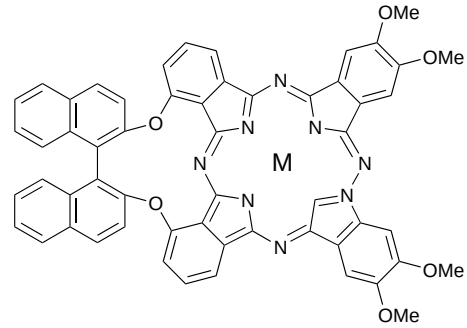

(*S*)-**$H_2$3**, (*R*)-**$H_2$3** M = H_2
(*S*)-**Zn3**, (*R*)-**Zn3** M = Zn
(*S*)-**Co3**, (*R*)-**Co3** M = Co

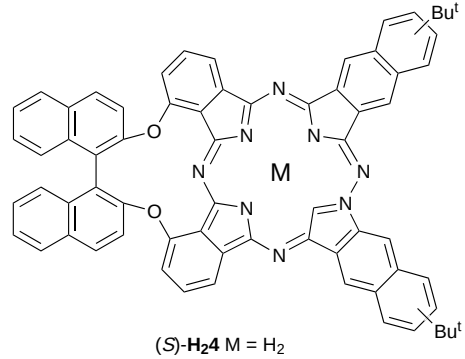

(*S*)-**$H_2$4** M = H_2
(*S*)-**Co4** M = Co

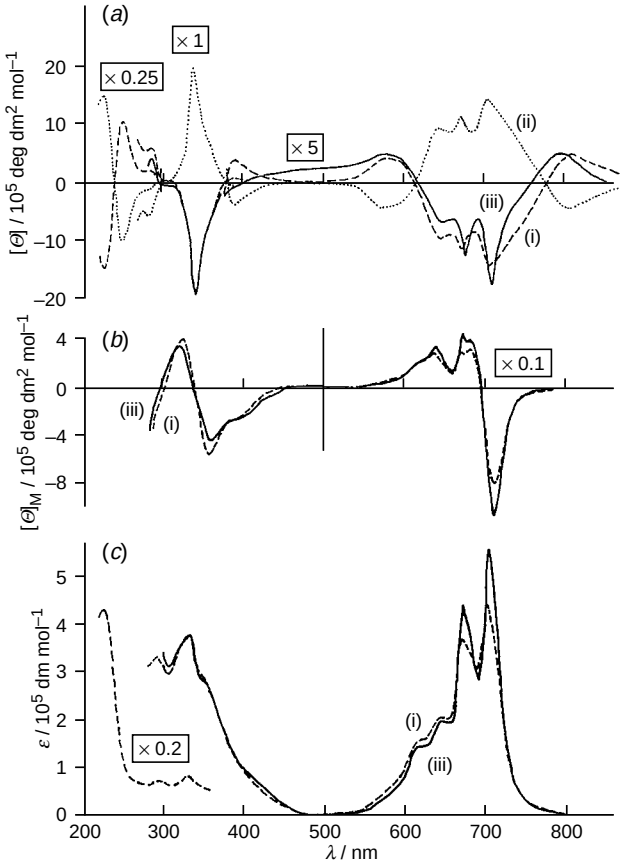

Fig. 1 (*a*) CD, (*b*) MCD and (*c*) electronic absorption spectra of (i) (*S*)-**H$_2$2** and (ii) (*R*)-**H$_2$2** in THF and (iii) (*S*)-**H$_2$2** in toluene

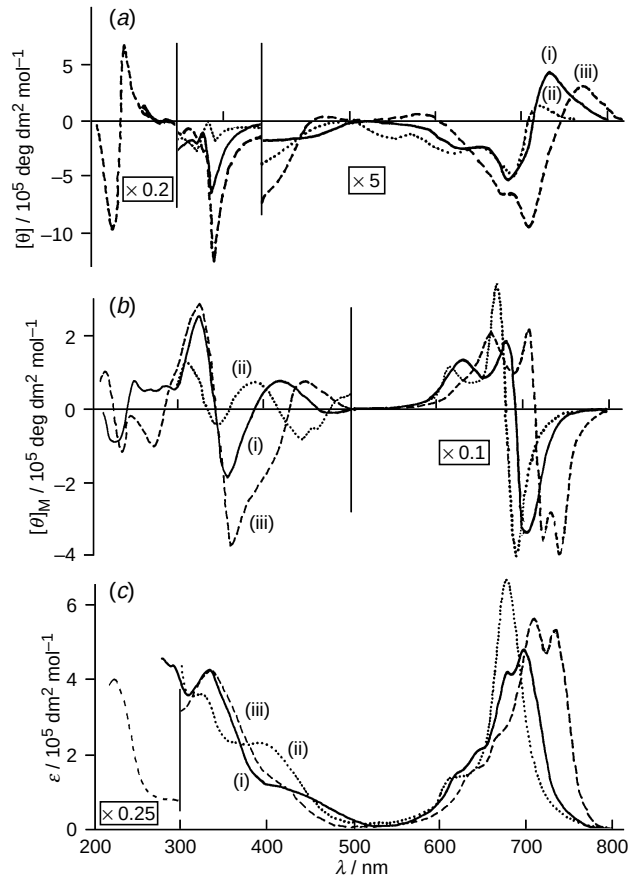

Fig. 2 (*a*) CD, (*b*) MCD and (*c*) electronic absorption spectra of (i) (*S*)-**H$_2$3**, (ii) its (pyrrole proton) deprotonated species and (iii) (*S*)-**H$_2$4** in THF

spectra are characteristic of the metal-free Pcs, producing Faraday *B*-terms approximately corresponding to the absorption maxima or shoulders.[9] Although the solvent effect is discernible in the absorption and MCD spectra, it is most clearly seen in the CD spectra. The shape of the spectrum in toluene is similar to that in the absorption spectrum, while in THF it deviates significantly, as seen typically in the Q band region, reflecting perhaps a tendency to higher aggregation trend in the latter solvent.[10] Thus, subtle differences in the absorption spectra are amplified in the CD spectra. Corresponding to the main Soret and Q band, the *R* and *S* enantiomers show mainly positive and negative CD envelopes, respectively.

The spectra of (*S*)-**H$_2$3** and its deprotonated species and (*S*)-**H$_2$4** are shown in Fig. 2. Compared with the spectra in Fig. 1, the Q bands are broadened and shifted to longer wavelength, and the CD spectra are mostly negative in sign through the Q and Soret regions. The Q band of (*S*)-**H$_2$4** lies at longer wavelength and is stronger than that of (*S*)-**H$_2$3**. (*S*)-**Co4** also shows the Q_{0-0} band at longer wavelength (708 nm in CH_2Cl_2) than is usual for CoPcs.[9] In compounds **1**–**4**, the binaphthyl moiety of all the *S* isomers is right-handed while that of the *R* isomers is left-handed, judging from the CD pattern in the 220–270 nm region.

The method shown here has general applicability, and the yields are very high for a reaction of this type. Diphthalonitriles linked by short chains (*ca*. 5–6 atoms) can be used as precursors of non-centrosymmetic Pcs such as **2**–**4**.

Notes and References

† E-mail: nagaok@mail.cc.tohoku.ac.jp

1 Reaction was carried out at room temperature for three days (C. C. Leznoff, S. M. Marcuccio, S. Greenberg and A. B. P. Lever, *Can. J. Chem.*, 1985, **63**, 623).

2 All compounds gave satisfactory elemental analytical data. *Selected data* for **1**: Off-white needle [silica, benzene–EtOAc (2 : 1 v/v), R_f 0.58], recrystallized from MeCN–Et_2O, mp 230–231 °C; yield: 95.2 and 90.4% for (*S*)-**1** and (*R*)-**1**, respectively. $[\alpha]_D$ −29.2 and 29.6 for (*S*)-**1** and (*R*)-**1**, respectively (*c* 1, CH_2Cl_2); δ (60 MHz, $CDCl_3$) 7.7–8.1 (m, 4 H), 7.0–7.6 (m, 14 H); *m/z* (EI) 538 (100%, $[M^+]$); For **H$_2$2**: δ_H (500 MHz, CD_2Cl_2) 6.0–9.2 (m, 36 H, arom), −4.54 (s, 2 H, pyrrole); *m/z* (FAB) 1078.3 (100%, $[M^+]$); a yield by direct methods was 35.7% for (*S*)-**H$_2$2**, recrystallized from CH_2Cl_2–MeOH. For **Co2**: *m/z* (FAB) 1135 (54%, $[M^+]$), 533 (41), 459 (100). For **H$_2$3**: *m/z* (FAB) 916 (100%, $[M^+]$). For **Zn3**: δ_H (500 MHz, CD_2Cl_2) 6.5–8.7 (m, 22 H, arom), 4.15 (br s, 12 H, OCH_3). For (*S*)-**H$_2$4**: δ (500 MHz, CD_2Cl_2) 6–9 (m, 28 H, arom), 1.3–1.8 (m, 18 H, CH_3), −2.40 (br s, H, pyrrole H at naphthalene site), −4.05 (br s, H, pyrrole H at benzene site). Since, as shown in Fig. 1, UV–VIS absorption, MCD and especially CD spectra change depending on the solvent the details of these spectra will be reported in a full paper.

3 P. J. Brach, S. J. Grammatica, O. A. Ossanna and L. Weinberger, *J. Heterocycl. Chem.*, 1970, **7**, 403.

4 J. Metz, O. Schneider and M. Hanack, *Inorg. Chem.*, 1984, **23**, 1065.

5 Compound (*S*)-**H$_2$2** and (*R*)-**H$_2$2** can be obtained from two molecules of (*S*)-**1** and (*R*)-**1** as a blue powder in 30–36% yield.

6 Compounds simimar to **2** but linked by two alkyl chains have been reported (C. C. Leznoff and D. M. Drew, *Can. J. Chem.*, 1996, **74**, 307).

7 N. Kobayashi, in *Phthalocyanines-Properties and Applications*, ed. C. C. Liznoff and A. B. P. Lever, VCH, Weinheim, New York, 1993, vol. 2, ch. 3.

8 N. Kobayashi, S. Minato and T. Osa, *Makromol. Chem.*, 1983, **184**, 2123.

9 M. J. Stillman and T. Nyokong, in *Phthalocyanines-Properties and Applications*, ed. C. C. Leznoff and A. B. P. Lever, VCH, Weinheim, New York, 1989, vol. 1, ch. 3.

10 In the absence of aggregation, the shapes of the CD spectra of allowed transitions are similar to that of the electronic absorption spectrum, aside from its sign (W. Moffitt and A. Moscowitz, *J. Chem. Phys.*, 1959, **30**, 648).

Received in Cambridge, UK, 19th November 1997; 7/08343B

Host–guest complexation: a new strategy for electrodeposition of processable polythiophene composites from aqueous medium

C. Lagrost, J. C. Lacroix, S. Aeiyach, M. Jouini, K. I. Chane-Ching and P. C. Lacaze*

Institut de Topologie et de Dynamique des Systèmes de l'Université Paris 7-Denis Diderot, associé au CNRS (URA 34), 1 rue Guy de la Brosse, 75005 Paris, France

For the first time host–guest complexation is used to (i) electrosynthesize polybithiophene in an aqueous medium and (ii) generate polybithiophene with electroactivity in water, enhanced solubility in common solvents and processability.

Electropolymerization of aromatic and heteroaromatic compounds, leading to anodic deposition of films, is one of the most valuable techniques for obtaining electrically conducting organic polymers which suffer from very low solubility and poor processability. With the exception of polyaniline and polypyrrole, which are sometimes electrosynthesized in aqueous solutions, most conducting polymers are synthesized in organic media.[1,2] The reasons are the very low water-solubility of monomers, whose oxidation potential is, moreover, higher than that of water decomposition, and the relatively high reactivity of the initially formed radical cations with water molecules.[2] For practical and industrial applications, however, water is the ideal solvent. Acidic solutions of various compositions[3–5] and anionic micellar media have been proposed for the electrosynthesis of polythiophene (PT) films in aqueous solution.[6] Furthermore, soluble and processable conducting polymers are needed in terms of industrial and practical applications. To enhance the processability of these materials, grafting long alkyl groups onto the polymer backbone has been used. This strategy induces modifications of the interchain interactions and makes, for instance, poly(octylthiophene) soluble in most common solvents.[7] We report here a new strategy which allows the synthesis of soluble polythiophene composites from an aqueous medium with no covalent modification of the polymer backbone. It uses host–guest complexation, without any covalent bonds being formed[8] prior to the electropolymerization step, cyclodextrin being the host, bithiophene being the guest.

Cyclodextrins have been widely studied because of their ability to form inclusion compounds with a large variety of molecules. They are cyclic oligosaccharides consisting of six, seven or eight glucose units (α-, β- and γ-cyclodextrins) with a hydrophobic inner cavity and a hydrophilic outer side. They, therefore, readily form inclusion compounds with hydrophobic species in aqueous media.[9] We have chosen to use hydroxypropyl-β-cyclodextrin (HPβCD), because of the size of its cavity and its good water-solubility, and bithiophene (BT) as the monomer, because it fits the β-cyclodextrin′s cavity, is a rather hydrophobic molecule and has a lower oxidation potential than water.

The water-solubility of BT is very low ($< 10^{-4}$ M) but is dramatically increased in the presence of HPßCD. Aqueous solutions of 10^{-3} and 10^{-2} M BT can be easily prepared with 10^{-1} M HPβCD, indicating the formation of an inclusion compound between BT and HPβCD. Fluorescence analyses were carried out by increasing the HPβCD concentration progressively. Emission spectra exhibit variations showing a change in the chemical environment of BT: the fluorescence intensity increases with the HPβCD concentration. This fluorescence amplification is typical of an inclusion phenomenon.[10]

BT was electropolymerized in aqueous HPβCD. Polybithiophene (PBT) thin films can be produced by electrooxidation of an aqueous solution of 10^{-2} M BT, 5.10^{-2} M HPβCD and 10^{-1} M $LiClO_4$ at platinum electrodes, using cyclic voltametry and the galvanostatic method. Multicycle voltammograms were recorded between −0.2 and 1.15 V *vs*. SCE at a scan rate of 100 mV s^{-1}. The first anodic sweep shows a wave at 1.0 V *vs.* SCE, corresponding to the oxidation of BT; additional anodic and cathodic peaks increase regularly with the number of successive cycles (Fig. 1). A thin, homogeneous and adherent film is obtained at the platinum electrode. It shows electroactive and electrochromic properties (Fig. 2) whereas PT and PBT films prepared from an organic solution (without cyclodextrins) do not show any electroactivity upon electrochemical cycling in aq. $LiClO_4$ solutions. Depending on the applied potential, the film is red (reduced state) or green (oxidized state). Similar films can be synthesized by applying constant current densities of 0.05, 0.1 and 0.2 mA cm^{-2} for 15 min. The chronopotentiometric responses of the electrode exhibits an instantaneous rise of the potential close to 1 V. Using higher current densities leads to non-adherent films.

The resonance Raman spectra (Fig. 3), performed *ex situ* with an excitation wavelength of 514.2 nm on a reduced film, are similar to those of PBT films formed in organic media. The most intense band at 1455 cm^{-1} is assigned to the symmetric stretching mode of the aromatic C=C band, while a weaker band at 1492 cm^{-1} is attributed to the antisymmetric stretching vibration. Other, weaker bands at 1364 and 1268 cm^{-1} are

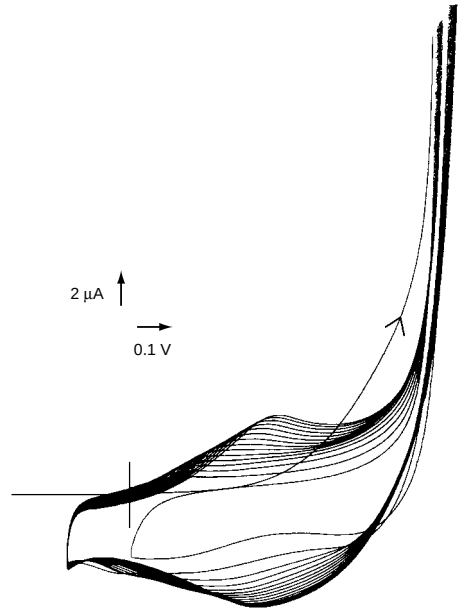

Fig. 1 Voltametric synthesis of PBT film from aq. BT (10^{-} M), HPβCD (5×10^{-2} M) and $LiClO_4$ (10^{-1} M) on Pt electrode (v = 100 mV s^{-1}): (arrow denotes first cycle)

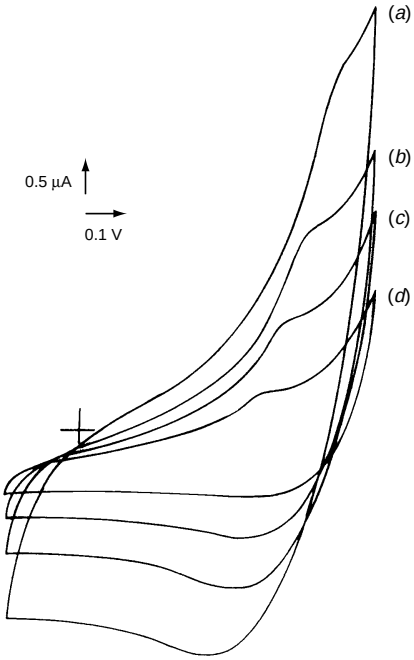

Fig. 2 Electroactivity of a PBT composite in aq. $LiClO_4$ (2.10–1.00 M) for various scan rates: (*a*) 200, (*b*) 100, (*c*) 50 and (*d*) 20 mVs^{-1}

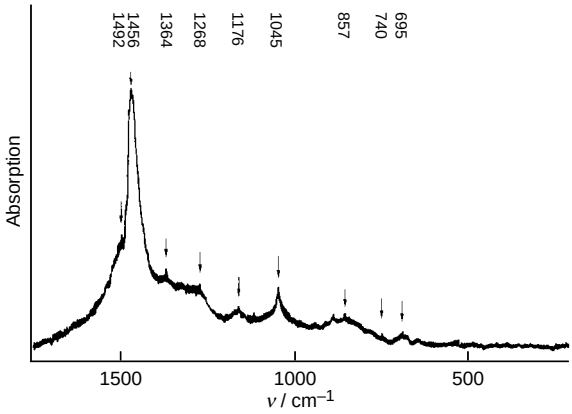

Fig. 3 Resonance Raman spectrum of PBT films deposited from aq. HPβCD

assigned to the stretching mode of the single C–C bond and the C–C inter-ring bond, respectively. The bands at 1045 and 695 cm^{-1} are attributed to the deformation modes of the C–H bond and the C–S–C aromatic bond (Fig. 3). The FT-IR spectra are also very similar to those of PBT films prepared in organic media but display strong bands at 3400, 2960 and 2930 cm^{-1} characteristic of cyclodextrins. A film washed in water for three days in order to eliminate residual cyclodextrins molecules still exhibits these strong bands, showing that cyclodextrins remain in the polymer film. The PBT films deposited from aq. HPßCD solutions are soluble in DMF, DMSO and THF, while PBT films prepared in MeCN are insoluble in these solvents. Since it is well-known that, for β-substituted oligothiophenes, the variation of the absorption maximum energy as a function of the inverse of the chain length is linear,[11] an average conjugation length of 15 thiophene units is estimated from UV–VIS spectroscopy (performed on the fully reduced film), indicating that the material does not consist of low molecular weight oligomers.

We have demonstrated that electropolymerization of BT in an aqueous solution of HPßCD is possible and leads to a homogeneous films similar to that produced in organic media. According to our first analyses, it seems that cyclodextrins persist in the film. The abnormal solubility in common solvents of PBT films electrosynthesized in aq. HPβCD, associated with a high conjugation length, strongly suggests that the polymer chains are partially encapsulated by cyclodextrins. Further work is in hand to confirm this interpretation.

Notes and References

† E-mail: lacaze@paris7.jussieu.fr

1 *Handbook of Conducting Polymers, Vol. 1 and 2*, ed. T.A. Skotheim, Marcel Dekker, New York, 1986.
2 R. J. Waltman, J. Bargon and A. F. Diaz, *J. Phys. Chem.*, 1983, **87**, 1459.
3 S. Dong and W. Zhang, *Synth. Met.*, 1989, **30**, 359.
4 M. Lapkowsky, G. Bidan and M. Fournier, *Synth. Met.*, 1991, **41**, 407.
5 E. A. Bazzaoui, S. Aeiyach and P. C. Lacaze, *J. Electroanal. Chem.*, 1994, **63**, 364.
6 N. Sakmeche, J. J. Aaron, M. Fall, S. Aeiyach, M. Jouini, J. C. Lacroix and P. C. Lacaze, *Chem. Commun.*, 1996, 2723.
7 M. Sato, S. Tanaka and K. Kaeriyama, *J. Chem. Soc., Chem. Commun.*, 1986, 873.
8 W. Saenger, *Angew. Chem., Int. Ed. Engl*., 1980, **19**, 344.
9 *Cyclodextrins in Pharmacy*, ed. J. Szejtli and K. A. Frömming, Kluwer, Dordrecht, 1993.
10 M. Hoshino, M. Imamura, K. Ikehara and Y. Hama, *J. Phys. Chem.*, 1981, **85**, 1820; A. Munoz de la Pena, F. Salinas, M. J. Gomez, M. I. Acedo and M. Sanchez-Pena, *J. Inclusion Phenom*., 1993, **15**, 131; S. Nigam and G. Durocher, *J. Phys. Chem.*, 1996, **100**, 7135.
11 A. Yassar, D. Delabouglise, M. Hmyene, B. Nessak, G. Horowitz and F. Garnier, *Adv. Mater.*, 1992, **4**, 490; R. A. Janssen, L. Smilowitz, N. S. Saricifti and D. Moses, *J. Chem. Phys.*, 1994, **228**, 1787.

Received in Cambridge, UK, 3rd November 1997; 7/07862E

Photogeneration of an *o*-quinone methide from pyridoxine (vitamin B_6) in aqueous solution

Darryl Brousmiche and Peter Wan*†

Department of Chemistry, Box 3065, University of Victoria, Victoria, British Columbia, Canada V8W 3V6

Photolysis (254, 266 or 308 nm) of pyridoxine (vitamin B_6) in aqueous solution gives an *o*-quinone methide efficiently which is trapped by MeOH and ethyl vinyl ether.

Over the past several years there has been a great deal of interest in the biological chemistry of quinone methides‡ (QMs), due mainly to their toxicological properties against both normal and cancerous cells, as well as their proposed intermediacy in the formation of many biologically important polymers (melanin, lignin and insect cuticles).[1,2] These properties have been attributed to the electrophilic nature of QMs which can result in both alkylation of DNA and amino acids, and in self polymerization. QM reactivity in biological systems has been studied extensively with QM precursors such as butylated hydroxytoluene (BHT), eugenol, mitomycin C and the anthracyclines.[1,2] The formation of these QMs has traditionally been *via* thermal reaction, through the use of enzymes *in vivo*, oxidation of phenols, or nucleophilic substitution of silyl or quartenary ammonium groups, amongst others.[1–5] Recently, however, our group has developed a clean and efficient photochemical method for the formation of *o*-, *m*- and *p*-QMs *via* UV (254 nm) photolysis of hydroxybenzyl alcohols.[6] Pyridoxine **1** (vitamin B_6) provides an ideal system for the continued study of photochemically generating QMs as it is a biologically relevant molecule and it contains the required hydroxybenzyl alcohol-type system. Moreover, it allows for a competition between the formation of an *o*-QM *vs*. a *m*-QM due to the presence of a second CH_2OH group *meta* to the aromatic hydroxy group. Formation of a QM from **1** *via* exposure to UV light§ could lead to cell and DNA damage which to the best of our knowledge has not been explored.

Photolysis of **1** and **5** (10^{-4} M; Rayonet photoreactor; 254 nm; *ca*. 15 °C; argon) in 1 : 1 MeOH–H_2O gave the corresponding methyl ethers **3** and **6** ($\phi \approx 0.2$ for reaction of **5**) cleanly (> 40%) at low conversion (Scheme 1). The location of the methoxy group was unambiguously assigned based on NOE data. Previous work by this group[6] has shown that the quantum yield of methyl ether formation from *m*-QMs is approximately half of that from the corresponding *o*-QM. Thus, if the *m*-QM was formed competitively with the *o*-QM of **1**, it would be easily discernable by formation of the corresponding methyl ether. Interestingly, none of the product studies show any evidence for the formation of the *m*-QM, thereby indicating that *o*-QM **2** is formed selectively.

Photolysis of **1** in 1 : 1 H_2O–MeCN with 0.26 M ethyl vinyl ether (EVE) gave the Diels–Alder adduct **4**¶ cleanly (> 70%) in a regioselective fashion (Scheme 1). Formation of **4** is only possible through the intermediacy of a 1,4-dipolar species and therefore provides conclusive evidence for the efficient photogeneration of *o*-QM **2**.

We have shown[6] that laser flash photolysis (LFP) provides an effective method for the direct detection of appropriately substituted *o*-, *m*- and *p*-QMs. The choice of **5** for these studies

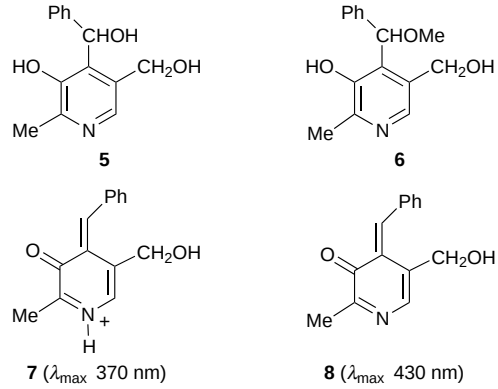

will enable the resulting QM to be more readily detectable due to the expected longer wavelength of absorption and correspondingly larger extinction coefficient. LFP of **5** (λ_{exc} = 266 or 308 nm, YAG or excimer lasers, < 20 mJ per pulse) in 100% H_2O (oxygen purged to remove triplet states and possible radical species) yielded a species at 370 nm, which is observed at pH 7 (τ > 10 ms) and 12 (τ *ca*. 2 ms) (Fig. 1). When LFP experiments were carried out at pH 1, this band can be seen

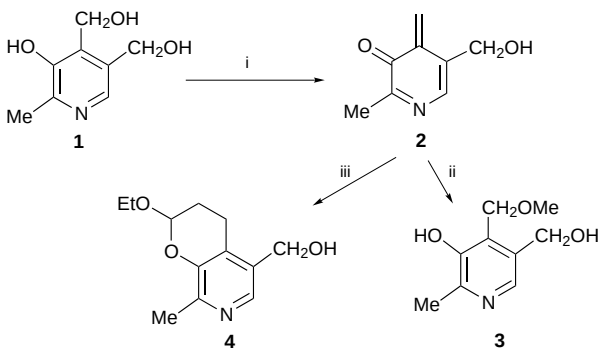

Scheme 1 *Reagents and conditions*: i, *hν*; ii, MeOH–H_2O (1 : 1); iii, EVE (0.26 M), MeCN–H_2O (1 : 1)

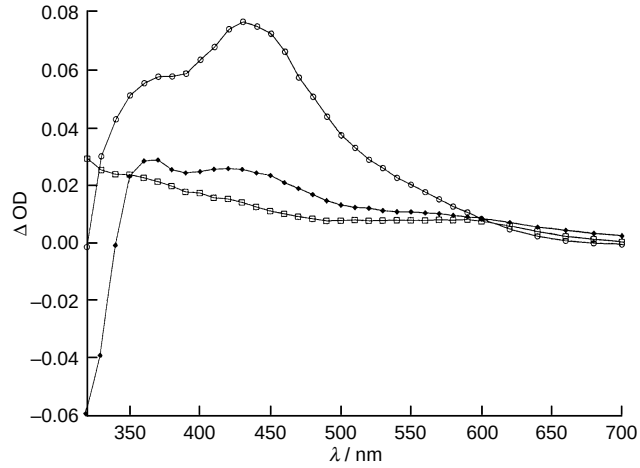

Fig. 1 LFP spectra (λ_{max} 308 nm; 100% H_2O; O_2 purged) of **5** at (□) pH 1, (◆) 7 and (○) 12

below 350 nm (τ < 50 μs). In all three cases, however, there is rapid drop-off signal (bleaching) as the wavelength of observation approaches the region where the ground state material absorbs,‖ thereby masking the true extent of this band. Another species with λ_{max} at 430 nm is apparent in the pH 7 (τ > 10 ms) and 12 (τ *ca*. 2 ms) spectra (Fig. 1). The relative intensities of the bands change with pH (there is no 430 nm band at pH 1), with an 'inflection' point in the pH 4–7 region. We have assigned the 370 nm band to *o*-QM **7** which is protonated at nitrogen. This is clearly the most basic site of the *o*-QM; protonation at oxygen (the other possible basic site) is unlikely at this pH as this would generate a highly reactive diarylmethyl carbocation. The 430 nm band is thus assigned to neutral *o*-QM **8**.

The lifetime of simple QMs is expected to be lower in basic and acidic media than at pH 7, due to attack by either H^+ or OH^- at the appropriate sites of the QM (carbonyl oxygen and exocyclic vinyl carbon, respectively). The transient lifetimes at pH 7 for both **7** and **8** are approximately five times longer than at pH 12, while the lifetime of **7** at pH 1 is approximately two hundred-fold shorter than in neutral solution, consistent with QM reactivity. The heteroatom present in the pyridine ring will also have an influence on the QM lifetime at low pH, where it is fully protonated: it should act a powerful electron-withdrawing group, making the QM more reactive, and this is consistent with the much shorter lifetime observed in pH 1.

It has been shown *via* LFP,[6] in the case of the simple hydroxybenzhydrol systems, that at elevated pH (> 10) QMs are formed more efficiently (higher quantum yields) than at neutral pH, as the phenolate is already present. This appears to be verified in our system as much stronger signals are observed when LFP experiments are carried out at pH 12. Moreover, product studies on the formation of **3** from **1** (1 : 1 MeOH–H_2O) at pH 7 and 12 gave yields of 9 and 15% (performed under low conversion conditions and in which samples received the same UV dose), respectively, consistent with the notion that the QM is more efficiently formed at high pH.

In summary, we have shown that the corresponding *o*-QMs of **1** and **5** can be formed readily in aqueous solution *via* irradiation with UV light. The *o*-QM is formed selectively in all cases, although *m*-QM formation is a possibility. The QM can exist as the free base or in the iminium ion form, which differ in reactivity. The pH of the solvent leads to significant differences in both the lifetime and amount of QM formed, with the QM being longest-lived at pH 7. These results suggest the possibility that **2** can be formed inside biological systems, leading to cell and DNA damage. We believe this to be the first example of the photogeneration of a quinomethane from an important biomolecule (*i.e.* **1**). Since pyridoxal is the active form of pyridoxine, and is known to be extensively hydrated in aqueous solution, we are investigating the possibility of analogous photochemistry for this compound.

We acknowledge support of this research by the Natural Sciences and Engineering Research Council (NSERC) of Canada. D. B. thanks the University of Victoria for a graduate fellowship.

Notes and References

† E-mail: pwan@uvic.ca

‡ IUPAC name: quinomethanes.

§ *o*-QM **2** has been generated thermally from **1** at 130–190 °C and trapped with various nucleophiles (ref. 7).

¶ *Selected data* for **4**: δ_H (300 MHz, $CDCl_3$) 1.07 (t, *J* 7.4, 3 H, CH_3CH_2O), 1.96 (m, 2 H, Ar CH_2CH_2), 2.25 (s, 3 H, $ArCH_3$), 2.70 (t, *J* 7.4, 2 H, $ArCH_2CH_2$), 3.65, 3.78 [two sets of dq (diastereotopic Hs), *J* 7.4, 10.3, 2 H, CH_3CH_2O), 4.50 (s, 2 H, $ArCH_2OH$), 5.33 (t, *J* 3.3, 1 H, CH_3CH_2OCH), 7.78 (s, 1 H, ArH).

‖ According to UV–VIS data, **5** is fully protonated (at the nitrogen) at pH 1 (λ_{max} 290 nm), is in its free base form at pH 7 (λ_{max} 325 nm) and is in its ArO^- form at pH 12 (λ_{max} 310 nm), in accordance with literature data for the parent **1** (ref. 8).

1 D. C. Thompson, J. A. Thompson, M. Sugumaran and P. Moldeus, *Chem. Biol. Interact.*, 1992, **86**, 129.
2 J. L. Bolton, H. Sevestre, B. O. Ibe and J. A. Thompson, *Chem. Res. Toxicol.*, 1990, **3**, 65; J. L. Bolton, L. G. Valerio Jr. and J. A. Thompson, *Chem. Res. Toxicol.*, 1992, **5**, 816; J. L. Bolton, N. M. Acay and V. Vukomanovic, *Chem. Res. Toxicol.*, 1994, **7**, 443; J. L. Bolton, G. R. J. Thatcher and P. G. McCracken, *J. Org. Chem.*, 1997, **62**, 1820.
3 K. Karabelas and H. W. Moore, *J. Am. Chem. Soc.*, 1990, **112**, 5372.
4 P. D. Gardner, H. Rafsanjani and L. Rand, *J. Am. Chem. Soc.*, 1959, **81**, 3364.
5 M. S. Chauhan, F. M. Dean, D. Matkin and M. L. Robinson, *J. Chem. Soc., Perkin Trans. 1*, 1973, 120.
6 P. Wan, L. Diao and C. Yang, *J. Am. Chem. Soc.*, 1995, **117**, 5369; P. Wan, B. Barker, L. Diao, M. Fischer, Y. Shi and C. Yang, *Can. J. Chem.*, 1996, **74**, 465.
7 M. Frater-Schröder and M. Mahrer-Busato, *Bioorg. Chem.*, 1975, **4**, 332.
8 S. A. Harris, T. J. Webb and K. Folkers, *J. Am. Chem. Soc.*, 1940, **62**, 3198.

Received in Corvallis, OR, USA, 6th October 1997; 7/07231G

Modified nucleosides from nitrones: a new and efficient stereoselective approach to isoxazolidinyl thymidine derivatives

Pedro Merino,*† Santiago Franco, Natalia Garces, Francisco L. Merchan and Tomas Tejero

Departamento de Quimica Organica, ICMA, Universidad de Zaragoza, Zaragoza, E-50009 Aragon, Spain

The addition of the sodium enolate of methyl acetate to the *N*-benzyl nitrone 4 derived from D-glyceraldehyde affords the 3-substituted isoxazolidin-5-one 6a with a high degree of *syn* selectivity and in quantitative chemical yield; its further elaboration leads to the preparation of the important isoxazolidine nucleoside analogue 2a in enantiomerically pure form.

Nucleoside analogues have aroused a considerable amount of attention because of their biological activity.[1,2] In particular, modified nucleosides, such as lamivudine **1a** and its 5-fluoro derivative **1b** show potent specific, competitive anti-HIV activities.[3] Also, nucleosides **2** and **3** containing an isoxazolidine moiety have been described to have promising

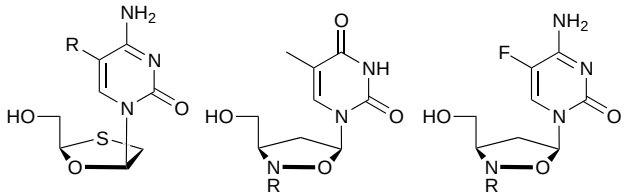

1a R = H **2a** R = Me **3a** R = Me
b R = F **b** R = Bn **b** R = Bn

therapeutic utility in the development of anti-AIDS agents.[4] As a consequence, syntheses of isoxazolidinyl nucleosides of type **2** and **3** have been recently reported.[5,6]

Recent investigations in this laboratory have revealed that chiral α-alkoxy and α-amino nitrones serve as versatile chiral building blocks in the preparation of several naturally occurring nitrogen-containing compounds.[7] Here we present a successful implementation of this strategy directed to the stereoselective synthesis of isoxazolidinyl nucleosides **2**.

The key step of our approach consists of the stepwise addition of an ester enolate to a chiral nitrone in order to construct the isoxazolidine ring. It had been described by Trombini and co-workers that both ketone silyl enol ethers and vinylketene acetals add to nitrones in the presence of trimethylsilyl triflate.[8] Kita and co-workers reported that α-alkoxy nitrones undergo nucleophilic additions with ketene silyl acetals to give the corresponding β-(siloxyamino) esters in good yields and stereoselectivity.[9] With this background in mind we felt that the ready availability of the enantiomerically pure nitrone derived from 1,2-di-*O*-isopropylidene-D-glyceraldehyde[10] and the well-precedented stereodirecting effect of the dioxolane group[7] made **4** an ideal starting material. The addition of nitrone **4** to 1.5 equiv. of the lithium enolate of methyl acetate (LDA and methyl acetate) afforded a 75:25 mixture of diastereomeric isoxazolidinones **6** in 60% isolated yield (Scheme 1).‡

The β-(hydroxyamino) ester was not observed in the crude product and only compounds **6**, coming from an intramolecular cyclization, were obtained. The stereochemistry of the obtained isoxazolidines **6** was ascertained by an X-ray crystallographic analysis of a single crystal of the major diastereomer *syn*-**6a**.§

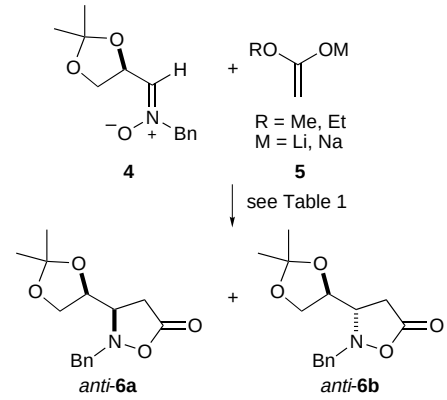

Scheme 1

The stereochemical outcome of the reaction is in accord with Kita's results[9] and our own previous data concerning the nucleophilic additions to α-alkoxy nitrones.[11] Efforts to improve both the diastereoselectivity and the chemical yield by variation of the counterion and the solvent, plus attempts of stereocontrol of the reaction by addition of a Lewis acid, are summarised in Table 1.

In all cases, sodium enolates afforded the *syn* adduct **6a** as the only product of the reaction (ds ⩾ 95%) in excellent chemical yield (Table 1, compare entries 1–4 with 5, 6 and 9), the solvent only having a slight influence on the chemical yield of the process. Guided by our previous results[11] on nucleophilic additions to **4** we next carried out the reaction in the presence of 1.0 equiv. of diethylaluminium chloride (Table 1, entries 7, 8 and 10). Unfortunately, the chemical yield was rather low (20–25%) in all cases, substantial amounts of starting nitrone being recovered. This behaviour suggests that the Lewis acid used as a pre-complexing agent of the nitrone eliminates the sodium enolate from the reaction mixture by forming the corresponding aluminium enolate, which is unable to react with **4**.

Thus, metal exchange should proceed rapidly at the expense of nucleophilic addition, which proceeds in only 20–25%

Table 1 Stereoselective addition of enolates to nitrone **4**

Entry	R	Base (solvent)	**6a**:**6b**	Yield[b] (%)
1	Me	LDA (THF)	75:25	60
2	Me	LDA (Et_2O)	70:30	54
3	Me	LiHMDS (THF)	86:14	68
4	Me	LiHMDS (Et_2O)	60:40	70
5	Me	NaHMDS (THF)	⩾95:5	100
6	Me	NaHMDS (Et_2O)	⩾95:5	95
7	Me	NaHMDS (THF)[a]	34:66	25
8	Me	NaHMDS (Et_2O)[a]	30:70	22
9	Et	NaHMDS (THF)	⩾95:5	93
10	Et	NaHMDS (Et_2O)[a]	32:68	20

[a] 1.0 equiv. of Et_2AlCl was used. [b] Isolated yield of the crude mixture of diastereomers.

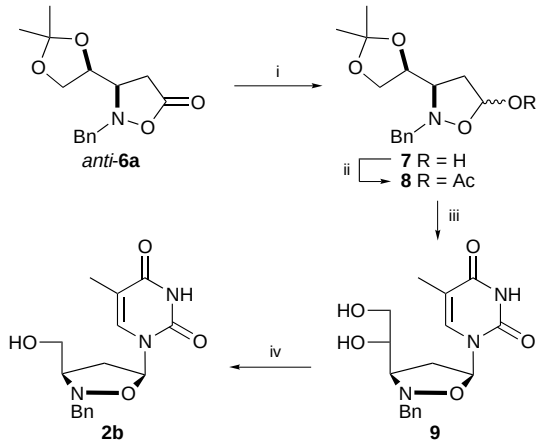

Scheme 2 *Reagents and conditions*: i, DIBAL-H, −80 °C, CH_2Cl_2, 2 h, 80%; ii, Ac_2O, Py, 0 °C, 1 h, 82%; iii, 2,4-bis(trimethylsilyloxy)-5-methylpyrimidine, TMSOTf, CH_2Cl_2, room temp., 2 h, 63%; iv, $NaIO_4$ (aq.), SiO_2, CH_2Cl_2, room temp., 20 min, then $NaBH_4$, MeOH, 0 °C, 90 min, 89%

yield.¶ The lower reactivity of aluminium enolates has been described in nucleophilic additions to imines.[12] A further confirmation of that hypothesis emerged from the fact that an identical result was obtained when nitrone **4** was made to react with the aluminium enolate of methyl acetate prepared *in situ* from methyl acetate and diethylaluminium chloride as described.[13] Nevertheless, despite these adverse results concerning the chemical yield, a reversal of the diastereofacial selectivity was observed (Table 1, entries 7, 8 and 10) and the *anti* isomer **6b** could be fully characterized‡ and used in further transformations.

Treatment of *syn*-**6a** with DIBAL-H in CH_2Cl_2 at −80 °C afforded lactols **7** as a 60 : 40 mixture of anomers. The first order 300 MHz ^{1}H NMR spectrum of the mixture provided unequivocal information on their structures.‖ Acetylation of **7** as described[6] afforded only unreacted starting material when stoichiometric amounts of reagents were used; on the other hand, an excess reagents led to deprotection of the acetonide moiety. If, however, compounds **7** were treated at 0 °C with Ac_2O and pyridine a 76 : 24 mixture of anomeric acetates **8** was formed in 82% combined yield, with the α anomer predominating. Coupling of **8** with 2,4-bis(trimethylsilyloxy)-5-methylpyrimidine[14] using the glycosylation methodology developed by Vörbruggen[15] afforded the N^1-nucleoside **9** as a 22 : 78 mixture of α/β anomers‖ in which the acetonide moiety had been hydrolysed (Scheme 2). The major β isomer (depicted in Scheme 2) was easily separated by column chromatography (100% EtOAc, R_f α-isomer = 0.13, R_f β-isomer = 0.23, visualized with UV at 254 nm). Finally, oxidative cleavage ($NaIO_4$) of the diol unit followed by *in situ* reduction with $NaBH_4$ generated the desired isoxazolidine nucleoside **2b** in good overall yield as summarised in Scheme 2.

As expected from these results, nitrone **4** behaved as an excellent precursor to other related isoxazolidinyl nucleosides, and thus further studies on its reactivity are underway.

This research was supported by MEC (Madrid, Spain). We are grateful to Professor S. Castillon for helpful discussions. One of us (S. F.) thanks the MEC (Madrid, Spain) for a contract.

Notes and References

† E-mail; pmerino@posta.unizar.es

‡ All new compounds exhibited consistent spectral (^{1}H and ^{13}C NMR, IR) and analytical data. Optical rotations: 20 ± 2 °C (*c* 1, $CHCl_3$). *Selected data* for **6a**: mp 60–62 °C, $[\alpha]_D$ + 122.6. For **6b**: mp 75–77 °C, $[\alpha]_D$ −9.7. For **9**: mp 182–183 °C, $[\alpha]_D$ −12.2 (*c* 0.34, MeOH). For **2b**: sticky foam, $[\alpha]_D$ +6.1 (*c* 0.80, MeOH); δ_H ($CDCl_3$) 1.70 (br s, 1 H, OH), 1.77 (d, 3 H, *J* 1.2, CH_3), 2.29 (ddd, 1 H, *J* 3.6, 8.5, 13.7, H_{2a}), 2.99 (dt, 1 H, *J* 7.4, 13.7, H_{2b}), 3.15 (ddt, 1 H, *J* 3.6, 5.2, 8.6, H_3), 3.68 (dd, 1 H, *J* 5.0, 11.7, H_{4a}), 3.79 (dd, 1 H, *J* 3.3, 11.7, H_{4b}), 3.92 (d, 1 H, *J* 13.9, CH_2Ph), 4.32 (d, 1 H, *J* 13.9, CH_2Ph), 4.32 (d, 1 H, *J* 13.9, CH_2Ph), 5.986 (dd, 1 H, *J* 3.6, 7.4, H_1), 7.23–7.50 (m, 6 H, ArH + CH), 8.47 (br s, 1 H, NH).

§ *Crystal data* for **6a**: $C_{15}H_{19}NO_4$, monoclinic, space group $P2_1$, a = 6.011(1), b = 8.039(1), c = 15.598 (2) Å, β = 92.680 (10)°, V = 752.9(2) Å^3, Z = 2, D_c = 1.223 g cm^{-3}, μ = 0.089 mm^{-1}. Of the 1452 unique measured reflections, 1182 with $I \geqslant 2\sigma(I)$ were used in the refinement. R(on F^2) = 3.83, R_w = 9.07. The data were collected on a Siemens P4 diffractometer with graphite monochromated Mo-Kα radiation ω–2θ scan technique (2.61 ⩽ θ ⩽ 23.99). The structure was solved by direct methods using the SHELXS-86 package.[16] All other calculations were accomplished by SHELXL-93.[17] CCDC 182/729.

¶ Similar results were observed with other Lewis acids such as $ZnCl_2$, $ZnBr_2$ or $MgBr_2$. In all cases the yield dropped considerably.

‖ The anomeric configurations were confirmed by ^{1}H NMR (300 MHz) and NOE experiments.

1 D. M. Huryn and M. Okabe, *Chem. Rev.*, 1992, **92**, 1745.
2 M. Kassou and S. Castillon, *J. Org. Chem.*, 1997, **62**, 3696; R. R. Talekar and R. H. Wightman, *Tetrahedron*, 1997, **53**, 3831 and references cited therein.
3 H. Jin, M. A. Siddiqui, C. A. Evans, H. L. A. Tse, T. S. Mansour, M. D. Goodyear, P. Ravenscroft and C. D. Beels, *J. Org. Chem.*, 1995, **60**, 262 and references cited therein.
4 J. M. J. Tronchet, M. Iznaden, F. Barbalatrey, H. Dhimane, A. Ricca, J. Balzarini and E. Declercq, *Eur. J. Med. Chem.*, 1992, **27**, 555; J. M. J. Tronchet, M. Iznaden, F. Barbalatrey, I. Komaromi, N. Dolatshami and G. Berbardinelli, *Nucleosides Nucleotides*, 1995, **14**, 1737.
5 U. Chiacchio, G. Gumina, A. Rescifina, R. Romero, N. Uccella, F. Casuscelli, A. Piperno and G. Romeo, *Tetrahedron*, 1996, **52**, 8889; G. Sindona, C. Siciliano, G. Giglio, A. Napoli, A. Leggio, A. Liguori and A. Procopio, *Synth. Commun.*, 1997, **26**, 4211.
6 Y. Xiang, Y. Gong and K. Zhao, *Tetrahedron Lett.*, 1996, **37**, 4877. During the refereeing process of this manuscript a similar approach based on the diastereoselective Michael addition of hydroxylamine to unsaturated esters has been reported by the same authors. See Y. Xiang, H.-J. Gi, D. Niu, R. F. Schinazi and K. Zhao, *J. Org. Chem.*, 1997, **62**, 7430.
7 P. Merino, A. Lanaspa, F. L. Merchan and T. Tejero, *Tetrahedron Lett.*, 1997, **38**, 1813; P. Merino, A. Lanaspa, F. L. Merchan and T. Tejero, *J. Org. Chem.*, 1996, **61**, 9028; A. Dondoni, F. Junquera, F. L. Merchan, P. Merino and T. Tejero, *J. Chem. Soc., Chem. Commun.*, 1995, 2127.
8 D. D. Dhavale and C. Trombini, *J. Chem. Soc., Chem. Commun.*, 1992, 1268; C. Camiletti, D. D. Dhavale, F. Donati and C. Trombini, *Tetrahedron Lett.*, 1995, **36**, 7293.
9 Y. Kita, F. Itoh, O. Tamura, Y. Y. Ke and Y. Tamura, *Tetrahedron Lett.*, 1987, **28**, 1431; Y. Kita, O. Tamura, F. Itoh, H. Kishino, T. Miki, M. Kohno and Y. Tamura, *J. Chem. Soc., Chem. Commun.*, 1988, 761.
10 P. Merino, S. Franco, F. L. Merchan and T. Tejero, *Tetrahedron: Asymmetry*, 1997, **8**, 3489.
11 P. Merino, E. Castillo, F. L. Merchan and T. Tejero, *Tetrahedron: Asymmetry*, 1997, **8**, 1725; P. Merino, S. Anoro, E. Castillo, F. L. Merchan and T. Tejero, *Tetrahedron: Asymmetry*, 1996, **7**, 1887.
12 T. Fujisawa, Y. Koorijama and M. Shimizu, *Tetrahedron Lett.*, 1996, **37**, 3881.
13 T.-J. Sturm, A. E. Marolewski, E. S. Rezenka and S. K. Taylor, *J. Org. Chem.*, 1989, **54**, 2039.
14 T. Niahimura and T. Iwai, *Chem. Pharm. Bull.*, 1964, **12**, 352.
15 H. Vorbruggen, K. Krolikiewicz and B. Bennua, *Chem. Ber.*, 1981, **114**, 1234.
16 G. M. Sheldrick, *Acta Crystallogr.*, 1990, **A46**, 467.
17 G. M. Sheldrick, SHELXL-93, *Program for the Refinement of Crystal Structures*, University of Gottingen, Germany, 1993.

Received in Glasgow, UK, 4th August 1997; 7/05673G

Facile and highly selective monoacylation of symmetric diols adsorbed on silica gel with acetyl chloride

Haruo Ogawa,*[a]† Misa Amano[a] and Teiji Chihara[b]

[a] *Department of Chemsitry, Tokyo Gakugei University, Koganei, Tokyo 184, Japan*
[b] *The Institute of Physical and Chemical Research (RIKEN), Wako, Saitama 351-01, Japan*

Monoacetylated alcohols of symmetric 1,*n*-diols are synthesized quantitatively by refluxing a suspension of the diols adsorbed on silica gel with acetylchloride.

The application of solid adsorbents such as alumina and silica gel as solid supports in organic synthesis affords a new procedure for selective reactions[1] involving oxidation,[2] alkylation,[3] condensation,[4] acetylation[5] and monomethyl esterification.[6] The significant potential of adsorbents is due to the milder reactions conditions and simpler work-up required and the selective organic transformations that they allow. It is important for organic chemists to develop methods that permit the selective protection or functionalization of one functional group of a bi- or multi-functional molecule. Monoprotection of polyols is achieved in some cases by carefully controlled reaction conditions,[7] continuous extraction,[8] the use of silica gel,[9] alumina,[10] phase-transfer catalysts[11] and insoluble polymer supports,[12] or *via* the formation of cyclic compounds.[13] Protection of hydroxy groups by acylation is common in organic syntheses and here we report the facile and highly selective monoacetylation of symmetric diols with acetyl chloride (AcCl) by use of silica gel.

Acetylation of symmetric diols adsorbed on silica gel was performed *via* the following method (adsorption method) (Scheme 1). Alcohols were adsorbed on silica gel (C-200, Wako Chemicals) as follows: 1 g of silica gel was added to a Et_2O solution of the alcohol; solvent was then eliminated under reduced pressure. The obtained solid (adsorption sample) and AcCl were introduced to 50–100 ml of cyclohexane and refluxed for 2 h. The reaction period of 2 h was sufficient for the reaction to reach completion. After the reaction the mixture was filtered and the solid was washed with distilled water and DMF. The washings plus the filtrate were concentrated, and the products were analyzed by GLC with higher hydrocarbons such as dodecane and heptadecane used as an internal standard. The products were spectrometrically identified *via* comparison with the authentic samples.

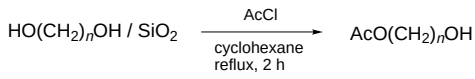

Scheme 1

The results of acetylation of symmetric diols are listed in Table 1. According to the adsorption method the monoacetylated products of 1,*n*-diols were quantitatively obtained, while in the case of cyclohexane-1,4-diol the products were obtained in lower yield. Even with a larger amount of decane-1,10-diol in the adsorption sample (3.2×10^{-3} mol g^{-1} SiO_2), the same result (quantitative monoacetylation) was observed. This adsorption method is insensitive to the amount of AcCl added, *e.g.* 2.5–20 equiv. of AcCl were effective for the quantitative formation of the monoacetylated alcohol of decane-1,10-diol.

The dependence of selectivity on reaction temperature was investigated in order to improve the selectivity in the reaction of cyclohexane-1,4-diol, which showed the lowest selectivity. Higher selectivity was observed with a decrease in the temperature. Selectivity was improved to 73% at 0 °C, and to 76% at 0 °C in hexane suspension (Table 2). Silica gel is considered to play a role as a protecting reagent for the counterpart hydroxy group of the symmetric diol, which is presumably adsorbed as a monomolecular layer on the surface of silica gel as in the case of the methylation of decan-1-ol on silica gel with CH_2N_2.[14] This explains why a large excess of AcCl yields only the monoacetylated alcohols of 1,*n*-diols. No further evidence has been obtained at the present time, however, this adsorption method should be applicable to the selective monoprotection or monofunctionalization of polyols.

Table 1 Monoacetylation of symmetric diols adsorbed on silica gel[a]

Substrate	Amount of AcCl[b] (in homogeneous reaction) (equiv.)	Yield (%)		Selectivity[c] (%)	Maximum yield in homogeneous reaction[d] (%)
		monoacetate	diacetate		
Butane-1,4-diol	9.0 (2.0)	99.5	0.0	100	52.3
Hexane-1,6-diol	5.0 (7.0)	99.5	0.0	100	58.6
Octane-1,8-diol	1.2 (7.0)	99.8	0.0	100	54.3
Decane-1,10-diol	2.5 (20.0)	99.8	0.0	100	56.5
Decane-1,10-diol[e]	2.5 (20.0)	98.3	1.7	98.3	56.5
Decane-1,10-diol[f]	3.0 (20.0)	99.0	1.0	99.0	56.5
Dodecane-1,12-diol	3.0 (3.0)	99.9	0.0	100	66.5
Hexadecane-1,16-diol	10.0 (5.0)	99.9	0.0	100	30.2
Cyclohexane-1,4-diol	4.0 (4.2)	29.9	40.8	42.7	32.6
trans-Cyclohexane-1,4-diol	4.0 (7.0)	39.9	30.1	50.1	43.1
Benzene-1,4-dimethanol	3.2 (3.0)	36.0	47.5	74.2	52.5

[a] Each experiment was carried out under reflux in cyclohexane for 2 h. Adsorption sample contains 3.2×10^{-4} mol g^{-1} SiO_2. [b] Minimum amount of AcCl. The same results were observed by the use of AcCl in the amount from the minimum to 20 equiv. [c] The value of [yield of the monoacetylated alcohol/(100 − intract diol)] × 100. [d] 2.5×10^{-2} M solution of diols in DMF in the presence of pyridine (1 equiv.). [e] Gas–solid phase reaction at room temperature in the bsence of cyclohexane solvent. [f] An adsorption sample containing 3.2×10^{-3} mol g^{-1} SiO_2 of the alcohol was used.

Table 2 Dependence of the monoacetylation of 1,4-cyclohexanediol on reaction temperature

	Yield (%)		
T/°C	monoacetate	diacetate	Selectivity[b] (%)
80.2 (reflux)	29.9	40.8	42.7
17.0	54.6	41.6	56.8
0.0	52.4	19.3	73.1
0.0[c]	61.4	19.4	76.0

[a] Adsorption sample of cyclohexane-1,4-diol (3.2×10^{-4} mol g^{-1} SiO_2) was used in cyclohexane suspension with 4.0 equiv. of AcCl. Other conditions as in the main text. [b] The value of [yield of the monoacetylated alcohol/(100 − intact diol)] × 100. [c] In hexane suspension.

Notes and References

† E-mail: ogawah@u-gakugei.ac.jp

1 J. H. Clark, A. P. Kybett, and D. J. Macquarrie, *Supported Reagents: Preparation, Analysis, and Applications*, VCH, N.Y., 1992; *Solid Supports and Catalysis in Organic Synthesis*, ed. K. Smith, Prentice Hall, West Sussex, 1992; *Preparative Chemistry Using Supported Reagents*, ed. by P. Laszlo, Academic Press, San Diego, 1987; A. McKillop and D. W. Young, *Synthesis*, 1979, 401; G. H. Posner, *Angew. Chem., Int. Ed. Engl.*, 1978, **17**, 487; A. Cornelis and P. Laszlo, *Synthesis*, **1985**, 909; H. Ogawa, M. Kodomari and T. Chihara, *PETROTECH*, 1996, **19**, 404.

2 Z. Cohen, E. Keinan, Y. Mazur and T. H. Varkony, *J. Org. Chem.*, 1975, **40**, 2141; E. Keinan and Y. Mazur, *J. Org. Chem.*, 1977, **42**, 844, and references cited therein.

3 G. Bram and T. Fillebeen-Khan, *J. Chem. Soc., Chem. Commun.*, 1979, 522.

4 E. Keinan and Y. Mazur, *J. Am. Chem. Soc.*, 1977, **99**, 3861; J. Muzard, *Synthesis*, 1982, 60.

5 T. Chihara, S. Teratani and H. Ogawa, *J. Chem. Soc., Chem. Commun.*, 1981, 1120; T. Chihara, Y. Takagi, S. Teratani and H. Ogawa, *Chem. Lett.*, 1982, 1451.

6 H. Ogawa, T. Chihara and K. Taya, *J. Am. Chem. Soc.*, 1985, **107**, 1365; H. Ogawa, *J. Phys. Org. Chem.*, 1991, **4**, 346; H. Ogawa, T. Chihara, S. Teratani and K. Taya, *J. Chem. Soc., Chem. Commun.*, 1986, 1337.

7 S. G. Wilkinson, in *Comprehensive Organic Chemistry*, ed. J. F. Stoddart, Pergamon, New York, 1979, vol. 1, p. 681; T. W. Greene and P. G. M. Wuts, *Protective Groups in Organic Synthesis*, Wiley, New York, 1991; J. Furhop and G. Penzlin, *Organic Synthesis*, Verlag Chemie, Weinheim, 1983, p. 143.

8 J. H. Babler and M. J. Coghlan, *Tetrahedron Lett.*, 1979, **22**, 1971.

9 T. Nishiguchi and K. Kawamine, *J. Chem. Soc., Chem. Commun.*, 1990, 1766; T. Nishiguchi, K. Kawamine and T. Ohtsuka, *J. Org. Chem.*, 1992, **57**, 312.

10 J. D. L. Zerda, G. Barak and Y. Sasson, *Tetrahedron*, 1989, **29**, 1533.

11 H. Ogawa, Y. Ichimura, T. Chihara, S. Teratani and K. Taya, *Bull. Chem. Soc. Jpn.*, 1986, **59**, 2481.

12 C. C. Lezonoff, *Acc. Chem. Res.*, 1978, **11**, 327.

13 M. Takasu, Y. Naruse and H. Yamamoto, *Tetrahedron Lett.*, 1988, **29**, 1947; S. Takano, M. Akiyama, S. Sato, and K. Ogasawara, *Chem. Lett.*, 1983, 1593.

14 H. Ogawa, T. Hagiwara, T. Chihara, S. Teratani and K. Taya, *Bull. Chem. Soc. Jpn.*, 1987, **60**, 627.

Received in Cambridge, UK, 28th October 1997; 7/07753J

Chiral dendrimers with backfolding wedges

H. W. I. Peerlings, D. C. Trimbach and E. W. Meijer*†

Laboratory of Macromolecular and Organic Chemistry, Eindhoven University of Technology, PO Box 513, 5600 MB Eindhoven, The Netherlands

Dendritic wedges with a substitution pattern that forces the growth inwards are introduced and the use of this new building strategy is exemplified in the synthesis and chiroptical properties of a chiral dendrimer.

The first reports on the synthesis and properties of dendrimers[1] initiated many studies towards this new class of highly branched macromolecules. A wide variety of synthetic routes have led to the production of a large number of new dendritic structures, even leading to structures that are now commercially available.[2] The branching pattern of many, if not all, of these dendrimers is designed to facilitate the growth of each next generation outwards. As a result, dendrimers can be obtained that possess a highly packed periphery and cavities in the interior, making for example, encapsulation of guest molecules possible.[3] Recently, however, it has been indicated that many of the structures studied so far have a rather flexible conformation, leading to an average density that is not different for interior and periphery. So far, conformational rigidity in these structures has only been found at higher generations of dendrimers.[3–6] Restricted flexibility at lower generations, however, has not been observed before and is of interest for many applications foreseen for dendrimers, *e.g.* molecular recognition and catalysis.[7] Also our search for an optically active chiral dendritic object, which owes its chirality to the presence of constitutionally different wedges attached to a central carbon atom, is hampered by this flexibility.[8] Recently, the enantiomerically pure dendrimer (*S*)-**1** was described (Fig. 1); however, no detectable optical activity was observed.[9] Here, we present the concept of backfolding wedges in the synthesis of dendrimers with restricted flexibility at lower generations. The effect of these wedges is exemplified in a chiroptical study based on the modification of the Fréchet-type poly(benzylether) wedges by changing from a 3,5- to a 2,6-dibenzyloxy substitution pattern.

2,6-Dihydroxybenzoic acid was used as a starting material for the synthesis of both desired backfolding dendritic wedges. The first generation was synthesized starting from a reaction of 2,6-dihydroxybenzoic acid with 3 equiv. of benzylbromide, yielding benzyl 2,6-dibenzyloxybenzoate **2**, which was reduced by a reaction with $LiAlH_4$ to 2,6-dibenzyloxybenzyl alcohol **3** (Scheme 1). Bromination of **3** was accomplished by a reaction with PBr_3, yielding 2,6-dibenzyloxybenzyl bromide **4**, the first generation bromide backfolding dendrimer. For the synthesis of the second generation of bromide backfolding dendritic wedge, first 2,6-dihydroxybenzoic acid was converted into methyl 2,6-dihydroxy benzoate **5** *via* reaction with methyl iodide in DMF in the presence of $NaHCO_3$. In our first approach to backfolding, the normal Fréchet-type dendritic wedge of the first generation was brought into reaction with **5**, yielding **6**. After reduction to the corresponding benzyl alcohol **7**, the desired benzyl bromide **8** was obtained *via* reaction with PBr_3. The crystalline benzyl bromides **4** and **8** proved to be rather acid sensitive and compound **8** even decomposes on standing in a $CHCl_3$ solution.

The effect of the backfolding dendritic wedges was tested in the synthesis of (*S*)-**9**, the conformationally more rigid analogue of (*S*)-**1** (Fig. 1). The assigned conformational flexibility in (*S*)-**1** is based on the chiroptical study, as there is no detectable optical activity in terms of optical rotatory dispersion (ORD), circular dichroism (CD) or optical rotation,[9] and therefore this compound can be referred to as being cryptochiral.[10]

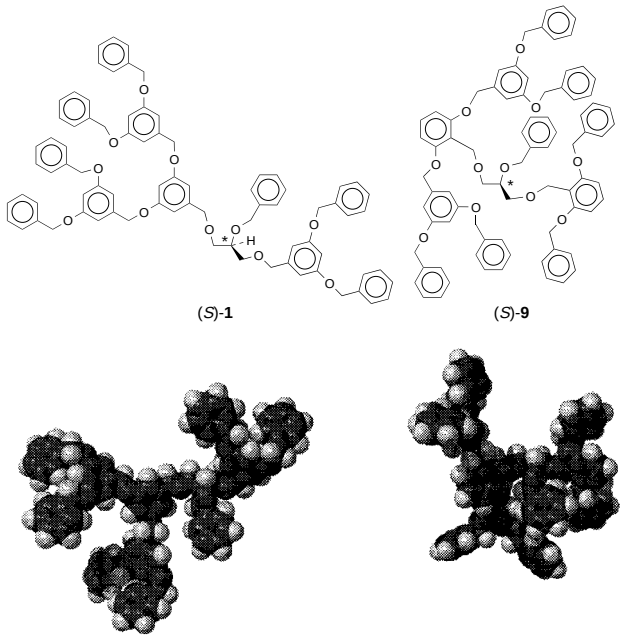

Fig. 1 Modelling study of (*S*)-**1** and (*S*)-**9**

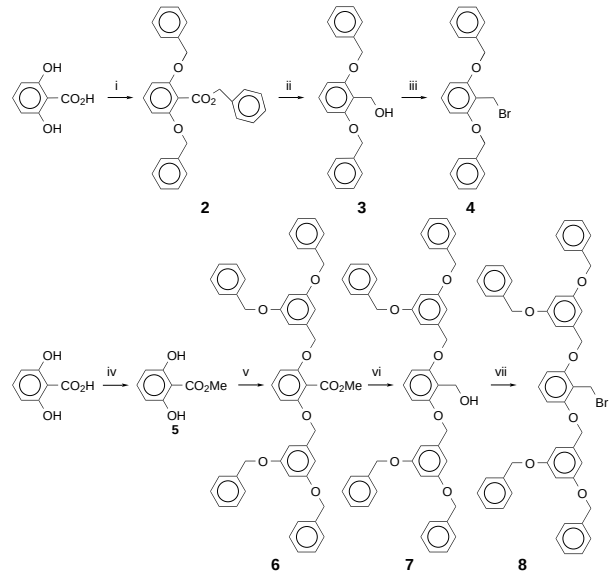

Scheme 1 *Reagents and conditions*: i, BnBr, K_2CO_3, 18-crown-6, acetone; ii, $LiAlH_4$, Et_2O, 65% for two steps; iii, PBr_3, Et_2O, 96%; iv, MeI, $NaHCO_3$, DMF, 77%; v, [G-1]Br, K_2CO_3, 18-crown-6, acetone, 67%; vi, $LiAlH_4$, THF, 75%; vii, PBr_3, Et_2O–THF, 74%

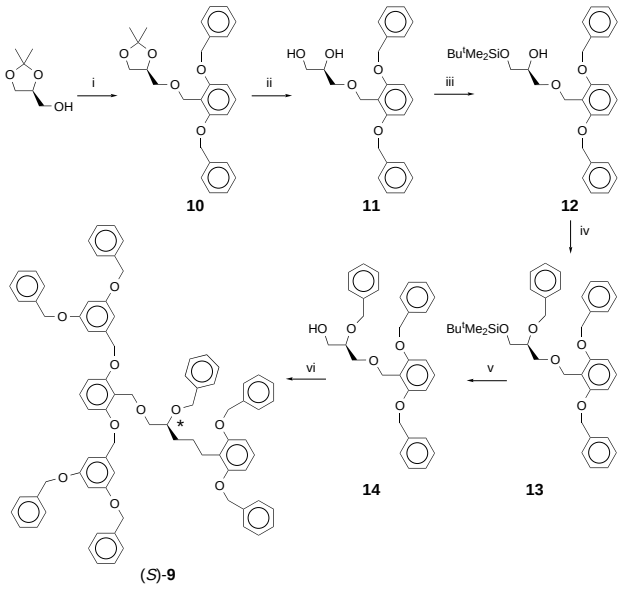

Scheme 2 *Reagents and conditions*: i, **4**, NaH, THF, 98%; ii, TsOH, MeOH, 75%; iii, NaH, Bu^{t}Me$_2$SiCl, THF, 54%; iv, NaH, BnBr, THF, 77%; v, Bu_4NF, THF, 77%; v, **8**, NaH, THF, 68%.

The synthetic approach to chiral dendrimer (*S*)-**9** is similar to the synthesis of (*S*)-**1**, with normal Fréchet-type wedges, as reported before.[9] However, due to the acid-sensitivity of the dendritic wedges the use of strong acidic conditions in the synthetic route had to be circumvented. Enantiomerically pure (*S*)-2,2-dimethyl-1,3-dioxolane-4-methanol [[α_D^{20}] +15.2 (neat, 25 °C)] was used as a starting material for the synthesis of the backfolding dendrimer (*S*)-**9**. The free alcohol functionality was brought into reaction with the first generation of backfolding bromide **4**, yielding **10**. Deprotection of the acetal protecting group was performed under mild acidic conditions, making use of a catalytic amount of toluene-*p*-sulfonic acid in MeOH, leading to diol **11**, which could be obtained as a white crystalline solid. In order to differentiate between the two alcohol functionalities a bulky protecting group was introduced *via* a reaction with NaH and Bu^{t}Me$_2$SiCl. Only the desired monosubstituted product **12** and unreacted product **11** could be obtained after the reaction, which could be separated by washing with hexane (in which only the product dissolved). The free secondary alcohol functionality was reacted with benzyl bromide (the zeroth generation of dendrimer), yielding **13**. Subsequently, the Bu^{t}Me$_2$Si group was removed by reaction with Bu_4NF to yield precursor molecule **14**. In the final step the free primary alcohol functionality of **14** was reacted with the second generation of backfolding bromide **8** in a Williamson synthesis, leading to target molecule (*S*)-**9**. Except for **11**, all chiral compounds were oils that had to be purified using column chromatography. All spectroscopic data are in full agreement with the compounds obtained.‡

Backfolding dendrimer (*S*)-**9** exhibited, in sharp contrast to (*S*)-**1**, an optical activity of $[\alpha]_D^{20}$ +0.8 (*c* = 2.2, CH_2Cl_2). A more thorough study was performed using ORD, UV and CD measurements. For the CD measurements, destilled CH_2Cl_2 was used and spectra were measured at λ = 320–220 nm. A very weak signal was found at λ = 280 nm, at a temperature of 15 °C, indicative of an induced chiral effect. However, at more elevated temperatures (30 °C) this signal vanished, indicating that the conformational flexibility/rigidity can be triggered by temperature. The difference in chiroptical effects for (*S*)-**1** and (*S*)-**9** are proposed to be the result of more conformational rigidity in the latter.

In conclusion, we present the concept of a backfolding dendritic wedge by modifying the branching pattern of Fréchet-type dendritic wedges. The backfolding character of this new type of dendrimers is illustrated in chiral dendrimer (*S*)-**9**, which exhibits optical activity. The chiroptical properties show that when introducing these conceptually new wedges an overall conformationally more rigid structure is obtained. The use of this new type of wedge enables us create more conformational rigidity at low generations, which up to now was only possible at very high generations.

The authors thank The Netherlands Foundation for Chemical Research (SON) and The Netherlands Organization for Scientific Research (NWO) for financial support. DSM Research is gratefully acknowledged for an unrestricted research grant. Sergey Nepogodiev and Peter Ashton are acknowledged for the LSIMS measurement of chiral dendrimer (*S*)-**9**.

Notes and References

† E-mail: tgtobm@chem.tue.nl

‡ *Selected data* for (*S*)-**9**: $\delta_H(CDCl_3)$ 3.58–3.69 (m, 4 H, C*HCH_2), 3.79 (q, *J* 5.5, 1 H, C*H), 4.51 and 4.67 (2*s, 4 H, CH_2OCH_2OAr), 4.71 and 4.73 (2d, *J* 10.3, C*HOCH_2Ph), 4.89 and 4.90 (2s, 8 H, $ArOCH_2Ph$, $ArOCH_2Ar'$), 4.91 (s, 8 H, Ar′OCH_2Ph), 6.44 and 6.48 (2d, *J* 8.4, 4 H, ArH-3,5), 6.51 (t, *J* 2.2, 2 H, Ar′H-4), 6.64 (d, *J* 2.2, 4 H, Ar′H-2,6), 7.03–7.35 (m, 37H, ArH-4 and PhH); $\delta_c(CDCl_3)$ 61.4, 69.8, 70.1, 70.9, 71.0, 71.8 (CH_2), 77.4 (C*H), 101.3 (Ar′C-4), 105.4 and 105.6 (ArC-3,5), 105.8 (Ar′C-2,6), 115.4, 115.5 (ArC-1), 126.8, 126.9, 127.2, 127.4, 127.5, 127.8, 128.3, 128.4, 129.3, 129.4 (PhCH), 129.3, 129.4 (ArC-4), 136.7 (Ar′-OCH_2Ph*C-ipso*), 137.1 ($ArOCH_2$Ph*C-ipso*), 139.1 (C*HOCH_2Ph*C-ipso*), 139.7 (Ar′C-1), 158.4 (ArC-2,6), 159.9 (Ar′C-3,5); ν_{max}(KBr)/cm^{-1} 3031 (=C–H), 2927 and 2872 (–CH_2–), 1596 and 1497 (C=C), 1452 (CH_2); 1115 (CH_2OCH_2). $[\alpha]_D^{20}$ +0.8 (*c* 2.2, CH_2Cl_2). *m/z* 1233 (M + Na^+), 1249 (M + K^+), 1343 (M + Cs^+).

1 G. R. Newkome, C. N. Moorefield and F. Vögtle, *Dendritic Molecules, Concepts, Syntheses, Perspectives*, VCH, Weinheim, 1996; D. A. Tomalia, N. Naylor and W. A. Goddard III, *Angew. Chem.*, 1990, **102**, 119; *Angew. Chem., Int. Ed. Engl.*, 1990, **29**, 138; G. R. Newkome, C. N. Moorefield, G. R. Baker, A. L. Johnson and R. K. Behera, *J. Org. Chem.*, 1992, **57**, 358; Z. Xu and J. S. Moore, *Angew. Chem.*, 1993, **105**, 1394; *Angew. Chem., Int. Ed. Engl.*, 1993, **32**, 1354; C. Wörner and R. Mülhaupt, *Angew. Chem.*, 1993, **105**, 1367; *Angew. Chem., Int. Ed. Engl.*, 1993, **32**, 1306; K. L. Wooley, C. J. Hawker and J. M. J. Fréchet, *J. Am. Chem. Soc.*, 1991, **113**, 4252; *Angew. Chem.*, 1994, **106**, 123; *Angew. Chem., Int. Ed. Engl.*, 1994, **33**, 82; T. M. Miller, T. X. Neenan, E. W. Kwock and S. M. Stein, *J. Am. Chem. Soc.*, 1993, **115**, 356; J. Issberner, R. Moore and F. Vögtle, *Angew. Chem.*, 1994, **106**, 2507; *Angew. Chem., Int. Ed. Engl.*, 1994, **33**, 2413.

2 D. A. Tomalia, A. Naylor and W. A. Goddard III, *Angew. Chem.*, 1990, **102**, 119; *Angew. Chem., Int. Ed. Engl.*, 1990, **29**, 138; E. M. M. de Brabander-van den Berg and E. W. Meijer, *Angew. Chem.*, 1993, **105**, 1370; *Angew. Chem., Int. Ed. Engl.*, 1993, **32**, 1308.

3 J. F. G. A. Jansen, E. M. M. de Brabander-van den Berg and E. W. Meijer, *Science*, 1994, **266**, 1226.

4 J. F. G. A. Jansen, H. W. I. Peerlings, E. M. M. de Brabander-van den Beg and E. W. Meijer, *Angew. Chem.*, 1995, **107**, 1321; *Angew. Chem., Int. Ed. Engl.*, 1995, **34**, 1206.

5 P. Murer and D. Seebach, *Angew. Chem.*, 1995, **107**, 2297; P. K. Murer, J.-M. Lapierre, G. Greiveldinger and D. Seebach, *Helv. Chim. Acta*, 1997, **80**, 1648.

6 D.-L. Jiang and T. Aida, *Nature*, 1997, **388**, 454.

7 H. W. I. Peerlings and E. W. Meijer, *Chem. Eur. J.*, 1997, **3**, 1643.

8 J. A. Kremers and E. W. Meijer, *J. Org. Chem.*, 1994, **59**, 4262; J. A. Kremers and E. W. Meijer, *Reactive & Functional Polymers*, 1995, **26**, 137.

9 H. W. I. Peerlings, M. P. Struijk and E. W. Meijer, *Chirality*, in the press.

10 K. Mislow and P. Bickart, *Isr. J. Chem.*, 1976, **15**, 1; H. Wynberg, G. L. Hekkert, J. P. M. Houbiers and H. W. Bosch, *J. Am. Chem. Soc.*, 1965, **87**, 2635; H. Wynberg and L. A. Hulshof, *Tetrahedron*, 1974, **30**, 1775; W. Ten Hoeve and H. Wynberg, *J. Org. Chem.*, 1980, **45**, 2754.

Received in Liverpool, UK, 12th November 1997; 7/08158H

HOBT immobilized on macroporous polystyrene beads: a useful reagent for the synthesis of amides

Kleanthis Dendrinos, Jeannie Jeong, Wei Huang and Aristotle G. Kalivretenos*†

Department of Chemistry and Biochemistry, University of Maryland, Baltimore County, Baltimore, MD 21250, USA

Polymer-supported 1-hydroxybenzotriazole (P-HOBT), prepared from macroporous polystyrene beads, was used to synthesize amides from primary and secondary amines.

Combinatorial chemistry has led to much research in the use of solid-phase organic synthesis techniques.[1] Polystyrene-supported 1-hydroxybenzotriazole (**P**-HOBT) was originally developed as a highly reactive *N*-acylating agent for the formation of peptide bonds.[2] Ongoing studies in our laboratory are directed at the development of **P**-HOBT as a generally useful acylating agent. We have utilized **P**-HOBT for the synthesis of medium-ring lactams from linear precursors,[3] the preparation of *N*-hydroxysuccinimide (NHS) esters[4] and the carbamate protection of amines.[5] A recent report describes the use of HOBT immobilized on an aminomethylated Merrifield resin for the synthesis of simple amides.[6] We are interested in utilizing **P**-HOBT for the derivatization of naturally occurring amines for improved chromatographic separation and identification properties. The use of HOBT immobilized on Merrifield type polystyrene resins, whose degree of swelling varies greatly depending on the solvent, would limit the variety of solvents utilized for amide formation. Herein, we report the use and advantages of HOBT immobilized on macroporous polystyrene beads for the amide derivatization of amines.

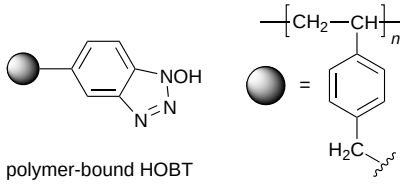

polymer-bound HOBT

We prepared **P**-HOBT using Bio-Rad SM-2 dried macroporous beads (polystyrene–divinylbenzene copolymer resin, 100–200 mesh, MW cutoff 2000) according to the method of Fridkin and Patchornik.[2]‡ We chose to use the macroporous SM-2 beads, designed as a chromatographic support for hydrophobic interaction chromatography, due to their ability to be used in aqueous, as well as organic solvents without swelling or contraction.[7] The number of active sites on the resin was determined by forming the polymer-bound acetate ester, followed by subsequent treatment with isopropylamine (large excess) to yield *N*-isopropylacetamide and recovered polymer. Based on the yield of recovered *N*-isopropylacetamide, three batches of polymer-bound reagent were prepared with activities of 0.27 (**1**) 0.25 (**2**) and 0.25 mmol g^{-1} (**3**), respectively.§ Polymers **1** and **2** were prepared and stored undessicated at room temperature for two years. At this time, both polymers retained *ca.* 90% of their original activity.

With the polymer in hand, the synthesis of a variety of amides was completed, as shown in Scheme 1. Acetamides, benzamides and amides of pyrene-1-carboxylic acid were chosen due to their potential for use as derivatization reagents for naturally occurring amines for improved chromatographic separation and detection properties. In general, the polymer-bound ester was formed by addition of the acid anhydride to the immobilized HOBT group in the presence of pyridine, or by coupling of the free carboxylic acid to the polymer using DCC as catalyst. The solvent in both cases was CH_2Cl_2. After washing the activated resin thoroughly, it was suspended in a solution of CH_2Cl_2 containing 0.8 equiv. of amine based on polymer activity. The reaction mixture was rocked for 4 h at room temperature, at which time filtration of the resin and subsequent concentration of the filtrate yielded the desired amide as the only observable product.¶‖ A summary of these results is given in Table 1. Of particular interest is entry **8**, in which water was used as a co-solvent to enhance the solubility of 6-aminohexanoic acid. The use of water did not have any deleterious effects on overall reactivity or diffusion through the polymer.

We have previously shown the **P**-HOBT reagent to be completely recyclable for the synthesis of NHS esters.[4] Here we have re-used the same batches of **P**-HOBT **2** and **3** for the synthesis of all amides *via* two protocols. The first method involves reactivation of used **P**-HOBT to synthesize amides utilizing the same carboxylic acid partner. Once used, the resin was washed with CH_2Cl_2, Pr^iOH–CH_2Cl_2 and Et_2O to remove any remaining unbound reagents. The washed **P**-HOBT was then reactivated using the carboxylic acid or the acid anhydride as described above, followed by subsequent treatment with an amine to yield the amide product. Alternately, the spent **P**-HOBT was used to synthesize amides utilizing a different acid coupling partner, following a two step reactivation procedure. The used polymer was reacted with a large excess of isopropylamine (based on polymer activity), followed by a rigorous washing protocol, utilizing CH_2Cl_2, Pr^iOH–CH_2Cl_2, DMF, CH_2Cl_2 and Et_2O to yield the clean polymer. The regenerated polymer was subsequently used to prepare amides *via* the general protocol described above.

In summary, polymer-supported HOBT, synthesized from macroporous polystyrene beads, has been utilized for the synthesis of amides from carboxylic acids and primary and

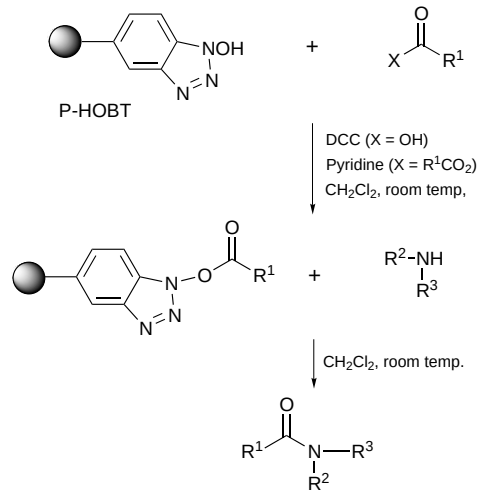

Scheme 1

Table 1 Amide formation utilizing P-HOBT

Entry	Carboxylic acid	Amine	Yield (%)[a]
1	AcOH	Pr^iNH_2	88
2	AcOH	Cyclohexylamine	97
3	AcOH	Piperidine	87
4	AcOH	*n*-Hexylamine	91
5	AcOH	$BnNH_2$	96
6	AcOH	Pr^nNH_2	96
7	AcOH	3-Aminopropan-1-ol	99
8	AcOH	6-Aminohexanoic acid[b]	83
9	AcOH	Pyrrolidine	85
10	AcOH	1,5-Diaminopentane[a]	96
11	BzOH	Pr^iNH_2	83
12	BzOH	Cyclohexylamine	99
13	BzOH	Piperidine	96
14	BzOH	*n*-Hexylamine	94
15	BzOH	$BnNH_2$	86
16	BzOH	Pr^nNH_2	91
17	BzOH	3-Aminopropan-1-ol	63
18	BzOH	Pyrrolidine	77
19	BzOH	1,5-Diaminopentane[c]	72
20	Pyrenecarboxylic acid	Pr^iNH_2	92
21	Pyrenecarboxylic acid	Piperidine	99
22	Pyrenecarboxylic acid	3-Aminopropan-1-ol	79

[a] The amides were recovered as the only product (purity determined by ^1H NMR spectroscopy) and the yields were based on the amount of amine used. [b] DMF–H_2O (70 : 30) used as solvent in place of CH_2Cl_2. [c] Formed *N*,*N*′-diacetyl-1,5-diaminopentane.

secondary amines. The polymeric reagent displays high reactivity, is recyclable and can be used with a variety of solvents, including water. We feel that this reagent provides an efficient and facile pathway to prepare amides in high yields and purity. We are currently utilizing this method for the derivatization of amines from biological sources, and for the preparation of small molecule amide libraries.

The authors thank the University of Maryland, Baltimore County for financial support.

Notes and References

† E-mail kalivret@umbc.edu

‡ *Immobilization of HOBT on polystyrene beads* (ref. 2): A suspension of 3-nitro-4-chlorobenzyl alcohol (5.01 g, 26.7 mmol), dried BioRad SM-2 macroporous beads (5.00 g, polystyrene–divinylbenzene copolymer resin, 100–200 mesh, MW cutoff 2000, Bio-Rad Laboratories) and anhydrous $AlCl_3$ (5.01 g, 37.6 mmol) in 30 ml of nitrobenzene was heated at 65–70 °C for 3 days. The suspension was cooled to room temperature and filtered. The polymer was then washed with a solution of 1 M HCl in dioxane (3 × 25 ml), DMF (3 × 25 ml), MeOH (3 × 25 ml) and CH_2Cl_2 (3 × 25 ml), and finally dried *in vacuo*. The 3-nitro-4-chloro benzylated polystyrene was heated to reflux in a mixture of hydrazine monohydrate and ethylene glycol monoethyl ether (4 : 6, v/v; 30 ml) for 20 h. The reaction mixture was cooled to room temperature and the polymer was filtered and washed with H_2O (3 × 25 ml) and CH_2Cl_2 (3 × 25 ml). The polymer was resuspended in a mixture of concentrated aq. HCl and dioxane (1 : 1, v/v; 50 ml) and the suspension was heated at reflux for 20 h. At this time, the polymer was filtered and washed with H_2O (5 × 50 ml), MeOH (3 × 50 ml) and Et_2O (3 × 25 ml), and finally dried *in vacuo* at room temperature to yield 4.90 g of **P**-HOBT.

§ *Assay of hydroxy group content in P-HOBT* **2**: To a suspension of **P**-HOBT **2** (0.450 g) in CH_2Cl_2 (5 ml) was added Ac_2O (0.32 g, 0.30 ml, 3.1 mmol) and pyridine (0.20 g, 0.20 ml, 2.5 mmol). The suspension was subsequently rocked for 1 h at 25 °C. At this time, the polymer was filtered, washed with CH_2Cl_2 (25 ml), DMF (2 × 40 ml), CH_2Cl_2 (3 × 25 ml) and anhydrous Et_2O (3 × 25 ml). The polymer was re-suspended in CH_2Cl_2 (5 ml) followed by the addition of isopropylamine (0.208 g, 0.300 ml, 3.52 mmol). The suspension was rocked at 25 °C for 3.5 h. The polymer was then filtered and washed with CH_2Cl_2 (3 × 25 ml). The filtrate and washings were combined and concentrated to yield 0.0113 g of *N*-isopropyl acetamide as a clear oil. This gave an activity of 0.248 mmol g^{-1} for **P**-HOBT **2**. All other polymers were tested in this fashion.

¶ *Typical experimental procedure for the synthesis of amides:* A suspension of **P**-HOBT **2** (0.33 g, 0.25 mmol g^{-1}, 0.083 mmol), Ac_2O (0.026 g, 0.024 ml, 0.25 mmol, 3.0 equiv.) and pyridine (0.021 g, 0.021 ml, 0.26 mmol, 3.2 equiv.) in CH_2Cl_2 (10 ml) was rocked for 1 h at 25 °C. At this time, the polymer was filtered, washed with DMF (2 × 10 ml), CH_2Cl_2 (3 × 10 ml) and anhydrous Et_2O (3 × 10 ml). The polymer was resuspended in CH_2Cl_2 (10 ml) followed by the addition of 3-aminopropan-1-ol (0.0051 g, 0.0052 ml, 0.068 mmol, 0.82 equiv. based on **P**-HOBT **2**). The suspension was rocked at 25 °C for 3.5 h. The polymer was then filtered and washed with CH_2Cl_2 (3 x 15 ml). The filtrate and washings were combined and concentrated to yield 0.0079 g (99%) of *N*-acetyl-3-aminopropan-1-ol as a white solid.

‖ All other amides were formed in an analogous fashion as *N*-acetyl-3-aminopropan-1-ol. The ^1H NMR and mass spectral data of all of the prepared compounds were consistent with the expected structures.

1 *Combinatorial Chemistry: synthesis and application*, ed. S. R. Wilson, and A. W. Czarnik, Wiley, New York, 1997; *Combinatorial peptide and nonpeptide libraries: a handbook*, ed. G. Jung, VCH, New York, 1996.
2 R. Kalir, A. Warshawsky, M. Fridkin and A. Patchornik, *Eur. J. Biochem.*, 1975, **59**, 55.
3 W. Huang, and A. G. Kalivretenos, *Tetrahedron Lett.*, 1995, **36**, 9113.
4 K. G. Dendrinos and A. G. Kalivretenos, *Tetrahedron Lett.*, in the press.
5 K. G. Dendrinos, and A. G. Kalivretenos, *J. Chem. Soc., Perkin Trans. 1*, in the press.
6 I. E. Pop, B. P. Déprez and A. L. Tartar, *J. Org. Chem.*, 1997, **62**, 2594.
7 *Life Science Research Products Catalog*, Bio-Rad Laboratories, 1997, pp. 81-82.

Received in Corvallis, OR, USA, 17th November 1997; 7/08273H

Adsorption of carbon monoxide on a SmO_x film

Takashi Kuriyama,[a] Kimio Kunimori[a] and Hisakazu Nozoye*[b]

[a] *Institute of Materials Science, University of Tsukuba, 1-1-1 Tennodai, Tsukuba, Ibaraki 305, Japan*
[b] *National Institute of Materials and Chemical Research, 1-1 Higashi, Tsukuba, Ibaraki 305, Japan*

A weak adsorption state of CO, characterized by extremely high binding energy photoemission features, was formed on samarium oxide film prepared in UHV.

Molecule/surface interactions on metal oxides are of interest owing to the importance of metal oxides in catalysis. A number of investigations of the chemisorption properties of metal oxides have been carried out under ultrahigh vacuum (UHV) conditions.[1] Little work, however, has dealt with molecular adsorbates on rare earth oxide surfaces,[2,3] since it is difficult to obtain well defined surfaces of such materials. In order to investigate the chemisorption property of a rare earth oxide in detail with surface science techniques, we prepared a samarium oxide (SmO_x) film in UHV. Here, we report the interaction of CO with the surface of the SmO_x film, using ultraviolet photoelectron spectroscopy (UPS), X-ray photoelectron spectroscopy (XPS) and temperature programmed desorption (TPD).

All experiments were performed in a commercial UHV apparatus (ESCALAB Mark II) with a base pressure of $< 1 \times 10^{-8}$ Pa. The SmO_x film was prepared in the UHV system by oxidizing a Sm overlayer, which was vapor-deposited on a Ru(001) single crystal sample (*ca*. 10 mm diameter and 1 mm thickness). Since the SmO_x films obtained here completely covered the Ru(001) surface, we did not have to take into account any effect of the Ru surface or the Ru/SmO_x interface on CO adsorption. UP and XP spectra were recorded at *ca*. 105 K using He II and Al-Kα radiation, respectively.

Fig. 1(*a*) shows the UP spectrum for the SmO_x film on Ru(001), which was prepared by repeating cycles of Sm deposition at 300 K and heating to 800 K in O_2 (*ca*. 10^{-5} Pa). The thickness of the SmO_x film was determined to be *ca*. 4.5 nm from the attenuation of Ru 3d signal intensity. Fig. 1(*b*) was recorded after the surface was saturated with CO at *ca*. 105 K. The difference spectrum, (*b*) − (*a*), shows the appearance of a pair of peaks at *ca*. 11.8 and 14.3 eV below E_F. These two peaks disappeared after heating to 150 K and desorption of CO was observed at *ca*. 125 K in TPD measurements at a heating rate of 5 K s^{-1}. These results suggest that the two observed peaks are attributed to CO species, which adsorbs weakly on the SmO_x surface. Supposing a first-order desorption, the activation energy of desorption of *ca.* 31 kJ mol^{-1} was obtained for this CO species from the desorption temperature of 125 K and a frequency factor of 10^{13} s^{-1}.

As shown in Fig. 1(*e*), two peaks at *ca*. 8.0 and 11.0 eV were observed for CO on the Ru(001) surface, which have been assigned to 5σ/1π and 4σ emissions, respectively.[4] The binding energies of the two peaks from CO on SmO_x are remarkably larger than those of CO on Ru(001) as well as on other metal surfaces. Similar very high binding energy features have been reported for CO on a partially reduced Cr_2O_3(111) surface.[5] This CO species interacts weakly with chromium atoms, and was not observed on a completely oxidized Cr_2O_3(111) surface. The higher binding energies of photoemissions compared with those of CO on metal surfaces were explained by σ bonding between CO and chromium atoms without π* back-donation, which plays an important role in CO adsorption on most metal surfaces. The bonding character of this distinct CO species is essentially different from that of CO on a metal surface.

Fig. 1(*c*) and (*d*) were recorded for an Ar^+-ion-bombarded SmO_x surface before and after CO adsorption, respectively. In the difference spectrum, (*d*) − (*c*), two peaks also appear, at *ca*. 11.8 and 14.3 eV. The intensities of these two peaks are apparently larger than those observed in (*b*) − (*a*) for the non-bombarded surface, suggesting that the Ar^+-ion-bombardment of the surface caused an increase in the number of CO adsorption sites. An explanation for this result is that the adsorbed CO molecules interact with defect sites, which are likely to increase for the rough ion-bombarded surface.

According to a previous report for a TiO_2 surface,[1] the lower part of the valence band (*ca*. 4 eV below E_F) is mostly composed of non-bonding 2p orbitals of oxygen in the oxide. Comparing Fig. 1(*c*) with (*a*), the non-bonding O 2p peak decreases in intensity significantly as a result of the ion bombardment. This fact suggests that the population of the oxygen atoms located at the SmO_x surface, which are less coordinated compared with bulk oxygen atoms, are reduced by the ion bombardment. Therefore, the ion-bombarded surface has a number of oxygen vacancy defect sites, where samarium

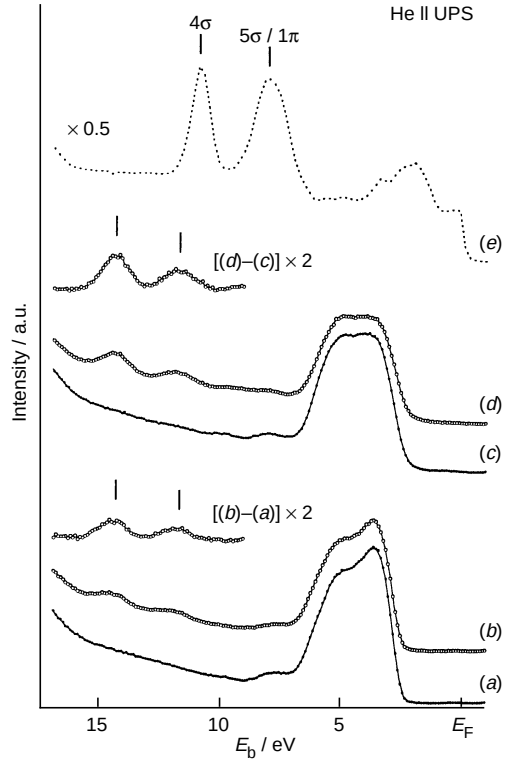

Fig. 1 He II UP spectra recorded on a SmO_x film surface (*a*) before and (*b*) after saturating with CO at *ca*. 105 K and on the Ar^+ ion bombarded SmO_x surface (*c*) before and (*d*) after saturating with CO. Spectrum (*e*) was recorded for CO on Ru(001).

atoms are exposed and probably exhibit an ability to bond to CO.

Fig. 2(*a*) and (*b*) show XP spectra in the O 1s region, which were recorded on a SmO_x film before and after CO adsorption at *ca*. 105 K, respectively. The main O 1s peak at *ca*. 529.6 eV is due to oxygen atoms in the SmO_x film. Comparing the peak area of this O 1s feature with that of Sm 3d, we obtained the stoichiometry of SmO_x : *ca*. 1.44 for *x*. This result is consistent with a previous report for the oxidation of a Sm metal surface by O_2 exposure in UHV system, where Sm_2O_3 was obtained.[6] The difference spectrum (*b*) − (*a*) has a small peak at *ca*. 537.8 eV. Since this O 1s feature disappeared after heating the sample to 150 K, it can be attributed to the weakly adsorbed CO species described above. The binding energy of this O 1s feature is much larger than that of CO on most metal surfaces, as well as those of the valence level emissions. Additionally, a high binding energy feature of C 1s was also observed at *ca*. 291.8 eV for this CO species. These higher binding energies must result mainly from poor screening of the holes induced by photoemission processes, and suggest a lack of π* back-donation and a very weak interaction of CO with the SmO_x surface.

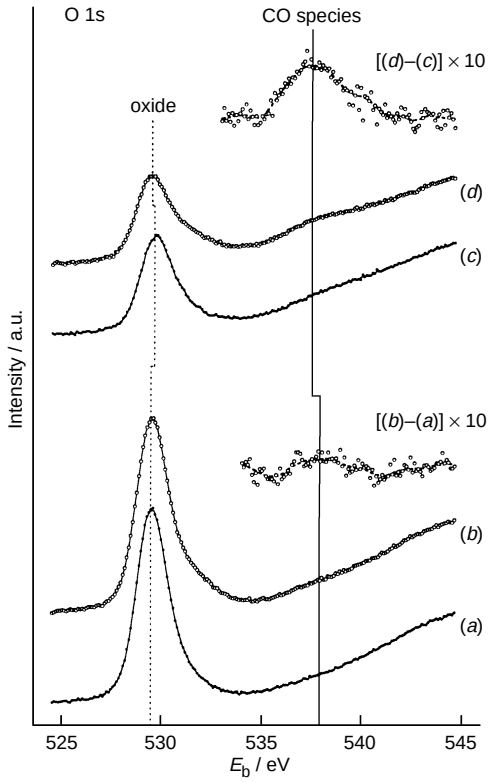

Fig. 2 O 1s XP spectra recorded on a SmO_x film prepared by oxidation of Sm with O_2, (*a*) before and (*b*) after saturating with CO at *ca*. 105 K and on the SmO_x film, which was prepared by oxidation of Sm with CO, (*c*) before and (*d*) after saturating with CO

Fig. 2(*e*) was recorded on a SmO_x film which was prepared by the reaction of deposited Sm with CO in UHV. In this spectrum, the O 1s feature at *ca*. 529.6 eV is obviously smaller than that in Fig. 2(*a*) for the SmO_x produced by O_2 exposure, although the amounts of deposited Sm were almost the same (*ca*. five monolayers). For this CO-produced SmO_x film, which probably consists of the corresponding amount of carbon as a component, the stoichiometry was determined to be *ca*. 0.73 for *x*. It is expected that the CO-produced SmO_x film has a larger number of exposed Sm atoms on the surface than the O_2-produced SmO_x film.

Fig. 2(*d*) was recorded on the surface of this SmO_x film after exposure to CO at *ca*. 105 K. In this spectrum, a more intense O 1s feature at *ca*. 537.6 eV was observed than in Fig. 2(*b*). Comparing the O 1s peak area with that of a saturated CO layer on Ru(001), the coverage of CO observed here was estimated to be *ca*. 0.2 with respect to the Ru(001) substrate. The SmO_x film produced by CO exposure has a larger number of weak CO bonding sites than that produced by O_2 exposure. This result also supports the fact that the weakly bound CO species interact with samarium atoms at oxygen vacancy defect sites.

With respect to the catalytic abilities of rare earth oxides for CO hydrogenation, Sakata *et al.* have studied CO adsorption on a practical Sm_2O_3 catalyst, using *in situ* IR spectroscopy.[7] They have reported that CO chemisorbed reactively on a Sm_2O_3 surface to form several types of species, which were also detected on other rare earth oxides.[8] On the other hand, under UHV conditions, no CO chemisorption was observed on rare earth oxide films[2] or single crystal surfaces of a rare earth oxide[3] at room temperature. The characteristic weak adsorption state of CO observed here on the SmO_x surface was not stable at room temperature under UHV condition. Under atmospheric pressure, however, it may be possible that this CO species becomes a precursor of the species such as those reported by Sakata *et al.*, or plays other important roles in catalytic reactions.

Notes and References

* E-mail: nozoye@nimc.go.jp

1 *The Surface Science of Metal Oxides*, ed. V. E. Henrich and P. A. Cox, Cambridge University Press, Cambridge, 1994.
2 G. Strasser, E. Bertel and F. P. Netzer, *J. Catal.*, 1983, **79**, 420.
3 J. Stubenrauch and M. Vohs, *J. Catal.*, 1996, **159**, 50.
4 J. C. Fuggle, T. E. Mady, M. Steinkilberg and D. Menzel, *Surf. Sci.*, 1975, **52**, 521.
5 C. Xu, B. Dillmann, H. Kuhlenbeck and H.-J. Freund, *Phys. Rev. Lett.*, 1991, **67**, 3551.
6 D. D. Sarma, M. S. Hegde and C. N. R. Rao, *J. Chem. Soc., Faraday Trans.*, 1981, **77**, 1509.
7 Y. Sakata, Y. Kancchika, H. Imamura and S. Tsuchiya, *Chem. Lett.*, 1994, 1829.
8 K. V. Topchieva, S. E. Spiridonov and A. Y. Logninov, *J. Chem. Soc., Chem. Commun.*, 1986, 636.

Received in Cambridge, UK, 4th November 1997; 7/07932J

Synthesis and extraction studies of 1,2- and 1,3-disubstituted butylcalix[4]arene amides with oxyions; geometric and conformational effects

Olusegun M. Falana,[a] H. Fred Koch,[a] D. Max Roundhill,*[a] Gregg J. Lumetta[b] and Benjamin P. Hay[b]

Department of Chemistry and Biochemistry, Texas Tech University, Lubbock, Texas 79409-1061, USA
Pacific Northwest National Laboratory, P.O. Box 999, Richland, Washington 99352, USA

26,28-(Dibutylcarbamoyl)methoxy-5,11,17,23-*tert*-butylcalix[4]arene and two geometric isomers of 27,28-(dibutylcarbamoyl)methoxy-5,11,17,23-*tert*-butylcalix[4]arene have been used to extract U^{VI}, Mo^{VI}, Cr^{VI} and Se^{VI} from aqueous solution into toluene or isooctane.

The selective extraction of metal cations and anions from aqueous solution into an organic phase is an important goal, especially if the particular ions are toxic and present in the environment in significant quantities.[1,2] Three such metals are uranium,[3] chromium[4–10] and selenium,[11] all of which exist primarily in their hexavalent forms. Although there is considerable diversity between these species there are also some similarities. The main difference is that whereas Se^{VI} and Cr^{VI} are anions in strongly acidic solution, U^{VI} is a cation. An important similarity, however, is that these species are high valent oxophiles, and an amide functionality can potentially act as a complexant for each of these species. This premise is based on the logic that such a functionality should not only coordinate as a hard N,O-donor ligand to such high-valent centers, but should also function as a neutral host to hydrogen bond with the protonated form of the oxyanion.

In developing extractants it is important to target specific solvent systems as well as complexants. Although in earlier work with calix[4]arenes we have used chloroform as the organic phase,[12–19] we have always been aware that it would be advantageous to use a less toxic organic such as an alkane. We have now prepared the geometrically isomeric 1,2- and 1,3-calix[4]arene amides having appended *n*-butyl substituents in order that they can be more compatible with such an alkane phase. In addition to solvent selectivity, the effect of both geometric and conformational properties of the complexant needs also to be considered. Since the 1,2 isomer has been obtained as a separable mixture of geometric isomers, the availability of such a pair of isomers affords us the opportunity to compare their relative extraction properties.

These three new calix[4]arene amides have been synthesized using the same general procedures.[20] The precursor compound *N*,*N*-dibutyl-2-bromoacetamide has been synthesized in 82% yield by stirring a mixture of bromoacetic acid and *N*,*N*-dibutylamine in dichloromethane with 1,3-dicyclohexylcarbodiimide for 12 h.

The synthetic route of the calix[4]arene amides involves reacting 5,11,17,23-*tert*-butylcalix[4]arene with *N*,*N*-dibutyl-2-bromoacetamide (2.2 equiv.) in the presence of a base. For the case of 26,28-(dibutylcarbamoyl)methoxy-5,11,17,23-*tert*-butylcalix[4]arene **1** the conditions use potassium carbonate in refluxing acetone for 18 h (Scheme 1), and for the two isomers of 27,28-(dibutylcarbamoyl)methoxy-5,11,17,23-*tert*-butylcalix[4]arene (**2**, **3**), sodium hydride in DMF at 60 °C for 26 h is used (Scheme 2). Compounds **2** and **3** were obtained in the same reaction mixture and separated by column chromatography.

These compounds have been structurally characterized by NMR spectroscopy. Compound **1** (yield 65%; mp 130–132 °C) is characterized as being in the cone conformation by the presence of a single triplet resonance in the ^{1}H NMR spectrum

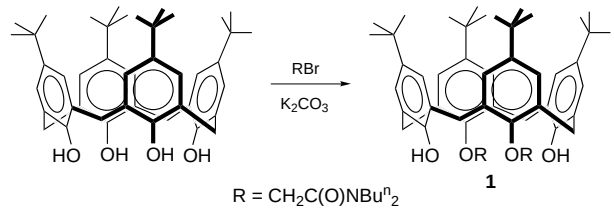

Scheme 1

due to the NCH_2 group at δ 3.36, a singlet at δ 4.81 due to $OCH_2C(O)$ and an AB pair for the bridging methylenes at δ 3.27 and 4.46 [^2J(HH) 13 Hz]. The $^{13}C\{^1H\}$ NMR spectrum shows the amide carbonyl resonance at δ 168.0. Compound **2** (yield 9.0%; mp 130 °C) is characterized as being in the partial cone conformation with the bis-(dibutylcarbamoyl)methoxy groups on opposite rims by the presence of a multiplet resonance due to NCH_2 groups at δ 3.21–3.42, two inequivalent singlets at δ 5.24 and 5.29 due to the pair of $OCH_2C(O)$ groups, and two sets of AB pairs for the inequivalent bridging methylenes at δ 4.34 and 4.96 [^2J(HH) 13 Hz], and at δ 4.68 and 4.70 [^2J(HH) 14 Hz]. The $^{13}C\{^1H\}$ NMR spectrum shows the amide carbonyl resonance at δ 170.0. Compound **3** (yield 9.6%; mp 174–175 °C) is characterized as being in the partial cone conformation with the bis-(dibutylcarbamoyl)methoxy groups on the same side of the upper rim by the presence of a multiplet resonance due to the NCH_2 group at δ 3.39–3.49, a singlet for $OCH_2C(O)$ at δ 4.98, along with two sets of AB pairs for the inequivalent bridging methylenes at δ 3.41 and 4.63 [^2J(HH) 13 Hz] and at δ 3.43 and 4.37 [^2J(HH) 14 Hz]. The OH resonances are found at δ 9.76 and 10.48. The $^{13}C\{^1H\}$ NMR spectrum shows the amide carbonyl resonance at δ 169.0. Both the ^{1}H NMR and ^{13}C NMR spectra show additional corresponding resonances for the other functional groups in these structures of **1**–**3**.

Extraction studies have been carried out with isooctane and toluene, along with the compounds **1**, **2** and **3** (1 mM solutions of each), and aqueous solutions of the metal salts (1 mM in

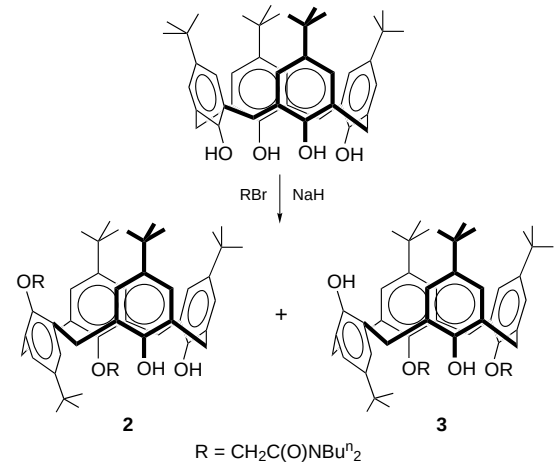

Scheme 2

Table 1 Extraction of oxyions by **1**, **2** and **3**

Compound	Solvent	Extraction (%)[a]			
		UO_2^{2+}	MoO_3(aq)	$Cr_2O_7^{2-}$	$HSeO_4^-$
1	Toluene	3	< 1	20(2)[b]	1
	Isooctane	31(3)	20(2)	< 1	< 1
2	Toluene	13(1)	7(1)	20(2)	11(1)
	Isooctane	25(2)	20(2)	< 1	< 1
3	Toluene	14(1)	< 1	32(3)	13(1)
	Isooctane	39(4)	40(4)	< 1	15(1)

[a] Extractions were carried out by vigorous shaking for 1 min with both the calix[4]arene and the metal salt as 1 mM solutions. The aqueous solution is at pH 0.85. [b] The initial and final metal concentrations were measured by ICP and the errors are estimated from multiple measurements.

0.14 M HNO_3). Equal volumes of the organic and aqueous solutions are then shaken for 1 min. The resultant aqueous layer is then separated and the remaining metal concentration in that layer analyzed by ICP. These data with estimated errors in parentheses are collected in Table 1. From these data it is apparent that the oxyions can be extracted into toluene or isooctane from an aqueous solution at pH 0.85 in the presence of these three hydrophobic calix[4]arene amides. These data also show differences between both these two solvents and the isomers of **1**, **2** and **3**. Although these data may not represent equilibrium conditions, they are viable because for an extractant to be useful the phase transfer of the species must be rapid, therefore these data reflect this property. From these preliminary data with these compounds it appears that both UO_2^{2+} and molybdenum trioxide have a slight preference for isooctane over toluene, with the reverse trend being observed for the two oxyanions. The differences between **1**, **2** and **3** are less apparent, but it does appear that there may be a preference of **3** being an extractant for transferring these oxyions into isooctane. Interestingly, this particular isomer is the one that has the amides in a potentially chelating geometry, with a hydrophobic *tert*-butyl group projecting into this lower rim binding cavity. Further use of these compounds as extractants will be reported in due course.

We thank the US Army Research Office and the US Department of Energy, through the Pacific Northwest Laboratory, for financial support.

Notes and References

* E-mail: uldmr@ttacs.ttu.edu

† Satisfactory elemental analyses have been obtained for these calix[4]arenes. The calix[4]arenes were purified on a silica column using the eluents dichloromethane and ethyl acetate for **1** and ethyl acetate and light petroleum (bp 40–50 °C) for **2** and **3**.

1 For an overview, see: *Heavy Metals*, ed. W. Salomons, U. Förstner and P. Mader, Springer, New York, 1995.
2 A. T. Yordanov and D. M. Roundhill, *Coord. Chem. Rev.*, in press.
3 R. A. Bulman, *Coord. Chem. Rev.*, 1980, **31**, 221.
4 D. Burrows, *Chromium: Metabolism and Toxicity*, CRC Press, Boca Raton, FL, 1983.
5 J. A. H. Waterhouse, *Br. J. Cancer*, 1975, **32**, 262.
6 S. Bonatti, M. Meini and A. Abbondandolo, *Mutat. Res.*, 1976, **39**, 147.
7 V. Bianchi, A. Zantedeschi, A. Montaldi and J. Majone, *Toxicol. Lett.*, 1984, **8**, 279.
8 S. De Flora and K. E. Wetterhahn, *Life Chem. Rep.*, 1989, **7**, 169.
9 D. M. Stearns, L. J. Kennedy, K. D. Courtney, P. H. Giangrande, L. S. Phieffer and K. E. Wetterhahn, *Biochemistry*, 1995, **34**, 910.
10 P. R. Wittbrodt and C. D. Palmer, *Environ. Sci. Technol.*, 1995, **29**, 255.
11 T. Jukes, *Nature*, 1985, **316**, 673.
12 A. T. Yordanov, J. T. Mague and D. M. Roundhill, *Inorg. Chem.*, 1995, **34**, 5084.
13 A. T. Yordanov, J. T.Mague and D. M. Roundhill, *Inorg. Chim. Acta*, 1995, **240**, 441.
14 A. T. Yordanov and D. M. Roundhill, *New J. Chem.*, 1996, **20**, 447.
15 A. T. Yordanov, D. M. Roundhill and J. T. Mague, *Inorg. Chim. Acta*, 1996, **250**, 295.
16 N. Wolf, E. M. Georgiev and D. M. Roundhill, *Polyhedron*, 1997, **16**, 1581.
17 A. T. Yordanov, B. R. Whittlesey and D. M. Roundhill, *Supramol. Chem.*, in press.
18 A. T. Yordanov and D. M. Roundhill, *Inorg. Chim. Acta*, in press.
19 A. T. Yordanov, O. M. Falana, H. F. Koch and D. M. Roundhill, *Inorg. Chem.*, 1997, **36**, 6468.
20 D. M. Roundhill, E. Georgiev and A. T. Yordanov, *J. Inclusion Phenom. Mol. Recog. Chem.*, 1994, **19**, 101.

Received in Bloomington, IN, USA, 29th October 1997; 7/07786F

Large optical limiting properties of the pentanuclear 'open' structural cluster compound $[WS_4Cu_4(SCN)_2(py)_6]$

Michael K. M. Low,[a] Hongwei Hou,[a] Hegen Zheng,[b] Wingtak Wong,[c] Guoxin Jin,[b] Xinquan Xin[b] and Wei Ji*[a]

[a] *Departments of Physics and Chemistry, National University of Singapore, 10 Kent Ridge Crescent, Singapore 119260, Singapore*
[b] *State Key Laboratory of Coordination Chemistry, Nanjing University, Nanjing 210093, P.R. China*
[c] *Department of Chemistry, University of Hong Kong, Pokfulam Road, Hong Kong, P.R. China*

Optical limiting properties of a pentanuclear 'open' structural inorganic cluster have been studied with 7 ns laser pulses of 532 nm wavelength; the limiting threshold of the cluster $[WS_4Cu_4(SCN)_2(py)_6]$ is 0.3 J cm^{-2}, which is about five times better than that observed in C_{60}.

Optical limiting materials are substances whose transmission is high when they are illuminated by low-intensity light but low when exposed to intense laser radiation. Because of their potential applications in the protection of optical sensors from high-intensity laser beams, the search for better optical limiting materials has become increasingly intensive. The most frequently reported materials are fullerenes (C_{60})[1,2] and phthalocyanine complexes,[3,4] which are generally regarded as the best compounds for optical limiting. Recently, large non-linear optical effects have also been found in inorganic clusters.[5–22] The structures of these clusters vary widely, they include butterfly-shaped clusters,[6] trinuclear linear clusters,[7] nest-shaped clusters,[8–10] 'half-open' cubane-like clusters,[11,12] cubane-like clusters,[13–16] hexagonal prism-shaped clusters,[17,18] twin-nest-shaped clusters[19,20] and twenty-nuclear supracage-shaped cluster.[21]

A good optical-limiting material should possess strong limiting responses to ns laser pulses in the visible and near-IR spectral regions. This is because the most likely encountered powerful light sources are Q-switched Nd : YAG lasers. In this regard, the optical limiting properties of cubane-like clusters and hexagonal prism-shaped clusters have been found to be the best amongst all the clusters studied, with limiting threshold in the order of *ca.* 0.1 J cm^{-2}.[13–15,17] This is comparable to those of phthalocyanine derivatives and better than that of C_{60}.[2,3] However, such performances were achieved under the single-shot condition; and when the pulse repetition rate exceeded 1 Hz, photodegradation occurred.[13] To overcome this problem, we have investigated different structural types of inorganic clusters. Here, we report the observation of superior limiting behavior in a pentanuclear 'open' structural cluster $[WS_4Cu_4(SCN)_2(py)_6]$ with a pulse repetition rate of up to 10 Hz.

The preparation of the cluster $[WS_4Cu_4(SCN)_2(py)_6]$ was reported elsewhere.[23,24] We obtained the cluster $[WS_4Cu_4(SCN)_2(py)_6]$ by the reaction of $[NH_4]_2WS_4$, CuSCN and KSCN with py. The structure was identified from IR spectra, elemental analysis and unit cell parameters.† The cluster has an 'open' structure with five metal atoms (one W and four Cu atoms) in the same plane. Four S–S edges of the tetrahedral WS_4^{2-} core are coordinated by four Cu atoms, giving a WS_4Cu_4 aggregate of approximate D_{2h} symmetry, as shown in the inset of Fig. 1. Its electronic spectrum in Fig. 1 illustrates that there is a relatively low linear absorption in the visible and near-IR region. A broad transparent range is an important criterion in the assessment of optical limiting materials.

Fig. 2 displays measurements of optical limiting effects in a DMF solution of $[WS_4Cu_4(SCN)_2(py)_6]$‡ with 532 nm laser pulses of 7 ns duration. The transmittance defined here is the ratio of the transmitted pulse energy to the incident pulse energy at 532 nm. It is obvious that the solution transmittance is independent of the incident fluence at < 0.1 J cm^{-2}. (The linear transmittance is 63%, which includes the Fresnel reflection losses of the two surfaces of the cell. If the surface losses are excluded, the transmittance of the solution is 69%.) When the

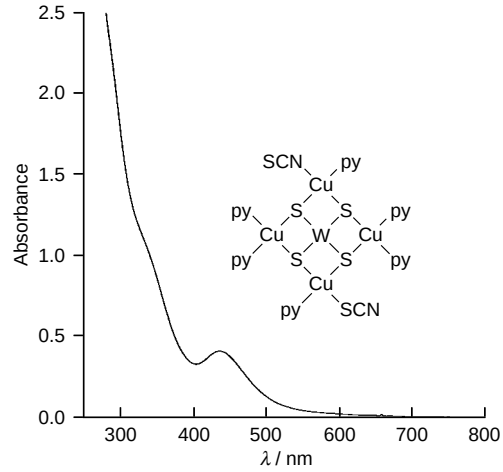

Fig. 1 Electronic spectrum of $[WS_4Cu_4(SCN)_2(py)_6]$ in DMF (1.3×10^{-3} M). Optical path: 1 mm. The inset shows the structure of $[WS_4Cu_4(SCN)_2(py)_6]$.

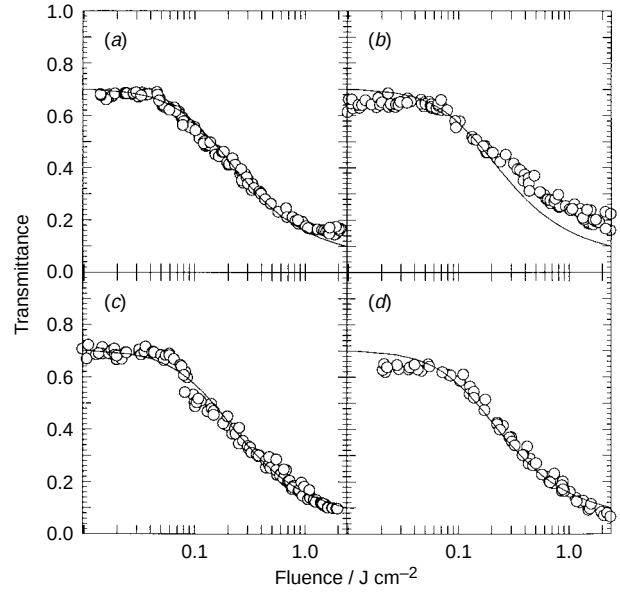

Fig. 2 Energy dependent transmittance of a $[WS_4Cu_4(SCN)_2(py)_6]$ DMF solution (1.1×10^{-3} M). Optical path: 1 mm; laser wavelength: 532 nm; pulse duration: 7 ns; and repetition rates: (*a*) 10, (*b*) 5, (*c*) 1 Hz and (*d*) single shots (30 s interval)

Table 1 The limiting thresholds of compounds measured at 532 nm with ns laser pulses

Compound	Solvent	Linear transmission (%)	Limiting threshold/ J cm^{-2}	Ref.
C_{60}	Toluene	62	1.6	2
$[NBu^n_4]_3[WCu_3Br_4S_4]$	MeCN	70	1.1	15
$[NBu^n_4]_3[WAg_3Br_4S_4]$	MeCN	70	0.6	15
$[NBu^n_4]_3[WAg_3BrI_3S_4]$	MeCN	70	0.5	15
$[NBu^n_4]_3[WAg_3BrCl_3S_4]$	MeCN	70	0.6	15
$[WS_4Cu_4(SCN)_2(py)_6]$	DMF	69	0.3	This work
Phthalocyanine derivatives	Toluene	85	≈0.1	3, 4
$[Mo_2Ag_4S_8(PPh_3)_4]$	MeCN	92	≈0.1	17

incident fluence exceeds 0.1 J cm^{-2}, the solution transmittance decreases as the incident fluence is increased, thus exhibiting a typical optical limiting effect. The limiting threshold is defined as the incident fluence at which the solution transmittance falls to 50% of the linear transmittance. From Fig. 2, we determine the limiting threshold of the $[WS_4Cu_4(SCN)_2(py)_6]$ DMF solution to be *ca.* 0.3 J cm^{-2}.

Fig. 2 also displays the optical limiting performance of the cluster measured with the pulse repetition rate ranging from single shots to 10 Hz. Within our experimental errors, no significant difference is found among these measurements, thereby indicating that the photostability of $[WS_4Cu_4(SCN)_2(py)_6]$ is considerably better compared to the cubane-like and hexagonal prism-shaped clusters.[13–15,17]

It is interesting to compare this new cluster with other well known optical limiting materials for 7 ns pulsed radiation of 532 nm wavelength. Table 1 shows the limiting thresholds of the cluster $[WS_4Cu_4(SCN)_2(py)_6]$, cubane-like clusters, hexagonal prism-shaped clusters, C_{60} and phthalocyanine derivatives. It is clear that the limiting performance in the $[WS_4Cu_4(SCN)_2(py)_6]$ DMF solution is five times better than that displayed in C_{60} and three times higher than that in phthalocyanine derivatives. It should be emphasized, however, that the Q absorption band in phthalocyanine derivatives makes them narrow-band limiters, while the spectrum of $[WS_4Cu_4(SCN)_2(py)_6]$ shown in Fig. 1 indicates that the new cluster should be a broad-band limiter.

It should be pointed out that our measurement of the transmitted pulse energy was conducted with a full collection of the transmitted pulse, and no aperture was used. Therefore, the observed optical limiting originates from a non-linear absorptive process. The limiting mechanism in cubane-like clusters has been studied in detail.[15] The initial linear absorption promotes electrons from the ground to an excited singlet state. These excited electrons are transferred to the lowest triplet state mainly by a process of ionization and germinate recombination. If the absorption cross-section of the triplet state is greater than that of the ground state, then reverse saturable absorption occurs, resulting in the optical limiting effect.

We have found that this non-linear process can be approximately expressed by[15]

$$T = \frac{(1-R)^2 \exp(-\alpha L)}{\sqrt{1 + B[1-\exp(-\alpha L)]F_{in}^2}}$$

where T is the transmittance, R is the reflectance of the cell surface, L is the optical path, α is the linear absorption coefficient, F_{in} is the incident fluence, and B is a parameter determined by the product of the lifetime and ionization cross-section of the excited singlet state, the absorption cross-section of the excited triplet state, and the probability of the germinate recombination. The solid curves in Fig. 2 are calculated by this expression with $B = 4.3 \times 10^4$ cm^4 J^{-2}. Nearly perfect fits indicate that the optical limiting in the cluster is caused by the absorption of the excited triplet state whose population is generated mainly by the process of ionization and germinate recombination.

This research was supported by the National Natural Science Foundation of China, the Hong Kong Research Grants Council, the University of Hong Kong, and the National University of Singapore.

Notes and References

* E-mail: phyjiwei@nus.edu.sg

† IR spectra: ν(W–S_{br}), 435 cm^{-1}; ν(SCN), 2081 cm^{-1}; ν(py), 1595, 1441, 752, 695 cm^{-1}. Anal. Calc. for $C_{32}H_{30}Cu_4N_8S_6W$: C, 33,22; H, 2.61; Cu, 21.97; N, 9.68; W, 15.9. Found: C, 33.00; H, 2.40; Cu, 21.78; N, 9.80; W, 16.3%. The cluster is orthorhombic, space group *Pbcn* (no. 60) with a = 19.786(2), b = 13.629(2), c = 15.080(2) Å.

‡ The optical limiting effects were observed with 532 nm wavelength laser pulses of 7 nanosecond duration. The laser pulses were produced by a frequency-doubled, Q-switched Nd:YAG laser operated with multiple axial modes. The pulse energy was spatially filtered to be a nearly Gaussian profiles and then was split into two parts: one was used as a reference for the incident energy and the other was focused onto the sample. The sample was a solution of $[WS_4Cu_4(SCN)_2(py)_6]$ dissolved in DMF (1.1×10^{-3} M) and contained in a 1 mm thick quartz cell. Both incident and transmitted pulse energy were measured with two pyroelectric probes (RjP-735, Laser Precision), simultaneously. The measurements were conducted over *ca.* 8 h.

1 L. W. Tutt and A. Kost, *Nature*, 1992, **356**, 224.
2 McLean, R. L. Sutherland, M. C. Brant, D. M. Brandelik, P. A. Fleitz and T. Pottenger, *Opt. Lett.*, 1993, **18**, 858.
3 J. W. Perry, K. Mansour, S. R. Marder, K. J. Perry, Jr., D. Alvarez and I. Choong, *Opt. Lett.*, 1994, **19**, 625.
4 J. W. Perry, K. Mansour, I.-Y. S. Lee, X.-L. Wu, P. V. Bedworth, C. T. Chen, D. Ng, S. R. Marder, P. Miles, T. Wada, M. Tian and H. Sasabe, *Science*, 1996, **273**, 1533.
5 L. W. Tutt and S. W. McCahon, *Opt. Lett.*, 1990, **15**, 700.
6 S. Shi, H. W. Hou and X. Q. Xin, *J. Phys. Chem.*, 1995, **99**, 4050.
7 H. G. Zheng, W. Ji, Michael, L. K. Low, G. Sakane, T. Shibahara and X. Q. Xin, *J. Chem. Soc., Dalton Trans.*, 1997, 2357.
8 H. W. Hou, X. R. Ye, X. Q. Xin, J. Liu, M. Q. Chen and S. Shi, *Chem. Mater.*, 1995, **7**, 472.
9 S. Shi, W. Ji, W. Xie, T. C. Chong, H. C. Zeng, J. P. Lang and X. Q. Xin, *Mater. Chem. Phys.*, 1995, **39**, 298.
10 P. Ge, S. H. Tang, W. Ji, S. Shi, H. W. Hou, D. L. Long, X. Q. Xin, S. F. Lu and Q. J. Wu, *J. Phys. Chem.*, 1997, **101**, 27.
11 H. W. Hou, B. Liang, X. Q. Xin, K. B. Yu, P. Ge, W. Ji and S. Shi, *J. Chem. Soc., Faraday Trans.*, 1996, **92**, 2343.
12 Z. R. Chen, H. W. Hou, X. Q. Xin, K. B. Yu and S. Shi, *J. Phys. Chem.*, 1995, **99**, 8717.
13 S. Shi, W. Ji, S. H. Tang, J. P. Lang and X. Q. Xin, *J. Am. Chem. Soc.*, 1994, **116**, 3615.
14 S. Shi, W. Ji, J. P. Lang and X. Q. Xin, *J. Phys. Chem.*, 1994, **98**, 3570.
15 W. Ji, H. J. Du, S. H. Tang and S. Shi, *J. Opt. Soc. Am. B*, 1995, **12**, 876.
16 P. E. Hoggard, H. W. Hou, X. Q. Xin and S. Shi, *Chem. Mater.*, 1996, **8**, 2218.
17 W. Ji, S. Shi, H. J. Du, P. Ge, S. H. Tang and X. Q. Xin, *J. Phys. Chem.*, 1995, **99**, 17 297.
18 G. Sakane, T. Shibahara, H. W. Hou, X. Q. Xin and S. Shi, *Inorg. Chem.*, 1995, **34**, 5363.
19 H. W. Hou, D. L. Long, X. Q. Xin, X. X. Huang, B. S. Kang, P. Ge, W. Ji and S. Shi, *Inorg. Chem.*, 1996, **35**, 5363.
20 H. W. Hou, X. Q. Xin, J. Liu, M. Q. Chen and S. Shi, *J. Chem. Soc., Dalton Trans.*, 1994, 3211.
21 S. Shi, W. Ji and X. Q. Xin, *J. Phys. Chem.*, 1995, **99**, 894.
22 S. Banerjee, G. R. Kumar, P. Mathur and P. Sekar, *Chem. Commun.*, 1997, 299.
23 G. X. Jin, Dissertation, Nanjing University, China, 1988.
24 Y. Jeannin, F. Secheresse, S. Bernes and R. Robert, *Inorg. Chim. Acta*, 1992, **198–200**, 493.

Received in Cambridge, UK, 17th November 1997; 7/08230D

Novel reactivity of photoexcited iron porphyrins caged into a polyfluoro sulfonated membrane in catalytic hydrocarbon oxygenation

A. Maldotti,* A. Molinari, L. Andreotti, M. Fogagnolo and R. Amadelli

Dipartimento di Chimica, Centro di Studio su Fotoreattività e Catalisi del CNR, Università degli Studi di Ferrara, Via L. Borsari 46, 44100, Ferrara, Italy

Heterogenization of iron porphyrins inside Nafion creates new photocatalytic systems which can be used to oxidize cyclohexene and cyclohexane with sunlight and O_2 under mild conditions (room temperature, atmospheric pressure); the polymeric matrix makes the iron porphyrin a good photocatalyst for the monooxygenation of the substrate and increases both its photocatalytic efficiency (about ten times) and its stability (turnover values > 1000).

As a development of an important field of research dealing with photoexcited iron porphyrins in the catalytic oxygenation of hydrocarbons,[1] we have recently investigated photocatalytic composite systems in which the porphyrin complexes are confined inside cross linked polystyrene,[2] bound on semiconducting transition metal oxides such as TiO_2[3] or interacting with polyoxotungstates.[4] Generally speaking, the use of heterogeneous media or organized systems is a suitable means to control the reaction environment in order to promote specific processes of interest in biomimetic catalysis by iron porphyrins.[5]

This work deals with composite systems in which iron porphyrin complexes are caged inside Nafion,[6] a commercial polyfluorosulfonated membrane consisting of sulfonic groups connected to a polymeric structure of polytetrafluoroethylene. We have chosen this support because (*i*) it is chemically inert also in strong oxidizing media; (*ii*) it is totally transparent to the light of interest in metal porphyrin photochemistry; (*iii*) it is expected to cage the monocationic porphyrin complexes inside its large anionic cavities where the SO_3^- groups are located; and (*iv*) dioxygen concentration inside Nafion is more than ten times higher than in organic solvent.[7]

The photocatalytic activity of these composite systems is demonstrated in the oxygenation of cyclohexene and cyclohexane by O_2 and sunlight under mild conditions (20 °C, 760 Torr of O_2). A comparison with the photocatalytic properties of the same iron porphyrins in homogeneous solution reveals that the polymeric matrix strongly affects the chemioselectivity of the oxidation process and increases both the photochemical efficiency and the stability of the iron porphyrin.

The following iron(III) porphyrins have been chosen on the basis of their well known[1] behaviour in homogeneous solution: iron(III) *meso*-tetraphenylporphyrin $[Fe^{III}(tpp)]^+$, iron(III) *meso*-tetrakis(2,6-dichlorophenyl)porphyrin $[Fe^{III}(tdcpp)]^+$, iron(III) *meso*-tetrakis(pentafluorophenyl)porphyrin $[Fe^{III}(tf_5pp)]^+$. Their absorption into Nafion was carried out in CH_2Cl_2–alcohol at 40 °C after swelling the membrane in EtOH or Pr^{i}OH. Typically the uptake of 0.5–0.8 μmol of complex in 1 g of resin occurs in a few minutes.

The UV–VIS spectra of the modified resin after swelling with EtOH or Pr^{i}OH are exactly those of the starting iron porphyrin dissolved in acidified alcohol media, which an extensive literature[8] ascribes to the monocationic species having an alcohol molecule bound to the axial position.† We then infer that heterogenization does not affect the nature of the iron porphyrin axial ligand. In support of this conclusion, an EPR spin-trapping investigation indicates that heterogenization does not affect even the primary photochemical process consisting of the homolytic cleavage of the Fe^{III} axial ligand bond according to step (*a*) in Scheme 1, which is a type of reaction already observed for many other iron porphyrin complexes in homogeneous solution.[1*a*,*b*,8,9] In fact, photoirradiation‡ of the iron porphyrin/Nafion composite systems in alcohol in the presence of the spin trap phenyl-*tert*-butylnitrone (PBN) inside the cavity of an EPR spectrometer yields spectra exhibiting the typical signals of the adducts between PBN and alkoxy radicals [step (*b*)].[10]

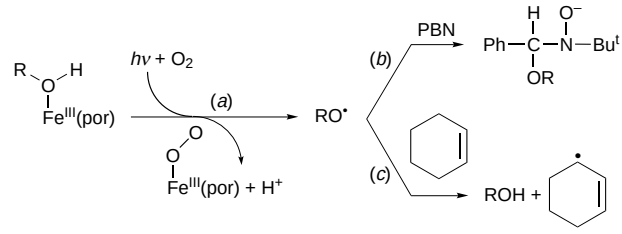

Scheme 1

Since the substituents on the *meso*-aryl groups of $[Fe^{III}(tdcpp)]^+$ and $[Fe^{III}(tf_5pp)]^+$ prevent the formation of a μ-oxo dimer complex,[11] the very fast reaction of the iron(II) porphyrin with O_2 is expected to restore the starting Fe^{III} complex, so inducing the reductive activation of O_2 itself[1*b*,12] (Scheme 1). In this way, using dioxygen and sunlight, the iron porphyrin/Nafion systems are able to form, in a cyclic way, reactive intermediates which are expected to induce the oxidation of hydrocarbons. The results obtained in the oxidation of cyclohexene and cyclohexane are summarized in Table 1.

Table 1 shows that irradiation of $[Fe^{III}(tdcpp)^+$ in EtOH–cyclohexene (25% v/v) results in the formation of cyclohex-2-en-1-one, cyclohex-2-en-1-ol and *trans*-cyclohexane-1,2-diol monoethyl ether. Interestingly, if the same experiment is carried out using Pr^{i}OH instead of EtOH, the ether represents about 90% of the overall oxidized alkene, and allylic oxidation products are formed only in very minor amounts. The presence of the ether indirectly reveals the formation of cyclohexene epoxide which, in the strong acidic environment inside Nafion, likely undergoes a nucleophilic attack by the alcohol, leading to the epoxide ring opening.§ Oxidation of cyclohexene is also observed with $Fe^{III}(tf_5pp)$/Nafion even though the ratio of allylic oxidation products increases significantly in Pr^{i}OH. For the latter system we obtain the maximum initial oxidation rate of *ca.* 8.5 turnovers min^{-1}.

Photoexcitation of $[Fe^{III}(tdcpp)]^+$ in homogeneous alcoholic solution gives totally different results: (*i*) the photooxidation is slower than in heterogeneous conditions; (*ii*) no ether is obtained; (*iii*) in addition to allylic oxidation products, cyclohexanol and cyclohexanone are formed, as we discussed earlier.[13]

The turnover values reported in Table 1 indicate that heterogenization significantly increases (about ten times) the stability of $[Fe^{III}(tdcpp)]^{3+}$. The Nafion matrix does not undergo any degradation and can be utilised several times. $[Fe^{III}(tpp)]^+$ is much less stable inside Nafion than both $[Fe^{III}(tdcpp)]^+$ and $[Fe^{III}(tf_5pp)]^+$. This indicates that, as in homogeneous sol-

Table 1 Photocatalytic[a] oxygenation of cyclohexene and cyclohexane

Photocatalytic system	Substrates	Products[b] and related turnover[c]		
Fe^{III}(tdcpp)/Nafion EtOH		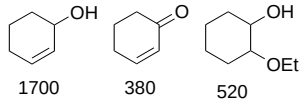		
		1700	380	520
Fe^{III}(tdcpp)/Nafion Pr^iOH		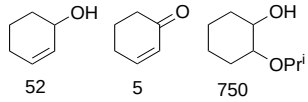		
		52	5	750
Fe^{III}(tf_5pp)/Nafion EtOH		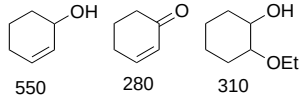		
		550	280	310
Fe^{III}(tf_5pp)/Nafion Pr^iOH		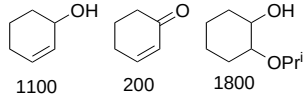		
		1100	200	1800
Fe^{III}(tpp)/Nafion Pr^iOH		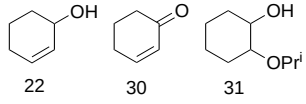		
		22	30	31
Fe^{III}(tdcpp)/EtOH (homogeneous solution)		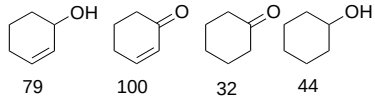		
		79	100	32 44
Fe^{III}(tdcpp)/Nafion Pr^iOH		$< 10^{-5}$ mol dm^{-3}		
Fe^{III}(tdcpp)/Nafion Pr^iOH		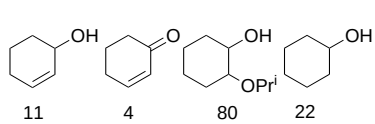		
		11	4	80 22

[a] Six hours photoirradiation, see footnote ‡. [b] Reaction products were determined by gas chromatography and gas mass analyses. Reported values are ±10%. Cyclohexane-1,2-diol monoethers have been separated on an SiO_2 column and characterised by proton NMR spectroscopy. [c] Mol of product formed per mol of consumed iron porphyrin.

utions,[1c,9] halogen substituents on the *meso* aryl groups play a fundamental role in restoring the starting iron porphyrin during the photocatalytic cycle, avoiding both a too fast oxidative degradation of the porphyrin ring and the formation of μ-oxo-dimers.

Upon irradiation of Fe^{III}(tdcpp)/Nafion in Pr^iOH containing cyclohexane (25% v/v) the concentration of oxidation products was $< 10^{-5}$ mol dm^{-3}, on the same timescale as for cyclohexene. On the other hand, the alkane undergoes hydroxylation when cyclohexene is present as a co-substrate (cyclohexane 12.5% v/v, cyclohexene 12.5% v/v). This suggests that cyclohexene plays a dominant role in the formation of active monooxygenating species during the photocatalytic process.

Cyclohexene is expected to capture efficiently alkoxy radicals originating from the photochemistry of iron porphyrins through an allylic hydrogen abstraction process [step (*c*) in Scheme 1].[14] This hypothesis is confirmed by experiments in which the intensity of the EPR signal of the adduct between PBN and alkoxy radicals is followed as a function of irradiation time. We observed that the signal intensity is unchanged in the presence of cyclohexane, while it is reduced by about 75% if cyclohexene is present. Apparently, the latter is able to compete efficiently with PBN in the reaction with the radical intermediates giving relatively stable cyclohexenyl radicals. Reaction of O_2 with these radicals in the presence of the iron porphyrin can give efficient monooxygenating species[1b] as in the catalytic cycle of cytochrome P450.[15] As a tentative explanation, the polymeric matrix may favour the above reactions in the proximity of the metal centre and, at the same time, inhibit the escape of radical intermediates that initiate autooxidation processes.¶ Our previous work in the homogeneous phase shows that photoexcited porphyrins under aerobic conditions can oxidise cyclohexane even in the absence of cyclohexene.[1c] However, in that case, the active species are OH· radicals which are more reactive than alkoxy radicals in extracting hydrogen atom from hydrocarbons.[16]

Notes and References

* E-mail: mla@ifeuniv.unife.it

† Exchange of the acid membrane with NaCl causes a red shift of the Soret band, in keeping with the deprotonation of the coordinated alcohol molecule and the formation of a neutral porphyrin complex. In fact, in this case we observe experimentally that the complex is released by the membrane after a few hours in alcohol. The spectral variations described are exactly the same as those for the starting iron porphyrin in alcohol with added CF_3SO_3H or $HClO_4$. In the acidified alcohol medium one should reasonably have an equilibrium among more species, with the anions or the alcohol molecules as axial ligands in the porphyrin complex.

‡ Irradiation was carried out at 20 ± 1 °C with a Hanau Q 400 mercury lamp (15 mW cm^{-2}), under oxygen at 760 Torr. Selection of wavelength between 330 and 400 nm was performed by use of a glass cut-off filter.

§ This statement is confirmed by the observation that the epoxide in acidic solution undergoes a nucleophilic attack with the formation of the same *trans*-cyclohexane-1,2-diol monoalkyl ether during the photocatalytic oxidation.

¶ The effect of the matrix is not just that of providing an acid environment. In fact, photooxidation of the cycloalkenes by $[Fe^{III}(tdcpp)]^+$ dissolved in EtOH or Pr^iOH acidified with trifluoromethanesulfonic acid leads to the formation of a mixture of various oxygenation products which, on the other hand, does not include the ethers.

1 (*a*) K. S. Suslick and R. A. Watson, *New. J. Chem.*, 1992, **16**, 633; (*b*) A. Maldotti, C. Bartocci, G. Varani, A. Molinari, P. Battioni and D. Mansuy, *Inorg. Chem.*, 1996, **35**, 1126; (*c*) L. Weber, R. Hommel, J. Behling, G. Haufe and H. Hennig, *J. Am. Chem. Soc.*, 1994, **116**, 2400.

2 E. Polo, R. Amadelli, V. Carassiti and A. Maldotti, *Inorg. Chim. Acta*, 1992, **192**, 1.

3 R. Amadelli, M. Bregola, E. Polo, V. Carassiti and A. Maldotti, *J. Chem. Soc., Chem. Commun.*, 1992, 1355.

4 A. Maldotti, A. Molinari, R. Argazzi, R. Amadelli, P. Battioni and D. Mansuy, *J. Mol. Catal.*, 1996, **114**, 141.

5 E. I. Stiefel, in *Bioinorganic Catalysis*, ed. J. Reedijk, Marcel Dekker, New York, Basel, Hong Kong, 1993, pp. 21–27; L. Barloy, P. Battioni and D. Mansuy, *J. Chem. Soc., Chem. Commun.*, 1990, 1365; J. T. Groves and S. B. Ungashe, *J. Am. Chem. Soc.*, 1990, **112**, 7796.

6 Nafion is a Du Pont Nemours registered trademark.

7 Z. Ogumi, T. Kuroe and Z. Takehara, *J. Electrochem. Soc.*, 1985, **132**, 2601.

8 C. Bizet, P. Morliere, D. Brault, O. Delgado, M. Bazin and R. Santus, *Photochem. Photobiol.*, 1981, **34**, 315; A. Maldotti, C. Bartocci, R. Amadelli and V. Carassiti, *J. Chem. Soc., Dalton Trans.*, 1989, 1197.

9 C. Bartocci, A. Maldotti, G. Varani, P. Battioni, V. Carassiti and D. Mansuy, *Inorg. Chem.*, 1991, **30**, 1255.

10 A. Ledwith, P. J. Russel and L. M. Sutcliffe, *Proc. R. Soc. London, Ser. A*, 1973, **332**, 151; A. Maldotti, C. Bartocci, R. Amadelli and V. Carassiti, *Inorg. Chim. Acta*, 1983, **74**, 275.

11 R. Cheng, L. Latos-Grazynsky and A. L. Balch, *Inorg. Chem.*, 1982, **21**, 2412.

12 A. Maldotti, C. Bartocci, C. Chiorboli, A. Ferri and V. Carassiti, *J. Chem. Soc., Chem. Commun.*, 1985, 881.

13 A. Maldotti, C. Bartocci, R. Amadelli, G. Varani, E. Polo and V. Carassiti, in *Chemistry and Properties of Biomolecular Systems*, ed. E. Rizzarelli and T. Theophanides, Kluwer Academic, Dordrecht, Boston, London, 1991.

14 D. N. Hendrickson, M. G. Kinnard and K. S. Suslick, *J. Am. Chem. Soc.*, 1987, **109**, 1243.

15 D. Mansuy, *Pure Appl. Chem.*, 1990, **62**, 741; B. Meunier, *Chem. Rev.*, 1992, **92**, 1411; M. Sono, M. P. Roach, E. D. Coulter and J. H. Dawson, *Chem. Rev.*, 1996, **96**, 2841.

16 S. W. Benson, *J. Chem. Educ.*, 1965, **42**, 503.

Received in Basel, Switzerland, 26th August 1997; 7/06237K

Synthesis and electrochemistry of a tetrathiafulvalene $(TTF)_{21}$–glycol dendrimer: intradendrimer aggregation of TTF cation radicals

Christian A. Christensen,[a] Leonid M. Goldenberg,[b] Martin R. Bryce*[b]† and Jan Becher[a]

[a] *Department of Chemistry, Odense University, DK-5230 Odense M, Denmark*
[b] *Department of Chemistry, University of Durham, Durham, UK DH1 3LE*

The convergent synthesis of a TTF–glycol dendrimer is reported: thin layer cyclic voltammetric studies on $(TTF)_{21}$ system 11 show that all the TTF units undergo two single-electron oxidations to produce the 42+ redox state spectroelectrochemical studies establish that there are intradendrimer interactions between partially-oxidised TTF units.

The study of dendrimers is a burgeoning topic.[1] These macromolecules possess well-defined, three-dimensional structural order, and they provide unique frameworks for placing functional groups in predetermined spatial arrangements in a polymeric structure. In the context of functional dendrimers,[2] a variety of redox-active groups have been incorporated into the structures.[3]

Tetrathiafulvalene (TTF) dendrimers should be very interesting materials as the TTF system possesses a unique combination of properties,[5] *viz*. (i) oxidation to the cation radical and dication species occurs sequentially and reversibly, (ii) the oxidation potentials can be finely tuned by substituents on the TTF ring system, (iii) TTF cation radicals are thermodynamically very stable, and (iv) oxidised TTF units have a high propensity to form dimers or higher aggregates. A large number of multi-TTF derivatives[5] and some main- and side-chain polymeric TTFs[6] are known, but dendrimeric TTFs are largely unexplored.[7] Here we present the synthesis of a novel $(TTF)_{21}$ dendrimer with TTF units placed at peripheral sites and within the branches of the structure, and we report the electrochemistry and spectroelectrochemistry of this polymer. Glycol chains were incorporated into the branches to impart solubilty in organic solvents, and air stability, and to provide a flexible structure to facilitate interactions between the TTF units.

The synthesis of dendrimer **11** uses a convergent strategy, with the caesium salts of TTF thiolate anions (Scheme 1) (generated by the *in situ* deprotection of their cyanoethyl derivatives)[8] as key intermediate species in the iterative steps. Compound **1** was deprotected by reaction with CsOH, and the resulting dithiolate reacted *in situ* with glycol derivative **2** to yield compound **3** in 63% yield. Cross-coupling of thione **3** with ketone **4**[8b] in the presence of $P(OEt)_3$ gave the TTF derivative **5** in 67% yield. Halogen exchange to yield diiodide **6** (NaI, 84% yield) was followed by reaction of **6** with 2 equiv. of the thiolate anion derived from **7**,[8c] to afford tris(TTF) system **8** in 77% yield. In an iterative procedure, the thiolate anion derived from **8** (2 equiv.) reacted with **6** to furnish the heptakis(TTF) dendron wedge **9** in 79% yield. Finally, the thiolate anion derived from **9** (3 equiv.) smoothly displaced the benzylic bromides of the core reagent **10** to furnish the dendrimer **11** possessing 21 TTF units (75% yield) as an air-stable, orange toffee-like solid, which has good solubility in a range of organic solvents (*e.g.* CH_2Cl_2, $CHCl_3$, THF, toluene, dichlorobenzene and CS_2) and was insoluble in water.‡

The solution electrochemistry of **11** in CH_2Cl_2 was studied using thin layer cyclic voltammetric (TLCV) techniques in which the current is not limited by mass transport to the electrode.[9] Integrating the voltammetric waves against the one-electron reduction peak of the internal standard 2,3-dichloronaphthoquinone (DCNQ) provided clear evidence that complete oxidation occurs for all the TTF units, thus ultimately generating the 42+ oxidation state of the dendrimer.§ We note that the second TTF oxidation wave was slightly narrower than the first wave, which was probably due to adsorption phenomena. Fig. 1 shows the TLCV of **11** in the presence of DCNQ.

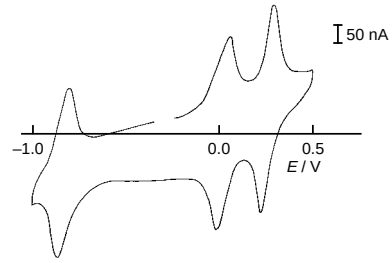

Fig. 1 TLCV of dendrimer **11** (0.5×10^{-4} M) and DCNQ (1.05×10^{-3} M) in Bu_4NClO_4 (1 M)/CH_2Cl_2, solution, *vs*. Ag/Ag^+, scan rate 2 mV s^{-1}

The spectroelectrochemistry of dendrimer **11** is shown in Fig. 2. The spectrum obtained at 0 V [Fig. 2(*a*)] is consistent with neutral TTF units; upon oxidation at 0.7 V, the characteristic absorptions of TTF cation radicals are seen: the new band at λ_{max} 425 nm is assigned to isolated (non-interacting) TTF cation radicals, while the absorption at λ_{max} 800 nm is diagnostic of interacting TTF cation radicals (π–π dimers).[10] On increasing the potential [Fig. 2(*c*)], as oxidation of the system proceeds the higher energy absorption decreases in intensity while there is a concomitant increase in the lower energy absorption, suggesting more of the partially-oxidised TTF units are now dimerised. Even when the spectrum was obtained at the threshold potential for oxidation, both bands were always present, which suggests that the cation radicals interact even when they are present in very low concentration: we therefore assign this to an intradendrimer interaction, achieved due to the flexibility of the glycol spacers. To the best of our knowledge, this is the first observation of π–π interactions (either intra- or inter-molecular) in oxidised dendrimers. This is timely in the light of studies of π–π stacking at the periphery of functionalised PAMAM dendrimers,[12] and the intermolecular self-association of dendrimers mediated by hydrogen bonding[13] or coordinative bonds.[14]

This work was funded by the EPSRC and NATO (C. A. C.) and the Royal Society (L. M. G.).

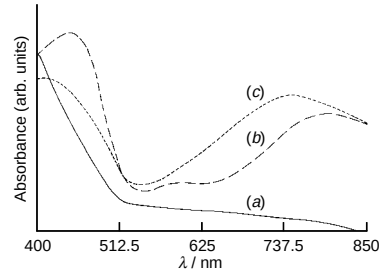

Fig. 2 Spectroelectrochemistry of **11** at (*a*) 0.0, (*b*) 0.7 and (*c*) 1.0 V

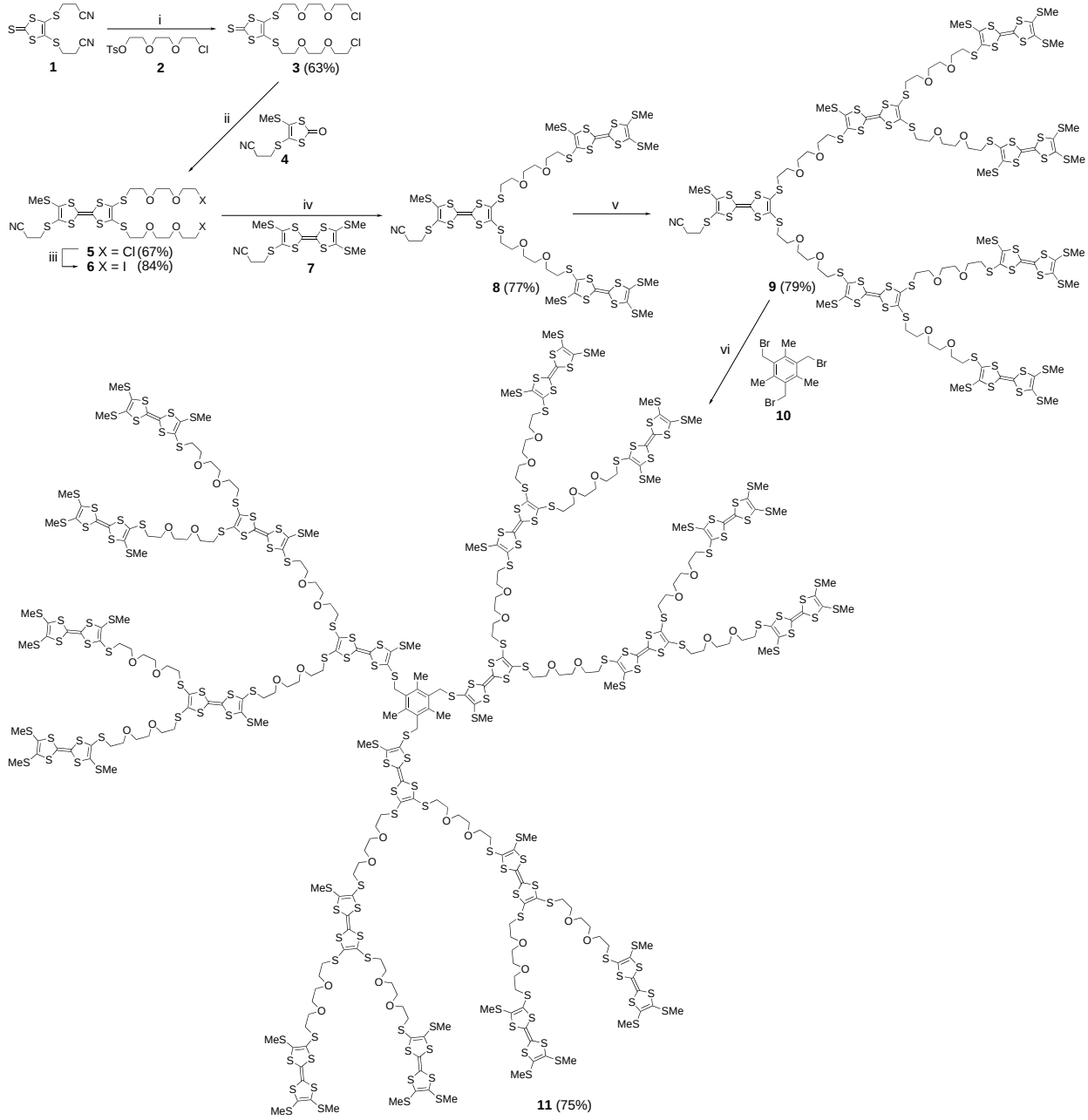

Scheme 1 *Reagents and conditions*: i, **2** (2 equiv.), $CsOH{\cdot}H_2O$, MeCN, reflux, 17 h; ii, **4**, $P(OEt)_3$, 120 °C, 5 h; iii, NaI, acetone, reflux, 3 d; iv, **7** (2 equiv.), $CsOH{\cdot}H_2O$, DMF, room temp., 16 h; v, **6** (0.5 equiv.), $CsOH{\cdot}H_2O$, DMF, room temp., 16 h; vi, **10** (0.33 equiv.), $CsOH{\cdot}H_2O$, DMF, room temp.

Notes and References

† E-mail: m.r.bryce@durham.ac.uk

‡ All new compounds gave satisfactory ^{1}H NMR spectra, mass spectra (FAB, plasma desorption or MALDI-TOF) and analytical data.

§ Allowing for the very small quantities of compound used and the large number of TTF groups present, we estimate that these data are accurate to within ±2 electrons for each TTF wave of compound **11**. CV data obtained in both CH_2Cl_2 and MeCN solutions gave two reversible redox waves at $E_1^{1/2}$ +0.56 and $E_2^{1/2}$ +0.86 V *vs.* Ag/AgCl.

1 G. R. Newkome, C. N. Moorefield and F. Vögtle, *Dendritic Molecules: Concepts, Synthesis, Perspectives*, VCH, Weinheim, 1996.
2 Review: J. Issberner, R. Moors and F. Vögtle, *Angew. Chem., Int. Ed. Engl.*, 1994, **33**, 2413.
3 Reviews: M. R. Bryce and W. Devonport, in *Advances in Dendritic Macromolecules*, ed. G. R. Newkome, JAI, London, 1996, vol. 3, p. 115.
4 Reviews: T. Jørgensen, T. K. Hansen and J. Becher, *Chem. Soc. Rev.*, 1994, 41; M. R. Bryce, *J. Mater. Chem.*, 1995, **5**, 1481.
5 Review: M. Adam and K. Müllen, *Adv. Mater.*, 1994, **6**, 439.
6 S. Frenzel, S. Arndt, R. M. Gregorious and K. Müllen, *J. Mater. Chem.*, 1995, **5**, 1529.
7 (*a*) M. R. Bryce, W. Devonport and A. J. Moore, *Angew. Chem., Int. Ed. Engl.*, 1994, **33**, 1761; (*b*) C. Wang, M. R. Bryce, A. S. Batsanov, L. M. Goldenberg and J. A. K. Howard, *J. Mater. Chem.*, 1997, **7**, 1189.
8 (*a*) J. Lau and J. Becher, *Synthesis*, 1997, 1015; (*b*) K. B. Simonsen, N. Svenstrup, J. Lau, O. Simonsen, P. Mørk, G. J. Kristensen and J. Becher, *ibid.*, 1996, 407; (*c*) J. Lau, O. Simonsen and J. Becher, *ibid.*, 1995, 521.
9 A. T. Hubbard and F. C. Anson, in *Electroanalytical Chemistry*, ed. A. J. Bard, Marcel Dekker, New York, 1970, vol. 4, pp. 129–210.
10 J. B. Torrance, B. A. Scott, B. Welber, F. B. Kaufman and P. E. Seiden, *Phys. Rev. B*, 1979, **19**, 730.
11 I. Tabakovic, L. L. Miller, R. G. Duan, D. C. Tully and D. A. Tomalia, *Chem. Mater.*, 1997, **9**, 736.
12 F. Osterod and A. Kraft, *Chem. Commun.*, 1997, 1435; P. Thiyagarajan, F. Zeng, C. Y. Ku and S. C. Zimmerman, *J. Mater. Chem.*, 1997, **7**, 1221.
13 W. T. S. Huck, F. C. J. M. van Veggel and D. N. Reinhoudt, *J. Mater. Chem.*, 1997, **7**, 1213.

Received in Liverpool, UK, 17th October 1997; 7/07504I

Luminescent europium tetraazamacrocyclic complexes with wide range pH sensitivity

Thorfinnur Gunnlaugsson and David Parker*

Department of Chemistry, University of Durham, South Road, Durham, UK DH1 3LE

The complexes $[EuL^1]^{3+}$ and $[EuL^2]$ function as luminescent pH sensors over an extended pH range; two distinguishable pH switching ranges are observed: the delayed europium emission is switched on in acidic solution, whereas the fluorescence emission spectra show a pronounced pH dependence only in alkaline media.

Luminescent chemosensors offer an attractive method for the detection of various physiological ions and molecules.[1] Fluorescent sensors may be adversely affected by autofluorescence and by light scattering from an active physiological environment.[2] Delayed luminescence affords an attractive means of overcoming some of these obstacles.[3] In solution, the application of lanthanide luminescence, has generated a great deal of interest owing to the long wavelength of the emission (large Stokes' shifts) and the long lifetimes (in the ms range).[4] An example of such a Tb^{III} and Eu^{III} sensory PET (photoinduced electron transfer) system has been reported recently for pH measurement in aqueous solution.[5] Various lanthanide complexes of tetra-substituted derivatives of 1,4,7,10-tetraazacyclododecane (cyclen) have been synthesised either as contrast agents in magnetic resonance imaging[6] or as luminescence probes.[7] In water, these complexes are kinetically stable with respect to dissociation and possess low hydration numbers ($q \leqslant 1$). In further developing this work, we have recently demonstrated the effect of protons, oxygen and halide anions on the luminescence emission spectra of some Eu^{III} phenanthridinium conjugates.[8] Here we introduce the cationic Eu^{III}–tetraamide $[EuL^1]^{3+}$ and the neutral monoamide $[EuL^2]$ quinolyl derived conjugates. In addition to acting as an efficient antenna sensitiser[4,6,7] the chromophore can reversibly switch, *via* an energy transfer mechanism,[4] the lanthanide emission on and off as a function of pH. At the same time, the fluorescence emission spectrum is only dependent on the hydroxide ion concentration, so that these conjugates show a dual pH dependence spanning a wide pH range.

The tetraamide ligand L^1 was synthesised by reaction of the α-haloamide **1** with 1,4,7,10-tetraazacyclododecane in DMF at 80 °C (4.1 equiv. Cs_2CO_3). The tribasic ligand H_3L^2 was synthesised by reacting the molybdenum tricarbonyl complex of cyclen with the same amide (1 : 1) in DMF–Cs_2CO_3, with a subsequent phosphinoxymethylation in THF followed by basic hydrolysis. The Eu^{III} complexes of L^1 and L^2 were made by reaction of the ligand with equimolar quantities of europium triflate in acetonitrile.[9]

The absorption spectra in water of $[EuL^1]^{3+}$ and $[EuL^2]$, were similar to those observed for the intermediate amide **1**. The spectra showed a pH dependent bathochromic shift (λ_{max} = 314 nm, log ε = 4.18) with an isosbestic point at 296 nm, and revealed the formation of a new band at 261 nm (log ε = 4.0) following protonation with CF_3CO_2H. The fluorescence emission spectrum of **1** did not show any substantial pH dependence below pH 8 when excited at 330 nm.† The same trend was observed for $[EuL^1]^{3+}$ and $[EuL^2]$, when excited at 330 nm; the fluorescence emission spectra decreased in intensity in alkaline media, as shown in the pH–luminescence profile of $[EuL^1]^{3+}$ (Fig. 1). In contrast, when excited at the isosbestic wavelength, the fluorescence emission spectra increased in intensity in

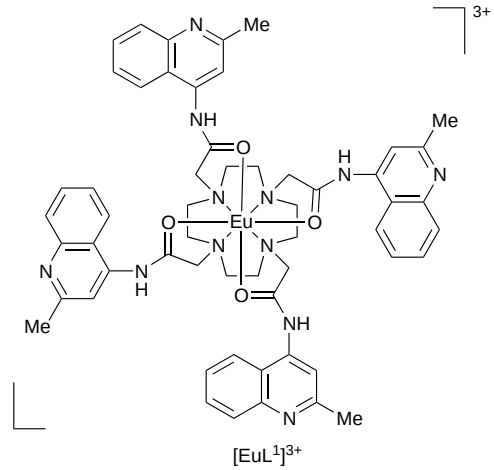

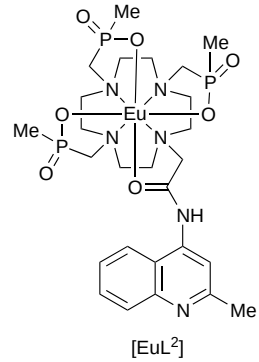

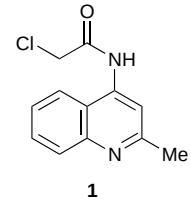

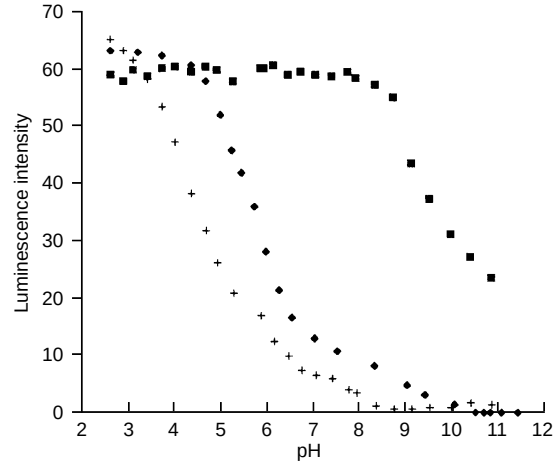

Fig. 1 Enhancement of the luminescence of europium complexes as a function of pH: (■) quinolyl fluorescence in $[EuL^1]^{3+}$; (+) metal-based emission (594 nm) in $[EuL^1]^{3+}$; (◆) metal-based emission in $[EuL^2]$

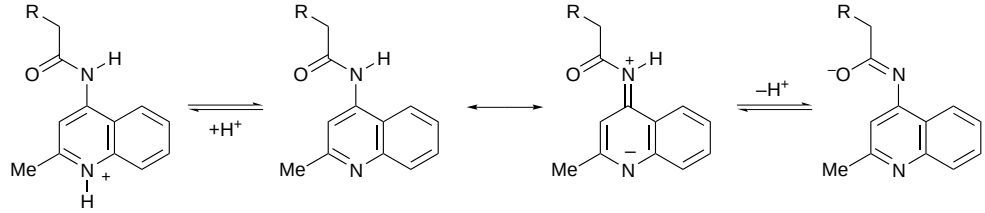

Scheme 1

alkaline solution. In both cases, λ_{max}(fluor.) shifted to longer wavelength in the presence of base, and pH titrations revealed formation of an isoemissive point, for $[EuL^1]^{3+}$ at 377 nm and [for EuL^2] at 375 nm. The estimated pK_a values of 9.4(3) and 9.6(3) were determined from these changes for $[EuL^1]^{3+}$ and $[EuL^2]$, respectively, which relate to the deprotonation of the aryl amide nitrogen.

The largest and the most significant pH dependence was observed in the delayed europium emission. The emission was independent of pH in alkaline solution (above pH 10) for $[EuL^1]^{3+}$, with only very small changes observed for $[EuL^2]$ (overall, contributing around 8–12% of the total emission). Significant 'off–on' luminescence switching was observed when the quinolyl nitrogen was protonated {Fig. 1 for $[EuL^1]^{3+}$}. The luminescence enhancement was at least 250 for $[EuL^2]$ (λ_{exc} = 330 nm), while a more modest factor of 30 was obtained with $[EuL^1]$, in each case observing Eu emission at 594 nm (ΔJ = 1).‡ The europium emission therefore signals the protonation of the remote chromophore, a feature which is not seen in the fluorescence emission spectrum.

Upon protonation of the quinolyl nitrogen atom the n–π* transition is removed, and the π–π* shifts to lower energy (as revealed by the excitation spectra for $[EuL^2]$ and $[EuL^1]^{3+}$ as a function of pH). The internal charge transfer (ICT) excited state which is populated in the neutral chromophore is probably modified upon protonation and deprotonation (Scheme 1). The switching between pH 4.5 and 6.5 for $[EuL^2]$ is in accordance with simple ion-binding equilibria[1,5,8] and a pK_a value of 5.8(2) was determined. The pH switching of the cationic complex $[EuL^1]^{3+}$ is over a broader range and is shifted by one pH unit lower. In addition a small inflection in the metal-based luminescence is apparent at *ca*. pH 7 for $[EuL^1]^{3+}$ and 8.5 for $[EuL^2]$: this feature, apparently not ligand based, could be related to the deprotonation of the proximate water molecule. The extended pH sensitivity range of the tricationic complex, *i.e.* in the region between pH 6.5 and 2.5, may be related to the successive protonation of each of the four nitrogens of the chromophore. The overall pH dependence is then a function of four stepwise equilibria, taking place over almost 4 pH units, rather than the pH range of two associated with a single protonation. In accord with this observation a pH-metric titration of fully protonated $[EuL^1]^{3+}$ revealed that 4 equivalents of base were consumed in the range 2.5–6. Similar behaviour has previously been observed for some fluorescent anthrylaza-macrocycle PET systems,[10] where the switching was considered to be linear over five pH units, although a detailed investigation into this behaviour has not subsequently been reported. In water at pH = 1.80, the luminescence emission lifetimes τ_{H2O}, for $[EuL^1]^{3+}$ and $[EuL^2]$ were measured to be 0.55 and 0.71 ms, respectively, while in D_2O, the lifetimes were 1.55 and 1.98 ms, respectively, consistent with an overall hydration state of 0.8 (inner + outer sphere) for both $[EuL^1]^{3+}$ and $[EuL^2]$ (after correcting for the quenching effect of the amide NH oscillators).[9,11]

In summary, the two europium complexes possess distinctly different pH sensitivity. The delayed europium emission is highly dependent on pH changes over the range 3–7 making these complexes interesting candidates for pH measurement in competitive media.

We gratefully acknowledge the BBSRC for grant support, and Drs Stephen Faulkner and Gareth Williams for helpful discussions.

Notes and References

* david.parker@durham.ac.uk

† The fluorescence emission spectrum of **1** gave spectra consistent with a weak internal charge transfer excited state. In solvents of increasing polarity (CH_2Cl_2, Et_2O, MeCN, MeOH, H_2O) a bathochromic shift was observed in λ_{max} and at pH 3 the ICT band was less apparent.

‡ These large enhancement factors are not explained simply by the suppression of photoinduced electron transfer following N-protonation (although this effect contributes a factor of *ca*. 3 per N, as seen by excitation at the isosbestic wavelength). Only when protonated, do the Eu complexes significantly absorb photons at 330 nm.

1 *Fluorescent Chemosensors for Ions and Molecular Recognition*, ed. A. W. Czarnik, *ACS Symp. Ser.*, Washington DC, 1993; R. A. Bissell, A. P. de Silva, H. Q. N. Gunaratne, P. L. M. Lynch, G. E. M. Maguire and K. R. A. S. Sandanayake, *Chem. Soc. Rev.*, 1992, **21**, 187; R. A. Bissell, A. P. de Silva, H. Q. N. Gunaratne, P. L. M. Lynch, G. E. M. Maguire, C. P. McCoy and K. R. A. S. Sandanayake, *Top. Curr. Chem.*, 1993, **168**, 223; A. W. Czarnik, *Acc. Chem. Res.*, 1994, **27**, 302.

2 A. Mayer and S. Neuenhofer, *Angew. Chem., Int. Ed. Engl.*, 1994, **33**, 1044; E. F. G. Dickson, A. Pollak and E. P. Diamandis, *J. Photochem. Photobiol. B*, 1995, **27**, 3.

3 R. A. Bissell, A. P. de Silva, *J. Chem. Soc., Chem. Commun.*, 1991, 1148; R. Grigg, J. M. Holmes, S. K. Jones and W. D. J. A. Norbert, *J. Chem. Soc., Chem. Commun.*, 1994, 185.

4 J.-C. G. Bunzli, in *Lanthanide Probes in Life, Chemical and Earth Sciences, Theory and Practice*, ed. J.-C. G. Bunzli and G. R. Choppin, Elsevier, New York, 1989, p. 219; D. Parker and J. A. G. Williams, *J. Chem. Soc., Dalton Trans.*, 1996, 3613; *J. Chem. Soc., Perkin Trans. 2*, 1995, 1305; A. Beeby and S. Faulkner, *Chem. Phys. Lett.*, 1997, **266**, 116; A. Beeby, R. S. Dickins, S. Faulkner, D. Parker and J. A. G. Williams, *Chem. Commun.*, 1997, 1401.

5 A. P. de Silva, H. Q. N. Gunaratne and T. E. Rice, *Angew. Chem., Int. Ed. Engl.*, 1996, **35**, 2116.

6 D. Parker, in *Comprehensive Supramolecular Chemistry*, ed. J.-M. Lehn, D. D. Macnicol, J. L. Atwood, J. E. Davis, D. N. Reinhoudt and F. Vogtle, Pergamon, Oxford, 1996, vol. 10, ch. 17, pp. 487–536; D. Parker, *Chem. Br.*, 1994, 818.

7 A. Beeby, D. Parker and J. A. G. Williams, *J. Chem. Soc., Perkin Trans. 2*, 1996, 1565; A. Beeby, M. Murru, D. Parker and J. A. G. Williams, *J. Chem. Soc., Chem. Commun.*, 1993, 1116; S. Aime, M. Botta, D. Parker and J. A. G. Williams, *J. Chem. Soc., Dalton Trans.*, 1996, 17.

8 D. Parker, K. Senanayake and J. A. G. Williams, *Chem. Commun.*, 1997, 1777; D. Parker and J. A. G. Williams, *Chem. Commun.*, 1998, 245.

9 D. Parker and J. A. G. Williams, *J. Chem. Soc., Perkin Trans. 2*, 1996, 1581.

10 E. U. Akkaya, M. E. Huston and A. W. Czarnik, *J. Am. Chem. Soc.*, 1990, **112**, 3590.

11 R. S. Dickins, D. Parker, A. S. de Sousa and J. A. G. Williams, *Chem. Commun.*, 1996, 697.

Received in Cambridge, UK, 19th November 1997; 7/08342D

Reaction of aromatic amines and ethyl acetoacetate promoted by zeolite HSZ-360. Phosgene-free synthesis of symmetric diphenylureas

Franca Bigi, Raimondo Maggi, Giovanni Sartori*† and Elena Zambonin

Dipartimento di Chimica Organica e Industriale dell'Università, Viale delle Scienze, I-43100 Parma, Italy

Reaction of aromatic amines 1 with ethyl acetoacetate 2 in the presence of the commercially available acid zeolite HSZ-360 gives symmetric diphenylureas 3 in good yields and excellent selectivities.

Zeolites and other solid acids have opened new perspectives in synthetic organic chemistry not only in terms of yield and selectivity, but also concerning the work-up and the effluent pollution.[1] The use of both solid acids and non-toxic reagents leads to a substantial reduction in cost and environmental impact of the production processes.[2] Here we report preliminary results of our study concerning the synthesis of symmetric diphenylureas (DPUs) from aromatic amines and ethyl acetoacetate under solid acid catalysis.

Substituted ureas have received considerable attention due to their wide range of applications, *e.g.* for use as antidiabetic and tranquillizing drugs, antioxidants in gasoline, corrosion inhibitors and herbicides.[3] The conventional methods reported for the urea synthesis are essentially based on phosgene and isocyanates,[4] phosgene substitutes,[5] carbonates and carbamates[6] or carboxylic acid derivatives.[7] However, phosgene and isocyanates are toxic and expensive to handle and the above methods are often difficult to apply. There is, thus, a continuing interest in the catalytic synthesis of ureas *via* phosgene-free reactions. Our strategy, utilizing ethyl acetoacetate as carboxylating agent in place of phosgene and solid acids as catalysts represents an efficient, innovative and environmentally safe method for the synthesis of DPUs.

The reaction of aromatic amines **1** with ethyl acetoacetate **2** has been described in the literature to produce ethyl β-arylaminocrotonates or acetoacetoanilides,[8] depending on the temperature. We found that DPUs could be obtained as the sole reaction products by heating the same mixture in the presence of different solid acids (Table 1).

The reaction of *p*-anisidine, selected as the model substrate, with **2** in the presence of zeolite HSZ-360[9] in *o*-dichlorobenzene at 180 °C for 5 h gave *N*,*N*′-bis(4-methoxyphenyl)urea which was isolated in 60% yield and 93% selectivity (entry g). Zeolite HSZ-330,[10] with higher acidity and comparable surface area, was less effective (entry f). The use of two montmorillonites, K10 and KSF,[11] gave the product with lower yield and similar, high selectivity independent of surface area and acidity (entries d and e).

The acidity of the catalyst is likely to play an important role in the activation of **2**. Note that the present system seems to require an optimum acidity level with respect to both strength and nature of the individual Brønsted and Lewis sites. Indeed, the more active zeolite HSZ-360 has a lower concentration of acid sites than HSZ-330, but the individual sites are more strongly acidic.[9,10] Moreover the use of typical hard Brønsted and Lewis acids such as TsOH, $ZnCl_2$ and $AlCl_3$ results in the production of untractable mixtures of compounds (entries a, b and c).

The best result was achieved by carrying out the reaction with zeolite HSZ-360 under solventless conditions (76% yield, 95% selectivity) (entry h). This result is of particular interest since *o*-dichlorobenzene is on the 'black list' of the environmentally incompatible solvents.[12]. In the control experiment with no zeolite catalyst only *p*-methoxyacetoacetanilide was recovered as reported above.[8] The general applicability of the present

Table 1 Formation of DPUs in the presence of different solid acid catalysts

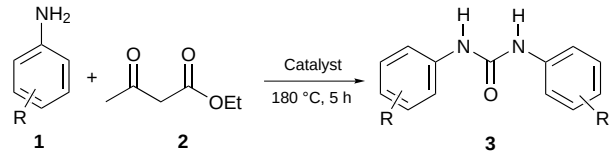

1 **2** **3**

Entry	R	Catalyst	Surface area/ $m^2\ g^{-1}$	Surface acidity/ mequiv. $H^+\ g^{-1}$	Solvent	Yield (%)	Selectivity (%)
a	4-OCH_3	TsOH			1,2-$Cl_2C_6H_4$	*a*	—
b	4-OCH_3	$ZnCl_2$			1,2-$Cl_2C_6H_4$	*a*	—
c	4-OCH_3	$AlCl_3$			1,2-$Cl_2C_6H_4$	*a*	—
d	4-OCH_3	KSF	15 ± 10	0.85 ± 0.03	1,2-$Cl_2C_6H_4$	43	92
e	4-OCH_3	K10	200 ± 10	0.70 ± 0.03	1,2-$Cl_2C_6H_4$	45	90
f	4-OCH_3	HSZ-330	460 ± 10	1.39 ± 0.03	1,2-$Cl_2C_6H_4$	52	94
g	4-OCH_3	HSZ-360	500 ± 10	0.51 ± 0.03	1,2-$Cl_2C_6H_4$	60	93
h	4-OCH_3	HSZ-360	500 ± 10	0.51 ± 0.03	None	76	95
i	H	HSZ-360	500 ± 10	0.51 ± 0.03	None	66	95
j	3-CH_3	HSZ-360	500 ± 10	0.51 ± 0.03	None	77	93
k	4-CH_3	HSZ-360	500 ± 10	0.51 ± 0.03	None	73	94
l	4-Cl	HSZ-360	500 ± 10	0.51 ± 0.03	None	58	96

[a] Untractable mixture of compounds.

DPU synthesis was demonstrated by extending the reaction to different aromatic amines **1** and recovering the products **3** with good yields and excellent selectivities (entries h–l).

A representative procedure for the preparation of DPUs is as follows: a flask containing a mixture of the selected aromatic amine **1** (10 mmol) and zeolite HSZ-360 (0.5 g) was placed in a hot oil bath (180 °C) and **2** (0.8 g, 0.8 ml, 6 mmol) was added dropwise during 1 min. The mixture was efficiently stirred at the same temperature for 5 h.[13] After cooling to room temp. the slurry was washed with boiling MeOH containing 5% water (2 × 100 ml). After filtration the product was recovered from the solution by addition of more water and cooling.[14] Alternatively, hot DMSO could be successfully utilized under the same conditions.

The formation of compounds **3** could be attributed to the initial production of acetoacetanilides and their subsequent reaction with a second molecule of aromatic amine to give DPUs and acetone. This hypothesis was in part confirmed by quantitative production of diphenylurea by heating a 1 : 1 mixture of acetoacetanilide and aniline in the presence of zeolite HSZ-360. We then estimated the catalyst activity on reuse. Our results confirmed that the activity of HSZ-360 recovered by filtration, washed with acetone and reactivated by heating at 500 °C for 8 h was the same for 5 runs.

In conclusion the above reported method of utilizing **2** as carboxylating agent, zeolite HSZ-360 as solid catalyst and avoiding the use of any solvent, represents an innovative phosgene-free route for the selective synthesis of symmetric diphenylureas.

Thanks are due to the Ministero dell'Università e della Ricerca Scientifica e Tecnologica (MURST), Italy, and the Consiglio Nazionale delle Ricerche (CNR), Italy, for financial support. The authors are also grateful to the Centro Interfacoltà Misure (C.I.M.) for the use of NMR and mass spectrometry instruments and to Mr Pier Antonio Bonaldi for technical assistance.

Notes and References

† E-mail: sartori@ipruniv.cce.unipr.it

1 I. E. Maxwell, *J. Inclusion Phenom.*, 1986, **4**, 1; W. F. Holderich, M. Hesse and F. Naumann, *Angew. Chem., Int. Ed. Engl.*, 1988, **27**, 226; H. Van Bekkum, *Recl. Trav. Chim. Pays-Bas*, 1989, **108**, 283; M. Balogh and P. Laszlo, *Organic Chemistry using Clays*, Springer Verlag, New York, 1993; A. Cornelius and P. Laszlo, *Synlett*, 1994, 155; J. H. Clark, S. R. Cullen, S. J. Barlow and T. W. Bastock, *J. Chem. Soc., Perkin Trans. 2*, 1994, 1117; A. Corma, *Chem. Rev.*, 1995, **95**, 559; J. H. Clark and J. Macquarrie, *Chem. Soc. Rev.*, 1996, 303; G. Eder-Mirth and J. A. Lercher, *Recl. Trav. Chim. Pays-Bas*, 1996, **115**, 157; W. F. Holderich, *Comprehensive Supramolecular Chemistry*, ed. G. Alberti and T. Bein, Pergamon, Oxford, 1996, vol. 7, pp. 671–692; G. W. Kabalka and R. M. Pagni, *Tetrahedron*, 1997, **53**, 7999.

2 J. M. Thomas and K. I. Zamaraev, *Angew. Chem., Int. Ed. Engl.*, 1994, **33**, 308; *New. J. Chem.*, 1996, **20**, issue dedicated to the 'Environmentally Benign Chemistry and Chemical Technology'; R. A. Sheldon, *Chem. Ind.* (*London*), 1997, 12.

3 T. P. Vishnyakova, I. A. Golubeva and E. V. Glebova, *Russ. Chem. Rev.* (*Engl. Transl.*), 1985, **54**, 249.

4 J. March, *Advanced Organic Chemistry*, Wiley, New York, 1985, p. 370; H.-J. Knölker, T. Braxmeier and G. Schlechtingen, *Angew. Chem., Int. Ed. Engl.*, 1995, **34**, 2497.

5 P. Majer and R. S. Randad, *J. Org. Chem.*, 1994, **59**, 1937.

6 T. M. Flyes, T. D. James, A. Pryhitka and M. Zojsji, *J. Org. Chem.*, 1993, **58**, 7456; M. Lamothe, M. Perez, V. Colovray-Gotteland and S. Halazy, *Synlett*, 1996, 507.

7 L. E. Overman, G. F. Taylor, C. B. Petty and P. J. Jessup, *J. Org. Chem.*, 1978, **43**, 2164.

8 W. Werner, *Tetrahedron*, 1969, **25**, 255; W. Werner, *Tetrahedron*, 1971, **27**, 1755.

9 Zeolite HSZ-360 is a commercial (Tosoh Corp.) acid faujasitic-type catalyst with 13.9 SiO_2–Al_2O_3 molar ratio, pore size 7.4 Å, surface area 500 ± 10 $m^2\ g^{-1}$ (determined in our laboratory by the BET method: S. Brunauer, P. H. Emmett and E. Teller, *J. Am. Chem. Soc.*, 1938, **60**, 309), acidity 0.51 mequiv. $H^+\ g^{-1}$ [determined in our laboratory by temperature programmed desorption of ammonia gas (NH_3-TPD): P. Berteau and B. Delmon, *Catal. Today*, 1989, **5**, 121] and with the following chemical composition (wt% dry basis): SiO_2 89.0, Al_2O_3 10.9, Na_2O 0.06.

10 Zeolite HSZ-330 is a commercial (Tosoh Corp.) acid faujasitic-type catalyst with 5.9 SiO_2–Al_2O_3 molar ratio, pore size 7.4 Å, surface area 460 ± 10 $m^2\ g^{-1}$ (determined in our laboratory by the BET method), acidity 1.59 mequiv. $H^+\ g^{-1}$ [determined in our laboratory by temperature programmed desorption of ammonia gas (NH_3-TPD)] and with the following chemical composition (wt% dry basis): SiO_2 86.1, Al_2O_3 13.7, Na_2O 0.19.

11 KSF is a commercial (Fluka) montmorillonite with surface area 15 ± 10 $m^2\ g^{-1}$, acidity 0.85 mequiv. $H^+\ g^{-1}$ [determined in our laboratory by temperature programmed desorption of ammonia gas (NH_3-TPD)] and with the following chemical composition (average value): SiO_2 (54.0%), Al_2O_3 (17.0%), Fe_2O_3 (5.2%), CaO (1.5%), MgO (2.5%), Na_2O (0.4%), K_2O (1.5%); K10 is a commercial (Fluka) montmorillonite with surface area 200 ± 10 $m^2\ g^{-1}$, acidity 0.70 mequiv. $H^+\ g^{-1}$ [determined in our laboratory by temperature programmed desorption of ammonia gas (NH_3-TPD)] and with the following chemical composition (average value): SiO_2 (73.0%), Al_2O_3 (14.0%), Fe_2O_3 (2.7%), CaO (0.2%), MgO (1.1%), Na_2O (0.6%), K_2O (1.9%).

12 See for example: R. A. Sheldon, *Chem. Ind.* (*London*), 1992, 903; R. A. Sheldon, *J. Mol. Catal., A*, 1996, **107**, 75; D. C. Dittmer, *Chem. Ind.* (*London*), 1997, 779.

13 By carrying out the reaction for longer times the same value of yield (~ 70%) was observed.

14 A. F. M. Iqbal, *Helv. Chim. Acta*, 1976, **59**, 655. **3g**: pale brown solid, mp 237–238 °C (lit., 236–238 °C); **3h**: pale brown solid, mp 237–283.5 °C (lit., 239 °C); **3i**: pale brown solid, mp 218–220 °C (lit., 219–220 °C); **3j**: pale brown solid, mp 263–264 °C (lit., 263–265 °C); **3k**: pale brown solid, mp 283–284.5 °C (lit., 284 °C).

Received in Liverpool, UK, 6th November 1997; 7/08019K

Synthesis and chemical and enzymatic reactivity of thymidine 3′-*O*- and 5′-*O*-phosphorofluoridothioates

Konrad Misiura, Daria Szymanowicz and Wojciech J. Stec*†

Polish Academy of Sciences, Centre of Molecular and Macromolecular Studies, Department of Bioorganic Chemistry, Sienkiewicza 112, 90-363 Lódź, Poland

5′-*O*- or 3′-*O*-Protected thymidine 3′-*O*- or 5′-*O*-(2-thiono-1,3,2-oxathiaphospholanes) react with triethylammonium fluoride in a presence of DBU and furnish, after deprotection, thymidine 3′-*O*- and 5′-*O*-phosphorofluoridothioates; the latter undergoes stereoselective hydrolysis by *snake venom* phosphodiesterase.

Within the course of our studies on the development of oxathiaphospholane methodology for phosphorylation,[1] phosphorothioylation[2] and phosphorodithioylation[3] of biomolecules we have found that the endocyclic P–S bond of a 2-thio-substituted 1,3,2-oxathiaphospholane ring attached to nucleoside moiety can be easily broken in the presence of DBU by fluoride ions leading, after spontaneous episulfide elimination, to 3′-*O*-methoxyacetyl nucleoside 5′-*O*-phosphorofluoridothioates or 5′-*O*-dimethoxytrilyl nucleoside 3′-*O*-phosphorofluoridothioates.[4,5] Thus, 5′-*O*-dimethoxytritylthymidine 3′-*O*-(2-thiono-1,3,2-oxathiaphospholane) **1** (ratio of diastereomers *ca.* 1:1), after treatment with triethylammonium fluoride‡ in a presence of DBU gives 5′-*O*-dimethoxytritylthymidine 3′-*O*-phosphorofluoridothioate **2**§ in 78% yield (Scheme 1). The dimethoxytrityl protecting group was removed by the treatment of **2** with 80% AcOH. The final product, thymidine 3′-*O*-phosphorofluoridothioate **3**,¶ was purified by anion-exchange chromatography on Sephadex A-25 using triethylammonium hydrogen carbonate buffer (pH 7.5, 0.02–0.5 M) as eluent. Pure **3** has also been obtained from **1** in 68% yield in a one-pot synthesis. Reaction of **1** with triethylammmonium fluoride in a presence of DBU is, unlike the 1,3,2-oxathiaphospholane ring-opening condensation with alcohols[2] or amines,[6] a non-stereospecific process. Starting from a mixture of partially separated diastereomers of **1** [ratio 73:27, δ_P (CD_3CN), 105.78 and 105.83] diastereomers of **2** were obtained in a ratio of 54:46 [δ_F (CD_3CN), −30.06 and −29.96]. The epimerisation at phosphorus was not unexpected in the light of published earlier results on the stereochemistry of nucleophilic substitution at phosphorus by fluoride ion.[7,8] Also, thymidine 5′-*O*-phosphorofluoridothioate **4** has been synthesized according to the reaction sequence presented in the Scheme 2. Phosphitylation of 3′-*O*-methoxyacetylthymidine with *N*,*N*-diisopropylamino-1,3,2-oxathiaphospholane[2] in a presence of 1*H*-tetrazole, followed by sulfurization yielded oxathiaphospholane **5**. Reaction of **5** with triethylammonium fluoride–DBU furnished intermediate 3′-*O*-methoxyacetylthymidine 5′-*O*-phosphorofluoridothioate **6** which subsequently was deprotected with a concentrated solution of ammonia providing, after purification on Sephadex A-25, the final product **4**** in 75% yield. The phosphorofluoridothioate monoesters **3** and **4** were hydrolytically stable even under basic conditions (conc. ammonia, room temp., 1 h), as proven by ^{31}P NMR assay. Similarly, the resistance of **3** and **4** towards methanolysis, attempted in the presence of triethylamine or pyridine, has been observed. Attempts at internucleotide bond formation in reaction of **2** with 3′-*O*-acetylthymidine in the presence of strong bases such as Bu^{t}OK, DBU and 2-*tert*-butylimino-2-diethylamino-1,3-dimethyl-1,3,2-diazaphosphinane (BEMP) have failed. Reactions were performed in DMF and their progress was followed by ^{31}P NMR spectroscopy. Under these conditions, even after 18 h, formation of dithymidylyl (3′,5′)phosphorothioate ($T_{PS}T$) was not observed. Instead, both **3** and **4** underwent intramolecular cyclization in the presence of an excess of Bu^{t}OK (five-fold molar excess) leading to thymidine cyclic (3′,5′)phosphorothioate (cTMPS). Similarly, as previously observed[9] for Bu^{t}OK-catalyzed cyclization of nucleoside 5′-*O*-*p*-nitrophenyl phosphorothioates, in the reactions of phosphorofluoridothioates **3** and **4** [S_P]-cTMPS[10] was also formed preferentially (ratio of [S_P]-: [R_P]-cTMPS *ca.* 2:1). Yields of Sephadex-purified cTMPS obtained from **3** and **4** were 57 and 38%, respectively. The lack of formation of $T_{PS}T$ in Bu^{t}OK assisted condensation of **2** with 3′-*O*-acetylthymidine was rather unexpected in the light of the results of von Tigerstrom and Smith[11] on effective formation of T_PT and other medium-sized oligothymidylates in the reaction of protected thymidine 3′-*O*-phosphorofluoridate with 3′-*O*-acetylthymidine.

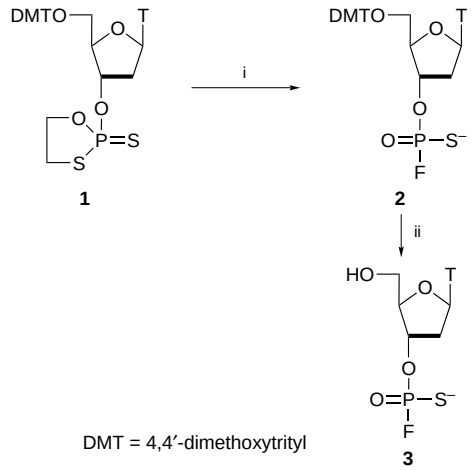

Scheme 1 *Reagents and conditions*: i, Et_3NHF, DBU, MeCN, 15 min; ii, 80% AcOH, 1 h

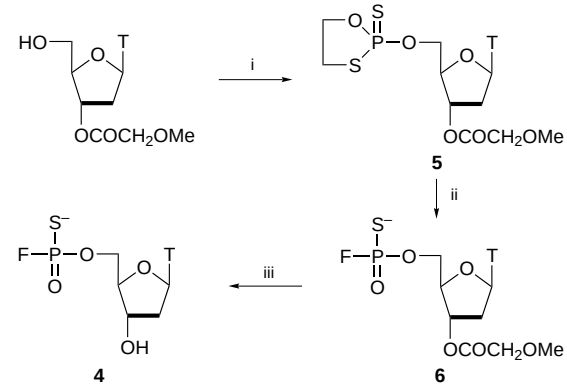

Scheme 2 *Reagents and conditions*: i, *N*,*N*-diisopropylamino-1,3,2-oxathiaphospholane, 1*H*-tetrazole, 2 h, then elemental sulfur, 18 h; ii, Et_3NHF, DBU, CH_2Cl_2 MeCN, 15 min; iii, conc. NH_4OH, EtOH, 2.5 h

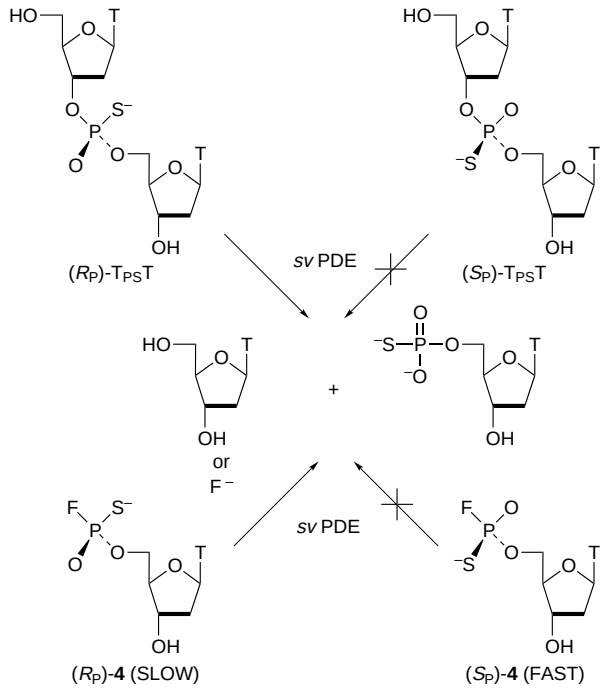

Fig. 1 Tentative assignment of absolute configuration of diastereomers of **4**

In the light of earlier results on an enzymatic cleavage of thymidine 5′-*O*- or 3′-*O*-phosphorofluoridate assisted by *snake venom* (*sv* PDE)[12,13] and *spleen*[12] phosphodiesterases (*spleen* PDE) it was tempting to study the thio analogues **4** and **3** as substrates for these enzymes. From the pioneering work of Eckstein[14] and Benkovic[15] demonstrating the stereoselectivity of *sv* PDE towards P-chiral diesters of phosphorothioic acid it was of interest to check if this enzyme can discriminate between the diastereomers of **3** or **4**.

5′-*O*-Phosphorofluoridothioate **4** was incubated with *sv* PDE†† and the progress of the enzymatic digestion was analyzed by RP-HPLC. It was found that *sv* PDE, if added to a diastereomeric mixture of **4**, causes the stereoselective hydrolysis of the P–F bond of slow-eluted **4** leaving the fast-eluted diastereomer intact. Also, in the case of diastereomeric mixture of **3**†† only slow-eluted **3** underwent hydrolysis in a presence of *sv* PDE, albeit the reaction proceeded much slower than that observed for slow-eluted **4**. Interestingly, under analogous conditions, the rate of hydrolysis of slow-**4** by *sv* PDE was similar to that obtained during digestion of dithymidylyl (3′,5′)phosphate (T_PT). In the presence of *spleen* PDE both diastereomers of **3** were hydrolyzed while both diastereomers of **4** were resistant to this enzyme.** It was also found that **3** and **4** have no inhibitory activity§§ towards either phosphodiesterase. Results on the use of **4** for inhibition of thymidylate synthase will be published separately.[16]

In conclusion, we have found that the 1,3,2-oxathiaphospholane ring can be opened in the presence of DBU by fluoride anion leading to the appropriate phosphorofluoridothioates. The nucleoside 5′-*O*- or 3′-*O*-phosphorofluoridothioates obtained can be used in studies of the mode of action of nucleolytic enzymes. Comparative topological analysis of diastereomers of $T_{PS}T$ and **4** undergoing *sv* PDE- assisted hydrolysis allows the tentative assignment of absolute configuration of the slow-eluted **4** as R_P (Fig. 1). *Spleen* and *sv* PDE-assisted hydrolysis of P–F bonds in compounds **3** and **4** is in agreement with earlier findings[12,13] that these enzymes split nucleoside 3′-*O*- or 5′-*O*-phosphorofluoridate, respectively, giving rise to the appropriate nucleoside phosphates. From this perspective our data on enzymatic hydrolyses of **3** and **4** disagree with the results of Dabkowski *et al.*,[17] who characterized thymidine 3′-*O*-phosphorofluoridate as the product of *spleen* PDE-assisted degradation of thymidin-3′-yl 2′-deoxyadenosin-5′-yl phosphorofluoridate. Adenosine 5′-*O*-phosphorofluoridate was found as the product of *sv* PDE-assisted hydrolysis of the same substrate. Besides the hydrolytic instability of the P–F bond of dinucleoside (3′,5′)phosphorofluoridates in buffered aqueous media[18] yielding appropriate phosphates, even if thymidine 3′-*O*-phosphorofluoridate or adenosine 5′-*O*-phosphorofluoridate were the respective products of PDE-catalyzed hydrolyses, they would necessarily undergo further enzymatic degradation to phosphomonoesters.

Studies presented here were financially supported by the State Committee of Scientific Research (KBN), grant no 4 PO5F 023 10.

Notes and References

† E-mail: wjstec@bio.cbmm.lodz.pl

‡ Triethylammonium fluoride (1 M solution in THF) was obtained by mixing triethylamine tris(hydrofluoride) (1 equiv.) with triethylamine (2 equiv.).

§ Compound **2** consists of a 1 : 1 mixture of diastereomers, δ_P(CD_3CN, 81 MHz) 54.52 ($^1J_{P–F}$ 1043 Hz), 54.58 ($^1J_{P–F}$ 1046 Hz); *m/z* (−FAB) 641.4 ($M^{+\cdot}$ −1).

¶ Compound **3** consists of a mixture of diastereomers (ratio 48 : 52), δ_P(D_2O, 81 MHz) 53.72, ($^1J_{P–F}$ 1053 Hz), 53.74 ($^1J_{P–F}$ 1055 Hz); δ_F(D_2O, 188 Mz) −31.4 ($^1J_{P–F}$ 1043 Hz), −31.2 ($^1J_{P–F}$ 1046 Mz); *m/z* (−FAB) 339.1 ($M^{+\cdot}$ −1).

‖ Compound **5** was obtained as a mixture of diastereomers, δ_P($CDCl_3$, 81 MHz) 106.64, 106.82 (ratio 1 : 1); *m/z* (+FAB) 453.2 ($M^{+\cdot}$ +1).

Compound **4 consists of mixture of diastereomers (ratio 59 : 41), δ_P(D_2O, 81 Mz) 54.17, 54.20 ($^1J_{P–F}$ 1053 Hz); δ_F(D_2O, 188 Mz) −35.6, −35.7 ($^1J_{P–F}$ 1053 Hz); *m/z* (−FAB) 339.2 ($M^{+\cdot}$ −1).

†† The reaction mixture consists of 0.1 mM **4** or **3**, 100 mM Tris–HCl pH 8.0, 20 mM $MgCl_2$, and *sv* PDE (0.01 U ml^{-1}); 37 °C; incubation time: 0.5 h for **4** and 16 h for **3**.

‡‡ The reaction mixtures consist of 0.1 mM **3** (or **4**), 50 mM acetate buffer pH 5.0, and *spleen* PDE (0.15 U ml^{-1}), 37 °C; incubation time: 1 h for **3** and 16 h for **4**.

§§ Enzymatic digestions were performed under conditions mentioned above. T_PT and **3** (or **4**) were used at equimolar concentrations (0.1 mM).

1 W. J. Stec, B. Karwowski, P. Guga, M. Koziolkiewicz, M. Boczkowska, M. W. Wieczorek and J. Blaszczyk, *J. Am. Chem. Soc.*, submitted for publication.
2 W. J. Stec, A. Grajkowski, M. Koziolkiewicz and B. Uznanski, *Nucleic Acids Res.*, 1991, **19**, 5883; W. J. Stec, A. Grajkowski, B. Karwowski, A. Kobylanska, M. Koziolkiewicz, K. Misiura, A. Okruszek, A. Wilk, P. Guga, M. Boczkowska, *J. Am. Chem. Soc.*, 1995, **117**, 12 019.
3 A. Okruszek, M. Olesiak, D. Krajewska, W. J. Stec, *J. Org. Chem.*, 1997, **62**, 2269; A. Okruszek, A. Sierzchala, M. Sochacki and W. J. Stec, *Tetrahedron Lett.*, 1992, **33**, 7585; A. Okruszek, A. Sierzchala, K. L. Fearon and W. J. Stec, *J. Org. Chem.*, 1995, **60**, 6998.
4 W. Dabkowski and I. Tworowska, *Chem. Lett.*, 1995, 727.
5 M. Bollmark and J. Stawinski, *Tetrahedron Lett.*, 1996, **37**, 5739.
6 K. Misiura, M. Olesiak and W. J. Stec, unpublished results.
7 M. Mikolajczyk and M. Witczak, *J. Chem. Soc., Perkin Trans. 1*, 1977, 2213.
8 R. J. P. Corriu, J. P. Dutheil and G. F. Lanneau, *J. Am. Chem. Soc.*, 1984, **106**, 1060.
9 F. Eckstein, L. P. Simonson and M. P. Baer, *Biochemistry*, 1974, **13**, 3806.
10 W. S. Zielinski and W. J. Stec, *J. Am. Chem. Soc.*, 1977, **99**, 8365.
11 R. G. von Tigerstrom and M. Smith, *Science*, 1970, **167**, 1266.
12 R. Wittmann, *Chem.Ber.*, 1963, **96**, 771.
13 Z. Kucerova and J. Skoda, *Biochim. Biophys. Acta*, 1971, **247**, 194.
14 P. M. J. Burgers, F. Eckstein and D. H. Hunneman, *J. Biol. Chem.*, 1979, **254**, 7476.
15 F. R. Bryant and S. J. Benkovic, *Biochemistry*, 1979, **18**, 2825.
16 B. Golos, K. Misiura, M. Olesiak, A. Okruszek, W. J. Stec and W. Rode, *Acta Biochim. Pol.*, 1998, in the press.
17 W. Dabkowski, F. Cramer and J. Michalski, *J. Chem. Soc., Perkin Trans. 1*, **1992**, 1447; W. Dabkowski, J. Michalski, J. Wasiak and F. Cramer, *ibid.*, **1994**, 817.
18 K. Misiura, D. Pietrasiak and W. J. Stec, *J. Chem. Soc., Chem. Commun.*, **1995**, 613; K. Misiura, D. Szymanowicz and W. J. Stec, *Collect. Czech. Chem. Commun.*, 1996, **61**, S101; M. Bollmark and J. Stawinski, *Chem. Commun.*, 1997, 991.

Received in Glasgow, UK, 12th September 1997; 7/06636H

Tetrahedral chlorometal derivatives of redox-active cyanomanganese ligands: synthesis, structures and solvatochromic properties of a new class of cyanide-bridged complexes

Neil G. Connelly,* Owen M. Hicks, Gareth R. Lewis, A. Guy Orpen and Andrew J. Wood

School of Chemistry, University of Bristol, Bristol, UK BS8 1TS

First row transition metal (M = Mn–Ni) dichlorides react with cyanomanganese(I) carbonyl ligands to give novel paramagnetic bi- and poly-nuclear cyanide-bridged complexes, X-ray structural studies on which are consistent with $Fe^{III}Mn^{I}$, $Fe^{III}Mn^{II}$ and $Mn^{II}Mn^{II}$ core oxidation states for $[Cl_3M(\mu\text{-NC})Mn(CO)(dppm)_2]^z$ (M = Fe, z = 0, 1; M = Mn, z = 0) respectively; $Fe^{III}Mn^{I}$ complexes show strong solvatochromism, consistent with low spin d^6 octahedral Mn^{I} to tetrahedral d^5 Fe^{III} charge transfer.

The archetypal mixed valence complex Prussian Blue, $Fe_4^{III}[Fe^{II}(CN)_6]_3$, has been known since the early 18th century,[1] yet the origin of its unusually intense colour was not understood until the 1960s.[2] Now it, analogues such as $Mn^{II}[Mn^{IV}(CN)_6]$, $CsM[Cr^{III}(CN)_6]$ (M = Mn^{II}, Ni^{II}) and $M_3[Fe^{III}(CN)_6]_2$ (M = Co^{II}, Ni^{II}),[3] and other novel cyanide-bridged complexes[4] are under intensive investigation as substances with novel electrochemical, opto-electronic and magnetic properties.

Our studies of cyanide-bridged[5] complexes are based on the systematic construction of bi- and poly-nuclear species by *N*-binding a second metal centre ML'_x to the redox-active, low spin Mn^{I} cyanomanganese carbonyl ligands *trans*-$[Mn(CN)(CO)(dppm)_2]$ and *cis*- and *trans*-$[Mn(CN)(CO)_2\{P(OR)_3\}(dppm)]$ (R = Et, Ph).[6] The resulting complexes are of interest not only in that one-electron oxidation of the Mn^{I} centre of $Mn(\mu\text{-CN})ML'_x$ may induce reactivity at M, but also in allowing studies of the interactions between two or more Mn^{I}–Mn^{II} redox centres within the cyanide-bridged cores $\{Mn(\mu\text{-CN})\}_nML'_x$ (n = 2–4, *etc.*). Our synthetic strategy may be viewed as complementary to that based on the use of $[M(CN)_6]^{z-}$ (M = Mn, Fe, Co, *etc.*) as building blocks where *N*-binding to other metal sites leads to three-dimensional solid-state arrays by a divergent pathway. The binding of two or more monocyanide donors, such as *trans*-$[Mn(CN)(CO)_2\{P(OEt)_3\}(dppm)]$ to M can be viewed as a convergent route to polynuclear molecular species.

Our previous studies have centred on systems where M is a low oxidation state metal centre such as Rh^{I},[7] Fe^{-I}[8] and Au^{I}.[9] Here, we describe simple species in which the cyanomanganese ligands bind to high spin, tetrahedral 3d metal centres in 'normal' oxidation states, and for which unusual electronic and magnetic properties may be anticipated.

Treatment of $MCl_2{\cdot}nH_2O$ (M = Mn, Co, Ni) with $[Mn(CN)L_x]$ [L_x = *cis*- or *trans*-$(CO)_2\{P(OR)_3\}(dppm)$; R = Et, Ph] gave $[Cl_2M\{(\mu\text{-NC})MnL_x\}_2]$ which show room temperature magnetic moments consistent with the presence of tetrahedral M. (Representative examples of the new complexes† are shown in Table 1.) These complexes are precursors to higher nuclearity species or can be oxidised to products in which low spin, paramagnetic Mn^{II} is bound to high spin tetrahedral centres. Thus, for example, treatment of $[Cl_2Co\{(\mu\text{-NC})MnL_x\}_2]$ [L_x = *trans*-$(CO)_2\{P(OEt)_3\}(dppm)$] **1** with 1 equiv. of $[Mn(CN)L_x]$ in the presence of $TlPF_6$ gives $[ClCo\{(\mu\text{-NC})MnL_x\}_3][PF_6]$ **2** [L_x = *trans*-$(CO)_2\{P(OEt)_3\}(dppm)$]; use of 2 equiv. gives $[Co\{(\mu\text{-NC})MnL_x\}_4][PF_6]_2$ **3**. Complexes **1**–**3** show room temperature magnetic moments in accord with the presence of tetrahedral, d^7 Co^{II}.[10] In CH_2Cl_2 the cyclic voltammograms of complexes **1** and **2** show two oxidation waves the separation of which (*ca.* 100 mV) is consistent with weak interactions between the manganese centres in the oxidation products. Chemical oxidation of **1** with $[N(C_6H_4Br\text{-}4)_3][SbCl_6]$ gives deep blue $[Cl_2Co\{(\mu\text{-NC})MnL_x\}_2][SbCl_6]_2$ [L_x = *trans*-$(CO)_2\{P(OEt)_3\}(dppm)$] $\mathbf{1}^{2+}$ the room temperature magnetic moment of which (μ_{eff} = 5.0 μ_B) indicates some spin pairing between the d^7 Co^{II} and two low spin d^5 Mn^{II} centres.

The reactions of $MCl_2{\cdot}nH_2O$ with the more electron-rich and sterically demanding ligand *trans*-$[Mn(CN)(CO)(dppm)_2]$ in thf give $[Cl_2(thf)M(\mu\text{-NC})Mn(CO)(dppm)_2]$ (M = Mn, Co, Ni)

Table 1 Representative IR spectroscopic data and room temperature magnetic moments

Complex	μ_{eff}/μ_B	Colour	Yield (%)	IR[a]/cm^{-1} ν(CN)	IR[a]/cm^{-1} ν(CO)[b]
$[Cl_2Mn\{(\mu\text{-NC})Mn(CO)_2[P(OPh)_3](dppm)\text{-}cis\}_2]$	5.7	Cream	52	2105w	1973, 1919ms
$[Cl_2Co\{(\mu\text{-NC})Mn(CO)_2[P(OEt)_3](dppm)\text{-}trans\}_2]$ **1**	4.6	Green	63	2095mw	1924vs (2008)
$[Cl_2Co\{(\mu\text{-NC})Mn(CO)_2[P(OEt)_3](dppm)\text{-}trans\}_2][SbCl_6]_2$ $\mathbf{1}^{2+}$	5.0	Dark blue	79	2137vw	2003vs (2071)
$[ClCo\{(\mu\text{-NC})Mn(CO)_2[P(OEt)_3](dppm)\text{-}trans\}_3][PF_6]$ **2**	4.5	Green	82	2088m	1926s (2008)
$[Co\{\mu\text{-NC})Mn(CO)_2[P(OEt)_3](dppm)\text{-}trans\}_4][PF_6]_2$ **3**	4.6	Green	68	2075m	1925s (2008)
$[Cl_2Ni\{(\mu\text{-NC})Mn(CO)_2[P(OEt)_3](dppm)\text{-}cis\}_2]$	3.5	Blue	40	2123w	1960, 1903ms
$[Cl_3Fe(\mu\text{-NC})Mn(CO)(dppm)_2]$ **5**	5.6	Deep blue–green	55	2017mw	1889
$[Cl_3Fe(\mu\text{-NC})Mn(CO)(dppm)_2][BF_4]$ **7**	5.8	Deep purple	67	2085m	1961
$[PPN][Cl_3Mn(\mu\text{-NC})Mn(CO)(dppm)_2]$	6.0	Orange	81	2085mw	1871
$[Cl_3Mn(\mu\text{-NC})Mn(CO)(dppm)_2]$ **6**	5.8	Deep red	56	2117w	1944
$[Cl_2(thf)Ni(\mu\text{-NC})Mn(CO)(dppm)_2]$	3.3	Brown	56	2098w[c]	1878[c]

[a] In CH_2Cl_2. Strong absorptions unless stated otherwise; vs = very strong, m = medium, w = weak, vw = very weak. [b] Very weak A-mode given in parentheses. [c] In thf.

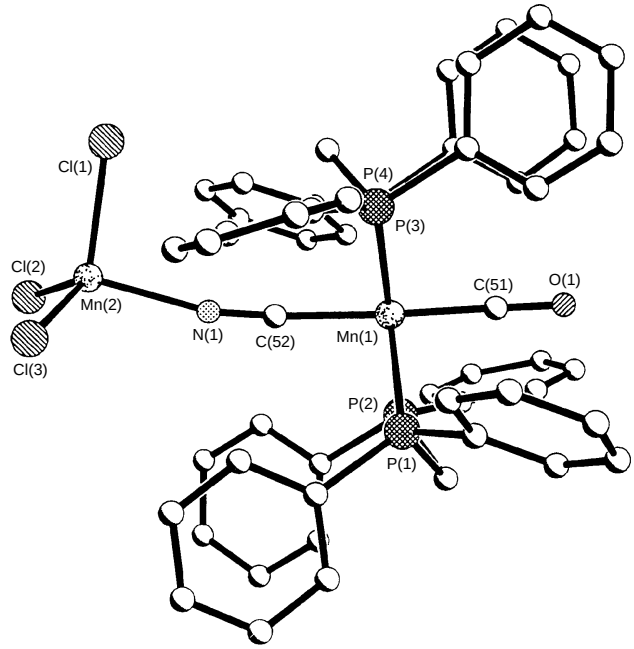

Fig. 1 Structure of **6** (hydrogen atoms and solvent molecule omitted for clarity); the molecular structures of **4** {as its $[FeCl_4]^-$ salt} and **5** are similar. Important bond lengths and angles: **4**, Fe–Cl 2.166, Mn–P 2.345; **5**, Fe–Cl 2.193, Mn–P 2.283; **6**, Mn–Cl 2.341, Mn–P 2.345. (Individual bond lengths have estimated standard uncertainties in the range 0.001–0.005 Å.)

which can be converted into $[PPN][Cl_3M^{II}(\mu\text{-}NC)Mn^{I}(CO)(dppm)_2]$ {PPN = $[N(PPh_3)_2]^+$} and $[Cl_3M^{II}(\mu\text{-}NC)Mn^{II}(CO)(dppm)_2]$ (M = Mn, Ni) by successive reactions with [PPN]Cl and $[Fe(\eta\text{-}C_5H_5)_2][PF_6]$.

Anhydrous $FeCl_2$ reacts with $[Mn(CN)L_x]$ [L_x = *cis*- or *trans*-$(CO)_2\{P(OR)_3\}(dppm)$, R = Et, Ph] in air to give very different products from those of the other metals noted above, namely the intensely coloured (blue to purple) complexes $[Cl_3Fe^{III}(\mu\text{-}NC)Mn^{I}L_x]$. The reaction of *trans*-$[Mn(CN)(CO)(dppm)_2]$ with $FeCl_2$ in air gives $[Cl_3Fe^{III}(\mu\text{-}NC)Mn^{II}(CO)(dppm)_2][Fe^{III}Cl_4]$ which can be reduced by $[Fe(\eta\text{-}C_5Me_5)_2]$ to $[Cl_3Fe^{III}(\mu\text{-}NC)Mn^{I}(CO)(dppm)_2]$. The presence of Mn^{I} and Fe^{III} in the neutral species is in marked contrast to the $M^{II}Mn^{II}$ cores of $[Cl_3M(\mu\text{-}NC)Mn(CO)(dppm)_2]$ (M = Mn, Co, Ni).

The assignments of oxidation state, based on the IR carbonyl spectra, are supported by X-ray structural studies of $[Cl_3Fe(\mu\text{-}NC)Mn(CO)(dppm)_2][FeCl_4]\cdot 2.5CHBr_3$ **4**, $[Cl_3Fe(\mu\text{-}NC)Mn(CO)(dppm)_2]\cdot CH_2Cl_2$ **5** and $[Cl_3Mn(\mu\text{-}NC)Mn(CO)(dppm)_2]\cdot CH_2Cl_2$ **6** (all three show similar structures‡). The structure of **6** is shown in Fig. 1, together with important bond lengths for **4**–**6**. As noted previously,[11] the Mn–P bond distances of the $(\mu\text{-}NC)MN(CO)(dppm)_2$ fragment are diagnostic of the oxidation state of Mn. Thus, **4** and **6** contain Mn^{II} and **5** contains Mn^{I}.

The intense colours of $[Cl_3Fe(\mu\text{-}NC)MnL_x]$ are in striking contrast to that of $[FeCl_4]^-$ (pale yellow) despite the presence of tetrahedral Fe^{III} in all cases. These intense colours arise from strong absorptions (ε_{max} *ca.* 3000 $dm^3\ mol^{-1}\ cm^{-1}$) in the visible spectrum which are highly solvatochromic (*e.g.* $[Cl_3Fe(\mu\text{-}NC)MnL_x]$ [L_x = *cis*-$(CO)_2\{P(OPh)_3\}(dppm)$ (λ_{max} = 508 nm in *n*-hexane; λ_{max} = 599 nm in 1,2-$C_2H_4Cl_2$), implying extensive intramolecular charge transfer.

Cyclic voltammetry provides some insight into the origin of the very different oxidation state distribution in the iron complexes compared with that in $[Cl_3M^{II}(\mu\text{-}NC)Mn^{II}(CO)(dppm)_2]$ (M = Mn, Co, Ni). Thus, **5** shows one oxidation wave ($E^{0\prime}$ = 0.43 V) and one reduction wave ($E^{0\prime}$ = 0.02 V) associated with the Mn^{I}–Mn^{II} and Fe^{II}–Fe^{III} couples respectively; no equivalent wave for the M^{II}–M^{III} couple is observed for M = Mn, Co or Ni. These results also suggest that the colour and solvatochromism of the iron complexes result from Mn^{I} to Fe^{III} charge transfer through the cyanide bridge. {In this respect, it is noteworthy that $[Cl_3Fe^{III}(\mu\text{-}NC)Mn^{II}(CO)(dppm)_2]^+$, where Mn^{II}-to-Fe^{III} charge transfer is impossible, is not solvatochromic.}

The magnetic behaviour of the iron complexes is also of interest. The magnetic moments of **4**, **5** and $[Cl_3Fe(\mu\text{-}NC)Mn(CO)(dppm)_2][BF_4]$ **7** {prepared by $[Fe(\eta\text{-}C_5H_4COMe)Cp][BF_4]$ oxidation of **5**} are 8.2, 5.6 and 5.8 μ_B respectively at 295 K. Detailed studies of the magnetic and electronic properties of these complexes are in progress.

We thank the EPSRC for studentships (to O. M. H., G. R. L. and A. J. W.).

Notes and References

* E-mail: Neil.Connelly@bristol.ac.uk

† All new complexes had satisfactory elemental analyses (C, H, N).

‡ Crystal structures were determined from data collected on a Siemens SMART diffractometer ($\bar{\lambda}$ = 0.71073 Å) at 173 K. The structures were solved by direct and Fourier methods and refined by least-squares against all F^2 data corrected for absorption. *Crystal data*: $[Cl_3Fe(\mu\text{-}NC)Mn(CO)(dppm)_2][FeCl_4]\cdot 2.5CHBr_3$ **4**: $C_{52}H_{44}Cl_7Fe_2MnNOP_4\cdot C_{2.5}H_{2.5}Br_{7.5}$, M = 1869.451, monoclinic, space group $C2/c$ (no. 15), a = 46.157(3), b = 12.612(2), c = 24.455(4) Å, β = 104.721(14)°, U = 13769(3) Å^3, Z = 4, D_c = 1.658 Mg m^{-3}, μ = 5.351 mm^{-1}, 9577 unique data, $\theta \leqslant 23°$, R_1 = 0.0994; $[Cl_3Fe(\mu\text{-}NC)Mn(CO)(dppm)_2]\cdot CH_2Cl_2$ **5**: $C_{52}H_{44}Cl_3FeMnNOP_4\cdot CH_2Cl_2$, M = 1124.898, triclinic, space group $P\bar{1}$ (no. 2), a = 14.092(3), b = 14.489(2), c = 14.791(3) Å, α = 89.111(17), β = 75.367(16), γ = 63.011(11)°, U = 2586.4(7) Å^3, Z = 2, D_c = 1.444 Mg m^{-3}, μ = 0.95 mm^{-1}, 8818 unique data, $\theta \leqslant 25°$, R_1 = 0.0479; $[Cl_3Mn(\mu\text{-}NC)Mn(CO)(dppm)_2]\cdot CH_2Cl_2$ **6**: $C_{52}H_{44}Cl_3Mn_2NOP_4\cdot CH_2Cl_2$, M = 1123.989, monoclinic, space group $P2_1/n$ (no. 14), a = 12.629(3), b = 23.525(4), c = 18.306(4) Å, β = 104.306(17)°, U = 5270.0(2) Å^3, Z = 2, D_c = 1.417 Mg m^{-3}, μ = 0.89 mm^{-1}, 8253 unique data, $\theta \leqslant 24°$, R_1 = 0.0521. CCDC 182/730.

1 J. Woodward, *Philos. Trans.*, 1724, **33**, 15; J. Brown, *Philos. Trans.*, 1724, **33**, 17 (cited in *Mixed-Valence Compounds*, ed. D. B. Brown, D. Reidel, Boston, MA, 1979).
2 M. B. Robin, *Inorg. Chem.*, 1962, **1**, 337.
3 K. R. Dunbar and R. A. Heintz, *Prog. Inorg. Chem.*, 1997, **45**, 283.
4 H. Vahrenkamp, A. Geiss and G. N. Richardson, *J. Chem. Soc., Dalton Trans.*, 1997, 3643.
5 G. A. Carriedo, N. G. Connelly, M. C. Crespo, I. C. Quarmby, V. Riera and G. H. Worth, *J. Chem. Soc., Dalton Trans.*, 1991, 315; A. Christofides, N. G. Connelly, H. J. Lawson, A. D. Loyns, A. G. Orpen, M. O. Simmonds and G. H. Worth, *J. Chem. Soc., Dalton Trans.*, 1991, 1595; M. Bardaji, N. C. Brown, A. Christofides and N. G. Connelly, *J. Chem. Soc., Dalton Trans.*, 1996, 2511.
6 G. A. Carriedo, V. Riera, N. G. Connelly and S. J. Raven, *J. Chem. Soc., Dalton Trans.*, 1987, 1769; N. G. Connelly, K. A. Hassard, B. J. Dunne, A. G. Orpen, S. J. Raven, G. A. Carriedo and V. Riera, *J. Chem. Soc., Dalton Trans.*, 1988, 1623.
7 F. L. Atkinson, A. Christofides, N. G. Connelly, H. J. Lawson, A. C. Loyns, A. G. Orpen, G. M. Rosair and G. H. Worth, *J. Chem. Soc., Dalton Trans.*, 1993, 1441.
8 F. L. Atkinson, N. C. Brown, N. G. Connelly, A. G. Orpen, A. L. Rieger, P. H. Rieger and G. M. Rosair, *J. Chem. Soc., Dalton Trans.*, 1996, 1959.
9 N. C. Brown, G. B. Carpenter, N. G. Connelly, J. G. Crossley, A. Martin, A. G. Orpen, A. L. Rieger, P. H. Rieger and G. H. Worth, *J. Chem. Soc., Dalton Trans.*, 1996, 3977.
10 D. Nicholls, in *Comprehensive Inorganic Chemistry*, ed. J. C. Bailar, Jr., H. J. Emeleus, R. Nyholm and A. F. Trotman-Dickenson, Pergamon, Oxford, vol. 3, 1973, p. 1092.
11 G. A. Carriedo, N. G. Connelly, E. Perez-Carreno, A. G. Orpen, A. L. Rieger, P. H. Rieger, V. Riera and G. M. Rosair, *J. Chem. Soc., Dalton Trans.*, 1993, 3103.

Received in Basel, Switzerland, 20th October 1997; 7/07541C

Molecular recognition of a tris(histidine) ligand

Shuguang Sun, Jennifer Saltmarsh, Sanku Mallik*†‡ and Kathryn Thomasson

Department of Chemistry, Box: 9024, University of North Dakota, Grand Forks, ND 58202, USA

Design and synthesis of a tri-Hg^{2+} complex to selectivity recognize a tris(histidine) ligand is presented.

We are interested in the design and synthesis of transition metal ion based receptors for histidine-containing peptides.[1] Histidine-to-metal ion interactions (Cu^{2+}, Ni^{2+}, Zn^{2+} *etc*.) have been used for various applications, *e.g*. protein purification,[2] cross-linking,[3] targeting proteins to lipid bilayers.[4] It is these strong, directed metal ion-to-histidine interactions that we are using as the basis of the recognition process.[5]

As a model system for peptide recognition, we have chosen the ligand **L** to position three (*S*)-histidines 12 Å apart (Fig. 1). The compound **C**, with one histidine, served as the control for our studies. **L′** and **C′** were tested as histidine-mimetic ligand and control, respectively. Three-dimensional structures for the receptor and ligands were constructed using the molecular modelling software INSIGHT II and DISCOVER (ver. 95.0, BioSym Technologies/MSI, San Diego, CA) and energy-minimized in the gas phase using the consistent valence force field (cvff).

Syntheses of the receptor **R**, ligands **L**, **L′** and the control **C**, **C′** are shown in Scheme 1. Selective protection of three nitrogens of the cyclam (1,4,8,11-tetraazacyclotetradecane) ring **1** was carried out following a literature procedure.[6]

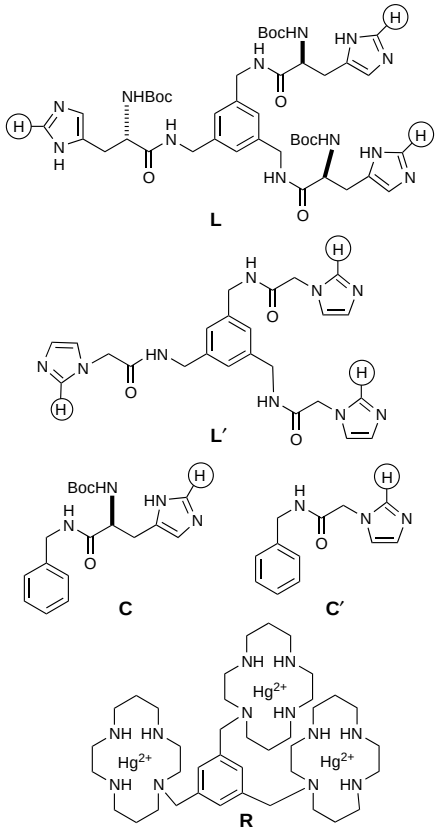

Fig. 1 Structures of the tris(histidine) ligand **L**, histidine mimetic ligand **L′**, controls **C**, **C′** and the designed receptor **R**. Hydrogens monitored in the titration studies are circled.

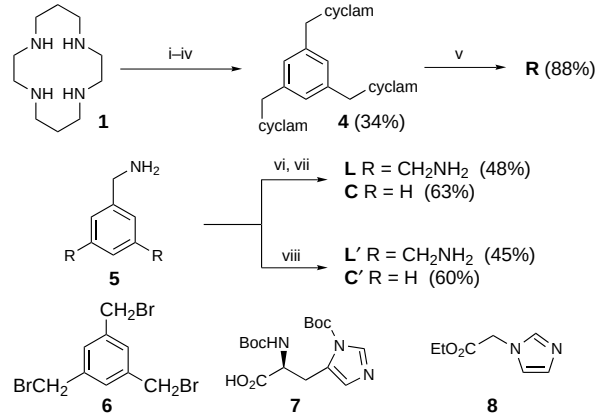

Scheme 1 *Reagents and conditions*: TsCl, Et_3N, $CHCl_3$; ii, **6**, K_2CO_3, MeCN, sonication; iii, HBr, AcOH, 70 °C; iv, ion exchange; v, $Hg(ClO_4)_2.3H_2O$, MeOH–MeCN; vi, *N*-hydroxysuccinimide, DCC, Et_3N, THF, **7**; vii, NaOH; viii, **8**, EtOH, sonication

Reaction of cyclam tritosylate **2** with 1,3,5-tris(bromomethyl)benzene **6**[7] proceeded smoothly in MeCN (using powdered K_2CO_3 as the base) under sonication (8 h). The crude product was purified by flash chromatography, using 5% MeOH–CH_2Cl_2 as the solvent (R_f 0.3). This reaction was found to yield a complex mixture of products under reflux. Removal of the tosyl groups was carried out in HBr–AcOH at 70 °C (10 h). Free ligand **4** was isolated by ion-exchange chromatography (IRA-400 column, hydroxide form) using water as eluent. Receptor **R** was synthesized by adding a solution of the free ligand **4** in MeCN to a methanolic solution of $Hg(ClO_4)_2.3H_2O$. Receptor **R** was isolated as the air-stable perchlorate salt after addition of Et_2O to the reaction mixture. (**Note**: we did not observe any explosive tendency for this compound.)§

Ligand **L** is known in the literature[8] and control **C** was synthesized by an analogous procedure. Reactions for the synthesis of **L′** and **C′** gave higher yields under sonication compared to refluxing conditions. Control **C′** was purified by recrystallization from $CHCl_3$–hexane and **L′** was purified by flash chromatography using MeOH as the eluent (R_f = 0.3).§ In the binding studies, a diamagnetic metal ion (Hg^{2+}) with strong affinity for histidine ($> 10^3$ M^{-1}) was used so that the binding could be monitored by ^{1}H NMR spectroscopy. Since the receptor **R** contains the embedded distance information, cyclam was used to hold the metal ions. Cyclam has very high affinities ($> 10^{20}$ M^{-1}) for transition metal ions. This ensures that the metal ions will not get displaced from **R** at high histidine concentrations. Cyclam also gives us the flexibility to synthesize the receptor with a variety of transition metal ions and to optimize the recognition properties.

Recognition studies were conducted in highly polar [$^2H_6$]DMSO, and were followed by ^{1}H NMR spectroscopy. The C-2-H of the imidazole moieties (indicated in Fig. 1) of **C** and **C′** were found to be shifted downfield (0.80 ppm for **C**; 0.87 ppm for **C′**) upon complexation with the Hg^{2+} ions of the receptor **R** (10 mM in **R**, 0–60 mM in **C** or **C′**). Both of these controls were in fast exchange with the receptor and an average signal was observed in each case. Resultant titration curves are

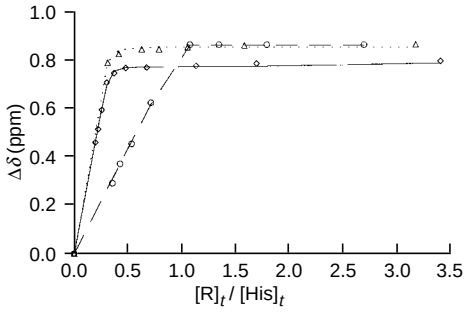

Fig. 2 Titration curves for (◇)C, (△)**C′** and (○) **L′**. The curves indicate the calculated titration curves with the reported binding constants.

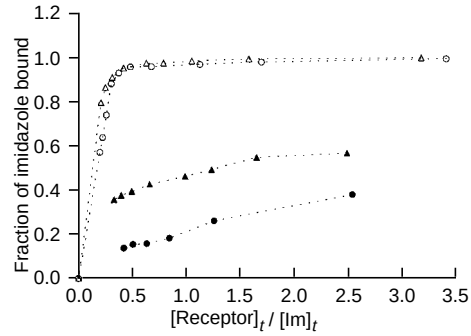

Fig. 3 Fraction of bound (●) **C** and (▲) **C′** in the competition experiments. The corresponding fractions bound in the titration experiments for (○) **C** and (△) **C'** are also plotted.

shown in Fig. 2. The turning of the titration curves at a 3 : 1 ratio of $[R]_t/[His]_t$ indicated a 3 : 1 stoichiometry of binding between **R** and **C** (or **C′**).[9]

For data analysis, the three metal ions were taken as interacting independently. Also shown in Fig. 2 are the calculated titration curves with the best-fit estimates of the binding constants. Non-linear regression analysis of the binding data following a previously-developed procedure[5] (SIGMA PLOT 4.0 for Windows, Jandel Scientific Inc.) provided the value of the binding constants (K_{RC} = 1.1 × 10^4 M^{-1}, $[\mathbf{R}]_t$ = 10.25–6.5 mM; $[\mathbf{C}]_t$ = 0–32 mM; $K_{RC'}$ = 10^4 M^{-1}, $[\mathbf{R}]_t$ = 9.6–6.6 mM; $[\mathbf{C'}]_t$ = 0–32 mM; in both regressions, error: < 10%). The regression analysis converged to these numbers starting from either a smaller or a larger value as the initial estimate.

Ligand **L′** was also in fast exchange with the receptor (Fig. 2). The sharp turning of the titration curve at [**R**]/[**L′**] = 1 indicated a 1 : 1 stoichiometry of the complex and a high affinity. Due to the high affinity, only a lower limit of *K* can be estimated from the binding data ($K_{RL'} > 10^5$ M^{-1}).

Similar titration experiments (10 mM in **R**, 3–30 mM in **L**) showed that **R** interacts differently with **L** compared to **C**. The ligand **L** was found to be in slow exchange with **R**.[10] Two different C-2-H signals were observed for the free (δ 7.67) and bound (δ 8.605) ligand. The amounts of free **L** (measured by the integration of bound and free C-2-H resonances) were very small up to 1 : 1 stoichiometry and then the amount of free **L** increased rapidly. The aromatic hydrogens of **L** were shifted upfield by 0.8 ppm in the presence of the receptor **R**. These observations indicated that **R** is forming a 1 : 1 complex with **L** and that the benzene rings of **R** and **L** are stacking. This was corroborated by the observance of a cross-peak between the aromatic ring hydrogens of the two benzene rings of **R** and **L** in a NOESY spectra and by molecular modeling. The binding constant was estimated from the integration of bound and free signals of **L**.[11] Owing to inherent errors in the integration of very small peaks in ^{1}H NMR spectra, only a lower limit of K_{RL} can be obtained ($K_{RL} > 10^5$ M^{-1}).

In order to determine the binding selectivity of **R** and **L** (or **L′**) over **C** (or **C′**), competitive titration experiments were conducted (Fig. 3).[5] A 10 mM solution of **R**.**L** (or **R**.**L′**) was titrated with **C** or **C′** (1–30 mM). The C-2–H chemical shift of **C** (or **C′**) was followed to measure the concentration of **C** (or **C′**) bound to **R**. The fraction of **R** bound to **L** (or **L′**) compared to the fraction of **R** bound to **C** (or **C′**) was taken as the measure of selectivity. **R** was found to be selective for **L** compared to **C** by a factor of 20; its selectivity for **L′** over **C′** was 10. This difference in selectivity may be due to the difference in inter-imidazole distances of **L** and **L′** and the resultant strain in the complexes arising from non-optimal distance matching between the receptor and the ligand. We are currently probing this by synthesizing tris(histidines) with varying inter-imidazole distances.

Thus, the designed receptor **R** is indeed selective for pattern matched tris(histidine) ligand **L** compared to the control **C**. Studies are currently underway to optimize the selectivity by changing the spacer of the tris(histidine) ligand **L**.

This work is supported by grants from the NIH (1R15 GM/OD 54321-01) and from the NSF (CAREER award to S. M.).

Notes and References

† E-mail: mallik@badlands.nodak.edu

‡ Present address: Department of Chemistry, North Dakota State University, Fargo, ND 58105, USA

§ All new compounds gave satisfactory characterization data. *Selected data* for **4** (*J* values in Hz): glassy solid (80%); mp 88–90 °C; $\delta_H(D_2O)$ 7.15 (s, 3H), 3.47 (s, 6H), 2.71–2.41 (m, 22H), 1.76–1.61 (m, 4H), 1.55–1.42 (m, 4H). HRMS (M^+) Calc. for $C_{39}H_{78}N_{12}$: 714.6472. Found: 714.6471. For **R**: white solid (88%); mp 165–167 °C; $\delta_H([^2H_6]$ DMSO): 7.09 (s, 3H), 5.36 (br s, 2H), 5.25 (br s, 2H), 4.58 (br s, 2H), 4.19 (d, 2H, *J* 15.0), 3.85 (d, 2H, *J* 15.0); the rest of the hydrogens appear as multiplets between 3.05–2.99, 2.88–2.83, 2.47–2.20, 1.90–1.77 and 1.72–1.67. Calc. for $C_{39}H_{78}N_{12}Hg_3(ClO_4)_6.3H_2O$: C, 23.80; H, 4.30; N, 8.54. Found: C, 24.01, H, 4.29; N, 8.51%. For **L**: white foamy solid; $\delta_H([^2H_6]$DMSO) 7.55 (s, 3H, Im-C_2H), 6.99 (s, 3H, Im-C_5H), 6.87 (s, 3H, Ar-H), 4.21 (3H, C_α-H), 4.17 (6H, $ArCH_2$), 2.80 (m, 6H, His- β-CH_2), 1.35(s, 27H, Bu^t); $\delta_C([^2H_6]$DMSO) 171.5, 155.2, 139.2, 134.7, 124.3, 78.1, 54.6, 42.1, 33.4, 28.2. HRMS M^+ Calc. for $C_{42}H_{60}N_{12}O_9$: 876.4605. Found: 876.4610. For **C**: white solid (85%); TLC (R_f 0.24, 3% MeOH–CH_2Cl_2); mp 150–152 °C; $[\alpha]_D^{21}$ +58 (MeOH, *c* 7.6); $\delta_H([^2H_6]$DMSO) 7.53 (s, 1H, Im-C_2H), 7.20 (m, 5H, Ar), 6.75 (s, 1H, Im-C_5H), 4.24 (s, 2H, $ArCH_2N$), 4.18 (m, 1H, C_α-H), 2.82 (m, 2H, His-β-CH_2), 1.35 (s, 9H, Bu^t); $\delta_C([^2H_6$DMSO) 171.6, 155.1, 139.4, 134.6, 128.1, 126.8, 126.5, 78.1, 54.6, 41.9, 28.1; HRMS (MH^+) Calc. for $C_{18}H_{24}N_4O_3$: 345.1926. Found 345.1911.

1 S. Mallik and I. Mallik, *Synlett*, 1996, 734. For examples of amino acid recognition based metal–ligand interactions, see K. Konishi, K. Yahara, H. Toshishige, T. Aida and S. Inoue, *J. Am. Chem. Soc*., 1994, **116**, 1337; T. Mizutani, T. Ema, T. Yoshisa, Y. Kuroda and H. Ogoshi, *Inorg. Chem*., 1993, **32**, 2072.

2 A. V. Terskikh, J. M. Ledoussal, R. Crameri, I. Fisch and J. P. Mach, *Proc. Natl. Acad. Sci. USA*, 1997, **94**, 1663; A. Gambero, L. T. Kubota, Y. Gushikem, C. Airoldi and J. M. Granjeiro, *Colloid Interfacial Sci*., 1997, **185**, 313.

3 D. A. Fancy, K. Melcher, S. A. Johnston and T. Kodadek, *Chem. Biol*., 1996, **3**, 551.

4 K. M. Malony, D. R. Shnek, D. Y. Sasaki and F. H. Arnold, *Chem. Biol*., 1996, **3**, 185; L. Schmitt, T. M. Bohanon, S. Denzinger, H. Ringsdorf and R. Tempw, *Angew. Chem., Int. Ed. Engl*., 1996, **35**, 317.

5 S. Mallik, R. D. Johnson and F. H. Arnold, *J. Am. Chem. Soc*., 1994, **116**, 8902.

6 I. M. Helps, D. Parker, J. R. Morphy and J. Chapman, *Tetrahedron*, 1989, **45**, 219.

7 W. P. Cochrane, P. L. Pauson and T. S. Stevenes, *J. Chem. Soc. (C)*, 1968, 630.

8 D. Goldfarb, J.-M. Fauth, Y. Tor and A. Shanger, *J. Am. Chem. Soc*., 1991, **113**, 1941.

9 R. S. Macomber, *J. Chem. Ed*., 1992, **69**, 375; Z.-X. Wang, N. Ravi Kumar and D. K. Srivastrava, *Anal. Biochem*., 1992, **206**, 376.

10 This may or may not indicate a very strong association constant. A. Bosti, B. Perley and E. Hadjoudis, *J. Chem. Soc., Perkin Trans. 2*, 1997, 89.

11 K. A. Connors, *Binding Constants*, Wiley, New York, 1987, pp.189–216.

Received in Corvallis, OR, USA, 10th September 1997; 7/06711I

ChemComm
FEATURE ARTICLE

Understanding structure and reactivity of new fundamental inorganic molecules: metal sulfides, metallocarbohedrenes, and nitrogenase

Ian Dance

School of Chemistry, University of New South Wales, Sydney 2052, Australia

A large number of new and unexpected molecules, fundamentally inorganic and containing just metal and sulfur, or metal and carbon, can be synthesised in the gas phase, and their reactivities investigated. In the absence of bulk samples and definitive characterisation data they can be very profitably investigated using density functional calculations. A valuable perspective places these new and unprotected molecules in the context of related non-molecular solids, and terminally ligated molecules. The Fe_7MoS_9 cluster which effects the mild reduction of N_2 at the active site of nitrogenase is similarly undercoordinated, floppy, and reactive. Density functional calculations reveal the characteristics of the Fe_7MoS_9 site and elucidate postulated mechanisms for the reduction.

Introduction

Consider this experiment: cobalt sulfide, as the familiar black insoluble solid, is energised with a high power pulse of a 1064 nm laser, in a high vacuum chamber. A plasma occurs at the surface, and after collisional cooling the products formed are trapped as negative ions, and assayed mass spectrometrically. The resulting mass spectrum reveals 83 binary species $[Co_xS_y]^-$, ranging in size up to $[Co_{38}S_{24}]^-$.[1]

What have we done? We have prepared 83 structurally-molecular forms of a fundamental inorganic binary compound, cobalt sulfide, which previously had been known only with non-molecular structure. This experiment is the metal sulfide analogue of the better known laser ablation of a non-molecular allotrope of carbon (graphite) to generate the family of fullerenes, which are elemental carbon in molecular form.

This feature article is about newly discovered inorganic molecules which are comprised of just two (or at most a few) elements, and yet which are unprecedented in composition and structure and reactivity. These molecules are at the core of inorganic chemistry, but they do not adhere to the traditional notions of composition or oxidation state or valence, and they require new concepts of structure and bonding. Very often these new molecules have their genesis in the gas phase (like the fullerenes). However, as described below, metal sulfide cores are also deployed by evolved biological chemistry to effect significant reactivity which is beyond current human capability in the laboratory.

Molecular binary metal chalcogenides

By gas phase experiments like that already outlined, the generation of metal sulfide (and selenide and telluride) molecular clusters $[M_xE_y]^-$ has been achieved for all of the first row transition metals, and others.[2–4] We know that these new molecules are formed in the gas phase by associative processes involving atoms, ions and/or electrons generated in a high energy plasma, and that our experiment does not merely excise various fragments from the solid metal sulfide. This conclusion derives from the result that the distributions of product ions are largely independent of the properties of the solid precursor, and the fact that laser ablation of a mixture of elemental copper and selenium gives the same distribution as copper selenide precursors.[5,6] Through this experimental program we now know of the existence of many hundreds of unprecedented molecular metal sulfides $[M_xS_y]^-$, and have information about their relative abundances, stabilities, and reactivities.[1,2,4,6–13]

Before considering the position of these metal sulfide molecules in the menagerie of chemistry, it is worth mentioning a related inorganic experiment also performed in the cell of the Fourier transform ion cyclotron resonance (FTICR) mass spectrometer: this cell can be regarded as a gas-phase 'beaker', in which we can undertake controlled synthesis and purification of new species, and investigate their reactivities, reactions, and dissociations.[13,14] All of the metals (except Tc) can be isolated as M^+ in this cell, and reacted with the elemental reagent $S_{8\,(g)}$, forming numerous cations $[MS_n]^+$. This is comparative inorganic chemistry *par excellence*: it compares all metals, in the same oxidation state, reacting with the same reagent under the same conditions.[14,15]

Inorganic perspectives: non-molecules, exposed molecules, and protected molecules

What structural perspective best serves the numerous questions which arise for these and related newly discovered molecules? A threefold overall classification is valuable. At one extreme are binary and ternary compounds which are structurally non-molecular (in one, two or three dimensions) and which therefore occur only in the solid state, and for which detailed structural data are available crystallographically. At the other extreme are conventional molecular compounds in which a metal cluster core is terminally ligated by ligands: this is the class of 'protected molecules'. In the third class, the new molecules considered here have only the cluster core, and no ligand termination, and so are named 'exposed molecules'. This classification is illustrated in Fig. 1 for nickel chalcogenide systems, by NiS (the mineral millerite) as the non-molecular solid, by $[Ni_{11}S_8]$[12] as the exposed molecule and by $[Ni_{34}Se_{22}(PPh_3)_{10}]$[16] as the protected molecule. To illustrate again with the familiar carbon systems, diamond is non-molecular carbon, C_{60} is exposed molecular carbon, and the hydrocarbon dodecahedrane $C_{20}H_{20}$ represents protected C_{20}. This tripartite perspective is valuable and stimulates research in other fields of contemporary inorganic chemistry: some examples from metal–carbon systems are developed below. The concepts of non-molecularity, exposure and protection also pervade surface chemistry.

Metallocarbohedrenes

In 1992 a class of naked metal carbide clusters known as metallocarbohedrenes (or met-cars) was discovered.[17] These metallocarbohedrenes are synthesised when reactive metal clusters dehydrogenate hydrocarbons in the gas phase. The prototypical species was $[Ti_8C_{12}]^+$, but now more than a hundred metal–carbon molecules have been detected for metals

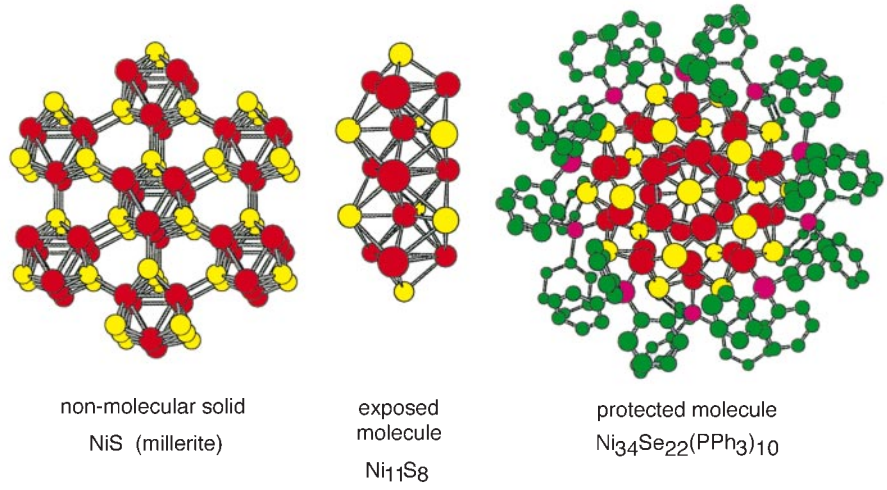

Fig. 1 Illustrations of the classification of non-molecular solids, exposed molecules, and protected molecules. Non-molecular NiS in the mineral millerite, the exposed molecule [$Ni_{11}S_8$] observed in the gas phase,[12] and the phosphine-protected nickel selenide core of [$Ni_{34}Se_{22}(PPh_3)_{10}$] prepared in solution and characterised crystallographically:[16] Ni red, S, Se yellow, P magenta, C green.

in groups 4–8 and 11. While many of these M_xC_y molecules have $y > x$ and an even number of C atoms and are believed to contain C_2 groups, there is a subset with $y \approx x$, believed to be fragments of a cubic metal carbide lattice containing C atoms.[18] The reactivities and transformations of metallocarbohedrenes are now well known,[18,19] but no pure bulk sample has been prepared. In the classification of Fig. 1, these exposed metal–carbon molecules lie between the non-molecular metal carbides[20] and organometallic clusters containing C_n moieties.[21]

Nitrogenase

Nitrogenase is the enzyme which reduces dinitrogen to ammonia, under conditions (ambient) which are far milder than those of the best industrial practice for reduction of N_2 with H_2 to form ammonia (the Haber–Bosch process, 400–500 °C, 100–1000 atm). The crystal structure of the FeMo protein of nitrogenase was determined in 1992, and subsequently improved,[22] revealing that the metal sulfide cluster (Fe_7MoS_9) at the active site is different from the many predictions, and unprecedented. The tantalising chemical question is 'how can a metal sulfide cluster enclosed in protein reduce one of the most recalcitrant molecules of chemistry under such mild conditions?' This question is another mantra in the philosophy of biognosis which holds that sophisticated chemistry can be learned from evolved biology.

The essential features of the Fe_7MoS_9 cluster at the active site are shown in Fig. 2. A six-coordinate Mo atom is coordinated by a side-chain histidine, bidentate homocitrate and three triply bridging sulfide ions to one triangular end of a trigonal prism of Fe atoms. The opposite end of this trigonal prism is connected through three triply bridging sulfides to the seventh Fe atom, whose tetrahedral coordination is completed by a cysteine residue. Around the equatorial belt of the trigonal prism there are three doubly-bridging sulfide ions. The significant features of the cluster are the threefold coordination of each of the six Fe^3 atoms† in the trigonal prism, the doubly-bridging S^2 atoms bridging the axial edges of the trigonal prism, and the connection of the cluster to the protein only at two end positions. The nakedness of the central Fe^3 and S^2 atoms is a conceptual link with the exposed metal sulfide clusters in the gas phase. Of course the essential Fe_7MoS_9 cluster is enclosed by protein, and the sophistication of the catalysis effected by nitrogenase depends on the cooperative action of cluster and protein, and the hydrogen bonds which link them. The Fe_7MoS_9 cluster participates in a rich sequence of reactions which probably depend, at least in part, on the reactivity of nakedness. There is another conceptual link between nitrogenase and the

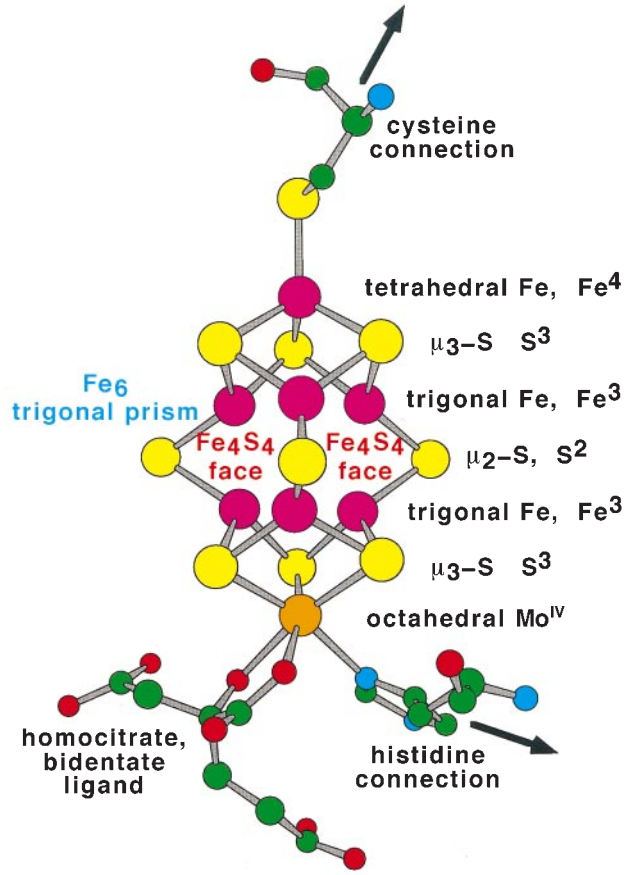

Fig. 2 The essential features of the Fe_7MoS_9(cysteine)(histidine)(homocitrate) cluster at the active site of the enzyme nitrogenase: Fe magenta, Mo orange, S yellow, C green, N blue, O red

gas phase metallocarbohedrene chemistry, in that the C_2^{2-} ligand of the metallocarbohedrenes is isoelectronic with the primary substrate N_2 of nitrogenase.

Determination of the crystal structure of the key protein of nitrogenase revealed the stage on which the marvellous molecular dance occurs, but provided no direct information about the dancers or the choreography.[23] The question now is how to determine that choreography.

Similar questions arise for the new exposed inorganic molecules. Their compositions and reactions are known mass

spectrometrically, but not their structures. In all of these contexts, powerful density functional theory provides valuable insights.

Calculating the structures and reactions of big molecules

Density functional theory (DFT) is now well established as a valuable quantum method for the calculation of the electronic structure and energy, and derived properties, of large molecules and molecules containing atoms which contribute many electrons.[11,24] DFT includes a computationally efficient account of the correlation and exchange energies (the electron–electron energies) which have complicated and prolonged traditional quantum chemical calculations. Apart from the selection of functionals to describe exchange and correlation, the DFT method is *ab initio*.

The performance of DFT calculations is impressive for molecules like those introduced above. For a calculational effort which scales with the number of electrons more favourably than any comparable method, optimised geometries are obtained with an accuracy sufficient to address the big-picture questions. As illustration, Fig. 3 shows the optimised structure of

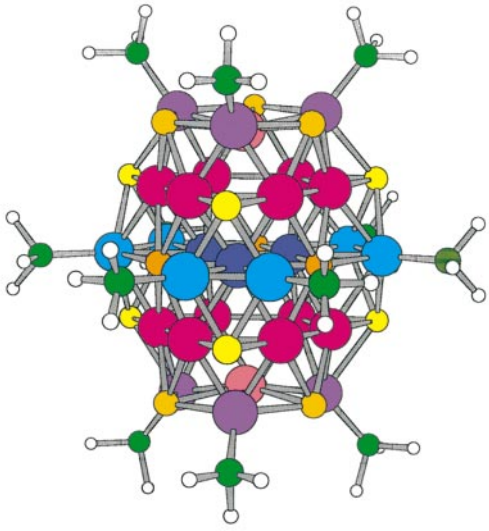

Bond	Obs	R=H: vwn/b88e
$Cu^h - Se^6$	2.56–2.62	2.52–2.56
$Cu^h - Se^4$	2.36–2.39	2.43, 2.44
$Cu^e - Se^4$	2.45–2.50	2.51, 2.52
$Cu^h - Se^5$	2.39–2.41	2.45, 2.46
$Cu^p - Se^5$	2.52–2.56	2.49–2.53
$Cu^a - Se^5$	2.48–2.53	2.55, 2.58
$Cu^h - Cu^h$	2.50–2.69	2.51–2.72
$Cu^h - Cu^p$	2.63–2.70	2.52–2.55
$Cu^p - Cu^a$	2.59–2.62	2.50, 2.51
$Cu^e - Cu^e$	2.63–2.74	2.52–2.56
$Cu^e - P$	2.23–2.26	2.23–2.25
$Cu^p - P$	2.22–2.25	2.20, 2.21

Fig. 3 The structure of $Cu_{29}Se_{15}(PR_3)_{12}$: large spheres are Cu atoms, colour coded according to chemical type and connectivity (point group D_{3h}), small yellow and orange spheres are Se, green P and white H. The tabulation of colour-coded bond types compares the distance range observed for R = Pr^i with the distances calculated (in C_{2v}) for R = H, using the Vosko–Wilke–Nusair local density functional[28] for correlation and Becke's gradient-corrected exchange functional.[29]

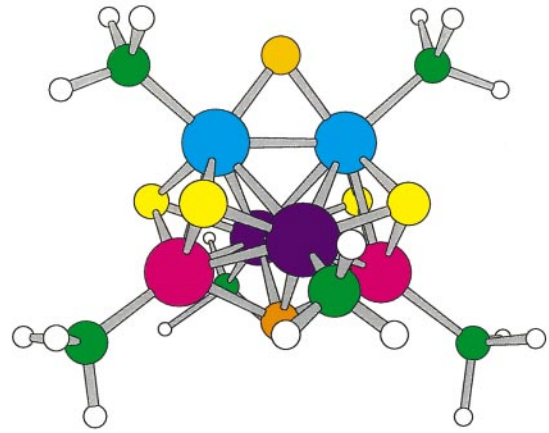

Bond	Obs	R=H: lyp/b88e
$Fe^a - S^2$	2.15	2.15
$Fe^a - S^3$	2.22, 2.23	2.20
$Fe^b - S^3$	2.19, 2.20	2.20
$Fe^c - S^3$	2.22	2.18
$Fe^c - S^4$	2.28, 2.30	2.25
$Fe^b - S^4$	2.23	2.19
$Fe^a - Fe^a$	2.63	2.62
$Fe^b - Fe^a$	2.72	2.73
$Fe^b - Fe^b$	2.97	3.00
$Fe^b - Fe^c$	2.63, 2.65	2.61
$Fe^a - P$	2.27, 2.29	2.32
$Fe^b - P$	2.28	2.31
$Fe^c - P$	2.36, 2.38	2.31

Fig. 4 The structure of $[Fe_6S_6(PR_3)_6]^{2+}$: large spheres are Fe atoms, colour coded according to chemical type and connectivity (point group C_{2v}), small yellow, light orange and deep orange spheres are S, green P and white H. The tabulation of colour-coded bond types compares the distances observed for R = Et with the distance calculated (in C_{2v}) for R = H, using the Lee–Yang–Parr gradient-corrected correlation functional[30] and Becke's gradient-corrected exchange functional.[29]

$Cu_{29}Se_{15}(PH_3)_{12}$ (which contains 1566 electrons) in comparison with the observed (X-ray crystal structure[25]) geometry for $Cu_{29}Se_{15}(PPr^i_3)_{12}$, and Fig. 4 shows the results for the 'basket cluster' $[Fe_6S_6(PR_3)_6]^{2+}$ (R = H calculated, R = Et observed[26]). In both molecules it can be seen that the calculated interatomic distances are generally within 0.05 Å (and often 0.02 Å) of those observed, and that the variability of bond type and length is reproduced, including long Fe–Fe distances which are not bonds. This augurs well for application to molecular metal sulfide clusters and to nitrogenase. There are extensive checks of calculated energies against experimental data.[27]

In exploring the geometry–energy hypersurface for new chemical systems it is also desirable to locate transition states (saddle points) and to calculate reaction profiles. The method used here is to postulate a saddle geometry, then follow the geometry change on its steepest downhill energy path, and then to iterate through a cycle of geometry adjustment and energy minimisation until the lowest energy transition state is found.

Answering the questions: transferring concepts

The new inorganic molecules and their reactions present innumerable questions. In DFT we have a powerful tool for answering those questions, or at least for the design of fruitful further experiments. The key challenge—and the exciting appeal of this research—is in devising the best hypotheses. In

my view the quality of research of this type is determined more by the quality of the ideas to be tested than by the computational methodology to be deployed.

In the following sections I outline some responses to the questions raised, with emphasis on the transferability of ideas and insight from metal sulfides to metallocarbohedrenes to nitrogenase, and the incorporation of structural data and principles from related non-molecular solids and protected molecules.

Structures of molecular metal sulfides

The compositions of the observed molecules $[M_xS_y]$ are plotted on maps of y *vs.* x, and show several significant general characteristics. Firstly, the x/y distribution is a continuous extended domain which is relatively narrow in y. In the case of $[Cu_xS_y]^-$, the main sequence of larger species can be described by the equations $x = 2y - 1$ and $x = 2y - 2$,[4,6] while for $[Mn_xS_y]^-$ the ions are described by $x = y$ and $x = y - 1$.[8] The continuous narrow regions of observability accentuate in contrast the emptiness of the composition maps and the many species which are not observed. Secondly, while for any metal there are variations in intensity along these sequences, there are no pronounced discontinuities in abundance which might signify special stability or structure. Thirdly, it must be remembered that observability on the composition map need not represent inherent stability, and could be due to favourable electron affinity in the competition for electrons during the formation of the anions. Fourthly, the slopes (y/x) of the domains of observability correlate with the number of valence electrons provided by M, and a qualitative electron counting pattern has been identified.[1,4]

The first issue for the new molecules is geometry: what is $[Mn_{20}S_{20}]^-$, or $[Fe_{11}S_{10}]^-$, or $[Co_{38}S_{24}]^-$, or $[Ni_{15}S_{10}]^-$, or . . .? And then, is there a fundamental structural principle for each metal? And are there structural principles which allow almost continuous growth, rather than special stability at certain sizes? In answering questions about geometry, knowledge of the many structures of terminally ligated metal chalcogenide clusters[2] provides inspiration for postulates to be tested.

In the case of $[Cu_xS_y]^-$ clusters, the enhanced stability of $[Cu_3S_3]^-$, $[Cu_6S_4]^-$ and $[Cu_{10}S_6]^-$ has been traced to cluster structures which contain local S–Cu–S linear (or near-linear) coordination, and the other reactive clusters are those which have exposed Cu atoms without this geometry.[4] For the $[Mn_xS_y]^-$ set,[8] 61 isomers for 23 compositions up to $[Mn_{15}S_{15}]^-$ have been evaluated by DFT in terms of optimised geometrical structure, electronic structure, and electron affinity.[7] Structures based on stacks of Mn_3S_3 triangles are favourable, as are regular Mn_x polyhedra with (μ_3-S) caps, and trigonal MnS_3 local coordination occurs in the more stable isomers.

Structures of metallocarbohedrenes

The prototypical metallocarbohedrene Ti_8C_{12} was postulated to have a structure (symmetry T_h) in which six C_2 units cap the faces of a Ti_8 cube, with the C_2 parallel to the edges of Ti_4 squares.[17] In this, the Ti–C and C–C bonds constitute a pentagonal dodecahedron, with analogy to C_{20}. My idea that there could be alternative stable structures came from a quite different field, metal thiolate clusters. The $M_8(SR)_{12}$ based clusters had been investigated earlier, when it was recognised that the M_8 polyhedron could be either a cube or a tetracapped tetrahedron, and that the bridging S atoms could constitute either a cuboctahedron or an icosahedron.[31,32] Therefore I explored alternatives for Ti_8C_{12}, and recognised a high symmetry (T_d) structure in which the Ti_8 set was a tetracapped tetrahedron, with the six C_2 groups bonded diagonally on each of the six folded Ti_4 rhombuses (or butterflies) on the Ti_8 surface (see Fig. 5). DFT calculations readily showed that the T_d structure was very much more stable than the T_h structure,[33] and this was confirmed by other theoretical investigations.[18,34] There are other isomers for M_8C_{12} which have lower symmetry arrangements of the diagonally bound C_2.[34] Subsequently I characterised the barrierless transformation of T_h-Ti_8C_{12} to T_d-Ti_8C_{12}, outlined in Fig. 5.[35]

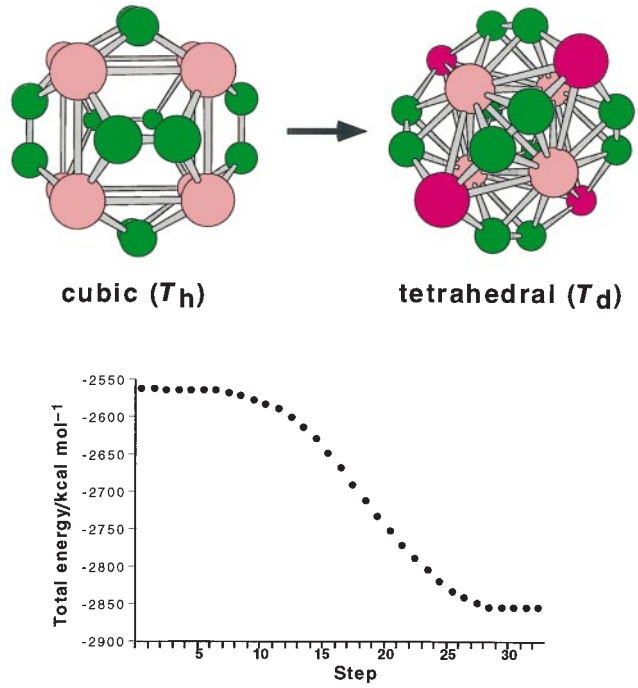

Fig. 5 The T_h and T_d isomers of Ti_8C_{12} (C green), and the barrierless energy change of 300 kcal mol^{-1} (1 cal = 4.184 J) in the transformation (in point group D_2) of T_h to T_d. In the T_d isomer the inner and outer Ti atoms are coloured pink and purple, respectively.

The concept of C_2 bonded diagonally across an M_4 rhombus rather than parallel to edges of an M_4 quadrilateral is entrenched in the models of many other metcars, such as the photodissociative transformation of $Ti_{14}C_{13}$ to Ti_8C_{13},[36] the structures of the unusual niobium carbohedrenes,[37] and the copper carbohedrenes.[38] Copper is unique in being the only late-transition metal reported to form metallocarbohedrenes: carbohedrenes are not known for metals in groups 9 or 10.

Copper carbohedrenes Cu_xC_y were observed in the series $[Cu_{2n+1}C_{2n}]^+$ for $1 \leqslant n \leqslant 10$, as well as $[Cu_7C_8]^+$, $[Cu_9C_{10}]^+$, $[Cu_{12}C_{12}]^+$, $[Cu_{16}C_{16}]^+$ and $[Cu_{20}C_{18}]^+$.[18] I noted a similarity between these compositions and those of the naked copper sulfide clusters $[Cu_xS_y]^-$, if C_2 was stoichiometrically equivalent to S. This similarity is shown on the composition map in Fig. 6. This is reasonable because both S^{2-} and C_2^{2-} can be isovalence-electronic in their bonding in metal clusters, both providing four donor electron pairs and having empty acceptor orbitals, as shown diagrammatically in Fig. 7.

Figs. 8 and 9 illustrate analogies between copper sulfide structures and copper carbohedrenes. The high symmetry structures of $Cu_{12}S_7$ (point group O_h) and $Cu_{13}(C_2)_6$ (point group T_h) have the same connectivity with either S or C_2 bound to the Cu_4 units of a cuboctahedron (see Fig. 8): the stoichiometry difference is accounted for by the presence of S at the centre of $Cu_{13}S_7$ and Cu at the centre of $Cu_{13}(C_2)_6$. This structural homology can be extended through larger clusters, to $Cu_{24}S_{13}$ and $Cu_{25}C_{24}$,[38] shown in Fig. 9.

While much further investigation is required to reveal the structures of the large numbers of exposed metal sulfide and metallocarbohedrene molecules, some guiding principles are becoming clear, and the analogies between the sulfide and carbide clusters stimulate hypotheses.

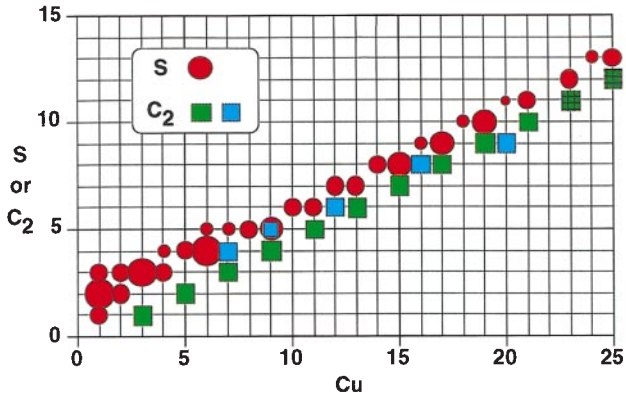

Fig. 6 Map of the compositions of $[Cu_xS_y]^-$ (red) and $[Cu_x(C_2)_y]^+$ (green, blue) in the gas phase: the vertical axis plots the number of S atoms or C_2 groups. The green compositions belong to the series $[Cu_{2n+1}C_{2n}]$, but the hatched green species were not observed.[18]

Fig. 7 Comparison (diagrammatic, not stereochemical) of the electronic components of sulfide S^{2-} and acetylide C_2^{2-} available for bonding participation in metal clusters. Both have four donor electron pairs marked as heavy lines (for C_2^{2-} these are the terminal σ pairs and the two π bonding pairs) and both have empty orbitals marked as lobes, being d orbitals at S and π* orbitals on C_2^{2-}: not all of these empty orbitals are shown.

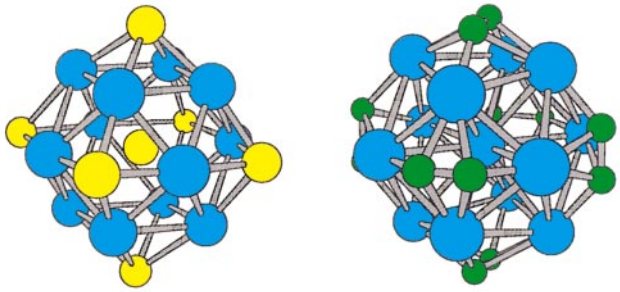

Fig. 8 Comparison of the optimised structures of $[Cu_{12}S_7]$ and $[Cu_{13}(C_2)_6]^+$, in which S and C_2 groups interchangeably cap the faces of a Cu_{12} cuboctahedron

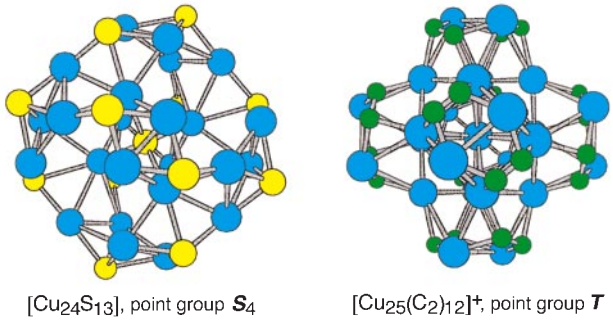

Fig. 9 Comparison of the optimised structures for $Cu_{24}S_{13}$ and $[Cu_{25}(C_2)_{12}]^+$, in which S and C_2 groups occupy similar positions on the surface of a Cu_{24} framework which is a distorted hexacapped cuboctahedron. The differences are due to tetrahedral coordination of the central S in $Cu_{24}S_{13}$ but cuboctahedral coordination of the central Cu in $[Cu_{25}(C_2)_{12}]^+$.

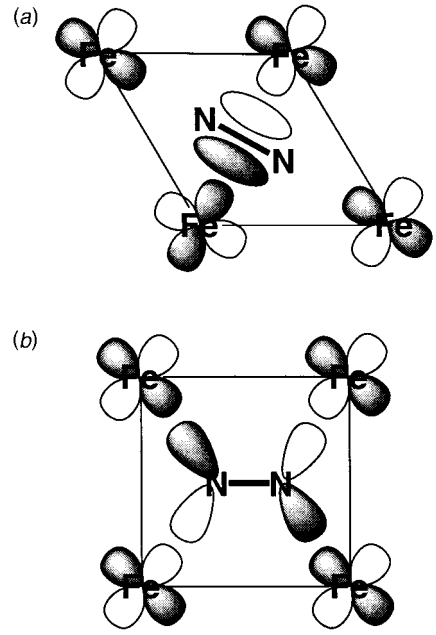

Fig. 10 Hypotheses for N_2 binding to an $(Fe^3)_4$ face of the Fe_7MoS_9 cluster of nitrogenase. (*a*) The twist or rhombus configuration allowing overlap between the Fe orbitals and N_2 π-bonding orbitals. (*b*) The parallel or rectangle configuration in which the Fe orbitals overlap with N_2 π-antibonding orbitals.

Tantalising nitrogenase

As already mentioned, the structure of the resting FeMo protein revealed nothing about the mechanism for conversion of N_2 to NH_3. There is however a very large amount of data on the kinetics and spectroscopy (mainly EPR) of the enzyme with various substrates and inhibitors, impressive model chemistry, and information about the effects of site-directed mutations.[22,39] An issue is how to incorporate the new structural data into a more detailed and chemical description of the mechanism. More specifically there are questions about the location and geometry for the initial binding of N_2, the bonding geometry which activates N_2, the effects of introduction of electrons, the proton approach pathways, details of the binding of the intermediates, and the pathway for egress of products. Nitrogenase reduces protons in amounts determined by the availability of N_2, and H_2 inhibits N_2 reduction, and so there are related key questions about the binding of H^+, H and H_2 at the active site.

The first question (although not necessarily the first step in the mechanism) concerns the binding of N_2. In 1993, a lecture by Doug Rees about the cluster structure triggered the idea that the metallocarbohedrene experience was relevant. The hypothesis was:[40]

(*i*) metallocarbohedrenes have C_2 bound most stably along the long diagonal of a M_4 rhombus, while C_2 bonding parallel to the edges of an M_4 rectangle is less stable;
(*ii*) the $(Fe^3)_6$ trigonal prism of nitrogenase has three $(Fe^3)_4$ rectangular faces;
(*iii*) rotation of a trigonal prism about its threefold axis changes the rectangular faces to rhombuses;
(*iv*) N_2 is isoelectronic with C_2^{2-};
(*v*) therefore the N_2 could be bound stably to an $(Fe^3)_4$ rhombus face of a twisted form of the $(Fe^3)_6$ trigonal prism [Fig. 10(*a*)];
(*vi*) rotation back to the trigonal prismatic $(Fe^3)_6$ geometry with a rectangular $(Fe^3)_4$ face could weaken the N–N bond [Fig. 10(*b*)], which is the objective.

This hypothesis was fully consistent with the binding of the Fe_7MoS_9 cluster to the protein, because the cluster is anchored at the six-coordinate Mo end, but able to rotate the other end

about the pseudo-threefold axis coincident with the Fe–S_{cys} bond.

The feasibility of an $(Fe^3)_4$ face of the cluster as N_2 binding site was developed by examination of the protein surrounds and hydrogen bonds, revealing that the $(Fe^3)_4$ face capped by the extended side chain of arginine-359 was much better positioned than the other two for substrate binding:[79] this full $[(Fe^3)_4(S^2)_2(S^3)_2]$ face proposed for action is named the front face. DFT calculations demonstrated the feasibility of N_2 binding at this face, and also revealed that reduction of the cluster concentrated negative electron density on the S (rather than Fe or Mo) atoms, and particularly on the S^2 atoms flanking the binding face. Since these two flanking S^2 atoms are hydrogen bonded to protein from behind the front face, this result inspired the important mechanistic concept of proton transfer to bound substrate *via* these S^2 atoms according to their redox-moderated basicity, along the pathway illustrated in Fig. 11.

Continued application of DFT to the questions about nitrogenase structure and mechanism has provided further insight[41] into: (*a*) the flexibility of the Fe_7MoS_9(cys)(his)(cit) core structure; (*b*) the influence of redox level (both electronation and hydrogenation) on the geometry of the core; (*c*) the optimum geometries for N_2 bound to the core in various ways, and their relative energies; (*d*) the sliding of H atoms around the cluster atoms, in relation to the $2e^- + 2\,H^+ \rightleftharpoons H_2$ processes and the exchangeable and non-exchangeable hydrogen binding sites; (*e*) the binding of inhibitor CO and alternative substrates; and (*f*) the formation of NH_3.

The initial idea of the trigonal prism twisting about its threefold axis has been expanded to include and explore all of the conformational freedom of the Fe_7MoS_9 cluster. Because this cluster is undercoordinated it was expected to be floppy. Using the distortions shown in Fig. 12, DFT calculations with the 38-atom asymmetric model (Fig. 12) show that the energy surface for these distortions is relatively flat. Variations of Fe–Fe distances by up to 1 Å involve energy changes of < 10 kcal mol^{-1}: the flatness of the energy surface is dependent on the redox level.

A number of geometries for N_2 binding to the Fe_7MoS_9 cluster have been investigated theoretically.[40,42] My DFT calculations show that terminal η^1 binding of N_2 to one of the Fe^3 atoms is energetically favourable, and draws the Fe^3 atom out of the cluster to achieve local trigonal pyramidal coordination. However this does not elongate N–N as much as does η^2, μ_4 binding of both N atoms of N_2 to an $(Fe^3)_4$ face. The lowest energy η^2, μ_4 geometry is the conformation shown in Fig. 13(*left*), and dubbed 'oblique arrow' to describe the approach of N_2 to the $(Fe^3)_4$ face. One N atom, labelled $N^{proximal}$, is bonded to all four Fe^3 atoms, while the other (N^{distal}) is bonded to two Fe^3. This configuration is *ca.* 27 kcal mol^{-1} more stable than the symmetrical configuration of Fig. 13(*right*), and the N–N bond in the oblique arrow geometry is 1.29 Å relative to 1.10 Å in free N_2. The 'direct arrow' configuration in which N_2 is bound symmetrically to $(Fe^3)_4$ through only one N atom is not an energy minimum.

The N^{distal} atom in the oblique arrow conformation is positioned between three S atoms (two S^3, one S^2) on the front face, with N···S distances of 2.7–3.0 Å. Electronation of the cluster is calculated to increase the basicity of these S atoms, allowing H^+ ions to be transferred to them *via* hydrogen bonds, and after inversion at S^2 the resulting bound H atoms are within hydrogen bonding distance of the N^{distal} atom. This suggested a

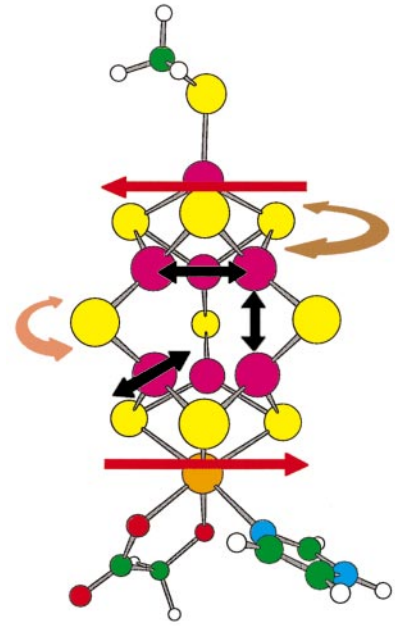

Fig. 12 Conformational freedom of the Fe_7MoS_9(cys)(his)(cit) cluster. The red arrows represent lateral shear, the brown arrow represents torsional twist about the pseudo-threefold axis, the orange arrow represents flapping of the S^2 atoms, and the black arrows represent various expansions and/or contractions of the $(Fe^3)_6$ trigonal prism.

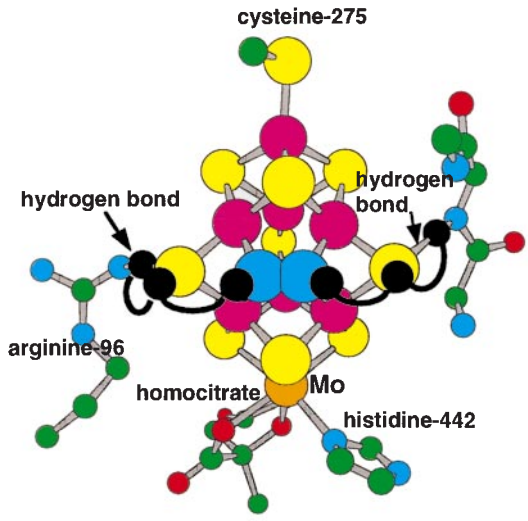

Fig. 11 The Fe_7MoS_9(cysteine)(histidine)(homocitrate) cluster, showing hydrogen bonds from behind the S^2 atoms flanking the front face, and the postulated transfer of H to bound N_2 by inversion of (S^2–H)

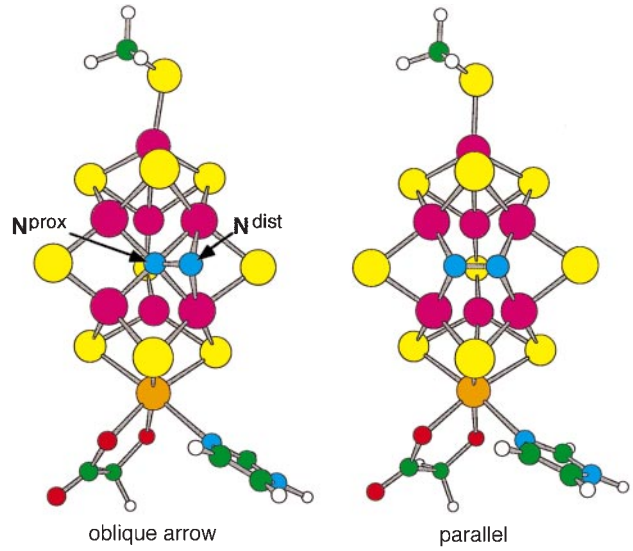

Fig. 13 The oblique arrow and parallel binding geometries for N_2 on the $(Fe^3)_4$ face of the Fe_7MoS_9(cys)(cit)(his) cluster. The calculated N–N distances are 1.29 and 1.25 Å, respectively.

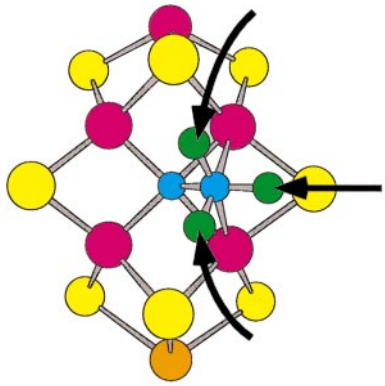

Fig. 14 Part of the front face of the Fe_7MoS_9(cys)(his)(cit) cluster showing N_2 bound in the oblique arrow configuration, the proposed trajectories for protonation of N^{distal}, and the H atom locations in the postulated transition state

mechanism for hydrogenation of N^{distal}. The transition state shown in Fig. 14 for transfer of these H atoms to N^{distal} was postulated, and on energy minimisation the N–N bond broke and NH_3 formed as N^{distal} separates.[43] This process is calculated to be exergonic by many tens of kcal mol^{-1}. Similar protonation of $N^{proximal}$ *via* the closest S atoms, in concert with electronation *via* the cluster, is postulated for subsequent formation of the second NH_3 product.[43]

The chemistry of hydrogen at the active site, while not as dramatic as the breaking of a very strong triple bond, is almost as intriguing. Some facts[39] are that proton reduction always accompanies N_2 reduction, in amounts depending on the availability of N_2; $H_{2\,(g)}$ inhibits N_2 reduction; the reductive formation of $HD_{(g)}$ from protons in the presence of $D_{2\,(g)}$ occurs in the presence of N_2 and with the same kinetics as N_2 reduction. A mechanistic requirement is that H atoms from the gas phase must always remain distinguishable from H atoms from water.[39]

The bonding and sliding of H atoms over the Fe and S atoms of the cluster can be investigated by DFT. One result is that H atoms bound to S atoms weaken their ligating ability, lengthening Fe^3–S bonds and shortening Fe^3–Fe^3 distances, while H atoms bonded to Fe^3 lengthen Fe^3–Fe^3 distances.[41] Other calculations show how H_2 can bind to Fe. Various $2H \rightleftharpoons H_2$ interconversions on the Fe_7MoS_9 cluster can be demonstrated.[41] As an illustration of the type of calculation which can inform this cluster–hydrogen chemistry, Fig. 15 outlines the main features of a calculated reaction coordinate for a symmetrical $2(S^2\text{–}H) \rightleftharpoons H_2$ interconversion on a $Fe_8S_9(SMe)_2$ model.

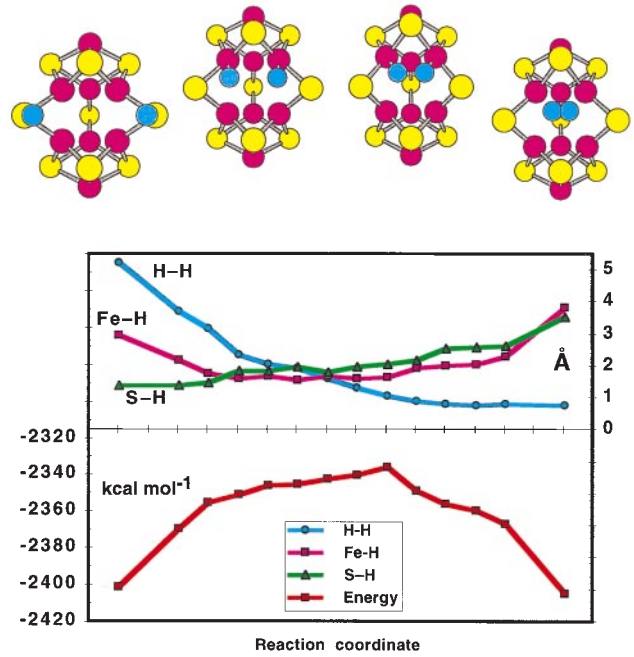

Fig. 15 Calculated reaction coordinate for a $2(S^2\text{–}H) \rightleftharpoons H_2$ transformation occurring on an $Fe_8S_9(SMe)_2$ model with C_s symmetry. Four structures in the sequence are shown at the top (with SMe groups omitted): in the left diagram two H atoms (blue) are bound to S^2 atoms, then move together *via* the mediation of Fe^3–H bonds, and then form H_2 which separates from the cluster. Interatomic distances and total energy through 14 points around the transition state are presented in the box.

Prospectives

This short account has provided glimpses of (1) the new chemistry which occurs for unprotected fundamental inorganic molecules, (2) consideration of this new molecular chemistry in the context of the more familiar non-molecular and protected analogous compounds, (3) the value of DFT, and (4) the value of concept-transfer between rather different chemical systems. But overall this has raised more questions than answers, and so I conclude with some prospectives for further research.

Continuing investigations of the formation and reactions of fundamental inorganic molecules in the gas phase, free of the ameliorating influences of solvation or crystal surrounds, will reveal more rule-breakers and expand the conceptual basis of fundamental inorganic chemistry.

A key objective is the preparation of bulk samples of the new molecules: this can be approached by condensation from the gas phase (*cf.* the fullerenes), or by planned reactions in relatively inert solution. The preparation of phosphine-protected copper sulfide clusters inspired by the gas phase results has been reported.[44] Preparation from the gas phase is likely to require condensation into a milieu which is inert or contains protecting ligands, to restrict conversion to non-molecular solids. On the basis of observed reactivities in the gas phase, the demonstrated successes of Dehnen and Fenske[44] using protecting ligands, and the calculated correlations of structure and reactivity, copper appears to be the most promising metal for preparation of the new molecules.

The Fe_7MoS_9 molecule at the catalytic site of nitrogenase is unprotected, in the sense of being undercoordinated, and is calculated to be reactive like other exposed metal sulfide molecules. It is also calculated to be floppy. The Fe_7MoS_9 cluster probably requires its protein cage for restraint of distortions, as well as restraint of some reactivity. The concerted enhancement of the catalytic reactivity of the Fe_7MoS_9 molecule by the protein surrounds is likely to occur primarily through the S atoms.

In an experimentally complex system such as the active site of nitrogenase, powerful DFT methods can provide insight and guidance to the experimental program.

Acknowledgments

I thank my coworkers and colleagues named in the references for their experimental efforts, vigorous discussions, and provision of information in advance of publication. This research is funded by the Australian Research Council and the University of NSW, and the Australian Nuclear Science and Technology Organisation provided computational resources.

Ian Dance is Professor of Inorganic Chemistry at the University of New South Wales. His formative research was under the direction of Professors Hans Freeman (Sydney), Jack Lewis (Manchester) and Richard Holm (MIT). He served on the faculty of the University of Wisconsin, Madison before joining the University of New South Wales in 1975. He won the Inorganic Award of the Royal Australian Chemical Institute in

1996, and was elected to Fellowship of the Australian Academy of Science in 1997.

Notes and References

* E-mail: i.dance@unsw.edu.au

† In the notation E^n the superscript *n* is the coordination number of E.

1 J. H. El Nakat, K. J. Fisher, I. G. Dance and G. D. Willett, *Inorg. Chem.*, 1993, **32**, 1931.
2 I. G. Dance and K. J. Fisher, *Prog. Inorg. Chem.*, 1994, **41**, 637.
3 I. G. Dance and K. J. Fisher, *Mater. Sci. Forum*, 1994, **152**, 137.
4 K. J. Fisher, I. G. Dance, G. D. Willett and M. Yi, *J. Chem. Soc., Dalton Trans.*, 1996, 709.
5 H. J. El-Nakat, I. G. Dance, K. J. Fisher and G. D. Willett, *J. Chem. Soc., Chem. Commun.*, 1991, 746.
6 J. H. El Nakat, I. G. Dance, K. J. Fisher and G. D. Willett, *Inorg. Chem.*, 1991, **30**, 2957.
7 I. G. Dance and K. J. Fisher, *J. Chem. Soc., Dalton Trans.*, 1997, 2563.
8 I. G. Dance, K. J. Fisher and G. D. Willett, *J. Chem. Soc., Dalton Trans.*, 1997, 2557.
9 K. Fisher and I. G. Dance, *J. Chem. Soc., Dalton Trans.*, 1997, 2381.
10 K. J. Fisher, I. G. Dance and G. D. Willett, *Polyhedron*, 1997, **16**, 2731.
11 I. G. Dance, in *Transition Metal Sulfur Chemistry: Biological and Industrial Significance*, ed. E. I. Stiefel and K. Matsumoto, American Chemical Society, Washington, DC, 1996, pp. 135–152.
12 J. H. El Nakat, I. G. Dance, K. J. Fisher, D. Rice and G. D. Willett, *J. Am. Chem. Soc.*, 1991, **113**, 5141.
13 K. J. Fisher, I. G. Dance and G. D. Willett, *Rapid Commun. Mass Spectrom.*, 1996, **10**, 106.
14 I. G. Dance, K. J. Fisher and G. D. Willett, *Inorg. Chem.*, 1996, **35**, 4177.
15 I. G. Dance, K. J. Fisher and G. D. Willett, *J. Chem. Soc., Chem. Commun.*, 1995, 975.
16 D. Fenske, J. Ohmer and J. Hachgenei, *Angew. Chem., Int. Ed. Engl.*, 1985, **24**, 993.
17 B. C. Guo, K. P. Kerns and A. W. Castleman, *Science*, 1992, **255**, 1411; A. W. Castleman, B. C. Guo, S. Wei and Z. Y. Chen, *Plasma Phys. Controlled Fusion*, 1992, **34**, 2047; Z. Y. Chen, G. J. Walder and A. W. Castleman, *J. Phys. Chem.*, 1992, **96**, 9581; S. Wei, B. C. Guo, J. Purnell, S. Buzza and A. W. Castleman, *Science*, 1992, **256**, 818.
18 J. S. Pilgrim and M. A. Duncan, *J. Am. Chem. Soc.*, 1993, **115**, 6958; Y. Yamada and A. W. Castleman, *Chem. Phys. Lett.*, 1993, **204**, 133; A. W. Castleman and K. H. Bowen, *J. Phys. Chem.*, 1996, **100**, 12 911; M. M. Rohmer, M. Benard and J. M. Poblet, in *Metal Clusters in Chemistry*, ed. P. Braunstein, VCH-Wiley, New York, 1997, in press; J. S. Pilgrim and M. A. Duncan, *Adv. Met. Semicond. Clusters*, 1995, **3**, 181; J. S. Pilgrim and M. A. Duncan, *J. Am. Chem. Soc.*, 1993, **115**, 9724; J. S. Pilgrim and M. A. Duncan, *Int. J. Mass Spectrom Ion Process.*, 1994, **138**, 283.
19 C. S. Yeh, S. Afzaal, S. A. Lee, G. Byun and B. S. Freiser, *J. Am. Chem. Soc.*, 1994, **116**, 8806; Y. G. Byun and B. S. Freiser, *J. Am. Chem. Soc.*, 1996, **118**, 3681; H. T. Deng, K. P. Kerns and A. W. Castleman, *J. Am. Chem. Soc.*, 1996, **118**, 446; B. C. Guo, K. P. Kerns and A. W. Castleman, *J. Am. Chem. Soc.*, 1993, **115**, 7415; H. T. Deng, B. C. Guo, K. P. Kerns and A. W. Castleman, *J. Phys. Chem.*, 1994, **98**, 13 373.
20 R. B. King, *J. Organomet. Chem.*, 1997, **536**–**537**, 7.
21 C. J. Adams, M. I. Bruce, B. W. Skelton and A. H. White, *J. Chem. Soc., Chem. Commun.*, 1993, 446; C. J. Adams, M. I. Bruce, B. W. Skelton and A. H. White, *Chem. Commun.*, 1996, 969; T. Bartik, B. Bartik, M. Brady, R. Dembinski and J. A. Gladysz, *Angew. Chem., Int. Ed. Engl.*, 1996, **35**, 414; W. Weng, T. Bartik and J. A. Gladysz, *Angew. Chem., Int. Ed. Engl.*, 1994, **33**, 2199.
22 J. Kim and D. C. Rees, *Nature*, 1992, **360**, 553; M. M. Georgiadis, H. Komiya, P. Chakrabarti, D. Woo, J. J. Kornuc and D. C. Rees, *Science*, 1992, **257**, 1653; J. Kim and D. C. Rees, *Science*, 1992, **257**, 1677; D. C. Rees, M. K. Chan and J. Kim, *Adv. Inorg. Chem.*, 1993, **40**, 89; J. T. Bolin, A. E. Ronco, T. V. Morgan, L. E. Mortenson and N. H. Xuong, *Proc. Nat. Acad. Sci. USA*, 1993, **90**, 1078; M. K. Chan, J. Kim and D. C. Rees, *Science*, 1993, **260**, 792; J. B. Howard and D. C. Rees, *Chem. Rev.*, 1996, **96**, 2965; J. W. Peters, M. H. B. Stowell, S. M. Soltis, M. G. Finnegan, M. K. Johnson and D. C. Rees, *Biochem.*, 1997, **36**, 1181.
23 R. J. Deeth, *New Sci.*, July 5, 1997, 24.
24 B. B. Laird, R. B. Ross and T. Ziegler, *Chemical Applications of Density Functional Theory*, American Chemical Society, Washington, DC, 1996; R. J. Deeth, *Struct. Bonding* (*Berlin*), 1995, **82**, 1; L. Fan and T. Ziegler, in *Density Functional Theory of Molecules, Clusters and Solids*, ed. D. E. Ellis, Kluwer, Dordrecht, 1995, pp. 67–95.
25 D. Fenske, H. Krautscheid and S. Balter, *Angew. Chem., Int. Ed. Engl.*, 1990, **29**, 796.
26 B. S. Snyder and R. H. Holm, *Inorg. Chem.*, 1990, **29**, 274.
27 A. C. Scheiner, J. Baker and J. W. Andzelm, *J. Comput. Chem.*, 1997, **18**, 775.
28 S. H. Vosko, L. Wilke and M. Nusair, *Can. J. Phys.*, 1980, **58**, 1200.
29 A. D. Becke, *Phys. Rev. A*, 1988, **38**, 3098.
30 C. Lee, W. Yang and R. G. Parr, *Phys. Rev. B*, 1988, **37**, 785.
31 I. G. Dance, *Aust. J. Chem.*, 1985, **38**, 1391.
32 I. G. Dance, *Polyhedron*, 1986, **5**, 1037.
33 I. G. Dance, *J. Chem. Soc., Chem. Commun.*, 1992, 1779.
34 M. M. Rohmer, M. Benard, C. Henriet, C. Bo and J. M. Poblet, *J. Chem. Soc., Chem. Commun.*, 1993, 1182; M. M. Rohmer, M. Benard, C. Bo and J. M. Poblet, *J. Am. Chem. Soc.*, 1995, **117**, 508; L. Lou, T. Guo, P. Nordlander and R. E. Smalley, *J. Chem. Phys.*, 1993, **99**, 5301.
35 I. G. Dance, *J. Am. Chem. Soc.*, 1996, **118**, 6309.
36 I. G. Dance, *J. Am. Chem. Soc.*, 1996, **118**, 2699.
37 I. G. Dance and H. H. Harris, *17th International Conference on Organometallic Chemistry*, Brisbane, Australia, 1996, Abstract PA65.
38 I. G. Dance, *J. Chem. Soc., Chem. Commun.*, 1993, 1306; I. G. Dance, *J. Am. Chem. Soc.*, 1993, **115**, 11 052.
39 B. K. Burgess, *Chem. Rev.*, 1990, **90**, 1377; G. J. Leigh, *New J. Chem.*, 1994, **18**, 157; G. J. Leigh and C. N. McMahon, *J. Organomet. Chem.*, 1995, **500**, 219; G. J. Leigh, *Eur. J. Biochem.*, 1995, **229**, 14; J. W. Peters, K. Fisher and D. R. Dean, *Annu. Rev. Microbiol.*, 1995, **49**, 335; G. J. Leigh, in *Nitrogen Fixation: Fundamentals and Applications*, ed. A. Tikhonavich *et al.*, Kluwer Academic, Dordrecht, 1995, pp. 129–135; B. K. Burgess and D. J. Lowe, *Chem. Rev.*, 1996, **96**, 2983 and references therein; R. H. Holm, P. Kennepohl and E. I. Solomon, *Chem. Rev.*, 1996, **96**, 2239; D. Sellmann and J. Sutter, *J. Biol. Inorg. Chem.*, 1996, 587; R. R. Eady, *Chem. Rev.*, 1996, **96**, 3013; C. J. Pickett, *J. Biol. Inorg. Chem.*, 1996, **1**, 601; R. N. F. Thorneley and D. J. Lowe, *J. Biol. Inorg. Chem.*, 1996, **1**, 576.
40 I. G. Dance, *Aust. J. Chem.*, 1994, **47**, 979.
41 I. G. Dance, in preparation.
42 H. Deng and R. Hoffmann, *Angew. Chem., Int. Ed. Engl.*, 1993, **32**, 1062; W. Plass, *J. Mol. Struct.*, 1994, **315**, 53; I. G. Dance, *J. Biol. Inorg. Chem.*, 1996, **1**, 581; K. K. Stavrev and M. C. Zerner, *Chem. Eur. J.*, 1996, **2**, 83.
43 I. G. Dance, *Chem. Commun.*, 1997, 165.
44 S. Dehnen, A. Schafer, D. Fenske and R. Ahlrichs, *Angew. Chem., Int. Ed. Engl.*, 1994, **33**, 746; S. Dehnen and D. Fenske, *Chem. Eur. J.*, 1996, **2**, 1407; S. Dehnen and D. Fenske, *Angew. Chem., Int. Ed. Engl.*, 1994, **33**, 2287.

7/08218E

Reappraisal of the spin-forbidden unimolecular decay of the methoxy cation†

Massimiliano Aschi, Jeremy N. Harvey, Christoph A. Schalley, Detlef Schröder and Helmut Schwarz‡

Institut für Organische Chemie der Technischen Universität Straße des 17. Juni 135, D-10623 Berlin, Germany

The mechanism of the unimolecular loss of H_2 from triplet methoxy cations ($^3CH_3O^+$) is revised.

The mental representation of chemical reactions relies on the paradigm of the potential energy surface (PES): the reactive system moves from the reactant minimum of the PES through a transition state to the product minimum. Reactions which involve a change in total spin appear to violate this paradigm, since they must necessarily occur on two or more PESs. For this reason, they have been difficult to understand, both qualitatively and quantitatively.[1] A typical example which has been the subject of numerous studies[2] is the unimolecular decomposition of triplet methoxy cation ($^3CH_3O^+$) to form H_2 and formyl cation (HCO^+), both singlet species. The present consensus (path A) is that this process occurs in a *stepwise* manner, *i.e.* first

$$^3CH_3O^+ \rightarrow {}^1CH_2OH^+ \rightarrow {}^1HCO^+ + H_2 \qquad \text{Path A}$$

$$^3CH_3O^+ \rightarrow {}^1HCO^+ + {}^1H_2 \qquad \text{Path B}$$

hydrogen shift, concurrent with spin change, to form *singlet* hydroxymethyl cation ($^1CH_2OH^+$), then the well documented[3] [1,2]-elimination to yield HCO^+ and H_2. The main support for this mechanistic scheme is derived from the observation of almost identical kinetic energy releases associated with the losses of molecular hydrogen from both $[C,H_3,O]^+$ cations.[2e] However, neither this experimental nor the computational evidence are conclusive. Indeed, a *concerted* pathway (path B) involving simultaneous spin change and [1,1]-elimination from $^3CH_3O^+$ has been suggested, but not established.[2f] Here we present experimental results[4–6] for the H/D isotope effect on unimolecular hydrogen loss from $[C,H_2,D,O]^+$ isotopomers of the methoxy and hydroxymethyl cations,[7] and discuss the mechanistic implications on the basis of supporting computational results in order to clear up the long-standing questions concerning the unimolecular decay of methoxy cation.

Assuming that only the *stepwise* mechanism occurs, Scheme 1 implies that the observed kinetic isotope effect KIE_{obs} for loss of molecular hydrogen from $^3CH_2DO^+$ is expected to be smaller than the kinetic isotope effect for loss of hydrogen from the intermediate $CHDOH^+$ (KIE_2), *whatever* the actual values of KIE_1 and KIE_2.[8] Assuming that KIE_2 does not depend much on the way in which $CHDOH^+$ is formed,[9] it can be obtained from the decay of independently generated $CHDOH^+$ cations. The relevant metastable ion (MI) spectra[4] (Fig. 1) lead to $KIE_{obs} = 8.0 \pm 1.0$ and $KIE_2 = 1.3 \pm 0.1$, respectively.[10] This value of KIE_{obs} is inconsistent with the above analysis, therefore

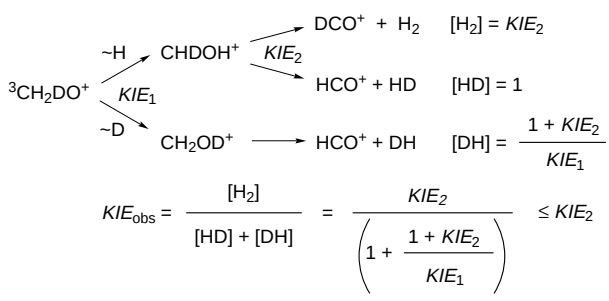

Scheme 1

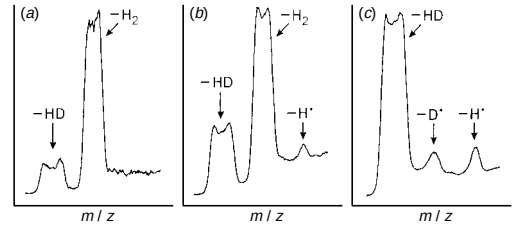

Fig. 1 MI spectra of (*a*) $^3CH_2DO^+$, (*b*) $CHDOH^+$ and (*c*) CH_2OD^+. Note that weak H/D atom losses are observed for the hydroxymethyl cations, which can be distinguished from H_2 loss by their peak shapes.

the stepwise path A alone cannot account for the experimental findings. Other mechanisms must strongly contribute; an obvious candidate is the *concerted* pathway B which could well have a kinetic isotope effect larger than KIE_2.

Further evidence comes from eqns. (1) and (2) for the relative yields of ideal *stepwise* and *concerted* mechanisms, respectively.[11] The experimental kinetic isotope effect for HD *vs.*

$$[HD] = 0.5\,([H_2] + [D_2]) \qquad (1)$$

$$[HD] = \sqrt{[H_2] \cdot [D_2]} \qquad (2)$$

D_2 loss from $^3CHD_2O^+$ cations[2e] is 10 ± 2, which, together with a kinetic isotope effect of 8.0 for H_2 *vs.* HD loss from $^3CH_2DO^+$, gives a branching ratio of $[H_2] : [HD] : [D_2] = 100 : 12.5 : 1.25$. Based on the measured $[H_2]$ and $[D_2]$ abundances, eqns. (1) and (2) predict [HD] values of 51 and 11 for *stepwise* and *concerted* pathways, respectively. Within the error margins, the observed [HD] figure of 12.5 is identical with the latter value, again suggesting that dehydrogenation of methoxy cation occurs in a concerted manner.

The $[C,H_3,O]^+$ hypersurfaces have been the subject of several computational studies.[2,3] The key events in the present reactions are, however, the spin changes, which can be assumed to proceed through surface hopping in the vicinity of the minimum energy crossing points (MECPs) between the PESs of different spin. Any computational description of unimolecular reactivity must therefore also consider the MECPs for paths A and B. This can be done with several methods which use analytical energy gradients.[1,12] The MECP corresponding to the *concerted* pathway (MECP1) has been described in the literature,[2f] but not that for the hydrogen migration in the *stepwise* route (MECP2).

Table 1 and Fig. 2 show the calculated[14] PESs for singlet and triplet $[C,H_3,O]^+$, including both MECPs. The key point is that MECP1 is slightly lower than MECP2 at each of the three levels of theory considered, although the relative energies of the two MECPs compared to $^3CH_3O^+$ vary somewhat. Further, the surface-hopping probability at the MECPs depends strongly on the spin-orbit coupling constant H^{SO} between the two wavefunctions. In fact, if the values of H^{SO} were very different at MECP1 and MECP2, the pathway with the larger H^{SO} could dominate, whatever the energies. To evaluate this possibility, we calculated[16] the value of H^{SO} at both MECPs, and obtained similar results, 50 cm^{-1} for H^{SO} (MECP1) and 56 cm^{-1} for H^{SO} (MECP2). With the present energies and H^{SO} values for MECP1 and MECP2, it is thus reasonable to expect that the

Table 1 Calculated (ref. 14) energies relative to $^3CH_3O^+$ at different points on the $[CH_3O^+]$ PESs, based on total energies[a] with no zero-point energy corrections

Species	UMP2	B3LYP	CCSD(T)	G2[b]
$HCO^+ + H_2$	−65.1	−38.4	−51.8	−54.5
CH_2OH^+	−92.4	−76.5	−85.6	−88.3
TS for H_2 loss	−6.4	11.7	2.5	−0.5
MECP1[c]	11.6	17.6	13.2	—
MECP2[c]	13.7	19.4	14.3	—

[a] Total energies (in Hartrees) for methoxy cation are −114.37456 (UMP2/BSI), −114.70013 (B3LYP/BSI), −114.47930 (CCSD(T)/BSII//B3LYP/BSI) and −114.50621 (G2). [b] G2 total energies are taken for comparison from ref. 13. [c] The calculated geometries for each MECP are very similar at all levels. The results for MECP1 reported in ref. 2(*f*) are similar to those obtained here.

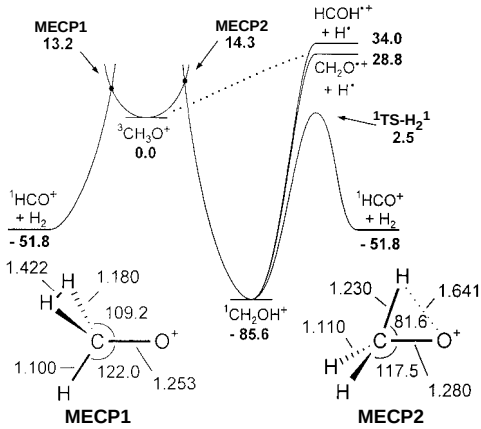

Fig. 2 Relevant parts of the triplet and singlet potential energy surfaces of $[C,H_3,O]^+$ cations calculated at the CCSD(T)/BSII//B:3LYP/BSI level (ref. 14). Bond lengths are given in Å and angles in degrees. Energies relative to the methoxy cation are given in kcal mol^{-1}.

concerted mechanism should at least be favoured over the *stepwise* pathway, although precise quantitative predictions would require a much more thorough analysis.[18]

The observation of nearly identical kinetic energy releases from both $[C,H_3O]^+$ cations[2e] is an argument in favour of the *stepwise* mechanism. However, if one considers that the height of MECP1 is less than 11 kcal mol^{-1} higher than ^{1}**TS-H$_2$**$^+$ (see Fig. 2), then it can be seen that these identical kinetic energy releases could come from different mechanisms.

In conclusion, the kinetic isotope effect results reported here provide very strong support for a reappraisal of the mechanism of unimolecular decomposition of the triplet methoxy cation and the present results suggest a [1,1]-elimination in which dehydrogenation and spin crossover occur in concert.[19,20]

Financial support by the Deutsche Forschungsgemeinschaft, the Fonds der Chemischen Industrie and the Volkswagen-Stiftung is acknowledged. M. A. and J. N. H. thank the CNR (Italy) and the Alexander-von-Humboldt-Stiftung, respectively, for research scholarships. The authors thank M. W. Schmidt and A. A. Granovsky for providing them with a copy of GAMESS for PC. Dedicated to Professor D. H. Williams FRS, Cambridge, on the occasion of his 60th birthday.

Notes and References

† This ChemComm is also available in expanded form *via* the World Wide Web: http://www.rsc.org/ccenhanced

‡ E-mail: schw0531@www.chem.tu-berlin.de

1 D. R. Yarkony, *J. Phys. Chem*., 1996, **100**, 18 612.

2 Selected references: (*a*) M. S. B. Munson and J. L. Franklin, *J. Phys. Chem*., 1964, **68**, 3191; (*b*) R. D. Bowen and D. H. Williams, *J. Chem. Soc., Chem. Commun*., 1977, 378; (*c*) P. v. R. Schleyer, A. D. Jemmis and J. A. Pople, *J. Chem. Soc., Chem. Commun*., 1978, 190; (*d*) M. M. Bursey, J. R. Hass, D. J. Harvan and C. E. Parker, *J. Am. Chem. Soc*., 1979, **101**, 5485; (*e*) P. C. Burgers and J. L. Holmes, *Org. Mass Spectrom*., 1984, **19**, 452; (*f*) D. R. Yarkony, *J. Am. Chem. Soc*., 1992, **114**, 5406; (*g*) S.-C. Kuo, Z. Zhang, R. B. Klemm, J. F. Liebman, L. J. Stief and F. L. Nesbitt, *J. Phys. Chem*., 1994, **98**, 4026.

3 (*a*) E. Uggerud, T. Helgaker, *J. Am. Chem. Soc*., 1992, **114**, 4265; (*b*) C. A. Schalley, M. Dieterle, D. Schröder, H. Schwarz and E. Uggerud, *Int. J. Mass Spectrom. Ion. Processes*, 1997, **163**, 101.

4 The experiments were carried out with a four-sector ZAB-2F-HF/AMD604 mass spectrometer (ref. 5). Methoxy cations were generated by charge reversal (CR) of the corresponding anions [ref. 2(*d*)]. Hydroxymethyl cations were formed by electron ionization of labelled ethanols. The ions' connectivities were checked by collisional activation (CA) and CR/CA experiments [refs. 2(*e*), 3(*b*)]. The metastable ion decomposition products were monitored in MI and CR/MI experiments by scanning the fourth sector.

5 C. A. Schalley, D. Schröder and H. Schwarz, *Int. J. Mass Spectrom. Ion Processes*, 1996, **153**, 173.

6 B. A. Rumpf, C. E. Allison and P. J. Derrick, *Org. Mass Spectrom*., 1986, **21**, 295.

7 The MI mass spectra of $[C,H_3,O]^+$ and $[C,D_3,O]^+$ were also recorded, and the results are consistent with the present analysis.

8 KIE_1 and KIE_2 are product determining. Intermolecular kinetic isotope effects have not been taken into account, but, of course, would not affect the qualitative conclusions made here.

9 The effect of different internal energies of non-ergodicity on KIE_2 is probably small; an *enormous* change would anyway be needed to modify the conclusions outlined in Scheme 2.

10 For evaluation of the kinetic isotope effects, several experiments were averaged and the intensities were corrected for mass discrimination (see ref. 6) and for the statistical weights of H_2, HD and D_2.

11 G. Hvistendahl and D. H. Williams, *J. Chem. Soc., Chem. Commun*., 1975, 4.

12 J. N. Harvey, M. Aschi, H. Schwarz and W. Koch, *Theor. Chem. Acc*., in the press, and references cited therein.

13 N. L. Ma, B. J. Smith, J. A. Pople and L. Radom, *J. Am. Chem. Soc*., 1991, **113**, 7903.

14 Calculations at the UMP2 and B3LYP levels of theory were performed with GAUSSIAN94 [ref. 15(*a*)] and the 6-311+G(d,p) (BSI) basis set. The MECPs were located using our recently described method (ref. 12), and the gradients at these points were inspected to verify that they connect to the relevant minima. The CCSD(T) calculations at B3LYP optimized geometries were performed in MOLPRO [ref. 15(*b*)] with the cc-pVTZ basis set, omitting the *d* functions on hydrogen (BSII). At this level, the MECPs were optimized using the hybrid method of ref. 12 with B3LYP/BSI gradients.

15 (*a*) GAUSSIAN 94, Revision E.1, Gaussian, Inc., Pittsburgh, PA, 1995; (*b*) MOLPRO 96.4 is a package of *ab initio* programs written by H.-J. Werner and P. J. Knowles; (*c*) GAMESS USA (18th March 1997 version), M. W. Schmidt, K. K. Baldridge, J. A. Boatz, S. T. Elbert, M. S. Gordon, J. H. Jensen, S. Koseki, N. Matsunaga, K. A. Nguyen, S. J. Su, T. L. Windus, M. Dupuis and J. A. Montgomery, *J. Comput. Chem*., 1993, **14**, 1347. PC version compiled by A. A. Granovsky, Moscow State University.

16 These calculations were performed using an approximate one-electron Hamiltonian (ref. 17), as implemented in GAMESS [ref. 15(*c*)]. The GAMESS TZV basis set was used with one heavy atom d-polarisation function; the singlet and triplet states were described by CI wavefunctions expanded within a basis of HF orbitals generated either for the singlet or the triplet; the effective nuclear charges used were those recommended in ref. 17. The CI expansion included all possible determinants formed by allocating the eight valence electrons into five orbitals, and by allowing single excitations into the virtual orbitals. The value reported is the magnitude of the H^{SO} complex matrix element between coupled substates.

17 S. Koseki, M. S. Gordon, M. W. Schmidt and N. Matsunaga, *J. Phys. Chem*., 1995, **99**, 12 764.

18 The relative slope of the two surfaces at the MECP also affects the surface hopping probability. This factor is very similar at the two MECPs.

19 Spin crossover is also important in transition and metal chemistry. See, for example S. Shaik, M. Filatov, D. Schröder and H. Schwarz, *Chem. Eur. J*., 1998, **4**, 193.

20 Proton transfer reactions involving spin changes were recently reported: J. Hu, B. T. Hill and R,. R. Squires, *J. Am. Chem. Soc*., 1997, **119**, 11 699; P. A. Janaway, M. Zhing, P. P. Gater, M. L. Chabinye and J. I. Brennan, *J. Am. Chem. Soc*., 1997, **119**, 11 697.

Received in Cambridge, UK, 1st December 1997; 7/08642C

Stereoselective synthesis of a new optically active phosphinoacyloxazolidinone *via* enantioselective hydrogenation

Pierre Le Gendre, François Jérôme, Christian Bruneau* and Pierre H. Dixneuf*†

Laboratoire de Chimie de Coordination et Catalyse, UMR 6509, CNRS-Université de Rennes, Campus de Beaulieu, F-35042 Rennes, France

The preparation of a new optically active phosphinoacyloxazolidinone, based on the enantioselective hydrogenation of a 4-methylene-*N*-propionyloxazolidinone in the presence of [(*R*)-BINAP]Ru(O_2CCF_3)$_2$ catalyst followed by stereoselective phosphinylation, is reported.

Chiral diphosphines coordinated to a transition metal centre have demonstrated their power in asymmetric catalysis.[1] More recently, optically active heterobidentate ligands containing only one phosphorus group have proved to be very efficient in a variety of catalytic reactions. Thus, the diphenylphosphino group attached to a functional group such as an amine,[2] an oxazoline,[3] a pyrazole[4] or a quinoline[5] moiety has led to a variety of new P–N ligand–metal catalysts which have contributed to the improvement of enantioselectivity in various catalytic reactions. Other heterobidentate functional phosphine ligands with an additional coordinating oxygen atom have also been used successfully in asymmetric catalysis.[6–9]

Here we report the preparation of a new P–O heterobidentate ligand of high optical purity based on the synthesis of an optically active acyloxazolidinone followed by its phosphinylation. This synthesis does not involve substrates from the natural chiral pool but is based on two successive selective reactions: (i) the enantioselective hydrogenation of a 4-methylene-*N*-propionyloxazolidin-2-one **1**, and (ii) the stereoselective phosphinylation of the resulting optically active acyloxazolidinone **2**, according to Scheme 1.

Whereas optically active acyloxazolidinones are usually prepared by acylation of oxazolidinones arising from optically active natural amino acids *via* multistep syntheses,[10,11] we have shown that it is possible to obtain both enantiomers of the acyloxazolidinone **2** *via* enantioselective hydrogenation of the 4-methylene-*N*-acyloxazolidinone **1** in the presence of a ruthenium catalyst containing an optically pure diphosphine ligand.

The bubbling of ammonia through an EtOAc solution of the carbonate **4**[12] at room temperature led to 95% yield of the hydroxyoxazolidinone **5**. The treatment of this cyclic carbamate with an excess of propionyl chloride in refluxing CH_2Cl_2 in the presence of $CaCl_2$ led to the isolation of the acyloxazolidinone **1** (80% yield) in a one pot acylation–dehydration reaction. The enantioselective hydrogenation of **1** was performed under 10 MPa of H_2 in MeOH at 50 °C for 18 h in the presence of 1 mol% of [(*R*)-BINAP]Ru(O_2CCF_3)$_2$ as catalyst and led to the (*R*)-*N*-propionyloxazolidinone (*R*)-**2** in 95% yield. Thus, in a four step synthesis involving only small simple molecules (prop-2-ynylic alcohol, CO_2, NH_3, AcCl and H_2), the (*R*)-*N*-propionyloxazolidinone (*R*)-**2** was isolated with an enantiomeric excess

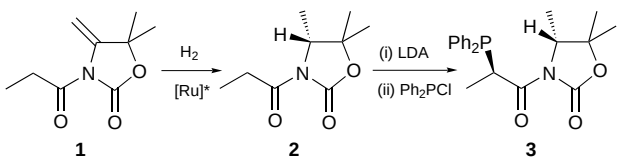

Scheme 1

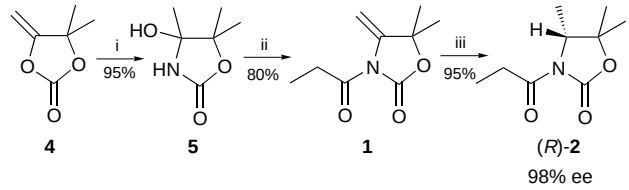

Scheme 2 *Reagents and conditions*: i, NH_3, room temp.; ii, EtCOCl, CH_2Cl_2 reflux; iii, H_2, [(*R*)-BINAP]Ru(O_2CCF_3)$_2$, MeOH, 50 °C

of 98%, according to Scheme 2.‡ Compound (*R*)-**2** appears to be the simplest (*R*)-enantiomer of the family of Superquats, the (*S*)-enantiomer of which has already been prepared from an amino acid.[11]

Advantage was taken of the asymmetric induction offered by chiral acyloxazolidinones to stereoselectively introduce an electrophile on the acyl group.[10,11] We thus attempted to transform (*R*)-**2** into a functional phosphine of type **3** by addition of the electrophilic diphenylphosphino group after deprotonation of the acyl moiety of (*R*)-**2** (Scheme 3).

The *N*-propionyloxazolidinone (*R*)-**2** (4.3 mmol) was first deprotonated in THF at −90 °C using LDA (1 equiv.). Then, chlorodiphenylphosphine (4.3 mmol) was added and the reaction mixture was kept at −90 °C for 15 h before warming to room temperature. The resulting phosphinoacyloxazolidinone (*R*,*R*)-**3** was purified by chromatography over alumina and isolated in 87% yield. The ^{31}P NMR spectrum of the crude oil showed two singlets at δ 5.84 and 4.87, indicating the presence of the two diastereoisomers in the ratio 95 : 5. This result shows that the novel transformation of acyloxazolidinones by phosphinylation is stereoselective and that the optically pure *N*-propionyloxazolidinone (*R*)-**2** provides efficient asymmetric induction as already observed for the alkylation with BnBr, of (*S*)-**2** prepared *via* a different route.[11]

This functional phosphine is very air-sensitive and it is preferable to stabilize it as a phosphine–borane adduct. The addition of BH_3·SMe at −80 °C at the end of the reaction leading to **3** made possible the preparation of the corresponding phosphine–borane (*R*,*R*)-**6**.§ Chromatography over silica gel allowed the isolation of only the major diastereoisomer in 47% yield (100% de).

Cleavage of the *N*-acyl bond of (*R*,*R*)-**3** was carried out under mild conditions in MeOH at room temperature in the presence of K_2CO_3 and led to the chiral oxazolidinone auxiliary (*R*)-**8** and

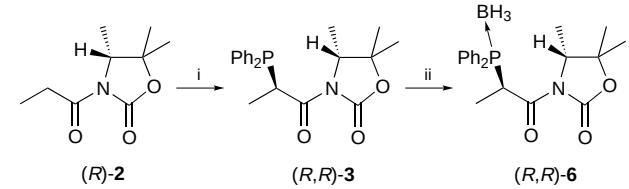

Scheme 3 *Reagents and conditions*: i, LDA, THF, −90 °C, then Ph_2PCl, −90 °C to room temp.; ii, BH_3·SMe_2

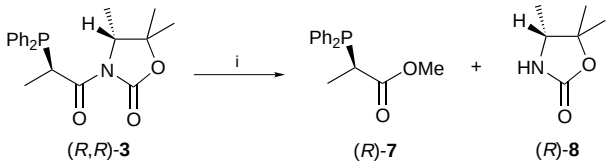

Scheme 4 *Reagents and conditions*: i, MeOH, K_2CO_3, room temp.

the optically active phosphine methyl ester (*R*)-**7** in 90% yield after column chromatography under N_2 (Scheme 4).

In conclusion, we report the selective preparation of an optically pure phosphinoacyloxazolidinone. The synthesis involves the preparation of an optically active acyloxazolidinone *via* catalytic enantioselective hydrogenation and its use as chiral inductor for stereoselective phosphinylation. This type of new compound has potential as a new heterobidentate ligand in asymmetric catalysis, and as a building block for access to a variety of optically active phosphorus derivatives *via* cleavage of the oxazolidinone ring.

Notes and References

† E-mail: pierre.dixneuf@univ-rennes1.fr

‡ *Selected data* for (*R*)-**2**: δ_H (300 MHz, $CDCl_3$) 1.14 (3 H, t, *J* 7.3, *Me*CH_2), 1.26 (3 H, d, *J* 6.6, *Me*CH), 1.39 and 1.41 (2 × 3 H, 2 s, Me_2C), 2.88 and 2.90 (2 H, m, *J* 16.0, 7.35, MeCH_2CO), 4.16 (1 H, q, *J* 6.6, *CH*Me); δ_C(75.5 MHz, $CDCl_3$) 8.35 (q, *J* 128), 14.69 (q, *J* 128), 21.55 (q, *J* 127), 27.83 (q, *J* 128), 29.33 (t, *J* 128), 58.88 (d, *J* 147), 81.41 (s), 152.79 (s), 174.34 (s); Calc. for $C_9H_{15}NO_3$: C, 58.36; H, 8.16; N, 7.56. Found: C, 58.07; H, 8.45; N, 7.60%. $[\alpha]_D$ −51 (*c* 0.9, $CHCl_3$).

§ *Selected data* for (*R*,*R*)-**6**: mp 141 °C; δ_P(121.5 MHz, $CDCl_3$) 26.76 (q, *J* 48.8); δ_H(300 MHz, $CDCl_3$) 1.09 (3 H, d, *J* 6.6, NCHCH_3), 1.17 (3 H, s, CMe_2), 1.35 (3 H, s, CMe_2), 1.42 [3 H, dd, *J* 15.5, 6.9, *Me*CH(PPh_2)], 4.03 (1 H, q, *J* 6.6, N*CH*CH_3), 5.50 [1 H, dq, *J* 12.7, 6.9, *CH*(PPh_2)], 7.39–7.90 (10 H, Ph); δ_C(75.5 MHz, $CDCl_3$) 13.39 (q, *J* 131.2), 13.68 (q, *J* 128.2), 21.59 (q, *J* 127.5), 27.51 (q, *J* 127.5), 34.75 (dd, *J* 137.9, 25.5), 59.37 (d, *J* 141.6), 81.46 (s), 126.65–133.72 (m), 152.87 (s), 171.09 (s); Calc. for $BC_{21}H_{27}NO_3P$: C, 65.81; H, 7.10; N, 3.65; P, 8.08. Found: C, 65.81; H, 7.14; N, 3.65; P, 7.93%. $[\alpha]_D$ + 58 (*c* 1.0, $CHCl_3$).

1 R. Noyori, *Asymmetric Catalysis in Organic Synthesis*, Wiley, New York, 1993; I. Ojima, *Catalytic Asymmetric Synthesis*, VCH, New York, 1993.
2 I. Hayashi, M. Konishi, M. Fukushima, T. Mise, M. Kagotani, M. Tajika and M. Kumada, *J. Am. Chem. Soc.*, 1982, **104**, 180; P. Wimmer and M. Widhalm, *Tetrahedron: Asymmetry* , 1995, **6**, 657; H. Kubota and K. Koga, *Tetrahedron Lett.*, 1994, **95**, 6689.
3 J. Spring and G. Helmchen, *Tetrahedron Lett.*, 1993, **34**, 1769; P. von Matt and A. Pfaltz, *Angew. Chem., Int. Ed. Engl.*, 1993, **32**, 566; G. J. Dawson, C. G. Frost and J. M. J. Williams, *Tetrahedron Lett.*, 1993, **34**, 3149.
4 A. Togni, U. Burckhardt, V. Gramlich, P. S. Pregosin and R. Salzmann, *J. Am. Chem. Soc.*, 1996, **118**, 1031.
5 J. M. Brown, D. J. Hulmes and P. J. Guiry, *Tetrahedron*, 1994, **50**, 4493.
6 Y. Uozumi and T. Hayashi, *J. Am. Chem. Soc.*, 1991, **113**, 9887; J. F. Marcaux, S. Wagaw and S. L. Buchwald, *J. Org. Chem.*, 1997, **62**, 1568.
7 T. Minami, Y. Okada, T. Otaguro, S. Tawaraya, T. Furiuki and T. Okauchi, *Tetrahedron: Asymmetry*, 1995, **6**, 2469.
8 Y. Nagagawa, M. Kanai, Y. Nagaoka and K. Tomioka, *Tetrahedron Lett.*, 1996, **37**, 7805.
9 D. Enders and T. Berg, *Synlett*, 1996, 796.
10 D. J. Ager, I. Prakash and D. R. Schaad, *Chem. Rev.*, 1996, **96**, 835.
11 S. G. Davies, M. E. C. Polywka and H. J. Sanganee, *Int. Appl.* WO 95/18112, 1995.
12 J.-M. Joumier, J. Fournier, C. Bruneau and P. H. Dixneuf, *J. Chem. Soc., Perkin Trans. 1*, 1991, 3271.

Received in Liverpool, UK, 14th November 1997; 7/08223A

Meerwein–Ponndorf–Verley reduction of carbonyl compounds catalysed by Mg–Al hydrotalcite

Pramod S. Kumbhar,† Jaime Sanchez-Valente, Joseph Lopez and François Figueras*‡

Institut de Recherches sur la Catalyse, 2 Av. A. Einstein, 69626 Villeurbanne, France

Properly activated Mg–Al hydrotalcite (Mg : Al = 3 : 1) is found to be a highly active, selective and regenerable heterogeneous catalyst for Meerwein–Ponndorf–Verley reduction of carbonyl compounds in the liquid phase.

The reduction of carbonyl compounds is one of the most widely practised operations in the synthetic organic, fine and perfumery chemical industries. Of particular importance is selective reduction of carbonyl groups in the presence of other functional groups. New methods, new catalysts and new reagents which offer greater activity, selectivity and reusability are constantly being sought.

The Meerwein–Ponndorf–Verley (MPV) reduction of aldehydes and ketones is one such reaction when high selectivities are obtained using metal alkoxides as catalysts, such as $Al(OPr^i)_3$ and $La(OPr^i)_3$.[1] However, the metal alkoxide catalysts are homogeneous, create problems during separation and are not reusable. Hence, reusable heterogeneous catalysts will have a distinct advantage if they can match the performance of homogeneous catalysts. In this regard, Posner *et al.*[2] were first to report the use of Al_2O_3 as a catalyst. However, a large amount of catalyst needed to be used (1–2 g Al_2O per mmol substrate) to achieve high conversions. Recently, Van Bekkum[3] showed that properly activated zeolite β was a highly active and stereoselective catalyst for the reduction of 4-*tert*-butylcyclohexanone to *cis*-4-*tert*-butylcyclohexanol. However, the use of zeolite β has limitations due to its pore size (7.4 × 6.5 Å). Kaspar *et al.*[4] have reported the use of MgO as a moderately selective catalyst for the reduction of α,β-unsaturated ketones in a fixed bed reactor using vapour phase conditions. In a fundamental study Ivanov *et al.*[5] have shown that MPV reductions can be catalysed by both basic and acid sites. Niyama *et al.*[6] reported that catalysts having adequate acidity and basicity show high activity in this reaction.

Here we report that properly activated Mg–Al hydrotalcite having a Mg/Al ratio of 3 : 1 is a highly active, selective and regenerable catalyst for MPV reduction of carbonyl compounds in the liquid phase. The high activity of these catalysts is attributed to the presence of both strongly basic and mildly acidic sites.

Mg–Al hydrotalcites having different ratios were synthesised using the procedure reported by Miyata *et al.*[7] The presence of pure hydrotalcite structure was confirmed by PWXRD. The catalysts activated in N_2 upto 550 °C showed a MgO pattern by X-ray diffraction indicating the formation of a solid solution of Al in MgO. The catalytic test was carried out using propan-2-ol as the hydrogen donor at 82 °C. The catalyst was pre-treated in N_2 at the desired temperature and carefully transferred to the reactor containing propan-2-ol without exposure to air, after which the substrate was introduced. Periodically withdrawn samples were analysed by gas-liquid chromatography.

The preliminary testing of hydrotalcites having different Mg/Al ratios and different calcination temperatures was carried out for the reduction of 4-*tert*-butylcyclohexanone to 4-*tert*-butylcyclohexanol. The hydrotalcite having a Mg : Al ratio of 3 : 1, calcined at 450 °C, was found to be the most active (Table 1). Hence all further studies were carried out using this catalyst.

Table 1 Effect of Mg : Al ratio and calcination temperature on the activity of Mg–Al hydrotalcites for MPV reduction of 4-*tert*-butylcyclohexanone[a]

Mg : Al ratio	Activation temperature/°C	Initial rate/10^4[b]
2 : 1	450	0.27
3 : 1	350	0.85
3 : 1	450	4.12
3 : 1	550	2.22
5 : 1	450	0.73
3 : 1[c]	450	4.09

[a] Reaction conditions: 4-*tert*-butylcyclohexanone (13 mmol), propan-2-ol (10 ml), catalyst (0.15 g) activated in N_2, reaction temperature 82 °C; [b] In mol per min per g catalyst. [c] Catalyst regenerated after one use in N_2 at 450 °C.

To allow comparison with the results reported by Van Bekkum[3] the same reaction was carried out using similar conditions on a reduced scale. Under these conditions, even with a lower catalyst loading (0.075 g instead of 0.1 g), 98% conversion was reached within 4 h with selectivity for alcohol greater than 95% (Fig. 1) (*trans* to *cis* alcohol ratio: 85 : 15). This shows that the activity of the catalyst prepared from hydrotalcite precursor is substantially higher than that reported for alumina, silica–alumina and Y-zeolite.[3]

The reusability of the catalyst was checked *via* solid separated by filtration and reactivated in N_2 at 450 °C. The reused catalyst showed similar activity to a fresh sample (Table 1).

The study was extended to the reduction of some industrially important unsaturated carbonyl compounds, such as cinnamaldehyde, citral and citronellal, to the corresponding unsaturated alcohols, which are high value perfumery chemicals. The results are summarised in Table 2. As can be seen, the catalyst is both active and highly selective.

The higher selectivities obtained are rather unexpected as hydrotalcites are strongly basic and one would have expected the aldol condensation reaction to be predominant. However, as we have already shown in our previous publication, the aldol

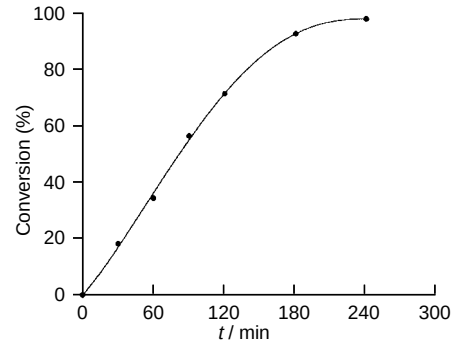

Fig. 1 Conversion *versus* time plot for reduction of 4-*tert*-butylcyclohexanone using Mg–Al hydrotalcite (Mg : Al = 3 : 1). Reaction conditions: same as Table 1 except 4-*tert*-butylcyclohexanone (1 mmol) catalyst (0.075 g) activated in N_2 at 450 °C.

Table 2 MPV reduction of unsaturated aldehydes to unsaturated alcohols over Mg–Al hydrotalcite (Mg : Al = 3 : 1)[a]

Aldehyde	*t*/h	Conversion (%)	Selectivity for unsaturated alcohol (%)
Citronellal	4	90	95[b]
Cinnamaldehyde	5	75	92[c]
Citral	5	83	70[d]

[a] Reaction conditions: aldehyde (1 mmol) catalyst (0.14 g) activated in N_2 at 450 °C, propan-2-ol (10 ml), T = 82 °C, stirring speed = 900 rpm. [b] Citronellol. [c] Cinnamyl alcohol. [d] Nerol + geraniol.

condensation reaction is catalysed by Brönsted bases (OH^- groups) and calcined hydrotalcites, which are Lewis bases, do not catalyse this reaction.[8] As we have used catalysts activated in N_2 at 450 °C having only Lewis basicity, they do not give aldol products under the mild reaction conditions used; this is consistent with the previous work.

The high activity of calcined hydrotalcites probably comes from the synergetic effect of strong Lewis basicity and mild acidity, as shown in Fig. 2. This mechanism agrees with that proposed by Ivanov *et al.*[5] based on *in situ* IR experiments.

In summary, we have shown that properly activated Mg–Al hydrotalcite (Mg : Al = 3 : 1) is a highly active, selective and regenerable catalyst for Meerwein–Ponndorf–Verley reduction of carbonyl compounds under liquid phase conditions.

We thank the Indo-French Centre for Promotion of Advanced Research (IFCPAR project no. IFC/1106-2696-2460) for financial support. J. S. V. thanks Conacyt de Mexico for a PhD grant.

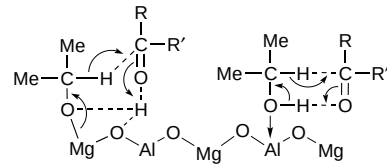

Fig. 2 Proposed mechanism of the MPV reduction over Mg–Al hydrotalcite

Notes and References

† On leave from Herdillia Chemicals Ltd., Navi Mumbai, India.
‡ E-mail: figueras@catalyse.univ-lyon1.fr

1 For a review, see: C. F. Grauw, J. A. Peters, H. Van Bekkum and J. Huskens, *Synthesis*, 1994, **10**, 1007.
2 G. H. Posner, A. W. Runquist and M. J. Chapdelaine, *J. Org. Chem.*, 1977, **42**, 1202.
3 E. J. Creyghton, S. D. Ganeshie, R. S. Downing and H. Van Bekkum, *J. Chem. Soc., Chem. Commun.*, 1995, 1859; *J. Mol. Catal., A: Chem.*, 1997, **115**, 457.
4 J. Kaspar, A. Trovarelli, M. Lenarda and M. Graziani, *Tettrahedron Lett.*, 1989, **30**, 2705.
5 V. A. Ivanov, J. Bachelier, F. Audry and J. C. Lavalley, *J. Mol. Catal.*, 1994, **91**, 45.
6 H. Niyama and E. Echigoya, *Bull. Chem. Soc. Jpn.*, 1972, **45**, 938.
7 S. Miyata, T. Kumura and M. Shimada, *US Pat.*, 1975, 3 879 523.
8 K. Rao, F. Figueras, J. Sanchez and M. Gravelle, *J. Catal.*, in the press.

Received in Liverpool, UK, 21st November 1997; 7/08431E

Liquid-crystalline mixed [60]fullerene–ferrocene materials

Robert Deschenaux,*[a] Michael Even[a] and Daniel Guillon[b]

[a] *Institut de Chimie, Université de Neuchâtel, Av. de Bellevaux 51, 2000 Neuchâtel, Switzerland*
[b] *Institut de Physique et Chimie des Matériaux de Strasbourg, Groupe des Matériaux Organiques, 23 Rue du Loess, 67037 Strasbourg Cédex, France*

[60]Fullerene was functionalized with a mesomorphic malonate derivative containing two ferrocene units; the targeted compound showed thermotropic liquid-crystalline properties.

Recently, we reported the first [60]fullerene-containing thermotropic liquid crystal.[1] The C_{60} core was functionalized with a twin cholesterol malonate derivative following well established literature procedures.[2] The targeted fullerene derivative showed a monotropic smectic A phase.[1] This finding is of interest regarding the increasing activity which is currently devoted to the design of fullerene-based new materials.[3] On the other hand, photoinduced electron transfer reactions in fullerene–ferrocene dyads have been investigated[4] (intramolecular quenching of C_{60} singlet excited state by the ferrocene framework was observed). Such studies are interesting with a view to elaborating new optical and electronic molecular devices.[3,4] The design of fullerene–ferrocene compounds showing liquid-crystalline behavior is attractive as such structures would lead to new multicomponent mesomorphic materials.

This communication describes the synthesis and liquid-crystalline properties of the mixed fullerene–ferrocene thermotropic liquid crystal **1** which represents the first member of this new family of mesomorphic materials. Malonate derivative **2** was selected to functionalize the C_{60} core owing to the high mesomorphic character of the twin cholesterol liquid crystals.[1]

The synthesis of **1** is presented in Scheme 1. 1-Carboxybenzyloxy-1′-chlorocarboxyferrocene[5] (**3**) was reacted with cholest-5-en-3β-yl-4-(10-hydroxydecyloxy)benzoate[1] to give protected ferrocene **4**. Deprotection of the latter species gave acid **5**, the esterification of which with hydroquinone monobenzyl ether led to benzyl derivative **6**. Removal of the benzyl protecting group furnished phenol intermediate **7**, which was subsequently *O*-alkylated with 6-bromohexanol to give **8**. Condensation of **8** with malonyl chloride led to **2**. Finally, treatment of **2** with [60]fullerene adapting a literature procedure[6] gave the targeted structure **1**, as a dark solid. The latter species was purified by column chromatography (silica gel, eluent: toluene–AcOEt 20 : 1 v/v) and precipitation (dissolution in CH_2Cl_2 and precipitation in MeOH). Its structure and purity were confirmed by NMR spectroscopy, UV–VIS spectroscopy and elemental analysis.† As expected, the [6,6]-closed methanofullerene derivative was obtained.[1,2]

The thermal and liquid-crystalline properties of **1**, **2**, **7** and **8** were investigated by a combination of polarized optical microscopy (POM), differential scanning calorimetry (DSC) and X-ray diffraction studies.‡ Compounds **2** (Cr 73 S_A 134 I)§ and **7** (Cr 112 S_A 151 I)§ gave an enantiotropic smectic A phase and **8** (Cr 63 S_A 125 N* 127 I)§ showed enantiotropic smectic A and chiral nematic phases. The liquid-crystalline phases were identified by POM from the observation of typical textures (smectic A phase: focal conic texture and homeotropic areas; chiral nematic phase: plane texture). The POM observations were confirmed by X-ray diffraction analysis.

During the first heating, DSC analysis of **1** gave two endotherms at 66 (onset, ΔH = 12.9 kJ mol^{-1}) and 118 °C (onset, ΔH = 11.7 kJ mol^{-1}), which were indicative of the formation of a liquid-crystalline phase. On cooling an exotherm was obtained at 113 °C (onset, ΔH = 10.5 kJ mol^{-1}) as well as a T_g at 61 °C (onset). Reversibility of the cooling transitions was observed during the second heating run. POM observations supported the DSC data: a viscous liquid-crystalline phase formed between the two endotherms (fluidity increased from *ca*. 80 °C). The transition at 118 °C corresponded to the clearing point, whereas the transition at 66 °C reflected softening of the sample. The low enthalpy value which is associated to this latter transition could be the consequence of a semicrystalline character of the sample, which was precipitated during the purification process (see above). Neither slow cooling of the sample from the isotropic liquid nor annealing of the sample near the clearing point led to the formation of a typical texture. This is often the case for viscous materials. Careful examinations of small droplets revealed the presence of a focal-conic texture and homeotropic zones.

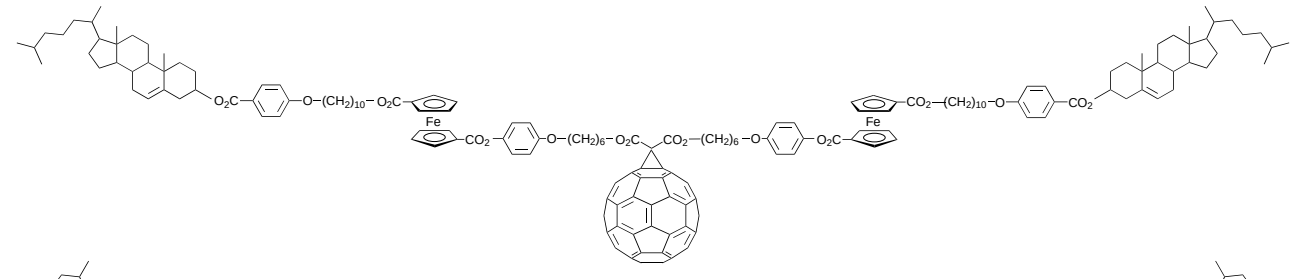

1

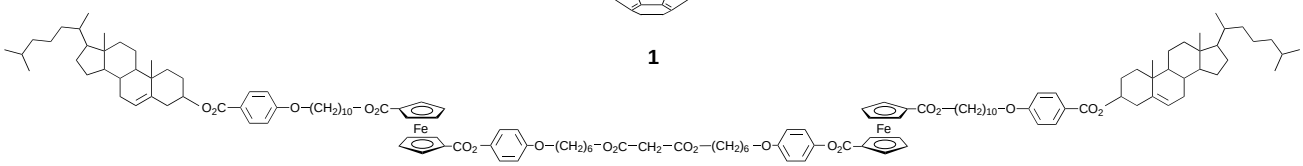

2

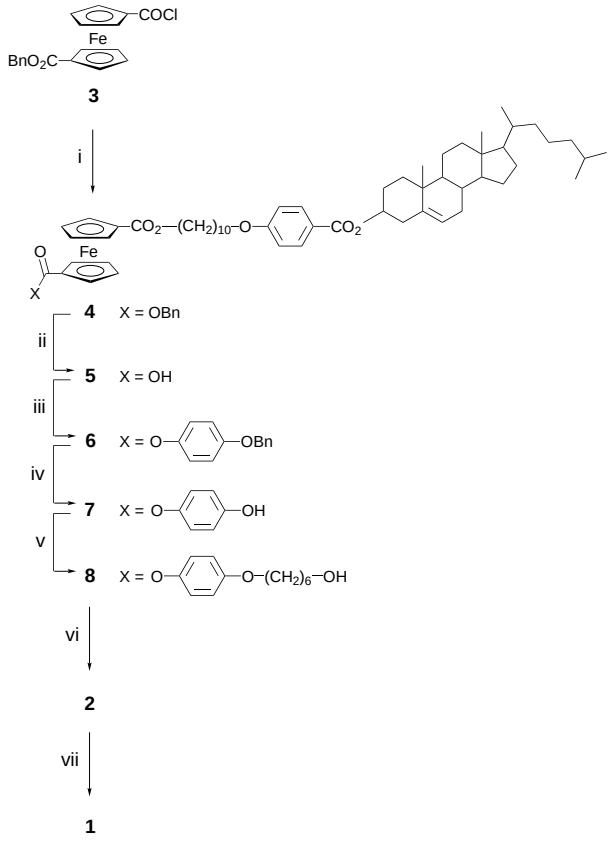

Scheme 1 *Reagents and conditions*: i, cholest-5-en-3β-yl-4-(10-hydroxydecyloxy)benzoate,[1] triethylamine (Et_3N), CH_2Cl_2, room temp. (16 h) and then reflux (overnight), 61%; ii, H_2, Pd/C, CH_2Cl_2–EtOH, room temp., 4 bar, overnight, 85%; iii, hydroquinone monobenzyl ether, *N*,*N*′-dicyclohexylcarbodiimide (DCC), 4-pyrrolidinopyridine, CH_2Cl_2, room temp., 3 h, 76%; iv, H_2, Pd/C, CH_2Cl_2–EtOH, room temp., 4 bar, overnight, 93%; v, 6-bromohexanol, K_2CO_3, acetone–THF, 60 °C, 24 h, 36%; vi, malonyl chloride, Et_3N, CH_2Cl_2, room temp., 2 h, 76%; vii, [60]fullerene, I_2, 1,8-diazabicyclo[5.4.0]undec-7-ene (DBU), toluene, room temp., 3 h, under N_2, 35%

To further investigate the nature of the liquid-crystalline phase displayed by **1**, X-ray diffraction studies were performed from 120 to 30 °C (the sample was heated into the isotropic fluid and then cooled to the desired temperature). Diffraction patterns typical of disordered smectic phases (*i.e.* smectic A or C) were recorded. They consisted, in the low-angle region, of two sharp diffraction peaks, the corresponding spacings of which are in a 1 : 2 ratio, and in the wide-angle region, of a diffuse signal. A representative diffractogram is shown in Fig. 1. The *d*-layer spacing was found to be independent of the temperature (a *d*-value of 74.5 Å was measured at 110 °C; from CPK molecular models, an approximate molecular length of 120 Å was measured for **2** in its fully extended conformation). The layered structure was retained at room temperature. The X-ray diffraction data and POM observations suggest that the liquid-crystalline phase could be smectic A in nature.

Finally, thermogravimetry (10 °C min^{-1}, under N_2) revealed good thermal stability for **1**: mass losses of 1, 5 and 10% were detected at 270, 295 and 309 °C, respectively.

The possibility to exploit the properties of the fullerene[3] and ferrocene[7] units within the same liquid-crystalline molecular framework represents an important step towards the development of multifunctional new materials.

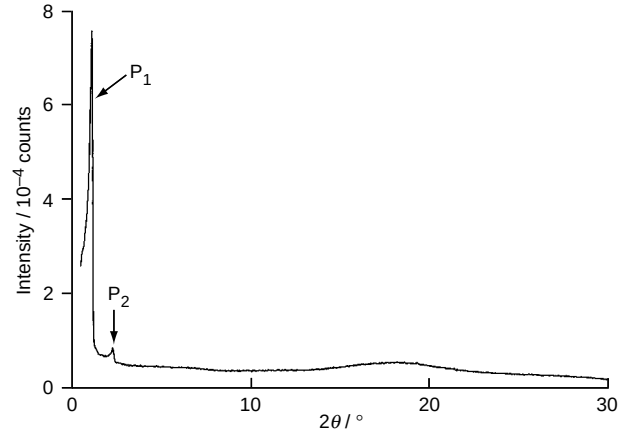

Fig. 1 X-Ray diffraction pattern of **1** recorded at 110 °C. P_1 and P_2 refer to the first and second order signals corresponding to the layer periodicity. The diffuse signal at large angles corresponds to the liquid-like arrangement of the molecules within the smectic layers.

R. D. acknowledges financial support from the Swiss National Science Foundation. We thank Dr B. Heinrich for his assistance with X-ray experiments.

Notes and References

* E-mail: robert.deschenaux@ich.unine.ch

† *Selected data* for **1**: VIS [λ_{max}/nm (ε/dm^3 mol^{-1} cm^{-1})]: 426 (3080), 476 (1990), 686 (246). ^{1}H NMR (400 MHz, $CDCl_3$): δ 7.97 (d, 4 H, arom.), 7.11 (d, 4 H, arom.), 6.92–6.87 (2 × d, 8 H, arom.), 5.41 (d, 2 H, CH=C, cholesteryl), 4.94 (t, 4 H, Cp), 4.89 (t, 4 H, Cp), 4.83–4.81 (m, 2 H, CHO, cholesteryl), 4.52 (t, 4 H, $C_{60}CCO_2CH_2$), 4.49–4.47 (m, 8 H, Cp), 4.19 (t, 4 H, $CpCO_2CH_2$), 4.00–3.93 [2 × t, 8 H, $(CH_2)_8CH_2O$ and $(CH_2)_4CH_2O$], 2.45 (d, 4 H, cholesteryl), 2.03–0.65 (series of m, 130 H, 82 cholesteryl protons and 48 aliphatic protons). Anal. Calc. for $C_{199}H_{186}Fe_2O_{20}$ (3009.34): C, 79.43; H, 6.23. Found: C, 79.37; H, 6.21%.

‡ For instrumentation, see: R. Deschenaux, F. Turpin and D. Guillon, *Macromolecules*, 1997, **30**, 3759.

§ Cr = Crystal state, S_A = smectic A phase, N* = chiral nematic (cholesteric) phase, I = isotropic liquid. The transition temperatures (onset point, rate 10 °C min^{-1} under N_2) reported (in °C) are taken from the first DSC heating run. Upon cooling from the isotropic liquid, none of compounds **2**, **7** and **8** crystallized. In each case, a T_g was detected by DSC.

1 T. Chuard and R. Deschenaux, *Helv. Chim. Acta*, 1996, **79**, 736.
2 A. Hirsch, *Synthesis*, 1995, 895; F. Diederich, L. Isaacs and D. Philp, *Chem. Soc. Rev.*, 1994, **23**, 243; C. Bingel, *Chem. Ber.*, 1993, **126**, 1957.
3 M. Prato, *J. Mater. Chem.*, 1997, **7**, 1097; H. Imahori and Y. Sakata, *Adv. Mater.*, 1997, **9**, 537.
4 D. M. Guldi, M. Maggini, G. Scorrano and M. Prato, *J. Am. Chem. Soc.*, 1997, **119**, 974.
5 R. Deschenaux, M. Rama and J. Santiago, *Tetrahedron Lett.*, 1993, **34**, 3293.
6 J.-F. Nierengarten, A. Herrmann, R. R. Tykwinski, M. Rüttimann, F. Diederich, C. Doudon, J.-P. Gisselbrecht and M. Gross, *Helv. Chim. Acta*, 1997, **80**, 293.
7 *Ferrocenes: Homogeneous Catalysis, Organic Synthesis, Materials Science*, ed. A. Togni and T.Hayashi, VCH, Weinheim, 1995.

Received in Bath, UK, 18th December 1997; 7/09092G

Electroreductive coupling of vinylpyridines and vinylquinolines: radical anion–substrate cycloaddition?

Robert G. Janssen, Majid Motevalli and James H. P. Utley*†

Department of Chemistry, Queen Mary & Westfield College, University of London, Mile End Road, London, UK E1 4NS

Cathodic reduction of 2- and 4-vinylpyridine and of 2-vinylquinoline gives *trans*-1,12-di(heteroaryl)cyclobutanes as major products; they arise *via* radical anion–substrate cycloaddition.

Much recent evidence[1,2] is in favour of electrohydrodimerisation (EHD) proceeding through the coupling of the initially-formed radical anions (the radical anion–radical anion route). An alternative, less well supported, is attack on the starting material by conjugate addition (the radical anion–substrate route) or, much less discussed, by cycloaddition between radical anion–substrate. Oxidative analogues of this possibility are well-known,[3] and there is one report[4] of the formation of cyclobutanes from aryl vinyl sulfones in a cathodically initiated reaction.

In examining templating effects on the stereoselectivity of EHD reactions[2] we explored the controlled potential cathodic

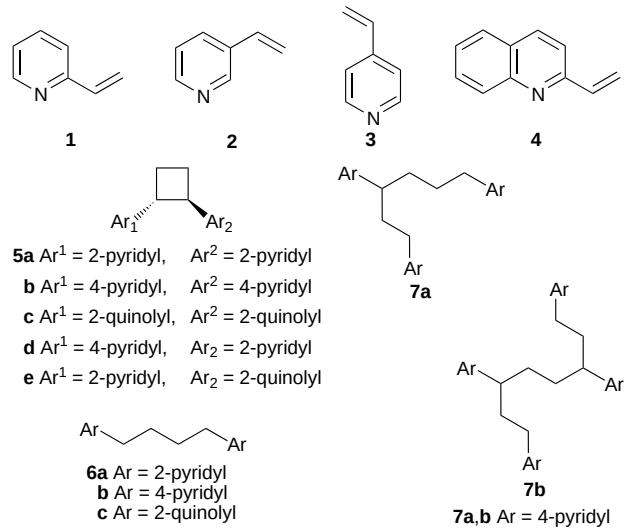

reduction of 2-vinylpyridine **1** at a mercury cathode in DMF (see Table 1). Compound **1** has a potentially ligating nitrogen atom which is close to the reaction centre for EHD. Previously the EHD reactions of both **1** and 4-vinylpyridine (**3**) were reported[5] to give, respectively, only the linear hydrodimers **6a** and **6b**. However, we discovered that substantial amounts of pyridine-substituted cyclobutanes were formed, together with the expected linear hydrodimers **6a** and **6b**. We now find that cyclobutane formation is quite general for vinylpyridines **1** and **3** and the vinylquinoline **4**. We present here compelling evidence for the proposed cycloaddition between radical anion–substrate.

Controlled potential electrolysis (CPE) of alkenyl-substituted pyridines and quinolines gave the *trans*-1,2-di(heteroaryl)-cyclobutanes **5a-e**. For two examples **5b** and **5c** this conclusion was established by X-ray crystallography,[6] which in turn allowed unambiguous interpretation of high-field NMR spectroscopic data used to characterise all of the cyclobutane products.[7] The other major products of the electrolyses were the linear hydrodimers **6a**–**c**.

From **3** and **4** substantial amounts (*ca*. 30%) of oligomers were formed and found, for **3**, to be the trimer **7a** and the tetramer **7b**. The position of vinyl-substitution is important; electrolysis of 3-vinylpyridine **2** gave predominantly cathodic hydrogenation of the double bond with only a 22% yield of an inseparable mixture of the corresponding cyclobutane and linear hydrodimer (3 : 7 ratio). The results of controlled potential electrolyses and the conditions used are summarised in Table 1.

The cyclobutanes **5a**–**c** have also been made[8] by a photochemical method which gave in our hands inseparable mixtures of the *cis*- and *trans*-isomers in case of cyclobutanes **5a** and **5b** with overall yields substantially lower than those reported. In addition to its mechanistic significance the electrochemical method is superior with regard to yield and product selectivity.

The cyclobutanes are electroactive at potentials close to the reduction potentials of the starting materials. Similar reduction, with ring opening, of cyclobutanes occurs in pulse radiolysis[9] of the methyl esters of truxillic acids. Cyclic voltammetry typically indicates an irreversible reduction followed by reversible reduction of the corresponding linear hydrodimer. Controlled potential electrolysis of cyclobutane **5c** gave linear hydrodimer **6c** quantitatively in a 2 F process. Electrolysis was therefore carried out at the foot of the relevant cyclic voltammetric wave, usually at low current density (1–3 mA

Table 1 Preparative scale controlled potential electrolyses[a]

	Cyclobutane	Yield (%)[b]	E_{work}/V[c]	Charge/F mol^{-1}
	5a	49	−2.0	0.80
		63	−1.75	0.43[d]
	5b	trace	−2.0	0.81
		15	−1.6	0.16
	5c	trace	−1.6	0.75
		53	−1.4	0.30
	5d	8	−1.6	
	5e	14	−1.4	

[a] Hg pool cathode, DMF–Et_4NBr (0.1 M), divided cell. [b] Isolated yields. [c] Ag wire reference electrode; $E°$ (Ag/AgBr) = −0.170 V *vs.* SCE. [d] Electrolysis followed by GC analysis of reactant and products.

Table 2 Reduction potentials[a] of vinylheteroaromatics and cyclobutanes

Vinylhetero-aromatic	$E°$/V	Cyclo-butane	$E_{pc}(1)$/V	$E°(2)$/V
1	−2.313	**5a**	−2.585[b]	
2	−2.322	**5b**	−2.441[b]	
3	−2.147	**5c**	−2.118[c]	−2.182
4	−1.915	**5d**	−2.495[b]	
		5e		−2.154[d]

[a] Hg–Pt microelectrode, DMF–Et_4NBr, V *vs.* SCE; concentration for $E°$ values = 4 mM, for E_p values = 2 mM. [b] ν = 10 V s^{-1}. [c] ν = 1 V s^{-1}; shoulder on second reduction wave. [d] First irreversible reduction wave was cathodically shifted under reversible second reduction wave.

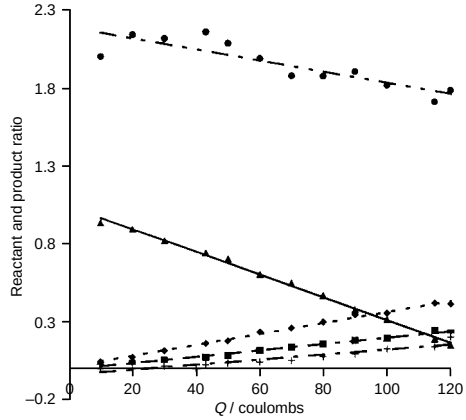

Fig. 1 Reaction profile for controlled potential electrolysis of **1** (see Table 1); (●) (CB)/(EHD), (▲) (VP)/[Total], (◆) (CB)/[Total], (■) (EHD)/[Total], (+) (VPH_2)/[Total]. [Total] = (VD) + (CB) (EHD) + (VPH_2).

cm^{-2}) for concentrations in the range 60 mM–0.3 M. Relevant reduction potentials[10] are given in Table 2.

Vinylpyridines **1** and **3** give chemically irreversible reduction on cyclic voltammetry at low scan rates but reversibility is apparent for the reductions of **2** and **4** at modest scan rates (< 10 V s^{-1}). Thus, apart from direct further reduction of the cyclobutanes it is possible that electron transfer from the persistent first-formed radical anions will take place to give redox-catalyzed cleavage of the cyclobutanes.

A reaction profile was constructed (Fig. 1) for cathodic constant potential reduction of **1** by using GLC analysis to follow relative concentrations of reactant and products as a function of charge passed. The results show clearly that **1** (VP) was consumed using 0.70 F. Furthermore cyclobutane **5a** (CB) and linear hydrodimer **6a** (EHD) were formed in almost constant proportion (2 : 1) throughout the electrolysis. A third product was that of 2 F cathodic hydrogenation (2-ethylpyridine). The profile and coulometry are consistent with consumption of the first-formed radical anion in parallel reactions; dimerisation leading to linear EHD, cycloaddition leading in a catalytic chain process to the cyclobutane, and cathodic hydrogenation leading to 2-ethylpyridine. The final molar proportions of products were **6a** (0.29), **5a** (0.51) and 2-ethylpyridine (0.20). Consequently the proportion of charge consumed, given that EHD is a 1 F process and hydrogenation a 2 F process, must be linear hydrodimer (0.29 F) and 2-ethylpyridine (0.4 F), totalling 0.69 F. 2-Vinylpyridine **1** was consumed in 0.70 F, which indicates that the cyclobutane is formed without overall charge consumption. This experiment is reproducible and repeated experiments gave similar results.

The possibilities are detailed in Scheme 1, which illustrates formation of the linear hydrodimer by the usual radical anion–radical anion route (A), by disproportionation of the first product of cycloaddition, the radical anion route (B), and by subsequent 2e reduction of the cyclobutanes. The 1,2-di(hetero-

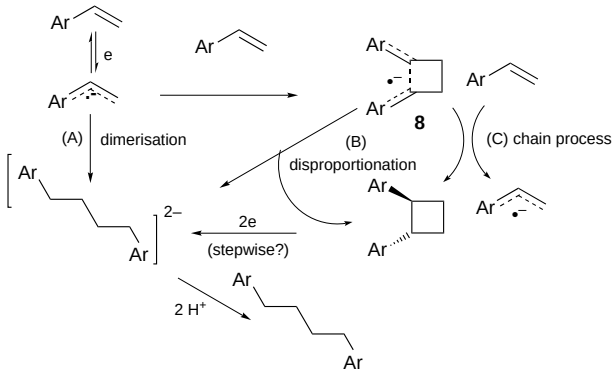

Scheme 1

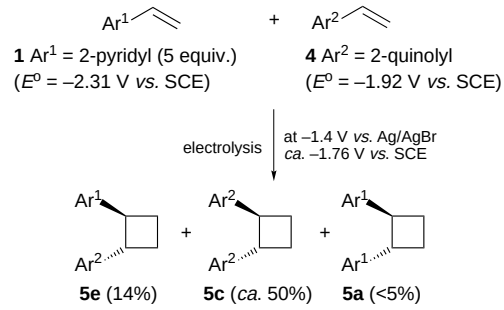

Scheme 2

aryl)cyclobutanes are formed by oxidation of the intermediate radical anion (tentatively represented as **8**); in principle this could be the result of disproportionation (route B) or of a chain process as in the vinyl-sulfone case[3] (route C). The results from the reaction profile (Fig. 1) indicate cyclobutane formation *via* the chain process with no overall consumption of charge.

Co-electrolysis gives further insight (Scheme 2 and Table 1). Co-electrolysis of **3** in the presence of a five-fold excess of **1**, at the potential of the more easily reduced substrate **3**, gave the cross-coupled cyclobutane **5d** and the homo-coupled cyclobutane and linear dimer **6b**, respectively. Cyclobutane **5a** was found in only trace amounts. Similar behaviour was observed for the co-electrolysis of **4** and **1**. Cross-coupled cyclobutanes are therefore formed by reaction between the radical-anion formed at the lower potential and the other, unreduced, component. Formation of both radical anions, *e.g.* by homogeneous electron transfer, would give all three possible cyclobutanes in comparable amounts.

Thus there is compelling evidence for the formation of the cyclobutanes by allowed cycloaddition between vinylpyridines or vinylquinolines and the radical anions derived from them. A detailed mechanistic and kinetic examination is underway, aimed at distinguishing conclusively between the possibilities for the follow-up reactions as outlined in Scheme 1.

We acknowledge support from the EPSRC and from the EU Human Capital & Mobility Institutional Grant # ERBCH-BGCT940590.

Notes and References

† E-mail: j.utley@qmw.ac.uk

1 F. Zhou and A. J. Bard, *J. Am. Chem. Soc*., 1994, **116**, 393.
2 I. Fussing, M. Güllü, O. Hammerich, A. Hussain, M. F. Nielsen and J. H. P. Utley, *J. Chem. Soc., Perkin Trans. 2*, 1996, 649.
3 N. L. Bauld, *Advances in Electron Transfer Chemistry*, 1992, vol. 2, pp. 1–61 and references cited therein.
4 J. Delaunay, G. Mabon, A. Orliac and J. Simonet, *Tetrahedron Lett*., 1990, **31**, 667. See also, J. Delaunay, A. Orliac and J. Simonet, *J. Electrochem. Soc*., 1995, **142**, 3613.
5 J. D. Anderson, M. M. Baizer and E. J. Prill, *J. Org. Chem*., 1965, **30**, 1645.
6 *Crystal data* for **5b**: colourless crystal, monoclinic, $P2_1n$, a = 26.095(10), b = 7.138(2), c = 6.134(3) Å, β = 92.59(3)°, V = 1141.4(8) $Å^3$, Z = 4, R = 0.0706, GOF = 0.677. CCDC 182/719.
7 All cyclobutanes were characterised by high resolution mass spectrometry, ^1H NMR (250 and 600 MHz) and ^{13}C NMR (62.5 MHz) spectroscopy; signal assignments were made using 600 MHz TOCSY, NOESY and HMQC spectroscopy. Satisfactory elemental analyses were obtained from all crystalline compounds, while the purity of oils was checked by GC analysis.
8 T. Nakano, A. Martin, C. Rivas and C. Pérez, *J. Heterocycl. Chem*., 1977, **14**, 921.
9 S. Takamuku, B. R. Dih-Nghoe and W. Schnabel, *Z. Naturforsch, Teil A*, 1978, **33**, 1281; S. Takamuku, H. Kighawa, S. Suematsu, S. Tokai, K. Tsumoni and H. Sakurai, *J. Phys. Chem*., 1982, **86**, 1861.
10 Formal reduction potentials ($E°$) were measured in collaboration with O. Hammerich and M. F. Nielsen (University of Copenhagen).

Received in Cambridge, UK, 16th October 1997; 7/07460C

Diastereomer-differentiating photoisomerization of 5-(cyclopent-2-en-1-yl)-2,5-dihydro-1*H*-pyrrol-2-ones

Matthias N. Wrobel and Paul Margaretha*

Institut für Organische Chemie, Universität Hamburg, D-20146 Hamburg, Germany

The diastereomeric *l*- and *u*-dihydropyrroles 1 and 2 photoisomerize to azatetracyclodecanones 3 and 4, respectively.

According to the reactant-based Izumi–Tai classification,[1] reactions wherein a *l*(ike) and an *u*(nlike) diastereomer exhibit differing behaviour are termed 'diastereomer differentiating'. Here we report the first example of a photochemical reaction where two diastereomeric hexa-1,5-dienes undergo photoisomerization to a crossed and a straight cycloadduct,[2] respectively. The 1 : 1 diastereomeric mixture of *tert*-butyl 5-(cyclopent-2-en-1-yl)-2-oxo-2,5-dihydro-1*H*-pyrrole-1-carboxylates **1** and **2** was available in 36% yield by alkylation of *tert*-butyl 2-*tert*-butyldimethylsilyloxy-1*H*-pyrrole-1-carboxylate[3] with 3-bromocyclopentene. Separation was achieved by chromatography (SiO_2, Et_2O–hexane 1 : 1) affording the *u*-diastereomer **1**, mp 86 °C, whose structure was confirmed by X-ray analysis, and the *l*-diastereomer **2**, mp 104 °C. Both $(CD_3)_2CO$-sensitized[4] (300 nm) or direct (254 nm) irradiation of **1** afford the Boc-protected 5-azatetracyclo[4.4.$0^{2,8}$.$0^{3,7}$]decan-4-one **3** (mp 94 °C) in nearly quantitative yield. In contrast, sensitized irradiation of **2** affords the Boc-protected 4-azatetracyclodecan-3-one **4** (oil) selectively (9 : 1) in 75% yield, but on direct irradiation a 1 : 1 mixture of **3** and **4** is formed. In both sets of experiments the conversion of **2** to product(s) proceeds slower than that of **1**.

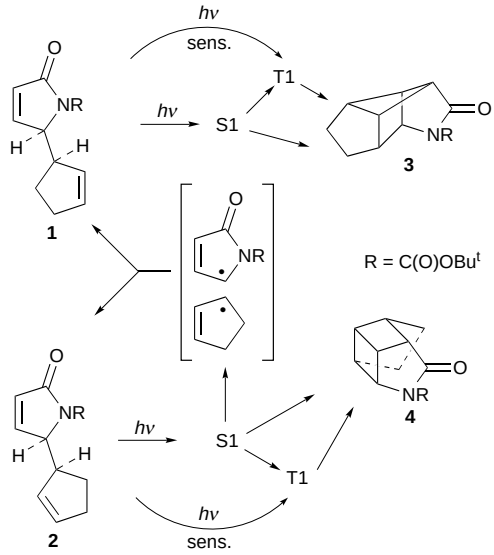

Scheme 1

The fact that in the sensitized runs both diastereomers undergo regioselective intramolecular [2 + 2]cycloaddition but on direct irradiation only **1**, and not **2**, exhibit this behaviour can be explained in terms of differential ratios of efficiencies of cycloadduct formation *vs.* cleavage to a radical pair for singlet and triplet excited states of **1** and **2**, respectively. The results indicate that only for singlet excited **2** does this racemization, which causes cleavage, become competitive, most probably reflecting the higher activation energy barrier in the formation of a bicyclo[2.2.0]hexane unit, as in **4**, compared to the less strained[5] bicyclo[2.1.1]hexane moiety of **3**. This differential behaviour is expected to be typical for all compounds containing a 3-(cyclopent-2-en-1-yl)cyclopentene framework.

The new compounds **1**–**4** have been fully characterized and have spectroscopic properties compatible with the structures assigned.

We thank the Deutsche Forschungsgemeinschaft and the Fonds der Chemischen Industrie for support.

Notes and References

* E-mail: margpaul@chemie.uni.hamburg.de

1 Y. Izumi and A. Tai, *Stereo-Differentiating Reactions*, Academic Press, New York, 1977; G. Helmchen, *Nomenclature and Vocabulary of Organic Stereochemistry*, in *Houben–Weyl, Methods of Organic Chemistry*, Thieme, Stuttgart, 1995, vol. E 21a, p. 1.

2 A. R. Matlin, C. F. George, S. Wolff and W. C. Agosta, *J. Am. Chem. Soc.*, 1986, **108**, 3385; S. A. Fleming, C. L. Bradford and J. J. Gao, *Regioselective and Stereoselective [2 + 2] Photocycloadditions*, in *Organic Photochemistry*, ed. V. Ramamurthy and K. S. Schanze, Marcel Dekker, New York, 1997, p. 187.

3 F. Zanardi, L. Battistini, G. Rassu, M. Cornia and G. Casiraghi, *J. Chem. Soc., Perkin Trans. 1*, 1995, 2471.

4 In (hexaprotio)acetone H-abstraction products from the solvent are formed as by-products, *cf.* M. N. Wrobel and P. Margaretha, *J. Photochem. Photobiol., A*, 1997, **105**, 35.

5 A. Greenberg and J. Liebman, *Strained Organic Molecules*, Academic Press, New York, 1978, p. 72.

Received in Liverpool, UK, 19th November 1997; 7/08365C

Heterogeneous $Cs_3PW_{12}O_{40}$ photocatalysts

Duane A. Friesen, David B. Gibson and Cooper H. Langford*

Department of Chemistry, University of Calgary, 2500 University Drive NW, Calgary, Alberta, Canada T2N 1N4

Colloidal $Cs_3PW_{12}O_{40}$ shows promise as a heterogeneous photo-oxidant, oxidizing alcohols in aqueous solution upon UV irradiation.

Polyoxotungstate clusters such as the Keggin ion ($XW_{12}O_{40}^{n-}$, where X is a heteroatom such as P or Si) are well known thermal catalysts for the oxidative transformation of various organic molecules in solution.[1,2] These species can also function as photocatalysts upon UV irradiation, promoting the oxidation of alcohols to aldehydes or ketones,[3–5] the functionalization of alkanes to form alkenes or ketones,[6] and the dimerization of alkenes.[7] Recent interest in the photochemical properties of these compounds has included the degradation of chlorophenols *via* oxidative processes.[8]

Much work has been done studying polyoxometalates as heterogeneous thermal catalysts and applying them for industrial purposes.[2] However, studies of the photo-oxidative behaviour of polyoxometalates have been with homogeneous solutions. Comparisons of the photo-oxidative activity of these solutions with conventional heterogeneous photocatalysts (*e.g.* TiO_2) have been made.[2d] For many applications, it is desirable to have the photoactive agent in a more recoverable form. Recently, progress has been made with placing polyoxotungstates (soluble forms such as $H_3PW_{12}O_{40}$ or insoluble forms such as $Cs_{2.5}H_{0.5}PW_{12}O_{40}$) on solid supports for liquid phase reactions in order to enhance recovery from the reaction mixture.[9] The utility of the Cs^+ salt for heterogeneous thermal catalysis has been proven.[2,10] There is a need for the potential of these systems for heterogeneous photo-oxidation to be investigated. Here, we demonstrate that a water-insoluble colloid, $Cs_3PW_{12}O_{40}$, can function as an effective photo-oxidative agent for the oxidation of propan-2-ol to acetone.

Colloidal $Cs_3PW_{12}O_{40}$ was synthesized by metathesis of $H_3PW_{12}O_{40}{\cdot}nH_2O$ and CsCl in H_2O. The precipitate was centrifuged, washed twice with water, and dried at 85 °C. Silica-supported photocatalyst materials were made using the sol–gel procedure of Izumi *et al.*[9a,b] A mixture of 1 g $Cs_3PW_{12}O_{40}$, 3 ml ethanol, 3.5 g tetraethoxysilane (TEOS), and 1.5 g H_2O was heated at 80 °C until dry. The resulting granular material was calcined at 300 °C for 4 h and washed with hot H_2O to separate soluble and fine colloidal materials.

Filtration and light scattering experiments suggested that a large fraction of the unsupported $Cs_3PW_{12}O_{40}$ powder was submicrometer in size, *i.e.* 300 nm in diameter. This value probably represents the size of aggregates of smaller particles as noted previously.[9a] The powder X-ray diffraction patterns of the uncalcined colloid and the calcined $Cs_3PW_{12}O_{40}$–SiO_2 composite were the same, indicating that the crystallinity of the polyoxometalate was not altered significantly during the calcination procedure.[2b,9d] From nitrogen adsorption measurements, it was determined that the $Cs_3PW_{12}O_{40}$ powder had a specific surface area of 126 $m^2\ g^{-1}$, in agreement with previous values.[10c] In comparison, the surface area for TiO_2 (Degussa P25) is 55 $m^2\ g^{-1}$. The calcined, sol–gel supported tungstate material was extremely porous, with a pore size distribution centered at 23 Å, a surface area of 677 $m^2\ g^{-1}$, and a total pore volume of 0.46 ml g^{-1}. This compares favorably with values obtained for the supported thermal catalyst $Cs_{2.5}H_{0.5}PW_{12}O_{40}$–$SiO_2$ and silica gel itself.[9a,b,11]

The insolubility of the $Cs_3PW_{12}O_{40}$ material in water is a critical factor for its potential use for the photo-oxidation of organic species in water, considering the solubility of $H_3PW_{12}O_{40}$. When the granular $Cs_3PW_{12}O_{40}$–SiO_2 composite (several hundred mg in 2 ml H_2O) was stirred at room temperature for *ca.* 3 h, the amount of $PW_{12}O_{40}^{3-}$ in the water at the end of this period was *ca.* 3×10^{-7} M as determined by UV–VIS spectroscopy. This was a factor of 100 less than the solubility of uncalcined $Cs_3PW_{12}O_{40}$ in H_2O at natural pH (5–6) and represented a leakage of $< 0.01\%$.

The photochemical oxidation of alcohols by dissolved $PW_{12}O_{40}^{3-}$ upon UV irradiation is well documented.[3–5] We demonstrate here that desolubilized polyoxometalate colloids also show photocatalytic behavior. Reflectance spectroscopy was used to observe reduction of the photoexcited $Cs_3PW_{12}O_{40}$ colloid suspended in neat propan-2-ol. An opaque suspension of $Cs_3PW_{12}O_{40}$ in N_2-purged propan-2-ol was irradiated in a 2 mm quartz cell using the output from a 200 W Xe(Hg) arc lamp with a 300 nm cutoff filter. UV–VIS spectral changes in the suspension were monitored using a fibre-optic diffuse reflectance probe coupled to an Ocean Optics S1000 absorption spectrometer. Fig. 1 shows changes in the reflectance spectrum upon irradiation of the slurry. Absorptions in the red region of the visible spectrum are those of the reduced tungstate.[3,4,6d,12] At early irradiation times the absorption maximum is at 760 nm, corresponding to the production of $PW_{12}O_{40}^{4-}$. Longer irradiation periods resulted in a blue-shift of the spectral maximum which may be due to > 1 electron reduction at some sites. After irradiation, the blue colloid was allowed to settle. The propan-2-ol liquid phase was uncolored, indicating that bleeding of the desolubilized metalate into solution remained negligible for the reduced forms. Subsequent experiments with silica-supported $Cs_3PW_{12}O_{40}$ yielded similar results under the same conditions. As shown in the figure, reduction is stoichiometrically significant.

This system was also investigated for product formation *via* photo-oxidation of the alcohol. Granules of $Cs_3PW_{12}O_{40}$–SiO_2 (200 mg) were added to 2 ml of 0.5 M aqueous propan-2-ol

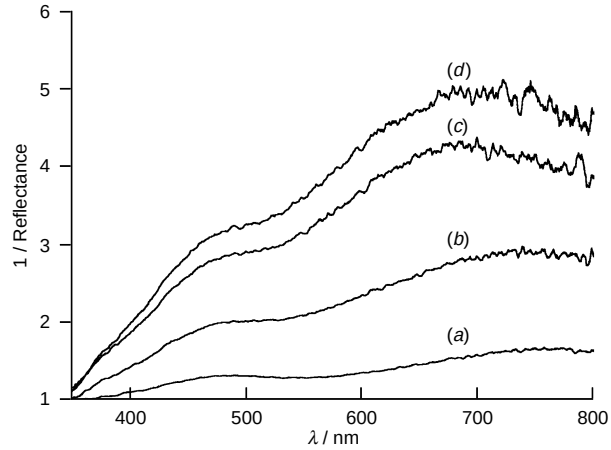

Fig. 1 Visible reflectance spectra for the irradiation (> 300 nm) of an N_2-purged slurry of $Cs_3PW_{12}O_{40}$ in propan-2-ol: (*a*) 7 min, (*b*) 12 min, (*c*) 17 min, (*d*) 22 min

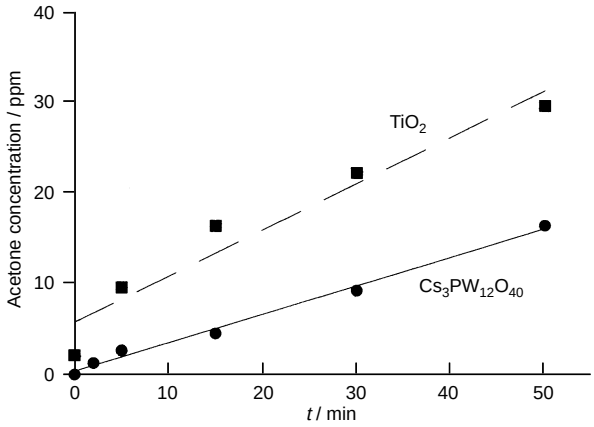

Fig. 2 Production of acetone by the irradiation (254 nm) of $Cs_3PW_{12}O_{40}$ and TiO_2 (2 g l^{-1}) in an aqueous solution (pH 3, $HClO_4$) of propan-2-ol (610 ppm)

(aerated) in a 1 cm quartz cell. The mixture was irradiated with the output of a 200 W Xe(Hg) lamp and 300 nm cutoff filter. The solution was sampled at regular intervals using an HP 5880 GC with FI detector and a 0.53 mm i.d. fused silica column with DB-WAX polyethylene glycol stationary phase (J&W Scientific). Acetone was produced steadily during the irradiation as found previously for dissolved solutions of $PW_{12}O_{40}^{3-}$. In this case formation of the heteropoly blue was not visually evident, due to reoxidation of the metalate by dissolved O_2.[13]

Determination of an accurate quantum yield is not facile, as demonstrated by Sun and Bolton for TiO_2 colloids.[14] However, we have performed a comparative study of the unsupported tungstate with TiO_2 (Degussa-P25), a commercially-available material for photocatalytic oxidations. Equal mass loadings of $Cs_3PW_{12}O_{40}$ or TiO_2 powder (2 g l^{-1}) in a 610 ppm solution of propan-2-ol were placed in an annular quartz cell irradiated by a low pressure mercury lamp (Philips TUV, 15 W, λ = 254 nm). The 4 mm pathlength and irradiation wavelength ensured near-total absorption of photons by the colloidal photocatalysts. The solutions, after allowing 1 h for dark adsorption, were irradiated. Samples were withdrawn and analyzed (GC–FID) for the production of acetone and loss of propan-2-ol. Fig. 2 illustrates the production of acetone by both species. From the data, it appears that the rate of conversion of propan-2-ol to acetone is approximately one-half for $Cs_3PW_{12}O_{40}$ colloid relative to TiO_2. That is, a first unoptimized preparation of a heterogeneous polyoxometalate is very competitive with a widely used form of TiO_2 for photo-oxidation. The apparent reactivity of the tungstate per unit area of catalyst is approximately one quarter that of TiO_2. This is very approximate due to the difficulty of determining the actual surface area illuminated.

The photo-oxidative ability is not limited to alcohols; upon broad-band irradiation [1000 W Xe(Hg) lamp, Pyrex cutoff], an aqueous solution of a model aromatic compound, acetophenone, shows > 99% degradation to hydroxy- and dihydroxyacetophenones over a 3 h period using $Cs_3PW_{12}O_{40}$. This underlines the possible importance of these systems for contaminant degradation, parallel to TiO_2.

In summary, desolubilized polyoxotungstates can function as heterogeneous photocatalysts for the oxidation of organic species in solution. These materials show promise as easily-recovered materials for photochemical oxidations.

The authors would like to thank Dr Alex Starosud for N_2 adsorption and determinations and Mr Fred Henselwood for light scattering measurements. The support of the Natural Sciences and Engineering Research Council of Canada is greatly appreciated.

Notes and References

* E-mail: chlangfo@acs.ucalgary.ca

1 C. L. Hill and C. M. Prosser-McCartha, *Coord. Chem. Rev.*, 1995, **143**, 407; D. C. Duncan, R. C. Chambers, E. Hecht and C. L. Hill, *J. Am. Chem. Soc.*, 1995, **117**, 681; C. L. Hill, D. C. Duncan and M. K. Harrup, *Comments Inorg. Chem.*, 1993, **14**, 367; R. C. Chambers and C. L. Hill, *Inorg. Chem.*, 1991, **30**, 2776; R. F. Renneke, M. Pasquali and C. L. Hill, *J. Am. Chem. Soc.*, 1990, **112**, 6585.

2 (*a*) T. Okuhara, N. Mizuno and M. Misono, *Adv. Catal.*, 1996, **41**, 113; (*b*) T. Okuhara, T. Nishimura, H. Watanabe, K. Na and M. Misono, *Stud. Surf. Sci. Catal.*, 1994, **90**, 419; (*c*) M. Misono, *Stud. Surf. Sci. Catal.*, 1993, **75**, 69; (*d*) K. Y. Lee, T. Arai, S. Nakata, S. Asaoka, T. Okuhara and M. Misono, *J. Am. Chem. Soc.*, 1992, **114**, 2836; (*e*) M. Misono, *Catal. Rev.-Sci. Eng.*, 1987, **29**, 269; (*f*) M. T. Pope and A. Müller, *Angew. Chem., Int. Ed. Engl.*, 1991, **30**, 34.

3 E. Papaconstantinou, *Chem. Soc. Rev.*, 1989, **18**, 1; D. Dimotikali and E. Papaconstantinou, *Inorg. Chim. Acta*, 1984, **87**, 177; E. Papaconstantinou, *J. Chem. Soc., Chem. Commun.* 1982, 12.

4 M. A. Fox, R. Cardona and E. Gaillard, *J. Am. Chem. Soc.*, 1987, **109**, 6347.

5 C. L. Hill and D. A. Bouchard, *J. Am. Chem. Soc.*, 1985, **107**, 5148.

6 (*a*) C. L. Hill, M. Kozik, J. Winkler, Y. Hou and C. M. Prosser-McCartha, in *Photosensitive Metal-Organic Systems—Mechanistic Principles and Applications*, ed. C. Kutal and N. Serpone, *ACS Symp. Ser.*, 1993, **238**, 243; (*b*) R. F. Renneke, M. Kadkhodayan, M. Pasquali and C. L. Hill, *J. Am. Chem. Soc.*, 1991, **113**, 8357; (*c*) R. F. Renneke, M. Pasquali and C. L. Hill, *J. Am. Chem. Soc.*, 1990, **112**, 6585; (*d*) R. F. Renneke and C. L. Hill, *J. Am. Chem. Soc.*, 1988, **110**, 5461; (*e*) R. F. Renneke and C. L. Hill, *J. Am. Chem. Soc.*, 1986, **108**, 3528.

7 T. Yamase and T. Usami, *J. Chem. Soc., Dalton Trans.*, 1988, 183.

8 A. Mylonas and E. Papaconstantinou, *J. Photochem. Photobiol. A*, 1996, **94**, 77; *J. Mol. Catal.*, 1994, **92**, 261.

9 (*a*) Y. Izumi, M. Ono, M. Kitagawa, M. Yoshida and K. Urabe, *Microporous Mater.*, 1995, **5**, 255; (*b*) Y. Izumi, M. Ono, M. Ogawa and K. Urabe, *Chem. Lett.*, 1993, 825; (*c*) Y. Izumi, N. Natsume, H. Takamine, I. Tamaoki and K. Urabe, *Bull. Chem. Soc. Jpn.*, 1989, **62**, 2159; (*d*) Y. Izumi, R. Hasebe and K. Urabe, *J. Catal.*, 1983, **84**, 402; (*e*) Y. Izumi and K. Urabe, *Chem. Lett.*, 1981, 663.

10 (*a*) Y. Izumi, M. Ogawa and K. Urabe, *Appl. Catal. A*, 1995, **132**, 127; (*b*) Y. Izumi, M. Ogawa, W. Nohara and K. Urabe, *Chem. Lett.*, 1992, 1987; (*c*) S. Tatematsu, T. Hibi, T. Okuhara and M. Misono, *Chem. Lett.*, 1984, 865.

11 D. M. Ruthven, *Principles of Adsorption and Adsorption Processes*, Wiley, New York, 1984, pp. 5–7.

12 G. M. Varga, Jr., E. Papaconstantinou and M. T. Pope, *Inorg. Chem.*, 1970, **9**, 662.

13 A. Hiskia and E. Papaconstantinou, *Inorg. Chem.*, 1992, **31**, 163.

14 L. Sun and J. R. Bolton, *J. Phys. Chem.*, 1996, **100**, 4127.

Received in Bloomington, IN, USA, 23rd September 1997; revised manuscript received 6th October 1987; 8/00381E

Unique ligand imposed distortions in a nickel(II) 1,5,9-triphospha-cyclododecane complex

Peter G. Edwards,* Florent Ingold, Simon J. Coles and Michael B. Hursthouse

Department of Chemistry, University of Wales Cardiff, PO Box 912, Cardiff, UK CF1 3TB

1,5,9-Triethyl-1,5,9-triphosphacyclododecane ([12]ane-P_3Et_3, L) reacts with $NiBr_2$ to afford the salt [NiLBr]Br which is shown by X-ray crystallography to have an unusually distorted structure as a result of constraints imposed by the ligand L.

Triaza and trithia cycloalkanes are well known to form stable nickel compounds in a variety of oxidation states and with properties that are unique to complexes of these ligand sets.[1] There are few examples of Ni complexes of macrocyclic polyphosphines and none with macrocyclic triphosphines. In view of the coordination control as well as the relative kinetic stability that may arise in complexes of phosphorus macrocycles, we have studied reactions of 1,5,9-triethyl-1,5,9-triphosphacyclododecane ([12]aneP_3Et_3, L) and report preliminary results of this study here.

Reactions of L with $NiBr_2$ in ethanol give rise to deep red solutions from which red crystals of **1** may be isolated and for which analytical data indicate the formula $NiLBr_2$.† The crystals are only slightly air-sensitive but solutions are readily oxidised by air giving rise to oxides of L. **1** is readily soluble in Me_2SO but is insoluble in hydrocarbons and aliphatic ethers and only poorly soluble in relatively polar organic solvents such as THF, CH_2Cl_2 and $MeNO_2$. **1** has only been isolated in reasonable yield when prepared in alcohols, black oils are formed in THF or CH_2Cl_2. **1** is a conductor in Me_2SO (Λ_M = 21 cm^2 ohm^{-1} mol^{-1}), a value close to other monocationic Ni^{II} complexes such as $[Ni(NP_3)I]BF_4$ [Λ_M = 14 cm^2 ohm^{-1} mol^{-1}, NP_3 = $N(CH_2PPh_2)_3$][2a] and is thus better formulated as the salt $[NiLBr]^+Br^-$. **1** is also diamagnetic, giving rise to sharp NMR spectra and so presumably does not have a tetrahedral Ni^{II} atom. The $^{31}P\{^1H\}$ NMR spectrum consists of a singlet (δ −3.0) indicating fluxionality in solution since a static distorted four-coordinate geometry would not have magnetically equivalent phosphorus atoms. The spectrum is temperature invariant (25 to −70 °C). This fluxionality may in part be due to halide lability since warming solutions of **1** in Me_2SO gives rise to solutions for which conductivity measurements indicate the solute to be dicationic (Λ_M = 229 cm^2 ohm^{-1} mol^{-1}) by comparison to related dicationic Ni complexes {*e.g.* for [Ni{η^2-1,2-$C_6H_4(PEt_2)_2$}$_2$], Λ_M = 182 cm^2 ohm^{-1} mol^{-1}}.[3]

The structure of the cation of **1** is presented in Fig. 1.‡ The geometry around the four-coordinate d^8 Ni atom is heavily distorted from either of the common, regular four-coordinate geometries.

Whereas the Ni–P distances are all similar [av. 2.151(1) Å] $[Ni(NP_3)I]^+$ [av. 2.22(1) Å],[8] the distortion is manifested in the bond angles around Ni where one of the P–Ni–P angles is considerably larger than the other two [126.43(4)° *vs*. 94.80(4) and 96.29(4)°]; similarly one of the Br–Ni–P angles is much larger than the other two [155.60(4)° *vs*. 94.52(3) and 96.19(3)°]. Distortions from square planar towards tetrahedral structures arising from steric encumbrance of the ligands are well known for Ni^{II} phosphine complexes. Examples are $[Ni(CH_2SiMe_3)Cl(PMe_3)_2]^+$ and $[Ni(CH_2SiMe_3)(PMe_3)_3]^+$ where the substitution of Cl, in the former, by PMe_3 increases the distortion around Ni, albeit less severe, approaches that in **1**.[4] Other than the direct bonding contacts between Ni and the three phosphorus and one bromine atoms in **1**, the closest intramolecular interaction with the nickel is to a P–Et hydrogen atom on C(15) at 2.85 Å and is thus considered to be non-bonding. There are no other interactions that could explain the distortion. A striking comparison is with the related ligands [12]aneN_3 and [12]aneS_3 which both form high-spin octahedral complexes with Ni^{II}, the latter forms a bis-macrocycle sandwich with six coordinated S atoms.[1,5] The related 9-membered nitrogen macrocycles, [9]aneN_3 and [9]aneN_3Me_3, also favour octahedral geometries, although the latter is reported not to form a bis-ligand complex of Ni^{II} owing to steric interactions between the methyl substituents.[1] It appears then that steric crowding is not responsible for forcing the distortion observed in **1** unlike in the PMe_3 complexes above, however space filling models[6] give a better view of its coordination sphere (Fig. 2) showing the apparent coordination vacancy arising from the distortion. This vacancy is highlighted by rotation of the P–Et[C(14)] bond [Fig. 2(*b*)], which might be expected to be facile in solution, such that the methyl group [C(15)] is removed from the proximity of the nickel atom. These views indicate that the structure might best be described as a distorted trigonal bipyramid with a vacant vertex. Although this behaviour is unexpected and unique for d^8 Ni^{II} phosphine complexes, there are other examples of four-coordinate d^8 complexes that show distortions from either square-planar or tetrahedral geometries as a result of electronic influences.[7] A relevant comparison with **1** in this context is the structure of $[Ru(CO)_2(PBu^t_2Me)_2]$ **2** which exhibits a similar distortion from a square-planar geometry and whose structure was also described as trigonal bipyramidal in which one equatorial ligand is absent; the '*transoid*' (P–Ru–P) and '*cisoid*' (C–Ru–C) angles are

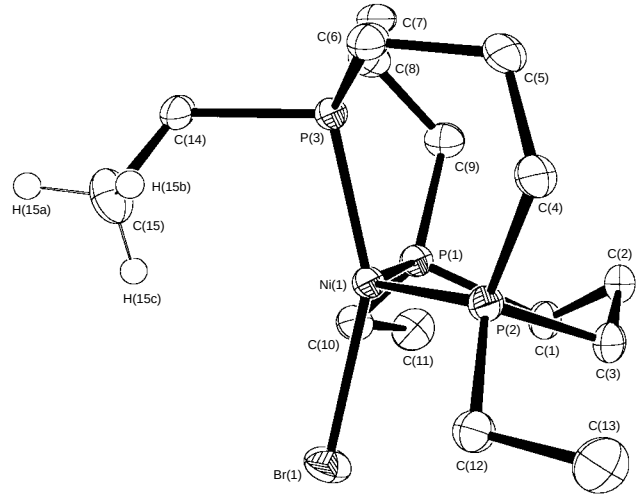

Fig. 1 The molecular structure and atom labelling scheme of [NiLBr]Br **1**. Isotropically refined hydrogen atoms closest to Ni [on C(15)] are included, all others are excluded for clarity. Selected bond lengths (Å) and angles (°): Br(1)–Ni(1) 2.329(1), Ni(1)–P(3) 2.124(1), Ni(1)–P(1) 2.163(1), Ni(1)–P(2) 2.167(1), P(3)–Ni(1)–P(1) 94.80(4), P(3)–Ni(1)–P(2) 96.29(4), P(1)–Ni(1)–P(2), 126.43(4), P(3)–Ni(1)–Br(1) 155.60(4), P(1)–Ni(1)–Br(1) 94.52(3), P(2)–Ni(1)–Br(1) 96.19(3).

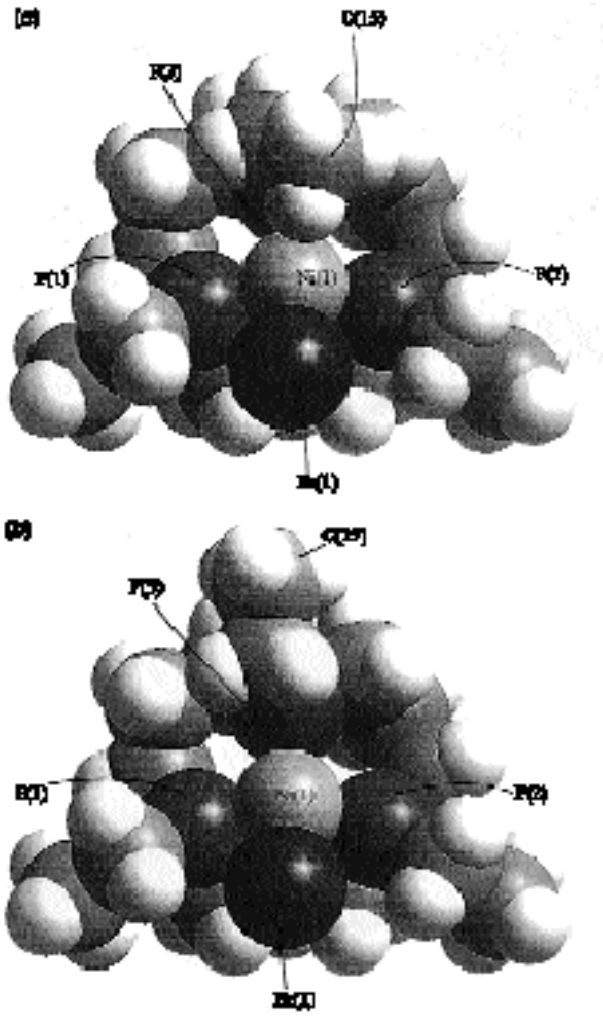

Fig. 2 Space filling models of $[Ni([12]aneP_3Et_3)Br]^+$; (*a*) crystallographically determined configuration, (*b*) ethyl group rotated away from Ni [around P(3)–C(14)]

165.56(8) and 133.3(4), respectively.[8] In this case, *ab initio* calculations (on the PH_3 analogue) at the RHF/MP2 level indicated that the observed structure was very close to the most stable ground state configuration and a more regular square-planar geometry was disfavoured. This is in contrast to analogous Rh^I complexes where the reverse is true; this difference was said to arise from a π-bonding stabilisation in the Ru carbonyl that is not as significant in Rh^I owing to differences in d-orbital energies. This explanation also implies that related Ni^{II} compounds would favour regular square-planar geometries in the ground state and especially in **1** where the tertiary alkyl phosphine donors are expected to be less efficient π acceptors than CO in **2**. The electronic preference for a square-planar ground state configuration in **1** is further supported by EHMO calculations[9] on the idealised system, $[Ni(PH_3)_3Br]^+$. Three geometries were studied: square planar, trigonal bipyramidal having a vacant equatorial site, and tetrahedral. The square-planar geometry is found to be the most stable owing to minimisation of antibonding Ni–Br interactions; the bipyramid and tetrahedron are destabilised by 133 and 204 kJ mol^{-1} respectivley.

The structure of **1** also contrasts with Ni^{II} complexes of tripodal ligands such as $N(CH_2L')_3$ (L′ = PPh_2, SH) for which trigonal-bipyramidal geometries predominate.[2] A related tripodal tris-amidate ligand $\{N[CH_2C(O)NBu^t]_3{}^{3-}\}$ has been shown to support a high-spin trigonal monopyramidal structure in its Ni^{II} complex although the absence of one axial ligand (*trans* to tertiary N) was explained as due to the steric bulk of the tertiary butyl groups precluding coordination of the fifth ligand.[10]

It appears then that the distortion observed in **1** is not due to either electronic influences or steric factors arising from ligand substituents but rather to the unique feature of the macrocycle in restricting the freedom of the phosphorus donors, forcing them to adopt the coordination configuration observed. The strong preference of the nickel for a low-spin configuration in the presence of the three high-field phosphorus ligands also clearly dominates, destabilising tetrahedral or octahedral coordination geometries. This demonstrates a marked difference in the coordination behaviour of this [12]aneP_3 macrocycle in comparison to directly analogous N_3 and S_3 macrocycles as well as related tripodal ligands; it also indicates that the properties of its complexes will differ markedly from those of other ligands.

The synthesis of other Ni complexes and their reactions with small molecules and unsaturated substrates are currently being studied; preliminary results indicate that tetrahedral Ni^0 carbonyl complexes of L $\{[NiL(CO)_3]_3$, $[NiL(CO)]$ and $[NiL(CO)]^+\}$ are readily formed.

We thank the EPSRC for a research grant (GR/L06508) and for support of the X-ray crystallography unit in Cardiff.

Notes and References

* E-mail: edwardspg@cardiff.ac.uk

† **1** was prepared by addition of an ethanolic solution of L to $NiBr_2$ in EtOH, followed by stirring (5 h) and evaporation of the solvent *in vacuo*. The residue was extracted into CH_2Cl_2; red crystals of crystallographic quality were obtained from CH_2Cl_2 by slow diffusion into light petroleum (bp 40–60 °C) in 23% yield. Analytical data, found (calc.): C, 34.24 (34.33); H 5.97 (6.34%).

‡ *Crystal data*: $C_{15}H_{33}Br_2NiP_3$, M = 524.85, monoclinic, space group $P2_1/c$, a = 14.950(3), b = 7.9648(4), c = 17.3117(7) Å, β = 95.679(9)°, U = 2051.3(5) Å^3. D_c = 1.699 g cm^{-3}, μ(Mo-Kα) = 5.069 mm^{-1}, $F(000)$ = 1064, λ = 0.710 69 Å, T = 150(2) K. All crystallographic measurements were made using a FAST area detector diffractometer following previously described procedures.[11] The structure was solved by direct methods (SHELXS-86[12]) and refined on F^2 by full-matrix least squares (SHELXL-93[13]) using all unique data. Hydrogens were included in idealised postions and refined with group isotropic thermal parameters. Final R (on F with $F_o > 3\sigma F$) = 0.0299 and wR (on all F^2) = 0.073. CCDC 182/742.

1 P. Chaudhuri and K. Wieghardt, *Prog. Inorg. Chem.*, 1987, **35**, 329; A. J. Blake and M. Schröder, *Adv. Inorg. Chem.*, 1990, **35**, 1.
2 (*a*) P. Dapporto and L. Sacconi, *J. Chem. Soc. A*, 1970, 1804; L. Sacconi and I. Bertini, *J. Am. Chem. Soc.*, 1968, **90**, 5443; (*b*) L. Sacconi, C. A. Ghilardi, C. Mealli and F. Zanobini, *Inorg. Chem.*, 1975, **14**, 1380; P. Stavropoulos, M. C. Muetterties, M. Carrie and R. H. Holm, *J. Am. Chem. Soc.*, 1990, **112**, 5385.
3 J. Chatt, F. A. Hart and H. R. Watson, *J. Chem. Soc.*, 1962, 2537.
4 M. Bochmann, I. Hawkins, M. B. Hursthouse and R. L. Short, *J. Chem. Soc., Dalton Trans.*, 1990, 1213.
5 W. N. Setzer, C. A. Ogle, G. S. Wilson and R. S. Glass, *Inorg. Chem.*, 1983, **22**, 266.
6 Using the program Cerius^2, Biosym/Molecular Simulations Ltd.
7 R. Poli, *Chem. Rev.*, 1996, **96**, 2135.
8 M. Ogasawara, S. A. Macgregor, W. E. Streib, K. Folting, O. Eisenstein and K. G. Caulton, *J. Am. Chem. Soc.*, 1995, **117**, 8869.
9 C. Mealli and D. M. Prosperio, *J. Chem. Educ.*, 1990, **167**, 389; R. Hoffmann, *J. Chem. Phys.*, 1963, **39**, 1397; R. Hoffmann and W. N. Lipscomb, *J. Chem. Phys.*, 1962, **36**, 1397; **37**, 2872.
10 M. Ray, G. P. A. Yap, A. L. Reingold and A. S. Borovik, *J. Chem. Soc., Chem. Commun.*, 1995, 1777.
11 J. A. Darr, S. R. Drake, M. B. Hursthouse and K. M. A. Malik, *Inorg. Chem.*, 1993, **32**, 5704.
12 G. M. Sheldrick, *Acta Crystallogr., Sect. B*, 1990, **46**, 467.
13 G. M. Sheldrick, SHELXL93, Program for Crystal Structure Refinement, University of Göttingen, 1993.

Received in Cambridge, UK, 29th September 1997; 7/07006C

Structural authentication of an N-functionalised disecondary diphosphane

Philip C. Andrews, Simon J. King, Colin L. Raston* and Brett A. Roberts

Department of Chemistry, Monash University, Clayton, Victoria 3168, Australia

The reaction of $RPCl_2$ [R = (6-Me-2-pyridyl)$(SiMe_3)_2C^-$] with $LiAlH_4$ in Et_2O gives the novel N-functionalised disecondary diphosphane compound [R(H)P–P(H)R] rather than the expected phosphorus dihydride complex RPH_2; the *meso* and *rac* isomers of the diphosphane crystallise separately with the *meso* isomer being structurally authenticated.

Disecondary diphosphanes,† $(R'PH)_2$ (R′ = alkyl or aryl) normally formed in the equilibration reaction of organophosphide oligomers, $(R'P)_n$, with organophosphorus hydrides, $n\,R'PH_2$, have been studied extensively in solution by NMR spectroscopy.[1] However in the solid state examples are limited to those where they have been synthesised *in situ* and isolated as Lewis base donors, bonding through phosphorus, and bridging two metal centres; namely Cr in {[$Cr(CO)_5$][MesP(H)P(H)Mes][$Cr(CO)_5$]}[2] (Mes = 2,4,6-$Me_3C_6H_2$), Mn in {[$MnCp(CO)_2$][PhP(H)P(H)Ph][$MnCp(CO)_2$]}[3] and Ag in $[PhPH_2Ag\{\mu\text{-}(PhPH)_2\}]_2[AsF_6]_2$.[4] The mechanism of formation of the diphosphanes is in each case unknown but has been attributed to the dimerisation of the reactive radical [R′(H)P]· species which is also accessible from the deprotonation of protic and/or polar solvents by a reactive phosphinidene intermediate [R′P:].[5]

Herein we report the synthesis and characterisation of the first non-complexed N-functionalised disecondary diphosphane, **1**. In attempting to synthesise the simple phosphorus dihydride derivative of the bulky alkyl ligand (6-Me-2-pyridyl)-$(SiMe_3)_2C^-$, R, *via* the reduction of $RPCl_2$ with $LiAlH_4$ we observed that on each occasion the product obtained by crystallisation was not the dihydride but the diphosphane, [(6-Me-2-pyridyl)$(SiMe_3)_2$CPH]$_2$ **1**. This was totally unexpected given that $LiAlH_4$ is an almost ubiquitous reagent used in the formation of $R'PH_2$ species from various phosphine, phosphinous and phosphonic sources.[6]

In a typical reaction (Scheme 1) an Et_2O solution of a slight stoichiometric excess of $LiAlH_4$ was added to a pale orange Et_2O solution of the crystals of the dichloride complex $RPCl_2$, formed from the metathetical reaction of $RLi\cdot Et_2O$ and PCl_3, at −78 °C and the reaction mixture allowed to warm slowly to ambient temperature over 4 h. Filtration followed by *in vacuo* concentration of the solution and cooling to −30 °C allowed for the growth of a moderate yield of **1** as colourless needles.‡

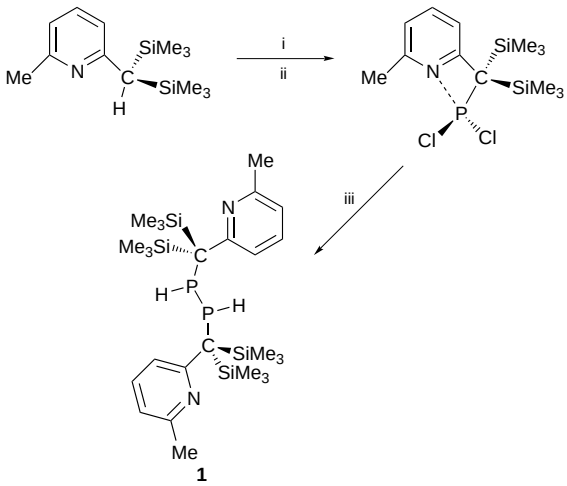

Scheme 1 *Reagents and conditions*: i, Bu^nLi, Et_2O, −78 °C; ii, PCl_3, Et_2O, −78 °C, 2 h; iii, $LiAlH_4$, Et_2O, −78 °C, 4 h

The structure (Fig. 1) of the single crystal analysed by X-ray techniques proved to be the *meso* isomer: crystallising in the triclinic space group $P\bar{1}$ (no. 2) with two molecules in the unit cell, each molecule possessing a centre of inversion.§ The P–P bond distance of 2.222(3) Å is comparable with that of 2.258(3) Å in the Mn complex, 2.253(2) Å in the Cr complex and 2.202(4) Å in the Ag complex. The pyridyl nitrogens are located away from the P centre indicating there are no N···P interactions.

Two significantly different melting points, 122–123 and 177–178 °C with decomposition to dark red products, were obtained for different crystals taken from the same sample. This coupled with the fact that NMR data obtained on several different samples was consistent and reproducible is indicative that both the *meso* and the *rac* (DL) isomers co-crystallise from solution. The NMR data also revealed that the *meso* and *rac* isomers were always present in solution in 1 : 0.6 ratio, respectively; a ratio which did not change in the temperature range −90 to 80 °C. There was no spectroscopic evidence that the target dihydride complex was formed either directly as originally proposed or by the disproportionation of the diphosphane into higher phosphide oligomers and the accompanying hydride species. This implies that the diphosphane is

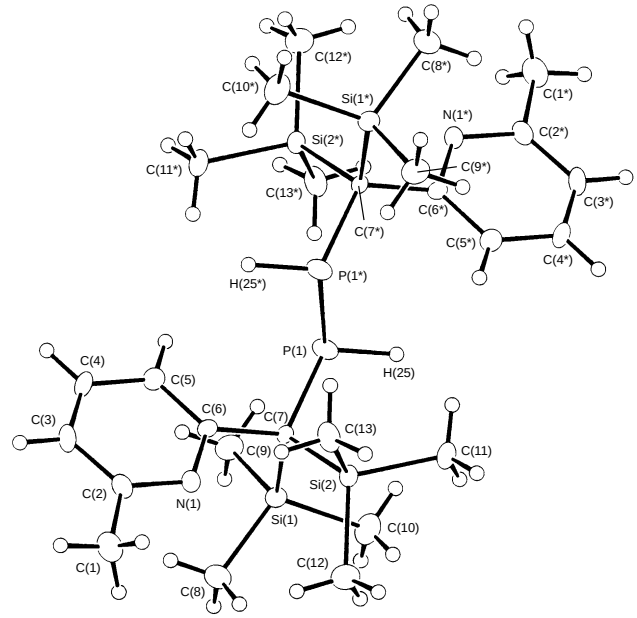

Fig. 1 Crystal structure of **1**. Selected distances (Å) and angles (°): P(1)–P(1*) 2.222(3), P(1)–C(7) 1.872(4), C(7)–C(6) 1.528(6), C(7)–Si(1) 1.931(4), C(7)–Si(2) 1.934(5), P(1*)–P(1)–C(7) 104.5(2), P(1)–C(7)–Si(1) 103.8(2), P(1)–C(7)–Si(2) 111.1(2), P(1)–C(7)–C(6) 116.4(2).

thermally robust and requires greater temperatures to force the creation of the equilibrium observed for other diphosphanes.

The NMR data on **1** can be compared with those obtained and compiled by Albrand and Taïeb[1] on a series of disecondary diphosphanes, R′ = Ph, Me, Et, cyclohexyl, CF_3, all relating to an AA′XX′ spin system. The $^{31}P\{^1H\}$ spectrum has two peaks at δ −99.5 (*rac*) and −91.5 (*meso*). The undecoupled ^{31}P spectrum has the two peaks split into two symmetrical sets of doublets of doublets, the coupling constants for the peaks centred at δ −99.5 being $^1J_{PH}$ 128 and $^2J_{PH}$ 74 Hz and for the peaks centred at δ −91.5 being $^1J_{PH}$ 152 and $^2J_{PH}$ 61 Hz. While the ^{31}P chemical shifts correlate most closely with those for R′ = Et (δ −99.6 and −93.8) the $^1J_{PH}$ and $^2J_{PH}$ values of 192.9, 192.9 and 11.2, 6.5 Hz, respectively, are clearly very different, as they are for all of the diphosphanes investigated, and must relate to the increased polarisation of the C–P bonds induced by the proximity of the two $SiMe_3$ groups.

The ^1H NMR spectrum also shows the high degree of P–H coupling. Two sets of doublets of doublets are present, one centred on δ 3.82 with coupling constants corresponding to those of the *meso* isomer at δ 91.5 in the ^{31}P spectrum and the other at δ 4.48 with coupling constants relating to the *rac* isomer at δ 99.5 in the ^{31}P spectrum. The two inner peaks of the doublet of doublets at δ 3.82 also show $^3J_{HH}$ splitting with a coupling constant of 4.89 Hz while those centred on δ 4.48 are smaller at 1.6 Hz. The differing electronic environments of the isomers are highlighted by the four signals present for the four $SiMe_3$ groups in both the ^1H and the ^{13}C spectra with the largest chemical shift separation (*cf.* δ 0.51 and δ 0.24 with δ 0.42 and δ 0.34) occurring for those relating to the *rac* isomer.

The mechanism of formation of the diphosphane can as yet only be speculated upon but two possibilities exist; dimerisation of a monohydride species, [R(H)P], radical or otherwise, occurring more rapidly than replacement of a remaining chloride by a hydride or formation of the diphosphene [RP=PR] which is subsequently hydrogenated by the $LiAlH_4$. Why this should occur for (6-Me-2-pyridyl)$(SiMe_3)_2CPCl_2$ and not, for example, 2,4,6-$Bu^t_3C_6H_2PCl_2$,[7] is puzzling though in several EPR studies we have shown that it is possible for the pyridyl system to stabilise a radical species for a significant amount of time. Thus [(2-pyridyl)$(SiMe_3)_2CHg]^{\cdot}$,[8] generated from {(2-pyridyl)$(SiMe_3)_2C_2$}M on exposure to unfiltered UV light at 100 K, gave a decaying EPR signal with $t_{0.5}$ = 300 s while $t_{0.5}$ for the radicals [{(2-pyridyl)$(SiMe_3)_2C$}$_2$M]$^{\cdot}$ (M = Al, Ga)[9] generated by the Na/K reduction of the {(2-pyridyl)(Si-$Me_3)_2C$}$_2$MCl complexes were of the order of 3600 s, though coupling in this case occurred, not unexpectedly, through the γ position of the pyridyl ring. Clearly in the absence of metallic centres and the absence of unfavourable M–M bond formation the possibility of [R(H)P]$^{\cdot}$ coupling exists as a viable mechanism. The attempt to form the As analogue by the same route resulted in crystallisation of only the thermally unstable $RAsH_2$ complex.

Compound **1** should prove to be a valuable, flexible and interesting new ligand having, with the added functionality of the two pyridyl nitrogens, four possible donating sites. We are currently investigating the potential of forming novel metal complexes of **1**.

We thank the Australian Research Council for financial support.

Notes and References

* E-mail: c.raston@sci.monash.edu.au

† Also referred to in the literature as diphosphines.

‡ *Analytical data* for **1**: colourless needle crystals. typical yield, after three crystallisations, 63%. Two isomers in 1 : 0.6 ratio (*rac* : *meso*). Mp 122–123 °C (decomp.) and 177–178 °C (decomp.). ^1H NMR (400 MHz, C_6D_6, 25 °C) δ 7.40 (d, 1 H, α), 7.33 (d, 0.6 H, α), 7.23 (m, 1.6 H, β), 6.51 (m, 1.6 H, γ), 4.48 (dd, 0.6 H, $^1J_{PH}$ 128, $^2J_{PH}$ 75 Hz), 3.82 (dd, 1 H, $^1J_{PH}$ 149, $^2J_{PH}$ 63 Hz) 2.36 (s, 3 H, Me), 2.33 (s, 1.8 H, Me) 0.51 (s, 0.6 × 9 H, $SiMe_3$), 0.42 (s, 9 H, $SiMe_3$), 0.34 (s, 9 H, $SiMe_3$) 0.27 (s, 0.6 × 9 H, $SiMe_3$). ^{13}C NMR (50.3 MHz, C_6D_6, 25 °C) δ 162.8, 156.4, 135.7, 120.1, 118.5, 28.9, 23.9, 2.42, 1.83, 1.80, 1.32. $^{31}P\{^1H\}$ NMR (81 MHz, C_6D_6, 25 °C) δ −99.5, −91.5. ^{31}P NMR (81 MHz, C_6D_6, 25 °C) δ −99.5 (dd $^1J_{PH}$ 128, $^2J_{PH}$ 74 Hz), −91.5 (dd, $^1J_{PH}$ 152, $^2J_{PH}$ 61 Hz). Elemental analysis (%); required (found) C, 55.32 (55.30); H, 8.86 (9.05); N, 4.96 (4.97).

§ *Crystallographic data* for **1**: Nicolet R3m diffractometer, crystals mounted in oil under N_2, $[RP(H)]_2$, $C_{26}H_{50}N_2P_2Si_4$, M = 564.98, triclinic, space group $P\bar{1}$, a = 8.790(5), b = 9.184(6), c = 11.735(6) Å, α = 93.99(5), β = 101.16(4), γ = 112.86(4)°, U = 845.3(10) Å^3, D_c = 1.110 g cm^{-3}, T = 173 K, Z = 2, F(000) = 306.00. μ_{Mo} = 2.87 cm^{-1}, $A^*_{min,max}$ = 0.79, 1.00. $2\theta_{max}$ = 45°, final R,R_w = 0.052, 0.038 (statistical weights), GOF 2.08, N_o = 1552 'observed' [$I > 2\sigma(I)$] reflections out of N = 2203 unique. The positions of all H atoms were calculated and included as invariants; fixed temperature and constrained in x, y, z, U_{iso}. CCDC 182/740.

1 J. P. Albrand and C. Taïeb, *Phosphorus Chemistry, Proceedings of the 1981 International Conference*, ed. L. D. Quin and J. G. Verkade, ACS Symp. Ser. 171, American Chemical Society, Washington, DC, 1981.
2 R. A. Bartlett, H. V. R. Dias, K. M. Flynn, H. Hope, B. D. Murray, M. M. Olmstead and P. Power, *J. Am. Chem. Soc.*, 1987, **109**, 5693.
3 G. Huttner, H.-D. Müller, V. Bejenke and O. Orama, *Z. Naturforsch., Teil B*, 1976, **31**, 1166.
4 P. G. Jones, H. B. Roesky, H. Grützmacher and G. M. Sheldrick, *Z. Naturforsch. Teil B*, 1985, **40**, 590; J. P. Albrand and D. Gagnaire, *J. Am. Chem. Soc.*, 1972, **94**, 8630.
5 C. Couret, J. Escudie, H. Ranaivonjatovo and J. Satgé, *Organometallics*, 1986, **5**, 113.
6 D. E. C. Corbridge, *Phosphorus, An Outline of its Chemistry, Biochemistry and Technology*, Elsevier, 1990, 4th edn., section 4.2.
7 S. Kurz and E. Hey-Hawkins, *Organometallics*, 1992, **11**, 2729.
8 M. J. Henderson, Honours Thesis, University of Western Australia, 1985.
9 U. Kynast, B. W. Skelton, A. H. White, M. J. Henderson and C. L. Raston, *J. Organomet. Chem.*, 1990, **384**, C1.

Received in Columbia, MO, USA, 4th September 1997; 7/06481K

Aggregation of lithium and mixed thallium(I)–lithium amides through η^3- and η^6-π-arene interactions in the solid

Konrad W. Hellmann,[a] Christian Galka,[a] Lutz H. Gade,*[a] Alexander Steiner,[b] Dominic S. Wright,[b] Thomas Kottke[a] and Dietmar Stalke[a]

[a] *Institut für Anorganische Chemie der Universität Würzburg, Am Hubland, D-97074 Würzburg, Germany*
[b] *University Chemical Laboratory, Lensfield Road, Cambridge, UK CB2 1EW*

The mixed Li–Tl amide $[C_{10}H_6\{N[Li(thf)_2]SiMe_3\}\{N(Tl)SiMe_3\}]$ has been synthesized and shown to aggregate *via* η^6-arene–thallium coordination in the solid; a related pattern of aggregation is found for the partially solvated homometallic Li amide $[C_{10}H_6\{N[Li(thf)]SiMe_3\}\{N(Li)SiMe_3\}]$ which displays an unusual η^3-arene–lithium interaction.

A comparison of the structural patterns observed in the solid state structures of lithium and thallium(I) amides reveals marked differences in the bonding patterns. Mainly ionic forms of aggregation controlled by electrostatic interactions and the steric demand of the organic periphery occur in the case of lithium amides (and other alkali metal amides).[1] However, the few structurally characterized thallium(I) amides known to date are not well described by the electrostatic model but rather display attractive intermolecular contacts between the heavy metal atoms which appear to arise from weak dispersion forces.[2,3] Another significant difference is the tendency for solvation of the metal atoms, with lithium being most readily coordinated by donor solvents while monovalent thallium appears to be more resistant to increasing its coordination number by donor solvation.

Here, we give a first account of our systematic attempts to break-up the hitherto established structural patterns in Tl^I–amide chemistry by incorporating potentially coordinating molecular units into the ligands employed, and to obtain mixed alkali metal–thallium amides which combine the characteristics of the two structural regimes mentioned above. As the ligand precursor we chose the known 1,8-bis(trimethylsilylamino)naphthalene **1** containing an aryl backbone[4] which may potentially interact with the metal centres and thus generate novel forms of aggregation. In this context it should be noted that MO calculations reported for the related dilithiated α-naphthylamine already suggested metal–C-8 interactions in the gas phase which were, however, not found in the decameric solid state structure $[(C_{10}H_7NLi_2)_{10}(Et_2O)_6]$.[5] With this in mind, we assumed that the formal addition of a donor functionality in or close to the C-8 position of the naphthyl unit would generate a significantly different structural pattern.

Lithiation of **1** in thf cleanly yielded the solvated Li–amide $[C_{10}H_6\{N[Li(thf)_2]SiMe_3\}_2]$ **2** which was isolated and employed as a starting material. Stirring **2** with 1 equiv. of TlCl in thf for 5 h followed by work-up by removal of the solvent, extraction with toluene and crystallization at −35 °C gave an orange crystalline solid in moderate yield. The analytical data and the ^1H and ^{13}C NMR spectra were consistent with its formulation as $[C_{10}H_6\{N[Li(thf)_2]SiMe_3\}\{N(Tl)SiMe_3\}]$ **3**, *i.e.* the first example of a mixed Tl^I–Li amide.† While cryoscopy in benzene indicated the presence of monomeric units in solution, its crystal structure revealed an intriguing dimeric aggregation in the solid (Fig. 1.)‡

The two halves of the dimer, in which a Tl^I atom and a $(thf)_2Li^+$ cation bridge the amido-N atoms, are related by a crystallographic centre of symmetry. The Tl···Tl distance of 3.982(2) Å does not indicate a significant metal–metal interaction. Instead, the interaction between the Tl centres and one of the naphthalene arene rings appears to provide the driving force for the dimeric aggregation in the solid. The distance between the Tl atom and the centroid of the η^6-coordinated arene ring of 3.5106 Å is somewhat greater than some of the previously reported Tl–arene contacts, in particular that found in $[\{2,6\text{-}Pr^i_2C_6H_3N(Tl)SiMe_3\}_4]$ (3.11 Å),[6a] but clearly within the range expected for a heavy metal arene coordination.[6b–d] The crystal structure of **3** nicely illustrates the structural principles outlined above, the solvation of the 'peripheral' Li atoms and aggregation involving the arene unit in the ligand backbone.

When the Li–Tl exchange is carried out with 2 molar equiv. of TlCl the completely transmetallated amide $[C_{10}H_6\{N(Tl)SiMe_3\}_2]$ **4** is formed which has a much decreased solubility in hydrocarbon solvents. It is therefore thought to be polymeric in the solid possibly as a result of metal···arene interactions similar to those established for **3**.

That the 1,8-naphthadiyl backbone of the bidentate amido ligand may strongly influence the aggregation of its metallated derivatives became apparent upon stirring the Li–amide **2** for

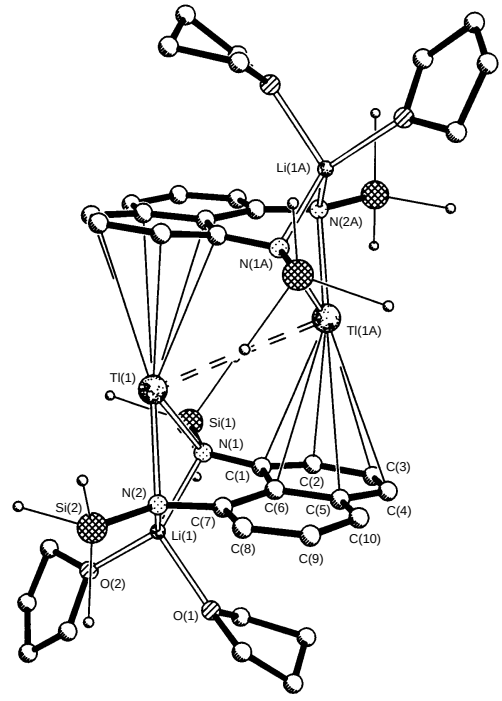

Fig. 1 Molecular structure of **3**. Selected atomic distances (Å) and interbond angles (°): Tl(1)–N(1) 2.467(11), Tl(1)–N(2) 2.497(10), Tl(1)–Li(1) 3.24(3), Tl(1)–C(2A) 3.628(14), Tl(1)–C(6A) 3.810(13), Tl(1)–C(3A) 3.82(2), Tl(1)–C(4A) 3.90(2), Tl(1)–C(5A) 3.91(2), Tl(1)–Tl(1A) 3.982(2), Li(1)–N(2) 1.97(3), Li(1)–N(1) 2.02(3), Li(1)–O(2) 2.06(3), Li(1)–O(1) 2.06(3); N(1)–Tl(1)–N(2) 69.8(3), N(1)–Li(1)–N(2) 90.4(11), Li(1)–N(1)–Tl(1) 91.8(9), Li(1)–N(2)–Tl(1) 92.3(9).

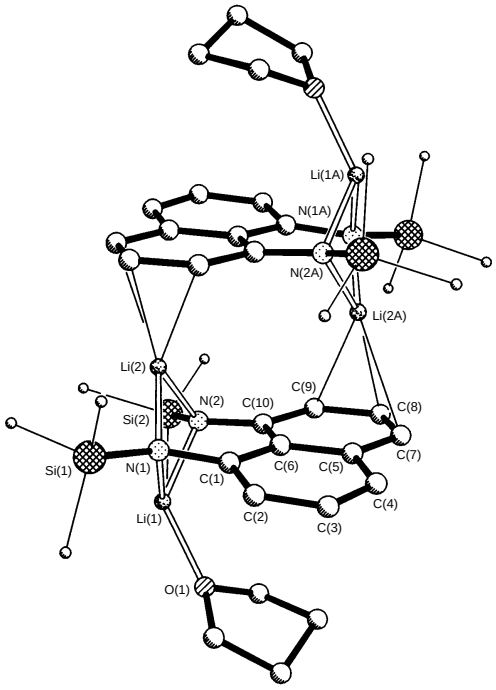

Fig. 2 Molecular structure of **5**. Selected atomic distances (Å) and interbond angles (°): N(1)–Li(1) 1.989(6), N(2)–Li(1) 1.995(6), N(1)–Li(2) 1.987(6), N(2)–Li(2) 1.861(4), Li(1)–O(1) 1.917(5), Li(2)–Li(2A) 4.117(6), Li(2)–C(9A) 2.596(6), Li(2)–C(8A) 2.399(6), Li(2)–C(7A) 2.577(6); Li(1)–N(1)–Li(2) 86.3(2), Li(1)–N(2)–Li(2) 86.3(2), N(1)–Li(1)–N(2) 89.2(2), N(1)–Li(2)–N(2) 89.6(2).

ca. 15 h in dioxane or toluene in the absence of TlCl. Instead of the disolvated Li–amide **2** large single crystals of a monosolvate $[C_{10}H_6\{N[Li(thf)]SiMe_3\}\{N(Li)SiMe_3\}]$ **5** were obtained.† The displacement of three of the thf ligands under these conditions was unexpected and indicated the formation of an unusual amide structure. This was confirmed by the single crystal X-ray structure analysis of the compound which revealed a dimeric structure closely related to that of **3** (Fig. 2).‡

The two molecular units are again related by a centre of inversion which generates a structural array which closely parallels that of the mixed metal amide **3**. The Li cation which has lost all of its donor ligands is coordinated by one of the naphthalene arene rings in an η^3-fashion [Li(2)–C(9A) 2.596(6), Li(2)–C(8A) 2.399(6), Li(2)–C(7A) 2.577(6) Å; nearest non-bonding Li–arene distances: Li(2)–C(5A) 2.956(6), Li(2)–C(10A) 2.992(6) Å]. The second Li atom which is located at the periphery is coordinated by only one thf molecule. At the vacant coordination site, which is occupied by a second thf molecule in **3**, a methyl group of the neighbouring dimeric unit is located [Li(1)–C(14′) 3.656(6) Å]. Although π-interactions of lithium cations with arene rings are known,[7] the η^3-mode of π-coordination observed in **5** is unprecedented in lithium amide chemistry.

Since lithium has a smaller ionic radius than thallium(I) and, consequently, forms shorter metal–arene distances, the two naphthalene ring systems are considerably closer in **5** than in **3** (lengths of the normal vectors between the arene planes in **3**: 5.41, **5**: 3.60 Å).

In conclusion, these first results indicate that the use of polydentate amido ligands containing potentially ligating backbone units generates structural arrays which differ markedly from those previously obtained with amido ligands containing an 'inactive' alkyl or silyl periphery.[3]

We thank the Deutsche Forschungsgemeinschaft, the Fonds der Chemischen Industrie, the Stiftung Volkswagenwerk, the EPSRC and the Deutscher Akademischer Austauschdienst for funding and Professor H. Werner for support of this work.

Notes and References

* E-mail: lutz.gade@mail.uni-wuerzburg.de

† *Selected spectroscopic and analytical data*: **3**: ^{1}H NMR (200.13 MHz, C_6D_6, 295 K) δ 0.38 [s, 18 H, $Si(CH_3)_3$], 0.85 (m, 8 H, CH_2CH_2O), 3.05 (m, 8 H, CH_2CH_2O), 6.74–7.30 (m, 6 H, $C_{10}H_6$); $\{^1H\}^7$Li NMR (77.78 MHz, C_6D_6, 295 K) δ 3.98; $\{^1H\}^{29}$Si NMR (39.76 MHz, C_6D_6, 295 K) δ −6.0; $C_{24}H_{40}LiN_2O_2Si_2Tl$ (656.09). Calc: C 43.94, H 6.14, N 4.27. Found: C 43.46, H 5.95, N 4.01%. **5**: ^{1}H NMR (200.13 MHz, C_6D_6, 295 K). δ 0.39 [s, 18 H, $Si(CH_3)_3$], 0.88 (m, 4 H, CH_2CH_2O), 3.08 (m, 4 H, CH_2CH_2O), 6.77 (dd, 2 H, $^3J_{HH}$ 7.3, $^4J_{HH}$ 1,1 Hz, $C_{10}H_6$), 7.13–7.32 (m, 4 H, $C_{10}H_6$); $\{^1H\}^7$Li NMR (77.78 MHz, C_6D_6, 295 K) δ −0.68; $\{^1H\}^{29}$Si NMR (39.76 MHz, C_6D_6, 295 K) δ −12.6; $C_{20}H_{32}Li_2N_2OSi_2$ (386.54). Calc. C 62.15, H 8.34, N 7.25. Found: C 61.88, H 8.05, N 7.19%.

‡ *Crystal data*: **3**: $C_{24}H_{40}LiN_2O_2Si_2Tl$, red blocks, crystal dimensions 0.2 × 0.2 × 0.2 mm, M = 656.07, triclinic, space group $P\bar{1}$, a = 10.912(4), b = 11.162(4), c = 12.662(5) Å, α = 92.43(5), β = 101.47(5), γ = 110.90(4)°, U = 1401.1(9) Å^3, Z = 2, D_c = 1.555 g cm^{-3}, μ = 5.871 mm^{-1}, F(000) = 652, 4504 reflections collected (4.03 < θ < 22.50°) at 153(2) K, 3640 independent (R_{int} = 0.090), 3625 used in the structure refinement; R_1 = 0.058 [$I > 2\sigma(I)$], wR_2 = 0.189 (all data), GOF = 1.104 for 328 parameters and 297 restraints, largest difference peak, hole = 1.624, −1.787 e Å^{-3}. The comparatively high residual electron density is due to absorption by Tl and to a third component of disorder of a thf molecule which could not be refined.

5: $C_{20}H_{32}Li_2N_2OSi_2$, yellow blocks, crystal dimensions 0.3 × 0.3 × 0.2 mm, M = 386.54, monoclinic, space group $P2_1/n$, a = 10.646(2), b = 11.918(1), c = 17.687(3) Å, β = 93.40(1)°, U = 2240.2(6) Å^3, Z = 4, D_c = 1.146 g cm^{-3}, μ = 0.169 mm^{-1}, F(000) = 832, 3918 reflections collected (3.42 < θ < 24.99°) at 173(2) K, 3325 independent (R_{int} = 0.027), 3325 used in the structure refinement; R_1 = 0.052 [$I > \sigma(I)$], wR_2 = 0.113 (all data), GOF = 1.015 for 269 parameters and 37 restraints, largest difference peak, hole = 0.222, −0.191 e Å^{-3}.[8–10] CCDC 182/751.

1 The systematic use of bulky substituent in amides was pioneered by Lappert *et al.* For a survey of early work, see: M. F. Lappert, P. P. Power, A. R. Sanger and R. C. Srivastava, *Metal and Metalloid Amides*, Ellis Horwood-Wiley, Chichester 1980. Recent reviews: K. Gregory, P. v. R. Schleyer and R. Snaith, *Adv. Inorg. Chem.*, 1991, **37**, 47; R. E. Mulvey, *Chem. Soc. Rev.*, 1991, **20**, 167.

2 M. Veith, A. Spaniol, J. Pöhlmann, F. Gross and V. Huch, *Chem. Ber.*, 1993, **126**, 2625.

3 K. W. Hellmann, L. H. Gade, I. J. Scowen and M. McPartlin, *Chem. Commun.*, 1996, 2515; K. W. Hellmann, L. H. Gade, A. Steiner, D. Stalke and F. Möller, *Angew. Chem., Int. Ed. Engl.*, 1997, **36**, 160; K. W. Hellmann, L. H. Gade, R. Fleischer and D. Stalke, *Chem. Commun.*, 1997, 527.

4 J. L. Smith, J. L. Beck and W. J. A. VandenHeuvel, *Org. Mass. Spectrom.*, 1971, **5**, 473; C. D. Schaeffer, Jr. and J. J. Zuckerman, *J. Am. Chem. Soc.*, 1974, **96**, 7160.

5 D. R. Armstrong, D. Barr, W. Clegg, S. R. Drake, R. J. Singer, R. Snaith, D. Stalke and D. S. Wright, *Angew. Chem., Int. Ed. Engl.*, 1991, **30**, 1707.

6 (*a*) S. D. Waezsada, T. Belgardt, M. Noltemeyer and H. W. Roesky, *Angew. Chem., Int. Ed. Engl.*, 1994, **33**, 1351; (*b*) W. Frank, D. Kuhn, S. Müller-Becker and A. Ravazi, *Angew. Chem., Int. Ed. Engl.*, 1993, **32**, 90; (*c*) M. D. Noirot, O. P. Anderson and S. H. Strauss, *Inorg. Chem.*, 1987, **26**, 2216; (*d*) H. Schmidbaur, W. Bublak, B. Huber, J. Hofmann and G. Müller, *Chem. Ber.*, 1989, **122**, 102.

7 B. Schiemenz and P. P. Power, *Angew. Chem., Int. Ed. Engl.*, 1996, **35**, 2150; K. Ruhland-Senge, J. J. Ellison, R. J. Wehmschulte, F. Power and P. P. Power, *J. Am. Chem. Soc.*, 1993, **115**, 11 353; S. Kurz and E. Hey-Hawkins, *Organometallics*, 1992, **11**, 2729.

8 T. Kottke and D. Stalke, *J. Appl. Crystallogr.*, 1993, **26**, 615; T. Kottke, R. J. Lagow and D. Stalke, *J. Appl. Crystallogr.*, 1996, **29**, 465.

9 G. M. Sheldrick, *Acta Crystallogr., Sect. A*, 1990, **46**, 467.

10 G. M. Sheldrick, program for crystal structure refinement, Göttingen 1993.

Received in Basel, Switzerland, 11th November 1997; 7/08139A

Structural control of ferromagnetic interactions in nickel(II) complexes based on a tetradentate biradical

Francisco M. Romero,[a] Dominique Luneau[b] and Raymond Ziessel[a]

[a] *Laboratoire de Chimie, d'Électronique et de Photonique Moléculaires, École de Chimie, Polymères et Matériaux (UPRES-A 7008), 1 rue Blaise Pascal, 67008 Strasbourg, France*

[b] *Département de Recherche Fondamentale sur la Matière Condensée, Service de Chimie Inorganique et Biologique, Laboratoire de Chimie de Coordination (URA CNRS 1194), CEA-Grenoble, 38054 Grenoble, France*

Complexation of a bipyridine-based nitronyl nitroxide biradical with nickel(II) affords two complexes that differ by the nature of one axial ligand and by their magnetic behaviour: in both cases ferromagnetic interactions between high-spin nickel(II) and the radicals are observed.

A key concept for the design of molecular ferromagnets involves the pre-programmed overlap of magnetic orbitals.[1] Thus far interest has focused on the preparation of multi-dimensional inorganic assemblies,[2,3] hybrid inorganic/organic systems[4] and organic radicals.[5] Coordination of nitroxide radicals to acidic paramagnetic metal centres provides valuable magnetic properties and, in certain cases, ferromagnetic ordering has been attained.[6,7] Surprisingly, chelating radicals have received scant attention despite the fact that they introduce important stereochemical constraints concerning the overlap of magnetic orbitals while favouring utilization of metal centres that are not strongly acid.[8,9] Here we report on the preparation, crystallographic analysis and magnetic properties of two nickel(II) complexes obtained from NIT-bpy, these being the first complexes to exhibit ferromagnetic Ni^{II}–radical interactions.

Complexes **1** and **2** were synthesised (Scheme 1), respectively, by mixing NIT-bpy with $[Ni(H_2O)_6][ClO_4]_2$ in methanol or in a mixture of dichloromethane–ethyl acetate.†

Single crystals of **1** were grown by slow evaporation of methanol.‡ Both the ORTEP view and the magnetic properties are shown in Fig. 1. It is seen that the NIT-bpy behaves as a pincer occupying the basal plane of the nickel octahedron. Two ancilliary ligands [H_2O molecules at a distance of 2.08(1) Å] complete the cation coordination sphere. Relevant structural features which have an impact on the magnetic properties are as follows: the O(1)N(1)C(1)N(2)O(2) mean plane containing one unpaired electron makes an angle of 14.07° with the equatorial plane N(5)N(6)O(1)O(3), 86.10 and 77.60°, respectively, with the N(5)O(w1)O(3)O(w2) and N(6)O(w1)O(1)O(w2) planes. The second O(3)N(3)C(12)N(4)O(4) mean plane exhibits an angle of 2.74° with the equatorial plane N(5)N(6)O(1)O(3), 89.50 and 88.97°, respectively, with N(5)O(w1)O(3)O(w2) and N(6)O(w1)O(1)O(w2) planes. The tilt angle about the exocyclic central C–C bond in the bpy subunit is 11.09°.

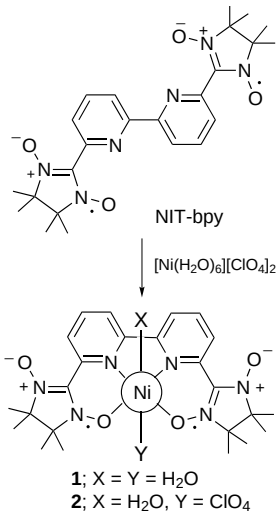

Scheme 1

The magnetic properties of these two nickel(II) complexes were studied by use of a SQUID susceptometer. For **1**, the product of molar susceptibility and temperature (χT) at 300 K corresponds to the calculated value expected for three uncorrelated spins (Ni^{II} $S = 1$ and two radicals $S = 1/2$) (Fig. 1). With decreasing temperature, χT shows a shallow decrease until a sharp breakdown occurs at around 220 K, presumably due to a phase transition. Then a continuous decrease is observed until a plateau is reached around 50 K, where $\chi T = 1.13$ emu K mol^{-1}. At still lower temperature an abrupt decrease occurs, indicating the onset of weak intermolecular antiferromagnetic interactions. A good fit of these experimental data could be obtained by allowing for the fact that coupling between each radical and the metal centre is different. One radical is coupled

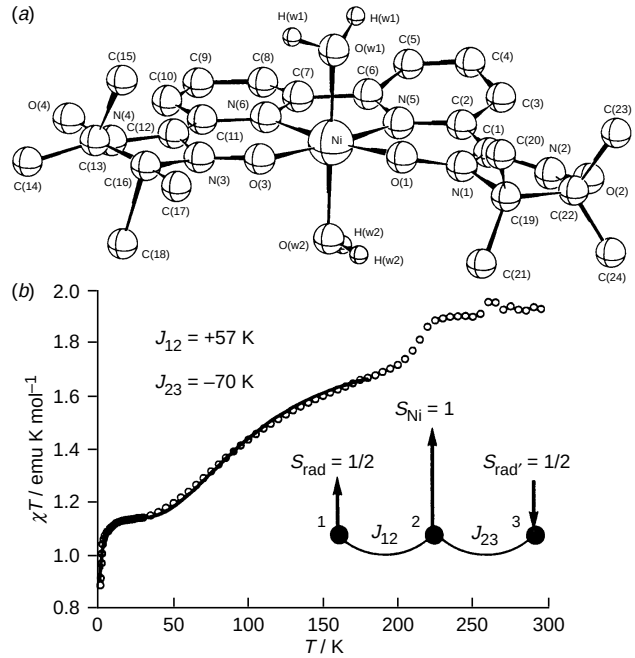

Fig. 1 (*a*) ORTEP view of the $[Ni(NIT\text{-}bpy)\cdot 2H_2O]^{2+}$ cation in complex **1** and (*b*) temperature dependence of the product of the magnetic susceptibility with temperature, χT *vs.* T, for **1**. The solid line represents the best-fit calculated values. Inset: magnetic interations network and values of the coupling constants.

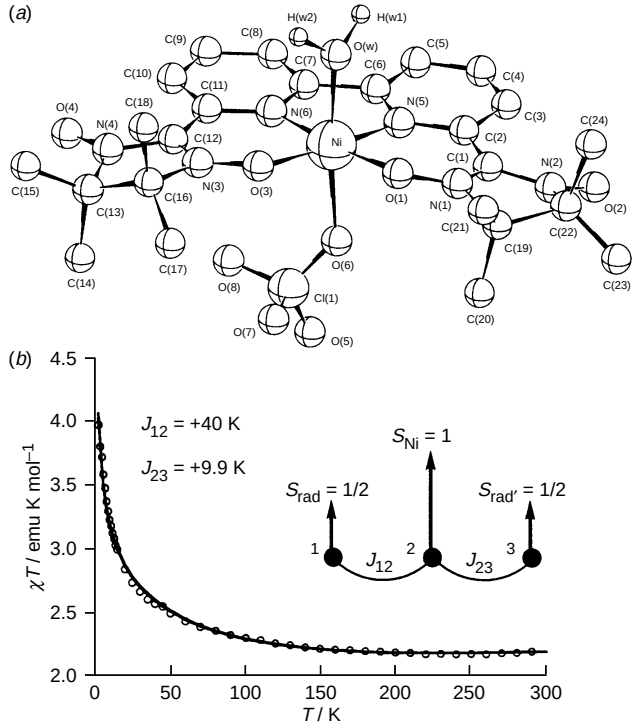

Fig. 2 (*a*) ORTEP view of the $[Ni(NIT\text{-}bpy)\cdot H_2O\cdot ClO_4]^{2+}$ cation in complex **2** and (*b*) temperature dependence of the product of the magnetic susceptibility with temperature, χT *vs.* T, for **2**. The solid line represents the best-fit calculated values. Inset: Magnetic interactions network and values of the coupling constants.

ferromagnetically (J_{12} = +57 K) while the second interaction (J_{23} = −70 K) is antiferromagnetic. The value obtained for the plateau corresponds to the value calculated for an S = 1 ground spin state arising from antiferromagnetic coupling between a spin 3/2 and a spin 1/2 of the second radical. The best fit in the low temperature regime was obtained with a mean field approximation (zJ' = −0.47 K).

At a first glance the crystal structure of complex **2**‡ looks very close to that of **1** (Fig. 2). However, careful examination of these structures reveals some important differences concerning relevant angles. Indeed, for **2** the O(1)N(1)C(1)N(2)O(2) system containing one unpaired electron is planar and makes an angle of 14.20° with the equatorial plane N(5)N(6)O(1)O(3), 81.48 and 78.68°, respectively, with the N(5)O(w)O(3)O(6) and the N(6)O(w)O(1)O(6) planes. The O(3)N(3)C(12)N(4)O(4) plane makes an angle of 9.43° with the equatorial plane N(5)N(6)O(1)O(3), 78.20 and 84.44°, respectively, with the N(5)O(w)O(3)O(6) and the N(6)O(w)O(1)O(6) planes. The tilt angle between both pyridine rings in the bpy subunit is only 2.54°. The axial ligands in **2** comprise a water molecule, located at 2.085(4) Å, and a perchlorate anion located at 2.178(4) Å.

Complex **2** exhibits disparate magnetic properties when compared to **1** (Fig. 2). The χT product measured at 300 K is somewhat higher than that calculated for three uncorrelated spins. With decreasing temperature, χT continuously increases over the entire temperature range reaching a value of 3.96 emu K mol^{-1} around 1.8 K. This value is higher than that calculated for two radicals ferromagnetically coupled to Ni^{II} (3.63 emu K mol^{-1}). This reveals that intermolecular ferromagnetic interactions are effective in this complex. The experimental data could be well explained by taking into account two intramolecular ferromagnetic interactions between the radicals and the Ni^{II} centre (J_{12} = +40 K and J_{23} = +9.9 K) as well as a weak intermolecular ferromagnetic interaction calculated by using a mean field approximation (zJ' = + 1.0 K). In **1** and **2**, as well as in the corresponding diamagnetic zinc(II) complex, intramolecular spin coupling between the radicals is insignificant since no sizeable magnetic interactions are observed when χ is measured in a frozen and dilute solution.

Analysis of the overlap between magnetic orbitals indicates that ferromagnetic interactions should be observed for the ideal case where the N_2O_2 ligand is planar. In fact, this conformation forces overlap between the π^* orbital of each radical and the magnetic orbitals of Ni^{II} to be orthogonal (for $d_{x^2-y^2}$) or symmetry forbidden (for d_{z^2}). However, slight deviation from orthogonality should induce the appearance of antiferromagnetic components. One radical in **1** is almost planar along the basal plane of the octahedron, thereby favouring ferromagnetic interaction. The second radical exhibits a prominent deviation from planarity, giving rise to strong antiferromagnetic interaction. Consequently, the overall magnetic behaviour of **1** is antiferromagnetic. The two radical centres in **2**, however, deviate only slightly from planarity and remain ferromagnetically coupled to the Ni^{II} centre.

This study has demonstrated that effective ferromagnetic coupling between Ni^{II} and nitronyl nitroxide radicals belonging to a tetradendate N_2O_2 tweezer ligand is possible. This is due to near orthogonality of the magnetic orbitals and was previously observed only for Cu^{II} complexes of nitronyl nitroxides in axial positions.[10] It is further shown that chelating ligands provide an excellent structural scaffold on which to assemble molecular ferromagnets. Future work will concentrate on the optimisation of these ligands both for their coordinative properties and for their ability to maintain strict orthogonality between the magnetic orbitals.

Notes and References

* E-mail: ziessel@chimie.u-strasbg.fr

† On the basis of spectroscopic evidence, including FAB$^+$ MS and elemental analysis, the structures of the new complexes were unequivocally authenticated.

‡ *Crystal data*: CAD4 Enraf-Nonius diffractometer (Mo-Kα), λ = 0.710 73 Å, graphite monochromator, T = 293 K. **1**, $C_{24}H_{30}Cl_2N_6NiO_{14}$, triclinic, space group $P\bar{1}$, a = 8.501(2), b = 12.815(3), c = 16.086(3) Å, α = 87.35(1), β = 84.86(1), γ = 71.18(1)°, Z = 2, V = 1651.8 Å^3, 2739 independent reflections with $F > 4\sigma(F)$, $R(F_o)$ = 0.0717, $R_w(F_o)$ = 0.0655. **2**, $C_{26}H_{35}Cl_2N_7NiO_{13}$, monoclinic, space group $P2_1/c$, a = 10.732(3), b = 20.823(3), c = 14.742(3) Å, β = 93.22(1)°, Z = 4, V = 3289.2 Å^3, 2780 independent reflections with $F > 4\sigma(F)$, $R(F_o)$ = 0.0417 and $R_w(F_o)$ = 0.0369. The structure was solved and refined on F factors using SHELX86[11a] and SHELX76[11b] packages, respectively. CCDC 182/746.

1 *Molecular Magnetism: From Molecular Assemblies to the Devices*, ed. E. Coronado, P. Delhaès, D. Gatteschi and J. S. Miller, Nato ASI Series, vol. 321, Kluwer Academic, Dordrecht, 1996.
2 M. Ohba, H. Okawa, N. Fukita and Y. Hashimoto, *J. Am. Chem. Soc.*, 1997, **119**, 1011 and references therein.
3 G. De Munno, M. Julve, G. Viau, F. Lloret, J. Faus and D. Viterbo, *Angew. Chem., Int. Ed. Engl.*, 1996, **35**, 1807.
4 M. Clemente-Leon, E. Coronado, J.-R. Galan-Mascaros and C. J. Gomez-Garcia, *Chem. Commun.*, 1997, 1727.
5 F. M. Romero, R. Ziessel, M. Drillon, J.-L. Tholence, C. Paulsen, N. Kyritsakas and J. Fischer, *Adv. Mater.*, 1996, **8**, 826.
6 A. Caneschi, D. Gatteschi and P. Rey, *Prog. Inorg. Chem.*, 1991, **39**, 331.
7 K. Inoue, T. Hayamizu, H. Iwamura, D. Hashizume and Y. Ohashi, *J. Am. Chem. Soc.*, 1996, **118**, 1803.
8 D. Luneau, G. Risoan, P. Rey, A. Grand, A. Caneschi, D. Gatteschi and J. Laugier, *Inorg. Chem.*, 1993, **32**, 5616.
9 D. Luneau, J. Laugier, P. Rey, G. Ulrich, R. Ziessel, P. Legoll and M. Drillon, *J. Chem. Soc., Chem. Commun.*, 1994, 741.
10 D. Gatteschi, J. Laugier, P. Rey and C. Zanchini, *Inorg. Chem.*, 1987, **26**, 938.
11 (*a*)G. M. Sheldrick, *Crystallographic Computing 3*, ed. G. M. Sheldrick, C. Kruger and R. Goddard, Oxford University Press, Oxford, 1985, p. 175; (*b*) G. Sheldrick, System of Computing Programs, University of Cambridge, 1976.

Received in Cambridge, UK, 13th October 1997; 7/07350J

Dioxygen binding to immobilized Co^{II} complexes in porous organic hosts: evidence for site isolation

John F. Krebs[b] and A. S. Borovik*[a]

[a] *Department of Chemistry, University of Kansas, Lawrence, KS 66045, USA*
[b] *Department of Chemistry, Kansas State University, Manhattan, KS 66504, USA*

To model channel motifs and site isolation properties found in metalloproteins, a series of Co^{II} Schiff base complexes have been immobilized in porous organic hosts which stabilize Co–O_2 species at room temperature.

Immobilization of metal complexes in porous hosts is an effective way to regulate metal-based chemistry. In natural systems, this is exemplified by metalloproteins where the microenvironments around the metal-based active sites are controlled by protein structure.[1] In most cases, the active sites are located within the interior of the proteins, isolated from each other to prevent undesirable interactions. Access to external ligands (or substrates) is provided by channels that connect the active sites to the surface of the protein. To mimic these two structural properties in synthetic systems, *i.e.* site isolation and channel structure, we are using template polymerization techniques to immobilize metal complexes within porous organic hosts.[2,3] Results described herein show the feasibility of this approach in isolating metal sites in porous hosts *via* the stabilization of Co–O_2 adducts at room temperature.[4]

Incorporating metal sites with polymeric materials to model the dioxygen binding properties of metalloproteins has been reported.[5–7] While some promising results have been obtained, several of these systems use < 10% crosslinked polymers that do not sufficiently isolate the metal sites or utilize only a small percentage of their immobilized metal sites in the binding of dioxygen.[8] Our approach for site isolating metal complexes is modeled after methods developed to make templated network polymers.[9] We have modified these published methods by using substitution-inert metal complexes as templates. Utilizing kinetically inert metallo-templates that are synthesized prior to polymerization is advantageous because they provide a way of controlling the architecture of the metal sites in the porous hosts. Copolymerization of the metallo-template with a large excess of an organic crosslinker in the presence of a porogenic agent results in materials with immobilized metal complexes that are dispersed throughout highly crosslinked hosts. In addition, the porous structure of the host permits the immobilized complexes to be chemically modified to bind dioxygen. To evaluate the extent of site isolation achieved by this approach, we have examined dioxygen binding to immobilized Co Schiff base complexes: these complexes are known to bind dioxygen to form superoxide adducts, yet at room temperature most complexes undergo rapid reactions to yield Co^{III}_2–peroxide species.[10] Thus monitoring the formation and stability of the cobalt–superoxide species in the porous hosts at room temperature will indicate whether the metal sites have the appropriate architecture to bind additional ligands, and provide a measure of the number of metal sites isolated within the host.

The kinetically inert six-coordinate $[Co\mathbf{1}(dmap)_2]^+$ containing the styrene-modified salen ligand **1**[11] and two axially coordinated dimethylaminopyridine (dmap) ligands was immobilized into a methacrylate host by the procedure shown in Scheme 1. After grinding and sieving a dark red solid P-**1**$[Co(dmap)_2]$([Co] = 180 μmol g^{-1})[12] was obtained with a particle size of ⩽125 μm and an average pore diameter of 80 Å. The nearly quantitative (> 90%) removal of Co^{III} ions and the dmap ligands was achieved by refluxing P-**1**$[Co(dmap)_2]$ in an aqueous solution of 0.1 M Na_2H_2edta at a pH *ca.* 4. This metal ion removal process hydrolyzes the immobilized salen ligand to yield sites composed of two salicylaldehyde moieties covalently attached to the organic host [P-**1**$(saI)_2$]. This assignment is based on (i) the almost complete loss of nitrogen content in the polymer, (ii) the loss of the signature salen absorbance band at 380 nm, and (iii) the appearance of the characteristic carbonyl signal of salicylaldehyde at 1653 cm^{-1} in the DRIFT spectrum. The predisposition of the salicylaldehyde groups allows for regeneration of the salen ligands within the porous host by treating a suspension of P-**1**$(sal)_2$ in methanol with ethylenediamine under N_2 which affords P-**1**.

The immobilized sites in P-**1** can rebind metal ions to form four-coordinate complexes: the EPR spectra of P-**1**[Co] and P-**1**[Cu] are consistent with the immobilized complexes having the expected square-planar arrangement of donors around the metal ions.[13] Note that these immobilized sites also have sufficient axial space for the coordination of external ligands, such as nitrogeneous bases and dioxygen. This space is a consequence of the $[Co\mathbf{1}(dmap)_2]^+$ complex used in the copolymerization. Hence, > 80% of the immobilized Co^{II} sites are converted to five-coordinate complexes when P-**1**[Co] is treated with *ca.* 15 equiv. of either pyridine or dmap under an Ar atmosphere. Fig. 1(*a*) shows the rhombic EPR spectrum of P-**1**[Co(dmap)] measured at 77 K which is indicative of a low-spin Co^{II} complex where the dmap ligand binds axially to afford a square-pyramidal coordination geometry around the Co^{II} ions.[11,14,15] These five-coordinate Co sites in P-**1**[Co(dmap)] and P-**1**[Co(py)] form 1 : 1 Co–O_2 adducts at room temperature under 1 atm of O_2: the EPR spectra of both systems contain the characteristic EPR signals of Co–superoxide complexes (Fig. 1).[10] Double integration of the 77 K EPR signal for P-**1**$[Co(dmap)(O_2)]$, shows that 70% of the immobilized five-coordinate Co^{II} sites in P-**1**[Co(dmap)] form Co–O_2 adducts.[16] For P-**1**$[Co(py)(O_2)]$, the percentage of stable Co–O_2 sites is

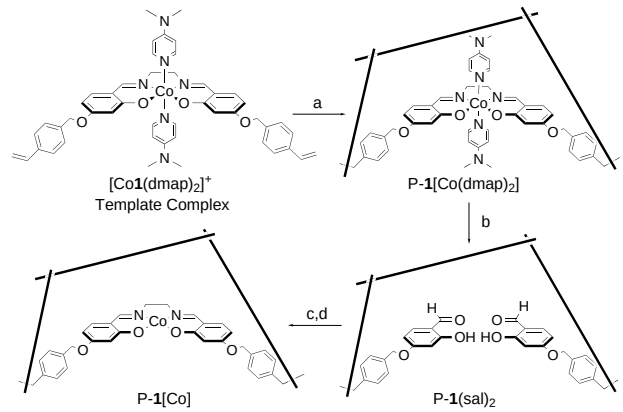

Scheme 1 a: ethylene glycol dimethacrylate; azobis(isobutyronitrile), DMF, Ar, 60 °C; b: EDTA, H_2O, heat; c: $C_2H_8N_2$, MeOH; d: $Co(OAc)_2$, MeOH, Ar

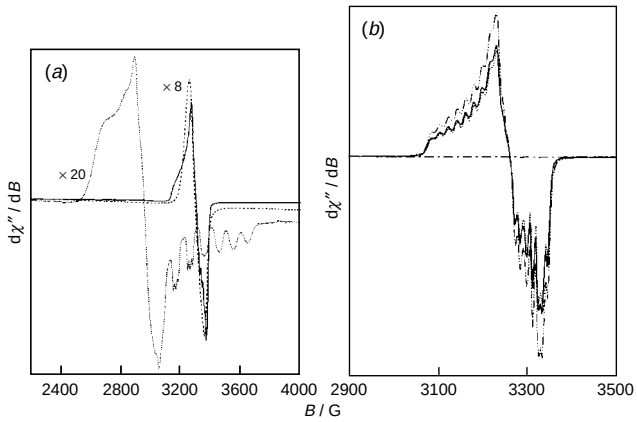

Fig. 1 (*a*) X-Band EPR spectra of P-**1**[Co(dmap)] collected at 77 K (···); P-**1**[Co(dmap)(O_2)] 1 hour after exposure to O_2 and collected at 77 K (—) and collected at 298 K (- - - -). EPR parameters for P-**1**[Co(dmap)]: g_1 = 2.45; g_2 = 2.25; g_3 = 2.20; A_3 = 96 G, d_3^N = 16 G; P-**1**[Co(dmap)$_2$(O_2)]: 77 K $g_\parallel$ = 2.10; $g_\perp$ = 2.02; $A_\parallel$ = 17 G; $A_\perp$ = 13 G; (298 K) g_{iso} = 2.02. (*b*) X-Band EPR spectra collected at 77 K of P-**2**[Co(O_2)] 1 hour after exposure to O_2 (-···-); P-**2**[Co(O_2)] after 40 h (——); P-**2**[Co] generated by flushing the sample after 40 h with N_2 (- — -); and rebinding of O_2 by P-**2**[Co] (···). EPR parameters for P-**2**[Co(O_2)]: $g_\parallel$ = 2.09; $g_\perp$ = 2.02; $A_\perp$ = 18 G; $A_\perp$ = 12 G.

slightly less at 52%. In contrast to these results, monomeric Co**1**(dmap) and Co**1**(py) complexes dissolved in a 1 : 1 CH_2Cl_2–toluene mixture yield < 10% of the Co–O_2 adducts 1 h after exposure to dioxygen at room temperature.

The above results demonstrate that the porous organic host can influence the chemistry of the immobilized metal complexes compared to that observed in solution. The design of P-**1** requires the binding of an external base to efficiently bind dioxygen. To circumvent the need for an external base, immobilized sites containing the pentadentate Schiff base ligand bis(2-hydroxybenzyliminopropyl)methylamine (smdpt) were synthesized using [Co**2**(1-MeIm)]$^+$ as the template complex. [Co**2**(1-MeIm)]$^+$, modeled after a similar complex

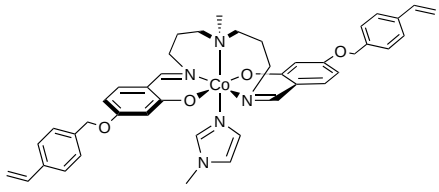

[Co**2**(1-MeIm)]$^+$

reported by Marzilli *et al.*,[17] was copolymerized into a methacrylate host following the procedure used for P-**1**[Co(dmap)$_2$]. P-**2**[Co],[18] having a cobalt concentration of 150 μmol g^{-1} readily forms Co–O_2 adducts: double integration of the EPR signal obtained for P-**2**[Co–O_2] shows that 88% of the immobilized cobalt sites bind O_2 at room temperature and 1 atm of O_2 [Fig. 1(*b*)]. After 40 h at room temperature, the Co–O_2 EPR signal corresponds to 62% of the immobilized sites Co–O_2 adducts.[19] Reversion of P-**2**[Co–O_2] to P-**2**[Co] (40 h after the initial O_2 exposure) is accomplished by flushing the system with N_2 for 30 min. Rebinding of O_2 to P-**2**[Co] produces an identical EPR spectrum to that obtained after 40 h [Fig. 1(*b*)].[20]

The room temperature dioxygen binding properties of P-**1**[Co] and P-**2**[Co] illustrates that this approach for immobilization of metal complexes in porous organic hosts is a useful method for designing functional metal complexes. For comparison, the large number of cobalt sites that stabilize Co–O_2 adducts in these materials are a significant improvement over results reported for similar complexes immobilized in zeolite cages: only 1% of the immobilized [Co(salen)(py)] in zeolite NaY form Co–O_2 adducts and 25% of the immobilized Co(smdpt) in zeolite NaEMT bind O_2.[7] The highly crosslinked porous hosts in P-**1**[Co] and P-**2**[Co] provide robust matrices that are sufficiently rigid to retain the metal site architecture and isolate the metal sites. This type of porous host thus prevents unwanted metal–metal interactions that are observed in solution. Extension of this technique toward the design of new reactive metal complexes is underway.

We thank the donors of Petroleum Research Fund administered by the American Chemical Society (26743-G3), NSF (OSR-9255223) and ONR (N00014-96-1-1216) for financial support of this work.

Notes and References

1 W. H. Armstrong, in *Metal Clusters in Proteins, ACS Symposium Series 372*, ed. L. Que, Jr., Am. Chem. Soc., Washington, DC, 1988, p. 1; Y. Lu and J. S. Valentine, *Curr. Opin. Struct. Biol.*, 1997, **7**, 495; L. Regan, *Trends Biochem. Sci.*, 1995, **20**, 280.
2 J. F. Krebs and A. S. Borovik, *J. Am. Chem. Soc.*, 1995, **117**, 10 593.
3 Recent examples of immobilized metal complexes in organic hosts: P. K. Dhal and F. H. Arnold, *Macromolecules*, 1992, **25**, 7051; B. B. De, B. B. Lohray, S. Sivaram and P. K. Dhal, *Macromolecules*, 1994, **27**, 1291; J. H. Golden, H. Deng, F. J. DiSalvo, J. M. J. Fréchet and P. M. Thompson, *Science*, 1995, **268**, 1463.
4 Evidence for site isolation has been reported in a titanocene/divinylbenzene-styrene copolymer: R. Grubbs, C. P. Lau, R. Cukier and C. Brubaker Jr., *J. Am. Chem. Soc.*, 1977, **99**, 4517.
5 J. H. Wang, *Acc. Chem. Res.*, 1970, **3**, 90; J. P. Collman and C. A. Reed, *J. Am. Chem. Soc.*, 1973, **95**, 2048; O. Leal, D. L. Anderson, R. G. Bowman, F. Basolo and R. L. Burwell, Jr., *J. Am. Chem. Soc.*, 1975, **97**, 5125; R. S. Drago, J. Gaul, A. Zombeck and D. K. Straub, *J. Am. Chem. Soc.*, 1980, **102**, 1033; D. Wöhrle and H. Bohlen, *Makromol. Chem.*, 1986, **187**, 2081.
6 T. Aida and D.-L. Jiang, *Chem. Commun.*, 1996, 1523; J. P. Collman, L. Fu, A. Zingg and F. Diederich, *Chem. Commun.*, 1997, 193.
7 R. F. Howe and J. H. Lunsford, *J. Am. Chem. Soc.*, 1975, **97**, 5156; N. Herron, *Inorg. Chem.*, 1986, 4714; P. K. Dutta and C. Bowers, *Langmuir*, 1991, **7**, 937; R. J. Taylor, R. S. Drago and J. P. Hage, *Inorg. Chem.*, 1992, **31**, 253; D. E. De Vos, E. J. P. Feijen, R. A. Schoonheydt and P. A. Jacobs, *J. Am. Chem. Soc.*, 1994, **116**, 4746.
8 Selected examples of metal complexes with cavity motifs that in solution reversibly bind dioxygen at room temperature: J. P. Collman, *Acc. Chem. Res.*, 1977, **10**, 265; M. Momenteau and C. A. Reed, *Chem. Rev.*, 1994, **94**, 659; D. H. Busch and N. W. Alcock, *Chem. Rev.*, 1994, **94**, 585.
9 Selected reports: G. Wülff, *Angew. Chem., Int. Ed. Engl.*, 1995, **34**, 1812 and references therein: K. Mosbach, *Trends Biochem. Sci.*, 1994, **19**, 92; K. J. Shea, *Trends Polym. Sci. A*, 1994, **32**, 166; B. B. De, B. B. Lohray, S. Sivaram and P. K. Dhal, *Tetrahedron Asymmetry*, 1995, **9**, 2105.
10 R. D. Jones, D. A. Summerville and F. Basolo, *Chem. Rev.*, 1979, **79**, 139.
11 Y. Fujii, K. Matsutani and K. Kikuchi, *J. Chem. Soc., Chem. Commun.*, 1985, 415.
12 The concentration of cobalt in P-**1**[Co(dmap)$_2$] ranges from 180 to 200 μmol g^{-1} in samples prepared independently.
13 P-1[Co]: [Co] = 170 μmol g^{-1}; EPR parameters: g = 1.98 and a broad feature centered at g = 3.28. P-**1**[Cu]: EPR parameters: $g_\parallel$ = 2.21; $g_\perp$ = 2.04; $A_\parallel$ = 202 G at 77 K.
14 EPR spectra recorded on samples of polymer suspended in toluene for 1 h after exposure to O_2.
15 X-Band EPR parameters for: P-**1**[Co(py)] at 77 K: g_1 = 2.48; g_2 = 2.26; g_3 = 2.01; A_3 = 99 G; a_3^N = 16 G; P-**1**[Co(py)(O_2)] at 77 K: $g_\parallel$ = 2.08; $g_\perp$ = 2.02; $A_\perp$ = 16 G; P-**1**[Co(py)(O_2)] at 298 K: g_{iso} = 2.02.
16 Exposure of O_2 to P-**1**[Co(dmap)] results in an immediate color change (orange–brown to purple) and formation of P-**1**[Co(dmap)(O_2)] is completed in < 4 min (the concentration of dioxygen is saturating at *ca.* 0.009 M in toluene). Similar results were observed for P-**1**[Co(py)] and P-**2**[Co].
17 T. J. Kristenmacher, L. G. Marzilli and P. A. Marzilli, *Inorg. Chem.*, 1974, **13**, 2089.
18 P-**2**[Co] was synthesized by same procedure used for P-**1**[Co] (Scheme 1) substituting 3,3′-diamino-*N*-methyldipropylamine for ethylenediamine.
19 The EPR spectrum of P-**2**[Co-O_2] obtained 125 h after initial O_2 exposure was identical to that measured after 40 h.
20 P-**1**[Co(py)] also reversibly binds O_2 at room temperature.

Received in Bloomington, IN, USA, 3rd November 1997; 7/07909E

Synthesis of copper(I) complexes with a novel naphthyl-appended macrocyclic ligand, including the crystal and molecular structure of the first copper(I)–η^2-naphthyl complex

William S. Striejewske and Rebecca R. Conry*

Department of Chemistry/216, University of Nevada, Reno, Nevada, 89557 USA

A new ligand, *N*-[2-(1-naphthyl)ethyl]-1-aza-4,8-dithiacyclodecane (L), and two of its copper(I) complexes [CuL(MeCN)]PF_6 and [CuL]PF_6, have been synthesized and characterized, including crystal structures of the two copper complexes.

Organocopper compounds are among the most widely used organometallic reagents in the synthetic organic chemist's arsenal, valued for diversity and versatility in effecting transformations.[1] However, knowledge of the structural chemistry for organocopper compounds is as yet underdeveloped.[1a] While a number of σ-bonded alkyl- and aryl-copper(I)[1a,2] as well as copper(I) π-alkene complexes[3] have been structurally characterized, there are only a handful of such reports for copper(I) π-arene and π-aryl complexes. These include a couple of η^5-cyclopentadienyl-ligated copper complexes,[4] and two η^2-benzene complexes, $(C_6H_6)CuAlCl_4$[5] and $(CuO\text{-}SO_2CF_3)_2C_6H_6$.[6] There are also accounts of weak interactions in the solid state between a Cu^I center and an arene ring, with long distances, typically in the range 2.7–3.0 Å.[7] Here, we report the synthesis and characterization of the first example, to our knowledge, of a structurally characterized copper complex containing a π-bound naphthalene ligand, plus details for a related complex, where an acetonitrile ligand is ligated instead of the naphthyl group, and the synthesis of the naphthyl-appended, macrocyclic-NS_2 ligand.

The novel ligand L, *N*-[2-(1-naphthyl)ethyl]-1-aza-4,8-dithiacyclodecane, consists of the NS_2-macrocyclic ligand reported by Chandrasekhar and McAuley[8] to which we have added a pendant naphthalene group. L was synthesized in two steps from the parent macrocycle, Scheme 1. The first step involves formation of a precursor amide by reaction of 8-aza-1,5-dithiacyclodecane with 1-naphthylacetyl chloride (prepared from 1-naphthylacetic acid and PCl_5 by literature methods[9]). The amide was isolated and purified by column chromatography [silica gel, ethyl acetate–hexanes (35 : 65)] and was then, in the second step, reduced to L with borane. The ligand L was isolated as an oil after purification by column chromatography [silica gel, ethyl acetate–hexanes (30 : 70)], in 44% overall yield for the two steps.†

The acetonitrile complex, [CuL(MeCN)]PF_6 **1**, was synthesized by the stoichiometric reaction of $[Cu(MeCN)_4]PF_6$[10] with

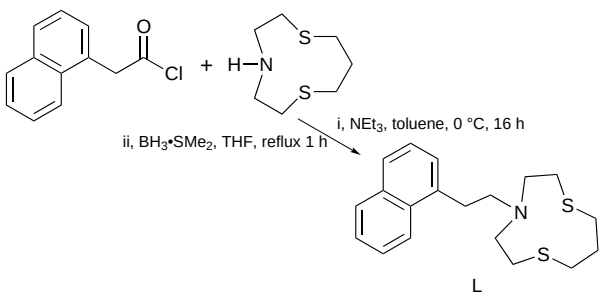

Scheme 1

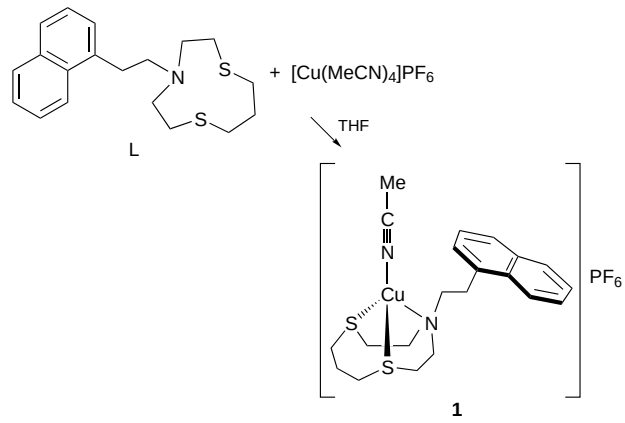

Scheme 2

L in THF at ambient temperature, Scheme 2. Recrystallization from acetonitrile–diethyl ether gave a 61% yield of **1** as yellow crystals. Elemental analysis, as well as ^1H and ^{13}C NMR and IR spectroscopic results are consistent with the formulation for **1**.‡ The solid-state structure (Fig. 1) shows that the geometry about the copper ion is slightly distorted from tetrahedral,§ with unexceptional bond lengths and angles.

In order to open a coordination site on the copper center, we wanted to remove the acetonitrile ligand from **1**. We first accomplished this, to synthesize [CuL]PF_6 **2**, by stirring **1** in CH_2Cl_2 under a CO atmosphere, followed by removal of the solvent and CO *in vacuo*. Thus, we were taking synthetic advantage of the tendency many copper(I) complexes have to bind CO weakly and reversibly.[11] However, we found that the CO was not necessary; the acetonitrile ligand from **1** was sufficiently labile that several of cycles of stirring the complex in CH_2Cl_2 followed by removal of the solvent *via* vacuum distillation also yielded **2** in > 85% isolated yield, Scheme 3.¶

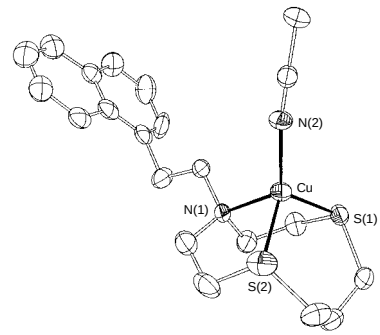

Fig. 1 Thermal ellipsoid plot of the solid-state structure of $[CuL(MeCN)]^+$ at the 25% probability level (hydrogens omitted for clarity). Selected bond distances (Å) and angles (°): Cu–N(1) 2.167(4), Cu–S(1) 2.2687(14), Cu–S(2) 2.260(2), Cu–N(2) 1.923(4); N(1)–Cu–N(2) 118.0(2), S(1)–Cu–N(2) 119.32(14), S(2)–Cu–N(2) 121.73(14), N(1)–Cu–S(1) 90.26(11), N(1)–Cu–S(2) 90.76(12), S(1)–Cu–S(2) 109.04(6).

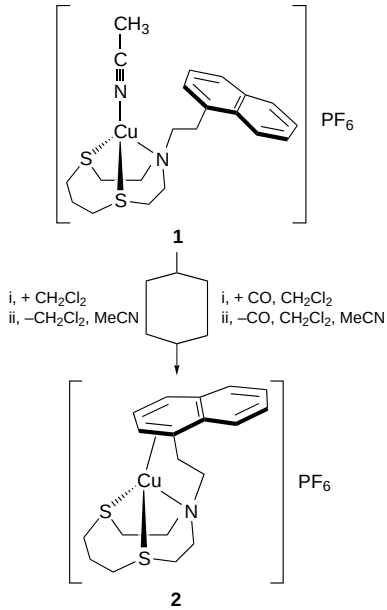

Scheme 3

Slow diffusion of hexane into a saturated CH_2Cl_2 solution of **2** yielded crystals suitable for X-ray diffraction.§

The solid state structure of **2** (Fig. 2) shows that the copper ion attains a distorted tetrahedral geometry by coordination of the pendant naphthyl group in an η^2-fashion. This binding occurs at the position adjacent to the ethylene linker chain and is unsymmetrical, with the Cu–C(10) and Cu–C(11) distances being 2.414(6) and 2.129(6) Å, respectively [the distance from the Cu to the center of the C(10)–C(11) bond is 2.168 Å]. These distances are comparable to the Cu–C distances in the two known Cu^I–η^2-benzene complexes,[5,6] which range from 2.09 to 2.30 Å. The binding in the previously reported complexes is also unsymmetrical, although it is less pronounced (differences in the pairs of Cu–C distances of 0.03–0.15 Å). Presumably the more accentuated unsymmetrical binding of the η^2-arene in **2** is at least partially due to the relatively short tether chain.

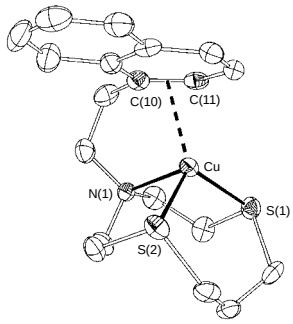

Fig. 2 Thermal ellipsoid plot of the solid-state structure of $[CuL]^+$ at the 25% probability level (hydrogens omitted for clarity). Selected bond distances (Å) and angles (°): Cu–N 2.146(5), Cu–S(1) 2.268(2), Cu–S(2) 2.233(2), Cu–C(10) 2.414(6), Cu–C(11) 2.129(6); N–Cu–S(1) 90.5(2), N–Cu–S(2) 91.89(14), S(1)–Cu–S(2) 111.08(7), N–Cu–C(10) 81.3(2), N–Cu–C(11) 105.4(2), S(1)–Cu–C(10) 133.8(2), S(1)–Cu–C(11) 108.2(2), S(2)–Cu–C(10) 114.5(2), S(2)–Cu–C(11) 136.7(2).

The C(10)–C(11) distance is essentially no longer in **2** [1.384(9) Å] than in **1** [1.343(11) Å]; no discernible differences in the coordinated C–C distances were observed in the two copper–benzene structures either.[5,6] Close comparison of the IR spectra of L and **2** shows that two bands, 1596 and 1509 cm^{-1}, are present in both spectra. In addition, there is a third band that has shifted from 1574 cm^{-1} for L to 1586 cm^{-1} for **2**; we tentatively assign these bands as C=C stretches. The C=C stretches for Cu–alkene complexes have been reported to shift from 15 to 170 cm^{-1} upon coordination.[3c,i,12]

We are currently exploring the properties of these novel complexes, to offer further insights into the chemistry of this interesting system.

The authors are grateful to the University of Nevada, Reno, the National Science Foundation, NSF Nevada EPSCoR, and the American Chemical Society-Petroleum Research Fund for funding. In addition, we thank Quynh Anderson, Angela Caffaratti and Lew Cary for technical assistance.

Notes and References

* E-mail: conry@chem.unr.edu

† *Selected characterizational data* for L: ^{1}H NMR ($CDCl_3$): δ 8.05 (d, 1 H), 7.86 (dd, 1 H), 7.72 (dd, 1 H), 7.51 (m, 2 H), 7.39 (m, 2 H), 3.30 (m, 2 H), 3.19 (m, 4 H), 2.89 (m, 4 H), 2.87 (m, 2 H), 2.73 (m, 4 H), 1.90 (m, 2 H).

‡ *Selected characterizational data* for **1**: ^{1}H NMR ($CDCl_3$ + 4 equiv. MeCN): δ 7.94 (d, 1 H), 7.88 (d, 1 H), 7.77 (d, 1 H), 7.54 (m, 2 H), 7.42 (m, 1 H), 7.29 (d, 1 H), 3.35 (m, 2 H), 3.21 (m, 4 H), 3.12 (m, 4 H), 3.00 (m, 4 H), 2.77 (m, 2 H), 2.23 (m, 2 H); IR: 2278 mw ν(C≡N).

§ *Crystal data*: **1**: M = 581.08, triclinic, space group $P\bar{1}$ (no. 2), a = 11.1901(10), b = 11.2735(12), c = 12.1350(10) Å, α = 98.996(8), β = 117.188(6), γ = 105.354(7)°, U = 1242.6(2) Å^3, Z = 2, μ(Mo-Kα) = 1.169 mm^{-1}. The structure was solved using Patterson methods and refined on F^2 to R_1 = 0.0505 and R_w = 0.1291 with $I > 2\sigma(I)$, using 3202 unique reflections and 382 parameters. **2**: M = 582.11, monoclinic, space group $P2_1/c$ (no. 14), a = 15.732(2), b = 8.9164(10), c = 17.205(2) Å, β = 102.431(6)°, U = 2356.8(4) Å^3, Z = 4, μ(Mo-Kα) = 1.231 mm^{-1}. The structure was solved using Patterson methods and refined on F^2 to R_1 = 0.0587 and R_w = 0.1285 with $I > 2\sigma(I)$, using 4153 unique reflections and 320 parameters. CCDC 182/742.

¶ *Selected characterizational data* for **2**: ^{1}H NMR ($CDCl_3$): δ 8.00 (d, 1 H), 7.92 (d, 1 H), 7.83 (d, 1 H), 7.63 (m, 2 H), 7.45 (t, 1 H), 7.28 (d, 1 H), 3.40 (br s, 2 H), 3.2–2.4 (br m, 12 H), 2.10 (m, 2 H), 1.46 (m, 2 H).

1 (*a*) G. van Koten, S. L. James and J. T. B. H. Jastrzebski, in *Comprehensive Organometallic Chemistry II*, ed. E. W. Abel, F. G. A. Stone and G. Wilkinson, Pergamon, New York, 1995, vol. 3, pp. 57–133; (*b*) G. H. Posner, *An Introduction to Synthesis Using Organocopper Reagents*, Wiley-Interscience, New York, 1980; (*c*) B. H. Lipshutz and S. Sengupta, *Org. React. (New York)*, 1992, **41**, 135; (*d*) *Organocopper Reagents: A Practical Approach*, ed. R. J. K. Taylor, Oxford University Press, New York, 1994.

2 G. van Koten, *J. Organomet. Chem.*, 1990, **400**, 283; A. Camus, N. Marsich, G. Nardin and L. Randaccio, *Inorg. Chim. Acta*, 1977, **23**, 131; P. P. Power, *Prog. Inorg. Chem.*, 1991, **39**, 75.

3 (*a*) V. V. Olijnik and E. A. Goreshnik, *J. Struct. Chem.*, 1994, **35**, 668; (*b*) T. Nickel, K.-R. Pörschke, R. Goddard and C. Krüger, *Inorg. Chem.*, 1992, **31**, 4428; (*c*) J. H. Van Den Hende and W. C. Baird, Jr., *J. Am. Chem. Soc.*, 1963, **85**, 1009; (*d*) M. Håkansson, S. Jagner, E. Clot and O. Eisenstein, *Inorg. Chem.*, 1992, **31**, 5389; (*e*) I. Sanyal, N. N. Murthy and K. D. Karlin, *Inorg. Chem.*, 1993, **32**, 5330; (*f*) H. Eriksson, M. Örtendahl and M. Håkansson, *Organometallics*, 1996, **15**, 4823; (*g*) P. Ganis, U. Lepore and G. Paiaro, *Chem. Commun.*, 1969, 1054; (*h*) M. Pasquali, C. Floriani, A. Gaetani-Manfredotti and A. Chiesi-Villa, *Inorg. Chem.*, 1979, **18**, 3535; (*i*) L. M. Engelhardt, P. C. Healy, J. D. Kildea and A. H. White, *Aust. J. Chem.*, 1989, **42**, 185; (*j*) T. C. W. Mak, H. N. C. Wong, K. H. Sze and L. Book, *J. Organomet. Chem.*, 1983, **255**, 123 and refs. therein.

4 C. Zybill and G. Müller, *Organometallics*, 1987, **6**, 2489 and refs. therein.

5 R. W. Turner and E. L. Amma, *J. Am. Chem. Soc.*, 1966, **88**, 1877.

6 M. B. Dines and P. H. Bird, *J. Chem. Soc., Chem. Commun.*, 1973, 12.

7 P. F. Rodesiler and E. L. Amma, *J. Chem. Soc., Chem. Commun.*, 1974, 599; M. Pasquali, C. Floriani and A. Gaetani-Manfredotti, *Inorg. Chem.*, 1980, **19**, 1191.

8 S. Chandrasekhar and A. McAuley, *Inorg. Chem.*, 1992, **31**, 2234.

9 J. C. Sheehan, D. W. Chapman and R. W. Roth, *J. Am. Chem. Soc.*, 1952, **74**, 3822; M. Pomerantz and A. S. Ross, *J. Am. Chem. Soc.*, 1975, **97**, 5850.

10 G. J. Kubas, *Inorg. Synth.*, 1979, **19**, 90.

11 B. J. Hathaway, in *Comprehensive Coordination Chemistry*, ed. G. Wilkinson, Pergamon, New York, 1987, vol. 5, pp. 533–774.

12 M. Håkansson, K. Wettström and S. Jagner, *J. Organomet. Chem.*, 1991, **421**, 347; B. W. Cook, R. G. J. Miller and P. F. Todd, *J. Organomet. Chem.*, 1969, **19**, 421 and refs. therein.

Received in Bloomington, IN, USA, 16th October 1997; 7/07480H

The structure of the S_6-symmetric methanol hexamer assembled in a supramolecular hydrophobic cavity

Frank Nils Penkert, Thomas Weyhermüller and Karl Wieghardt*

Max-Planck-Institut für Strahlenchemie, P.O. Box 10 13 65, D-45413 Mülheim an der Ruhr, Germany

The structure of the cyclic S_6-symmetric hexamer of methanol has been established by X-ray crystallography in crystals of $[GaLF_3](MeOH)_{6/2}\cdot(MeOH)_3\cdot CH_2Cl_2$ 1; the hexamer has been proposed to be the dominant species in liquid methanol.[4]

Crystalline, solid methanol consists of infinite zigzag chains of hydrogen bonded methanol molecules with an O···O distance of 2.66 Å at −110 °C.[1] Upon melting long chains and/or cyclic oligomers $(MeOH)_n$ form (n = 3–20).[2] In his famous book *The Nature of the Chemical Bond*, Pauling has depicted the cyclic hexamer $(MeOH)_6$ with six O–H···O bonding contacts as an example.[3] This cluster has later been proposed to be the dominant species in liquid methanol at room temperature[4] and its structure and vibrational spectrum in the gas phase have been repeatedly calculated.[5] Two conformers of nearly equal energy apparently exist: an S_6 and a C_2 symmetric form (Scheme 1) both of which have been generated by the method of size selection of clusters by momentum transfer in a scattering experiment with atoms in the gas phase.[5a,6] Upon vaporization of methanol the tetramer $(MeOH)_4$ has been shown to be the major component of the vapour.[7] To date none of these cyclic structures has been found in the solid state and, consequently, they have not been characterized by single crystal X-ray crystallography.

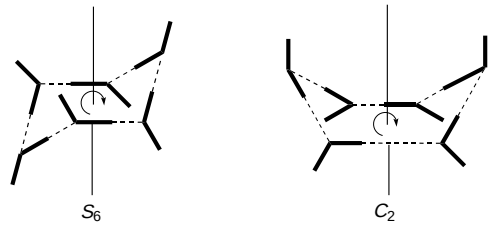

Scheme 1

We report here the crystal structure of $[GaLF_3](MeOH)_{6/2}\cdot(MeOH)_3\cdot CH_2Cl_2$ **1**† where L represents the neutral pendent arm macrocycle 1,4,7-tris(2-amino-3,5-di-*tert*-butylbenzyl)-1,4,7-triazacyclononane. In crystals of **1** the cyclic $(MeOH)_6$ hexamer is assembled in a hydrophobic ligand cavity.

The reaction of L with $GaF_3\cdot 3H_2O$ (1 : 2) in refluxing ethanol produces colourless microcrystals of $[GaLF_3]$ upon addition of water to the above mixture. Colourless crystals of **1** were obtained from a dichloromethane–methanol (1 : 5 v/v) solution of $[GaLF_3]$ at −20 °C. Details of the ligand and complex syntheses will be reported elsewhere.

The solid state structure of **1** consists of neutral $[GaLF_3]$ molecules shown in Fig. 1 where the 1,4,7-triazacyclononane backbone of the macrocycle L is bound to a GaF_3 fragment. The three 2-amino-3,5-di-*tert*-butylbenzyl arms are not coordinated. A *cis*-N_3F_3Ga octahedron is formed. The molecule possesses C_3 symmetry. The three uncoordinated pendent arms adopt a conformation where they are folded upwards toward the coordinated nine-membered 1,4,7-triazacyclononane ring. An approximately circular bowl-shaped hydrophobic 'surface' is formed with six bulky tertiary butyl groups at the rim of this

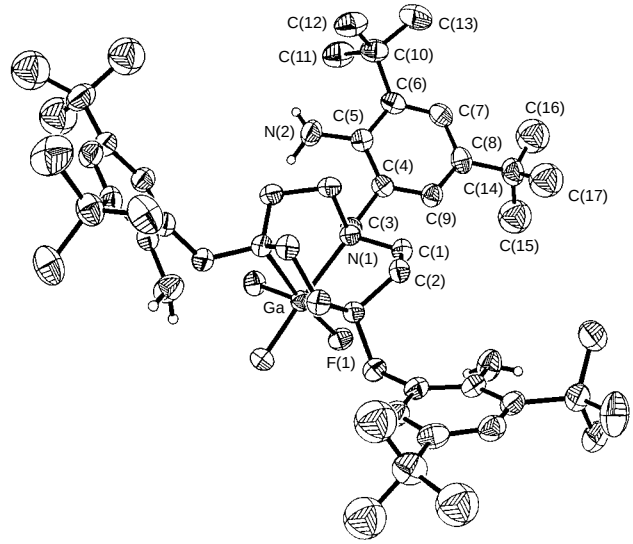

Fig. 1 Molecular structure of the neutral $[GaLF_3]$ complex in crystals of **1**. Selected distances (Å) and angles (°): Ga–N(1) 2.147(3), Ga–F(1) 1.849(2), C(5)–N(2) 1.397(6), F(1)–Ga–F(1′) 94.1(1), N(1)–Ga–N(1′) 82.8(1), N(1)–Ga–F(1) 88.7(1).

bowl. Two such $[GaLF_3]$ molecules are then packed together in a fashion which brings the two hydrophobic bowl-shaped surfaces facing each other. The two sets of three pendent arms are staggered. This 'dimer' is held together by van der Waals forces only. Roughly, its shape may be viewed as clam-like with S_6 symmetry. The inner surface of this clam is of purely hydrophobic nature since it comprises exclusively phenyl rings and methylene hydrogen atoms of the two ligands L. The discus-shaped cavity inside is filled with six methanol molecules as is shown in Fig. 2. Fig. 3 shows the six MeOH molecules forming a cyclic structure *via* six O–H···O hydrogen bonding contacts [O···O 2.62(1) Å]. The methyl groups are staggered; the hexamer adopts S_6 symmetry. The methyl groups form weak van der Waals contacts to the hydrophobic inner

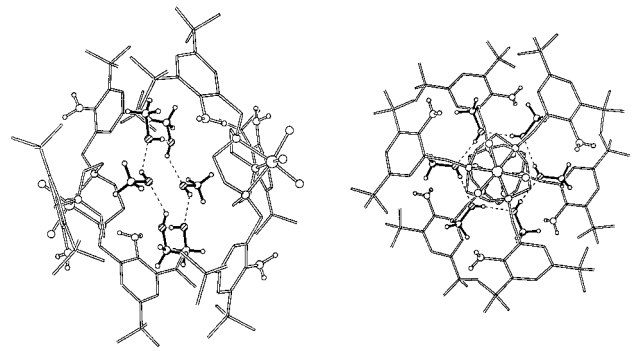

Fig. 2 Schematic representation of the $[GaLF_3]_2\cdot(MeOH)_6$ unit in **1**. Left: side-view looking into the 'clam' composed of two $[GaLF_3]$ shells. Right: view down the S_6 axis on which the two Ga^{3+} ions (only one is seen) lie.

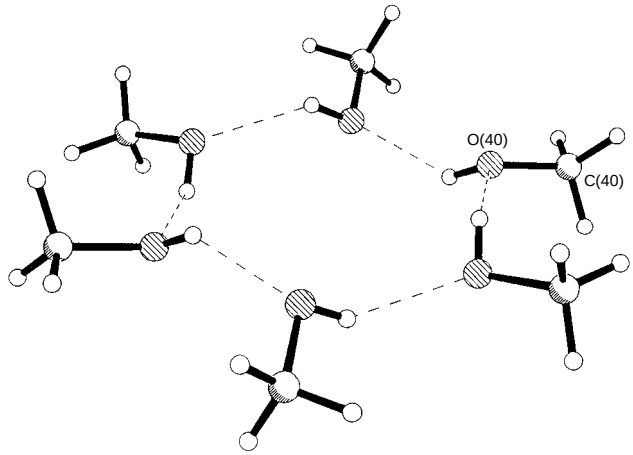

Fig. 3 Schematic representation of the S_6 symmetric methanol hexamer in **1**. Selected distances (Å): O(40)···O(40′) 2.62(1), O(40)–C(40) 1.394(9).

surface of the cavity only. The O–H···O bonds are asymmetric and the twelve-membered ring is puckered.

The outer surface of the clam exposes two sets of (*a*) three fluoro ligands and (*b*) of three amino groups; it is 'sticky'. Three additional methanol molecules per $GaLF_3$ unit form each a strong O–H···F contact at 2.58(1) Å and two somewhat weaker O···H–N interactions with the amino groups at 2.94(1) and 3.39(1) Å. The latter two interactions enforce an ordered packing of the clams relative to each other in the solid state ('inter-clam' contacts).

The authors gratefully acknowledge financial support of this work by the Fonds der Chemischen Industrie.

Notes and References

* E-mail: wieghardt@mpi-muelheim.mpg.de

† *Crystal data*: **1**: $C_{58}H_{110}Cl_2F_3GaN_6O_6$, M = 1185.14, trigonal, space group $R\bar{3}$, $a = b$ = 18.940(3), c = 33.672(6) Å, U = 10461(3) Å^3, Z = 6, D_c = 1.129 Mg m^{-3}, μ(Mo-Kα) = 0.53 mm^{-1}, F(000) = 3840. A transparent colorless block of 0.56 × 0.49 × 0.28 mm was mounted in a sealed capillary. 3517 independent reflections were collected on an Enraf-Nonius CAD4 diffractometer [graphite monochromated Mo-Kα radiation, 293(2) K] using ω-scan technique. The structure was solved by direct methods and all non-hydrogen atoms were refined anisotropically using full-matrix least squares based on F^2. Carbon atoms C(15), C(16), C(17) belonging to a *tert*-butyl group were disordered by rotation and a split atom model was applied. The CH_2Cl_2 solvent molecule was found to be disordered on a crystallographic threefold axis. Owing to evaporation, its occupancy factor was reduced to one third of the complete molecule (1/9 for carbon and 2/9 for chlorine). The methyl, methylene and phenyl ring hydrogen atoms were placed at calculated positions whereas all OH and NH_2 hydrogen atoms were located in a difference electron density map around a circle which represents the possible loci for a fixed O–H, or N–H distance and C–N(O)–H angle. Final R_1 = 0.072, wR_2 = 0.196, 2740 $F_o > 4\sigma(F_o)$, $2\theta \leqslant 50°$, 233 parameters. CCDC 182/747.

1 J. K. Tauer and W. N. Lipscomb, *Acta Crystallogr.*, 1952, **5**, 606.
2 D. L. Wertz and R. K. Kruh, *J. Chem. Phys.*, 1967, **47**, 388; A. H. Narten and A. Habenschuss, *J. Chem. Phys.*, 1984, **80**, 3387; M. Magini, G. Paschina and G. Piccaluga, *J. Chem. Phys.*, 1982, **77**, 2051.
3 L. Pauling, in *The Nature of the Chemical Bond*, Cornell University Press, Ithaca, NY, 1962, p. 474.
4 S. Sarkar and R. N. Joarder, *J. Chem. Phys.*, 1993, **99**, 2032.
5 (*a*) U. Buck, B. Schmidt and J. G. Siebers, *J. Chem. Phys.*, 1993, **99**, 9428; (*b*) U. Buck, *Ber. Bunsenges. Phys. Chem.*, 1992, **96**, 1275; (*c*) U. Buck and B. Schmidt, *J. Chem. Phys.*, 1993, **98**, 9410; (*d*) U. Buck and I. Ettischer, *J. Chem. Phys.*, 1994, **100**, 6974.
6 U. Buck, *J. Phys. Chem.*, 1994, **98**, 5190.
7 W. Weltner, Jr. and K. S. Pitzer, *J. Am. Chem. Soc.*, 1951, **73**, 2606.

Received in Basel, Switzerland, 4th December 1997; 7/08730F

Synthesis of mesoporous aluminophosphates using surfactants with long alkyl chain lengths and triisopropylbenzene as a solubilizing agent

Tatsuo Kimura,[a] Yoshiyuki Sugahara[a] and Kazuyuki Kuroda*[a,b]

[a] *Department of Applied Chemistry, School of Science and Engineering, Waseda University, Ohkubo-3, Shinjuku-ku, Tokyo 169, Japan*

[b] *Kagami Memorial Laboratory for Materials Science and Technology, Waseda University, Nishiwaseda-2, Shinjuku-ku, Tokyo 169, Japan*

Mesostructured organo-aluminophosphates were prepared by using surfactants with long alkyl chain lengths (C_{16} and C_{22}) and by utilizing solubilization of triisopropylbenzene; calcination of the mesostructured materials yielded thermally stable mesoporous aluminophosphates with surface areas > 700 m^2 g^{-1} and with pore diameters in the range 1.8–3.9 nm.

Mesoporous silicas, denoted FSM[1] and M41S,[2] are very attractive materials for catalysts, catalyst supports and adsorbents for larger molecules than those treated in microporous crystals. Since microporous $AlPO_4$-*n* materials are known,[3] it is expected that mesostructured organo-aluminophosphates are useful for the formation of mesoporous aluminophosphates to enlarge the variety and possible applications of mesoporous materials. We have already reported the successful formation of a hexagonal mesostructured aluminophosphate (AlPO) by using hexadecyltrimethylammonium chloride.[4] Feng *et al.* also reported a hexagonal mesostructured material prepared in the presence of F^- ions, however, the porous structure collapsed upon calcination.[5] Recently a mesoporous aluminophosphate with large surface area (790 m^2 g^{-1}) was reported by Zhao *et al.*[6] Although the pore diameter of the product was reported to be *ca.* 4.0 nm, this value is somewhat questionable because it is too large judging from the values observed for ordered mesoporous silicas.[1,2] On the other hand, Holland *et al.*[7] and Cheng *et al.*[8] reported mesoporous aluminophosphate-based materials *via* layered intermediates; the porous materials, prepared by solvent extraction, are thermally unstable.

The hexagonal mesostructured AlPO reported by us had a less condensed framework, so that a microporous material formed after calcination in air.[4] Based on this result, it is expected that mesoporous AlPOs can be obtained by utilizing mesostructured AlPOs with larger hexagonal arrays. Here, we report the successful synthesis of thermally stable mesoporous AlPOs, based on this strategy.

Hexagonal mesostructured AlPOs were prepared by using $C_{16}H_{33}NMe_3Cl$ (C_{16}TMACl) and $C_{22}H_{45}NMe_3Cl$ (C_{22}TMACl), denoted as C_{16}-AlPO and C_{22}-AlPO, respectively. C_{16}-AlPO was prepared according to our previous paper.[4] C_{22}-AlPO was prepared as follows: C_{22}TMACl (containing a small amount of shorter alkyl chains), tetramethylammonium hydroxide (TMAOH, 25 mass% in water), 85% H_3PO_4, and water were mixed for several hours. Aluminium triisopropoxide was added to this mixture under vigorous stirring, and the stirring was continued for 1 day. The composition of the starting mixture was $Al_2O_3 : P_2O_5 : C_{22}$-TMACl : 2.0 TMAOH : 65.0 H_2O. The starting mixture was dispersed in distilled water at 70 °C, with formation of a white solid. This solid was washed with distilled water heated at 70 °C repeatedly, and dried at 80 °C. Solubilization of 1,3,5-triisopropylbenzene (TIPBz) into surfactant assemblage was also carried out for C_{22}TMACl; TIPBz has already been known to act as a solubilizing agent.[9] The synthesis procedure was the same as described above and TIPBz was added before the addition of aluminium triisopropoxide. The molar ratio of TIPBz/C_{22}TMACl in the starting mixture was 1, and this product was denoted as TIPBz/C_{22}-AlPO; the molar ratio of TIPBz/C_{22}TMACl in the TIPBz/C_{22}-AlPO was *ca.* 0.67 based on the CHN analysis, indicating that not all the TIPBz was solubilized in the surfactants. All the products were heated at 600 °C for 1 h in flowing N_2, followed by calcination at 600 °C for 1 h in flowing air. The calcined products were analyzed by XRD, N_2 adsorption, and ^{27}Al and ^{31}P MAS NMR spectroscopy performed on a JEOL GSX-400 with a spinning rate of 5 kHz (for ^{27}Al: frequency: 104.05 MHz; pulse angle: 45°; recycle time: 5 s, for ^{31}P: 161.70 MHz; 60°; 20 s, respectively).

The XRD patterns of all the products before calcination are shown in Fig. 1. The XRD peaks of the C_{16}-AlPO can be assigned to (100), (110) and (200) of a hexagonal phase. The XRD peaks of both C_{22}-AlPO and TIPBz/C_{22}-AlPO can also be assigned to (100), (110), (200) and (210) of hexagonal phases. The lattice parameters (a_0) of the C_{16}-AlPO, C_{22}-AlPO and TIPBz/C_{22}-AlPO were 4.8, 5.8 and 7.2 nm, respectively. These XRD results indicate the formation of mesostructured AlPOs with large hexagonal arrays by utilizing C_{22}TMA and solubilization of TIPBz.

In the XRD patterns of the calcined products (Fig.1), the d_{100} peak shifted from 4.1 to 2.8 nm for C_{16}-AlPO after calcination, and the XRD patterns showed a shift from 5.1 to 3.7 nm for C_{22}-AlPO and a shift from 6.2 to 4.6 nm for TIPBz/C_{22}-AlPO. The lattice parameters (a_0: $2d_{100}/\sqrt{3}$) of the calcined C_{16}-AlPO, calcined C_{22}-AlPO and calcined TIPBz/C_{22}-AlPO were 3.2, 4.3 and 5.3 nm, respectively, if we assume that the calcined products retain the hexagonal structures. The shrinkages are

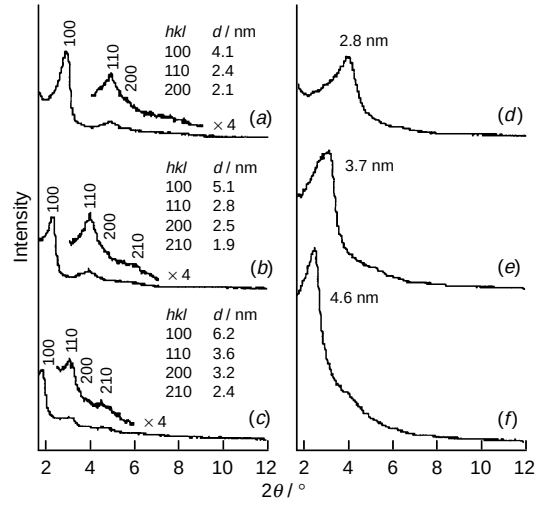

Fig. 1 XRD patterns of (*a*) C_{16}-AlPO, (*b*) C_{22}-AlPO and (*c*) TIPBz/C_{22}-AlPO, (*d*) calcined C_{16}-AlPO, (*e*) calcined C_{22}-AlPO and (*f*) calcined TIPBz/C_{22}-AlPO. These patterns were recorded on a Mac Science M03XHF[22] diffractometer with monochromated Fe-Kα radiation.

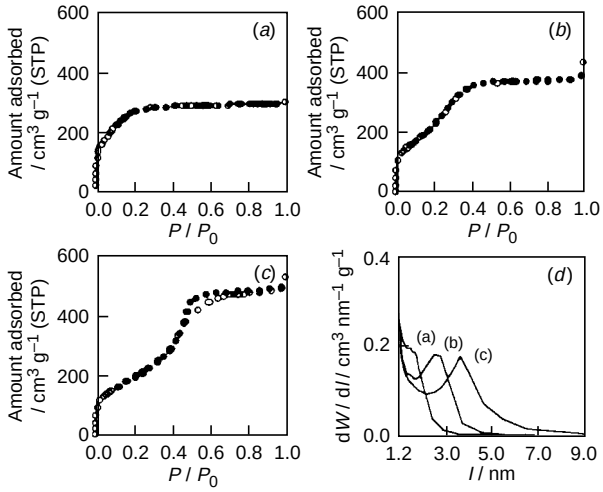

Fig. 2 N_2 adsorption isotherms of calcined (*a*) C_{16}-AlPO, (*b*) C_{22}-AlPO and (*c*) TIPBz/C_{22}-AlPO. Filled symbols denote desorption. Corresponding pore size distributions of the calcined products are shown in (*d*). These isotherms were obtained by a BELSORP 28 (Bel Japan, Inc.) at 77 K.

larger than those observed for silica-based mesoporous materials[2] because of less condensed frameworks as described below. In addition, the XRD peaks of all the products were broadened after calcination. These results suggest that the porous structures remained, although the sizes and the regularities of the hexagonal arrays decreased upon calcination.

Hexagonal arrays with relatively ordered arrangements were observed in the TEM images of all the products before calcination. After calcination, disordered arrays were obtained, and the periodic distances of these arrays decreased. These TEM images are in agreement with the XRD results. No other phases were detected in any TEM images.

The N_2 adsorption isotherms and the pore size distributions of the calcined products, calculated by the Horváth–Kawazoe method,[10] are shown in Fig. 2. The N_2 adsorption isotherm of calcined C_{16}-AlPO showed almost type I behavior, indicating the presence of micropores; the pore diameter was *ca.* 1.8 nm. In contrast, the isotherms of the calcined C_{22}-AlPO and TIPBz/C_{22}-AlPO showed type IV behavior. The calcined C_{22}-AlPO had a BET surface area of 760 $m^2\ g^{-1}$, a pore volume of 0.56 $cm^3\ g^{-1}$ and an average pore diameter of 2.8 nm. For the calcined TIPBz/C_{22}-AlPO, the BET surface area and the pore volume were 720 $m^2\ g^{-1}$ and 0.72 $cm^3\ g^{-1}$, respectively. The pore diameter was *ca*. 3.9 nm.

The structural changes during calcination can be monitored by ^{27}Al and ^{31}P MAS NMR measurements before and after calcination. The ^{31}P MAS NMR spectra of the uncalcined products showed several peaks in the range δ 0 to −20, indicating the uncalcined products had less condensed frameworks.[4,11,12] A broad peak centered at δ −21 was observed after calcination indicating condensation of the frameworks.[11,12] The ^{27}Al MAS NMR spectra of the uncalcined products showed that signals due to both four- (Al^{IV}) and six-coordinate Al (Al^{VI}) at δ *ca.* 43 and 1, respectively. Based on the Al^{IV}/Al^{VI} intensity ratios, varying from *ca.* 0.6 (C_{16}-AlPO) to *ca*. 0.3 (C_{22}-AlPO and TIPBz/C_{22}-AlPO), a large amount of Al^{VI} is present in the uncalcined products and they may be coordinated with not only PO_4 units but also water molecules,[4] being related to less condensed frameworks. Only a broad signal due to Al^{IV} was observed at *ca*. δ 39 for each calcined product; the chemical shift strongly suggesting that the $Al^{IV}O_4$ units are surrounded by mainly P.[11,13] Although the Al/P ratios (1.5), discussed below, might suggest the presence of Al–O–Al bonds, such bonds are unlikely, judging from very different chemical shifts expected for [$Al^{IV}O_4$(*n*Al)] (*n* = 1–4).[13]

Both N_2 adsorption and NMR results indicate that the pore sizes can be controlled although shrinkage must be taken into consideration, so that the C_{22}-AlPO and TIPBz/C_{22}-AlPO changed to mesoporous materials after calcination owing to the larger hexagonal arrays.

The C_nTMA/(Al + P) ratios were 0.25 (C_{16}-AlPO), 0.19 (C_{22}-AlPO) and 0.16 (TIPBz/C_{22}-AlPO), and the Al/P ratios of all the products were *ca.* 1.5. This Al/P value is different from unity which would be expected for an ideal three-dimensional $AlPO_4$-*n*.[3] The Al/P ratios of mesostructured and/or mesoporous aluminophosphates reported by Feng *et al.*,[5] Zhao *et al*.,[6] Holland *et al.*,[7] and Cheng *et al*.[8] are 2.9, 0.64, 1.5, and 1.0, respectively. Although the Al/P ratios of mesoporous AlPOs reported here are similar to those reported by Holland *et al.*,[7] the coordination of Al atoms is six for their materials while it is mainly four for ours. For the other three materials, the Al/P ratios are clearly different. Nevertheless, the coordination of Al atoms in the material reported by Feng *et al*.[5] is similar to ours. However, because there is little information on the aluminophosphate frameworks in those reports, appropriate comparison with our materials is not possible at present.

In conclusion, thermally stable mesoporous AlPOs were obtained by calcination of hexagonal mesostructured AlPOs prepared by using both C_{22}TMA as a micelle aggregate and TIPBz as a solubilizer. This method can be applicable for the preparation of various mesoporous materials from less condensed inorganic units–surfactant mesostructured materials, which normally afford microporous materials owing to substantial shrinkage. A study on the surface structure of these mesoporous AlPO is now in progress.

The authors acknowledge Mr M. Fuziwara, MCCL, Waseda University for TEM measurements. K. K. acknowledges the financial assistance from Grant-in-Aid for the Special Priority Area by the Ministry of Education, Science, and Culture of the Japanese Government.

Notes and References

*E-mail: kuroda@mn.waseda.ac.jp

1 T. Yanagisawa, T. Shimizu, K. Kuroda and C. Kato, *Bull. Chem. Soc. Jpn.*, 1990, **63**, 988; S. Inagaki, A. Koiwai, N. Suzuki, Y. Fukushima and K. Kuroda, *Bull. Chem. Soc. Jpn.*, 1996, **69**, 1449.
2 C. T. Kresge, M. E. Leonowicz, W. J. Roth, J. C. Vartuli and J. S. Beck, *Nature*, 1992, **359**, 710.
3 S. T. Wilson, B. M. Lok, C. A. Messina, T. R. Cannan and E. M. Flanigen, *J. Am. Chem. Soc.*, 1982, **104**, 1146.
4 T. Kimura, Y. Sugahara and K. Kuroda, *Book of Abstracts, 11th Int. Zeolite Conf.*, Seoul, Korea, 1996, RP45; T. Kimura, Y. Sugahara and K. Kuroda, *Chem. Lett.*, 1997, 983.
5 P. Feng, Y. Xia, J. Feng, X. Bu and G. D. Stucky, *Chem. Commun.*, 1997, 949.
6 D. Zhao, Z. Luan and L. Kevan, *Chem. Commun*., 1997, 1009; D. Zhao, Z. Luan and L. Kevan, *J. Phys. Chem.*, 1997, **101**, 6943.
7 B. T. Holland, P. K. Isbester, C. F. Blanford, E. J. Munson and A. Stein, *J. Am. Chem. Soc.*, 1997, **119**, 6796.
8 S. Cheng, J.-N. Tzeng and B.-Y. Hsu, *Chem. Mater*., 1997, **9**, 1788.
9 A. Mochizuki, M. Yamai and S. Namba, *Book of Abstracts, 11th Int. Zeolite Conf.*, Seoul, Korea, 1996, RP29.
10 G. Horváth and K. Kawazoe, *J. Chem. Eng. Jpn.*, 1983, **16**, 470.
11 D. Müller, E. Jahn, G. Ladwig and U. Haubenreisser, *Chem. Phys. Lett.*, 1984, **109**, 33.
12 R. F. Mortlock, A. T. Bell and C. J. Radke, *J. Phys. Chem.*, 1993, **97**, 767.
13 D. Müller, W. Gessner, A. Samoson, E. Lippmaa and G. Scheler, *J. Chem. Soc., Dalton Trans.*, 1986, 1277.

Received in Cambridge, UK, 24th November 1997; 7/08463C

Sonophotoluminescence: pyranine emission induced by ultrasound

Muthupandian Ashokkumar and Franz Grieser*

Advanced Mineral Products Research Centre, School of Chemistry, University of Melbourne, Parkville, 3052, Australia

Sonoluminescence has been used to excite the water soluble acid–base fluorescent indicator trisodium 8-hydroxy-1,3,6-pyrenetrisulfonate, leading to light emission (sonophotoluminescence) from the dye.

The acoustic driven collapse of microbubbles in solution results in a phenomenon referred to as sonoluminescence.[1] The emission spectrum obtained from multibubble sonoluminescence (SL) in water is quite broad, ranging from 200 to above 800 nm, with a maximum in the region of 250–350 nm.[1–3] In addition to SL, emission stemming from the ground state chemical reaction of ultrasonically generated oxidising radicals with luminol has also been observed.[4] In the latter case the spectrum obtained is similar to the chemiluminescence of luminol.

The broad band emission from SL raises the question of whether it can be conveniently used as an internal light source to excite other molecules in solution. To explore this possibility we have examined the 'trivial' excitation of trisodium 8-hydroxy-1,3,6-pyrenetrisulfonate (pyranine, POH), by SL, and the ensuing emission, which can be referred to as sonophotoluminescence (SPL).

Details of the experimental system used are given elsewhere.[5] Briefly, a modified Undatim D-Reactor (515 kHz) was fitted into the cavity of a spectrofluorimeter (Hitachi, F-4500) and spectra recorded directly. A full scan (200–800 nm) could be measured in *ca.* 2 min. The sonication of the aqueous solutions was carried out in pulsed mode using 4 ms pulses with a 1 : 3 duty cycle. The reactor was operated at *ca.* 15 W into 50 ml solutions. Under these conditions the temperature rise of the solutions sonicated was *ca.* 1° min^{-1}.

All solutions were made with Milli-Q water and used on the day of preparation. Pyranine was obtained from Molecular Probes Inc. and used as received. The UV-VIS spectrum of pyranine in water agreed with that reported by others.[6] The temperature of the solutions remained in the range of 20–25 °C while spectra were recorded.

Pyranine is a highly water soluble compound with well characterised photophysical properties.[6,7] Its chemical structure is shown below.

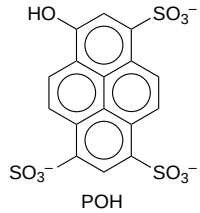

POH

Pyranine has a ground state pK_a = 7.2 but on excitation pK_a* = 0.5.[7] Its excited state lifetime is also sufficiently long (5 ns) such that deprotonation occurs over a wide pH range.[7] It is only when the pH is < *ca.* 2 that the emission from the POH* form begins to dominate. These photophysical properties of pyranine are evident in the absorption and fluorescence spectra (Fig. 1), at pH values above and below its ground state pK_a.

Fig. 2 shows the emission observed when pyranine solutions (at several pH values) are sonicated. These spectra can be compared with the equivalent pH fluorescence spectra shown in Fig. 1. Close correspondence of the two sets of spectra is evident although there are some differences. Fig. 3 directly compares the standardised fluorescence and SPL from pyranine at pH = 6.4. Also shown is the SL signal obtained from water in the absence of pyranine. As can be seen, the SPL signal is slightly broader than the fluorescence band with a shoulder at 450 nm. The broadness and the shoulder are both due to the residual SL emission that has not been absorbed by ground state pyranine. It can be seen from Fig. 1 that at pH = 6.4 there is no substantial light absorption by ground state pyranine above *ca.* 440 nm.

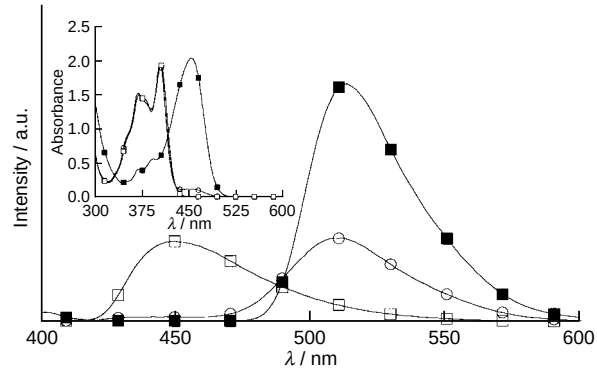

Fig. 1 Emission spectra (λ_{ex} = 350 nm) of 0.1 mM pyranine in water at various pH. Insert shows the absorption spectra obtained from the same solutions. Emission and absorption spectra were measured in standard 1 cm pathlength cuvettes. (Emission spectra are uncorrected.) pH = 10.7 (■), 6.4 (○), 0.7 (□).

At a pH of 10.7 all the pyranine exists in its ionised form, PO^-, and its absorption spectrum extends to *ca.* 500 nm (Fig. 1). Under these conditions all of the SL is absorbed at wavelengths below 500 nm and therefore the shoulder seen at 450 nm is no longer present.

At pH = 0.7 the reaction,

$$PO^{-}* + H^{+} \rightarrow POH* \quad (1)$$

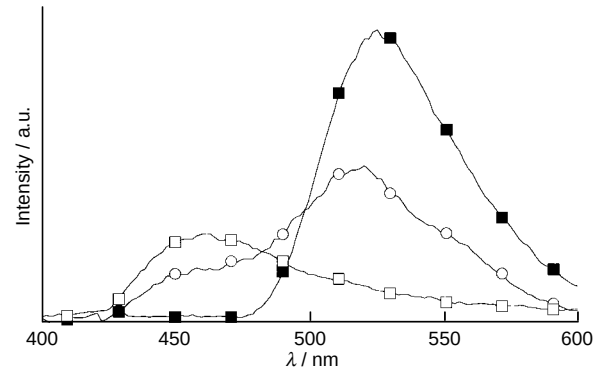

Fig. 2 Sonophotoluminescence of 0.1 mM pyranine in water at various pH. The emission is produced in a 4 cm diameter cell using a 3.5 cm diameter transducer plate. (Emission spectra are uncorrected.) pH = 10.7 (■), 6.4 (○), 0.7 (□).

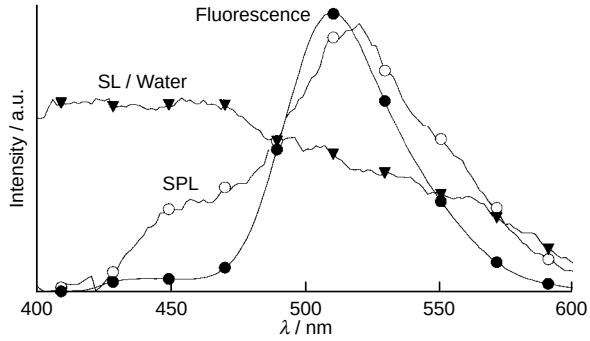

Fig. 3 A comparison of the fluorescence and SPL spectra of pyranine at pH = 6.4. The intensity maxima of the bands have been normalised to allow a better comparison. Under the quite different excitation conditions used the fluorescence intensity is *ca.* 600 times stronger than the SPL. Also shown is the SL from water. The intensity is on the same scale as that of the SPL. (Emission spectra are uncorrected.)

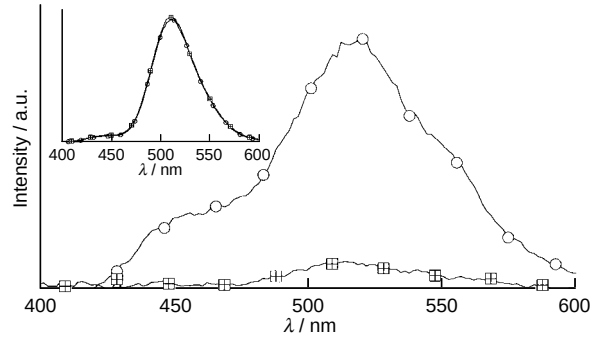

Fig. 4 Sonophotoluminescence spectra of 0.1 mM pyranine in water in the absence (○) and presence ⊞ of 0.1 M butan-1-ol at pH = 6.4. Insert shows the fluorescence spectra (λ_{ex} = 350 nm) of the same solutions. (Emission spectra are uncorrected.)

prevents emission from the PO^{-}* form and the emission recorded is a combination of SL and SPL from the POH* species.

In order to confirm that it is sonoluminescence that excites pyranine and not some thermal activation from heat leaking away from the acoustically collapsed bubble some experiments were carried out in the presence of butan-1-ol. Butanol has been found to quench the SL intensity from water[5] while enhancing sonochemical reactions in solution.[8,9] The latter indicates that bubble collapse in the presence of butanol still occurs and local heating still produces radicals that are responsible for the chemical reactions in solution.

Fig. 4 shows the effect that 0.1 M of butan-1-ol has on pyranine fluorescence and its SPL signal. It can be seen that butanol has a minimal effect on the fluorescence signal but almost completely quenches the SPL emission. This is consistent with butan-1-ol quenching the SL and hence eliminating photon excitation of pyranine.

The results presented clearly show that SL can be used to excite solution solutes. One of the advantages offered by this method is that no external light source is required and photon excitation can, in principle, be achieved in optically opaque and remote sites. For example, photosensitizing drugs within a human body could be activated using SPL generated by an ultrasound source external to the body. We note also that since sonoluminescence is observed in a wide range of liquids[1,10,11] it should be possible to generate SPL in systems other than water.

Notes and References

* E-mail: f.grieser@chemistry.unimelb.edu.au

1 F. R. Young, *Cavitation*, McGraw-Hill Book Company, London, 1989.
2 T. G. Leighton, *The Acoustic Bubble*, Academic Press, London, 1994.
3 Y. T. Didenko and S. P. Pugach, *J. Phys. Chem.*, 1994, **98**, 9742.
4 E. N. Harvey, *J. Am. Chem. Soc.*, 1939, **61**, 2392; A. Henglein, R. Ulrich and J. Lilie, *J. Am. Chem. Soc.*, 1989, **111**, 1974.
5 M. Ashokkumar, R. Hall, P. Mulvaney and F. Grieser, *J. Phys. Chem. B*, 1997, **101**, 10 845.
6 O. S. Wolfbeis, E. Fürlinger, H. Kroneis and H. Marsoner, *Fresenius Z. Anal. Chem.*, 1983, **314**, 119.
7 M. J. Politi, O. Brandt and J. H. Fendler, *J. Phys. Chem.*, 1985, **89**, 2345.
8 J. Z. Sostaric, P. Mulvaney and F. Grieser, *J. Chem. Soc., Faraday Trans.*, 1995, **91**, 2843.
9 S. Au Yeung, R. A. Hobson, S. Biggs and F. Grieser, *J. Chem. Soc., Chem. Commun.*, 1993, 823.
10 E. B. Flint and K. S. Suslick, *J. Am. Chem. Soc.*, 1989, **111**, 6987.
11 R. D. Finch, *Ultrasonics*, 1963, **1**, 87.

Received in Cambridge, UK, 3rd December 1997; 7/08708J

A new type of allylation: synthesis of β,γ-unsaturated ketones from α-halogenated aryl ketones using an allyltributyltin(IV)–tin(II) dichloride–acetonitrile system

Makoto Yasuda, Makihiro Tsuchida and Akio Baba*†

Department of Applied Chemistry, Faculty of Engineering, Osaka University, 2-1 Yamadaoka, Suita, Osaka 565, Japan

Allylation of α-halogenated aryl ketones with an allyltributyltin–tin dichloride–acetonitrile system gave β,γ-unsaturated ketones in high yields *via* selective aryl rearrangement.

Allylation of carbonyl compounds has been intensively studied for carbon–carbon bond formation, affording homoallylic alcohols.[1] We have recently reported an allylic tin(II) species as powerful allylation reagents toward aldehydes, ketones or imines in preference to the corresponding tin(IV) species.[2] The tin(II) species, which have vacant orbitals to accept electrons, contribute to the selective carbonyl allylation *via* a cyclic transition state owing to the strong affinity between the tin(II) atom and the carbonyl oxygen.[2] The tin(II) center would be expected to interact even with a halogen atom because the latter bears unshared electron pairs for coordination to tin(II). Herein, we report a new type of allylation system for α-halogenated aryl ketones.[3] This reaction proceeds *via* carbonyl allylation and subsequent aryl rearrangement to give β,γ-unsaturated ketone derivatives in high yields, in which reaction the tin(II) species characteristically effects the rearrangement.

A mixture of tin dichloride ($SnCl_2$) and 2-bromopropiophenone **2a** in MeCN was treated with allyltributyltin **1** at room temperature for 10 min to afford, unexpectedly, the β,γ-unsaturated ketone **3a**, whereas general activation by a Lewis acid, boron trifluoride–diethyl ether,[1,4] gave the homoallyl alcohol **4a** exclusively (Scheme 1). In the allyltributyltin–$SnCl_2$ system, migration of the phenyl group takes place as shown in Scheme 2. The homoallylic tin alkoxide **A** is a key intermediate

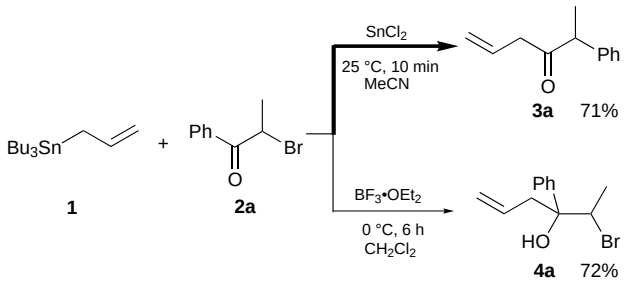

Scheme 1

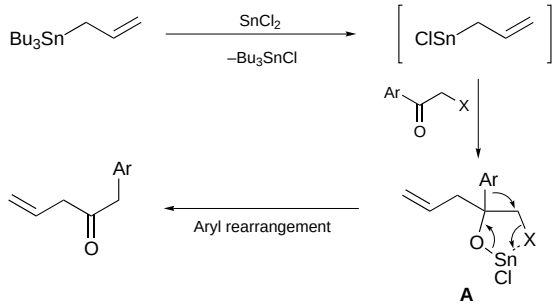

Scheme 2

in which the interaction between the tin(II) atom and the halogen directs the aryl rearrangement.[5] This type of interaction is unlikely to occur using allyltin(IV) reagents, which have a weaker affinity for halogen than the tin(II) species. Allylation using tin(IV) reagents of α-halo ketones proceeds *via* cyclization of the intermediate tin alkoxides to give oxiranes exclusively, and no rearrangement is observed.[6–8] Other solvents examined (THF, toluene, CH_2Cl_2, $CHCl_3$) in the presence of $SnCl_2$ gave low yields of **3a** (0–24% yield) at room temperature for 1 h. These facts strongly support the participation of the allylic tin(II) species in the rearrangement, because our previous report[2] has already shown the efficiency of MeCN as the solvent of choice for transmetalation of allyltributyltin **1** with $SnCl_2$. Allylaton of **2a** in MeCN for 24 h without $SnCl_2$ did not proceed at all. Considering these results, we suppose that this new type of allylation system giving the β,γ-unsaturated ketone evolves from the unique character of the tin(II) reagents.

We then explored the generality of the reaction by varying the aryl halo ketones. As shown in Table 1, β,γ-unsaturated ketones

Table 1 Synthesis of β,γ-unsaturated ketones **3**

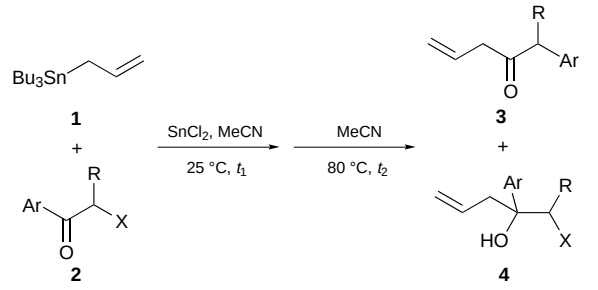

	Halo ketone **2**					Yield (%)	
Entry	Ar	R	X	t_1/h	t_2/h	**3**	**4**
1	4-$MeOC_6H_4$	H	Br	1	0	98	0
2	4-MeC_6H_4	H	Br	1	0.5	81	0
3	4-PhC_6H_4	H	Br	1	0.5	65	0
4	4-PhC_6H_4	H	Br	1	0	0	89
5	Ph	H	Br	1	0.5	60	0
6	4-ClC_6H_4	H	Br	1	0.5	26	27[a]
7	4-$O_2NC_6H_4$	H	Br	1	0.5	0	16
8	2-naphthyl	H	Br	1	1	74	0
9	2-naphthyl	H	Br	1	0	0	95
10	2-thienyl	H	Br	0.25	0.5[b]	72	0
11	2-thienyl	H	Br	1	0	0	76
12	3-thienyl	H	Br	1	0.5	61	0
13	3-thienyl	H	Br	1	0	0	83
14	Ph	Me	Br	24	0	98	0
15	Ph	Me	Cl	1	0.5	71	0
16	Ph	Me	Cl	0.25	0	0	90[c]
17	Ph	Ph	Cl	1	0	86	0

[a] 2-(*p*-Chlorophenyl)pent-4-enal (*ca*. 10% yield) was obtained as a side product (see ¶). [b] 50 °C. [c] Isomeric ratio = 61 : 39.

3 were effectively obtained.‡ The aryl rearrangement often required high temperature conditions (80 °C) because homoallyl alcohols **4** were formed exclusively at 25 °C (entries 4, 9, 11, 13 and 16). This result suggests that the reaction includes the intermediate **A** illustrated in Scheme 2. The effect of different aromatic substituents was interesting. Generally, the allylation of aryl-substituted carbonyls is enhanced by an electron-withdrawing group on the aromatic substituents since the electrophilicity of the carbonyl group is increased. The opposite effect was observed in entries 1–3 and 5–7 in regard to the synthesis of **3**. The unrearranged products **4** were observed in the reaction with the substrates bearing chloro or nitro groups (entries 6 and 7). These substituent effects are explainable by the rate-determining migration of the aryl groups,[9] as the allyltin(II) species have an adequate ability to promote carbonyl allylation.[2] The thienyl ring is tolerated in this reaction system (entries 10–13), in which sulfur did not reduce the activity of the tin(II) reagent at all. The secondary bromo or chloro ketones also gave **3** exclusively (entries 14, 15 and 17). The rearrangement took place readily without the need for high temperatures (entries 14 and 17). The interaction of tin(II) with the halogen (in **A**) would generate cationic halide carbon species, which are more stable for secondary substrates.

On the other hand, α-halogenated alkyl ketones showed a different reaction course, without any rearrangement; allyloxazolines were formed by the addition of solvent nitriles to the tin alkoxide intermediate, albeit in low yields.§

This work describes a new allylation system for the synthesis of β,γ-unsaturated carbonyl compounds, in which an unusual reaction course, including aryl rearrangement, is proposed. The selective rearrangement is promoted by the properties of the tin(II) species. Further investigaton of allylic tin(II) species is in progress.

This work was supported by a Grant-in-Aid for Scientific Research on Priority Area No. 09231229 from the Ministry of Education, Science, Sports, and Culture, of the Japanese Government. Thanks are due to Mr H. Moriguchi, Faculty of Engineering, Osaka University, for assistance in obtaining mass spectra.

Notes and References

† E-mail: baba@ap.chem.eng.osaka-u.ac.jp

‡ *Typical experimental procedure*: Allyltributyltin **1** (1.0 mmol) was added to a stirred suspension of $SnCl_2$ (1.0 mmol) and α-halo ketone **2** (1.0 mmol) in dry MeCN (1.0 ml), and the mixture was stirred under the conditions noted in the text. Et_2O (100 ml) and aq. NH_4F (15%; 40 ml) were added, the organic layer was separated and washed with water (50 ml × 2), dried ($MgSO_4$) and evaporated to give β,γ-unsaturated ketone **3**. The crude product was further purified by flash chromatography on silica gel.

§ Since the alkyl group has a low aptitude for migration, reaction of the intermediate with the solvent nitrile occurred.

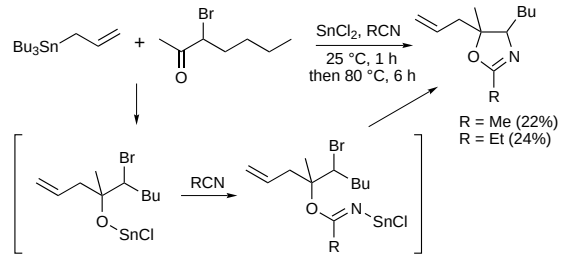

¶ The aldehyde, 2-(*p*-chlorophenyl)pent-4-enal, was formed *via* 2-allyl-2-(*p*-chlorophenyl)oxirane. The transformation of oxirane to aldehyde commonly proceeds in acidic conditions.

1 A recent review: Y. Yamamoto and N. Asao, *Chem. Rev.*, 1993, **93**, 2207.
2 M. Yasuda, Y. Sugawa, A. Yamamoto, I. Shibata and A. Baba, *Tetrahedron Lett.*, 1996, **37**, 5951.
3 α-Halogenated ketones are an important class of organic compound and detailed information on their synthesis has been reported. N. De Kimpe and R. Verhé, *The Chemistry of α-Haloketones, α-Haloaldehydes and α-Haloimines*, ed. S. Patai and Z. Rappoport, Wiley, Chichester, 1988.
4 Y. Naruta, S. Ushida and K. Maruyama, *Chem. Lett.*, 1979, 919.
5 We have recently reported a similar rearrangement of a 2-oxoalkyl group promoted by $ZnCl_2$. In this case, however, there was no observation of the aryl rearrangement even with the use of an aromatic substrate. M. Yasuda, S. Tsuji, I. Shibata and A. Baba, *J. Org. Chem.*, 1997, **62**, 8282.
6 I. Pri-Bar, P. S. Pearlman and J. K. Stille, *J. Org. Chem.*, 1983, **48**, 4629.
7 K. Yano, Y. Hatta, A. Baba and H. Matsuda, *Synlett*, 1991, 555.
8 K. Yano, Y. Hatta, A. Baba and H. Matsuda, *Synthesis*, 1992, **7**, 693.
9 The migratory aptitude for pinacol rearrangement of various aromatic substituents has been reported. W. E. Bachmann and J. W. Ferguson, *J. Am. Chem. Soc.*, 1934, **56**, 2081.

Received in Cambridge, UK, 2nd December 1997; 7/08679B

First characterisation of zirconium enolate radical cations in solution and their mesolytic bond cleavage to zirconocene cations

Michael Schmittel* and Rolf Söllner

Institut für Organische Chemie, Universität Würzburg, Am Hubland, D-97074 Würzburg, Germany

Zirconocene enolate radical cations are generated and characterised in solution for the first time; the sterically congested radical cations undergo a mesolytic Zr–O bond cleavage process yielding zirconocene cations, the kinetics of which are determined.

In light of the importance of transition metal enolates for organic synthesis[1] we have recently become interested in the redox umpolung of these nucleophilic species.[2] We were able to show that titanium enolate radical cations can undergo carbon–carbon bond formation to 1,4-diketones, a reaction which can even be conducted in a diastereoselective fashion.[3] In the present paper we describe for the first time the properties and reactions of zirconium enolate radical cations and their clean mesolytic† bond cleavage to zirconocene cations. The latter are well known as the catalytic active species in the Ziegler–Natta polymerization of α-alkenes.[4]

Since zirconium enolates constitute highly reactive compounds with a high sensitivity towards hydrolysis, only a small number of zirconium enolates[5] has been isolated and investigated. The kinetic stability of zirconium enolates should be largely increased by starting from sterically bulky β,β-dimesitylenols.[6] These were deprotonated quantitatively with sodium hydride in THF at room temperature and subsequentially reacted with stoichiometric amounts of zirconocene dichloride. All chloro zirconocene enolates could be obtained as bright yellow crystals by crystallisation from *n*-hexane or *n*-hexane–toluene.

A route leading to the methyl zirconocene enolates was realised by reacting dimethyl zirconocene with the corresponding β,β-dimesitylenols accompanied by elimination of methane. The zirconocene enolates **4**–**6** could be obtained in analytically pure form as pale yellow solids by crystallization from acetonitrile–dichloromethane mixtures (Scheme 1).

In standard cyclic voltammetry (CV) experiments all zirconocene enolates showed irreversible oxidation waves (E_{pa}; Table 1) in acetonitrile at 100 mV s^{-1}. By changing the solvent to dichloromethane and increasing the scan rates up to 1000 V s^{-1} reversible waves could be obtained. We observed partially reversible waves for **1**–**3** and **5** already at scan rates $\nu \geqslant 100$ V s^{-1}, for **4** at $\nu \geqslant 200$ V s^{-1}, and for **6** at $\nu \geqslant 50$ V s^{-1}. This represents the first direct observation of zirconium enolate radical cations in solution, allowing for the determination of their thermodynamically relevant redox potentials $E_{\frac{1}{2}}^{Ox}$ (Table 1). The oxidation potentials fall in the range +0.35 to +0.57 V *vs.* ferrocene–ferrocenium† and are *ca.* 100 mV more anodic than those of structurally analogous titanocene enolates,[2] an effect which is already known from simple titanocene and zirconocene compounds.[7]

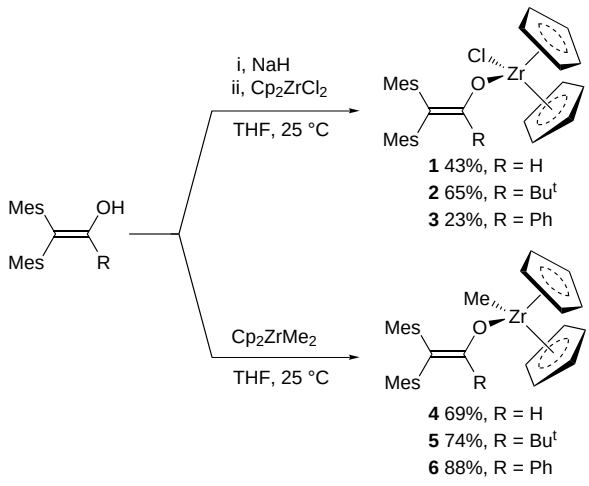

Scheme 1

Table 1 Oxidation potentials of zirconocene enolates determined by CV

Zirconocene enolate	E_{pa}[a,b]/V	$E_{\frac{1}{2}}^{Ox}$[a,c]/V	Yield of benzofuran
1	+0.45	+0.57	95% of **7**
2	+0.32	+0.43	90% of **8**
3	+0.41	+0.44	88% of **9**
4	+0.51	+0.46	82% of **7**
5	+0.30	+0.35	86% of **8**
6	+0.35	+0.36	80% of **9**

[a] *vs.* Fc–Fc†. [b] In acetonitrile at ν = 100 mV s^{-1}. [c] In dichloromethane at ν = 1000 V s^{-1}.

The chemical one-electron oxidations of the zirconium enolates **1**–**6** which were performed on a preparative scale using tris(1,10-phenanthroline)iron(III) hexafluorophosphate ($E_{\frac{1}{2}}$ = +0.69 V), as a well-defined outer-sphere one-electron oxidant, or nitrosonium hexafluorophosphate ($E_{\frac{1}{2}}$ = +0.89 V) in acetonitrile–dichloromethane afforded the benzofuran derivatives **7**–**9** in good yields (Scheme 2, Table 1).

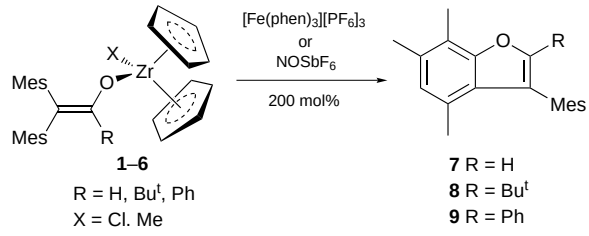

Scheme 2

Formation of benzofurans by one-electron oxidation of stable enols[8] and various enol derivatives[9] (including titanium enolates[2]) is known to be initiated by a mesolytic bond cleavage of the O–X bond followed by several reaction steps that are well established (Scheme 3).

For the zirconocenes the Zr–O bond must have been broken at the stage of the enolate radical cation since the direct cyclization is highly unfavourable because of steric reasons. Equally, a dissociative electron transfer process can be ruled out since all the radical cations could be characterised at high scan rates in the CV experiment. Hence, we conclude that mesolytic Zr–O bond cleavage is the primary follow-up reaction of the

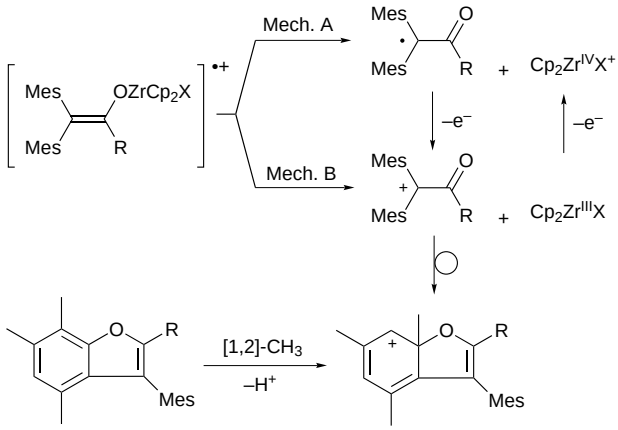

Scheme 3

radical cations **1**$^{\bullet+}$–**6**$^{\bullet+}$ which can follow two distinct mechanistic pathways:[9d] the heterolytic scission (Mech. A) would result in the formation of an α-carbonyl radical and a zirconocene cation, the homolytic variant (Mech. B) would lead to an α-carbonyl cation and a zirconocene(III) species. Both cleavage selectivities are known for enol radical cations: homolytic cleavage can be observed for radical cations of enol esters,[9a] enol carbonates and enol carbamates[9d] whereas the radical cations of enols, silyl enol ethers,[9b] enol phosphites and enol phosphinates[9c] and of the structurally very closely related titanium enolates[2] follow the heterolytic variant.

When the oxidation potentials of the homolytic cleavage fragments (α-carbonyl radicals and $Cp_2Zr^{III}X$) are known then the selectivity of such fragmentation processes can be determined by using a simple thermochemical cycle calculation. The fragments which are split off in a cationic form must have the lower redox potential. We hence measured the oxidation potential of $Cp_2Zr^{III}Me$ to $E_{pa} = -1.9$ V§ and compared it with those of the relevant α-carbonyl radicals. Since the latter are much more positive (0.15–0.36 V)[8a] it is clear that mesolytic bond cleavage of the methyl zirconocene enolates **4**–**6** takes place according to the heterolytic pathway (Mech. A). This result is in analogy to Jordan's findings, who performed one-electron oxidations of dimethyl zirconocene and other dialkyl zirconocenes with equimolar amounts of ferrocenium and isolated the cationic complexes $[Cp_2ZrR]^+$ after Zr–C bond cleavage.[10] Owing to the much larger differences of the oxidation potentials between oxidant and substrate the desired reaction time of this conversion is much longer (10 h) than in our experiments (1 min). In case of the chlorine substituted model compounds **1**–**3** simple considerations¶ propose that their fragmentation should follow the same pathway.

The knowledge of the exact mechanism of this process enabled us to determine the lifetime of zirconocene enolate radical cations by following the kinetics of the mesolytic bond cleavage through fast scan cyclic voltammetry at ultramicro electrodes in dichloromethane. From the ratio of cathodic to anodic peak current I_{pc}/I_{pa} the kinetic parameter kt was evaluated according to the method of Nicholson and Shain[11] applying a working curve for an $EC_{irr}E$ mechanism (electron transfer–chemical reaction–electron transfer). The working curve had been obtained from digital simulation of cyclic voltammograms using the implicit Crank–Nicholson technique.[12] This kinetic analysis at room temperature provided a first order-rate constant of $k_f = 3.3 \times 10^2$ s^{-1} ($t_{\frac{1}{2}} = 2.1 \times 10^{-3}$ s) for the mesolytic bond cleavage of **2**$^{\bullet+}$, $k_f = 3.1 \times 10^2$ s^{-1} ($t_{\frac{1}{2}} = 2.2 \times 10^{-3}$ s) for that of **3**$^{\bullet+}$, $k_f = 8.3 \times 10^2$ s^{-1} ($t_{\frac{1}{2}} = 8.4 \times 10^{-4}$ s) for that of **4**$^{\bullet+}$ and $k_f = 5.0 \times 10^2$ s^{-1} ($t_{\frac{1}{2}} = 1.4 \times 10^{-3}$ s) for that of **5**$^{\bullet+}$.

In conclusion, we have characterised for the first time zirconium enolate radical cations in solution and identified them as rapidly cleaving precursors for zirconocene cations. Work is in progress to use this mesolytic cleavage reaction in photoinduced electron transfer reactions for triggering polymerisation.

We gratefully acknowledge the financial support by the Deutsche Forschungsgemeinschaft (SFB 347: 'Selective Reactions of Metal Activated Molecules'). In addition, we are most indebted to the Fonds der Chemischen Industrie for the ongoing support of our research as well as to Degussa for a generous gift of electrode materials.

Notes and References

* E-mail: mjls@chemie.uni-wuerzburg.de

† The expression mesolytic was coined by Maslak to describe bond cleavage of radical ions to yield radical and ionic products: P. Maslak and J. N. Narvaez, *Angew. Chem., Int. Ed. Engl.*, 1990, **29**, 283.

‡ All potentials are referenced to the ferrocene–ferrocenium (Fc) redox couple unless otherwise noted. To obtain values *vs.* SCE, simply add +0.39 V.

§ We determined the reduction potential of the corresponding cation $[Cp_2Zr^{IV}Me(MeCN)_2]BPh_4$ to $E_{pc} = -1.94$ V (in acetonitrile at 100 mV s^{-1}; supporting electrolyte: $NaBPh_4$). The preparation of this cation is described in: R. F. Jordan, C. S. Bajgur, W. E. Dasher and A. L. Rheingold, *Organometallics*, 1987, **6**, 1041.

¶ The difference between the oxidation potentials of $Cp_2Zr^{III}Me$ and $Cp_2Zr^{III}Cl$ can be approximated by the difference between the half-wave potentials of Cp_2ZrMe_2 ($E_{\frac{1}{2}} = -3.06$ V) and Cp_2ZrCl_2 ($E_{\frac{1}{2}} = -2.04$ V). As the potential of $Cp_2Zr^{III}Me$ is $E_{pa} \approx -1.9$ V we assume that that of $Cp_2Zr^{III}Cl$ is $E_{pa} \approx -0.9$ V_{Fc} being distinctly lower than those of the α-carbonyl radicals.

1 I. Paterson, in *Comprehensive Organic Synthesis*, ed. C. H. Heathcock, Oxford, 1991, vol. 2, p. 301; D. A. Evans, F. Urpi, T. C. Somers, J. S. Clark and M. T. Bilodeau, *J. Am. Chem. Soc.*, 1990, **112**, 8215; M. P. Bonner and E. R. Thornton, *J. Am. Chem. Soc.*, 1991, **113**, 1299; D. A. Evans, D. L. Rieger, M. T. Bilodeau and F. Urpi, *J. Am. Chem. Soc.*, 1991, **113**, 1047; R. Mahrwald, *Chem. Ber.*, 1995, **128**, 919; R. O. Duthaler and A. Hafner, *Chem. Rev.*, 1992, **92**, 807.

2 M. Schmittel and R. Söllner, *Angew. Chem., Int. Ed. Engl.*, 1996, **35**, 2107; *Chem. Ber./Recueil*, 1997, **130**, 771.

3 M. Schmittel, A. Burghart, W. Malisch, J. Reising and R. Söllner, *J. Org. Chem.*, 1998, **63**, 396.

4 *Cf.* H. H. Brintzinger, D. Fischer, R. Mülhaupt, B. Rieger and R. Waymouth, *Angew. Chem., Int. Ed. Engl.*, 1995, **34**, 1143 and references therein.

5 J. M. Manriquez, D. R. McAlister, R. D. Sanner and J. E. Bercaw, *J. Am. Chem. Soc.*, 1978, **100**, 2716; R. S. Threlkel and J. E. Bercaw, *J. Am. Chem. Soc.*, 1981, **103**, 2650; E. J. Moore, D. A. Straus, J. Armantrout, B. D. Santasiero, R. H. Grubbs and J. E. Bercaw, *J. Am. Chem. Soc.*, 1983, **105**, 2068; M. D. Curtis, S. Thanedar and W. M. Butler, *Organometallics*, 1984, **3**, 1855; S. Gambarotta, S. Strologo, C. Floriani, A. Chiesi-Villa and C. Guastini, *Inorg. Chem.*, 1985, **24**, 654; M. F. Lappert, C. L. Raston, L. M. Engelhardt and A. H. White, *J. Chem. Soc., Chem. Commun.*, 1985, 521; R. Beckhaus, I. Strauß and T. Wagner, *J. Organomet. Chem.*, 1994, **464**, 155.

6 M. Schmittel, H. Werner, O. Gevert and R. Söllner, *Chem. Ber./Recueil*, 1997, **130**, 195.

7 P. G. Gassman, D. W. Macomber and J. W. Hershberger, *Organometallics*, 1983, **2**, 1470; M. J. Burk, W. Tumas, M. D. Ward and D. R. Wheeler, *J. Am. Chem. Soc.*, 1990, **112**, 6133.

8 (*a*) M. Röck and M. Schmittel, *J. Chem. Soc., Chem. Commun.*, 1993, 1739; (*b*) M. Schmittel, G. Gescheidt and M. Röck, *Angew. Chem., Int. Ed. Engl.*, 1994, **33**, 1961.

9 (*a*) M. Schmittel, J. Heinze and H. Trenkle, *J. Org. Chem.*, 1995, **60**, 2726; (*b*) M. Schmittel, M. Keller and A. Burghart, *J. Chem. Soc., Perkin Trans. 2*, 1995, 2327; (*c*) M. Schmittel, J.-P. Steffen and A. Burghart, *Chem. Commun.*, 1996, 2349; (*d*) M. Schmittel and H. Trenkle, *Chem. Lett.*, 1997, 299.

10 S. L. Borkowsky, R. F. Jordan and G. D. Hinch, *Organometallics*, 1991, **10**, 1268.

11 R. S. Nicholson and I. Shain, *Anal. Chem.*, 1964, **36**, 706.

12 A. Lasia, *J. Electroanal. Chem., Interfacial Electrochem.*, 1983, **146**, 397; J. Heinze, M Störzbach and M. Mortensen, *J. Electroanal. Chem., Interfacial Electrochem.*, 1984, **165**, 61; J. Heinze and M. Störzbach, *J. Electroanal. Chem.*, 1993, **346**, 1.

Received in Cambridge, UK, 25th November 1997; 7/08495A

Extended rim redox active tris-metallodioxolene derivatives of cyclotricatechylene

D. Scott Bohle* and Daniel Stasko

Department of Chemistry, University of Wyoming, Laramie, WY 82071-3838, USA

Triple metallation of cyclotricatechylene (CTC) results in new cavitands with significantly extended rims and three reversible redox couples as determined by single-crystal X-ray diffraction and electrochemistry.

Supramolecular constructs based on cyclotriveratrylene (CTV) **1** are versatile cavitands which form inclusion compounds for a diverse group of guests ranging from buckministerfullerene[1] and carboranes[2] to halocarbons,[3] anions,[4] and cationic organometallic sandwich complexes.[5] As has been recently recognized, the solid state structures of these host–guest complexes are either columnar, with the guests often packing between the CTV units, much like a typical solvate, or, as in the case of the fullerene inclusion compounds, the cavity is fully utilized to maximize the non-covalent interactions in the $C_{60}\subset$CTV aggregate.[1,5,6] One strategy to more fully utilize the cavitand scaffold offered by the CTV unit is to extend the rim by building off from the three catechol moieties; while a wide range of alkyl and pendant ligand derivatives have been so prepared,[7–9] we are unaware of any reports where transition metal complexes have been used to directly extend the rim of the CTV cavity. Herein, we describe (*i*) the preparation and characterization of two such derivatives; (*ii*) the structure of one as its bisdimethylacetamide (DMA) inclusion adduct; and (*iii*) the redox activity of these new hosts. These compounds provide unusual new examples of a redox active hosts where the redox units are incorporated directly into the framework of the host.

Cyclotriveratrylene, **1** was converted into the tris-catechol derivative, cyclotricatechylene **2** with boron tribromide.[10] Compound **2** was then treated for several hours in deoxygenated DMA solutions with a slight excess of $LPtCl_2$ [(L = diphenylphosphinobenzene (dppb) or diphenylphosphinoferrocene (dppfc)] in the presence of a methanol/potassium carbonate mixture acting as a base. The product was isolated as an orange solid collected by precipitation with diethyl ether and recrystallization from dichloromethane–acetone. The two materials, (CTC)[Pt(dppb)]$_3$ **3** and (CTC)[Pt(dppfc)]$_3$ **4**, were both obtained in moderate yields and appear indefinitely stable in air in the solid state; the latter slowly decomposes in solution after a few days.

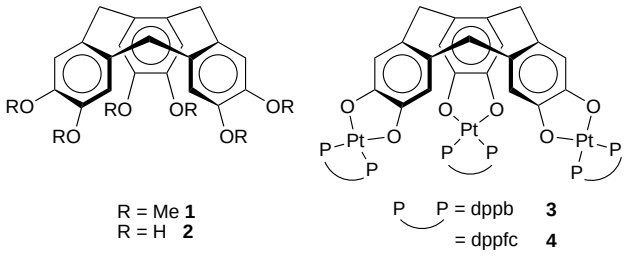

Characterization† of these compounds has led to the formulation of the materials as the triply metallated platinum(II)–tris-catecholate species. Support for this assignment comes from the presence of a strong IR active band at 1270 cm^{-1} attributable to a ν(C–O–M) mode. In addition, the ^{31}P NMR spectral data for these species are indicative of complete

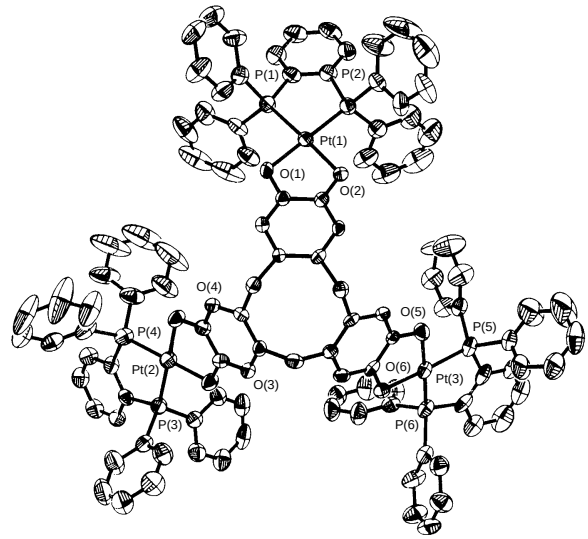

Fig. 1 Structure of (CTC)[Pt(dppb)]$_3$ **3** viewed looking down from the top of the bowl, ORTEP (50% thermal ellipsoids); solvent and hydrogens removed for clarity. Average Pt–Pt distance 9.85 Å.

substitution, showing only one phosphorus signal with corresponding platinum satellites. The ^{1}H NMR spectrum also shows this symmetrical substitution, indicated by a singlet representing the aromatic CTC protons. The geminal coupling of the protons on the methylene bridgehead carbons, characteristic CTC markers due to the rigid conformation of the bowl,[7] also suggests that the sterically bulky phosphine ligands do not significantly perturb the shape.

Structural characterization of **3** by single-crystal X-ray diffraction‡ confirms that the tris-catecholate complex retains the original bowl structure of the cavitand (Fig. 1). Moreover, the square planar coordination of the platinum centers within the molecule and their metrical data are consistent with the formulation of the compound as a Pt^{II} catecholate.[11] As shown in the graphical abstract a crystallographic inversion center leads to the formation of a cage in the solid state. The resulting shell incorporates four DMA molecules, disordered over eight positions, within its interior. While this is expected from the known ability of CTV compounds to form inclusion type complexes,[7,8] what is especially striking is that the guests are now completely enclosed within the rim of the host; derivatization at the rim of the CTV bowl with LPt extends the depth of the cavity while also maintaining the host character of the parent compound.

The electrochemical properties of the two compounds, **3** and **4**, were examined by cyclic voltammetry.§ Upon sweeping the voltage to oxidizing potentials, a three wave voltammogram (Fig. 2) appears, with the first oxidation taking place at approximately 50 mV (*vs.* NHE). These reversible oxidations corresponds to the three separate one-electron oxidations of each catecholate (cat) moiety of the CTC unit to a semiquinoid (sq) species (Table 1). This behavior is quite different to that of the parent CTV compound which shows two irreversible waves

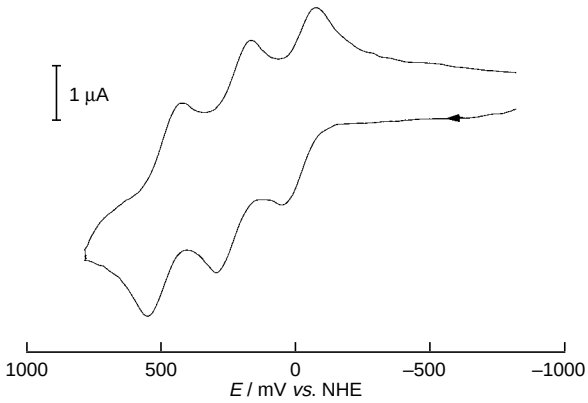

Fig. 2 Cyclic voltammogram of (CTC)[Pt(dppfc)]$_3$ **4** reversible cat–sq couples. Referenced *vs*. NHE, scan rate = 100 mV s^{-1}. See Table 1 for experimental conditions.

Table 1 Electrochemical data

Compound	$E_{1/2}$[a]/mV	Assignment
3	40	cat–sq
	240	
	490	
	≈ 1050 (irr.)	sq–quin (decomp.)
4	60	cat–sq
	230	
	470	
	≈ 1150 (irr.)	sq–quin (decomp.)

[a] Experiments were carried out using CH_2Cl_2 as the solvent with 0.1 M $NBu^n_4PF_6$ as the supporting electrolyte, Pt disc working and Pt wire auxiliary electrodes, and an Ag–$AgNO_3$ non-aqueous reference electrode. Half-cell potentials were calibrated against an internal Fc–Fc$^+$ standard. Reported values are referenced *vs*. NHE.

at much higher potential, 1670 and 1830 mV (*vs*. NHE).[12] Though the electrochemical properties of **3** and **4** are very different from **1**, the first oxidation potentials are similar to those observed for the first oxidation of simple platinum catecholate derivatives.[13] Sweeping to greater oxidizing potentials produces a fourth irreversible couple resulting in decomposition of the CTC complex. This fourth oxidation is observed at *ca*. 1100 mV and most likely is attributed to quinoid formation and loss of coordination of the CTC moiety to the platinum center. For **4**, this oxidation and decomposition appears to be coincident with oxidation of the ferrocene moiety of the chelating phosphine. The three cat–sq waves indicate communication between the metal centers; since the potential is characteristic of CTC based catecholate oxidations, this communication is likely to be mediated primarily by the CTC framework itself, either through a through-space interaction from the increased charge density on the aromatic ring, or from a through-bond interaction at the bridging methylene spacers. The electron rich CTV based cryptophanes are known to form radical cations which are thought to be stabilized through extended delocalization of the unpaired electron over the CTV units.[12] The communication observed between the redox centers of **3** and **4** may be attributed to a similar phenomenon.

This set of compounds extends the family of known CTC derivatives to include the new dioxolene species which incorporate a previously unexamined aspect of metallated host–guest chemistry. Current efforts are directed towards exploring the range of complexes that can be created and characterizing their binding and catalytic properties.

We gratefully acknowledge support from the DOE (Grant DE-FCO2-91ER) and the Camille and Henry Dreyfus Foundation teacher/scholar award (D. S. B). We would also like to thank Dr Navamoney Arulsamy for assistance with the crystallography.

Footnotes and References

* E-mail: bohle@uwyo.edu

† *Selected spectroscopic data*: IR **3**, 1271 cm^{-1}; **4**, 1274 cm^{-1} (aryl C–O–M stretch). NMR [$CDCl_3$–CD_3OD (5 : 1), 23 °C]: **3**, δ(^{1}H) 6.7 (s, 6 H, CTV aromatic), 4.6 (d, *J* 12 Hz, 3 H, CTV methylene bridge), 3.3 (d, *J* 12 Hz, 3 H, CTV methylene bridge). δ(^{31}P) 33.2 ($^1J_{PPt}$ 3492 Hz). **4**, δ(^{1}H) 6.7 (s, 6 H, CTV aromatic), 4.8 (d, *J* 12 Hz, 3 H, CTV methylene bridge), 3.4 (d, *J* 12 Hz, 3 H, CTV methylene bridge). δ(^{31}P) 10.2 ($^1J_{PPt}$ 3640 Hz). Complete details are available in supplementary data available from the authors.

‡ *Selected crystallographic data* for **3** (193 K): $C_{143}H_{156}N_8O_{14}P_6Pt_3$, dark orange rhombus from DMA–isopropyl alcohol, triclinic, space group $P\bar{1}$, *a* = 17.2442(3), *b* = 20.98140(10), *c* = 21.3249(3) Å, α = 69.876(1), β = 85.997(1), γ = 66.325(1)°, *U* = 6613.8(2) Å^3, *Z* = 2; R_1 (*wR*$_2$) [$I > 2\sigma(I)$] = 0.046 (0.095), All non-hydrogen atoms refined anisotropically. Complete details are available in supplementary material available from the authors. CCDC 182/725.

§ Anaerobic dichloromethane solutions of **3** and **4**, with 0.1 M $NBu^n_4PF_6$ as supporting electrolyte, were examined using a Pt disk working electrode, a Pt wire auxiliary electrode, and a nonaqueous Ag/$AgNO_3$ reference electrode. Potentials and corresponding currents were examined at various scan rates, ranging from 25 to 1000 mV s^{-1}. Reversibility was determined by examination of cathodic and anodic peak current ratios as well as peak symmetry and by examination of the linearity of plots of $\Delta E = E_{ox} - E_{red}$ *vs*. the square root of the scan rate. Measured potentials were calibrated through the use of an internal Fc–Fc$^+$ standard, with the reported values referenced against NHE.

1 J. L. Atwood, M. J. Barnes, M. G. Gardiner and C. L. Raston, *Chem. Commun.*, 1996, 1449.
2 R. J. Blanch, M. Williams, G. D. Fallon, M. G. Gardiner, R. Kaddour and C. L. Raston, *Angew. Chem., Int. Ed. Engl.*, 1997, **36**, 504.
3 D. J. Cram, J. Weiss, R. C. Helgeson, C. B. Knobler, A. E. Dorigo and K. N. Houk, *J. Chem. Soc., Chem. Commun.*, 1988, 407.
4 J. L. Atwood, K. T. Holman and J. W. Steed, *Chem. Commun.*, 1996, 1401.
5 K. T. Holman, J. W. Steed and J. L. Atwood, *Angew. Chem., Int. Ed. Engl.*, 1997, **36**, 1736.
6 J. W. Steed, H. Zhang and J. L. Atwood, *Supramol. Chem.*, 1996, **7**, 37.
7 A. Collet, *Tetrahedron*, 1987, **43**, 5725.
8 A. Collet, in *Comprehensive Supromolecular Chemistry*, ed. D. D. MacNicol, F. Toda and R. Bishop, Pergamon, Oxford, 1996, vol. 6, pp. 281–303.
9 J. A. Wytko, C. Boudon, J. Weiss and M. Gross, *Inorg. Chem.*, 1996, **35**, 4469.
10 A. S. Lindsey, *J. Chem. Soc.*, 1965, 1685.
11 J. M. Clemente, C. Y. Wong, P. A. Bhattacharya, M. Z. Slawin, D. J. Williams and J. D. Woollins, *Polyhedron*, 1994, **13**, 261; G. A. Fox, S. Bhattacharya and C. G. Pierpont, *Inorg. Chem.*, 1991, **30**, 2895.
12 A. Renault, D. Talham, J. Canceill, P. Batail, A. Collet and J. Lajzerowicz, *Angew. Chem., Int. Ed. Engl.*, 1989, **28**, 1249.
13 D. S. Bohle and D. Stasko, unpublished work.

Received in Columbia, MO, USA, 23rd October 1997; 7/07649E

Model investigations for vanadium–protein interactions: first vanadium(III) complexes with dipeptides and their oxovanadium(IV) analogues

Anastasios J. Tasiopoulos,[a] Yiannis G. Deligiannakis,[b] J. Derek Woollins,[c] Alexandra M. Z. Slawin*[c] and Themistoklis A. Kabanos*[a]

[a] *Department of Chemistry, Section of Inorganic and Analytical Chemistry, University of Ioannina, 45110 Ioannina, Greece*
[b] *NRPCS Demokritos, Institute of Materials Science, 15 310Agia Paraskevi Attikis, Greece*
[c] *Department of Chemistry, Loughborough University, Loughborough, Leicestershire, UK LE11 3TU*

Reaction of the dipeptides H_2Gly-Tyr and H_2Gly-Phe with VCl_3 and 1,10-phenanthroline affords the compounds [V(Gly-Tyr)(phen)]Cl·3MeOH 1 and [V(Gly-Phe)(phen)]Cl-·3MeOH 2; aerial oxidation of the complexes 1 and 2 gives their oxovanadium(IV) analogues [VO(Gly-Tyr)(phen)] 3 and [VO(Gly-Phe(phen)] 4, respectively; the X-ray crystal structure of 3 is reported.

Vanadium is an essential nutrient for higher animals,[1] although this has not yet been clearly established as such to human life.[2] Nevertheless, vanadium *in vivo* generates significant physiological responses;[3] for example, vanadate inhibits ion transport ATP-ases,[4] phosphotyrosine phosphatase,[5] *etc.* Beyond dispute, the most important physiological response of vanadium is its insulin-mimetic properties.[6] Our understanding of the mechanism of vanadium insulinomimetic action is still in its infancy.[6] In addition to the above mentioned roles of vanadium, the oxovanadium(IV) center is an excellent EPR spectroscopic probe for various naturally occurring vanadoproteins and oxovanadium(IV)-substituted protein systems.[7] Detailed structural, physicochemical and kinetic investigations on synthetic model complexes of vanadium with peptides, that are the most closely related models to proteins, will contribute greatly to our understanding of the mechanism of insulinomimetic action of vanadium as well as of its biological role in general. To date, there are only two vanadium(V) complexes structurally characterized with the dipeptide glycylglycine.[8a,b] The preparation of two vanadium(IV) compounds with the dipeptides glycylglycine and glycylalanine has also been reported.[8c] Herein, we describe the synthesis of the first vanadium(III) complexes with dipeptides, namely, with glycyl-L-tyrosine (Gly-Tyr) and glycyl-L-phenylalanine (Gly–Phe) and their oxovanadium(IV) analogues. The X-ray crystal structure of VO^{2+} with Gly-Tyr is reported, as well as the electrochemistry and the EPR spectra of the VO^{2+} compounds. To our knowledge, the structure of VO^{2+} with the dipeptide Gly-Tyr is the first example of a structurally characterized vanadium(IV) complex with a peptide.

Vanadium(III) chloride (2 mmol) was dissolved in methanol at ambient temperature, then the solution was cooled to −20 °C. Sequential addition of 1,10-phenanthroline (2 mmol), of the dipeptide (2 mmol) and an excess of triethylamine (10 mmol) to the vanadium solution, followed by slow warming under magnetic stirring to room temperature, induced a sequence of color changes (from red through red-brown to brown-purple) and resulted in the formation of the complexes [V(Gly-Tyr)(phen)]Cl·3MeOH **1** (yield 70%) and [V(Gly-Phe)-(phen)]Cl·3MeOH **2** (yield 50%). Air oxidation of **1** and **2** gives their oxovanadium(IV) analogues, [VO(Gly-Tyr)(phen)] **3** (yield 80%) and [VO(Gly-Phe)(phen)] **4** (yield 65%), respectively. The elemental analyses for complexes **1**–**4** are in accord with the formulas given above.

The molecular structure of the complex **3** (Fig. 1), shows the vanadium atom possessing a severely distorted octahedral coordination. The vanadium atom is **3** is ligated to a tridentate Gly-Tyr^{2-} ligand at the N_{amine} atom N(11) the deprotonated $N_{peptide}$ atom N(12) and one of the $O_{carboxylato}$ atoms O(14), as well as an oxo group O(1) and two phenanthroline nitrogens N(1) and N(10) and is 0.33 Å, above the mean equatorial plane, defined by the three ligating atoms of the dipeptide [N(11), N(12), O(14)] and a phenanthroline nitrogen N(1), in the direction of the oxo ligand. The peptide functionality N(12)C(12)O(12)C(11) [maximum deviation of C(12) is 0.02 Å] is planar within the limits of precision. The ligand Gly-Tyr^{2-} forms two five-membered fused chelate rings and is meridionally ligated to VO^{2+} center with the amine nitrogen and carboxylato oxygen atoms lying in *trans* position. The $V–N_{peptide}$ bond length [1.927(7) Å] is indicative of a very strong bond of the deprotonated peptide nitrogen to vanadium, and may reflect some V=N character[9] due to donation of electron density from the deprotonated peptide nitrogen into metal d orbitals. The oxovanadium(IV)–amidate N distance in complex **3** is significantly shorter (*ca.* 0.07 Å) than seen in the related complex $[NHEt_3][V^{IV}O(mpg)(phen)]CH_3OH$[8c,10] **5** [$V–N_{amide}$ = 1.997(4) Å] which is the only other oxovanadium(IV) complex which contains an aliphatic $V–N_{amide}$ bond. This significant difference could be ascribed to ligand constraints in **3** and to the weaker dianionic ligand set (Gly-Tyr^{2-}) in complex **3**, compared to trianionic ligand set (mpg^{3-}) in complex **5**, which results in a higher effective charge on the vanadium center and shorter V–N distances. Nevertheless, the $V–N_{amide}$ and $V–N_{amine}$ bond lengths in **3** are longer (*ca.* 0.03 and 0.06 Å, respectively) from the analogous distances found in the complexes $[Cu(Gly-Tyr)(H_2O)_2]·2H_2O$ **6**[11] [Pd(Gly-Tyr)-(cyd)]·$6.5H_2O$ **7**[12] [complexes **6** and **7** are the only two other Gly-Tyr compounds with transition metal ions] but the $V–O_{carboxylato}$ bond distance in **3** is shorter (*ca.* 0.03 and 0.07 Å for **6** and **7** respectively); this is expected[13] as the $V^{IV}O^{2+}$ center

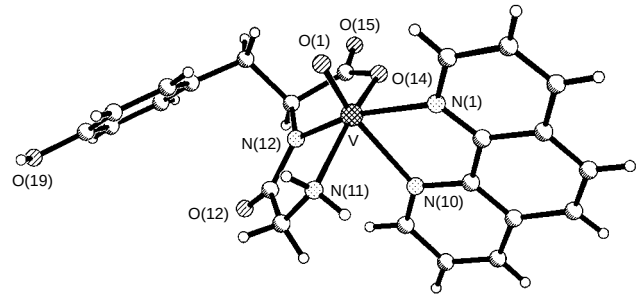

Fig. 1 The X-ray structure of **3**. Selected interatomic distances (Å) and angles (°): V–O(1) 1.574(5), V–O(14) 1.946(5), V–N(1) 2.105(7), V–N(12) 1.927(7), V–N(11) 2.075(7), V–N(10) 2.351(7); O(1)–V–N(12) 106.9(3), N(12)–V–O(14) 80.2(2), N(12)–V–N(11) 78.8(3), O(1)–V–N(1) 91.5(3), O(14)–V–N(1) 91.6(2), O(1)–V–N(10) 162.7(3), O(14)–V–N(10) 82.7(2), N(1)–V–N(10) 72.0(2), O(1)–V–O(14) 103.5(3), O(1)–V–N(1) 98.0(3), O(14)–V–N(11) 153.4(3), N(12)–V–N(1) 161.1(3), N(11)–V–N(1) 103.3(3), N(12)–V–N(10) 90.0(2), N(11)–V–N(10) 81.3(2).

Table 1 EPR parameters for the complexes **3** and **4**

Compound	Donor set	g_x	g_y	g_z	10^{-4} A/cm^{-1} A_x	A_y	A_z	$A_{z,amide}$
3	N_3O	1.982	1.984	1.952	53.0	58.0	160.0	35
4	N_3O	1.981	1.983	1.951	54.0	58.0	159.0	34

is considered a 'hard acid', Cu^{2+} a borderline acid and Pd^{2+} a soft acid and oxygen a harder base than nitrogen. The side chain aromatic ring is tilted to the equatorial coordination plane of vanadium (the dihedral angle between these planes is 31°) and in the opposite direction from it, in marked contrast to complexes **6** and **7** where the aromatic ring is roughly above the coordination plane of the metal atom; this conformation of the tyrosine residue in **3** may be imposed by the presence of the axial ligand (O^{2-}), that pushes away the aromatic ring.

The V–Cl stretch is absent from the IR spectra of complexes **1** and **2**. This, in combination with the molar conductance of these complexes in methanol, which is characteristic of 1 : 1 electrolytes led us to the conclusion that the chloride atom is not coordinated to vanadium. The magnetic moments of complexes **1**, **2** and **3**, **4** are in accord with the spin-only value expected for d^2 and d^1 systems, respectively.

The redox properties of **4** in acetonitrile (complexes **1**, **2** and **3** are not soluble enough to be studied in MeCN) have been studied by cyclic voltametric and polarographic techniques. The complex displays a reversible one-electron redox process [eqn. (1); $E_{\frac{1}{2}}$ *vs.* NHE].

$$[V^{IV}O(Gly\text{-}Phe)(phen)] + e^- \rightarrow [V^{III}O(Gly\text{-}Phe)(phen)]^- \; E_{1/2} = -1.26 \text{ V} \quad (1)$$

The continuous wave (cw) EPR parameters for the two oxovanadium(IV) complexes **3** and **4** (Table 1) were determined by computer simulation of the experimental cw EPR spectrum. Comparison of the cw EPR data of the complexes **3** and **4** with those reported for various oxovanadium(IV) species[14] with different equatorial donor sets (*e.g.*, O_4, N_2O_2, N_2S_2, *etc.*) indicates that their equatorial donor set should be N_3O. Application of the additivity relationship[15] for complexes **3** and **4** gives an A_z value of 159.6×10^{-4} cm^{-1} [= $(40.1 + 42.7 + 35 + 41.8) \times 10^{-4}$ cm^{-1}] which is almost identical to the experimental values for both complexes (Table 1). Electron spin echo envelope modulation (ESEEM) experiments, that were performed on complexes **3** and **4** verified the existence of three different ^{14}N atoms ligated to the equatorial plane of the oxovanadium(IV) center. Thus, it was concluded that in solution, as well as in the solid state, the VO^{2+} center is coordinated to three nitrogen atoms in the equatorial plane. The experimental values for $A_{z,amide}$ (35×10^{-4} and 34×10^{-4} cm^{-1} for complexes **3** and **4**, respectively) do not deviate from the average $A_{z,amide}$ value (34×10^{-4} cm^{-1}) reported by Cornman *et al.*[16] for oxovanadium(IV) complexes with various aromatic amides and from the $A_{z,amide}$ for the complexes $[V^{IV}O(Gly\text{-}Gly)(phen)]\cdot 2MeOH$ and $[V^{IV}O(Gly\text{-}Ala)(phen)]\cdot MeOH$ (36×10^{-4} cm^{-1}). Solution studies (water) of the VO^{2+} with a number of peptides[17] also gave a value of *ca.* 35×10^{-4} cm^{-1} for $A_{z,amide}$.

We gratefully acknowledge support of this research by the Greek General Secretariat of Research and Technology (Grant no. 1807/95) and Mrs F. Masala for typing the manuscript.

Notes and References

* E-mail: mlouloud@cc.uoi.gr

† *Crystal data*: **3**, $C_{23}H_{20}N_4O_5V$, M = 483.36, orthorhombic, space group $P2_12_12_1$, a = 6.9130(2), b = 12.4343(5), c = 23.7833(9) Å, U = 2044.37(13) Å^3, Z = 4, D_c = 1.57 g cm^{-3}; crystal dimensions 0.04 × 0.12 × 0.27 mm, μ = 0.53 mm^{-1}; 8496 data collected, 3049 data unique, 2999 data used; $F(000)$ = 992, 303 parameters, R_1 = 0.0714, wR_2 = 0.1491 with $I > 2\sigma(I)$. Data were collected using small slices on a Siemens SMART system. The absolute chirality was established by the Flack parameter, 0.03(6). CCDC 182/750.

1 M. Anke, B. Groppel, K. Gruhn, T. Kosla and M. Szilagyi, *Spurelement-Symposium: New Trace Elements*, ed. M. Anke, W. Bauman, H. Braunlich, C. Bruckner and B. Groppel, Jena, Friedrich-Schiller-Universitat, pp. 1266–1275; E. O. Uthus and F. H. Nielsen, *FASEB J.*, 1988, **2**, A841.
2 B. F. Harland and B. A. Harden-Williams, *J. Am. Diet Assoc.*, 1994, **94**, 891.
3 D. Rehder, in *Metal Ions in Biological Systems*, ed. H. Sigel and A. Sigel, Marcel Dekker, New York, 1995, vol. 31, pp. 1–43.
4 B. R. Nechay, *Annu. Rev. Pharmacol.*, 1984, **24**, 501.
5 G. Swarup, K. V. Speeg, S. Cohen and D. L. Garbers, *J. Biol. Chem.*, 1982, **257**, 7298.
6 C. Orving, K. H. Thompson, M. Battell and J. H. McNeil, in *Metal Ions in Biological Systems*, ed. H. Siegel and A. Sigel, Marcel Dekker, New York, 1995, vol. 31, pp. 576–594.
7 B. J. Hamstra, A. L. P. Houseman, G. J. Colpas, J. W. Kampf, R. L. Brutto, W. O. Frasch and V. L. Pecoraro, *Inorg. Chem.*, 1997, **36**, 4866 and references therein.
8 (*a*) A. D. Keramidas, S. M. Miller, O. P. Anderson and D. C. Crans, *J. Am. Chem. Soc.*, 1997, **119**, 8901; (*b*) F. W. B. Einstein, R. J. Batchlor, S. J. Angus-Dunne and A. S. Tracey, *Inorg. Chem.*, 1996, **35**, 1680; (*c*) A. J. Tasiopoulos, A. T. Vlahos, A. D. Keramidas, T. A. Kabanos, Y. G. Deligiannakis, C. P. Raptopoulou and A. Terzis, *Angew. Chem., Int. Ed. Engl.*, 1996, **35**, 2531.
9 P.. V. Bernhardt, G. A. Lawrence, B. Comba, L. L. Martin and T. W. Hambley, *J. Chem. Soc., Dalton Trans.*, 1990, 2859.
10 H_3mpg is the pseudopeptide *N*-(2-mercaptopropionyl)glycine.
11 A. Mosset and J.-J. Bonnet, *Acta Crystallogr., Sect. B*, 1977, **33**, 2807.
12 M. Sabat, K. A. Satyshur and M. Sundaralingam, *J. Am. Chem. Soc.*, 1983; **105**, 976.
13 R. G. Pearson, *J. Chem. Educ.*, 1968, **45**, 581; *Inorganic Chemistry, Principles of Structure and Reactivity*, ed. J. E. Huheey, E. A. Keiter and R. L. Keiter, Harper Collins, College Publishers, New York, 1993, pp. 344–348.
14 G. R. Hanson, T. A. Kabanos, A. D. Keramidas, D. Mentzafos and A. Terzis, *Inorg. Chem.*, 1992, **31**, 2587 and references therein.
15 N. D. Chasteen in *Biological Magnetic Resonance*, ed. L. Berliner and J. Reuben, Phenum Press, New York, 1981, vol. 3, p. 53.
16 C. R. Cornman, E. P. Zovinka, Y. D. Boyajian, K. M. Geiser-Busch, P. D. Boyle and P. Singh, *Inorg. Chem.*, 1995, **34**, 4213.
17 J. C. Pessoa, S. M. Luz and R. D. Gillard, *J. Chem. Soc., Dalton Trans.*, 1997, 569.

Received in Basel, Switzerland, 3rd November 1997; 7/07910I

Covalently supported porphyrins as ligands for the preparation of heme a_3/Cu_B binuclear active site analogues of heme–copper terminal oxidases and metallation under mild conditions

Jin-Ook Baeg and R. H. Holm*

Department of Chemistry and Chemical Biology, Harvard University, Cambridge, Massachusetts 02138, USA

New covalently supported binucleating porphyrins have been prepared as potential structural and/or functional ligands for the iron–copper (heme a_3/Cu_B) active sites of heme–copper oxidases, and the introduction of iron and copper into one porphyrin under mild reaction conditions has been developed.

Essential to the elucidation of the mechanism of dioxygen reduction to water and its inhibition at the binuclear heme a_3/Cu_B active sites of heme–copper oxidases[1–5] is the construction of a functional enzyme analogue system. This can presumably be achieved by synthesizing covalently supported binucleating heme ligands whose iron–copper arrangement approaches the enzyme active site stereochemistry. Collman *et al.*[6–9] have reported the synthesis of several such ligands by a congruent Michael multiple addition method, including one ligand whose Co^{II}–Cu^{I} derivative shows catalytic activity in the four-electron reduction of dioxygen to water.[9,10] These systems primarily contain 1,4,7-triazacyclononane-, cyclen-, or cyclam-adapted copper binding sites. Our previous investigations of binuclear heme–Cu bridged assemblies have featured a variety of unsupported bridges suitable for structural and electronic elucidation.[11–20] To extend our investigation to reactivity with dioxygen and inhibiting ligands such as cyanide, we have undertaken the design and synthesis of covalent binucleating ligands and their complexes capable of sustaining various Fe–X–Cu bridges. Here we report the preparation of three new porphyrin ligands, using Michael addition methodology for one of them, with structural features somewhat different than those previously described.[6–9]

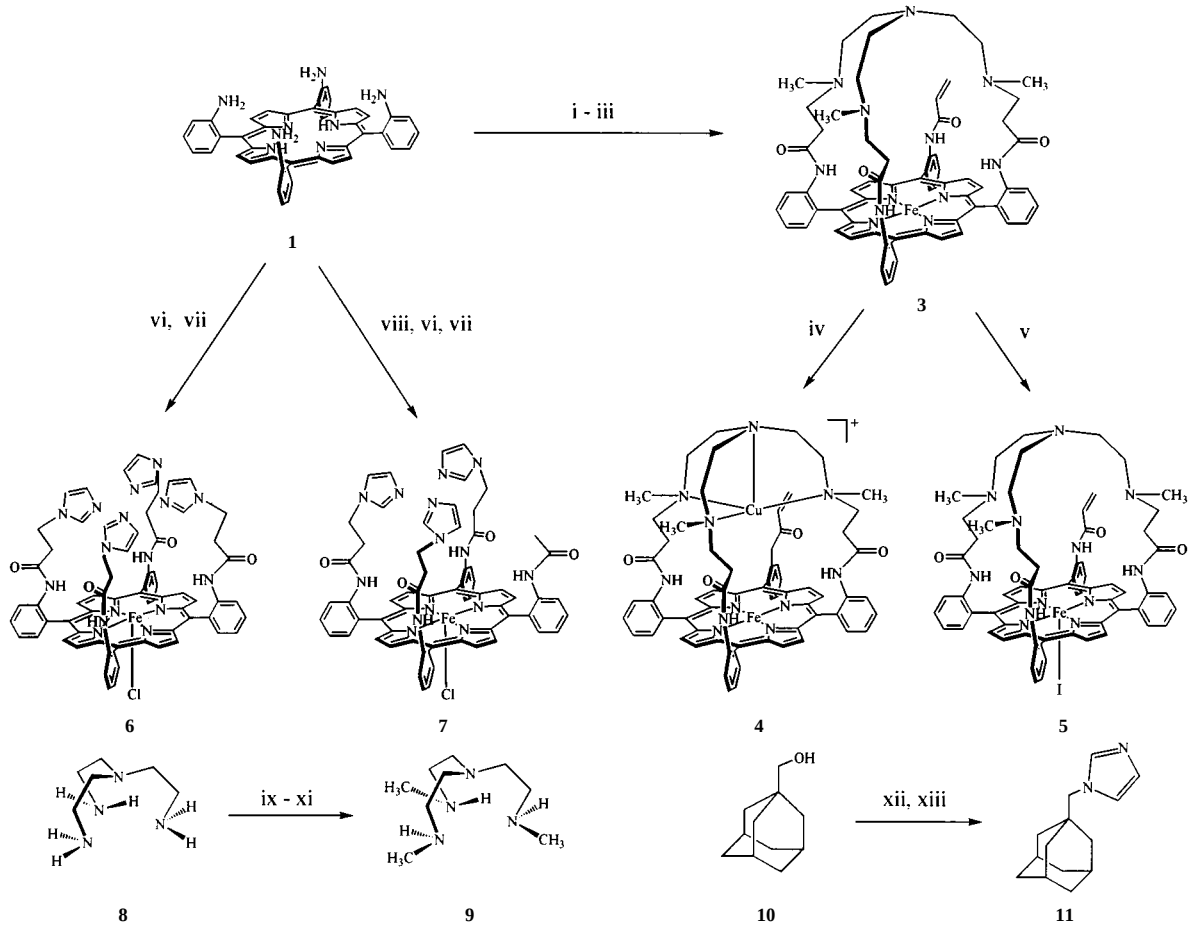

Scheme 1 *Reagents and conditions*: i, H_2C=CHCOCl, Et_3N, CH_2Cl_2, 46%; ii, $[Fe(OH_2)_6][BF_4]_2$, 2,6-dimethypyridine, THF, 90%; iii, **9**, CH_2Cl_2, MeOH, 48 h, 32%; iv, $[Cu(MeCN)_4]PF_6$, THF, 24 h, 70%; v, I_2, THF, 12 h, 82%; vi, **15**, $SOCl_2$, DMF, 20 h, 60%; vii, $FeSO_4$, HOAc, O_2, NaOH, HCl, 57–60%; viii, MeCOCl, Et_3N, CH_2Cl_2, 2 h, 50%; ix, PhCHO, 1 N HCl, benzene, molecular sieves, $NaBH_3CN$, 85%; x, HCO_2H, HCHO, 110 °C, 12 h, 76%; xi, $Pd(OH)_2$ on carbon, MeOH, H_2 (1 atm), 60 °C, 20 h, 90%; xii, PBr_3, quinoline, bromobenzene, 24 h, 165 °C, 65%; xiii, sodium imidazolate, Me_2SO, 150 °C, 20 h, 84%

Synthetic pathways for ligands and complexes are depicted in Scheme 1.† Reactions were carried out at ambient temperature unless noted otherwise. A key starting material, as in related work,[6–8] is *meso*-α,α,α,α-tetrakis(*o*-aminophenyl)porphyrin **1**.[21] Treatment of **1** with acryloyl chloride and triethylamine in dichloromethane affords the corresponding tetrakis(acryloylamidophenyl)porphyrin **2**[6] (46%). The new tetraamine **9** was prepared in three steps from tris(2-aminoethyl)amine **8** in 58% overall yield. Reaction of **8** with benzaldehyde in dry benzene containing ethereal 1 M HCl and molecular sieves, followed by reduction with $NaBH_3CN$, gave tris[2-(benzylamino)ethyl]amine **12** (85%). Subsequent reaction of **12** with formic acid and formaldehyde solution afforded tris[2-(benzylmethylamino)ethyl]amine **13** (76%). Palladium hydroxide catalyzed the selective debenzylation of **13** under 1 atm of dihydrogen at room temperature for 20 h to afford **9** (90%). Iron(II) was inserted into **2** at room temperature by reaction of $Fe[BF_4]_2$ in the presence of 2,6-dimethylpyridine to give [Fe^{II}(**2**)] (90%). Metal insertion under these mild conditions is necessary to minimize undesirable porphyrin isomerization. In the next step, reaction of the Michael acceptor [Fe^{II}(**2** −2H)] with tetraamine **9** in dichloromethane for 48 h gave the covalently capped iron(II) porphyrin **3** (32%, λ_{max} 426 nm, *m/z* 1133) with a vacant tetraaza binding site. The free ligand of **3** (λ_{max} 424 nm, *m/z* 1079) was obtained by the same reaction in comparable yield using **2**. Treatment of **3** with 1 equiv. of $[Cu(MeCN)_4]PF_6$ in THF for 24 h afforded the binuclear Fe^{II}–Cu^{I} assembly **4** (70%, λ_{max} 426 nm, *m/z* 1196). Complex **3** was readily oxidized by excess iodine in THF to give the iron(III) complex **5** (82%, λ_{max} 417 nm, *m/z* 1260) in which the iodide ligand is presumed to occupy an axial position on the unhindered heme face as shown. The EPR spectrum shows **5** to be high spin ($g_{\|}$ = 2.03, $g_{\perp}$ = 5.73; acetonitrile, 10 K).

Ligand binding by complexes **3**–**5** at the iron site could introduce ligands internal to the tetraaza cavity or on the unhindered face. To direct ligands to the desired internal venue, an exceptionally bulky axial base, incapable of residing in the cavity, has been prepared. Selective bromination of 1-adamantylmethanol using PBr_3 gave 1-bromomethyladamantane **14** (65%). Reaction of **14** with equimolar sodium imidazolate in Me_2SO at 150 °C yielded the *N*-adamantylimidazole **11** (84%).

Spectroscopic evidence has supported the coordination of three imidazole groups from histidyl residues by Cu_B,[1,2,5] a matter recently confirmed by the X-ray structures of two enzymes in the oxidized form.[3,4] To our knowledge, no binucleating porphyrin having this type of binding potentiality with copper is available, the closest approach being those with pyrazolyl binding sites.[22] We have sought binucleating ligands of this sort from the reactions of **1** and the acyl chloride of 3-(*N*-imidazolyl)propionic acid **15**.[23] Treatment of **1** with an excess (5 equiv.) of **15** and $SOCl_2$ in DMF for 20 h produced the free base of **6** (60%, λ_{max} 421 nm, *m/z* 1163). In another experiment, **1** was monoprotected by reaction with 1 equiv. of acetyl chloride in dichloromethane for 2 h to give the triphenyl(*o*-methylamidophenyl)porphyrin, which was resolved from an isomeric mixture by preparative TLC (acetone–chloroform, 3 : 7 v/v; 50%). This compound was subjected to reaction with 4 equiv. of **15** and $SOCl_2$ in DMF to give the desired free base of **7** (58%, λ_{max} 420, *m/z* 1083) containing three imidazole groups. Both free bases could be metalated by the $FeSO_4$/HOAc method:[24] **6** [60%, λ_{max} 425 nm, *m/z* 1252]; **7** [57%, λ_{max} 424 nm, *m/z* 1172].

In summary, we have prepared three new types of binucleating porphyrin ligands and their iron complexes capable of covalently supporting Fe–X–Cu bridges. The ligand of **3**–**5** furnishes a trigonal four-coordinate tetraaza binding site, one feature of which is direction of the magnetic orbital of Cu^{II} toward a bridging ligand such as dioxygen, hydroxide or cyanide, thereby optimizing magnetic coupling of the iron atom across the bridge.[20] Complex **6** is favorable to planar coordination by Cu^{II}, while **7** provides the tris(imidazole) binding site of the native oxidases. The binding sites in **3**–**5** and **7** are necessarily displaced off a perpendicular through the iron atom normal to the heme plane, as is the case for two crystalline oxidases.[3,4] The sterically demanding ligand **11** has been developed as a promotor of the bridging *vs*. terminal ligand binding mode.

This research was supported by National Science Foundation Grant CHE 94-23830.

Notes and References

* E-mail: holm@chemistry.harvard.edu

† Full experimental details will be published in due course. All new compounds were fully characterized by spectroscopic methods. UV–VIS spectra were measured in THF. Masses quoted are from FAB or electrospray mass spectral measurements and apply to the principal ion $(M + H)^+$. Stated yields refer to isolated compounds.

1 G. T. Babcock and M. Wikström, *Nature*, 1992, **356**, 301.
2 O. Einarsdottir, *Biochim. Biophys. Acta*, 1995, **1229**, 129.
3 S. Iwata, C. Ostermeier, B. Ludwig and H. Michael, *Nature*, 1995, **376**, 660.
4 T. Tsukihara, H. Aoyama, E. Yamashita, T. Tomizaki, H. Yamaguchi, K. Shinzawa-Itoh, R. Nakashima, R. Yaono and S. Yoshikawa, *Science*, 1995, **269**, 1069.
5 S. Ferguson-Miller and G. T. Babcock, *Chem. Rev.*, 1996, **96**, 2889.
6 J. P. Collman, X. Zhang, P. C. Herrman, E. S. Uffelman, B. Boitrel, A. Straumanis and J. I. Brauman, *J. Am. Chem. Soc.*, 1994, **116**, 2681.
7 J. P. Collman, P. C. Herrman, B. Boitrel, X. Zhang, T. A. Eberspacher and L. Fu, *J. Am. Chem. Soc.*, 1994, **116**, 9783.
8 J. P. Collman, P. C. Herrman, L. Fu, T. A. Eberspacher, M. Eubanks, B. Boitrel, P. Hayoz, X. Zhang, J. I. Brauman and V. W. Day, *J. Am. Chem. Soc.*, 1997, **119**, 3481.
9 J. P. Collman, *Inorg. Chem.*, 1997, **36**, 5145.
10 J. P. Collman, L. Fu, P. C. Herrman and X. Zhang, *Science*, 1997, **275**, 949.
11 S. C. Lee and R. H. Holm, *J. Am. Chem. Soc.*, 1993, **115**, 5833; 11 789.
12 S. C. Lee and R. H. Holm, *Inorg. Chem.*, 1993, **32**, 4745.
13 S. C. Lee, M. J. Scott, K. Kauffmann, E. Münck and R. H. Holm, *J. Am. Chem. Soc.*, 1994, **116**, 401.
14 M. J. Scott and R. H. Holm, *J. Am. Chem. Soc.*, 1994, **116**, 11 357.
15 M. J. Scott, S. C. Lee and R. H. Holm, *Inorg. Chem.*, 1994, **33**, 4651.
16 M. J. Scott, H. H. Zhang, S. C. Lee, B. Hedman, K. O. Hodgson and R. H. Holm, *J. Am. Chem. Soc.*, 1995, **117**, 568.
17 M. J. Scott, C. A. Goddard and R. H. Holm, *Inorg. Chem.*, 1996, **35**, 2558.
18 M. T. Gardner, G. Deinum, Y. Kim, G. T. Babcock, M. J. Scott and R. H. Holm, *Inorg. Chem.*, 1996, **35**, 6878.
19 H. H. Zhang, A. Filipponi, A. Di Cicco, S. C. Lee, M. J. Scott, R. H. Holm, B. Hedman and K. O. Hodgson, *Inorg. Chem.*, 1996, **35**, 4819.
20 K. Kauffmann, C. A. Goddard, Y. Zang, R. H. Holm and E. Münck, *Inorg. Chem.*, 1997, **36**, 985.
21 J. P. Collman, R. R. Gagne, C. A. Reed, T. R. Halbert, G. Lang and W. T. Robinson, *J. Am. Chem. Soc.*, 1975, **97**, 1427.
22 T. Sasaki and Y. Naruta, *Chem. Lett.*, 1995, 663.
23 C. K. Chang and R. Young, *J. Am. Chem. Soc.*, 1985, **107**, 898.
24 *Porphyrins and Metalloporphyrins*, ed. K. M. Smith, Elsevier, New York, 1975, p. 803.

Received in Bloomington, IN, USA, 29th October 1997; 7/07785H

Electrostatic investigation of metal cation binding to DNA bases and base pairs

Shridhar R. Gadre,[a] Savita S. Pundlik,[a] Ajay C. Limaye[b] and Alistair P. Rendell[b]

[a] *Department of Chemistry, University of Pune, Pune 411007, India*
[b] *Supercomputer Facility, Australian National University, Canberra, ACT 0200, Australia*

Various binding sites in DNA bases and base pairs as predicted by rigorous analysis of the molecular electrostatic potential (MESP) are explored for coordination with Li^+ and Ca^{2+} cations; the electrostatics is generally seen to provide an explanation for the observed trends in binding upon subjecting the anticipated structures to optimization at a high level *ab initio* theory.

The interactions between metal cation and the bases of DNA are being widely studied for gaining insights into the origin of stabilization or destabilization of DNA due to the presence of such ions.[1] In the polynucleotide DNA sequence, most of the cations predominantly interact with the backbone phosphate groups,[2] the charge neutralization leading to an enhancement of stabilization of the sequence. However, the cation–base interaction is not negligible.[1] In fact, some transition metal ions like Zn^{2+} and Cd^{2+} are found[2] to interact extensively with the bases facilitating renaturation of thermally denatured DNA.

Theoretical Hartree–Fock calculations carried out for the Watson–Crick (WC) base pairs with minimal basis[3] revealed that metal ion binding, in general, leads to an increased stability of the complementary base pairs. It is observed experimentally that the purine–purine–pyrimidine (PuPuPy) type triplexes respond differently to various cations.[4] For example, the GGC triplexes are found to be stabilized by divalent alkaline earth as well as transition metal cations while AAT triads are stabilized exclusively by the latter. The observed differential stabilization also finds support from the recent high level *ab initio* calculations by Sponer *et al*.[5] who have explained the phenomenon on the basis of missing lone-pair interactions with d orbitals in the case of alkaline earth cations.

An important issue concerning DNA–metal cation interactions is the relative energetic preference of the various lone-pair sites in the bases. There seems to be a general consensus that the N^7 site in guanine is the most favored one among all the bases for a given cation,[1,6] although the recent theoretical treatment[1] also emphasizes the influence of the O^6 atom in stabilizing the cation. The larger stabilization in G–cation complexes has been[1] accounted for by the large dipole moment of the base.

The interactions of DNA with the metal cation are mostly driven by electrostatics. However, an analysis of the binding sites in terms of the complete electrostatic description of bases and base pairs is conspicuous by its absence from the earlier literature. The MESP,[7] V, at a point $\boldsymbol{r}$ due to nuclear charges $\{Z_\Lambda\}$ at $\{\boldsymbol{R}_\Lambda\}$ and the electronic charge density $\rho(\boldsymbol{r})$ is defined as

$$V(\boldsymbol{r}) = \sum_{\mathrm{A}} \frac{Z_{\mathrm{A}}}{|\boldsymbol{R}_{\mathrm{A}} - \boldsymbol{r}|} - \int \frac{\rho(\boldsymbol{r}')}{|\boldsymbol{r}' - \boldsymbol{r}|} d^3r'$$

$V(\boldsymbol{r})$ can assume both positive and negative values and can provide useful information regarding electron-rich sites. It is interesting to see[8a,b] whether all the negative valued critical points (CPs) in MESP of the base (and the base pair) turn out to be the binding sites for cations and also whether any of the amino-lone pair sites are accessed by them. Since the reported findings[1,3] are based on calculations with either the effective core potentials or basis sets of limited extent for the metal species, there is a need for employing better quality basis sets including polarization functions. Here, we report the findings of base–cation as well as WC base pair–cation interactions using an electrostatic approach at a high level *ab initio* theory.

Planar optimized structures at 6-31G** basis set are used for the bases A, G, T, C and the WC base[9] pairs AT and GC. A 6-31G* basis set is employed for Li while for Ca, use is made of TZV* basis. The topography of MESP[10] of the organic molecules is used for initial positioning of Li^+ or Ca^{2+}. The cation is docked by keeping the base (or base pair) geometry fixed until the electrostatic interaction energy[11] attains a minimum. The resultant structure obtained by electrostatic docking is consequently subjected to full *ab initio* geometry optimization carried out on Fujitsu VPP300 with the GAUSSIAN94 package tuned for this platform. The single point energy (ΔE_S) values as well as the interaction energies of the fully optimized structures (ΔE_F) are reported in Table 1.

It can be seen that the relative ordering of the interaction energies for Li^+ and Ca^{2+} with various hosts is according to the depth of negative potential at the CP positions. On *ab initio* optimization, it is found that the distance of the cation from the nearest atom in the host is similar to the distance of the

Table 1 Interaction energies [kcal mol^{-1} (1 cal = 4.184 J)] with single point SCF calculations at the electrostatically docked geometry, ΔE_S, and full optimization, ΔE_F for various DNA···cation interactions[a]

Host	Site	ΔE_S with Li^+	ΔE_F with Li^+	ΔE_S with Ca^{2+}	ΔE_F with Ca^{2+}
A	a_1	−42.83	−45.80	−66.52	−70.97
	a_2	−42.85	−46.54	−65.70	−72.35
	a_3	−24.94	−45.80[b]	−41.62	−92.31[c]
	a_4	−39.28	−41.41	−56.15	−61.90
G	g_1	−19.00	−40.85[c]	−38.73	−62.74
	g_2	−27.11	−33.10	−40.31	−47.01
	g_5, g_6, g_7	−68.13	−78.24	−124.31	−133.78
T	t_2	−44.68	−51.90	−70.86	−81.40
	t_4	−46.45	−53.63	−71.25	−86.06
C	c_3, c_4, c_5	−70.20	−76.02	−108.16	−123.33
AT	at_1	−57.49	−62.82	−85.13	−142.63[d]
			(−4.47)		
	at_2	−44.34	−56.98[b]	−67.52	−161.81[b,d]
	at_3	−49.67	−56.98	−72.68	Not
			(−5.81)		converged
	at_4, at_5, at_6	−68.04	−68.97	−99.75	−111.70
			−5.26		−18.35
	at_7	−56.31	−63.77	−84.91	−161.81[d]
			(−10.13)		
GC	gc_1	−58.58	−100.56[d]	−53.62	−138.13[d]
	gc_2	−66.91	−73.12	−62.63	−74.06
			(−13.97)		(−27.05)
	gc_3, gc_4, gc_5	−103.79	−110.57	−142.74	−143.63
			(−6.28)		(−10.45)
	gc_6	−66.89	−79.19	−58.45	−200.05[d]

[a] The relevant CPs in MESP (Fig. 1) of the bases and the WC base pairs are employed as starting positions of the cations. The numbers in parentheses for AT and GC are the base pair stabilization energies on cation binding. [b] These structures are similar to those obtained from different starting guess. [c] Amino group is twisted to facilitate manifold coordination of the cation. [d] Cation is sandwiched between two bases splitting the base pair.

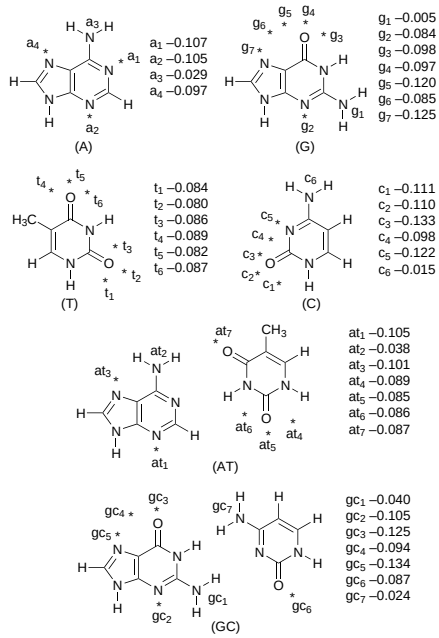

Fig. 1 MESP topographical features of DNA bases A, G, T and C as well as Watson–Crick base pairs AT and GC. The CPs are marked by * and corresponding MESP values given alongside.

corresponding MESP CP. Whereas the binding energies at various sites in A as well as in T are quite close, the region between the O^6 and N^7 atoms in G shows much more binding strength than other sites. From an electrostatic point of view, it is natural to expect that the extensive negative MESP region constituted by a number of CPs stabilizes the cation to a greater extent in G and C. In T, the cation enjoys a surrounding negative MESP region when it is close to t_2 or t_5, the saddles in MESP. Thus, rather than relying upon the partial information such as moments of various orders, the MESP topography leads to a more complete picture of these interactions. This is evident from the fact that all the negative MESP regions which are disjoint give rise to distinct optimum structures.

Electrostatic energy minimization predicts off-plane binding for both the cations with A and G near the amino nitrogen but not for C, probably due to the high negative potential region being concentrated only near O^2 and N^3 in C. Further optimization at the SCF level leads Li^+ to converge to the position a_1 (rather than a_4) in A without affecting the geometry of the NH_2 group. In G, however, full optimization leads Li^+ to the g_2 site with an out of plane twisting of the amino group. The cation is thus able to coordinate with the N^2 as well as N^3 atoms forming a bidentate structure. Using the wavefunction of this twisted amino-G, it is observed that the MESP minimum at N^3 (g_2) deepens to $-0.100\ E_h$. This is reflected in the improvement in the stabilization energy ΔE_F which is much more than the value for the monodentate structure at the N^3 site. The differential behavior of Li^+ towards N^6 in A and N^2 in G could arise due to a relatively deep negative MESP region in the former and a very weak one in the latter (*cf.* Fig. 1). Similar bidentate structure is formed by Ca^{2+} with A (coordinating with N^1 and N^6) while the optimized structure for G–Ca^{2+} has the cation occupying the off-plane site. The discrimination between the two purine bases by the divalent cation could arise due to higher ionic charge as well as polarization effects.

From Table 1, the coordination of cations at various sites in WC base pairs is enhanced as compared to individual bases. This appears to be due to increased charge concentration upon base pairing, which is reflected in the MESP topography (Fig. 1). Thus MESP seems to govern the relative binding affinities of various sites in base pairs. In some cases (site at_7 in AT accessed by Li^+ and gc_4 in GC accessed by Ca^{2+}), the interaction energy at the electrostatically docked geometries is < 2 kcal mol^{-1} ($< 2\%$) away from the value for the final optimized structure. There are other instances when ΔE_S and ΔE_F differ substantially owing to large changes in the geometrical orientation of the bases within the pair upon optimization. These structures, however, may not have much significance in biological systems. Geometry optimization could not be achieved for Ca^{2+} at the N^7 position of A in AT. This observation is consistent with the finding of Sponer *et al.*[5] resulting in the inability of alkaline earth cations to stabilize the AAT triplex.

Base pair stabilization due to cation binding is calculated according to Anwander *et al.*,[3] although the interaction energies are not corrected for basis set superposition error. The earlier calculations[3] are based upon optimization of a cation bound to a single base and the use of inter-base geometry determined by X-ray crystallography, though their trends generally agree with our results for GC. Thus, the largest stabilization occurs at the purine N^3 site in GC for both cations. For AT, the present full optimization at higher level does not lead to binding of Ca^{2+} at N^7 and N^3 positions (the base pair is split) which may be interpreted as a destabilization effect. The AT pair is stabilized due to the cation only if it binds near the O^2 of thymine, reports[3] also predict this site to be the most stabilizing.

The outcome of this work is that the strength of MESP at CPs can be meaningfully employed for predicting the sites of cation coordination in bases and base pairs as well as the respective binding energies. In general, Li^+ and Ca^{2+} do not prefer to occupy amino-nitrogen lone pair sites with the exception of G–Ca^{2+} complex. In all those structures where the base pair geometry does not alter much, the initial site predicted by electrostatics is very close to the final optimized one. In conclusion, electrostatics may be used as a powerful tool for a qualitative and semiquantitative prediction of cation coordination sites in DNA bases and base pairs.

The financial assistance by Council of Scientific and Industrial Research [CSIR 80(0022) 96-EMR-II and 9/137 (271)/95 EMR-I, New Delhi] is gratefully acknowledged by S. R. G. and S. S. P. A. C. L. and A. P. R. thank Fujitsu, Japan for financial assistance.

Notes and References

* E-mail: gadre@parcom.ernet.in

1 J. V. Burda, J. Sponer and P. Hobza, *J. Phys. Chem*., 1996, **100**, 7275.
2 M. Langlais, H. A. Tajmir-Riahi and R. Savoie, *Biopolymers*, 1990, **30**, 743.
3 E. H. S. Anwander, M. M. Probst and B. M. Rode, *Biopolymers*, 1990, **29**, 757.
4 V. N. Potaman and V. N. Soyfer, *J. Biomol. Struct. Dynam*., 1994, **11**, 1035.
5 J. Sponer, J. V. Burda, J. Leszczynski and P. Hobza, *J. Biomol. Struct. Dynam*., 1997, **14**, 613.
6 R. B. Martin, *Acc. Chem. Res*., 1985, **18**, 32.
7 P. Politzer and D. G. Truhlar, *Chemical Applications of Atomic and Molecular Electrostatic Potentials*, Plenum, New York, 1981; J. Tomasi, R. Bonaccorsi and R. Cammi, in *Theoretical Methods of Chemical Bonding*, ed. Z. B. Maksic, Springer, 1990, vol. 3.
8 (*a*) S. R. Gadre, S. A. Kulkarni and I. H. Shrivastava, *J. Chem. Phys*., 1992, **96**, 5253; (*b*) R. N. Shirsat, S. V. Bapat and S. R. Gadre, *Chem. Phys. Lett*., 1992, **200**, 373; (*c*) S. R. Gadre and S. S. Pundlik, *J. Am. Chem. Soc*., 1995, **117**, 9559; (*d*) S. R. Gadre, P. Bhadane, S. S. Pundlik and S. S. Pingale, in *Molecular Electrostatic Potentials: Theory and Applications*, ed. J. S. Murray and K. D. Sen, Elsevier, Amsterdam, 1996, vol. 3.
9 J. Sponer, J. Leszczynski and P. Hobza, *J. Phys. Chem*., 1996, **100**, 1965. The optimized planar structures of WC base pairs are kindly made available by Dr Sponer.
10 S. R. Gadre and S. S. Pundlik, *J. Phys. Chem*., 1997, **101**, 3298.
11 See S. P. Gejji, C. H. Suresh, L. J. Bartolotti and S. R. Gadre, *J. Phys. Chem*., 1997, **101**, 5678 and references therein for a discussion of electrostatic docking.

Received in Cambridge, UK, 20th November 1997; 7/08372F

[2 + 2] Cycloaddition derivatives of stiba(III)alkene (Sb=C) and arsa(III)imine (As=N) intermediates

Philip C. Andrews,[a] Colin L. Raston,*[a] Brian W. Skelton,[b] Vicki-Anne Tolhurst[a] and Allan H. White[b]

[a] *Department of Chemistry, Monash University, Clayton, Victoria 3168, Australia*
[b] *Department of Chemistry, University of Western Australia, Nedlands, WA 6907, Australia*

Mild thermolysis of (2-pyridyl)$(SiMe_3)_2CSbCl_2$ and [2-(6-Me)pyridyl](SiMe$_3$)$NAsCl_2$ affords, respectively, the chloro-bridged polymeric geminal C-centred distibine(III) complex $[(2\text{-pyridyl})(SiMe_3)CSbCl]_\infty$ 1 and the geminal N-centred arsenic(III) amide $[\{2\text{-(6-Me)pyridyl}\}NAsCl]_2$ 2; the proposed mechanism involves the elimination of Me_3-SiCl and a [2 + 2] stereospecific *cis*-cycloaddition of the stibaalkene (Sb=C) and arsaimine (As=N) intermediates.

In developing the main group chemistry of the bulky alkyl ligand, (2-pyridyl)$(SiMe_3)_2C^-$, R_{py}, and the related amido ligand, {2-(6-Me)pyridyl}$(SiMe_3)N^-$, L_{py}, the presence of the Me_3Si group has been important in the kinetic protection of any metal(loid) centre.[1] However another important aspect of this chemistry is the potential present for the low energy β-elimination of Me_3SiCl from substituted metal(loid) chloride complexes resulting in novel and/or rare multiply bonded species. As such the elimination of halosilane from $R_{py2}SbCl$ proved useful in synthesising the novel geminal Al^{III}/Sb^{III} bimetallic heterocycle[2] and has been important in the preparation of phosphaalkenes and alkynes.[3] In contrast to N, and to a lesser degree P, the multiply bonded species of the heavier group 15 elements have a tendency to oligomerise unless this thermodynamically favoured process is offset by the presence of bulky ligands.[4] However this can be utilised in the formation of C-centred geminal organodimetallics which are receiving increasing attention as a result of their potential in developing new synthetic routes to complex organic molecules.[5]

Herein, we report the synthesis and characterisation of the chloro-bridged polymeric C-centred geminal distibine, $[(2\text{-pyridyl})(SiMe_3)CSbCl]_\infty$ **1** and the dimeric N-centred amidoarsine, $[\{2\text{-(6-Me)-pyridyl}\}NAsCl]_2$ **2** derived from the doubly bonded intermediate species [(2-pyridyl)$(SiMe_3)$C=SbCl] and [{2-(6-Me)pyridyl}N=AsCl] *via* the elimination of Me_3SiCl from $R_{py}SbCl_2$ and $L_{py}AsCl_2$.

In contrast to its As and P analogues, which undergo Me_3SiCl elimination at below −20 °C, $R_{py}SbCl_2$ can be prepared, as previously described,[6] from the 1:1 metathesis reaction of $R_{py}Li\cdot tmen$ and $SbCl_3$. However Me_3SiCl elimination can be achieved in two ways, as shown in Scheme 1, to give bright yellow rod-like crystals of **1**.† The crystals, which melt at 201–203 °C after gradually becoming opaque and then blackening, are relatively stable to air and atmospheric moisture, slowly becoming white and opaque, On melting further Me_3SiCl elimination occurs giving the appearance of effervescence.

Pale yellow prismatic crystals of **2** were obtained in a similar manner to the thermal elimination synthesis of **1**.† These crystals also decompose slowly in air, and melt in the range 187–189 °C.

X-Ray diffraction studies on **1**‡ revealed a geminal distibine structure. Such geminal distibine complexes are extremely rare with only a few structurally authenticated Sb^V and Sb^{III} methylene bridged complexes.[7] The repeating unit of the polymer contains, as its core, an almost square, but buckled, C_2Sb_2 ring internally bridged by a single Cl lying on a 2-symmetry axis, as does the other Cl which provides the

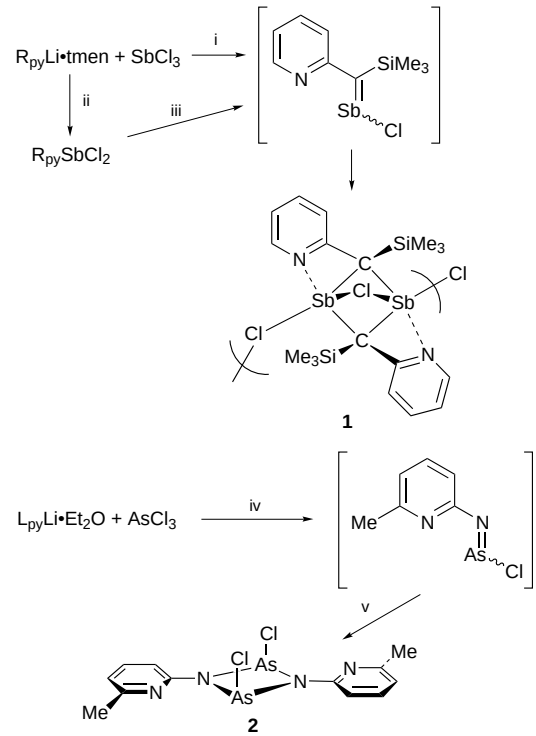

Scheme 1 *Reagents and conditions*: i, thf, −78 °C to room temp., 3 days; ii, Et_2O, −78 °C; iii, toluene, 50 °C, 4 h; iv, Et_2O, −78 °C; v, toluene, 80 °C, 4 h

connecting points along the chain (Fig. 1). The geminal carbon is formally bonded to two Sb^{III} centres with bond distances of 2.180(9) and 2.219(9) Å. Furthermore each Sb centre is bound to a pyridyl N [2.220(8) Å] a ring bridging Cl(1), [2.850(3) Å] and a linking Cl(2) [3.054(2) Å] making each Sb five coordinate. The stereochemically active lone pairs occupy a position *trans* to one of the geminal C-centres. The Sb–Cl distances in **1** are much longer than those found in $R_{py}SbCl_2$, 2.373(2) and 2.469(2) Å, while the Sn–N distance is actually

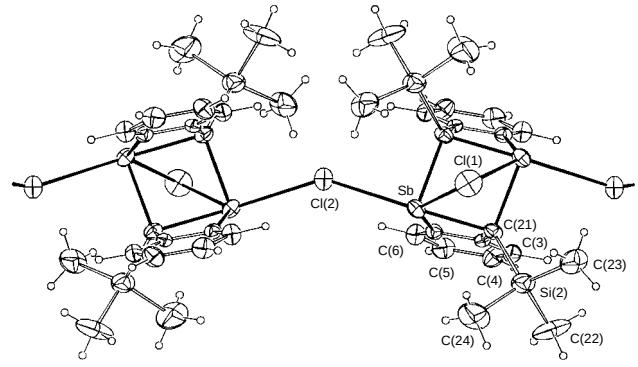

Fig. 1 Crystal structure of **1**

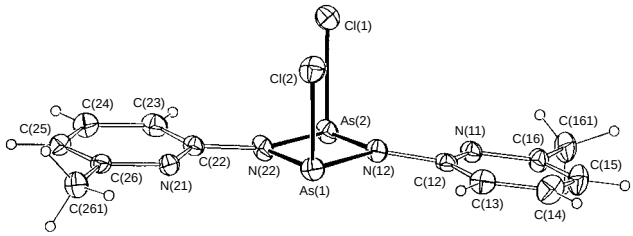

Fig. 2 Crystal structure of **2**

shorter, *cf*. 2.317(7) Å. The C(21)–Sb–N(1) angle of 63.1(3)° is comparable with that of 61.4(2)° found in $R_{py}SbCl_2$. The Sb–C distance of 2.213(5) Å in $R_{py}SbCl_2$[4] is only comparable with the longer Sb–C bond distance found in **1** despite the greater coordinative saturation at the Sb centre, *i.e.* five over four, while the Sb–C(–Al) distance in the recently reported Sb/Al geminal metallocycle,[2] in which Sb is only three coordinate, is shorter than both Sb–C bonds in **1**, being 2.167(7) Å. The bridging Cl(1) directly straddles the two Sb centres in the repeating unit at an angle of 67.4(1)° while the linking Cl(2) forms an angle of 149.3(1)° between the Sb centres of two different repeating units. Surprisingly the pyridyl rings are *cis* to the $(CSb)_2$ ring and almost eclipse each other.

The symmetry of bond distances and angles, and hence charge distribution, within the dimeric repeating unit must be the result of an initial [2 + 2] cycloaddition reaction of the stibene units, [(2-pyridyl)($SiMe_3$)C=SbCl], prior to polymerisation through the linking chlorides (Scheme 1). The concomitant stereochemical requirements of such a reaction may explain the *cis* arrangement of the pyridyl rings. However, it is noted that such reactions for alkenes are photolytically induced. The presence of the metal and thus some ionic character may render the cycloaddition more facile.

This argument can also be proposed in explaining the dimeric structure of the amidoarsine, **2**. The sp^2 geometry at the amido N requires that the $(NAs)_2$ ring and the (Me)pyridyl fragments are coplanar (Fig. 2), dihedral angles 8.6(3) and 4.4(2)°, though from an examination of the bond lengths there is no evidence of delocalisation. The unusual *cis* orientation of the Cl atoms relative to the $(NAs)_2$ ring is most likely, once again, a result of the stereochemical outcome of the [2 + 2] cycloaddition. Olah and Oswald[8] noted that the reaction of Bu^tNH_2 with $AsCl_3$ resulted in the formation, *via* HCl elimination, of the imidochloroarsenite $Bu^tN{=}AsCl$. The subsequent crystal structure[9] showed the complex to be dimeric, $(Bu^tNAsCl)_2$ **3** sharing the same structural features as **2**; the geometry around N being essentially planar and the Cl atoms *cis* to the $(NAs)_2$ planar ring. There is a great deal of similarity in the bond distances and angles of the $As_2N_2Cl_2$ cores: As–N bond lengths in **2** range from 1.809(7)–1.857(7) Å compared with 1.799(5)–1.827(4) Å in **3**, however the As–Cl bond distances in **2** of 2.228(2) and 2.233(2) Å are shorter than those in **3**, 2.249(3) and 2.252(2) Å, while the As···As–Cl angles in **2** are 103.72(8) and 103.75(8)° and 111.1(1) and 110.5(1)° in **3**. To date the only structurally characterised compound containing an $As^{III}{=}N$ bond is [2,4,6-$Bu^tC_6H_2N$(H)–As=$NC_6H_2Bu^t_3$-2,4,6],[10] the aryl groups of which are significantly more bulky than L_{py}. Dimerisation in **2** is not unexpected given the loss of a bulky Me_3Si moiety.

At room temperature the ^1H and ^{13}C NMR spectra of **2** suggest one dominant species (> 95%) with only one other set of minor signals indicating other possible oligomeric species. At low temperature these two species integrate almost equally. No coalescence occurs so it is unlikely that there is restricted rotation around the C–N bond. A more reasonable assumption is the presence of either monomers or higher oligomers. The NMR spectra of **1** show no evidence of polymer disintegration in solution but reveal that the polymer crystals often retain residual solvents in their structure. The structure shown in Fig. 1 contains 0.5 toluene situated between layers of the polymeric chain in the interstices formed by four $R_{py2}Sb_2Cl_2$ units.

We thank the Australian Research Council for financial support.

Notes and References

* E-mail: c.raston@sci.monash.edu.au

† (*i*) $R_{py}SbCl_2$ was prepared as previously described.[4] The *in vacuo* removal of Et_2O from this reaction, followed by the addition of toluene, subsequent filtration to remove LiCl and heating to 50 °C for 4 h leads to the precipitation of a pale yellow powder. Removal of toluene and recrystallisation at 4 °C from thf–toluene results in bright yellow rod-like crystals of **1**. (*ii*) Alternatively, the metathesis reaction of $R_{py}Li$ and $SbCl_3$ can be carried out in thf at −78 °C, allowed to warm slowly to room temp. and stirred for 3 days. The thf is removed *in vacuo* and a CH_2Cl_2 extraction of the remaining solids allows for the crystallisation of **1**, again at 4 °C. Yield 63% (not maximised). Mp 201.203 °C. ^1H NMR (300 MHz, CD_2Cl_2, 25 °C) δ 7.76 (d, br, 1 H), 7.57 (t, 1 H), 7.14 (br, d, 1 H), 6.73 (t, 1 H), 0.34 (s, 9 H), residual thf (0.25) 3.68 (m, 1 H), 1.80 (m, 1 H), residual toluene (0.33) 7.17 (m, 1.7 H) 2.11 (s, 1 H). ^{13}C NMR (100.6 MHz, CD_2Cl_2, 25 °C) δ 160.6, 144.1, 138.0, 128.1, 119.1, 45.7 (CH_2), 2.8. Satisfactory elemental analysis obtained.

2. A toluene solution of $L_{py}AsCl_2$, prepared from the metathesis reaction of $L_{py}Li{\cdot}Et_2O$ with $AsCl_3$, was heated at 80 °C for 4 h. The *in vacuo* reduction of the solution and cooling slowly from 50 °C to room temp. resulted in pale yellow prismatic crystals of **2**. Yield 94%. Mp 187–189 °C. ^1H NMR (300 MHz, C_7D_8, 25 °C) (major component, > 95%) δ 6.89 (m, 1 H), 6.45 (d, 1 H, *J* 8 Hz), 6.30 (d, 1 H, *J* 8 Hz), 2.26 (s, 3 H, Me), (minor component) 6.73 (t), 6.50 (d), 6.40 (d), 2.19 (s). ^{13}C NMR (100.6 MHz, C_7D_8, 25 °C) δ 169.0, 156.5, 139.0, 115.0, 105.6. 23.8. Satisfactory elemental analysis obtained.

‡ *Crystallographic data* for **1**. (CAD4 diffractometer, crystals mounted in capillaries) $(R_{py}SbCl)_2{\cdot}C_7H_8$, $C_{25}H_{34}Cl_2N_2Sb_2Si_2$, M = 733.15, orthorhombic, space group *Pnna* (D_{2h}^6, no. 52) a = 10.015(3), b = 15.746(13), c = 18.996(3) Å, U = 2996(3) Å^3, D_c = 1.625 g cm^{-3}, Z = 4, F(000) = 1448. μ_{Mo} = 20.8 cm^{-1}, specimen 0.08 × 0.32 × 0.25 mm, $A^*_{min,max}$ = 1.35, 1.72. $2\theta_{max}$ = 50°, final R,R_w = 0.047, 0.039 (statistical weights). N_o = 1339 'observed' [$I > 3\sigma(I)$] reflections out of N = 2640 unique. Toluene disordered with a site occupancy factor of 0.5. **2**. $C_{12}H_{12}As_2Cl_2N_4$, M = 443.08, monoclinic, space group $P2_1/c$ (C_{2h}^5, no. 14), a = 9.926(4), b = 13.005(3), c = 14.224(4) Å, β = 122.61(2)°, U = 1546.6(9) Å^3, D_c = 1.859 g cm^{-3}, Z = 4, F(000) = 848, μ_{Mo} = 46.6 cm^{-1}, specimen 0.58 × 0.24 × 0.28 mm, $A^*_{min,max}$ = 2.64, 3.60, $2\theta_{max}$ = 50°, final R,R_w = 0.055, 0.051 (statistical weights). N_o = 2144 'observed' [$I > 2\sigma(I)$] reflections out of N = 3540 unique. CCDC 182/724.

1 T. R. van den Ancker and C. L. Raston, *J. Organomet. Chem.*, 1995, **500**, 289; L. M. Engelhardt, G. E. Jacobsen, W. C. Patalinghug, B. W. Skelton, C. L. Raston and A. H. White, *J. Chem. Soc., Dalton Trans.*, 1991, 2895.
2 P. C. Andrews, C. L. Raston, B. W. Skelton and A. H. White, *Chem. Commun.*, 1997, 1183.
3 A. C. Gaumont and J. M. Denis, *Chem. Rev.*, 1994, **94**, 1413.
4 N. C. Norman, *Polyhedron*, 1993, **20**, 2431.
5 I. Marek and J.-F. Normant, *Chem. Rev.*, 1996, **96**, 3241.
6 C. Jones, L. M. Engelhardt, P. C. Junk, D. S. Hutchings, W. C. Patalinghug, C. L. Raston and A. H. White, *J. Chem. Soc., Chem. Commun.*, 1991, 1560.
7 W. Kolandra, W. Schwarz and J. Weidlein, *Z. Anorg. Allg. Chem.*, 1983, **501**, 137; *J. Organomet. Chem.*, 1984, **260**, C1; H. Schmidbaur, B. Milewski-Mahrla, G. Muller and C. Kruger, *Organometallics*, 1984, **3**, 38; A. F. Chiffey, J. Evans, W. Levason and M. Webster, *Organometallics*, 1995, **14**, 1522.
8 G. A. Olah and A. A. Oswald, *Can. J. Chem.*, 1960, **38**, 1428.
9 R. Bohra, H. W. Roesky, M. Noltemeyer and G. M. Sheldrick, *Acta Crystallogr., Sect. C*, 1984, **40**, 1150.
10 P. B. Hitchcock, M. F. Lappert, A. K. Rai and H. D. Williams, *J. Chem. Soc., Chem. Commun.*, 1986, 1633.

Received in Columbia, MO, USA, 5th August 1997; 7/05711C

New insights into the formation of extended supramolecular architectures from simple building blocks

Hany Hassaballa,[a] Jonathan W. Steed*[a] and Peter C. Junk[b]

[a] *Department of Chemistry, King's College London, Strand, London, UK WC2R 2LS*
[b] *Department of Chemistry, James Cook University, Townsville, Qld, 4811, Australia*

Reaction of uranyl acetate with HCl and 15-crown-5 in toluene results in the formation of a liquid clathrate phase from which crystals of $(H_5O_2)[UO_2Cl_3(H_2O)_2]\cdot(15\text{-crown-}5)_2$ 1 are deposited; on standing, loss of HCl results in the isolation of a second product $[UO_2Cl_2(H_2O)_3]_{16}\cdot(15\text{-crown-}5)_{16}$ 2 which displays an extremely complex hydrogen bonded chain structure in the solid state.

In crystal growth the task presented to Nature is one of three dimensional tesselation. Often irregular molecular shapes must be fitted together in such a way as to minimise the amount of wasted space (vacuum) within the crystal.[1] In some cases, particularly those in which the molecule to be crystallised possesses a molecular cavity or cleft, the occurrence of vacant space is difficult to avoid and adventitious molecules of solvent, other species present in the reaction mixture or even gases[2,3] are incorporated within the crystalline lattice. The study of this phenomenon has given birth to the rich field of inclusion chemistry.[4,5]

A significant amount of work within the field of crystal engineering has been devoted in attempts to predict how Nature will solve the crystal 'tesselation' problem for a wide range of solid compounds.[6,7] Many synthetic chemists are, however, familiar with compounds which 'just will not crystallise'. The amorphous nature of such solids, which are often found to form oils in which a well defined ratio of solvent and solute comprises a separate phase from the bulk solvent, may often be rationalised in terms of molecular size and shape and its consequences on the lattice energy of the crystalline solid.[1] An excellent, and well studied example of this phenomenon is the formation of liquid clathrates in which an aromatic solvent serves to separate anions and cations of widely differing shape and size.[8–10] Under certain circumstances however, liquid clathrates may be decomposed by, for example, loss of HCl from the reaction medium and a consequent gradual decrease in polarity. In this way, studies of crown ether/metal salt mixtures in liquid clathrate media[8] have resulted in the isolation of a wide range of crystalline arrays of type '$H(H_2O)_n^+$(crown ether)-(anion)' in which the oxonium ion acts as a hydrogen bond donor and the crown ether as a hydrogen bond acceptor, thus giving insight into the precursor solution species.[11–14] In the case of the larger crown ethers such as 18-crown-6 and 21-crown-7 the oxonium cation is encapsulated by the macrocycle.[11,12,15] For 15-crown-5 and 12-crown-4, extended hydrogen bonded arrays are formed involving alternating hydrogen bond donors and acceptors, as a result of the inability of the small crown ether to surround the oxonium cation.[16]

The key to the production of materials with predictable crystal structures lies in the engineering of complementary crystal building blocks either by consideration of molecular shape,[17,18] electronic properties,[19] or hydrogen bond donor/acceptor ability.[20] We report herein the preliminary results of crystal engineering studies carried out in liquid clathrate media between hydrogen bond donor–acceptor pairs, which are not sterically complementary, and exhibit a symmetry mismatch.

The reaction of uranyl acetate with HCl and 15-crown-5 in toluene was carried out as shown in Scheme 1. This resulted in the formation of a large, yellow liquid clathrate layer over a period of *ca*. 12 h. Upon standing for a further 12 h gradual loss of HCl resulted in the deposition of crystals of formula $(H_5O_2)[UO_2Cl_3(H_2O)_2]\cdot(15\text{-crown-}5)_2$ **1**. The X-ray crystal structure† of this complex is shown in Fig. 1 and consists of an infinite chain comprising alternating $H_5O_2^+$ and $[UO_2Cl_3(H_2O)_2]^-$ anions linked by hydrogen bonding *via* 15-crown-5 molecules. Within the $H_5O_2^+$ cation the O···O distance is extremely short at 2.371(8) Å (*cf*. typical values of O···O separations 2.40–2.45 Å[11,15,21–23]) although distances as low as 2.336(14) Å have been noted.[24] Oxonium–crown contacts are in the range 2.70–3.20 Å, while the opposite face of each crown ether is hydrogen bonded to coordinated water molecules at distances of 2.92–3.04 Å. The $[UO_2Cl_3(H_2O)_2]^-$ anion itself exhibits normal bond lengths and angles with U=O 1.743(6), U–OH_2 2.37(3), 2.45(5) [O(2) and O(3) are disordered] and U–Cl 2.708(3), 2.709(3). This may be compared to typical distances of 1.763, 2.455 and 2.653 respectively.[25] The $[UO_2Cl_3(H_2O)_2]^-$ anion adopts a pentagonal bipyramidal geometry resulting in the hydrogen bond donating H_2O ligands both residing in the equatorial plane with a O–U–O angle of 146.4(9)°. This, in turn, enforces a zigzag structure to the $[UO_2Cl_3(H_2O)_2]^-\cdots$15-crown-5 chain.

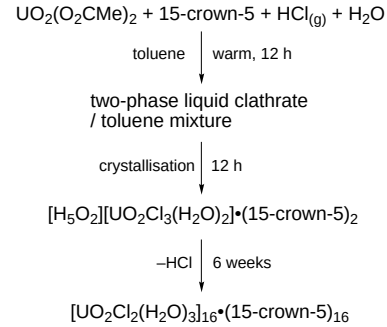

Scheme 1 Formation of the hydrogen bonded array $[UO_2Cl_2(H_2O)_3]_{16}\cdot(15\text{-crown-}5)_{16}$

Over a period of six weeks continued loss of HCl from the same reaction mixture results in the replacement of the yellow rectangular crystals of complex **1** by large, multifaceted crystals of a second product of empirical formula $[UO_2Cl_2(H_2O)_3]\cdot$15-crown-5. X-Ray crystallographic analysis† revealed a striking structure of trigonal symmetry, space group $P3_2$, consisting of sixteen unique uranium complexes and 15-crown-5 molecules, Fig. 2. The structure is arranged in sheets consisting of approximately linear, infinite hydrogen bonded strands, which

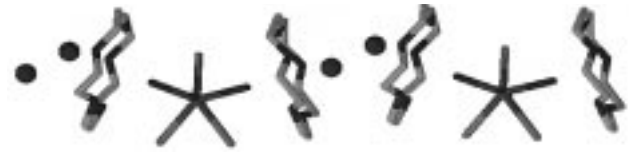

Fig. 1 Infinite chain structure of $H_5O_2^+$ and $[UO_2Cl_3(H_2O)_2]^-$ linked by 15-crown-5

Fig. 2 The asymmetric unit of $[UO_2Cl_2(H_2O)_3]_{16}\cdot(15\text{-crown-}5)_{16}$ **2** comprising four parallel, helical columns of alternating $[UO_2Cl_2(H_2O)_3]$ and 15-crown-5 (end and side views)

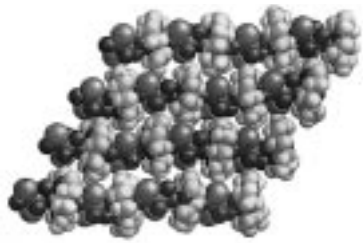

Fig. 3 Space filling plot of **2** showing the interlocking of the chains

repeat every four uranium centres. The strands are held together by interactions between the crown oxygen atoms and water molecules O(*n*3) and O(*n*4) (where *n* represents the number of the uranium centre to which the atom is attached) which form the most nearly linear H_2O–U–OH_2 angle of *ca*. 152° [the analogous O(*n*3)–U–O(*n*5) angle is *ca*. 140°]. Typically both O(*n*3) and O(*n*4) form two hydrogen bonds to an adjacent crown ether with a wide range of $O_{water}\cdots O_{crown}$ distances of between 2.60(2) and 2.92(2) Å highlighting the individual nature of each of the sixteen crown–metal complex pairs. In addition, O(*n*5) forms a single short hydrogen bond to a further crown oxygen on the same side as O(*n*4) with distances ranging from 2.49(2) to 2.71(2) Å. While some disorder was evident in the 15-crown-5 molecules of **1**, complex **2** is ordered at −100 °C with each of the sixteen 15-crown-5 units exhibiting a structure in which three oxygen atoms point towards O(*n*4) and O(*n*5) of one metal complex and two others interact with O(*n*3) on the next. It is the unsymmetrical nature of this conformation with three donor atoms one side and two on the other, which, in the absence of oxonium ions, leads to such a complicated structure. In forming the interactions to water ligands O(*n*4) and O(*n*5) with three of the crown oxygen atoms, two are left for forming the next interaction to an adjacent anion [*via* O(*n*3)]. This results in the docking of this anion in such a way as to maximise O(*n*3)···crown interactions, in the process fixing its orientation. Hydrogen bonding from O(*n*4) and O(*n*5) to the next crown ether must now necessarily occur in a different orientation to the previous member of the chain. This results in a rotation perpendicular to the chain direction of *ca*. 25–35° accompanied by a tilt along the chain axis of *ca*. 10°. The net result is that it is not until the fifth such donor–acceptor pair that the crown has rotated back to its starting point. Furthermore, the displacement of the uranium centres to one side of the chain axis as a consequence of the non-linear O(*n*3)–U–O(*n*4) axis results in the formation of grooves in the chain into which the crown ethers of adjacent stacks slot. Again, the steric requirements of one chain dictate the orientation of the next such that each chain is rotated with respect to its neighbour. This pattern also does not repeat itself until the fifth chain resulting in a unique 4 × 4 array of donor acceptor pairs, Fig. 3.

In summary, the rigid and uncomplementary nature of both uranyl species in **1** and **2** results in interesting crystal packing motifs. In the former case the presence of a linear oxonium ion serves to simplify the crystal packing. For **2** a highly complex crystalline array is required before the problem of three-dimensional tessellation of such mismatched building blocks can be solved.

We thank the EPSRC and King's College London for funding of the diffractometer system. Grateful acknowledgement is also given to the Nuffield Foundation for the provision of computing equipment.

Footnotes and References

* E-mail: jon.steed@kcl.ac.uk

† *Crystal data*: **1**: $C_{20}H_{29}Cl_3O_{16}U$, M = 869.81, orthorhombic, *Pmcn*, a = 12.1740(5), b = 14.7740(7), c = 18.4920(11) Å, U = 3325.9(3) Å^3, Z = 4, data 2434, parameters 204, R_1 = [$F^2 > 2\sigma(F^2)$] = 0.042, wR_2 (all data) = 0.111. **2**: $C_{10}H_{26}Cl_2O_{10}U$, M = 615.24, trigonal, $P3_2$, a = 35.3500(2), c = 21.3755(2) Å, U = 23 132.7(3) Å^3, Z = 48, data 51 913, parameters 3305, R_1 [$F^2 > 2\sigma(F^2)$] = 0.072, wR_2 (all data) = 0.158. CCDC 182/735.

1 J. Hulliger, *Angew. Chem., Int. Ed. Engl.*, 1994, **33**, 143.
2 E. Weber, *Top. Curr. Chem.*, 1987, **140**, 2.
3 C. D. Gutsche, *Calixarenes*, ed. J. F. Stoddart, Royal Society of Chemistry, 1989.
4 J. L. Atwood, J. E. Davies and D. D. MacNicol, in *Inclusion Compounds*, Academic, London, 1984.
5 J. L. Atwood, J. E. D. Davies and D. D. MacNicol, in *Inclusion Compounds*, OUP, Oxford, 1991.
6 A. Gavezzotti, *Acc. Chem. Res.*, 1994, **27**, 309.
7 G. Desiraju, *Angew. Chem., Int. Ed. Engl.*, 1995, **34**, 2311.
8 J. L. Atwood, in *Inclusion compounds*, ed. J. L. Atwood, J. D. Davies and D. D. MacNicol, Academic, London, 1984.
9 J. L. Atwood, in *Chemical Separations*, ed. C. J. King and J. D. Navratil, Denver, 1986.
10 J. L. Atwood, in *Separation Technology*, ed. N. N. Li and H. Strathmann, United Engineering Trustees, New York, 1988.
11 P. C. Junk and J. L. Atwood, *J. Chem. Soc., Chem. Commun.*, 1995, 1551.
12 J. L. Atwood, S. G. Bott, P. C. Junk and M. T. May, *J. Organomet. Chem.*, 1995, **487**, 7.
13 J. L. Atwood, S. G. Bott, P. C. Junk and M. T. May, *J. Coord. Chem.*, 1996, **37**, 89.
14 J. L. Atwood and P. C. Junk, *J. Chem. Soc., Dalton Trans.*, 1997, 4393.
15 J. L. Atwood, S. G. Bott, K. D. Robinson, E. J. Bishop and M. T. May, *J. Cryst. Spectros. Res.*, 1991, **21**, 459.
16 J. L. Atwood and P. C. Junk, *Chem. Commun.*, submitted.
17 J. W. Steed, P. C. Junk, J. L. Atwood, M. J. Barnes, C. L. Raston and R. L. Burkhalter, *J. Am. Chem. Soc.*, 1994, **116**, 10 346.
18 J. L. Atwood, G. A. Koutsantonis and C. L. Raston, *Nature*, 1994, **368**, 229.
19 J. S. Miller and A. J. Epstein, *Angew. Chem., Int. Ed. Engl.*, 1994, **33**, 385.
20 M. J. Zaworotko, *Chem. Soc. Rev.*, 1994, **23**, 283.
21 R. D. Rogers, A. H. Bond, W. G. Hipple, A. N. Rollina and R. F. Henry, *Inorg. Chem.*, 1991, **30**, 2671.
22 R. Attig and J. M. Williams, *Inorg. Chem.*, 1976, **15**, 3057.
23 C. I. Ratcliffe and D. E. Irish, in *The Nature of the Hydrated Proton*, ed. F. Franks, CUP, Cambridge, 1988, vol. 3.
24 A. Bino and F. A. Cotton, *J. Am. Chem. Soc.*, 1979, **101**, 4150.
25 G. Orpen, L. Brammer, F. H. Allen, O. Kennard, D. G. Watson and R. Taylor, *J. Chem. Soc., Dalton Trans.*, 1989, S1.

Received in Columbia, MO, USA; 27th October 1997; 7/07744K

Synthesis of Si and Ti-Si-MCM-48 mesoporous materials with controlled pore sizes in the absence of polar organic additives and alkali metal ions

Avelino Corma,* Qiubin Kan and Fernando Rey

Instituto de Tecnologia Química, UPV-CSIC, Universidad Politécnica, Avda. de los Naranjos, S/N, 46022 Valencia, Spain

A new route for the synthesis of Si- and Si-Ti-MCM-48 has been developed which allows these materials to be obtained without using polar organic additives and alkali metal ions; this procedure not only produces more active and selective Ti-MCM-48 oxidation catalysts than those reported before, but also permits the synthesis of MCM-48 with controlled pore diameters.

The development of ordered mesoporous materials (M41S) containing different atoms in the pore walls has opened up new possibilities for the use of mesoporous molecular sieve materials in the field of catalysis.[1–7] These materials have large channels with regular pores which can be varied in some cases from 1.5 to 7.0 nm, and which are ordered in a hexagonal (MCM-41), cubic (MCM-48), or laminar (MCM-50) array. All these materials are characterised by extremely narrow pore size distributions in the mesoporous region, long range order, high surface areas (> 700 m^2 g^{-1}) and are stable after calcination. From the point of view of catalytic activity the most interesting materials are the MCM-48 array, because its pore structure is built up of two independent tridirectional channel systems.[8] However, little research has been carried out on MCM-48, probably due to the difficulty of its synthesis compared with the more studied MCM-41, and also the difficulty of controlling its pore size. In general, MCM-48 is prepared with high surfactant to silicon ratios (0.65–1.5),[9] and the presence of polar organic additives in the reaction mixture is believed to be essential for a successful synthesis of MCM-48[10,11] when cetyltrimethylammonium ion (CTA^+) surfactant is used as the structure-directing agent. To achieve the latter, tetraethylorthosilicate (TEOS) is usually used as the silicon source for preparation of MCM-48 since in this case the ethanol produced from the hydrolysis of TEOS acts as the required polar organic additive. When sodium silicate or other silica sources were used without addition of polar organics, MCM-41 was produced instead.[10,12] Furthermore, in most of the reported syntheses of pure siliceous MCM-48 materials and their metal derivates, NaOH was introduced in the synthesis gel.[9,12–14] It is known however, that there is a detrimental effect of alkali metal ions on the catalytic properties of titanium silicate molecular sieves.[15,16] We have found only one report in which pure siliceous and titanium-containing MCM-48 were prepared in absence of sodium ions by using TEOS as the silicon source.[17] Unfortunately, the synthesis was poorly reproducible due to the ill defined and critical ethanol evaporation step, which is required for the synthesis. While MCM-41 can be prepared with a large range of pore diameters, even in the absence of added organics,[18] this is not the case for the MCM-48 structure where relatively small changes in the pore diameter could only be achieved by using surfactants with different chain length, and pore sizes larger than *ca.* 2.8 nm have not been reported.

It is possible to overcome the above synthetic shortcomings and to produce high quality MCM-48 samples in the absence of polar organics and alkali metal ions, as well as enabling the pore diameter to be increased to *ca.* 3.8 nm. These achievements certainly open more possibilities for the use of MCM-48 as catalysts as is illustrated for Ti-MCM-48.

The hydrothermal synthesis of Si-MCM-48 was carried out with the following molar composition: 1.0 SiO_2 : x CTAOH/Br : 32.0 H_2O, x = 0.18–0.35; the source of silicon was amorphous silica (Aerosil 200, Degussa) and an aqueous solution of CTAOH/Br with a OH/Br ratio of 90/10 was used. The homogenous gel was sealed in Teflon-lined stainless steel autoclaves and heated at 60–150 °C under static conditions. The time of synthesis was varied from 1 to 7 days depending on the temperature of synthesis and the pore size to be obtained. The resulting solid products were recovered by filtration, washed and dried at 60 °C for 24 h. The occluded organic was removed by heating the samples at 540 °C under a continuous flow of N_2 for 2 h, followed by calcination in a flow of air at 540 °C for 6 h.

From the XRD patterns presented in Fig. 1 it can be seen that highly ordered MCM-48 mesoporous materials consistent with an *Ia*3*d* cubic symmetry were obtained. In our procedure we succeeded in synthesising the MCM-48 structure at low surfactant to silicon ratios (0.20–0.28), unlike in the synthesis reported by Mobil Researchers where higher ratios seem to be mandatory to obtain the cubic structure.[9] However, following our synthesis procedure it is critical to stay in between the limits given above for the surfactant/silicon ratio, since when this ratio reached 0.35, a lamellar phase (MCM-50) was formed under the same reaction conditions, and MCM-41 was produced when the ratio was lower than 0.18. The reaction temperature and crystallisation time were the key variables to control the pore diameter of the resultant samples. For instance, two different MCM-48 samples with cell parameters a_0 = 92.8 Å and a_0 = 98.6 Å were obtained after 24 h crystallization at 135 °C and 150 °C, respectively. Longer reaction times at 150 °C, *e.g.* 3 or 5 days, resulted in the swelling of the unit cell volume of the MCM-48 to a_0 = 112.7 and 116.8 Å, respectively. Moreover, after 5 days of crystallization a lamellar structure starts to appear due to a phase transition of MCM-48 (Fig. 1), producing a pure lamellar phase after 7 days of synthesis. The nitrogen

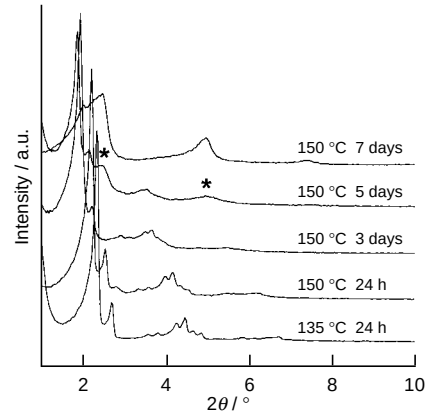

Fig. 1 X-Ray diffraction patterns of mesophases (MCM-48) synthesised at various temperatures and different reaction times. The phase transition from MCM-48 to the lamellar structure (*) upon extended synthesis times can be clearly seen.

Table 1 Unit cell parameter a_0 upon calcination at 540 °C, pore diameter, BET surface area and pore volume of MCM-48

Sample	Synthesis conditions		Unit cell, a_0/Å		Unit cell contraction/ Å	Pore diameter, d/Å	Surface area, s/m^2 g^{-1}	Pore volume, v/cm^3 g^{-1}
	T/°C	t/h	as[a]	ca[a]				
1	135	24	92.8	84.6	8.2	24	1121	0.87
2	150	24	98.6	92.1	5.5	28	1026	1.00
3	150	72	112.7	110.9	1.8	36	961	1.09
4[b]	150	120	116.8	115.4	1.4	38	800	0.93

[a] as = as-synthesized, ca = calcined. [b] Containing lamellar phase (see Fig. 1).

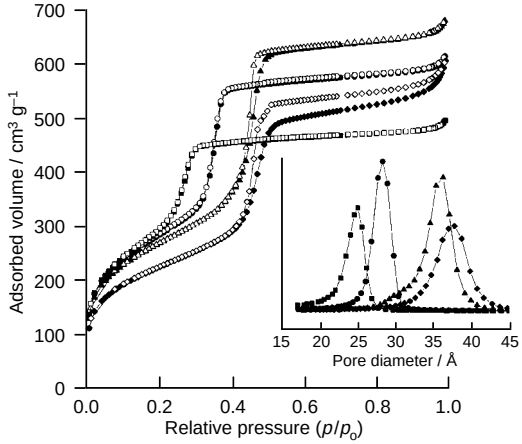

Fig. 2 Nitrogen adsorption–desorption isotherms of calcined MCM-48 materials with unit cell a_0 = 84.6 Å (■), a_0 = 92.1 Å (●), a_0 = 110.9 Å (▲) and a_0 = 115.4 Å (◆); inset: pore distribution of calcined MCM-48 materials with different unit cell parameters (calculated from N_2 adsorption isotherm branch)

adsorption–desorption isotherms of the corresponding calcined samples and the pore size distribution deduced from them are illustrated in Fig. 2. Table 1 lists the physicochemical characteristics of the as-synthesised and calcined samples, showing that swelling of the pore diameter occurs when the unit cell parameter increases.

If lower reaction temperatures are used the formation of MCM-41 is favoured. For instance, mesoporous materials with the MCM-41 structure were generated at 60 and 100 °C after 3 days when the synthesis gel composition given above was used. The effect of temperature on the structure of the mesoporous products is probably associated with the modification of the packing parameter g ($g = V/A_0l$) of the surfactant organisation,[19,20] where V is the surfactant tail volume, l is the length of surfactant chain and A_0 is the effective head group area at the micelle surface. At lower temperatures, *e.g.* at 60 or 100 °C, where MCM-41 is produced, the effective g value for CTA^+ ions is smaller[21] than that at 135 to 150 °C when MCM-48 is generated.

By following the above procedure for the synthesis of Si-MCM-48, Ti-MCM-48 with Si/Ti = 100 has been successfully obtained. UV–VIS spectra for the as-synthesised and calcined Ti-MCM-48 show a main band at *ca.* 200–210 nm assigned to isolated framework titanium in tetrahedral coordination. The catalytic reactions for epoxidation of cyclohexene with *tert*-butyl hydroperoxide (TBHP) over the Ti-MCM-48 was carried out at 60 °C with an alkene/TBHP ratio of 4.0 and 5 mass% of catalyst and following the reaction and analytical procedure described previously.[4] The Ti-MCM-48 prepared here in the absence of alkali metal ions shows an initial reaction rate of 1.642 mol g^{-1} h^{-1}. The sample with the same Si/Ti ratio obtained in the presence of sodium ions using the method described in ref. 15 gives an initial reaction rate four times lower (0.448 mol g^{-1} h^{-1}) than that over the Ti-MCM-48 reported here, illustrating the beneficial effect of the novel synthesis procedure presented here.

In conclusion, it has been proven that it is possible to carry out the synthesis of mesoporous materials having the MCM-48 structure without using polar organics and alkali metal cations in the synthesis mixture. When the synthesis is carried out in the absence of alkali metal ions, the Ti-MCM-48 produced is a more active epoxidation catalyst than the Ti-MCM-48 synthesised following the conventional procedure in the presence of Na^+. Finally, by precisely controlling the synthesis conditions, *i.e.* composition of the gel, synthesis temperature and time, it was possible to produce MCM-48 samples with different pore diameters up to 3.8 nm.

The authors thank CICYT for financial support (MAT97-1207-C03-01).

Notes and References

* E-mail: itq@upvnet.upv.es

1 C. T. Kresge, M. E. Leonowicz, W. J. Roth, J. C. Vartuli and J. S. Beck, *Nature*, 1992, **359**, 710.
2 C. Y. Chen, S. L. Burkett, H. X. Li and M. E. Davis, *Microporous Mater.*, 1993, **2**, 27.
3 A. Corma, V. Fornes, M. T. Navarro and J. Perez-Pariente, *J. Catal.*, 1994, **148**, 569.
4 A. Corma, M. T. Navarro and J. Perez-Pariente, *J. Chem. Soc., Chem. Commun.*, 1994, 147; T. Blasco, A. Corma, M. T. Navarro and J. P. Pariente, *J. Catal.*, 1995, **156**, 65.
5 K. M. Reddy, I. L. Moudrakouski and A. Sayari, *J. Chem. Soc., Chem. Commun.*, 1995, 973.
6 F. Rey, G. Sankar, T. Maschmeyer, J. M. Thomas and R. G. Bell, *Top. Catal.*, 1996, **3**, 121.
7 A. Corma, *Chem. Rev.*, 1997, **97**, 2373.
8 A. Monnier, F. Schuth, Q. Huo, D. Kumar, D. Margolese, R. S. Maxwell, G. D. Stucky, M. Krishnamurty, P. Petroff, A. Firouzi, M. Janicke and B. F. Chmelka, *Science*, 1993, **261**, 1299.
9 J. C. Vartuli, K. D. Schmitt, C. T. Kresge, W. J. Roth, M. E. Leonowicz, S. B. McCullen, S. D. Hellring, J. S. Beck, J. L. Schlenker, D. H. Olson and E. W. Sheppard, *Chem. Mater.*, 1994, **6**, 2317.
10 Q. Huo, D. Y. Margolese and G. D. Stucky, *Chem. Mater.*, 1996, **8**, 1147.
11 K. W. Gallis and C. C. Landry, *Chem. Mater.*, 1997, **9**, 2035.
12 D. Zhao and D. Goldfarb, *J. Chem. Soc., Chem. Commun.*, 1995, 875.
13 M. Morey, A. Davidson and G. Stucky, *Microporous Mater.*, 1996, **6**, 99.
14 W. Zhang and T. J. Pinnavaia, *Catal. Lett.*, 1966, **38**, 261.
15 C. B. Khouw and M. E. Davis, *J. Catal.*, 1995, **151**, 77.
16 M. A. Camblor, A. Corma and J. Pérez-Pariente, *Zeolites*, 1993, **13**, 82.
17 K. A. Koyano and t. Tatsumi, *Chem. Commun.*, 1996, 145.
18 A. Corma, Q. Kan, M. T. Navarro, J. Perez-Pariente and F. Rey, *Chem. Mater.*, 1997, **9**, 2123.
19 J. Chavrolin and J. F. Srdoc, *J. Phys.*, 1987, **48**, 189.
20 S. M. Grunner, *J. Phys. Chem.*, 1989, **93**, 7562.
21 G. D. Stucky, A. Monnier, F. Schüth, Q. Huo, D. Margolese, D. Kumar, M. Krishnamurty, P. Petroff, A. Firouzi, M. Janicke and B. F. Chmelka, *Mol. Cryst. Liq. Cryst.*, 1994, **240**, 187.

Received in Bath, UK, 18th December 1997; 7/09093E

Self-assembly of coordination polymeric chains: crystal structures of silver(I) complexes with 3,6-bis(diphenylphosphino)pyridazine and 2,6-bis(diphenylphosphino)pyridine

Shan-Ming Kuang,[a] Zheng-Zhi Zhang,*[b] Qi-Guang Wang,[a] and Thomas C. W. Mak*†[a]

[a] *Department of Chemistry, The Chinese University of Hong Kong, Shatin, New Territories, Hong Kong, PR China*
[b] *Elemento-Organic Chemistry Laboratory, Nankai University, Tianjin, China*

Site-specific metal–ligand interactions lead to self-assembly of coordination polymeric chains in the crystal structures of silver(I) complexes with 3,6-bis(diphenylphosphino)pyridazine and 2,6-bis(diphenylphosphino)pyridine.

The design of solid-state architectures has become an area of increasing interest in recent years.[1–6] Much attention has centered upon the use of supramolecular contacts, particularly hydrogen bonding, between suitable molecules to generate multidimensional arrays or networks.[1,3,4] In comparison, the design of inorganic networks is less well developed though catching up fast in recent years.[7–11]

The self-assembly of coordination polymeric chains presents an interesting challenge. We reasoned that, with judicious design, it should be possible to assemble linear chains in a single process involving simple mixing of metals and ligands. Such a strategy requires the design of a ligand with two or more coordination sites that are juxtaposed in such a way that they cannot all coordinate to the same metal ion, and interaction between the ligand and a linear sequence of metal ions must occur in a logical fashion to form a polymeric chain.

With this in mind, we decided to conduct a test case with N,P-donor ligands with suitable binding sites and idealized C_{2v} molecular symmetry. The substituted pyridazine ligand 3,6-bis-(diphenylphosphino)pyridazine (L^1), which was synthesized in

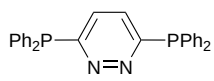

L^1

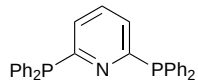

L^2

an earlier study,[13] is constrained by its connectivity to act as a tetranucleating ligand, presenting a pair of N,P-bridging sites to a linear arrangement of four metal ions. Here we report the self-assembly reaction of L^1 with $[Ag(MeCN)_4]ClO_4$ to generate a zigzag polymeric chain in the silver(I) complex $\{[Ag_2(MeCN)_2(\mu\text{-}L^1)]\}_n[ClO_4]_{2n}$ **1**. In contrast, the use of the related ligand 2,6-bis(diphenylphosphino)pyridine (L^2)[14] in the same reaction gave $\{[Ag(MeCN)_2(\mu\text{-}L^2)]\}_n[ClO_4]_n$ **2** with a different metal : ligand molar ratio and exhibiting a simple linear chain.

The reaction of $[Ag(MeCN)_4]ClO_4$[15] with L^1 in MeCN at room temperature (Scheme 1) leads to the rapid formation of a colorless solution from which $\{[Ag_2(MeCN)_2(\mu\text{-}L^1)]\}_n[ClO_4]_{2n}$ **1** was isolated.‡ Elemental analysis results are consistent with the stoichiometric formula $Ag_2(MeCN)_2(L^1)(ClO_4)_2$. Slow diffusion of diethyl ether into an acetonitrile solution afforded colorless crystals of **1**, the structure of which was determined by single crystal X-ray analysis.§

As anticipated, the L^1 ligand bridges between metal centers *via* coordination by its P,N-donor sets (Fig. 1). Each silver(I) center is bound to a P atom from one L^1 ligand and a N atom from the other, resulting in the formation of a polymeric zigzag chain running in the direction of the *c* axis (Scheme 1, left); note that the centers of eight-membered $(PCNAg)_2$ rings are located at successive inversion centers. The highly distorted trigonal-planar coordination sphere about each Ag^I atom is completed by an acetonitrile ligand that stabilizes the resulting 16-electron configuration, so that the repeating structural unit is $Ag_2(MeCN)_2(\mu\text{-}L^1)$. The sums of the three bond angles at Ag(1) and Ag(2) are 358.3 and 357.8°, respectively. The intermolecular Ag(1)···Ag(1a) and Ag(2)···Ag(2b) distances are 3.005(2) and 3.184(2) Å, respectively, which are in agreement with those [3.162(1)–3.223(1) Å] in $[Ag\{HC(PPh_2)_3\}_2Cl][ClO_4]_2\cdot 2MeCN$,[16] and those [2.943(2)–3.014(2) Å] in $[Ag_3(dppp)_2(MeCN)_2(ClO_4)_2]^+$ [dppp = bis(diphenylphosphinophenylphosphine)],[17] but much shorter than that [3.641(2) Å] in $\{[AgL^3(MeCN)_2]\}_n[BF_4]_n$ (L^3 = 2,7-diazapyrene).[9] The Ag(1)···Ag(2) contact is 3.535(2) Å.

The silver(I) complex $\{[Ag(MeCN)_2(\mu\text{-}L^2)]\}_n[ClO_4]_n$ **2** was obtained from the reaction of $[Ag(MeCN)_4]ClO_4$ with L^2 in 1 : 1 molar ratio. The crystal structure of **2**§ consists of a packing of linear chains of alternating Ag^I and L^2 units (Fig. 2 and Scheme 1, right) and perchlorate ions. In each coordination polymeric chain the repeating unit $Ag(MeCN)_2(\mu\text{-}L^2)$ is held together by the P atoms of ligand L^2, whose pyridyl N atom takes no part in metal coordination. The coordination geometry of the silver(I) center is distorted tetrahedral, stabilization being achieved by linkage to two acetonitrile ligands. The Ag–N distances of 2.332(8) and 2.419(9) Å are much shorter than those [2.871(4), 2.926(4) Å] found in $\{[AgL^3(MeCN)_2]\}_n[BF_4]_n$.[9]

In summary, we have taken advantage of the different site-specific ligating capacities of P,N-donor ligands L^1 and L^2 in generating coordination polymeric chains with $[Ag(MeCN)_4]ClO_4$. In complex **1**, successive L^1 ligands lie on alternate sides of the zigzag silver(I) chain, while in **2** the L^2 ligand is repeated by the *a* translation to generate a simple linear chain. The latter case contrasts sharply with the related one-dimensional gold(I) polymer $\{[Au_2(\mu\text{-}L^2)(C{\equiv}CPh)_2]\}_n$ in which the L^2 ligands are arranged in a zigzag fashion along the chain.[18] That the silver(I) and gold(I) complexes of L^2 adopt different linear polymeric structures can be attributed to the difference in number, charge and bulkiness of the respective acetonitrile and phenylacetylide

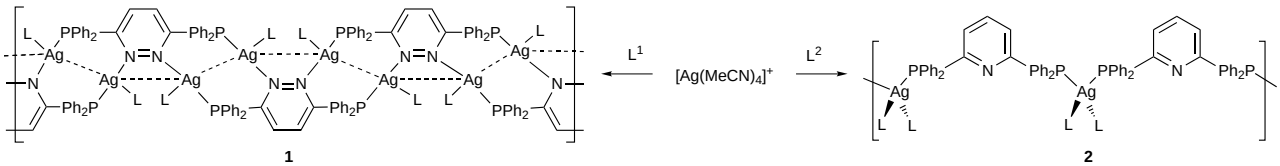

Scheme 1

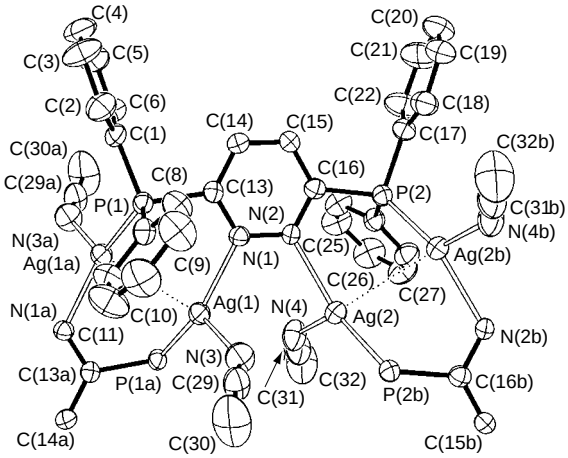

Fig. 1 Perspective view (35% thermal ellipsoids) of the cationic $[Ag_2(MeCN)_2(\mu\text{-}L^1)]^{2+}$ unit in complex **1**. Selected bond lengths (Å) and angles (°): Ag(1)–N(1) 2.299(5), Ag(1)–N(3) 2.300(7), Ag(1)–P(1a) 2.387(2), Ag(1)–Ag(1a) 3.005(2), Ag(2)–N(4) 2.274(7), Ag(2)–N(2) 2.309(5), Ag(2)–P(2b) 2.384(2), Ag(2)–Ag(2b) 3.185(2); N(1)–Ag(1)–N(3) 89.9(2), N(1)–Ag(1)–P(1a) 147.30(13), N(3)–Ag(1)–P(1a) 121.1(2), N(1)–Ag(1)–Ag(1a) 89.15(13), N(3)–Ag(1)–Ag(1a) 135.4(2), P(1a)–Ag(1)–Ag(1a) 75.99(5), N(4)–Ag(2)–N(2) 91.7(2), N(4)–Ag(2)–P(2b) 126.6(2), N(2)–Ag(2)–P(2b) 139.50(12), N(4)–Ag(2)–Ag(2b) 142.3(2), N(2)–Ag(2)–Ag(2b) 86.89(12), P(2b)–Ag(2)–Ag(2b) 70.86(5). Symmetry codes: a, $-x$, $1-y$, $2-z$; b, $-1-x$, $1-y$, $2-z$.

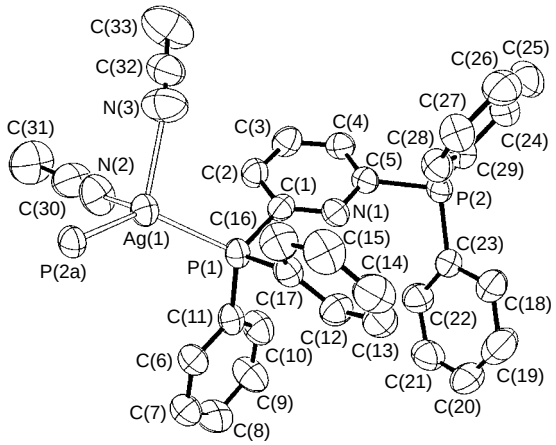

Fig. 2 Perspective view (35% thermal ellipsoids) of cation $[Ag(MeCN)_2(\mu\text{-}L^2)]^+$ in complex **2**. Selected bond lengths (Å) and angles (°): Ag(1)–P(1) 2.441(2), Ag(1)–N(2) 2.332(8), Ag(1)–N(3) 2.419(9), Ag(1)–P(2a) 2.423(2); P(1)–Ag(1)–N(2) 107.6(2), P(1)–Ag(1)–N(3) 102.8(3), P(1)–Ag(1)–Ag(2a) 127.5(1), N(2)–Ag(1)–N(3) 86.7(4), N(2)–Ag(1)–P(2a) 111.2(2), N(3)–Ag(1)–P(2a) 113.2(2). Symmetry code: a, $1-x$, y, z.

coligands, as well as the tendency for weak intermolecular interaction between adjacent gold(I) centres.[19]

This work is supported by Hong Kong Research Grants Council Earmarked Grant Ref. No. CUHK 4179/97P and the National Natural Science Foundation of China.

Notes and References

† E-mail: tcwmak@cuhk.edu.hk

‡ *Preparations*: polymeric complex **1**: to a solution of $[Ag(MeCN)_4]ClO_4$ (0.19 g, 0.5 mmol) in 20 ml of MeCN was added L^1 (0.23 g, 0.5 mmol). The resulting solution was stirred at room temperature for 3 h after which the colorless solution was filtered and subsequent diffusion of diethyl ether into the concentrated solution gave **1** as air-stable colorless crystals, 0.40 g (85.1%). (Found: C, 40.73; H, 3.01; N, 6.00. $C_{32}H_{28}AgCl_2N_4O_8P_2$ requires: C, 40.66; H, 2.99; N, 5.93%). $^{31}P(^1H)$ NMR ($CDCl_3$, external standard: 85% H_3PO_4, 298 K): δ 15.9.

Polymeric complex **2**: the procedure was similar to that above, except that 0.23 g (0.5 mmol) of L^2 was used instead of L^1. Recrystallization from MeCN–diethyl ether afforded **2** as colorless crystals. Yield: 0.32 g (86.5%) (Found: C, 53.99; H, 3.60; N, 5.60. $C_{35}H_{35}CuNP_2S_2O_3\cdot H_2O$ requires: C, 53.79; H, 3.97; N, 5.70%). $^{31}P(^1H)$ NMR ($CDCl_3$, external standard: 85% H_3PO_4, 298 K): δ 10.1.

§ *Crystal data*: $\{[Ag_2(MeCN)_2(\mu\text{-}L^1)]\}_n[ClO_4]_{2n}$, $C_{32}H_{28}Ag_2Cl_2N_4O_8P_2$ **1**, M = 945.16, triclinic, space group $P\bar{1}$ (no. 2), a = 12.294(2), b = 12.999(3), c = 13.679(3) Å, α = 62.98(3), β = 73.74(3), γ = 74.63(3)°, U = 1845.1(7) Å^3, Z = 2, μ(Mo-Kα) = 1.342 mm^{-1}; Rigaku RAXIS-IIC imaging plate, 5639 observed data [$|F_o| > 4\sigma(F_o)$] out of 5964 unique reflections converged (SHELXTL-PC[19]) to $R(F) \equiv \Sigma(||F_o| - |F_c||)/\Sigma|F_o|$ = 0.053 and $R_w(F^2) \equiv [\{\Sigma w(|F_o| - |F_c|)^2\}/\{\Sigma w|F_o|^2\}]^{1/2}$ = 0.057.

$\{[Ag(MeCN)_2(\mu\text{-}L^2)]\}_n[ClO_4]_n$, $C_{33}H_{29}AgClN_3O_4P_2$ **2**, M = 736.85, orthorhombic, space group $P2_12_12_1$ (no. 22), a = 9.465(1), b = 14.116(1), c = 25.596(2) Å, U = 3419.8(5) Å^3, Z = 4, μ(Mo-Kα) = 0.801 mm^{-1}; Rigaku RAXIS-IIC imaging plate, 5687 observed data out of 6025 unique reflections converged (SHELXTL-PC[20]) to $R(F)$ = 0.065 and $R_w(F^2)$ = 0.070. CCDC 182/749.

1 G. R. Desiraju, in *Crystal Engineering: Design of Organic Solids*, Elsevier, Amsterdam, 1989.
2 R. Robson, B. F. Abrahams, S. R. Batten, R. W. Gable, B. F. Hoskins and J. Liu, *Supramolecular Architecture*, ACS Publications, Washington DC, 1992, ch. 19.
3 *The Crystal as a Supramolecular Entity*, ed. G. R. Desiraju, Wiley, New York, 1995.
4 G. R. Desiraju, *Angew. Chem., Int. Ed. Engl.*, 1995, **34**, 2311.
5 J.-M. Lehn, *Supramolecular Chemistry—Concepts and Perspectives*, VCH, Weinhein, 1995.
6 D. Philip and J. F. Stoddart, *Angew. Chem., Int. Ed. Engl.*, 1996, **35**, 1155.
7 S. B. Copp, S. Subramanian and M. J. Zaworotko, *J. Am. Chem. Soc.*, 1992, **114**, 8719; S. B. Copp, S. Subramanian and M. J. Zaworotko, *J. Chem. Soc., Chem. Commun.*, 1993, 1078; L. R. MacGillivary, S. Subramanian and M. J. Zaworotko, *J. Chem. Soc., Chem. Commun.*, 1994, 1325; S. B. Copp, K. T. Holman, J. O. S. Sangster, S. Subramanian and M. J. Zaworotko, *J. Chem. Soc., Dalton Trans.*, 1995, 2233; S. Subramanian and M. J. Zaworotko, *Angew. Chem., Int. Ed. Engl.*, 1995, **34**, 2127; P. Losier and M. J. Zaworotko, *Angew. Chem., Int. Ed. Engl.*, 1995, **35**, 2779.
8 B. F. Abrahams, S. R. Batten, H. Hamit, B. F. Hoskins and R. Robson, *Angew. Chem., Int. Ed. Engl.*, 1995, **35**, 1691; D. M. L. Goodgame, S. Menzer, A. M. Smith and D. J. Williams, *Angew. Chem., Int. Ed. Engl.*, 1995, **34**, 574; P. C. M. Duncan, D. M. L. Goodgame, S. Menzer and D. J. Williams, *Chem. Commun.*, 1996, 2127.
9 A. J. Blake, N. R. Champness, S. S. M. Chung, W.-S. Li and M. Schröder, *Chem. Commun.*, 1997, 1005; A. J. Blake, N. R. Champness, A. N. Khlobystov, D. A. Lemenovskii, W.-S. Li and M. Schröder, *Chem. Commun.*, 1997, 1339; A. J. Blake, N. R. Champness, S. S. M. Chung, W.-S. Li and M. Schröder, *Chem. Commun.*, 1997, 1675.
10 M. Fujita, J. Yazaki and K. Ogura, *J. Am. Chem. Soc.*, 1990, **112**, 5645; M. Fujita, Y. J. Kwon, S. Washizu and K. Ogura, *J. Am. Chem. Soc.*, 1994, **116**, 1151; M. Fujita, S. Nagao and K.Ogura, *J. Am. Chem. Soc.*, 1995, **117**, 1649.
11 M. J. Hannon, C. L. Paiting and W. Errington, *Chem. Commun.*, 1997, 307; M. J. Hannon, C. L. Paiting and W. Errington, *Chem. Commun.*, 1997, 1805.
13 Z.-Z. Zhang, H.-K. Wang, Y.-J. Shen, H.-G. Wang and R. J. Wang, *J. Organomet. Chem.*, 1990, **381**, 45.
14 G. R. Newkome and D. C. Hager, *J. Org. Chem.*, 1978, **43**, 947.
15 B. Akermark and A. Vitagliano, *Organometallics*, 1985, **4**, 1281.
16 C.-M. Che, H.-K. Yip, V. W.-W. Yam, P.-Y. Cheung, T.-F. Lai, S.-J. Shieh and S.-M. Peng, *J. Chem. Soc., Dalton Trans.*, 1992, 427.
17 C.-M. Che, H.-K. Yip, D. Li, S.-M. Peng, G.-H. Lee, T.-F., Lai, Y.-M. Wang and S.-T. Liu, *J. Chem. Soc., Chem. Commun.*, 1991, 1615.
18 S.-J. Shieh, X. Hong, S.-M. Peng and C.-M. Che, *J. Chem. Soc., Dalton Trans.*, 1994, 3067.
19 P. Pyykkö, *Chem. Rev.*, 1988, **88**, 563; 1997, **97**, 597; T. C. W. Mak and G.-D. Zhou, *Crystallography in Modern Chemistry: A Resource Book of Crystal Structures*, Wiley-Interscience, New York, 1992, pp. 463–472.
20 *SHELXL/PC V5.0 Reference Manual*, Siemens Analytical X-Ray Instruments, Inc., Madison, Wisconsin, 1995.

Received in Cambridge, UK, 14th November 1997; 7/08216I

N-Methyl-1,3,5,2-trioxazinane, a possible spontaneous ignition sensitiser†

Wai-To Chan, DeLin Shen‡ and Huw O. Pritchard*§

Department of Chemistry, York University, Downsview, Ontario, Canada M3J 1P3

***N*-Methyl-1,3,5,2-trioxazinane (or *N*-methyl-2,4,6-trioxapiperidine), by analogy with *s*-trioxane, should decompose thermally into MeNO + $2CH_2O$; this substance does not appear to have been made, but molecular orbital calculations show that it should be almost as stable as *s*-trioxane.**

Nitrogen dioxide, from the thermal decomposition of alkyl nitrates, sensitises the spontaneous ignition of fuel in a diesel engine;[1] likewise, so does formaldehyde, from the thermal decomposition of *s*-trioxane.[2] Synergy occurs between CH_2O and NO_2, so that if both are released simultaneously, the ignition quality of the fuel is even more enhanced. The efficiency of 2-ethylhexyl nitrate as a sensitiser of diesel-fuel ignition arises because following its dissociation into NO_2 and an alkoxy radical, a fraction[3] of these radicals goes on to eliminate CH_2O. However, with increasing legislative pressure to minimise NO_x emissions,[4] strategies for increasing the ratio of CH_2O/NO_2 formation could be beneficial.

An obvious choice is the thermal decomposition of phenethyl nitrate [eqn. (1)], not only giving the desired

$$PhCH_2CH_2ONO_2 \rightarrow PhCH_2CH_2O + NO_2 \rightarrow PhCH_2 + CH_2O + NO_2 \quad (1)$$

products in equal amounts, but yielding also benzyl radicals, which are powerful ignition sensitisers.[5] The hoped-for advantage, however, does not materialise in engine measurements[6] because in the temperature range of interest (*ca.* 650–800 K), phenethyl nitrate[7] decomposes an order of magnitude more slowly than does 2-ethylhexyl nitrate[3a]

(phenethyl nitrate: $k = 5.0 \times 10^{13} e^{-35,600/1.987T}$ s^{-1};
2-ethylhexyl nitrate: $k = 2.5 \times 10^{15} e^{-37,500/1.987T}$ s^{-1}).

N-Methyl-1,3,5,2-trioxazinane, by analogy with the thermal decomposition of *s*-trioxane into three CH_2O molecules (or other symmetrically substituted alkyltrioxanes into three aldehyde molecules),[8] should yield two CH_2O molecules and MeNO, the latter decomposing rapidly to give NO and thence NO_2 in the presence of excess oxygen [eqn. (2)].

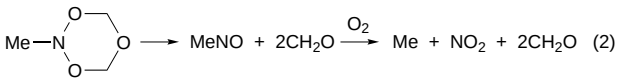

(2)

Thus, we explored a parallel set of GAUSSIAN 94 molecular orbital calculations[9] for these two molecules. Their equilibrium geometries were found at the RHF/6-31G** level of theory, as were the transition states for the concerted dissociations [eqns. (3) and (4)], with key energies further

$$(CH_2O)_3 \rightarrow 3CH_2O \quad (3)$$

$$MeNO(CH_2O)_2 \rightarrow MeNO + 2CH_2O \quad (4)$$

refined at the MP2 and/or MP4 levels. All characteristic structures were verified by harmonic vibration analysis, and by demonstrating that equivalent structures could be found by non-local density functional calculations; in the case of *s*-trioxane, all of the reported structures were duplicated with both the B3LYP and BHandHLYP functionals, but for brevity only the latter results are presented. Also, for the *N*-methyl-1,3,5,2-trioxazinane molecule, because of its increased size and complexity, slightly less demanding levels of approximation were used, and extensive searches were made for both singlet and triplet configurations to eliminate the possibility of a lower energy path for the breakup or structural rearrangement. The results of these calculations are collected together in Tables 1 and 2.

For *s*-trioxane, the minimum energy configuration is, as expected, in the chair form, with C–O and C–H bond lengths each within 1% of 1.40 and 1.08 Å, respectively, in all levels of approximation. Also, there is always a local minimum for the $(CH_2O)_2$ configuration, with bond lengths approximately 1% longer than in *s*-trioxane. The transition state for the dissociation was characterised by an imaginary vibrational degree of freedom which corresponds precisely to a concerted dissociation into three CH_2O molecules. At the energy maximum, the C–O bonds now alternate between 1.25 and 1.90 Å in length, compared with the calculated C–O distance in formaldehyde itself of *ca.* 1.20 Å. Concerted dissociations of six-membered ring compounds into three identical fragments, *viz*. 1,3,5-triaza-

Table 1 RHF/6-31G** energies for the reaction systems $(CH_2O)_3 \rightarrow 3CH_2O$ and $MeNO(CH_2O)_2 \rightarrow MeNO + 2CH_2O$

System[a]	Symmetry	*E*/a.u.[b]	zpe/a.u.[b]
CH_2O	C_{2v}	−113.8697	0.0290
$(CH_2O)_2$	D_{2h}	−227.7374	0.0689
‡$(CH_2O)_3$	C_3	−341.5580	0.0989
$(CH_2O)_3$	C_{3v}	−341.6649	0.1079
MeNO	C_s	−168.8344	0.0471
‡$MeNO(CH_2O)_2$	C_s	−396.5941	0.1242
$MeNO(CH_2O)_2$	C_1	−396.5021	0.1163

[a] ‡ Signifies the transition state. [b] 1 a.u. = $2I_H$ = 27.2 eV = 627.5 kcal mol^{-1} = 2625.5 kJ mol^{-1}.

Table 2 Density functional, MP2 and MP4 estimates of energy differences in the $(CH_2O)_3$ and $MeNO(CH_2O)_2$ reaction systems

System[a]	*E*/a.u.[b]	zpe/a.u.[b]	ΔE_0/a.u.[b]
BHandHLYP/6-311+G**			
$3CH_2O$	−343.4202	0.0828	+0.0434 (+27)
‡$(CH_2O)_3$	−343.3937	0.0944	+0.0815 (+51)
$(CH_2O)_3$	−343.4841	0.1033	0
BHandHLYP/6-311G*			
$MeNO + 2CH_2O$	−398.6663	0.1008	+0.0206 (+13)
‡$MeNO(CH_2O)_2$	−398.6392	0.1195	+0.0664 (+42)
$MeNO(CH_2O)_2$	−398.6981	0.1120	0
RMP2/6-31G**//RHF/6-31G**			
‡$(CH_2O)_3$	−342.5221	0.0989	+0.0783 (+49)
$(CH_2O)_3$	−342.6094	0.1079	0
‡$MeNO(CH_2O)_2$	−397.6463	0.1242	+0.0619 (+39)
$MeNO(CH_2O)_2$	−397.7161	0.1163	0
RMP4/6-311G**//RHF/6-31G**			
‡$(CH_2O)_3$	−342.7541	0.0989	+0.0717 (+45)
$(CH_2O)_3$	−342.8348	0.1079	0

[a] ‡ Signifies the transition state. [b] 1 a.u. = $2I_H$ = 27.2 eV = 627.5 kcal mol^{-1} = 2625.5 kJ mol^{-1}. Figures in parentheses in kcal mol^{-1}.

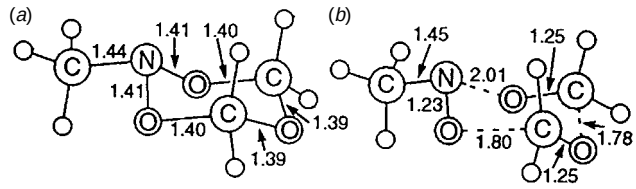

Fig. 1 Structures of (*a*) the lowest energy conformer of *N*-methyl-1,3,5,4-trioxazinane and (*b*) the transition state for dissociation. Distances are in Å.

cyclohexane → $3H_2C{=}NH$, trinitro-1,3,5-triazacyclohexane → $3H_2C{=}N{-}NO_2$ and *sym*-triazine → 3HCN, have been studied previously by molecular orbital methods.[10]

The thermochemical results for dissociation into three CH_2O molecules are typical of what one can expect at the present time for a reaction with unequal numbers of reactants and products. The latest thermochemical data for *s*-trioxane[11] and for formaldehyde[12] give $\Delta H_{298} \simeq +33$ kcal mol^{-1}, or about +30 kcal mol^{-1} at 0 K; an alternative datum for formaldehyde[13] gives values of +28 and +25 kcal mol^{-1} respectively. The results for 0 K from these calculations are +22, +27, +28 and +20 kcal mol^{-1} from the RHF, DFT, MP2 and MP4 calculations respectively; unscaled zero point energies (zpe) are used in all calculations.

For *N*-methyl-1,3,5,2-trioxazinane there are six conformers, with the one of lowest energy being again in a chair configuration; we did not examine the other five structures beyond RHF/6-31G**. Again, all the C–H distances are about 1.08–1.09 Å and the lowest path to dissociation is a concerted one, but the structure of the transition state is slightly asymmetric; the two structures are shown in Fig. 1. Comparison of the energies given in Table 2 would suggest that both the enthalpy and activation energy for the dissociation into three fragments are about 10 kcal mol^{-1} less for this molecule than for *s*-trioxane.

There have been several kinetic studies of the thermal decomposition of *s*-trioxane: in the 500–800 K temperature range, three conventional studies[14] all gave activation energies of between 47–48 kcal mol^{-1}, and frequency factors of $10^{14.80}$ to $10^{15.28}$ s^{-1}; in addition, a high-temperature shock tube study[15] gives results that extrapolate nicely into this body of measurements. By comparison, our MP2 and MP4 results for the activation energy at 0 K are 49 and 45 kcal mol^{-1} respectively.

A straightforward transition state calculation[16] of the rate constant for the thermal dissociation of *s*-trioxane over the temperature range 500–800 K yields an Arrhenius *A* factor of $10^{15.56}$ s^{-1}, and an activation energy of 52.1 or 48.1 kcal mol^{-1}, depending upon which value of the critical energy is used.¶ These results compare favourably with the experimental ones quoted above.

Likewise, for *N*-methyl-1,3,5,2-trioxazinane decomposing into $2CH_2O$ + MeNO, we find an Arrhenius *A* factor of $10^{15.25}$ s^{-1}, and an activation energy of 41.7 kcal mol^{-1}, using the frequency data and the MP2 result for the critical energy of activation.¶ These rate parameters are rather similar to those for 2-ethylhexyl nitrate, noted above, making this new substance an ideal candidate for a diesel-fuel ignition sensitiser.

The close parallels between the various structures in the two systems, and moderate acceptability of the *s*-trioxane results (both for the thermochemistry and the reaction rate), tend to suggest that the calculations on *N*-methyl-1,3,5,2-trioxazinane can be accepted with a reasonable degree of confidence. Thus, *N*-methyl-1,3,5,2-trioxazinane should be a stable molecule, with an activation energy for concerted dissociation into nitrosomethane and formaldehyde in the region of 35–40 kcal mol^{-1}. In which case, it may seem surprising that this heterocycle has apparently never been reported, particularly since quite a number of examples of *N*,*N*-dialkoxy-*N*-alkylamines or *N*,*N*-dialkoxybenzamides are known.[17]

This work was supported both by the Natural Sciences and Engineering Research Council of Canada and by Imperial Oil Products Division, Sarnia. We also thank Dr D. N. Butler for suggesting this idea, and for many helpful comments.

Notes and References

† This ChemComm is also available in enhanced multi-media format *via* the World Wide Web: http://rsc.org/ccenhanced

‡ Present address: Emulsion Research Laboratory, Eastman Kodak Company, Rochester, NY, USA, 14650-1736.

§ E-mail: huw@yorku.ca

¶ The following are the vibrational and rotational constants, at the DFT-RHF/6-311G* level of approximation, used in the transition state calculations; vibrational degeneracies, if any, are in parentheses.

s-Trioxane, ground state: vibration: 298(2), 468, 555(2), 803, 1009(2), 1033, 1059, 1130(2), 1265(2), 1295, 1309, 1390(2), 1460, 1504(2), 1566(2), 1585, 3041(2), 3058, 3245(2), 3248 cm^{-1}; rotation: 0.1793, 0.1793, 0.09938 cm^{-1}.

s-Trioxane, transition state: vibration: 176(2), 276(2), 315, 461(2), 547, 911, 943(2), 1178, 1278(2), 1289, 1290(2), 1473, 1511(2), 1644, 1691(2), 3071(2), 3072, 3210(2), 3212 cm^{-1}; rotation: 0.1451, 0.1451, 0.07979 cm^{-1}.

N-Methyl-1,3,5,2-trioxazinane, ground state: vibration: 192, 251, 345, 371, 398, 512, 594, 618, 821, 888, 900, 1024, 1050, 1145, 1146, 1203, 1219, 1239, 1275, 1320, 1360, 1406, 1479, 1505, 1519, 1547, 1560, 1564, 1582, 3112, 3120, 3142, 3231, 3259, 3263, 3265 cm^{-1}; rotation: 0.1777, 0.09097, 0.06509 cm^{-1}.

N-Methyl-1,3,5,2-trioxazinane, transition state: vibration: 149, 189, 213, 253, 280, 307, 341, 488, 517, 589, 629, 975, 1036, 1067, 1141, 1214, 1257, 1290, 1309, 1347, 1456, 1474, 1493, 1504, 1546, 1550, 1639, 1667, 3066, 3114, 3138, 3177, 3226, 3227, 3286 cm^{-1}; rotation: 0.1429, 0.08135, 0.05610 cm^{-1}.

1 P. Q. E. Clothier, B. D. Aguda, A. Moise and H. O. Pritchard, *Chem. Soc. Rev.*, 1993, **22**, 101.
2 P. Q. E. Clothier, H. O. Pritchard and M.-A. Poirier, *Combust. Flame*, 1993, **95**, 427.
3 (*a*) H. O. Pritchard, *Combust. Flame*, 1989, **75**, 415; (*b*) M. A. R. Al-Rubaie, J. F. Griffiths and C. G. W. Sheppard, *Some observations on the effectiveness of additives for reducing the ignition delay period of diesel fuels*, SAE Technical Paper Series, 1991, 912333.
4 G. Baumbach, *Air Quality Control*, Springer, Berlin, 1996, ch. 2, 7 and 8.
5 P. Q. E. Clothier, D. Shen and H. O. Pritchard, *Combust. Flame*, 1995, **101**, 383.
6 P. Q. E. Clothier and H. O. Pritchard, unpublished work.
7 M. A. Hiskey, K. R. Brower and J. C. Oxley, *J. Phys. Chem.*, 1991, **95**, 3955.
8 C. C. Coffin, *Can. J. Res. (B)*, 1932, **7**, 75; 1933, **9**, 603.
9 See M. J. Frisch, A. Frisch and J. B. Foresman, *GAUSSIAN 94 User's Reference*, Gaussian, Inc., Pittsburgh PA, 1996, p. 2, for complete citation.
10 D. Habibollahzadeh, M. Grodzicki, J. M. Seminario and P. Politzer, *J. Phys. Chem.*, 1991, **95**, 7699; S. V. Pai, C. F. Chabalowski and B. M. Rice, *ibid*., 1996, **100**, 15 368.
11 M. Mansson, E. Morowetz, Y. Nakase and S. Sunner, *Acta Chem. Scand.*, 1969, **23**, 15.
12 R. A. Fletcher and G. Pilcher, *Trans. Faraday Soc.*, 1970, **66**, 794.
13 *JANAF Thermochemical Tables*, 2nd edn., NSRDS-NBS 37, National Bureau of Standards, Washington, D.C., 1971.
14 R. Le G. Burnett and R. P. Bell, *Trans. Faraday Soc.*, 1938, **34**, 420; W. Hogg, D. M. McKinnon, A. F. Trotman-Dickenson and G. J. O. Verbeke, *J. Chem. Soc.*, 1961, 1403; S. Hochgreb and F. L. Dryer, *J. Phys. Chem.*, 1992, **96**, 295.
15 E. A. Irdam and J. H. Kiefer, *Chem. Phys. Lett.*, 1990, **166**, 491.
16 S. Glasstone, K. J. Laidler and H. Eyring, *The theory of rate processes*, McGraw-Hill, New York, 1941, p. 192.
17 V. F. Rudchenko, S. M. Ignatov and R. G. Kostyanovskii, *J. Chem. Soc., Chem. Commun.*, 1990, 261; J. J. Campbell and S. Glover, *J. Chem. Soc., Perkin Trans. 2*, 1992, 1661 and references cited therein.

Received in Cambridge, UK, 11th November 1997; 7/08108A

On the 'Novel two-phase oxidative cross-coupling of the two-component molecular crystal of 2-naphthol and 2-naphthylamine'[1]

Štěpán Vyskočil,*[a,b] Martin Smrčina,[a] Miroslav Lorenc,[a] Vladimír Hanuš,[c] Miroslav Polášek[c] and Pavel Kočovský*[b]†

[a] *Department of Organic Chemistry, Charles University, 128 40, Prague 2, Czech Republic*
[b] *Department of Chemistry, University of Leicester, Leicester, UK LE1 7RH*
[c] *J. Heyrovský Institute of Physical Chemistry, Academy of Sciences of the Czech Republic, 182 23 Prague 8, Czech Republic*

The $FeCl_3$-mediated, heterogeneous cross-coupling of the title compounds (1 + 2 → 3) has been re-examined and formation of the molecular crystal (1 + 2) shown to be irrelevant to the selectivity observed; a comparison of Fe^{III} and Cu^{II} as reagents is presented.

Oxidative self-coupling of 2-naphthol **1** is a well known reaction; the resulting BINOL **4** constitutes a pivotal intermediate in the synthesis of numerous chiral ligands, such as BINAP and MOP.[2] A number of mild oxidants have been reported to effect this coupling, in particular Cu^{II}, Fe^{III} and Mn^{III} salts.[3]

In a recent paper, Ding *et al.*[1] reported on the Fe^{III}-mediated, two-phase oxidative cross-coupling of the title compounds to produce (±)-2-amino-2′-hydroxy-1,1′-binaphthyl (NOBIN) (**1** + **2** → **3**, Scheme 1) and rationalised this outcome as being due to the unique formation of the molecular crystal **1** + **2** prior to the reaction. We challenge this communication for the following reasons. Firstly, in 1991, we had published the very same cross-coupling (**1** + **2** → **3**), mediated by Cu^{II} in a methanolic solution,[4,5] which demonstrates that this selectivity is not exclusive to the heterogeneous system. Secondly, this is not the only case of a highly selective cross-coupling; there are about twenty examples of this kind known to date which all occur in a homogeneous solution.[4–8] Thirdly, Ding's mechanism[1] is in conflict with that proposed by us.[6] Here we present a direct comparison of Ding's protocol with our published procedure and offer evidence which does not support the mechanism proposed by Ding.

We have shown that 2-naphthol **1** and 2-naphthylamine **2** can be cross-coupled by treatment with a complex generated *in situ* from $CuCl_2$ and an amine, such as $BnNH_2$ or Bu^tNH_2; in a methanolic solution and under anaerobic conditions, the resulting NOBIN **3** is obtained in up to 85% yield. As by-products, we have detected the diol **4** (6%) and diamine **5** (2%). The presence of an amine is crucial for high conversion and selectivity;[4–7] if a chiral amine is employed, acceptable enantioselectivity is attained (46% ee in the case of **3** and up to ⩾99% ee for **4**).[5]

In contrast to the previous experiments, which were carried out in homogeneous solutions,[3–8] Ding *et al.*[1] used a suspension of the pre-formed mixture of **1** and **2** in water and $FeCl_3$ as the oxidant. At 55 °C the conversion was practically quantitative and the yields fo **3** were in the range of 71–82% in typical instances; **4** (13–19%) was identified as the only by-product, while **5** was not detected.

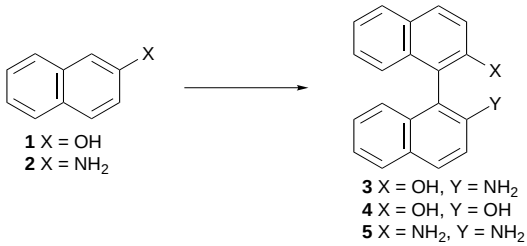

1 X = OH
2 X = NH_2

3 X = OH, Y = NH_2
4 X = OH, Y = OH
5 X = NH_2, Y = NH_2

Scheme 1

We have rationalised the striking preference for the cross-coupling as follows: in the pair to be cross-coupled, one partner has to be prone to a ready, one-electron oxidation (as documented by cyclic voltammetry and *ab initio* calculations) and the other should be capable of trapping the radical-like species thus generated;[6]‡ the coupling itself apparently occurs in the co-ordination sphere of the metal (*vide infra*).[5b,6,8d,8e] If the redox potentials of the two partners differ sufficiently (as is the case for **1** and **2** and several other combinations), high preference for the cross-coupling can be anticipated. On the other hand, if the latter difference is small, the reaction becomes non-selective and mixtures of cross- and self-coupled products are obtained.[6] Ding *et al.* proposed a different mechanism, according to which **1** and **2** form a molecular crystal (or a molecular compound) and the coupling occurs either in the solid state or at the boundary between the solid and liquid phases.[1] The favourable orientation of **1** and **2** in the latter crystal is then assumed to control the coupling reaction to produce mainly **3**, whereas the self-coupling processes, which would lead to **4** and **5**, are suppressed.[1]

Ding's molecular crystal (or compound) is, presumably, formed as a result of interaction of a weak Brønsted acid **1** with a weak base **2**. Therefore, the differences in the IR spectra and in the powder X-ray diffraction characteristics he reported for the crystal and the individual components[1] are not unexpected.§

In a typical experiment, carried out with a suspension of the molecular crystal in an aqueous solution of $FeCl_3$ at 55 °C, high preference for the cross-coupling was observed (82% of **3** and 14% of **4**), ¶‖ which was interpreted by Ding as evidence for the crucial role of the molecular crystal in controlling the chemoselectivity.[1] On the other hand, when solid **1** and **2** were added separately to an aqueous solution of $FeCl_3$ at 55 °C, very similar selectivity was observed (78% of **3** and 20% of **4**).[1] To account for this result, Ding suggested a rapid formation of the molecular crystal prior to the coupling.[1]**

We find little support for the proposed mechanism on the grounds of the experiments[1] presented. First of all, neither **1** nor **2** is entirely insoluble in water: 1 g of **1** is dissolved in 1 l of water at ambient temperature, while the same amount will dissolve in 80 ml of boiling water.[9] According to our experience, the solubility of **2** is similar to that of **1**.†† Hence, appreciable amounts of each of **1** and **2** must be dissolved under the reaction conditions both at room temp. and, especially, at 55 °C. This alone casts doubts on Ding's mechanism and suggests that the oxidative coupling does, in fact, occur in the aqueous phase and is controlled by the factors[6] we have identified. Furthermore, Ding observed a loss of selectivity when $FeCl_3$ was replaced by other Fe^{III} salts, namely $Fe_2(SO_4)_3$ or NH_4FeCl_4, as oxidants. We believe this is further in conflict

with Ding's hypothesis. Should the selectivity originate from the molecular crystal, the nature of the metal ligands would be irrelevant.‡‡

To address these issues, we have carried out the following experiment: equimolar amounts of **1** and **2** were dissolved in CH_2Cl_2 and stirred vigorously with an aqueous solution of $FeCl_3$ at room temp. for 48 h. With this two-phase system we obtained similar selectivity to that reported by Ding¶‖ (the ratio of **3**, **4** and **5** was 79 : 9 : 12, as revealed by GC), although the conversion (*ca*. 50%) was not as high, presumbably owing to the lower temperature and the lower concentration of the reactants in the aqueous phase in our case.

In conclusion, we have shown that the cross-coupling of **1** and **2**, suspended in an aqueous solution of $FeCl_3$, most likely occurs in solution (note that the reactants are sparingly soluble in water). The selectivity observed does not originate from the existence of the molecular crystal and can be attributed to the different redox properties of the reaction partners, as proposed earlier by us.[6] Since the product **3** is much less soluble than the reactants, its formation siphons off the reactants from the solution and the system obeys the Le Chatelier–Braun principle. Under these conditions, BINOL **4** is the main contaminant. When carried out in a methanolic solution with Cu^{II}, less BINOL is formed but some diamine **5** can be detected (*vide supra*).[6] These marginal differences between the two methods are presumably associated with the nature of the oxidant (Fe *vs.* Cu) rather than with the homogeneity or non-homogeneity of the reaction mixture. Carrying out the reaction in aqueous suspension appears to have the advantage of simplicity if racemic NOBIN **3** is required. However, its asymmetric verison remains to be developed if this method is to be competititve with the homogeneous protocol. The same conclusion holds for the synthesis of BINOL **4** by the self-coupling of **1**.

We thank the GAČR for grant No 203/97/1009, GAUK for grant No 86/95 and the Britisch Council and the University of Leicester for additional support.

Notes and References

† E-mail: pk10@le.ac.uk

‡ Ding *et al.* [ref. 3(*k*)] proposed an analogous mechanism for the self-coupling of **1** to give **4** after our original communication (ref. 6).

§ Ding has reported the following IR peaks: **1**, 3250; **2**, 3375, 3290, 3170; **1** + **2**, 3350, 3260 cm^{-1}. Our values (obtained in substance by means of the 'Golden Gate' technique) were as follows: **1**, 3197; **2**, 3390, 3302, 3197; **1** + **2**, 3363, 3275 cm^{-1} (or 3364, 3357 sh, 3283 cm^{-1} for a suspension of the latter mixture in fluorolube). On the other hand, a 10^{-3} M solution of the mixture in CCl_4 represented a clear superposition of the spectra of the two components. All this indicates a strong intermolecular hydrogen bonding between **1** and **2** in the solid state, which disappears on dissolving in a nonpolar solvent; therefore, selective pairing in protic solvents, such as water or alcohols, is unlikely.

¶ A rigorous, quantitative interpretation of Ding's experiments is difficult. Based on the HPLC analysis, he claimed to obtain **3** (82%) and **4** (14%) at 100% consumption of **1**. Since *two* molecules of **1** are required to form **4**, these yields would appear to be impossible since the total would exceed 100% (see note ‖).

‖ We have repeated Ding's experiment. A capillary GC (using a DB5 column, 15 m × 0.5 mm, at 220 °C) with FID gave a 90 : 8 : 2 ratio of **3**, **4** and **5** in the crude product.

** In this instance, the molecular crystal is presumably formed in an equilibrium process that involves partial dissolving of each of the components and crystallisation of the less soluble molecular crystal.

†† Note that both **1** and **2** can be purified by crystallisation from hot water.

‡‡ The ligands' crucial role is further evidenced by asymmetric induction, observed in the presence of enantiopure amines (ref. 5). Moreover, this effect indicates that the coupling does occur in the co-ordination sphere of the metal (or, at least, in its vicinity) (ref. 5), rather than *via* a free-radical species. For details and further discussion, see refs. 5(*b*), 8(*d*) and 8(*e*).

1 K. Ding, Q. Xu, Y. Wang, J. Liu, Z. Yu, B. Du, Y. Wu, H. Koshima and T. Matsuura, *Chem. Commun.*, 1997, 693.

2 For reviews, see: C. Rosini, L. Franzini, A. Raffaelli and P. Salvadori, *Synthesis*, 1992, 503; R. Noyori, *Asymmetric Catalysis in Organic Synthesis*, Wiley, New York, 1994; T. Hayashi, *Acta Chem. Scand.*, 1996, **50**, 259.

3 Cu^{II}: (*a*) B. Ferringa and H. Wynberg, *Tetrahedron Lett.*, 1977, 4447; (*b*) B. Ferringa and H. Wynberg, *Bioorg. Chem.*, 1978, **7**, 397; (*c*) K. Kushioka, *J. Org. Chem.*, 1983, **48**, 4948; (*d*) K. Yamamoto, H. Fukushima and M. Nakazaki, *J. Chem. Soc., Chem. Commun.*, 1984, 1490; (*e*) J. Brussee, J. L. G. Groenendijk, J. M. te Koppele and A. C. A. Jansen, *Tetrahedron*, 1985, **41**, 3313; (*f*) T. Sakamoto, H. Yonehara and C. Pac, *J. Org. Chem.*, 1994, **59**, 6859. Cu^{II}/O_2: (*g*) M. Noji, M. Nakajima and K. Koga, *Tetrahedron Lett.*, 1994, **35**, 7983; (*h*) B. H. Lipshutz, B. James, S. Vance and I. Carrico, *Tetrahedron Lett.*, 1997, **38**, 753. Fe^{III}: (*i*) R. Pummerer and A. Rieche, *Chem. Ber.*, 1926, 59; (*j*) F. Toda, K. Tanaka and S. Iwata, *J. Org. Chem.*, 1989, **54**, 3007 and references cited therein; (*k*) K. Ding, Y. Wang, L. Zhang, Y. Wu and T. Matsuura, *Tetrahedron*, 1996, **52**, 1005. Mn^{III}: (*l*) M. J. S. Dewar and T. Nakaya, *J. Am. Chem. Soc.*, 1968, **90**, 7134; (*m*) K. Yamamoto, H. Fukushima, Y. Okamoto, K. Hatada and M. Nakazaki, *J. Chem. Soc., Chem. Commun.*, 1984, 1111; (*n*) F. Diederich, M. R. Hester and M. Uyeki, *Angew. Chem., Int. Ed. Engl.*, 1988, **27**, 1705. Other methods involve melting the reactant or ball-milling in the presence of $FeCl_3.6H_2O$: (*o*) J. Bao, W. D. Wulff, J. B. Dominy, M. J. Fumo, E. B. Grant, A. C. Rob, M. C. Whitcomb, S. M. Yeung, R. L. Ostrander and A. L. Rheingold, *J. Am. Chem. Soc.*, 1996, **118**, 3392; (*p*) M. O. Rasmussen, O. Axelson and D. Tanner, *Synth. Commun.*, 1997, **27**, 4027.

4 M. Smrčina, M. Lorenc, V. Hanuš and P. Kočovský, *Synlett*, 1991, 231.

5 (*a*) M. Smrčina, M. Lorenc, V. Hanuš, P. Sedmera and P. Kočovský, *J. Org. Chem.*, 1992, **57**, 1917; (*b*) M. Smrčina, J. Poláková, Š. Vyskočil and P. Kočovský, *J. Org. Chem.*, 1993, **58**, 4534.

6 M. Smrčina, Š. Vyskočil, B. Máca, M. Polášek, T. A. Claxton, A. P. Abbott and P. Kočovský, *J. Org. Chem.*, 1994, **59**, 2156.

7 M. Smrčina, Š. Vyskočil, J. Polívková, J. Poláková and P. Kočovský, *Collect. Czech. Chem. Commun.*, 1996, **61**, 1520.

8 (*a*) K. Yamamoto, H. Yumioka, Y. Okamoto and H. Chikamatsu, *J. Chem. Soc., Chem. Commun.*, 1987, 168; (*b*) M. Hovorka, J. Günterová and J. Závada, *Tetrahedron Lett.*, 1990, **31**, 413; (*c*) M. Hovorka and J. Závada, *Org. Prep. Proceed. Int.*, 1991, **23**, 200; (*d*) M. Hovorka, J. Ščigel, J. Günterová, M. Tichý and J. Závada, *Tetrahedron*, 1992, **48**, 9503; (*e*) M. Hovorka and J. Závada, *Tetrahedron*, 1992, **48**, 9517.

9 *The Merck Index*, 12th edn., Merck & Co., Inc., Whitehouse Station, NJ, 1996, p. 1096.

Received in Cambridge, UK, 14th November 1997; 7/08213D

A chlorophobic pocket in the *p-tert*-butylcalix[4]arene cavity: a test site for molecular recognition investigated by ^{13}C CP MAS NMR and X-ray crystallography†

Eric B. Brouwer,[a,b] Konstantin A. Udachin,[a] Gary D. Enright,[a] Christopher I. Ratcliffe[a] and John A. Ripmeester*[a,b]

[a] *Steacie Institute for Molecular Sciences, National Research Council of Canada, Ottawa, Ontario K1A 0R6, Canada*
[b] *Ottawa-Carleton Chemistry Institute, Carleton University Campus, 1125 Colonel By Drive, Ottawa, Ontario K1S 5B6, Canada*

Five-membered aliphatic guests X(CH$_2$)$_3$Y (X, Y = Me, OH, Cl, Br) adopt equilibrium positions in the asymmetric *p-tert*-butylcalix[4]arene cavity formed in the solid state and reveal a marked aversion of the host pocket for halogen end-groups.

Weak interactions are expected to play an important role in the construction of complex materials *via* self-assembly processes.[1] Although there are many studies of interactions involving H-bonding or π-stacking, there appear to be few methods where the relative importance of other weak interactions can be gauged in an unambiguous way.[2] Here we report on the use of the deep pocket in solid *p-tert*-butylcalix[4]arene host–guest materials as a site for testing relative interaction strengths, a concept also explored for guests in channel clathrates.

Recently we have reported the preparation and structural characterization of *p-tert*-butylcalix[4]arene (*t*-BC) compounds with aliphatic guests.[3] One example is the compound with pentane where the diffraction studies show that the guest molecule is inserted along the four-fold symmetry axis of the calix in the all-*trans* conformation with one methyl group deeply inserted in the calix cavity. It is therefore quite interesting that the ^{13}C NMR spectrum of the solid shows the presence of a single methyl resonance with a chemical shift close to where it is expected for pentane in solution (**1**, Table 1) rather than resonances for inequivalent methyls with one resonance shifted upfield by *ca*. 5 ppm owing to ring current effects from the four proximate aromatic rings of the calix.[4,5] The conclusion is that the pentane molecule can invert itself in the cavity on an NMR timescale. This process probably involves low concentrations of transient *gauche* isomers invisible in the diffraction experiment. The important conclusion is that linear molecules with an equivalent length of up to five carbon atoms are free to take up equilibrium orientations and conformations inside the calix cavity. This differs from monosubstituted and *para*-disubstituted aromatic guests in *t*-BC,[5,6] where the orientation of the guest is locked in during crystallization. The strongly asymmetric calix cavity therefore offers the unique possibility of using the deep pocket as a test site for molecular recognition for molecules of the type X(CH$_2$)$_3$Y (Table 1). A somewhat similar strategy has been followed in the pursuit of end group interaction energies for guests in channel clathrates.[12]

Table 1 45.3 MHz ^{13}C CP MAS NMR chemical shifts for the guest in *p-tert*-butylcalix[4]arene·guest compounds **1**–**5**; $\Delta\delta$ refers to the difference in the guest carbon chemical shift between $CDCl_3$ solution and the host

Guest X(CH$_2$)$_3$Y	X	Y	Carbon chemical shifts			
			Carbon	δ(calix)[a]	δ(solution)	$\Delta\delta$
1	CH_3	CH_3	CH_3	12.3	13.7	−1.4
			C^2	15.9	15.9	0.0
			C^3	—[b]	34.6	—[b]
2	CH_3	Cl	CH_3	8.7	13.0	−4.3
			C^3	23.5	23.0	+0.5
			C^2	35.6	34.7	+0.9
			C^1	45.0	44.3	+0.7
3	CH_3	Br	CH_3	9.0	13.0	−4.0
			C^3	22.3	21.2	+1.1
			C^2	—[b]	33.0	—[b]
			C^1	36.0	34.7	+1.3
4	Cl	Cl	C^2	29.0	34.4	−4.4
			C^1	40.4	41.1	−0.7
5	CH_3	OH	CH_3	12.2	13.6	−1.4
			C^2	—[b]	35.0	—[b]
			C^3	18.4	19.1	−0.7
			C^1	59.1	61.4	−1.7

[a] Solid-state NMR spectra were obtained on a Bruker CXP-180 spectrometer under cross-polarization and magic angle spinning conditions. Probe: Bruker 7 mm; number of acquisitions 200–500; recycle time 4 s; 90° pulse 3.5 μs; contact time 3–5 ms; 4 K data points acquired and zero-filled to 16 K before processing; spectral width = 20 kHz; ν = 3.5 kHz. [b] The guest resonance in the solid is hidden under host resonances.

Examination of the ^{13}C NMR spectra of the guest inclusions with 1-chlorobutane and 1-bromobutane indicates that in this case the methyl resonances show the expected high field shifts for methyl groups inserted deeply inside the cavity (Table 1). This implies that the halogens are excluded from the cavity. A single-crystal X-ray diffraction study of the 1-chlorobutane compound confirms that this is indeed the case (Fig. 1).‡ The alkyl chain is inserted in the pocket, with the chlorine outside the cavity and situated just off the calixarene four-fold axis. The depth of penetration is limited by the unusual conformation of the chain which places C^2 and C^3 in close contact with the calix walls. We can exclude the influence of Cl···Cl interactions on the guest orientation,[2,7] as the Cl atoms are at least 6 Å apart. Although the X-ray structure is not of as high a quality as the

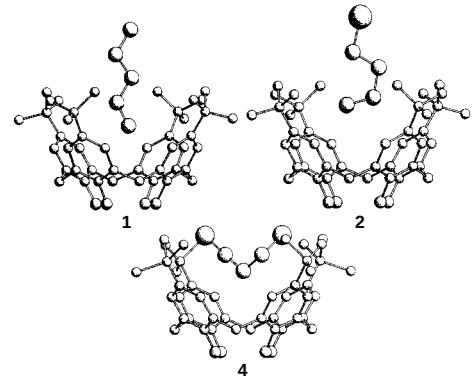

Fig. 1 Geometry of *p-tert*-butylcalix[4]arene inclusion compounds with pentane (**1**), 1-chlorobutane (**2**) and 1,3-dichloropropane (**4**). Only one of four symmetry-related guests is shown for **1** and **2**. For **4**, there is a second independent guest orientation, giving eight positions in all.

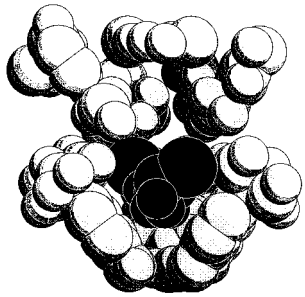

Fig. 2 A cutaway view of the highly anisotropic *p-tert*-butylcalix[4]arene cavity, showing the location of the 1,3-dichloropropane guest (**4**). The chlorophobic pocket is at the bottom in the cleft between aromatic rings.

others, the orientation of the guest is certain. Placing the chain with Cl in the cavity decreases the quality of the refinement.

Examination of the crystal structure of the compound with 1,3-dichloropropane (Fig. 1) is even more instructive, as now both chlorine atoms are excluded in favour of penetration of the cavity by a methylene group. The guest molecule is disordered equally over two orientations not related by symmetry which are in turn disordered equally about the compound's fourfold symmetry axis. Well defined positions for all guest atoms can be found, thus yielding eight possible orientations for the 1,3-dichloropropane guest. The carbon chemical shifts show only two guest lines (Table 1), indicating that the observed guest conformations are able to interchange. Considerable mobility of the guests is confirmed by dipolar dephasing experiments,[8] which show that both the terminal and central methylenes are mobile on an NMR timescale. It is interesting to note that the central methylene resonance is shifted by *ca*. 4 ppm, consistent with considerable penetration of the deep pocket by this group as observed in the diffraction study. This is also illustrated in Fig. 2, which shows a cutaway view of the calixarene cavity and illustrates its highly anisotropic nature. For the structure in question, the upper part of the cavity is occupied by a water molecule for about half the cages in the structure.

Since the steric requirements for a chlorine atom and a methyl group are very similar, one must conclude that there are very specific electronic effects that cause the exclusion of the chlorine atom. It is clear that the approach presented here is able to distinguish quite small energy differences. For instance, for **2**, complete exclusion of Cl requires that the energy difference between Cl_{in} and Cl_{out} is at least *ca*. 4 *kT*, *ca*. 10 kJ mol^{-1}.

It is not expected that dipole moments play a determining role in orienting the guest. This was checked by studying a *t*-BC compound with an *n*-butanol guest. It is clear from the NMR results that for this guest (**5**) there is little or no preference for either CH_3 or OH in the deep pocket (Table 1). The diffraction results indicate that the guest is located in the structure as a *gauche* conformer with the penetrating group on the axis (as in **2**). It makes no difference to the refinement whether OH or CH_3 is taken to be the penetrating group. Interactions involving acidic H such as O–H$\cdot\cdot\pi$ and alkyne C–H$\cdot\cdot\pi$ interactions have been duly studied.[2,9,10] More specifically, interactions between electron-rich calix[4]resorcarene hosts and CH-containing guests have been described in terms of a polarization-induced dipole interaction between a soft base (the host) and soft acid (the guest).[11] In the *n*-butanol case, the O–H$\cdot\cdot\pi$ interaction seems to be no stronger than the interaction of the aliphatic methyl group with the calix pocket. As well as being polarizable (*i.e.* soft) the *t*-BC cavity is also basic due to the electron-donating CH_2, Bu^t and OH substituents on the aromatic rings that form the deep pocket. While the OH group is more acidic than the CH_3 group, it is also less polarizable (*i.e.* harder) and the observed lack of specificity likely reflects a balance between the hard/soft and acid/base characteristics of the guest end groups. For the Cl-bearing groups in **2** and **4**, Cl is a hard base that does not show any attractive interaction with the soft and basic host, and thus gives rise to the observed orientations.

We note that the study of *t*-BC compounds with guests that have one more carbon atom per chain also are likely to give new insight, as preliminary X-ray diffraction evidence suggests that the hexane molecule forms a 2 : 1 compound with both ends inserted deeply in the *t*-BC pocket.

In conclusion, pentane-like linear guest molecules are free to take up equilibrium orientations and conformations inside the *p-tert*-butylcalix[4]arene cavity. The soft and basic *t*-BC pocket includes the guest deep in the cavity with the preference: $CH_3 \approx OH > CH_2 > Br, Cl$. It is hoped that modelling calculations should be able to provide significant new insight into the detailed nature of the interactions governing the guest orientations.

Notes and References

* E-mail: jar@ned1.sims.nrc.ca

† Issued as NRCC no. 40856. E. B. B. and J. A. R. thank NSERC for partial support of this work and K. A. U. thanks the NATO Science Program for a Research Visit Grant.

‡ *Crystal data:* for **1**–**5**, space group *P*4/*n* (*Z* = 2). For **1** and **2**: Enraf Nonius CAD4 (Cu-Kα), *T* = 150 K, refinement against F_o. For **1**, $C_{44}H_{56}O_4{\cdot}C_5H_{12}$, *M* = 721.08, *a* = 13.0230(19), *c* = 12.6190(12) Å, *V* = 2140.2 Å^3, D_c = 1.119 g cm^{-3}, μ = 0.50 mm^{-1}, *F*(000) = 790.04, 2154 reflections measured, 2045 unique, 1641 with $I > 2.5\sigma(I)$, *R* = 0.048, R_w = 0.070, residual density −0.200 to 0.190 e Å^{-3}. For **2**, $C_{44}H_{56}O_4{\cdot}C_4H_9Cl$, *M* = 741.48, *a* = 13.0571(19), *c* = 12.5986(15) Å, *V* = 2144.4 Å^3, D_c = 1.148 g cm^{-3}, μ = 1.09 mm^{-1}, *T* = 150 K, *F*(000) = 806.73, 4048 reflections measured, 2046 unique, 1549 with $I > 2.5\sigma(I)$, *R* = 0.090, R_w = 0.131, residual density −0.84 to 1.37 e Å^{-3}. For **4** and **5**, Siemens SMART CCD, (Mo-Kα), *T* = 273 K, refined against F_o^2. For **4**: $C_{44}H_{56}O_4{\cdot}C_3H_6Cl_2$, *M* = 761.87, *a* = 12.8869(12), *c* = 13.1494(13) Å, *V* = 2183.8 Å^3, D_c = 1.159 g cm^{-3}, μ = 0.189 mm^{-1}, *F*(000) = 820, 8398 reflections measured, 1591 unique, 1113 with $I > 2\sigma(I)$, *R* = 0.039, R_w = 0.138, residual density −0.106 to 0.126 e Å^{-3}. For **5**: $C_{44}H_{56}O_4{\cdot}\ C_4H_{10}O$, *M* = 723.01, tetragonal, space group *P*4/*n*, *a* = 12.9590(3), *c* = 13.1041(15) Å, *V* = 2200.6 Å^3, D_c = 1.091 g cm^{-3}, μ = 0.069 mm^{-1}, *F*(000) = 488, 14494 reflections measured, 2845 unique, 1843 with $I > 2\sigma(I)$, *R* = 0.099, R_w = 0.239, residual density −0.215 to 0.366 e Å^{-3}. CCDC. 182/745.

1 G. R. Desiraju, in *Comprehensive Supramolecular Chemistry*, ed. J. L. Atwood, J. E. D. Davies, D. D. MacNicol and F. Vogtle, Pergamon/Elsevier, Oxford, 1996, p. 1.

2 G. R. Desiraju, *Angew. Chem., Int. Ed. Engl.*, 1995, **34**, 2133.

3 E. B. Brouwer, G. D. Enright and J. A. Ripmeester, *Supramol. Chem.*, 1996, **7**, 143.

4 T. Komoto, I. Ando, Y. Nakamoto and S. Ishida, *J. Chem. Soc., Chem. Commun.*, 1988, 135.

5 E. B. Brouwer, G. D. Enright, C. I. Ratcliffe and J. A. Ripmeester, *Supramol. Chem.*, 1996, **7**, 79.

6 G. Andreetti, R. Ungaro and A. Pochini, *J. Chem. Soc., Chem. Commun.*, 1979, 1005; R. Ungaro, A. Pochini, G. D. Andreetti and P. Domiano, *J. Chem. Soc., Perkin Trans. 2*, 1985, 197; M. Prager, R. Caciuffo, G. Amoretti, C. J. Carlile, G. Coddens, F. Fillaux, O. Francescangeli and F. Ugozzoli, *Mol. Phys.*, 1994, **81**, 609; G. D. Andreetti and F. Ugozzoli, in *Calixarenes*, ed. J. Vicens and V. Bohmer, Kluwer, Dordrecht, 1990, p. 87; E. B. Brouwer, G. D. Enright and J. A. Ripmeester, *Supramol. Chem.*, 1996, **7**, 7.

7 J. L. Atwood, L. J. Barbour, E. S. Dawson, P. C. Junk and J. Kienzle, *Supramol. Chem.*, 1996, **7**, 271; F. H. Allen, J. A. K. Howard, V. J. Hoy, G. R. Desiraju, D. S. Reddy and C. C. Wilson, *J. Am. Chem. Soc.*, 1996, **118**, 4081.

8 S. J. Opella and M. H. Frey, *J. Am. Chem. Soc.*, 1979, **101**, 5854.

9 S. A. Bourne, L. R. Nassimbeni, M. L. Niven, E. Weber and A. Weirig, *J. Chem. Soc., Perkin Trans. 2*, 1994, 1215; V. R. Pedireddi, D. S. Reddy, B. S. Goud, D. C. Craig, A. D. Rae and G. R. Desiraju, *J. Chem. Soc., Perkin Trans. 2*, 1994, 2353; H. Krupitsky, Z. Stein and I. Goldberg, *J. Inclusion Phenom.*, 1994, **20**, 211.

10 T. Steiner, E. B. Starikov, A. N. Amado and J. J. C. Teixeira-Dias, *J. Chem. Soc., Perkin Trans. 2*, 1995, 1321.

11 T. Fujimoto, R. Yanagihara, K. Kobayashi and Y. Aoyama, *Bull. Chem. Soc. Jpn.*, 1995, **68**, 2113; R. G. Pearson, *J. Chem. Educ.*, 1987, **64**, 561.

12 M. D. Hollingsworth and A. R. Palmer, *J. Am. Chem. Soc.*, 1993, **115**, 5881.

Received in Columbia, MO, USA, 29th September 1997; 7/05508K

Enantioselective epoxidation catalysed by ruthenium complexes with chiral tetradentate bisamide ligands

Nicole End and Andreas Pfaltz*

Max-Planck-Institut für Kohlenforschung, Kaiser-Wilhelm-Platz 1, D-45470 Mülheim an der Ruhr, Germany

Ruthenium complexes with chiral bis(dihydrooxazolylphenyl)oxalamide ligands catalyse the epoxidation of (*E*)-stilbene and (*E*)-1-phenylpropene with 69 and 58% ee, respectively, using $NaIO_4$ as oxidant.

The development of efficient catalytic methods for the enantioselective preparation of epoxides is an important objective of current research.[1–6] The most general and most effective catalysts available today are titanium–tartrate complexes for the epoxidation of allylic alcohols[6] and manganese–salen complexes[3,5] which allow the preparation of epoxides from certain *cis*-disubstituted, tri- and tetra-substituted alkenes with high ees. However, for other important classes of substrates such as terminal and *trans*-disubstituted olefins efficient enantioselective epoxidation catalysts are still lacking.

A method for the epoxidation of alkenes using $RuCl_3$, 2,2′-bipyridyl and $NaIO_4$ in a two-phase reaction medium has been reported.[7] Several attempts were made to render this system enantioselective by replacing bipyridyl with chiral ligands.[8,9] However, only low enantioselectivities have been obtained so far.

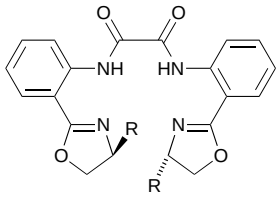

1a–e

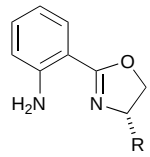

2a–e

a R = Me, **b** R = Pr^i, **c** R = Bu^t, **d** R = Bn, **e** R = Ph

We have recently developed an efficient synthesis of chiral C_2-symmetric oxalamides **1**, starting from readily available 2-(2-aminophenyl)oxazolines **2** and oxalyl chloride.[10] Oxalamides of this type possess a number of features which make them attractive ligands for enantiocontrol of metal-catalysed reactions, in particular for oxidations. A variety of differently substituted derivatives can be readily prepared in both enantiomeric forms starting from commercially available enantiopure precursors. The doubly deprotonated oxalamide **1** can act as a tetradentate ligand. Due to the π-acceptor properties of the α-dicarbonyl unit and the oxazoline rings, these ligands are expected to be quite resistant to oxidation and hence suitable for the formation of stable high-valent metal complexes. Here we report that ligands **1** can be used for the enantiocontrol of ruthenium-catalysed epoxidations.

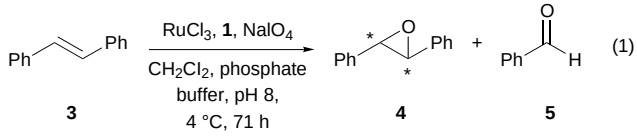

In preliminary experiments, following Balavoine's procedure,[7a] with 2 mol% of $RuCl_3 \cdot H_2O$ and 2 equiv. of $NaIO_4$ in the presence of 12 mol% of ligand **1b**, (*E*)-stilbene was epoxidised in 31% yield with an ee of 43%. Higher ees and somewhat better yields were obtained when an aqueous buffer was used instead of water [Table 1, reaction (1)]. In addition to the desired

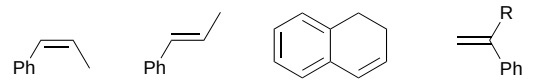

6 **7** **8** **9** R = H **10** R = Me

epoxide, significant amounts of benzaldehyde were formed. Control experiments showed that the epoxide **4** is stable under the reaction conditions. This implies that benzaldehyde is formed directly by oxidative cleavage of the olefin rather than by degradation of the epoxide.

Among the different oxalamides **1a–e**, the isopropyloxazoline derivative **1b** was found to be the most effective ligand. In contrast, the *tert*-butyloxazoline derivative **1c** gave poor ees and low yields of epoxide due to the formation of benzaldehyde, which is the main reaction in this case. Ligands **1a** and **1d** gave similar yields of epoxides as **1b** but somewhat lower ees. Interestingly, with ligand **1e** the opposite enantiomer of **4** was formed in 21% ee. In the absence of catalyst, (*E*)-stilbene was not oxidised by $NaIO_4$ under otherwise identical conditions. Replacing $NaIO_4$ by NaOCl resulted in very low yield and enantiomeric excess.

One of the problems in this reaction is the formation of benzaldehyde, which is rapid in the beginning (Fig. 1). In the initial period up to *ca*. 60% conversion, the alkene is consumed at about the same rate as benzaldehyde is formed while the formation of epoxide is much slower. The ee is very low in the beginning but increases significantly during the course of the reaction. We thought that these problems could possibly be overcome if the catalyst was treated with the oxidant prior to addition of the substrate. Indeed, the catalytic performance could be significantly improved using the following protocol. A suspension of $RuCl_3 \cdot H_2O$ (3.5 mg, 14 μmol) and ligand **1**

Table 1 Ruthenium-catalysed epoxidation of **3** using ligands **1a–e**

Entry	Ligand	Conversion (%)	Yields[a] (%) **4**	Yields[a] (%) **5**	Ee[b] (%)	Abs. Config.[c]
1	**1a**	> 99	42	21	42	(1*R*,2*R*)
2	**1b**	> 99	37	31	62	(1*R*,2*R*)
3	**1c**	> 99	4	65	21	(1*R*,2*R*)
4	**1d**	> 99	43	27	38	(1*R*,2*R*)
5	**1e**	69	19	34	21	(1*S*,2*S*)

[a] Determined by GC integration based on tridecane as internal standard. The yields of **4** and **5** are based on the conversion of alkene. [b] Determined by GC using a chiral capillary column (Chiraldex γ-CD-TFA, 30 m × 0.25 mm, 1 bar H_2, 150–157 °C (0.5° min^{-1}), 157 °C (1 min), 157–180 °C (30° min^{-1}), t_R = 11.9/12.1 min). [c] The absolute configuration was determined based on the sign of the optical rotation, see ref. 13.

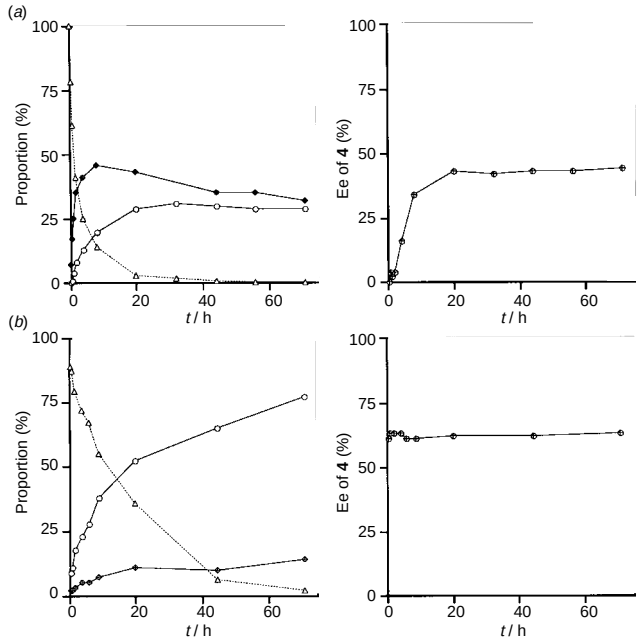

Fig. 1 Epoxidation of (*E*)-stilbene using ligand **1b** under (*a*) non-optimised (see text) and (*b*) optimised conditions: (△) **3**, (○) **4** and (◇) benzaldehyde **5**

(80 μmol) in aqueous buffer (2 ml, pH 8, 20 mM sodium phosphate) was stirred for 30 min at 4 °C. Subsequently, CH_2Cl_2 (3 ml) was added, followed by $NaIO_4$ (300 mg, 1.403 mmol). The resulting two-phase system was vigorously stirred for 4 h at 4 °C. Then (*E*)-stilbene (**3**) (125 mg, 0.694 mmol) was added and stirring continued for another 67 h. As shown in Fig. 1(*b*), the epoxide is now the major product and the enantiomeric excess remains constant during the reaction. Under these conditions **3** was converted to **4** in 74% yield (determined by GC based on tridecane as internal standard) with 69% ee. In a larger scale experiment with 3.5 mmol of **3**, the product **4** was isolated in 60% yield with the same ee after column chromatography. This is the best result obtained so far in the ruthenium-catalysed epoxidation of **3** with $NaIO_4$. After completion of this work, a ruthenium catalyst derived from a chiral bis(oxazolinyl)pyridine ligand was reported which gave up to 74% ee in the epoxidation of **3** with $PhI(OAc)_2$.[11] Interestingly, only benzaldehyde formation but no epoxidation was observed in this case when $NaIO_4$ was used as oxidant.

Using the same procedure, other alkenes were tested as substrates in the ruthenium-catalysed epoxidation with ligand **1b**. The epoxidation was found to be stereospecific for both (*E*)- and (*Z*)-alkenes. (*Z*)-1-Phenylpropene **6** was converted to the *cis*-epoxide in 50% yield with 25% ee. Significantly higher enantioselectivity was achieved for the epoxidation of the corresponding (*E*)-isomer **7** (58% ee, 40% yield). In this respect the ruthenium–oxalamide complexes resemble chromium–salen complexes[12] which also give higher ees with **7** than with the (*Z*)-isomer **6**, but differ from related manganese–salen or –porphyrin complexes[3–5] which afford higher ees for (*Z*)- than for (*E*)-olefins. Olefins **8**–**10** could not be used as substrates because the corresponding epoxides were not stable under the reaction conditions.

Notes and References

* E-mail: pfaltz@mpi-muelheim.mpg.de

1 B. E. Rossiter, in *Asymmetric Synthesis*, ed. J. D. Morrison, Academic Press, New York, 1985, vol. 5, ch. 7, pp. 193–246.
2 *Asymmetric Catalysis in Organic Synthesis*, ed. R. Noyori, Wiley, New York, 1994, pp. 137–150.
3 E. N. Jacobsen, in *Catalytic Asymmetric Synthesis*, ed. I. Ojima, VCH, New York, 1993, pp. 159–202.
4 J. T. Groves and R. S. Myers, *J. Am. Chem. Soc.*, 1983, **105**, 5791; J. P. Collman, X. Zhang, V. J. Lee, E. S. Uffelman and J. I. Brauman, *Science*, 1993, **261**, 1404; J. P. Collman, V. J. Lee, C. J. Kellen-Yuen, X. Zhang, J. A. Ibers and J. I. Brauman, *J. Am. Chem. Soc.*, 1995, **117**, 692.
5 T. Katsuki, *Coord. Chem. Rev.*, 1995, **140**, 189; T. Katsuki, *J. Mol. Catal.*, 1996, **113**, 87.
6 T. Katsuki and K. B. Sharpless, *J. Am. Chem. Soc.*, 1980, **102**, 5974; Y. Gao, R. M. Hanson, J. M. Klunder, S. Y. Ko, H. Masamune and K. B. Sharpless, *J. Am. Chem. Soc.*, 1987, **109**, 5765.
7 (*a*) G. Balavoine, C. Eskenazi, F. Meunier and H. Rivière, *Tetrahedron Lett.*, 1984, **25**, 3187; C. Eskénazi, G. Balavoine, F. Meunier and H. Rivière, *J. Chem. Soc., Chem. Commun.*, 1985, 1111; (*b*) for a review on Ru-catalysed epoxidations, see: G. A. Barf and R. A. Sheldon, *J. Mol. Catal.*, 1995, **102**, 23.
8 R.-Y. Yang and L.-X. Dai, *J. Mol. Catal.*, 1994, **87**, L1; (*b*) C. Augier, L. Malara, V. Lazzeri, and B. Waegell, *Tetrahedron Lett.*, 1995, **36**, 8775.
9 For stoichiometric enantioselective epoxidations with a chiral mono-oxoruthenium(IV) complex, see: W.-H. Fung, W.-C. Cheng, W.-Y. Yu, C.-M. Che and T. C. W. Mak, *J. Chem. Soc., Chem. Commun.*, 1995, 2007.
10 N. End, Dissertation, University of Basel, 1997; N. End and A. Pfaltz, *Chem. Eur. J.*, in the press.
11 H. Nishiyama, T. Shimada, H. Itoh, H. Sugiyama and Y. Motoyama, *Chem. Commun.*, 1997, 1863.
12 C. Bousquet and D. G. Gilheany, *Tetrahedron Lett.*, 1995, **36**, 7739.
13 H.-T. Chang and K. B. Sharpless, *J. Org. Chem.*, 1996, **61**, 6456.

Received in Cambridge, UK, 10th December 1997; 7/08874D

Binding of the uranyl moiety by an Amavadin-style complex; synthesis and characterisation of $[\{UO_2(H_2O)_3\}\{\Delta\text{-}V(hida)_2\}\cdot 2H_2O]_n$

Robert E. Berry, Paul D. Smith, Spencer M. Harben, Madeleine Helliwell, David Collison and C. David Garner*

Department of Chemistry, The University of Manchester, Oxford Road, Manchester, UK M13 9PL

$[\Delta\text{-}V(hida)_2]^{2-}$ (H_3hida = *N*-hydroxyiminodiacetic acid) and UO_2^{2+} form the solid $[\{UO_2(H_2O)_3\}\{\Delta\text{-}V(hida)_2\}\cdot 2H_2O]_n$ which is comprised of left-handed helical arrays, linked by H-bonding networks, in which the V^{IV} is eight-coordinate and the U^{VI} seven-coordinate.

Recent studies in these laboratories have established that 2,2′-(*N*-hydroxyimino)dicarboxylic acid proligands form a range of distinctive eight-coordinate complexes with early d-transition metal centres such as Ti^{IV}, V^{IV}, V^{V}, Nb^{V}, Ta^{V} and Mo^{V}.[1–5] This work was initiated by the discovery of Amavadin,[6] originally isolated from mushrooms of the genus *Amanita* and constituted as a 1 : 2 complex of V^{IV} with (*S*,*S*)-2,2′-(*N*-hydroxyimino)dipropionic acid (H_3hidpa).[7] Amavadin possesses a novel eight-coordinate geometry, with each $hidpa^{3-}$ ligand bonding *via* an η^2-NO group and two unidentate carboxylate groups. This coordination geometry leads to chirality at the vanadium and the isolated natural product Amavadin contains an approximately equimolar mixture of the Δ- and Λ-isomers of $[V\{(S,S)\text{-}hidpa\}_2]^{2-}$.[1,8] Amavadin-style anions form extended structures with cations such as Ca^{2+} *via* bridging caboxylate groups.[4,5] We have explored the possibility of extending this 'cation-trapping' by Amavadin-style complexes to other metals and, herein, we report the synthesis and characterisation of $[\{UO_2(H_2O)_3\}\{\Delta\text{-}V(hida)_2\}\cdot 2H_2O]_n$ **I** [H_3hida = 2,2′-*N*-hydroxyimino(diacetic acid)].

I was formed by the addition of $UO_2(O_2CMe)_2\cdot 2H_2O$ to an aqueous solution of $H_2[\Delta,\Lambda\text{-}V(hida)_2]$[9] and obtained as brown prismatic crystals.† The V^{IV} centres (Fig. 1) consist exclusively of $[\Delta\text{-}V(hida)_2]^{2-}$ moieties, each with the eight-coordinate geometry characteristic of Amavadin[1] with two mutually *trans* η^2-NO groups and four unidentate carboxylate groups. The dimensions of the V^{IV} centres are very similar to those obtained previously for this anion and its close relatives.[1,4,8,12] A striking aspect of **I** is that only the Δ-form of $[V(hida)_2]^{2-}$ was observed in the crystal subjected to X-ray crystallographic analysis; no vanadium-containing material remained in solution after crystallisation and we presume that a racemic mixture of 'left' and 'right' handed crystals was produced and one hand was arbitrarily selected for study.

In **I**, each U^{VI} centre is seven-coordinate (Fig. 1) with a pentagonal bipyramidal coordination geometry; the *trans* oxo-groups [O(11) and O(15)] are the axial ligands and the equatorial plane is comprised of three H_2O molecules [O(12), O(13) and O(14)] and two carboxylate oxygens from different $[\Delta\text{-}V(hida)_2]^{2-}$ centres [O(2*) and O(9)]. An approximate twofold axis of symmetry is located along the U–O(13) bond; O(11)–U–O(15) is effectively linear [177.1(6)°] and perpendicular (90.0°) to the least-squares plane of U and the five equatorial oxygen atoms; O(9) and O(14) sit above (0.05 and 0.06 Å, respectively) and U, O(12), O(13) and O(2*) sit below (−0.01, −0.02, −0.02, −0.06 Å, respectively) the least-squares plane. This coordination geometry is well known for seven-coordinate U^{VI} compounds[13] and may be directly compared with that of $[UO_2(orotato)_2(H_2O)_3]$‡,[14] which involves two orotato ligands in *cis* positions in the equatorial plane each coordinated *via* a unidentate carboxylate group. The U–O distances of **I** are similar to those in $[UO_2(orotato)_2(H_2O)_3]$ and related U^{VI} complexes.[13,14]

The unit cell of **I** is comprised of four identical and parallel left-handed helical chains centred on cell edges, each contributing its atoms to four unit cells; each turn of the helix is composed of six V^{IV} and six U^{VI} centres (Fig. 2). There are four solvent fragments in the lattice beyond the helical chains which, in the crystallographic refinement, were assumed to be H_2O molecules at 0.5 occupancy each. There is a network of short interhelix contacts, consistent with extensive H-bonding throughout the lattice, in particular: the uranyl *trans* oxo-groups H-bond to protons on different anions in neighbouring chains, O(15)···H(6b) and O(11)···H(3b) (2.4, 2.4 Å, respectively); and the water molecule O(13) coordinated to the U^{VI} has close contacts with carboxylates on different helical chains, O(13)···O(4) and O(13)···O(7) (2.5, 2.5 Å, respectively); these carboxylates also have close contacts with hydrogens on neighbouring anions, O(4)···H(7b) and O(7)···H(2b) (2.6, 2.7 Å, respectively); uncoordinated water molecules also have close contacts with water molecules coordinated to U^{VI}, O(12)···O(17) and O(14)···O(16) (2.7, 2.7 Å, respectively).

The IR spectrum of **I** contains ν(C=O) bands at 1637, 1617, and 1587 cm^{-1} and the different frequencies are consistent with the different roles of the carboxylate groups in bridging to the U^{VI} centres (Fig. 1). The ν(O=U=O) asymmetric stretching

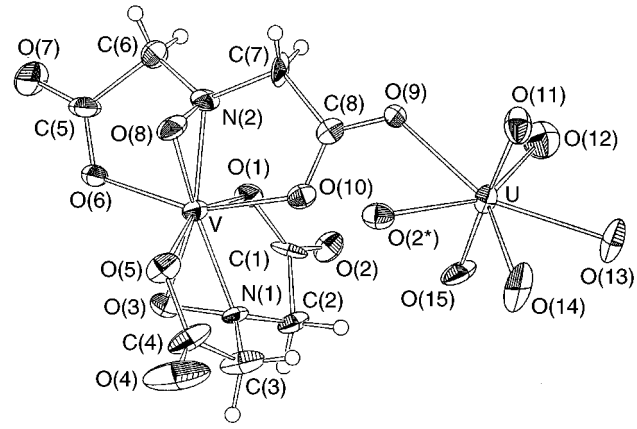

Fig. 1 V^{IV} and U^{VI} centres of **I**: selected bond lengths (Å) and interbond angles (°) U–O(2*) 2.36(1), U–O(9) 2.35(1), U–O(11) 1.71(2), U–O(12) 2.42(2), U–O(13) 2.39(1), U–O(14) 2.47(1), U–O(15) 1.69(2), V–O(1) 2.06(1), V–O(3) 1.95(2), V–O(5) 2.08(1), V–O(6) 2.07(1), V–O(8) 1.89(2), V–O(10) 2.05(2), V–N(1) 2.01(2), V–N(2) 1.95(2); O(2*)–U–O(9) 76.0(4), O(2*)–U–O(11) 92.1(7), O(2*)–U–O(14) 71.1(5), O(2*)–U–O(15) 90.3(7), O(9)–U–O(11) 88.9(7), O(9)–U–O(12) 72.2(5), O(9)–U–O(15) 93.1(6), O(11)–U–O(12) 90.1(8), O(11)–U–O(13) 89.8(7), O(11)–U–O(14) 88.5(8), O(12)–U–O(13) 69.0(6), O(12)–U–O(15) 88.6(8), O(13)–U–O(14) 71.9(6), O(13)–U–O(15) 87.3(8), O(14)–U–O(15) 90.9(8). The dihedral angle between {VNO} planes is 85.34°. * Indicates an atom derived by symmetry.

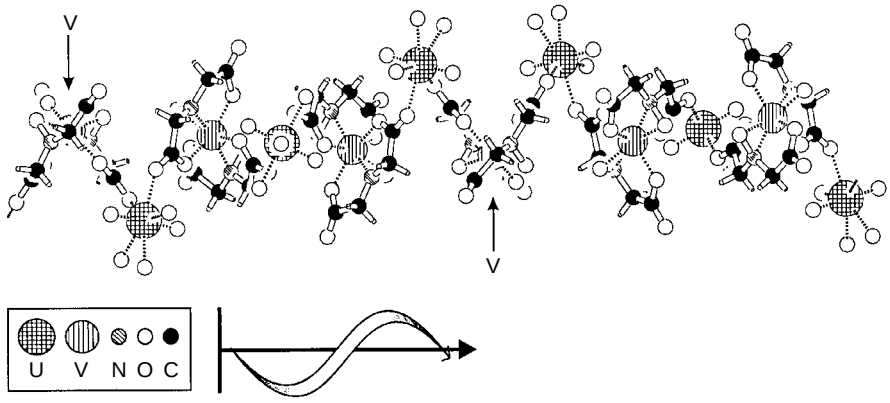

Fig. 2 Representation of a left-hand helical chain of **I**

frequency is manifest in the IR spectrum by a sharp absorption at 930 cm^{-1}.

Solid state reflectance UV–VIS data reveal absorptions due to the uranyl moiety, composed of progressions (average separation 625 cm^{-1}) arising from UO_2^{2+} symmetric stretching centred at 22 700 cm^{-1}; as well as d–d bands due to the V^{IV} centre at 12 100, 14 400 and 18 800 cm^{-1} and charge transfer transitions at $>26\,300$ cm^{-1}.

The EPR spectrum of a polycrystalline powder of **I** at Q-band frequency at room temp. comprises a single broad (ΔB_{p-p} 235 G) line with a very asymmetric derivative shape indicative of axial symmetry with $g_{\|} = 1.932$, $g_{\perp} = 1.979$. This is consistent with a magnetically concentrated sample arising from the relatively short inter- and intra-helix V–V distances.

The 'trapping' of metal cations by Amavadin-style anions may allow the selective binding of cations, either to immobilise them or for ion exchange.[15] In this context it is of interest to note that competition experiments have demonstrated the preferential precipitation of UO_2^{2+} by the diffusion of MeOH into an aqueous solution of $H_2[V(hida)_2]$ containing equimolar amounts of UO_2^{2+} and Ca^{2+}.

We thank BNFL plc (R. E. B., P. D. S., S. M. H.), EPSRC (R. E. B.) and The Royal Society (D. C.) for financial support, Dr E. J. L. McInnes (EPSRC CW EPR Service Centre, Department of Chemistry, The University of Manchester) for the EPR spectrum and Dr P. Harston (BNFL) and Messrs. P. R. Silverwood and Y. Zhang for valuable discussions.

Notes and References

* E-mail: dave.garner@man.ac.uk

† [VO(pentane-2,4-dionate)$_2$] (0.13 g, 0.5 mmol) was added to a stirred solution of H_3hida (0.15 g, 1 mmol) in H_2O (5 cm^3) at room temp.;[9] after dissolution, $UO_2(O_2CMe)_2{\cdot}2H_2O$ (0.21 g, 0.5 mmol) was added and the solution stirred for *ca.* 3 h. Crystals of **I** suitable for X-ray diffraction were grown by slow vapour diffusion of MeOH into the reaction solution at 275 K. Analysis. Found: C, 14.2; H, 2.5; N, 4.0; U, 33.1 V, 7.4. Calc. for $C_8H_{18}N_2O_{17}UV$: C, 13.7; H, 2.6; N, 4.0; U, 33.9; V, 7.2%. *X-Ray crystal data for* **I**: $C_8H_{20}N_2O_{17}UV$, M = 705.22, hexagonal, space group $P6_5$ (no. 170), a = 9.534(2), c = 38.300(3) Å, U = 3014(1) $Å^3$ (by least squares refinement on diffractometer angles of 25 automatically centred reflections), λ = 0.710 69 Å, Z = 6, $F(000)$ = 1998, D_c = 2.330 g cm^{-3}, μ = 85.99 cm^{-1}, brown prismatic crystal of dimensions 0.20 × 0.22 × 0.25 mm. Data were collected at 296 K using a Rigaku AFC5R diffractometer with graphite monochromated Mo-Kα radiation and a rotating anode generator. A total of 3988 reflections were measured in the ω scan mode to a $2\theta_{max}$ of 50.1°, which gave 1849 independent reflections (R_{int} = 0.035). An empirical absorption correction was applied, based on the azimuthal scans of several reflections (transmission factors: 0.6784–1.00). A decay correction was also applied (1.39% decline). 1587 reflections had $I > 1.50\sigma(I)$. The structure was solved by direct methods[10] and expanded using Fourier techniques.[11] The non-hydrogen atoms were refined anisotropically except for O(12) and the disordered water molecules O(16)–O(19), which were refined isotropically. Hydrogen atoms were included but not refined. Refinement of the 255 variables converged with R = 0.044, R_w = 0.037. Max., min. peaks in the final difference map 0.96, −0.93 e^- $Å^{-3}$.

Careful consideration was given to the space group symmetry. There were four possible options, $P6_1$ and $P6_122$ and the alternative hands $P6_5$ and $P6_522$. The absolute configuration was determined by carrying out refinements in each space group using all of the observed data, including equivalent reflections. The detailed arguments which led to the selection of $P6_5$ as the correct space group are available as supplementary material from the corresponding author. CCDC 182/752.

‡ $[UO_2(orotato)_2(H_2O)_3]$ = dioxobis(1,2,3,6-tetrahydro-2,6-dioxo-4-pyrimidinecarboxylato)triaquauranium(VI).

1 E. M. Armstrong, R. L. Beddoes, L. J. Calviou, J. M. Charnock, D. Collison, S. N. Ertok, J. H. Naismith and C. D. Garner, *J. Am. Chem. Soc.*, 1993, **115**, 807.
2 P. D. Smith, S. M. Harben, R. L. Beddoes, M. Helliwell, D. Collison and C. D. Garner, *J. Chem. Soc., Dalton Trans.*, 1997, 685.
3 H. S. Yadav, E. M. Armstrong, R. L. Beddoes, D. Collison and C. D. Garner, *J. Chem. Soc., Chem. Commun.*, 1994, 605.
4 P. D. Smith, R. E. Berry, S. M. Harben, R. L. Beddoes, M. Helliwell, D. Collison and C. D. Garner, *J. Chem. Soc., Dalton Trans.*, 1997, 4509.
5 S. M. Harben, P. D. Smith, R. L. Beddoes, D. Collison and C. D. Garner, *Angew. Chem., Int. Ed. Engl.*, 1997, **36**, 1897; S. M. Harben, P. D. Smith, M. Helliwell, D. Collison and C. D. Garner, *J. Chem. Soc., Dalton Trans.*, 1997, 4517.
6 E. Bayer and H. Kneifel, *Z. Naturforsch., Teil B*, 1972, **27**, 207.
7 H. Kneifel and E. Bayer, *Angew. Chem., Int. Ed. Engl.*, 1973, **12**, 508; *J. Am. Chem. Soc.*, 1986, **108**, 3075.
8 E. M. Armstrong, M. S. Austerberry, R. L. Beddoes, R. E. Berry, D. Collison, S. N. Ertok, C. D. Garner, M. Helliwell and F. E. Mabbs, manuscript in preparation; S. N. Ertok, PhD Thesis, The University of Manchester, 1993.
9 J. Felcman, M. Cândida, T. A. Vaz and J. J. R. Fraústo da Silva, *Inorg. Chim. Acta*, 1984, **93**, 101; E. Koch, H. Kneifel and E. Bayer, *Z. Naturforsch., Teil B*, 1986, **41**, 359; G. Anderegg, E. Koch and E. Bayer, *Inorg. Chim. Acta*, 1987, **127**, 183.
10 SHELXS86: G. M. Sheldrick, in *Crystallographic Computing 3*, ed. G. M. Sheldrick, C. Kruger and R. Goddard, Oxford University Press, 1985, pp. 175–189.
11 DIRDIF94: P. T. Beurskens, G. Admiraal, G. Beurskens, W. P. Bosman, R. de Gelder, R. Israel and J. M. M. Smits. The DIRDIF-94 program system, Technical Report of the Crystallography Laboratory, University of Nijmegen, The Netherlands, 1994.
12 M. A. A. F. de C. T. Carrondo, M. T. L. S. Duarte, J. C. Pessoa, J. A. L. Silva, J. J. R. Fraústo da Silva, M. C. T. A. Vaz and F. L. Vilas-Boas, *J. Chem. Soc., Chem. Commun.*, 1988, 1158.
13 R. L. Lintredt, M. J. Heeg, N. Ahmad and M. D. Glick, *Inorg. Chem.*, 1982, **21**, 2350.
14 D. Mentzafos, N. Katsaros and A. Terzis, *Acta Crystallogr., Sect. C*, 1987, **43**, 1905.
15 A. J. Stemmler, J. W. Kampf and V. L. Pecoraro, *Angew. Chem., Int. Ed. Engl.*, 1996, **35**, 2841.

Received in Cambridge, UK, 6th October 1997; 8/00213D

Novel color isomerism and catalytic activities of Cu(salen) complex encapsulated in a zeolitic matrix

Subratanath Koner*

Catalysis Division, National Chemical Laboratory, Pune 411 008, India

The green zeolite encapsulated Cu(salen) complex on treatment with MeCN turns red and is found to be catalytically active towards oxidation reactions whereas the green species is inactive.

The development of efficient biomimetic oxidation catalysts containing metal complexes of porphyrins, phthalocyanines, Schiff-bases, *etc.* which mimic the active sites of metalloenzymes has received a lot of attention.[1] The oxidation reactions catalyzed by metal complexes are often impeded due to oxidative degradation of the complex and/or the formation of μ-oxo dimers.[1c] Several strategies, *viz.* encapsulation of those complexes within zeolitic[2,3] or polymeric matrices[4] or intercalation in clays,[2] have been adopted to enhance the stability and reactivity of such catalysts. It is now well understood that encapsulation of these complexes in zeolitic hosts can enhance the catalytic performance of the complexes in comparison to their homogeneous counterparts used in solution.[1c]

Here, we report the preparation, novel physicochemical properties and unique catalytic behavior of a zeolite (NaY) encapsulated Cu(salen) [salen = *N*,*N*′-bis(salicylaldehyde)-ethylenediimine] complex [Cu(salen)-NaY].

To prepare Cu(salen)-NaY, 2 g of calcined Cu-NaY† zeolite was mixed with 2 g of salen and placed in a sealed glass tube containing dry N_2 and heated at 150 °C with occasional stirring for 5–6 h. The green mass thus formed was then pulverized and subjected to Soxhlet extraction with MeOH and Me_2CO. The extracted green solid was then stirred with the portions of fresh MeCN several times. To our surprise during the stirring with MeCN the green mass transformed in to a red solid within a few min whereas treatment of Cu(salen) with MeCN or recrystallization of the complex from the same solvent gave no such color change. Although there is ample evidence of metal complexes recrystallized from different solvents giving different colors owing to the formation of different isomers or conformers[5,6] the present type of color isomerism among zeolite encapsulated metal complexes is rarely observed. No color change is observed when the green species is treated with other sovlents such as EtOH, Pr^iOH, CH_2Cl_2, $CHCl_3$, *etc.* Elemental analysis showed the Cu content of this solid was *ca.* 0.06%, which corresponds to encapsulation of *ca.* 26 molecules of [Cu(salen)] per 100 supercages in this solid. The Cu content of the green solid is virtually the same.

A relatively weak band in the visible region in the electronic spectra of the prepared catalysts and pure complex {590 nm for [Cu(salen)] and Cu(salen)-NaY(green); 558 nm for Cu(salen)-NaY(red)} is assigned to d–d transitions whereas two fairly strong bands appearing in the range 410–280 nm are assigned to ligand charge transfer bands {370 and 286 nm for the red and green species and 406 and 355 for the [Cu(salen)] complex} (Fig. 1).[5] All the prominent IR bands for ligand vibrations appearing in the region 1700–1250 cm^{-1} of the [Cu(salen)] species are also present in Cu(salen)-NaY. The ligand vibration bands in the other regions are obscured by the presence of zeolitic vibration bands. The principal *g* values calculated by usual methods from EPR spectra (Fig. 2) are in agreement with those reported for Cu^{II} Schiff base complexes.[7] The $g_{\|}$ and $g_{\perp}$ values of the red and green species of Cu(salen)-NaY and for [Cu(salen)] are 2.189, 2.178, 2.176 and 2.041, 2.039, 2.044, respectively.

All the above results convincingly demonstrate the presence of the [Cu(salen)] chromophore in both varieties of Cu(salen)-NaY catalysts. The shifting of the d–d transition band to shorter wavelength in electronic spectra of the red species in comparison to the green species clearly indicates that the axial ligand field around the Cu^{II} ion is weaker in the former.[6b,8b] EPR spectra are in accord with this as $g_{\|}$ values of the red species are higher than that of the green species whereas the $g_{\perp}$ values are almost the same. It is well documented that a decrease of axial ligand interaction with Cu^{II} in these types of complexes leads to a red-shift of d–d transition bands and an increase in $g_{\|}$.[6b,8] It is also noteworthy that the resolution of IR spectral bands for ligand vibrations of the red species is higher than the green species suggesting that the Cu(salen) moiety in the red species is more comfortably enclosed inside the zeolitic supercage than in the green species; which also indirectly indicates that the interaction between the Cu(salen) moiety and the zeolitic matrix in the red species is much weaker than in the green species. Therefore, it can be proposed that in the green species, Cu^{II}

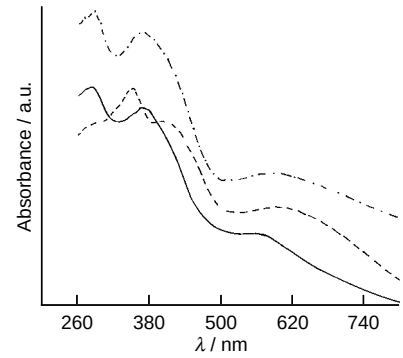

Fig. 1 UV–VIS diffuse reflectance spectra of Cu(salen)-NaY(red) (———) Cu(salen)-NaY(green) (-·-·-·-) and Cu(salen) (- - - -)

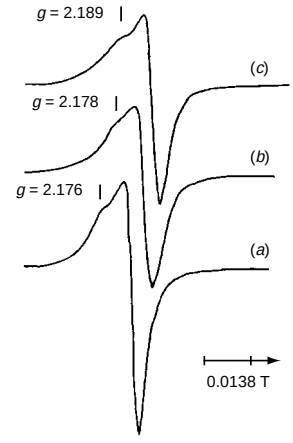

Fig. 2 EPR spectra of Cu(salen) (*a*), Cu(salen)-NaY(green) (*b*) and Cu(salen)-NaY(red) (*c*)

Table 1 Catalytic performance of zeolite encapsulated Cu(salen)

Catalyst	Substrate	*t*/h	Conversion (mass%)	Product
Cu(salen)-NaY(red)	Norbornene	3	23.1	*exo*-Epoxynorbornane[a]
		12	66.7	*exo*-Epoxynorbornane[a]
	1-Naphthol	12	16.8	1,4-Naphthoquinone[a]
Cu(salen)-NaY(green)	Norbornene	12	0.1	—[b]
	1-Naphthol	12	0.2	—[b]

[a] Selectivity = 100 (mass%). [b] No expected oxidized products are detected.

forms weak Cu–O bonds with zeolitic oxygen to give either square-pyramidal or octahedral geometry around the Cu^{II} ion, which upon treatment with MeCN becomes square planar. The formation of weak Cu–O bonds between the Cu^{II} ion and zeolitic oxygen can not be ruled out since recently it has been shown by single crystal X-ray analysis that Cu(salen) forms dimers through weak Cu–O (O-salen) bonds in the solid state.[5]

The epoxidation of norbornene and hydroxylation of 1-naphthol were carried out in a glass batch reactor using TBHP (*tert*-butyl hydroperoxide) as oxidant. MeOH was used as solvent for Cu(salen)-NaY(green) while MeCN was used for Cu(salen)-NaY(red). In a typical reaction, 0.1 g of catalyst was slurried in a batch reactor with 10 g of MeCN or MeOH. To this, 0.5 g of oxidant was added and the mixture allowed to equilibrate at 50 °C in oil bath. After *ca.* 10 min the substrate was added and products collected at different time intervals and identified and quantified by GC and verified by GC–MS.

Results for both reactions (Table 1) established that the Cu(salen)-NaY(red) catalyst showed excellent product selectivity as well as activity towards oxidation reactions with exclusively one oxidized product being obtained in each case. Selectivity of products to this extent is rare among zeolite encapsulated metal complex catalysts. For the 1-naphthol hydroxylation reaction 1,4-naphthoquinone is selectively obtained among the three possible products (1,4-naphthoquinone, 1,4-dihydroxynaphthalene, 1,2-dihydroxynaphthalene)[9] whereas for norbornene only *exo*-epoxynorbornane is obtained, where *exo*- and *endo*-epoxynorbornane, cyclohexene-4-carbaldehyde and norcamphor are all possible products.[10] On the other hand Cu(salen)-NaY(green) does not show any activity towards these reactions. It should be noted that Cu is not detected in the liquid phase of the reaction mixtures (the solid catalyst is separated from the mixture by filtration at *ca.* 50 °C) after completion of experiment. Therefore, the Cu complex is not leached from the catalysts during reaction.

In conclusion, it can be stated that the catalytic activity of Cu(salen)-NaY changes dramatically with change in the coordination geometry around the Cu^{II} ion in the zeolite. The Cu(salen)-NaY(red) catalyst where Cu^{II} ion appears to possess vacant axial positions shows activity[1e,5] towards oxidation reactions whereas the green variety, where Cu^{II} ion is either five- or six-coordinate, is inactive. Further this work is a novel example where a metal complex encapsulated in a zeolitic matrix shows color isomerism upon treatment with a specific solvent.

The author acknowledges CSIR, India for an award of a Senior Research Associateship (Pool Officer). The author also thanks Dr S. Sivasanker for his encouragement and interest in this work.

Notes and References

* Present Address and Address for Communication: Biomolecular Engineering Department, National Institute of Bioscience and Human Technology, 1-1 Higashi, Tsukuba, Ibaraki 305, Japan. Fax: +81-298-54-6161; E-mail: skoner@ccmail.nibh.go.jp

† Cu-NaY was prepared by stirring a slurry of NaY in $Cu(NO_3)_2$ solution [1 g NaY with 0.25 g $Cu(NO_3)_2$ dissolved in 200 ml of water] at room temp. In order to control the quantity of Cu^{II} exchange in NaY-zeolite a relatively dilute $Cu(NO_3)_2$ solution was used and the stirring time was fixed at 30 min. The Cu content in the solid is found to be *ca.* 0.075%. Cu(salen)-NaY(green) was prepared following the same procedure as above (main text) avoiding treatment with MeCN. The catalysts were calcined at 120 °C for 8–10 h in dry N_2 before use in reactions. To re-exchange the unreacted Cu^{II} present in both the green and red solids by Na^+ ions they were repeatedly stirred in $NaNO_3$ solution for several hours.

1 (*a*) S. B. Ogunwumi and T. Bein, *Chem. Commun.*, 1997, 901; (*b*) R. Robert and P. Ratnasamy, *J. Mol. Catal. A*, 1996, **100**, 93; (*c*) K. Balkus, Jr., M. Eissa and R. Levedo, *J. Am. Chem. Soc.*, 1995, **117**, 10 753; (*d*) J. T. Groves and T. E. Nemo, *J. Am. Chem. Soc.*, 1983, **105**, 5786; (*e*) B. M. Weckhuysen, A. A. Verberckmoes, I. P. Vannijvel, J. A. Pelgrims, P. L. Buskens, P. A. Jacobs and R. A. Schoonheydt, *Angew. Chem., Int. Ed. Engl.*, 1995, **34**, 2652.
2 F. Bedioui, *Coord. Chem. Rev.*, 1995, **144**, 39 and references therein.
3 K. Balkus, Jr., A. G. Gabrilov, S. L. Bell, F. Bedioui, L. Roué and J. Devynck, *Inorg. Chem.*, 1994, **33**, 67.
4 R. F. Parton, I. F. J. Venkelecom, M. J. A. Casselman, C. P. Bezouhanova, J. B. Uytterhoeven and P. A. Jacobs, *Nature*, 1994, **370**, 541.
5 M. M. Bhadbhade and D. Srinivas, *Inorg. Chem.*, 1993, **32**, 6122.
6 (*a*) S. Koner, A. Ghosh and N. Ray Chaudhuri, *Transition Met. Chem.*, 1988, **13**, 291; S. Koner, A. Ghosh and N. Ray Chaudhuri, *J. Chem. Soc., Dalton Trans.*, 1990, 1563; (*b*) D. R. Bloomquist and R. D. Willett, *Coord. Chem. Rev.*, 1982, **47**, 125.
7 A. H. Maki and B. R. McGarvey, *J. Chem. Phys.*, 1958, **29**, 35; E. Hasty, T. J. Colburn and D. N. Hendrickson, *Inorg. Chem.*, 1973, **12**, 2414.
8 (*a*) H. Yokoi, M. Sai and T. Isobe, *Bull. Chem. Soc. Jpn.*, 1969, **42**, 2232; (*b*) R. L. Belford, M. Calvin and G. Belford, *J. Chem. Phys.*, 1957, **26**, 1165.
9 T. K. Das, K. Chaudhari, A. J. Chandwadkar and S. Sivasanker, *J. Chem. Soc., Chem. Commun.*, 1995, 2495.
10 T. L. Siddall, N. Miyaura, J. C. Huffman and J. K. Kochi, *J. Chem. Soc., Chem. Commun.*, 1983, 1185; T. G. Traylor and A. R. Miksztal, *J. Am. Chem. Soc.*, 1989, **111**, 7443.

Received in Cambridge, UK, 24th October 1997; 7/07681I

X-Ray crystal structure of $\{Cu[1,2\text{-bis}(4\text{-pyridyl})ethane]_2(NO_3)_2\}_n$: the first example of a coordination polymer that exhibits the NbO 3D network architecture†

K. Nicole Power, Tracy L. Hennigar and Michael J. Zaworotko*

Department of Chemistry, Saint Mary's University, Halifax, Nova Scotia, B3H 3C3, Canada

The coordination polymer $\{Cu[1,2\text{-bis}(4\text{-pyridyl})ethane]_2(NO_3)_2\}_n$ does not exist as a square grid network, rather it is the first example of a twofold NbO type 3D network. A twofold level of interpenetration does not preclude the presence of 11 × 11 Å channels which contain benzene and methanol guest molecules.

Recent activity in crystal engineering has afforded several examples of coordination polymers which have open framework network structures and therefore have the potential to be functionally related to zeolites.[1–3] The architectures of coordination polymers can be either mineralomimetic or, more commonly, without precedence in naturally occurring solids. If simple linear spacer ligands such as 4,4′-bipyridine (4,4′-bipy) are utilized, the architecture of a coordination polymer is strictly limited by the stoichiometry. For example, a 1 : 1.5 ratio of T-shape, square planar or octahedral metal to 4,4′-bipy affords ladder,[4–7] brick-wall,[4] 3D frame[8,9] or bilayer structures.[7,10] These architectures, which can be regarded as being supramolecular isomers of one another,[7,10] are without precedence in naturally occurring compounds. If one considers a 1 : 2 ratio of square planar or octahedral metal to linear spacer ligand, there

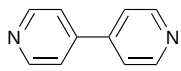

4,4′-bipy

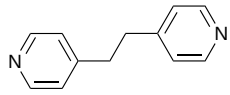

bpye

would appear to be only two likely supramolecular isomers, square 2D grids or 3D frames (Scheme 1). These supramolecular isomers could occur for either square planar or suitably substituted octahedral complexes. The former has been widely encountered in Hoffman clathrates[11] and 4,4′-bipy sustained networks[12–15] whereas the latter has to our knowledge only hitherto been observed in NbO.[16] In this contribution we report the structure of a copper(II) coordination polymer based upon the spacer ligand 1,2-bis(4-pyridyl)ethane (bpye) which represents, to our knowledge, the first example of a coordination polymer which exhibits the NbO type structure, $[Cu(bpye)_2(NO_3)_2]_n$ **1**.

Blue crystals of **1** were grown by carefully layering a methanol solution of $Cu(NO_3)_2 \cdot 6H_2O$ onto a benzene solution of bpye under ambient conditions. The ligand bpye is capable of adopting either *gauche* or *anti* conformations and can therefore act as either an angular or a linear spacer ligand, respectively.[7] As revealed by single crystal X-ray crystallography, the bpye ligands in **1** are *anti* and they sustain a 3D framework motif with channels of effective cross-section 11 × 22 Å.‡ In the structure there is a single network of **1**.† The large channels in a single framework of **1** facilitate twofold interpenetration with a second independent framework but do not result in a close-packed structure, rather, large square channels with effective cross-sectional area of 11 × 11 Å exist parallel to the crystallographic *a*-axis; these channels contain two ordered benzene molecules and one disordered methanol/benzene molecule per metal centre and crystals appear to lose solvent and crystallinity within minutes of their removal from the mother liquor.†

The coordination geometry around the Cu^{II} moiety can be regarded as pseudo-square planar since the nitrate anions are only weakly coordinated, Cu–O distances being 2.366(4) and 2.486(4) Å, significantly longer than those seen for octahedral Ni^{II} or Co^{II} analogues.[14] Other bond distances are within expected ranges. It is not clear from this study why **1** exists as a 3D NbO type framework rather than a 2D square grid framework of the type commonly exhibited by 4,4′-bipy analogues of **1**.[12–15] Indeed, we have now prepared more than twenty 4,4′-bipy square grid compounds and we have prepared more than ten bpye square grid compounds. The title compound still remains the only one that exhibits the NbO framework. It would not appear that the Jahn–Teller induced distortion from octahedral geometry is a likely factor for the observed structure since, in principle, both square planar and octahedral metal moieties should be able to sustain the NbO network. However, the length of bpye compared to 4,4′-bipy might be a factor. It is

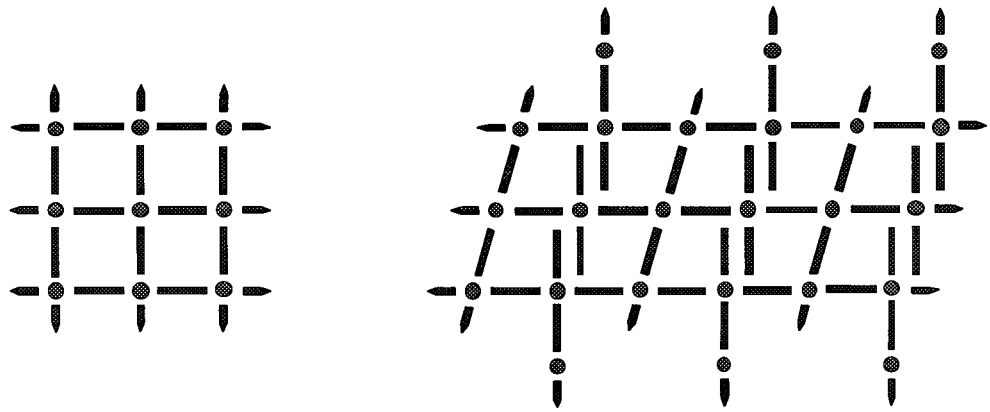

Scheme 1

known that 4,4′-bipy sustained square grid coordination polymers can form close packed structures *via* interpenetration[12] or stable open framework structures through inclusion of aromatic molecules.[13–15] The larger cavity that would be formed by bype might not be as amenable to such behaviour. It should also be noted that bpye inherently possesses conformational flexibility and other supramolecular isomers based upon conformational isomerism[7] are therefore likely for **1**. The factors that affect the generation of supramolecular isomers of **1** and related coordination polymers, in particular the influence of guest and solvent, are currently being investigated further.

We acknowledge Dr C. Campana of Siemens Industrial Automation Ltd. for furnishing the X-ray data and the generous financial support of the NSERC (Canada) in the form of a research grant (M. J. Z.).

Notes and References

* Present address: Faculty of Arts and Science, University of Winnipeg, 515 Portage Avenue, Winnipeg, Manitoba, R3B 2E9, Canada. E-mail: mike.zaworotko@uwinnipeg.ca

† This ChemComm is also available in enhanced multi-media format *via* the World Wide Web: http://www.rsc.org/ccenhanced. Figs. 1 and 2 are shown in the enhanced version.

‡ *Crystal data* for **1**: $C_{41}H_{48}CuN_6O_{8.5}$, orthorhombic, space group *Pccn*, a = 14.7097(18), b = 21.832(3), c = 26.719(3), U = 8580.4(18) Å^3, Z = 8, D_c = 1.281 Mg m^{-3}, λ = 0.709 30 Å, $F(000)$ = 3464. 6639 reflections out of 8443 unique reflections with $I_{net} > 3.5I$ measured at 173 K for a crystal of dimensions 0.2 × 0.3 × 0.4 mm on a Siemens SMART/CCD diffractometer using the θ scan mode ($4 < 2\theta < 52°$) afforded on convergence final R-factors of R_f = 0.114 and R_w = 0.117. Two independent benzene and two independent MeOH guest molecules were observed to have high thermal motion and a third benzene guest was observed to be disordered with a water or methanol molecule. H atoms of the framework were placed in calculated positions (C–H 1.0 Å) whereas H atoms of the disordered guest molecules were not placed. All non-hydrogen atoms were anisotropically refined. The crystallographic calculations were conducted using the NRCVAX program package. CCDC 182/734.

1 D. Venkataraman, G. B. Gardner, S. Lee and J. S. Moore, *J. Am. Chem. Soc.*, 1995, **117**, 11 600.
2 O. M. Yaghi, G. Li and H. Li, *Nature*, 1995, **378**, 703.
3 S. Subramanian and M. J. Zaworotko, *Angew. Chem., Int. Ed. Engl.*, 1994, **35**, 2127.
4 M. Fujita, Y. J. Kwon, O. Sasaki, K. Yamaguchi and K. Ogura, *J. Am. Chem. Soc.*, 1995, **117**, 7287.
5 G. A. Doyle, D. M. L. Goodgame, S. P. W. Hill and D. J. Williams, *J. Chem. Soc., Chem. Commun.*, 1993, 207.
6 P. Losier and M. J. Zaworotko, *Angew. Chem., Int. Ed. Engl.*, 1996, **35**, 2779.
7 T. Hennigar, D. C. MacQuarrie, P. Losier, R. D. Rogers and M. J. Zaworotko, *Angew. Chem., Int. Ed. Engl.*, 1997, **36**, 972.
8 F. Robinson and M. J. Zaworotko, *Chem. Commun.*, 1995, 2413.
9 O. Yaghi and H. Li, *J. Am. Chem. Soc.*, 1996, **118**, 295.
10 K. N. Power, T. L. Hennigar and M. J. Zaworotko, *New J. Chem.*, in press.
11 T. Iwamoto, in *Inclusion Compounds*, ed. J. L. Atwood, J. E. D. Davies and D. D. MacNicol, Academic Press, London, vol. 1, 1984, ch. 2, pp. 29–57.
12 R. W. Gable, B. F. Hoskins and R. Robson, *J. Chem. Soc., Chem. Commun.*, 1990, 1677.
13 M. Fujita, Y. J. Kwon, S. Washizu and K. Ogura, *J. Am. Chem. Soc.*, 1994, **116**, 1151.
14 J. L. Atwood, T. L. Hennigar, C. M. Hogg, K. T. Holman, P. Losier, L. R. MacGillivray, K. N. Power, R. D. Rogers and M. J. Zaworotko, unpublished work.
15 J. Lu, T. Paliwals, S. C. Lim, C. Yu, T. Niu and A. J. Jacobsen, *Inorg. Chem.*, 1997, **36**, 923.
16 A. F. Wells, *Structural Inorganic Chemistry*, Clarendon Press, Oxford, 4th edn., 1975.

Received in Columbia, MO, USA, 19th May 1997, revised manuscript received 29th October 1997; 7/08943K

The first stable copper(II) complex containing four sulfide ligands: synthesis and structural characterization of $[Pt_2(dppe)_2(\mu\text{-}S)_2]$ and $[Cu\{Pt_2(dppe)_2(\mu_3\text{-}S)_2\}_2]^{2+}$

Mercè Capdevila,[a] Yolanda Carrasco,[a] William Clegg,[b] Robert A. Coxall,[b] Pilar González-Duarte,*[a] Agustí Lledós,*[a] Joan Sola[a] and Gregori Ujaque[a]

[a] *Departament de Química, Universitat Autònoma de Barcelona, 08193 Bellaterra, Barcelona, Spain*
[b] *Department of Chemistry, University of Newcastle, Newcastle upon Tyne, UK NE1 7RU*

The synthesis and crystal structure of the novel heteropolymetallic aggregate $[\{Pt_2(dppe)_2(\mu_3\text{-}S)_2\}_2Cu][PF_6]_2$ 2 and of its precursor $[Pt_2(dppe)_2(\mu\text{-}S)_2]$ 1 are reported; 2 has been further characterized by EPR and electronic spectroscopies and the hinged Pt_2S_2 rings in 1 and 2 have been rationalized by *ab initio* MP2 calculations.

The ability of $[Pt_2L_4(\mu\text{-}S)_2]$ (L = phosphine) to behave as a metalloligand towards Lewis acids of p- and d-block elements is well reflected in the literature by a wide range of homo- and hetero-metallic aggregates with various nuclearities and structures.[1] However, structural data in dimeric platinum sulfide complexes are scarce and contradictory. The partially determined X-ray structure of $[Pt_2(PMe_2Ph)_4(\mu\text{-}S)_2]$ shows a hinged Pt_2S_2 ring (θ = 121°),[2] but the ring is strictly planar in $[Pt_2(dppy)_4(\mu\text{-}S)_2]$ (dppy = 2-diphenylphosphanopyridine).[3] Theoretical *ab initio* studies found a bent structure for the $[Pt_2(PH_3)_4(\mu\text{-}S)_2]$ complex.[4] Stimulated by the difficulty of stabilizating Cu^{II} in S_4 environments, relevant for the study of copper proteins, and based on the coordinative versatility of $[Pt_2L_4(\mu\text{-}S)_2]$, we targeted the synthesis of a copper(II) complex containing four sulfide ligands. The only X-ray structure of a heterometallic platinum sulfide aggregate, $[\{Pt_2(PPh_3)_4(\mu_3\text{-}S)_2\}Cu(PPh_3)]PF_6$,[1a] contains copper as Cu^{I}. The closest precedents to copper(II) complexes contain alkyl persulfide[5] and disulfide[6] ligands. We report the synthesis and X-ray structure of $[Pt_2(dppe)_2(\mu\text{-}S)_2]$ **1** and pentametallic $[Cu\{Pt_2(dppe)_2(\mu_3\text{-}S)_2\}_2](PF_6)_2$ **2**, MP2 *ab initio* calculations for the $[Pt_2(H_2PCH_2CH_2PH_2)_2(\mu\text{-}S)_2]$ complex **3** that can be taken as a model for **1**, and spectroscopic and magnetic features of **2**.

The preparation of $\mathbf{1}\cdot 2C_6H_6$ from $[PtCl_2(dppe)]$ and an excess of Na_2S in benzene by a standard method[7] led to a mixture of products. ^{31}P NMR measurements on aliquots of the reaction mixture allowed the determination of a satisfactory $[PtCl_2(dppe)]:Na_2S:$benzene ratio and of the appropriate reaction time. Slow evaporation of the mother-liquor gave orange crystals of $\mathbf{1}\cdot 2C_6H_6$ in *ca.* 90% yield,† whose structure‡ consists of neutral dinuclear molecules devoid of crystallographic symmetry elements (Fig. 1). Each molecule shows a hinged Pt_2S_2 central ring (θ = 140.2°) with the two platinum atoms bridged by two sulfide anions, coordination being completed by chelating dppe ligands. The geometries at the individual Pt sites are approximately square planar.

To understand the preference for the bent structure of **1** we have optimized complex **3** at the MP2 level§ yielding a hinged structure with θ = 118.8°. This result indicates the intrinsic preference of **3** to adopt a bent structure and allows us to disregard crystal packing effects as the cause for hinging. The energy difference with respect to an optimized structure with a fixed θ = 180° is 30.1 kJ mol^{-1} in favour of the former. This energy difference between the bent and planar forms is small enough for changes in the size of the terminal ligands to cause significant variations in the dihedral angle. Thus, **3** is more hinged (θ = 118.8°) than **1** (140.2°) and a further increase in the steric hindrance about P atoms, as happens in $[Pt_2(dppy)_4(\mu\text{-}S)_2]$, leads to planarity. Optimization of **3** with a fixed θ = 140° gives an energy only 10.0 kJ mol^{-1} above than that for θ = 118.8°. It is likely that the great coordinative versatility of $[Pt_2L_4(\mu\text{-}S)_2]$ is due to the low energy cost associated with the bending process. Moreover, this low energy cost would allow a ring reversal process and thus a fluxional behaviour in solution.[11]

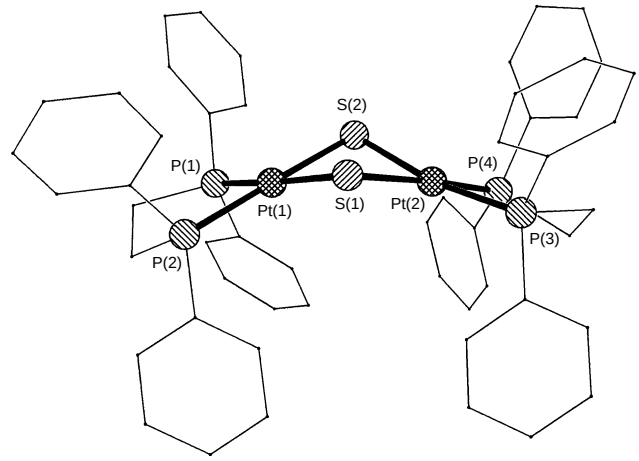

Fig. 1 View of the structure of $[Pt_2(dppe)_2(\mu\text{-}S)_2]$ in **1** with hydrogen atoms omitted, showing labelling of key atoms. Selected bond lengths (Å) and angles (°) of the Pt_2S_2 ring: Pt(1)–S(2) 2.3412(12), Pt(1)–S(1) 2.3554(12), S(1)–Pt(2) 2.3581(13), S(2)–Pt(2) 2.3437(12); S(2)–Pt(1)–S(1) 83.73(4), Pt(1)–S(1)–Pt(2) 88.60(4), Pt(1)–S(2)–Pt(2) 89.28(4), S(2)–Pt(2)–S(1) 83.61(4).

Mixing $Cu(PF_6)_2$ with **1** (1 : 2 molar ratio) in methanol gave rise to a dark solution that afforded red crystals of $\mathbf{2}\cdot 0.5Et_2O$.‡ As shown in Fig. 2, the crystallographically non-symmetrical cation $[Cu\{Pt_2(dppe)_2(\mu_3\text{-}S)_2\}_2]^{2+}$ comprises two $\{Pt_2S_2\}$ butterflies linked through sulfur to the Cu^{II} ion. The long S···S distance (3.1 Å) in each Pt_2S_2 moiety indicates the lack of a disulfido bond. The deviations from square-planarity around all platinum atoms are small and the hinge angles between PtS_2P_2 planes are 118.4 and 121.1°. There is a near-symmetrical chelation of both disulfide metalloligands **1** to the Cu^{II} centre. The distorted tetrahedral environment about the heterometal is shown by the two acute S–Cu–S bite angles of *ca.* 83.6° and by a torsion angle, ω = 60°, between the two S–Cu–S planes. Among the numerous geometries of the heterometal in the environment of $[Pt_2L_4(\mu\text{-}S)_2]$ there is no example where the former is tetrahedrally coordinated to two $[Pt_2L_4(\mu\text{-}S)_2]$ molecules.

The EPR spectrum of **2** in CH_2Cl_2 solution displays a signal at g_{iso} = 2.056. The hyperfine coupling constant to the copper ion (I = 3/2) A_{iso} was determined to be 58.5 × 10^{-4} cm^{-1}. The spectrum of a powdered sample of **2**, which consists of a nearly axial signal with no appreciable changes either at room

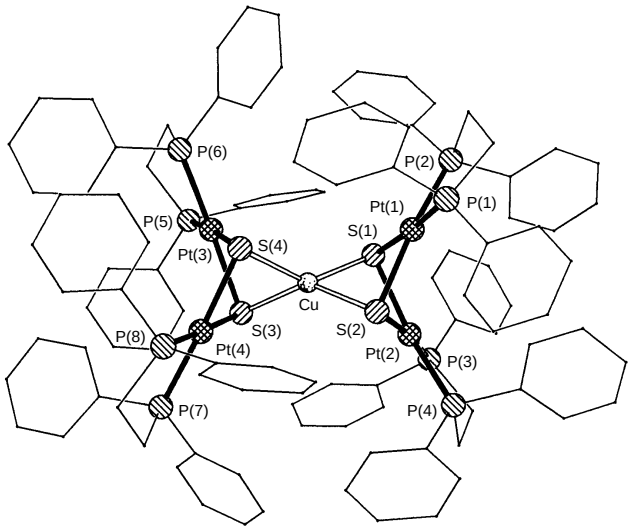

Fig. 2 The structure of the $[Cu\{Pt_2(dppe)_2(\mu_3\text{-}S)_2\}_2]^{2+}$ cation in **2** with key atoms labelled. Selected bond lengths (Å) and angles (°) of the $Cu\{Pt_2S_2\}_2$ core: Pt(1)–S(2) 2.355(2), Pt(1)–S(1) 2.375(3), S(1)–Pt(2) 2.362(2), S(2)–Pt(2) 2.365(2), S(1)–Cu 2.320(2), S(2)–Cu 2.318(3), S(4)–Cu 2.303(3), S(3)–Cu 2.316(3), S(3)–Pt(4) 2.359(3), S(3)–Pt(3) 2.364(3), S(4)–Pt(4) 2.366(2), S(4)–Pt(3) 2.372; S(2)–Pt(1)–S(1) 81.66(8), Pt(1)–S(1)–Pt(2) 80.86(7), Pt(1)–S(2)–Pt(2) 81.20(7), S(2)–Pt(2)–S(1) 81.75(8), S(2)–Cu–S(1) 83.65(8), S(4)–Cu–S(3) 83.54(9), S(3)–Pt(3)–S(4) 81.02(9), Pt(3)–S(3)–Pt(4) 82.98(8), Pt(3)–S(4)–Pt(4) 82.65(8), S(3)–Pt(4)–S(4) 81.26(8).

temperature or at 115 K, shows a partially good resolution of the copper hyperfine splitting, probably brought about by magnetic dilution afforded by the bulky phenyl groups of the dppe ligands on the diamagnetic $[Pt_2(dppe)_2(\mu\text{-}S)_2]$ moieties. Simple first-order spectral analysis yielded $g_z = 2.114$, $g_y = 2.055$ and $g_x = 1.994$, and $A_z = 124.4 \times 10^{-4}$, $A_y = 37 \times 10^{-4}$ and $A_x = 36 \times 10^{-4}$ cm^{-1}. These results agree with the distorted tetrahedral geometry and show that the heterometal is a copper(II) ion rather than copper(I) coordinated to a $[Pt_2(dppe)_2(\mu\text{-}S)_2]^+$ radical moiety. The unpaired electron resides in the d_{xy} orbital of the metal centre (with sulfur donor-atoms between the *x* and *y* axes).[12] No evidence of delocalization of the unpaired electron onto the platinum(II) ions has been found. Comparison of these features with EPR spectral patterns of the blue copper sites[13] indicates that $g_{x,y}$ and $A_{x,y}$ are similar, but those of the corresponding parallel parameters deviate significantly. This can be attributed to the different nature of the donor atoms bound to Cu and to the more flattened tetrahedral geometry about this metal centre in the case of the $[Cu\{Pt_2(dppe)_2(\mu_3\text{-}S)_2\}_2]^{2+}$ cation.[14]

The electronic spectrum of **2** in acetonitrile solution shows a very broad band with maximum intensity at $\nu_1 = 8550$ cm^{-1} (1170 mm, $\varepsilon = 740$ dm^3 mol^{-1} cm^{-1}), a band at $\nu_2 = 17\,700$ cm^{-1} (565 nm, $\varepsilon = 4400$ dm^3 mol^{-1} cm^{-1}), and a very strong absorption between 320 and 220 nm ($\varepsilon > 20\,000$ dm^3 mol^{-1} cm^{-1}). The position of ν_1 reveals that the distorted tetrahedral geometry of the copper ion in complex **2** is preserved in solution and compares well with the estimated value of 9800 cm^{-1} for the higher energy d–d band of a tetrahedral $CuCl_4$ core with the same degree of distortion ($\omega = 61°$) as **2**.[15] On the basis of an idealized D_2 symmetry the ν_1 band is assigned to the $^2B_1 \rightarrow {}^2A$ ($d_{z^2} \rightarrow d_{xy}$) transition. Following the EPR behaviour, both the position and the intensity of ν_2 are close to those of the characteristic band of the blue copper sites appearing at *ca.* 600 nm in stellacyanin, plastocyanin and azurin proteins. Therefore, ν_2 is assigned to a $\sigma(S) \rightarrow d_{xy}(Cu)$ LMCT transition.[13]

The authors acknowledge the DGICYT through projects PB94-0695 and PB95-0639-C02-01, and the UK EPSRC for financial support. R. A. C. thanks Siemens plc for CASE studentship support. We are grateful to Dr J. Vidal from ICMAB for the EPR measurements.

Notes and References

† $^{31}P\{^1H\}$ NMR [101.2 MHz, $(CD_3)_2SO$, 25 °C]: δ 40.48 [t, ^1J(PPt) 2696, ^3J(PPt) 48 Hz]; $^{195}Pt\{^1H\}$ NMR [85.6 MHz, $(CD_3)_2SO$, 25 °C]: δ −4297.6 [t, ^1J(PtP) 2721, ^2J(PtPt) 784 Hz].

‡ **1**·2C_6H_6: $C_{64}H_{60}P_4Pt_2S_2$; $M = 1407.3$; monoclinic, space group $P2_1/c$; $a = 14.6661(9)$, $b = 25.359(2)$, $c = 15.0660(10)$ Å, $\beta = 95.386(2)°$; $U = 5578.6(6)$ Å^3, $Z = 4$, $D_c = 1.676$ g cm^{-3}; Mo-Kα ($\lambda = 0.710\,73$ Å), $\mu = 5.24$ mm^{-1}; $T = 160$ K. 34 054 (12 524 unique, $\theta < 28.5°$, $R_{int} = 0.0337$) data were collected on a Siemens SMART CCD, and were corrected for absorption (SADABS, G. M. Sheldrick, University of Göttingen, Germany, 1997), transmission 0.397–0.673. Refinement on F^2 values of all data (G. M. Sheldrick, SHELXTL manual, Siemens Analytical X-ray Instruments Inc., Madison WI, USA, 1994, version 5) gave $wR = \{\Sigma[w(F_o^2 - F_c^2)^2]/\Sigma[w(F_o^2)^2]\}^{1/2} = 0.0796$, conventional $R = 0.0338$ for F values of 10 865 reflections with $F^2 > 2\sigma(F^2)$, $S = 1.198$ for 650 parameters. Residual electron density extrema are 1.57 and −1.69 e Å^{-3}.

2·0.5Et_2O: $C_{106}H_{101}CuF_{12}O_{0.50}P_{10}Pt_4S_4$; $M = 2892.7$; monoclinic, space group $C2$; $a = 33.9929(11)$, $b = 13.6034(4)$, $c = 23.4524(7)$ Å, $\beta = 90.374(2)°$; $U = 10844.6(6)$ Å^3; $Z = 4$; $D_c = 1.772$ g cm^{-3}; $\mu = 5.63$ mm^{-1}; $T = 160$ K; 35 148 (19 241 unique, $\theta < 28.7°$, $R_{int} = 0.0347$) data, transmission 0.490–0.810. Experimental and computational methods were as above. $wR = 0.0943$, $R = 0.0404$ (18 847 F values), $S = 1.263$ for 1241 parameters. Residual electron density extrema are 1.72 and −1.72 e Å^{-3}. CCDC 182/759.

§ *Ab initio* calculations were performed with the GAUSSIAN 94 series of programs.[8] Geometry optimizations were carried out at the second level of the Möller–Plesset theory (MP2)[9] with a basis set of valence double-ζ quality for the metal atoms[10a] and valence double-ζ[10b] + *d* polarization functions[10c] for the atoms attached to the metal. Effective core potentials (ECP) were used to represent the innermost electrons of the metal atoms[10a] as well as the electron core of the P and S atoms.[10b] A minimal basis set was used for the H and C atoms of the $H_2PCH_2CH_2PH_2$ ligands.[10d]

1 (*a*) H. Liu, A. L. Tan, Y. Xu, K. F. Mok and T. S. A. Hor, *Polyhedron*, 1997, **16**, 377 and references therein; (*b*) V. W. W. Yam, P. K. Y. Yeung and K. K. Cheung, *Angew. Chem., Int. Ed. Engl.*, 1996, **35**, 739.
2 C. E. Briant, C. J. Gardner, T. S. A. Hor, N. D. Howells and D. M. P. Mingos, *J. Chem. Soc., Dalton Trans.*, 1984, 2645.
3 V. W. W. Yam, P. K. Y. Yeung and K. K. Cheung, *J. Chem. Soc., Chem. Commun.*, 1995, 267.
4 M. Capdevila, W. Clegg, P. González-Duarte, A. Jarid and A. Lledós, *Inorg. Chem.*, 1996, **35**, 490.
5 E. John, P. K. Bharadwaj, K. Krogh-Jespersen, J. A. Potenza and H. J. Schugar, *J. Am. Chem. Soc.*, 1986, **108**, 5015.
6 K. Fujisawa, Y. Moro-oka and N. Kitajima, *J. Chem. Soc., Chem. Commun.*, 1994, 623.
7 R. Ugo, G. La Monica, S. Cenini, A. Segre and F. Conti, *J. Chem. Soc. A*, 1971, 522.
8 M. J. Frisch, G. W. Trucks, H. B. Schlegel, P. M. W. Gill, B. G. Johnson, M. A. Robb, J. R. Cheeseman, T. A. Keith, G. A. Petersson, J. A. Montgomery, K. Raghavachari, M. A. Al-Laham, V. G. Zakrzewski, J. V. Ortiz, J. B. Foresman, J. Cioslowski, B. B. Stefanov, A. Nanayakkara, M. Challacombe, C. Y. Peng, P. Y. Ayala, W. Chen, M. W. Wong, J. L. Andrés, E. S. Replogle, R. Gomperts, R. L. Martin, D. J. Fox, J. S. Binkley, D. J. De Frees, J. Baker, J. P. Stewart, M. Head-Gordon, C. Gonzalez and J. A. Pople, Gaussian 94; Gaussian Inc., Pittsburg PA, 1995.
9 C. Möller and M. S. Plesset, *Phys. Rev.*, 1934, **46**, 618.
10 (*a*) P. J. Hay and W. R. Wadt, *J. Chem. Phys.*, 1985, **82**, 299; (*b*) W. R. Wadt and P. J. Hay, *J. Chem. Phys.*, 1985, **82**, 284; (*c*) A. Höllwarth, M. Böhme, S. Dapprich, A. W. Ehlers, A. Gobbi, V. Jonas, K. F. Köhler, R. Stegmann, A. Veldkamp and G. Frenking, *Chem. Phys. Lett.*, 1993, **208**, 237; (*d*) W. J. Hehre, R. E. Stewart and J. A. Pople, *J. Chem. Phys.*, 1969, **51**, 2657.
11 N. Duran, P. González-Duarte, A. Lledós, T. Parella, J. Sola, G. Ujaque, W. Clegg and K. A. Fraser, *Inorg. Chim. Acta*, 1997, **265**, 89.
12 B. J. Hathaway and D. E. Billing, *Coord. Chem. Rev.*, 1970, **5**, 143.
13 K. W. Penfield, R. R. Gay, R. S. Himmelwright, N. C. Eickman, V. A. Norris, H. C. Freeman and E. I. Solomon, *J. Am. Chem. Soc.*, 1981, **103**, 4382.
14 U. Sakaguchi and A. W. Addison, *J. Chem. Soc., Dalton Trans.*, 1979, 600.
15 L. P. Battaglia, A. Bonamartini Corradi, G. Marcotrigiano, L. Menabue and G. C. Pellacani, *Inorg. Chem.*, 1979, **18**, 148.

Received in Cambridge, UK, 14th October 1997; 7/07398D

Identification of the precursor of singlet oxygen ($^1O_2$, $^1\Delta_g$) involved in the disproportionation of hydrogen peroxide catalyzed by calcium hydroxide

Véronique Nardello,[a] Karlis Briviba,[b] Helmut Sies[b] and Jean-Marie Aubry*[a]

[a] *Equipe de Recherches sur les Radicaux Libres et l'Oxygène Singulet, URA CNRS 351, Faculté de Pharmacie de Lille, BP 83, F-59006 Lille Cedex, France*

[b] *Institut für Physiologische Chemie I, Heinrich-Heine-Universität Dusseldorf, Postfach 101007, D-40001 Düsseldorf, Germany*

Catalytic disproportionation of hydrogen peroxide by calcium hydroxide generates singlet molecular oxygen $^1O_2$ ($^1\Delta_g$) through the diperoxohydrate peroxide $CaO_2{\cdot}2H_2O_2$ with a 50% yield based on the calcium peroxide.

Many inorganic compounds are known to induce the disproportionation of hydrogen peroxide into singlet oxygen ($^1O_2$, $^1\Delta_g$).[1] Among them, calcium hydroxide appears both attractive for its environmental friendly feature and amazing on account of the simplicity of the catalyst involved [eqn. (1)].

$$2\ H_2O_2 \xrightarrow{Ca^{II}} 2\ H_2O + \alpha\ {}^1O_2 + (1-\alpha)\ {}^3O_2 \qquad (1)$$

Although the formation of $^1O_2$ during reaction (1) has been established,[1] several points remain unclear: (*i*) the traps of $^1O_2$ bore carboxylate functions which precipitated partially in presence of the calcium salts, (*ii*) the calcium hydroxide did not have the highest purity commercially available, (*iii*) the influence of the main parameters on the reaction were not studied, (*iv*) no information was provided with regard to the nature of the precursor of $^1O_2$. Therefore, the system H_2O_2/Ca^{II} has been reinvestigated by resorting to two complementary techniques: the detection of the IR luminescence of $^1O_2$ at 1270 nm and the chemical trapping with a more suitable trap. In a second step, the nature of the precursor and the yield of $^1O_2$ were determined.

The monomol emission of $^1O_2$ was detected with a liquid-nitrogen cooled germanium diode equipped with a bandpass filter for 1270 ± 10 nm.[2] The assays were carried out in a thermostated cell at 50 °C filled with an aqueous (H_2O or D_2O) solution of H_2O_2 (1.0 M). After recording the baseline, solid CaO (0.2 M) of high purity (99.995%) was added and the photoemission of $^1O_2$ was monitored. The maximum values of the luminescence intensy I_p are reported in Table 1.

The luminescence intensity I_p was found to be strongly dependent on the deuteration of the solvent (Table 1, entries 1 and 2) as a ten-fold increase was observed in deuterated water (95%), in good agreement with the longer lifetime of $^1O_2$ in D_2O than in H_2O.[3] In a control experiment (Table 1, entry 3), it was shown that the disproportionation of H_2O_2 (1 M) induced by NaOH (0.4 M) did not provide any detectable signal in contrast with the finding of Smith and Kulig.[4] Accordingly, $^1O_2$ arises from the interaction between Ca^{II} and H_2O_2 and not from the base-catalyzed disproportionation of H_2O_2.

Table 1 Experimental conditions and emission intensity I_p of $^1O_2$ luminescence[a]

Entry	Calcium compound	$[H_2O_2]$/ mmol	[NaOH]/ mmol	Solvent	I_p/mV
1	CaO	5.0	—	H_2O	0.4 ± 0.1
2	CaO	5.0	—	D_2O	4.4 ± 0.5
3	—	5.0	2.0	D_2O	No signal
4	$CaO_2{\cdot}8H_2O$	—	—	D_2O	0.3 ± 0.1
				CD_3OD	0.5 ± 0.1
5	$CaO_2{\cdot}2H_2O_2$	—	—	D_2O	10 ± 0.5
				CD_3OD	98 ± 2

[a] Experiments were carried out with 1.0 mmol of calcium compounds at 50 °C in 5 ml of solvent.

The detection of $^1O_2$ *via* its IR luminescence requires a relatively high steady-state concentration of $^1O_2$.[5] Thus, experiments with the system H_2O_2/Ca^{II} were carried out in D_2O and with gentle warming (50 °C). On the other hand, specific chemical trapping worked in ordinary water, at room temperature, and was found to be more reliable for the quantification of $^1O_2$ than the spectral method. The new cationic water-soluble trap, 9,10-bis(4-trimethylphenylammonium) anthracene dichloride (BPAA), which efficiently reacts with $^1O_2$ giving a specific endoperoxide $BPAAO_2$ as the sole product,[6] was particularly suitable for these trapping experiments since it did not interfere with the catalytic reaction as the tetrapotassium rubrene-2,3,8,9-tetracarboxylate (RTC) did.[1] In presence of BPAA, $^1O_2$ arising from reaction (1) can either be quenched by water [eqn. (2)] and by BPAA [eqn. (3)] or react with this trap [eqn. (4)].[7]

$$^1O_2 \xrightarrow[\text{water}]{k_d} {}^3O_2 \qquad (2)$$

$$\text{BPAA} + {}^1O_2 \xrightarrow{k_q} \text{BPAA} + {}^3O_2 \qquad (3)$$

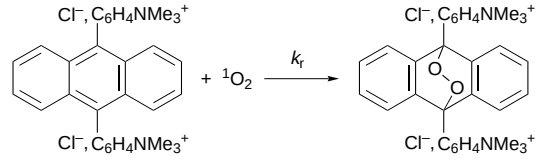

(4)

Under pseudo-stationary conditions ($d[^1O_2]/dt = 0$), processes (1)–(4) lead to eqn. (5) giving the rate of the disappearance of BPAA:

$$\frac{d[BPAA]}{dt} = -v(^1O_2)\frac{k_r[BPAA]}{k_d + (k_r + k_q)[BPAA]} \qquad (5)$$

where $v(^1O_2)$ is the rate of $^1O_2$ generation from reaction (1).

The concentration of BPAA used was very low (10^{-4} M) in order to minimize the disturbance of the process under study. Under these conditions, the quenching of $^1O_2$ by water is the main pathway for $^1O_2$ decay. Thus, $k_d \gg (k_r + k_q)$ [BPAA] and eqn. (5) reduces to eqn. (6) which allows calculation of $v(^1O_2)$ from the initial rate of BPAA disappearance, d[BPAA]/d*t*:

$$v(^1O_2) = -\frac{d[BPAA]}{dt}\frac{k_d}{k_r[BPAA]} \qquad (6)$$

In control experiments, it was shown that the oxidation of BPAA (10 mM) gives the expected endoperoxide $BPAAO_2$ identified by ^1H and ^{13}C NMR spectroscopy.[6] Accordingly, the

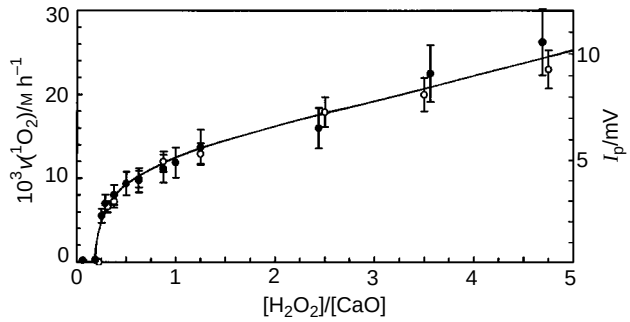

Fig. 1 $^1O_2$ formation as a function of [H_2O_2] detected by chemical trapping (○) (200 mM CaO, 0.1 mM BPAA, H_2O, 25 °C) or by IR luminescence at 1270 nm (●) (same conditions except D_2O, 50 °C)

disappearance of BPAA could be confidently assigned to an oxidation through $^1O_2$. It was also shown that 50 mM CaO was able to disproportionate 500 mM H_2O_2 indicating that the Ca^{II} involved in process (1) acts as a catalyst. It is noteworthy that, whereas no H_2O_2 could be detected in the aqueous phase at the end of the reaction, the precipitate was found to contain exactly one peroxide group per Ca^{II} whatever the starting concentrations of H_2O_2 and CaO were. The final product is then probably the hydrated calcium monoperoxide $CaO_2{\cdot}8H_2O$ which is known to be stable in water.[8,9] The rate of $^1O_2$ formation was measured for various initial concentrations of H_2O_2 (Fig. 1).

This figure shows that the formation of $^1O_2$ requires at least 1 equiv. of H_2O_2. The reaction rate increases steeply at first and then moderately when the concentration of H_2O_2 is increased suggesting that the main precursor of $^1O_2$ is probably the calcium complex which bears the highest number of peroxo groups. It is noteworthy that chemical trapping and detection of the luminescence provided similar results since a mere standardization allowed the fitting of both curves.

Although numerous calcium peroxides are reported in the literature,[8–10] Karelin *et al.* have recently established that only two well defined compounds may be obtained by reaction of H_2O_2 with CaO in aqueous solution. The first is the stable octahydrate peroxide $CaO_2{\cdot}8H_2O$ and the other is the unstable diperoxohydrate peroxide $CaO_2{\cdot}2H_2O_2$ which decomposes spontaneously releasing oxygen.[10] Up to now, no report has dealt with the multiplicity of the oxygen. We looked for the possible $^1O_2$ luminescence emitted by thermolysis at 50 °C of the calcium peroxides $CaO_2{\cdot}8H_2O$ and $CaO_2{\cdot}2H_2O_2$ dispersed in deuterated methanol and water (Table 1). Deuterated solvents were preferred to take advantage of the longer lifetime of $^1O_2$ which provides an enhanced intensity of the luminescence. $CaO_2{\cdot}8H_2O$ did not emit any significant luminescence (Table 1, entry 4) whereas a similar amount of $CaO_2{\cdot}2H_2O_2$ emitted a huge signal (98 ± 2 mV) in CD_3OD. In D_2O, the signal was significant but lower probably owing to hydrolysis of the

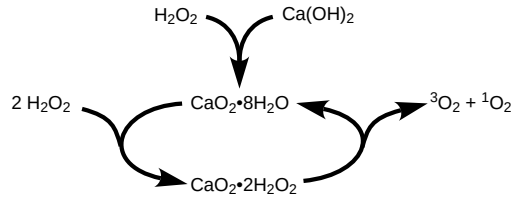

Scheme 1

complex as for the peroxomolybdates.[11] Accordingly, we can assert that $CaO_2{\cdot}2H_2O_2$ is a precursor of $^1O_2$. A catalytic scheme may be drawn from this conclusion (Scheme 1).

In a first step, $Ca(OH)_2$ is converted into $CaO_2{\cdot}8H_2O$ which binds two molecules of H_2O_2 giving $CaO_2{\cdot}2H_2O_2$. On thermolysis at moderate temperature, this latter peroxide splits up into $^1O_2$ and $CaO_2{\cdot}8H_2O$. This catalytic cycle would operate until complete disproportionation of H_2O_2 and would leave $CaO_2{\cdot}8H_2O$ as a final product.

In order to assess the efficiency of $CaO_2{\cdot}2H_2O_2$ to generate $^1O_2$, the oxidation of 250 mM α-terpinene was performed by warming at 50 °C a suspension of 400 mM $CaO_2{\cdot}2H_2O_2$ in CD_3OD. α-Terpinene is known to trap efficiently all the $^1O_2$ released giving mainly ascaridol.[12] ^1H NMR analysis of the reaction mixture showed that, under these conditions, $CaO_2{\cdot}2H_2O_2$ converts 85% of α-terpinene into ascaridol providing a yield of $^1O_2$ formation equal to 50 ± 3% based on this calcium peroxide.

This work was supported by the CNRS (program 'Catalysis and catalysts for industry and environment').

Notes and References

* E-mail: jmaubry@phare.univ-lille2.fr

1 J. M. Aubry, *J. Am. Chem. Soc.*, 1985, **107**, 5844.
2 P. Di Mascio and H. Sies, *J. Am. Chem. Soc.*, 1989, **111**, 2909.
3 A. A. Gorman and M. A. J. Rodgers, *Singlet Oxygen, in Handbook of Organic Photochemistry*, ed. J. C. Scaiano, CRC Press, Boca Raton, 1989, vol. 2, pp. 229–247.
4 L. L. Smith and M. J. Kulig, *J. Am. Chem. Soc.*, 1976, **98**, 1027.
5 K. Böhme and H.-D. Brauer, *Inorg. Chem.*, 1992, **31**, 3468.
6 V. Nardello and J. M. Aubry, *Tetrahedron Lett.*, 1997, **38**, 7361.
7 F. Wilkinson and J. G. Brummer, *J. Phys. Chem. Ref. Data*, 1995, **24**, 663.
8 I. I. Vol'nov, in *Peroxides, Superoxides and Ozonides of Alkali-Earth Metals*, ed. A. W. Petrocelli, Plenum, New York, 1966.
9 N. G. Vannerberg, *Prog. Inorg. Chem.*, 1962, **4**, 125.
10 A. I. Karelin, D. G. Lemesheva and N. F. Gladyshev, *Russ. J. Inorg. Chem.*, 1995, **40**, 371.
11 V. Nardello, J. Marko, G. Vermeersch and J. M. Aubry, *Inorg. Chem.*, 1995, **34**, 4950.
12 J. M. Aubry, B. Mandard-Cazin, M. Rougee and R. V. Bensasson, *J. Am. Chem. Soc.*, 1995, **117**, 9159.

Received in Liverpool, UK, 12th November 1997; 7/08161H

Strong negative thermal expansion in siliceous faujasite

Martin P. Attfield and Arthur W. Sleight*†

Department of Chemistry and Center for Advanced Materials Research, Oregon State University, Corvallis, OR 97331-4003, USA

Strong isotropic negative thermal expansion ($\alpha = -4.2 \times 10^{-6}$ K^{-1}) found for siliceous faujasite over a temperature range of 25 to 573 K is attributed to transverse vibrations of the bridging oxygen atoms, a model supported by structural refinements of X-ray diffraction data as a function of temperature.

Negative thermal expansion is not a common phenomenon in solid materials. When it does arise, it is usually of small magnitude and displayed over a limited temperature range. Such thermal expansion is most usually found in anisotropic materials, for example, $LiAlSiO_4$,[1] $NbZrP_3O_{12}$[1] and $Sc_2W_3O_{12}$,[2] where the intrinsic linear thermal expansion is not more negative than -2.2×10^{-6} K^{-1}. Ceramic bodies made from such materials can show greater negative thermal expansion owing to microcracking effects which tend to become larger at lower temperatures. For instance a ceramic body of $Sc_2W_3O_{12}$, depending on how it is processed, can give a thermal expansion of up to -11×10^{-6} K^{-1}. Problems with microcracking in such ceramic bodies can be avoided if the material shows isotropic negative thermal expansion as is the case for the cubic material ZrW_2O_8 which exhibits strong isotropic negative thermal expansion (-8.7×10^{-6} K^{-1}) over a broad temperature range.[3,4]

An apparent requirement for an oxide material to have strong intrinsic negative thermal expansion is that it has an open framework structure with two-coordinate oxygen atoms. Several classes of such framework structures exist, including those of the family of SiO_2 structures and their derivatives. Various forms of the more condensed polymorphs of SiO_2 are known to exhibit negative thermal expansion over limited temperature ranges which do not include room temperature. Amorphous SiO_2 shows this behaviour below room temperature, and certain crystalline forms (quartz, cristobalite and tridymite) show weak negative thermal expansion above 1000 °C.[5] Zeolites are a group of open framework structures that derive from the SiO_2 family of structures in which some aluminium replaces the silicon atoms in the framework structure. The presence of aluminium atoms in the framework causes complications when considering thermal expansion properties. The charge of the aluminium in the framework is balanced by extraframework cations which influence the thermal expansion in several ways. In particular, bonds between framework oxygen atoms and alkali or alkaline earth cations exhibit large positive thermal expansion so these cations will provide a positive contribution to the expansion of the zeolite as the temperature increases. The position of the extraframework cations is also known to vary with temperature, as has been shown for Ca-mordenite,[6] again affecting the thermal expansion properties of the zeolite. The presence of the extraframework cations also increases the amount of water taken up by the zeolite. This water is often difficult to fully remove and can influence the thermal expansion properties of the system. These difficulties appear to play a large factor in the experimental data for the thermal expansion of Na-zeolite X, (the only data reported for the faujasite family that the authors are aware of) which has a net negative thermal expansion between 25 and 200 K and appears to expand above 200 K.[8,9]

In this work, we chose to study the thermal expansion of a purely siliceous zeolite, thus avoiding the complications associated with the extraframework cations and greatly reducing the water content of the zeolite. Here, we report the thermal expansion properties of siliceous faujasite from 25 to 573 K, it being strongly negative (-4.2×10^{-6} K^{-1}) over the entire range.

The sample of dealuminated Y (DAY) was kindly supplied by Amoco Chemical Company and was prepared as described previously.[9,10] The Al content was 120 ppm by ICP analysis. DAY was heated to 550° for 8 h in air to produce what has been referred to[9,10] as 'zero defect' DAY or ZDDAY. This treatment removes the defects caused by dealumination as determined by ^{29}Si MAS NMR; only one type of ^{29}Si is observed in ZDDAY. The sample was dehydrated for 12 h at 330 °C under a vacuum of *ca.* 10^{-5} Torr and transferred to an argon-filled glovebox where it was loaded, and sealed, into 0.5 mm and 0.3 mm diameter Lindemann glass capillary tubes. Before dehydration, the water content can be indicated as $SiO_2 \cdot xH_2O$ with $x = 0.08$. After dehydration, water was undetected indicating that x was < 0.005. Synchrotron X-ray powder diffraction data were collected on the sample at beamline X7A, National Synchrotron Light Source, Brookhaven National Laboratory. The diffractometer set up included the use of a Si(111) monochromator and a krypton filled position sensitive detector (p.s.d.). All data were collected at a wavelength of 1.099 32(6) Å. The temperature of the sample for each data collection was controlled using an Air Products Displex, and data were collected at seven temperatures between 25.16 and 297.5 K, inclusive. X-Ray data on the sample from 303 to 573 K were collected on an INEL XRG 3000 diffractometer using Cu-Kα_1 radiation monochromated by a Ge(111) crystal and adjustable vertical slits. The detector used was an INEL CPS 90 p.s.d. filled with an ethane–argon mixture. The sample was held within a capillary furnace fitted with resistive heating elements.

The synchrotron X-ray data sets were refined using the Rietveld method.[11] The refinement at each temperature was performed using the same procedure. The first four peaks were excluded from each refinement owing to their highly asymmetric peak shape. All backgrounds were fitted by linear interpolation using the same number of points in each case. The starting model for the siliceous faujasite was taken from that described by Hriljac *et al.*[10] The last cycle of least-squares refinement included the histogram scale factor, zero point, lattice parameter, five peak shape parameters, and the coordinates and isotropic temperature factors of each atom. The X-ray data sets collected on the laboratory diffractometer were fitted using the Le Bail method only.[12] Again, the background was fitted by linear interpolation and the last cycle of least-squares refinement included the zero point, lattice parameter, and five peak shape parameters. All refinements were carried out using the GSAS suite of programs.[13]

The negative thermal expansion properties of siliceous faujasite are shown in Fig. 1. An approximately linear decrease in cell dimension is seen over the entire temperature range 25.16–572.0 K. The overall coefficient of thermal expansion {defined as $(l_{T2} - l_{T1})/[l_{T1}(T_2 - T_1)]$} calculated for the whole temperature range is -4.2×10^{-6} K^{-1}. This value is in good

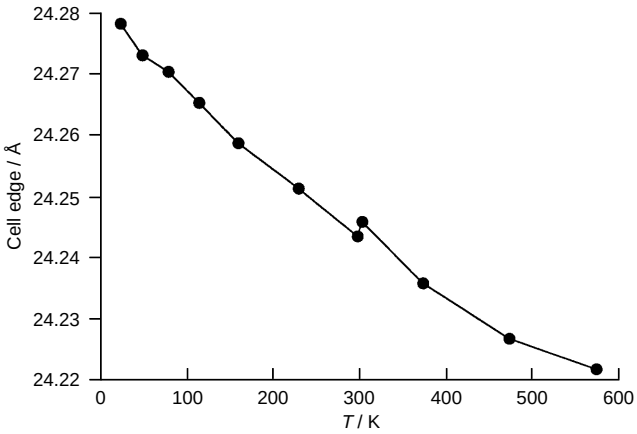

Fig. 1 Cubic cell edge as a function of temperature for siliceous faujasite

agreement with that calculated for siliceous faujasite by Couves *et al.* (-4.1×10^{-6} K^{-1}), but is significantly more negative than the values obtained from their computational and experimental studies on Na-zeolite X (-3.0×10^{-6} K^{-1} and -0.7×10^{-6} K^{-1}, respectively).[7,8]

The results from the Rietveld refinements at the seven temperatures between 25 and 298 K enable us to gain some insight into the structural changes giving rise to the negative thermal expansioin of siliceous faujasite. As in other negative thermal expansion materials,[2–4] the overall changes in bond distances and angles are small relative to their e.s.d.s. A cell dimension change of that observed between 25.16 and 297.5 K (24.2782–24.2442 Å), when placed on the same scale as a typical Si–O bond represents a change of only 1.600–1.598 Å, where a typical Rietveld e.s.d. on a bond length is only 0.002 Å.

The observed O–Si–O and Si–O–Si angles varied from 107 to 113° and 137 to 149°, respectively, with no detectable change with temperature in either case. There was an apparent decrease in the average Si–O bond distance of 1.614 to 1.610 Å from 25 to 298 K. However, after correcting for the thermal motion of oxygen,[14] there was no detectable change in the Si–O bond length over this temperature range. The fact that the bond angles and corrected bond distances within the SiO_4 tetrahedra remain essentially constant over the temperature range studied allows the latter to be considered as rigid tetrahedra.

The results from the structure refinements lead us to believe that the negative thermal expansion of this material is related to the transverse vibrations to the two-coordinate bridging oxygen atoms, a mode of lattice vibration that is of low enough energy to be readily excited at low temperatures. These vibrations lead to coupled rotations of the essentially rigid tetrahedra making up the structure of the zeolite. The lack of any systematic changes in atomic coordinates and bond angles over the temperature range studied implies that the transverse vibrations of the bridging oxygen atoms are essentially harmonic in nature and the bending of the Si–O–Si bonds is dynamic rather than static in nature. As the temperature of the material is increased, the magnitude of the transverse vibrations of the bridging oxygen atoms, as well as the resulting coupled rotations of the tetrahedra, increases, which manifests itself in the structure refinement results as a decrease in the average Si–O distance. With the decrease in the Si–O bond length accompanying the increase in temperature, a decrease in the average Si–Si non-bonding distance occurs, resulting in the negative thermal expansion observed. Again we emphasise that the apparent reduction of the Si–O bond length results from the increased thermal motion and not from actual changes in the magnitude of the Si–O vector. The explanation of the mechanism of negative thermal expansion for siliceous faujasite is the same as that suggested for other materials such as ZrW_2O_8[3,4] and the usual forms of SiO_2.[15]

The strong negative thermal expansion found in siliceous faujasite indicates that other zeolites and ALPOs might exhibit similar behaviour, as has been suggested qualitatively by computational methods.[7,8] However, the latter also predicts that some such framework materials exhibit positive thermal expansion. The reasons for the difference in behaviour for similar materials remain unclear and merit further investigation.

We thank G. J. Ray, Amoco Chemical Company, for provision of the dealuminated zeolite-Y sample. This work was supported through NSF grant No. DMR-9308530. Some data were collected at the National Synchrotron Light Source, Brookhaven National Laboratory, which is supported by the US Department of Energy, Division of Materials Sciences and Division of Chemical Sciences, under Contract No. DE-AC02-76CH00016.

Notes and References

† E-mail: Sleighta@chem.orst.edu

1 A. W. Sleight, *Endeavour*, 1995, **19**, 64.
2 J. S. O. Evans, T. A. Mary and A. W. Sleight, *J. Solid State Chem.*, 1997, **133**, 580.
3 J. S. O. Evans, T. A. Mary, T. Vogt, M. A. S. Subramanian and A. W. Sleight, *Chem. Mater.*, 1996, **8**, 2809.
4 J. S. O. Evans, T. A. Mary, A. W. Sleight and T. Vogt, *Science*, 1996, **272**, 90.
5 D. Taylor, *Br. Ceram. Trans. J.*, 1984, **83**, 129.
6 W. J. Mortier, *J. Phys. Chem.*, 1977, **81**, 1334.
7 J. W. Couves, R. H. Jones, S. C. Parker, P. Tschaufeser and C. R. A. Catlow, *J. Phys.: Condens. Matter*, 1993, **5**, L329.
8 P. Tschaufeser and S. C. Parker, *J. Phys. Chem.*, 1995, **99**, 10 600.
9 G. J. Ray, A. G. Nerheim and J. A. Donohue, *Zeolites*, 1988, **8**, 458.
10 J. A. Hriljac, M. M. Eddy, A. K. Cheetham, J. A. Donohue and G. J. Ray, *J. Solid State Chem.*, 1993, **106**, 66.
11 H. M. Rietveld, *J. Appl. Crystallogr.*, 1969, **2**, 65.
12 A. C. Le Bail, H. Duroy and J. L. Fourquet, *Mater. Res. Bull.*, 1988, **23**, 447.
13 A. C. Larson and R. B. Von Dreele, GSAS, Tech. Rept. LA-UR-86-748, Los Alamos National Laboratory, NM, 1987.
14 D. W. J. Cruickshank, *Acta Crystallogr.*, 1956, **9**, 757.
15 T. H. K. Barron, J. G. Collins and G. K. White, *Adv. Phys.*, 1980, **29**, 609.

Received in Bloomington, IN, USA, 2nd October 1997; 7/07141H

Asymmetric synthesis of dimethyl swazinecate and structural confirmation of its parent alkaloid (−)-swazine

James D. White,*† John C. Amedio, Jr., Peter Hrnciar, Nadine C. Lee, Susumu Ohira and Alexandre F. T. Yokochi

Department of Chemistry, Oregon State University, Corvallis, OR 97331-4003, USA

Synthesis of dimethyl swazinecate, a principal component of the pyrrolizidine alkaloid swazine, was completed from (*S*)-(−)-β-citronellal; an X-ray crystallographic analysis of natural swazine confirmed its absolute stereostructure.

Pyrrolizidine alkaloids are widespread among plants of the *Senecio* family, many of which possess toxic properties that pose serious risk to human and animal health.[1] (−)-Swazine **1**, first isolated from *Senecio swaziensis* Compton,[2] is among the more complex members of this class of alkaloids, consisting of a functionalized adipic acid derivative **2** (swazinecic acid) that bridges the C7 and C9 hydroxy groups of the pyrrolizidine retronecine to form a twelve-membered dilactone. Neither acidic nor careful basic hydrolysis of **1** has permitted isolation of intact **2**. Instead, the constitution of this dicarboxylic (necic) acid was inferred from the spirolactone **3** obtained upon treatment of **1** with hot, 1.5 M sulfuric acid. The structure of **3** was established by X-ray crystallographic analysis of its *p*-bromobenzoate.[2] Initially, swazine was formulated as the dilactone isomeric with **1**, in which swazinecic acid **2** was connected to retronecine in the reverse orientation to that shown. This assignment was subsequently revised,[3] and the revision was accepted after a more complete degradative and spectroscopic investigation.[4] Herein, we report the first synthesis of swazinecic acid, characterized as its dimethyl ester, which confirms its absolute stereostructure as **2**. We also describe an X-ray crystallographic analysis of natural swazine which now substantiates the designation of this alkaloid as **1**.

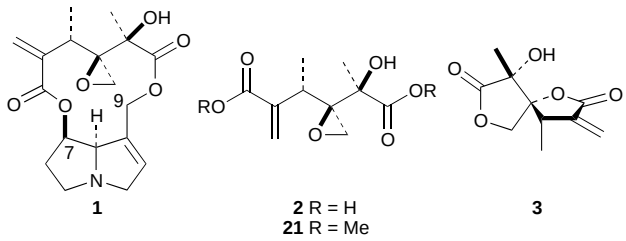

1 **2** R = H, **21** R = Me **3**

Our approach, which employs β-citronellal as the starting material,[5] hinges upon oxidative truncation of an elaborated terpenoid structure to generate a dicarboxylic acid having the requisite functionality and configuration of the necic acid.[6–10] Since our planned route to **2** involved early introduction of a relatively sensitive epoxide, it was essential that later steps in the sequence avoid reagents which would destroy this function.

α-Methylenation of (−)-**4**, followed by Luche reduction of the resultant α,β-unsaturated aldehyde (as described for the enantiomeric series),[9] gave the allylic alcohol **5** (Scheme 1). The trisubstituted olefin of this diene underwent selective methoxyselenation using Toshimitsu's conditions,[11] and the intermediate alkyl selenide was oxidized to afford **6** in good yield. Asymmetric epoxidation of **6** using (*S*,*S*)-(+)-diisopropyl tartrate (DIPT) as the chiral adjuvant[12] gave **7** and **8** in the ratio 6.5 : 1.

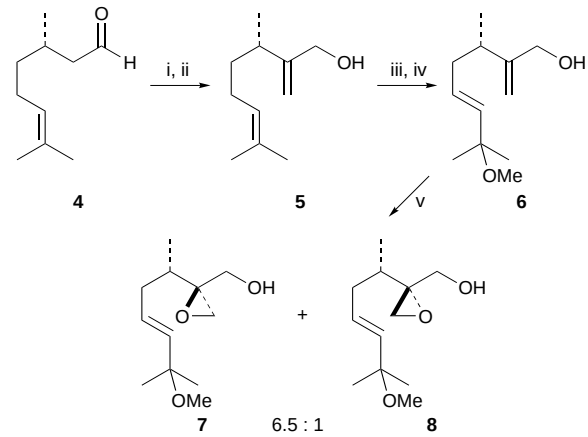

Scheme 1 *Reagents and conditions*: i, LDA, $CH_2{=}N^+Me_2I^-$, MeI, $NaHCO_3$, 94%; ii, $NaBH_4$, $CeCl_3{\cdot}7H_2O$, 93%; iii, PhSeCl, $NaHCO_3$, THF–MeOH; iv, H_2O_2, $NaHCO_3$, THF–H_2O, 82% (from **5**); v, Bu^tOOH, $Ti(OPr^i)_4$, (+)-DIPT, CH_2Cl_2, 92%

After chromatographic separation, **7** was oxidized to aldehyde **12** which was converted to alcohol **13** upon treatment with vinylmagnesium bromide at low temperature (Scheme 2). Further oxidation with Dess–Martin periodinane produced α,β-unsaturated ketone **14**. Chelation-controlled Grignard addition to this ketone was expected to occur selectively at the *re* face of the carbonyl group, and when **14** was treated carefully with methylmagnesium bromide at low temperature a single alcohol,

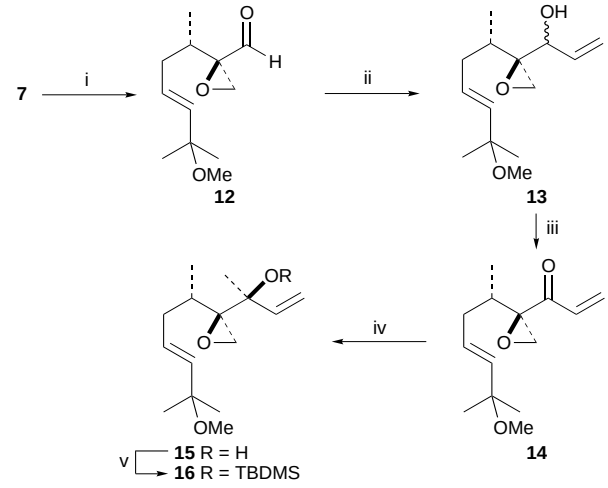

Scheme 2 *Reagents and conditions*: i, $(COCl)_2$, DMSO, Et_3N, CH_2Cl_2, 95%; ii, vinylmagnesium bromide, THF, −78 °C, 72%; iii, Dess–Martin periodinane, 100%; iv, methylmagnesium bromide, Et_2O, −78 °C, 60%; v, TBDMSOTf, 2,6-lutidine, CH_2Cl_2, −35 °C, 76%

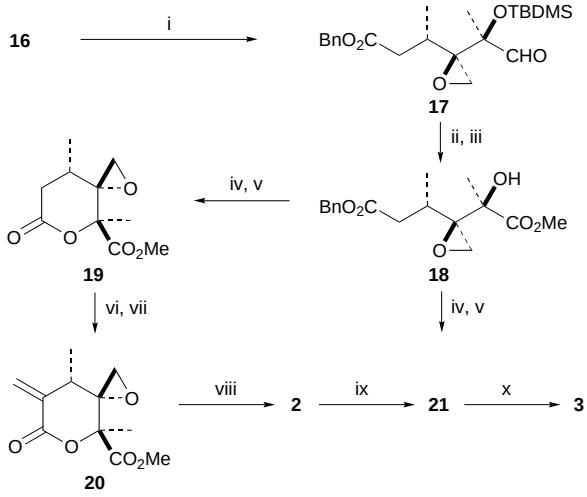

Scheme 3 *Reagents and conditions*: i, O_3, $(CF_3CO)_2O$, BnOH–CH_2Cl_2, $NaHCO_3$, Et_3N, −78 °C; ii, $NaClO_2$, Bu^{t}OH, Me_2C=CHMe; iii, CH_2N_2, Et_2O, 65% from **16**; iv, H_2, Pd/C; v, 2-chloro-1-methylpyridinium iodide (Mukaiyama's reagent), 99% from **18**; vi, LDA, CH_2O, 55%; vii, MsCl, Et_3N, 96%; viii, KOH, MeOH–H_2O; ix, CH_2N_2, Et_2O, 63% from **20**; x, H_2SO_4

assigned structure **15**, was obtained accompanied by the product of conjugate addition.

Alcohol **15** was protected as its *tert*-butyldimethylsilyl ether **16** in a process that retained the epoxide intact. Ozonolytic cleavage of **16** in the presence of benzyl alcohol, trifluoroacetic anhydride and triethylamine at low temperature gave the aldehyde ester **17** in excellent yield (Scheme 3).[13] Unfortunately, the inherent instability of **17** resulting from its propensity towards intramolecular aldol condensation demanded immediate oxidation of this aldehyde to a carboxylic acid, during which the silyl ether was cleaved. Treatment of the resultant α-hydroxy acid with diazomethane afforded **18** which underwent hydrogenolysis of the benzyl ester followed by lactonization with Mukaiyama's reagent[14] to give **19**. Condensation of the lithium enolate of **19** with formaldehyde produced a stereoisomeric mixture of hydroxymethyl lactones which, when exposed to methanesulfonyl chloride and base, led directly to *exo* methylene δ-lactone **20**. Saponification of **20** furnished swazinecic acid **2** which was characterized as its dimethyl ester **21**.‡

Since there is no record of either **2** or **21** having been obtained by degradation of swazine **1**, the structure of synthetic dimethyl swazinecate was confirmed by its conversion to the spirodilactone **3** upon treatment with sulfuric acid in hot THF. The spectroscopic properties of **3** obtained by this method matched those recorded for the same substance derived from **1**.

Final confirmation of the structure, including absolute configuration, of swazinecic acid was obtained by X-ray crystallographic analysis of swazine itself (Fig. 1).§ Since hydrolysis of swazine is known to yield (+)-retronecine, whose absolute configuration has been determined by independent synthesis,[15] the full structure of **1** and hence **2** is as shown.

We are indebted to Professor S. E. Drewes, University of Natal, South Africa, for a sample of natural swazine. Financial support was provided by the National Institute of Environmental Health Sciences (ES03334).

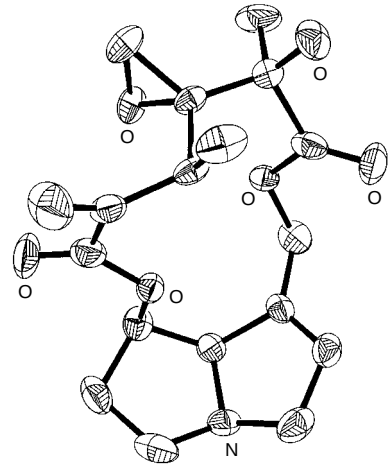

Fig. 1 ORTEP plot of the crystal structure of swazine **1**. Thermal ellipsoids are drawn at the 50% probability level.

Notes and References

† E-mail: whitej@ccmail.orst.edu

‡ *Selected data* for **21**: $[\alpha]_D^{27}$ −38.4 (*c* 0.25, $CHCl_3$); δ_H (400 MHz, $CDCl_3$) 1.19 (3 H, d, *J* 7), 1.47 (3 H, s), 2.44 (1 H, d, *J* 4), 2.91 (1 H, d, *J* 4), 3.62 (1 H, q, *J* 7), 3.77 (3 H, s), 3.81 (3 H, s), 5.52 (1 H, s), 6.17 (1 H, s); δ_C (100 MHz, C_6D_6) 17.2, 22.8, 30.5, 45.2, 51.9, 52.7, 63.8, 77.8, 123.0, 141.3, 168.0, 175.0; ν_{max}/cm^{-1} 3472, 2959, 1733, 1450, 1269, 1156, 1103, 1035; *m*/*z* (CI) 259 (M^+ + 1), 241, 227, 209, 199, 181, 177, 167, 155, 125.

§ *Crystal data* for **1**: $C_{18}H_{23}NO_6$, (MW = 349.37), orthorhombic, space group $P2_12_12_1$ (No. 19), *a* = 8.940(2), *b* = 12.229(2), *c* = 16.706(3) Å, *V* = 1826.4(6) Å^3, *Z* = 4, D_c = 1.271 Mg m^{-3}. A total of 1936 data were collected on a Siemens P4 diffractometer equipped with Cu-Kα radiation (λ = 1.54178 Å, μ = 0.795 mm^{-1}) of which 1775 were unique (R_{int} = 0.0335). A solution was obtained using direct methods as programmed in SHELXS-90 and refined against all data using the program SHELXL 97. The final residuals are *R*1 = 0.0366 (all data), *wR*2 = 0.0990 (all data) with a GoF = 1.071. Supplementary materials in electronic format (CIF file) are available from the authors upon request. CCDC 182/758.

1 A. R. Mattocks, *Chemistry and Toxicology of Pyrrolizidine Alkaloids*, Academic Press, Orlando, Florida, 1986.
2 C. G. Gordon-Gray, R. B. Wells, N. Hallak, M. B. Hursthouse, S. Neidle and T. B. Toube, *Tetrahedron Lett.*, 1972, 707.
3 M. Laing and P. Sommerville, *Tetrahedron Lett.*, 1972, 5183.
4 C. G. Gordon-Gray and R. B. Wells, *J. Chem. Soc., Perkin Trans. 1*, 1974, 1556.
5 T. L. Ho, *Enantioselective Synthesis of Natural Products from Chiral Terpenes*, Wiley, New York, 1992, p. 16.
6 J. D. White and S. Ohira, *J. Org. Chem.*, 1986, **51**, 5492.
7 J. D. White and L. R. Jayasinghe, *Tetrahedron Lett.*, 1988, **29**, 2139.
8 J. D. White, J. C. Amedio, Jr., S. Gut and L. R. Jayasinghe, *J. Org. Chem.*, 1989, **54**, 4268.
9 J. D. White, J. C. Amedio, Jr., S. Gut and L. R. Jayasinghe, *J. Org. Chem.*, 1992, **57**, 2270.
10 M. P. Dillon, N. C. Lee, F. Stappenbeck and J. D. White, *J. Chem. Soc., Chem. Commun.*, 1995, 1645.
11 A. Toshimitsu, T. Aoai, H. Owada, S. Menwra and M. Okano, *Tetrahedron*, 1985, **41**, 5301.
12 Y. Gao, R. M. Hanson, J. M. Klunder, A. Y. Do, H. Masamune and K. B. Sharpless, *J. Am. Chem. Soc.*, 1987, **109**, 5765.
13 S. L. Schreiber, R. E. Claus and J. Reagan, *Tetrahedron Lett.*, 1982, **23**, 3867.
14 T. Mukaiyama, *Angew. Chem., Int. Ed. Engl.*, 1979, **18**, 707.
15 H. Rüeger and M. Benn, *Heterocycles*, 1983, **20**, 1331.

Received in Cambridge, UK, 2nd January 1998; 8/00011E

Synthesis of DNA-binding heteroaromatic oligoamides on liquid solid support

Burkhard König*† and Martin Rödel

Institut für Organische Chemie der Technischen Universität Braunschweig, Hagenring 30, D-38106 Braunschweig, Germany

Heteroaromatic oligoamides as building blocks for the synthesis of sequence specific DNA binding molecules are obtained from nitro carboxylic acids on polyethylene glycol without the use of protecting groups

Mimicking the sequence specific DNA recognition of gene regulation proteins[1] with small molecules is not only an academic challenge: such molecules are highly desirable as regulatory factors in biotechnology or as gene specific drugs.[2] Several sequence-specific DNA-binding compounds[3] have been discovered over the last 10 years, such as triplex-forming oligonucleotids, peptide nucleic acids and minor groove binding heteroaromatic oligoamides.[3b] The stability and simple structure of the latter compounds renders them especially suitable for most applications. However, compared to the synthesis of aliphatic peptides, that of heteroaromatic imidazole/pyrrole oligoamides is difficult: the heteroaromatic amines are unstable and the carboxy group is less reactive in amide formation. To address these problems, Baird and Dervan recently reported a solid phase synthesis protocol for the synthesis of even complex hairpin oligoamides.[4] Unfortunately, the employed solid support together with the required protecting groups now make the synthesis of larger quantities of heteroaromatic oligoamides an expensive venture. In addition the current protocol is restricted to *N*-methylpyrrole and *N*-methylimidazole, so that new building blocks and coupling conditions must be developed for the introduction of each new heterocycle.[5] To remedy this situation we report here a versatile 'protecting group free' synthesis of short heteroaromatic oligoamides on polyethylene glycol 'liquid' solid support.[6]

Methoxypoly(ethylene glycol) (MeO-PEG-OH) with an average molecular weight of 5000 g mol^{-1} was used as an inexpensive solid support. By the reaction of 1-methyl-4-nitro-1*H*-pyrrole-2-carbonyl chloride **1** with MeO-PEG-OH under standard conditions the first heterocyclic unit of the peptide synthesis is introduced quantitatively *via* ester linkage (Scheme 1). A sample of 100 g of MeO-PEG-OH can so accommodate *ca.* 2.5 g of the first heterocycle. Using the advantage of a soluble solid support, the nitro group is then reduced with NH_4HCO_2–Pd/C in MeOH over 1 h at room temperature. For work-up the heterogeneous catalyst is removed by filtration and the polymer-bound amine is precipitated by the addition of Et_2O. The solid is dissolved in CH_2Cl_2, rendering it ready for the next coupling step and leaving behind excess NH_4HCO_2. Either the reaction of **2** in the presence of pyridine or the coupling of the corresponding carboxylic acid **5** with DCC–HOBt can be used to introduce the next heterocycle in excellent yield.[7] Repetition of the reduction-coupling cycle gives trimers and tetramers. Finally, treatment with base[8] allows the quantitative cleavage of the oligoamide from the polymer.‡ The so obtained molecules§ are most suitable starting materials for the construction of DNA recognizing structures: solution phase peptide chemistry allows the large scale synthesis of hairpin structures,[9] immobilization leads to new stationary chromatography phases[10] and further functionalization gives DNA markers.[11]

The described procedure allows the large scale synthesis of heteroaromatic oligoamides without the use of protecting groups and chromatography. On top of that it facilitates reaction monitoring when new analogs are prepared. Using available nitro carboxylic acids[12] a variety of carbo- or hetero-cyclic units can be introduced, whereby the successful incorporation is confirmed by NMR spectroscopy.¶ With aromatic nitro isocyanates as building blocks the amide linkage is replaced by a urea moiety. Such peptidomimetic heteroaromatic compounds may also have interesting DNA-binding properties, but this remains to be established. Examples of structures that were prepared by the reported route, including yields, are: **11** (61%), **12** (56%) and **13** (62%).

In conclusion we have shown that heteroaromatic oligoamides can be prepared in a most economical way on MeO-PEG polymer support avoiding the use of protecting groups. The procedure facilitates both large scale synthesis and reaction optimization for known and new heteroaromatic oligoamides. This will make this interesting class of compounds more easily available for the further investigation of specific molecular recognition of biological structures.

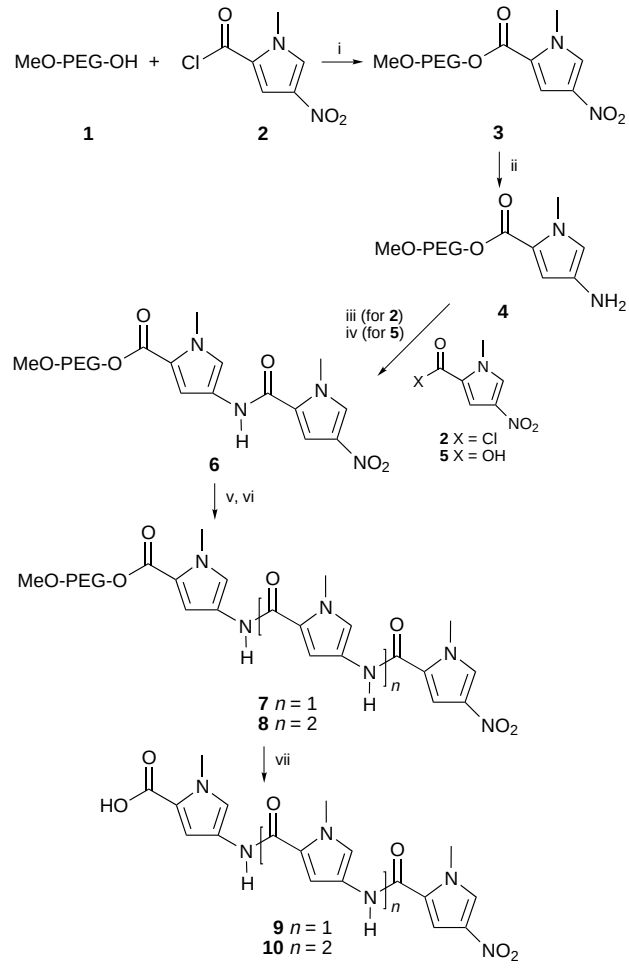

Scheme 1 *Reagents and conditions*: i, CH_2Cl_2, Py, quant.; ii, NH_4HCO_2, Pd/C, MeOH, room temp., 1 h; iii, CH_2Cl_2, Py, quant.; iv, DCC, HOBt, quant.; v, NH_4HCO_2, MeOH, Pd/C; vi, DCC, HOBt, 83%; vii, 2 M, NaOH, 50 °C, 6 h, quant.

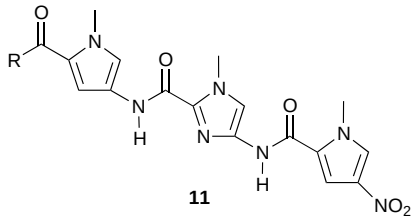

11

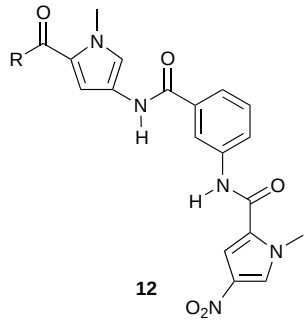

12

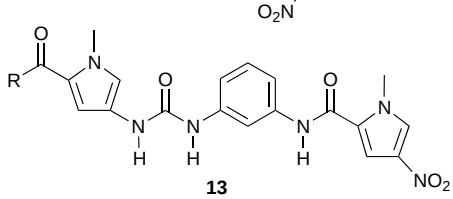

13

Notes and References

† E-mail: B.KOENIG@tu-bs.de

‡ *General procedure* for the reduction-coupling cycle on MeO–PEG-support: A mixture of **3** (5 g, 1 mmol), Pd/C (10%, 100 mg, 9 mol%) and NH_4HCO_2 (1 g, 16 mmol) in MeOH (50 ml) was stirred for 1 h at room temp. The catalyst was removed by filtration, Et_2O (400 ml) was added to the solution and the precipitate was collected by filtration. The white solid was dissolved in CH_2Cl_2 (25 ml), leaving behind excess NH_4HCO_2 that was filtered of. Either **2** (570 mg, 3.3 mmol) and pyridine (1 ml) or a solution of **5** (560 mg, 3.3 mmol), $HOBt·H_2O$ (510 mg, 3.3 mmol) and DCC (680 mg, 3.3 mmol) in DMF (25 ml) were added and the mixture was stirred for 12 h. The reaction mixture was filtered, the polymer-bound product was precipitated by addition of Et_2O (400 ml) and collected by filtration. The crude product was redissolved, precipitated twice and dried *in vacuo*.

§ *Selected data* for **9**: δ_H(400 MHz, [$^2H_6$]DMSO) 3.82 (s, 3 H), 3.86 (s, 3 H), 3.96 (s, 3 H), 6.85 (d, ^4J 1.9, 1 H), 7.05 (d, ^4J 1.8, 1 H), 7.26 (d, ^4J 1.6, 1 H), 7.42 (d, ^4J 1.8, 1 H), 7.59 (d, ^4J 1.9, 1 H), 8.18 (d, ^4J 1.8, 1 H), 9.94 (s, 1 H), 10.28 (s, 1 H); 12.16 (s, 1 H); δ_C(100 MHz, [$^2H_6$]DMSO) 36.1 (+), 36.2 (+), 37.5 (+), 104.6 (+), 107.6 (+), 108.4 (+), 118.7 (+), 119.6 (C_{quart}), 120.3 (+), 121.5 (C_{quart}), 122.6 (C_{quart}), 122.9 (C_{quart}), 126.3 (C_{quart}), 128.3 (+), 133.8 (C_{quart}), 156.9 (C_{quart}), 158.3 (C_{quart}), 162.0 (C_{quart}); *m*/*z* (70 eV) 370 (74%) [$M^+ - CO_2$], 275 (100).

¶ For NMR analysis, 100 mg of the polymer bound product were dissolved in 0.5 ml of $CDCl_3$. The terminal methoxy group of MeO-PEG was used to calibrate polymer loading and reaction yields. *Selected data* for **11**: δ_H(400 MHz, [$^2H_6$]DMSO) 3.52 (3 H), 4.05 (3 H), 4.10 (3 H), 6.89 (1 H), 7.44 (1 H), 7.48 (1 H), 7.49 (1 H), 7.64 (1 H), 9.05 (1 H), 9.16 (1 H). For **12**: 3.92 (3 H), 4.07 (3 H), 6.90 (1 H), 7.44 (1 H), 7.57 (1 H), 7.65 (1 H), 7.70 (1 H), 8.09 (1 H), 8.15 (1 H), 9.01 (1 H), 9.14 (1 H). For **13**: 3.87 (3 H), 4.02 (3 H), 6.69 (1 H), 7.2–7.3 (3 H), 7.42 (1 H), 7.53 (1 H), 7.60 (1 H), 7.68 (1 H), 7.73 (1 H), 7.92 (1 H), 8.73 (1 H). Signals of the resin are omitted. All integrals are relative to the methoxy group of the resin.

1 There are five main peptide structural motifs for DNA-binding that have been identified: helix-turn-helix, zinc finger, leucine zipper, helix-loop-helix and antiparallel β-sheets (β-ribbon). D. S. Johnson and D. L. Boger, in *Comprehensive Supramolecular Chemistry*, ed. J. L. Atwood, J. E. Davies, D. D. Macnicol, F. Vögtle and J.-M. Lehn, Elsevier Science, Oxford, 1996, vol. 4, p. 77.

2 For a recent example of the regulation of genes expression by small molecules, see: J. M. Gottesfeld, L. Neely, J. W. Trauger, E. E. Baird and P. B. Dervan, *Nature*, 1997, **387**, 202.

3 (*a*) P. E. Nielsen, *Chem. Eur. J.* 1997, **3**, 505 and references cited therein; (*b*) The structure of the heteroaromatic peptides was inspired by DNA-binding natural products, such as distamycin or netropsin: D. S. Johnson and D. L. Boger, in *Comprehensive Supramolecular Chemistry*, ed. J. L. Atwood, J. E. Davies, D. D. Macnicol, F. Vögtle and J.-M. Lehn, Elsevier Science, Oxford, 1996, vol. 4, p. 73; (*c*) *New J. Chem.*, 1997, **21**, 1 (special issue).

4 E. E. Baird and P. B. Dervan, *J. Am. Chem. Soc*., 1996, **118**, 6141.

5 Heteroaromatic oligopeptides with terminal pyridine, thiazole and furan units have been synthesized. These derivatives were expected to bind preferentially G-C rich regions. However, in most cases they still show a preference for A-T regions; K. E. Rao, R. G. Shea, B. Yadagiri and J. W. Lown, *Anti-Cancer Drug Des*., 1990, **5**, 3 (terminal thiazol); M. Lee, R. G. Shea, J. W. Lown and R. T. Pon, *J. Mol. Recogn*., 1989, **2**, 6 (furan); a terminal pyridine has been found to be G-C specific in certain cases: W. S. Wade, M. Mrksich and P. B. Dervan, *J. Am. Chem. Soc.*, 1992, **114**, 8783.

6 For the use of poly(ethylene glycol) as support in synthesis, see: M. Mutter, H. Hagenmaier and E. Bayer, *Angew. Chem.*, 1971, **83**, 883; *Angew. Chem., Int. Ed. Engl*., 1971, **10**, 811; R. N. V. Pillai and M. Mutter, *Top. Curr. Chem.*, 1982, **106**, 119; D. J. Gravert and K. D. Janda, *Chem. Rev.*, 1997, **97**, 489; combinatorial libraries: H. Han, M. M. Wolfe, S. Brenner and K. D. Janda, *Proc. Natl. Acad. Sci. USA*, 1995, **92**, 6419.

7 The coupling with DCC–DMAP gave **6** in a lower yield of 92%.

8 M. A. Tilak and C. S. Hollinden, *Tetrahedron Lett*., 1968, 1297.

9 M. Mrksich, M. E. Parks and P. B. Dervan, *J. Am. Chem. Soc*., 1994, **116**, 7983. MeO-PEG support is not suitable for a direct synthesis of extended structures due to the known alteration of its physical properties with growing oligoamide chain length. This leads to incomplete precipitation.

10 B. König, H. Buchholz, M. Rödel and M. Schulze, patent pending.

11 Recent example: S. M. Touami, C. C. Poon and P. A. Wender, *J. Am. Chem. Soc*., 1997, **119**, 7611.

12 Many carbo- or hetero-cyclic aromatic nitro carboxylic acids are readily available; 4-nitrothiophene-2-carboxylic acid: M. Römer, *Chem. Ber*., 1887, **20**, 116; ethyl-1-methyl-4-nitroimidazole- 2-carboxylate: K. Krowicki and J. W. Lown, *J. Org. Chem*., 1987, **52**, 3493; 5-nitrothiophene-2-carboxylic acid: P. Cogolli, F. Maiolo, L. Testaferri, M. Tiecco and M. Tingoli, *J. Chem. Soc., Perkin Trans. 2*, 1980, 1331; 2-nitrothiazole-5-carboxylic acid: W. Knauf, *Eur. J. Med. Chem. Chim. Ther*., 1975, **10**, 533.

Received in Liverpool, UK, 17th November 1997; 7/08270C

Resorcin[4]arene dimer linked by eight water molecules and incorporating a tetraethylammonium ion: guest-driven capsule formation *via* cation–π interactions

Kazutaka Murayama and Katsuyuki Aoki*†

Department of Materials Science, Toyohashi University of Technology, Tempaku-cho, Toyohashi 441, Japan

X-Ray analysis of the co-crystallization compound formed between tetraethylresorcin[4]arene 1 and tetraethylammonium ion, $Et_4N^+\cdot\mathbf{1}\cdot\mathbf{1}^-\cdot 8H_2O\cdot 2EtOH$, has shown that the two 'head-to-head' arranged resorcinarenes are linked by eight water molecules and encapsulate a tetraethylammonium ion within the cavity *via* cation–π interactions.

Molecular containers,[1–7] which have the ability to encapsulate substrates, have attracted much attention in supramolecular chemistry because of their numerous applications: the design of artificial receptors, transport and storage of small organic guests, design of chemical sensor devices, removal of pollutants from water, and use as reaction chambers. A variety of container compounds whose interior cavities are constructed by covalently linked structures, typically involving carcerands,[1,2] cryptophanes[3] or cucurbiturils,[4] have been synthesized and well characterized. More recently, self-assembly through non-covalent interactions such as hydrogen bonding has proved to give novel types of molecular containers, which we here tentatively call 'molecular capsules', the still-limited examples being glycolurils,[5] urea-substituted calix[4]arenes[6] and tetrols.[7] Most recently, MacGillivray and Atwood have reported[8] a self-assembled resorcin[4]arene hexamer, forming a shell-like molecular capsule, held together by eight water bridges in addition to direct hydrogen bonds between the substructures. We report here the preparation and crystal structure of a dimeric resorcin[4]arene molecular capsule, linked by eight water bridges and incorporating a tetraethylammonium ion inside the cavity. The formation of the capsule might be guest-driven through the cation–π interaction, an important mechanism for molecular recognition that is not yet sufficiently explored.[9]

Tetraethylresorcin[4]arene **1**‡ (0.1 mmol) and tetraethylammonium perchlorate (1 mmol) were dissolved in EtOH–H_2O (5 : 3, 8 ml). The mixture (pH 5) was allowed to stand at room temperature for three weeks to give colourless crystals with a yield of 60%,§ the structure of which has been determined.¶

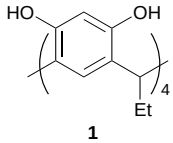

1

The molecular structure of the compound with the composition of $Et_4N^+\cdot\mathbf{1}\cdot\mathbf{1}^-\cdot 8H_2O\cdot 2EtOH$‖ is shown in Fig. 1, where, coinciding with crystallographic symmetries, each macrocyclic resorcinol tetramer **1** has four-fold symmetry and the two macrocycles are related to each other by a mirror plane. The resorcinarene molecule adopts a bowl-shaped conformation with the usually observed intramolecular hydrogen bonds between neighbouring hydroxy groups: the crystallographically independent hydrogen bond O(1)···O(2′) = 2.767(9) Å. The most interesting structural feature is the formation of a molecular capsule constructed of two 'head-to-head' arranged substructures which captures a tetraethylammonium ion within the cavity.** The Et_4N^+ nitrogen atom is located at a crystallographic centre of symmetry, the point that the four-fold axis and the mirror plane intersect, and thus the ethyl groups of the cation are disordered over two sets of sites related by the mirror plane on which the central nitrogen and terminal carbon atoms ride. The architecture of the capsule structure is unique in that the two substructures are not directly but indirectly connected to each other *via* eight water bridges, because in so far reported molecular capsules[5–7] the two substructures are directly hydrogen-bonded to each other *via* functional groups, *e.g.* urea-substituents,[6] that are designed to form complementary hydrogen bonds. Thus each water molecule, which lies on the mirror plane noted above, is hydrogen-bonded to two hydroxy groups, one from each substructure, summing to a total of 16 hydrogen bonds in the capsule unit: the crystallographically independent hydrogen bonds O(3)···O(1) = 2.76(1) and O(4)···O(2) = 2.753(10) Å. The water linking is engaged also in the assembly of the tetramethylresorcin[4]arene hexamer,[8] in addition to, in this case, direct hydrogen bonds between the hydroxy groups of the 'head-to-head' arranged resorcinarenes. As shown in Fig. 2, the Et_4N^+ ion is arranged in such a way that its ethyl groups project toward the bridging C(7) carbons of **1**, where each ethyl group makes close contacts with the phenyl rings through, we suggest, multiple cation–π interactions. Since the capsule unit is negatively (monovalently) charged, the presence of the cation–π interactions between the quaternary cationic Et_4N^+ group and the aromatic rings of **1** is

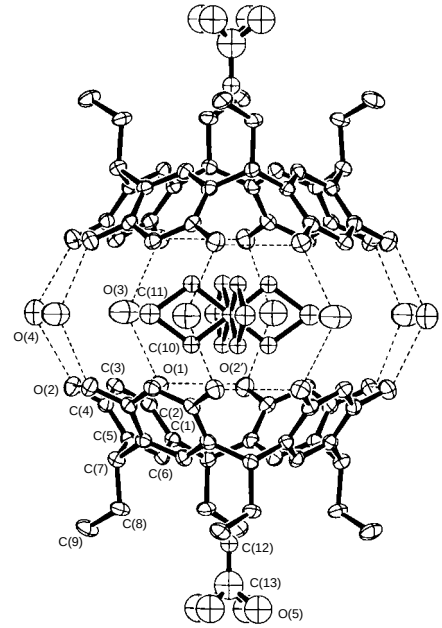

Fig. 1 Molecular structure of the capsule molecule [the ethanol solvate is disordered at four positions due to the four-fold axis passing through it, where the thermal ellipsoid of the C(12) atom is given at arbitrary scale for clarity]. O(2′) is related to O(2) by four-fold symmetry. Broken lines denote hydrogen bonds.

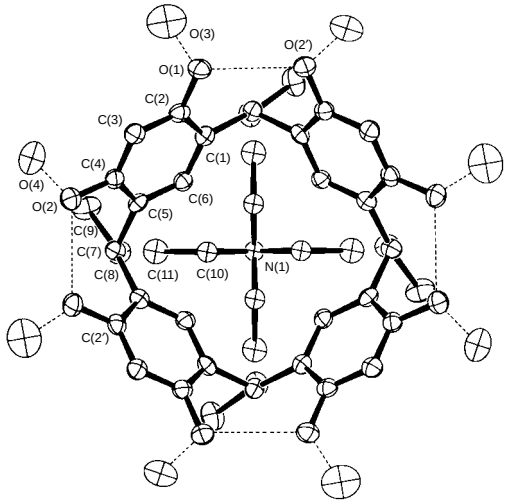

Fig. 2 A top view of the capsule molecule along the four-fold axis, showing the disposition of the Et_4N^+ ion within the cavity. Close contacts: C(2′)···C(10) = 3.58(2), C(2′)···C(11) = 3.59(1), C(4)···C(10) = 3.59(2), and C(4)···C(11) = 3.59(1) Å. O(2′) and C(2′) are related to O(2) and C(2), respectively, by four-fold symmetry. Broken lines denote hydrogen bonds.

not self-evident. However, X-ray evidence for such an interaction between the Me_3N^+ group of acetylcholine and the π-rings of the *neutral* resorcin[4]arene is available.[10] The bond lengths and angles of the resorcin[4]arene molecule are in good agreement with those in the literature.[10]

Crystallization of **1**, in the absence of tetraethylammonium ion, from EtOH–H_2O or EtOH–acetone–H_2O gave compounds, 2(**1**)·2EtOH·10H_2O or **1**·Me_2CO·EtOH·2H_2O, respectively, and their X-ray analyses have shown that in both compounds no molecular capsule is formed.[11] The lack of formation of a molecular capsule for *neutral* substrates in these two and, to the best of our knowledge, six other cases such as MeCN–H_2O,[12] acetone–EtOH–H_2O,[12] ethyl methyl ketone,[13] EtOH,[14] pyridine,[15] and MeCN–4,4′-bipyridine[15] may give circumstantial evidence for the important role of the cation–π interaction in the formation of the present resorcinarene molecular capsule, suggesting that capsule formation might be guest-driven through cation–π interactions. This is in contrast to the usually observed[5–7] host-driven capsule formation by direct hydrogen bonding between two substructures that are predesigned to form self-complementary hydrogen bonds.

The ^{1}H NMR spectrum (270 MHz, CD_3OD) of the capsule complex (1 mmol dm^{-3}) shows a quartet at δ 3.130 and a triplet at δ 1.173 for the CH_2 and CH_3 protons of Et_4N^+, respectively, whereas the corresponding signals of Et_4N^+ alone appear at δ 3.321 and 1.289. These upfield shifts for the complex are probably due to the shielding effect of the aromatic rings, indicating that the quaternary tetraethylammonium group associates preferentially with the π-rings of **1** in solution.††

In conclusion, the synthesis and isolation of the resorcin[4]arene molecular capsule incorporating an Et_4N^+ ion are straightforward, giving a moderate yield by simply mixing starting materials which are readily available. Unlike other molecular capsules,[5–7] the two substructures are *not directly* hydrogen-bonded but are *indirectly* bonded *via* water bridges. The architecture is simple and elegant: the two hemispherical resorcin[4]arenes are attached *via* their upper rims with eight water molecules to form a spherical capsule having C_{4h} symmetry. The present study provides additional X-ray evidence[10] for cation–π interaction between the quaternary ammonium group and the π-electrons of the aromatic rings, a novel type of binding force that is important in the function of biological systems.[9,16] The cation–π interaction could also play a major role in the process of the capsule formation, by forcing simultaneous interactions between a tetraethylammonium ion and two resorcinarenes. The guest-driven host construction observed here could offer a promising approach for building new supramolecular compounds.

Notes and References

† E-mail: kaoki@tutms.tut.ac.jp

‡ 2,8,14,20-Tetraethyl-4,6,10,12,16,18,22,24-octahydroxycalix[4]arene **1** was synthesized according to a literature procedure (ref. 17).

§ Elemental microanalysis of the compound was not possible due to its rapid decomposition out of solution. The molecular formula was determined by X-ray analysis.

¶ *Crystal data*: $C_{10.5}H_{15.875}N_{0.125}O_{3.25}$, M = 195.80, colourless columns, tetragonal, space group *P*4/*mnc*, a = 13.927(2), c = 22.434(2) Å, U = 4351.5(10) Å^3, Z = 16, D_c = 1.195 g cm^{-3}, μ(Mo-Kα) = 0.88 cm^{-1}, T = 293 K, F(000) = 1692. A crystal was sealed in a glass capillary with a drop of mother liquor. Of 2926 unique data in the range $4 < 2\theta < 45°$, 1052 data with $I > 3\sigma(I)$ were used in the refinement. Residuals of R = 0.104 and R_w = 0.115 were obtained after 127 parameters had been refined to convergence, where only the resorcinarene and water atoms were treated anisotropically while all the other atoms were treated isotropically. No attempt was made to locate the H atoms. Extensive disordering of Et_4N^+ and EtOH caused the rather high R values. CCDC 182/753.

‖ The Et_4N^+ : **1** : EtOH composition of 1 : 2 : 2 for the compound formed was consistent with its ^{1}H NMR spectra. The absence of ClO_4^- was ascertained *via* IR spectroscopy. Any one of the sixteen hydroxy substituents belonging to the two resorcin[4]arenes constituting the capsule could be deprotonated.

** Resorcin[4]arenes as receptors for tetraalkylammonium ions have been demonstrated in alkaline solution (ref. 18), where, however, a tetradeprotonated host anion is assumed to form a 1 : 1 complex with an ammonium cation.

†† A study to clarify the solution structure or structures involved in the capsule formation remains to be carried out.

1 D. J. Cram and J. M. Cram, *Container Molecules and Their Guests*, The Royal Society of Chemistry, Cambridge, UK, 1994; R. C. Helgeson, C. B. Knobler and D. J. Cram, *J. Am. Chem. Soc.*, 1997, **119**, 3229 and references cited therein.
2 B.-H. Huisman, D. M. Rudkevich, F. C. J. M. van Veggel and D. N. Reinhoudt, *J. Am. Chem. Soc.*, 1996, **118**, 3523 and references cited therein.
3 A. Collet, *Cryptophanes*, in *Comprehensive Supramolecular Chemisry*, ed. F. Vögtle, Pergamon, 1996, vol. 2, ch. 11, pp. 325–365.
4 Y.-M. Jeon, J. Kim, D. Whang and K. Kim, *J. Am. Chem. Soc.*, 1996, **118**, 9790.
5 R. Wyler, J. de Mendoza and J. Rebek, Jr., *Angew. Chem., Int. Ed. Engl.*, 1993, **32**, 1699; J. Kang and J. Rebek, Jr., *Nature*, 1997, **385**, 50 and references cited therein.
6 K. D. Shimizu and J. Rebek, Jr., *Proc. Natl. Acad. Sci. USA*, 1995, **92,** 12 403; R. K. Castellano, D. M. Rudkevich and J. Rebek, Jr., *J. Am. Chem. Soc.*, 1996, **118**, 10 002 and references cited therein; O. Mogck, M. Pons, V. Böhmer and W. Vogt, *J. Am. Chem. Soc.*, 1997, **119**, 5706 and references cited therein.
7 R. G. Chapman and J. C. Sherman, *J. Am. Chem. Soc.*, 1995, **117**, 9081; K. Nakamura, C. Sheu, A. E. Keating, K. N. Houk, J. C. Sherman, R. G. Chapman and W. L. Jorgensen, *J. Am. Chem. Soc.*, 1997, **119**, 4321.
8 L. R. MacGillivray and J. L. Atwood, *Nature*, 1997, **389**, 469.
9 D. A. Dougherty, *Science*, 1996, **271**, 163.
10 K. Murayama and K. Aoki, *Chem. Commun.*, 1997, 119 and references cited therein.
11 K. Murayama and K. Aoki, unpublished results.
12 L. M. Tunstad, J. A. Tucker, E. Dalcanale, J. Weiser, J. A. Bryant, J. C. Sherman, R. C. Helgeson, C. B. Knobler and D. J. Cram, *J. Org. Chem.*, 1989, **54**, 1306.
13 G. Mann, L. Hennig, F. Weinelt, K. Müller, R. Meusinger, G. Zahn and T. Lippmann, *Supramol. Chem.*, 1994, **3**, 101.
14 F. Davis and C. J. M. Stirling, *J. Am. Chem. Soc.*, 1995, **117**, 10 385.
15 L. R. MacGillivray and J. L. Atwood, *J. Am. Chem. Soc.*, 1997, **119**, 6931.
16 Z. Lin and M. E. Johnson, *FEBS Lett.*, 1995, **370**, 1; D. Barak, A. Ordentlich, Y. Segall, B. Velan, H. P. Benshop, L. P. A. D. Jong and A. Schafferman, *J. Am. Chem. Soc.*, 1997, **119**, 3157.
17 Y. Aoyama, Y. Tanaka and S. Sugahara, *J. Am. Chem. Soc.*, 1989, **111**, 5397.
18 H.-J., Schneider, D. Güttes and U. Schneider, *J. Am. Chem. Soc.*, 1988, **110**, 6449.

Received in Cambridge, UK, 25th November 1997; revised manuscript received 13th January 1998; 8/00340H

Unusual C→N migration of phosphoryl group; synthesis of *N*′-phosphorylated amidines

Won Bum Jang, Kilsung Lee, Chi-Wan Lee and Dong Young Oh*†

Department of Chemistry, Korea Advanced Institute of Science and Technology, 373-1, Kusung-Dong, Yusung-Gu, Taejon, Korea

Synthetically and structurally interesting *N*′-phosphoryl amidines were obtained by the reaction of lithiated alkyl phosphonates with *N*,*N*-dialkylcyanamide *via* an unprecedented migration of the phosphoryl group.

We have been interested in recent years in the reaction of α-lithioalkylphosphonates with nitriles, and we have used these as synthetic intermediates in the preparation of β-keto phosphonates,[1] α,β-unsaturated ketones,[2] deoxybenzoines[3] and *E*-allylic amines.[4] Following on from this work, we turned our attention to the question of whether the reaction of α-lithioalkylphosphonates with cyanamides (instead of nitriles) would generate intermediates **6**, in the hopes of thereby obtaining α,β-unsaturated amides.

To this end, we examined the reaction of α-lithioalkylphosphonates, derived from dialkyl alkylphosphonates, with cyanamides **2** followed by hydrolysis (Scheme 1), and we were surprised to find that the expected compounds **7** were not obtained. Good yields of compounds **5** were obtained instead. Looking closer, we found no evidence for formation of β-carbonyl phosphonate and/or enamine phosphonates on monitoring by TLC. Thus, the most reasonable explanation for the formation of **5** would be the migration of phosphoryl group (**3**→**4**). This unusual C→N migration of a phosphoryl group was observed in all other dialkyl alkylphosphonates and amides tested.‡

As shown in Table 1, the migration works well and gives good yields. All the products were characterized *via* ^{1}H, ^{13}C and ^{31}P NMR spectroscopy and HRMS. The C→N migration is so fast that the reaction was completed within 5 min at −78 °C. The α-lithio anion derived from a benzylphosphonate (**5h** in Table 1) did not give the migration product, and the starting material was recovered. This could be due to the lithiated benzylphosphonate being possibly less nucleophilic than other alkylphosphonates.

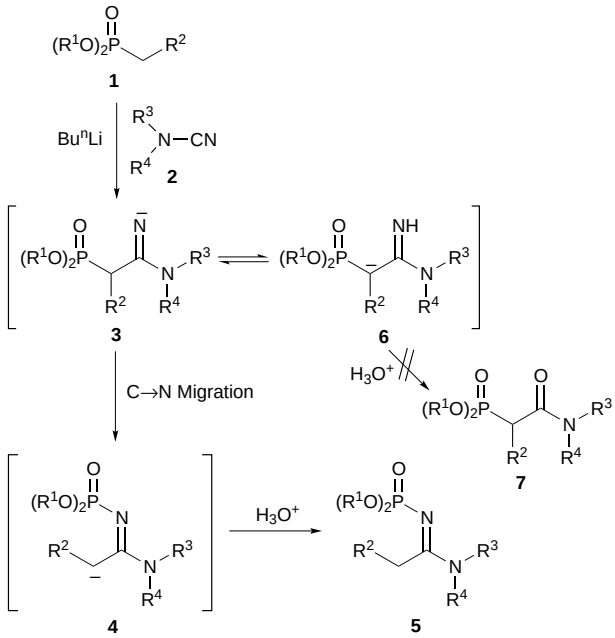

Scheme 1

Table 1 Synthesis of *N*′-phosphorylated amidines **5**

Compound	R^1	R^2	R^3	R^4	Yield (%)[a]
5a	Me	H		–(CH$_2$)$_4$–	79
5b	Me	H		–(CH$_2$)$_5$–	82
5c	Et	H		–(CH$_2$)$_4$–	81
5d	Et	H		–(CH$_2$)$_5$–	80
5e	Et	H	Me	Me	87
5f	Et	Allyl	Me	Me	71
5g	Et	Me		–(CH$_2$)$_5$–	73
5h	Et	Ph		–(CH$_2$)$_5$–	No reaction[b]
5i	Pr^i	H		–(CH$_2$)$_5$–	84

[a] Isolated yield. [b] Starting materials were recovered.

Intermediate **3** (or its tautomeric form **6**) seems to be very unstable. In general, amidine derivatives have a zwitterionic character but, in the case of intermediate **3**, the anion interrupts the zwitterionic resonance in the N–C=N linkage, so the migration of the phosphoryl group may not only initiate the zwitterionic resonance, but also stabilize the zwitterionic structure due to p_π–d_π interaction in the P–N bond.[5]§

In order to prepare various *N*′-phosphorylated amidine derivatives **8**, we carried out the reaction shown in Scheme 2 with several electrophiles. Our results are summarized in Table 2. All of the electrophiles gave good yields, even in the one-pot procedure.¶

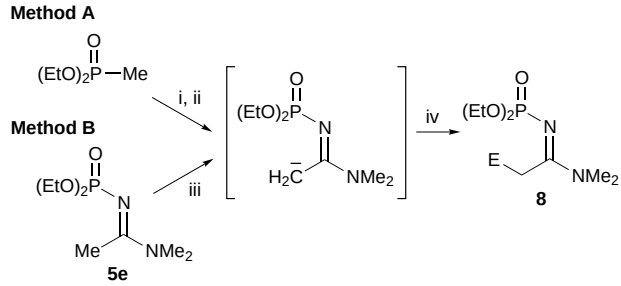

Scheme 2 *Reagents and conditions*: i, Bu^{n}Li, THF, −78 °C, 1 h; ii, Me$_2$NCN, −78 °C, 10 min; iii, LDA, THF, −78 °C, 1 h; iv, electrophile, −78 °C to room temp., 1 h

Table 2 Synthesis of various *N*′-phosphorylated amidine derivatives **8**

Compound	Electrophile	E in **8**	Method[a]	Yield (%)[b]
8a	D$_2$O	D	A	78
8b	MeI	Me	A	73
8c	Allyl bromide	Allyl	A	68
8d	TMSCl	TMS	A	62
8e	PhCHO	PhCH(OH)	A	41
8e	PhCHO	PhCH(OH)	B	92

[a] See footnote ¶. [b] Isolated yield.

Rearrangements of the phosphoryl groups and other phosphorus containing functional groups are known.[6] Their mechanisms and resulting products are of importance, not only for their synthetic applications and biological activities, but also for understanding the reactivity of the phosphorus atom. However, this is to the best of our knowledge the first example of the C→N migration of a phosphoryl group.

In summary, we have developed an interesting and synthetically useful C→N migration. A study of phosphorylated amidine and its synthetic application is in progress.

Notes and References

† E-mail: s_opmc@cais.kaist.ac.kr

‡ *Typical reaction procedure*: To a stirred solution of $(EtO)_2P(O)Me$ (0.167 g, 1.1 mmol) in dry THF (4 ml) was added Bu^nLi (0.68 ml, 1.1 mmol, 1.6 M in hexanes) at −78 °C under N_2. After stirring for 1 h at −78 °C, Me_2NCN (0.070 g, 1.0 mmol) was added, and the mixture warmed to room temp. After 30 min, saturated aqueous NH_4Cl (5 ml) was added, and stirring continued for 10 min. Extraction with Et_2O (3 × 20 ml), drying and removal of the solvent under reduced pressure gave the crude product. Pure **5e** was obtained (0.1933 g, 87%) by flash column chromatography (EtOAc–MeOH, 10 : 1): δ_H(300 MHz, $CDCl_3$) 1.07–1.12 (t, *J* 17.45, 6 H), 2.16 (s, 3 H), 2.86 (s, 3 H), 2.87 (s, 3 H), 3.83 (dt, J_{P-H} 7.14, J_{H-H} 7.14, 4 H); δ_C(75 MHz, $CDCl_3$) 15.88 (d, J_{P-C} 6.9), 19.40 (d, *J* 4.72), 37.55, 38.23, 61.36 (d, J_{P-C} 6.525), 166.32 (d, J_{P-C} 14.1); δ_P(120 MHz, $CDCl_3$) +6.157; HRMS (EI) calc. 222.1133, found 222.1127.

§ In general, the rotational barrier of the C–N single bond in the amidine moiety is due to its zwitterionic structure. The C–N single bond in *N*′-aryl-*N*,*N*-dimethylacetamidines, which are known for having aryl groups strongly conjugated to the N=C–N moiety, shows a relatively low coalescence temperature (T_c, −60 to 33 °C; ref. 7). However, in the case of *N*′-phosphorylated amidines, the coalescence temperature is about 80 °C (ref. 8), evidence of the extension of the conjugation in the N=C–N linkage to the phosphoryl group, involving strong p_π–d_π conjugation of the P–N bond.

¶ *Method A*: To a stirred solution of $(EtO)_2P(O)Me$ (0.167 g, 1.1 mmol) in dry THF (4 ml) was added Bu^nLi (0.68 ml, 1.1 mmol, 1.6 M in hexanes) at −78 °C under N_2. After stirring for 1 h at −78 °C, Me_2NCN (0.070 g, 1.0 mmol) was added, and the mixture warmed to −5 °C for 30 min. Allyl bromide (0.106 g, 1.0 mmol) was added dropwise and the mixture was warmed to room temp. After 1 h saturated aqueous NH_4Cl (5 ml) was added and stirring continued for 10 min. Extraction with Et_2O (3 × 20 ml), drying and removal of the solvent under reduced pressure gave the crude product. Pure **8c** was obtained (0.178 g, 68%) by flash column chromatography (EtOAc–MeOH, 10 : 1): δ_H(200 MHz, $CDCl_3$) 1.27–1.34 (t, *J* 7.06, 6 H), 2.34–2.46 (m, 2 H), 2.84–2.96 (m, 2 H), 3.00 (s, 3 H), 3.01 (s, 3 H), 4.05 (dq, J_{P-H} 5.02, J_{H-H} 5.02, 4 H), 4.98–5.14 (m, 1 H), 5.77–5.97 (m, 1 H); δ_C(50 MHz, $CDCl_3$) 16.19 (J_{P-C} 6.77), 30.71, 31.91 (J_{P-C} 6), 38.01, 38.31, 115.42, 136.42, 169.01 (J_{P-C} 15.05); HRMS (EI) calc. 262.1446, found 262.1436.

Method B: To a stirred solution of **5e** (0.244 g, 1.1 mmol) in dry THF (4 ml) was added LDA (0.53 ml, 1.1 mmol, 2.0 M in THF) at −78 °C under N_2. After stirring for 1 h at −78 °C, benzaldehyde (1.06 g, 1.0 mmol) was added dropwise. After 1 h, saturated aqueous NH_4Cl (5 ml) was added, and stirring continued for 10 min. Extraction with Et_2O (3 × 20 ml), drying and removal of the solvent under reduced pressure gave the crude product. Pure **8e** was obtained (0.302 g, 92%) by flash column chromatography (EtOAc–MeOH, 10 : 1): δ_H(300 MHz, $CDCl_3$) 1.14–1.18 (t, J_{H-H} 7.09 Hz), 1.18–1.23 (t, J_{H-H} 7.05), 2.88–2.94 (m, 1 H), 2.94 (s, 3 H), 2.96 (s, 3 H), 3.13–3.21 (m, 1 H), 3.87–3.99 (m, 4 H), 4.86 (br d, 1 H), 6.09 (br s, 1 H), 7.09–7.22 (m, 3 H), 7.30–7.33 (m, 2 H); δ_C(75 MHz, $CDCl_3$) 15.99 (d, J_{P-C} 6.975), 38.20, 38.40, 42.63 (d, J_{P-C} 6.375), 61.919 (t, *J* 5.625), 71.04, 125.10, 127.09, 128.15, 144.54, 166.59 (d, J_{P-C} 15.6); δ_P(120 MHz, $CDCl_3$) +8.083; HRMS (EI) calc. 328.1552, found 328.1579.

1 K. Lee and D. Y. Oh, *Bull. Korean Chem. Soc.*, 1989, **10**, 613.
2 K. Lee and D. Y. Oh, *Synthesis*, 1991, 213.
3 K. Lee and D. Y. Oh, *Bull. Korean Chem. Soc.*, 1991, **12**, 254.
4 W. S. Shin, K. Lee and D. Y. Oh, *Tetrahedron Lett.*, 1995, **36**, 281.
5 S. Patai, *The Chemistry of Amidines and Imidates*, Wiley, London, 1975, p. 60.
6 Some examples of phosphoryl group migration: (*a*) O→C migration, B. Dhawan and D. Redmore, *J. Org. Chem.*, 1986, **51**, 179; Y.-Z. An and D. F. Wiemer, *J. Org. Chem.*, 1992, **57**, 317; (*b*) S→C migration, G. Sturtz, B. Corbel and J. P. Paugam, *Tetrahedron Lett.*, 1976, **32**, 47; S. Masson, J.-F. Saint-Clair and M. Saquet, *Tetrahedron Lett.*, 1994, **35**, 3083; (*c*) C→O migration, F. Hammerschmidt and E. Zbiral, *Chem. Ber.*, 1980, **113**, 3891; C. E. Burgos-Lepley, S. A. Mizsak, R. A. Nugent and K. A. Johnson, *J. Org. Chem.*, 1993, **58**, 4159; (*d*) S→N migration, C. Blonski, M. B. Gasc, A. F. Hegarty and J. J. Perie, *J. Org. Chem.*, 1984, **106**, 7523; (*e*) O→O′ migration, S. N. Mikhailov, M. Oivanen, P. Oksman and H. Lönnberg, *J. Org. Chem.*, 1992, **57**, 4122; (*f*) other related phosphorus-containing functional group migration, M. J. P. Harger, *Chem. Commun.*, 1997, 403; M. J. P. Harger, *J. Chem. Soc., Perkin Trans. 1*, 1989, 563; C. Earnshaw, J. I. Grayson and S. Warren, *J. Chem. Soc., Perkin Trans. 1.*, 1979, 1506.
7 D. Leibfritz, Dissertation, Universität Tübingen, 1970.
8 C. K. Tseng and F. M. Pallos, *Spectroscopy Lett.*, 1972, **5**, 43.

Received in Cambridge, UK, 16th December 1997; 7/09026I

Novel porphyrin–viologen rotaxanes

Alan E. Rowan,*† Patrick P. M. Aarts and Koen W. M. Koutstaal

Department of Organic Chemistry, NSR Center, University of Nijmegen, Toernooiveld 6525 ED Nijmegen, The Netherlands

A new porphyrin-containing host has an exceptionally high affinity for viologen guests, with binding constants as high as K_{ass} = 7 × 10^6 M^{-1} in organic solvents, allowing the construction of porphyrin–viologen rotaxanes.

The design and construction of rotaxanes and catenanes using a 'self-assembling' approach is now regularly reported in literature.[1] In general, however, few systems have been assembled which possess addressable cyclic components, with an eye toward the construction of functional devices.[2] An interesting functional species for incorporation in a rotaxane is a porphyrin. Somewhat surprisingly the inclusion of a porphyrin in such a system has only been preliminarily explored and mainly only as a photoactive endgroup.[3,4] Reported here is a new porphyrin-clip macrocycle **1** which binds methyl viologen (*N*,*N*′-dimethyl-4,4′-bipyridinium) and a variety of *N*-substituted derivatives with the highest binding constants reported to date and is an ideal basic building block for rotaxane synthesis.

Compound **1** was synthesized as depicted in Scheme 1.[5] Catechol was converted in three steps into 1,2-bis(2-*p*-tolylsulfonylethoxy)benzene (in 57% yield) which was then coupled with tetrachloromethyldiphenylglycoluril,[6] to generate the tetratosylate molecular clip. This U-shaped molecule was converted to the tetraaldehyde derivative and subsequently cyclized with pyrrole to give the porphyrin clip **1** (6%). NOESY and COSY 2D spectra revealed that the porphyrin moiety is situated rigidly and symmetrically, directly above the cavity.[5]

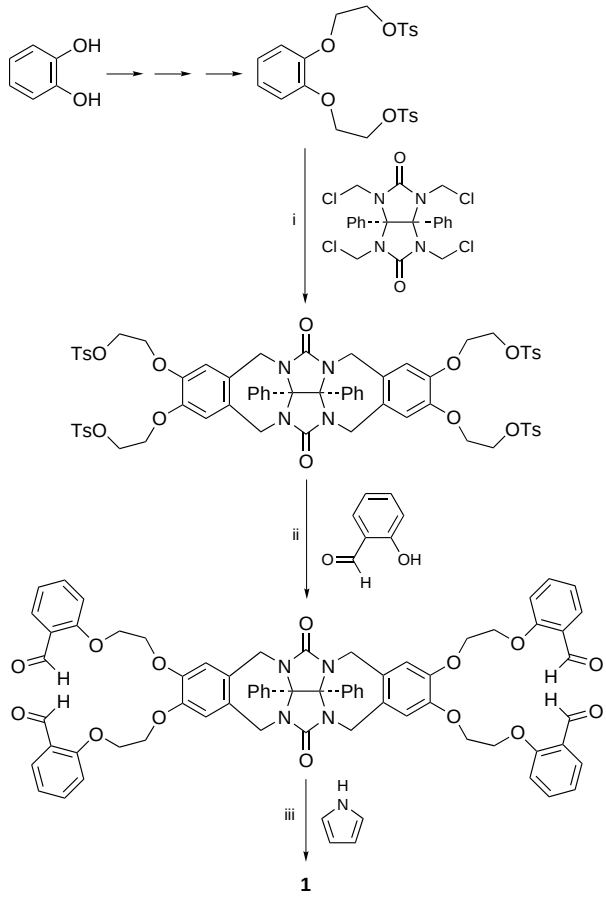

Scheme 1 *Reagents and conditions*: i, $SnCl_4$, $ClCH_2CH_2Cl$, 72%; ii, MeCN, K_2CO_3, 59%; iii, $BF_3{\cdot}Et_2O$, CH_2Cl_2, *p*-chloranil, 6%

The affinity of this new host for complexation with *N*,*N*′-derivatized 4,4-bipyridinium guests was investigated by UV–VIS spectroscopy. Host–guest titrations in MeCN–$CHCl_3$ (1 : 1, v/v) revealed the formation of exceptionally strong 1 : 1 charge-transfer complexes with all the viologen guests **2**. The strength and geometry of binding is strongly dependent upon the N-functionality of the guest. In the case of the methyl derivative **2a** the association constant, K_{ass} = (6.0 ± 0.9) × 10^5 M^{-1}, is several orders of magnitude higher than previously reported association constants for similar complexes.[3,7] Complexation of porphyrin clip **1** with *N*,*N*′-bis(2-hydroxyethyl)-4,4′-bipyridinium **2b**,[8] resulted in one of the strongest host–guest complexes in organic solvents reported to date [K_{ass} = (7.4 ± 0.8) × 10^6 M^{-1}]. The complex between **1** and the propylamine derivative **2c** displayed an association constant, K_{ass} = (9.0 ± 1) × 10^5 M^{-1}, which is more similar to that of the complex between **1** and **2a**.

^{1}H NMR studies on an equimolar solution of **1** and **2b** in CD_3CN–$CDCl_3$ (1 : 1, v/v) revealed large complexation shifts (see structure **1**). In the case of the porphyrin host, the central NH resonance was shifted significantly upfield by 1.16 ppm (from δ −2.79 to −3.95) implying that this proton is situated over the centre of an aromatic ring of the guest. Both sets of CH_2 protons, which link the porphyrin with the aromatic side-walls of the cavity, (ArOCH_aH_b and PorOCH_aH_b) were shifted downfield by identical amounts (+0.4 and +0.7 ppm), suggesting that these protons are at the side of an aromatic ring which is situated symmetrically between the two sets of protons. In the case of the resonances for the bipyridinium guest **2b** even larger shifts were observed, with the value of the shift diminishing as one goes from the centre of the bipyridinium ring to the end of the hydroxyethyl functions (see structure **2b** for $\Delta\delta$s). The exceptionally large upfield shifts for the β and α protons (−3.51 and −1.99 ppm) confirm that the guest sits in the cavity parallel to the porphyrin ring.

The ^{1}H NMR spectra (500 MHz) of an equimolar solution of **2a** and porphyrin clip **1** in contrast showed three broad resonances at δ 6.20, 4.13 and 3.35 for the α, β and methyl protons of the guest, respectively. The complexation shifts are even larger than those for the complex with **2b**: $\Delta\delta_\alpha$ = −2.66, $\Delta\delta_\beta$ = −4.24 and $\Delta\delta_{methyl}$ = −1.05 ppm. In contrast to the complex of **1** with **2b**, upon the addition of **2a** to the host only a very small upfield shift of the central NH proton (−0.17 ppm) was observed. The host protons ArOCH_2 of the complex with **2a** were now shifted upfield (−0.16 and −0.69 ppm) with the protons PorOCH_2 being unaffected by the complexation of the guest. The geometry of complexation of **2a** is such that the bipyridinium rings sit between the two aromatic walls of **1**, perpendicular with respect to the porphyrin. This binding geometry is different from that of **2b** but the same as that observed for complexation of this guest in a molecular basket derived from diphenylglycoluril.[7]

The difference in binding geometry of the two guests is also reflected in the UV–VIS spectra of the complexes. Upon

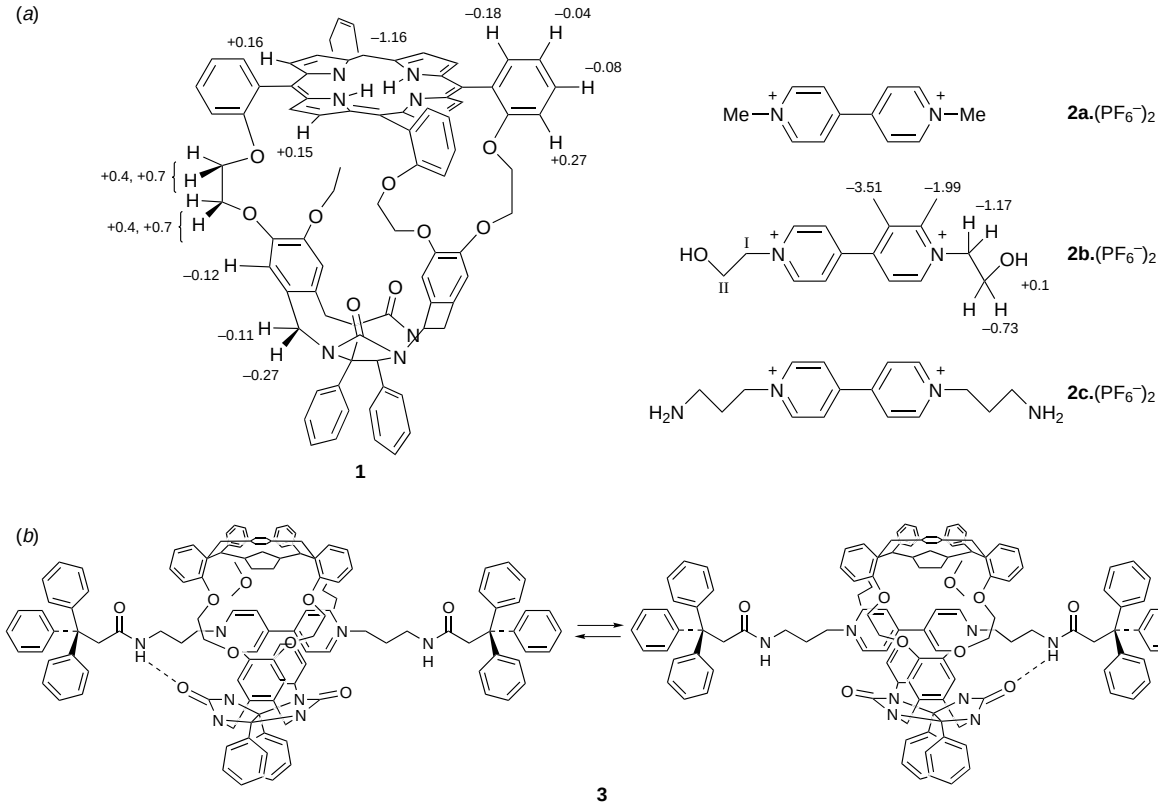

Fig. 1 (*a*) Porphyrin clip **1** and viologen guests **2**. The observed ^{1}H NMR complexation shifts for the 1 : 1 complex of **1** and **2b** ($CDCl_3$–CD_3CN) are indicated. (*b*) Rotaxane **3** assembled by the condensation reaction of 3,3,3-triphenylpropionyl chloride and the pseudo-rotaxane complex of **1** and **2c**.

addition of excess guest, the porphyrin Soret band in the UV–VIS spectrum was shifted to the red by 5 nm in the case of **2b** and only by 2 nm in the case of **2a**. The Q-bands remained unaffected. The addition of 10 equiv. of guest **2b** or 100 equiv. of the methyl derivative **2a** to the porphyrin clip caused an almost complete quenching of the porphyrin fluorescence $\{I/I_0$ at 645 nm (excitation 418 nm) = 0.02; [Host] = 2.9×10^{-6} mol l^{-1}, CH_3CN–$CHCl_3$ (1 : 1, v/v)$\}$, confirming the close proximity of the guest to the porphyrin.

Toward the construction of [*n*]rotaxanes assemblies it was decided to use the 1 : 1 complex of bis(aminopropyl)bipyridinium **2c** and porphyrin clip **1** as the basic building block. NMR studies showed that guest **2c** forms a pseudo-rotaxane complex with the NH_2 functions sticking outside the cavity. Simple condensation reactions of this 1 : 1 complex with acid chloride derivatives should enable a variety of amide rotaxanes to be formed.[9] Using the bulky stopper 3,3,3-triphenylpropionyl chloride a condensation reaction was carried out with the 1 : 1 complex of **1** and **2c**, to give molecule **3·(PF$_6$)$_2$** in 30% yield after column chromatography and counter-ion exchange. The resulting rotaxane was, surprisingly, very soluble in $CHCl_3$. ^{1}H NMR studies confirmed that the viologen is bound in the cavity, in an asymmetric geometry, rapidly exchanging between two equivalent sites in which the amide function of the thread hydrogen bonds to the carbonyl of the porphyrin clip (see structure **3**).[5]

As shown here the strong complexation between porphyrin clip **1** and bipyridinium guests **2** generates stable pseudo-rotaxane complexes. The cyclic porphyrin component allows the system to be potentially addressed by a variety of means: chemically,[3] electrochemically or photochemically.[4] Current studies are directed towards the construction of larger [*n*]rotaxane systems and arrays of porphyrin–viologens and the study of their properties.

We thank Professor R. J. M. Nolte and Professor J. F. Stoddart for discussions and their interest in this work.

Footnotes and References

† E-mail: rowan@sci.kun.nl

1 D. Philip and J. F. Stoddart, *Angew. Chem., Int. Ed. Engl.*, 1996, **35**, 1154; F. Vögtle, M. Handel, S. Meier, S. Ottens-Hildebrandt, F. Ott and T. Schmidt, *Liebigs. Ann.*, 1995, 739.
2 P. R. Aston, R. Ballardini, V. Balzani, S. E. Boyd, A. Credi, M. T. Gandolfi, M. Gomez-Lopez, S. Iqbal, D. Philip, J. A. Preece, L. Prodi, H. G. Ricketts, J. F. Stoddart, M. S. Tolley, M. Venturi, A. J. P. White and D. J. Williams, *Chem. Eur. J.*, 1997, **3**, 152.
3 M. J. Gunter and M. R. Johnston, *J. Chem. Soc., Perkin Trans. 1*, 1994, 995; M. J. Gunter, D. C. R. Hockless, M. R. Johnston, B. W. Skelton and A. H. White, *ibid.*, 1994, 1008; M. J. Gunter, D. C. R. Hockless, M. R. Johnston, B. W. Skelton and A. H. White, *J. Am. Chem. Soc.*, 1994, **116**, 4810.
4 Porphyrins in rotaxanes; D. B. Amabillino and J.-P. Sauvage, *Chem. Commun.*, 1996, 2441; F. Vögtle, F. Ahuiis, S. Baumann and J. L. Sessler, *Liebigs, Ann.*, 1996, 921; M. C. Feiters, M. C. T. Fyfe, M.-V. Martinez-Diaz, S. Menzer, R. J. M. Nolte, J. F. Fraser, P. J. M. van Kan and D. J. Williams, *J. Am. Chem. Soc.*, 1997, **119**, 8119; R. B. Hannak, G. Farber, R. Konrat and B. Krautler, *J. Am. Chem. Soc.*, 1997, **119**, 2313.
5 The full synthesis and characterization of all compounds will be reported in full in a forthcoming paper.
6 J. N. H. Reek, J. A. A. W. Elemans and R. J. M. Nolte, *J. Org. Chem.*, 1997, **62**, 2234.
7 A. P. H. J. Schenning, B. de Bruin, A. E. Rowan, H. Kooijman, A. L. Spek and R. J. M. Nolte, *Angew. Chem., Int. Ed. Engl.*, 1995, **34**, 2132.
8 P. R. Aston, D. Philip, M. V. Reddington, A. M. Z. Slawin, N. Spencer, J. F. Stoddart and D. J. Williams, *J. Chem. Soc., Chem. Commun.*, 1991, 1680.
9 A. G. Johnston, D. A. Leigh, A. Murphy, J. P. Smart and M. D. Deegan, *J. Am. Chem. Soc.*, 1966, **118**, 10 662; F. Vögtle, T. Duennwald, M. Haendel, R. Jaeger, S. Meier and G. Harder, *Chem. Eur. J.*, 1996, **2**, 640.

Received in Cambridge, UK, 20th November 1997; 7/08373D

Ligand and H/D exchange of $Mn(H_2O)_6^{2+}$ and $Cu(OH)(H_2O)_4^{+}$ in the gas phase

Steen Brøndsted Nielsen[a] and Gustav Bojesen*[b]

[a] *Department of Chemistry, Odense University, DK-5230 Odense, Denmark*
[b] *Department of Chemistry, University of Copenhagen, The H.C. Ørsted Institute, DK-2100 København Ø, Denmark*

When ligand exchange of aqua complexes in the gas phase is examined by reaction with D_2O it is not accompanied by H/D exchange.

In solution, aqua complexes undergo exchange of intact ligands as well as proton exchange.[1] In the present work it is shown that whereas ligand exchange occurs in the gas phase, doubly charged aqueous complexes do not undergo proton exchange in the gas phase. Formation by electrospray of aqua complexes of doubly charged metal ions is well known.[2] However, only a few studies of ligand exchange in complexes of doubly charged metal ions in the gas phase have appeared.[3,4]

The spectra obtained when $Mn(H_2O)_6^{2+}$ is allowed to react with D_2O are shown in Fig. 1 for two different pressures of D_2O.[5] The parent ions occur at *m/z* 81.5 and the products of consecutive ligand exchange reactions occur at intervals of one *m/z* value above the parent ion. At low pressure the unexchanged reactant is the most abundant ion whereas the product of four ligand exchanges is the most abundant at high pressure. Since the ions are doubly charged, this shows that the exchange reaction leads to an increase in the mass of two Daltons. Hence the products have been formed by exchange of intact water molecules, and no evidence of hydrogen exchange is observed. The spectra shown in Fig. 1(*a*) and (*b*) include a group of peaks at *m/z* 72.5 and above which must arise from reactant ions which have lost one or more ligands. This is due to the poorly defined collision conditions when ion–molecule reactions (IMRs) are studied in a multipole. In order to optimize the yield of IMRs the axial velocity of the ions is kept low, and under such circumstances the radial RF field in the multipole may contribute significantly to the kinetic energy which is available in the collisions.[6] When the pressure of D_2O is increased, products of addition as well as ligand exchange reactions are observed [Fig. 1(*b*)]. The six equidistant peaks above that from the reactant show that at this pressure all six water molecules in the parent ion can be exchanged. The abundance of the products formed by loss of a ligand is increased, and products of addition reactions are observed. In the observed addition products all the ligands have been exchanged. This phenomenon is well known from studies of H/D exchange reactions in quadrupole instruments.[7–10] Briefly it is a consequence of the instability of the addition product relative to dissociation back into the reactants. The addition product can be stabilized by different mechanisms but these all require a pressure at which all the ligands in the parent ion have been exchanged. For most of the aqueous complexes the largest clusters which we have observed under high-pressure conditions have nine water molecules, independently of the size of the parent complex.[11] This shows that the binding of a tenth ligand is very weak. A structure which is in agreement with this is shown in Scheme 1.

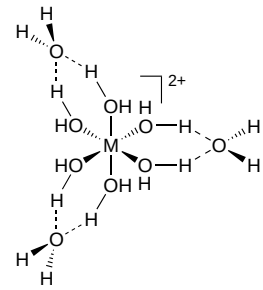

Scheme 1

Whereas H/D exchange has not been observed in the doubly charged ions, it is readily observed in singly charged ions. Fig. 2 shows the spectrum obtained when $^{63}Cu(OH)(H_2O)_4^{+}$ is allowed to react with D_2O. Such hydroxidoaqua complexes are

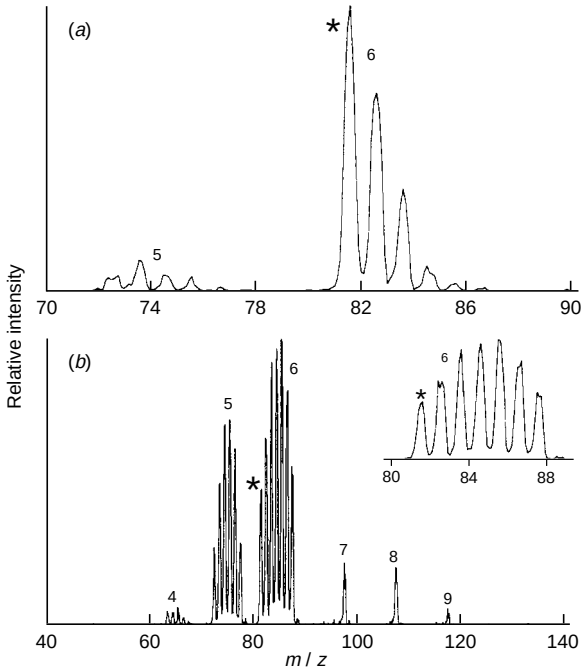

Fig. 1 Spectra obtained from the reaction between $Mn(H_2O)_6^{2+}$ and D_2O at two different pressures; (*a*) 0.20 (*b*) 0.40 mTorr. The reactant ion is indicated by *. The number at each group of peaks indicates the number of aqua ligands in the complex assigned to the peaks.

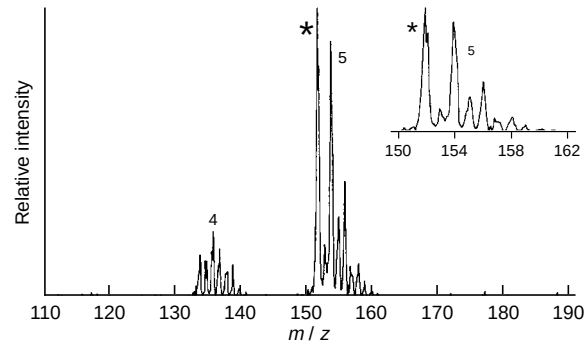

Fig. 2 Spectrum obtained from the reaction between $^{63}Cu(OH)(H_2O)_4^{+}$ and D_2O at 0.20 mTorr. The reactant ion is indicated by *. The number at each group of peaks indicates the number of ligands (including one hydroxido) in the complex assigned to the peaks.

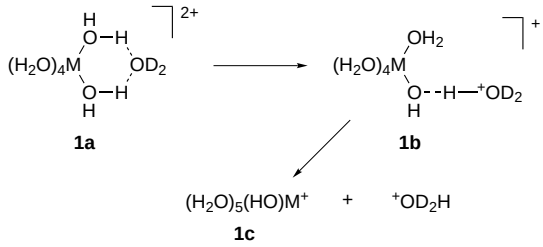

Scheme 2

formed in the source along with the aqua complexes. The equivalent complex with manganese could not be generated in sufficiently high abundance to study its reactivity in IMRs. This difference in acidity of copper and manganese aqua complexes in the gas phase has been noticed before.[2] The reactant ion $^{63}Cu(OH)(H_2O)_4^+$ gives a peak at *m/z* 152, and the products of the exchange reaction are observed at intervals of one *m/z* value above. Products of exchange and ligand loss are observed at *m/z* 134 and above. The most abundant products occur at *m/z* 154 and *m/z* 156. This seems to indicate that exchange of the intact ligand is preferred for the singly charged complex, but the observation of peaks at *m/z* 153, 155, 157 shows that in the singly charged complex the hydrogen atoms can be exchanged one at a time.

The absence of H/D exchange in the reaction between the doubly charged complex $Mn(H_2O)_6^{2+}$ and D_2O is in agreement with the model which previously has been used to rationalize the reactivity of ligated doubly charged metal ions and of doubly charged molecular ions.[12–14] Excluding exchange of hydrogen radicals or simultaneous exchange reactions, the mechanism giving exchange of a singly hydrogen would have to proceed by intermediates in which the two charges are partially separated. The overall product of the reaction will be proton transfer rather than exchange as is observed at high D_2O pressures. A possible mechanism is shown in Scheme 2.

Protonation of inner-sphere ligands has been proposed to play a role in the exchange of water complexes.[15] However, in the gas phase formation of ions such as **1b** must be energetically disfavoured.[12,13] The absence of H/D exchange indicates that when an intermediate such as **1b** is formed in an IMR, the electrostatic repulsion prevents the incipient hydroxonium ion and the complex from remaining together for long enough for back exchange of a deuteron to occur. The overall outcome of the reaction will then be transfer of a proton rather than H/D exchange.

The structure of hydrated doubly charged metal ions and the dynamics of the exchange reaction are being very actively studied both experimentally and theoretically.[16–19] In aqueous solutions of $Mn(H_2O)_6^{2+}$ ligand exchange is faster than proton exchange.[20] The results presented here show that the exchange of the intact ligand has its parallel in the gas phase, but that the very different influence of electrostatic interactions prevents the occurrence of H/D exchange reactions.

Notes and References

* E-mail: bojesen@kiku.dk

1 J. Burgess, *Metal ions in solution*, Ellis Horwood, Chichester, 1978.
2 A. T. Blades, P. Jayaweera, M. G. Ikonomou and P. Kebarle, *J. Chem. Phys.*, 1990, **92**, 5900.
3 Y. D. Hill, B. S. Freiser and C. W. Bauschlicher, *J. Am. Chem. Soc.*, 1991, **113**, 1507.
4 U. N. Andersen and G. Bojesen, *Int. J. Mass Spectrom. Ion Process*, 1996, **153**, 1.
5 The experiments were carried out with a Finnigan TSQ700 tripelquadrupole instrument in which the collision region is in fact an octapole. The complexes were generated by electrospray ionization from 0.20 mM aqueous solutions of appropriate salts, and the ion–molecule reactions were conducted as described in ref. 4.
6 K. M. Ervin and P. B. Armentrout, *J. Chem. Phys.*, 1985, **83**, 166.
7 N. N. Dookeran and A. G. Harrison, *J. Mass Spectrom.*, 1995, **30**, 666.
8 J. A. Stone, *Org. Mass Spectrom.*, 1993, **28**, 1119.
9 N. N. Dookeran and A. G. Harrison, *J. Am. Soc. Mass Spectrom.*, 1994, **6**, 19.
10 A. Ranasinghe, R. G. Cooks and S. K. Sethi, *Org. Mass Spectrom.*, 1992, **27**, 77.
11 S. B. Nielsen and G. Bojesen, unpublished work.
12 R. Tonkyn and J. C. Weisshaar, *J. Am. Chem. Soc.*, 1986, **108**, 7128.
13 L. M. Roth and B. S. Freiser, *Mass Spectrom. Rev.*, 1991, **10**, 303.
14 S. D. Price, M. Manning and S. R. Leone, *J. Am. Chem. Soc.*, 1994, **116**, 8673.
15 T. J. Swift and T. A. Stephenson, *Inorg. Chem.*, 1966, **5**, 1100.
16 R. Åkesson, L. G. M. Pettersson, M. Sandström and U. Wahlgren, *J. Am. Chem. Soc.*, 1994, **116**, 8705.
17 A. K. Katz, J. P. Glusker, S. A. Beebe and C. W. Bock, *J. Am. Chem. Soc.*, 1996, **118**, 5752.
18 F. P. Rotzinger, *J. Am. Chem. Soc.*, 1997, **119**, 5230.
19 E. D. Glendening and D. Feller, *J. Phys. Chem.*, 1996, **100**, 4790.
20 T. J. Swift and R. E. Connick, *J. Chem. Phys.*, 1962, **37**, 307.

Received in Basel, Switzerland, 11th November 1997; 7/08136G

High catalytic efficiency of transition metal complexes encapsulated in a cubic mesoporous phase

M. Eswaramoorthy, Neeraj and C. N. R. Rao,*

Chemistry and Physics of Materials Unit, Jawaharlal Nehru Centre for Advanced Scientific Research, Jakkur Post, Bangalore 560 064, India

Copper(II) acetate dimer and $[Mn^{II}(bipy)_2]^{2+}$ encapsulated in cubic Al-MCM-48 show high catalytic activity in the oxidation of phenol to catechol by oxygen activation, and of styrene to styrene oxide by singlet oxygen, respectively.

Transition metal complexes encapsulated in the cavities of zeolites are known to exhibit high catalytic activity in certain oxidation reactions, suggesting that these catalytic systems are good enzyme mimics.[1] Oxidation of phenols with O_2 by copper acetate dimer incorporated in MCM-22 or VPI-5 is a case in instance wherein the copper(II) complex mimics the phenolase activity of tyrosinase.[2,3] Besides the activation of O_2, there have been studies of the oxidation of organic compounds with singlet oxygen sources such as H_2O_2, by metal complexes encapsulated in molecular sieves. Selective oxidation of alkenes by bis(2,2′-bipyridyl)manganese, $[Mn(bipy)_2]^{2+}$, encapsulated in zeolites X and Y is one such example.[4] The $[Mn^{II}(bipy)_2]^{2+}$ complex immobilized in mesoporous Al-MCM-41 has been recently shown to exhibit high catalytic activity for styrene oxidation.[5] Based on the geometry of the pore structures of mesoporous solids, it was our view that the cubic phase should be an excellent host for enhancing the catalytic activity of metal complexes. We have therefore investigated the catalytic activity of two transition metal complexes incorporated in mesoporous Al-MCM-48, in oxidation reactions. The metal complexes examined are copper(II) acetate dimer which has the structural features of Cu-containing monooxygenase enzymes[2,3] and $[Mn^{II}(bipy)_2]^{2+}$. While copper(II) acetate incorporated in Al-MCM-48 was primarily meant to examine the catalytic activity for oxygen activation at ambient conditions, the manganese(II) complex system was intended to study the oxidation of styrene by singlet oxygen.

Al-MCM-48 was prepared by employing a modified procedure. To a solution of 2.9 g of cetyltrimethylammonium bromide in 40 ml of deionised water, 2.8 ml of 5 M NaOH was added and the solution stirred for 30 min. To this, a solution containing 0.09 g of aluminium sulfate dissolved in 10 ml of water was added followed by the dropwise addition of 6.2 ml of tetraethylorthosilicate. The mixture was stirred for 1 h, transferred to a stainless steel autoclave and kept at 383 K for 5 days. The final product was filtered, washed several times with deionised water, dried at 353 K for 3 h and calcined at 773 K for 10 h in air to remove the template. The Si/Al ratio in the product was *ca*. 50. The cubic nature of the mesoporous phase was confirmed by X-ray diffraction (Fig. 1). Distinct (211), (220), (321), (400) and (332) reflections were seen in the pattern. Cu-acetate-Al-MCM-48 was prepared by stirring 0.4 g of Al-MCM-48 with 0.2 g of copper acetate monohydrate in distilled, deionised water for 12 h. The product was filtered, washed with water and dried at 383 K for 24 h in vacuum. The Cu/Al ratio in the final product was 0.15. The XRD pattern given in Fig. 1 shows the cubic mesoporous nature of the catalyst. The surface area of the catalyst was 600 $m^2\ g^{-1}$. Al-MCM-48-$[Mn(bipy)_2]^{2+}$ was prepared by the treatment of Al-MCM-48 (0.3 g) with a solution of 0.3 g of $[Mn(bipy)_2][NO_3]_2$ in 20 ml of 1:9 (by volume) DMF–acetonitrile mixture at room temperature for 48 h. The sample was filtered, washed with acetonitrile and dried at 353 K under vacuum for 1 h. Chemical analysis showed that the Mn/Al ratio in the product was 0.14. The XRD pattern (Fig. 1) confirmed that the cubic mesoporous structure was retained. The surface area of the catalyst was 770 $m^2\ g^{-1}$.

The second derivative EPR spectrum of Cu-acetate-Al-MCM-48 ($g_\perp$ = 2.06, $g_\parallel$ = 2.18) exhibited the expected

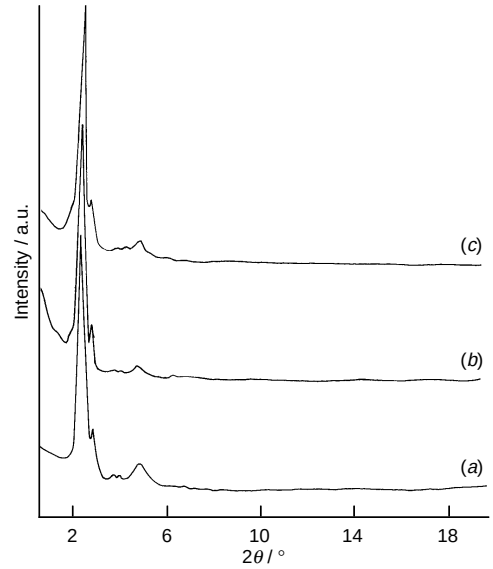

Fig. 1 X-Ray diffraction patterns of (*a*) calcined Al-MCM-48, (*b*) copper acetate dimer encapsulated Al-MCM-48 and (*c*) $[Mn(bipy)_2]^{2+}$ encapsulated Al-MCM-48

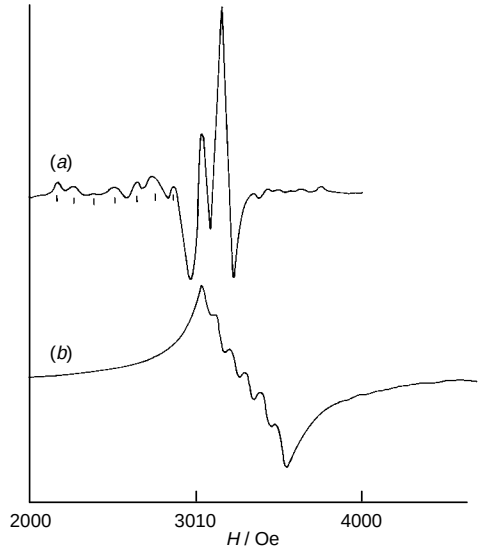

Fig. 2 EPR spectra of (*a*) copper acetate dimer and (*b*) $[Mn(bipy)]^{2+}$ encapsulated in Al-MCM-48

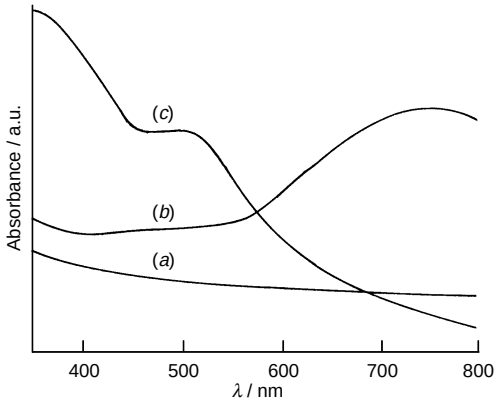

Fig. 3 Electronic absorption spectra of (*a*) Al-MCM-48, (*b*) copper acetate dimer encapsulated in Al-MCM-48

hyperfine structure [Fig. 2(*a*)], establishing the presence of the copper(II) acetate dimer.[3] The IR spectrum showed the carboxylate absorption at 1629 cm^{-1}. The diffuse reflectance spectrum [Fig. 3(*b*)] gave a band around 740 nm, just as in the case of the copper acetate encapsulated zeolites. Oxidation of phenol by the Cu-Al-MCM-48 catalyst was studied by stirring 100 mg of the catalyst in a phosphate buffer solution with 0.57 mmol of phenol in an oxygen atmosphere at 303 K. Gas chromatographic analysis of the product indicated 36% conversion, with catechol as the primary product. The turnover number was 37, a value considerably higher than that found (*ca*. 4) with copper(II) acetate alone. This result demonstrates the high catalytic activity of Cu-Al-MCM-48 in the orthohydroxylation of phenol by oxygen activation.

The Al-MCM-48-$[Mn(bipy)_2]^{2+}$ gave an EPR spectrum with the expected hyperfine structure due to Mn^{2+} [Fig. 2(*b*)]. It was pink with a broad band around 490 nm in its DRS, due to the metal–ligand charge transfer transition [Fig. 3(*c*)]. The IR spectrum showed bands at 760 and 773 cm^{-1} due to the out-of-plane C–H deformation of the bipy. Oxidation of styrene was studied by taking 100 mg of the catalyst in a solution of 0.87 mmol of styrene in 5 ml of acetonitrile, to which 3.5 mmol of H_2O_2 was added. Gas chromatographic analysis showed the conversion to be *ca*. 40% with styrene oxide as the primary product. The turnover number was 82 compared with *ca*. 7 for the $[Mn(bipy)_2]^{2+}$ complex alone. In the hexagonal mesoporous host, Al-MCM-41, the maximum turnover number was 58.[5] This result establishes Al-MCM-48-$[Mn(bipy)_2]^{2+}$ to be an excellent catalyst for such oxidation reactions. It is to be noted that the turnover number for styrene oxidation with Cu-acetate-Al-MCM-48 catalyst was 46, but there was hardly 5% conversion to styrene oxide, the main product being benzaldehyde. Similarly, the turnover number of the manganese catalyst for the oxidation of phenol through the activation of molecular oxygen was 14 and the product contained almost no catechol. These results reveal the specificity of the metal complexes encapsulated in the cubic mesoporous phase.

The present study not only demonstrates the high catalytic potential of transition metal complexes encapsulated in cubic mesoporous phases in oxidation reactions, but also the need to explore other reactions as well as mesophase compositions with different Si/Al ratios.

Notes and References

* E-mail: cnrrao@jncasr.ac.in

1 D. R. Corbin and N. Herron, *J. Mol. Catal.*, 1994, **86**, 343.
2 L. M. Sayre and D. V. Nadkarni, *J. Am. Chem. Soc.*, 1994, **116**, 3157.
3 R. Robert and P. Ratnasamy, *J. Mol. Catal.*, 1995, **100**, 93.
4 P. P. Knops-Gerrits, D. D. Vos, F. Thibault-Starzyk and P. A. Jacobs, *Nature*, 1994, **369**, 543.
5 S. S. Kim, W. Zhang and T. J. Pinnavaia, *Catal. Lett.*, 1997, **43**, 149.

Received in Cambridge, UK, 18th December 1997; 7/09095A

Amphiphilic poly(sugar amino acid)s: a novel class of glycoclusters for supramolecular materials[1]

Shin-Ichiro Nishimura,*† Shinnosuke Nomura and Kuriko Yamada

Laboratory for Bio-Macromolecular Chemistry, Division of Biological Sciences, Graduate School of Science, Hokkaido University, Sapporo 060, Japan

A poly(sugar amino acid) having self-assembling properties was efficiently synthesised by simple polymerisation of 1-*O*-dodecyl-2-amino-2-deoxy-β-D-glucopyranosiduronic acid 7 derived from D-glucofuranurono-6,3-lactone as the key starting material.

The growing importance of glycoconjugates in biology[2] and the emergence of libraries[3] for the construction of glycodrugs prompted us to design and synthesise a series of carbohydrate analogues and glycomimetics.[4] Carbopeptoids[5] (peptide-bond linked carbohydrates) are also potential candidates for functional glycomimetics having interesting biological activity as carbohydrate or peptide mimetics. Sugar amino acids (SAAs)[6,7] and their derivatives are important synthons for the preparation of a series of carbopeptoids.[8] One of the synthetic SAAs has been incorporated into a cyclic peptide with the β-turn motif of somatostatin containing Phe-Trp-Lys-Thr.[9] Poly(sugar amino acid)s [poly (SAA)s],[10] peptide-bond linked polysaccharide mimetics (polyamides[11]) derived from the SAAs, are regarded as one of the potential starting points for the synthesis of a novel class of biocompatible and/or biodegradable materials. As part of our ongoing efforts in designing artificial glycoclusters with specific functions,[12] we report herein the first synthesis of poly(sugar amino acid)s able to self-assemble to form stable monomolecular layers using the readily available D-glucofuranurono-6,3-lactone **1** ($194 per 1 kg, Aldrich Chemical Company, Inc.) as a key starting material.

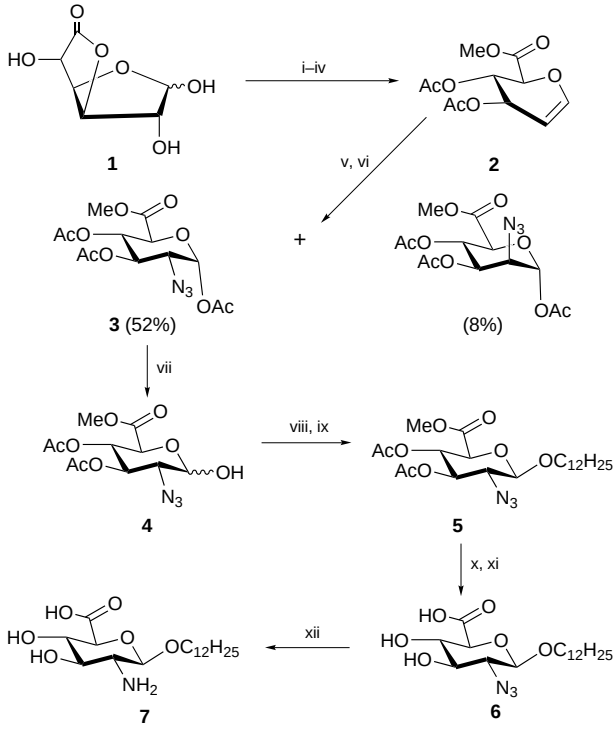

Scheme 1 *Reagents and conditions*: i, NaOH, MeOH; ii, Ac_2O, C_5H_5N; iii, HBr–AcOH; iv, Zn, AcONa, $CuSO_4$, 60% from **1**; v, NaN_3 (1.4 equiv.), $Ce(NO_3)_6(NH_4)_2$ (2.3 equiv.), MeCN, −15 °C, 20 h; vi, NaOAc (3 equiv.), AcOH, 100 °C, 1 h, 52% from **2**; vii, $BnNH_2$ (1.5 equiv.), THF, 20 °C, 3 h, 99%; viii, DAST (1.2 equiv.), THF, −20 °C, 15 min; ix, $C_{12}H_{25}OH$ (2.0 equiv.), Cp_2ZrCl_2 (2.5 equiv.), $AgClO_4$ (5.0 equiv.), C_6H_6, 4 Å molecular sieves, 25 °C, 16 h, 45% from **4**; x, NaOMe (0.2 equiv.), MeOH, 25 °C, 1.5 h; xi, 1 M NaOH (aq.) (1.0 equiv.), MeOH, 25 °C, 3 h, then 1 M HCl (aq.) (pH 3), 79% from **5**; xii, Pd–C, H_2 gas, MeOH, 25 °C, 48 h, 55%

For the construction of the amphiphilic poly(sugar amino acid) we designed a D-glucosaminuronic acid derivative **7** as an amphiphilic SAA monomer. Scheme 1 summarises the synthetic route to the target compound **7** starting from **1**. Thus, manipulation of **1** by a known sequence afforded glucal derivative **2** in large quantities.[13] The latter compound was then converted to 2-azido derivative **3**, under standard conditions for the azidonitration of glucals,[14] in 52% overall yield.‡ Removal of the C-1 acetyl group of **3** was accomplished *via* treatment with benzylamine to afford hemiacetal **4** in quantitative yield. Fluorination of the 1-OH group of **4** with DAST, followed by direct glycosylation with dodecan-1-ol in the presence of Cp_2ZrCl_2–silver perchlorate (1 : 2) in benzene gave β-glycoside **5** in 45% yield from **4**.‡§ Successive treatment of **5** with NaOMe–MeOH and aq. NaOH afforded intermediate **6** in 79% overall yield.¶ Hydrogenolysis of **6** over Pd–C gave amphiphilic SAA monomer **7** in 55% yield.‡

Polymerisation of monomer **7** having two unprotected hydroxy groups at the C-3 and C-4 positions proceeded smoothly using diphenylphosphoryl azide (DPPA) according to the published procedure[15] and gave new poly(SAA) in 72% yield (Scheme 2).‖ The molecular weight of the poly(SAA) was estimated to be in the range 700–4500 (DP = 2–13) by the MALDI-TOF mass spectrum.‖ This polymer forms a stable monolayer *via* spreading of a dilute DMSO–$CHCl_3$ solution on a pure water surface. The surface pressure–area diagram shows a steep increase of the surface pressure at around 1.8 nm^2 per molecule [Fig. 1(*a*)]. This indicates that the poly(SAA) molecules are closely packed. Upon further compression the monolayer collapses, at 50 mN m^{-1}. On the other hand, compound **7**, the repeating unit of this polymeric amphiphile, exhibited a poor ability to form a monomolecular layer,

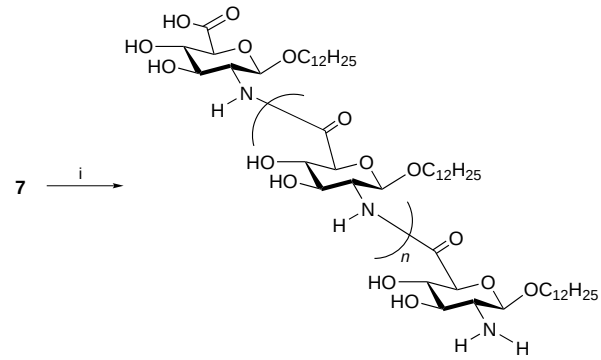

Scheme 2 *Reagents and conditions*: i, $Ph_2P(O)N_3$ (2.3 equiv.), Et_3N (2.3 equiv.), DMSO, 25 °C, 15 h, 72%

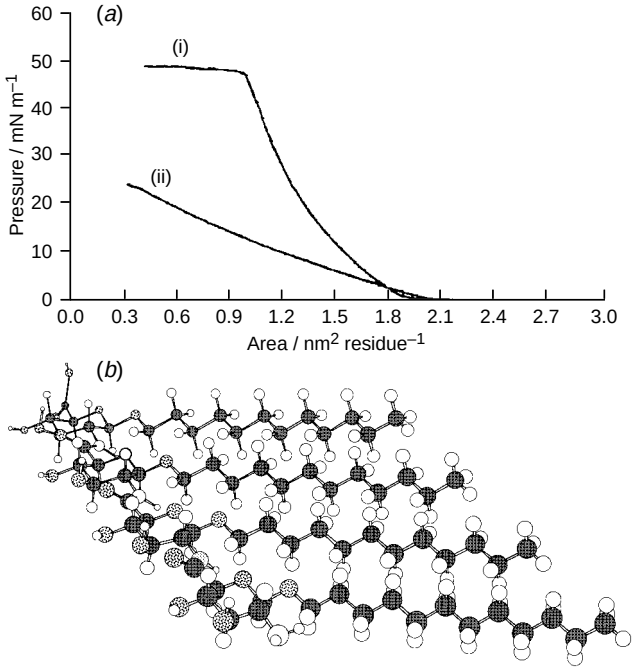

Fig. 1 (*a*) Surface pressure–area isotherms of (i) poly(SAA) and (ii) monomer **7**. (*b*) Possible molecular arrangements of the amphiphilic poly(SAA).

suggesting that the stable peptide bond-type linkages of poly(SAA) are efficient triggers for control of the orientation of the hydrophilic sugar head groups and the hydrophobic alkyl tails, as indicated in the possible molecular arrangements of the polymer [Fig. 1(*b*)]. It should also be noted that the highly ordered structure of the amphiphilic poly(SAA) will favour further chemical and/or enzymatic modification of the two hydroxy groups at the C-3 and C-4 positions. The versatility of the synthetic strategy using poly(SAAs) as 'scaffolds' allows monolayers to be applied to a variety of novel supramolecular materials[16] having specific molecular recognition sites, such as galactose and sialic acid residues.

The authors are indebted to Dr A. Yamagishi, Dr N. Nishi and Dr S. Tokura of Hokkaido University for their valuable suggestions and discussions. This work was partly supported by grants from the Association for the Progress of New Chemistry and the Kato Memorial Bioscience Foundation.

Notes and References

† E-mail: nishimura@polymer.sci.hokudai.ac.jp

‡ *Selected data* for **3**: $\delta_H(CDCl_3)$ 6.37 (d, 1 H, *J* 3.7, H-1), 5.51 (t, 1 H, *J* 9.8, H-4), 5.20 (t, 1 H, *J* 9.8, H-3), 4.37 (d, 1 H, *J* 10.3, H-5), 3.75 (s, 3 H, Me), 3.69 (dd, 1 H, *J* 11.0 and 10.2, H-2), 2.21, 2.12 and 2.05 (each s, 3 H, MeCO). For **5**: $\delta_H(CDCl_3)$ 5.12 (t, 1 H, *J* 9.8, H-4), 5.02 (t, 1 H, *J* 10.2, H-3), 4.41 (d, 1 H, *J* 8.1, H-1), 3.98 (d, 1 H, *J* 9.9, H-5), 3.95 and 3.58 (each q, 1 H, *J* 6.5, OCH_2), 3.75 (s, 3 H, Me), 3.56 (dd, 1 H, *J* 9.4 and 9.2, H-2), 2.09 and 2.01 (each s, 3 H, MeCO) 1.64–1.26 (m, 20 H, CH_2), 0.88 (t, 3 H, *J* 7.0, CH_3). For **7**: $\delta_H([^2H_6]DMSO)$ 5.75 (br s, 2 H, NH_2), 4.30 (d, 1 H, *J* 8.0, H-1), 3.72 and 3.40 (each q, 1 H, *J* 6.5, OCH_2) 3.56 (t, 1 H, *J* 10.0, H-4), 3.49 (t, 1 H, *J* 10.0, H-3), 3.34 (d, 1 H, *J* 9.8, H-5), 3.20 (q, 1 H, *J* 9.8, H-2), 1.56 and 1.23 (m, 20 H, CH_2), 0.84 (t, 3 H, *J* 7.9, CH_3).

§ Glycosyl fluoride derived from **4** was directly employed for the glycosidation reaction without further chromatographic purification owing to its unstable nature.

¶ The versatility of compound **6** as a carboxyl component for the synthesis of the sequential poly(SAAs) should also be noted, and some examples will be reported shortly.

‖ *Polymerisation* of **7**: To a solution of **7** (100 mg, 0.277 mmol) in Me_2SO (5 ml) was added DPPA (137 μl, 0.637 mmol) and Et_3N (89 μl, 0.637 mmol). The mixture was stirred at room temp. for 15 h. The precipitate obtained by addition of EtOH–Et_2O (1 : 1) was collected and dried over P_2O_5 under reduced pressure to give the poly(SAA); ν_{max}/cm^{-1} 3350, 2930, 2850, 1660 and 1545; δ_H ($[^2H_6]$DMSO) 4.48 (br d, 1 H, *J* 8, H-1), 3.85–3.35 (br m, H-2, 3, 4, 5 and OCH_2), 1.55 and 1.22 (m, 20 H, CH_2), 0.85 (br t, 3 H, CH_3). *m/z* 727.9, 1071.4, 1414.9, 1758.3, 2101.8, 2445.25, 2788.7, 3132.2, 3475.7, 3819.1, 4162.6 and 4506.0.

1 Synthetic Glycoconjugates, part 10. For part 9, see M. Ohmae, S. Suzuki, S. Tokura, N. Nishi and S.-I. Nishimura, *J. Biochem.*, 1996, **119**, 367.
2 Y. C. Lee and R. T. Lee, *Acc. Chem. Res.*, 1995, **28**, 321.
3 P. Arya and R. N. Ben, *Angew. Chem., Int. Ed. Engl.*, 1997, **36**, 1280 and references cited therein.
4 For leading references: D. Rouzaud and P. Sinay, *J. Chem. Soc., Chem. Commun.*, 1983, 1353; H. Dietrich and R. R. Schmidt, *Liebigs Ann. Chem.*, 1994, 975; T. Haneda, P. G. Goekjian, S. H. Kim and Y. Kishi, *J. Org. Chem.*, 1992, **57**, 490; H. Ishida, H. Hosokawa, H. Kondo, M. Kiso and A. Hasegawa, *Carbohydr. Res.*, 1997, **303**, 131.
5 K. C. Nicolaou, H. Florke, M. G. Egan, T. Barth and V. A. Estevez, *Tetrahedron Lett.*, 1995, **36**, 1775.
6 K. Heyns and H. Paulsen, *Chem. Ber.*, 1995, **88**, 188.
7 E.-F. Fuchs and J. Lehmann, *Chem. Ber.*, 1975, **108**, 2254.
8 J. Yoshimura, H. Ando, T. Sato and S. Tsuchida, *Bull. Chem. Soc. Jpn.*, 1976, **49**, 2511; C. Muller, E. Kitas and H. P. Wessel, *J. Chem. Soc., Chem. Commun.*, 1995, 2425; Y. Suhara, J. E. K. Hildreth and Y. Ichikawa, *Tetrahedron Lett.*, 1996, **37**, 1575; R. A. Goodnow, S. Tam, D. L. Pruess and W. W. McComas, *Tetrahedron Lett.*, 1997, **38**, 3199; J. Gervay, T. M. Flaherty and C. Nguyen, *Tetrahedron Lett.*, 1997, **38**, 1493.
9 E. G. Von Roedern, E. Lohof, G. Hessler, M. Hoffmann and H. Kessler, *J. Am. Chem. Soc.*, 1996, **118**, 10156.
10 S. Tokura, Y. Ikeuchi, S.-I. Nishimura and N. Nishi, *Int. J. Biol. Macromol.*, 1983, **5**, 249.
11 A polyamide containing a sugar mimetic bicyclic oxalactam has also been reported, see H. Sumitomo and K. Hashimoto, *Macromolecules*, 1977, **10**, 1327.
12 S.-I. Nishimura and Y. C. Lee, in *Structural Diversity and Functional Versatility of Polysaccharides*, ed. S. Dumitriu, Marcel Dekker, NY, 1997, pp. 523–537 and references cited therein.
13 P. C. Wyss, J. Kiss and W. Arnold, *Helv. Chim. Acta*, 1975, **58**, 204.
14 R. U. Lemieux and R. M. Ratcliffe, *Can. J. Chem.*, 1979, **57**, 1244.
15 T. Tsuda and S.-I. Nishimura, *Chem. Commun.*, 1996, 2779.
16 J.-M. Lehn, in *Supramolecular Chemistry, Concepts and Perspectives*, VCH, Weinheim, 1995, p. 173.

Received in Cambridge, UK, 27th November 1997; 7/08555I

Isolation and characterisation of the two major isomers of [84]fullerene (C_{84})

T. John S. Dennis, Tsutomu Kai, Tetsuo Tomiyama and Hisanori Shinohara*†

Department of Chemistry, Nagoya University, Nagoya 464-8602, Japan

We report the first successful separation of the two major isomers of C_{84}, *i.e.* [84-D_2]fullerene and [84-D_{2d}(II)]-fullerene, and ^{13}C NMR and UV–VIS–near IR absorption spectra of the purified materials.

[84]Fullerene, C_{84}, is one of the first higher fullerenes found in arc-processed soot, and solvent extracted in macroscopic amounts.[1] C_{84} has 24 structural isomers obeying the isolated pentagon rule (IPR).[2] Early ^{13}C NMR studies[3,4] indicated that the two major isomers of [84]fullerene have D_2 and D_{2d}(II) symmetry and a 2 : 1 abundance ratio. Theoretical calculations[5,6] predict that the D_2(IV) and D_{2d}(II) isomers are the most stable of the 24 IPR isomers. A number of spectroscopic and structural studies have been carried out on [84]fullerene during the last seven years.[7] However, since the separation of the D_2 and D_{2d}(II) isomers had not been achieved, none of these experiments have been carried out on isomer-free samples. Here we report the first successful isolation of the two major isomers of [84]fullerene.

Separation of C_{84} isomers was achieved by recycling HPLC using a Cosmosil *5PYE* column and toluene as eluent (20 mm × 250 mm; 10 ml injections of C_{84} solution; 18 ml min^{-1} flow rate).[8] Fig. 1 shows the resulting first-recycling-phase HPLC profile. In this figure, the D_2 and D_{2d} isomers are seen to be partially separated. Complete separation could not be achieved at this stage by continuing to recycle due to peak spreading. However, by cutting the sample at the line marked in Fig. 1, fractions greatly enriched in each of the two isomers were obtained. Further enrichment resulted from repeating the 20 cycle HPLC and cutting technique, and pure D_2 isomer was obtained after a third treatment. The D_2 isomer has the shorter retention time on this column, and because of the tailing of the D_2 fraction into the D_{2d}, two further recycling HPLC treatments are required to produce pure D_{2d} isomer.

Fig. 2 shows the ^{13}C NMR spectra of the purified D_2 and D_{2d} fractions. These spectra give a good indication of the purity of our samples, as there is no detectable contamination of the D_2 C_{84} fraction by the D_{2d}, or *vice versa*. Fig. 2(*a*) contains 21 lines of almost equal intensity, and Fig. 2(*b*) contains 11 lines with one being of roughly half the intensity of the others. These correspond to the D_2 and D_{2d}(II) isomers, respectively. We can confirm that the previous ^{13}C NMR spectra[3,4] of the mixture are convolutions of the present isomer-free spectra. However, owing to the 2 : 1 D_2 : D_{2d} isomer abundance ratio, in the spectrum of the mixture all lines due to the D_2 isomer and ten of the eleven lines due to the D_{2d} isomer have the same intensity. Therefore, we are also able to show for the first time which lines belong to which isomer. Since the submission of the present communication, an attempt to assign these 31 lines, on the basis of a comparison of ^{13}C NMR spectra of a central and tail cut from the main C_{84} band in an HPLC profile, has appeared in the literature.[9] This was only moderately successful, having six incorrect assignments.

Among the 24 possible IPR isomers of C_{84}, four have D_2 symmetry and two have D_{2d} symmetry. The present D_{2d} isomer can be unambiguously assigned to C_{84} isomer II. This isomer possesses 11 different carbon atom environments. One of these

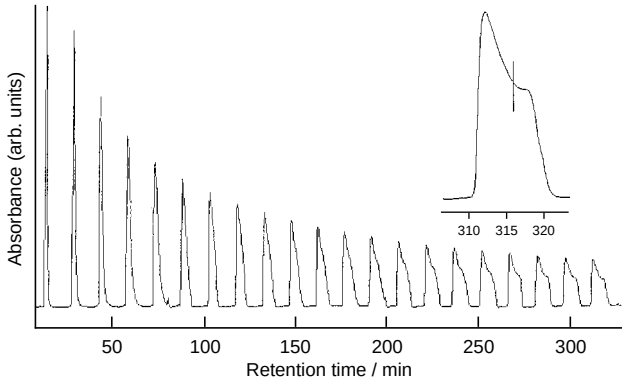

Fig. 1 HPLC profile taken from the second recycling-phase. The insert is an expanded view of the 20th cycle. Partial separation of the two major isomers of C_{84} has occurred, and by cutting at the line shown in the insert, fractions enriched in the D_2 and D_{2d} isomers are obtained. Several more recycling HLPC treatments are required to produce pure materials.

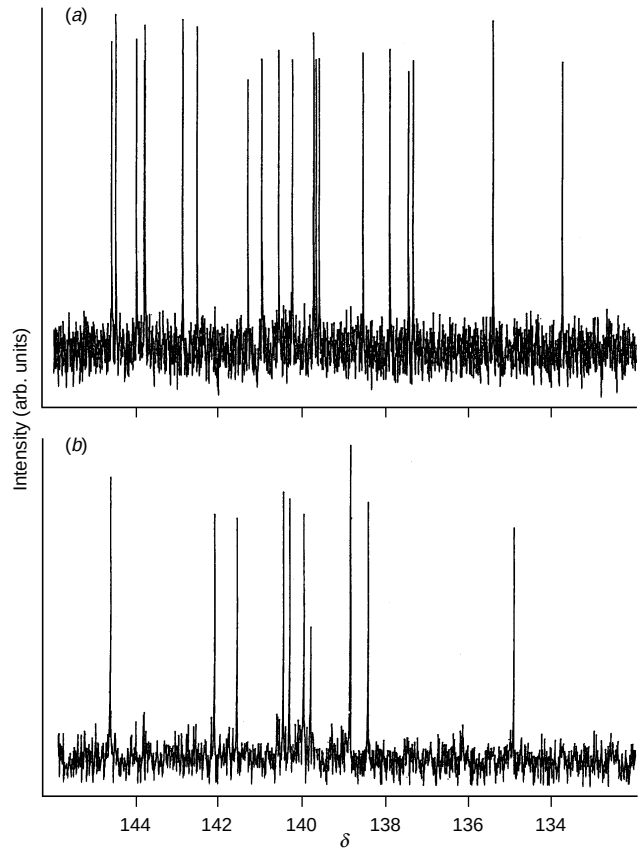

Fig. 2 ^{13}C NMR spectra of the purified two major isomers C_{84}: (*a*) one of the four D_2 IPR isomers, and (*b*) [84-D_{2d}(II)]fullerene. The measured chemical shifts for the present C_{84} isomers are: D_2 δ 133.81, 135.48, 137.39, 137.50, 137.91, 138.58, 139.63, 139.74, 139.77, 139.79, 140.32, 140.60, 141.00, 141.33, 142.58, 142.89, 143.78, 143.81, 143.98, 144.48, 144.58; D_{2d}; δ 134.98, 138.48, 138.87, 138.88, 139.82, 140.00, 140.37, 140.50, 141.57, 142.13, 144.60.

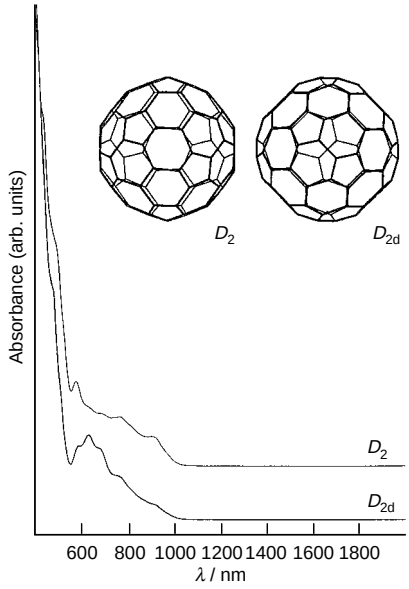

Fig. 3 UV–VIS–near IR absorption spectra of the D_2 and D_{2d}(II) isomers of C_{84}

occurs four times, and the other ten each occur eight times. This fits perfectly with the spectrum given in Fig. 2(*b*), both in terms of the number of lines and their relative intensities. An unambiguous assignment cannot be given to the D_2 isomer, as all four IPR D_2 isomers would have a one-dimensional ^{13}C NMR spectrum consisting of 21 equal-intensity lines. However, a recent two-dimensional ^{13}C NMR study[10] suggests that the present sample corresponds to $C_{84}\{D_2(IV)\}$.

Fig. 3 shows the UV–VIS–near IR absorption spectra of the purified C_{84} D_2 and D_{2d}(II) isomers. The absorption dip near 600 nm in the spectrum of the present D_{2d}(II) C_{84} sample accounts for this isomer being green; the D_2 isomer is yellow–brown in CS_2 solution.

The UV–VIS–near IR absorption spectrum of [84-D_2(II)] fullerene is considerably different from the discandium *incar*-fullerene *i*$Sc_2C_{84}\{D_2(II)\}$,[11,12] even though they share the same C_{84} isomer. This indicates that metal encapsulation alters substantially the electronic structure of the host fullerene.

T. J. S. D. thanks the Japan Society for the Promotion of Science for a Fellowship for Foreign Researchers. H. S. thanks the Japanese Ministry of Education, Science, Sport and Culture for Grants-in-Aid for Scientific Research on Scientific Research (A)(2)(No.08554020) for the financial support of this study.

Notes and References

† E-mail: nori@chem2.chem.nagoya-u.ac.jp

1 H. Ajie, M. M. Alvarez, S. J. Anz, R. D. Beck, F. Diederich, F. Fostiropoulos, D. R. Huffman, W. Krätschmer, Y. Rubin, K. E. Schrivens, D. Sensharma and R. L. Whetten, *J. Phys. Chem.*, 1990, **94**, 8630.
2 P. W. Fowler and D. E. Manolopoulos, *An Atlas of Fullerenes*, Clarendon, Oxford, 1995, pp. 73–80.
3 K. Kikuchi, N. Nakahara, T. Wakabayashi, S. Suzuki, H. Shiromaru, Y. Miyake, K. Saito, I. Ikemoto, M. Kainosho and Y. Achiba, *Nature* 1992, **357**, 142.
4 D. E. Manolopoulos, P. W. Fowler, R. Taylor, H. W. Kroto and D. R. M. Walton, *J. Chem. Soc., Faraday Trans.*, 1992, **88**, 3117.
5 B. L. Zhang, C. Z. Wang and K. M. Ho, *J. Phys. Chem.*, 1992, **96**, 7183.
6 K. Raghavachari, *Chem. Phys, Lett.*, 1992, **190**, 397.
7 M. S. Dresselhaus, G. Dresselhaus and P. C. Ekland, *Science of Fullerenes and Carbon Nanotubes*, Academic Press, New York, 1996, pp. 730–733.
8 T. J. S. Dennis and H. Shinohara, *Chem. Phys. Lett.*, 1997, **278**, 107.
9 A. G. Avent, D. Dobois, A. Pénicaud and R. Taylor, *J. Chem. Soc., Perkin Trans. 2*, 1997, 1907.
10 K. Kikichi, Y. Miyake and Y. Achiba, private communication.
11 E. Yamamoto, M. Tansho, T. Tomiyama, H. Shinohara, H. Kawahara and Y. Kobayashi, *J. Am. Chem. Soc.*, 1996, **118**, 2293.
12 E. Yamamoto, T. Tomiyama, Y. Kobayashi and H. Shinohara, unpublished work.

Received in Cambridge, UK, 7th November 1997; 7/08025E

Catalytic enantioselective epoxidation of alkenes with a tropinone-derived chiral ketone

Alan Armstrong*† and Barry R. Hayter

Department of Chemistry, University of Nottingham, University Park, Nottingham, UK NG7 2RD

α-Fluoro-*N*-ethoxycarbonyltropinone is an efficient catalyst for the epoxidation of alkenes by Oxone® with good enantioselectivity.

The development of catalytic methods for the asymmetric epoxidation of unfunctionalised alkenes continues to be an important goal in organic chemistry.[1] The chiral manganese salen complexes developed by Jacobsen and Katsuki provide a solution to this problem for certain alkene substitution patterns, but these catalysts generally give poor enantioselectivity for epoxidation of, for example, *trans*-disubstituted alkenes.[1] Recently, attention has focused on the catalysis of Oxone® epoxidation of alkenes[2] by chiral ketones[3–6] (*via* a dioxirane[7]‡) and by chiral iminium salts[8] (*via* an oxaziridinium species) as a possible solution to this problem, and some impressive advances have been recorded. Yang and co-workers described a catalytic binaphthyl-based ketone which, with appropriate substitution, can give high selectivity [up to 84% ee for the epoxidation of (*E*)-stilbene].[3] Shi has reported a D-fructose-derived chiral ketone which gives extremely high enantioselectivities, but is destroyed under the Oxone® epoxidation conditions, presumably by Baeyer–Villiger reaction.[4] It must therefore be used in relatively large quantities, although modified pH conditions have improved the catalytic efficiency of the process.[4b] The enantiomeric catalyst derived from L-fructose is less readily available, however. Here we describe some of our own results in the development of new ketone catalysts which have led to the discovery of a new class of chiral ketone which can be used catalytically and recycled if required, as well as affording high enantioselectivities for alkene epoxidation.

Recognising the need for an efficient ketone catalyst to be activated electronically towards attack,[3,9] we initially examined several classes of α-functionalised ketone. Of these, α-amido ketones were attractive with regard to the easy introduction of asymmetry, but were prone to decomposition by Baeyer–Villiger reaction.[9] We therefore turned our attention to β-amido ketones and in particular, in view of the need eventually to prepare conformationally well-defined chiral catalysts, tropinone derivatives. Commercially available *N*-ethoxycarbonyltropinone **1** provided promising initial results: using **1** (10 equiv.) and Oxone® (10 equiv.) under the Yang MeCN–H_2O conditions,[10] (*E*)-stilbene was epoxidised completely within 3 h. Importantly, there was no evidence for decomposition of **1** under these conditions. Reasoning that electron-withdrawing substituents should further increase the activity of the catalyst,[11] we prepared the α-fluoro derivative **2** from **1** by treatment of the derived trimethylsilyl enol ether with a Selectfluor reagent.[12]§ Racemic **2** proved to be an excellent catalyst for the epoxidation of (*E*)-stilbene (Table 1): using 10 mol% **2**, reaction was complete in less than 2 h (entry 4), while reasonable conversions were possible at the 1 mol% level over longer time periods (entry 6).¶ There was no evidence for Baeyer–Villiger reaction by ^{1}H NMR spectroscopy, and the catalyst could be recovered (*ca*. 70% yield) by column chromatography.

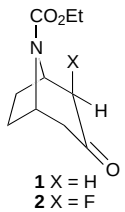

1 X = H
2 X = F

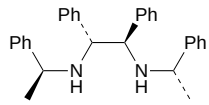

3

In view of the extremely promising catalytic activity of **2**, we then attempted its synthesis in enantiomerically pure form. Following the work of the Simpkins group on desymmetrisation of tropinones using chiral lithium amide bases,[13] treatment of **1** with the lithium amide base derived from **3**[14] (1 equiv.) and Bu^nLi (2 equiv.) in the presence of Me_3SiCl (5 equiv.) and LiCl (1 equiv.) gave the crude silyl enol ether which was reacted without purification with the Selectfluor reagent. The resulting sample of **2** (36% yield, unoptimised), *ca*. 60% ee, was recrystallised once from Et_2O–light petroleum and then once from CH_2Cl_2–light petroleum to provide ketone **2** in > 98% ee according to chiral HPLC.‖ The relative stereochemistry of **2** was proven by X-ray crystallography;** the absolute stereochemistry is assigned based on the precedent of Simpkins, who converted the same intermediate silyl enol ether into (−)-anatoxin-a.[13] It should be noted that the antipodal form of the chiral amine **3** is also readily available,[14] and so it should be possible to access the other enantiomer of **2** by this route. We are also currently exploring resolution methods.

Enantiomerically enriched **2** was used as catalyst for the Oxone® epoxidation of a range of alkenes (Table 2) and the results are extremely promising. Enantioselectivities of up to 83% have been obtained. Interestingly, all our results to date fit a simple transition state model (Fig. 1), which assumes attack on the sterically less hindered *exo*-oxygen of the dioxirane intermediate and a spiro transition state (in accord with Yang[3] and Shi[4]). The hydrogen substituent on the alkene occupies the region of the fluorine substituent of the catalyst. In accord with this model, the epoxidation of styrene, where there are two possible hydrogens on the terminal carbon of the alkene that can occupy the catalyst fluorine region, proceeds with lower enantioselectivity (entry 5). Amongst the other substrates examined so far, it is noteworthy that α,β-unsaturated esters can be epoxidised under these conditions with moderate (but

Table 1 Oxone® epoxidation of (*E*)-stilbene catalysed by ketone **2**[a]

Entry	(±)-**1** (mol%)[b]	Conversion (%)[c]	*t*/h
1	100	100	< 0.25
2	50	100	< 0.25
3	25	100	< 0.5
4	10	100	2
5	5	100	⩽20
6	1	62[d]	24

[a] Alkene (0.1 mmol), Oxone® (1.0 mmol $KHSO_5$), $NaHCO_3$ (1.55 mmol), MeCN (1.5 ml), aq. Na_2EDTA (1 ml of 0.4 mmol dm^{-3} solution). [b] Relative to alkene. [c] By TLC analysis. [d] Measured by ^{1}H NMR spectroscopy.

Table 2 Asymmetric epoxidation of alkenes catalysed by ketone (+)-**2**[a]

Entry	Alkene	(+)-**2** (mol%)[b]	Conversion (%)[c]	*t*/h	Yield (%)[d]	Ee (%)[e] configuration[f]
1	(*E*)-Stilbene	10	100	< 3	88	76[g] *R,R*
2	(*E*)-α-Methylstilbene	10	100	< 4	100	73 *R,R*
3	Phenylstilbene	10	100	< 4	100	83 *R*
4	1-Phenylcyclohexene	10	100	< 6	97	69 *R*
5	Styrene	10	100	< 2	33	29 *R*
6	(*E*)-Methylcinnamate	25	64[h]	24	33	64[i]

[a] Alkene (0.1 mmol), Oxone® (1.0 mmol $KHSO_5$), $NaHCO_3$ (1.55 mmol), MeCN (1.5 ml), aq. Na_2EDTA (1 ml of 0.4 mmol dm^{-3} solution), (+)-**2**. [b] Relative to alkene. [c] Estimated by TLC. [d] Isolated yield of epoxide product. [e] Enantiomeric excesses were measured by ^1H NMR spectroscopy in the presence of $Eu(hfc)_3$ as chiral shift reagent. [f] Absolute configurations were determined by comparison to literature data (refs. 3 and 4). [g] Determined by HPLC (Chiracel OD). [h] Measured by ^1H NMR spectroscopy. [i] Absolute configuration not assigned.

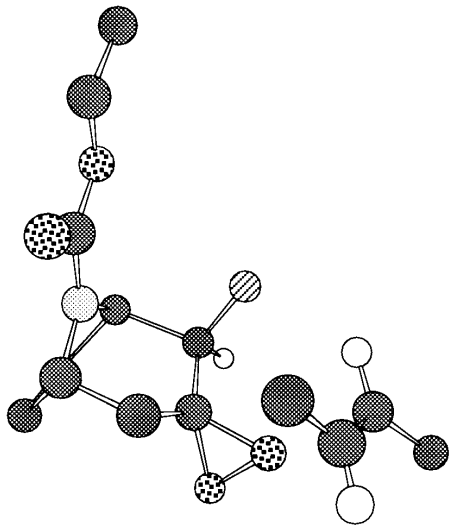

Fig. 1 Model for the approach of a *trans*-disubstituted alkene to the dioxirane derived from ketone (+)-**2**

promising) enantioselectivity (entry 6), albeit requiring longer reaction times and higher catalyst loadings.

In conclusion, we have found that α-fluoro-*N*-ethoxycarbonyltropinone is an efficient catalyst for the epoxidation of alkenes by Oxone®; it can be used in low loadings and recovered and recycled. Moreover, when prepared in enantiomerically pure form, it affords high enantioselectivity for alkene epoxidation. Attempts to prepare related bicyclo[3.2.1]octanone derivatives with alternative α-substitution, in order to improve enantioselectivity further and to clarify the factors responsible for asymmetric induction, are underway.

We thank the EPSRC, the DTI and a consortium of chemical companies for funding this work through the LINK Asymmetric Synthesis Second Core Programme. We also thank Mr T. Lowdon (Hicksons) and Dr N. Johnson (Chiroscience) for helpful discussions. We are grateful to Professor N. S. Simpkins and Mr C. D. Jones of this Department for supplies of *N*-ethoxycarbonyltropinone and of the chiral base **3**, and for helpful advice concerning the asymmetric deprotonation chemistry.

Notes and References

† E-mail: alan.armstrong@nottingham.ac.uk

‡ A dioxirane is almost certainly the active species in the monophasic MeCN–H_2O solvent system: A. Armstrong, B. R. Hayter and P. A. Clarke, unpublished results. See also ref. 5 for ^{18}O labelling experiments in support of this. Earlier ^{18}O labelling experiments (A. Armstrong, P. A. Clarke and A. Wood, *Chem. Commun.*, 1996, 849) were performed in a two phase, CH_2Cl_2–H_2O solvent system.

§ 1-Chloromethyl-4-fluoro-1,4-diazoniabicyclo[2.2.2]octane bis(tetrafluoroborate).

¶ It is probable that the lower conversions at the 1 mol% level are due to decomposition of the Oxone® over the extended reaction times rather than decomposition of the catalyst.

‖ The ketone had mp 57.5 °C, $[\alpha]_D^{27}$ +7.3 (*c* 1.16, CH_2Cl_2). Chiral HPLC was performed using a Chiracel OD column with 100 : 1 hexane–Pr^iOH + 0.1% TFA as eluent; detection at 224 nm; flow rate 1 cm^3 min^{-1} retention time 27 min (minor enantiomer), 29.3 min (major enantiomer).

** Details will appear in a full account of this work. We thank Dr A. J. Blake and Dr Wan-Sheung Li of this Department for this structure determination.

1 T. Katsuki, *Coord. Chem. Rev.*, 1995, **140**, 189.
2 S. E. Denmark, D. C. Forbes, D. S. Hays, J. S. DePue and R. G. Wilde, *J. Org. Chem.*, 1995, **60**, 1391.
3 D. Yang, Y.-C. Yip, M.-W. Tang, M.-K. Wong, J.-H. Zheng and K.-K. Cheung, *J. Am. Chem. Soc.*, 1996, **118**, 491; D. Yang, X.-C. Wang, M.-K. Wong, Y.-C. Yip and M.-W. Tang, *J. Am. Chem. Soc.*, 1996, **118**, 11311.
4 (*a*) Y. Tu, Z.-X. Wang and Y. Shi, *J. Am. Chem. Soc.*, 1996, **118**, 9806; (*b*) Z.-X. Wang, Y. Tu, M. Frohn and Y. Shi, *J. Org. Chem.*, 1997, **62**, 2328.
5 C. E. Song, Y. H. Kim, K. C. Lee, S.-G. Lee and B. W. Jin, *Tetrahedron: Asymmetry*, 1997, **8**, 2921.
6 For earlier attempts to use chiral ketones as catalysts, see R. Curci, M. Fiorentino and M. R. Serio, *J. Chem. Soc., Chem. Commun.*, 1984, 155; R. Curci, L. D'Accolti, M. Fiorentino and A. Rosa, *Tetrahedron Lett.*, 1995, **36**, 5831; D. S. Brown, B. A. Marples, P. Smith and L. Walton, *Tetrahedron*, 1995, **51**, 3587.
7 For reviews of dioxirane chemistry, see R. W. Murray, *Chem. Rev.*, 1989, **89**, 1187; W. Adam, R. Curci and J. O. Edwards, *Acc. Chem. Res.*, 1989, **22**, 205; R. Curci, A. Dinoi and M. F. Rubino, *Pure Appl. Chem.*, 1995, **67**, 811; R. Curci, M. Fiorentino, L. Troisi, J. O. Edwards and R. H. Pater, *J. Org. Chem.*, 1980, **45**, 4758.
8 V. K. Aggarwal and M. F. Wang, *Chem. Commun.*, 1996, 191; A. Armstrong, G. Ahmed, I. Garnett and K. Goacolou, *Synlett*, 1997, 1075 and references cited therein; P. C. Bulman Page, G. A. Rassias, D. Bethell and M. B. Schilling, in the press.
9 A. Armstrong and B. R. Hayter, unpublished results; A. Armstrong and B. R. Hayter, *Tetrahedron: Asymmetry*, 1997, **8**, 1677.
10 D. Yang, M.-K. Wong and Y.-C. Yip, *J. Org. Chem.*, 1995, **60**, 3887.
11 S. E. Denmark, Z. Wu and C. M. Crudden, ACS Meeting Abstract 374-ORGN, vol. 214, Las Vegas, September, 1997.
12 G. S. Lal, *J. Org. Chem.*, 1993, **58**, 2791.
13 N. J. Newcombe and N. S. Simpkins, *J. Chem. Soc., Chem. Commun.*, 1995, 831 and references cited therein.
14 K. Bambridge, M. J. Begley and N. S. Simpkins, *Tetrahedron Lett.*, 1994, **35**, 3391.

Received in Liverpool, UK, 2nd December 1997; 7/08695D

Water-soluble cationic poly-*p*-phenylene polyelectrolytes with an exceptionally high charge density

Matthias Wittemann and Matthias Rehahn*†

Polymer-Institut, Universität Karlsruhe, Kaiserstrasse 12, D-76128 Karlsruhe, Germany

Rod-like poly-*p*-phenylene polyelectrolytes bearing four quaternized tetraalkylammonium functionalities per *p*-phenylene repeating unit are easily available *via* conversion of poly[2,5-di(6-iodohexyl)-1,4-phenylenes] with a large excess of TMEDA followed by the quaternization of the second TMEDA amino group with EtI.

Understanding polyelectrolyte behaviour in dilute solutions of low ionic strengths is an important objective in macromolecular science.[1–3] Despite much effort, however, a conclusive theoretical description of experimentally observed phenomena such as the polyelectrolyte effect is unavailable so far. One of the reasons for this is the fact that, in the case of the commonly investigated flexible-chain polyelectrolytes, various effects influence the measured quantities simultaneously whose contributions are difficult to separate properly. When, for example, measurements are carried out as a function of ionic strength, the radii of gyration of the polyelectrolytes change over the course of the experiment because the intramolecular Coulomb interactions change. However, not only do the radii of gyration increase with decreasing ionic strength but so also does the distance up to which the charged macromolecules repulse one another intermolecularly. For a more reliable interpretation of the obtained data it is therefore advantageous to additionally study polyelectrolytes which cannot change their shape. Because conformative and excluded volume effects are ruled out here, only the intermolecular Coulomb interactions will determine the solution properties. Based on these considerations, numerous studies have been performed using naturally occurring rod-like polyelectrolytes such as DNA.[4] At very low ionic strengths and at elevated temperatures, however, these systems fail because they lose their rod-like shape. Moreover, variation of the charge density, *i.e.* the number of ionic groups per unit length, is not possible with these biopolymers. To overcome the latter limitations, efficient routes to synthetic rod-like polyelectrolytes such as the poly(*p*-phenylene) (PPP) derivatives **1**–**3**[5] and **4**[6] have been developed which take advantage of both the concept of solubilizing side chains[7] and the efficient Pd-catalyzed aryl–aryl coupling reaction.[8–10] The polymers thus available combine exceptional hydrolytic, thermal and chemical stability with a high charge density of up to two ionic groups per *p*-phenylene repeating unit.

Nevertheless, further PPP polyelectrolytes having an even higher charge density would be important as well. We have now developed an efficient two-step quaternization route leading to PPP polyelectrolytes **9** with as many as four tetraalkylammonium groups per *p*-phenylene repeating unit and thus every 4.5 Å. Poly[2,5-di(6-iodohexyl)-1,4-phenylene] precursor PPP **7**, which is readily available *via* Pd-catalyzed polycondensation of 4-bromophenylboronic acid derivative **5** followed by an ether cleavage reaction, is first reacted with a 400-fold molar excess of TMEDA (Scheme 1). The large excess of TMEDA is essential in order to suppress quaternization of both TMEDA nitrogen atoms in this first step, which would lead to structural irregularities and crosslinks. Representative samples of the reaction mixture were analyzed at regular intervals using NMR spectroscopy to determine the reaction time required for a quantitative conversion. When the reaction was found to be

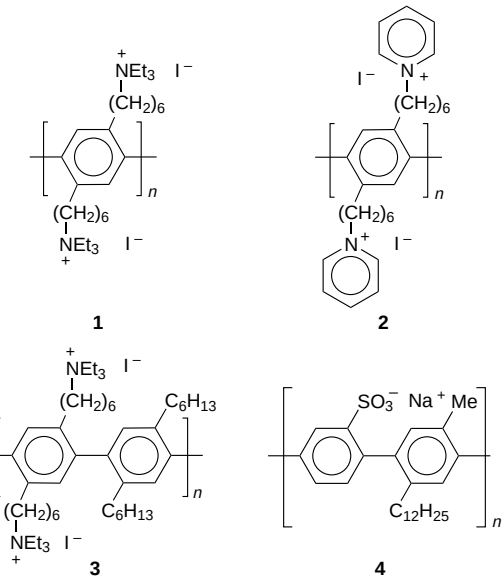

complete, solvents and the excess of TMEDA were removed by distillation. The residue was redissolved in water, and the last traces of organic solvents and TMEDA were carefully separated off by ultrafiltration using distilled water. Finally, PPP **8** was freeze-dried from the resulting aqueous solution. In order to quaternize the second TMEDA amino groups of **8**, the brownish, foamy materials thus obtained were redissolved in DMSO and heated in the presence of a slight excess of EtI. Here also the progress of the conversion was monitored using NMR spectroscopy. A prolonged reaction time and forcing conditions

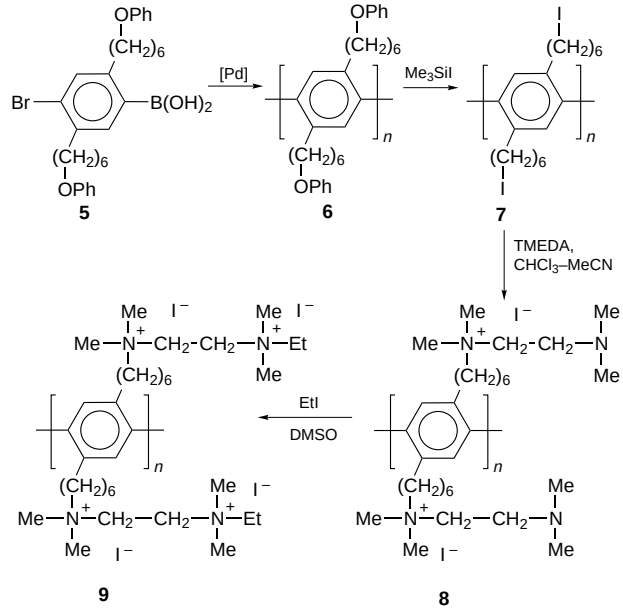

Scheme 1

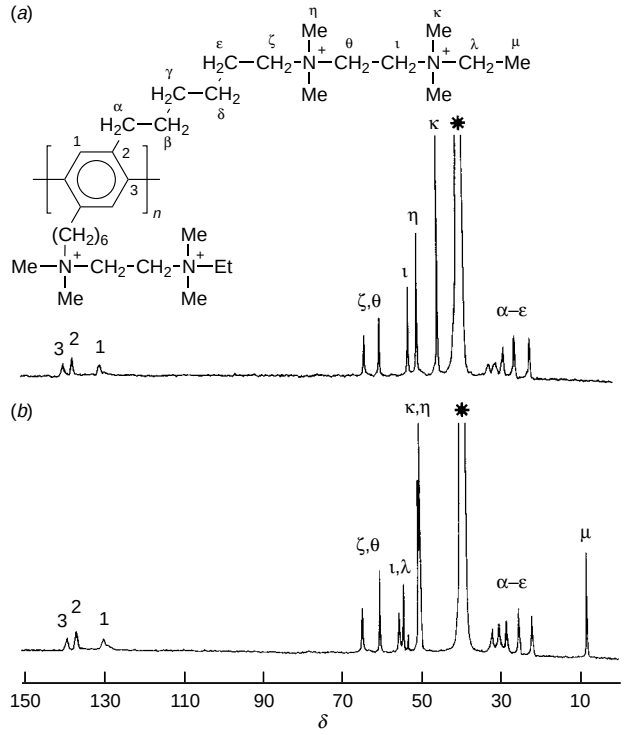

Fig. 1 100 MHz ^{13}C NMR spectra of (*a*) polymer **8** and (*b*) polymer **9** recorded in [$^2H_6$]DMSO (*) at room temperature. The signal assignment is based on the numbering given for polymer **9**.

were found to be necessary here to achieve complete conversion. Nevertheless, after heating the solutions to 60 °C for two days, complete conversion was reached. The obtained slurries were first diluted with DMSO to redissolve the formed precipitate, and a 20-fold excess of water was then added. Subsequently, the resulting polyelectrolyte solutions were purified by ultrafiltration and freeze-dried to give dark brown, foamy solids **9**.

As both the intermediate **8** and the doubly quaternized polyelectrolyte **9** readily dissolve not only in pure water but also in polar organic solvents, their homogeneous molecular constitution could be proved using NMR spectroscopy. Fig. 1 displays the ^{13}C NMR spectra of polyelectrolytes **8** and **9** together with the full signal assignment, which is based on tabulated increments and model compounds.

As is evident from these spectra, all observed absorptions are in full agreement with the expected polymer structures, and no absorptions can be detected which would point towards the formation of structural irregularities. However, not only is the homogeneous constitution of the polyelectrolytes of importance for the planned investigations, but so also is their molar masses. We therefore determined the degrees of polycondensation of precursor PPPs **6** using osmometry. Because no evidence of chain degradation was found during the conversions **6** → **7** → **8** → **9**, the only process that might result in a change of the molar masses is diffusion of low- molecular-weight polymer fractions through the membranes used for ultrafiltration. We therefore ensured that no polymeric material passed through the membranes, and we can thus also rule out any fractionation in the course of the polymer work-up processes. Consequently, the obtained polyelectrolytes **8** and **9** have the same degrees of polycondensation as the precursor PPPs **6** used for their preparation,[13] *i.e.* PPP polyelectrolytes became available in the present work with average degrees of polycondensation of P_n = 20–70 (M_n = 15 000–50 000 g mol^{-1}).

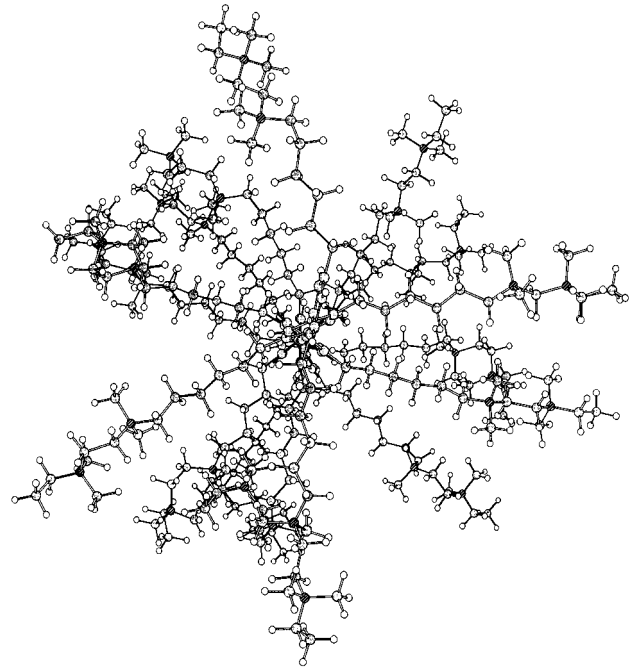

Fig. 2 Schematic illustration of the cylinder-like shape of polymers **9** (viewed along the polymer main chain), sketched according to the results of preliminary SAXS studies performed in salt-free aqueous solutions

Finally, we would like to emphasize that PPP polyelectrolytes **8** and **9** are very soluble in water, despite their highly hydrophobic skeleton. This is presumably due to the fact that these macromolecules represent cylinders of an average length of l_c = 90–300 Å and a diameter of $d_c \approx$ 10 Å whose hydrocarbon core is covered by the highly polar and thus hydrophilic shell of tetraalkylammonium groups (Fig. 2).

Presently, we are investigating the behaviour of PPP polyelectrolytes **8** and **9** in solution as a function of solvent, temperature, ionic strength and counter ion. The obtained results will be compared with those of other PPP polyelectrolytes such as **1**–**4** to gain a deeper insight into polyelectrolyte behaviour in dilute solution.

The authors are grateful to Professor M. Ballauff, Karlsruhe for his support of this work. We thank the Deutsche Forschungsgemeinschaft for financial support.

Notes and References

† E-mail: rehahn@polyibm2.chemie.uni-karlsruhe.de

1 S. Förster and M. Schmidt, *Adv. Polym. Sci.*, 1995, **120**, 51.
2 K. S. Schmitz, *Macroions in solution and colloid suspension*, VCH, New York, 1993.
3 S. Förster, M. Schmidt and M. Antonietti, *Polymer*, 1990, **31**, 781.
4 K. Kassapidou, W. Jesse, M. E. Kuil, A. Lapp, S. Egelhaaf and J. R. C. van der Maarel, *Macromolecules*, 1997, **30**, 2671.
5 G. Brodowski, A. Horvath, M. Ballauff and M. Rehahn, *Macromolecules*, 1996, **29**, 6962.
6 R. Rulkens, M. Schulze and G. Wegner, *Macromol. Rapid Commun.*, 1994, **15**, 669.
7 M. Ballauff, *Mater. Sci. Tech.*, 1993, **12**, 213.
8 A.-D. Schlüter and G. Wegner, *Acta Polym.*, 1993, **44**, 59.
9 I. U, Rau and M. Rehahn, *Acta Polym.*, 1994, **45**, 3.
10 S. Vanhee, R. Rulkens, U. Lehmann, C. Rosenauer, M. Schulze, W. Köhler and G. Wegner, *Macromolecules*, 1996, **29**, 5136.

Received in Cambridge, UK, 3rd December 1997; 7/08709H

Particle size and support effects on the activity and deactivation of Pt-based catalysts for the reduction of NO by *n*-octane under lean-burn conditions

Robert Burch,*† Paolo Fornasiero and Barry W. L. Southward

Catalysis Research Centre, Department of Chemistry, University of Reading, Whiteknights, Reading, UK RG6 6AD

Very high and stable activity for the reduction of NO by *n*-octane under lean-burn conditions may be achieved at temperatures as low as 180 °C by the use of supported Pt catalysts, providing the catalyst is clean and is comprised of large Pt particles.

The adverse environmental impact of NO_x is well known and is the subject of increasingly stringent emissions control legislation.[1,2] It is now accepted that diesel engines will soon require comparable exhaust emissions control to that used on petrol engines. However, despite intensive research into the field of lean $DeNO_x$,[3–6] no suitable material has yet been developed which will attain the levels of activity required under real operating conditions. The problems encountered range from SO_x poisoning to hydrothermal instability, particularly for zeolite-based materials.[1,5] In contrast, Pt-based materials are resistant to SO_x and have good hydrothermal stability.[2,4,5] However, the primary goal of obtaining stable low temperature activity has yet to be realised. Here, we address this problem and present preliminary data concerning highly active low temperature $DeNO_x$ catalysts.

The catalysts used in this study were prepared by incipient wetness impregnation using platinum dinitrodiammine precursor (ex Johnson Matthey), followed by drying (24 h, 120 °C) and calcination (12 h, 550 °C) to give nominal Pt loadings of 1%. The exception to this was the commercial catalyst Azko CK303 (0.3% Pt/Al_2O_3). All catalyst testing was performed in a standard microreactor system described elsewhere.[3] Prior to reaction all samples were aged overnight in standard reaction mixture (100 mg catalyst, 500 ppm NO, 500 ppm *n*-octane, 5% O_2, balance He, total flow 200 $cm^3\ min^{-1}$) at 500 °C. Subsequently, all samples were 'cleaned', *viz.* calcined at 550 °C in 5% O_2 in He for 1 h. *n*-Octane was chosen as a model reductant to simulate a component in a real fuel. NO_x conversions were determined by on-line analysis using a standard chemiluminescence detector (Signal series 4000), with data logged onto a PC at 6 s intervals. CO_2 analysis was performed using a Signal series 2000 IR analyser. No reaction was observed in the absence of a catalyst. H_2 chemisorption was performed in a facility constructed in-house using conditions described elsewhere.[3] Metal particle diameters were calculated assuming a spherical geometry. BET surface areas were determined by standard N_2 adsorption.

Previously much importance has been placed upon the analysis of temperature profiles for $DeNO_x$ catalysts.[4–6] Moreover, such studies have been performed upon 'aged' materials to simulate exhaust catalyst lifetime performance. Conversely, in the present study it was found that profile measurements were not a reliable indication of catalyst activity. Hence isothermal activity profiles of the catalysts were determined using 'clean' samples at temperatures in the region of the hydrocarbon light off (defined as the temperature required for > 20% hydrocarbon combustion, in these studies *ca.* 220 and 195 °C for 0.3% Pt/Al_2O_3 and 1% Pt/Al_2O_3, respectively). By this method it is possible to obtain information on the activity of catalysts in the absence of any surface deposition. This premise is reflected in Fig. 1 which compares the activity of a 0.3% Pt/Al_2O_3 catalyst at 198 °C. Trace 1, in which the catalyst was temperature profiled from 150 °C, exhibits a severe loss of activity *cf.* trace 2 obtained for the 'clean' surface. Thus it is clear that this frequently adopted procedure for evaluating catalysts may seriously underestimate their intrinsic activity.

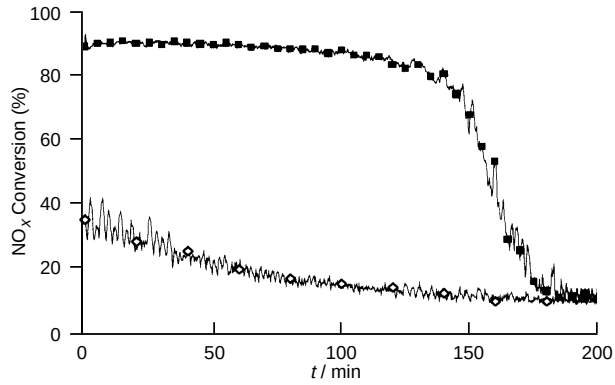

Fig. 1 Effect of surface retention upon activity of 0.3% Pt/Al_2O_3 at 198 °C. **1**, (◇), $DeNO_x$ activity after exposure to reaction mixture at lower temperatures; **2**, (■), $DeNO_x$ activity of 'clean' surface.

Fig. 2 illustrates the response of several 1% Pt catalysts under 'clean' reaction conditions. The data further demonstrate that high $DeNO_x$ activity is possible below the hydrocarbon light-off temperature. In all cases there was an initial period of high activity for NO reduction (> 90% NO_x) and for *n*-octane combustion (100% conversion of *n*-octane to CO_2). The high combustion activity resulted in a marked increase in catalyst temperature (at least 30 °C, as indicated by in-bed thermocouple).

The duration of the initial period of high activity (see Fig. 2) was found to be dependent on the reaction temperature and the choice of catalyst support as summarised in Table 1. Thus, while the SiO_2-supported catalyst exhibited very rapid deactivation below 190 °C, the activity of 1% Pt/ZrO_2 was constant at temperatures as low as 180 °C for > 10 h. Similarly for 1% Pt/Al_2O_3, decreasing the furnace temperature from 180 to 175 °C halved the catalyst lifetime. In all cases the decrease in $DeNO_x$ activity was mirrored by a loss of combustion activity.

Some of these features are attributed to variable metal/support interactions. With SiO_2 there is minimal support interaction and hence the catalysis occurs exclusively on unmodified metal particles. In contrast, both Al_2O_3 and ZrO_2 can interact with the Pt and facilitate surface reactions[7] and hence the reaction is not so constrained. Moreover chemisorption results (Table 1), indicate that both the SiO_2- and Al_2O_3-supported samples contain comparatively small Pt particles. Hence it appears that the combination of a non-interacting support and small Pt particles is responsible for the poor low temperature stability of the ex SiO_2 sample. Conversely the low temperature stability of 1% Pt/ZrO_2 is ascribed to the positive combination of these factors.

To test this hypothesis the 1% Pt/Al_2O_3 sample was subjected to a high temperature treatment in 5% O_2–He (740 °C for 24 h) to induce sintering. This increase in particle size was clearly beneficial to $DeNO_x$ activity (Fig. 3). Comparative studies of

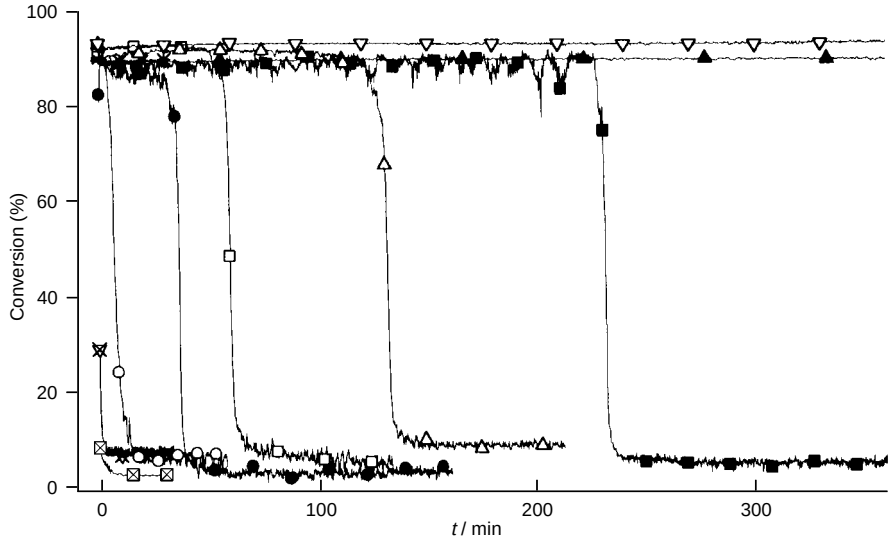

Fig. 2 Effect of the choice of the support and the temperature on the activity of supported Pt catalysts for NO reduction by *n*-octane (100 mg catalyst, 500 ppm NO, 500 ppm *n*-octane, 5% O_2–He, balance He, total gas flow rate was 200 cm^3 min^{-1}). Key: (⊠), SiO_2/175 °C; (⊠), SiO_2/185 °C; (*) SiO_2/190 °C; (○), Al_2O_3/170 °C; (□) Al_2O_3/175 °C; (△), Al_2O_3/180 °C (▽), Al_2O_3/185 °C; (●), ZrO_2/170 °C; (■), ZrO_2/175 °C; (▲), ZrO_2/180 °C.

Table 1 Characterisation and catalytic performance data for the materials under investigation

Catalyst 1% Pt	Pt size[a]/ nm	MSA[a]/ m^2 g^{-1}	BET/ m^2 g^{-1}	Lifetime @ temperature (°C)/min				
				170	175	180	185	190
Al_2O_3	2.0	1.4	218	5	60	130	∞[b]	∞
SiO_2	3.5	0.8	296	—	< 1	—	1	∞
ZrO_2	11	0.26	16	40	240	∞	∞	∞
Al_2O_3[c]	12	0.24	160	15	130	∞	∞	∞

[a] Metal surface area (MSA) and Pt particle size determined from H_2 chemisorption. [b] ∞ indicates beyond the end of the experiment. [c] Sample sintered at 740 °C, in 5% O_2–He for 24 h. In all cases lifetime is defined as the period for which NO_x conversion > 80%.

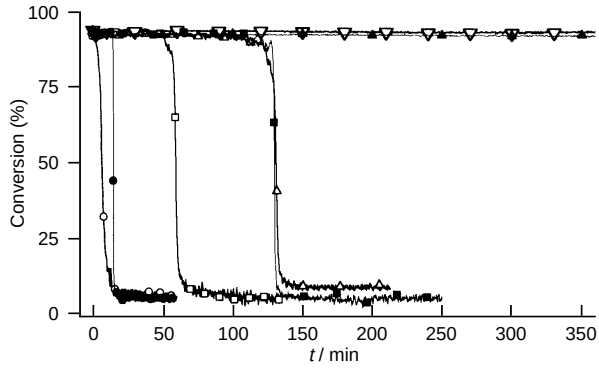

Fig. 3 Effect of sintering on the activity of 1% Pt/Al_2O_3 under standard reaction conditions. Key: (○), 170 °C; (□), 175 °C; (△), 180 °C; (▽), 185 °C; (●), sintered 170 °C; (■), sintered 175 °C; (▲), sintered 180 °C.

the original and the post-sintered samples demonstrated significant improvements in the performance at lower temperatures. The minimum operating temperature for high activity $DeNO_x$ without deactivation was lowered, and the stability of the sintered catalyst was far superior to that of the pre-sintered case with lifetimes at comparable temperatures being more than doubled.

This increased poison tolerance reflects the complex balance in these $DeNO_x$ catalysts owing to the competition for surface sites between the reductant and oxidants, as has been found previously.[8] It further reflects the adverse effects of the retention of reaction intermediates, whether derived from organic compounds or from NO_x, as clearly illustrated in the differences observed in isothermal and temperature-programmed studies. Future work will address the nature of the deposits responsible for deactivation. However at this stage any attempt to identify these poisoning species would be mere speculation and outside the scope of this communication.

These preliminary results have an important technological value concerning the evaluation of the real intrinsic activity of $DeNO_x$ catalysts. Three significant points emerge. First, the intrinsic activity of clean Pt catalysts for NO reduction by higher hydrocarbons may be much higher than would be observed under normal testing conditions because of the rapid and serious deactivation observed at temperatures (*ca.* < 170 °C) below the hydrocarbon light-off region. Second, the lowest apparent activity is observed for supports, such as SiO_2, which do not strongly interact with Pt particles and so perhaps do not provide any resistance to deactivation. Third, the intrinsic activity and stability of large Pt particles is much greater than that of small Pt particles. Hence for a specific support, Pt particle size rather than metal–support interaction seems to be dominant, since the available data suggest that deactivation is initiated at the Pt : support interface. Irrespective of the origin of the enhanced performance it is clear that this information may prove useful in the development of more active catalysts for NO reduction under lean-burn conditions.

We are grateful for financial support for this work through the EU Environment programme, contract number EV5V-CT94-0535.

Notes and References

† E-mail: R.Burch@reading.ac.uk

1 J. C. Frost and G. S. Smedler, *Catal. Today*, 1995, **26**, 207.
2 K. M. Adams, J. V. Catavaio and R. H. Hammerle, *Appl. Catal. B*, 1996, **10**, 157.
3 R. Burch, P. Fornasiero and B. W. L. Southward, *J. Catal.*, in press.
4 R. Burch and P. J. Millington, *Catal. Today*, 1995, **26**, 185.
5 A. P. Walker, *Catal. Today*, 1995, **26**, 107.
6 J. L. D'Itri and W. M. H. Sachtler, *Appl. Catal. B*, 1993, **2**, 7.
7 C. P. Hubbard, K. Otto, H. S. Gandhi and K. S. Ng, *J. Catal.*, 1993, **139**, 268.
8 R. Burch and T. C. Watling, *Catal. Lett.*, 1997, **43**, 19.

Received in Exeter, UK, 10th November 1997; 7/08055G

Hybrid Monte Carlo and lattice dynamics simulations: the enthalpy of mixing of binary oxides

John A. Purton,[a,b] Jon D. Blundy,[a] Mark B. Taylor,[b] Gustavo D. Barrera[b] and Neil L. Allan†[b]

[a] *CETSEI, Department of Geology, University of Bristol, Wills Memorial Building, Bristol, UK BS8 1RJ*
[b] *School of Chemistry, University of Bristol, Cantock's Close, Bristol, UK BS8 1TS*

We present two novel methods for the calculation of the enthalpies of mixing of oxides; both the sampling of many different configurations and the effects of ionic relaxation, which have been largely neglected in previous studies, are crucial.

Understanding the thermodynamics of solid solutions of oxides and phase stability is essential in many areas of solid-state chemistry and mineralogy, including the fabrication and design of ceramics, solid-state batteries, heterogeneous catalysis and high temperature superconductivity. However, experimental data are difficult to obtain and are often unavailable. This is particularly acute at high temperatures and/or pressures, where thermodynamic behaviour is important for sustained material performance and for the stability of minerals deep within the Earth's interior. The paucity of experimental data has led to possibly severe approximations such as the extrapolation of low temperature data and the assumption that enthalpies of mixing, ΔH_{mix}, are constant over wide ranges of temperature.

Advances in computational procedures are such that atomistic simulations[1] (*e.g.*, Monte Carlo, molecular dynamics, lattice statics and dynamics) are now capable of providing detailed information about the structure and thermodynamics of ordered inorganic materials and minerals over a wide range of *T* and *P*. The vast majority of calculations have studied the properties of perfect crystals, assuming a periodic system in a particular configuration; disorder has largely been investigated theoretically *via* point defect calculations, which refer only to the dilute limit. Such methods are not readily extended to solid solutions or disordered systems containing a finite impurity or defect content. Simulations have been largely restricted to the study of end-member compounds, excluding many industrially important ceramics and naturally occurring minerals.

The key objective of the present work is to show explicitly how (*i*) a modified Monte Carlo technique, that allows an efficient sampling of a large number of different configurations, and (*ii*) direct free energy minimisation *via* lattice dynamics can be used for the study of solid solutions, taking explicit account of relaxation and thermal effects. We do not resort to the use of a parameterised Hamiltonian which averages out local relaxation and cannot readily be extended to include the effects of lattice vibrations and pressure. In this way we remove the major limitations of the existing methods which restrict considerably the contact between experiment and theory, and extend the range of applications that can be tackled to include real rather than model systems.

In this preliminary communication we report results for the enthalpies of mixing of the paradigm system MnO/MgO. We use the ionic model and the set of potential parameters from the work of Lewis and Catlow.[2]

The motivation for our new hybrid Monte Carlo (HMC) approach has been the extensive use made by related techniques in the modelling of polymers and biomolecules.[3–5] During one HMC cycle, one of three options is chosen at random, with equal probability. The first of these is a short NVE molecular dynamics (MD) simulation (15 steps and a timestep of 1.5 fs) in which the last configuration is accepted or rejected by comparing its energy with the energy of the starting configuration and using the standard Metropolis algorithm. If the last configuration is rejected, the original configuration is included in the statistical averaging of thermodynamic properties. In the second, a short MD run follows a random exchange of atoms. Again, the difference in energy between the previous configuration and that immediately after the MD simulation is used in the Metropolis algorithm. This second option allows us to sample efficiently different configurations, while the first mainly takes account of vibrations. At the start of each MD run, velocities are chosen anew at random from a Maxwellian distribution. The third option is a random change of the volume of the box[6] which again is accepted or rejected using the Metropolis algorithm.

In Fig. 1(*a*) we show the values of ΔH_{mix} determined using HMC and a box-size of 216 ions at 1300 K. The enthalpy of mixing at 1300 K is symmetric with a maximum of *ca*. 5.4 kJ mol^{-1} at a concentration of 50% MgO–50% MnO. We have been able to find two sets of experimental data less than thirty years old.[7,8] Agreement with the data of Gripenberg *et al.*[7] is good, but we do not see the asymmetry reported by Raghavan.[8] For comparison we also show values calculated using mean field theory, a common approach to the modelling of solid solutions.[9] In this model, instead of distinct Mg^{2+} and Mn^{2+} ions, a 'hybrid' ion is introduced, for which the non-Coulombic potentials are a linear combination of the potentials for Mn^{2+} and Mg^{2+}, appropriately weighted by the site occupancies. If local relaxation or clustering is important then results from this approach will be poor. Fig. 1(*a*) shows that this is the case even in our relatively simple example, where the Mn^{2+} and Mg^{2+} ions are similar in size.

An alternative approach is to average over a limited set of calculations representing different arrangements of the cations within a supercell. Previous work has often assumed just one (the most regular) arrangement and calculated its energy, with or possibly without relaxation, either using lattice statics/dynamics, or by an *ab initio* method.[10] We have recently developed an efficient method which uses lattice statics and quasiharmonic lattice dynamics (QLD) for the fully dynamic structure optimisation of large unit cells *via* the analytic calculation of the free energy, *G*, and its derivatives with respect to all strains.[11] Given the free energy, G_k, for the relaxed structure of each possible cation arrangement *k* the enthalpy is properly averaged over all arrangements in the Gibbs ensemble using

$$< H >= \frac{\sum_k H_k \exp(-\beta G_k)}{\sum_k \exp(-\beta G_k)}$$

Fig. 1(*b*) shows the enthalpies thus calculated of disordered supercells containing 16, 32 and 64 ions of $Mg_xMn_{1-x}O$ (x = 0, 0.25, 0.5, 0.75, 1). For the 16-ion cell, the average was over all possible cation arrangements, whilst for the larger supercells 32

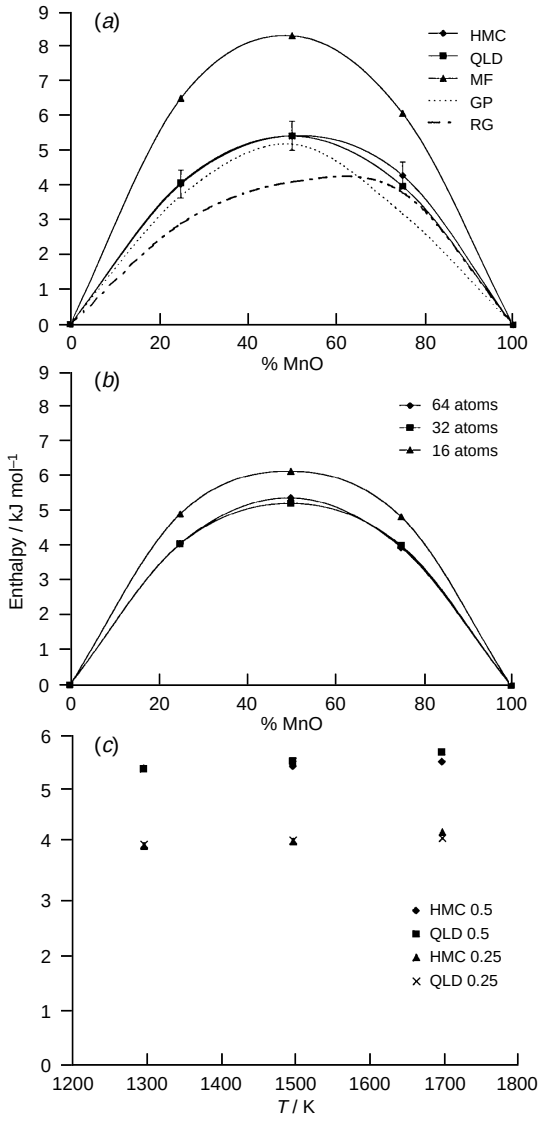

Fig. 1 (*a*) Calculated values of ΔH_{mix} at 1300 K using hybrid Monte Carlo (HMC), mean field theory (MF), and quasiharmonic lattice dynamics (QLD). Two sets of experimental data (GP from ref. 7, RG from ref. 8) are also shown. (*b*) The variation of ΔH_{mix}, calculated using QLD at 1300 K, with supercell size. (*c*) ΔH_{mix} *vs.* T for $Mg_xMn_{1-x}O$ (x = 0.25, 0.5), calculated using QLD and HMC.

arrangements were chosen at random for each concentration. The enthalpies for 32- and 64-ion cells are almost identical and are substantially smaller than those from the 16-ion cell. This highlights once again the importance of allowing for relaxation and clustering. The results for the 64-ion cells are also shown in Fig. 1(*b*) where it is clear that there is excellent agreement between the quasiharmonic lattice dynamics and HMC methods. This result suggests the future use of QLD for enthalpies of mixing at temperatures below the Debye temperature where classical Monte Carlo and molecular dynamics fail due to their neglect of quantum effects. Moreover, the Gibbs free energy can be calculated efficiently and accurately from the QLD, without resorting to lengthy thermodynamic integration.

Fig. 1(*c*) shows the calculated temperature dependence of ΔH_{mix} over the temperature range 1300–1700 K calculated using both HMC and QLD. ΔH_{mix} does not change significantly with temperature, supporting the common assumption that ΔH_{mix} is largely temperature independent.

In summary, we have demonstrated that both the proposed HMC and QLD methods provide an accurate description of the enthalpy of mixing of the binary oxides MgO–MnO. We reiterate that it is essential to take explicit account of ionic relaxation without any averaging out of local effects. The methodology we propose is general, easily extended to other ensembles, and applicable to a wide range of materials and minerals.

This work was funded by NERC grants GR3/09772 and GR9/02621, EPSRC grants GR/K05979 and GR/L31340. GDB's contribution was made possible by means of a grant from el Consejo Nacional de Investigaciones Científicas y Técnicas de la República Argentina.

Notes and References

† E-mail: n.l.allan@bristol.ac.uk

1 See for example: *Computer Modelling in Inorganic Crystallography*, ed. C. R. A. Catlow, Academic Press, San Diego–London, 1997.
2 G. V. Lewis and C. R. A. Catlow, *J. Phys. Solid State Phys.*, 1985, **18**, 1149.
3 S. Duane, A. D. Kennedy, B. J. Pendleton and D. Roweth, *Phys. Lett. B*, 1987, **195**, 216.
4 B. Mehlig, D. W. Heermann and B. M. Forrest, *Phys. Rev. B*, 1992, **45**, 679.
5 M. E. Clamp, P. G. Baker, C. J. Stirling and A. Brass, *J. Comput. Chem.*, 1994, **15**, 838.
6 Q. Wang, J. K. Johnson and J. Q. Broughton, *Mol. Phys.*, 1996, **89**, 1105.
7 H. Gripenberg, S. Seetharaman and L. I. Staffansson, *Chem. Scr.*, 1978–9, **13**, 162.
8 S. Raghavan, PhD Thesis, Indian Institute of Science, Bangalore, India, 1971.
9 See for example: D. De Fontaine, *Solid State Phys.*, 1979, **37**, 73.
10 K. D. Heath, W. C. Mackrodt, V. R. Saunders and M. Causà, *J. Mater. Chem.*, 1994, **4**, 825.
11 M. B. Taylor, G. D. Barrera, N. L. Allan and T. H. K. Barron, *Phys. Rev. B*, 1997, **56**, 14 380; M. B. Taylor, G. D. Barrera, N. L. Allan, T. H. K. Barron and W. C. Mackrodt, *Comput. Phys. Comm.*, 1998, in press.

Received in Bath, UK, 28th November 1997; 7/08907D

Conjugated polyrotaxanes containing coordinating units: reversible copper(I) metallation–demetallation using lithium as intermediate scaffolding

P. L. Vidal,[a] M. Billon,[a] B. Divisia-Blohorn,[a] G. Bidan,[a] J. M. Kern[b] and J. P. Sauvage[b]

[a] *CEA/CNRS/Université J. Fourier, UMR 585, Département de Recherche Fondamentale sur la Matière Condensée, CEA Grenoble, 17 rue des Martyrs, F-38054 Grenoble Cedex 9, France*

[b] *Laboratoire de Chimie Organo-Minérale, UMR 7513, Institut Le Bel, Université Louis Pasteur, 4 rue Blaise Pascal, F-67000 Strasbourg, France*

A new polyrotaxane containing a conjugated backbone has been synthesized *via* a copper(I) template and electropolymerisation; after decomplexation of Cu^{I}, remetallation is only possible if lithium is present during copper removal, as labile scaffolding able to prevent collapse of the free coordination sites and of the organic matrix.

Functionalised conducting polymers obtained by electropolymerisation of pyrrole or thiophene derivatives represent an important family of organic materials.[1] In parallel, rotaxanes have attracted much attention, in relation with photoinduced electron transfer[2] and electro- or photo-chemically driven molecular motions.[3–5]

Recently, the synthesis of a polymetallorotaxane[6] with a conjugated rod threaded through coordinating 30-membered rings has been reported, following a strategy similar to previous works from one of our groups.[7] This report prompts us to disclose our own results and we would like to describe a new coordinating polyrotaxane, with a conjugated –(phen–tph)–$_n$ backbone (phen = 1,10-phenanthroline, tph = thiophene) and its demetallation–remetallation behaviour.

As indicated in Scheme 1, the Cu^{I} template used to assemble the fragments of the precursor could be removed but, interestingly, subsequent remetallation was only possible if lithium was present during demetallation. The function of lithium is assumed to be that of an ionic scaffolding, maintaining the topography of the coordination site after copper removal, though forming a labile complex.

The molecules used are depicted in Scheme 2. The bithienyl-2,9 disubstituted compound **1**† was chosen as the key ligand and the dpphen-containing macrocycle **2**[8] (dpphen = 2,9-diphenyl-1,10-phenanthroline) as its partner for complexation (Scheme 1). The reaction between **2** and a slight deficit of $[Cu(MeCN)_4]BF_4$ followed by addition of **1** in CH_2Cl_2–MeCN at room temperature led to the intertwined heteroleptic copper complex $[Cu(\mathbf{1}\cdot\mathbf{2})]BF_4$ in 95% yield after purification by column chromatography. Analytical and spectroscopic data of this dark red, stable complex confirmed its structure.‡ Cyclic voltammetry (CV) of a 2×10^{-3} mol dm^{-3} complex solution in CH_2Cl_2–0.3 mol dm^{-3} $NBu^{n}_4PF_6$ showed a one electron reversible wave ($E_{1/2}$ = 0.51 V *vs.* 0.01 mol dm^{-3} Ag^+/Ag) corresponding to the redox reaction Cu^{II}–Cu^{I}.§

Electropolymerisation on a platinum electrode (S = 0.07 cm^2, Q = 26 mC cm^{-2}) by continuous cycling of this solution between −0.2 and +1.4 V led to the deposition of a thin red–orange film, characterized by CV measurements [Fig. 1(*a*)]. The presence of the Cu^{I} template is evidenced by the unchanged potential value compared to the monomer. A partial loss of reversibility was observed for this response, but at a slower potential sweep rate (10 mV s^{-1}), the ΔE_p value observed (20 mV) is typical of immobilized electroactive systems. The response between 0.8 and 1.4 V consists of two well defined waves, in agreement with the electrochemical behaviour of end-capped tetrathienylenes,[9] which confirms the electrochemical coupling of the terminal bithienyl units.

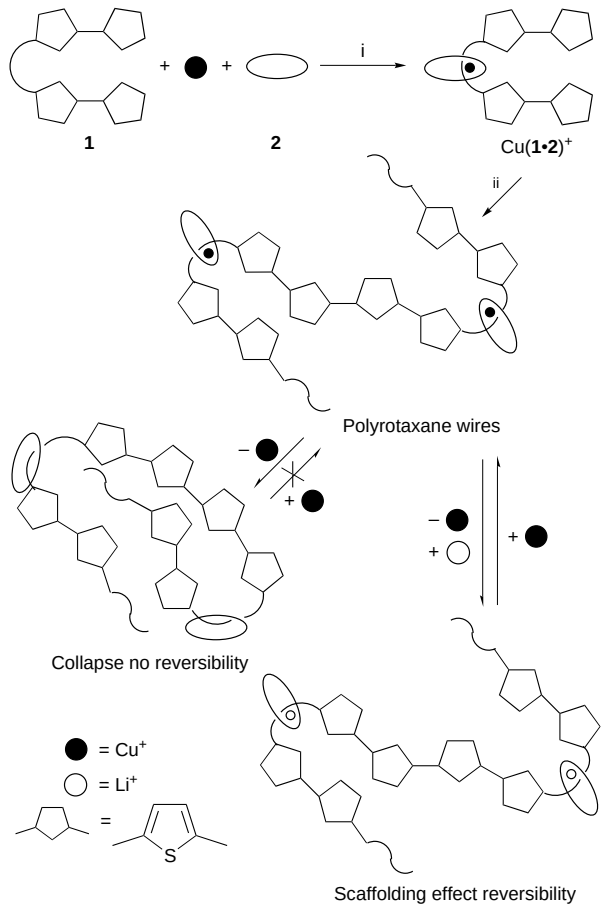

Scheme 1 i, Threading step; ii, electropolymerisation

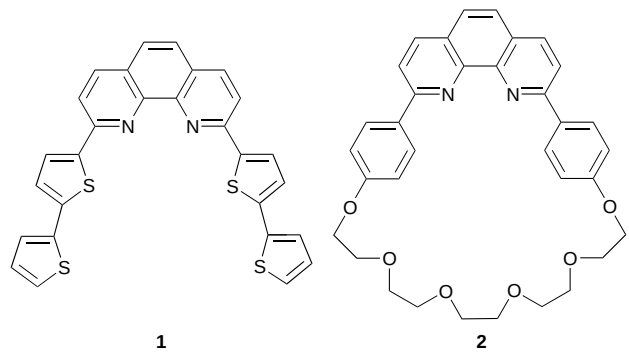

Scheme 2

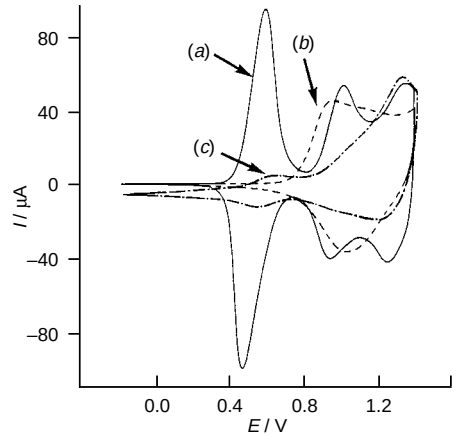

Fig. 1 Cyclic voltammetry in CH_2Cl_2 + 0.3 mol dm^{-3} $NBu^n_4PF_6$ (v = 50 mV s^{-1}) of (*a*) a freshly prepared poly[Cu(**1**·**2**)$^+$] film (solid line), (*b*) after dipping (20 min) in a 0.1 mol dm^{-3} NBu^n_4CN MeCN solution (dashed line) and (*c*) after dipping (4 h) in a 0.1 mol dm^{-3} $[Cu(MeCN)_4]BF_4$ MeCN solution (dot–dashed line)

On treating this film with the strong copper complexing agent CN^-, the signal due to the metallic centre disappeared, whereas those due to the oligothienyl wires dramatically changed with total loss of resolution [Fig. 1(*b*)]. The collapse of the polyrotaxane network was confirmed by the non-reincorporation of Cu^I [Fig. 1(*c*)] or other metallic centers.

Dipping another film freshly prepared under the same conditions in a 0.1 mol dm^{-3} Li^+ + 0.1 mol dm^{-3} CN^- MeCN solution resulted again in complete loss of the copper response but in this case a partial conservation of resolution of the oligothienyl response was observed [Fig. 2(*b*)], which could be attributed to the scaffolding effect induced by Li^+ complexation. Conservation of the topography of the network was spectacularly evidenced by the nearly quantitative reincorporation of Cu^I species [Fig. 2(*c*)] (shown by determination of the ratio of current quantities corresponding respectively to the metallic and the oligothienyl redox systems), probably due to a Li^+/Cu^+ exchange. The strong anodic shift (140 mV) of the electrochemical response of the wire when copper centres are present could be attributed to copper–phenanthroline interactions which induce an electroattracting effect onto the oligothienyl moiety.

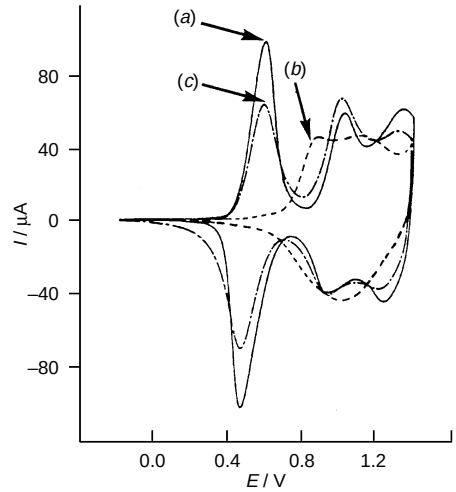

Fig. 2 Cyclic voltammetry in CH_2Cl_2 + 0.3 mol dm^{-3} $NBu^n_4PF_6$ (v = 50 mV s^{-1}) of: (*a*) a freshly prepared poly[Cu(**1**·**2**)$^+$] film (solid line), (*b*) after dipping (20 min) in a 0.1 mol dm^{-3} $LiClO_4$ + 0.1 mol dm^{-3} NBu^n_4CN MeCN solution (dashed line) and (*c*) after dipping (3 h) in a 0.1 mol dm^{-3} $[Cu(MeCN)_4]BF_4$ MeCN solutionn (dot–dashed line)

Reversibility of this demetallation–remetallation process is strongly dependent on the ratio r = $[Li^+]/[CN^-]$ (with $[CN^-]$ = 0.1 mol dm^{-3}) during the demetallation process: for r = 0.1, reincorporation of Cu^I is slower and of 80% compared to the case r = 1, with a loss of reversibility for both the metallic center and the oligothienyl wires, whereas for r = 0.01, collapse of the structure was observed.

In situ conductivity measurements are underway to evaluate the electronic properties of our conjugated structure.

Notes and References

* E-mail: sauvage@chimie.u-strasbg.fr

† **1** was prepared in two successive additions of a cold solution (0 °C) of 5-lithio-2,2′-bithiophene: first, onto a THF solution of 1,10-phenanthroline maintained at room temp. and then on the resulting 2-[5-(-2,2′bithienyl)]-1,10-phenanthroline. Each step was followed by hydrolysis and reoxidation with MnO_2.[8] 5-Lithio-2,2′-bithiophene itself was prepared by reacting at −78 °C 1 equiv. of LDA with bithiophene dissolved in THF. After addition of the base, the solution was raised to 0 °C. Overall yield: 18%. Attempts to obtain **1** in a single step were unsuccessful. ^{1}H NMR (CD_2Cl_2, 400 MHz): δ8.20 (d, 2 H), 7.95 (d, 2 H), 7.74 (d, 2 H), 7.70 (s, 2 H), 7.42 (dd, 2 H), 7.29 (dd, 2 H), 7.27 (d, 2 H), 7.09 (dd, 2 H).

‡ ^{1}H NMR (CD_2Cl_2, 400 MHz): δ8.54 (d, 2 H), 8.42 (d, 2 H), 8.17 (s, 2 H), 7.91 (s, 2 H), 7.89 (d, 2 H), 7.86 (d, 2 H), 7.32 (d, 4 H), 7.24 (d, 2 H), 7.10 (dd, 2 H), 6.78 (dd, 2 H), 6.65 (d, 2 H), 6.17 (dd, 2 H), 5.96 (d, 4 H), 3.85–3.40 (m, 20 H). FABMS: *m/z* 1137.2 ([M − BF_4]$^+$), 629.2 ([M − **1** − BF_4]$^+$), 570.9 ([M − **2** − BF_4]$^+$), 509.0 ([**1**H]$^+$).

§ $E_{1/2}$ (ferrocene) = 0.18 V *vs.* our reference electrode Ag^+/Ag. $E_{1/2}$ = 0.48 V for a 10^{-3} mol dm^{-3} solution of $Cu(dap)_2^+$ in the same supporting electrolyte [dap = 2,9-di(*p*-anisyl)-1,10-phenanthroline].

1 S. J. Higgins, *Chem. Soc. Rev.*, 1997, **26**, 247.
2 A. Harriman, V. Heitz and J.-P. Sauvage, *J. Phys. Chem.*, 1993, **97**, 5940; J.-C. Chambron, A. Harriman, V. Heitz and J.-P. Sauvage, *J. Am. Chem. Soc.*, 1993, **115**, 6109.
3 E. Cordova, A. E. Kaifer and J. F. Stoddart, *Nature*, 1994, **369**, 1330; P. R. Ashton, R. Ballardini, V. Balzani, S. E. Boyd, A. Credi, M. T. Gandolfi, M. Gomez-Lopez, S. Iqbal, D. Philp, J. A. Preece, L. Prodi, H. G. Ricketts, J. F. Stoddart, M. S. Tolley, M. Venturi, A. J. P. White and D. J. William, *Chem. Eur. J*, 1997, **3**, 152 and references therein.
4 J. P. Collin, P. Gavina and J. P. Sauvage, *New J. Chem.*, 1997, **21**, 525.
5 M. Belohradsky, F. M. Rayno and J. F. Stoddart, *Collect. Czech. Chem. Commun.*, 1996, **61**, 1.
6 S. Sherry Zhu, P. J. Carroll and T. M. Swager, *J. Am. Chem. Soc.*, 1996, **118**, 8713.
7 C. O. Dietrich-Buchecker, J. P. Sauvage and J. P. Kintzinger, *Tetrahedron Lett.*, 1983, **24**, 5095; C. O. Dietrich-Buchecker, J. P. Sauvage and J. M. Kern, *J. Am. Chem. Soc.*, 1984, **106**, 3043; J.-C. Chambron, C. O. Dietrich-Buchecker and J.-P. Sauvage, *Comprehensive Supramolecular Chemistry*, ed. J. L. Atwood, E. D. Davies, D. D. MacNicol, F. Vögtle, J.-M. Lehn, J.-P. Sauvage and M. W. Hosseini, 1996, vol. 9, pp. 43–83.
8 C.-O. Dietrich-Buchecker and J.-P. Sauvage, *Tetrahedron*, 1990, **46**, 503.
9 P. Bäuerle, *Adv. Mater.*, 1992, **4**, 102; G. Zotti, G. Schiavon, A. Berlin and G. Pagani, *Chem. Mater.*, 1993, **5**, 430.

Received in Basel, Switzerland, 2nd December 1997; 7/08662H

Novel ring-opened reaction of μ-(1–3-η : 4–7-η-cycloheptatrienyl)-tricarbonylirontricarbonylmanganese with aryllithium reagents

Beihan Wang, Ronghua Li, Jie Sun and Jiabi Chen*

Laboratory of Organometallic Chemistry, Shanghai Institute of Organic Chemistry, Chinese Academy of Sciences, 354 Fenglin Lu, Shanghai 200032, China

The reactions of μ-(1–3-η : 4–7-cycloheptatrienyl)tricarbonylirontricarbonylmanganese $[Mn(CO)_3Fe(CO)_3(C_7H_7)]$ 1, with aryllithium reagents, ArLi (Ar = Ph, *o*-, *m*-, *p*-MeC_6H_4), in ether at low temperature, followed by alkylation of the acylmetalate intermediates with Et_3OBF_4 in aqueous solution at 0 °C affords four novel ring-opened polyene complexes $[Mn(CO)_3Fe(CO)_3\{C_8H_7(OEt)Ar\}]$ (Ar = Ph 2, *o*-MeC_6H_4 3, *m*-MeC_6H_4 4, *p*-MeC_6H_4 5), of which the structure of 2 has been established by a single-crystal X-ray diffraction study.

In recent years, alkene-coordinated transition metal carbene and carbyne complexes and/or their isomerized products, as part of a broader investigation of transition metal carbene and carbyne complexes, have been examined extensively in our laboratory. We found that the isomerizations of the alkene ligands and resulting products depend not only on the alkene ligands but also on the central metals.[1–5] For instance, (cycloheptatriene)-tricarbonyliron $[Fe(C_7H_8)(CO)_3]$, reacted with aryllithium and subsequent alkylation with Et_3OBF_4 gave no product containing ethyl group but the novel compound $[(Cl_3C\text{-}cyclo\text{-}C_7H_8)(CO)_2Fe(COC_6H_4Me\text{-}o)]$, in which the Cl_3C group was derived from a metathetical reaction of solvent CH_2Cl_2 molecules aided by iron at Et_3OBF_4, or ring-opened diallyl-like compound $[(CO)_2Fe\{C(OEt)(C_6H_4Me\text{-}o)C_7H_8\}]$ depending on the alkylation conditions.[3] While the cycloheptatrienediiron hexacarbonyl $[Fe_2(C_7H_8)(CO)_6]$, where the two iron atoms are directly bonded to each other, reacted with aryllithium reagents under analogous conditions to yield the novel isomerized bridging carbyne complexes $[Fe_2(CO)_4\{\mu\text{-}\eta^4\text{:}\eta^3\text{-}C_7H_7C(OEt)\text{-}Ar(\mu\text{-}C(OEt)\}]$.[4] In order to further investigate the effect of different binuclear central metals on the isomerizations of the alkene ligands and the reaction products, we chose μ-(1–3-η : 4–7-η-cycloheptatrienyl)tricarbonylirontricarbonylmanganese, $[Mn(CO)_3Fe(CO)_3(C_7H_7)]$ **1**,[6] where the cycloheptatrienyl ligand is η^4 and η^3 respectively bonded to the $Mn(CO)_3$ and $Fe(CO)_3$ units, and the Mn and Fe atoms are directly bonded to each other, as the starting material for the reaction with aryllithium reagents. These reactions led to nucleophilic addition to and cleavage of the cycloheptatrienyl ring to afford novel ring-opened polyene complexes. We report herein these novel reactions and the structures of the resulting products.

$[Mn(CO)_3Fe(CO)_3(C_7H_7)]$ **1**, was treated with 2 molar equiv. of aryllithium reagents, ArLi (Ar = Ph, *o*-, *m*-, *p*-MeC_6H_4), in diethyl ether at −55 to −40 °C for 3–4 h. The acylmetalate intermediates were subsequently alkylated with Et_3OBF_4 in aqueous solution at 0 °C. After removal of the solvent under high vacuum at low temperature, the solid residue was chromatographed on an alumina column at −20 to −25 °C, and the crude product was recrystallized from light petroleum –CH_2Cl_2 solution at −80 °C to afford orange–red crystalline complexes $[Mn(CO)_3Fe(CO)_3\{C_8H_7(OEt)Ar\}]$ **2**–**5**† (Scheme 1) in 47–52% yields.

The mechanism of the reaction (Scheme 1) is as yet unclear, but it could involve unstable alkoxycarbene intermediates **b** and metalcyclobutane intermediates **c**.[7] The latter then gives intermediates **d** upon opening of the ring, as in the reactions of the tetrafluorobenzobicyclo[2.2.2]octatriene tricarbonyliron with aryllithium nucleophiles.[7] Subsequently, such an intermediate **d** can abstract one molecule of CO to satisfy an 18-electron configurational iron and be converted into the stable ring-opened polyene complexes **2**–**5**.

Complexes **2**–**5** are very sensitive to air and to heat in solution but are stable for short periods on exposure to air as solids. Their structures were established by elemental analyses, spectroscopic determination and single-crystal X-ray diffraction.

The X-ray structure of **2** (Fig. 1)‡ shows that the cycloheptatrienyl ring of **1** has been opened by cleavage of the original C(7)–C(13) σ bond, and in **2** the C(13) atom is now linked to the carbon C(14) forming a double bond C(13)–C(14) and the C(7) atom is linked to the iron atom constructing a MnFeC(7) three-membered ring. Along with the formation of the new π bond,

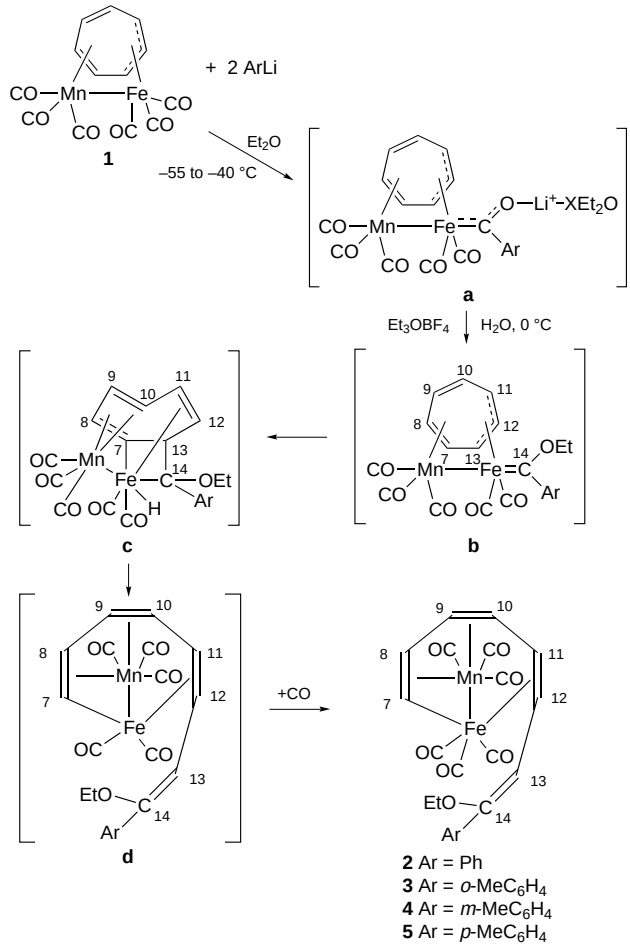

Scheme 1

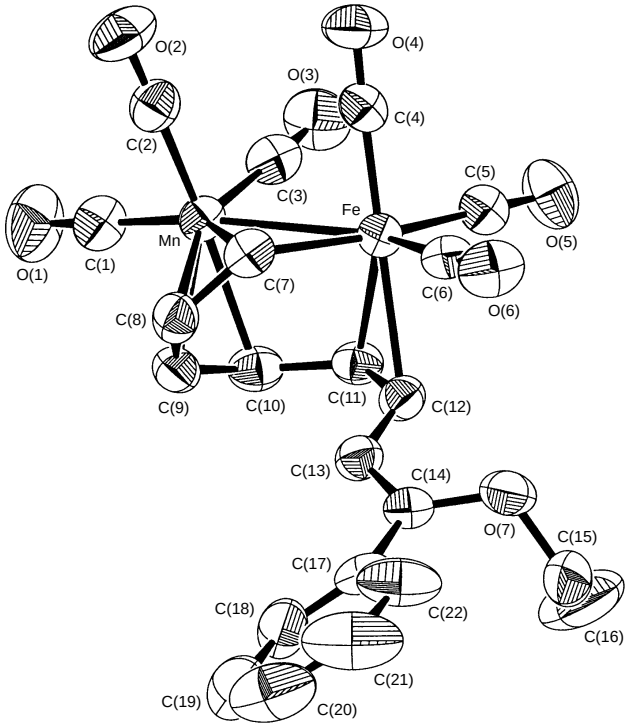

Fig. 1 Molecular structure (bond lengths in Å, angles in °) and labelling diagram for $[Mn(CO)_3Fe(CO)_3\{C_8H_7(OEt)Ph\}]$ **2**: Fe···Mn 2.7216(7), Fe–C(7) 1.967(4), Mn–C(7) 2.130(3), Fe–C(11) 2.211(3), Fe–C(12) 2.260(4), Mn–C(7) 2.130(3), Mn–C(8) 2.160(4), Mn–C(9) 2.144(4), Mn–C(10) 2.234(4), C(7)–C(8) 1.392(5), C(8)–C(9) 1.417(5), C(9)–C(10) 1.392(5), C(10)–C(11) 1.440(5), C(11)–C(12) 1.393(5), C(12)–C(13) 1.441(5), C(13)–C(14) 1.329(5); Fe–Mn–C(7) 45.84(10), Mn–Fe–C(7) 51.0(1), Fe–C(7)–Mn 83.2(1), Fe–C(7)–C(8) 130.3(3), C(7)–C(8)–C(9) 121.8(4), C(8)–C(9)–C(10) 122.7(4), C(9)–C(10)–C(11) 127.4(4), C(10)–C(11)–C(12) 127.3(4), C(11)–C(12)–C(13) 127.3(4), C(12)–C(13)–C(14) 124.9(4).

the alkene ligand became now a conjugated chain octatetraene with the OEt and Ph groups on the terminal carbon atom C(14), and the atomic chains C(7)C(8)C(9)C(10) and C(11)C(12) are coordinated to the orbitals of the Mn and Fe atoms in η^4- and η^2-bonding, respectively, to satisfy the 18-electron rule.

Notes and References

* E-mail: chenjb@pub.sioc.ac.cn

† Satisfactory elemental analyses were obtained for the compounds described. **2**: mp 94–96 °C (decomp.) IR [ν(CO)/cm^{-1}]: 2040s, 1998vs, 1989vs, 1950w, 1943s (br) (cyclohexane). ^{1}H NMR (CD_3COCD_3): δ 7.82 (d, 1 H), 6.27 (t, 1 H), 5.57 (dd, 1 H), 4.95 (t, 1 H), 4.62 (d, 1 H), 4.18 (t, 1 H), 3.78 (m, 1 H), 7.43–7.36 (m, 5 H), 1.29 (t, 3 H), 3.78 (m, 2 H). *m/z* 476 ($M^+ - CO$), 448 ($M^+ - 2CO$), 420 ($M^+ - 3CO$), 392 ($M^+ - 4CO$), 364 ($M^+ - 5CO$), 336 ($M^+ - 6CO$), 280 ($M^+ - 6CO - Fe$), 225 ($M^+ - 6CO - Fe - Mn$). **3**: mp 89–91 °C (decomp.). IR [ν(CO)/cm^{-1}]: 2048s, 2000vs, 1991vs, 1955w, 1945s (br) (cyclohexane). ^{1}H NMR (CD_3COCD_3): δ 7.83 (d, 1 H), 6.29 (t, 1 H), 5.57 (dd, 1 H), 4.95 (t, 1 H), 4.60 (d, 1 H), 4.20 (t, 1 H), 3.81 (m, 1 H), 7.27–7.09 (m, 4 H), 2.32 (s, 3 H), 1.29 (t, 3 H), 3.81 (m, 2 H). *m/z* 490 ($M^+ - CO$), 462 ($M^+ - 2CO$), 434 ($M^+ - 3CO$), 406 ($M^+ - 4CO$), 378 ($M^+ - 5CO$), 350 ($M^+ - 6CO$), 294 ($M^+ - 6CO - Fe$), 239 ($M^+ - 6CO - Fe - Mn$). **4**: mp 30–32 °C (decomp.). IR [ν(CO)/cm^{-1}]: 2060s, 2010vs, 1995vs, 1960w, 1950s (br) (cyclohexane). ^{1}H NMR (CD_3COCD_3): δ 7.84 (d, 1 H), 6.30 (t, 1 H), 5.59 (dd, 1 H), 4.96 (t, 1 H), 4.62 (d, 1 H), 4.22 (t, 1 H), 3.80 (m, 1 H), 7.25–7.16 (m, 4 H), 2.33 (s, 3 H), 1.31 (t, 3 H), 3.80 (m, 2 H). *m/z* 490 ($M^+ - CO$), 462 ($M^+ - 2CO$), 434 ($M^+ - 3CO$), 406 ($M^+ - 4CO$), 478 ($M^+ - 5CO$), 350 ($M^+ - 6CO$), 294 ($M^+ - 6CO - Fe$), 239 ($M^+ - 6CO - Fe - Mn$). **5**: mp 42–44 °C (decomp.). IR [ν(CO)/cm^{-1}]: 2050s, 2001vs, 1993vs, 1958w, 1948s (br) (cyclohexane); ^{1}H NMR (CD_3COCD_3): δ 7.85 (d, 1 H), 6.30 (t, 1 H), 5.59 (dd, 1 H), 4.97 (t, 1 H), 4.60 (d, 1 H), 4.22 (t, 1 H), 3.79 (m, 1 H), 7.37–7.21 (m, 4 H), 2.33 (s, 3 H), 1.31 (t, 3 H), 3.79 (m, 2 H). *m/z* 434 ($M^+ - 3CO$), 406 ($M^+ - 4CO$), 378 ($M^+ - 5CO$), 350 ($M^+ - 6CO$), 294 ($M^+ - 6CO - Fe$), 239 ($M^+ - 6CO - Fe - Mn$).

‡ *Crystal data* for **2**: $C_{22}H_{17}FeMnO_7$, monoclinic, space group $P2_1/n$, a = 6.823(1), b = 26.698(6), c = 11.767(2) Å, β = 91.86(2)°, U = 2142.4(8) Å^3, Z = 4, D_c = 1.563 g cm^{-3}, μ = 13.06 cm^{-1} (Mo-Kα). A total of 3826 unique reflections were collected within 5–50° in the conventional ω–2θ scan mode, of which 2553 observed reflections [$I > 3.00\sigma(I)$] were used in the structure solution (direct methods) and refinement (full-matrix least-squares method) to give final R = 0.031 and R_w = 0.032. CCDC 182/741.

1 J.-B. Chen, G.-X. Lei, W.-H. Xu, Z.-H. Pan, S.-W. Zhang, Z.-Y. Zhang, X.-L. Jin, M.-C. Shao and Y.-Q. Tang, *Organometallics*, 1987, **6**, 2461.
2 J.-B. Chen, D.-S. Li, Y. Yu, Z.-S. Jin, Q.-L. Zhou and G.-C. Wei, *Organometallics*, 1993, **12**, 3885.
3 J.-B. Chen, G.-X. Lei, Z.-H. Pan, Z.-Y. Zhang and Y.-Q. Tang, *J. Chem. Soc., Chem. Commun.*, 1987, 1273.
4 Y. Yu, J.-B. Chen, J. Chen and P.-J. Zheng, *Organometallics*, 1993, **12**, 4731.
5 Y. Yu, J. Sun and J.-B. Chen, *J. Organomet. Chem.*, 1997, **533**, 13.
6 M. J. Bennett, J. L. Pratt, K. A. Simpson, L. K. K. LishingMan and Josef Takats, *J. Am. Chem. Soc.*, 1976, **98**, 4810.
7 J.-B. Chen, J. G. Jin, W.-H. Xu, L.-H. Lai, Z.-Y. Zhang and M.-C. Shao, *Organometallics*, 1987, **6**, 2607.

Received in Cambridge, UK, 11th November 1997; 7/08122G

Typeset and printed by Black Bear Press Limited, Cambridge, England

ChemComm
FEATURE ARTICLE

Asymmetric routes to substituted piperidines

Patrick D. Bailey,† Paula A. Millwood and Peter D. Smith

Department of Chemistry, Heriot-Watt University, Riccarton, Edinburgh, UK EH14 4AS

An overview of the main asymmetric routes to substituted piperidines is presented. A wide range of synthetic strategies have been developed, because of the ubiquitous nature of the piperidine sub-unit in natural products, and because of the biological properties of natural and synthetic piperidine derivatives. This review concentrates on general methodologies that provide enantioselective routes to substituted piperidines, but also includes some specific target syntheses that illustrate the power of the methods that have been developed. The three approaches that have been most successful are: the use of the chiral pool, especially amino acids; the use of reagents that utilise a chiral catalyst; and the use of chiral auxiliaries in the asymmetric formation or derivatisation of the piperidine ring.

Introduction

The piperidine ring system **1** is one of the commonest structural sub-units in natural compounds, as exemplified by structures **2**–**6**. Moreover, piperidine alkaloids (*e.g.* **2**–**6**) and synthetic

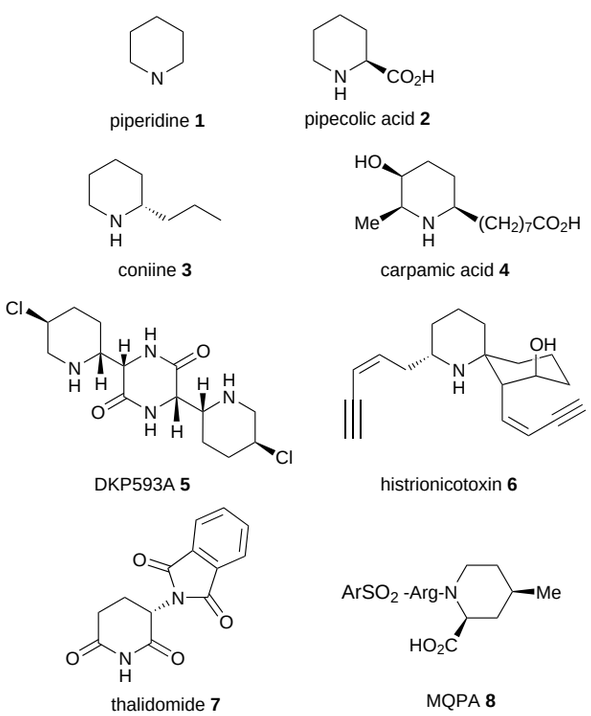

analogues (*e.g.* **7, 8**) are the focus of great interest in the pharmaceutical industry because they exhibit an extensive range of biological activities. The importance of this ring system makes short, versatile, stereocontrolled routes to substituted piperidines of tremendous potential value. This review outlines some of the recent developments in the asymmetric synthesis of piperidine systems;[1] it does not include resolution methods, although these are still very important, but focusses on the use of the chiral pool, chiral reagents and chiral auxiliaries. The examples selected are those that, in the view of the authors, offer the most reliable and flexible asymmetric routes to piperidines, and/or have the greatest potential for doing so.

Asymmetry from the chiral pool

Amino acids

Amino acids are particularly useful precursors for the asymmetric synthesis of piperidine alkaloids for several reasons. Firstly, many amino acids are cheap and homochiral; secondly, they already contain the nitrogen of the alkaloid target; thirdly, they usually lead to 2-substituted piperidines, which is the commonest position for substitution.

Lysine. Lysine is the biosynthetic precursor for many piperidine alkaloids, but there are two main problems with its use in a laboratory synthesis; firstly, the amino groups need to be differentiated and (one of them) converted into a leaving group; secondly, it is not easy to introduce additional substitution (other than the existing carboxylic acid of lysine) into the piperidine ring. Enantiomerically pure forms of pipecolic acid have been prepared from lysine *via* several synthetic pathways. Fujii *et al.* have reported a six step synthesis of L-pipecolic acid in 60% overall yield starting from L-lysine.[2] However, L-pipecolic acid has also been prepared in 39% yield in a one step reaction of L-lysine with disodium nitrosyl pentacyanoferrate(II).[3]

The 6-methoxypipecolate derivative **10**, which is of biological interest, can be synthesised from the lysine derivative **9** by electrochemical oxidation at a platinum electrode.[4] Subsequent conversion of the *cis* isomer into enantiomerically pure (−)-sedamine **12** and (−)-allosedamine **13** was achieved in five further steps as outlined in Scheme 1. (+)-*N*-Methylconiine **14** has also been synthesised from **10** by Shono *et al.*; exclusive formation of the *cis*-disubstituted intermediate **11** was followed by saponification, anodic decarboxylation and reduction to afford the pure enantiomer in good yield (Scheme 1).[5]

Several other methods for the preparation of piperidine derivatives from lysine and various lysine analogues have been

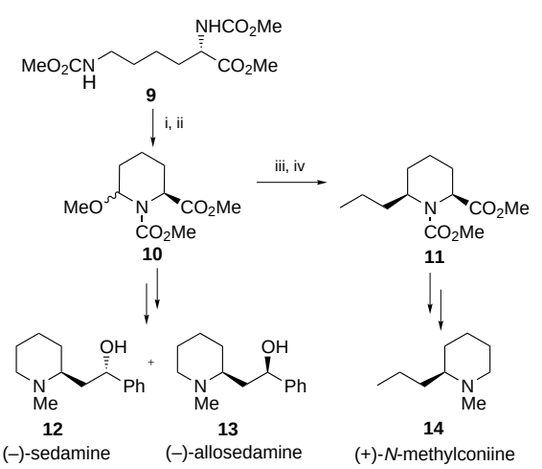

Scheme 1 *Reagents and conditions*: i, −2e⁻, MeOH; ii, MeOH, H_2SO_4; iii, CH_2=$CHCH_2SiMe_3$, $TiCl_4$; iv, H_2, Pd–C

reported,[6,7] including the use of an immobilised analogue of lysine to access piperidine derivatives attached to a polymeric support, providing the opportunity for preparing combinatorial libraries.[8]

Glutamic acid/glutamine. Glutamic and aspartic acids are attractive chiral building blocks for piperidine targets because the side-chain functionality can be readily derivatised. In both cases, additional carbon(s) need to be introduced, and this can be exploited as a means of introducing additional substituents into the piperidine ring. The side-chain carboxylic acid group is usually retained as a functionalised position, thus providing access to 5-substituted pipecolic acid derivatives in the case of glutamic acid.

For example, Bailey *et al.* have made use of L-glutamic acid in a stereo- and enantio-specific synthesis of the naturally occurring alkaloid, *cis*-5-hydroxy-L-pipecolic acid **20**.[9] The dense functionalisation led to a number of synthetic problems, but treatment of the trialkylsilyl-protected alcohol **18** with NaH in DMF at 85 °C induced an intramolecular cyclisation to form the piperidine unit in 60% yield (Scheme 2).

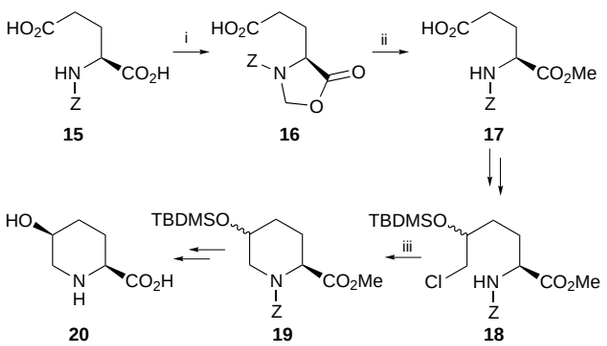

Scheme 2 *Reagents and conditions*: i, $(CH_2O)_n$, TsOH, benzene, reflux (94%); ii, NaOMe, MeOH, reflux (95%); iii, NaH, DMF, 85 °C (60%)

This route has been subsequently improved in two ways. Firstly, the problematic differentiation of the two carboxylic acid groups in glutamic acid has been overcome by selective hydrolysis of glutamine using *tert*-butyl nitrite, and the development of a rhodium(II) catalyzed carbene N–H insertion reaction has led to a short and efficient route to the piperidine ring. The substitution pattern is amenable to the synthesis of 2,5-disubstituted targets such as DKP593A **5**, and the monomer of this compound has been prepared in protected form (Scheme 3).[10]

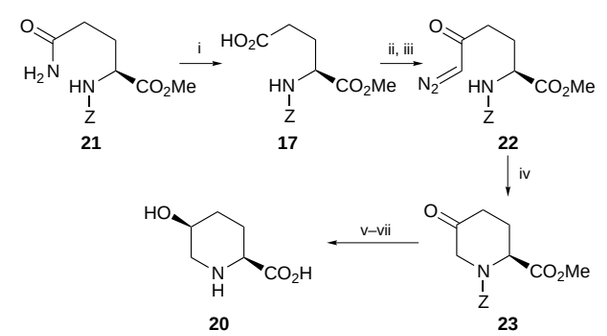

Scheme 3 *Reagents and conditions:* i, Bu^{t}ONO, MeCN, reflux (74%); ii, EtOCOCl; iii, CH_2N_2, Et_2O; iv, $[Rh(OAc)_2]_2$, benzene, reflux; v, $NaBH_4$, MeOH; vi, HO^- (aq); vii, H_2, Pd–C

The α-chiral centre can also be sacrificed after using it to control the stereochemistry elsewhere, such as in the synthesis of (*S*)- or (*R*)-3-hydroxypiperidine from D- or L-glutamic acid,[11] or in the formation of piperidines (and pyrrolidines) from glutamine.[12]

Aspartic acid/asparagine. In the same way that glutamic acid provides a route to 5-substituted pipecolic acids, aspartic acid can be used as a chiral precursor to 4-substituted pipecolic acids. For example, a range of 2,6-disubstituted piperidines can be prepared by extending the side-chain carboxylic acid group of Asp, using the attack of a sulfonamide on a ketone to effect the cyclisation.[12]

Differentiation of the α- and β-carboxylic groups in Asp can be tricky, but they were neatly distinguished in work by Golubev *et al. via* the formation of an oxazolidinone, which could be readily transformed into the hexafluoroacetone protected enone **25**.[13] A Lewis acid catalysed intramolecular Michael addition, followed by deprotection of the vicinal amino and carboxylic functions, gave the 4-oxo-L-pipecolic acid **26** which served as an intermediate in the synthesis of *cis*- and *trans*-4-hydroxy-L-pipecolates (Scheme 4).

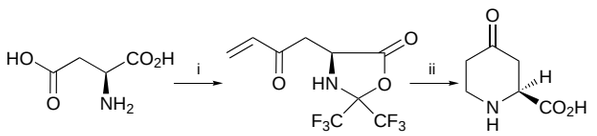

Scheme 4 *Reagents and conditions*: i, hexafluoroacetone, then $SOCl_2$, Δ, then CH_2=$CHSnMe_3$, $BnPd(PPh_3)_2Cl$, dimethoxyethane; ii, $BF_3{\cdot}OEt_2$, benzene, Δ, then H_2O–Pr^{i}OH

Using the side-chain of asparagine in a completely different way, Christie converted the amide of asparagine into a nitrile, and used this to construct the piperidine ring in an asymmetric synthesis of vincamine **31**, a known hypertensive agent.[12] Thus, L-asparagine was converted into the iodide **29**, which was cyclised in the presence of LDA and ethyl iodide to afford the piperidine derivative **30** equipped with two chiral centres at positions 2 and 3. Apovincamine, a known precursor to vincamine **31**, was synthesised from **30** in six further steps (Scheme 5).

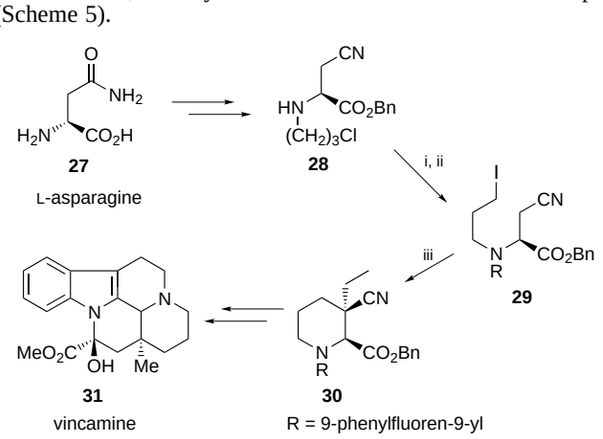

Scheme 5 *Reagents and conditions*: i, $NaHCO_3$, CH_2Cl_2, 9-phenylfluoren-9-yl bromide, K_3PO_4, $Pb(NO_3)_2$, MeCN; ii, NaI, MeCN, Δ; iii, LDA (excess), EtI (excess), −78 °C

Other amino acids. The amino acids discussed above all utilise the functionalised side-chains to become part of the piperidine ring. It is also possible to use both the α-amino and α-carboxylic acid groups of amino acids to form piperidine rings, in which case the amino acid side-chain becomes a piperidino subsituent. In such cases, the amino acid must be chosen so that the side-chain matches the target molecule. For example, starting from L-alanine, Angle *et al.* completed a nine step synthesis of (+)-monomorine, with the key step in the synthesis involving a Claisen rearrangement.[14]

Sugars

Sugars have been used extensively to prepare polyhydroxylated piperidines; these aza-analogues of pyranose sugars often have potent enzyme inhibitory properties, and are thus of medicinal

importance. There is clearly a wide range of sugar building blocks available that might provide much of the functionalisation and stereochemistry, and the one selected depends on the specific target. The major challenge is to successfully differentiate the hydroxy groups so that one of them can be converted into an amino group, and a second one can be converted into a leaving group. This field has been dominated by Fleet's group, and he has developed a number of elegant tactics for achieving the necessary selectivity for the synthesis of polyhydroxylated targets.[15] Less oxygenated targets can also be accessed relatively quickly, as exemplified by the work of Tadano *et al.*[16]

Other chiral building blocks

As many alkaloids incorporate one or more 'isoprene' units within their structure, terpenes are sometimes attractive chiral building blocks. For example, Honda *et al.* developed an efficient stereoselective route to nuphar piperidine alkaloids starting from the readily available chiral monoterpenes, (−)- or (+)-carvone;[17] stereoselective construction of the piperidine ring was achieved *via* an intramolecular aza-Wittig cyclisation. Many other chiral building blocks are specific to the target in question, rather than providing general routes to substituted piperidines; for example, the chiral epoxide **32a** allows a short efficient synthesis of the C_2-symmetric target (−)-2,6-lupetidine **35** (Scheme 6)[18] and elaboration of the oxygenated analogue **34b** might provide access to other C_2-symmetric piperidine derivatives.

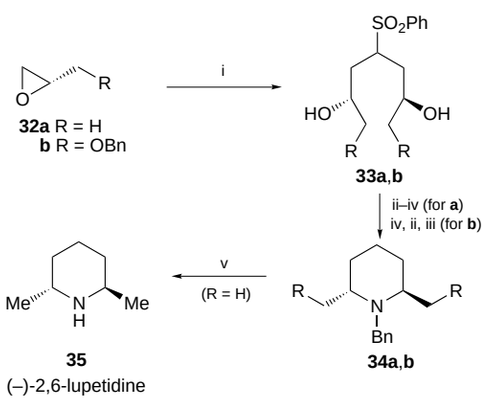

Scheme 6 *Reagents and conditions*: i, MesPh–BuLi; ii, TsCl, Py; iii, $PhNH_2$; iv, Na–Hg; v, Pd–C

Use of chiral reagents

There are now many chiral reagents that induce asymmetry, and some of these have found widespread applicability in the synthesis of substituted piperidines. In most of the examples below, the reagent utilises a chiral catalyst, with obvious economic advantages.

Sharpless asymmetric dihydroxylation

This procedure has been used quite widely, as exemplified by the asymmetric syntheses of *trans*-2,6-disubstituted piperidines, (+)-epidihydropinidine and (+)-solenopsin A, reported by Takahata *et al.*[19] The asymmetric dihydroxylation (ADH) reaction was exploited even more effectively by Takahata *et al.*, using the ADH reaction to provide access to the piperidine ring, and then employing it again to generate the dihydroxylated targets **40** and **41**; the ADmix control of absolute stereochemistry was able to override any diastereocontrol for dihydroxylation in the penultimate step (Scheme 7).[20]

Sharpless's more recent asymmetric aminohydroxylation procedure is certain to be used extensively for the synthesis of piperidine targets.[21]

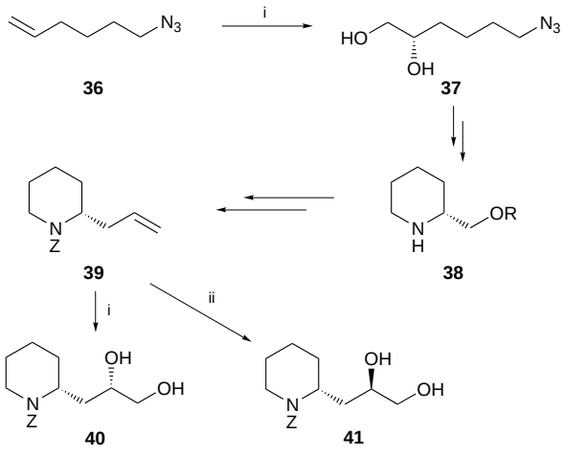

Scheme 7 *Reagents and conditions*: i, AD Mix-α; ii, AD Mix-β

Sharpless asymmetric epoxidation

The Sharpless asymmetric epoxidation reaction is now a well-established and reliable procedure for the epoxidation of allylic alcohols, and there are many asymmetric syntheses of piperidine targets that exploit the reaction. One recent example nicely demonstrates how Sharpless asymmetric epoxidation (SAE) can be used to control (ultimately) the stereochemistry of three substituents on the piperidine ring.[22] A much more general approach is demonstrated by Ahman and Somfai, who prepared the chiral vinylaziridine **43** (> 95% ee) in a straightforward manner from the known epoxy alcohol **42**, itself produced *via* Sharpless asymmetric epoxidation. They showed that these types of vinylaziridines undergo an aza-[2,3]-Wittig rearrangement yielding the corresponding *cis*-2,6-disubstituted tetrahydropyridines **44** as single diastereoisomers (Scheme 8).[23] This methodology has been extended, allowing access to many indolizidine and piperidine alkaloids.

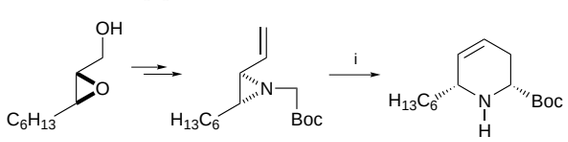

Scheme 8 *Reagents and conditions*: i, LDA, THF

Less conventional is the use of SAE conditions to effect kinetic resolution of the racemic furanyl sulfonamide **45**, which provided asymmetric routes to both enantiomers of **47** (Scheme 9).[24]

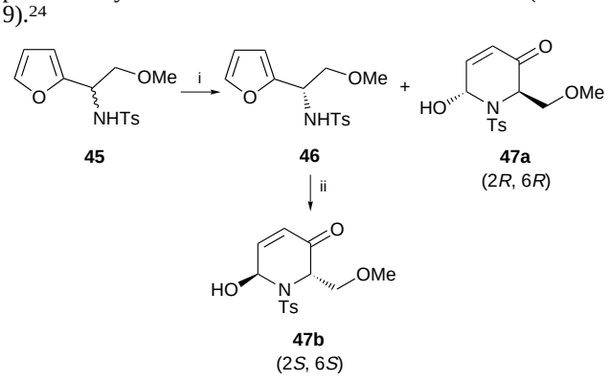

Scheme 9 *Reagents and conditions*: i, $Ti(OPr^i)_4$, L-(+)-DIPT, Bu^tOOH, SiO_2, CaH_2; ii, MCPBA

Chiral bases

Michael reactions using enolate nucleophiles can sometimes occur enantioselectively if triggered by a chiral base. For

example, the readily available achiral compound **49** has been shown to undergo an asymmetric intramolecular Michael reaction with the chiral base, (+)-1-phenylethylamine, to give the optically active cycloadduct **50** in good yield and 80% ee (Scheme 10).[25] This versatile chiral building block has been used in the synthesis of various alkaloids including kainic acid, (−)-tetrahydroalstonine and (−)-ajmalicine **51**.

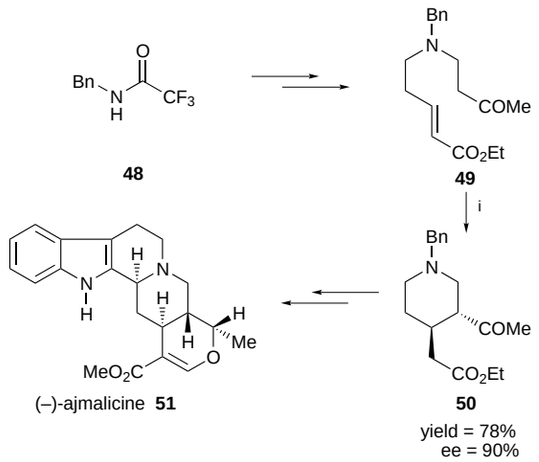

Scheme 10 *Reagents and conditions*: i, (+)-1-phenylethylamine, THF

Chiral boron reagents

The boron reagents developed by Brown are so efficient that their use in the asymmetric synthesis of substituted piperidines was inevitable. For example, the allylB(Ipc)$_2$ reagent can be reacted with a wide range of aldehydes, to provide homoallyl alcohols **53**; these can be elaborated to the diols **54**, from which the 2-substituted piperidines **55** are readily prepared. Not only does this provide a simple route to diverse 2-substituted piperidines, but either enantiomeric series is accessible by use of appropriate chiral boranes (Scheme 11).[26]

The use of chiral borane reagents as catalysts has been only moderately successful, but used in conjunction with a chiral auxiliary, the matched reagents can lead to very high asymmetric induction—see the section concerning Diels–Alder reactions of imines.

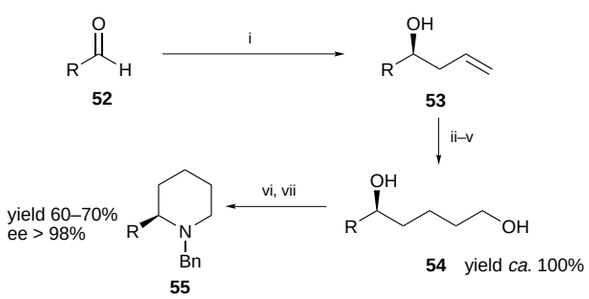

Scheme 11 *Reagents and conditions*: i, Ipc$_2$BAll, −100 °C; ii, BH_3·DMS; iii, MeOH; iv, $BrCH_2Cl$, −78 °C, then BuLi; v, H_2O_2–OH^-; vi, MsCl, NEt_3; vii, $BnNH_2$

Chiral auxiliaries

Chiral auxiliaries have been used with great success in the synthesis of piperidine ring systems. Perhaps the three most general and widely used methods are: the CN(*R,S*) method, the use of chiral lactams, and aza-Diels–Alder methodology.

The CN(R,S) *method*

The CN(*R,S*) method aptly derives its name from the Institut de Chemie des Substances Naturelles du C.N.R.S., where Husson *et al.* developed the use of chiral 2-cyano-6-oxazolopiperidine **59** for the asymmetric synthesis of functionalised piperidines; **59** can be readily obtained from a 'one-pot' condensation reaction between (−)-phenylglycinol, gluteraldehyde and KCN under acidic conditions (Scheme 12).

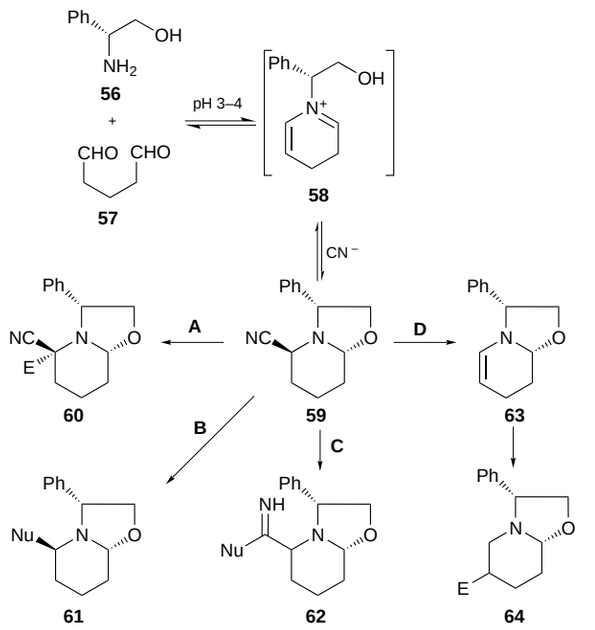

Scheme 12

The CN(*R,S*) method allows access to a wide range of 2,6-disubstituted piperidines of very high optical purity, exploiting the high functionality and facial selectivity in **59**. It possesses two non-equivalent reactive sites on the piperidine ring system; an α-amino nitrile at the C-2 position and an α-amino ether at the C-6 position. As summarised in Scheme 12, differential chemo- and stereo-selective reactions can be achieved at several positions, allowing access to a wide range of piperidine derivatives: (i) electrophilic attack at the C-2 position (route A); (ii) nucleophilic attack at the C-2 position (route B); (iii) attack at the cyano group (route C); and (iv) electrophilic attack at the C-3 position (route D).

To demonstrate the versatility of the CN(*R,S*) method, Husson *et al.* have completed the syntheses of numerous enantiopure piperidine alkaloids which exhibit biological activity including monomorine, perhydrohistrionicotoxin, various analogues of podophyllotoxin and cephalotaxine.

For example the α-amino nitrile anion, generated by treatment of **59** with LDA, can be alkylated by reaction with alkyl halides. Elimination of the cyano group in the presence of NaH results in the formation of a single diastereoisomer; stereoelectronic effects are responsible for the addition of hydride to the *si* face, so that only *cis* diastereoisomers are formed. This has been illustrated in the synthesis of (−)-coniine[27] (Scheme 13).

Alternatively, the nitrile can itself be incorporated into the target molecule, as in a four step synthesis of (*S*)-(−)-pipecolic acid **2** from the synthon **59**.[28] The cyanide was first converted into the ethyl ester, and reduction with Zn(BH$_4$)$_2$ gave the lactone **66** as a mixture of diastereoisomers. A deprotonation and reprotonation procedure converted **66** into a single diastereoisomer, from which (*S*)-(−)-pipecolic acid was subsequently isolated in 47% overall yield by a simple hydrogenation under acidic conditions (Scheme 20). The phosphonic acid analogue of **2** can also be accessed using the CN(*R,S*) method, as indicated in Scheme 13.[29]

Chiral lactams

The use of chiral lactams has been developed most effectively by Meyer's group,[30] and this approach has wide applicability to

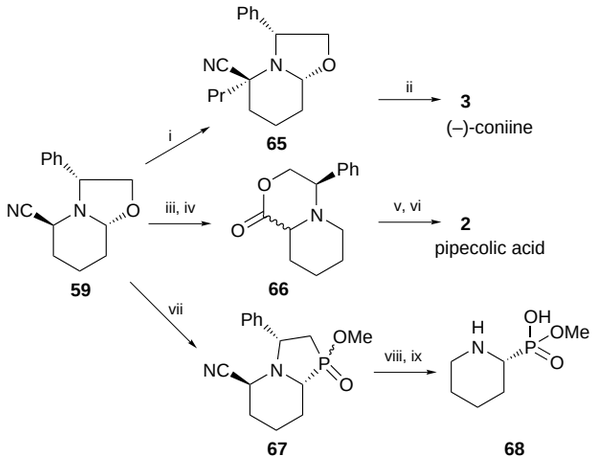

Scheme 13 *Reagents and conditions*: i, LDA, THF, −78 °C, then PrBr; ii, $NaBH_4$, then H_2SO_4; iii, HCl–EtOH, SiO_2, PhMe; iv, $Zn(BH_4)_2$, Et_2O; v, LDA, THF, AcOH; vi, H_2, Pd–C, HCl–MeOH; vii, $P(OMe)_3$–$SnCl_4$; viii, $NaBH_3CN$; ix, H_2, Pd–C

the synthesis of substituted piperidines, as indicated in Scheme 14. In particular: (i) the enolate of lactam **69** can be alkylated at the 3-position (A); (ii) the *N*-acyliminium intermediate allows introduction of C-6 substituents (B); and (iii) the amide carbonyl can be further functionalised (C). Overall, this provides access to 2,3,6-trisubstituted piperidines with excellent diastereo- and enantio-control.

In the course of their endeavours towards starting materials for the asymmetric synthesis of piperidine derivatives, Royer and Husson were also able to prepare **69** and epimeric **70** from **59**, as shown in Scheme 14.[31]

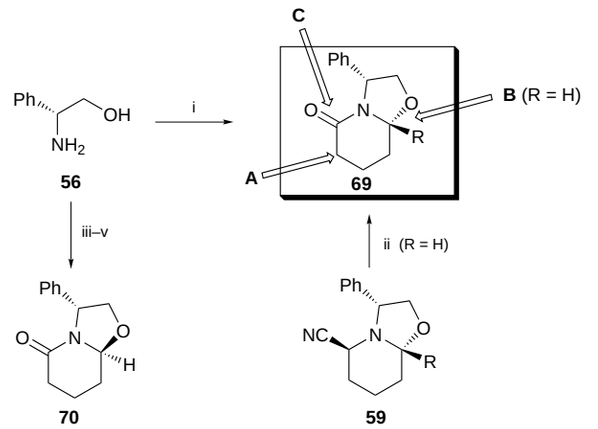

Scheme 14 *Reagents and conditions*: i, $RCO(CH_2)_3CO_2H$; ii, LDA, −78 °C, then O_2; iii, glutaric anhydride, AcCl; iv, $NaBH_4$; v, HCl–MeOH

Meyers has demonstrated the flexibility of his methodology in numerous syntheses.[30] For example, his approach readily allows access to 2,6-disubstituted piperidines (see Scheme 15),[32] whilst reduction of the (thio)lactam clearly provides a simple route to 2-substituted piperidines.

Aza-Diels–Alder reactions

The aza-Diels–Alder reaction has the potential to be a very effective method for the preparation of substituted piperidines.[33] The reaction potentially allows the rapid construction of quite complex piperidines, functionalised or derivatised at various positions, and there is the possibility of regio-, diastereo- and enantio-selectivity in the reaction. The aza-Diels–Alder reaction has therefore provided the key step in numerous syntheses of these compounds. Nevertheless, there

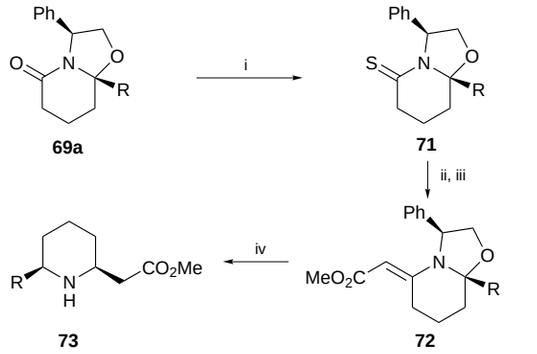

Scheme 15 *Reagents and conditions*: i, Belleau's reagent; ii, $BrCH_2CO_2Me$; iii, $P(OMe)_3$; iv, 3 atm. H_2, $Pd(OH)_2$–C

are problems associated with all of the possible aza-Diels–Alder routes to piperidines, and only recently has substantial progress been made concerning the general applicability of these reactions. The three basic variations of the aza-Diels–Alder reaction that can be used to form piperidine derivatives are shown in Scheme 16. An excellent recent review on 'Asymmetric Hetero-Diels–Alder Reactions' by Waldmann includes a valuable summary of asymmetric aza-Diels–Alder chemistry.[34]

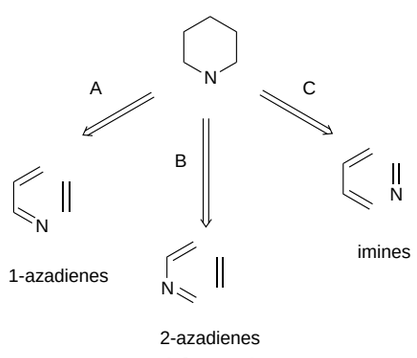

Scheme 16

1-Azadienes (route A). 1-Azadienes have proved particularly capricious in (4 + 2)π cycloaddition reactions, with competing imine chemistry often thwarting the intended reaction, and although chiral auxiliaries can be attached to the nitrogen atom, this has not proved to be a major asymmetric route to substituted piperidines.

2-Azadienes (route B). 2-Azadienes have also been extensively studied as starting materials for the synthesis of piperidine-based compounds *via* the Diels–Alder reaction. Unfortunately, general asymmetric versions of these reactions have been elusive, as there is no simple way by which a removable chiral auxiliary can be attached.

Imines as dienophiles (route C). The Diels–Alder reaction of imines or iminium salts with carbon dienes is probably the most efficient route to substituted piperidines reported to date. Intramolecular cycloadditions of *N*-acyl imines have been particularly useful in the synthesis of several natural products, including lupinine **76** and epilupinine **77** (Scheme 17).[35]

The chiral imine **79** can be readily produced by condensation of ethyl glyoxylate with 1-phenylethylamine, and the Diels–Alder reaction of **79** with a number of dienes has been investigated (Scheme 18).[36]

Bailey *et al.* have proposed a mechanism which explains why catalytic amounts of water are necessary to effect the cycloaddition under acidic conditions. It was suggested that intermolecular hydrogen-bonding between water and the imine formed a seven membered ring complex (Fig. 1) and that the diene approached this π-stabilised iminium intermediate from

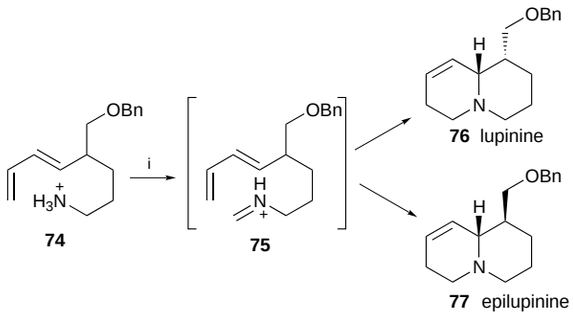

Scheme 17 *Reagents and conditions*: i, HCHO

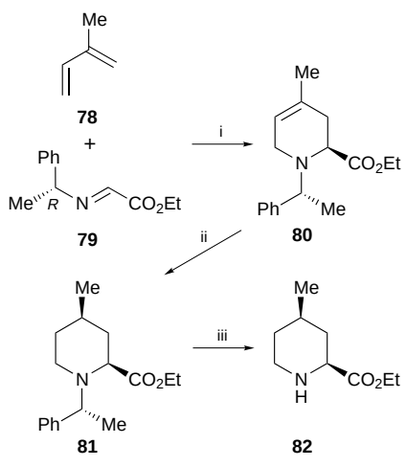

Scheme 18 *Reagents and conditions*: i, DMF, TFA (1 equiv.), H_2O (cat), 25 °C; ii, H_2, Pt–C, EtOAc; iii, H_2, $Pd(OH)_2$–C, EtOH

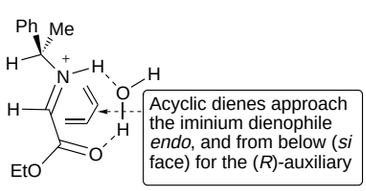

Fig. 1 Predictive model for the outcome of the aza-Diels–Alder reaction between acyclic dienes and **79**

the *si* face due to steric preferences induced by the chiral *N*-auxiliary.[37]

Stella and co-workers devised an alternative set of conditions in which the Diels–Alder reaction proceeded in the presence of TFA and $BF_3{\cdot}OEt_2$ in CH_2Cl_2 at low temperature. Application of these conditions in the cycloaddition of the chiral 1-phenylethylimine of methyl glyoxylate with cyclopentadiene led to total face selectivity and up to 98% *exo* selectivity in the cycloadduct, but extension to acyclic dienes was less successful.[38]

The Diels–Alder reaction of imines with *N*-chiral auxiliaries demonstrates that both high *endo*/*exo* selectivity and asymmetric induction can be achieved to allow access to a range of enantiopure piperidine derivatives. Moreover, the chiral Lewis acid **83**, derived from (*R*)-binaphthol and triphenyl borate, has been shown to catalyse the Diels–Alder reaction between chiral imines and Danishefsky's diene **84** with a very high degree of asymmetric induction (Scheme 19).[39] The use of lanthanide Lewis acid catalysts has been recently published in aza-Diels–Alder reactions of an imine derived from a chiral aldehyde,[40] and the addition of chiral ligands to these reactions has given very encouraging preliminary results—this may well turn out to be one of the most efficient and economical asymmetric routes to chiral piperidines.

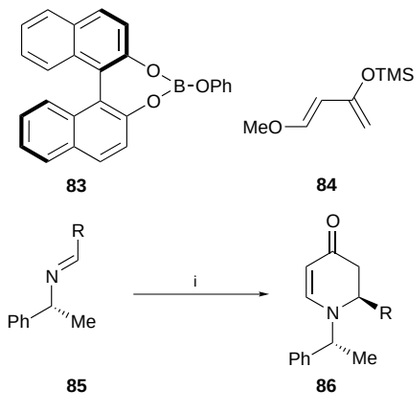

Scheme 19 *Reagents and conditiosn*: i, **83**, **84**, CH_2Cl_2, −78 °C

Holmes has investigated the participation of *N*-*p*-tolylsulfonyl imines **87**, carrying an chiral ester auxiliary, in the aza-Diels–Alder reaction with cyclopentadiene (Scheme 20).[41] The source of chirality on the ester moiety of the imines was from glyoxylate ester derivatives of (*R*)-pantolactone and ethyl (*S*)-lactate, which are known to coordinate Lewis acids in asymmetric cycloaddition reactions. The best results were obtained using Et_2AlCl in toluene at −78 °C. Use of the (*S*)-lactate auxiliary led to the formation of **88a** as the major diastereoisomer (76% de) whereas (*R*)-pantolactone predominantly yielded the diastereoisomer **88b** (70% de).

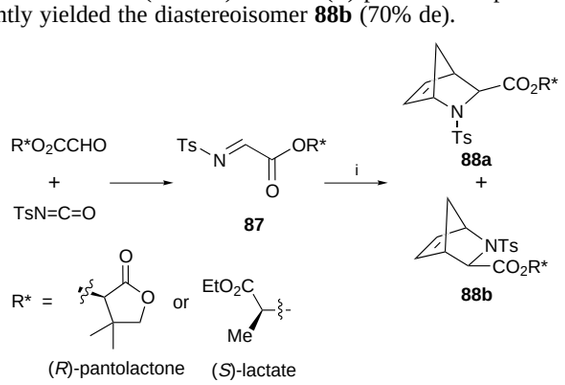

Scheme 20 *Reagents and conditions*: i, cyclopentadiene, Et_2AlCl, toluene, −78 °C

Several groups had sought to prepare the cyclic imines such as **90**, for which Diels–Alder reactions ought to proceed with excellent diastereo- (and hence enantio-)control. Routes in which the imine should have been generated by cyclisation of δ-amino aldehyde derivatives were singularly unsuccessful, but Harwood's group has successfully prepared **90** *via* an oxidative route, and the enantiocontrol in its aza-Diels–Alder reactions is (as expected) superb (Scheme 21).[42] The modest overall yield, and the cost of (unrecoverable) (*R*)- or (*S*)-phenylglycinol are limitations, but this method does provide the highest enantiocontrol from a single auxiliary, and (provided the reaction is sufficiently general) it offers to be a very attractive asymmetric route to a wide range of substituted piperidines.

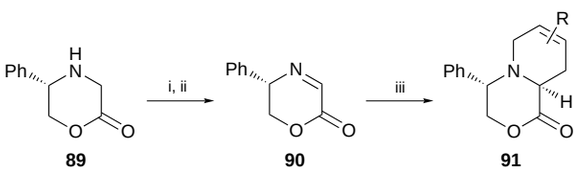

Scheme 21 *Reagents and conditions*: i, NBS; ii, propylene oxide; iii, substituted butadienes, TFA or AcOH (*ca.* 1.5 equiv.), $BF_3{\cdot}OEt_2$, −78 °C (yield *ca.* 35% from **89**)

Returning to the readily accessed glyoxylate imines, the groups of Bailey and Holmes were able to combine their

auxiliaries and explore the effect of matched and mismatched auxiliaries on the nitrogen and the ester moieties of the imine in aza-Diels–Alder reactions.[43] The imines derived from alcohols (*R*)-pantolactone, (−)-borneol and (−)-8-phenylmenthol in combination with (*R*)- and (*S*)-1-phenylethyl *N*-auxiliaries were studied (imines **92**–**94**) using 2,3-dimethylbutadiene as the 4π partner.

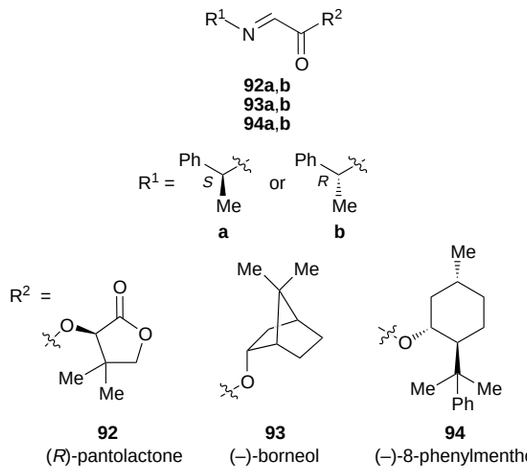

Optimum results were recorded for the Diels–Alder reaction using the imine PhMeCHN=CHCO$_2$PhMen* **94a** bearing matched auxiliaries, and the reaction provided single stereoisomeric products with a range of dienes. The reactions also occurred with complete regiospecificity in all cases, and acyclic dienes added *via* an *endo* transition state, whilst cyclic dienes yielded the *exo* adducts. Detachment of the (recoverable) ester auxiliary was achieved by saponification, and removal of the (cheap) 1-phenylethyl auxiliary could be achieved by catalytic hydrogenation, allowing access to piperidines of known absolute stereochemistry.

Other chiral auxiliaries

There are many other examples of syntheses involving chiral auxiliaries for the synthesis of piperidines, although most have yet to demonstrate that they are as reliable and versatile as the general methods outlined above. Nevertheless, the wide range of other approaches may provide the best method for a specific target. We have selected a dozen or so examples to illustrate the types of methodology available.

Oppolozer's group has led the way in the use of chiral sultams in asymmetric synthesis, and their methodology provides access to 2,6-*trans*-dialkylated piperidines.[44] Their approach can also be adapted to other substitution patterns, such as the 2,5-disubstituted piperidine (+)-pseudoconhydrine **98**, which has been prepared *via* a versatile deoxygenative decarboxylation–imine trapping route (Scheme 22). In most of the sultam work, the moderately high asymmetric induction can be improved by recrystallization, and the chiral sultam auxiliary can be efficiently recovered part way through the synthesis.

A similar camphor-like auxiliary has been developed by Wanner's group, providing access to 2-substituted piperidines.[45] The key step involves the conversion of an *N*-acyl 2,3-didehydropiperidine into an acyliminium derivative, which is susceptible to nucleophilic attack with high stereocontrol.

Alkylation of acyliminium intermediates has also been achieved, using a C_2-symmetric chiral hydrazone derivative as the source of asymmetry.[46] Hydrazones have also been used by Enders and Jegelka in a further development of RAMP/SAMP methodology, although the approach perhaps lacks generality.[47]

A rather unusual variation of the SAMP/RAMP auxiliary uses a cyclic hydrazine, and involves C–O bond cleavage that is reminiscent of Meyer's chiral lactam work.[48]

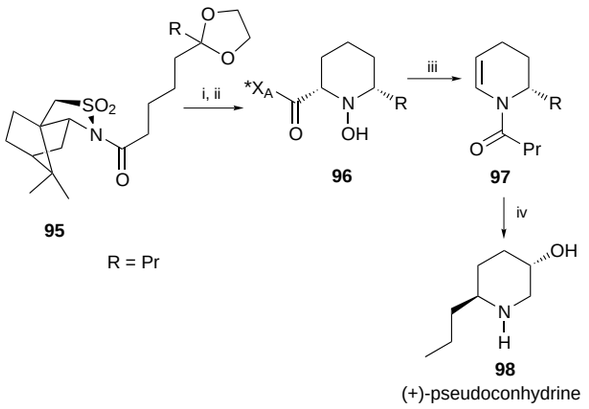

Scheme 22 *Reagents and conditions*: i, NaN(SiMe$_3$)$_2$, 1-chloro-1-nitrocyclohexane, H_3O^+; ii, $NaCNBH_3$; iii, NaH, 110 °C, PrC(O)X, base; iv, $BH_3.SMe_2$, THF, then H_2O_2, NaOH, then Pd(OH)$_2$–C, MeOH

The enantiospecific reduction of imines can be used to gain access to piperidines, as demonstrated by Moody's group.[49] The approach should be quite flexible, as a variety of alkyl derivatives could be introduced during the synthesis to yield a range of 2,6-disubstituted piperidines.

Using well-established auxiliaries, several groups have developed quite general asymmetric routes to substituted piperidines. For example, Agami *et al.* utilised an intramolecular ene-iminium cyclisation in which stereoselective control was exerted *via* a morpholinone auxiliary;[50] this gave access to *cis*-2,4-disubstituted piperidines, in which the solvent provided the nucleophile stereospecifically. Using the ephedrine auxiliary, hetero-Diels–Alder chemistry has also been used to gain rapid access to a linear piperidine precursor; although the stereocontrol was modest, the minor diastereoisomer was readily removed, and the second (and final) step provided 5-hydroxy-2-methylpiperidine as a single enantiomer, with full recovery of the auxiliary.[51] The aza-annulation of enamines is another general approach,[52] and asymmetric versions have been developed. In contrast, Jones' imidazoline chiral auxiliary effects complete stereocontrol, and provides access to a wide range of 2-substituted piperidines, but the auxiliary is lost upon final deprotection.[53] Finally, Meyer's formamidine chiral auxiliary, which labilises the proton α to nitrogen, can be used in the synthesis of piperidines.[54]

Conclusions

The huge amount of work on the synthesis of piperidines testifies to their importance. However, there are only a few really concise approaches that provide access to a wide range of substitution patterns. If 2-substituted piperidines are required, then there are many possible synthetic strategies. But for more complex targets, three main options dominate the literature: (i) a tailor-made synthesis using a chiral pool precursor (*e.g.* an amino acid or a sugar); (ii) the construction of a linear precursor using the best asymmetric reagents available (*e.g.* chiral AD-Mix or borane reagents), although such syntheses are often long; and (iii) the use of a chiral auxiliary to control the construction or derivatisation of a piperidine derivative. The last approach offers the potential of short, flexible, highly stereospecific syntheses, despite some limitations. The top methods are the CN(*RS*) approach, the use of Meyers' bicyclic lactam chemistry, and aza-Diels–Alder reactions.

Despite much success, the apparently simple piperidine ring system remains a demanding challenge for synthetic chemists, and there is still enormous scope for improvement. It seems certain the the biological properties of substituted piperidines will ensure that synthetic work on them continues apace.

Acknowledgements

We thank Quintiles for financial support towards an MPhil studentship (for P. A. M.) and a PhD studentship (to P. D. S.).

Patrick D. Bailey was born in 1959, and carried out his MA and DPhil at the University of Oxford, before taking up a lectureship at the University of York in 1983, and held a Yorkshire Cancer Research Campaign career development award from 1986–1991. He moved to Heriot-Watt University in 1993, to take up the Chair of Organic Chemistry, and was awarded the Zeneca Organic Chemist Researcher prize in 1994. His research interests are focussed on asymmetric synthesis of *N*-heterocycles, and the synthesis and properties of unusual peptides.

Paula A. Millwood was born in 1972, and carried out her BSc at the University of Strathclyde. She carried out an MPhil at Heriot-Watt University in 1995/96, working on aza-Diels–Alder reactions.

Peter D. Smith was born in 1972, and carried out his BSc at the University of Glasgow. After two years working with Zeneca Agrochemicals at Jealott's Hill, he returned to Scotland in 1996 to carry out a PhD at Heriot-Watt University on aza-Diels–Alder chemistry.

Notes and References

† E-mail: p.d.bailey@hw.ac.uk

1 For a recent review of the synthesis of saturated nitrogen heterocyles, see A. Nadin, *Contemp. Org. Synth*., 1997, **4**, 387.
2 T. Fujii and M. Miyoshi, *Bull. Chem. Soc. Jpn.*, 1975, 1341.
3 L. Kisfaludy and F. Korenczki, *Synthesis*, 1982, 163.
4 K. Irie, K. Aoe, T. Tanaka and S. Saito, *J. Chem. Soc., Chem. Commun.*, 1985, **10**, 633.
5 T. Shono, Y. Matsumura, K. Tsubata and K. Uchida, *J. Org. Chem.*, 1986, **51**, 2590.
6 S. A. Hermitage and M. Maloney, *Tetrahedron: Asymmetry*, 1994, **5**, 1463.
7 B. Ohtani, S. Tsuru, S. Nishimoto, T. Kagiya and K. Izawa *J. Org. Chem.*, 1990, **55**, 5551.
8 P. J. Murray and I. D. Starkey, *Tetrahedron Lett.*, 1996, **37**, 1875.
9 P. D. Bailey and J. S. Bryans, *Tetrahedron Lett.*, 1988, **29**, 2231.
10 D. R. Adams, P. D. Bailey, I. D. Collier, J. D. Heffernan and S. Stokes, *Chem. Commun.*, 1996, 349.
11 N. Huh and C. M. Thompson, *Tetrahedron*, 1995, **51**, 5935.
12 B. D. Christie and H. Rapoport, *J. Org. Chem.*, 1985, **50**, 1239.
13 A. Golubev, N. Sewald and K. Berger, *Tetrahedron Lett.*, 1995, **36**, 2037.
14 S. R. Angle and J. G. Breitenbucher, *Tetrahedron Lett.*, 1993, **34**, 3985.
15 For example, B. P. Bashyal, H.-F. Chow, L. E. Fellows and G. W. J. Fleet, *Tetrahedron*, 1987, **43**, 415.
16 K. Tadano, K. Takao, Y. Nigawara, E. Nishino, I. Takagi, K. Maeda and S. Ogawa, *Synlett*, 1993, **8**, 565.
17 T. Honda, F. Ishikawa and S. Yamane, *J. Chem. Soc., Chem. Commun.*, 1994, 499.
18 S. Najdi and M. J. Kurth, *Tetrahedron Lett.*, 1990, **31**, 3279.
19 H. Takahata, K. Inose, N. Araya and T. Momose, *Heterocycles*, 1994, **38**, 1961.
20 H. Takahata, M. Kubota and T. Momose, *Tetrahedron Lett.*, 1997, **38**, 3451.
21 G. Li, H.-T. Chang and K. B. Sharpless, *Angew. Chem., Int. Ed. Engl.*, 1996, **35**, 451.
22 Y. Hirai, J. Watanabe, T. Nozaki, H. Yokoyama and S. Yamaguchi, *J. Org. Chem.*, 1997, **62**, 776.
23 J. Ahman and P. Somfai, *J. Am. Chem. Soc.*, 1994, **116**, 9781.
24 Y.-M. Xu and W.-S. Zhou, *J. Chem. Soc., Perkin Trans. 1*, 1997, 741.
25 Y. Hirai, T. Terada and T. Yamazaki, *J. Am. Chem. Soc.*, 1988, **110**, 958.
26 T. Nguyen, D. Sherman, D. Ball, M. Solow and B. Singaram, *Tetrahedron: Asymmetry*, 1993, **4**, 189.
27 L. Guerrier, J. Royer, D. S. Grierson and H.-P. Husson, *J. Am. Chem. Soc.*, 1983, **105**, 7754.
28 J.-F. Berrien, J. Royer and H.-P. Husson, *J. Org. Chem.*, 1994, **59**, 3769.
29 C. Maury, Q. Wang, T. Gharbaoui, M. Chiadmi, A. Tomas, J. Royer and H.-P. Husson, *Tetrahedron*, 1997, **53**, 3627.
30 A. I. Meyers and G. P. Brengel, *Chem. Commun.*, 1997, 1.
31 J. Royer and H.-P. Husson, *Heterocycles*, 1993, **36**, 1493.
32 M. J. Munchhof and A. I. Meyers, *J. Am. Chem. Soc.*, 1995, **117**, 5399.
33 D. L. Boger and S. M. Weinreb, *Hetero-Diels–Alder Methodology in Organic Synthesis*, Academic Press, Orlando, 1987.
34 H. Waldmann, *Synthesis*, 1994, 535.
35 P. A. Grieco and D. T. Parker, *J. Org. Chem.*, 1988, **53**, 3325.
36 P. D. Bailey, G. R. Brown, F. Korber, A. Reid and R. D. Wilson, *Tetrahedron: Asymmetry*, 1991, **2**, 1263.
37 P. D. Bailey, R. D. Wilson and G. R. Brown, *J. Chem. Soc., Perkin Trans. I*, 1991, 1337.
38 L. Stella and H. Abraham, *Tetrahedron*, 1992, **48**, 9707; L. Stella, H. Abraham, J. Feneau-Dupont, B. Tinant and J. P. Declerq, *Tetrahedron Lett.*, 1990, **31**, 2603.
39 K. Hattori and H. Yamamoto, *Synlett*, 1993, 129.
40 L. Yu, J. Li, J. Ramirez, D. Chen and P. G. Wang, *J. Org. Chem.*, 1997, **62**, 903.
41 P. Hamley, G. Helmchen, A. B. Holmes, D. R. Marshall, J. W. M. MacKinnon, D. F. Smith and J. W. Ziller, *J. Chem. Soc., Chem. Commun.*, 1992, 786.
42 D. Ager, N. Cooper, G. G. Cox, F. Garro-Hélion and L. M. Harwood, *Tetrahedron: Asymmetry*, 1996, **7**, 2563.
43 P. D. Bailey, D. J. Londesborough, T. C. Hancox, J. D. Heffernan and A. B. Holmes, *J. Chem. Soc., Chem. Commun.*, 1994, 2543.
44 W. Oppolzer, C. G. Bochet and E. Merrifield, *Tetrahedron Lett.*, 1994, **35**, 7015; W. Oppolzer and C. G. Bochet, *Tetrahedron Lett.*, 1995, **36**, 2959.
45 K. T. Wanner and A. Kärtner, *Heterocycles*, 1987, **26**, 921.
46 H. Suzuki, S. Aoyagi and C. Kibayashi, *Tetrahedron Lett.*, 1994, **35**, 6119.
47 D. Enders and U. Jegelka, *Synlett*, 1992, 999.
48 N. Yamazaki and C. Kibayashi, *Tetrahedron Lett.*, 1997, **38**, 4623.
49 C. J. Moody, A. P. Lightfoot and P. T. Gallagher, *J. Org. Chem.*, 1997, **62**, 746.
50 C. Agami, F. Couty, M. Poursoulis and J. Vaissermann, *Tetrahedron*, 1992, **48**, 431.
51 A. Hussain and P. B. Wyatt, *Tetrahedron*, 1993, **49**, 2123.
52 J. R. Stille and N. S. Barta, *Stud. Nat. Prod. Chem*., 1996, **18**, 315.
53 R. C. F. Jones, I. Turner and K. J. Howard, *Tetrahedron Lett.*, 1993, **34**, 6329.
54 A. I. Meyers, D. A. Dickman and T. R. Bailey, *J. Am. Chem. Soc.*, 1985, **107**, 7974.

7/09071D

An anomalous Dakin–West reaction of *N*-carbamate substituted prolines and trifluoroacetic anhydride

Masami Kawase,*[a] Michitaka Hirabayashi,[a] Hiromi Koiwai,[a] Katsumi Yamamoto[a] and Hiroshi Miyamae[b]

[a] *Faculty of Pharmaceutical Sciences, Josai University, 1-1 Keyakidai, Sakado, Saitama 350-0290, Japan*
[b] *Faculty of Science, Josai University, 1-1 Keyakidai, Sakado, Saitama 350-0290, Japan*

A novel transformation of *N*-alkoxycarbonylprolines 1 to 4-trifluoroacetyl-2,3-dihydropyrroles 2 was efficiently realized by utilizing trifluoroacetic anhydride, in which probable intermediates were mesoionic 1,3-oxazolium-5-olates B.

The Dakin–West (D–W) reaction of α-amino acids usually produces α-amino ketones.[1] However, treatment of *N*-acyl-*N*-alkyl-α-amino acids or *N*-acylprolines with trifluoroacetic anhydride (TFAA) under the D–W reaction conditions can lead to trifluoromethylated oxazoles,[2] acyloins[3] or morpholines,[4] depending on the nature of the *N*-substituents of the amino acids and/or reaction conditions. In the course of our studies on the reactivities of mesoionic 1,3-oxazolium-5-olates,[5] we have now found that *N*-alkoxycarbonylprolines **1** led unexpectedly, by way of a novel decarboxylative dehydration followed by trifluoroacetylation, to 4-trifluoroacetyl-2,3-dihydropyrroles **2** under the D–W reaction conditions.

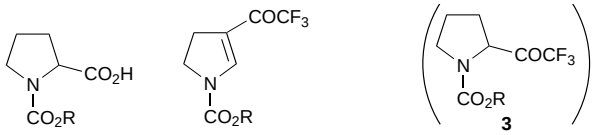

1a R = Me
b R = Et
c R = Bu
d R = Ph
e R = fluoren-9-yl
f R = Allyl
g R = Bn

2a R = Me
b R = Et
c R = Bu
d R = Ph
e R = fluoren-9-yl
f R = Allyl

3

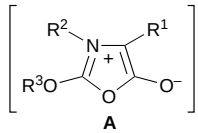

A

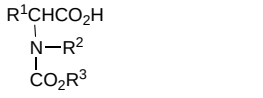

4a R^1 = Bn, R^2 = Me, R^3 = Me
b R^1 = Bn, R^2 = Me, R^3 = Bn
c R^1 = H, R^2 = Ph, R^3 = Et

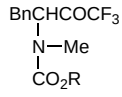

5a R = Me
b R = Bn

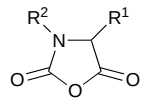

6a R^1 = Bn, R^2 = Me
b R^1 = H, R^2 = Ph

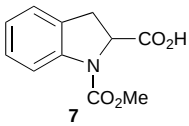

7

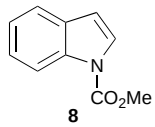

8

RNHAc
9a R = CH_2=$CHCH_2$
b R = Bn

Thus, treatment of **1a** (1 mmol) with TFAA (3 mmol) in MeCN (5 ml) at 80 °C for 5 h gave rise to *N*-methoxycarbonyl-4-trifluoroacetyl-2,3-dihydropyrrole **2a** in 66% yield. In the reaction, the D–W reaction product, *N*-methoxycarbonyl-2-trifluoroacetylpyrrolidine **3** (R = Me), was not isolated.

Reaction variables were briefly examined. Addition of pyridine (3 equiv.) to the reaction reduced the yield (**2c**; 22%). High temperatures (80 °C) were needed to obtain a high yield of **2c**, lower temperatures (60 °C) reducing the yield (**2c**; 46%). Various solvents such as MeCN, DMF, $ClCH_2CH_2Cl$, benzene, $MeNO_2$ and acetone are usable, and among them MeCN and DMF are the solvents of choice for this reaction, while little or no reaction takes place in THF, DME or dioxane. Several urethane-protected prolines **1a**–**f** were reacted in this way and the results are presented in Table 1. Among the *N*-alkoxycarbonyl groups examined, Me, Et and Bu proved to give a good yield of the product **2**. The low yields of **2d**–**f** could be attributable to the ease of cleavage of the alkoxy group in the mesoionic oxazole intermediate **B**. In the reaction of **1f**, *N*-allylacetamide **9a** was isolated in 58% yield as a side product.

Table 1 Reactions of *N*-alkoxycarbonylprolines with TFAA[a]

Entry	Starting material	Solvent	Product (% yield)[b]
1	**1a**	MeCN	**2a** (66)
2	**1a**	DMF	**2a** (67)
3	**1b**	MeCN	**2b** (61)
4	**1b**	DMF	**2b** (53)
5	**1c**	MeCN	**2c** (58)
6	**1c**	DMF	**2c** (68)
7	**1d**	MeCN	**2d** (32)
8	**1d**	DMF	**2d** (27)
9	**1e**	MeCN	**2e** (34)
10	**1f**	MeCN	**2f** (30) + **9a** (54)
11	**1g**	MeCN	**9b** (94)[c]
12	**7**	MeCN	**8** (86)

[a] The reactions were carried out according to the general procedure described in the text. [b] Isolated yields of pure products. All new compounds gave satisfactory spectroscopic data (IR, MS, ^1H and ^{13}C NMR) and analytical (combustion and/or high resolution mass) data. [c] Plus 54% of proline.

The structure of **2** was determined from analytical and spectral data† and was subsequently secured by single-crystal X-ray diffraction analysis of **2d** (Fig. 1).‡

A plausible mechanism for the formation of **2** is suggested in Scheme 1. The existence of the mesoionic oxazole **B** is supported by the following facts. (i) The reaction of Z-proline

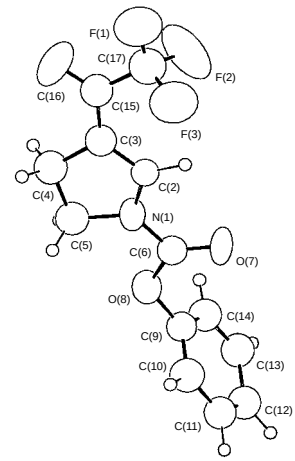

Fig. 1 X-Ray Crystal structure of **2d** (the probability level of the ellipsoids is 50%)

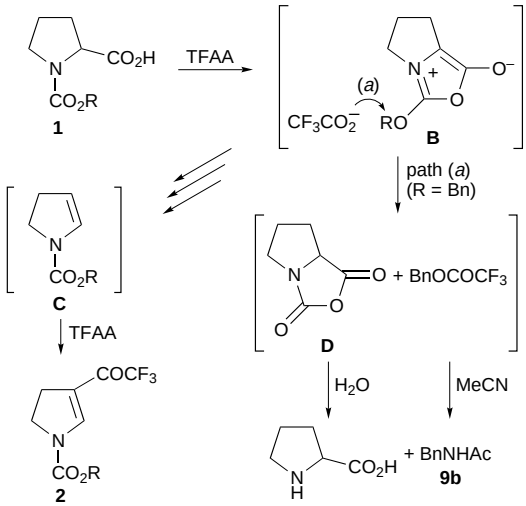

Scheme 1

1g with TFAA afforded proline (45%) and *N*-benzylacetamide **9b** (94%). Formation of proline is presumably due to hydrolysis of anhydride **D**,[6] which was produced by the attack of trifluoroacetate ion on the mesoionic oxazole intermediate **B** *via* path (*a*). *N*-Benzylacetamide **9a** was formed by the Ritter reaction of intermediary benzyl trifluoroacetate and the solvent MeCN. (ii) Treatment of *N*-methoxycarbonyl-*N*-methylphenylalanine **4a** with TFAA in the presence of pyridine gave the D–W reaction product, trifluoroacetyl derivative **5a**, in 93% yield.[7] In the case of *N*-benzyloxycarbonyl-*N*-methylphenylalanine **4b**, trifluoroacetyl derivative **5b** and the anhydride[8] of **6a** *N*-carboxyphenylalanine were obtained in 39 and 43% yields, respectively. (iii) In attempts to form the mesoionic oxazole **A** by treatment of *N*-ethoxycarbonyl-*N*-phenylglycine **4c** with $SOCl_2$, Potts *et al.* isolated the anhydride **6b** of *N*-carboxyglycine and ethyl chloride.[9] This suggests that ring closure to the mesoionic oxazole **A** actually occurred and that it underwent rapid deethylation. However, it is difficult to obtain a definitive explanation for the transformation of **B** to **2**. The existence of intermediary **C** is supported by the reaction of *N*-methoxycarbonyl-2,3-dihydroindole-1-carboxylic acid **7** with TFAA. Thus, the reaction yielded *N*-methoxycarbonylindole **8** in 86% yield and disclosed the probable intermediacy of **C**. Indeed, *N*-methoxycarbonylindole **8** cannot undergo trifluoroacetylation, whereas *N*-methoxycarbonyl-2-pyrroline **C** (R = Me)[10] prepared independently gave the trifluoroacetyl derivative **2a** in 65% yield under the same reaction conditions as described for **1a**. Finally, trifluoroacetylation of **C** leads to the product **2**.

In summary, this work describes the reaction of *N*-alkoxycarbonylprolines and TFAA, which has great practical potential because of the ready availability of the starting materials and reagents and the ease of manipulation. Our method makes novel compounds **2** readily accessible for further study as building blocks for the synthesis of fluorine-containing compounds, in view of the versatility of aminoenones (N–C=C–C=O) in synthetic as well as heterocyclic chemistry.[11] Detailed mechanistic studies and synthetic utilization of **2** as trifluoromethyl building blocks are now in progress.

Notes and References

† *Selected data* for **2d**: mp 99–101 °C (hexane); *m/z* 285 (M^+, 100%); ν_{max}/cm^{-1} 1670, 1740; δ_H(500 MHz; $CDCl_3$; Me_4Si) 3.04 (br s, 2 H), 4.12 (br s, 2 H), 7.17 (d, 2 H, *J* 7.9), 7.25–7.30 (m, 1 H), 7.40–7.43 (m, 2 H), 7.93 (s, 1 H); δ_C(125 MHz; $CDCl_3$; Me_4Si) 26.15 (CH_2), 46.77 (CH_2), 116.92 (C), 116.54 (CF_3, $^1J_{CF}$ 290.0), 121.16 (CH), 126.42 (CH), 129.61 (CH), 144.46 (CH), 145.85 (C), 150.15 (C), 176.49 (C, $^2J_{CF}$ 35.5).

‡ *Crystal data* for **2d**: ($C_{13}H_{10}NO_3F_3$), FW = 285.2, orthorhombic, $P2_12_12_1$, *a* = 8.409(7), *b* = 22.604(6), *c* = 6.774(6) Å, *V* = 1288(2) $Å^3$, *Z* = 4, μ(Mo-Kα) = 1.26 cm^{-1} by Rigaku AFC-5 diffractometer. Final *R* value was 0.074 for 1331 reflections (R_w = 0.044, *S* = 2.770). CCDC 182/754.

1 G. L. Buchanan, *Chem. Soc. Rev.*, 1988, **17**, 91.
2 M. Kawase, H. Miyamae, M. Narita and T. Kurihara, *Tetrahedron Lett.*, 1993, **34**, 859; M. Kawase, *Heterocycles*, 1993, **36**, 2441.
3 M. Kawase, *Tetrahedron Lett.*, 1994, **35**, 149.
4 M. Kawase, S. Saito, H. Kikuchi and H. Miyamae, *Heterocycles*, 1997, **45**, 2185.
5 M. Kawase, *Chem. Pharm. Bull.*, 1997, **45**, 1248.
6 T. S. Kaufman, V. L. Ponzo and J. Zinczuk, *Org. Prep. Proced. Int.*, 1996, **28**, 487 and references cited therein.
7 Full details of the D–W reaction of *N*-alkoxycarbonyl-*N*-alkyl-α-amino acids will be reported elsewhere.
8 R. Wilder and S. Mobashery, *J. Org. Chem.*, 1992, **57**, 2755; H. Collet, C. Bied, L. Mion, J. Tailades and A. Commeyras, *Tetrahedron Lett.*, 1996, **37**, 9043 and references cited therein.
9 K. T. Potts, D. Bhattacharjee and S. Kanemasa, *J. Org. Chem.*, 1980, **45**, 4985.
10 G. A. Kraus and K. Neuenschwander, *J. Org. Chem.*, 1981, **46**, 4791; Y. Nomura, K. Ogawa, Y. Takeuchi and S. Tomoda, *Chem. Lett.*, 1977, 693.
11 T. Nishio, C. Kashima and Y. Omote, *J. Synth. Org. Chem. Jpn.*, 1976, **34**, 526; J. V. Greenhill, *Chem. Soc. Rev.*, 1977, **6**, 277.

Received in Cambridge, UK, 18th November 1997; 7/08294K

Synthesis of transition metal–poly(yne) polymer possessing chiral acetylene bridges

Kiyotaka Onitsuka, Yuri Harada, Fumie Takei and Shigetoshi Takahashi*†

The Institute of Scientific and Industrial Research, Osaka University, Mihogaoka, Ibaraki, Osaka 567-0047, Japan

Treatment of C_2-symmetric chiral acetylenes, prepared from (*R*)-1,1′-bi-2-naphthol, with dichlorobis(trialkylphosphine)-platinum or -palladium in the presence of a Cu^{I} catalyst in amine gave high molecular-weight polynuclear complexes, which show a large negative optical rotation.

In recent years much attention has been drawn to molecular architecture incorporating coordination chemistry of transition metals.[1] We have been studying the chemistry of transition metal–poly(yne) polymers, in which metal atoms are linked by diynes such as butadiyne or *p*-diethynylbenzene to form rigid rod-like molecules.[2] Recently we showed that our methodology for the synthesis of multinuclear transition metal acetylides in one-dimension can be successfully applied to the synthesis of a three-dimension system giving a platinum–acetylide dendrimer.[3] Now we have expanded our methodology to the synthesis of polymers having a controlled main chain such as a helical structure. Since artificial polymers with a chiral backbone may maintain a stable single-handed helical conformation, they are of interest in view of their potential as new materials.[4] Here we report the first synthesis of a novel optically active poly(yne) polymer possessing a chiral acetylene bridge.

Bridging acetylene ligands **1** were easily prepared from 1,1′-bi-2-naphthol as shown in Scheme 1.[5] When optically active (*R*)-1,1′-bi-2-naphthol (commercially available, >99% ee determined by HPLC using a chiral column) was used as a starting material, optically active acetylenes [**1a**: $[\alpha]_D$ −69 (*c* 0.05, $CHCl_3$); **1b**: $[\alpha]_D$ −29 (*c* 0.05, $CHCl_3$); **1c**: $[\alpha]_D$ −8 (*c* 0.1, $CHCl_3$)] having C_2 symmetry were obtained. X-Ray crystallographic study of **1b** and **1c** showed that the two naphthyl groups make a dihedral angle of 112.8° in **1b** and 105.3° in **1c**, respectively.‡

As a model compound of the polymer we prepared optically active dinuclear complexes possessing a chiral acetylene bridge (Scheme 2). Treatment of **1a** with 2 equiv. of $Pd(PEt_3)_2Cl_2$ in the presence of a CuCl catalyst in Et_2NH at room temperature gave dipalladium complex **2a**. Similarly the reaction of **1b** with $Pd(PEt_3)_2Cl_2$ gave **2b**. Platinum analogs **3** were also prepared in a similar manner but at higher temperature (under piperidine reflux) because proportionation between platinum diacetylides and dichlorides takes place only at high reaction temperature.[2] These complexes were fully characterized by IR and NMR spectroscopy and elemental analysis.§ Yields and optical rotations are summarized in Table 1. The ^{1}H NMR spectrum of **3a** using the chiral shift reagent $Eu(fod)_3$ showed that no racemization took place during the conversion from chiral 1,1′-bi-2-naphthol.¶

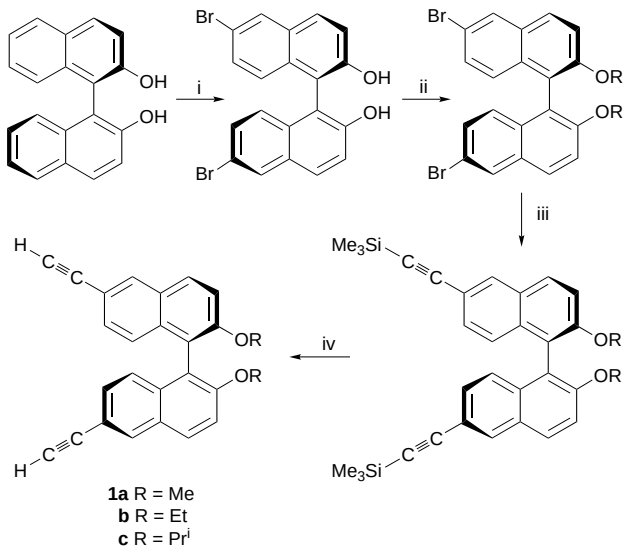

Scheme 1 *Reagents and conditions*: i, Br_2, CH_2Cl_2, −78 °C to room temp., 4 h, 91%; ii, RI, K_2CO_3, acetone, reflux, overnight, 85–89%; iii, $Me_3SiC{\equiv}CH$, $Pd(PPh_3)_2Cl_2$, CuI, Et_3N, reflux, overnight, 68–78%; iv, K_2CO_3, MeOH, overnight, 85–87%

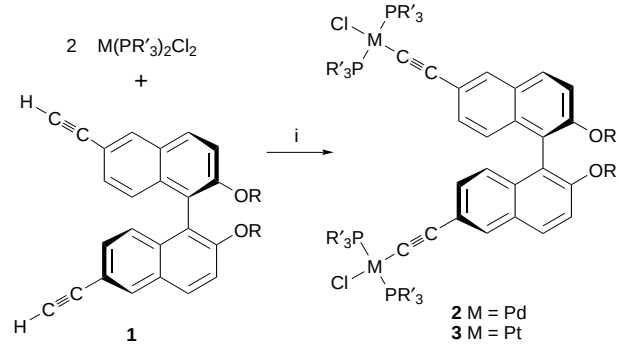

Scheme 2 *Reagents and conditions*: i, CuCl, Et_2NH, room temp., 4 h (M = Pd); CuCl, piperidine, reflux, overnight (M = Pt)

Reactions of chiral acetylene **1** with an equimolar amount of $M(PR'_3)_2Cl_2$ in the presence of a CuI catalyst in Et_2NH result in the formation of polynuclear complexes **4** and **5** having high molecular weight (Scheme 3). Experiments using ^{31}P NMR spectroscopy and GPC indicated the formation of dinuclear complexes **2** or **3** at an early stage, which slowly condense with terminal acetylene to propagate a metal–acetylide main chain. Since the resulting polymers are stable and soluble in common organic solvents, purification was performed by column chromatography on alumina followed by reprecipitation from CH_2Cl_2 into MeOH. The regular structures of **4** and **5** were

Table 1 Yields and optical rotations of dinuclear complexes **2** and **3**

Complex	M	R′	R	Yield (%)	$[\alpha]_D$[a]
2a	Pd	Et	Me	82	−142
2b	Pd	Et	Et	78	−150
3a	Pt	Et	Me	62	−147
3b	Pt	Et	Et	61	−148
3c	Pt	Bu	Me	76	−103
3d	Pt	Bu	Et	57	−87

[a] In 10^{-1} deg cm^2 g^{-1} (*c* 0.05, $CHCl_3$, 25 °C).

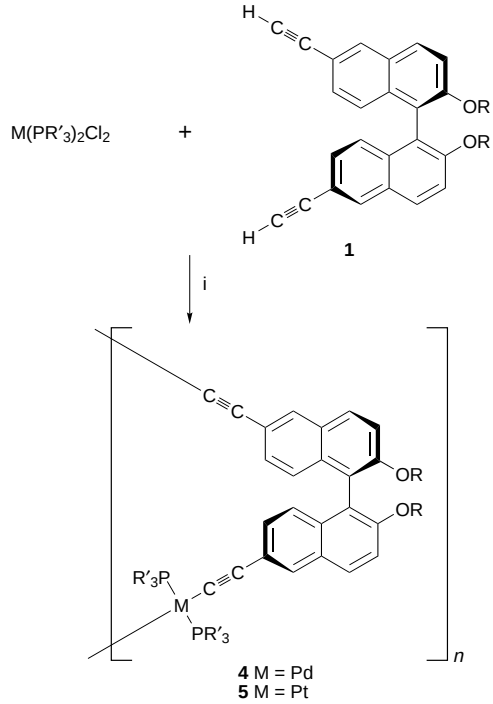

Scheme 3 *Reagents and conditions*: i, CuI, Et_2NH, room temp., 4 h (M = Pd); CuCl, Et_2NH, reflux, overnight (M = Pt)

Table 2 Yields, molecular weights and optical rotations of poly(yne) polymers **4** and **5**

Polymers	M	R′	R	Yield (%)	$M_w/10^3$ [a]	M_w/M_n	$[\alpha]_D$ [b]
4a	Pd	Et	Me	69	5.4	1.6	−370
4b	Pd	Et	Et	71	12	1.9	−227
4c	Pd	Et	Pr^i	73	11	1.9	−278
4d	Pd	Bu	Me	69	6.1	1.6	−265
4e	Pd	Bu	Et	63	9.8	1.6	−206
4f	Pd	Bu	Pr^i	59	7.4	1.6	−182
5a	Pt	Et	Me	73	12	2.7	−364
5b	Pt	Et	Et	73	30	2.9	−350
5c	Pt	Bu	Me	76	46	3.5	−331
5d	Pt	Bu	Et	92	100	4.0	−262
5e	Pt	Bu	Pr^i	71	22	2.2	−288

[a] Determined by GPC using poly(styrene) standards. [b] In 10^{-1} deg cm^2 g^{-1} [*c* 0.05 (R = Me, Et), *c* 0.10 (R = Pr^i), $CHCl_3$ at 25 °C].

confirmed by spectral analyses. For example, the ^{31}P NMR spectrum of **5d** exhibited one singlet signal at δ 3.27 with satellite signals (J_{Pt-P} = 2365 Hz). Only one set of signals, attributed to the naphthyl group, was observed in the ^1H and ^{13}C NMR spectra of **5d**.‖ Yields, molecular weights and optical rotations for **4** and **5** are shown in Table 2. The M_w values for palladium polymers **4** are in the range of 5400–12 000 regardless of the substituent on acetylene and the nature of the phosphine ligands, and are smaller than those of the platinum analogs **5**. A similar trend was observed in *p*-diethynylbenzene-bridged poly(yne) polymers.[2] In contrast, the M_w values of platinum polymers **5** were influenced to a certain extent by the substituent on the naphthyl group of the acetylene bridges and the nature of the phosphine ligands. Thus, the M_w values of ethoxy analogs **5b** and **5d** are much higher than those of the methoxy and isopropoxy variants. Since there is no significant difference in the structure of the bridging acetylene ligands **1b** and **1c** as determined *via* X-ray analysis, it is not clear why the molecular weights of the resulting polymers depend on the bridging acetylene ligands. Tributylphosphine analogs **5c** and **5d** have higher M_w values than triethylphosphine analogs **5a** and **5b**. It should be noted that all polymers prepared here showed larger specific optical rotations than both acetylene ligands **1** and model compounds **2** and **3**, which may indicate that the main chain of the polymers adopts a one-handed helical conformation and induces the helical chirality of the polymers.

In summary, we prepared novel optically active poly(yne) polymers of palladium and platinum possessing C_2-symmetric chiral acetylene bridges, which provide the first organometallic polymer with an optically active backbone, although some optically active organic acetylene polymers, in which chirality is similarly derived from 1,1′-bi-2-naphthol, have been reported very recently.[5]

This work was supported by a Grant-in-Aid for Scientific Research on Priority Areas, 'New Polymers and Their Nano-Organized Systems' (No. 277/08246103), and Encouragement of Young Scientists (No. 09740491) from the Ministry of Education, Science, Sports and Culture, Japan.

Notes and References

† E-mail: takahashi@sanken.osaka-u.ac.jp

‡ *Crystal data* for **1b**: $C_{28}H_{22}O_2$, orthorhombic, $P2_12_12_1$, a = 16.576(2), b = 18.193(3), c = 7.319(4) Å, V = 2207(1) Å^3, Z = 4, D_c = 1.175 g cm^{-3}, μ(Mo-Kα) = 0.73 cm^{-1}, 6 < 2θ < 55°, $R(R_w)$ = 0.054 (0.056) against 1420 reflections with $I > 2.0\sigma(I)$ out of 2914 unique reflections, GOF = 1.35. For **1c**: $C_{30}H_{26}O_2$, orthorhombic, $P2_12_12_1$, a = 16.359(7), b = 17.898(7), c = 8.025(9) Å, V = 2349(2) Å^3, Z = 4, D_c = 1.183 g cm^{-3}, μ(Mo-Kα) = 0.72 cm^{-1}, 6 < 2θ < 55°, $R(R_w)$ = 0.045 (0.046) against 2025 reflections with $I > 3.0\sigma(I)$ out of 3089 unique reflections, GOF = 1.44.

Data were measured on a Rigaku AFC5R diffractometer at −75 °C using the ω–2θ scan technique. The structure was solved by direct methods (SAPI91) and refined by full-matrix least-squares methods using anisotropic thermal parameters for all non-hydrogen atoms. Hydrogen atoms are located at calculated positions. CCDC 182/755.

§ *Selected data* for **3b**: ν_{max}(KBr)/cm^{-1} 2115 (C≡C); δ_H($CDCl_3$, $SiMe_4$) 1.06 (t, *J* 7.0, 6 H), 1.20 (dt, J_{P-H} 14.1, J_{H-H} 7.1, 36 H), 2.04–2.11 (m, 24 H), 4.01 (q, *J* 7.0, 4 H), 6.95 (d, *J* 8.8, 2 H), 7.07 (dd, *J* 8.8, 1.5, 2 H), 7.34 (d, *J* 9.0, 2 H), 7.70 (d, *J* 1.5, 2 H), 7.80 (d, *J* 9.0, 2 H); δ_C($CDCl_3$, $SiMe_4$) 8.06, 14.67, 16.53, 65.26, 81.53 (t, J_{Pt-C} 1432, J_{P-C} 14.9), 102.02 (J_{Pt-C} 407), 116.17, 120.73, 123.67, 125.06, 128.28, 129.01, 129.28, 129.59, 132.23, 154.06; δ_P($CDCl_3$, H_3PO_4) 15.35 (J_{Pt-P} 2393.

¶ Only one signal assignable to the protons of the methoxy group appeared in the ^1H NMR spectrum of **3a** using the chiral shift reagent Eu(fod)$_3$, while two signals of the methoxy protons were separately observed in a similar NMR experiment of the corresponding racemic mixture.

‖ *Selected data* for **5d**: ν_{max}(KBr)/cm^{-1} 2114 (C≡C); δ_H($CDCl_3$, $SiMe_4$) 0.90 (t, *J* 7.3, 18 H), 1.02 (t, *J* 6.8, 6 H), 1.43 (sextet, *J* = 7.4, 12 H), 1.60–1.61 (m, 12 H), 2.17–2.20 (m, 12 H), 3.96–4.02 (m, 4 H), 6.97 (d, *J* 9.0, 2 H), 7.11 (d, *J* 9.0, 2 H), 7.33 (d, *J* 9.0, 2 H), 7.73 (s, 2 H), 7.76 (d, *J* 9.0, 2 H); δ_C($CDCl_3$, $SiMe_4$) 13.84, 14.99, 23.86 (vt, *N* 16.7), 24.40 (vt, *N* 6.8), 26.36, 65.31, 107.81 (t, J_{Pt-C} 968, J_{P-C} 14.3), 109.28 (J_{Pt-C} 272), 116.05, 120.86, 124.10, 124.97, 128.13, 128.88, 129.38, 129.67, 132.00, 153.79; δ_P($CDCl_3$, H_3PO_4) 3.27 (J_{Pt-P} 2365).

1 For recent reviews, see: B. Linton and A. D. Hamilton, *Chem. Rev.*, 1997, **97**, 1669; M. M. Conn and J. Rebek, Jr., *Chem. Rev.*, 1997, **97**, 1647; J.-M. Lehn, *Supramolecular Chemistry: Concepts and Perspectives*, VCH, Weinheim, 1995; D. B. Amabilino and J. F. Stoddart, *Chem. Rev.*, 1995, **95**, 2725.

2 N. Hagihara, K. Sonogashira and S. Takahashi, *Adv. Polym. Sci.*, 1981, **41**, 149.

3 N. Ohshiro, F. Takei, K. Onitsuka and S. Takahashi, *Chem. Lett.*, 1996, 871.

4 O. Vogl and G. D. Jaycox, *CHEMTECH*, 1986, **16**, 698; G. Wulff, *Angew. Chem., Int. Ed. Engl.*, 1989, **28**, 21; Y. Okamoto and T. Nakano, *Chem. Rev.*, 1994, **94**, 349; R. J. M. Nolte, *Chem. Soc. Rev.*, 1994, 11.

5 L. Ma, Q.-S. Hu, K. Y. Musick, D. Vitharana, C. Wu, C. M. S. Kwan and L. Pu, *Macromolecules*, 1996, **29**, 5083; L. Ma, Q.-S. Hu, D. Vitharana, C. Wu, C. M. S. Kwan and L. Pu, *Macromolecules*, 1997, **30**, 204; C.-J. Li, W. T. Slaven IV, V. T. John and S. Bannerjee, *Chem. Commun.*, 1997, 1569.

Received in Cambridge, UK, 31st October 1997; revised manuscript received 13th January 1998; 8/00372F

Diastereoselective routes to side-chain truncated analogues of *N*-acetylneuraminic acid†

Martin Banwell,*[a]‡ Chris De Savi,[a] David Hockless[a] and Keith Watson[b]

[a] *Research School of Chemistry, Institute of Advanced Studies, The Australian National University, Canberra, ACT 0200, Australia*

[b] *Biota Chemistry Laboratory, Chemistry Department, Monash University, Clayton, Victoria 3168, Australia*

Vitamin C 3 has been converted, in a completely stereocontrolled manner, into the side-chain truncated analogues 4 and 5 of *N*-acetylneuraminic acid 1.

N-Acetylneuraminic acid **1** (Neu5Ac) and other members of the sialic acid class of carbohydrates play fundamental roles in many important biological processes, including cell adhesion and differentiation, immune responses, tumour metastasis and the development of neural cells.[1] In addition, they constitute a ligand commonly recognised by many infectious pathogens such as viruses, bacteria and parasites.[1] Consequently, sialic acids and various derivatives including the potent anti-influenza drug GG167 **2**[2] are assuming increasing importance as pharmacological tools and/or therapeutic agents.[3] In this regard there is now considerable interest[4] in side-chain truncated analogues of Neu5Ac which are currently only accessible *via* degradation of the natural product **1**.[3,4] Therefore, we report herein on the stereocontrolled conversion of abundant vitamin C **3** into compounds **4** and **5**, each of which embodies the sialic

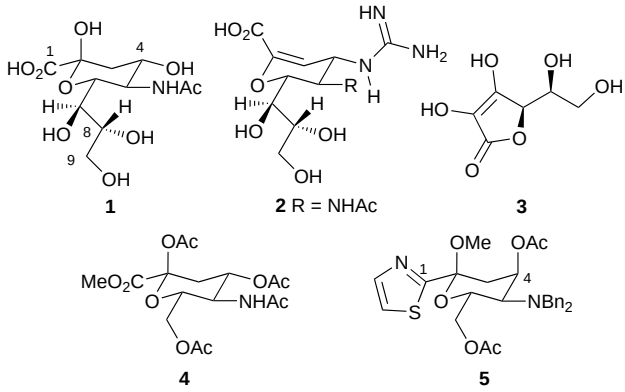

acid core but lacks the C-8/C-9 (side-chain) assemblage associated with the parent system **1**. The reaction sequences used for these conversions offer possibilities for the synthesis[5] of a range of novel sialic acid analogues which can vary in both the nature and stereochemistry of the substituents attached to the pyranose ring.

The reaction sequence (Scheme 1) leading to compound **4** starts with a literature procedure[6] for the oxidative degradation of vitamin C **3** to the α-hydroxy ester **6**. The triflate derivative **7** of the latter compound was then prepared in quantitative yield by standard methods[7] and underwent a smooth S_N2 reaction with lithium azide[8] in DMF at room temperature to give the azide **8** {80%, $[\alpha]_D$ −14.7 (*c* 2.6)§}. Reduction of this α-azido ester with LAH afforded the amino alcohol **9** {100%, $[\alpha]_D$ −10.5 (*c* 1.5)} which was immediately protected as its *N*,*N*-dibenzyl derivative **10** {90%, $[\alpha]_D$ +1.2 (*c* 2.1)}. Oxidation of compound **10** using the Swern reagent gave aldehyde **11**[9] {95%, $[\alpha]_D$ +3.9 (*c* 3.8)} which upon reaction with ethyl (2-bromomethyl)acrylate, zinc dust and saturated aq. NH_4Cl[10] in THF afforded the homoallylic alcohol **12** {87%, $[\alpha]_D$ −14.8 (*c* 2.1)} in a completely diastereoselective fashion.[11] Oxidation of the latter compound with the Swern reagent afforded ketone **13** {90%, $[\alpha]_D$ −72.9 (*c* 2.5)} and this was immediately reduced with $NaBH_4$ in EtOH to alcohol **14** {82%, $[\alpha]_D$ −5.9 (*c* 2.3)} which proved to be the only isolable product of the reaction. Attempts to cleave the C=C double bond[12] within this last compound using ozone failed because of competing reaction at the aromatic rings associated with the *N*,*N*-dibenzylamino moiety. Consequently, a somewhat more circuitous method was devised for achieving this end. Thus, compound **14** was

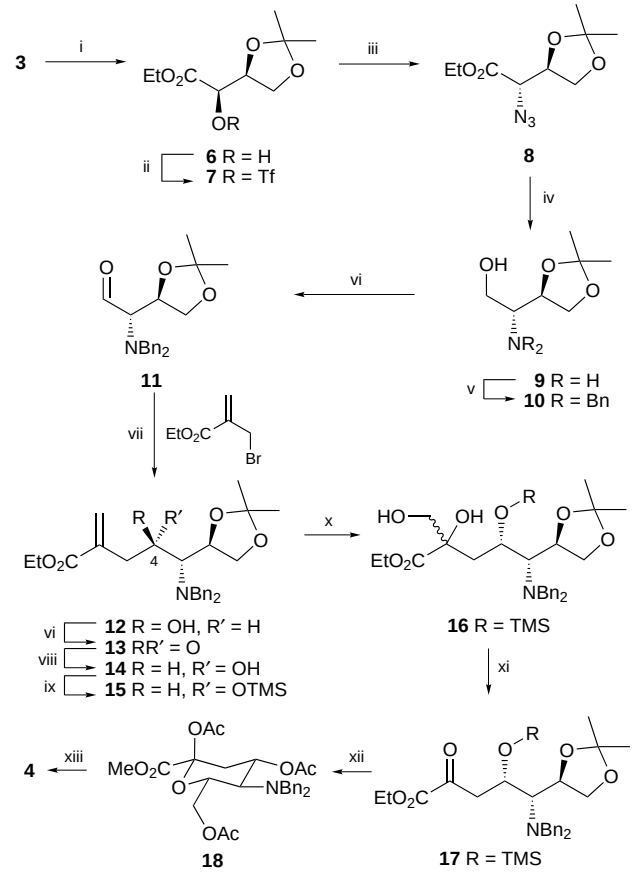

Scheme 1 *Reagents and conditions*: i, see ref. 6; ii, Tf_2O (1.3 equiv.), 2,6-lutidine (1.3 equiv.), CH_2Cl_2, −50 to −10 °C, 0.75 h; iii, LiN_3 (2.5 equiv.), DMF, 18 °C, 3 h; iv, LAH (3.5 equiv.), THF, 18 to 65 °C, 3 h; v, BnBr (2.2 equiv.), K_2CO_3 (2 equiv.), MeCN, 60 °C, 14 h; vi, $(COCl)_2$ (1.2 equiv.), DMSO, CH_2Cl_2, −78 to 0 °C, 1 h, then Et_3N (2.6 equiv.); vii, Zn dust (1.2 equiv.), sat. aq. NH_4Cl, THF, 60 °C, 0.75 h; viii, $NaBH_4$ (6 equiv.), EtOH, −10 °C, 1.5 h; ix, TMSCl (4.0 equiv.), hexamethyldisilazane (4.0 equiv.), pyridine, 0 to 18 °C, 19 h; x, AD-mix-α (2.2 equiv.), Bu^tOH, H_2O, 18 °C, 22 h; xi, $Pb(OAc)_4$ (0.9 equiv.), $CaCO_3$ (11 equiv.), CH_2Cl_2, 18 °C, 0.33 h; xii, 6% w/v HCl in MeOH, 18 °C, 18 h then Ac_2O (10 equiv.), DMAP (trace), pyridine, 18 °C, 20 h; xiii, Pd black, 5% w/v HCO_2H in MeOH, 18 °C, 0.5 h, then Ac_2O (10 equiv.), DMAP (trace), pyridine, 18 °C, 20 h

converted into the corresponding Me_3Si-ether **15** {83%, $[\alpha]_D$ −12.9 (*c* 3.0)} and the C=C double bond within this latter compound was dihydroxylated using AD-mix-α.[13] The resulting 1 : 1 mixture of diastereoisomeric diols **16** (83%) was then cleaved with lead tetraacetate to give the α-keto ester **17** {90%, $[\alpha]_D$ −21.7 (*c* 2.3)}. Treatment of compound **17** with 6% w/v methanolic HCl at room temperature for 18 h and subsequent peracetylation of the crude reaction mixture resulted in formation of the sialic acid analogue **18** {72%, $[\alpha]_D$ −81.3 (*c* 5.7)}. The benzyl protecting groups within this last compound could be removed using palladium black and formic acid[14] in MeOH and the resulting primary amine was acetylated to give the target compound **4** {80% at 80% conversion, $[\alpha]_D$ −97.1 (*c* 1.0)}, the structure of which follows from spectroscopic data.

Extension of this chemistry to the preparation of compound **5** is readily achieved. Thus, aldol condensation of the enolate anion derived from 2-acetylthiazole[15] with aldehyde **11** afforded the β-hydroxy ketone **19** {72%, $[\alpha]_D$ −58 (*c* 0.7)} in a completely stereoselective manner. Reaction of this last compound with 20% w/v methanolic HCl at room temperature for 18 h and subsequent peracetylation of the crude reaction mixture afforded compound **5** {70%. $[\alpha]_D$ −182.1 (*c* 1.0)} together with quantities (30%) of the open-chain dehydration product **20** {$[\alpha]_D$ −154.2 (*c* 0.6)}.

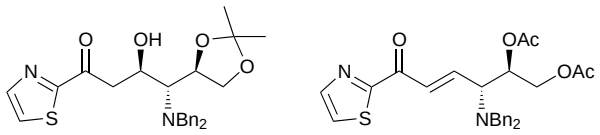

While the reaction sequence just described delivers a sialic acid analogue **5** which possesses the unnatural configuration at C-4, there are some constraints associated with the stereochemical variations that are available. This situation is highlighted by the outcome of the reaction sequence outlined in Scheme 2. Thus, treatment of triflate **7** with sodium azide in DMF at 75 °C for 6 h afforded azide **21** {85%, $[\alpha]_D$ +42.5 (*c* 2.7)} together with minor amounts (*ca*. 8%) of its C-2 epimer **8** which could be removed chromatographically. Reduction of compound **21** with LAH then provided the corresponding amino alcohol **22** {83%, $[\alpha]_D$ + 1.0 (*c* 5.7)} which was converted into the *N*,*N*-dibenzyl derivative **23** {92%, $[\alpha]_D$ −80.0 (*c* 6.8)}. Oxidation of this latter compound afforded the C-2 epimer of α-amino aldehyde **11**, namely compound **24** {88%, $[\alpha]_D$ +58.7 (*c* 7.9)}, which underwent stereoselective aldol condensation with the enolate anion derived from 2-acetylthiazole to give amino alcohol **25** {79%, $[\alpha]_D$ −5.5 (*c* 3.7)}. The stereochemistry at C-4 within compound **25** has not been rigorously proven but is assigned as illustrated on the basis of the well-known[9,11] directing effect of an α-(*N*,*N*-dibenzylamino) substituent on nucleophilic additions to aldehydes. In an effort to achieve a cyclisation reaction, compound **25** was treated with 8% w/v methanolic HCl, then the crude reaction mixture was subjected to exhaustive acetylation. However, no cyclisation products were observed. The only compound obtained was the open-chain dehydration product **26** {70%, mp 123–125 °C, $[\alpha]_D$ +106.3 (*c* 0.7)}, the structure of which was established by spectroscopic and X-ray crystallographic methods.¶

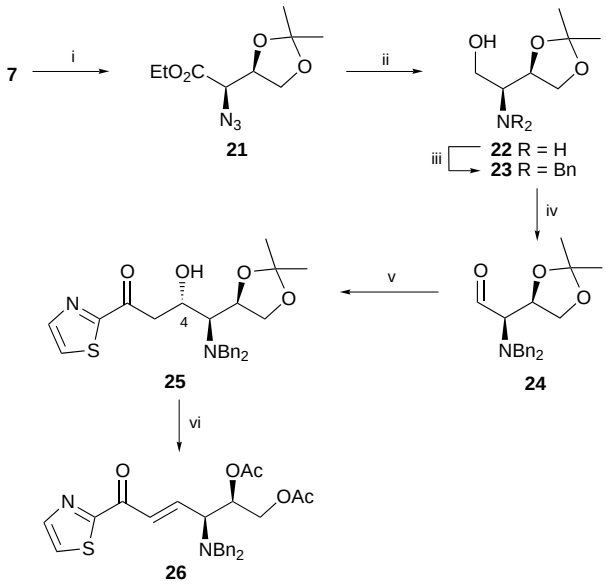

Scheme 2 *Reagents and conditions*: i, NaN_3 (2 equiv.), DMF, 75 °C, 6 h; ii, LAH (3.5 equiv.), THF, 18 to 65 °C, 3 h; iii, BnBr (2.2 equiv.), K_2CO_3 (2 equiv.), MeCN, 60 °C, 14 h; iv, $(COCl)_2$ (1.2 equiv.), DMSO, CH_2Cl_2, −78 to 0 °C, 1 h then Et_3N (2.6 equiv.); v, Bu^tOH (1 equiv.), Bu^nLi (1.2 equiv.), THF, 18 °C, 0.66 h, then 2-acetylthiazole (1.2 equiv.), −50 °C, 2.5 h; vi, 8% w/v HCl in MeOH, 18 °C, 18 h, then Ac_2O (10 equiv.), DMAP (trace), pyridine, 18 °C, 20 h

Notes and References

† The work described herein is the subject of a patent application (AIPO Patent Office Provisional Application No. PO8998, lodged September 5th, 1997).

‡ E-mail: mgb@rsc.anu.edu.au

§ All optical rotations were determined in $CHCl_3$ at 20 °C.

¶ *Crystal data* for **26**: $C_{27}H_{28}N_2O_5S$, M = 492.59, T = 193(1) K, monoclinic, space group $P2_1$, a = 11.346(4), b = 7.778(2), c = 15.473(6) Å, β = 109.34(3)°, U = 1288.4(3) Å^3, D_c (Z = 2) = 1.270 g cm^{-3}, F(000) = 520, μ(Cu-Kα) = 14.42 cm^{-1}, semi-empirical absorption correction; 2085 unique data ($2\theta_{max}$ = 120.1°), 1583 with $I > 3\sigma(I)$; R = 0.033, wR = 0.029, GOF = 1.44. CCDC 182/739.

1 S.-K. Choi, S. Lee and G. M. Whitesides, *J. Org. Chem.*, 1996, **61**, 8739 and references cited therein.
2 G. B. Kok, D. R. Groves and M. von Itzstein, *Chem. Commun.*, 1996, 2017 and references cited therein.
3 M. von Itzstein and R. J. Thomson, *Top. Curr. Chem.*, 1997, **186**, 119 and references cited therein.
4 M. J. Bamford, J. C. Pichel, W. Husman, B. Patel, R. Storer and N. G. Weir, *J. Chem. Soc., Perkin Trans. 1*, 1995, 1181.
5 For discussions of approaches to the total synthesis of sialic acid derivatives see ref. 3 and M. P. DeNinno, *Synthesis*, 1991, 583.
6 K. S. Kim, I. H. Cho, Y. H. Anh and J. I. Park, *J. Chem. Soc., Perkin Trans. 1*, 1995, 1783; E. Abushanab, P. Vemishetti, R. W. Leiby, H. K. Singh, A. B. Mikkilineni, D. C.-J. Wu, R. Saibaba and R. P. Panzica, *J. Org. Chem.*, 1988, **53**, 2598.
7 J. N. Vos, J. H. van Boom, C. A. A. van Boeckel and T. Beetz, *J. Carbohydr. Chem.*, 1984, **3**, 117. For a review on carbohydrate triflates, see R. W. Binkley and M. G. Ambrose, *ibid.*, 1984, **3**, 1.
8 N. Hofman-Bang, *Acta. Chem. Scand.*, 1957, **11**, 581.
9 Reetz and co-workers have highlighted the value of using *N*,*N*-dibenzyl-protected α-amino aldehydes in reactions (at the aldehyde carbon) with nucleophiles because of the configurational stability and high levels of diastereofacial control exerted by this protecting group (see M. T. Reetz, *Angew. Chem., Int. Ed. Engl.*, 1991, **30**, 1531 and, for example, R. V. Hoffman and J. Tao, *J. Org. Chem.*, 1997, **62**, 2292).
10 R. C. Anand and V. Singh, *Heterocycles*, 1993, **36**, 1333.
11 For related work see: S. Hanessian, H. Park and R.-Y. Yang, *Synlett*, 1997, 351 and 353.
12 In the reaction sequence culminating in this cleavage step, the organozinc species derived from ethyl (2-bromomethyl)acrylate is functioning as an equivalent for the pyruvate anion. For a review on, *inter alia*, pyruvate anion equivalents, see L. Kovács, *Recl. Trav. Chim. Pays-Bas*, 1993, **112**, 471.
13 K. B. Sharpless, W. Amberg, Y. L. Bennani, G. A. Crispino, J. Hartung, K.-S. Jeong, H.-L. Kwong, K. Morikawa, Z.-M. Wang, D. Xu and X.-L. Zhang, *J. Org. Chem.*, 1992, **57**, 2768.
14 B. ElAmin, G. M. Anantharamaiah, G. P. Royer and G. E. Means, *J. Org. Chem.*, 1979, **44**, 3442; B. D. Gray and P. W. Jeffs, *J. Chem. Soc., Chem. Commun.*, 1987, 1329; A. M. Diederich and D. M. Ryckman, *Tetrahedron Lett.*, 1993, **34**, 6169.
15 A. Dondoni and D. Perrone, *Aldrichim. Acta*, 1997, **30**, 35 and references cited therein.

Received in Cambridge, UK, 28th November 1997; 7/08594J

Ochratoxin A acts as a photoactivatable DNA cleaving agent

Ivan G. Gillman, Jennifer M. Yezek and Richard A. Manderville*

Department of Chemistry, Wake Forest University, Winston-Salem, North Carolina 27109-7486, USA

The ability of ochratoxin A to photoinduce DNA cleavage is described; in the presence of DNA the photoreaction yields the non-chlorinated derivative, ochratoxin B, while a hydroquinone derivative is produced under anaerobic conditions.

Ochratoxin A (OTA, **1**: X = Cl) is a fungal toxin produced by a species of Aspergillus and Penicillium.[1,2] It contaminates a wide range of foodstuffs and is implicated in the disease Balkan endemic nephropathy in which patients suffer from urinary tract tumors.[3] OTA induces single-strand DNA cleavage[4] and DNA adduction *in vivo*;[5] properties that establish a basis for its genotoxicity. However, the mechanism of OTA-induced DNA damage is currently not known.

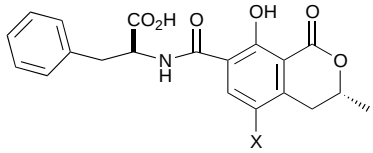

OTA, **1** X = Cl
OTB, **2** X = H
OTOH, **3** X = OH

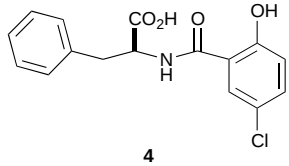

4

Despite this, it is known that the chlorine atom is essential[6] and antioxidants inhibit its genotoxic activities.[7] While activation of OTA appears to be oxidative,[3–7] we have found, using fluorescence spectroscopy (λ_{ext} = 380 nm, λ_{em} = 441 nm), that the toxin is particularly susceptible to light and decomposes over time unless a suitable filter is used to suppress light intensity. Since certain halogenated compounds have been shown to efficiently photocleave DNA,[8–10] we hypothesized that **1** may photoinduce DNA damage. Such activity was also expected to provide new insight into the toxin's DNA targeting activities as photoactivatable agents have proven useful as probes of DNA structure,[11] sequence,[12] and mechanism, both in terms of DNA strand-scission[13] and DNA alkylation.[14]

Here we describe our preliminary findings on the photonuclease activity of **1**. While *in vivo* activation of **1** may be mediated by cytochrome P450[15] with subsequent formation of hydroxyl radicals,[16,17] our results show that light can also activate **1** and the products from the photoactivation provide new insight into species that may participate in its *in vivo* DNA targeting activities.

The ability of **1** to facilitate DNA photocleavage was examined using supercoiled plasmid DNA and agarose gel electrophoresis. As shown in Fig. 1, no cleavage resulted in the absence of light (lane 2), highlighting that **1** alone does not induce DNA cleavage. However, in the presence of light, DNA cleavage by **1** occurred in a concentration dependent fashion (lanes 4–7). Table 1 shows the effect of various additives on the extent of photocleavage by **1**. In an ambiently oxygenated atmosphere, inhibition was provided by the oxygen radical scavengers, DMSO, *tert*-butyl alcohol and sodium azide. However, a marked increase in the extent of photocleavage occurred in an N_2-flushed atmosphere, precluding the requirement for activated oxygen species. Inhibition of photocleavage was also provided by copper(II) ions; a metal that binds **1** effectively and quenches its fluorescence spectrum.[18] That both Cu^{II} and O_2 inhibit DNA cleavage suggests that they quench the excited state of **1**.[19]

Additional insight into the mode of photocleavage by **1** was obtained from the finding that the non-chlorinated derivative, OTB (**2**: X = H), and the derivative **4**,† which lacks the dihydroisocoumarin (lactone) ring system of **1**, failed to photoinduce DNA strand-scission (Fig. 2). These findings are remarkably similar to the *in vivo* toxicity of **1** and indicate a requirement for both the chlorine atom[6] and the lactone.[20]

Product analysis from the photoreaction of **1** in aqueous buffered media also provided information regarding the mode of photocleavage by the toxin. In an ambiently oxygenated atmosphere, no products were identified in the photoreaction of **1** alone, even though the toxin was consumed as evidenced by

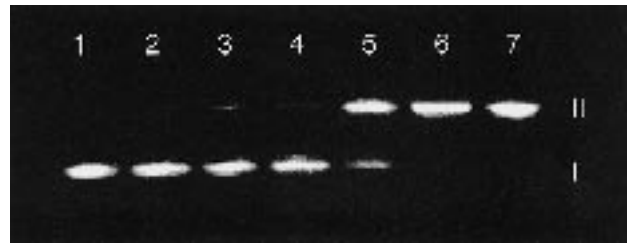

Fig. 1 Cleavage of supercoiled plasmid DNA by **1**. Reaction mixtures (20 μl total volume) contained 400 ng of plasmid DNA in 10 mM MOPS buffer, pH 7.4, and were irradiated on ice through a Pyrex filter with an ILC Technology 300 W Xenon arc lamp. After 5 min, the reaction mixtures were analyzed on a 1.2% agarose gel. Lane 1: DNA alone. Lane 2: DNA + 1000 μM **1**. Lane 3: irradiated DNA. Lane 4–7: irradiated DNA + 40, 200, 400 and 1000 μM **1**, respectively.

Table 1 Effect of additives on the extent of photocleavage of supercoiled DNA (Form 1) by **1**

Conditions[a]	Form I[b] (%)	Form II[c] (%)	Form III[d] (%)
Control	89	11	0
+**1**	27	73	0
+100 mM NaN_3	78	22	0
+1 μl DMSO	66	34	0
+1 μl Bu^tOH	62	38	0
+ SOD[e]	27	73	0
+ catalase[f]	27	73	0
+10 mM $Cu(OAc)_2$	74	26	0
Anaerobic[g]	0	61	39

[a] Reactions were run at pH 7.4 (10 mM MOPS buffer) using 200 μM **1** and 400 ng of supercoiled plasmid DNA in 20 μl total volume, and were irradiated in ice through a Pyrex filter with an ILC Technology 300 W Xenon arc lamp for 5 min. Densitometric quantitation of the gels was performed using a Microtek Scanmaker E_6 equipped with PhotoImpact and UTHSCSA Image Tool software. [b] Supercoiled DNA. [c] Nicked circular DNA. [d] Linear DNA. [e] 1000 units ml^{-1} super oxide dismutase. [f] 1000 units ml^{-1} catalase. [g] Reaction with **1** was purged with N_2 prior to photocleavage.

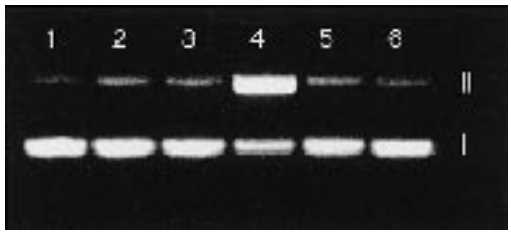

Fig. 2 Structure–activity relationships in DNA cleavage of supercoiled plasmid DNA by **1**. Reactions were carried out for 5 min as described in the caption below Fig. 1. Lane 1: DNA alone. Lane 2: DNA + 200 mM **1**. Lane 3: irradiated DNA. Lane 4: irradiated DNA + 200 μM **1**. Lane 5: irradiated DNA + 200 μM **2**. Lane 6: irradiated DNA + 200 μM 4.

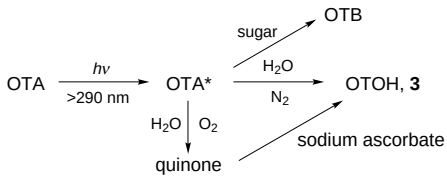

Scheme 1 Summary of the photoreaction of **1**. Excitation by light (> 290 nm) to produce **1*** is accompanied by production of **2** in the presence of a sugar. Under anaerobic conditions (N_2, H_2O) substitution of chlorine by H_2O yields the hydroquinone **3**, which is also produced under reducing conditions in the presence of O_2.

HPLC. However, in the presence of calf thymus DNA or dextrose, photoirradiation of **1** yielded the non-chlorinated derivative **2**.‡ Under anaerobic conditions in the absence of a sugar, photoreaction of **1** produced the hydroquinone derivative, OTOH (**3**: X = OH),§ a finding that we attribute to $S_{RN}1$ displacement[21] of the chlorine atom by H_2O. Interestingly, **3** was also detected in the presence of O_2 when a reducing agent (sodium ascorbate) was added to the photoreaction. This observation suggests that the hydroquinone **3** may have originated from a reactive quinone precursor, in analogy to photooxidation of halogenated phenols that yield benzoquinone derivatives in the presence of O_2.[22,23] The results of these studies are summarized in Scheme 1.

In conclusion, the fungal carcinogen **1** does not facilitate DNA cleavage alone. However, we have demonstrated that light is one way to activate **1** to induce DNA damage. The finding that **2** is a product of **1** photoirradiation in the presence of DNA, suggests that strand-scission is mediated by H-atom abstraction from deoxyribose sugars through initial C–Cl bond homolysis.[8–10] In the absence of a sugar and O_2, **1** is converted in high yield to the hydroquinone derivative, **3**. This species is also formed in the presence of O_2, provided that a suitable reducing agent is added to the photoreaction. This result suggests strongly that photooxidation of **1** produces a reactive quinone derivative, a species that may be responsible for the toxin's DNA adduction properties.[5] Presently, experiments are in progress to identify the cleavage sites and the mechanistic pathways for photocleavage. We are also studying the oxidation of **1** to determine the exact nature of oxidized **1**, its chemical reactivity and lifetime in aqueous buffered media and the potential of such a species to induce DNA adduction.

We thank Dr Fred W. Perrino (Department of Biochemistry, Wake Forest University) for the sample of plasmid DNA. This work was supported by Grant #IRG from the American Cancer Society and Wake Forest University.

Notes and References

* E-mail: manderra@wfu.edu

† The derivative **4** was prepared in 70% yield from 5-chloro-2-hydroxybenzoic acid and L-β-phenylalanine using a DCC coupling procedure; mp 172–173 °C, δ_H[$(CD_3)_2CO$, 200 MHz] 12.3 (br, 1 H), 8.62 (d, 1 H, *J* 7.9), 7.92 (m, 1 H), 7.54–7.10 (m, 6 H), 6.94 (d, 1 H, *J* 8.9), 5.01 (m, 1 H), 3.4–3.1 (m, 2 H); δ_C[$(CD_3)_2CO$] 173.0, 169.2, 160.6, 138.3, 134.6, 130.0, 129.2, 127.7, 127.5, 120.3, 116.7, 55.0, 37.7. (Calc. for $C_{16}H_{14}ClNO_4$; C, 60.10; H, 4.41; N, 4.38. Found C, 60.02; H, 4.47; N, 4.39%.)

‡ After 5 min irradiation time, the yield of **2** from the reaction of 100 μM **1** with 100 mM dextrose was *ca.* 20% based on HPLC analysis. The isolated sample was identical to authentic **2** purchased from Sigma.

§ The hydroquinone derivative **3** was obtained in 80% from the photoreaction of (100 μM) in N_2-flushed phosphate buffer (0.1 M, pH 7.4). δ_H[$^2H_6$]DMSO) 13.08 (s, 1 H), 12.04 (s, 1 H), 9.88 (s, 1 H), 8.95 (d, 1 H, *J* 6.0), 7.72 (s, 1 H), 7.29 (m, 5 H), 4.29 (m, 2 H), 3.12 (m, 3 H), 2.66 (dd, 1 H, *J* 11.9, 11.6), 1.43 (d, 3 H, *J* 6.2). δ_C([$^2H_6$]DMSO) 172.5, 169.9, 163.1, 152.2, 145.8, 136.9, 130.2, 129.3, 128.4, 126.7, 123.4, 118.3, 109.4, 76.2, 53.9, 36.7, 28.1, 20.3. These peaks are identical to a separately prepared sample starting from 4-methoxyphenol. Full details will be published elsewhere.

1 K. J. van der Merwe, P. S. Steyn, L. Fourie, D. B. Scott and J. J. Theron, *Nature*, 1965, **205**, 1112.
2 W. van Walbeek, P. M. Scott, F. S. Thatcher, *Can. J. Microbiol.*, 1968, **14**, 131.
3 R. R. Marquardt and A. A. Frohlich, *J. Anim. Sci.*, 1992, **70**, 3968.
4 J. C. Seegers, L. H. Bohmer, M. C. Kruger, M. L. Lottering and K. M. de, *Toxicol. Appl. Pharmacol.*, 1994, **129**, 1.
5 Y. Grosse, I. Baudrimont, M. Castegnaro, A.-M. Betbeder, E. E. Creppy, G. Dirheimer and L. A. Pfohl, *Chem.-Biol. Interact.*, 1995, **95**, 175.
6 C. Malaveille, G. Brun and H. Bartsch, *Mutation Res.*, 1994, **307**, 141.
7 I. Baudrimont, A.-M. Betbeder, A. Gharbi, L. A. Pfohl, G. Dirheimer and E. E. Creppy, *Toxicology*, 1994, **89**, 101.
8 T. Matsumoto, Y. Utsumi, Y. Sakai, K. Toyooka and M. Shibuya, *Heterocycles*, 1992, **34**, 1697.
9 J. C. Quada, Jr., M. J. Levy and S. M. Hecht, *J. Am. Chem. Soc.*, 1993, **115**, 12 171.
10 Saito, T. Sakurai, T. Kurimoto and M. Takayama, *Tetrahedron Lett.*, 1994, **35**, 4797.
11 J. K. Barton, *Science*, 1986, **233**, 727.
12 P. E. Nielsen, C. Hiort, S. H. Sönnichsen, O. Buchardt, O. Dahl and B. Norden, *J. Am. Chem. Soc.*, 1992, **114**, 4967.
13 D. Ly, Y. Kan, B. Armitage and G. B. Schuster, *J. Am. Chem. Soc.*, 1996, **118**, 8747.
14 G. Büchi, K. W. Fowler and A. M. Nadzan, *J. Am. Chem. Soc.*, 1982, **104**, 544.
15 R. J. Omar, H. V. Gelboin and A. D. Rahimtula, *Biochem. Pharmacol.*, 1996, **51**, 207.
16 B. B. Hasinoff, A. D. Rahimtula and R. F. Omar, *Biochim. Biophys. Acta*, 1990, **1036**, 78.
17 D. Hoehler, R. R. Marquardt, A. R. McIntosh and H. Xiao, *J. Biol. Chem.*, 1996, **271**, 27 388.
18 J. A. Ardus, I. G. Gillman and R. A. Manderville, *Can. J. Chem.*, in the press.
19 N. J. Turro, *Modern Molecular Photochemistry*, University Science Books, Sausalito, CA, 1991, pp. 589–591.
20 D. Hoehler, R. R. Marquardt, A. R. McIntosh and G. M. Hatch, *Biochim. Biophys. Acta*, 1997, **1357**, 225.
21 J. F. Bunnett, *Acc. Chem. Res.*, 1978, **11**, 413.
22 K. David-Oudjehani and P. Boule, *New J. Chem.*, 1995, **19**, 199.
23 C. Richard and P. Boule, *New J. Chem.*, 1994, **18**, 547.

Received in Corvallis, OR, USA, 17th November 1997, 7/08275D

Dihydropyran-2-carboxylic acid, a novel bifunctional linker for the solid-phase synthesis of peptides containing a C-terminal alcohol

Hsing-Pang Hsieh, Ying-Ta Wu, Shui-Tein Chen*† and Kung-Tsung Wang

Institute of Biological Chemistry, Academia Sinica, Taipei, 11529, Taiwan

Dihydropyran-2-carboxylic acid, a novel compound used to link an amino alcohol and an amine resin, is utilised for the solid-phase synthesis of peptide alcohols *via* the Fmoc strategy; this bifunctional linker was effectively applied to the synthesis of Octreotide.

Peptides that contain a C-terminal alcohol, such as Octreotide,[1] Enkephalins,[2] Gramicidin[3] and Trichoderma species,[4] have been the focus of recent research, because of these peptides bind with high affinity to their receptors and have a long half-life *in vivo*. Peptides containing a C-terminal alcohol cannot be synthesized by conventional solid-phase peptide synthesis (SPPS), because present protocols require a free carboxy group to attach onto the resin. Octreotide **1**, a metabolically stable somatostatin analog, inhibits the growth of tumor cells by binding to surface somatostatin receptors.[5] Many methods have been reported for its synthesis,[1a,6a,b,c] however[5,6] these methods have drawbacks including low yields and complicated procedures. We describe here a new procedure using dihydropyran-2-carboxylic acid as a bifunctional linker for the synthesis of peptide alcohols by SPPS.

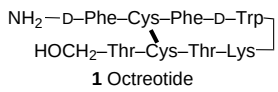

1 Octreotide

Sodium 3,4-dihydro-2*H*-pyran-2-carboxylate **2** was prepared according to established procedures.[7,8] Compound **2** is a key component of the bifunctional linker which easily undergoes self-lactonization under acidic conditions,[9,10] and the carboxy group of **2** must be protected before the dihydropyran portion couples with the amino alcohol. Compound **2** was reacted with BnBr in DMF at 25 °C in the presence of Cs_2CO_3 to form benzyl 3,4-dihydro-2*H*-pyran-2-carboxylate **3**, which was further reacted with Fmoc-Thr(Bu^t)OH[11] in the presence of TsOH in CH_2Cl_2 to yield Fmoc-Thr(Bu^t)-THP-2-CO_2Bn **4**. Selective catalytic transfer hydrogenation to remove the benzyl group of **4** using Pd/C–cyclohexa-1,4-diene yielded Fmoc-Thr(Bu^t)-THP-2-CO_2H **5** (90% yield) without interfering with the other three protection groups. Enzymes such as alcalases and lipases or chemical methods such as K_2CO_3 in THF–H_2O under mild hydrolytic conditions were ineffective for removal of the benzyl ester, due to low reactivity and low conversion. Catalytic hydrogen transfer, however, effectively cleaved the benzyl ester without deprotecting the Fmoc group, while the Fmoc group could be cleaved by hydrogenation over Pd/C or $Pd(OAc)_2$.[12] In a similar manner, Fmoc-Gly-THP-2-CO_2H **6** and Fmoc-Phe-THP-2-CO_2H **7**, the C-terminal amino alcohols of the Grami-

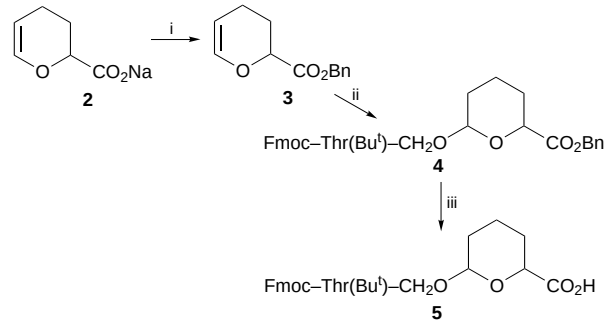

Scheme 1 *Reagents and conditions*: i, Cs_2CO_3, BnBr, room temp., 24 h (80%); ii, TsOH, CH_2Cl_2, Fmoc-Thr(Bu^t)-ol, 12 h (85%); iii, Pd/C, MeOH, cyclohexa-1,4-diene, 2 h (90%)

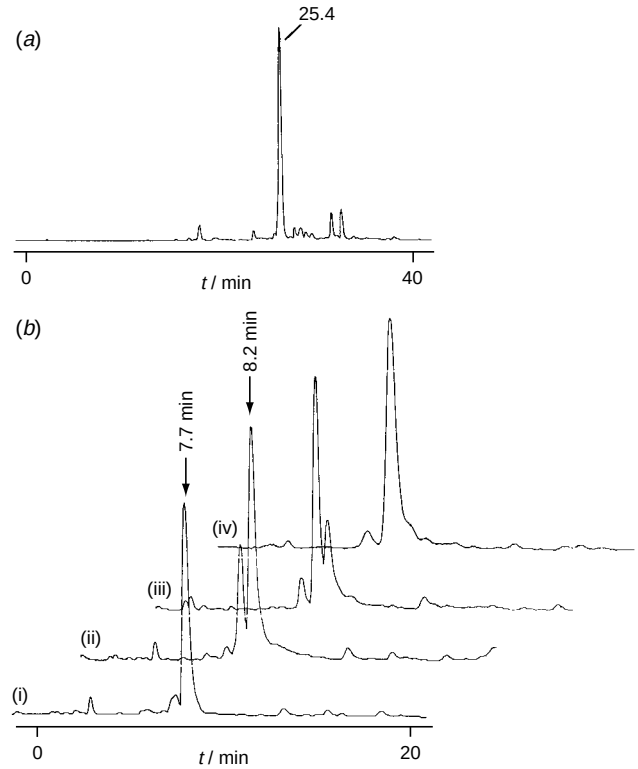

Fig. 1 (*a*) Analysis of reduced Octreotide (retention time 25.4 min) by HPLC. Sample was taken from the aq. AcOH (5%) used to extract the peptide immediately after the elongated peptide was cleaved from the resin. Conditions for HPLC: RP-18 column, 4.6 × 250 mm; gradient 0 → 30 min, 0 → 100% B; 30 → 35 min, 100% B; 35 → 40 min, 100 → 0% B; flow rate 1.0 ml min^{-1}; A = 5% MeCN in water containing 0.1% TFA; B = 90% MeCN in water containing 0.1% TFA; UV detection at 214 nm. (*b*) The time course for the folding of reduced Octreotide: (i) 0, (ii) 8, (iii) 32 and (iv) 46 h. The progress of the peptide folding was followed by analytic reverse-phase HPLC. The retention time for the reduced Octreotide was 8.2 min and for the folded Octreotide was 7.7 min. Conditions for HPLC: RP-18 column, 4.6 × 250 mm; gradient 0 → 20 min, 50 → 60% B; 20 → 25 min, 60% B; 25 → 30 min, 60 → 50% B; flow rate 1.0 ml min^{-1}; A = 50% MeCN in water containing 0.1% TFA; B = 90% MeCN in water containing 0.1% TFA; UV detection at 214 nm.

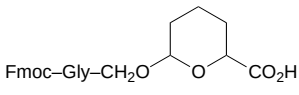

6

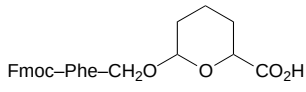

7

cidin[3] and Trichoderma species,[4] were also obtained from Fmoc-Gly-ol[13] and Fmoc-Phe-ol[13] in yields of 72 and 78%, respectively (see Scheme 1).

The novel linker was used successfully to synthesize Octreotide. Fmoc-Thr(Bu^t)-THP-2-CO_2H was attached to an amine resin and the peptide Fmoc-D-Phe-Cys(Trt)-Phe-D-Trp(Boc)-Lys(Boc)-Thr(Bu^t)-Cys(Trt)-Thr(Bu^t)-CH_2O-THP-CO-amide resin was synthesized stepwise using an Fmoc protocol. After completion of the peptide synthesis, simultaneous cleavage of Octreotide from the resin and deprotection of the side-chains was performed using the TFA method (TFA–thioanisole–ethanedithiol–H_2O = 0.9 : 0.5 : 0.25 : 0.25). Dilsulfide bond formation was achieved by air oxidation in aqueous phosphate buffer at 25 °C pH 7 for 48 h monitored by HPLC. Pure Octreotide was isolated *via* preparative reverse-phase HPLC (70% total yield). Fig. 1 illustrates the time course of the disulfide bond formation. The reduced form of Octreotide and the final product appeared as major peaks (Fig. 1). The presence of Octreotide was confirmed by amino acid analysis and FAB mass spectrometry (*m*/*z* 1019.5 [M^+ + 1]).

The high yields and purity (Fig. 1) of Octreotide produced using the novel bifunctional linker demonstrate that the linker is stable under basic Fmoc/Bu^t synthetic conditions as well as acid-labile and easily removed from the resin to regenerate the desired C-terminal alcohol. Furthermore, because the DHP-2-CO_2H linker first couples with the C-terminal amino alcohol to form the first residue for SPPS, the linker can more easily couple to any primary, secondary or even tertiary alcohols compared to Ellman's DHP-resin bound system.[6] In conclusion, the novel bifunctional linker can be used successfully in the synthesis of peptide C-terminal alcohols in addition to the preparation and screening of combinatorial peptide and non-peptide libraries *via* solid-phase synthesis techniques.[14]

Support for this research by the National Science Council, Taiwan, is gratefully acknowledged.

Notes and References

† E-mail: bcchen@gate.sinica.edu.tw

1 (*a*) J. Pless, W. Bauer, U. Briner, W. Doepfner, P. Marbach, R. Maurer, T. J. Petcher, J.-C. Reubi and J. Vonderscher, *Scand. J. Gastroenterol.*, 1986, **21** (Suppl. 119), 54; (*b*) W. Bauer, U. Briner, W. Doepfner, R. Haller, R. Hugenin, P. Marbach, T. J. Petcher and J. Pless, *Life Sci.*, 1982, **31**, 1133.

2 D. Roemer, H. H. Buescher, R. C. Hill, J. Pless, W. Bauer, F. Cardinaux, A. Closse, D. Hauser and R. Hugenin, *Nature* (*London*), 1977, **268**, 547; D. Roemer and J. Pless, *Life Sci.*, 1979, **24**, 621.

3 B. Cornell, *J. Bioemerg. Biomembr.*, 1987, **19**, 655; W. Neugebauer, R. Brzezinski and G. E. Willick, in *Peptide 1990*, ed. E. Giralt and D. Andreu, ESCOM, 1991, p. 188.

4 M. Solfrizzo, C. Altomare, A. Visconti, A. Bottalico and G. Perrone, *Nat. Toxins*, 1994, **2**, 360; S. Rebuffat, L. Conraux, M. Massias, C. Auvin-Guette and B. Bodo, *Int. J. Peptide Protein Res.*, 1993, **41**, 74.

5 G. Weckbecker, F. Raulf, B. Stolz and C. Bruns, *Pharmacol. Ther.*, 1993, **60**, 245.

6 (*a*) M. Mergler and R. Nyfeler, in *Peptide 1992*, ed. C. H. Schneider and A. N. Eberle, ESCOM, 1993, p. 177; (*b*) W. B. Edwards, C. G. Fields, C. J. Anderson, T. S. Pajeau, M. J. Welch and G. B. Fields, *J. Med. Chem.*, 1994, **37**, 3749; (*c*) M. A. Schmidt, R. R. Wilhelm and A. Srinivasan, in *Abstracts of the Fifteenth American Peptide Symposium*, June 14–19, 1997, Nashville, Tennessee, p. 2.

7 Compound **2** was prepared in two stages: (i) dimerization of acrolein was either carried out with the standard high-pressure method [ref. 8(*a*)] (37% yield) or with a recently described microwave-assisted method (91% yield) [ref. 8(*b*)]; (ii) 3,4-dihydro-2*H*-pyran-2-carboxaldehyde was oxidized and hydrolyzed to obtain sodium 3,4-dihydro-2*H*-pyran-2-carboxylate **2** [ref. 8(*c*)].

8 (*a*) T. Shiraishi, K. Ichimura and T. Haga, *Jpn. Kokai*, 74 86, 373; *Chem. Abstr.*, 1975, **82**, 156 072d; (*b*) H.-P. Hsieh, S.-T. Chen and K.-T. Wang, *J. Chim. Chem. Soc. (Taipei)*, 1997, **44**, 597; (*c*) M. Okada, H. Sumitomo and I. Tajima, *Macromolecules*, 1977, **10**, 505.

9 W. Neugebauer and E. Escher, *Helv. Chim. Acta*, 1989, **72**, 1319.

10 E. K. Kick and J. A. Ellman, *J. Med. Chem.*, 1995, **38**, 1427; L. A. Thompson and J. A. Ellman, *Tetrahedron Lett.*, 1994, **35**, 9333.

11 Purchased from BACHEM Inc., Switzerland.

12 L. A. Carpino and G. Y. Han, *J. Am. Chem. Soc.*, 1970, **92**, 5748; J. Martinez, J. C. Tolle and M. Bodanszky, *J. Org. Chem.*, 1979, **44**, 3596; E. Atherton, C. Bury, R. C. Sheppard and B. J. Williams, *Tetrahedron Lett.*, 1979, **32**, 3041.

13 Purchased from NOVA Biochem Inc., Switzerland.

14 L. A. Thompson and J. A. Ellman, *Chem. Rev.*, 1996, **96**, 555.

Received in Cambridge, UK, 4th November 1997; 7/07934F

CAN-mediated tandem 5-*exo*-cyclisation of tertiary aminocyclopropanes: novel accelerative effect of an *N*-benzyl group for oxidative ring-opening

Yoshiji Takemoto, Saori Yamagata, Syun-ichirou Furuse, Hiroki Hayase, Tomoki Echigo and Chuzo Iwata*†

Faculty of Pharmaceutical Sciences, Osaka University, 1-6 Yamada-Oka, Suita, Osaka 565, Japan

Treatment of tertiary cyclopropylamines with cerium(IV) ammonium nitrate (CAN) gave ring-opened ketones and/or bicyclic secondary amines *via* an oxidative cyclopropane cleavage followed by a hydrogen abstraction or 5-*exo* radical cyclization: an *N*-benzyl group plays a crucial role in these reactions.

Cyclopropylamines have attracted considerable interest from organic and biological chemists as conformationally constrained amino acids[1] and mechanism-based inhibitors of cytochrome P-450 and monoamine oxidase.[2] Thus far many facile preparations of cyclopropyl amines, such as the Simmons–Smith cyclopropanation of enamines[3] and the Ti^{II}-mediated coupling of *N*,*N*-dialkylamides and monosubstituted olefins,[4] have been developed. However, compared with these synthetic methods, few transformations of cyclopropylamines into more versatile synthetic intermediates have been reported.[3,5] Only the enzymatic oxidation of cyclopropylamines to clarify the mechanism for the inactivation of cytochrome P-450[6] and monoamine oxidase,[7] and ethylene formation from 1-aminocyclopropane carboxylic acid[8] have been examined. In these studies, it has been proposed that the ring-opening reaction proceeds *via* cyclopropylamine radical cations, whose existence have been proven by an EPR study.[9] Recently, we developed an efficient synthetic method for cyclic ethers and spirocyclic compounds by a single electron transfer (SET) promoted ring-opening of cyclopropyl sulfides with cerium(IV) ammonium nitrate (CAN).[10] Our recent efforts have been directed to the oxidative ring-opening of the tertiary cyclopropylamines. Herein we report a convenient method for cleaving a cyclopropyl bond‡ and an intramolecular [3 + 2]cycloaddition with a tethered olefin.[11]

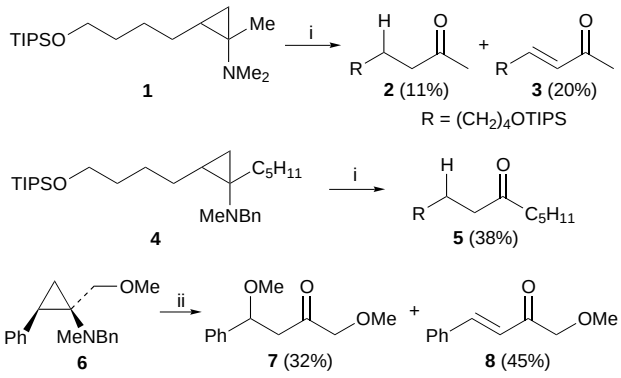

Scheme 1 *Reagents and conditions*: i, CAN, $NaHCO_3$, DMF, room temp.; ii, CAN, K_2CO_3, MeOH, 0 °C

The ring-opening of *N*,*N*-dimethyl- and *N*-methyl-*N*-benzylcyclopropylamines **1**§ and **4**§ was studied as a model reaction (Scheme 1). The CAN-promoted oxidation of **1** proceeded slowly (20 h) in DMF in the presence of $NaHCO_3$ to give the ring-opened ketone **2** and α,β-unsaturated ketone **3** in 11 and 20% yield, respectively. The use of MeOH as solvent in place of DMF slowed the reaction rate, resulting in the recovery of almost all the starting materials. On the other hand, the reaction of **4** under the same reaction conditions proceeded smoothly (2 h), irrespective to the reaction solvent, to give the ring-opened ketone **5** as the sole product in good yield. Although all products seem to be produced by cleaving the most substituted cyclopropyl bond of **1** and **4**, two-electron oxidation occurred simultaneously with single-electron oxidation in the former case. In addition, the oxidation of 2-phenylcyclopropylamine **6** took place only through two electron oxidation, giving the β-methoxy ketone **7** and the α,β-unsaturated ketone **8** in 32 and 45% yield, respectively. These results indicate that the CAN-mediated oxidation of the tertiary cyclopropylamines is affected by substituents on both the nitrogen and the cyclopropane ring. The reaction pathway shown in Scheme 2 clearly explains these phenomena. The SET oxidation of **1** and **4** generates the radical-

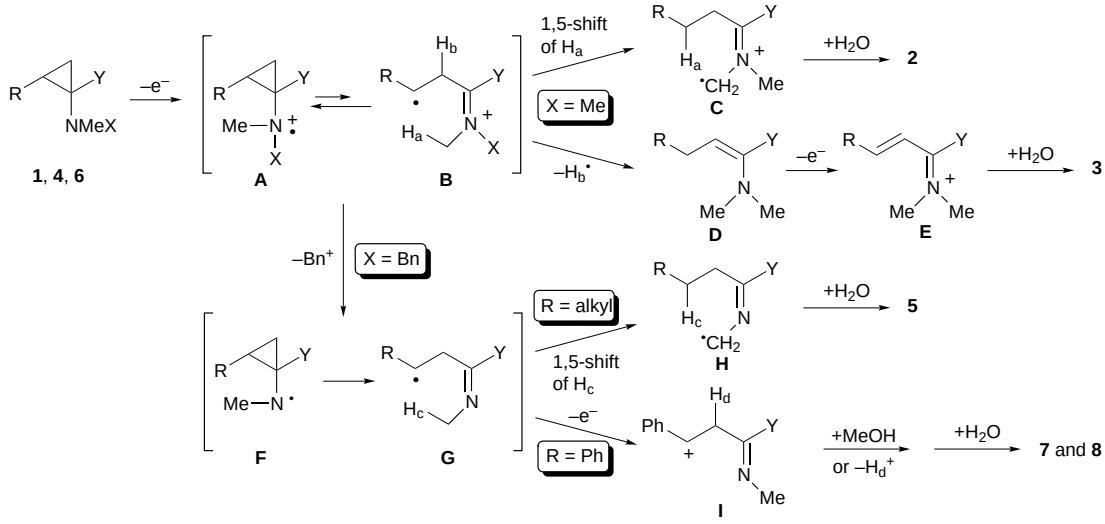

Scheme 2

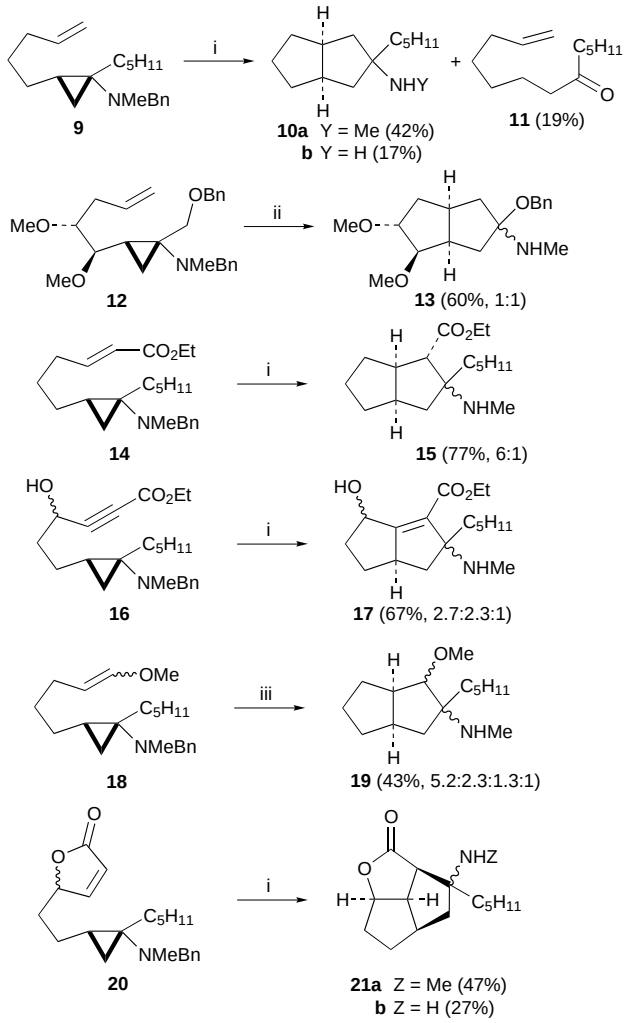

Scheme 3 *Reagents and conditions*: i, CAN, $NaHCO_3$, DMF, room temp.; ii, CAN, $NaHCO_3$, MeOH–THF (5 : 1), room temp.; iii, CAN, $NaHCO_3$, DMF, 0 °C

cation **A**, which is equilibrated to the ring-opened iminium radical **B**. In the case of **1** (X = Me), the following 1,5-hydrogen shift (**B** → **C**) and successive deprotonation and second SET oxidation (**B** → **D** → **E**) might proceed slowly because the equilibrium lies so far to **A**. On the other hand, in the case of **4** (X = Bn), the benzyl group of the radical-cation species **A** and **B** was rapidly lost from the nitrogen atom, giving the aminyl radical **F** and/or iminyl radical **G**. Because the aminyl radical **F** undergoes a very rapid ring-opening to **G**,[12] the next 1,5-hydrogen shift (**G** → **H**) occurs at a reasonable rate to afford **5**. However, in the case of **6** (R = Ph), another SET oxidation of **G** takes place at a rate faster than the 1,5-hydrogen shift due to the stability of the radical, producing **7** and **8** *via* the cation intermediate **I**.

To achieve an intramolecular trapping of the presumed radical **G** by a tethered olefin, we next examined the CAN oxidation of *N*-benzyl-*N*-methylcyclopropylamines bearing a suitably situated radical acceptor, typically a double or triple bond (Scheme 3). The oxidation of **9** bearing a terminal olefin was carried out with 5 equiv. of CAN in DMF at room temperature. The reaction was completed in 2 h and gave the bicyclic products **10a** and **10b** in a total yield of 59% along with the ketone **11** as a minor product, while no monocyclic products were obtained.¶ The cyclization of **12** was not influenced by the substituent on the tether, giving the desired products **13** in 60% yield. More interestingly, the α,β-unsaturated ester **14** and the α,β-acetylenic ester **16** cyclized more efficiently to give the corresponding bicyclic products **15** and **17** without the ketones, whereas the oxidation of the methyl enol ether **18** afforded **19** in only moderate yield with several over-oxidation products. The α,β-unsaturated lactone **20** was also investigated to examine whether the chirality of the cyclopropylamine moiety influences the diastereoselectivity of the products obtained by the tandem cyclization. Because the CAN-mediated oxidation of **20** (diasteromeric mixture of 1.1 : 1) gave rise to the tricyclic products **21a** and **21b** in a total yield of 74% as a single isomer, the chirality of the cyclopropylamine moiety of **20** appears to have no effect on the diastereoselectivity of the tandem [3 + 2]-type cycloaddition.[12]

In conclusion, we have developed a novel tandem [3 + 2]-type cycloaddition using the CAN-mediated ring-opening reaction of the cyclopropylamines. This transformation allows for the utilization of aminocyclopropanes as the synthetic equivalents of γ-imino radicals. In addition, the present research demonstrates that the γ-imino radicals possess a totally different reactivity with γ-keto radicals, which can be prepared from cyclopropyl alcohols and α,β-unsaturated ketones by SET oxidation and Bu^n_3SnH-mediated reduction, respectively.[13]

We thank the Research Foundation for Pharmaceutical Sciences for financial support.

Notes and References

† E-mail: iwata@phs.osaka-u.ac.jp

‡ During our study, Cha reported the oxidative ring-opening of tertiary cyclopropylamines by photooxidation to give the corresponding ring-opened ketones (see ref. 11).

§ Syntheses of **1** and **4** were conducted according to the procedure of ref. 4.

1 J. Salaün and M. S. Baird, *Cur. Med. Chem.*, 1995, **2**, 511; K. Burgess, K.-K. Ho and D. Moye-Sherman, *Synlett*, 1994, 575; C. H. Stammer, *Tetrahedron*, 1990, **46**, 2231.
2 R. B. Silverman, *Mechanism-Based Enzyme Inactivation: Chemistry and Enzymology*, CRC Press, Boca Raton, 1988, vol. 2, pp. 119–130; C. J. Suckling, *Angew. Chem., Int. Ed. Engl.*, 1988, **27**, 537.
3 M. E. Kuehne and J. C. King, *J. Org. Chem.*, 1973, **38**, 304.
4 V. Chaplinski and A. de Meijere, *Angew. Chem., Int. Ed. Engl.*, 1996, **35**, 413; J. Lee and J. K. Cha, *J. Org. Chem.*, 1997, **62**, 1584.
5 T. Itoh, K. Kaneda and S. Teranishi, *Tetrahedron Lett.*, 1975, 2801; Y. S. Park and P. Beak, *Tetrahedron*, 1996, **52**, 12 333.
6 M. R. Angelastro, M. E. Laughlin, G. L. Schatzman, P. Bey and T. R. Blohm, *Biochem. Biophys. Res. Commun.*, 1989, **162**, 1571; F. P. Guengerich, R. J. Willard, J. P. Shea, L. E. Richards and T. L. Macdonald, *J. Am. Chem. Soc.*, 1984, **106**, 6446.
7 R. B. Silverman and X. Lu, *J. Am. Chem. Soc.*, 1994, **116**, 4129; J.-M. Kim, S. E. Hoegy and P. S. Mariano, *J. Am. Chem. Soc.*, 1995, **117**, 100.
8 M. C. Pirrung, J. Cao and J. Chen, *J. Org. Chem.*, 1995, **60**, 5790; J. E. Baldwin, R. M. Adlington, G. A. Lajoie and B. J. Rawlings, *J. Chem. Soc., Chem. Commun.*, 1985, 1496; R. K. Hill, S. R. Prakash, R. Wiesendanger, W. Angst, B. Martinoni, D. Arigoni, H.-W. Liu and C. T. Walsh, *J. Am. Chem. Soc.*, 1984, **106**, 795.
9 X.-Z. Qin and F. Williams, *J. Am. Chem. Soc.*, 1987, **109**, 595.
10 Y. Takemoto, T. Ohra, S. Furuse, H. Koike and C. Iwata, *J. Chem. Soc., Chem. Commun.*, 1994, 1529; Y. Takemoto, T. Ohra, H. Koike, S. Furuse, C. Iwata and H. Ohishi, *J. Org. Chem.*, 1994, **59**, 4727.
11 J. Lee, J. S. U. S. C. Blackstock and J. K. Cha, *J. Am. Chem. Soc.*, 1997, **119**, 10 241.
12 Y. Takemoto, S. Furuse, H. Koike, T. Ohra, C. Iwata and H. Ohishi, *Tetrahedron Lett.*, 1995, **36**, 4085.
13 K. I. Booker-Milburn, B. Cox and T. E. Mansley, *Chem. Commun.*, 1996, 2577; N. Iwasawa, S. Hayakawa, M. Funahashi, K. Isobe and K. Narasaka, *Bull. Chem. Soc. Jpn.*, 1993, **66**, 819; E. J. Enholm and K. S. Kinter, *J.Org. Chem.*, 1995, **60**, 4850; G. Pandey, S. Hajra and M. K. Ghorai, *Tetrahedron Lett.*, 1994, **35**, 7837.

Received in Cambridge, UK, 5th December 1997; 8/00125A

Metal-bound chlorine often accepts hydrogen bonds

Gabriel Aullón,[a] Dena Bellamy,[a] Lee Brammer,*[b]† Eric A. Bruton[b] and A. Guy Orpen*[a]†

[a] *School of Chemistry, University of Bristol, Bristol, UK BS8 1TS*
[b] *Department of Chemistry, University of Missouri-St. Louis, 8001 Natural Bridge Road, St. Louis MO 63121-4499, USA*

Analysis of 6624 crystallographically characterised hydrogen bonds containing M–Cl, C–Cl or Cl⁻ and either HO or HN groups show that M–Cl moieties are good, anisotropic hydrogen-bond acceptors forming hydrogen bonds similar in length to those of the chloride anion, while C–Cl moieties are very poor hydrogen-bond acceptors.

In a recent article,[1] Dunitz and Taylor showed that the hydrogen bonding capability of the C–F moiety is very poor on the basis of a crystal structure database study and quantum mechanical calculations. The implication of that work is that hydrogen bonding D–H···F–C (D = O, N,*etc.*) interactions are too weak to be of great significance in molecular recognition processes in, for example, biological chemistry or crystal engineering. Here, we show that although C–Cl moieties and C–F have rather similar hydrogen-bonding characteristics, M–Cl moieties (M = transition metal) are much better hydrogen-bond acceptors. The ability of metal halide species to act as hydrogen-bond acceptors has been noted anecdotally by us and others on the basis of one or more crystal structures.[2] Braga, Desiraju and Grepioni and coworkers[3] have shown that ligands in organometallic complexes can be involved in hydrogen bonding. In the systems they have studied the ligands are either rather weak acceptors (*e.g.* carbon monoxide) or behave essentially as their organic analogues do. In the inorganic species studied here (those with terminal M–Cl bonds) the effects of the metal on the hydrogen-bonding ability of the ligand are much more dramatic, in a way not anticipated in recent authoritative texts on hydrogen bonding.[4] Indeed Jeffery states 'while halide ions are strong hydrogen-bond acceptors, there is no evidence from crystal structures supporting hydrogen bonds to halogens.[4a] Here we show that (as Dance has speculated)[5] in contrast, metal bound chlorine is a good hydrogen bond acceptor.

To assess the hydrogen-bonding capabilities of the M–Cl unit, the Cambridge Stuctural Database[6] was used to search for structures containing O–H or N–H fragments as well as M–Cl, Cl⁻ or C–Cl.‡ Our objective was to compare the geometry of D–H···Cl–M interaction in these crystal structures as well as to assess the relative probability of such contacts being formed to chlorine in these three different forms. The intermolecular contacts were categorised as 'short' (≤2.52 Å), intermediate

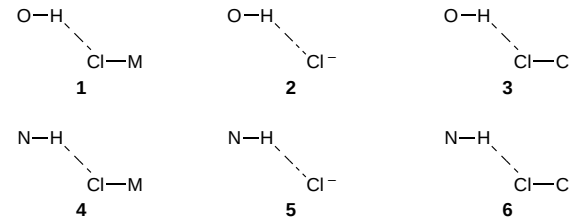

Scheme 1

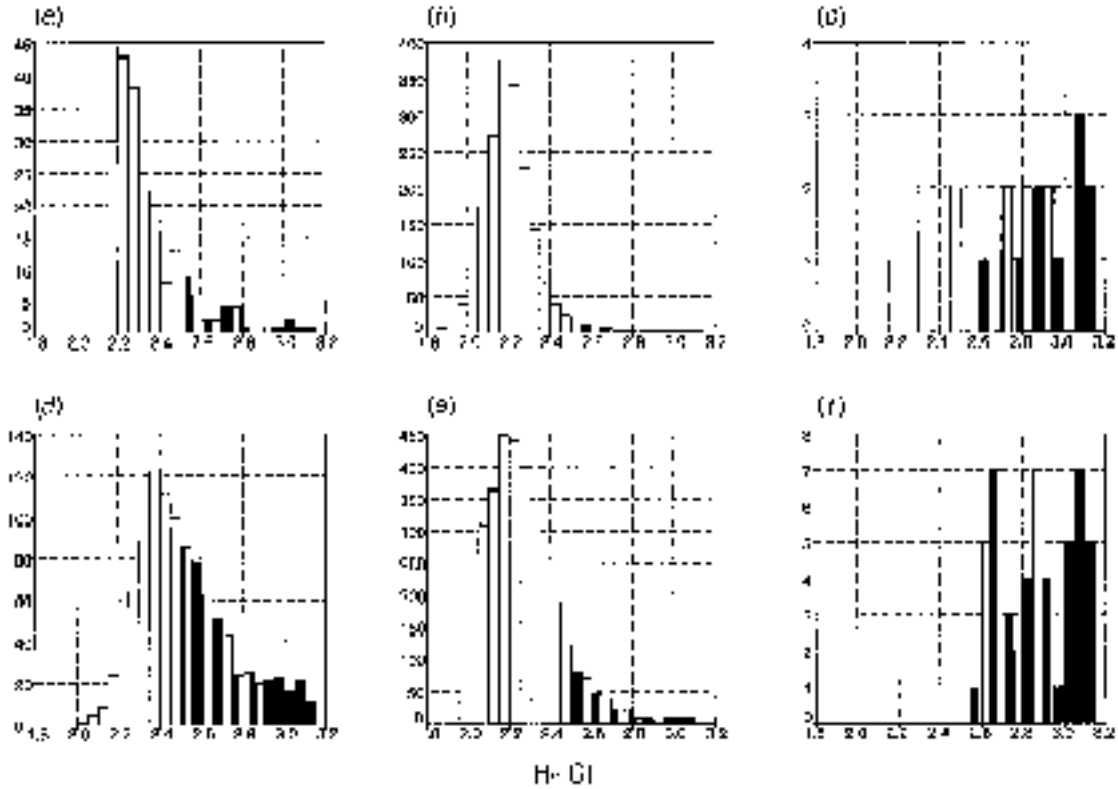

Fig. 1 Histograms of H···Cl distances for (*a*) **1**, (*b*) **2**, (*c*) **3**, (*d*) **4**, (*e*) **5**, (*f*) **6**. Short distances in light grey, intermediate in grey, long in black.

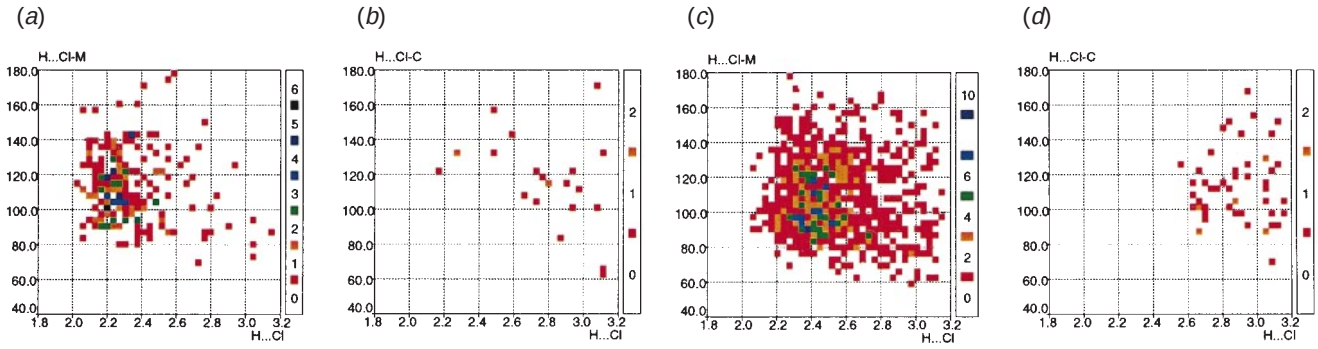

Fig. 2 Scattergrams of M–Cl···H or C–Cl···H angles *vs.* H···Cl distances in systems (*a*) **1**, (*b*) **3**, (*c*) **4**, (*d*) **6**. The number of cases in a given pixel are colour coded.

Table 1 Percentage of hydrogen-bond contacts (H···Cl ⩽ 3.15 Å) which were classified as short (H···Cl ⩽ 2.52 Å)

Interaction	D = O	D = N
D–H···Cl–M	86.5 **1**	57.4 **4**
D–H···Cl⁻	97.2 **2**	90.8 **5**
D–H···Cl–C	22.7[a] **3**	0.0 **6**

[a] Represents five observations (out of a total of 22 O–H···Cl–C contacts ⩽3.15 Å).

(2.52–2.95 Å) and long 2.95–3.15 Å (*cf.* sum of van der Waals radii for H and Cl = 1.2 + 1.75 = 2.95 Å).[7]

The range of H···Cl distances for the cases shown in Scheme 1 are illustrated in Fig. 1. It is clear that Cl^- forms many 'short' Cl···H interactions, as does the M–Cl group, whereas C–Cl moieties form almost no 'short' Cl···H interactions. The correlation of D–H···Cl angles with H···Cl distance (see Supplementary material§) is comparable to that typically observed for the corresponding parameters in both strong and weak hydrogen bonds, and shows a predominance of D–H···Cl angles close to 180° at short H···Cl separations[8]

Fig. 2 shows the spread of M–Cl···H and C–Cl···H angles with respect to H···Cl distance.¶ It is clear from examination of Fig. 2(*a*) that there is a clustering of structures for M–Cl acceptors, particularly in the short distance range, at angles of *ca.* 100–110°, suggesting some directional preference in these interactions. The C–Cl acceptors [Fig. 2(*b*),(*d*)] appear to favour a similar range of angular approaches, through there are fewer data, and almost no stronger, shorter Cl···H interactions.

The percentage of interactions formed that fall in the various categories (in particular the 'short' group, Table 1) may be taken as an indicator of the strength of the interactions of types **1**–**6**. These percentages confirm the expectation that in general O–H is a stronger donor than N–H, and more importantly that the sequence of acceptor strengths is Cl^- > M–Cl ≫ C–Cl.

The clear implication of these observations is that M–Cl containing complexes have the potential to interact with hydrogen-bond donors in both a strong (*i.e.* short) and anisotropic fashion. In the first respect they resemble the chloride ion and in the second organochlorine species. The shortness of D–H···Cl–M bonds presumably derives at least in part from the large negative charge on the chloride in these partially ionic M–Cl bonds. The poor hydrogen-bond acceptor qualities of C–Cl, C–F, *etc.* may in turn be associated with much lower charge accumulation at the halogen atom in these species.[1]

Rheingold, Crabtree and their coworkers showed that the structure of $[HNC_5H_3Ph_2\text{-}2,6][AuCl_4]$ was consistent with greater basicity of chlorine p than sp lone pairs,[2c] since there appeared to be preference for their involvement in the N–H···Cl–M bonds. In this work we have shown that this is not an isolated occurrence and that this phenomenon may be much more general than has hitherto been thought.

These observations may be extended to metal complexes of the other halides, which although less numerous show similar patterns of behaviour in structures in the CSD. We are exploring the application of these observations to the design and synthesis of crystal structures of metal halide complexes, as has been recently reported by Van Koten and coworkers.[10]

We are grateful to Todd Foust for writing utility programs to separate data for simple hydrogen bonds from those for bifurcated examples, and Dr F. H. Allen for useful discussions. We thank the Spanish Ministerio de Educación y Ciencia for an F.P.U. (Becas en el extranjero) grant (to G. A.), an NSF-REU grant (for partial support of E. A. B.), and the Universities of Bristol and Missouri-St Louis for financial support.

Notes and References

† E-mail: lee.brammer@umsl.edu; guy.orpen@bristol.ac.uk

‡ All N–H and O–H distances were normalised to standard neutron diffraction determined internuclear lengths, and only those structures containing intermolecular contacts with 1.80 ⩽ H···Cl ⩽ 3.15 Å and D–H···Cl angles ⩾ 110° were included in subsequent analyses. Data for bifurcated hydrogen bonds were removed after the initial search using locally written programs and will be discussed in a later paper.

§ Available upon request from the Authors.

¶ No spatial normalisation corrections[9] have been applied to these scattergrams. Such corrections, although widely recognised as appropriate, are not substantial in this case since there are few fragments for which the E–Cl···H angle (E = M, C) approaches 180°.

1 J. D. Dunitz and R. Taylor, *Chem. Eur. J.*, 1997, **3**, 89.
2 (*a*) L. Brammer, J. M. Charnock, P. L. Goggin, R. J. Goodfellow, T. F. Koetzle and A. G. Orpen, *J. Chem. Soc., Chem. Commun.*, 1987, 443, *J. Chem. Soc., Dalton Trans.*, 1991, 1789; (*b*) C. Xu, G. K. Anderson, L. Brammer, J. Braddock-Wilking and N. P. Rath, *Organometallics*, 1996, **15**, 3972; (*c*) G. P. A. Yap, A. L. Rheingold, P. Das and R. H. Crabtree, *Inorg. Chem.*, 1995, **34**, 3474; (*d*) T. G. Richmond, *Coord. Chem. Rev.*, 1990, **105**, 221.
3 D. Braga, F. Grepioni, P. Sabatino and G. R. Desiraju, *Organometallics*, 1994, **13**, 3532; D. Braga, F. Grepioni, K. Biradha and G. R. Desiraju, *J. Am. Chem. Soc.*, 1995, **117**, 3156; K. Biradha, D. Braga, F. Grepioni and G. R. Desiraju, *Organometallics*, 1996, **15**, 1284; D. Braga, F. Grepioni, E. Tedesco, K. Biradha and G. R. Desiraju, *Organometallics*, 1996, **15**, 2692.
4 (*a*) G. A. Jeffery *Introduction to Hydrogen Bonding*, Wiley, Chichester, 1997; (*b*) G. A. Jeffery and W. Saenger, *Hydrogen Bonding in Biology and Chemistry*, Springer Verlag, Berlin, 1993.
5 I. G. Dance, in *The Crystal as a Supramolecular Entity*, ed. G. R. Desiraju, *Perspectives in Supramolecular Chemistry*, *2*, Wiley, Chichester, 1996.
6 F. H. Allen, J. E. Davies, J. J. Galloy, O. Johnson, O. Kennard, C. F. Macrae, E. M. Mitchell, G. F. Mitchell, J. M. Smith and D. G. Watson, *J. Chem. Inf. Comput. Sci.*, 1987, **31**, 187.
7 A. J. Bondi, *J. Chem. Phys.*, 1964, **68**, 441.
8 See, for example: R. Taylor and O. Kennard, *Acc. Chem. Res.*, 1984, **17**, 320.
9 J. P. M. Lommerse, A. J. Stone, R. Taylor and F. H. Allen, *J. Am. Chem. Soc.*, 1996, **118**, 3108.
10 P. J. Davies, N. Veldman, D. M. Grove, A. L. Spek, B. T. G. Lutz and G. van Koten, *Angew. Chem., Int. Ed. Engl.*, 1996, **35**, 1959.

Received in Basel, Switzerland, 15th December 1997; 7/09014E

Enantioselective palladium catalyzed allylic substitution of acyloxypyrrolinones by alcohols

Agnes D. Cuiper, Richard M. Kellogg and Ben L. Feringa*†

Department of Organic and Molecular Inorganic Chemistry, Groningen Centre for Catalysis and Synthesis, University of Groningen, Nijenborgh 4, Groningen 9747 AG, The Netherlands

Chiral non-racemic acyloxypyrrolinones are converted into alkoxypyrrolinones with retention of configuration by a palladium catalyzed allylic substitution; this comprises a key step in a short chemo-enzymatic route to acyliminium ion precursors.

Enantiomerically pure alkoxypyrrolinones have been shown to be facile building blocks for a variety of stereoselective syntheses involving Diels–Alder cycloadditions, 1,3-dipolar reactions, conjugate additions and acyliminium ion intermediates.[1] In particular application in the asymmetric synthesis of alkaloids, based on *N*-acyliminium ion chemistry, is of great current interest.[2] For example, (*R*)-1-acetyl-5-isopropoxy-3-pyrrolin-2-one [compound (−)-**3a** (R^2 = Pr^i) in Scheme 1] has been used by Hiemstra and Speckamp as an intermediate in the synthesis of gelsemine.[3] However, the stereoselective synthesis from (*S*)-malic acid[4] is laborious and more practical routes would be desirable.

Recently we reported simple and efficient enzymatic methodology to obtain enantiomerically pure acyloxypyrrolinones **2** from hydroxypyrrolinones **1**.[5] In this process both enantiomers of an acyloxypyrrolinone can be obtained by the same enzyme (*Candida antarctica* lipase, CAL) using either an esterification (Scheme 1) or a transesterification. Although these compounds have been applied with success in various stereoselective transformations,[6] they are not suitable as acyliminium ion precursors. In order to generate an acyliminium ion the acyl group on nitrogen must be removed.[4] This is possible with an alkoxy group at the 5-position but not with a more sensitive acyloxy group. We now report that the enzymatic method can be combined with a palladium catalyzed allylic substitution to generate optically active alkoxypyrrolinones, which can readily be transformed to acyliminium ion precursors.[4]

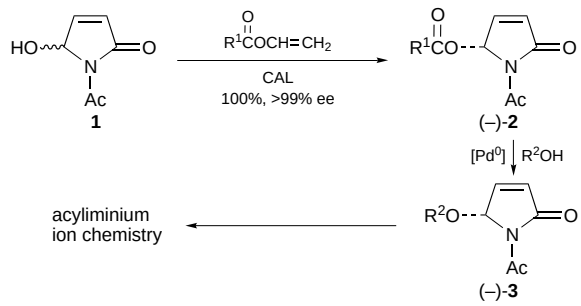

Scheme 1

When a solution of (*R*)-(−)-**2a** (R^1 = Me) in Pr^iOH is stirred at room temperature for 7 h in the presence of 0.5 mol% $Pd(PPh_3)_4$, 5-isopropoxy derivative (*R*)-(−)-**3a** (R^2 = Pr^i) is obtained in 99% yield with 95% ee (Table 1, entry 1).‡ The optically active acyloxypyrrolinone is thus converted into optically active alkoxypyrrolinone, *via* Pd^0 catalyzed allylic substitution with Pr^iOH as the nucleophile, with nearly complete *retention of configuration*. An allyl palladium intermediate **5** (Scheme 2) is presumably involved. When the reaction was performed in the presence of $Pd(OAc)_2$ (5 mol%) and PPh_3 (20 mol%) the reaction rate was appreciably lower (90% conversion after 3 d at 20 °C, > 95% ee). An essential feature is that the nucleophile Pr^iOH is also used as a solvent (roughly 13 M). In the presence of an additional solvent like THF (Pr^iOH *ca.* 10^{-1} M) no product was obtained after 18 h at room temp. When the allylic substitution was performed at higher temperatures, the reaction was very fast, but the enantioselectivity decreased in the course of the reaction (Table 2). This depletion of ee might be due either to loss of stereochemical integrity of the allyl palladium intermediate or partial racemization of acyloxypyrrolinone **1** or alkoxypyrrolinone **3**.

The substitution using $Pd(PPh_3)_4$ can easily be performed on a gram scale with equal efficiency (99%) and selectivity (94% ee). A lower rate was observed in the presence of additional PPh_3, probably because the equilibrium for the oxidative addition of the palladium complex is shifted to the left (Scheme 2).[7] The effect on the enantioselectivity is negligible.

When EtOH was used instead of Pr^iOH as a nucleophile the reaction was much faster, probably because of the higher

Table 1 Pd catalyzed nucleophilic substitution of (−)-**2** (> 99% ee)

Entry	R^1	R^2	*T*/°C	Catalyst	*t*/h	Conversion[a] (%)	Ee[b] (%)
1[c]	Me	Pr^i	25	$Pd(PPh_3)_4$ (0.5%)	7	99	95
2[c]	Me	Pr^i	25	$Pd(PPh_3)_4$ (0.5%)	5.5	72	97
3[c]	Me	Et	18	$Pd(PPh_3)_4$ (5%)	1	100	93
4[d]	Allyl	Pr^i	20	$Pd(OAc)_2 + PPh_3$ (5%)	63	100	83
5[d]	C_9H_{19}	Pr^i	20	$Pd(OAc)_2 + PPh_3$ (10%)	63	40	84
6[d]	Bu^t	Pr^i	20	$Pd(OAc)_2 + PPh_3$ (5%)	48	29	95
7[d]	Ph	Pr^i	20	$Pd(OAc)_2 + PPh_3$ (5%)	18	33	93
8	Me	Pr^i	25	$Pd(MeCN)_2Cl_2 + PPh_3$ (5%)	21	100	89
9	Me	Pr^i	25	$Pd(MeCN)_2Cl_2$ (5%)	3	99	> 99
10	Me	Et	25	$Pd(MeCN)_2Cl_2$ (5%)	3	94	99

[a] The conversion was determined by GC. [b] The ee of **3** was determined by chiral GC; > 99% indicates that the other enantiomer could not be detected. [c] (+)-**2** (> 99% ee) was used as starting material. [d] The ee of starting material **2** is unknown.

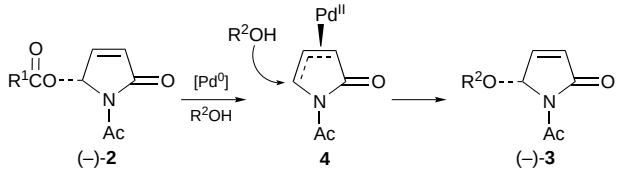

Scheme 2

Table 2 Pd catalyzed nucleophilic substitution of (+)-**2a** (R^1 = Me) at 70 °C[a]

Entry	*t*/min	Conversion[b] (%)	Ee[c] (%)
1	5	43	90
2	25	91	79
3	40	100	75

[a] $Pd(OAc)_2$ + PPh_3 (5%) was used as catalyst, Pr^iOH was used as solvent. [b] The conversion was determined by GC. [c] The ee of (+)-**3a** (R^2 = Pr^i) was determined by chiral GC.

solubility of the substrate in this solvent. A slight decrease in selectivity (93% ee) was observed (Table 1, entry 3).

This reaction can also be performed with acyloxypyrrolinones with other acyl groups (Table 1, entry 4–7). The optically active starting materials were obtained *via* enzymatic esterification, analogously to our reported procedure.[5] Because a method for direct ee determination of these 5-acyloxypyrrolinones has not yet been found, the palladium catalyzed allylic substitution and subsequent ee determination of the 5-isopropoxy pyrrolinone provides a useful alternative for determination of the ee of the starting materials.

Other palladium catalysts were also examined as the use of $Pd(PPh_3)_4$ did not result in complete stereoselectivity (95–97% ee). $PdBn(PPh_3)_2Cl$ gave, under the same conditions in Pr^iOH, less than 5% conversion in 23 h (71% ee), whereas with $Pd(dppe)_2$ no product was obtained. Palladium(II) complexes such as $Pd(OAc)_2$ were also tested without PPh_3. In this case the reaction did not proceed, but surprisingly when LiCl was added 22% conversion was found after 23 h (42% ee). A mixture of $Pd(MeCN)_2Cl_2$ (5 mol%) and PPh_3 (20 mol%) was also used, but although this reaction was faster than with $Pd(OAc)_2$ and PPh_3 (100% conversion in 21 h), the selectivity was not improved (Table 1, entry 8). A remarkable improvement was achieved when $Pd(MeCN)_2Cl_2$ (5 mol%) was used without PPh_3. With this catalyst the reaction is fast, quantitative and proceeds with complete stereoselectivity (Table 1, entries 9, 10). On 0.5 g scale with 5 mol% Pd^{II} catalyst, 96% yield of (*S*)-**3a** (R^2 = Pr^i, 99% ee) was obtained.

Palladium catalyzed nucleophilic substitution reactions of allylic substrates have found widespread use in organic synthesis and although a variety of nucleophiles has been employed emphasis has been on carbon–carbon bond formation.[8] On the contrary the use of alcohols as nucleophiles in Pd catalyzed allylic substitution is rare, because alcohols are generally considered poor nucleophiles. The few reported examples[9] are often either intramolecular substitutions or make use of derivatives of alcohols. The quantitative and stereoselective Pd catalyzed allylic substitution of 5-acyloxypyrrolinones by alcohols provides a key step in the new catalytic enantioselective, lipase and palladium based methodology for the preparation of enantiopure alkoxypyrrolinones.

We gratefully acknowledge stimulating discussions with Dr A. van Oeveren in the early stages of this work and financial support by the IOP catalysis.

Notes and References

† E-mail: feringa@chem.rug.nl

‡ Ee's were determined with a Hewlett Packard 5890 GC, equipped with a capillary column coated with CP cyclodextrin B-2,3,6-M-19 (for **3a**, R = Pr^i) or with a 30 m × 0.25 mm capillary column (ASTEC G9409-15) coated with B-TA (β-cyclodextrin, trifluoroacetyl) (for **3b**, R = Et).

Selected data for **3a**: $[\alpha]_D^{25}$ −149 (*c* 0.5, $CHCl_3$); $\delta_H(CDCl_3)$ 1.15 (d, 3 H, *J* 8.8), 1.18 (d, 3 H, *J* 8.8), 2.49 (s, 3 H), 4.23 (sept, 1 H, *J* 6.1), 5.92 (d, 1 H, *J* 2.0), 6.06 (d, 1 H, *J* 6.1), 6.97 (dd, 1 H, *J* 2.0, 6.1); $\delta_C(CDCl_3)$ 22.8 (q), 23.0 (q), 24.9 (q), 73.0 (d), 86.3 (d), 126.8 (d), 147.7 (d), 168.7 (s), 170.0 (s).

1 D. Romo and A. I. Meyers, *Tetrahedron*, 1991, **47**, 9503; A. H. Fray and A. I. Meyers, *Tetrahedron Lett.*, 1992, **33**, 3575; A. I. Meyers and L. Snyder, *J. Org. Chem.*, 1992, **57**, 3814; W.-J. Koot, H. Hiemstra and W. N. Speckamp, *Tetrahedron: Asymmetry*, 1993, **4**, 1941; W.-J. Koot, R. van Ginkel, M. Kranenburg, H. Hiemstra and W. N. Speckamp, *Tetrahedron Lett.*, 1991, **32**, 401.
2 P. Renaud and D. Seebach, *Helv. Chim. Acta*, 1986, **69**, 1704; M.-P. Heitz and L. E. Overman, *J. Org. Chem.*, 1989, **54**, 2591; M. Thaning and L.-G. Wistrand, *J. Org. Chem.*, 1990, **55**, 1406.
3 N. J. Newcombe, F. Ya, R. J. Vijn, H. Hiemstra and W. N. Speckamp, *J. Chem. Soc., Chem. Commun.*, 1994, 767.
4 W.-J. Koot, H. Hiemstra and W. N. Speckamp, *J. Org. Chem.*, 1992, **57**, 1059.
5 H. van der Deen, A. D. Cuiper, R. P. Hof, A. van Oeveren, B. L. Feringa and R. M. Kellogg, *J. Am. Chem. Soc.*, 1996, **118**, 3801.
6 A. D. Cuiper, R. M. Kellogg and B. L. Feringa, unpublished work.
7 B. M. Trost and T. R. Verhoeven, *J. Am. Chem. Soc.*, 1980, **102**, 4730.
8 J. Tsuji, in *Palladium Reagents and Catalysts*, Wiley, Chichester, 1995, ch. 4.
9 B. M. Trost and A. Tenaglia, *Tetrahedron Lett.*, 1988, **29**, 2927; R. C. Larock and N. H. Lee, *J. Org. Chem.*, 1991, **56**, 6253; F. Guibe and Y. Saint M'Leux, *Tetrahedron Lett.*, 1981, **22**, 3591; R. Lakhmiri, P. Lhoste and D. Sinou, *Synth. Commun.*, 1990, **20**, 1551; A. P. Davis, B. J. Dorgan and E. R. Mageean, *J. Chem. Soc., Chem. Commun.*, 1993, 492.

Received in Cambridge, UK, 16th January 1998; 8/00444G

Large variation of the luminescence energy from rhenium(v) complexes with oxo and nitrido ligands

Ueli Oetliker,[a] Carole Savoie,[a] Sandrine Stanislas,[a,b] Christian Reber,*[a]† Fabienne Connac,[a,b] André L. Beauchamp,[a] Frédérique Loiseau[b] and Michèle Dartiguenave[b]

[a] *Département de chimie, Université de Montréal, C.P. 6128, Succ. Centre-ville, Montréal (Québec) H3C 3J7, Canada*
[b] *Laboratoire de Chimie Inorganique, Université P.Sabatier, 118 route de Narbonne, 31062 Toulouse, France*

We observe visible and near-IR luminescence from oxo and nitrido compounds of rhenium(v) with chelating ligands combining soft (P) and hard (O) donors and show that the emitting state energy of the nitrido complexes is higher in energy by a factor of *ca*. two (8300 cm^{-1}) than for the oxo compounds, an unusually large difference.

Complexes of Re^{V} with metal–ligand multiple bonds have received considerable attention due to their reactivity, photochemical and spectroscopic properties.[1–4] We have studied a series of *trans*-dioxo complexes of Re^{V} and Os^{VI} with imidazole, carboxylate and ethylenediamine ligands[5,6] and have discovered near-IR (NIR) luminescence bands that are lower in energy by several thousand wavenumbers than the luminescence maximum of the well known *trans*-$[ReO_2(py)_4]^+$, a representative *trans*-dioxorhenium(v) compound.[7,8] Oxorhenium(v) complexes with low-energy emissions could lead to a novel spin-crossover transition expected for tetragonal 5d^2 complexes.[4]

A detailed comparative study of nitrido and *trans*-dioxo complexes of rhenium(v) reports a difference of 3000 cm^{-1} between the luminescence maxima of related *trans*-dioxo and nitrido compounds.[9] We report here that a significantly larger energy range is accessible to complexes of 5d^2 ions with metal–ligand multiple bonds. We present luminescence spectra of related Re≡O and Re≡N complexes with only one metal–ligand multiple bond and two chelating ligands.

The compounds used for our spectroscopic experiments are shown in Scheme 1. All Re^{V} centers have a triple bond to either an oxo or nitrido ligand and two anionic P–O$^-$ chelating ligands, 2-(diphenylphosphino)phenolate (**2**, **4**) or 1-phenyl-2-(diphenylphosphino)ethanolate (**1**, **3**). The distorted octahedral coordination sphere of the oxo compounds **1**, **2** is completed by chloride ligands.[10,11] The nitrido compound **3** has a triphenylphosphine ligand in its first coordination sphere[10,11] and compound **4** has a square-pyramidal structure, proposed from ^{31}P NMR, IR and elemental analysis data.

The instrumentation for luminescence measurements in the visible and near-IR wavelength range has been described previously.[12,13]‡

Fig. 1 shows low-temperature luminescence spectra of compounds **2**–**4**. Luminescence spectroscopy allows us to directly determine the energy of the lowest energy excited state for each compound. Band maxima and widths of all emission spectra are summarized in Table 1. The spectra of the oxo complexes **1** and **2** are almost identical and only the spectrum of **2** is shown. The band maxima of the oxo compound **2** and the nitrido compound **4** are separated by more than 8000 cm^{-1}, corresponding to emitting state energies that vary by a factor of two. The solid-state emissions are still observed at 200 K, but their integrated intensity decreases by approximately an order of magnitude for the compounds in Fig. 1. The spectrum of the oxo complex **2** shows barely resolved vibronic structure with a separation of *ca*. 800 cm^{-1} between peaks. This progression involves mainly the Re≡O vibrational mode observed at 958 cm^{-1} in the Raman spectrum. The nitrido compounds **3**, **4** do not show resolved structure involving the Re≡N vibrational mode, but their large bandwidths indicate that this high-frequency mode contributes significantly to the bandshape. The nitrido compound **4** shows weak vibronic structure with peaks separated by *ca*. 130 cm^{-1}. Progressions involving similar low-frequency modes have been observed for nitrido complexes of the isoelectronic Os^{VI}.[14]

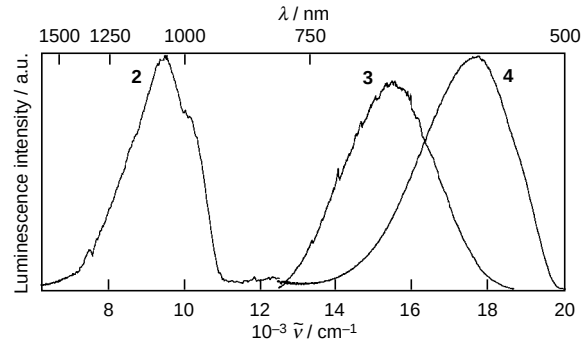

Fig. 1 Solid-state luminescence spectra of the oxorhenium(v) complex **2** and of the nitridorhenium(v) complexes **3**, **4** measured at 10 K

Table 1 Summary of spectroscopic data for the oxorhenium(v) complexes **1**, **2** and the nitridorhenium(v) complexes **3**, **4**

Complex	Luminescence (crystal, 10 K) E_{max}/cm^{-1}	Bandwidth/cm^{-1} [a]	Raman (crystal, 300 K) Re≡O,N mode/cm^{-1}	Absorption (solution, 300 K) λ_{max}/nm (ε/dm^3 mol^{-1} cm^{-1})
Re≡O, **1**	9250	2060	982	840 (10), 635 (75) 400 (260), 280 (3400)
Re≡O, **2**	9500	1990	958	830 (15), 610 (80) 400 (490), 280 (2080)
Re≡N, **3**	15350	2810	1034	450 (sh, 200) 320 (18 000)
Re≡N, **4**	17560	2940	1100	410 (800), 324 (10 200)

[a] Full width at half height.

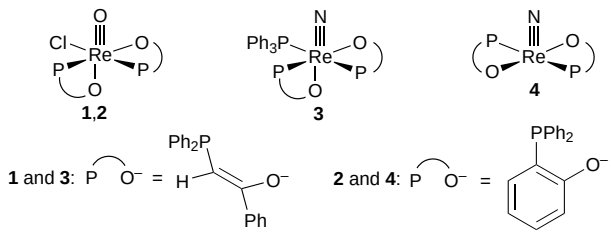

Scheme 1 Oxo (**1**, **2**) and nitrido (**3**, **4**) complexes of rhenium(v) used for spectroscopic measurements

The luminescence lifetimes of compounds **3**, **4** are shorter than 5 μs at 20 K, indicating a low quantum yield and important non-radiative relaxation processes even at low temperatures. The NIR luminescences from compounds **1**, **2** are too weak to be detected with fast Ge diodes and no lifetimes could be measured.

Absorption spectra of all compounds were measured in Me_2SO or CH_2Cl_2 solution. The onset of the lowest-energy absorption band occurs at wavelengths close to the high-energy onset of the luminescence spectra in Fig. 1, indicating that the observed solid-state emissions are not originating from deep traps. The molar absorptivities of the lowest-energy bands are low, characteristic for d–d transitions, but higher than those typically observed in *trans*-dioxo systems owing to the absence of inversion symmetry in compounds **1**–**4**. Absorption and Raman data for all compounds are included in Table 1.

We rationalize the observed large variation of the luminescence band maxima by comparing spectra and EHMO calculations based on crystal structures for compounds **1**–**3**.[10,11]§ The molecular *z* axis is chosen to coincide with the metal–ligand multiple bond and the calculations show predominant contributions from the $5d_{xy}$ and $5d_{xz,yz}$ atomic orbitals to the HOMO and LUMO, respectively. The lowest energy electronic transition therefore arises from a $5d_{xy} \rightarrow 5d_{xz,yz}$ orbital excitation, identical to the first electronic transition for *trans*-dioxo complexes of rhenium(V).[4,7] The energy of the HOMO ($5d_{xy}$) orbital depends mainly on the ancillary ligands and varies by less than 400 cm^{-1} within the series of compounds. The different LUMO energies are the most important reason for the variation of the emission energies of oxo and nitrido complexes. The calculated HOMO–LUMO gap for the nitrido compound **3** is 10 621 cm^{-1}, higher by approximately a factor of two than for the oxo complex **2**, where a gap of 4923 cm^{-1} is calculated. These orbital energy differences vary by 5700 cm^{-1}, surprisingly close to the difference of 5850 cm^{-1} between the emission maxima of compounds **2** and **3** given in Table 1. The comparison also indicates that interelectronic repulsions and other physical effects neglected in the EHMO calculations account for the discrepancy between observed transition energies and orbital energy differences. The separation of the $5d_{xz,yz}$ orbitals is calculated to be less than 1000 cm^{-1} for compounds **1**–**3**. These orbitals are degenerate in *trans*-dioxo compounds with D_{4h} symmetry and the small separations calculated for our compounds again underline the close similarity to the *trans*-dioxo systems. The MO calculations therefore confirm our d–d assignment for the lowest-energy electronic transition and are consistent with the spectroscopic data in Fig. 1 and Table 1. In addition, they qualitatively agree with *ab initio* calculations on a series of complexes with metal–ligand multiple bonds.[15]

Electronic spectra and EHMO calculations suggest that the character of the lowest-energy electronic transitions is essentially d–d. We have shown a first example for the large tuning range for the luminescence energies of related oxo and nitrido complexes.

This work was made possible by research grants from the NSERC (Canada) and from the Ministère de l'Enseignement Supérieur et de la Recherche (France).

Notes and References

† E-mail: reber@chimie.umontreal.ca

‡ Luminescence spectra of polycrystalline samples of all compounds were measured in a helium gas-flow cryostat. A Xe lamp and the 488.0 and 514.5 nm lines of an Ar^+ ion laser were used as excitation sources, and the emitted light was dispersed by either a 0.5 m or a 0.75 m monochromator. Photomultipliers and a photon counting system were used to detect the luminescence from the nitrido compounds, the emission from the oxo systems was measured with a cooled Ge detector and a lock-in amplifier, using an acquisition approach developed in our laboratory to minimize noise in the near-IR region.[13] A pulsed excimer laser and a digital oscilloscope were used to measure luminescence lifetimes. Raman spectra were measured with a Spex Ramalog system and Ar^+ ion laser, solution absorption spectra were recorded on a Varian Cary 5E spectrometer.

§ EHMO calculations were made with the program package YAeHMOP (version 2.0) by G. Landrum, 1997. YAeHMOP is available at http://overlap.chem.cornell.edu:8080/yaehmop.html.

1 W. A. Nugent and J. M. Mayer, *Metal–Ligand Multiple Bonds*, Wiley, New York, 1988.
2 V. W.-W. Yam and C.-M. Che, *Coord. Chem. Rev.*, 1990, **97**, 93.
3 D. M. Roundhill, *Photochemistry and Photophysics of Metal Complexes*, Plenum, New York, 1994.
4 V. M. Miskowski, H. B. Gray and M. D. Hopkins, *Adv. Transition Met. Coord. Chem.*, 1996, **1**, 159.
5 C. Savoie, C. Reber, S. Bélanger and A. L. Beauchamp, *Inorg. Chem.*, 1995, **34**, 3851.
6 C. Savoie and C. Reber, *Coord. Chem. Rev.*, 1998, in press.
7 J. R. Winkler and H. B. Gray, *Inorg. Chem.*, 1985, **24**, 346.
8 J. R. Winkler and H. B. Gray, *J. Am. Chem. Soc.*, 1983, **105**, 1373.
9 V. W.-W. Yam, K.-K. Tam, M.-C. Cheng, S.-M. Peng and Y. Wang, *J. Chem. Soc., Dalton Trans.*, 1992, 1717.
10 F. Loiseau, Y. Lucchese, M. Dartiguenave, F. Bélanger-Gariépy and A. L. Beauchamp, *Acta Crystallogr., Sect. C*, 1996, **52**, 1968.
11 F. Connac, Y. Lucchese, M. Dartiguenave and A. L. Beauchamp, *Inorg. Chem.*, 1997, **36**, 256.
12 M. J. Davis and C. Reber, *Inorg. Chem.*, 1995, **34**, 4585.
13 U. Oetliker and C. Reber, *J. Near Infrared Spectrosc.*, 1995, **3**, 63.
14 M. D. Hopkins, V. M. Miskowski and H. B. Gray, *J. Am. Chem. Soc.*, 1986, **108**, 6908.
15 A. Neuhaus, A. Veldkamp and G. Frenking, *Inorg. Chem.*, 1994, **33**, 5278.

Received in Bloomington, IN, USA, 25th November 1997; 7/08517F

Chiral relay auxiliary for the synthesis of enantiomerically pure α-amino acids

Steven D. Bull, Stephen G. Davies,*† Simon W. Epstein and Jacqueline V. A. Ouzman

The Dyson Perrins Laboratory, University of Oxford, South Parks Road, Oxford, UK OX1 3QY

Chiral auxiliary (3*S*)-*N*,*N*′-bis(*p*-methoxybenzyl)-3-isopropylpiperazine-2,5-dione employs a chiral relay network based on non-stereogenic *N*-benzyl protecting groups to enhance diastereocontrol during enolate alkylation.

The structural diversity of non-proteinogenic α-amino acids is reflected by the large number of different methods which have been developed for their asymmetric synthesis.[1] Those approaches that are based on chiral auxiliaries generally rely on alkylation of a masked glycine enolate where diastereofacial selectivity is controlled by an attached homochiral residue.[2] Schöllkopf's auxiliary **1** derived from *O*-methylation of diketopiperazine (DKP) **3** has been widely used in this area but there are problems associated with its use for synthesis (Scheme 1).[3] It is a volatile oil which is difficult to prepare, it exhibits poor diastereoselectivities with a linear or β-branched electrophiles and is also susceptible to acid catalysed hydrolysis.[4] It is known that *N*,*N*′-dialkylpiperazine-2,5-diones are robust, highly crystalline compounds[5] and we wished to exploit these characteristics to create a new chiral auxiliary **4** for the synthesis of enantiomerically pure α-amino acids.

Molecular modelling studies[6] revealed that enolate **5** derived by deprotonation of **4** adopts a conformation which enables the stereochemical information of the (3*S*)-isopropyl group to be relayed through space *via* non-stereogenic benzyl protecting groups. The ring system of enolate **5** is essentially planar with its isopropyl group fixing the conformation of the proximal N4 benzyl *anti*, which in turn directs the distal N1 benzyl group *syn* to the isopropyl group. This arrangement effectively blocks the *Si* face of enolate **5** towards alkylation at C6 (Fig. 1). We predicted that the proximity of the N1 benzyl group to C6 would result in significantly higher alkylation diastereoselectivities for DKP **4** than would be achieved for either Schöllkopf's auxiliary **1** or *N*,*N*′-dimethylated DKP **2** where, in both cases, the stereofacial control is only provided by the C3 isopropyl group.

Highly crystalline (3*S*)-*N*,*N*′-bis(*p*-methoxybenzyl)-3-isopropylpiperazine-2,5-dione **4** ($[\alpha]_D^{23}$ −53.7, *c* 1.0 in $CHCl_3$)‡ was prepared in 85% yield by dropwise addition of *p*-methoxybenzyl chloride to cyclo-[L-Val-Gly] **3**[4] and sodium hydride in DMF (Scheme 1). Enantiomerically pure (3*S*)-*N*,*N*′-dimethyl-3-isopropylpiperazine-2,5-dione **2** ($[\alpha]_D^{23}$ +84.4, *c* 1.0 in $CHCl_3$)‡ was prepared in a similar manner using methyl iodide as the electrophile (Scheme 1). The enantiomeric purities of both **2** and **4** were confirmed by comparison of their ^{1}H NMR spectra with authentic racemic materials in the presence of chiral shift reagent (*S*)-(+)-2,2,2-trifluoro-1-(9-anthryl)ethanol.[7]

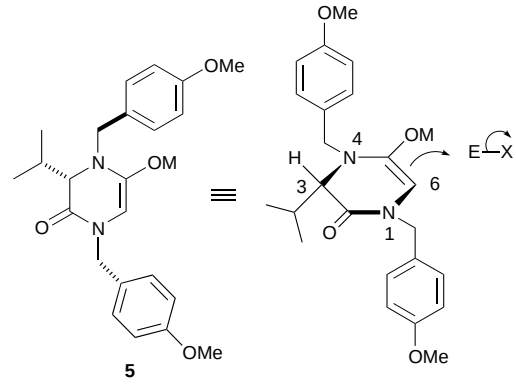

Fig. 1 Electrophile attacks *anti* to both the C3 isopropyl and N1 protecting group

DKP **4** was deprotonated with one equivalent of lithium hexamethyldisilazide in THF at −78 °C followed by addition of four equivalents of methyl iodide to afford a mixture of C6-methylated diastereoisomers **6** and **7** in 93% de (Scheme 2). The diastereoisomers were separated by chromatography [silica, diethyl ether–hexane (1 : 1)] and the configuration of the major diastereoisomer confirmed as *trans*-**7** by direct compar-

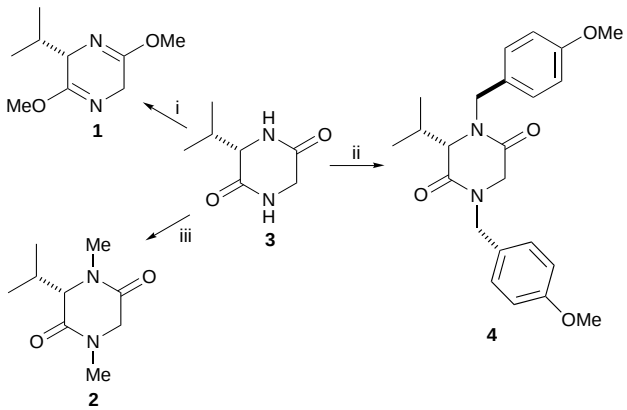

Scheme 1 *Reagents and conditions*: (i) $Me_3O^+BF_4^-$, CH_2Cl_2; (ii) NaH, *p*-methoxybenzyl chloride, DMF; (iii) NaH, MeI, DMF

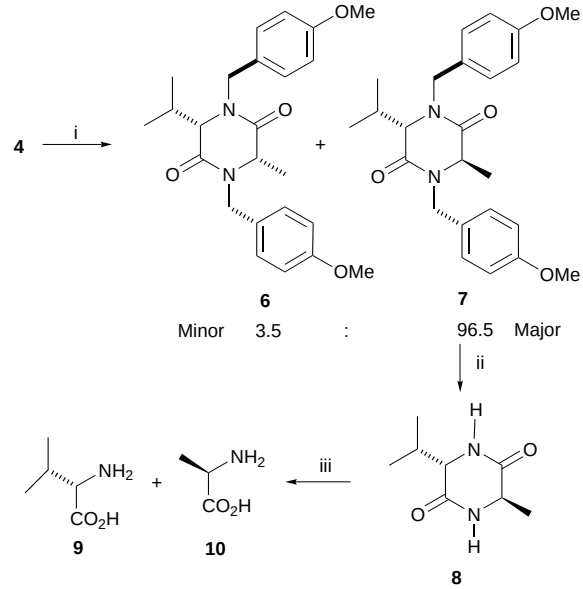

Scheme 2 *Reagents and conditions*: (i) LHMDS, THF, −78 °C; 10 equiv. MeI; (ii) CAN, CH_3CN–H_2O; (iii) 6 M HCl, Dowex 50-XH

Table 1 Comparison of diastereoselectivity and yield for alkylation of auxiliaries **1** and **4**[a]

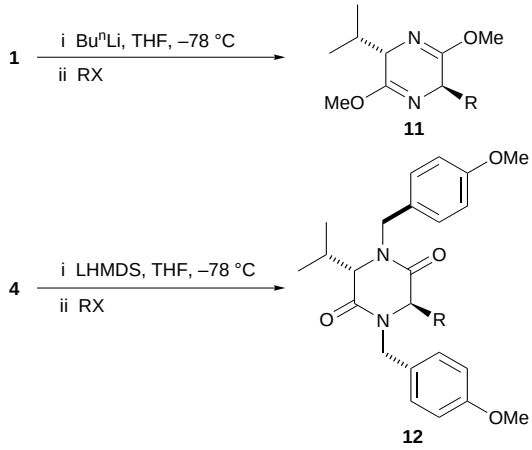

	De (%)		Yield (%)		
Electrophile RX	**11**	**12**	**11**	**12**	$[\alpha]_D^{23}$ **12** ($CHCl_3$)‡
Methyl iodide	50	93	54	72	+22.5 (*c* 0.98)
Benzyl bromide	91[b]	98	81[b]	88	+58.6 (*c* 0.99)
Allyl bromide	74	94	83[c]	63	+25.8 (*c* 0.99)
Prop-2-ynyl bromide	52[c]	89	70[d]	74	+14.6 (*c* 0.98)
Ethyl iodide	*d*	90	*a*	78	+46.1 (*c* 1.00)
Isopropyl iodide	*d*	96	*a*	90	0 (*c* 1.00)

[a] Ref. 13. [b] Ref. 3. [c] Ref. 11. [d] Ref. 12.

ison with an authentic sample prepared *de novo* by *N*-*p*-methoxybenzylation of the piperazine-2,5-dione **8** derived from L-valine **9** and D-alanine **10**.

Deprotection of *trans*-methylated auxiliary **7** was easily achieved *via* oxidative removal of the *p*-methoxybenzyl groups using cerium ammonium nitrate in CH_3CN–H_2O[8] followed by acid catalysed hydrolysis of **8** to afford a mixture of (*S*)-valine **9** and (*R*)-alanine **10**. This mixture was separated by ion exchange chromatography[9] to afford enantiomerically pure (*R*)-alanine, **10** ($[\alpha]_D^{23}$ −14.0, *c* 0.6 M in 1 M HCl)[10]‡ in 86% yield (Scheme 2).

Alkylation of **4** with a range of electrophiles afforded highly crystalline *trans*-alkylated products **12** in > 90% de (Table 1). Simple recrystallisation of the crude reaction product afforded the major *trans*-diastereoisomer pure in good yield. The non-basic character of enolate **5** is particularly noteworthy since reaction with electrophiles that are prone to β-elimination (ethyl iodide or isopropyl iodide) occurred in excellent yield.

It is clear that the alkylation diastereoselectivities observed for the new piperazine-2,5-dione auxiliary **4** compare favourably with those obtained using Schöllkopf's auxiliary **1** (Table 1). Evidence to suggest that the benzylic *N*,*N*′-protecting groups are directly responsible for the improved performance of **4** was obtained by methylating *N*,*N*′-dimethylated piperazine-2,5-dione **2** in which the *N*-methyl groups do not have the capacity to enhance the stereoselectivity *via* the proposed relay mechanism. DKP **2** was methylated under identical conditions

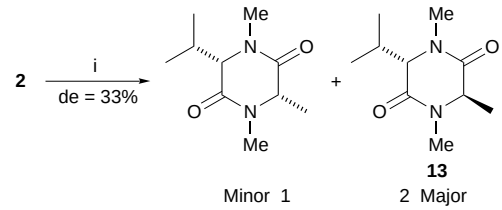

Scheme 3 *Reagents and conditions*: (i) LHMDS, THF, −78 °C; 10 equiv. MeI.

described for **4** to afford *trans*-(3*S*,6*R*)-6-methyl-**13** as the major diastereoisomer in a much reduced 33% de (Scheme 3).

The results obtained for methylation of the enolates of **2** and **4** are clearly consistent with the proposed chiral relay network operating to enhance the diastereoselectivity observed for alkylation of enolate **5**. Further investigations are currently underway to apply the proposed chiral relay concept to enhance stereocontrol in other scenarios.

We thank Zeneca Pharmaceuticals (J. V. A. O.) and Oxford Asymmetry Ltd (S. D. B.) for financial support, and the DTI and EPSRC for a LINK award.

Notes and References

† E-mail: steve.davies@chemistry.ox.ac.uk

‡ Given in 10^{-1} deg cm^2 g^{-1}.

1 R. M. Williams, *Synthesis of Optically Active* α*-amino acids*, Pergamon Press, Oxford, 1989; R. O. Duthaler, *Tetrahedron*, 1994, **50**, 1539.
2 Some of the more popular methods are (*a*) Seebach's imidazolidinone: D. Seebach, A. R. Sting and M. Hoffmann, *Angew. Chem., Int. Ed. Engl.*, 1997, **35**, 2708; (*b*) Williams' oxazinone: R. M. Williams and M. N. Im, *J. Am. Chem. Soc.*, 1991, **113**, 9276; (*c*) Evans' oxazolidinone: D. A. Evans, A. E. Weber, *J. Am. Chem. Soc.*, 1986, **108**, 6757; (*d*) Oppolzers' sultam: W. Oppolzer, R. Moretti and C. Zhou, *Helv. Chim. Acta.*, 1994, **77**, 2363; (*e*) Myers' pseudoephedrine auxiliary: A. G. Myers, J. L. Gleason and T. Yoon, *J. Am. Chem. Soc.*, 1995, **117**, 8488.
3 C. Deng, U. Groth and U. Schöllkopf, *Angew. Chem., Int. Ed. Engl.*, 1981, **20**, 798.
4 S. D. Bull, S. G. Davies and W. O. Moss, *Tetrahedron: Asymmetry*, 1997, in the press.
5 G. Porzi and S. Sandri, *Tetrahedron: Asymmetry*, 1996, **7**, 189.
6 Molecular modelling calculations were carried out using the MOPAC™ (CHEM3D™) suite of Molecular Mechanics programs using PM3 parameters.
7 W. H. Pirkle and P. E. Adams, *J. Org. Chem.*, 1980, **45**, 4117.
8 R. M. Williams, M. R. Sabol, H. Kim and A. Kwast, *J. Am. Chem. Soc.*, 1991, **113**, 6621.
9 S. Moor and W. H. Stein, *J. Biol. Chem.*, 1951, **192**, 663.
10 Identical specific rotation to an authentic sample purchased from Aldrich Chemical Company.
11 W. Karnbrock, H. J. Musiol and L. Moroder, *Tetrahedron*, 1995, **51**, 1187.
12 Only starting material **1** was obtained due to deprotonation of the electrophile.
13 All new compounds were fully characterised.

Received in Liverpool, UK, 14th January 1998; 8/00407B

Carboxylate and carboxylic acid recognition by tin(IV) porphyrins

Joanne C. Hawley,[a] Nick Bampos,[a] Raymond J. Abraham[b] and Jeremy K. M. Sanders*[a]†

[a] *Cambridge Centre for Molecular Recognition, University Chemical Laboratory, Lensfield Road, Cambridge, UK CB2 1EW*
[b] *Department of Chemistry, University of Liverpool, Liverpool, UK L69 3BX*

The scope of carboxylate binding by tin(IV) porphyrins and the solution geometries of the resulting complexes have been explored using ^{1}H NMR spectroscopy; ring current induced shifts and competition experiments indicate the operation of an attractive anthracene–porphyrin interaction; outer sphere carboxylic acid complexes of dihydroxy tin(IV) porphyrins have been characterised, apparently for the first time.

As part of a larger project[1,2] aimed at supramolecular catalysis we have been exploring the ligand recognition properties of tin(IV) porphyrins. We report here on the scope of carboxylate recognition and the solution state geometry of the resulting complexes, demonstrate that anthracene–porphyrin interactions can overcome the usual geometrical preference, and present what we believe is the first direct evidence for hydrogen-bonded carboxylic acid outer sphere complexes.

It has long been known[3,4] that the hard metal centre endows a strongly oxophilic character on tin(IV) porphyrins:‡ carboxylate complexes of acids with p$K_a \leqslant$ *ca*. 5 can be prepared rapidly and effectively quantitatively by mixing a large excess of the free carboxylic acid with dihydroxy tin(IV) porphyrins in non-polar solvents. However, by employing low concentrations of acids, following the reactions by ^{1}H NMR spectroscopy, and exploiting the fact that the ring currents associated with porphyrins lead to large upfield shifts for axially bound ligands, we have uncovered several previously unreported phenomena:

(*i*) The rate and extent of complex formation increases with acid strength: using 5 mM porphyrin and 5 mM propionic acid, complexation is complete in 30 min at room temperature, while carboxylate complex formation with dichloroacetic acid is complete within a few seconds.§ Fig. 1 shows the complexation shifts observed in several dicarboxylate complexes of Sn^{IV}(tpp).¶ The carboxylate complexes are in slow exchange on the NMR chemical shift timescale with any excess carboxylic acid that is present.

(*ii*) With weaker acids or in the presence of < 2 equiv. of stronger acids the monohydroxymonocarboxylate complex is readily observed as the major complex.

(*iii*) Stronger acids generally displace the carboxylates of weaker acids. However, in such competition experiments, anthracene-9-carboxylic acid (p$K_a \approx 3.6$) behaves as if it were intermediate in strength between monochloroacetic acid (p$K_a \approx$ 2.9) and dichloroacetic acid (p$K_a \approx 1.5$). This unusual result is discussed below.

(*iv*) 'Free' carboxylic acid resonances are broadened and shifted upfield unexpectedly: immediately after addition of 1 equiv. of propionic acid to a $CDCl_3$ solution of Sn^{IV}(tpp)$(OH)_2$, the methylene resonance of the added acid was upfield shifted by 1.02 ppm, but as carboxylate complex formation took place over a period of minutes the residual 'free' carboxylic acid signals shifted back towards their normal positions. This observation is consistent with the formation, in fast exchange on the chemical shift timescale, of a weak outer sphere complex between the Sn–OH and carboxylic acid. Such a complex is the first intermediate in the likely mechanism of formation of the final covalent complex (Fig. 2).‖ As the reaction proceeds the concentrations of Sn–OH sites and free carboxylic acids decrease, so the fraction of outer-sphere bound acid molecules also decreases. At low temperatures the formation of the covalent carboxylate complex of adamantane-1-carboxylic acid is slowed sufficiently that it does not interfere with observation of essentially complete formation of the hydrogen-bonded complex (Fig. 3). From analysis of the concentration dependence of shifts we estimate the apparent association constant for this hydrogen-bonded species to be *ca*. 10^4 dm^3 mol^{-1}, while analysis of the ring current-induced shift of H_A indicates a distance of *ca*. 5 Å from the carboxylate oxygen to the Sn centre. To our knowledge, such complexes have never been directly observed previously, although their existence has been

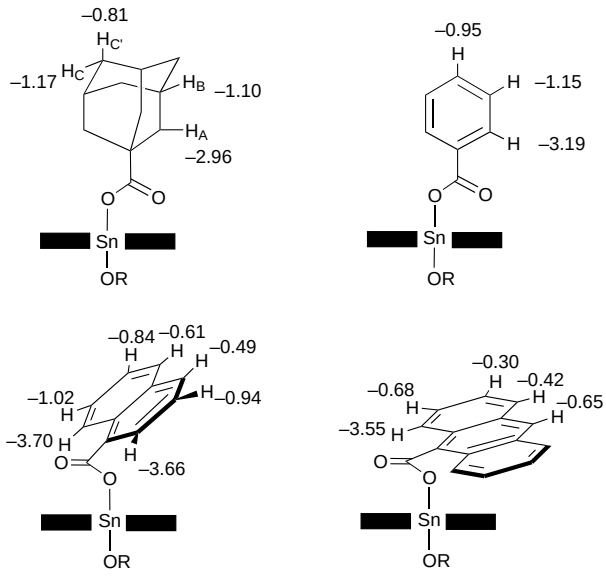

Fig. 1 Porphyrin-induced shifts ($\Delta\delta$/ppm) for some Sn^{IV}(tpp) dicarboxylate complexes. In each case $\Delta\delta = \delta$ (complex) $- \delta$ (free acid).

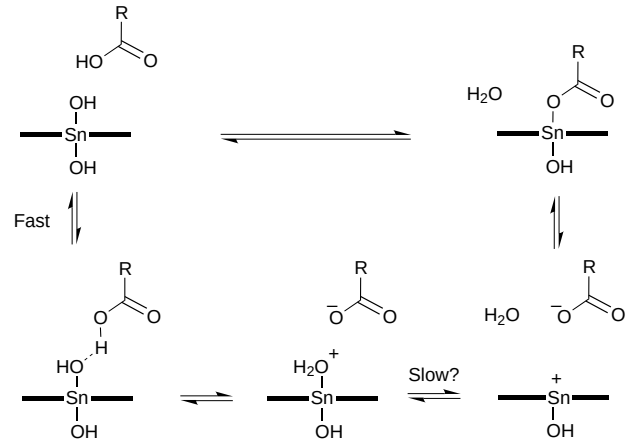

Fig. 2 Presumed mechanism of formation for tin–carboxylate complexes

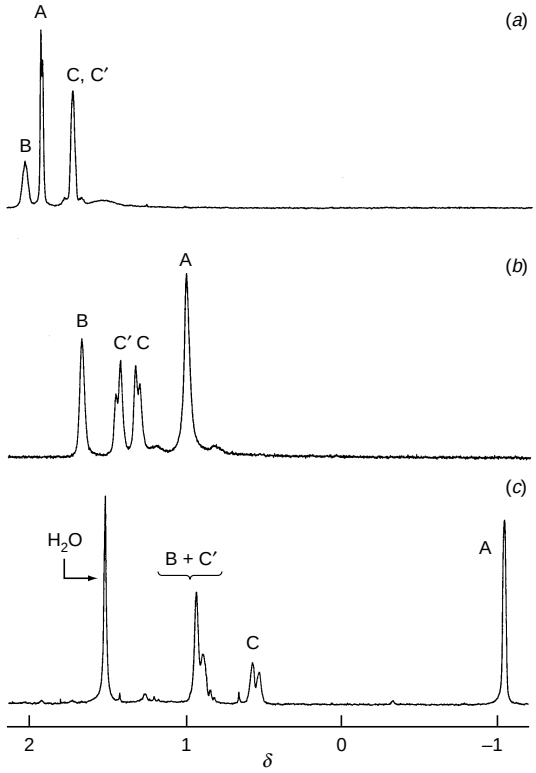

Fig. 3 Partial ^{1}H NMR spectra of adamantane acid (*a*) free, (*b*) hydrogen-bonded to $Sn^{IV}(tpp)(OH)_2$ and (*c*) as dicarboxylate complex. Traces (*a*) and (*c*) were obtained at 250 MHz, 20 °C, and trace (*b*) at 400 MHz, −53 °C.

postulated in connection with tin(IV) porphyrin electrochemistry.[5]

Since the porphyrin ring current is quite well characterised geometrically and has been applied to a range of metallo-porphyrin complexes,[6] we elected to apply the same approach to the tin(IV) systems. In the first instance, the known X-ray[7] structure for the dibenzoate complex was used to parametrise the ring current for our observed solution state NMR shifts in the same complex. With the ring current thus calibrated, the observed $\Delta\delta$ were fitted to give best-fit geometries. While it is not possible to obtain great precision it is clear that simple aromatic carboxylates are bound with their aryl rings effectively perpendicular to the porphyrin plane, with the dihedral angle Sn–O–C–C of *ca*. 180° and with an Sn–O bond length of *ca*. 2.1 Å.

However, the shifts observed in the anthracene complex do not match this geometry: they are consistent only with an arrangement where the Sn–O–C–C angle is reduced to *ca*. 100°, bringing the anthracene ring almost coplanar with the porphyrin as shown in Fig. 1. We attribute this geometry to an attractive π–π or donor–acceptor interaction with the porphyrin ring; this additional interaction also explains the unexpectedly strong binding described above. Naphthoic-1-carboxylic acid, perhaps unsurprisingly, displays a shift (and therefore spatial) behaviour that is intermediate between its anthracene and benzoic homologues (Fig. 1), but we cannot distinguish rapid exchange between 'vertical' and 'horizontal' conformations from a static conformation that is intermediate in geometry.

The exclusive oxophilicity of tin(IV) porphyrins complements perfectly the strong preference of zinc and ruthenium(II) porphyrins for nitrogen ligands. Pyridines do indeed bind to zinc or ruthenium(II) porphyrins in the same solution as carboxylic acids bind to Sn^{IV} porphyrins without mutual interference, so it is possible to construct mixed metal dimers and trimers with completely independent ligand specificities at each site.[9] This greatly expands the repertoire of recognition and catalytic processes that are now available. At a simpler level, $Sn^{IV}(tpp)(OH)_2$ may prove useful as a diamagnetic NMR shift reagent for carboxylates.

We thank Simon Webb for helpful discussions and advice, and the EPSRC and Unilever Research for financial support.

Notes and References

† E-mail: jkms@cam.ac.uk

‡ Tin(II) porphyrins bind soft ligands such as S and Se, but their sensitivity to air and moisture renders them unsuitable for routine molecular recognition studies.[8]

§ Detailed analysis of NMR shifts and couplings, and of X-ray structures, reveals that the Sn–O bond length increases slightly but systematically as the pK_a of the carboxylic acid decreases. Details will be discussed in a full paper, but the trends are broadly in line with those expected.[4,7]

¶ H_2tpp = 5,10,15,20-tetraphenylporphyrin.

‖ It is possible that the hydrogen bonding pattern is actually Sn–O–H···O=C rather than as shown. The pK_a dependent behaviour described above is also consistent with the suggested mechanism.

1 J. K. M. Sanders, *Comprehensive Supramolecular Chemistry*, ed. J. L. Atwood, J. E. D. Davies, D. D. Macnicol and F. Vögtle, Elsevier, Amsterdam, 1996, vol. 9, pp. 131–164.
2 Z. Clyde-Watson, A. Vidal-Ferran, L. J. Twyman, C. J. Walter, D. W. J. McCallien, S. Fanni, N. Bampos, R. S. Wylie and J. K. M. Sanders, *New J. Chem.*, 1998, in press.
3 J. W. Buchler and L. Puppe, *Liebigs Ann. Chem.*, 1974, 1046.
4 D. P. Arnold, E. A. Morrison and J. V. Hanna, *Polyhedron*, 1990, **9**, 1331.
5 C. E. Kibbey, S. B. Park, G. Deadwyler and M. E. Meyerhoff, *J. Electroanal. Chem.*, 1992, **335C**, 135.
6 P. Leighton, J. A. Cowan, R. J. Abraham and J. K. M. Sanders, *J. Org. Chem.*, 1988, **53**, 733; R. J. Abraham and C. J. Medforth, *Magn. Reson. Chem.*, 1990, **28**, 343; R. J. Abraham and I. Marsden, *Tetrahedron*, 1992, **48**, 7489.
7 G. Smith, D. P. Arnold, C. H. L. Kennard and T. C. W. Mak, *Polyhedron*, 1991, **10**, 509.
8 J.-M. Barbe, C. Ratti, P. Richard, C. Lecomte, R. Gerardin and R. Guilard, *Inorg. Chem.*, 1990, **29**, 4126.
9 S. J. Webb and J. C. Hawley, unpublished work.

Received in Cambridge, UK, 18th December 1997; 7/09069B

Electrophilic functionalization of a cyclometallated ruthenium complex, an easy entry to new organometallic synthons

Christophe Coudret,*† Sandrine Fraysse and Jean-Pierre Launay

Molecular Electronics Group, Centre d'Elaboration des Matériaux et d'Etudes Structurales, CNRS UPR 8011, BP 4347, 29 rue Jeanne Marvig, 31055 Toulouse Cedex, France

With the regiospecific halogenation of the complex [Ru(bpy)$_2$L^1]$^+$ (bpy = 2,2′-bipyridine, HL^1 = 2-phenylpyridine) new organometallic starting materials are now available.

Our long lasting interest into dinuclear mixed valence complexes originates from the fact that they are the best chemical models of molecular wires, the basic function of molecular electronics. Indeed, a simple spectroscopic study of the intervalence transition gives directly the ability of the bridging ligand to couple the two metallic centers.[1] Since it is usually achieved by a redox titration, the various species (reduced, mixed valence or oxidized) have to be stable for a long period of time, typically up to 1 h. Ruthenium cyclometallated complexes with a N_5C donor set were found to be among the best metallics ends for such purpose.[2]

In a recent report, the synthesis of such polynuclear complexes involved as 'building block' a brominated cyclometallated RuN_5C complex, which was prepared from a bromine containing ligand.[3] Such a synthesis could be advantageously shortened by a direct and regioselective halogenation of the metallated ligand *i.e.* after the complex is prepared.

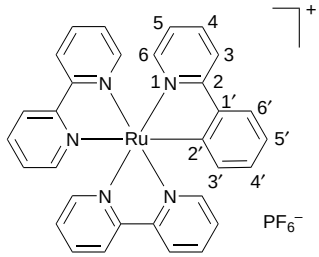

1

Apart from the typical cathodic shifts of all the redox potentials compared to the RuN_6 family,[4,5] few chemical properties of RuN_5C cyclometallated complexes have been reported. The presence of the C–Ru bond promotes oxidative dimerization,[5,6] but also nitration[3] or chlorination (albeit in low yield).[7] Since the cyclometallated analogue of [Ru(bpy)$_3$]$^{2+}$, *i.e.* [Ru(bpy)$_2$L^1]$^+$, was readily accessible from commercially available chemicals,[4] a systematic study of the electrophilic bromination and iodination of the complex [Ru(bpy)$_2$L^1]PF$_6$ **1** was undertaken on a preparative scale and the reactivity of the resulting complexes under Sonogashira alkynylation reaction was studied. We would like to report here our findings on these points.

Theoretical calculations using extended Hückel theory were first performed in an analogous manner as for [Ru(terpy)(dpb)]$^+$ [dpb = 1,3-bis(2-pyridyl)benzene].[8] As for this complex the HOMO was found to be not only mostly located on the metallated phenyl ring but also having an important coefficient on the C$^{5'}$.‡ Owing to its low oxidation potential (0.5 V *vs.* SCE) and rather high sensitivity to acidic medium, buffered, mildly oxidizing electrophilic conditions were selected.

Upon treatment of the complex with 1.1 equiv. of *N*-bromosuccinimide in MeCN at room temperature[9] and after a hydrazine quench, a single compound was isolated as a PF_6 salt by column chromatography (SiO_2/CH_2Cl_2). It was identified by FABMS as the expected bromo-substituted complex [Ru(bpy)$_2$L^2]PF$_6$ **2a**. Eventually the regioselectivity of the substitution was recognised by ^{1}H NMR spectroscopy since the pattern associated with the very shielded core hydrogen H$^{3'}$ was clearly simplifed. The bromination, easily scaled up, did not require anhydrous or anaerobic conditions to proceed and occurred within 4 to 6 h (Scheme 1).§

This result prompted us to prepare the iodo analogue, more interesting from a synthetic point of view. Surprisingly NIS[10] was found to be unreactive or lead to complex degradation in MeCN respectively at room or reflux temperature. We found that complex oxidation could be limited by using CH_2Cl_2 as solvent, the best iodinating agent being I_2/PhI(OAc)$_2$, at room temperature for 4 h.[11] Finally, column chromatography purification (SiO_2) after anion exchange using a 'basic eluent' $CHCl_3$–Et_3N–EtOH gave a reproducible isolated yield of *ca.* 50% of [Ru(bpy)$_2$L^3]PF$_6$ **3a**.

As expected, the electron-withdrawing nature of the substituent induced an anodic shift with respect to parent complex **1** for the Ru^{III}–Ru^{II} redox couple of complexes **2a** and **2b** (Table 1). Reactivity of complexes **2a** and **2b** towards Sonogashira's alkynylation [Pd(PPh$_3$)$_4$, CuI, Et_3N, DMF] was then investigated with protected acetylene, *i.e.* trimethylsilylacetylene and 3-methylbut-3-yn-2-ol, as substrates (Scheme 2). In all cases, compounds were isolated as PF_6 salts by column chromatography. A marked difference between **2a** and **2b** was observed

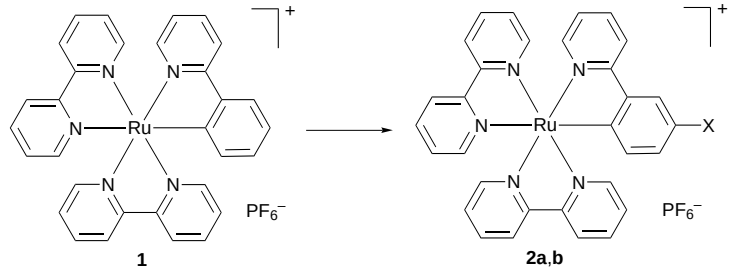

1 **2a**,**b**

Scheme 1 *Reagents and conditions*: X = Br: NBS, MeCN, room temp., 6 h, 95%, **2a**; X = I: PhI(OAc)$_2$, I_2, CH_2Cl_2, room temp., 6 h, 50%, **2b**

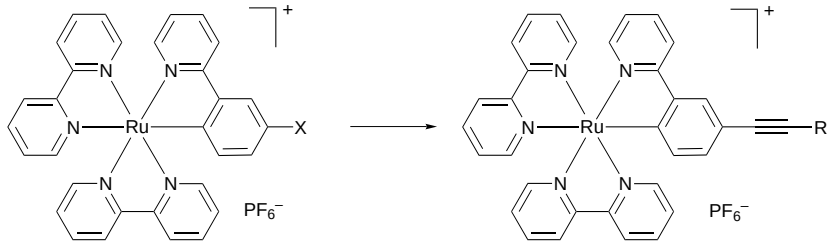

Scheme 2 *Reagents and conditions*: i, **2a**, DMF, Et_3N, CuI, $Pd(PPh_3)_4$, 80 °C, 18 h, 80%; ii, **2b**, DMF, Et_3N, CuI, $Pd(PPh_3)_4$, 20 °C, 18 h, 80%

Table 1 Ru^{III}–Ru^{II} redox couples *vs.* SCE (MeCN, 0.1 M $NBu^n_4PF_6$, Pt)

Complex	E^0 (Ru^{III}–Ru^{II})/mV
$[Ru(bpy)_2(L^1)]PF_6$ **1**	464
$[Ru(bpy)_2(L^2)]PF_6$ **2a**	520
$[Ru(bpy)_2(L^3)]PF_6$ **2b**	498

since the iodo complex reacted at room temperature with both alkynes, while the bromo complex required at least heating to 80 °C. Furthermore **2a** did not react with silylated acetylene ($SiMe_3$ or $SiEt_3$). These results, in sharp contrast with a RuN_6 analogue developed by Tzalis and Tor,[12] might indicate that the limiting step is the oxidative addition of the C–Br bond on the Pd^0 complex.

Hence we have shown that, despite the possibility of over-oxidation of the metal center, the presence of the C–Ru bond not only activates the metallated aromatic ring towards electrophilic substitution but also controls its regioselectivity. This *a posteriori* functionalization provides a simple and unique entry to synthetically interesting synthons which would have been difficult to prepare otherwise, especially for the iodo complex **2b**. We are currently studying their reactivity as building blocks in the preparation of more sophisticated architectures such as molecular wires or switches.

We thank the CNRS and EEC (CHRXCT-94-0538) for financial support, Dr G. Balacco for a free copy of Swan-MR,[13] and Drs J.-P. Collin and E. Ishow for fruitful discussions.

Notes and References

† E-mail: coudret@cemes.fr

‡ Since the HOMO is very close in energy to the two other orbitals belonging to the t_{2g} set of low-spin d^6 Ru^{II}, more complete information is given by the examination of net charges borne by carbon atoms, because they are determined by all occupied orbitals. Thus for carbon atoms *para* to pyridine nitrogens, values near +0.06 are found, while the carbon atom *para* to the C–Ru bond exhibits a −0.09 charge, confirming its better reactivity towards electrophiles. Calculations were performed with the CACAO program (CACAO PC Version 4.0, July 1994. C. Mealli and D. M. Proserpio, *J. Chem. Educ.*, 1990, **67**, 399 using −12.0 eV for Ru 4d energy). A related calculation by the Fenske Hall method has been reported (E. C. Constable and C. E. Housecroft, *Polyhedron*, 1990, **9**, 1939).

§ *Selected analytical data* for **2a**: ^{1}H NMR (CD_3CN, 250 MHz, $SiMe_4$): δ 6.36 (d, 1 H, 8.0 Hz), 6.93 (dd, 1 H, 8.0, 2.1 Hz), 6.97 (td, 1 H, 6.5, 1.4 Hz), 7.22 (td, 3 H, 6.6, 1.3 Hz), 7.41 (td, 1 H, 7.0, 1.2 Hz), 7.60 (dd, 1 H, 5.7, 1.3 Hz), 7.66–7.88 (m, 7 H), 7.94–8.10 (m, 4 H), 8.30 (dd, 2 H, 8.0, 3.4 Hz), 8.39 (d, 1 H, 8.0 Hz), 8.46 (d, 1 H, 8.2 Hz). Anal. Calc. for $C_{31}H_{23}BrF_6N_5RuP$, C, 47.04; H, 2.93; N, 8.85. Found: C, 46.94; H, 3.25; N, 8.66%. FABMS (NBA matrix) *m*/*z*: 648 $(M - PF_6)^+$, calc. 646.5.

1 A.-C. Ribou, J.-P. Launay, K. Takahashi, T. Nihira, S. Tarutani and C. W. Spangler, *Inorg. Chem.*, 1994, **33**, 1325; C. Patoux, C. Coudret, J.-P. Launay, C. Joachim and A. Gourdon, *Inorg. Chem.*, 1997, **36**, 5037.
2 M. Beley, S. Chodorowski-Kimmes, J.-P. Collin, P. Laine, J.-P. Launay and J.-P. Sauvage, *Angew. Chem., Int. Ed. Engl.*, 1994, **33**, 1775.
3 S. Chodorowski-Kimmes, M. Beley, J.-P. Collin and J.-P. Sauvage, *Tetrahedron Lett.*, 1996, **37**, 2963.
4 E. C. Constable and J. M. Holmes, *J. Organomet. Chem.*, 1986, **301**, 203.
5 M. Beley, J.-P. Collins and J.-P. Sauvage, *Inorg. Chem.*, 1993, **32**, 4539.
6 M. Beley, J.-P. Collin, R. Louis, M. Metz and J.-P. Sauvage, *J. Am. Chem. Soc.*, 1991, **113**, 8521.
7 J.-P. Sutter, D. Grove, M. Beley, J.-P. Collin, N. Veldman, A. Spek, J.-P. Sauvage and G. van Koten, *Angew. Chem., Int. Ed. Engl.*, 1994, **33**, 1282.
8 C. Patoux, J.-P. Launay, M. Beley, S. Chodorowski-Kimmes, J.-P. Collin, S. James and J.-P. Sauvage, *J. Am. Chem., Soc.*, in press.
9 M. C. Carreño, J. L. Garcia Ruano, G. Sanz, M. Toledo and A. Urbano, *J. Org. Chem.*, 1995, **60**, 5328.
10 M. C. Carreño, J. L. Garcia Ruano, G. Sanz, M. Toledo and A. Urbano, *Tetrahdron Lett.*, 1996, **37**, 4081.
11 E. B. Merkushev, N. D. Simakhina and G. M. Koveshnikova, *Synthesis*, 1980, 486; Y. Ogata and K. Aoki, *J. Am. Chem. Soc.*, 1968, **90**, 6187.
12 D. Tzalis and Y. Tor, *Chem. Commun.*, 1996, 1043; *J. Am. Chem. Soc.*, 1997, **119**, 852.
13 G. Balacco, *J. Chem. Comput. Sci.*, 1994, **34**, 1235.

Received in Basel, Switzerland, 19th December 1997; 7/09101J

Solid state and solution behaviour of novel transition metal containing surfactants

Ian A. Fallis,*† Peter C. Griffiths,* Paul M. Griffiths, David E. Hibbs, Michael B. Hursthouse and Angie L. Winnington

Department of Chemistry, University of Wales Cardiff, PO Box 912, Cardiff, UK CF1 3TB

The micellation properties of first row transition metal containing surfactants derived from aza-macrocyclic ligands is described; the structure of one of the surfactants in the solid state has been determined by X-ray crystallography; the dimensions and morphology of micelles formed by a nickel(II) surfactant have been investigated by small-angle neutron scattering (SANS).

Surfactants containing transition metal ions have only recently begun to be investigated, and to date no attempt has been made at the rigorous determination of their structure–property relationships. Typical cationic amphiphiles, such as cetyltrimethylammonium bromide (CTAB), display surface activity but are essentially 'innocent' in their chemical reactivity. Our interest in this area is ultimately directed towards the preparation and application of surfactants which contain 'non-innocent' transition metal complexes as the head-group. The use of a transition metal ion in the head-group not only imparts charge, but also permits the incorporation of useful properties such as colour (*i.e.* a chromophore), paramagnetism, variable charge and pH sensitivity. However, most importantly, transition metal complexes possess a wide range of reactivity, such as redox behaviour and catalytic activity. Thus transition metal containing surfactants provide a method for localising redox or catalytic activity at an interface.

Here, we report our preliminary results on the synthesis and characterisation of a range of nickel(II) and copper(II) based surfactants. For the purposes of this paper we define the systems under investigation as cationic metallo-surfactants in which a (transition) metal ion forms an integral part of the head-group. Earlier work by other groups on metallo-surfactants has tended to concentrate on the lyotropic phase behaviour of non-labile metal complexes for example a $[Ru^{II}(terpy)_2]^{2+}$ system.[1] An example of micellation in a $[Co^{II}(polyamine)]^{3+}$ system has been reported,[2] but again the metal centre is non-labile. Of systems with kinetically labile metal ions, there has also been an elegant investigation into the micellation of a diaza-18-crown-6 based surfactant (an annelide) in the presence of s-block cations by a range of techniques,[3] and a recent report of a copper(II) cryptand which forms unilamellar vesicles.[4] The work presented here describes the solution and solid state behaviour of a ligand system which produces surface active complexes from non-surface active ligands upon coordination of a labile metal centre.

Initially we sought simple ligand systems in which the various components of the resulting complex amphiphile could easily be modified to accommodate different alkyl chain lengths and numbers, variable head-group size and a range of d- and f-block metal ions. Also we required a ligand system which formed stable complexes in which the metal ion remained strongly bound to the head-group of the amphiphile. This prevents the complication of metal–ligand dissociation affecting the composition of the system. Metal–ligand dissociation would not only increase the ionic strength of the solution but would also lower c.m.c. values by the introduction of the largely hydrophobic free ligand. We therefore prepared the range of ligands L^1R based upon 1,4,7-triazacyclononane ([9]aneN_3). The synthesis of these ligands was achieved in gram quantitites

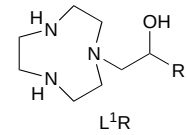

L^1R

$R = C_nH_{2n+1}$

n = 6, 8, 10, 12, 14, 16

by reacting 20 equiv. of 1,4,7-triazacyclononane with 1,2-epoxyalkanes in ethanol solution. The free ligands were isolated in quantitative yield after removing the excess 1,4,7-triazacyclononane by distillation. To date these ligands represent the first reported examples of aza-macrocycles bearing a single pendant alcohol donor.

The ligands L^1R are poorly soluble in water, but readily dissolve upon the addition of nickel(II) salts to afford blue/purple solutions. The electronic spectra of these solutions indicate that the coordination geometry at the metal centre is octahedral and it is probable that an N_3O_3 (*i.e.* L^1R and two molecules of water) donor atom set is present. The single crystal structure of $[Ni^{II}(L^1R)(H_2O)_2]Cl_2$ ($R = C_{10}H_{21}$) was determined.‡ The structure of the cation is illustrated in Fig. 1. This confirms the N_3O_3 coordination sphere at a slightly distorted octahedral metal centre, with the macrocycle in its typical face capping mode and the pendant-arm alcohol also coordinated to the metal centre. The alkyl chain is found to be in the fully extended conformation. The packing diagram (Fig. 2) indicates that a lamellar structure is formed with an antiparallel arrangement of the cations. We have prepared ligands L^1R in both racemic and optically active forms. The structure presented here was prepared with racemic material and the crystal structure contains alternating layers of (*R*) and (*S*) material. It is worth noting that single crystals of the complexes $[Ni^{II}(L^1R)(H_2O)_2]Cl_2$ were found to be remarkably easy to obtain by cooling or concentrating stock solutions containing an excess of $NiCl_2$(aq). The facile nature of the crystallisation process is attributed to a Krafft point effect, with the approximate Krafft temperatures for the complex $[Ni^{II}(L^1R)(H_2O)_2]Cl_2$ being 35 °C ($R = C_{10}H_{21}$) and 65 °C ($R = C_{16}H_{33}$).

Characterisation of the interfacial behaviour of $[Ni^{II}(L^1R)(H_2O)_2]Cl_2$ ($R = C_nH_{2n+1}$, n = 6, 8, 10, 12, 14, 16) has been undertaken to determine its critical micelle concentration, c.m.c. Surface tension measurements were determined by the Du Noüy platinum ring method. A typical plot of surface tension *vs.* concentration is illustrated in Fig. 3 for $[M^{II}(L^1R)(H_2O)_2]Cl_2$ ($R = C_{10}H_{21}$), ($M = Ni^{II}$, Cu^{II}). Using this method,

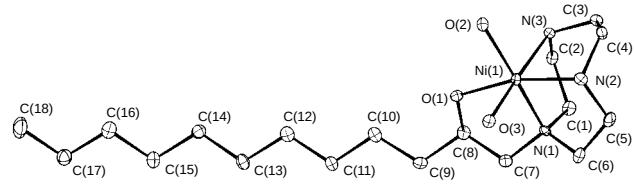

Fig. 1 Structure of the cation in $[Ni^{II}(L^1R)(H_2O)_2]Cl_2$ ($R = C_{10}H_{21}$). H-atoms are omitted. Ellipsoids are drawn at 50% probability.

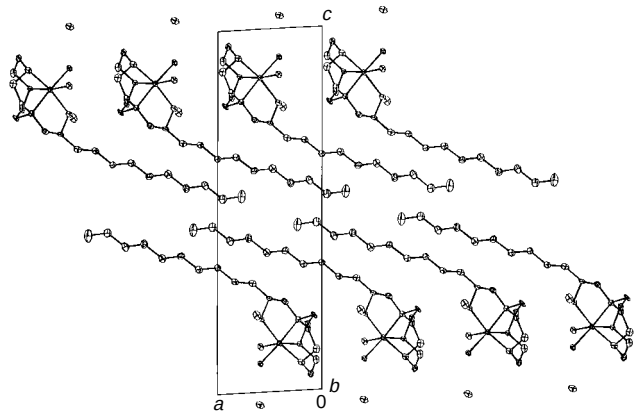

Fig. 2 Packing diagram in $[Ni^{II}(L^1R)(H_2O)_2]Cl_2$ (R = $C_{10}H_{21}$). View is along the *b* axis. Ellipsoids are drawn at 50% probability.

the c.m.c.s of the surfactants are 1.5 ± 0.2 mM (M = Ni^{II}) and 0.8 ± 0.1 mM (M = Cu^{II}). The adsorbed amount and hence, area per molecule at the surface, calculated *via* the Gibbs equation, $d\gamma/d \ln c = -\Gamma/RT$ is the same for both surfactants; 50 ± 5 Å^2. The c.m.c. values are lower than expected for a doubly charged amphiphile, which may be explained by noting that the head-group itself contains eight additional carbon centres, and hence reducing the overall hydrophilicity. The lower c.m.c. value of the copper complex is attributed to the tendency for Cu^{II} to adopt five-coordinate geometries. This would result in a marginally smaller head-group. Furthermore, it has been shown[5] that Cu^{II} can increase the acidity of a bound alcohol group so as to permit deprotonation. This process, even if occurring to a limited extent, would reduce the charge on the head-group and permit alkoxide to alcohol hydrogen bonding to occur between head-groups. This interaction between head-groups would reduce the effect of electrostatic repulsion of the head-groups, further lowering the c.m.c. value. Thus it can be seen that a very subtle change in the metal centre from Ni^{II} to Cu^{II} has a significant effect on the micellation properties of these surfactants.

The structures formed in the bulk solution slightly above the c.m.c. have been investigated by small-angle neutron scattering (SANS). The scattering from surfactant systems contains three important terms; the form factor, the structure factor and a constant term, essentially the intensity per micelle. The form factor describes the size and shape of the scattering body. The structure factor describes the spatial distribution of the scattering bodies and is determined by their interaction potential. For dilute cases, the structure factor may be neglected. A full analysis of the comprehensive SANS study will be presented shortly, but some data referring to the $[Ni^{II}(L^1R)(H_2O)_2]Cl_2$ (R = $C_{10}H_{21}$) surfactant are presented here.§ A typical set of scattering data and a fit to a spherical micelle model are shown

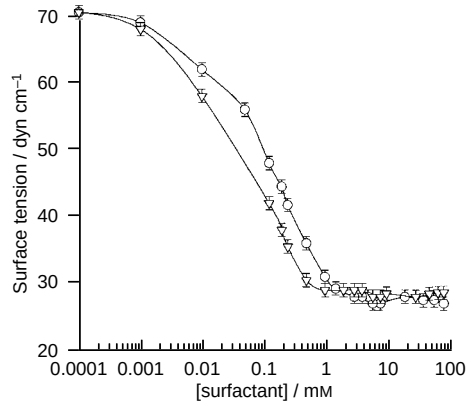

Fig. 3 Surface tension *vs.* concentration for $[M^1(L^1R)(H_2O)_2]Cl_2$(aq) (R = $C_{10}H_{21}$) where M = Ni^{II} (○) or Cu^{II} (▽)

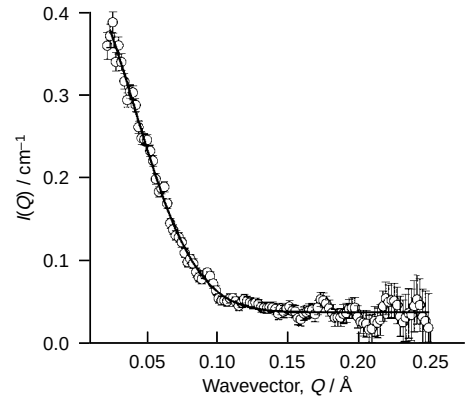

Fig. 4 SANS data for $[Ni^{II}(L^1R)(H_2O)_2]Cl_2$ (in D_2O) and the fit to a spherical micelle model. Concentration of $[Ni^{II}(L^1R)(H_2O)_2]Cl_2$ = 10 mM. (The quantity Q is given by $Q = (4\pi/\lambda)\sin(\theta/2)$, and is the modulus of the scattering vector, the resultant between the incident and scattered wavevectors.)

in Fig. 4. Given the resolution of the data, we have made no attempt to break the scattering down into its component 'core' (alkyl tails) and 'shell' (head-group) contributions. The radius of the micelle is found to be 34 ± 3 Å with an aggregation number of 50 ± 10. This radius is somewhat larger than might be expected from a surfactant which has an all-*trans* length of *ca.* 20 Å and it therefore appears that the micelles are either very diffuse in nature or display a degree of non-sphericity. This anomaly is currently the subject of further SANS experiments.

We wish to thank Dr. Stephen M. King (ISIS, Didcot). We also acknowledge the Engineering and Physical Sciences Research Council (P. M. G.) and the Nuffield Foundation (A. L. W.) for financial support.

Notes and References

† E-mail: fallis@cf.ac.uk

‡ *Crystal data* for $C_{18}H_{43}Cl_2N_3NiO_3$, M = 479.16, triclinic, space group $P\bar{1}$, a = 7.0430(6), b = 7.4080(8), c = 23.795(3) Å, α = 98.660(14)°, β = 90.670(14)°, γ = 106.010(5) (by least squares refinement of the setting angles for 250 reflections within θ = 2.60–25.13°). U = 1177.9(2) Å^3, Z = 2, D_c = 1.351 g cm^{-3}, T = 150 K, μ(Mo-Kα) = 10.72 cm^{-1}, $F(000)$ = 516, crystal size = 0.24 × 0.18 × 0.16 mm. Data were collected on a FAST TV Area detector diffractometer following previously described methods.[6] From the ranges scanned, 5038 data were recorded ($2.60 < \theta < 25.13°$; index ranges $-7 < h < 7$, $-6 < k < 8$, $-26 < l < 26$) and merged to give 3244 unique (R_{int}) = 0.0726). The structure was solved *via* direct methods[7] and refined on F_o^2 by full matrix least squares[8] using all unique data corrected for Lorentz and polarisation factors. All non-hydrogen atoms were anisotropic. The hydrogen atoms were inserted in idealised position with U_{iso} set at 1.5 U_{eq} of the parent. The weighting scheme used was $w = 1/[\sigma^2(F_o)^2 + (0.0219P)^2]$, where $P = [\text{Max.}(F_o)^2 + 2(F_c)^2]/3$; this gave satisfactory agreement analyses. Final R_1 (F) and $wR2$ (F_o^2) values were 0.0671 and 0.1016 for all 3244 data and 245 parameters. The corresponding R-values were 0.0419 and 0.0978 for 2038 data with $I > 2\sigma(I)$. Sources of scattering factors as in ref. 8. CCDC 182/756.

§ SANS measurements were performed on the LOQ diffractometer at the ISIS Spallation Source, Oxfordshire, UK.

1 J. D. Holbrey, G. J. T. Tiddy and D. W. Bruce, *J. Chem. Soc., Dalton Trans.*, 1995, 1769.
2 M. Yashiro, K. Matysumoto and S. Yoshikawa, *Chem. Lett.*, 1989, 985.
3 J. Le Moigne and J. Simon, *J. Phys. Chem.*, 1980, **84**, 170.
4 P. Ghosh, T. K. Khan and P. K. Bharadwaj, *Chem. Commun.*, 1996, 189.
5 A. J. Blake, T. M. Donlevy, P. A. England, I. A. Fallis, S. Parsons, S. A. Ross and M. Schröder, *J. Chem. Soc., Chem. Commun.*, 1994, 1981.
6 J. A. Darr, S. R. Drake, M. B. Hursthouse and K. M. A. Malik, *Inorg. Chem.*, 1993, **32**, 5704.
7 G. M. Sheldrick, *Acta. Crystallogr., Sect. A.*, 1990, **46**, 467.
8 G. M. Sheldrick, SHELXL-93, Program for Crystal Structure Refinement, University of Göttingen, Germany, 1993.

Received in Cambridge, UK, 24th November 1997; 7/08448J

Synthesis and characterisation of microporous titano-borosilicate ETBS-10

João Rocha,*[a] Paula Brandão,[a] Michael W. Anderson,[b] Tetsu Ohsuna[c] and Osamu Terasaki[d]

[a] *Department of Chemistry, University of Aveiro, 3810 Aveiro, Portugal*
[b] *Department of Chemistry, UMIST, PO Box 88, Manchester, UK M60 1QD*
[c] *Institute for Materials Research, Tohoku University, Sendai 980, Japan*
[d] *Department of Physics, Tohoku University, Aramaki Aoba, Sendai 980, Japan*

The synthesis and structural characterisation of microporous titanosilicate ETS-10 containing boron in the framework (ETBS-10) are reported.

Microporous titanosilicates known as ETS contain six-coordinate framework titanium atoms and are, thus, fundamentally different from other zeolite-type solids. The framework of ETS-10, the most prominent member of this new family, consists of 'TiO_2' rods, which run in two orthogonal directions, surrounded by tetrahedral silicate units.[1–3] The pore structure consists of 12-rings, 7-rings, 5-rings and 3-rings and has a three-dimensional wide-pore channel system whose minimum diameter is defined by 12-ring apertures. In an attempt to improve the acid characteristics of ETS-10, silicon has been isomorphously substituted by aluminium and gallium on sites which avoid Ti–O–Al(Ga) linkages.[4–6] We now wish to report the synthesis of boron-substituted ETS-10. Establishing the insertion of a light element, such as boron, in the framework of a zeolite-type material is, by no means, a trivial task. In order to gather as much evidence as possible for the substitution of silicon by boron in the framework of ETS-10 we have used a multi-technique approach.

ETBS-10 materials were prepared using a modification of the ETS-10 synthesis.‡ The samples were characterised by bulk chemical analysis (ICP), powder X-ray diffraction (XRD), high-resolution and scanning electron microscopies (HREM and SEM, respectively), FTIR and Raman spectroscopies, ^{29}Si and ^{11}B solid state NMR.

All ETBS-10 samples studied contain a single phase. The HREM images of this phase (not shown) are very similar to those previously reported for ETS-10.[2,3] The powder XRD patterns of ETS-10 and ETBS-10 samples (not shown) are almost identical, the only difference being a slight shift of the ETS-10 reflection at 2θ 24.63° to lower *d*-values when the boron content increases (2θ 24.72° for Si/B = 32). This is a first indication that the smaller boron atom replaces silicon in the structure of ETS-10.

The Raman spectrum of ETS-10 [Fig. 1(*a*)] contains a strong and sharp band at *ca.* 730 cm^{-1} associated with the TiO_6 octahedra. ETBS-10 samples display similar spectra [Fig. 1(*b*,*c*)] but this band broadens and shifts to higher frequency as the boron content increases. Similar effects have been observed with aluminium [Fig. 1(*d*)] and gallium (not shown) substituted ETS-10 samples. Hence, Raman spectroscopy provides further indication of the framework boron insertion.

Fig. 2 shows the ^{29}Si magic-angle spinning (MAS) NMR spectra of ETS-10 and ETBS-10 samples with different boron contents. In ETS-10 there are two types of silicon chemical environments, Si(3Si, 1Ti) and Si(4Si, 0Ti), which give the two groups of resonances at δ −94 to −97 and δ *ca.* −103.7, respectively.[3] The spectrum reveals a further crystallographic splitting of the Si(3Si, 1Ti) site. As the amount of boron in ETBS-10 increases, a new peak grows at δ *ca.* −99 and all the resonances broaden considerably. Owing to this broadening, the ETS-10 line splitting at δ *ca.* −96.5 is no longer resolved. This further suggests that boron has been incorporated into the framework of ETS-10. Indeed, detailed studies on aluminium-substituted ETS-10 have shown that the broadening of the ^{29}Si MAS NMR resonances (and concomitant loss of the δ *ca.* −96.5 line splitting) is due to lattice distortion upon Al incorporation.[3] At present we cannot give a detailed assignment of the ETBS-10 peak at δ *ca.* −99. However, since (*i*) it becomes stronger as the boron content increases and (*ii*) we have found no evidence for the presence in our samples of any other (siliceous) phase, we believe that this resonance is given by Si–O–B environments.

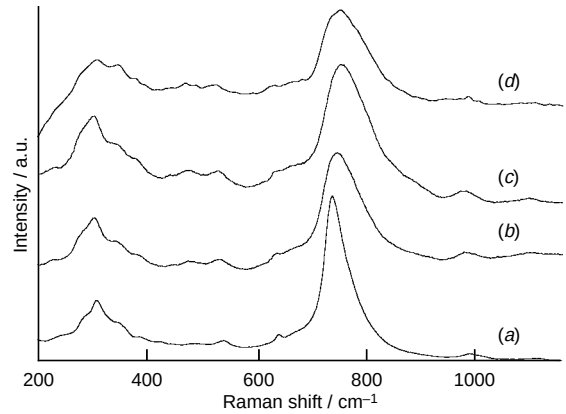

Fig. 1 Stokes shifted Raman spectra of (*a*) ETS-10, (*b*) ETBS-10 (Si/B = 45), (*c*) ETBS-10 (Si/B = 32) and (*d*) Al-substituted ETS-10 (Si/Al = 20). The spectra were measured using a Renishaw Raman imaging microscope model 2000.

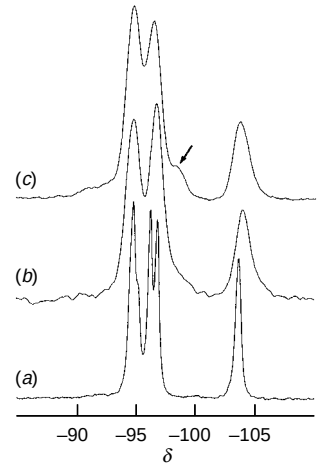

Fig. 2 ^{29}Si MAS NMR spectra of (*a*) ETS-10, (*b*) ETBS-10 (Si/B = 45) and (*c*) ETBS-10 (Si/B = 32). The spectra were recorded at 79.5 MHz on a Bruker MSL 400P spectrometer using 3.0 μs radio-frequency pulses, 40 s recycle delays and spinning rates of 5 kHz.

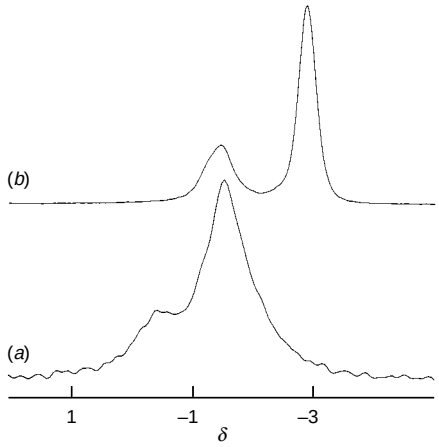

Fig. 3 (*a*) ^{1}H–^{11}B CP MAS and (*b*) ^{11}B MAS NMR spectra of ETBS-10 (Si/B = 32), recorded at 128.4 MHz, using 2 s recycle delays, a contact time of 1 ms and spinning rates of 7 kHz

The ^{11}B MAS NMR spectra [Fig. 3(*b*)] of ETBS-10 samples with different boron contents are similar and contain two groups of very sharp peaks (full width at half maximum, FWHM, *ca*. 78 Hz) at δ *ca*. −1.4 and −2.9. This implies that any electric field gradients created by the electronic cloud at the ^{11}B nuclei are very small and shows that boron is in tetrahedral, rather than trigonal, coordination[7,8] and, most likely, residing in the framework. Indeed, it has been reported that hydrated boron-substituted H-ZSM-5 zeolite gives a single sharp ^{11}B NMR peak at δ −3.[7] On the other hand, the local environment of any extraframework boron would, in principle, be more distorted or, at least, a dispersion of boron sites would occur leading to significantly broader ^{11}B NMR resonances. As prepared hydrated ETBS-10 and dehydrated ETBS-10 (500 °C for 2 h in air) display almost identical ^{11}B and ^{29}Si MAS NMR spectra. The parent gel gives a much broader (FWHM 360 Hz) ^{11}B resonance at δ *ca*. 1.1 (not shown). A second faint and broad peak is seen at δ *ca*. 3.2. The ^{1}H–^{11}B cross-polarization (CP) MAS NMR signal is very weak and the spectrum shown in Fig. 3(*a*) required the accumulation of 30 000 transients (500 for the MAS spectrum). We tentatively assign the two resonances at δ −1.4 and −0.5 to symmetric B–OH environments presumably associated with defect sites or on the surface of the crystallites. Since the former is broader than the δ −1.5 MAS NMR peak it is probably not given by the same boron site.

In order to be absolutely sure that the ^{11}B NMR spectrum of ETBS-10 does contain two separate resonances and that the peaks seen are not part of a second-order quadrupole powder pattern we have further recorded quadrupole nutation (QN)[8] and triple-quantum (3Q)[9] MAS NMR spectra. The latter (not shown) contains two ^{11}B resonances confirming the presence of two main boron sites (the peaks revealed by CP MAS are too faint to be detected). The QN spectrum (not shown) recorded with a radiofrequency, B_1, field of 28 kHz (non-selective excitation) again shows that two resonances are present. A second spectrum, recorded with B_1 = 10 kHz (small deviation from non-selective excitation) suggests that the δ −1.4 resonance has a larger quadrupole coupling constant (C_Q) and, hence, is given by a slightly more distorted boron site. However, both C_{QS} are estimated to be very small (40–80 kHz) confirming that boron is in tetrahedral coordination.

Since ETS-10 contains corner-sharing TiO_6 octahedra and corner-sharing SiO_4 tetrahedra for every framework titanium there is an associated −2 charge. In an analogous way, when SiO_4 is replaced by AlO_4 a −1 charge is introduced. The preferred framework site for silicon substitution by aluminium in ETS-10 has been recently modelled by lattice energy minimisation and semi-empirical quantum chemical calculations on model clusters.[10] The latter technique indicates that, compared to Al–O–Si–O–Ti linkages, Al–O–Ti direct linkages result in enhanced electronic repulsion between neighbouring negative charges associated with the AlO_4 and TiO_6 sites and higher lattice strains. Thus, both electronic and strain factors influence the observed preferential aluminium siting and it is difficult to decide which one plays a more important role. At present, we are performing similar calculations to ascertain whether it is possible to decide or not which one these two factors plays a more important role in the location of boron in ETBS-10.

J. R. and P. B. acknowledge Junta Nacional de Investigação Científica e Tecnológica, PRAXIS XXI and FEDER for funding. O. T. and T. O. thank CREST, Japan for financial support.

Notes and References

† E-mail: ROCHA@DQ.UA.PT

‡ *Synthesis* of ETBS-10 with Si/B = 45: an alkaline solution was made by mixing 11.32 g sodium silicate (Na_2O 8 mass%, SiO_2 27 mass%, Merck), 4.25 g H_2O, 1.62 g NaOH (Merck), 0.17 g KOH (Carlo Erba), 0.93 KF (Aldrich), 0.34 g KCl (Panreac), 8.96 g $TiCl_3$ (15 mass% solution of $TiCl_3$ in 10 mass% HCl, Merck) and 0.84 g $Na_2B_2O_4{\cdot}10H_2O$ (Panreac). 0.10 g seed of ETS-10 was added to the resulting gel. This gel, with a composition 2.41 Na_2O : 2.18 K_2O : 5.86 SiO_2 : TiO_2 : 0.51 B_2O_3 : 27.1 H_2O, was autoclaved under autogeneous pressure for 2 days at 230 °C. The crystalline product was filtered, washed with distilled water and dried at ambient temperature, the final product being an off-white microcrystalline (2–5 μm) powder. Chemical analysis by ICP of the two samples reported here yielded Si/Ti and Si/B molar ratios of 5.0, 5.2 and 32, 45, respectively, while TG revealed a mass loss from 50 to 350 °C of 13 ± 1%. FTIR spectra of ETBS-10 samples display a shoulder at 990 cm^{-1}, not seen in the spectrum of ETS-10, ascribed to tetrahedrally coordinated boron.

1 S. M. Kuznicki, *US Pat.*, 4 853 202, 1989.
2 M. W. Anderson, O. Terasaki, T. Ohsuna, A. Phillippou, S. P. Mackay, A. Ferreira, J. Rocha and S. Lidin, *Nature*, 1994, **367**, 347.
3 M. W. Anderson, O. Terasaki, O. Ohsuna, P. J. O'Malley, A. Philippou, S. P. MacKay, A. Ferreira, J. Rocha and S. Lidin, *Philos. Mag. B*, 1995, **71**, 813.
4 M. W. Anderson, A. Philippou, A. Ferreira, Z. Lin and J. Rocha, *Angew. Chem., Int. Ed. Engl.*, 1995, **34**, 1003.
5 J. Rocha, Z. Lin, A. Ferreira and M. W. Anderson, *J. Chem. Soc., Chem. Commun.*, 1995, 867.
6 M. W. Anderson, J. Rocha, Z. Lin, A. Philippou, I. Orion and A. Ferreira, *Microporous Mater.*, 1996, **6**, 195.
7 K. F. M. G. J. Scholle and W. S. Veeman, *Zeolites*, 1985, **5**, 118.
8 G. Engelhardt and Michel, *High Resolution Solid-State NMR of Silicates and Zeolites*, Wiley, New York, 1987.
9 A. Medek, J. S. Harwood and L. Frydman, *J. Am. Chem. Soc.*, 1995, **117**, 12 779.
10 M. E. Grillo and J. Carrazza, *J. Phys. Chem. B*, 1997, **101**, 6749.

Received in Cambridge, UK, 10th December 1997; 7/08878G

Isolation, structure and iridium-mediated decarbonylation of a sodium fluorenone dianion complex

Zhaomin Hou,*[a]† Akira Fujita,[b] Hiroshi Yamazaki[b] and Yasuo Wakatsuki*[a]

[a] *The Institute of Physical and Chemical Research (RIKEN), Hirosawa 2-1, Wako, Saitama 351-01, Japan*
[b] *Department of Applied Chemistry, Chuo University, Kasuga 1-13-27, Bunkyo, Tokyo 112, Japan*

Reaction of fluorenone with 2 equiv. of Na in THF at room temp. gave the polymeric Na–fluorenone dianion complex 1 in 79% isolated yield, which upon reaction with 0.5 equiv. of $[(C_5Me_5)IrCl(\mu\text{-}Cl)]_2$ afforded the decarbonylation product 2; both 1 and 2 have been structurally characterized.

The formation of ketone dianions by two-electron reduction of aromatic ketones with reducing metals such as alkali,[1] low-valent titanium,[2] and lanthanide metals[3] has been known for a long time. These dianionic species as unique nucleophiles have been extensively studied in the area of organic chemistry.[1–3] However, owing to their extreme air- and moisture-sensitivity, which makes them difficult to isolate, structurally characterized examples of this important class of compounds remain very scarce. To date, only two ketone dianion complexes, both of which are limited to those of benzophenone and adopt a dimeric structure, have been isolated and structurally characterized. One is the lithium complex $[Li_2(OCPh_2)(thf)(tmen)]_2$ (thf = tetrahydrofuran, tmen = tetramethylethylenediamine),[4] and the other is the ytterbium(II) complex $[Yb(\mu\text{-}\eta^1:\eta^2\text{-}OCPh_2)(hmpa)_2]_2$ (hmpa = hexamethylphosphoric triamide).[5] Here, we wish to report the isolation and structural characterization of a polymeric sodium fluorenone dianion complex, which constitutes the first example of a structurally characterized fluorenone dianion complex, as well as the first example of a structurally characterized sodium ketone dianion complex. Its reaction with $[(C_5Me_5)IrCl(\mu\text{-}Cl)]_2$ to cause unprecedented decarbonylation of the fluorenone unit is also described.

Reaction of fluorenone with 2 equiv. of fresh sodium chips in thf at room temp. yielded a green precipitate, which upon dissolving in dimethoxyethane (DME) gave a green solution. Evaporation of DME under reduced pressure yielded a green oily residue, which after addition of thf and standing at room temp. for several days afforded green blocks of **1** in 79% yield (Scheme 1).‡ An X-ray analysis has revealed that **1** is a thf-coordinated fluorenonedisodium complex in which one sodium atom [Na(1)] is bonded to the oxygen atom O(1), while the other sodium atom [Na(2)] is bonded to the O(1), C(1) and C(2) atoms of the fluorenone unit (Fig. 1).§ The bond distance of the Na(1)–O(1) bond [2.168(6) Å] is in the 2.14–2.39 Å range of the Na–OR bond distances found in $[NaOBu^t]_6$,[6] $[NaOBu^t]_9$,[6] $[Na\{\mu\text{-}OC_6H_2(CF_3)_3\text{-}2,4,6\}(thf)_2]_2$[7] and $[Na(\mu\text{-}OR)(hmpa)_2]_2$ (OR = fluorenone ketyl),[8] while the bond distances of the Na(2)–C(1) [2.644(7) Å] and Na(2)–C(2) [2.921(7) Å] bonds can be compared with those of the Na–η^{3-5}-Cp bonds (2.620–3.044 Å) found in the sodium fluorenide complexes Na(fluorenide)-$[Me_2N(CH_2)_2N(Me)(CH_2)_2NMe_2]$,[9] $[Na(fluorenide)\{Me_2N(CH_2)_3NMe_2\}]_4$,[9] and $[Na(fluorenide)\{Me_2N(CH_2)_2NMe_2\}]_\infty$.[9] These bond distances are consistent with the fact that **1** is a sodium fluorenone dianion species. The intermolecular interactions between the sodium atoms and part of the fluorenyl ring, the carbonyl unit, and the thf ligands in **1** constitute a unique polymeric structure, in which the fluorenone unit is bonded on one side to a Na atom *via* the Na(2)–η^3-O(1)C(1)C(2) (2.348–2.921 Å) interactions and on the other side to two Na atoms *via* the Na(1′)–η^6-C(8–13) (2.725–2.888 Å) and Na(2′)–η^3-O(1)C(1)C(13) (2.340–3.083 Å) interactions (Fig. 1). The carbonyl moiety interacts with the Na(2) and Na(2′) atoms in a $\mu\text{-}\eta^2$-fashion on two opposite sides (dihedral angle between the Na(2)O(1)C(1) and Na(2′)O(1)C(1) planes = 173°), while the C(13) atom is bonded to both Na(1′) and Na(2′) on the same side [Na(1′)–C(13)–Na(2′) 72.2(2)°]. These structural features are in sharp contrast with those observed in the dimeric benzophenone dianion complexes $[Li_2(OCPh_2)(thf)(tmen)]_2$[4] and $[Yb(\mu\text{-}\eta^1:\eta^2\text{-}OCPh_2)(hmpa)_2]_2$,[5] and apparently result from the planar configuration of the fluorenone unit. The formation of thf bridges in **1** is also noteworthy, since only very few precedents, such as $\{Na(\mu\text{-}thf)[(C_5Me_5)Gd(thf)]_2(\mu\text{-}Cl)(\mu_3\text{-}Cl)_2\}_2$[10] and $[K\{\mu\text{-}OC_6H_2(CF_3)_3\text{-}2,4,6\}(thf)_2(\mu\text{-}thf)]_2$,[7] could be found in the literature. The Na(1)–O(2) [2.371(6) Å] and Na(1)–O(3) [2.391(7) Å] bonds are respectively significantly shorter than the Na(2′)–O(2) [2.440(6) Å] and Na(2′)–O(3) [2.606(6) Å] bonds, showing that the thf bridges in the polymeric structure are unsymmetric, and the intramolecular interactions are stronger than the intermolecular ones. Similarly, the intramolecular Na(2)–C(1) [2.644(7) Å] and Na(2)–C(2) [2.921(7) Å] bonds are respectively much shorter than the intermolecular Na(2′)–C(1) [2.775(7) Å] and Na(2′)–C(13) [3.083(7) Å] bonds, though the Na(2)–O(1) bond distance [2.348(6) Å] is similar to that of the Na(2′)–O(1) bond [2.340(6) Å] (Fig. 1). The bond distance of the C–O bond of the fluorenone unit in **1** [1.379(8) Å] is comparable with those of the benzophenone dianion units found in $[Li_2(OCPh_2)(thf)(tmen)]_2$ (1.406 Å)[4] and $[Yb(\mu\text{-}\eta^1:\eta^2\text{-}OCPh_2)(hmpa)_2]_2$ [1.39(6) Å],[5] and significantly longer than those of free fluorenone [1.220(4) Å][11] and fluorenone ketyl (1.27–1.32 Å).[8,12]

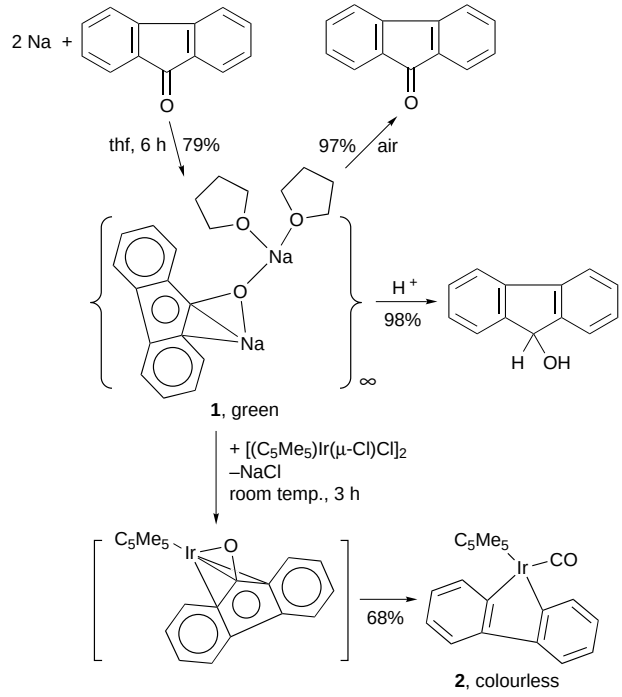

Scheme 1

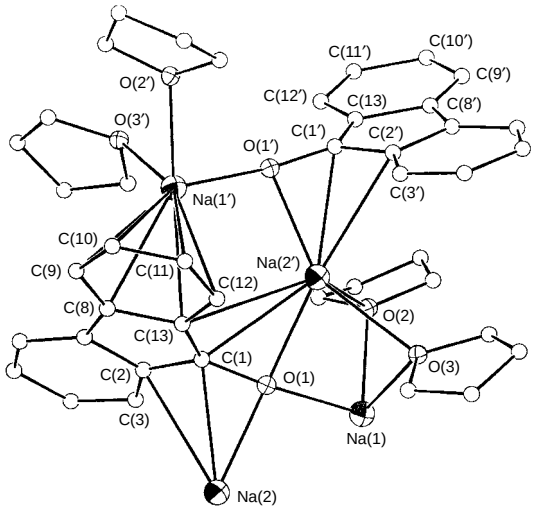

Fig. 1 Extended structure of **1**. Selected bond lengths (Å) angles (°) (′ = 1.5 − *x*, 0.5 + *y*, 1.5 − *z*): Na(1)–O(1) 2.168(6), Na(1)–O(2) 2.371(6), Na(1)–O(3) 2.391(7), Na(2)–O(1) 2.348(6), Na(2)–C(1) 2.644(7), Na(2)–C(2) 2.921(7), Na(2′)–O(1) 2.340(6), Na(2′)–C(1) 2.775(7), Na(2′)–C(13) 3.083(7), Na(2′)–O(2) 2.440(6), Na(2′)–O(3) 2.606(6), Na(1′)–C(8) 2.733(7), Na(1′)–C(9) 2.822(8), Na(1′)–C(10) 2.888(8), Na(1′)–C(11) 2.881(8), Na(1′)–C(12) 2.805(8), Na(1′)–C(13) 2.725(7), O(1)–C(1) 1.379(8); O(1)–Na(1)–O(2) 91.2(2), O(1)–Na(1)–O(3) 86.2(2), O(2)–Na(1)–O(3) 84.5(3), Na(1)–O(1)–C(1) 164.1(5), Na(2)–O(1)–C(1) 86.3(4), Na(1)–O(1)–Na(2) 98.9(2), Na(1)–O(1)–Na(2′) 83.6(2), Na(2′)–O(1)–C(1) 92.9(4), Na(2)–O(1)–Na(2′) 173.4(3), Na(1′)–C(13)–Na(2′) 72.2(2).

Reflecting the reactivity of a fluorenone dianion species,[1–3] hydrolysis of **1** yielded fluorenol, while air oxidation of **1** afforded fluorenone almost quantitatively. Moreover, when **1** was allowed to react with 0.5 equiv. of $[(C_5Me_5)IrCl(\mu\text{-}Cl)]_2$ at room temp. in DME, the decarbonylation product **2** was obtained as colorless crystals in 68% isolated yield (Scheme 1, Fig. 2).§¶ In contrast, the similar reaction of sodium benzophenone dianion with $[(C_5Me_5)IrCl(\mu\text{-}Cl)]_2$ did not give any C–C bond cleavage product, but instead afforded benzophenone and several unidentified iridium hydride species. These results again demonstrated the difference in behavior between fluorenone dianion and benzophenone dianion. Further studies on the decarbonylation reaction are in progress.

This work was partly supported by a grant-in-aid from the Ministry of Education, Science, Sports, and Culture of Japan.

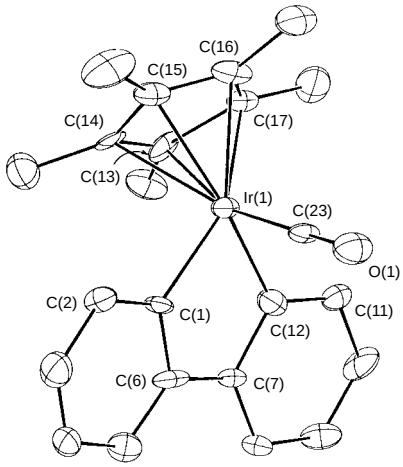

Fig. 2 ORTEP drawing of **2** (only one of the two independent molecules is shown for clarity). Selected bond lengths (Å) and angles (°): Ir(1)–C(1) 2.07(2), Ir(1)–C(12) 2.05(2), Ir(1)–C(13) 2.25(3), Ir(1)–C(14) 2.27(3), Ir(1)–C(15) 2.27(3), Ir(1)–C(16) 2.27(2), Ir(1)–C(17) 2.28(2), Ir(1)–C(23) 1.83(1), O(1)–C(23) 1.14(3); Ir(1)–C(23)–O(1) 179(2).

Notes and References

† E-mail: houz@postman.riken.go.jp

‡ A typical procedure for the synthesis of **1** is as follows. In a glove box, addition of a thf solution (5 ml) of fluorenone (180 mg, 1 mmol) to freshly-cut sodium chips (48 mg, 2.1 mmol) gave immediately a brown solution, which after being stirred at room temperature for *ca*. 1 h, changed to dark green and yielded gradually thf-insoluble green precipitates. The green mixture was further stirred at room temperature for 5 h. The thf was pumped off and DME (5 ml) was added to give a green solution. Evaporation of DME yielded a green oily residue, which after addition of thf and standing at room temperature for several days afforded thf-insoluble green blocks of **1** (292 mg, 0.79 mmol, 79% yield). Anal. Calc. for $C_{21}H_{24}Na_2O_3$: C, 68.10; H, 6.53. Found. C, 67.80, H, 6.44%.

§ *Crystal data*: for **1**: $C_{21}H_{24}Na_2O_3$, M = 370.40, monoclinic, space group $P2_1/n$ (no. 15), a = 12.6600(9), b = 8.5523(5), c = 17.8251(11) Å, β = 98.942(6)°, U = 1906.5(2) Å^3, Z = 4, D_c = 1.25 g cm^{-3}, μ(Cu-Kα) = 10.440 cm^{-1}, 3120 measured reflections, 2892 independent, R = 0.0847 (R_w = 0.0830) for 2387 data with $I > 3\sigma(I)$ and 301 variables. For **2** (two independent molecules in the unit cell): $C_{46}H_{46}Ir_2O_2$, M = 1015.32, orthorhombic, space group *Pcab* (no. 61), a = 16.476(5), b = 31.468(8), c = 14.645(4) Å, U = 7593(3) Å^3, Z = 8, D_c = 1.78 g cm^{-3}, μ(Mo-Kα) = 70.131 cm^{-1}, 9831 measured reflections, 7404 independent, R = 0.0580 (R_w = 0.0638) for 4071 data with $I > 3\sigma(I)$ and 451 variables. CCDC 182/761.

¶ ^{1}H NMR for **2** (CD_2Cl_2, 22 °C): δ 7.47 (d of d, J_1 7.26, J_2 1.32 Hz, 2 H, $C_{12}H_8$), 7.46 (d of d, J_1 7.26, J_2 1.32 Hz, 2 H, $C_{12}H_8$), 7.06 (d of t, J_1 7.26, J_2 1.32 Hz, 2 H, $C_{12}H_8$), 6.90 (d of t, J_1 7.26, J_2 1.32 Hz, 2 H, $C_{12}H_8$), 1.87 (s, 15 H, C_5Me_5). ^{13}C NMR (CD_2Cl_2, 22 °C): δ 169.3, 154.5, 141.1, 137.2, 125.8, 123.6, 120.3, 99.1, 8.8. IR (in thf): ν(CO) 1996.9 cm^{-1}. Anal. Calc. for $C_{23}H_{23}IrO$: C, 54.42; H, 4.57. Found. C, 54.24, H, 4.49%.

1 W. Schlenk and T. Weichel, *Ber.*, 1911, **44**, 1182; H. Schlubach, *Ber.*, 1915, **48**, 12; C. B. Wooster, *J. Am. Chem. Soc.*, 1928, **50**, 1388; W. E. Bachmann, *J. Am. Chem. Soc.*, 1933, **55**, 1179; P. J. Hamrick, Jr. and C. R. Hauser, *J. Am. Chem. Soc.*, 1959, **81**, 493; S. Selman and J. F. Easthan, *J. Org. Chem.*, 1965, **30**, 3804; E. L. Anderson and J. E. Casey, Jr., *J. Org. Chem.*, 1965, **30**, 3959; W. S. Murphy and D. J. Buckley, *Tetrahedron Lett.*, 1969, 2975; J. W. Huffman, in *Comprehensive Organic Synthesis*, ed. B. M. Trost and I. Fleming, Pergamon, New York, 1991, vol. 8, ch. 1.4; G. M. Robertson, in *Comprehensive Organic Synthesis*, ed. B. M. Trost and I. Fleming, Pergamon, New York, 1991, vol. 3, ch. 2.6.

2 J. E. McMurry and L. R. Krepiski, *J. Org. Chem.*, 1976, **41**, 3929; J. E. McMurry, M. P. Fleming, K. L. Kees and L. R. Krepiski, *J. Org. Chem.*, 1978, **43**, 3255; J. M. Pons and M. Santelli, *Tetrahedron Lett.*, 1982, **23**, 4937; J. E. McMurry, *Acc. Chem. Res.*, 1983, **16**, 405; 1974, **7**, 281; *Chem. Rev.*, 1989, **89**, 1513; A. Fürstner and B. Bogdanovic, *Angew. Chem., Int. Ed. Engl.*, 1996, **35**, 2442.

3 Z. Hou, K. Takamine, Y. Fujiwara and H. Taniguchi, *Chem. Lett.*, 1987, 2061; Z. Hou, K. Takamine, O. Aoki, H. Shiraishi, Y. Fujiwara and H. Taniguchi, *J. Chem. Soc., Chem. Commun.*, 1988, 668; *J. Org. Chem.*, 1988, **53**, 6077; H. Olivier, Y. Chauvin and L. Saussine, *Tetrahedron*, 1989, **45**, 165; Z. Hou, T. Yoshimura and Y. Wakatsuki, *J. Am. Chem. Soc.*, 1994, **116**, 11169; T. Yoshimura, Z. Hou and Y. Wakatsuki, *Organometallics*, 1995, **14**, 5382.

4 B. Bogdanovic, C. Kruger and B. Wermeckes, *Angew. Chem., Int. Ed. Engl.*, 1980, **19**, 817.

5 Z. Hou, H. Yamazaki, K. Kobayashi, Y. Fujiwara and H. Taniguchi, *J. Chem. Soc., Chem. Commun.*, 1992, 722; Z. Hou, H. Yamazaki, Y. Fujiwara and H. Taniguchi, *Organometallics*, 1992, **11**, 2711.

6 J. E. Davies, J. Kopf and E. Weiss, *Acta Crystallogr., Sect. B*, 1982, **38**, 2251.

7 S. Brooker, F. T. Edelmann, T. Kottke, H. W. Roesky, G. M. Scheldrick, D. Stalke and K. H. Whitmire, *J. Chem. Soc., Chem. Commun.*, 1991, 144.

8 Z. Hou, A. Fujita, H. Yamazaki and Y. Wakatsuki, *J. Am. Chem. Soc.*, 1996, **118**, 2503.

9 S. Corbelin, J. Kopf and E. Weiss, *Chem. Ber.*, 1991, **124**, 2417.

10 Q. Shen, M. Qi and Y. Lin, *J.Organomet. Chem.*, 1990, **399**, 247.

11 H. R. Luss and D. L. Smith, *Acta Crystallogr., Sect. B*, 1972, **28**, 884.

12 Z. Hou, T. Miyano, H. Yamazaki and Y. Wakatsuki, *J. Am. Chem. Soc.*, 1995, **117**, 4421; Z. Hou, A. Fujita, H. Yamazaki and Y. Wakatsuki, *J. Am. Chem. Soc.*, 1996, **118**, 7843.

Received in Cambridge, UK, 12th January 1998; 8/00291F

Biosynthesis of phytyl side-chain of chlorophyll *a*: apparent reutilization of carbon dioxide evolved during acetate assimilation in biosynthesis of chloroplastidic isoprenoid

Kensuke Nabeta,*† Tatsuto Saitoh, Kadzuya Adachi and Kaori Komuro

Department of Bioresource Science, Obihiro University of Agriculture and Veterinary Medicine, Obihiro 080, Japan

Equal incorporation of either acetyl methyl or carboxy carbons into all carbon atoms of the phytyl side-chain of chlorophyll *via* doubly labelled acetyl CoA, with complete loss of methyl hydrogens, indicated that CO_2 evolved from the carboxy carbon during acetate assimilation through the TCA cycle may be reutilized *via* the reductive pentose phosphate cycle followed by the glycolic pathway, while incorporation of [2-^{13}C]glycerol and [6,6-$^{2}H_2$]glucose into the phytyl chain demonstrated the simultaneous operation of two distinct pathways, both the mevalonate pathway and the 1-deoxy-D-xylulose mediating pathways (non-mevalonate pathway) in isopentenyl diphosphate formation within liverwort chloroplasts.

The labelling pattern of the phytyl side-chain of chlorophyll was determined by incorporation studies using ^{2}H- or ^{13}C-labelled acetates, glycerol and glucose into cultured cells of liverwort, *Heteroscyphus planus*. The most unexpected feature of the labelling pattern was that either acetyl methyl or carboxy carbons were equally incorporated into all carbon atoms of the phytyl side-chain *via* doubly labelled acetyl CoA with complete loss of methyl hydrogens. The labelling pattern of the phytyl side-chain incorporating [2-^{13}C]glycerol and [6,6-$^{2}H_2$]glucose together with ^{2}H- and ^{13}C-labelled mevalonate (MVA)[1,2] revealed the simultaneous operation of two distinct pathways, the classical acetate/MVA (mevalonate) pathway[3] and the novel 1-deoxy-D-xylulose (non-mevalonate) pathway,[4] in isopentenyl diphosphate (IPP) formation within liverwort chloroplasts.

Cell cultures of *Heteroscyphus planus* were grown in MSK-4 medium[5] (6–8 × 75 ml), and fed with sodium [1-^{13}C]-, [2-^{13}C]-, [1,2-$^{13}C_2$]-, [2,2,2-$^{2}H_3$, 1-^{13}C]- and [2,2,2-$^{2}H_3$, 2-^{13}C]-acetate, (> 99 atom%, 0.5 mmol), [2-^{13}C]glycerol (60 atom%, 0.5 mmol in 1 ml of 10% aq. EtOH) and [6,6-$^{2}H_2$]glucose (20 atom%, 11.1 mmol) under continuous light at 25 °C.[6] Chlorophyll *a* was isolated and hydrolyzed, and the isolated phytol was acetylated by the procedure reported previously.

The ^{13}C enrichment [sixteen ^{13}C-enriched peaks with doublets due to ^{13}C–^{13}C coupling (C-1–C-2, C-3–C-20, C-5–C-6, C-7–C-19, C- 9–C-10, C-11–C-18, C-13–C-14 and C-15–C-17) and four intense singlet peaks (C-4, C-8, C-12 and C-16) as shown in Fig. 1 and Table 1] in the phytols incorporating [1-^{13}C]-, [2-^{13}C]- and [1,2-$^{13}C_2$]-acetates was identical, indicating that the doubly ^{13}C-labeled acetyl CoA was formed from either two carboxy carbons of [1-^{13}C]acetate or two methyl carbons of [2-^{13}C]acetate. Transposition of ^{13}C label between the C-4 and C-5 carbons in IPP was also observed. The average intensity of the ^{13}C–^{13}C coupled peaks relative to the intense center peak in phytol incorporating [1,2-$^{13}C_2$]acetate (observed

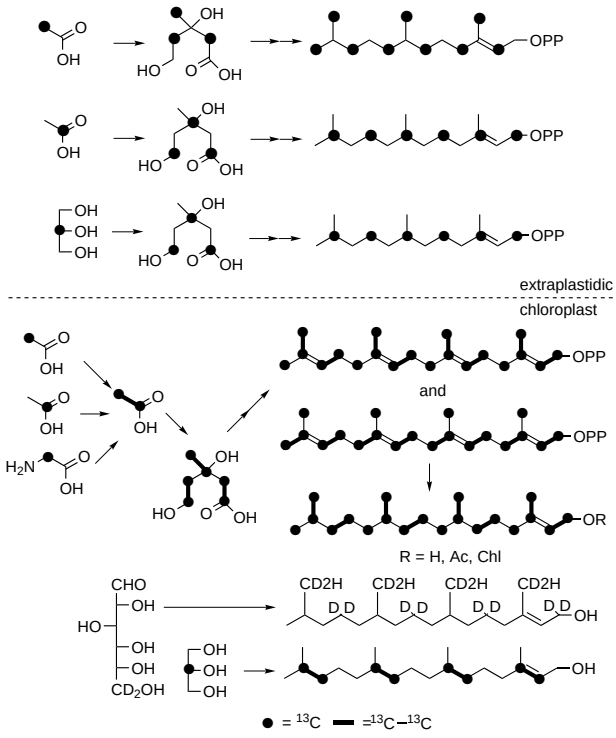

Fig. 1 Labelling patterns of the phytyl side-chain of chlorophyll *a* and sesquiterpenes incorporating ^{13}C labelled acetates, [2-^{13}C]glycerol and [6,6-$^{2}H_2$]glucose in cultured cells of *H. planus*

Table 1 ^{13}C enrichment of phytyl side-chain of chlorophyll *a* incorporating ^{13}C-labelled acetates

	Enrichment (atom% excess)		
Carbon	[1-^{13}C]acetic acid	[2-^{13}C]acetic acid	[1,2-^{13}C]acetic acid[a]
C-1	1.87	1.18	0.34
C-2	1.61	0.83	0.69
C-3	1.47	0.77	0.44
C-4	3.14	1.94	1.31
C-5	1.94	1.10	0.53
C-6	1.64	1.67	0.67
C-7	2.94	2.15	1.32
C-8	2.77	2.37	0.85
C-9	1.87	1.58	0.67
C-10	1.74	1.45	0.20
C-11	1.80	1.50	0.66
C-12	2.40	1.84	0.41
C-13	1.89	1.39	0.77
C-14	2.91	2.83	1.09
C-15	2.93	2.45	1.45
C-16	3.18	3.30	1.80
C-17	2.41	2.52	1.03
C-18	2.45	2.96	1.32
C-19	3.12	2.96	1.36
C-20	1.49	1.14	0.59
Average	2.28	1.90	0.89

[a] $J_{^{13}C-^{13}C}$/Hz: C-1–C-2, C-3–C-20, C-5–C-6, C-7–C-19, C-9–C-19, C-11–C-18, C-13–C-14, C-15–C-17 have been previously reported. C-3–C-4 = 34.2, C-7–C-8 = 34.2, C-11–C-12 = 35.4 and C-15–C-16 = 35.4.

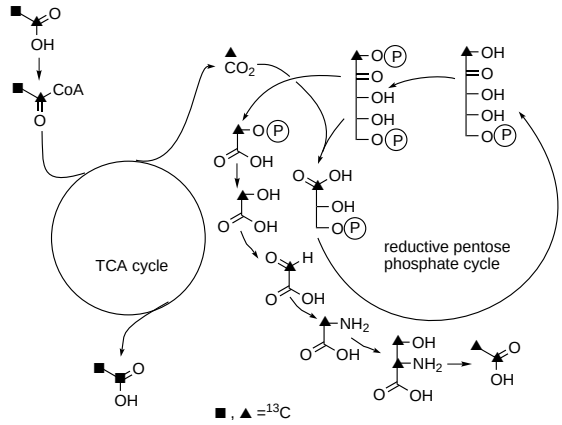

Fig. 2 Pathway for [1,2-$^{13}C_2$]acetate from [1-^{13}C]acetate *via* the TCA cycle, the reductive pentose phophate cycle and the glycollate pathway

relative intensity: 0.185) was much lower (× 4.5) than that estimated (0.82) on the basis of the natural abundance of ^{13}C (1.08%) and ^{13}C enrichment (0.89 atom% excess) indicating that reformed acetate, rather than intact acetate, was incorporated into MVA. The α-^{2}H and β-^{2}H isotopic peaks[6] were not observed in phytol incorporating [2,2,2-$^2H_3$, 2-^{13}C]- and [2,2,2-$^2H_3$, 1-^{13}C]-acetates, respectively, indicating the complete loss of ^{2}H of the acetate during formation of [1,2-$^{13}C_2$]acetate.

The pathway leading to two contiguously labelled acetate (or three contiguously labelled propionate) molecules from [2-^{13}C]acetate, which was detected in a rare actinomycetes, *Actinomadura azurea*,[7] and cell cultures of the vascular plants *Zea mays*[8] and *Morus alba*[9] was reasonably explained by the participation of the tricarboxylic acid cycle (TCA cycle). Formation of doubly labeled acetate from [1-^{13}C]acetate, however, has not yet been reported. The results of this as well as earlier studies in which we examined the incorporation of [2-^{13}C]glycine into the phytyl moiety of chlorophyll *a*[1,2] suggest that the ^{13}C-labelled carbon dioxide evolved during [1-^{13}C]acetate assimilation through the TCA cycle is reutilized *via* the reductive pentose phosphate cycle. Carbon-13 labelled CO_2 was incorporated into ribulose 1,5-bisphosphate at C-1 by the mechanism shown in Fig. 2. The ^{13}C label at C-1 in ribulose 1,5-bisphosphate was further translocated into the methylene carbon (C-2) of glycine *via* the glycolic pathway. The doubly labelled acetyl-CoA was formed from two C-2 carbons of the endogenously formed [2-^{13}C]glycine *via* the glycolic pathway. There is indirect evidence that reassimilation of CO_2 liberated during acetate photoassimilation could be reutilized in glycolate production in *Chlorella*[10] other eukaryotic algae and vascular plants.[11]

Label was detected at C-2, C-3, C-6, C-7, C-10, C-11, C-14 and C-15 of the phytyl side-chain incorporating [2-^{13}C]glycerol, all of which showed $J_{^{13}C-^{13}C}$ coupling ($J_{2,3}$ = 73.2, $J_{6,7}$ = 34.8, $J_{10,11}$ = 34.8 and $J_{14,15}$ = 34.2 Hz). When [6,6-$^2H_2$]glucose was added, the label was incorporated into C-1 (δ_D 4.15) and C-20 (δ_D 1.66) together with three methylene carbons (C-5, C-9 and C-13, δ_D 1.35–1.55, unresolved) and three methyl carbons (C-17, C-18, C-19, δ_D 0.8–0.9, unresolved). The labelling pattern indeed confirmed the operation of the non-mevalonate pathway in biosynthesis of the phytyl side-chain. We found that the phytyl side-chain was also formed from MVA.[1,2] Thus, it is suggested that biosynthesis of all compounds derived from geranylgeranyl diphosphate within liverwort chloroplasts proceeds *via* both the classical mevalonate pathway[1,2,12] and the novel non-mevalonate pathway. The simultaneous operation of the mevalonate and the non-mevalonate pathways has also been detected in microorganisms without organelles.[13]The labelling pattern of β-barbatene, a predominant sesquiterpene hydrocarbon in *H. planus*,[14] incorporating labelled glycerol and glucose revealed that biosynthesis of the cytoplasmic terpenoids proceeds *via* the mevalonate pathway but not *via* the non-mevalonate pathway.

We present here evidence that CO_2 evolved from acetate assimilation is reutilized to biosynthesize isoprenoids in chloroplasts. The enzymes involved in the TCA cycle, the reductive pentose cycle and the glycolic acid pathway are separately localized in mitochondria, chloroplasts and peroxisomes, respectively. Thus reconstruction of acetate in chloroplasts requires consideration of the flux of CO_2 and the intermediates through the TCA cycle in mitochondria.

We are grateful to Dr H. Koshino (The Institute of Physical and Chemical Research) for ^{2}H NMR analyses and to Professors H. Seto (Tokyo University) and K. Kakinuma (Tokyo Institute of Technology) for a generous gift of [6,6-$^2H_2$]glucose. These investigations were supported by the Suhara Memorial Foundation and Grants-in-aid for Scientific Research (A. No. 08306021 and C. No. 08660125) from the Ministry of Education, Science and Culture, Japan.

Notes and References

† E-mail: knabeta@obihiro.ac.jp

1 K. Nabeta, T. Kawae, T. Kikuchi, T. Saitoh and H. Okuyama, *J. Chem. Soc., Chem. Commun.*, 1995, 2539.
2 K. Nabeta. T. Kawae, T. Saitoh and T. Kikuchi, *J. Chem. Soc., Perkin Trans. 1*, 1997, 261.
3 L. Ruzicka, A. Eschenmoser and H. Heusser, *Experimentia*, 1953, **9**, 357; S. L. Spurgeon and J. W. Porter, *Biosynthesis of Isoprenoid Compounds*, ed. J. W. Porter and S. L. Spurgeon, Wiley, New York, 1981; vol. 1, pp. 1–47; N. Quereshi and J. W. Porter, in *Biosynthesis of Isoprenoid Compounds*, ed. J. W. Porter and S. L. Spurgeon, Wiley, New York, 1981; vol. 1, pp. 47–93.
4 T. Duvold, J.-M. Bravo, C. Pale-Grosdemage and M. Rohmer, *Tetrahedron Lett.*, 1997, **38**, 4769; D. Arigoni, S. Sagner, C. Latzel, W. Eisenreich, A. Bacher and M. H. Zank, *Proc. Natl. Acad. Sci. USA*, 1997, **94**, 10 600.
5 R. Takeda and K. Katoh, *Planta*, 1981, **151**, 525; K. Nabeta, K. Katayama, S. Nakagawara and K. Katoh, *Phytochemistry*, 1993, **32**, 117.
6 J. C. Vederas, *Nat. Prod. Rep.*, 1987, **4**, 277 and references cited therein.
7 M. Ubukata, J. Uzawa and K. Isono, *J. Am. Chem. Soc.*, 1984, **106**, 2213.
8 D. J. Aschworth, R. Y. Lee and D. O. Adams, *Plant. Physiol.*, 1987, **85**, 463.
9 Y. Hano, T. Nomura and S. Ueda, *Chem. Pharm. Bull.*, 1989, **37**, 554; Y. Hano, A. Ayukawa, T. Nomura and S. Ueda, *J. Am. Chem. Soc.*, 1994, **116**, 4189.
10 M. J. Merrett and K. H. Goulding, *Planta*, 1967, **75**, 275.
11 W. Wiessner, *Photosynthesis II. Photosynthetic Carbon Metabolism and Related Processes*, ed. M. Gibbs and E. Latzko, Springer-Verlag, Berlin, 1979, pp. 181–189.
12 K. Nabeta, T. Ishikawa, T. Kawae and H. Okuyama, *J. Chem. Soc., Chem. Commun.*, 1995, 681.
13 H. Seto, H. Watanabe and K. Furihata, *Tetrahedron Lett.*, 1996, **37**, 7979.
14 K. Nabeta, K. Komuro, T. Utoh, H. Tazaki and H. Koshino, *Chem. Commun.*, 1998, 169.

Received in Cambridge, UK, 24th December 1997; 7/09274A

Synthesis and X-ray crystal structure of a hexanuclear silver(I) complex with non-chelating tri- and tetra-dentate bridging *o*-(diphenylphosphino)benzoate ligands

Wai-Kwok Wong,*[a]† Lilu Zhang[a] and Wing-Tak Wong[b]

[a] *Department of Chemistry, Hong Kong Baptist University, Kowloon, Hong Kong, P.R. China*
[b] *Department of Chemistry, The University of Hong Kong, Pokfulam Road, Hong Kong, P.R. China*

Single crystal X-ray analysis of the hexanuclear silver(I) complex $Ag_6[o\text{-}Ph_2P(C_6H_4CO_2)\text{-}O,P]_6$, synthesized by treatment of $Ag(CF_3SO_3)$ with $N(CH_2CH_2NH_2)_3$, 1,3-dicyclohexylcarbodiimide (DCC) and $o\text{-}Ph_2PC_6H_4(CO_2H)$ in 1:1:3:3 molar ratio in ethanol, shows that the complex is centrosymmetric and consists of three independent silver(I) centres linking together *via* non-chelating tri- and tetradentate bridging *o*-(diphenylphosphino)benzoate groups.

We have been interested in the preparation of diimino-, diamino- and diamido-diphosphine ligands and demonstrated that these ligands do indeed exhibit a very rich coordination chemistry.[1,2] Recently, we have extended our study to the preparation of polydentate ligands containing three imino-phosphino groups and show that the heptadentate ligand $\{(o\text{-}Ph_2PC_6H_4)CH{=}NCH_2CH_2\}_3N$ can be prepared *via* template synthesis.[3] Here we report the result of our attempt to extend the template synthetic route for the preparation of the amidophosphino heptadentate ligand.

Treatment of $Ag(CF_3SO_3)$ with $N(CH_2CH_2NH_2)_3$, 1,3-dicyclohexylcarbodiimide (DCC) and $o\text{-}Ph_2PC_6H_4CO_2H$ in 1 : 1 : 3 : 3 molar ratio in refluxing ethanol affords, after work up, white crystals of stoichiometry $[Ag(o\text{-}Ph_2PC_6H_4CO_2)]_6$ **1**‡ in 10% yield. However, compound **1** could not be isolated from the reaction of $Ag(CF_3SO_3)$ with $o\text{-}Ph_2PC_6H_4CO_2H$ and 4-dimethylamino-pyridine (DMAP) in 1 : 1 : 1 molar ratio in the absence of DCC. The structure of **1** was established by X-ray crystallography. Crystals of $\mathbf{1}\cdot 2C_4H_8O\cdot C_6H_{14}$ suitable for X-ray diffraction study§ were grown by slow diffusion of hexane into a tetrahydrofuran solution of **1**. The molecular structure of **1** [Fig. 1(*a*)] shows that the hexameric system is embedded within an outer shell of aromatic rings formed by the phenyl rings of the phosphine and benzoate. The molecule is a centrosymmetric hexanuclear silver(I) complex with three independent Ag atoms linking together *via* the *o*-(diphenylphosphino)benzoate groups forming a $Ag_6[o\text{-}Ph_2P(C_6H_4CO_2)\text{-}O,P]_6$ cluster as shown in Fig. 2. The three independent Ag atoms in the asymmetric unit are four-coordinate and their coordination geometries can be described as highly distorted tetrahedra. The coordination environment of Ag(2) and Ag(3) are very similar. Both silver(I) centres are surrounded by two O atoms and one P atom from three different *o*-(diphenylphosphino)benzoate ligands and have a very long metal–metal distance [Ag(2)–Ag(3) 3.244(2) Å which is significantly shorter than the other two inter-silver distances; Ag(1)···Ag(2) 3.805, Ag(1)···Ag(3) 3.756 Å] between each other. The Ag(2)···Ag(3) distance is much longer than that (2.89 Å) found in metallic silver and is comparable to the long Ag–Ag distance [3.090(4) Å] in $[Ag_6L_2(HL)_2(H_2O)_4]$ (L = pyridine-2,3-dicarboxylate),[4] [3.194(2) Å] in $[Ag(\eta^2\text{-}O_2CMe)(\mu\text{-dppm})]_2$ (dppm = $Ph_2PCH_2PPh_2$),[5] and the inter-chain Ag–Ag distances [3.269(2) and 3.346(2) Å] in $[Ag_2L'_2(H_2O)]_n[ClO_4]_{2n}$ (L′ = trimethylammoniopropionate)[6] indicating a very weak metal–metal interaction. Ag(2) is approximately coplanar with O(1), O(6*) and P(2) [Ag(2)–O(1) 2.185(7), Ag(2)–O(6*) 2.411(8), Ag(2)–P(2) 2.376(4) Å] with a

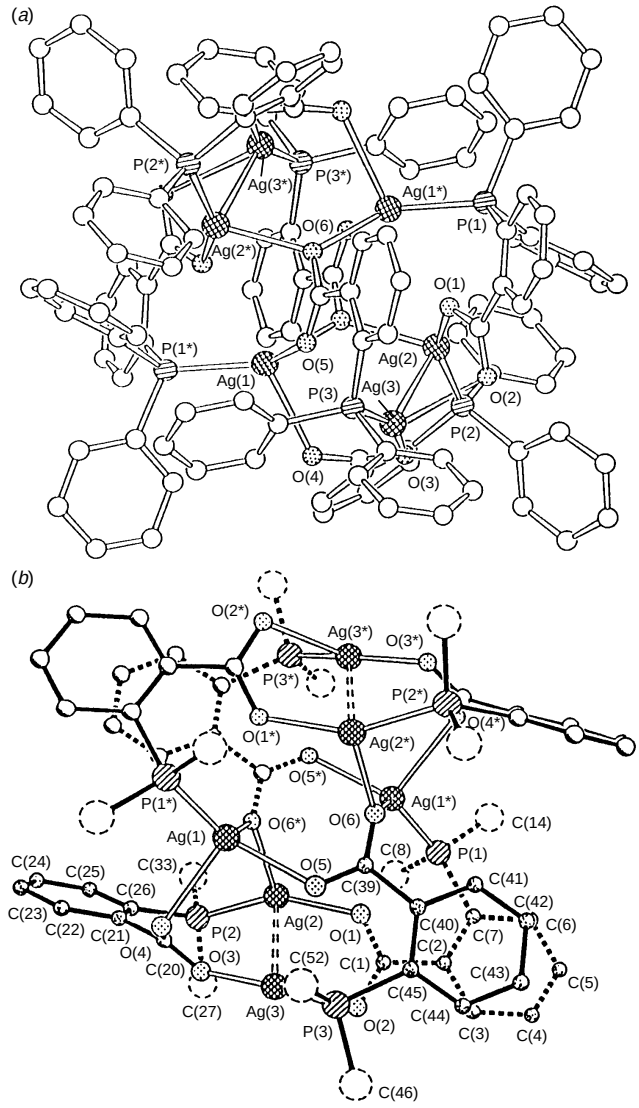

Fig. 1 (*a*) Overall molecular geometry of compound **1**. For clarity, the hydrogen atoms are omitted. (*b*) A perspective drawing of **1** with the phenyl rings of the PPh_2 groups each represented by a circle with broken outline. Selected bond lengths (Å) and angles(°): Ag(2)–Ag(3) 3.244(2), Ag(1)–P(1*) 2.381(4), Ag(2)–P(2) 2.376(4), Ag(3)–P(3) 2.378(4), Ag(1)–O(4) 2.598(9), Ag(1)–O(5) 2.261(9), Ag(1*)–O(6) 2.394(9), Ag(2)–O(1) 2.185(9), Ag(2*)–O(6) 2.411(9), Ag(3)–O(2) 2.619(9), Ag(3)–O(3) 2.176(9), P(1*)–Ag(1)–O(4) 108.8(2), P(1*)–Ag(1)–O(5) 129.5(2), P(1*)–Ag(1)–O(6*) 130.5(2), O(4)–Ag(1)–O(5) 100.4(3), O(4)–Ag(1)–O(6*) 87.9(3), O(5)–Ag(1)–O(6*) 89.9(3), O(1)–Ag(2)–O(6*) 98.6(3), P(2)–Ag(2)–O(6*) 108.0(2), Ag(3)–Ag(2)–P(2) 106.0(1), P(2)–Ag(2)–O(1) 152.8(2), O(2)–Ag(3)–P(3) 93.1(2), O(2)–Ag(3)–O(3) 105.4(3), O(3)–Ag(3)–P(3) 161.2(3), Ag(2)–Ag(3)–P(3), 134.6(1).

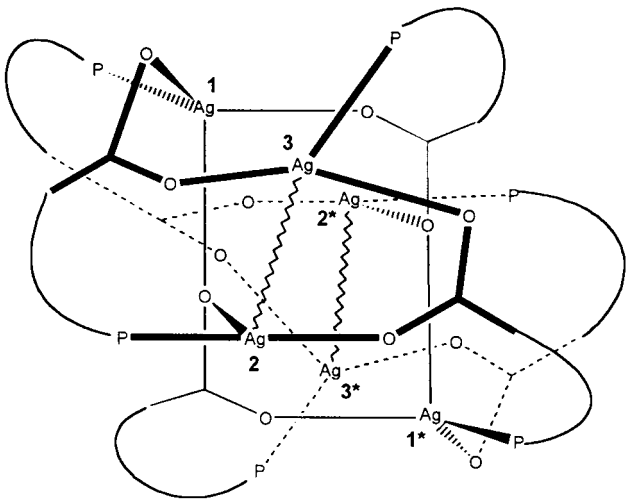

Fig. 2 $Ag_6[o\text{-}Ph_2P(C_6H_4CO_2)\text{-}O,P]_6$ cluster

deviation of 0.108 Å and equatorial bond angles [O(1)–Ag(2)–O(6*) 98.6(3), P(2)–Ag(2)–O(6*) 108.0(2), and P(2)–Ag(2)–O(1) 152.8(2)°] summing to *ca.* 360°. Ag(3) is *ca.* 0.250 Å above the least-squares plane formed by O(2), O(3) and P(3) [Ag(3)–O(2) 2.619(9), Ag(3)–O(3) 2.176(9), Ag(3)–P(3) 2.378(4) Å] with equatorial bond angles [O(2)–Ag(3)–P(3) 93.1(2), O(2)–Ag(3)–O(3) 105.4(3), O(3)–Ag(3)–P(3) 161.2(3)°] summing to *ca.* 360°. However, if one considers the long Ag–O [Ag(2)–O(6*) 2.411(8), Ag(3)–O(2) 2.619(9)] and Ag(2)–Ag(3) distances as insignificant and non-interacting, with the large P(2)–Ag(2)–O(1) [152.8(2)°] and P(3)–Ag(3)–O(3) [161.2(3)°] angles, Ag(2) and Ag(3) may be described as two-coordinate. Ag(1) is surrounded by three carboxylato-O atoms and a P atom from four different *o*-(diphenylphosphino)benzoate ligands [Ag(1)–O(4) 2.598(9), Ag(1)–O(5) 2.261(9), Ag(1)–O(6*) 2.394(9), Ag(1)–P(1*) 2.381(4) Å]. The coordination geometry of Ag(1) is highly distorted from tetrahedral with the Ag atom lying only 0.418 Å above the least-squares plane of O(5), O(6*) and P(1*) and the bond angles ranging from 89.9(3) to 130.5(2)°. The Ag–P distances are normal and comparable to the Ag–P distances [2.363(4), 2.390(4) Å] in $[Ag_2(\mu\text{-}O_2CMe\text{-}O,O')(\mu\text{-}O_2CMe\text{-}O)(dppm)]_2$[5] and [2.342(4)–2.378(5) Å] in $[(C_{12}H_6O_4)_2(Ph_3PAg)_4]$ ($C_{12}H_6O_4$ = 1,8-naphthalenedicarboxylate).[7]

Of the three independent carboxylate groups, two behave as bidentate and one as tridentate ligands. The coordination modes of the two bidentate carboxylate ligands are very similar. Both of them coordinate unsymmetrically to two different silver atoms with a short and a long Ag–O bond in a *syn–syn* bridging mode. For the carboxylato group C(2)C(1)O(1)O(2), the Ag(2)–O(1) distance [2.185(9) Å] is significantly shorter than that of Ag(3)–O(2) [2.619(9) Å] with comparable C–O distances [C(1)–O(2) 1.24(1), C(1)–O(1) 1.28(1) Å]. Similarly, for the carboxylato group C(21)C(20)O(3)O(4), the Ag(3)–O(3) distance [2.176(9) Å] is significantly shorter than that of Ag(1)–O(4) [2.598(9) Å] with similar C–O distances [C(20)–O(3) 1.26(1), C(20)–O(4) 1.24(1) Å]. The carboxylato group C(40)C(39)O(5)O(6) coordinates to three different Ag atoms with Ag–O [Ag(1)–O(5) 2.261(9), Ag(2*)–O(6) 2.411(9), Ag(1*)–O(6) 2.394(9) Å] and C–O [C(39)–O(5) 1.22(1), C(39)–O(6) 1.27(1) Å] distances comparable to those observed in $[Ag_2(\mu\text{-}O_2CMe\text{-}O,O')(\mu\text{-}O_2CMe\text{-}O)(dppm)]_2$ [Ag–O, 2.232(11)–2.485(10), C–O 1.238(21)–1.278(19) Å],[5] resulting a tridentate carboxylato-μ-*O,O′*;μ-*O,O* mode.

Unlike previous reported *o*-(diphenylphosphino)benzoate metal complexes in which the ligand behaves as a bidentate chelating ligand,[8,9] the *o*-(diphenylphosphino)benzoate-*O,P* ligands in **1** do not exhibit chelation with any Ag atom, neither do the carboxylato-*O,O′* groups, instead, both groups connect with different Ag atoms at different coordinating sites.

Thanks are due to the Hong Kong Baptist University, the University of Hong Kong and the Hong Kong Research Grants Council (HKBU 131/94P) for financial support.

Notes and References

† E-mail: wkwong@sci.hkbu.edu.hk

‡ $[Ag(o\text{-}Ph_2PC_6H_4CO_2)]_6\cdot 2C_4H_8O\cdot C_6H_{14}$ (**1**$\cdot 2C_4H_8O\cdot C_6H_{14}$): white crystals, mp > 300 °C. Found: C, 56.6; H, 4.3. Calc. for $C_{128}H_{114}P_6O_{14}Ag_6$: C, 56.7; H, 4.2%. IR ($cm^{-1}$, in KBr): 3058w, 2976w, 2932w, 2854w, 2128w, 1597vs, 1577vs, 1556vs, 1481m, 1360vs, 1287m, 1260m, 1097m, 1061m, 1028w, 841m, 757vs, 696vs, 535m, 510m. $^{31}P\{^1H\}$ NMR ($CDCl_3$): δ 10.6 (br) and 15.0 (br). ^1H NMR ($CDCl_3$): δ 7.25–7.69 (br, m).

§ *Crystal data*: **1**$\cdot 2C_4H_8O\cdot C_6H_{14}$: $C_{114}H_{84}P_6O_{12}Ag_6\cdot 2C_4H_8O\cdot C_6H_{14}$, M_w = 2709.35, triclinic, space group $P\bar{1}$ (no. 2), a = 14.973(2), b = 15.635(3), c = 14.740(3) Å, α = 116.77(1)°, β = 107.71(1)°, γ = 71.87(1)°, U = 2872(1) $Å^3$, Z = 1, $F(000)$ = 1366, D_c = 1.566 g cm^{-3}, μ = 11.46 cm^{-1}. Crystal dimensions: 0.10 × 0.20 × 0.27 mm. Intensity data were collected on a Rigaku AFC7R diffractometer with graphite monochromated Mo-Kα radiation (λ = 0.710 73 Å) using ω–2θ scans ($2\theta_{max} \leqslant 45°$) at room temperature. The data were corrected for Lorentz, polarization effects and absorption correction using ψ-scan method resulting in transmission factors ranging from 0.8482 to 1.0000. A total of 7503 (R_{int} = 0.066) unique reflections were measured; 3183 of these had $I \geqslant 3\sigma(I)$ and were considered to be observed. The structure was solved by direct methods (SIR92)[10] and refined by full matrix least-squares analysis to give R = 0.047, wR = 0.047. Silver and phosphorus atoms were refined anisotropically and the rest of the non-hydrogen atoms were refined isotropically. Hydrogen atoms were generated in their idealized positions (C–H bond fixed at 0.95 Å) and allowed to ride on their respective parent carbon atoms. These hydrogen atoms were assigned appropriate isotropic thermal parameters and included in the structure factor calculations but not in the refinement. All calculations were performed on a Silicon-Graphics computer using program package Texsan from MSC.[11] CCDC 182/774.

1 W. K. Wong, J.-X. Gao, Z.-Y. Zhou and T. C. W. Mak, *Polyhedron*, 1992, **11**, 2965; W. K. Wong, J.-X. Gao and W. T. Wong, *Polyhedron*, 1993, **12**, 1647; W. K. Wong, J.-X. Gao, Z.-Y. Zhou and T. C. W. Mak, *Polyhedron*, 1993, **12**, 1415; J.-X. Gao, H.-L. Wan, W. K. Wong, M. C. Tse and W. T. Wong, *Polyhedron*, 1996, **15**, 1241.
2 W. K. Wong, J.-X. Gao, W. T. Wong, W. C. Cheng and C. M. Che, *J. Organomet. Chem.*, 1994, **471**, 277; W. K. Wong, T. W. Chik, K. N. Hui, I. Williams, X. Feng, T. C. W. Mak and C. M. Che, *Polyhedron*, 1996, **15**, 4447.
3 W. K. Wong, L-L. Zhang, F. Xue and T. C. W. Mak, *Chem. Commun.*, 1997, 1525.
4 F. Jaber, F. Charbonnier and R. Faure, *Polyhedron*, 1996, **15**, 2909.
5 S. P. Neo, Z.-Y. Zhou, T. C. W. Mak and T. S. A. Hor, *Inorg. Chem.*, 1995, **34**, 520.
6 X.-M. Chen and T. C. W. Mak, *J. Chem. Soc., Dalton Trans.*, 1991, 3253.
7 A. F. M. J. van der Ploeg, G. van Koten and A. L. Spek, *Inorg. Chem.*, 1979, **18**, 1052.
8 H. Schumann, H. Hemling, V. Ravindar, Y. Badrieh and J. Blum, *J. Organomet. Chem.*, 1994, **469**, 213.
9 M. C. Bonnet, F. Dahan, A. Ecke, W. Keim, R. P. Schulz and I. Tkatchenko, *J. Chem. Soc., Chem. Commun.*, 1994, 615.
10 SIR92: A. Altomare, M. C. Burla, M. Camalli, M. Cascarano, C. Giacovazzo, A. Guagliardi and G. Polidori, *J. Appl. Crystallogr.*, 1994, **27**, 43.
11 Texsan: Crystal Structure Analysis Package, Molecular Structure Corporation, The Woodlands, TX, 1985 and 1992.

Received in Cambridge, UK, 14th November 1997; 7/08227D

Electrochemical dehydrodimerisation of a vinylenylamide ligand: formation of the binuclear group {Mo≡N$^+$CH=CHCH=CHCH=CHN$^+$≡Mo} which displays very strong electronic coupling in the {(Mo^{III})–(Mo^{IV})} mixed-valence state

Yatimah Alias,[a] Marie-Laurence Abasq,[a,b] Frédéric Barrière,[a,b] Sian C. Davies,[a] Shirley A. Fairhurst,[a] David L. Hughes,[a] Saad K. Ibrahim,[a] Jean Talarmin[b] and Christopher J. Pickett*[a]†

[a] *The Nitrogen Fixation Laboratory, John Innes Centre, Norwich Research Park, Colney, Norwich, UK NR4 7UH*
[b] *UMR CNRS 6521, Faculté des Sciences, Université de Bretagne Occidentale, BP 809, 29285 Brest, France*

Electrochemical dehydrodimerisation of an {Mo–N=CHCH=CH$_2$} group gives an all-*trans*-{≡N$^+$CH=CHCH=CHCH=CHN$^+$≡} ligand, bridging two Mo^{IV} centres; the {(Mo^{III})–bridge–(Mo^{IV})} mixed-valence state is accessible by electrochemical reduction and exhibits very strong electronic coupling over the 11.7 Å which separates the two metal centres; this accords with EHMO calculations which show that the SOMO has substantial (30%) bridging-ligand character; in its capacity to function as a molecular wire linking two metal centres, the eight-atom hexatriene di(imide) chain {N(CH)$_6$N} compares favourably with C$_8$ chains of acetylenic carbons bridging other metal centres.

An extensive and diverse chemistry of enylamide ligands (–N=CR$_2$; R = H or organic group) is developing, particularly at molybdenum(II) centres.[1] For example, recently it has been shown that incipient carbanionic character at the γ-carbon atom within the {Mo–N=CHCH=CH$_2$} group allows regio- and stereo-specific addition of carbon electrophiles.[2] We now report a new reaction of this vinylenylamide group: anodic dehydrodimerisation to give the hitherto unknown {≡N$^+$CH=CHCH=CHCH=CHN$^+$≡} bridging ligand.

Controlled potential oxidation of *trans*-[MoCl(N=CHCH=CH$_2$)(dppe)$_2$] **1** {dppe = Ph$_2$PCH$_2$CH$_2$PPh$_2$; vitreous carbon; −0.55 V *vs.* ferrocenium–ferrocene (Fc$^+$–Fc); 0.2 M [NBu$_4$][BF$_4$] in tetrahydrofuran(thf)–KOBu^t (2 equiv.)} gives all-*trans*-[Cl(dppe)$_2$Mo≡NCH=CHCH=CHCH=CHN≡MoCl(dppe)$_2$]$^{2+}$ **2**$^{2+}$ in an overall two-electron process, Scheme 1.

Cation **2**$^{2+}$ is formed in *ca.* 70% yield and was isolated from the anolyte as the tetrafluoroborate salt. Recrystallisation from CH$_2$Cl$_2$–EtO$_2$ gave **2**[BF$_4$]$_2$·solvent as dark-orange plates and the structure was determined by X-ray crystallography.‡ This established that the alternate-hydrocarbon bridge has the all-*trans* arrangement as shown in Fig. 1. The *trans*-Cl–Mo–N arrangement at each Mo atom, and the dimensions about the metal atoms, are similar to those found in the molybdenum(IV) methylimide cation *trans*-[MoCl(NMe)(dppe)$_2$]$^+$ **3**$^+$.[3]

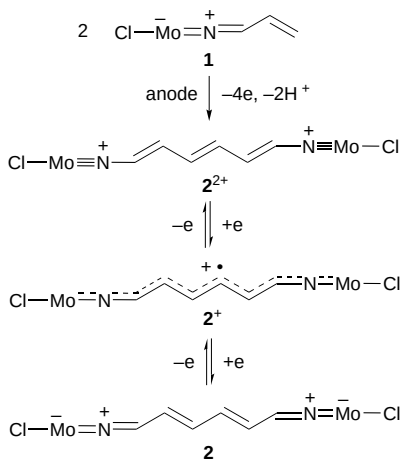

Scheme 1

The bridging ligand, which places the two Mo atoms 11.7 Å apart, is unique in that a polyene unit is linked to the metal centres by multiply bonding imide groups. The electronic consequences of this arrangement are considerable. EHMO calcualtions[4] indicate that the LUMO of **2**$^{2+}$ has both metal (30%, 30%) and bridging-ligand π*-character (30%).§ Populating this delocalised orbital by one-electron reduction leads to strong electronic coupling between the metal centres in the mixed-valence ion **2**$^+$ (Robin and Day, Class III behaviour[5]) as is borne out by the following experimental evidence.

Cyclic voltammetry {vitreous carbon; 0.2 M [NBu$_4$][BF$_4$]–CH$_2$Cl$_2$} shows that **2**$^{2+}$ undergoes two successive reversible one-electron reductions with $\Delta E°$ = 320 mV (K_{com} = 2.6 × 10^5) which is indicative of Class II or Class III behaviour, Fig. 2.

Controlled potential electrolysis {vitreous carbon; −1.35 V *vs.* Fc$^+$–Fc; 0.2 M [NBu$_4$][BF$_4$]–CH$_2$Cl$_2$} cleanly generates **2**$^+$ as a stable, paramagnetic solution species (S = 1/2; $g_\perp$ = 1.998, $g_\parallel$ = 1.960; frozen glass, 77 K). The electronic spectrum of electrogenerated **2**$^+$ shows an intense symmetric intervalence charge-transfer (IT) band in the near-IR at 12 820 cm^{-1} which is absent in **2**$^{2+}$.

The IT band-width at half-peak intensity ($\Delta\nu_{1/2}$) can be calculated for Class II systems from ν_{max} using the Hush equation.[6] This gives $\Delta\nu_{1/2}$ (calc.) = 5442 cm^{-1} whereas $\Delta\nu_{1/2}$ (exptl.) = 702 cm^{-1}: IT bands which are considerably sharper than predicted typify Class III character. The intensity of IT bands in Class II complexes are weak with ε_{max} typically in the order of 10^2 dm^3 mol^{-1} cm^{-1}; in addition ν_{max} is solvent dependent. In contrast, Class III complexes display intense solvent-independent IT bands. **2**$^+$ has ε_{max} = 9.5 × 10^4

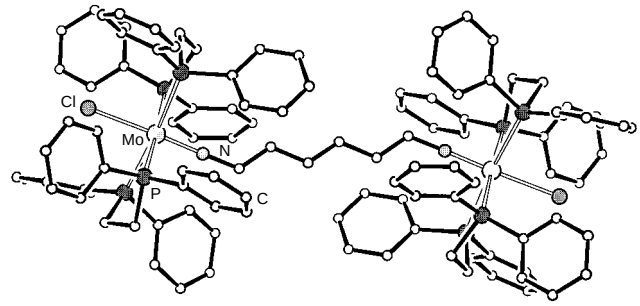

Fig. 1 View of cation [{MoCl(dppe)$_2$}$_2${μ-N(CH=CH–)$_3$N}]$^{2+}$; the two halves are related by a centre of symmetry. Selected molecular dimensions: Mo–Cl 2.521(4), Mo–N 1.752(11), mean Mo–P 2.551(7) Å; Mo–N–C 178.0(10)°.

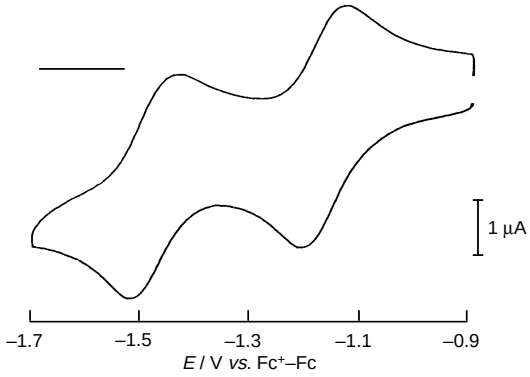

Fig. 2 Cyclic voltammogram at 293 K of $\mathbf{2}^{2+}$ at vitreous carbon electrode in 0.2 M $[NBu_4][BF_4]$–CH_2Cl_2 at a scan rate of 30 mV s^{-1} showing two successive reversible one-electron reductions. Electrode area = 0.0707 cm^2; concentration of complex = 0.26 mM.

$dm^3\ mol^{-1}\ cm^{-1}$ and ν_{max} is solvent independent, again consistent with Class III assignment.

The crystallographic distance between the metal centres, ν_{max} and $\Delta\nu_{1/2}$ can be used to estimate the degree of delocalisation (α^2) in the ground state of a mixed-valence system.[6] For $\mathbf{2}^+$, α^2 is 0.25 which compares favourably with $\alpha^2 = 0.26$ for the Class III system $[(\eta^5\text{-}C_5Me_5)(dppe)Fe{-}C{\equiv}CC{\equiv}CC{\equiv}CC{\equiv}C{-}Fe(\eta^5\text{-}C_5Me_5)(dppe)]^+$; this cation also has eight atoms separating the metal centres which are described as functioning as a 'molecular wire'.[7]

We thank the University of Malaya for providing a scholarship (to Y. A.); the Ministère de l'Enseignement Supérieur et de la Recherche for providing scholarships (to M. L. A. and F. B.); and the BBSRC for support of this work.

Notes and References

† Pickett@bbsrc.ac.uk

‡ Crystal structure analysis of $[\{MoCl(dppe)_2\}_2\{\mu\text{-}N(CH{=}CH{-})_3N\}][BF_4]_2{\cdot}nCH_2Cl_2{\cdot}mEt_2O$.

Crystal data: $C_{110}H_{102}B_2Cl_2F_8Mo_2N_2P_8{\cdot}CH_2Cl_2{\cdot}C_4H_{10}O$, assuming *n* and *m* are each 1.0, M = 2295.3, triclinic, space group $B\bar{1}$ (equiv. to no. 2), a = 12.533(1), b = 14.733(2), c = 30.206(3) Å, α = 83.818(8), β = 94.801(8), γ = 83.150(8)°, U = 5479.0(9) Å^3. Z = 2, D_c = 1.391 g cm^{-3}, $F(000)$ = 2360, T = 293 K, μ(Mo-Kα) = 5.1 cm^{-1}, λ(Mo-Kα) = 0.71069 Å.

Air-sensitive, thin, deep orange plate crystals. Preliminary photographic examination, then Enraf-Nonius CAD4 diffractometer (with monochromated radiation) for accurate cell parameters (25 reflections, θ = 10–11°) and diffraction intensities (5094 unique intensities (5094 unique reflections to θ_{max} = 20°; 2643 'observed' with $I > 2\sigma_I$).

Corrections applied for Lorentz-polarisation effects, crystal deterioration (*ca.* 14.3% overall), absorption (by semi-empirical ψ-scan methods) and to eliminate negative net intensities (by Bayesian statistical methods). Structure determined by automated Patterson routines; refinement by full-matrix least-squares methods, on F^2 values, in SHELXL.[8] In the cation, non-hydrogen atoms refined anisotropically, hydrogen atoms included with all parameters riding. Anion and solvent regions show disorder and not fully resolved. At conclusion of refinement, wR_2 = 0.182 and R_1 = 0.101[8] for 3881 reflections (with $I > \sigma_I$) weighted $w = [\sigma^2(F_o^2) + (0.0964P)^2]^{-1}$ with $P = (F_o^2 + 2F_c^2)/3$; for the 'observed' data, R_I = 0.068. In the final difference map, the highest peaks (*ca.* 0.67 e Å^{-3}) were close to the Mo centres. CCDC 182/766.

§ EHMO calculations[4] reveal that in $\mathbf{2}^{2+}$ a degenerate pair of occupied orbitals constitute two metal-based HOMOs each with 93% Mo character. Consistent with this, cyclic voltammetry (vitreous carbon; 0.2 M $[NBu_4][BF_4]$–CH_2Cl_2) shows that $\mathbf{2}^{2+}$ undergoes two successive and closely spaced ($\Delta E°$ = 100 mV) reversible one-electron oxidations indicative of a valence-trapped $\{Mo^{V}(bridge)Mo^{IV}\}$ system.

1 D. L. Hughes, M. Y. Mohammed and C. J. Pickett, *J. Chem. Soc., Chem. Commun.*, 1989, 1399; A. Hills, D. L. Hughes, C. J. Macdonald, M. Y. Mohammed and C. J. Pickett, *J. Chem. Soc., Dalton Trans.*, 1991, 121; D. L. Hughes, S. K. Ibrahim, C. J. Macdonald, H. Moh'd Ali and C. J. Pickett, *J. Chem. Soc., Chem. Commun.*, 1992, 1762; R. A. Henderson, S. K. Ibrahim and C. J. Pickett, *J. Chem. Soc., Chem. Commun.*, 1993, 392; D. L. Hughes, S. K. Ibrahim, H. Moh'd Ali and C. J. Pickett, *J. Chem. Soc., Chem. Commun.*, 1994, 425; Y. Alias, S. K. Ibrahim, M. A. Queiros, A. Fonseca, J. Talarmin, F. Volant and C. J. Pickett, *J. Chem. Soc., Dalton Trans.*, 1997, 4807.

2 S. A. Fairhurst, D. L. Hughes, S. K. Ibrahim, M.-L. Abasq, J. Talarmin, M. A. Queiros, A. Fonseca and C. J. Pickett, *J. Chem. Soc., Dalton Trans.*, 1995, 1873.

3 D. L. Hughes, D. L. Lowe, M. Y. Mohammed, N. M. Pinhal and C. J. Pickett, *J. Chem. Soc., Dalton Trans.*, 1990, 2021.

4 J. M. Ammeter, H. Bürgi, J. C. Thibeault and R. Hoffmann, *J. Am. Chem. Soc.*, 1978, **100**, 3686; C. Mealli and D. Proserpio, *J. Chem. Educ.*, 1990, **67**, 399.

5 M. B. Robin and P. Day, *Adv. Inorg. Chem. Radiochem.*, 1967, **10**, 247.

6 N. S. Hush, *Prog. Inorg. Chem.*, 1967, **8**, 391; 1984, **23**, 3002; R. J. Crutchely, *Adv. Inorg. Chem.*, 1994, **41**, 273.

7 F. Coat and C. Lapinte, *Organometallics*, 1996, **15**, 478.

8 G. M. Sheldrick, SHELX L—Program for crystal structure refinement, University of Göttingen, Germany, 1993.

Received in Cambridge, UK, 15th January 1998; 8/00419F

Selective electrochemical magnesium and calcium sensors based on non-macrocyclic nitrogen-containing ferrocene ligands

Antony Chesney, Martin R. Bryce,* Andrei S. Batsanov, Judith A. K. Howard and Leonid M. Goldenberg

Department of Chemistry, University of Durham, South Road, Durham, UK DH1 3LE

Ferrocene derivatives 1, 2a, 2b and 5 act as electrochemical sensors of Mg^{2+} and Ca^{2+} ions in acetonitrile solution in concentrations as low as 10 mol%: a new redox peak appears in the cyclic voltammogram, anodically shifted by 160–360 mV, with no interference from a large excess of several other metal salts; the single crystal X-ray structure of ligand 5 is reported.

The study of redox-active ligands in which a change in electrochemical behaviour can be used to monitor complexation of guest species is an increasingly important area of molecular recognition.[1] Ferrocene derivatives, most of which are substituted with macrocyclic ligands, have proved successful as ion sensors.[2] However, no selectivity towards magnesium or calcium ions has been reported for these systems: representative derivatives[3,4] show strong affinities for group 1 metals in solution (typically Li, Na or K) and selectivity for Li^+ has been observed for systems which are insensitive to Na^+ or K^+.[5] The electrochemical sensing of Mg^{2+} has been demonstrated in molten alloys[6] and in ferret ventricular muscle tissue,[7] and both fluorescent[8] and fibre-optical[9] devices have proved useful. However, no solution studies on efficient redox-active Mg^{2+} or Ca^{2+} sensors have been reported.

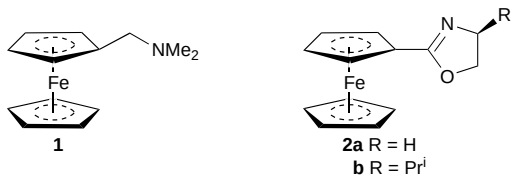

1 **2a** R = H **b** R = Pr^i

We now report the metal-binding properties of nitrogen-containing, non-macrocyclic derivatives of ferrocene. Commercially available (dimethylamino)methylferrocene **1** was employed initially. Titration studies using cyclic voltammetry (CV)† in acetonitrile indicated that compound **1** could detect the presence of Mg^{2+} and Ca^{2+} ions in concentrations as low as 10 mol%: on addition of $Mg(ClO_4)_2$ or $Mg(CF_3SO_3)_2$ a second redox peak appeared in the CV, anodically shifted by *ca.* 230 mV. The observation of approximately equal peak currents for the two redox waves after addition of 0.2 equiv. of $Mg(ClO_4)_2$ (Fig. 1) or $Mg(CF_3SO_3)_2$ suggests the formation of a complex with a ligand : metal ratio of *ca.* 2 : 1. Addition of $Ca(ClO_4)_2$, instead of $Mg(ClO_4)_2$, led to an anodic drift in the redox wave with no clearly defined new peak. Remarkably, the presence of a range of other metal ions in solution [$LiClO_4$, $NaClO_4$, $KClO_4$, $CsClO_4$, $Ba(ClO_4)_2$ and $AgClO_4$] had no effect on the CV, even in concentrations as high as 2500 mol%.‡

We next studied the known oxazolines **2a** and **2b**.[10] The oxygen atom of **2a** and **2b** could act as an alternative chelation site, and **2b** also possesses a potentially sterically demanding isopropyl group α to the nitrogen. Additionally, to assess the importance of the proximity of the binding site to the ferrocene core on the selectivity and strength of binding, the extended oxazoline ligand **5** was prepared from aldehyde **3** according to Scheme 1, utilising reagent **4**, prepared by analogy with the literature procedure.[11] X-Ray crystal structure analysis§ of **5** confirmed the expected *trans* configuration of the alkene bridge (in agreement with ^{1}H NMR data) and the (*S*)-configuration of the chiral centre at C(4) (Fig. 2).

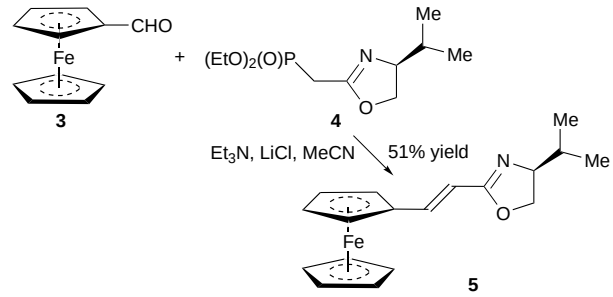

Scheme 1

Ligands **2a**, **2b** and **5** all demonstrated a selectivity towards Mg^{2+} and Ca^{2+} over other metal ions, similar to that observed for amine **1** and Mg^{2+} with a second redox peak emerging in the CV arising from ligand–metal complexation. This 'two-wave' behaviour is diagnostic of a large value ($> 10^4$) for the equilibrium constant for cation binding by the neutral (electrochemically unaltered) ligand.[12] Data comparing the redox behaviour of these systems in the presence of Mg^{2+} and Ca^{2+} ions are collated in Table 1. These ligands showed a significant binding enhancement[12] in the presence of Mg^{2+} and Ca^{2+} ions‡ and these data are quantitatively similar to those reported by Beer for the interaction of cations (Na^+, Li^+) with a macrocycle,

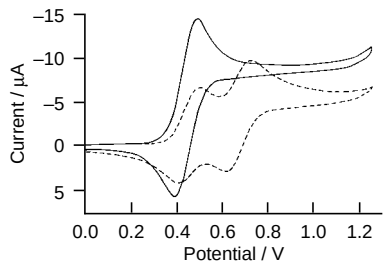

Fig. 1 Cyclic voltammogram of **1** in MeCN (———) and after the addition of $Mg(ClO_4)_2$ (0.2 equiv.) (- - - -)

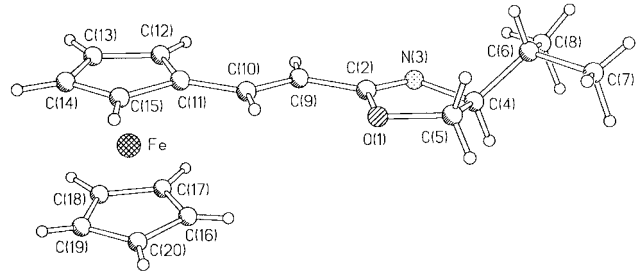

Fig. 2 X-Ray molecular structure of **5**

Table 1 Cyclic voltammetric data

Ligand/ M	$E^{\frac{1}{2}}_{free}$/ mV	$E^{\frac{1}{2}}_{complex}$/ mV	ΔE/ mV	min. equiv. M^{2+} [a]	max. equiv. M^{2+} [b]	K_1/K_2 [c]
1/Ca	490	—[d]		0.1	0.5	
1/Mg	490	720	230	0.1	3	3.8×10^5
2a/Ca	670	980	310	0.1	1	1.7×10^5
2a/Mg	670	1000	330	0.1	3	3.8×10^5
2b/Ca	680	1040	360	0.1	3	1.2×10^6
2b/Mg	680	1040	360	1	5	1.2×10^6
5/Ca	650	810	160	0.1	3	5.0×10^3
5/Mg	650	840	190	1	15	1.6×10^3

[a] Minimum equiv. of metal ClO_4^- salt required to produce a detectable second redox peak. [b] Equiv. of metal salt required for complete disappearance of original ligand redox peak (E free). [c] Binding enhancement for the complexation of a metal cation calculated using the equation in 12(*b*). The equilibrium constants K_1 and K_2 correspond to the complexation processes by the neutral and oxidised forms of the ligand. [d] A second redox peak was not observed; instead, an anodic drift occurred upon addition of Ca^{2+} which ceased when *ca.* 0.5 equiv. had been added. This behaviour is diagnostic of weak binding of the metal and the neutral ligand[12] and prevented the calculation of a binding enhancement.

monitored by changes in the cathodic electrochemistry of an appended anthraquinone substituent, although such systems do not often exhibit significant selectivity in the presence of other metals.[2a] Notably, compounds **1** and **2a** showed an identical affinity for Mg^{2+}, whereas only **2a** showed a strong affinity for Ca^{2+}. The presence of the isopropyl group in **2b** slightly increased the strength of binding of both Mg^{2+} and Ca^{2+} still further, presumably for electronic rather than steric reasons, whilst the amount of Mg^{2+} required to achieve a response was increased by a factor of 10 over that observed for **2a**: recognition of Ca^{2+}, however, suffered no such problem. For compound **5**, there was a considerably reduced anodic shift in the new redox peak and a lowering of the binding enhancement. The observed shift (160–190 mV) is consistent with the transmission of cation binding through a conjugated alkene link, with no contribution from a through-space effect.[3] System **5** required a considerably higher concentration of Mg^{2+} (15 equiv.) than the other ligands before the original ferrocene redox peak was lost.

Cation binding by systems **2a**, **2b** and **5** was also detected by changes in the UV–VIS spectra: on addition of Mg^{2+} or Ca^{2+} a new absorption peak appeared at lower energy. This was most striking for compound **5** which possesses an extended chromophore. Upon addition of $Mg(ClO_4)_2$ (1 equiv.) to a solution of compound **5** (10^{-3} M) in acetonitrile, the solution changed from pale yellow to purple, and the absorption peak of **5** at λ_{max} 449 nm entirely disappeared and was replaced by a new peak at λ_{max} 528 nm. For compounds **2a** and **2b** the colour change was less striking. For example, the absorption peak of **2b** at λ_{max} 446 nm in acetonitrile shifts to λ_{max} 472 nm on addition of $MgClO_4$ (1 equiv.): addition of more $Mg(ClO_4)_2$ gives no significant change in the spectra. A UV titration experiment suggested the formation of a complex of stoichiometry ligand : cation = 2 : 1. We presume that the electrochemical and spectrophotometric response observed for systems **2a**, **2b** and **5** arises from Mg^{2+} or Ca^{2+} coordination to the nitrogen atom of the substituent. The ligands can be recovered unchanged in *ca.* 60% yield from solutions containing the metal salts by aqueous workup.

We have discounted the fact that the electrochemical and spectrophotometric response is due to adventitious protonation or hydration of the ligands. The CV and UV–VIS spectra of ligands **2a** and **2b** in MeCN were unchanged by the addition of water to the solution. Protonation of the ligands (achieved by the addition of perchloric acid to the solution) was monitored by the appearance of a new redox wave at $E^{\frac{1}{2}}$ +680 mV (compound **2a**) and +980 mV (compound **2b**) which are decisively different potentials from those assigned to the metal complexes (Table 1). Moreover, ^{1}H NMR spectroscopic data supported these conclusions.¶

Oxazoline derivatives **2b** and **5** are chiral which may enable chiral recognition of magnesium-containing species, and may also offer a method for electrochemically modifying asymmetric reactions in which magnesium coordination plays a pivotal rôle.[13]

This work was funded by EPSRC (A. C.), Royal Society (L. M. G.) and the Leverhulme Trust (A. S. B.). We thank Dr C. J. Richards for details of the synthesis of **2a** and **2b** prior to publication of ref. 10(*c*).

Notes and References

* E-mail: m.r.bryce@durham.ac.uk

† Experiments used the ligand (10^{-3} M) and $NBu^n_4ClO_4$ (0.1 M) in HPLC grade MeCN, *vs.* Ag/AgCl with a platinum working electrode. Sequential additions of aliquots of 0.1 or 0.5 equiv. of 10^{-2} M solutions of the appropriate metal salt in MeCN were monitored by CV.

‡ In the presence of 1–4 equiv. of Zn^{2+} [$Zn(ClO_4)_2$ or $ZnCl_2$] an anodic drift (maximum 60 mV) in the redox potential for compounds **1**, **2** and **5** was observed. Addition of traces of Mg^{2+} ions to these mixtures resulted in the immediate appearance of the second redox peak listed in Table 1.

§ *Crystal data*: $C_{18}H_{21}FeNO$, M = 323.21, orthorhombic, space group $P2_12_12_1$ (no. 19), a = 5.8828(4), b = 10.948(1), c = 24.274(2) Å, U = 1563.4(3) Å^3, Z = 4, T = 150 K, μ = 9.6 cm^{-1}, $2\theta \leqslant 55.8°$, 8017 total data, 2840 unique, 2569 observed [$I \geqslant 2\sigma(I)$]; R_{int} = 0.052 before, 0.038 after numerical absorption correction (seven faces, T_{min} = 0.81, T_{max} = 0.93); $wR(F^2)$ = 0.061; $R(F$, obs. data) = 0.028; residual $\Delta\rho_{max}$ = 0.18, $\Delta\rho_{min}$ = −0.25 e Å^{-3}; absolute configuration was determined by Flack parameter, x = −0.01(2). CCDC 182/757.

¶ The data for ligand **2b** are representative; the most diagnostic protons are those at the chiral centre (H_a), the methylene group adjacent to oxygen (H_b) and the unsubtituted Cp ring (H_c). For the free ligand in CD_3CN these protons appear at δ 3.97, 4.08 and 4.24, respectively. Addition of $KClO_4$ to this solution led to no change in the spectrum, whereas on addition of $Mg(ClO_4)_2$ (2 equiv.) the peaks shifted to δ 4.38, 4.81 and 4.46. ^{1}H NMR titration curves, monitoring the shifts of H_a, H_b and H_c upon addition of $Mg(ClO_4)_2$ support the UV–VIS and CV data in suggesting a stoichiometry of 2 : 1. The spectrum in the presence of Mg^{2+} was different from that of protonated **2b**.

1 (*a*) G. W. Gokel, *Chem. Soc. Rev.*, 1992, **21**, 39; (*b*) P. D. Beer, *Chem. Soc. Rev.*, 1989, **18**, 409; (*c*) T. M. Swager and M. J. Marsella, *Adv. Mater.*, 1994, **6**, 595; (*d*) R. Dieing, V. Morisson, A. J. Moore, L. M. Goldenberg, M. R. Bryce, J.-M. Raoul, M. C. Petty, J. Garín, M. Savíron, I. K. Lednev, R. E. Hester and J. N. Moore, *J. Chem. Soc., Perkin Trans. 2*, 1996, 1587.

2 P. D. Beer, *Adv. Inorg. Chem.*, 1992, **39**, 79; P. D. Beer and K. Y. Wild, *Polyhedron*, 1996, **15**, 775.

3 M. P. Andrews, C. Blackburn, J. F. McAleer and V. D. Patel, *J. Chem. Soc., Chem. Commun.*, 1987, 1122; P. D. Beer, C. Blackburn, J. F. McAleer and V. D. Patel, *Inorg. Chem.*, 1990, **29**, 378.

4 P. D. Beer, H. Sikanyika, C. Blackburn and J. F. McAleer, *J. Chem. Soc., Chem. Commun.*, 1989, 1831.

5 (*a*) P. D. Beer, H. Sikanyika, C. Blackburn and J. F. McAleer, *J. Organomet. Chem.*, 1988, **350**, C15; (*b*) P. D. Beer, A. D. Keefe, H. Sikanyika, C. Blackburn and J. F. McAleer, *J. Chem. Soc., Dalton Trans.*, 1990, 3289.

6 B. L. Tiwari and B. J. Howie, *J. Met.*, 1988, **40**, 102.

7 L. A. Blatter, A. Buri and J. A. S. McGuigan, *J. Physiol.*, 1984, **418**, 154 and references therein.

8 Z. J. Zhang and W. R. Seitz, *Anal. Chim. Acta*, 1985, **171**, 251.

9 K. Suzuki, K. Tohda, Y. Tanda, H. Ohzora, S. Nishihama, H. Inoue and T. Shirai, *Anal. Chem.*, 1989, **61**, 382.

10 (*a*) C. J. Richards, T. Damalidis, D. E. Hibbs and M. B. Hursthouse, *Synlett.*, 1995, 74; (*b*) T. Sammakia, H. A. Latham and D. R. Schaad, *J. Org. Chem.*, 1995, **60**, 10; (*c*) C. J. Richards and A. W. Mulvaney, *Tetrahedron: Asymmetry*, 1996, **7**, 1419.

11 A. I. Meyers and M. Shipman, *J. Org. Chem.*, 1991, **56**, 7098.

12 (*a*) S. R. Miller, D. A. Gustowski, Z. C. Chen, G. W. Gokel, L. Echegoyen and A. E. Kaifer, *Anal. Chem.*, 1988, **60**, 2021; (*b*) A. E. Kaifer and S. Mendoza, in *Comprehensive Supramolecular Chemistry*, ed. G. Gokel, Pergamon, Oxford, 1996, vol. 1, p. 701.

13 E. J. Corey and K. Ishihara, *Tetrahedron Lett.*, 1992, **33**, 6807.

Received in Cambridge, UK, 10th September 1997; revised manuscript received 18th December 1997; 8/00436F

2,2′-Dimethylbiphenyl-6,6′-dicarboxylic acid enforces two attached valine molecules to form up a chiral host lattice

Claus Weigand[a] Martin Feigel*[a]† and Claudia Landgrafe[b]

[a] Institut für Organische Chemie and [b] Institut für Analytische Chemie, Ruhr-Universität Bochum, Universitätsstr. 150, D-44780 Bochum, Germany

Crystals of (*R*)-valyl 2,2′-dimethylbiphenyl-6,6′-dicarboxylate 3 and (*S*)-valyl 2,2′-dimethylbiphenyl-6,6′-dicarboxylate 4 are stabilised by a network of inter- and intramolecular hydrogen bonds; together with the space requirement of the biphenyl core, structures result which contain cavities filled by THF (3) or EtOH molecules engaged in hydrogen bridging (4).

The regular structural motifs of proteins, β-strands and α-helices have been imitated using artificial amino acids. β-Sheets, β-turns or unusual helices have been targets of recent research.[1] Other examples are cyclic peptides of alternating chirality which aggregate to dimers in the form of antiparallel or parallel β-sheets.[2] We used an organic dicarboxylic acid as spacer to provide the optimal geometry for a parallel β-sheet.[3] However, the active centers of natural peptide oligomers as the enzymes or catalytic antibodies[4] are often located in regions of irregular peptide conformations. While it may be very difficult to design such active centers from scratch it is promising to study organic spacer units which hold attached peptide chains in divergent directions so that regular sheets or helices cannot be formed by self-association. Here, we report the synthesis and the solid state structure of two small peptides where biphenyldicarboxylic acid **2** is used as nucleation point of an irregular peptide structure.

Methyl 2-iodo-3-methylbenzoate **1** was prepared from *m*-toluic acid.[5] The biaryl coupling forming the dimethyl ester of **2** was achieved in high yields using a specially activated copper catalyst (Scheme 1). (*S*)-**2** was isolated from the brucine salt of the carboxylic acid. The peptide coupling of (*S*)-**2** with 2 equiv. of (*R*) or (*S*)-valine methyl ester yields **3** and **4** (after hydrolysis of the valine ester groups) in almost quantitative yield. Diethyl cyanophosphonate was used for the sterically demanding peptide coupling.[6]

Crystals of **3** and **4** were grown from THF–EtOH and from EtOH. They contain THF and EtOH guest molecules. The X-ray determined solid state structures‡ of **3** and **4** shows that the attachment of four substituents in the *o*,*o*′-positions of the biphenyl core results in a divergence of the two peptide chains by almost 90° (Fig. 1).

The unit cell of **4** contains two different molecules with slightly different orientation of the valine side-chains. The dihedral angles ϕ in the peptide chains A and B of **3** and **4** [A(**3**): ϕ = 112.2°, B(**3**): ϕ = 121.7°, A(**4**)/A′(**4**): ϕ = −67.3/−93.4°, B(**4**)/B′(**4**): ϕ = −116.8/−137.4°] belong to regions of the Ramachandran diagram were extended and helical peptide structures have been located[6] (note the change in sign with the chirality of the amino acid). The biphenyl core obviously does not enforce energetically disfavoured geometries in attached peptides.

In both structures, an intramolecular hydrogen bond is formed between the Val-NH proton of one peptide chain (A) and the biphenylic-carbonyl oxygen of the other chain B. The chains A and B are however identical in the NMR spectra of **3** and **4** in DMSO at 30 °C. Even low temperature spectra of the corresponding dimethyl esters in $CDCl_3$ (−40 °C) contain only one set of signals for both peptide chains. So it can be assumed

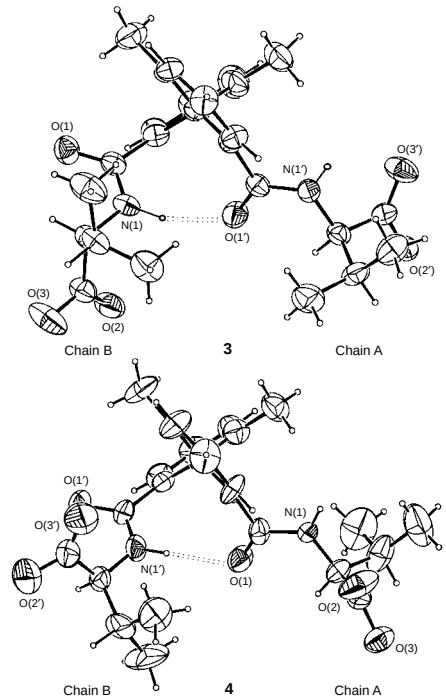

Fig. 1 ORTEP plot of the molecules **3** and **4** in the solid state. Both compounds develop the same intramolecular hydrogen bond, but the orientation of the valine side-chains is different.

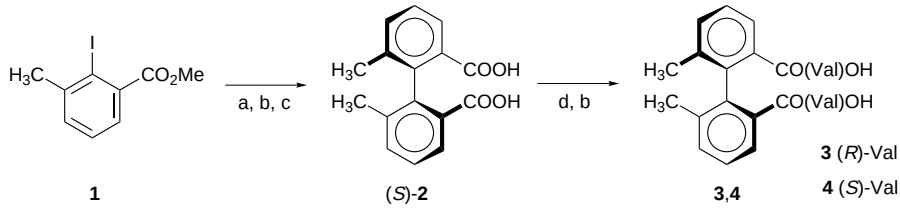

Scheme 1 *Reagents and conditions*: (*a*) **1** (10 g), dendritic copper (Aldrich, 3 μ, 6 g), DMF (20 ml), 150 °C; distill. 92%: (*b*) KOH, EtOH, H_2O (60 °C) then HCl, quant.: (*c*) acetone, MeOH, brucine, 40% (*S*)-**2**, see ref. 5: (*d*) D (or L)-valine methyl ester, diethyl cyanophosphonate, triethylamine, DMF, 90–92%

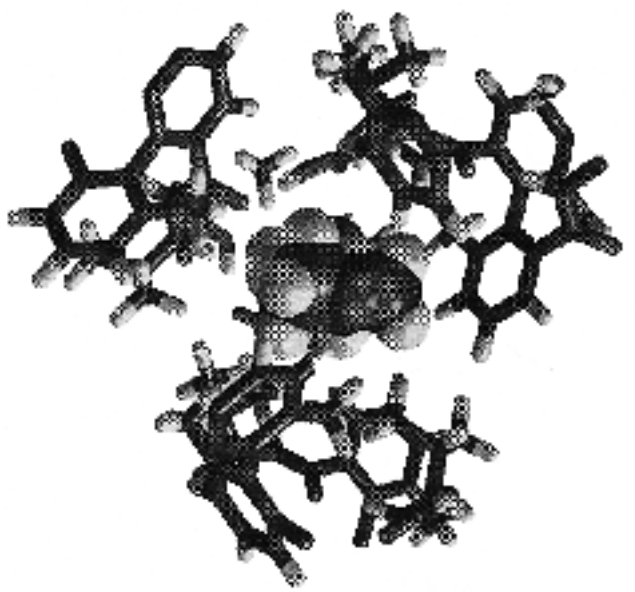

Fig. 2 Coordination of THF (drawn as CPK model) in the solid state structure of **3** (drawn as tubes). A second disordered THF molecule can be seen behind the THF in front.

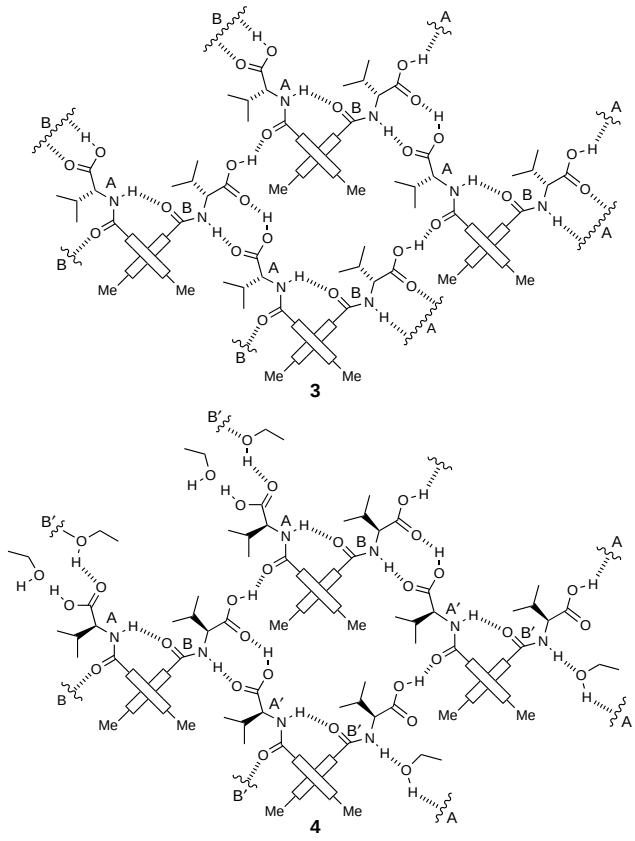

Fig. 3 Schematic two dimensional drawing of the hydrogen bond network in the solid state structure of **3** and **4**. The structure of **4** contains an EtOH molecule disordered over two sites.

that the chains A and B interconvert rapidly on the NMR timescale if the solid state conformation persists in solution.

The crystal lattice of **3** encapsulates THF molecules at two different positions. The THF guests are surrounded by a lipophilic environment of aromatic CH groups and CH_3 groups of valine and of the biphenyl unit (Fig. 2) One of the THF molecules is disordered (site occupation factor = 0.5) and fills only every second position available.

Whereas the conformations of the peptide chains differ in **3** and **4** (see above and Fig. 1), both molecules have an almost identical network of intermolecular hydrogen bonds (see Fig. 3). The carboxylic groups do not form carboxylic acid dimers but are engaged in hydrogen bonding to the amide groups. The carboxylic OH group of chain B is in contact with the CO group at the biphenyl core of chain A building an infinite structure of hydrogen bonded molecules (in **3** and **4**). The carboxylic group of chain A uses the HN–Cα–CO unit of chain B to build up another strand of hydrogen bonds almost orthogonal to the first one. Compound **4** uses EtOH molecules to complete this second strand of hydrogen bonds.

The biphenyl core **2** serves as a molecular cross for attached peptides. The intra- and inter-molecular hydrogen bonds found in the solid state structure of **3** and **4** do not resemble the common β-sheets or helical structures of peptides. Biaryl diacids are known to form inclusion complexes with several organic guests.[8] The peptides in **3** and **4** obviously do not reduce this tendency and may be ideal tools to alter the properties of these cavities. We are looking forward to synthesising host–guest lattices of biphenyl peptides containing longer peptide chains.

Notes and References

† E-mail: feigel@indi-f.orch.ruhr-uni-bochum.de

‡ *Crystal data* for $C_{26}H_{32}N_2O_6{\cdot}2C_4H_8O$ (**3**): Siemens P4 diffractometer, Mo-Kα radiation, M = 612.74, 0.68 × 0.52 × 0.48 mm, orthorhombic, space group $P2_12_12_1$, a = 11.107(5), b = 15.013(6), c = 20.813(7) Å, U = 3471(2) Å^3, F(000) = 1320, Z = 4, D_c = 1.173 g cm^{-3}, R = 0.086 [for data with $I > 2\sigma(I)$], wR_2 = 0.269 for 5958 reflections (Θ_{max} = 25.14°). The asymmetric unit contains an THF molecule disordered over two sites (site occupation factors = 0.5). The structure was resolved with SHELXS and refined with SHELXL.

Crystal data for $C_{26}H_{32}N_2O_6{\cdot}0.5\ C_2H_5OH$ (**4**): Siemens P4 diffractometer, Mo-Kα radiation, M = 983.14, 0.68 × 0.36 × 0.10 mm, monoclinic, space group $P2_1$, a = 11.480(8), b = 10.186(4), c = 25.274(9) Å, β = 100.18(5)°, U = 2909 Å^3, F(000) = 1052, Z = 4, D_c = 1.122 g cm^{-3}, R = 0.083 [for data with $I > 2\sigma(I)$], wR_2 = 0.272 for 4012 unique reflections (Θ_{max} = 25.51°).The asymmetric unit contains an EtOH molecule disordered over two sites (site occupation factors = 0.5). The structure was resolved with SHELXS and refined with SHELXL. CCDC 182/748.

1 J. D. Nowick, M. Pairish, I. Q. Leen, D. L. Holmes and J. W. Ziller, *J. Am. Chem. Soc.*, 1997, **119**, 5413; D. S. Kemp, B. R. Bowen and C. C. Muendel, *J. Org. Chem*., 1990, **55**, 4650; E. Graf von Roedern, E. Lohof, G. Hessler, M. Hoffmann and H. Kessler, *J. Am. Chem. Soc*., 1996, **118**, 10 156; D. H. Appella, L. A. Christianson, I. L. Karle, D. R. Powell and S. H. Gellman, *J. Am. Chem. Soc*., 1996, **118**, 13 071; D. Seebach, M. Overhand, F. N. M. Kühnle, B. Martinoni, L. Oberer, U. Hommel and H. Widmer, *Helv. Chim. Acta*., 1996, **79**, 913; I. L. Karle, A. Pramanik, A. Banerjee, S. Bhattacharjya and P. Balaram, *J. Am. Chem. Soc*., 1997, **119**, 9087.

2 M. R. Ghadiri, K. Kobayashi, J. R. Granja, R. K. Chadha and D. E. McRee, *Angew. Chem., Int. Ed. Engl.*, 1995, **34** 93; K. Kobayashi, J. R. Granja and M. R. Ghadiri, *Angew. Chem., Int. Ed. Engl*., 1995, **34**, 95.

3 G. Wagner and M. Feigel, *Tetrahedron*, 1993, **49**, 10 831.

4 P. G. Schultz and R. A. Lerner, *Acc. Chem. Res*., 1993, **26**, 391.

5 S. Kandi, H. Muramato, N. Kabayashi, M. Motoi and H. Suda, *Bull. Chem. Soc. Jpn.*, 1987, **60**, 3559.

6 S. Yamada, Y. Kasai and T. Schioiri, *Tetrahedron Lett.*, 1973, **18**, 1595; T. Shioiri, Y. Yokoyama, Y. Kasai and S. Yamada, *Tetrahedron*, 1976, **32**, 2211.

7 G. N. Ramachandran and V. Sasisekharan, *Adv. Protein. Chem*., 1968, **23**, 283.

8 E. Weber, I. Csoregh, B. Stensland and M. Czugler, *J. Am. Chem. Soc*., 1984, **11**, 3297.

Received in Liverpool, UK, 12th November 1997; 7/08162F

Single-feed one-step block copolymerization of *n*-octyloxyallene with phenylallene using π-allylnickel as initiator

Koji Takagi,[a] Ikuyoshi Tomita[b]† and Takeshi Endo*[a]

[a] *Research Laboratory of Resources Utilization, Tokyo Institute of Technology, Nagatsuta 4259, Midori-ku, Yokohama, 226-8502 Japan*

[b] *Department of Electronic Chemistry, Interdisciplinary Graudate School of Science and Engineering, Tokyo Institute of Technology, Nagatsuta 4259, Midori-ku, Yokohama, 226-8503 Japan*

The π-allylnickel initiated block copolymerization of *n*-octyloxyallene and phenylallene takes place in one step from a single-feed mixture of the two monomers.

The living polymerization technique is the most prominent method to obtain well-defined block copolymers.[1] Generally, two monomers are fed stepwise as the polymerization progresses, except in a few examples. Saegusa *et al*. reported the 'one-shot block copolymerization' of 2-alkyl-2-oxazoline with 2-perfluoroalkyl-2-oxazoline,[2] which involves the change of the propagating species from the ionic to the covalent form. Feast *et al*. also reported the successful one-shot block copolymerization of *syn*- and *anti*-7-methylnorbornene using a Schrock molybdenum alkylidene initiator,[3] where the large difference in polymerizability of the two monomers assisted the block copolymerization.

Herein, we describe the π-allylnickel complex initiated block copolymerization of *n*-octyloxyallene **2** with phenylallene **3** in one step from a single-feed mixture of the two monomers[4,5] (Scheme 1).

A mixture of **2** and **3** (50 equiv. each) was added to a toluene solution of $[(\pi\text{-allyl})NiOCOCF_3]_2$ **1** and the polymerization was performed for 12 h. As a result, a copolymer (M_n = 20 100, M_w/M_n = 1.15) was obtained in 94% yield, whose composition was poly(**2**):poly(**3**) = 49 : 51 (determined by ^{1}H NMR spectroscopy) in good accordance with the monomer feed ratio. The monomer conversion, determined by GC, gave interesting information on the copolymerization process (Fig. 1).†

The specific consumption of **2** took place at the initial stage of the polymerization, meanwhile **3** was not converted at all. However, when **2** had been consumed completely, the slow polymerization of **3** started to give a copolymer with a high block sequence. By quenching the copolymerization of **2** with **3** (50 equiv. each) in the initial stages (*i.e.* at 0 °C for 10 min) by pouring the reaction mixture into large amount of MeOH–H_2O (1 : 1), a polymer (M_n = 9450, M_w/M_n = 1.15) was obtained in 54% yield, which was composed solely of a poly (**2**) segment (determined by ^{1}H NMR spectroscopy).[6] This experiment also supports the efficient formation of a block copolymer.

The unexpected formation of the block copolymer cannot be explained fully by the difference in polymerization rate of the two monomers [k_{obs} (**2**) = 9.94×10^3 and k_{obs} (**3**) = 0.14×10^3 l mol^{-1} h^{-1}; k_{obs} (**2**)/k_{obs} (**3** = *ca.* 70]. The observed kinetic coefficient of **2** is not influenced by **3**, because k_{obs} (**2**) in the early stage of the copolymerization (9.94×10^3 l mol^{-1} h^{-1}) is comparable to that in the homopolymerization of **2**. The result clearly indicates that the concentration of the active species (most probably the nickel complex coordinated with **2**) is not affected by **3**. Namely, it can be taken to mean that the coordination equilibrium of the nickel complex with the monomers is shifted considerably to coordinated with **2** in the copolymerization, which promotes the specific polymerization of **2** in the initial stages. Further work on the copolymerization of various monomer combinations and a mechanistic investigation are in progress.

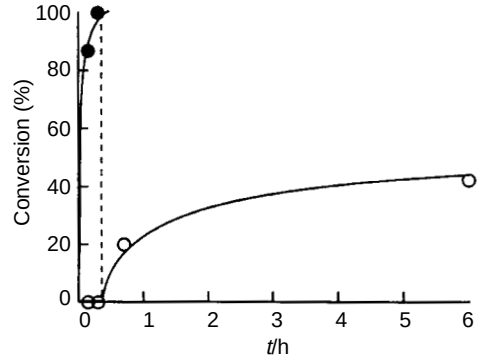

Fig. 1 Time *vs*. conversion curves for (●) **2** and (○) **3** in the copolymerization by **1** at 0 °C ($[\mathbf{2}]_0 = [\mathbf{3}]_0 = 5.0 \times 10^{-2}$ M, [Ni] = 1.0×10^{-3} M)

Notes and References

† E-mail: itomita@res.titech.ac.jp

‡ Estimation of the kinetic coefficients (typical procedure): The copolymerization of **2** with **3** ($[\mathbf{2}]_0/[Ni] = [\mathbf{3}]_0/[Ni]$ = 50, [Ni] = 1.0×10^{-3} M) by **1** was performed at 0 °C in toluene containing *n*- tetradecane (2.0×10^{-3} M) as an internal standard. After designated reaction periods, a small portion of the reaction mixture was sampled with the syringe (*ca.* 10 μl) and the monomer conversions were estimated by GC analysis.

1 See, for example: A. S. Hoffmann and R. Bacckai, in *Highpolymers, Vol. XVIII, Copolymerization*, ed. G. E. Ham, Wiley, New York, 1964, ch. 6, p. 135; I. Goodman, in *Development in Block Copolymer I*, ed. I. Goodman, Elsevier, Essex, 1982, ch. 5, p. 127; D. B. Johns, R. W. Lenz, and A. Luick, in *Ring-Opening Polymerization, Vol. I*, ed. K. J. Ivin and T. Saegusa, Elsevier, London, 1984, ch. 5, p. 218; R. N. Young, *Trends Polym. Sci.*, 1993, **1**, 149.

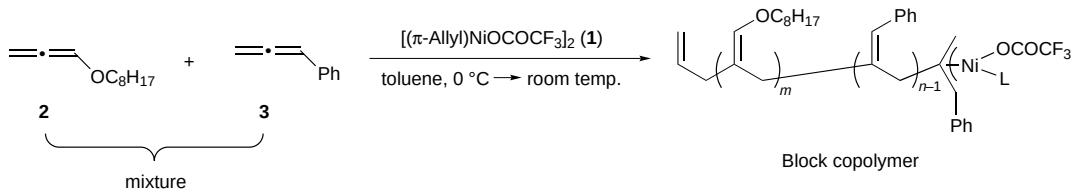

Scheme 1

2 T. Saegusa, Y. Chujo, K. Aoi, and M. Miyamoto, *Makromol. Chem., Macromol. Symp*., 1990, **32**, 1.
3 W. J. Feast, V. C. Gibson, K. J. Ivin, E. Khosravi, A. M. Kenwright, E. L. Marshall and J. P. Mitchell, *Makromol. Chem*., 1992, **193**, 2103.
4 For the living polymerization of allene derivatives, see: I. Tomita, Y. Kondo, K. Takagi and T. Endo, *Macromolecules*, 1994, **27**, 4413; K. Takagi, I. Tomita and T. Endo, *Maclomolecules*, 1997, **30**, 7386.
5 We have recently reported the two-feed block polymerization of alkoxyallenes with phenylallene by a π-allylnickel catalyst, in which block copolymers with controlled segment lengths could be successfully obtained by using additives (PPh_3 or CuI) over the course of the polymerization. See: K. Takagi, I. Tomita and T. Endo, *Polym. Bull*., in the press.
6 The yield of 54% corresponds to 91 wt% of **2**. Namely, **3** was untouched at least until the conversion of **2** reached to 91%.

Received in Cambridge, UK, 8th December 1997; 7/08786A

Dioxygenase-catalysed *cis*-dihydrodiol formation in the carbo- and hetero-cyclic rings of quinolines

D. R. Boyd,*[a]† N. D. Sharma,[a] J. G. Carroll,[a] J. F. Malone,[a] D. G. Mackerracher[a] and C. C. R. Allen[b]

[a] *The School of Chemistry, The Queen's University of Belfast, Belfast, UK BT9 5AG*
[b] *The QUESTOR Centre, The Queen's University of Belfast, Belfast, UK BT9 5AG*

Evidence of enzyme-catalysed *cis*-dihydroxylation in the pyridine (3,4-bond) and benzene rings (5,6- and 7,8-bonds) of quinoline and 2-substituted quinolines is examined in light of the isolation of a heterocyclic *cis*-diol derivative of 2-quinolone, as a single enantiomer of opposite absolute configuration to that found for the enantiopure carbocyclic *cis*-diol metabolites from quinolines.

Dioxygenase-catalysed *cis*-dihydroxylation of arenes to yield the corresponding carbocyclic *cis*-dihydrodiol metabolites is well-established in the mono- and poly-cyclic aromatic hydrocarbon series.[1] Recently the first *cis,trans*-dihydrodiol metabolites from a heterocyclic aromatic ring, *e.g.* thiophene, benzothiophene and benzofuran, were isolated using the toluene-dioxygenase (TDO) system present in a mutant strain of the bacterium *Pseudomonas putida* UV4.[2,3] To date, however, no direct evidence for the formation of a *cis*-dihydrodiol metabolite from a pyridine ring has been reported. Indeed, the mechanism of bacterial metabolism of pyridine rings is not clearly understood.[4]

As part of an earlier study of the bacterial metabolism of bicyclic azaarenes using *P. putida* UV4, *cis*-dihydroxylation of the carcinogen quinoline **1** was observed to occur at the carbocyclic ring to yield *cis*-dihydrodiols **2** and **3** in very low yields (Scheme 1).[5] The major metabolites formed in the pyridine ring of **1** were 3-hydroxyquinoline and anthranilic acid. The phenolic metabolite was postulated to be derived from the initially formed unstable *cis*-dihydrodiol **5** of unknown absolute configuration,[5] while anthranilic acid could have been derived from either **5** or **4**. Previous studies[6] of the metabolism of **1** with different strains of *P. putida, P. fluorescens* and a *Rhodococcus* species did not indicate the formation of any *cis*-dihydrodiols, *e.g.* **2** or **3**, but reported oxidation of the pyridine ring to yield **4**.

Encouraged by the recent isolation of *cis*-dihydrodiol metabolites of five-membered aromatic heterocycles[2,3] and of 3-hydroxyquinoline (from bacterial metabolism of **1**),[5] a new approach to obtain direct evidence of *cis*-diol formation in a pyridine ring was sought. It was assumed that our earlier, unsuccessful, efforts to isolate the *cis*-diol **5** from **1** was due to its instability, and to competition from oxidation at position 2 in the pyridine ring yielding **4** and anthranilic acid. To test this assumption the alternative approach of using 2-substituted quinolines **7** and **10** as substrates was adopted. It was hoped that the chloro and methoxy groups present at the 2-position might be readily replaced by OH groups as a result of spontaneous hydrolysis of the initial unstable *cis*-dihydrodiol metabolites **13** and **14**, respectively, to yield the more stable *cis*-diol **6** (Scheme 1). Furthermore it was anticipated that substitution would block oxidation at the 2-position and formation of **4**, thus increasing the yields of other metabolites. Oxidation at C-2 is a common initial step in the bacterial metabolism of quinoline *via* either the 'coumarin' or '*meta*-cleavage' pathways.[4,6]

Addition of **7** to growing cultures of *P. putida* UV4 yielded two carbocyclic *cis*-dihydrodiols **8** (R_f 0.3, 8%) and **9** (R_f 0.45, 30%) as major metabolites (Scheme 1) which were separated using PLC (MeOH–$CHCl_3$, 7 : 93). Formation of the cyclic boronate derivatives using (*S*)-(−)- and (*R*)-(+)-2-(1-ethoxyethyl)phenylboronic acid (MPBA)[7] and their ^{1}H NMR analysis proved that *cis*-dihydrodiols **8** and **9** were both enantiopure, *i.e.* ⩾98% ee. The absolute configurations of the *cis*-dihydrodiols **8** (5*R*,6*S*) and **9** (7*S*,8*R*) were established by comparison of CD spectra and by stereochemical correlation with the corresponding *cis*-dihydrodiols **2** and **3** of known configuration[5] (Table 1).

On the basis of NMR, mass and IR spectroscopy and elemental microanalysis, the least abundant (2%) and most polar metabolite **6** (R_f 0.14) proved to be a *cis*-diol ($J_{3,4}$ = 3.7 Hz) within a δ-lactam ring. The enantiopurity (⩾98% ee) of diol **6** was determined by formation of a monocamphanate derivative from esterification of the hydroxy group at C-4. The structure, relative configuration and absolute configuration of

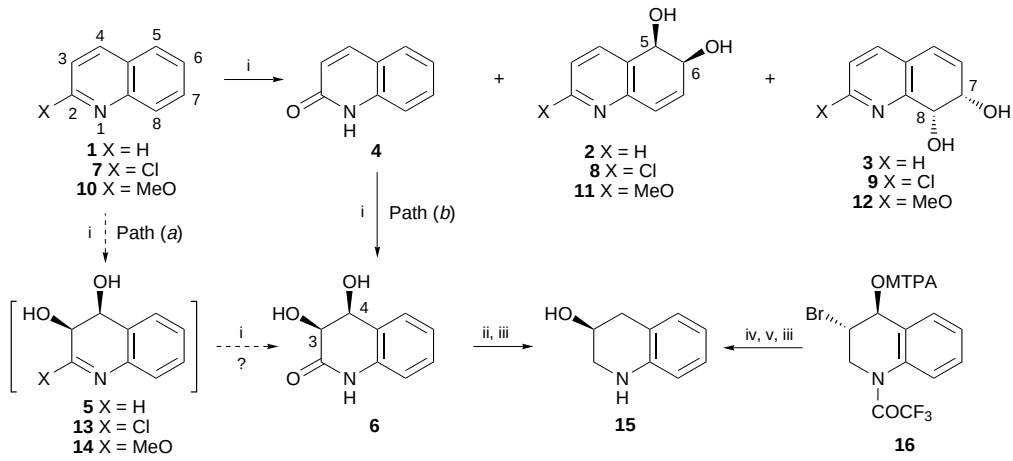

Scheme 1 *Reagents and conditions*: i, *P. putida* UV4, O_2; ii, TBDMS OTf; iii, $LiAlH_4$; iv, Ac_2O, AgOAc; v, NaOH, MeOH

Table 1 Data for *cis*-diol metabolites and derivatives from **7** and **10**

Compound	$[\alpha]_D$ (MeOH)/ 10^{-1} deg cm^2 g^{-1}	Configuration
8	+140	5*R*,6*S*
9	+148	8*R*,7*S*
11	+8	5*R*,6*S*
12	+20	8*R*,7*S*
6	+6[a]	3*S*,4*S*
15	+39	3*S*

[a] Pyridine solvent

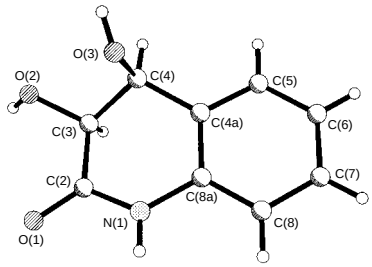

Fig. 1 Crystal structure of metabolite **6**

cis-diol **6** was established by X-ray crystal structure analysis.‡ The preferred conformation of **6** in the crystalline state (Fig. 1) contains the OH groups at C-3 and C-4 in pseudo-equatorial and -axial positions, respectively. The (3*S*,4*S*) absolute configuration deduced from the X-ray study was confirmed by stereochemical correlation with **15** (Scheme 1) which, in turn, has been correlated to the known configuration of the 2-methoxy-2-trifluoromethyl-2-phenylacetate (MTPA) ester derivative **16**.[8] In solution the OH group at C-3 could not be readily converted to a TBDMS ether or camphanate ester derivative, suggesting that *intramolecular* H-bonding to the amide C=O might be present. In the solid state, however, only *intramolecular* H-bonding was observed, each molecule being involved in a total of six H-bonding interactions to three different neighbours. Diol **6** proved to be remarkably stable compared with *cis*-dihydrodiols **2**, **3**, **8** and **9**. Thus while the latter compounds were found to aromatise under acidic conditions (dilute HCl), **6** remained unchanged. An earlier report on the bacterial metabolism of **7** described only the formation of a single *cis*-dihydrodiol **9** in the carbocyclic ring of unspecified ee and absolute configuration.[9]

Addition of **10** as substrate to *P. putida* UV4 also yielded two carbocyclic *cis*-dihydrodiols, **11** (R_f 0.30, 2%) and **12** (R_f 0.4, 7%) (Scheme 1). Similar stereochemical analysis methods to those used for **8** and **9** (NMR and CD spectroscopy) again showed that single enantiomers of configuration indicated in Table 1 [(5*R*,6*S*) and (8*R*,7*S*), respectively] had been formed. The more abundant (13%) and more polar *cis*-diol metabolite from **10** was found to be of identical structure, ee and absolute configuration [(3*S*,4*S*)] to **6** derived from **7**. The optical rotations and absolute configurations of **6**, **8**, **9**, **11** and **12**, and the derived monol **15**, are shown in Table 1.

The formation of the stable (3*S*,4*S*) enantiomer of *cis*-diol **6** as a bacterial metabolite from both **7** and **10** may be explained by a metabolic sequence involving (i) stereoselective *cis*-dihydroxylation to yield the unstable diols **13** and **14**, respectively, and (ii) hydrolysis to yield the stable diol **6** [Scheme 1, path (*a*)]. However, past work on the dioxygenase-catalysed *cis*-dihydroxylations of a range of carbocyclic and five-membered heterocyclic arenes had shown an exclusive or marked preference for the opposite absolute configuration (*e.g.* *cis*-diols **8**, **9**, **11** and **12**), which could be considered as the normal absolute configuration for arene *cis*-diols.

Based on several additional observations an alternative sequence involving partial hydrolysis of substrates **7** and **10** to yield **4**, followed by dioxygenase-catalysed *cis*-dihydroxylation to yield *cis*-diol **6**, appears to be more plausible [Scheme 1, path(*b*)]. Thus, traces of **4** were detected (using GC–MS and ^{1}H NMR analysis) during the biotransformation of **10**, and when **4** was added to *P. putida* UV4 under the normal biotransformation conditions, *cis*-diol **6** (10% isolated yield) of identical ee and absolute configuration to that obtained from **7** and **10** was isolated as a metabolite.

The (3*S*,4*S*) absolute configuration of *cis*-diol **6** derived from the TDO-catalysed dihydroxylation of the pyridine ring in **4**, **7** and **10** seems to be abnormal when compared with that found during TDO-catalysed *cis*-dihydroxylation of arenes in general. The opposite absolute configuration had been observed for the *cis*-diol metabolites of a series of benzocycloalkenes, *e.g.* 1,2-dihydronaphthalene, and the heterocyclic analogues, *e.g.* chromene and thiochromene, using the TDO biocatalyst.[1] The (3*S*,4*S*) configuration of *cis*-diol **6** would be expected if the substrates **7** and **10** were to undergo partial hydrolysis to yield **4**, and if it were to be accepted as a benzocycloalkene-type substrate by the TDO system.

Enzyme-catalysed oxidation of pyridine rings containing alkyl,[4] aryl[8] and thioalkyl substituents[10] has generally been found to occur at the exocyclic substituents, indicating that *cis*-dihydroxylation of a pyridine ring is not a preferred metabolic step, and hence the formation of the *cis*-diol **6** appears to be unusual. Although the formation of compound **6** is still consistent with either TDO-catalysed *cis*-dihydroxylation of the 2-substituted quinoline substrates **7** and **10** [Scheme 1, path (*a*)] or the derived 2-quinolone **4** [Scheme 1, path (*b*)], the currently available evidence is strongly in favour of the latter pathway.

We thank the BBSRC (N. D. S.) and the Queen's University Environmental Science and Technology Research (QUESTOR) Centre (C. C. R. A., J. C.) for financial support, and Eric Becker (Mannheim) and David Clarke (QUESTOR) for valuable assistance with the biotransformations.

Notes and References

† E-mail: dr.boyd@qub.ac.uk

‡ *Crystal data* for **6**: $C_9H_9NO_3$, M = 179.2, monoclinic, $P2_1$, a = 5.453(4), b = 11.039(8), c = 6.762(5) Å, β = 100.14(6)°, V = 400.7(5) Å^3, Z = 2, D_c = 1.485 g cm^{-3}, $F(000)$ = 188, μ(CuKα) = 0.95 mm^{-1}, 828 unique data (and Friedel opposites) (θ_{max} = 50°), 735 with $I > 2\sigma(I)$, R_1 = 0.057, wR_2 (all data) = 0.097, GOF = 0.99, absolute structure parameter −0.3(4). Data were collected on a Siemens P3 diffractometer at 293 K using Cu-Kα radiation, λ = 1.5418 Å; structure determination and refinement using SHELXS-86 and SHELXL-93, respectively; full-matrix least-squares refinement with allowance for anisotropic thermal parameters for non-hydrogen atoms; hydrogens included as riding atoms at positions calculated from the geometry of the molecule, except for the hydrogens of the OH groups, which were included at positions located in a difference Fourier map and refined as free atoms. CCDC 182/770

1 D. R. Boyd and G. N. Sheldrake, *Nat. Prod. Rep.*, 1998, in the press.
2 D. R. Boyd, N. D. Sharma, R. Boyle, B. T. McMurray, T. A. Evans, J. F. Malone, H. Dalton, J. Chima and G. N. Sheldrake, *J. Chem. Soc., Chem. Commun.*, 1993, 49.
3 D. R. Boyd, N. D. Sharma, I. N. Brannigan, D. A. Clarke, H. Dalton, S. A. Haughey and J. F. Malone, *Chem. Commun.*, 1996, 2361.
4 J.-P. Kaiser, Y. Feng and J.-M. Bollag, *Microbiol. Rev.*, 1996, 483.
5 D. R. Boyd, N. D. Sharma, M. R. J. Dorrity, M. V. Hand, R. A. S. McMordie, J. F. Malone, H. P. Porter, J. Chima, H. Dalton and G. N. Sheldrake, *J. Chem. Soc., Perkin Trans. 1*, 1993, 1065.
6 G. Schwartz, R. Bauder, M. Speer, T. O. Rommel and F. Lingens, *Biol. Chem. Hoppe-Seyler*, 1989, **370**, 1183.
7 S. M. Resnick, D. S. Torok and D. T. Gibson, *J. Org. Chem.*, 1995, **60**, 3546.
8 D. R. Boyd, N. D. Sharma and J. F. Malone, unpublished data.
9 S. Fetzner, B. Vogler and F. Lingens, *FEMS Microbiol. Lett.*, 1993, **112**, 151.
10 D. R. Boyd, H. Dalton, N. D. Sharma, S. A. Haughey, R. A. S. McMordie, B. T. McMurray, K. Sproule and G. N. Sheldrake, *J. Chem. Soc., Chem. Commun.*, 1995, 119.

Received in Cambridge, UK, 22nd December 1997; 7/09138I

Synthesis of pentaarabinofuranosyl structure motif A of *Mycobacterium tuberculosis*

Hari Babu Mereyala, Srinivas Hotha and Mukund K. Gurjar

Indian Institute of Chemical Technology, Hyderabad 500 007, India

The first synthesis of motif A, the branched chain arabinofuranosyl pentasaccharide [t-β-Ara*f*-(1 → 2)-α-D-Ara*f*]$_2$-3,5-α-D-Ara*f*-(1 → 5) which constitutes the major humoral immunological epitope in the arabinogalactan cell wall of *Mycobacterium tuberculosis* is described.

Tuberculosis (TB) continues to affect developing countries as 8 000 000 new cases and 3 000 000 deaths occur every year.[1] As a consequence of the HIV epidemic, the occurrence of TB particularly in developed countries has risen sharply. The etiological agent, *Mycobacterium* (*M.*) *tuberculosis* has been extensively investigated and Fig. 1 represents a schematic diagram of macro structural motifs (A–E) of cell wall arabinogalactan.[2a] The fine structure of the cell wall of mycobacteria allows us to understand drug and solute impenetrability, antigen processing and presentation by accessory cells, and aspects of immunopathogenesis. The structurally unusual and biologically significant arabinofuranosyl residue of motif A (**1**, Fig. 1) is responsible for the antigenicity of arabinogalactan.[2a] It is speculated that, in part or complete, structural motif A is the major humoral immunological epitope of arabinogalactan *vis a vis* whole mycobacteria.[2d] Our interest in the chemistry of compounds derived from *M. tuberculosis* has previously resulted in the synthesis[3] of oligosaccharide fragments of glycolipids and glycopeptide cell wall segments. In this report, we communicate the first synthesis of the branched chain arabinofuranosyl pentasaccharide [t-β-Ara*f*-(1 → 2)-α-D-Ara*f*]$_2$-3,5-α-D-Ara*f*-(1 → 5) which forms the crucial part of structural motif A of the *M. tuberculosis* cell wall.

Synthesis of **1a** was initiated from D-arabinose which was transformed into 5-*O*-*tert*-butyldiphenylsilyl-1,2-*O*-(propane-2,2-diyl)-β-D-arabinofuranose (**2**) in two steps.[4] Subsequent desilylation using Bu$^n_4$NF in THF at ambient temperature gave 1,2-*O*-(propane-2,2-diyl)-β-D-arabinofuranose (**3**).[5] Reaction of **3** with NaH–BnBr in DMF protected both the hydroxy groups to afford the 3,5-di-*O*-benzyl derivative **4**. Conversion of **4** into the *n*-pentenyl glycoside was effected with pent-4-en-1-ol in the presence of TsOH to obtain a 1 : 1 anomeric mixture of α,β-*n*-pentenyl glycosides (**5** and **6**) which were separated by silica gel column chromatography (Scheme 1). In another sequence,

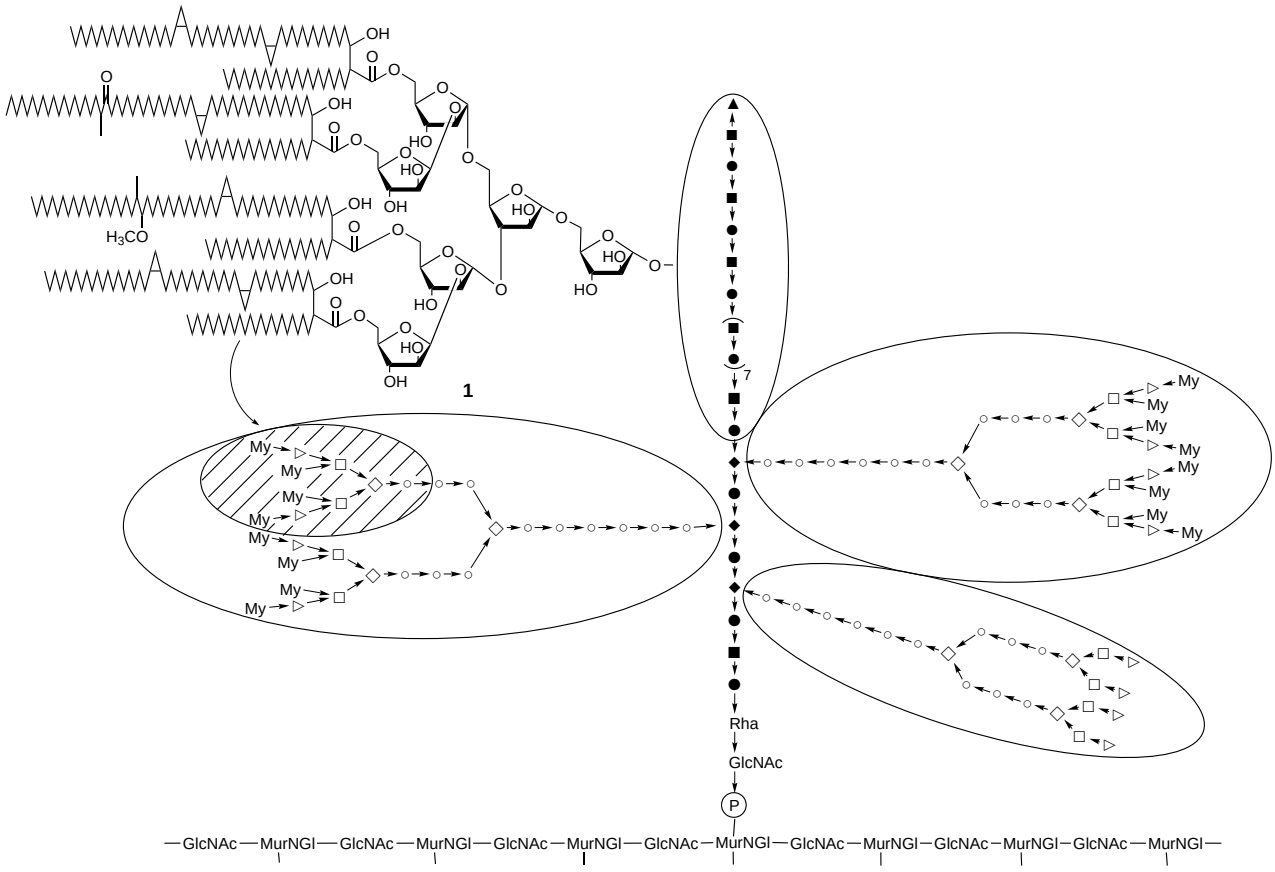

Fig. 1 Schematic diagram of the proposed illustration of the macro structural motifs of the cell wall arabinogalactan. My, Mycolic acid; (▼) t-β-D-Ara*f*; (□) 2-α-D-Ara*f*; (◇) 3, 5-α-D-Ara*f*; (▲) t-β-D-Gal*f*; (■) 6-β-D-Gal*f*; (●) 5-β-D-Gal*f*; (◆) 5,6-β-D-Gal*f*; GlcNAc, *N*-acetylglucosamine; Rha, rhamnose; MurNGl, *N*-glycolylmuramic acid.

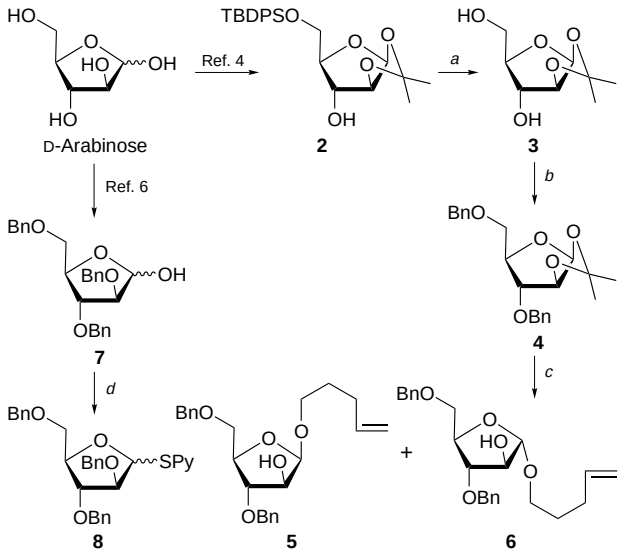

Scheme 1 *Reagents and conditons*: (*a*) Bu^n_4NF, THF, room temp., 2 h, 96%; (*b*) NaH,BnBr, DMF, 0 °C–room temp., 83%; (*c*) Pent-4-en-1-ol, TsOH, CH_2Cl_2, 60 °C, 2 h, 85%; (*d*) PySSPy, Bu^n_3P, CH_2Cl_2, room temp., 30 min, 98%

2,3,5-tri-*O*-benzyl-α,β-D-arabinofuranose (**7**)[6] was transformed into the corresponding *S*-(2-pyridyl)-1-thiofuranoside **8** by reacting with 2,2′-dithiodipyridyl and Bu^n_3P in CH_2Cl_2.[7]

The coupling reaction of **5** with **8** was promoted[8] by the protocol developed in our laboratory, according to which 5% MeI in dry CH_2Cl_2 was used as an activator to give the β-disaccharide **9**. Its structure was confirmed by ^1H and ^{13}C NMR spectroscopy (Scheme 2).

The *O*-glycosylation of **2**[4] with the above formed *n*-pentenyl disaccharide **9** was induced in the presence of iodonium dicollidine perchlorate (IDCP)[9] in CH_2Cl_2, followed by desilylation of the coupled product with Bu^n_4NF in THF, resulted in the isolation of the trisaccharide **10** whose newly formed glycosidic linkage was confirmed as having an α-configuration by the ^1H NMR spectrum. For example, the characteristic resonances due to H-1′ was located at δ 5.05 as a singlet, whereas H-1 and H-1″ protons appeared as doublets at δ 4.90 and 5.75, respectively, as expected for β-anomeric configurations. In addition, the ^{13}C NMR spectrum of **10** showed resonances due to anomeric carbons at $\delta_{C\text{-}1}$ 100.1, $\delta_{C\text{-}1'}$ 105.3 and $\delta_{C\text{-}1''}$ 105.5.

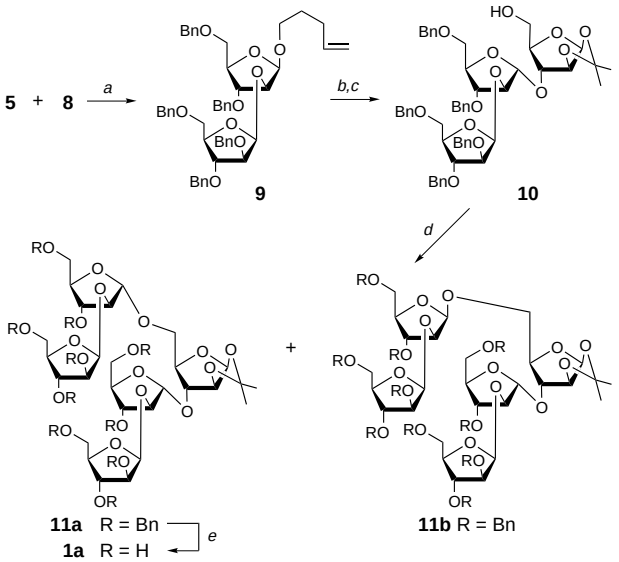

Scheme 2 *Reagents and conditions*: (*a*) 5% MeI in CH_2Cl_2, 57 °C, 4 Å MS powder, 15 h, 69%; (*b*) IDCP CH_2Cl_2, 4 Å MS powder, 24 h, 62%; (*c*) Bu^n_4NF, THF, room temp., 3 h, 95%; (*d*) I(*s*-Collidine)$_2ClO_4$, CH_2Cl_2, 4 Å MS powder, 12 h, 70%; (*e*) $Pd(OH)_2$/C, MeOH,H_2, room temp., 12 h, 97%

The OH group at C-5 of compound **10** was glycosylated again with donor **9** under the conditions reported above. However, in this reaction, a 3 : 2 mixture of α- and β-pentasaccharides (**11a** and **11b**) was formed. The major α-anomeric product (**11a**) was isolated by silica gel column chromatography, hydrogenolysis of which over $Pd(OH)_2$/C at normal temperature and pressure for 12 h gave the required pentasaccharide **1a**. The structure of **1a** was fully characterised by ^1H, ^{13}C NMR and FABMS analysis.[9]

In conclusion it is pertinent to mention that resistance to the current regime of anti-TB drugs is developing rapidly and therefore there is a constant need to discover new drugs. It is reported that (*S*,*S*)-ethambutol inhibits arabinan biosynthesis and therefore the arabinan segment of the cell wall provides an attractive target for development of new drugs because of the xenobiotic status of the human host. The present synthesis of the pentaarabinofuranoside of structure motif A of *M. tuberculosis* cell wall opens a new vista in this direction.

S. H. thanks CSIR, New Delhi, for a Junior Research Fellowship.

Notes and References

* E-mail: gurjar@csiict.ren.nic.in

1 *Current Topics in Microbiology and Immunology: Tuberculosis*, ed. T. M. Shinnick, Springer-Verlag, Berlin, 1996, vol. 215.

2 (*a*) G. S. Besra, K.-H. Khoo, M. R. McNeil, A. Dell, H. R. Morris and P. J. Brennan, *Biochemistry*, 1995, **34**, 4257; (*b*) B. A. Wolucka, M. R. McNeil, E. de Hoffmann, T. Chojnacki and P. J. Brennan, *J. Biol. Chem.*, 1994, **269**, 23 328; (*c*) M. R. McNeil, M. Daffe and P. J.Brennan, *J. Biol. Chem.*, 1990, **265**, 18 200; (*d*) M. Daffe, P. J. Brennan, M. McNeil, *J. Biol. Chem.*, 1990, **265**, 6734; (*e*) M. McNeil, S. J. Wallner, S. W. Hunter, P. J. Brennan, *Carbohydr. Res.*, 1987, **166**, 299; (*f*) R. E. Lee, K. Mikusova, P. J. Brennan and G. S. Besra, *J. Am. Chem. Soc.*, 1995, **117**, 11 829.

3 M. K. Gurjar and S. Adhikari, *Tetrahedron*, 1997, **53**, 8629; H. B. Mereyala and B. R. Gaddam, *Proc. Indian Acad. Sci.* (*Chem. Sci.*), 1994, **106**, 1225; M. K. Gurjar and K. R. Reddy, *J. Chem. Soc., Perkin Trans. 1*, 1993, 1269; M. K. Gurjar and U. K. Saha, *Bioorg. Med. Chem. Lett.*, 1993, **3**, 697; M. K. Gurjarand P. S. Mainkar, *Carbohydr. Res.*, 1993, **239**, 297; M. K. Gurjar and U. K. Saha, *Tetrahedron Lett.*, 1992, **33**, 4979; M. K. Gurjar and A. S. Mainkar, *Tetrahedron*, 1992, **48**, 6729; M. K. Gurjar and U. K. Saha, *Tetrahedron*, 1992, **48**, 4039; M. K. Gurjar and K. R. Reddy, *Carbohydr. Res.*, 1992, **226**, 232; M. K. Gurjar and G. Viswanadham, *Tetrahedron Lett.*, 1991, **32**, 6191; M. K. Gurjar and G. Viswanadham, *J. Carbohydr. Chem.*, 1991, **10**, 481.

4 O. Dahlman, P. J. Garegg, H. Mayer and S. Schramek, *Acta Chem. Scand., Ser. B*, 1986, **40**, 15.

5 C. Genu-Dellac, G. Gosselin and J.-L. Imbach, *Carbohydr. Res.*, 1991, **216**, 249.

6 P. Finch, G. M. Iskander and A. H. Siriwardena, *Carbohydr. Res.*, 1991, **210**, 319.

7 H. B. Mereyala and G. V. Reddy, *Tetrahedron*, 1991, **47**, 6435.

8 R. U. Lemieux and A. R. Morgan, *Can. J. Chem.*, 1965, **43**, 2190.

9 *Selected data* for **9**: δ_H(200 MHz, $CDCl_3$) for anomeric protons: 5.05 (d, *J* 4.6), 5.15 (d, *J* 4.1); δ_C(50 MHz, $CDCl_3$) for anomeric carbons: 98.5, 100.2; FABMS: 823 $(M + Na)^+$. For **10**: δ_H(200 MHz, $CDCl_3$) for anomeric protons: 4.90 (d, *J* 4.6), 5.05 (s), 5.76 (d, *J* 4.6); δ_C(50 MHz, $CDCl_3$) for anomeric carbons: 100.1, 105.3, 105.5; FABMS: 928 $(M + Na)^+$. For **11a**: δ_H(200 MHz, $CDCl_3$) for anomeric protons: 4.92 (d, *J* 4.6), 5.04 (s), 5.18 (d, *J* 4.7), 5.29 (s), 5.70 (d, *J* 4.8); δ_C(50 MHz, $CDCl_3$) for anomeric carbons: 100.1, 100.4, 105.2, 105.5, 106.0; FABMS: 1643 $(M + Na)^+$. For **11b**: δ_H(200 MHz, $CDCl_3$) for anomeric protons: 4.90 (d, *J* 4.70), 5.02 (s), 5.09 (d, *J* 4.65), 5.29 (d, *J* 4.8), 5.70 (d, *J* 4.7); δ_C (50 MHz, $CDCl_3$) for anomeric carbons: 98.3, 100.2, 100.6, 105.1, 105.5; FABMS: 1643 $(M + Na)^+$. For **1a**: δ_H(400 MHz, D_2O) for anomeric protons: 4.90 (d, *J* 4.20), 5.10 (d, *J* 4.65), 5.15 (s), 5.28 (s), 6.00 (d, *J* 4.8); δ_C(50 MHz, D_2O) for anomeric carbons: 102.0, 102.1, 106.3, 106.5, 106.9; FABMS: 741 $(M + Na)^+$.

Received in Cambridge, UK, 29th October 1997; 7/07796C

Catalytic selective cleavage of a strong C–C single bond by rhodium in solution

Shyh-Yeon Liou, Milko E. van der Boom and David Milstein*†

Department of Organic Chemistry, The Weizmann Institute of Science, Rehovot 76100, Israel

Reaction of $[RhCl(C_8H_{14})_2]_2$ with an excess of the diphosphine 1,3-bis(diisopropylphosphinomethylene)mesitylene 1 in dioxane under mild H_2 pressure (25 psi) or with an excess of $HSi(OEt)_3$ results in catalytic selective cleavage of a strong C–C single bond.

Activation and functionalization of strong C–C single bonds by soluble transition metal complexes is of considerable current interest.[1–6] Most challenging is the search for the underlying mechanisms and homogeneous catalysis based on such relatively inert bonds. While several examples of homogeneous catalytic activation of C–H bonds of hydrocarbons are known,[2] the few reports of catalytic C–C bond activation in solution are limited to weak C–C bonds α to a carbonyl group,[3] strained systems,[4] or a combination of both.[5] Selective transition metal insertion into a strong, unstrained C–C single bond in solution and details related to the mechanism were reported by us only recently.[6] We report here on the catalytic hydrogenolysis and hydrosilylation of a strong sp^2–sp^3 C–C bond. This rhodium catalyzed process is unprecedented, occurs under homogeneous reaction conditions and is highly selective.

Reaction of $[RhCl(C_8H_{14})_2]_2$ (C_8H_{14} = cyclooctene) with 50 equiv. of the phosphine substrate **1** under mild H_2 pressure (25 psi; 1 psi ≈ 6.894757×10^3 Pa) in dioxane at 180 °C for one day leads to catalytic formation of the demethylated phosphine **2** and CH_4 (Scheme 1; 16 turnovers based on rhodium and 32% yield). The CH_4 was collected by standard vacuum line techniques and was identified and quantified by GC. Compound **2** was identified spectroscopically by various NMR and MS techniques and by comparison with an added authentic sample.[6b] Reactions were also performed in [$^2H_8$]dioxane to record ^1H, $^{13}C\{^1H\}$, ^{13}C-DEPT-135 and $^{31}P\{^1H\}$ NMR spectra. Formation of product **2** is highly selective, the other two arylmethyl groups remaining unaffected and no other organic products were formed. Addition of another 50 equiv. of **1** to the reaction mixture and applying the same reaction conditions resulted in another 15 turnovers, demonstrating that the catalyst remains active. Similar results were obtained by performing the reaction for two days with 100 equiv. of **1** (31 turnovers and 31% yield). Using 500 equiv. of substrate **1** leads to 106 turnovers after three days. The hydrogenolysis proceeds also at lower temperatures (150 °C), but it is much slower, leading to only 15 turnovers after one week.

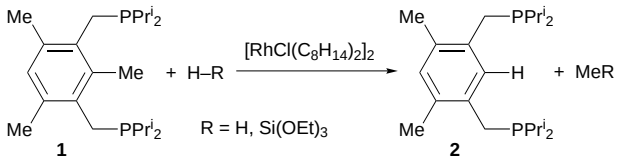

1 **2**

Scheme 1

To probe the possibility of catalytic hydrosilylation of a C–C single bond, we used an excess of $HSi(OEt)_3$ instead of H_2. Reaction of $[RhCl(C_8H_{14})_2]_2$ with 50 equiv. of **1** and an excess of $HSi(OEt)_3$ in dioxane (or toluene) at 150 °C for two days resulted in 10 turnovers to form **2** and $MeSi(OEt)_3$ (Scheme 1), which were unambiguously characterized by ^1H, $^{13}C\{^1H\}$, ^{13}C-DEPT, $^{29}Si\{^1H\}$ NMR and by GC–MS.[6b] Thus, catalytic transfer of a CH_2 group from an arene to a silane was observed. Again the reaction is completely selective.

Reaction of 50 equiv. of the ethyl aromatic phosphine **3** with $[RhCl(C_8H_{14})_2]_2$ at 180 °C under mild H_2 pressure in dioxane for 3 days resulted in formation of compound **4** and C_2H_6, although only 4 turnovers were obtained (Scheme 2). Compound **4** was fully identified by comparison with an authentic sample. The expected amount of C_2H_6 was observed by GC analysis of the gas phase. Control reactions showed that **1** and **3** were stable under the same reaction conditions in the absence of rhodium.

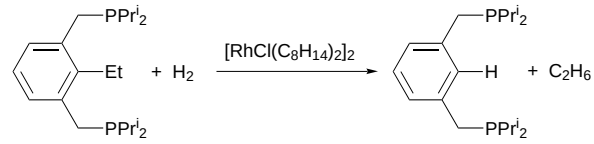

3 **4**

Scheme 2

A postulated catalytic cycle is outlined in Scheme 3. The high selectivity of the catalytic processes, only one alkyl group being affected, provides strong evidence that both phosphines are coordinated to the metal centre prior to the C–C bond activation. Intermediates such as **A** have been observed with platinum and ruthenium.[7] At this stage competitive C–H and C–C oxidative addition might occur.[6f] C–H activation would result in the reversible formation of a benzylic rhodium species.[6] Metal insertion into the strong Ar–C bond was observed in a stoichiometric reaction of **1** (0.031 mmol) with 0.5 equiv. of $[RhCl(C_8H_{14})_2]_2$ in [$^2H_6$]benzene (2 ml) in a sealed tube for 2 h

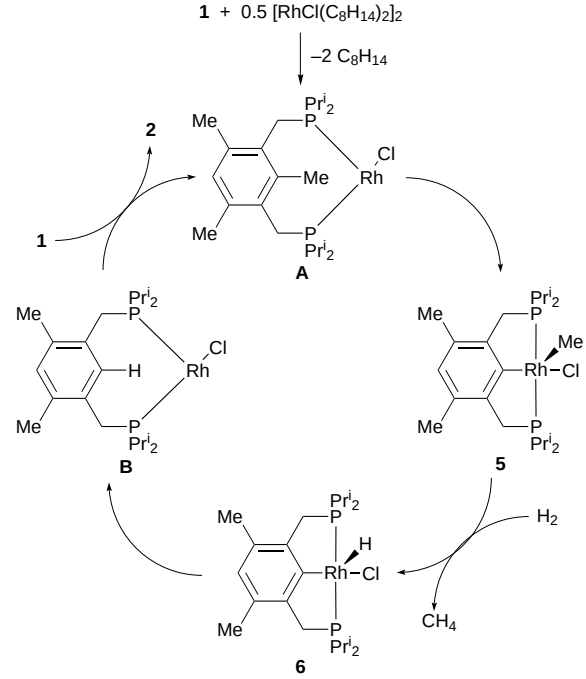

Scheme 3 Proposed catalytic hydrogenolysis cycle for **1** with rhodium

at room temperature. ^{1}H, ^{31}P{^{1}H} and ^{13}C{^{1}H} NMR analysis of the reaction solution showed the formation of **5** in 75% yield. The Rh–Me group is clearly observed in the ^{13}C{^{1}H} NMR at δ −4.3 [dt, ^1J(RhC) 30.2, ^2J(PC) 6.4 Hz] and the *ipso* carbon at δ 166.7 [dt, ^1J(Rh, C) 33.6, ^2J(PC) ≈ 1.0 Hz]. An isostructural rhodium(III) complex was recently fully characterized by X-ray analysis.[6f]

Subsequently, complex **5** reacts with H_2 to yield complex **6**. Indeed, reaction of **5** with H_2 (25 psi) at 80 °C for 1 day and analysis by ^{1}H, ^{31}P{^{1}H}, ^{13}C{^{1}H} NMR, IR and GC analysis showed the quantitative formation of complex **6** and CH_4.§ This reaction may proceed through a rhodium(V) intermediate or *via* σ-bond metathesis. Complex **6** can also be used as catalyst under the same reaction conditions. Release of the aryl phosphine **2** from **6** probably proceeds *via* **B**, which undergoes phosphine exchange with substrate **1** giving back **A**. This is likely to be the rate-determining step. Such a process was demonstrated by treating a dioxane solution of complex **6** with 20 equiv. of PEt_3 at 80 °C overnight, which resulted in formation of the PCP ligand **2** and $RhCl(PEt_3)_3$ by phosphine exchange. Replacement of a cyclometalated terdentate diamino ligand of a ruthenium(II) complex by a phosphorus analogue was reported very recently.[7b] The liberated arene **2** most probably strongly competes with substrate **1**, slowing down the catalytic process. It is well known that α,α′-diphosphine-*m*-xylenes such as **2** and **4** undergo readily Ar–H oxidative addition with rhodium forming thermally stable, isolable complexes such as **6**.[6c,8]

In summary, a novel catalytic process has been presented using simple diphosphine substrates. For the first time, an unstrained, strong Ar–C bond is selectively activated by a metal centre in solution in a catalytic fashion. Moreover, catalytic transfer of a methylene group to a primary silane has been observed using a rhodium complex. Stoichiometric reactions involved in the catalysis were directly demonstrated. Although the catalytic reactions were not optimized and the reactions are at present slow, more than one hundred turnovers were observed.

The research was supported by the US-Israel Binational Science Foundation, Jerusalem, Israel. D. M. is the holder of the Israel Matz Professorial Chair of Organic Chemistry.

Notes and References

† E-mail: comilst@wiccmail.weizmann.ac.il

‡ Catalytic hydrogenolysis of an unstrained C–C single bond. A [$^2H_8$]dioxane solution (1.5 ml) of substrate **1** (106 mg, 0.278 mmol) was added dropwise to a [$^2H_8$]dioxane solution (1.5 ml) of $[RhCl(C_8H_{14})_2]_2$ (2 mg, 0.00278 mmol), loaded into a 90 ml Fischer porter pressure bottle equipped with a stirring bar and pressurized with H_2 (20–25 psi) (toluene can be used as well). After heating the reaction solution at 180 °C for 1 day, the gas phase was collected by standard vacuum line techniques and analyzed by GC using a molecular sieve column. The formed CH_4 was identified and quantified using authentic samples (13.6 turnovers). ^{31}P{^{1}H} NMR of the reaction mixture shows two signals at δ 5.6 (s, 2 P, **1**) and 3.20 (s, 2 P, **2**). The ratio of the signals (100 : 54) indicated 17.5 turnovers and a yield of 35%. Addition of trioctylphosphine oxide to the reaction mixture as an internal standard indicated 15.3 turnovers and a yield of 31%. The addition of authentic samples **1**, **2** to the reaction mixture resulted in overlap of resonances in ^{31}P{^{1}H} and ^{13}C{^{1}H} NMR.[6b] The same reaction conditions and analysis of the reaction mixture were used for substrate **3**. Similar reaction conditions were applied for the catalytic hydrosilylation, only an excess of $HSi(OEt)_3$ (91 mg, 0.556 mmol) was used instead of H_2.

§ *Spectral data* for **6**. ^{1}H NMR (C_6D_6, 400.1 MHz): δ 6.56 (s, 1 H, *p*-H of C_6HRh), 3.24 [m, ^3J(HH) 7.2 Hz, 2 H, C*H*Me$_2$], 3.14 [dvt, left part of ABq, ^2J(HH) 15.7 Hz, ^2J(HP) not resolved, 2 H, CH_2P], 2.95 [dvt, right part of ABq, ^2J(HH) 15.7 Hz, ^2J(HP) not resolved, 2 H, CH_2P], 2.28 [m, ^3J(HH) 7.1 Hz, 2 H, C*H*Me$_2$], 2.14 (s, 6 H, *Me*$_2$C$_6$HRh), 1.89, 1.72, 1.38, 1.24 [all q, ^3J(HH) ≈ 7.0 Hz, 6 H, CH*Me*$_2$], −19.36 [dt, ^1J(RhH) 31.1, ^2J(PH) 12.3 Hz, 1 H, HRh]. ^{31}P{^{1}H} NMR (C_6D_6, 161.9 MHz): δ 65.7 [d, ^1J(RhP) 113.6 Hz]. ^{13}C NMR (C_6D_6, 100.1 MHz): δ 161.1 [dm, ^1J(RhC) 31.9, ^2J(PC) ≈ 1.0 Hz, C_{ispo}], 142.8 [t, *J*(PC) 12.3 Hz, Ar], 129.7 [dt, *J*(PC) 7.4, *J*(RhC) 1.4 Hz, Ar], 126.5 (s, Ar), 32.8 [dt, *J*(PC) 12.6 Hz, CH_2P], 26.6 [t, *J*(PC) 10.0 Hz, CHMe$_2$], 23.2 [t, *J*(PC) 10.2 Hz, *C*HMe$_2$], 22.6 (s, *Me*$_2$Ar), 22.1, 19.7, 19.5 (all s, CH*Me*$_2$). IR (neat): ν 2071 cm^{-1}.

1 R. H. Crabtree, *Chem. Rev.*, 1985, **85**, 245; H. Suzuki, Y. Takaya and T. Takemori, *J. Am. Chem. Soc.*, 1994, **116**, 10 779; C.-H. Jun, J.-B. Kang and Y.-G. Lim, *Tetrahedron Lett.*, 1995, **36**, 277; K. McNeill, R. A. Andersen and R. G. Bergman, *J. Am. Chem. Soc.*, 1997, **119**, 11 244.

2 For example: M. Trost, K. Imi and I. W. Davies, *J. Am. Chem. Soc.*, 1995, **117**, 5371; S. Murai, F. Kakiuchi, S. Sekine, Y. Tanaka, A. Kamatani, M. Sonoda and N. Chatani, *Nature*, 1993, **366**, 529.

3 J. W. Suggs and C.-H. Jun, *J. Chem. Soc., Chem. Commun.*, 1985, 92.

4 C. Perthuisot and W. D. Jones, *J. Am. Chem. Soc.*, 1994, **116**, 3647; C. Perthuisot, B. L. Edelbach, D. L. Zubris and W. D. Jones, *Organometallics*, 1997, **16**, 2016; F. Fujimura, S. Aoki and E. Nakamura, *J. Org. Chem.*, 1991, **56**, 2809; R. Noyori, T. Odagi and H. Takaya, *J. Am. Chem. Soc.*, 1970, **92**, 5780.

5 M. A. Huffman and L. S. Liebeskind, *J. Am. Chem. Soc.*, 1991, **113**, 277; M. Murakami, H. Amii and Y.Ito, *Nature*, 1994, **370**, 540; M. Murakami, H. Amii, K. Shigeto and Y. Ito, *J. Am. Chem. Soc.*, 1996, **118**, 8285; M. Murakami, K. Takahashi, H. Amii and Y. Ito, *J. Am. Chem. Soc.*, 1997, **119**, 9307.

6 (*a*) M. Gozin, A. Weisman, Y. Ben-David and D. Milstein, *Nature*, 1993, **364**, 699; (*b*) M. Gozin, M. Aizenberg, S.-Y. Liou, A. Weisman, Y. Ben-David and D. Milstein, *Nature*, 1994, **370**, 42; (*c*) S.-Y. Liou, M. Gozin and D. Milstein, *J. Chem. Soc., Chem. Commun.*, 1995, 1965; (*d*) S.-Y. Liou, M. Gozin and D. Milstein, *J. Am. Chem. Soc.*, 1995, **117**, 9774; (*e*) M. E. van der Boom, H.-B. Kraatz, Y. Ben-David and D.Milstein, *Chem. Commun.*, 1996, 2167; (*f*) B. Rybtchinski, A. Vigalok, Y. Ben-David and D. Milstein, *J. Am. Chem. Soc.*, 1996, **118**, 12 406; (*g*) M. Gandelman, A. Vigalok, L. J. W. Shimon and D. Milstein, *Organometallics*, 1997, **16**, 3981.

7 (*a*) M. E. van der Boom, M. Gozin, Y. Ben-David, L. J. W. Shimon, F. Frolow, H.-B. Kraatz and D. Milstein, *Inorg. Chem.*, 1996, **35**, 7068; (*b*) P. Dani, T. Karlen, R. A. Gossage, W. J. J. Smeets, A. L. Spek and G. van Koten, *J. Am. Chem. Soc.*, 1997, **119**, 11 317.

8 C. J. Moulton and B. L. Shaw, *J. Chem. Soc., Dalton Trans.*, 1976, 1020; A. Weisman, M. Gozin, H.-B. Kraatz and D. Milstein, *Inorg. Chem.*, 1996, **35**, 1792.

Received in Cambridge, UK, 20th January 1998; 8/00537K

Design, synthesis and structural studies on polynucleating ligands based on atropoisomerism of catechol bearing porphyrins

Cathy Drexler,[a] Mir Wais Hosseini,*[a]† Jean-Marc Planeix,[a] Gilles Stupka,[a] André De Cian[b] and Jean Fischer[b]

[a] *Laboratoire de Chimie de Coordination Organique (UMR 7513 CNRS), Université Louis Pasteur, F-67000 Strasbourg, France*
[b] *Laboratoire de Cristallochimie et Chimie Structural (UMR 7513), Université Louis Pasteur, F-67000 Strasbourg, France*

High yield syntheses of all four atropoisomers of the *meso*-tetrakis(*o*-catecholamidophenyl)porphyrin has been achieved; all four atropoisomers were isolated and characterised by NMR spectroscopy; for the methyl protected $2_{\alpha\beta\alpha\beta}$ and $2_{\alpha 4}$ atropoisomers obtained as water and chloroform solvates respectively, X-ray analysis was used to assign their structure.

Porphyrins, used in chemistry, biology, medicine and material science, are among the most fascinating organic molecules. These tetradentate macrocycles bind a large variety of metal cations and exhibit interesting redox as well as photochemical properties. Furthermore their functionalisation either at the β-pyrrolic or *meso* positions has been well established. The porphyrin backbone may be used as a preorganised complexing core for the elaboration of di- and poly-nucleating ligands. Examples of porphyrins bearing neutral bidentate ligands such as bipyridine and phenanthroline have been reported.[1] So far, two examples of porphyrins bearing dianionic bidentate catecholate units have been published.[2,3] Whereas in the first case, two catechols were directly incorporated at the meso positions,[2] in the second example, the porphyrin was functionalised by one to four *m*-catecholamidophenyl units at the *meso* positions.[3] On the other hand, diaza-,[4] triaza- and tetraaza-macrocycles[5] as well as a calix[4]arene derivative[6] bearing pendant catechol units have been also reported.

In our search for polynuclear complexes, we thought that one could take advantage of atropoisomerism,[7] previously elegantly used for the preparation of picket fence porphyrins,[8] for the design of new polynucleating ligands. Thus, the *meso*-tetrakis(*o*-catecholamidophenyl)porphyrin atropoisomers appeared to be interesting targets. Indeed, owing to high rotational barriers, one would expect four atropoisomers designated as

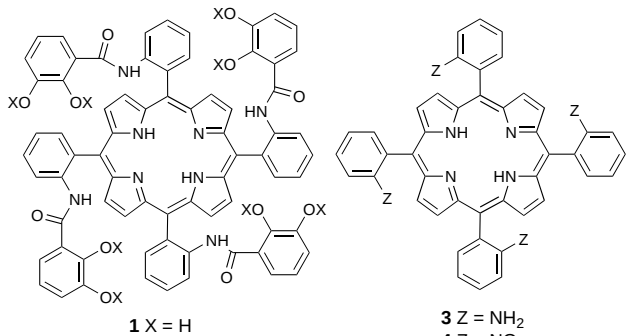

1 X = H
2 X = Me

3 Z = NH_2
4 Z = NO_2

$\mathbf{1}_{\alpha 4}$, $\mathbf{1}_{\alpha 3\beta}$, $\mathbf{1}_{\alpha 2\beta 2}$ and $\mathbf{1}_{\alpha\beta\alpha\beta}$ for the *meso*-tetraphenylporphyrin bearing bulky catecholamido groups at the *ortho* position on the phenyl groups (Fig. 1).

Whereas the $\mathbf{1}_{\alpha 4}$ atropoisomer may lead to heterodinuclear complexes by simultaneous binding of transition and lanthanide cations, the $\mathbf{1}_{\alpha 2\beta 2}$ and $\mathbf{1}_{\alpha\beta\alpha\beta}$ isomers may form homo- or heterotrinuclear species with transition metals. Furthermore, for the $\mathbf{1}_{\alpha\beta\alpha\beta}$ atropoisomer, the formation of infinite coordination polymers with metals adopting octa-coordination around cubic arrangements may also be envisaged. Here, we report the synthesis and structural analysis of the above mentioned ligands.

The synthesis of all four protected atropoisomers $\mathbf{2}_{\alpha 4}$, $\mathbf{2}_{\alpha 3\beta}$, $\mathbf{2}_{\alpha 2\beta 2}$ and $\mathbf{2}_{\alpha\beta\alpha\beta}$ was first achieved by condensation of a statistical mixture of the *meso*-tetrakis(*o*-aminophenyl)-porphyrin **3** isomers with the acyl chloride derivative of the methyl protected catechol[9] in THF in the presence of NEt_3. **3** was obtained as a statistical mixture by reduction of the nitro compound **4** prepared from *ortho*-nitrobenzaldehyde and pyrrole.[8] Although the condensation reaction proceeded quantitatively, the separation of the mixture appeared to be extremely tedious. Indeed, whereas based on TLC analysis [SiO_2, CCl_4–ethyl acetate (1/1)], the separation of atropoisomers could have been straightforward, because of their low solubility, the purification on a preparative silica column yielded, after at least three passages, only small quantities of the pure isomers. The separation of the zinc complexes, obtained by treatment of the mixture by zinc acetate, was as difficult as for the free prophyrin derivatives. Attempts to reach better results using chromatotron or preparative HPLC also failed. An alternative strategy, consisting of the separation of all four atropoisomers of **3**[8] and then condensation with the acyl chloride derivative of the methyl protected catechol, was followed to avoid the purification difficulties mentioned above. In order to minimise the atropoisomerisation, the reactions were carried out at −15 °C in THF and in the presence of NEt_3. Again, the condensation reaction proceeded with almost quantitative yields. After chromatography on silica and crystallisation from $CHCl_3$–ethyl acetate mixtures, the protected atropoisomers $\mathbf{2}_{\alpha\beta\alpha\beta}$ [CH_2Cl_2; CH_2Cl_2–AcOEt (96 : 4); $CHCl_3$], $\mathbf{2}_{\alpha 2\beta 2}$ [CH_2Cl_2; CH_2Cl_2–AcOEt (96 : 4); $CHCl_3$], $\mathbf{2}_{\alpha 3\beta}$ [toluene–$CHCl_3$–MeOH (25 : 5 : 5)] and $\mathbf{2}_{\alpha 4}$ [toluene–$CHCl_3$–AcOEt (25 : 5 : 5)–

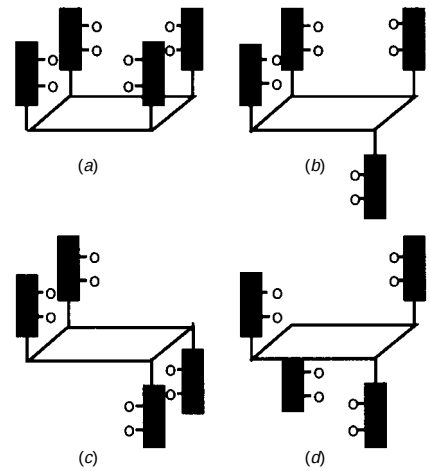

Fig. 1 Schematic representations of α_4 (a), $\alpha_3\beta$ (b), $\alpha_2\beta_2$ (c) and $\alpha\beta\alpha\beta$ (d) atropoisomers of the porphyrins **1**–**4**

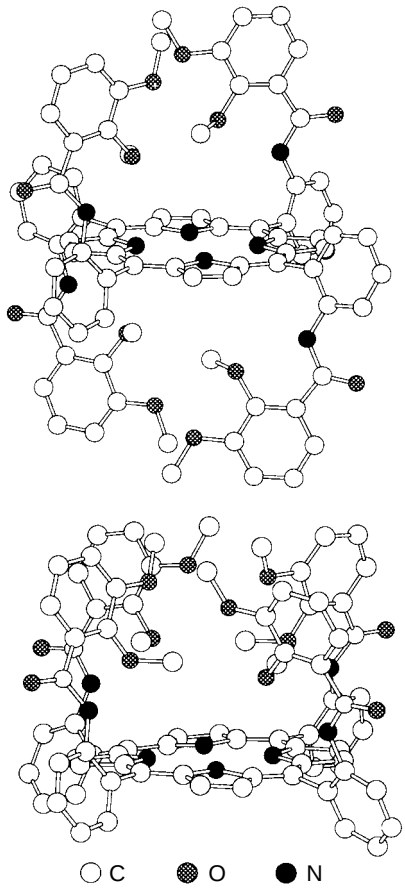

Fig. 2 X-Ray crystal structures of $\mathbf{2}_{\alpha4}$ (top) and $\mathbf{2}_{\alpha\beta\alpha\beta}$ (bottom); solvent molecules as well as H atoms are not shown for clarity. In both cases, the core of the porphyrin was almost planar, the amide groups were in *trans* configuration and the catechol units were found to be oriented in a convergent manner.

(25 : 10 : 5)] could be obtained in 57, 63, 70 and 60% isolated yields, respectively.

Based on symmetry, the ^{1}H NMR signals for $\mathbf{2}_{\alpha3\beta}$ (C_s) could be unambiguously assigned. For the other three $\mathbf{2}_{\alpha4}$ (C_{4v}), $\mathbf{2}_{\alpha\beta\alpha\beta}$ (D_{2d}) and $\mathbf{2}_{\alpha2\beta2}$ (C_{2h}) atropoisomers, only the latter could be identified by the observation of two singlets for the β-pyrrolic protons, whereas for the remaining atropoisomers the assignments could not be achieved without taking into account their polarity. In order to confirm the structural assignment, both $\mathbf{2}_{\alpha4}$ and $\mathbf{2}_{\alpha\beta\alpha\beta}$ atropoisomers were studied by X-ray diffraction (Fig. 2).‡ In both cases, suitable monocrystals were obtained as water and chloroform solvates respectively upon slow liquid–liquid diffusion of MeOH into a chloroform solution of either $\mathbf{2}_{\alpha4}$ or $\mathbf{2}_{\alpha\beta\alpha\beta}$. The X-ray analysis revealed the following common features: (*i*) the core of the porphyrin was almost planar, however, owing to steric reasons, the deformation was slightly greater for $\mathbf{2}_{\alpha4}$; (*ii*) the amide groups were in *trans* configuration with NH hydrogen atoms inwardly oriented towards oxygen atoms belonging to the catechol units and the CO groups oriented in divergent fashion towards the periphery of the porphyrin backbone; (*iii*) both in the case of $\mathbf{2}_{\alpha4}$ for which all four protected catechol units were localised on the same face of the molecule [Fig. 2(top)] and of $\mathbf{2}_{\alpha\beta\alpha\beta}$ for which the two sets of two protected catechols were localised below and above the mean plane of the porphyrin [Fig. 2(bottom)], the catechol units were found to be oriented in a convergent manner. Dealing with the $\mathbf{2}_{\alpha3\beta}$ isomer, although its structure was also established by X-ray analysis which revealed the same common features as for the above two isomers, the data are not reported because of rather low resolution.

The deprotection of $\mathbf{2}_{\alpha4}$, $\mathbf{2}_{\alpha3\beta}$, $\mathbf{2}_{\alpha2\beta2}$ and $\mathbf{2}_{\alpha\beta\alpha\beta}$ atropoisomers at −78 °C using the classical BBr_3–CH_2Cl_2 method[10] afforded the desired compounds $\mathbf{1}_{\alpha4}$, $\mathbf{1}_{\alpha3\beta}$, $\mathbf{1}_{\alpha2\beta2}$ and $\mathbf{1}_{\alpha\beta\alpha\beta}$ as the hydrobromide salts after several precipitations from MeOH–ethyl–ether mixtures. Whereas in the solid state all four atropoisomers were stable, in solution the protonated $\mathbf{1}_{\alpha4}$, $\mathbf{1}_{\alpha3\beta}$ and $\mathbf{1}_{\alpha2\beta2}$ isomers were found to undergo atropoisomerisation. Interestingly, probably due to steric reasons, all three isomers were converted into the lowest energy atropoisomer $\mathbf{1}_{\alpha\beta\alpha\beta}$ under heating at 50 °C for 48 h. This observation is not unprecedented since it has been previously reported for another porphyrin derivative[11] that the protonation of the porphyrin core induces considerable deformation[12] leading to thermal atropoisomerisation.

In summary, high yield syntheses of all four atropoisomers $\mathbf{1}_{\alpha4}$, $\mathbf{1}_{\alpha3\beta}$, $\mathbf{1}_{\alpha2\beta2}$ and $\mathbf{1}_{\alpha\beta\alpha\beta}$ of *meso*-tetrakis(*o*-catecholamidophenyl)porphyrin was achieved and their structures assigned based on X-ray and NMR analysis. Furthermore, it has been established that all three protonated $\mathbf{1}_{\alpha4}$, $\mathbf{1}_{\alpha3\beta}$, $\mathbf{1}_{\alpha2\beta2}$ atropoisomers may be converted into the most stable $\mathbf{1}_{\alpha\beta\alpha\beta}$ isomer upon heating. The formation of the bi- and tri-nuclear complexes using different atropoisomers of **1** with a variety of transition metal cations as well as the formation of coordination polymers are under current investigation.

We thank Dr. R. Ruppert for the initial preparation of the mixture of protected atropoisomers, Dr. I. Huc for his help with the HPLC separation, the Institut Universitaire de France (IUF), and the CNRS for financial support.

Notes and References

† E-mail: hosseini@chimie.u-strasbg.fr

‡ *Crystallographic data*: for $\mathbf{2}_{\alpha4}$ (dark red crystals, 294 K): $C_{80}H_{66}N_8O_{12}\cdot2H_2O$, M = 1367.5, monolcinic, space group $C2/c$, a = 29.447(2), b = 10.672(1) c = 27.067(3) Å, β = 123.449(6), U = 7096(2) Å^3, Z = 4, D_c = 1.28 g cm^{-3}, T = 294 K, μ = 0.083 mm^{-1}, Mo-Kα graphite monochromated radiation, 3111 data with $I > 3\sigma(I)$, R = 0.087, R_w = 0.129. For $\mathbf{2}_{\alpha\beta\alpha\beta}$ (red crystals, 173 K): $C_{80}H_{66}N_8O_{12}\cdot2CHCl_3$, M = 1570.2, triclinic, space group $P\bar{1}$, a = 16.305(5), b = 17.578(5), c = 13.881(4) Å, α = 105.29(2), β = 100.09(2), γ = 98.28(2), U = 3701.7 Å^3, Z = 2, D_c = 1.409 g cm^{-3}, T = 173 K, μ = 2.72 mm^{-1}, Cu-Kα, graphite monochromated radiation, 6342 data with $I > 3\sigma(I)$, R = 0.063, R_w = 0.099. Both structures were solved using OpenMoleN 2.2. CCDC 182/775.

1 S. G. DiMagno, V. S.-Y. Lin and M. J. Therein, *J. Am. Chem. Soc.*, 1993, **115**, 2513; A. D. Hamilton, H.-D. Rubin and A. B. Bocarsly, *J. Am. Chem. Soc.*, 1984, **106**, 7255; J. A. Wytko, E. Graf and J. Weiss, *J. Org. Chem.*, 1992, **57**, 1016.
2 L. D. Sarson, K. Ueda, M. Takeuchi and S. Shinkai, *Chem. Commun.*, 1996, 619.
3 C. Drexler, M. W. Hosseini, A. De Cian and J. Fischer, *Tetrahedron Lett.*, 1997, **38**, 2993.
4 E. Graf, M. W. Hosseini and R. Ruppert, *Tetrahedron Lett.*, 1994, **35**, 7779; E. Graf, M. W. Hosseini, R. Ruppert, N. Kyritsakas, A. De Cian, J. Fischer, C. Estournès and F. Taulelle, *Angew. Chem., Int. Ed. Engl.*, 1995, **34**, 1115; F. Bockstahl, E. Graf, M. W. Hosseini, D. Suhr, A. De Cian and J. Fischer, *Tetrahedron Lett.*, 1997, **38**, 7539.
5 F. L. Weitl and K. N. Raymond, *J. Am. Chem. Soc.*, 1980, **102**, 2289; K. N. Raymond, G. Müller and B. F. Matzanke, *Top. Curr. Chem.*, 1984, **123**, 49.
6 G. Mislin, E. Graf and M. W. Hosseini, *Tetrahedron Lett.*, 1996, **37**, 4503.
7 L. K. Gottwald and E. F. Ullman, *Tetrahedron Lett.*, 1969, 619; F. A. Walker, *Tetrahedron Lett.*, 1971, 4949.
8 J. P. Collman, R. R. Gagne, C. A. Reed, T. R. Halbert, G. Lang and W. T. Robinson, *J. Am. Chem. Soc.*, 1975, **97**, 1427.
9 F. L. Weitl, K. N. Raymond, W. L. Smith and T. R. Howard, *J. Am. Chem. Soc.*, 1978, **100**, 1170.
10 J. F. W. McOmie and M. L. Watts, *Tetrahedron*, 1968, **24**, 2289; E. H. Vickery, L. F. Pahler and E. J. Eisenbraun, *J. Org. Chem.*, 1979, **44**, 4444.
11 R. A. Freitag and D. G. Whitten, *J. Phys. Chem.*, 1983, **87**, 3918.
12 E. B. Fleischer and A. L. Stone, *J. Am. Chem. Soc.*, 1968, **90**, 2725.

Received in Basel, Switzerland, 4th November 1997; 7/07949D

Reaction of ketones with the organotitanium oxide [{TiCp*(μ-O)}$_3$(μ$_3$-CMe)] *via* the hydride–vinylidene [{TiCp*(μ-O)}$_3$(μ-C=CH$_2$)(H)] intermediate‡

Mikhail Galakhov, Miguel Mena*† and Cristina Santamaría

Departamento de Química Inorgánica de la Universidad de Alcalá, E-22871 Alcalá de Henares, Madrid, Spain

Thermal and/or photochemical treatment of [{TiCp*(μ-O)}$_3$(μ$_3$-CMe)] 1 (Cp* ≡ η^5-C$_5$Me$_5$) with organic ketones affords the new oxo derivatives [{TiCp*(μ-O)}$_3$(μ-C=CH$_2$)(OCHRR′)] (R = R′ = Me 2, Ph 3; R = Ph, R′ = Me 4, Et 5); these reactions take place by insertion of the ketones CO group into the Ti–H bond of the *in situ* formed [{TiCp*(μ-O)}$_3$(μ-CCH$_2$)(H)] intermediate.

We have reported the unprecedented oxotitanium complexes, [{TiCp*(μ-O)}$_3$(μ$_3$-CR)] (R = H, Me),[1] possessing a μ$_3$-alkylidyne sp^3-carbon similar to that found for the early-transition-metal clusters [M$_3$(μ$_3$-CR′)(OR)$_9$] (M = Mo, W)[2] and in contrast with the sp-hybridized alkylidyne carbon of the species as [Co$_3$(μ$_3$-CR)(CO)$_9$].[3] The chemistry of these μ$_3$-alkylidynetrimetal clusters have been extensively explored.[3a,4] Meanwhile, to our knowledge, the [{CrCp(μ-Cl)}$_3$(μ$_3$-CH)],[5] [{TiCp*(μ-O)}$_3$(μ$_3$-CR)][1] and [{TiCp*}$_4$(μ$_3$-CH)$_4$][6] complexes are the only reported examples of μ$_3$-alkylidyne units supported on trinuclear cores without metal–metal bonds and their reactivity is, as yet, practically unknown.[7] This chemistry might be of great current interest, imitating the behaviour of the alkylidyne groups attached to metal or metal oxide surfaces and establishing a clear connection between organometallic and solid surface systems.[8] Here, we report the surprising reactivity of diverse ketones and the μ$_3$-ethylidyne group on an organotitanium oxide.

Treatment of [{TiCp*(μ-O)}$_3$(μ$_3$-CMe)] **1** with 1 equiv. of RCOR′ (R = R′ = Me, Ph; R = Ph, R′ = Me, Et) in toluene or hexane, heating at temperatures between 100 and 120 °C or irradiating with a sunlamp for several days, leads to the formation (46–77% yield) of blue–violet complexes characterised as [{TiCp*(μ-O)}$_3$(μ-CCH$_2$)(OCHRR′)] (R = R′ = Me **2**, Ph **3**; R = Ph, R′ = Me **4**, Et **5** (Scheme 1).§

The IR spectra of these complexes show a weak band at 1580 (**2**) and 1598 cm^{-1} (**3**, **4**, **5**) assigned to the *ν*(C=C) of the μ-vinylidene moiety, as in the case of the bimetallic systems [Ru$_2$(CO)$_3$Cp$_2$(μ-C=CH$_2$)] (1586 cm^{-1})[9] and [ClNi(μ-dppm)$_2$(μ-C=CH$_2$)NiCl] (1580 cm^{-1}).[10] The NMR spectra (Table 1) are consistent with the proposed structure and reveal the presence of the characteristic signals for μ-vinylidene, alkoxide and Cp* ligands.

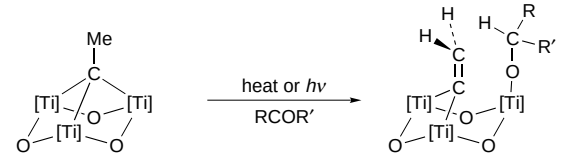

1
[Ti] = Ti(η^5-C$_5$Me$_5$)

R = R′ = Me **2**, Ph **3**
R = Ph; R′ = Me **4**, Et **5**

Scheme 1

The ^{13}C NMR spectra of **2**–**5** reveal triplets at δ_{av} 317.5 (^2J 5 Hz) attributed to the C$_\alpha$ resonance of the bridging vinylidene fragment >C$_\alpha$=C$_\beta$H$_2$, which are very similar to those found for other known vinylidene complexes.[11] The terminal moiety (=C$_\beta$H$_2$) of this fragment appear, in both ^{1}H and ^{13}C NMR spectra, in the typical range for organic alkenes. The NMR spectra also display the clear presence of the OC*H*RR′ signals whose chemical shifts and multiplicity depend on the nature of the ketone substituents (Table 1) and the values of $^1J_{CH}$ ≈ 142 Hz are according to the proximity of the oxygen atom. Additionally, the NMR spectra of **4** and **5** show signals for three different Cp* ligands in 1 : 1 : 1 ratio and AB spin systems for the vinylidene protons due to the chiral carbon atoms of the alkoxy groups.

A plausible pathway for these reactions involves initial β-hydrogen elimination in the μ$_3$-ethylidyne ligand to generate the intermediate [{TiCp*(μ-O)}$_3$(μ-CCH$_2$)(H)]. Similar conversion of μ$_3$-alkylidyne complexes to vinylidenes has been found for many trinuclear clusters[11a] and may be responsible of the H/D exchange reactions in ethylidynes on metal surfaces.[8a,c] Interestingly, we have also observed that the complex **1** incorporate deuterium in the μ$_3$-ethylidyne group when a C$_6$D$_6$ solution of **1** is heated above 200 °C,¶ and this H/D exchange is easy to explain if we assume the participation of the above mentioned hydride intermediate.[12] Finally the insertion of the ketones into the Ti–H bond of [{TiCp*(μ-O)}$_3$(μ-CCH$_2$)(H)] takes place (Scheme 2).[13]

Table 1 Selected NMR data (*δ*, *J*/Hz) for complexes [{TiCp*(μ-O)}$_3$(μ-CCH$_2$)(OCHRR′)] (R = R′ = Me **2**, Ph **3**; R = Ph, R′ = Me **4**, Et **5**)[a]

	^{1}H				^{13}C			
Assignment	**2**	**3**	**4**	**5**	**2**	**3**	**4**	**5**
C$_5$*Me*$_5$	2.11 (s, 15 H) 1.99 (s, 30 H)	2.03 (s, 15 H) 1.97 (s, 30 H)	2.07 (s, 15 H), 2.03 (s, 15 H), 1.97 (s, 15 H)	2.05 (s, 15 H), 2.04 (s, 15 H), 1.97 (s, 15 H)	11.7, 11.4	11.9, 11.7	11.6, 11.7, 11.9	11.6, 11.7, 11.8
C$_5$Me$_5$					120.4, 122.3	120.7, 123.1	120.6, 122.6 125.7	120.5, 122.6, 126.0
μ-C=*CH*$_2$	6.04 (s, 2 H)	5.78 (s, 2 H)	5.93$_{av}$ (2 H, ^2J 4.5)	5.97$_{av}$ (2 H, ^2J 4.8)	120.9 (t, ^1J 154.9)	122.0 (t, ^1J 155.6)	121.6 (t, ^1J 155.4)	121.1 (t, ^1J 154.8)
μ-*C*=CH$_2$					317.3 (t, ^2J 5.2)	317.2 (t, ^2J 5.7)	317.5 (t, ^2J 4.8)	318.0 (t, ^2J 4.9)
–O*CH*RR′	4.80 (spt, 1 H, ^3J 6.0)	6.80 (s, 1 H)	5.78 (q, 1 H, ^3J 6.6)	5.46 (dd, 1 H, ^3J 4.5, 8.4)	74.9 (dm, ^1J 140.9)	85.3 (dm, ^1J 141.4)	79.5 (dm, ^1J 144.2)	85.5 (dm, ^1J 140.2)

[a] Recorded on Varian Unity 300 or 500 Plus in C$_6$D$_6$ at 20 °C.

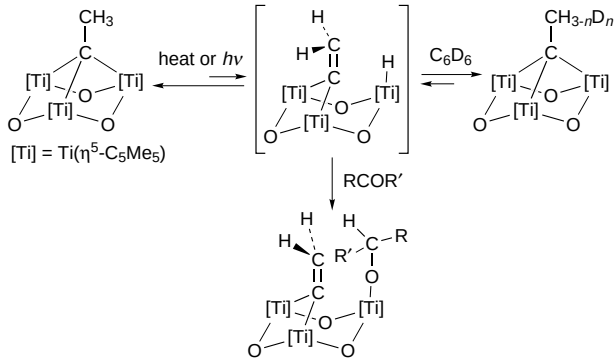

Scheme 2

Thus the incorporation of the ketones onto the organometallic titanium oxide [{TiCp*(μ-O)}$_3$(μ$_3$-CMe)] can be best interpreted in terms of an insertion process of the carbonyl groups into a Ti–H bond of the hydride–vinylidene species [{TiCp*(μ-O)}$_3$(μ-CCH$_2$)(H)]. Further studies are required in order to determine the behaviour of other carbonyl derivatives and unsaturated molecules against these μ$_3$-alkylidyne complexes.

We wish to thank the DGICYT (project PB93-0476) and the Universidad de Alcalá for financial support of this research. C. Santamaría also thanks the MEC for a Predoctoral Fellowship.

Notes and References

† E-mail: mmena@inorg.alcala.es

‡ Dedicated to Professor Pascual Royo on the occasion of his 60th birthday.

§ *Preparations*: **2**: a solution of **1** (0.50 g, 0.80 mmol) and acetone (0.06 ml, 2.40 mmol) in toluene (50 ml) were transferred by cannula to a Carius tube (volume 100 ml), cooled to −78 °C, and flame-sealed. This tube was heated at 100 °C for 12 h to obtain a blue–violet lather (0.42 g, 77%). EI mass spectrum: *m*/*z* 624 (M$^+$ − MeCOMe, 9%), 613 (M$^+$ − MeCHMe − C$_2$H$_2$, 25%). **3**: this derivative was obtained analogously to **2** from 0.80 g (1.28 mmol) of **1** and 0.23 g (1.28 mmol) of benzophenone heating at 125 °C for 24 h to obtain a blue–violet crystalline solid (0.73 g, 71%). EI mass spectrum: *m*/*z* 624 (M$^+$ − PhCOPh, 6%), 613 (M$^+$ − PhCHPh − C$_2$H$_2$, 28%). **4**: acetophenone (0.16 ml, 1.33 mmol) diluted in 15 ml of hexane was added to a solution of **1** (0.80 g, 1.28 mmol) in hexane (100 ml). The reaction mixture was irradiated at room temp. for 45 h with a sunlamp. The solution was concentrated and a crystalline blue solid was obtained at room temp. (0.50 g, 52%). EI mass spectrum: *m*/*z* 624 (M$^+$ − PhCOMe, < 1%), 613 (M$^+$ − PhCHMe − C$_2$H$_2$, 3%). **5**: the preparation of this complex is similar to **4** from 0.80 g (1.28 mmol) of **1** and 0.17 ml (1.33 mmol) of ethyl phenyl ketone irradiating for 68 h with a sunlamp; 0.44 g (46%) of a blue solid was obtained. EI mass spectrum: *m*/*z* 624 (M$^+$ − PhCOEt, 5%), 613 (M$^+$ − PhCHEt − C$_2$H$_2$, < 1%).

Full NMR and analytical data for the new compounds **2**–**5** can be acquired as supplementary material upon request from the authors.

¶ In the ^{1}H NMR spectra we have detected the presence of μ$_3$-CCH$_2$D and μ$_3$-CCHD$_2$ isotopomers.

1 (*a*) R. Andrés, M. Galakhov, A. Martín, M. Mena and C. Santamaría, *Organometallics*, 1994, **13**, 2159; (*b*) R. Andrés, M. Galakhov, A. Martín, M. Mena and C. Santamaría, *J. Chem. Soc., Chem. Commun.*, 1995, 551; (*c*) R. Andrés, Doctoral Thesis, Universidad de Alcalá, Madrid, 1995.

2 M. H. Chisholm, D. L. Clark, J. Hampden-Smith and D. H. Hoffman, *Angew. Chem., Int. Ed. Engl.*, 1989, **28**, 432.

3 (*a*) D. Seyferth, *Adv. Organomet. Chem.*, 1976, **14**, 97; (*b*) B. E. R. Schilling and R. Hoffman, *J. Am. Chem. Soc.*, 1979, **101**, 3456; (*c*) P. T. Chesky and B. M. Hall, *Inorg. Chem.*, 1981, **20**, 4419.

4 R. D. W. Kemmitt and D. R. Russell, in *Comprehensive Organometallic Chemistry*, ed. G. Wilkinson, F. G. A. Stone and E. W. Abel, Pergamon, Oxford, UK, 1982, vol. 5, p. 162; (*b*) M. I. Bruce, *ibid*, vol. 4, p. 843; (*c*) J. B. Keister, in *Encyclopedia of Inorganic Chemistry*, ed. R. B. King, Wiley, Chichester, UK, 1994, p. 3348; (*d*) M. Akita, in *Comprehensive Organometallic Chemistry II*, ed. G. Wilkinson, F. G. A. Stone and E. W. Abel, Pergamon, Oxford, UK 1995, vol. 7, p. 259; (*e*) A. K. Smith, *ibid*, vol. 7, p. 747; (*f*) C. E. Barnes, *ibid*, vol. 8, p. 419; (*g*) Y. Chi and D.-K. Hwang, *ibid*, vol. 10, p. 85 (see also references therein).

5 D. S. Richeson, S.-W. Hsu, N. H. Fredd, G. V. Duyne and K. H. Theopold, *J. Am. Chem. Soc.*, 1986, **108**, 8273.

6 R. Andrés, P. Gómez-Sal, E. de Jesús, A. Martín, M. Mena and C. Yélamos, *Angew. Chem., Int. Ed. Engl.*, 1997, **36**, 115.

7 We have communicated some aspects about the reactivity of the [{TiCp*(μ-O)}$_3$(μ$_3$-CR)] derivatives: see ref. 1(*b*), R. Andrés, M. Galakhov, M. P. Gómez-Sal, A. Martín, M. Mena and C. Santamaría, *XIth FECHEM Conference on Organometallic Chemistry*, Parma, Italy, 1995, p. 172; *XIIth FECHEM Conference on Organometallic Chemistry*, Prague, Czech Republic, 1997, PB118.

8 (*a*) G. A. Somorjai, *Introduction to Surface Chemistry and Catalysis*, Wiley, New York, 1994, p. 400; (*b*) B. C. Gates, *Catalytic Chemistry*, Wiley, New York, 1992, (*c*) F. Zaera, *Chem. Rev.*, 1995, **95**, 2651; (*d*) B. E. Bent, *Chem. Rev.*, 1996, **96**, 1361; (*d*) H. H. Kung, *Transition Metal Oxides: Surface Chemistry and Catalysis*, Elsevier Science Publ., Amsterdam, The Netherlands, 1989; (*e*) M. A. Barteau, *Chem. Rev.*, 1996, **96**, 1413; (*f*) P. M. Maitlis, H. C. R. Long Quyoum, M. L. Turner and Z.-Q. Wang, *Chem. Commun.*, 1996, 1.

9 J. Evans and G. S. McNulty, *J. Chem. Soc., Dalton Trans.*, 1983, 639.

10 X. L. R. Fontaine, S. J. Higgins, B. L. Shaw, M. Thornton-Pett and W. Yichang, *J. Chem. Soc., Dalton Trans.*, 1987, 1501.

11 (*a*) M. I. Bruce, *Chem. Rev.*, 1991, **91**, 197; (*b*) R. Beckhaus, *Angew. Chem., Int. Ed. Engl.*, 1997, **36**, 686.

12 Comparable deuterium incorporation in the β position of an alkyl complex (Cp*$_2$ScCH$_2$CH$_2$CH$_2$CH$_3$) *via* a hydride intermediate (Cp*$_2$ScH) has been reported: B. J. Burger, M. E. Thompson, W. D. Cotter and J. E. Bercaw, *J. Am. Chem. Soc.*, 1990, **112**, 1566.

13 In an analogous manner, it is known that Cp*$_2$TiEt reacts with Me$_2$C=O through a Cp*$_2$TiH intermediate to give the product of migratory insertion into the Ti–H bond: G. A. Luinstra, J. Vogelzang and J. H. Teuben, *Organometallics*, 1992, **11**, 2273.

Received in Basel, Switzerland, 23rd December 1997; 7/09194J

Direct conversion of perfluoroalkanes and perfluoroarenes to perfluoro Grignard reagents

Christopher M. Beck, You-Jung Park and Robert H. Crabtree*†

Yale University, Department of Chemistry, 225 Prospect Street, New Haven, CT 06511, USA

Magnesium anthracene selectively reduces C_6F_{12} or C_6F_6 and $CF_3C_6F_{11}$ or $CF_3C_6F_5$ to C_6F_5MgF and $CF_3C_6F_4MgF$, respectively

Magnesium anthracene[1] $MgC_{14}H_{10}$ **1**, has found a wealth of applications in organic chemistry.[2] This compound is believed to act as a soluble, activated form of magnesium metal,[2a,b] and is often the compound of choice for the preparation of Grignard reagents that are difficult or impossible to obtain directly from magnesium metal.[2] Here, we describe the use of **1** in new synthetic routes to perfluoroaromatic Grignard reagents from both perfluoroaromatic compounds as well as from the less costly analogous saturated fluorocarbons.

Rare cases are known in which perfluoro Grignard reagents have been synthesized from perfluoroaromatic compounds (but not from perfluoroalkanes) and magnesium by entrainment with a more reactive organic bromide, with[3] or without[4] transition metal catalysis. Important work by Richmond and Pez and their coworkers has shown that transition metal compounds[5] and arene anions[6] can reduce saturated perfluorocarbons in solution but never previously to give such useful species as Grignard reagents.

We now find that hexafluorobenzene **2a** reacts cleanly with 1 equiv. of the orange species **1** in THF solution at −41 °C to afford a solution, the blue color of which is believed to be associated with the anthracene monoanion. Treatment of this solution with CO_2 followed by acid work-up, yielded pentafluorobenzoic acid **5a** in moderate yield (34%), along with unreacted **2a**. The reaction appears to proceed *via* net insertion of a Mg atom into the aromatic C–F bond, forming a Grignard reagent which subsequently reacts with CO_2 to form the carboxylic acid (Scheme 1). Since **1** exists in a temperature dependent equilibrium with anthracene and magnesium metal,[1b] it is unclear if the formation of the Grignard reagent occurs directly or by prior production of a highly active form of magnesium metal.

The reaction of perfluorotoluene **2b** with 1 equiv. of **1** at −41 °C produced perfluorotoluic acid **5b**‡ exclusively as the *para* isomer but in low yield (8.5%). The yields did not change significantly between −78 and 0 °C or in the presence of an excess of **1**. Perfluoronaphthalene gave no identifiable organic products in the presence of **1** at −78 °C. For comparison, Mg powder (Aldrich Co., 50 mesh) was exposed to **2a** or **2b** under analogous conditions. In this case, no reaction was observed between the perfluoroarene and magnesium, further illustrating the necessity for using **1** in Grignard synthesis.

Our success with these perfluoroarenes led us to look at the corresponding perfluoroalkanes. When a THF solution of 4 equiv. of **1** at 0 °C was treated with perfluorocyclohexane **3a**, the initial orange solution rapidly turned dark brown. Subsequent work-up with CO_2, then acid, followed by extraction with dilute base afforded dark brown solids after removal of the solvent. Direct sublimation of these solids at 115 °C *in vacuo* afforded white crystals which proved to be an inseparable mixture of $C_6F_5CO_2H$ and 2,3,5,6-$C_6HF_4CO_2H$§ by ^{19}F NMR spectroscopy in 14 and 4% overall chemical yield based on fluorocarbon. This result is consistent with initial reduction of perfluorocyclohexane to hexafluorobenzene which would then be expected to react with an additional equivalent of **1** to yield the corresponding Grignard reagent. Similarly, perfluoromethylcyclohexane **3b** upon treatment with 4 equiv. of **1** yielded **5b** in 5.7% yield, exclusively as the *para* isomer. As in the case of the perfluoroarenes, no products were observed when commercial Mg powder was treated with **3a** or **3b** in an analogous manner. These transformations constitute, to our knowledge, the only known conversions of perfluoroalkanes directly to Grignard reagents. **CAUTION**: Fluorinated Grignards can spontaneously explode;[8] appropriate care must therefore be exercised.

The authors are grateful to the Department of Energy and the 3M corporation for financial support.

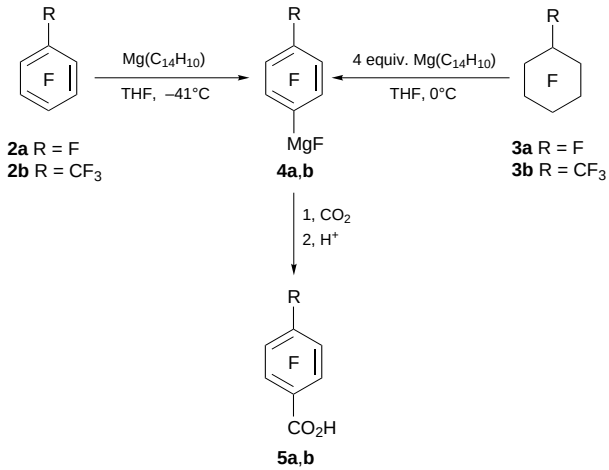

Scheme 1

Table 1 Yields of **5** and reaction temperature for the reactions of **2** and **3** with **1**[a]

Fluorocarbon	*T*/°C	Yield (%)
2a	−41	34.3
2b	−41	8.5
3a	0	14.0[b]
3b	0	5.7

[a] Fluorocarbon was added to a pre-cooled THF solution of **1** and allowed to stir for 15–40 min. Dry CO_2 was introduced for *ca*. 40 min at the reaction temperature and allowed to warm to room temperature under a CO_2 flow. The mixture was then quenched with dilute H_2SO_4 and the THF removed *in vacuo*. The product was extracted with Et_2O, and then extracted by shaking with 1 M (aq) KOH. The basic extracts were acidified with dilute H_2SO_4 and extracted with Et_2O to yield the product. Yields reported here are for the doubly sublimed, analytically pure solids. [b] Isolated as a mixture which also contained 2,3,5,6-$C_6HF_4CO_2H$ in 4% yield based on fluorocarbon.

Notes and References

† E-mail: robert.crabtree@yale.edu

‡ *Data* for **5b**: ^{19}F NMR (461 MHz, [$^2H_6$]acetone, 20 °C, $CFCl_3$); δ −56.5 (t, 3F, $^4J_{FF}$ 22 Hz), −138.9 (m, 2 F), −140.7 (m, 2 F); mp 109–112 °C, lit:[7] 110–111.5 °C. Anal. Calc. for $C_8HF_7O_2$: C, 36.64; H, 0.38; F, 50.76. Found: C, 36.62; H, 0.36; F, 50.74%.

§ This compound was identified by ^{19}F NMR in comparison with an authentic sample. Occasionally, traces of this species could be distinguished in the crude solids obtained from the reaction of **2a** with **1**, but was absent after purification.

1 (*a*) B. Bogdanovic, N. Janke, H. Kinzelmann, K. Seevogel and J. Treber, *Chem. Ber.*, 1990, **123**, 1529; (*b*) B. Bagdanovic, S. Liao, R. Mynott, K. Schlichte and U. Westeppe, *Chem. Ber.*, 1984, **117**, 1378.

2 (*a*) M. Gallagher, S. Harvey, C. Raton and R. Sue, *J. Chem. Soc., Chem. Commun.*, 1988, 289; (*b*) B. Bogdanovic, *Acc. Chem. Res.*, 1988, **21**, 261; (*c*) S. Harvey and C. Raston, *J. Chem. Soc., Chem. Commun.*, 1988, 652 (*d*) T. Hudlicky, M. Natchus and G. Sinai-Zingde, *J. Org. Chem.*, 1987, **52**, 4644.

3 W. Respess and C. Tamborski, *J. Organomet. Chem.*, 1969, **18**, 263.

4 W. Respess, J. Ward and C. Tambroski, *J. Organomet. Chem.*, 1969, **19**, 191.

5 J. Kiplinger, T. Richmond and C. Osterberg, *Chem. Rev.*, 1994, **94**, 373, and references within; B. Bennett, R. Harrison and T. Richmond, *J. Am. Chem. Soc.*, 1994, **116,** 11 165; J. Kiplinger and T. Richmond, *J. Am. Chem. Soc.*, 1996, **118**, 1805; *Chem. Commun.*, 1996, 1115.

6 J. Marsella, A. Gilicinski, A. Coughlin and G. Pez, *J. Org. Chem.*, 1992, **57**, 2856; A. Oku., J. Nishimura, S. Nakagawa and K. Yamada, *Nippon Kagaku Kaishi*, 1985, **10**, 1985; *Chem. Abstr.*, 1986, **105**, 97074z.

7 C. Tamborski and E. Soloski, *J. Org. Chem.*, 1966, **31**, 746.

8 E. C. Ashby and D. Al-Fekri, *J. Organomet. Chem.*, 1990, **390**, 275.

Received in Bloomington, IN, USA, 25th November 1997; 7/08515J

Photochemistry and magnetic resonance spectroscopy as probes of supramolecular structures and migration pathways of organic molecules and radicals adsorbed on zeolites

Nicholas J. Turro,*[a]† Xuegong Lei,[a] Wei Li,[a] Ann McDermott,[a] Lloyd Abrams,[b] M. Francesca Ottavianai[c] and Hege Støgård Beard[d]

[a] *Chemistry Department, Columbia University, New York, NY 10027, USA*
[b] *E. I. duPont de Nemours and Co., Central Research Department, Experimental Station, Wilmington, DE 19880, USA*
[c] *University of Florence, Department of Physical Chemistry, Via Gino Capponi, 9, 50121 Florence, Italy*
[d] *Chemistry Department, University of Oslo, Oslo, Norway*

Magnetic resonance, surface area measurements and computational techniques have been integrated to elucidate the supramolecular photochemistry of two isomeric ketones adsorbed on two MFI zeolites (silicalite and ZSM-5) and to demonstrate that common factors proportional to the available external surface area operate to determine the measured parameters in each case.

We report here examples of supramolecular photochemistry[1,2] of ketones adsorbed on molecular sieve zeolites (possessing MFI topology). The systems employed are two isomeric ketones, *o*ACOB and *p*ACOB, whose molecular photochemistries are essentially identical,[3] but whose supramolecular photochemistries[4] (Scheme 1) are a strong function of supramolecular composition, structure and dynamics.

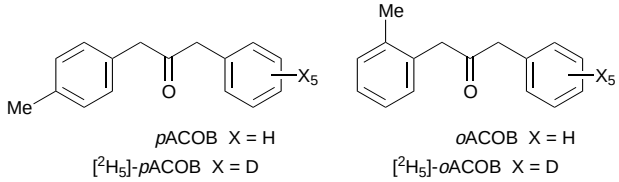

As shown in Scheme 1, the external surface of ZSF-5 zeolites[5] possesses two sites for binding of *o*ACOB molecules: (i) the holes on the external surface (*ca.* 30% of the external surface area) and (ii) the remaining 'solid framework' of the external surface (*ca.* 70% of the external surface area). As ketone is loaded, a monolayer of ketone will form at some point and loading of ketone beyond this point will cause the formation of multilayers.

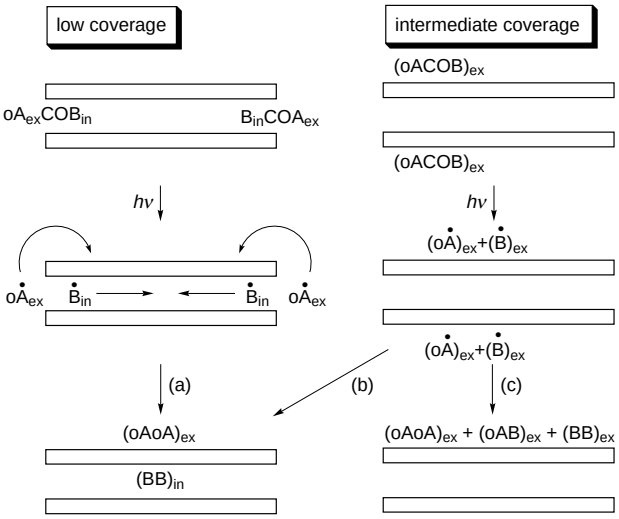

Scheme 1 Schematic description of the supramolecular photochemistry of *o*MeDBK/MFI complexes and *p*MeDBK/MFI complexes at loadings corresponding to less than a monolayer. The holes are filled first (left) and then the solid framework.

According to the paradigm[4] of Scheme 1, the products of the photochemistry of *o*ACOB adsorbed on MFI zeolites will depend both on the initial siting of the ketone and on the dynamics of the radicals produced by photolysis of *o*ACOB adsorbed at these sitings.

The photolyses of *o*ACOB and *p*ACOB adsorbed on two MFI zeolites,[5] silicalite (surface area = 5 m^2 g^{-1})[6] and ZSM-5 (surface area = 16 m^2 g^{-1}),[6] were investigated as a function of loading of ketone in the range *ca.* 0.1 to *ca.* 5% w/w. Fig. 1 summarizes the results of the 'cage effect'[7] as a function of loading. The product mixture from the photolysis of the *p*ACOB/zeolite sysem was found to exhibit a strong positive cage effect (CE)[7] *over the entire loading range* investigated for both silicalite and ZSM-5. In contrast, the product mixture from the photolysis of the *o*ACOB/zeolite system depends strongly on the loading, exhibiting a strong negative cage effect[7] at low loadings, and an increasingly positive cage effect[7] reaching a

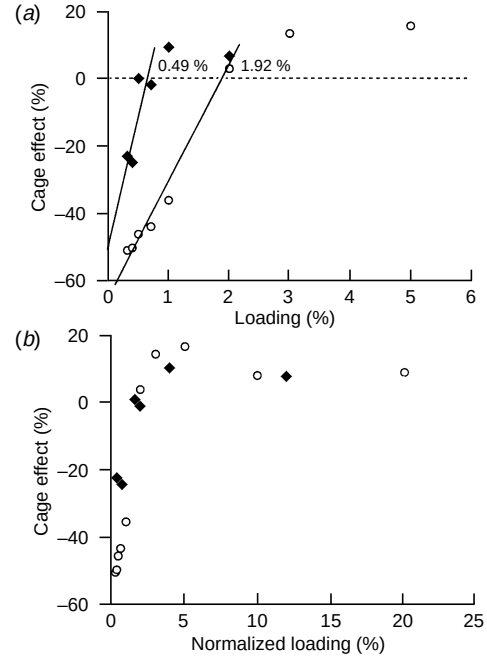

Fig. 1 (*a*) Loading and (*b*) normalized loading dependence of the cage effect for the photolysis of *o*MeDBK on (○) 25M-5 and (◆) silicalite zeolites

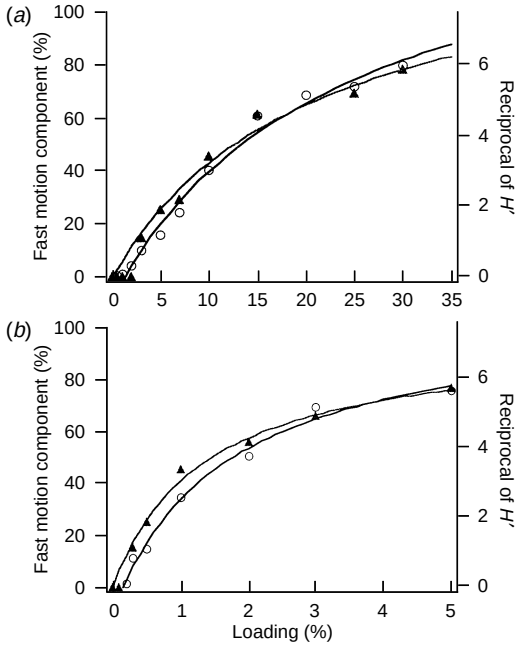

Fig. 2 Values for (*a*) ZSM-5 and (*b*) silicalite zeolites of (○) the reciprocal of H' from ^{2}H NMR spectra and (▲) the fast motion component extracted from EPR spectra, as a function of loading of *o*ACOB

maximum and progressing towards a limiting cage effect of zero at the highest loadings [Fig. 1(*a*)].

For low loadings (conditions for which the surface area and number of holes determine the CE), a linear fit of the data in Fig. 1 yields values of 0.49 and 1.92% for the loadings at which a CE of *ca.* 0% is achieved (assumed to correspond approximately to the formation of the monolayer). The ratio of these loadings is 3.9 and is strikingly similar to the observed ratio (3 : 2) of the experimentally measured surface areas of the two zeolite samples.[6] These results demonstrate that the external surface area is a key parameter in understanding the results.

The reciprocal of the half width of the signal ($H' = 1/\Delta H_{1/2}$) in the solid state ^{2}H NMR of [$^2H_5$]-*o*ACOB was determined as a function of loading (Fig. 2). The values of H' are related to the motion[8] of ring B. If the ring is plugged in a hole on the external surface, its motion is expected to be more constrained than when it is adsorbed on the solid external surface.[8] Finally, if the ring is in a liquid-like multilayer, the motion is expected to be effectively isotropic and unconstrained.

For the lowest loadings, the values of H' for both zeolite samples are small (motion constrained) and constant, as expected if the ketones first occupy the holes on the external surface. The value of H' begins to increase, and then plateau as expected if the ketones begin to occupy a liquid-like environment.

The form of the graph of the ^{2}H NMR data in Fig. 2 may be described by a Langmuir expression such as eqn. (1), where Y is

$$Y = M(k)x/(1 + kx) \quad (1)$$

the value of a parameter proportional to coverage, x is the loading of *o*ACOB (w/w), M is the maximum value of Y [computed from fitting the data to eqn. (1)], and k is related to the equilibrium constant for adsorption of the ketone on the external surface.

If we assume that the motion of the adsorbed *o*MeDBK molecules is directly related to the external surface coverage, then the reciprocal of the half-widths[8] of the ^{2}H NMR data serves as parameter Y in eqn. (1). At loadings below 0.3% the ^{2}H NMR signal is relatively broad and constant, implying that the first *o*ACOB molecules adsorbed are more tightly bound to the holes than subsequently adsorbed molecules which bind to the solid external surface.[9] However, for values of H' plotted as a function of loadings greater than *ca.* 1%, the data fit eqn. (1) within experimental error (solid curves in Fig. 2). Values of $k = 0.041 \pm 0.010$ and 0.56 ± 0.50 for ZSM-5 and silicalite, respectively, are evaluated from the fit to eqn. (1). The data for both zeolite samples overlap within experimental error if the data for silicalite are scaled by a factor of *ca.* 5, which is of the order of the ratio of the measured external surface area of the two zeolites and the ratio of the linear portions of the slopes of the photochemical data in Fig. 1(*a*).

A second experiment employing EPR spectroscopy confirms indirectly the results of the photochemical and ^{2}H NMR experiments. In these experiments 4-oxo-TEMPO (T) was employed as an EPR probe of binding of *o*ACOB to the external surface. A small amount (0.1%) of T was added to the zeolite samples and the influence of the addition of *o*ACOB on the EPR signal of the probe was observed. In the absence of *o*ACOB, the EPR spectrum consists of only a broad signal characteristic peak, a strongly motion-constrained (slow component) probe bound to the external surface. Addition of ketone causes the conversion of the broad signal to a sharp, three line signal (fast component) characteristic of a mobile probe displaced by the ketone to a weaker binding region of the external surface. The resulting spectra could be simulated[10] as the sum of a fast and slow component. Under the assumption that the ketone is displacing the constrained probe, the percent of fast component is proportional to the adsorbed ketone. Fig. 2 shows a plot of the percent of fast component as a function of loading for the two zeolites examined.

A plot of the percent of fast component as a function of loading fits eqn. (1) within the experimental error [Fig. 2(*a*)]. Values of $k = 0.048 \pm 0.010$ and 0.76 ± 0.11 for ZSM-5 and silicalite, respectively, are evaluated from the fit to eqn. (1). Strikingly, these values are experimentally indistinguishable from the k values evaluated from the ^{2}H NMR data ($k = 0.041 \pm 0.010$ and 0.56 ± 0.50 for ZSM-5 and silicalite, respectively). Furthermore, the EPR data in Fig. 2 for the two zeolites overlap the data for the ^{2}H NMR data of Fig. 2 when the data for silicalite are scaled by the same factor (*ca.* 5) which corrects for the different surface areas of the two zeolites.

The authors at Columbia thank the National Science Foundation for its generous support of this research and Dr Zhi Liu for performing preliminary ^{2}H NMR experiments. X. G. L. and W. L. thank the Kanagawa Academy of Science and Technology for funding.

Notes and References

† E-mail: turro@chem.columbia.edu

1 *Supramolecular Chemistry*, J. M. Lehn, VCH, New York, 1995.
2 E. G. Derouane and Z. Gabelica, *J. Catal.*, 1980, **65**, 486.
3 N. J. Turro, M.-F. Chow, C.-J. Chung, G. Weed and B. Kraeutler, *J. Am. Chem. Soc.*, 1980, **102**, 4843 and references cited therein.
4 N. J. Turro, C. C. Cheng, L. Abrams and D. R. Corbin, *J. Am. Chem. Soc.*, 1987, **109**, 2449.
5 The external area available to a *o*MeDBK molecule on the [010] MFI external surface was determined by computer simulation.
6 The surface area of the samples was determined by mercury porosimetry.
7 The cage effect is defined empirically in terms of the ratio of *o*A*o*A, *o*AB and BB measured experimentally (ref. 4).
8 R. J. Wittebort, E. T. Olejniczak and R. G. Griffin, *J. Chem. Phys.*, 1987, **86**, 5411.
9 Adsorption of *o*ACOB on porous silica, a model for a flat version of the MFI external surface, results in only a sharp signal (*ca.* 5 kHz).
10 D. J. Schneider and J. H. Freed, in *Biological Magnetic Resonance. Spin Labeling. Theory and Applications*, ed. L. J. Berliner and J. Reuben, Plenum, New York, 1989, vol. 8, p. 1.

Received in Corvallis, OR, USA, 1st December 1997; 7/08688A

Photochemistry of ketones adsorbed on size/shape selective zeolites. A supramolecular approach to persistent carbon centered radicals

Nicholas J. Turro,*[a]† Ann McDermott,[a] Xuegong Lei,[a] Wei Li,[a] Lloyd Abrams,[b] M. Francesca Ottaviani,[c] Hege Støgård Beard,[d] Kendall N. Houk,[e] Brett R. Beno[e] and Patrick S. Lee[e]

[a] *Chemistry Department, Columbia University, New York, NY 10027, USA*
[b] *E. I. duPont de Nemours, Central Research Department, Experimental Station, Wilmington, DE 19880, USA*
[c] *University of Florence, Department of Physical Chemistry, Via Gino Capponi, 9, 50121 Florence, Italy*
[d] *Chemistry Department, University of Oslo, Oslo, Norway*
[e] *Department of Chemistry and Biochemistry, University of California, Los Angeles, CA 90095-1569, USA*

^{2}H NMR, EPR, computational and product analyses of the photolysis of 2,4-diphenylpentan-3-one (DPP) adsorbed on MFI size/shape selective zeolites are consistent with supramolecular structural changes as a function of surface coverage that provide a novel method for the generation of persistent diffusing organic free radicals.

The MFI topology zeolites (*e.g.* silicalite and ZSM-5) are of technical significance in both size/shape selective catalysis and in molecular sieve separations.[1] The technically attractive properties of MFI zeolites originate from supramolecular, structural (substrates as guests, zeolite crystal as host) and dynamic (shape/size dependent supramolecular molecular diffusion) characteristics, *i.e.* substrates possess 'effective' molecular diameters comparable to the size/shape of the holes on the external surface of the zeolite crystal and/or the channels and intersections on the internal surface.[2] The siting and diffusion of a substrate are vital in determining the product selectivity in catalysis and the resolution efficiency in separations.[3]

Understanding the role of diffusion and siting requires the uncoupling of both supramolecular, structural and dynamic features from the effects of activation at active sites and rearrangements of reactive intermediates. The effects of activation are pronounced at high temperatures with zeolites possessing strongly acidic sites (*e.g.* HZSM-5).

We report a supramolecular photochemical investigation[4] at room temperature in which the activation and diffusional/siting effects of zeolite catalysis are uncoupled. Activation of the substrate towards reaction is provided by photochemical methods which (i) excite adsorbed substrates whose sitings and reaction products are directly determined by ^{2}H NMR analysis and (ii) produce persistent[5,6] adsorbed carbon-centred radical intermediates whose structure and mobility are directly determined by EPR spectroscopy. Computational methods are employed for (i) analysis of the plausibility of the siting and diffusional processes on the external and internal surfaces, (ii) rationalization of the variation of product distribution as a function of supramolecular structure, and (iii) simulation of the EPR spectra of the persistent supramolecular radical species formed upon photoexcitation of the adsorbed substrates.

In the molecular (solution) photochemistry [eqns. (1)–(3)] of 2,4-diphenylpentan-3-one (DPP) α-cleavage from T_1 produces,

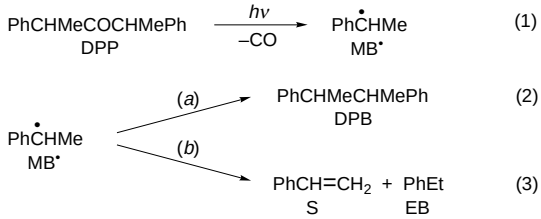

after rapid loss of CO, α-methylbenzyl radicals (MB•) [eqn. (1)], which undergo random radical combination to produce 2,3-diphenylbutane (DPB) (*ca.* 95%) and disproportionates to styrene (S) and ethylbenzene (EB) (*ca.* 5%). The rates of the radical–radical reactions in eqns. (2) and (3) are close to diffusion controlled[5,8] and, in the absence of radical scavengers, determine the lifetime of the 'molecular' radicals MB•.

Results of product analysis and EPR measurements as a function of coverage [DPP/(Na)ZSM-5 (w/w), Si/Al = 80, average particle size *ca.* 0.1 μ] showed that (i) the dominant products depend on the coverage, with disproportionation to form S and EB being favored by low coverage (< 0.3%) and combination to form DPB being increasingly favored as the coverage increases,[9] and (ii) the maximum EPR intensity of the signal of the persistent MB• radicals is insensitive to loading. For example, the ratio of disproportionation to combination of MB• radicals in solution is typically of the order of 0.1; at 0.3% loading of DPP the ratio is 3.1.

The values of the half-widths ($\Delta H_{1/2}$) of the ^{2}H NMR spectra of $C_6D_5CHMeCOCHMeC_6D_5$ ([$^2H_{10}$]-DPP) as a function of coverage are shown in Fig. 1. These provide information[10] concerning both the supramolecular structure and dynamics of the [$^2H_{10}$]-DPP/ZSM-5 system as a function of coverage: (i) a 'sharp' signal (< 1 kHz) indicates rapid, isotropic motion and the lack of constraints of the molecular structure of [$^2H_{10}$]-DPP by the host ZSM-5 structure, *i.e.* the system is essentially molecular (very weak intermolecular bonds between guest and host); (ii) a 'relatively broad' signal (*ca.* 40 kHz) indicates an anisotropic and partial constraint of a weakly bonded supramolecular structure of a DPP/ZSM-5 system; (iii) a 'limiting broad' signal (*ca.* 130 kHz) indicates relatively strong intermolecular bonds which result in inhibition of motion of a supramolecular [$^2H_{10}$]-DPP/ZSM-5 system. If the ketone were located on the flat part of the external surface, its motion would be essentially isotropic, and $\Delta H_{1/2}$ would be expected to be of the

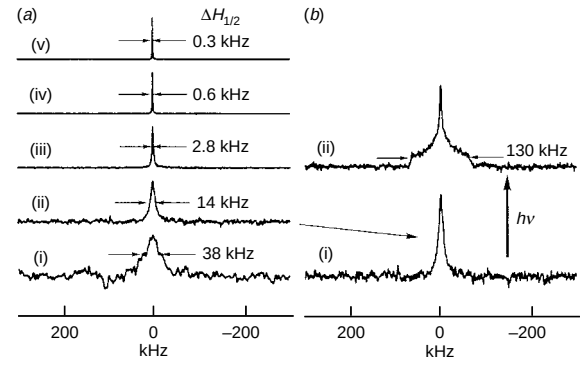

Fig. 1 (*a*) ^{2}H NMR spectra of ([$^2H_{10}$]-DPP) at (i) 0.3, (ii) 1, (iii), 2, (iv) 5 and (v) 10 wt% loading on zeolite. (*b*) Result of 1% loading sample (i) before and (ii) after photolysis.

order of 1 kHz. If the ketone were located on the inside of the zeolite $\Delta H_{½}$ would be of the order of 130 kHz. The observed value of 40 kHz is consistent with the ketone being moderately constrained in the holes on the external surface.

Before photolysis (Fig. 1), the ^{2}H NMR spectrum of the DPP/ZSM-5 system at low loading (< 1% loading) exhibits a half width of *ca*. 40 kHz, characteristic of a moderately constrained [$^2H_{10}$]-DPP molecule. Thus, we conclude that the DPP molecules at low coverage are adsorbed in the holes at the interface of the external and internal surfaces of the ZSM-5 crystal. Photolysis of [$^2H_{10}$]-DPP at room temperature results in a change in the ^{2}H NMR spectrum and the appearance of a new broad feature (*ca*. 130 kHz) which grows as the extent of photolysis increases (Fig. 2).

For high coverage before photolysis the spectrum shows mainly a sharp peak ($\Delta H_{1/2}$ < 1 kHz), with the broad peak being buried in the base line due to the [$^2H_{10}$]-DPP molecules in the holes. We conclude that photolysis of [$^2H_{10}$]-DPP at high coverage does not lead to a significant increase of the broad peak because most of the photolyzed [$^2H_{10}$]-DPP molecules occur in multilayers at high coverage, and the radicals produced in these fluid multilayers are very mobile and undergo random radical–radical combination [eqn. (2)]. This view is supported by the fact that the major product of photolysis at high coverage is that expected from 'molecular' or solution conditions, *i.e.* DPB (*ca*. 95%); most of the absorbed light excites the large excess of ketones in the multilayers rather than the relatively smaller number adsorbed in the holes at the interface.

The steady state photolysis of DPP adsorbed on ZSM-5 produced intense, long lived (many hours) EPR signals at all coverages studied. The observed spectrum fits a simulation[12] of a powder spectrum of MB$^{\bullet}$ as expected from the restricted mobility of MB$^{\bullet}$ adsorption on the internal surface. Computational analysis indicates that the lowest energy supramolecular structure of MB$^{\bullet}$ has the Ph group placed in an intersection between the channels, and the alkyl radical moiety placed in a channel between the intersections. This supramolecular geometry possesses a substantial barrier to motion, but allows the achievement of a roughly planar structure at the radical center. The hyperfine coupling constants computed and determined experimentally,[11,12] taking into account anisotropies due to restricted motion, are sufficient for the simulation. Finally, computations were made of the external surface area available for adsorption of DPP in order to estimate the relationship between the macroscopic composition (loading w/w) and the surface coverage. The measured external surface area of the ZSM-5 sample[9] is of the order of 16 $m^2\ g^{-1}$, which, when compared to the computations, implies that a monolayer of DPP will be formed when the coverage is *ca*. 0.4%, the coverage at which the experimentally observed salient effects on products and spectroscopic properties begin to change. As the coverage increases to values of *ca.* 1% and greater, the results become characteristic of a molecular, two dimensional film rather than of an adsorbed layer, because the bulk of the ketone molecules are in the multilayer and not adsorbed on the zeolite external surface. As the coverage increases, the lifetime of the radicals decreases and the ratio of disproportionation to combination decreases, *i.e.* the product distribution becomes more like that in homogeneous solution. These results are also consistent with the formation of multilayers of ketones on the external surface, so that ketone molecules finds themselves increasingly in a 'two-dimensional' liquid as the loading increases, and the results tend toward those for homogeneous solutions.

The persistence,[6,7] or lifetime, of MB$^{\bullet}$ is limited by either (i) the diffusion of two MB$^{\bullet}$ radicals into the vicinity of an intersection, or (ii) disproportionation, the lowest energy supramolecular reaction of the system within the intersection. Thus, as a consequence of their supramolecular structure, two encountering MB$^{\bullet}$ radicals to not undergo the 'molecularly favored' radical–radical combination, but instead undergo disproportionation to S and EB [eqn. (3)]. The structural basis for this selectivity may be either a supramolecular 'steric' or 'dynamic' effect. The steric effect would result from the high energy required for a C–C bond to form DPB at an intersection, as indicated by computation, and resulting from the supramolecular steric effects associated with the compression of a DPB molecule into the limited space available in the vicinity of the intersections and channels. The less sterically demanding radical–radical disproportionation in the vicinity of the intersections becomes the default supramolecularly-allowed radical–radical reaction, but even this reaction is still remarkably slow and allows the supramolecular MB$^{\bullet}$/ZSM-5 radicals to become persistent for hours at room temperature. A dynamic mechanism, termed a diffusional 'maze' effect, could also cause the persistence of otherwise reactive radicals. In the maze effect, the molecular traffic patterns of the radicals lead to rate limiting infrequent encounters in the vicinity of the intersection. In the extreme form of the maze effect an encounter leads to a 'diffusion controlled' reaction.

The ^{2}H NMR, EPR, computational and photochemical product analyses are all supported by the same supramolecular structural and dynamic interpretation of the results at high and low coverages. The supramolecular photochemistry of DPP adsorbed on ZSM-5 molecular sieve zeolites depends dramatically on the composition of the DPP/ZSM-5 system, because the supramolecular constitutional structure (connectivity relationship of the guest and host structures) depends on the system's composition. At low loading (< 0.3%) DPP is mainly adsorbed in the holes on the external surfaces that provide access to the internal surface. At intermediate loadings (*ca*. 1%), when the limited amount of holes is plugged with DPP molecules, as the coverage increases, the external framework surface between the holes becomes covered with DPP molecules until a monolayer is formed. At 'high' loadings (> 1%), both the holes and the framework's external surface are covered (a monolayer is formed) so that, as the coverage increases, multilayers or two dimensional films of DPP are formed on the external surface.

The authors thank Dr Paul Krusic (DuPont), Professors Hans Fischer and Henning Paul for enlightening discussions, and the NSF for financial support. X. G. L. and W. L. thank the Kanagawa Academy of Science and Technology for funding.

Notes and References

† E-mail: turro@chem.columbia.edu

1 See, for example, R. M. Dessau, *Selective Sorption Properties of Zeolties, ACS Symp. Ser.*, 1980, **135**, 123.
2 V. R. Choudhary, V. S. Nayak and T. V. Chaudhary, *Ind. Eng. Chem. Res.*, 1997, **36**, 1812.
3 P. B. Weisz, *Pure Appl. Chem.*, 1980, **52**, 2091; P. B. Weisz, *Ind. Eng. Chem. Fundam.*, 1986, **25**, 53.
4 For a review of the photochemistry of organic molecules adsorbed on zeolites, see N. J. Turro, *Pure Appl. Chem.*, 1986, **58**, 1219.
5 (*a*) D. Griller and K. U. Ingold, *Acc. Chem. Res.*, 1976, **9**, 13; (*b*) G. D. Mendenhall and K. U. Ingold, *J. Am. Chem. Soc.*, 1973, **95**, 3422.
6 Self reaction *via* combination or disproportionation determines the persistence of radicals inert to rearrangement and reaction with the environment.
7 N. D. Ghatlia and N. J. Turro, *J. Photochem. Photobiol. A: Chem.*, 1991, **57**, 7; B. H. Baretz and N. J. Turro, *J. Am. Chem. Soc.*, 1983, **105**, 1309.
8 H. Fischer, *J. Am. Chem. Soc.*, 1986, **108**, 3925 and references therein.
9 The surface area of the ZSM-5 samples was determined to be *ca*. 15 $m^2\ g^{-1}$ by mercury porosimetry.
10 For a discussion of the relationship between motion and line shape or ^{2}H NMR spectroscopy, see R. J. Wittebort, E. T. Olejniczak and R. G. Griffin, *J. Chem. Phys.*, 1987, **86**, 5411.
11 R. Batra, B. Giese, B. M. Spichty, G. Gescheidt and K. N. Houk, *J. Phys. Chem.*, 1996, **100**, 1837.
12 M. S. Conradi, H. Zeldes and R. Livingston, *J. Phys. Chem.*, 1979, **83**, 633.

Received in Corvallis, OR, USA, 1st December 1997; 7/08691A

Ruthenium-catalyzed ring-closing reaction of α,ω-bis(vinylsilyl) compounds *via* a silyl transfer mechanism

Takaya Mise,*[a]† Yutaka Takaguchi,[a] Takeshi Umemiya,[b] Shoichi Shimizu[b] and Yasuo Wakatsuki[a]

[a] *The Institute of Physical and Chemical Research (RIKEN), Wako-shi, Saitama 351-0198, Japan*
[b] *Department of Industrial Chemistry, College of Industrial Technology, Nihon University, Narashino, Chiba 275, Japan*

Compounds having a vinyldimethylsilyl group at both terminals have been successfully cyclized by ruthenium hydride catalysts to give selectively disilacycles of various ring sizes *via* a metathetical reaction, *i.e.* ethene elimination from the two terminal vinyl groups, not involving metallocarbene–metallacyclobutane type intermediates.

In 1991 we reported ruthenium hydride catalyzed homo- and cross-disproportionation reactions between CH_2=CH-SiR_3 and CH_2=CHR′ (R′ = SiR_3, Me, Ph, CO_2Me, OBu^n) to yield CH_2=CH_2 and R′CH=CHSiR_3.[1] When R = Me and R′ = $SiMe_3$ (homo-disproportionation), one of the disubstituted products originally assigned as the (*Z*)-isomer was subsequently identified by Marciniec and Pietrasuk as 1,1-bis(silyl)ethene.[2] We have also confirmed by NMR studies that in the case of cross disproportionations, *e.g.* R = R′ = Me, a minor product originally referred to as the (*Z*)-isomer is actually the 1,1-isomer. As a result, the catalytic sequence is now written as outlined in Scheme 1.

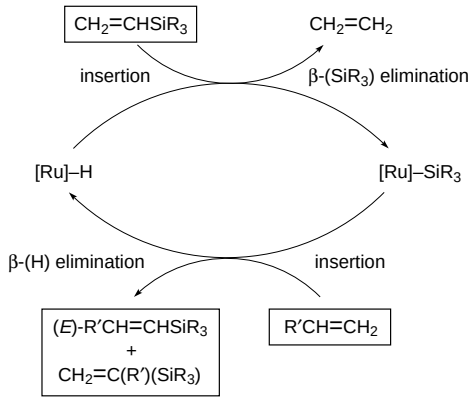

Scheme 1

The reaction mechanism involving β-silyl elimination and insertion of a C=C double bond into the resulting Ru–Si bond was established in the original report based on isolation of the ruthenium–silyl intermediate [RuCl(CO)$(PPh_3)_2$($SiMe_3$)] and its reaction with ethene.[1] This mechanism has been reconfirmed by a series of elaborate experiments by Marciniec and co-workers, who pointed out the possibility of involvement of metallocarbene and metallacyclobutane intermediates.[2–5] A remaining problem is that the regioselectivity of this reaction is poor in some cases, particularly for self-disproportionation-type reactions, where almost equal amounts of (*E*)-R_3SiCH=CHSiR_3 and CH_2=C$(SiR_3)_2$ are formed.[1] Apparently, the regioselection is controlled simply by the direction of insertion of the second olefin molecule into the Ru–Si bond.

Our efforts to improve the regioselectivity of the self-disproportionation of vinyltrimethylsilane, by modifying the electronic character and bulkiness of the ligands or by using coordinating additives, met with only partial success, yielding the (*E*)-1,2- and 1,1-isomers in an 88 : 12 ratio in one case and a 15 : 85 ratio at the other extreme (Scheme 2). The catalyst precursor used in the former was [RuCl(CNC_6H_4-NO_2)$(PPh_3)_3$(H)] while in the latter case, a small amount of MeCN was added to the initial reaction mixture containing [RuCl(CO)$(PPh_3)_3$(H)]: without MeCN, the isomer ratio was 44 : 56.

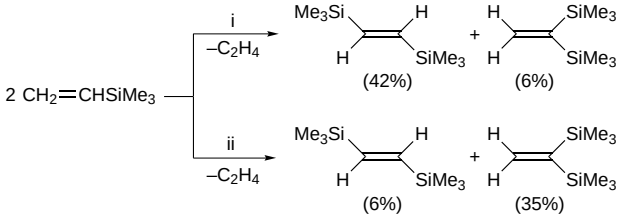

Scheme 2 *Reagents and conditions*: i, [RuCl$(PPh_3)_3$(CNC_6H_4-4-NO_2)(H)] (20 mg), vinylsilane (0.2 ml), toluene (2 ml), 100 °C, 20 h; ii, [RuCl$(PPh_3)_3$(CO)(H)] (20 mg), MeCN (0.1 ml), vinylsilane (0.2 ml), toluene (2 ml), 100 °C, 20 h. GLC yields in parentheses.

Table 1 Disproportionation of α,ω-bis(vinylsilyl) compounds

Entry, Catalyst[a]	Substrate	Product	Yield (%)
1[b], A	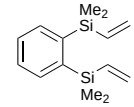 **1**	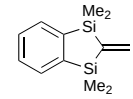 **2**	87[c]
2[d], A	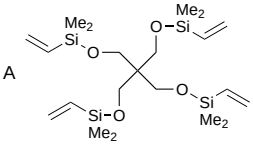 **3**	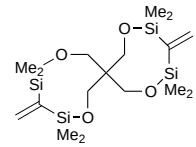 **4**	75[e]
3[f], B	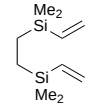 **5**	 **6**	83[c]
4[g], A	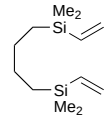 **7**	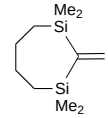 **8**	97[c]
5[h], B	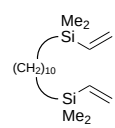 **9**	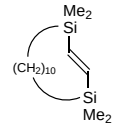 **10**	76[e]

[a] A: [RuCl(CO)$(PPh_3)_3$(H)], B: [RuCl(CO)$(PPr^i_3)_2$(H)]. [b] 80 °C, 24 h, toluene. [c] GLC yield. [d] 100 °C, 15 h, THF. [e] Isolated yield. [f] 60 °C, 24 h, THF. [g] 80 °C, 25 h, toluene. [h] 110 °C, 42 h, toluene.

Application of this catalytic system for intramolecular disproportionation of α,ω-bis(vinylsilyl) compounds was found to be more successful, giving disilacycles of various ring sizes: in particular, the regioselectivity was almost perfect (Table 1).‡ Only very small amounts of intermolecular reaction products was formed at normal concentrations of the reaction mixture, as detected by GC–MS, and they could be easily separated. By using either $[RuCl(CO)(PPh_3)_3(H)]$ or Werner's hydride $[RuCl(CO)(PPr^i_3)_2(H)]$ as the catalyst precursor,[6] the cyclic compounds with an *exo*-methylene unit were obtained as the sole cyclization products (Table 1, entries 1–4); the existence of the methylene unit in the products was confirmed by NMR DEPT studies. In contrast, a product which corresponds to the (*E*)-isomer, *i.e.* a 14-membered disilacycloolefin, was obtained selectively when the substrate had a longer aliphatic chain spacer (entry 5).§ In all of the cases examined, no isomeric material could be detected. Werner's hydride is in general more active as catalyst than the PPh_3 analog, but separation of the product from the catalyst and its residues is easier for the latter due to its low solubility.

The products in entries 1–4 correspond to the 1,1-isomer depicted in Scheme 2 and should not be formed in principle by the Grubbs type ring-closing metathesis using ruthenium–carbene initiators.[7] Obviously, the insertion–β-elimination mechanism shown in Scheme 1, is operating in an intramolecular fashion.

Further application of this novel ring-closing reaction to the synthesis of mono- and di-silamacrocycles, as well as to silicone-containing polymers, is now under investigation.

Notes and References

† E-mail: tmise@postman.riken.go.jp

‡ All new compounds gave satisfactory microanalytical data and mass spectra. *Selected data* for **2**: δ_H (270 MHz, $CDCl_3$) 6.53 (=CH_2); δ_C 154.2 (C=), 140.9 (=CH_2). For **4**: δ_H 6.33 (=CH_2); δ_C 154.2 (C=), 142.8 (=CH_2). For **6**: δ_H 6.37 (=CH_2); δ_C 156.5 (C=), 138.4 (=CH_2). For **8**: δ_H 6.28 (=CH_2); δ_H 155.4 (C=), 139.4 (=CH_2). For **10**: δ_H 6.53 (HC=CH); δ_C 150.4 (HC=CH).

§ The (*E*)-confuguration of **10** was confirmed by preparing the product by another route, *i.e.* the reaction of (*E*)-$Me_2ClSiCH{=}CHSiClMe_2$ with $BrMg(CH_2)_{10}MgBr$ under diluted conditions. This route, however, also gives by-products.

1 Y. Wakatsuki, H. Yamazaki, M. Nakano and Y. Yamamoto, *J. Chem. Soc., Chem. Commun.*, 1991, 703.
2 B. Marciniec and C. Pietraszuk, *J. Chem. Soc., Chem. Commun.*, 1995, 2003.
3 B. Marciniec, Z. Foltynowicz, C. Pietraszuk, J. Gulínski and H. Maciejewski, *J. Mol. Catal.*, 1994, **90**, 213.
4 B. Marciniec, C. Pietraszuk and Z. Foltynowicz, *J. Organomet. Chem.*, 1994, **474**, 83.
5 B. Marciniec and C. Pietraszuk, *Organometallics*, 1997, **16**, 4320.
6 M. A. Esteruelas and H. Werner, *J. Organomet. Chem.*, 1986, **303**, 221.
7 For example, see P. Schwab, M. B. France, J. W. Ziller and R. H. Grubbs, *Angew. Chem., Int. Ed. Engl.*, 1995, **34**, 2039. For a recent review on olefin metathesis, see M. Schuster and S. Blechert, *Angew. Chem., Int. Ed. Engl.*, 1997, **36**, 2037.

Received in Cambridge, UK, 12th January 1998; 8/00293B

Highly enantioselective synthesis of dialkyl and alkyl aryl *N*-tosylsulfimides

Giuseppe Celentano, Stefano Colonna,† Nicoletta Gaggero* and Carlo Richelmi

Centro CNR and Istituto di Chimica Organica, Facoltà di Farmacia, via Venezian 21, 20133 Milano, Italy

Enantiomerically pure *S*-alkyl-*S*-[(4*S*)-4-benzyl-2-oxo-1,3-oxazolidin-3-yl]-*N*-tosylsulfimides react with Grignard reagents affording dialkyl and alkyl aryl sulfimides in high chemical yield and enantiomeric excess.

Sulfimides are a class of compounds potentially of interest in the field of medicine,[1] because of their different pharmacological properties: several families of structurally related sulfimides have shown antimicrobial, diuretic and hypotensive properties, inhibitor effects on tumor growth and activity as antidepressants and stimulants of the central nervous system.

In organic synthesis sulfimides are versatile reagents due to the presence of an S^{IV}=N moiety which provides two reaction sites susceptible to attack by both nucleophilic and electrophilic reagents. Moreover, like sulfoxides, sulfimides form stable α-carbanions. This property has recently been exploited in asymmetric methylidene transfer from the sodium salt of (*S*)-*S*-methyl-*S*-*p*-tolyl-*N*-tosylsulfimide to prochiral carbonyl groups yielding epoxides with ees of up to 70%.[2] Wider applications of sulfimides are limited, however, because of the dearth of general synthetic methodologies affording high ees. The first procedure for the preparation of optically active sulfimides took advantage of the stereospecific reaction of chiral sulfoxides with various iminating species, such as bis(*N*-tosylsulfur diimine), *N*-sulfinyltoluene-*p*-sulfonamide and toluene-*p*-sulfinyl nitrene.[3] More recently Uemura[4] reported the asymmetric synthesis of alkyl aryl sulfimides by imidation of the corresponding prochiral sulfides with [*N*-(toluene-*p*-sulfonyl)imino]phenyliodinane (PhI=NTs) in the presence of a catalytic amount of Cu^{I} salts and chiral 4,4′-disubstituted bis(oxazoline) ligands, the ee being in the range 10–71%.

N-Functionalized chiral oxazolidinones are commonly employed auxiliaries which afford excellent degrees of asymmetric induction in reactions ranging from alkylations to aldol condensations and Diels–Alder additions.[5] Their use has been highly successful in the stereoselective construction of a number of natural products, antibiotics, macrolides and other pharmacologically important compounds. Recently chiral *N*-sulfinyloxazolidinones were used by Evans[6] as sulfinylating agents of a series of organometallic nucleophiles for the synthesis of sulfoxides, sulfinate esters and sulfinamides with up to 100% ee.

Now we report a new enantioselective synthesis of dialkyl and alkyl aryl *N*-tosyl sulfimides *via S*-alkyl-*S*-[(4*S*)-4-benzyl-2-oxo-1,3-oxazolidin-3-yl]-*N*-tosylsulfimides **3** and **4** prepared from the corresponding *N*-(alkylthio)oxazolidinones[6] by reaction with chloramine T (Scheme 1).

Reagents **3** and **4**, separated by flash chromatography, reacted with a series of Grignard reagents to give the corresponding sulfimides (Tables 1 and 2).‡ The displacement reaction occurred with good chemical yields even with bulky organometallic reagents such as cyclohexylmagnesium bromide (Table 1, entry 7; Table 2, entry 7) and 2-naphthylmagnesium bromide (Table 1, entry 4; Table 2, entry 4). However, *tert*-butylmagnesium bromide did not react, even when used in a large excess (four-fold excess) and for longer reaction time. In all the cases examined, no racemization of the recovered chiral auxiliary was observed.

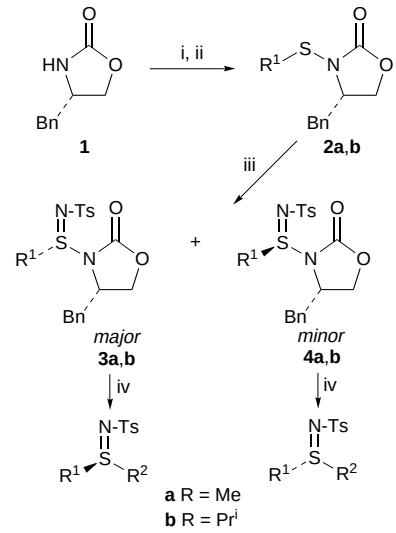

Scheme 1 *Reagents and conditions:* i, $Bu^{n}Li$ (1 equiv.), THF, 0 °C, 0.5 h; ii, R′S–SO_2Me (1.2 equiv.), room temp., 1 h; iii, Chloramine T (1.1 equiv.), toluene, $C_{16}H_{33}Bu_3PBr$ (0.05 equiv.), room temp., 4 h; iv, R^2MgBr (2 equiv.), THF, −78 °C, 1 h

The enantioselectivity in the formation of sulfimides was almost unaffected by the reaction temperature, indeed the ee of *S*-methyl-*S*-phenyl-*N*-tosylsulfimides obtained from diastereoisomers **3a** and **4a** with phenylmagnesium bromide was unchanged at both −78 and 0 °C. Therefore, intermediates **3a** and **4a** did not undergo epimerization, unlike *N*-sulfinyloxaz-

Table 1 Chemical yields and ees for nucleophilic displacement reactions on diastereoisomers **3a** and **3b**

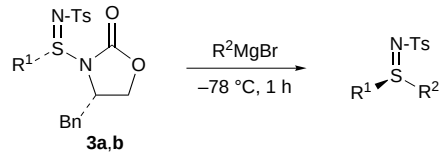

Entry	R^1	R^2	Yield (%)	Ee (%)[a]
1	Me	Ph	91	94
2[b]	Me	Ph	72	81
3	Me	*p*-tolyl	89	87 (*R*)
4	Me	2-naphthyl	75	> 98
5	Me	Bn	86	84
6	Me	vinyl	89	98
7	Me	Cy	85	98
8	Me	Pr^{i}	80	85
9[c]	Me	Bu^{t}	—	—
10[c]	Pr^{i}	Ph	39	96

[a] Determined by HPLC using a Chiralcel OD (entries 5, 6, 7, 8), Chiralcel OJ (entries 1, 2, 10) or Chiralpack AS column (entry 3) with different mixtures of *n*-hexane–EtOH as the mobile phase. The optical purity of *S*-methyl-*S*-naphthyl-*N*-tosylsulfimide (entry 4) was obtained by ^{1}H NMR analysis using $Eu(tfc)_3$. [b] For 1 h at 0 °C. [c] For 8 h at 25 °C.

Table 2 Chemical yields and ees for nucleophilic displacement reactions on diastereoisomers **4a** and **4b**

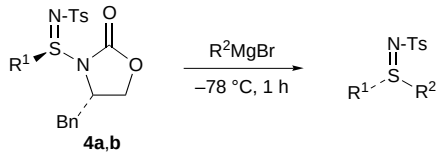

4a,**b**

Entry	R^1	R^2	Yield (%)	Ee (%)[a]
1	Me	Ph	88	85
2[b]	Me	Ph	69	83
3	Me	*p*-tolyl	91	94 (*S*)
4	Me	2-naphthyl	72	> 98
5	Me	Bn	87	92
6	Me	vinyl	92	98
7	Me	Cy	84	96
8	Me	Pr^i	84	88
9[c]	Me	Bu^t	—	—
10[c]	Pr^i	Ph	40	78

[a] Determined by HPLC using a Chiralcel OD (entries 5, 6, 7, 8), Chiralcel OJ (entries 1, 2, 10) or Chiralpack AS columns (entry 3) with different mixtures of *n*-hexane–EtOH as the mobile phase. The optical purity of *S*-methyl-*S*-naphthyl-*N*-tosylsulfimide (entry 4) was obtained by ^{1}H NMR analysis using $Eu(tfc)_3$. [b] For 1 h at 0 °C. [c] For 8 h at 25 °C.

olidinones, which are configurationally unstable at the sulfur atom.[6] This could explain the high imidation stereoselectivity with respect to overall chemical yield.

Increasing the steric hindrance at the sulfur atom in diastereoisomers **3b** and **4b** affected the yield but not the ee of the sulfimides formed (Table 1, entries 1, 10; Table 2, entries 1, 10), thus extending this methodology to *S*-alkyl-*S*-[(4*S*)-4-benzyl-2-oxo-1,3-oxazolidin-3-yl]-*N*-tosylsulfimides having *S*-alkyl substituents other than methyl.

Diastereoisomer **3a** yielded *S*-methyl-*S*-*p*-tolyl-*N*-tosylsulfimide (Table 1, entry 2) with 87% ee and (*R*) absolute configuration according to the literature,[3] the opposite enantiomer [94% ee, (*S*)] being obtained from diastereoisomer **4a**. If we assume that the nucleophilic displacement occurred with inversion of configuration, as in the case of the *N*-sulfinyloxazolidinones,[6] the absolute configuration at the sulfur atom should be (*R*) for the diastereoisomer **3a** and (*S*) for the diastereoisomer **4a**.

In summary, this study represents a further example of the synthetic versatility of chiral oxazolidinones and describes a new approach to optically active sulfimides with good chemical yields and high ees.

Notes and References

† E-mail: colonna@imiucca.csi.unimi.it

‡ *Experimental procedure*: *S*-Methyl-*S*-[(4*S*)-4-benzyl-2-oxo-1,3-oxazolidin-3-yl]-*N*-tosylsulfimides **3a** and **4a** were prepared by adding chloramine T (1.1 equiv.) to *N*-(methylthio)oxazolidinone (ref. 6) (1 equiv.) and hexadecyltributylphosphonium bromide (0.05 equiv.) in toluene as solvent. After 4 h at room temperature, normal work-up afforded the diastereoisomers **3a** and **4a**. Purification by flash silica gel column chromatography (hexane–ethyl acetate 3 : 7) gave pure **3a** and **4a** in the ratio 2.3 : 1 (yield 80%.) Sulfimides were obtained by reacting diastereoisomers **3a** and **4a** (1 equiv.) with the Grignard reagents (2 equiv.) at −78 °C for 1 h in THF as solvent (ref. 6) and purification by flash silica gel column chromatography (Et_2O–MeOH 9 : 1). Diastereoisomers **3b** and **4b** were prepared in an analogous way and obtained in the ratio 1.3 : 1 (yield 72%). MeS–SO_2Me was purchased from Aldrich, and Pr^iS–SO_2Me was prepared according to the literature (ref. 7).

1 T. L. Gilchrist and C. J. Moody, *Chem. Rev.*, 1977, **77**, 409.
2 P. C. Baird and P. C. Taylor, *J. Chem. Soc., Chem Commun.*, 1995, 893.
3 D. J. Cram, J. Day, D. R. Rayner, Don M. von Schriltz, D. J. Duchamp and D. C. Garwood, *J. Am. Chem. Soc.*, 1970, **92**, 7369.
4 H. Takada, Y. Nishibayashi, K. Ohe and S. Uemura, *Chem Commun.*, 1996, 931. H. Takoda, Y. Nishibayashi, K. Ohe, S. Uemura, C. P. Baird, T. J. Sparey and P. C. Taylor, *J. Org. Chem.*, 1997, **62**, 6512.
5 D. J. Ager, I. Prakash and D. R. Schaad, *Aldrichim. Acta*, 1997, **30**, 3.
6 D. A. Evans, M. M. Faul, L. Colombo, J. J. Bisaha, J. Clardy and D. Cherry, *J. Am.Chem. Soc.*, 1992, **114**, 5977.
7 M. D. Bentley, I. B. Douglass and J. A. Lacadie, *J. Org. Chem.*, 1972, **37**, 633.

Received in Liverpool, UK, 15th December 1997; 7/08977E

Chlorine abstraction by laser pyrolysis of $W(CO)_6$; a mild route to gas-phase organic radical chemistry

Grant R. Allen, Noel D. Renner and Douglas K. Russell*†

Department of Chemistry, University of Auckland, Private Bag 92019, Auckland, New Zealand

SF_6-photosensitised IR laser pyrolysis of $W(CO)_6$ in the gas phase at moderate temperatures leads to unsaturated $W(CO)_n$ species; these prove to be very effective and selective abstractors of Cl atoms from a wide range of organic substrates, and offer a low energy and clean route into gas phase organic radical chemistry.

IR laser powered homogeneous pyrolysis (LPHP)[1,2] has been successfully exploited for over 20 years in the investigation of the mechanisms of thermal decomposition of volatile organometallic[3] and organic compounds.[4] In IR LPHP, the vapour of the target species is mixed with SF_6, and the mixture exposed to the output of a CO_2 IR laser. The SF_6 strongly absorbs the laser energy, which is rapidly converted to heat *via* efficient intra- and inter-molecular relaxation.[2] The advantages of this technique are well documented; very small quantities of material are required, initiation of reaction is unambiguously homogeneous and short-lived intermediates are readily trapped (physically or chemically). Progress of reaction may be monitored by conventional analytical techniques, in the present work FTIR spectroscopy or GC–MS. The pyrolysis of many organochlorine compounds has been studied using IR LPHP, principally by Pola.[5] As in conventional pyrolysis, the chemistry of these compounds is dominated by the themes of HCl elimination (where available) and C–Cl bond homolysis.

LPHP of $W(CO)_6$ at much lower laser powers (*i.e.*, temperatures) than those required for the organochlorine compounds described below leads to copious amounts of CO and a grey deposit, shown elsewhere to be more or less pure tungsten.[6] It is usually assumed that these products result from the successive homolytic loss of carbonyl groups. In the presence of vapours of chlorinated organic compounds, the deposits also contain chlorine, XPES and reflectance IR spectroscopy indicating a composition approximating to $W(CO)_4Cl_2$. It appears, therefore, that unsaturated $W(CO)_n$ (n < 6) species are highly efficient abstractors of Cl from such compounds. Where the target compound contains both Cl and F, abstraction of Cl occurs preferentially, in accord with the relative strengths of W–X and C–X bonds.[7] Moreover, the secondary product of the $W(CO)_6$ (namely CO) is chemically inert, and highly reactive Cl atoms are effectively removed from the system. These factors lead to end products that may be ascribed unambiguously to subsequent reactions of the resultant organic radicals. Here, we report preliminary results using simple and familiar systems which confirm this point of view, and which illustrate the potential of this route into gas phase organic radical chemistry.

The thermal decomposition of the refrigerant CF_2HCl (Freon 22) has been extensively studied by both conventional methods and IR LPHP in the light of its role in destruction of stratospheric ozone.[1,8] In all cases, the observed products were HCl and C_2F_4, with further breakdown of the latter at higher temperatures. This has been ascribed to unimolecular elimination of HCl followed by recombination of the resultant difluorocarbene $:CF_2$. In the present work, the $:CF_2$ intermediate was detected directly by IR spectroscopy in an Ar matrix (dilution 100 : 1). At 15 K, a strong peak at 1220 cm^{-1} attributable to CF_2 was observed; on annealing to 40 K, this peak decayed, to be replaced by two assignable to C_2F_4 at 1178 and 1328 cm^{-1}. On co-pyrolysis with $W(CO)_6$ at much lower laser power (*i.e.*, temperature), the major products were SiF_4 and 1,1,2,2-tetrafluoroethane; no traces of HCl or C_2F_4 (or its breakdown products) were detected. These results are consistent with the selective abstraction of Cl to yield the $\cdot CF_2H$ radical; this either recombines or migrates to the cell wall, where reaction with silica results in the observed SiF_4. The decomposition of CF_2Cl_2 (Freon 12) and CH_2Cl_2 led to corresponding results, in particular the production of 1,2-dichlorotetrafluoroethane in copyrolysis of the former, and of 1,2-dichloroethane in the latter. Neither of these compounds is a major product in conventional pyrolysis, as a result of competing elimination processes and extensive secondary reactions.

The series of halogenated acetic acids provides an interesting example of a change in pyrolysis mechanism down a series.[9] Decarbonylation of the intermediate oxiranone formed by elimination of HCl from CH_2ClCO_2H yields formaldehyde, CO and HCl as the observed end products. On the other hand, C–I homolysis in CH_2ICO_2H, followed by a hydrogen shift and decarboxylation, results in CH_4 and CO_2 as the stable products; CH_2BrCO_2H follows both routes concurrently. On co-pyrolysis with $W(CO)_6$ at very low temperatures, CH_2ClCO_2H also yields the radical abstraction end-products CH_4 and CO_2. Similarly, IR LPHP of CH_3COCl alone largely follows the HCl elimination pathway, yielding the ketene observed in conventional pyrolysis.[10] Low temperature co-pyrolysis with $W(CO)_6$ completely suppresses formation of ketene, resulting instead in the CH_4 and CO characteristic of the radical route. These results are illustrated in Fig. 1.

The IR LPHP of 1,2-dichloroethene has been studied by Kubat and Pola,[11] with the conclusion that pyrolysis at low temperature leads to *Z*–*E* isomerisation; at higher laser power, this is followed by elimination of HCl yielding chloroacetylene (and, to a small extent, of Cl_2 to yield acetylene). In the present work, a sample of the slightly less stable *E*-1,2-$C_2H_2Cl_2$ alone was initially exposed to low laser power to yield an approximately equimolar mixture of the *Z* and *E* isomers. $W(CO)_6$ was then admitted to the cell, and further IR LPHP at powers insufficient to lead to further isomerisation led to decay of IR features of the two isomers at different rates. The first-order kinetic plots of Fig. 2 are consistent with reactions whose

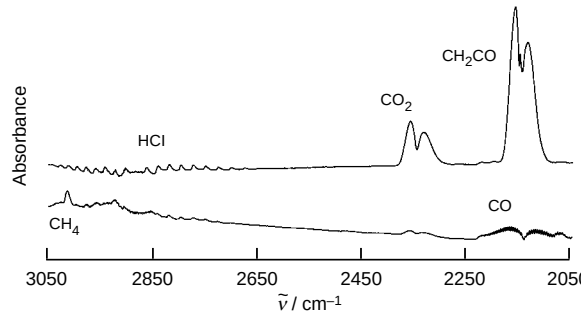

Fig. 1 Partial FTIR spectra of the products of laser pyrolysis of CH_3COCl in the absence (upper) and presence (lower) of $W(CO)_6$; the small amount of HCl evident in the lower trace was present in the original sample

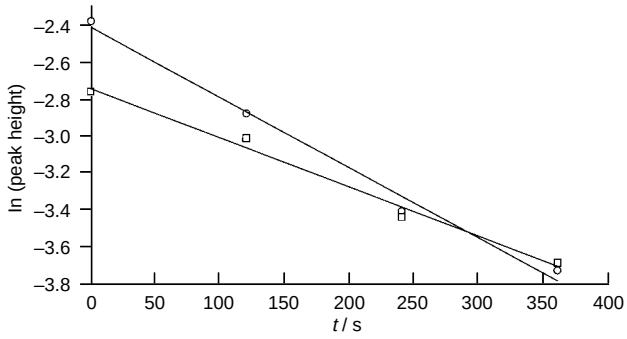

Fig. 2 First-order kinetic plots for the decay of *E*-1,2-$C_2H_2Cl_2$ (○) and *Z*-1,2-$C_2H_2Cl_2$ (□) on laser pyrolysis in the presence of $W(CO)_6$

activation energies differ by the known zero point energy difference[12] of 1840 J mol^{-1}, and an effective temperature of 650 ± 150 K. This 'kinetic isomer effect' suggests that loss reactions of the two isomers involve Cl abstraction pathways whose transition states differ little in energy.

The above preliminary results confirm that $W(CO)_n$ species do indeed act as efficient and selective abstractors of Cl from a range of organochlorine compounds under comparatively mild conditions, and that the subsequent chemistry is dominated by the resulting organic radical species. In this sense, this system may serve as a gas phase analogue of well known solution abstractors such as tri-*n*-butyltin[13] and tris(trimethylsilyl)silyl.[14] In future work, we shall investigate more complex systems; preliminary results on chlorinated xylenes, for example, have already indicated that substantially new reaction routes are opened in such species.[15]

We thank the University of Auckland for assistance with the purchase of equipment and a doctoral scholarship to G. R. A.

Notes and References

† E-mail: d.russell@auckland.ac.nz

1 W. M. Shaub and S. H. Bauer, *Int. J. Chem. Kinet.*, 1975, **7**, 509.
2 D. K. Russell, *Chem. Soc. Rev.*, 1990, **19**, 407; *Chem. Vap. Deposition*, 1996, **2**, 223.
3 A. S. Grady, R. D. Markwell and D. K. Russell, *J. Chem. Soc., Chem. Commun.*, 1991, 929; R. E. Linney and D. K. Russell, *J. Mater. Chem.*, 1993, **3**, 587; D. K. Russell, I. M. T. Davidson, A. M. Ellis, G. P. Mills, M. Pennington, I. M. Povey, J. B. Raynor, S. Saydam and A. D. Workman, *Organometallics*, 1995, **14**, 3717.
4 H. Hettema, N. R. Hore, N. D. Renner and D. K. Russell, *Aust. J. Chem.*, 1997, **50**, 363; N. R. Hore and D. K. Russell, *J. Chem. Soc., Perkin Trans. 2*, 1998, 269.
5 J. Pola, *Spectrochim. Acta, Part A*, 1990, **46**, 607.
6 K. E. Lewis, D. M. Golden and G. P. Smith, *J. Am. Chem. Soc.*, 1986, **106**, 3905.
7 *CRC Handbook of Chemistry and Physics*, ed. R. C. Weast, CRC Press Inc., Roca Baton, FL, 60th edn., 1979, p. F220.
8 S. S. Kumaran, K. P. Lim, J. V. Michael, M. C. Su and A. F. Wagner, *J. Phys. Chem.*, 1996, **100**, 15827 and references therein.
9 H. Hettema, N. R. Hore, N. D. Renner and D. K. Russell, *Aust. J. Chem.*, 1997, **50**, 363.
10 H. Bock, T. Hirabayashi, S. Mohmand and B. Solouki, *Angew. Chem., Int. Ed. Engl.*, 1977, **16**, 105; V. R. Stimson and J. W. Tilley, *Aust. J. Chem.*, 1977, **30**, 81.
11 P. Kubat and J. Pola, *Z. Phys. Chem.*, 1987, **268**, 849.
12 N. C. Craig, L. G. Piper and V. L. Wheeler, *J. Phys. Chem.*, 1971, **75**, 1453.
13 W. P. Neumann, *Synthesis*, 1987, 665.
14 C. Chatgilialoglu, *Acc. Chem. Res.*, 1992, **25**, 188.
15 G. R. Allen and D. K. Russell, unpublished work.

Received in Exeter, UK, 4th December 1997; 7/08737C

Two-step phosphorus-mediated substitution of hydroxy groups in selected primary alcohols for fluorinated alkyl or aryl substituents: the molecular structure of 1,1-bis(fluorosulfonyl)-1-fluoro-2-phenylethane

Alexander Kolomeitsev,*[a] Alexander Shtarev,[a] Kyrill Chabanenko,[a] Tatjana Savina,[a] Yurii Yagupolskii,[a] Michaela Görg,[b] Jan Przyborowski,[b] Enno Lork[b] and Gerd-Volker Röschenthaler*[b]†

[a] *Institut of Organic Chemistry, Ukrainian National Academy of Sciences, Murmanskaya 6, Kiev-94, 253660, Kiev, Ukraine*
[b] *Institut für Anorganische und Physikalische Chemie, Universität Bremen, Leobener Strasse, D-28334, Bremen, Germany*

In an Arbuzov type reaction, amido phosphites $(Et_2N)_2POR^1$ and a broad range of halofluoro organic halides (X = Cl, Br) formed the corresponding alkylated derivatives R^1–R^2 [R^1 = Bn, R^2 = $C(SO_2F)_3$, CCl_2F, CCl_2CF_3, CBr_2F, $C(CF_3)_3$, C_6F_5; R^1 = Et, CH_2CF_3, Me, R^2 = CCl_2CF_3], whereas with $FC(SO_2F)_3$ and loss of SO_2, $BnCF(SO_2F)_2$ was obtained, as shown by X-ray crystallography.

Owing to the chemical and biological properties of organofluorine compounds,[1] considerable efforts have been made to find new reagents and methods for the fluorination of alcohols, oxy acids and glucosides. Nucleophilic fluoroalkylation is one of the most attractive routes for introducing fluorinated moieties.[2] However, to the best of our knowledge, there are no methods for substituting oxy groups in alcohols (directly or using their corresponding tosylates or triflates) for fluorinated carbon-centered anions. Phosphorus-containing reagents, *e.g.* the three component system $CF_3Br/P(NEt)_3$/electrophile or trifluoromethyl tris(dialkylamino)phosphonium salts,[3] have proven to be versatile reactants for trifluoromethylation of a variety of organic and organoelement compounds, *e.g.* Me_3SiCF_3, in its turn a powerful CF_3 transfer agent, too.[3,4] As we have recently shown, the phosphitylation of alcohols and oxy acid esters with $(Et_2N)_2PCl$, followed by the low temperature reaction of $(CF_3S)_2$ with the diamido phosphites formed, is an effective route for addition of the lipophilic SCF_3 moiety to sp^3-hybridized carbon atoms under mild reaction conditions;[5] in the case of CCl_4 and some Cl_3C group-containing species, trichloromethylated alkanes, 1,1-dichloromethyl esters and 1,1-dichloroethyl substituted phosphines were obtained.[6–8] Our preliminary results show that the reaction of $(Et_2N)_2POR^1$ (R^1 = Bn) with $XC(SO_2F)_3$ (X = F, Cl), X_3CF (X = Cl, Br), Cl_3CCF_3 and $BrC(CF_3)_3$, BrC_6F_5, and of $(Et_2N)_2POR^1$ (R^1 = Et, CH_2CF_3, Me) with Cl_3CCF_3 is a novel, convenient and generally applicable method for a two step substitution of hydroxy groups in primary alcohols for wide range of different fluorinated species; respective literature syntheses give fairly different and preparatively demanding approaches with low yields, *e.g.* $MeC(SO_2F)_3$ has been synthesized from MeI and $AgC(SO_2F)_3$,[9] $BnCCl_2CF_3$ by electrochemical cross-coupling,[10] $MeCCl_2CF_3$ from 2,2-dichloropropionic acid and SF_4,[11] $EtCCl_2CF_3$ and $CF_3CH_2CCl_2CF_3$ have been prepared photolytically,[12,13] and $BnC(CF_3)_3$ has been prepared from 1,1,3,3,3-pentafluoro-2-trifluoromethylpropene, CsF and $PhCHCl_2$.[14] For BnC_6F_5, BnCl and pentafluorobenzoyl chloride were required.[15]

In a superior general alternative to the already known methods, mentioned above, bis(diethylamido) phosphites, $(Et_2N)_2POR^1$, **1** (R^1 = Bn)[5] and the fluoro species $ClC(SO_2F)_3$ **2a**,[9] CCl_3F **2b**, CCl_3CF_3 **2c**, CBr_3F **2d**, $BrC(CF_3)_3$ **2e** and BrC_6F_5 **2f** underwent an Arbuzov type reaction to give in good yields R^1–R^2 **4a–f** [R^1 = Bn, R^2 = $C(SO_2F)_3$ (**4a**), CCl_2F (**4b**) CCl_2CF_3 (**4c**), CBr_2F (**4d**), $C(CF_3)_3$ (**4e**), C_6F_5 (**4f**)] and the corresponding halogeno amidates, $(Et_2N)_2P(O)X$ (X = Cl, Br),‡ (see Table 1). Gaseous SO_2 was formed when $FC(SO_2F)_3$ **3** was allowed to interact with **1** yielding $BnCF(SO_2F)_2$ **5**§ and $(Et_2N)_2P(O)F$. (Scheme 1) Reacting $(Et_2N)_2POR^1$ (R^1 = Et (**6**), CH_2CF_3 (**8**),[16] Me (**10**)] with **2c** gave the corresponding alkanes R^1–CCl_2CF_3 [R^1 = Et (**7c**),[12] CH_2CF_3 (**9c**),[13] Me (**11c**)[11]]. The products, either colorless liquids or low melting point solids, were easily separated from the phosphorus-containing substances by distillation or column chromatography on silica. The fluoro species R^1–$C(SO_2F)_3$ **4a**, R^1–CCl_2F **4b**, R^1–CBr_2F **4d** and R^1–$CF(SO_2F)_2$ **5** (R^1 = Bn) have not been described previously.¶ THF or triglyme were required as solvent; however, in the case of $XC(SO_2F)_3$ (X = F, Cl)[9] the reaction exclusively proceeds in aprotic, non-polar media, such as pentane. If *no* solvent is used, either no reaction occurs or products with P–C bond formation were obtained.[17]

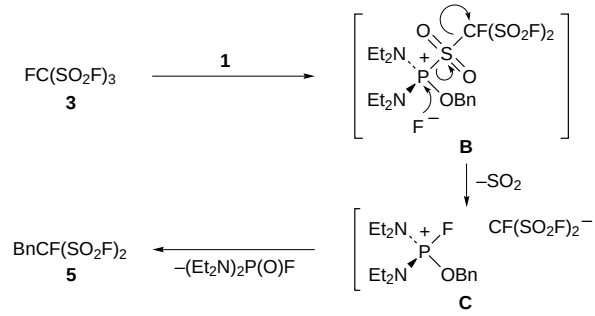

Scheme 1

It is possible that, in a two step Arbuzov reaction *via* halogenophilic attack of phosphorus at R²–X (X = Cl, Br),

Table 1 Preparation of R^1–R^2

Reactants $R^1OP(NEt_2)_2/R^2$–X[a]	Product R^1–R^2	Yield (%)
1/2a	**4a**[b,c]	80
1/2b	**4b**[b,d]	40
1/2c	**4c**[b,d]	90
1/2d	**4d**[b,d]	40
1/2e	**4e**[b,e]	81
1/2f	**4f**[d,f]	80
1/3	**5**[b,d]	86
6/2c	**7c**[b,d]	80
8/2c	**9c**[b,d]	70
10/2c	**11c**[b,e]	85

[a] $R^1OP(NEt_2)_2$ (10 mmol) in 10 ml solvent was added to a 10 ml solution of R^2–X (10 mmol), cooled to −50 to −78 °C within 5 min. [b] Reaction time: 15–30 min at −50 to −78 °C. [c] In pentane. [d] In THF. [e] In triglyme. [f] Reaction time: 90 min at −50 to −78 °C.

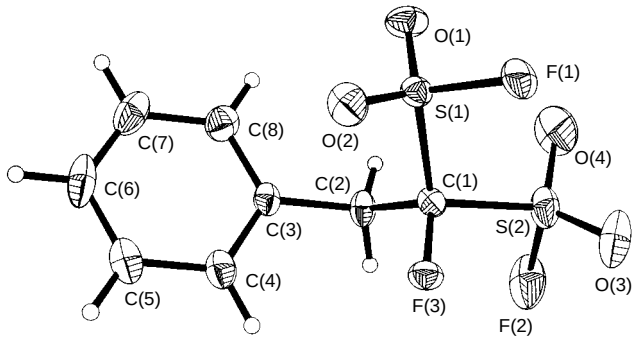

Fig. 1 Crystal structure of **5** with thermal ellipsoids. Selected bond distances (pm) and angles (°): C(1)–S(1) 183.8(3), C(1)–S(2) 183.3(3), C(1)–C(2) 151.5(4), C(2)–C(3) 151.7(4), C(3)–C(4) 138.3(4), S(1)–O(1) 140.5(1), S(2)–O(3) 141.8(2), S(1)–F(1) 154.7(2), S(2)–F(2) 152.0(2), C(1)–F(3) 137.3(3); C(2)–C(1)–S(1) 110.7(2), C(2)–C(1)–S(2) 111.8(2), F(3)–C(1)–C(2) 112.1(2), C(1)–C(2)–C(3) 114.3(2), F(3)–C(1)–S(1) 105.7(2), F(3)–C(1)–S(2) 106.2(2), S(2)–C(1)–S(1) 110.1(2), O(1)–S(1)–F(1) 107.02(12), O(3)–S(2)–F(2) 106.9(2), O(1)–S(1)–O(2) 122.36(14), O(4)–S(2)–O(3) 121.0(2), F(1)–S(1)–C(1) 100.51(12), F(2)–S(2)–C(1) 98.49(12).

unstable quasi-phosphonium intermediates $[(Et_2N)_2P(OR^1)X]^+$ $[R^2]^-$ **A** are formed, which in turn yield R^1–R^2 and $(Et_2N)_2P(=O)X$. For the reaction of **3** with **1**, a halogenophilic pathway seemed unlikely. However, the λ^3,σ^3 phosphorus nucleophile might attack sulfur (intermediate **B**) displacing a fluoride anion, which induced loss of SO_2 (intermediate **C**) and the proposed formation of $[CF(SO_2F)_2]^-$ (Scheme 1). Despite being the conjugated base of super acid (pK_a −12),[18] the tris(fluorosulfonyl)methanide anion[19] was able to be alkylated under mild conditions in pentane. Attempts to react this anion, as tetrabutylammonium tris(fluorosulfonyl)methanide, with alkyl tosylates and BnBr failed, even at elevated temperature.[18] The intermediate **A** probably exists as a tight ion pair, which facilitates the trapping of the incipient $[C(SO_2F)_3]^-$ anion *via* an intramolecular Arbuzov rearrangement. In THF or triglyme no methanide alkylation could be observed. In the case of $BrC(CF_3)_3$ **2e**, no perfluorobutene or its reaction products were found. No substitution of fluorine in the C_6F_5 moiety occurred. With C_6F_5Br **2f** the reaction was slower and accompanied by C_6F_5H formation, originating from the interaction of the corresponding anion with the solvent.[17] A concerted mechanism with λ^5,σ^5 phosphorane intermediates or a radical pathway could not be ruled out.[20]

The single crystal X-ray structure determination§ of **5** (Fig. 1), the first carried out on an alkyl derivative of $HCF(SO_2F)_2$, showed a slightly distorted tetrahedral geometry at C(1) bearing the SO_2F groups and C(2). The bond length of C(1)–S(1) corresponds to a single bond,[9] and the bond lengths C(1)–F(3), C(1)–C(2), C(2)–C(3), C(3)–C(4), S(1)–O(1) and S(1)–F(1) are all in the expected ranges.[21]

The outlined synthetic approach for introducing carbon-centered anions with a broad range of nucleophilicity to the sp^3-hybridized carbon of BnOH can be considered a simple alternative, superior to already known procedures. Preliminary positive results for EtOH, CF_3CH_2OH and MeOH promise extension of the procedure to various alkanes $R^FCCl_2(Br_2)CH_2R$, which, when successively dehydrohalogenated, offer an easy access to fluoroalkylated alkenes $R^FCCl(Br)=CHR$ and alkynes $R^FC\equiv CR$, which are in turn building blocks for fluoro heterocycles and other versatile precursors.[22]

We acknowledge financial support of the Deutsche Forschungsgemeinschaft for A. A. K. J. Ortlam is thanked for his assistance in compound preparation.

Notes and References

† E-mail: jl8j@zfn.uni-bremen.de

‡ All new compounds gave satisfactory elemental analyses and mass spectra.

§ *Crystal data* for **5**: $C_8H_7F_3O_4S_2$, M = 288.3, orthorhombic, space group *Pbca*, a = 1010.7(3), b = 1100.5(2), c = 1984.7(3) pm, V = 2.2075(8) nm^3, Z = 8, D_c = 1.735 Mg m^{-3}, λ(Mo-Kα) = 71.073 pm, Siemens P4 m/v diffractometer, θ region 2.88 ⩽ θ ⩽ 27.51°, T = 173(2) K; 3323 reflections collected, 2536 independent (R_{int} = 0.0485), full-matrix least-squares refinement at F^2 (SHELXL 93); goodness of fit on F^2 0.857, final R-values [$I > 2\sigma(I)$] $R1$ = 0.0461, wR_2 = 0.0978; R-values (all data) $R1$ = 0.0847, wR_2 = 0.1065, extinction coefficient 0.0065(7), difference electron density 422 and −494 e nm^{-3}. CCDC 182/767.

¶ *Selected data* for **4a**: mp 86–87 °C; δ_H 4.2 (CH_2, 2 H, $^3J_{HF}$ 1.9), 7.3 (C_6H_5, 5 H); δ_F 65.7 (SO_2F). For **4b**: bp 102–103 °C/0.05 mbar; δ_H 3.7 (CH_2, 2 H, $^3J_{HF}$ 17.0), 7.3 (C_6H_5, 5 H); δ_F −55.8. For **4d**: bp 125 °C/14 mbar; δ_H 3.9 (CH_2, 2 H, $^3J_{HF}$ 18.0), 7.3 (C_6H_5, 5 H); δ_F − 52.1. For **5**: mp 34–35 °C; δ_H 3.9 (CH_2, 2 H, $^3J_{HF}$ 23.6, $^4J_{HF}$ 1.9), 7.3 (C_6H_5, 5 H); δ_F 51.2 (SO_2F, 2 F, $^3J_{FF}$ 3.7), −139.8 (1 F).

1 J. T. Welch and S. Eswarakrishnan, *Fluorine in Bioorganic Chemistry*, Wiley, New York, 1991; *Organofluorine Compounds in Medicinal Chemistry and Biomedical Applications*, ed. R. Filler, Y. Kobayashi and L. M. Yagupolskii, Elsevier, Amsterdam, 1993.
2 G. K. Surya Prakash and A. K. Yudin, *Chem. Rev*., 1997, **97**, 757; M. Yoshida, D. Suzuki and M. Iyoda, *J. Chem. Soc., Perkin Trans. 1*, 1997, 643; F. Hong and C.-M. Hu, *Chem. Commun*., 1996, 57.
3 I. Ruppert, K. K. Schlich and W. Volbach, *Tetrahedron Lett*., 1984, **25**, 2195.
4 A. N. Chernega, A. A. Kolomeitsev, Yu. L. Yagupolskii, A. Gentzsch and G.-V. Röschenthaler, *J. Fluorine Chem.*, 1995, **70**, 271.
5 A. A. Kolomeitsev, K. Y. Chabanenko, G.-V. Röschenthaler and Yu. L. Yagupolskii, *Synthesis*, 1994, 145.
6 V. S. Abramov and N. A. Il'ina, *Zh. Obshch. Khim*., 1971, **41**, 100.
7 J. H. Hargis and W. D. Alley, *J. Am. Chem. Soc.*, 1974, **96**, 5927.
8 A. P. Marchenko, G. N. Kojdan, G. O. Baram, A. N. Chernega and A. N. Pinchuk, *Zh. Obshch. Khim*., 1994, **64**, 821.
9 G. Klöter, H. Pritzkow and K. Seppelt, *Angew. Chem*., 1980, **92**, 954.
10 J. Y. Nedelec, H. Ait-Haddou-Mouloud, J. C. Folest and J.Perichon, *Tetrahedron Lett*., 1988, **29**, 1699.
11 W. Dmowski and R. Kolinski, *Rocz. Chem*., 1973, **47**, 1211.
12 X.-Z. Qin, Q.-C. Meng and F. Williams, *J. Am. Chem. Soc*., 1987, **109**, 6778.
13 R. N. Haszeldine and F. Nyman, *J. Chem. Soc*., 1959, 387.
14 W. B. Farnham and J.C. Calabrese, *J. Am. Chem. Soc*., 1986, **108**, 2449.
15 *Synthesis of Fluoroorganic Compounds*, ed. I. L. Knunyants and G. G. Yakobson, Springer, Berlin, 1985, p. 129.
16 M. Görg, A. A. Kolomeitsev and G.-V. Röschenthaler, *Phosphorus Sulfur Silicon Relat Elem.*, in the press.
17 A. A. Kolomeitsev and G.-V. Röschenthaler, unpublished results.
18 Yu. L. Yagupolskii, T. I. Savina, N. V. Pavlenko, A. A. Pankov and S. V. Pazenok, *Zh. Obshch. Khim.*, 1991, **61**, 1512.
19 N. S. Zefirov and D. I. Makhon'kov, *Chem. Rev*., 1982, **82**, 615.
20 A. K. Bhattacharya and G. Thyargarayan, *Chem. Rev*., 1981, **81**, 415; J. Michalski, A. Skowronska and R. Bodalski, in *Phosphorus-31 Spectroscopy in Stereo-chemical Analysis*, ed. J. G. Verkade and L. D. Quin, VCH, Deerfield Beach, 1987, p. 255.
21 *International Tabels for Crystallography, Vol. C*, ed. A. J. C. Wilson, Kluwer, Dordrecht, 1995, p. 691.
22 M. Van Der Puy, *J. Fluorine Chem*., 1997, **81**, 187; J. E. Bunch and C. L. Bumgardner, *ibid*, 1987, **36**, 313; W. Dmowski, *ibid*, 1985, **29**, 287; M. Makosza, H. Plienkiewicz, *ibid*, 1984, **24**, 387; Y. Kobayashi, T. Yamashita, K. Takahashi, H. Kuroda and I. Kumadaki, *Tetrahedron Lett*., 1982, **23**, 343; H. F. Koch, W. Tumas and R. Knoll, *J. Am. Chem. Soc*., 1981, **103**, 5323; L. M. Yagupolskii and Y. A. Filyakov, *Zh. Obshch. Khim*., 1960, **30**, 1291.

Received in Cambridge, UK, 28th October 1997; 7/07757B

Synthesis and crystal structure determination of sodium ozonide

Wilhelm Klein, Klaus Armbruster and Martin Jansen*†

Institut für Anorganische Chemie der Rheinischen Friedrich-Wilhelms-Universität Bonn, Gerhard-Domagk-Straße 1, 53121 Bonn, Germany

So-far-unknown ionic ozonides are accessible by a new method of synthesis; the new binary compound NaO_3 crystallizes isostructural to $NaNO_2$.

Recently, the alkali metal ozonides KO_3,[1] RbO_3[2] and CsO_3[3] have become available as bulk and pure materials, and a generally applicable route for the syntheses of ionic ozonides with relatively bulky organic group-15-'onium' cations has been developed.[4] All ozonides known so far are metastable and decompose *via* exothermal reactions.[5] Within the group of the alkali metal ozonides the stability decreases with decreasing diameter of the respective cation. As a consequence, unlike KO_3, RbO_3 and CsO_3, the lithium and sodium ozonides are not accessible *via* direct ozonisation of their peroxides or hyperoxides. However, solutions of LiO_3 and NaO_3 in liquid ammonia can be obtained by ion exchange. From these solutions the solid ozonides Li[2.2.1]O_3 and Na[2.2.2]O_3 precipitate after complexation of the cations by the appropriate cryptands.[6] In the absence of a cryptand, NaO_3 decomposes into a mixture of solid NaOH and NaO_2 upon removing the solvent. Presumably, in an initial step a proton is transferred to the ozonide anion from ammonia, which shows an increased acidity because of its coordination to the smaller and thus more strongly polarizing sodium cation, compared to K^+, Rb^+ and Cs^+. In order to circumvent this complication, we have added methylamine, which, being a stronger base than ammonia, would be the preferred ligand for the coordination of sodium, and at the same time, is less proton acidic. When evaporating the solvent mixture at −78 °C, first ammonia is removed, and upon increasing the temperature slowly up to −20 °C, pure sodium ozonide precipitates. The intensively red, air sensitive polycrystalline samples decompose slowly at room temperature into solid NaO_2 and oxygen. However, at a temperature of −18 °C, NaO_3 can be stored undecomposed for months. Surprisingly, the temperature at which rapid spontaneous decomposition starts is slightly higher for NaO_3 (37 °C) than for KO_3 (35 °C).[1]

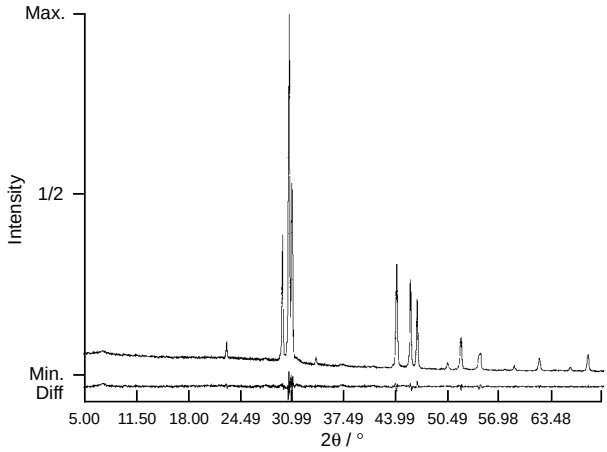

Fig. 1 Measured and calculated powder diffraction pattern of sodium ozonide and difference plot

According to a crystal structure determination by Rietveld's technique of refinement of X-ray powder data[7] (Fig. 1), NaO_3 is isostructural to sodium nitrite.‡ Thus, sodium ozonide is the first alkali metal ozonide exhibiting a ferroelectric arrangement of the anions. Generally, the crystal structure of NaO_3 can be related to the rock salt type of structure (*cf.* Fig. 2), each sodium being surrounded octahedrally by six ozonide groups. However, six negatively polarized terminal oxygen atoms belonging to only five complex anions coordinate sodium at a distance (242–244 pm) as would be expected for the first coordination sphere[8–10] (*cf.* Fig. 3). The ozonide ion exhibits the longest O–O bonds and the smallest O–O–O angle that have been seen so far. The newly determined data confirm the trend that with decreasing ionic radius of the cation the bond lengths increase and the bond angles decrease within the ozonide ion (see Table 1). Note that the differences among these values are rather close to the limits of experimental error. However, they are consistent with considerations based on Walsh's rules.[11] As in KO_3 (300.5

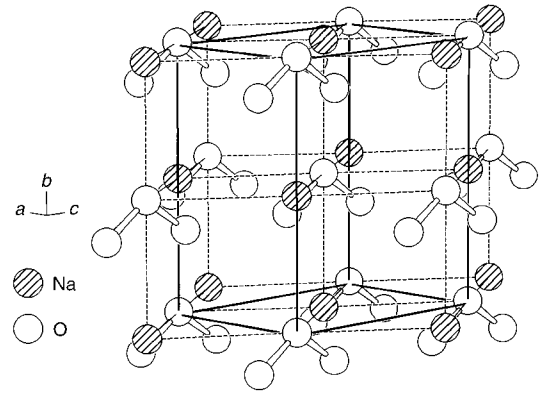

Fig. 2 Perspective view of the crystal structure of NaO_3. Bold lines: conventional unit cell, dashed lines emphasize the relation to the rock salt type of structure.

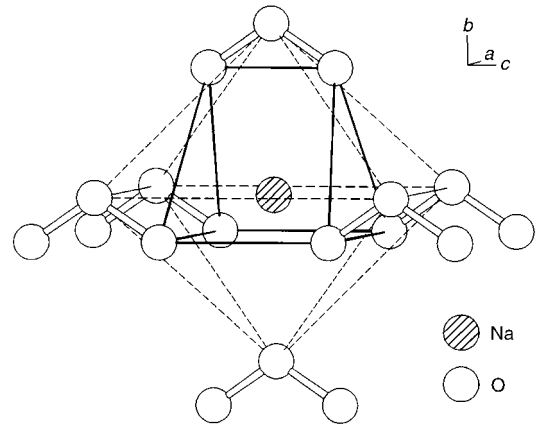

Fig. 3 Trigonal prismatic coordination of the sodium cation by six terminal oxygen atoms (bold lines), octahedral surrounding by six ozonide anions (dashed lines)

Table 1 Selected bond lengths and angles for ionic ozonides

	O–O/Å	O–O–O/°
NaO_3	135.3(3)	113.0(2)
KO_3[a]	134.6(2)	113.5(1)
RbO_3[a]	134.3(7)	113.7(5)
CsO_3[b]	133.3(9)	114.6(6)

[a] Ref. 2. [b] Ref. 13.

pm),[12] the shortest distances between different anions in NaO_3 are 301.5 pm. In contrast, for the first time the nearest oxygen atoms of different ozonide groups are terminal and negatively polarized,[13] instead of one terminal and one less negatively polarized bridging atom like in the other alkali ozonides.

Somewhat unexpectedly, the difficulties in preparing pure NaO_3 are not caused by its supposed higher intrinsic instability as compared with, *e.g.* KO_3, but probably by a stronger activation of ammonia with respect to a proton transfer when coordinated to sodium instead of potassium. Thus the synthesis method employed here might represent a general procedure for the synthesis of so far unknown ozonides. According to preliminary results $Ba(O_3)_2$ seems to be accessible *via* this novel route.

Notes and References

† E-mail: mjansen@snchemie2.chemie.uni-bonn.de

‡ X-Ray structure determination of NaO_3: space group *Im*2*m* (no. 44), a = 3.5070(2), b = 5.7703(3), c = 5.2701(3) Å, U = 106.777(1) Å^3, Z = 2, D_c = 2.2078 g cm^{-3}, X-ray scattering experiments were carried out on a Stoe Stadi P diffractometer with germanium monochromated Cu-Kα_1 radiation, small PSD, 2θ = 5–70°, T = −60 °C. The crystal structure was refined supposing the structure model of $NaNO_2$ with the CSD program package[7] by application of Rietveld method: no. of observed reflections 19, no. of parameters 8, Na, O(1) on 2a, O(2) on 4d, R_{int} = 0.0371, R_{prof} = 0.0922. Atomic parameters are listed in Table 2.

Table 2 Atomic parameters for NaO_3

	x	y	z	B_{eq}/Å^2
Na	0	0.5074(3)	0	2.20(5)
O(1)	0	0.0106(6)	0	4.97(8)
O(2)	0	−0.1189(3)	0.2139(4)	2.87(6)

1 W. Schnick and M. Jansen, *Rev. Chim. Miner.*, 1987, **24**, 446.
2 W. Schnick and M. Jansen, *Z. Anorg. Allg. Chem.*, 1986, **532**, 37.
3 M. Jansen and W. Assenmacher, *Z. Kristallogr.*, 1991, **194**, 315.
4 N. Korber and M. Jansen, *Chem. Ber.*, 1992, **125**, 1383.
5 W. Hesse, M. Jansen and W. Schnick, *Prog. Solid State Chem.*, 1989, **19**, 47.
6 N. Korber and M. Jansen, *Chem. Ber.*, 1996, **129**, 773.
7 L. G. Akselrud, J. N. Grin, P. Y. Zavalii, V. K. Pecharskii, V. S. Fundamenskii, CSD-Universal Program Package for Single Crystal and/or Powder Structure Data Treatment, 12. European Crystallographic Meeting, Collected Abstracts, Moskau, 1989, vol. 3, p. 155.
8 E. Zintl, A. Harder and B. Dauth, *Z. Elektrochem.*, 1934, **40**, 588.
9 R. L. Tallmann, J. L. Margrave and S. W. Bailey, *J. Am. Chem. Soc.*, 1957, **79**, 2979.
10 M. Ziegler, M. Rosenfeld, W. Kaenzig and P. Fischer, *Helv. Phys. Acta*, 1976, **49**, 57.
11 H. D. Walsh, *J. Chem. Soc.*, 1953, 2266.
12 W. Schnick and M. Jansen, *Angew. Chem., Int. Ed. Engl.*, 1985, **24**, 54.
13 T. Kellersohn, N. Korber and M. Jansen, *J. Am. Chem. Soc.*, 1993, **115**, 11 254.

Received in Cambridge, UK, 27th November 1997; 7/08570B

Response to steric constraint by d^{10} cations: an 'A-frame' disilver cryptate

Joanne L. Coyle,[a,b] Vickie McKee*[a]† and Jane Nelson*[a,b]†

[a] *School of Chemistry, Queens University, Belfast, UK BT9 5AG*
[b] *Chemistry Department, Open University, Milton Keynes, UK MK7 6AA*

A pair of silver(I) cations is accommodated within a small azacryptand which adopts an A-frame conformation, allowing both intra- and inter-cryptate bonding of silver cations.

In recent years we have successfully used the strategy of constraining copper ions within small azacryptand hosts in coordination geometry appropriate to overlap of d_{z^2} bonding orbitals, to generate, *via* one-electron oxidation of the dicopper(I) cryptates, metal–metal bonded dicopper cryptates of average-valence $Cu^{1.5}$ redox state.[1] This unprecedented copper–copper bond has unusual and possibly applicable spectroscopic and electrochemical properties.[1,2] The isomorphism observed between copper(I) and silver(I) cryptates elsewhere in our azacryptate series[3] encouraged us to examine the silver(I) analogues of the dicopper(I) precursors to see if similarly enforced proximity would generate delocalized metal–metal bonding in the disilver(I) pair on oxidation. This is of interest not just from the point of view of metal–metal bonding theory, but because higher redox states of silver may be of interest as replacements for chlorine-based oxidants for some specialist purposes. However, as the coordination geometry preferences of silver and copper are known to be different, a necessary first step was the structural characterisation of any disilver(I) cryptate isolated. Treatment of the free ligand imBT with silver perchlorate in either 1:2 or 1:1 stoichiometry resulted in the isolation of a pale yellow microcrystalline product $[Ag_2(imBT)][ClO_4]_2$ **2** which could be recrystallised from acetonitrile to generate X-ray quality crystals.

When copper(I) cations coordinate the tren-derived N_4 caps within the small azacryptand host imBT, steric constraint brings this pair of cations to within 2.45 Å[1] of each other, within the internuclear distance of *ca*. 2.56 Å in elemental copper. In the average-valence dicopper(1.5) state, this distance reduces only slightly, to 2.38 Å,[4] whereas within the larger (trispropylene capped) cryptate host, imbistrpn, the contraction in going from the dicopper(I) state to the average-valence $Cu^{1.5}{}_2$ state is sizeable (> 0.5 Å).[4] The lack of significant increase of internuclear distance on going to the dicopper(I) state within the imBT host suggests that the 2.45 Å separation is near the maximum achievable when the cryptand caps are used as coordination sites. As 2.45 Å would represent an improbably short Ag^I–Ag^I internuclear distance, isomorphism of polycrystalline $[Cu_2(imBT)][ClO_4]_2$ **1** and $[Ag_2(imBT)][ClO_4]_2$ **2** did not appear likely and was not, indeed, observed. Although, unexpectedly, CD_3CN solution ^1H NMR spectra of **1** and **2** show a good deal of similarity,[5] their solid state MAS NMR spectra[6] are quite different. The ^{13}C solid state NMR for **1** is simple, consistent with high symmetry of the cryptand conformation while for the disilver(I) analogue **2** it is complex, indicating lower symmetry for the cryptand host. The structure obtained by X-ray crystallography reveals the reason for these differences; the silver(I) cations have not chosen the 'pre-organised' N_4 site used by copper in its imBT, amBT and imbistrpn cryptates and adopted also in other, less constrained, disilver(I) cryptates.[7]

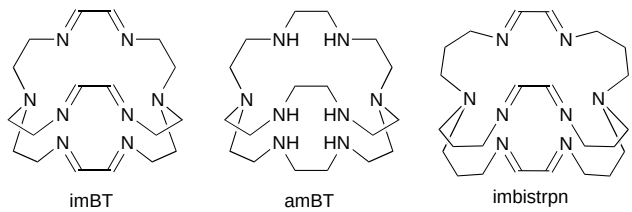

Fig. 1 illustrates the alternative site selected by Ag^I. The asymmetric unit contains two independent cations and four perchlorate anions. The cations are very similar to one another, differing only in the minor details of conformation in the cryptand strands. The Ag–Ag distances are 2.8314(8) and 2.8545(8) for Ag(1a)–Ag(2a) and Ag(1d)–Ag(2d) respectively. Two of the three strands act as bidentate diimine donors to a silver ion, while the third strand bridges the two silver ions. The bridgehead nitrogen atoms are not coordinated (Fig. 2) and the overall $N_{br}\cdots N_{br}$ distance is 6.05 Å, *vs.* 5.88 Å in **1**. The three

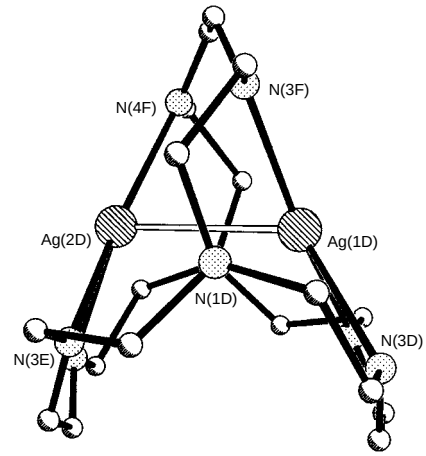

Fig. 1 View of the disilver(I) cryptate looking down the $N_{bridgehead}$ axis

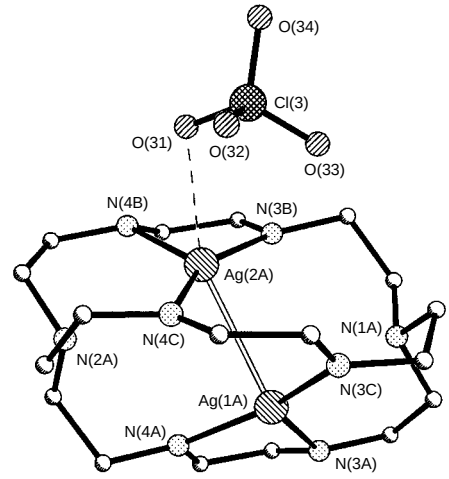

Fig. 2 View of the disilver cryptate looking sideways on to the $N_{bridgehead}$ axis. (One of the two very similar cations existing independently in the unit cell.)

imine donors take up an irregular trigonal geometry with the silver ion close to the mean plane of the nitrogen donors. The chelating diimine groups are necessarily restricted to a bite angle of *ca*. 72°. They are also asymmetric: one of the Ag–N distances is long (mean 2.405 Å) and the second is considerably shorter (mean 2.283 Å). The more tightly bound imine of the chelating imine group makes a large N–Ag–N angle [mean 158.6(2)°] with the third nitrogen donor, reflecting the preference of silver(I) for linear-based coordination.

The exposed position of the silver ions: on the outer surface of the ligand cage rather than cryptated along the main axis, allows interaction with the perchlorate anions. Ag(2a) and Ag(2d) form Ag–$OClO_3$ bonds of 2.681(6) and 2.731(5) Å, respectively while there are longer interactions with the remaining silver ions [Ag(1a)–O(22) 3.335, Ag(1d)–O(34) 3.087, Ag(2a)–O(33) 3.319 Å]. These interactions link the disilver cations in zigzag perchlorate-bridged chains, using two of the four independent perchlorate anions.

Viewed along the bridgehead–bridgehead vector the cations show A-frame geometry (Fig. 1). The top (hinge) angle is provided by the bridging diimine strand and requires a large torsion angle [46(1)° for N(3c)–C(3c)–C(4c)–N(4c) and 45(1)° for N(3f)–C(3f)–C(4f)–N(4f)]. The equivalent torsion angles for the bidentate diimine strands are in the range 28–31°.

Whether some degree of metal–metal bonding is to be implied from the observation of Ag–Ag internuclear distances shorter than those (2.89 Å) in elemental silver is a matter of debate. The rationale for the close approach of d^{10} ions observed in many systems[8] has remained a longstanding puzzle in bonding theory. To quote Hoffman[9] 'One has difficulty in seeing why two or more d^{10} ions should come near each other; after all they are filled shells'. His explanation of this behaviour relies on hybridisation of 4d with higher energy 5s and 5p orbitals which converts the closed shell repulsions into weak attractive interactions. In the case of Au^{I}, relativistic effects reduce the d–s energy gap to allow Au–Au interaction[10] of around 6–8 kcal mol^{-1} (cal = 4.184 J), but this mechanism cannot be invoked for Ag^{I}. Oxidation of the d^{10} cation should however allow stronger interaction, of the order of a one-electron bond. Preliminary electrochemical study[11] of **2** reveals a pair of overlapped and poorly reversible waves in the range 1.0–1.5 V *vs*. Ag/AgCl indicating that this disilver cryptate can be oxidised at accessible potential, apparently generating $Ag^{I}Ag^{II}$ and $Ag^{II}Ag^{II}$ products, at least in solution. Should cryptates of these redox states be isolable, the comparison of the weak $d^{10}d^{10}$ interaction with that existing in $d^{9}d^{10}$, or $d^{9}d^{9}$ where formal metal–metal bonding is theoretically possible, will assist understanding of the $d^{10}d^{10}$ situation.

The significance of the novel and unusual conformation adopted in this cryptate is that linkage of metal–metal intra-cryptate bonded entities becomes possible, *via* bridging donors coordinated at the vacant axial positions on the face of the A. Such a possibility, illustrated by the perchlorate bridging of Fig. 3, could be exploited by the use of efficient bridging ligands. In this way, cryptand-enforced metal–metal bonds could be linked together *via* unsaturated bridging groups such as CN^{-} to generate potentially exploitable oligomeric or continuous solid materials. These would still incorporate the valuable properties of the cryptand host such as steric constraint and cryptand cavity protection, while enabling propagation of bulk electronic properties such as conductivity or magnetism through the extended structure.

We thank EPSRC for support (to J. C.) and also for access to facilities: FABMS at Swansea and solid state NMR at Durham.

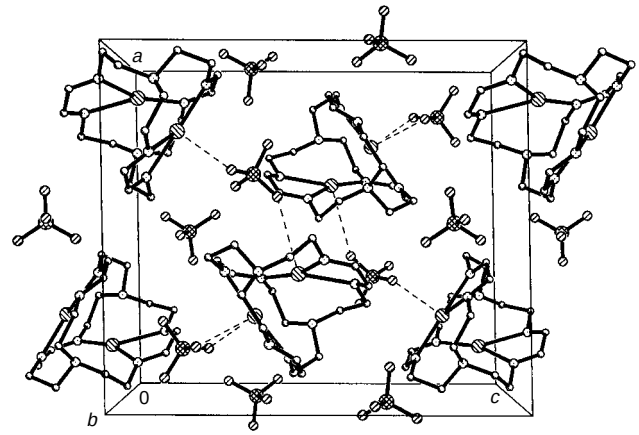

Fig. 3 Linkage of cryptate units *via* anion (perchlorate) bridging

Notes and References

† E-mail: v.mckee@qub.ac.uk, m.j.nelson@open.ac.uk

‡ *Crystal data*: $[Ag_2(imBT)][ClO_4]_2$, $C_{18}H_{30}Ag_2Cl_2N_8O_8$, pale yellow lath, dimensions 0.80 × 0.37 × 0.17 mm, monoclinic, space group $P2_1/n$, a = 14.467(2), b = 11.194(1), c = 16.555(2) Å, β = 91.29(1)°, U = 2682.0(5) $Å^{-3}$, space group $P2_1$, Z = 4, μ = 1.718 mm^{-1}, $F(000)$ = 1544. Using Mo-Kα radiation, (λ = 0.71073 Å) at 153(2) K, a total of 7680 reflections was collected in the range $4 < 2\theta < 52°$. Data were corrected for a 2% drop in intensity as well as for Lorentz and polarisation effects and an empirical absorption correction was applied. The structure was solved by direct methods (TREF[12]) and refined by full-matrix least squares on F^2, using all 5608 independent reflections (R_{int} = 0.0365). All the non-hydrogen atoms were refined with anisotropic atomic displacement parameters and hydrogen atoms were inserted at calculated positions. Refinement of 685 parameters, converged with wR_2 = 0.0706, GOF = 1.065 (all data) and conventional R_1 = 0.0300 (2σ data). There were no significant residual peaks in the electron density map. All programs used in the structure refinement are contained in the SHELXL-97 package.[13] CCDC 182/780.

1 C. J. Harding, V. McKee and J. Nelson, *J. Am. Chem. Soc.*, 1991, **113**, 9684; C. J. Harding, J. Nelson, J. Wyatt and M. C. R. Symons, *J. Chem. Soc., Chem. Commun.*, 1994, 2499.
2 J. A. Farrar, V. McKee, A. H. R. Al-Obaidi, J. J. McGarvey, J. Nelson, A. J. Thomson, *Inorg. Chem.*, 1995, **34**, 1302; J. A. Farrar, R. Grinter, F. Neese, J. Nelson and A. J. Thomson, *J. Chem. Soc., Dalton Trans.*, 1997, 4083.
3 M. G. B. Drew, J. Hunter, C. Harding, D. Marrs and J. Nelson, *J. Chem. Soc., Dalton Trans.*, 1992, 3235.
4 A. Al-Obaidi, G. Baranovich, J. L. Coyle, C. Coates, J. J. McGarvey, V. McKee and J. Nelson, *Inorg. Chem.*, submitted.
5 M. G. B. Drew, B. Maubert, N. Martin and J. Nelson, *J. Chem. Soc., Dalton Trans.*, submitted.
6 D. Apperly and J. Nelson, work in progress.
7 M. G. B. Drew, C. J. Harding, Q. Lu, V. McKee and G. G. Morgan, *J. Chem. Soc., Dalton Trans.*, 1996, 3021; M. G. B. Drew, D. McDowell and J. Nelson, *Polyhedron*, 1988, **7**, 2229; G. Morgan, V. McKee and J. Nelson, *Inorg. Chem.*, 1994, **24**, 4427.
8 G. Smith, A. N. Reddy, K. A. Byriel and C. H. L. Kennard, *J. Chem. Soc., Dalton Trans.*, 1995, 3565; D.-D. Wu and T. C. W. Mak, *J. Chem. Soc., Dalton Trans.*, 1995, 2671; R. I. Papasergio, C. L. Raston and A. H. White, *J. Chem. Soc., Chem. Commun.*, 1984, 612.
9 A. deDieu and R. Hoffman, *J. Am. Chem. Soc.*, 1978, **100**, 2074.
10 H. Schmidbaur, W. Graf and G. Muller, *Angew. Chem., Int. Ed. Engl.*, 1988, **27**, 417.
11 R. M. Town, V. McKee and J. Nelson, work in progress.
12 G. M. Sheldrick, SHELXS-86, *Acta Crystallogr., Sect. A*, 1990, **46**, 467.
13 G. M. Sheldrick, SHELXL-97 Version 97-1, University of Göttingen.

Received in Basel, Switzerland, 21st November 1997; 7/08408K

The reductive coupling of tertiary amides to give enediamines using $PhMe_2SiLi$

Ian Fleming,*[a]† Usha Ghosh,[a] Stephen R. Mack[a] and Barry P. Clark[b]

[a] *Department of Chemistry, Lensfield Road, Cambridge, UK CB2 1EW*
[b] *Eli Lilly and Co., Lilly Research Centre, Erl Wood Manor, Windlesham, Surrey, UK GU20 6PH*

$PhMe_2SiLi$ reacts with tertiary amides to give enediamines, which can be isolated in good yield when the α-carbon is branched; the enediamines can be hydrolysed more or less easily to α-amino ketones, isomerised from *Z* to *E*, oxidised to dienediamines and isomerised to amino enamines.

We have been studying the reactions of $PhMe_2SiLi$[1] with a variety of substrates, including carbon electrophiles at the oxidation state of a carboxylic acid. One goal in this work had been to find a synthesis of acylsilanes that might be even easier than the reaction between an acid chloride and a silyl cuprate.[2] We reported almost no success, and several surprises, in the reaction between the silyllithium reagent and nitriles,[3] some success in the reaction with esters,[4] and some success with tertiary amides **1a**→**2**, *provided that the reaction is carried out and quenched at dri ice–acetone temperatures*.[4] To avoid this delicate operation, the standard device when synthesising aldehydes or ketones from amides is to use a Weinreb amide,[5] but we find that this does not work for the synthesis of acylsilanes, because the Weinreb amide **1b** gives N–O cleavage instead (Scheme 1), presumably by elimination of methoxide from the tetrahedral intermediate **3** giving the secondary amide **4**.[6] Among the variety of unexpected reactions of the silyllithium reagent that we have already reported, none has been as surprising as the reactions with tertiary amides carried out at higher temperatures, which we report here and in the following two papers.

When we treated the same *N*,*N*-dimethylamide **1a** with a little over 1 equiv. of the silyllithium reagent at −20 °C, and quenched the mixture with aq. $NaHCO_3$ at that temperature, we obtained a good yield of the crystalline enediamine **5** (Scheme 2). Although there is one precedent for this type of reaction, where a 14% yield of an enediamine was obtained from *N*,*N*-diethylbenzamide with Et_3SiLi,[7] we were at first uneasy about the structure of this compound, since it had survived dissolution in dilute hydrochloric acid overnight at room temperature—conditions that are far more vigorous than those usually needed for the hydrolysis of an enamine. An X-ray crystal structure

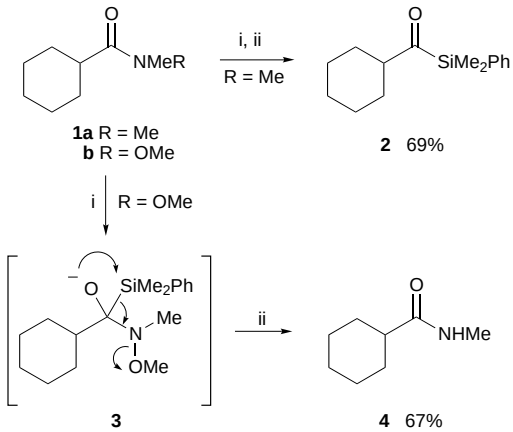

Scheme 1 *Reagents and conditions*: i, $PhMe_2SiLi$ (1.2 equiv.) THF, −78 °C, 1.5 h; ii, NH_4Cl, H_2O, −78 °C → room temp.

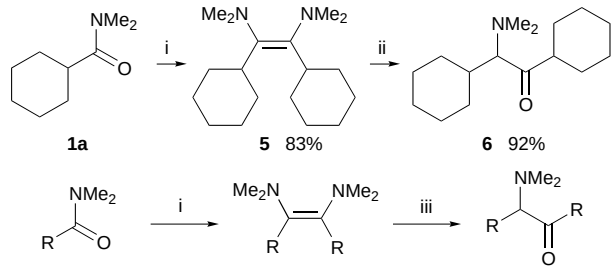

7a R = Pr^i **8a** 80% **9a** 79%
b R = Bu^t **9b** 6%
c R = Pr^n **9c** 81%
d R = $Me(CH_2)_8$ **9d** 72%
e R = $CH_2{=}CH(CH_2)_2$ **9e** 75%
f R = $CH_2{=}CH(CH_2)_3$ **9f** 59%
g R = Bn **9g** 52%
h R = $Ph(CH_2)_2$ **9h** 69%
i R = $PH(CH_2)_3$ **9i** 60%
j R = $Ph(CH_2)_4$ **9j** 46%
k R = Ph **9k** 51%

Scheme 2 *Reagents and conditions*: i, $PhMe_2SiLi$ (1.1 equiv.) THF, −78 → −20 °C, 1 h; ii, 3 M HCl, 70 °C, 18 h; iii, 3 M HCl, various times and temperatures

(Fig. 1) confirmed that it was the enediamine and showed also that it was the *Z* isomer.[8]‡

The stability in acid was now convincingly explained—the lone pairs on both nitrogen atoms are in the plane of the double bond, and not conjugated to it as they are in a typical enamine. Hydrolysis of the enediamine **5** required heating to 70 °C in dilute hydrochloric acid for 18 h in order to obtain the α-amino ketone **6**. Clearly, in contrast to the one precedent, the reductive coupling of amides can be a high-yielding reaction. We find that the amides **7a**–**k** undergo reductive coupling followed by hydrolysis to give the α-amino ketones **9a**–**k**, but the enediamines **8a**–**k**, although detectably intermediates, were only easily isolated when they carry branched substituents, as with **8a**, to confer on them this remarkable hydrolytic stability.

The enediamines **5** and **8a** showed a number of unexpected reactions (Scheme 3). When we treated the enediamine **5** with methyl acrylate, attempting to induce a cycloaddition characteristic of enamines,[9] it isomerised to the *E* isomer **11a**, which was remarkable for the substantial difference in its properties from the *Z* isomer: the R_f value on silica gel eluting with hexane changed from 0.1 to 0.7 and the mp changed from 89–90 °C to 175–176 °C. The isomerisation from the *Z* isomers **5** and **8a** to

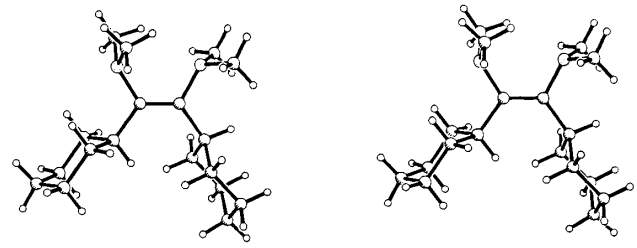

Fig. 1 Stereoview of the enediamine **5**

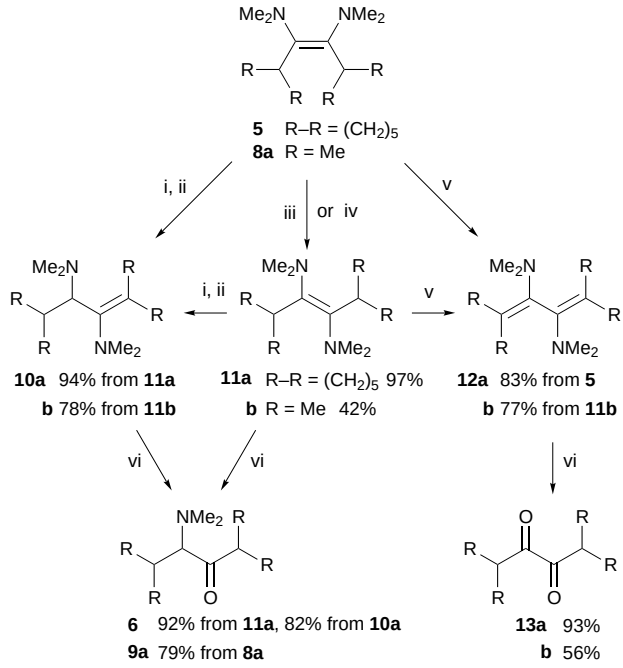

Scheme 3 *Reagents and conditions*: i, $(CO_2H)_2$, recrystallise from EtOAc; ii, NaOH, H_2O; iii, CH_2=$CHCO_2Me$, 60 °C, 24 h; iv, PtO_2, MeOH, 50 °C, 15 min; v, Pd/C, MeOH, room temp., 4 h; vi, 3 M HCl, 70 °C, 18 h

the *E* isomers **11a**, **b**, respectively, is actually better carried out using a short treatment with Adams' catalyst. The enediamines, both the *Z* and *E* isomers, gave oxalate salts, but simple recrystallisation of these salts, followed by basification, gave the isomers **10a** and **10b** of the enediamines in which the double bond had moved. All of the enediamines could be hydrolysed to the α-amino ketones **6** and **9a**, but all attempts to reduce any of them to the saturated vicinal diamine failed. Most remarkable amongst our attempts was the oxidation of the enediamines **5** or **11a** *using hydrogen and palladium on charcoal*, which gave the dienediamine **12a**. Needless to say, this oxidation was better performed without the hydrogen, and the first step, when carried out on the *Z* isomers, appears to be isomerisation to the *E* isomers. Hydrolysis of the dienediamines **12** gave the α-diketones **13**.

The reductive coupling of the amide carbonyls resembles the McMurry coupling of aldehydes and ketones, and even more closely the reductive coupling of amides using samarium and its iodide,[10] and other lanthanides and their salts.[11] While an electron transfer mechanism might be operating in our reaction, the very different reagent that we have used led us to suspect otherwise. We describe our investigations into the mechanism of the coupling in the following paper.

We thank Dr P. R. Raithby, Dr H. R. Powell and C. Wilson for carrying out the X-ray structure determination, the EPSRC and Lilly Industries for a CASE studentship for S. R. M., and Duckhee Lee for the experiment with the Weinreb amide.

Notes and References

† E-mail: if10000@cam.ac.uk

‡ *Crystal data* for **5**: $C_{18}H_{34}N_2$, FM = 278.47, monoclinic, *P*2(1)/*n*, *a* = 6.3930(6), *b* = 13.3934(11), *c* = 20.962(2) Å, β = 91.6833(11)°, *T* = 293(2) K, *Z* = 4, μ = 0.443 mm^{-1}, 5035 reflections collected, of which 3621 were independent, *R*1 = 0.0884, *wR*2 = 0.1811. CCDC 182/765.

1 M. V. George, D. J. Peterson and H. Gilman, *J. Am. Chem. Soc.*, 1960, **82**, 403; A. S. Guram and G. A. Krafft, in *Encyclopaedia of Reagents for Organic Synthesis*, ed. L. A. Paquette, Wiley, Chichester, 1995, p. 2113; I. Fleming, in *Synthetic Methods of Organometallic and Inorganic Chemistry (Hermann/Brauer)*, ed. N. Auner and U. Klingebiel, Georg Thieme, Stuttgart, 1996, vol. 2, p. 167.

2 B. F. Bonini, F. Busi, R. C. de Laet, G. Mazzanti, J.-W. J. F. Thuring, P. Zani and B. Zwanenburg, *J. Chem. Soc., Perkin Trans. 1*, 1993, 1011; B. F. Bonini, M. Comes-Franchini, G. Mazzanti, U. Passamonti, A. Ricci and P. Zani, *Synthesis*, 1995, 92. For some related reactions see also: J. Kang, J. H. Lee, K. S. Kim, J. U. Jeong and C. Pyun, *Tetrahedron Lett.*, 1987, **28**, 3261; A. G. Brook, A. Baumegger and A. J. Lough, *Organometallics*, 1992, **11**, 310; K. Yamamoto, A. Hayashi, S. Suzuki and J. Tsuji, *Organometallics*, 1987, **6**, 974; A. Ricci, A. Degl'Innocenti, S. Chimichi, M. Fiorenza, G. Rossini and H. J. Bestmann, *J. Org. Chem.*, 1985, **50**, 130; F. Jin, B. Jiang and Y. Xu, *Tetrahedron Lett.*, 1992, **33**, 1221; M. Nakada, S. Nakamura, S. Kobayashi and M. Ohno, *Tetrahedron Lett.*, 1991, **32**, 4929; P. Bourgeois, J. Dunoguès and N. Duffaut, *J. Organomet. Chem.*, 1974, **80**, C25; J.-P. Picard, R. Calas, J. Dunoguès, N. Duffaut, J. Gerval and P. Lapouyade, *J. Org. Chem.*, 1979, **44**, 420; P. Bourgeois, *J. Organomet. Chem.*, 1974, **76**, C1; N. Kise, H. Kaneko, N. Uemoto and J. Yoshida, *Tetrahedron Lett.*, 1995, **36**, 8839.

3 I. Fleming, M. Solay and F. Stolwijk, *J. Organomet. Chem.*, 1996, **521**, 121.

4 I. Fleming and U. Ghosh, *J. Chem. Soc., Perkin Trans. 1*, 1994, 257.

5 S. Nahm and S. M. Weinreb, *Tetrahedron Lett.*, 1981, **22**, 3815.

6 D. Lee, Ph.D., Thesis, Cambridge, 1997.

7 D. A. Bravozhitivitovsk, S. D. Pigarev, I. D. Kalikhman, O. A. Vyazankina and N. S. Vyazankin, *J. Organomet. Chem.*, 1983, **114**, 51.

8 P. R. Raithby, H. R. Powell and C. Wilson, unpublished work, Cambridge, 1994.

9 K. C. Brannock, A. Bell, R. D. Burpitt and C. A. Kelly, *J. Org. Chem.*, 1964, **29**, 801; K. C. Brannock, R. D. Burpitt, V. W. Goodlett and J. G. Thweatt, *J. Org. Chem.*, 1964, **29**, 813; I. Fleming and J. Harley-Mason, *J. Chem. Soc.*, 1964, 2165.

10 A. Ogawa, N. Takami, M. Sekiguchi, I. Ryu, N. Kambe and N. Sonoda, *J. Am. Chem. Soc.*, 1992, **114**, 8729.

11 A. Ogawa, T. Nanke, N. Takami, M. Sekiguchi, N. Kambe and N. Sonoda, *Appl. Organomet. Chem.*, 1995, **9**, 461.

Received in Liverpool, UK, 12th November 1997; revised manuscript received, 21st January 1998; 8/00648B

α-Amino carbene or carbenoid formation in the reaction of a tertiary amide with $PhMe_2SiLi$ and its insertion into the Si–Li bond of a second equivalent

Ian Fleming,*[a]† Stephen R. Mack[a] and Barry P. Clark[b]

[a] *Department of Chemistry, Lensfield Road, Cambridge, UK CB2 1EW*
[b] *Eli Lilly and Co., Lilly Research Centre, Erl Wood Manor, Windlesham, Surrey, UK GU20 6PH*

$PhMe_2SiLi$ reacts with tertiary amides, $RCONMe_2$, to give a carbene, $RCNMe_2$, or an equivalent carbenoid, which gives enediamines, $R(Me_2N)C{=}C(NMe_2)R$, in the absence of a strong nucleophile, but is attacked by strong nucleophiles, NuLi, to give lithium reagents $R(Me_2N)CLiNu$.

In the preceding paper[1] and its predecessor,[2] we described the reaction between 1 equiv. of $PhMe_2SiLi$ and the amide **1** giving the acylsilane **6** when the mixture was quenched at −78 °C, but giving the enediamine **2** when the mixture was warmed to −20 °C before quenching. Neither in those papers, nor in the paper describing the one precedent for this type of reaction,[3] has there been any discussion of the mechanism of the formation of the enediamine.

Among other possibilities, such reductive coupling implies that a species electrophilic at the carbonyl carbon has been attacked by an umpolung species nucleophilic at the carbonyl carbon. The latter is easily identified as the consequence of a Brook rearrangement,[4] which can be formulated as an equilibrium between an α-silyl alkoxide **3** and the α-silyloxy anion **5**,[5] with the latter the umpolung species (Scheme 1). Alternatively, it can be formulated as a single hypervalent species **4**,[6] which can react as an oxygen or a carbon (**4** arrow) nucleophile, depending upon the circumstances. It is, however, much less easy to identify the electrophilic species. Several candidates present themselves: the amide **1**, the acylsilane **6**, an iminium ion **7**, and a carbene **8**. We now report that all the evidence suggests that the carbene is the electrophile.

The amide itself cannot have been the electrophile—if we simply warmed the solution of the tetrahedral intermediate **3** from −78 to −20 °C, and then quenched the mixture, we obtained the enediamine **2** in good yield. The tetrahedral intermediate **3** was fully formed at the lower temperature, since on quenching it, the acylsilane **6** was obtained in reasonably good yield. It does not revert to amide and the silyllithium reagent, since adding *N*,*N*-dimethylcyclohexanecarboxamide before warming up from −78 °C gave only the homo-coupled product **2**.[7] The tetrahedral intermediate must have provided both the nucleophilic and the electrophilic species for the coupling reaction.

To trap the electrophile, we carried out the same reaction as before but with rather more than 2 equiv. of the silyllithium reagent, in the hope that the intermediate would be trapped by the second equivalent of nucleophile. The product was the α-silyl amine **9** (Scheme 2), analogous to a minor product in the Russian work.[3] If the iminium ion **7** had been an intermediate, it ought to have led to a product with two silyl groups, not just one, and the easy loss of one seems unlikely. We showed that this was not the case, by treating the tetrahedral intermediate **3** with $Ph_2MeSiLi$, and obtained this time only the α-silyl amine **11** having the Ph_2MeSi group rather than the original $PhMe_2Si$ group. We also carried out the experiment the other way round, adding $Ph_2MeSiLi$ to the amide **1** at −100 °C to give the tetrahedral intermediate **10**. This then reacted with $PhMe_2SiLi$ on warming to −20 °C to give the α-silyl amine **9**, showing that neither an α,α-disilyl amine nor the iminium ion **7** could have been intermediates—only the silyl group from the second silyllithium reagent delivered was incorporated into the product.

The formation of the products **9** and **11** was, however, compatible with the carbene **8** being an intermediate—it could be expected to insert into the Si–Li bond of the second lithium reagent to give an intermediate lithium reagent **12**, which would be protonated before or during the workup. Our attempts to detect the intermediate **12a** were thwarted by its evident strong basicity—it did not incorporate a deuterium label when quenched with D_2O, having already found a proton somewhere else. Nor were we at first successful in finding where that proton came from, but eventually we showed that an organolithium intermediate had been involved by trapping the corresponding Ph_2MeSi intermediate **12b** at −78 °C (Scheme 3). It is known that the more phenyl groups there are on a silyl group, effectively the faster the Brook rearrangement takes place.[8] In consequence, the intermediate **12b** was formed between −100

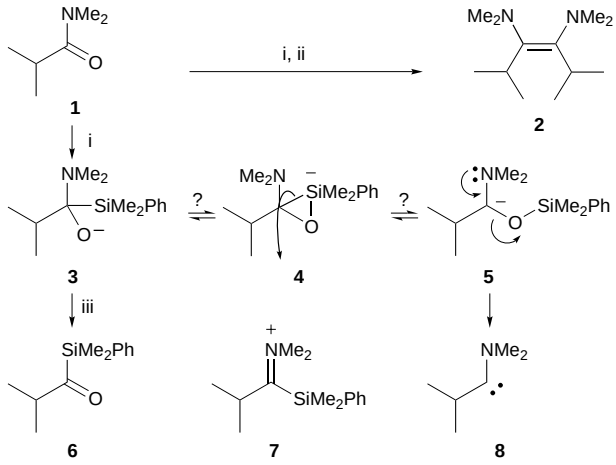

Scheme 1 *Reagents and conditions*: i, $PhMe_2SiLi$ (1.2 equiv.) THF, −78 °C, 1.5 h; ii, −20 °C, then $NaHCO_3$, H_2O; iii, NH_4Cl, H_2O, −78 °C → room temp.

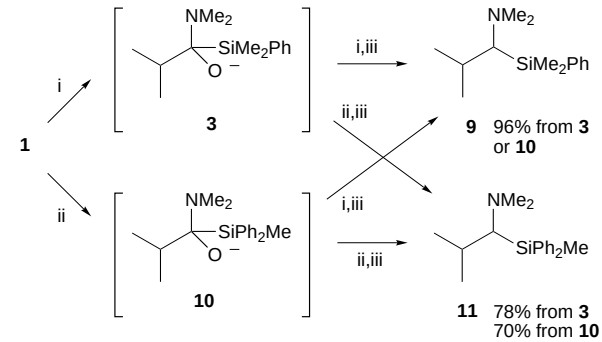

Scheme 2 *Reagents and conditions*: i, $PhMe_2SiLi$ (1.2 equiv.) THF, −78 °C, 1.5 h; ii, $Ph_2MeSiLi$ (1.2 equiv.) THF, −100 °C, 1.5 h; iii, −20 °C, then $NaHCO_3$, H_2O

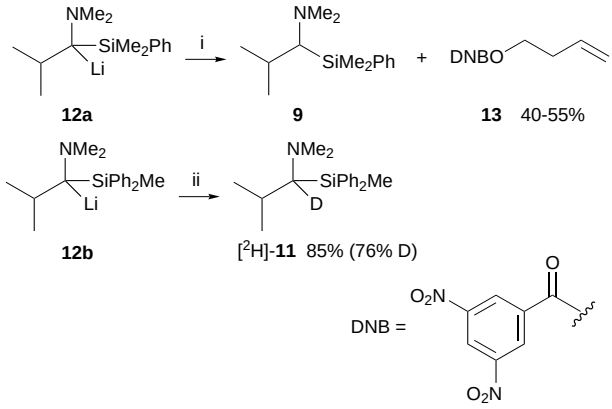

Scheme 3 *Reagents and conditions*: i, 3,5-$(O_2N)_2C_6H_3COCl$; ii, D_2O

and −78 °C, at which temperature it survived long enough to be quenched with D_2O to give the deuterated α-silyl amine [^{2}H]**11**. The $PhMe_2Si$ intermediate **12a**, having been formed at higher temperature, somewhere between −78 and −20 °C, evidently found a proton before it could be quenched with D_2O. The source of that proton appears to be, at least in part, THF, which is known to react with strong bases like BuLi, losing the proton on C-2 and undergoing a retro-cycloaddition to give the enolate of acetaldehyde.[9] We detected a low level of deuterium incorporation when the reaction was carried out in [$^2H_8$]THF, and, expecting to trap the enolate of acetaldehyde, we added 3,5-dinitrobenzoyl chloride, and obtained instead the 3,5-dinitrobenzoate **13** in yields of 40–55%, with no trace of the expected product. As far as we are aware, the apparently simple E2 elimination from THF losing the proton from C-3 has not been seen before in solution chemistry, although it is thoroughly established with hydroxide ion and amide ion as bases in the gas phase,[10] and the formation of but-3-enol from the reaction between sodium and 3-chlorotetrahydrofuran is also known.[11] It is presumably unfavourable because the elimination is a retro-5-*endo*-*trig* reaction.

We also found that the presence of a phenyl group in the *N*,*N*-dimethylbenzamide **14** stabilised the corresponding intermediate **15**, which survived even at −20 °C, and gave a deuterated α-silyl amine **16** on quenching with D_2O (Scheme 4). The intermediate **15** also reacted with alkyl halides giving the amines **17a** and **17b**, and with isobutyraldehyde giving, initially, an alkoxide **18** that undergoes a Peterson elimination giving the enamine **19**, which is easily hydrolysed to the ketone **20**. These reactions illustrate an umpolung of reactivity in the amide **14**.

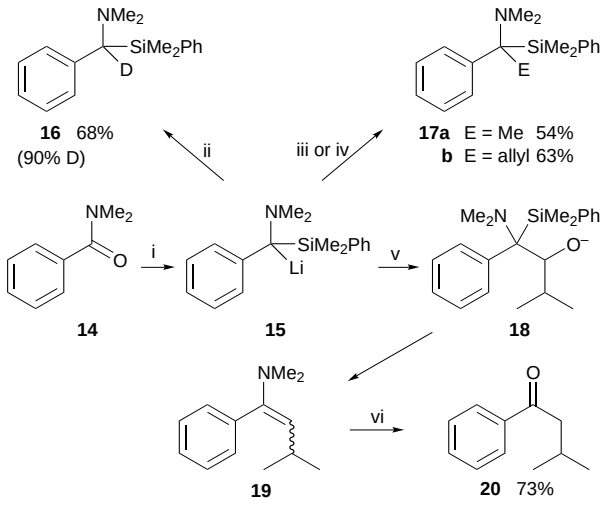

Scheme 4 *Reagents and conditions*: i, $PhMe_2SiLi$ (2.4 equiv.) THF, −78 → −20 °C, 1.5 h; ii, D_2O; iii, MeI; iv, allylBr; v, Pr^{i}CHO; vi, HCl, H_2O

The carbene intermediate **8** could be formed by Brook rearrangement, followed by or concerted with the elimination of silane oxide (Scheme 1). This pathway is, as far as we are aware, a new one for reactions taking place within the Brook rearrangement manifold, and is a new route to carbene or carbene-like intermediates. The nearest analogy is the formation of an oxygen-stabilised carbene when the acetals of acylsilanes are heated to 190 °C.[12] Our reaction takes place, presumably, because of the extra electronic push (**5**, arrows) from the Me_2N lone pair. It could equally be derived by cheletropic extrusion of $PhMe_2SiO^-$ directly from the intermediate **4**. It is not clear what the structure of the carbene is in detail—it could be the carbene itself **8**, as we have drawn it here for simplicity, or it could be an equivalent species such as an α-lithio iminium ion. A carbene was also invoked by Ogawa and Sonoda in their work using samarium iodide induced coupling of amides.[13] Whatever its nature, our carbene was not trapped by a silicon hydride—only the enediamine **2** was formed, and not the silyl amine **9**, when the tetrahedral intermediate **3** was warmed to −20 °C in the presence of $PhMe_2SiH$, nor have we found at any stage products that might have been derived by insertion of the carbene into the neighbouring C–H bond, nor into a well-placed C=C bond, as described in the following paper. The enediamine could be produced from the carbene or carbenoid by dimerisation, or, more likely in view of the probable low concentration of such a species, by attack upon it by the *C*-nucleophilic intermediate **4** or **5** of the Brook rearrangement, followed by β-elimination of a second silyloxy anion.

The following paper describes some other remarkable reactions that can be ascribed to the presence of intermediate lithium reagents like **12** and **15**. They add further support to this being the correct mechanism, at least in outline.

We thank the EPSRC and Lilly Industries for a CASE studentship for S. R. M.

Notes and References

† E-mail: if10000@cam.ac.uk

1 I. Fleming, U. Ghosh, S. R. Mack and B. P. Clark, *Chem. Commun.*, 1998, 711.
2 I. Fleming and U. Ghosh, *J. Chem. Soc., Perkin Trans. 1*, 1994, 257.
3 D. A. Bravozhitivitovsk, S. D. Pigarev, I. D. Kalikhman, O. A. Vyazankina and N. S. Vyazankin, *J. Organomet. Chem.*, 1983, **114**, 51.
4 A. G. Brook, *Acc. Chem. Res.*, 1974, **7**, 77.
5 A. Wright and R. West, *J. Am. Chem. Soc.*, 1974, **96**, 3214, 3222 and 3227.
6 R. J. Linderman and A. Ghannam, *J. Am. Chem. Soc.*, 1990, **112**, 2392; I. Fleming, *Chemtracts: Org. Chem.*, 1996, **9**, 121.
7 Similarly, carrying out the original reaction with the cyclohexanecarboxamide and adding the isobutyramide before warming gave only the homo-coupled product (**5** in the preceding paper).
8 A. G. Brook, G. E. LeGrow and D. M. MacRae, *Can. J. Chem.*, 1967, **45**, 239.
9 R. B. Bates, L. M. Kroposki and D. E. Potter, *J. Org. Chem.*, 1972, **37**, 560.
10 C. H. DePuy and V. M. Bierbaum, *J. Am. Chem. Soc.*, 1981, **103**, 5034; C. H. DePuy, E. C. Beedle and V. M. Bierbaum, *J. Am. Chem. Soc.*, 1982, **104**, 6483.
11 L. Crombie, J. Gold, S. H. Harper and B. J. Stokes, *J. Chem. Soc.*, 1956, 136; M. Jurjew, *Zh. Obshch. Khim.*, 1948, **18**, 1807.
12 A. G. Brook and P. J. Dillon, *Can. J. Chem.*, 1969, **47**, 4347.
13 A. Ogawa, N. Takami, M. Sekiguchi, I. Ryu, N. Kambe and N. Sonoda, *J. Am. Chem. Soc.*, 1992, **114**, 8729; A. Ogawa, T. Nanke, N. Takami, M. Sekiguchi, N. Kambe and N. Sonoda, *Appl. Organomet. Chem.*, 1995, **9**, 461.

Received in Liverpool, UK, 12th November 1997; revised manuscript received, 21st January 1998; 8/00650D

Formation of α-dialkylamino alkyllithium intermediates in the reaction of *N*,*N*-dialkylamides with $PhMe_2SiLi$ followed by a second lithium reagent, and their alkylation, fragmentation, cyclisation and rearrangement by proton transfer

Ian Fleming,*[a]† Stephen R. Mack[a] and Barry P. Clark[b]

[a] *Department of Chemistry, Lensfield Road, Cambridge, UK CB2 1EW*
[b] *Eli Lilly and Co., Lilly Research Centre, Erl Wood Manor, Windlesham, Surrey, UK GU20 6PH*

Tertiary amides ($RCONMe_2$) react with $PhMe_2SiLi$, followed by a second lithium reagent NuLi, to give α-dialkylamino alkyllithium intermediates $R(Me_2N)CLiNu$ that undergo protonation 2 → 3, alkylation 2a → 3ab, β-elimination 5 → 6, intramolecular attack on an isolated double bond 9 → 10, intramolecular proton transfer 12, 17 and 22 (arrows), and fragmentation 28 and 34 (arrows), depending upon the structures of the various components R and Nu.

In the preceding paper[1] we described how an intermediate carbene **1** derived from the remarkable reaction between 1 equiv. of $PhMe_2SiLi$ and *N*,*N*-dimethylisobutyramide could be trapped by a second equivalent of the silyllithium reagent. We now report that when we prepared the tetrahedral intermediate from the amide with 1 equiv. of $PhMe_2SiLi$ at −78 °C as usual, and then added PhLi, Bu^nLi or Bu_3SnLi, before warming the mixture to −20 °C, we obtained the amines **3aa**, **3ba** and **3ca**, presumably by way of the intermediate lithium reagents **2a**–**c**. We also quenched the phenyl-stabilised lithium reagent **2a** with allyl bromide to give the amine **3ab** (Scheme 1). These reactions establish a new way of assembling secondary alkyl and, more remarkably, tertiary alkyl tertiary amines, and an α-stannyl tertiary amine.

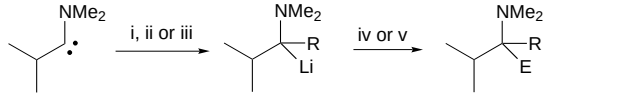

1

2a R = Ph
b R = Bu^n
c R = $SnBu_3$

3aa R = Ph, E = H 68%
ab R = Ph, E = allyl 60%
ba R = Bu^n, E = H 42%
ca R = $SnBu_3$, E = H 21%

Scheme 1 *Reagents and conditions*: i, PhLi; ii, Bu^nLi; iii, Bu_3SnLi; iv, $NaHCO_3$, H_2O; v, allylBr

We achieved umpolung in another way, by building a leaving group into the nucleophile (Scheme 2). We treated *N*,*N*-dimethylcyclohexanecarboxamide with 1 equiv. of the silyllithium reagent, followed by 1 equiv. of $PhSCH_2Li$, and then warmed to −20 °C to give the lithium reagent **5**, drawn here and from now on as an anion, in order to allow us to use uncomplicated curly arrows. β-Elimination gave the enamine **6**, and hence the ketone **7** on hydrolysis. We also intercepted the intermediate anion **9**, setting it up with 2 equiv. of the silyllithium reagent, and found that nucleophilic attack by the anion (arrows) is possible on the isolated double bond built in to be at the appropriate distance for a known[2] type of 5-*exo*-*trig* reaction of α-amino alkyllithium reagents (Scheme 2). The isolated cyclopentane product **10** was a single diastereoisomer, but we do not know which one. These simple extensions of the pathways recorded in the preceding paper confirm the intermediacy of α-amino alkyllithium intermediates **2**, **5** and **9**.

We also report that the generality of these routes is compromised by the ease with which the intermediate anion, suitably constituted, undergoes proton transfer to give better stabilised anions, and how other similarly constituted anions suffer extraordinary elimination reactions with a benzyl anion leaving group. The intermediate lithium reagents are evidently unstable, and find a disconcerting variety of ways to decompose.

Thus, the phenylacetamide **11** gave, as well as the normal product **13**, small amounts of a cyclic product **15** (Scheme 3). This appears to be a result of a proton transfer **12** → **14**, to give a phenyl anion, followed by displacement of the phenyl group from silicon (**14** → **15**). Displacement of a phenyl group from silicon with an oxy anion nucleophile is well established,[3] and there are a few examples of the displacement of a phenyl or vinyl group by a carbon–lithium reagent.[4]

Similarly, the bis-homologue **16** gave the normal product **18** together with a product of proton transfer (**20**) in this case with a benzyl anion displacing the phenyl group (**19** → **20**) (Scheme 4).

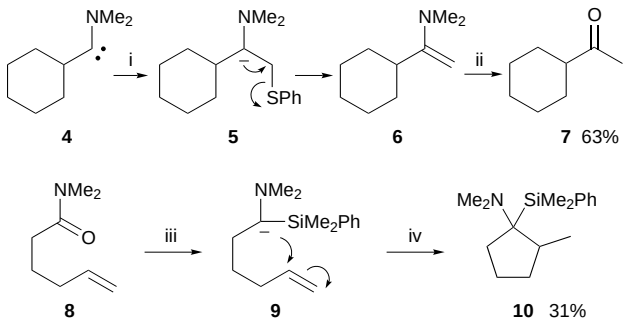

4 **5** **6** **7** 63%

8 **9** **10** 31%

Scheme 2 *Reagents and conditions*: i, $PhSCH_2Li$, −20 °C; ii, HCl, H_2O; iii, $PhMe_2SiLi$ (2.4 equiv.) THF, −78 → −20 °C, 1.5 h; iv, $NaHCO_3$, H_2O

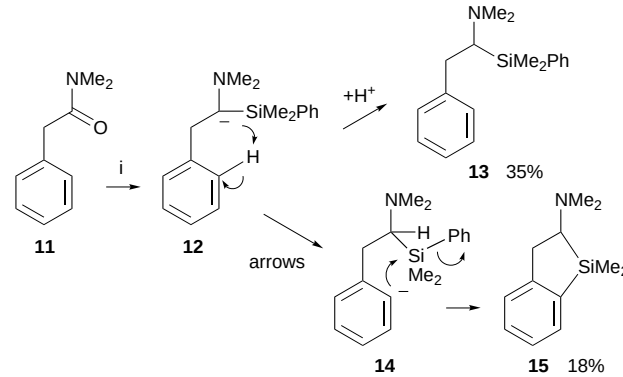

11 **12** **13** 35%

14 **15** 18%

Scheme 3 *Reagents and conditions*: i, $PhMe_2SiLi$ (2.4 equiv.), THF, −78 → −20 °C, 1.5 h

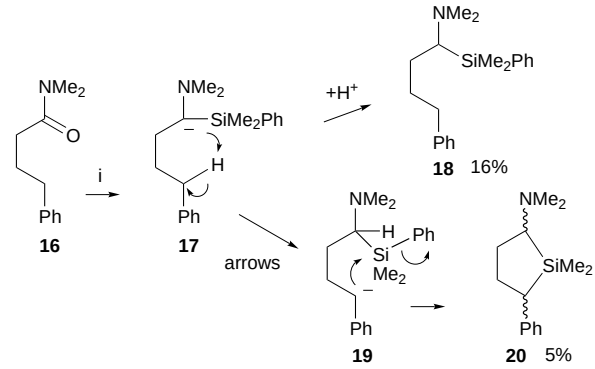

Scheme 4 *Reagents and conditions*: i, $PhMe_2SiLi$ (2.4 equiv.), THF, −78 → −20 °C, 1.5 h

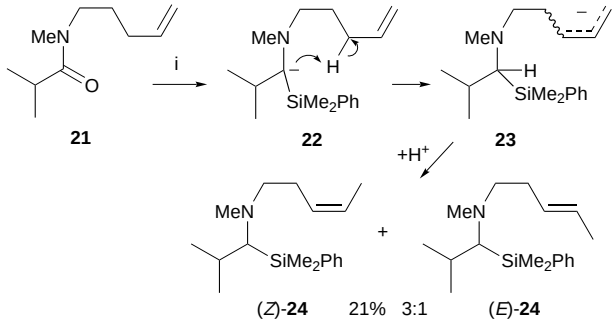

Scheme 5 *Reagents and conditions*: i, $PhMe_2SiLi$ (2.4 equiv.), THF, −78 → −20 °C, 1.5 h

Proton transfer within a five-membered ring also took place from the pentenyl substituent in the amide **21**, where the minor, but the only recognisable, basic products were the pent-3-enylamines (*Z*)-**24** and (*E*)-**24**, similar to what we might call the normal product, except that the double bond had moved (Scheme 5). Proton transfer **22** → **23**, with the formation, as usual,[5] of more of the sickle-shaped allylic anion than of the W-shaped anion, accounts for this curious reaction.

We saw yet another pathway in the reaction with *N*-benzyl-*N*-methylamide **25** (Scheme 6), where the only basic product that we were able to identify from the reaction with 2 equiv. of $PhMe_2SiLi$ was the tertiary amine **27**. This can be accounted for by elimination **28** → **30** to release a benzyl anion **29**, followed by the attack of the benzyl anion on the carbene intermediate **26** and subsequent protonation.

Elimination to give a benzyllithium intermediate also explains what is perhaps the most remarkable reaction in the

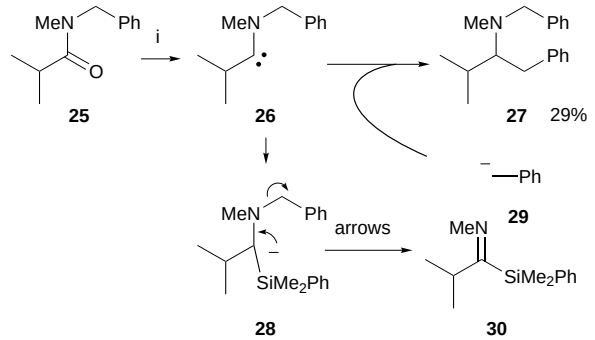

Scheme 6 *Reagents and conditions*: i, $PhMe_2SiLi$ (2.4 equiv.), THF, −78 → −20 °C, 1.5 h

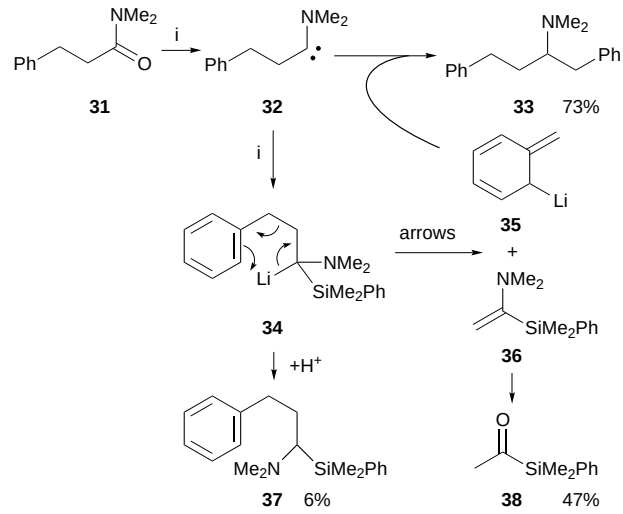

Scheme 7 *Reagents and conditions*: i, $PhMe_2SiLi$ (2.4 equiv.), THF, −78 → −20 °C, 1.5 h

cornucopia of remarkable reactions, both those described in this series of papers and those for which we have no room here. When we treated the amide **31**, intermediate between the amides **11** and **16**, with 2 equiv. of $PhMe_2SiLi$, the major basic product was the amine **33** (Scheme 7). Elimination from the usual intermediate **34** would give the enamine **36**. The elimination is drawn here (**34** arrows) as a retro metalla-ene reaction, and the elimination product is drawn as the 'allylic' isomer **35** of benzyllithium, to illustrate an alternative perception to that drawn for the related elimination **28** → **29** + **30** in Scheme 6. The benzyllithium or its allylic isomer **35** might then trap the carbene **32** to give, after protonation, the major product **33**. In support of this sequence, we also isolated the acylsilane **38** from the basic fraction, into which, presumably, it had been extracted as the enamine **36**. We are not aware of any precedent for carbon–carbon bond cleavage with a benzyllithium leaving group.

We thank the EPSRC and Lilly Industries for a CASE studentship for S. R. M.

Notes and References

† E-mail: if10000@cam.ac.uk

1 I. Fleming, S. R. Mack and B. P. Clark, *Chem. Commun.*, 1998, 713.
2 I. Coldham and R. Hufton, *Tetrahedron Lett.*, 1995, **36**, 2157 and references cited therein.
3 K. Tamao, T. Yamauchi and Y. Ito, *Chem. Lett.*, 1987, 171; I. Fleming, *Pure Appl. Chem.*, 1990, **62**, 1879; P. F. Hudrlik, Y. M. Abdallah and A. M. Hudrlik, *Tetrahedron Lett.*, 1992, **33**, 6747; M. Murakami, M. Suginome, K. Fujimoto, H. Nakamura, P. G. Anderson and Y. Ito, *J. Am. Chem. Soc.*, 1993, **115**, 6487; S. C. Archibald and I. Fleming, *Tetrahedron Lett.*, 1993, **34**, 2387; A. Barbero, D. C. Blakemore, I. Fleming and R. N. Wesley, *J. Chem. Soc., Perkin Trans. 1*, 1997, 1329.
4 H. Gilman, R. A. Benkeser and G. E. Dunn, *J. Am. Chem. Soc.*, 1950, **72**, 1689; S. M. Sieburth and L. Fensterbank, *J. Org. Chem.*, 1993, **58**, 6314; J. G. Duboudin, B. Jousseaume and M. Pinet-Vallier, *J. Organomet. Chem.*, 1979, **172**, 1.
5 S. Bank, A. Schriesheim and C. A. Rowe, *J. Am. Chem. Soc.*, 1965, **87**, 3244; D. A. Hutchinson, K. R. Beck, R. A. Benkeser and J. B. Grutzner, *J. Am. Chem. Soc.*, 1972, **95**, 7075; R. A. Benkeser, *Synthesis*, 1971, 347; M. Schlosser, J. Hartmann and V. David, *Helv. Chim. Acta*, 1974, **57**, 1567.

Received in Liverpool, UK, 12th November 1997; revised manuscript received, 21st January 1998; 8/00651B

Hybridization properties of nucleic acid analogs containing β-aminoalanine modified with nucleobases

Masayuki Fujii,*[a]† Kohya Yoshida,[a] Jinsai Hidaka[a] and Takayuki Ohtsu[b]

[a] *Department of Industrial Chemistry, Faculty of Engineering in Kyushu, Kinki University, 11-6 Kayanomori, Iizuka, Fukuoka 820, Japan*

[b] *Department of General Education, Faculty of Biological Science and Engineering, Kinki University, 930 Nishimitani, Uchida, Naka-gun, Wakayama 649-64, Japan*

Oligopeptides containing *N*β-(thymin-1-ylacetyl)-β-aminoalanine and *N*β-(cytosin-1-ylacetyl)-β-aminoalanine moieties synthesized on a solid phase using standard Boc chemistry showed hybridization properties with single stranded DNA and RNA, and also with double stranded DNA, at pH 7.0.

The development of artificial regulatory molecules for specific gene expression is of special interest from the medicinal and biological points of view.[1] In particular, nucleic acids and their analogs, such as antisense or triple-helix forming oligonucleotides, ribozymes and decoy RNAs, are promising reagents as genetic medicines. In spite of intensive efforts to improve their chemical and biological properties, several problems still remain to be solved, which include degradability by cellular nucleases, impermeability through cell membranes and low hybridization affinity caused by electrostatic repulsion between phosphate backbones.[2]

Among various chemical modifications that could be performed on such synthetic DNAs and RNAs, introduction of a peptide backbone into such molecules seems to be attractive because peptide compounds can be expected to have such preferable properties as nuclease resistance, membrane permeability and a good affinity and specificity to nucleic acids, as can be seen in a number of DNA binding proteins.

In this study, oligopeptides **1** containing β-aminoalanine bearing a nucleobase were synthesized and their hybridization properties with ssDNA, ssRNA and dsDNA were examined *via* T_m measurement.

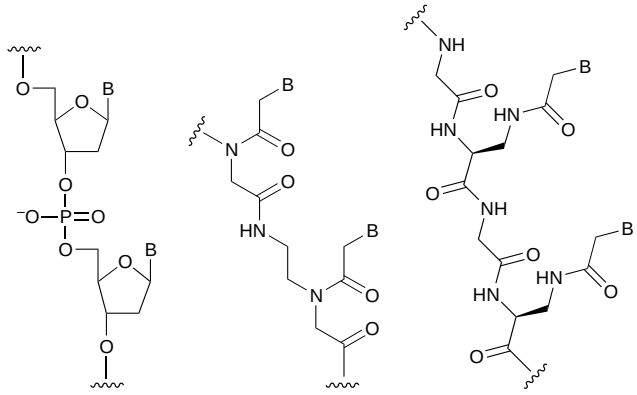

Syntheses of *N*-*tert*-butoxycarbonylglycyl-*N*β-(thymin-1-ylacetyl)-L-β-aminoalanine **7** (T*) and *N*-*tert*-butoxycarbonylglycyl-*N*β-(cytosin-1-ylacetyl)-L-β-aminoalanine **8** (^{Z}C*) were achieved as shown in Scheme 1.[3] These protected amino acids **7** and **8** were readily applicable to solid-phase peptide synthesis using standard Boc chemistry on methylbenzhydrylamine (MBHA) resin.[4] The obtained 20-mer peptide T^*_{10} (**P**) and 30-mer peptide $T^*_5(C^*T^*)_5$ (**Q**) were purified by RP HPLC and confirmed by FAB mass spectrometry {**P**: $C_{122}H_{154}N_{52}O_{51}$ calc. 3164.9, found 3165.9 $[(M + H)^+]$; **Q**: $C_{177}H_{224}N_{82}O_{71}$ calc. 4636.2, found 4637.2 $[(M + H)^+]$}.

As shown in Table 1, formation of a hybrid double strand by **P** and dA_{10} was confirmed by observing a hypochromic effect at pH 7.0. It should be noted that the melting temperature (T_m) was higher than that for the natural DNA double strand by 13.5 °C (1.35 °C base^{-1}).[5] The stability of the hybrid was not affected by salt concentration. The peptide **P** also formed a double strand with rA_{10}, and the T_m was 21 °C. Moreover, it was shown that **P** could bind to double stranded DNA by triple helix

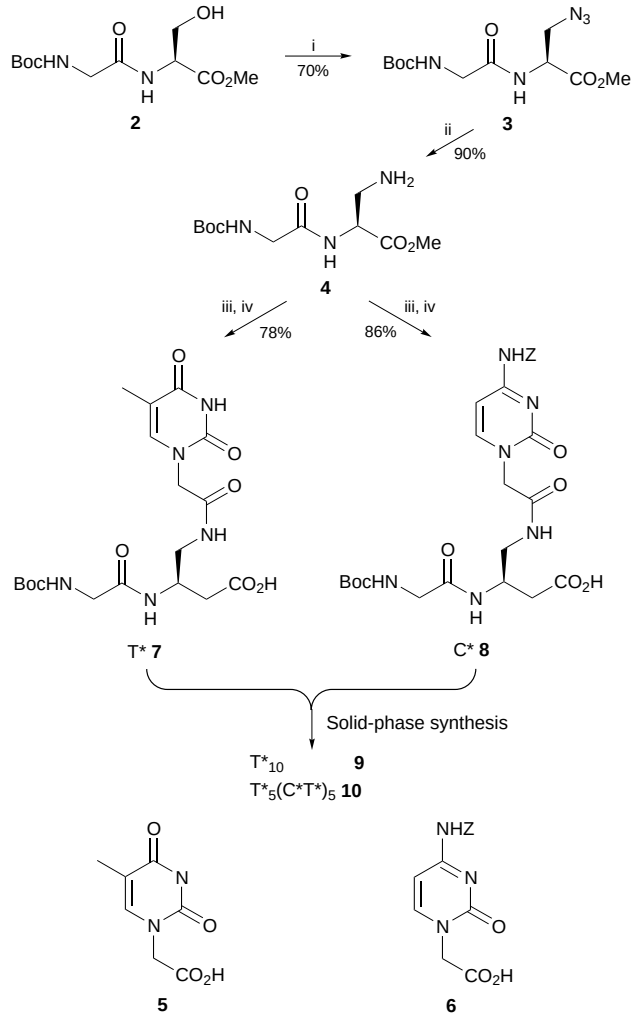

Scheme 1 *Reagents and conditions*; i, Ph_3P, NaN_3, CBr_4, DMF, room temp., 24 h; ii, Pd/C, H_2, MeOH, room temp., 20 h; iii, **5** or **6**, HOBt, DCC, CH_2Cl_2, 0 °C to room temp., 5 h; iv, 1 M NaOH, room temp., 12 h

Table 1 Double and triple helix formation by peptide DNA analogs **P** and **Q**

Strand	Target	T_m[a]/°C	Δ T_m/°C
dT_{10}	dA_{10}	23	—
PNA	dA_{10}	73[b]	+50
P	dA_{10}	36.5	+13.5
P	dA_{10}	36.2[c]	+13.2
P	dA_{10}	36.4[d]	+13.4
P	rA_{10}	21.4	—
dT_{10}	5′-GCTA_{10}TCG-3′/3′-CGAT_{10}AGC-5′	20.9	—
P	5′-GCTA_{10}TCG-3′/3′-GCAT_{10}AGC-5′	19.3	−0.4
5′-T_5-$(CT)_5$-3′	5′-GCT$A_5$$(GA)_5$TCG-3′/3′-CGA$T_5$ $(CT)_5$AGC-5′	21.3	
Q	5′-GCT$A_5$$(GA)_5$TCG-3′/3′-CGA$T_5$ $(CT)_5$AGC-5′	22.8	+1.5

[a] Measured in a buffer containing 50 mM Tris, pH 7.0, 20 mM $MgCl_2$, 100 mM NaCl, [Strand] = [Target] = 0.5 mM. [b] 140 mM NaCl, 10 mM sodium phosphate, pH 7.2. [c] 20 mM $MgCl_2$, 1.0 M NaCl, pH 7.0. [d] 0 M $MgCl_2$, 0 M NaCl, pH 7.0.

formation with comparable affinity (T_m = 19.3 °C, ΔT_m = −0.7 °C).

Oligopeptide **Q** containing mixed pyrimidine bases was also shown to form a triple helix with double stranded DNA (T_m = 22.8 °C, ΔT_m = +1.5 °C).[6]

Studies on the pH dependence of these hybridization properties revealed that the peptide **P**, which contains only thymine bases, binds to ssDNA and dsDNA with an affinity independent of pH, whereas the peptide **Q**, which contains thymine and cytosine bases, binds to dsDNA with less affinity as the pH value increased (Fig. 1). This pH dependency was interpreted to mean that triple helix formation by **Q** with dsDNA required protonation of the cytidine bases in **Q**. These results strongly suggested that **P** and **Q** are binding to dsDNA in the major groove by Hoogsteen hydrogen bonding.

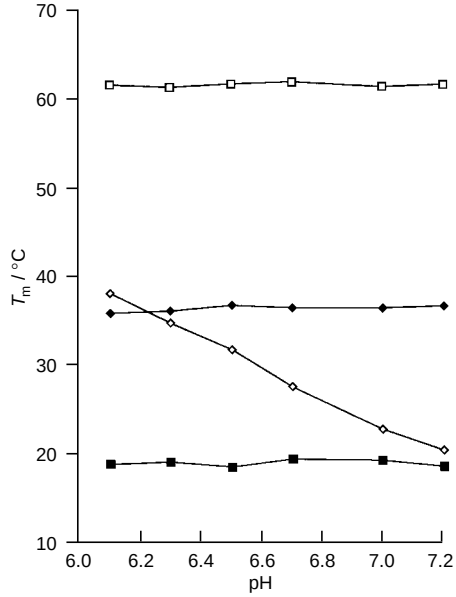

Fig. 1 pH dependence of hybridization: (□) dsDNA, (◆) **P**/ssDNA, (◇) **Q**/dsDNA and (■) **P**/dsDNA

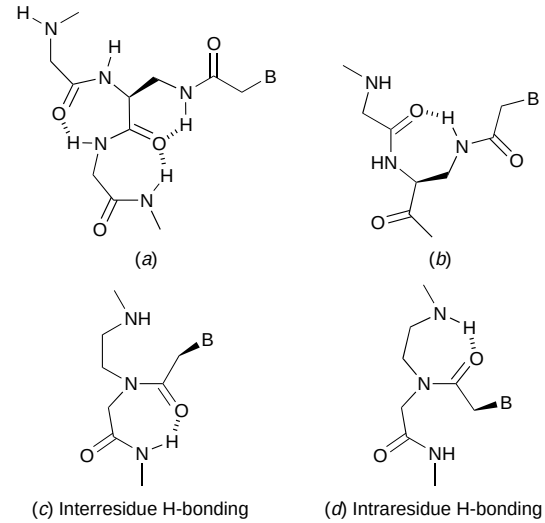

Fig. 2 Intramolecular hydrogen bonding in **1** [(*a*) and (*b*)] and PNA [(*c*) and (*d*)]

The oligopeptides **P** and **Q** were designed to have nucleobase moieties at an interval of six atoms on the backbone, which was previously demonstrated to be critical for hybrid formation with DNA or RNA by Nielsen.[7] The linkage between the nucleobase and the backbone in **P** and **Q** is longer than that in DNA or PNA by two atoms. It was also pointed out by Nielsen's group that the linkage is slightly flexible. It can be postulated that Watson–Crick base pairing in the duplex and Hoogsteen base pairing in triplex by **P** and **Q** is made possible because of the favorable orientation of the base moieties caused by intramolecular hydrogen bond, as shown in Fig. 2.[8]

The present study demonstrates that these novel peptide DNA analogs are promising candidates for antisense and triple helix forming molecules. Further studies to reveal the chemical and biological properties of the peptide DNA analogs are now in progress in our laboratory.

The authors are grateful for financial support from the Chugai Pharmaceuticals Award in Synthetic Organic Chemistry, Japan and from the Fukuoka Industry, Science and Technology Foundation (IST).

Notes and References

† E-mail: mfujii@fuk.kindai.ac.jp

1 C. Helene and J.-J. Toulme, *Biochim. Biophys. Acta*, 1990, **1049**, 99.
2 U. Englisch and D. H. Gauss, *Angew. Chem., Int. Ed. Engl.*, 1991, **30**, 613.
3 M. Fujii, K. Yoshida, J. Hidaka and T. Ohtsu, *Bioorg. Med. Chem. Lett.*, 1997, **7**, 637.
4 E. Atherton and R. C. Sheppard, *Solid phase peptide synthesis, a practical approach*, ed. D. Rickwood and B. D. Hames, IRL Press, Oxford, 1989.
5 P. E. Nielsen, M. Egholm, R. H. Berg and O. Buchardt, *Science*, 1991, **254**, 1497.
6 H. E. Moser and P. B. Dervan, *Science*, 1987, **238**, 645.
7 B. Hyrup, M. Egholm, P. E. Nielsen, P. Witung, B. Norden and O. Buchardt, *J. Am. Chem. Soc.*, 1994, **116**, 7964.
8 O. Almarsson and T. C. Bruice, *Proc. Natl. Acad. Sci. USA*, 1990, **90**, 9542.

Received in Cambridge, UK, 2nd December 1997; 7/08674A

Efficient near IR sensitization of nanocrystalline TiO_2 films by ruthenium phthalocyanines

Md. K. Nazeeruddin,†[a] R. Humphry-Baker,[a] M. Grätzel*[a] and Barry A. Murrer[b]

[a] *Laboratory for Photonics and Interfaces, Institute of Physical Chemistry, Swiss Federal Institute of Technology, CH-1015 Lausanne, Switzerland*

[b] *Technology Centre, Johnson Matthey, Reading, UK RG4 9NH*

Bis(3,4-dicarboxypyridine)(1,4,8,11,15,18,22,25-octamethylphthalocyaninato)ruthenium(II) (JM3306) anchored to nanocrystalline TiO_2 films through the axial pyridine 3,4-dicarboxylic acid ligands is an efficient near IR sensitizer for photovoltaic injection cells based on nanocrystalline TiO_2 films.

Nanocrystalline solar cells have attracted significant attention as low cost alternatives to conventional solid state photovoltaic devices.[1] The most successful charge transfer sensitizers employed so far in these cells are polypyridyl-type complexes of ruthenium[2,3] yielding overall AM 1.5 solar to electric power conversion efficiencies of up to 10–11% and stable operation for millions of turnovers.[4] In order to improve further the performance of these devices it is imperative to enhance their near IR response which is weak owing to the small absorption coefficient of such ruthenium complexes above 650 nm. Phthalocyanines possess intense absorption bands in the near IR region and are known for their excellent stability rendering them attractive for photovoltaic applications.[5] They have been repeatedly tested in the past as sensitizers of wide band gap oxide semiconductors.[6,7] However, poor incident photon to electric current conversion yields were obtained remaining under 1% with these systems which is insufficient for solar cell applications. Here we report on the use of ruthenium phthalocyanines (RuPC) as a charge transfer sensitizer. While RuPC derivatives have been tested as agents for photodynamic cancer therapy[8,9] they have not been employed as redox sensitizers so far. The choice of Ru as a central metal offers the advantage to attach the chromophore through axial ligands to the surface of the oxide semiconductor. Using 3,4-dicarboxypyridine to anchor the dye to mesoscopic TiO_2 films we have achieved for the first time strikingly high photocurrent yields with phthalocyanines exceeding 60% in the near-IR region.

Bis(3,4-dicarboxypyridine)(1,4,8,11,15,18,22,25-octamethylphthalocyaninato)ruthenium(II) (JM3306) was synthesized according to literature procedure[10] and isolated as $[(PCMe_8)Ru\{3,4\text{-}py(CO_2)_2H\}_2]\cdot 3THF$. Elemental analysis (calculated mass% in parentheses): C, 62.05 (62.11); H, 4.86 (4.86); N, 10.79 (10.98). The absorption and emission spectra of an ethanol solution of this dye are shown in Fig. 1. The absorption band in the visible [Fig. 1(*a*)] has a maximum at 650 nm (ε = 49 000 $dm^3\ mol^{-1}\ cm^{-1}$) and that of the phosphorescence [Fig. 1(*b*)] is located at 895 nm the triplet state lifetime being 474 ± 5 ns under anaerobic conditions. The emission is entirely quenched [Fig. 1(*c*)] when JM3306 is adsorbed onto a nanocrystalline TiO_2 film. The dye was deposited by dipping a mesoscopic anatase film (thickness *ca.* 10 μm, coated onto conducting glass, LOF TEC 10, fluorine doped SnO_2 sheet resistance 10 $\Omega\ \square^{-1}$) as previously described[2] for several hours in a 2×10^{-5} M solution in ethanol containing 40 mM 3α,7α-dihydroxy-5β-cholic acid (Cheno) and 2.5% Me_2SO. The presence of Cheno is necessary to avoid surface aggregation of the sensitizer. The vibible band in the absorption spectrum of JM3306 is red shifted by 10 nm upon adsorption.

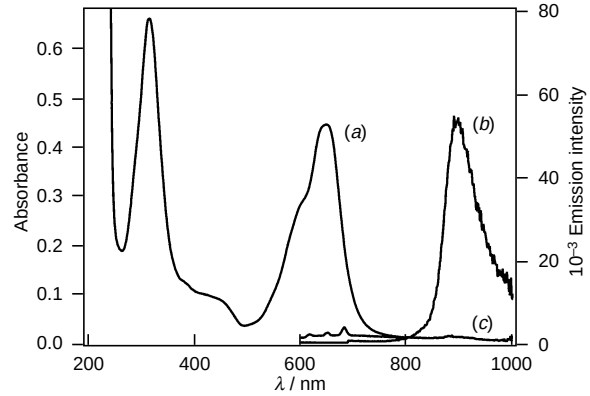

Fig. 1 Absorption (*a*) and emission (*b*) spectra of JM3306 in ethanol, concentration = 9×10^{-6} M; (*c*) quenched emission of JM3306 adsorbed onto the nanocrystalline TiO_2 film

The very efficient quenching of the emission of JM3306 was found to be due to electron injection from the excited triplet state of the phthalocyanine into the conduction band of the TiO_2. The photocurrent action spectrum is shown in Fig. 2 where the incident photon to current conversion efficiency (IPCE) is plotted as a function of wavelength. The feature is extending well into the near IR region displaying a maximum

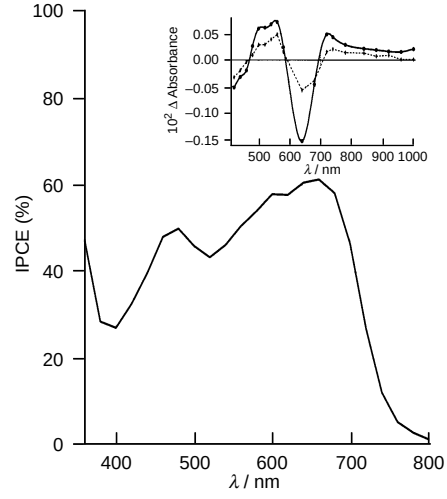

Fig. 2 Photocurrent action spectrum obtained with a nanocrystalline TiO_2 film supported onto a conducting glass sheet and derivatized with a monolayer of JM3306 and coadsorbed with Cheno. The incident photon to current conversion efficiency is plotted as a function of wavelength. A sandwich type cell configuration was used to measure this spectrum. The redox electrolyte was 0.5 M LiI–0.05 M LiI_3 in propylene carbonate solvent. Insert shows the transient spectra of JM3306 on a TiO_2 film, at time slices of 8 and 32 μs after the 532 nm (0.3 mJ) exciting pulse from a Nd-YAG laser.

around 660 nm where the IPCE exceeds 60%. Despite the fact that the pyridyl orbitals do not participate in the π–π*-excitation which is responsible for the 650 nm absorption band of JM3306, electronic coupling of its excited state to the Ti 3d conduction band manifold is strong enough through this mode of attachment to render charge injection very efficient. Bignozzi and coworkers[11] achieved very recently sensitization of TiO_2 with ruthenium polypyridyl type complexes where the coupling of the MLCT excited state to the conduction band manifold was through space and did not involve the anchoring group.

The occurrence of electron transfer was further confirmed by time resolved nanosecond laser experiments shown in the inset of Fig. 2. The end of the pulse transient spectrum indicates bleaching of the ground state absorption of JM3306 and the appearance of new features in the wavelength range 700–800 and 480–580 nm. These bands are attributed to the formation of the cation radical of the phthalocyanine.[9] The recovery of the ground state specrum due to charge recombination occurs on a time scale of several hundred microseconds indicating that recapture of the conduction band electron by the oxidized dye is a relatively slow process.

Our results establish a new pathway for grafting phthalocyanines to oxide surfaces through axially attached pyridine ligands. Using such a film in a sandwich type cell configuration[2] in conjunction with a 1 M LiI–0.05 M LiI_3 redox electrolyte photocurrents close to 10 mA cm^{-2} were readily obtained under simulated AM 1.5 solar radiation. These are by far the highest conversion efficiencies obtained with phthalocyanine type sensitizers. These findings open up new avenues for improving the near IR response of our nanocrystalline injection solar cell. In addition, important applications can be foreseen for the development of photovoltaic windows transmitting part of the visible light. Such devices would remain transparent to the eye, while absorbing enough solar photons in the near IR to render efficiencies acceptable for practical applications.

Partial financial support of this work by the Swiss Federal Institute for Energy is gratefully acknowledged.

Notes and References

† E-mail: nazeer@igcsun3.epfl.ch

1 B. O'Regan and M. Grätzel, *Nature*, 1991, **353**, 737.
2 Md. K. Nazeeruddin, A. Kay, I. Rodicio, R. Humphry-Baker, E. Müller, N. Vlachopoulos and M. Grätzel, *J. Am. Chem. Soc.*, 1993, **115**, 6382.
3 P. Péchy, F. P. Rotzinger, M. K. Nazeeruddin, Oliver Kohle, S. M. Zakeeruddin, R. Humphry-Baker and M. Grätzel, *J. Chem. Soc., Chem. Commun.*, 1995, 65.
4 N. Papageorgiou, Y. Athanassov, P. Bonhôte, H. Pettersson, A. Azam and M. Grätzel, *J. Electrochem. Soc.*, 1996, **143**, 3099.
5 D. Wöhrle and D. Meissner, *Adv. Mater.*, 1991, **3**, 129.
6 A. Giraudeau, Fu-Ren F. Fan and A. J. Bard, *J. Am. Chem. Soc.*, 1980, **102**, 5137.
7 H. Yanagi, S. Chen, P. A. Lee, K. W. Nebesny, N. R. Armstrong and A. Fujishima, *J. Phys. Chem.*, 1996, **100**, 5447.
8 M. J. Abrams, *Platinum Met. Rev.*, 1995, **39**, 14.
9 P. Charlesworth, T. G. Truscott, R. C. Brooks and B. C. Wilson, *J. Photochem. Photobiol. B: Biol.*, 1994, **26**, 277.
10 Johnson Matthey, *Int. Pat. Appl.*, PCT/GB-92/02061.
11 R. Argazzi, A. R. Chiarati, M. T. Indelli, F. Scandola and C. A. Bignozzi, Book of Abstracts L-09, *Eleventh International Conference on Photochemical Conversion and Storage of Solar Energy*, Bangalore, India, 1996.

Received in Basel, Switzerland, 8th December 1997; 7/08834E

Single-molecule magnets: out-of-phase ac susceptibility signals from tetranuclear vanadium(III) complexes with an $S = 3$ ground state

Ziming Sun,[a] Craig M. Grant,[b] Stephanie L. Castro,[b] David N. Hendrickson*[a] and George Christou*[b]†

[a] *Department of Chemistry-0358, University of California at San Diego, La Jolla, CA 92093-0358, USA*
[b] *Department of Chemistry, Indiana University, Bloomington, IN 47405-4001, USA*

The salts of the tetranuclear vanadium(III) ions $[V_4O_2(O_2CEt)_7(L–L)_2]^z$ (L–L = bpy, $z = +1$; L–L = pic$^-$, $z = -1$) with a V_4 butterfly topology and a $S = 3$ ground state have been found to exhibit out-of-phase ac susceptibility signals, a signature of single-molecule magnets.

The study of molecules possessing unusually large spin values in their ground state is an area of intense current research, particularly since the realisation in recent years that some species with this property exhibit the new phenomenon of single-molecule magnetism.[1–4] Such molecules provide a new approach to nanoscale magnets, and one with the major advantage that it provides 'magnetic particles' that are both soluble and are composed of a single, sharply defined size. As such, they hold the promise of numerous technological applications, including access to the ultimate high-density memory device.

The first single-molecule magnet (SMM) to be discovered was $[Mn_{12}O_{12}(O_2CMe)_{16}(H_2O)_4]\cdot 2MeCO_2H\cdot 4H_2O$ with $S = 10$.[1–6] The related complexes $[Mn_{12}O_{12}(O_2CR)_{16}(H_2O)_x]$ (R = Et, $x = 3$;[2] R = Ph, $x = 4$[2]) with $S = 9$ or 10 also show SMM properties, as does $[PPh_4][Mn_{12}O_{12}(O_2CEt)_{16}(H_2O)_4]$, the first ionic SMM.[2] More recently, a second class of SMM has been discovered, the family of Mn molecules of formulation $[Mn_4O_3X(O_2CMe)_3(dbm)_3]$ (X = various; dbm = anion of dibenzoylmethane) with a $[Mn_4(\mu_3\text{-}O)_3(\mu_3\text{-}X)]^{6+}$ highly distorted cubane core and an $S = 9/2$ ground state.[7] Additionally, $[Fe_8O_2(OH)_{12}(tacn)_6]^{8+}$ (tacn = 1,4,7-triazacyclononane) has been reported to exhibit SMM behaviour.[8] We recently reported the synthesis of $[V_4O_2(O_2CEt)_7(bpy)_2][ClO_4]$ **1** (bpy = 2,2′-bipyridine)[9] with a $[V_4O_2]^{8+}$ butterfly core and a $S = 3$

ground state, and we have now discovered that **1** and the related complex $[NEt_4][V_4O_2(O_2CEt)_7(pic)_2]$ **2** (pic = 2-picolinate) are new additions to this small family of SMMs.

Ac magnetic susceptibility studies, which monitor the response of a material's magnetic moment to an applied oscillating magnetic field, are an excellent way to detect the slow relaxation of magnetisation characteristic of a SMM. Ac susceptibility data were collected on **1** and **2** in a 1.0 G ac field oscillating at 250, 500 or 1000 Hz with a dc field of zero. In the range 10–30 K, the value of χ'_mT (χ'_m is the in-phase ac susceptibility) for **1** is constant at $\sim$4.8 cm^3 K mol^{-1} (μ_{eff} = 6.20 μ_B) consistent with an $S = 3$ ground state and $g \approx 1.8$. Below 4.0 K, χ'_mT decreases from 4.13 cm^3 K mol^{-1} at 4.0 K to 3.47 cm^3 K mol^{-1} at 1.7 K [Fig. 1(top)] suggesting that at these temperatures the magnetisation of the complex cannot reverse its direction fast enough to keep in phase with the oscillating ac field. If this is the case, an out-of-phase magnetic susceptibility (χ''_m) signal should be seen; indeed, a χ''_m signal is observed [Fig. 1(bottom)] and found to be frequency dependent. Such behaviour is characteristic of single-molecule magnets, corresponding to superparamagnet-like behaviour normally associated with large, but single-domain collections of interacting spin carriers. However, the χ''_m signal for **1** is quite weak at the lowest temperature attainable with present instrumentation, the χ''_m value at 1.7 K being only *ca.* 1–2% of the χ'_m signal. Complex **2** gives similar results but a stronger χ''_m signal of *ca.* 0.05 cm^3 K mol^{-1} at 1.7 K and a 1000 Hz ac field oscillation frequency.

As was the case for the $[Mn_{12}O_{12}]$ and $[Mn_4O_3X]$ complexes, the slow relaxation of **1** and **2** can be rationalized as due to a barrier to magnetisation reversal arising from a sufficiently large S coupled with negative magnetic anisotropy ($D < 0$, where D is the zero-field splitting (ZFS) parameter). For **1** and **2**, the potential energy plot of Fig. 2 then applies and indicates that the barrier to magnetisation reversal from, say, 'up' ($M_s = -3$) to down ($M_s = +3$) is $|9D|$. Fitting of dc magnetisation *vs.* field data (not shown) collected in the 0.500–50.0 kG and 2.00–30.0 K ranges gave $S = 3$, $g = 1.93$ and $D = -1.52$ cm^{-1} for **1**, and $S = 3$, $g = 2.00$ and $D = -1.50$ cm^{-1} for **2**. Thus, the barrier to magnetisation reversal in the ac experiments is $|9D| \approx 13.5$ cm^{-1}, a relatively small number that rationalises only a weak χ''_m signal at 1.7 K. In contrast, the $S = 10$ and $D \approx -0.5$ cm^{-1} values for certain $[Mn_{12}O_{12}]$ complexes give a barrier of $|100D| \approx 50$ cm^{-1} and χ''_m signals in the range 6–8 K under comparable conditions.[1–6]

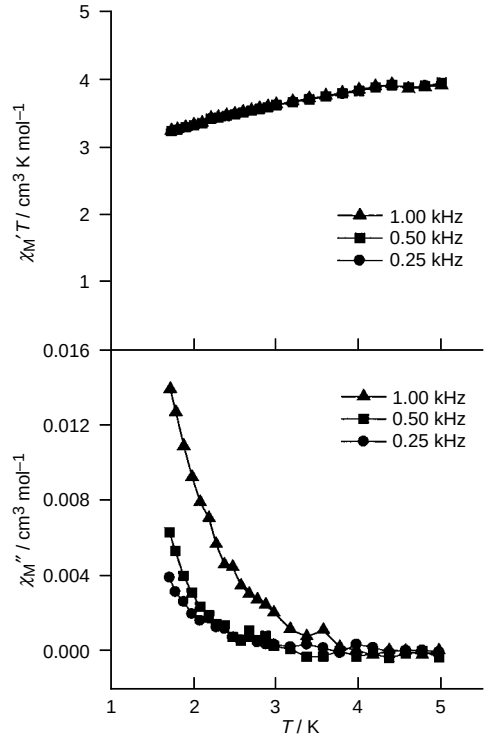

Fig. 1 Plots of χ'_mT *vs.* T (top) and χ''_m *vs.* T (bottom) for $[V_4O_2(O_2CEt)_7(bpy)_2][ClO_4]$ **1** in a 1.0 G ac field oscillating at the indicated frequencies (and with no applied dc field)

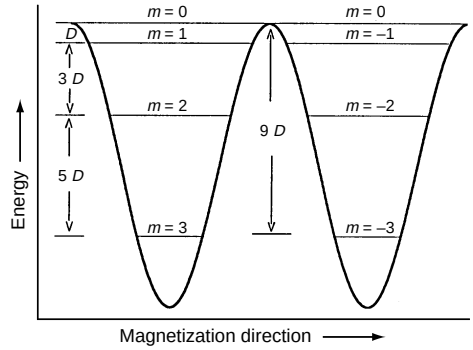

Fig. 2 Double-well potential energy *vs.* magnetisation direction diagram for an $S = 3$ system with a negative ZFS parameter D

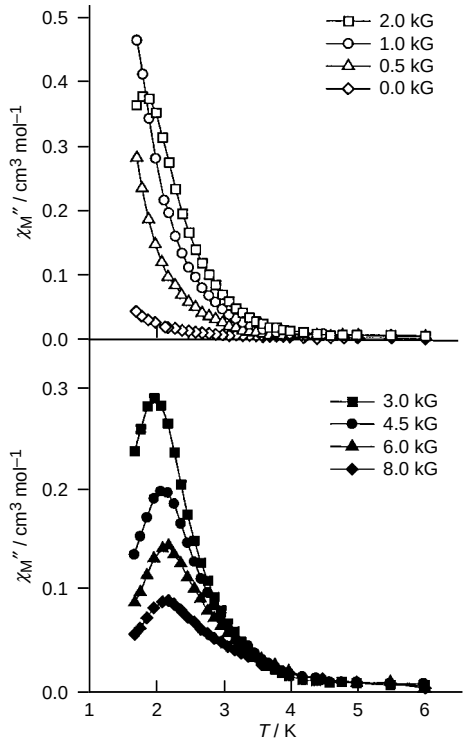

Fig. 3 Plots of χ''_m *vs.* T for $[NEt_4][V_4O_2(O_2CEt)_7(pic)_2]$ **2** in a 1.0 G ac field oscillating at 1000 Hz and applied dc fields of 0–2.0 kG (top) and 3.0–8.0 kG (bottom)

To better observe the χ''_m signals at $\geqslant$1.7 K, an external dc field was applied: this makes the double-well potential energy diagram of Fig. 2 asymmetric and slows down the relaxation rate by (*i*) increasing the barrier to (thermally activated) relaxation (originally $|9D|$), and (*ii*) making the energy levels on one side of the double-well no longer equienergetic to those on the other side, thus decreasing the rate of resonant quantum tunneling of magnetisation through the barrier. As a result, the χ''_m signal should move to higher temperatures. This is indeed observed for **1** and **2**. The data for **2** at different dc fields are shown in Fig. 3 and it can be seen that the χ''_m signal at 1.7 K increases in strength with increasing dc field, presumably as a χ''_m peak moves closer to the observable temperature range. Eventually, a peak does become visible at 1.8 K at 2.0 kG dc field, moving to 2.2 K at 8.0 kG field. The peak position represents the temperature at which the relaxation rate equals the ac field frequency.

To probe the stability of complex **1** in solution, ^{1}H NMR spectra were recorded in CD_2Cl_2. A total of 20 peaks were observed in the range δ +90 to −50 assignable to the $[V_4O_2(O_2CEt)_7(bpy)_2]^+$ cation. This is exactly the number expected for effective C_2 solution symmetry: eight bpy resonances, four CH_3 resonances in a 2:2:2:1 relative integration ratio, and eight CH_2 resonances in a 2:2:2:2:2:2:1:1 relative ratio resulting from the diastereotopic nature of the CH_2 hydrogen atoms. The resonances were fully assigned by 2D COSY and T_1 studies, together with Me-substitution on the bpy rings: full details will be provided elsewhere.[10] Similar results were obtained for **2**. The ^{1}H NMR studies thus show that these cations retain their structures on dissolution.

The combined data described above establish that the $[V_4O_2]^{8+}$ complexes are new examples of single-molecule magnets and that they retain their structural and therefore magnetic integrity in solution. The latter is noteworthy, given that, in addition to a small, sharply defined size, solubility is one of the greatest advantages of SMMs over conventional magnetic particles of nanoscale dimensions.

This work was supported by the US National Science Foundation.

Notes and References

† E-mail: christou@indiana.edu

1 R. Sessoli, H.-L. Tsai, A. R. Schake, S. Wang, J. B. Vincent, K. Folting, D. Gatteschi, G. Christou and D. N. Hendrickson, *J. Am. Chem. Soc.*, 1993, **115**, 1804; R. Sessoli, D. Gatteschi, A. Caneschi and M. A. Novak, *Nature*, 1993, **365**, 141.
2 H. J. Eppley, H.-L. Tsai, N. De Vries, K. Folting, G. Christou and D. N. Hendrickson, *J. Am. Chem. Soc.*, 1995, **117**, 301.
3 M. A. Novak, R. Sessoli, A. Caneschi and D. Gatteschi, *J. Magn. Magn. Mater.*, 1995, **146**, 211.
4 H.-L. Tsai, H. J. Eppley, N. De Vries, K. Folting, G. Christou and D. N. Hendrickson, *Mol. Cryst. Liq. Cryst.*, 1995, **274**, 167; H. J. Eppley, S. M. J. Aubin, M. W. Wemple, D. M. Adams, H.-L. Tsai, V. A. Grillo, S. L. Castro, Z. Sun, K. Folting, J. C. Huffman, D. N. Hendrickson and G. Christou, *Mol. Cryst. Liq. Cryst.*, 1997, **305**, 267.
5 J. R. Friedman, M. P. Sarachik, J. Tejada, J. Maciejewski and R. Ziolo, *J. Appl. Phys.*, 1996, **79**, 6031; J. R. Friedman, M. P. Sarachik, J. Tejada and R. Ziolo, *Phys. Rev. Lett.*, 1996, **76**, 3830.
6 J. M. Hernandez, X. X. Zhang, F. Luis, J. Bartolomé, J. Tejada and R. Ziolo, *Europhys. Lett.*, 1996, **35**, 301; E. M. Chudnovsky, *Science*, 1996, **274**, 938; J. M. Hernandez, X. X. Zhang, F. Luis, J. Tejada, J. R. Friedman, M. P. Saarachik and R. Ziolo, *Phys. Rev. B*, 1997, **55**, 5858.
7 M. W. Wemple, D. M. Adams, K. S. Hagen, K. Folting, D. N. Hendrickson and G. Christou, *J. Chem. Soc., Chem. Commun.*, 1995, 1591; S. M. J. Aubin, M. W. Wemple, D. M. Adams, H.-L. Tsai, G. Christou and D. N. Hendrickson, *J. Am. Chem. Soc.*, 1996, **118**, 7746.
8 A. L. Barra, P. Debrunner, D. Gatteschi, C. E. Schultz and R. Sessoli, *Europhys. Lett.*, 1996, **35**, 133.
9 S. l. Castro, Z. Sun, J. C. Bollinger, D. N. Hendrickson and G. Christou *J. Chem. Soc., Chem. Commun.*, 1995, 2517.
10 S. L. Castro, Z. Sun, C. M. Grant, J. C. Bollinger, D. N. Hendrickson and G. Christou, *J. Am. Chem. Soc.*, in press.

Received in Bloomington, IN, USA, 7th October 1997; 7/07266J

Reversible five-component assembly of a [2]catenane from a chiral metallomacrocycle and a dinaphtho-crown ether

Andrew C. Try,[a] Margaret M. Harding,*[a]† Darren G. Hamilton[b] and Jeremy K. M. Sanders*[b]†

[a] *School of Chemistry, University of Sydney, Sydney, NSW 2006, Australia*
[b] *Cambridge Centre for Molecular Recognition, University Chemical Laboratory, Lensfield Road, Cambridge, UK CB2 1EW*

Addition of a dinaphtho-crown ether to the components of a chiral metallomacrocycle affords a [2]catenane as the exclusive thermodynamic product; the reversible assembly process is driven by a combination of zinc(II)–bipyridyl ligation and π-donor/π-acceptor interactions between the electronically complementary aromatic components.

In recent years a range of non-covalent interactions have been employed in the template directed kinetically controlled syntheses of wholly organic catenated structures, including π-association of aromatic rings,[1] metal–ligand coordination[2] and hydrogen-bonding interactions.[3–5] The application of these strategies results in mechanically interlocked ring systems, whose separation would require the cleavage of a covalent bond.[6] Catenanes incorporating an organic ring and a magnesium metallomacrocycle,[7] as well as interlocked metallomacrocyclic structures,[8,9] have also been reported: incorporation of labile metal coordination sites into the ring introduces the possibility of reversibility into the threading process, although this feature has not hitherto been fully explored.[10] We now report the use of both metal ligation and donor–acceptor interactions to achieve quantitative catenane synthesis under reversible, thermodynamically controlled conditions.

We reported the design and synthesis of ligand L which assembles exclusively into a helical [2 + 2] metallomacrocycle in the presence of zinc(II) ions and a complementary aromatic substrate.[11,12] The π-electron rich aromatic guest plays a crucial role in the assembly process, effecting the selection of its optimal metallomacrocycle host from the range of geometries and oligomers present in solutions containing only L and Zn^{II}. The driving force for the formation of the supramolecular complex is provided by the π-donor/π-acceptor stacking interactions present in the final complex. Similar programmed recognition features between π-electron deficient aromatic diimides and the π-electron rich dinaphtho-crown ether **1** have been used to prepare neutral [2]catenanes in good yield *via* irreversible acetylenic couplings.[13–15] In light of these results we have utilised the electron-deficient diimide present in L and the electron-rich diethers of crown **1** to promote the assembly of a chiral [2]catenane in a thermodynamically controlled association process.

Titration of a solution of **1** into a CD_3CN solution of $L_2Zn_2OTf_4$ (in equilibrium with other oligomers)[11,12] resulted in a change from pale yellow to purple–maroon, indicative of the formation of a π-donor/π-acceptor complex (Scheme 1). Electrospray mass spectrometry of the complex was consistent with formation of the catenane, with peaks at *m/z* 530.8 $[L_2Zn_2\cdot\mathbf{1}]^{4+}$, 757.8 $[L_2Zn_2OTf\cdot\mathbf{1}]^{3+}$ and 1210.8 $[L_2Zn_2OTf_2\cdot\mathbf{1}]^{2+}$; no peaks corresponding to the individual components were detected.

Unambiguous evidence for formation of the catenane‡ was obtained by analysis of the ^1H NMR spectra obtained on titration of **1** into a solution of L and zinc(II) triflate. The resulting spectrum exhibits a new set of sharp signals [Fig. 1(*b*)]; an identical spectrum was also obtained upon dissolution of equimolar amounts of L, zinc(II) triflate and 0.5 equiv. of **1** in CD_3CN. Two distinct environments for the 'inner' and 'outer' naphthyl protons of **1** were detected,‡ both sets of signals resonating at higher field to those of 'free' **1**, an observation consistent with slow exchange of the crown naphthyl rings on the NMR chemical shift timescale. In the methylene region of the spectrum the predominant AB system of the $L_2Zn_2OTf_4$ host [Fig. 1(*a*)] is split into two AB systems upon interlocking with **1** [Fig. 1(*b*)], consistent with the helical catenated structure§ being templated out of the equilibrating mixture of complexes. Similar distinct changes were observed in the aromatic region of the spectrum where the protons of the naphthalenediimide spacer evolved from a singlet in the equilibrating pre-complexation mixture [Fig. 1(*a*)] to four doublets in the interlocked complex [Fig. 1(*b*)]. These observations taken in isolation suggest that the two diimide units of $L_2Zn_2OTf_4\cdot\mathbf{1}$, like the crown naphthyl rings, exist in 'inner' and

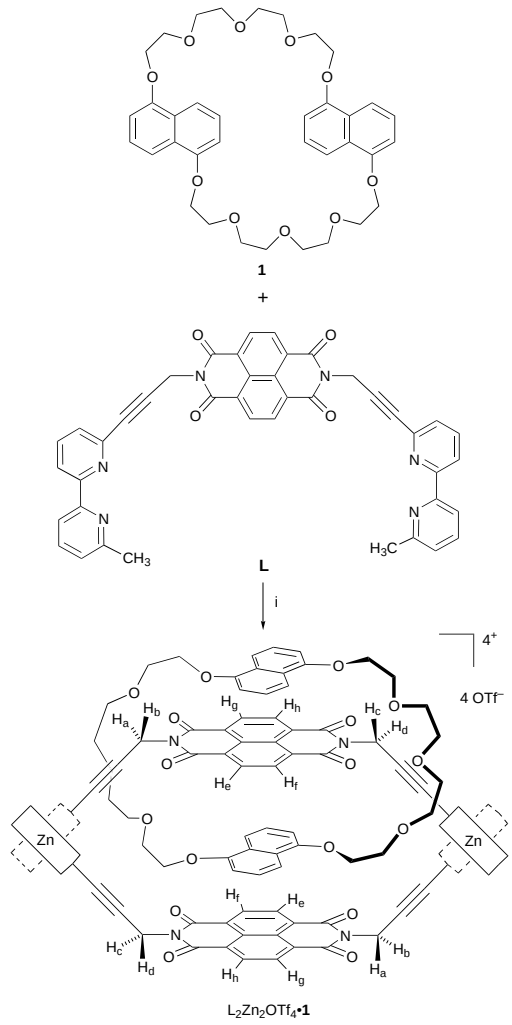

Scheme 1 *Reagents and conditions*: i, $Zn(OTf)_2$, acetonitrile

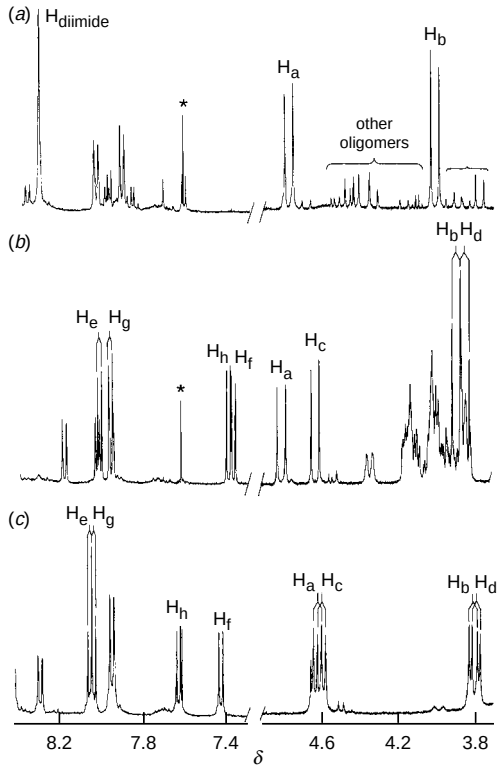

Fig. 1 ^{1}H NMR spectra (400 MHz, CD_3CN) of the methylene and aromatic regions of (*a*) $L_2Zn_2OTf_4$ (in equilibrium with oligomers) at 300 K, (*b*) $L_2Zn_2OTf_4$·**1** at 300 K and (*c*) $L_2Zn_2OTf_4$·**2** at 235 K; * impurity

'outer' environments (with respect to **1**). However, the appearance of similar splitting patterns in the complex formed between $L_2Zn_2OTf_4$ host and 1,5-dimethoxynaphthalene **2** at 235 K [Fig. 1(*c*)] indicates that the two diimide units of $L_2Zn_2OTf_4$·**1** are in the same environment (assigned as shown in Scheme 1).¶‖ This observation is consistent with an exchange process in which the 'outer' naphthyl ring of **1** is able to sweep around the periphery of $L_2Zn_2OTf_4$, rendering the two diimide components equivalent. This behaviour parallels that displayed by our recently reported neutral [2]catenanes.[13,14]

The catenane is remarkably stable: up to 350 K the maroon colour of the interlocked complex is retained and no signal coalescence is observed in the NMR spectrum. For comparison, the analogous complex formed with **2** contained exchange broadened resonances at room temperature; these coalesce on heating to 350 K to give two methylene doublets and a broad signal for the diimide protons, while at 235 K sharp, slowly-exchanging multiple resonances are observed [Fig. 1(*c*)]. Although the exact orientation of the bound naphthyl rings between the two aromatic diimide spacers is unknown, the optimal stacking of **1**, and also **2** (at 235 K), with $L_2Zn_2OTf_4$ results in overall asymmetry in this system.

We have shown that a stable [2]catenane can be non-covalently assembled from five components using pre-programmed recognition sites. The lability of the zinc(II)–bipyridyl coordination complex is an important feature of this system as it facilitates opening of the [2 + 2] metallomacrocycle to allow the thermodynamically favourable interlocking process in the presence of the crown. The access to a range of coordination geometries for zinc(II) is probably also important in optimising the electrostatic interactions between the π-complementary components. The principles embodied in the reversible nature of this assembly process should facilitate template-directed syntheses of more complex organic and supramolecular structures that would otherwise be difficult to obtain, and dynamic combinatorial libraries of mechanically interlocked structures.[16]

We acknowledge financial support from the Australian Research Council (M. M. H.) and EPSRC (J. K. M. S.).

Notes and References

† E-mail: harding@chem.usyd.edu.au, jkms@cam.ac.uk

‡ *Selected data* for $L_2Zn_2OTf_4$·**1**: ^{1}H NMR (CD_3CN, 300 K): $L_2Zn_2OTf_4$ resonances, δ 2.51 (6 H, s, 2 × CH_3), 2.63 (6 H, s, 2 × CH_3), 3.82 and 4.62 (4 H, AB system, *J* 17.3 Hz, H_a and H_b), 3.87 and 4.79 (4 H, AB system, *J* 17.2 Hz, H_c and H_d), 7.37 (2 H, d, *J* 7.6 Hz, H_f), 7.40 (2 H, d, *J* 7.6 Hz, H_h), 7.96 (2 H, d, *J* 7.8 Hz, 2 × H$^{5''}$), 7.97 (2 H, d, *J* 7.6 Hz, H_g), 8.02 (2 H, d, *J* 7.6 Hz, H_e), 8.03 (2 H, d, *J* 7.8 Hz, 2 × H$^{5''}$), 8.19 (2 H, d, *J* 8.1 Hz, 2 × H$^{5'}$), 8.42 (2 H, d, *J* 8.1 Hz, 2 × H$^{5'}$), 8.52 (2 H, app t, 2 × H$^{4''}$), 8.62 (2 H, app t, 2 × H$^{4''}$), 8.76 (2 H, d, *J* 7.9 Hz, 2 × H$^{3''}$), 8.81–8.85 (4 H, m, 2 × H$^{3''}$ and 2 × H$^{4'}$), 8.98–9.04 (4 H, app t, 4 × H$^{3'}$), 9.14 (2 H, app t, 2 × H$^{4'}$). **1**, δ 3.54–3.60 (2 H, m, CH_2), 3.63–3.70 (2 H, m, CH_2), 3.80–4.18 (26 H, m, 13 × CH_2), 5.29 [2 H, dd, *J* 2.3, 6.1 Hz, H^2 and H^6 (inner)], 5.68–5.73 [4 H, m, H^3, H^4, H^7 and H^8 (inner)], 5.94 [2 H, d, *J* 7.6 Hz, H^2 and H^6 (outer)], 6.42 [2 H, app t, H^3 and H^7 (outer)], 6.52 [2 H, d, *J* 8.4 Hz, H^4 and H^8 (outer)]; *m/z* 530.8 (L_2Zn_2·**1**, $C_{120}H_{96}N_{12}O_{18}Zn_2$, M^{4+}), 758.7 (L_2Zn_2OTf·**1**, $C_{121}H_{96}F_3N_{12}O_{21}SZn_2$, M^{3+}) 1210.8 ($L_2Zn_2OTf_2$·**1**, $C_{122}H_{96}F_6N_{12}O_{24}S_2Zn_2$, M^{2+}).

§ The helical configuration was assigned by comparison with our previous studies in which the metallomacrocycle host was characterised in both solution and the solid state.[11,12]

¶ The labelling of spin systems in Scheme 1 is arbitrary; unequivocal assignment of $H_{a,b}$ and $H_{c,d}$ was not possible as NOE crosspeaks to $H_{e,f,g,h}$ were not detected.

‖ Two-dimensional NOESY spectra of the catenane complex revealed the expected proton connectivities and additional cross-peaks from the inner naphthyl protons to the two bipyridyl H$^{5'}$ environments as well as to some of the naphthalene diimide protons.

1 D. B. Amabilino and J. F. Stoddart, *Chem. Rev.*, 1995, **95**, 2725.
2 J. C. Chambron, C. O. Dietrich-Buchecker, J. F. Nierengarten and J.-P. Sauvage, *Pure Appl. Chem.*, 1994, **66**, 1543.
3 C. A. Hunter, *J. Am. Chem. Soc.*, 1992, **114**, 5303.
4 F. Vögtle, S. Meier and R. Hoss, *Angew. Chem., Int. Ed. Engl.*, 1992, **31**, 1619.
5 A. G. Johnston, D. A. Leigh, L. Nezhat, J. P. Smart and M. D. Deegan, *Angew. Chem., Int. Ed. Engl.*, 1995, **34**, 1212.
6 A polyether lactone has been used to template the synthesis of cyclobis(paraquat-4,4′-biphenylene) in a catenated structure. Degradation of the catenane *via* ester hydrolysis afforded the free cyclobis(paraquat-4,4′-biphenylene), see: F. M. Raymo and J. F. Stoddart, *Pure Appl. Chem.*, 1996, **68**, 313; M. Asakawa, P. R. Ashton, S. Menzer, F. M. Raymo, J. F. Stoddart, A. J. P. White and D. J. Williams, *Chem. Eur. J.*, 1996, **2**, 877.
7 G.-J. M. Gruter, F. J. J. de Kanter, P. R. Markies, T. Nomoto, O. S. Akkerman and F. Bickelhaupt, *J. Am. Chem. Soc.*, 1993, **115**, 12 179.
8 M. Fujita, F. Ibukuro, H. Hagihara and K. Ogura, *Nature*, 1994, **367**, 720; M. Fujita, M. Aoyagi, F. Ibukuro, K. Ogura and K. Yamaguchi, *J. Am. Chem. Soc.*, 1998, **120**, 611.
9 D. J. Cárdenas and J.-P. Sauvage, *Inorg. Chem.*, 1997, **36**, 2777.
10 M. Fujita and K. Ogura, *Bull. Chem. Soc. Jpn.*, 1996, **69**, 1471.
11 A. Bilyk and M. M. Harding, *J. Chem. Soc., Chem. Commun.*, 1995, 1697.
12 M. A. Houghton, A. Bilyk, M. M. Harding, P. Turner and T. W. Hambley, *J. Chem. Soc., Dalton Trans.*, 1997, 2725.
13 D. G. Hamilton, J. K. M. Sanders, J. E. Davies, W. Clegg and S. J. Teat, *Chem. Commun.*, 1997, 897.
14 D. G. Hamilton, J. E. Davies, L. Prodi and J. K. M. Sanders, *Chem. Eur. J.*, 1998, in press.
15 D. G. Hamilton, N. Feeder, L. Prodi, S. J. Teat, W. Clegg and J. K. M. Sanders, *J. Am. Chem. Soc.*, 1998, **120**, 1096.
16 P. A. Brady and J. K. M. Sanders, *Chem. Soc. Rev.*, 1997, **26**, 327; S. J. Rowan and J. K. M. Sanders, *Chem. Commun.*, 1997, 1407; B. Hasenknopf, J.-M. Lehn, N. Boumediene, A. Dupont-Gervais, A. van Dorselaar, B. Kneisel and D. Fenske, *J. Am. Chem. Soc.*, 1997, **119**, 10 956; B. Klekota, M. H. Hammond and B. L. Miller, *Tetrahedron Lett.*, 1997, **38**, 8639.

Received in Cambridge, UK, 22nd December, 1997; 7/09112E

$Rb_2Au_6Sb_4S_{10}$: a novel sulfosalt with two different interpenetrating anionic frameworks: $[Au_3Sb_4S_8]^-$ and $[Au_3S_2]^-$

Jason A. Hanko and Mercouri G. Kanatzidis*†

Department of Chemistry and Center for Fundamental Materials Research, Michigan State University, East Lansing, Michigan 48824, USA

The layered compound $Rb_2Au_6Sb_4S_{10}$ consisting of two interpenetrating $[Au_3Sb_4S_8]^-$ and $[Au_3S_2]^-$ frameworks was prepared from the reaction of Au with a polythioantimonate flux.

Polychalcoantimonate fluxes can be used for the synthesis of new ternary and quaternary thioantimonate and selenoantimonate compounds.[1–4] This method is complementary to conventional direct combination of the binary sulfides[5] or hydro(solvento)thermal synthesis.[6] The polychalcoantimonate fluxes are formed by the *in situ* fusion of $A_2Q/Sb/Q$ and contain $[Sb_xQ_y]^{n-}$ ligands (A = Na, K, Rb, Cs; Q = S, Se) as well as polychalcogenide ligands. The key feature of this method is that the polychalcoantimonate units form and coordinate to metal ions to build up extended lattices. Examples include A_2AgSbS_4 (A = K, Rb, Cs),[3,4] $Cs_3Ag_2Sb_3Q_8$ (Q = S, Se),[3,4] $KThSb_2Se_6$,[2] A_2AuSbS_4 (A = Rb, Cs)[3b] and $KHgSbS_3$.[7] Continuing our investigations of the coinage metals, particularly Au, we report here, the synthesis, structural characterization, and physical properties of a novel quaternary gold thioantimonate compound, $Rb_2Au_6Sb_4S_{10}$.‡ The novelty in this two-dimensional compound derives from the fact that its layers are comprised of two different and independent interwoven frameworks. The only other structurally characterized example of two interpenetrating frameworks is K_2PdSe_{10}.[8]

The strikingly complex structure of $Rb_2Au_6Sb_4S_{10}$§ is composed of two different interpenetrating layered frameworks, $[Au_3Sb_4S_8]^-$ and $[Au_3S_2]^-$, Fig. 1. As a result, $Rb_2[Au_3Sb_4S_8][Au_3S_2]$ is a more descriptive formula, and to the best of our knowledge, represents the first reported example of a compound in which a binary framework is interpenetrating with a ternary one. The $[Au_3Sb_4S_8]^-$ layer is strongly undulating and consists of infinite $[Sb_4S_7]^{2-}$ one-dimensional chains bound to $[Au_3S]^+$ units. The $[Sb_4S_7]^{2-}$ chain [Fig. 2(*a*)] is comprised of four condensed SbS_3 pyramids forming a twelve membered Sb–S ring. Two of the SbS_3 units share two corners leaving one terminal sulfide while the other two SbS_3 units share all three corners. The dimensions of the ring are 6.49(3) Å [Sb(4)–Sb(2)] by 7.83(3) Å [Sb(1)–Sb(3)]. The chains alternate above and below the layer in a staggered fashion [Fig. 2(*b*)]. The Sb atoms are in pyramidal coordination with Sb–S distances in the range from 2.21(6) to 2.65(6) Å [mean 2.46(3) Å] and compare well with those reported for $Cs_2Sb_4S_8$[1] and $Cs_3Ag_2Sb_3S_8$.[3,4] The discrete $[Au_3S]^+$ unit has a pyramidal sulfide linked to three linear Au^+ cations. The Au–S distances range from 2.28(4) to 2.46(5) Å and compare well with those found in $CsAu_3S_2$,[9a] AAuS[9b] (A = Na, K, Rb, Cs), $KAuS_5$[10] and $AAuSbS_4$[3] (A = Rb, Cs). The S–Au–S angles range from 170 to 174°.

The second framework, which is interwoven with the one described above is a $[Au_3S_2]^-$ layer. The $[Au_3S_2]^-$ layer is puckered with twelve-membered Au–S rings in an *anti*-B_2O_3 motif {ring dimensions: 6.91(2) Å [Au(4)···Au(4)] by 7.19(3) Å [Au(3)···Au(3)]}. Fig. 3(*a*) highlights the pyramidal sulfide and the puckered nature of the layer and Fig. 3(*b*) shows a perpendicular view. The Au–S distances are in the range from 2.25(4) to 2.46(5) Å and the S–Au–S angles range from 165 to 178°. The $[Au_3S_2]^-$ layered structure is similar but not identical to that observed in $CsAu_3S_2$.[9a]

Upon further inspection, it was observed that the Au^+ centers in $Rb_2Au_6Sb_4S_{10}$ aggregate to form a column that runs along the *c*-axis. There are two types of Au···Au interactions: those at ≤3.25 Å and those between 3.25 and 3.6 Å. Fig. 3(*c*) shows a view perpendicular to these Au-based columns. In Fig. 3(*c*) the interactions ≤3.25 Å are represented as solid lines while the Au···Au interactions between 3.25 and 3.60 Å are represented as dashed lines. The layers are separated by ten-coordinate $Rb(1)^+$ [Rb(1)–S (mean) 3.59(3) Å] and eight-coordinate Rb(2) [$Rb(2)^+$ [Rb(2)–S (mean) 3.50(3) Å].

The optical spectrum of $Rb_2Au_6Sb_4S_{10}$ reveals the presence of a sharp optical gap of 1.37 eV, suggesting the material is a semiconductor.

The far-IR spectrum¶ of $Rb_2Au_6Sb_4S_{10}$ displays absorptions at *ca*. 377 and 350 cm^{-1} which can be tentatively assigned to Sb–S stretching modes in the 'Sb_2S_4'-like backbone of the $[Au_3Sb_4S_8]^-$ framework.[1,3] Absorptions in the range 381–347 cm^{-1} are tentatively assigned to the Sb–S vibrational stretching modes by analogy with the $Cs_2Sb_4S_8$[1] and $Cs_3Ag_2Sb_3S_8$.[3] Absorptions below 347 cm^{-1} are assigned to Au–S vibrations as compared to Rb_2AuSbS_4.[3] By comparison with $KAuS_5$ the absorption at *ca*. 323 cm^{-1} is assigned as an Au–S stretching vibration.[10] The Raman spectrum¶ of $Rb_2Au_6Sb_4S_{10}$ displays absorptions in the range 377–350 cm^{-1} which are assigned to

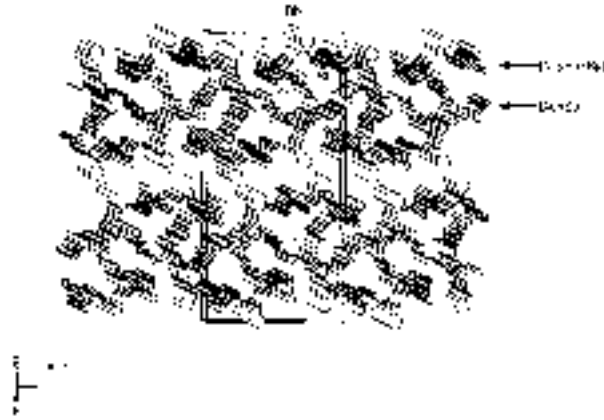

Fig. 1 Structure of $Rb_2Au_6Sb_4S_{10}$ viewed down the *c*-axis. Selected distances (Å) and angles (°) with esds in parentheses: Au(1)–S(3) 2.32(1), Sb(1)–S(6) 2.43(2), Au(1)–S(5) 2.30(1), Sb(1)–S(8) 2.47(1) (×2), Au(2)–S(2) 2.28(2), Sb(2)–S(5) 2.54(2), Au(2)–S(4) 2.30(2), Sb(2)–S(1) 2.48(1) (×2), Au(3)–S(3) 2.32(1), Sb(3)–S(6) 2.58(2), Au(3)–S(7) 2.31(1), Sb(3)–S(1) 2.48(1) (×2), Au(4)–S(3) 2.29(2), Sb(4)–S(4) 2.40(2), Au(4)–S(7) 2.30(2), Sb(4)–S(8) 2.47(1) (×2), Au(1)–Au(3) 3.192(3), Au(1)–Sb(1) 3.393(5), Au(1)–Au(4) 3.060(4), Au(1)–Sb(3) 3.233(5), Au(2)–Au(4) 3.593(1), Au(2)–Sb(2) 3.091(6), Au(1)–Au(1′) 3.588(4), Au(2)–Au(3) 3.389(4), Au(3)–Au(3′) 3.461(5), Au(3)–Au(4) 3.558(3); S(2)–Au(1)–S(5) 170.9(7), S(1)–Sb(3)–S(1′) 89.4(7), S(2)–Au(2)–S(4) 173.9(8), S(1)–Sb(3)–S(6) 95.6(5), S(3)–Au(3)–S(7) 178.4(7), S(1′)–Sb(3)–S(6) 95.6(5), S(3)–Au(4)–S(7) 170.0(8).

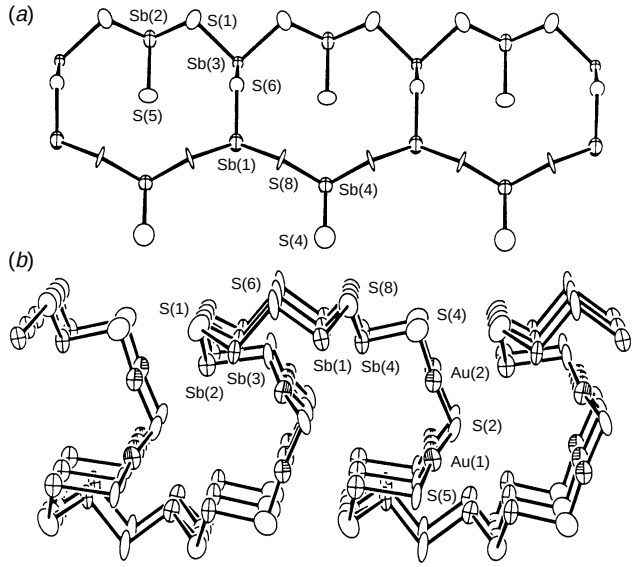

Fig. 2 (*a*) ORTEP view of the $[Sb_4S_7]^{2-}$ chain with labelling; (*b*) ORTEP view of the complete $[Au_3Sb_4S_8]^-$ framework with labelling

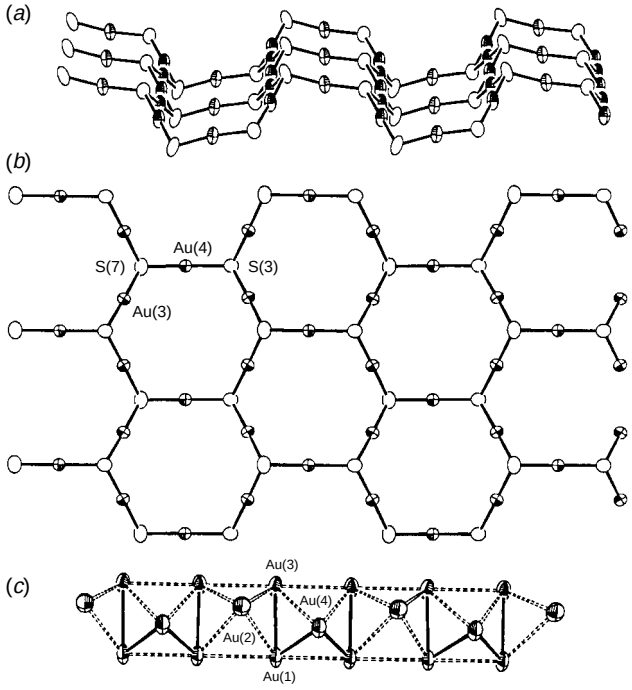

Fig. 3 (*a*) ORTEP view of the $[Au_3S_2]^-$ layer highlighting the pyramidal sulfides in the undulating layer; (*b*) perpendicular view of the $[Au_3S_2]^-$ layer with labelling; (*c*) Au···Au interactions of the Au column

Sb–S modes and the absorptions below 350 cm^{-1} are assigned to Au–S stretching vibrations.

DTA data, followed by careful XRD analysis of the residues, show that $Rb_2Au_6Sb_4S_{10}$ melts incongruently at *ca*. 442 °C. Examination of the residue by powder XRD revealed that the compound decomposes to an amorphous material and Au metal.

In conclusion, $Rb_2Au_6Sb_4S_{10}$ represents the first example of a sulfosalt with two different interpenetrating anionic frameworks. Although one of the frameworks $[Au_3S_2]^-$ can exist by itself, efforts to isolate the second framework alone are in progress.

Financial support from the National Science Foundation DMR-9527347 is gratefully acknowledged. M. G. K. is an A. P. Sloan Foundation, and a Camille and Henry Dreyfus Teacher Scholar 1993–98. The authors are grateful to the X-ray Crystallography Laboratory of the University of Minnesota and to Dr Victor G. Young, Jr. for collecting the single crystal X-ray data set. This work made use of the SEM facilities of the Center for Electron Optics at Michigan State University.

Notes and References

† E-mail: kanatzid@argus.cem.msu.edu

‡ $Rb_2Au_6Sb_4S_{10}$ was synthesized from a mixture of Rb_2S (0.102 g, 0.5 mmol), Au (0.098 g, 0.5 mmol), Sb (0.031 g, 0.25 mmol) and S (0.064 g, 2 mmol) sealed under vacuum in a Pyrex tube and heated to 350 °C for 4 days followed by cooling to 150 °C at 4 °C h^{-1}. The excess $Rb_x[Sb_yS_z]$ flux was removed by washing with DMF to reveal analytically pure black needles in low yield (20% yield based on Sb). The crystals are air- and water-stable. Microprobe analysis carried out on several randomly selected crystals gave an average composition of $RbAu_{4.6}Sb_{2.7}S_9$. This technique tends to underestimate the amount of Rb.

§ *Crystallography*: A Siemens SMART Platform CCD diffractometer equipped with Mo-Kα was used for a crystal of 0.400 × 0.010 × 0.005 mm. An empirical radiation (λ = 0.710 73 Å) absorption correction was applied to the data during data processing. *Crystal data* at −120 °C: a = 12.4402(2), b = 26.0790(4), c = 6.9614(1) Å, U = 2258.3(7) $Å^3$, Z = 4, D_c = 4.043 g cm^{-3}, space group *Pnnm* (no. 63), μ = 48.83 cm^{-1}, index ranges $-14 \leqslant h \leqslant 14$, $-31 \leqslant k \leqslant 28$, $-8 \leqslant l \leqslant 8$; total data 15609; unique data 2340 (R_{int} = 0.146), data with $F_o^2 > 3\sigma(F_o^2)$ 1181; no. of variables, 124; final R, R_w = 0.080, 0.096; GOF 2.66; max. peak in difference electron density map = 7.97 e^- $Å^{-3}$. The structure was solved with SHELXS-86 and refined with the TEXSAN Structure Analysis Package (Molecular Structure Corporation, 1985) of crystallographic programs. CCDC 182/760.

¶ Far-IR (CsI matrix) gave absorptions at *ca*. 381w, *ca.* 359w (sh), 347m, 325m, 306w, 295w, 270s and 233w cm^{-1}. Raman spectra (ground crystals) gave absorptions at *ca*. 377w, 350s, 323m, 285w, 266m and 250s cm^{-1}.

1 T. J. McCarthy and M. G. Kanatzidis, *Inorg. Chem.*, 1994, **33**, 1205.
2 K.-S. Choi, L. Iordanidis, K. Chondroudis and M. G. Kanatzidis, *Inorg. Chem.*, 1997, **36**, 3804.
3 (*a*) J. A. Hanko and M. G. Kanatzidis, Abstract No. 0413 from 210th Fall ACS Meeting, Chicago Il 1995; (*b*) J. A. Hanko and M. G. Kanatzidis, submitted.
4 P. T. Wood, G. L. Schimek and J. W. Kolis, *Chem. Mater.*, 1996, **8**, 721; G. L. Schimek, T. L. Pennigton, P. T. Wood and J. W. Kolis, *J. Solid State Chem.*, 1996, **123**, 272.
5 For example see: G. Cordier and H. Schäfer, *Rev. Chem. Miner.*, 1981, **18**, 218; W. Dorrscheidt and H. Schäfer, *Z. Naturforsch., Teil B*, 1981, **36**, 410; G. Cordier, C. Schwidetzky and H. Schäfer, *Rev. Chem. Miner.*, 1982, **19**, 179.
6 W. Sheldrick and M. Wachhold, *Coord. Chem. Rev.*, in press; G. W. Drake and J. W. Kolis, *Coord. Chem. Rev.*, 1994, **137**, 131.
7 M. Imafuku, I. Nakai and K. Nagashima, *Mater. Res. Bull.*, 1986, **21**, 493.
8 K.-W. Kim and M. G. Kanatzidis, *J. Am. Chem. Soc.*, 1992, **114**, 4878.
9 (*a*) K. O. Klepp and C. Weithhaler, *J. Alloys Compd.*, 1996, **243**; (*b*) K. O. Klepp and C. Weithhaler, *J. Alloys Compd.*, 1996, **243**, 12; (*c*) W. Bronger and H. U. Kathage, *J. Alloys Compd.*, 1992, **184**; 87; (*d*) K. O. Klepp and W. Bronger, *J. Less-Common Met.*, 1987, **127**, 65; (*e*) K. O. Klepp and W. Bronger, *J. Less-Common Met.*, 1987, **132**, 173; (*f*) K. O. Klepp and W. Bronger, *J. Less-Common Met.*, 1988, **137**, 13; (*g*) K. O. Klepp and G. Brunnbauer, *J. Alloys Compd.*, 1992, **183**, 252.
10 Y. Park and M. G. Kanatzidis, *Angew. Chem., Eng. Ed. Engl.*, 1990, **29**, 914.

Received in Bloomington, IN, USA, 17th June 1997; 7/04254J

Typeset and printed by Black Bear Press Limited, Cambridge, England

ChemComm
FEATURE ARTICLE

Crystal engineering: molecular networks based on inclusion phenomena

Mir Wais Hosseini*[a] and André De Cian[b]

[a] *Laboratoire de Chimie de Coordination Organique, Université Louis Pasteur, Institut Le Bel, Strasbourg, France*
[b] *Laboratoire de Cristallochimie et Chimie Structurale, Université Louis Pasteur, Institut Le Bel, Strasbourg, France*

Inclusion processes based on molecular recognition processes may be used as a design principle for the generation of molecular networks in the solid state. Hollow tuneable molecular modules (koilands) based on fusion of pre-organised cavities were shown to be assembled in the solid state into one-dimensional molecular arrays (koilates) either by self-inclusion or by interconnection using connector molecules. The formation of the molecular networks in the crystalline phase was established by X-ray studies.

Introduction

Molecular solids are defined by the chemical nature of their molecular components and by their interactions with respect to each other in the crystalline phase. With our present level of knowledge, the complete understanding and therefore prediction of all intermolecular interactions in the crystalline phase seems unreachable. Therefore, it appears that crystal structures are not predictable.[1] However, following the statement by Jack Dunitz:[2] 'A crystal is, in a sense, the supramolecule *par excellence*', using appropriate molecular modules, one may predict some of the intermotive interactions. Molecular networks are defined as supramolecular structures, theoretically composed of infinite number of molecules, possessing translational symmetry.[3] Whereas molecules are described as assemblies of atoms interconnected by covalent bonds, by analogy, one may describe molecular networks as hypermolecules in which the connectivity between the elementary components (molecular modules) is ensured by non-covalent intermotive interactions.

The construction of large molecular networks (10^{-6}–10^{-3} m scale) with predicted and programmed structure may hardly be envisaged through step by step type strategy. However, the preparation of such higher-order materials may be reached through iterative self-assembling processes engaging individual modules. This strategy relies on a double analysis. One is at the molecular level, dealing with the individual modules composing the solid, and the other is at the supramolecular level, dealing with the intermotive or intermolecular interactions.[4,5] Obviously the latter type of analysis is more subtle. For the design and synthesis of molecular networks, the approach called molecular tectonics,[6] which is based on the self-assembly[7] of structurally defined and energetically programmed complementary tectons[8] (from Greek *tekton*: builder), seems to be the most viable one. The synthesis of solids based on iterative assembling of individual complementary tectons still remains a challenge. A strict control of the self-assembly of molecular modules in the solid state should lead to structurally strictly controlled molecular networks (one-, two- and three-dimensional solids).

Dealing with design, whereas an endo molecular receptor forms discrete molecular complexes with a selected exo-substrate, an exo-receptor may form either discrete species with substrates acting as stoppers or molecular networks in the presence of appropriate connectors (Fig. 1). Thus, in order to achieve an iterative assembling process, the building blocks or tectons must fulfil both structural and energy criteria. In particular, the complementary tectons must recognise each other (molecular recognition) and furthermore should allow the repetition of the recognition patterns which may be designed as assembling cores. These two requirements lead to molecular modules possessing connecting points or interaction sites located in a divergent fashion. We have previously reported exo-ligands based on mercaptocalix[4]arenes,[9a] calix-[4]arene,[9b] tetraarylporphyrin[9c] bearing bidentate catechol units and macrocyclic frameworks containing bipyridine units.[9d]

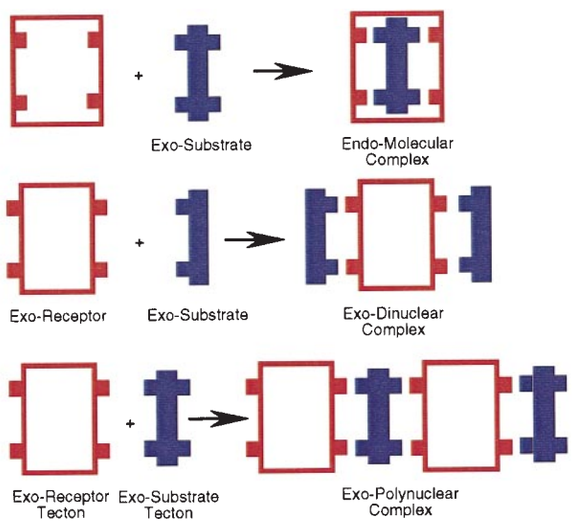

Fig. 1 Schematic representation of the formation of discrete molecular complexes by an endo-receptor and a substrate (top), by an exo-receptor and two stoppers (middle) or of a linear molecular network by an exo-receptor and a connector (bottom)

Thus, the most important operational concepts in molecular tectonics are molecular recognition between tectons and geometrical features, encoded within their frameworks, allowing the iteration of the recognition processes. Molecular networks may be obtained by an iterative assembling process of either self-complementary, or of several complementary tectons.

In terms of interaction energy between molecular modules governing the recognition and assembling processes, hydrogen[10] and coordination[11] bonds have been almost exclusively used for the formation of molecular networks. However, some time ago, we proposed the use of rather weak van der Waals interactions responsible for the inclusion processes between concave and convex molecules.[12,13] Although, based on the above mentioned approach, molecular networks were obtained using all three types of interactions, *i.e.* hydrogen bond,[14] coordination bond[15] and van der Waals interactions[12,13] the present article shall be mainly devoted to molecular networks based on inclusion phenomena in the solid state.

Design of koilands

The chemistry of inclusion complexes based on concave and convex molecules, *i.e.* the inclusion of a substrate within the cavity of a receptor molecule, is an established area. One may extend the concept of inclusion in solution to the construction of new networks in the solid state. Koilands[12,13] (from Greek *koilos*: hollow) were defined as multicavity receptor molecules composed of at least two cavities arranged in a divergent fashion. Since each individual cavity offers the possibility of forming inclusion complexes with a convex molecules, fusing, in a rigid framework, two or more of such cavities may lead in the presence of an appropriate connector to a non-covalently assembled polymeric species which may be called a koilate. For example, linear koilates (one dimensional linear molecular arrays or α-networks) may be assembled in the solid state using non-covalent van der Waals interactions between a rigid and compact direceptor possessing two divergent cavities with an angle of 180° between them (linear koiland) and a linear connector, possessing two extremities each capable of being included within the cavities of the direceptor (Fig. 2).

For the design of koilands, calix[4]arene derivatives[16] appeared to be candidates of choice (Fig. 3). Indeed, these compounds offer a preorganised and tuneable hydrophobic pocket surrounded by four aryl moieties as well as four hydroxy groups for further functionalisation. Furthermore, both the entrance and the depth of the preorganised cavity of calixarenes may be controlled by the nature of the substituent R at the *para* position (Fig. 4), *i.e.* Bu^t (**1**), H (**2**), Me (**3**), Ph (**4**). Whereas for the parent compounds **1**, **2** and **4** the cone conformation was established in the solid state by X-ray studies, to our knowledge, for compound **3** no X-ray data are available so far. The basket-type cavity of calix[4]arene derivatives such as **1** resulting from the cone conformation has been shown to accommodate in the solid state a variety of neutral guests.[17]

The design of koilands was based on the fusion of two calix[4]arenes derivatives in the cone conformation by two silicon atoms (Fig. 4).[12] Examples of fused calix[4]arenes using titanium(IV), niobium(V), aluminium(IV) and more recently zinc have been reported.[18] Two calix[4]arenes have also been interconnected by organic[19] and organometallic bridges.[20]

Tuning the cavity

The general strategy for the synthesis of koilands was based on treatment of the calix derivatives by NaH in dry THF followed by addition of $SiCl_4$. The desired compounds were usually obtained after chromatography on silica or by crystallisation. The starting material for the synthesis of all koilands reported was the *p-tert*-butylcalix[4]arene **1** prepared according to the published procedure.[21] The calix[4]arene **2** was obtained by aluminium chloride de-*tert*-butylation of **1**.[22] The latter was the common starting material for the synthesis of both *p*-methylcalix[4]arene **3** and *p*-phenylcalix[4]arene **4**. Although the syntheses of **3**[23] and **4**[24] were first reported by Gutsche *et al.*, the procedures by Ungaro and coworkers[25] and by Atwood and coworkers[26] respectively were found to be more convenient. The koilands **9**[27] (42%), **12**[12] (60%) and **14**[27] (17%) based on the double fusion of two *p*-methylcalix[4]arenes **3**, *p-tert*-butylcalix[4]arene **1** and *p*-phenylcalix[4]arenes **4**, respectively

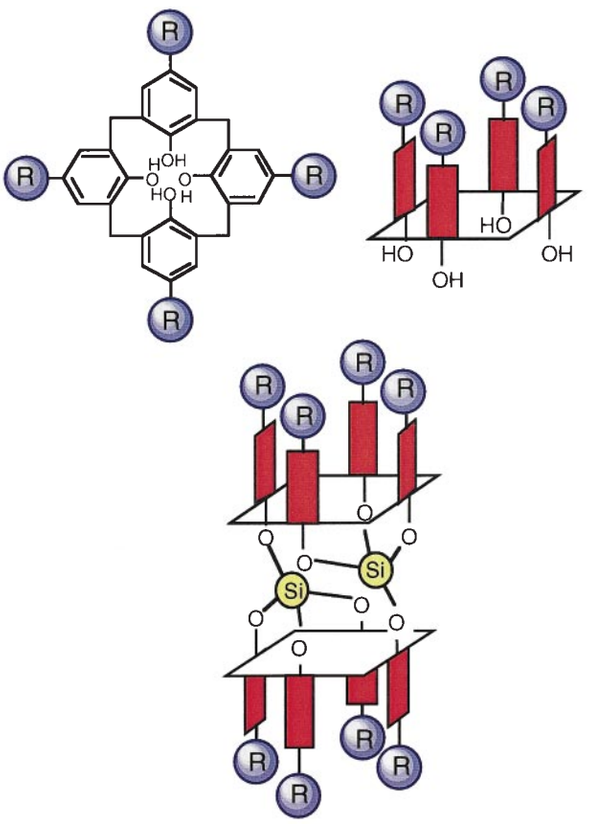

Fig. 3 Calix[4]arene derivatives (top left) and schematic representations of its cone conformation (top right) and of linear koilands obtained by fusion of two such units by two silicon atoms (bottom)

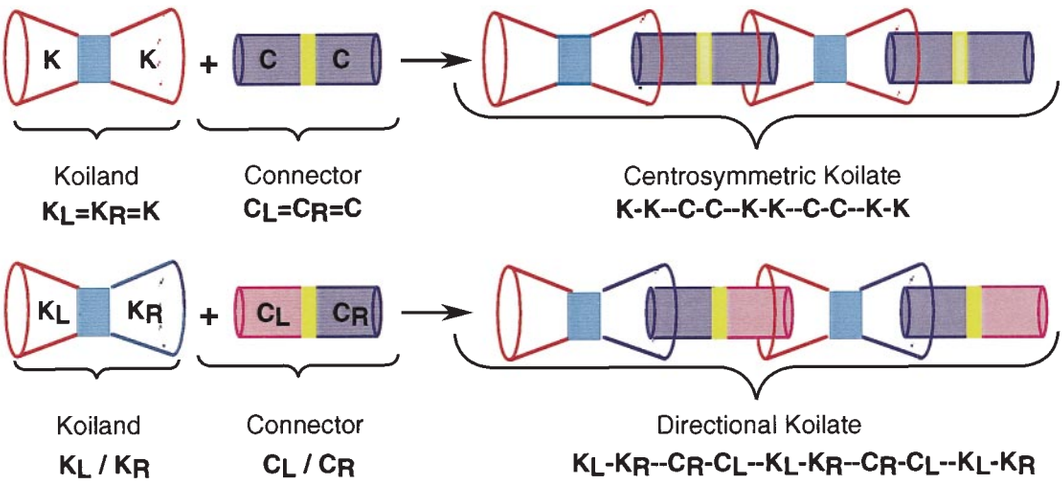

Fig. 2 Schematic representation of the formation of centrosymmetric (top) and directional (bottom) koilates (linear molecular network) by centrosymmetric (top) or non-centrosymmetric (bottom) linear koilands and connectors

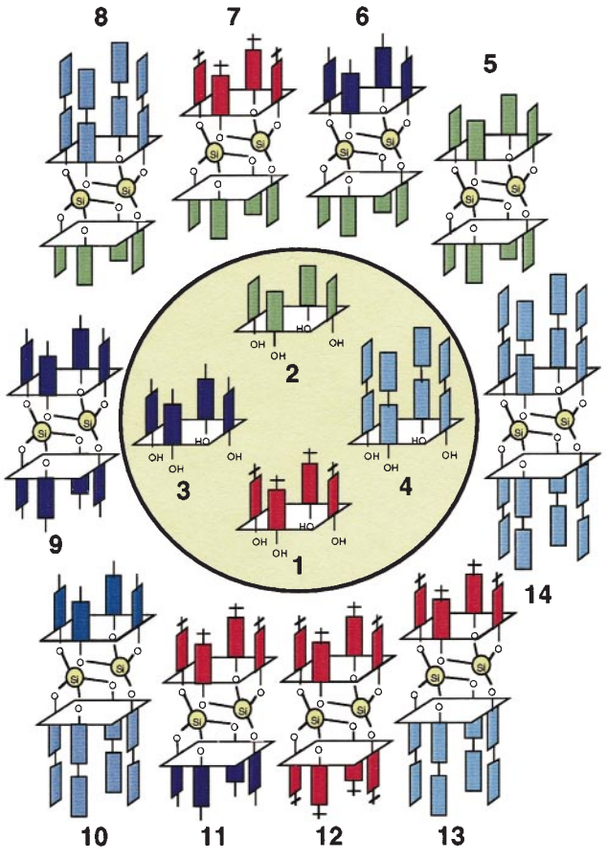

Fig. 4 Schematic representation of parent calix[4]arene derivatives **1**–**4** used as preorganised cavities and of centro-symmetric (**5**, **9**, **12**, **14**) and non-centrosymmetric (**6**–**8**, **10**, **11**, **13**) koilands formed by fusion of two calix units by two silicon atoms

with two silicon atoms were obtained as colourless stable crystalline solids.

The solid state structures of **9**[27] and **12**[12] were confirmed by X-ray studies which revealed that both compounds were indeed centrosymmetric aryloxy dimers consisting of two Si and two calixarenes. Both calixarene units were in cone conformation, thus presenting two divergent cavities (Fig. 5).

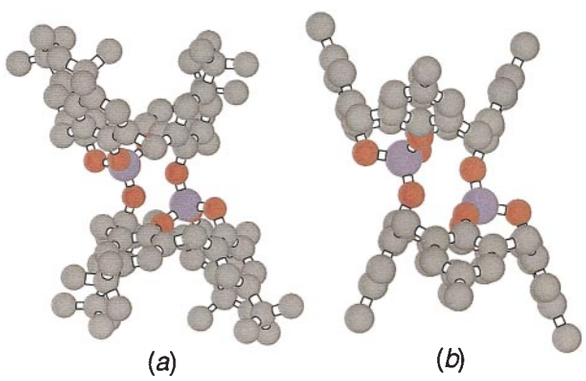

Fig. 5 X-Ray structures of linear koilands **9** (*a*) and **12** (*b*) showing the interconnection of two cavities in a linear fashion. For the sake of clarity, solvent molecules and hydrogen atoms are not presented.

Formation of discrete binuclear inclusion complexes

In order to ascertain the possibility of double inclusion, discrete binuclear complexes composed of koiland **12** and $CHCl_3$,[12] anisol[28] and *p*-xylene[28] were prepared (Fig. 6). The crystal study showed that in all three cases, each cavity accommodates,

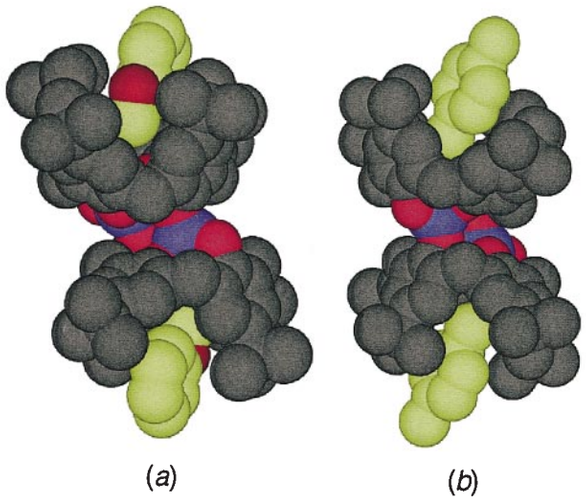

Fig. 6 X-Ray structures of discrete binuclear inclusion complexes formed by the linear koiland **12** and anisol (*a*) and *p*-xylene (*b*). For the sake of clarity, the carbon atoms of the substrate are coloured in green and the hydrogen atoms are not presented.

in a inclusive fashion, a solvent molecule. For the anisol co-crystals, amongst the four anisol molecules present in the lattice, only two of them, one at each side, were deeply inserted through their Me groups into the cavities of the hollow module [Fig. 6(*a*)]. In the case of *p*-xylene, although a sandwich complex composed of the parent compound **1** and the solvent with a 1 : 1 ratio was reported in the solid state,[29] with the koiland **12**, again a discrete binuclear inclusion complex in the solid state was obtained [Fig. 6(*b*)]. Again, amongst the three *p*-xylene molecules present, two of them penetrate deeply into the cavities of **12** through one of their Me groups. Whereas the formation of discrete binuclear complexes with $CHCl_3$ and anisol may be explained by their restricted dimension and unfavourable geometry, in the case of *p*-xylene possessing the right topology, one could, *a priori*, expect the formation of a koilate. However, it appeared from the X-ray study that the distance between the two Me groups ($d_{C–C}$ = 5.83 Å) was too short to allow the interconnection of two consecutive units and thus the formation of the koilate.

Formation of koilates

Hexadiyne, a rod type molecule, possessing both the requested linear geometry and distance between its two terminal Me groups ($d_{C–C}$ = 6.65 Å) leads indeed to the formation of the desired koilate (Fig. 7). The latter crystallises out from either

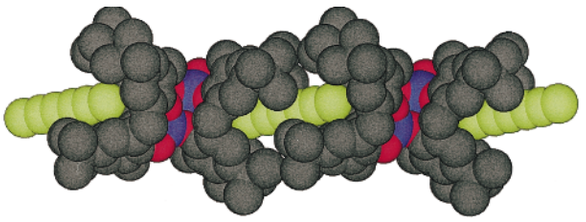

Fig. 7 A portion of the X-ray structure of the koilate formed between the koiland **12** and hexadiyne as the connector. The one-dimensional network is obtained by a single translation of the assembling core defined by the inclusion of the connector into the cavity of the receptor. For the sake of clarity, the carbon atoms of the connector are coloured in green and the hydrogen atoms are not presented.

$CHCl_3$–MeOH or $CHCl_3$–hexane mixtures of koiland **12** and hexadiyne in large excess.[28] The X-ray analysis revealed that in the crystal, in addition to **12** and hexadiyne present in 1 : 1 ratio, two $CHCl_3$ molecules were also present. The lattice is indeed composed of molecular linear arrays of koilates formed between

koilands **12** and hexadiyne as connectors. Each connector bridges two consecutive hollow bricks by penetrating their cavities through its terminal Me groups. The methyl groups of hexadiyne are deeply inserted into the cavity of the koiland. Indeed, the shortest distance between the Me group of the connector and the aromatic carbon atom (CO) of the koiland is 3.64 Å. It is worth noting that the hexadiyne molecules are extremely well encapsulated by two consecutive koilands **12** forming a sandwich, the shortest distance between the Me groups of the *tert*-butyl moieties of **12** being 3.51 Å.

Functionalisation of koilands

Calix[4]arene, in addition to the features stated above, presents further advantages by being readily modified at the *para* position by a large variety of substituents bearing functionalities. In particular, one may introduce at the *para* position functional groups such as allyl moieties.[30] It has been shown previously that although the compound **15** shows temperature-dependent conformational mobility, below room temperature it adopts a cone conformation.[30] The design of the new koiland **16** [Fig. 8(*a*)] possessing functional groups at both faces of the

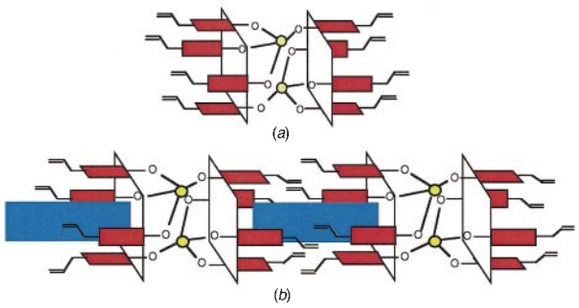

Fig. 8 Schematic representations of the doubly fused tetraallylcalix[4]arene **16** (*a*) and of the linear koilate formed in the presence of connector molecules (*b*)

molecule was based on the double fusion of the parent compound **15** with two silicon atoms.[31] Compound **15** was prepared according to published procedures[30] starting from compound **1**[21] which was dealkylated leading thus to the compound **2** and the latter was first converted into the allyl ether and then, by a Claisen rearrangement, to the desired compound **15**. The doubly fused compound **16** was obtained after column chromatography in 53% yield upon treatment of compound **15** in dry THF by NaH followed by addition of $SiCl_4$.[31]

Since it has been previously observed that *p*-xylene, a rigid, compact and ditopic molecule, forms in the solid mononuclear and binuclear inclusion complexes with *p-tert*-butylcalix[4]arene[17,29] **1** and with the koiland **12**[28] respectively, the formation of a one-dimensional network using compound **16** as the koiland and *p*-xylene as the connector was investigated [Fig. 8(*b*)]. Suitable crystals were obtained from a mixture of compound **16** and *p*-xylene in excess and Pr^iOH at room temperature. The X-ray analysis[31] showed the following features (Fig. 9). The crystals were composed exclusively of **16** and *p*-xylene disposed in an alternate fashion. Both the connector and the koiland were centrosymmetric, the latter offering two divergent cavities. The coordination geometry around the silicon atoms was tetrahedral. As predicted, a linear koilate was formed through the interconnection of two cavities belonging to consecutive koilands **16** with the *p*-xylene molecule. In the crystal one could identify an assembling core which could be defined as the inclusion of a Me group of the connector within a cavity of **16**. The shortest C–C distance of 3.63 Å between the Me groups of the connector and one of the carbon atoms belonging to one of the phenolic group at the bottom of the cavity indicated a high degree of inclusion. The formation of the α-network resulted from a single translation of the assembling core.

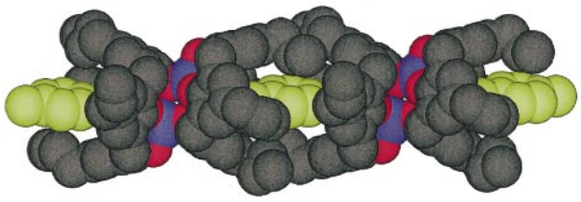

Fig. 9 A portion of the X-ray structure of the koilate formed between the koiland **16** and *p*-xylene as the connector. The one-dimensional network is obtained by a single translation of the assembling core defined by the inclusion of the connector into the cavity of the receptor. For the sake of clarity, the carbon atoms of the connector are coloured in green and the hydrogen atoms are not presented.

Although the formation of the α-network was predicted, the X-ray analysis revealed another unexpected feature. Due to the large number of rotations available for the allyl moieties, one cannot in fact predict their conformations in the crystal lattice. Interestingly, when looking at lateral packing of consecutive linear koilates, it was observed that among the eight allyl groups present in each koiland **16**, two of them were oriented centrosymmetrically in a peculiar manner (Fig. 10). Indeed, two

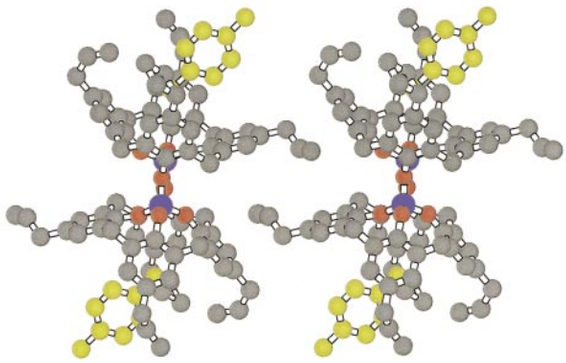

Fig. 10 A portion of the X-ray structure of the koilate formed between the koiland **16** and *p*-xylene as the connector showing the lateral packing of linear koilates leading to parallel disposition of the allyl moieties

alkene moieties belonging to two consecutive koilands were located perfectly parallel to each other with a alkene-to-alkene distance of 4.52 Å between them. Although the observed distance seems slightly too long, the proximity of the two double bonds suggests the possibility to interconnect covalently the koilates by performing a [2 + 2] cycloaddition reaction in the solid state.

It is interesting to notice that although, using compound **12** and hexadiyne, the first fully characterised linear koilate was obtained in the solid state,[28] one could nevertheless argue that, owing to the presence of $CHCl_3$ molecules in the lattice, the formation of the koilate was governed by solvent molecules. The formation of the koilate with compound **16** and *p*-xylene precludes this objection since in that case the linear koilate was formed in the solid without the presence of any solvent molecules in the lattice.

Formation of koilates by self-inclusion

As demonstrated above, koilands may lead in the solid state either to discrete molecular complexes in the presence of molecules acting as stoppers [Fig. 11(*a*)] or to linear molecular networks in the presence of appropriate connectors [Fig. 11(*b*)]. Another alternative route to the formation of linear koilate may be based on the use of self-complementary koilands possessing simultaneously two divergent cavities and connecting moieties [Fig. 11(*c*)]. Compound **16** fulfils these requirements. Indeed, the latter possesses two preorganised cavities resulting from the fusion of two calix units in cone conformation, as well as allyl groups at both faces of the molecule which may act as connectors.[32]

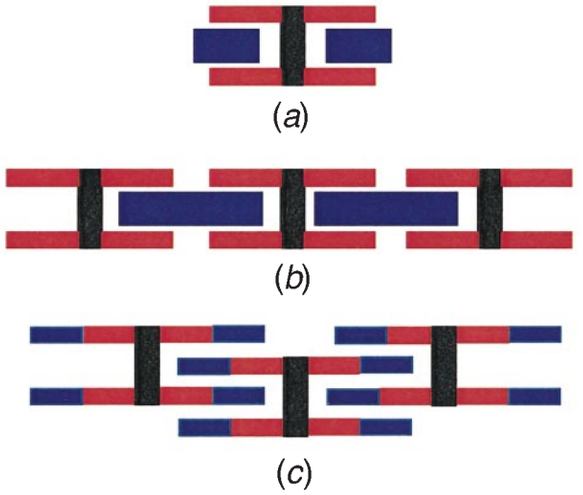

Fig. 11 Schematic representation of discrete binuclear inclusion complexes formed between koilands and stopper molecules (*a*) or of infinite linear molecular networks formed by koilands in the presence (*b*) and absence (*c*) of connector molecules

A study based on X-ray diffraction on single crystals obtained under various conditions for the compound **16** revealed indeed the formation of an α-network in the solid state. Upon slow liquid–liquid diffusion at room temperature of EtOH into a $CHCl_3$ solution of compound **16**, suitable large, colourless, air stable at room temperature, mono-crystals of the same morphology (rhombic) were obtained. The X-ray analysis revealed that the crystal was exclusively composed of compound **16**. The latter, offering two divergent cavities, was centrosymmetric. As in the case of other koilands presented above, the coordination geometry around the silicon atoms was tetrahedral. In the crystalline phase, the self-complementary koiland **16** formed a linear koilate (Fig. 12) through the

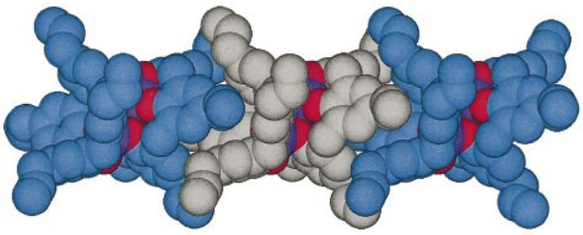

Fig. 12 A portion of the X-ray structure of the koilate formed by self-inclusion of the koiland **16**. The one-dimensional network is obtained by a single translation of the assembling core defined by the inclusion of the allyl moieties acting as internal connector into the cavity of the consecutive koiland **16**. For the sake of clarity, the carbon atoms of the consecutive koilands are differentiated by colour and the hydrogen atoms are not presented.

interconnection of two cavities belonging to consecutive koilands **16** by van der Waals interactions. The assembling core leading by a single translation to the α-network, could be identified as the inclusion of one of the four allyl groups located at one of the two faces of the molecule **16** by one of the two cavities of the consecutive self-complementary compound **16**. The shortest C–C distance between the terminal CH_2 of the allyl group acting as connector and carbon atoms of one of the aromatic moieties of the cavity belonging to the next unit varied from 3.63 to 3.92 Å, including a rather high degree of inclusion. Interestingly, when crystals of compound **16** were grown from other solvent systems such as toluene–EtOH, $CHCl_3$–Pr^iOH and toluene–Pr^iOH, in all cases, crystals of the same morphology and stability were obtained and their investigation by X-ray (lattice parameters) confirmed that they were the same. However, when crystals of **16** were grown by the same technique from a CH_2Cl_2–EtOH mixture, two types of crystals, one with a rod-type morphology and the other with rhombic shape, were observed. Whereas the crystals with rhombic morphology were stable at room temperature and proved by X-ray analysis to be of the same type as those mentioned above, the rod-shape crystals were unstable outside the solution. Their analysis by X-ray diffraction revealed the presence of **16** and three molecules of CH_2Cl_2. In the lattice two types of discrete inclusion complexes were present and therefore no network based on inclusion processes could be identified (Fig. 13). The

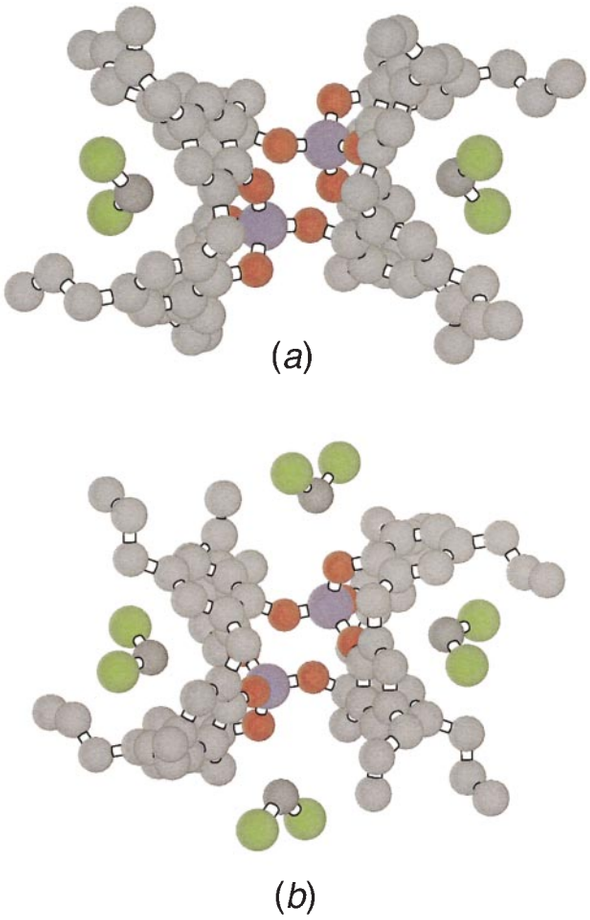

Fig. 13 X-Ray structures of the discrete bi- (*a*) and tetra-nuclear (*b*) inclusion complexes formed by the linear koiland **16** and CH_2Cl_2. For the sake of clarity, the hydrogen atoms are not presented.

two types of units were a binuclear [Fig. 13(*a*)] and a tetranuclear [Fig. 13(*b*)] CH_2Cl_2 inclusion complex. For the binuclear complex, both cavities of compound **16** were occupied by a CH_2Cl_2 molecule. For the tetranuclear species, among the four CH_2Cl_2 present, as in the case of the binuclear complex, two of them occupied the two preorganised cavities, whereas the remaining solvent molecules were located within the two 'pockets' resulting from the positioning of the allyl groups. The difference between the two discrete complexes observed in the lattice may be assigned to two different conformations adopted by the allyl groups.

It is worth noting that in the case of the self-complementary compound **16** depending on composition of the solution, all three situations (Fig. 11), *i.e.* discrete inclusion complexes and one-dimensional networks formed either by interconnection of consecutive units by connectors or by self-interconnection, were obtained.

Towards directional koilates

In dealing with one-dimensional networks, the control of the directionality of the assembly remains an important and

challenging issue. In all cases of koilates mentioned above, although the dimensionality of the molecular assembly could be controlled (α-network) by the geometrical features of the building blocks, due to their centrosymmetric nature, no particular directionality could be obtained (Fig. 1). In order to control both the dimensionality and the directionality of koilates, one may use non-symmetric koilands (Fig. 14). The design of non-centrosymmetric koilands may be based either on electronic or on geometric differentiation.

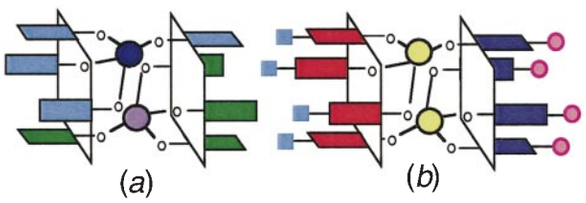

Fig. 14 Schematic representation of non-centrosymmetric koiland based either on electronic (*a*) or geometric (*b*) differentiation of the two cavities

Electronic differentiation [Fig. 14(*a*)] may be achieved by using two different fusing atoms with the same oxidation state IV such as Si and Ti or with different oxidation states III and IV such as B and Si. The non-symmetric nature of the Si–Ti heterobinuclear koiland is based on the induced difference between the two calix units by their coordination to two different metals with different electronegativity. Indeed, one of the calixes is triply coordinated to a Si atom whereas the other unit is triply coordinated to a Ti atom. The synthesis of the Si–Ti heterobinuclear koiland **17** [Fig. 15(*a*)] was achieved.[33] The stepwise strategy used was based on the preparation of the mono-fused compound **18** [Fig. 15(*b*)] which was shown by NMR ROESY experiments to adopt a face to face '*syn*' conformation. Upon treatment of the latter by $TiCl_4$ the desired compound **17** was obtained in high yield.

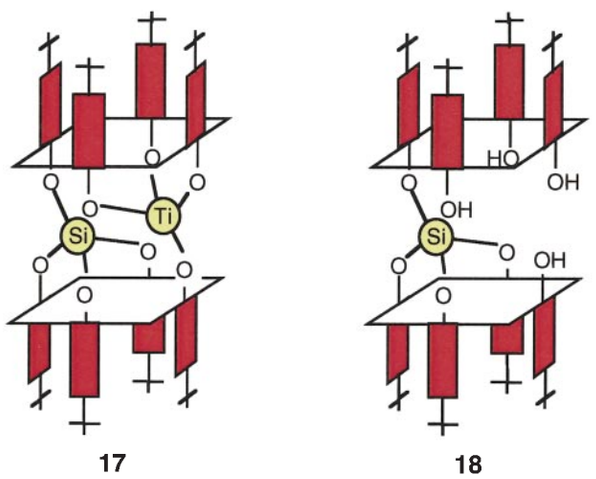

Fig. 15 Schematic representation of the koiland obtained by double fusion of two *p-tert*-butylcalix[4]arenes by silicon and titanium atoms **17** and of the mono-fused compound **18**

Geometric differentiation [Fig. 14(*b*)] may be accomplished, while keeping the same fusing element such as Si, by connecting two different calix units. Mixed compounds based on the double fusion of two different calix units by two Si atoms have been prepared. The general strategy for the preparation of non-symmetric koilands **6**–**8**, **10**, **11** and **13** (Fig. 4) was based on a combinatorial approach. Upon treatment of a combination of two different calix[4]arenes [X,Y] (X = Y = **1**–**4**) with base, followed by reaction with $SiCl_4$, as expected, three different koilands [X–X], [Y–Y] of the homo type (centrosymmetric) and [X–Y] of the hetero type (non-centrosymmetric) were obtained.[34]

In solution, as expected, ^{29}Si NMR studies revealed the presence of two signals for the non-centrosymmetric heterodimers, whereas for the centrosymmetric koilands a unique signal was observed. In the solid state structures of compounds **6** and **7** were confirmed by X-ray analysis (Fig. 16). For both

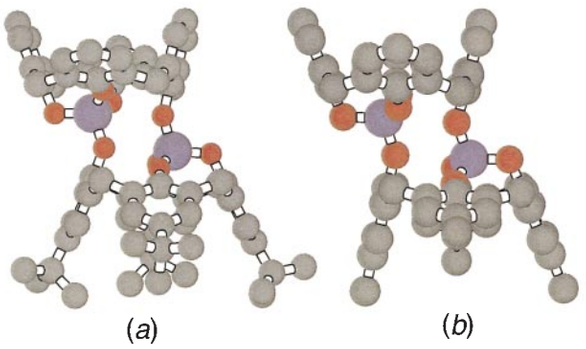

Fig. 16 X-Ray structures of linear koilands **6** (*a*) and **7** (*b*) showing the interconnection of two different calix units by two silicon atoms. For the sake of clarity, solvent molecules and hydrogen atoms are not presented.

compounds, the coordination geometry around the silicon atoms was tetrahedral. The Si–Si distance varied only slightly from 3.84 Å for **6** to 3.77 Å for **7**. These values are similar to those previously observed for compounds **9** and **12**.

Formation of directional koilates using the non-centrosymmetric koilands mentioned above is under current investigation.

Conclusions

In conclusion, it has been demonstrated that hollow molecular modules may be assembled in the solid state into one-dimensional molecular arrays either by self inclusion or by interconnection using connector molecules. Thus, inclusion processes based on van der Waals interactions may be used as a design principle for the generation of molecular networks in the solid state. Although at the present state of affairs, this approach remains essentailly structural, by using molecular building blocks possessing specific magnetic, photonic or electric properties, one may extend this strategy to the preparation of functional solids. Work along these lines is in progress.

This work was supported by the Université Louis Pasteur, Institut Universitaire de France and Centre National de la Recherche Scientifique. Thanks are also due to F. Hajek, Dr. E. Graf, Dr. X. Delaigue, Prof. J. Fischer and N. Kyritsakas.

Mir Wais Hosseini was born in 1955 in Kaboul, Afghanistan. In 1972 he moved to Strasbourg. He was mainly educated at the Louis Pasteur University, Strasbourg where he obtained his PhD degree in 1983 working with Jean-Marie Lehn. In 1981 he joind the French National Research Centre as a permanent member. After a postdoctoral fellowship spent in 1985 with Kenneth Raymond at Berkeley, he returned to Strasbourg where he continued to work with Jean-Marie Lehn. In 1990 he was appointed as a Professor of Organic Chemistry at Louis Pasteur University. In 1992 he was nominated for a period of five years at the Institut Universitaire de France. He was invited Professor at the University of Western Australia at Perth, University of Geneva, The Institute of Materials and Chemical Research, Tsukuba, Japan and University of Tokyo. His main research interests are in the area of molecular architecture and range from molecular receptors and catalysts to molecular networks and molecular materials.

André De Dian was born in 1942 in Aumetz, France. He completed his undergraduate and graduate studies at Louis Pasteur University, Strasbourg, he obtained his PhD degree at the same institution in 1972 working with Raymond Weiss.

After a postdoctoral fellowship with M. L. H. Green at Oxford, he returned to Strasbourg as a permanent researcher (French National Research Centre, CNRS). He is a chemist and crystallographer and his main scientific interests are in the area of porphyrins and mixed porphyrin/phthalocyanine derivatives as well as in the field of crystal engineering.

Notes and References

1 A. Gavezzotti, *Acc. Chem. Res.*, 1994, **27**, 309.
2 J. D. Dunitz, *Pure Appl. Chem.*, 1991, **63**, 177.
3 M. C. Etter, *Acc. Chem. Res.*, 1990, **23**, 120; G. M. Whitesides, J. P. Mathias and T. Seto, *Science*, 1991, **254**, 1312; F. W. Fowler and J. W. Lauher, *J. Am. Chem. Soc.*, 1993, **115**, 5991. X. Delaigue, E. Graf, F. Hajek, M. W. Hosseini and J.-M. Planeix, in *Crystallography of Supramolecular Compounds*, ed. G. Tsoucaris, J. L. Atwood and J. Lipkowski, NATO ASI, Kluwer, 1996, **C480**, 159; G. Brand, M. W. Hosseini, O. Félix, P. Schaeffer and R. Ruppert, in *Magnetism a Supramolecular Function*, ed. O. Kahn, NATO ASI, Kluwer, 1996, **C484**, 129.
4 J.-M. Lehn, *Supramolecular Chemistry, Concepts and Perspectives*, VCH, Weinheim, 1995.
5 G. R. Desiraju, *Angew. Chem., Int. Ed. Engl.*, 1995, **34**, 2311.
6 S. Mann, *Nature*, 1993, **365**, 499.
7 J. S. Lindsey, *New J. Chem.*, 1991, **15**, 153; D. S. Lawrence, T. Jiang and M. Levett, *Chem. Rev.*, 1995, **95**, 2229; D. Philip and J. F. Stoddart, *Angew. Chem., Int. Ed. Engl.*, 1996, **35**, 1155.
8 M. Simard, D. Su and J. D. Wuest, *J. Am. Chem. Soc.*, 1991, **113**, 4696.
9 (*a*) X. Delaigue, J. McB. Harrowfield, M. W. Hosseini, A. De Cian, J. Fischer and N. Kyritsakas, *J. Chem. Soc., Chem. Commun.*, 1994, 1579; X. Delaigue, M. W. Hosseini, A. De Cian, N. Kyritsakas and J. Fischer, *J. Chem. Soc., Chem. Commun.*, 1995, 609 (*b*) G. Mislin, E. Graf and M. W. Hosseini, *Tetrahedron Lett.*, 1996, **37**, 4503; (*c*) C. Drexler, M. W. Hosseini, A. De Cian and J. Fischer, *Tetrahedron Lett.*, 1997, **38**, 2993; (*d*) C. Kaes, M. W. Hosseini, R. Ruppert, A. De Cian and J. Fischer, *Tetrahedron Lett.*, 1994, **35**, 7233; C. Kaes, M. W. Hosseini, R. Ruppert, A. De Cian and J. Fischer, *J. Chem. Soc., Chem. Commun.*, 1995, 1445; C. Kaes, M. W. Hosseini, A. De Cian and J. Fischer, *Tetrahedron Lett.*, 1997, **38**, 3901; 4389; *Chem. Commun.*, 1997, 2229.
10 C. B. Aakeröy and K. R. Seddon, *Chem. Soc. Rev.*, 1993, **22**, 397; S. Subramanian and M. J. Zaworotko, *Coord. Chem. Rev.*, 1994, **137**, 357; D. Braga and F. Grepioni, *Acc. Chem. Res.*, 1994, **27**, 51; V. A. Russell and M. D. Ward, *Chem. Mater.*, 1996, **8**, 1654.
11 R. Robson, in *Comprehensive Supramolecular Chemistry*, ed. J. L. Atwood, J. E. D. Davies, D. D. Macnicol and F. Vögtle, Pergamon, New York, vol. 6 (ed. D. D. Macnicol, F. Toda and R. Bishop), 1996, p. 733.
12 X. Delaigue, M. W. Hosseini, A. De Cian, J. Fischer, E. Leize, S. Kieffer and A. Van Dorsselaer, *Tetrahedron Lett.*, 1993, **34**, 3285.
13 X. Delaigue, M. W. Hosseini, R. Graff, J.-P. Kintzinger and J. Raya, *Tetrahedron Lett.*, 1994, **35**, 1711.
14 G. Brand, M. W. Hosseini, R. Rupert, A. De Cian, J. Fischer and N. Kyritsakas, *New J. Chem.*, 1995, **19**, 9; M. W. Hosseini, R. Rupert, P. Schaeffer, A. De Cian, N. Kyritsakas and J. Fischer, *J. Chem. Soc., Chem. Commun.*, 1994, 2135; M. W. Hosseini, G. Brand, P. Schaeffer, R. Ruppert, A. De Cian and J. Fischer, *Tetrahedron Lett.*, 1996, **37**, 1405; O. Félix, M. W. Hosseini, A. De Cian and J. Fischer, *Angew. Chem., Int. Ed. Engl.*, 1997, **36**, 102; O. Félix, M. W. Hosseini, A. De Cian and J. Fischer, *Tetrahedron Lett.*, 1997, **38**, 1755; 1933; *New J. Chem.*, 1997, **21**, 285.
15 C. Kaes, M. W. Hosseini, C. E. F. Rickard, B. W. Skelton and A. H. White, *Angew. Chem.*, 1998, in press.
16 C. D. Gutsche, *Calixarenes, Monographs in Supramolecular Chemistry*, ed. J. F. Stoddart, Royal Society of Chemistry, London, 1989; *Calixarenes. A Versatile Class of Macrocyclic Compounds*, ed. J. Vicens and V. Böhmer, Kluwer Academic, Dordrecht, 1991; V. Böhmer, *Angew. Chem., Int. Ed. Engl.*, 1995, **34**, 713.
17 C., D. Gutsche, B. Dhawan, K. H. No and R. Muthukrishnan, *J. Am. Chem. Soc.*, 1981, **103**, 3782; G. D. Andreetti, R. Ungaro and A. Pochini, *J. Chem. Soc., Chem. Commun.*, 1979, 1005; R. Ungaro, A. Pochini, G. D. Andreetti and P. Domiano, *J. Chem. Soc., Perkin Trans. 2*, 1985, 197; M. Coruzzi, G. D. Andreetti, V. Bocchi, A. Pochini and R. Ungaro, *J. Chem. Soc., Perkin Trans. 2*, 1982, 1133.
18 M. M. Olmstead, G. Sigel, H. Hope, X. Xu and P. Power, *J. Am. Chem. Soc.*, 1985, **107**, 8087; F. Corazza, C. Floriani, A. Chiesti-Villa and C. Guastini, *J. Chem. Soc., Chem. Commun.*, 1990, 1083; J. L. Atwood, S. G. Bott, C. Jones and C. L. Raston, *J. Chem. Soc., Chem. Commun.*, 1992, 1349; J. L. Atwood, P. C. Junk, S. M. Lawrence and C. L. Raston, *Supramol. Chem.*, 1996, **7**, 15.
19 D. Kraft, J.-D. van Loon, M. Owens, W. Verboom, W. Vogt, M. A. McKervey, V. Böhmer and D. N. Reinhoudt, *Tetrahedron Lett.*, 1990, **31**, 4941; J.-D. van Loon, D. Kraft, M. J. K. Ankoné, W. Verboom, S. Harkema, V. Böhmer and D. N. Reinhoudt, *J. Org. Chem.*, 1990, **55**, 5176.
20 P. D. Beer, A. D. Keefe, A. M. Z. Slawin and D. J. Williams, *J. Chem. Soc., Dalton Trans.*, 1990, 3675.
21 C. D. Gutsche and M. Iqbal, *Org. Synth.*, 1989, **68**, 234.
22 C. D. Gutsche and J. A. Levine, *J. Am. Chem. Soc.*, 1982, **104**, 2652.
23 C. D. Gutsche and K. C. Nam, *J. Am. Chem. Soc.*, 1988, **110**, 6153.
24 C. D. Gutsche and K. H. No, *J. Org. Chem.*, 1982, **47**, 2708; K. H. No and C. D. Gutsche, *J. Org. Chem.*, 1982, **47**, 2713.
25 M. Almi, A. Arduini, A. Casnati, A. Pochini and R. Ungaro, *Tetrahedron*, 1989, **45**, 2177.
26 R. K. Juneja, K. D. Robinson, C. P. Johnson and J. L. Atwood, *J. Am. Chem. Soc.*, 1993, **115**, 3818.
27 F. Hajek, E. Graf and M. W. Hosseini, *Tetrahedron Lett.*, 1996, **37**, 1409.
28 F. Hajek, E. Graf, M. W. Hosseini, X. Delaigue, A. De Cian and J. Fischer, *Tetrahedron Lett.*, 1996, **37**, 1401.
29 M. Perrin, F. Gharnati, D. Oehler, R. Perrin and S. Lecocq, *J. Inclusion Phenom.*, 1992, **14**, 257.
30 C. D. Gutsche and J. A. Levine, *J. Am. Chem. Soc.*, 1982, **104**, 2653.
31 F. Hajek, E. Graf, M. W. Hosseini, A. De Cian and J. Fischer, *Angew. Chem., Int. Ed. Engl.*, 1997, **36**, 1760.
32 F. Hajek, E. Graf, M. W. Hosseini, A. De Cian and J. Fischer, *Mater. Res. Bull.*, 1998, in press.
33 X. Delaigue, M. W. Hosseini, E. Leize, S. Kieffer and A. Van Dorsselaer, *Tetrahedron Lett.*, 1993, **34**, 7561.
34 F. Hajek, E. Graf, M. W. Hosseini, A. De Cian and J. Fischer, *Tetrahedron Lett.*, 1997, **38**, 4555.

7/07355K

Novel ferrocene-based chiral Schiff's base derivative with a twist-grain boundary phase (TGBA) and a blue phase

Tarimala Seshadri*† and Hans-Jürgen Haupt

Department of Inorganic and Analytical Chemistry, University of Paderborn, Warburger Straße 100, 33098 Paderborn, Germany

Synthesis of a monosubstituted ferrocene-based chiral Schiff's base derivative with unusual mesomorphic behavior is reported namely the first metallomesogen which exhibits TGBA and blue phases apart from S_C*, S_A and N* phase transformations.

Chirality in ordered fluids has become one of the most fascinating and innovative fields of current research in liquid crystals. The quest to develop new chiral mesomorphic compounds led to the serendipitous discovery of new types of physical behavior namely the twist grain boundary (TGB)[1] and the blue phases[2] apart from the ferri- and antiferro-electric[2,3] liquid crystalline phases. The TGBA phase first discovered by Goodby *et al.*,[4] in 1989 was initially predicted by Gennes[5] in 1972. The appearance of the TGB phase[6] has induced enormous interest due to the formal analogy of its Landau free energy to that of the Shubnikov phase occurring in the type II superconductors.[5,7] Renn and Lubensky[7] in 1988 described this phase as a frustrated intermediate between N* and S_A phases. Since then, several new organic compounds showing such a phase were synthesized by different workers and their phase sequences were identified.[6]

Both the TGB and the blue phases are two kinds of frustrated phases which are found exclusively in chiral organic compounds. None of the chiral metallomesogens reported until now exhibited such phase formation, although several of their Pd, Cu and V complexes bearing one or more stereocenters were synthesized.[8] Nevertheless, incorporation of metals into the structures of low molar mass chiral liquid crystals to attain such phases must be a very challenging and attractive subject for study from both the academic and the applications point of view. Especially, introduction of ferrocene units as components of chiral liquid-crystalline materials may bring about high thermal stability and other additional properties among which its ability to undergo reversible one-electron transfer processes is one of the most important.[9]

However, studies on the synthesis of chiral smectic C mesophases comprising monosubstituted ferrocenyl group are scanty except the one reported by Imrie and Loubser.[10] The limited studies in this direction are attributed to the fact that monosubstituted ferrocenes, because of their unfavourable molecular shape (L-shape) and also due to repulsive steric effects of the ferrocene unit which hinders the ability of the molecules to pack in layers thus favouring mostly the formation of nemetic phases.[11–13]

We therefore attempted to prepare several ferrocene based chiral mesophases and surprisingly synthesized a compound that exhibits enantiotropic S_C*, S_A, a twist grain boundary phase (TGBA), a cholesteric as well as a blue phase. This is the first chiral metallomesogen which exhibits a TGBA and a blue phase.

The synthesis of the chiral Schiff's base derivative **8** is described in Scheme 1. To start with, we used the readily available (*S*)-(−)-2-methylbutan-1-ol for this purpose. In **8** the chiral centre with a small terminal chain is located adjacent to the rigid molecular core in order to couple strongly with the

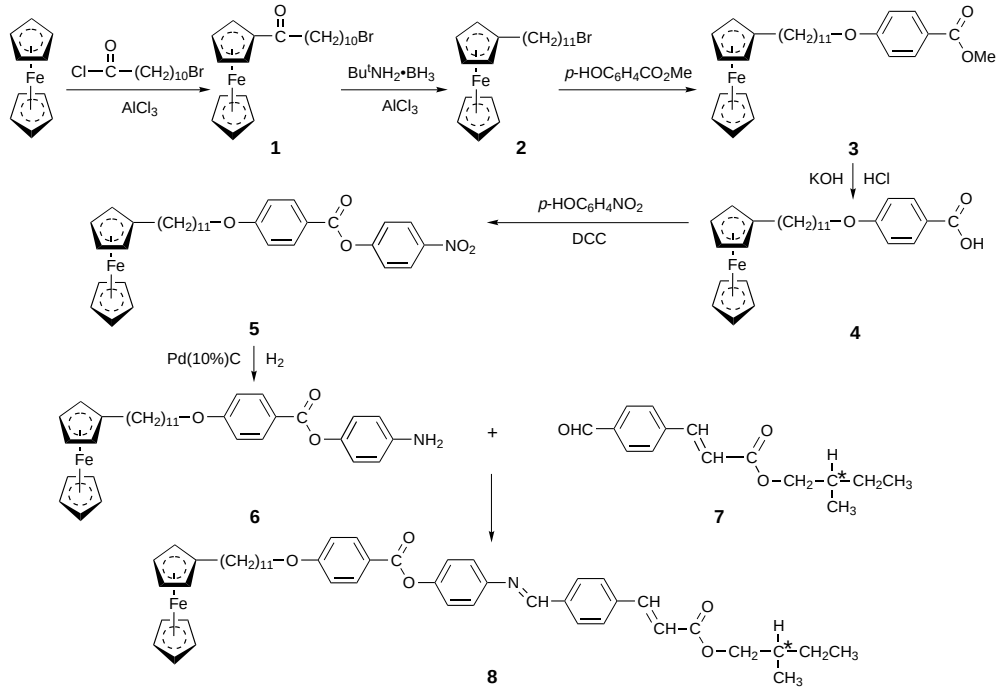

Scheme 1

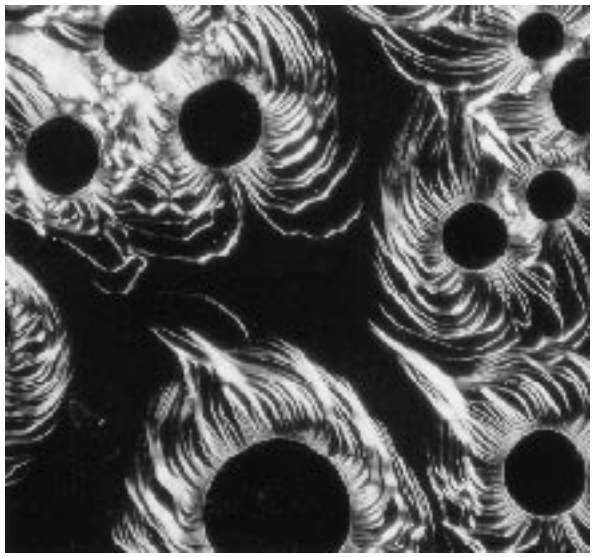

Fig. 1 Polarized optical micrograph of the TGBA phase on heating to 143.8 °C; magnification × 100

dipolar regions of the core. The phase assignments and transition temperatures (°C) of **8** shown below were determined by polarized optical microscopy using clean, untreated glass microscopic slides and cover slips as well as by differential scanning calorimetry (DSC) measurements.

C 116 S_C* 136 S_A 143.8 TGBA 144.9 N* 158 BP 159.2 I
I 157.2 BP 154.6 N* 143.1 TGBA 141.2 S_A 132.6 S_C* 77.9 C

At the S_A–S_C* transition, a dramatic textural change was observed whereby the dark homeotropic texture of the S_A phase gives rise to a *schlieren* texture characteristic of the S_C phase. The thermogram indicates that owing to the small enthalpy associated with these transitions, some of the peaks could not be detected. The calculated enthalpies (kJ mol^{-1}) are as follows. S_C*–S_A, 0.28; S_A–TGBA–N*, 0.55 and BP–I, 0.81.

When heating slowly (0.2° min^{-1}), the filament structure of the TGBA phase shown in Fig. 1, grows slowly in the homeotropic regions of the smectic A phase and ends up in a fire ball which coalesces into a cholesteric phase with a fan-shaped texture. Also oily streaks are seen upon subjecting the preparation to mechanical stress.

Both during heating and cooling cycles (0.2° min^{-1}), the formation of the blue phase is clearly seen as a platelet texture which is shown in Fig. 2.

The influence of orientation of ester linkages which directs the electron delocalization and the coplanarity of the two aromatic rings of benzylideneaniline (the angle between the two planes of these rings deduced from X-ray[14] and UV data[15] was found to be 66°) probably enhances the polarisability of the rigid core due to extended conjugation. This in turn enhances the preponderance of smectic phases and also creates favourable packing conditions. Furthermore, the presence of the flexible spacer between the phenyl ring and the ferrocenyl unit in **8** is primarily responsible for the formation of highly ordered phases, in the absence of which only a cholesteric phase was observed.

Compound **8** is very stable and no decomposition was seen during repeated heating and cooling cycles. Furthermore, a free-standing film can be prepared by heating the compound into its smectic state (130 °C) without any decomposition.

In conclusion, we report here a monosubstituted ferrocene-based metallomesogen with a chiral Schiff's base which shows for the first time a relatively long S_C* domain, a TGBA phase which mediates between S_A and N* and a blue phase just before the clearing point, in spite of a bulky pendant ferrocene unit on the one side and a relatively small terminal group appended to the chiral centre on the other side. This ferrocene derivative and derivatives thereof should be interesting candidates for preparing ferroelectric smectic C* materials useful in fast switching electro-optic devices.

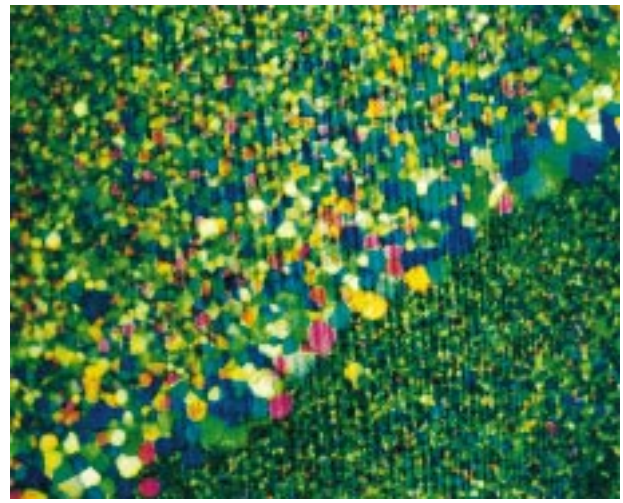

Fig. 2 Polarized optical micrograph of the blue phase platelet texture on cooling from the isotropic liquid to 156.1 °C; magnification × 100.

Notes and References

† E-mail: ts@chemie.uni-paderborn.de

‡ Detailed synthetic procedures for the intermediate ferrocenyl derivatives **1**–**6** will be reported separately. The final Schiff's base compound **8** is obtained by refluxing equimolar amounts of **6** and **7** in ethanol containing a few drops of acetic acid for 1 h and filtered hot through a sintered glass. The precipitate obtained after cooling was dissolved in dichloromethane and reprecipitated by the addition of heptane. Yield: 82%. Anal. Calc. for $C_{49}H_{57}FeNO_5$: C, 73.95; H, 7.22; N, 1.76. Found: C, 74.32; H, 7.27, N. 1.89%. FTIR (KBr) ν/cm^{-1}: 2919, 2848, 1714, 1606, 1513, 1311, 1253, 1188, 1162, 1068. ^{1}H NMR ($CDCl_3$), δ 0.90–0.99 (m, 6 H, CH_3), 1.20–1.70 (m, 18 H, 8 × CH_2, 1 CH_2), 1.85 (m, 3 H, 1 CH_2, 1 CH), 2.35 (m, 2 H, CH_2), 4.03–4.09 (m, 4 H, C_5H_4 + 4 H, 2 × OCH_2), 6.57 (d, 1 H, =CH), 7.75 (d, 2 H, Ar), 7.93–7.96 (d, 1 H, =CH), 7.14–7.17 (d, 2 H, Ar), 8.50 (s, 1 H, N=CH)

1 J. W. Goodby, M. A. Waugh, S. M. Stein, E. Chin, R. Pindak and J. S. Patel, *Nature*, 1989, **337**, 449.
2 J. W. Goodby, I. Nishiyama, J. Slaney, C. J. Booth and K. J. Toyne, *Liq. Cryst.*, 1993, **14**, 37.
3 A. Fukuda, Y. Takanishi, T. Isozaki, K. Ishikawa and H. Takezoe, *J. Mater. Chem.*, 1994, **4**, 997.
4 J. W. Goodby, M. A. Waugh, S. M. Stein, E. Chin, R. Pindak and J. S. Patel, *J. Am. Chem. Soc.*, 1989, **111**, 8119.
5 P. G. De Gennes, *Solid State Commun.*, 1972, **10**, 753.
6 H. S. Kitzerow, A. J. Slaney and J. W. Goodby, *Ferroelectrics*, 1996, **179**, 61; M. H. Li, V. Laux, H. T. Nguyen, G. Sigaud, P. Barois and N. Isaert, *Liq. Cryst.*, 1997, **23**, 389 and refs. therein.
7 S. R. Renn and T. C. Lubensky, *Phys. Rev. A*, 1988, **38**, 2132.
8 J. Buey, L. Diez, P. Espinet, H. S. Kitzerow and J. A. Miguel, *Chem. Mater.*, 1996, **8**, 2375 and refs. therein.
9 R. Deschenaux, M. Schweissguth and A. M. Levelut, *Chem. Commun.*, 1996, 1275.
10 C. Imrie and C. Loubser, *J. Chem. Soc., Chem. Commun.*, 1994, 2159.
11 R. Deschenaux and J. W. Goodby, in *Ferrocenes*, ed. A. Togni and T. Hayasi, VCH, Weinheim, 1995, ch. 9.
12 C. Loubser and C. Imrie, *J. Chem. Soc., Perkin Trans. 2*, 1997, 399.
13 T. Seshadri and H.-J. Haupt, *J. Mater. Chem.*, in press.
14 H. B. Bürgi and J. D. Dunitz, *Helv. Chim. Acta*, 1970, **53**, 1747.
15 J. Van Der Veen and A. H. Grobben, *Mol. Cryst. Liq. Cryst.*, 1971, **15**, 239.

Received in Cambridge, UK, 22nd December 1997; 7/09140K

Surprises in enolate binding at high valent molybdenum

Paul A. Cameron, George J. P. Britovsek, Vernon C. Gibson,*† David J. Williams and Andrew J. P. White

Department of Chemistry, Imperial College of Science, Technology and Medicine, Exhibition Road, London, UK SW7 2AY

Treatment of $[Mo(NAr)_2Cl_2(DME)]$ (Ar = 2,6-diisopropylphenyl; DME = 1,2-dimethoxyethane) with $LiOC(O\text{-}Bu^t)CMe_2$ at low temperature affords the unexpected carbon-bound molybdenum(VI) enolate complex $[Mo(N\text{-}Ar)_2Cl\{\eta^2\text{-}C(Me_2)CO_2Bu^t\}]$ 1; the novel α-aminoenolate derivative $[Mo(NAr)_2Cl\{\eta^2\text{-}CH(NMe_2)CO_2Et\}]$ 2 is obtained under analogous conditions using $LiNPr^i_2/Me_2NCH_2CO_2Et$; the structures of 1 and 2 confirm the carbophilic nature of the $[Mo(NAr)_2]$ core.

Transition metal enolate chemistry nowadays features prominently in organic synthetic methodology. The enolate ligand, an intermediate between an allyl and an acetate unit, has two different binding modes. Depending on the oxophilicity/carbophilicity of the metal centre, the enolato functionality can bind either *via* the 'CH_2' unit or *via* its oxygen atom [Scheme 1(*a*)], giving rise to different reactivity in further transformations. In general, the oxygen binding mode **I** predominates for early transition metals, whereas M–C bonding **III** is favoured by the softer late transition metals. A number of oxygen bound enolate complexes of early transition metals have been isolated and structurally characterised.[1–4] For molybdenum, only low valent molybdenum enolate complexes as in $[MoCp(CO)_3R]$ (R = enolate ligand) have been made and these are exclusively carbon bound.[5–9]

With a view to exploiting the isolobal relationship between the Cp_2M^{IV} and the $(RN)_2M^{VI}$ cores,[10,11] we became interested in establishing whether or not the relatively 'hard' high valent molybdenum centre would promote a switch from a carbon-bound to an oxygen-bound enolate binding mode, since oxygen-bound enolate complexes of early transition metal[12,13] and rare earth metallocenes[14,15] are implicated as the active species in the polymerisation of methyl methacrylate (MMA). Here, we describe the first examples of high valent molybdenum enolate complexes and their unusual and unanticipated structures.

Complex **1** was prepared according to Scheme 1(*b*), from $[Mo(NAr)_2Cl_2(DME)]$ and $[LiOC(OBu^t)CMe_2]$[16] at −78 °C. Recrystallisation from pentane at −30 °C afforded **1** as an orange crystalline product.‡ A second recrystallisation from heptane gave X-ray quality crystals of **1** and the molecular structure is shown in Fig. 1.§ Compound **1** decomposes slowly in solution ($t_{1/2}$ *ca.* 1 week) but can be stored for weeks in the solid state at −20 °C.

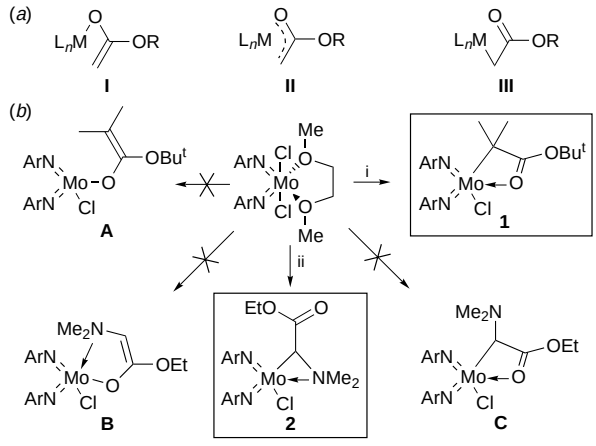

Scheme 1 (*a*) Potential binding modes of the ester enolate ligand. (*b*) *Reagents and conditions*: i, $LiOC(OBu^t)CMe_2$ (1 equiv.), Et_2O, −78 °C → room temp.; ii, LDA, $Me_2NCH_2CO_2Et$, THF, −78 °C → room temp.

The X-ray analysis of **1** reveals the unexpected bidentate coordination of the enolate ligand *via* the carbonyl oxygen atom O(2) and the α-carbon atom C(1). The geometry at Mo, although five-coordinate, is probably best described as distorted tetrahedral with the chelating enolate ligand occupying one of the tetrahedral sites; the angles subtended at Mo by the two imido N atoms and the Cl atom range between 105.4(4) and 111.3(3)°. The Mo–N distances are typical of 'linear' imido ligands, the angles at the N atoms being 157.6(8) [N(10)] and 158.5(8)° [N(23)].[17,18] The feature of most interest is the pattern of bonding to, and within, the enolate ligand. The 'stronger' coordination is to the α-C atom [Mo–C(1) 2.208(11) Å] whereas that to the carbonyl O atom is 2.370(6) Å. The C(1)–C(2) linkage [1.50(2) Å] has lost all its double bond character, though there is not a full pyramidalisation at C(1), the sum of the C–C(1)–C angles being *ca.* 342°. There is evidence for delocalisation between the two O atoms of the ester, the C(2)–O(2) and C(2)–O(3) distances being 1.24(2) and 1.29(2) Å, respectively.

Interestingly, complex **1** unveils a fundamental difference between the isolobal Cp_2M^{IV} and the $(ArN)_2M^{VI}$ cores. Whereas the analogous Cp_2M^{IV} complex $[Cp_2Ti\{O\text{-}C(OMe)CMe_2\}Cl]$ was found to be an O-bound enolate complex,[4] complex **1** does not bind similarly *via* the O atom as in complex **A**, but clearly establishes the carbophilic nature of the $(ArN)_2Mo^{VI}$ core.

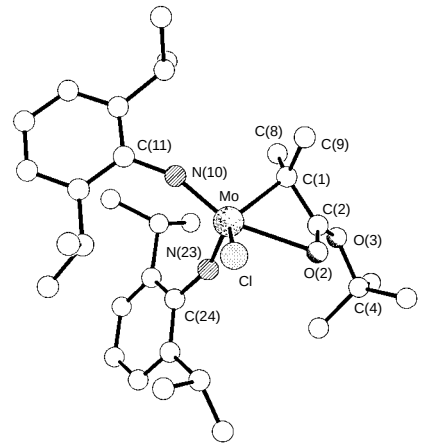

Fig. 1 Molecular structure of **1**. Selected bond lengths (Å) and angles (°); Mo–C(1) 2.208(11), Mo–C(2) 2.579(12), Mo–N(10) 1.754(9), Mo–N(23) 1.730(9), Mo–Cl 2.362(3), C(1)–C(2) 1.50(2), C(2)–O(2) 1.24(2), C(2)–O(3) 1.29(2); C(1)–Mo–O(2) 60.6(4), C(1)–Mo–Cl 128.1(3), C(1)–Mo–N(10) 101.4(4), C(1)–Mo–N(23) 105.4(5), O(2)–Mo–Cl 82.4(2), O(2)–Mo–N(10) 158.2(4), O(2)–Mo–N(23) 92.0(4), Cl–Mo–N(10) 102.6(3), Cl–Mo–N(23) 111.3(3), N(10)–Mo–N(23) 105.4(4), Mo–C(1)–C(2) 85.9(7), C(1)–C(2)–O(2) 115.1(11), C(2)–O(2)–Mo 85.1(6), C(11)–N(10)–Mo 157.6(8), C(24)–N(23)–Mo 158.5(8).

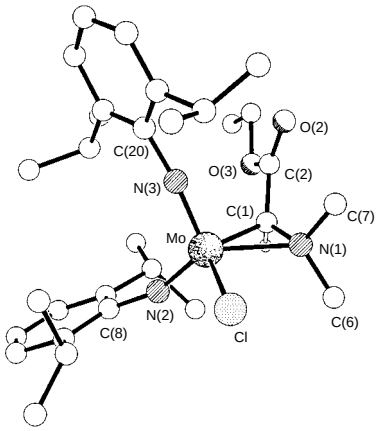

Fig. 2 Molecular structure of **2**. Selected bond lengths (Å) and angles (°); Mo–C(1) 1.149(6), Mo–N(1) 2.198(4), Mo–N(2) 1.753(4), Mo–N(3) 1.746(4), Mo–Cl 2.336(1), C(1)–N(1) 1.452(7), C(1)–C(2) 1.477(7), C(2)–O(2) 1.219(7), C(2)–O(3) 1.337(7), C(1)–Mo–N(1) 39.0(2), C(1)–Mo–N(2) 103.8(2), C(1)–Mo–N(3) 101.4(2), C(1)–Mo–Cl 124.3(2), N(1)–Mo–N(2) 125.8(2), N(1)–Mo–N(3) 112.4(2), N(1)–Mo–Cl 85.8(1), N(2)–Mo–N(3) 113.2(2), N(2)–Mo–Cl 105.9(1), N(3)–Mo–Cl 108.3(2), Mo–C(1)–N(1) 72.3(3), Mo–N(1)–C(1) 68.7(3), C(8)–N(2)–Mo 171.1(4).

Subsequently, an attempt was made to force the enolate ligand into an O-bound coordination mode, by using an α-aminoester enolate ligand [Scheme 1(*b*)]. It was anticipated that this ligand should produce a five-membered chelate, bound *via* the N and the carbonyl O donor to the metal centre as in complex **B** [Scheme 1(*b*)]. However, the strong carbophilic nature of the $(ArN)_2Mo^{VI}$ fragment again became apparent, resulting in the C-bound enolate complex **2**. Moreover, a three-membered chelate with an intramolecular coordination of the amine donor is formed. Thus, chelation of the carbonyl O to give a four-membered ring as in complex **C** is not observed [Scheme 1(*b*)]. Similar preferred arrangements have been reported previously for low valent Mo complexes.[19,20]

The preparation of complex **2** involved the *in situ* formation of the lithium enolate from LDA and $Me_2NCH_2CO_2Et$ in THF at −78 °C. Addition to $[Mo(NAr)_2Cl_2(DME)]$ at this temperature and extraction of the product with pentane at room temp. gave complex $[Mo(NAr)_2\{CH(NMe_2)CO_2Et\}Cl]$ **2** as a dark red crystalline solid.‡ Suitable crystals for X-ray analysis were obtained from pentane, and the molecular structure is given in Fig. 2.§

The X-ray structure of **2** again reveals an unexpected coordination of the α-aminoenolate ligand, with chelation *via* the amino atom N(1) and the α-C atom C(1) [with consequent loss of double bond character for C(1)–C(2)], rather than the carbonyl O atom O(2). As in **1**, the coordination at Mo can be considered as distorted tetrahedral, the enolate occupying a single coordination site [the N–Mo–N and N–Mo–Cl angles are in the range 106.9(1)–113.2(2)°]. The Mo–N(imido) distances are again typical of 'linear' species, with angles at N of 161.0(4) and 171.1(4)° for N(2) and N(3) respectively. As in **1**, the 'strong' bond to the α-aminoenolate ligand is to the α-C atom [2.149(6) Å] whereas that to N(1) is 2.198(4) Å. This contrasts with the pattern observed for related chelation to a Mo^{II} centre where the Mo–C bond is noticeably longer than that to N.[20] In the absence of coordination to the ester carbonyl O atom there is no delocalisation between the two O atoms.

In conclusion, we have shown that enolate complexes of the bis(imido)Mo^{VI} core are readily accessible and that the metal–carbon bonded form is favoured over the oxygen-bonded arrangement, confirming the surprisingly carbophilic nature of the Mo^{VI} centres in these complexes.

ICI Acrylics (CASE Award to P. A. C.) and EPSRC are gratefully acknowledged for financial support.

Notes and References

† E-mail: V.gibson@ic.ac.uk

‡ Satisfactory microanalyses and MS data were obtained for complexes **1** and **2**. *Selected spectroscopic data*: for **1**: IR (CsI, Nujol, cm^{-1}): 1567 [ν(C=O)]; ^{1}H NMR (C_6D_6, 250 MHz, 298 K), δ 6.99–6.91 (m, 6 H, *m*- and *p*-$C_6H_3Pr^i_2$-2,6), 3.92 [spt, 4 H, $^3J_{HH}$ 6.8 Hz, C*H*$(CH_3)_2$], 1.73 [s, 6 H, $C(CH_3)_2$], 1.34 [s, 9 H, $C(CH_3)_3$], 1.20 [d, 12 H, $^3J_{HH}$ 6.8 Hz, CH(C*H*$_3)_2$], 1.13 [d, 12 H, $^3J_{HH}$ 6.8 Hz, CH(C*H*$_3)_2$]; ^{13}C NMR (C_6D_6, 62.5 MHz, 298 K), δ 185.7 (s, O–C=O), 153.3 (s, *ipso*-$C_6H_3Pr^i_2$-2,6), 143.5 (s, *o*-$C_6H_3Pr^i_2$-2,6), 127.0 (d, *p*-$C_6H_3Pr^i_2$-2,6), 123.1 (d, *m*-$C_6H_3Pr^i_2$-2,6), 86.4 [s, Mo–$C(CH_3)_2$], 56.7 [s, *C*$(CH_3)_3$], 28.8, 28.0, 24.6, 24.0 (4s, 2Pr^i *Me*, Bu^t *Me*, Mo–C(*Me*)$_2$, 23.0 [d, *C*H$(CH_3)_2$]. For **2**: IR: 1718m [ν (C=O)]; ^{1}H NMR (C_6D_6, 250 MHz, 298 K), δ 7.1–6.8 (m, 6 H, Ar-H), 4.0–3.8 [4 spt., 4 H, $^3J_{HH}$ 6.8 Hz, C*H*$(CH_3)_2$], 3.85–3.57 (q, 2 H, $^3J_{HH}$ 7.1 Hz, OC*H*$_2CH_3$), 3.73 [s, 1 H, $(CH_3)_2$NC*H*], 3.12, 2.33 [2s, 6 H, (C*H*$_3)_2$NCH], 1.37, 1.24, 1.20, 1.14 [4d, 24 H, $^3J_{HH}$ 6.8 Hz, CH(C*H*$_3)_2$], 0.75 (t, 3 H, $^3J_{HH}$ 7.1 Hz, OCH_2CH_3). ^{13}C NMR (C_6D_6, 62.5 MHz, 298 K), δ 170.0 (s, C=O), 154.2, 153.0, 146.6, 140.9, 128.3, 127.6, 125.3, 122.5 (8s, ArC), 60.2 (s, OCH_2CH_3), 58.8 (s, NCH), 51.0, 42.8 [2s, $(CH_3)_2$N], 28.9, 28.5 [2s, *C*H$(CH_3)_2$], 24.4, 23.9, 23.4, 23.2 [4s, CH(*CH*$_3)_2$], 14.1 (s, OCH_2CH_3).

§ *Crystal data*: for **1**: $C_{32}H_{49}ClMoN_2O_2$, M = 625.1, monoclinic, space group $P2_1$ (no. 4), a = 9.376(2), b = 11.061(4), c = 16.496(3) Å, β = 103.18(2)°, U = 1665.8(7) Å^3, Z = 2, D_c = 1.25 g cm^{-3}, μ(Mo-Kα) = 5.0 cm^{-1}, F(000) = 660. An orange plate of dimensions 0.33 × 0.32 × 0.07 mm was used. For **2**: $C_{30}H_{46}ClMoN_3O_2$, M = 612.1, monoclinic, space group $C2/c$ (no. 15), a = 22.823(1), b = 8.981(1), c = 30.877(4) Å, β = 90.34(1)°, U = 6329(1) Å^3, Z = 8, D_c = 1.29 g cm^{-3}, μ(Cu-Kα) = 43.9 cm^{-1}, F(000) = 2576. An orange–red prism of dimensions 0.18 × 0.10 × 0.07 mm was used. 2661 (4325) Independent reflections were measured at 203 K on Siemens P4 diffractometers with graphite monochromated Mo-Kα and Cu-Kα (rotating anode source) radiation for **1** and **2** respectively using ω-scans. The structures were solved by direct methods and all the non-hydrogen atoms were refined anisotropically (with absorption corrected data for **2**) using full-matrix least squares based on F^2 to give R_1 = 0.057 (0.046), wR_2 = 0.097 (0.098) for 2088 (3430) independent observed reflections [$|F_o| > 4\sigma|F_o|$), $2\theta \geqslant 47°$ (115°)] and 343 (339) parameters for **1** and **2** respectively. The absolute chirality of **1** could not be unambiguously determined. CCDC 182/776.

1 M. David Curtis, S. Thanedar and W. M. Butler, *Organometallics*, 1984, **3**, 1855.
2 M. Schmittel, H. Werner, O. Gevert and R. Söllner, *Chem. Ber./Recueil*, 1997, **130**, 195.
3 P. Veya, C. Floriani, A. Chiesi-Villa and C. Rizzoli, *Organometallics*, 1993, **12**, 4892.
4 K. Hortmann, J. Diebold and H.-H. Brintzinger, *J. Organomet. Chem.*, 1993, **445**, 107.
5 J. Hillis, M. Ishaq, B. Gorewit and M. Tsutsui, *J. Organomet. Chem.*, 1976, **116**, 91.
6 R. B. King, M. B. Bisnette and A. Fronzaglia, *J. Organomet. Chem.*, 1966, **5**, 341.
7 M. Ishaq, *J. Organomet. Chem.*, 1968, **12**, 414.
8 J. K. P. Ariyaratne, A. M. Bierrum, M. L. H. Green, M. Ishaq, C. K. Prout and M. G. Swanwick, *J. Chem. Soc. A*, 1969, 1309.
9 E. R. Burkhardt, J. J. Doney, R. G. Bergman and C. H. Heathcock, *J. Am. Chem. Soc.*, 1987, **109**, 2022.
10 V. C. Gibson, *J. Chem. Soc., Dalton Trans.*, 1994, 1607.
11 D. S. Williams, M. H. Schofield and R. R. Schrock, *Organometallics*, 1993, **12**, 4560.
12 S. Collins, D. G. Ward and K. H. Suddaby, *Macromolecules*, 1994, **27**, 7222.
13 H. Deng, T. Shiono and K. Soga, *Macromolecules*, 1995, **28**, 3067.
14 M. A. Giardello, Y. Yamamoto, L. Brard and T. J. Marks, *J. Am. Chem. Soc.*, 1995, **117**, 3276.
15 H. Yasuda, H. Yamamoto, K. Yokota, S. Miyake and A. Nakamura, *J. Am. Chem. Soc.*, 1992, **114**, 4908.
16 Y.-J. Kim, M. P. Bernstein, A. S. Galiano Roth, F. E. Romesberg, P. G. Williard, D. J. Fuller, A. T. Harrison and D. B. Collum, *J. Org. Chem.*, 1991, **56**, 4435.
17 V. C. Gibson, E. L. Marshall, C. Redshaw, W. Clegg and M. R. J. Elsegood, *J. Chem. Soc., Dalton Trans.*, 1996, 4197.
18 W. A. Nugent and J. M. Mayer, *Metal–Ligand Multiple Bonds*, Wiley-Interscience, New York, 1988.
19 M. W. Creswick and I. Bernal, *Inorg. Chim. Acta*, 1983, **71**, 41.
20 H. Adams, N. A. Bailey, C. E. Tattershall and M. J. Winter, *J. Chem. Soc., Chem. Commun.*, 1991, 912.

Received in Cambridge, UK, 5th January 1998; 8/00116B

A method for obtaining stable, high activity for NO_x reduction at low temperatures

Robert Burch,*† Paolo Fornasiero and Barry W. L. Southward

Catalysis Research Centre, Department of Chemistry, University of Reading, Whiteknights, Reading, UK RG6 6AD

Very high and stable low temperature activity for the reduction of NO by *n*-octane on a 0.3 mass% Pt/Al_2O_3 catalyst operating under lean burn conditions may be achieved by secondary injection of micropulses of clean-burning thermal promoters into the gas stream.

Oxides of nitrogen (NO_x) formed in the combustion of diesel fuel are recognised as severe atmospheric pollutants and are the subject of increasingly stringent emissions control legislation[1,2] and so diesel engines will soon require comparable exhaust emissions technology to that used for petrol engines. However, although there has been much research on NO_x removal in fuel-lean exhaust streams,[3–6] to date no suitable material has been developed which will attain the levels of activity required under diesel operating conditions. Of the various materials examined, supported Pt catalysts appear to offer the best low temperature activity, are resistant to poisoning by SO_x, and are hydrothermally stable.[1,2,4,5] However, the goal of obtaining high activity at low temperatures, without rapid deactivation, has yet to be realised. Here, we address this problem and present preliminary data concerning the use of microinjection techniques to achieve highly active low temperature $DeNO_x$ catalysts.

The catalyst used in this study was the commercial catalyst CK303, ex Akzo (0.3 mass% Pt on Al_2O_3, pre-reaction surface area 226 $m^2\ g^{-1}$, metal surface area 0.48 $m^2\ g^{-1}$, Pt particle diameter 1.7 nm). It was chosen primarily as a low cost material having modest low temperature activity.[3,4] All catalyst testing was performed in a standard microreactor system described elsewhere.[3] Prior to testing, all samples were aged overnight in a standard reaction mixture (100 mg catalyst, 500 ppm NO, 500 ppm *n*-octane, 5% O_2, balance He, total flow 200 ml min^{-1}) at 500 °C and then 'cleaned' (550 °C in 5% O_2 in He for 1 h). *n*-Octane was chosen as a reductant to simulate a real fuel. NO_x conversions were determined by on-line analysis using a standard chemiluminescence detector (Signal series 4000), with samples logged onto a PC at 6 s intervals. CO_2 analysis was performed using a Signal series 2000 IR analyser. No reaction was observed in the absence of a catalyst.

The profile for the $DeNO_x$ reaction over a range of temperatures was analysed and gave results typical of those found in the literature with the conversion to N_2 rising to a maximum at *ca*. 220 °C[3,4–8] (results not shown). However we have previously shown that temperature programming studies may not be a reliable measure of catalyst activity[7] because of deactivation as the catalysts is heated up from lower temperatures. Therefore we have examined the lifetime of clean catalysts under isothermal conditions at temperatures close to the *n*-octane light-off point (*ca*. 220 °C when using CK303 as the catalyst, defined as the temperature required for >20% conversion of *n*-octane). The activity was clearly sensitive to temperature (Fig. 1). Indeed, only at 220 °C was the activity stable, whilst at lower temperatures the timescale for steady activity became increasingly small. Hence at 170 °C catalyst deactivation occurred so rapidly that reactor response lag and NO_x adsorption mask any NO_x reduction. This was reflected in the low amount of CO_2 produced, and the absence of an in-bed exotherm.[3,7] In contrast, reaction at 185 °C [steady activity for *ca*. 65 min, see Fig. 1(*c*) and Fig. 2(*a*)] was ascribed to catalytic reaction only. The decline in activity is ascribed to surface deposition of unreacted (carbonaceous) intermediates.

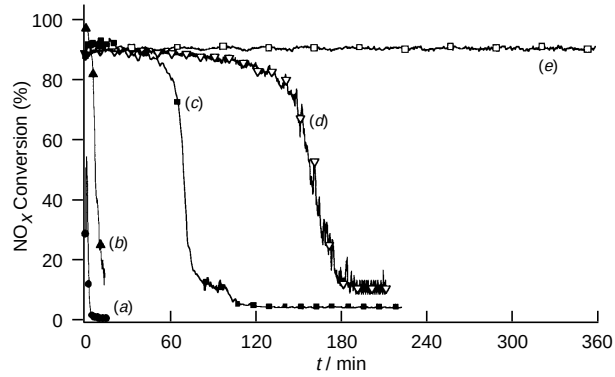

Fig. 1 Effect of temperature on the activity of CK303 (0.3 mass% Pt on Al_2O_3) under standard reaction conditions (100 mg catalyst, 500 ppm NO, 500 ppm *n*-octane, 5% O_2–He, balance He, total flow 200 ml min^{-1}). (*a*) 170 °C (●), (*b*) 180 °C (▲), (*c*) 185 °C (■), (*d*) 200 °C (▽), (*e*) 220 °C (□)

To circumvent this process of deposition leading to deactivation the method of micropulse injection was devised. This entailed injection of minute quantities of 'thermal promoters', *i.e.* readily combustible molecules, into the standard reaction mixture. It was envisioned that the combustion of these molecules would create an exotherm within the catalyst bed, and more specifically at the reaction centres. The ensuing temperature rise would promote reaction/desorption of any deposits located thereon.

The injection of small quantities of H_2 [Fig. 2(*b*)], gave no significant improvement in lifetime. However a bed exotherm of *ca*. 20 °C was recorded some 10 s after the injection, although it is clear that the temperature rise at any active site would be significantly larger, with associated desorption of surface NO_x as evidenced by the sharp (negative) peaks. However, the use of

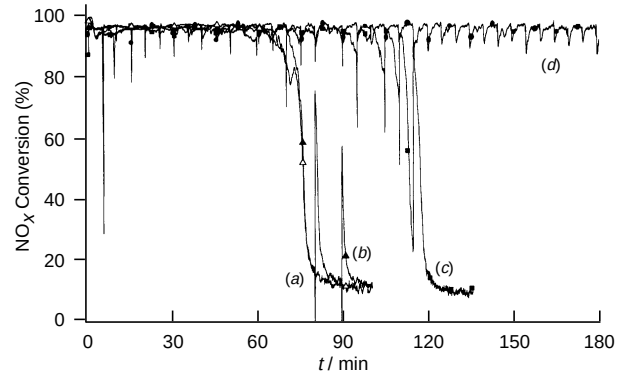

Fig. 2 Effect of microinjection on the activity of CK303 under standard reaction conditions, at 185 °C. (*a*) No injection (▽), (*b*) 0.5 ml H_2 every 10 min (▲), (*c*) 2 ml of H_2 every 5 min (■), (*d*) 1 μl of MeOH every 5 min-(●)

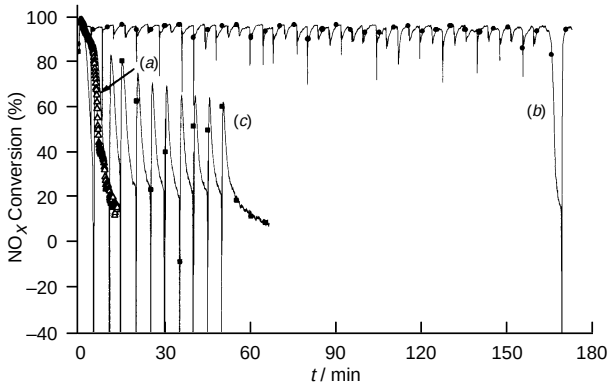

Fig. 3 Effect of microinjection on the activity of CK303 under standard reaction conditions at 180 °C. (*a*) No injection (▽), (*b*) pulse feed of 2 μl MeOH only every 4 min (■), (*c*) 2 μl MeOH every 4 min (●). Note after 160 min injections stopped and then recommenced at 169 min.

larger, more regular pulses of H_2 was found to be beneficial [Fig. 2(*c*)], and increased catalyst lifetime by *ca*. 30 min. This was consistent with the increased and more regular exotherm (bed temperature increase of *ca*. 30 °C) and associated desorption/reaction of NO_x and other adsorbates.

The use of pulses of methanol was even more successful [Fig. 2(*d*)] with no deactivation being observed for > 4 h on line (associated bed exotherm 40–45 °C). This is clearly a very significant result and suggested a means for obtaining high activity with no deactivation at low temperatures.

Given the successful application of methanol micropulsing at 185 °C its use at 180 °C was attempted. Previously, complete deactivation of CK303 had been observed in *ca*. 6 min [Fig. 3(*a*)] but by pulse injection (2 μl every 4 min, bed exotherm *ca*. 45 °C) deactivation was circumvented [Fig. 3(*b*)]. Injection was ceased after 160 min and deactivation occurred within 6 min in exactly the same manner as observed earlier with the clean catalyst [Fig. 3(*a*)]. Injection of MeOH at 169 min however, resulted in complete recovery of activity. These data confirm that the methanol effectively cleans the Pt surface to enable $DeNO_x$ to occur.

The methanol pulse itself is not the primary reductant as can be seen from the reaction of MeOH pulses in the absence of the *n*-octane feed [Fig. 3(*c*)]. In this case there is some $DeNO_x$ activity but this decreases rapidly to a low value. Thus it is clear that the very high activity obtained when MeOH is injected into a gas stream containing *n*-octane is due to the micropulsing in conjunction with the *n*-octane feed.

These results provide a novel, practical method for obtaining high activity for $DeNO_x$ reactions under diesel exhaust conditions at low temperatures.

We are pleased to acknowledge the financial support for this work through EU grant EV5V-CT94-0535.

Notes and References

† E-mail: r.burch@reading.ac.uk

1 J. C. Frost and G. S. Smedler, *Catal Today*, 1995, **26**, 207.
2 K. M. Adams, J. V. Catavaio and R. H. Hammerle, *Appl. Catal. B*, 1996, **10**, 157.
3 R. Burch, P. Formasiero and B. W. L. Southward, *J. Catal.*, submitted.
4 R. Burch and P. J. Millington, *Catal Today*, 1995, **26**, 185.
5 A. P. Walker, *Catal Today*, 1995, **26**, 107.
6 J. L. D'Itri and W. M. H. Sachtler, *Appl. Catal. B*, 1993, **2**, 7.
7 R. Burch, P. Fornasiero and B. W. L. Southward, *Chem. Commun.*, 1998, 625.
8 R. Burch and T. C. Watling, *Catal. Lett.*, 1997, **43**, 19.

Received in Exeter, UK, 23rd January 1998; 8/00719E

Solvolysis of 1-oxo-2,8-diphenyl-2,5,8-triaza-1λ⁵-phosphabicyclo[3.3.0]octane: new rearrangement of an eight- to a five-membered phosphodiamidate system

Xavier Y. Mbianda, Tomasz A. Modro*† and Petrus H. Van Rooyen

Centre for Heteroatom Chemistry and Department of Chemistry, University of Pretoria, Pretoria 0002, South Africa

The alcoholysis of the title compound with RO⁻/ROH gives the 1,3,2-diazaphospholidine derivative *via* the cleavage of the P–N(2) bond, while under acidic catalysis the P–N(5) bond is broken leading to the eight-membered monocyclic product, which can isomerize *via* a new type of rearrangement to the former five-membered system.

We have recently reported the preparation of the bicyclic phosphoric triamides **1** *via* the base-promoted cyclization of the corresponding 3-(2-chloroethyl)-2-oxo-1-aryl-2-arylamino-1,3,2-diazaphospholidines.[1] Nucleophilic cleavage of one of the P–N bonds in **1** can lead to another 1,3,2-diazaphospholidine derivative ['*exo*' departure of N(2)], or to a novel, eight-membered heterocyclic system **2** ['*endo*' departure of N(5)] (Scheme 1). We present here the results of the acid-catalyzed or base-promoted alcoholysis of **1a** (Ar = Ph). It was expected that under acidic conditions the regioselectivity governed by the first protonation site of the substrate[2] should involve the departure of the more basic N(5) atom. Our recent ^{15}N NMR spectroscopic studies[3] indicated a high degree of 'p³' character, hence high basicity, of N(5) in **1**. Alcoholysis of **1a** carried out in an alcohol containing 1 equiv. of dry HCl led, as expected, to the exclusive cleavage of the P–N(5) bond, yielding the corresponding 1-oxo-1-alkoxy-2,8-diphenyl-2,5,8-triaza-1λ⁵-phosphacyclooctane **2a** (Ar = Ph; Nu = OMe) or **2b** (Ar = Ph; Nu = OEt).‡ Amido esters **2** are, however, rather unstable compounds and undergo further changes upon purification (*vide infra*); they could be converted into stable derivatives *via* acylation of the N(5) atom.§ Unambiguous evidence for the structure of the primary product of the solvolysis was obtained from the crystal structure of the *N*⁵-Bz derivative of **2b** (Fig. 1).¶ Structural parameters of the phosphodiamidate function in *N*⁵-Bz**2b** are similar to those reported for related structures, except for two points. First, we observe the short P···N(2) non-bonded distance of 3.242 Å, which should be even shorter in free, nonbenzoylated **2b**. Second, the two P–N bonds are non-equivalent: while one (1.651 Å) lies well within a typical bond distance for phosphoramidates,[4] the other (1.688 Å) indicates a significantly lower bond order.

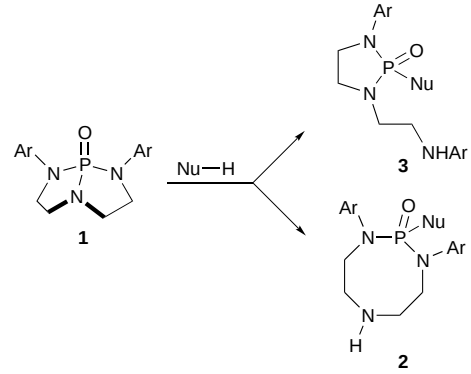

Scheme 1

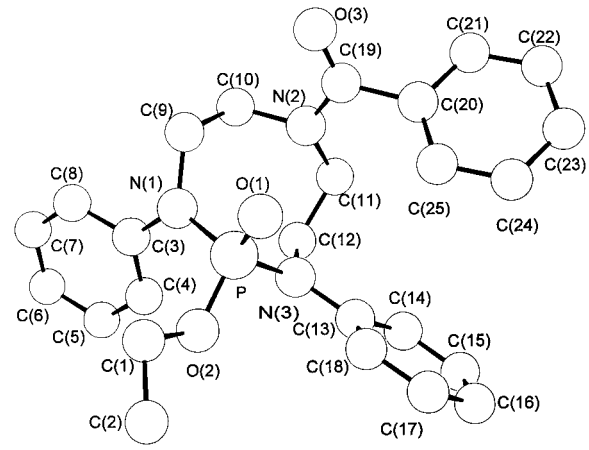

Fig. 1 ORTEP plot of the structure of the *N*-benzoyl derivative of **2b**

When free cyclic diamido phosphates **2** were stored as neat substances, or as solutions in aprotic solvents, they underwent slow change yielding another phosphorus-containing product. Full conversion could be achieved by refluxing **2** in benzene or THF and, for **2b**, the product, after isolation and purification, was identified as the isomeric 3-[2-(phenylamino)ethyl]-2-oxo-2-ethoxy-1-phenyl-1,3,2λ⁵-diazaphospholidine **3b**.‖ The structure of this product was determined by X-ray diffraction (Fig. 2),** demonstrating unambigously the 8 → 5 ring contraction nature of the rearrangement. The only reported structure closely related to **3b** is that of Jones *et al.*,[5] the molecular parameters of both compounds correspond well to each other.

This new ring contraction **2b** → **3b** can be conveniently followed *via* ^{31}P NMR spectroscopy ($\Delta\delta_P$ = 6.4 ppm). Reactions carried out in refluxing THF with variable initial concentrations of **2b** showed clearly the first order kinetics, with $k_1 = (4.1 \pm 0.1) \times 10^{-5}$ s^{-1}. The rearrangement can be explained in terms of intramolecular 1,5-nucleophilic attack of the amine nitrogen at the phosphoryl centre, followed by proton transfer and P–N bond cleavage (Scheme 2); this mechanism is also supported by the structural characteristics of *N*⁵-Bz**2a** discussed above. Similar transannular N–P interaction in an eight-membered heterocyclic system was postulated for the

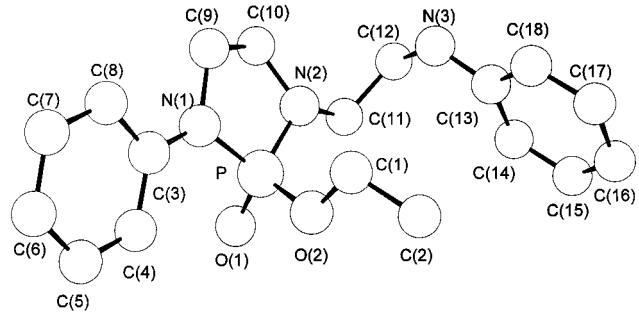

Fig. 2 ORTEP plot of the structure of **3b**

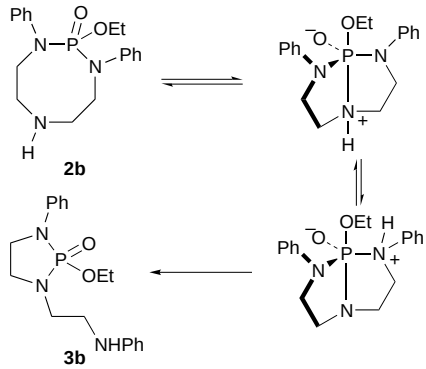

Scheme 2

mechanism of the hydrolysis of medium-ring phosphate esters.[6] In that case, however, as well as in other cases of transannular interactions involving nitrogen and a carbonyl group,[7] the ring structure of the substrate remains intact, while for **2** we observe a change in the cyclic skeleton of the molecule. To the best of our knowledge, this is the first reported case of a rearrangement of this type.

Methanolysis of **1a** in MeO^-/MeOH led directly to the formation of **3a** (Ar = Ph; Nu = OMe) as a result of nucleophilic cleavage of the P–N(Ph) bond. In the absence of the activation of the N(5) atom in **1** *via* protonation, it is the leaving ability of the departing nitrogen (NPh) that determines the regioselectivity of the P–N bond cleavage. In the presence of an excess of MeO^- ions, **3a** undergoes the opening of the second 1,3,2λ^5-diazaphospholidine ring, yielding dimethyl di(2-phenylaminoethyl)phosphoramidate **4a**.††

The **2** → **3** rearrangement reported here indicates greater thermodynamic stability of the latter heterocyclic system. The structure and conformational behaviour of **2**, as well as the mechanism of its rearrangement to **3**, is currently being studied in this laboratory.

Notes and References

† E-mail: tamodro@scientia.up.ac.za

‡ *Acid-catalysed alcoholysis* of **1a**: a solution of **1a** (0.50 g, 1.67 mmol) in anhydrous alcohol (15 ml) containing dry HCl (1.67 mmol) was kept at room temperature for 16 h, diluted with water (10 ml) and neutralised with aq. Na_2CO_3. The solution was extracted with $CHCl_3$ (3 × 10 ml), dried (Na_2SO_4) and evaporated under reduced pressure yielding **2** as a solid (**2a**) or a viscous oil (**2b**). Data for **2a** (0.55 g, 100%): mp 91.5–92.7 °C; δ_H (300 MHz, $CDCl_3$) 2.04 (1 H, br s), 2.87 (4 H, ddd, *J* 14.6, 6.7, 3.1), 3.50 (3 H, d, *J* 5.6), 3.60–3.85 (4 H, m), 7.08–7.50 (10 H, m); δ_C 47.4 (s), 51.8 (s), 53.2 (d, *J* 5.7 Hz), 123.5 (s), 124.1 (s), 129.2 (s), 143.3 (d, *J* 4.2); δ_P 13.6. For **2b** (0.58 g, 100%): oil; δ_H 0.99 (3 H, t, *J* 7.1), 2.06 (1 H, br s), 2.87 (4 H, ddd, *J* 14.6, 6.7, 3.1), 3.55–3.80 (4 H, m), 3.87 (2 H, dt, *J* 7.1), 7.08–7.50 (10 H, m); δ_C 15.6 (d, *J* 6.7), 47.3 (s), 51.5 (s), 62.9 (d, *J* 5.4), 123.4 (s), 123.9 (s), 129.1 (s), 143.2 (d, *J* 4.2); δ_P 12.1.

§ *Selected data* for N^5-Bz**2a**: (66%), mp 148.2–149.7 °C (from MeCN–hexane, 1 : 1); δ_P 12.0; Found: C, 66.22; H, 6.17; N, 9.50; $C_{24}H_{26}N_3O_3P$ requires: C, 66.19; H, 6.01; N, 9.64%. For N^5-Bz**2b**: (74%), mp 144.2–145.6 °C (from MeCN); δ_P 10.6; Found: C, 67.07; H, 6.29; N, 9.34. $C_{25}H_{28}N_3O_3P$ requires: C, 66.80; H, 6.27; N, 9.34%.

¶ *Crystal data* for N^5-Bz**2b**: $C_{25}H_{28}N_3O_3P$, *M* = 449.49, monoclinic, space group $P2_1/n$ (No. 14), *a* = 9.743(1), *b* = 12.443 (2), *c* = 19.334(2) Å, β = 104.34(1)°, *U* = 2271(1) Å^3, *F*(000) = 952, λ(Mo-Kα) = 0.7107 Å, μ(Mo-Kα) = 1.13 cm^{-1}, *T* = 295(1) K, *Z* = 4, D_c = 1.30 g cm^{-3}. Data were collected on an Enraf Nonius CAD4 diffractometer in the range $3 \leqslant \theta \leqslant 30°$ (7072 reflections). The structure was solved by direct methods (ref. 8) and refinement, based on *F*, was by full-matrix least-squares methods (ref. 9) to R = 0.057, R_w = 0.065 {weighting scheme $[\sigma^{-2}(F_o) + 0.000699F^2]$} for 293 parameters using 4047 unique reflections with $I > 3\sigma(I)$.

‖ *Rearrangement* of **2b** to **3b**: **2a** (0.345 g, 1 mmol) in dry benzene (15 ml) was heated under reflux for 18 h. After concentrating to *ca*. 1/4 volume, the solution was poured into dry Et_2O (20 ml) with vigorous stirring. The precipitate (0.318 g, 92%) was filtered off and crystallized from MeCN. 1-Phenyl-2-ethoxy-2-oxo-3-[2-(phenylamino)ethyl]-1,2,3λ^5-diaza-phospholidine **3b**, mp 129.4–130.1 °C; δ_H 1.17 (3 H, t, *J* 7.1), 3.24–3.46 (6 H, m), 3.57–3.70 (2 H, m), 3.97 (2 H, dt, *J* 7.1), 6.60–7.30 (10 H, m); δ_C 16.2 (d, *J* 7.2), 41.6 (d, *J* 2.4), 43.1 (s), 43.3 (s), 44.4 (d, *J* 4.9), 63.6 (d, *J* 7.2), 112.5 (s), 115.9 (s), 122.9 (s), 129.2 (s), 129.3 (s), 141.3 (d, *J* 6.3), 148.0 (s); δ_P 18.5; Found: C, 62.18; H, 7.16; N, 12.08; $C_{18}H_{24}N_3O_2P$ requires: C, 62.59; H, 7.00; N, 12.16%.

** *Crystal data* for **3b**: $C_{18}H_{24}N_3O_2P$, *M* = 345.38, monoclinic, space group $P2_1/n$ (No. 14), *a* = 13.902(2), *b* = 6.046(5), *c* = 22.110(5) Å, β = 94.59(3)°, *U* = 1852(1) Å^3, *F*(000) = 736, λ(Mo-Kα) = 0.7107 Å, μ(Mo-Kα) = 1.24 cm^{-1}, *T* = 295(1) K, *Z* = 4, D_c = 1.22 g cm^{-3}. Data were collected on an Enraf Nonius CAD4 diffractometer in the range $3 \leqslant \theta \leqslant 30°$ (6077 reflections). The structure was solved by direct methods (ref. 8) and refinement, based on F^2, was by full-matrix least-squares methods (ref. 9) to R = 0.063, R_w = 0.040 {weighting scheme $[\sigma^2(f_o)]$} for 221 parameters using 2522 unique reflections with $I > 3\sigma(I)$. An intermolecular bond O(1)···H–N(3) of 2.042 Å is observed. Perspective drawings were prepared using ORTEP (ref. 10). CCDC 182/772.

†† *Base-promoted alcoholysis* of **1a**: a solution of **1a** (0.300 g, 1 mmol) and MeONa (3 mmol) in MeOH (20 ml) was kept at room temperature for 28 days (full conversion, as shown by ^{31}P NMR spectroscopy), neutralised with methanolic HCl, filtered and evaporated under reduced pressure. The crude product (0.336 g, oil) consisted of two phosphorus-containing compounds (δ_P 19.9, 55%; δ_P 14.4, 45%) which were separated by column chromatography (SiO_2, Et_2O). *Selected data* for **3a**, oil; δ_H 3.39 (6 H, m), 3.61 (3 H, d, *J* 12.3), 3.63 (2 H, m), 4.42 (1 H, br s), 6.63 (2 H, d, *J* 7.6), 6.68 (1 H, t, *J* 7.5), 6.98 (1 H, t, *J* 7.3), 7.15 (4 H, m), 7.29 (2 H, t, *J* 7.9); δ_C 41.7 (s), 43.2 (d, *J* 7.7), 43.4 (d, *J* 6.5), 44.5 (s), 54.3 (d, *J* 7.8), 112.8 (s), 115.7 (s), 117.4 (s), 121.7 (s), 129.3 (s), 129.4 (s), 137.6 (d, *J* 5.2), 147.8 (s); δ_P 19.9; Found: C, 63.20; H, 7.48; N, 11.45. $C_{19}H_{26}N_3O_2P$ requires: C, 63.50; H, 7.29; N, 11.69%. For **4a**: oil; δ_H 3.28 (8 H, m), 3.69 (6 H, d, *J* 11.2), 6.56 (4 H, d, *J* 7.7), 6.68 (2 H, t, *J* 7.4), 7.15 (4 H, m); δ_C 41.5 (s), 45.8 (d, *J* 4.4), 53.5 (d, *J* 6.2), 112.7 (s), 117.9 (s), 129.3 (s), 147.8 (s); δ_P 14.2.

1 H. Wan and T. A. Modro, *Synthesis*, 1996, 1227.
2 J. Rahil and P. Haake, *J. Am. Chem. Soc.*, 1981, **103**, 1723 and references cited therein.
3 A. M. Modro, T. A. Modro, P. Bernatowicz, W. Schilf and L. Stefaniak, *Magn. Reson. Chem.*, 1997, **35**, 774.
4 S. A. Bourne, X. Y. Mbianda, T. A. Modro, L. R. Nassimbeni and H. Wan, *J. Chem. Soc., Perkin Trans. 2*, 1998, 83.
5 P. G. Jones, H. Thönnessen, A. Fischer, I. Neda, R. Schmutzler, J. Engel, B. Kutscher and U. Niemeyer, *Acta Crystallogr., Sect. C*, 1996, **52**, 2359.
6 R. K. Sharma and R. Vaidyanathaswamy, *J. Org. Chem.*, 1982, **47**, 1741.
7 *Conformational Analysis of Medium-Sized Heterocycles*, ed. R. S. Glass, VCH, New York, 1988, ch. 3.8.
8 G. M. Sheldrick, *SHELX86. A program for the solution of crystal structures*, University of Göttingen, 1986.
9 G. M. Sheldrick, *SHELX76. Program for crystal structure determination*, University of Cambridge, 1976.
10 C. K. Johnson, ORTEP, Report ORNL-3794, Oak Ridge National Laboratory, Tennessee, USA, 1965.

Received in Cambridge, UK, 13th November 1997; revised manuscript received 30th January 1998; 8/00836A

Dicephalic surfactants

Nico A. J. M. Sommerdijk,† Theo L. Hoeks, Kees Jan Booy, Martinus C. Feiters, Roeland J. M. Nolte* and Binne Zwanenburg*

Department of Organic Chemistry, NSR-Institute for Molecular Structure, Design and Synthesis, University of Nijmegen, Toernooiveld, 6525 ED Nijmegen, The Netherlands

Two examples of dicephalic surfactants, a new class of two-headed amphiphiles, were prepared and demonstrated to exhibit unexpected aggregation behaviour.

Recently several research groups have studied the aggregation behaviour of surfactants with unusual structural features in order to further understand the relationship between the structure of the amphiphile and the type of aggregates it forms. Examples include surfactants with hyperextended[1] and spiro[2] hydrocarbon chains, gemini surfactants[3] and super surfactants, *e.g.* block copolymers of polystyrene and poly(propyleneimine) dendrimers.[4] Gemini surfactants, a new class of amphiphilic molecules with two hydrocarbon chains and two polar head groups connected by a linker, display aggregation behaviour that is distinctly different from that of the constituting 'parent' surfactants.[5] The interesting properties of gemini surfactants prompted us to design and synthesise another type of amphiphilic molecule for which we propose the name dicephalic (two-headed) surfactant. Molecules of this type consist of a single hydrocarbon chain and two polar head groups (**1** and **2**).‡ Both compounds can complex metal ions: the former binds transition metals to its imidazole groups, the latter calcium ions to its phosphate functions.[6] Here we report on the unusual self-assembling properties of the dicephalic surfactants.

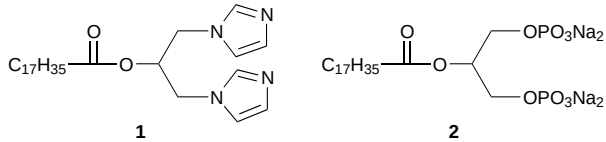

1 **2**

The synthesis of compound **1** was initially tried by treating 1,3-dibromopropan-2-yl stearate **3**§ with imidazole in MeCN. Instead of the desired product **1** a mixture of compounds **4** and **6** was isolated. A mechanistic explanation is presented in Scheme 1A. Direct nucleophilic replacement of the second halogen atom in **3** by imidazole is difficult due to considerable steric hindrance as was evident from examination of CPK models.¶ During aqueous work-up a hydroxy group is probably introduced which gives **5** and after acyl migration[7] the α-hydroxystearate **6**. Compound **1** could, however, be synthesised *via* a double nucleophilic attack of sodium imidazolide on epibromohydrin, followed by acylation of the alkoxide intermediate (Scheme 1B).

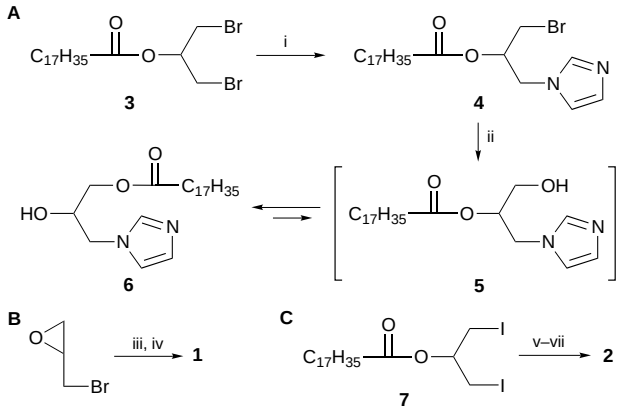

Scheme 1 (i) Imidazole–CH_3CN; (ii) aqueous work-up; (iii) NaH–imidazole–DMF; (iv) $C_{17}H_{35}COCl$; (v) $AgOP(O)(OBn)_2$–toluene, reflux; vi H_2/Pd/C; (vii) Dowex-Na^+

Reaction of **3** with tetraalkylammonium salts of mono- and di-benzyl phosphate, for similar steric reasons as mentioned above, did not lead to satisfactory yields of the respective desired bis-phosphates.‖ Compound **2** was prepared therefore by phosphorylation of the diiodide **7**§ with silver dibenzyl phosphate[8] followed by catalytic hydrogenation over Pd/C and subsequent cation exchange (Scheme 1C). This indirect displacement of the halogen atoms by the dibenzyl phosphate ions is promoted by the formation of an AgI complex and the neighbouring group participation of the ester carbonyl function.

Inspection of CPK models of **1** and **2** revealed that both compounds have a very large head group section compared to their lipophilic part. According to the structure–shape concept,[9] the formation of micelles may therefore be expected when these compounds are dispersed in water. Dispersion of **1** in water at pH 7.0 (0.1%, w/w) did not, however, lead to the formation of micelles, but to well defined multilayered platelets of micrometer size [Fig. 1(*a*)]. Powder diffraction experiments revealed a repetitive distance of 31 Å, indicating a structure in which the hydrocarbon chains are interdigitated. Electron diffraction showed several bands, indicative of the polycrystalline nature of the sample, and a strong phase transition at 58 °C (ΔH = 60 J g^{-1}) was observed by DSC. The pK_a values of **1** (3.6 and *ca.* 7), make it likely that the platelets consist of a mixture of protonated and deprotonated surfactant molecules. The possibility of intermolecular hydrogen bond formation over long distances, may account for the remarkable stability of these lamellar structures.

When 0.25 equiv. of $CuSO_4$ were added to a dispersion of **1** in water, vesicles with diameters of 50–250 nm were formed [Fig. 1(*b*)]. EPR and FTIR titration experiments showed that a complex of the type $Cu(Imidazole)_4^{2+}$ had been formed,** but it was not possible to differentiate between a monomeric Cu^{II} $\mathbf{1}_2$

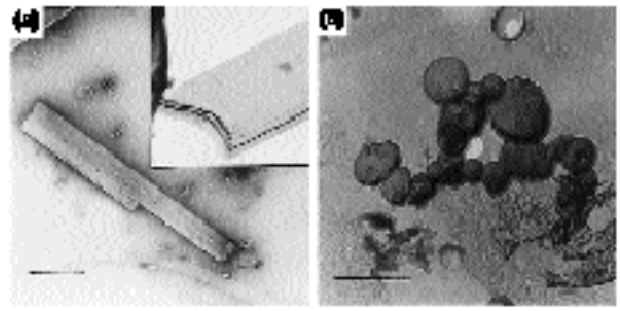

Fig. 1 Electron micrographs of (*a*) **1** (negative staining, inset Pt shadowing technique) and (*b*) a 2:1 complex of **1** and $CuSO_4$ (freeze fracture technique) in water. Bars represent 250 nm.

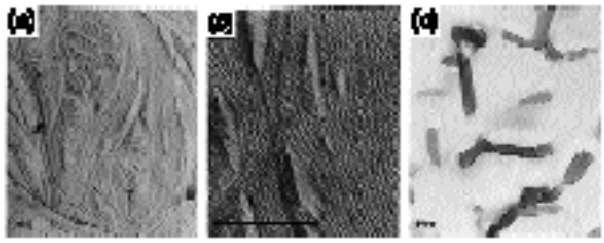

Fig. 2 Electron micrographs of **2** in (*a*, *b*) aqueous 2 mM PIPES buffer (pH 7.0, freeze fracture technique) and (*c*) aqueous 2 mM PIPES buffer containing 0.5 mM $CaCl_2$ (pH 7.0, Pt shadowing technique). Bars represent 100 nm.

complex and a polymeric coordination network. According to powder X-ray diffraction these vesicles had an interdigitated bilayer with a thickness of 32 Å. DSC revealed a phase transition at 15 °C (ΔH = 15 J g^{-1}), indicating that copper complex formation caused a dramatic change in the molecular packing.

For 0.1% (w/w) dispersions of **2** in an aqueous buffer of pH 7.0, electron microscopy [Fig. 2(*a*),(*b*)] revealed the formation of bundles of fibres each with a diameter of 65 Å, (approximately twice the molecular length) and lengths up to 15 μm (aspect ratio >2000). These fibres showed a faint phase transition at 23 °C (ΔH = 1.5 J g^{-1}) in DSC. The formation of very long structures suggests that intermolecular interactions must also play an important role in stabilising these aggregates. Since at pH 7.0 the phosphate groups will be in their monoprotonated form,[10] a network of hydrogen bonds can be formed between protonated and unprotonated P–OH groups of neighbouring molecules (Fig. 3), which could account for the observed stability of these large structures.

Compound **2** is expected to form a 1:1 complex with calcium, either intramolecularly by chelation or intermolecularly by formation of a linear polymeric complex.[11] Addition of calcium chloride ([Ca^{2+}] = 0.5 mM) to aqueous dispersions of **2** led to the formation of a precipitate consisting of small (200–500 nm) and irregularly shaped multilayered platelets [Fig. 2(*c*)]. These platelets were shown to be polycrystalline by electron diffraction and displayed a sharp phase transition at 148 °C (ΔH = 17 J g^{-1}) in DSC. Considering the relative volumes of the hydrophilic and hydrophobic parts of **2** it is reasonable to assume that the lamellar structures formed upon complexation of calcium ions consist of intercalated bilayers.

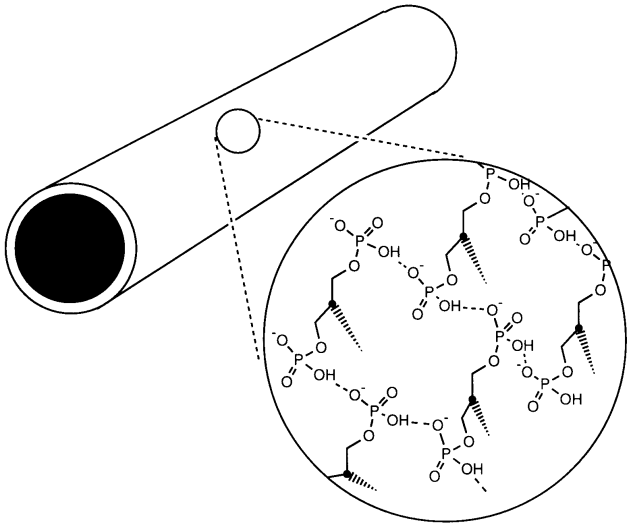

Fig. 3 Schematic representation of the possible hydrogen bonding arrangement of molecules of **2** in the fibers presented in Fig. 2(*a*,*b*). The dashed lines represent the lipophilic parts of the molecules, pointing towards the interior of the fiber.

In summary, **1** and **2** are examples of a new class of amphiphiles whose aggregation behaviour in water does not follow the structure–shape concept.[9] The extended intermolecular interactions which are possible because of the dicephalic character of the molecules lead to the formation of lamellar platelets in the case of **1** and fibres in the case of **2**. Complexation of metal ions, *i.e.* Cu^{II} ions to **1** and Ca^{2+} ions to **2**, gives rise to a change in molecular organisation resulting in the generation of lamellar structures in both cases. Further studies are underway and will be presented elsewhere.

Notes and References

† E-mail: tijdink@sci.kun.nl

‡ *Physical data* for **1**: mp 88 °C (Calc. for $C_{27}H_{46}N_4O_2$: C, 70.70; H, 10.11; N, 12.21. Found: C, 70.67; H, 10.20; N, 11.99%.); *m/z* (EI) 458 (M^+); $\delta_H(CDCl_3)$ 0.88 (t, *J* 6.7, 3 H, C*H*$_3$), 1.25 [m, 28 H $CH_2(CH_2)_{14}CH_3$], 1.56 [m, 3 H, C(O)CH_2CH_2], 2.31 [t, *J* 7.5, 2 H, C(O)CH_2], 4.07 (*ABX*, 4 H, CH_2N), 5.33 (AB*X*, 1 H, C*H*–O), 6.92 (s, 1 H, 5-ImH), 7.11 (s, 1 H, 4-ImH), 7.47 (s, 1 H, 2-ImH); ν(KBr)/cm^{-1} 3100 (C–H_{Im}), 2910, 2840 (C–H), 1740 (C=O), 1530–1490 (Im).

Physical data for **2**: R_f 0.17 (silica, BuOH–AcOH–H_2O 4:1:1) (Calc. for $C_{21}H_{40}P_2O_{10}Na_4 \cdot H_2O$: C, 39.2; H, 6.84; Na, 14.3. Found: C, 39.0; H, 6.74; Na, 14.0%.); *m/z* (FB^+, free acid) 541 ($M + Na^+$); $\delta_{31P}(D_2O)$ −2.27; ν(KBr)/cm^{-1} 2910, 2860 (C–H), 1740 (C=O), 1200 (P=O).

§ **3** and **7** were prepared by acylation of the corresponding alcohols using stearoyl chloride and a catalytic amount of $AlCl_3$ (ref 12). The alcohols were prepared according to literature procedures (refs. 13, 14).

¶ The molecular structure of **3** is such that one of the bulky groups on the C(2) atom, *i.e.* the stearoyloxy group or the methylene imidazole group, blocks the incoming second imidazole group.

‖ Tetra-*n*-butylammonium dibenzyl phosphate (ref. 15) and tetraethylammonium (ref. 16) monobenzyl phosphate were used, respectively, following modified literature procedures.

** The stoichiometry of the complex was determined by monitoring the intensity of a new imidazole vibration at 1521 cm^{-1} in the FTIR spectrum upon addition of Cu^{II} ions. In addition a signal attributed to free $CuSO_4$ was observed in the EPR spectrum when the Cu^{II}:**2** ratio exceeded 0.5.

1 F. M. Menger and Y. Yamasaki, *J. Am. Chem. Soc.*, 1993, **115**, 3840.
2 F. M. Menger and J. Ding, *Angew. Chem., Int. Ed. Engl.*, 1996, **35**, 2137.
3 F. M. Menger and C. A. Littau, *J. Am. Chem. Soc.*, 1991, **113**, 1451; R. Zana, M. Benrraou and R. Rueff, *Langmuir*, 1991, **7**, 1072; R. Zana and Y. Talmon, *Nature*, 1993, **362**, 228.
4 J. C. M. van Hest, M. W. P. L. Baars, D. A. P. Delnoye, M. H. P. van Genderen and E. W. Meyer, *Science*, 1995, **268**, 1592.
5 S. Karaborni, K. Esselink, P. A. J. Hilbers, B. Smit, J. Karthauser, N. M. van Os and R. Zana, *Science*, 1994, **266**, 5183; Q. Hue, R. Leon, P. M. Petroff and G. D. Stucky, *Science*, 1995, **268**, 5215; L. Perez, J. L. Torres, A. Manresa, C. Solans and M. R. Infante, *Langmuir*, 1996, **12**, 5296.
6 J. M. P. M. Borggreven, T. H. L. Hoeks, F. C. M. Driessens and B. Zwanenburg, *Caries Res.*, 1992, **26**, 84.
7 O. E. van Lohuizen and P. E. Verkade, *Recl. Trav. Chim. Pays-Bas*, 1960, **79**, 133; E. S. Lutton, *J. Am. Oil Chem. Soc.*, 1967, **44**, 1.
8 L. Zervas, *Naturwissenschaften*, 1939, **27**, 317.
9 J. N. Israelachvilli, S. Marcelja and R. G. Horn, *Quart. Rev. Biophys.*, 1980, **13**, 2.
10 N. A. J. M. Sommerdijk, M. C. Feiters, R. J. M. Nolte and B. Zwanenburg, *Rec. Trav. Chem. Pays-Bas*, 1994, **113**, 194.
11 N. A. J. M. Sommerdijk, T. H. L. Hoeks, M. Synak, M. C. Feiters, R. J. M. Nolte and B. Zwanenburg, *J. Am. Chem. Soc.*, 1997, **119**, 4338.
12 M. E. Hill, *J. Am. Chem. Soc.*, 1953, **75**, 3020.
13 A. R. Jones and G. Fakhouri, *Xenobiotica*, 1979, **9**, 595.
14 A. Fairbourne and D. W. Stephens, *J. Chem. Soc.*, 1932, 1972.
15 (*a*) A. Zwierzak and M. Kluba, *Synthesis*, 1978, 770; (*b*) F. R. Atherton, H. T. Howard and A. R. Todd, *J. Chem. Soc.*, 1948, 1106.
16 F. Kramer and G. Weiman, *Chem. Ber.*, 1964, **94**, 126; R. A. Bauman, *Synthesis*, 1974, 870.

Received in Cambridge, UK, 14th January 1998; 8/00395E

Promiscuous recognition of the hexapyranose epimers α,β-D-glucuronic and α,β-D-galacturonic acids between corrugated brucine sheets

Fokke J. J. Dijksma,[a] Robert O. Gould,*[a]† Simon Parsons,[a] Paul Taylor[b] and Malcolm D. Walkinshaw[b]

[a] *Department of Chemistry, University of Edinburgh, West Mains Road, Edinburgh, Scotland, UK EH9 3JJ*
[b] *Department of Biochemistry, University of Edinburgh, Michael Swann Building, Edinburgh, Scotland, UK EH9 3JR*

The crystal structures of brucinium glucuronate and galacturonate are reported, both of which show layers of uronate between identical corrugated brucine sheets; the change of configuration at C(4) of the acid engineers a reversal in the packing mode of these sheets, while differences at C(1) appear to be relatively unimportant.

For many years the alkaloid brucine **1** has been used to separate racemic mixtures by co-crystallisation, generally with molecules containing acidic functional groups. We have previously reported a motif common to many brucine co-crystals;[1,2] this feature makes it attractive to examine the possibilities of using brucine as a co-crystallising agent for determining the structures of molecules which crystallise on their own with difficulty or not at all. Carbohydrates provide many examples of this type, and in a preliminary study, we have crystallised glucuronic **2** and galacturonic **3** acids with brucine to examine the specific interactions made. The acids **2** and **3** differ only in the configuration of the OH group at C(4). In addition, both exist in aqueous solution as an equilibrium of anomers [opposite configuration at C(1)] with the approximate anomeric ratio[3] α:β = 3:2. Advances in methods of crystal structure determination, particularly as applied to those structures containing substantial fragments of fixed and known stereochemistry,[4] make the use of brucine as a co-crystallising agent particularly attractive.

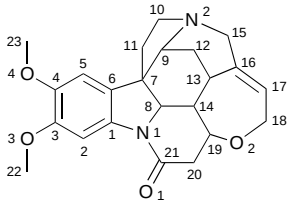

1

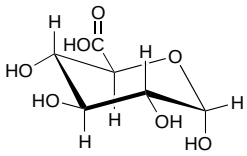

2

α-D-Glucuronic acid

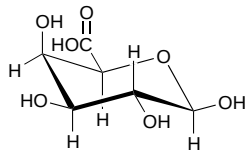

3

β-D-Galacturonic acid

Crystals of brucinium D-glucuronate **4** and brucinium D-galacturonate **5** were obtained from an aqueous solution of an equimolar mixture of **1** and **2** or **1** and **3**. Crystals of **5** were readily obtained within two days as well-formed colourless blocks. Crystals of **4** were only obtained with much greater difficulty as colourless laths after acetonitrile was added to the solution. Both give monoclinic crystals, space group $P2_1$, with unit cell dimensions for **4**: a = 7.946(1), b = 12.660(1), c = 14.814(2) Å, β = 93.676(9)°; and for **5**: a = 7.958(4), b = 12.366(5), c = 27.639(10) Å, γ = 93.57(3)° (in order to emphasise the relationship of the two structures, **5** has been referred to a cell with c as the unique axis).‡

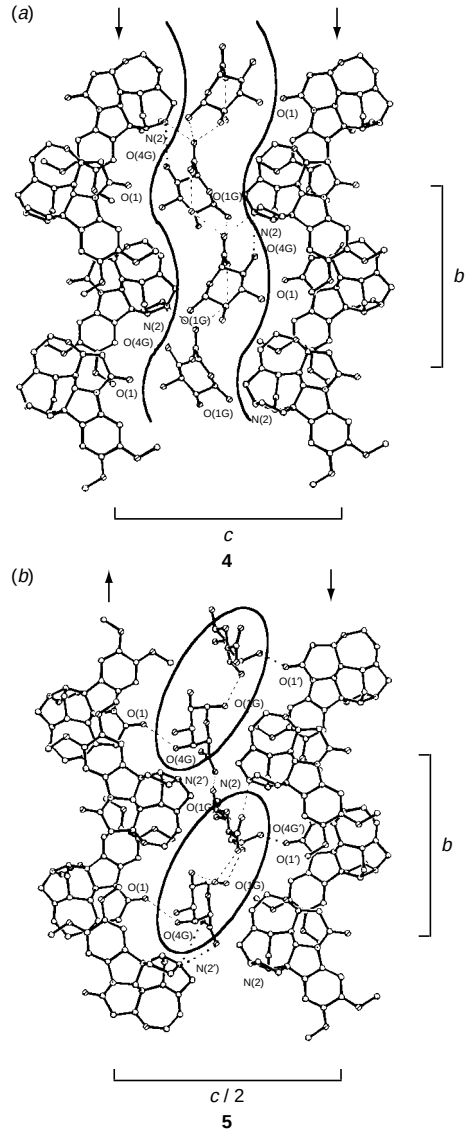

Fig. 1 A view parallel to a brucinium layer (along the *a*-axis) of the major components of **4** and **5** showing the relative polarities of the brucine sheets, the interstices between them and significant hydrogen bonds. (*a*) **4**: N(2)···O(6G): 2.851(4), N(2)···O(4G): 3.065(4), O(3W)···O(1) [$\bar{1}-x, \frac{1}{2}+y, -z$]: 2.812(4),[a] O(1G)···O(6G) [$1-x, \frac{1}{2}+y, 1-z$]: 2.794(4) O(4G)···O(3W) [$x-1, y, z$]: 2.796(4)[a]. (*b*) **5**: N(2)···O(6G): 2.719(5), N(2)···O(5G): 2.976(5), N(2′)···O(6G) [$2-x, 1-y, \frac{1}{2}+z$]: 2.781(5), N(2′)···O(7G) [$2-x, 1-y, \frac{1}{2}+z$]: 3.184(5), O(1G′)···O(7G): 2.656(5), O(4G′)···O(1) [$x, y-1, z$]: 3.035(5), O(1G)···O(3G) [$x, 1+y, z$]: 2.731(5), O(4G)···O(1) [$1-x, 1-y, z-\frac{1}{2}$]: 2.832(5), O(1W)···O(1) [$\bar{1}-x, 1-y, z-\frac{1}{2}$]: 3.169(5)[a].

[a] Not shown in figure.

Both structures show layers of brucinium ions reported previously,[1,2] with anions and solvent between the layers as shown in Fig. 1. While the uronates give many opportunities for donation and acceptance of hydrogen bonds, the brucinium ions are limited to two: donation by N(2) and acceptance by O(1) (see Fig. 1). In both structures, O(1) in brucine accepts from water, and in **5** additionally from the hydroxy group (axial) at C(4) of both independent galacturonates, which do not accept hydrogen bonds. In **4** these hydroxy groups (equatorial) donate to water and accept bifurcated bonds from N(2) of a brucinium. This proton is shared in both structures by the O(6) of a uronate; it is shared in **5** with O(5) or O(7) of a uronate. The only disorder in the crystal structures is in the region of the anomeric carbon atoms. In **4** the glucuronate ion is 82.7(8)% in the α-anomeric form. In **5** one of the galacturonate ions is essentially all in the α-anomer, while the other exists as 89.3(8)% β-anomer. These hydroxy groups show hydrogen bonding only with neighbouring uronate ions or water molecules. The water molecules are present mainly as a connecting medium for the uronates. In **5** there are three molecules of water for every one in **4**, and they partially compensate for the poorer fit of glucuronate to brucinium layers. Their requirement may explain the much slower formation of **5**.

In **4**, with one brucinium ion per asymmetric unit, the layers simply repeat along the *c*-axis, giving parallel sheets of brucinium ions and an interstice of roughly uniform thickness [Fig. 1(*a*)]. In **5**, with the unit cell nearly twice as large, there are two bruciniums in the asymmetric unit, the layers being related by the 2_1 axis parallel to the *c*-axis, while the two crystallographically independent ions in each layer are related by an approximate screw axis parallel to the *b*-axis. This antiparallel packing of layers results in the division of the interstices into channels [Fig. 1(*b*)].

The crystal structures are remarkable in showing a conserved packing of brucine moieties, although the packing and the hydrogen bonding of the sheets of water and uronate ions is very different. The configuration at C(4), which distinguishes the two ions, is crucial while the configuration at C(1) is practically irrelevant.

Notes and References

† E-mail: gould@ed.ac.uk

‡ *Crystal data* for $C_{23}H_{26}N_2O_4 + C_6H_{10}O_7 + H_2O$ **5**: $V = 2714.6(9)$ Å^3 [cell dimensions from 31 reflections with $40 \leqslant 2\theta/° \leqslant 44$ and $\lambda = 1.54184$ Å], $Z = 4$, $D_c = 1.484$ Mg m^{-3}, $T = 220(2)$ K, colourless block, $\mu = 0.976$ mm^{-1}.

Crystal data for $C_{23}H_{26}N_2O_4 + C_6H_{10}O_7 + 3\ H_2O$ **4**: $V = 1487.8(5)$ Å^3 [cell dimensions from 56 reflections with $40 \leqslant 2\theta/° \leqslant 44$ and $\lambda = 1.54184$ Å], $Z = 2$, $D_c = 1.435$ Mg m^{-3}, $T = 220(2)$ K, colourless lath, $\mu = 0.973$ mm^{-1}.

Data collection and processing: Stoë STADI-4 four circle diffractometer, graphite-monochromated Cu-Kα X-radiation, ω-θ scans, $6.0 < 2\theta < 120.0°$. **4** gave 4246 independent data, including 1929 Friedel pairs ($-8 \leqslant h \leqslant 8$, $-14 \leqslant k \leqslant 13$, $0 \leqslant l \leqslant 16$) and **5** 4171 (155 Friedel pairs), ($-8 \leqslant h \leqslant 8$, $-1 \leqslant k \leqslant 13$, $0 \leqslant l \leqslant 31$). Both structures were solved by DIRDIF-96[4] and refined anisotropically to give: **4**: $R_1 = 0.0465$ for 3977 data (1785 Friedel pairs), $F > 4\sigma(F)$, $wR_2 = 0.1261$ for all data; **5**: $R_1 = 0.0306$ for 4037 data (133 Friedel pairs), $F > 4\sigma(F)$, $wR_2 = 0.0801$ for all data. All calculations used SHELXL-97.[5] All hydrogen atoms were placed in calculated positions except those in water molecules, which were placed, and then constrained to give normal geometry. CCDC 182/771.

1 S. B. B. Glover, R. O. Gould and M. D. Walkinshaw, *Acta Crystallogr., Sect. C*, 1985, **41**, 990.
2 R. O. Gould and M. D. Walkinshaw, *J. Am. Chem. Soc.*, 1984, **106**, 7840.
3 L. W. Jaques, J. Burns Macaskill and W. Weltner, Jr., *J. Phys. Chem.*, 1979, **83**, 1412.
4 P. T. Beurskens, G. Beurskens, R. de Gelder, S. Garcia-Granda, R. O. Gould, R. Israel and J. M. M. Smits, the DIRDIF-96 program system, Crystallography Laboratory, University of Nijmegen, The Netherlands.
5 G. M. Sheldrick, SHELXL-97, University of Göttingen, Germany, 1997.

Received in Cambridge, UK, 7th January 1998; 8/00219C

Reaction of phosphinoyl-activated imines: stereocontrolled synthesis of either *trans*- or *cis*-vinylaziridines

Xue-Long Hou,*† Xiao-Fang Yang, Li-Xin Dai and Xian-Feng Chen

Laboratory of Organometallic Chemistry, Shanghai Institute of Organic Chemistry, Chinese Academy of Sciences, 354 Fenglin Lu, Shanghai 200032, PR China

Phosphinoyl imines react with allylsulfonium ylide to provide *trans*-aziridines at room temperature and *cis*-aziridines at low temperature, in high yields and good to excellent stereoselectivities.

Aziridines are versatile building blocks that have found many uses in organic synthesis.[1] They are also an important subunit in many natural products.[2] All these factors make the synthesis of aziridines an active field of research, and recently, a number of methods have appeared in the literature for the preparation of these useful compounds. Among them the direct approach to ring formation *via* a carbene or nitrene route is more attractive because of its efficiency.[3] Similar to the carbene approach, ylide attack at a C=N bond is another useful possibility,[1b] however, the synthesis of substituted aziridines *via* an ylide route is less well explored. For example, only a few procedures have been reported for the synthesis of vinyl-substituted aziridines,[4] although the versatility in synthesis of this kind of aziridine is well documented.[5] As part of a programme aimed at the application of imines to organic synthesis, we studied the aziridination reaction using normal and *N*-tosyl-activated imines as starting materials and semi-stabilized and stabilized sulfonium ylides as reagents,[3a,b,6] and found that the ylide route is a convenient way to prepare aziridine derivatives.

In the presence of Lewis acids, aldimines reacted with allyl- and prop-2-ynyl-sulfonium ylides to deliver the corresponding *cis*-aziridines as the sole products when the substituent at nitrogen was an aryl group.[6] On the other hand, the reaction of *N*-tosyl imines with allyl- and prop-2-ynyl-sulfonium ylides also provided the corresponding aziridines, but high stereoselectivities were obtained only in the case of prop-2-ynylsulfonium ylides;[3b] *cis*- and *trans*-aziridines were afforded with lower selectivity when trimethylsilylallylsulfonium ylide was used as the starting material.[3a] Unlike the ylide epoxidation reaction, where the *trans* isomer is usually the preferred configuration, the former reaction afforded the *cis*-isomer exclusively. In order to improve the stereoselectivity of the latter reaction another imine activation group was sought. It was found that when phosphinoyl-activated imines reacted with allylsulfonium ylides, both *cis*- and *trans*-aziridines were formed with high stereoselectivity. Here we disclose the results of our studies on the stereocontrolled aziridination of phosphinoyl-activated imines *via* the ylide route.

N-Phosphinoyl imines **1**[7] reacted with [3-(trimethylsilyl)-allyl]dimethylsulfonium bromide **2** in the presence of base at room temperature to provide *trans*-vinylaziridines **3** predominantly. On the other hand, *cis*-vinylaziridines **4** were the main products when the preformed ylide prepared from [3-(trimethylsilyl)allyl]diphenylsulfonium perchlorate **5** reacted with the same imines **1** (Scheme 1, Table 1). The operation was simple and the yields of both reactions were excellent.‡

From Table 1, it can be seen that all reactions furnished the desired aziridines in satisfactory yields. Stereocontrol is realized *via* simply changing the ligands on the sulfur atom (that is, Ph or Me) and the reaction conditions. Reaction at room

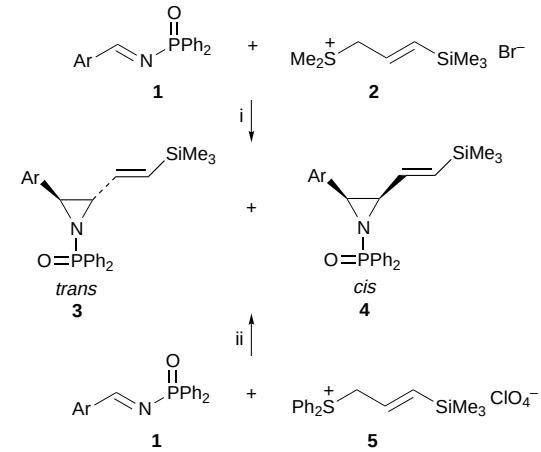

Scheme 1 *Reagents and conditions*: i, base, CH_2Cl_2, room temp.; ii, base, THF, the **1**, −100 °C

Table 1 Stereoselective preparation of aziridines

Entry	Ar	Ylide	Base	*T*/°C	Yield (%)[a]	*cis*:*trans*[b]
1	Ph	**2**	NaH	room temp.	92	10 : 90
2	Ph	**2**	KOH	room temp.	78	24 : 76
3	*p*-ClC_6H_4	**2**	NaH	room temp.	93	12 : 88
4	*p*-$MeOC_6H_4$	**2**	NaH	room temp.	95	20 : 80
5	1-Naphthyl	**2**	NaH	room temp.	86	22 : 78
6	Ph	**5**	NaHMDS[c]	−100	93	91 : 9
7	*p*-$MeOC_6H_4$	**5**	NaHMDS[c]	−100	90	99 : < 1
8	*p*-MeC_6H_4	**5**	NaHMDS[c]	−100	94	99 : < 1
9	*p*-ClC_6H_4	**5**	NaHMDS[c]	−100	84	85 : 15
10	2-Furyl	**5**	NaHMDS[c]	−100	90	99 : < 1
11	*p*-$CF_3C_6H_4$	**5**	NaHMDS[c]	−100	72	85 : 15
12	Ph	**5**	NaHMDS[c]	−78	91	87 : 13
13	Ph	**5**	NaHMDS	−78	93	85 : 15

[a] Isolated yield. [b] Determined by 300 MHz ^{1}H NMR spectroscopy. [c] 1 equiv. of LiBr was added.

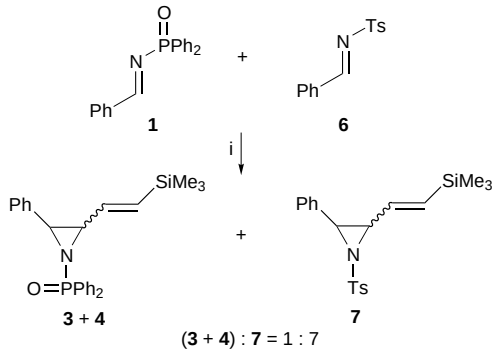

Scheme 2 *Reagents and conditions*: i, **2**, NaH, CH_2Cl_2, room temp.

temperature with the dimethylsulfonium salt provided *trans*-aziridines **3** (*trans* : *cis* = 78 : 22 to 90 : 10), even though *cis*-aziridines are considered thermodynamically more stable.[8] In this reaction, the selection of base is important. High stereoselectivity is obtained when NaH is used (entry 1), but it is lowered if KOH is used (entry 2). This might be because the use of NaH avoids the formation of water in the reaction. It was also observed that the stereoselectivity of the reaction in CH_2Cl_2 was better than that in MeCN or benzene. At low temperature, reaction of the ylide preformed from diphenyl sulfide with imines **1** gave rise to *cis*-aziridines with high stereoselectivity. Lower temperatures favored the *cis*-isomers (entries 6 and 12). In some cases the reaction furnished the *cis*-products almost exclusively (entries 7, 8 and 10). Unlike epoxidation and cyclopropanation reactions,[9] the presence of LiBr is not crucial and the stereochemistry of this reaction does not depend on whether LiBr is present or not (entries 12 and 13).

The improvement of stereoselectivity in the case of the *N*-diphenylphosphinoyl imines as compared with the *N*-tosyl imines is probably due to their different reactivity toward the attack of the allylsulfonium ylide. A competition reaction involving phosphinoylimine, tosylimine and allylsulfonium ylide shows that phosphinoylimine is less reactive than tosylimine (Scheme 2).

In summary, the $Ph_2P(O)$ moiety is a good activating group of imines for the reaction with sulfonium ylides. The advantages are (i) the stereochemistry can be greatly improved and tuned to either the *cis*- or *trans*-isomer, (ii) the *cis*- and *trans*-aziridines are easily separated by simple chromatography and (iii) the $Ph_2P(O)$ group is easily removed using acid.[10] Further investigations on the reaction mechanism and asymmetric synthesis of aziridines using *N*-phosphinoyl imines are underway.

Financial support from the National Sciences Foundation of China (Project 29790127) and Chinese Academy of Sciences is gratefully acknowledged. Dedicated to Professor Dr Emanuel Vogel on the occasion of his 70th Birthday.

Notes and References

† E-mail: xlhou@pub.sioc.ac.cn

‡ *General experimental procedure* for room temperature reaction: To a solution of sulfonium salt **2** (0.44 mmol) and phosphinoyl imine **1** (0.4 mmol) in CH_2Cl_2 (4 ml) was added NaH (15 mg, 0.6 mmol) at room temp. The resulting mixture was stirred at room temp. until the starting material **1** disappeared (monitored by TLC). Water (10 ml) was added and the mixture was extracted with CH_2Cl_2 (15 ml × 3). The organic solutions were combined and dried ($MgSO_4$). Removal of solvent under reduced pressure and chromatography (silica gel, light petroleum–EtOAc 5 : 1) afforded pure *trans*-aziridine **3** and *cis*-aziridine **4**.

General procedure for low temperature reaction: To a solution of sulfonium salt **5** (0.48 mmol) in THF (6 ml) under argon at −100 °C was added NaHMDS (2 M in THF, 0.24 ml, 0.48 mmol). The resulting mixture was stirred for 10 min. A solution of imine **1** (0.4 mmol) in THF (2 ml) was added and the stirring continued for another 1 h. The reaction temperature was then allowed to rise to room temp. Work up as above and chromatography provided pure *trans*-aziridine **3** and *cis*-aziridine **4**.

1 (*a*) D. Tanner, *Angew. Chem., Int. Ed. Engl.*, 1994, **33**, 599; (*b*) A. H. Li, L. X. Dai and V. K. Aggarwal, *Chem. Rev.*, 1997, **97**, 2341.
2 For reviews, see: W. A. Remers and B. S. Iyengar, *Recent Progress in the Chemical Synthesis of Antibiotics*, ed. G. Lukacs and M. Ohno, Springer, Berlin, 1990, p. 415; F. E. Ziegler and M. Belema, *J. Org. Chem.*, 1997, **62**, 1083; T. Fukuyama, F. Nakatsubo, A. J. Cocuzza and Y. Kishi, *Tetrahedron Lett.*, 1977, 295.
3 For example: (*a*) A. H. Li, Y. G. Zhou, L. X. Dai, X. L. Hou, L. J. Xia and L. Lin, *Angew. Chem., Int. Ed. Engl.*, 1997, **36**, 1317; (*b*) A. H. Li, L. X. Dai, X. L. Hou and M. B. Chen, *J. Org. Chem.*, 1996, **61**, 4641; (*c*) Y. G. Zhou, A. H. Li, X. L. Hou and L. X. Dai, *Tetrahedron Lett.*, 1997, **38**, 7225; (*d*) V. K. Aggarwal, A. Thompson, R. V. H. Jones and M. C. H. Standen, *J. Org. Chem.*, 1996, **61**, 8368; (*e*) R. S. Atkinson, M. P. Coogan and I. S. T. Lochrie, *Chem. Commun.*, 1996, 789; (*f*) D. A. Evans, M. M. Faul, M. T. Bilodeau, B. A. Anderson and D. M. Barnes, *J. Am. Chem. Soc.*, 1993, **115**, 5328; (*g*) Z. Li, K. R. Conser and E. N. Jecobsen, *J. Am. Chem. Soc.*, 1993, **115**, 5326; (*h*) K. B. Hansen, N. S. Finney and E. N. Jacobsen, *Angew. Chem., Int. Ed. Engl*, 1995, **34**, 676; (*i*) L. Casarrubios, J. A. Pérez, M. Brookhart and J. L. Templeton, *J. Org. Chem.*, 1996, **61**, 8358; (*j*) J. M. Mohan, B. S. Uphade, V. R. Choudhary, T. Ravindranathan and A. Suddalai, *Chem. Commun.*, 1997, 1429; (*k*) K. G. Rasmussen and K. A. Jørgensen, *J. Chem. Soc., Perkin Trans. 1*, 1997, 1287.
4 A. A. Cantrill, A. N. Jarvis, H. M. I. Osborn, O. A. Ouadi and J. B. Sweeney, *Synlett*, 1996, 847.
5 For example: U. M. Lindstrom and P. Somfai, *J. Am. Chem. Soc.*, 1997, **119**, 8385; J. Ahman, T. Jarevang and P. Somfai, *J. Org. Chem.*, 1996, **61**, 8148; I. Coldham, A. J. Collis, R. J. Mould and R. E. Rathmell, *J. Chem. Soc., Perkin Trans. 1*, 1995, 2739.
6 D. K. Wang, L. X. Dai and X. L. Hou, *Chem. Commun.*, 1997, 1231.
7 B. Krzyzanowska and W. J. Stec, *Synthesis*, 1978, 521; B. Krzyanowska and W. J. Stec, *Synthesis*, 1982, 270; A. Zweierzak and A. Napieraj, *Tetrahedron*, 1996, **52**, 8789.
8 T. Ibuka, N. Mimura, H. Ohno, K. Nakai, M. Akaji, H. Habashita, H. Tamamura, Y. Miwa, T. Taga, N. Fuji and Y. Yamamoto, *J. Org. Chem.*, 1997, **62**, 2982 and references cited therein; A. A. Canttrill, L. D. Hall, A. N. Jarvis, H. M. I. Osborn, J. Rappy and J. B. Sweeney, *Chem. Commun.*, 1996, 2631.
9 T. Yong, Ph.D. Thesis, Shanghai Institute of Organic Chemistry, Chinese Academy of Sciences, 1995; Y. G. Zhou, A. H. Li, X. L. Hou and L. X. Dai, *Chem. Commun.*, 1996, 1353.
10 R. Ramage, D. Hopton and M. Parrott, *J. Chem. Soc., Perkin Trans. 1*, 1984, 1357; G. W. Kenner, G. A. Noore and R. Ramage, *Tetrahedron Lett.*, 1976, 3623.

Received in Cambridge, UK, 16th January 1998; 8/00438B

Highly efficient photometathesis in a proximate, synperiplanar diazene-diazene oxide substrate: retention of optical purity, mechanistic implications

Kai Exner and Horst Prinzbach*†

Institut für Organische Chemie und Biochemie, Universität Freiburg, Albertstr. 21, D-79104 Freiburg, Germany

In a specifically designed proximate and almost perfectly synperiplanar diazene–diazene oxide substrate, metathesis is the exclusive photoreaction and occurs with retention of optical purity, providing support for the [π2 + π2]photocycloaddition pathway (tetrazetidine oxide intermediate).

An intriguing discrepancy between rigid, proximate (*d*), synperiplanar (*ω*) dienes **A** (X = CR) and bisdiazenes **A** (X = N) is the contrasting propensity for [π2 + π2] photocycloaddition (**A** → **B**).[1] The ease of N_2 extrusion is the main reason for the repeated failure to achieve diazene + diazene → tetrazetidine photocycloaddition [reaction (1)].[2,3]

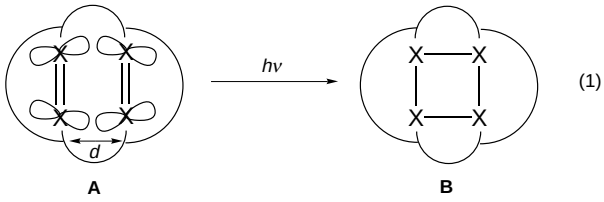

(1)

We have recently reported that in the specifically designed very proximate and nearly synperiplanar bisdiazene **1** with its very favourable stereoelectronic prerequisites (*d* = 2.822 Å, *ω* = 174.2°, X-ray), N_2 elimination still precludes the [π2 + π2] photocycloaddition, but that some photometathesis of its oxide **2** (→ **3**) does occur (2%) [reaction (2)], most probably through the tetrazetidine oxide.[4] Given the quantum yields Φ_{-N_2} of 1.00 and 0.02, respectively, for the N_2 elimination from the parent 2,3-diazabicyclohept-2-ene (DBH) and 2,3-diazabicyclooct-2-ene (DBO),[5] the cycloaddition (metathesis) of the isomeric oxide **4** with its oxidized DBH- and 'reluctant' DBO-subunits was expected to be more successful [reaction (3)]. The synthesis of **4** as a racemate and as the (+)-enantiomer and the experimental verification of the above hypotheses are the subjects of this communication.[6]

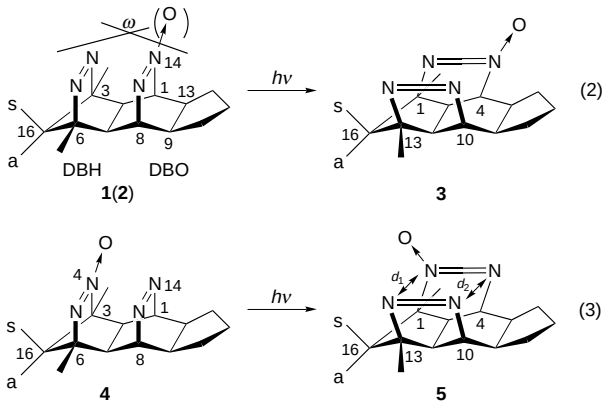

(2)

(3)

Since monooxidation of bisdiazene **1** had exclusively occurred in the DBO section to give **2**, the isomer **4** was prepared starting with **6**[4] (Scheme 1). The quantitatively obtained oxide *rac*-**7** [λ_{max} (CH_3CN)/nm 230 (ε/dm^3 mol^{-1} cm^{-1} 5980)] was then transformed into the diazene-diazene oxide **10** (mixture of diastereomers [λ_{max} (CH_3CN)/nm 236 (ε 3340), 387 (82)] *via* dialdehyde **8** and dihydropyridazine **9** (mixture of trimers) following the procedure for the preparation of **1**. Yet, hydrogenation (catalytic, N_2H_2) of the cyclopentene ring in **10** could not be effected without partial deoxygenation (→ **1**). Typical for the rigid, colourless, crystalline *rac*-**4**, obtained in *ca.* 50% yield after chromatography and crystallisation ($CHCl_3$–*n*-hexane), are *inter alia* the small H,H coupling constants ($J_{1,2\ (1,13)}$ = $J_{7,8\ (8,9)}$ = 1.6 Hz) and the *m*/*z* = 141 fragment in the EIMS spectrum (3,4,4,5-tetramethyl-4*H*-pyrazole 1-oxide + H$^+$, 100%). In the UV spectra (CH_3CN) of **10** (**4**) the distinct N=NO π,π* maxima at 237(236) nm [ε 3780(2340)] and the N=N n,π* maxima at 387(387) nm [ε 82(81)], when compared with the N=NO absorption of **7** and the n,π* maximum for the parent DBO [λ_{max}(*n*-hexane)/nm 378 (ε 182)], can be taken as evidence for a weak transannular N=N/N=NO interaction. Note that **2** and **4**, upon heating to their melting temperature (260/264 °C), remained unchanged; there was no indication for their interconversion or for their common [4 + 2] oxazolidine cycloadduct;[7] at even higher temperatures neat N_2 elimination (**2**) or oligomerization (**4**) occurred.

In line with expectation n,π* excitation (solidex vessel, CH_3OH, 150 W Hg high pressure lamp, 25 °C) for several hours left **4** unchanged; denitrogenation was obviously very much slower than in isomer **2**. Monochromatic π,π* excitation (254 nm, quartz vessel, CH_3OH, Hanau TNN 15 lamp, 25 °C)

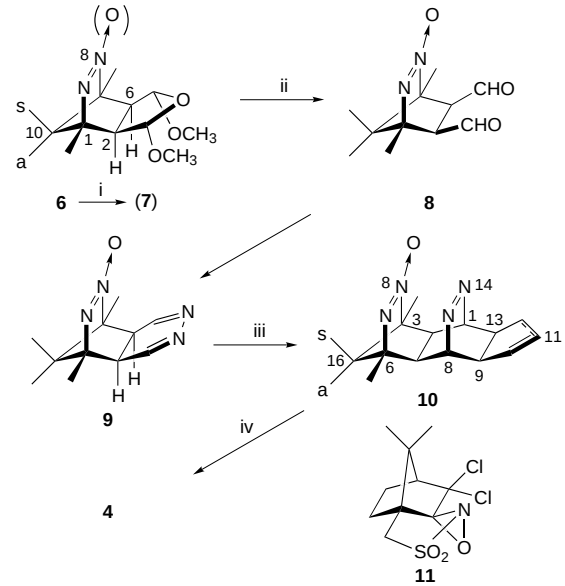

Scheme 1 *Reagents and conditions*: i, (±)-**7**: DMDO, CH_2Cl_2–Me_2CO, rt, quant.; (+)-**7**: (+)-**11**, 14 kbar, 65 °C, 12 d, ethyl acetate, 75%, 92–95% ee; ii, 1 M H_2SO_4, reflux, used as CH_2Cl_2 solution of the hydrate; N_2H_4, 10 equiv., K_2CO_3, 100 equiv. CH_2Cl_2, 0 °C; iii, TFA (1 equiv.), cyclopentadiene (*ca.* 500 equiv.), CH_2Cl_2, 4 °C, 62%; iv, H_2/MeOH/Pd/C (10%), rt, 66%

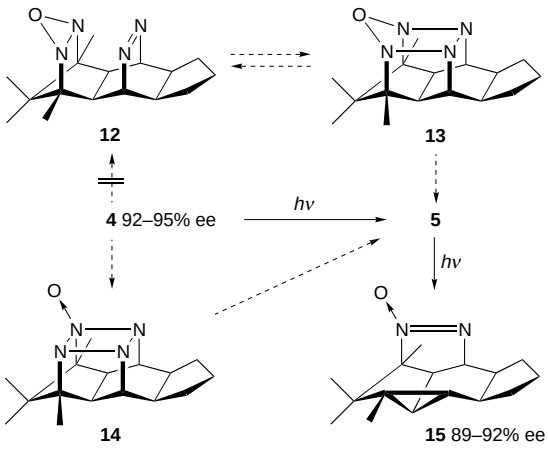

Scheme 2 Photochemistry of (chiral) bisdiazene oxide **4** and its isomer **5** (254 nm low pressure Hg lamp, MeOH, rt)

generated, in up to *ca.* 10% conversion exclusively, the metathesis isomer **5** (TLC, NMR) which was chromatographically isolated as colourless crystals [λ_{max} (CH_3CN)/nm 239 (ε 5510, π,π* N=NO), 346 (ε 172, n,π* N=N)]. With increasing conversion, denitrogenation of **5** to give **15** (70–75% was isolated in the crystalline form) and oligomers (25–30%) became important (Scheme 2). By separate irradiation of **5** it was ascertained that **15** indeed was a secondary photoproduct. The skeletal changes in going from **4** to the more mobile **5** with the most stable calculated (B3LYP/6-31G*) conformation at d_1 = 3.142 and d_2 = 2.950 Å (ω = 161.4°) are manifested *inter alia* by the relatively large H,H coupling constants $J_{4,5}$ = 5.9, $J_{4,15}$ = 6.4, $J_{9,10}$ = 9.2, $J_{10,14}$ = 7.0 Hz and the hypsochromic displacement of the N=N n,π* absorption.[8]

Of the two pathways shown in Scheme 2 for the metathesis **4** → **5**, the route featuring the C_s symmetrical **12** and **13** as intermediates could be put to experimental test with optically active **4**. After futile attempts to oxidize **6** enantioselectively using Sharpless[9] and Jacobsen[10] methods, with percamphanic acid[11] or the chiral oxaziridine **11**,[12] the application of high pressure to the reaction of **6** with **11** brought the solution: chiral oxide **7** was isolated with 92–95% ee (Chiralcel AD, propan-2-ol–*n*-hexane 1 : 3). After standard synthesis of (+)-**4** and photolysis, the retention of the optical purity was established for (−)-**15** (89–92% ee, Chiralcel AD, the enantiomers of **4** and **5** could not be sufficiently separated). Experiments for the low-temperature (matrix) characterisation of the tetrazetidine oxide **14** as the most plausible intermediate are in progress.[13]

This work was supported by the Deutsche Forschungsgemeinschaft, the Fonds der Chemischen Industrie, and BASF AG. We thank B. Geiser for technical assistance.

Notes and References

† E-mail: prinzbach@oca.chemie.uni-freiburg.de

1 Another fundamental difference is the readiness of these 'proximate' bisdiazenes to undergo one- and two-electron reduction with generation of so far unknown cyclically delocalised, highly persistent 4N/5e radical anions and 4N/6e dianions. K. Exner, O. Cullmann, D. Hunkler, H. Prinzbach, G. Gescheidt and V. Peron, unpublished results.

2 H. Prinzbach, G. Fischer, G. Rihs, G. Sedelmeier, E. Heilbronner and Z.-Z. Yang, *Tetrahedron Lett.*, 1982, **23**, 1251, *c.f.* E. Tauer and R. Machinek, *Liebigs Ann. Chem.*, 1996, 1213; E. Tauer, K.-H. Grellmann and A. Heinrich, *Chem. Ber.*, 1991, **124**, 2053; G. Ritter, G. Häfelinger, H. Rau and E. Lüdecke, *J. Am. Chem. Soc*., 1989, **111**, 4627.

3 E. Beckmann, N. Bahr and H. Prinzbach, *Tetrahedron Lett.*, 1990, **31**, 1125.

4 K. Exner, D. Hochstrate, M. Keller, F.-G. Klärner and H. Prinzbach, *Angew. Chem., Int. Ed. Engl.*, 1996, **35**, 2256.

5 P. S. Engel, *Chem. Rev*., 1980, **80**, 99; M. A. Anderson and C. B. Grissom, *J. Am. Chem. Soc*., 1995, **117**, 5041 and references therein.

6 All compounds have been fully characterized (^{1}H, ^{13}C NMR, MS, UV, IR). *Selected data* for **4**: δ_H($CDCl_3$, 400 MHz) 5.47 (dd, $J_{7,8}$ = $J_{8,9}$ 1.6, 8-H), 5.31 (dd, $J_{1,2}$ = $J_{1,13}$ 1.6, 1-H), 2.35 (*AB*XY, J_{AB} 10.4, 7-H), 2.27 (A*B*XY, J_{AB} = 10.4, 2-H), 2.32–2.25 (dddd, 9-H), 2.23–2.15 (dddd, 13-H), 1.80–1.70 (m, 10a-H, 12a-H), 1.47 (s, 6-Me), 1.45–1.35 (m, 10s-H, 11a-H, 12s-H), 1.39 (s, 3-Me), 1.23–1.10 (m, 11s-H), 0.92 (s, 16s-Me), 0.72 (s, 16a-Me); δ_C($CDCl_3$, 100.6 MHz) 91.0 (C-3), 75.6 (C-6), 64.0 (C-8), 63.6 (C-1), 59.8 (C-16), 48.3 (C-7), 44.6 (C-13), 43.7 (C-9), 43.3 (C-2), 30.2/29.9 (C-10, C-12), 26.2 (C-11), 17.4 (16-Me *anti*), 15.6 (16-Me *syn*), 12.1 (6-Me), 9.7 (3-Me); *m*/*z* (EI) 201 [M^+ − Me − N_2 − N_2O] (5%), 141 [tetramethyl-4*H*-pyrazole *N*-oxide + H^+] (100), 125 [tetramethyl-4*H*-pyrazole + H^+] (26), 91 (39); λ_{max}(CH_3CN)/nm 204 (ε/dm^3 mol^{-1} cm^{-1} 4620), 237 (3780), 387 (81). ν (KBr)/cm^{-1} 1509 (NNO). *Selected data* for **5**: δ_H($CDCl_3$, 400 MHz) 4.38 (dd, $J_{9,10}$ 9.2, $J_{10,14}$ 7.0, 10-H), 4.10 (dd, $J_{4,5}$ 5.9, $J_{4,15}$ 6.4, 4-H), 2.79–2.69 (dddd, 9-H), 2.58 (dd, $J_{4,15}$ = 6.4, $J_{14,15}$ 10.4, 15-H), 2.45–2.35 (m, i. a. 5-H), 2.25–2.19 (m, 8-H), 2.15 (dd, $J_{10,14}$ = 7.0, $J_{14,15}$ 10.4, 14-H), 2.11–1.96 (m, 2 H), 1.93–1.85 (m, 1 H), 1.84 (s, Me), 1.59–1.48 (m, 7-H), 1.40 (s, Me), 1.05 (s, Me), 1.02 (s, Me): δ_C($CDCl_3$, 100.6 MHz) 105.4 (C-13), 98.5 (C-1), 86.5 (C-10), 65.7 (C-4), 49.3 (C-16), 45.4 (C-15), 41.0 (C-14), 37.2 (C-9), 36.7 (C-5), 31.5/30.1 (C-6, C-8), 26.1 (C-7), 25.2/17.2/16.9/15.0 (CH_3); *m*/*z* (EI) 288 [M^+] (2%), 244 [M^+−N_2O] (1), 216 [M^+ − N_2 − N_2O] (28), 201 [M^+ − N_2 − N_2 O − Me] (100), 133 (60); λ_{max}(CH_3CN)/nm 239 (ε/dm^3 mol^{-1} cm^{-1} 5510), 346 (172); ν_{max}(KBr)/cm^{-1} 1509 (NNO).

7 For related ene-diazene oxide cycloadditions see, G. Fischer, D. Hunkler and H. Prinzbach, *Tetrahedron Lett*., 1984, **25**, 2459; S. Hünig and M. Schmitt, *Liebigs Ann. Chem.*, 1995; 1801, and references therein.

8 N. Bahr, E. Beckmann, K. Mathauer, D. Hunkler, M. Keller, H. Prinzbach and H. Vahrenkamp, *Chem. Ber*., 1993, **126**, 429; O. Cullmann, Ph.D. Dissertation, University of Freiburg, 1998.

9 The modified procedure used to oxidize sulfides to sulfones was applied: P. Pitchen, E. Dunach, M.N. Deshmukh and H.B. Kagan, *J. Am. Chem. Soc.*, 1984, **106**, 8188.

10 E. N. Jacobsen, W. Zhang, A. R. Muci, J. R. Ecker and L. Deng, *J. Am. Chem. Soc.*, 1991, **113**, 7063.

11 F. D. Greene and St. S. Hecht, *Tetrahedron Lett.*, 1969, **18**, 575.

12 F. A. Davis, M. C. Weismiller, C. K. Murphy, R. T. Reddy and B.-C. Chen, *J. Org. Chem*., 1992, **57**, 7274.

13 Together with M. Schweizer, J. Wirz (Basel), H.-P. Reisenauer and G. Maier (Gießen).

Received in Liverpool, UK, 23rd December 1997; 7/09232F

The synthesis and structure of $\{[\eta^4\text{-}Me_8taa]Sn(\mu\text{-}O)\}_2$: a bridging oxo complex in a system that yields terminal sulfido and selenido counterparts

Matthew C. Kuchta, Tony Hascall and Gerard Parkin*†

Department of Chemistry, Columbia University, New York, New York 10027, USA

Oxo transfer from N_2O to divalent $[\eta^4\text{-}Me_8taa]Sn$ (Me_8taaH_2 = octamethyldibenzotetraaza[14]annulene) yields the oxo complex, $\{[\eta^4\text{-}Me_8taa]Sn(\mu\text{-}O)\}_2$; the bridging nature of the oxo ligand provides a marked contrast with the terminal sulfido and selenido counterparts, $[\eta^4\text{-}Me_8taa]SnE$ (E = S, Se).

Terminal chalcogenido complexes of the transition[1] and main group[2] elements are presently a major focus of our research. For example, with respect to the main group elements, we have employed (*i*) the sterically demanding tris(3,5-di-*tert*-butyl)pyrazolylhydroborato ligand to enable the isolation of terminal chalcogenido complexes of gallium and indium, *i.e.* $[Tp^{Bu^t_2}]GaE$ (E = S, Se, Te),[3] and $[Tp^{Bu^t_2}]InSe$,[4] and (*ii*) the macrocyclic octamethyldibenzotetraaza[4]annulene ligand to support terminal chalcogenido complexes of germanium and tin, *i.e.* $[\eta^4\text{-}Me_8taa]GeE$ (E = S, Se, Te)[5] and $[\eta^4\text{-}Me_8taa]SnE$ (E = S, Se).[6,7] In this paper, we report the synthesis of the tin oxo counterpart, and describe X-ray diffraction studies which demonstrate that, unlike the [Sn=S] and [Sn=Se] functionalities, the corresponding terminal [Sn=O] moiety is unstable with respect to bridging.

Considering that the terminal sulfido and selenido complexes, $[\eta^4\text{-}Me_8taa]SnE$ (E = S, Se) are readily obtained by reaction of $[\eta^4\text{-}Me_8taa]Sn$ with the elemental chalcogens,[6] it was anticipated that the related oxo species could be generated by the reaction of $[\eta^4\text{-}Me_8taa]Sn$ with an appropriate oxo transfer reagent. Indeed, $[\eta^4\text{-}Me_8taa]Sn$ was found to react cleanly with N_2O to give the orange oxo complex, $\{[\eta^4\text{-}Me_8taa]Sn(\mu\text{-}O)\}_2$ (Scheme 1).[8] However, in contrast to the monomeric terminal sulfido and selenido complexes, X-ray diffraction studies revealed that the oxo counterpart is dimeric, with bridging oxo ligands (Fig. 1).[9,10] Tin complexes with bridging oxo ligands are common, as illustrated by the cyclic 'stannoxanes', $[R_2Sn(\mu\text{-}O)]_n$, but are typically obtained by hydrolysis of tetravalent halide precursors, R_2SnX_2,[11] rather than by reactions of divalent precursors with oxo transfer reagents. A notable exception, however, is Lappert's synthesis of $\{[(Me_3Si)_2CH]_2Sn(\mu\text{-}O)\}_2$ by reaction of $[(Me_3Si)_2CH]_2Sn$ with Me_3NO.[12,13] In addition to the similar method of synthesis, another feature that is common to both $\{[\eta^4\text{-}Me_8taa]Sn(\mu\text{-}O)\}_2$ and $\{[(Me_3Si)_2CH]_2Sn(\mu\text{-}O)\}_2$ is the presence of a four-membered $[Sn_2O_2]$ ring. More typically, stannoxanes exist as cyclic trimers with six-membered $[Sn_3O_3]$ rings, as exemplified by $[Mes_2Sn(\mu\text{-}O)]_3$,[14] $[R_2Sn(\mu\text{-}O)]_3$ (R = Bu^t, Me_2EtC),[15] $[(Me_3Si)_3C(Me)Sn(\mu\text{-}O)]_3$,[16] $[\{2,4,6\text{-}(CF_3)_3C_6H_2\}_2Sn(\mu\text{-}O)]_3$,[17] and $[(2,6\text{-}Et_2C_6H_3)Sn(\mu\text{-}O)]_3$.[18,19]

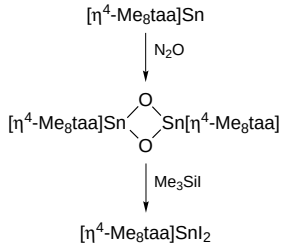

Scheme 1

The observation that the oxo ligand in the $\{[\eta^4\text{-}Me_8taa]SnE\}$ system bridges more readily than does either the sulfido or selenido ligands is particularly interesting, especially in view of the notion embodied by the so-called 'classical double bond rule', one version of which cites: 'elements having a principal quantum number greater than 2 should not be able to form $(p\text{–}p)\pi$ bonds to themselves or with other elements.[20] Furthermore, it is noteworthy that all other structurally characterized multiply bonded terminal chalcogenido complexes of tin are restricted to the heavier congeners,[21] with no examples of terminal oxo derivatives; as noted above, however, bridging oxo complexes of tin are well precedented. Regardless of whether or not monomeric $\{[\eta^4\text{-}Me_8taa]SnO\}$ is an intermediate in the reaction of $[\eta^4\text{-}Me_8taa]Sn$ with N_2O, the structures of $\{[\eta^4\text{-}Me_8taa]SnE\}_n$ suggest that the terminal [Sn=O] moiety is significantly more prone to participate in bridging than is either the [Sn=S] or [Sn=Se] functionalities. Albeit limited, there are other observations which also suggest that the oxo ligand shows a greater propensity to act as a bridging functionality in main group chemistry than do the heavier chalcogenido ligands. For example, the germanium sulfido complex $[\eta^3\text{-}\{(\mu\text{-}Bu^tN)_2(SiMeNBu^t)_2\}]GeS$ exists as a monomer, whereas the oxygen analogue is dinuclear with oxo bridges.[22] Likewise, the sulfido and selenido complexes $Ph(\eta^2\text{-}C_{10}H_6NMe_2)SiE$ (E = S, Se) are monomeric, while the oxygen counterpart is trinuclear with a six-membered Si_3O_3 ring.[23] Such behaviour is completely counter to that observed in transition metal systems, where the oxo ligand shows the least tendency to bridge,[24] with terminal oxo complexes being considerably more abundant than terminal sulfido, selenido, and tellurido derivatives.[1] A possible explanation for this difference between oxo complexes of the main group and transition elements is associated with the polarity of

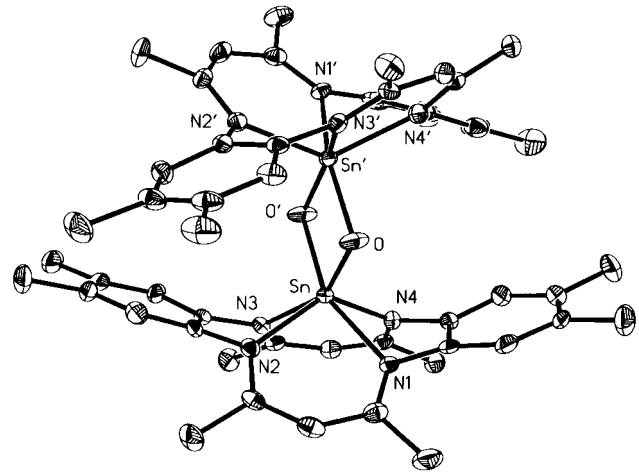

Fig. 1 Molecular structure of $\{[\eta^4\text{-}Me_8taa]Sn(\mu\text{-}O)\}_2$. Selected bond lengths (Å) and angles (°): Sn–O 2.001(5), Sn–O′ 1.987(5), Sn–N1 2.220(6), Sn–N2 2.142(7), Sn–N3 2.256(7), Sn–N4 2.169(7); O–Sn–O′ 80.1(2), Sn–O–Sn′ 99.8(2).

the M–O bonds. Specifically, oxo ligands bound to electropositive main group elements may be expected to bear a substantial negative charge,[25,26] especially if the metal center has a coordination number greater than three, such that p_π–p_π overlap is unfavourable. For such a situation, the resonance structure $[\overset{+}{M}–\overline{O}]$ is an appropriate description of the bonding, and the existence of this dipole would be expected to promote oxo bridging. Transition metal oxo complexes, however, do not normally exhibit such a high degree of polarity due to favourable d_π–p_π overlap (*i.e.* a contribution from the resonance structure $[\overset{-}{M}\equiv\overset{+}{O}]$) which serves to reduce the $[\overset{\delta+}{M} \sim \overset{\delta-}{O}]$ polarity of the bond.[27,28] Since the $[\overset{+}{M}–\overline{E}]$ resonance structure for main group chalcogenido complexes would be expected to be most significant for oxo derivatives,[29] the propensity for bridging is likewise expected to be greater for oxo complexes than for the heavier chalcogenido counterparts.

Finally, it is noteworthy that the bridging oxo ligand of $\{[\eta^4\text{-}Me_8taa]Sn(\mu\text{-}O)\}_2$ is readily abstracted by treatment with excess Me_3SiI to give $[\eta^4\text{-}Me_8taa]SnI_2$ (Scheme 1), a complex that has previously been synthesized by oxidative addition of I_2 to $[\eta^4\text{-}Me_8taa]Sn$.[30]

In summary, oxo transfer from N_2O to divalent $[\eta^4\text{-}Me_8taa]Sn$ yields the bridging oxo complex, $\{[\eta^4\text{-}Me_8taa]Sn(\mu\text{-}O)\}_2$. Since the sulfido and selenido counterparts are mononuclear, it is evident that the oxo ligand in this system shows the greatest propensity to bridge. Such behavior is in marked contrast to that typically observed in transition metal systems.

We thank the National Science Foundation (CHE 96-10497) for support of this research. G. P. is the recipient of a Presidential Faculty Fellowship Award (1992–1997).

Notes and References

† E-mail: parkin@chem.columbia.edu

1 T. M. Trnka and G. Parkin, *Polyhedron*, 1997, **16**, 1031; G. Parkin, *Prog. Inorg. Chem.*, 1998, **47**, 1.

2 M. C. Kuchta and G. Parkin, *Coord. Chem. Rev.*, in press.

3 M. C. Kuchta and G. Parkin, *Inorg. Chem.*, 1997, **36**, 2492 and unpublished results.

4 M. C. Kuchta and G. Parkin, *J. Am. Chem. Soc.*, 1995, **117**, 12 651.

5 M. C. Kuchta and G. Parkin, *J. Chem. Soc., Chem. Commun.*, 1994, 1351.

6 M. C. Kuchta and G. Parkin, *J. Am. Chem. Soc.*, 1994, **116**, 8372.

7 Related porphyrin complexes (POR)SnE (E = S, Se) have also been synthesized; see: R. Guilard, C. Ratii, J.-M. Barbe, D. Dubois and K. M. Kadish, *Inorg. Chem.*, 1991, **30**, 1537.

8 ^{1}H NMR data (C_6D_6): δ 1.89 (4 CH_3), 2.23 (4 CH_3), 4.44 (2 CH), 6.68 (4 C*H*).

9 $\{[\eta^4\text{-}Me_8taa]Sn(\mu\text{-}O)\}_2$ monoclinic, space group *C*2/*c* (no. 15), *a* = 19.199(2), *b* = 19.12(2), *c* = 17.263(1) Å, α = 90, β = 110.019(7)°, γ = 90°, *U* = 5954.7(8) Å^3, *Z* = 4, R_1 = 0.0505, wR_2 = 0.0983 [$I > 2\sigma(I)$], room temp. CCDC 182/787.

10 The Sn–O bond lengths in $\{[\eta^4\text{-}Me_8taa]Sn(\mu\text{-}O)\}_2$ [1.987(5) and 2.001(5) Å] compare favorably with the CSD mean (1.98 Å). The search was performed using CSD Version 5.13 for Sn–O interactions with two-coordinate oxygen. 3D Search and Research Using the Cambridge Structural Database, E. H. Allen and O. Kennard, *Chem. Des. Automat. News*, 1993, vol. 8(1), pp. 1 and 31–37.

11 A. G. Davies and P. J. Smith, in *Comprehensive Organometallic Chemistry*, ed. G. Wilkinson, F. G. A. Stone and E. W. Abel, Pergamon, New York, 1982, vol. 2, ch. 11, p. 573.

12 M. A. Edelman, P. B. Hitchcock and M. F. Lappert, *J. Chem. Soc., Chem. Commun.*, 1990, 1116.

13 Some bridging peroxo complexes that have been synthesized by oxidation of divalent tin complexes include $\{[(Me_3Si)_2N]_2Sn(\mu\text{-}O_2)\}_2$[13a] and $\{[(Me_3Si)_2CH]_2Sn(\mu\text{-}O)(\mu\text{-}O_2)Sn[CH(SiMe_3)_2]\}$.[13b] (*a*) R. W. Chorley, P. B. Hitchcock and M. F. Lappert, *J. Chem. Soc., Chem. Commun.*, 1992, 525; (*b*) C. J. Cardin, D. J. Cardin M. M. Devereux and M. A. Convery, *J. Chem. Soc., Chem. Commun.*, 1990, 1461.

14 U. Weber, N. Pauls, W. Winter and H. B. Stegmann, *Z. Naturforsch., Teil B*, 1982, **37**, 1316.

15 H. Puff, W. Schuh, R. Sievers and R. Zimmer, *Angew. Chem., Int. Ed. Engl.*, 1981, **20**, 591; H. Puff, W. Schuh, R. Sievers, W. Wald and R. Zimmer, *J. Organomet. Chem.*, 1980, **186**, 213.

16 V. K. Belsky, I. V. Zemlyansky, I. V. Borisova, N. D. Kolosova and I. P. Beletskaya, *J. Organomet. Chem.*, 1983, **254**, 189.

17 J. F. Van der Maelen Uria, M. Belay, F. T. Edelmann and G. M. Sheldrick, *Acta Crystallogr., Sect. C*, 1994, **50**, 403.

18 S. Masamune, L. R. Sita and D. J. Williams, *J. Am. Chem. Soc.*, 1983, **105**, 630.

19 There are, however, some structurally characterized tin complexes with four-membered rings which incorporate only a single oxygen atom, *e.g.* $[(2,4,6\text{-}Pr^i_3C_6H_2)_2Sn(\mu\text{-}O)(\mu\text{-}S)Sn(2,4,6\text{-}Pr^i_3C_6H_2)_2]$[19a] and $[\{(2,6\text{-}Et_2C_6H_3)_2Sn\}_3O]$.[19b] (*a*) P. Brown, M. F. Mahon and K. C. Molloy, *J. Chem. Soc., Chem. Commun.*, 1989, 1621; (*b*) C. J. Cardin, D. J. Cardin, M. A. Convery and M. M. Devereux, *J. Organomet. Chem.*, 1991, **411**, C3.

20 P. Jutzi, *Angew. Chem. Int. Ed. Engl.*, 1975, **14**, 232.

21 For example, Richeson and co-worker[21a] have synthesized the sulfido complex $[\eta^2\text{-}CyNC(Bu^t)NCy]_2SnS$ and Leung *et al.*[21b] have reported the tellurido complex $\{\eta^2\text{-}[(C_9H_6N)(Me_3Si)CH]\}_2SnTe$. (*a*) Y. Zhou and D. S. Richeson, *J. Am. Chem. Soc.*, 1996, **118**, 10 850; (*b*) W.-P. Leung, W.-H. Kwok, L. T. C. Law, Z.-Y. Zhou and T. C. W. Mak, *Chem. Commun.*, 1996, 505.

22 M. Veith, S. Becker and V. Hutch, *Angew. Chem., Int. Ed. Engl.*, 1989, **28**, 1237.

23 P. Arya, J. Boyer, F. Carré, R. Corriu, G. Lanneau, J. Lapasset, M. Perrot and C. Priou, *Angew. Chem., Int. Ed. Engl.*, 1989, **28**, 1016.

24 For example, compare the terminal oxo complexes $[Cp^{Me}]_2MoO$[24a] and $[Cp^{Bu^t}]_2MoO$[24b] with the bridging chalcogenido complexes $\{[Cp^{Bu^t}]_2\text{-}Mo(\mu\text{-}E)\}_2$ (E = S, Se, Te). (*a*) N. D. Silavwe, M. Y. Chiang and D. R. Tyler, *Inorg. Chem.*, 1985, **24**, 4219. (*b*) J. H. Shin and G. Parkin unpublished results.

25 Furthermore, theoretical studies on three-coordinate $H_2M{=}O$ (M = Ge, Sn, Pb) complexes have indicated that both the σ- and π-bonds are polarized towards oxygen. See: J. Kapp, M. Remko and P. v. R. Schleyer, *J. Am. Chem. Soc.*, 1996, **118**, 5745; G. Trinquier, M. Pelissier, B. Saint-Roch and H. Lavayssiere, *J. Organomet. Chem.*, 1981, **214**, 169; G. Trinquier, J.-C. Barthelat and J. Satge, *J. Am. Chem. Soc.*, 1982, **104**, 5931.

26 For additional theoretical studies on $H_2M{=}O$ (M = Si, Ge, Sn, Pb), see: J. Kapp, M. Remko and P. v. R. Schleyer, *Inorg. Chem.*, 1997, **36**, 4241.

27 W. A. Nugent and J. M. Mayer, *Metal–Ligand Multiple Bonds*, Wiley-Interscience, New York, 1988.

28 Certain early and late transition metal oxo complexes are, however, believed to be best represented by the $[\overset{+}{M}–\overline{O}]$ resonance structure, *e.g.* $Cp^*_2Zr(O)(NC_5H_5)$[28a] and (dppp)(L)PtO.[28b] (*a*) W. Howard and G. Parkin, *J. Am. Chem. Soc.*, 1994, **116**, 606; (*b*) M. A. Andrews, G. L. Gould and E. J. Voss, *Inorg. Chem.*, 1996, **35**, 5740.

29 The relative contribution of the $[\overset{+}{M}–\overline{E}]$ resonance structure would be most significant for the oxo derivative due to (*i*) the greater electronegativity of oxygen which stabilizes the negative charge, and (*ii*) the shorter M–O bond length which results in a greater Coulombic stabilization. See ref. 28(*a*).

30 M. C. Kuchta and G. Parkin, *Polyhedron*, 1996, **15**, 4599.

Received in Bloomington, IN, USA, 18th December 1997; 7/09065J

A Ga_4N_8 cage structure formed by reaction of trimethylgallium with phenylhydrazine

David W. Peters,[a,b] Maurice P. Power,[a] Edith D. Bourret[b] and John Arnold*[a,b]†

[a] *Department of Chemistry, University of California, Berkeley, California 94720-1460, USA*
[b] *Materials Sciences Division, Lawrence Berkeley National Laboratory, California 94720, USA*

Methane elimination during thermolysis of $GaMe_3$ with $PhHNNH_2$ yields sequentially dimeric $[Me_2Ga\{\mu\text{-}N(H)N(H)Ph\}]_2$, tetrameric $[MeGa\{\mu\text{-}N(H)NPh\}]_4$ and, ultimately, GaN; the X-ray structure of the tetramer shows a novel Ga_4N_8 cage.

A number of research groups have investigated the chemistry of molecules containing Ga–N bonds,[1–5] with most of the recent emphasis directed at using these compounds as single-source precursors to the wide bandgap semiconductor GaN.[6–13] Here we describe some new results on the use of hydrazines as a source of nitrogen including the formation of two intermediates formed on elimination of 1, then 2 equiv. of methane during the thermolysis reaction between $GaMe_3$ and $PhHNNH_2$. Both complexes have been isolated and fully characterized and the latter is shown to have an unusual structure featuring a cage with a Ga_4N_8 core;[14] this species eliminates a final equivalent of methane to form GaN at higher temperatures.

As shown in Scheme 1, 1 equiv. of methane is eliminated in the reaction of $GaMe_3$ and $PhHNNH_2$ at room temperature in toluene. We saw no evidence for the presumed monomeric intermediate 'Me_2Ga–N(H)N(H)Ph', instead the colorless dimeric product was isolated in 88% yield.[15]

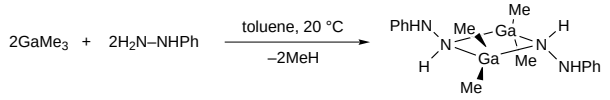

Scheme 1

The solid-state structure of the dimer is very similar to that of the closely related species $[Et_2Ga\{\mu\text{-}N(H)NPh_2\}]_2$, prepared by the metathesis reaction between Et_2GaCl and $LiN(H)NPh_2$,[11] with both compounds crystallizing as *anti* conformers.[16]

Upon further heating, the dimer undergoes a second methane elimination reaction as shown in Scheme 2.

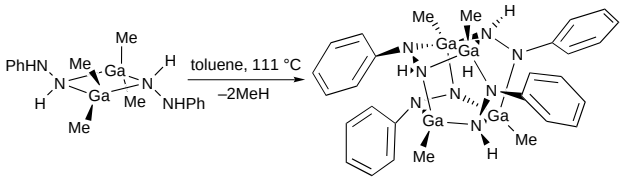

Scheme 2

As monitored by ^1H NMR spectroscopy, the reaction proceeds in a quantitative fashion and microcrystalline product, which is much less soluble than the starting material, precipitates from the reaction solvent in 84% yield.[15] The ^1H NMR spectrum shows a simple pattern consistent with only single methyl, N–H and phenyl environments[15] and we saw no evidence of fluxional behavior between −80 and 110 °C. Since these data were insufficient to unambiguously determine the structure of the molecule, an X-ray study was carried out.

Crystals of $[MeGaN(H)NPh]_4$ were grown by thermolysis of $[Me_2GaN(H)N(H)Ph]_2$ in toluene at 105 °C.[17] The solid state structure, shown in Fig.1, consists of a tetrameric unit that resides on the intersection of three mutually perpendicular mirror planes. The geometry about gallium is distorted tetrahedral, with angles ranging from 121.3(1) [N(1)–Ga(1)–C(1)] to 94.4(1) [N(2*)–Ga(1)–N(2*)]. The bond length of Ga to the four-coordinate N(2*) [1.993 (3) Å] is longer than that to the three-coordinate N(1) [1.914(2) Å], although the mean Ga–N distance of 1.966(3) Å falls within the reported range for gallium amido complexes.[1–5] The N–N bond length of 1.489(3) Å is longer than in the only other crystallographically characterized Ga hydrazide complex $[Et_2Ga\{\mu\text{-}N(H)NPh_2\}]_2$, [1.457(8) and 1.446(8) Å][11] and is somewhat longer than predicted for a N–N single bond (1.454 Å), a result that may be attributed to the bridging nature of the hydrazine ligand[18] in the cage species. Owing to the high quality of the data obtained, the hydrazine hydrogen was located in the Fourier difference map and refined isotropically. Fig. 2 shows a view of the unit cell which highlights the rather large open core of the structure (*ca.* 4.5 Å) and the fact that there are no unusually short intermolecular contacts. We are unaware of previous reports of such a cage structure for Ga, although we note that a related boron compound $[Bu^tBN(H)N(H)]_4$ was characterized some time ago.[19]

Thermolysis of the cage complex at 700 °C under a hydrogen atmosphere leads to the formation of hexagonal GaN (identified

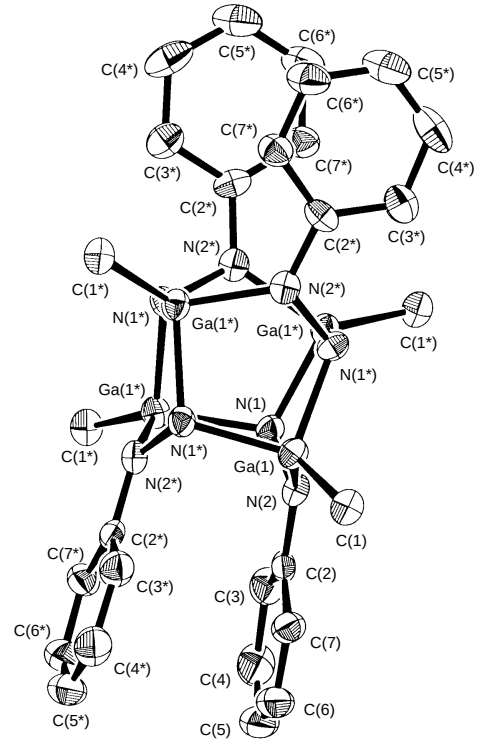

Fig. 1 X-Ray crystal structure of $[MeGaN(H)NPh]_4$

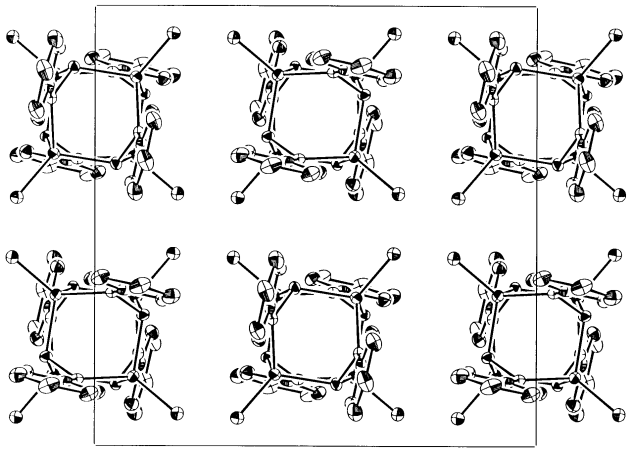

Fig. 2 Unit cell of $[MeGaN(H)NPh]_4$

by powder X-ray diffraction by comparison to a standard sample in the JCPDS database) along with a mixture of unidentified volatile organic fragments. Further studies are in progress and will be described in a more detailed account.

We thank the donors of the Petroleum Research Fund (administered by the American Chemical Society) for partial support of this work.

Notes and References

†E-mail: arnold@violet.berkeley.edu

1 S. Amirkhalili, P. B. Hitchcock and J. D. Smith, *J. Chem. Soc., Dalton Trans*., 1979, 1206.
2 T. Belgardt, S. D. Waezsada, H. W. Roesky, H. Gornitzka, L. Haming and D. Stalke, *Inorg. Chem.*, 1994, **33**, 6247.
3 F. Cordeddu, H. D. Hausen and J. Weidlein, *Z. Anorg. Allg. Chem.*, 1996, **622**, 573.
4 K. M. Waggoner, M. M. Olmstead and P. P. Power, *Polyhedron*, 1990, **9**, 257.
5 D. A. Atwood, V. O. Atwood, A. H. Cowley, R. A. Jones, J. L. Atwood and S. G. Bott, *Inorg. Chem.*, 1994, **33**, 3251.
6 D. A. Atwood, R. A. Jones, A. H. Cowley, J. L. Atwood and S. G. Bott, *J. Organomet. Chem.*, 1990, **394**, C6.
7 J. W. Hwang, J. P. Campbell, J. Kozubowski, S. A. Hanson, J. F. Evans and W. L. Gladfelter, *Chem. Mater*., 1995, **7**, 517.
8 J. Janik and R. Wells, *Chem. Mater*., 1996, **8**, 2708.
9 J. Kouvetakis, J. McMurran, P. Matsunaga, M. OKeefe and J. Hubbard, *Inorg. Chem.*, 1997, **36**, 1792.
10 J. Mcmurran, M. Todd, J. Kouvetakis, and D. J. Smith, *Appl. Phys. Lett.*, 1996, **69**, 203.
11 D. A. Neumayer, A. H. Cowley, A. Decken, R. A. Jones, V. Lakhotia and J. G. Ekerdt, *Inorg. Chem.*, 1995, **34**, 4698.
12 A. Miehr, M. R. Mattner, and R. A. Fischer, *Organometallics*, 1996, **15**, 2053.
13 D. A. Neumayer, A. H. Cowley, A. Decken, R. A. Jones, V. Lakhotia and J. G. Ekerdt, *J. Am. Chem. Soc.*, 1995, **117**, 5893.
14 M. Veith, *Chem., Rev*., 1990, **90**, 3.
15 Satisfactory elemental analyses (C, H, N) were obtained for all compounds. Experimental details and spectroscopic data are provided as supplementary information.
16 Details will be given in a full paper.
17 *Crystallographic data* $[MeGaN(H)NP]_4$, $C_{28}H_{36}Ga_4N_8$, M_w = 763.53, tetragonal, space group $I4_1/a$ (no. 88), a = 14.0460(2), c = 15.581(2) Å, U = 2970.81(6) Å^3, Z = 4, D_c = 1.71 g cm^{-3}, graphite monochromated Mo-Kα radiation (λ = 0.710 69 Å), μ(Mo-Kα) = 36.3 cm^{-1}. A total of 6973 reflections (1433 unique, R_{int} = 2.73%) were collected on a colourless crystal of dimensions 0.24 × 0.29 × 0.31 mm at −111 °C on a Siemens SMART diffractometer/CCD area detector; an empirical absorption correction was applied. The structure was solved by direct methods and refined by full matrix least squares procedures. All non-hydrogen atoms were refined isotropically. The hydrogen atom on N(1) was located from the Fourier difference map and refined isotropically. Final residuals at convergence were R = 0.0227 and R_w = 0.0281 for 1046 data with $F^2 > 3\sigma(F^2)$ and GOF = 1.23. CCDC 182/782.
18 N–N bond lengths of 1.512 and 1.517 Å have been observed in dinuclear ruthenium complexes with bridging hydrazines: J. F. Corrigan, S. Doherty, N. J. Taylor and A. J. Carty, *J. Chem. Soc., Chem. Commun.*, 1991, 1640; T. V. Ashworth, M. J. Nolte, R. H. Reimann and E. Singleton, *J. Chem. Soc., Dalton Trans*., 1978, 1043.
19 P. C. Thomas and I. C. Paul, *Chem. Commun.*, 1968, 1130.

Received in Bloomington, IN, USA, 9th January 1998; 8/00266E

Side-chain hydrophobicity controls the activity of proton channel forming rigid rod-shaped polyols

Chiyou Ni and Stefan Matile*†

Department of Chemistry, Georgetown University, Washington, D.C. 20057-1227, USA

Increased activity, facile incorporation into lipid bilayers and intact active structure and transport selectivity are the consequences of modifications of the side-chain hydrophobicity of a proton channel-forming octa(*p*-phenylene).

Rigid-rod molecule **1**[1,2] represents a promising new class of non-peptide ion channel models[3–5] with unique properties, but unfortunately it does not incorporate well into lipid bilayers (Fig. 1). Although the incorporation of artificial ion channels into lipid bilayers is a general problem, it is often bypassed by using high temperatures or constructing the entire supramolecular assay system in the presence of the test sample for every new experiment. Rational design strategies to tune partition without changing desired properties of a parent model have not been established so far, in spite of the fact that poor incorporation may prevent potential biological studies and pharmaceutical applications. Here we present our efforts to solve this problem by increasing the hydrophobicity of lateral side-chains attached to oligo(*p*-phenylene)s without destructive effects on active structure or transport selectivity.

In addition to the general aim to increase the lipophilicity of octamer **1**, the following considerations were taken into account for the design of the new side-chains in **2** and **3** (Fig. 1). We anticipated that length and flexibility of the propylene spacer in polyol **2** could facilitate the arrangement of the diols to form the transmembrane hydrogen-bonded chain[6] essential for proton selectivity.[2] It further may enlarge the ionophoric tube between the rigid-rod scaffold and 'proton wire'. The additional propyl group at the terminus of each side-chain in **3** possibly covers the hydrophilic 'proton wire' with an external lipophilic layer.

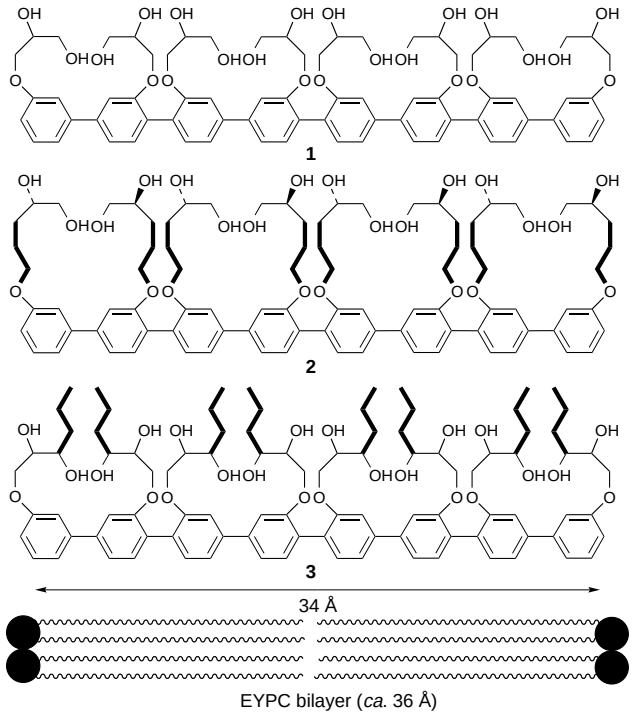

Fig. 1 In-scale planar structures of membrane-bound octa(*p*-phenylene)s **1**–**3**. Structural modifications of the side-chains are emphasized with bold lines.

Syntheses of the octamers **2** and **3** are shown in Scheme 1. For **2**, bromide **4** was subjected to Sharpless asymmetric dihydroxylation,[7]‡ and the resulting diol **5** was converted to acetonide **6**. For **3**, the diastereomeric mixture of triol **7** was selectively tosylated, and protection of the resulting diol **8** afforded **9**. Williamson ether synthesis using **6**/**9** and the crude octaphenol prepared by treatment of **10** with BBr_3,[1] followed by deprotection of **11**/**12**, yielded the polyols **2**/**3**, respectively. The corresponding hexamers **13** and **14** were prepared identically from hexaanisole **15**.§

The interaction of the fluorophores **1**–**3** with lipid bilayers was examiend using uniformly sized (68 ± 3 nm) EYPC-SUVs labeled with either 2 mol% 5- or 12-DOXYL-PC.[8,2]¶ Quenching of *ca.* 60% of the red-shifted emission of **2** and **3** by 5-DOXYL-PC labeled EYPC-SUVs proved facile incorporation compared to **1** (Fig. 2). Nearly identical quenching of **1**–**3** by 5-DOXYL-PC and 12-DOXYL-PC (not shown) confirmed that variation of side-chain hydrophobicity does not disturb the preferred transmembrane orientation of **1**–**3**.

In sharp contrast to the membrane-spanning octamers **1**–**3** (34 Å), the side-chain structure governs the organization of the corresponding hexamers (26 Å) in EYPC-bilayers. Namely, **16** was found at the membrane/water interface (quenching by 12-DOXYL-PC < 5-DOXYL-PC),[2] **13** in transmembrane orientation [12-DOXYL-PC (67%) ≈ 5-DOXYL-PC (69%)], and **14** between the two leaflets of the lipid bilayer [12-DOXYL-PC (49%) > 5-DOXYL-PC (26%)].

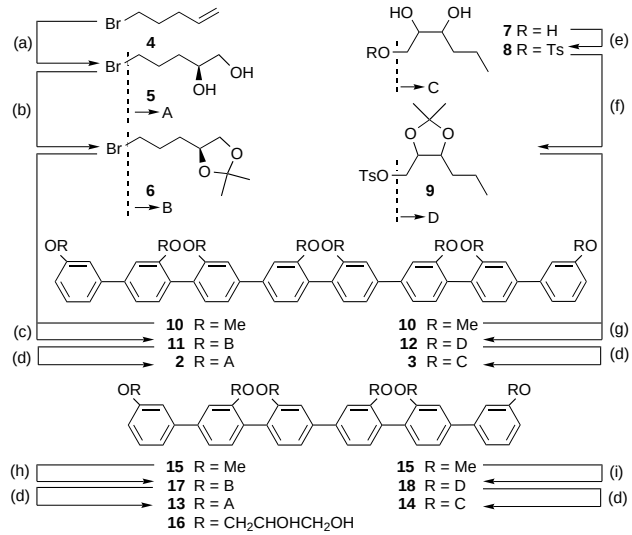

Scheme 1 *Reagents and conditions*: (a) AD-mix-α, 71%; (b) 2,2-dimethoxypropane, H_2SO_4, 80%; (c) (1) BBr_3; (2) **6**, Cs_2CO_3, 66%; (d) TFA (quant.); (e) TsCl, pyridine, 65%; (f) 2,2-dimethoxypropane, H_2SO_4, 83%; (g) (1) BBr_3; (2) **9**, Cs_2CO_3, 27%; (h) see (c), 15%; (i) see (g), 27%

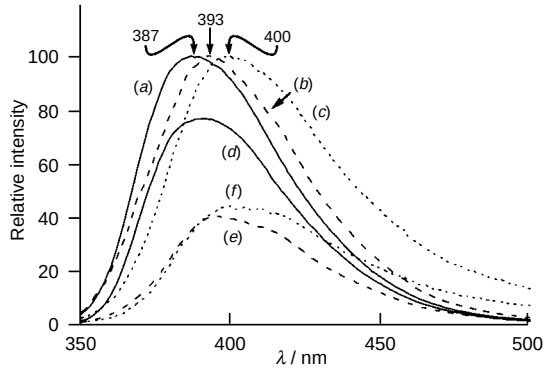

Fig. 2 Relative emission intensities [I/I (λ^{e}_{max}) × 100%, λ_{ex} = 328 nm) of 5 μM solutions of **1** (*a*), **2** (*b*), and **3** (*c*) with 0.5 mM of unlabeled EYPC-SUVs, and of **1** (*d*), **2** (*e*) and **3** (*f*) with 5-DOXYL-PC labeled EYPC-SUVs (100 mM KCl, 100 mM HEPES, pH 7.1)

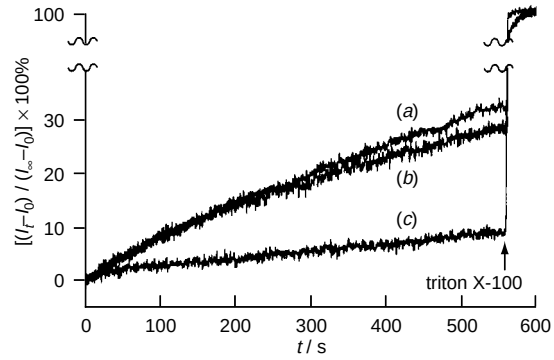

Fig. 3 Change in fluorescent intensity {[(I_t–I_0)/(I_∞–I_0)] × 100%, λ_{ex} = 460 nm, λ_{em} = 510 nm} of EYPC-SUV-entrapped HPTS (100 mM KCl, 100 mM HEPES, pH_{in} = 7.0, pH_{out} = 7.6) as a function of time after the addition of 10 nmoles of octa(*p*-phenylene)s **1** (*c*), **2** (*b*) and **3** (*a*) in 20 μl MeOH followed by 40 μl of 1.2% triton X-100¶

The ion transport activity of polyol **1** was originally assessed in comparison with the structurally related antifungal polyol amphotericin B (AmB).[1] Both mediated intravesicular pH changes with comparable exchange rates (**1** > AmB) when added to EYPC-SUVs having entrapped pH sensitive fluorophore HPTS and a transmembrane pH gradient.[1] The K^+/Na^+ > H^+ selectivity of AmB was shown by accelerated internal pH changes in the presence of a selective H^+ carrier,[9,1] while similar enhancements induced by the presence of the K^+ carrier valinomycin demonstrated proton selectivity for **1**.[2]

For direct comparison with incorporation efficiencies of polyols **1**–**3** (Fig. 2), we conducted the activity measurements summarized above under the conditions used for fluorescence quenching, *i.e.* reduced polyol and increased lipid concentrations compared to previous reports.[1,2] Under these conditions, the transport activity of **1** without additional valinomycin is nearly identical with the negative control ($k = 9.0 \times 10^{-6}$ s^{-1}, Fig. 3).‖ Improved incorporation (Fig. 2) resulted in significantly increased ion flux rates for octamer **2** ($k = 2.2 \times 10^{-4}$ s^{-1}) and **3** ($k = 2.4 \times 10^{-4}$ s^{-1}, Fig. 3). For all octamers (**1**–**3**), accelerated internal pH changes in the presence of 12 nM valinomycin were observed as reported before for polyol **1** (not shown).[2] Thus, the difference in side-chain lipophilicity of **2** and **3** does not significantly alter the proton selectivity previously observed for **1**.‖

These results demonstrate that the incorporation of proton channel forming rigid-rod octa(*p*-phenylene)s into lipid bilayers can be precisely tuned without significant disturbance of active structure and transport selectivity. The erratic interactions of identically modified hexa(*p*-phenylene)s with lipid bilayers further corroborate the importance of the length of the rigid-rod scaffold for controlled, transmembrane binding of substituted oligo(*p*-phenylene)s. Ion channel formation of octamers **1**–**3**, but not hexamer **16** in planar lipid bilayers supports these conclusions and will be reported in due course.

We thank NIH (GM56147-01), the donors of the Petroleum Research Fund, administered by the American Chemical Society, Suntory Institute for Bioorganic Research (SUNBOR Grant), and Georgetown University for support of this work. Both authors thank Dr Naomi Sakai for invaluable discussions and experimental advise.

Notes and References

† E-mail: matiles@gusun.georgetown.edu

‡ The stereochemistry of the side-chain is with all likelihood irrelevant for the transport activity of rigid-rod polyols.[2] However, judging from the outcome of osmium-catalyzed asymmetric dihydroxylation of terminal olefins, formation of the *S*-enantiomer **5** in 78–97% ee can be expected using AD-mix-α.[7]

§ All final products were purified by reverse-phase HPLC and gave satisfactory spectroscopic data.

¶ Abbreviations: AmB: amphotericin B; 5-DOXYL-PC: 1-palmitoyl-2-stearoyl(5-DOXYL)-*sn*-glycero-3-phosphocholine; 12-DOXYL-PC: 1-palmitoyl-2-stearoyl(12-DOXYL)-*sn*-glycero-3-phosphocholine; EYPC: egg yolk phosphatidylcholine; HPTS: 8-hydroxypyrene-1,3,6-trisulfonic acid; SUV: small unilamellar vesicle.

‖ In all experiments conducted with HPTS, the intensity change was confirmed to be the consequence of internal pH change by simultaneous measurement of the time course of emission intensity at 510 nm due to excitation at 460 nm as well as 405 nm. The contribution of the negative control was eliminated for the calculation of the initial first-order rate constants. The effect of valinomycin further corroborates the absence of HPTS-leakage.[2]

1 N. Sakai, K. C. Brennan, L. A. Weiss and S. Matile, *J. Am. Chem. Soc.*, 1997, **119**, 8726.
2 L. A. Weiss, N. Sakai, B. Ghebremariam, C. Ni and S. Matile, *J. Am. Chem. Soc.*, 1997, **119**, 12 142.
3 G. W. Gokel and O. Murillo, *Acc. Chem. Res.*, 1996, **29**, 425 and citations in ref. 2.
4 J.-C. Meillon and N. Voyer, *Angew. Chem., Int. Ed. Engl.*, 1997, **36**, 967.
5 H. Wagner, K. Harms, U. Koert, S. Meder and G. Boheim, *Angew. Chem., Int. Ed. Engl.*, 1996, **35**, 2643.
6 J. F. Nagle and S. Tristram-Nagle, *J. Membr. Biol.*, 1983, **74**, 1.
7 K. B. Sharpless, W. Amberg, Y. L. Bennani, G. A. Crispino, J. Hartung, K.-S. Jeong, H.-L. Kwong, K. Morikawa, Z.-M. Wang, D. Xu and X. L. Zhang, *J. Org. Chem.*, 1992, **57**, 2768.
8 A. S. Ladokhin, *Method Enzymol.*, 1997, **278**, 462.
9 J. Bolard, P. Legrand, F. Heitz and B. Cybulska, *Biochemistry*, 1991, **30**, 5707.

Received in Corvallis, OR, USA, 9th December 1997; 7/08841H

Novel synthesis and new chemistry of naphthochlorins

Bénédicte Krattinger, Daniel J. Nurco and Kevin M. Smith*†

Department of Chemistry, University of California, Davis, CA 95616, USA

Reactions of 2-nitro-5,10,15,20-tetraphenylporphyrin with alkyl α-isocyanoacetates afford naphthochlorins (in addition to the expected pyrroloporphyrins) which undergo free radical dimerization; the X-ray structure of one such naphthochlorin dimer is reported.

Tetrapyrrole macrocycles bearing fused aromatic rings have attracted considerable attention, with examples including benzoporphyrins,[1] benzochlorins,[2] pyrroloporphyrins,[3a,b] naphthoporphyrins,[4] naphthochlorins[5] and others.[6] Many of these possess long wavelength absorptions and are therefore potential candidates as second generation photodynamic therapy photosensitizers.[7] The approaches to naphthochlorins described to date have involved acid-catalyzed intramolecular cyclizations. Thus, naphthochlorins were prepared from Ni^{II} and Cu^{II} 2-formyl-TPPs[5b–d] and from Ni^{II} 2-vinyl-TPPs.[5a] Herein we report a novel base-promoted reaction which affords naphthochlorins; we also show that naphthochlorins possess novel free-radical chemistry wherein, in the presence of oxygen, a unique covalently linked naphthochlorin dimer is obtained. This naphthochlorin dimer represents the first example of a β–β′ linked bis(chlorin).

Nitroalkenes have been shown to react with α-isocyanoacetates to give pyrroles.[3c] Treatment of nitroporphyrin **1** with methyl or ethyl α-isocyanoacetate has been shown to afford pyrroloporphyrins **2** and **3**.[3a,b] Under similar reaction conditions we have now discovered that reaction of **1** with *tert*-butyl α-isocyanoacetate affords the expected pyrroloporphyrin **4**‡ in 32% yield and an additional porphyrinic product, the naphthochlorin **5**,‡ in 19% yield. Since our reaction conditions involved basic rather than acidic conditions it is necessary to postulate a new mechanistic route for naphthochlorin formation (Scheme 1). We propose that addition of the *tert*-butyl α-isocyanoacetate anion to nitroporphyrin **1** gives nitrochlorin **6** which eliminates HNO_2 to afford porphyrin **7**. Further reaction of DBU with porphyrin **7** yields chlorin **8** which subsequently undergoes two electrocyclic rearrangements (Scheme 1) to afford naphthochlorin **5**. Test reactions confirmed that naphthochlorin **5** did not arise from pyrroloporphyrin **4**. Further reaction of nitroporphyrin **1** [refluxing 10 : 1 THF–EtOH, DBU (4 equiv.)] with ethyl α-isocyanoacetate (2 equiv.) yielded a mixture of naphthochlorin **10** and pyrroloporphyrin **3**; when EtOH was replaced with BnOH a mixture of naphthochlorin **11** and pyrroloporphyrin **12** was obtained. A test reaction to prepare naphthochlorin free of pyrroloporphyrin was undertaken; isopropyl cyanoacetate (2 equiv.) was used instead of an alkyl α-isocyanoacetate [refluxing 10 : 1 THF–Pr^iOH, nitroporphyrin **1**, DBU (4 equiv.)] and formation of naphthochlorin **13** was observed. Although we were able to isolate naphthochlorins **10**, **11** and **13**, yields for each were < 1% [λ_{max}/nm (rel. int.) (CH_2Cl_2); **10**: 440 (1), 604 (0.08), 662 (0.15); **11**: 444 (1), 606 (0.08), 662 (0.18); **13**: 440 (1), 604 (0.08), 668 (0.16); these optical data agree well with those of naphthochlorin **5** (the structure of which has been confirmed by the crystal structure of naphthochlorin dimer **14**) and with those of previously reported naphthochlorins[5]]. Full characterization of naphthochlorins **10**, **11** and **13** was not possible owing to the scarcity and instability of these compounds.

Attempted crystallization of naphthochlorin **5** from $CDCl_3$–MeOH afforded crystals of naphthochlorin dimer **14**.‡ We were able to reproduce the dimerization *via* the following methods. A solution of naphthochlorin **5** in 1 : 1 CH_2Cl_2–MeOH (MeOH optional) was stirred while exposed to the air. After 5 days the presence of **5** was no longer detectable and naphthochlorin dimer **14** was isolated in 37% yield. Alternatively, refluxing **5** in dry benzene under argon with benzoyl peroxide (0.5 equiv.) afforded **14** in 53% yield. The reaction presumably proceeds by way of a π-stabilized radical on the non-aromatic β-carbon, followed by a radical dimerization. There is ample precedent for this type of reaction in the porphyrin literature; π-stabilized radicals have been obtained from oxophlorins[8] and some of them dimerize[9] by a mechanism similar to those involved in phenolic chemistry.[10]

The identity of naphthochlorin dimer **14**‡ was confirmed by a crystal structure, as shown in Fig. 1. This structure is unique among porphyrinoid crystal structures in that the dimeric linkage features a direct C_β–$C_{\beta'}$ bond. The macrocycles are both

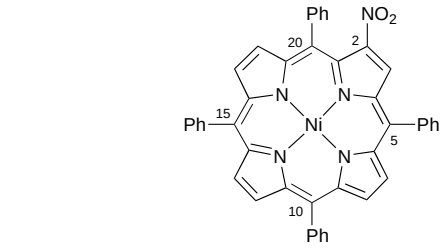

1

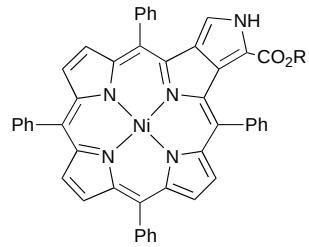

2 R = Me
3 R = Et
4 R = Bu^t
12 R = Bn

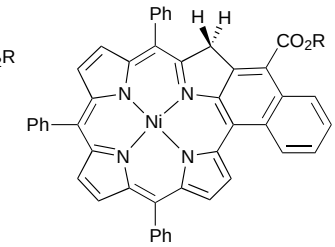

5 R = Bu^t
10 R = Et
11 R = Bn
13 R = Pr^i

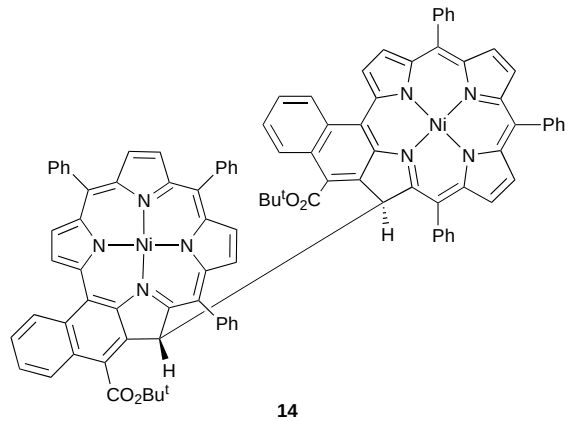

14

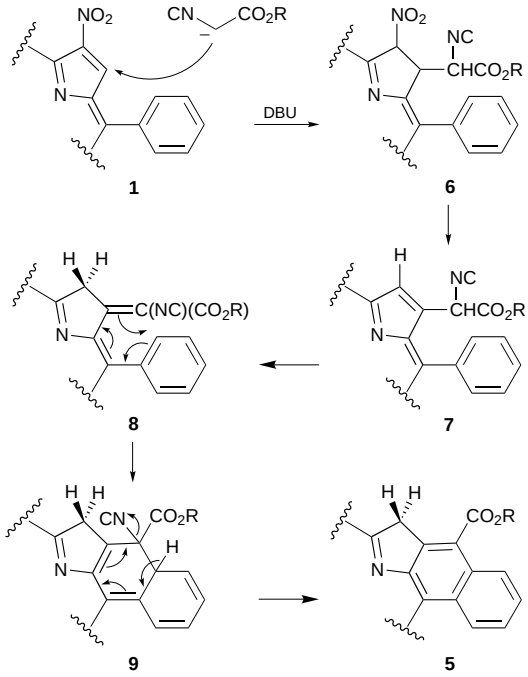

Scheme 1

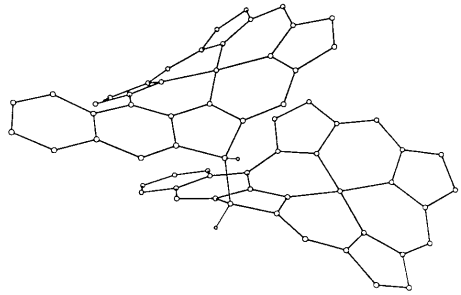

Fig. 1 Molecular structure of naphthochlorin dimer **14**;‡ esters, non-fused phenyl rings and hydrogen atoms (with the exception of those associated with the direct dimer link) have been omitted for clarity

significantly ruffled[11] with 0.33 and 0.36 Å mean deviations of the macrocyclic atoms from their least-squares planes (calculated based upon the 24 core carbon and nitrogen atoms); the average Ni–N bond length was 1.914(6) Å. The two macrocycles were nearly coplanar and exhibited an interplanar angle of 30.1°, a mean plane separation of 3.70(14) Å, and a metal to metal distance of 5.68 Å. Macrocyclic overlap was limited to one pyrrolic subunit of each naphthochlorin monomer. A lateral shift of 4.54 Å and a slip angle of 53(13)° were observed; in this regard this structure bears a marked similarity to the bacterial PRC 'special pair' which exhibits an overall geometry which is generally similar and a lateral shift of *ca*. 6.6 Å.[12]

This work was supported by grants from the National Science Foundation (CHE-96-23117) and the National Institutes of Health (HL-22252). We thank Dr Timothy P. Forsyth for carrying out the cyclic voltammetry experiments.

Notes and References

† E-mail: kmsmith@ucdavis.edu

‡ *Selected data* for **4**: $\lambda_{max}(CH_2Cl_2)$/nm 444 (ε 182 000), 538 (9400), 558 (9800), 606 (14 200); *m/z* (LSIMS) 809.3 (M^+ 100%). C,H,N combustion analysis satisfactory.

For **5**: $\lambda_{max}(CH_2Cl_2)$/nm 444 (ε 153 000), 614 (11 000), 662 (29 000); $\delta_H(CDCl_3)$ 5.19 (s, 2 H, reduced pyrrole ring H); *m/z* (LSIMS) 782.3 (M^+ 100). C,H,N combustion analysis satisfactory. Cyclic voltammetric measurements were carried out with a Cypress Systems CS-1087 computer controlled potentiostat. Naphthochlorin **5** undergoes two one electron oxidations at $E_{1/2} = -1.14$ and 0.74 V; a single compartment cell was used with a platinum disk working electrode, Ag/AgCl reference electrode, and silver wire auxiliary electrode. Measurements (scan rate 110 mV s^{-1}) were made in CH_2Cl_2, with Bu_4NPF_6 as supporting electrolyte. Ferrocene was added as an internal reference.

For **14**: $\lambda_{max}(CH_2Cl_2)$/nm 440 (ε 109 000), 668 (16 500), 712 (6800). Crystals of *meso*-**14** ($C_{100}H_{70}N_8O_4Ni_2 \cdot 3.4CHCl_3 \cdot 0.5MeOH$) were grown by the slow diffusion of MeOH into a $CHCl_3$ solution of **5**. The selected crystal (0.20 × 0.25 × 0.50 mm) had a triclinic unit cell, space group $P\bar{1}$ and cell dimensions a = 14.925(3), b = 17.025(3), c = 18.395(3) Å, α = 90.896(12), β = 99.902(13), γ = 105.083(13)°, V = 4436.9(12) Å^3 and Z = 2 (FW = 1987.0). Data were collected on a Siemens P4 diffractometer with a rotating anode [λ(Cu-Kα) = 1.54178 Å] at 130(2) K in $\theta/2\theta$ scan mode to $2\theta_{max}$ = 112°. Of 12 130 reflections measured ($+h,\pm k,\pm l$) 11 578 were independent (R_{int} = 0.090) and 8509 had $I > 2\sigma$ (T_{min} = 0.50, T_{max} = 0.56, ρ_{calc} = 1.487 g cm^{-3}, μ = 3.85 mm^{-1}). The structure was solved by direct methods and refined (based on F^2 using all independent data except for two suppressed reflections) by full-matrix least-squares methods with 1038 parameters (Siemens SHELXTL V. 5.03). Hydrogen atom positions were generated by their idealized geometry and refined using a riding model. An empirical absorption correction was applied (ref. 13). All of the solvate molecules were disordered; further description of the solvate disorder and how it was treated is given in the supplementary material. Final R factors were $R1$ = 0.092 (observed data) and $wR2$ = 0.25 (all data). CCDC 182/768.

1 P. S. Clezy and C. W. F. Leung, *Aust. J. Chem.*, 1993, **46**, 1705; E. W. Baker, T. F. Yen, J. P. Dickie, R. E. Rhodes and L. F. Clark, *J. Am. Chem. Soc.*, 1967, **89**, 3631.
2 R. T. Holmes, J. J. Lin, R. G. Khoury, C. P. Jones and K. M. Smith, *Chem. Commun.*, 1997, 919; D. Arnold, R. Gaete- Holmes, A. W. Johnson and A. R. P. Smith, *J. Chem. Soc., Perkin Trans. 1*, 1978, 1660.
3 (*a*) L. Jaquinod, C. Gros, M. M. Olmstead, M. Antolovich and K. M. Smith, *Chem. Commun.*, 1996, 1475; (*b*) C. P. Gros, L. Jaquinod, R. G. Khoury, M. M. Olmstead and K. M. Smith, *J. Porphyrins Phthalocyanines*, 1997, **1**, 201; (*c*) D. H. R. Barton, J. Kervagoret and S. Z. Zard, *Tetrahedron*, 1990, **46**, 7587;
4 T. D. Lash and C. P. Denny, *Tetrahedron*, 1995, **51**, 59.
5 (*a*) M. A. Faustino, M. G. P. M. S. Neves, M. G. H. Vicente, A. M. S. Silva and J. A. S. Cavaleiro, *Tetrahedron Lett.*, 1995, **36**, 5977; (*b*) Y. V. Ishkov and Z. I. Zhilina, *Zh. Org. Khim.*, 1995, **31**, 136; (*c*) L. Barloy, D. Dolphin, D. Dupre and T. P. Wijesekera, *J. Org. Chem.*, 1994, **59**, 7976; (*d*) H. J. Callot, E. Schaeffer, R. Cromer and F. Metz, *Tetrahedron*, 1990, **46**, 5253.
6 T. D. Lash and B. H. Novak, *Angew. Chem., Int. Ed. Engl.*, 1995, **34**, 683; K. Henrick, P. G. Owston, R. Peters and P. A. Tasker, *Inorg. Chim. Acta*, 1980, **45**, L161.
7 S.-J. H. Lee, N. Jagerovic and K. M. Smith, *J. Chem. Soc., Perkin Trans. 1*, 1993, 2369; D. Dolphin, *Can. J. Chem.*, 1994, **72**, 1005.
8 R. G. Khoury, L. Jaquinod, A. M. Shachter, N. Y. Nelson and K. M. Smith, *Chem. Commun.*, 1997, 215; J.-H. Fuhrhop, S. Besecke and J. Subramanian, *J. Chem. Soc., Chem. Commun.*, 1973, 1; J.-H. Fuhrhop, S. Besecke, J. Subramanian, C. Mengersen and D. Riesner, *J. Am. Chem. Soc.*, 1975, **97**, 7141.
9 R. G. Khoury, L. Jaquinod, D. J. Nurco, R. K. Pandey and K. M. Smith, *Angew. Chem., Int. Ed. Engl.*, 1996, **35**, 2496.
10 M. L. Mihailovic and C. Cekovic, in *The Chemistry of the Hydroxyl Group*, Part 1, ed. S. Patai, Wiley, New York, 1971, pp. 505–592.
11 D. J. Nurco, C. J. Medforth, T. P. Forsyth, M. M. Olmstead and K. M. Smith, *J. Am. Chem. Soc.*, 1996, **118**, 10 918.
12 T. E. Clement, D. J. Nurco and K. M. Smith, *Inorg. Chem.*, in the press.
13 S. R. Parkin, B. Moezzi and H. Hope, *J. Appl.Crystallogr.*, 1995, 28, 53.

Received in Corvallis, OR, USA, 4th December 1997; 7/08765I

Dodecasubstituted metallochlorins (metallodihydroporphyrins)

Kalyn M. Shea, Laurent Jaquinod, Richard G. Khoury and Kevin M. Smith*†

Department of Chemistry, University of California, Davis, CA 95616, USA

Regioselective bromination of 2-nitro-5,10,15,20-tetraphenylporphyrin, cyclopropa[*b*]chlorins, or *trans*-bis-(dicyanomethyl)chlorins occurs in the pyrrole subunit opposite the substituted ring; exhaustive bromination of functionalized tetraphenylchlorins provides a route to dodecasubstitued dihydroporphyrins for the first time.

The existence of nonplanar hydroporphyrins in photosynthetic chromophores is increasingly evident in X-ray structures of protein complexes.[1] A series of synthetic nonplanar porphyrin models, obtained by steric crowding of β- and *meso*-positions, has established that such conformational variations can have significant effects on the physical and chemical properties of nonplanar porphyrins.[2,3] Results show that the excited state properties of some of these chromophores are exquisitely sensitive to structural and vibrational variations.[4] The synthesis of such model systems often requires the relatively inaccessible 3,4-disubstituted pyrrole for condensation with aldehydes.[5] Nonplanar β-brominated porphyrins, on the other hand, are easily accessed *via* controlled bromination of porphyrins[6] or metalloporphyrins,[7] and have since provided intermediates for a range of nonplanar β-arylporphyrin syntheses.[8] Extension of these synthetic efforts to hydroporphyrin systems will allow facile entry into highly nonplanar dihydroporphyrins (chlorins) and thus provide a means to more effectively test the theoretical predictions[9] of the consequences of nonplanar distortions in this biologically important class of compounds.

2-Nitro-5,10,15,20-tetraphenylporphyrins have been shown to undergo nucleophilic attack at the β–β′ bond bearing the nitro group leading to a range of β-substituted porphyrins,[10] and more recently, work completed in our laboratory has provided new methodology for the preparation of a wide range of highly substituted dihydroporphyrin systems by way of nucleophilic attack of 2-nitro-5,10,15,20-tetraphenylporphyrin **1** (2-nitroTPP), with 'active' methylene compounds.[11] It has also been shown that regiospecific functionalization of pyrrolic positions on the porphyrin periphery occurs *via* fixation of the delocalization pathway.[12]

Here we show that either a nitro group or a reduced pyrrole substituents directs the bromination to the antipodal pyrrolic ring, leading to 12,13-dibromoporphyrin products. We also demonstrate that, *via* hexabromination of metallated dihydroporphyrins, highly nonplanar dodecasubstitued dihydroporphyrins can be prepared for the first time.

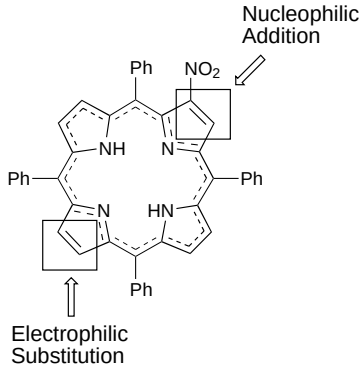

Fig. 1 Regioselective reactivity in 2-nitroTPP

Treatment of 2-nitroTPP **1** (2 g scale) with 2.5 equiv. of NBS in refluxing $CHCl_3$ afforded 2-nitro-12,13-dibromoTPP **3** in good yield (82%). Reaction of **3** (100 mg scale) with malononitrile (10 equiv.) and K_2CO_3 in THF afforded the cyclopropyl derivative **7** in 65% yield. The ^{1}H NMR spectrum of **7** displayed a singlet at δ 5.08, characteristic of the reduced pyrrole protons, and two doublets at δ 8.43 and 8.71. Similar treatment of **3** at 60 °C led to a second chlorin compound, **6**, in 62% yield. This set of reactions reveals the bimodal reactivity of 2-nitroTPP: (i) nucleophilic attack at the double bond bearing the nitro group and (ii) electrophilic regiospecific attack at the antipodal double bond (Fig. 1). The molecular structure of compound **6** was further confirmed by X-ray crystallography [Fig. 2(*a*)].‡

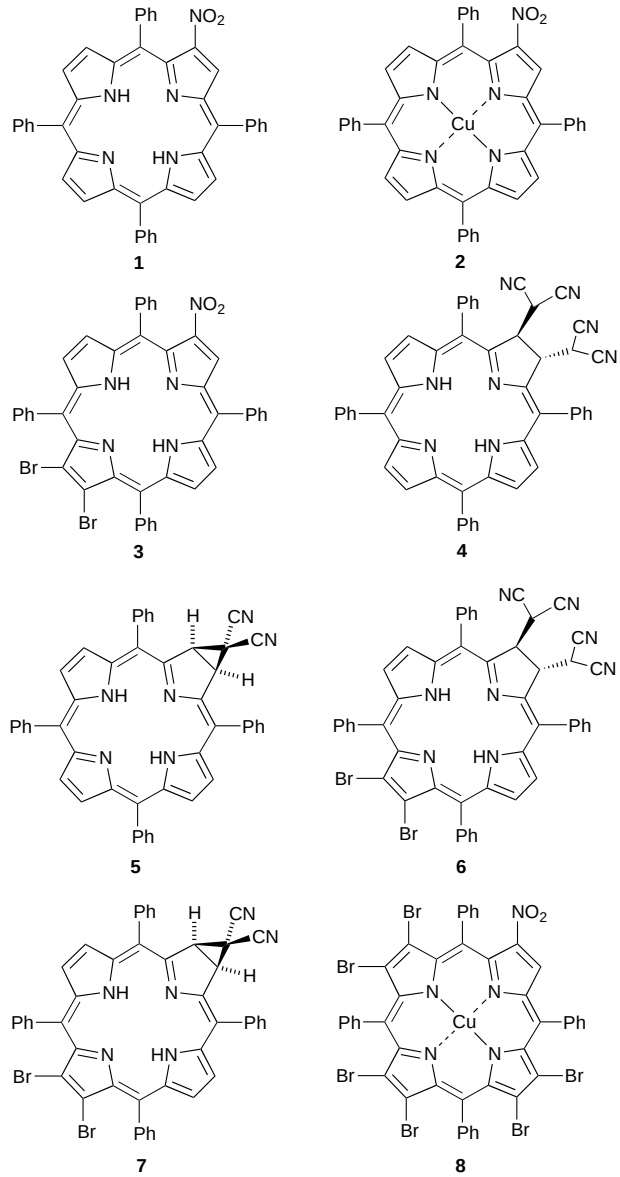

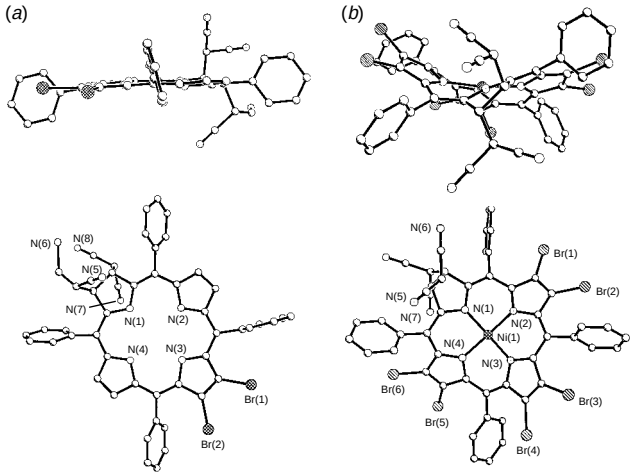

Fig. 2 Molecular structure of (*a*) **6** (below: from top; above: edge-on view) and (*b*) **11** (below: from top; above: edge-on view). Hydrogen atoms have been omitted for clarity.

A second route leading to dibromochlorin compounds involves initial formation of the chlorin chromophore.[11] In this case, the reduced pyrrole functionality induces a favored delocalization pathway, *via* thermodynamically more stable N(22)H–N(24)H tautomerism, allowing regiospecific bromination to take place. Treatment of **5** (200 mg scale) with 2.5 equiv. of NBS in $CHCl_3$ at 65 °C afforded **7** quantitatively. Dropwise addition of bromine (2.5 equiv. in $CHCl_3$) to **4** afforded the desired brominated product **6** in 91% yield. A characteristic 10 nm red shift of the Soret band was observed (λ_{max} 408 to 418 nm) as a result of this reaction. As expected, reaction of a Ni–chlorin **7** with 2.5 equiv. of bromine led to a mixture of brominated products.[12]

Reaction of the metal-free nitroporphyrin **1** with excess NBS (or chlorin **4**, with excess bromine, 10 equiv.) afforded only dibrominated products **3** (or **6**). In contrast, subjecting metallated 2-nitroTPP and metallated dihydroporphyrins to excessive bromination conditions produced the desired hexabrominated products. When Cu-nitroTPP **2** was allowed to react with 16 equiv. of NBS in refluxing 1,2-dichloroethane, hexabromo-2-nitroTPP **8** was produced in 70% yield.

Initial preparation of Ni^{II}–chlorins **9** and **10**,[11] followed by excessive bromination, afforded the desired hexabromochlorins, providing the first route to dodecasubstituted dihydroporphyrins. Dropwise addition of bromine (10 equiv.) in $CHCl_3$ to **9** and **10** (100 mg scale) produced **11** and **12** in 88 and 84% yields, respectively. Hexabromination of **11** resulted in a 26 nm red shift of the Soret band (λ_{max} 414 to 440 nm) and a 56 nm shift for the Q band (λ_{max} 604 to 660 nm). The ^{1}H NMR spectrum of **11** displayed two doublets at δ 3.52 and 4.83, characteristic of the *trans* chlorin functionality, and no peaks in the aromatic β proton region. The molecular structure of compound **11** was further confirmed by X-ray crystallography (Fig. 2).‡ The macrocycle exhibits a ruffled-type conformation with a mean deviation of 0.536 Å for the 24 core atoms from their least-squares plane, and is significantly more nonplanar than dibromochlorin **6** [Fig. 2(*a*)].

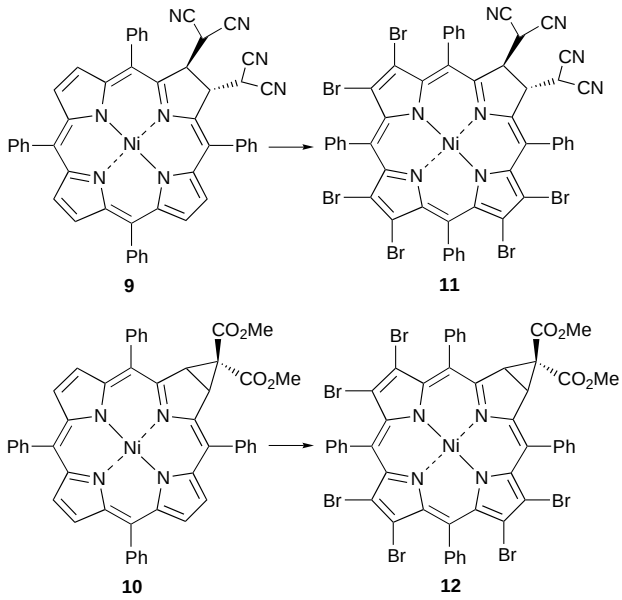

This work was supported by grants from the National Science Foundation (CHE-96-23117) and the National Institutes of Health (HL-22252).

Notes and References

† E-mail: kmsmith@ucdavis.edu

‡ *Crystal data* for **6**: $C_{50}H_{30}Br_2N_8\cdot(CHCl_3\cdot 0.25MeOH)$, MW = 1030.0, monoclinic, a = 33.329(5), b = 10.193(3), c = 27.787(4) Å, β = 103.28(3)°, V = 9187(3) Å^3 (by least-square refinement on diffractometer angles for 40 centered reflections), λ = 1.54178 Å, space group $C2/c$, Z = 8, D_c = 1.489 g cm^{-3}, $F(000)$ = 4148. The single, purple parallelipiped crystal with cell dimensions 0.36 × 0.04 × 0.02, μ = 4.215 mm^{-1}, was collected on a Siemens P4 rotating anode diffractometer, scan type 2θ–θ, T = 130(2) K, $2\theta_{max}$ = 112°, 10 227 data, 6074 unique [R(int) = 0.079], 4030 > 2σ(I). The number of parameters was 529. Final R factors were wR (all data) = 0.2206 and R (obs. data) = 0.085; the maximum residual electron density was 0.883 e Å^{-3}.

For **11**: $C_{50}H_{24}Br_6N_8Ni\cdot 2(CHCl_3)$, MW = 1513.68, triclinic, a = 12.911(3), b = 13.085(3), c = 18.383(4) Å, α = 75.47(3)°, β = 71.60(3)°, γ = 65.27(3)°, V = 2651.03(1) Å^3 (by least-squares refinement on diffractometer angles for 29 centered reflections), λ = 0.71073 Å, space group $P\bar{1}$, Z = 2, D_c = 1.896 g cm^{-3}, $F(000)$ = 1468. The single, purple parallelipiped crystal with cell dimensions 0.50 × 0.30 × 0.20, μ = 5.236 mm^{-1}, was collected on a Siemens R3m/V diffractometer, scan type ω, T = 130(2) K, $2\theta_{max}$ = 55°, 12 887 data, 12 269 unique [R(int) = 0.039], 9104 > 2σ(I). The number of parameters was 658. Final R factors were wR (all data) = 0.1939 and R (obs. data) = 0.067; the maximum residual electron density was 1.358 e Å^{-3}. Both structures **6** and **11** were solved by direct methods and refined (based on F^2 using all independent data) by full-matrix least-squares methods (Siemens SHELXTL ver. 5.03). Hydrogen atom positions were located by their idealized geometry and refined using a riding model. An absorption correction was applied using XABS2 (ref. 13). CCDC 182/769.

1 J. Deisenhofer, O. Epp, I. Sinning and H. Michel, *J. Mol. Biol.*, 1995, **246**, 429; E. Antonini, *Eur. J. Biochem.*, 1990, **187**, 287; D. E. Tronrud, M. F. Schmid and B. W. Matthews, *J. Mol. Biol.*, 1986, **188**, 443.
2 M. Ravikanth and T. K. Chandrashekar, *Struct. Bonding* (*Berlin*), 1995, **82**, 105.
3 J. A. Shelnutt, X. Song, W. Jentzen and C. J. Medforth, *Chem. Soc. Rev.*, 1998, in the press.
4 S. Gentemann, C. J. Medforth, T. Ema, N. Y. Nelson, K. M. Smith, J. Fajer and D. Holten, *Chem. Phys. Lett.*, 1993, **245**, 441.
5 B. L. Bray, P. H. Mathies, R. Naef, D. R. Solas, T. T. Tidwell, D. T. Artis and J. M. Muchowski, *J. Org. Chem.*, 1990, **55**, 6317.
6 H. J. Callot, *Tetrahedron Lett.*, 1973, **50**, 4987.
7 P. Bhyrappa and V. Krishnan, *Inorg. Chem.*, 1991, **30**, 239.
8 K. S. Chan, X. Zhou, M. T. Au and C. Y. Tam, *Tetrahedron*, 1995, **51**, 3129.
9 H. Treutlein, K. Schulten, A. T. Brunger, M. Karplus, J. Deisenhofer and H. Michel, *Proc. Natl. Acad. Sci. USA*, 1992, **89**, 75; K. M. Barkigia, L. Chantranupong, K. M. Smith and J. Fajer, *J. Am. Chem. Soc.*, 1988, **110**, 7566.
10 M. J. Crossley, M. M. Harding and C. W. Tansey, *J. Org. Chem.*, 1994, **59**, 4433.
11 K. M. Shea, L. Jaquinod and K. M. Smith, submitted for publication; L. Jaquinod, C. Gros, R. G. Khoury and K. M. Smith, *Chem Commun.*, 1996, 2581.
12 M. J. Crossley, P. L. Burn, S. S. Chew, F. B. Cuttance and I. A. Newsom, *J. Chem. Soc., Chem. Commun.*, 1991, 1564.
13 S. R. Parkin, B. Moezzi and H. Hope, *J. Appl. Cryst.*, 1995, **28**, 53.

Received in Corvallis, OR, USA, 4th December 1997; 7/08766G

Total synthesis of (+)-furanomycin

Sung Ho Kang*† and Sung Bae Lee

Department of Chemistry, Korea Advanced Institute of Science and Technology, Taejon 305-701, Korea

A highly enantioselective total synthesis of (+)-furanomycin 24 has been achieved *via* the mercury cation-mediated cyclizations of γ-hydroxy alkene 4 and homoallylic trichloroacetimidate 11 to install the *trans*-2,5-disubstituted tetrahydrofuran and the (α*S*)-amino acid side chain, respectively.

In 1967 Katagiri *et al.* discovered a novel antibiotic (+)-furanomycin from a culture filtrate of *Streptomyces threomyceticus* (ATCC 15795),[1] which binds to *E. coli* isoleucyl-tRNA synthetase, to be charged to *E. coli* isoleucine tRNA and subsequently incorporated into protein.[2] Biosynthetically it is believed to be derived from two acetetes and one propionate.[3] The antibiotic also functions as a competitive antagonist of isoleucine and suppresses the growth of T-even coliphage more effectively than T-odd.[1] Originally its molecular structure was assigned as (+)-(2*R*)-2-amino-2-[(2*R*,5*R*)-2,5-dihydro-5-methyl-2-furyl]acetic acid by spectroscopic data and chemical degradation experiments,[1] but later revised as (+)-(2*S*)-2-amino-2-[(2*R*,5*S*)-2,5-dihydro-5-methyl-2-furyl]-acetic acid by X-ray crystallography[4] and a stereodefined synthesis.[5] Although (+)-furanomycin **24** has a seemingly simple structure, its highly enantiospecific synthesis has not been established, in part due to the difficulties in assembling the *trans*-2,5-dihyrofuran and (*S*)-amino carboxylic acid units. Here we describe a highly enantiocontrolled total synthesis of (+)-furanomycin **24** employing mercury cation-promoted cyclizations of γ-hydroxy alkene **4** and homoallylic trichloroacetimidate **11** to construct the aforementioned functionalities.

The known silyl ether **1**, prepared from dimethyl L-tartrate in 83% overall yield,[6] was desilylated using TBAF, and the resulting alcohol **2**, $[\alpha]_D^{23}$ −3.1 (*c* 1.01, $CHCl_3$), was treated with I_2, PPh_3 and imidazole in THF[7] to yield the corresponding iodide **3**, $[\alpha]_D^{22}$ −10.1 (*c* 1.01, $CHCl_3$), quantitatively from **1** (Scheme 1). The substitution reaction of **3** was conducted with vinylmagnesium bromide, which should be generated freshly, in the presence of $CuBr{\cdot}SMe_2$ and HMPA in THF at −50 °C.[8] The somewhat volatile diene acetonide, without purification, was hydrolyzed with methanolic HCl to give diene diol **4**, $[\alpha]_D^{23}$ −11.6 (*c* 1.01, $CHCl_3$), in 75% overall yield. For the stereoselective formation of *trans*-2,5-disubstituted tetrahydrofuran, the cyclization[9] of **4** was attempted using I_2, IBr or *N*-iodosuccinimide (NIS) under various reaction conditions to provide a 1–3 : 1 mixture of *trans*- and *cis*-isomers. However, when $Hg(OCOCF_3)_2$ was employed as an electrophile, the stereoselectivity was improved significantly. Accordingly, **4** was treated with $Hg(OCOCF_3)_2$ in the presence of K_2CO_3 in THF at −78 °C to afford a mixture of *trans*- and *cis*-2,5-disubstituted tetrahydrofurans **5** and **6**, which was found to revert to the starting material **4** during work-up with brine or aq. KBr and chromatographic purification. In order to elude the reversion, the *in situ* demercuration of the crude organomercurials **5** and **6** was attempted with various reducing reagents[10] in the absence or presence of phase transfer catalyst, NaOAc, NaOH or AcOH to furnish the expected *trans*- and *cis*-tetrahydrofurans **7** and **8**, accompanied by variable amounts of the starting diol **4** and alcohols **9** and **10**. After intensive experimentation, reproducible demercuration conditions were established, involving treating the cyclization reaction mixture *in situ* with BEt_3 and $LiBH_4$ at −78 °C to produce an inseparable 8.5–9 : 1 mixture of **7**, $[\alpha]_D^{22}$ +57.0 (*c* 1.00, $CHCl_3$), and **8** in 83% overall yield from **4** without appreciable formation of side products.

The mixture of **7** and **8** was converted into the readily separable trichloroacetimidates **11** and **12**, which provided after chromatographic purification the requisite imidate **11**, $[\alpha]_D^{22}$ +47.0 (*c* 1.00, $CHCl_3$), in 83% yield. While the proposed cyclization[11] of **11** hardly proceeded with I_2 or NIS, the use of IBr resulted in poor stereoselectivity,[12] yielding a 2.5 : 1 mixture of iodides **13** and **14**, of which the relative stereochemistries were determined by NOE difference experiments, *i.e.* irradiation at H–C(6) showed enhancements at H–C(4) for the former and at H_2–C(10) for the latter (Scheme 2). On the other hand, when the intramolecular amination of **11** was performed with $Hg(OCOCF_3)_2$ in the presence of K_2CO_3 in THF at 0 °C, only the desired organomercury bromide **15** could be isolated in higher than 95% yield after work-up with aq. KBr. Its stereochemistry was corroborated by converting it into iodide **13** with I_2 in THF. For the oxidation of **15** to alcohol **16**, oxygen was bubbled vigorously through a solution of **15** and $NaBH_4$ in DMF,[13] but only the reductive demercuration product **17** was generated. Alternatively exposure of **15** to TEMPO and $LiBH_4$ in the presence of BEt_3 in THF provided the oxidized product **18**, mp 134.5–135.5 °C, $[\alpha]_D^{23}$ −32.0 (*c* 0.99, $CHCl_3$), in 76% yield. It is noted that without BEt_3 the chemical yield decreased to 50–55%. The dihydro-1,3-oxazine heterocycle of **18** was hydrolyzed with HCl and then the unmasked amino alcohol was

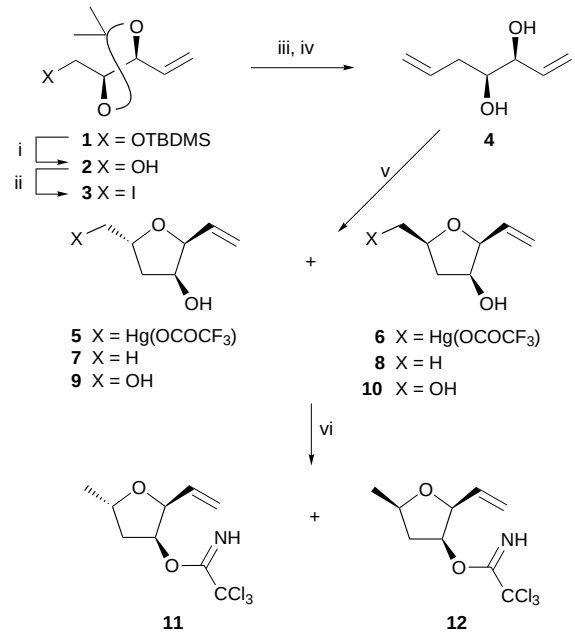

Scheme 1 *Reagents and conditions*: i, Bu_4NF, H_2O, THF, 20 °C; ii, I_2, PPh_3, imidazole, THF, 20 °C; iii, CH_2=CHMgBr, $CuBr{\cdot}SMe_2$, HMPA, THF, −50 °C; iv, 6 M HCl, MeOH, 20 °C; v, $Hg(OCOCF_3)_2$, K_2CO_3, THF, −78 °C, then Et_3B, $LiBH_4$, −78 °C; vi, Cl_3CCN, DBU, MeCN, −30 °C

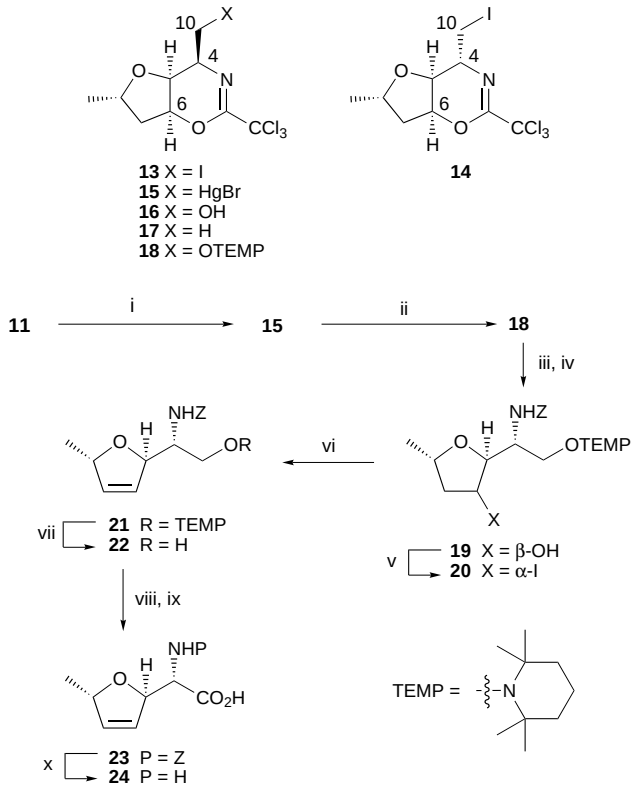

Scheme 2 *Reagents and conditions*: i, $Hg(OCOCF_3)_2$, K_2CO_3, THF, 0 °C, then aq. KBr; ii, TEMPO, Et_3B, $LiBH_4$, THF, 20 °C; iii, 6 M HCl, MeOH, THF, reflux; iv, BnOCOCl, K_2CO_3, MeOH, 20 °C; v, I_2, PPh_3, DMAP, PhH, CH_2Cl_2, 0 °C, then 60 °C; vi, DBU, DMF, 80 °C; vii, Zn, NH_4Cl, H_2O, MeOH, 80 °C; viii, $(COCl)_2$, DMSO; ix, $NaClO_2$, NaH_2PO_4, 2-methylbut-2-ene, Bu^{t}OH, H_2O, 20 °C; x, PhSMe, TFA, 50 °C

protected with benzyl chloroformate to afford carbamate **19**, $[\alpha]_D^{25}$ −12.0 (*c* 1.00, $CHCl_3$), in 95% overall yield.

The dihydrofuryl ring could not be formed by the basic or pyrolytic elimination reaction of the mesylate, triflate or xanthate derivatives of **19**. In addition their substitution reaction with iodide or phenylselenide anion did not yield the expected product. Various experimental attempts revealed that iodide **20**, $[\alpha]_D^{25}$ −65.2 (*c* 0.99, $CHCl_3$) could be prepared in 76% yield by treating **19** with I_2 and PPh_3 in the presence of DMAP in a mixture of benzene and CH_2Cl_2, while the reaction using imidazole[7] instead of DMAP resulted in a poor chemical yield of 35%. The ensuing elimination reaction was effected by heating **20** with DBU in DMF to provide dihydrofuran **21**, $[\alpha]_D^{27}$ +105.3 (*c* 1.02, $CHCl_3$), regioselectively in 89% yield. The TEMP group of **21** was reductively removed with zinc dust in methanolic NH_4Cl to afford the primary alcohol **22**, $[\alpha]_D^{28}$ +195.8 (*c* 0.99, $CHCl_3$), in 92% yield. Since Jones oxidation of **22** proceeded inefficiently, it was oxidized using Swern conditions[14] followed by sodium chlorite[15] to give carboxylic acid **23**, $[\alpha]_D^{27}$ +175.4 (*c* 0.57, MeOH), in 89% yield. Finally removal of the BnOCO group of **23** with thioanisole in TFA produced (+)-furanomycin **24**, mp 222–224 °C, $[\alpha]_D^{26}$ +136.0 (*c* 0.4, H_2O), in 97% yield, the physical and spectroscopic data of which were identical with those previously reported.

Financial support from the Korea Science and Engineering Foundation (971-0302-010-2) is gratefully acknowledged.

Notes and References

† E-mail: shkang@kaist.ac.kr

1 K. Katagiri, K. Tori, Y. Kimura, T. Yoshida, T. Nagasaki and H. Minato, *J. Med. Chem.*, 1967, **10**, 1149.
2 T. Kohno, D. Kohda, M. Haruk, S. Yokoyama and T. Miyazawa, *J. Biol. Chem.*, 1990, **265**, 6931.
3 R. J. Parry and H. P. Buu, *J. Am. Chem. Soc.*, 1983, **105**, 7446; R. J. Parry, R. Turakhia and H. P. Buu, *J. Am. Chem. Soc.*, 1988, **110**, 4035.
4 M. Shiro, H. Nakai, K. Tori, J. Nishikawa, Y. Yoshimura and K. Katagiri, *J. Chem. Soc., Chem. Commun.*, 1980, 375.
5 M. M. Joullie, P. C. Wang and J. E. Semple, *J. Am. Chem. Soc.*, 1980, **102**, 887; J. E. Semple, P. C. Wang, Z. Lysenko and M. M. Joullie, *J. Am. Chem. Soc.*, 1980, **102**, 7505.
6 I. Savage and E. J. Thomas, *J. Chem. Soc., Chem. Commun.*, 1989, 717; S. H. Kang and H.-W. Choi, *Chem. Commun.*, 1996, 1521.
7 P. J. Garegg and B. Samuelsson, *J. Chem. Soc., Chem. Commun.*, 1979, 978; P. J. Garegg and B. Samuelsson, *J. Chem. Soc., Perkin Trans. 1*, 1980, 2866; P. J. Garegg, R. Johansson, C. Ortega and B. Samuelsson, *J. Chem. Soc., Perkin Trans. 1*, 1982, 682.
8 H. O. House, C.-Y. Chu, J. M. Wilkins and M. J. Umen, *J. Org. Chem.*, 1975, **40**, 1460; E. Erdik, *Tetrahedron*, 1984, **40**, 641.
9 T. L. B. Boivin, *Tetrahedron*, 1987, **43**, 3309; J.-C. Harmange and B. Figadere, *Tetrahedron: Asymmetry*, 1993, **4**, 1711.
10 R. P. Quirk and R. E. Lea, *J. Am. Chem. Soc.*, 1976, **98**, 5973; M. C. Benhamou, G. Etemad-Moghadam, V. Speziale and A. Lattes, *Synthesis*, 1979, 891; K. E. Harding, R. Stephens and D. R. Hollingsworth, *Tetrahedron Lett.*, 1984, **25**, 4631.
11 G. Cardillo and M. Orena, *Tetrahedron*, 1990, **46**, 3321.
12 A. R. Chamberlin, R. M. Mulholland, Jr., S. D. Kahn and W. J. Hehre, *J. Am. Chem. Soc.*, 1987, **109**, 672.
13 C. L. Hill and G. M. Whitesides, *J. Am. Chem. Soc.*, 1974, **96**, 870.
14 A. J. Mancuso and D. Swern, *Synthesis*, 1981, 165.
15 B. S. Bal, W. E. Childers and H. W. Pinnik, *Tetrahedron*, 1981, **37**, 2091.

Received in Cambridge, UK, 27th January 1998; 8/00727F

ESIPT-Induced photocyclization of *N,N′*-diphenyl-1,5-dihydroxy-9,10-anthraquinone diimine

Keiji Kobayashi,*[a]† Mayumi Iguchi,[a] Tatsuro Imakubo,[a] Koichi Iwata[b] and Hiro-o Hamaguchi[b]

[a] *Department of Chemistry, Graduate School of Arts and Sciences, The University of Tokyo, Komaba, Meguro-ku, Tokyo 153 Japan*

[b] *Department of Chemistry, Graduate School of Sciences, The University of Tokyo, Hongo, Bunkyo-ku, Tokyo 113 Japan*

Photolysis of *N,N′*-diphenyl-1,5-dihydroxy-9,10-anthraquinone diimine affords acridine-condensed aromatic compounds *via* excited-state intramolecular proton-transfer, as revealed by time-resolved IR spectroscopy.

Excited-state intramolecular proton-transfer (ESIPT) has been extensively investigated in relation with photochromic materials and UV stabilizers.[1] In ESIPT phenomena, mostly observed in salicylates[2] and salicylideneanilines,[3] the photoexcited keto form is produced by rapid proton transfer from the photoexcited enol form and undergoes deactivation nonradiatively and/or radiatively to the ground-state keto form, which regenerates thermally the original enol. In such a reversible phototautomeric cycle, the ESIPT-induced excited enol is fated to follow the tautomeric pathway and other relaxation processes have rarely been encountered. We report herein a novel photochemical reaction which is, to the best of our knowledge, the first irreversible transformation *via* ESIPT in a phototautomeric system.

N,N′-diphenyl-1,5-dihydroxy-9,10-anthraquinone diimine **1a** in benzene was irradiated at room temperature, using a 100 W high pressure Hg lamp through a Pyrex filter, under argon for 48 h (Scheme 1). The photoproducts were chromatographed on silica gel and acridine-condensed compounds **2a** and **3** were obtained in 64 and 14% yields, respectively. Irradiation of **2a** under the same conditions as used for **1a** gave rise to **3**, indicating that **3** is a secondary photoproduct of **1a**. The photocyclization was also accomplished in monohydroxy derivative **1b**; irradiation of **1b** in benzene for 54 h led to the formation of **2b** (18%). The structure of **2a** was deduced from an X-ray crystallographic analysis‡ and that of **2b** was proved on the basis of its spectral properties. The formation of **2a** and **2b** is ascribed to aromatic cyclization at C(4) accompanied by enol-to-keto tautomerization of the hydroxy group at C(1). These common characteristics of the photoproducts indicate that the same type of the photoreaction occurred in **1a** and **1b**.

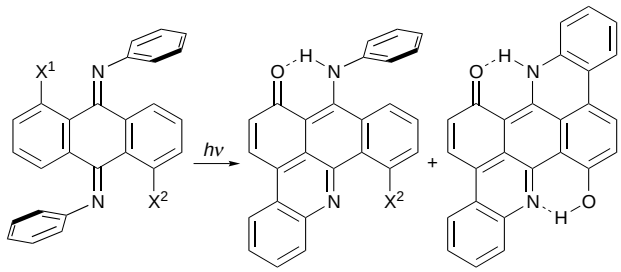

1a $X^1 = X^2 = OH$ **2a** $X^2 = OH$ **3**
b $X^1 = OH$, $X^2 = H$ **b** $X^2 = H$
c $X^1 = X^2 = H$
d $X^1 = X^2 = OMe$

Scheme 1

The irradiation of **1c** and **1d**, which have no hydroxy groups at the peri positions, caused no photoreactions even after irradiation for 60 h. The absence of photoreactivity in **1c** and **1d** clearly shows that the hydroxy group at the peri position plays an essential role in promoting the photocyclization. Furthermore, the role of the hydroxy group cannot be ascribed to its electron-donating nature, since the methoxy derivative was not photoreactive. The above results provide chemical evidence for the involvement of ESIPT in the photocyclization. It should also be noted here that compound **1a** exists almost completely in the enol form (96%) under the fast equilibrium with the keto form in the ground state, as monitored by temperature dependent ^1H and ^{13}C NMR spectroscopy.

The intervention of the ESIPT in the photocyclization was probed by means of sub-microsecond time-resolved IR spectroscopy,[4] which can detect the increase in the ground-state keto form upon irradiation. Fig. 1 shows the transient IR spectra of **1a** in CCl_4 following excitation at 262 nm with 5 ns pulses.§ Several new positive absorption bands appear following excitation, in addition to negative peaks due to the ground-state depletion. Those are ascribed to two transient species; one (**A**: ~1550 cm^{-1}) decays rapidly and almost disappears after 200–300 μs, while the other (**B**: 1630 and 1240 cm^{-1}) decays very slowly and still remains after 800 μs. The lifetimes of transient species **A** and **B** were estimated to be 80–90 μs and 1.3 ms, respectively, by the curve fitting of Fig. 2, assuming a simple exponential decay.

Transient species **B** could be assigned to the keto imine tautomer in the ground-state, since its absorptions 1630 and 1240 cm^{-1} are attributed to vibration of the hydrogen bonded C=O group and the C–N stretching, respectively. With respect to transient species **A**, we postulate an intramolecular cycloadduct as the most plausible candidate based on its IR absorption at *ca*. 1550 cm^{-1}, corresponding to the absorption

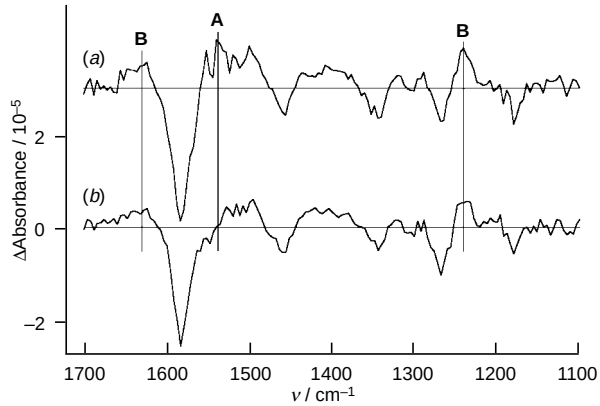

Fig. 1 Time-resolved IR spectra of **1a** after (*a*) 0–20 and (*b*) 200–800 μs of excitation. The figure is represented as a difference spectrum. Negative peaks represent a decrease in the infrared absorption due to the depletion of the ground state and positive peaks correspond to an increase in the absorption by the photogenerated transient species.

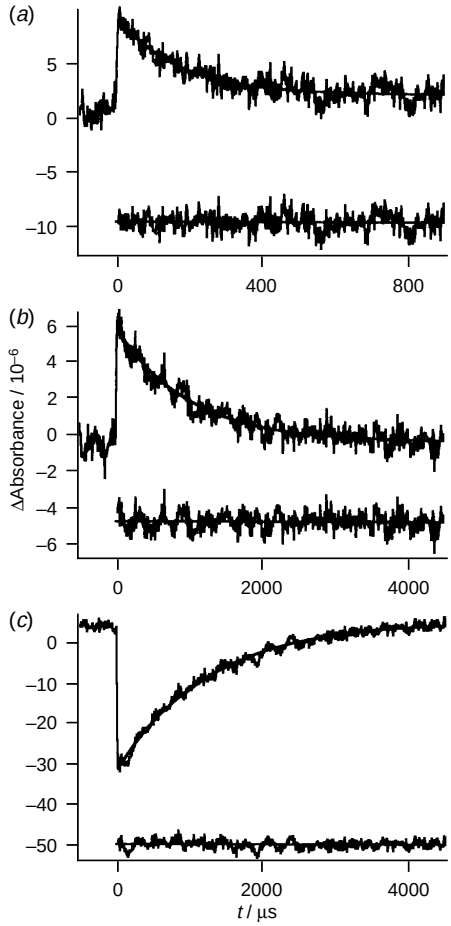

Fig. 2 Decay curves of the absorption bands at (*a*) 1550 (**A**) and (*b*) 1630 cm^{-1} (**B**), and (*c*) recovery curve of the absorption band at 1584 cm^{-1} (**1a**)

band of a C=N bond incorporated in the cyclic framework. Thus we can depict the fate of the ESIPT as shown in Scheme 2.

No photoproduct **2a** could be detected after the time-resolved measurements. The bubbling of argon through the reaction is considered to work effectively to prevent oxidation of transient species **A** to give **2a**. Thus, all the spectral changes were reversible. However, when argon was not bubbled through the reaction, the formation of **2a** was confirmed by its UV absorption at 530 and 460 nm; the formation of **2a** upon photolysis of **1a** on a preparative scale is ascribed to inefficient argon bubbling. Irradiation of a cautiously degassed sample of **1a** in an NMR sample tube suppressed the formation of **2a** down to a few percent.

The formation of polycyclic systems by intramolecular photocyclization is a common process for several types of aromatic compound. However, benzilideneanilines and azo-

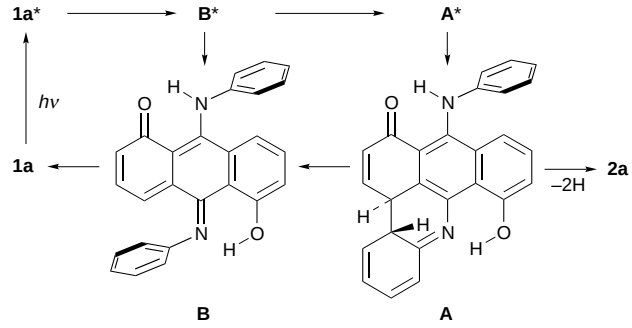

Scheme 2

benzenes fail to undergo aromatic photocyclization under the usual conditions; it has been reported that addition of sulfuric acid or Lewis acids promotes the heteroaromatic cyclization.[5] Thus this work demonstrates a novel photocyclization promoted by ESIPT and hence provides an example of deactivation other than phototautomerization that is possible for the ESIPT of a tautomeric system.

Notes and References

† E-mail: ckobak@komaba.ecc.u-tokyo.ac.jp

‡ *Crystal data* for **2a**: Rigaku AFC-5S diffractometer, Mo-Kα radiation, λ = 0.71073 Å, graphite monochrometer, T = 295 K. Data collection, solution and refinement: ω–2θ, direct methods using the SIR 88 program, followed by Fourier synthesis, TEXSAN computer program. $C_{26}H_{16}N_2O_2$, M_w = 388.43, triclinic, space group $P\bar{1}$, a = 11.0202(14), b = 11.3768(14), c = 8.7455(10) Å, α = 110.652(9), β = 94.004(11), γ = 113.733(9)°, U = 910.0(2) Å^3, Z = 2, D_c = 1.417 g cm^{-3}, crystal size 0.40 × 0.15 × 0.10 mm. 4399 reflections measured in the range $4 < 2\theta < 55°$, 1436 unique reflections with $|F_o| > 3\sigma|F_o|$. 335 parameters. R = 0.045 and R_w = 0.026. CCDC 182/764.

§ We also carried out time-resolved experiments at 349 nm, despite some experimental difficulties associated with low absorbance at this wavelength, and confirmed the formation of **2a** when argon was not bubbled. Thus we observe the same photoexcited process in the time-resolved experiments and in the preparative-scale experiments.

1 For reviews, see special issues: *Chem. Phys.*, 1989, **136**; *J. Phys. Chem.*, 1991, **95**; W. Klopffer, in *Advances in Photochemistry*, ed. J. N. Pitts, Jr., G. S. Hammond and K. Gollnick, Wiley, New York, 1997, vol. 10, p. 311.
2 D. Le Gourrierec, S. M. Ormson and R. G. Brown, *Prog. React. Kinet.*, 1994, **19**, 211.
3 S. M. Ormson and R. G. Brown, *Prog. React. Kinet.*, 1994, **19**, 45.
4 T. Yuzawa, C. Kato, M. W. George and H. Hamaguchi, *Appl. Spectrosc.*, 1994, **48**, 684; K. Iwata and H. Hamaguchi, *Appl. Spectrosc.*, 1990, **44**, 1431.
5 G. Zimmerman, L. Chow and U. Paik, *J. Am. Chem. Soc.*, 1958, **80**, 3528; F. B. Mallory and C. S. Wood, *Tetrahedron Lett.*, 1965, 2643; G. M. Badger, C. P. Joshua and G. E. Lewis, *Tetrahedron Lett.*, 1964, 3711; H. H. Perkampus and B. Behjati, *J. Heterocycl. Chem.*, 1974, **11**, 511; G. M. Thompson and S. Docter, *Tetrahedron Lett.*, 1988, **29**, 5213; C. P. Joshua and V. N. R. Pillai, *Tetrahedron*, 1974, **30**, 3333.

Received in Cambridge, UK, 16th December 1997; 7/09022F

Relative M–X bond dissociation energies in 16-, 17- and 18-electron organotransition-metal complexes (X = halide, H)

Mats Tilset,*[a]† Jean-René Hamon*[b] and Paul Hamon[b]

[a] *Department of Chemistry, University of Oslo, PO Box 1033 Blindern, N-0315 Oslo, Norway*
[b] *UMR CNRS 6509, 'Organométalliques et Catalyse: Chimie et Electrochimie Moléculaires', Université de Rennes 1, Campus de Rennes-Beaulieu, F-35042 Rennes Cedex, France*

The Fe–halide bonds in Cp*Fe(dppe)X (X = F, Cl, Br, I) complexes are weakened as a consequence of one and two-electron oxidations; the bond weakening decreases in the order F << Cl < Br < I and is much less pronounced for F than the other halides, indicating a pronounced effect of apparent fluoride-to-metal backbonding as a consequence of the removal of electrons.

Knowledge of the nature and energetics of metal–ligand bonding in organotransition-metal complexes is crucial to the understanding of organometallic reactions and catalysis.[1] Recently, the nature of the bonding between organotransition-metal centers and electronegative σ-bonded ligands such as halide, alkoxide, and amido groups has received considerable attention.[2] In addition to forming covalent M–X bonds, these ligands are capable of acting as π donors towards the metal. A ligand p_π to metal d_π electron-pair donation generally serves to destabilize electronically saturated complexes *via* filled–filled repulsive interactions, whereas coordinatively unsaturated species may achieve considerable stabilization through partial π bond formation.[3–9] A substantial line of evidence,[2] including IR ν_{CO} spectroscopy data,[4,5] electrode potentials,[6,10] chemical reactivity,[4,7] and theoretical calculations,[3,4,8] suggests that among the halides, it is the fluoride ligand that is the most efficient electron-pair donor towards the metal.‡

The presence of significant π bonding from halide to metal should be reflected in bond dissociation energy (BDE) changes when this bonding is 'switched on'[3a] by the generation of coordinative unsaturation. To the best of our knowledge, there exist no quantitative data on the homolytic M–X BDEs of metal–halide bonds in closely related pairs of coordinatively saturated (18 electron) and unsaturated (16 electron) species. Here we present the first data concerning the relative M–X bond strengths in 18-, 17- and 16-electron complexes which differ only in their number of valence electrons and thence charge of the central atom. The data establish a pronounced 'fluorine effect', and suggest that a specific electronic or ionic effect of the fluorine is evident already in the 17-electron systems.

Thermochemical cycles that incorporate electrode potential data, introduced by Breslow and Chu,[11] have been frequently used in organic[12] and organometallic[13–15] chemistry to obtain bond-energy data that are not available by direct methods. We have employed this technique to establish a bond-weakening effect of *ca.* 25–33 kJ mol^{-1} when 18-electron metal hydrides were oxidized to their 17-electron cation radicals.[13c,d] Eqn. (1) derived from the thermochemical cycle in Scheme 1, was used to quantify this effect for X = H.

$$\mathrm{BDE(MX)} - \mathrm{BDE(MX^+)} = F[E_{ox}(\mathrm{MX}) - E_{ox}(\mathrm{M})] \quad (1)$$

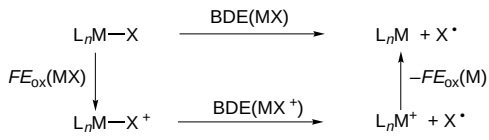

Scheme 1

Scheme 1 is quite general and eqn. (1) can therefore be applied for any other X, and also to evaluate relative BDEs between multiply oxidized species.§ The pertinent 16- and 17-electron species M^+ amd MX^+ are usually so short-lived that electrode potential data, and thereby BDE data, are inaccessible. However, it has been recently demonstrated that the sterically crowded and electron-rich Cp*Fe(dppe) moiety¶ supports metal complexes in a great number of oxidation states, and compounds have been isolated with electron counts ranging from 16 to 19.[16] The persistent 15-electron $Cp^*Fe(dppe)^{2+}$ has even been generated in solution.[16d] The Cp*Fe(dppe) derivatives therefore are particularly well suited for the application of thermochemical cycles.

Table 1 summarizes electrochemical data obtained by cyclic voltammetry for the Cp*Fe(dppe)X–$Cp^*Fe(dppe)X^+$ and $Cp^*Fe(dppe)X^+$–$Cp^*Fe(dppe)X^{2+}$ couples for X = H, F, Cl, Br, I. All neutral–monocation redox couples in Table 1 were chemically reversible, near-Nernstian processes (ΔE_p = 67–75 mV). Remarkably, except for X = H, the cation–dication couples were also reversible.

The electrochemical data for these halides constitute the first example of reversible electrode potentials for a complete organometallic L_nMX series (X = F, Cl, Br, I). Interestingly, the reversible oxidation to monocation occurs most readily for the most electronegative halide and becomes progressively more difficult in the series F < Cl < Br < I.[17,18] The trend is the opposite of that predicted on the basis of halide electronegativities alone, and most likely is a manifestation of the importance of apparent π donation from halide to metal. The particularly large jump, > 0.2 V, in the $E°$ value for F relative to Cl and the other halides support the idea that F acts as an exceptionally good donor.‡

The electrochemical data are used in conjunction with eqn. (1) to give the differences in M–X BDEs between $Cp^*Fe(dppe)X^{n+}$ complexes when *n* changes from 0 to 1 to 2. The results are summarized in Table 2. It is important to keep in mind that the data show only the net change in the bond energies caused by oxidation state changes. The data carry no information about

Table 1 Cyclic voltammetry data for the oxidation of Cp*Fe(dppe) derivatives[a]

Compound M	E_1 (M/M^+)[b]	E_2 (M^+/M^{2+})[b]
$Cp^*Fe(dppe)$[c]	−1.272	−0.290
Cp*Fe(dppe)H	−0.747	0.75[d]
Cp*Fe(dppe)F[e]	−0.824	0.688
Cp*Fe(dppe)Cl	−0.618	0.823
Cp*Fe(dppe)Br	−0.582	0.811
Cp*Fe(dppe)I	−0.540	0.780

[a] THF–0.2 M $NBu_4^+PF_6^-$, T = 20 °C, Pt disk electrode (d = 0.4 mm), voltage sweep rate v = 1.0 s^{-1}. [b] Oxidation potential, V *vs.* Cp_2Fe–Cp_2Fe^+. The voltammograms were reversible unless otherwise stated. [c] Measurements were done on $Cp^*Fe(dppe)^+PF_6^-$ which, contrary to Cp*Fe(dppe)•, is stable in THF at room temperature. [d] Peak potential for irreversible process. [e] Measurements were performed on $Cp^*Fe(dppe)F^{\bullet+}PF_6$ (ref. 19).

Table 2 Relative bond dissociation energies for $Cp^*Fe(dppe)X^{n+}$ complexes (kJ mol^{-1})[a]

Compound M–X	ΔBDE ($MX–MX^+$)	ΔBDE ($MX^+–MX^{2+}$)	ΔBDE ($MX–MX^{2+}$)
$Cp^*Fe(dppe)H$	51	100[b]	151[b]
$Cp^*Fe(dppe)F$	43	94	138
$Cp^*Fe(dppe)Cl$	63	107	171
$Cp^*Fe(dppe)Br$	67	106	173
$Cp^*Fe(dppe)I$	71	103	174

[a] Obtained using the data in Table 1 and eqn. (1). [b] Minimum value. The corresponding value for $E_{ox}(MX^+–MX^{2+})$ is a minimum value due to the unknown kinetic potential shift that is imposed by the irreversible nature of this electrode process for X = H.

absolute BDEs. The observed bond energy changes result from the combined σ and π effects.‡ For all X, overall bond weakening occurs as a consequence of oxidation of the neutral $Cp^*Fe(dppe)X$ to their monocations. A further bond weakening, almost twice as large, results when the monocations are oxidized to dications. Thus, the data unambiguously demonstrate that for all X studied, Fe–X bond energies decrease in the order $Fe–X > Fe–X^{\bullet+} > Fe–X^{2+}$.

For both oxidation processes, there is a very interesting and obvious trend in the bond activation for the halides. The oxidatively induced bond weakening decreases in the order I > Br > Cl > F and is particularly less pronounced for F than for the other halides. In particular, for the overall two-electron oxidation (which in principle corresponds to the generation of a vacant coordination site) the difference between F and the other halides is > 30 kJ mol^{-1}. It is tempting to attribute this phenomenon to a more efficient donation from F to the metal. This quantity may be viewed as an extra stabilization of the unsaturated 16-electron complex $Cp^*Fe(dppe)X^{2+}$ that is provided by F, relative to the other halides.

Interestingly, whereas the bond weakening is less pronounced for X = F than for H, a pure σ donor, the opposite is true when Cl, Br and I are compared to H. For a pure σ donor, $E_{ox}(MX)$ should be more positive than for $E_{ox}(M)$ when X is more electronegative than M, and eqn. (1) shows that an oxidation in this case should lead to a weakening of the σ bond. In particular, this situation applies to X = H. For X = F, π donation to the metal is enhanced by the oxidation, and this in part compensates for the σ bond weakening. On the other hand, for X = Cl, Br, and I, a combination of a greater σ bond weakening and a poorer π donation to the metal leads to an overall bond weakening that exceeds even that found for X = H. As noted in the introduction, metal–halide bonding can be rather complex, and we plan to further develop these issues in an extended study that includes theoretical aspects of the Fe–X bonding.**

M. T. gratefully acknowledges support from Statoil under the VISTA program, administered by the Norwegian Academy of Science and Letters, from the Norwegian Research Council, and from Université de Rennes 1 during a sabbatical (1996/97). J.-R. H. is deeply grateful to Mrs M. H. Lorrilleux for her generous and valuable assistance in reading articles. We thank Professor J.-Y. Saillard and K. Costuas for their assistance and helpful discussions.

Notes and References

† E-mail: mats.tilset@kjemi.uio.no

‡ The theoretical results[3b,4,8] imply that π-effects, σ-effects and the ionicity of the M–X bond must all be taken into account when trends in ν_{CO} and other observable parameters are to be explained.

§ The ΔBDE data obtained from eqn. (1) are in reality free energy based. However, the enthalpic ΔBDE values will be identical to the free-energy ones if ΔS for the top and bottom homolytic processes in Scheme 1 cancel. This will be the case here since M and MX have the same charges and the different X groups are small in comparison to the M fragment. Thus, one might anticipate MX and M to have nearly identical solvation properties. The same applies to MX^+ *vs.* M^+.

¶ Abbreviations: Cp^* = η^5-C_5Me_5; dppe = η^2-$Ph_2PCH_2CH_2PPh_2$.

‖ The X-ray crystal structures of $Cp^*Fe(dppe)^{n+}$ (n = 0, 1) have been reported. The cation does not bind THF or counter anion. There was no indication of stabilization by agostic interactions with ligand C–H bonds.[16d]

** Preliminary DFT calculations on the halide series indicate that the MX and MX^+ BDEs defined in Scheme 1 include, in addition to the energy necessary to break the M–X bond, a significant component associated with electronic reorganization of the L_nM fragment. However, the reorganization energy barely varies in the halogen series, so that the big jump observed in the ΔBDE values from F to the other halogens is essentially associated with variations on the M–X bond.

1 J. A. M. Simões and J. L. Beauchamp, *Chem. Rev.*, 1990, **90**, 629; *Energetics of Organometallic Species*, ed. J. A. M. Simões, NATO ASI Series, Kluwer Academic, Dordrecht, 1992; *Bonding Energetics in Organometallic Compounds*, ed. T. J. Marks, ACS Symp. Ser. No. 428, American Chemical Society, Washington, DC, 1990.
2 For recent reviews, see: K. G. Caulton, *New J. Chem.*, 1994, **18**, 25; N. Doherty and N. W. Hoffman, *Chem. Rev.*, 1991, **91**, 553.
3 (*a*) J. T. Poulton, K. Folting, W. E. Streib and K. G. Caulton, *Inorg. Chem.*, 1992, **31**, 3190; (*b*) T. J. Johnson, K. Folting, W. E. Streib, O. Eisenstein and K. G. Caulton, *Inorg. Chem.*, 1995, **34**, 488; (*c*) M. Ogasawara, D. Huang, W. E. Streib, J. C. Huffman, N. Gallego-Planas, F. Maseras, O. Eistenstein and K. G. Caulton, *J. Am. Chem. Soc.*, 1997, **119**, 8642.
4 J. T. Poulton, M. P. Sigalas, K. Folting, W. E. Streib, O. Eisenstein and K. G. Caulton, *Inorg. Chem.*, 1994, **33**, 1476.
5 L. Vaska and J. Peone, *Chem. Commun.*, 1971, 418.
6 G. Schiavon, S. Zecchin, G. Pilloni and M. Martelli, *Inorg. Nucl. Chem.*, 1977, **39**, 115.
7 D. J. Darensbourg, K. K. Klausmeyer and J. H. Reibenspies, *Inorg. Chem.*, 1995, **34**, 4933.
8 F. Abu-Hassayan, A. S. Goldman and K. Krogh-Jespersen, *Inorg. Chem.*, 1994, **33**, 5122;
9 M. D. Butts, B. L. Scott and G. J. Kubas, *J. Am. Chem. Soc.*, 1996, **118**, 11 831.
10 S. S. P. R. Almeida and A. J. L. Pombeiro, *Organometallics*, 1997, **16**, 4469.
11 R. Breslow and W. Chu, *J. Am. Chem. Soc.*, 1973, **95**, 411.
12 E. M. Arnett, R. A. Flowers, II, R. T. Ludwig, A. Meckhof and S. Walek, *Pure Appl. Chem.*, 1995, **67**, 729; F. G. Bordwell, A. V. Satish, S. Zhang and X.-M. Zhang, *Pure Appl. Chem.*, 1995, **67**, 735; D. D. M. Wayner and V. D. Parker, *Acc. Chem. Res.*, 1993, **26**, 287.
13 (*a*) M. Tilset and V. D. Parker, *J. Am. Chem. Soc.*, 1989, **111**, 6711; 1990, **112**, 2843; (*b*) O. B. Ryan, M. Tilset and V. D. Parker, *J. Am. Chem. Soc.*, 1990, **112**, 2618; (*c*) M. Tilset, *J. Am. Chem. Soc.*, 1992, **114**, 2740; (*d*) V. Skagestad and M. Tilset, *J. Am. Chem. Soc.*, 1993, **115**, 5077.
14 E. P. Cappellani, S. D. Drouin, G. Jia, P. A. Maltby, R. H. Morris and C. T. Schweitzer, *J. Am. Chem. Soc.*, 1994, **116**, 3375; M. Schlaf, A. J. Lough, P. A. Maltby and R. H. Morris, *Organometallics*, 1996, **15**, 2270.
15 D. Wang and R. J. Angelici, *J. Am. Chem. Soc.*, 1996, **118**, 936; J. Protasiewicz and K. H. Theopold, *J. Am. Chem. Soc.*, 1993, **115**, 5559; H. A. Trujillo, C. M. Casado and D. Astruc, *J. Chem. Soc., Chem. Commun.*, 1995, 7; M. E. Kerr, X.-M. Zhang and J. W. Bruno, *Organometallics*, 1997, **16**, 3249.
16 (*a*) C. Roger, P. Hamon, L. Toupet, H. Rabaâ, J.-Y. Saillard, J.-R. Hamon and C. Lapinte, *Organometallics*, 1991, **10**, 1045. (*b*) P. Hamon, L. Toupet, J.-R. Hamon and C. Lapinte, *Organometallics*, 1992, **11**, 1429. (*c*) P. Hamon, J.-R. Hamon and C. Lapinte, *J. Chem. Soc., Chem. Commun.*, 1992, 1602; (*d*) P. Hamon, L. Toupet, J. R. Hamon and C. Lapinte, *Organometallics*, 1996, **15**, 10.
17 This trend has been commonly found for the heavier halides (Cl, Br, I). See for example: R. Poli, *J. Coord. Chem.*, 1993, **29**, 121.
18 A similar trend for the heat of protonation of a series of $CpOs(PR_3)_2X$ complexes (decrease in $-\Delta H$ in the order Cl > Br > I) has been reported: M. K. Rottink and R. J. Angelici, *J. Am. Chem. Soc.*, 1993, **115**, 7267.
19 The compound $Cp^*Fe(dppe)F^{\bullet+}PF_6^-$ is isolated after oxidation of the 16-electron $Cp^*Fe(dppe)^+PF_6^-$ with $Cp_2Fe^+PF_6^-$ in THF at −90 °C: C. P. Hamon, J.-R. Hamon and C. Lapinte, unpublished work.

Received in Basel, Switzerland 27th October 1997; revised manuscript received 21st January 1998; 8/00742J

1-Benzostannepines: first synthesis and novel conversion into 1-benzo-borepines, -stibepines and -tellurepines[1]

Haruki Sashida,*† Atsuhiro Kuroda and Takashi Tsuchiya

Faculty of Pharmaceutical Sciences, Hokuriku University, Kanagawa-machi, Kanazawa 920-11, Japan

2-Alkyl-1-benzostannepines 3 were prepared in one pot from (*Z*)-1-(*o*-bromophenyl)but-1-en-3-ynes 1 *via* tin hydride intermediates 2 and easily converted into 1-benzo-borepines 4 and 5, -stibepines 6, 7 and 8, and -tellurepines 9 by tin–metal exchange reaction in moderate to good yields.

3-Benzostannepines,[2] fully unsaturated seven-membered tin-containing heterocycles, were synthesized by hydrostannation of *o*-diethynylbenzenes more than 30 years ago. Monocyclic,[3] thiophene ring-,[4] pyrrole ring-[5] and cyclopentane ring-fused[6] stannepines have also been prepared by extension of this reaction. It is well-known that these parent stannepines can be converted into the corresponding derivatives of borepine[2b,3b,4–7] and stibepine.[8] However, no 1-benzostannepines **3**, a theoretically possible structural isomer, have been prepared until now, in spite of much synthetic effort. Recently, we reported the synthesis of 1-benzotellurepines **9**,[9] novel tellurium-containing seven-membered heterocycles, *via* the successive intramolecular addition of telluroles to a triple bond. In our continuing studies[10] on the synthesis of new heterocyclic ring systems using efficient intramolecular cyclization reactions with a participating acetylenic group, we herein describe the preparation of novel stable 1-benzostannepines **3** and the transformation of **3** into 1-benzoborepines **4** and **5**, 1-benzostibepines **6**, **7** and **8**, and also 1-benzotellurepines **9**; the former compounds are new heterocyclic ring systems.

(*Z*)-1-(*o*-Bromophenyl)but-1-en-3-ynes **1**[11] were lithiated with Bu^tLi in the presence of tetramethylethylenediamine in *n*-hexane, followed by hydrostannation with Bu^n_2ClSnH[12] to give the desired 2-alkyl-1-benzostannepines **3**‡ as a sole product in 30–40% yield. The intermolecular hydrostannation of acetylene compounds induced by radical initiators,[13] transition metal catalysts,[14] base catalysts[2] or Lewis acid catalysts[15] to form vinylstannanes has been given extensive attention, and this hydrostannation frequently proceeds in the absence of a catalyst.[16] Therefore, the stannepines **3** may probably be obtained by the intramolecular *endo*-mode ring closure of stannyl hydride intermediates **2** at the sp carbon of the ethynyl moiety, as shown in Scheme 1. These compounds are quite stable and are not sensitive to air, light or even moisture.

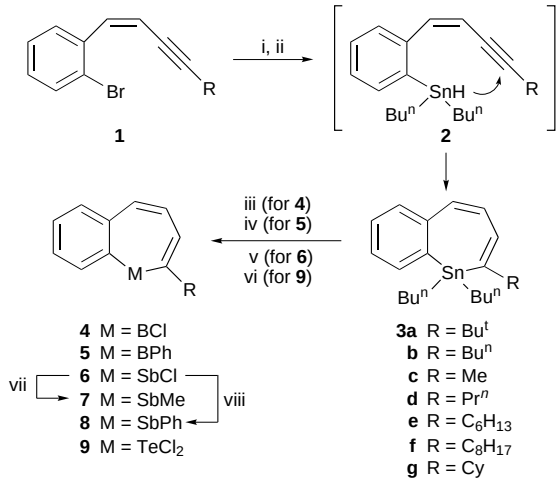

Scheme 1 *Reagents and conditions*: i, Bu^tLi (2.2 equiv.), $Me_2NC_2H_4NMe_2$, hexane, −80 °C, then room temp., 3 h; ii, Bu^n_2SnHCl, room temp., 1 h; iii, BCl_3 (1 equiv.), hexane, room temp., 1 h; iv, $PhBCl_2$ (1 equiv.), hexane, room temp., 1 h; v, $SbCl_3$ (1 equiv.), $CHCl_3$, room temp., 30 min; vi, $TeCl_4$ (1 equiv.), PhH, room temp., 1 h; vii, MeLi (1.2 equiv.), Et_2O, −20 °C, 30 min; PhLi (1.2 equiv.), Et_2O, −20 °C, 30 min

The reaction of the 1-stannepine **3a** with 1.0 equiv. of BCl_3 in *n*-hexane at room temperature afforded 2-*tert*-butyl-1-chloro-1-benzoborepine **4a**,§ which could be purified by distillation under reduced pressure in spite of being air- and moisture-sensitive. A 1-phenyl derivative **5a** was similarly obtained.

The stannepines **3a**,**b** also reacted readily with 1.0 equiv. of $SbCl_3$ in $CHCl_3$ at 0 °C to give the corresponding 1-chlorostibepines **6a**,**b**¶ almost quantitatively, but these compounds were too unstable to be isolated. Thus, we have examined the conversion of **6** to the Sb-alkyl or -phenyl substituted derivatives. Treatment of the 1-chlorostibepines **6**, which were freshly prepared without purification after removal of the solvent and $Bu^n_2SnCl_2$ under reduced pressure, with a small excess of MeLi in Et_2O at −20 °C gave the 1-methylstibepines **7**. The phenyl derivative **8** was prepared in a similar manner. Compounds **7** and **8**‖ were more stable than the 1-chloro derivatives **6**, and could be chromatographed on silica gel, contrary to our expectation. However, the 3-alkyl-3-benzostibepines are thermally labile. The structure of **6** was determined by comparison of its NMR spectra with those of **7** and **8**.

1,1-Dichlorotellurepines **9a**,**b** were formed from the parent stannepines **3** by tin–tellurium replacement reaction in 77–82% yield and were identical with authentic samples.[11] To the best of our knowledge, this tin–tellurium exchange reaction, accompanied by fission of a tin–carbon single bond and the simultaneous formation of a tellurium–carbon bond, is a new discovery.

Monocyclic fully unsaturated borepines, 3-benzoborepines and other ring-fused derivatives have now been recognized and established as aromatic compounds[4–7,17] by ^1H and ^{13}C NMR spectropic studies, molecular orbital calculations and X-ray crystal analyses. The ^1H NMR chemical shift values of the borepine ring protons in **4** and **5** appear rather lower than those of the other seven-membered heterocycles obtained in this work; in particular, the proton signals of 4-H of **4** and **5** are shifted 0.34–0.64 ppm downfield. These results suggest that the 1-borepines **4** and **5** are aromatic.

Further detailed studies on the ring transformation and reactivities of these novel 1-benzostannepines and its analogues, and on the aromaticity of the 1-benzoborepines, are in progress.

Notes and References

† Fax: +81-76-229-29810

‡ All new compounds exhibited satisfactory spectroscopic data. *Selected data* for **3a**: 39%, colorless oil; δ_H(400 MHz, $CDCl_3$) 0.97, 1.21–1.48 and 1.59–1.68 (6 H, t, *J* 7.3, 8 H, m, 4 H, $Bu^n \times 2$), 1.14 (9 H, s, Bu^t), 6.25 (1 H, dd, *J* 5.9 and 13.6, 4-H), 6.53 (1 H, d, *J* 5.9, 3-H), 6.84 (1 H, d, *J* 13.6, 5-H), 7.31–7.37 and 7.51–7.53 (3 H, m, and 1 H, m, Ar-H); δ_C(100 MHz,

$CDCl_3$) 10.55 (t), 13.64 (q), 27.36 (t), 29.43 (t), 30.59 (q), 38.37 (s), 127.03 (d), 127.81 (d), 128.32 (d), 128.40 (d), 130.24 (d), 134.45 (d), 134.49 (d), 142.81 (s), 143.85 (s), 163.29 (s); HRMS: Calc. for $C_{22}H_{34}Sn$ (M^+) 418.1682. Found 418.1775. For **3b**: 33%. For **3c**: 24%. For **3d**: 23%. For **3e** 37%. For **3f**: 35%. For **3g**: 36%. Compounds **3b–g** are also colorless oils.

§ *Selected data* for **4a**: 44%, pale yellow oil, bp 90–100 °C (2 mmHg); δ_H(400 MHz, $CDCl_3$) 1.43 (9 H, s, Bu^t), 6.75 (1 H, dd, *J* 8.4 and 11.0, 4-H), 7.25 (1 H, d, *J* 8.4, 5-H), 7.49 (1 H, d, *J* 11.0, 3-H), 7.40–7.60 and 8.30–8.40 (3 H, m and 1 H, m, Ar–H); HRMS: Calc. for $C_{14}H_{16}BCl$ (M^+) 230.1034, 232.1004. Found 230.1031, 232.1011. For **5a**: 54%, colorless oil, bp 80–100 °C (4×10^{-6} mmHg); δ_H(400 MHz, $CDCl_3$) 1.19 (9 H, s, Bu^t), 6.50 (1 H, dd, *J* 7.0 and 11.7, 4-H), 6.75 (1 H, d, *J* 7.0, 3-H), 6.88 (1 H, d, *J* 11.7, 5-H), 7.17–7.52 and 7.71–7.80 (6 H, m and 3 H, m, Ar-H); HRMS: Calc. for $C_{20}H_{21}B$ (M^+) 272.1736. Found 272.1734.

¶ The reaction of **3a** with $SbCl_3$ was carried out in $CDCl_3$, and the formation of **6a** was characterized by ^{1}H NMR spectroscopy. *Selected data* for **6a**: δ_H(400 MHz, $CDCl_3$) 1.25 (9 H, s, Bu^t), 6.41 (1 H, dd, *J* 5.5 and 13.0, 4-H), 6.68 (1 H, d, *J* 5.5, 3-H), 7.07 (1 H, d, *J* 13.0, 5-H), 7.25–7.54 and 7.92 (3 H, m and 1 H, d, *J* 6.4, Ar–H).

‖ *Selected data* for **7a**: 57% from **3a**, colorless oil; δ_H(400 MHz, $CDCl_3$) 0.95 (3 H, s, Sb–Me), 1.18 (9 H, s, Bu^t), 6.28 (1 H, dd, *J* 6.0 and 13.2, 4-H), 6.69 (1 H, d, *J* 6.0, 3-H), 6.82 (1 H, d, *J* 13.2, 5-H), 7.29–7.49 and 7.61–7.71 (3 H, m and 1 H, m, Ar-H); δ_C(100 MHz, $CDCl_3$) −6.18 (q), 30.59 (q), 39.36 (s), 127.43 (d), 127.86 (d), 128.14 (d), 129.43 (d), 129.57 (d), 132.62 (d), 133.81 (s), 137.05 (d), 142.80 (s), 157.20 (s); HRMS: Calc. for $C_{15}H_{19}Sb$ (M^+) 320.0525. Found 320.0533. For **7b**: 41% from **3b**, colorless oil. For **8a**: 36% from **3a**, colorless oil. For **8b**: 41% from **3b**, colorless oil.

1 Studies on Tellurium-Containing Heterocycles. Part 8. For Part 7, see H. Sashida, S. Yasaike and T. Tsuchiya, *J. Heterocycl. Chem.* in the press.

2 (*a*) A. L. Leusink, J. G. Noltes, H. A. Budding and J. M. van der Kerk, *Recl. Trav. Chim. Pays-Bas*, 1964, **83**, 1036; (*b*) A. J. Ashe III, J. W. Kampf, C. M. Kausch, H. Konishi, M. O. Kristen and J. Kroker, *Organometallics*, 1990, **9**, 2944.

3 (*a*) Y. Nakadaira, R. Sato and H. Sakurai, *Chem. Lett.*, 1987, 1451; (*b*) A. J. Ashe III, J. W. Kampf, Y. Nakadaira and J. M. Pace, *Angew. Chem., Int. Ed. Engl.*, 1992, **31**, 1255.

4 Y. Sugihara, T. Yagi and I. Murata, *J. Am. Chem. Soc.*, 1992, **114**, 1479; Y. Sugihara, R. Miyatake and T. Yagi, *Chem. Lett.*, 1993, 933.

5 Y. Sugihara, R. Miyatake, I. Murata and A. Imamura, *J. Chem. Soc., Chem. Commun.*, 1995, 1249.

6 A. J. Ashe III and F. Drone, *J. Am. Chem. Soc.*, 1987, **109**, 1879.

7 A. L. Leusink, J. G. Noltes and J. M. van der Kerk, *Tetrahedron Lett.*, 1967, 1263.

8 A. J. Ashe III, L. Goossen, L. W. Kampf and H. Konishi, *Angew. Chem., Int. Ed. Engl.*, 1992, **31**, 1642.

9 H. Sashida, K. Ito and T. Tsuchiya, *J. Chem. Soc., Chem. Commun.*, 1993, 1493.

10 H. Sashida, H. Kurahashi and T. Tsuchiya, *J. Chem. Soc., Chem. Commun.*, 1991, 802.

11 H. Sashida, K. Ito and T. Tsuchiya, *Chem. Pharm. Bull.*, 1995, **43**, 19.

12 A. K. Sawyer and H. G. Kuviila, *Chem. Ind.*, 1961, 260.

13 K. Nozaki, K. Oshima and K. Uchimoto, *J. Am. Chem. Soc.*, 1987, **109**, 2547 and references cited therein.

14 Y. Ichinose, H. Oda, K. Oshima and K. Uchimoto, *Bull. Chem. Soc. Jpn.*, 1987, **60**, 3468 and references cited therein.

15 N. Asao, J.-X. Liu, T. Sudoh and Y. Yamamoto, *J. Chem. Soc., Chem. Commun.*, 1995, 2405 and references cited therein.

16 A. J. Leusink, H. A. Budding and J. W. Marsman, *J. Organomet. Chem.*, 1967, **9**, 285; A. J. Leusink, H. A. Budding and W. Drenth, *J. Organomet. Chem.*, 1967, **9**, 295.

17 S. M. van der Kerk, J. Boersma and G. M. van der Kerk, *J. Organomet. Chem.*, 1981, **215**, 303; A. J. Ashe III, F. J. Drone, C. M. Kausch, J. Kroker and S. M. Al-Taweel, *Pure Appl. Chem.*, 1990, **62**, 513; A. J. Ashe III, J. W. Kampf, W. Klein and R. Rousseau, *Angew. Chem., Int. Ed. Engl.*, 1993, **32**, 1065.

Received in Cambridge, UK, 4th December 1997; 7/08739J

Tetraphenyldihydrocyclobutaarenes—what causes the extremely long 1.72 Å C–C single bond?

Holger F. Bettinger,[a,b] Paul v. R. Schleyer*[a]† and Henry F. Schaefer III[b]

[a] *Computer Chemie Center, Institut für Organische Chemie, Universität Erlangen-Nürnberg, Henkestr. 42, D-91054 Erlangen, Germany*

[b] *Center for Computational Quantum Chemistry, The University of Georgia, Athens, GA, 30602, USA*

The exceptional 0.19 Å lengthening (to 1.720 *vs.* 1.53 Å in ethane) of the C_{sp^3}–C_{sp^3} bond in tetraphenyldihydrocyclobutaarenes is attributed to a combination of cyclobutene ring strain (0.04 Å), through-bond coupling (0.08 Å) and steric repulsion (0.07 Å) by comparison with model systems.

The 1.720(4) Å C_{sp^3}–C_{sp^3} distance in 3,8-dichloro-1,1,2,2-tetraphenylcyclobuta[*b*]naphthalene **1** is currently the longest

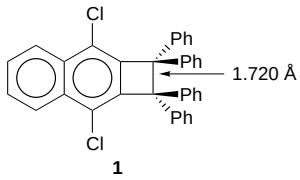

1

known single bond length in hydrocarbons.[1–3] Since semiempirical methods (PM3 and MNDO) underestimate the C_{sp^3}–C_{sp^3} bond length in **1** by as much as 0.05 Å,[3] it was suggested that 'special bonding effects exist'[2] in **1**. Moreover, recent studies concluded that through-bond coupling 'never has more than a 2–3 pm effect'[4] on the length of the mediating single bond.[4,5] Hence, we agree that the extremely long C–C single bonds in 1,1,2,2-tetraphenyldihydrocyclobutaarenes[3] 'are of utmost importance for our understanding of chemical bonding.'[2] Choi and Kertesz recently showed that electron correlation effects have to be included in order to give agreement between quantum mechanical calculations and experiment.[6]

We computed the geometry of C_2 symmetric **1** at various levels of theory.‡ Since B3LYP/6-31G** gives the best agreement with the X-ray data of **1** (Fig. 1), all subsequent

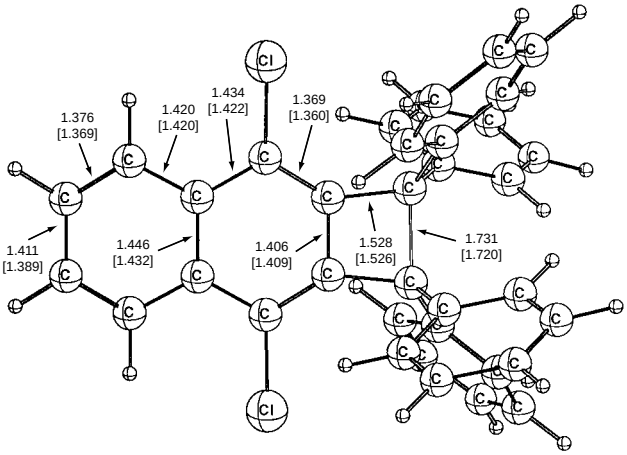

Fig. 1 The structure of 3,8-dichloro-1,1,2,2-tetraphenylcyclobuta[*b*]-naphthalene **1** optimized at the B3LYP/6-31G** level of theory. Bond lengths are in Å, experimental bond lengths are given in brackets.

calculations on model systems **2**–**6** were carried out with this hybrid functional.[9,12] Note that at HF/6-31G** the C_{sp^3}–C_{sp^3} bond length of **1** is underestimated by 0.06 Å. The C_{2v} symmetric form of **1** is a transition state at HF/STO-3G (81*i* cm^{-1}) and 9.4 kcal mol^{-1} higher in energy at B3LYP/6-31G** than the C_2 ground state.

Which effects cause the extremely long bond in **1**? A very similar C_{sp^3}–C_{sp^3} distance (1.718 Å) as for **1** (1.731 Å) is computed for 1,1,2,2-tetraphenylbenzocyclobutene **2** (Fig. 2). Obviously, the two chlorine atoms and the presence of the annelated naphthalene (instead of benzene) ring have only a small influence on the C_{sp^3}–C_{sp^3} bond length. Ring strain in the cyclobutane moiety engenders elongated C_{sp^3}–C_{sp^3} bonds in cyclobutane **3** (1.555 Å),[13] in cyclobutene **4** (1.566 Å, *via* microwave analysis)[14] and in benzocyclobutene **5** (1.580 Å, *via* X-ray analysis)[15] with respect to ethane (1.535 Å; 1.530 Å at B3LYP/6-31G**).[16] the C_{sp^3}–C_{sp^3} bonds in **1** and **2** are 0.14–0.15 Å longer than in the parent compound **5**. However, abnormally long C–C single bonds in the 1.64–1.66 Å range have been observed previously for cyclobutane derivatives with vicinal phenyl groups.[1,2]

The lengthening of a mediating C–C single bond by vicinal phenyl groups has been attributed to through-bond interactions[17] of the favorably aligned π-oribtals of the benzene rings.[1] The benzene rings in **1**, *trans*-1,2-diphenylbenzocyclobutene **6** and **2** are orientated ideally, and due to the low lying σ*(C_{sp^3}–C_{sp^3}) orbital of the cyclobutane ring, the through-bond interaction is expected to be enhanced.[1]

A distance of 1.622 Å between the C_{sp^3} centers is obtained for **6**. Inspection of the MOs reveals an orbital ordering similar to the one reported for *anti*-1,2-diphenylethane.[4] Through-bond coupling is indicated by the reversal of the conventional out-of-phase above in-phase MO ordering,[5] and through-space coupling is not observed due to the 3.72 Å separation of the benzene rings. Thus, the bond elongation of 0.042 Å in **6** with respect to **5** can only be ascribed to through-bond interaction, and is significantly larger than the 0.02–0.03 Å limit of Baldridge *et al.*[4]

Assuming that the elongation effect is additive, a C_{sp^3}–C_{sp^3} bond length of 1.58 + 2 × 0.04 = 1.66 Å, based on through-

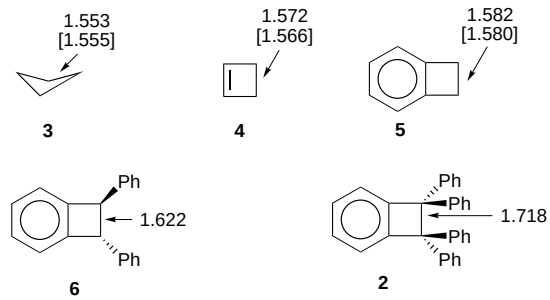

Fig. 2 Calculated (B3LYP/6-31G**) and experimental [in brackets, where available] bond lengths (Å) in molecules **2** to **6**

bond interaction, is expected for **2**. The difference of 0.07 Å with the calculated 1.73 Å length can be ascribed to repulsive steric interactions (and perhaps to through-space interactions) among the phenyl groups.

Indeed, the MM2[18] value for the C_{sp^3}–C_{sp^3} bond length in **2** is 1.651 Å, 0.08 Å shorter than the B3LYP/6-31G** result. As MM2 includes ring strain effects and steric congestion, but not through-bond interactions, our estimate of 0.08 Å as the contribution of the latter effect seems to be reasonable. The C_{sp^3}–C_{sp^3} bond in **1** is 0.18 Å longer than in cyclobutane **3**. Of this, the benzoannelation strain (*i.e.* in **5**) contributes 0.03 Å. Through-bond interaction elongates the bond by an additional 0.08 Å, and repulsion and possible through-space interaction of the phenyl groups contributes another 0.07 Å.

The elongation of a bond is in general associated with the decrease of the corresponding force constant. Thus, a perturbation's effect on the bond length is larger for an already elongated bond than for a 'normal' bond. We conclude that bonds which are weakened (elongated) by other influences are more prone to further bond lengthening by through-bond coupling than concluded recently.[4]

The work in Erlangen was supported by the Deutsche Forschungsgemeinschaft, the Stiftung Volkswagenwerk, and the Fonds der Chemischen Industrie. The work in Georgia was supported by the National Science Foundation, Grant CHE-9527468. H. F. B. thanks the Freistaat Bayern and the Deutsche Akademische Austauschdienst (DAAD) for fellowships.

Notes and References

† E-mail: pvrs@organik.uni-erlangen.de

‡ The C_{sp^3}–C_{sp^3} bond lengths of **1** are 1.658 Å at AM1 (ref. 7), 1.686 Å at HF/6-31G**, 1.788 Å at BLYP/6-31G** (refs. 8(*a*), 9], 1.757 Å at BP86/6-31G** [refs. 8(*a*), 10], 1.692 Å at BHLYP [ref. 8(*b*)] and 1.731 Å at B3LYP/6-31G** [refs. 8(*c*), 9]. All computations employed GAUSSIAN 94 (ref. 11).

1 E. Osawa and K. Kanematsu, in *Molecular Structure and Energetics*, ed. J. F. Liebman and A. Greenberg, VCH, Deerfield Beach, 1986, vol. 3, p. 329.
2 G. Kaupp and J. Boy, *Angew. Chem., Int. Ed. Engl.*, 1997, **36**, 48.
3 F. Toda, K. Tanaka, Z. Stein and I. Goldberg, *Acta Crystallogr., Sect. C*, 1996, **52**, 177; F. Toda, K. Tanaka, I. Sano and T. Isozaki, *Angew. Chem., Int. Ed. Engl.*, 1994, **33**, 1757.
4 K. K. Baldridge, T. R. Battersby, R. VernonClark and J. S. Siegel, *J. Am. Chem. Soc.*, 1997, **119**, 7048.
5 S. Osawa, M. Sakai and E. Osawa, *J. Phys. Chem. A*, 1997, **101**, 1378.
6 C. H. Choi and M. Kertesz, *Chem. Commun.*, 1997, 2199.
7 M. J. S. Dewar, E. G. Zoebisch, E. F. Healy and J. P. Stewart, *J. Am. Chem. Soc.*, 1985, **107**, 3902.
8 (*a*) A. D. Becke, *Phys. Rev. A*, 1988, **38**, 3098; (*b*) A. D. Becke, *J. Chem. Phys.*, 1993, **98**, 1372; (*c*) A. D. Becke, *J. Chem. Phys.*, 1993, **98**, 5648.
9 C. Lee, W. Yang and R. G. Parr, *Phys. Rev. B*, 1988, **37**, 785.
10 J. P. Perdew, *Phys. Rev. B*, 1986, **33**, 8822.
11 GAUSSIAN 94, Revision C.3, M. J. Frisch, G. W. Trucks, H. B. Schlegel, P. M. W. Gill, B. G. Johnson, M. A. Robb, J. R. Cheeseman, T. Keith, G. A. Petersson, J. A. Montgomery, K. Raghavachari, M. A. Al-Laham, V. G. Zakrzewski, J. V. Ortiz, J. B. Foresman, J. Cioslowski, B. B. Stefanov, A. Nanayakkara, M. Challacombe, C. Y. Peng, P. Y. Ayala, W. Chen, M. W. Wong, J. L. Andres, E. S. Replogle, R. Gomperts, R. L. Martin, D. J. Fox, J. S. Binkley, D. J. Defrees, J. Baker, J. P. Stewart, M. Head-Gordon, C. Gonzalez and J. A. Pople, Gaussian, Inc., Pittsburgh PA, 1995.
12 A. D. Becke, *J. Chem. Phys.*, 1993, **98**, 5648.
13 *Landolt-Börnstein, Structure Data of Free Polyatomic Molecules*, ed. K.-H. Hellwege,, Springer-Verlag, Berlin, 1976, vol. 7, p. 285.
14 B. Bak, J. J. Led, L. Nygaard, J. Rastrup-Andersen and G. O. Sørensen, *J. Mol. Struct.*, 1969, **3**, 369.
15 R. Boese and D. Bläser, *Angew. Chem., Int. Ed. Engl.*, 1988, **27**, 304.
16 M. D. Harmony, *J. Chem. Phys.*, 1990, **93**, 7522.
17 R. Hoffmann, A. Imamura and W. J. Hehre, *J. Am. Chem. Soc.*, 1968, **90**, 1499; R. Hoffmann, *Acc. Chem. Res.*, 1971, **4**, 1; R. Gleiter, *Angew. Chem., Int. Ed. Engl.*, 1974, **13**, 696.
18 N. L. Allinger, *J. Am. Chem. Soc.*, 1977, **99**, 8127.

Received in Corvallis, OR, USA, 29th August 1997; revised manuscript received, 16th January 1998; 8/00741A

Versatile pentadentate 1,5-bis(salicylideneamino)pentan-3-ol type ligands yield novel tri- and tetra-manganese(II) complexes: structure and properties

Lutz Stelzig,[a] Alexander Steiner,[b] Benoît Chansou[a] and Jean-Pierre Tuchagues*[a]†

[a] *Laboratoire de Chimie de Coordination du CNRS, UP 8241, 205 route de Narbonne, 31077 Toulouse Cedex, France*
[b] *Department of Chemistry, University of Liverpool, Crown Street, Liverpool, UK L69 7ZD*

Novel manganese–oxygen cores observed in trinuclear $[Mn^{I}I_3(L^3)_2(\mu_2\text{-OAc})]Na$ and tetranuclear $[Mn^{II}_2L^3(\mu_3\text{-OMe})(MeOH)]_2$ complexes [H_3L^3 = 1,5-bis(3-Cl,5-NO_2-salicylideneamino)pentan-3-ol] illustrate the coordination versatility of the 1,5-bis(salicylideneamino)pentan-3-ol type of trianionic pentadentate Schiff bases.

The coordination versatility of 1,3-bis(salicylideneamino)propan-2-ol type ligands towards transition metal ions, particularly manganese,[1] has prompted us to further explore the possible coordination modes of the related 1,5-bis(salicylideneamino)pentan-3-ol Schiff bases. The ligands in both series are potentially dinucleating pentadentate with two imine nitrogen, two phenolate and one alcoholate oxygen donors. Owing to the difference in aliphatic chain-length between their imine nitrogens, their dinucleating coordination mode results in five- and six-membered central chelate rings in the first and second series, respectively. As illustrated by work of Mikuryia *et al.*[2] with 1,5-bis(salicylideneamino)pentan-3-ol, H_3L^1, and manganese(III), the resulting increased flexibility allows formation of approximately planar dinuclear M_2L species which may be stabilized either with two additional bridges (one in-plane monoatomic and one out-of-plane triatomic), or through dimerization when two monoatomic μ_3-oxo and two triatomic bridges are provided. From the 3,5-NO_2-salicylidene substituted ligand H_3L^2, we have recently obtained a bis-dinuclear manganese(II) structure where two approximately planar dinuclear M_2L units are bridged by two μ_3-hydroxy anions.[3] Our efforts are directed towards exploration of the different types of manganese polynuclear structures obtainable from these flexible dinucleating pentadentate ligands, depending upon the electronic influence of the salicylaldimine-ring substituents, manganese oxidation state, and nature of the ancillary ligands.

As part of this project, we report here the first data concerning the novel bis-dinuclear $[Mn^{II}_2L^3(\mu_3\text{-OMe})(MeOH)]_2$ **1** and trinuclear Na $[Mn^{II}_3(L^3)_2(\mu_2\text{-OAc})]\cdot H_2O\cdot 0.25$thf **2** complexes based on the same 1,5-bis(3-Cl,5-NO_2-salicylideneamino)pentan-3-ol pentadentate ligand, H_3L^3. Reaction of $Mn(OAc)_2\cdot 2H_2O$ with H_3L^3 and NaOH (2 : 1 : 3 molar ratio) in methanol yields a very air-sensitive orange precipitate within hours. Isolation and subsequent crystallisation from dmf–MeOH yields **1** as well shaped orange–red crystals. Treatment of the initial mother-liquor with water induces precipitation of a second compound. Crystallisation of this complex from thf–pentane gives red crystals of **2**.

The X-ray crystallographic study of **1**‡ revealed a bis-dinuclear structure related to that of $[Mn^{II}_2L^2(\mu_3\text{-OH})(thf)]_2\cdot 2$thf **3**:[3] two layered M_2L^3 dinuclear units bridged by two μ_3-methoxo anions and two L^3-phenolato oxygen atoms are related by a crystallographic inversion centre (Fig. 1). The significant differences between **1** and **3** are the presence of μ_3-methoxo (**1**) instead of μ_3-hydroxo (**3**) bridges, and of a Mn(2)-bonded methanol molecule (**1**) instead of thf (**3**). The two manganese atoms within the M_2L^3 unit have different coordination spheres: Mn(1) is in a square pyramidal NO_4 ligand environment while the NO_5 environment of Mn(2) is distorted octahedral. The Mn–L bond lengths and angles, and the intra- and inter-dinuclear Mn···Mn separations (Fig. 1) differ significantly from those in related Mn^{III}_4 and $Mn^{II}_2Mn^{III}_2$ species,[2,4] but are similar to those reported for **3** and characteristic of the +2 oxidation state of the Mn ions.[3] Two strong hydrogen bonds (Fig. 1) involving the coordinated Me*OH* molecules and N*O*$_2$ substituents of L^3 link each dinuclear unit to its nearest neighbour, thus generating infinite 1D chains of bis-dinuclear molecules.

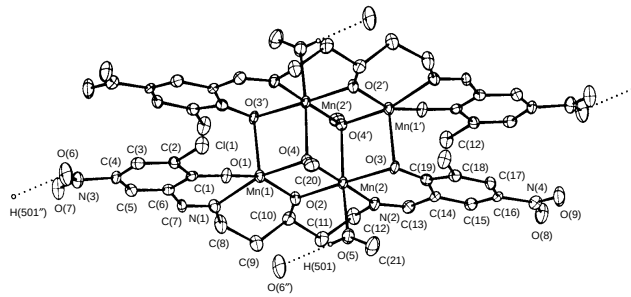

Fig. 1 Molecular structure of $[Mn^{II}_2(L^3)(\mu_3\text{-OMe})(MeOH)]_2$ **1**. Selected distances (Å): Mn(1)–O(1) 2.080(3), Mn(1)–O(2) 2.032(3), Mn(1)–O(3′) 2.200(3), Mn(1)–O(4) 2.131(3), Mn(1)–N(1) 2.206(3), Mn(2)–O(2) 2.077(3), Mn(2)–O(3) 2.157(3), Mn(2)–O(4) 2.162(3), Mn(2)–O(4′) 2.237(3), Mn(2)–O(5) 2.271(3), Mn(2)–N(2) 2.216(4), Mn(1)···Mn(2) 3.154(1), Mn(1)···Mn(2′) 3.240(1), Mn(2)···Mn(2′) 3.372(1), Mn(1)···Mn(1′) 5.432(1) (′ = $-x$, $-y$, $-z$).

The X-ray crystallographic study of **2**‡ reveals an unprecedented surpamolecular array of trinuclear $[Mn^{II}_3(L^3)_2(\mu_2\text{-OAc})]^-$ anions bonded to Na^+ cations (Fig. 2 and 3). The core of the complex anion, a triangle of Mn^{II} cations bridged by the alkoxo μ_3-O atoms of both L^3 ligands, is reminiscent of a [1.1.1]-

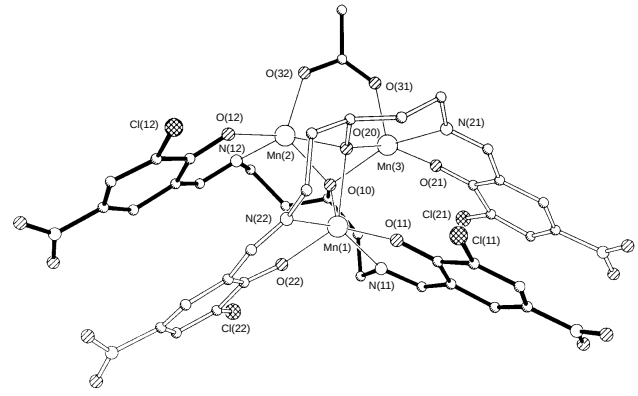

Fig. 2 Molecular structure of the trinuclear $[Mn^{II}_3(L^3)_2(\mu_2\text{-OAc})]^-$ complex anion of **2**. Selected distances (Å): Mn(1)–O(10) 2.285(8), Mn(1)–O(11) 2.064(10), Mn(1)–O(20) 2.254(9), Mn(1)–O(22) 2.166(19), Mn(1)–N(11) 2.287(11), Mn(1)–N(22) 2.17(2), Mn(2)–O(10) 2.164(8), Mn(2)–O(12) 2.030(8), Mn(2)–O(20) 2.181(8), Mn(2)–O(32) 2.094(10), Mn(2)–N(12) 2.181(11), Mn(3)–O(10) 2.112(8), Mn(3)–O(20) 2.129(7), Mn(3)–O(21) 2.083(8), Mn(3)–O(31) 2.084(9), Mn(3)–N(21) 2.172(11), Mn(1)···Mn(2) 3.174(3), Mn(1)···Mn(3) 3.121(2), Mn(2)···Mn(3) 3.067(3).

propellane. The +2 oxidation state of the Mn ions is deduced from stoichiometric and structural considerations, further confirmed by the EPR and magnetic studies. In addition to the two alkoxo μ_3-oxygens, the trigonal prismatic Mn(1) coordination sphere includes one imine-N and one phenolate-O from each L^3 ligand. The basal plane of the square pyramidal ligand environment of Mn(2) and Mn(3) includes one imine-N, one phenolate-O and the alkoxo μ_3-O atoms from one L^3 ligand, in addition to the alkoxo μ_3-O atom from the second L^3 ligand. The apical position of each square pyramid is occupied by one oxygen atom of the bridging acetate. As a result, Mn(1) is doubly bridged to Mn(2) and Mn(3) while Mn(2) and Mn(3) are triply bridged, which is reflected in the 3.067(3) Å Mn(2)···Mn(3) distance compared to the 3.174(3) [Mn(1)···Mn(2)] and 3.121(2) Å [Mn(1)···Mn(3)] separations. Both L^3 ligands are helically arranged around the trinuclear metal core, and show π-stacking interactions between their aromatic rings (Fig. 2). Interestingly, additional aromatic-ring interactions operate between adjacent trinuclear units throughout the crystal lattice, resulting in a 1D supramolecular array of alternating pairs of $[Mn^{II}_3(L^3)_2(\mu_2\text{-OAc})]^-$ anions and Na^+ cations (Fig. 3). Sodium cations interact with terminal 5-nitro and central alkoxo functions of L^3 and bridging acetate anions of the anionic trinuclear units. In addition each Na cation also interacts with one water molecule.

The structure of **2** is unique among the trinuclear manganese complexes reported: those including three Mn^{II} ions are linear[5] or triangular,[6] $Mn^{II}Mn^{III}_2$ complexes include the extensively studied oxo-centred carboxylato compounds,[7] and linear species;[8] Mn^{III}_3 complexes include oxo-centred carboxylato compounds,[9] and a triangular species including a double methoxo μ-oxygen bridge and two single alkoxo μ-oxygen bridges;[10] Mn^{IV}_3 complexes include the $[Mn_3O_4]^{4+}$ core with a double μ-oxo and two single μ-oxo bridges.[11]

The 300–80 K X-band powder spectra of complex **1** exhibit an extremely broad (*ca.* 3500 G) and featureless $g \approx 2$ centred resonance. At variance with the reasonably broad absorption typical of tetranuclear Mn^{II} complexes,[3] the broadness of this EPR absorption indicates the presence of weak extended interactions in the solid state.[12] This agrees with the crystallographic observation of 1D chains of tetramanganese(II) units. The 100 K dmf–toluene X-band glass spectrum of **1** exhibits a reasonably broad (*ca.* 700 G) $g \approx 2$ centred isotropic resonance devoid of any fine or hyperfine structure. This indicates that, (*i*) the tetranuclear structure is retained in solution, and (*ii*) the weak extended interactions are not operating in solution, *i.e.* the 1D chains of hydrogen-bonded tetranuclear molecules are broken. The 300–80 K X-band powder spectra of **2** are similar to those reported for **3**,[3] and typical of magnetically interacting Mn^{II} ions. On the other hand, the 100 K dmf–toluene glass X-band EPR spectrum of **2** indicates dissociation, not only of its supramolecular architecture, but also of the trinuclear Mn^{II} complex anions. Two resulting Mn^{II} species are clearly identified: (*i*) a mononuclear one showing the usual ^{55}Mn six-line hyperfine pattern at $g \approx 2$, and (*ii*) a dinuclear one showing the typical 11-line hyperfine pattern superimposed on several fine structure absorptions (0–5000 G).[13] The magnetic susceptibilities of complexes **1** and **2** have been measured in the 300–2 K temperature range. For both complexes, μ_{eff} mol^{-1} at 300 K is lower than the spin-only value for non-interacting spin systems (11.83 μ_B for four $S = 5/2$ spins and 10.25 μ_B for three $S = 5/2$ spins) and decreases from 10.50 to 4.89 μ_B (**1**) and 9.00 to 4.91 μ_B (**2**) at 2 K, indicating overall antiferromagnetic coupling of the $S = 5/2$ spins of the Mn^{II} ions in both complexes.

Owing to the possible role of the vacant coordination sites at the Mn^{II} centres of both novel complexes, their redox behaviour and reactivity are currently under study.

This work was supported by a postdoctoral grant from the European community to L. S. (Human Capital and Mobility Programme, Contract No ERBCHBGCT 93-0417).

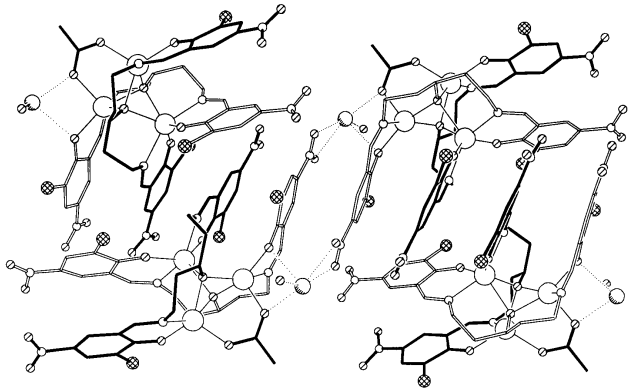

Fig. 3 View of four $[Mn^{II}_3(L^3)_2(\mu_2\text{-OAc})]^-$, $Na^+\cdot H_2O$ ion pairs **2** emphasizing the infinite π-stackings perpendicular to [001]. The intramolecular π-stacking distances are 3.4 and 3.5 Å. The two crystallographically independent intermolecular π-stacking distances are 3.3 and 3.4 Å.

Notes and References

† E-mail: tuchague@lcc-toulouse.fr

‡ *Crystal data*: for **1**: $C_{21}H_{22}Cl_2Mn_2N_4O_9$, crystal size: 0.5 × 0.3 × 0.05 mm, triclinic, space group, $P\bar{1}$, a = 9.203(1), b = 11.071(1), c = 13.50(1) Å, U = 1270.3(2) Å^3, Z = 2, D_c = 1.71 g cm^{-3}, μ(Mo-Kα) = 12.23 cm^{-1}, 8646 reflections collected at 180 K (STOE-IPDS diffractometer) in the 2.8–48.4° 2θ range, 3373 unique, 2576 used with $I > 1.0\sigma(I)$, 348 parameters refined on F to final R indices: R = 0.042, and R_w = 0.042. For **2**: $C_{40}H_{35}Cl_4Mn_3NaN_8O_{17}\cdot 0.25$thf, crystal size: 0.45 × 0.25 × 0.13 mm, tetragonal, space group, $P4/ncc$, a = 30.296(3), c = 28.362(3) Å, U = 26032(5) Å^3, Z = 16, D_c = 1.273 g cm^{-3}, μ(Mo-Kα) = 8.05 cm^{-1}, 17511 reflections collected at 180 K (STOE-IPDS diffractometer) in the 3.2–36.8° 2θ range, 4709 unique, 825 parameters refined on F^2 to final R indices: R_1 [$I > 2\sigma(I)$] = 0.0921, $wR2$ (all data) = 0.2789. Crystals of **2** were poorly shaped and weakly diffracting, giving low resolution data and relatively high R-values. One reason for this might be the high amount of disorder in the crystal structure. One half of one L^3 ligand is disordered and could be refined onto two positions using distance and ADP-restraints. The lattice bound thf molecule is disordered on a four-fold axis. CCDC 182/788.

1 Z. Zhang, C. Brouca-Cabarrecq, C. Hemmert, F. Dahan and J.-P. Tuchagues, *J. Chem. Soc., Dalton Trans.*, 1995, 1453 and refs. therein.

2 M. Mikuriya, Y. Yamato and T. Tokii, *Bull. Chem. Soc. Jpn.*, 1992, **65**, 2624 and references therein.

3 L. Stelzig, B. Donnadieu and J.-P. Tuchagues, *Angew. Chem., Int. Ed. Engl.*, 1997, **36**, 2221.

4 V. McKee and S. S. Tandon, *J. Chem. Soc., Chem. Commun.*, 1988, 1334.

5 *E.g.*: Z. L. Zhong, X.-Z. You and T. C. W. Mak, *Polyhedron*, 1994, **13**, 2157 and references therein.

6 *E.g.*: N. H. Buttrus, C. Eaborn, M. N. A. El-Kheli, P. B. Hitchcock, J. D. Smith, A. C. Sullivan and K. Tavakkoli, *J. Chem. Soc., Dalton Trans.*, 1988, 381; R. A. Reynolds III, W. O. Yu, W. R. Dunham and D. Coucouvanis, *Inorg. Chem.*, 1996, **35**, 2721 and refs. therein.

7 *E.g.*: C. J. Gomez-Garcia, E. Coronado, R. Georges and G. Pourroy, *Physica B*, 1992, **182**, 18; J. K. McCusker, H. G. Jang, S. Wang, G. Christou and D. N. Hendrickson, *Inorg. Chem.*, 1992, **31**, 1874.

8 *E.g.*: D. A. Malamatari, P. Hitou, A. G. Hatzidimitriou, F. E. Inscore, A. Gourdon, M. L. Kirk and D. P. Kessissoglou, *Inorg. Chem.*, 1995, **34**, 2493, and references therein.

9 *E.g.*: J. B. Vincent, H.-R. Chang, K. Folting, J. C. Huffman, G. Christou and D. N. Hendrickson, *J. Am. Chem. Soc.*, 1987, **109**, 5703.

10 M. Mikuriya, K. Majima and Y. Yamato, *Chem. Lett.*, 1992, 1929.

11 *E.g.*: S. Pal, M. K. Chan and W. H. Armstrong, *J. Am. Chem. Soc.*, 1992, **114**, 6398 and references therein.

12 R. D. Dowsing, J. F. Gibson, M. Goodgame and P. J. Hayward, *J. Chem. Soc. A*, 1969, 187; B. A. Goodman and J. B. Raynor, *Adv. Inorg. Chem. Radiochem.*, 1970, **13**, 205 and references therein.

13 B. Mabad, P. Cassoux, J.-P. Tuchagues and D. N. Hendrickson, *Inorg. Chem.*, 1986, **25**, 1420, and references therein.

Received in Basel, Switzerland, 15th December 1997; 7/09015C

Effects of the arrangement of a distal histidine on regioselectivity of the coupled oxidation of sperm whale myoglobin mutants

Tatsuya Murakami,[a] Isao Morishima,*[a]† Toshitaka Matsui,[b] Shin-ichi Ozaki[c] and Yoshihito Watanabe*[c]‡

[a] *Department of Molecular Engineering, Graduate School of Engineering, Kyoto University, Kyoto 606-01, Japan*
[b] *Department of Structural Molecular Science, The Graduate University for Advanced Studies, Okazaki, Myodaiji, 444 Japan*
[c] *Institute for Molecular Science, Okazaki, Myodaiji, 444, Japan*

The arrangement of a distal histidine of sperm whale myoglobin alters the regioselectivity of the heme degradation by coupled oxidation.

Heme oxygenase (HO), a monooxygenase of the heme catabolism,[1] utilizes electrons from NADPH and molecular oxygen to transform heme into biliverdin (Scheme 1). The formation of an oxy complex[2] is followed by the hydroxylation of the α-*meso*-carbon presumably *via* a ferric hydroperoxide intermediate.[3] The release of carbon monoxide from hydroxyheme and subsequent ring opening affords biliverdin.[1] Therefore, α-*meso*-hydroxyheme formation from the oxy complex is a key step for the regiospecific opening of the tetrapyrrole macrocycle. Recently, Torpey and co-workers reported that the regiochemistry of the reaction is primarily controlled by the electronic effect of the heme.[4] However, resonance Raman studies suggested that an oxygen molecule of the O_2-bound heme–HO complex had a bent structure and that the terminal oxygen atom was in van der Waals contact with the α-*meso*-carbon of the porphyrin ring.[5] These results might imply that orientation of the bound oxygen also affects the regioselective heme degradation by HO.

Myoglobin (Mb), normally an oxygen storage protein, is also known to transform its prosthetic heme into mainly biliverdin IXα in the presence of ascorbate under aerobic conditions, the so-called coupled oxidation of Mb.[6] Although the coupled oxidation of Mb is much slower than the heme degradation catalyzed by HO, Mb and heme–HO complex both have a histidine residue as a ligand of the heme iron.[7] Furthermore, the crystal structure of oxyMb indicates that the molecular oxygen bound to the heme is restricted by the distal histidine (His-64) toward the α-*meso*-position, and the oxy complex is stabilized by a hydrogen bond with His-64 (Fig. 1). In order to examine whether or not the reorientation of the bound oxygen caused by removal or relocation of the distal histidine affects the regiospecific degradation of heme in Mb, we have constructed H64L, L29H/H64L, F43H/H64L and I107H/H64L Mb and analyzed the biliverdin regioisomers generated by the coupled oxidation of the MBs.§

The high-pressure liquid chromatograph (HPLC) trace of the biliverdin regioisomers prepared from protoheme IX [Fig. 2(*a*)] exhibits four separate peaks. Comparison of the elution profiles of authentic biliverdins allows us to identify the peaks at 8.4, 9.8, 10.4, and 13.6 min as the α-, β-, δ- and γ-isomers, respectively. Wild type Mb affords mainly biliverdin IXα with a trace amount of the β-isomer, as reported previously [Fig. 2(*b*)].[8] Elimination of the distal histidine does not alter the major product [Fig. 2(*c*)]; however, a small amount of the γ-isomer, which is absent in the case of wild type Mb, is observed presumably because the replacement of His-64 with a smaller residue such as Leu allows the bound oxygen to be directed toward the γ-*meso* position (Fig. 1). Interestingly, the His-64 → Leu/Phe-43 → His double mutation significantly alters the product distribution [Fig. 2(*d*)]. Although one of the major degradation products for F43H/H64L Mb is still biliverdin IXα (40%) as observed for the wild type and H64L mutant, a significant amount of the β- (16%) and γ-isomers (44%) are accumulated (Table 1). More importantly, the L29H/H64L mutant is almost regiospecifically oxidized to biliverdin IXγ [Fig. 2(*e*)]. Finally, the substitution of Ile-107 of the H64L mutant with a histidine residue does not change the regioselectivity with respect to H64L Mb [Fig. 2(*f*) and (*d*)].

We have for the first time observed changes in the regioselectivity of the coupled oxidation process of Mb by relocating the distal His.¶ In particular, L29H/H64L Mb is almost regiospecifically oxidized to biliverdin IXγ, although the distal His at position 29 is located too far from the heme iron (6.6 Å)[9] to directly interact with the bound oxygen. The increased amount of the γ-isomer for H64L Mb can be explained by elimination of His-64, which sterically blocked the γ-*meso*-position.[10] Introduction of the His at various positions in H64L Mb tends to further enhance γ-isomer formation. Although the mechanism is not clear at this moment, these observations could imply that the distal His, except for His-64

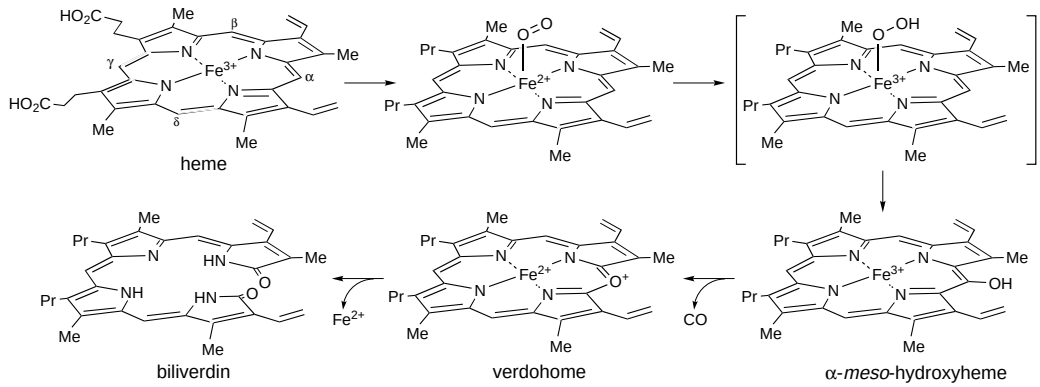

Scheme 1

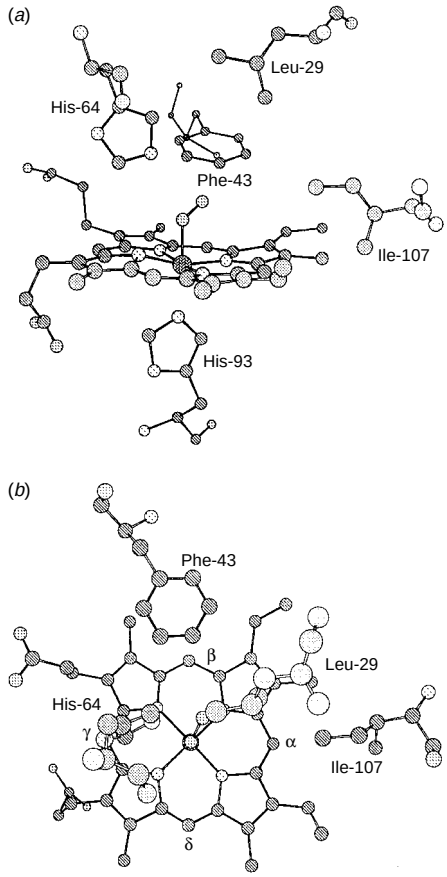

Fig. 1 Heme environmental structure of myoglobin. Heme and some selected residues are shown. (*a*) Side view. (*b*) Top view.

in the wild type, enhances orientation of the bound oxygen toward the γ-*meso*-position by an indirect effect, *e.g.* a biased polarity in the distal site. As discussed before, His-64 in wild type Mb forces the oxygen toward the α-position, thus preventing γ-isomer formation.

Very recently, we have shown that F43H/H64L Mb reacts with H_2O_2 much faster than wild type Mb to form compound I as an observable species.[11] Detailed kinetic studies support the participation of His-43 in F43H/H64L Mb as a general acid/base catalyst, *i.e.* the hydrogen peroxide bound to heme interacts with His-43 *via* a hydrogen bond. In fact, the distance between the terminal oxygen atom and the N_ε atom of His-43 is estimated to be approximately 3 Å, within the range of normal hydrogen bond distances, based on calculations using DISCOVER.[12] Thus, the increase in the ratio of the β-isomer for the oxidation of F43H/H64L Mb would be due to a hydrogen bond between the terminal oxygen atom and the His-43 near the β-*meso*-position in the oxy complex.

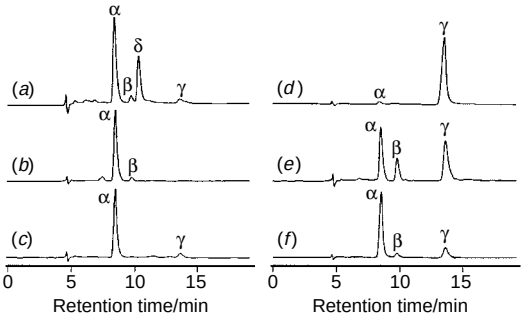

Fig. 2 HPLC analysis of the biliverdin regioisomers isolated from the coupled oxidation of Mbs with ascorbate at 37 °C for 3 h: (*a*) hemin, (*b*) wild type Mb, (*c*) H64L Mb, (*d*) L29H/H64L Mb, (*e*) F43H/H64L Mb and (*f*) I107H/H64L Mb

Table 1 Ratio of four biliverdin isomers produced by the coupled oxidation of Mbs[a]

	Ratio (%)			
Mb	α :	β :	γ :	δ
Wild-type	95 :	5 :	0 :	0
H64L	94 :	0 :	6 :	0
L29H/H64L	3 :	0 :	97 :	0
F43H/H64L	40 :	16 :	44 :	0
I107H/H64L	72 :	6 :	22 :	0

[a] Ratio of the peak area.

In summary, the arrangement of a distal histidine of Mb alters the regioselectivity of the heme degradation even without direct interaction of histidine with the peroxide bound to heme. This type of effect on the regioselectivity in HO reaction has never been considered. Introduction of a more polar or even charged residue in the active site to study the basis for regioselectivity of the coupled oxidation of Mb is now under way.

The authors thank Dr Satoshi Takahashi for his helpful discussions. This study was supported by a Grant-in-Aid for Scientific Research on Priority Areas, Molecular Biometallics, by the Ministry of Education, Science, Sports and Culture (I. M. and Y. W.).

Notes and References

† E-mail: morisima@mds.moleng.kyoto-u.ac.jp
‡ E-mail: yoshi@ims.ac.jp

§ To a 250 μl solution of ferric Mb or its mutants (40 μm) was added sodium ascorbate (2 mg) and the resulting solution was incubated at 37 °C for 3 h. Extraction of the biliverdin regioisomers was previously reported by Brown and Docherty.[13] The products dissolved in MeOH were loaded onto a HPLC (Waters 600) apparatus equipped with Waters 741 data module and a TOSOH CO-8020 column oven. A reversed-phase HPLC column (Whatmann Partisil 5 ODS-3) was employed at 40 °C at a flow rate of 0.7 ml min^{-1} with 75 : 25 (v/v) MeOH–25 mM ammonium phosphate buffer (pH 3.5) and monitored at 380 nm. A mixture of four biliverdin regioisomers was prepared from protoheme IX according to the method previously reported [ref. 4(*a*)].

¶ We assumed that the structural framework of the mutant proteins remained unchanged.

1 R. Tenhunen, H. S. Marver and R. Schmid, *J. Biol. Chem.*, 1969, **244**, 6388.
2 T. Yoshida, M. Noguchi and G. Kikuchi, *J. Biol. Chem.*, 1980, **255**, 4418.
3 M. Noguchi, T. Yoshida and G. Kikuchi, *J. Biochem.* (*Tokyo*), 1983, **93**, 1027; A. Wilks, J. Torpey and P. R. Ortiz de Montellano, *J. Biol. Chem.*, 1994, **269**, 29 553.
4 (*a*) J. Torpey and P. R. Ortiz de Montellano, *J. Biol. Chem.*, 1996, **271**, 26 067; (*b*) J. Torpey and P. R. Ortiz de Montellano, *J. Biol. Chem.*, 1997, **272**, 22 008; (*c*) J. Torpey, A. D. Lee, K. M. Smith and P. R. Ortiz de Montellano, *J. Am. Chem. Soc.*, 1996, **118**, 9172.
5 S. Takahashi, K. Ishikawa, N. Takeuchi, M. Ikeda-Saito, T. Yoshida and D. L. Rousseau, *J. Am. Chem. Soc.*, 1995, **117**, 6002.
6 R. Lemberg, *Rev. Pure. Appl. Chem.*, 1956, **6**, 1.
7 S. Takahashi, J. Wang, D. L. Rousseau, K. Ishikawa, T. Yoshida, J. R. Host and M. Ikeda-Saito, *J. Biol. Chem.*, 1994, **269**, 1010; J. Sun, M. Loehr, A. Wilks and P. R. Ortiz de Montellano, *Biochemistry*, 1994, **33**, 13 734.
8 K. Hirota, S. Yamamoto and H. A. Itano, *Biochem. J.*, 1985, **229**, 477.
9 Manuscript in preparation.
10 S. B. Brown, A. A. Chabot, E. A. Enderby and A. C. T. North, *Nature*, 1981, **289**, 93.
11 S.Ozaki, T. Matsui and Y. Watanabe, *J. Am. Chem. Soc.*, 1997, **119**, 6666.
12 DISCOVER was obtained from Molecular Simulations Inc.
13 S. B. Brown and J. C. Docherty, *Biochem. J.*, 1978, **173**, 985.

Received in Cambridge, UK, 14th November 1997; 7/08214B

Structure–activity relationship for quantifying aromatic interactions†

Fiona J. Carver,[a] Christopher A. Hunter*[a]‡ and Eileen M. Seward[b]

[a] *Krebs Institute for Biomolecular Science, Department of Chemistry, University of Sheffield, Sheffield, UK S3 7HF*
[b] *Merck Sharp and Dohme, Terlings Park, Harlow, UK*

The magnitudes of a range of intermolecular edge-to-face aromatic interactions are measured using chemical double mutant cycles in synthetic H-bonded molecular zipper complexes, and good correlations are obtained with the Hammett substituent constants, suggesting that the results can be extrapolated to other functional group combinations.

Molecular recognition events are complex processes which are influenced by a large number of different factors that make it difficult to quantify the thermodynamic properties of the basic functional group interactions involved.[1–10] We have adapted the double mutant cycle approach developed to quantify side chain–side chain interactions in proteins[5] to quantify functional group interactions in a synthetic supramolecular system. Here we apply this method to derive a quantitative structure–activity relationship for aromatic interactions.[2,8,11,12] The results not only yield a molecular explanation for the properties of these interactions, they also allow us to make quantitative predictions about the influence of chemical structure on the magnitudes of aromatic interactions.

The chemical version of the double mutant cycle which enables us to dissect out and isolate the contribution of the terminal aromatic interaction to the overall free energy of binding for zipper complex **A** is shown in Scheme 1.[13,14] Chemical mutation of one aromatic ring to a Bu^t group (**A** → **B**) removes the aromatic interaction of interest, but this change also removes secondary interactions between the aromatic ring and the core of the complex. In addition, the mutation alters the strength of the neighbouring H-bond. However, the magnitude of the secondary interactions and the change in H-bond strength can be measured directly by carrying out the same chemical mutation in complex **C** (**C** → **D**). Thus by determining association constants for all four complexes and constructing the cycle in Scheme 1, we can quantify the aromatic interaction of interest. The advantages offered by this synthetic system are that the two interacting groups are attached to a relatively rigid framework which determines the geometry of the interaction, and that a wide range of different functional groups can be studied. The geometry of interaction is probably not the optimum orientation for all combinations of functional group, but it will be essentially identical in each case. This means that electronic structure–activity relationships are not buried by differences in conformation. A limitation of the approach is that we assume that the magnitudes of the core interactions in all four complexes in a cycle are insensitive to changes in the overall binding energy.[1,6] The magnitude of entropy–enthalpy compensation effects in such systems has not yet been established, but even if they are large enough to affect our measurements, they will not alter the trends in the magnitudes of the functional group interaction energies.

Using the system in Scheme 1, we have carried out a quantitative study of substituent effects on the magnitudes of edge-to-face aromatic interactions. The required compounds were synthesised using standard protocols and characterised by a range of spectroscopic and analytical techniques. The complexes were characterised using ^{1}H NMR spectroscopy in $CDCl_3$. ^{1}H NMR titrations were used to determine the association constants and hence free energies of complexation for use in the thermodynamic cycles. The final results are

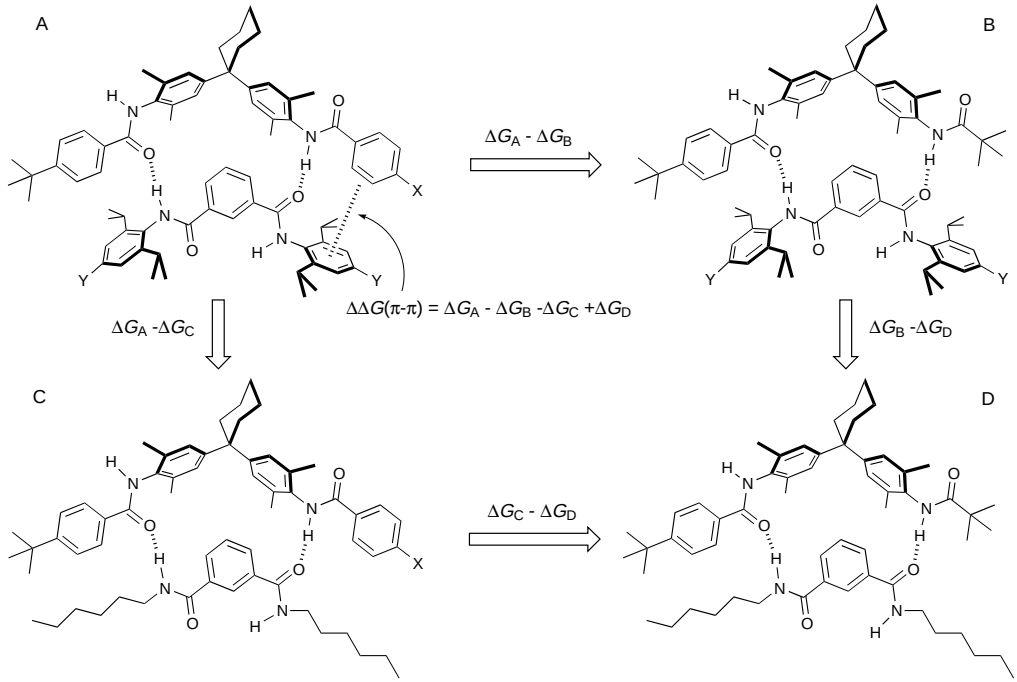

Scheme 1 Chemical double mutant cycles used to measure the magnitude of edge-to-face aromatic interactions, $\Delta\Delta G(\pi–\pi)$. X, Y = NO_2, H, NMe_2

Table 1 Magnitudes of edge-to-face aromatic interactions [$\Delta\Delta G(\pi–\pi)$ in kJ mol^{-1}] measured in $CDCl_3$ at 295 K using the chemical double mutant cycles shown in Fig. 1. Errors are ± 0.5–0.8 kJ mol^{-1}

Y	X = NO_2	X = H	X = NMe_2
NO_2	+1.2	−0.2	−1.4
H	−3.4	−1.4	−1.1
NMe_2	−4.6	−1.8	−0.9

summarised in Table 1. Intermolecular NOEs from ROESY experiments and the magnitudes of the complexation-induced changes in chemical shift from the titrations show that all four complexes in each of the nine double mutant cycles adopt essentially the same conformation in solution, *i.e.* the chemical mutations do not grossly alter the three-dimensional structure of the core of the complex. More detailed information about the geometry of the edge-to-face aromatic interactions under investigation was obtained from X-ray structures of model compounds such as **1** which corresponds to half of the zipper complex and crystallises with the same H-bonds and edge-to-face aromatic interactions inferred from our solution studies.[13,14]

The magnitude of the aromatic interaction, $\Delta\Delta G(\pi–\pi)$, is clearly sensitive to the nature of the substituents and varies from +1.0 kJ mol^{-1} repulsive to −4.9 kJ mol^{-1} attractive (more than an order of magnitude in binding strength). The ability to measure both repulsive and attractive interactions allows us to properly characterise the potential energy surface in this system. The trends in Table 1 are difficult to interpret, and so we have analysed the results using the Hammett substituent parameters (σ) which quantify the electronic effects of the substituents on the aromatic ring.[15] The correlation is remarkable and allows us to describe the experimental results using eqn. (1) (Fig. 1).

$$\Delta\Delta G(\pi–\pi) = 5.2\ \sigma_X\ \sigma_Y - 1.9\ \sigma_X + 1.4\ \sigma_Y - 1.5 \qquad (1)$$

This equation gives some insight into the molecular basis for the variations in interaction energy in Table 1. The last three terms in eqn. (1) are interpreted as an electrostatic interaction between the positively-charged CH groups on the edge ring and the negatively charged π-electron density on the face ring [Fig. 2(*a*)].[16] This part of the interaction is sensitive to changes in the local charge distributions on the two rings. The first term in eqn. (1) is attractive when the two groups X and Y exert opposite effects which reflects an interaction between the global charge distributions across the two aromatic rings, *i.e.* an electrostatic interaction between the overall dipoles caused by the polarising effects of the substitutents [Fig. 2(*b*)].

Eqn. (1) implies that although we have only studied nine interactions, the results can be extrapolated to a wide range of functional group combinations provided the Hammett parameters are available from the literature. It is unlikely that eqn. (1) will accurately predict ΔG values for aromatic interactions in other systems, but we expect it to provide a reasonable estimate of the magnitudes of substituent effects, *e.g.* if an edge-to-face aromatic interaction is implicated in a drug-receptor complex,[17] there is no point looking at lots of different Y groups if X is electron donating (NMe_2), because the magnitude of the interaction is relatively insensitive to Y. However if X is electron withdrawing (NO_2), the nature of Y is likely to have a dramatic effect on the interaction energy.

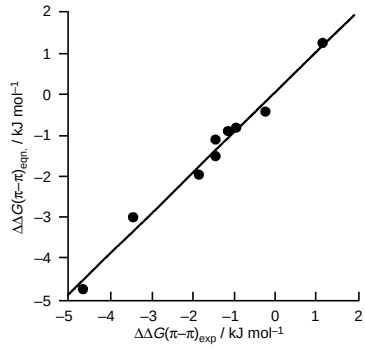

Fig. 1 Correlation of the experimental measurements of the aromatic interaction energies from Table 1 with the interaction energies calculated using eqn. (1) and the Hammett substituent parameters

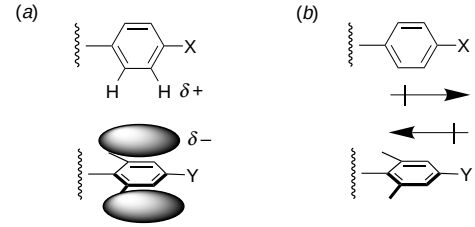

Fig. 2 Molecular interpretation of eqn. (1). (*a*) Electrostatic interactions between the CH groups of the edge ring and the π-electron density of the face ring are sensitive to changes in the local charge distributions on the two aromatic rings. (*b*) Electrostatic interactions between the overall dipoles of the π-systems are sensitive to changes in the global charge distributions on the two aromatic rings.

The generality of these results remains to be tested in different contexts, using alternative molecular frameworks and solvents, but the approach is clearly a promising method for dissecting out individual contributions to the overall thermodynamic stability of a particular molecular recognition event. By studying different interaction geometries and types, we hope to develop a database of thermodynamic measurements that can be used alongside the structural data from crystallography for understanding the chemical basis of complex molecular recognition phenomena and ultimately for rational design.

We thank the Lister Institute (C. A. H.), the EPSRC and Merck Sharp & Dohme (F. J. C.) for funding.

Notes and References

† This ChemComm is also available in enhanced multi-media format *via* the World Wide Web: http://www.rsc.org/ccenhanced

‡ E-mail: C. Hunter@Sheffield.ac.uk

1 D. H. Williams, B. Bardsley, W. Tsuzuki and A. J. Maguire, *Chem. Biol.*, 1997, **4**, 507.
2 S. B. Ferguson, E. M. Sanford, E. M. Seward and F. Diederich, *J. Am. Chem. Soc.*, 1991, **113**, 5410.
3 S. Mecozzi, A. P. West and D. A. Dougherty, *J. Am. Chem. Soc.*, 1996, **118**, 2307.
4 J. Rebek, *Acc. Chem. Res.*, 1990, **23**, 399.
5 A. R. Fersht and L. Serrano, *Curr. Opin. Struct. Biol.*, 1993, **3**, 75.
6 A. E. Mark and W. F. Vangunsteren, *J. Mol. Biol.*, 1994, **240**, 167.
7 T. J. Murray and S. C. Zimmerman, *J. Am. Chem. Soc.*, 1992, **114**, 4010.
8 A. V. Muehldorf, D. Vanengen, J. C. Warner and A. D. Hamilton, *J. Am. Chem. Soc.*, 1988, **110**, 6561.
9 H. J. Schneider, *Chem. Soc. Rev.*, 1994, **23**, 227.
10 Y. Aoyama, M. Asakawa, Y. Matsui and H. Ogoshi, *J. Am. Chem. Soc.*, 1991, **113**, 6233.
11 F. Cozzi and J. S. Siegel, *Pure Appl. Chem.*, 1995, **67**, 683.
12 S. Puliwal, S. Geib and C. S. Wilcox, *J. Am. Chem. Soc.*, 1994, **116**, 4497.
13 H. Adams, F. J. Carver, C. A. Hunter, J. C. Morales and E. M. Seward, *Angew. Chem., Int. Ed. Engl.*, 1996, **35**, 1542.
14 H. Adams, K. D. M. Harris, G. A. Hembury, C. A. Hunter, D. Livingstone and J. F. McCabe, *Chem. Commun.*, 1996, 2531.
15 σ_p parameters from N. S. Isaacs, *Physical Organic Chemistry*, Longman, London, 1995, p. 152.
16 C. A. Hunter and J. K. M. Sanders, *J. Am. Chem. Soc.*, 1990, **112**, 5525.
17 T. M. Fong, M. A. Cascieri, H. Yu, A. Bansal, C. Swain and C. D. Strader, *Nature*, 1993, **362**, 350.

Received in Cambridge, UK, 21st January 1998; 8/00567B

Synthesis, luminescence and electrochemistry of novel pentanuclear rhenium(I)–copper(I) mixed-metal acetylide complexes. X-Ray crystal structure of $[Cu_3(\mu\text{-dppm})_3\{\mu_3\text{-}\eta^1\text{-}C{\equiv}CC_6H_4C{\equiv}C\text{-}p\text{–}Re(bpy)(CO)_3\}_2]^+$

Vivian Wing-Wah Yam,*† Wendy Kit-Mai Fung, Keith Man-Chung Wong, Victor Chor-Yue Lau and Kung-Kai Cheung

Department of Chemistry, The University of Hong Kong, Pokfulam Road, Hong Kong, PR China

A series of luminescent mixed-metal acetylide complexes $[Cu_3(\mu\text{-LL})_3\{\mu_3\text{-}\eta^1\text{-}C{\equiv}C\text{–}C_6H_2R_2\text{-}2,5\text{–}C{\equiv}C\text{-}p\text{–}Re(NN)(CO)_3\}_2]^+$, (LL = dppm, Pr^nPNP; NN = bpy, Bu^t_2bpy; R = H, Me) have been synthesized and their electrochemical properties studied; the X-ray crystal structure of $[Cu_3(\mu\text{-dppm})_3\{\mu_3\text{-}\eta^1\text{-}C{\equiv}C\text{–}C_6H_4C{\equiv}C\text{-}p\text{–}Re(bpy)(CO)_3\}_2]^+$ has also been determined.

The highly conjugated polyynes and their transition metal complexes have attracted enormous attention in recent years owing to their potential technological applications as precursors for non-linear optical materials and rigid-rod molecular wires.[1] With our recent interest in the design and synthesis of luminescent Re^I[2] and Cu^I acetylide complexes,[3] it would be interesting to extend our studies to mixed-metal acetylide complexes using the 'metal complex as ligand' or metalloligand approach.[1c,4] Here, we report the synthesis of a series of Re^ICu^I mixed-metal acetylide complexes (**1**–**5**), $[Cu_3(\mu\text{-LL})_3\{\mu_3\text{-}\eta^1\text{-}C{\equiv}C\text{–}C_6H_2R_2\text{-}2,5\text{–}C{\equiv}C\text{-}p\text{–}Re(NN)(CO)_3\}_2]^+$, {LL = bis(diphenylphosphino)methane (dppm), bis(diphenylphosphino)-*n*-propylamine (Pr^nPNP); NN = 2,2′-bipyridine (bpy), 4,4′-di-*tert*-butyl-2,2′-bipyridine (Bu^t_2bpy); R = H, Me} with a rigid-rod acetylide backbone employing Re^I acetylide as the metalloligand. We believe that these mixed-metal acetylide complexes would be ideal building blocks for the design of luminescent rigid-rod oligomers.

$[Cu_3(\mu\text{-LL})_3\{\mu_3\text{-}\eta^1\text{-}C{\equiv}C\text{–}C_6H_2R_2\text{-}2,5\text{–}C{\equiv}C\text{-}p\text{-}Re(NN)(CO)_3\}_2]^+$ {LL = dppm, NN = bpy, R = H (**1**); LL = dppm, NN = bpy, R = Me (**2**); LL = dppm, NN = Bu^t_2bpy, R = H (**3**); LL = Pr^nPNP, NN = bpy, R = H (**4**); LL = Pr^nPNP, NN = bpy, R = Me (**5**)} were prepared by reaction of the corresponding $[Cu_2(\mu\text{-LL})_2(MeCN)_2]X_2$ (X = BF_4, PF_6)[3c,5] with $[Re(NN)(CO)_3(C{\equiv}C\text{–}C_6H_2R_2\text{-}2,5\text{–}C{\equiv}CH\text{-}p)$[6] in a 3 : 4 molar ratio in the presence of an excess of KOH in CH_2Cl_2–MeOH at room temp. Recrystallization from CH_2Cl_2–Et_2O gave orange crystals of **1**–**5**. Complexes **1**–**5** have been characterized by elemental analyses, ^1H NMR, IR and Raman spectroscopy. The X-ray crystal structure of **1** has been determined.‡

Fig. 1 shows a perspective drawing of the complex cation of **1**. It consists of an isosceles triangular array of Cu atoms with a dppm ligand bridging each edge to form a roughly planar Cu_3P_6 core, with two Re acetylide metalloligands capping the triangular Cu^I in a μ_3-η^1 fashion. The bridging mode of the alkynyl group is asymmetric with Cu–C bond distances in the range 2.10(1)–2.34(2) Å. The C≡C bond distances are 1.17(2)–1.23(2) Å, typical of metal–acetylide σ bond.[7] The Cu···Cu separations in the range 2.556(2)–2.674(3) Å, which are shorter than the sum of van der Waals radii for Cu are suggestive of the presence of weak Cu···Cu interactions.

The electronic absorption spectra of **1**–**5** in CH_2Cl_2 show high-energy absorption bands at *ca*. 250–300 nm, tentatively assigned as ligand-localized transitions. Absorptions at *ca*. 348–378 nm appear as vibronically structured bands with vibrational progressional spacings of *ca*. 1350–1500 cm^{-1}, typical of ν(C··C) stretching modes of the aromatic ring in the excited state. In addition, a low-energy absorption is observed at *ca*. 440 nm, which is likely to arise from a $[d_\pi(Re) \rightarrow \pi^*(NN)]$ MLCT transition,[8] since the mononuclear Re^I diimine acetylide complexes $HC{\equiv}C\text{–}C_6H_2R_2\text{-}2,5\text{–}C{\equiv}C\text{-}p\text{-}Re(NN)(CO)_3$ (NN = bpy, Bu^t_2bpy; R = H, Me) absorb in a similar region.[2,6]

Excitation of **1**–**5** in the solid state and in fluid solutions resulted in strong orange luminescence. The photophysical data are summarized in Table 1. All spectra showed a low-energy emission band at *ca*. 600–660 nm. With reference to previous spectroscopic studies on Re^I diimine acetylide systems,[2,6] the low-lying emission band in **1**–**5**, which resembles that of the corresponding mononuclear Re^I diimine acetylide, is assigned as derived from an emissive state of $[d_\pi(Re) \rightarrow \pi^*(NN)]$ MLCT character. The shift in emission energy upon changing the bipyridine and the acetylide ligands lends further support to the MLCT assignment. A blue shift in energy of the lowest lying emission band of 0.09 eV from **1** to **3** in CH_2Cl_2 is in accord with the higher π^* orbital energy of Bu^t_2bpy than bpy. A similar blue shift in emission energy (0.11 eV) has also been observed

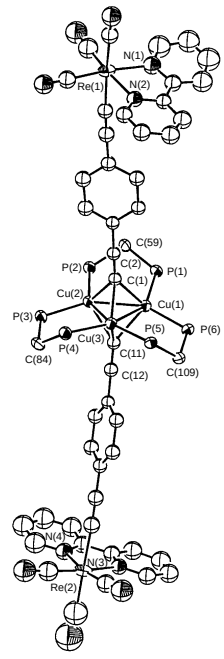

Fig. 1 Perspective drawing of the complex cation of **1** with the atomic numbering scheme. Hydrogen atoms and phenyl rings have been omitted for clarity. Thermal ellipsoids are shown at the 40% probability level. Selected bond lengths (Å) and angles (°): C(1)–C(2) 1.20(2), C(11)–C(12) 1.21(2), Cu(1)···Cu(2) 2.556(2), Cu(2)···Cu(3) 2.674(3), Cu(1)···Cu(3) 2.674(3); Cu(1)–Cu(2)–Cu(3) 61.44(7), Cu(2)–Cu(1)–Cu(3) 61.47(7), Cu(1)–Cu(3)–Cu(2) 57.09(6).

Table 1 Photophysical and electrochemical data for complexes **1**–**5**

Complex	Medium (T/K)	λ_{abs}/nm (ε_{max}/dm^3 mol^{-1} cm^{-1})	λ_{em}[a]/nm (τ_o/μs)	$E_{1/2}^{ox,c}$	$E_{1/2}^{red,c}$
1	CH_2Cl_2 (298)	262sh (102 600), 300sh (78 400), 354sh (69 300), 372 (77 400), 440sh (5110)	642 (< 0.1)	+0.39	−1.82
	Solid (298)		616 (< 0.1)		
	Solid (77)		605		
2	CH_2Cl_2 (298)	298 (51 800), 360sh (50 700), 378 (53 000), 440sh (4920)	650 (< 0.1)	+0.31	−1.83
	Solid (298)		615 (0.14)		
	Solid (77)		608		
3	CH_2Cl_2 (298)	296 (103 100), 356sh (101 200), 374 (117 000), 440sh (9230)	615 (< 0.1)	+0.33	−1.91
	Solid (298)		613 (0.1)		
	Solid (77)		605		
4	CH_2Cl_2 (298)	276sh (91 800), 292 (94 300), 348sh (95 400), 370 (145 100), 440sh (5310)	660 (< 0.1)	+0.34	−1.90
	Solid (298)		616 (0.12)		
	Solid (77)		623[b]		
5	CH_2Cl_2 (298)	244sh (23 400), 278sh (41 600), 294 (16 100), 350sh (15 500), 372 (22 100), 440sh (950)	650 (< 0.1)	+0.30	−1.93
	Solid (298)		618 (0.13)		
	Solid (77)		615		

[a] Excitation at 400 nm. [b] Excitation at 510 nm. [c] In MeCN (0.1 M $NBu^n_4PF_6$), glassy carbon electrode, scan rate 100 mV s^{-1}, 298 K. $E_{1/2}$ (V *vs.* Fc–Fc$^+$) is taken to be the average of E_{pa} and E_{pc}.

on going from $[Re(bpy)(CO)_3Cl]$[8b] to $[Re(Bu^t_2bpy)(CO)_3Cl]$.[2a] A comparison of the emission energies for the complexes with the same Re acetylide but different bidentate phosphine ligands, that is, between **1** and **4** and **2** and **5**, showed that a slight red shift in energy occurred on going from **1** to **4** and **2** to **5**. Such a trend may be rationalized by the fact that the Pr^nPNP ligand is more electron rich than dppm, which upon coordination to Cu^I would render the Cu^I-coordinated acetylide more electron rich, which in turn raises the energy of the Re d orbitals, causing a lower energy ^{3}MLCT emission. Similar findings have been reported in Re^I-acetylide and Re^I-alkyl systems.[2,9] On the contrary, an acetylide-to-Cu LMCT origin would predict an opposite trend since a more electron rich diphosphine on Cu^I would lower the electron-accepting ability of Cu, raising its acceptor orbital energy, leading to a higher emission energy. Furthermore, the lifetime in the range of submicroseconds is typical of ^{3}MLCT emission.

The electrochemistry of complexes **1**–**5** has been studied by cyclic voltammetry and the electrochemical data are listed in Table 1. Complexes **1**–**5** in MeCN (0.1 M $NBu^n_4PF_6$) show both a quasi-reversible oxidation couple and a quasi-reversible reduction couple. In general, complexes with electron rich ligand are found to be more easily oxidized, with the potential values decreasing for the series with dppm as bridging ligand: **1** > **3** > **2** and the series with Pr^nPNP as bridging ligand: **4** > **5**. These trends are consistent with the greater electron richness of the 2,5-dimethyl-1,4-diethynylbenzene than the unsubstituted 1,4-diethynylbenzene and Bu^t_2bpy than bpy. The oxidation couples are tentatively assigned as the one-electron oxidation of the Cu^I center, with the more electron rich ligands preferentially stabilizing the Cu^{II} center to a larger extent. Oxidation couples at similar potential values have also been observed in the trinuclear Cu^I acetylide systems.[3a–c]

The quasi-reversible reduction couple for **1**–**5** has been assigned as the one-electron reduction couple of bpy ligands[10] on the basis of the similarity of their reduction potential. The greater ease of reduction in **1** and **2** than **3** is in line with the greater π-acceptor ability of bpy than Bu^t_2bpy.

V. W. W. Y. acknowledges financial support from the Research Grants Council and The University of Hong Kong. W. K. M. F. acknowledges the receipt of a postgraduate studentship and a Hung Hing Ying Scholarship, both of which are administered by The University of Hong Kong. K. M. C. W. acknowledges the receipt of a Croucher Studentship and a postgraduate studentship, and V. C. Y. L. acknowledges the receipt of a Croucher Studentship and Croucher Scholarship.

Notes and References

† E-mail: wwyam@hkucc.hku.hk

‡ *Crystal data* for **1**: $\{[Re_2Cu_3P_6O_6N_4C_{121}H_{90}]^+PF_6^-\}$; M_w = 2589.92, triclinic, space group $P\bar{1}$ (no. 2), a = 19.635(3), b = 22.083(4), c = 14.703(3) Å, α = 92.82(2), β = 102.04(2), γ = 89.06(2)°, U = 6227(2) Å^3, Z = 4, μ(Mo-Kα) = 25.91 cm^{-1}, $F(000)$ = 1352, T = 301 K. Convergence for 1040 variable parameters by least-squares refinement on F with $w = 4\ F_o^2/\sigma^2(F_o^2)$, where $\sigma^2(F_o^2) = [\sigma^2(I) + (0.040F_o^2)^2]$ for 10 336 reflections with $I > 3\sigma(I)$ was reached at R = 0.067 and wR = 0.103 with a goodness-of-fit of 2.88. CCDC 182/784.

1 (*a*) T. B. Marder, G. Lesley, Z. Yuan, I. R. Jobe, N. J. Taylor, I. D. Williams and S. K. Kurtz, *ACS Symp. Ser.*, 1991, **455**, 605; (*b*) R. M. Laine, in *Inorganic and Organometallic Polymers with Special Properties*, ed. H. B. Fyfe, M. Mlekuz, G. Stringer, N. J. Taylor and T. B. Marder, Kluwer, Netherlands, 1992, p. 331; (*c*) A. Harriman, M. Hissler, R. Ziessel, A. D. Cian and J. Fisher, *J. Chem. Soc., Dalton Trans.*, 1995, 4067.

2 V. W. W. Yam, V. C. Y. Lau and K. K. Cheung, *Organometallics*, (*a*) 1995, **14**, 2749; (*b*) 1996, **15**, 1740.

3 (*a*) V. W. W. Yam, W. K. Lee and T. F. Lai, *Organometallics*, 1993, **12**, 2383; (*b*) V. W. W. Yam, W. K. Lee, K. K. Cheung, B. Crystall and D. Phillips, *J. Chem. Soc., Dalton Trans.*, 1996, 3283; (*c*) V. W. W. Yam, W. K. M. Fung and M. T. Wong, *Organometallics*, 1997, **16**, 1772; (*d*) V. W. W. Yam, W. K. M. Fung and K. K. Cheung, *Chem. Commun.*, 1997, 963.

4 V. Grosshenny and R. Ziessel, *J. Chem. Soc., Dalton Trans.*, 1993, 817; M. Hissler and R. Ziessel, *ibid.*, 1995, 893; V. Balzani, S. Campagna, G. Denti, A. Juris, S. Serroni and M. Venturi, *Coord. Chem. Rev.*, 1994, **132**, 1; F. Barigelletti, L. Flamigni, V. Balzani, J.-P. Collin, J.-P. Sauvage, A. Sour, E. C. Constable and A. M. W. C. Thompson, *J. Am. Chem. Soc.*, 1994, **116**, 7692; V. W. W. Yam, V. W. M. Lee and K. K. Cheung, *Organometallics*, 1997, **16**, 2833.

5 J. Diéz, M. P. Gamasa, J. Gimeno, A. Tiripicchio and M. T. Camellini, *J. Chem. Soc., Dalton Trans.*, 1987, 1275.

6 V. W. W. Yam, K. M. C. Wong and V. C. Y. Lau, unpublished work.

7 R. Nast, *Coord. Chem. Rev.*, 1982, **47**, 89; E. Sappa, A. Tiripicchio and P. Braunstein, *ibid.*, 1985, **65**, 219.

8 (*a*) S. M. Fredericks, J. C. Luong and M. S. Wrighton, *J. Am. Chem. Soc.*, 1979, **101**, 7415, 147; (*b*) J. V. Caspar and T. J. Meyer, *J. Phys. Chem.*, 1983, **87**, 952; (*c*) G. Tapolsky, R. Duesing and T. J. Meyer, *Inorg. Chem.*, 1990, **29**, 2285; (*d*) R. Lin, Y. Fu, C. P. Brock and T. F. Guarr, *Inorg. Chem.*, 1992, **31**, 4346.

9 L. A. Lucia, R. D. Burton and K. S. Schanze, *Inorg. Chim. Acta*, 1993, 208; D. J. Stufkens, J. W. M. van Outersterp, A. Oskam, B. D. Rossenaar and G. J. Stor, *Coord. Chem. Rev.*, 1994, **132**, 147.

10 Y. Kawanishi, N. Kitamura and S. Tazuke, *Inorg. Chem.*, 1989, **28**, 2968; B. P. Sullivan, C. M. Bolinger, D. Conrad, W. J. Vining and T. J. Meyer, *J. Chem. Soc., Chem. Commun.*, 1984, 1244; A. I. Breikss and H. D. Abruna, *J. Electroanal. Chem.*, 1986, **201**, 347.

Received in Cambridge, UK, 15th December 1997; 7/08989I

Synthesis of silica-pillared layered titanium niobium oxide

Wenfeng Shangguan, Kozo Inoue and Akira Yoshida*†

Inorganic Materials Department, National Industrial Research Institute, Shuku-machi, Tosu-shi, Saga-ken, 841, Japan

A silica-pillared layered titanium niobium oxide with high thermal stability has been synthesized and characterized for the first time.

The successful methods for preparation of pillared materials that were first developed from pillaring clays and clay minerals,[1–3] led to many attempts to prepare new classes of porous materials, which can be used as shape-selective catalysts and molecular sieves.[4,5] There are also a wide variety of layered metal oxides that have the potential to undergo ion-exchange reactions similarly to clays, but the pillaring procedures developed for smectite clays are not generally applicable to these laminar metal oxides that do not spontaneously delaminate in aqueous media owing to their high charge densities on the frameworks. Recently, the preparation of alumina-pillared layered sodium trititanate, $Na_2Ti_3O_7$[6] and silica-pillared layered tetratitanate $K_2Ti_4O_9$[7] have been reproted. Silica is one of the most commonly used pillars. Silica-pillared layered lanthanum–niobium oxides were also prepared and investigated as catalysts.[8,9] As for titanium–niobium oxides, Wadsley[10] first prepared potassium titanoniobate $KTiNbO_5$ and found that it had a layered structure. Raveau and coworkers[11–13] studied the ion-exchange properties of potassium titanoniobate $KTiNbO_5$ and the intercalation of organic materials into titanoniobic acid. Nakato *et al.*[14] reported the preparation of a methyl viologen–$HTiNbO_5$ intercalation compound. We report here the preparation of silica-pillared layered titanoniobate with high porosity and good thermal stability by a novel pillaring method, in which *n*-hexylamine and tetraethylorthosilicate [$Si(OEt)_4$] are employed as an interlayer exchange guest and a pillar precursor, respectively.

The starting material, layered potassium titanoniobate $KTiNbO_5$ was prepared by heating a mixture of K_2CO_3 (Katayama), TiO_2 (Katayama) and Nb_2O_5 (Wako) (molar ratio = 1 : 2 : 1) at 1060 °C in air. Ion exchange of $KTiNbO_5$ was carried out with 6 M HNO_3 at room temperature for 72 h to afford $HTiNbO_5$. Since $HTiNbO_5$ cannot react directly with tetraethylorthosilicate to form an intercalate, the *n*-hexylamine–$HTiNbO_5$ intercalation compound was prepared first in order to increase the interlayer distance and lower the charge density.

n-Hexylamine-intercalated titanoniobate was obtained by adding $HTiNbO_5$ to a 50% *n*-hexylamine (Wako)–ethanol (Wako) solution and stirring at room temperature for one week, followed by filtering off the product and washing successively with ethanol–water (1 : 1) and distilled water. The obtained *n*-hexylamine-intercalated titanoniobate (3.0 g) was then added to 120 ml of tetraethylorthosilicate (Wako). Having failed to obtain a silica-pillared titanoniobate by reaction between *n*-hexylamine-intercalated titanoniobate and tetraethylorthosilicate at room temperature, the present operation was performed by stirring for one week at *ca.* 65 °C with two additions of tetraethylorthosilicate (40 ml) during this period. After the reaction, the product was separated and washed as above and finally dried at room temperature. Obtained products were studied by X-ray diffraction (Gigaku Geigerflex, Cu-Kα radiation). In $KTiNbO_5$, units consisting of two MO_6 (M = Ti, Nb) octahedra are linked in the *b*-direction to form layers with the potassium ions in the interlayer spaces. XRD analysis shows [Fig. 1(*a*), 2(*b*)] that obtained $KTiNbO_5$ has an interlayer distance of 9.01 Å by measuring the first diffraction peak (2θ = 9.82°) which decreases to 8.28 Å (2θ = 10.69°) upon exchanging K^+ with H^+ in HNO_3 solution, which is comparable to the value of 8.35 Å[11] but is smaller than 8.5 Å[4] published previously. These differences may be due to the differential preparation conditions. As shown in Fig. 1(*c*), *n*-hexylamine readily intercalates layered titanoniobate and leads to an extremely strong peak at 2θ = 4.08 Å. This interlayer distance is 21.7 Å, which is more than twice that of $HTiNbO_5$. The *n*-hexylamine intercalated titanoniobate had rather low thermal stability, and collapses after calcination at 400 °C [Fig. 1(*d*)]. However, the opened layers can facilitate the reaction of layered-hexylamine intercalated titanoniobate with tetraethylorthosilicate, which gives rise to a lower 2θ (3.68°) and a larger layer distance [24.01 Å, Fig. 1(*e*)]. Fig. 1(*f*) shows that the interlayer distance of the product calcined at 400 °C decreases remarkably to 15.61 Å (2θ = 5.66°) as a result of decomposition of organic matter. The peak is still retained upon heat treatment at 600 °C with only slightly increased 2θ and lower intensity [Fig. 1(*h*)]. TG–DTA analysis at a heating rate of 5 °C min^{-1} for the product intercalated with tetraethylorthosilicate indicated that the interlayer organic matter was decomposed between 300 and 440 °C, and no mass loss was observed at higher temperatures. From these results, it is concluded that silica-like clusters are formed in the interlayer, which act as pilalrs to prop up the titanoniobate layers after interlayer

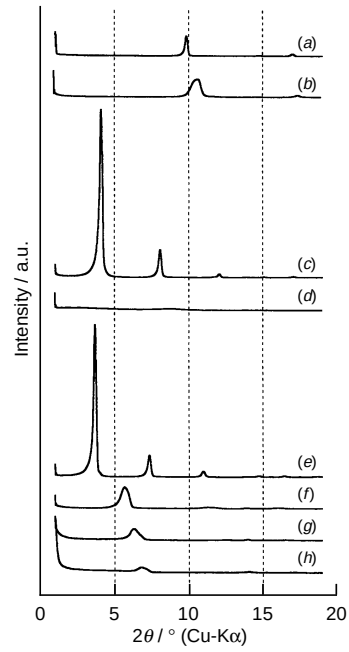

Fig. 1 Cu-Kα X-ray diffraction patterns of (*a*) $KTiNbO_5$ synthesized at 1060 °C; (*b*) as (*a*), proton-exchanged by 6 M HNO_3 at room temperature for 72 h; (*c*) reaction product of $HTiNbO_5$ with *n*-hexylamine solution; (*d*) as (*c*), calcined in air at 400 °C for 2 h; (*e*) reaction product of *n*-hexylamine-intercalated titanoniobate with tetraethylorthosilicate; (*f*) as (*e*), calcined in air at 400 °C for 2 h; (*g*) as (*f*), calcined in air at 500 °C for 2 h; (*h*) as (*g*), calcined in air at 600 °C for 2 h.

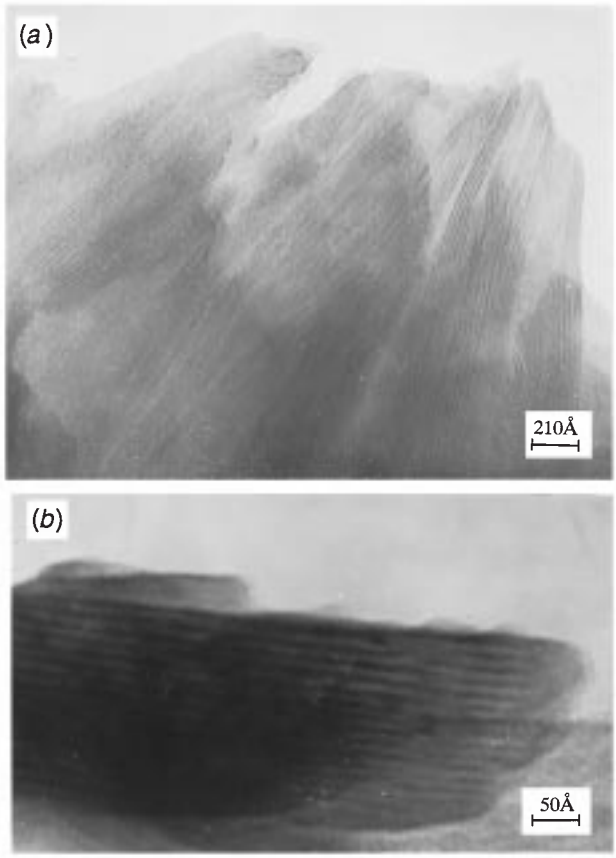

Fig. 2 TEM image of layered silica-pillared titanium niobium oxide with no calcination (*a*) and calcined at 500 °C for 2 h (*b*)

organic matter is removed. The interlayer spacing of the product calcined at 500 °C is found to be 14.05 Å [2θ = 6.29°, Fig. 1(*g*)], which is nearly twice that of $HTiNbO_5$. Fig. 2 shows transmission electron microscopy (TEM, recorded with a JEOL JEM-200CX microscope) images of untreated silica-pillared layered titanoniobate [Fig. 2(*a*)] and a sample calcined at 500 °C [Fig. 2(*b*)]. The layer structures are clearly visible, and the interlayer separations observed by TEM are consistent with those obtained from XRD. While the interlayer spacing of the material increases, the BET surface area of the titanoniobates increases from 1.8 $m^2\ g^{-1}$ for the original $KTiNbO_5$ to 20.0 $m^2\ g^{-1}$ for pillared SiO_2–$TiNbO_5$ calcined at 500 °C, and decreases to 11.3 $m^2\ g^{-1}$ at 600 °C. Elemental analysis results showed that the SiO_2 content in this silica-pillared material is *ca*. 56 mass%. The BET surface area is perhaps lower than expected due to a large amount of SiO_2 incorporated into the interlayers and the weak Bronsted acidity of $HTiNbO_5$ as compared to some layered compounds.[15]

The UV–VIS spectra of SiO_2–$TiNbO_5$ shifted into the visible region as compared to those of $KTiNbO_5$ and $HTiNbO_5$. Hydrogen evolution from the photocatalytic decomposition of water on the pillared layered titanoniobate was observed under a mercury lamp and sunlight. Thus, the new material is expected to show photocatalytic activity. Future investigation on its systematic characterization and catalytic properties is being undertaken.

Notes and References

† E-mail: yosidaa@kniri.go.jp

1 R. M. Barrer and D. M. Macload, *Trans. Faraday Soc.*, 1955, **52**, 1290.
2 G. W. Brindley and R. E. Sepples, *Clay Miner.*, 1977, **12**, 229.
3 S. Yamanaka and G. W. Brindley, *Clay Miner.*, 1979, **27**, 119.
4 F. Figueras, *Catal. Rev. Sci. Eng.*, 1988, **30**, 457.
5 T. J. Pinnavaia, *Science*, 1983, **220**, 365.
6 M. W. Anderson and J. Klinowski, *Inorg. Chem.*, 1990, **29**, 3260.
7 W. Hou, Q. Yan and X. Fu, *J. Chem. Soc., Chem. Commun.*, 1994, 1371.
8 T. Matsuda, M. Udagawa and I. Kunou, *J. Catal.*, 1997, **168**, 26.
9 C.-X. Guo, W.-H. Hou, M. Guo, Q.-J. Yan and Y. Chen, *Chem. Commun.*, 1997, 801.
10 A. D. Wadsley *Acta Crystallogr.*, 1964, **17**, 623.
11 H. Rebbah, G. Desgardin and B. Raveau, *Mater. Res. Bull.*, 1979, **14**, 1125.
12 H. Rebbah, M. M. Borel, M. Bernard and B. Raveau, *Rev. Chim. Miner.*, 1981, **18**, 109.
13 A. Grandin, M. M. Borel and B. Raveau, *Rev. Chim. Miner.*, 1987, **24**, 351.
14 T. Nakato, H. Miyata, K. Kuroda and C. Kato, *React. Solids*, 1988, **6**, 231.
15 J. Gopalakrishnan, V. Bhat and B. Raveau, *Mater. Res. Bull.*, 1987, **22**, 413.

Received in Cambridge, UK, 22nd December 1997; 7/09108G

Non-planar structures of Et_3N and Pr^i_3N: a contradiction between the X-ray, and NMR and electron diffraction data for Pr^i_3N

Roland Boese,*[a]† Dieter Bläser,[a] Mikhail Y. Antipin,*[a,b] Vladimir Chaplinski[c] and Armin de Meijere[c]

[a] *Institut für Anorganische Chemie, Universität Essen, Universitätsstraße 3-5, D-45117, Essen, Germany*
[b] *Institute of Organoelement Compounds Russian Academy of Sciences, Vavilov St. 28, B-334, Moscow, 117813, Russia*
[c] *Institut für Organische Chemie, Georg-August-Universität Göttingen, Tammanstraße 4, D-37077 Göttingen, Germany*

The crystal structures of Et_3N and Pr^i_3N were determined by X-ray analysis using the *in situ* crystallization technique for single crystal growth on the diffractometer; both have a pyramidal configuration of the nitrogen atom, even Pr^i_3N, which was considered to be planar in accord with electron diffraction and NMR data.

Aliphatic amines represent an important class of compounds widely used in organic chemistry. One of the dominant characteristics of saturated amines is that in the absence of steric congestion their ground state is pyramidal, whereas the exited state is planar. Sterically hindered tertiary amines are particularly interesting in this respect because strong steric effects of substituents can be used to change the geometry around the nitrogen atom. The stereodynamics of simple tertiary amines has been the subject of a few reviews[1] and original publications.[2–9] Most of these studies dealt with investigations into the dynamics of the inversion-rotation processes in amines and/or energetic molecular mechanics and quantum calculations.[9b]

The molecular structures of $MeNH_2$, Me_2NH, Me_3N and Me_2EtN were studied by the gas electron diffraction (GED) and microwave techniques,[10] Me_3N was also studied in the solid state.[11] All compounds have pyramidal configuration around the nitrogen, with C–N–C angles of 110.4–111.8° and C–N lengths of 1.451–1.471 Å $(CF_3)_3N$.[12] has a larger C–N–C angle [117.9(4)°] and a shorter C–N length [1.426(6) Å]. The GED and theoretical studies of Et_3N showed[13] that it exists as a mixture of three conformers with C_3, C_s and C_1 symmetry having very similar energies [angle around N = 112.6(26)°, N–C = 1.466(1) Å]. The structure of the partially fluorinated analogue, $(CH_2CF_3)_3N$, was studied *via* GED and X-ray analysis.[14] The GED investigation[15] of $(CF_2CF_3)_3N$ detected only one conformer having C_3 symmetry with almost planar configuration around the nitrogen atom (C–N–C = 119.3°) and rather a long C–N bond length [1.482(7) Å].

Amongst all known structures of noncyclic trialkylamines there is only one other example where a planar configuration around nitrogen was assumed. This is a GED study of Pr^i_3N by Bock *et al.*[16] [C–N–C = 119.2(3)°, C–N = 1.460(5) Å, C_3 symmetry with C–N–C′–H′ = 5.0(18)°.] Although these data are mostly in line with NMR studies of this compound in solution and in the solid state,[2,7] there are some contradictions with the results of quantum chemical calculations of its molecular structure.[9] Thus, AM1 and PM3 methods predict a nonplanar structure (C–N–C = *ca.* 116.3°) with rather small inversion barriers. In contrast, STO-3G, 3-21G and 6-31G calculations predict a planar structure, while a 6-31G** calculation yields a nearly planar structure (bond angle at N = 119.01°).

Here we compare the X-ray crystal structure of Me_3N **1**[11] with those of Et_3N **2** and Pr^i_3N **3**, the latter two being reported here for the first time; for **1** we present a redetermination based on data which covers a wider 2θ range and twice as many unique reflections.§

In the crystal structure of **1**, the pyramidal molecules have effective C_{3v} symmetry.[11] Those C–H bonds which have an *anti* orientation with respect to the N atom lone pair have a slightly longer bond length [0.997(10) Å] in comparison with the two others [0.959(18) and 0.957(11) Å], which may be attributed to the hyperconjugation effect. Geometrical parameters around the N atom in the crystal [C–N–C = 110.7(1)°, height of N pyramid = 0.450 Å and C–N = 1.448(1) Å] almost coincide with those in the gas phase (110.6° and 1.451 Å)[9] and the previous X-ray determination (110.4° and 1.454 Å). The charge density distribution (Fig. 1), using a quasi-high-order refinement with the Seiler and Dunitz weight scheme,[17] contains the DED maximum at the nitrogen lone pair position at a distance about 0.58 Å from its nuclei, as well as DED peaks at the N–C and C–H bonds. The DED maximum at the N–C bond is slightly shifted from the N–C line inside the NC_3 tetrahedron, which may reflect bending of this bond due to repulsion between the electron density of the lone pair and the covalent N–C bond. Very similar bond bending was found in crystals of NH_3.[18]

The crystal structure of Et_3N **2** is characterized by a rather complicated disorder phenomenon related with the crystallographic m-plane passing through the nitrogen and Me C(1) atoms, such that each CH_2 group has two distinguishable orientations in the crystal, while the carbon atoms of the Me groups have only one position with differing orientations of their hydrogens. The nitrogen has the usual pyramidal configuration [C–N–C = 107.9–112.1(1)°, height of N pyramid = 0.467 Å, and C–N = 1.422–1.497(2) Å; their relatively large scatter is related to the disordering]. As expected, the orientation of all Me groups with respect to the N atom lone pair was found to be *gauche*. We cannot exclude, however, the possibility that the complicated crystal disordering in **2** may be a result of some crystal twinning that was not resolved.

X-Ray diffraction data for Pr^i_3N **3** were collected at 203, 168, 118 and 84 K in order to reveal the nature of the structural disordering. The crystals are hexagonal, space group $P6_3/m$, $Z = 3$, and no indication of a phase transition was found in the temperature interval studied. The structure was solved and refined first at 203 K in this space group with the strictly planar

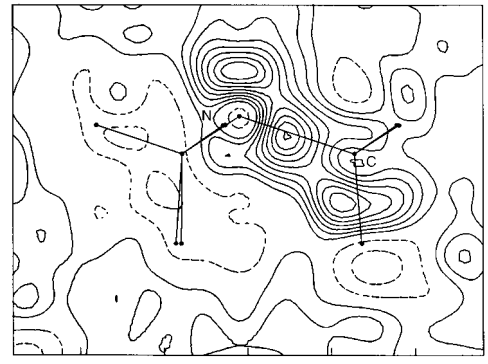

Fig. 1 Deformation electron density in the plane of the three-fold axis and N–C bond. Positive and negative contours are given through 0.025 and −0.05 e Å^{-3}, negative contours dashed.

configuration around the N atom in the special position $\bar{6}$ (2/3, 1/3, 1/4). In accord with this symmetry, the central C and methine H atoms of the Pr^i groups must be in the crystallographic m-plane together with nitrogen, while two Me groups of each Pr^i substituent are above and below this plane and perpendicular to it. The refinement of this model, however, resulted in an unreasonably large U_{33} component of the nitrogen thermal ellipsoid, indicating some kind of disordering, therefore its position was split into two 'halves' below and above the m-plane with a distance of 0.529(8) Å between them. This model was found to be more significant than the previous one and resulted in 'normal' thermal ellipsoids of all atoms and a nonplanar geometry around nitrogen (Table 1). Because these data alone could not give an answer about the nature of the crystal disordering (whether it is dynamic and related to the inversion of the N atom in the crystal, or it is static and the crystal structure represents a superposition of two pyramidal molecules having so-called 'crystal-imposed' symmetry), additional diffraction data at 168, 118 and 84 K were analyzed. We expected that in the case of a dynamic disorder a lowering of the temperature would result in a proportional decrease of the nitrogen thermal ellipsoid (mostly of its U_{33} component), but even at 84 K this ellipsoid still was very large (Fig. 2) and the split model with two 'halves' of the nitrogen atom was found to be significant. These additional data therefore give a definite proof of the pyramidal structure of Pr$^i_3$N in the crystal and the static nature of the disordering.

Our X-ray data for Pr$^i_3$N to a certain extent contradict earlier GED and NMR measurements[2,7,16] but they agree well with AM1, PM3 and *ab initio* calculations[9] giving a nonplanar structure for this molecule. However, we cannot totally exclude the possibility that the nonplanar structure of **3** may be enhanced by the crystal field effect. On the other hand, for tricyclopropylamine[19] which has the same spatial requirements as Pr$^i_3$N, effective C_s symmetry was found, it was not planar (height of N pyramid = 0.467 Å with C–N–C = 110°) and it is not disordered,[20] thus being very similar to Me_3N. In all three structures the intermolecular contacts are significantly larger than the sum of van der Waals radii (H···H > 2.75 Å). In comparison with the structures of **1** and **2**, the height of the N atom pyramid in **3** is the smallest (0.27–0.29 Å) and the inversion barrier is probably not very high.

Table 1 Geometry of Pr$^i_3$N in the crystal at different temperatures

Parameter	203 K	168 K	118 K	84 K
Bond length/Å				
N–C(1)	1.461(2)	1.468(1)	1.469(1)	1.469(1)
C(1)–C(2)	1.511(2)	1.519(1)	1.520(1)	1.522(1)
N–N′	0.529(8)	0.543(4)	0.564(3)	0.583(3)
Bond angle (°)				
C(1)–N–C(1′)	116.8(1)	116.7(1)	116.4(1)	116.2(1)
N–C(1)–C(2)	122.3(2)	122.5(1)	122.8(1)	123.0(1)
N–C(1)–C(2A)	103.8(2)	103.6(1)	103.2(1)	102.7(1)
C(2)–C(1)–C(2A)	109.8(2)	109.8(1)	109.7(1)	109.8(1)

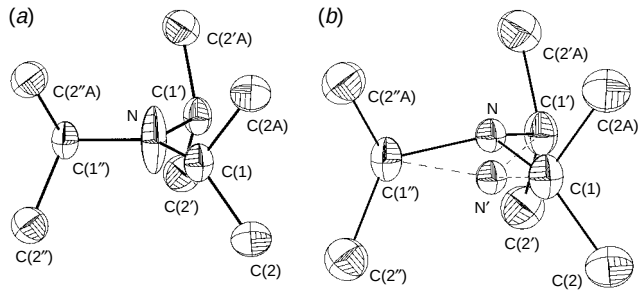

Fig. 2 View of Pr$^i_3$N in the crystal at 84 K (H atoms are not shown): (*a*) N atom in the special position $\bar{6}$ (2/3, 1/3, 1/4) and (*b*) split model with two 'halves' of the pyramidal N below and above the m-plane

Notes and References

† E-mail: boese@structchem.uni-essen.de
‡ E-mail: mishan@xray.ineos.ac.ru

§ *Crystal data* for **1**: C_3H_9N, trigonal, space group $P\bar{3}$, T = 143 K, a = 6.143(1), c = 6.979(2) Å, V = 228.10 Å^3, Z = 3, 2767 measured reflections $2\theta_{max}$ = 80°, 944 unique and 570 observed unique reflections with $F_o > 4.0\,\sigma(F)$, 25 parameters, R = 0.0454, Rw = 0.0687.

For **2**: $C_6H_{15}N$, orthorhombic, space group *Pnma* (*Pna*2$_1$ was excluded by parallel refinements, giving the same type of disorder) T = 138 K, a = 7.337(1), b = 11.797(2), c = 8.470(2) Å, V = 733.1(3) Å^3, Z = 4, 1958 measured reflections $2\theta_{max}$ = 60°, 757 observed unique reflections with $F_o > 4.0\,\sigma(F)$, 56 parameters, R = 0.0506, Rw = 0.0534.

For **3** (ref. 19): $C_9H_{21}N$, hexagonal, space group $P6_3$/m (removing the mirror plane and refinement at all temperatures with a fully occupied N atom in $P6_3$, starting at a position of the split atoms, resulted in the same picture as for $P6_3$/m), Z = 3, data collection at T = 203 K, 168, 118 and 84 K with the total number of the collected reflections = 1786, 2253, 4217 and 3269, respectively, up to $2\theta_{max}$ = 50, 60 and 80° (at 118 and 84 K), the number of unique observable reflections with $F_o > 4.0\,\sigma(F)$ = 270, 422, 640 and 769, 35 refined parameters, refinement at 203 and 84 K to R = 0.037 and 0.042, Rw = 0.087 and 0.060. At 203 and 84 K, a = 7.200(1) and 7.138(2), c = 11.460(2) and 11.365(2) Å, V = 514.5(1) and 501.5(2) Å^3. All single crystals were grown *in situ* on the diffractometer using a zone-melting crystallization technique (ref. 21). Measurements were performed on a Nicolet R3m/V diffractometer using Mo-Kα-radiation, graphite monochromator and the Wyckoff scan method. All calculations were made with the SHELX program package. CCDC 182/762.

1 Review: C. H. Bushweller, in *Acyclic Organonitrogen Stereodynamics*, ed. J. B. Lambert and Y. Takeuchi, VCH, New York, 1992.
2 J. E. Anderson, D. Casarini and L. Lunazzi, *J. Org. Chem.*, 1996, **61**, 1290.
3 J. H. Brown and C. H. Bushweller, *J. Am. Chem. Soc.*, 1992, **114**, 8153.
4 J. H. Brown and C. H. Bushweller, *J. Am. Chem. Soc.*, 1995, **117**, 12 567.
5 J. H. Brown and C. H. Bushweller, *J. Phys. Chem.*, 1994, **98**, 11 411.
6 J. H. Brown and C. H. Bushweller, *J. Phys. Chem.*, 1997, **101**, 5700.
7 T. C. Wong, L. R. Colazzo and F. S. Guziec, Jr., *Tetrahedron*, 1995, **51**, 649.
8 A. M. Belostotskii, P. Aped and A. Hassner, *J. Mol. Struct.* (*THEOCHEM*), 1997, **398**, 427.
9 (*a*) A. M. Halpern and R. R. Ramachandran, *J. Phys. Chem.*, 1992, **96**, 9832; (*b*) C. Kölmel, C. Ochsenfeld and R. Ahlrichs, *Theor. Chim. Acta*, 1991, **82**, 271.
10 For details, see L. V. Vilkov and N. I. Sadova, in *Stereochemical Applications of Gas-Phase Electron Diffraction, Part 2*, ed. I. Hargittai and M. Hargittai, VCH Weinheim, 1988, pp. 35–92.
11 A. J. Blake, E. A. V. Ebsworth and A. J. Welch, *Acta Crystallogr., Sect. C.*, 1984, **40**, 413.
12 H. Bürger, H. Niepel, G. Pawelke and H. Oberhammer, *J. Mol. Struct.*, 1979, **54**, 159.
13 H. Takeuchi, T. Kojima, T. Egawa and S. Konaka, *J. Phys. Chem.*, 1992, **96**, 4389.
14 A. Dimitrov, H.-G. Mack, S. Rüdiger, K. Seppelt and H. Oberhammer, *J. Phys. Chem.*, 1994, **98**, 11 401.
15 M. Gaensslen, U. Gross, H. Oberhammer and S. Rüdiger, *Angew. Chem.*, 1994, **104**, 1525; *Angew. Chem., Int. Ed. Engl.*, 1992, **31**, 1467.
16 H. Bock, I. Göbel, Z. Havlas, S. Liedle and H. Oberhammer, *Angew. Chem.*, 1991, **103**, 193; *Angew. Chem., Int. Ed. Engl.*, 1991, **30**, 187.
17 J. D. Dunitz and P. Seiler, *Acta Crystallogr., Sect. B*, 1973, **29**, 589.
18 R. Boese, N. Niederprüm, D. Bläser, A. Maulitz, M. Antipin and P. Mallinson, *J. Phys. Chem. B*, 1997, **101**, 5794.
19 The sample was prepared according to the procedure described by F. Kuffner and W. Koechlin, *Monatsh. Chem.*, 1962, **93**, 476, with an overall yield of 17%; using MeMgBr instead of MeMgCl increases the yield in the last step from 45 to 89%.
20 A. de Meijere, V. Chaplinski, P. Rademacher, R. Boese, T. Haumann, P. v. R. Schleyer, T. Zywietz, H. Jiao, P. Merstetter and F. Gerson, *Angew. Chem.*, 1998, submitted for publication.
21 R. Boese and M. Nussbaumer, *Organic Crystal Chemistry*, ed. D. W. Jones, Oxford University Press, Oxford, England, 1994, p. 20.

Received in Cambridge, UK, 21st November 1997; 7/08399H

First enantiocontrolled synthesis of sceletium alkaloid A-4: determination of the absolute configuration

Takashi Kamikubo and Kunio Ogasawara*†

Pharmaceutical Institute, Tohoku University, Aobayama, Sendai 980-8578, Japan

Sceletium A-4, a pyridine alkaloid isolated from the *Sceletium* species, has been synthesized for the first time in an enantiocontrolled manner along with (−)-mesembrine, an alkaloid isolated from the same plant, starting from a chiral cyclohexadienone synthon to determine the absolute configuration.

The alkaloid (+)-sceletium A-4[1,2] **1** is a minor constituent of various *Sceletium* species of the family *Aizonaceae* and was

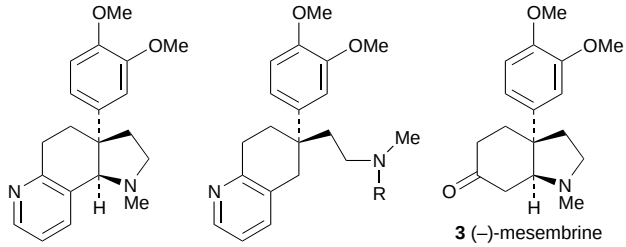

isolated with congeners such as (−)-tortuosamine[2b,d] **2a**, (−)-*N*-formyltortuosamine[2d] **2b** and (−)-mesembrine[1] **3**. (+)-Sceletium A-4 **1** afforded (−)-tortuosamine **2a** on hydrogenolysis[2b,d] while the latter afforded (−)-*N*-formyltortuosamine **2b** on formylation, indicating that they possess the same absolute configuration at the benzylic quaternary centers. The structure determination, both by a single-crystal X-ray analysis[2c] and by racemic syntheses,[3] revealed that (+)-sceletium A-4 **1** possesses the same relative stereochemistry as (−)-mesembrine **3** with respect to two stereogenic centers. However, the absolute configuration of the former alkaloid has not been correlated to the latter, whose absolute configuration has been determined both by X-ray analysis[4] and by enantioselective syntheses.[5]

In order to determine the absolute configuration of (+)-sceletium A-4 **1** as well as of the two congeners **2** by correlation to the stereochemistry of (−)-mesembrine **3**, we examined enantiocontrolled synthesis of Sceletium A-4 **1** along with (−)-mesembrine **3** using the common tricyclic chiral building block (+)-**4**, serving as a chiral cyclohexadienone.[6,7] We report here the first enantiocontrolled synthesis of (+)-sceletium A-4 **1** and a new synthesis of (−)-mesembrine **3** leading to the unambiguous determination of the absolute configuration of (+)-sceletium A-4 **1** and its two congeners, (−)-tortuosamine **2a** and (−)-*N*-formyltortuosamine **2b**.

We have recently demonstrated[8] that the tricyclic enone **4** may be β-alkylated to furnish the β-substituted enone **7** by a single-flask sequential Michael–Wittig process[9] *via* the phosphonium trifrate **5** and the 1,3-diene **6** (Scheme 1). Employing this procedure, we prepared the β-substituted enone‡ **7** (R = CH_2OBn), $[\alpha]_D^{28}$ +164.3 (*c* 1.13, $CHCl_3$), in 71% yield from (+)-**4** and 2-benzyloxyacetaldehyde. Reaction of **7** with 3,4-dimethoxyphenylmagnesium bromide in the presence of copper(I) bromide–dimethyl sulfide complex[10] proceeded from the convex face to give the β,β-disubstituted ketone **8** after acid workup, which on thermolysis afforded the cyclohexenone **9**, $[\alpha]_D^{28}$ +64.2 (*c* 1.38, $CHCl_3$). To transpose its 5,5-disubstituted cyclohex-2-enone structure to the 4,4-disubstituted cyclohex-2-enone structure **14**, **9** was first transformed into the α-diketone monothioketal **11** *via* the cyclohexanone **10**, by sequential 1,4-reduction,[11] debenzylation, silylation and α,α-thioketalization.[12] On reduction of the ketone functionality, followed by the thioketal–methyl ketal exchange reaction,[13] **11** furnished the secondary alcohol **12** which was then transformed to the methyl xanthate **13** after acid hydrolysis. Finally, **13** was heated to give the 4,4-disubstituted cyclohex-2-enone **14**, $[\alpha]_D^{29}$ −21.7 (*c* 0.62, $CHCl_3$).

To produce (−)-mesembrine **3**, **14** was first transformed into the ketal alcohol **16** *via* **15**. Employing the Mitsunobu reaction,[14] **16** was next converted to the secondary amine **19**, *via* the imide **17**, and the carbamate **18**. Finally, **18** was treated with perchloric acid in THF to give (−)-mesembrine **3**, $[\alpha]_D^{29}$ −55.4 (*c* 1.16, MeOH) [lit.,[5b] $[\alpha]_D^{30}$ −57.5 (*c* 0.146, MeOH) (Scheme 2).

Having obtained (−)-mesembrine **3**, we investigated the transformation of the same enone **14** into (+)-sceletium A-4 **1** to correlate the stereochemistry (Scheme 3). The enenone **14** was exposed to I_2 in CH_2Cl_2 containing pyridine[15] to furnish the α-iodo ketone **21**. Palladium-mediated cross-coupling reaction[16] between the iodo ketone **21** and *N*-*tert*-butylcarbamoylprop-1-yne yielded the enyne **22** which was converted into the ketal **24** *via* **23** by sequential ketalization and desilylation. Employing a five-step sequence including the Mitsunobu reaction,[14] **24** was transformed into the bis-carbamate **27** *via* the imide enyne **25** and the imide diene **26**. On standing in diluted hydrochloric acid in THF at room temperature, **27** collapsed gradually to the pyridine **30** through a concurrent deketalization, chemoselective decarbamoylation, double cyclization and dehydrogenation, presumably through the allyl amine **28** and the dihydropyridine **29**. The pyridine **30** was exposed to TFA to give the secondary amine **31**, which was immediately subjected

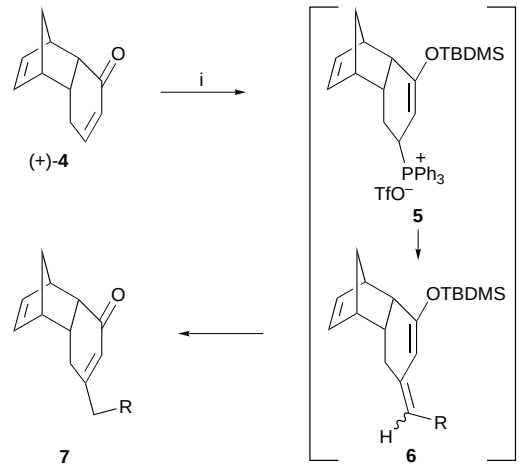

Scheme 1 *Reagents and conditions*: i, PPh_3, TBDMSOTf, THF, −78 °C, then Bu^nLi, −78 °C, then RCHO, 10% HCl

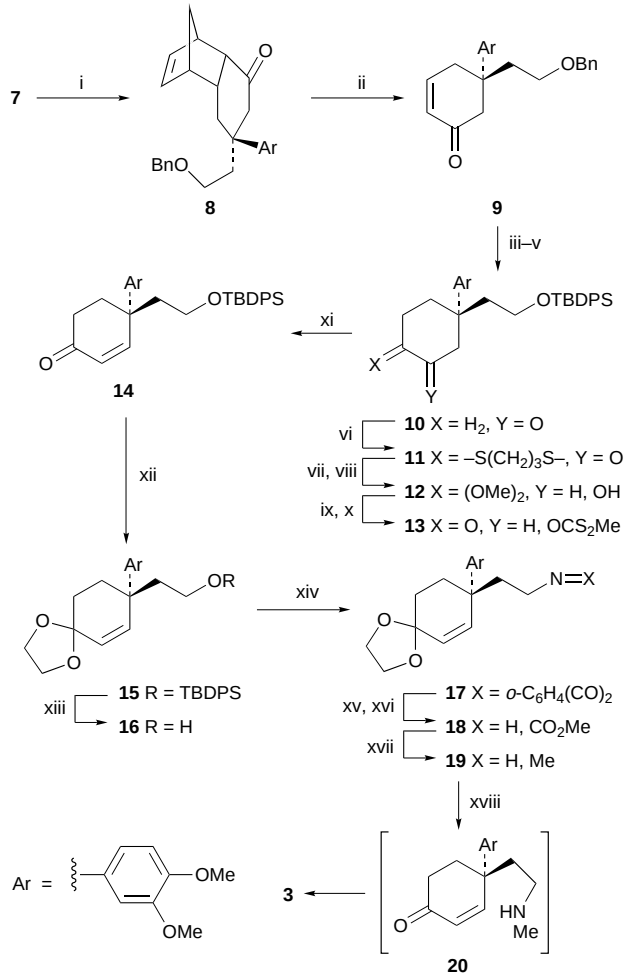

Scheme 2 *Reagents and conditions*: i, 3,4-$(MeO)_2C_6H_3MgBr$, $CuBr{\cdot}SMe_2$, Me_3SiCl, HMPA, THF; ii, Ph_2O, *ca.* 260 °C (77% from **7**); iii, DIBAL-H, CuI, HMPA, THF; iv, H_2, 10% Pd–C; v, Bu^tPh_2SiCl, imidazole, DMF (72% from **9**); vi, $TsS(CH_2)_3STs$, Bu^tOK, THF–Bu^tOH (70%); vii, $NaBH_4$, $CeCl_3{\cdot}7H_2O$; viii, $(CF_3CO_2)IPh$, MeOH (87% from **11**); ix, NaH, CS_2, MeI, THF; x, 70% $HClO_4$–THF (1 : 20); xi, *o*-$C_6H_4Cl_2$, *ca.* 180 °C (77% from **12**); xii, $(CH_2OH)_2$, TsOH, C_6H_6, (100%); xiii, Bu_4NF, THF (94%); xiv, phthalimide, PPh_3, $Pr^iO_2CN{=}NCO_2Pr^i$ (DIPAD), THF (94%); xv, hydrazine·H_2O, EtOH, reflux; xvi, $ClCO_2Me$, Et_3N, CH_2Cl_2 (79% from **17**); xvii, $LiAlH_4$, THF, reflux; xviii, aq. $HClO_4$, THF (66% from **18**)

to the Eschweiler–Clarke reaction[17] to afford (+)-Sceletium A-4 **1**, mp 153.5–154.5 °C, $[\alpha]_D^{27}$ + 120.5 (*c* 1.10, MeOH) (lit.,[2a] mp 153.5–154.5; lit.,[2b] 132–134 °C, lit.,[2c] $[\alpha]_D$ +131 (MeOH); lit.,[2d] $[\alpha]_D$ +131 (EtOH)). The synthetic material had a circular dichroism (CD) spectrum (in 95% EtOH) showing the first cotton effect (positive) at 278 nm, the second (positive) at 274 nm and the third (negative) at 247 nm which was identical to that reported[2d] for (+)-sceletium A-4 **1** (positive at 278 nm, positive at 274 nm and negative at 247 nm in 95% EtOH). Since (+)-**1** thus obtained has the same CD spectrum as the natural product, the absolute configuration of natural (+)-Sceletium A-4 **1** as well as its two natural congeners, (+)-tortuosamine **2a** and (−)-*N*-formyltortuosamine **2b**, has now been established as that shown by correlation to (−)-mesembrine **3**.

Notes and References

† E-mail: konol@mail.cc.tohoku.ac.jp

‡ Satisfactory analytical (high resolution mass) and spectral (IR, ^1H NMR and mass) data were obtained for all new isolable compounds.

1 A. Popelak and G. Lettenbauer, in *The Alkaloids*, ed. R. H. F. Manske, Academic Press, New York, 1967, vol. IX, p. 467.

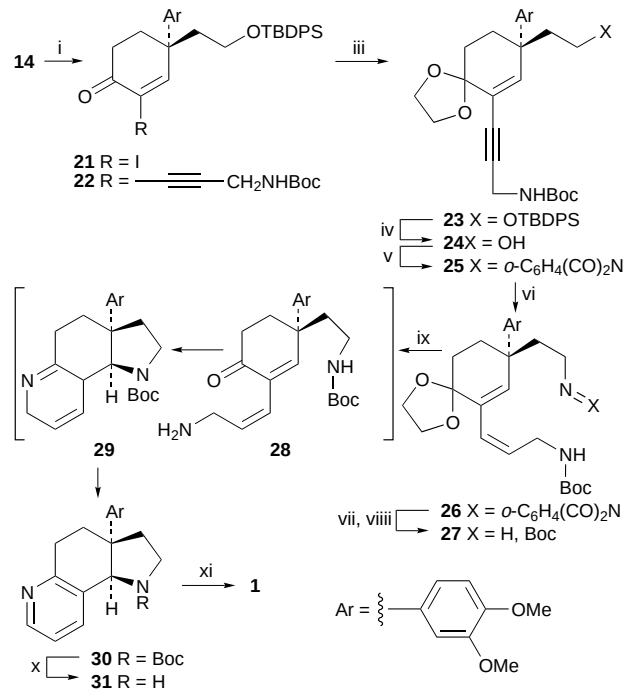

Scheme 3 *Reagents and conditions*: i, I_2, Py, CH_2Cl_2 (97%); ii, $HC{\equiv}CCH_2NHBoc$, $PdCl_2(PPh_3)_2$ (cat), CuI, Et_3N (91%); iii, $(CH_2OH)_2$, TsOH, C_6H_6 (71%); iv, Bu_4NF, THF (100%); v, phthalimide, PPh_3, DIPAD, THF (90%); vi, H_2, Lindlar catalyst, MeOH (86%); vii, hydrazine·H_2O, EtOH, reflux; viii, Boc_2O, Et_3N, CH_2Cl_2 (85% from **26**); ix, 10% HCl–THF (1 : 4) (42%); x, TFA, $CHCl_3$; xi, 35% HCHO, HCO_2H (67%)

2 (*a*) P. W. Jeffs, P. A. Luhan, A. T. McPhail and N. H. Martin, *J. Chem. Soc., Chem. Commun.*, 1971, 1466; (*b*) F. O. Snyckers, F. Strelow and A. Wiechers, *J. Chem. Soc., Chem. Commun.*, 1971, 1467; (*c*) P. A. Luhan and A. T. McPhail, *J. Chem. Soc., Perkin Trans. 2*, 1972, 2006; (*d*) P. W. Jeffs, T. Capps, D. B. Johnson, J. M. Karle, N. H. Martin and B. Rauckman, *J. Org. Chem.*, 1974, **39**, 2703.

3 R. V. Stevens, P. M. Lesko and R. Lapalme, *J. Org. Chem.*, 1975, **40**, 3495; P. N. Confalone and E. M. Huie, *J. Am. Chem. Soc.*, 1984, **106**, 7175.

4 P. Coggon, D. S. Farrier, P. W. Jeffs and A. T. McPhail, *J. Chem. Soc.* (*B*), 1970, 1267.

5 S. Takano, Y. Imamura and K. Ogasawara, *Tetrahedron Lett.*, 1981, **22**, 4479.

6 K. Ogasawara, *Pure Appl. Chem.*, 1994, **66**, 2119.

7 S. Takano, Y. Higashi, T. Kamikubo, M. Moriya and K. Ogasawara, *Synthesis*, 1993, 948; K. Hiroya, Y. Kurihara and K. Ogasawara, *Angew. Chem., Int. Ed. Engl.*, 1995, **34**, 2287.

8 M. Shimizu, T. Kamikubo and K. Ogasawara, *Tetrahedron: Asymmetry*, 1997, **8**, 2519.

9 A. P. Kozikowski and S. H. Jung, *J. Org. Chem.*, 1986, **51**, 3402.

10 Y. Horiguchi, S. Matsuzawa and I. Kuwajima, *Tetrahedron Lett.*, 1986, 4025.

11 S. Takano, K. Inomata and K. Ogasawara, *J. Chem. Soc., Chem. Commun.*, 1992, 169.

12 M. Saito, M. Kawamura, K. Hiroya and K. Ogasawara, *Chem. Commun.*, 1997, 765.

13 G. Stork and K. Zhao, *Tetrahedron Lett.*, 1989, **30**, 287.

14 O. Mitsunobu, *Synthesis*, 1981, 1; D. L. Hughes, *Org. React.*, 1972, **42**, 335.

15 C. R. Johnson, P. A. Adams, M. P. Braun, C. B. W. Senanayake, P. M. Wovkulich and M. R. Uskokovic, *Tetrahedron Lett.*, 1992, **33**, 917.

16 K. Sonogashira, Y. Toda and N. Hagiwara, *Tetrahedron Lett.*, 1975, 4467.

17 W. S. Emerson, *Org. React.*, 1948, **4**, 174.

Received in Cambridge, UK, 23rd December 1997; 7/09212A

Solution-phase combinatorial synthesis of 4-hydroxyquinolin-2(1*H*)-ones

Bheemashankar A. Kulkarni and A. Ganesan*†

Institute of Molecular and Cell Biology, National University of Singapore, 30 Medical Drive, Singapore 117609

Ion-exchange resins catalyse an intramolecular Claisen-type condensation leading to the title compounds, and also serve to purify the products.

In recent years, much effort has been devoted to the synthesis of chemical libraries, particularly for the generation and optimisation of biologically active compounds.[1] High-throughput synthesis by traditional solution-phase chemistry (as opposed to solid-phase techniques) is gaining in popularity with the advent of efficient methods for compound purification. One approach employs polymer-supported reagents[2] that can be readily removed by filtration. Recent examples include immobilized Sc^{III},[3] hydroxybenzotriazole,[4] carbodiimides[5] and guanidines.[6] Another application[5,7] of polymer-supported functional groups is to scavenge unreacted or excess starting materials in solution. Conventional ion exchange resins have been used both as a reagent[8] as well as a purification aid,[9] and we have recently reported[10] a synthesis of tetramic acids in which the resin performs both functions. Here, we demonstrate the application of this technique to the preparation of a pharmacologically important heterocyclic ring system.

4-Hydroxyquinolin-2(1*H*)-ones have attracted considerable attention for various therapeutic areas including antimicrobial and antitumour activity,[11] local anaesthetics[12] and antiinflammatory agents,[13] as well as being antagonists of thyroid hormone,[14] *N*-methyl-D-aspartate[15] and serotonin.[16] A common route to these compounds is the intramolecular Claisen-type condensation of *N*-acylated anthranilate esters. Various bases were used[17] for the cyclization (*e.g.* NaOH, alkoxides, lithium amides, TBAF), but removing these and other impurities is relatively tedious in the context of parallel synthesis. We envisioned that an insoluble quaternary ammonium resin would be more suitable, as in our tetramic acid synthesis.

We prepared a set of Claisen-type condensation precursors from methyl anthranilate by Schotten–Baumann two-phase acylation to give primary amides **1a**–**d** (Scheme 1). For increased diversity, additional examples were first reductively alkylated[18] before acylation to afford secondary amides **1e**–**j**. Treatment of compounds **1** with Amberlyst A-26 resin (OH^- form) uniformly resulted in cyclization. As expected, the 4-hydroxyquinolin-2(1*H*)-ones **2** remain tightly bound to the quaternary ammonium resin, enabling impurities to be removed by simple filtration. Subsequent acidification then releases the product in high yield and purity (Table 1). These cyclizations proceed more readily than with the tetramic acids, as shown by the ability of R^2 = Ph and SPh to be sufficiently activating.

We have further extended this procedure to substituted anthranilic acids (for examples, see Table 2, entries **1k**–**p**). Finally, the selectivity of product sequestration by the resin after the Claisen-type condensation enables the use of crude precursors **1** (Table 2, entries **1q**–**t**). These were obtained without purification after the reductive alkylation or acylation steps, the workup consisting of only aqueous washing. The ability to carry forward intermediates without full purification facilitates the overall sequence for high-throughput synthesis.

In summary, this protocol is suitable for the preparation of diverse 4-hydroxyquinolin-2(1*H*)-ones from commercially available building blocks, while permitting wide variations in the substitution pattern.

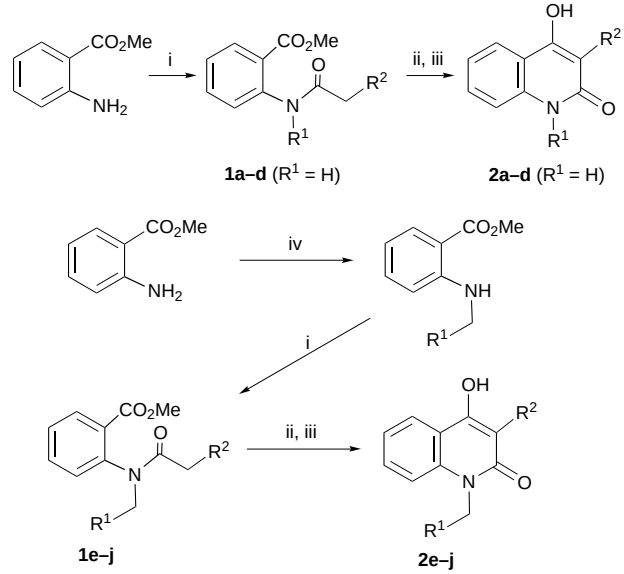

Scheme 1 *Reagents and conditions*: i, R^2CH_2COCl, 10% aq. Na_2CO_3–CH_2Cl_2, room temp., 30 min; ii, Amberlyst A-26 (OH^- form), MeOH, room temp., 16 h; iii, TFA, MeOH, room temp., 30 min; iv, R^1CHO, $NaBH(OAc)_3$, CH_2Cl_2, room temp., 18 h

Table 1 Yield and purity of 4-hydroxyquinolin-2(1*H*)-ones prepared by the intramolecular Claisen-type condensation

Precursor	R^1	R^2	Product	Yield (%)	Purity[a] (%)
1a	H	CN	**2a**	82	98
1b	H	3-pyridyl–S	**2b**	78	97
1c	H	SPh	**2c**	80	99
1d	H	Ph	**2d**	86	85
1e	4-$MeOC_6H_4$	SPh	**2e**	94	94
1f	4-$MeOC_6H_4$	2-$NO_2C_6H_4$	**2f**	96	95
1g	4-$MeOC_6H_4$	CO_2Me	**2g**	89	95
1h	CH_2CHMe_2	2-$NO_2C_6H_4$	**2h**	96	94
1i	4-$MeOC_6H_4$	Ph	**2i**	89	95
1j	Ph	SPh	**2l**	91	99

[a] Assessed by HPLC analysis with UV detection (254 nm). All compounds were characterised spectroscopically (NMR, MS).

Table 2 Yield and purity of additional 4-hydroxyquinolin-2(1*H*)-ones prepared

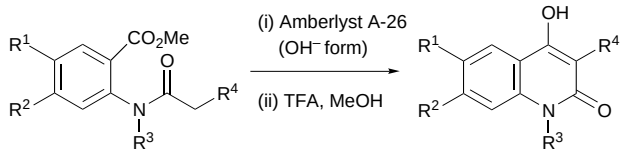

1k–t **2k–t**

Precursor	R^1	R^2	R^3	R^4	Product	Yield (%)	Purity[a] (%)
1k	H	H	Me	Ph	**2k**	86	98
1l	H	H	Ph	SPh	**2l**	91	97
1m	H	Cl	Bn	CO_2Me	**2m**	89	79
1n	F	F	Bn	CO_2Me	**2n**	90	95
1o	H	CO_2Me	Bn	Ph	**2o**	88[a]	97
1p	OMe	OMe	4-$MeOC_6H_4CH_2$	CO_2Me	**2p**	72	91
1q[b]	H	H	H	CO_2Me	**2q**	84	90
1r[b]	H	H	Me	CO_2Me	**2r**	97	97
1s[b]	H	H	4-$MeOC_6H_4CH_2$	SPh	**2s**	83	91
1t[b]	H	H	Bn	SPh	**2t**	92	95

[a] Two products were isolated (*ca.* 1 : 1 ratio), due to the partial hydrolysis of the ester (R^2 = CO_2Me to CO_2H). [b] Crude material used without chromatographic purification after either the reductive alkylation or acylation.

This work was supported by funds from the National Science and Technology Board of Singapore. Dedicated to Professor M. Vandewalle on the occasion of his 65th Birthday.

Notes and References

† E-mail: mcbgane@imcb.nus.edu.sg

1 For recent journal issues devoted to combinatorial chemistry, see: *Chem. Rev.*, 1997, **97**, Issue 2; *Curr. Opin. Chem. Biol.*, 1997, **1**, Issue 1.
2 For a review on functionalised polymers including combinatorial chemistry applications, see S. J. Shuttleworth, S. M. Allin and P. K. Sharma, *Synthesis*, 1997, 1217.
3 S. Kobayashi and S. Nagayama, *J. Am. Chem. Soc.*, 1996, **118**, 8977; S. Kobayashi, S. Nagayama and T. Busujima, *Tetrahedron Lett.*, 1996, **37**, 9221.
4 I. E. Pop, B. P. Déprez and A. L. Tartar, *J. Org. Chem.*, 1997, **62**, 2594.
5 D. L. Flynn, J. Z. Crich, R. V. Devraj, S. L. Hockerman, J. J. Parlow, M. S. South and S. Woodard, *J. Am. Chem. Soc.*, 1997, **119**, 4874; J. J. Parlow, D. A. Mischke and S. S. Woodard, *J. Org. Chem.*, 1997, **62**, 5908.
6 W. Xu, R. Mohan and M. M. Morrissey, *Tetrahedron Lett.*, 1997, **38**, 7337.
7 S. W. Kaldor, M. G. Siegel, J. E. Fritz, B. A. Dressman and P. J. Hahn, *Tetrahedron Lett.*, 1996, **37**, 7193; S. W. Kaldor, J. E. Fritz, J. Tang and E. R. McKinney, *Bioorg. Med. Chem. Lett.*, 1996, **6**, 3041; R. J. Booth and J. C. Hodges, *J. Am. Chem. Soc.*, 1997, **119**, 4882;J. J. Parlow, W. Naing, M. S. South and D. L. Flynn, *Tetrahedron Lett.*, 1997, **38**, 7959; M. M. Sim, C. L. Lee and A. Ganesan, *J. Org. Chem.*, 1997, **62**, 9358.
8 J. J. Parlow, *Tetrahedron Lett.*, 1996, **37**, 5257.
9 L. M. Gayo and M. J. Suto, *Tetrahedron Lett.*, 1997, **38**, 513; R. M. Lawrence, S. A. Biller, O. M. Fryszman and M. A. Poss, *Synthesis*, 1997, 553; M. G. Siegel, P. J. Hahn, B. A. Dressman, J. E. Fritz, J. R. Grunwell and S. W. Kaldor, *Tetrahedron Lett.*, 1997, **38**, 3357; A. J. Shuker, M. G. Siegel, D. P. Matthews and L. O. Weigel, *Tetrahedron Lett.*, 1997, **38**, 6149.
10 B. A. Kulkarni and A. Ganesan, *Angew. Chem., Int. Ed. Engl.*, 1997, **36**, 2454.
11 M. Rideau, C. Verchere, P. Hibon, J.-C. Cheniéux, P. Maupas and C. Veil, *Phytochemistry*, 1979, **18**, 155.
12 I. V. Ukrainets, S. V. Slobodzyan, V. I. Krivobok, P. A. Bezuglyi, V. I. Treskach, A. V. Turov, S. V. Gladchenko and G. V. Obolenteseva, *Farm. Zh. (Kiev)*, 1991, **2**, 78.
13 I. V. Ukrainets, O. V. Gorokhava, S. G. Taran and A. V. Turov, *Khim. Geterotsikl. Soedin.*, 1994, 1397.
14 I. V. Ukrainets, P. A. Bezugly, O. V. Borokhova, V. I. Treskach and A. V. Turov, *Khim. Geterotsikl. Soedin.*, 1993, 105.
15 P. D. Leeson, R. Baker, R. W. Carling, J. J. Kulagowski, I. M. Mawer, M. P. Ridgill, M. Rowley, J. D. Smith, I. Stansfield, G. I. Stevenson, A. C. Foster and J. A. Kemp, *Bioorg. Med. Chem. Lett.*, 1993, **3**, 299; M. Rowley, P. D. Leeson, G. I. Stevenson, A. M. Moseley, I. Stansfield, I. Sanderson, L. Robinson, R. Baker, J. A. Kemp, G. R. Marshall, A. C. Foster, S. Grimwood, M. D. Tricklebank and K. L. Saywell, *J. Med. Chem.*, 1993, **36**, 3386; J. J. Kulagowski, R. Baker, N. R. Curtis, P. D. Leeson, I. M. Mawer, A. M. Moseley, M. P. Ridgill, M. Rowley, I. Stansfield, A. C. Foster, S. Grimwood, R. G. Hill, J. A. Kemp, G. R. Marshall, K. L. Saywell and M. D. Tricklebank, *J. Med. Chem.*, 1994, **37**, 1402.
16 H. Hayashi, Y. Miwa, S. Ichikawa, N. Yoda, I. Miki, A. Ishii, M. Kono, T. Yasuzawa and F. Suzuki, *J. Med. Chem.*, 1993, **36**, 617.
17 A. Detsi, V. Bardakos, J. Markopoulos and O. Igglessi- Markapoulou, *J. Chem. Soc., Perkin Trans. 1*, 1996, 2909 and references cited therein.
18 A. K. Szardenings, T. S. Burkoth, G. C. Look and D. A. Campbell, *J. Org. Chem.*, 1996, **61**, 6720.

Received in Cambridge, UK, 22nd December 1997; 7/09125G

Polymer induced multiphase generation in water/organic solvent mixtures. Strategies towards the design of triphasic and tetraphasic liquid systems

Luis H. M. da Silva† and Watson Loh*‡

Instituto de Química, Universidade Estadual de Campinas, Campinas, SP 13083-970, Brazil

The addition of polyethylene oxide to mixtures of CH_2Cl_2 and heptane caused the formation of a biphase liquid system, allowing the attainment of triphase and tetraphase liquid systems upon addition of aqueous salt solutions.

It has been known since the beginning of this century,[1] that ternary mixtures of water and certain pairs of polymers, such as polyethylene oxide (PEO) and Dextran, may form aqueous two-phase systems, each phase being rich in one of the polymers. The same phenomenon has been observed when some inorganic salts, like alkaline sulfates, carbonates or phosphates, are added to aqueous solutions of polymers like PEO.[2] Again, one of the phases is rich in the polymer and the other in the salt. Many theoretical models have been proposed to account for such phenomena,[3] but a comprehensive explanation is not yet available. In general, the current view assumes mutual segregation between the two polymers or the polymer and the inorganic anion, associated with their competition for the water molecules, leading to the exclusion of one of the components to another aqueous phase. Owing to the biocompatibility of their components and to the predominance of water as solvent, these systems have been extensively studied in bioseparation processes involving proteins, nucleic acids and even whole cells.[4]

CH_2Cl_2 and heptane are miscible over their whole composition range. However, upon addition of small amounts of polyethylene oxide (PEO 3350, Sigma) to a mixture of these solvents (CH_2Cl_2: Merck, p.a., previously distilled over CaH_2 and stored over molecular sieves; *n*-heptane: Merck, extra pure), we observed the formation of a stable two-phase liquid system. PEO is almost insoluble in alkanes,[5] but it is very soluble in polar organic solvents like CH_2Cl_2. Therefore, adding heptane to a CH_2Cl_2 solution of PEO should lead to polymer precipitation, as commonly performed in polymer fractionation. The occurrence of liquid–liquid demixing might be explained by the exclusion of PEO from the alkane solution associated with the carrying of CH_2Cl_2 molecules due to their strong interaction with the polymer, similar to what is observed for the aqueous two-phase systems. This view is in accordance with literature reports on solvent preferential adsorption onto polymers in ternary mixture.[6–9] The phase diagram for PEO, CH_2Cl_2 and heptane at 298 K is shown in Fig. 1.

Fig. 1 reveals that the biphase system forms even at low polymer fractions and is favoured by the addition of heptane, whereas an excess of CH_2Cl_2 (more than 60 mol%) leads to a homogeneous system. As PEO is strongly solvated by CH_2Cl_2, the bottom phase is expected to contain solvent molecules which are somewhat bound to the polymer, as they would otherwise mix with heptane. In fact, analysis of the phases' composition,§ performed for the systems represented in Fig. 1 as A and B, supported this view and the segregation between PEO and heptane. The upper phases of systems A and B were composed of 59.7 and 56.3% heptane, 40.3 and 43.7% CH_2Cl_2 and negligible amounts of PEO, respectively. The bottom phases contained 38.2 and 36.1% CH_2Cl_2, 61.8 and 63.9% PEO and no detectable heptane. As more polymer was added, more CH_2Cl_2 was extracted into the bottom phase. In addition, the volume of the bottom phase was observed to increase with the polymer content, agreeing with the proposed polymer solvation role of CH_2Cl_2.

Other polymers were investigated in order to verify the generality of this phenomenon. This behaviour was not observed with polypropylene oxide (1000, Aldrich), poly(tetrahydrofuran) (Terathane 1000, Aldrich) or poly(vinyl alcohol) PVA (13 000–23 000, 98% hydrolysed, Aldrich). For the first two only homogeneous systems were observed, probably because the polymers are less polar than PEO and do not interact so strongly with CH_2Cl_2, or are not so strongly segregated by heptane. For PVA, the addition of heptane led to polymer precipitation, probably due to its higher polarity. For poly(*N*-vinyl-2-pyrrolidone) (PVP, 10000, Aldrich), however, liquid–liquid demixing was observed, but the volume of the bottom phase (which contained PVP and CH_2Cl_2) was much smaller than the one formed with PEO. This suggests that, although PVP interacts sufficiently strongly with CH_2Cl_2 to carry some solvent molecules to another phase, these solvation molecules are fewer in number than those of PEO. Preliminary studies with PEO 10000 produced a phase diagram very similar to that of PEO 3350.

In addition to the water/organic solvent systems widely used for liquid extraction, these organic biphase systems provide two phases without the use of water, which might be harmful to some chemical compounds, and which do not have such extreme polarity differences and thus might overcome solubility problems for some extracts. Furthermore, the strong interaction between the polymer and CH_2Cl_2 could be used to extract this chlorinated solvent from mixtures with other less polar organic solvents, without the need for distillation.

This phenomenon also allows the generation of other multiphase systems. Addition of small amounts of water to this biphase system causes the appearance of a third phase, containing water and PEO. For this system, 77.0% of the

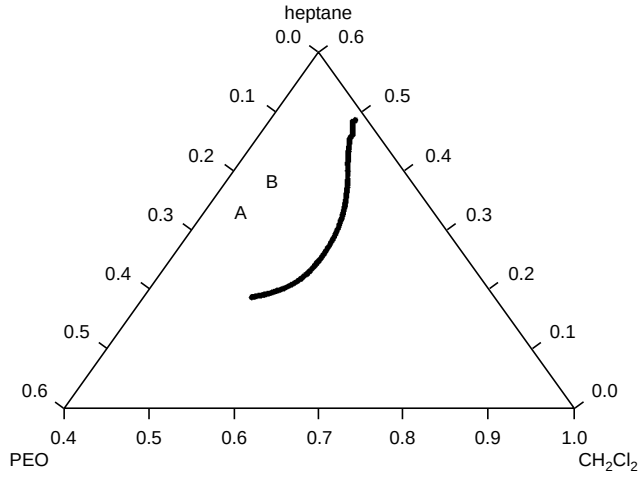

Fig. 1 Phase diagram for mixtures of PEO, CH_2Cl_2 and heptane; the polymer fraction is expressed in terms of monomer units. The two-phase region is the area containing points A and B (see text for the phase compositions).

polymer is in the aqueous phase. As more water is added, more PEO is transferred from the CH_2Cl_2 phase to the aqueous phase. At higher water contents (more than 74.0%), the system becomes biphasic again.

To avoid the destruction of the three-phase system due to polymer extraction, a salt solution may be used, taking advantage of its incompatibility with PEO. This has been observed for a three-phase system with an overall composition of 9.5% PEO, 21.7% CH_2Cl_2, 16.3% heptane, 0.1% sodium sulfate and 51.5% water. The upper phase contained heptane (58.5%) and CH_2Cl_2. The middle phase contained PEO (43%) and CH_2Cl_2. The bottom phase is constituted by the aqueous salt solution containing small amounts of CH_2Cl_2. No polymer was detected in this phase, confirming its segregation from the salt solution.

Other three-phase systems can be obtained by adding an organic solvent such as heptane to an aqueous biphase system, and might be useful in extracting apolar components in bioseparation processes designed for aqueous biphasic systems.

With the addition of larger amounts of salt, it is possible to obtain a four-phase liquid system, with an overall composition of 7.1% PEO, 15.5% CH_2Cl_2, 10.9% heptane and 66.5% sodium sulfate and water. In general, this system may be rationalised as a mixture of aqueous and organic biphasic systems. In fact, the upper phase of the above system contains only heptane (50.2%) and CH_2Cl_2. The second upper phase is composed predominantly of an aqueous solution of PEO (containing 66.3% of the total polymer). The third phase occurs as a sphere and contains PEO and CH_2Cl_2, with a little water. Addition of more salt turns this phase turbid and, by optical microscopy and addition of Methylene Blue, it was verified to consist of a water-in-oil emulsion, probably stabilised by PEO molecules. The spherical shape of this phase is determined by the attainment of the smallest area to volume ratio, in order to minimise the unfavourable interfacial energy due to the contact with the aqueous phase. Finally, the bottom phase of this four-phase system contains an aqueous salt solution, with no polymer due to its mutual incompatibility with sulfate.

These multiphasic liquid systems allow much higher selectivities than the usual water/oil or aqueous biphasic systems, providing phases with a wide range of polarities and chemical properties to suit different purposes. Furthermore, the presented general procedure may be extended to include other polymers or organic solvents and opens a variety of possibilities for improvement of liquid extraction processes.

The authors thank the Brazilian Agencies FAPESP and CNPq for financial support. L. H. M. S. thanks CAPES/PICDT for a scholarship and the Universidade Federal de Viçosa for a leave of absence. We also thank R. G. da Rosa and R. Buffon for their help in the gas chromatography measurements.

Notes and References

† On leave of absence from Departamento de Química, Universidade Federal de Viçosa, Viçosa, MG, Brazil.
‡ E-mail: wloh@iqm.unicamp.br
§ These compositions were determined by weighing the carefully separated phases and assaying heptane by gas chromatography (HP 5890 chromatograph, using N_2 as carrier, a FID detector and cyclooctane as internal standard) and PEO by dry weight. All compositions are expressed on the basis of mol% and, for PEO, mol refers to moles of monomer units.

1 M. W. Beijernick, *Kolloidn. Zh*., 1910, **7**, 16.
2 K. P. Ananthapadmanabhan and E. D. Goddard, *Langmuir*, 1987, **3**, 25.
3 H. J. Cabezas, *J. Chromatogr. B*, 1996, **680**, 3.
4 P.-A. Albertsson, *Partition of Cell Particles and Macromolecules*, Wiley, New York, 3rd. edn., 1986.
5 F. E. Bailey and J. V. Koleske, *Alkylene Oxides and their Polymers*, Marcel Dekker, New York, 1991, p. 153
6 Z. Tan and G. J. Vancso, *Macromolecules*, 1997, **30**, 4665.
7 M. J. Solomon and S. J. Muller, *J. Polym. Sci. B*, 1996, **34**, 181.
8 C. A. Khatri, Y. Pavlova, M. M. Green and H. Morawetz, *J. Am. Chem. Soc*., 1997, **119**, 6991.
9 F. Muller-Plathe and W. F. Van Gunsteren, *Polymer*, 1997, **38**, 2259.

Received in Cambridge, UK, 2nd January 1998; 8/00082D

NMR evidence for the nucleation of a β-hairpin peptide conformation in water by an Asn-Gly type I′ β-turn sequence

Samuel R. Griffiths-Jones, Allister J. Maynard, Gary J. Sharman and Mark S. Searle*†

Department of Chemistry, University of Nottingham, University Park, Nottingham, UK NG7 2RD

The contribution of the β-turn sequence to the folding and stability of a peptide β-hairpin in water has been analysed from studies of a truncated peptide lacking one β-strand and hence the majority of the interstrand hydrophobic interactions; NMR analysis shows that the Asn-Gly type I′ β-turn conformation is significantly populated, suggesting that the intrinsic conformation preference of the turn sequence may play an important role in nucleating hairpin folding.

Hydrogen bonding,[1] hydrophobic interactions[2,3] and conformational preferences[4,5] (largely associated with the β-turn sequence) have been variously proposed to play key roles in the folding of peptide and protein fragments into β-hairpin structures. Given the prominent position of anti-parallel β-sheets in the architecture of globular proteins, autonomously folding β-hairpin peptides provide useful model systems for probing β-sheet stabilisation in solution, for assessing their possible role in nucleating protein folding and as novel motifs in molecular recognition.[6–8]

We have recently described a 16-residue model peptide that folds into a β-hairpin in water (50% populated at 303 K) without the need for cross-links or incorporation of non-natural amino acids [Fig. 1(*a*)].[8] Our sequence was designed, and subsequently shown, to adopt a β-hairpin with a type I′ two-residue β-turn forming at the Asn-Gly sequence. This choice of β-turn sequence was based upon statistical analyses of two-residue turns in the Protein Data Bank which are predominantly of the type I′ variety (and to a lesser extent type II′ variety) with the Asn-Gly sequence having a high abundance.[3,9,10] To understand further the origin of the stability of the hairpin in water we have investigated the conformational properties of several shorter peptide fragments to assess the role of the turn sequence in nucleating the folding and in stabilising the β-hairpin conformation. Thermodynamic analysis of the intact β-hairpin has shown that the folded conformation in water is stabilised by cross-strand hydrophobic interactions between the residue side chains of the two β-strands.[8] Such interactions give rise to an entropy-driven folding process which is associated with a large negative change in the heat capacity (ΔC_p^o) between the folded and unfolded states. Both of these features are hallmarks of the hydrophobic effect playing a key role in the self-assembly process.[11] Here we assess whether these hydrophobic contacts are pivotal to the formation of the adopted conformation or whether they act to stabilise an intrinsic conformational preference nucleated by the residues in the turn sequence.

In the peptide shown in Fig. 1(*b*), residues 1–5 of the N-terminal β-stand have been deleted leaving only residues immediately adjacent to the turn sequence on the N-terminal strand and all residues of the C-terminal strand. The majority of interstrand hydrophobic contacts previously identified[8] (involving Y^3, T^4 and V^5) have now been removed such that any tendency for the β-turn to form must now reflect, in large part, the intrinsic conformational preference of the turn sequence and the immediately flanking residues. The residues flanking the Asn-Gly turn sequence on the N-terminal strand (namely S^6 and I^7) were retained in the sequence of the truncated peptide (**1b**) to provide convenient NMR 'handles' for detecting turn formation. In the hairpin (**1a**), cross-strand Hα–Hα (S^6–K^{11}) and NH–NH (I^7–K^{10}) medium range NOEs are detected that are consistent with this conformation.[8]

Analysis of the 200 ms ROESY spectrum of **1b** at 278 K reveals the presence of both of these cross-strand interactions [S^6 Hα–K^{11} Hα, Fig. 2(*a*); I^7 NH–K^{10} NH, Fig. 2(*b*)], providing convincing evidence that the two-residue turn conformation is populated in water in the absence of the interstrand hydrophobic interactions that appear to stabilise the intact hairpin. While these medium range ROEs provide evidence for secondary structure formation, the intensity of the ROEs between protons

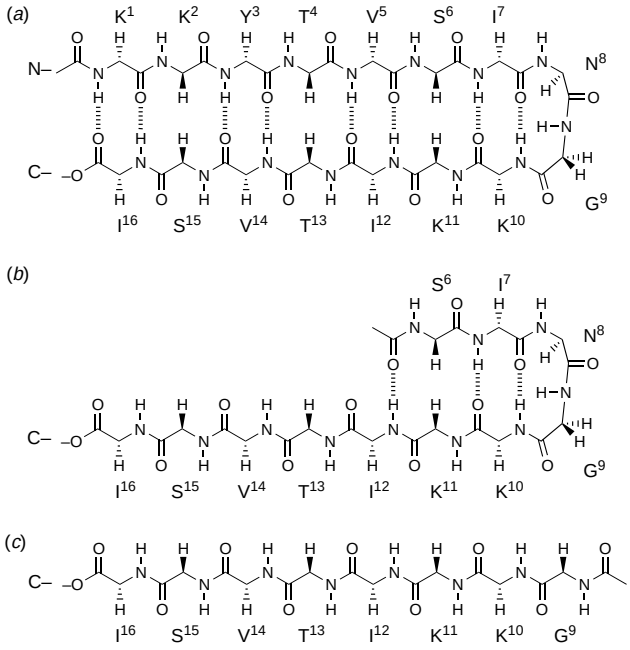

Fig. 1 Amino acid sequences (one letter code, numbering from the N-terminus) and the proposed folded conformations. Side chains are excluded for clarity.

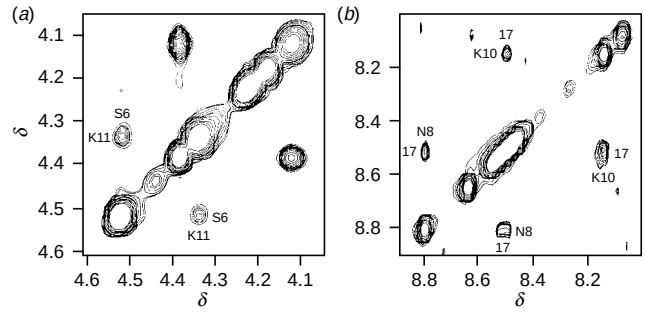

Fig. 2 Portions of the 200 ms ROESY spectrum of peptide **1b** at 278 K recorded at 500 MHz on a Bruker DRX500 spectrometer: (*a*) Hα–Hα and (*b*) NH–NH cross-strand interactions are highlighted that are consistent with the folded conformation shown in Fig. 1(*b*)

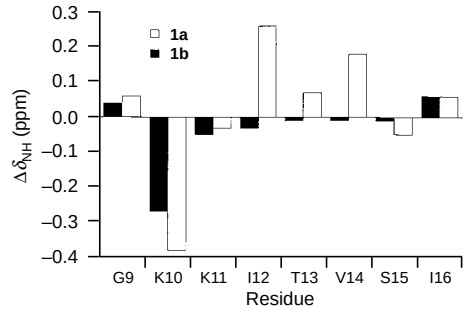

Fig. 3 Plot of difference in NH chemical shift ($\Delta\delta_{NH}$) for residues 9–16 of the folded hairpin peptide **1a** and the truncated analogue **1b** with respect to reference peptide **1c**

of neighbouring residues provide additional support for local order in the peptide backbone, consistent with the population of a type I′ turn conformation. For example, a significant NH–NH interaction is detected for I^7–N^8, while all other sequential NH–NH ROEs are too weak to observe [Fig. 2(*b*)]. In general, sequential Hα–NH ROEs are stronger than the equivalent intraresidue Hα–NH interaction (ratio of intensities > 4),[12] but for N^8 and G^9 the ratio of intensities is very close to 1, again characteristic of the reverse turn conformation found for the hairpin (**1a**).[8]

To what extent is the turn formed under these conditions? Perturbations to the Hα and NH chemical shifts are characteristic of secondary structure formation and can provide a method of estimating the population of folded structures.[8] To this end we have examined perturbations to the chemical shifts of residues on the C-terminal strand of the hairpin and peptide **1b** to estimate relative populations. As a reference state we have used the corresponding Hα and NH chemical shifts of the isolated C-terminal strand (**1c**) to fully account for any sequence-dependent effects on chemical shifts. Thus, differences in chemical shifts between **1a** and **1c**, and between **1b** and **1c**, are expected, in large part, to reflect perturbations due to secondary structure formation. The data in Fig. 3 show the difference in NH chemical shifts ($\Delta\delta_{NH}$) at 278 K for residues 9–16 of the hairpin (**1a**) and truncated peptide (**1b**) with respect to the reference state **1c**, and illustrate convincingly the folding pattern of the two peptides. The NH of K^{10} shifts upfield for both peptides reflecting the anisotropic effect from the carbonyl group of G^9 in the folded structure. T^{12}, V^{14} and I^{16} of the hairpin are proposed to form hydrogen bonds to the opposite strand and significant downfield shifts are observed for the NHs of these residues that are consistent with this model. In contrast, only the NH of I^{12} of the truncated peptide (**1b**) has the opportunity to form a hydrogen bond, but no significant perturbation is observed suggesting a very weak interaction that probably reflects the more dynamic nature of its hydrogen bonding partner, the *N*-acetyl carbonyl of S^6 at the N-terminus.

Since both peptides are able to form the same β-turn conformation, as is evident from the ROE data described above, we interpret the larger change in shift for K^{10} NH of the hairpin (**1a**) as reflecting a greater population of the folded conformation than is present for the truncated peptide (**1b**). We estimate the population of turn conformation of **1b** to be *ca*. 70% of that of the hairpin under the same conditions (278 K). We have previously estimated the folded population of the hairpin at this temperature to be *ca*. 32% *versus* 68% 'random coil';[8] on this basis the population of the folded conformation of **1b** is *ca*. 22%. Quantitative estimates of the intensity of the cross-strand ROEs shown in Fig. 2 similarly suggest a folded population in the range 20–30%, indicating some agreement between the different methods of estimation.

The data show convincingly that the sequence INGK at the core of the β-hairpin peptide used in these studies has a natural propensity to form a two-residue β-turn conformation in water *alone*, in the absence of significant structure stabilising hydrophobic interactions or a conformationally restricted proline residue. The INGK turn sequence is likely to play an important role in nucleating hairpin formation through association of the two β-strands.

We thank the EPSRC, BBSRC, Roche Ltd, the Nuffield Foundation and the Department of Chemistry for financial support. We are grateful to John Keyte in the Department of Biochemistry for peptide synthesis.

Notes and References

† E-mail: mark.searle@nottingham.ac.uk

1 K. L. Constantine, L. Mueller, N. H. Andersen, H. Tong, C. F. Wandler, M. S. Friedrichs and R. E. Bruccoleri, *J. Am. Chem. Soc.*, 1995, **117**, 10 841.
2 M. S. Searle, D. H. Williams and L. C. Packman, *Nat. Struct. Biol.*, 1995, **2**, 999.
3 M. Ramirez-Alvarado, F. J. Blanco and L. Serrano, *Nat. Struct. Biol.*, 1996, **3**, 604.
4 E. De Alba, M. A. Jimenez and M. Rico, *J. Am. Chem. Soc.*, 1997, **119**, 175.
5 T. S. Haque and S. H. Gellman, *J. Am. Chem. Soc.*, 1997, **119**, 2303.
6 J. D. Puglisi, L. Chen, S. Blanchard and A. D. Frankel, *Science*, 1995, **270**, 1200.
7 X. M. Ye, R. A. Kumar and D. J. Patel, *Chem. Biol.*, 1995, **2**, 827.
8 A. J. Maynard and M. S. Searle, *Chem. Commun.*, 1997, 1297; A. J. Maynard, G. J. Sharman and M. S. Searle, *J. Am. Chem. Soc.*, 1998, in the press.
9 E. G. Hutchinson and J. M. Thornton, *Protein Sci.*, 1994, **3**, 2207.
10 B. L. Sibanda and J. M. Thornton, *Methods Enzymol.*, 1991, **202**, 59.
11 R. L. Baldwin, *Proc. Natl. Acad. Sci. USA*, 1986, **83**, 8069; K. P. Murphy, P. L. Privalov and S. J. Gill, *Science*, 1990, **247**, 559; K. P. Murphy and S. J. Gill, *J. Mol. Biol.*, 1991, **222**, 699.
12 L. J. Smith, K. M. Fiebig, H. Schwalbe and C. M. Dobson, *Folding Des.*, 1996, **1**, R95.

Received in Cambridge, UK, 28th January 1998; 8/00749G

A new feature in the chemistry of nitrobenzofuroxans: ambident reactivity in Diels–Alder condensations

Dominique Vichard,[a]† Jean-Claude Hallé,*[a]‡ Boris Huguet,[a] Marie-José Pouet,[a] Didier Riou[b] and François Terrier*[a]§

[a] *Laboratoire SIRCOB, CNRS EP 102, Université de Versailles-Saint Quentin, Bâtiment Lavoisier, 45 Avenue des Etats-Unis, 78035 Versailles Cedex, France*

[b] *Laboratorie IREM, CNRS CO173, Université de Versailles-Saint Quentin, Bâtiment Lavoisier, 45 Avenue des Etats-Unis, 78035 Versailles Cedex, France*

The 4,6-dinitrobenzofuroxan (DNBF) structure is shown to act both as a dienophile and a heterodiene upon treatment with 1-trimethylsilyloxybuta-1,3-diene and vinyl ethyl ether, providing in two steps a highly functionalised stereoselective compound.

In recent years, a large body of evidence has been accumulated showing that 4,6-dinitro-2,1,3-benzoxadiazole 1-oxide, commonly known as 4,6-dinitrobenzofuroxan (DNBF), is a neutral 10π-electron heteroaromatic substrate which, in many processes, exhibits extremely high electrophilic character.[1–5] In fact, recent studies have shown that DNBF is a stronger electrophile than the 4-nitrobenzenediazonium cation.[2] This makes DNBF a remarkable probe to assess the reactivity of such weak carbon nucleophiles as benzenoid aromatics or π-excessive heteroaromatics with large negative pK_a^{CH} values, *e.g.* 1,3-dimethoxybenzene (pK_a^{CH} = −9) or 3-methoxythiophene (pK_a^{CH} = −6.5).[6,7] In all of the above processes, covalent addition of the carbon nucleophile takes place at C(7) of the carbocyclic ring of DNBF to give stable anionic σ-complexes, *e.g.* **1**.[6] The same principle applies in all reported interactions of DNBF with oxygen, nitrogen or sulfur nucleophiles.[1,3,4,8–10]

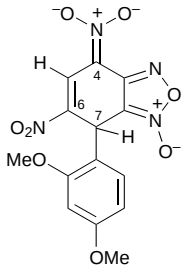

1

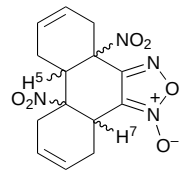

2

Interestingly it has been argued that the low aromatic character of the benzofuroxan system should be one of the major factors responsible for the exceptional electrophilic reactivity of DNBF and nitrobenzofuroxans in general.[1,2,9] Should this be true, the idea that these compounds might be involved in Diels–Alder type reactions under some experimental conditions could not be excluded. In 1973, Kresze and Bathelt reported the very slow formation of the diadduct **2** upon reaction of DNBF with butadiene.[11] Although the most reasonable explanation for the formation of this adduct was in terms of a Normal Electron Demand Diels–Alder (NEDDA) mechanism, this finding did not lead to further investigation and the stereochemistry was not investigated. Here we present the first evidence that the DNBF structure can in fact exhibit an ambident Diels–Alder reactivity, acting as a dienophile in NEDDA reactions or as a heterodiene in Inverse Electron Demand Diels–Alder (IEDDA) reactions, depending upon the experimental conditions and the reaction partners employed.

Treatment of DNBF with 1-trimethylsilyloxybuta-1,3-diene **3** (used as the solvent at room temperature) (Scheme 1) results in the rapid and nearly quantitative formation of a product which we readily isolated as a pale yellow solid. Based on ^{1}H NMR and electrospray mass spectroscopy data,¶ this product can be formulated as the cycloadduct **4** in racemic form, resulting from a regioselective NEDDA process involving the C(6)=C(7) double bond of DNBF as the dienophile contributor. Strong support for the regioselectivity of the condensation comes from ^{15}N labelling of the 4- and 6-NO_2 groups in **4**. In this instance, only the H(5) proton appears to be coupled with both ^{15}N atoms [$J_{N(4)H(5)}$ = 3.1 and $J_{N(6)H(5)}$ = 0.7 Hz]. Interestingly, the ^{1}H NMR spectra of **4**, recorded in $CDCl_3$, consisted of only one set of signals, indicating that the reaction is also diastereoselective and affords only the cycloadduct resulting from an *endo* condensation, as will be confirmed in the second step. In contrast with Kresze and Bathelt's finding that the addition of butadiene to DNBF eventually afforded the diadduct **2** within a few weeks at low temperature,[11] further reaction of **3** with **4** to give the related bis-NEDDA adduct did not occur in our case.

Most interestingly, we found that a second cycloaddition process takes place readily on treatment of **4** with vinyl ethyl ether **5** (Scheme 1). In this cycloaddition process, the DNBF moiety does not act as a dienophile but clearly as a heterodiene, according to an IEDDA process, to give the dihydrooxazine *N*-oxide **6**‖ in 92% yield. As found for the formation of **4**, the reaction is highly stereoselective, affording only the diastereomer **6**, shown in Scheme 1, whose stereochemistry could be safely attributed *via* ^{1}H NMR and NOE experiments in solution. A determination of the crystallographic structure of **6** by X-ray analysis** confirmed the consecutive NEDDA and the IEDDA

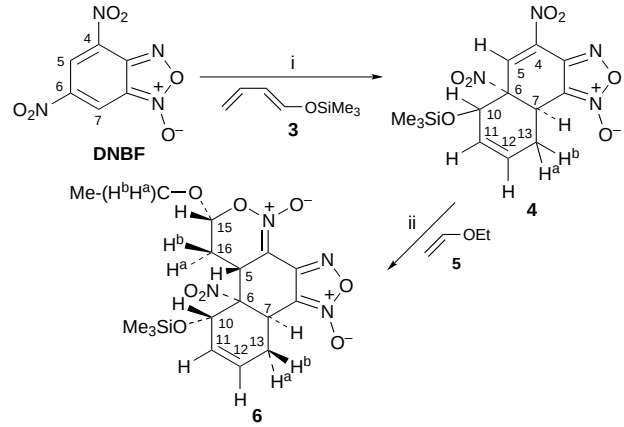

Scheme 1 *Reagents and conditions*: i, 1-trimethylsilyloxybuta-1,3-diene **3** (50 equiv., no solvent), 84%; ii, vinyl ethyl ether **5** (50 equiv., no solvent), 92%

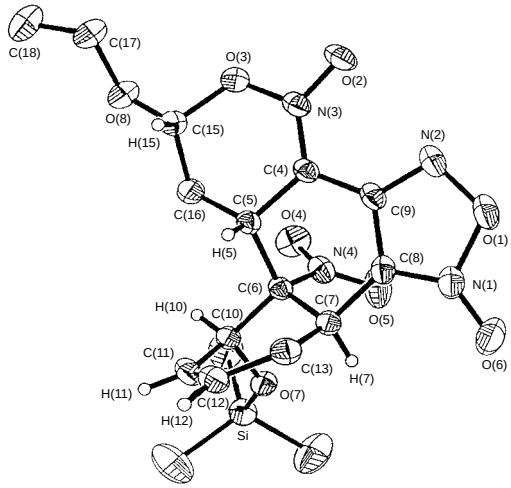

Fig. 1 ORTEP view of **6** (only one enantiomer is represented). Bond lengths (Å): C(4)–N(3) 1.321(3), C(6)–N(4) 1.544(3), C(15)–O(3) 1.476(3), C(15)–O(8) 1.360(3), N(3)–O(2) 1.245(2), N(3)–O(3) 1.404(3), N(4)–O(4) 1.215(3), N(4)–O(5) 1.208(3).

additions as well as the stereochemistry assignment in the solid state (Fig. 1). This ORTEP view shows that H(7), the 6-NO_2 group and the $OSiMe_3$ substituent are located on the same side of the molecule, *trans* to both H(5) and H(15). This clearly indicates that both Diels–Alder condensations proceed through *endo* processes which take place *via* consecutive *trans* addition.

Such nitro group participation has previously been observed in the reaction of DNBF with indene.[12] Recently, we found that direct treatment of DNBF with **5** affords the bis(dihydrooxazine *N*-oxide) adduct **7**.[13] In this instance, both experimental and

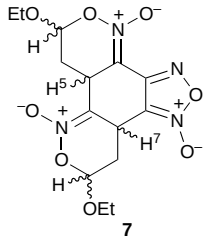

7

theoretical studies indicated that **7** was the result of two consecutive IEDDA processes involving the 4-NO_2 and 6-NO_2 heterodienyl moieties of DNBF, respectively.[13,14] In the present work we extend considerably the scope of the reactivity of DNBF by showing that this compound may also be consecutively involved in NEDDA and IEDDA cycloadditions to give a functionalised diadduct which is formed with high stereoselectivity. Interestingly, this ambident reactivity of DNBF in Diels–Alder condensations is a feature of general significance, being a promising new approach to synthesis in heterocyclic chemistry. Also such behaviour is in itself evidence that DNBF has a low resonance energy, a feature which has been commonly accepted but has not yet been specifically addressed.[1]

Further experimental and theoretical work towards a better understanding of how one can modulate the dienophile or heterodiene behaviour of DNBF with respect to the structure of the opposed electron-rich substrate is currently underway.

Notes and References

† E-mail: vichard@chimie.uvsq.fr
‡ E-mail: halle@chimie.uvsq.fr
§ E-mail: terrier@chimie.uvsq.fr

¶ *Synthetic procedure* for **4**: 2 ml of 1-trimethylsilyloxybuta-1,3-diene (11.4 mmol) were added to 48 mg of DNBF (0.212 mmol) charged in a tube. The mixture was maintained under stirring at room temperature for 30 mn. A pale yellow precipitate rapidly appeared. The precipitation was complete after addition of a large excess of pentane. The precipitate was isolated by centrifugation, washed with pentane and dried *in vacuo* (84%). For **6**: A similar procedure was applied, under 4 h stirring in the presence of vinyl ether ether (92%). A single crystal was obtained by slow diffusion of pentane into a THF solution of **6**.

‖ *Selected data* for **4**: δ_H(300 MHz, $CDCl_3$) 0.13 [s, 9 H, $OSi(CH_3)_3$], 1.93 (ddt, 1 H, H-13b, $J_{11–13b}$ 2.3, $J_{12–13b}$ 3.2, $J_{13a–13b}$ 19.2, $J_{7–13b}$ 9.2), 3.03 (dddd, 1 H, H-13a, $J_{11–13a}$ 1.7, $J_{12–13a}$ 3.7, $J_{7–13a}$ 8.0), 4.40 (dt, 1 H, H-7, $J_{5–7}$ 1.0), 4.88 (d, 1 H, H-10, $J_{10–11}$ 5.4), 5.99 (ddt, 1 H, H-11, $J_{11–12}$ 9.9), 6.07 (dt, 1 H, H-12), 7.33 (d, 1 H, H-5); mp 148 °C (decomp.); *m*/*z* (electrospray) 391.1 $(M + Na)^+$. For **6**: (Found C, 46.58; H, 5.36; N, 12.73. $C_{17}H_{24}SiN_4O_8$ requires C, 46.36; H, 5.45; N, 12.73%) δ_H(300 MHz, $CDCl_3$) 0.11 [s, 9 H, $OSi(CH_3)_3$], 1.28 (t, 3 H, CH_3, $J_{H17–H18}$ 7.2), 2.19 (m, 1 H, H-13b, $J_{13a–13b}$ 19.8, $J_{7–13b}$ 9.9), 2.41 (ddd, 1 H, H-16b, $J_{16a–16b}$ 13.4, $J_{5–16b}$ 7.5, $J_{15–16b}$ 3.0), 2.80 (ddd, 1 H, H-16a, $J_{5–16a}$ 10.3, $J_{15–16a}$ 7.4), 3.10 (ddd, 1 H, H-13a, $J_{12–13a}$ 2.3, $J_{13a–7}$ 8.1), 3.35 (dd, 1 H, H-5), 3.76 (dq, 1 H, H-17a-b, $J_{H17a,b}$ 9.5), 4.06 (dq, 1 H, H-17a-b), 4.18 (dd, 1 H, H-7), 4.71 (m, 1 H, H-10), 5.56 (dd, 1 H, H-15), 5.95 (m, 2 H, H-11 and -12); mp 187 °C (decomp.); *m*/*z* (electrospray) 441.3 $(M + H)^+$, 463.0 $(M + Na)^+$, 479.0 $(M + K)^+$.

** *Crystal data* for **6**: $C_{17}H_{24}SiN_4O_8$, M = 440.5, monoclinic, space group $P2_1/c$ (no. 14), a = 12.2186(3), b = 7.1267(1), c = 24.5675(2) Å, β = 98.979(1)°, U = 2113.08(6) Å^3, Z = 4, D_c = 1.385 g.cm^{-3}, μ(Mo-Kα) = 1.63 cm^{-1}, λ = 0.71073 Å, graphite monochromator, crystal dimensions: 0.3 × 0.12 × 0.04 mm. The data were collected up to 2θ = 62° on a Siemens SMART three-circle diffractometer equipped with a bidimensional CCD detector. The exposure time was 60 s by frame. A total of 15 314 reflections corresponding to the whole reciprocal space were collected of which 6197 were unique (R_{int} = 0.0546) with $I \geqslant 2\sigma(I)$. The data were corrected for absorption effects by the SADABS program (G. Sheldrick, unpublished) specific to the CCD detector. The structure was solved by direct methods using SHELX-TL and the hydrogen atoms were located using geometrical constraints. Refinement (276 parameters) was performed by full-matrix least-squares analysis of SHELX-TL up to $R_1(F_o)$ = 0.0554 and $wR_2(F_o^2)$ = 0.1334. CCDC 182/777.

1 F. Terrier, in *Nucleophilic Aromatic Displacement*, ed. H. Feuer, VCH, New York, 1991, p. 18 and 138; E. Buncel, M. R. Crampton, M. J. Strauss and F. Terrier, in *Electron-Deficient Aromatic and Heteroaromatic Base Interactions*, Elsevier, Amsterdam, 1984, p. 166 and 296.
2 F. Terrier, E. Kizilian, J. C. Hallé and E. Buncel, *J. Am. Chem. Soc.*, 1992, **114**, 1740; F. Terrier, M. J. Pouet, J. C. Hallé, S. Hunt, J. R. Jones and E. Buncel, *J. Chem. Soc., Perkin Trans. 2*, 1993, 1665; F. Terrier, F. Millot and W. S. Norris, *J. Am. Chem. Soc.*, 1976, **98**, 5883.
3 M. J. Strauss, R. A. Renfrow and E. Buncel, *J. Am. Chem. Soc.*, 1983, **105**, 2473; E. Buncel, R. A. Renfrow and M. J. Strauss, *J. Org. Chem.*, 1987, **52**, 488; E. Buncel, R. A. Manderville and J. M. Dust, *J. Chem. Soc., Perkin Trans. 2*, 1997, 1019; E. Buncel, J. M. Dust and R. A. Manderville, *J. Am. Chem. Soc.*, 1996, **118**, 6072.
4 R. J. Spear, W. P. Norris and R. W. Read, *Tetrahedron Lett.*, 1983, **23**, 1555; W. P. Norris, R. J. Spear and R. W. Read, *Aust. J. Chem.*, 1989, **36**, 297.
5 J. Kund and H. J. Niclas, *Synth. Commun.*, 1993, **23**, 1569; H. J. Niclas, B. Göhrmann and E. Gründemann, *ibid*, 1991, **333**, 909.
6 F. Terrier, E. Kizilian, J. C. Hallé, M. J. Pouet and E. Buncel, *J. Phys. Org. Chem.*, 1998, in the press.
7 F. Terrier, E. Kizilian, K. Gzouli, M. J. Pouet and J. C. Hallé, *J. Chem. Soc., Perkin Trans. 2*, 1997, 2667.
8 F. Terrier, A. P. Chatrousse, Y. Soudais and M. Hlaibi, *J. Org. Chem.*, 1984, **49**, 4176.
9 M. J. Strauss, A. De Fusco and F. Terrier, *Tetrahedron Lett.*, 1981, **32**, 1945.
10 J. H. Atherton, M. R. Crampton, G. L. Duffield and J. A. Stevens, *J. Chem. Soc., Perkin Trans. 2*, 1995, 443.
11 G. Kresze and H. Bathelt, *Tetrahedron*, 1973, **29**, 1043.
12 P. Mac Cormack, J. C. Hallé, M. J. Pouet and F. Terrier, *J. Org. Chem.*, 1988, **53**, 4407.
13 J. C. Hallé, D. Vichard, M. J. Pouet and F. Terrier, *J. Org. Chem.*, 1997, **62**, 7178.
14 S. Pugnaud, D. Masure, J. C. Hallé and P. Chaquin, *J. Org. Chem.*, 1997, **62**, 8687.

Received in Cambridge, UK, 13th January 1998; 8/00343B

Palladium-catalyzed allylic substitution on solid support

Lutz F. Tietze,*† Thomas Hippe and Adrian Steinmetz

Institut für Organische Chemie, Georg-August-Universität, Tammannstr. 2, D-37077 Göttingen, Germany

Different polymer-bound 1,3-dicarbonyl compounds react as nucleophiles in Pd-catalyzed allylic substitutions on solid support with a variety of allylic acetates, chlorides and carbonates.

Combinatorial chemistry is regarded as a powerful tool to improve the search for new pharmacologically interesting compounds.[1] In most of the cases solid phase synthesis is used to generate combinatorial libraries, which are subsequently tested for their biological activity. Therefore, the development of basic carbon–carbon bound-forming reactions on the solid phase is an important task, especially in combinatorial synthesis of organic compounds of low molecular weight.

In the course of our studies on the use of resin-linked 1,3-dicarbonyl compounds to build up combinatorial libraries, we have previously reported on a two-component domino–Knoevenagel–ene reaction[2] and a three-component domino–Knoevenagel-hetero-Diels–Alder reaction[3] to afford structurally diverse cycloalkanes and 3,4-dihydro-2*H*-pyrans, respectively. Furthermore, we established an efficient method to synthesise highly diverse pyrazolones by treatment of a variety of polymer-bound β-keto esters with hydrazine derivatives, resulting in concomitant release of the final products from the support.[4]

Herein, we report on the use of polymer-bound 1,3-dicarbonyl compounds in Pd^0-catalyzed allylic substitution reactions with a variety of allylic substrates **1a**–**g**, **5** and **8a**,**b**. The Pd-catalyzed allylation[5] is well known for its high control of stereoselectivity and functional group tolerance, as well as good yields, and is therefore of great interest for combinatorial chemistry.[6]

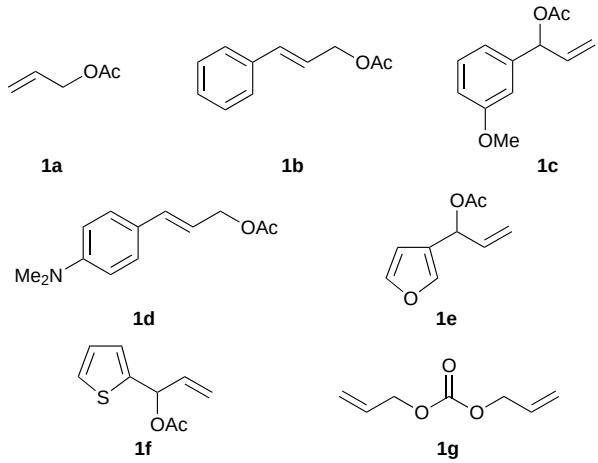

Polymer-bound malonate **2a** and acetoacetates[2,3] **2b** and **2c** reacted with a variety of aliphatic and aromatic allylic acetates **1a**–**f** (5 equiv., Scheme 1) in the presence of 20 mol% of tetrakis(triphenylphosphine)palladium as a catalyst and bis-(trimethylsilyl)acetamide (BSA)[7] as a base (5 equiv.) in THF at reflux temperature for 6–15 h. The resin-bound products **3** were cleaved under reductive conditions with DIBAL-H (10 equiv., toluene, 0 °C, 12 h) to afford the desired diols **4a**–**h** in 20–57% overall yield based on the concentration of free hydroxy groups

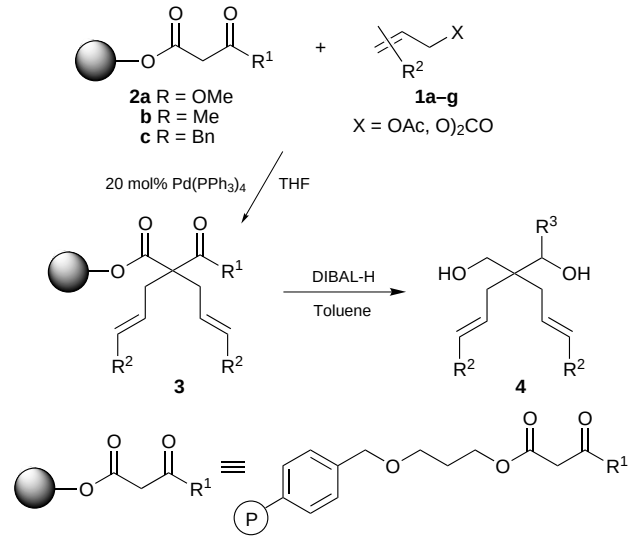

Scheme 1

in the spacer-modified polystyrene-resin (0.75 mmol per gram resin)[2] (Table 1). Using the sterically less hindered allylic acetates **1a**–**f** dialkylation was observed in all cases, showing the expected high reactivity of the polymer-bound β-keto esters **2a**,**b** towards allylic substitution.

In addition to the allylic acetates, allylic chlorides and carbonates were also used. Employing allylic carbonates, no addition of base is required since the carbonate moiety reacts as a leaving group and simultaneously forms an alkoxide as a base after loss of carbon dioxide.[5] Thus, reaction of diallyl carbonate **1g** (3 equiv.) with the polymer-bound benzyl-substituted acetoacetate[4] **2c** was performed at room temperature in THF for 1 h using 10 mol% Pd catalyst. After cleavage from the resin the dialkylated product **4i** was obtained in 76% yield, showing the very high reactivity of allylic carbonates (Table 1). In the case of β-methallyl chloride **5**, Bu^nLi (1 equiv.) was used as base and the reaction was performed at room temperature for 21 h. In this

Table 1 Synthesised 1,3-diols **4**

Substrates		Products				
1	**2**	**4**	R^1	R^2	R^3	Overall yield (%)[a]
a	**a**	**a**	OMe	H	H	30
b	**a**	**b**	OMe	Ph	H	57
b	**b**	**c**	Me	Ph	Me	40
c	**b**	**d**	Me	3-$MeOC_6H_4$	Me	23
d	**b**	**e**	OMe	4-$Me_2NC_6H_4$	Me	34
e	**a**	**f**	OMe	3-Furyl	H	20
e	**b**	**g**	Me	3-Furyl	Me	23
f	**b**	**h**	Me	2-Thienyl	Me	20
g	**c**	**i**	Bn	H	Bn	76[b]

[a] The products were purified by flash chromatography. The yields are based on the concentration of free hydroxy groups in the spacer-modified polystyrene-resin (0.75 mmol per gram resin) (ref. 2). [b] No base was used. The reaction was performed at room temperature.

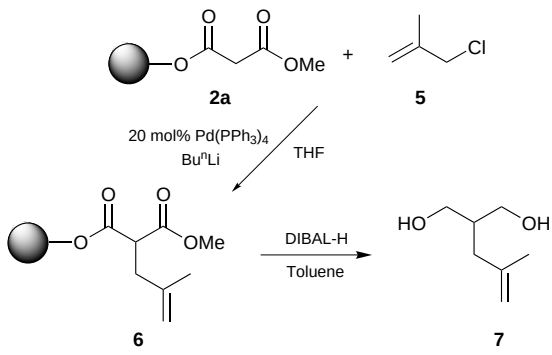

Scheme 2

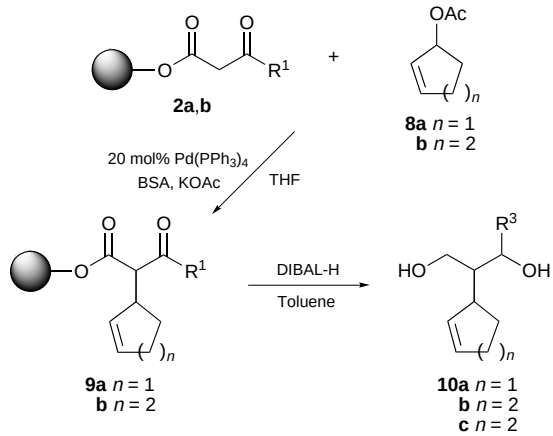

Scheme 3

reaction only monoalkylation was observed. Thus, after reductive cleavage product **7** was obtained in 28% yield (Scheme 2).

Selective monoalkylation could also be achieved using sterically more hindered cyclic allylic acetates (Scheme 3). Under the conditions described for **1a**–**f** [20 mol% $Pd(PPh_3)_4$, BSA, KOAc, THF, reflux, 10 h] the reaction of the cyclic acetates **8a**,**b** and **2a**,**b** gave after reductive cleavage the desired diols **10a**–**c**, respectively, in 40–59% yield (Table 2). The formation of the dialkylated products was not observed.

Table 2 Synthesis of the 1,3-diols **10**

Substrates		Products				
2	**8**	**10**	*n*	R^1	R^3	Overall yield (%)[a]
a	**a**	**a**	1	OMe	H	53
a	**b**	**b**	2	OMe	H	40
b	**b**	**c**	2	Me	Me	59

[a] The products were purified by flash chromatography. The yields are based on the concentration of free hydroxy groups in the spacer-modified polystyrene-resin (0.75 mmol per gram) (ref. 2).

A further possibility to increase diversity in a one-pot procedure is shown in Scheme 4. As previously described by our group,[4] γ-alkylation of polymer-bound acetoacetate **2b** can be achieved by generating the dianion **11** with LDA at 0 °C and subsequent treatment with an alkylating reagent in THF at 0 °C, *e.g.* iodoethane **12**. The resulting monoanion **13** can now react as a nucleophile in an allylic substitution with **8b** to give the

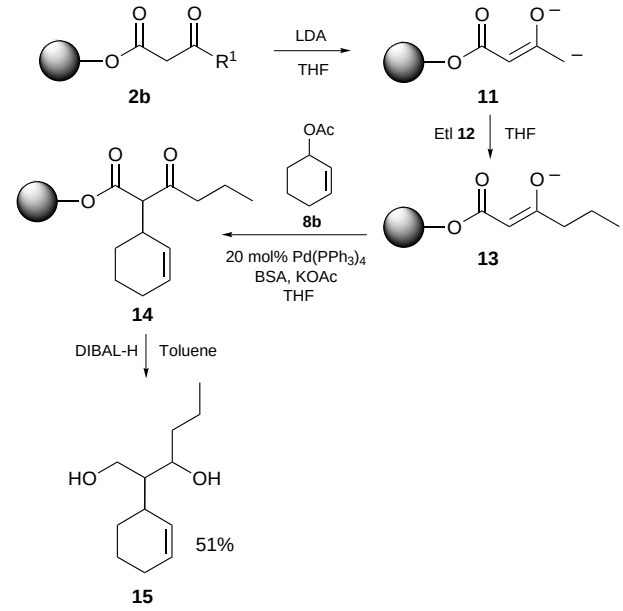

Scheme 4

resin-bound product **14**, which was reductively cleaved as described above to afford the diol **15** in 51% overall yield.

In conclusion, we have shown that the Pd-catalyzed allylic substitution of allylic substrates such as acetates, chlorides and carbonates with different polymer-bound 1,3-dicarbonyl compounds is a very efficient C–C bond-forming reaction. Since allylic substrates are readily available building blocks, the solid phase reaction presented above should be amenable for combinatorial synthesis. Furthermore, the development of a one-pot protocol consisting of γ-alkylation and α-allylation of solid supported acetoacetate provides an even greater diversity of the desired products. We are currently investigating the possibility of using vinylic epoxides and bisallylic templates as substrates and resin-bound allylated 1,3-dicarbonyl compounds for further transformations.

This work was supported by BASF AG, the Fonds der Chemischen Industrie and the Bundesministerium für Bildung, Wissenschaft, Forschung und Technologie (Grants No. 03 D0056 2).

Notes and References

† E-mail: ltietze@gwdg.de

1 F. Balkenhohl, C. von dem Bussche-Hünnefeld, A. Lansky and C. Zechel, *Angew. Chem.*, 1996, **108**, 2436; *Angew. Chem., Int. Ed. Engl.*, 1996, **35**, 2288; L. A. Thompson and J. A. Ellman, *Chem. Rev.*, 1996, **96**, 555; J. S. Früchtel and G. Jung, *Angew. Chem.*, 1996, **108**, 19; *Angew. Chem., Int. Ed. Engl.*, 1996, **35**, 17.
2 L. F. Tietze and A. Steinmetz, *Angew. Chem.*, 1996, **108**, 682; *Angew. Chem., Int. Ed. Engl.*, 1996, **35**, 651.
3 L. F. Tietze, T. Hippe and A. Steinmetz, *Synlett*, 1996, 1043.
4 L. F. Tietze and A. Steinmetz, *Synlett*, 1996, 667; L. F. Tietze, A. Steinmetz and F. Balkenhohl, *Bioorg. Med. Chem. Lett.*, 1997, **7**, 1303.
5 B. M. Trost and D. L. Van Vranken, *Chem. Rev.*, 1996, **96**, 395; C. G. Frost, J. Howath and J. Williams, *Tetrahedron: Asymmetry*, 1992, **3**, 1089; J. Tsuji, *Tetrahedron*, 1986, **42**, 4361.
6 Z. Flegelová and M. Pátek, *J. Org. Chem.*, 1996, **61**, 6735.
7 B. M. Trost and D. J. Murphy, *Organometallics*, 1985, **4**, 1143.

Received in Glasgow, UK, 23rd October 1997; 7/07670C

Linked arene clusters: the interaction of tetracobalt nonacarbonyl with [2.2.2]paracyclophane

Paul Schooler,[a] Brian F. G. Johnson,*[a]† Caroline M. Martin,[a] Paul J. Dyson[b] and Simon Parsons[c]

[a] *University Chemical Laboratory, Lensfield Road, Cambridge, UK CB2 1EW*
[b] *Department of Chemistry, Imperial College of Science, Technology and Medicine, South Kensington, London, UK SW7 2AY*
[c] *Department of Chemistry, University of Edinburgh, West Mains Road, Edinburgh, UK EH9 3JJ*

The thermolysis of [2.2.2]paracyclophane in the presence of an excess of $[Co_4(CO)_{12}]$ yields three new arene clusters $[\{Co_4(CO)_9\}_n(C_{24}H_{24})]$ (n = 1, 2 and 3): the molecular structures of the mono- and bis-cluster complexes have been established by single crystal X-ray diffraction while the tris-complex has been characterised by spectroscopy.

The interaction of the $[2_n]$cyclophanes with transition and main group metals has received much attention since their conception by Cram several decades ago.[1] These complexes were initially used to probe the unusual electronic properties of the $[2_n]$cyclophane ligands, which stem from the interpenetration of arene π molecular orbitals, giving rise to unusual and unique effects.[2] More recently, interest has been stimulated by the potential for the $[2_n]$cyclophane ligands to serve as bridging units between metal centres in organometallic polymers and networks which should have interesting electrical and non-linear optical properties.[3]

Metal atoms and ions may bond to [2.2.2]paracyclophane by either endo- or exo-coordination. In the former the metal atom resides in or near the ligand cavity such as in the π cryptates formed with gallium(I) and silver(I) salts[4] while in the latter the metal atom interacts with the external face of the aromatic rings as in the piano-stool complexes formed with $[M(CO)_3]$ (M = Cr, Mo or W) fragments.[5] There are few reports concerning the coordination of more than one metal atom to [2.2.2]paracyclophane; only recently has diffraction data become available for the mono- and bis-$[Cr(CO)_3]$ complexes,[6] and structural data for the tris-chromium tricarbonyl has not yet been obtained. Here, we report the molecular structure of the complexes $[Co_4(CO)_9(\eta\text{-}C_{24}H_{24})]$ **1** and $[\{Co_4(CO)_9\}_2(\eta:\eta\text{-}C_{24}H_{24})]$ **2** in which one and two of the C_6-rings of [2.2.2]paracyclophane are coordinated to $[Co_4(CO)_9]$ cluster units respectively. Spectroscopic characterisation of the tris-$[Co_4(CO)_9]$ complex, $[\{Co_4(CO)_9\}_3(\eta:\eta:\eta\text{-}C_{24}H_{24})]$ **3**, is also reported. These latter two compounds represent the first examples of clusters linked *via* a cyclophane ligand.

The thermolysis of [2.2.2]paracyclophane with 10 molar equiv. of $[Co_4(CO)_{12}]$ in hexane under reflux over 5 h affords three new complexes $[Co_4(CO)_9(\eta\text{-}C_{24}H_{24})]$ **1** (20%), $[\{Co_4(CO)_9\}_2(\eta:\eta\text{-}C_{24}H_{24})]$ **2** (2%) and $[\{Co_4(CO)_9\}_3(\eta:\eta:\eta\text{-}C_{24}H_{24})]$ **3** (*ca.* 0.1%) which were separated by thin layer chromatography on silica using dichloromethane–hexane (1 : 3 v/v) as the eluent. These complexes can be conveniently interconverted (Scheme 1) by either adding cluster units to compounds **1** and **2** by thermolysis with $[Co_4(CO)_{12}]$ in hexane or by the thermolysis of compounds **2** and **3** in toluene whereby cluster units are removed from the cyclophane ligand *via* arene exchange. The molecular structures of compounds **1** and **2** are shown in Figs. 1 and 2, respectively. In both molecules the coordinated rings of the cyclophane ligands lie parallel to, and staggered with respect to, the metal triangle defined by Co(2)Co(3)Co(4). The cobalt–ring carbon distances indicate that the coordinated rings are not planar as the average distances involving the bridgehead carbon atoms are slightly longer than the remaining four carbon atoms [*cf.* 2.174(6) and 2.107(8) Å in **1** and 2.174(5) and 2.120(12) Å in **2**]. Although the coordinated rings of the cyclophane in both compounds are expanded owing

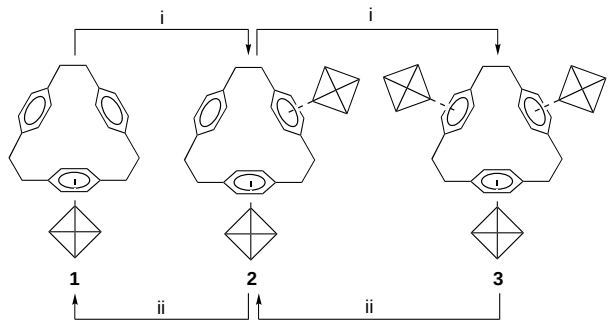

Scheme 1 The interconversion of compounds **1**, **2** and **3**. *Reagents and Conditions* i, $[Co_4(CO)_{12}]$, heat in hexane; ii, heat in toluene.

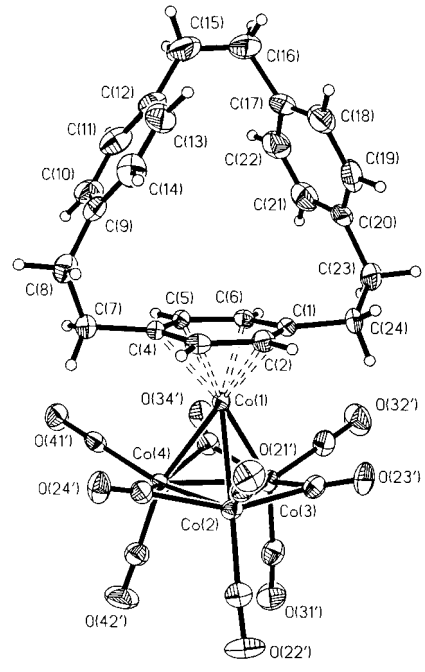

Fig. 1 The molecular structure of $[Co_4(CO)_9(\eta\text{-}C_{24}H_{24})]$ **1**. Important bond lengths (/Å): Co(1)–Co(2) 2.4614(13), Co(1)–Co(3) 2.4823(11), Co(1)–Co(4) 2.4626(10), Co(2)–Co(3) 2.4823(11), Co(2)–Co(4) 2.4740(12), Co(3)–Co(4) 2.4552(11), Co(1)–C(1) 2.175(4), Co(1)–C(2) 2.131(4), Co(1)–C(3) 2.103(4), Co(1)–C(4) 2.172(4), Co(1)–C(5) 2.115(4), Co(1)–C(6) 2.095(4), C(1)–C(2) 1.402(6), C(1)–C(6) 1.408(5), C(2)–C(3) 1.397(6), C(3)–C(4) 1.397(5), C(4)–C(5) 1.400(5), C(5)–C(6) 1.405(5), C(9)–C(10) 1.363(7), C(9)–C(14) 1.362(6), C(10)–C(11) 1.376(7), C(11)–C(12) 1.367(7), C(12)–C(13) 1.371(7), C(13)–C(14) 1.367(7), C(17)–C(18) 1.369(7), C(17)–C(22) 1.366(7), C(18)–C(19) 1.394(7), C(19)–C(20) 1.390(7), C(20)–C(21) 1.359(7), C(21)–C(22) 1.341(7), average C–O (terminal) 1.133(12) and average C–O (bridging) 1.164(8).

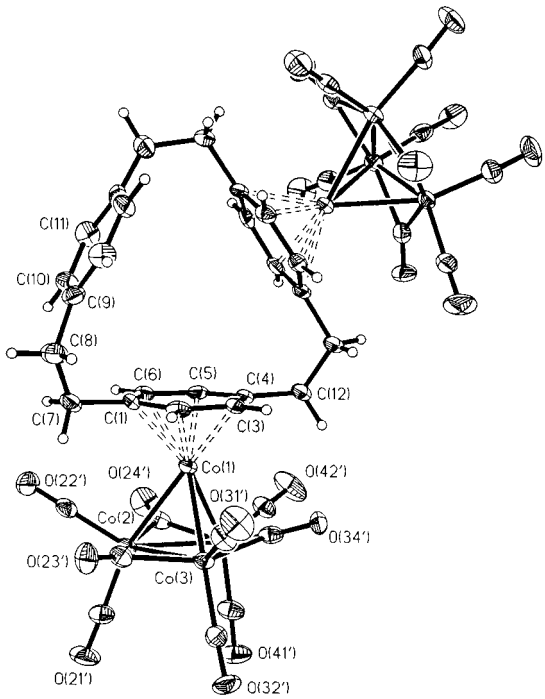

Fig. 2 The molecular structure of [{$Co_4(CO)_9$}$_2$(η-$C_{24}H_{24}$)] **2**. Important bond lengths (/Å): Co(1)–Co(2) 2.5078(12), Co(1)–Co(3) 2.4646(12), Co(1)–Co(4) 2.4758(12), Co(2)–Co(3) 2.4628(13), Co(2)–Co(4) 2.4413(14), Co(3)–Co(4) 2.4513(13), Co(1)–C(1) 2.166(7), Co(1)–C(2) 2.104(6), Co(1)–C(3) 2.141(6), Co(1)–C(4) 2.179(6), Co(1)–C(5) 2.111(6), Co(1)–C(6) 2.122(6), C(1)–C(2) 1.396(10), C(1)–C(6) 1.398(10), C(2)–C(3) 1.409(10), C(3)–C(4) 1.408(11), C(4)–C(5) 1.429(11), C(5)–C(6) 1.387(10), C(9)–C(10) 1.346(11), C(10)–C(11) 1.389(11), average C–O (terminal) 1.13(2) and average C–O (bridging) 1.173(16).

to the electron-withdrawing nature of the cluster [*cf.* average C–C distances of 1.401(13) and 1.37(2) Å in **1** and 1.40(2) and 1.36(3) Å in **2**], little significance can be placed upon this observation owing to the magnitude of the electron shift densities. It should be noted that the cyclophane ligand in compound **1** is much less symmetrically coordinated than in **2**; this is reflected in the dihedral angles made between the bow and stern of the C_6 rings of 5.9° (coordinated), 2.8 and 0.9° while the ethano bridge C(15)–C(16) lies some 2.17 Å out of the plane defined by Co(1)C(1)C(4)C(7)C(24).

The average Co–Co bond distances in the base of the clusters are short compared to the sides owing to the contracting action of the bridging CO groups [2.459(2), 2.469(2) Å in **1** and 2.452(2), 2.483(2) Å in **2**, respectively]. Both bridging and equatorial terminal carbonyl ligands point upwards toward the cyclophane.

Compounds **2** and **3** are of particular interest as precursors to organometallic one and two-dimensional networks and polymers since the [2.2.2]paracyclophane ligands in these complexes bridge cluster units. However, it should be noted that we have been unable to introduce a second cyclophane ligand to a Co_4 cluster in order to sustain chain growth: the weakness of the metal–arene interaction (as demonstrated by arene exchange reactions with toluene) permits multiple complexation of clusters by a single ligand but is too weak to allow the substitution of further carbonyl ligands with poorer π-acceptors upon the arene cluster. We have also found that, for example in compound **1**, the cobalt cluster is unwilling to share the cyclophane ligand with more electronically demanding subunits such as [$Ru_6C(CO)_{14}$], Ga^I or Ag^I. Although the linkage of cobalt clusters through arene systems in itself is not novel (this has been previously achieved using diphenylmethane),[7] the combination of the unique electronic properties of clusters and cyclophanes may allow novel types of electronic communication. Our preliminary electrochemical analyses, although complex, indicate this and our investigation is ongoing.

We wish to thank the EPSRC, Cambridge University, and the Newton Trust (P. S.) for financial support. P. J. D. would like to thank the Royal Society for a University fellowship.

Notes and References

† E-mail: bfgj1@cus.cam.ac.uk

‡ *Spectroscopic data*: **1**, IR (CH_2Cl_2) ν_{CO}/cm^{-1} 2072s, 2046w, 2028vs, 2009s, 1995w (sh) and 1814m (br). FABMS: *m*/*z* 800 (calc. 800) with the loss of all nine CO ligands observed. ^{1}H NMR ($CDCl_3$): δ 6.53 (d, 4 H, *J* 7.2 Hz, free aromatic), 6.45 (d, 4 H, *J* 7.2 Hz, free aromatic), 5.66 (s, 4 H, bound aromatic), 3.28 (m, 4 H), 2.90 (m, 4 H) and 2.81 (s, 4 H).

2, IR (CH_2Cl_2) ν_{CO}/cm^{-1} 2069s, 2026vs, 2007s, 1992w (sh) and 1815m (br). FABMS: *m*/*z* 1290 (calc. 1288) with the loss of all eighteen CO ligands and four cobalt atoms observed. ^{1}H NMR ($CDCl_3$): δ 6.28 (s, 4 H, free aromatic), 5.48 (d, 4 H, *J* 7.0 Hz, bound aromatic), 5.38 (d, 4 H, *J* 7.0 Hz, bound aromatic), 3.20 (s, 4 H), 3.12 (m, 4 H) and 2.75 (s, 4 H).

3, IR (CH_2Cl_2) ν_{CO}/cm^{-1} 2072s, 2028vs, 2008s, 1996w (sh) and 1837m (br). FABMS: *m*/*z* 1778 (calc. 1777) with the loss of eight CO ligands observed.

§ *Crystal data*: Structures solved by direct methods (SIR92) and refined by full-matrix least squares on F^2 (SHELXTL version 5).

1, $C_{33}H_{24}Co_4O_9$, *M* = 800.24, triclinic, space group $P\bar{1}$, *a* = 10.594(4), *b* = 12.060(5), *c* = 14.506(6) Å, α = 110.37(2), β = 111.20(2), γ = 93.78(2), *U* = 1580.4(11) Å^3, *Z* = 2, D_c = 1.682 Mg m^{-3}, *T* = 250(2) K, *F*(000) = 804, R_1 = 0.0371 [3977 reflections with $F_o > 4\sigma(F_o)$], wR_2 = 0.0800 for 5576 independent reflections corrected for adsorption [μ(Mo-Kα) = 2.177 mm^{-1}] and 416 parameters 0.39 × 0.38 × 0.29 mm black block obtained from dichloromethane at −20 °C. The crystal lattice contained no solvent. The final difference map extrema were +0.67 and −0.40 e Å^{-3}.

2, $C_{42}H_{24}Co_8O_{18}$·0.43CH_2Cl_2, *M* = 1324.57, trigonal, space group $P3_121$, α = 15.4261(12), *c* = 18.282(3), *U* = 3767.7(8) Å^3, *Z* = 3 (the molecule lies on a two-fold axis), D_c = 1.751 Mg m^{-3}, *T* = 220(2) K, *F*(000) = 1962, R_1 = 0.0460 [3598 reflections with $F_o > 4\sigma(F_o)$], wR_2 = 0.1069 for 4358 independent reflections corrected for adsorption [μ(Mo-Kα) = 2.687 mm^{-1}] and 308 parameters. The Flack absolute structure parameter was 0.01(3). 0.39 × 0.38 × 0.29 mm dark green block obtained from dichloromethane at −20 °C. The crystal lattice contained disordered solvent molecules which were treated in the manner described by van der Sluis and Spek.[8] This amounted to 36 e per cell or 0.43 CH_2Cl_2 per formula unit. The final difference map extrema were +0.05 and −0.62 e Å^{-3}. CCDC 182/783.

1 D. J. Cram, in *Cyclophanes I*, ed. P. M. Keehn and S. M. Rosenfeld, Academic Press, New York, 1983.
2 D. J. Cram and D. I. Wilkinson, *J. Am. Chem. Soc.*, 1960, **82**, 5721.
3 E. D. Laganis, R. H. Voegeli, R. T. Swann, R. G. Finke, H. Hopf and V. Boekelheide, *Organometallics*, 1982, **1**, 1415.
4 H. Schidbaur, R. Hager, B. Huber and G. Muller, *Angew. Chem., Int. Ed. Engl.*, 1987, **26**, 338; J.-L. Pierre, P. Baret, P. Chautemps and M. Armand, *J. Am. Chem. Soc.*, 1981, **103**, 2986.
5 C. Elschenbroich, J. Schneider, M. Wünsch, J.-L. Pierre, P. Baret and P. Chautemps, *Chem. Ber.*, 1988, **121**, 177.
6 P. J. Dyson, D. G. Humphrey, J. E. McGrady, P. Suman and D. Tocher, *J. Chem. Soc., Dalton Trans.*, 1997, 1601.
7 A. I. Yanovsky, F. M. Dolgushin, Y. T. Struchov, V. S. Kaganovich and M. I. Rybinskaya, *Russ. Chem. Bull.*, 1995, **44**, 1072; E. Kolehmainen, K. Laihia, J. Kaganovich, M. I. Rybinskaya and Z. A. Kezerina, *J. Organomet. Chem.*, 1995, **485**, 109.
8 P. van der Sluis and A. L. Spek, *Acta Crystallogr., Sect. A*, 1990, **46**, 194.

Received in Cambridge, UK, 26th January 1998; 8/00715B

The first stable scandocene: synthesis and characterisation of bis(η-2,4,5-tri-*tert*-butyl-1,3-diphosphacyclopentadienyl)scandium(II)

Polly L. Arnold, F. Geoffrey N. Cloke*† and John F. Nixon*

School of Chemistry, Physics and Environmental Sciences, University of Sussex, Brighton, UK BN1 9QJ

The first isolable example of a molecular scandium(II) complex, the dark purple scandocene [Sc(η^5-P$_2$C$_3$Bu$^t_3$)] 1, has been isolated from the cocondensation of scandium vapour with *tert*-butylphosphaalkyne, Bu^{t}CP at 77 K.

To date the only stable divalent lanthanoid metallocenes are those of the elements Sm, Eu and Yb for reasons which have been well documented.[1] These metallocenes are all highly reactive, showing strong reducing properties and consequent unusual reaction chemistry.[2] Very recently, two lanthanum species that are intermediates in the potassium reduction of [La(Cp″)$_3$] {Cp″ = η-C$_5$H$_3$(SiMe$_3$)$_2$} have been observed and characterised, by EPR spectroscopy, as containing a La^{II} centre; one of the latter has been shown to be a dme solvated metallocene, La(Cp″)$_2$(dme).[3]

In recent years metal vapour synthetic techniques have afforded a variety of novel and reactive low valent organometallic complexes of group 3 and the lanthanides directly from the elements; the technique remains the only route to zero-valent molecular lanthanide complexes.[4] Cyclisation reactions undergone by 2,2-dimethylpropylidynephosphine (*tert*-butylphosphaalkyne, Bu^{t}CP) at metal atoms during cocondensation reactions are of considerable current interest since the choice of metal clearly dictates the nature of ring or rings formed.[5] The most common cyclisation observed to date is the combination of five phosphaalkyne units resulting in the isolation of sandwich complexes such as [(V(η^5-P$_3$C$_2$Bu$^t_2$)(η^5-P$_2$C$_3$Bu$^t_3$)].[6] Here, we report the synthesis of [Sc(η^5-P$_2$C$_3$Bu$^t_3$)$_2$] **1**, which represents only the second reported scandium(II) complex. The first example, also described by our laboratory, resulted from ligand metallation during the cocondensation of scandium vapour with tri-*tert*-butylbenzene; this product was unfortunately not separable from the admixture with [Sc(η-C$_6$H$_3$Bu$^t_3$-1,3,5)$_2$].[7] The present work is thus the first instance in which we have been able to isolate, and thus fully characterise, a complex of scandium in this oxidation state.

Cocondensation of electron beam vaporised scandium with an excess of Bu^{t}CP at 77 K affords a dark brown matrix which is soluble in hexanes. Two products are separable from the dark solution by flash sublimation (220 °C, 10^{-5} mbar), Scheme 1.‡ The dark purple microcrystalline [Sc(η^5-P$_2$C$_3$Bu$^t_3$)$_2$] **1** may be obtained from the sublimate by repeated sublimation and removal of by-product volatile oils. The forest-green triple-decker complex [(η^5-P$_3$C$_2$Bu$^t_2$)Sc(μ-η^6:η^6-P$_3$C$_3$Bu$^t_3$)Sc(η^5-P$_3$C$_2$Bu$^t_2$)], can be extracted from the sublimant and has been the subject of a recent communication.[8]

The 1,2,4-triphospha-3,5-di-*tert*-butylcyclopentadienyl ring is regularly formed in conjunction with the 1,3-diphospha-2,4,5-di-*tert*-butylcyclopentadienyl ring in cyclisation reactions at a number of both transition elements and main group metal centres.[5b] Since the yield of **1** is approximately the same as that of the scandium(I) triple-decker complex [(η^5-P$_3$C$_2$Bu$^t_2$)Sc(μ-η^6:η^6-P$_3$C$_3$Bu$^t_3$)Sc(η^5-P$_3$C$_2$Bu$^t_2$)], which contains a greater proportion of ligated phosphorus, the number of phosphaalkyne monomers is preserved between the two complexes. This leads us to believe, at least in this case, that the fusion of a number of Bu^{t}CP molecules around the metal does not simply involve one metal centre.

Complex **1** is extremely air- and moisture-sensitive and is soluble in pentane and other non-polar solvents; a solution in thf decomposes immediately giving no tractable products, precluding electrochemical studies. Unfortunately, single crystals of **1** suitable for X-ray structural determination could not be obtained owing to its extreme solubility in solvents with which it does not react. The intense purple colour of **1**, due to an absorption maximum observed at 571 nm in the UV–VIS spectrum, is characteristic of a charge transfer band and appears to be a common feature in low- and zero-valent group 3 and lanthanide complexes.[4a]

Magnetic and EPR studies have been employed to study the d^1 electronic configuration of **1**. The EPR spectrum of **1** in toluene at 295 K is broad and shows coupling only to the ^{45}Sc nucleus, presumably due to rapid relaxation at this temperature, characterised by g_{iso} 1.9823 and A_{iso}(^{45}Sc) 3.757 mT (I = 7/2, 100%). Upon cooling the sample to a glass at 120 K, well resolved coupling to scandium is observed, accompanied by further hyperfine coupling to the four phosphorus nuclei (I = ½, 100%) which are equivalent on the EPR timescale at this temperature, Fig. 1. The resonance is characterised by $g_\perp$ 2.0098 with a calculated value of $g_\parallel$ 1.9273 and is well simulated using values of $A_\perp$(^{45}Sc) 2.99 mT, $A_\parallel$(^{45}Sc) 5.29 mT and A(^{31}P) 0.72 mT. The solution magnetic moment is found to be 1.70 μ_B at room temperature,[9] showing no evidence for any orbital contribution to the spin only value (μ_{eff} = 1.73 μ_B).

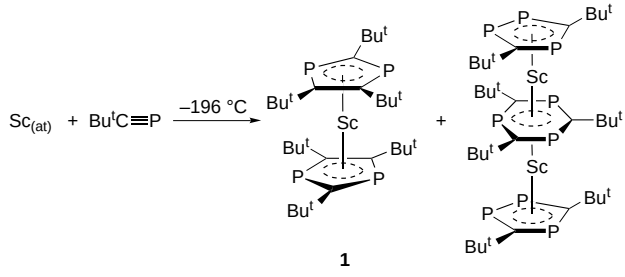

Scheme 1 Synthesis of **1**

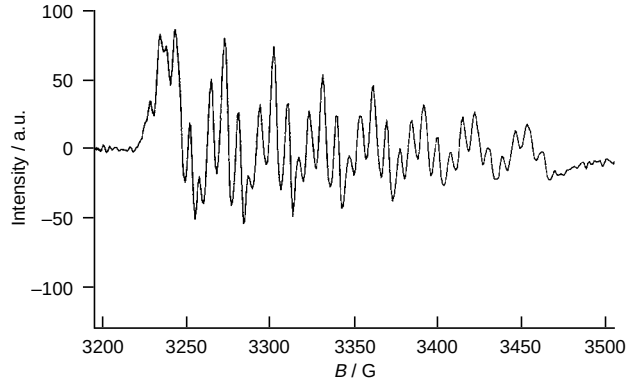

Fig. 1 EPR spectrum of **1** (toluene glass, 120 K)

Warren has suggested,[10] in a review of the ligand field theory for pseudo-axially symmetric metallocenes that a distortion and subsequent lowering to C_{2v} symmetry occurs since the degenerate ground state is necessarily Jahn–Teller unstable. The majority of d^1 metallocene systems extant in the literature are bent from pseudo-axial symmetry and the resulting quenching of any orbital contribution results in isotropic *g* values close to 2.00 and near spin-only values of the magnetic moment.[11] A similar argument is appropriate here since **1** is not modelled well as axial, owing to the unsymmetric substitution of the cyclopentadienyl rings.[12] The phosphorus atom in the diphosphatri-*tert*-butylcyclopentadienyl ligands provides a second magnetic nucleus, thus the resolution of coupling to the ligand nuclei by the electron, particularly at lower temperatures when the relaxation processes are slowed, strongly suggests that the single electron resides in the degenerate d_{xy} or $d_{x^2-y^2}$ orbitals (rather than the d_{z^2} orbital), as predicted.

The existence and stability of **1**, which thus completes the series of divalent metallocenes for the 3d elements, presumably result from a combination of steric shielding of the diphosphatri-*tert*-butylcyclopentadienyl rings and the increased π-electron accepting properties of the rings induced by phosphorus incorporation.

The authors are grateful to Dr A. Abdul-Sada for determination of the mass spectrum of **1**, to Mr C. Dadswell for recording of the EPR spectrum of **1** and to the EPSRC (ROPA) for funding.

Notes and References

† E-mail: f.g.cloke@sussex.ac.uk

‡ Scandium (0.30 g, 0.66 mol) was vaporised (power input 200 W) and cocondensed with Bu^tCP (10 g, 0.1 mol, M : L ratio 1 : 10) at 77 K.[1] The dark brown matrix formed over a period of 2.5 h persisted on warming to room temperature under an inert atmosphere. The product was washed from the reactor with hexanes (2 l), filtered through a bed of Teflon powder (20 μm), and evaporated to dryness. Flash sublimation (by introduction of the sublimer into a tube furnace pre-heated to 220 °C) at 10^{-5} mbar of the resultant solid yielded a purple oil. From this, **1** is obtained pure in 5–10% yield, *ca*. 30 mg (based on scandium) after resublimation. UV–VIS for **1**: λ_{max}/nm (pentane) 571 (ε/dm^3 mol^{-1} cm^{-1} 15 000). MS (EI): *m/z* 583 (90%, M^+), 269 (43, $P_2C_3Bu^t{}_3^+$); HRMS: *m/z* found 583.273922. $C_{30}P_4H_{54}Sc$ requires 583.273519. Solution state magnetism (Evans method, [$^2H_8$]toluene): μ_{eff} = 1.70 μ_B.

1 W. J. Evans, *Polyhedron*, 1987, **6**, 803.
2 W. J. Evans, J. W. Grate, L. A. Hughes, H. Zhang and J. L. Atwood, *J. Am. Chem. Soc*., 1985, **107**, 3728; P. B. Hitchcock, J. A. K. Howard, M. F. Lappert and S. Prashar, *J. Organomet. Chem.*, 1992, **437**, 177; W. J. Evans, L. A. Hughes and T. P. Hanusa, *Organometallics*, 1987, **5**, 1285; W. J. Evans, T. A. Ulibarri and J. W. Ziller, *J. Am. Chem. Soc.*, 1988, **110**, 6877; C. J. Burns and R. A. Andersen, *J. Am. Chem. Soc.*, 1987, **109**, 5853.
3 M. C. Cassani, M. F. Lappert and F. Laschi, *Chem. Commun.*, 1997, 1563.
4 (*a*) F. G. N. Cloke, *Chem. Soc. Rev.*, 1993, 17; (*b*) P. L. Arnold, F. G. N. Cloke and P. B. Hitchcock, *Chem. Commun.*, 1997, 481.
5 J. F. Nixon, A. G. Avent, F. G. N. CLoke, K. R. Flower, P. B. Hitchcock and D. M. Vickers, *Angew. Chem.*, 1994, **106**, 2406; *Angew. Chem., Int. Ed. Engl.*, 1994, **33**, 2330; J. F. Nixon, *Chem. Soc. Rev*., 1995, 319 and references therein; D. M. Vickers, D.Phil. Thesis, University of Sussex, 1997.
6 F. G. N. Cloke, K. R. Flower, P. B. Hitchcock and J. F. Nixon, *J. Chem. Soc., Chem. Commun.*, 1995, 1659.
7 F. G. N. Cloke, K. Khan and R. N. Perutz, *J. Chem. Soc., Chem. Commun.*, 1991, 1372.
8 P. L. Arnold, F. G. N. Cloke, P. B. Hitchcock and J. F. Nixon, *J. Am. Chem. Soc*., 1996, **118**, 7630.
9 NMR method; [$^1H_8$]toluene solution, 190–320 K.
10 K. D. Warren, *J. Phys. Chem.*, 1973, **77**, 1681.
11 K. D. Warren, *Struct. Bonding* (*Berlin*), 1976, **27**, 45; K. D. Warren, *Inorg. Chem.*, 1974, **13**, 1317; B. A. Goodman and J. B. Raynor, *Adv. Inorg. Radiochem.*, 1970, 218; R. Couttes and P. C. Wailes, *Inorg. Nucl. Chem. Lett.*, 1967, **3**, 1.
12 A. H. Maki and T. E. Berri, *J. Am. Chem. Soc.*, 1965, **87**, 4437.

Received in Basel, Switzerland, 5th January 1998; 8/00089A

Catalytic deoxygenation of epoxides with $(Cp^*ReO)_2(\mu\text{-}O)_2$ and catalyst deactivation

Kevin P. Gable,*† Fedor A. Zhuravlev and Alexandre F. T. Yokochi

Department of Chemistry, Orgeon State University, Corvallis, OR 97331-4003, USA

***In situ* reduction of Cp^*ReO_3 by PPh_3 to form $(Cp^*ReO)_2(\mu\text{-}O)_2$ allows catalytic deoxygenation of epoxides, however, conproportionation between the Re^{V} and Re^{VII} species to form clusters of $\{(Cp^*Re)_3(\mu\text{-}O)_6\}^{2+}(ReO_4^-)_2$ and new compound $\{(Cp^*Re)_3(\mu^2\text{-}O)_3(\mu^3\text{-}O)_3ReO_3\}^+(ReO_4^-)$ leads to removal of rhenium from the catalytic cycle and loss of activity.**

A primary focus of recent work with metal oxo systems has been formation of new C–O bonds.[1] However, cleavage of C–O bonds with concomitant formation of one or more new M=O bonds is also a useful transformation. One example of this is deoxygenation of epoxides, wherein removal of an oxygen atom generates a new C=C π bond. Given that most methodology for making epoxides begins with the alkene, the combination epoxidation/deoxygenation would provide a useful protection/deprotection sequence for the multiple bond. Few such sequences now exist,[2] and many of these risk loss of stereochemical integrity or remain incompatible with other functional groups in the organic substrate.

We recently observed that $(Cp^*ReO)_2(\mu\text{-}O)_2$ reacted stereospecifically with epoxides to form alkene plus Cp^*ReO_3, presumably *via* the monomeric form Cp^*ReO_2.[3] Cook and Andrews recently reported catalytic deoxygenation of vicinal diols with this rhenium system,[4] so we decided to explore the catalytic deoxygenation of epoxides.

Conditions similar to stoichiometric deoxygenation reactions were used: toluene solvent, sealed under vacuum, heated to 90–120 °C. An initial study of deoxygenation of 1,2-epoxydodecane using 5 mol% Re gave only traces of alkene after extensive reaction times. As seen in Table 1, increasing the porportion of rhenium led to improved yields, but very little turnover. However, catalytic turnover could be achieved if the electronic properties of the epoxide were properly tuned.‡ The optimum turnover was seen in the case of electron-withdrawing substituents (Table 1).

It was evident from these experiments that catalyst turnover was being impeded by an interfering reaction. Further, in cases where poor turnover was observed (Table 1, entries 1, 2, 7), a green solid was seen to precipitate. The rapid reduction of Cp^*ReO_3 to $(Cp^*ReO)_2(\mu\text{-}O)_2$ at room temperature[5a] implied the two compounds did not react with each other, but this might not be true under the fairly severe reaction conditions of the deoxygenation (> 100 °C). Indeed, heating equimolar amounts of the two at 110 °C for 14 h formed a precipitate (sealed tube; isolated yield 5% from $CHCl_3$). This green solid was isolated by filtration and washing with benzene, and was identified as $\{(Cp^*Re)_3(\mu\text{-}O)_6\}^{2+}(ReO_4^-)_2$ **1**, first characterized by Herrmann *et al.*[5] The IR spectrum (908s cm^{-1}, 609, 650w cm^{-1}) and ^1H NMR spectrum (δ 2.22, s; CD_3CN) were identical to reported values. As expected, this salt was unreactive toward epoxides at elevated temperatures. Anion exchange with NaI in water gave the iodide salt; the perrhenate band disappeared from the IR spectrum, though the weak μ-O bands remained. Oxidation of the iodide salt with aqueous H_2CrO_4 (Jones' reagent) gave a 37% yield of Cp^*ReO_3 [based on formulating the salt as $\{(Cp^*Re)_3(\mu\text{-}O)_6\}I_2$].

In epoxide reductions and in conproportionation of Cp^*ReO_3 with $(Cp^*ReO)_2(\mu\text{-}O)_2$, this compound was accompanied by formation of an air-stable purple compound **2** that was insoluble in benzene. This second compound became predominant at relatively high rhenium concentrations (Table 1, entries 4, 5); and it was isolated from the conproportionation reaction by precipitation from benzene in 28% yield. Aside from the dramatically different visible spectrum, the only other significant spectroscopic difference from **1** was a new IR peak at 736 cm^{-1} and weak shoulder on the very strong perrhenate Re–O stretch at 908 cm^{-1}. A single sharp peak appeared in the ^1H NMR (δ 2.23 in CD_2Cl_2). We obtained high quality crystals of this compound for X-ray diffraction analysis;[6]§ the structure of the cation is shown in Fig. 1.

This compound is formulated as $\{(Cp^*Re)_3(\mu^2\text{-}O)_3(\mu^3\text{-}O)_3ReO_3\}^+(ReO_4^-)$, a monoperrhenate salt of a cluster. Formally, it can be represented by the coordination of ReO_3^- to **1**, although a more useful interpretation is to view it as the neutral $(Cp^*Re)_3(\mu\text{-}O)_6$ coordinated to ReO_3^+. (The latter is consistent with the theoretical prediction that compound **1** should be a ground-state triplet,[7] and similar to other reported structures.[8]) The ReO_3 unit is a slightly distorted octahedral rhenium in a typical $LReO_3$ environment: the terminal oxo bond lengths are normal [1.668(10), 1.685(13), 1.707(12) Å] as are the O–Re–O angles [103.2(6)°, 105.9(6), 104.1(6)°]. The $Re_3(\mu\text{-}O)_6$ core is similar to the trinuclear dication; the Re–Re distances are 2.750(1) and 2.759(1) Å. There is significant distortion of the

Table 1 Reaction of epoxides with catalytic Cp^*ReO_3 + excess PPh_3[a]

	Epoxide	*c*/M	$[Cp^*ReO_3]$/M	*t*/h	*T*/°C	Conversion (%)	Turnover
1	1,2-Epoxydecane	0.16	0.007	20	116	5%	1.1
2	1,2-Epoxydodecane	0.14	0.007	18	112	< 5%	—
3	1,2-Epoxydodecane	0.14	0.029	13	112	20%	0.9
4	1,2-Epoxydodecane	0.14	0.056	13	112	70%	1.6
5	1,2-Epoxydodecane	0.14	0.14	13	112	> 90%	0.9
6	1,2-Epoxydodecane	0.14	0.007†	13	112	50%	10
7	2,3-Epoxynorbornane	0.23	0.009	6	116	< 5%	—
8	*p*-Bromostyrene Oxide	0.12	0.007	16	90	20%	3.4
9	3-Fluoropropylene Oxide	0.28	0.005	3	116	23%	12.9

[a] $[PPh_3]$ = 0.17 M except entry 6, $[PPh_3]$ = 0.35 M.

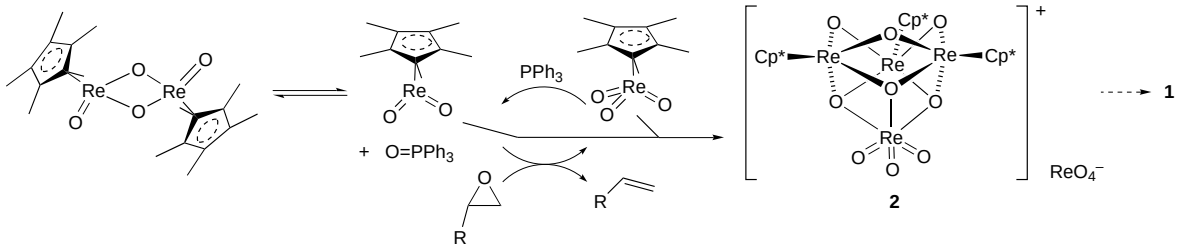

Scheme 1

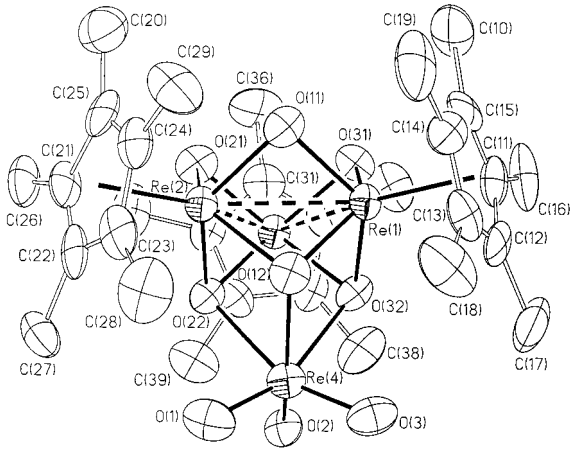

Fig. 1 Crystal structure of the cation for **2**

two sets of bridging oxo ligands compared to compound **1**, with bond lengths averaging to 1.94 Å (μ_2) and 2.02 Å (μ_3). The O–(ReO_3) distances are long at an average of 2.18 Å.

Compound **2** is a precursor to the trinuclear cluster **1**. Heating a Me_2SO solution of **2** in air to 100 °C for 2 h results in quantitative conversion. (Under conditions of the conproportionation or epoxide deoxygenation, Cp^*ReO_3 can play the same chemical role as Me_2SO in converting the ReO_3 unit to perrhenate.)[9] It is still not clear what the origin of the trinuclear core is, nor the fate of the Cp* ligands lost in formation of **1** and **2**. We have seen NMR evidence for monomeric Cp^*ReO_2,[3] but do not see evidence for a trimeric species. It is possible that Cp^*ReO_2 can condense with Cp^*ReO_3, and that this dimeric species initiates a cascade resulting in **2**. Alternatively, if indeed the trinuclear Re^V cluster forms as an equilibrium aggregate of Cp^*ReO_2 units, it may attack Cp^*ReO_3 irreversibly.

Clearly, the success of the catalytic cycle for epoxide deoxygenation (or any other system involving this chemistry) depends on a careful balance of reaction rates (Scheme 1). Cp^*ReO_2 must react with the epoxide substrate rapidly, or else conproportionation will lead to inactivation. The rate of O-atom transfer from epoxide is controlled by the reactivity of the substrate, as seen by the impact of substituent on turnover number. Likewise, Cp^*ReO_3 must be rapidly reduced to Cp^*ReO_2; there is again a competition between reduction and cluster formation. We tested this by increasing the concentration of PPh_3; a 2.4-fold excess led to an increase in conversion from < 5% to 50% (Table 1, Entry 6)! It must be noted that this required an almost saturated solution of PPh_3. Although this modification interferes with the practicality of this catalytic cycle, it shows that the key to an improved system is to design a kinetically more reactive stoichiometric reductant that does not interact with the epoxide.

We wish to thank the donors to the Petroleum Research Fund, administered by the American Chemical Society, and the National Science Foundation (CHE-9619296, CHE-9015466) for support of this work. A. F. T. Y. thanks the National Science Foundation (grant CHE-9711187) for support.

Notes and References

† E-mail: gablek@chem.orst.edu

‡ Examination of the stoichiometric O-atom transfer from substituted styrene oxides shows that reaction is accelerated by electron deficient substituents: K. P. Gable and M. A. Gartman, unpublished work.

§ *Crystal data* for $\{Cp^*Re)_3(\mu^2\text{-}O)_3(\mu^3\text{-}O)_3ReO_3\}ReO_4\cdot NCMe$ (**2**·NCMe). Data were collected on a block shaped (0.5 × 0.3 × 0.2 mm) dark brown crystal of $C_{32}H_{48}NO_{13}Re_5$ (M = 1585.71) on a Siemens P4 equipped with graphite monochromated Cu radiation (μ = 30.002 mm^{-1}) at room temperature. Automated search and indexing routines revealed that the crystals belong to the monoclinic space group $P2_1/c$ (no. 14) with a = 11.180(1), b = 15.631(1), c = 22.612(3) Å, β = 98.614(8)°, U = 3906.8(7) $Å^3$, Z = 4, D_c = 2.696 Mg m^{-3}. Of 10 677 data collected, 5191 were unique (R_{int} = 9.10%), and of these 4997 had $I > 2\sigma(I)$. Data were corrected for the effects of absorption anisotropy by analytical methods (face indexing). The structure was solved using a Patterson map search using SHELXS-90, and expanded by Fourier techniques and refined (full-matrix least-squares refinement on F^2) using SHELXL-93. Refinement of 492 parameters using all data yielded final residuals of R_1 = 0.661, wR_2 = 0.1768. The largest residual electron density peaks (3.28 e^- $Å^{-3}$) were all very close to the Re atoms and are not of chemical significance. CCDC 182/789.

1 W. A. Nugent and J. M. Mayer, *Metal–Ligand Multiple Bonds*, Wiley-Interscience, New York, 1988; R. A. Sheldon and J. K. Kochi, *Metal Catalyzed Oxidations of Organic Compounds*, Academic Press, New York, 1981; *Organic Synthesis by Oxidation with Metal Compounds*, ed. W. J. Mijs, C. R. H. I. deJonghe, Plenum, New York, 1986; K. P. Gable, *Adv. Organomet. Chem.*, 1997, **41**, 127.

2 *Encyclopedia of Reagents for Organic Synthesis*, ed. L. A. Paquette, Wiley, New York, 1995 vol. 3, pp. 1649, 2078; K. G. Molloy, *Inorg. Chem.*, 1988, **27**, 677; P. K. Chowdhury, *J. Chem. Res.*, 1990, (*S*) 192; J. March, *Advanced Organic Chemistry: Reactions, Mechanisms and Structure*, Wiley, New York, 4th edn., 1992, pp. 1029–1030.

3 K. P. Gable, J. J. J. Juliette and M. A. Gartman, *Organometallics*, 1995, **14**, 3138.

4 G. K. Cook and M. A. Andrews, *J. Am. Chem. Soc.*, 1996, **118**, 9448.

5 (*a*) W. A. Herrmann, R. Serrano, M. L. Ziegler, H. Pfisterer and B. Nuber, *Angew. Chem., Int. Ed. Engl.*, 1985, **24**, 50; (*b*) W. A. Herrmann, R. Serrano, U. Küsthardt, E. Guggolz, B. Nuber and M. L. Ziegler, *J. Organomet. Chem.*, 1985, **287**, 329.

6 G. M. Sheldrick, *Acta Crystallogr., Sect. A*, 1990, **46**, 467; G. M. Sheldrick, in *Crystallographic Computing 6*, ed. H. D. Flack, L. Parkanyi and K. Simon, Oxford University Press, Oxford, 1993.

7 P. Hoffmann, N. Rösch and H. R. Schmidt, *Inorg. Chem.*, 1986, **25**, 4470; P. Hoffmann and N. Rösch, *J. Chem. Soc., Chem. Commun.*, 1986, 843.

8 K. Wieghardt, C. Pomp, V. Nuber and J. Weiss, *Inorg. Chem.*, 1986, **25**, 1659; C. Pomp and K. Wieghardt, *Polyhedron*, 1988, **7**, 2537; W. A. Hermann, P. W. Roesky, F. E. Kühn, M. Elison, G. Artus, W. Scherer, C. C. Romão, A. Lopes and J.-M. Basset, *Inorg. Chem.*, 1995, **34**, 4701; J. Xiao, R. J. Puddephatt, L. Manojlović-Muir, K. W. Muir and A. A. Torabi, *J. Am. Chem. Soc.*, 1994, **116**, 1129.

9 K. P. Gable, J. J. J. Juliette, C. Li and S. P. Nolan, *Organometallics*, 1996, **15**, 5250.

Received in Bloomington, IN, USA, 25th November 1997; 7/08516H

Triamidoamine complexes of scandium, yttrium and the lanthanides

Paul Roussel, Nathaniel W. Alcock and Peter Scott*†

Department of Chemistry, University of Warwick, Coventry, UK CV4 7AL

Synthesis of the simple triamidoamine complexes of the group 3 and lanthanide elements is achieved for the first time by reaction of $[Li_3(NN'_3)(thf)_3]$ [NN'_3 = $N(CH_2CH_2NSiMe_3)_3$] with the metal trichlorides; the 'ate' complexes $[M(NN'_3)ClLi(thf)_3]$ (M = Sc, Y, La) thus produced are converted smoothly to $[M(NN'_3)]$ on sublimation *in vacuo*.

The quadridentate triamidoamines $[N(CH_2CH_2NR)_3]^{3-}$ are established as an important class of ligand for the main group, transition and actinide elements. The complexes formed have unique properties as a result, for example, of the formation of a single, sterically protected fifth coordination site.[1] Most recently we have reported the complexation of dinitrogen to a (triamidoamine)uranium centre; an unprecedented feat for an actinide element.[2]

Reported attempts to synthesise the group 3 and lanthanide triamidoamines have thus far led to isolation of a novel trigonal monopyramidal lithium compound,[3] or the formation of the unusual product **I** below.[4]

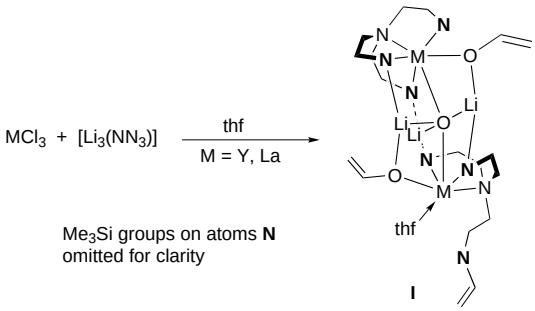

The triamidoamine ligand $[N(CH_2CH_2NR)_3]$ (R = $SiMe_3$) would be expected to have a lower steric demand than the closely related fragment $\{N(SiMe_3)_2\}_3$ because of the constraints of the tripodal chelate structure. The actinide complexes $[U\{N(CH_2CH_2NSiMe_3)_3\}X]$ for example tend to have dimeric or distorted structures unless strong π-donor ligands X are used[5] while the compounds $[U\{N(SiMe_3)_2\}_3X]$ are monomeric.[6] The more sterically demanding triamidoamines R = $SiPr^i_3$ and $SiMePh_2$ form complexes which, in our experience, are difficult to isolate and unreactive. The ligand R = $SiMe_2Bu^t$[7] (henceforth NN'_3) however represents a suitable compromise between steric demand and synthetic utility. In its complexes with the actinides, three *tert*-butyl groups are oriented such that they encircle the equatorial plane in three-fold symmetric (trigonal pyramidal) structures and thus stabilise this geometry while allowing reactivity at the remaining axial site.[8] The complexes are crystalline, soluble and volatile. Using this type of ligand we have synthesised for the first time the simple group 3 and lanthanide triamidoamines.

Reaction of pure $[Li_3(NN'_3)(thf)_3]$ **1** with anhydrous $[MCl_3(thf)_n]$ (M = Sc, Y, La) in thf leads to rapid dissolution of the metal halide and formation of the analytically pure, colourless 'ate' complexes $[M(NN'_3)ClLi(thf)_3]$ (M = Sc **2**, Y **3**, La **4**) in near quantitative yields (Scheme 1).‡

Single crystals of the yttrium compound **3** were grown by slow cooling of a concentrated solution in pentane. The

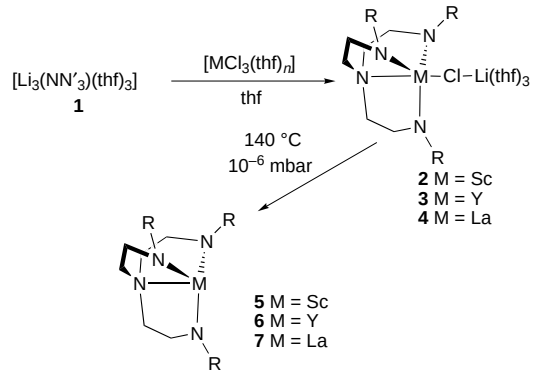

Scheme 1 Synthesis of complexes **2**–**7**

molecular structure shown in Fig. 1 was determined by X-ray diffraction.§ The crystallographically threefold symmetric (triamidoamine)yttrium fragment is distorted from trigonal monopyramidal geometry by the displacement of the yttrium atom 0.67 Å out of the plane defined by the three amido nitrogen atoms. In the related triamides $[M\{N(SiMe_3)_2\}_3]$ (M = Sc, Eu[9] Y,[10] Nd,[11] Yb[12]) the metal atoms all lie 0.4 Å above the plane regardless of the ionic radius of the metal.[13] The apical amino N(1)–Y bond length in **3** is 2.588(4) Å. The amido N(1)–Y bond length of 2.231(2) Å is comparable to 2.226(6) Å found in $[Y\{N(SiMe_3)_2\}_3]$. The Y–Cl bond of 2.6526(16) Å is slightly longer than 2.55 and 2.598(2) Å observed in the 'ate' complexes $[Y\{N(SiMe_3)_2\}_3Cl][Li(thf)_4]$ and $[YR_3ClLi(Et_2O)_3]$ [R = $CH(SiMe_3)_2$], respectively,[10] presumably as a result of the *trans* effect of the amino N(1).

Heating compounds **2**–**4** to 140 °C and 10^{-6} mbar led to the distillation of pure colourless $[M(NN'_3)]$ (M = Sc **5**, Y **6**, La **7**) which solidified on cooling.‡ Trigonal monopyramidal triamidoamine complexes of the first row transition metals have been

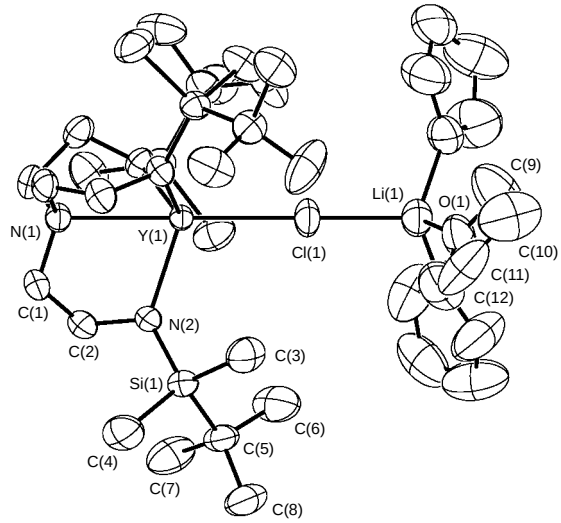

Fig. 1 Thermal ellipsoid plot of the molecular structure of **3**; hydrogen atoms omitted

synthesised,[7,14] but similar complexes of the second and third row have not been detected despite their implication in dinitrogen activation processes.[15] We cannot at present exclude the possibility of an agostic C–H–Y interaction in the apical coordination site, although no unusual NMR or IR shifts were observed.

Variable temperature NMR spectra of **2** in [$^2H_8$]toluene solution show that an equilibrium is established between the 'ate' complex [Sc(NN′$_3$)ClLi(thf)$_3$] **2** and [Sc(NN′$_3$)] **5** with the ratio [**5**] : [**2**] = 1 : 2.0 at 293 K. For the yttrium compounds, the ratio [**6**] : [**3**] is 1 : 22 while for lanthanum the base-free compound [La(NN′$_3$)] is not observed up to *ca*. 373 K. Thus the increase in atomic radius from Sc^{III} (0.89 Å) to Ln^{III} (1.17 Å) is accompanied by increased stability of the 'ate' complex; a good example of the prevalence of steric over electronic effects in lanthanide chemistry.

Complexes analogous to **2**–**7** are readily prepared for all of the stable lanthanides; we will report the trends in magnetic and spectroscopic properties of these compounds in due course. They have potential applications as regioselective Lewis acid catalysts by virtue of their single, sterically protected coordination site; related chiral titanatranes are effective enantioselective catalysts.[16] For the moment, we have shown that with suitable choice of ligand substituent, the elusive triamidoamine complexes of scandium and the rare earth elements can be synthesised.

P. S. wishes to thank the EPSRC for a Project Studentship, BNFL for a CASE award (to P. R.), and Pfizer Ltd. and SmithKline Beecham for support.

Notes and References

* E-mail: peter.scott@warwick.ac.uk

† *Characterising data*: for **2**: ^{1}H NMR (293 K, [$^2H_6$]benzene, see text), δ 3.7 (br m, 12 H, thf), 3.56 (t, 6 H, CH_2), 2.68 (t, 6 H, CH_2), 1.40 (m, 12 H, thf), 1.23 (s, 27 H, Bu^t), 0.43 (s, 18 H, $SiMe_2$). ^{13}C{^{1}H} NMR (293 K, [$^2H_6$]benzene), δ 68.59 (thf), 65.91 (CH_2), 45.99 (CH_2), 28.61 (C*Me*$_3$), 25.48 (thf), 21.65 (*C*Me$_3$), −2.41 ($SiMe_2$). ^{7}Li{^{1}H} NMR (293 K, [$^2H_6$]benzene), δ 1.80 (br s). MS (EI) as for **5**. For **3**: ^{1}H NMR (293 K, [$^2H_6$]benzene, see text), δ 3.56 (m, 15 H, CH_2 and thf), 2.64 (t, 6 H, CH_2), 1.4 (m, 12 H, thf), 1.22 (s, 27 H, Bu^t), 0.41 (s, 18 H, $SiMe_2$). ^{13}C{^{1}H} NMR (293 K, [$^2H_6$]benzene), δ 68.69 (thf), 65.15 (CH_2), 46.01 (CH_2), 28.67 (C*Me*$_3$), 25.46 (thf), 21.34 (*C*Me$_3$), −3.32 ($SiMe_2$). ^{7}Li{^{1}H} NMR (293 K, [$^2H_6$]benzene), δ 0.38 (s). MS (EI) as for **6**. For **4**: ^{1}H NMR (293 K, [$^2H_8$]toluene, see text), δ 3.62 (br m, 12 H, thf), 3.54 (t, 6 H, CH_2), 2.72 (t, 6 H, CH_2), 1.36 (m, 12 H, thf), 1.11 (br s, 27 H, Bu^t), 0.16 (br s, 18 H, $SiMe_2$). ^{13}C{^{1}H} NMR (293 K, [$^2H_8$]toluene), δ 68.44 (thf), 47.25 (CH_2), 27.96 (C*Me*$_3$), 25.45 (thf), 20.89 (*C*Me$_3$), 14.27 (CH_2), −4.32 ($SiMe_2$). ^{7}Li{^{1}H} NMR (293 K, [$^2H_6$]benzene), δ 1.80 (br s). ^{139}La{^{1}H} (298 K, [$^2H_6$]benzene), δ 1035.2 (s). MS (EI) as for **7**. For **5**: ^{1}H NMR (293 K, [$^2H_8$]toluene), δ 3.32 (t, 6 H, CH_2), 2.56 (t, 6 H, CH_2), 1.01 (s, 27 H, Bu^t), 0.13 (s, 18 H, $SiMe_2$). ^{13}C{^{1}H} NMR (293 K, [$^2H_8$]toluene), δ 58.84 (CH_2), 45.11 (CH_2), 27.61 (C*Me*$_3$), 20.40 (C*Me*$_3$), −3.82 ($SiMe_2$). MS (EI) *m/z* 530 (63%, M$^+$), 515 (14%, M$^+$ − Me), 473 (100%, M$^+$ − Bu^t). For **6**: ^{1}H NMR (293 K, [$^2H_8$]toluene), δ 3.39 (t, 6 H, CH_2), 2.57 (t, 6 H, CH_2), 1.00 (s, 27 H, Bu^t), 0.08 (s, 18 H, $SiMe_2$). ^{13}C{^{1}H} NMR (293 K, [$^2H_8$]toluene), δ 57.23 (CH_2), 45.88 (CH_2), 27.49 (C*Me*$_3$), 20.40 (*C*Me$_3$), − 4.23 ($SiMe_2$). MS (EI) *m/z* 574 (45%, M$^+$), 559 (12%, M$^+$ − Me), 517 (80%, M$^+$ − Bu^t). For **7**: ^{1}H NMR (293 K, [$^2H_8$]toluene), δ 3.57 (t, 6 H, CH_2), 2.71 (t, 6 H, CH_2), 1.00 (s, 27 H, Bu^t), 0.08 (s, 18 H, $SiMe_2$). ^{13}C{^{1}H} NMR (293 K, [$^2H_8$]toluene), δ 57.48 (CH_2), 47.65 (CH_2), 27.44 (C*Me*$_3$), 20.37 (*C*Me$_3$), −4.59 ($SiMe_2$). MS (EI) *m/z* 624 (16%, M$^+$), 609 (7%, M$^+$ − Me), 567 (33%, M$^+$ − Bu^t).

§ *Crystal data* for **3**. $C_{36}H_{81}ClLiN_4O_3Si_3Y$, M = 833.62, cubic, space group $Pa\bar{3}$, a = 21.486(2) Å, U = 9919.0(16) Å^3 (by least squares refinement on 6602 reflection positions), Z = 8, D_c = 1116 Mg m^{-3}, F(000) = 3600. Colourless needle 0.52 × 0.16 × 0.14 mm at 180(2) K, final R_1, wR_2 and S were 0.0486, 0.0961 and 1.070. CCDC 182/797.

1 J. G. Verkade, *Acc. Chem. Res.*, 1993, **26**, 483; *Coord. Chem. Rev.*, 1994, **137**, 233; R. R. Schrock, *Acc. Chem. Res.*, 1997, **30**, 9; *Pure Appl. Chem.*, 1997, **69**, 2197.
2 P. Roussel and P. Scott, *J. Am. Chem. Soc.*, 1998, **120**, 1070.
3 D. Zhibang, V. G. Young and J. G. Verkade, *Inorg. Chem.*, 1995, **34**, 2179.
4 H. C. Aspinall and M. R. Tillotson, *Inorg. Chem.*, 1996, **35**, 2163.
5 P. Scott and P. B. Hitchcock, *J. Chem. Soc., Dalton Trans.*, 1995, 603; *J. Chem. Soc., Chem. Commun.*, 1995, 579; P. Roussel, P. B. Hitchcock, N. D. Tinker and P. Scott, *Inorg. Chem.*, 1997, **36**, 5716.
6 H. W. Turner, R. A. Andersen, A. Zalkin and D. H. Templeton, *Inorg. Chem.*, 1979, **18**, 1221.
7 C. C. Cummins, J. Lee, R. R. Schrock and W. M. Davis, *Angew. Chem., Int. Ed. Engl.*, 1992, **31**, 1501.
8 P. Roussel, P. B. Hitchcock, N. D. Tinker and P. Scott, *Chem. Commun.*, 1996, 2053.
9 J. S. Ghotra, M. B. Hursthouse and A. J. Welch, *J. Chem. Soc., Chem. Commun.*, 1973, 669.
10 M. Westerhausen, M. Hartmann, A. Pfitzner and W. Schwarz, *Z. Anorg. Allg. Chem.*, 1995, **621**, 837.
11 R. A. Andersen, D. H. Templeton and A. Zalkin, *Inorg. Chem.*, 1978, **17**, 2317.
12 P. J. Eller, D. C. Bradley, M. B. Hursthouse and D. W. Meek, *Coord. Chem. Rev.*, 1977, **24**, 1.
13 K. N. Raymond and C. W. Eigenbrot, *Acc. Chem. Res.*, 1980, **13**, 276.
14 C. Rosenberger, R. R. Schrock and W. M. Davis, *Inorg. Chem.*, 1997, **36**, 123.
15 K.-Y. Shih, R. R. Schrock and R. Kempe, *J. Am. Chem. Soc.*, 1994, **116**, 8804.
16 W. A. Nugent, T. V. Rajanabu and M. J. Burk, *Science*, 1993, **259**, 479.

Received in Basel, Switzerland, 8th December 1997; 7/08785C

Resonant magnetization tunnelling in the half-integer-spin single-molecule magnet $[PPh_4][Mn_{12}O_{12}(O_2CEt)_{16}(H_2O)_4]$

Sheila M. J. Aubin,[a] Stefano Spagna,[b] Hilary J. Eppley,[c] Ronald E. Sager,[b] George Christou*[c] and David N. Hendrickson*[a]

[a] *Department of Chemistry and Biochemistry-0358, University of California at San Diego, La Jolla, CA 92093, USA*
[b] *Quantum Design, 11578 Sorrento Valley Road, Suite 30, San Diego, CA 92121, USA*
[c] *Department of Chemistry, Indiana University, Bloomington, IN 47405-4001, USA*

Steps are observed on the magnetization hysteresis loop for an oriented crystal sample of $[PPh_4][Mn_{12}O_{12}(O_2CEt)_{16}(H_2O)_4]$ and these are taken as evidence for field-tuned resonant magnetization tunnelling between quantum levels of the $S = 19/2$ ground state.

The interest in single-molecule magnets (SMM) is growing.[1,2] A SMM has a large spin ground state with such a large magnetic anisotropy that an individual molecule exhibits hysteresis in its magnetization *vs.* external field response. The first SMM reported[3–5] is neutral $[Mn_{12}O_{12}(O_2CMe)_{16}(H_2O)_4]\cdot 2(HO_2CMe)\cdot 4H_2O$ **1** (denoted Mn_{12}-acetate), which has an $S = 10$ ground state. Molecules possessing Mn_{12},[6] Mn_4,[7] Fe_8,[8] and V_4[9] metal contents have been found to function as SMM. Recently, Friedman *et al.*[10] reported the initial observation of resonant magnetization tunnelling for Mn_{12}-acetate; steps were observed at regular intervals of magnetic field in the magnetization hysteresis loop for oriented crystals. Here, we report the observation of steps in the hysteresis loop for oriented crystals of the salt $[PPh_4][Mn_{12}O_{12}(O_2CEt)_{16}(H_2O)_4]$ **2**. In previous work we have shown[11] the $[Mn_{12}]^-$ anions in **2** have an $S = 19/2$ ground state. The observation of resonant quantum tunnelling in this salt is of considerable interest since a half-integer-spin system should not tunnel coherently in the absence of a magnetic field.[12,13]

In solution, it is possible to add a single electron to a Mn_{12} molecule, and the X-ray crystal structure[11] for complex **2** shows that the added electron is localized on an outer (originally Mn^{3+}) ion rather than an inner (cubane) Mn^{4+} ion, producing a trapped-valence Mn^{2+}, $Mn^{3+}{}_7$, $Mn^{4+}{}_4$ anion in the crystal. The $[Mn_{12}]^-$ anion has an $S = 19/2$ ground state with the double-well potential energy diagram shown in Fig. 1. There are 20 different states with $m_s = \pm 19/2, \pm 17/2 \ldots, \pm 1/2$. The double well represents the change in potential energy of one $[Mn_{12}]^-$ anion in zero field as the anion changes the direction of its magnetic moment from 'spin up' (parallel to *z*-axis) where $m_s = +19/2$ to 'spin down' (antiparallel to *z*-axis) where $m_s = -19/2$. The barrier height U is $90|D|$, where D is the parameter characterizing the axial zero-field splitting (DS_z^2) in the $S = 19/2$ ground state.

The rate of relaxation of the magnetization was measured for a polycrystalline sample of **2** equilibrated at one of five temperatures in the range 1.8–2.5 K in an external magnetic field of 3.5 T; the latter was then quenched to zero. The decrease in the magnetization measured at each temperature was fitted to a distribution of single exponentials to give the relaxation rate. Relaxation rates were also determined in the range 3.2–7.2 K by means of ac magnetic susceptibility measurements in zero dc field. At a fixed temperature, the in-phase (χ_M') and out-of-phase (χ_M'') components of magnetic susceptibility were measured as the frequency of the ac field (0.05 Oe) was varied from 0.01 to 1500 Hz. The relaxation time (τ) at a given temperature was determined by fitting the data to eqn. (1),[14] where ω is the angular frequency ($2\pi\nu$), χ_S is the adiabatic susceptibility (*i.e.* $\omega \rightarrow \infty$) and χ_T is the isothermal

$$\chi_M' = \chi_S + (\chi_T - \chi_S)/(1 + \omega^2\tau^2) \quad (1)$$

susceptibility (*i.e.* $\omega \rightarrow 0$). The relaxation rates vary from 3.94×10^4 s^{-1} at 7.2 K to 6.19×10^{-6} s^{-1} at 1.8 K. Fig. 2 shows an Arrhenius plot of $\ln(1/\tau)$ *vs.* $1/T$. These data were fit to the Arrhenius law to give a barrier height, U, of 60.2 K with a pre-exponential ($1/\tau_0$) of 1.31×10^8 s^{-1}. This compares with $U = 61$–67 K and $1/\tau_0 \simeq 10^7$ s^{-1} found[4,5] for the $S = 10$ molecule, Mn_{12}-acetate.

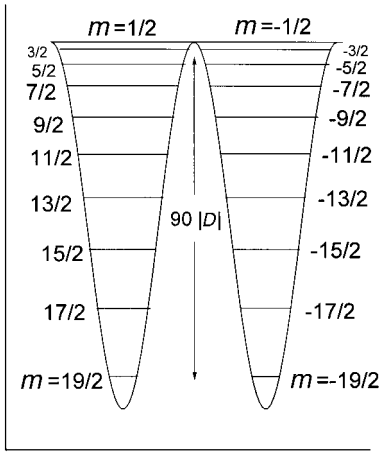

Fig. 1 Plot of potential energy *vs.* the magnetization direction for a single molecule with an $S = 19/2$ ground state in zero magnetic field. Axial zero-field interactions split the $S = 19/2$ state into $m = \pm 19/2, \pm 17/2, \ldots, \pm 1/2$ levels.

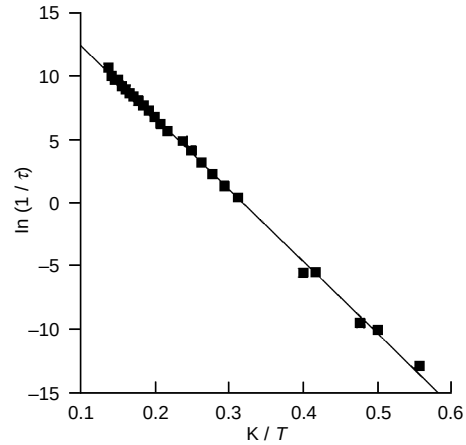

Fig. 2 Plot of the logarithm of the rate of relaxation *vs.* the inverse absolute temperature for $[PPh_4][Mn_{12}O_{12}(O_2CEt)_{16}(H_2O)_4]$ **2**

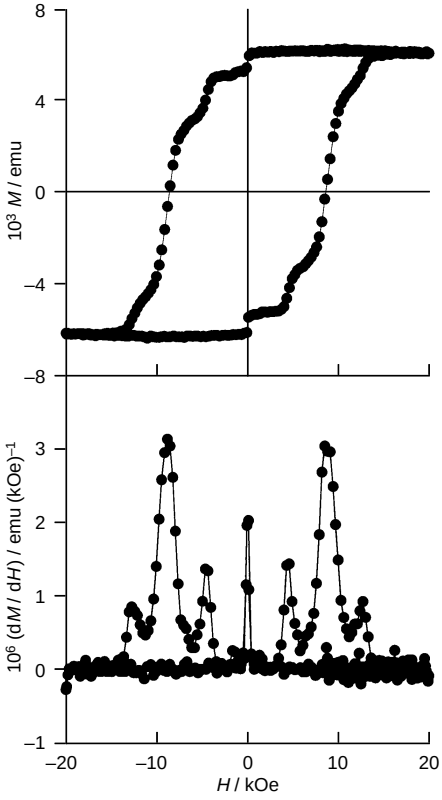

Fig. 3 The top plot shows the magnetization hysteresis loop measured at 1.85 K for five crystals of $[PPh_4][Mn_{12}O_{12}(O_2CEt)_{16}(H_2O)_4]$ **2** oriented in an eicosane wax matrix. In the lower plot is shown a plot of the first derivative of the magnetization hysteresis loop.

Five small crystals (3 × 0.1 × 0.1 mm) of **2**, grown from CH_2Cl_2–hexanes, were suspended in eicosane held at 40 °C and the suspension introduced into a 5.5 T field, whereupon the five crystals were oriented each with its easy axis parallel to the field. The eicosane was then cooled to room temperature, to give a solid wax cube with the five crystals oriented with parallel easy axes. Fig. 3 shows the hysteresis loop taken at 1.85 K with the magnetic field applied along the easy axes of the crystals. The sample was first saturated in a field of +2.0 T, and the field then swept down to −2.0 T, and cycled back to +2.0 T. The rate of change of the field was 25 Oe s^{-1} and each data point was measured within a few milliseconds. The whole hysteresis loop was collected in 1 h. Steps can clearly be seen on the hysteresis loop, as was reported[10] for the neutral molecule, Mn_{12}-acetate. In the lower part of Fig. 3 is shown the first derivative of the hysteresis plot. As the field is decreased from +2.0 T, the first step is seen at zero field, followed by steps at −0.4686, −0.9022 and −1.262 T. The steps correspond to increases in the rate of change of the magnetization, and are attributable to resonant tunnelling between quantum spin states. With reference to Fig. 1, a +2.0 T field leads to a stabilization in energy of the m_s = −19/2 and a destabilization of the m_s = +19/2 state. When there is saturation, all of the molecules are in the m_s = −19/2 state. As the field is decreased, the first step in the hysteresis loop is seen at zero field. Resonant tunneling occurs because the m_s levels on the right-hand side of the double well have the same energies as the m_s levels on the left.

The simplest Hamiltonian for $[PPh_4][Mn_{12}O_{12}(O_2CEt)_{16}(H_2O)_4]$ **2** is given by eqn. (2).

$$\hat{H} = -D\hat{S}_z^2 - g\mu_B\hat{S}\cdot\hat{H} \quad (2)$$

If the field is applied along the easy axis, then the eigenstates are $|S, m_s>$. The first term in the Hamiltonian gauges the axial zero-field splitting of the S = 19/2 ground state. Physically, this zero-field splitting of the ground state is largely due to the single-ion zero-field splitting at the Mn^{3+} ions in the $[Mn_{12}]^-$ anion. With the above Hamiltonian, it can be shown that the spacings between the steps in the hysteresis loop are given as $\Delta H = -Dn/g\mu_B$, where n = 0, 1, 2, 3, ... From Fig. 3, we calculate the average step size to be ΔH = 0.42 T, which gives a value of D/g of 0.20 cm^{-1}, identical to the value obtained for **2** by fitting variable-field magnetization data,[11] and high-field EPR data more recently.

Friedman *et al.*[10] observed six steps for the neutral Mn_{12}-acetate, including the step at zero field, as the field was swept from zero to −3 T after saturation in a +3 T field. We have observed only four steps for the salt **2**, presumably due to the faster relaxation rate of the latter complex. At lower temperatures, more steps should be seen since the relaxation rate will decrease. For both molecular systems, each successive step is seen. This is interesting because the Mn_{12}-acetate molecule has an integer spin ground state with S = 10, whereas the $[Mn_{12}]^-$ anion has a half-integer-spin ground state with S = 19/2. There have been several papers[12,13] addressing the fact that a molecule with an odd number of unpaired electrons (such as S = 19/2) should not exhibit resonant tunnelling in the absence of a magnetic field. For such a molecule, each pair of $\pm m_s$ levels in zero-field exhibits Kramers degeneracy. An S = 19/2 molecule should not be able to tunnel coherently between the m_s = −19/2 and m_s = +19/2 levels, or for that matter, between any m_s and $-m_s$ pair in the absence of a magnetic field. However, clearly the salt of $[Mn_{12}]^-$ shows steps on the hysteresis loop. A possible mechanism for resonant tunneling in this S = 19/2 molecule centers around the nuclear spins in the molecule. The ^{55}Mn and ^1H nuclei have spins of I = 5/2 and I = 1/2, respectively, and this will give rise to a small internal magnetic field (10–200 G) in the molecule. A transverse component of this internal magnetic field may lead to resonant tunnelling for an oriented collection of $[Mn_{12}]^-$ molecules in zero external field.

This work was supported by the National Science Foundation. The W. M. Keck Foundation provided funds for the SQUID magnetometer used in the ac susceptibility experiments.

Notes and References

† E-mail: christou@indiana.edu

1 B. Schwarzschild, *Physics Today*, January 1997, 17.
2 E. M. Chudnovsky, *Science*, 1995, **274**, 938.
3 R. Sessoli, D. Gatteschi, A. Caneschi and M. A. Novak, *Nature*, **365**, 141; D. Gatteschi, A. Caneschi, L. Pardi and R. Sessoli, *Science*, 1994, **265**, 1054.
4 R. Sessoli, H.-L. Tsai, A. R. Schake, S. Wang, J. B. Vincent, K. Folting, D. Gatteschi, G. Christou and D. N. Hendrickson, *J. Am. Chem. Soc.*, 1993, **115**, 1804.
5 F. Lionti, L. Thomas, R. Ballou, B. Barbara, A. Sulpice, R. Sessoli and D. Gatteschi, *J. Appl. Phys.*, 1997, **81**, 4608.
6 S. M. J. Aubin, Z. Sun, I. A. Guzei, A. L. Rheingold, G. Christou and D. N. Hendrickson, *Chem. Commun.*, 1997, 2239.
7 S. M. J. Aubin, M. W. Wemple, D. M. Adams, H.-L. Tsai, G. Christou and D. N. Hendrickson, *J. Am. Chem. Soc.*, 1996, **118**, 7746.
8 C. Sangregorio, T. Ohm, C. Paulsen, R. Sessoli and D. Gatteschi, *Phys. Rev. Lett.*, 1997, **78**, 4645.
9 S. L. Castro, Z. Sun, C. M. Grant, J. C. Bollinger, D. N. Hendrickson and G. Christou, *J. Am. Chem. Soc.*, in press.
10 J. R. Friedman, M. P. Sarachik, J. Tejada and R. Ziolo, *Phys. Rev. Lett.*, 1996, **76**, 3830.
11 H. J. Eppley, H.-L. Tsai, N. de Vries, K. Folting, G. Christou and D. N. Hendrickson, *J. Am. Chem. Soc.*, 1995, **117**, 301.
12 D. Loss, D. P. Di Vincenzo, G. Grinstein, D. Awschalom and J. F. Smyth, *Physica B*, 1993, **189**, 189.
13 D. P. Di Vincenzo, *Physica B*, 1994, **197**, 109.
14 R. L. Carlin, *Magnetochemistry*, Springer-Verlag, Berlin, 1986.

Received in Bloomington, IN, USA, 21st January 1998; 8/00586I

Solar light induced carbon–carbon bond formation *via* TiO_2 photocatalysis

Laura Cermenati,[a] Christoph Richter[b] and Angelo Albini[a]†

[a] *Department of Organic Chemistry, University of Pavia, via. Taramelli 10, 27100 Pavia, Italy*
[b] *Plataforma Solar de Almeria, PO Box, 22, 04200 Tabernas, Almeria, Spain*

Solar light irradiation of a TiO_2 suspension in MeCN containing maleic anhydride and 4-methoxybenzyl(trimethyl)silane gives benzylated succinic acid (or anhydride) on a gram scale.

Irradiation of a semiconductor ($\lambda \geqslant \Delta E_{bg} = E_{cb} - E_{vb}$, see Scheme 1) causes charge separation. If a significant part of the solar emission is absorbed, methods for solar energy conversion based on this principle can be devised. Most of the research in this field makes use of titanium dioxide, an inexpensive, chemically stable and atoxic semiconductor which absorbs all of the UV component of the solar spectrum.[1–4] Photoelectrochemical solar cells have been devised and their efficiencies have been considerably improved over the years. However, solar light is diffuse, and electrical power produced in this way remains expensive.[5] The same holds for the production of fuels, *e.g.* hydrogen, which is also feasible using this principle.[5] On the other hand, the production of fine chemicals may be rewarding. We report here an example of the use of solar light for the most typical reaction of organic synthesis, carbon–carbon bond formation, *via* TiO_2 photocatalysis. The reaction considered is the radical alkylation of electron-withdrawing substituted olefins.

When planning a synthesis based on TiO_2 photocatalysis, the problem is to translate a *transient* charge separation (electron-hole recombination on the semiconductor surface takes place in *ca*. 30 ps)[6] into an irreversible and selective reaction. The system we used is outlined in eqns. (1)–(4). The solution

$$TiO_2(h^+, e^-) + R^1X + R^2Z \rightarrow TiO_2 + R^1X^{+\cdot} + R^2Z^{-\cdot} \quad (1)$$

$$R^1X^{+\cdot} + TiO_2(e^-) \rightarrow TiO_2 + R^1X \quad (2)$$

$$R^1X^{+\cdot} + R^2Z^{-\cdot} \rightarrow R^1X + R^2Z \quad (3)$$

$$R^1X^{+\cdot} \rightarrow R^{\cdot} \rightarrow \text{Products} \quad (4)$$

must contain *both* a donor and an acceptor with the suitable redox potential [see eqn. (1)] since return electron transfer to the surface [*e.g.* eqn. (2)] would otherwise immediately quench the key intermediate. One of the radical ions should react rapidly in order to prevent back electron transfer after diffusion [eqn. (3)] from quenching the reaction. In our case, the reaction is cleavage of the radical cation leading to a radical, which is then trapped in the desired chemical reaction [eqn. (4)]. This implies that the radical anion should not fragment, because otherwise statistical radical coupling ($R^{1\cdot} + R^{2\cdot}$) would result, and that efficient trapping prevents dimerisation of $R^{1\cdot}$.

In the present case, 4-methoxybenzyl(trimethyl)silane (see Scheme 1, E_{ox} 1.31 V *vs*. SCE in MeCN, *cf.* E_{vb} 2.2 V for TiO_2) functions as the fragmentable donor and either maleic acid or maleic anhydride (E_{red} −0.84 V, *cf.* E_{cb} −0.8 V) has the double role of electron acceptor and radical trap.

Thus, an MeCN solution (1 l) of the silane (3.88 g, 0.02 M) and maleic anhydride (2.16 g, 0.022 M) containing TiO_2 (1.4 g) (untreated Degussa P25 pigment) was pumped by means of a peristaltic pump through a refrigerated tube sitting in the focus of a parabolic mirror (surface exposed to the sun 0.2 m^2), while maintaining a slow flux of nitrogen and keeping the temperature at 15 °C. This arrangement was sufficient for maintaining a uniform suspension of TiO_2 in the tube. After 10 h (July, Almeria, sunny day) of exposure to solar light, the suspension was filtered, the solvent evaporated and the residue recrystallized to give 2.86 g (65%) of 2-(4-methoxybenzyl)succinic anhydride. Minor products were 4,4′-bis(4-methoxy)bibenzyl and 2,3-bis(4-methoxybenzyl)succinic anhydride.

Monitoring the reaction by GC showed that it followed the expected zero-order kinetics, and reagent consumption and

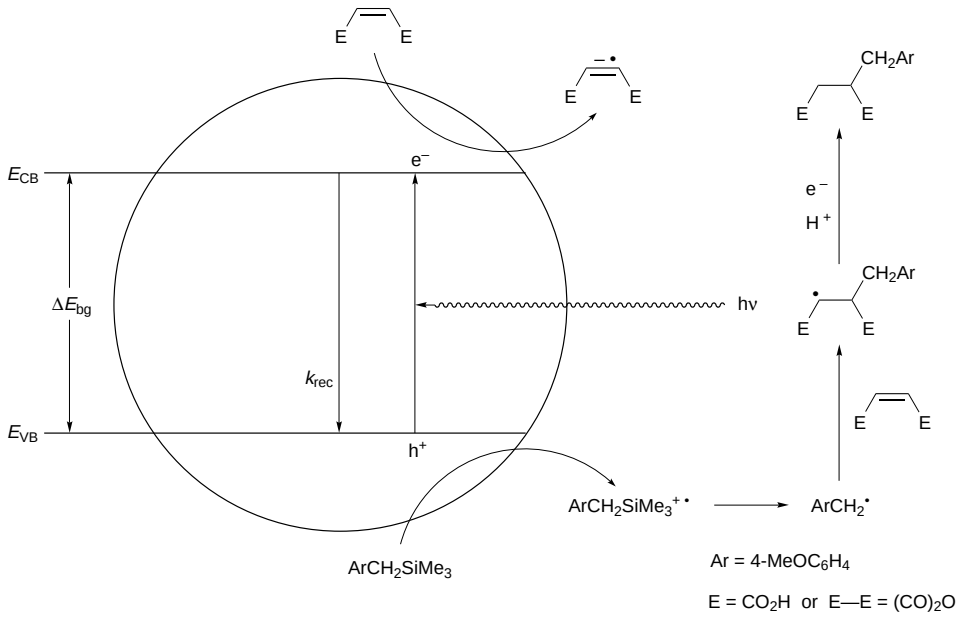

Scheme 1

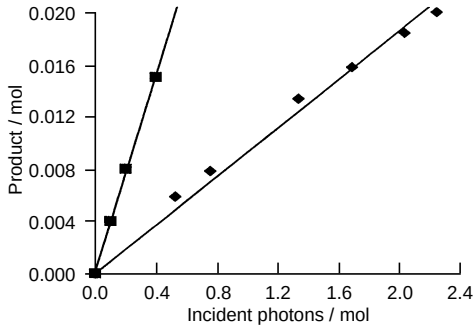

Fig. 1 Formation of (■) 4-Methoxybenzylsuccinic anhydride or (◆) acid *vs.* incident UV photons

product formation were proportional to the integrated incident flux‡ (Fig. 1). A similar reaction course and a similar yield of the benzylated succinic acid was obtained when maleic acid was used in the place of the anhydride, although this required 22 h exposure overall. Furthermore, the alkylation could be effected with other donors, *e.g.* 4-methoxyphenylacetic acid.

These reactions are initiated by hole/electron transfer to produce a pair of radical ions (see Scheme 1). The alkene radical anion is stable, while the silane radical cation fragments and gives the 4-methoxybenzyl radical. Under the present conditions this is mainly trapped by maleic anhydride (or acid), rather than coupling. The adduct radical is reduced by the persistent radical anion of the acceptor or by electron transfer at the semiconductor surface, and protonated by water present in MeCN to give the final products. Operation of a similar mechanism for photoinduced electron transfer initiated alkylation of unsatured acid derivatives had been previously demonstrated to occur when a soluble sensitizer was used (although in that case no benzylation was observed),[7] but has no precedent in photocatalysis.§ The change to a heterogeneous sensitiser simplifies the method, since introduction of other species into the solution is avoided, work-up is simpler and the semiconductor can be recovered.

Exploitation of solar light in this way is not efficient (at the present stage 'apparent'¶ quantum yields are *ca*. 3% for the anhydride and 1% for the acid, see Fig. 1, and the literature shows that in general this quantity does not exceed 10% with TiO_2 sensitised reactions,[9] in part due to reflection). However, a good yield of alkylated products is obtained on a reasonable scale by this simple method, both solvent and semiconductor are easily recovered and reused, and little excess reagents or by-products remain. This may induce further exploration of heterogeneous photocatalysis for organic synthesis beyond the few cases that are known to date,[8,10] and lead to its use, along with homogeneous photoreactions,[11] for the exploitation of solar light.

Support of this work by the EC under the TMR program is gratefully acknowledged.

Notes and References

† E-mail: albini@chifis.unipv.it

‡ This was measured by means of a calibrated photometer (λ < 400 nm).

§ A 30% yield of dihydrofuranyldiphenylhydrazine (also on a gram scale) has been obtained by Kish *via* CdS photocatalysis from azobenzene and dihydrofuran; in that case, however, the key step is radical coupling (see ref. 8).

¶ Based on the total flux incident on the reflecting mirror surface exposed to the sun, 0.2 m²) and the fact that this is concentrated on a Pyrex tube (∅ 3 cm, length 1 m), coaxial with the mirror, in which the solution flows. No account is taken of any loss by refraction or reflection.

1 A. Fujishima and K. Honda, *Nature*, 1972, **238**, 37.
2 K. C. Chang, A. Heller, B. Schwartz, S. Menezes and B. Miller, *Science*, 1977, **196**, 1097.
3 A. Heller, *Acc. Chem. Res.*, 1995, **28**, 503.
4 M. Graetzel, *J. Sol-Gel Sci. Technol.*, 1994, **2**, 673.
5 L. Jacob, E. Oliveros, O. Legrini and A. M. Braun, *Trace Met. Environ.*, 1993, **3**, 511.
6 D. E. Skinner, D. P. Colombo, J. A. Cavalieri and R. M. Bowman, *J. Phys. Chem.*, 1995, **99**, 7853; N. Serpone, D. Lawless, R. Khairutdinov and E. Pelizzetti, *J. Phys. Chem.*, 1995, **99**, 16 655.
7 M. Fagnoni, M. Mella and A. Albini, *J. Am. Chem. Soc.*, 1995, **117**, 7877; M. Mella, M. Fagnoni, M. Freccero, E. Fasani and A. Albini, *Chem. Soc. Rev.*, 1998, 81.
8 R. Kuenneth, C. Feldmer, F. Knoch and H. Kisch, *Chem. Eur. J.*, 1995, **1**, 441; W. Schindler, F. Knoch and H. Kisch, *Chem. Ber.*, 1996, **129**, 925.
9 N. Serpone, *J. Photochem. Photobiol. A*, 1997, **97**, 1.
10 M. A. Fox, *Top. Curr. Chem.*, 1987, **142**, 71; M. A. Fox and M. T. Dulay, *Chem. Rev.*, 1993, **93**, 417; H. Kish, *J. Prakt. Chem.*, 1994, **336**, 635.
11 P Esser, B. Pohlmann and H. D. Scharf, *Angew. Chem., Int. Ed. Engl.*, 1994, **33**, 2009; *Angew. Chem.*, 1994, **106**, 2085.

Received in Cambridge, UK, 22nd December 1997; 7/09172I

New type formation of 1,3-enynes (or internal alkynes) *via* coupling of organoboranes with alkynylcopper compounds mediated by copper(II)

Yuzuru Masuda,*† Miki Murata, Kaname Sato and Shinji Watanabe

Department of Materials Science, Kitami Institute of Technology, Kitami 090-8507, Japan

The copper(II)—mediated coupling reaction of alkenyldialkyl- or trialkyl-boranes with alkynylcopper compounds (generated *in situ*), in the presence of appropriate solvents and a small amount of water, gives (*E*)-1,3-enynes (or disubstituted alkynes) with various functional groups in reasonable yields.

Conjugated enynes are attractive organic compounds,[1,2] and in recent years[3] have been mainly constructed *via* coupling reactions[4] of organometallic compounds (alkynyl[5] or alkenyl[6,7]) with organic halides (alkenyl[5] or alkynyl[6,7]) respectively. They can also be synthesized *via* the internal coupling of lithium (dialkyl) (alkenyl)(alkynyl)borates by I_2[8a] or of (alkyl)-(alkenyl) (alkynyl)boranes by I_2 and MeOK.[8b] Internal alkynes can also be formed in a similar manner.[4,8c]

Previously we found a synthesis of alkenyl[9a] or alkyl[9b] cyanides *via* copper(II) acetate—mediated reactions of alkenyl- or alkyl-boranes[10] with copper(I) cyanide. This observation led us to investigate a synthetic approach to 1,3-enynes (or substituted alkynes) *via* a similar reaction employing copper(I) acetylides, regarding them simply as copper(I) cyanide analogues.

Thus, although the reaction of (*E*)-hex-1-enylbis(1,2-dimethylpropyl)borane[11] **1a** with neat hexynylcopper (prepared and isolated *via* the generally known method), in the presence of copper(II) acetate, HMPT and a small amount of water, generated (*E*)-dodec-5-en-7-yne **2a** in unsatisfactory yield (35%), accompanied with dodeca-5,7-diyne (10%), the introduction of copper(II) nitrate trihydrate to the reaction mixture provided the enyne **2a** in 77% yield (GC) and the diyne in 3% yield. In a similar reaction employing hexyldicyclohexylborane[11] **1a′**, the introduction of $Cu(acac)_2$[9b] along with $Cu(OAc)\cdot H_2O$ afforded dodec-5-yne **2a′** in 70% yield [in the absence of $Cu(acac)_2$, the yield was 25%].

In order to obtain more practical synthesis, further improvements of the reaction procedures were attempted. Consequently, the sequence shown in Scheme 1, which probably proceeds *via in situ* generation[12] of the alkynylcopper species [from alk-1-ynes with copper(I) iodide], was used instead of that previously described which utilised neat reactants prepared separately. DMA–pyridine was the solvent system of choice for enynes **2** (or DMA alone for internal alkynes **2′**).

For the synthesis of internal alkynes **2′**, the participation of CuI was not always essential (suggesting that copper acetate might take the place of the copper iodide).[13] However, for the syntheses of enynes **2**, its absence always led to poor results. In this manner, conjugated (*E*)-alkenynes **2** or disubstituted alkynes **2′** were produced easily‡ and isolated§ with high selectivities [*E*-isomers > 99%; the diynes (by-product) were present in trace amounts] and in reasonable yields as shown in Table 1 (entries 1–3 and 13–14).

The present reaction tolerates various functional groups on the alkyne moiety (R^2) to afford **2d** (entry 4), **2e** (entry 5), **2f** (entry 6), **2g**¶ (entry 7), **2h**‖ (entry 8), **2l** (entry 12), **2d′** (entry 15) and **2m′** (entry 16), in a similar manner to that for the reaction using alkynylcopper.[5a] In contrast, the reaction using lithium alkynylborate[8a] would have some problems in this aspect. Also, the toleration of functional groups on the boron

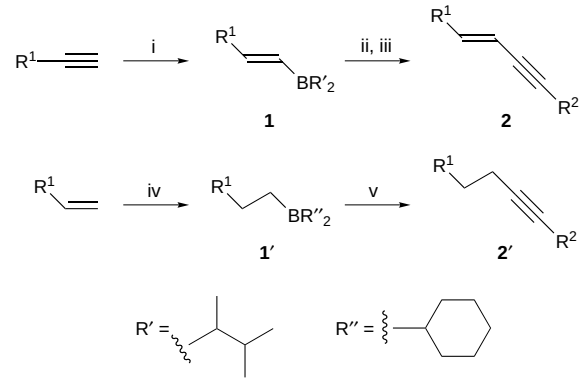

Scheme 1 *Reagents and conditions*: i, R'_2BH (1 equiv.), THF, −15 °C, then 0 °C, 3 h; ii, $R^2C{\equiv}CH$ (1 equiv.), CuI (1.1 equiv.), pyridine (2 equiv.), DMA, 0 °C, then 20 °C, 3 h; iii, $Cu(OAc)_2$ (2 equiv.), $Cu(NO_3)_2\cdot 3H_2O$ (2 equiv.), THF, 0 °C, then 20 °C, 18 h; iv, R''_2BH (1 equiv.), THF, 0 °C, 2 h; v, $R^2C{\equiv}CH$ (1 equiv.), $Cu(OAc)_2\cdot H_2O$ (2 equiv.), $Cu(acac)_2$ (0.25 equiv.), DMA–THF, 0 °C, then 20 °C, 18 h

reagent (R^1)[15] was confirmed by the reactions which gave **2i** (entry 9), **2j** (entry 10), **2k** (entry 11), **2l** (entry 12) and **2n′** (entry 17).

We feel that the organocopper species (*i.e.* alkenyl- or alkylcopper) is probably generated *via* a transmetalation of the organoborane. However, the detailed mechanism of the present reaction is unclear due to the absence of direct or obvious evidence, like many organocopper reactions to date.

In summary, the present reaction is not only interesting as a new method for formation of (*E*)-1,3-enynes (or disubstituted alkynes), but is also remarkably useful for the synthesis of such

Table 1 Products and their yields

	Product (enyne) **2** or (alkyne) **2′**			
Entry		R^1	R^2	Yield (%)[a]
1	**2a**	Bu	Bu	85 (90)[b]
2	**2b**	Bu	Ph	70
3	**2c**	Bu^t	Bu^t	76
4	**2d**	Bu	$(CH_2)_2COMe$	84
5	**2e**	Bu	$(CH_2)_2CN$	87
6	**2f**	Bu	$(CH_2)_2CO_2Et$	79
7	**2g**	Bu	$(CH_2)_4OH$	86
8	**2h**	Ph	$C(Me)_2OH$	72
9	**2i**	$(CH_2)_2CN$	Bu	80
10	**2j**	$(CH_2)_2CO_2Et$	Bu	75
11	**2k**	$(CH_2)_2OH$	Bu	86[c]
12	**2l**	$(CH_2)_2COMe$	CH_2OH	72
13	**2a′**	Bu	Bu	76 (83)[b]
14	**2b′**	Bu	Ph	72
15	**2d′**	Bu	$(CH_2)_2COMe$	77
16	**2m′**	Bu	CH_2OH	75
17	**2n′**	$(CH_2)_2COMe$	Bu	73

[a] Isolated, based on **1** or **1′** employed: *E*-isomers > 99%. [b] By GC. [c] Using 2 equiv. of R'_2BH.

compounds having a variety of functional group. Further investigations are underway.

This work was supported by a Grant-in-Aid for Scientific Research from the Ministry of Education, Japan (No. 04650763).

Notes and References

† E-mail: masuda@kaimen4.mtrl.kitami-it.ac.jp

‡ It was observed that galvinoxyl (a radical scavenger) depressed the formation of the disubstituted alkyne **2′** but not that of the enyne **2**.

§ After filtration the reaction mixture was washed and extracted, followed by oxidation with $NaBO_3 \cdot 4H_2O$ in H_2O and THF (ref. 14). The mixture was then worked up as usual. The pure product, isolated from the mixture (consisting of **2** or **2′** and an almost quantitative amount of R′OH or R″OH derived from the residual dialkylboryl groups) by column chromatography or Kugelrohr distillation, gave satisfactory spectral data (IR, ^{1}H NMR, ^{13}C NMR, mass).

¶ This would be applicable to the synthesis of the pheromone of the tent caterpillar *Malacosoma disstria* [(5*Z*,7*E*)-dodeca-5,7-dien-1-ol] [ref. 8(*b*)].

‖ Such enynes are known to be converted into terminal enynes (RCH=CHC≡CH) *via* the elimination of acetone using alkali (ref. 16).

1 Review: J. F. Normant and A. Alexakis, *Synthesis*, 1981, 841.
2 For example: E. J. Corey and A. Tramontano, *J. Am. Chem. Soc.*, 1984, **106**, 462; P. J. Stang and T. Kitamura, *J. Am. Chem. Soc.*, 1987, **109**, 7561; M. M. Salter, V. Gevorgyan, S. Saito and Y. Yamamoto, *Chem. Commun.*, 1996, 17; S. Saito, M. M. Salter, V. Gevorgyan, N. Tsuboya, K. Tando and Y. Yamamoto, *J. Am. Chem. Soc.*, 1996, **118**, 3970.
3 For more recent example: P. Ramiandrasoa, B. Bréhon, A. Thivet, M. Alami and G. Cahiez, *Tetrahedron Lett.*, 1997, **38**, 2447; R. Hara, Y. Liu, W.-H. Sun and T. Takahashi, *Tetrahedron Lett.*, 1997, **38**, 4103.
4 G. Pattenden, in *Comprehensive Organic Chemistry*, ed. J. F. Stoddart, Pergamon, Oxford, 1979, vol. 1, p. 171; R. C. Larock, in *Comprehensive Organic Transformations*, VCH, New York, 1989.
5 For representative example: (*a*) K. Sonogashira, Y. Tohda and N. Hagihara, *Tetrahedron Lett.*, 1975, 4467; (*b*) J. K. Still and J. H. Simpson, *J. Am. Chem. Soc.*, 1987, **109**, 2138.
6 For representative example: J. F. Normant, A. Commerçon and J. Villiéras, *Tetrahedron Lett.*, 1975, 1465.
7 H. C. Brown and G. A. Morandar, *J. Org. Chem.*, 1981, **46**, 645; N. Miyaura, K. Yamada and A. Suzuki, *Tetrahedron Lett.*, 1979, **20**, 3437; M. Hoshi, Y. Masuda and A. Arase, *Bull. Chem. Soc. Jpn.*, 1983, **56**, 2855; 1985, **58**, 1683.
8 (*a*) E.Negishi, G. Lew and T. Yoshida, *J. Chem. Soc., Chem. Commun.*, 1973, 874; (*b*) H. C. Brown, N. G. Bhat and Basavaiah, *Synthesis*, 1986, 674; (*c*) A. Suzuki, N. Miyaura, S. Abiko, M.Itoh, H. C. Brown, J. A. Sinclair and M. M. Midland, *J. Am. Chem. Soc.*, 1973, **95**, 3080.
9 (*a*) Y. Masuda, M. Hoshi and A. Arase, *J. Chem. Soc., Chem. Commun.*, 1991, 748; (*b*) 1989, 266.
10 Recent reviews: A. Pelter, K. Smith and H. C. Brown, *Borane Reagents*, Academic Press, London, 1988; D. S. Matteson, *Stereodirected Synthesis with Organoboranes*, Springer, Berlin, 1995; M. Vaultier and B. Carboni, *Comprehensive Organometallic Chemistry II*, ed. A. Mckillop, Pergamon, Oxford, 1995, vol. 11, p. 191.
11 H. C. Brown, in *Organic Synthesis* via *Boranes*, Wiley, New York, 1975.
12 J. F. Normant, *Synthesis*, 1972, 63.
13 Alk-1-ynes are known to couple in the presence of copper(II) acetate: G. Eglinton and A. R. Galbrath, *Chem. Ind.*, 1956, 737.
14 G. W. Kabalka, T.M. Shoup and N. G. Goudgaon, *Tetrahedron Lett.*, 1989, 1483.
15 For more recent report: G. W. Kabalka, S. Yu and N.-S. Li, *Tetrahedron Lett.*, 1997, **38**, 5455; 7681.
16 B. P. Andreini, A. Carpita, R. Rossi and B. Scamuzzi, *Tetrahedron*, 1989, **45**, 5621.

Received in Cambridge, UK, 8th January 1998; 8/00242H

Total syntheses of palmarumycins CP_1 and CP_2 and CJ-12,371: novel spiro-ketal fungal metabolites

Anthony G. M. Barrett,*† Dieter Hamprecht and Thorsten Meyer

Department of Chemistry, Imperial College of Science, Technology and Medicine, London, UK SW7 2AY

Total syntheses of palmarumycins CP_1 1 and CP_2 9 and the structurally related CJ-12,371 11 are reported, thereby establishing a strategy for the synthesis of further natural products in the palmarumycins, diepoxines and preussomerines family.

The palmarumycins,[1] diepoxines[2] and preussomerines[3] are a structurally remarkable class of natural products isolated from various fungi cultures. They all are graced with a spiro-ketal entity formally derived from naphthalene-1,8-diol **6** and 1,4-naphthoquinone, yet at rich and varied oxidation levels. All three classes of fungal metabolites are undoubtedly closely interrelated biosynthetically and may well be derived from a naphthalene-1,8-diol spiro-ketal with late introduction of the unusual oxygenation patterns. These secondary metabolites are

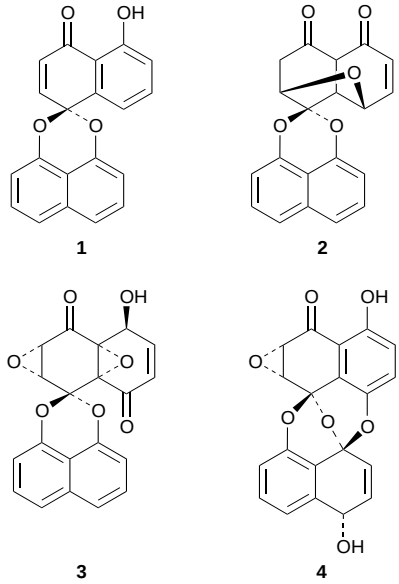

exemplified by palmarumycin CP_1 **1**, palmarumycin CP_3 **2**, diepoxine σ **3** and preussomerine E **4**, which show diverse biological effects including selective antifungal and antibacterial activities.[4] Although Wipf and Jung have reported studies towards the synthesis of diepoxine σ **3**[5] and Krohn *et al.* have reported an elegant biomimetic cyclisation approach to a model spiro-ketal array,[6] there have been no reports on the total synthesis of any natural product in this intriguing series. Herein we now report the total syntheses of three natural products palmarumycins CP_1 **1** and CP_2 **9** and CJ-12,371 **11**.

Condensation of 5-methoxytetralone **5** and diol **6**[7] under acid catalysis gave spiro-ketal **7**‡ in an 86% yield (Scheme 1). Subsequent benzylic oxidation using bipyridinium chlorochromate[8] and a 30-fold excess of *tert*-butyl hydroperoxide gave the corresponding ketone **8** in 61% yield. Alternative oxidants including Jones' Reagent or potassium permanganate were much less efficient for the preparation of ketone **8**. Reaction of

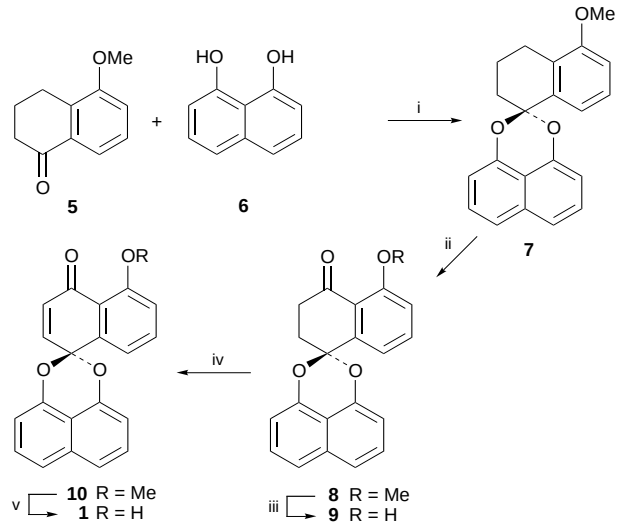

Scheme 1 *Reagents and conditions*: i, TsOH (cat), PhH, Dean–Stark, 48 h, reflux, 86%; ii, CrO_3·HCl·bipy, BtOOH, Celite, PhH, 10 h, room temp., 61%; iii, MgI_2, PhH, 1.5 h, reflux, 84%; iv, DDQ, PhH, 10 h, reflux, 65%; v, *B*-bromocatecholborane, DBU, CH_2Cl_2, 10 min, 5 °C, 50%

the methyl ether **8** with a freshly prepared solution of magnesium iodide[9] in benzene gave palmarumycin CP_2 **9** (84%). Deprotection using magnesium iodide was found to be far superior to trimethylsilyl iodide (32%) or sodium ethanethiolate (63%).[10] Oxidation of ketone **8** with DDQ[11] followed by deprotection of the methyl ether with *B*-bromocatecholborane[12] gave palmarumycin CP_1 **1**, the dehydro analogue of **9**, in 33% yield over two steps.

Finally, palmarumycin CP_2 **9** was converted into its corresponding dihydro derivative **11** (60% yield, 93% ee)§ by asymmetric reduction using (+)-*B*-chlorodiisopinocampheylborane **12**[13] (Scheme 2). It is germane to mention that reduction presumably takes place *via* intramolecular hydride delivery thereby reversing the absolute stereochemistry of reaction seen

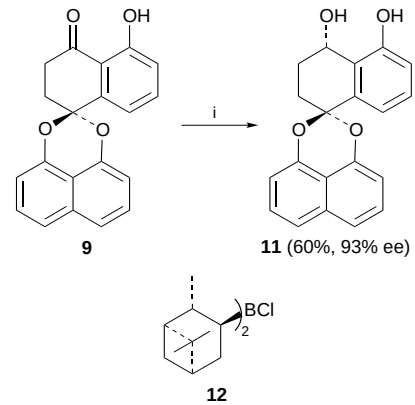

Scheme 2 *Reagents and conditions*: i, (+)-**12**, THF, room temp., 18 h, then H_2O_2, KOH

with simple alkyl aryl ketones.[13] The product of reduction, alcohol **11**, is a natural product in its own right named CJ-12,371 **11**,[14] a DNA-gyrase inhibitor isolated from an unidentified fungus (N983-46). The authenticity of both palmarumycins CP_1 **1** and CP_2 **9** were established by comparison of the synthetic compounds with authentic samples (^1H and ^{13}C NMR spectroscopy). Unfortunately, we have been unable to obtain an authentic sample of CJ-12,371 **11** and the characterisation of our synthetic material rests on comparison of our data with those published for the natural product.[14]

It is clear that the spiro-ketal **7** is a useful intermediate for further redox manipulations and the synthesis of simple palmarumycins. Further studies towards the total synthesis of the more challenging and higher oxidation level diepoxines and preussomerines are currently under investigation and will be reported in due course.

We thank SmithKline Beecham for support of our research, Glaxo Wellcome Research Ltd. for an endowment (to A. G. M. B.), the Wolfson Foundation for establishing the Wolfson Centre for Organic Chemistry in Medical Science at Imperial College and Professor Karsten Krohn for authentic samples of palmarumycins CP_1 **1** and CP_2 **9**.

Notes and References

† E-mail: m.stow@ic.ac.uk

‡ All new compounds were fully characterised by spectroscopic data, microanalysis and HRMS

§ The enantiomeric excess was determined by chiral HPLC while the absolute stereochemistry was determined by comparison of the optical rotation $[\alpha]_D^{24}$ −42.2, (*c* 0.45 in MeOH)] with the isolated natural product $[\alpha]_D^{24}$ −46.8 (*c* 0.23, MeOH)].

1 K. Krohn, A. Michel, U. Flörke, H.-J. Aust, S. Draeger and B. Schulz, *Liebigs Ann. Chem.*, 1994, 1093; 1994, 1099.

2 G. Schlingmann, R. R. West, L. Milne, C. J. Pearce and G. T. Carter, *Tetrahedron Lett.*, 1993, **34**, 7225; F. Petersen, T. Moerker, F. Vanzanella and H. H. Peter, *J. Antibiot.*, 1994, **47**, 1098; R. Thiergardt, P. Hug, G. Rihs and H. H. Peter, *Tetrahedron Lett.*, 1994, **35**, 1043; *Tetrahedron*, 1995, **51**, 733.

3 H. A. Weber, N. C. Baezinger and J. B. Gloer, *J. Am. Chem. Soc.*, 1990, **112**, 6718; H. A. Weber and J. B. Gloer, *J. Org. Chem.*, 1991, **56**, 4355; S. B. Singh, D. L. Zink, J. M. Liesch, R. G. Ball, M. A. Goetz, E. A. Bolessa, R. A. Giacobbe, K. C. Silverman, G. F. Bills, F. Pelaez, C. Cascales, J. B. Gibbs and R. B. Lingham, *J. Org. Chem.*, 1994, **59**, 6296.

4 M. Chu, I. Truumees, M. G. Patel, V. P. Gullo and M. S. Puar, *J. Org. Chem.*, 1994, **59**, 1222; M. Chu, I. Truumees, M. G. Patel, V. P. Gullo, C. Blood, I. King, J.-K. Pai and M. S. Puar, *Tetrahedron Lett.*, 1994, **35**, 1343; M. Chu, I. Truumees, M. G. Patel, C. Blood, P. R. Das and M. S. Puar, *J. Antibiot.*, 1995, **48**, 329; M. Chu, M. G. Patel, J.-K. Pai, P. R. Das and M. S. Puar, *Biorg. Chem. Lett.*, 1996, **6**, 579; G. Schlingmann, S. Matile, N. Berova, K. Nakanishi and G. T. Carter, *Tetrahedron*, 1996, **52**, 435; G. Bringmann, S. Busemann, K. Krohn and K. Beckmann, *Tetrahedron*, 1997, **53**, 1655; K. Krohn, K. Beckmann, U. Flörke, H.-J. Aust, S. Draeger, B. Schulz, S. Busemann and G. Bringmann, *Tetrahedron*, 1997, **53**, 3101.

5 P. Wipf and J.-K. Jung, *Angew. Chem., Int. Ed. Engl.*, 1997, **36**, 764.

6 K. Krohn, K. Beckmann, H.-J. Aust, S. Draeger, B. Schulz, S. Busemann and G. Bringmann, *Liebig Ann. Recl.*, 1997, 2531.

7 H. Erdmann, *Ann. Chem.*, 1888, **247**, 356.

8 For examples of benzylic oxidations using chromium reagents, see: N. Chidambaram and S. Chandrasekaran, *J. Org. Chem.*, 1987, **52**, 5048; R. Rathore, N. Saxena and S. Chandrasekaran, *Synth. Comm.*, 1986, **16**, 1493; J. Muzart, *Tetrahedron Lett.*, 1987, **28**, 2131; R. Rangarajan and E. J. Eisenbraun, *J. Org. Chem.*, 1985, **50**, 2435; B. M. Choudary, A. D. Prasad, V. Bhuma and V. Swapna, *J. Org. Chem.*, 1992, **57**, 5841.

9 B. W. Bycroft and J. C. Roberts, *J. Chem. Soc.*, 1963, 4868.

10 M. V. Bhatt and S. U. Kulkarni, *Synthesis*, 1983, 249.

11 D. R. Buckle, in *Reagents for Organic Synthesis*, Wiley, Chichester 1995, vol. 3, p. 1699.

12 P. F. King and S. G. Stroud, *Tetrahedron Lett.*, 1985, **26**, 1415.

13 P. V. Ramachandran, B. Gong and H. C. Brown, *Tetrahedron Lett.*, 1994, **35**, 2141.

14 S. Sakemi, T. Inagaki, K. Kaneda, H. Hirai, E. Iwata, T. Sakakibara, Y. Yamauchi, M. Norcia, L. M. Wondrack, J. A. Sutcliffe and N. Kojima, *J. Antibiot.*, 1995, **48**, 134.

Received in Liverpool, UK, 8th January 1998; 8/00237A

Laser-induced molecular mixing of electron donor and acceptor in poly(ethyl methacrylate)

Guillaume Gery, Hiroshi Fukumura*† and Hiroshi Masuhara

Department of Applied Physics, Osaka University, Suita, Osaka 565, Japan

Dicyanoanthracene molecules are ejected from a polymer film by pulsed UV laser irradiation and are transferred into another polymer film containing hexamethylbenzene, resulting in the formation of the charge-transfer complex in a polymer solid.

Intense irradiation with UV laser pulses has been considered to decompose organic molecules in polymer solids by multiphotonic chemical reactions.[1] However, we have recently shown that aromatic molecules dispersed in polymers hardly decompose by nanosecond laser irradiation and can be ejected from the polymer surfaces without decomposition.[2–4] The evidence that a large thermal jump dominates in laser ablation of doped polymers has been provided by transient thermal expansion of the polymer surfaces.[5] Based on these mechanistic studies of dopant-sensitized laser ablation, we have developed laser molecular implantation (LMI) as an innovative method to generate patterns of intact molecules on polymer surfaces.[6–8] The process involves the overlay of two polymer films: the source film, which contains dopant molecules absorbing the laser light, and the target film, which may be a neat polymer film. Molecules embedded in the source film are excited by a pulsed excimer laser and implanted into the target film in contact. From fluorescence measurements under total internal reflection conditions, the thickness of the implanted layer is estimated to be of a few tens of nanometers.[7] Our attention is now focused on space-selective chemical reactions in a controlled volume beneath a polymer surface by transferring reactants by LMI. This method can be applied for the fabrication of devices using a variety of organic functional molecules. The successful attempt described in this report is opening new prospects for nano-scale chemistry in solid macromolecular structures.

Poly(ethyl methacrylate) (PEMA, $\overline{M}_w = 3.4 \times 10^5$, Aldrich) films were prepared by spin coating on glass plates from chloroform (Nacalai Tesque Inc. HPLC grade) solutions. The typical thickness of the films was 3 μm when the concentration of PEMA in chloroform was 6 wt% and the spin speed was 1000 rpm. Source films were prepared from a saturated solution of 9,10-dicyanoanthracene (DCNA, Kodak) in PEMA–chloroform. Micro-crystals were removed by syringe filters (PTFE 0.2 μm, DISMIC-25 JP, Advantec Toyo). The concentration of hexamethylbenzene (HMB, Nacalai Tesque Inc.) in target films was 0.4 M. For each measurement a neat PEMA target film was irradiated under the same conditions and used as a reference. Only DCNA exhibited an absorption band in the spectral region above 320 nm and a XeF excimer laser pulse (351 nm, fwhm ≈ 30 ns) allowed the selective excitation of DCNA molecules. After irradiation, the fluorescence spectrum of the target film was recorded on a conventional spectrofluorometer (Hitachi F-4500) and the surface was observed by both a fluorescence microscope (Olympus BX 50) with a U-MWU filter unit (λ_{ex} < 400 nm; observation: 400–700 nm) and a scanning electron microscope (SEM) (JEOL JXA-8600X). In the case of repetitive irradiation, it was carried out at 1 Hz or less in order to avoid any cumulative heating effect.

DCNA and HMB are known to form exciplexes in solution and in the gas phase.[9–12] Fluorescence spectra of polymer films doped with DCNA and of films doped with both DCNA and HMB were recorded and used as standards. DCNA films emitted blue fluorescence with a maximum at 430 nm when excited at 380 nm. When HMB was introduced, the monomer fluorescence was quenched, and a broad and structureless band appeared at *ca*. 500 nm (green emission). The excitation spectrum of this compound corresponded to the superposition of the vibrational structure of DCNA monomer fluorescence and a broad charge-transfer band indicating complex formation in ground state between DCNA and HMB.

Laser-implanted area was first examined by fluorescence microscopy. With the first laser shot, the surface was implanted with a gold–yellow emissive compound. This compound was

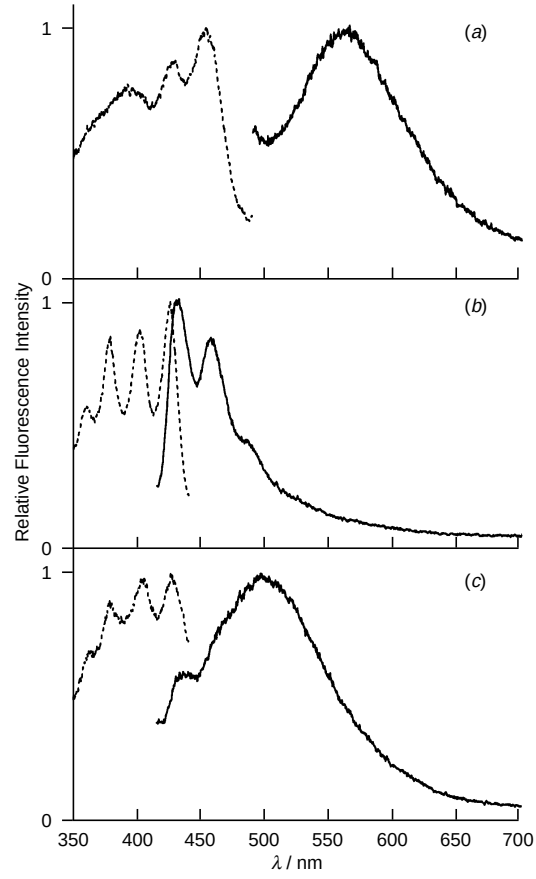

Fig. 1 Fluorescence (——, excited at 380 nm) and their excitation (- - -, observed at 550 nm) spectra of the target films after laser irradiation (laser fluence, 200 mJ cm^{-2}; source film ablation threshold, 400 mJ cm^{-2}). (*a*) The emission band of the yellow compound formed by the first laser shot appeared at *ca*. 560 nm. The excitation spectrum was shifted to longer wavelengths compared to monomeric DCNA. (*b*) After 10 shots irradiation, the emission spectrum of the implanted area almost corresponded to the monomer emission and the excitation spectrum was identical to the DCNA monomer absorption spectrum. (*c*) When HMB was involved in the target film a clear charge transfer band of the DCNA–HMB complex appeared at *ca*. 500 nm.

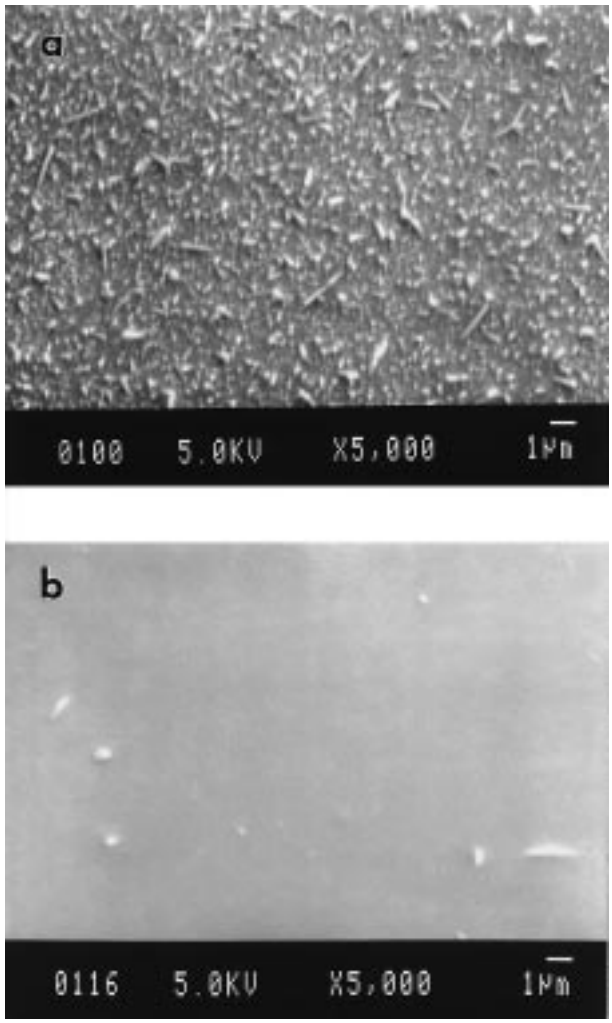

Fig. 2 SEM micrographs of the target film surfaces. (a) With the first laser pulse nano-crystals were formed on the surface of the target film. (b) By repetitive irradiation (10 shots), the nano-crystals almost disappeared and the surface recovered the original flatness.

always formed with the first laser shots irrespective of the existence of HMB in the target film. By increasing the number of laser shots, the yellow fluorescence disappeared and instead blue monomer fluorescence was observed for the target film not including HMB. When the target film contained HMB, the color of the implanted pattern turned to green fluorescence suggesting the formation of the charge transfer complex.

In order to confirm the complex formation in the polymer matrix, we also measured fluorescence spectra of those implanted polymer films (Fig. 1). After the first laser shot, the emission spectrum of the target film exhibited a broad band centered at *ca*. 560 nm and the excitation spectrum was shifted to a longer wavelength region compared to the DCNA monomer absorption band [Fig. 1(*a*)]. The emission changed to that of the DCNA monomer after 10 laser shots and then its excitation spectrum was almost coincident with the DCNA absorption spectrum [Fig. 1(*b*)]. When the target film was doped with HMB, an emission band centered around 500 nm clearly ascribed to the charge transfer emission emerged [Fig. 1(*c*)].

The origin of the yellow emissive compound should be solely ascribed to DCNA as it was found to be independent of HMB. Scanning electron microscope images of the surface revealed the presence of aggregates of a few hundreds of nanometers after the first laser shot [Fig. 2(a)]. The amount of those aggregates decreased with increasing the laser shot number [Fig. 2(b)]. This suggests that upon repetitive irradiation the nano-aggregates absorbed light, reached a high temperature, melted a thin layer of the polymer surface and were dispersed into deeper layers of the surface, which resulted in the recovery of a smooth surface of the polymer. Changes in the fluorescence spectra of the target film also supports the aggregate dispersion by repetitive irradiation.

The yellow emissive aggregates formed by the first laser shot may be attributed to a specific crystal form of DCNA. Meso-substituted anthracene derivatives generally have two crystal forms, α and β, depending on the overlapping of aromatic rings[13,14] and some spectral changes have been reported in the case of thermal treatment of DCNA[15] The α-form is produced by recrystallization from solution while the β-form is obtained either by sublimation or by heating the α-form at temperatures above 453 K for 24 h. A similarity in the fluorescence spectra of the aggregates and the β-form crystal suggests that DCNA in the source film was sublimated by a high transient temperature rise and condensed on the surface of the target film to crystallize as the yellow emissive β-form.

Since the two films in contact were irradiated from the backside of the target film, the crystals formed on the surface of the target film absorb light efficiently, transform it into thermal energy by non-radiative processes and diffuse into a deeper layer of the film. The curve of the fluorescence intensity of the target films as a function of the shots number reached a constant value after a few laser shots indicating that most of the molecules are transferred by the first laser shots. The following shots provide the energy required to dissociate molecular aggregates and release the monomer into deeper layers of the target film where complex formation occur.

In this paper, light has been used for the first time to transfer molecules from one film to another and to mix two components in a polymer matrix without the transfer of the source film polymer matrix itself. LMI appears as a promising tool to induce a chemical reaction in a limited volume of macro-molecular solids leading to a wide range of applications, from the manufacturing of biochemical sensors to that of optical and electronic circuits by using organic functional molecules.

The authors wish to thank the Japanese Ministry of Education, Science, Sports and Culture for financial support in the form of Grant-in-Aids (07554063, 08454223). G. G. is indebted to the Ministry for a Japanese government scholarship.

Notes and References

† E-mail: fukumura@ap.eng.osaka-u.ac.jp; Fax: +81-6-879-7840.

1 R. Srinivasan and R. Braren, *Chem. Rev.*, 1989, **89**, 1303.
2 H. Fukumura, N. Mibuka, S. Eura, H. Masuhara and N. Nishi, *J. Phys. Chem*., 1993, **97**, 13 761.
3 H. Fukumura and H. Masuhara, *Chem. Phys. Lett.*, 1994, **221**, 373.
4 H. Fujiwara, H. Fukumura and H. Masuhara, *J. Phys. Chem*., 1995, **99**, 11 844.
5 H. Furutani, H. Fukumura and H. Masuhara, *J. Phys. Chem.*, 1996, **100**, 6871.
6 H. Fukumura, Y. Kohji, K. Nagasawa and H. Masuhara, *J. Am. Chem. Soc*., 1994, **116**, 10 304.
7 H. Fukumura, Y. Kohji and H. Masuhara, *Appl. Surf. Sci*., 1996, **96–98**, 569.
8 G. Gery, H. Fukumura and H. Masuhara, *J. Phys. Chem. B*, 1997, **101**, 3698.
9 S. Hirayama and D. Phillips, *J. Phys. Chem.*, 1981 **85**, 643.
10 I. R., Gould, R. H. Young, R. E. Moody and S. Farid, *J. Phys. Chem*., 1991, **95**, 2068.
11 P. Jacques, E. Haselbach, E. Henseler, D. Pilloud and P. Suppan, *J. Chem. Soc., Faraday Trans*., 1991, **87**, 3811.
12 I. R. Gould, R. H. Young, L. J. Mueller and S. Farid, *J. Am. Chem. Soc*., 1994, **116,** 8176.
13 H. Kuwano and M. Kondo, *Bull. Chem. Soc. Jpn*., 1966, **39,** 2779.
14 J. Tanaka and M. Shibata, *Bull. Chem. Soc. Jpn*., 1968, **41,** 34.
15 M. Martinaud and Ph. Kottis, *J. Phys. Chem*., 1978, **82**, 1497.

Received in Cambridge, UK, 26th November 1997; 7/08539G

Poly(alkylbenzyls), a promising new polymeric material

D. Baudry-Barbier, A. Dormond,*† F. Dumont and F. Duriau-Montagne

Laboratoire de Synthèse et d'Electrosynthèse Organométalliques (L.S.E.O.), U.M.R. 5632-C.N.R.S., Université de Bourgogne, 6 bd Gabriel, 21000 Dijon, France

The reaction of mesitylene substituted by alkyl or alkoxy chains of various lengths and α,α′-dichloro-*p*-xylene with K10 Montmorillonite as catalyst affords a new class of poly(alkylbenzyls) soluble in common organic solvents.

The synthesis of thermostable and water resistant polymers has been widely investigated, but remains even today an important economical challenge. For this purpose, polybenzyls, first reported in 1885,[1] were reinvestigated in the 1970s by several groups.[2–5] These polymers obtained in Friedel–Crafts type polyalkylation reactions[6–8] were found to be thermally stable up to 400 °C,[5,9] but the molecular weights were often very low[5] and little information about their nature and their properties was available. All these materials were described as insoluble in organic solvents, this insolubility preventing any possibility of industrial use. Moreover, it was noted that although *para* substitution in the main chain was predominant,[5,9] the possibility of lateral substitution on the polybenzyl skeleton leading to branched polymers is not excluded.[10] Then, it was interesting to synthesize non-crosslinked, linear polybenzyls, with a high solubility in usual organic solvents.

To obtain a linear and defined material, the polycondensation of α,α′-dichloro-*p*-xylene on 1,2,4,5-tetramethylbenzene has been performed using K10 Montmorillonite as catalyst. This acidic clay is widely used as a Friedel–Crafts alkylation and acylation supported catalyst.[11–13] The alkylation is then expected to occur preferentially at the two *para* positions of durene[14] rather than on the disubstituted ring. A linear polymer (**P1**) was effectively obtained: the ^{1}H NMR spectrum showed only one singlet due to the four protons of the methylene groups and only one sharp signal due to the four protons of the equivalent aromatic protons. But the solubility was low in usual solvents ($CHCl_3$ THF, toluene, CH_2Cl_2, *etc.*). The molecular weight of the THF soluble fraction ranged from 7000 to 10 000.

The solubility may be increased by replacing one of the methyl groups by a long aliphatic chain to obtain a polymer containing flexible segments after condensation. Moreover both the interactions between side-chains and the free volume created by the side-chains in the material influence the physical properties. Two alkyl and three alkoxy side-chains were chosen and the starting materials were synthesized from mesitylene by a Friedel–Crafts reaction (**2** and **2′**) or from sodium 2,4,6,trimethylphenolate and the appropriate alkyl bromide by a Williamson (**3**,**3′** and **3″**) reaction. These substrates were characterized by elemental analysis, mass, IR, ^{1}H and ^{13}C NMR spectroscopy.

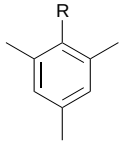

2 R = $C_{16}H_{31}$
2′ R = C_8H_{17}

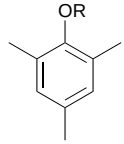

3 R = $C_{16}H_{31}$
3′ R = C_8H_{17}
3″ R = Bu

The stoichiometric (1 : 1) reaction between the substrate (**2**, **2′**, **3**, **3′** or **3″**) and α,α′-dichloro-*p*-xylene was performed in refluxing decane (174 °C) during 24 h in the presence of K10 Montmorillonite. After usual work up, removal of the catalyst and of the solvent, dissolution in the appropriate solvent and precipitation by MeOH, the polymers **P2**, **P2′**, **P3**, **P3′** and **P3″**

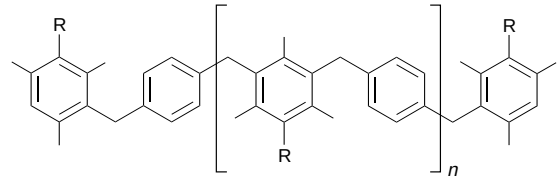

P2 R = $C_{16}H_{31}$
P2′ R = C_8H_{17}
P3 R = $OC_{16}H_{31}$
P3′ R = OC_8H_{17}
P3″ R = OBu

were obtained respectively as white powders in *ca*. 60% yield. The solubility of these compounds increases with the length of the chain:

P3″ (THF, moderately) < **P2′** (Et_2O, moderately) < **P3′**, **P2** (Et_2O) < **P3** (heptane)

Elemental analyses and the IR, ^{1}H and ^{13}C NMR spectra of the crude materials are in agreement with the proposed formulae.‡ Note that these compounds contain a small amount of chlorine (*ca*. 0.1%), which could be due to terminal $-CH_2Cl$ groups of the macromolecular chains which were not quenched. The signal at 4.5 ppm due to a terminal $-CH_2Cl$ group is either extremely weak or not depicted. Consequently, the small amount of chlorine implies that most of the terminal groups are substituted phenyl groups.

The apparent volume of these polymers is strongly dependent on the length and the spatial position of the side-chains. It was thus very difficult to establish their molecular weight (M_w) by steric exclusion chromatography (SEC) using polystyrene samples as calibration standards. The polydispersity index (I_p) of the soluble fraction ranged from 1.3 to 2. Therefore, M_w values were estimated from the NMR data: to each signal of the substituted phenyl group are joined signals of *ca*. 10 times lower intensity whereas the signal of the C_6H_4 protons is virtually unique: only a shoulder and two extremely weak signals (nearly 1% of the total integral value) were observed. The molecule is therefore linear, with a level of branching which does not exceed a few percent. The weak signals of the substituted phenyl group are due to the terminal groups (traces of residual polyalkylbenzene might also give such signals) and the minimal chain length and indeed the minimal averaged molecular weight can be deduced from the signals rate: *ca*. 20 units and 7000, respectively, for **P3′**. These results are also in good accordance with the molecular weight of **P1** (7000–10 000) determinated by SEC.

In conclusion, soluble polybenzyls can be synthesized by Friedel–Crafts polycondensation, using a non-toxic, mineral and removable catalyst. Their solubility should permit easy

casting of thin films or coatings. Further experiments are in progress to enhance the macromolecular chain length of these polymers.

Notes and References

† E-mail: baudryd@satie.u-bourgogne.fr

‡ Melting points were determined on a Kofler hot-stage apparatus. The weight-average molecular weight (M_w) of **P1** was obtained on a gel permeation chromatograph (Spectra Physics P200) connected to a Spectra Series UV 100 detector (λ = 254 nm) after calibration of the column using polystyrene standards (Polymer Laboratories). The column was a mixed PL-Gel column (particle size: 5 μm, pore type: 10 000 Å, length: 300 mm, internal diameter: 7.5 mm) with THF as solvent. The GPC Plus program was used to calculate the polydispersity index (I_p). ^{1}H and ^{13}C NMR spectra were recorded in $CDCl_3$ as internal reference (δ 7.25) on Bruker AC 200 (200 MHz) or DRX 500 (500 MHz) spectrometers. Mass spectra of the substrates were obtained on a GC–MS coupled spectrometer (Hewlett Packard G1800A) and elemental analyses on a EA 1108 CHNS-O (Fisons Instruments). The FTIR absorbance spectra were performed on a IFS 66v apparatus. The reactions were performed in a two necked-flask connected to a condenser. This flask was heated by a sand-bath and the mixture stirred by a magnetic stirrer. The condenser was connected to a drying tube for the substrates synthesis and to a HCl-trap for the polycondensations.

1 C. Friedel and J. M. Crafts, *Bull. Soc. Chim. Fr.*, 1885, **43**, 53.
2 G. Montaudo, F. Bottino, S. Caccamese, P. Finocchiario and G. Bruno, *J. Polym. Sci., Part A1*, 1970, **8**, 2453.
3 N. Grassie and I. G. Meldrum, *Eur. Polym. J.*, 1971, **7**, 629.
4 J. Kuo and R. W. Lenz, *J. Polym. Sci., Part A: Polym. Chem.*, 1976, **14**, 2749.
5 K. Arata, A. Fukui and I. Toyoshima, *J. Chem. Soc., Chem. Commun.*, 1978, 121.
6 J. Skura and R. W. Lenz, *Polym. Bull.*, 1980, **2**, 31.
7 M. Olazar, J. Bilbao, A. T. Aguayo and A. Romero, *Ind. Eng. Chem. Res.*, 1987, **26**, 1956.
8 T. R. Baumberger and N. F. Woolsey, *J. Polym. Sci., Part A: Polym. Chem.*, 1992, **30**, 1717.
9 M. Hino and K. Arata, *Chem. Lett.*, 1979, **9**, 1141.
10 C. P. Tsonis, *J. Mol. Catal.*, 1990, **57**, 313.
11 D. R. Brown and C. N. Rhodes, *Catal. Lett.*, 1997, **45**, 35.
12 J. H. Clark, S. R. Cullen, S. J. Barlow and T. W. Bastock, *J. Chem. Soc., Perkin Trans. 2*, 1994, 1117.
13 D. Baudry, A. Dormond, F. Montagne and J. R. Desmurs, *FR Pat. 96024*, 1996.
14 B. N. Hendy, K. H. Patterson, D. M. Smith, S. E. Gardner and N. J. Nicolson, *J. Mater. Chem.*, 1995, **5**, 199.

Received in Liverpool, UK, 14th January 1998; 8/00409I

Radical reaction of *S*-phenyl chlorothioformate with alkyl iodides: free radical-mediated carboxylation approach

Sunggak Kim*† and Sang Yong Jon

Department of Chemistry, Korea Advanced Institute of Science and Technology, Taejon 305-701, Korea

Free radical-mediated carboxylation is achieved by treatment of alkyl iodides with *S*-phenyl chlorothioformate and bis(tributyltin) with irradiation at 300 nm.

Since a free radical-mediated carboxylation reaction was reported by Kharasch and co-workers in the 1940s,[1] no further developments in this area have been noted during the last 50 years, although a free radical carboxylation approach involving carbonylation and iodine atom transfer has recently been reported.[2] This could be due to the fact that alkyl radical additions to C=O bonds are inefficient due to the reversibility of the addition step and the high π-bond strengths of C=O bonds.[3] Thus, intermolecular addition of alkyl radicals to C=O and C=N bonds[4,5] is relatively rare, as compared to C=C bonds. Recently, we have shown that alkyl radical additions to phenylsulfonyl oxime ethers are highly efficient, suggesting the importance of the substituent at the C=N bond.[6] We conceived that the success of alkyl radical additions to C=O bonds would depend very much on the nature of the substituent, which would be closely related to the LUMO energy of carbonyl derivative **1**. We have studied the possibility of developing a free radical carboxylation reaction utilizing carbonyl derivative **1** as a carboxyl equivalent radical acceptor [eqn. (1)].

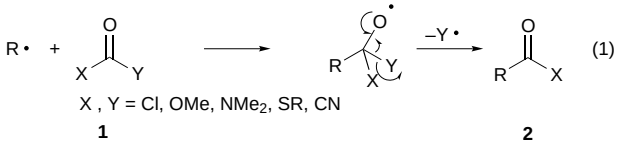

Before we began our studies with carbonyl derivatives, AM1 calculations for several carbonyl derivatives were performed, as nucleophilic alkyl radicals would react more rapidly with radical acceptors having lower LUMO energy.[7] According to the computational studies, *S*-phenyl chlorothioformate exhibited the lowest LUMO energy among carbonyl derivatives tested in this study. To see whether the computational results are in accordance with experimental results, free radical carboxylation reactions were carried out with 4-phenoxybutyl iodide, carbonyl derivative **1** and bis(tributyltin) using irradiation at 300 nm.[8] As shown in Table 1, dimethylcarbamoyl chloride, methyl chlorofomate and phosgene were totally ineffective.

Table 1 LUMO energy of **1** and chemical yields of **2**

	Carbonyl derivative **1**	LUMO energy[a]/eV	Product **2**	Yield (%)
1a	$ClC(O)NMe_2$	0.1377	$RCONMe_2$	0
1b	$ClCO_2Me$	0.0039	RCOOMe	0
1c	$C(O)Cl_2$	−0.7740	RCOCl	0
1d	$C(O)(SPh)_2$	−1.0911	RCOSPh	31
1e	ClC(O)SMe	−1.1810	RCOSMe	32
1f	ClC(O)SPh	−1.3863	RCOSPh	60
1g	NCC(O)SPh	−1.2635	RCOCN	0[b]

[a] The LUMO energy was calculated using MOPAC. [b] 4-Phenoxybutyl cyanide (75%) was obtained.

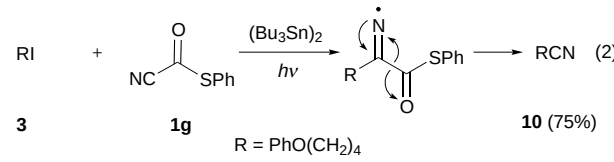

Table 2 Preparation of *S*-phenyl thioates from alkyl iodides with *S*-phenyl chlorothioformate

Substrate	Product	Yield (%)
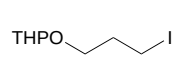	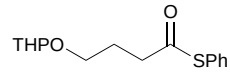	53 (5)[a] (20)[b]
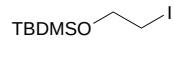	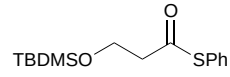	55 (5)[a]
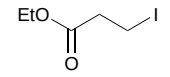	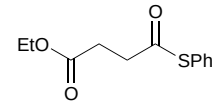	44 (11)[a]
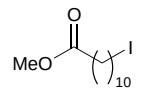	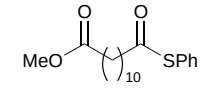	52 (12)[a] (27)[b]
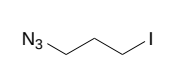	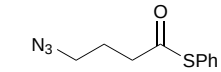	48 (9)[a]
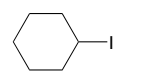	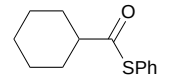	56
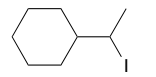	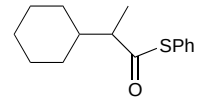	51 (8)[a]
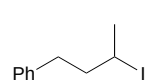	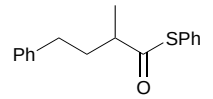	53
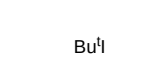	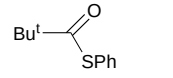	49
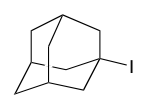	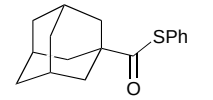	56 (4)[a]

[a] Sulfide product. [b] Direct reduction product.

S-Phenyl chlorothioformate **1f** gave the best result, although bis(thiophenyl) carbonate **1d** and *S*-methyl chlorothioformate **1e** were effective to some extent. Furthermore, it is noteworthy

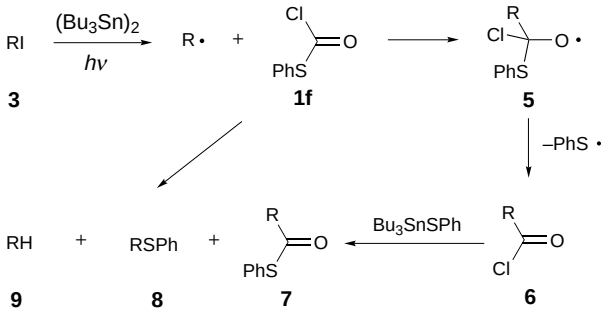

Scheme 1

that the radical reaction with *S*-phenyl cyanothioformate **1g** afforded 4-phenoxybutyl cyanide **10** [eqn. (2)]. Apparently, the 4-phenoxybutyl radical attacked the cyano group rather than the carbonyl group. The present result clearly indicates that the LUMO energy is a very important factor in predicting and designing the radical reactions. Treatment of 4-phenoxybutyl iodide with **1f** and bis(tributyltin) in benzene with irradiation at 300 nm for 10 h afforded *S*-phenyl thioate **7** in 60% yield. In addition, 4-phenoxybutane **9** was obtained in 15% yield along with 4-phenoxybutyl phenyl sulfide **8** (8%) due to homolytic substitution by the alkyl radical at the sulfur atom.[9] When the same reaction was carried out in the presence of an equimolar amount of isobutyryl chloride, a mixture of **7** (26%) and *S*-phenyl thioisobutyrate (52%) was obtained.

According to our experimental results, the present approach involves an alkyl radical addition to the C=O bond to generate alkoxy radical **5**, which undergoes β-fragmentation to afford acid chloride **6** (Scheme 1). Reaction of acid chloride **6** with tri-*n*-butyltin phenylthiolate would provide *S*-phenyl thioate **7**.[10]

Table 2 summarizes the experimental results and illustrates the efficiency of the present method. For most of the cases observed, the reaction required 10 h for completion of the reaction and afforded the *S*-phenyl thioates in reasonably good yield. Sterically hindered tertiary alkyl iodides gave similar results. We also studied sequential radical reactions involving cyclization and carboxylation. Radical reaction of olefinic iodide **11** under similar conditions afforded the desired product **12** in 53% yield along with **13** (9%) and **14** (30%) [eqn. (3)]. When a similar reaction was carried out with **15**, cyclopentanone **16** was obtained in 40% yield along with *S*-phenyl thioate **17** (27%) [eqn. (4)]. Further studies on free radical carboxylation related reactions are underway.[11]

We thank The Korea Research Foundation for financial support.

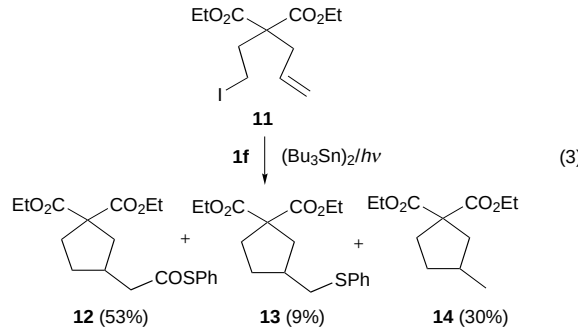

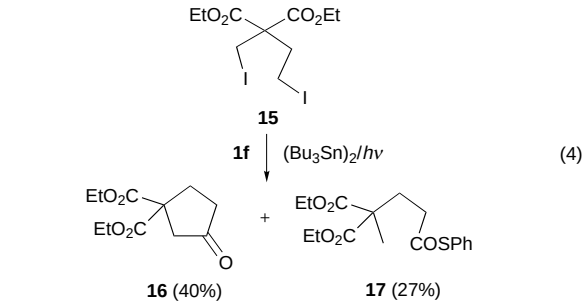

Notes and References

† E-mail: skim@sorak.kaist.ac.kr

1 H. C. Brown and M. S. Kharasch, *J. Am. Chem. Soc.*, 1942, **64**, 329; H. C. Brown and M. S. Kharasch, *J. Am. Chem. Soc.*, 1942, **64**, 333; H. C. Brown and M. S. Kharasch, *J. Am. Chem. Soc.*, 1942, **64**, 5621.

2 I. Ryu, K. Nagahara, M. Komatsu and N. Sonoda, *J. Am. Chem. Soc.*, 1997, **119**, 5465.

3 A. L. J. Beckwith and B. P. Hay, *J. Am. Chem. Soc.*, 1989, **111**, 230; A. L. J. Beckwith and B. P. Hay, *J. Am. Chem. Soc.*, 1989, **111**, 2674; R. Walton and B. Fraser-Reid, *J. Am. Chem. Soc.*, 1991, **113**, 5791.

4 M. Oyama, *J. Org. Chem.*, 1965, **30**, 2429; W. G. Bentrude and K. R. Darnall, *J. Am. Chem. Soc.*, 1968, **90**, 3588; F. Minisci, R. Galli, M. Cecere, V. Malatasta and T. Caronna, *Tetrahedron Lett.*, 1968, 5609.

5 A. Citterio and L. Filippini, *Synthesis*, 1986, 473; D. J. Hart and F. L. Seely, *J. Am. Chem. Soc.*, 1988, **110**, 1631.

6 S. Kim, I. Y. Lee, J.-Y. Yoon and D. H. Oh, *J. Am. Chem. Soc.*, 1996, **118**, 5138; S. Kim and J.-Y. Yoon, *J. Am. Chem. Soc.*, 1997, **119**, 5982; S. Kim, J.-Y. Yoon and I. Y. Lee, *Synlett*, 1997, 475.

7 B. Giese, in *Radicals in Organic Synthesis: Formation of Carbon–Carbon Bonds*, Pergamon, New York, 1986, ch. 2; I. Fleming, in *Frontier Orbitals and Organic Chemical Reactions*, Wiley, London, 1976, ch. 4 and 5.

8 M. Harendza, J. Junggebauer, K. Lebmann, W. P. Neuman and H. Tews, *Synlett*, 1993, 286.

9 M. Tada and H. Nakagiri, *Tetrahedron Lett.*, 1992, **33**, 6657; M. Tada and K. Kaneko, *Chem. Lett.*, 1995, 843; C. H. Schiesser and L. M. Wild, *Tetrahedron*, 1996, **52**, 13265.

10 D. N. Harpp, T. Aida and T. H. Chan, *Tetrahedron Lett.*, 1979, **20**, 2853.

11 A typical procedure for the radical reaction of *S*-phenyl chlorothioformate with an alkyl iodide is as follows. A benzene solution (0.5 ml, 0.4 M in the iodide) of cyclohexyl iodide (42 mg, 0.2 mmol), *S*-phenyl chlorothioformate (70 mg, 0.4 mmol) and bis(tributyltin) (140 mg, 0.24 mmol) in a quartz tube was degassed for 10 min and then irradiated at 300 nm in a photochemical reactor for 9 h. The reaction mixture was concentrated under reduced pressure. EtOAc (3 ml), water (2–3 drops) and KF (116 mg, 2 mmol) were then added and the mixture was stirred at room temperature for 30 min. After the mixture was filtered through a short column of silica gel, the filtrate was concentrated under reduced pressure. The crude product was purified by flash silica gel column chromatography to give *S*-phenyl cyclohexanecarbothioate (25 mg, 56%) as a colorless oil: δ_H (200 MHz, $CDCl_3$) 1.23–1.54 (m, 4 H), 1.56–1.87 (m, 4 H), 1.88–2.13 (m, 2 H), 2.53–2.68 (m, 1 H), 7.38 (s, 5 H); δ_C (50 MHz, $CDCl_3$) 25.4, 25.5, 29.5, 52.4, 127.8, 129.1, 129.2, 134.4, 200.6; ν_{max}(NaCl)/cm^{-1} 2928, 1708, 1066, 950.

Received in Cambridge, UK, 26th January 1998; 8/00664D

Synthesis of a novel pseudodisaccharide glycoside as a potential glycosidase inhibitor

Alan H. Haines*† and Ivone Carvalho‡

School of Chemical Sciences, University of East Anglia, Norwich, UK NR4 7TJ

An *N*-linked pseudodisaccharide 2 containing an inositol moiety in place of a glycopyranosyl residue has been synthesised to mimic the disaccharide unit, 3-*O*-(α-D-glucopyranosyl)-D-glucopyranose, cleaved by Glucosidase II during glycoprotein processing; an attempt to prepare the analogous 2-*N*-linked compound 1 as an inhibitor of Glucosidase I led to the novel *N*-phenyl derivative 10 of 2-amino-2-deoxy-D-glucopyranose.

Glycoprotein processing, a key step in the formation of cell surface oligosaccharides, initially involves the action of Glucosidase I and II on the *N*-linked oligosaccharide $Glc_3Man_9GlcNAc_2$ for sequential removal of the α(1 → 2)- and α(1 → 3)-linked glucose residues.[1] Inhibition of either of these two key enzymes leads to incorrect modification of nascent oligosaccharides.[2] Malformation of gp 120 on the surface of the AIDS virus is the likely reason why glycosidase inhibitors such as 1-deoxynojirimycin (DNJ) or castanospermine exhibit anti-HIV activity.[3]

We wished to design potential glycosidase inhibitors which mimic the *disaccharide units* which form the substrates for Glucosidase I and II, 2-*O*-(α-D-glucopyranosyl)-D-glucopyranose and 3-*O*-(α-D-glucopyranosyl)-D-glucopyranose, respectively. There are clear advantages in introducing nitrogen into such structures at strategic points[4] but in view of the likely hydrolytic instability of simple *N*-linked mimics, which are glycosylamines, and the efficacy of *N*-linked monocarba-oligosaccharide inhibitors such as acarbose[5] and oligostatin,[6] we decided to prepare the corresponding *N*-linked pseudodisaccharides **1** and **2** in which the non-reducing glycosyl moiety is imitated by an inositol unit, which only fails in its ability to mimic the α-D-glucopyranose unit in having an OH in place of the usual 5-CH_2OH group and a –CH(OH)– group in place of the ring oxygen atom. We report an unexpected result in our attempt to synthesise **1**,§ the synthesis of **2**, and a

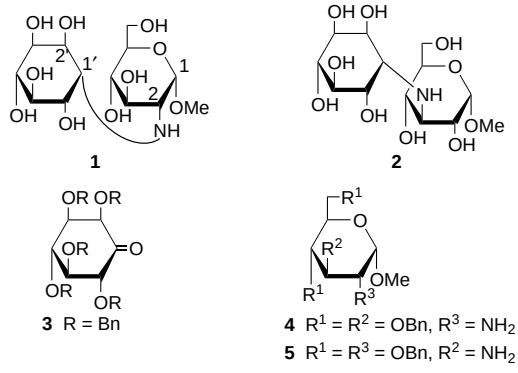

preliminary result on inhibition studies with **2** on yeast α-glucosidase.

Our proposed syntheses were based on the reaction between the chiral penta-*O*-benzylinosose **3**[7] and either methyl 2-amino-3,4,6-tri-*O*-benzyl-2-deoxy-α-D-glucopyranoside **4** or methyl 3-amino-2,4,6-tri-*O*-benzyl-3-deoxy-α-D-glucopyranoside **5** to afford corresponding imines, which we aimed to reduce stereoselectively, creating a chiral centre which, in the final product **1** and **2**, mimics the α-anomeric link in the oligosaccharide.

To prepare amine **4**, 2-amino-2-deoxy-D-glucopyranose **6** was *N*-protected by reaction with 2,2,2-trichloroethoxycarbonyl chloride, and the resultant amide **7** was converted by reflux in MeOH containing HCl into the corresponding methyl α-D-glycoside **8** (Scheme 1). Attempted *O*-benzylation of the latter compound using NaH–BnBr led to extensive decomposition, but treatment with benzyl trichloroacetimidate[8] under acidic catalysis gave the required protected benzyl ether **9** which was de-*N*-protected by treatment[9] with Zn/Cu couple in KH_2PO_4–THF–H_2O to give **4**.

Storage of **4** with an equimolar quantity of inosose **3** in benzene over molecular sieves at 20 °C for several days gave no reaction, but repeated evaporation of benzene from the mixture at 60 °C under reduced pressure afforded a new product with a characteristic single at δ 6.25 in its ^{1}H NMR spectrum. NMR spectral data and elemental analysis indicated the compound to be methyl 3,4,6-tri-*O*-benzyl-2-(2,4,6-tribenzyloxyphenylamino)-2-deoxy-α-D-glucopyranoside **10** which can arise from an initially formed imine by elimination of two molecules of benzyl alcohol followed by aromatisation of the imino quinone so formed.¶ Subjecting **10** to catalytic transfer hydrogenation conditions without careful exclusion of air led to the initial formation of a purple solution followed by extensive decomposition as evidence by TLC, presumably because of oxidation of the initially formed aminophloroglucinol derivative. Hydrogenation with subsequent manipulations under an atmosphere of argon gave material with the expected ^{1}H and ^{13}C NMR spectra of methyl 2-deoxy-2-(2,4,6-trihydroxyphenylamino)-α-D-glucopyranoside **11**.

In contrast, our related strategy for the preparation of **2** was successful. Amine **5** was prepared in three steps from methyl 2,3-anhydro-α-D-allopyranoside **12** by reaction with azide ion, followed by conventional benzylation (NaH–BnBr in DME) of the 3-azido-*gluco* product **13**, chromatographically isolated from the simultaneously formed 2-azido-*altro* isomer, and then

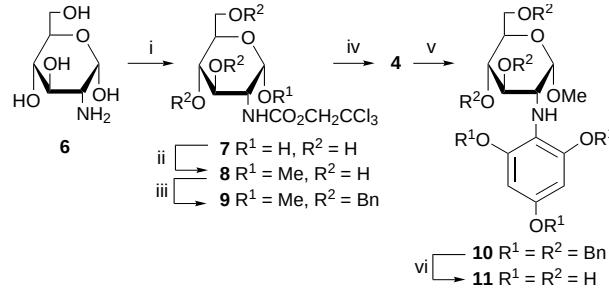

Scheme 1 *Reagents and conditions*: i, CCl_3CH_2OCOCl, aq. $NaHCO_3$, 10 °C for 2 h, then 20 °C for 19 h, 72%; ii, 2.5% w/v HCl in MeOH, reflux 8.5 h, 96%; iii, $CCl_3C(NH)OBn$, CH_2Cl_2–cyclohexane (1 : 2), TFA, 20 °C, 2.5 h, 78%; iv, Zn/Cu, THF–1 M aq. KH_2PO_4 (5 : 1), 20 °C, 8.5 h, 51%; v, **3**, C_6H_6 (addition and evaporation, ×5), 60 °C, 79%; vi, EtOH–cyclohexene (2 : 1), Pd black, reflux under Ar, 38 h, yield not determined (air-unstable product)

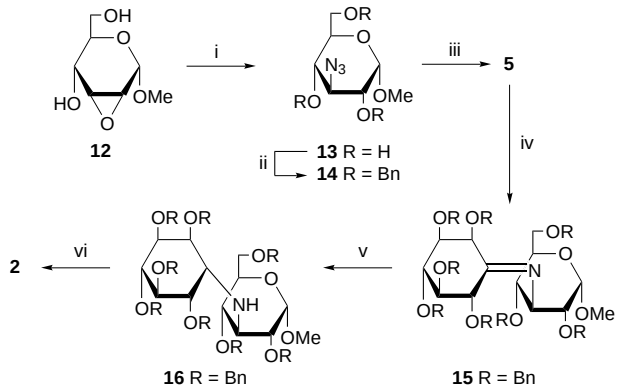

Scheme 2 *Reagents and conditions*: i, NaN_3, $(NH_4)_2SO_4$, DMF, 110 °C, 3 h, 47%; ii, NaH, BnBr, DMF, 20 °C, 1 h, 91%; iii, Ph_3P, THF–H_2O (10 : 1), 80 °C, 7 h, 70%; iv, **3**, C_6H_6, 4 Å molecular sieves under N_2, 20 °C, 70 h; v, $NaBH_3CN$, DMF, 20 °C, 70 h and 100 °C, 1 h, 61%; vi, EtOH–cyclohexene (2 : 1), Pd black, reflux 24 h, 67%

reduction (Ph_3P–THF–H_2O) of the so-produced azido benzyl ether **14** (Scheme 2). Condensation of **5** with the protected chiral inosose **3** to give imine **15** occurred on storage of a mixture of the two reactants in a 1.2 : 1 molar ratio in benzene solution over molecular sieves at 20 °C for 70 h. Surprisingly, attempted formation of the imine **15** by an aza-Wittig reaction of **3** with the iminophosphorane obtained by treatment of azide **13** with PPh_3 under anhydrous conditions proved unsuccessful.

Reduction of imine **15** with sodium cyanoborohydride in DMF occurred with the required stereoselectivity, the major product being shown by ^{1}H NMR spectroscopy at 600 MHz to be the amine **16**. Thus, on the reasonable assumption that the inositol ring in **16** adopts a chair conformation with four equatorial substituents, an assumption supported by the vicinal coupling constants, the signal for the proton (1′-H) on the inositol carbon carrying the nitrogen substituent would be expected to be an overlapping doublet of doublets, each with $J \sim 3$ Hz, resulting in an apparent triplet with ~ 3 Hz splitting. The alternative stereoisomer would be expected to show for the same proton a true doublet of doublets with component splittings of ~ 9 and 3 Hz. The observed apparent triplet with a J value of 4.4 Hz confirmed structure **16**. Signal allocation for 1′-H on the inositol ring was confirmed by measurement of the ^{1}H NMR spectrum of the analogous deuterated compound obtained by reduction of imine **15** with sodium borodeuteride.

De-*O*-benzylation was achieved by catalytic transfer hydrogenation (cyclohexene–Pd black–EtOH) at reflux temperature for 24 h. Purification of the product by chromatography on silica gel with 1 : 1 EtOAc–MeOH gave the required pseudodisaccharide **2** as a foam. Inspection of the ^{1}H NMR spectrum of the crude hydrogenolysis product indicated a 'satellite' doublet at δ 4.64 to that of the anomeric proton at δ 4.67, with an integrated intensity $\leqslant$5% of the major signal, but no other difference from the spectrum of **2** could be observed. That the benzyl ether **16** appeared 'anomerically pure' results from the very small amount of the diastereoisomer present and extensive overlap of the absorption region for anomeric protons with that of the benzylic CH_2 resonances.

Preliminary inhibition studies on yeast α-glucosidase indicate that **2** is a much poorer inhibitor of the enzyme than DNJ. Thus, under identical conditions (30 °C, pH 6.5, PIPES buffer), an approximately 100-fold greater molar concentration of **2** was required compared to that for DNJ to bring about a 20% reduction in the rate of enzyme-catalysed release of 4-nitrophenol from 4-nitrophenyl α-D-glucopyranoside. This result reflects, most likely, a different inhibitory mechanism for **2** compared to that of DNJ;[5] the latter carries an endocyclic N-atom in contrast to **2**, in which the N-atom replaces the usual glycosidic O-atom.

We thank C. MacDonald for expert help in obtaining ^{1}H NMR spectra at 600 MHz, A. W. R. Saunders for microanalysis, and the Mass Spectrometry Service Centre at Swansea for high resolution mass spectra.

Notes and References

† E-mail: a.haines@uea.ac.uk
‡ On leave from the Departamento de Ciências Farmacêuticas, Faculdade de Ciências Farmacêuticas de Ribeirão Preto, Universidade de São Paulo, Ribeirão Preto, Brasil.

§ All new compounds, except for the unstable imine **15**, gave satisfactory elemental analyses or high resolution mass spectral data and gave NMR spectra in accord with expected structures.

¶ Although the isomeric 3,4,5-tribenzyloxy isomer cannot be ruled out, the structural allocation is based on the combined considerations of: (i) a comparison of the observed ^{13}C NMR chemical shifts for Ar-C in the tetrasubstituted aromatic ring of **10** with those estimated for the two isomers; (ii) a comparison of the observed ^{1}H NMR chemical shift for Ar-H at δ 6.25 with those for 3,4,5-trimethoxyaniline (δ 5.91) and 2,4,6-trimethoxyaniline (δ 6.05), all measured in $CDCl_3$; (iii) the likely mechanism of elimination from the supposed intermediate imine.

1 R. Kornfeld and S. Kornfeld, *Annu. Rev. Biochem.*, 1985, **54**, 631.
2 A. D. Albein, *Annu. Rev. Biochem.*, 1987, **56**, 497.
3 G. B. Karlsson, T. D. Butters, R. A. Dwek and F. M. Platt, *J. Biol. Chem.*, 1993, **268**, 570.
4 G. Legler, *Adv. Carbohydr. Chem. Biochem.*, 1990, **48**, 317.
5 E. Truscheit, W. Frommer, B. Junge, L. Müller and D. D. Schmidt, *Angew. Chem., Int. Ed. Engl.*, 1981, **20**, 744.
6 J. Itoh, S. Omoto, T. Shomura, H. Ogino, K. Iwamatsu and S. Inouye, *J. Antibiot.*, 1981, **34**, 1424.
7 Inosose **3**, $[\alpha]_D$ +9.2 (*c* 1.0, $CHCl_3$), was prepared by Swern oxidation of the corresponding known (−)-penta-*O*-benzyl-*myo*-inositol derivative; R. Aneja, S. Aneja, V. P. Pathak and P. T. Ivanova, *Tetrahedron Lett.*, 1994, **35**, 6061; G. R. Baker, D. C. Billington and D. Gani, *Tetrahedron*, 1991, **47**, 3895.
8 T. Iversen and D. R. Bundle, *J. Chem. Soc., Chem. Commun.*, 1981, 1240.
9 G. Just and K. Grozinger, *Synthesis*, 1976, 457.

Received in Glasgow, UK, 9th January 1998; 8/00279G

Fluorene acceptors with intramolecular charge-transfer from 1,3-dithiole donor moieties: novel electron transport materials

Igor F. Perepichka,*[a] Dmitrii F. Perepichka,[a] Martin R. Bryce,*[b]† Leonid M. Goldenberg,[b] Lyudmila G. Kuz'mina,[c] Anatolii F. Popov,[a] Antony Chesney,[b] Adrian J. Moore,[b] Judith A. K. Howard[b] and Nikolai I. Sokolov[d]

[a] *L. M. Litvinenko Institute of Physical Organic and Coal Chemistry, National Academy of Sciences of Ukraine, Donetsk 340114, Ukraine*
[b] *Department of Chemistry, University of Durham, Durham, UK DH1 3LE*
[c] *Institute of General and Inorganic Chemistry, Russian Academy of Sciences, Moscow 117907, GSP-1, Russian Federation*
[d] *Laboratory of Holography, Natural Faculty, University 'Kievo-Mogilyanskaya Academy', Kiev 254145, Ukraine*

The synthesis, solution redox behaviour and intramolecular charge transfer properties of novel D(=CH–CH)$_n$=A compounds (n = 0, 1, 3; D and A are 1,3-dithiole and nitrofluorene moieties, respectively) are reported.

Organic compounds with asymmetric π-electron delocalization exhibit properties such as non-linear optical effects (NLO), photoconductivity and electron transport properties.[1] Electron acceptors of the fluorene series are widely used for optical information recording.[2] It has been shown that fluorene acceptors substituted with a donor moiety can efficiently sensitise the photoconductivity of carbazole-containing polymers in the spectral region of intramolecular charge transfer (ICT) of the acceptors.[3] Although 1,3-dithiole electron donor are well-known building blocks in conductive charge transfer salts,[4] there are few reports of 1,3-dithioles as components of π-conjugated push-pull compounds.[5] Herein we report a new series of D(=CH–CH)$_n$=A compounds containing 1,3-dithioles and nitrosubstituted fluorenes as D and A moieties, respectively.

Compounds **2**–**9** were synthesised (Scheme 1) by condensation of the substituted fluorenes **1** with the appropriate dithiolium salts (for **2**–**5**) or aldehydes (for **6**–**9**) in DMF, (20–70 °C, 0.5–50 h; 30–90%). The intramolecular charge transfer (ICT) in these compounds is manifested in the appearance of long-wavelength absorbance bands in their electronic spectra (Fig. 1, Table 1). Increasing the acceptor character of the fluorene fragment with electron withdrawing substituents results in a bathochromic shift of the ICT band that can be described quantitatively by eqn. (1), where $h\nu_{ICT}$ is the

$$h\nu_{ICT} = h\nu^0_{ICT} + \rho^-_{ICT}\,\Sigma\sigma^-_p \qquad (1)$$

ICT energy defined by the maxima of the ICT band (λ_{ICT}), $h\nu^0_{ICT}$ is $h\nu_{ICT}$ for the reference compound (unsubstituted benzene rings in fluorenes, $\Sigma\sigma^-_p = 0$), ρ^- is a parameter showing ICT energy sensitivity to substituents, and $\Sigma\sigma^-_p$ is a sum of σ^-_p (nucleophilic constants of the substituents in the fluorene nucleus).

The sensitivity parameter ρ^-_{ICT} shows only minor changes with changing the substituents in the 1,3-dithiole ring (**2** → **3** → **4**) or with lengthening the C=C chain between the D and A moieties (**2** → **6** → **7**) (Table 1). The values of ρ^-_{ICT} ≈ 0.14–0.17 eV are higher than that reported for 9-(4-phenyl-1,2-dithiol-3-ylidene)fluorenes (0.12 ± 0.01 eV).[6]

The structure of **3g** was determined by X-ray analysis (Fig. 2).§ As a result of ICT, the exocyclic C(9)=C(14) double bond is lengthened [1.395(5) Å] and is close to that observed in another ICT compound of the fluorene series, *i.e.* 9-(α-cyano-α-dimethylaminomethylene)-2,4,5,7-tetranitrofluorene [1.388(4) Å].[3b] The distortions of the substituents in the fluorene ring are a result of the close contact between the nitro groups in positions 4 and 5. The dihedral angle between the planes of the fluorene five-membered ring and the 1,3-dithiole ring is 21.3°. Fig. 2 shows that the acceptor moieties in the molecules related by symmetry centres form stacks (interplanar distance 3.58 Å). Interstack interactions occur through weak contacts of the donor fragments; S(2b)···S(3a) and S(2a)···S(3b) distances are slightly shortened (3.543 Å) compared to double

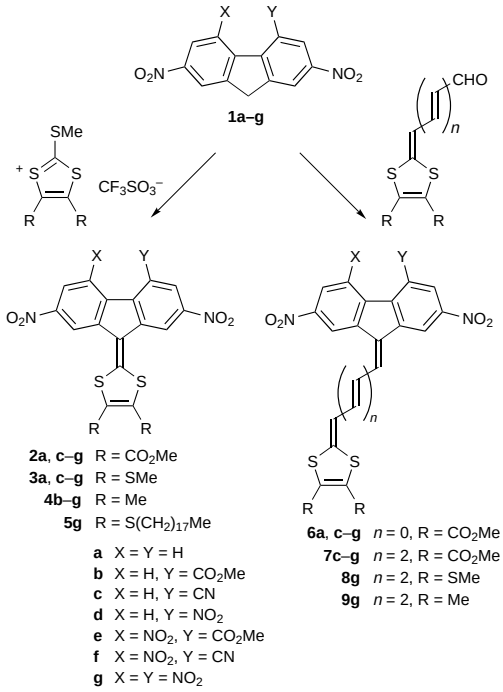

Scheme 1

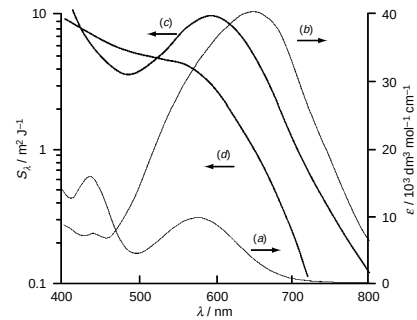

Fig. 1 Electron absorption spectra for (*a*) **3g** and (*b*) **8g** in acetone, (25 °C) and spectral distribution of $S_{\Delta V}$ for PEPC films sensitized by 5 mass% of electron acceptors (*c*) **5g** and (*d*) TNF

Table 1 Correlations[a] of ICT energies of acceptors **2**–**4**, **6** and **7** using eqn. (1), spectral data for **2g**–**4g** and **6g**–**9g** and CV data for **2g**–**4g** and **6g**

Compound	$h\nu^0_{ICT}$/eV[b]	ρ^-_{ICT}/eV[b]	$\lambda_{ICT/nm}$[b,c]	$\lambda_{ICT/nm}$[c,d]	ε_{ICT}/dm^3 mol^{-1} cm^{-1}	$E^{\frac{1}{2}}_{1red}$/V[e]	$E^{\frac{1}{2}}_{2red}$/V[e]
2	3.00 ± 0.05	−0.138 ± 0.012	544	535	9800	−0.80	−1.02
3	2.88 ± 0.02	−0.153 ± 0.008	592	578	9700	−0.81	−1.04
4	2.81 ± 0.02	−0.150 ± 0.011	611	595	8600	−0.83	−1.05
6	2.98 ± 0.02	−0.169 ± 0.006	587.5	572	21 000	−1.11	−1.32
7	2.79 ± 0.02	−0.164 ± 0.011	636	590	39 000		
8			707	650	40 000		
9			753	700			

[a] $r \geqslant 0.985$. [b] In 1,2-dichloroethane. [c] Spectral data for compounds **2g**–**4g** and **6g**–**9g**. [d] In acetone. [e] CV data for **2g**–**4g** and **6g** (see footnote ¶).

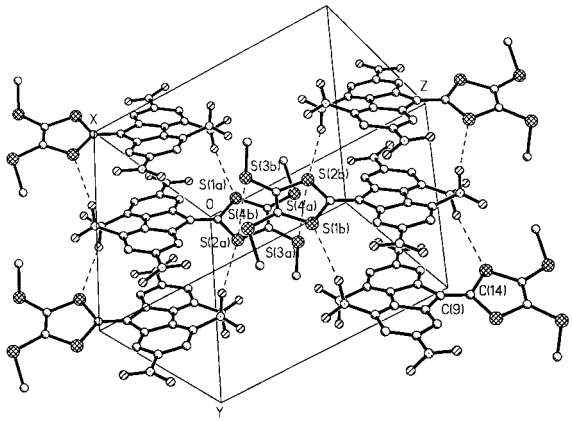

Fig. 2 Crystal packing of compound **3g**; short intermolecular S···S and S···O contacts are shown by dashed lines

the van der Waals radius of sulfur (3.6–3.7 Å).[7] There are also weak intermolecular S···O contacts (3.25–3.42 Å).

The electrochemical redox properties of the compounds **2**–**4** and **6** have been studied by cyclic voltammetry (Table 1).¶ Compounds **2**–**4** display two reversible single-electron reduction waves ($E^{\frac{1}{2}}_{1red}$ = −1.44 → −0.81 V, $E^{\frac{1}{2}}_{2red}$ = −1.60 → −1.02 V in the sequence **a** → **g**). Third quasi-reversible or irreversible single-electron reduction [$E^{\frac{1}{2}}_{3red}$ = −(1.88–2.15) V] and oxidation ($E^{\frac{1}{2}}_{ox}$ = +0.63–0.70 V) processes were observed in some, but not all, cases. Insertion of an additional double bond between the A and D moieties (**6**) leads to a shift of both $E^{\frac{1}{2}}_{1red}$ and $E^{\frac{1}{2}}_{2red}$ by *ca* . 0.3 V to more cathodic potentials. Correlation analyses of $E^{\frac{1}{2}}_{1red}$ and $E^{\frac{1}{2}}_{2red}$ for compounds **2**–**4** by eqn. (2), where $E^{\frac{1}{2}}$ is the half-wave potential of reduction or

$$E^{\frac{1}{2}} = E^{\frac{1}{2}}_0 + \rho^-_{CV}\,\Sigma\sigma^-_p \qquad (2)$$

oxidation of a compound, $E^{\frac{1}{2}}_0$ is $E^{\frac{1}{2}}$ for the reference compound (unsubstituted benzene rings in fluorenes, $\Sigma\sigma^-_p = 0$), and ρ^- is a parameter showing electrochemical potential sensitivity to substituents, gave good linear relationships (r = 0.98–0.999); sensitivity parameters ρ^-_{CV} for the first and second reduction steps of compounds **2**–**4** were close and lay in the region of 0.20–0.24 V, which is slightly higher compared to ρ^-_{CV} for nitrosubstituted 9-aminomethylenefluorenes.[3b] The electron affinities obtained for compounds **2**–**4** from their $E^{\frac{1}{2}}_{1red}$ potentials[8] are *ca.* 0.2 eV lower than for the corresponding 4,5-X,Y-2,7-dinitrofluoren-9-ones, and for tetranitro substituted derivatives **2g**–**4g** are *ca.* 2 eV. This characterises compounds **2**–**4** as moderate acceptors.

Due to the low solubility of compound **3g** we tested the more soluble long-chain homologue **5g** as a sensitiser in photothermoplastic storage media (PTSM) based on poly[*N*-(2,3-epoxypropyl)carbazole] (PEPC).‖ Fig. 1 shows the spectral distribution of the electrophotographic sensitivity ($S_{\Delta V}$) of PTSM on the basis of PEPC films sensitized by **5g** and by 2,4,7-trinitrofluoren-9-one (TNF) which is widely used for these purposes.[2b] In contrast to TNF, for which $S_{\Delta V}$ decreases with increasing wavelength in the visible region, **5g** displays increased sensitivity in its ICT region. Excellent rheological properties of PTSM sensitised with **5g** (diffraction efficiency for plane lightwave holograms η_{max} = 25%) allowed the attainment of extremely high values of holographic sensitivity, S_η = 250–300 m^2 J^{-1} at the level of η = 1% (He-Ne laser, λ = 632.9 nm),** suggesting that this type of acceptor is extremely promising as sensitisers for hologram recording.

We thank the EPSRC the Royal Society for funding (I. F. P., L. M. G. and L. G. K.), and the Royal Society for a Leverhulme Senior Research Fellowship (to J. A. K. H.).

Notes and References

† E-mail: m.r.bryce@durham.ac.uk

‡ All new compounds gave satisfactory mass spectra, ^{1}H NMR spectra and elemental analysis.

§ *Crystal data* for **3g**: $C_{18}H_{10}N_4O_8S_4$, M = 538.54, triclinic, $P\bar{1}$, a = 9.079(1), b = 10.014(1), c = 12.806(2) Å, α = 108.61(1), β = 102.30(1), γ = 103.06(1)° , V = 1022.4(4) Å^3, Z = 2, D_c = 1.749 g cm^{-3}, F(000) = 548, λ = 0.71073 Å, T = 150.0(2) K, R = 0.0580, wR = 0.1345 and goodness-of-fit 1.096, $\Delta\rho_{max}$ = 0.665 e Å^{-3}, $\Delta\rho_{min}$ = −0.588 e Å^{-3}. CCDC 182/778.

¶ *ca.* 10^{-4} mol dm^{-3} compound in dry DMA (**2**–**4**) or CH_2Cl_2 (**6**), Pt working electrode, 0.2 mol dm^{-3} $Bu_4N^+PF_6^-$; all potentials were measured *vs.* Fc^0/Fc^+ couple as internal reference.

‖ Details are the same as described in refs. 2(*c*) and 3(*b*).

** PTSM with 5 mass% TNF gave η_{max} = 15% and S_η = 20 m^2 J^{-1} under the same conditions [ref. 2(*b*)].

1 D. R. Kanis, M. A. Ratner and T. J. Marks, *Chem. Rev.*, 1996, **94**, 195; M.Matsui, K. Fukuyasu, K. Shibata and H. Muramatsu, *J. Chem. Soc., Perkin Trans. 2*, 1993, 1107; M. Matsui, K. Shibata, H. Muramatsu and H. Nakazumi, *J. Mater. Chem.*, 1996, **6**, 1113.

2 (*a*) D. F. Eaton, *Top. Curr. Chem.*, 1990, **156**, 200; (*b*) I. F. Perepichka, D. D. Mysyk and N. I. Sokolov, in *Current Trends in Polymer Photochemistry*, ed. N. S. Allen, M. Edge, I. R. Bellobono and E. Selli, Ellis Horwood, London, 1995, ch. 18, p. 318; (*c*) D. D. Mysyk, I. F. Perepichka and N. I. Sokolov, *J. Chem. Soc., Perkin Trans. 2*, 1997, 537.

3 (*a*) N. G. Kuvshinskii, N. G. Nakhodkin, N. A. Davidenko, A. M. Belonozhko and D. D. Mysyk, *Ukr. Phis. Zh.*, 1989, **34**, 1100; (*b*) I. F. Perepichka, A. F. Popov, T.V. Orekhova, M. R. Bryce, A. N. Vdovichenko, A. S. Batsanov, L. M. Goldenberg, J. A. K. Howard, N. I. Sokolov and J. L. Megson, *J. Chem. Soc., Perkin Trans. 2*, 1996, 2453.

4 T. Jørgensen, T. K. Hansen and J. Becher, *Chem. Soc. Rev.*, 1994, **23**, 41; M. R. Bryce, *J. Mater. Chem.*, 1995, **5**, 1481; V. Khodorkovsky and J. Y. Becker, in *Organic Conductors. Fundamentals and Applications*, ed. J.-P. Farges, Marcel Dekker, New York, 1994, ch. 3, p. 75.

5 H. E. Katz, K. D. Singer, J. E. Sohn, C. W. Dirk, L. A. King and H. M. Gordon, *J. Am. Chem. Soc.*, 1987, **109**, 6561; M. Blanchard-Desce, I. Ledoux, J.-M. Lehn, J. Malthete and J. Zyss, *J. Chem. Soc., Chem. Commun.*, 1988, 737; S. Inoue, Y. Aso and T. Otsubo, *Chem. Commun.*, 1997, 1105 and references cited therein.

6 D. D. Mysyk and I. F. Perepichka, *Phosphorus, Sulfur, Silicon, Relat. Elem.*, 1994, **95**–**96**, 527.

7 Y. V. Zefirov and P. M. Zorkii, *Russ. Chem. Rev.*, 1989, **58**, 421; R. S. Rowland and R. Taylor, *J. Phys. Chem.*, 1996, **100**, 7384.

8 D. D. Mysyk, I. F. Perepichka, A. S. Edzina and O. Ya. Neilands, *Latvian J. Chem.*, 1991, 727 (in Russian).

Received in Cambridge, UK, 6th November 1997; revised manuscript received, 2nd February 1998; 8/00912K

On the mechanism of the synergistic oxidation of saturated hydrocarbons and hydrogen sulfide under Gif conditions

Derek H. R. Barton*† and Tingsheng Li*

Department of Chemistry, Texas A & M University, PO Box 300012, College Station, TX 77842, USA

It is demonstrated by a study of cyclohexane phenylselenation that the synergistic oxidation of cyclohexane with H_2S and O_2 does not involve carbon or oxygen radicals.

Recently we reported a new reaction in which saturated hydrocarbons were oxidized synergistically with H_2S and O_2.[1] This unusual reaction is an extension of Gif chemistry that should be of industrial importance. We now present further evidence on the mechanism of this reaction.

The bond strength[2] in the H–SH bond is 90.5 (±1.1) kcal mol^{-1}. Thus any secondary or primary carbon radical would be immediately reduced by H-atom transfer. When we photolyzed the Barton ester of adamantane-1-carboxylic acid in the presence of H_2S it was converted quantitatively into adamantane. Similarly, oxidation of adamantane in the presence of H_2S gave a *normalized* secondary/tertiary ratio of about 1. This is three times as great as normal and corresponds to the reduction of tertiary radicals back to hydrocarbon.[3] Since there are no secondary radicals, secondary position oxidation proceeded normally.

Cyclohexane gave a mixture of cyclohexanone and cyclohexanol. The latter was produced by reduction of the intermediary hydroperoxide[4] by H_2S.

The formation of alcohol and ketone at the same time enabled us to determine the kinetic isotope effect (KIE) for alcohol formation. It was of the order 1.1–1.2.

Recently[5] we showed that phenylselenation of saturated hydrocarbons[6a] involves PhSeH, an excellent trap for radicals.[6b] In fact the earlier work[6a] involved reduction with Zn^0–Fe^{II} catalyst. Methylation showed that all the PhSeSePh had been reduced to PhSeH.[7] This was, in fact, a proof of the non-involvement of carbon radicals. Our recent work[5] has shown that selenide anion is not involved.[8] Another factor to consider is the relative rates of reaction (3×10^9 and 2.3×10^7 M^{-1} s^{-1}) for radicals with PhSeH and PhSeSePh, respectively.[6b]

In the present study, PhSeSePh was added to a system where H_2S and O_2 were being passed through a mixture of cyclohexane and picolinic acid (Table 1). This afforded ketone, alcohol and a very high yield of phenylselenocyclohexane with respect to the amount of PhSeSePh added (entries 1 and 2). Unlike in the earlier study[5] using H_2O_2, when H_2S was used the picolinic acid was no longer needed. The phenylselenocyclohexane was then produced in quantitative yield (entries 3, 4 and 5).

We consider that phenyselenocyclohexane must be produced by the same type of mechanism that we proposed before[5] (Scheme 1).

In our first publication on the H_2S–O_2 reaction[1] we did not comment on the mechanism except to classify it as 'Gif chemistry'. We suggested that the oxidant was superoxide and that this reacted with Fe^{II} to furnish the species Fe^{III}–OOH. The species can also be produced by displacement on Fe^{III} with H_2O_2. Without hydrocarbon this has $t_{\frac{1}{2}}$ *ca*. 45 min. Upon addition of hydrocarbon it is rapidly inserted into the Fe–C bond, which slowly ($t_{\frac{1}{2}}$ *ca*. 45 min) affords ketone or, with iodide, rapidly gives the iodide of the hydrocarbon.[9] In order to explain why the selective functionalization of saturated hydrocarbons takes place in the presence of H_2S, Ph_2S, Ph_3P, $(MeO)_3P$, PhSH and even PhSeH, we proposed in 1992 that it was the contact of a relatively inert iron species with the hydrocarbon which created the active iron species, which then reacted immediately with the hydrocarbon. We cited the agostic effect[10] as an explanation. It is the reactivity of PhSeH, produced by[5] PhSeSePh and Bu_3P, that gives real substance to our proposal. We now suggest that Fe^{IV} and Fe^{V} are only produced at the moment of contact with the hydrocarbon and that these species react instantly with their hydrocarbon activator. We offer the same explanation for the KIE of close to 1 (see above).

Thus the Fe^{III}–Fe^{V} manifold can be modified according to Scheme 2. The H_2S–O_2 chemistry then takes place by H_2S reduction of Fe^{V} to Fe^{IV}.

The alternative route for phenylselenation is from Fe^{II} and H_2O_2, which we have used in our work with PhSeSePh and Bu_3P already cited. We modify our concept of the Fe^{II}–Fe^{IV} manifold as shown in Scheme 3. Normally, the Fe^{IV}–CHR_2 species can fragment into Fe^{III} and a carbon radical. This, however, does not happen when $PhSe^-$ is one of the ligands.

In our recent work on the phenylselenation reaction we showed by ^{77}Se NMR spectroscopy that the reaction of PhSeSePh and Bu_3P (50% excess) with a drop of water was an excellent method for quantitative synthesis of PhSeH *in situ*. The presence of the excess Bu_3P guaranteed that there was no

Table 1 Effect of selenide on Gif oxidation[a]

Entry	Ligand (mmol)	Selenide (mmol)	$FeCl_2·4H_2O$/ (mmol)	Cyclohexane/ (mmol)	Ketone/ (mmol)	Alcohol/ (mmol)	$PhSeC_6H_{11}$/ (mmol)	Conversion[b] (%)	Yield[c] (%)
1	Picolinic acid (3)	PhSeSePh (1)	1	20	0.75	2.31	1.81	24.35	90.5
2	Picolinic acid (3)	PhSeH (1.5)	1	20	0.15	0.51	1.46	10.6	97.3
3	—	PhSeH (2.5)	1	20	0.74	1.32	2.51	22.85	100
4	—	PhSeSePh (1.5)	1	20	1.28	2.50	3.03	30.85	100
5	—	PhSeSePh (1)	1	20	1.00	2.19	1.98	25.85	99
6	—	PhSeSePh (1)	1	5	0.19	0.40	0.95	30.8	47.5
7	—	PhSeSePh (1)	1	2	0.10	0.15	0.75	50	37.5

[a] Ligand (0–3 mmol), $FeCl_2·4H_2O$ (0.3–1 mmol), cyclohexane (2–20 mmol), selenide (1–2.5 mmol), 4-*tert*-butylpyridine (2 ml), MeCN (31 ml). O_2 (g) and H_2S (g) were passed at atmospheric pressure through the reaction mixture at room temperature for 3–4 h. The products were analyzed by GC, naphthalene was used as internal standard. [b] Conversion based on cyclohexane. [c] Yield based on selenide.

Table 2 Phenyselenation in the presence of Bu_3P[a]

Entry	PhSeSePh/ mmol	Bu_3P/ mmol	LiCl/ mmol	Conditions	Chloride/ mmol	Ketone/ mmol	Alcohol/ mmol	$PhSeC_6H_{11}$/ mmol
1[b]	1	8	—	H_2S–O_2	—	0.73	1.98	1.85
2[b]	2	60	—	H_2S–O_2	—	0.39	1.07	0.83
3[c]	2	3	—	H_2S–H_2O_2 (1)	—	—	—	0.74
4[c]	2	3	—	H_2S–H_2O_2 (2)	—	—	—	1.30
5[c]	4	6	—	H_2S–H_2O_2 (1)	—	—	—	0.85
6[c]	4	6	—	H_2S–H_2O_2 (2)	—	—	—	1.54
7[c]	4	6	—	H_2S–H_2O_2 (3)	—	—	—	1.92
8[c]	4	6	—	H_2S–H_2O_2 (4)	—	—	—	2.55
9[d]	1	2	20	H_2O_2 (1)	0.23	—	—	0.69
10[d]	1	2	20	H_2O_2 (2)	0.34	—	—	1.05

[a] Picoline acid (3 mmol), $FeCl_2{\cdot}4H_2O$ (1 mmol), cyclohexane (20 mmol), PhSeH (0.5–4 mmol), 4-*tert*-butylpyridine (2 ml), MeCN (31 ml). The products were analyzed by GC, naphthalene was used as internal standard. [b] O_2 (g) and H_2O (g) were passed through the reaction mixture at room temperature for 3–4 h. [c] H_2S (g) was passed through the reaction mixture at 0 °C when H_2O_2 (1–4 mmol) was added. [d] H_2O_2 (1–2 mmol) was added at 0 °C.

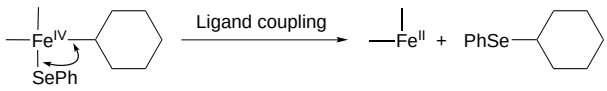

Scheme 1

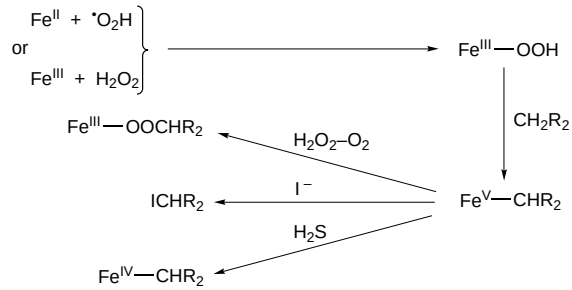

Scheme 2

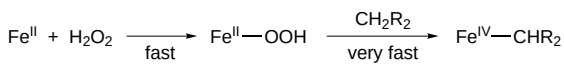

Scheme 3

adventitious oxidation of PhSeH back to PhSeSePh. We studied this reaction by ^{31}P NMR spectroscopy and showed that the reduction was complete in 2 min (experiment by Dr J. A. Smith). Before adding H_2O_2 we waited for 10–20 min to make sure that the reduction was complete.

Table 2 shows further experiments in which Bu_3P is used in the presence of PhSeSePh. Entries 1 and 2 used the H_2S–O_2 system as studied in Table 1. For entry 1 the yield of phenylselenocyclohexane was 92%, whilst the total activation including ketone and alcohol was 4.56 mmol. This is a good conversion as judged by past experiments.[1] All the selenium was present as PhSeH prior to reaction with the hydrocarbon yet the ketone and alcohol were formed in significant amounts. So not only are no radicals present but also the Bu_3P does not react with the iron species prior to activation by the hydrocarbon.

Using H_2O_2 as a minor component in the presence of an excess of PhSeH, the yield of the phenylselenocyclohexane (the only product) was 74 and 85% for entries 3 and 5, respectively (for 1 mmol of H_2O_2), and 65 and 77% for entries 4 and 6, respectively (for 2 mmol of H_2O_2). The increased yields in entries 5 and 6 were due to an increase in the available PhSeH. A further increase in the amount of H_2O_2 (entries 7 and 8) reduced the yield with respect to H_2O_2 to 64%.

The formation of cyclohexyl chloride in the Fe^{II}–Fe^{IV} manifold is usually accepted[11] to imply the reaction of a carbon radical with an Fe^{III}–Cl bond. The reaction can also be considered as a ligand-coupling reaction with an Fe^{IV}–C bond as in formation of the selenide (Scheme 1). The formation of cyclohexyl chloride using H_2O_2, like the phenylselenation reaction, requires the presence of the right carboxylic acid (here picolinic acid) and the correct amount of a suitable pyridine base (here 4-*tert*-butylpyridine). If the formation of the chloride can only take place *via* radical formation then the presence of PhSeH would remove the radical and no chloride would be formed. In fact entries 9 and 10 show that chloride formation is in competition with the phenylselenation reaction.

Finally we examined an oxidant, *tert*-butyl hydroperoxide (TBHP), that always reacts with Fe^{II} to make *tert*-butoxy radicals.[12–14] When TBHP (3 mmol) was added to cyclohexane (20 mmol) in MeCN (31 ml) and 4-*tert*-butylpyridine (2 ml) containing $FeCl_2{\cdot}4H_2O$ (1 mmol) and picolinic acid (3 mmol) with passage of H_2S, only traces of oxidation (0.05 mmol) were seen. From workup, 3 mmol of *tert*-butyl alcohol were recovered. This result is in keeping with the reduction of *tert*-butoxy radicals by H_2S. We conclude that carbon and oxygen radicals do not play a role in the synergistic oxidation of saturated hydrocarbons.

We thank Unilever, for support of this work. We thank Dr J. A. Smith for the ^{31}P NMR experiment.

Notes and References

† E-mail:dhrbarton@tamu.edu

1 D. H. R. Barton, T. Li and J. MacKinnon, *Chem. Commun.*, 1997, 557.
2 *Handbook of Chemistry and Physics*, ed. R. C. Weast, 67th edn., CRC Press, Boca Raton, Florida, 1986, pp. F-178–184.
3 D. H. R. Barton and D. Doller, *Acc. Chem. Res.*, 1992, **25**, 504.
4 D. H. R. Barton, D. Crich and W. B. Motherwell, *J. Chem. Soc., Chem. Commun.*, 1984, 242.
5 D. H. R. Barton, G. Lalic and J. A. Smith, *Tetrahedron*, in the press.
6 D. H. R. Barton, J. Boivin and P. Le Coupanec, *J. Chem. Soc., Chem. Commun.*, 1987, 1379; G. Balavoine, D. H. R. Barton, J. Boivin, P. Le Coupanec and P. Lelandais, *New J. Chem.*, 1989, **13**, 691; D. H. R. Barton and B. Chabot, *Tetrahedron*, 1996, **52**, 10 287; (*b*) M. Newcomb and M. B. Marek, *J. Am. Chem. Soc.*, 1990, **112**, 9662; M. Newcomb, *Tetrahedron*, 1993, **49**, 1151.
7 D. H. R. Barton, S. D. Bévière, W. Chavasiri, E. Csuhai, D. Doller and W.-G. Liu, *J. Am. Chem. Soc.*, 1992, **114**, 2147.
8 M. J. Perkins, *Chem. Soc. Rev.*, 1996, **25**, 229.
9 D. H. R. Barton, M. Costas Salgueiro and J. MacKinnon, *Tetrahedron*, 1997, **53**, 7417.
10 F. A. Cotton and A. G. Stanislowski, *J. Am. Chem. Soc.*, 1974, **96**, 5074.
11 D. H. R. Barton, B. Hu, D. K. Taylor and R. U. Rojas Wahl, *J. Chem. Soc., Perkin Trans. 2*, 1996, 1031.
12 F. Minisci and F. Fontana, *Tetrahedron Lett.*, 1994, **35**, 1427; F. Minisci, F. Fontana, S. Araneo and F. Recupero, *J. Chem. Soc., Chem. Commun.*, 1994, 1823; *Tetrahedron Lett.*, 1994, **35**, 3759.
13 I. W. C. E. Arends, K. U. Ingold and D. D. M. Wayner, *J. Am. Chem. Soc.*, 1995, **117**, 4710; P. A. MacFaul, I. W. C. E. Arends, K. U. Ingold and D. D. M. Wayner, *J. Chem. Soc., Perkin, Trans 2*, 1997, 135.
14 D. H. R. Barton, V. N. Le Gloahec, H. Patin and F. Launay, *New J. Chem.*, in the press; D. H. R. Barton, V. N. Le Gloahec and H. Patin, *ibid.*, in the press.

Received in Corvallis, OR, USA, 14 November 1997; revised manuscript received, 15th January 1998; 8/00552D

Porous copper(I) coordination polymers containing both the cyclic ion ligating agent methylcycloarsoxane $(MeAsO)_4$ and rigid aromatic heterocycles as spacers

Iris M. Müller, Thomas Röttgers and William S. Sheldrick*†

Lehrstuhl für Analytische Chemie, Ruhr-Universität Bochum, D-44780 Bochum, Germany

Porous lamellar networks with flexible $[Cu_xI_y\{cyclo\text{-}(MeAsO)_4\}]$ ribbons bridged by either π–π stacked terminal benzonitrile ligands ($x = y = 2$), rigid *p*-diaminobenzene spacers ($x = y = 2$) or ionic $[Cs\{cyclo\text{-}(MeAsO)_4\}_2]^+$ sandwiches ($x = 3$, $y = 4$) may be constructed by self-assembly from CuI and $(MeAsO)_n$ in the presence of the respective structure-directing agents.

The rational design of porous solid-state coordination networks with potential ion exchange or molecular sieving properties has aroused considerable current interest.[1] Although the majority of known examples involve Ag^I or Cu^I centres separated by rigid organic spacers (*e.g.* piperazine, pyrazine, 4,4′-bipyridine and 4,4′-biphenyldicarbonitrile), a few encouraging reports of the employment of more flexible connecting ligands such as methylene bridged dichalcogeno ethers,[2] thioether macrocycles[3] or alkylcycloarsoxanes $(RAsO)_n$ (R = Me, Et; n = 4, 5)[4] have recently appeared. In analogy both to zeolites[5] and porous group 14 or 15 chalcogenidometalates,[6] such layers or frameworks might be expected to be capable of undergoing elastic deformations in response to different structure-directing agents or imbibed molecular guests. Our current extension of this line of coordination polymer design to networks containing both ion ligating alkylcycloarsoxanes and aromatic heterocycles has been motivated by the desire to construct multifunctional materials. To our knowledge, only one previous report of the self-assembly of an extended solid-state structure with both flexible and rigid spacers has appeared, namely that of $^2_\infty[\{Cu_2(C_3H_2O_4)_2(4,4'\text{-bipy})(H_2O)_2\}\cdot H_2O]$, in which small cyclic $[Cu(C_3H_2O_4)]_4$ tetramers ($C_3H_2O_4^{2-}$ = malonate) are linked through 4,4′-bpy ligands into a 4^4 net.[7]

We have recently demonstrated that ribbons of the type $^1_\infty[Cu_2X_2\{cyclo\text{-}(MeAsO)_4\}]$ (X = Cl, Br, I) can be joined into comparable square networks by employment of additional bridging $(MeAsO)_4$ ligands.[4c] When the self-assembly reaction‡ between CuI and $(MeAsO)_n$ is performed in PhCN instead of MeCN, the connectivity role of these linking cyclic tetramers is taken over by terminally coordinated solvent molecules, whose aromatic π-systems stack to generate the large channels depicted in Fig. 1.§ The pore size increases significantly from 0.41 × 0.72 nm (shortest transannular H···H contacts) in $^2_\infty[Cu_2I_2\{cyclo\text{-}(MeAsO)_4\}_2]$[4c] to 0.82 × 0.82 nm in $^1_\infty[\{Cu_2I_2(PhCN)_2[cyclo\text{-}(MeAsO)_4]\}\cdot PhCN]$ **1**, with the result that relatively large guest PhCN molecules can now be accommodated in the extended structure. In a second 4^4 net shown in Fig. 2, this design principle has been extended to bridging 1,4-diaminobenzene spacers. Deep-red crystals of the layered structure $^2_\infty[Cu_2I_2(p\text{-}H_2NC_6H_4NH_2)\{cyclo\text{-}(MeAsO)_4\}]$ **2** may be grown by carefully underlayering a $p\text{-}H_2NC_6H_4NH_2$–$(MeAsO)_n$ solution in MeCN with a CuI solution in the same solvent at 0 °C. Optical properties of zeolites with analogous imbibed parallel chromophore molecules such as *p*-nitroaniline are of considerable current interest.[8] The identical building principles of the triclinic lattices of **1** and **2** suggest that the construction of larger pores should be possible by employing longer rigid bidentate aromatic spacer molecules.

Alkylcycloarsoxanes $(RAsO)_n$ coordinate alkali metal ions M in sandwich complexes of the type $[M\{cyclo\text{-}(RAsO)_n\}_2]$, that are reminiscent of those formed by macrocyclic polyethers. The ring size of the crown-shaped $(RAsO)_n$ ligands is controlled by the volume of the central cation (M = Na, n = 4; M = NH_4, K, Cs, n = 5).[4b,9] Attachment of crown polyethers to solid supports such as silica gel has successfully been employed in commer-

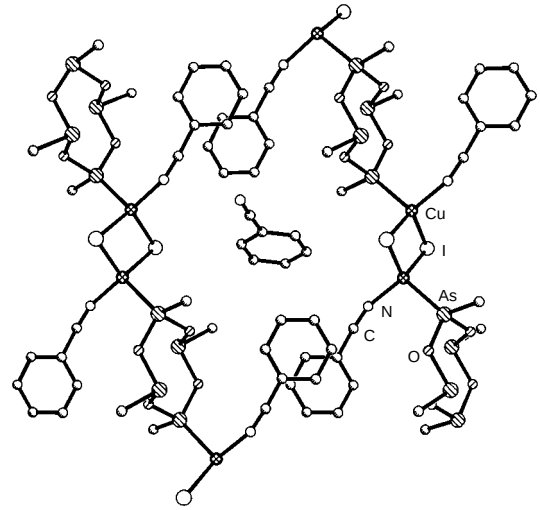

Fig. 1 Packing diagram for the π–π stacked $^1_\infty[Cu_2I_2(PhCN)_2\{cyclo\text{-}(MeAsO)_4\}]$ chains of **1**. Methyl groups have been omitted for clarity.

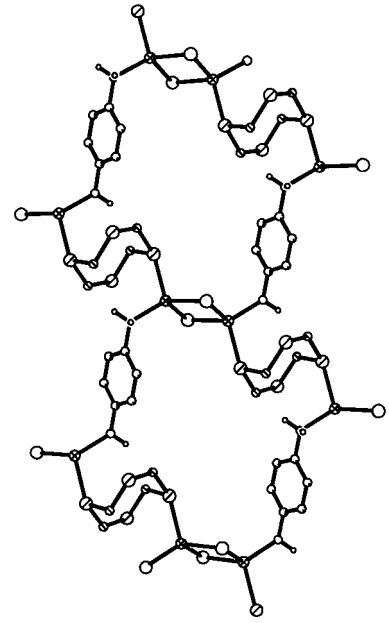

Fig. 2 Packing diagram for the lamellar $^2_\infty[Cu_2I_2(p\text{-}H_2NC_6H_4NH_2)\{cyclo\text{-}(MeAsO)_4\}]$ 4^4 net of **2**. Methyl groups have been omitted for clarity.

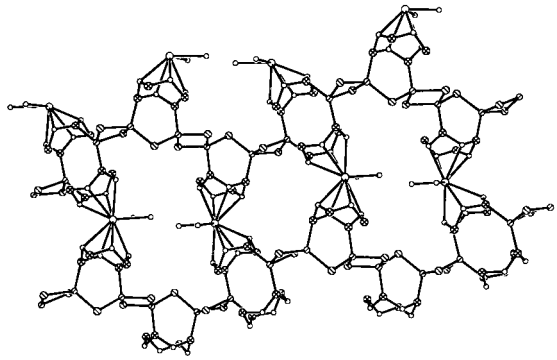

Fig. 3 Packing diagram for anionic $^1_\infty[Cu_3I_4\{cyclo\text{-}(MeAsO)_4\}_2]$ chains that are linked together through $[Cs\{cyclo\text{-}(MeAsO)_4\}_2]^+$ sandwiches into the porous sheet of **3**. Methyl groups have been omitted for clarity.

cially available solid-phase extraction systems (SPE).[10] Designed incorporation of such ion ligating agents into ordered solid-state networks offers, therefore, an attractive assignment for crystal engineering, that has been realized in the anionic $^1_\infty[Cu_3I_4\{cyclo\text{-}(MeAsO)_4\}_2]$ chains depicted in Fig. 3. Two water ligands were found to be necessary to complete the tenfold κ^1O coordination spheres of the Cs^+ cations, which were used to direct the self-assembly of this structure, $[Cs(H_2O)_2][Cu_3I_4\{cyclo\text{-}(MeAsO)_4\}_2]$ **3**, from CuI and $(MeAsO)_n$ in MeCN–MeOH–H_2O. The presence of these H_2O molecules lends the larger cavities a degree of polar character and these contain disordered methanol molecules.

A DTA trace for **3** reveals initial endothermic loss of methanol and water (35–120 °C) followed by exothermic collapse of the solid-state network in the temperature range 122–149 °C. This indicates that the flexible sheet structure of **3**, whose individual $(MeAsO)_4$ and $[Cu_6I_8]^{2-}$ building blocks are illustrated in a schematic manner in Fig. 4, could be capable of imbibing a range of small polar molecules whilst retaining its integrity. We are currently studying whether this and similar anionic networks could be suitable for selective cation exchange.

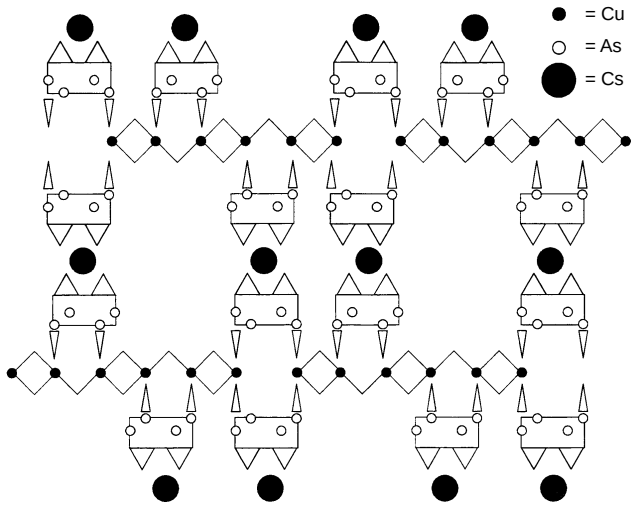

Fig. 4 A schematic diagram of the building principle of **3**, showing the μ-1 $\kappa As^1:2\kappa As^2$ and μ-1$\kappa As^1:2\kappa As^3$ bridging of $[Cu_6I_8]^{2-}$ units by different crown-shaped $(MeAsO)_4$ ligands which also simultaneously coordinate Cs^+ cations in a κ^4O fashion. Two water ligands complete the tenfold coordination sphere to the Cs^+ cations in the actual structure (Fig. 3).

Notes and References

† E-mail: shel@anachem.ruhr-uni-bochum.de

‡ $^1_\infty[\{Cu_2I_2(PhCN)_2[cyclo\text{-}(MeAsO)_4]\}\cdot PhCN]$ **1**: CuI (285.2 mg, 1.50 mmol) and $(MeAsO)_n$ (53.5 mg, 0.51 mmol for n = 1) were heated in 1.5 ml PhCN for 16 h in a sealed glass tube at 100 °C. The resulting yellow solution was left to stand at 4 °C to afford colourless crystals (81.2 mg, 64.3% yield).

$^2_\infty[Cu_2I_2(p\text{-}H_2NC_6H_4NH_2)\{cyclo\text{-}(MeAsO)_4\}]$ **2**: 1,4-diaminobenzene (21.6 mg, 0.2 mmol) and $(MeAsO)_n$ (84.7 mg, 0.8 mmol for n = 1) were dissolved in 10 ml MeCN and the solution cooled to 0 °C. An acetonitrile solution (5 ml) of CuI (38.1 mg, 0.2 mmol) was layered under this solution leading to the formation of deep-red crystals (39.8 mg, 43% yield).

$[Cs(H_2O)_2][Cu_3I_4\{cyclo\text{-}(MeAsO)_4\}_2]\cdot 0.5MeOH$ **3**. A solution of CsI (95.2 mg, 0.5 mmol) in 1 ml H_2O–MeOH (1 : 4) was unified with 5 ml of an acetonitrile solution of CuI (65.0 mg, 0.25 mmol) and $(MeAsO)_n$ (211.9 mg, 2.0 mmol for n = 1) and left to stand at 20 °C to afford colourless crystals (130.0 mg, 46.5% yield). Satisfactory elemental analyses (C, H, As) were obtained for all compounds.

§ Siemens P4 diffractometer, graphite-monochromated Mo-Kα radiation, ω scans. The structures were solved using direct methods[11] and refined against F_o^2 by full-matrix least squares.[12] Hydrogen atoms were placed at calculated positions and allowed to ride on their parent atoms.

Crystal data: **1**: $C_{25}H_{27}As_4Cu_2I_2N_3O_4$, M = 1114.06, triclinic, space group $P\bar{1}$ (no. 2), a = 8.740(2), b = 9.254(2), c = 11.732(2) Å, α = 101.84(3), β = 101.24(3), γ = 105.54(3)°, U = 862.8(3) Å^3, Z = 1, $F(000)$ = 526, D_c = 2.145 g cm^{-1}, μ(Mo-Kα) = 6.86 mm^{-1}. Colourless tablet (0.37 × 0.39 × 0.54 mm), ψ-scan absorption corrections (T_{min} = 0.30, T_{max} = 0.49), 4603 unique reflectiions ($2\theta_{max}$ = 60°) of which 3442 had $I \geqslant 2\sigma(I)$. Terminal reliability indices were R_1 = 0.061 [$I \geqslant 2\sigma(I)$], wR_2 = 0.202 for 207 refined parameters, S = 1.12, $\Delta\rho_{max}$ = 2.65 e Å^{-3}, $\Delta\rho_{min}$ = −1.89 e Å^{-3}.

2: $C_{10}H_{20}As_4Cu_2I_2N_2O_4$, M = 912.84, triclinic, space group $P\bar{1}$ (no. 2), a = 7.861(2), b = 9.021(2), c = 9.199(2) Å, α = 63.19(3), β = 84.64(3), γ = 69.99(3)°, U = 545.7(2) Å^3, Z = 1, $F(000)$ = 422, D_c = 2.778 g cm^{-1}, μ(Mo-Kα) = 10.81 mm^{-1}. Deep-red plate (0.12 × 0.17 × 0.32 mm), ψ-scan absorption corrections (T_{min} = 0.27, T_{max} = 0.67), 1840 unique reflections ($2\theta_{max}$ = 50°) of which 1362 had $I \geqslant 2\sigma(I)$. Terminal reliability indices were R_1 = 0.048 [$I \geqslant 2\sigma(I)$], wR_2 = 0.114 for 111 refined parameters, S = 1.02, $\Delta\rho_{max}$ = 3.11 e Å^{-3}, $\Delta\rho_{min}$ = −1.30 e Å^{-3}.

3: $C_{8.5}H_{30}As_8CsCu_3I_4O_{10.5}$, M = 1730.31, triclinic, space group $P\bar{1}$ (no. 2), a = 8.992(2), b = 13.685(3), c = 17.129(3) Å, α = 104.48(3), β = 91.43(3), γ = 107.21(3)°, U = 1938.3(7) Å^3, Z = 2, $F(000)$ = 1565, D_c = 2.965 g cm^{-1}, μ(Mo-Kα) = 12.55 mm^{-1}. Colourless prism (0.39 × 0.49 × 0.60 mm), ψ-scan absorption corrections (T_{min} = 0.080, T_{max} = 0.160), 8768 unique reflections ($2\theta_{max}$ = 55°) of which 5341 had $I \geqslant 2\sigma(I)$. Terminal reliability indices were R_1 = 0.069 [$I \geqslant 2\sigma(I)$], wR_2 = 0.203 for 302 refined parameters, S = 1.03, $\Delta\rho_{max}$ = 1.95 e Å^{-3}, $\Delta\rho_{min}$ = −2.05 e Å^{-3}. CCDC 182/793.

1 R. Robson, B. F. Abrahams, S. R. Batten, R. W. Gable, B. F. Hoskins and J. Liu, *Supramolecular Architecture*, ACS Publications, Washington, DC, 1992, ch. 19; M. J. Zaworotko, *Chem. Soc. Rev.*, 1994, **23**, 283; C. Janiak, *Angew. Chem., Int. Ed. Engl.*, 1997, **36**, 1499.
2 J. R. Black, N. R. Champness, W. Levason and G. Reid, *Inorg. Chem.*, 1996, **35**, 4432.
3 A. J. Blake, D. Collins, R. O. Gould, G. Reid and M. Schröder, *J. Chem. Soc., Dalton Trans.*, 1993, 521; A. J. Blake, W.-S. Li, V. Lippolis and M. Schröder, *Chem. Commun.*, 1997, 1943.
4 (*a*) W. S. Sheldrick and T. Häusler, *Z. Anorg. Allg. Chem.*, 1994, **620**, 334; (*b*) T. Häusler and W. S. Sheldrick, *Chem. Ber.*, 1997, **130**, 371.
5 *Introduction to Zeolite Science and Practice*, ed. H. van Bekkum, E. M. Flanigen and J. C. Jansen, Elsevier, Amsterdam, 1991.
6 G. A. Ozin, *Supramol. Chem.*, 1995, **6**, 125; W. S. Sheldrick and M. Wachhold, *Angew. Chem., Int. Ed. Engl.*, 1997, **36**, 206.
7 J. Li, H. Zeng, J. Chen, Q. Wang and X. Wu, *Chem. Commun.*, 1997, 1213.
8 P. Behrens and G. D. Stucky, *Comprehensive Supramolecular Chemistry*, ed. J. L. Atwood, D. D. MacNicol, J. E. D. Davies and F. Vögtle, vol. 7, ed. G. Alberti and T. Bein, Pergamon, Oxford, 1996, ch. 25.
9 W. S. Sheldrick and T. Häusler, *Z. Anorg. Allg. Chem.*, 1993, **619**, 1984.
10 J. S. Bradshaw and R. M. Izatt, *Acc. Chem. Res.*, 1997, **30**, 338.
11 G. M. Sheldrick, SHELXS-86, *Acta Crystallogr., Sect. A*, 1990, **46**, 467.
12 G. M. Sheldrick, SHELXL-93, Universität Göttingen, 1993.

Received in Basel, Switzerland, 5th December 1997; 7/08767E

Potassium cation induced switch in anion selectivity exhibited by heteroditopic ruthenium(II) and rhenium(I) bipyridyl bis(benzo-15-crown-5) ion pair receptors

Paul D. Beer*† and Simon W. Dent

Inorganic Chemistry Laboratory, University of Oxford, South Parks Road, Oxford, UK OX1 3QR

Cl^- and $H_2PO_4^-$ anion selectivity properties of new heteroditopic Ru^{II} and Re^{I} bipyridyl bis(benzo-15-crown-5) receptors are remarkably dependent upon the presence of co-bound intramolecular sandwich crown ether complexed K^+.

The design of new multisite ion pair receptors that contain covalently linked binding sites for both cations and anions is a new topical area of coordination chemistry.[1–6] In addition to being potential selective extraction/membrane transportation reagents for metal salts these ditopic ligand systems can be tailored to exhibit novel cooperative and allosteric behaviour whereby the complexation of one charged guest can influence, through electrostatic and conformational effects, the subsequent coordination of the pairing ion. We report here the synthesis of new heteroditopic Ru^{II} and Re^{I} bipyridyl bis(benzo-15-crown-5) receptors whose selectivity towards Cl^- and $H_2PO_4^-$ anionic guest species is remarkably dependent upon allosteric conformational and electrostatic effects of co-bound intramolecular sandwich crown ether complexed K^+ cations.

The synthetic routes to preparing the bipyridyl amide functionalised mono- and bis(benzo-15-crown-5) ligands and 3,4′-dimethoxyphenyl appended analogues are shown in Scheme 1. Reaction with $[RuCl_2(bipy)_2]$ followed by NH_4PF_6 and with $[Re(CO)_5Br]$, respectively, afforded the new receptors L^1–L^4 in good yields (Scheme 2). The K^+ cation and both Cl^- and $H_2PO_4^-$ anion coordination properties of the receptors were investigated by ^1H and in some instances by ^{13}C NMR titration experiments in $(CD_3)_2SO$ solution. The addition of KPF_6 to solutions of L^1 and L^3 caused the crown ether methylene carbons of the ^{13}C NMR spectra to significantly shift upfield by up to 0.6 ppm. Analysis of the resulting titration curves using the computer program EQNMR[7] suggested both receptors were forming 1 : 1 stoichiometric intramolecular sandwich bis crown ether complexes with K^+ with respective stability constant values of 350 and 540 M^{-1} for L^1 and L^3. The relatively smaller value of stability constant for L^1 may reflect the positively charged Ru^{II} centre electrostatically destabilising the crown ether bound K^+. Negligible shifts were observed with L^2 and L^4 suggesting K^+ complexation only takes place at the crown ether binding sites. Significant downfield perturbations of the respective receptor's amide and H^3-bipyridyl protons were observed on the addition of NBu_4Cl and $H_2PO_4^-$ salts to $(CD_3)_2SO$ solutions of L^1–L^4 indicating the amide-bipyridyl vicinity of the receptor is the site of anion binding. In all cases with Cl^- the titration curves suggested 1 : 1 complex stoichiometry which was also observed with $H_2PO_4^-$ and L^1, L^3. Precipitation problems unfortunately prevented complete $H_2PO_4^-$ titration curves from being obtained with receptors L^2 and L^4. Where possible titrations with both anions were repeated in the presence of 2 equiv. of KPF_6 and EQNMR determined stability constant values for all these titration experiments are presented in Tables 1 and 2. As found previously with related simple acyclic transition metal bipyridyl amide derivatives[8] a comparison of Tables 1 and 2 reveals L^1 and L^3 exhibit a pronounced selectivity preference for $H_2PO_4^-$ over Cl^-. It is noteworthy that Table 1 explicitly shows that the bis crown ether containing receptors L^1 and L^3 exhibit substantial increases in the magnitudes of stability constant for Cl^- binding on addition of KPF_6 by nearly sixfold for L^3. Interestingly no such increase in stability constant value is displayed by receptors L^2 and L^4 which do not contain crown ether binding sites. In contrast Table 2 displays a dramatic decrease in the stability constant values for $H_2PO_4^-$ binding for L^1 and L^3 on addition of KPF_6. The important consequence of which is the presence of K^+ can in principle induce a novel switch in the anion selectivity properties of both receptors. Tables 1 and 2 clearly illustrate the free receptors L^1, L^3 are $H_2PO_4^-$ selective whereas initial coordination of K^+ changes their anion selectivity preference to Cl^-. Repeating the titrations in the presence of tenfold excess of NBu_4PF_6 resulted in virtually no change in the determined stability constant values which negates simple ion pairing as a possible explanation for these positive and negative cooperative binding effects.

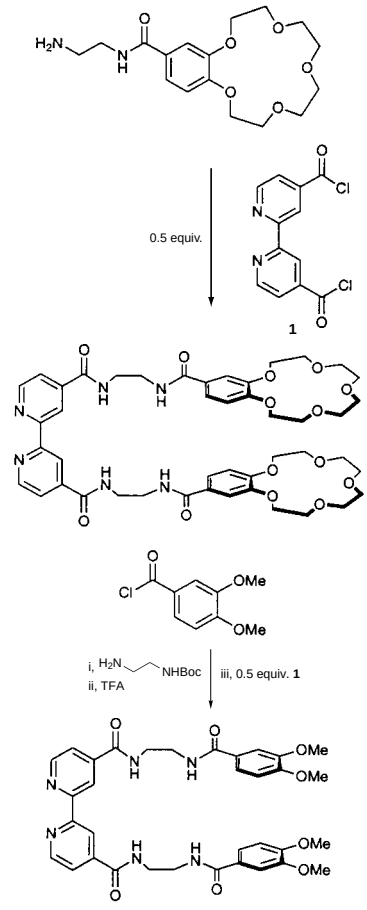

Scheme 1

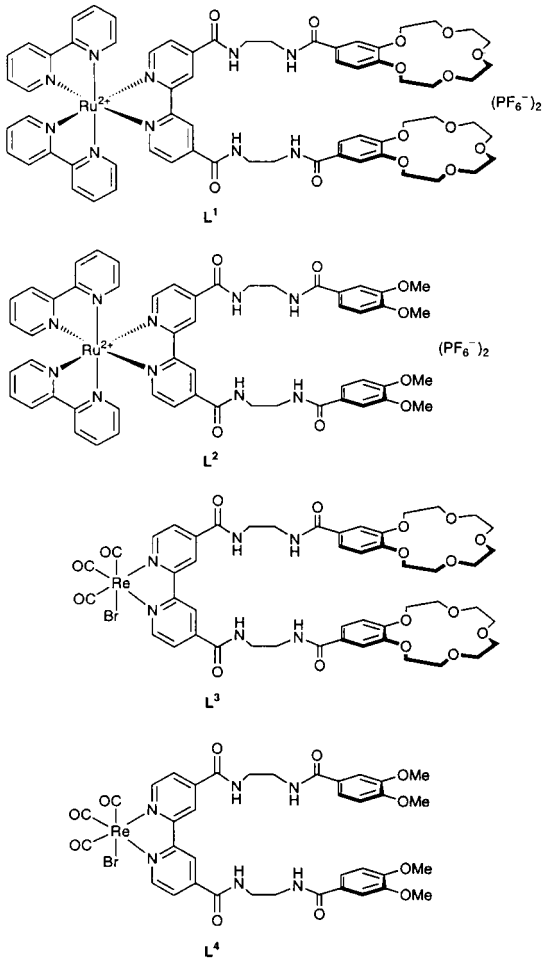

Scheme 2

Table 1 Stability constants for Cl^- binding in the presence and absence of K^+ in $(CD_3)_2SO$

Receptor	K^a/M^{-1}
L^1	190
L^1 + 2 equiv. KPF_6	660
L^2	195
L^2 + 2 equiv. KPF_6	165
L^3	55
L^3 + 2 equiv. KPF_6	300
L^4	46
L^4 + 2 equiv. KPF_6	55

[a] Errors estimated to be ≤10%.

The K^+ induced positive cooperativity of Cl^- binding may be a consequence of favourable electrostatic attraction between the crown ether bound K^+ and bipyridyl amide complexed anion, and, in addition be due to a favourable allosteric K^+ induced conformational effect. Solution formation of the 1 : 1 bis-benzo-15-crown-5 potassium cation intramolecular sandwich complex results in L^1 and L^3 forming a pseudo-macrocyclic preorganised structure which enhances Cl^- recognition but disfavours the binding of $H_2PO_4^-$ (Fig. 1). Of particular note is the structurally related macrocyclic receptor L^5 which exhibits remarkable thermodynamic stability and selectivity for Cl^- and does not bind $H_2PO_4^-$ phosphate at all in $(CD_3)_2SO$ solutions.[9]

Preliminary fluorescence emission spectroscopic measurements corroborate the NMR binding studies. The addition of Cl^- and $H_2PO_4^-$ to MeCN solutions of L^1 caused significant increases of up to 140% in luminescence intensity of the MLCT emission band (λ_{max} = 640 nm) with a concomitant hypsochromic shift of 7 nm. However in the presence of 1 equiv. of KPF_6 the subsequent addition of $H_2PO_4^-$ had very little effect on either the emission intensity or λ_{max}. In contrast with Cl^- a significant enhancement of intensity was observed.

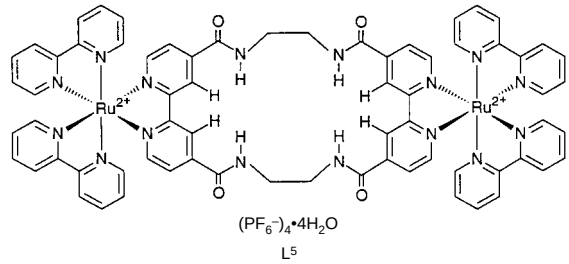

Table 2 Stability constants for $H_2PO_4^-$ binding in the presence and absence of K^+ in $(CD_3)_2SO$

Receptor[a]	K^b/M^{-1}
L^1	900
L^1 + 2 equiv. KPF_6	60
L^3	205
L^3 + 2 equiv. KPF_6	35

[a] Precipitation problems prevented complete titration curves from being obtained with L^2 and L^4 in presence and absence of KPF_6. [b] Errors estimated to be ≤10%.

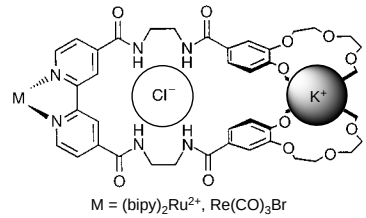

Fig. 1 Proposed solution structure of K^+Cl^- ion pair complex of L^1 and L^3. M = $Ru(bipy)_2^{2+}$ or $Re(CO)_3Br$

In summary the anion selectivity properties of new Ru^{II} and Re^{I} bipyridyl bis(benzo-15-crown-5) receptors can be dramatically switched *via* the binding of K^+ cations. In the absence of K^+ the receptors are selective for $H_2PO_4^-$ over Cl^-, whereas following the formation of the intramolecular K^+ bis crown sandwich complex the reverse selectivity Cl^- over $H_2PO_4^-$ is exhibited.

We thank Kodak Ltd for a studentship (S. W. D.), the EPSRC for use of the mass spectrometry service at University College Swansea and Johnson Matthey for a generous loan of ruthenium salts.

Notes and References

† E-mail: paul.beer@chem.ox.ac.uk

1 M. T. Reetz, C. M. Niemeyer and K. Harris, *Angew. Chem., Int. Ed. Engl.*, 1991, **30**, 1472.
2 D. M. Rudkevich, Z. Brzozka, M. Palys, H. C. Visser, W. Verboom and D. N. Reinhoudt, *Angew. Chem., Int. Ed. Engl.*, 1994, **33**, 467.
3 K. I. Kinnear, D. P. Mousley, E. Arafar and J. C. Lockhart, *J. Chem. Soc., Dalton Trans.*, 1994, 3637.
4 P. D. Beer, M. G. B. Drew, R. J. Knubley and M. I. Ogden, *J. Chem. Soc., Dalton Trans.*, 1995, 3117.
5 J. Scheerder, J. P. M. van Duynhoven, J. F. J. Engbersen and D. N. Reinhoudt, *Angew. Chem., Int. Ed. Engl.*, 1996, **35**, 1090.
6 J. E. Redman, P. D. Beer, S. W. Dent and M. G. B. Drew, *Chem. Commun.*, 1998, 231.
7 M. J. Hynes, *J. Chem. Soc., Dalton Trans.*, 1993, 311.
8 F. Szemes, D. Hesek, Z. Chen, S. W. Dent, M. G. B. Drew, A. J. Goulden, A. R. Graydon, A. Grieve, R. J. Mortimer, J. S. Weightman and P. D. Beer, *Inorg. Chem.*, 1996, **35**, 5868.
9 P. D. Beer, F. Szemes, V. Balzani, C. M. Salà, M. G. B. Drew, S. W. Dent and M. Maestri, *J. Am. Chem. Soc.*, 1997, **119**, 11 864.

Received in Cambridge, UK, 13th January 1998; 8/00356D

Formation of 1,11-bis(pendant donor)-cyclam derivatives *via* the formamidinium salt (cyclam = 1,4,8,11-tetraazacyclotetradecane)

Philip J. Davies, Max R. Taylor and Kevin P. Wainwright*†

Department of Chemistry, The Flinders University of South Australia, GPO Box 2100, Adelaide, South Australia 5001, Australia

When reacted in chloroform, the dimethyl acetal of dmf and cyclam (1,4,8,11-tetraazacyclotetradecane) forms a stable formamidinium salt which can be used as an intermediate for very simple formation of 1,11-bis(pendant donor)-cyclam derivatives.

Some years ago we reported that reaction of the dimethyl acetal of dmf, dmfdma, with 1,4,8,11-tetraazacyclotetradecane (cyclam) in ethanol generates the electron rich alkene **1** which can subsequently undergo atmospheric oxidation to the bis(urea) derivative of cyclam **2**.[1] In a recent adaptation of that work we had cause to change the solvent from ethanol to chloroform and found that the outcome of the reaction is totally changed. The serendipitous result of this is that we have now found a simple means for producing 1,11-dialkylated derivatives of cyclam which upon deprotection can be used to afford mixed pendant donor ligands.

Reaction of cyclam with an equimolar amount of dmfdma in refluxing chloroform (instead of ethanol) for a period of 18 h gives a 75% yield, after crystallisation from aqueous acetonitrile, of the previously unreported formamidinium salt, **3**.‡ The formation of stable formamidinium salts from triaza macrocycles having secondary amines separated by trimethylene units (1,5,8-triazacyclododecane and some derivatives) has been reported,[2] but those derived from tetraaza macrocycles have only been invoked as reactive intermediates formed along the hydrolysis pathways between the orthoamide and formyl structures.[3] In the case of the triaza ligands the formamidinium salt forms upon treatment of the similarly stable orthoamide with HCl, but in the case of cyclam we did not observe the orthoamide, despite vigorous attempts to dehydrate **3**.

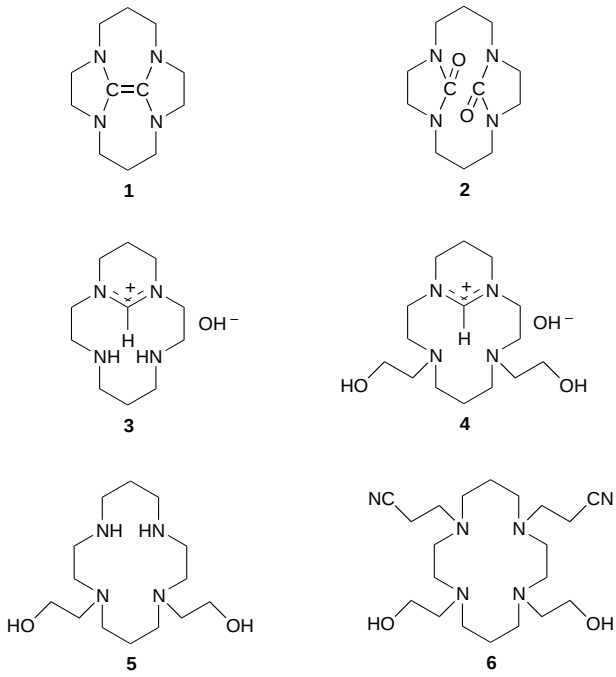

Formation of **3** affords protection of one pair of 1,11-related amine sites on the cyclam moiety whilst allowing alkylation at the other two. Thus, in reaction with ethylene oxide the substituted salt **4** was generated quantitatively and then converted to the free base, **5**, in 79% yield, by reaction with 10 M sodium hydroxide for 6 h.

As an illustration of the utility of this sequence, **5** was quantitatively derivatised by reaction with acrylonitrile giving the bis(cyanoethyl) ligand, **6**. The zinc(II) complex of **6** was formed through the reaction of **6** with $Zn(ClO_4)_2 \cdot 6H_2O$ in ethanol. Recrystallisation of the crude complex from hot water gave crystals of sufficiently high quality for structure determination by X-ray diffraction.§ This revealed that the complex is a rare example of a macrocyclic complex in which a pendant hydroxyethyl group coordinated to a divalent metal ion has undergone deprotonation at neutral pH.[4] The complex has the trigonal bipyramidal structure, shown in Fig. 1, in which the four nitrogen atoms of the macrocycle and one deprotonated pendant hydroxyl group coordinate. The macrocycle is in the *trans*-I configuration (the four pendant arms project in the same direction). The axial sites are occupied by a nitrogen atom [N(4)] carrying a pendant 2-cyanoethyl group and by the nitrogen atom [N(11)] carrying the pendant alkoxide. The N(4)–Zn–N(11) angle is 169.8(2)° and the equatorial angle, N(1)–Zn–N(8), internal to the macrocycle, is 138.7(2)°. The Zn–O^- bond length is 1.923(4) Å which is significantly shorter than the 1.994 Å separation seen for a Zn–neutral pendant alcohol bond in the zinc(II) complex of

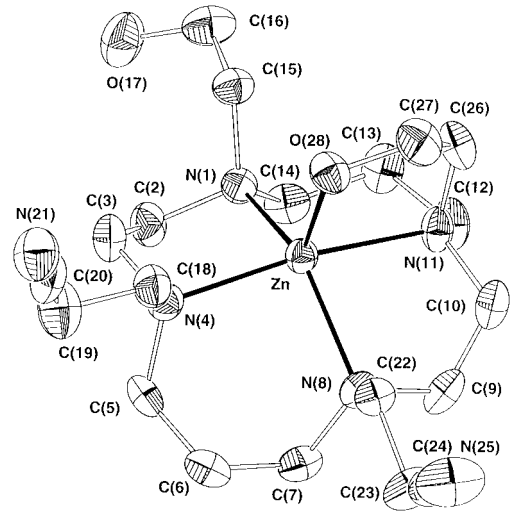

Fig. 1 Molecular structure of the cation in [Zn(**6** − H)]$ClO_4 \cdot H_2O$. Displacement ellipsoids are drawn at the 50% probability level. Important bond distances (Å) and angles (°): Zn–N(1) 2.155(5), Zn–N(4) 2.200(4), Zn–N(8) 2.204(5), Zn–N(11) 2.187(4), Zn–O(28) 1.923(4); N(1)–Zn–N(4) 85.0(2), N(1)–Zn–N(8) 138.7(2), N(1)–Zn–N(11) 93.4(2), N(1)–Zn–O(28) 110.0(2), N(4)–Zn–N(8) 91.6(2), N(4)–Zn–N(11) 169.8(2), N(4)–Zn–O(28) 104.3(2), N(8)–Zn–N(11) 83.0(2), N(8)–Zn–O(28) 110.7(2), N(11)–Zn–O(28) 85.7(2).

N-(2-hydroxyethyl)cyclen (cyclen = 1,4,7,10-tetraazacyclododecane).[5]

Notes and References

† E-mail: chkpw@flinders.edu.au

‡ IR (Nujol) 1650 cm^{-1} [amidinium ν(C–N)]; ^{13}C (D_2O), δ 155.8 (amidinium C), 51.8, 47.0, 45.5, 42.3, 26.2, 18.8; ^1H NMR (D_2O), δ 7.96 (s, amidinium H), 3.60 (t, 4 H), 3.37 (t, 4 H), 2.95 (t, 4 H), 2.69 (t, 4 H), 2.15 (qnt., 2 H), 1.71 (qnt., 2 H).

§ *Crystal data* for [Zn(**6** −H)]$ClO_4 \cdot H_2O$: $C_{20}H_{39}ClN_6O_7Zn$, M = 576.4, orthorhombic, space group $P2_12_12_1$, a = 8.409(1), b = 16.180(1), c = 18.886(1) Å, U = 2569.6(4) $Å^3$, Z = 4, $F(000)$ = 1216, T = 293(1) K, D_c = 1.490 Mg m^{-3}, μ(Mo-Kα) = 1.11 mm^{-1}, λ(Mo-Kα) = 0.71069 Å. Data were measured on an Enraf-Nonius CAD/PC diffractometer using graphite-monochromated Mo-Kα X-radiation, θ_{max} = 27.5°. Absorption corrections were calculated by Gaussian integration, crystal size 0.10 × 0.13 × 0.41 mm, T_{min}, T_{max} = 0.710, 0.906. Reflections measured; 6468 (ω–2θ scans), unique 3347, R_{int} = 0.039. The structure was solved by direct methods and refined using XTAL 3.5 (ref. 6). Hydrogen atoms were placed at geometrically calculated positions, but the hydroxyl and the water molecule hydrogen atoms were not included. The perchlorate ion was found to be disordered in two orientations and was modelled as two rigid groups. Refinement of a group population parameter indicated equal occupancy of the two orientations. Refinement on F^2, with individual anisotropic displacement parameters for all atoms except hydrogen, which were held fixed, converged at $R(F)$ = 0.069, $wR(F^2)$ = 0.093, S = 1.063 for 3100 reflections with $F^2 > 0$ and 345 variable parameters. Final shift/σ(max.) = 0.001 and $\Delta\rho$(min., max.) = −0.62, +0.62 e $Å^{-3}$.

1 P. B. Hitchcock, M. F. Lappert, P. Terreros and K. P. Wainwright, *J. Chem. Soc., Chem. Commun.*, 1980, 1180.

2 G. R. Weisman, D. J. Vachon, V. B. Johnson and D. A. Gronbeck, *J. Chem. Soc., Chem. Commun.*, 1987, 886.

3 P. L. Anelli, L. Calabi, P. Dapporto, M. Murru, L. Paleari, P. Paoli, F. Uggeri, S. Verona and M. Virtuani, *J. Chem. Soc., Perkin Trans. 1*, 1995, 2995.

4 A. J. Blake, I. A. Fallis, R. O. Gould, S. Parsons, S. A. Ross and M. Schröder, *J. Chem. Soc., Chem. Commun.*, 1994, 2467.

5 T. Koike, S. Kajitani, I. Nakamura, E. Kimura and M. Shiro, *J. Am. Chem. Soc.*, 1995, **117**, 1210.

6 *XTAL User's manual*, ed. S. R. Hall, G. S. D. King and J. M. Stewart, University of Western Australia, Lamb, Perth, 1995.

Received in Cambridge, UK, 6th February 1998; 8/01089G

X-Ray reflection studies on the monolayer-mediated growth of mesostructured MCM-41 silica at the air/water interface

Stephen J. Roser, Harish M. Patel, Michael R. Lovell, Jane E. Muir and Stephen Mann*†

Department of Chemistry, University of Bath, Bath, UK BA2 7AY

X-Ray reflection has been used to study the nucleation and growth of thin films of a silica–surfactant mesophase (MCM-41) at the air/water interface in the presence and absence of an insoluble lipid monolayer of phosphatidylcholine; the rate of self-assembly and structural order of films comprising up to four micellar layers were enhanced under the lipid monolayer.

One of the most promising routes to new silica-based mesostructured materials with pore diameters greater than those of conventional materials such as zeolites involves the co-operative assembly of inorganic precursors with supramolecular organic templates.[1–7] The resulting silica–surfactant liquid crystalline mesophases can have a range of symmetries, including hexagonal (MCM-41) or cubic (MCM-48), and can be processed to produce mesoporous replicas consisting of an ordered array of channels with 1 nm thick silica walls. Several studies have recently shown that thin films of MCM-41 materials can be formed under acidic conditions at the air/water,[8] mica/water,[9] or graphite/water interface,[10] as well as on Au substrates that had been chemically patterned.[11] In a recent study,[12] X-ray reflection (XRR) was used to investigate the time-dependent growth of MCM-41 under acidic conditions at the air/water interface. In this report we use X-ray reflectivity to probe the nucleation and growth of thin films of MCM-41 under alkaline conditions at the air/water interface in the presence of an insoluble lipid monolayer that acts as a secondary template in the self-assembly process.

MCM-41 silica was synthesised at room temperature from a dilute basic solution *via* condensation of tetraethoxysilane (TEOS) in the presence of hexadecyltrimethylammonium bromide (C_{16}TMABr).‡ The films were grown slowly at the air/water interface from a quiescent solution contained within a Teflon trough which was sealed in a Perspex box with thin Mylar windows for X-ray transmission. In experiments involving phosphatidylcholine (PC) monolayers, a known volume of PC in chloroform was spread onto the air/water interface prior to recording of the XRR data.§ Analysis of X-ray reflection data was performed according to established procedures.¶

Fig. 1 shows the fitted reflectivity profile and calculated scattering density (inset) for the initial measurements for MCM-41 films grown from alkaline solutions under a PC monolayer. The zero-time fit has a fringe periodicity which corresponds to a thickness of 4 nm and demonstrates that the electron density profile perpendicular to the surface has two maxima, both of which have similar electron density values. The presence of the fringes indicates that a single micellar layer of a silicate–surfactant film is nucleated under the lipid monolayer. Similar data were obtained for the zero-time measurements for MCM-41 grown at an unmodified air/water interface, except that the peak values of the scattering length density profiles were slightly lower, suggesting that the presence of the PC monolayer induced the nucleation of a more densely packed arrangement of silicated rod-like micelles. In both cases, the model used to fit the data was based on a layer of amorphous silica-coated cylindrical micelles with an overall diameter of 4 nm. Interestingly, the data could not be fitted with a model corresponding to a primary surface layer of hemispherical micelles, as has been recently proposed as the initial stage in the nucleation of MCM-41 films from acidic solutions.[8] Thus, under alkaline conditions, mineralized micellar cylinders are considered to constitute the first layer of MCM-41 nuclei formed at the air/water or monolayer/solution interfaces.

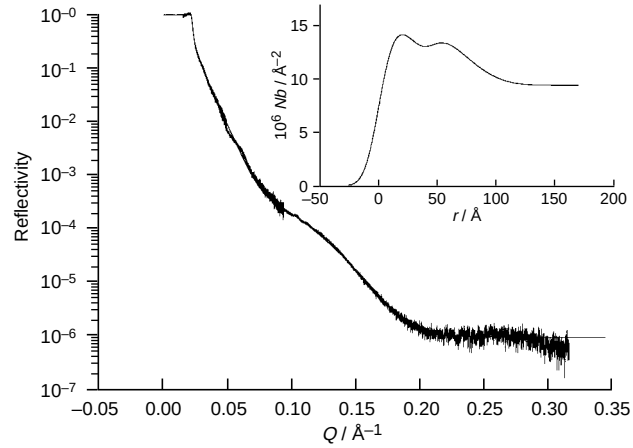

Fig. 1 Fitted reflectivity profile and calculated scattering length density (*Nb*, inset) for MCM-41 films grown for 1 h under a PC monolayer

Significant differences were observed in the XRR scattering length density profiles for thin films grown for 3 days under a PC monolayer (Fig. 2). The complex profile shows five distinct peaks with a repeat spacing of 3.9 nm in the density plot, leading to a broad Bragg peak centred at $\boldsymbol{Q}$ *ca.* 0.16 Å^{-1}. If the cylinders are hexagonally close packed, this corresponds to a film consisting of four silica–surfactant micellar layers, but with the scattering length density less than that expected from a perfectly ordered structure. The Bragg peak was consistent with small angle powder XRD and electron diffraction data of the retrieved thin films which confirmed the formation of the hexagonal mesophase.‖ In contrast, the MCM-41 silica prepared at the unmodified air/water interface showed a less well developed

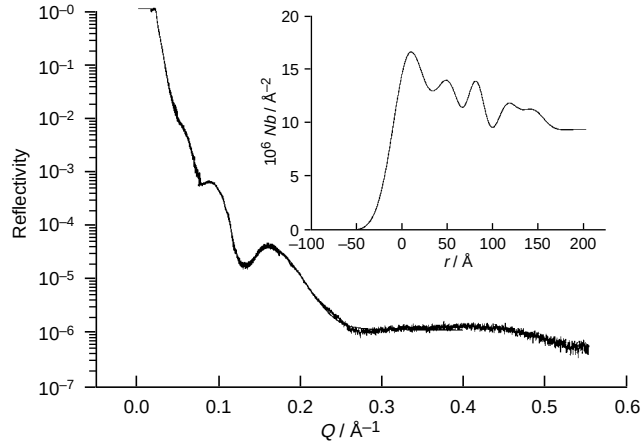

Fig. 2 Fitted reflectivity profile and calculated scattering density (inset) for MCM-41 films grown for 3 days under a PC monolayer

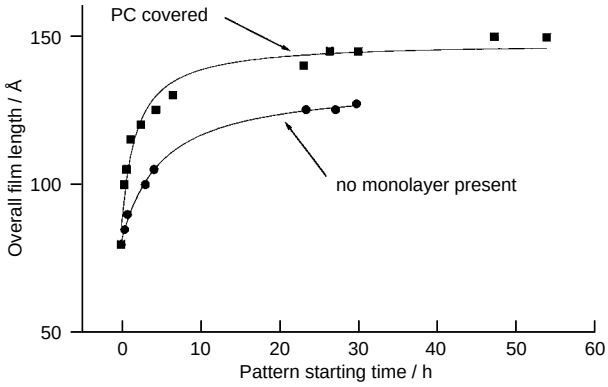

Fig. 3 Plot of film thickness *vs*. time for MCM-41 deposition from monolayer-covered and uncovered reaction solutions

fringe structure, and no Bragg peak after 48 h (data not shown). This indicates that under these conditions the silica–surfactant mesophase was significantly less ordered perpendicular to the air/water interface than the thin film nucleated under the lipid monolayer.

We also undertook preliminary studies on the time-dependence of the Bragg peak and scattering length profiles. In the presence of the PC monolayer, a Bragg peak at 0.16 $Å^{-1}$ was discernible after 4 h and clearly visible after 1 day. After this time, the peak did not change in position, width or intensity, indicating that the ordered internal structure was stable at the monolayer/solution interface. The scattering length profiles were used to determine the rate of growth in thickness of the MCM-41 films and clearly indicated that the presence of the PC monolayer results in faster growth and a more ordered mesophase (Fig. 3).

In conclusion, we have demonstrated that it is possible to obtain detailed information on the growth and structure of mesostructured MCM-41 silica films at the air/water interface using X-ray reflection. Spreading of a PC monolayer at the air/water interface enhances the rate of formation and quality of the thin films, suggesting that interactions between the lipid headgroups and molecular or supramolecular silica/surfactant species facilitate the assembly of the first layer of the nucleus. Further work using a range of lipids and their associated phase behaviour is underway to elucidate these interfacial processes.

Notes and References

† E-mail: s.mann@bath.ac.uk

‡ In a typical experiment, 0.16 g of C_{16}TMABr was dissolved in 318.0 g of H_2O and stirred continuously. 2.0 g of 1 M NaOH were added, followed by 0.828 cm^3 of TEOS, (molar composition = 0.001 C_{16}TMABr : 0.11 NaOH : 0.009 TEOS : 40.2 H_2O). The solution was left to stir for 3 min before being placed in the Teflon trough of the X-ray reflectometer. Growth of the MCM-41 film was extremely slow because of the constant vapour pressure of ethanol in the sealed environment which arose from the initial condensation reactions. In contrast, the results of ref. 12 were obtained from an evaporative environment. Measurements were made using an in-house energy-dispersive X-ray reflectometer, and typically consisted of three separate runs at different angles, lasting in total for 1 h. Measurements of MCM-41 growth were taken over a period of several days.

§ 124 μl of a chloroform solution of PC (100 mg cm^{-3}) were spread at the air/water interface using a micro-syringe. The volume added was calculated to produce a solid phase monolayer after solvent evaporation.

¶ In general, each discontinuity in scattering length density ($Nb/Å^{-2}$) between thin layers lying parallel to the interface under investigation contributes to the X-ray reflectivity, given by the well known Fresnel coefficient. This is modified by a factor, which allows for the roughness of the interface. The contributions from each layer are then combined using a matrix method. The usual procedure in fitting a reflectivity profile is to assume a model profile, and allow variation of numerous parameters, until the best fit between the model and the real $R(\boldsymbol{Q})$ is found. The layer electron density in $Å^{-3}$ can be determined by dividing Nb by the scattering length of a single electron (2.8×10^{-5} Å). Thus, the experiment measures the change in electron density perpendicular to the air/water interface, but averages information in the plane of the surface. Further details can be found in ref. 13.

‖ Samples for SAXRD, electron diffraction, ^{13}C and ^{29}Si solid state NMR, FTIR and TGA were collected from the air/water or monolayer/water interfaces after growth for 3 days in an unsealed environment. Data for monolayer-mediated synthesis; SAXRD *d* spacings, 4.0, 2.31, 1.99, 1.51 nm (as-synthesized), 3.16, 1.97, 1.75 nm (calcined); ^{29}Si NMR, δ −89.7 (Q^2), −99.6 (Q^3), −109.4 (Q^4) (as-synthesized); ^{13}C NMR, δ 14.46, 23.25, 26.99, 30.68, 32.62, 54.04, 66.91 (as-synthesized); FTIR, ν(Si–O–Si) 1000–1200 cm^{-1}, $\nu(CH_2)$ 1460–1490, 2850–2950 cm^{-1}; CHN analysis, 32 mass% C (as-synthesized). Hexagonal arrays of 4 nm spaced lattice fringes were observed by TEM.

1 C. T. Kresge, M. E. Leonowicz, W. J. Roth, J. C. Vartuli and J. S. Beck, *Nature*, 1992, **359**, 710.
2 J. S. Beck, J. C. Vartuli, W. J. Roth, M. E. Leonwicz, C. T. Kresge, K. D. Schmitt, C. T. Chu, D. H. Olsen, E. W. Sheppard, S. B. McCullen, J. B. Higgins and J. L. Schlenker, *J. Am. Chem. Soc.*, 1992, **114**, 10 834.
3 A. Firouzi, D. Kumar, L. M. Bull, T.Besier, P. Sieger, Q. Hue, S. A. Walker, J. A. Zasadzinski, C. Glinka, J. Nicol, D. Margolese, G. D. Stucky and B. F. Chemelka, *Science*, 1995, **267**, 1138.
4 Q. S. Huo, D. I. Marglose, U. Ciesla, D. G. Demuth, P. Y. Feng, T. E. Gier, P. Sieger, A. Firouzi, B. F. Chmelka, F. Schüth and G. D. Stucky, *Chem. Mater.*, 1994, **6**, 1176.
5 D. Khushalani, A. Kuperman, G. A. Ozin, K. Tanaka, J. Garces, M. M. Olken and N. Coombs, *Adv. Mater.*, 1995, **7**, 842.
6 J. H. Koegler, H. W. Zandbergen, J. L. N. Harleveld, M. S. Nieuwenhuizen, J. C. Jansen and H. Vanbekkum, *Stud. Surf. Sci. Catal.*, 1994, **84**, 307.
7 J. C. Jansen and G. M. Vandrosmalen, *J. Cryst. Growth*, 1994, **128**, 1150.
8 H. Yang, N. Coombs, I. Sokolov and G. A. Ozin, *Nature*, 1996, **381**, 589.
9 H. Yang, A. Kuperman, N. Coombs, S. Mamiche-Afara and G. A. Ozin, *Nature*, 1996, **379**, 703; I. A. Aksay, M. Trau, S. Manne, I. Hunma, N. Yao, L. Zhou, P. Fenter, P. M. Eisenberger and S. M. Gruner, *Science*, 1996, **273**, 892.
10 H. Yang, N. Coombs, I. Sokolov and G. A. Ozin, *J. Mater. Chem.*, 1997, **7**, 1285.
11 H. Yang, N. Coombs and G. A. Ozin, *Adv. Mater.*, 1997, **9**, 811.
12 A. S. Brown, S. A. Holt, Thien Dam, M. Trau and J. W. White, *Langmuir*, 1997, **13**, 6363.
13 J. Penfold and R. K. Thomas, *J. Phys: Condens. Matter.*, 1990, **2**, 1369.

Received in Cambridge, UK, 1st December 1997; revised manuscript received 28th January 1998; 8/00777B

In situ synthesis and the catalytic properties of platinum colloids on polystyrene microspheres with surface-grafted poly(*N*-isopropylacrylamide)‡

Chun-Wei Chen, Ming-Qing Chen, Takeshi Serizawa and Mitsuru Akashi*†

Department of Applied Chemistry and Chemical Engineering, Faculty of Engineering, Kagoshima University, 1-21-40 Korimoto, Kagoshima 890-0065, Japan

Well dispersed platinum colloids were synthesized *in situ* on polystyrene microspheres with surface-grafted poly(*N*-isopropylacrylamide) *via* the reduction of $PtCl_6^{2-}$ by ethanol, and found to be active and stable heterogeneous catalysts for the hydrogenation of allyl alcohol in water.

There is currently much interest in the preparation of colloidal noble-metal particles with a diameter of a few nanometers or less, not only owing to their unique physical and chemical properties, but for widespread applications such as in catalysis.[1,2] The synthesis of catalytically active metal colloids by aqueous alcohol reduction of metal salts in the presence of a protective polymer was firstly reported by Hirai and coworkers.[3,4] In a proportion of cases the polymer-protected metal colloids have been immobilized on a support,[5–7] thus giving the advantages of a truly heterogeneous catalytic system. These synthesis routes are based on a two-step process involving synthesis of colloidal nanoparticles and immobilization *via* covalent interaction or ligand coordination between the protective polymers and supports. These methods obviously suffer from special design of the protective copolymer and/or complex steps for the immobilization. Here, we report an alternative approach involving the synthesis *in situ* of the platinum colloids on polystyrene microspheres with surface-grafted poly(*N*-isopropylacrylamide) (PS-PNIPAAm). The catalyst, separated from the reaction mixture by centrifugation, retains high activity on recycling in the aqueous hydrogenation of allyl alcohol.

A range of monodispersed microspheres have been prepared by emulsifier-free dispersion copolymerization of styrene with a PNIPAAm macromonomer of molecular mass 3600. The average diameter and polydispersity index of the microspheres showed here, as determined from TEM image, are 500 nm and 1.01, respectively. The PNIPAAm branches covalently attached on the surface of microspheres provide a steric stabilization for the long-term water dispersibility of microspheres. The details concerning the synthesis and characterization of such microspheres have been given elsewhere.[8] We have already reported the formation of platinum colloids with an average diameter of 20.9 Å by ethanol reduction of $PtCl_6^{2-}$ in the presence of PNIPAAm with a mean molecular mass of 4000.[9] By using the PNIPAAm branch on the surface of the microspheres as the capping polymer, we have firstly synthesized *in situ* the well dispersed platinum colloids on the surfaces of polystyrene microspheres.

The synthesis *in situ* of platinum colloids on polystyrene microspheres by alcohol reduction of $PtCl_6^{2-}$ is similar to that of PNIPAAm-protected colloidal Pt sol.[9] For example, $H_2PtCl_6{\cdot}6H_2O$ (0.01 mmol Pt) and PS-PNIPAAm (45.2 mg, 0.4 mmol as PNIPAAm monomeric unit) were added in an ethanol–water mixed solvent (6/4, v/v, 38 ml), and the solution was then refluxed at 90 °C for 1.5 h. After separating the dark brown microspheres from the reaction mixture by centrifugation (7000 rpm, 10 min) and redispersing them in water, we studied the activity and stability of the Pt colloids on the microspheres for the aqueous hydrogenation of allyl alcohol.

The ESCA data for the Pt colloids on PS-PNIPAAm showed that the platinum appears to be in a zero-valent state after the recycling processes and a coordination interaction exists between the platinum colloid and the nitrogen atoms in PNIPAAm. Therefore, PNIPAAm branches of a polystyrene microsphere are adsorbed on the surface of the Pt colloids by both the hydrophobic interaction of the main chain and the coordination interaction of the amide group in the side chain. As a consequence, the strong interaction of PNIPAAm branches with Pt particles prevents or slows the migration and agglomeration of the metal particles by steric stabilization.

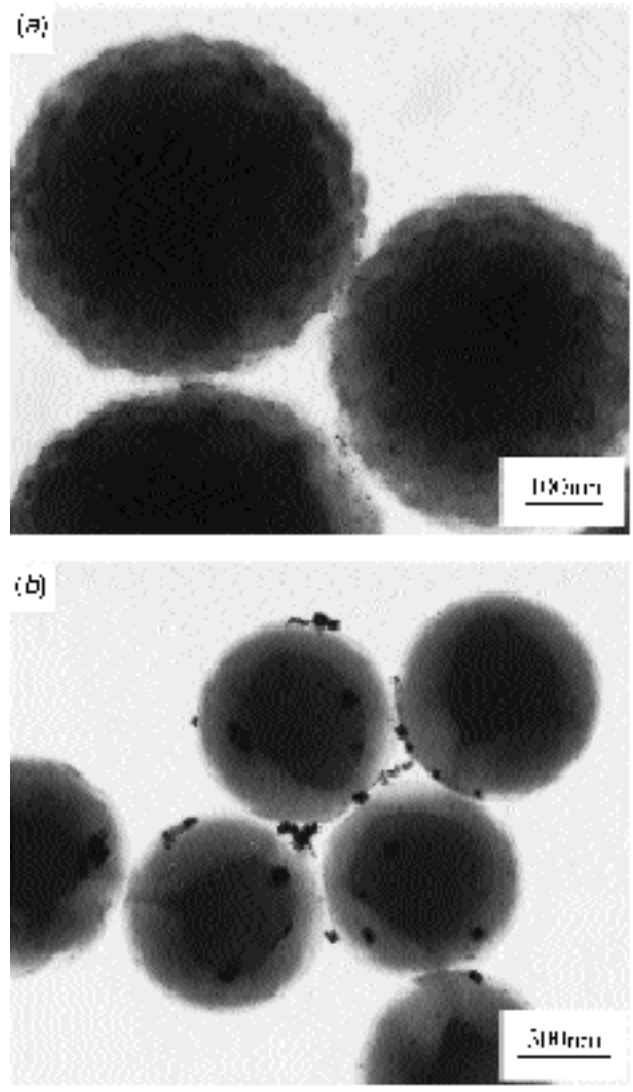

Fig. 1 TEM images of the platinum colloids on (*a*) PS-PNIPAAm after seven recycles and (*b*) commercial polystyrene beads

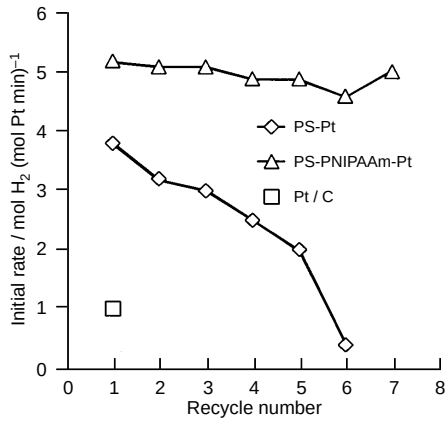

Fig. 2 Recycling of platinum colloids on PS-PNIPAAm and commercial PS beads in the hydrogenation of allyl alcohol (recovered by centrifugation). Conditions: Pt, 0.004 mmol (PS-Pt, 0.005 mmol); allyl alcohol, 2 mmol; solvent, water, 20 ml; 25 °C; H_2, 1 atm.

The PNIPAAm branches not only stabilize the platinum colloids by steric repulsion, but also immobilize them on polystyrene microspheres. TEM images of the platinum colloids on polystyrene microspheres showed that the particles have been immobilized in a well dispersed manner on the polymeric supports. The average particle size (diameter) and size distribution (standard deviation) of the fresh catalyst were 15.0 and 5.6 Å, respectively, which are smaller than those of the platinum colloids protected by free PNIPAAm (20.9 and 6.3 Å, respectively).[9] This may suggest that the migration and agglomeration of the metal colloids can be further prevented by covalently bonding the protective polymer to the surface of the polystyrene microspheres. The immobilized Pt colloids on the surfaces of the microspheres were in a very stable state and little change in the measured size distributions after seven recycling times was observed. Fig. 1(*a*) shows that the immobilized colloids are located at the surface of microspheres, and the vast majority of particles are isolated from each other after seven catalytic runs. Here, the average diameter and standard deviation of the Pt colloids are 15.2 and 5.7 Å, respectively. However, the TEM image of platinum colloids on the commercial PS beads shows that most of the Pt particles agglomerated together owing to the total lack of steric stabilization of the polymer [Fig. 1(*b*)].

The platinum colloid on the commercial PS beads or synthesized PS-PNIPAAm was employed as a heterogeneous catalyst for the hydrogenation of allyl alcohol in water. The data in Fig. 2 show the initial hydrogenation rate, with the same sample of catalyst recycled seven times. It can be seen that a PS-PNIPAAm-Pt catalyst showed higher activity than the catalysts of commercial platinum-activated carbon and Pt colloids on PS beads, and retained high activity in the hydrogenation on recycling seven times. We have previously seen the unusual temperature dependence of activity of the PNIPAAm-protected Pt sol for the same reaction.[9] The reported catalytic properties of the platinum colloids on PS-PNIPAAm in the hydrogenation are therefore most encouraging. We have evaluated thermosensitive properties of the microspheres,[8] and suggest that the activity of the catalyst must be moderated through a temperature change.

This work was financially supported in part by a Grant-in-Aid for Scientific Research in Priority Areas of New Polymers and Their Nano-Organized Systems (277/09232249) and a Grant-in-Aid for Scientific Research (08651055) from the Ministry of Education Science, Sports and Culture, Japan. The authors thank the Ministry of Education, Science, Sports and Culture, Japan for scholarships to C.-W. C. and M.-Q. C.

Notes and References

† E-mail: akashi@apc.eng.kagoshima-u.ac.jp

‡ This paper is part XIX in the series of the study on Graft Copolymers Having Hydrophobic Backbone and Hydrophilic Branches. Part XVIII is as follows: T. Serizawa, M.-Q. Chen, M. Akashi, Poly(styrene) Nanospheres with Novel Thermosensitive Poly(*N*-vinylisobutyramide)s on Their Surfaces. *J. Polym. Sci. Part A: Polym. Chem. Ed.*, in press.

1 L. N. Lewis, *Chem. Rev.*, 1993, **93**, 2693.
2 *Clusters and Colloids*, ed. G. Schmid, VCH, Weinheim, 1994; L. Troger, H. Hunefeld, S. Nunes, M. Oehring and D. Fritsch, *J. Phys. Chem. B*, 1997, **101**, 1279.
3 H. Hirai, Y. Nakao and N. Toshima, *J. Macromol. Sci., Chem.*, 1978, **12**, 1117; H. Hirai, H. Chawanya and N. Toshima, *Reactive Polym.*, 1985, **3**, 127.
4 N. Toshima, T. Takahashi, T. Yonezawa and H. Hirai, *J. Macromol. Sci., Chem.*, 1988, **25**, 669.
5 M. Ohtaki, M. Komiyama, H. Hirai and N. Toshima, *Macromolecules*, 1991, **24**, 5567.
6 Q. Wang, H. Liu and H. Wang, *J. Colloid Interf. Sci.*, 1997, **190**, 380.
7 Y. Wang, H. Liu and Y. Jiang, *J. Chem. Soc., Chem. Commun.*, 1989, 1878.
8 M.-Q. Chen, A. Kishida and M. Akashi, *J. Polym. Sci. Part A: Polym. Chem.*, 1996, **34**, 2213.
9 C.-W. Chen and M. Akashi, *Langmuir*, 1997, **13**, 6465.

Received in Cambridge, UK, 6th January 1998; 8/00203G

Deposition of thin films of CdSe or ZnSe by MOCVD using simple air stable precursors

M. Chunggaze, J. McAleese, P. O'Brien*† and D. J. Otway

Department of Chemistry, Imperial College of Science Technology and Medicine, South Kensington, London, UK SW7 2AY

The air-stable bis-complexes of methyl (*n*-hexyl)diselenocarbamate with cadmium or zinc have been shown to be effective precursors for the deposition of the metal chalcogenides by MOCVD; studies of their thermal decomposition mechanism provide possible explanations as to why these complexes are effective whilst simpler ones are not.

Cadmium and zinc selenide are compound semiconductors with optoelectronic and/or photovoltaic applications.[1] There are many reports in the literature of attempts to develop effective single-source precursors for the deposition of such materials by MOCVD (metal organic chemical vapour deposition).[1,2] We have developed one such approach using dithio-[3,4] monothio-[5] and diseleno-carbamates.[6,7] One striking observation has concerned differences between the behavior of the simple bis-diethyldithio- and bis-diethyldiseleno-carbamates of zinc and cadmium. The bis-diethyldithiocarbamates are effective precursors for materials such as CdS and films of good quality can be deposited.[4,8] However, attempts to use the related selenium compounds lead to films of elemental selenium or metal selenide films heavily contaminated with elemental selenium.[9] In efforts to increase the volatility of this family of precursors we have used bulkier substituents on the amine parent of the carbamate.[4] Here, we report that we have now discovered that some of these air stable compounds are effective precursors for the deposition of the metal selenides. This unexpected result can be understood in terms of quite subtle changes in the mechanism of thermal decomposition of the complexes.

Fig. 1 Typical thin film of CdSe on glass from $[Cd\{Se_2CNMe(C_6H_{13})\}_2]$, T_{source} = 250 °C, T_{growth} = 450 °C, 2 h growth run; bar is 10 μm

The complexes used as precursors, bis[methyl(*n*-hexyl)-diselenocarbamato]-zinc **1** or -cadmium **2**, are air stable solids melting at 151–152 and 130–132 °C respectively.‡ Thin films of CdSe and ZnSe were deposited by low pressure (LP)–MOCVD as described previously.[10] Films were deposited on glass microscope slides and growth runs were typically for times between 30 min and 2 h. After 2 h, thick, *ca.* 3 μm films were deposited (T_{source} = 200–250 °C, T_{growth} = 400–450 °C). Growth rates were *ca.* 1 μh^{-1} for ZnSe and 1.5 μh^{-1} for CdSe. The films formed were all of substantial thickness, adherent and fully dense; Fig. 1 shows a typical electron micrograph. The surface of all these films tended to be featureless. Cross-sectional microscopy of thicker samples revealed a columnar structure.§ EDAX analysis results of the selenide films gave a metal : chalcogenide ratio approximating 1 : 1; in the case of zinc there appeared to be a significant, but small, oxygen content (*ca.* 3% of total). The optical band gaps of the as-

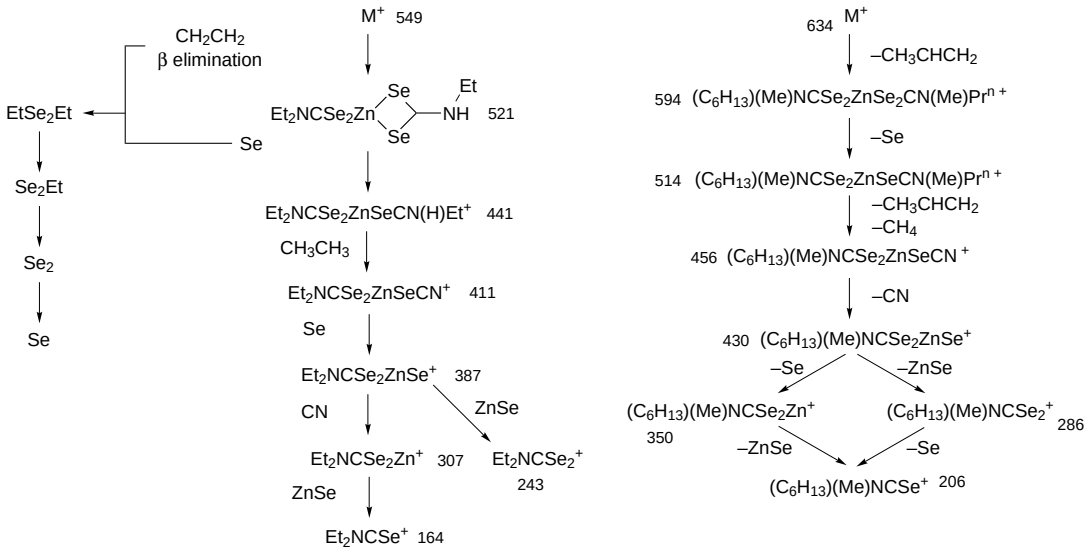

Scheme 1 Plausible decomposition mechanism for $[Zn(Se_2CNEt_2)_2]$ and $[Zn\{Se_2CNMe(C_6H_{13})\}_2]$ combining the steps observed from GC–MS and EI^+ studies of the precursors

deposited films were estimated by using the direct band gap method (from plots of absorbance^2 *vs.* energy) as 1.70 eV for CdSe and 2.58 eV for ZnSe (literature 1.74 and 2.58 eV). The films were further characterized by X-ray diffraction.¶

Compounds **1**, **2** and the analogous bis-diethyldiselenocarbamate were studied by pyrolysis GC–MS (pyrolysis temperature of 370 °C) and EIMS to develop plausible decomposition pathways/mechanisms for both sets of precursors.‖ These methods give valuable information concerning probable stable decomposition products and the results of these studies are summarized in Scheme 1. The gas chromatogram of the bis-diethyldiselenocarbamates for both cadmium and zinc shows the formation of a number of organoselenide products of which the most abundant is diethyl diselenide, $EtSe_2Et$. At the higher GC-column temperature (*ca.* 240 °C) elemental selenium fragments Se_n (n = 1–7) are observed which indicates that clusters of selenium are being formed on the pyrolysis of the precursor. These species may be responsible for the formation of selenium films during MOCVD. The selenium clusters were probably formed *via* an intermediate organoselenium complex on the column, $EtSe_2Et$ is a likely candidate as the mass spectrum of $EtSe_2Et$ shows it to dissociate to elemental selenium. In contrast to the diethyl derivative, the GC–MS traces of **1** and **2** show no evidence for the formation of selenium clusters, or the volatile organoselenium compound $EtSe_2Et$.[11]

We believe that by changing the alkyl groups on the parent amine of the diselenocarbamates from the symmetric diethyl to the asymmetric methyl(*n*-hexyl) derivative, the formation of diethyl diselenide is hindered and thus the deposition of selenium during film growth is inhibited. This subtle change results in the successful deposition of the ZnSe and CdSe from **1** and **2**.

Paul O'Brien is the Royal Society Amersham International Research Fellow and the Sumitomo/STS Professor of Materials Chemistry. We thank the EPSRC and the Leverhulme foundation for grants supporting work on single molecule precursors. M. C. thanks the EPSRC for a studentship. We thank the ULIRS mass spectrometry service at Kings College for pyrolysis GC–MS studies and J. Barton for other mass spectra. We would also like to thank Dr J. R. Walsh for earlier studies on the precursors.

Notes and References

† E-mail: p.obrien@ic.ac.uk

‡ The compounds were prepared by adaptations of the literature methods[3,4] for metal bis-dithiocarbamates and have been fully characterized by: NMR, mass spectrometry, microanalysis and IR spectroscopy.

§ For the purposes of analysis, samples were carbon coated and electron microscopy/EDAX was performed on a JEOL Superprobe 733 microscope.

¶ X-Ray diffraction of the films gave intense peaks with *d* values (% relative intensity, *hkl*) of 3.26 Å (100, 111), 2.00 Å (20, 220) and 1.71 Å (12, 311) for ZnSe (corresponding to cubic zinc selenide with a preferred orientation of 111; 3.27 (100), 2.00 (70), 1.71 Å (44) {ASTMS}) and 3.72 Å (21, 100), 3.51 Å (100, 002), 3.28 Å (18, 101), 2.54 Å (14, 102) 2.15 Å (15, 110), 1.98 Å (36, 103), 1.83 Å (11, 112), 1.45 (4, 203) Å for CdSe (corresponding to hexagonal CdSe with a preferred orientation of 001; 3.72 (100), 3.51 (70), 3.29 (75), 2.55 (36), 2.15 (85), 1.98 (70), 1.83 (51), 1.45 Å (20) {ASTMS}).

‖ EI-MS: a micromass AutoSpec-Q, using Micromass OPUS software was used. An electron impact energy of 70 eV at 10^{-7} Torr was used to initiate mass fragmentation. GC-MS: analysis of the samples was carried out using a Hewlett Packard Series II Gas/Liquid chromatograph linked to a JEOL JMS AX505W mass spectrometer. The chromatography conditions were as follows: column BP1 (supplied by SGE). Bonded phase methyl siloxane, length of 25 m, inner diameter of 0.22 mm, Phase thickness 0.25 μm. The temperature program employed for analysis was, initial temperature 30 °C, initial time 2 min, 8 °C min^{-1} to 100 °C (first ramp rate), 12 °C min^{-1} (second ramp rate), final temperature 280 °C. The pyrolysis injector temperature was 370 °C. Carrier gas helium pressure of 12 psi, flow 1 cm^3 min^{-1}. MS settings were a 3 kV accelerating voltage, 100 μA beam current and a detector voltage of 2 kV. Mass spectra were recorded between 10 and 600 u with a scan speed of 0.9 s. The precursor was dissolved in chloroform and 1 μl aliquots were injected onto the heated injector with a 30 : 1 split where pyrolysis occurred. Mass spectra of the volatile pyrolyzates were recorded as described above.

1 R. Nomura and P. O'Brien, *J. Mater. Chem.*, 1995, **5**, 1761.
2 M. Bochmann, *Adv. Mater., Chem. Vap. Dep.*, 1996, **2**, 86.
3 P. O'Brien, J. R. Walsh, I. M. Watson, M. Motevalli and L. Henriksen, *J. Chem. Soc., Dalton Trans.*, 1996, 2491.
4 M. Motevalli, P. O'Brien, J. R. Walsh and I. M. Watson, *Polyhedron*, 1996, **15**, 2801.
5 M. Chunggaze, M. A. Malik and P. O'Brien, *Adv. Mater. Opt. Electron.*, 1997, **7**, 311.
6 M. B. Hursthouse, M. A. Malik, M. Motevalli and P. O'Brien, *J. Mater. Chem.*, 1992, **2**, 949.
7 P. O'Brien, D. J. Otway and J. R. Walsh, *Adv. Mater., Chem. Vap. Dep.*, 1997, **3**, 227.
8 P. O'Brien, J. R. Walsh, I. M. Watson, L. Hart and S. R. P. Silva, *J. Cryst. Growth*, 1996, **167**, 133.
9 M. B. Hursthouse, M. A. Malik, M. Motevalli and P. O'Brien, *Polyhedron*, 1992, **11**, 45.
10 M. A. Malik and P. O'Brien, *Adv. Mater. Opt. Electron.*, 1994, **3**, 171.
11 R. Nomura, K. Migawaki, T. Toyasaki and H. Matsuda, *Adv. Mater. Chem. Vap. Dep.*, 1996, **2**, 174.

Received in Cambridge, UK, 24th December 1997; 7/09273C

Magnetic communication in acyclic mixed-valence trimolybdenum complexes mediated by redox switching

Eleftheria Psillakis, John P. Maher, Jon A. McCleverty* and Michael D. Ward*

School of Chemistry, University of Bristol, Cantocks Close, Bristol, UK BS8 1TS

Reversible one-electron reduction converts the 'V-shaped' [Mo(NO)[HB(dmpz)$_3$]{OC$_6$H$_4$XpyMo(NO)[HB(dmpz)$_3$]-Cl}$_2$] (dmpz = 3,5-dimethylpyrazolyl; X = nothing, CH=CH or CH$_2$CH$_2$; py = pyridyl) with two unpaired electrons on the peripheral metals, whose magnetic exchange properties depend on X, into a monoanion having three unpaired paired spins on each metal centre which engage in magnetic exchange in solution irrespective of X.

Molecular magnets are materials which may be derived either from organic radicals or from oligonuclear metal complexes containing at least one paramagnetic transition metal centre.[1] The construction of stable multicentre high-spin organic molecules remains a difficult synthetic challenge and the confirmation of interesting magnetic behaviour has been elusive.[2] However, the assembly of two or more transition metal components of differing spin, whose 'magnetic' orbitals are orthogonal and which are embedded in chain-like structures incorporating relatively short rigid organic bridges, has been more successful leading, for example, to solids exhibiting bulk ferromagnetic behaviour.[3]

The identification of paramagnetic transition metal components which can be easily linked within a rigid carbon-based architectural framework and which may couple magnetically is an important objective in the design and assembly of 'molecular magnets'. Central to this type of work is the control of the sign and magnitude of the magnetic exchange interaction J which depends critically on the nature of the pathway linking the interacting spins. We have recently shown that in paramagnetic isovalent dinuclear molybdenum nitrosyl complexes containing bipyridyl ligands (metal configuration 17 valence electrons), the sign of J can be predicted using a spin-polarisation mechanism,[4] and ferromagnetic behaviour has been detected in [{Mo(NO)-[HB(dmpz)$_3$]Cl}$_2$(3,4′-bpe)] (bpe = bipyridylethene; J = +2.4 cm^{-1}).[5] Furthermore, we have demonstrated that antiferromagnetic coupling can occur over surprisingly long distances, as in the isovalent [{Mo(NO)[HB(dmpz)$_3$]Cl}$_2${py(CH=CH)$_4$py}] (*ca.* 20 Å; J *ca.* −6.6 cm^{-1}).[6]‡ We have also shown that spin correlation, a manifestation in solution of magnetic coupling detected by EPR spectroscopy, occurs in the trinuclear species [1,3,5-{Mo(NO)[HB(dmpz)$_3$]Cl(pyCH=CH)}$_3$C$_6$H$_3$] and [1,3,5-{Mo(NO)[HB(dmpz)$_3$]Cl(pyC≡C)}$_3$C$_6$H$_3$] although we have not yet determined the relative signs of J.[7]

The mixed-valence/mixed donor atom species [{Mo(NO)-[HB(dmpz)$_3$]Cl}$_2$(OC$_6$H$_4$CH=CHpy)] which we prepared earlier contains a diamagnetic 16e$^-$ and a paramagnetic 17e$^-$ metal centre. The solution EPR spectrum shows A_{Mo} = 5.0 mT, consistent with valence-trapped behaviour, but on reduction to the isovalent monoanion, the EPR spectrum revealed that the two unpaired spins correlate strongly (A_{Mo} = 2.5 mT). The reduced species is isoelectronic and probably 'isomagnetic' with [{Mo(NO)[HB(dmpz)$_3$]Cl}$_2$(4,4′-bpe)] (A_{Mo} = 2.5 mT, J = −18 cm^{-1}),[5] the magnetic interaction between the two molybdenum centres being 'switched on' by reversible reduction of the molybdenum phenolate terminus from a 16e$^-$ to a 17e$^-$ configuration.

By substitution of both chlorides in [Mo(NO){HB(dmpz)$_3$}Cl$_2$] by the appropriate pyridine–phenol the diamagnetic bis-phenoxides [Mo(NO){HB(dmpz)$_3$}(4-OC$_6$H$_4$py)$_2$] **1**, [Mo(NO){HB(dmpz)$_3$}(4-OC$_6$H$_4$CH=CHpy)$_2$] **2** and [Mo(NO){HB(dmpz)$_3$}(4-OC$_6$H$_4$CH$_2$CH$_2$py)$_2$] **3**, have been obtained. Further reaction of these with [Mo(NO){HB(dmpz)$_3$}Cl$_2$] in the presence of NEt$_3$ afforded a mixture of di- and tri-metallic species which were separated by chromatography. The trimetallic species, [Mo(NO){HB-(dmpz)$_3$}{4-OC$_6$H$_4$pyMo(NO)[HB(dmpz)$_3$]Cl}$_2$] **4**, [Mo(NO)-[HB(dmpz)$_3$]{4-OC$_6$H$_4$CH=CHpyMo(NO)[HB(dmpz)$_3$]Cl}$_2$] **5** and [Mo(NO)[HB(dmpz)$_3$]{4-OC$_6$H$_4$CH$_2$CH$_2$pyMo(NO)-[HB(dmpz)$_3$]Cl}$_2$] **6**, contain a mixed-valence 17 : 16 : 17e$^-$ trimetal core in a 'V-shaped' array because of the *cis*-disposition of the phenoxide groups at the central molybdenum atom.§ Cyclic voltammetry¶ of **4**, **5** and **6** in dichloromethane revealed two synchronous one-electron oxidations of the molybdenum–pyridyl terminal groups and two reduction processes, one one-electron process associated with the central bis-phenolato molybdenum group and two synchronous one-electron reductions of the molybdenum–pyridyl termini. The formation potentials for the generation of the monoanion fall in the range −1.05 to −1.29 V *vs*. ferrocene–ferrocenium couple, entirely consistent with the reduction of {Mo(OC$_6$H$_4$–)$_2$} cores and with the cyclic voltammetric behaviour of **1**, **2** and **3**,[8] and are well-separated from the reduction processes of the terminal molybdenum–pyridyl groups.

The EPR spectrum (room temp., CH_2Cl_2 solution) of **5** is typical of significant spin exchange coupling in dinuclear molybdenum nitrosyl systems (g_{iso} = 1.977, A_{Mo} = 2.4 mT), *i.e.* strong spin correlation with $|J| \gg A_{Mo}$.[5] The spectrum of **4** is different from that of **5** (Fig. 1), being probably second order and characteristic of significant reduction in the exchange interaction, $|J| \approx A_{Mo}$, perhaps brought about by twisting of the rings within the bipyridyl fragments.‖ We have observed similar effects in related molecules.[9] However, the EPR spectrum of **6** reveals no spin correlation and therefore negligible magnetic interaction between the paramagnetic termini, *i.e.* $|J| \ll A_{Mo}$; A_{Mo} = 4.9 mT. This is probably a consequence of the insertion of saturated hydrocarbon links in the bridging ligands, of the number of bonds between the peripheral Mo centres (in ligands with extensive delocalisation,

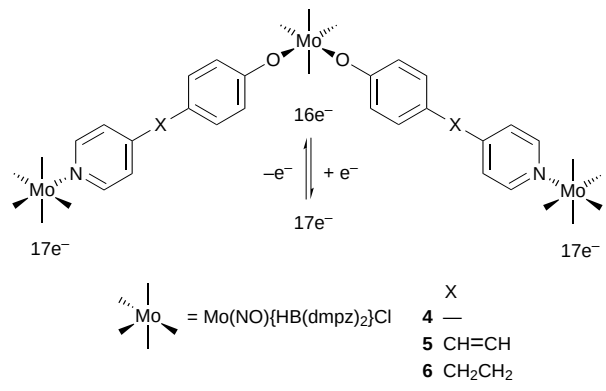

Fig. 1

strong correlation seems to persist up to about 20 atoms), and of possible twisting which degrades π-delocalisation.[10]

Reduction of the monometallic precursors **1**, **2** and **3** gave EPR spectra entirely similar to that of **6**, namely characteristic of one unpaired electron on an isolated 17-valence electron molybdenum nitrosyl group. However, the EPR spectra of $\mathbf{4}^-$ and $\mathbf{5}^-$, produced by chemical or electrochemical reduction of **4** and **5**, provided EPR spectra revealing strong correlation between all three 17-electron metal centres, g_{iso} = 1.976, A_{Mo} = 1.7 mT, very similar to the data obtained from the symmetrical [1,3,5-{Mo(NO)[HB(dmpz)$_3$]Cl(pyCH=CH)}$_3$-C_6H_3]. Even more remarkably, the EPR spectrum of $\mathbf{6}^-$ also revealed strong spin correlation (large $|J|$) between all three metal centres (g_{iso} = 1.973, A_{Mo} = 1.7 mT).

It appears, therefore, that reduction of the central molybdenum bis(phenoxy) moiety from a 16- to a 17-valence electron unit is essential to facilitate strong spin-correlation and so strong magnetic interaction between all three 17-electron metal centres. The EPR spectral consequences of the correlation in these 'V-shaped' molecules appear to be broadly similar to those in the more symmetrical [1,3,5-{Mo(NO)-[HB(dmpz)$_3$]Cl(pyCH=CH)}$_3$C$_6$H$_3$] and its analogues. Thus the reversible conversion of **6** to $\mathbf{6}^-$ can be interpreted as an example of a simple molecular magnetic or '*J* switch' in that changing the redox level of the central atom increases spin correlation (*i.e.* magnetic exchange) between the terminal groups.

While the molecular components and the effects described here are of themselves small by molecular electronic standards, by elaboration of the design of these mixed phenoxy–pyridine complexes into oligomeric and polymeric species, it should be possible to build up an extended array of mixed-oxidation state metal systems which may be switched to isovalent species whose magnetic properties may be sufficiently strong to constitute useful devices.

Notes and References

† E-mail: jon.mccleverty@bristol.ac.uk

‡ Earlier magnetic susceptibility results obtained over the range 80–300 K indicated $J = -41$ cm^{-1} (ref. 6), but more recent results measured down to 2 K give $J = -6.6$ cm^{-1}; D. Moryusef, J. Boinvoisin, J.-P. Launay, J. A. McCleverty and M. D. Ward, unpublished work; D. Moryusef, DEA Thesis, Université Paul Sabatier, 1996–7.

§ All compounds analysed correctly for C, H and N; ν_{NO} (KBr discs) of **1**, **2** and **3**: 1656, 1655 and 1651, respectively; **4**, **5** and **6**: 1616, 1670; 1611, 1670 and 1617, 1656 cm^{-1}, respectively.

¶ In CH_2Cl_2, *vs.* ferrocene–ferrocenium couple, using Pt wire and [NBu$^n_4$][PF$_6$] as supporting electrolyte: **1**, $E_f = -1.10$ V; **2**, $E_f = -1.14$ V; **3**, $E_f = -1.30$ V; **4**, $E_f = +0.03, -1.05, -2.11$ V; **5**, $E_f = +0.04, -1.06, -1.99$ V; **6**, $E_f = +0.05, -1.29, -2.12$ V.

‖ Typical first and second order spectra of these types of molybdenum nitrosyl complexes have been illustrated in refs. 7 and 9.

1 R. J. Rushby and J.-L. Pauillaud, in *An Introduction to Molecular Electronics*, ed. M. C. Petty, M. R. Bryce and D. Bloor, Edward Arnold, London, 1995, p. 72; O. Kahn, O. Cador, J. Larionova, C. Mathoniere, J. P. Sutter and L. Ouahab, *Mol. Cryst. Liq. Cryst., Sect. A*, 1997, **305**, 1.

2 H. Tanaka, T. Tokuyama, T. Sato and T. Ota, *Chem. Lett.*, 1990, 1813; P. M. Allemand, K. C. Khemani, A. Koch, F. Wudl, K. Holczer, K. Donovan, G. Grüner and J. D. Thompson, *Science*, 1991, **253**, 301; Y. Nakazawa, M. Tamura, N. Shirakawa, D. Shiomi, M. Takahashi, M. Kinoshita and M. Ishikawa, *Phys. Rev. B*, 1992, **46**, 8906; J. Veciana, C. Rovira, N. Ventosa, M. I. Crespo and F. Palacio, *J. Am. Chem. Soc.*, 1993, **115**, 57; A. Lang, H. Naarmann, G. Rosler, B. Gotschy, H. Winter and E. Dormann, *Mol. Phys.*, 1993, **79**, 1051; T. Nogami, K. Tomioka, T. Ishida, H. Yoshikawa, M. Yasui, F. Iwasaki, H. Iwamura, N. Takeda and M. Ishikawa, *Chem. Lett.*, 1994, 29; S. Rajca and A. Rajca, *J. Am. Chem. Soc.*, 1995, **117**, 9172; M. M. Matsushita, A. Izuoka, T. Sugawara, T. Kobayashi, N. Wada, N. Takeda and M. Ishikawa, *J. Am. Chem. Soc.*, 1997, **119**, 4369; K. Matsuda, T. Yamagata, T. Seta, H. Iwamura and K. Hori, *J. Am. Chem. Soc.*, 1997, **119**, 8058; J. Cirujeda, O. Jurgens, J. Vidal Cancedo, C. Rovira, P. Turek and J. Veciana, *Mol. Cryst. Liq. Cryst., Sect. A*, 1997, **305**, 367.

3 J. K. McCusker, E. A. Schmitt and D. N. Hendrickson, in *Magnetic Molecular Materials*, NATO ASI Series, ed. D. Gatteschi, O. Kahn, J. S. Miller and F. Palacio, Kluwer Academic Press, 1991, vol. E198, p. 297; O. Kahn, *Molecular Magnetism*, VCH, New York, 1993; M. L. Allan, J. H. F. Martens, A. T. Coomber, R. H. Friend, I. Marsden, E. A. Marseglia, A. E. Underhill and A. Charlton, *Mol. Cryst. Liq. Cryst.*, 1993, **230**, 387; P. J. Vankoningsruggen, J. N. Koga, Y. Ishimaru and H. Iwamura, *Angew. Chem., Int. Ed. Engl.*, 1996, **35**, 755; H. L. Nie, S. M. J. Aubin, M. S. Matshuta, R. A. Porter, J. F. Richardson and D. N. Hendrickson, *Inorg. Chem.*, 1996, **35**, 3325.

4 J. McConnell, *J. Chem. Phys.*, 1963, **39**, 1910.

5 A. M. W. Cargill Thompson, D. Gatteschi, J. A. McCleverty, J. A. Navas, E. Rentschler and M. D. Ward, *Inorg. Chem.*, 1996, **35**, 2701; V. An Ung, A. M. W. Cargill Thompson, D. A. Bardwell, D. Gatteschi, J. C. Jeffery, J. A. McCleverty, F. Totti and M. D. Ward, *Inorg. Chem.*, 1997, **36**, 3447.

6 S. L. W. McWhinnie, J. A. Thomas, T. A. Hamor, C. J. Jones, J. A. McCleverty, D. Collison, F. E. Mabbs, C. J. Harding, L. J. Yellowlees and M. G. Hutchings, *Inorg. Chem.*, 1996, **35**, 760.

7 A. J. Amoroso, A. M. W. Cargill Thompson, J. P. Maher, J. A. McCleverty and M. D. Ward, *Inorg. Chem.*, 1995, **34**, 4828.

8 N. Al-Obaidi, M. Chaudhury, D. Clague, C. J. Jones, J. C. Pearson, J. A. McCleverty and S. S. Salam, *J. Chem. Soc., Dalton Trans.*, 1987, 1733; A. Das, J. C. Jeffery, J. P. Maher, J. A. McCleverty, E. Schatz, M. D. Ward and G. Wollerman, *Inorg. Chem.*, 1993, **32**, 2145.

9 R. Cook, J. P. Maher, J. A. McCleverty, M. D. Ward and A. Wlodarczyk, *Polyhedron*, 1993, **12**, 2111.

10 R. Shonfield, A. A.Jouaiti, J. P. Maher, J. A. McCleverty and M. D. Ward, unpublished work.

Received in Basel, Switzerland, 26th January 1998; 8/00660A

Selective electrochemical recognition of mercury in water by a redox-functionalised aza-oxa crown derivative

José M. Lloris, Ramón Martínez-Máñez,*† Teresa Pardo, Juan Soto and Miguel E. Padilla-Tosta

Departamento de Química, Universidad Politécnica de Valencia, Camino de Vera s/n, 46071 Valencia, Spain

The ability of the new cyclic aza-oxa redox-active receptor *N*-ferrocenylmethyl-1,4,7-trioxa-10-azacyclododecane to selectively and electrochemically recognize Hg^{2+} in water over other commonly water-present metal ions is reported.

The design and synthesis of promising new materials from supramolecular chemistry for the development of novel chemical sensors is a field of current interest. Of special interest are novel functionalised molecules which are able to change an easily measurable physical property by coordination with a target substrate. Among these new molecules are redox-functionalised receptors able to display a shift of the redox potential upon addition of particular substrates.[1] We have recently been involved in the synthesis of electroactive water soluble receptors for the electrochemical recognition of toxic heavy metal cations. A combination of well known molecular properties and suitable redox groups could prove to be a good method to strategically design new molecules for the selective electrochemical recognition of target substrates. The design strategy was inspired by two well known properties; (*i*) macrocyclic receptors compared to acyclic structures generally provide more selective complexation, and (*ii*) the presence of central oxygen donors in macrocycles has been used to control the selectivity for large metal ions over small ones.[2,3] Taking these two principles into account the aza-oxa crown derivative 1,4,7-trioxa-10-azacyclododecane ([12]-aneNO$_3$),[4] which has been reported to display higher stability constants with mercury than with other common metal ions, was chosen and functionalised with ferrocenyl groups. Synthesis of L^1 was carried out by reaction of [12]-aneNO$_3$ with (ferrocenylmethyl)-trimethylammonium iodide in acetonitrile (Scheme 1).

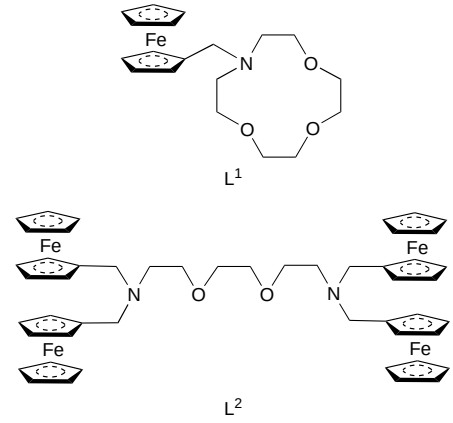

Scheme 1

L^1 is an oil but can be obtained as a solid by adding [NH$_4$][PF$_6$] to a solution of L^1 in ethanol and further addition of water to give [HL^1][PF$_6$]. Crystals‡ were obtained by slow diffusion of hexane into dichloromethane solutions of [HL^1][PF$_6$]. Fig. 1 shows the molecular structure of the $[HL^1]^+$ cation. The protonation constants of the free ligand and the stability constants for the formation of the Cu^{2+}, Zn^{2+}, Cd^{2+}, Pb^{2+} and Hg^{2+} complexes of L^1 have been determined using potentiometric methods (25 °C, 0.1 mol dm^{-3} KClO$_4$; titration was carried out with KOH from previously acidified solutions with HClO$_4$ of L^1 and the corresponding metal ion).[6] Stability constants are gathered in Table 1. The formation of the $[ML^1(OH)]^+$ and $[ML^1(OH)_2]$ complexes has been observed for all the metal ions. Additionally, for Pb^{2+} and Hg^{2+}, $[ML^1]^{2+}$ species have also been found to exist. Functionalisation with the ferrocenyl group does not basically appear to modify the coordination behaviour of the cyclic oxa-aza cavity. Fig. 2 displays the distribution diagrams of the L^1–H^+–Cu^{2+} and L^1–H^+–Hg^{2+} systems. Hg^{2+} shows a quite different diagram and, when the $[HgL^1]^{2+}$ complex is predominant (near pH 5), there is not interaction between the receptor and Cu^{2+}, Zn^{2+}, Cd^{2+} and Pb^{2+} ions. This can be explained taking into account

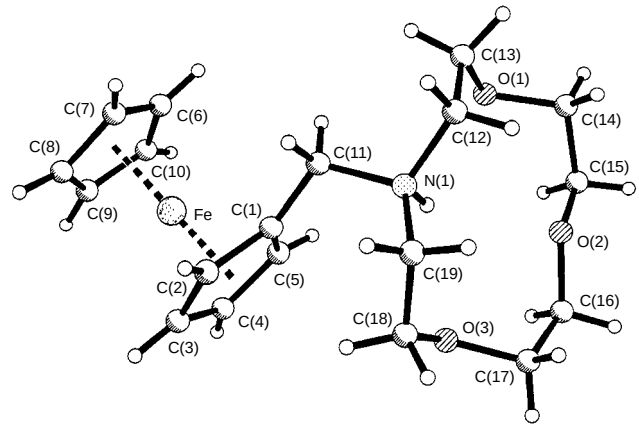

Fig. 1 Molecular structure of the $[HL^1]^+$ cation

Table 1 Stability constants (log *K*) for the formation of Cu^{2+}, Zn^{2+}, Cd^{2+}, Pb^{2+} and Hg^{2+} complexes of L^1 in H_2O at 25 °C in 0.1 mol dm^{-3} KClO$_4$[a]

	M				
Reaction	Cu^{2+}	Zn^{2+}	Cd^{2+}	Pb^{2+}	Hg^{2+}
$M^{2+} + L^1 \rightleftharpoons [ML^1]^{2+}$	—	—	—	5.29(5)[b]	10.03(4)
$M^{2+} + L^1 + H_2O \rightleftharpoons [ML^1(OH)]^+ + H^+$	−0.72(2)	−3.49(3)	−6.19(2)	−3.47(7)	3.0(1)
$M^{2+} + L^1 + 2H_2O \rightleftharpoons [ML^1(OH)_2] + 2H^+$	−10.10(4)	−13.10(4)	−16.52(2)	−13.23(6)	−4.08(7)

[a] The titration curves were merged and treated simultaneously to give the stability constants: L^1–H^+–Hg^{2+}, three titration curves, pH 3–8; L^1–H^+–M^{2+} (M = Cu^{2+}, Zn^{2+}, Cd^{2+}, Pb^{2+}), three titration cures, pH 3–9. [b] Values in parentheses are standard deviations on the last significant figure.

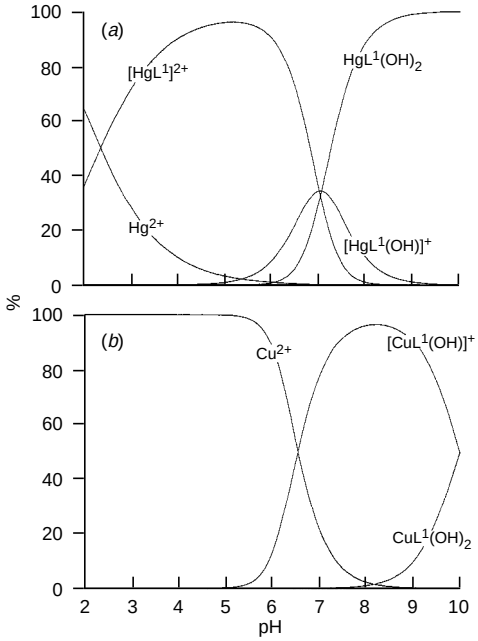

Fig. 2 Distribution diagram for the systems (*a*) L^1–H^+–Hg^{2+} and (*b*) L^1–H^+–Cu^{2+}

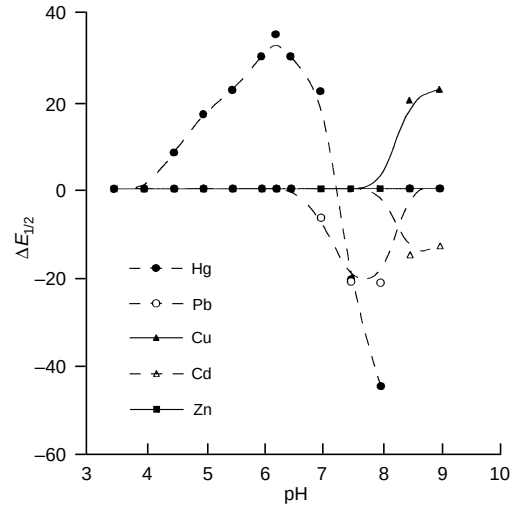

Fig. 3 Plot of $\Delta E_{1/2}$ *vs.* pH as a function of the pH for L^1–H^+–M^{2+} (M^{2+} = Cu^{2+}, Zn^{2+}, Cd^{2+}, Pb^{2+} and Hg^{2+})

the larger affinity of Hg^{2+} for L^1, which is able to produce the reaction $Hg^{2+} + HL^{1+} \rightleftharpoons [HgL^1]^{2+} + H^+$ at a lower pH value than the remaining metal ions. To determine if the ferrocenyl group is able to amplify the selective mercury-binding behaviour found at molecular level into a macroscopic signal using electrochemical methods, the oxidation potential of the free receptor and the oxidation potential of L^1–M^{2+} systems (M = Cu^{2+}, Zn^{2+}, Cd^{2+}, Pb^{2+}, Hg^{2+}) has been monitored as a function of the pH in water. $E_{1/2}$ of the free receptor is pH-dependent. $E_{1/2}$ is *ca.* 175 mV at pH = 10. When the pH decreases there is an anodic shift until pH = 8 ($E_{1/2}$ = 375). In the pH range 8–3 the potential remains constant with a total shift between basic and acid pH of near 200 mV. Fig. 3 shows $\Delta E_{1/2}$ found in the presence of metal ions [M = Cu^{2+}, Zn^{2+}, Cd^{2+}, Pb^{2+}, Hg^{2+}; $\Delta E_{1/2}$ is defined for a particular pH as $E_{1/2}$(L^1–H^+–M^{2+}) − $E_{1/2}$(L^1–H^+), studies have been carried out using 1 : 1 metal-to-ligand molar ratios; typical metal concentrations were 3–4 × 10^{-4} mol dm^{-3}]. It can be observed that there is a selective electrochemical recognition of Hg^{2+} over other common typically water-present metal ions as was predicted from the potentiometric results. At pH 6 there is no interaction between L^1 and Cu^{2+}, Zn^{2+}, Cd^{2+} or Pb^{2+}, and the addition of these metal ions (*ca.* 3 × 10^{-4} mol dm^{-3}) to solutions of L^1 and Hg^{2+} ([Hg^{2+}] *ca.* 3 × 10^{-4} mol dm^{-3}) does not shift $E_{1/2}$. Additionaly L^1–M^{2+}–H^+ curves in Fig. 3 are transformed into the L^1–Hg^{2+}–H^+ curve by adding equimolecular amounts of mercury to L^1–M^{2+} solutions (M^{2+} = Cu^{2+}, Zn^{2+}, Cd^{2+} or Pb^{2+}), indicating that Hg^{2+} is able to displace other metal ions in pre-formed $[ML^1]^{2+}$ complexes. L^1 behaves as a selective sensing molecule for Hg^{2+}.

To study the role played by the cyclic nature of L^1 similar experiments have been carried out using L^2 as receptor, which has been isolated after condensation of 2,2′-(ethylenedioxy)-bis(ethylamine) and (ferrocenylmethyl)trimethylammonium iodide. Electrochemical data showed, in contrast with L^1, that the values of $E_{1/2}$ *vs.* pH found for the free receptor and $E_{1/2}$ *vs.* pH obtained in the presence of metal ions (M^{2+} = Cu^{2+}, Zn^{2+}, Cd^{2+}, Pb^{2+} and Hg^{2+}; 1 : 1 metal-to-ligand molar ratios) were the same within the experimental error, pointing out the importance of the molecular architecture in L^1.

We should like to thank the DGICYT (proyecto PB95-1121-C02-02) for support.

Notes and References

† E-mail: rmaez@qim.upv.es

‡ $C_{19}H_{28}F_6FeNO_3P$, M = 512.24, monoclinic, space group $P2_1$, a = 8.049(3), b = 10.353(4), c = 13.905(6) Å, β = 104.24(3)°, U = 1123.2(7) $Å^3$, Z = 2, D_c = 1.54 g cm^{-3}, λ(Mo–Kα) = 0.710 69 Å, T = 293(2) K, μ(Mo-Kα) = 8.12 cm^{-1}. A well shaped crystal with approximate dimensions 0.15 × 0.15 × 0.25 mm was mounted on a Siemens P4 single-crystal diffractometer. A total of 2925 independent reflections were collected (R_{int} = 0.021) (4.9 ⩽ 2θ ⩽ 45.1°). Lorentz and polarization corrections were applied and absorption was corrected from ψ-scans. The structure was solved by direct methods and refined by full-matrix least-squares analysis on F^2 (SHELXTL).[5] The refinement converged at R_1 = 0.0524 [$F > 4\sigma(F)$] and wR_2 0.1500 (all data). Largest peak and hole in the final difference map = +0.42, −0.20 e $Å^{-3}$. CCDC 182/785.

1 See for example: P. D. Beer, *Chem. Soc. Rev.*, 1989, **18**, 409; M. E. Padilla-Tosta, R. Martínez-Máñez, T. Pardo, J. Soto and M. J. L. Tendero, *Chem. Commun.*, 1997, 887.
2 K. A. Byriel, K. R. Dunster and L. R. Gahar, *Inorg. Chim. Acta.*, 1993, **205**, 191.
3 V. J. Thöm and R. D. Harcock, *Inorg. Chem.*, 1986, **25**, 2992.
4 J. E. Richman and T. J. Atkins, *J. Am. Chem. Soc.*, 1974, **96**, 2268
5 SHELXTL, Program version 5.03. Siemens Analytical X-Ray Instruments, Madison, WI, 1994.
6 For experimental details see for example; M. J. L. Tendero, A. Benito, R. Martínez-Máñez, J. Soto, J. Payá, A. J. Edwards and P. R. Raithby, *J. Chem. Soc., Dalton Trans.*, 1996, 343.

Received in Cambridge, UK, 2nd January 1998; 8/00053K

Amplified microgravimetric quartz-crystal-microbalance analyses of oligonucleotide complexes: a route to a Tay–Sachs biosensor device

Amos Bardea,[a] Arie Dagan,[a] Iddo Ben-Dov,[a] Boaz Amit[b] and Itamar Willner*[a]†

[a] *Institute of Chemistry, The Hebrew University of Jerusalem, Jerusalem, 91904, Israel*
[b] *General Biotechnology, Kiryat Weizmann, Rehovot, Israel*

An oligonucleotide monolayer acts as an active interface for the microgravimetric, quartz-crystal-microbalance analysis of the complementary oligonucleotide.

The formation of specific double-stranded (ds)-oligonucleotide complexes on solid supports has evoked substantial recent research activities directed to the nanoscale architecture of metal-colloid arrays by means of oligonucleotide bridges[1] and to the tailoring of functionalized surfaces for gene detection.[2,3] Electrochemical DNA-sensors based on the intercalation or interaction of redox-active transition metal complexes,[4,5] *e.g.* $Co(bpy)_3^{3+}$, or dyes[6] such as acridine or Hoechst 33258, were reported. Microgravimetric quartz-crystal-microbalance (QCM) analyses, that use oligonucleotide sensing interfaces, were recently initiated to identify oligonucleotide–protein[7] or oligonucleotide–DNA complexes.[8] Although oligonucleotide–protein interactions were reported to reveal specificity,[7] the sensitivity of the oligonucleotide–oligonucleotide or DNA sensors is low and the specificity of these devices needs to be established. Recently, we applied antigen or antibody monolayer-functionalized Au–quartz crystals for the microgravimetric analyses of the complementary antibodies[9] or antigens.[10]

The assembly of biologically active monolayers on Au-supports *via* thiol bridging units has been extensively developed by our laboratory.[11] Enzyme-electrodes,[12] photoactive enzyme-electrodes,[13] immunosensors[9,10] and reversible immunosensors[14] were developed by this method. Here we wish to report on the development of an active oligonucleotide interface for the microgravimetric, piezoelectrical analysis of the complementary oligonucleotide. The method is exemplified for the analysis of the oligonucleotide residue characterizing the Tay–Sachs genetic disorder.[15] We demonstrate means to confirm and amplify the formation of the oligonucleotide–oligonucleotide complex at the crystal interface.

The 41-mer oligodeoxynucleotide **1** includes ten successive thiophosphate thymine residues linked to the 5′-terminus and acts as thiol-tag for attachment to the Au surface.[16] The remaining 31-mer oligonucleotide includes the complementary characteristic base-order of the normal Tay–Sachs gene. The 31-mer oligodeoxynucleotide **2** includes the base sequence of TS 4I-N in the gene in which mutations lead to the Tay–Sachs genetic disorder.[15] The thiol-tagged oligonucleotide **1** was assembled on a Au–quartz crystal (AT-cut, 9 MHz, EG&G) by interaction of the crystal with a phosphate buffer (0.01 M, pH 7.3) solution of **1**, 50 μg ml for 12 h at 4 °C.

Fig. 1(*b*)–(*e*) show the frequency changes of different crystals exposed to different concentrations of the complementary oligonucleotide **2**. Interaction of the monolayer-functionalized crystal with **2** yields a frequency decrease, implying a mass increase on the crystal surface as a result of the formation of the ds-oligonucleotide between **1** and **2**, Scheme 1. The extent of the crystal frequency decrease is enhanced as the bulk concentration of **2** increases, consistent with the increased surface coverage of the sensing interface by **2**. At a bulk concentration of **2** corresponding to 11.5 μg ml^{-1} [Fig. 1(*e*)], the crystal frequency decreases by 11 Hz and it levels-off to a constant value after *ca.* 200 s. Exposure of the monolayer-functionalized crystal to higher concentrations of **2** does not enhance the crystal frequency change, and the value of $\Delta f = -(11 \pm 1)$ Hz is preserved. This implies that the **1**–monolayer interface is saturated by **2** as a result of the formation of the ds-oligonucleotide. Using the observed frequency change, we estimate the surface coverage of the ds-oligonucleotide or the surface density of the base monolayer of **1** to be *ca.* 4.4×10^{-12}

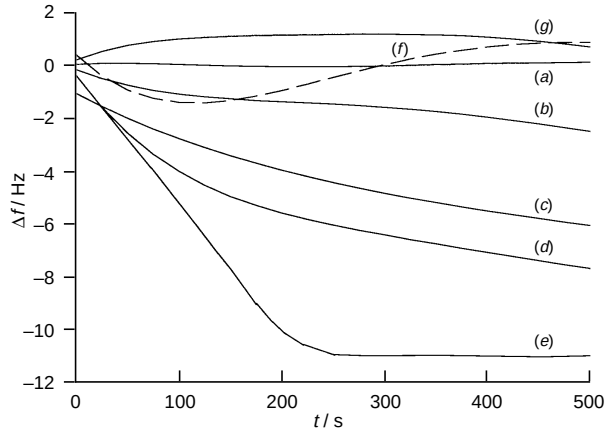

Fig. 1 Time-dependent frequency changes of a **1**-functionalized Au–quartz crystal upon addition of: (*a*) SSC buffer solution, pH = 7.0; (*b*) **2**, 0.6 μg ml^{-1}; (*c*) **2**, 2.4 μg ml^{-1}; (*d*) **2**, 3.5 μg ml^{-1}; (*e*) **2**, 11.5 μg ml^{-1}; (*f*) **3**, 11.5 μg ml^{-1}, (*g*) **2a** 2.4 μg ml^{-1}. Oligonucleotides are dissolved in SSC buffer, pH = 7.0, SSC = 30 mM Na–citrate and 300 mM NaCl.

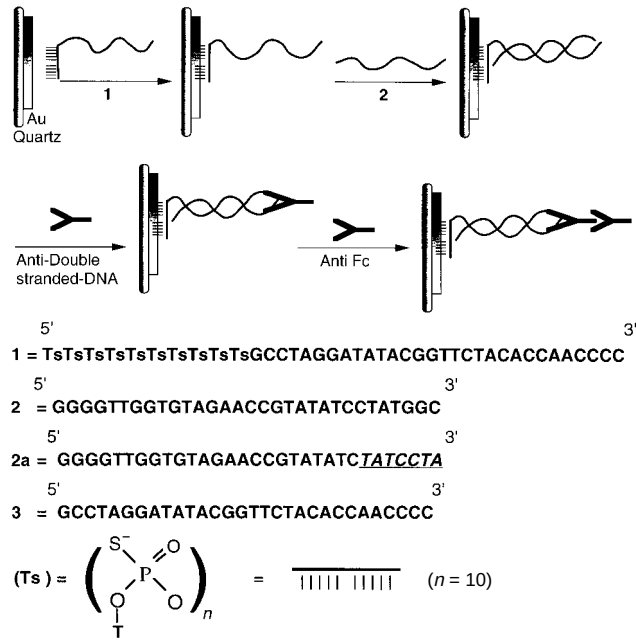

Scheme 1 Schematic amplified microgravimetric analysis of an oligonucleotide

mol cm^{-2}. This corresponds to *ca*. 50% of a densely packed monolayer of the ds-oligonucleotide. Control experiments reveal that the frequency of a bare Au–quartz crystal is unaffected upon interaction with **2**, (0.6 μg ml^{-1}), $\Delta f = -(1 \pm 1)$ Hz. Also, treatment of the **1**-functionalized crystal with a pure buffer solution [Fig. 1(*a*)] or with the 31-mer oligonucleotide solution **3**, (11.5 μg ml^{-1}), [Fig. 1(*f*)], does not yield any significant change in the crystal frequency. Note that the oligonucleotide **3** is essentially complementary to **2**. Thus, the lack of frequency changes upon interaction of the **1**-functionalized crystal with **3** indicates that non-specific oligonucleotide binding interactions are not operative on the interface. The frequency change observed upon interactions of the **1**-modified crystal with **2** originates from specific complementary interactions that generate the ds-assembly. A major concern in the development of the microgravimetric DNA-sensor relates to the specificity of interactions of the sensing interface with oligonucleotide mutants. Accordingly the quartz-crystal functionalized with the oligonucleotide **1** was interacted with the 31-mer oligonucleotide **2a**. The latter oligonucleotide includes the characteristic mutation differentiating the normal gene and 75% of the Tay–Sachs genetic disorder carriers. Note, that a seven-base mutation occurs in **2** as compared to **2a**. Fig. 1(*g*) shows the crystal frequency response upon interaction of the sensing interface with **2a** (2.4 μg ml^{-1}). No detectable crystal frequency decrease is observed, indicating that the removal of the seven-base pair recognition between the sensing interface and **2a** is sufficient to eliminate significant binding interactions. Thus, the sensing interface reveals sufficient specificity to distinguish between the normal and mutated DNA-sequences involved with Tay–Sachs genetic disorder.

At a bulk concentration of **2** corresponding to 0.6 μg ml^{-1}, a frequency change of only 2 Hz is observed after 500 s. This seems to be the sensitivity limit. In order to confirm that the frequency change observed in Fig. 1(*b*) originates from specific complementary interactions, and to amplify the transduced sensing signal, the resulting ds-assembly was interacted with a mouse anti-ds-DNA antibody (Ab). Fig. 2(*a*) shows the crystal frequency changes upon the interaction of **1**-functionalized crystal with **2** (0.6 μg ml^{-1}). A frequency change of $\Delta f = -(2 \pm 1)$ Hz is observed. Fig. 2(*b*) shows the crystal frequency changes upon interaction of the ds-assembly with the anti-ds-DNA antibody. Note that although the coupling of **2** results in a frequency change of only $\Delta f = -(2 \pm 1)$ Hz, the association of the Ab results in a frequency change of $\Delta f = -(14 \pm 1)$Hz. This is consistent with the fact that the mass ratio of **2** : Ab is 1 : 15. Challenging of the supramolecular ds-oligonucleotide/anti-ds-DNA antibody with the goat anti-mouse Fc-antibody results in a further decrease in the crystal frequency of $\Delta f = -(8 \pm 1)$ Hz, Fig. 2(*c*). This originates from the association of the secondary antibody to the Fc-part of the anti-ds-DNA antibody, Scheme 1. The frequency decrease in the presence of the secondary antibody is only half of the frequency decrease observed with the primary anti-ds-DNA antibody. This originates from the fact that the secondary antibody includes two binding sites for the primary antibody. Control experiments reveal that the anti-ds-DNA antibody or the anti-mouse-Fc-antibody do not bind to the **1**-functionalized interface [$\Delta f = -(2 \pm 1)$ Hz]. Thus, the ds-assembly formed by the interaction between the functionalized crystal and **2** specifically associates the anti-ds-DNA antibody. The latter complex with the mouse antibody binds the secondary goat anti-mouse antibody.

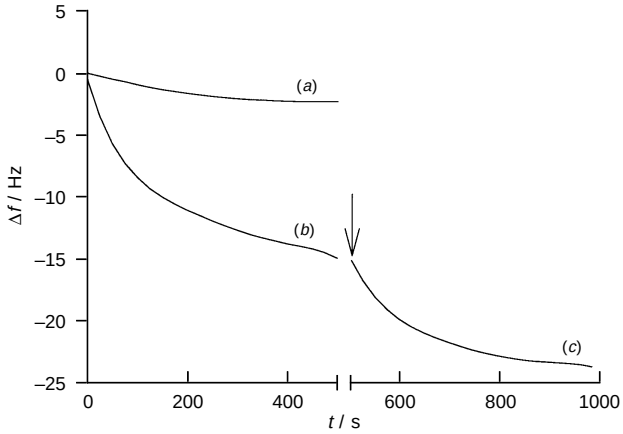

Fig. 2 Time-dependent frequency changes of the **1**-functionalized Au–quartz crystal upon addition of: (*a*) **2**, 0.6 μg ml^{-1}; (*b*) addition of anti-ds-DNA-Ab, 1.2 μg ml^{-1}, to the **1** and **2** double stranded complex on the surface; (*c*) addition of anti-Fc-Ab, 21 ng ml^{-1} to the **1** and **2** ds-complex with linked anti-ds-DNA-Ab. Arrow indicates the time of anti-Fc-Ab addition. Prior to addition of the anti-Fc-Ab, the cell was rinsed with PBS buffer.

Thus, we have developed a novel means to assemble an interface for the specific microgravimetric analysis of complementary oligonucleotides. The interaction of the resulting surface-bound ds-oligonucleotide assembly with the anti-ds-DNA antibody and with the respective anti-antibody provides means to confirm and amplify the primary formation of the complementary oligonucleotide complexes. Further attempts to regenerate the sensing interface by unfolding of the ds-oligonucleotide complex by thermal or chemical treatments are underway in our laboratory.

Parts of this research were supported by the Bundesministerium für Bildung Wissenschaft, Forschung und Technologie, Germany, (BMBF) The Israel Ministry of Science, MOS, and The Szold Foundation, The Hebrew University of Jerusalem.

Notes and References

† E-mail: willnea@vms.huji.ac.il

1 C. A. Mirkin, R. L. Letsinger, R. C. Mucic and J. J. Storhoff, *Nature*, 1996, **382**, 607; A. P. Alivisatos, K. P. Johnsson, X. Peng, T. E. Wilson, C. J. Loweth, M. P. Bruchez, Jr. and P. G. Schultz, *Nature*, 1996, **382**, 609.
2 M. Yang, M. E. McGovern and M. Thompson, *Anal. Chim. Acta*, 1997, **346**, 259; H. Su, M. R. Kallury, M. Thompson and A. Roach, *Anal. Chem*., 1994, **66**, 763.
3 D-W. Pang, M. Zhaug, Z.-L. Wang, Y.-P. Qi, J.-K. Cheng and Z.-Y. Liu, *J. Electroanal. Chem*., 1996, **403**, 183.
4 A. J. Bard and M. T. Carter, *J. Am. Chem. Soc*., 1987, **109**, 7528; A. J. Bard and M. Rodriguez, *Anal. Chem*., 1990, **62**, 2658.
5 K. M. Millan and S. R. Mikkelsen, *Anal. Chem*., 1993, **65**, 2317.
6 K. Hashimoto, K. Ito and Y. Ishimori, *Anal. Chem*., 1994, **66**, 3830.
7 K. Niikura, K. Nagata and Y. Okahata, *Chem. Lett*., 1996, 863.
8 K. Ito, K. Hashimoto and Y. Ishimori, *Anal. Chim. Acta*, 1996, **327**, 29; F. Caruso, E. Rodda and D. Furlong, *Anal. Chem*., 1997, **69**, 2043; N. C. Fawcett, J. A. Evans, L. C. Chien and N. Flowers, *Anal. Lett*., 1988, **21**, 1099.
9 Y. Cohen, S. Levi, S. Rubin and I. Willner, *J. Electroanal. Chem*., 1996, **417**, 65; R. Blonder, E. Katz, Y. Cohen, N. Itzhak, A. Riklin and I. Willner, *Anal. Chem*., 1996, **68**, 3151.
10 I. Ben-Dov, I. Willner and E. Zisman, *Anal. Chem*., 1997, **69**, 3506.
11 I. Willner, A. Riklin, R. Shoham, D. Rivenzon and E. Katz, *Adv. Mater*., 1993, **5**, 912.
12 I. Willner, V. Heleg-Shabtai, R. Blonder, E. Katz, G. Tao, A. F. Bückmann and A. Heller, *J. Am. Chem. Soc*., 1996, **118**, 10 321; A. Riklin and I. Willner, *Anal. Chem*., 1995, **67**, 4118.
13 I. Willner and B. Willner, *Adv. Mater*., 1995, **7**, 587; I. Willner, *Acc. Chem. Res*., 1997, **30**, 347.
14 I. Willner, R. Blonder and A. Dagan, *J. Am. Chem. Soc*., 1994, **116**, 9365; R. Blonder, S. Levi, G. Tao, I. Ben-Dov and I. Willner, *J. Am. Chem. Soc*., 1997, **119**, 10 467.
15 R. A. Gravel, J. T. R. Clarke, M. M. Kaback, D. Mahuran, K. Sandhoff and K. Suzuki, in *The Metabolic and Molecular Basis of Inherited Disease*, ed. C. R. Scriver, A. L. Beaudet, W. S. Sly and D. Valle, McGraw Hill, New York, 1995, vol. 2, pp. 2839–2879.
16 Prepared by the application of Beaucage's reagent, *cf*. R. P. Iyer, W. Egan, J. B. Regen and S. L. Beaucage, *J. Am. Chem. Soc*., 1990, **112**, 1253.

Received in Cambridge, UK, 2nd January 1998; 8/00215K

Practical route to high activity enzyme preparations for synthesis in organic media

Johann Partridge,*† Peter J. Halling and Barry D. Moore*

Department of Pure and Applied Chemistry, University of Strathclyde, Thomas Graham Building, 295 Cathedral Street, Glasgow, Scotland, UK G1 1XL

A single pot method to rapidly prepare immobilised subtilisin Carlsberg and α-chymotrypsin gives 1000-fold greater catalytic activities in polar organic solvents than freeze-dried powders.

The application and utility of enzymes such as serine proteases and esterases in organic synthesis is well established. This has led to increased demand for enzyme preparations which exhibit high activity and reproducible selectivity, particularly in organic solvents.[1–4] The commonly used freeze-dried powders are known to exhibit low activity,[5,6] but are often used because they can be obtained in one step from commercially supplied enzymes. Enzymes immobilised onto a support often show higher activity in organic media but the types of support material reported may not always be readily available and well controlled immoblisation procedures are often required.[7–11] Recently, commercial cross-linked enzyme crystals (CLECs) have been introduced and these exhibit high activity, good stability and excellent reproducibility but are only currently available for certain enzymes.[12]‡ Here we demonstrate how enzyme preparations of very high activity can be rapidly and economically produced in a normal chemistry laboratory utilising a novel dehydration process.

The procedure employed is summarised in Fig. 1. The enzyme is first immobilised onto a support and for convenience we have used adsorption onto a standard silica chromatography gel.[13,14]§ For the enzymes tested the adsorption takes place quantitatively on stirring the protein with the silica in aqueous buffer solution at pH 7.8.¶ The immobilisation process disperses the biocatalyst over a large surface area and ensures good active site accessibility is obtained when the preparation is transferred to an organic solvent.‖ Following adsorption most of the aqueous solution is decanted from the silica–enzyme preparation ensuring the solid remains wetted. The key dehydration step is then achieved simply by rinsing the silica–enzyme preparation with successive aliquots of dry *n*-propanol, again keeping the solid wetted with solvent at all times. Where required, a final rinse with the reaction solvent of choice can be used to remove the propanol before the reactants are added. The propanol rinse rapidly removes water associated with the protein by a mechanism which minimises denaturation and appears to leave the majority of enzyme molecules in an active conformation. Ethanol and longer chain alcohols can also be used for the rinse, but methanol produces a much less active preparation.

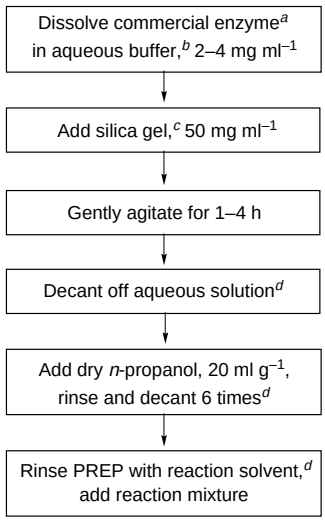

Fig. 1 Typical preparation of enzyme for use in organic solvent. [a] Highest purity available. [b] pH of maximum activity. [c] No special treatment required. [d] Ensure silica remains immersed.

The propanol rinsed enzyme preparations (PREPs) of subtilisin Carlsberg and α-chymotrypsin are found to exhibit very high activities in synthetically useful polar organic solvents such as acetonitrile (ACN) and THF.** Table 1 shows a comparison of the initial reaction rates obtained for a standard transesterification reaction in ACN using subtilisin Carlsberg prepared in different forms. At water levels of 1% (v/v) and above, the rates for the PREP are found to be comparable to the CLEC, and over 1000 times greater than the commonly used freeze-dried powders. Cross-linked enzyme crystals of chymotrypsin are not commercially available but under the same reaction conditions described in Table 1 the PREP of this enzyme exhibited transesterification activities of 21 and 131 nmol mg^{-1} min^{-1} in ACN, containing 1 and 4.5% v/v water, respectively. Again this is two orders of magnitude better than the freeze-dried powder.

If the PREP is removed from propanol and dried in air prior to assaying in the organic solvent most of the activity is lost and the residual level approaches that obtained for the lyophilised powder (see Table 1). However, aqueous suspensions of the silica adsorbed enzymes can be stored in the fridge for at least

Table 1 Effect of preparation type on subtilisin Carlsberg activity. Reaction conditions: 10 mM *N*-acetyl-L-tyrosine ethyl ester, 1 M propan-1-ol, in ACN containing water added as shown (% v/v). The mixture was incubated at 24 °C with constant reciprocal shaking (150 min^{-1}). Samples were analysed by HPLC on a Gilson 715 equipped with an ODS2 reversed phase column (Hichrom)

	Rate[a]/nmol mg^{-1} min^{-1}		
Enzyme form	0% H_2O v/v in ACN[b] (a_w < 0.01)	1% H_2O v/v in ACN (a_w = 0.22)	4.5% H_2O v/v in ACN (a_w = 0.55)
Freeze-dried powder	< 0.01	0.13	0.28
Cross-linked crystal (CLEC)	226	172	105
Propanol rinsed (PREP)	0.82	142	124
Propanol rinsed, air dried[c]	—	0.60	—

[a] mg refers to weight of enzyme in preparation. [b] Water content of dry ACN was < 0.007% v/v. [c] Sample prepared as in Fig. 1, placed in sealed jar over molecular sieves for 3 days, then equilibrated for a further 3 days over H_2O-saturated potassium acetate (a_w = 0.22).

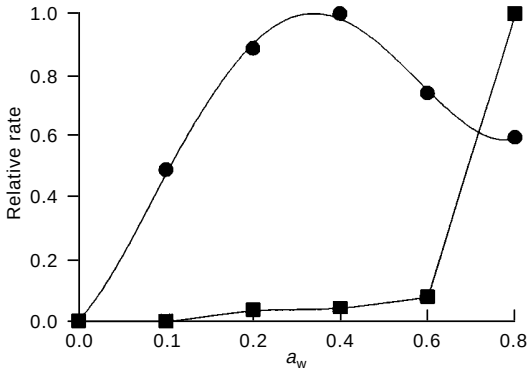

Fig. 2 Relative rate as a function of a_w for the transesterification reaction catalysed by subtilisin PREP (●) and freeze dried subtilisin Carlsberg (■). Rates for each preparation were normalised relative to the maximum value. These were 159.7 nmol mg^{-1} min^{-1} at a_w of 0.44 for the PREP and 3.3 nmol mg^{-1} min^{-1} at a_w of 0.76 for the freeze-dried powder. Reaction conditions as for Table 1.

3 weeks with negligible loss of activity and converted to the PREP as required.

It is perhaps surprising the method described here for preparing biocatalysts for reactions in low water media has not been reported previously. However, until recently the large hydration hysteresis effects obtainable with enzymes had not been fully recognised.[15,16] This work and that previously with CLECs[15] has shown that different methods of water removal can dramatically affect the enzyme activity obtained. Two possible explanations are (*i*) different dehydration protocols effect the amount of water left bound to the enzyme, or (*ii*) the conformation of the dried enzyme is very sensitive to the method of water removal. Most probably these two effects are intimately related.

According to previous studies the amount of water bound to a protein in solvent would be expected to be controlled by the thermodynamic water activity, a_w.[17,18] We therefore compared the catalytic activities of a freeze-dried powder and a PREP of subtilisin as a function of this parameter. Under these conditions differences in the amount of residual bound water should be eliminated and hence similar rate *vs*. a_w profiles might be expected for the PREP and powder. As can be seen in Fig. 2 this is not the case. The activity of the lyophilised powder continues to increase even up to a_w 0.76 while a maximal but much higher rate is obtained with the subtilisin PREP at a_w 0.44.†† Note that since the activity per unit weight of enzyme is much lower in the lyophilised powder (see Table 1), the rate profiles for the two preparations compared in Fig. 2 are relative rates normalised to the maximum value.

The different rate profiles could arise because the two forms of the enzyme differ in either water binding or the water required for catalytic activity. A large difference in water binding isotherms is unlikely, but kinetic factors may be significant. The water content of the lyophilised powder will be determined by its adsorption isotherm. In contrast, the treatment of the PREP imposes a water desorption process, for which the isotherm will be different due to hysteresis, and even the apparent equilibrium value may not be reached in the time allowed. An alternative hypothesis is that the PREP requires less water because the propanol dehydration process leaves a large proportion of the enzyme molecules in a conformation close to the active form. Only low levels of water may then be needed to promote catalysis and further increases in water availability provide no beneficial effect. With the dry freeze-dried powder the very low rates suggest most of the enzyme is initially inactive. In this case a water catalysed reorganisation process is probably required to convert the enzyme back to an active state since much greater water levels are needed to obtain high activity. The difference in profiles in Fig. 2 therefore reflects the fact that water plays different roles in promoting enzyme catalysis depending on the hydration history of the system.

We have shown here that very high activity propanol rinsed enzyme preparations (PREPs) can be obtained with both subtilisin Carlsberg and α-chymotrypsin, enzymes with very different secondary and tertiary protein structures. This suggests the procedure may find widespread application as a simple and economical way of preparing biocatalysts for reactions in organic media.

We would like to thank the BBSRC for funding this work.

Notes and References

† E-mail: j.partridge@strath.ac.uk

‡ Other enzyme forms recently reported to exhibit high activity in organic media include enzymes entrapped in sol-gels[19] and dissolved enzymes.[20]

§ Silica gel was Sigma S-0507, 230–400 mesh, 60 Å pores.

¶ The adsorption pH used corresponds to the optimum activity of the enzymes in aqueous solution. Typical adsorption conditions used; 20 ml of subtilisin Carlsberg (2 mg ml^{-1}) in 20 mM sodium phosphate buffer, pH 7.8, was mixed with 1 g of silica gel and the mixture shaken for 1 h at 25 °C. 20 ml of α-chymotrypsin (4 mg ml^{-1}) in 25 mM tris buffer, pH 7.8, containing 10 mM calcium chloride (to minimise autolysis) was shaken for 4 h at 25 °C. After mixing the adsorbed enzymes were stored in aqueous buffer at 4 °C.

‖ Since enzymes are generally insoluble in most organic solvents a heterogeneous reaction mixture is obtained and diffusion limitations can become important.

** It is often useful to carry out reactions at known thermodynamic water activity, a_w.[18] In polar solvents, in order to achieve a fixed a_w, a known concentration of water can be conveniently added to the system.[21] For ACN, a_w values of 0.11, 0.22, 0.44, 0.55 and 0.76 can be achieved by adding 0.5, 1.0, 2.7, 4.5 and 13% water (v/v) to the solvent.

†† Similarly, for freeze-dried chymotrypsin the rate increases with a_w, whereas an optimum rate is achieved at a_w of 0.55 for the PREP of this enzyme. The shift in rate *vs*. a_w for the chymotrypsin PREP in comparison to subtilisin PREP is interesting. This is also apparent when comparing profiles for the lyophilised powders of the two enzymes.

1 C. R. Wescott and A. M. Klibanov, *Biochim. Biophys. Acta*, 1994, **1206**, 1.
2 J. Broos, J. F. J. Engbersen, I. K. Sakodinskaya, W. Verboom and D. N. Reinhoudt, *J. Chem. Soc., Perkin Trans.* 1, 1995, 2899.
3 J. O. Rich and J. S Dordick, *J. Am. Chem. Soc.*, 1997, **119**, 3245.
4 G. A. Hutcheon, M. C. Parker, A. James and B. D. Moore, *Chem. Commun.*, 1997, 931.
5 K. Dabulis and A. M. Klibanov, *Biotechol. Bioeng.*, 1993, **41**, 566.
6 O. Almarsson and A. M. Klibanov, *Biotechnol. Bioeng.*, 1996, **49**, 87.
7 A. O. Triantafyllou, D. B. Wang, E. Wehtje and P. Adlercreutz, *Biocat. Biotrans.*, 1997, **15**, 185.
8 Z. Yang, A. J. Mesiano, S. Venkatasubramanian, S. H. Gross, J. M. Harris and A. J. Russell, *J. Am. Chem. Soc.*, 1995, **117**, 4843.
9 E. Wehtje, P. Adlercreutz and B. Mattiasson, *Biotechnol. Bioeng.*, 1993, **41**,171.
10 J. F. Diaz and K. J. Balkus, *J. Mol. Cat.*, 1996, **2**, 115.
11 M. T. Reetz, A. Zonta, A. and J. Simpelkamp, *Biotechnol. Bioeng.*, 1996, **49**, 527.
12 Y. F. Wang, K. Yakovlevsky and A. L. Margolin, *Tetrahedron Lett.*, 1996, **37**, 5317.
13 T. Zoungrana, G. H. Findenegg and W. Norde, *J. Colloid Interface Sci.* 1997, **190**, 437.
14 V. M. Stepanov, E. Y. Terenteva, T. L. Voyushina and M.Y. Gololobov, *Bioorg. Med. Chem.*, 1995, **3**, 479.
15 J. Partridge, G. A. Hutcheon, B. D. Moore and P. J. Halling, *J. Am. Chem. Soc.*, 1996, **118**, 12 873.
16 F. X. Yang and A. J. Russell, *Biotechnol Bioeng.*, 1996, **49**, 700.
17 G. A. Hutcheon, P. J. Halling and B. D. Moore, *Methods Enzymol.*, 1997, **286**, 465.
18 G. Bell, P. J. Halling, B. D. Moore, J. Partridge and D. G. Rees, *Trends Biotechnol.*, 1995, **13**, 468.
19 S. Sato, T. Murakata, M. Ochifuji, M. Fukushima and T. Suzuki, *J. Chem. Eng. Jpn.*, 1994, **27**, 732.
20 V. M. Paradkar and J. S. Dordick, *J. Am. Chem. Soc.*, 1994, **116**, 5009.
21 G. Bell, A. E. M. Janssen and P. J. Halling, *Enzyme Microb. Technol.*, 1997, **20**, 471.

Received in Liverpool, UK, 14 January 1998; 8/00408K

Solid state polymerization of the unsymmetrical [1]ferrocenophane Fe(η-C_5H_4)$_2$SiMePh; synthesis of the first stereoregular organometallic polymer

John Rasburn, Daniel A. Foucher, William F. Reynolds, Ian Manners*† and G. Julius Vancso*‡

Department of Chemistry, University of Toronto, 80 St. George St., Toronto, Ontario M5S 3H6, Canada

Solid state polymerization of the [1]ferrocenophane Fe(η-C_5H_4)$_2$SiMePh yields a stereoregular poly(ferrocenylmethylphenylsilane), the first example of a stereoregular organometallic polymer.

Although stereoregular organic polymers (*e.g.* isotactic or syndiotactic polypropylene) are well studied materials of considerable industrial importance, stereoregular inorganic polymers are virtually unknown.[1] A rare recent report describes the preparation of poly(methylphenylsilane) [SiMePh]$_n$ using a chiral dehydrocoupling catalyst.[2] In this case the tacticity was not deduced unequivocally, but a syndiotactic microstructure was tentatively proposed on the basis of NMR data. Here, we report the first synthesis of a stereoregular organometallic polymer using the technique of solid-state polymerisation.

Owing to the possibility of accessing processable materials with novel electronic and optical properties, the synthesis and study of inorganic and organometallic polymers has attracted increasing recent interest.[3] Significant among these are the poly(ferrocenylsilanes), unusual polymers with a main-chain comprising alternating ferrocene and organosilane units.[4] A common method of polymerisation involves thermal ring-opening polymerization (ROP) of strained, silicon-bridged [1]ferrocenophanes to give high molecular mass materials (M_w = 10^5–10^6 Da).[5–10] More recently, anionic and transition metal catalyzed ROP has also been reported.[11] However, by analogy with the well known case of the topotactic polymerisation of trioxane and tetroxane to produce polyoxymethylene,[12–14] strained [1]ferrocenophanes would also seem to be excellent candidates for topotactic or solid-state polymerisation. Indeed, recently we showed that the symmetrically substituted [1]ferrocenophane Fe(η-C_5H_4)$_2$SiMe$_2$ yielded a high-molecular-weight poly(ferrocenyldimethylsilane) [Fe(η-C_5H_4)$_2$SiMe$_2$]$_n$ with properties similar to the thermally ring-opened materials on ^{60}Co γ-irradiation of symmetrically-substituted monomer crystals.[15] Nevertheless, important issues such as whether the reaction was topotactic remained open.

To gain further insight, we have investigated the use of an unsymmetrically-substituted [1]ferrocenophane monomer, Fe(η-C_5H_4)$_2$SiMePh **1**.[16] The resulting microstructure can be examined by solution NMR and hence represents an alternative approach to reliance on X-ray scattering methods, although not as detailed. In the reaction scheme (Scheme 1) **2a** refers to the solid-state polymerised polymer, to be compared with **2b**, the thermally ring-opened material.

For our study, large maroon single-crystals of **1** were synthesised as described previously,[10] purified by repeated high-vacuum sublimations, and then sealed (0.65 g) in a Pyrex tube. The crystal structure of this monomer is well established.[16] The tube was then irradiated *via* placement close to a ^{60}C γ-ray source at 25 °C at 0.71 MRad for 24 h (for a total dosage of 17 MRad). On removal from the source, the temperature was measured to be 38 °C, well below the melting temperature of the crystals.[10,16] Any post-irradiation heat-treatment was avoided. The tube was then returned to the N_2 atmosphere and the contents extracted with an excess of

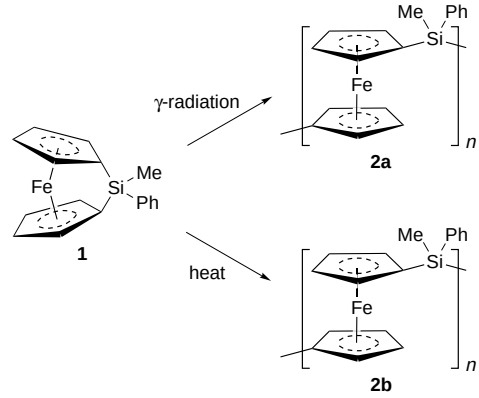

Scheme 1

hexanes to remove unreacted monomer and oligomeric species. The product **2a** was obtained as 0.30 g (46%) of yellow–orange platelets on which the original superstructure of the monomer crystals could be vaguely discerned. The platelets could be teased apart into fibrils. For solution NMR analysis, the product was purified by reprecipitation from THF into chilled *n*-propanol to give a pale yellow powder (M_w was determined to be 90 000 Da with a polydispersity of 1.4 by gel permeation chromatography *vs.* polystyrene standards). The thermally ring-opened polymer **2b** was synthesised as described previously.[10]

Wide-angle X-ray analysis of **2a** revealed three main scattering peaks at d = 7.81, 5.69 and 4.26 Å, all rather broad and suggestive of small and imperfect crystallites. By contrast, samples of **2b** give broad and featureless amorphous halos characteristic for this amorphous polymer. This suggested a different and more regular stereochemistry for **2a** compared to **2b**. Moreover, conspicuous differences in the ^{1}H and ^{13}C NMR spectra were evident when the solid state polymerized material **2a** was compared with the thermally generated product **2b**. In both the ^{1}H and the ^{13}C NMR spectra the methyl resonance of **2a** was a singlet. This implies stereoregularity when compared to the three observed resonances for **2b** where the approximate 1 : 2 : 1 intensity ratio can be assigned to mm (or rr), mr/rm, and rr (or mm) triads for an atactic polymer [see Fig. 1(*b*) *cf.* 1(*d*) and 2(*c*) *cf.* 2(*f*), respectively].[17] Similarly, the observed ^{1}H NMR resonances for the cyclopentadienyl group for **2a** [shown in Fig. 1(*a*)] constitute a subspectrum of that of **2b** [Fig. 1(*c*)]. Interestingly, the *ipso*-carbon atoms in the cyclopentadienyl groups show tetrad resolution with six ^{13}C NMR resonances in Fig. 2(*e*). In striking contrast, only one of the tetrad sequences is present in **2a** [Fig. 2(*b*)].[17,18]

The actual tacticity of **2a** (syndiotactic or isotactic) has not yet been definitively elucidated. The assignment is not straightforward, particularly as there is negligible *J*-coupling across the iron centres, and therefore some interpretation of the chemical shifts or dipolar couplings in terms of likely rotational isomeric states is required.[17,18] However, we tentatively assign

a syndiotactic architecture. Thus, for the melt polymerized polymer **2b** although atactic triads (mr/rm) clearly predominate, syndiotactic triads (mm§) would be expected to be slightly more favoured than isotactic triads (rr§) based on steric arguments. This suggests the assignment of the ^{1}H NMR resonances at δ 0.772 in Fig. 1(*d*) and the ^{13}C NMR resonance at δ −3.17 in Fig. 2(*f*) to syndiotactic (mm) triads. Consideration of Fig. 1(*b*) *cf.* 1(*d*) and 2(*c*) *cf.* 2(*f*) shows that the ^{1}H and ^{13}C NMR resonances assigned to the methyl groups of **2a** correspond to these resonances of **2b** which we tentatively assign to syndiotactic triads.

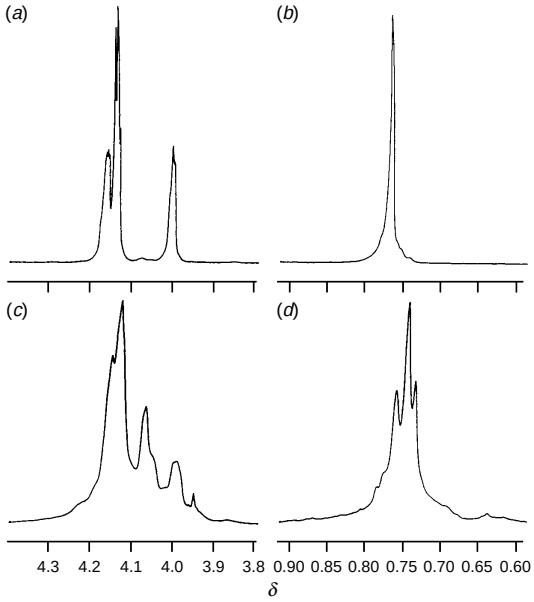

Fig. 1 ^{1}H NMR spectra (300 MHz, C_6D_6, 20 °C) of **2a** [(*a*), (*b*)] and **2b** [(*c*), (*d*)]. Spectra (*a*) and (*c*) compare cyclopentadienyl resonances, and (*b*) and (*d*) methyl resonances.

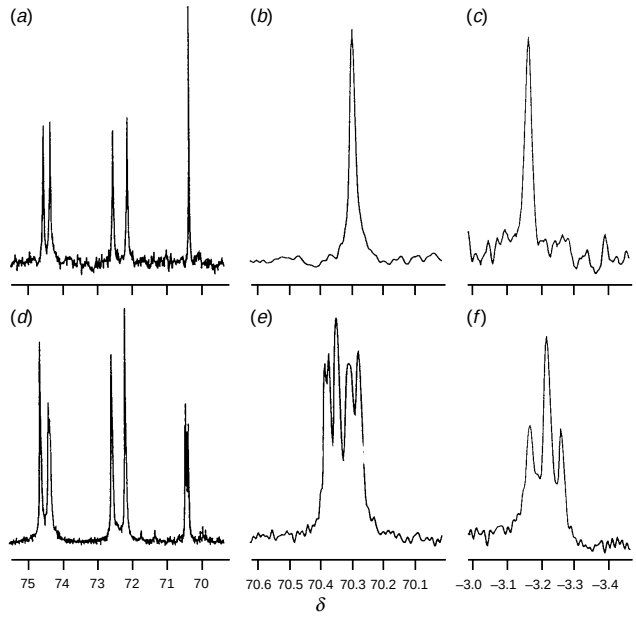

Fig. 2 Quantitative ^{13}C NMR spectra (75 MHz, C_6D_6, 20 °C) of **2a** [(*a*)–(*c*)] and **2b** [(*d*)–(*f*)]. Spectra (*a*) and (*d*) show resonances for cyclopentadienyl carbons, (*b*) and (*e*) show resonances for *ipso* cyclopentadienyl carbons, and (*c*) and (*f*) show resonances for methyl carbons.

Further work is aimed at definitively determining the stereochemistry of **2a** (isotactic or syndiotactic) as well as obtaining further insight into the kinetics and topotaxis of this novel solid-state reaction.

The authors would like to thank Dr J. K. Pudelski for provision of the thermally polymerised polymer sample. G. J. V. and I. M. are grateful to the Natural Science and Engineering Research Council (NSERC) and Institute for Chemical Sciences and Technology (ICST) for funding this research. I. M. also thanks NSERC for an E. W. R. Steacie Fellowship (1997–99), the Alfred P. Sloan Foundation for a Fellowship (1994–98), and the University of Toronto for a McLean Fellowship (1997–2003).

Notes and References

† E-mail: imanners@alchemy.chem.utoronto.ca
‡ Present address: University of Twente, Department of Chemical Technology, Drienerlo Laan 5, NL 7522 NB Enschede, The Netherlands.
§ For an isotactic poly(ferrocenylsilane) (*i.e.* a chain comprising repeat units of identical stereochemistry) inspection of the asymmetic center by Newman projections from within a given dyad indicates that both have the same handedness and hence isotactic dyads are r and syndiotactic dyads are m, in contrast to the situation with vinyl and silane polymers.

1 H. H. Brintzinger, D. Fischer, R. Mülhaupt, B. Rieger and R. M. Waymouth, *Angew. Chem., Int. Ed. Engl.*, 1995, **34**, 1143.
2 J. P. Banovetz, K. M. Stein and R. M. Waymouth, *Organometallics*, 1991, **10**, 3430.
3 I. Manners, *Angew. Chem., Int. Ed. Engl.*, 1996, **35**, 1602.
4 I. Manners, *Adv. Organomet. Chem.*, 1995, **37**, 131.
5 D. A. Foucher, B.-Z. Tang and I. Manners, *J. Am. Chem. Soc.*, 1992, **114**, 6246.
6 D. A. Foucher, R. Ziembinski, B.-Z. Tang, P. M. Macdonald, J. Massey, C. R. Jaeger, G. J. Vancso and I. Manners, *Macromolecules*, 1993, **26**, 2878.
7 M. T. Nguyen, A. F. Diaz, V. V. Dement'ev and K. H. Pannell, *Chem. Mater.*, 1993, **5**, 1389; M. Hmyne, A. Yasser, M. Escorne, A. Percheron-Guegan and F. Garnier, *Adv. Mater.*, 1994, **6**, 564.
8 S. Barlow, A. L. Rohl, S. Shi, C. M. Freeman and D. O'Hare, *J. Am. Chem. Soc.*, 1996, **118**, 7578.
9 A. G. Osborne, R. H. Whiteley and A. E. Meads, *J. Organomet. Chem.*, 1980, **193**, 345.
10 D. A. Foucher, R. Ziembinski, R. Petersen, J. K. Pudelski, M. Edwards, Y. Ni, J. Massey, C. R. Jaeger, G. J. Vancso and I. Manners, *Macromolecules*, 1994, **27**, 3992.
11 R. Rulkens, A. J. Lough and I. Manners, *J. Am. Chem. Soc.*, 1994, **116**, 797; Y. Ni, R. Rulkens and I. Manners, *J. Am. Chem. Soc.*, 1996, **118**, 4102; P. Gómez-Elipe, P. M. Macdonald and I. Manners, *Angew. Chem., Int. Ed. Engl.*, 1997, **36**, 762.
12 M. Thakur, *Solid-state Polymerisation* in *Encyclopaedia of Polymer Science and Engineering*, ed. J. I. Kroshwitz, Wiley, New York, 1989, vol. 15.
13 J. Schultz, *Polymer Materials Science*, Prentice-Hall Inc., New Jersey, 1975, ch. 2, p. 113.
14 Y. Chatani, T. Uchida, H. Tadokoro, K. Hayashi, M. Nishi and S. Okamura, *J. Macromol. Sci. B: Phys.*, 1968, **2**, 567.
15 J. Rasburn, R. Petersen, T. Jahr, R. Rulkens, I. Manners and G. J. Vancso, *Chem. Mater.*, 1995, **7**, 871.
16 D. A. Foucher, A. J. Lough, I. Manners, J. Rasburn and G. J. Vancso, *Acta. Crystallogr., Sect. C*, 1995, **51**, 580.
17 F. A. Bovey, *High Resolution NMR of Macromolecules*, Academic Press, New York, 1972.
18 A. E. Tonelli, *NMR and Polymer Microstructure: The Conformational Connection*, VCH, New York, 1989.

Received in Bath, UK, 5th February 1998; 8/01042K

$[NBu^n_4]_4[(Re_6S_5OCl_7)_2O]$, an oxo-bridged siamese twin cluster of two hexanuclear oxochalcohalide rhenium clusters

Falk Simon, Kamal Boubekeur, Jean-Christophe P. Gabriel and Patrick Batail*†

Institut des Matériaux de Nantes, UMR 6502 CNRS-Université de Nantes, 2, rue de la Houssinière, 44322 Nantes, France

A report of the solid state synthesis and X-ray crystal structure analysis of $[NBu^n_4]_4[(Re_6S_5OCl_7)_2O]$, the first oxo-bridged, tetravalent hexanuclear oxochalcohalide rhenium cluster.

The potassium and rubidium salts of hexanuclear chalcohalide rhenium clusters, $M[Re_6(Q_5Cl_3)Cl_6]$ (M = Rb, Q = S; M = K, Q = Se), obtained from high temperature solid state reactions, are soluble in a variety of organic solvents,[1] and have been shown to be splendid starting materials for a variety of heterosubstituted or functionalized rhenium clusters.[2–5] These reactions, performed at room temperature and in organic solvents, always lead to the cluster dianions, $[NBu^n_4]_2[Re_6(Q^i_5E^iCl^i_2)Cl^a_6]^{2-}$ (E = O, S, Se, Te, NH, NMe, NBz), and involve the substitution of one of the μ_3-face-capping chloride ligand of the Re_6L_8 cluster core in $[NBu^n_4][Re_6(Q_5Cl_3)Cl_6]$ (Q = S, Se), with a divalent anion or its synthetic equivalent, for example the silylated main group reagents $E(SiMe_3)_2$.[4,5] We now report a novel high temperature solid state reaction, in the presence of minute amounts of water which (*i*) achieves the concomitant solid state synthesis and former transformation of the cluster monoanion form into the corresponding dianion upon a single core ligand substitution, and (*ii*) involves a single apical-chloride displacement and a subsequent linkage of two clusters across an oxo-bridge, both unprecedented in this chemistry.

The compound $[NBu^n_4]_4[(Re_6S_5OCl_7)_2O]$ was synthesized by mixing Re (206 mg, 1.11 mmol), $ReCl_5$ (200 mg, 0.55 mmol), KCl (30 mg, 0.40 mmol) and S (35 mg, 1.09 mmol) in an inert gas atmosphere. The powder was then pressed into a pellet and placed in a silica tube (inner diameter 10 mm, external diameter 12 mm; *ca*. 105 mm long), into which H_2O (0.014 ml, 0.78 mmol) was carefully condensed (the hydrolysis of $ReCl_5$ leads to the formation of $HReO_4$, ReO_2 and HCl).[6] After 10 min the system was evacuated to 10^{-2} Torr, sealed and heated for 4 days at 850 °C in a furnace, using a 30 °C h^{-1} rate for heating and cooling ramps. The crude material was washed with water and dissolved in ethanol. An ethanolic solution of NBu^n_4Cl was then added, forming rapidly an orange precipitate, which was recrystallized from acetone to give 470 mg of dark red crystals [Yield = 42% (based on Re). Anal. for $C_{64}H_{144}Cl_{14}N_4O_3S_{10}Re_{12}$. Calc. C, 18.89; H, 3.57; N, 1.38; Cl, 12.20; S, 7.88. Found: C, 16.95; H, 3.10; N, 1.33; Cl, 12.21; S, 8.13%].

The structure was solved by single crystal X-ray diffraction.‡ The asymmetric unit contains one cluster tetra-anion and four tetrabutylammonium cations. The cluster anion (Fig. 1) consists of two identical $[Re_6(S_5OCl_2)]^{4+}$ cores linked by an apical oxygen ligand [O(2)], the ten other apical positions being occupied by chlorine atoms. Thus, the charge of each cluster moiety is 2−. The average rhenium to apical chloride bond length (Re–Cl^a, where Cl^a denotes such a chlorine atom in Schäfer's notation)[7] is 2.380(4) Å [range 2.367(4)–2.389(3) Å], as expected for a cluster dianion.[3,4] The Re–Q distances observed for the μ_3-bridging, disordered Cl and S inner atoms (Q = S^i, Cl^i) are in the range of 2.385(3)–2.450(3) Å, whereas the μ_3-bridging oxo ligands are much closer to the Re atoms [2.090(7)–2.105(8) Å]. This distance is similar to that found in the oxygen substituted cluster, $[NBu^n_4]_2[Re_6S_5OCl_8]$ [average Re–(S^i, Cl^i) 2.415(11) Å, Re–O 2.087(6) Å].[4] It is important to note that there is no evidence for disorder in the position of the oxo ligands, a rare event in this type of chemistry.[4,5] Finally, the rhenium octahedra are slightly distorted, a manifestation of the closer approach of the face capping oxo ligand, consistent with the shortening of the Re–Re bond lengths observed for rhenium octahedra when one goes from the Re–Se–Cl to Re–S–Cl system.[3,8,9] In the structure of $[NBu^n_4]_4[(Re_6S_5OCl_7)_2O]$, the three rhenium atoms capped by the μ_3-oxo ligands have regular Re–Re distances [$< d_{Re-Re} >$ = 2.530(6) Å], whereas the opposing triangular Re_3 face is also regular, $< d_{Re-Re} >$ = 2.595(8) Å, but with Re–Re distances similar to those observed in all hexanuclear clusters in the Re–S–Cl system.[3,9] The remaining Re–Re bond lengths, that connect these two Re_3 triangles, are intermediate to the two former, $< d[Re_3(O)–Re_3(S)] >$ = 2.585(8) Å, very close to the barycentre calculated as [(2.530 × 1 + 2.595 × 7)/8] = 2.587 Å.

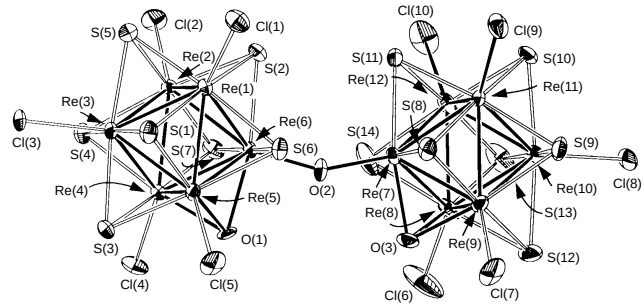

Fig. 1 ORTEP drawing and numbering scheme for the cluster $[(Re_6S_5OCl_7)_2O]^{4-}$ in $[NBu^n_4]_4[(Re_6S_5OCl_7)_2O]$. The thermal ellipsoids are drawn at the 50% probability level. Face-capping ligands S are composite S/Cl atoms (ratio: 5/2), the two face-capping O ligands are located. The cluster molecule is totally asymmetric. The relevant bond lengths are described in the text.

The present oxo-bridged siamese twin cluster compound differs from $[Re_{12}Se_{16}(PEt_3)_{10}][SbF_6]_4$, which was recently reported by Zheng *et al.*,[10] since, in the latter case, the two rhenium clusters are connected *via* two bonds, one Re–Se^{a-i} and the other Re–Se^{i-a}, in a similar fashion to the Chevrel phases.[11] The novel class of solid state reaction disclosed in this work opens the way for an infinite oxo-bridged cluster polymer.

F. S. thanks the Région Pays de Loire for a Post-Doctoral fellowship.

Notes and References

† E-mail: patrick.batail@cnrs-imn.fr

‡ *Crystal structure analysis* for $[NBu^n_4]_4[(Re_6S_5OCl_7)_2O]$: A dark red crystal (0.25 × 0.15 × 0.20 mm) of the title compound was selected for X-ray diffraction analysis and mounted on a Stoe IPDS single ϕ-axis diffractometer with a 2D area detector based on imaging plate technology. 289 images (frames) were recorded at 150 K using the rotation method ($0 \leqslant \phi \leqslant 260.1°$) with $\Delta\phi$ = 0.9° increments, an exposure time of 3 min and a crystal-to-plate distance of 60 mm (program EXPOSE).[12] The images were processed with the suite of programs provided by Stoe (DISPLAY, INDEX, PROFILE, INTEGRATE).[12] *Crystal data* for $C_{64}H_{144}Cl_{14}N_4O_3Re_{12}S_{10}$, *M* = 4069.13, *F*(000) = 7512, monoclinic, space group $P2_1/c$ (no. 14),

a = 24.378(3), b = 18.025(2), c = 24.044(3) Å, β = 93.69(1)°, U = 10544(2) Å^3, Z = 4, graphite monochromated Mo-Kα radiation (λ = 0.710 73 Å), T = 150 K, D_c = 2.563 Mg m^{-3}; 132 608 reflections measured (3.8 ⩽ 2θ ⩽ 56.3°; −32 ⩽ h ⩽ 31, −23 ⩽ k ⩽ 23, −31 ⩽ l ⩽ 31), 25 138 were unique (R_{int} = 0.093) and 13 071 have $I > 2\sigma(I)$, no decay was observed. Corrections were made for absorption [μ(Mo-Kα) = 14.3 mm^{-1}] by empirical methods (max. and min. transmission 0.2033 and 0.0690). The structure was solved by direct methods (SHELXS-86)[13] and subsequent Fourier difference techniques and refined by full-matrix least squares, on F^2 (program SHELXL-93).[14] All non-hydrogen atoms were refined anisotropically except for a few carbon atoms for which thermal motion precluded such refinement. The positions of the H atoms were calculated for idealized positions. The final $wR(F^2)$ was 0.0777, with conventional $R(F)$ = 0.0373 (R factors defined in ref. 14), for 909 parameters, GOF = 0.629, $w^{-1} = \sigma^2(F_o^2) + (0.0001\,p)$,[2] where p = [max $(F_o^2, 0) + 2\,F_c^2)/3$], $(\Delta/\sigma)_{max}$ = 0.000. Minimum and maximum $\Delta\rho$ were −4.047 and 3.285 e Å^{-3}, respectively, in the vicinity of Re atoms. The cluster core face-capping chlorine and sulfur atoms were disordered and were refined as sulfur atoms. CCDC 182/790.

1 P. Batail, L. Ouahab, A. Pénicaud, C. Lenoir and A. Perrin, *C. R. Acad. Sci., Ser. 2*, 1987, **304**, 1111.
2 O. M. Yaghi, M. J. Scott and R. H. Holm, *Inorg. Chem.*, 1992, **31**, 4778.
3 J.-C. Gabriel, K. Boubekeur and P. Batail, *Inorg. Chem.*, 1993, **32**, 2894.
4 S. Uriel, K. Boubekeur, P. Batail, J. Orduna and E. Canadell, *Inorg. Chem.*, 1995, **34**, 5307.
5 S. Uriel, K. Boubekeur, P. Batail and J. Orduna, *Angew. Chem., Int. Ed. Engl.*, 1996, **35**, 1544.
6 F. A. Cotton and G. Wilkinson, *Advanced Inorganic Chemistry*, Wiley, New York, 5th edn., 1988.
7 H. Schäfer and H. G. von Schnering, *Angew. Chem.*, 1964, **20**, 833.
8 K. Boubekeur, PhD Thesis, Université de Rennes I, 1989.
9 C. B. Guilbaud, J.-C. P. Gabriel, K. Boubekeur and P. Batail, unpublished work.
10 Z. Zheng, J. R. Long and R. H. Holm, *J. Am. Chem. Soc.*, 1997, **119**, 2163.
11 R. Chevrel, M. Sergent and J. Prigent, *J. Solid State Chem.*, 1971, **3**, 515.
12 Stoe IPDS Software manual V2.75, Stoe & Cie, Darmstadt, 1996.
13 G. M. Sheldrick, SHELXS 86, Program for structure solution, University of Göttingen, 1986.
14 G. M. Sheldrick, SHELXL 93, Program for structure refinement, University of Göttingen, 1993.

Received in Basel, Switzerland 2nd December 1997; date accepted 13th February 1998; 8/01260A

A unique and highly facile method for synthesising disulfide linked neoglycoconjugates: a new approach for remodelling of peptides and proteins

Wallace M. Macindoe, Anita H. van Oijen and Geert-Jan Boons*

School of Chemistry, The University of Birmingham, Edgbaston, Birmingham, UK B15 2TT

An asymmetric disulfide linkage, formed by conjugation of a 5-nitropyridine-2-sulfenyl activated thioglycoside and a protein or pre-assembled peptide sequence, represents a good structural mimic of natural asparagine glycosylation.

Most eukaryotic cellular proteins with the exception of some hormones and enzymes are reliant on the sugar units bound to them to confer a broad range of important biological functions, including immunogenicity, solubility, recognition, protection from proteolytic attack, and induction and maintenance of the protein conformation in a biologically active form.[1] The biosynthesis of *N*-linked glycoproteins is complex and results in micro-heterogeneity in the carbohydrate structure (formation of glycoforms).[2] Several studies have highlighted that each glycoform should be seen as a unique population of molecular species with particular biological properties.[3]

Much effort has been directed to alter the constitution of the carbohydrate protion of particular glycoproteins.[4] Saccharide glycoprotein remodelling (GPR) originally relied on cumbersome and inefficient means of adding carbohydrate structures, either by chemical or enzymatic methods, to proteins.[5] This approach has been supplanted by a technique using recombinant proteins to alter the intrinsic glycosylation pattern of cells.[6] However, the drawback of this technology is that it has the propensity to produce either inactive, undesired or missing glycoforms as part of the protein product.[7]

We report here an approach to the GPR problem which is based on asymmetric disulfide conjugation (an S–S glycosidic linkage) between a 5-nitropyridine-2-sulfenyl activated thioglycoside (*e.g.* **3**, Scheme 1) and a protein or pre-assembled peptide sequence having its natural asparagine glycosylation site replaced with a cysteine residue (R′SH). The merit of such an asymmetric disulfide linkage is that it represents a good structural mimic for natural *N*-linked glycoproteins[9] since the disulfide linkage is flexible enough to adopt conformations imposed by natural amide linkages at glycosylation sites.[10]

The synthesis of compound **3** was executed in five steps (25% yield overall) from commercially available *N*-acetylglucosamine *via* a modified procedure precedent for preparing 2-acetamido-2-deoxy-1-thio-β-D-glucose **2**.[11] Compound **1** decomposed during both Zemplén and KOBu^t mediated deacetylation conditions, but quantitatively gave thiol sugar **2** by a mild saponification procedure (Et_3N–MeOH–H_2O). The 5-nitropyridine-2-sulfenyl (pNpys) function was easily introduced onto mercapto-sugar **2** by treating the latter with 2,2′-dithiobis(5-nitropyridine) (DTNP) in AcOH–water[12] to yield compound **3** in a satisfactory yield of 58%. We anticipate the synthesis to be amenable for preparing oligosaccharide analogues thereof as judged by the mildness of the procedure.

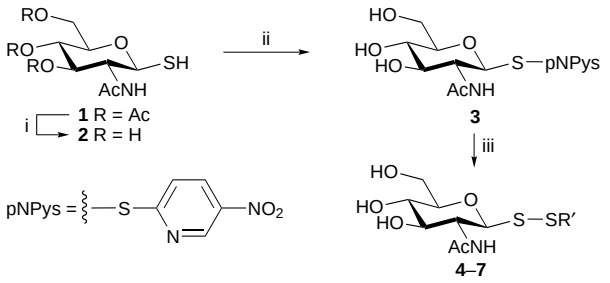

Scheme 1 *Reagents and conditions*: i, Et_3N–MeOH–H_2O (2 : 5 : 5), 0.5 h, quant.; ii, DTNP, AcOH–water (12 : 1), 6 h, 58%; iii, R′SH, NH_4OAc (1 M) pH 5, 2–15 min

The activated thio-*N*-acetylglucosamine **3** under mild buffered conditions (1 M NH_4OAc, pH 5) is able to form asymmetric disulfide conjugates with a variety of free thiol-containing substrates. Reaction times are in the range of 2–15 min and yields are quantitative with excesses of **3** (*e.g.* product **7**). The generality thus far encompasses peptide, protein and polymer substrates, as shown in Table 1. Certainly, model conjugate **6** is of high immunological importance, in that the pentapeptide moiety represents that of a human IgG2 sequence[13] with Cys in place of Asn-297. Unfortunately, the ^{1}H NOESY spectra of both conjugate **6** and the natural glycopentapeptide equivalent (in this case Cys is replaced by Asn and thus becomes a structural motif for the natural *N*-glucoasparagine linkage found in wild-type human IgG2) did not reveal any cross peaks between sugar-peptide protons. Therefore the structural similarities between the disulfide and natural amide glycopeptide linkages of the neoglycotripeptide AcPhe(1-thio-β-GlcNAc-1→*S*)CysSerNHCH$_3$ **8** were examined by molecular modelling. Thus, a starting structure of compound **8** was built based on the tripeptide moiety of the same IgG2 sequence[13] (*vide supra*) with Cys in place of Asn-297 [AcPhe(β-GlcNAc-1→*N*)AsnSerNHCH$_3$ **9**] and subjected to Monte Carlo multi-

Table 1 Generality of synthesis of disulfide linked neoglycoconjugates

Mole ratio **3**/R′SH	Product R′	Yield (%)
1 : 1	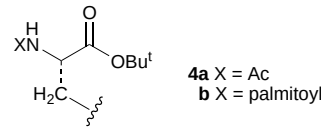 **4a** X = Ac **b** X = palmitoyl	53–65[a]
5 : 1	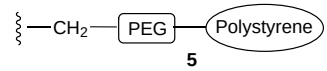 **5**	63[b]
2 : 1	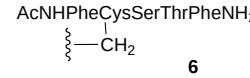 **6**	77
50 : 1	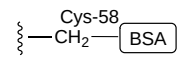 BSA = Bovine serum albumin **7**	quant.[c]

[a] Yields are representative for two different *N*-acylated cysteine derivatives prepared, X = Ac (65%) and X = Palmitoyl (53%). [b] Determined by the amount of **1** cleaved from the support (1,2-dithioerythritol–CH_2Cl_2) after treatment with Ac_2O–pyridine. [c] Absolute yield determined by HPAEC-PAD analysis of thio-*N*-acetylglucosamine **2** deconjugated from **7** using 1,2-dithioerythritol–water.

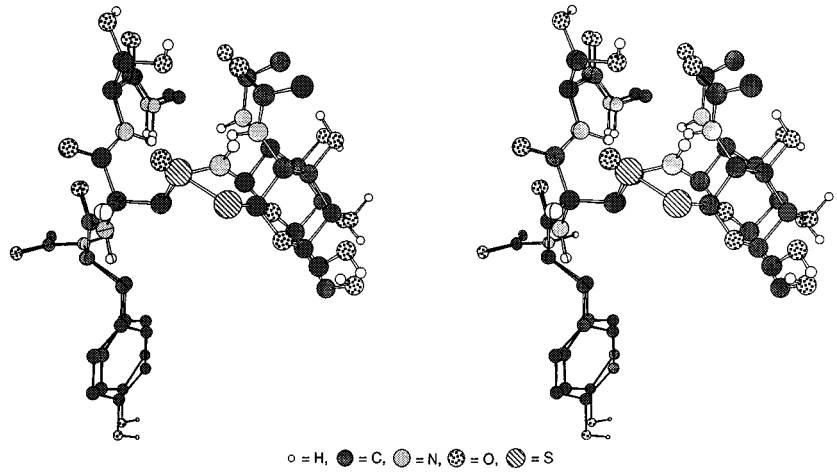

Fig. 1 Stereoviews showing superimposition of neoglycotripeptide **8** and neoglycotripeptide **9** as present in human IgG2

conformer analysis in combination with molecular mechanics calculations.[14] The global minimum of neoglycotripeptide **8** as well as all conformations lying within a 50 kJ mol^{-1} energy window were investigated using both filtering and clustering analysis resulting in families of conformers. Overlays of the resulting families of these conformations with glycopeptide **9** demonstrate that a similar spatial orientation as present at the glycosylation site of human IgG2[15] can be adopted by disulfide analogue **8** (see Fig. 1).

Bovine serum albumin (BSA) was chosen as a model protein on the merit of its availability and the convenience of having a single cysteinyl function at Cys-58 of its protein sequence. After 15 min of reacting **3** with BSA, the BSA-containing fractions were quickly isolated free from the excess amount of **3** and other low molecular weight thiol by-products (Sephadex G-15; eluent, water). Ellman analysis[16] of the isolated conjugate **7** against a blank sample of non-reacted BSA gave a zero absorbance reading at 412 nm, showing the conjugation to be complete. Further spectroscopic corroboration of conjugate **7** came from electrospray mass spectrometry. The mass increase for conjugate **7** over the BSA sample was 160 ± 100 while the theoretical difference is 235.[17]

The conjugate **7** was treated with a 50-fold excess of glutathione. After 7 days, the MALDI-TOF spectra of test sample aliquots showed only molecular ion peaks of the conjugate and no exchange products, which supports the idea that the disulfide bond contained in the conjugates are of considerable stability.

Currently, we are involved in the construction of an aglycosylated IgG recombinant antibody by site-directed mutagenesis which bears a cysteine residue in lieu of Asn-297. Covalent introduction of defined and activated oligosaccharide thiol derivatives will provide neoglycoconjugates that will enable us to study in detail the relationship between carbohydrate microstructure and biological properties of IgG molecules.

Financial support for this project was provided by the Engineering and Physical Sciences Research Council.

Notes and References

† E-mail: gjboons@chemistry.bham.ac.uk

1 A. Varki, *Glycobiology*, 1993, **3**, 97.
2 A. Kobata and S. Takasaki, in *Structure and Biosynthesis of Cell Surface Carbohydrates*, ed. M. Fukuda, CRC Press, London, 1992, pp. 1–24.
3 P. Knight, *Biotechnology*, 1989, **7**, 35.
4 I. Meynial-Salles and D. Combes, *J. Biotechnol.*, 1996, **46**, 1.
5 C. Roth-Robbins, *BioVenture View*, 1990, June/July, 25.
6 N. Jenkins and E. M. A. Curling, *Enzym. Microb. Technol.*, 1994, **16**, 354.
7 J. C. Paulson, *TIBS*, 1989, **14**, 272; R. B. Parekh, *Curr. Opin. Biotechnol.*, 1991, **2**, 730.
8 A. Wright and S. L. Morrison, *TIBTECH.*, 1997, **15**, 26.
9 In a similar approach, other workers have favored the attachment of iodoacetate-sugar derivatives to the cysteine residues of proteins: N. J. Davis and S. L. Flitsch, *Tetrahedron Lett.*, 1991, **32**, 6793. This approach however suffers the drawback that the resulting *N*-thioacetamide linkage is longer by a CH_2S group than the natural glycopeptide linkage; thus it can be anticipated that many of the protein–oligosaccharide interactions that would normally be in place will be annihilated.
10 A. Imberty and S. Pérez, *Protein Eng.*, 1995, **8**, 699.
11 B. Paul and W.Korytnyk, *Carbohydr. Res.*, 1984, **126**, 27.
12 F. Rabanal, W. F. DeGrado and P. L. Dutton, *Tetrahedron Lett.*, 1996, **37**, 1347.
13 L. Carayannopoulos and J. D. Capra, in *Fundamental Immunology*, ed. W. E. Paul, Raven Press, 1993, pp. 283–314.
14 Molecular modelling was carried out using MACROMODEL version 5.0 (G. Chang, W. C. Guida and W. C. Still, *J. Am. Chem. Soc.*, 1988, **9**, 343) on a Silicon Graphics Indigo 2 Powerx2 computer. The energy minimisation method was PRCG (relative permittivity = 10) with the United Atom Amber Force field (S. J. Weiner, P. A. Kollman, D. A. Case, U. C. Sigh, C. Ghio, G. Alagona, S. Profeta and P. Weiner, *J. Am. Chem. Soc.*, 1984, **106**, 765; S. J. Weiner, P. A. Kollman, D. T. Nguyen and D. A. Case, *J. Comput. Chem.*, 1986, **7**, 230) in BATCHMIN version 5.0. The torsion angles of the pyranose-ring and the peptide-backbone were maintained during energy minimisation and conformational searches. Using the filter option all conformations with a distance between C-1 and Cys-C^2 of 4.7–5.1 Å were selected. Conformational families were obtained for these conformations using XCLUSTER version 1.2 (P. S. Shenkin and D. Q. McDonald, *J. Comput. Chem.*, 1994, **15**, 899). The distance between corresponding atoms (C-1, C-2, O-5, Cys-C^1, Cys-C^2 and Cys-N) in pairs of structures was used as the criterion. Superimposition of conformations was achieved by selecting pairs of atoms (Cys-C^1, Cys-C^2 and Cys-N).
15 Deisenhofer, *J. Biochem.*, 1981, **20**, 2361.
16 G. L. Ellman, *Arch. Biochem. Biophys.*, 1959, **82**, 70.
17 *Selected data* for **7**: MALDI-TOF MS: *m/z* (delayed extraction) 66532 $[M + H]^+$ (BSA: 66431 $[M + H]^+$); Electrospray MS: *m/z* 66591 $[M + H]^+$ (BSA: 66430 $[M + H]^+$).

Received in Glasgow, UK, 2nd December 1997; 7/08701B

Novel olefin polymerization catalysts based on iron and cobalt

George J. P. Britovsek,[a] Vernon C. Gibson,*[a]† Brian S. Kimberley,[b] Peter J. Maddox,[b] Stuart J. McTavish,[a] Gregory A. Solan,[a] Andrew J. P. White[a] and David J. Williams[a]

[a] *Department of Chemistry, Imperial College, Exhibition Road, South Kensington, London, UK SW7 2AY*
[b] *BP Chemicals, Sunbury Research Centre, Chertsey Road, Sunbury on Thames, Middlesex, UK TW16 7LN*

A new family of olefin polymerization catalysts, derived from iron and cobalt complexes bearing 2,6-bis(imino)pyridyl ligands, is described.

Metallocene catalyst technology has made a dramatic impact on the polyolefins industry, providing access to polyolefinic materials with new or improved performance parameters.[1–7] There is thus great interest in the discovery and development of new families of catalysts for α-olefin polymerisation with a view to obtaining ever greater control over the properties of the resultant polymers and to extending the family of products to new monomer combinations. Late transition metal catalysts are particularly attractive because of their potential for tolerating heteroatom functionalities, which may open up the possibility for copolymerizations of polar comonomers. A significant development in late transition metal polymerization technology was reported by Brookhart and co-workers who showed that catalysts based on nickel and palladium could be used to access a range of linear and branched polyethylenes.[8–11]

Here we describe a new, strikingly active family of ethylene polymerization catalysts based on iron and cobalt bearing 2,6-bis(imino)pyridyl ligands. To the best of our knowledge these are the first iron based catalysts to show significant activities for the polymerization of ethylene. The precursor complexes are prepared by treatment of $FeCl_2$ or $CoCl_2$ with the 2,6-bis(imino)pyridines in excellent yields according to Scheme 1.‡ Derivatives containing a variety of bulky aryl substituents are accessible, the iron compounds **1a**–**d** being blue, while the aldimine complex **1e** and the cobalt compound **2** are green; all are paramagnetic. The magnetic moment of 5.34 μ_B (Evans balance) of complex **1a** indicates a high spin electronic configuration with four unpaired electrons for the d^6 iron(II) centres in these complexes.

Crystals of **1a** suitable for an X-ray structure determination§ were grown from a layered CH_2Cl_2–pentane (1 : 1) solution; the molecular structure is shown in Fig. 1. The complex has molecular C_S symmetry about a plane containing the iron, the two chlorides and the pyridyl nitrogen atom. The geometry at the Fe^{II} centre can probably be best described as distorted square pyramidal, with Cl(1) occupying the apical position. The four basal atoms are co-planar to within 0.02 Å, the iron atom lying 0.59 Å out of this plane. The Fe–Cl bonds are noticeably asymmetric, with that to the apical chloride being significantly longer [at 2.311(2) Å] than that to its basal counterpart [2.266(2) Å]. The Fe–N(imino) distances [av. 2.244(4) Å] are noticeably longer than the Fe–N(pyridyl) bond length [2.088(4) Å], probably as a consequence of satisfying the tridentate chelating constraints of the ligand. The bis(imino)pyridine unit is co-planar to within 0.19 Å, the plane extending to include the basal chloride Cl(2) with the 2,6-diisopropylphenyl rings each being inclined by 79° to this plane. There is no apparent delocalisation of the imino double bonds into the pyridyl ring system, the C(7)–N(7) and C(9)–N(9) bond lengths being 1.285(6) and 1.280(6) Å, respectively.

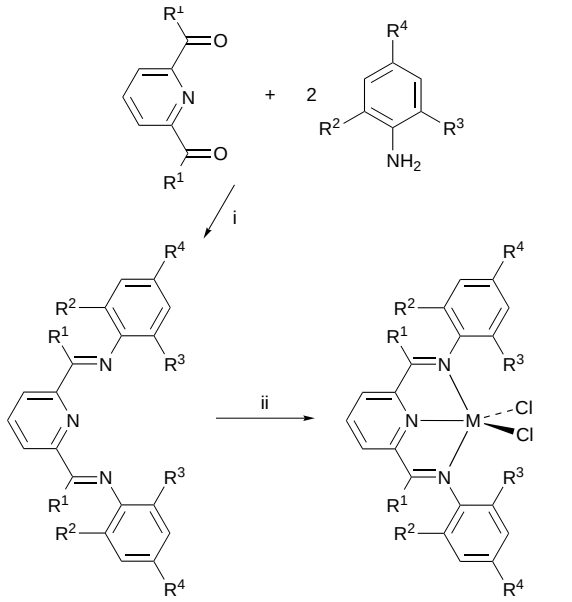

	M	R^1	R^2	R^3	R^4
1a	Fe	Me	Pr^i	Pr^i	H
1b	Fe	Me	Me	Me	H
1c	Fe	Me	Me	Me	Me
1d	Fe	Me	Me	H	Me
1e	Fe	H	Me	Me	H
2	Co	Me	Pr^i	Pr^i	H

Scheme 1 *Reagents and conditions*: i, EtOH, AcOH; ii, MCl_2, Bu^nOH, 80 °C, 10 min

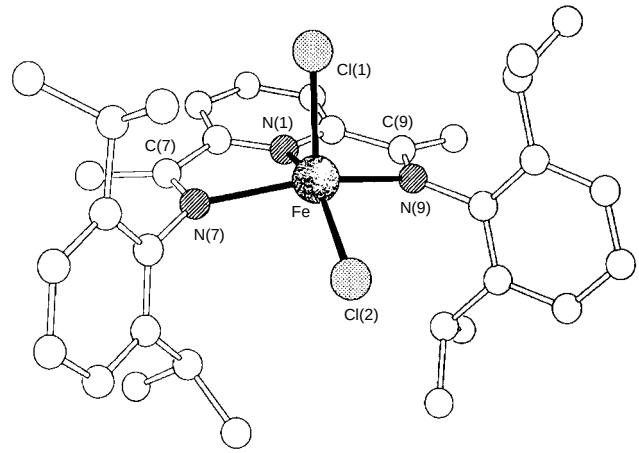

Fig. 1 The molecular structure of **1a**. Selected bond lengths (Å) and angles (°): Fe–Cl(1) 2.311(2), Fe–Cl(2) 2.266(2), Fe–N(1) 2.088(4), Fe–N(7) 2.238(4), Fe–N(9) 2.250(4), C(7)–N(7) 1.285(6), C(9)–N(9) 1.280(6); N(1)–Fe–N(7) 73.2(1), N(1)–Fe–N(9) 72.9(1), N(7)–Fe–Cl(2) 98.6(1), N(9)–Fe–Cl(2) 98.9(1), N(1)–Fe–Cl(2) 147.9(1), N(7)–Fe–N(9) 140.1(1)

Table 1 Results of ethylene polymerisation runs using procatalysts **1** and **2**[a]

Run	Procatalyst (μmol)	Activator (mmol/equiv)	*T*/°C	Solvent	Pressure C_2H_4/bar	Yield PE/g	Activity/ g mmol^{-1} h^{-1} bar^{-1}	M_w
1	**1a** (10)	MAO (1.0/100)	25	toluene	1	5.8	1170	203 000
2	**1a** (0.5)	MAO (0.5/1000)	50	isobutane	10	26.9	5430	611 000
3	**1b** (20)	MAO (8.0/400)	25	toluene	1	5.7	570	29 000
4	**1b** (0.6)	MAO (0.6/1000)	50	isobutane	10	56.5	9340	242 000
5	**1c** (10)	MAO (1.0/100)	25	toluene	1	6.2	1230	52 000
6	**1c** (0.6)	MAO (0.6/1000)	50	isobutane	10	63.1	11 020	562 000
7	**1d** (20)	MAO (8.0/400)	25	toluene	1	1.2	120	260
8	**1d** (0.6)	MAO (0.6/1000)	50	isobutane	10	7.8	1280	470
9	**1e** (10)	MAO (1.0/100)	25	toluene	1	3.7	740	15 000
10	**2** (10)	MAO (1.0/100)	25	toluene	1	2.3	460	26 000
11	**2** (0.5)	MAO (0.5/1000)	50	isobutane	10	3.7	450	14 000

[a] General conditions: 1 atm Schlenk tests carried out in toluene over 30 min, reaction quenched with dil. HCl and the solid PE washed with MeOH (50 cm^3) and dried in a vacuum oven at 50 °C. 10 atm tests performed in 1 l autoclave, procatalyst dissolved in toluene, isobutane solvent, triisobutylaluminium scavenger, runs carried out over 60 min.

The results of ethylene polymerization tests are collected in Table 1. Several features are noteworthy. In general, the activities of the iron catalysts are exceptionally high, in many cases comparable or even higher than those seen by metallocenes under analogous conditions. All of the catalysts produce essentially linear polyethylene with molecular weights that are dependent upon the aryl substitution pattern. Most notable is a dramatic fall-off in molecular weight to α-olefin oligomers for derivatives with one *o*-methyl substituent (runs 7,8) compared with derivatives that contain methyl substituents in both *ortho* positions. Clearly steric protection of the active site is a crucial factor in controlling molecular weight.

There is also a marked dependence of the polymer molecular weight on ethylene pressure for the iron catalyst system, an effect that is not seen for the cobalt catalyst **2** (runs 10, 11); the cobalt catalyst also displays a considerably lower activity than its iron analogue. ^{13}C NMR end-group analysis of the polymers generated by **1a**–**c** (runs 2, 4, 6) reveals isopropyl end-groups in addition to low levels of vinyl unsaturation. This is consistent with a termination mechanism involving alkyl group transfer from the $AlBu^i_3$ scavenger in addition to β-H transfer. The polymers formed from **1d** and the aldimine catalyst **1e** contain a larger proportion of vinyl end-groups (> 4 per 1000 carbons) indicating that β-H transfer plays a more dominant role in chain termination for these catalysts.

The new catalyst family described herein represents a significant addition to the growing armoury of technologically important olefin polymerization catalysts.

BP Chemicals Ltd is thanked for financial support. Dr J. Boyle and Dr G. Audley are thanked for NMR and GPC measurements, respectively.

Notes and References

† E-mail: v.gibson@ic.ac.uk

‡ Satisfactory elemental analyses have been obtained.

§*Crystal data* for **1a**: $C_{33}H_{43}N_3Cl_2Fe{\cdot}0.5H_2O$, M = 617.5, triclinic, $P\bar{1}$ (no. 2), a = 8.779(1), b = 9.876(1), c = 20.976(1) Å, α = 83.70(1), β = 88.18(1), γ = 65.67(1)°, V = 1646.9(3) Å^3, Z = 2, D_c = 1.245 g cm^{-3}, μ(Cu-Ka) = 53.6 cm^{-1}, F(000) = 654. A deep blue platy needle of dimensions 0.40 × 0.20 × 0.03 mm was used. 4878 independent reflections were measured on a Siemens P4/PC diffractometer with Cu-Kα radiation using ω-scans. The structure was solved by direct methods and all of the non-hydrogen atoms were refined anisotropically using full-matrix least-squares based on F^2 to give R_1 = 0.061, wR_2 = 0.144 for 3595 independent observed, absorption corrected reflections [$|F_o| > 4\sigma(|F_o|)$, $2\theta \leqslant 120°$] and 362 parameters. CCDC 182/812.

1 K. B. Sinclair and R. B. Wilson, *Chem. Ind.*, 1994, 857.
2 A. M. Thayer, *Chem. Eng. News*, Sept 11, 1995, 15.
3 R. G. Harvan, *Chem. Ind.*, 1997, 212.
4 H. H. Brintzinger, D. Fischer, R. Mülhaupt, B. Rieger and R. M. Waymouth, *Angew. Chem., Int. Ed. Engl.*, 1995, **34**, 1143.
5 M. Bochmann, *J. Chem. Soc., Dalton Trans.*, 1996, 255.
6 T. J. Marks, *Acc. Chem. Res.*, 1992, **25**, 57.
7 R. F. Jordan, *Adv. Organomet. Chem.*, 1991, **32**, 325.
8 L. K. Johnson, C.M. Killian and M. Brookhart, *J. Am. Chem. Soc.*, 1995, **117**, 6414.
9 L. K. Johnson, S. Mecking and M. Brookhart, *J. Am. Chem. Soc.*, 1996, **118**, 267.
10 C. M. Killian, D. J. Tempel, L. K. Johnson and M. Brookhart, *J. Am. Chem. Soc.*, 1996, **118**, 11 664.
11 L. K. Johnson, C. M. Killian, S. D. Arthur, J. Feldman, E. F. McCord, S. J. McLain, K. A. Kreutzer, A. M. A. Bennett, E. B. Coughlin, S. D. Ittel, A. Parthasarathy, D. J. Tempel and M. S. Brookhart, Pat. Appl. WO 96/23010, 1996, DuPont.

Received in Liverpool, UK, 10th March 1998; 8/01933I

ChemComm
FEATURE ARTICLE

Catalysis of liquid phase organic reactions using chemically modified mesoporous inorganic solids

James H. Clark* and Duncan J. Macquarrie

Department of Chemistry, University of York, Heslington, York, UK YO1 5DD

The modification of silicas and related materials by attachment of organic functionalities to their surface is an important area of research in heterogeneous catalysis and green chemistry. The methods available for the preparation of these hybrid organic–inorganic materials are reviewed, as are their applications as catalysts in a range of reactions.

Catalysts played a major role in establishing the economic strength of the chemical industry in the first half of the 20th century. As we approach the first half of the 21st century increasingly demanding environmental legislation, public and corporate pressure and the resulting drive towards clean technology in the industry will provide new opportunities for catalysis and catalytic processes. Some of the major goals of 'Green Chemistry' are to increase process selectivity, to maximise the use of starting materials (aiming for 100% atom efficiency), to replace stoichiometric reagents with catalysts and to facilitate easy separation of the final reaction mixture including the efficient recovery of the catalyst.[1] The use of efficient solid catalysts can go a long way towards achieving these goals.[2] Polymer-supported catalysts have been widely used.[3] Their popularity comes mainly from the fact that product isolation is simplified and that milder conditions and higher selectivity can be attained although they can suffer from limited thermo-oxidative stability. Catalysts based on high surface area inorganic support materials should have better thermal stability and have also attracted a lot of interest as solid catalysts and reagents in liquid phase organic reactions. They form the basis of some new industrial catalysts which are used as replacements for toxic and corrosive traditional reagents.[4] The mesoporous nature of silicas and acid-treated clays for example, allows reasonably good molecular diffusion rates and can lead to activity enhancement through the concentration of active centres.[5] These first generation supported reagent catalysts are, however, based on physisorbed reagents, are frequently unstable in polar media and, consequently, often cannot be reused. An emerging area of research which seeks to retain the 'green benefits' of heterogenisation and enhanced activity and/or product selectivity while avoiding the drawbacks of catalyst instability and limited reusability is the development and use as catalysts of mesoporous inorganic support materials with chemically bound active centres.

Preparative methodology

A range of possible methodologies exists for attaching organic functionality to the surface of a support. We will concern ourselves primarily with those methods which result in covalent attachment to a silica surface. Thus, purely electrostatic methods, such as those used to attach porphyrins to supports (*via e.g.* sulfonate-supported pyridinium ion pairs) will not be described. Nor will concepts such as the supported aqueous phase catalysts pioneered by Davis amongst others.

Several routes exist for the covalent attachment of organic functionality to the surface of a silica. These include grafting of functional organosilanes, surface chlorination and subsequent displacement, direct sol–gel preparation of organomodified silicas (especially micelle templated versions) and post-functionalisation of existing organic groups at the surface.

Grafting

This remains the most popular method, mostly due to its simplicity, at least in terms of experimental procedures. The silica is reacted with an appropriate organosilane in a suitable solvent, typically toluene at reflux, although ethanol at room temperature is also effective in some cases. The resulting solid is collected and washed (Scheme 1).

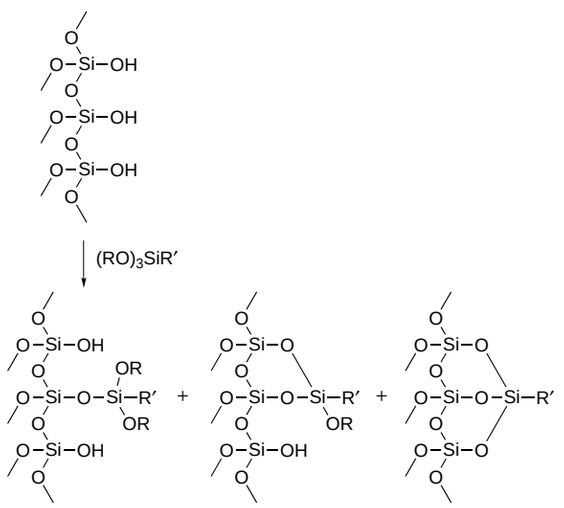

Scheme 1 Simplified grafting reaction at a silica surface

This method is versatile and relatively rapid, with many silanes being commercially available. Loadings of organic groups on the surface vary from *ca.* 0.3 mmol g^{-1} for cyanoethyl groups to *ca.* 1 mmol g^{-1} for amine-containing silanes. Loadings for the more recent controlled porosity MCM-based materials† can be significantly higher (1–1.7 mmol g^{-1}). Pore size distributions vary little from the original silica used, although surface areas can drop by a significant amount.[6] While this is a good method for initial studies, drawbacks can include the formation of several surface species resulting from binding *via* one, two or three Si–O–Si groups, attachment of oligomeric silanes, and the presence of physisorbed material, which must be thoroughly washed off before the catalyst can be used in reactions. Loading can often be low, resulting in the need for relatively large amounts of catalyst. Nonetheless, many catalysts have been successfully prepared by this method, and it remains the most commonly used route to new catalysts. The catalytically active group can be present in the silane which is attached to the surface, or can be introduced by subsequent post-modification reactions.

Surface chlorination and subsequent displacement

This is a much less frequently used method, although it has advantages of forming a direct Si–C bond at the surface and precludes the formation of surface bound oligomers and

variable modes of attachment. Groups are robustly bound, and are typically less prone to leaching than those attached *via* grafting. The technique is less easy to use, requiring the reaction of silica with the chlorinating agent, converting surface hydroxyls to Si–Cl bonds, and is typically achieved using thionyl chloride at reflux,[7] or with CCl_4 in a fluidised bed reactor[8] at 400–450 °C. The Si–Cl material thus produced is reacted with a solution of a Grignard reagent or an organolithium species, leading to displacement of the Cl and the formation of a Si–C surface bond. The main drawback in this method is that the requirement for strongly nucleophilic reagents limits the functionality which can be successfully attached. This approach has been used for silicas[8,9] and clays.[7,10] One article describes the exchange of Si–Cl for Si–Li,[10] rather than the normal Si–R, although no reason for this inverted reactivity was given.

Templated sol–gel techniques

This methodology is essentially the co-polymerisation of a silica precursor (typically a tetraalkylorthosilicate) with an organosilicate precursor [typically a trialkoxy(organo)silane] (Scheme 2).

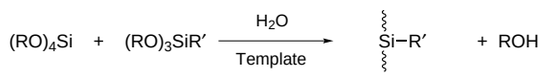

Scheme 2 Templated sol–gel synthesis of organofunctionalised silicas

The most important impetus for this approach has come from the discovery of the MCMs, which has allowed the predictable formation of very regular mesoporous materials, which show a great deal of promise as highly selective catalysts. This technique, which was initially used for the preparation of purely inorganic materials, has been successfully extended to include organomodified materials.[11–13]

Reaction conditions are very mild and the procedure is remarkably simple. The materials produced are very thermally stable; organic groups do not detach from the surface at temperatures lower than *ca.* 450 °C, and, as the groups are intimately bound into the surface, they are also solvolytically stable. Loadings can be very high, and are essentially independent of the silane used. We have recently prepared a material with a loading of 3.0 mmol g^{-1}, much higher than those obtainable by grafting. Loading is controlled by the ratio of silanes in the preparation. The surface areas reported are very high, ranging from 700 to *ca.* 1600 m^2 g^{-1}. Typical silica supported reagents have surface areas of *ca.* 75–300 m^2 g^{-1}.

Post modification

This is often a necessary step in the synthesis of chemically modified surfaces, since the range of silanes available is limited (they are also moisture sensitive and can be difficult to work with) and the use of Grignard or organolithium reagents means that the chlorination methodology can only be used with a few functional groups. One of the commonest grafted functions is the primary amine, usually *via* the cheap 3-aminopropyl-(trimethoxy)silane. This group behaves like a typical amine function, and can thus be derivatised by formation of amides or imines, and by alkylation. Nucleophilic aromatic substitution of suitable activated rings is also possible (Scheme 3).

The formation of amides can be carried out with anhydrides, acids or acid chlorides. Esters will also form amides, although slowly.[14] A particularly attractive option is to use acids without solvent in a vapour phase reaction at 150–170 °C. For example, 4-aminobenzoic acid can be reacted to form the silica-bound amide by mixing with the amine-functionalised silica in the absence of solvent and heating to 170 °C under vacuum.[15] This allows the vapour to enter the pores of the catalyst and react. Water and excess acid are removed under the reaction conditions, leaving the surface bound amide. The supported aniline thus formed can be further functionalised *via* diazonium

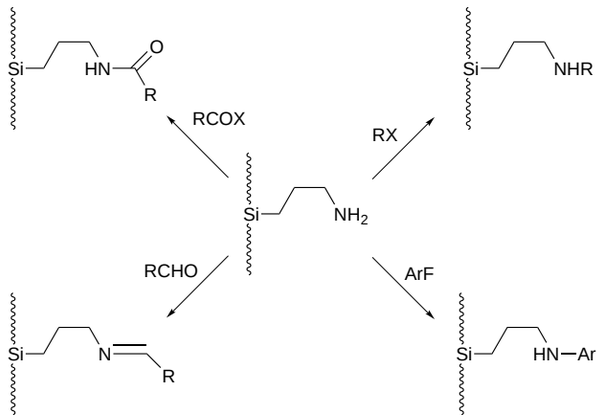

Scheme 3 Reactions of aminopropyl-functionalised silica

chemistry, and forms the basis for an effective base catalyst.[16] The attachment of a silane to a surface often allows the selective monofunctionalisation of a doubly functional molecule. This approach has been used in the synthesis of the supported metal salt depicted in Scheme 6, a very versatile and active oxidation catalyst (see following section).[17]

Newer methods for the functionalisation of surface bound alkenes (from chlorination/displacement routes) include the Heck reaction.[18] This methodology allows the attachment of a variety of aryl groups to the surface under solvent free conditions at temperatures between 130 and 150 °C (Scheme 4).

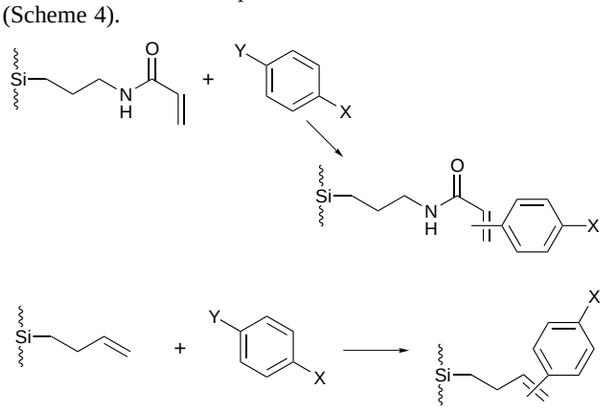

Scheme 4 The functionalisation of surface alkenes *via* the Heck reaction: X = H, CHO, CO_2H, CN; Y = Br, I

The use of the resulting materials in catalysis is currently under study.

Catalysis of oxidation reactions

Oxidation is the area where chemically modified surfaces have found most use. A wide variety of materials have been prepared, using several methods for attaching the organics to the surface, with many areas of oxidation chemistry benefiting from the materials thus derived.

We recently reported a simple immobilised form of $Co(OAc)_2$ which is capable of the epoxidation of alkenes.[19] This material was prepared according to Scheme 5.

This is a remarkable result, since the organo-functionalised silica is shown to survive the harsh conditions required to

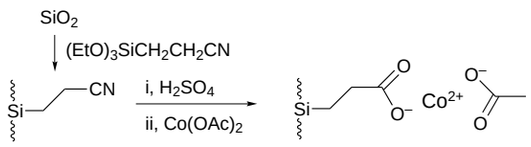

Scheme 5 Preparation of supported $Co(OAc)_2$

hydrolyse the nitrile group (50% H_2SO_4 at reflux, 24 h). The materials was found to efficiently catalyse the epoxidation of alkenes using sacrificial aldehydes and oxygen (Table 1).

Table 1 Epoxidation of alkenes using supported cobalt acetate

Alkene	*t*/h	Yield of epoxide[a]
Cyclohexene	5	85
Oct-1-ene	5	45
Octa-1,7-diene	24	48[b]
2,4,4-Trimethylpentene	5	95
Hex-1-ene	24	30
Styrene	3	32[c]

All reactions were carried out at 19 °C in dichloromethane with isobutyraldehyde as sacrificial aldehyde. [a] GC yield with internal standard. [b] Monoepoxide; 7% of diepoxide was also formed. [c] 5% PhCHO and 21% polymer also formed.

A related catalyst type has been recently reported,[17] where the metal centre is supported by a longer spacer chain (Scheme 6). This material was prepared from aminopropyl-silica by reaction with terephthalaldehyde to form the monoimine (attachment of the amine to the surface precludes reaction at both ends of the dialdehyde), followed by formation of a second imine with *p*-aminobenzoic acid. The supported acid was then treated with metal acetates to generate the active catalyst.

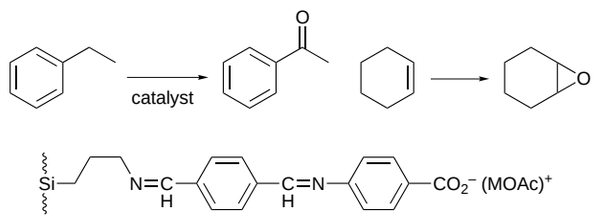

Scheme 6 Reactions catalysed by supported metal acetates

The catalyst is active in the same epoxidation reaction as the supported Co acetate above. Interestingly, the Ni version is most active, followed closely by Cr and Cu, with Mn and Co being distinctly poorer. Of particular interest is the ability of this catalyst to carry out the oxidation of alkyl aromatics. In this case the Cr version is the best, and allows a conversion rate of 370 turnovers h^{-1} to be achieved.

Kurusu and Neckers have also prepared simple complexed metal species on silica, based on the salicylimine species **I**:

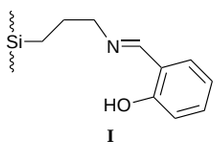

I

The metals complexes show some activity in the oxidation of cyclohexane[20,21] and in alkylaromatics.[21]

Jacobs and coworkers have prepared an active epoxidation catalyst based on supported metal complexes with the triazacyclononane ligand system.[22] Both silicas and MCMs were used as supports. The catalysts were prepared by the reaction of the cyclic ligand with a supported glycidyl material, in the case of the MCM, and with both glycidyl and chloropropyl in the case of the silica. The ligand system was then modified by reacting the two free amines with propylene oxide, and subsequent metal complexation. The epoxidation of styrene was used as a test reaction. Selectivities and turnover numbers (mol h^{-1}) were higher in the case of the MCM-derived materials than the silicas, regardless of the nature of the supported ligand.

Metalloporphyrins have also been the subject of much work, and several routes have been developed to attach them to heterogeneous supports. Porphyrins are expensive, and thus recovery becomes economically important. It is also possible that attachment to a surface may hinder destructive oxidation of the electron rich ring system, a factor which traditionally limits their useful lifetime. The use of charged groups, typically ammonium or sulfonate attached to the periphery has been used to enhance adsorption to polar supports such as silica and magnesium oxide.[23,24] Direct covalent binding to silica surfaces has been achieved by coordinative binding of the metal centre to supported imidazoles, pyridines, *etc*.[25,26] The second mode of attachment is *via* aryl groups attached to the periphery of the ring system. Thus, Mansuy and coworkers have used aminopropyl silica to tether a perfluorophenyl-substituted porphyrin.[27] These approaches are summarised in Fig. 1.

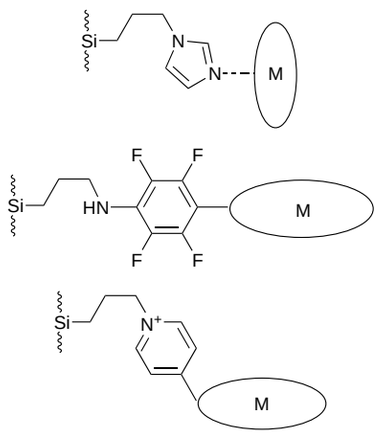

Fig. 1 Examples of covalently bound porphyrins

A second approach is the nucleophilic displacement of chloride from chloropropylsilica with a pyridine-substituted porphyrin.[28] These materials are active in the epoxidation of alkenes, where iodosylbenzene is the preferred oxidant, and in the oxidation of alkanes to alchols and ketones.

A further example of this approach is the copolymerisation of a porphyrin containing four attached trimethoxysilane groups with tetraethoxysilane, leading to an active hybrid silica–porphyrin.[29]

Finally, one problem relating to the oxidation of hydrocarbons with hydrogen peroxide is the difficulty of having appreciable concentrations of the non-polar substrate and the polar oxidant together at the catalytic centre. One elegant solution has recently been published by Neumann and Wange.[30] They have shown that attachment of a mixture of poly(ethylene oxide) and poly(propylene oxide) to a silica, followed by the physisorption of methylrhenium trioxide allows the efficient mixing of both reaction partners (Fig. 2). The catalyst allows the efficient epoxidation of alkenes with hydrogen peroxide.

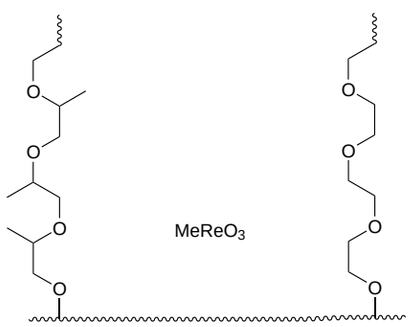

Fig. 2 Polyether modified supported methylrhenium oxide

A mix of the two polymeric chains was shown to be better than a single type of chain. This is attributed to a combination

of the relatively hydrophilic poly(ethylene oxide) and the more hydrophobic poly(propylene oxide) giving the right balance of properties, and allowing optimum mixing of the two reagents.

Solid acid catalysts

Solid acids are the most widely studied and commonly used heterogeneous catalysts. Their use however, is heavily biased towards large-scale continuous vapour phase processes such as catalytic cracking and alkane isomerisations. There is also a great need for solid acid catalysts which are effective in liquid phase organic reactions such as those employed in many batch-type reactors by fine, speciality and pharmaceutical intermediate chemical manufacturers. These include Friedel–Crafts alkylations, acylations and sulfonylations, isomerisations, dehydrations, oligomerisations and aromatic halogenations and nitrations. At present these reactions are commonly catalysed by mineral acids such as H_2SO_4 and HF and by Lewis acids such as $AlCl_3$ and BF_3. These traditional reagents suffer from many drawbacks including hazards in handling, corrosiveness, and difficulty in separation along with the inevitable production of often large volumes of toxic and/or corrosive waste. Solid acids based on organic polymers such as ion-exchange resins and Nafion are available but suffer from poor stability or high cost whereas supported reagents such as 'clayzic' (acid-treated clay supported zinc chloride)[31] have a limited range of applications and their weak support–reagent interaction may result in leaching of metal ions into polar media. The development of active and truly catalytic, heterogeneous alternatives to traditional soluble or liquid acids is a very important goal in green chemistry and while solid acids based on organically modified supports are relatively uncommon, significant progress using supports which have been chemically modified by reaction with Lewis acids has recently been made in our laboratory and elsewhere.

Aluminium chloride is one of the most widely used inorganic reagents in organic chemistry, being highly soluble and very active. However, its many drawbacks, such as its corrosive nature, difficulties in separation and recovery, and the large volumes of environmentally hazardous waste associated with its use, make it a prime target for heterogenisation.[4,32] We have reported an active heterogeneous form of aluminium chloride which is highly effective at least in Friedel–Crafts alkylation reactions.[33] The material **II**, which is believed to contain a mixture of $OAlCl_2$ and O_2AlCl sites, is prepared by reaction of a surface-hydroxylated high surface area mesoporous inorganic solid such as silica gel or acid-treated montmorillonite with aluminium chloride in a low-polarity aprotic organic solvent (Scheme 7).

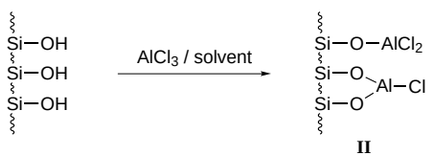

II

Scheme 7 Preparation of supported aluminium chloride

The optimum loading is support dependent with the higher surface area mesoporous silica gel having an optimum loading (1.5 mmol g^{-1}) twice as high as that of K10 montmorillonite. The former catalyst is also a little more active and selective towards monoalkylation although K10 is a less expensive support material.

Previous attempts at preparing immobilised aluminium chloride have met with limited success. Catalysts prepared in the vapour phase or from a CCl_4 solution have proved to be active in the gas phase (*e.g.* in cracking reactions) but their activity in liquid phase reactions has generally been poor.[34] Catalysts of this type should be differentiated from those which undergo a final high temperature calcination stage after treatment with a soluble aluminium salt. Thus various mesoporous materials such as MCM-41, MCM-48, SBA-1 and KIT-1 have been treated with reagents including ethanolic solutions of $AlCl_3$ and $Al(NO_3)_3$ and slurries of $Al(OPr^i)_3$ in non-polar solvent (*e.g.* hexane) followed by calcination of the resulting solid at temperatures of > 800 K to give solid acids.[35,36] This typically results in the formation of tetrahedral (framework) and octahedral (non-framework) Al. Such materials are more commonly associated with vapour phase reactions such as cracking.[36]

The catalyst represented by **II** shows excellent activity in the room temperature alkylation of benzene with alkenes.[33] Its activity is comparable to that of aluminium chloride but it shows improved selectivity towards monoalkylation compared to $AlCl_3$ itself and is readily recoverable and reusable (unlike $AlCl_3$ which need to be removed from the reaction after one use, typically by a water quench). The reaction can be extended to alkylbenzenes but halobenzenes are considerably less reactive presumably because of complexation of the polarisable halogen centre to active catalyst centres (Table 2).

Table 2 Activity of (optimised) supported aluminium chloride solid acids in the alkylation of aromatic substrates [2 : 1 mol ratio of ArH to alkene; 10 g catalyst (mol ArH)$^{-1}$]

Substrates	Catalyst	Reaction conditions *t*/h (*T*/°C)	Monoalkyl-aromatic yield (GC%)
PhH + oct-1-ene	$AlCl_3$	2(20)	61.6
PhH + oct-1-ene	SiO_2(70 Å)-$AlCl_3$	1.25(20)	78.3
PhH + oct-1-ene	K10-$AlCl_3$	2(20)	76.3
PhH + hex-1-ene	K10-$AlCl_3$	2(20)	69.2
PhH + dodec-1-ene	K10-$AlCl_3$	2(20)	77.3
PhH + hexadec-1-ene	K10-$AlCl_3$	2(20)	71.0
PhMe + oct-1-ene	K10-$AlCl_3$	1.5(20)	80.9
PhEt + oct-1-ene	K10-$AlCl_3$	3.5(20)	74.3
PhF + oct-1-ene	K10-$AlCl_3$	4(20)	29.6
PhCl + oct-1-ene	K10-$AlCl_3$	4.5(20)	14.2

It is interesting that reaction of mesoporous silica gel with $MeAlCl_2$ under similar conditions gives a catalyst with comparable activity to that prepared using $AlCl_3$. In contrast, reaction of $MeAlCl_2$ with K10 gives an appreciably less active catalyst, an observation that is consistent with the theory that the HCl released during the reaction of $AlCl_3$ with the clay helps to convert the more microporous clay structure into a more mesoporous silica structure[37] ($MeAlCl_2$ reacts with the surface hydroxyls by elimination of CH_4). Remarkably, $MeAlCl_2$ itself is less active again[33] suggesting that the methyl group is more deactivating than the support surface although the presence of isolated Lewis acid sites on the surface, rather than dimers in solution, may be a more important factor.

We have shown that it is possible to extend the methodology for supported aluminium chloride for liquid phase applications to the relatively new hexagonal mesporous silicas as supports (HMSs).[38,39]† Activity in the alkene alkylation of alkylaromatics is again comparable to that of $AlCl_3$ itself, and the solid acids are also easily recovered and can be reused. Most significantly, the increase in selectivity towards monoalkylation through the use of the heterogenised Lewis acid is further enhanced (Fig. 3). By using external site poisons such as Ph_3N (to block external acid sites through complexation) or Ph_3SiCl (to destroy external hydroxyl groups), there is a still greater increase in selectivity with close to 100% monoalkylation being achievable with hexadec-1-ene. This may be the first significant illustration of zeolitic like effects (in-pore selectivity) in catalysts based on these structured mesoporous materials operating in the liquid phase. The extension of this phenomenon from the small molecules transformed by zeolites to large molecules is clearly very important. It promises significant improvements in product selectivity, while maintaining the

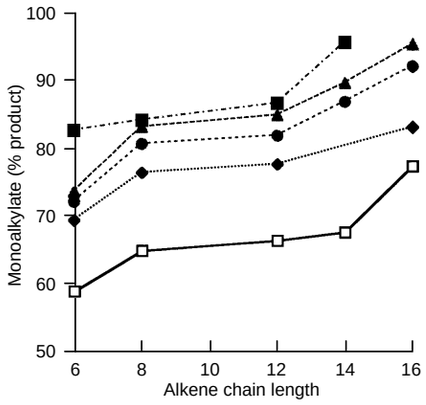

Fig. 3 Selectivity *vs*. chain length for a series of alkenes with HMS catalysts. (□) $AlCl_3$, (◆) $AlCl_3$/K10, (●) $AlCl_3$/HMS24, (▲) $AlCl_3$/HMS24-TPS, (■) $AlCl_3$/HMS24-Ph_3N; TPS = triphenylsilyl. HMS24 refers to a parent HMS with av. pore diameter 24 Å.

relatively fast reaction rates that mesoporous catalysts can give in liquid phase organic reactions.

It seems likely that heterogeneous versions of other very active Lewis acids can be prepared by similar methods although there are few other references to this in the existing literature. Iron(III) chloride should be reactive enough to form surface $OFeCl_2$ bonds for example and a stable form of supported $FeCl_3$ has been recently reported.[40] The material has been used to catalyse liquid phase Friedel–Crafts benzoylations[40] reminiscent of a commercial catalyst[41] although the surface structure and activity on reuse of the catalyst have not been described.

Brønsted acids can also be fixed to the hydroxylated surfaces of support materials. Most spectacularly surface attached perfluorosulfonic acids have been reported[42] which supercede the perfluorinated sulfonic acid resin (Nafion)-silica composites reported a year earlier.[43] The route to these requires the preparation of the new reagent $(OH)_3Si(CH_2)_3(CF_2)_2O(CF_2)_2SO_3^-M^+$ which is then bonded to an existing support or incorporated in an *in situ* sol–gel technique to give the novel silica based solid acid **III**.

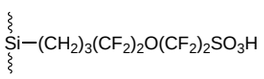

III

The materials are catalytically active for a number of typically acid-catalysed liquid phase organic reactions such as alkene alkylations of aromatics (although they are considerably less active than the supported aluminium chloride described above) and the benzoylation of activated aromatics such as *m*-xylene. They are orders of magnitute more active than conventional acidic ion exchange resins.

On a somewhat more mundane level, there are various reports of solid Brønsted acids derived from reaction of support materials with conventional liquid acids although the nature of the support–acid interaction and catalyst stability are generally not well understood. Thus simple treatment of silica gel with sulfuric acid followed by mild drying gives a solid acid that is active in various aromatic nitrations (nitric acid or isopropyl nitrate as nitrating agent).[44] Activity of the solid acid is comparable to the more expensive Nafion-H.

Heterogeneous versions of heteropoly acids have also been prepared. Apart from direct deposition into support materials, they can be more firmly bonded to the surface through chemical surface modification. Acids such as 12-tungstophosphate (PW_{12}) will react with silica gels which have been treated with aminoalkylsilanes.[45] The acidic site of PW_{12} reacts with the surface-bound amino group. The activities of such catalysts are generally higher than those of supported reagents prepared by direct deposition[45] and it is likely that further improvements are achievable by using the structured hexagonal mesoporous materials.[46]

Base catalysis

The use of supported basic groups as heterogeneous catalysts has been researched by a few groups over the last decade. The majority of work has been carried out on the simple 3-aminopropyl-derivatised silica. A variety of papers has been published describing the use of this material as an efficient catalyst for the Knoevenagel reaction.[47–49] Most of the papers deal with the relatively facile reaction of benzaldehyde with nucleophiles such as ethyl cyanoacetate and malononitrile. We have carried out an indepth study of this reaction system with a variety of aldehydes and ketones, and have shown that this simple material is indeed a versatile and active catalyst.[14] Several important features have emerged. One of the most important parameters is the solvent, a recurrent theme in heterogeneous liquid phase catalysis. In this case the solvent must play two roles. Firstly it must remove water from the system. The reaction is reversible, and the rates of all but the simplest reactions are significantly reduced by the presence of water. Secondly, the partitioning of reactants between the solvent phase and the catalyst surface is important. Since the catalyst surface is probably the most polar phase in the system, the use of non-polar solvents will allow the reagent to preferentially adsorb onto the catalyst surface (polar solvents will compete for the surface). Both these criteria are met by hydrocarbon solvents such as alkanes. Indeed it was found that the rates of reaction varied with solvent according to the following order: cyclohexane > toluene > 1,2-dichloroethane > chlorobenzene when the reaction was performed at the boiling point of each solvent. Even the higher temperature used with toluene and chlorobenzene did not bring about a rate close to that of cyclohexane (Fig. 4).

Interestingly, the much more polar[50] catalysts based on aminopropyl groups incorporated into hexagonal mesoporous silicates (HMS)[51,†] show essentially the same trend, although

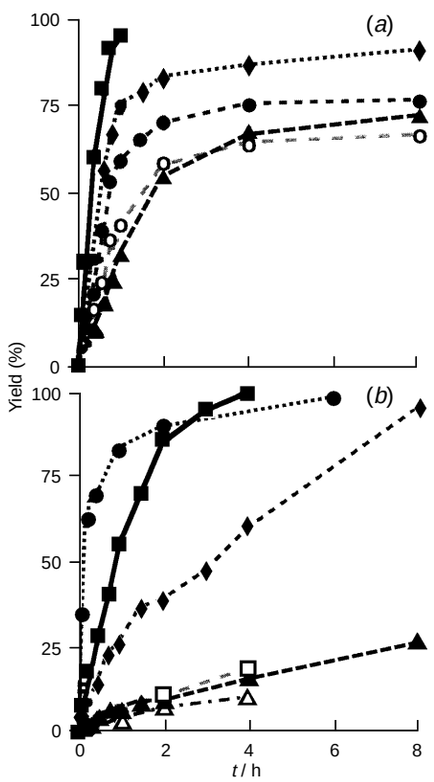

Fig. 4 Solvent effects in the Knoevenagel reaction using aminopropyl silica (*a*) and aminopropyl HMS catalysts (*b*); (■) cyclohexane, (●) toluene, (◆) hexane, (▲) 1,2-dichloroethane, (□) chloroform, (○) chlorobenzene, (△) ethyl acetate

the more polar surfaces of the HMS materials mean that toluene is the optimum solvent, with partition onto the catalyst surface still being favourable even with the more polar solvent. Increasing the solvent polarity further again reduces the rate dramatically.

Reaction studies on both sets of catalysts showed that both materials were active for a variety of reactions (Table 3).

Table 3 Knoevenagel reactions catalysed by aminopropyl substituted catalysts

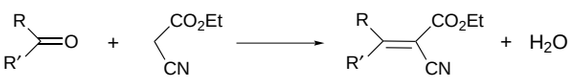

R, R′	Catalyst	*T*/°C	*t*/h	Yield[a] (%)	TON[b]
Ph, H	**1**	82	0.1	99	—
Ph, H	**2**	82	36	94	—
n-C_5H_{11}, H	**1**	82	0.2	97	—
n-C_5H_{11}, H	**2**	82	0.1	99	> 6000
n-C_7H_{15}, H	**1**	82	0.2	98[a]	—
n-C_7H_{15}, H	**2**	82	0.15	98	> 6000
c-C_5H_{10}	**1**	82	1	98	650
c-C_5H_{10}	**2**	110	2	92	2450
Et, Et	**1**	82	2	97	265
Et, Et	**2**	82	4	97	1127
n-C_4H_{10}, Me	**1**	82	4	98	350
n-C_4H_{10}, Me	**2**	110	4	95	1244
t-C_4H_{10}, Me	**1**	82	24	22	—
Me, Ph	**1**	82	24	68	250
Me, Ph	**2**	110	36	48	47
Ph, Ph	**1**	82	72	8	—

[a] GC yields with *n*-dodecane as internal standard. Isolated yields are 5–10% lower. [b] Number of mol product per mol of NH_2 groups. Catalyst **1** is aminopropyl-silica; catalyst **2** is aminopropyl-HMS.

Aldehydes and ketones (aliphatic and aromatic) both react readily, as had been shown by previous authors and turnover numbers are generally good (200–600). The poisoning mechanism was also shown to be due to amide formation by reaction of the amine with the ester group of ethyl cyanoacetate. The HMS catalysts are generally slightly less active when compared directly, but their ability to function well in toluene, and the much higher loadings achievable (2.5 *cf.* 1.0 mmol g^{-1}) means that under optimum conditions they can match the silica catalysts in terms of rate. Their turnover numbers are typically higher by a factor of 4–5, and the poisoning mechanism is different. These materials thus display a great deal of promise as novel catalysts. Rates, selectivity and conversion were found to be much higher than for typical homogeneous conditions (piperidine as base).

Brunel and coworkers[52] have studied aminopropyl-grafted MCMs as catalysts for this reaction. They used Me_2SO as solvent, and achieved complete conversion of reactants (benzaldehyde and ethyl cyanoacetate) after 100 min. They also found that a supported piperidine catalyst (prepared by reaction of piperidine with chloropropyl-MCM) was significantly less active as a catalyst. Unfortunately, the different conditions used preclude meaningful comparison with the materials mentioned above at this time.

We have recently described the preparation and use of two novel base catalysts (Fig. 5) which have phenolates as the basic centre.[16] One was prepared using the amidation/diazonium chemistry described above, the other using alkylation of surface bound amine groups with a polyether tosylate. The catalysts are active in the Michael addition, and extension of the methodology to enantioselective catalysis is currently underway.

Solid catalysts for other applications

The concept of triphase catalysis, whereby a phase transfer catalyst (PTC) is immobilised onto a support material and the

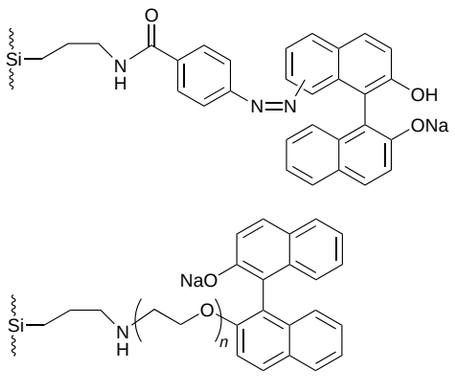

Fig. 5 Supported phenolates derived from diazotisation of surface bound aniline and from alkylation of surface bound amine

resulting supported PTC is then used in a biphasic aqueous–organic solvent reaction mixture is well established. We have recently reported a series of supported tetraarylphosphonium PTCs which show particularly high thermal stabilities and useful activities in nucleophilic substitution reactions and aromatic oxidative brominations.[9,53,54] The catalysts are often reusable and are effective in non-polar solvents such as hydrocarbons even when the unsupported phosphonium salt is inactive (owing to poor solubility, the supported catalysts are believed to operate at the aqueous–organic interface). The catalysts can be prepared by a variety of methods as shown in Scheme 8.

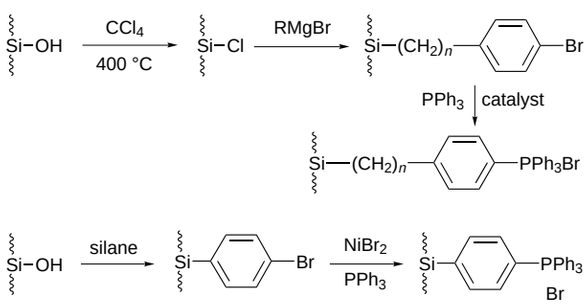

Scheme 8 Preparation of heterogeneous phase transfer catalysts

The most remarkable of these catalysts is the mesoporous silica based material which contains two adjacent phosphonium centres referred to as a 'bicipital supported phosphonium phase transfer catalyst' IV.[9]

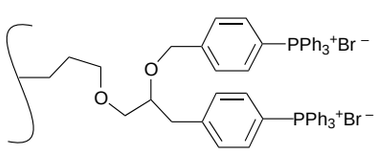

IV

This catalyst is considerably more active than other supported phosphonium salts in the model nucleophilic substitution reaction of 1-bromooctane with potassium iodide. It is also very dependent on the pore size of the silica with an average pore diameter of *ca.* 100 Å giving the highest activity; this is consistent with more simple physisorbed silica-based supported reagents and seems to support the view that for liquid phase reactions catalysed by porous solids, a reasonably large pore is required to give a good molecular diffusion rate.[2,5] Most significantly, the analogous material with only one of the aromatic rings substituted with a phosphonium group is significantly less active per phosphonium centre than the bicipital material. It is likely that the neighbouring centres can

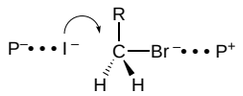

Scheme 9

produce a synergistic effect through simultaneous polarisation of the C–Br bond by one phosphonium centre and attack by the I^- delivered by the other cation (Scheme 9).

This is supported by the unusually low activation enthalpy and entropy found for reactions catalysed by the bicipital material, which are consistent with a lower energy pathway and a more ordered transition state.[9]

Chemically modified solid supports can also make very effective ligands for metal ions enabling heterogenisation of many valuable catalyst structures. These are to be distinguished from the very many examples of supported metals and metal oxides which are often prepared *via* metal complexes which are then decomposed in a final, typically high temperature stage.[55] The immobilisation of palladium and applications of the resulting solid catalysts in important reactions such as carbonylation, amidation and carbon–carbon forming coupling reactions are good examples of this.[56–58] Apart from organic polymer based materials, catalytically active clay and silica supported palladium complexes are known. These include a silica-supported sulfur palladium complex which can be used to catalyse the arylation of styrene and acrylic acid at 100 °C[57] (Scheme 10).

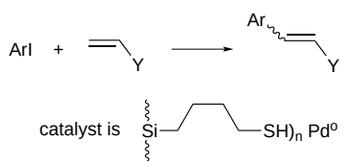

Scheme 10 Arylation reactions catalysed by supported Pd centres

Other metals can be similarly immobilised. Remarkably, the heterogenisation process can confer dramatically enhanced activity on the metal complex. Thus, the dimolybdenum complex $[Mo_2(MeCN)_8]BF_4$-SiO_2 prepared by direct reaction of the silica with the metal complex is unusual in its ability to catalyse the polymerisation of norbornene in the absence of an aluminium co-catalyst and at moderate temperatures.[59] Catalysts can be made directly by sol–gel methods. Thus sol–gel processing of the ruthenium complex *cis*-$[RuCl(H)(CO)(P)_3]$ (where P is a coordinated ether–phosphine) with tetraethoxysilane and $[Al(OPr^i)_3]$ gives a stable material with moderate surface area which is active in the hydrogenation of *trans*-crotylaldehyde with reasonable chemoselectivity to the carbonyl reduced products, *cis*- and *trans*-crotyl alcohol.[60]

Non-metallic chemically modified solids have also been developed for liquid phase catalytic applications. Silica-supported guanidinium chloride for example, has been shown to have high efficiency in the decomposition of methyl chloroformate (into MeCl + CO_2) and electrophilic reactions of carboxylic acids and epoxides.[61]

Recent advances in solid state synthesis offer some interesting possibilities for the future. Thus the preparation of a biomolecular tether device based on a silica support chemically modified with 4,4′-azodianiline units and its successful use in binding a peptide residue[62] suggests potential for biocatalysis. Covalently bound calixarenes[63] help demonstrate complex surface structures which could be used to bind catalytically active metal ions. Our recently reported highly fluorinated materials derived from the reaction of perfluorocarboxylic acids with aminopropyltrimethoxysilated silica may also point the way forwards.[64] These materials are capable of reversibly binding perfluorocarboxylates to the exclusion of other salts. Clearly the improved selectivity that could result from adding molecular recognition to the already impressive list of attributes of chemically modified mesoporous solids will further enhance their growing popularity.

Acknowledgements

J. H. C. thanks the Royal Academy of Engineering/EPSRC for a Clean Technology Fellowship. D. J. M. thanks the Royal Society for a University Research Fellowship. We are both indebted to the members of the Green Chemistry group at York, whose efforts have produced much of the work described in this article.

James Clark is a graduate of Kings College, London. Following Postdoctoral Fellowships in Canada and England he joined the academic staff at York in 1979. He currently holds a Chair in Industrial and Applied Chemistry as well as the RAEng-EPSRC Clean Technology Fellowship in Heterogeneous Catalysis. The *York Green Chemistry Group* which he leads, has won several national and international awards for its research and will soon move into a new purpose-built Centre for Clean Technology at York.

Duncan Macquarrie gained BSc and PhD degrees at the University of Strathclyde (1982 and 1985). He then moved to York where he carried out research into phase transfer catalysis and heterogeneous catalysis. After moving to Ciba–Geigy and then Lonza AG, he has returned to York to take up a Royal Society University Research Fellowship, where he is researching into chemically modified surfaces as novel heterogeneous catalysts.

Notes and References

* E-mail: jhc1@york.ac.uk

† MCMs are silicas or aluminosilicates, prepared by polymerisation of silicon (and aluminium) containing monomers around micelles of quaternary ammonium surfactants. HMS refers to analogous materials prepared using micelles of long chain amines. We originally called the organomodified materials MCMs. According to the above scheme of nomenclature, these materials should be referred to as derivatives of hexagonal mesoporous silicas (HMS).

1 *Chemistry of Waste Minimisation*, ed. J. H. Clark, Chapman and Hall, London, 1995.
2 J. H. Clark and D. J. Macquarrie, *Chem. Soc. Rev.*, 1996, 303.
3 D. C. Sherrington, *Polymer Supported Synthesis*, p. 141 in ref. 1.
4 T. W. Bastock and J. H. Clark, in *Speciality Chemicals*, ed. B. Pearson, Elsevier, London, 1992.
5 J. H. Clark, S. R. Cullen, S. J. Barlow and T. W. Bastock, *J. Chem. Soc., Perkin Trans. 2*, 1994, 1117.
6 E. F. Vansant, P. Van Der Voort and K. C. Vrancken, *Stud. Surf. Sci. Catal.*, Elsevier, Amsterdam, 1995, **93**, ch. 9.
7 K. R. Kumar, B. M. Choudhary, Z. Jamil and G. Thayagarajan, *J. Chem. Soc., Chem. Commun.*, 1986, 130.
8 J. H. Clark and C. Williamson, *J. Mater. Chem.*, 1993, **3**, 575.
9 J. H. Clark, S. J. Tavener and S. J. Barlow, *Chem. Commun.*, 1996, 2429.
10 B. M. Choudhary and P. Barathi, *J. Chem. Soc., Chem. Commun.*, 1987, 1505.
11 S. L. Burkett, S. D. Sims and S. Mann, *Chem. Commun.*, 1996, 1367.
12 S. Mann and C. E. Fowler, *Chem. Commun.*, 1997, 1769.
13 D. J. Macquarrie, *Chem. Commun.*, 1996, 1961.
14 D. J. Macquarrie, J. H. Clark, A. Lambert, A. Priest and J. E. G. Mdoe, *Reactive Funct. Polym.*, 1997, **35**, 153.
15 V. Basiuk and A. A. Chuiko, *J. Chromatogr.*, 1990, **529**, 29.
16 D. J. Macquarrie, *Chem. Commun.*, 1997, 601.
17 J. H. Clark, D. J. Macquarrie, J. Chisem (née Bovey), I. C. Chisem and J. S. Rafelt, *Chem. Commun.*, 1997, 2203.
18 D. J. Macquarrie and S. E. Fairfield, *J. Mater. Chem.*, 1997, **7**, 2201.
19 A. Butterworth, J. H. Clark, P. H. Walton and S. J. Barlow, *Chem. Commun.*, 1996, 1859.
20 Y. Kurusu and D. C. Neckers, *J. Org. Chem.*, 1991, **56**, 1981.
21 Y. Kurusu, *React. Polym.*, 1995, **25**, 63.

22 Y. V. Subba Rao, D. E. De Vos, T. Bein and P. A. Jacobs, *Chem. Commun.*, 1997, 355.
23 L. Barloy, J.-P. Lallier, P. Battoni and D. Mansuy, *New J. Chem.*, 1992, **16**, 71.
24 P. Battoni, J.-P. Lallier, L. Barloy and D. Mansuy, *J. Chem. Soc., Chem. Commun.*, 1989, 1149.
25 P. R. Cooke and J. R. Lindsay-Smith, *Tetrahedron Lett.*, 1992, **33**, 2737.
26 C. Gilmartin and J. R. Lindsay-Smith, *J. Chem. Soc., Perkin Trans. 2*, 1995, 243.
27 P. Battoni, J. F. Bartoli, D. Mansuy, Y. S. Byun and T. G. Traylor, *J. Chem. Soc., Chem. Commun.*, 1992, 1051.
28 H. S. Hilal, C. Kim, M. L. Sito and A. F. Schreiner, *J. Mol. Catal.*, 1991, **64**, 133.
29 P. Battoni, E. Cardin, M. Louloudi, B. Schoellhorn, G. Spyroulias, D. Mansuy and T. G. Traylor, *Chem. Commun.*, 1996, 2031.
30 R. Neumann and T.-J. Wang, *Chem. Commun.*, 1997, 1915.
31 J. H. Clark, *Catalysis of Organic Reactions using Supported Inorganic Reagents*, VCH, New York, 1994.
32 J. H. Clark, in *Waste Minimisation: A Chemists Approach*, ed. K. Martin and T. W. Bastock, Royal Society of Chemistry, Cambridge, 1994.
33 J. H. Clark, K. Martin, A. J. Teasdale and S. J. Barlow, *J. Chem. Soc., Chem. Commun.*, 1995, 2037.
34 R. S. Drago, S. C. Petrosius and P. B. Kaufman, *J. Mol. Catal.*, 1994, **89**, 317.
35 R. Ryoo, S. Jun, J. Man Kim and M. Jeong Kim, *J. Chem. Soc., Chem. Commun.*, 1997, 2225.
36 R. Mokaya and W. Jones, *J. Chem. Soc., Chem. Commun.*, 1997, 2185.
37 J. B. Butrille and T. J. Pinnavaia, *Catal. Today*, 1992, **14**, 141.
38 J. H. Clark, P. M. Price, K. Martin, D. J. Macquarrie and T. W. Bastock, *J. Chem. Res.*, 1997, 430.
39 J. H. Clark, P. M. Price, K. Martin, D. J. Macquarrie and T. W. Bastock, *UK Pat. Appl.*, 1996.
40 B. M. Khadilkar and S. D. Borkar, *Tetrahedron Lett.*, 1997, **38**, 1641.
41 *Envirocats*, Contract Catalysts Ltd., Knowsley, Merseyside, England.
42 M. A. Harmer, Q. Sun, M. J. Michalczyk and Z. Yang, *Chem. Commun.*, 1997, 1803.
43 Q. Sun, M. A. Harmer and W. E. Farneth, *Chem. Commun.*, 1996, 1201.
44 J. M. Riego, Z. Sedin, J. M. Zaldivar, N. C. Marziano and C. Tortato, *Tetrahedron Lett.*, 1996, 513.
45 M. Kamada, H. Nishijima and Y. Kera, *Bull. Chem. Soc. Jpn.*, 1993, **66**, 3565.
46 A. Corma, *Chem. Rev.*, 1997, **97**, 2373.
47 E. Angeletti, C. Canepa, G. Martinetti and P. Venturello, *J. Chem. Soc., Perkin Trans. 1*, 1989, 105.
48 E. Angeletti, C. Canepa, G. Martinetti and P. Venturello, *Tetrahedron Lett.*, 1988, 2261.
49 R. H. Jin and Y. Kurusu, *J. Mol. Catal.*, 1982, **73**, 218.
50 D. J. Macquarrie, S. J. Tavener, G. Gray, P. A. Heath and J. H. Clark, *Chem. Commun.*, 1997, 1147.
51 D. J. Macquarrie and D. B. Jackson, *Chem. Commun.*, 1997, 1781.
52 M. Lasperas, T. Lloret, L. Chaves, I. Rodriguez, A. Cauvel and D. Brunel, *Stud. Surf. Sci., Catal.*, 1997, **108**, 75.
53 J. H. Clark, S. J. Tavener and S. J. Barlow, *J. Mater. Chem.*, 1995, **5**, 827.
54 J. H. Clark, A. J. Butterworth, S. J. Tavener, A. J. Teasdale, S. J. Barlow, T. W. Bastock and K. Martin, *J. Chem. Technol. Biotechnol.*, 1997, **68**, 367.
55 C. P. Mehnert and J. Y. Ying, *Chem. Commun.*, 1997, 2215.
56 M.-Z. Cai, C.-S. Song and X. Huang, *Synth. Commun.*, 1997, **27**, 361.
57 M.-Z. Cai, C.-S. Song and X. Huang, *Synthesis*, 1997, 521.
58 M.-Z. Cai, C.-S. Song and X. Huang, *J. Chem. Soc., Perkin Trans. 1*, 1997, 2273.
59 M. McCann, E. M. G. Coda and K. Maddock, *J. Chem. Soc., Dalton Trans.*, 1994, 1489.
60 E. Lindner, A. Jager, M. Kemmler, F. Auer, P. Wegner, H. A. Mayer and E. Plies, *Inorg. Chem.*, 1997, **36**, 862.
61 P. Gros, P. Le Perchec and J.-P. Senet, *J. Chem. Res.*, 1995, 196.
62 J. Ching, K. I. Voivodov and T. W. Hutchens, *J. Org. Chem.*, 1996, **61**, 3582.
63 G. Arena, A. Casnati, A. Contino, L. Mirone and D. Sciotto, *Chem. Commun.*, 1996, 2277.
64 J. H. Clark, J. E. Johnstone and M. S. White, *Chem. Commun.*, 1996, 2253.

7/09143E

Highly stereoselective indium trichloride-catalysed asymmetric aldol reaction of formaldehyde and a glucose-derived silyl enol ether in water

Teck-Peng Loh,*† Guan-Leong Chua, Jagadese J. Vittal and Meng-Wah Wong

Department of Chemistry, National University of Singapore, 10 Kent Ridge Crescent, Singapore 119260

The yield and stereochemical outcome of the reaction between D-glucose-derived silyl enol ether 1 (*Z* and *E* isomers) and commercial formaldehyde in water catalysed by indium(III) choride was studied.

The many possible advantages of performing carbon–carbon bond formation in aqueous media has resulted in studies by several groups. This relatively unfamiliar territory, especially reactions that are done without organic solvents, lends itself to exploration in terms of reaction characteristics and stereochemical behaviour.[1]

Here we report an efficient and highly stereoselective aldol reaction between commercially available aqueous formaldehyde (37% in water) and silyl enol ether **1**, which can be easily obtained using glucose as starting material (Scheme 1). The reaction conditions chosen have allowed for formaldehyde to be used without prior dissolution or *in situ* generation in highly basic or acidic conditions from paraformaldehyde, as compared to reactions in organic solvents.

The use of **1** has allowed for the study of asymmetric induction *via* the chiral centers and steric bulk of the various groups. In addition, we aim to provide a stereoselective one-carbon extension of glucose under mild conditions employing readily available starting materials, in contrast to existing methodologies.[2] Previously reported use of commercial formaldehyde solution for Mukaiyama aldol reactions using lanthanide triflates was unable to be carried out efficiently in the absence of organic solvents.[3] Our aim in completely excluding organic solvents had led us to our choice of $InCl_3$ as a water-stable Lewis acid from our earlier work.[4] We had also studied the characteristics of the unexplored $In(OTf)_3$ and did a comparative study with the lanthanide triflate $Yb(OTf)_3$. Our study demonstrated the superiority of $InCl_3$ in terms of yield and selectivity.

Ketone **5**, precursor of silyl enol ether **1**, was derived from diacetone D-glucose in two steps (Scheme 2). Deprotonation of C-6 using LDA and subsequent trapping of the enolate with trimethylsilyl chloride gave (*Z*)-**1** and (*E*)-**1** in an approximate ratio of 80 : 20 [Scheme 3, reaction conditions (i)]. The ratio of the isomers was determined *via* ^{1}H NMR spectroscopy, through integration of the α-vinylic proton resonances, with the *Z*-isomer at a lower field than the *E*-isomer.[5]‡

The aqueous Mukaiyama aldol-type reaction was performed by first activating the formaldehyde (commercial solution, 37% in water, 2 equiv.) using Lewis acid (0.4 equiv. $InCl_3$, 0.02 equiv. $In(OTf)_3$ or 0.4 equiv. $Yb(OTf)_3$) and then adding this solution to the silyl enol ether. The reaction mixture was then stirred vigorously§ at room temperature and monitored by TLC for complete consumption of **1**. Aqueous workup followed by flash chromatography gave the desired products. The results are shown in Table 1 (entries 1 to 3). The low yield observed for the reaction catalysed by triflates was due to the significant conversion of **1** to the ketone, particularly with 0.4 equiv. of $In(OTf)_3$, and deprotection of C-6 hydroxy group from the product **2**. Diastereoselectivities obtained were good, with catalysis by $InCl_3$ proceeding with excellent selectivity.¶ The stereochemistry about C-6 of product (*R*)-**2** was determined by X-ray crystallographic analysis of (*R*)-6 obtained from deprotection of the C-6 hydroxy group (Scheme 4).‖

The lack of correlation between the isomer ratio of **1** and the diastereoselectivities of the products suggests that both isomers gave the same major product *via* conformational preference

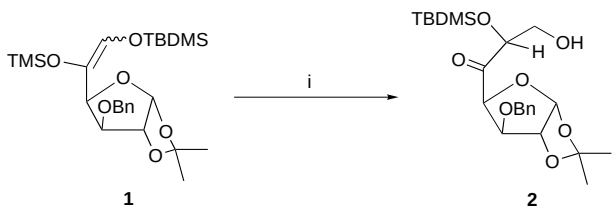

Scheme 1 *Reagents and conditions*: i, CH_2O (37% in H_2O), Lewis acid, room temp.

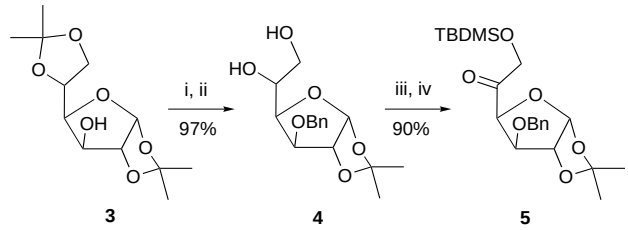

Scheme 2 *Reagents and conditions*: i, NaH, BnBr, Bu_4NI, THF, room temp., 48 h; ii, 0.06 M HCl, MeOH, room temp., 3 days; iii, TBDMSCl, Et_3N, DMAP, CH_2Cl_2, room temp., 18 h; iv, DMSO, $(COCl)_2$

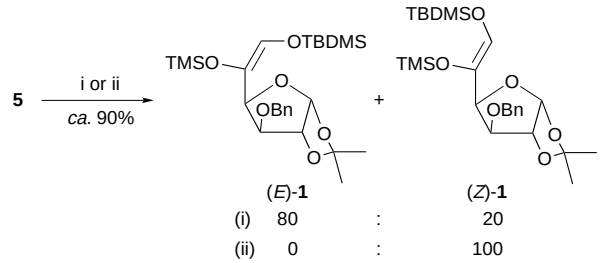

Scheme 3 *Reagents and conditions*: i, LDA, $SiMe_3Cl$, THF, −78 °C to room temp.; ii, Et_3N, $SiMe_3Cl$, DMF, 70 °C, 2 days

Table 1 Yields and diastereoselectivities for reactions described in Scheme 1

Entry	*E* : *Z*	Lewis acid (equiv.)	*t*	Yield[a] (%)	*R* : *S*
1	80 : 20	$InCl_3$ (0.4)	4–7 d	73	96 : 4
2	80 : 20	$In(OTf)_3$ (0.4)	30 min	0[b]	—
3	80 : 20	$In(OTf)_3$ (0.02)	0.5–1 d	38	93 : 7
4	80 : 20	$Yb(OTf)_3$ (0.4)	2–3 d	40	88 : 12
5	0 : 100	$InCl_3$ (0.4)	4–7 d	68	82 : 18
6	0 : 100	$In(OTf)_3$ (0.02)	0.5–1 d	37	70 : 30
7	0 : 100	$Yb(OTf)_3$ (0.4)	2–3 d	35	54 : 46

[a] Purified yield. [b] Extensive decomposition occurs.

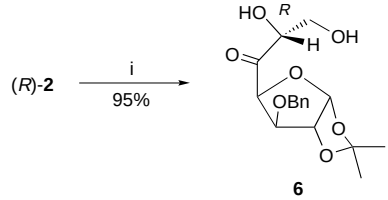

Scheme 4 *Reagents and conditions*: i, TBAF, THF, 0 °C, 1 h

governed by thermodynamic factors. To further investigate this, we managed to obtain exclusively (Z)-**1** by use of Et_3N as base instead of LDA [Scheme 3, reaction conditions (ii)].[6] Reaction of (Z)-**1** with formaldehyde using $InCl_3$ as catalyst results in a (*R*)-**2** : (S)-**2** ratio of 82 : 18 (Table 1, entry 5), a lower diastereoselection from that previously obtained. Similar trends were also observed with the triflates as Lewis acids (Table 1, entries 6 and 7).

To rationalise our results, we propose the existence of a preferred path of approach of the formaldehyde nucleophile owing to the steric requirements imposed by the rigid silyl enol ether. Hence, diastereofacial selection would depend on the favoured conformation of the silyl enol ether. Standard *ab initio*[7,8] studies carried out for the four possible conformers of silyl enol ether **4** are in good accord with the experimental finding that the *R*-isomer is the preferred observed product (Fig. 1).

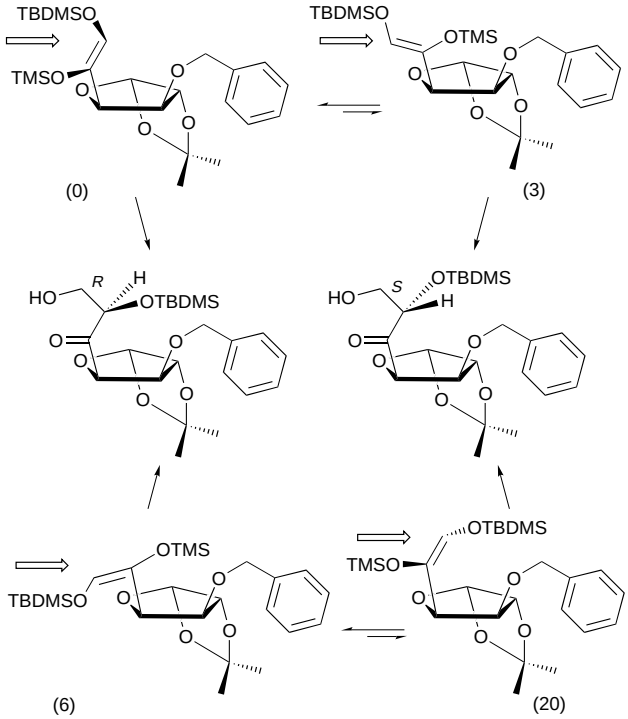

Fig. 1 Numbers in parentheses denote the calculated relative energies in kJ mol^{-1}

In effect, this methodology exploits the structure provided by the glucose derivative to achieve a highly stereoselective means of one carbon extension under mild and readily accessible reaction conditions. This, together with the well-established chemistry of the carbohydrates, would provide for its adaptation to natural product syntheses.

We acknowledge financial support for this project from the National University of Singapore (Grant RP 9300657, RP 940633 and RP 950609).

Notes and References

† E-mail: chmlohtp@nus.edu.sg

‡ Chemical shifts of α-vinylic protons: (*Z*)-**1** (s, 1 H, δ 6.21); (*E*)-**1** (s, 1 H, δ 6.08).

§ The heterogeneous nature of the mixture demands good continuous mixing.

¶ Selectivities were determined from ^{13}C NMR analysis of the purified product through comparison of the signal intensities due to the carbonyl carbon at δ 205 for (*R*)-**2** and δ 206 for (*S*)-**2**.

‖ The assignment of the stereochemistry *via* X-ray crystallography is based on the known and unchanged stereochemistry of the four chiral centres in the furanose ring. *Crystal data* for (*R*)-**6**: $C_{17}H_{22}O_7$, M = 338.35, T = 296(2) K, orthorhombic, space group $P2_12_12_1$, a = 6.0536(1), b = 13.5051(1), c = 21.8795(5) Å, U = 1788.75(5) $Å^3$, Z = 4, D_c = 1.256 Mg m^{-3}, μ(Mo-Kα radiation, λ = 0.71073 Å) = 0.098 mm^{-1}, $2\theta_{max}$ = 58.76°, F(000) = 720. Absorption correction: SADABS (Sheldrick, 1996), independent reflections = 4327, final R indices [$I > 2\sigma(I)$]: $R1$ = 0.0566, $wR2$ = 0.1413, R indices (all data): $R1$ = 0.0899, $wR2$ = 0.1596, GOF on F^2 = 1.051.

1 C. J. Li, *Chem. Rev.*, 1993, **93**, 2023.
2 A. Dondoni and A. Marra, in *Preparative Carbohydrate Chemistry*, ed. S. Hanessian, Marcel Dekker, New York, 1997, p. 173.
3 S. Kobayashi and I. Hachiya, *J. Org. Chem.*, 1994, **59**, 3590.
4 T. P. Loh, J. Pei and G. Q. Cao, *Chem. Commun.*, 1996, 1819.
5 D. A. Evans, in *Asymmetric Synthesis*, *Vol. 3*, *Part B*, ed. J. D. Morrison, Academic Press, New York, 1984, p. 12.
6 M. E. Garst, J. N. Bonfiglio, D. A. Grudoski and J. Marks, *J. Org. Chem.*, 1980, **45**, 2307.
7 W. J. Hehre, L. Radom, P. V. R. Schleyer and J. A. Pople, *Ab Initio Molecular Theory*, Wiley: New York, 1986.
8 Calculations were performed using the GAUSSIAN 92/DFT program: M. J. Frisch, G. W. Tucks, H. B. Schlegel, P. M. Gill, B. G. Johnson, M. W. Wong, J. B. Foresman, M. A. Robb, M. Head-Gordon, E. S. Replogle, R. Gomperts, J. L. Andres, K. Raghavachari, J. S. Binkley, C. Gonzalez, R. L. Martin, D. J. Fox, D. J. DeFrees, J. Baker, J. J. P. Stewart and J. A. Pople, GAUSSIAN 92/DFT, Gaussian Inc., Pittsburgh PA, 1992.

Received in Cambridge, UK, 19th January 1998; 8/00486B

Biogenesis of sex pheromones in the female olive fruit-fly

Natasha L. Hungerford,[a] Basilis E. Mazomenos,[b] Maria A. Konstantopoulou,[b] Fragoulis D. Krokos,[b] George E. Haniotakis,[b] Achim Hübener,[a] Mary T. Fletcher,[a] Christopher J. Moore,[c] James J. DeVoss[a] and William Kitching*[a]†

[a] *Department of Chemistry, The University of Queensland, Brisbane, Qld. 4072 Australia*
[b] *Biology Department, NCSR 'Demokritos', Aghia Paraskeri, Attikis, Greece*
[c] *Department of Primary Industries, Yeerongpilly, Qld. 4105, Australia*

A likely pathway to the sex pheromones of *Bactrocera oleae* (olive fruit-fly) is presented, based mainly on feeding experiments with deuterium labelled precursors.

There is little knowledge of the chemistry, enzymology or molecular biology of the biosynthesis of fruit-fly pheromones which could be linked with the known chemistry[1,2] of these species to facilitate species-specific monitoring and control. We now describe experiments with the pestilent species, *Bactrocera oleae* (olive fruit-fly),[1,3] that permit a proposal for the biogenesis of the (female) pheromone, which is essentially one component.[4] This suggests the operation of a single, major biosynthetic pathway for study, and possible disruption.

The major component of the pheromone is racemic 1,7-dioxaspiro[5.5]undecane **1**[5] which is accompanied by low levels (*ca.* 3%) of hydroxy derivatives **2**–**4**.[6] We selected 6-*n*-butyl-3,4-dihydro-2*H*-pyran **5**[7] for investigation as an advanced precursor of **1**[8] for the following reasons. Although **5** has not been identified in the olive fruit-fly, it co-occurs with **1** in *B. cacuminata*,[9] in which keto alcohol **6a** also occurs; dehydration of the corresponding hemiketal **6b** would afford **5**. Secondly, 2-methyl-6-*n*-pentyl-3,4-dihydro-2*H*-pyran **8**[10] and keto alcohol **9** accompany isomers of 2,8-dimethy-1,7-dioxaspiro[5.5]undecane **10** in *B. halfordiae* and *B. kraussii*,[2] so that the nexus that applies to **5** and **1** also applies to **8** and **10**. Appropriate side-chain hydroxylation of these dihydropyrans (**5** and **8**) followed by cyclisation would yield the corresponding spiroacetals **1** and **10**.

A [$^2H_3$]-labelled analogue of **5**, *viz* **11**, was prepared from [$^2H_6$]-propanone,[11] and essentially complete deuteration at the indicated positions in **11** was confirmed by ^{1}H and ^{13}C NMR and mass spectral analyses.‡ Examination by GC–MS of the rectal glandular contents of female olive flies, subsequent to the receipt of diet-administered **11**, established that **1** was now significantly ^{2}H-enriched, as were the accompanying hydroxyspiroacetals **2**–**4**, and the fragmentation patterns confirmed that deuterium was located at the anticipated positions α to the spiro centre. In this and in other cases described here, variation is isotopic composition for **1** was observed by progressive mass spectral examination from the foreside to the centre of the GC peak. More highly deuterated species elute earlier.[11] These examinations showed at least 40% of **1** incorporated deuterium. It is possible that *in vivo* hydration of **5** to form the hydroxy ketone **6a** (or the corresponding cyclic hemiketal **6b**) provided the real substrate for methyl oxidation. Thus, **7** (a deuterium analogue of **6**) was synthesised and administered and resulted in efficient formation of labelled **1**, indicating that **6** is also a possible penultimate precursor of **1**.

To explore the nature and specificity of the presumed side-chain oxidation, dihydropyrans **12** and **14** were also administered to female olive flies and inefficient oxidation (compared with **11**) occurred, to provide low levels of the known spiroacetals **13** and **15**,[2] respectively (Scheme 1). To the best of our knowledge these have never been detected in olive fruit-flies under natural conditions. Labelled alkenes **16** and **17**, which correspond to possible precursors of the hydroxyspiroacetals **2** and **3**, were also administered to whole female *B. oleae*. Analyses confirmed that deuterium from **16** or, more effectively, **17** was specifically incorporated into **2** and **3**, but not **4** or the parent spiroacetal **1**. This outcome is shown in Scheme 2.

The proportion of labelled **2** and **3** relative to **1** and **4** increased to a level twenty times higher when **17**, but not **16**, was administered. This supports the view that the penultimate step in the biosynthesis of **1** in *B. oleae* is ω-oxidation of **6**, followed by cyclisation. Significantly, the results for **12**, **14**, **16** and **17** demonstrate that exogenous compounds can access the enzymes of the biosynthetic sequence, a crucial feature if enzyme inhibitors[12] are to be devised for pest control.

With respect to the origin of the minor co-occurring hydroxyspiroacetals **2**–**4**, we considered these might arise from hydroxylation of intact, initially formed spiroacetal **1**. To test this proposal, [5,5,11,11-$^2H_4$]-**1** was synthesised[13] and administered, and GC–MS analysis confirmed the efficient formation

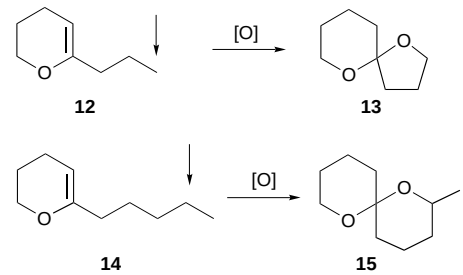

Scheme 1

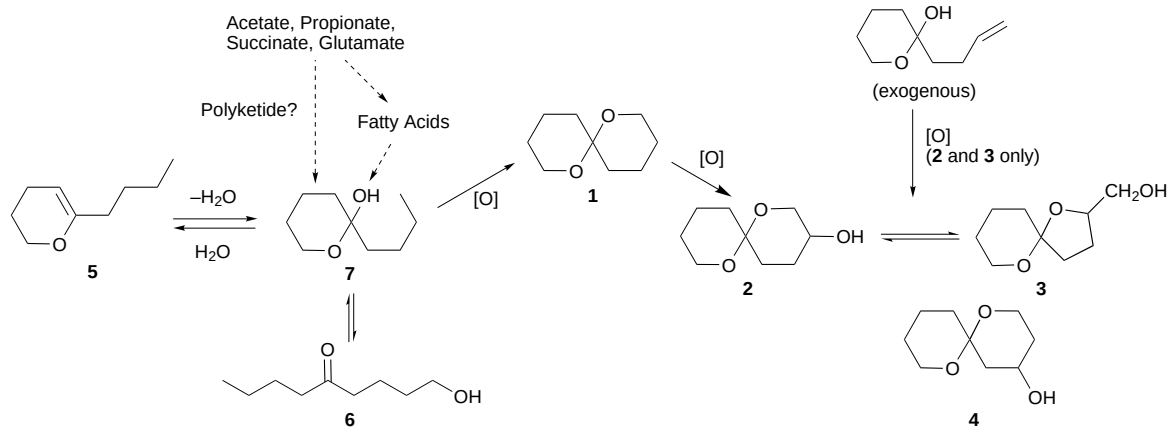

Scheme 3

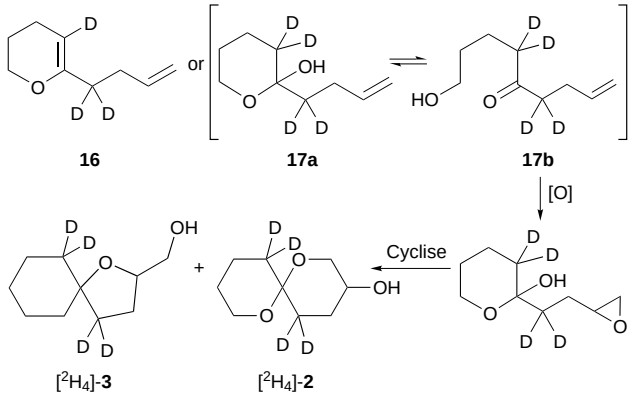

Scheme 2

of labelled **2**–**4**. The enantiomeric compositions of the hydroxy spiroacetals from this trial group closely matched those from the control group.[13,14] In contrast to this, the enantiomeric profile of the hydroxy derivatives resulting from administration of **16** or **17** was quite different. For example, **3** from the control group was predominantly (2*R*,5*R*) and (2*R*,5*S*) (20% ee), but was predominantly (2*S*,5*S*) and (2*S*,5*R*) (60% ee) for those derived from **17**.[13] This indicates that epoxidation of an unsaturated precursor is an unlikely natural route to **2** and **3**. We believe that **2**–**4** are hydroxylation products of intact **1** (or a chemically equivalent species).[15]

In summary, the above results are consistent with ω-hydroxylation of **6** (or possibly **5**) followed by dehydrative spirocyclisation to yield **1**. The remarkable, highly regioselective oxidation (compare results from **5**, **12** and **14**) of a remote Me or CH_2 group is reminiscent of similar oxidations mediated by cytochrome P450s in other eucaryotic systems.[16] This class of enzymes is known to occur in insects, mediating important transformations such as pesticide detoxification.[17]

With this framework established (Scheme 3), we are now directing attention to the origin of **6**, the likely precursor of **1**, and to establishing the generality of the biosynthetic relationship between keto alcohols and the corresponding spiro acetals, *e.g.* **9** and **10**. Keto alcohols **6** and **9** could conceivably arise by either a fatty acid or polyketide pathway and experiments to differentiate these are being conducted. In this context, it is of interest that labelled nonanoic acid and 5-oxononanoic acid were not incorporated into **1** in *B. oleae*. The isolation and characterisation of the likely P450 enzyme in *B. oleae* and *B. cacuminata* are also being pursued.

We are grateful to the Australian Research Council for financial support.

Notes and References

† E-mail: kitching@chemistry.uq.edu.au

‡ All new compounds exhibited appropriate ^{1}H and ^{13}C NMR spectra and high resolution mass spectra.

1 H. Kuba, *Proc. Internat. Symp. Biological Control of Fruit Flies*, ed. K. Kawasaki, O. Iwahashi and K. Y. Kaneshiro, Okinawa, Japan, 1991, p. 214. See also *Pheromone Biochemistry*, ed. G. D. Prestwich and G. J. Blomquist, Academic Press, Orlando, 1987.
2 M. T. Fletcher and W. Kitching, *Chem. Rev.*, 1995, **95**, 789.
3 B. E. Mazomenos, *World Crop Pests: Fruit Flies. Their Biology, Natural Enemier and Control*, ed. A. S. Robinson and G. H. S. Cooper, Elsevier, Amsterdam, 1989.
4 For a summary, see ref. 2.
5 R. Baker, R. Herbert, P. E. Howse, O. T. Jones and W. Francke, *J. Chem. Soc., Chem. Commun.*, 1980, 52.
6 R. Baker and R. H. Herbert, *J. Chem. Soc., Perkin Trans. 1*, 1987, 1123.
7 W. Francke, W. Mackenroth, W. Schröder, S. Schulz, J. Tengö, E. Engels, W. Engels, R. Kittmann and D. Schneider, *Z. Naturforsch. Teil C*, 1985, **40**, 145.
8 Previously, Mazomenos had reported that the sodium salts of [2-^{14}C]-acetate, [2-^{14}C]malonate, [2-^{14}C]propionate and [2,3-^{14}C]succinate and L-[U-^{14}C]glutamate were incorporated into **1** from *B. oleae*, and a biosynthetic proposal based on 5-oxo-1,9-nonanedioic acid was presented. See ref. 3 and J. G. Pomonis and B. E. Mazomenos, *Int. J. Invert. Reprod. Devel.*, 1986, **10**, 169.
9 S. Krohn, M. T. Fletcher, W. Kitching, R. A. I. Drew, C. J. Moore and W. Francke, *J. Chem. Ecol.*, 1991, **17**, 485.
10 M. V. Perkins, M. F. Jacobs, W. Kitching, P. J. Cassidy, J. A. Lewis and R. A. I. Drew, *J. Org. Chem.*, 1992, **57**, 365; M. T. Fletcher, J. A. Wells, M. F. Jacobs, S. Krohn, W. Kitching, R. A. I. Drew, C. J. Moore and W. Francke, *J. Chem. Soc., Perkins Trans. 1*, 1992, 2827.
11 A. B. Attygalle, J. Meinwald and T. Eisner, *Tetrahedron Lett.*, 1991, **37**, 4849.
12 Terminal alkynes are mechanism-based irreversible inhibitors of cytochrome P-450s (see P. R. Ortiz de Montellano and M. Correia, *Inhibition of Cytochrome P450 Enzymes*, in *Cytochrome P450*, ed. P. R. Ortiz de Montellano, Plenum, New York, 1995, ch. 9, p. 305 and experiments with the alk-1-yne anologue of **17** are being planned.
13 For a discussion, see N. L. Hungerford, PhD Thesis, The University of Queensland, 1997.
14 M. T. Fletcher, M. F. Jacobs, W. Kitching, S. Krohn, R. A. I. Drew, G. E. Haniotakis and W. Francke, *J. Chem. Soc., Chem. Commun.*, 1992, 1457.
15 G. D. Prestwich, *Pure Appl. Chem.*, 1989, **61**, 551; W. Francke, F. Schröder, P. Philipp, H. Meyer, V. Sinwell and G. Gries, *Bioorg. Med. Chem.*, 1996, **4**, 363.
16 R. Feyeresien, *Cytochrome P450*, ed. J. B. Schenkmna and H. Greim, Springer, Heidelberg, 1993, pp. 311–314.
17 E. Hodgson, *Microsomal Mono-Oxygenases*, in *Comprehensive Insect Physiology, Biochemistry and Pharmacology*, ed. G. A. Kerkut and L. I. Gilbert, 1985, vol. 11, p. 225; P. F. Dowd, C. M. Smith and T. C. Sparks, *Insect Biochem.*, 1983, **13**, 453.

Received in Cambridge, UK, 26th January 1998; 8/00691A

Use of antibodies to dissect the components of a catalytic event. The cyclopropenone hapten

Flavio Grynszpan[a] and Ehud Keinan*[a,b]†

[a] *The Scripps Research Institute, Department of Molecular Biology and the Skaggs Institute for Chemical Biology, 10550 North Torrey Pines Road, La Jolla, California 92037, USA*

[b] *Department of Chemistry, Technion—Israel Institute of Technology, Technion City, Haifa 32000, Israel*

Antibodies elicited against the planar cyclopropenone hapten 1 efficiently catalyze ester hydrolysis, highlighting the importance of charge rather than shape complementarity as a design element of hydrolytic antibodies.

In the most common approach to the design of antibody catalysts the experimenter simultaneously incorporates a series of parameters that will operate in concert to achieve a catalytic event. A less frequently discussed but equally important approach is to apply special hapten design to induce only selected parameters and thereby assess their role in catalysis. Here we take the less common approach in order to examine the relative importance of two key parameters—charge *vs.* shape complementarity in the antibody active site. The relative importance of these parameters is of central significance not only in hapten design but also in immunochemistry in general.

Mechanistic and X-ray crystallographic studies of both esterolytic enzymes[1] and catalytic antibodies highlight the importance of three design elements when planning inhibitors and haptens. I. *Tetrahedral geometry*, needed to mimic the rehybridization of the carbonyl carbon in the transition state. II. *Negative charge*, needed to create a stabilizing environment for the developing oxyanion. III. *Positive charge*, needed to generate a general base residue in the active site. Haptens with design elements I and II, *e.g.* phosphonates, amidophosphonates, phosphates, have been extensively used to elicit antibodies that catalyze various interconversion reactions of carboxylic acid derivatives.[2] Design elements I and III were also used to generate hydrolytic antibodies.[3] Few attempts to simultaneously employ all design elements, I, II and III, in order to achieve polyfunctional catalytic antibodies have been reported.[4,5]

A common assumption that lies at the basis of all of the above mentioned studies is that the shape complementarity element I is an indispensable feature to be considered in the design of hydrolytic antibodies. Here we report on esterolytic antibodies that were raised against the cyclopropenone functionality. Hapten **1** reflects the electrostatic design elements II and III but lacks the geometrical design element I, thereby allowing us to examine the importance of charge complementarity alone.

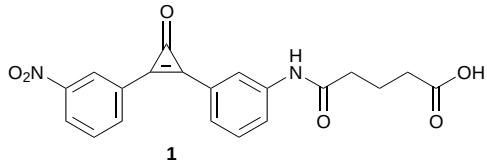

1

Hapten **1** presents a cyclopropenone ring as well as two aromatic recognition elements. Diphenylcyclopropenone, **2**,[6] may be described by two canonical resonance forms **2a** and **2b**. The solid state structure of **2** indicates that its carbonyl bond is highly polarized, suggesting a significant contribution of the aromatic (2π electrons) zwitterionic structure **2b**. This polarization may be enhanced by the formation of hydrogen bonds.[7] The physical properties of **2** (^{17}O NMR, IR and dipole moment) provide supporting evidence for the existence of a negative charge on the oxygen atom.[5] The remarkable chemical stability of **2** under acidic conditions is also attributed to the aromatic nature of the cyclopropenium moiety.

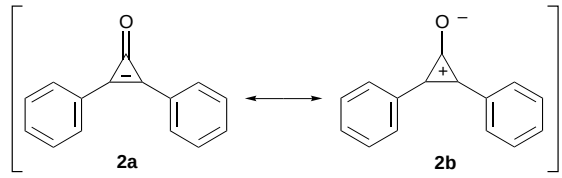

2a **2b**

The synthesis of **1** was achieved in four steps starting with mono-nitration of **2** (Aldrich) to give 2-(3-nitrophenyl)-3-phenylcyclopropenone **3**.[8] The nitro group was reduced with Ti^{III} to the corresponding amine, **4**. Reaction with glutaric anhydride to produce the monoamide **5** (**3**–**5** not shown),[9] followed by nitration of the unsubstituted phenyl ring, afforded hapten **1**.[10]

The five substrate esters **6**–**8** were prepared by acid catalyzed esterification of the substituted phenylacetic acid with the appropriate phenol.

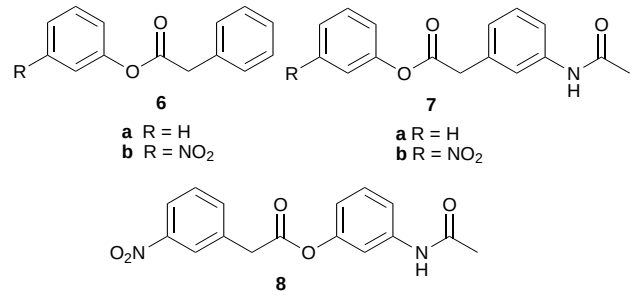

6 **7** **8**

a R = H
b R = NO_2

a R = H
b R = NO_2

Following immunization of 129^{IX+} mice with the Keyhole Limpet Hemocyanin (KLH) conjugate of **1**, 15 hybridoma cells producing anti-**1** antibodies were selected for further studies. Antibodies from each cell-line were purified by ammonium sulfate precipitation, anion exchange, and protein-G affinity chromatography. The antibodies were screened for catalytic activity by monitoring the release of *m*-nitrophenol (λ_{max} = 330 nm) in the hydrolysis of **6b** and **7b** using a microplate reader. Antibodies 10E8, 11G4, 12G2, 13B6 and 15D3 were found to be catalytic and antibody 12G2 was selected for this study.

The antibody catalyzed reactions were carried out by mixing a phosphate-buffered saline (PBS) solution (50 mM phosphate, 100 mM NaCl, at different pHs) of antibody 12G2 (12 μM, 0.045 ml) with MeCN solutions (0.005 ml) of the substrate **6b** at different concentrations (0.04–0.6 mM) and monitoring them

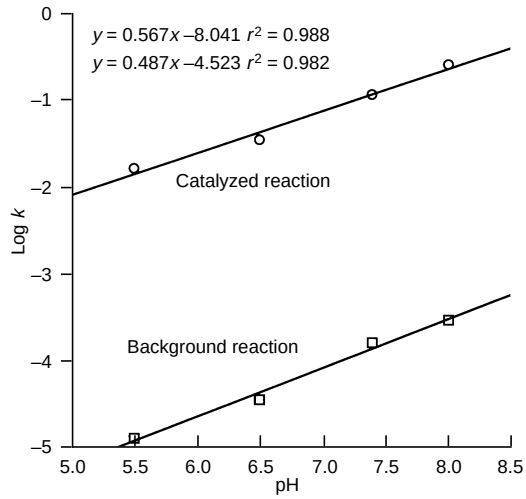

Fig. 1 pH–rate profile of 12G2-catalyzed hydrolysis of **6b**

Table 1 Kinetic parameters 10^{-5} for the 12G2 catalyzed hydrolysis of the studied substrates

Substrate	$k_{un}/10^{-5}$ min^{-1}	K_m/μM	$k_{cat}/10^{-2}$ min^{-1}	k_{cat}/k_{un}
6b	3.6	100	3.5	970
7b	7.0	480	1.4	200
8	2.7	90	0.3	110

by HPLC. The background (uncatalyzed) reaction rate constants (k_{un}) were determined in the presence of 12G2 and **1** (0.001 ml, EtOH solution, equimolar to the substrate).[11] The catalyzed reaction rate constants (k_{cat}) were obtained from Lineweaver–Burk plots of the kinetic data.

The pH rate profiles (log *k vs.* pH) of the catalyzed and uncatalyzed hydrolysis of **6b** between pH 5.5 and 8 (Fig. 1) show that both reactions have the same linear dependence on pH. The fact that both lines in Fig. 1 exhibit the same slope suggests that catalysis does not involve any strain/rehybridization effect and both reactions proceed along the same mechanism, namely, general base catalysis.

A comparative study of the substrate range was carried out at pH 6.5. The kinetic parameters for three different substrates, derived from the corresponding Lineweaver–Burk plots are given in Table 1. While rate enhancement of 2–3 orders of magnitude is achieved with substrates **6b**, **7b** and **8**, no catalysis is observed with **6a** and **7a**, a fact that highlights the importance of the nitro group as a substrate recognition element. Comparison of the kinetic data of **6b** and **7b** indicates that the presence of an acetamido group in the substrate decreases both substrate binding and catalytic efficiency. This observation supports the above-mentioned conclusion that the antibody cannot distort the substrate to fit the binding pocket of 12G2. Ester **8** binds to 12G2 as well as **6b** does but its catalyzed hydrolysis is one order of magnitude slower.

Interestingly, very little is known about natural products containing a cyclopropenone fragment.[12] A papain inhibitor possessing a cyclopropenone moiety exhibits a K_i in the submicromolar level. The mechanism for the action of this unique protease inhibitor still remains unclear.[13]

Catalytic antibodies offer unique opportunities to examine mechanistic hypotheses and the relative importance of individual design elements in catalysis. We have shown here that antibodies elicited against hapten **1** catalyze ester hydrolysis with a 1000-fold rate enhancement. As hapten **1** does not mimic the shape of the transition state, yet elicits efficient catalysts, it is likely to generate the necessary charge complementarity in the active site. Thus, haptenic tetrahedral geometry is a desirable feature but not a prerequisite to generating hydrolytic antibodies. This study, together with the information reported about a cyclopropenone-containing protease inhibitor, highlights the potential applications of the rarely used cyclopropenone functionality in the future design of both haptens and enzyme inhibitors.

We are grateful to Dr S. C. Sinha for early contributions to this work and to D. M. Kubitz for antibody preparation. We thank Pharmore Therapeutics and The Skaggs Institute for Chemical Biology for financial support. F. G. thanks the Lady Davis foundation for a postdoctoral fellowship.

Notes and References

† E-mail: keinan@scripps.edu

1 G. Fisher, *Enzyme Mechanisms*, ed. M. I. Page and A. Williams, The Royal Society of Chemistry, London, 1987, p. 227.
2 P. G. Schultz and R. A. Lerner, *Science*, 1995, **269**, 1835; J. R. Jacobsen and P. G. Schultz, *Curr. Opin. Struct. Biol.*, 1995, **5**, 818; G. MacBeath and D. Hilvert, *Chem. Biol.*, 1996, **3**, 433; E. Keinan and R. A. Lerner, *Israel J. Chem.*, 1996, **36**, 113; N. R. Thomas, *Nat. Prod. Rep.*, 1996, 479.
3 K. D. Janda, M. I. Weinhouse, D. M. Schloeder, R. A. Lerner and S. J. Benkovic, *J. Am. Chem. Soc.*, 1990, **112**, 1274; A. I. Khalaf, G. R. Proctor, C. J. Suckling, L. H. Bence, J. I. Irvine and W. H. Stimson, *J. Chem. Soc., Perkin Trans. 1*, 1992, 1475.
4 For the use of haptens with trimethylammonium and phosphate groups on two vicinal carbon atoms, see: H. Suga, O. Ersoy, T. Tsumuraya, J. Lee, A. J. Sinskey and S. Masamune, *J. Am. Chem. Soc.*, 1994, **116**, 487.
5 For the use of two differently charged haptens in heterologous immunization to generate two catalytic residues in the antibody's active site, see: H. Suga, O. Ersoy, S. F. Williams, T. Tsumuraya, M. N. Margolies, A. J. Sinskey and S. Masamune, *J. Am. Chem. Soc.*, 1994, **116**, 6025; T. Tsumuraya, H. Suga, S. Meguro, A. Tsunakawa and S. Masamune, *J. Am. Chem. Soc.*, 1995, **117**, 11 390.
6 K. T. Potts and J. S. Baum, *Chem. Rev.*, 1974, **74**, 189.
7 H. Tsukada, H. Shimanouchi and Y. Sasada, *Tettrahedron Lett.*, 1973, **27**, 2455; H. Tsukada, H. Shimanouchi and Y. Sasada, *Chem. Lett.*, 1974, 639.
8 C. W. Bird and A. F. Hamer, *Org. Prep. Proced. Int.*, 1970, **2**, 79.
9 Preparation of **5**: **4** (0.55 g, 2.5 mmol) was dissolved in dry THF (25 ml). Glutaric anhydride (1.42 g, 12.5 mmol) was added and the mixture was stirred at room temp. for 12 h. Work-up and purification by column chromatography (silica gel, EtOAc–hexane 4 : 1) afforded **5** (0.21 g, 25%) in the form of a colorless solid. δ_H($CDCl_3$ with 2 drops CD_3OD) 8.05 (s 1 H), 7.90 (s br, 2 H), 7.84 (s br, 1 H), 7.59 (d, *J* 9.72, 1 H), 7.50 (s, 3 H), 7.41 (t, *J* 7.48, 1 H), 2.35 (t, *J* 7.68, 2 H), 2.31 (t, *J* 6.76, 2 H), 1.91 (t, *J* 7.80, 2 H); *m/z* (ESI) 334 ($M - H^+$).
10 Preparation of **1**: sodium nitrate (0.025 g, 0.298 mmol) was added to a stirred solution of 2-[3-(4-carboxybutanamido)phenyl]-3-phenylcyclopropenone (0.1 g, 0.298 mmol) in conc. sulfuric acid (1 ml). The mixture was stirred for 1 h at room temp., then heated to 100 °C for 1 h and poured into ice–water. The precipitate was washed with water, dissolved in EtOAc and passed through a silica gel bed using EtOAc to give **1** (0.053 g, 31%) in the form of a colorless solid. δ_H(CD_3OD) 8.87 (s, 1 H), 8.52 (d br, 1 H, *J* 8.28), 8.50 (s, 1 H), 8.44 (d br, 1 H, *J* 7.04), 7.95 (t, 1 H, *J* 7.72), 7.82 (d, 1 H, *J* 8.04), 7.76 (d, 1 H, *J* 7.44), 7.66 (s, 1 H), 7.61 (t, 1 H, *J* 7.80); *m/z* (LSI) 381 (MH^+).
11 No change in the rate of the 12G2-catalyzed hydrolysis of **6b** could be detected in the presence of ethanol (0.001 ml). Partial inhibition of the reaction was observed in the presence of compounds **2**, **3** and **5** (1 equiv. with respect to the substrate).
12 T. Okuda, K. Yokose, T. Furumai and H. Maruyama, *J. Antibiot.*, 1984, **37**, 718; H. Tokuyama, M. Isaka, E. Nakamura, R. Ando and Y. Morinaka, *J. Antibiot.*, 1992, **45**, 1148.
13 R. Ando, Y. Morinaka, H. Tokuyama, M. Isaka and E. Nakamura, *J. Am. Chem. Soc.*, 1992, **115**, 1174.

Received in Cambridge, UK, 9th January 1998; 8/00274F

Synthesis and crystal structure of a bis(phosphiren-1-yl)–iron complex[1]

J. Simon, U. Bergsträßer and M. Regitz*†

Fachbereich Chemie der Universität Kaiserslautern, Erwin-Schrödinger-Straße, D-67663 Kaiserslautern, Germany

1-Chloro-1*H*-phosphirenes 5 react with disodium tetracarbonylferrate to furnish the novel mono-complexed bis(phosphirenyl)s 7 which, in turn, are converted to the doubly-complexed species 8 by treatment with nonacarbonyldiiron.

Investigations on the synthesis and reactivity of λ³-phosphinines **1** in the 1960s played a major role in the development of

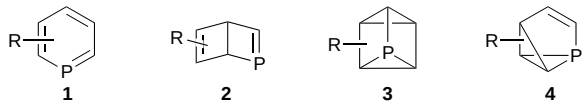

the chemistry of low-coordinated phosphorus.[2,3] Somewhat later, their classical valence isomers such as, for example, λ³,σ²-Dewar-benzenes **2**,[4] phosphaprismanes **3**[5] and λ³,σ³-benzvalenes **4**[5] were also prepared.

The Dewar-benzene derived from 2,4,6-tri-*tert*-butyl-1,3,5-triphosphinine was recently added to this list.[6] In contrast, very little information about the diphosphinines is available,[7] and the valence isomers derived from them are still unknown. We now report the first synthesis of a complexed bis(phosphirenyl), representing a new type of phosphinine valence isomer.

The starting materials for the syntheses of the bis(phosphirenyl)s **7a**,**b** were the 1-chloro-1*H*-phosphirenes **5a**,**b** (Scheme 1).[8] Reactions of the latter with disodium tetracarbonylferrate (0.5 equiv.) furnished the mono-complexed bis(phosphirenyl)s **7a**,**b** in good yields (60%). The composition and constitution of the products were elucidated with the help of NMR and mass spectroscopy.‡ Because of the presence of centres of chirality at the two phosphorus atoms and their configurational stability, these reactions give rise to two diastereomers which, however, cannot be separated by column chromatography. One of the diastereomers in each case can be enriched up to a ratio of 8:1 (**7a**) or 4:1 (**7b**) (as determined from their ^{1}H NMR spectra) by crystallization.

The formation of **7** is reflected in the ^{31}P NMR spectra by a significant $^1J_{P,P}$ coupling constant of 427 Hz. The complexed ring phosphorus atom gives rise to a signal at considerably lower field than that of the uncomplexed ring (δ −88, as compared to −132). Complexation with the tetracarbonyliron fragment is also apparent in the ^{13}C NMR spectra from a drastic reduction in the intracyclic $^1J_{C,P}$ coupling constant of the complexed phosphirene to 22–27 Hz, in comparison to 50–57 Hz for the uncomplexed ring. A similar phenonemon has also been reported for complexation reactions of other 1*H*-phosphirenes.[9c] The signals for the ring carbon atoms of **7a**,**b** occur in the typical region for 1*H*- phosphirenes.[9]

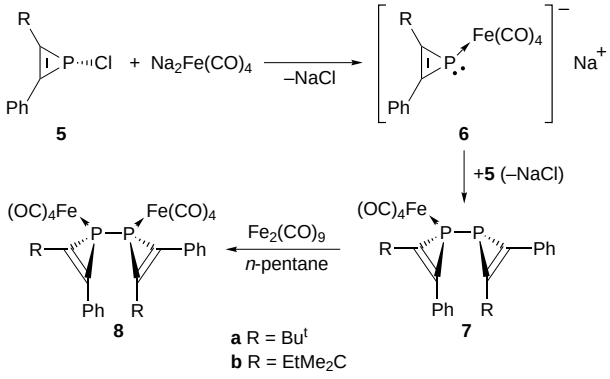

Scheme 1

The initial reductive substitution of the chlorine atom of **5** by the tetracarbonyliron fragment results in the anionic phosphirene complex **6** which participates in an immediate nucleophilic substitution with a second molecule of **5** to afford **7**.

Treatment of the compounds **7a**,**b** with nonacarbonyldiiron results in the formation of the symmetrical, doubly-complexed bis(phosphirenyl)s **8a**,**b** in yields of 63% (**8a**) and 54% (**8b**).§ As a consequence of the high symmetry of compounds **8** their ^{31}P NMR spectra each contain only one singlet signal. Complexation of the additional tetracarbonyliron fragments effects further shifts to lower field [δ −69.3 (**8a**) and −70.5 (**8b**)].

The ^{13}C NMR spectra of **8** do not show any significant changes in chemical shifts due to the additional complex fragments in comparison to those of **7**.

An X-ray crystallographic analysis of the complex **8a** confirmed the proposed structure (Fig. 1).¶ In the crystal the two tetracarbonyliron fragments and, respectively, the two phosphirene rings have *syn* orientations to each other. Because of the extreme steric situation, the two phosphirene rings are somewhat twisted, as reflected in torsional angles of 39.4° [Fe(1)–

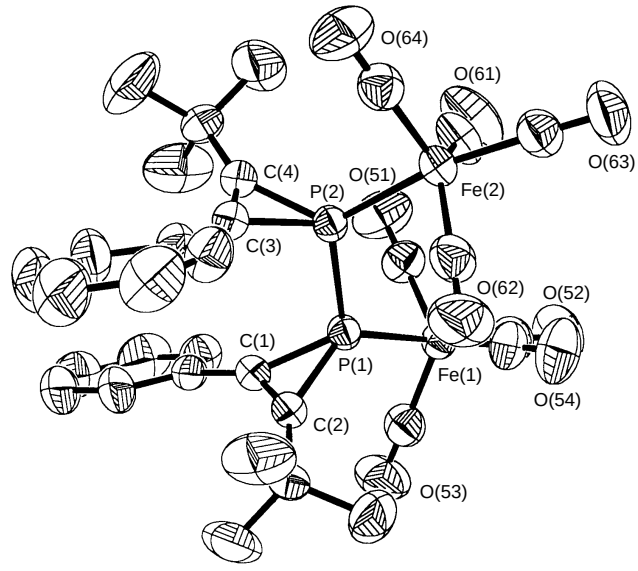

Fig. 1 Crystal structure of **8a**. Selected bond lengths (Å) and angles (°): Fe(1)–P(1) 2.2311(7), Fe(2)–P(2) 2.2185(7), P(1)–P(2) 2.2516(10), P(1)–C(1) 1.793(2), P(1)–C(2) 1.796(2), P(2)–C(3) 1.793(2), P(2)–C(4) 1.797(2), C(1)–C(2) 1.317(3), C(3)–C(4) 1.319(3); C(1)–P(1)–C(2) 43.05(11), C(1)–P(1)–P(2) 108.23(8), C(2)–P(1)–P(2) 108.97(8), C(3)–P(2)–C(4) 43.11(11), C(3)–P(2)–P(1) 108.55(8), C(4)–P(2)–P(1) 109.05(8), C(2)–C(1)–P(1) 68.60(14), C(1)–C(2)–P(1) 68.3(2), C(3)–C(4)–P(2) 68.3(2), C(4)–C(3)–P(2) 68.58(14).

P(1)–P(2)–Fe(2)] and 33.9° [C(1)–P(1)–P(2)–C(4)]. The P(1)–P(2) bond length amounts to 2.2516(10) Å and is thus somewhat lengthened as a result of the spatially demanding substitution pattern. The intracyclic P–C bond lengths of 1.793 to 1.797 Å, as well as the carbon–carbon double bond length of 1.317 Å, are of the expected sizes for a complexed 1*H*-phosphirene.[9c] Similary, the C–P–C bond angles of 43.05(11) and 43.11(11)° are comparable with those of other 1*H*-phosphirenes.[9]

We thank the Landesregierung von Rheinland-Pfalz for a graduate grant (to J. S.) and the Fonds der Chemischen Industrie for generous financial support.

Notes and References

† E-mail: regitz@rhrk.uni-kl.de

‡ *Selected data* for **7a** (only values for the major diastereomer are given): mp 97–99 °C; δ_P (81 MHz, $CDCl_3$) −88.1 (d, $^1J_{P,P}$ 427.3, P-1), −134.2 (d, $^1J_{P,P}$ 427.3 P-2); δ_H(200 MHz, $CDCl_3$) 1.44 [br s, 18 H, $C(CH_3)_3$], 7.40–7.51 (m, 6 H, *m*/*p*-Ph), 7.57–7.65 (m, 4 H, *o*-Ph); δ_C (50 MHz, $CDCl_3$) 29.22 [d, $^3J_{C,P}$ 1.7, $C(CH_3)_3$], 29.53 [s, $C(CH_3)_3$], 33.86 [dd, $^2J_{C,P}$ 6.4, $^3J_{C,P}$ 3.0, $C(CH_3)_3$], 34.24 [d, $^2J_{C,P}$ 6.8, $C(CH_3)_3$], 120.33 (d, $^1J_{C,P}$ 50.8, C-5), 124.80 (dd, $^1J_{C,P}$ 22.0, $^2J_{C,P}$ 4.2, C-3), 127.30 (d, $J_{C,P}$ 7.6, Ph), 128.62 (s, Ph), 128.87 (s, Ph), 129.73 (d, $J_{C,P}$ 5.1, Ph), 130.41 (d, $J_{C,P}$ 4.2, Ph), 131.33 (s, Ph), 138.50 (d, $^1J_{C,P}$ 57.7, C-6), 140.51 (dd, $^1J_{C,P}$ 27.1, $^2J_{C,P}$ 5.1, C-4), 213.94 [d, $^2J_{C,P}$ 19.5, $Fe(CO)_4$]; *m*/*z* (EI, 70 eV) 546 (8) [M^+], 276 (100) [$M^+ - 4CO - C_{12}H_{14}$] (Calc. for $C_{28}H_{28}FeP_2O_4$: C, 61.56; H, 5.17. Found: C, 60.90; H, 5.07%) (HR-MS: calc. for M^+: 546.0813. Found: 546.0813). For **7b**: δ_P (81 MHz, $CDCl_3$) −90.6 (d, $^1J_{P,P}$ 427.6, P-1), −132.2 (d, $^1J_{P,P}$ 427.6, P-2); δ_H (200 MHz, $CDCl_3$) 0.96 (t, 3 H, $^3J_{H,H}$ 7.6, CH_2CH_3), 1.12 (t, 3 H, $^3J_{H,H}$ 7.0, CH_2CH_3), 1.42 [s, 3 H, $C(CH_3)_2$], 1.43 [s, 3 H, $C(CH_3)_2$], 1.46 [s, 3 H, $C(CH_3)_2$], 1.47 [s, 3 H, $C(CH_3)_2$], 1.63–1.92 (m, 4 H, CH_2CH_3), 7.37–7.53 (m, 6 H, Ph), 7.57–7.77 (m, 4 H, Ph); δ_C (100 MHz, $CDCl_3$) 8.67 (d, $^4J_{C,P}$ 6.3, CH_2CH_3), 9.13 (d, $^4J_{C,P}$ 4.5, CH_2CH_3), 25.66 [s, $C(CH_3)_2$], 26.28 [d, $^3J_{C,P}$ 5.4, $C(CH_3)_2$], 26.45 [s, $C(CH_3)_2$], 26.88 [s, $C(CH_3)_2$], 34.36 (d, $^3J_{C,P}$ 5.4, CH_2CH_3), 34.39 (s, CH_2CH_3), 37.01 [s, $C(CH_3)_2Et$], 37.65 [d, $^2J_{C,P}$ 5.4, $C(CH_3)_2Et$], 120.89 (d, $^1J_{C,P}$ 51.2, C-5), 125.12 (d, $^1J_{C,P}$ 22.4, C-3), 127.03 (d, $^3J_{C,P}$ 8.3, *o*-Ph), 127.16 (d, $^3J_{C,P}$ 7.2, *o*-Ph), 128.32 (s, Ph), 128.58 (s, Ph), 129.41 (d, $^2J_{C,P}$ 16.2, *i*-Ph), 129.48 (d, $^2J_{C,P}$ 14.4, *i*-Ph), 130.12 (s, Ph), 131.18 (s, Ph), 138.25 (d, $^1J_{C,P}$ 57.5, C-6), 141.38 (dd, $^1J_{C,P}$ 28.3, $^2J_{C,P}$ 4.0, C-4), 213.73 [d, $^2J_{C,P}$ 18.0, $Fe(CO)_4$]; *m*/*z* (EI, 70 eV): 574 (1) [M^+], 143 (100) [$C_{11}H_{11}^+$] (HR-MS: calc. for M^+: 574.1135. Found 574.1130).

§ *Selected data* for **8a** (only values for the major diastereomer are given): mp 135 °C (decomp.); δ_P (81 MHz, $CDCl_3$) −69.3 (s); δ_H (200 MHz, $CDCl_3$) 1.52 [s, 18 H, $C(CH_3)_3$], 7.41–7.54 (m, 6 H, *m*/*p*-Ph), 7.55–7.61 (m, 4 H, *o*-Ph); δ_C (50 MHz, $CDCl_3$) 29.27 [pseudo t, $^3J_{C,P}$ + $^4J_{C,P}$ 4.2, $C(CH_3)_3$], 34.82 [pseudo t, $^2J_{C,P}$ + $^3J_{C,P}$ 3.4, $C(CH_3)_3$], 126.07 (pseudo t, $^3J_{C,P}$ + $^4J_{C,P}$ 3.4, *o*-Ph), 128.52 (pseudo t, $^1J_{C,P}$ + $^2J_{C,P}$ 15.2, C-2/C-2′), 128.93 (s, *m*-Ph), 130.38 (pseudo t, $^2J_{C,P}$ + $^3J_{C,P}$ 5.9, *i*-Ph), 130.55 (d, $^5J_{C,P}$ 1.7, *p*-Ph), 142.20 (pseudo t, $^1J_{C,P}$ + $^2J_{C,P}$ 22.0, C-3/C-3′), 213.11 [pseudo t, $^2J_{C,P}$ + $^3J_{C,P}$ 17.0, $Fe(CO)_4$]; *m*/*z* (EI, 70 eV): 714 (0.02) [M^+], 332 (100) [$M^+ - 8CO - C_{12}H_{14}$] (Calc. for $C_{32}H_{28}Fe_2P_2O_8$: C, 53.82; H, 3.95. Found: C, 53.12; H, 4.20%). For **8b**: δ_P (81 MHz, $CDCl_3$) −70.5 (s); δ_H (400 MHz, $CDCl_3$) 0.90 (t, 6 H, CH_2CH_3), 1.42 [s, 6 H, $C(CH_3)_2Et$], 1.45 [s, 6 H, $C(CH_3)_2Et$], 1.80 (q, 4 H, CH_2CH_3), 7.34–7.46 (m, 6 H, *m*/*p*-Ph), 7.67–7.73 (m, 4 H, *o*-Ph); δ_C (100 MHz, $CDCl_3$) 8.79 (d, $^4J_{C,P}$ 8.8, CH_2CH_3), 26.00 [s, $C(CH_3)_2Et$], 26.21 [s, $C(CH_3)_2Et$], 34.24 (d, $^3J_{C,P}$ 10.4, CH_2CH_3), 38.28 [d, $^2J_{C,P}$ 14.5, $C(CH_3)_2Et$], 126.32 (d, $^1J_{C,P}$ 20.0, C-2/C-2′), 128.93 (s, *m*-Ph), 129.87 (pseudo t, $^2J_{C,P}$ + $^3J_{C,P}$ 7.2, *i*-Ph), 130.38 (d, $^3J_{C,P}$ 6.4, *o*-Ph), 130.54 (d, $^5J_{C,P}$ 3.2, *p*-Ph), 141.61 (pseudo t, $^1J_{C,P}$ + $^2J_{C,P}$ 12.0, C-3/C-3′), 213.74 [d, $^2J_{C,P}$ 4.8, $Fe(CO)_4$]; *m*/*z* (EI, 70 eV) 742 (0.04) [M^+], 143 (100) [$C_{11}H_{11}^+$]. (Calc. for $C_{32}H_{28}Fe_2P_2O_8$: C, 55.02; H, 4.35. Found: C, 53.95; H, 4.10%).

¶ *Crystal data* for **8a**: $C_{32}H_{28}Fe_2O_8P_2$, M = 714.18 g mol^{-1}, monoclinic, space group $P2_1/n$, a = 10.102(2), b = 18.273(4), c = 18.775(4) Å, β = 99.86(3)°, V = 3414.7(12) Å^3, Z = 4, D_c = 1.389 Mg m^{-3}, μ = 0.989 mm^{-1}, $F(000)$ = 1464. Crystal dimensions 0.35 × 0.20 × 0.15 mm^3, 26 734 reflections collected, 6321 independent reflections (R_{int} = 0.0382), 4511 reflections with $I > 2\sigma(I)$, goodness-of-fit on F^2 = 1.205, R [$I > 2\sigma(I)$] = 0.0370, wR_2 = 0.0896; R (all data) = 0.0534, wR_2 = 0.0945; maximum residual density 0.420 e Å^{-3}. Data were collected on a STOE Imaging Plate Diffraction System at room temperature with Mo-Kα radiation (λ = 0.71073 Å). The structure was solved with SHELXS-86 [ref. 10(*a*)] and refined with SHELXL-93 [ref. 10(*b*)]. CCDC 182/787.

1 Part 128 of the series of papers on Organophosphorus Compounds. For part 127, see: T. W. Mackewitz and M. Regitz, *Synthesis*, 1998, in the press.
2 O. J. Scherer and M. Regitz, in *Multiple Bonds and Low Coordination in Phosphorus Chemistry*, ed. M. Regitz and O. J. Scherer, Thieme, Stuttgart, 1990, p. 1.
3 G. Märkl, in *Multiple Bonds and Low Coordination in Phosphorus Chemistry*, ed. M. Regitz and O. J. Scherer, Thieme, Stuttgart, 1990, p. 220.
4 J. Fink, W. Rösch, U.-J. Vogelbacher and M. Regitz, *Angew. Chem.*, 1986, **98**, 265; *Angew. Chem., Int. Ed. Engl.*, 1986, **25**, 280.
5 K. Blatter, W. Rösch, U.-J. Vogelbacher, J. Fink and M. Regitz, *Angew. Chem.*, 1987, **99**, 67; *Angew. Chem., Int. Ed. Engl.*, 1987, **26**, 85.
6 P. Binger, S. Leininger, J. Stannek, B. Gaber, R. Mynott, J. Bruckmann and C. Krüger, *Angew. Chem.*, 1995, **107**, 2411; *Angew. Chem., Int. Ed. Engl.*, 1995, **34**, 2227
7 D. Böhm, F. Knoch, S. Kummer, U. Schmidt and U. Zenneck, *Angew. Chem.*, 1995, **107**, 251.
8 O. Wagner, M. Ehle and M. Regitz, *Angew. Chem.*, 1989, **101**, 227; *Angew. Chem., Int. Ed. Engl.*, 1989, **28**, 225; O. Wagner, M. Ehle, M. Birkel, J. Hoffmann and M. Regitz, *Chem. Ber.*, 1991, **124**, 1207.
9 (*a*) F. Mathey and M. Regitz, in *Comprehensive Heterocyclic Chemistry II*, ed. A. R. Katritzky, C. W. Rees and E. F. V. Scriven, Pergamon, Oxford, 1996, p. 277; (*b*) H. Memmesheimer and M. Regitz, *Rev. Heteroatom Chem.*, 1994, **10**, 61; (*c*) F. Mathey, *Chem. Rev.*, 1990, **90**, 997.
10 (*a*) G. M. Sheldrick, SHELXS-86, a program for the solution of crystal structures, Göttingen, Germany 1986; (*b*) G. M. Sheldrick, SHELXL-93, a program for structure refinement, Göttingen, Germany 1993.

Received in Liverpool, UK, 22nd December 1997; 7/09127C

Synthesis, crystal and molecular structure of the first indium trihydride complex, $[InH_3\{\overline{CN(Pr^i)C_2Me_2N(Pr^i)}\}]$

David E. Hibbs,[a] Michael B. Hursthouse,[a] Cameron Jones*[b] and Neil A. Smithies[b]

[a] *EPSRC X-ray Crystallography Service, Department of Chemistry, University of Wales, Cardiff, PO Box 912, Park Place, Cardiff, UK CF1 3TB*

[b] *Department of Chemistry, University of Wales, Swansea, Singleton Park, Swansea, UK SA2 8PP*

The reaction of either $[InH_3(NMe_3)]$ or $LiInH_4$ with an excess of the imidazol-2-ylidene carbene, $:\overline{CN(Pr^i)C_2Me_2N(Pr^i)}$, affords the first example of an indium trihydride complex, $[InH_3\{\overline{CN(Pr^i)C_2Me_2N(Pr^i)}\}]$, the X-ray crystal structure of which is described.

The chemistry of the binary hydrides of aluminium and gallium, $[(MH_3)_n]$ (M = Al, Ga), and their Lewis base adducts is now a well established field that derives its current importance from the application such compounds have in areas ranging from organic synthesis to chemical vapour deposition.[1] Despite early claims,[2] it seems unlikely that the corresponding indium trihydride $[(InH_3)_n]$ has yet been synthesised although monomeric InH_3 has been isolated and studied in a solid argon matrix.[3] In fact, the weakness of the In–H bond has meant that to date only five indium hydride compounds have been structurally characterised (*viz.* $[Li(thf)_2][\{(Me_3Si)_3C\}_2In_2H_5]$ **1**,[4] $K[H\{In(CH_2CMe_3)_3\}_2]$ **2**,[5] $K_3[K(Me_2SiO)_7]$ $[InH(CH_2CMe_3)_3]_4$ **3**,[6] $[InH\{2\text{-}Me_2NCH_2(C_6H_4)\}_2]$ **4**[7] and $[Me_2InB_3H_8]$ **5**[8]). In our laboratory we have become interested in extending this field to the stabilisation of indium trihydride complexes, which are as yet unknown. With this goal in mind we saw imidazol-2-ylidene carbenes as potentially useful ligands, primarily because their AlH_3 complexes (*e.g.* $[AlH_3\{\overline{CN(Mes)C_2H_2N(Mes)}\}]$ **6**, Mes = $C_6H_2Me_3$-2,4,6, mp 246 °C[9]) are known to be considerably more stable than normal AlH_3 adducts (*e.g.* $[AlH_3(NMe_3)]$ decomp. at 100 °C[10]). This stability stems from the high nucleophilicity of such carbenes which we have previously exploited in the preparation of a series of complexes between $:\overline{CN(Pr^i)C_2Me_2N(Pr^i)}$ **7** and indium trihalides, *viz.* $[InX_3\{\overline{CN(Pr^i)C_2Me_2N(Pr^i)}\}_n]$ (n = 1, **8**; 2, **9**) and $[HCN(Pr^i)C_2Me_2N(Pr^i)]^+[InX_4\{\overline{CN(Pr^i)C_2Me_2N(Pr^i)}\}]^-$ **10** (X = Cl, Br).[11] We now wish to report the use of **7** in the synthesis of the first structurally authenticated indium trihydride complex.

Treatment of an ethereal solution of $[InH_3(NMe_3)]$[12] (generated *in situ* from $LiInH_4$[2] and $NMe_3{\cdot}HCl$ at −30 °C) with 2 equiv. of **7** at −40 °C led to a moderate yield (42%) of $[InH_3\{\overline{CN(Pr^i)C_2Me_2N(Pr^i)}\}]$ **11** after recrystallisation from diethyl ether (Scheme 1). Complex **11** is an extremely air sensitive, colourless material that decomposes, depositing indium metal and generating hydrogen gas, at temperatures greater than −20 °C in solution and −5 °C in the solid state. Interestingly, treatment of $LiInH_4$ with 2 equiv. of **7** also gave **11** in a moderate yield (38%). This is not surprising and has a precedent in aluminium chemistry with the reaction of $LiAlH_4$ with tertiary amines which can yield alane adducts, $[AlH_3(NR_3)]$, and Li_3AlH_6.[13] It seems likely that in the present reaction a related complex indium hydride is being generated as a by-product in the formation of **11**. Unfortunately attempts to characterise this by-product have so far proved fruitless owing to its thermal instability. It is noteworthy that the aluminium analogue of **11**, *viz.* $[AlH_3\{\overline{CN(Pr^i)C_2Me_2N(Pr^i)}\}]$ **12**, can also be prepared in high yield by the reaction of **7** with either $[AlH_3(NMe_3)]$ or $LiAlH_4$.[12]

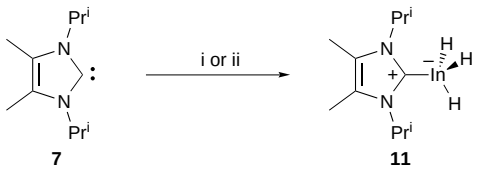

7 **11**

Scheme 1 *Reagents and conditions*: i, $[InH_3(NMe_3)]$, Et_2O, −30 °C, 2 h; ii, $LiInH_4$, Et_2O, −30 °C, 5 h

It is interesting that only a 1 : 1 complex is formed in the reaction of an excess of **7** with $[InH_3(NMe_3)]$ despite the fact that 2 : 1 complexes of the same carbene with indium halides, *e.g.* **9**, are readily formed.[11] This is presumably because the InH_3 unit is less Lewis acidic than InX_3 (X = Cl, Br), and therefore more easily electronically satisfied. Indeed, treatment of **11** with tertiary amines did not lead to the formation of five-coordinate complexes and no other reaction occurred.

The molecular structure of **11** is depicted in Fig. 1. During the course of refinement it was found that the methyl groups attached to C(6) were disordered over two sites, each having a 50% occupancy (only one disordered set is depicted in Fig. 1). The molecule is monomeric, sits on a mirror plane and does not display any intermolecular interactions. Unfortunately the hydride ligands attached to In could not be located from difference maps but their presence can be assumed from spectroscopic evidence (*vide infra*). By contrast the hydride ligands were located in the crystal structure of the isostructural

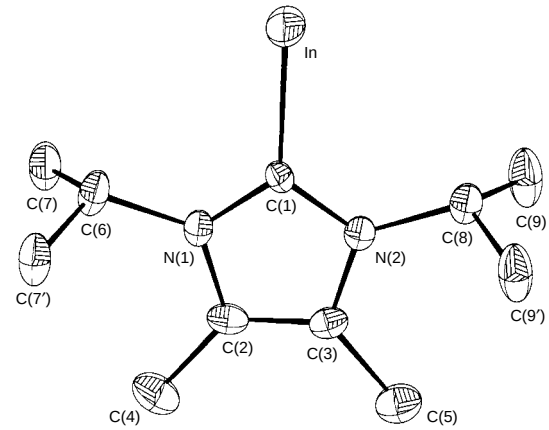

Fig. 1 Molecular structure of $[InH_3\{\overline{CN(Pr^i)C_2Me_2N(Pr^i)}\}]$ **11**. Selected bond lengths (Å) and angles (°): In–C(1) 2.260(6), N(1)–C(1) 1.354(9), N(1)–C(2) 1.402(8), N(2)–C(1) 1.331(9), N(2)–C(3) 1.413(9), C(2)–C(3) 1.340(11); N(2)–C(1)–N(1) 105.8(6), N(2)–C(1)–In 125.6(5), N(1)–C(1)–In 128.6(5), C(1)–N(1)–C(2) 110.2(6), C(1)–N(2)–C(3) 110.9(6), C(3)–C(2)–N(1) 106.9(7), C(2)–C(3)–N(2) 106.2(6).

compound **12**, the aluminium centre of which was found to have a distorted tetrahedral environment.[12] The In–C(1) distance in **11** is longer than is normally seen for In–C bonds [*e.g.* 2.174 Å av. in trimethyl(quinuclidine)indium].[14] Similar trends in M–C (carbene) bond lengths have been observed in other group 13–carbene complexes.[9,11] In addition, the bond lengths and angles within the carbene heterocycle are close to those in **8** and suggest a degree of delocalisation within the ring. Of particular note is the N–C(carbene)–N angle of 105.8(6)° which lies between the normal value for free imadazolylidene carbenes (*ca.* 102°) and imadazolium cations (*ca.* 108°).[9]

The solution NMR data for **11** support its proposed structure. Its ^{1}H NMR spectrum is similar to that of **8** but also displays a very broad resonance at δ 5.58 which integrates for three hydrogens and has been assigned as the hydride resonance. The broadness of this peak is due to the high quadrupole moment of the indium centre (^{115}In 95%, I = 9/2, ^{113}In 5%, I = 9/2) to which the hydrides are attached. This also accounts for the fact that no resonance was observed for the indium coordinated carbene centre, C(1), in the ^{13}C NMR spectrum of **11**, as was the case in the ^{13}C NMR spectrum of **8**.[11] Additionally, no signal was seen in its ^{115}In NMR spectrum which is not surprising considering the lack of spherical symmetry about In. The IR spectrum of **11** (Nujol mull) displays a strong, broad absorbance centred at 1640 cm^{-1} which has been attributed to its In–H stretching modes. This is at a significantly lower frequency than in free InH_3 (1754.5 cm^{-1}),[3] presumably because the nucleophilic carbene donor is weakening the In–H bonds in **11** relative to those in InH_3. Moreover, the In–H stretching absorbance for **11** is at a lower wavenumber than the corresponding Al–H stretching regions for its aluminium counterparts **6** (1743 cm^{-1})[9] and **11** (1730 cm^{-1}).[12] A similar trend is seen for the uncoordinated, monomeric hydrides, InH_3 (1754.5 cm^{-1}) and AlH_3 (1882.9 cm^{-1}).[3]

The indium trihydride complex **11** represents the first example of a new class of compound, the chemistry of which should prove fruitful. To establish this we are currently examining its further reactivity and the preparation of a series of related indium trihydride complexes. The results of these studies will be presented in a later publication.

We gratefully acknowledge financial support from the EPSRC (studentship for N. A. S.).

Notes and References

† E-mail: c.a.jones@swansea.ac.uk

‡ *Spectroscopic data* for **11**: ^{1}H NMR (250 MHz, $C_6D_5CD_3$, $SiMe_4$, 243 K) δ 1.04 [d, 12 H, CH(CH_3)$_2$, $^3J_{HH}$ 6 Hz], 1.54 (s, 6 H, Me), 5.05 [br, 2 H, CH(CH$_3$)$_2$], 5.58 (br s, 3 H, In–H), ^{13}C NMR (100.6 MHz, $C_6D_5CD_3$, 243 K) δ 10.0 (Me), 20.7 [CH(*C*H$_3$)$_2$], 46.3 [*C*H(CH$_3$)$_2$], 121.0 (C=C); IR ν 1640 cm^{-1} (s, br, In–H str.).

§ *Crystal data* for **11**: $C_{11}H_{23}InN_2$, M = 298.13, orthorhombic, space group *Pnma*, a = 15.1920(10), b = 9.5780(9), c = 9.7010(9) Å, U = 1411.6(2) Å^3, Z = 4, D_c = 1.403 g cm^{-3}, F(000) = 608, μ = 16.46 cm^{-1}, crystal 0.15 × 0.25 × 0.20 mm, Mo-Kα radiation (λ = 0.710 69 Å), 150(2) K.

All crystallographic measurements were made using a FAST area detector diffractometer following previously described procedures.[15] The structure was solved by direct methods (SHELXS86)[16] and refined on F^2 by full matrix least squares (SHELX93)[17] using all unique data. All non-hydrogen atoms are anisotropic with H-atoms [except those attached to In] included in calculated positions (riding model). Neutral-atom complex scattering factors were employed.[18] Empirical absorption corrections were carried out by the DIFABS method.[19] Final R (on F) and wR (on F^2) were 0.0425 and 0.1004 for $I > 2\sigma(I)$, and 0.0752 and 0.1074 for all data. CCDC 182/799.

1 *Chemistry of Aluminium, Gallium, Indium and Thallium*, ed. A. J. Downs, Blackie, Glasgow, 1993; C. Jones, G. A. Koutsantonis and C. L. Raston, *Polyhedron*, 1993, **12**, 1829; A. J. Downs and C. R. Pulham, *Chem. Soc. Rev.*, 1994, 175 and references therein.
2 E. Wiberg and M. Schmidt, *Z. Naturforsch., Teil B*, 1957, **12**, 54.
3 P. Pullumbi, Y. Bouteiller, L. Manceron and C. Mijoule, *Chem. Phys.*, 1994, **185**, 25.
4 A. G. Avent, C. Eaborn, P. B. Hitchcock, J. D. Smith and A. C. Sullivan, *J. Chem. Soc., Chem. Commun.*, 1986, 988.
5 O. T. Beachley, S. L. Chao, M. R. Churchill and R. F. See, *Organometallics*, 1992, **11**, 1486.
6 M. R. Churchill, C. H. Lake, S. L. Chao and O. T. Beachley, *J. Chem. Soc., Chem. Commun.*, 1993, 1577.
7 C. Kümmel, A. Meller and M. Noltemeyer, *Z. Naturforsch., Teil B*, 1996, **51**, 209.
8 S. Aldridge, A. J. Downs and S. Parsons, *Chem. Commun.*, 1996, 2055.
9 A. J. Arduengo, H. V. R. Dias, J. C. Calabrese and F. Davidson, *J. Am. Chem. Soc.*, 1992, **114**, 9724.
10 J. K. Ruff and M. F. Hawthorne, *J. Am. Chem. Soc.*, 1960, **82**, 2141.
11 S. J. Black, D. E. Hibbs, M. B. Hursthouse, C. Jones, K. M. A. Malik and N. A. Smithies, *J. Chem. Soc., Dalton Trans.*, 1997, 4313.
12 C. Jones and N. A. Smithies, unpublished work.
13 E. M. Marlett and W. S. Park, *J. Org. Chem.*, 1990, **55**, 2968.
14 D. C. Bradley, H. Dawes, D. Frigo, M. B. Hursthouse and B. Hussain, *J. Organomet. Chem.*, 1987, **325**, 55.
15 J. A. Darr, S. A. Drake, M. B. Hursthouse and K. M. A. Malik, *Inorg. Chem.*, 1993, **32**, 5704.
16 G. M. Sheldrick, *Acta Crystallogr., Sect. A*, 1990, **46**, 467.
17 G. M. Sheldrick, SHELXL-93 Program for Crystal Structure Refinement, University of Göttingen, Germany, 1993.
18 *International Tables for X-ray Crystallography*, ed. J. A. Ibers and W. C. Hamilton, Kynnoch Press, Birmingham, England, 1974, vol. 4.
19 N. P. C. Walker and D. Stuart, *Acta Crystallogr., Sect. A*, 1983, **39**, 158, adapted for FAST geometry by A. I. Karavlov, University of Wales, Cardiff, 1991.

Received in Cambridge, UK, 9th February 1998; 8/01118D

Stereoselective synthesis of *O,O*-dimethylkorupensamine A *via* palladium(0)-mediated cross-coupling of a planar chiral (arene)$Cr(CO)_3$ complex with naphthylboronic acid

Takashi Watanabe and Motokazu Uemura*†

Department of Chemistry, Faculty of Integrated Arts and Sciences, Osaka Prefecture University, Sakai, Osaka 599-8531, Japan

***O,O*-Dimethylkorupensamine A was stereoselectively synthesized by using the palladium(0)-mediated cross-coupling of the enantiomerically pure tricarbonylchromium complex of 3,5-dimethoxy-2-bromobenzene having a functional group at C-1 position with naphthylboronic acid as a key step.**

Korupensamines and michellamines have been isolated from the tropical liana *Ancistrocladus korupensis* in Cameroon and some of these alkaloids possess significant pharmacological activities such as antimalarial properties,[1] and remarkable antiviral activity against human immunodeficiency virus strains HIV-1 and HIV-2.[2] Structurally, the korupensamines have a naphthyltetrahydroisoquinoline skeleton with an axial chirality between the naphthalene and tetrahydroisoquinoline rings, and the michellamines are atropisomerically dimeric alkaloids of the korupensamines. These alkaloids have been previously synthesized *via* construction of the axial bond between the naphthalene and tetrahydroisoquinoline rings as a key step.[3,4] However, the palladium(0)-catalyzed cross-coupling[3] of two arene rings or nucleophilic addition[4] of aryl Grignards to the *o*-methoxyaryl oxazoline compounds for the central bond formation of the naphthalene and tetrahydroisoquinoline rings gave unfortunately various ratios of the atropisomeric mixture in the previous reports. In continuation of our studies on development of the planar chiral (arene)chromium complexes in the asymmetric reactions, we have recently reported[5,6] that both enantiomers of the axial biaryls could be stereoselectively prepared from a single planar chiral (arene) chromium complex by the palladium(0)-mediated cross-coupling of (2,6-disubstituted 1-bromobenzene)chromium complexes with arylboronic acids and following axial isomerization of the cross-coupling products under thermal conditions. This paper describes the asymmetric synthesis of (−)-*O,O*-dimethylkorupensamine A (**1**, R = Me) utilizing the stereoselective palladium(0)-catalyzed cross-coupling of the planar chiral (arylhalide)$Cr(CO)_3$ with napthylboronic acid as the key step.

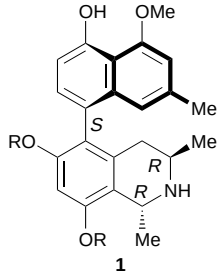

1

R = H; Korupensamine A
R = Me; *O,O*-Dimethylkorupensamine A

The planar chiral tricarbonylchromium complex of 3,5-dimethoxyphenylbromide having a functional group at C-1 position as a coupling partner was initially prepared as follows (Scheme 1). An asymmetric catalytic dihydroxylation of (*E*)-(3,5-dimethoxyphenyl)propene **2** was treated with AD-mix-α,[7] and the resulting diol was subsequently protected with acetone dimethylacetal to give the acetonide **4** ($[\alpha]_D^{27}$ +23.8)‡ in 96% yield with > 98% ee. Tricarbonylchromium complexation of **4** with $Cr(CO)_6$ in dibutyl ether and THF (10 : 1) at reflux gave the corresponding (arene)chromium complex **5** ($[\alpha]_D^{26}$ −4.0) in 89% yield. In order to introduce the bromine atom at either *ortho*-position of the C-1 side-chain group regioselectively, the C-4 position was initially protected by the introduction of the easily removable Me_3Si group. Thus, the lithiation of **5** with Bu^nLi followed by treatment with trimethylsilylchloride afforded the trimethylsilylated complex **6** ($[\alpha]_D^{27}$ −36.0) in 97% yield. Subsequent lithiation§ of **6** followed by quenching with 1,2-dibromo-1,1,2,2-tetrafluoroethane gave the bromination complex **8** ($[\alpha]_D^{26}$ −93.0) at the H^a-position without the regioisomeric complex after detrimethylsilylation in 95% overall yield. The planar chirality of **8** was determined by X-ray crystallography.¶

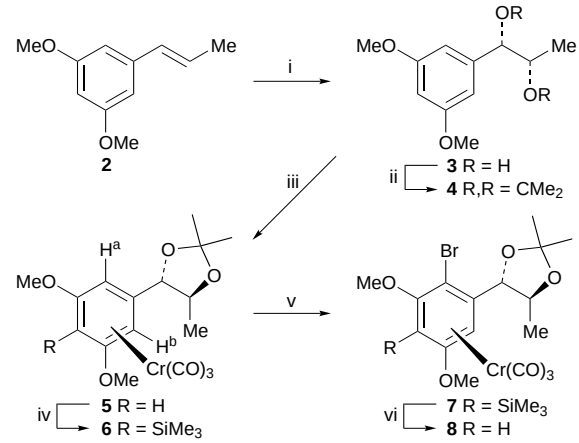

Scheme 1 *Reagents and conditions*: i, AD-mix-α, $CH_3SO_2NH_2$, Bu^tOH, H_2O, 99%, > 98% ee; ii, $Me_2C(OMe)_2$, TsOH, 97%; iii, $Cr(CO)_6$, dibutyl ether, THF, reflux, 20 h, 89%, > 99% ee; iv, Bu^nLi, THF, TMEDA, −78 °C, then Me_3SiCl, THF, −78 °C, 97%; v, Bu^nLi, THF, TMEDA, −78 °C, then $BrCF_2CF_2Br$, THF, −78 °C, 98%; vi, $Bu^n{}_4NF$, THF, AcOH, 97%

The palladium(0)-catalyzed cross-coupling of the planar chiral (arene)$Cr(CO)_3$ complex **8** with 4-benzyloxy-5-methoxy-6-methylnaphthylboronic acid **9**[8] in the presence of sodium carbonate in aqueous MeOH at reflux for 30 min produced a single atropisomeric coupling product **10** ($[\alpha]_D^{28}$ −142.9) in 90% yield without any formation of the atropisomers (Scheme 2). The axial stereochemistry of the coupling product **10** was assigned to be the (*S*)-configuration by ^1H NMR spectra, in which the *peri*-proton of the naphthalene ring appeared at lower field (δ 8.62) due to the anisotropic effect of the *syn*-$Cr(CO)_3$ fragment.[5] An oxidative demetallation of **10** and subsequent treatment with dilute HCl afforded the dihydroxyl compound **12** ($[\alpha]_D^{27}$ +3.5). Selective protection of the hydroxyl at the homobenzylic position of **12** with *tert*-butyltrimethylsilyl chloride gave the monosilylated compound **13** ($[\alpha]_D^{25}$ +35.8) in

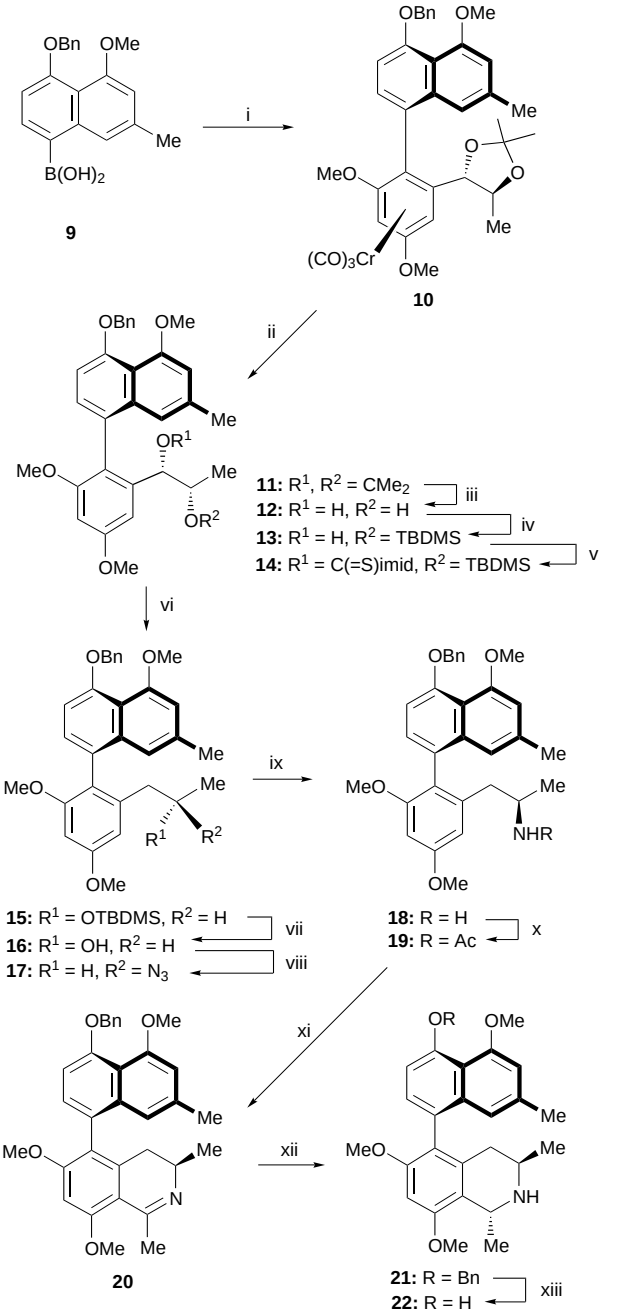

Scheme 2 *Reagents and conditions*: i, **8**, $Pd(PPh_3)_4$ (0.05 mol equiv.), aq. Na_2CO_3, MeOH, 75 °C, 30 min, 90%; ii, *hν*, O_2, diethyl ether, 92%; iii, 1 M aq. HCl, THF, 50 °C, 96%; iv, Bu^tMe_2SiCl, imidazole, DMF, 84%; v, $(imid)_2C{=}S$, THF; vi, Bu^n_3SnH, AIBN, toluene, 62% from **13**; vii, Bu^n_4NF, THF, 96%; viii, $(PhO)_2PON_3$, DEAD, PPh_3, THF; ix, $SnCl_2$, MeOH; x, Ac_2O, py, 66%, from **16**; xi, $POCl_3$, MeCN; xii, $LiAlH_4$, Me_3Al, THF, −78 to 0 °C, 70% from **19**; xiii, Pd-black, HCO_2H, MeOH, 45 °C, 91%

84% yield. The benzylic hydroxyl of **13** was removed by the Barton method[9] to give the deoxygenation compound **15** ($[\alpha]_D^{26}$ +11.9) in 62% yield. The substitution of the hydroxyl to nitrogen atom with stereochemical inversion was achieved under Mitsunobu conditions.[10] Thus, deprotection of the silyl ether **15** and subsequent treatment with $(PhO)_2PON_3$ in the presence of DEAD and PPh_3 produced the azide compound **17** which was reduced with $SnCl_2$ followed by acetylation to give the amide compound **19** ($[\alpha]_D^{26}$ +8.1) in 66% overall yield. Bischler–Napieralski cyclization of **19** with $POCl_3$ in acetonitrile gave the naphthyldihydroisoquinoline compound **20**. Reduction[11] of the imine double bond of **20** with $LiAlH_4$ in the presence of Me_3Al afforded *trans*-dimethyl compound **21** ($[\alpha]_D^{23}$ −20.6) along with a small amount of the corresponding *cis*-isomer (ratio, 93 : 7) in 70% overall yield. Finally, debenzylation with Pd-black in a solution of 8.8% formic acid in MeOH gave *O*,*O*-dimethylkorupensamine A **22** (R = H) ($[\alpha]_D^{22}$ −29.1) in 91% yield.

In conclusion, we have demonstrated the asymmetric synthesis of *O*,*O*-dimethylkorupensamine A *via* a stereoselective Pd^0-mediated cross-coupling method for the construction of the highly hindered biaryl bond as the key bond forming reaction. This procedure should have broad utility for the stereoselective synthesis of structural analogs of the atropisomeric naphthyltetrahydroisoquinoline alkaloids.

Partial financial support for this work was provided by a Grant-in-Aid for Scientific Research from the Ministry of Education, Science, Sports and Culture of Japan. We acknowledge the financial support by the Ciba-Geigy Foundation (for Japan) and The Asahi Glass Foundation.

Notes and References

† E-mail: uemura@ms.cias.osakafu-u.ac.jp

‡ All optical rotation values were measured in $CHCl_3$ solution.

§ The corresponding di-MOM ether chromium complex analog instead of the dimethoxy ether complex **6** resulted in a regioisomeric mixture of the bromination compounds in a 85 : 15 ratio by the *ortho*-lithiation with Bu^nLi followed by bromination.

¶ *Crystal data* for **10**: $C_{17}H_{19}BrCrO_7$, M = 467.23, yellow prismatic, triclinic, space group $P\bar{1}$, a = 9.829(2), b = 13.393(3), c = 7.996(2) Å, α = 98.27(2), β = 110.31(2), γ = 94.38(2)°, U = 967.7(4) Å^3, Z = 2, D_c = 1.603 g cm^{-3}, $F(000)$ = 472.00, μ = 26.96 cm^{-1}, $R(R_w)$ = 0.039 (0.053). A total of 4729 data were collected using ω scans with $22.35 < 2\theta < 24.98°$. Of these 4467 were unique (R_{int} = 0.085). CCDC 182/795.

1 Y. F. Hallock, K. P. Manfredi, J. W. Blunt, J. H. Cardellina II, M. Schäffer, K.-P. Gulden, G. Bringmann, A. Y. Lee, J. Clardy, G. François and M. R. Boyd, *J. Org. Chem.*, 1994, **59**, 6349.

2 K. P. Manfredi, J. W. Blunt, J. H. Cardellina II, J. B. McMahon, L. L. Pannell, G. M. Cragg and M. R. Boyd, *J. Med. Chem.*, 1991, **34**, 3402; M. R. Boyd, Y. F. Hallock, J. H. Cardellina II, J. W. Blunt, J. B. McMahon, R. W. Buckheit, Jr., G. Bringmann, M. Schäffer, G. M. Cragg, D. W. Thomas and J. G. Jato, *J. Med. Chem.*, 1994, **37**, 1740; J. B. McMahon, M. J. Currens, R. J. Gulakowski, R. W. Buckheit, Jr., C. Lackman-Smith, Y. F. Hallock and M. R. Boyd, *Antimicrob. Agents Chemother.*, 1995, **39**, 484.

3 T. R. Hoye, M. Chen, L. Mi and O. P. Priest, *Tetrahedron Lett.*, 1994, **35**, 8747; T. R. Hoye and L. Mi, *Tetrahedron Lett.*, 1996, **37**, 3097; T. R. Hoye and M. Chen, *Tetrahedron Lett.*, 1996, **37**, 3099; T. R. Hoye and M. Chen, *J. Org. Chem.*, 1996, **61**, 7940; G. Brignmann, R. Götz, P. A. Keller, R. Walter, P. Henschel, M. Schäffer, M. Stäblein, T. R. Kelly and M. R. Boyd, *Heterocycles*, 1994, **39**, 503; P. D. Hobbs, V. Upender, J. Liu, D. J. Pollart, D. W. Thomas and M. I. Dawson, *Chem. Commun.*, 1996, 923; P. D. Hobbs, V. Upender and M. I. Dawson, *Synlett*, 1997. 965.

4 M. A. Rizzacasa and M. V. Sargent, *J. Chem. Soc., Chem. Commun.*, 1990, 894; B. N. Leighton and M. A. Rizzacasa, *J. Org. Chem.*, 1995, **60**, 5702.

5 K. Kamikawa, T. Watanabe and M. Uemura, *J. Org. Chem.*, 1996, **61**, 1375.

6 K. Kamikawa, T. Watanabe and M. Uemura, *Synlett*, 1996, 1040.

7 K. B. Sharpless, W. Amberg, Y. L. Bennani, G. A. Crispino, J. Hartung, K.-S. Jeong, H.-L. Kwong, K. Morikawa, Z.-M. Wang, D. Xu and X.-L. Zhang, *J. Org. Chem.*, 1992, **57**, 2768.

8 Compound **11** was prepared by a modified procedure of the following reference; M. Watanabe, S. Hisamatsu, H. Hotokezaka and S. Furukawa, *Chem. Pharm. Bull.*, 1986, **34**, 2810.

9 D. H. R. Barton and S. W. McCombie, *J. Chem. Soc., Perkin Trans. 1*, 1975, 1574.

10 O. Mitsunobu, *Synthesis*, 1981, 1.

11 G. Bringmann, J. R. Jansen and H.-P. Rink, *Angew. Chem., Int. Ed. Engl.*, 1986, **25**, 913; G. Bringmann, R. Weirich, H. Reuscher, J. R. Jansen, L. Kinzinger and T. Ortmann, *Liebigs. Ann. Chem.*, 1993, 877; R. Jansen and H.-P. Rink, *Angew. Chem., Int. Ed. Engl.*, 1986, **25**, 913; K. Maruoka and H. Yamamoto, *Angew. Chem., Int. Ed. Engl.*, 1985, **24**, 668.

Received in Cambridge, UK, 2nd January 1998; 8/00075A

Synthesis of poly(anthra-9,10-quinone-2,6-diyl)

Gerald Power, Philip Hodge,*† Ian D. Clarke, Michael A. Rabjohns and Ian Goodbody

Chemistry Department, University of Manchester, Oxford Road, Manchester, UK M13 9PL

The synthesis, *via* a precursor polymer, of poly(anthra-9,10-quinone-2,6-diyl) 1 is described and some of its properties are reported.

Poly(anthra-9,10-quinone-2,6-diyl) **1** is of interest for several reasons. For example, it is expected to have novel redox properties and these might lead to applications of the polymer in electrochromic displays and/or as charge injection layers in electroluminescent displays. A previous attempt[1,2] to synthesise polymer **1** directly from 2,6-dichloroanthraquinone **2**, by nickel(0)-mediated couplings, led only to very small oligomers because of the extremely low solubilities of compounds of this general type in all common organic solvents. Even the dimer **3** has very low solubilities.[3] We now report a synthesis of polymer **1**, *via* the soluble precursor polymer **4**, which produces a product with a number average molecular weight corresponding to an average degree of polymerisation, $\overline{DP}$, of 13.

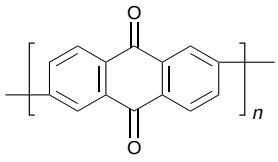

1

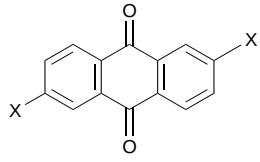

2 X = Cl
7 X = NH_2
8 X = Br

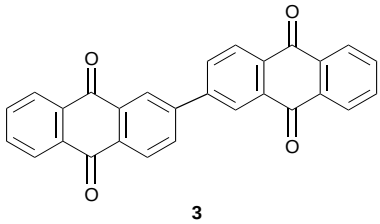

3

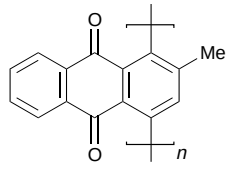

5

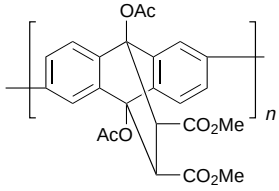

4

Quinone-containing polymers have been described before,[1,2,4] but most are electron-transfer polymers.[4] The latter are usually crosslinked polymers with quinone-containing pendant groups.[5] Very few quinone-containing polymers that have been described actually have the quinone moiety in the main chain and conjugated with the π-electron systems of the neighbouring units. The work most relevant to the present is the synthesis of poly(2-methylanthra-9,10-quinone-1,4-diyl) **5** and several very closely related polymers by nickel(0)-mediated couplings of dichloroquinones.[1,2] For steric reasons, the neighbouring anthraquinone moieties in these polymers are essentially orthogonal to each other.

The basic strategy of the present synthesis was to prepare Diels–Alder adduct **6**, carry out a nickel(0)-mediated coupling to give the soluble precursor polymer **4**, then, after characterisation of the latter, convert it into polymer **1**. Thus, commercial 2,6-diaminoanthraquinone **7** was converted into 2,6-dibromoanthraquinone **8**, mp 282–283 °C (lit.,[6] 289–290 °C) (60% yield) using a Sandmeyer reaction.[7,8] Reductive acetylation of quinone **8** by treatment with zinc dust, Ac_2O and NaOAc at reflux temperature gave the anthracene **9**, mp 310 °C (decomp.)‡ (81% yield), and treatment of this with an excess of maleic anhydride in xylene at reflux temperature for 18 h gave the Diels–Alder adduct. The latter was treated with MeOH at reflux temperature to give the half esters. These reacted smoothly with ethereal CH_2N_2 to give compound **6**, mp 195–200 °C (decomp.)‡, (35% overall yield of recrystallised product from compound **9**).

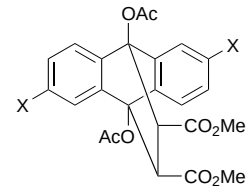

6 X = Br
11 X = H

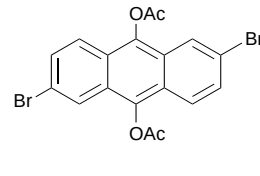

9

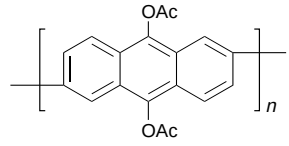

10

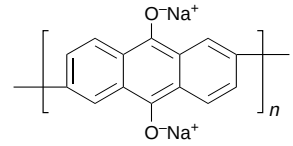

12 Very dark green

Treatment of compound **6** in DMA at 80 °C with 1.2 equiv. of $Ni^0[cod]_2$ in the presence of cod (1.0 equiv.) and 2,2′-bipyridyl (1.2 equiv.)[2,8–11]gave precursor polymer **4**‡ in 82% yield. The polymer was highly soluble in many organic solvents including $CHCl_3$ and THF. The infrared and ^1H NMR spectra of the product were consistent with structure **4**. By gel permeation chromatography polymer **4** had, relative to polystyrene standards, a number average molecular weight M_n, of 5690, a weight average molecular weight M_w, of 8980 and a peak molecular weight M_p, of 6830. The $\overline{M}_n$ value corresponds to a DP of 13.

Heating polymer **4** to 240 °C did not bring about a clean retro-Diels–Alder reaction to give polymer **10** even though analogous reactions in syntheses of related polymers proceed cleanly.[8,12] However, model studies showed that the dimethyl maleate-9,10-diacetoxyanthracene Diels–Alder adduct **11**‡ reacts readily with 5 equiv. of NaOEt and EtOH in NMP at 20 °C under nitrogen to give a deep red solution of the disodium salt of 9,10-dihydroxyanthracene, and that exposure of this to air rapidly gives anthra-9,10-quinone in essentially 100% yield. We suggest that the key steps in this overall conversion are, successively, (i) a retro-aldol reaction, (ii) a retro-Michael reaction and (iii) an esterolysis (see Scheme 1). Treatment of polymer **4** with NaOEt under similar conditions to those used above gave a very dark green *solution* which we attribute to the formation of polymer **12**. Passage of air through the green solution precipitated polymer **1**, as a pale brown solid, in 95% overall yield from the precursor polymer **4**.

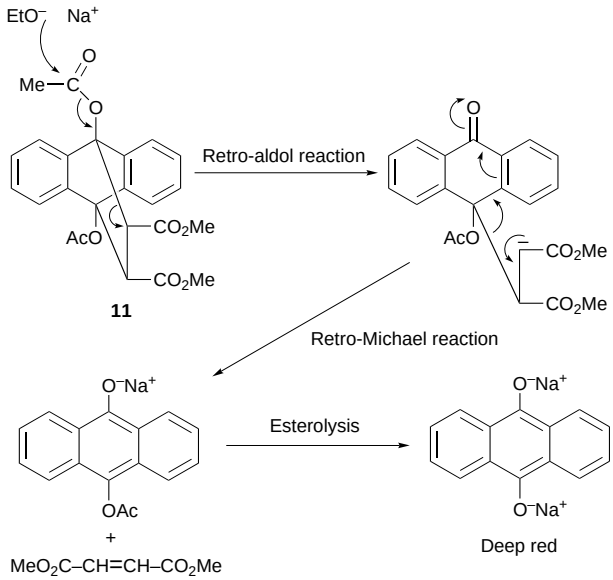

Scheme 1

Polymer **1**, like most anthraquinones, is soluble in concentrated sulfuric acid and trifluoromethanesulfonic acid but it is insoluble in all common organic solvents. The product had an elemental analysis consistent with structure **1**. The FT-IR spectrum of polymer **1** displayed the expected bands at 1679 and at 1592 cm^{-1}: there were no bands which could be attributed to the presence of either maleate or aryl acetate groups. Thermogravimetric analysis of the polymer in air showed no significant weight loss up to 175 °C, then a steady weight loss up to 480 °C by which temperature 35% of the weight had been lost. There was no further significant loss up to 600 °C, the temperature limit of the instrument. A very similar pattern of weight loss was observed when the polymer was heated under nitrogen.

These results demonstrate a practical synthesis of polymer **1**. They also indicate how closely related polymers with these or other anthraquinone moieties might be prepared. Optimisation of the synthesis to obtain a higher $\overline{DP}$ and a more detailed study of the properties of polymer **1**, including its redox properties, are currently under investigation.

We thank the EPSRC for financial support.

Notes and References

† E-mail: philip.hodge@man.ac.uk

‡ All new compounds had satisfactory FT-IR and ^{1}H NMR spectra and elemental analyses.

1 H. Etori, T. Kanbara and T. Yamamoto, *Chem. Lett.*, 1994, 461.
2 T. Yamamoto and H. Etori, *Macromolecules*, 1995, **28**, 3371.
3 I. Goodbody and P. Hodge, unpublished results.
4 H. C. Cassidy and K. A. Kun, *Oxidation-Reduction Polymers*, Wiley-Interscience, New York, 1965.
5 See, for example, G. Manecke, *Angew. Makromol. Chem.*, 1968, **2**, 86.
6 *Rodd's Chemistry of Carbon Compounds*, 2nd edition, ed. S. Coffey, vol. III, part H , Elsevier, Amsterdam, 1979.
7 M. P. Doyle, B. Siegfried and J. F. Dellaria, *J. Org. Chem.*, 1977, **42**, 2426.
8 P. Hodge, G. A. Power and M. A. Rabjohns, *Chem. Commun.*, 1997, 73.
9 I. Colon and G. T. Kwiatkowski, *J. Polym. Sci., Polym. Chem. Ed.*, 1990, **28**, 367.
10 M. Ueda and F. Ichikawa, *Macromolecules*, 1990, **23**, 926.
11 V. Chaturvedi, S. Tanaka and K. Kaeriyama, *J. Chem. Soc. Chem. Commun.*, 1992, 1658; *Macromolecules*, 1993, **26**, 2607.
12 G. A. Power, P. Hodge and N. B. McKeown, *Chem. Comm.*, 1996, 655.

Received in Liverpool, UK, 2nd February 1998; 8/00883C

Cp_2TiPh-coordinated cyano and ester groups as efficient ketyl radical acceptors in the reductive radical cyclization of γ- and δ-cyano ketones and δ-keto esters

Yoshihiko Yamamoto, Daisuke Matsumi and Kenji Itoh*†

Department of Applied Chemistry, Graduate School of Engineering, Nagoya University, Chikusa, Nagoya 464-8603, Japan

Cp_2TiPh promotes the reductive radical cyclization of γ- and δ-cyano ketones and δ-keto esters to give α-hydroxycycloalkanones in moderate to good yields; the titanium reagent coordinates to both the ketone and the cyano or ester terminus, the LUMO of the cyano or ester group is thus lowered, and cyclization proceeds irreversibly without formation of the unstable iminyl or alkoxy radical intermediates.

Radical cyclizations have been extensively utilized as powerful tools for the construction of carbocyclic skeletons, especially five-membered ring systems.[1] In these processes, C–C bonds are generally formed by the addition of a carbon-centered radical to a non-polar carbon–carbon multiple bond. On the other hand, radical additions to a carbonyl or cyano group are generally not efficient because they generate highly unstable alkoxy or iminyl radicals.[1] However, radical addition to these polar multiple bonds might be successful if the resulting unstable radical intermediates are effectively scavenged and converted into the desired products. With this in mind, we have developed a Ti^{III}-mediated reductive coupling of γ- and δ-cyano ketones leading to α-hydroxycycloalkanones, in which the Ti^{III} complex Cp_2TiPh coordinates to the cyano group so that the ketyl radical efficiently cyclizes to the coordinated cyano group without formation of the undesired iminyl radical intermediate (Scheme 1).[2] In addition, coordination of the Ti^{III} species lowers the LUMO of the cyano group and increases its ketyl trapping ability.[3]

Cp_2TiPh was prepared according to the reported procedures[4] and used for further reactions without isolation. Typically, commercial Cp_2TiCl_2 (3 mmol) was treated sequentially with dry, degassed Et_2O solutions of Pr^iMgCl (3.3 mmol) and PhMgBr (3.3 mmol) in dry, degassed toluene (10 ml) under Ar at ambient temperature.[5] To the resultant dark green solution of Cp_2TiPh was added dropwise a 0.1 M toluene solution of 2-cyanoethylcyclopentanone **1a** (1 mmol) and the reaction mixture was stirred for 1 h at ambient temperature. Acid hydrolysis followed by silica gel chromatography afforded the 5-*exo* cyclization product **2a**[6] in 77% yield. The phenyl–titanium bond is essential, since analogous Ti^{III} species generated by the reduction of Cp_2TiCl_2 by Pr^iMgCl did not promote the cyclization under the same conditions. Similarly, intramolecular coupling product **2b**[6] was obtained from cycloalkanones **1b** in 70% yield. Acyclic ketone **1c** also gave **2c**,[6] but the yield was lower than those of the above cyclic precursors due to conformational flexibility around the carbonyl group. High dilution (0.04 M) and prolonged reaction time (2 h) was required to increase the yield to 50%. In contrast, the inverse addition of the Ti^{III} reagent to **1c** decreased the yield (17%). Thus the concentration of the Ti^{III} reagent is critical for the present cyclization. It is noteworthy that the present method is applicable to aryl-substituted ketone **1d** to afford tricyclic α-hydroxy ketone **2d**[6] in 58% yield, whereas the reported electrochemical reduction gave cyano alcohol due to simple reduction of the carbonyl group.[7,8] In the same manner, 6-*exo* cyclization of δ-cyano ketones **1e**,**f** and acyclic δ-cyano ketones **1g** gave the desired α-hydoroxycyclohexanones **2e**–**g**[6] in 45, 69 and 42% yields, respectively. It is interesting that the *trans*-fused product was selectively obtained from **1f**, whereas the *cis*-fused isomer was obtained for **2a**,**b**,**d** and **e**.

In addition to the cyano group, the ester group is an effective ketyl radical accepting group when coordinated by Cp_2TiPh.[2] Aromatic keto esters **3a** and **3b** were treated with the Ti^{III} reagent under high dilution conditions to afford 5-*exo* cyclization products **2d** and **2h** in 49 and 38% yields, respectively.

Recently, Molander and Kenny reported the SmI_2-promoted reductive cyclization of δ,ε-unsaturated keto esters, demonstrating that the ketyl-trapping ability of nitriles is lower than those of alkenes, alkynes, ketones and aldehydes.[9] In our hands, the double coordination to both carbonyl and cyano or ester groups by the Ti^{III} complex resulted in efficient reductive cyclization of a variety of keto nitriles and keto esters under mild conditions. In this context, alkenyl groups are no longer superior to the cyano group as a ketyl radical acceptor. In fact,

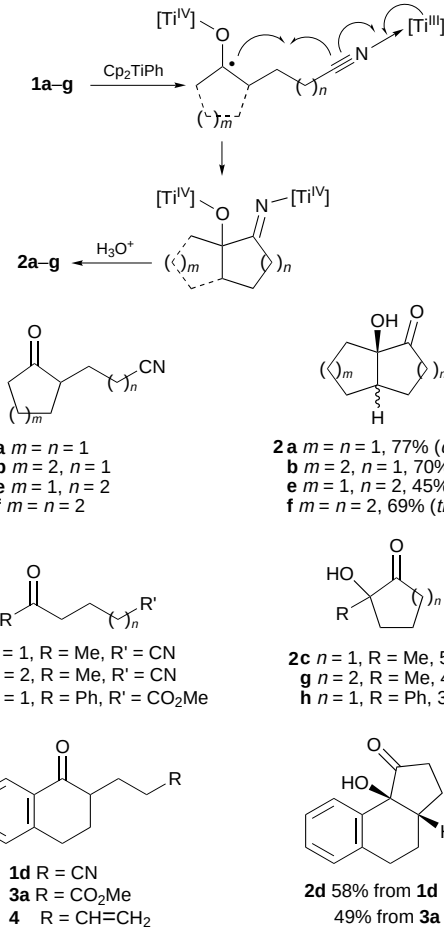

Scheme 1

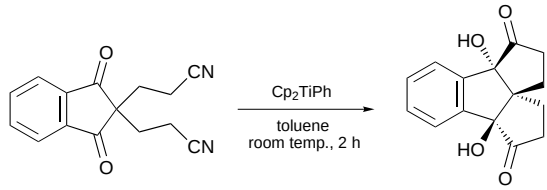

5 **6** 75%

Scheme 2

α-butenyl ketone **4** did not give the expected cyclization product after treatment for 24 h with the Ti^{III} reagent, and the starting material was recovered with the carbonyl group intact (75% recovery).[10] This result shows that ketyl radical formation is reversible and this reversibility combined with the steric hindrance of the Cp_2TiPh-coordinated ketyl moiety makes the 5-*exo*-*trig* cyclization of **4** ineffective.

In conclusion, the Cp_2TiPh-mediated reductive radical cyclization of cyano ketones in both 5- and 6-*exo* modes was successful to provide an easy entry to 5- and 6-membered α-hydroxycycloalkanones. The coordination to the cyano group plays a key role in the present cyclization, *i.e.* the titanium reagent coordinates to both carbonyl and cyano moieties, and therefore, a low concentration of the Ti^{III} reagent is unfavorable. As a result, the LUMO of the cyano group is lowered and cyclization proceeds irreversibly without formation of the unstable iminyl radical intermediates. To the best of our knowledge, the intramolecular reductive coupling of keto nitriles is quite rare, and thus far only a few examples using one-electron reducing agents such as Zn[11] and SmI_2[9] have been reported in addition to the electroreductive method.[7] In our hands, intramolecular reductive radical cyclization of aromatic keto esters also gave the corresponding α- hydroxycycloalkanones, in which the Cp_2TiPh-coordinated ester group functions as a ketyl radical acceptor. Such an effect did not operate for the α-butenyl ketone, producing no reductive cyclization product. The synthetic utility of the cyano ketone cyclization was also demonstrated in the double cyclization of dicyano diketone **5**, giving rise to an interesting angular triquinane derivative **6**[6] in 75% yield (Scheme 2).

We gratefully acknowledge financial support (09750947 and 09305059) from the Ministry of Education, Science Sports and Culture, Japan.

Notes and References

† E-mail: itohk@apchem.nagoya-u.ac.jp

1 D. P. Curran, in *Comprehensive Organic Synthesis*, ed. B. M. Trost, Pergamon, Oxford, 1991, vol. 4, ch. 4.
2 Neither radical coupling products nor reduced products were obtained from the treatment of BnCN and $BnCO_2Et$ with Cp_2TiPh, demonstrating that no radical species are generated from aliphatic nitriles or esters with Cp_2TiPh.
3 PM3 theoretical calculations (Wavefunction, Inc. MacSpartan plus) for free and Cp_2TiPh-coordinated acetonitriles suggested that the LUMO level of MeCN (1.4 eV: RHF/PM3) is higher than the β-LUMO of Cp_2TiPh(MeCN) (0.3 eV: UHF/PM3).
4 E. J. M. de Boer and J. H. Teuben, *J. Organomet. Chem.*, 1978, **153**, 53.
5 Although only 2 equiv. of the Ti^{III} reagent is theoretically required, 3 equiv. of Cp_2TiCl_2 was used to ensure completion of cyclization.
6 The structures and stereochemistry of cyclized products **2a**–**c**, **e**–**g** were determined by comparison of their spectral features with those of reported compounds (ref. 7), and new compounds were characterized by the usual means.
7 T. Shono, N. Kise, T. Fujimoto, N. Tominaga and H. Morita, *J. Org. Chem.*, 1992, **57**, 7175.
8 In the presence of a large excess of Pr^iOH, the cyclization of **1d** afforded cyclized product **2** in 41% yield without formation of the simple reduced product cyano alcohol. This indicates that anionic species generated by the reduction of ketyl radicals are not involved in the present cyclization.
9 G. A. Molander and C. Kenny, *J. Am. Chem. Soc.*, 1989, **111**, 8236.
10 Similar results were reported in the reaction of hex-5-enal with SmI_2, where only a pinacol coupling product was obtained instead of a 5-*exo* cyclization product (E. J. Enholm and A. Trivellas, *Tetrahedron Lett.*, 1989, **30**, 1063.).
11 E. J. Corey and S. G. Pyne, *Tetrahedron Lett.*, 1983, **24**, 2821.

Received in Cambridge, UK, 26th January 1998; 8/00661J

Efficient aerobic epoxidation of alkenes in perfluorinated solvents catalysed by chiral (salen) Mn complexes

Gianluca Pozzi,*† Flavio Cinato, Fernando Montanari and Silvio Quici

Centro CNR and Dipartimento di Chimica Organica e Industriale dell'Università, Via Golgi 19, I-20133 Milano, Italy

Chiral complexes selectively soluble in perfluorocarbons have been synthesized for the first time and tested as catalysts for the epoxidation of alkenes under fluorous biphasic conditions.

The use of perfluorocarbons as reaction media in preparative organic chemistry and homogeneous catalysis is a topic of growing interest.[1] In particular, the value of a new phase-separation and immobilization technique known as FBS (Fluorous Biphase Systems), developed by Horváth and Rábai,[2] is now becoming evident to both academic and industrial researchers. Principles and current achievements of this technique have been recently reviewed.[3] The introduction of FBS raises a number of questions, among them the possible application to enantioselective reactions. Besides helping recovery and reuse of precious chiral reagents or catalysts, it has been repeatedly proposed that the unique solvation environment provided by perfluorocarbons might have unforeseen beneficial effects on the selectivity of the reactions.[4] However, neither examples of enantioselective FBS reactions nor feasibility studies have been reported so far. Metal complexes of salen ligands are able to catalyse the epoxidation of unfunctionalized alkenes.[5] The synthetic route to salen ligands is straightforward and can be adapted to the preparation of many different compounds, including chiral ones.[6] This offers the opportunity to increase the very limited number of known catalysts for FBS oxidations,[7,8] and also to begin assessing the true potential of FBS in enantioselective catalysis. For these reasons we have synthesized two optically active (salen)Mn^{III} complexes (Jacobsen–Katsuki catalysts) selectively soluble in fluorocarbons (Scheme 1). They were tested as catalysts in the epoxidation of alkenes under FBS conditions, in the presence of various oxygen donors.

Both C_2 symmetric salen ligands **1** and **2** were obtained in good yields (75 and 82%, respectively) by the condensation of 2 equiv. of the perfluoroalkylated salicylaldehyde **3** with the proper chiral 1,2-diamine (Scheme 1).‡ The synthesis of the key compound **3** was easily achieved following the pathway reported in the same scheme. The free OH groups of 3,5-diiodosalicyclic acid were protected by methylation with Me_2SO_4 (quantitative yield) before the coupling reaction with 2 equiv. of $C_8F_{17}I$ mediated by Cu powder (65% yield).[9] The ester **4** was converted into **3** by reduction to benzylic alcohol (70% yield) followed by oxidation (85% yield) and demethylation (88% yield). The use of trifluoromethylbenzene as solvent greatly improved the yield of the oxidative step,[10] which was conveniently carried out under aqueous-organic two-phase conditions according to a procedure already reported by us.[11] The free salen ligands were soluble in cold perfluorocarbons,§ CCl_2FCF_2Cl and Et_2O, soluble in hot EtOH and only sparingly soluble in cold halogenated solvents. The corresponding manganese complexes (Mn–**1** and Mn–**2**), obtained in quantitative yield by refluxing an ethanolic solution of ligand with an excess of $Mn(OAc)_2{\cdot}4H_2O$, were soluble in cold perfluorocarbons and CCl_2FCF_2Cl, but completely insoluble in common organic solvents.

Mukaiyama and co-workers have shown that optically active (salen)Mn complexes catalyse the enantioselective epoxidation of alkenes in the presence of molecular oxygen and a sacrificial aldehyde.[12] Fluorocarbons dissolve large quantities of molecular oxygen and this property has been exploited in oxidation reactions, including the epoxidation of alkenes under FBS conditions in the presence of aliphatic aldehydes.[7a,8b] Complexes Mn–**1** and Mn–**2** were thus first tested adapting Mukaiyama conditions to a typical FBS procedure (see Table 1 for results and conditions). Reactions were carried out in the dark at 20 °C under atmospheric pressure of O_2, with Mn–**1** and Mn–**2** immobilized in the fluorinated phase. In the absence of the catalyst, conversions were negligible. As already reported in

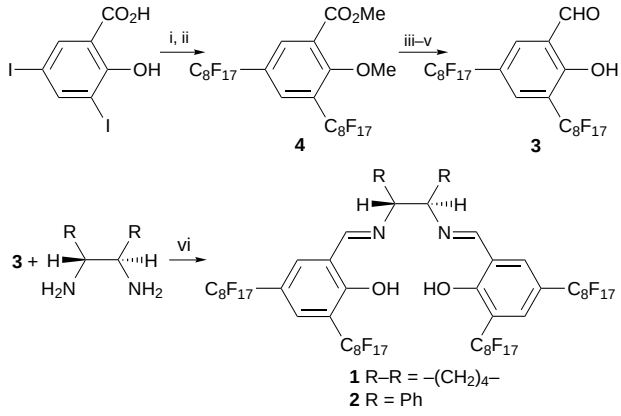

Scheme 1 *Reagents and conditions*: i, Me_2SO_4, K_2CO_3, acetone, reflux; ii, $C_8F_{17}I$, Cu, DMF, 125 °C; iii, LAH, Et_2O, 0 °C; iv, aq. NaOCl, KBr (10 mol%), TEMPO, $PhCF_3$, 5 °C; v, BBr_3, CH_2Cl_2 −78 °C, then toom temp.; vi, EtOH, reflux

Table 1 Expoxidation of alkenes with O_2–pivalaldehyde catalysed by chiral (salen)Mn complexes under FBS conditions[a]

Catalyst	Substrate	*t*/h	Conversion (%)[b]	Yield (%)[c]	Ee (%)
Mn–**1**[d]	Indene	2	100	83	92[e]
Mn–**1**[d]	1,2-Dihydronaphthalene	8	85	70	10[e]
Mn–**1**[d]	Styrene	5	100	86	n.d.[e]
Mn–**1**[f]	3-Nitrostyrene	12	70	36	n.d.[e]
Mn–**1**[d]	*trans*-β-Methylstyrene	5	100	75	n.d.[g]
Mn–**1**[d]	*trans*-Stilbene	12	80	78	n.d.[g]
Mn–**1**[d]	*cis*-Stilbene	12	88	85[h]	—
Mn–**2**[d]	Indene	3	100	77	90[e]
Mn–**2**[d]	1,2-Dihydronaphthalene	8	95	73	13[e]
Mn–**2**[d]	Styrene	5	100	81	n.d.[e]

[a] Conditions: [catalyst] = 0.005 M in D-100; [substrate] = 0.33 M in CH_2Cl_2; [pivalaldehyde] = 1 M in CH_2Cl_2; [*N*-hexylimidazole] = 0.033 M in CH_2Cl_2; volume of D-100 = 3 ml; volume of CH_2Cl_2 = 3 ml. T = 20 °C. Stirring rate = 1300 rpm. [b] Determined by capillary GC integration against an external standard (dichlorobenzene). [c] Isolated epoxide. [d] A second run with the recovered perfluorocarbon layer gave almost the same results. [e] Determined by capillary GC using a Cyclodex-B chiral column. n.d. = not detected. [f] The catalyst bleached in the first run. [g] Determined by ^1H NMR spectroscopy in the presence of Eu(hfc)$_3$. [h] *cis* : *trans* epoxide = 3 : 1.

Table 2 Epoxidation of 1,2-dihydronaphthalene catalysed by Mn–**1** under FBS conditions[a]

Oxidant	Solvent	*t*/h	*T*/°C	Conversion (%)[b]	Yield (%)[b]	Ee (%)[c]
30% H_2O_2[d]	MeCN	0.5	20	—	—	—
PhIO	MeCN	24	20	85	65	6
Bu_4NHSO_5	CH_2Cl_2	10	20	95	89	8
MCPBA–NMO[e]	CH_2Cl_2	4	−78	10	9	5
MCPBA–NMO[e]	CH_2Cl_2	6	−50	70	56	7
MCPBA–NMO[e]	CH_2Cl_2	6	−20	98	86	5
MCPBA–NMO[e,f]	CH_2Cl_2	4	−50	90	85	71

[a] Conditions: [catalyst] = 0.005 M in D-100; [substrate] = 0.1 M in CH_2Cl_2; volume of D-100 = 1 ml; volume of CH_2Cl_2 = 1 ml; oxidant: 0.2 mmol. Stirring rate = 1300 rpm. [b] Determined by capillary GC integration against an internal standard (dichlorobenzene). [c] Determined by capillary GC using a Cyclodex-B chiral column. [d] The catalyst bleached in 30 min. [e] NMO = *N*-methylmorpholine *N*-oxide (0.5 mmol). Addition of the oxidant was carried out according to the procedure described in ref. 13. [f] Substrate = indene.

the case of the cobalt complex of a perfluoroalkylated tetraarylporphyrin, the presence of two distinct phases did not preclude the oxidation of the substrate dissolved in the organic solvent.[7a] Both complexes were found to be active catalysts, affording epoxides in isolated yields up to 85%. Moreover we were able to use the catalysts in substantially lower amounts than those required under homogenous conditions (catalyst = 1.5% with respect to the alkene, instead of 12%).[12] The brown perfluorocarbon layer recovered by simple decantation could be generally recycled in a second run without appreciable decrease of activity. Rather surprisingly, only indene was epoxidized with high enantioselectivity (> 90%). All the other alkenes that we tested gave low (15%) or even 0% ee. The same trend was observed when reactions were carried out in the presence of other oxygen donors more commonly used in combination with chiral (salen)Mn. Results are exemplified in Table 2 for the epoxidation of 1,2-dihydronaphthalene and indene catalysed by Mn–**1**. Epoxidations with the couple *m*-chloroperbenzoic acid–*N*-methylmorpholine *N*-oxide (MCPBA–NMO) were very slow at −78 °C, probably because of hindered mass-transfer between the two liquid phases. Although still lower than in the case of homogeneous systems,[13] reaction rates in the FBS became reasonable at −50 °C. Catalyst Mn–**2** gave lower ee (58%) and conversion (50%) with respect to Mn–**1** in the MCPBA–NMO epoxidation of indene. In the case of 1,2-dihydronaphthalene ee was improved (15 *vs*. 7%), but conversion of the substrate was not satisfactory (45% after 5 h).

Despite the low enantioselectivities generally observed with our prototype catalysts, the FBS approach described here offers distinct advantages over other reported methods of immobilization of salen complexes. Note that in just one case the reported activities, chemoselectivities and ees of heterogenized Jacobsen–Katsuki catalysts were as high as those obtained with one of the best homogeneous chiral (salen)Mn complexes.[14] Stability of the catalyst immobilized in the fluorocarbon layer toward bleaching is increased and its activity remains high. The easy separation of the products from the catalyst which can be readily reused is another considerable benefit that was not given, for instance, by embedding salen complexes into the pores of zeolites.[15] The present results show that an improvement in enantioselectivity does not necessarily follow from the use of FBS versions of chiral catalysts. In this context, the behaviour of Mn–**1** and Mn–**2** is coherent with a strong electron-withdrawing effect exerted by the four perfluoroalkyl chains on the Mn–oxo intermediate responsible for the oxygen transfer.[16,17] Further synthetic efforts are required in order to improve enantiofacial discrimination, still maintaining the peculiar solubility of the catalysts in fluorocarbons.

We thank Ausimont S.p.A. (Milano) for a kind gift of Galden®-D100 and the Progetto Strategico per la Difesa dai Rischi Chimico-Industriali ed Ecologici, CNR (Rome) for financial support.

Notes and References

† E-mail: lupo@iumchz.chimorg.unimi.it

‡ *Selected data* for **1**: mp 108–109 °C; $[\alpha]_D^{20}$ −105.2 (*c* 0.5 in Et_2O); δ_H(300 MHz, $CDCl_3$) 13.45 (br s, 2 H), 8.29 (s, 2 H), 7.65 (d, *J* 2.1, 2 H), 7.47 (d, *J* 2.1, 2 H), 3.48–3.37 (m, 2 H), 2.16–1.68 (m, 8 H); δ_F(282 MHz, $CDCl_3$) −81.3 (t, *J* 10, 3 F), −106.9 (t, *J* 15, 2 F), −120.2 (br s, 2 F), −122.1 (m, 6 F), −123.2 (br s, 2 F), −126.6 (br s, 2 F). For Mn–**1**: $[\alpha]_D^{20}$ −780 (*c* 0.01 in CCl_2FCF_2Cl); λ_{max}(CCl_2FCF_2Cl)/nm 465, 385, 335. For **2**: mp 48–50 °C; $[\alpha]_D^{20}$ −8.8 (*c* 0.5 in Et_2O); δ_H($CDCl_3$) 13.24 (br s, 2 H), 8.44 (s, 2 H), 7.65 (d, *J* 2.1, 2 H), 7.52 (d, *J* 2.1, 2 H), 7.27–7.05 (m, 10 H), 4.82 (s, 2 H); δ_F(282 MHz, $CDCl_3$) −81.1 (t, *J* 10, 3 F), −106.8 (t, *J* 14, 2 F), −120.3 (br s, 2 F), −121.9 (m, 6 F), −123.8 (br s, 2 F), −126.6 (br s, 2 F). For Mn–**2**: $[\alpha]_D^{20}$ +90 (*c* 0.01 in CCl_2FCF_2Cl); λ_{max}(CCl_2FCF_2Cl)/nm 480, 385, 330.

§ The following commercially available perfluorocarbons were tested as solvents: FC-72 (3M, mainly perfluorohexanes, bp 56 °C), FC-75 (3M, mainly perfluoro-*n*-butyltetrahydrofuran, bp 102 °C), D-100 (Ausimont, mainly *n*-perfluorooctane, bp 100 °C).

1 Early work in this field; M. Vogt, Ph.D. Thesis, Rheinisch-Westfälischen Technischen Hochschule, Aachen, Germany, 1991; D.-W. Zhu, *Synthesis*, 1993, 953; I. T. Horváth and J. Rábai, (Exxon Comp.), US Pat. 5 463 082, 1995.
2 I. T. Horváth and J. Rábai, *Science*, 1994, **266**, 72.
3 D. P. Curran, *Chemtracts: Org. Chem.*, 1996, **9**, 75; B. Cornils, *Angew. Chem., Int. Ed. Engl.*, 1997, **36**, 2057.
4 A. Gladysz, *Science*, 1994, **266**, 55; J. J. J. Juliette, I. T. Horváth and J. A. Gladysz, *Angew. Chem., Int. Ed. Engl.*, 1997, **36**, 1610.
5 E. G. Samsel, K. Srinivasan and J. K. Kochi, *J. Am. Chem. Soc.*, 1985, **107**, 7606.
6 E. N. Jacobsen, *Catalytic Asymmetric Synthesis*, ed. I. Ojima, VCH, Weinheim, 1993, p. 159; T. Katsuki, *J. Mol. Cat.*, 1996, **113**, 87 and references cited therein.
7 (*a*) G. Pozzi, F. Montanari and S. Quici, *Chem. Commun.*, 1997, 69; (*b*) G. Pozzi, M. Cavazzini, S. Quici and S. Fontana, *Tetrahedron Lett.*, 1997, **38**, 7605.
8 (*a*) S. G. DiMagno, P. H. Dussault and J. A. Schultz, *J. Am. Chem. Soc.*, 1996, **118**, 5312; (*b*) I. Klement, H. Lütjens and P. Knochel, *Angew. Chem., Int. Ed. Engl.*, 1997, **36**, 1454; (*c*) J.-M. Vincent, A. Rabion, V. K. Yachandra and R. H. Fish, *Angew. Chem., Int. Ed. Engl.*, 1997, **36**, 2346.
9 V. C. R. McLoughlin and J. Thrower, *Tetrahedron*, 1969, **25**, 5921; G. Pozzi, I. Colombani, M. Miglioli, F. Montanari and S. Quici, *Tetrahedron*, 1997, **53**, 6145.
10 A. Ogawa and D. P. Curran, *J. Org. Chem.*, 1997, **62**, 450.
11 P. L. Anelli, F. Montanari and S. Quici, *Org. Synth.*, 1993, **Coll. Vol. VIII**, 367.
12 T. Yamada, K. Imagawa, T. Nagata and T. Mukaiyama, *Chem. Lett.*, 1992, 2231; K. Imagawa, T. Nagata, T. Yamada and T. Mukaiyama, *Chem. Lett.*, 1994, 527.
13 M. Palucki, G. J. McCormick and E. N. Jacobsen, *Tetrahedron Lett.*, 1995, **36**, 5457.
14 I. F. J. Vankelecom, D. Tas, R. F. Parton, V. Van de Vyver and P. A. Jacobs, *Angew. Chem., Int. Ed. Engl.*, 1996, **35**, 1346.
15 S. B. Ogunwumi and T. Bein, *Chem. Commun.*, 1997, 901; M. J. Sabater, A. Corma, A. Domenech, V. Fornés and H. Garcìa, *Chem. Commun.*, 1997, 1285; L. Frunza, H. Kosslick, H. Landmesser, E. Höft and R. Friecke, *J. Mol. Catal.*, 1997, **123**, 179.
16 A. Robert, A. Tsapara and B. Meunier, *J. Mol. Catal.*, 1993, **85**, 13; P. J. Pospisil, D. H. Carsten and E. N. Jacobsen, *Chem. Eur. J.*, 1996, **2**, 974.
17 M.-A. Guillevic, A. M. Arif, I. T. Horváth and J. A. Gladysz, *Angew. Chem., Int. Ed. Engl.*, 1997, **36**, 1612.

Received in Liverpool, UK, 20th January 1998; 8/00558C

Recognition-induced control of a Diels–Alder reaction

Douglas Philp*† and Andrew Robertson

School of Chemistry, University of Birmingham, Edgbaston, Birmingham, UK B15 2TT

The rational design of a system which is capable of controlling the stereochemical outcome of a Diels–Alder reaction between a maleimide and a furan is presented.

The acceleration of chemical reactions and the control of their regio- and/or stereo-chemical outcome by the intervention of recognition processes in solution—achieved so elegantly by enzymes—has prompted synthetic chemists to design a variety[1] of unnatural systems which are capable of performing similar tasks. We are interested in achieving acceleration and control in solution phase reaction processes *via* the use of molecular recognition. In particular, we wished to investigate the acceleration and control of the Diels–Alder reaction[2] between a maleimide and a furan. In principle, this reaction can give rise to two products—the *endo* and the *exo* adducts—depending on the orientation of the approach of the diene to the dienophile. Normally, the *endo* adduct is the kinetic product and the *exo* adduct is the thermodynamic product of this reaction. In principle, rate acceleration[3]‡ can be achieved by transforming the bimolecular reaction between the diene and dienophile in solution into a unimolecular reaction within a non-covalently bound complex.

The objective can be accomplished most readily by locating complementary recognition sites on the diene and dienophile. Accordingly, we designed (Fig. 1) the maleimide **1**, which bears an amidopicoline moiety, and the furan **2**, which bears a carboxylic acid. These two species would be expected to bind to each other through the mutual recognition between the amidopicoline and the carboxylic acid. Molecular mechanics calculations§ suggested that we could expect the furan and maleimide rings to be positioned (Fig. 1) in an orientation which should accelerate the rate of the Diels–Alder cycloaddition and/or control its stereochemical outcome. The benzene ring used as a rigid spacer between the recognition site and the maleimide ring in **1** might be expected to function in a manner which would permit discrimination between the *endo* and *exo* transition states, hence generating stereoselectivity. Here, we report the observation of the control of the Diels–Alder reaction between **1** and **2** and the rationalisation and analysis of this control by kinetic simulation.

Maleimide **1** was synthesised¶ by standard methods in five steps from 4-(aminomethyl)benzoic acid in an overall yield of 32%. Furan **2** was synthesised in 88% yield by catalytic hydrogenation of commercially-available 3-furylacrylic acid.

In order to assess the efficiency of the rate acceleration and control induced by the formation of a complex betwen **1** and **2**, we followed the course of the reaction between these components in $CDCl_3$ at 30 °C. The initial concentrations of the reactants were 5 mM and the emergence of the resonances arising from **3** and **4** were monitored by 400 MHz ^{1}H NMR spectroscopy over a period of 60 h. The reaction between **2** and benzyl maleimide was chosen as the control reaction and was performed and monitored under identical conditions. The data obtained (Fig. 2) indicates that the recognition-mediated (RM) reaction proceeds significantly faster than the control reaction at this concentration and with high stereoselectivity.

Kinetic simulation and optimisation[4] of the model parameters (Fig. 1) afforded best fit values for the rate constants (Table 1) for the control reaction which, in turn, were used in the kinetic model for the RM reaction. The ratio k_7/k_3 for the *endo* product gives an estimate of 64 mM for the effective molarity (EM) achieved within the [**1**·**2**] complex. The corresponding value for the *exo* isomer (k_5/k_1) is only 6 mM. The *endo* reverse reaction is significantly slower (k_4/k_8 = 170) in the RM system. This observation is consistent with stabilisation of the *endo* product by a strong intramolecular hydrogen bond. The value of k_5/k_6 suggests that there is little or no net product of the *exo* product *via* the recognition mediated pathway.

The kinetic data shown in Table 1 can be converted into an energy profile for the recognition mediated reaction (Fig. 3) by application of standard thermodynamic relationships. In the absence of any stabilising or destabilising effect on the transition states induced by complexation, the activation barrier for the reaction within the complex [**1**·**2**] should simply be the sum of the bimolecular activation barrier and the free energy of binding. For the *exo* isomer, this relationship holds suggesting that the formation of the [**1**·**2**] complex has no net effect on the reaction leading to the *exo* isomer. By contrast, the transition state leading to the *endo* isomer is stabilised by 6.1 kJ mol^{-1}. This stabilisation is not enough to offset the increase (13.1

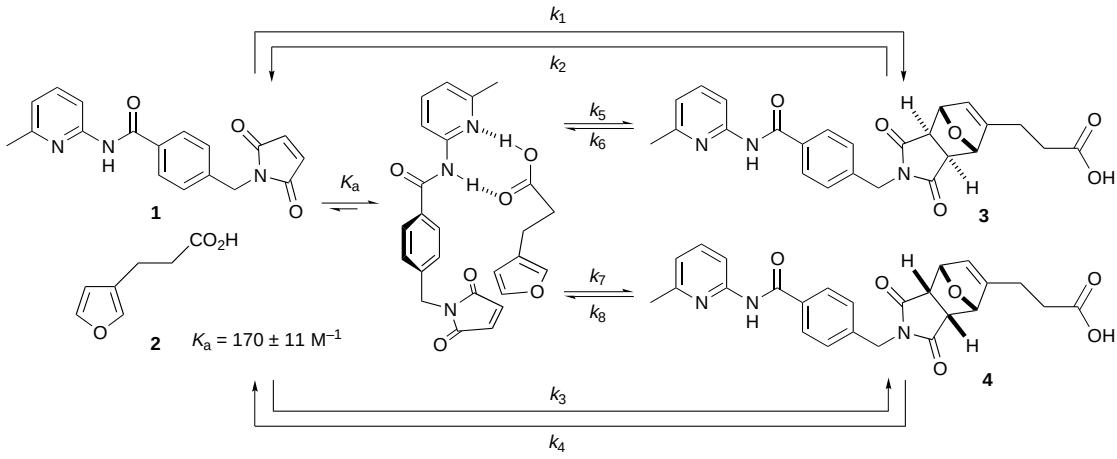

Fig. 1 The design and kinetic scheme for the recognition-mediated Diels–Alder cycloaddition between **1** and **2**. Rate constants are given in Table 1.

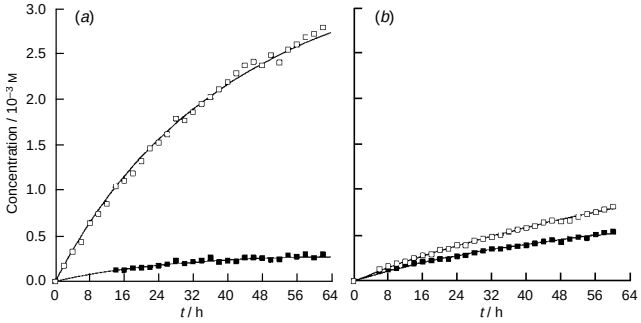

Fig. 2 Concentration–time profiles for (*a*) the reaction between **1** and **2** in $CDCl_3$ at 30 °C and (*b*) the reaction between benzyl maleimide and **2** in $CDCl_3$ at 30 °C. In both cases, the starting concentrations of the reactants were 5 mM. In both plots, the open squares represent the concentration of the *endo* product and the filled squares represent the concentration of the *exo* product. The solid lines represent the best fit of the appropriate kinetic model to the experimental data. For clarity, error bars are omitted from the graphs (errors in concentration are ±3%).

Table 1 Kinetic parameters for the recognition-mediated reaction obtained from the simulation and fitting of the experimental data to the kinetic scheme shown in Fig. 1

$k_1/10^{-5}$ M^{-1} s^{-1}	160 ± 3
$k_2/10^{-5}$ s^{-1}	1.68 ± 0.13
$k_3/10^{-5}$ M^{-1} s^{-1}	209 ± 4
$k_4/10^{-5}$ s^{-1}	0.34 ± 0.03
$k_5/10^{-5}$ s^{-1}	0.99 ± 0.06
$k_6/10^{-5}$ s^{-1}	0.89 ± 0.04
$k_7/10^{-5}$ s^{-1}	13.3 ± 0.11
$k_8/10^{-5}$ s^{-1}	0.002

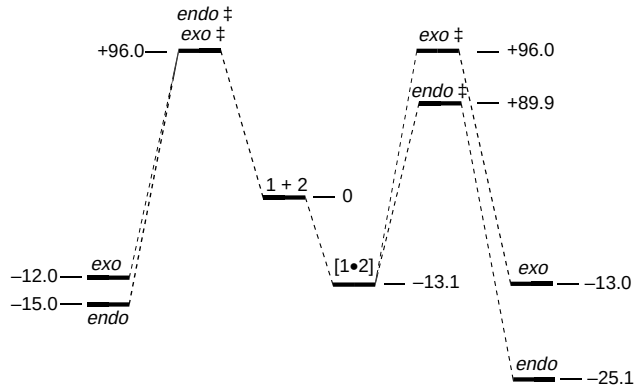

Fig. 3 Thermodynamic profile for the recognition-mediated reaction obtained by the simulation and fitting of the experimental data. The zero point for energy comparisons is set at the energy of the uncomplexed reactants **1** and **2**. All energy values are in kJ mol^{-1}. Data shown to the left of the zero energy point refer to the bimolecular reaction (k_1 to k_4). Data shown to the right of the zero energy point refer to the recognition-mediated reaction (k_5 to k_8).

kJ mol^{-1}) in activation barrier brought about by complexation (thus reflecting the fact that EM < 1 M), however, it does ensure that the *endo* product is produced at a faster rate than the *exo* product within the [**1**·**2**] complex. A more profound effect is observed on the stabilities of the products themselves. Molecular mechanics calculations indicate that the most stable conformation of the *endo* isomer contains an intramolecular hydrogen bond. The *exo* product is incapable of forming an intramolecular hydrogen bond—mechanics calculations indicate that the closest approach of the acid to the amidopyridine is 6.9 Å. This intramolecular interaction is the source of the large discrimination (12.1 kJ mol^{-1}) between the product ground states and, hence, in conjunction with the difference in activation barriers, the selectivity expressed by the reaction for the *endo* isomer.

In conclusion, we have demonstrated that by attaching appropriate recognition sites to a diene and a dienophile, it is possible to exert a high degree of stereocontrol on a Diels–Alder cycloaddition reaction between maleimide and a furan. This control is achieved through the intermediacy of the mutual recognition between reactive partners and by ensuring that only one product—in this case, the *endo* product—is capable of forming stabilising intramolecular hydrogen bonds. The reaction reported here is accelerated only modestly (EM = 64 mM for the *endo* isomer). We are currently addressing this matter and exploring the use of the methodology reported here in the regio- and stereo-control of other [4 + 2] and [3 + 2] cycloaddition reactions.

This research was supported by the University of Birmingham and the EPSRC (Quota Award to A. R.). We thank Professor G. von Kiedrowski for providing us with a copy of his SimFit program. We thank Mr P. Ashton for performing mass spectrometric analyses and Dr Neil Spencer and Mr Malcolm Tolley for the acquisition of the NMR data.

Notes and References

† E-mail: d.philp@birmingham.ac.uk

‡ In the present context, we are not concerned with catalysis in the sense of turnover, but rather ensuring that, by encoding the appropriate recognition features within the reagents, the Diels–Alder reaction is accelerated and its stereochemical outcome controlled.

§ Molecular mechanics calculations on the [**1**·**2**] complex were carried out using the AMBER* forcefield as implemented in Macromodel (Version 5.0, F. Mohamadi, N. G. J. Richards, W. C. Guida, R. Liskamp, M. Lipton, C. Caufield, G. Chang, T. Hendrickson and W. C. Still, *J. Comput. Chem*., 1990, **11**, 440) together with the GB/SA solvation model (W. C. Still, A. Tempczyk, R. C. Hawley and T. Hendrickson; *J. Am. Chem. Soc*., 1990, **112**, 6127) for $CHCl_3$. Conformational searching was carried out using 10 000 step Monte Carlo simulations and all conformations generated within 10 kcal mol^{-1} of the global minimum were minimised. The sets of low energy conformations generated were then filtered to locate those conformations where the maleimide and furan were in close proximity (centroid–centroid distance < 5 Å). This produced a significant number (> 10% of total set size) of conformations corresponding to the pro-*endo* complex.

¶ *Selected data* for **1**: δ_H(300 MHz, $CDCl_3$) 8.75 (1 H, br s), 8.18–8.12 (1 H, m), 7.89–7.81 (2 H, m), 7.65–7.56 (1 H, m), 7.43–7.37 (2 H, m), 6.90–6.85 (1 H, m), 6.72 (2 H, s), 4.70 (2 H, s), 2.39 (3 H, s); δ_C(75 MHz, $CDCl_3$) 170.2, 165.2, 156.9, 150.8, 140.3, 138.8, 134.3, 133.9, 128.6, 127.7, 119.5, 111.1, 41.0, 23.9 [EIMS: *m/z* 321 (70%), 214 (100%)].

1 For excellent general reviews, see A. J. Kirby, *Angew. Chem., Int. Ed. Engl*., 1996, **35**, 707; H. Dugas, *Bioorganic Chemistry—A Chemical Approach to Enzyme Action*, Springer-Verlag, New York, 3rd edn., 1996. For some efficient examples, see M. W. Hosseini, J. M. Lehn, K. C. Jones, K. E. Plute, K. B. Mertes and M. P. Mertes, *J. Am. Chem. Soc*., 1989, **111**, 6330; I. Huc, J. Pieters and J. Rebek, Jr., *J. Am. Chem. Soc*., 1994, **116**, 10 296; P. Tecilla, V. Jubian and A. D. Hamilton, *Tetrahedron*, 1995, **51**, 435.

2 M. C. Carreno, J. L. G. Ruano and A. Urbano, *J. Org. Chem*., 1996, **61**, 6136; D. S. Millan, T. T. Pham, J. A. Lavers and A. G. Fallis, *Tetrahedron Lett*., 1997, **38**, 795; M. J. Lilly and M. S. Sherburn, *Chem. Commun*., 1997, 967; T. Wong, P. D. Wilson, S. Woo and A. G. Fallis *Tetrahedron Lett*., 1997, **38**, 7045; E. J. Bush and D. W. Jones, *J. Chem. Soc., Perkin Trans. 1*, 1997, 3531.

3 T. R. Kelly, V. S. Ekkundi and P. Meghani, *Tetrahedron Lett*., 1990, **31**, 3381; S. C. Hirst and A. D. Hamilton, *J. Am. Chem. Soc*., 1991, **113**, 382; C. J. Walter and J. K. M. Sanders, *Angew. Chem., Int. Ed. Engl*., 1995, **34**, 217; H. L. Anderson and J. K. M. Sanders, *J. Chem. Soc., Perkin Trans. 1*, 1995, 2223; J. Rebek, Jr. and J. Kang, *Nature*, 1997, **385**, 50; B. Wang and I. O. Sutherland *Chem. Commun*., 1997, 1495.

4 SimFit, A Program for the Analysis of Kinetic Data, Version 1.0, G. von Kiedrowski, 1994.

Received in Liverpool, UK, 20th January 1998; 8/00559A

New approach to the solution chemistry of bismuth citrate antiulcer complexes

John A. Parkinson,* Hongzhe Sun and Peter J. Sadler*†

Department of Chemistry, University of Edinburgh, West Mains Road, Edinburgh, UK EH9 3JJ

The use of ^{13}C-labelled citrate together with diffusion-ordered 2D [^{1}H,^{13}C] HSQC NMR spectroscopy has allowed the detection of cluster complexes formed by a bismuth(III) antiulcer complex in aqueous solution at pH 7.4.

Citrate is an important biological ligand for metal ions. It is present at high concentration (*ca.* 200 μM) in blood plasma and forms strong complexes not only with natural metal ions such as Ca^{II}, Mg^{II} and Fe^{III}, but also with ions of toxic (*e.g.* Al^{III}),[1] therapeutic (*e.g.* Bi^{III}) and diagnostic (*e.g.* $^{67}Ga^{III}$)[2] importance. Notable features of the chemistry of citrate are the low pK_a values of its three carboxyl groups (3.13, 4.76 and 5.40 at 25 °C, I = 0.1 M),[3] and, consequently, its existence as a trianion at biological pH (7.4), and the ability of the more highly charged metal ions to deprotonate the hydroxyl group (pK_a *ca.* 11.0)[4] giving rise to very strong metal–alkoxide bonds. Since citrate is a dendritic ligand with seven potential oxygen donors, it is perhaps not surprising that both solution equilibria and solid-state structures of metal citrate complexes are complicated, and often dominated by oligomer formation.

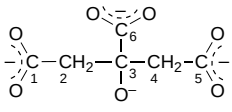

citrate

For example, X-ray crystallography has demonstrated the existence of an iron(III) citrate dimer,[5] an aluminium(III) citrate trimer[6] and a wide variety of structures (dimers, cubes, chains, sheets) for bismuth(III) citrate containing additional hydroxide and oxide ligands.[7] These form the basis of antiulcer drugs such as Colloidal Bismuth Subcitrate (CBS) and Ranitidine Bismuth Citrate (RBC).[8] Equilibria between different types of bismuth citrate complexes in aqueous solution are poorly understood and difficult to study. We show here that the combined use of ^{13}C-labelled citrate and a novel 2D diffusion-ordered [^{1}H,^{13}C] HSQC NMR method provides new insights into the structures and dynamics of bismuth(III) citrate complexes in aqueous solution and can readily be applied to studies of a wide range of other metal citrate complexes.

The normal 1D ^{1}H NMR spectrum of ranitidine bismuth citrate in the region δ 2.0–3.4 is characterized by a combination of sharp intense resonances from ranitidine (which is not bound directly to Bi^{III}),[9] some relatively intense AB quartets and some very broad peaks close to the baseline assignable to citrate. In order to investigate the types of Bi-bound citrate present in ranitidine bismuth citrate solutions at pH* 7 (pH meter reading for D_2O solution), we prepared the complex using citrate labelled at C2 and C4 with >95% ^{13}C.‡ As can be seen in Fig. 1, the peaks in the 2D [^{1}H,^{13}C] HSQC NMR spectrum cover a remarkably large chemical shift range in both the ^{1}H (δ 2.3–3.4) and ^{13}C (δ 47–57) dimensions. The appearance of the spectrum was the same at ranitidine bismuth citrate concentrations of 2 and 5 mM. At a given ^{13}C shift, the ^{1}H peaks appear as doublets of doublets due to the presence of $^{13}C_XH_AH_B$ spin systems, and the two CH_2 groups within one citrate ligand can be non-equivalent, as has been observed for $Na_2[Bi_2(cit)_2]$ by solid-state ^{13}C CP MAS NMR spectroscopy.[7e] The peaks in region 1 of the 2D [^{1}H,^{13}C] HSQC NMR spectrum (Fig. 1) have shifts close to those of free (unbound) citrate, whereas the marked high frequency ^{13}C shifts and pronounced separation of H_A and H_B peaks in region 3 suggest that these cross-peaks arise from rigidly-bound citrate ligands which place H_A and H_B in markedly different environments (*e.g.* bridging ligands in clusters). To investigate the dynamic properties of these bismuth(III) citrate species we measured their self-diffusion coefficients using 2D diffusion-edited heteronuclear single quantum coherence NMR spectroscopy (DOSY-HSQC).

Although DOSY-HSQC has been alluded to in the literature,[10] the present use appears to be the first direct application. One-dimensional homonuclear and heteronuclear diffusion-ordered NMR methods have been used recently to correlate chemical shifts and molecular self-diffusion coefficients. In view of the limitation of peak overlap in 1D ^{1}H NMR spectra, techniques have been developed which combine diffusion methods with standard 2D homonuclear techniques *e.g.* DOSY-COSY,[11] DOSY-NOESY[12] and diffusion-ordered TOCSY.[13] These depend on the existence of either scalar or dipolar coupling between spins and are useful only if cross-peaks from different species are not degenerate. The heteronuclear DOSY-HSQC method in combination with specific ^{13}C labelling can overcome the problem of overlap of ^{1}H resonances, and also provides greatly increased sensitivity in the ^{13}C dimension compared to direct heteronuclear observation.

Self-diffusion coefficients (D) were evaluated from measurements of volume integrals [$A(g_d)$] of peaks in 2D [^{1}H,^{13}C] DOSY-HSQC NMR spectra acquired using the pulse sequence

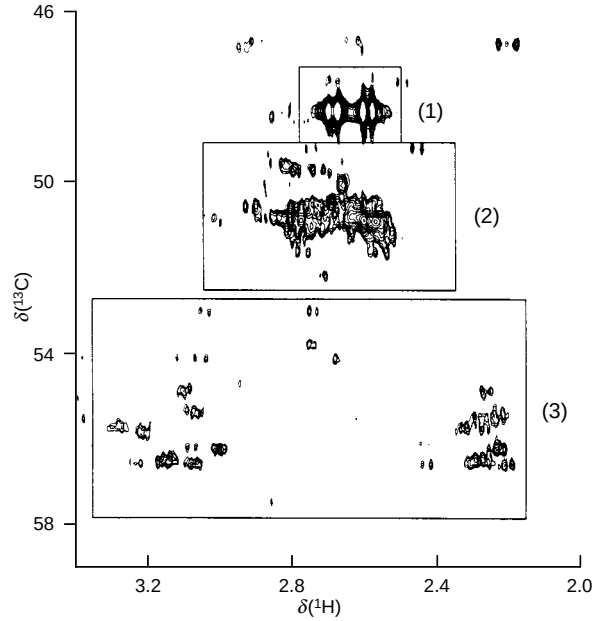

Fig. 1 2D [^{1}H,^{13}C] HSQC NMR spectrum of 5 mM ranitidine bismuth citrate (pH* 7.4) with diffusion weighting at a bipolar gradient strength of 25.05 mT m^{-1} acquired using the scheme in Fig. 2. The volume integrals of peaks in areas labelled 1–3 were used to measure self-diffusion coefficients. The total areas of each region were determined but the behaviour of the individual peaks in each region appear to be similar.

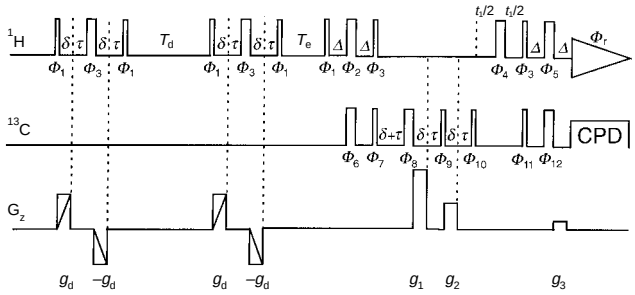

Fig. 2 Pulse sequence used for 2D [^{1}H,^{13}C] DOSY-HSQC experiments. Along the ^{1}H and ^{13}C schemes, narrow and wide vertical bars represent 90° and 180° pulses, respectively. Phase cycling: $\phi_1 = \phi_2 = \phi_5 = \phi_6 = \phi_8 = \phi_{10} = x$; $\phi_3 = y$; $\phi_4 = x, x, -x, -x$; $\phi_7 = 4(y), -4(y)$; $\phi_{11} = x, -x$; $\phi_r = x, -x, x, -x, -x, x, -x, x$. An XY32 composite pulse (CPD) decoupling scheme was applied during acquisition. Diffusion period T_d = 120 ms; settling period prior to the start of the HSQC section of the experiment T_e = 30 ms; gradient duration δ = 2 ms; gradient recovery period t = 100 μs; $\Delta = 1/4J_{HC}$ = 1.84 ms; gradients g_1, g_2 and g_3 were set in the ratio 80 : 30 : 20 with gradient strengths of 60.7, 24.1 and 15.17 mT m^{-1}, respectively. Rectangular gradients were used throughout.

shown in Fig. 2. This uses gradients to select for the correct quantum transitions. The peak volumes vary with the applied gradient strength (g_d) according to eqn. (1):[13c]

$$A(g_d) = \exp[-D(2\gamma g_d \delta)^2(T_d + \tau/2 + 4\delta/3)] \quad (1)$$

where γ is the gyromagnetic ratio of the observed nucleus, T_d the diffusion time, τ the time interval between bipolar gradients, and δ the gradient duration.

As can be seen from Fig. 3, the diffusion coefficients associated with peaks in regions 2 and 3 are less than half that associated with region 1, which in turn is less than half of the value measured for citrate itself. If we make the assumption that the molecules concerned are approximately spherical (with radius, r) then, according to the Stokes–Einstein equation, the diffusion coefficient is proportional to r^{-1}. If free citrate is assumed to have a diameter of *ca*. 4 Å then the bismuth(III) citrate complexes giving rise to the peaks in regions 2 and 3 have diameters of *ca*. 20 Å. This is close to the size of the dodecanuclear cluster $[Bi_{12}O_8(cit)_8]^{12-}$ in the crystalline state.[7d] In this structure some of the citrate ligands form bridges between three Bi^{III} ions and such a coordination mode might

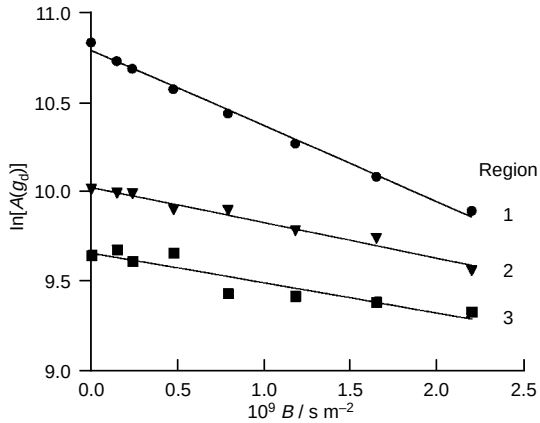

Fig. 3 Plots of ln[$A(g_d)$] *vs.* $B = q^2(T_d + \tau/2 + 4\delta/3)$ where $A(g_d)$ is the (arbitrary) volume integral at a diffusion gradient strength g_d, and $q = (2\gamma g_d \delta)$, and g_d varies from 8.35 to 125.25 mT m^{-1} in increments of 16.7 mT m^{-1}, for peaks in region 1 (●), region 2 (▼) and region 3 (■) of Fig. 1. The slope is proportional to D, the self-diffusion coefficient, giving the values: 4.3, 1.9, 1.7 and 10.2 × 10^{-10} m^2 s^{-1} for regions 1, 2, 3 and free citrate, respectively.

give rise to the unusual shifts we observe, although several types of cluster species appear to be present in solution.

In conclusion we have shown that the use of diffusion-ordered 2D [^{1}H,^{13}C] HSQC NMR spectroscopy, together with ^{13}C-enriched citrate, allows the sensitive detection of a wide range of types of bound citrate in aqueous solutions of the antiulcer drug ranitidine bismuth citrate at pH* 7.4. The unusual ^{1}H,^{13}C shifts and slow diffusional behaviour of some of these species provide a new method of characterising citrate cluster complexes. The identification of cluster species in solution is particularly important since they may be taken up by cells by a different mechanism compared to low molecular mass complexes. We are applying similar methods to the study of a range of biologically important citrate complexes.

We thank GlaxoWellcome for their support of this work, the EPSRC for access to the 600 MHz NMR Service Instrument in Edinburgh and Professor John Lindon (Birkbeck College) for helpful discussions.

Notes and References

† E-mail: p.j.sadler@ed.ac.uk

‡ Bismuth citrate was prepared by mixing 16 mg [^{13}C2,^{13}C4]citric acid (0.08 mmol, supplied by GlaxoWellcome) with 35.6 mg bismuth nitrate (0.076 mmol, Sigma) in 2 ml water and heating at 80 °C for 1 h, followed by filtering and washing three times with water, and drying in a desiccator. Ranitidine bismuth [^{13}C]citrate was prepared by dissolving 8 mg of bismuth [^{13}C]citrate and 1.6 mol equiv. of ranitidine in 1 ml D_2O and adjusting the pH* to 7.4 by addition of ranitidine. NMR experiments were performed on a Varian ^{Unity}INOVA 600 NMR spectrometer operating at a ^{1}H resonance frequency of 599.613 MHz using a triple resonance [^{1}H,^{13}C,^{15}N] probe equipped with a *z*-field gradient capability. The *z*-field gradients were accurately calibrated with a sample of doped water at 25 °C using a 1D diffusion experiment. 2D [^{1}H,^{13}C] DOSY-HSQC data were typically acquired with 16 transients into 512 complex data points over a ^{1}H frequency width of 1 kHz for each of 2 × 64 t_1 increments over a ^{13}C frequency width of 2.5 kHz using an XY32 decoupling scheme during t_2.

1 S. J. A. Fatemi, F. H. A. Kadir, D. J. Williamson and G. R. Moore, *Adv. Inorg. Chem.*, 1991, **36**, 409.
2 J. D. Glickson, T. P. Pitner, J. Webb and R. A. Gams, *J. Am. Chem. Soc.*, 1975, **97**, 1679.
3 G. Pettit and L. D. Pettit, *IUPAC Stability Constants database*, 1993, IUPAC/Academic Software, Otley, UK.
4 L. G. Sillén and A. E. Martell, *Stability Constants of Metal Ion Complexes*, Chemical Society Spec. Publ. 17, The Chemical Society, London, 1964.
5 I. Shweky, A. Bino, D. P. Goldberg and S. J. Lippard, *Inorg. Chem.*, 1994, **33**, 5161.
6 T. L. Feng, P. L. Gurian, M. D. Healy and A. R. Barron, *Inorg. Chem.*, 1990, **29**, 408.
7 (*a*) W. A. Herrmann, E. Herdtweck and L. Pajdla, *Inorg. Chem.*, 1991, **30**, 2579; (*b*) E. Asato, W. L. Driessen, R. A. G. de Graaff, F. B. Hulsburgen and J. Reedijk, *Inorg. Chem.*, 1991, **30**, 4210; (*c*) E. Asato, K. Katsura, M. Mikuriya, T. Fujii and J. Reedijk, *Inorg. Chem.*, 1993, **32**, 5322; (*d*) E. Asato, K. Katsura, M. Mikuriya, U. Turpeinen, I. Mutikainen and J. Reedijk, *Inorg. Chem.*, 1995, **34**, 2447; (*e*) P. J. Barrie, M. I. Djuran, M. A. Mazid, M. McPartlin, P. J. Sadler, I. J. Scowen and H. Sun, *J. Chem. Soc., Dalton Trans.*, 1996, 2417.
8 H. Sun, H. Li and P. J. Sadler, *Chem. Ber.*, 1997, **130**, 669.
9 P. J. Sadler and H. Sun, *J. Chem. Soc., Dalton Trans.*, 1995, 1395.
10 D. Wu, A. Chen and C. S. Johnson Jr., *Abstracts of the 37th Experimental Nuclear Magnetic Resonance Conference*, Asilomar, USA, 1996, Abstr. p. 74.
11 D. Wu, A. Chen and C. S. Johnson Jr., *J. Magn. Reson. A*, 1996, **121**, 88.
12 E. K. Gozansky and D. G. Gorenstein, *J. Magn. Reson. B*, 1996, **111**, 94.
13 (*a*) A. Jershow and N. Muller, *J. Magn. Reson. A*, 1996, **123**, 222; (*b*) M. Lin and M. J. Shapiro, *J. Org. Chem.*, 1996, **61**, 7617; (*c*) M. Liu, J. K. Nicholson, J. A. Parkinson and J. C. Lindon, *Anal. Chem.*, 1997, **69**, 1504.

Received in Cambridge, UK, 3rd December 1997; 7/08710A

Production and isolation of the C_{80}-based group 2 *incar*-fullerenes: *i*CaC_{80}, *i*SrC_{80} and *i*BaC_{80}

T. John S. Dennis and Hisanori Shinohara*†

Department of Chemistry, Nagoya University, Nagoya 464-8602, Japan

We report the first production and isolation of mono-*incar*-fullerenes based on the missing fullerene C_{80}, and their characterisation by UV–VIS–NIR absorption spectroscopy.

Mass spectroscopic measurements of solvent-extracted fullerenes obtained from arc-processed carbon reveal good signals from C_{76}, C_{78}, C_{82}, C_{84}, C_{86} *etc*., but the signal from C_{80} is meagre. Small quantities of C_{80} were isolated only recently by Hennrich *et al.*[1] Thus at first sight, it seems surprising that C_{80}-based *incar*-fullerenes are isolated in yields similar to other *incar*-fullerenes. The dilanthanum *incar*-fullerene, *i*La_2C_{80}, was first produced and solvent extracted by Whetten and coworkers.[2] Isolation of *i*La_2C_{80}[3,4] and *i*Ce_2C_{80}[5] has recently been achieved, and their UV–VIS–NIR absorption spectra,[3,5] and their ^{139}La and ^{13}C NMR[4] spectra were reported.

In our continuing efforts to elucidate structures and electronic properties of group 2 element-based *incar*-fullerenes,[6–13] we have fortuitously found C_{80}-based *incar*-fullerenes in arc-processed soot. Here we present the first successful production, isolation, and characterisation of mono *incar*-fullerenes based on C_{80}: namely *i*MC_{80} (M = Ca, Sr, Ba). The yields of these materials are relatively high; comparable to those of *i*MC_{82} and *i*MC_{84}.[6–9]

Fullerene-soot containing group 2 element-based *incar*-fullerenes is produced by the direct-current contact-arc method using graphite–metal carbide composite rods.[9,12] The fullerenes are extracted using ultrasonication and CS_2 solvent. Although the extracted *incar*-fullerenes are air stable, they are air sensitive prior to extraction, and are collected and extracted under totally anaerobic conditions.[12]

Isolation schemes for all three *incar*-fullerenes are very similar, being achieved by our three stage HPLC treatment. Stage 1 is a rough separation step used primarily to remove C_{60} and C_{70}. A Cosmosil Buckyprep column (28 mm × 250 mm) is used with a high injection volume (100 ml; 30 ml min^{-1} flow rate, toluene eluent). LD-TOF mass spectroscopy reveals that for each case *i*MC_{80} elutes from the column with the C_{86}-containing fraction. Following concentration, the *i*MC_{80}-containing fraction is subjected to further HPLC treatment. In stage 2, recycling HPLC, a Cosmosil 5PYE column (20 × 250 mm; 10 ml injections, 18 ml min^{-1} flow rate, toluene eluent) is used as retention times on this column are approximately half those on the buckyprep, yet its resolution is similar. After typically four cycles separation into several subfractions is complete. The final eluting sub-fraction contains C_{86}, *i*MC_{84},[7–9] and *i*MC_{80}; all other sub-fractions contain minor isomers of C_{84}. In stage 3, again recycling HPLC, a Regis Buckyclutcher column (20 × 300 mm) is used to separate the materials that cannot be resolved on either Buckyprep or 5PYE columns (5 ml injections; 9.3 ml min^{-1} flow rate, toluene eluent). After 9 recycles three fractions are observed to be completely separated. These contain, in order of increasing retention time, empty C_{86}, *i*MC_{84},[7–9] and *i*MC_{80}. To ensure the purity of the sample, stage 3 HPLC was repeated on the *i*MC_{80} fractions. The result was fine black powders of mass 0.60, 0.30 and 0.10 mg for *i*CaC_{80}, *i*SrC_{80} and *i*BaC_{80}, respectively. Complete isolation is confirmed by HPLC analysis and laser-desorption time-of-flight mass spectrometry. Fig. 1 shows a stage 3 recycling-HPLC chromatogram for *i*BaC_{80}.

Fig. 2 shows the UV–VIS–NIR absorption spectra of *i*CaC_{80}, *i*SrC_{80} and *i*BaC_{80}, recorded between 400 and 2000 nm in CS_2 solution. All three spectra are remarkably similar, being characterised by onsets near 1400 nm, three characteristic and sharp absorption bands at *ca*. 500, 600 and 700 nm, and a broad feature around 1050 nm. These particularly sharp absorption bands may arise from electron transfers from the encased metals to the C_{80} cages. They have not been observed in any absorption spectrum of any previous *incar*-fullerene,[12] suggesting unique electronic and structural properties for these C_{80}-based mono *incar*-fullerenes. These spectra differ considerably from the UV–VIS–NIR spectrum of empty C_{80}.[1] That spectrum has an onset near 900 nm, and contains weak broad absorption bands near 600, 800 and 880 nm. The present spectra can also be contrasted with those of other C_{80}-based *incar*-fullerenes. For *i*Ce_2C_{80}[5] and *i*La_2C_{80},[3] both spectra have onsets near 600 nm, but are otherwise practically featureless.

There are seven structural isomers (D_2, D_{5d}, C_{2v}, C_{2v}', D_3, D_{5h} and I_h) for the empty C_{80} fullerene that satisfy the isolated pentagon rule (IPR).[14] A ^{13}C NMR study on C_{80} indicates the most abundant isomer has D_2 symmetry.[1] However, *ab initio* calculations[15] predict encapsulation of two La atoms in the I_h isomer is much more stable than the D_2 or other isomers. Confirmation of I_h symmetry for *i*La_2C_{80} has come from recent ^{13}C NMR measurements.[4] [80-I_h]Fullerene has two electrons in a fourfold degenerate HOMO. Accommodation of six further electrons forms a closed shell electronic state, *i*$La_2^{6+}C_{80}^{6-}\{I_h\}$.[15,16] The late onsets and featureless nature of the UV–VIS–NIR absorption spectra of *i*La_2C_{80} and *i*Ce_2C_{80} have been attributed to the closed-shell nature of the icosahedral *incar*-fullerene cage.[3,5]

Our studies suggest two electrons are transferred to the cage of group 2 element-based *incar*-fullerenes.[6–11] If *i*Ca/Sr/BaC_{80}

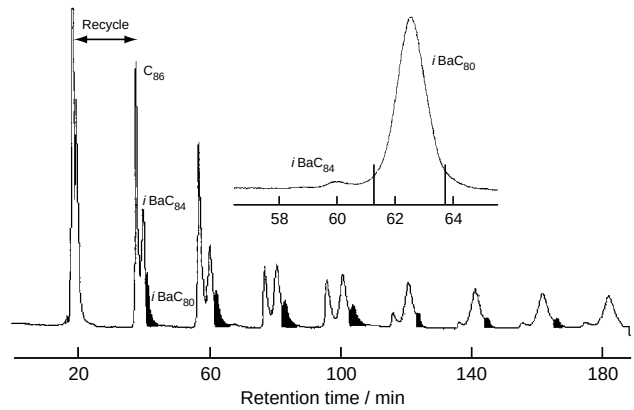

Fig. 1 Stage 3 recycling HPLC chromatogram for the purification of *i*BaC_{80}. The three peaks, in order of increasing retention time, are C_{86}, *i*BaC_{84} and *i*BaC_{80} (highlighted) (the changing relative intensities after the third cycle is due to peak cutting by the experimenter). Inset, the third-cycle chromatogram for *i*BaC_{80} from the repeat stage 3 separation, indicates the high sample purity.

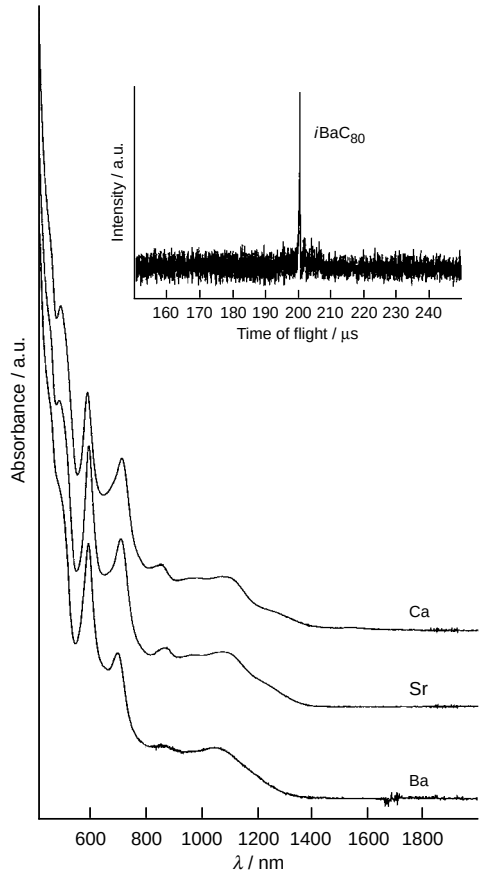

Fig. 2 The UV–VIS–NIR absorption spectra of *i*Ca/Sr/BaC_{80}. The absorption dips at *ca*. 500 and 700 nm account for three CS_2 solutions being greenish brown. The three sharp peaks appearing between 500 and 700 nm are particularly salient (see text). The LD-TOF mass spectrum (inset) of isolated *i*BaC_{80} confirms sample purity.

also has I_h symmetry, these materials may possess novel solid state properties, high-T_c superconductors, for example, because the transfer of two electrons to the fullerene cage would result in forming a half-filled degenerate HOMO: a situation strikingly similar to the half-filled threefold degenerate HOMO of superconducting A_3C_{60} (A = K, Rb).

The great similarity between the UV–VIS–NIR absorption spectra of the present samples (Fig. 2), coupled with their near identical HPLC retention times, strongly suggests that all three *incar*-fullerenes share the same C_{80} isomer.

T. J. S. D. thanks the Japan Society for the Promotion of Science, and H. S. thanks the Japanese Ministry of Education, Science, Sports and Culture for Grants-in-Aid for Scientific Research on Scientific Research (A)(2) (No. 08554020), for financial support of the present study.

Notes and References

† E-mail: nori@chem2.chem.nagoya-u.ac.jp

1 F. H. Hennrich, R. H. Michel, A. Fischer, S. Richard-Schneider, S. Gilb, M. K. Kappes, D. Fuchs, M. B. Ÿrk, K. Kobayashi and S. Nagase, *Angew. Chem., Int. Ed. Engl.*, 1996, **35**, 1732.
2 M. M. Alvarez, E. G. Gillan, K. Holczer, R. B. Kaner, K. S. Min and R. L. Whetten, *J. Phys. Chem.*, 1991, **95**, 10 561.
3 T. Suzuki, Y. Maruyama, T. Kato, K. Kikuchi, Y. Yakao, Y. Achiba, K. Kobayashi and S. Nagase, *Angew. Chem., Int. Ed. Engl.*, 1995, **107**, 1228; *Angew. Chem.*, 1995, **34**, 1094.
4 J. Ding and S. Yang, *Angew. Chem., Int. Ed. Engl.*, 1996, **35**, 2234.
5 T. Akasaka, S. Nagase, K. Kobayashi, M. Wlscli, K. Yamamoto, H. Funasaka, M. Kako, T. Hoshino and T. Erata, *Angew. Chem., Int. Ed. Engl.*, 1997, **36**, 1643.
6 Z. Xu, T. Nakane and H. Shinohara, *J. Am. Chem. Soc.*, 1996, **118**, 11 309.
7 T. J. S. Dennis and H. Shinohara, *Chem. Phys. Lett.*, 1997, **278**, 107.
8 T. J. S. Dennis and H. Shinohara, *Fullerenes: Recent Advances in the Chemistry and Physics of Fullerenes and Related Materials*, ed. K. M. Kadish and R. S. Ruoff, The Electrochemical Society Inc., NJ, 1997, vol. 4, p. 507.
9 T. J. S. Dennis and H. Shinohara, *Appl. Phys. A*, 1998, **66**, 243.
10 T. Nakane, Z. Xu, E. Yamamoto, T. Kai, T. Tomiyama and H. Shinohara, *Electronic Properties on Novel Materials: Molecular Nanostructures*, ed. H. Kuzmany, J. Fink, M. Mehring and S. Roth, World Scientific, London, 1997, p. 193.
11 T. S. M. Wan, H. W. Zhang, T. Nakane, Z. Xu, H. Shinohara, K. Kobayashi and S. Nagase, *J. Am. Chem. Soc.*, submitted.
12 H. Shinohara, M. Takata, M. Sakata, T. Hashizume and T. Sakurai, *Mater. Sci. Forum*, 1996, **232**, 207.
13 H. Shinohara, H. Yamaguchi, N. Hayashi, H. Sato, M. Ohkohchi, Y. Ando and Y. Saito, *J. Phys. Chem.*, 1993, **97**, 4259.
14 P. W. Fowler and D. E. Manolopoulos, *An Atlas of Fullerenes*, Oxford University Press, Oxford, 1995, p. 73.
15 K. Kobayashi, S. Nagase and T. Akasaka, *Chem. Phys. Lett.*, 1995, **245**, 230.
16 S. Nagase, K. Kobayashi and T. Akasaka, *Bull. Chem. Soc. Jpn.*, 1996, **69**, 2131.

Received in Cambridge, UK, 7th January 1998; 8/00218E

Bi- and tri-nuclear ruthenium(II) complexes containing tetrapyridophenazine as a rigid bridging ligand

Pierre Bonhôte,*[a]† Ariane Lecas[b] and Edmond Amouyal*[b]‡

[a] *Department of Chemistry, Massachusetts Institute of Technology, Cambridge, MA 02139, USA and Laboratoire de Photonique et Interfaces, Ecole Polytechnique Fédérale de Lausanne, CH-1015 Lausanne, Switzerland*
[b] *Laboratoire de Physico-Chimie des Rayonnements (CNRS, URA 75), Bât. 350, Université de Paris-Sud, F-91405 Orsay, France*

The rigid, aromatic bis-tridentate bridging ligand tetrapyrido[2,3-a:3′,2′-c:2″,3″-h:3‴,2‴-j]phenazine (tpp) allowed the preparation of linear, stable bi- and tri-nuclear complexes of ruthenium(II) exhibiting low energy Ru → tpp MLCT absorptions and a strong electronic coupling in the mixed-valence state.

Following the pioneering work of Creutz and Taube,[1] much interest has been devoted to the bridged bi- and poly-nuclear ruthenium complexes, particularly in their mixed valence state.[2,3] The short bridging ligands such as pyrazine,[1] *tert*-butylmalonitrile, dinitrogen, cyanogen[2] or 4,4-dithiodipyridine[4] provide often a strong enough coupling between ruthenium–amine centers to allow complete electronic delocalization in the mixed-valence (MV) state (class III MV complexes). On the other hand, polynuclear ruthenium–polypyridine complexes usually show weaker electronic coupling and are valence-trapped (class II).[5] Tetrakis(2-pyridyl)pyrazine (tppz) was up to now the only polyazine bridging ligand allowing a Ru–Ru coupling of a similar intensity as in the Creutz–Taube ion.[5–8] Polynuclear complexes of ruthenium(II) are valuable sensitizers for the conversion of light into chemical or electrical energy[9] as they are efficient MLCT chromophores in which the absorption maximum can be tuned to almost any wavelength of the visible spectrum.[10] In order to ensure a potentially good charge separation from an excited state in a donor–chromophore–acceptor triad, it is suitable to aim at linear, rigid assembly.[11] It is thus obvious that the most promising bridging ligands are the bis-tridentate ones, like tppz. In that class of polyazines, tetrapyrido[2,3-a:3′,2′-c:2″,3″-h:3‴,2‴-j]phenazine (tpp), is the representative which is at the same time the most rigid and the shortest intermetallic spacer. We have developed a straightforward synthesis of this compound[12] and report here on its outstanding properties as a bridging ligand between ruthenium–terpyridine units.

Attempts to react directly a blue solution of ruthenium(II) chloro complexes with tpp in various ratios in refluxing ethylene glycol led only to the mononuclear complex $[Ru(tpp)_2]Cl_2$ **1**. For the elaboration of polynuclear Ru–tpp complexes, we used $RuCl_3$(ttp) (ttp = 4′-*p*-tolyl-2,2′-6′,2″-terpyridine) as a starting ruthenium containing unit.[5,7,8,11,13] The advantage of ttp[14] over terpyridine is the availability of a methyl group for further linkage with electron donors or acceptors[11] and as a useful internal standard for NMR integration. Reaction of $RuCl_3$(ttp) with an excess of tpp in refluxing ethanol–water–triethylamine, followed by precipitation by NH_4PF_6 afforded the orange $[Ru(tpp)(ttp)][PF_6]_2$ **2** in 52% yield (Scheme 1). This complex reacted under the same conditions with $RuCl_3$(ttp) to give, after chromatography over SiO_2, the green binuclear complex $[(ttp)Ru(ttp)Ru(ttp)][PF_6]_4$ **3** in 39% yield. The same product was obtained by reacting tpp with $RuCl_3$(ttp) (28% yield). In the reductive solvents mentioned above, the main product obtained by reaction of **1** with 3 equiv. of $RuCl_3$(ttp) was surprisingly the binuclear complex **3**, and not the expected trinuclear species $[(ttp)Ru(tpp)Ru(tpp)Ru(ttp)][PF_6]_6$ **4**. Similarly, the reaction of $RuCl_3$(ttp) with a slight excess of **1** afforded **2** only instead of the expected $[(ttp)Ru(tpp)Ru(tpp)][PF_6]_4$. The use of a less reducing mixture [water–methanol (3:1)] allowed finally the synthesis of **4** in 16% yield by reaction of **1** with $RuCl_3$(ttp). Even in this case, a small amount of the binuclear complex was formed. It appears thus that $RuCl_3$(ttp) is able to abstract a tpp ligand from $[Ru(tpp)_2]^{2+}$ under reducing conditions.§

For all the investigated compounds, the first one-electron cathodic wave observed by cyclic voltammetry¶ was attributed to the tpp-centered reduction. It shifts from −1.23 V *vs.* SCE in the free ligand to −0.80 V in **2** and further to −0.38 V in **3**. The oxidation waves corresponding to the $Ru^{2+/3+}$ couple appeared at 1.52 V in **2** but at 1.32 and 1.71 V in **3**. This splitting ΔE of 0.39 V between the $(Ru–Ru)^{4+/5+}$ and the $(Ru–Ru)^{5+/6+}$ redox potentials, symmetrically above and below the potential of **2**, indicates a strong degree of interaction between the two metallic centers. It corresponds to a comproportionation constant $K_c = [(Ru–Ru)^{5+}]^2/\{[(Ru–Ru)^{6+}][(Ru–Ru)^{4+}]\} = \exp(\Delta EF/RT) = 4 \times 10^6$ which is identical to the value reported for the Creutz–Taube ion[1] and higher than the value obtained for $[(ttp)Ru(tppz)Ru(ttp)]^{5+}$ ($K_c = 10^5$).[5] The insolubility of **1** and **4** in the presence of supporting electrolytes prevented any determination of their electrochemical properties.

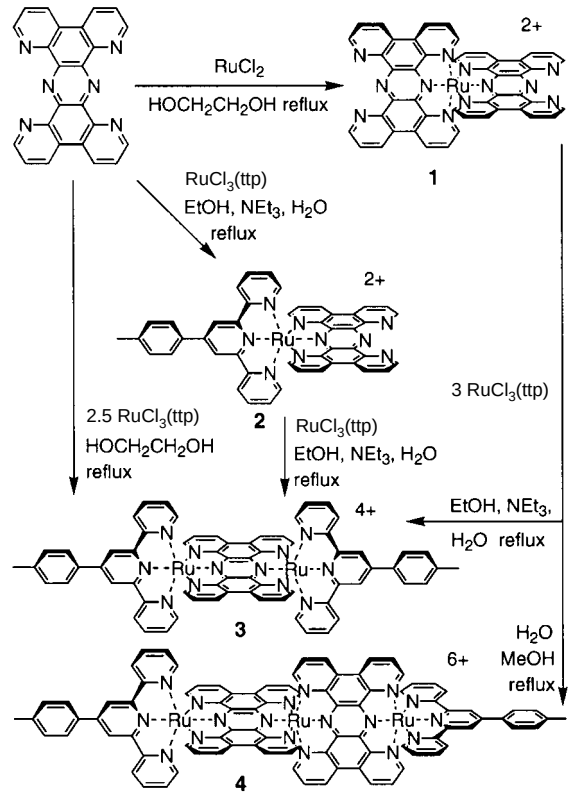

Scheme 1

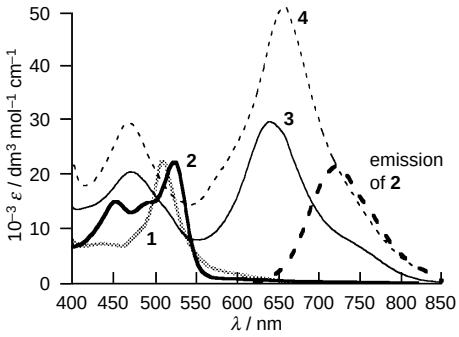

Fig. 1 Visible absorption spectra of **1**, **2**, **3** and **4** as well as emission spectrum of **2** (arbitrary units), in acetonitrile

Table 1 UV–VIS spectral data in MeCN and attribution

	λ_{max}/nm (10^{-3} ε/dm³ mol^{-1} cm^{-1})		
Complex	LC	Ru→ttp	Ru→tpp
1[a]	254(92.0) 276(87.4) 316(82.3) 364(48.1)		508(22.6)
2	251(61.0) 280(79.4) 306(75.3) 366(40.2)	450(15.1)	522(22.2)
3	282(103.2) 309(112.1) 371(33.8)	470(20.7)	644(29.9)
4	230(110.0) 276(148.0) 310(156.0) 376(58.4)	470(29.5)	658(50.7)

[a] As hexafluorophosphate.

The visible absorption spectra of **1**, **2**, **3** and **4** as well as the emission spectrum of **2** are shown in Fig. 1 and the corresponding parameters are given in Table 1. The monometallic complexes show a sharp Ru→tpp MLCT band around 520 nm. In **2**, an additional Ru→ttp MLCT band appears at 450 nm and the complex emits at room temperature at 738 nm, with a yield of $1.2 \pm 0.2 \times 10^{-4}$ and a lifetime $\tau = 60$ ns. No emission was detected from **1**. In **3** and **4**, the low-energy absorption band is attributed to the Ru→tpp MLCT. It is strongly red-shifted compared to those of the monometallic species, while the Ru→ttp band is only slightly affected. This shift is attributed both to the strong stabilization of the π* orbital of the tpp ligand by the chelation of the second Ru^{II}, as shown by the associated low reduction potential, and to the splitting of the t_{2g} orbitals, the d_{xy} set engaged in the bonds with the π* orbital on the pyrazine ring of tpp being destabilized by the metal–metal interaction, while the other sets linked to ttp are less (d_{yz}) or not at all (d_{xz}) affected. From **3** to **4**, the Ru→tpp MLCT band only red-shifts by 14 nm but grows by 70%, which means that the set of t_{2g} orbitals does not undergo a significant additional splitting by addition of a third Ru^{II} center, certainly because the environment is different for the central and for the two terminal metals. While solutions of **3** in acetonitrile could be stored for weeks at room temperature without degradation, **4** was observed to break down quite rapidly, its solution showing after 7 days essentially the spectrum of **2**. No emission was detected below 900 nm for **3** and **4** which could emit further in the IR. The photophysical study of these complexes will be published elsewhere. Oxidation of **3** by Ce^{4+} in acetonitrile acidified by 0.5 M CF_3CO_2H led to the disappearance of the Ru→tpp MLCT band accompanied by the rise of a new absorption at 592 nm, attributed to a tpp→Ru ligand-to-metal charge transfer. Concomitantly, an 'intervalence' absorption band appeared at 1388 nm (7206 cm^{-1}). Its width at half-intensity $\Delta\nu_{1/2}$ is only 2000 cm^{-1}, half the value calculated by the Hush model for a class II complex (4080 cm^{-1}).[2,15] This discrepancy indicates that **3** is a class III complex. In such a case, the electron coupling matrix element V_{ab} is half the energy of the band maximum, *i.e.* 0.447 eV.

In conclusion, tpp appears to form stable mono- and binuclear ruthenium complexes and to mediate a strong interaction between the metallic centers. The intense low-energy Ru→tpp MLCT absorption could prove useful for the development of supramolecular systems and for the photochemical conversion of solar energy.

P. B. thanks the Ciba-Geigy Jubiläums Stiftung and the Fonds National Suisse de la Recherche Scientifique for their postdoctoral grant as well as Prof. Mark S. Wrighton (MIT) for offering the research facilities. A. L. and E. A. thank the CNRS for its support.

Notes and References

† The work by P. B. was carried out in part at MIT and in part at EPFL. Present address: EPFL. E-mail: pierre.bonhote@dcqm.epfl.ch
‡ E-mail: edmond.amouyal@lpcr.u.psud.fr
§ All compounds gave satisfactory elemental and/or FABMS and/or plasma-desorption MS analyses. The corresponding data and NMR spectra will be published elsewhere.
¶ Medium: MeCN + 0.1 M NBu_4BF_4; working electrode: glassy carbon disk; reference: SCE. The given half-wave potentials correspond to reversible processes.

1 C. Creutz and H. Taube, *J. Am. Chem. Soc.*, 1973, **95**, 1086.
2 C. Creutz, *Prog. Inorg. Chem.*, 1983, **30**, 1 and references therein.
3 D. E. Richardson and H. Taube, *Coord. Chem. Rev.*, 1984, **60**, 107; M. J. Powers and T. J. Meyer, *J. Am. Chim. Soc.*, 1980, **102**, 1289; M. J. Powers, R. W. Callahan, D. J. Salmon and T. J. Meyer, *Inorg. Chem.*, 1976, **15**, 894; M. Haga, *Inorg. Chim. Acta*, 1980, **45**, L183; M. Haga, T. Ano, K. Kano and S. Yamabe, *Inorg. Chem.*, 1991, **30**, 3843; T. Ono, K. Nozaki and M. Haga, *Inorg. Chem.*, 1992, **31**, 4256; A.-C. Ribou, J.-P. Launay, K. Takahashi, T. Nihira, S. Tarutani and C. W. Spangler, *Inorg. Chem.*, 1994, **33**, 1325; E. Constable, A. M. W. Cargill Thompson and S. Greulich, *J. Chem. Soc., Chem. Commun.*, 1993, 1444; M. Beley, P.-P. Collin and J.-P. Sauvage, *Inorg. Chem.*, 1993, **32**, 4539; E. Constable and A. M. W. Cargill Thompson, *J. Chem. Soc., Dalton Trans.*, 1995, 1615; V. Balzani, A. Juris, M. Venturi, S. Campagna and S. Serroni, *Chem. Rev.*, 1996, **96**, 759.
4 I. de Sousa Moreira and D. W. Franco, *J. Chem. Soc., Chem. Commun.*, 1992, 450; I. de Sousa Moreira and D. W. Franco, *Inorg. Chem.*, 1994, **33**, 1607.
5 J.-P. Collin, P. Lainé, J.-P. Launay, J.-P. Sauvage and A. Sour, *J. Chem. Soc., Chem. Commun.*, 1993, 434.
6 C. R. Arana and H. D. Abruña, *Inorg. Chem.*, 1993, **32**, 194.
7 R. P. Thummel and S. Chirayil, *Inorg. Chim. Acta*, 1988, **154**, 77.
8 L. M. Vogler, B. Scott and K. J. Brewer, *Inorg. Chem.*, 1993, **32**, 898.
9 M. K. Nazeeruddin, P. Liska, N. Vlachopoulos and M. Grätzel, *Helv. Chim. Acta*, 1990, **73**, 1788; B. O'Regan and M. Grätzel, *Nature*, 1991, **335**, 737; E. Amouyal, in *Homogeneous Photocatalysis*, ed. M. Chanon, Wiley, Chichester, 1997, pp. 263–307; V. Balzani and F. Scandola, *Supramolecular Photochemistry*, Ellis Horwood, Chichester, 1991.
10 A. von Kameke, G. M. Tom and H. Taube, *Inorg. Chem.*, 1978, **17**, 1790.
11 J. P. Collin, S. Guillerez, J. P. Sauvage, F. Barigelletti, L. De Cola, L. Flamigni and V. Balzani, *Inorg. Chem.*, 1991, **30**, 4230.
12 P. Bonhôte and M. S. Wrighton, *Synlett*, 1997, 897; a similar synthesis of tpp, with a lower yield, was described almost simultaneously by A. Gourdon, *Synth. Commun.*, 1997, **27**, 2893.
13 B. P. Sullivan and J. M. Calvert and T. J. Meyer, *Inorg. Chem.*, 1980, **19**, 1404.
14 E. Amouyal, M. Mouallem-Bahout and G. Calzaferri, *J. Phys. Chem.*, 1991, **95**, 7641.
15 G. C. Allen and N. S. Hush, *Prog. Inorg. Chem.*, 1967, **8**, 357; N. S. Hush, *Prog. Inorg. Chem.*, 1967, **8**, 391.

Received in Basel, Switzerland, 15th December 1997; 7/09013G

Hydrogen evolution and oxygen reduction at a titanium sonotrode

H. N. McMurray, D. A. Worsley*† and B. P. Wilson

The Department of Materials Engineering, University of Wales Swansea, Singleton Park, Swansea, UK SA2 8PP

A titanium sonotrode is used to demonstrate that ultrasonic irradiation significantly enhances the rate of electrochemical oxygen reduction and hydrogen evolution reactions in neutral aqueous electrolyte.

The effect of ultrasound in the 15–40 kHz frequency range on the kinetics and mechanism of electrochemical reactions is a topic of rapidly growing interest. Power ultrasound produces cavitation in solution which may influence electrode processes through four distinct modes of interaction: (*i*) mass transport enhancement owing to turbulence and microstreaming,[1–4] (*ii*) continuous activation of the electrode surface,[5] (*iii*) the formation of ions, radicals and other high energy intermediates,[1] (*iv*) the mediation of chemical processes associated with heterogeneous electron transfer steps[6] and (*v*) product desorption.[7] Ultrasound baths or probes may be used to irradiate electrodes indirectly.[8] However, recent studies have demonstrated greater rate enhancement using directly stimulated 'sonotrodes' in which the solution contacting end of a ultrasonic transducer horn acts as the electrode surface.[9,10] In the work described here a titanium sonotrode was used to investigate the effect of ultrasound on electrochemical hydrogen evolution [reaction (1)] and oxygen reduction [reaction (2)] in aqueous electrolyte.

$$2H^+_{(aq)} + 2e^- \rightarrow H_{2(g)} \quad (1)$$

$$O_{2(aq)} + 2H_2O + 4e^- \rightarrow 4OH^-_{(aq)} \quad (2)$$

Reactions (1) and (2) are the cathodic reactions most commonly associated with metallic corrosion in aqueous systems and acceleration of corrosion rates in the presence of cavitation is a significant technological problem.[11] Both reactions have complex multistep mechanisms involving chemisorbed intermediates,[12,13] and reaction rates could potentially be influenced through any one of modes (*i*)–(*v*) above. In the current study we aim to determine the extent to which the cathodic processes associated with metallic corrosion are influenced by the presence of intense cavitation.

The titanium (Ti) tip sonotrode and sono-electrochemical cell arrangement, used in this work is illustrated in Fig. 1. A 20 kHz ultrasound generator (Branson Ultrasonics Sonifier 250) was used with a standard flat 10 mm titanium tip. The ultrasonic power level used throughout was 26 W cm^{-2}, as determined using calorimetry.[4] The circulation of water from a thermostated bath through a stainless steel cooling coil,[9] allowed the electrolyte temperature to be kept constant to within 1 °C during all experiments. All voltammetric measurements were carried out at 30 °C using a Solartron 1280 potentiostat under computer control. The electrolyte used was a 0.7 mol dm^{-3} aqueous Na_2SO_4 adjusted to pH 7 using 0.1 M NaOH. All chemicals were obtained from BDH at Analar grade purity and doubly distilled water was used throughout. Prior to measurement under deaerated conditions the electrolyte was purged with prepurified argon (BOC) for 30 min. Linear sweep voltammograms were recorded by sweeping the sonotrode potential from −2.5 to 0 V *vs.* SCE at 0.014 V s^{-1}. Prior to recording voltammetric data the sonotrode potential was cycled between −2.5 and 0 V at ±0.014 V s^{-1} in the absence of ultrasound until the voltammogram became reproducible (< three cycles).

The voltammetric response of the Ti sonotrode in deaerated and aerated electrolyte is shown as a series of Tafel plots in Fig. 2(*a*) and (*b*) respectively; H_2 evolution occurred visibly at potentials < −1.6 V. It may be seen from Fig. 2 that the characteristic shapes of the Tafel plots remained similar under silent and sonicated conditions but that current density values were higher at all potentials in the presence of ultrasound. The magnitude of the sono-electrochemical effect, its reproducibility and reversible nature are highlighted in Fig. 3(*a*) and (*b*) for the deaerated and aerated solutions, respectively which illustrates the transient (time dependent) current responses of the sonotrode when subject to short (1–5 s) pulses of sonication at constant potential. Fig. 3(*a*) shows the response at −1.3 V in deaerated electrolyte and Fig. 3(*b*) shows the response at −1.25 V in aerated electrolyte. In both cases it can be seen that the

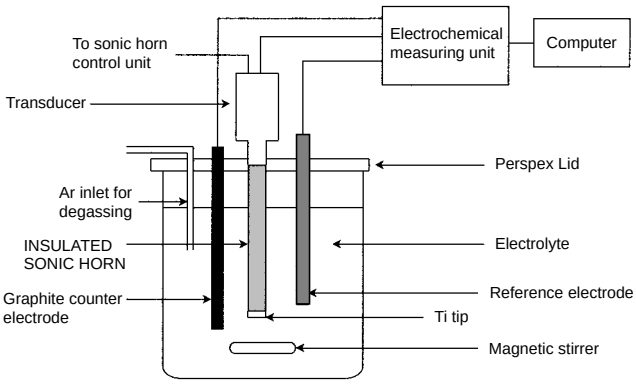

Fig. 1 Schematic diagram of sonotrode and electrochemical cell arrangement

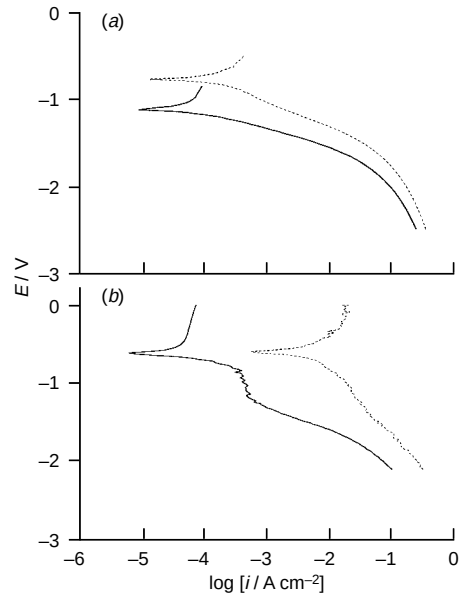

Fig. 2 Tafel plots of titanium sonotrode voltammetric response under silent (—) and sonicated (---) conditions in (*a*) deaerated and (*b*) aerated neutral 0.7 M aqueous Na_2SO_4 at 30 °C. Potential sweep rate = 0.014 V s^{-1}.

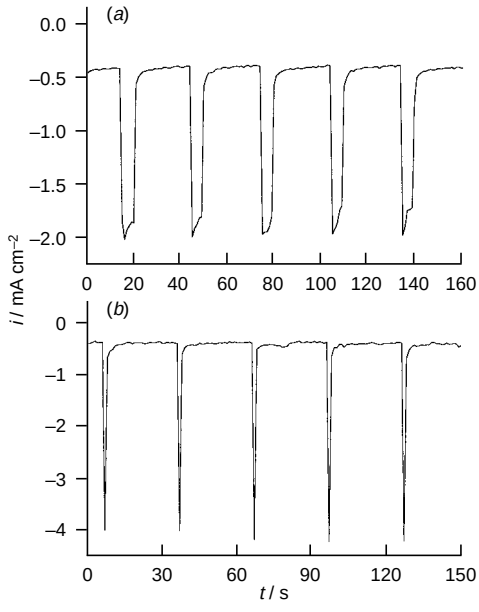

Fig. 3 Transient (time dependent) current response of titanium sonotrode in neutral 0.7 M aqueous Na_2SO_4 at 30 °C. (*a*) Deaerated, 5 s ultrasound pulses at −1.3 V *vs.* SCE. (*b*) Aerated, 1 s ultrasound pulses at −1.25 V *vs.* SCE.

changes in current density resulting from sonication are instantaneous and reversible. This finding rules out the possibility that bulk heating by ultrasound contributes significantly to the observed current density increases. The n-type semiconducting TiO_2/Ti_2O_3 layer, which rapidly forms on Ti exposed to air, can limit the rate of electrochemical reactions (especially anodic reactions) at Ti sonotrodes.[9] However, Figs. 2 and 3 suggest that the Ti sonotrode is an adequate cathode for reactions (1) and (2) at the potentials indicated and that reaction rates are significantly enhanced by sonication.

Considering the deaerated case first, it is assumed that the cathodic currents in Fig. 2(*a*) are entirely due to reaction (1). Under silent conditions the Tafel plot is approximately linear over the range −1.25 to −1.6 V which is consistent with reaction (1) being activation controlled; the Tafel slope is 190 mV decade^{-1}. At potentials cathodic of −1.7 V the Tafel plots curve in a manner suggestive of current limiting. Under sonicated conditions the Tafel plot is shifted anodically by approximately 500 mV and the Tafel slope in the linear region increases to 280 mV decade^{-1}. The change in Tafel slope is consistent with ultrasound producing a change in mechanism or rate determining step for reaction (1). Ultrasonic current density enhancement at constant potential is greatest in the linear, activation controlled region (a factor of *ca*. five) and smaller in the current limiting region (a factor of *ca*. two). Since the effect of ultrasound is greatest when reaction (1) is activation controlled it is probable that interaction with the electrochemical process occurs primarily through modes (*ii*)–(*v*) above.

Considering the aerated case, under silent conditions the Tafel plot in Fig. 2(*b*) shows a well developed current plateau between −0.9 and −1.4 V due to reaction (2) becoming limited by mass transport of O_2 to the sonotrode surface.[15] It is therefore assumed that the cathodic currents in Fig. 2(*b*) result predominantly from reaction (2) at potentials cathodic of −1.4 V, and from a combination of reactions (1) and (2) at potentials anodic of −1.4 V. Ultrasonic current density enhancement at constant potential is greatest (more than one order of magnitude) at potentials anodic of −1.4 V and the diffusion limited current plateau becomes indistinct in the sonicated Tafel plot. The current density increase between −0.9 and −1.4 V must arise primarily through mode (*i*) above and implies a decrease of at least tenfold in the effective thickness of the Nernst diffusion layer under sonicated conditions. Modes (*ii*)–(*v*) may be significant at potentials anodic of −0.9 V where reaction (2) is not mass transport limited, but mode (*i*) probably remains an important contribution to the current increase observed on sonication.

These preliminary results show that the rates of electrochemical O_2 reduction and H_2 evolution at a titanium surface are significantly increased by power ultrasound. Ultrasonically enhanced mass transport appears to be the principle cause of rate increase in the case of O_2 reduction but significant rate increase also occurs in the case of activation controlled H_2 evolution. The acceleration of both these cathodic processes may contribute to the increased rates of metallic corrosion observed in the presence of intense cavitation. Furthermore, the finding that activation overpotentials for H_2 evolution may be reduced by ultrasound suggests that electrocatalytic sonotrodes might usefully be investigated as a means of increasing the efficiency of technologically important gas evolving electrolyses.

We thank Maysonic Ultrasonics Ltd, Briton Ferry, West Glamorgan for supporting this work and Duncan McDonald (M. D.) for permission to publish.

Notes and References

† E-mail: D.A.Worsley@swansea.ac.uk

1 R. G. Compton, J. C. Eklund and S. D. Page, *J. Phys. Chem.*, 1995, **99**, 4211.
2 J. Klima, C. Bernard and C. Degrand, *J. Electroanal. Chem.*, 1994, **367**, 297.
3 K. S. Suslick, *Science*, 1990, **247**, 1439.
4 D. J. Walton, S. S. Phull, A. Chyla, J. P. Lorimer, T. J. Mason, L. D. Burke, M. Murphy, R. G. Compton, J. C. Eklund and S. D. Page, *J. Appl. Electrochem.*, 1995, **25**, 1083.
5 R. G. Compton, J. C. Eklund, S. D. Page. G. H. W. Sanders and J. Booth, *J. Phys. Chem.*, 1995, **98**, 12 410.
6 R. G. Compton, J. C. Eklund, S. D. Page and T. O. Rebbitt, *J. Chem. Soc., Dalton Trans.*, 1995, 389.
7 D. J. Walton, L. D. Burke and M. M. Murphy, *Electrochemica Acta*, 1996, **41**, 2747.
8 C. G. Jung, F. Chapelle and A. Fontana, *Ultrasonics Sonochem.*, 1997, **4**, 117.
9 R. G. Compton, J. C. Eklund, F. Marken and D. N. Waller, *Electrochem. Acta*, 1996, **41**, 315.
10 J. Reisse, H. Francois, J. Vandercammen, O. Fabre, A. Kirche-de Mesmaeker, C. Maerschalk and J. L. Delplanke, *Electrochem. Acta*, 1994, **39**, 37.
11 D. J. Godfrey, in *Corrosion*, ed. L. L. Shreir, Newnes–Butterworth, 1976, vol. 1, pp. 124–132.
12 A. Damjanovic, in *Modern Aspects of Electrochemistry*, ed. J. O'M. Bockris and B. E. Conway, Butterworths, 1969, no. 5, pp. 369–485.
13 J. O'M. Bockris and Sum Shah, *Surface Electrochemistry*, Plenum, New York, 1993.
14 T. J. Mason, *Practical Sonochemistry*, Ellis Horwood Publ., 1991, p. 45.
15 H. S. Wroblowa and S. B. Qaderi, *J. Electroanal. Chem.*, 1990, **279**, 231.

Received in Cambridge, UK, 29th January 1998; 8/00801I

Evidence for the presence of dual emission in a ruthenium(II) polypyridyl mixed ligand complex

Tia E. Keyes, Christine O'Connor and Johannes G. Vos*†

Inorganic Chemistry Research Centre, School of Chemical Sciences, Dublin City University, Dublin 9, Ireland

The complex $[Ru(bpy)_2(pztr)]^+$ 1 [bpy = 2,2′-bipyridyl, Hpztr = 3-(pyrazin-2-yl)-1,2,4-triazole] exhibits two emission maxima in fluid solution [ethanol–methanol (4 : 1)] over the temperature range 120–260 K; from fluorometric studies two well resolved emission maxima are observed at 590 and 700 nm, accompanied by two different lifetimes; the observations suggest the presence of two emitting states in this compound, one bpy and one pyrazine based.

The photophysical properties of ruthenium(II) polypyridyl complexes make them attractive building blocks for supramolecular assemblies and as a result several thousands of homo- and hetero-leptic compounds have been reported in the literature.[1] It is generally accepted that emission in ruthenium polypyridyl complexes originates from a triplet metal-to-ligand charge-transfer (^{3}MLCT) state.[1] In the case of a mixed ligand complex this excited state can in principle be located on any of the ligands. Many detailed studies have therefore been carried out to determine the location of the emitting state in such compounds. From theoretical considerations one would predict that emission will occur from the lowest triplet state only[2] and indeed this is observed in almost all cases. In rigid media a number of dual emissions have been documented.[3] However, in solution such reports are rare,[4] and to our knowledge no clear-cut cases have been reported in solution for ruthenium polypyridyl type compounds.

In this contribution, we wish to present direct evidence for dual emission in solution over a wide temperature range for the mononuclear mixed ligand ruthenium(II) polypyridyl complex $[Ru(bpy)_2(pztr)]PF_6$, **1** [bpy = 2,2′-bipyridyl, Hpztr = 3-(pyrazin-2-yl)-1,2,4-triazole].

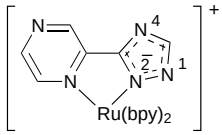

The compound under investigation was synthesised as described previously.[5] The N^2 and N^4 isomers were separated by semi-preparative HPLC and characterized by ^{1}H NMR spectroscopy, analytical diode array HPLC, and elemental analysis. These techniques confirm that the purity of **1** is > 99%. In this study only the N^2 isomer, shown above, was investigated.

Earlier work on these compounds has shown that isomerisation, photoinduced or otherwise, of the deprotonated N^2 and N^4 isomers does not occur,[5c,d] while pK_a values obtained for the ground state and excited state for the N^2 isomer are between 3.5 and 4 and as a result, protonation of **1** under the experimental conditions discussed here is unlikely.[5a]

One can therefore be confident that in the experiments carried out in this contribution only one species will be present. It is furthermore important to note that pK_a values, electrochemical experiments and resonance Raman data have shown that bpy and pyrazine based excited states are similar in energy. In **1** the bpy state is lower in energy, while in the complex containing a protonated triazole the emitting state is pyrazine based.[5b,d] Finally, emission and absorption maxima of **1** in its protonated and deprotonated states are very similar.[5a]

Selected temperature dependent luminescence spectra for **1** [ethanol–methanol (4 : 1), containing 1% diethylamine or ammonia to assure deprotonation of the triazole ring] are shown in Fig. 1. At 90 K, the spectrum obtained [Fig. 1(*a*)] is typical for compounds of this type with a single emission being observed at 617 nm. After laser excitation at 355 nm the luminescence decays according to a single exponential with a lifetime of 3200 ns (all lifetimes ±10%). On increasing the temperature to 145 K, [Fig. 1(*b*)] the emission spectrum of **1** is resolved into two distinct bands; one, as expected, at 710 nm and an additional feature at 590 nm. The luminescent signal obtained at this temperature monitored at 650 nm cannot be fitted as a single exponential. Normal curve fitting procedures yield lifetimes of 2400 and 800 ns with ratios of 60 and 40%, respectively. Measurements monitored out at 700 and 590 nm yield single exponential decays and identify the long lifetime as belonging to the 700 nm signal. At higher temperatures the contribution from the higher energy component decreases. The temperature dependence of the emission decay for the two signals is therefore different. Excitation spectra obtained at both emission maxima are sufficiently similar to suggest that both emissions are based on MLCT emissions. The excitation spectrum of the 590 nm emission shows an absorption maximum at 440 nm, while for the 700 nm band a maximum is observed at 465 nm.

In cases where a dual emission is observed, the contribution from impurities is always a concern. However, we do not believe that the data above can be attributed to the presence of an impurity. First of all, the lifetimes and intensities observed for the two emission components (see above) suggest that the concentration of an impurity would have to be high and this is not observed. Also, the same results were obtained for various samples of **1**. Finally, when the triazole is protonated a normal single exponential behavior is obtained over the entire temperature range [77 K (2200 ns), 175 K (800 ns) and room temperature (230 ns)].

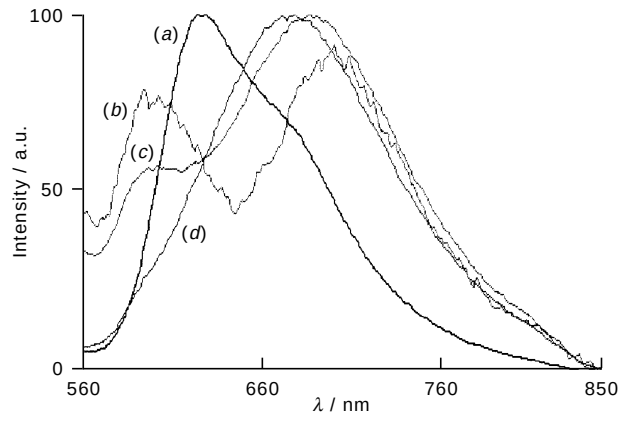

Fig. 1 Temperature dependent luminescent spectra of **1** in ethanol–methanol (4 : 1) and 1% diethylamine, at (*a*) 90, (*b*) 145, (*c*) 220 and (*d*) 298 K

On the basis of these considerations we are confident that the results obtained are best explained by the presence in the title compound of two weakly coupled emitting states. As pointed out above, earlier work has shown that bpy and pyrazine based MLCT states are similar in energy. For example, the energy separation between these two emitting states of 2400 cm^{-1} which at 145 K is consistent with the electrochemistry of this complex which shows a potential difference of 0.33 eV between the first two bpy and pyrazine based reductive steps of **1**. We therefore propose, based on our earlier results,[5] that the highest energy emitting state observed between 120 and 260 K, is pyrazine based. After excitation to the ^{1}MLCT level, efficient intersystem crossing to the lowest, strongly coupled bpy based triplet state is observed. Up to 260 K it is the lowest energy manifold of the bpy triplet that is populated. Population of the pyrazine based triplet state can in this model only occur by thermal means. The lower energy components of this manifold are weakly coupled to a pyrazine state, and population of the pyrazine state occurs thermally between *ca*. 120 and 260 K. Above this temperature the upper, fourth ^{3}MLCT of the bpy triplet manifold is thermally populated,[6] such population is observed in the temperature dependent luminescent lifetimes of related[5c] complexes, where population of this state was observed to occur from around 240 K. This upper state, which contains more singlet character, is not coupled to the pyrazine, and therefore a single emission primarily based on the fourth ^{3}MLCT is observed. Further investigations are at present in progress to further develop this picture.

The authors thank the EC Training and Mobility Programme (Contract CT96-0076), the EC Joule programme, Forbairt and the Electricity Supply Board for financial assistance. Johnson Matthey are thanked for a generous loan of $RuCl_3 \cdot xH_2O$.

Notes and References

† E-mail: vosh@ccmail.dcu.ie

1 A. Juris, V. Balzani, F. Barigelletti, S. Campagna, P. Belser and A. von Zelewsky, *Coord. Chem. Rev.*, 1988, **84**, 85; V. Balzani, A. Juris, M. Venturi, S. Campagna and S. Serroni, *Chem. Rev.*, 1996, **96**, 759.
2 M. Kasha, *Discuss. Faraday Soc.*, 1950, **9**, 14.
3 R. L. Blakley and M. K. DeArmond, *J. Am. Chem. Soc.*, 1987, **109**, 4895; A. P. Wilde, K. A. King and R. J. Watts, *J. Phys. Chem.*, 1991, **95**, 629; E. Taffarel, S. Chirayil, W. Y. Kim, R. P. Thummel and R. H. Schmehl, *Inorg. Chem.*, 1996, **35**, 2127.
4 R. J. Watts, *Inorg. Chem.*, 1981, **20**, 2302; L. Wallace, D. C. Jackman, D. P. Rillema and J. W. Merkert, *Inorg. Chem.*, 1995, **34**, 5210.
5 (*a*) R. Hage, J. G. Haasnoot, H. A. Nieuwenhuis, J. Reedijk, R. Wang and J. G. Vos, *J. Chem. Soc., Dalton Trans.*, 1991, 3271; (*b*) H. A. Nieuwenhuis, J. G. Haasnoot, R. Hage, J. Reedijk, T. L. Snoeck, D. J. Stufkens and J. G. Vos, *Inorg. Chem.*, 1991, **30**, 48; (*c*) R. Wang, J. G. Vos, R. H. Schmehl and R. Hage, *J. Am. Chem. Soc.*, 1992, **114**, 1964; (*d*) H. Hughes, Thesis, Dublin City University, 1993.
6 J. V. Casper and T. J. Meyer, *Inorg. Chem.*, 1983, **22**, 2444; E. M. Kober and T. J. Meyer, *Inorg. Chem.*, 1984, **23**, 3877.

Received in Cambridge, UK, 3rd February 1998; 8/00921J

Distinction between the weak hydrogen bond and the van der Waals interaction

Thomas Steiner*[a] and Gautam R. Desiraju*[b]†

[a] *Institut für Kristallographie, Freie Universität Berlin, Takustraße 6, D-14195 Berlin, Germany*
[b] *School of Chemistry, University of Hyderabad, Hyderabad 500 046, India*

The angular distributions of C–H···O interactions for different types of C–H groups show that the directionality decreases with decreasing C–H polarisation, but that it is still clearly recognisable for methyl groups; for C–H···H–C van der Waals contacts, in contrast, isotropic angular characteristics are observed.

It is by now well-recognised that C–H groups can act as weak hydrogen bond donors.[1,2] While vibrational spectroscopy shows that the C–H donor strength depends on the carbon hybridisation as C(sp)–H > C(sp^2)–H > C(sp^3)–H,[3] early crystallographic data suggests some donor potential even for the weakly polarised methyl groups.[4] Statistical database surveys demonstrate that mean C···O distances in C–H···O contacts correlate convincingly with conventional C–H acidities,[5] and even for methyl groups R–CH_3, mean H···O distances have been found to depend on the nature of the R group.[6] All these experimental studies indicate that most kinds of C–H groups can donate weak hydrogen bonds. While the bonds formed by acidic C–H groups (alkynes, haloforms) are moderately strong, those that involve weakly polarised C–H groups are much weaker. Many studies have concentrated on the stronger of the C–H···O hydrogen bonds, possibly because they are associated with more dramatic structural and spectroscopic effects, and this has meant that experimental information on weakly polarised C–H donors is relatively scarce. Still, theoretical calculations have been published for weakly polarised C–H groups,[7] estimating C–H···O hydrogen bond energies to be around 0.5 to 1 kcal mol^{-1}.

Despite this wealth of experimental and theoretical work, the concept of the C–H···O hydrogen bond, and that of the weak hydrogen bond in general, has been persistently questioned. The strong disapproval that was published[8] in the 1960s has, over the years,been steadily diluted into oral objections that may best be described as stationary. It is therefore of some interest that a recent paper in this journal states that the typical C–H···O/N hydrogen bond represents 'nothing more than a classical van der Waals interaction.[9] Here this claim will be directly falsified.

A fundamental difference between hydrogen bonds and the van der Waals interaction lies in their different directionality characteristics. Hydrogen bonds are inherently *directional*, with linear or close to linear geometries favoured energetically over bent ones. In contrast, van der Waals contacts are *isotropic*, with interaction energies independent of the contact angle θ. This difference allows one, in principle, to distinguish between hydrogen bonds and the van der Waals interaction. However, hydrogen bond directionality is soft,[10] and even for moderately strong bonds it cannot be characterised from single examples or small data samples. A proper description of angular preferences, or lack thereof, requires statistical analysis of large quantities of structural data, such as may be retrieved from the Cambridge Structural Database (CSD).[11] Database analysis is complicated by factors such as steric hindrance and chemical inhomogeneity, which in adverse situations can completely smear structural trends.‡ However, one can plan and perform CSD analyses so as to minimise these complicating factors.

The angular characteristics of the weakest kinds of C–H···O hydrogen bonds have not yet been described. Therefore, we report here a CSD study of these characteristics in conjunction with those for van der Waals contacts of the type C–H···H–C. Structural data were retrieved§ for C–H···O contacts involving the prototypes of the C(sp)–H, C(sp^2)–H and C(sp^3)–H groups, that is ethynyl, vinyl and ethyl groups. For comparison, data for conventional hydrogen bonds from hydroxy donors is also presented. To reduce chemical inhomogeneity, only organic carbonyl acceptors were considered. For the H···O distance cutoff, a long value of 3.0 Å was selected; this is greater than the van der Waals sum by 0.3 Å.[12] Initial tests showed that this cutoff value is not critical for the subsequent analysis. Data for C–H···H–C van der Waals contacts were also retrieved to the distance limit of the van der Waals sum plus 0.3 Å (= 2.7 Å). Numerical data giving mean hydrogen bond distances and angles are listed in Table 1. To examine the degree to which linear contact geometries are preferred, histograms of angular C–H···O distributions were generated (Fig. 1). Since the solid angle covered by an angular interval $\Delta\theta$ is smaller for nearly linear angles θ than for bent ones (Fig. 2), the angular distribution must be weighted by a correction factor of $1/\sin\theta$ to properly reflect angular preferences. This is termed the 'cone correction'.[13]

The histogram for hydroxy donors shows the well-known directional behaviour of conventional hydrogen bonds [mean θ = 154.0(4)°].[10,13] For the acidic ethynyl donors C≡C–H, the mean C–H···O angle θ is only slightly smaller, 152(2)°, and the angular distribution is only slightly broader. For vinyl donors, the mean angle θ falls to 143(1)° and the angular distribution widens considerably. For the very weakly polarised methyl donor of the ethyl group, the mean angle θ falls further to 137.1(7)° and the angular distribution is correspondingly softened, *but it still shows directional behaviour with linear contact geometries being favoured*. Finally, the mean C–H···H angle for C–H···H–C contacts of methyl groups is 128.6(3)°. Here, however, the angular distribution is almost ideally isotropic in the range 120 to 180°, while for θ < 120°, the frequencies fall because side-on contacts are sterically disfavoured [Fig. 1(*e*)]. This is exactly the picture that is expected for the non-directional van der Waals interaction.

The sequence of histograms in Fig. 1 clearly shows a gradual decrease of directionality for C–H···O interactions with decreasing C–H polarisation. For alkyne donors, the directionality

Table 1 Numerical data for X–H···Y contacts with H···Y< 3.0 Å (2.7 Å for H···H contacts). Data for normalised H-atom positions

Contact type	Number	Mean H···Y (Å)	Mean X···Y (Å)	Mean X–H···Y (°)
C(*sp*^{3})–O–H···O=C	3330	1.974(6)	2.837(4)	154.0(4)
C≡C–H···O=C	44	2.36(4)	3.31(2)	152(2)
C=CH_2···O=C	124	2.67(1)	3.56(2)	143(1)
CH_2–CH_3···O=C	767	2.761(6)	3.590(7)	137.1(7)
CH_2–CH_3···H–C	3975	2.500(2)	3.246(4)	128.6(3)

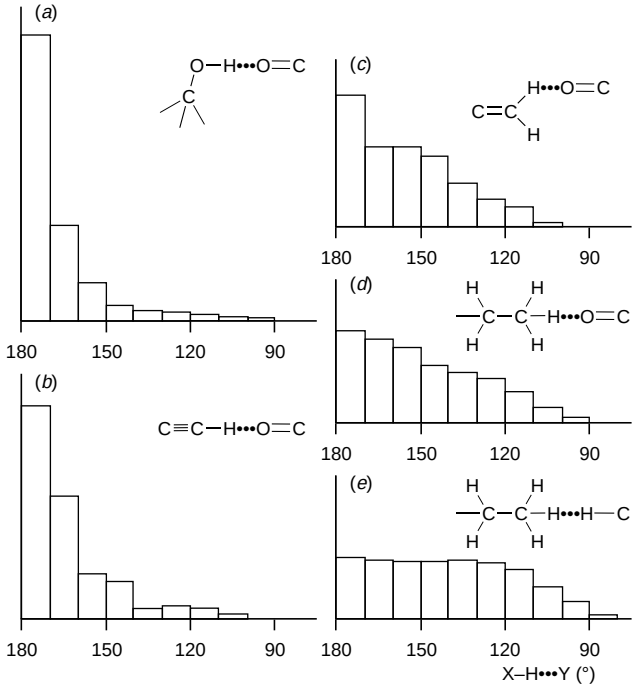

Fig. 1 CSD results. Histograms with angular frequencies of X–H···O=C contacts for different donor types, and of C–H···H–C van der Waals contacts: (*a*) hydroxy, (*b*) ethynyl, (*c*) vinyl and (*d*) ethyl donors and (*e*) van der Waals contacts. The distributions are 'cone-corrected' (ref. 13) (*i.e.* weighted by 1/sinθ) and scaled in such a way that they cover the same area.

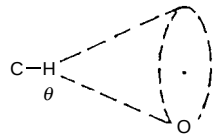

Fig. 2

behaviour is that of conventional hydrogen bonds such as those formed by hydroxy groups. For vinyl donors, the directionality is weaker, but is still clearly pronounced. For methyl groups, the directionality is the weakest, but is still clearly different from the perfectly isotropic behaviour for C–H···H–C contacts. Since C–H···O interactions of alkyl groups are *not* isotropic (even at the long distance cutoff of 3.0 Å), they should definitely not be classified as mere van der Waals contacts. The observed differences in directionality behaviour between any kind of C–H···O hydrogen bond and the van der Waals interaction is a consequence of the fundamentally different distance and angle fall-off characteristics of these interactions.

It is important to note that weak hydrogen bonds encompass a wide scale of strengths just as do carbon acidities. It is therefore misleading to consider all kinds of C–H···O hydrogen bonds as being exactly alike, even as it is misleading to assign hydrogen bond character only to a certain class of C–H···O contacts and consider the rest as nothing more than classical van der Waals interactions. *A C–H···O hydrogen bond does not become a van der Waals contact just because the H···O distance crosses an arbitrary threshold.* It is pointed out, however, that this does not mean that every C–H···O contact of a methyl group is 'automatically' a hydrogen bond: it has been shown theoretically and also experimentally that some C–H···O geometries formed by methyl groups have zero or possibly even positive interaction energies.[7,14]

In this light, the more interesting question is the nature of the interface between the weak hydrogen bond and the van der Waals interaction. Recent experiments indicate that this grey area is shrinking.[15] Investigating such matters will undoubtedly be difficult, but given the continuous spectrum of these structural phenomena, it is not hard to conceive of a domain wherein the distance falloff characteristics of an interaction X–H···A varies between those expected for a hydrogen bond and for a van der Waals interaction. Exploration of this region will surely yield new insights.

T. S. thanks Professor Wolfram Saenger for giving him the opportunity to carry out a part of this work in his laboratory. G. R. D. acknowledges financial support from the Department of Science and Technology, Government of India (SP/S1/G-19/94) and discussions with Dr Ashwini Nangia.

Notes and References

† E-mail: grdch@uohyd.ernet.in

‡ When studying the correlation of carbon acidity with mean C···O distances in C–C–H···O interactions, it was observed that this correlation is clearcut for sterically unhindered donor types, but completely smeared for sterically hindered groups (ref. 5). The finer effect of acceptor basicity on mean distances could subsequently be shown *only* in chemically homogeneous sets of sterically unhindered C–H···O hydrogen bonds (ref. 6).

§ Database analysis: Cambridge Structural Database, June 1997 update with 167 797 entries, ordered and error-free organic crystal structures with R values < 0.05 (for alkynes: R < 0.07), H-atom positions normalised. Distance cutoff values: H···O < 3.0 Å for hydrogen bonds, H···H < 2.7 Å for van der Waals contacts. No angle restriction.

1 G. R. Desiraju, *Acc. Chem. Res.*, 1991, **24**, 290; 1996, **29**, 441.
2 T. Steiner, *Chem. Commun.*, 1997, 727.
3 A. Allerhand and P. von P. Schleyer, *J. Am. Chem. Soc.*, 1963, **85**, 1715.
4 D. J. Sutor, *Nature*, 1962, **195**, 68; *J. Chem. Soc.*, 1963, 1105.
5 V. R. Pedireddi and G. R. Desiraju, *J. Chem. Soc., Chem. Commun.*, 1992, 988 and references cited therein.
6 T. Steiner, *J. Chem. Soc., Chem. Commun.*, 1994, 2341.
7 J. J. Novoa, B. Tarron, M.-H. Whangbo and J. M. Williams, *J. Chem. Phys.*, 1991, **95**, 5179; X. Yan, S. Wang, M. Hodoscek and G. W. A. Milne, *J. Mol. Struct.: THEOCHEM*, 1994, **309**, 279; T. van Mourik and F. B. van Duijneveldt, *J. Mol. Struct.: THEOCHEM*, 1995, **341**, 63.
8 J. Donohue, in *Structural Chemistry and Molecular Biology*, ed. A. Rich and N. Davidson, Freeman, San Francisco, 1968, p. 443.
9 F. A. Cotton, L. M. Daniels, G. T. Jordan IV and C. A. Murillo, *Chem. Commun.*, 1997, 1673.
10 G. A. Jeffrey and W. Saenger, *Hydrogen Bonding in Biological Structures*, Springer, Berlin, 1991.
11 F. H. Allen and O. Kennard, *Chem. Des. Autom. News*, 1993, **8**, 1.
12 A. Bondi, *J. Phys. Chem.*, 1964, **68**, 441.
13 J. Kroon and J. A. Kanters, *Nature*, 1974, **248**, 667.
14 P. Seiler, L. Isaacs and F. Diederich, *Helv. Chim. Acta*, 1996, **79**, 1047.
15 N. N. L. Madhavi, A. K. Katz, H. L. Carrell, A. Nangia and G. R. Desiraju, *Chem. Commun.*, 1997, 1953.

Received in Columbia, MO, USA, 11th November 1997; 7/08099I

Triple fluorescence of 4-(1,4,8,11-tetraazacyclotetradecyl)benzonitrile

Ling-Siu Choi and Greg E. Collins*†

Naval Research Laboratory, Chemistry Division, Washington, DC 20375-5000, USA

Triple fluorescence is observed for DMABN-cyclam in EtOH, corresponding to a locally excited (LE) singlet state, a twisted intramolecular charge transfer (TICT) state, and an intramolecular exciplex (E).

More than 30 years ago, Lippert investigated the dual fluorescence of 4-(dimethylamino)benzonitrile (DMABN) in polar solvent.[1] Several models have been proposed to address the cause of the anomalous long-wavelength fluorescence, including bending of the cyano group,[2] solute–solvent exciplex formation,[3] and twisted intramolecular charge transfer (TICT).[4] The concept put forward by Grabowski of a TICT state, or charge transfer reaction which is accompanied by a twisting motion and orbital decoupling of the phenyl acceptor ring from the dimethylamino donor group, is generally favored.[4] In addition to TICT state formation, benzonitriles bearing flexible, alkylamino chains, *e.g.* 3-(4-cyanophenyl)-1-dimethylaminopropane (CNP3NM), can form intramolecular exciplexes which arise due to the conformational flexibility of the alkylamino chain, and its ability to form a sandwich configuration promoting excited state, charge transfer.[5] Van der Auweraer *et al.*[6] observed a correlation between intramolecular exciplex formation and Hirayama's rule,[7] which states that the most stable sandwich conformation will arise when $n = 3$ for a $Ph(CH_2)_nNMe_2$ system. We report here the triple fluorescence of 4-(1,4,8,11-tetraazacyclotetradecyl)benzonitrile (DMABN-cyclam), corresponding to the LE state, a TICT state, and an intramolecular exciplex (E) (Fig. 1).

The UV spectrum for DMABN-cyclam in EtOH shows a single absorption peak at 295 nm. Excitation at this wavelength leads to three emission peaks: 352 (LE state), 421 and 473 nm (Fig. 2). Intensity contributions from the three individual excited states were estimated using the Voigt Amplitude function of Jandel's PEAKFIT 4.0. Recently, Létard *et al.* reported the dual fluorescence of two compounds structurally similar to DMABN-cyclam, 4-(1-aza-4,7,10-trioxacyclododecyl)benzonitrile (DMABN-crown4) and 4-(1-aza-4,7,10,13-tetraoxacyclopentadecyl)benzonitrile (DMABN-crown5).[8] DMABN-crown5 exhibited a TICT emission that red-shifted and increased in intensity as the solvent polarity increased from hexane (where the emission band was too weak to be measured accurately) to toluene (λ_{max} = 406 nm), to acetonitrile (λ_{max} = 466 nm). Similarly, DMABN-cyclam, which differs from DMABN-crown4 primarily in the replacement of nitrogen binding sites for the oxygen atoms of the crown ether, reports a similar trend in the emission spectra (Fig. 2): hexane (λ_{max} = 390 nm), toluene (λ_{max} = 413 nm) and EtOH (λ_{max} = 473 nm). We, therefore, attribute the third emission band in EtOH at 473 nm to a TICT state. Unlike DMABN-crown4, however, DMABN-cyclam has two pendant amine groups linked by a short chain (n = 3 and 4) to the benzonitrile acceptor. Despite the cyclic nature of cyclam, this molecule exhibits sufficient flexibility to form a sandwich complex in the excited state that gives rise to an intramolecular exciplex peak (E) (Fig. 1). The peak position identified for the exciplex peak of DMABN-cyclam in hexane (λ_{max} = 392 nm) compares favorably with that found for CNP3NM in isopentane (λ_{max} = 390 nm).[9]

Several trends are evident from Fig. 2 with regards to the effect of solvent polarity on the triple fluorescence of DMABN-cyclam. The TICT emission band red-shifts by more than 80 nm and increases in intensity relative to the LE emission as solvent polarity is increased. The relative intensity of the TICT band increases with solvent polarity due to a stabilization of the charge separation. The exciplex emission does not red-shift quite as severely (34 nm), due to a smaller dipole moment compared with the TICT configuration, and reflects a maxima in the solvent, toluene. Apparently, a ground state sandwich configuration is promoted for DMABN-cyclam in toluene, fostering enhanced intramolecular exciplex formation despite

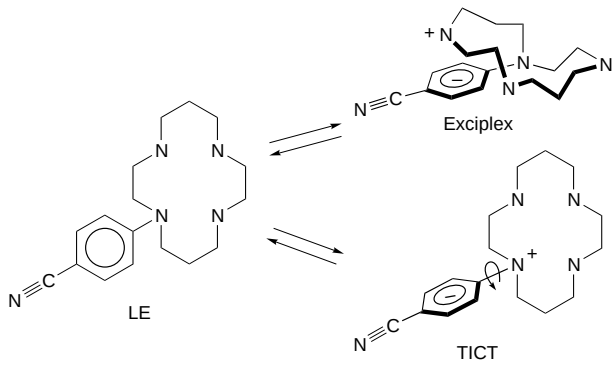

Fig. 1 Proposed structures and equilibria existing between the three excited state species, LE, TICT and E, generating the observed triple fluorescence

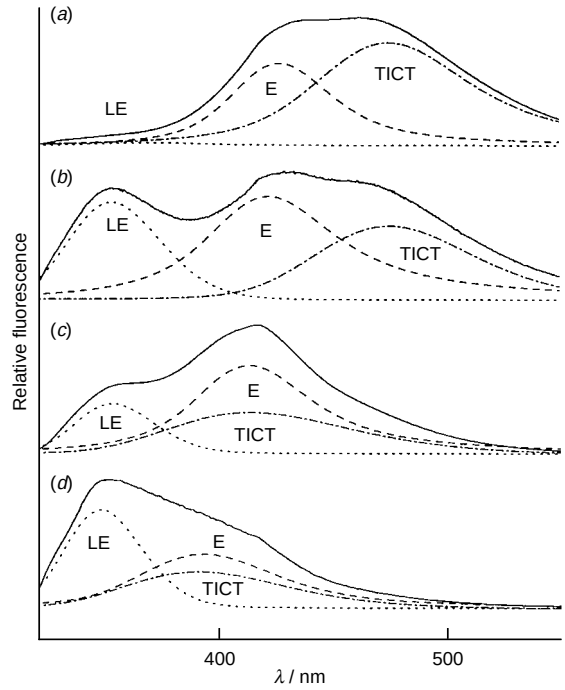

Fig. 2 Solvent effect on the triple fluorescence of DMABN-cyclam: (*a*) water, (*b*) EtOH, (*c*) toluene and (*d*) hexane

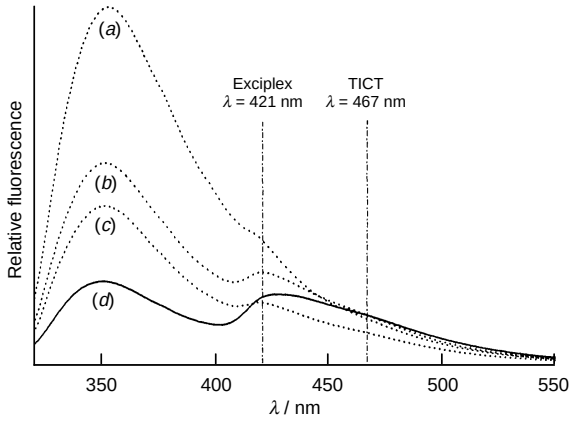

Fig. 3 Emission spectra of DMABN-cyclam in poly(vinyl alcohol) at (*a*) 20, (*b*) 40, (*c*) 60 and (*d*) 80 °C

the lower polarity of this solvent. The LE band exhibits an intensity minimum in water because of the high polarity of this solvent, and its capability for stabilizing the two charge transfer complexes.

Temperature studies of the fluorescence arising from thin films of DMABN-cyclam in poly(vinyl alcohol) (PVA) indicate the dependence of the two excited-state charge-transfer emission peaks (E and TICT) on the conformational mobility of the molecule.[9] PVA was chosen as a support material for DMABN-cyclam because it provides a solid matrix with similar polarity to EtOH. PVA is hydrophilic and absorbs moisture from the air, decreasing the glass transition temperature (T_g) and facilitating the conformational transitions in the excited state at higher temperatures. At room temperature, DMABN-cyclam in PVA shows only a single peak at 357 nm, with a slight shoulder evident at 421 nm (Fig. 3). As the temperature increases, the overall fluorescence intensity correspondingly decreases. However, as the temperature approaches 80 °C (above the T_g for PVA), the exciplex shoulder at 421 nm becomes a more prominent peak, and there is evidence for the formation of the TICT state at 467 nm. This result verifies the dependence of these excited-state charge transfer bands on the conformational mobility of DMABN-cyclam in PVA as it transitions from a glass to a rubbery state.

In conclusion, DMABN-cyclam is a unique molecule which exhibits triple fluorescence arising from the LE state and two excited state complexes, a TICT state and an intramolecular exciplex (E). All three emission bands are strongly perturbed by solvent polarity and conformational mobility.

The authors gratefully acknowledge J. H. Callahan and M. Shahgholi for the mass spectroscopic identification of DMABN-cyclam, and the Office of Naval Research for funding this study.

Notes and References

† E-mail: gcollins@ccf.nrl.navy.mil

1 E. Lippert, W. Lüder, F. Moll, H. Nagele, H. Boos, H. Prigge and I. Siebold-Blankenstein, *Angew. Chem.*, 1961, **73**, 695.
2 A. L. Sobolewski and W. Domcke, *Chem. Phys. Lett.*, 1996, **250**, 428.
3 M. C. C. de Lange, D. Thorn Leeson, K. A. B. Van Kuijk, A. H. Huizer and C. A. G. O. Varma, *Chem. Phys.*, 1993, **177**, 243.
4 K. Rotkiewicz, K. H. Grellmann and Z. R. Grabowski, *Chem. Phys. Lett.*, 1973, **19**, 315.
5 Z. R. Grabowski, *Pure Appl. Chem.*, 1992, **64**, 1249.
6 M. Van der Auweraer, Z. R. Grabowski and W. Rettig, *J. Phys. Chem.*, 1991, **95**, 2083.
7 F. Hirayama, *J. Chem. Phys.*, 1965, **42**, 3163.
8 J.-F. Létard, S. Delmond, R. Lapouyade, D. Braun, W. Rettig and M. Kreissler, *Recl. Trav. Chim. Pays-Bas*, 1995, **114**, 517.
9 M. Van der Auweraer, A. Vannerem and F. C. de Schryver, *J. Mol. Struct.*, 1982, **84**, 343.

Received in Columbia, MO, USA, 10th June 1997; revised manuscript received, 26th February 1998; 8/01749B

Complexation of C_{60} with hexahomooxacalix[3]arenes and supramolecular structures of complexes in the solid state

Kazunori Tsubaki,[a] Kiyoshi Tanaka,[a] Takayoshi Kinoshita[b] and Kaoru Fuji*[a]†

[a] *Institute for Chemical Research, Kyoto University, Uji, Kyoto 611-0011, Japan*
[b] *Basic Research Laboratories, Fujisawa Pharmaceutical Co., Ltd., Kashima, Yodogawa, Osaka 532-8514, Japan*

Hexahomooxacalix[3]arenes 1–5, which possess a variety of substituents on their upper rim, have captured fullerene C_{60} in toluene with association constants of K_a = 9.1–35.6 dm^3 mol^{-1}; X-ray analysis of the complex of C_{60} and 4 indicated that a van der Waals attractive interaction is the dominant driving force which brings the hexagonal faces of the C_{60} close to both the aromatic rings and the dibenzyl ether oxygen of 4.

Supramolecular complexes with C_{60} as the guest molecule have provoked a great deal of interest in the field of host–guest chemistry.[1–8] Recent studies on this complexation have focused on the inclusion phenomena of C_{60} with so-called 'dish-shaped' hosts in solution.[9–15] Among these studies, X-ray analyses of the complexes of C_{60} with calix[5]arenes[14,16,17] and with cyclotriveratrylene (CTV)[12,15] have been reported. Quite recently, Shinkai reported the inclusion complex of C_{60} and *tert*-butylhexahomooxacalix[3]arene **2** in organic solution.[11] However, the precise details of the structural features of the inclusion complex are still ambiguous. Here we report the first X-ray analyses of the complexes of C_{60} with hexahomooxacalix[3]arenes **2** and **4**, and the formation of supramolecular complexes of C_{60} with hexahomooxacalix[3]arenes possessing different substituents on their upper rims.

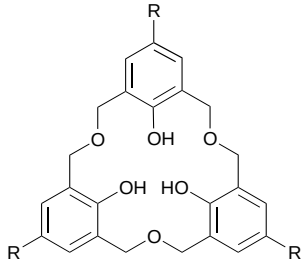

1 R = H
2 R = Bu^t
3 R = OMe
4 R = Br
5 R = $CMe_2C_6H_4$-*p*-OMOM

We have developed a stepwise synthesis for a variety of hexahomooxacalix[3]arenes having different substituents on their upper rim portion, revealing that some hexahomooxacalix[3]arenes adopt a cone conformation owing to an intramolecular hydrogen-bonding network in the solid state.[18] The interaction between hexahomooxacalix[3]arenes **1**–**5**‡ and C_{60} was examined using UV–VIS spectroscopy. Thus, upon addition of hexahomooxacalix[3]arenes to a solution of C_{60} in toluene, a slight change in color (from purple to pale brown), based on an increase in the absorption band at *ca*. 430 nm, was observed. The UV–VIS titration method allowed us to determine the association constants, which were determined by the Rose–Drago method[19] to be those of a 1 : 1 complex (λ = 425 or 430 nm, 298 K, toluene solution, $[C_{60}]_0 = 5.1 \times 10^{-4}$ M). The composition ratio of C_{60} and **2** has been reported,[11] and that of C_{60} and **5** was determined by Job plot, but this was not effective for the determination of the composition ratios of C_{60} and **1**, **3** and **4** due to both the very small K_a and the change in absorption. These results are shown in Table 1. Generally, neither the magnitude of nor the difference between association constants for the five hosts **1**–**5** is particularly large. Consequently, it might be concluded that the strength of complexation is not affected by the electron density of the aromatic rings of the host compounds.

Table 1 Association constants for hexahomooxacalixarene–C_{60} complexation in toluene at 298 K[a]

Compound	K_a/dm^3 mol^{-1}
1	9.1 ± 1.0
2	35.6 ± 0.3
3	20.7 ± 0.9
4	14.9 ± 2.0
5	13.3 ± 0.4

[a] Association constants were determined by the Rose–Drago method (ref. 19) for a 1 : 1 complex at 425 or 430 nm.

The inclusion complexes were obtained as dark brown crystals by allowing a toluene solution of C_{60} and the corresponding hexahomooxacalix[3]arenes **2**–**5** in a molar ratio of 1 : 10–20 to stand for a couple of weeks. The crystal structure of the complex of C_{60} and **4** was clarified by X-ray analysis and is shown in Fig. 1.§ As a result of the suppression of the rotational disorder of C_{60} in the solid state, all the atoms of the inclusion complex can be identified. The inclusion complex has a C_{3d} symmetric structure in the solid state, in which a six-membered ring of C_{60} is disposed parallel to the mean plane composed of the three phenolic oxygens of **4**. In addition, three six-membered rings around the above-mentioned six-membered ring at the bottom position of C_{60} are approximately parallel to three six-membered rings of **4**, where the closest distance [3.615 (6) Å] between two sp^2 carbons is very close to those reported for related complexes (3.51 Å[15] and 3.60–3.62 Å[16]). The inclination angle (θ) of the three phenol rings from the mean plane composed of three phenol oxygens in **4** is 147°, which is consistent with the dihedral angle between the six-membered ring at the bottom and the neighboring five- and six-membered rings of C_{60} (average angle of 145°). The additional striking feature of this complex is that the closest distance from the dibenzyl ether oxygens of **4** to the six-membered ring at the bottom of C_{60} is only 3.290 (5) Å. Taking into account these close contacts, as well as the weak electrostatic effect mentioned above, it can be suggested that van der Waals forces are the predominant attractive forces for complexation. The packing arrangement of C_{60} and **4** is shown in Fig. 2. The closest intermolecular distance of 3.51 (3) Å between carbons of C_{60} suggests some attractive interactions between C_{60} molecules, which is comparable to that observed in graphite (3.35 Å).

Similarly, X-ray analysis of the crystals of the complex of C_{60} with **2** indicated a complexation pattern with a 1 : 1 ratio, in which **2** is ordered, whereas the packing of the guest C_{60} molecules is rotationally disordered in the solid state. This packing arrangement is shown in Fig. 3.¶

The authors are grateful to Professor Y. Tobe and Dr K. Hirose (Osaka University) and Dr T. Hayashi (Kyoto University) for their useful suggestions.

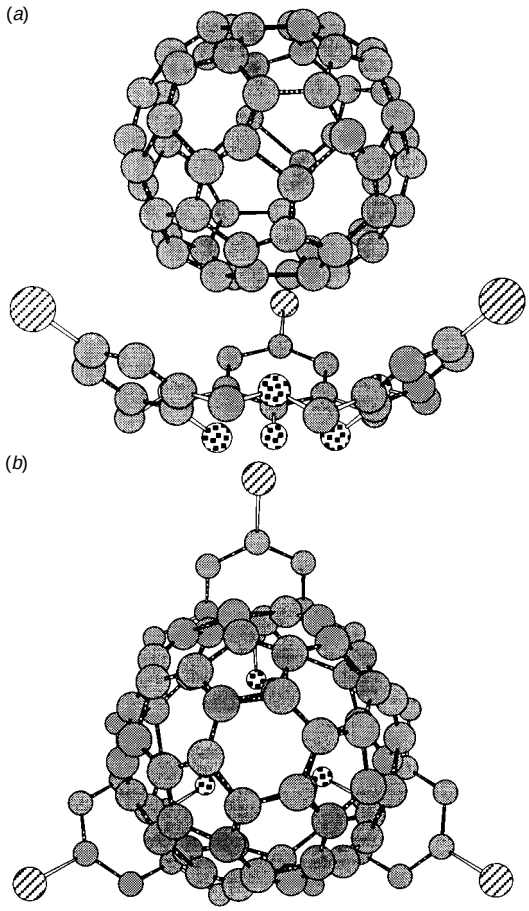

Fig. 1 Crystal structure of C_{60} and **4** generated by CHEM3D; (*a*) side view and (*b*) top view. Hydrogen atoms are excluded for clarity.

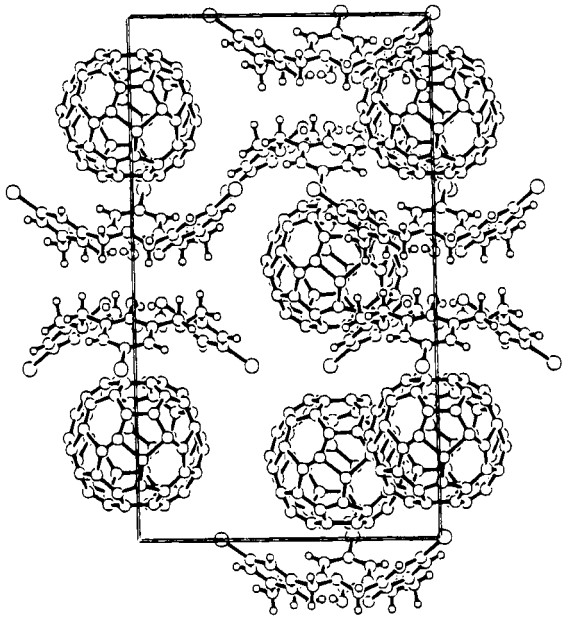

Fig. 2 Packing arrangement for the complex of C_{60} and **4**

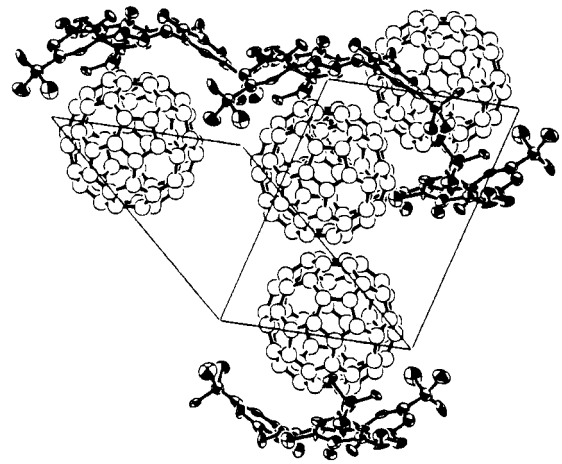

Fig. 3 Packing arrangement for the complex of C_{60} and **2**; the illustrated orientation of C_{60} has been optimized using the information obtained from the X-ray analysis of the complex of C_{60} and **4**

Notes and References

† E-mail: fuji@scl.kyoto-u.ac.jp

‡ Syntheses of hexahomooxacalix[3]arenes **1**–**4** have been reported (ref. 18). The hexahomooxacalix[3]arene **5** was prepared by cyclotrimerization according to the procedure of Gutsche (ref. 20).

§ *Crystal data* for **4**·C_{60}; $C_{28}H_7O_2Br$, M = 455.27, trigonal, $a = b$ = 18.104(1), c = 26.624(2) Å, V = 7556.8(9) Å^3, space group $R\bar{3}$ (#148), Z = 18, D_c = 1.801 g cm^{-3}, μ(Cu-Kα) = 35.59 cm^{-1}, λ(Cu-Kα) = 1.54178 Å, T = 293 K, R = 0.105, Rw = 0.163 for 3088 reflections.

¶ *Crystal data* for **2**·C_{60}; $C_{96}H_{48}O_6$, M = 1297.43, triclinic, a = 14.316(4), b = 16.88(1), c = 14.292(6) Å, α = 108.23(5)° β = 111.90(2), γ = 90.62(5)°, V = 3010(3) Å^3, space group $P\bar{1}$ (#2), Z = 2, D_c = 1.431 g cm^{-3}, μ(Cu-Kα) = 6.97 cm^{-1}, λ(Cu-Kα) = 1.54178 Å, T = 293 K, R = 0.205, Rw = 0.198 for 6473 reflections.

1 Z. Yoshida, H. Takekuma, S. Takekuma and Y. Matsubara, *Angew. Chem., Int. Ed. Engl.*, 1994, **33**, 1597.
2 T. Andersson, G. Westman, G. Stenhagen, M. Sundahl and O. Wennerström, *Tetrahedron Lett.*, 1995, **36**, 597.
3 T. Suzuki, K. Nakashima and S. Shinkai, *Chem. Lett.*, 1994, 699.
4 J. L. Atwood, G. A. Koutsantonis and C. L. Raston, *Nature*, 1994, **368**, 229.
5 F. Diederich, J. Effing, U. Jonas, L. Jullien, T. Plesnivy, H. Ringsdorf, C. Thilgen and D. Weinstein, *Angew. Chem., Int. Ed. Engl.*, 1992, **31**, 1599.
6 J. D. Crane, P. B. Hitchcoch, H. W. Kroto, R. Taylor and D. R. M. Walton, *J. Chem. Soc., Chem. Commun.*, 1992, 1764.
7 J. D. Crane and P. B. Hitchcoch, *J. Chem. Soc., Dalton Trans.*, 1993, 2537.
8 D. M. Eichhorn, S. Yang, W. Jarrell, T. F. Baumann, L. S. Beall, A. J. P. White, D. J. Williams, A. G. M. Barrett and B. M. Hoffman, *J. Chem. Soc., Chem. Commun.*, 1995, 1703.
9 C. L. Raston, J. L. Atwood, P. J. Nichols and I. B. N. Sudria, *Chem. Commun.*, 1996, 2615.
10 K. Araki, K. Akao, A. Ikeda, T. Suzuki and S. Shinkai, *Tetrahedron Lett.*, 1996, **37**, 73.
11 A. Ikeda, M. Yoshimura and S. Shinkai, *Tetrahedron Lett.*, 1997, **38**, 2107.
12 J. L. Atwood, M. J. Barnes, M. G. Gardiner and C. L. Raston, *J. Chem. Soc., Chem. Commun.*, 1996, 1449.
13 N. S. Isaacs, P. J. Nichols, C. L. Raston, C. A. Sandova and D. J. Young, *Chem. Commun.*, 1997, 1839.
14 T. Haino, M. Yanase and Y. Fukazawa, *Angew. Chem., Int. Ed. Engl.*, 1997, **36**, 259.
15 J. W. Steed, P. C. Junk, J. L. Atwood, M. J. Barnes, C. L. Raston and R. S. Burkhalter, *J. Am. Chem. Soc.*, 1994, **116**, 10 346.
16 T. Haino, M. Yanase and Y. Fukazawa, *Tetrahedron Lett.*, 1997, **38**, 3739.
17 For a review on calix[*n*]arenes, see A. Ikeda and S. Shinkai, *Chem. Rev.*, 1997, **97**, 1713.
18 K. Tsubaki, T. Otsubo, K. Tanaka, K. Fuji and T. Kinoshita, unpublished work.
19 N. J. Rose and R. S. Drago, *J. Am. Chem. Soc.*, 1959, **81**, 6138.
20 B. Dhawan and C. D. Gutsche, *J. Org. Chem.*, 1983, **48**, 1536.

Received in Cambridge, UK, 2nd January 1998; 8/00078F

Recognition of 1,2-diazines by a bidentate Lewis acid

François P. Gabbaï,*[a]† Annette Schier,[a] Jürgen Riede[a] and Michael J. Hynes[b]

[a] *Anorganisch-chemisches Institut der Technischen Universität München, Lichtenbergstrasse 4, D-85747 Garching, Germany*
[b] *Department of Chemistry, National University of Ireland, Galway, Ireland*

Dimeric *ortho*-phenyleneindium bromide 1 shows a higher affinity for 1,2-diazines than for 1,3- and 1,4-diazines; as shown by the X-ray crystal structure analysis of the host–guest complex 3 the observed selectivity results from subtle structural variation which can bring the indium p orbitals to converge.

The chemistry of group 13-based bidentate Lewis acids, while still in its infancy, appears to have a promising future. Research activity in this area has mainly focussed on the use of these compounds as anion receptors.[1,2] More scarcely, those compounds have been used as catalysts[3,4] or as selective receptors for neutral nucleophiles.[5,6] We have recently reported the synthesis of dimeric *ortho*-phenyleneindium bromide **1**.[7] The specific arrangement of the two indium centers of this derivative indicates that selectivity in the binding of bifunctional bases might be attainable. In order to verify this assumption, we have investigated the ligative behavior of **1** toward the different diazine structural isomers and report that **1** is a selective 1,2-diazine receptor.

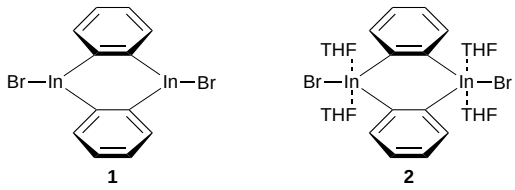

1 **2**

Compound **1** was isolated as a tetrakis(tetrahydrofuran) adduct **2**, which dissolves only in polar solvents. Addition of 1 or 2 equiv. of pyrazine (1,4-diazine) or pyrimidine (1,3-diazine) to a [$^2H_8$]THF solution of **2** at 25 °C did not result in any detectable changes of the ^{1}H NMR features of **2** thus indicating weak association between **1** and pyrazine or pyrimidine under those conditions.‡ In contrast, incremental addition of pyridazine (1,2-diazine) or phthalazine (2,3-benzodiazine) to a [$^2H_8$]THF solution of **2** at 25 °C resulted in an up-field shift of the H^{2,3,6,7} NMR resonances of the diindacycle **1** (Fig. 1).‡

These observations reflect the formation of complexes between **1** and the 1,2-diazines (pyridazine or phthalazine). Moreover, the inflection observed in the titration curve of **1** by phthalazine occurs at an added amount of base of one equivalent, thus suggesting the formation of a 1 : 1 host–guest complex, possibly **1**·phthalazine·2THF. Based on this hypothesis, the stability constants of the 1 : 1 complexes **1**·pyridazine·2THF and **1**·phthalazine·2THF can be derived and are respectively equal to 80 ± 10 and 1000 ± 150 M^{-1} (Scheme 1).[8] These data as a whole indicate that **1** is a selective receptor for 1,2-diazines.[9,10]

While the 1 : 1 complex **1**·phthalazine·2THF seems to be the preferred species in solution, colorless pale yellow crystals of the less soluble 1 : 2 complex **1**·2(phthalazine)·THF **3** spontaneously formed in a saturated THF solution containing equimolar amounts of **2** and phthalazine.‡§ Compound **3** crystallizes in the monoclinic space group $P2_1/n$ with one solvate THF.¶ As shown in Fig. 2, the diindacycle acts as a ditopic receptor for one phthalazine molecule. Each indium atom adopts a trigonal bipyramidal coordination geometry. As in the parent compound,[7] the equatorial sites are occupied by the two phenylene rings and the bromine atoms. The two nitrogen atoms of the chelated phthalazine molecule [N(21) and N(22)] occupy one of the axial sites of each indium center [In(2) and In(1), respectively]. The coordination sphere of each indium atom is completed by axial ligation of one THF molecule [In(2)] and one phthalazine [In(1)]. The chelation of one phthalazine molecule by the diindacycle has some noteworthy structural consequences. The two indium atoms are displaced towards their respective coordinated nitrogen atoms N(21) and N(22), respectively. As a result, the six-membered ring containing the two indium atoms has a boat-like conformation rather than being planar as in **2**.[7] The two phenylene rings of **3** are not coplanar (dihedral angle of 16.5°) and the dimeric *ortho*-phenylene indium moiety adopts a saddle shape. There is one metrical parameter, which merits comment. The N(22)–In(1) distance [2.824(5) Å] is significantly longer than the other In–N bond lengths observed in **3** [2.398(5) and 2.446(5) Å]. While one could question the existence of a N(22)–In(1) interaction, examination of the bond angles at In(1) and N(22) indicates

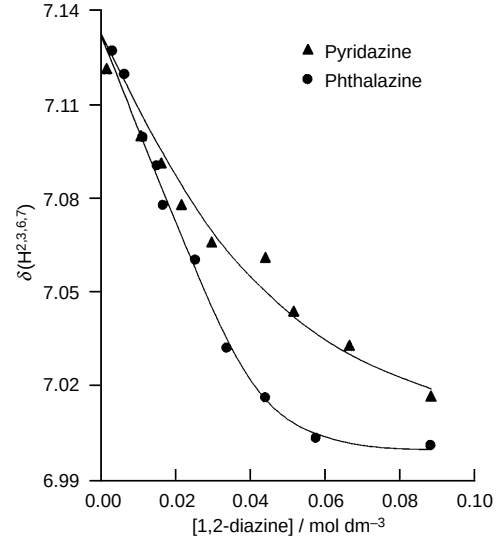

Fig. 1 ^{1}H chemical shift of H^{2,3,6,7} of **1** *vs*. the concentration of 1,2-diazines; [**1**] = 0.044 mol dm^{-3}

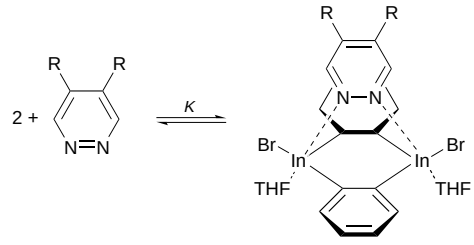

R = H, K = 80 M^{-1}
RR = *o*-C_6H_4, K = 1000 M^{-1}

Scheme 1

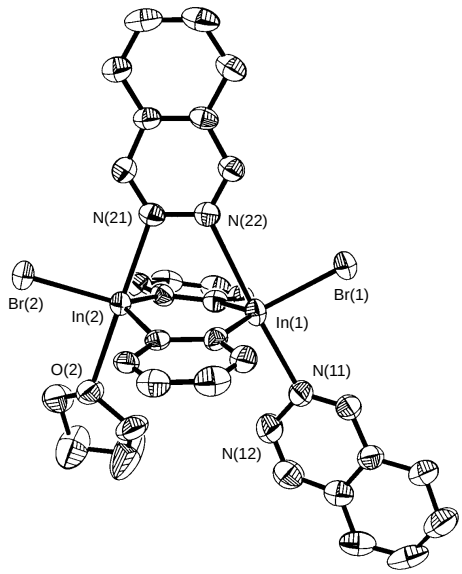

Fig. 2 Structure of **3**. ORTEP drawing with 50% probability ellipsoids; H atoms omitted for clarity. Selected bond lengths (Å) and angles (°): In(2)–O(2) 2.480(4), In(2)–N(21) 2.446(5), In(1)–N(11) 2.398(5), In(1)–N(22) 2.824(5); N(21)–In(2)–O(2) 179.5(2), N(11)–In(1)–N(22) 173.3(2).

clearly that N(22) is positioned at an axial site of the indium coordination sphere. Moreover, the N(22)–In(1) distance is much shorter than the sum of the van der Waals radii [r_{vdw}(N) = 1.5 Å,[11] r_{vdw}(In) = 1.9 Å][12] and just slightly longer than the previously reported longest In–N bond of 2.776 Å.[13] Altogether, these observations suggest the presence of a weak N(22)–In(1) dative bond.

In conclusion, as a result of subtle structural variations, the indium p orbitals of **1** can be brought to converge thus allowing chelation of bifunctional bases with adjacent electrophilic centers. The observed selectivity (phthalazine > pyridazine > pyrimidine ≅ pyrazine) follows the basicity order phthalazine (pK_a 3.5) > pyridazine (pK_a 2.3) > pyrimidine (pK_a 1.23) > pyrazine (pK_a 0.6).[14] It has however been noted previously that pK_a values are poor indicator of the donor ability of nitrogen ligands.[15] Hence, the ability of **1** to chelate 1,2-diazines can be taken as an alternative explanation for the observed selectivity.

We thank Professor H. Schmidbaur who made this work possible. Financial support from the European Commission (Training and Mobility of Researcher Program), the Deutsche Forschungsgemeinschaft and the Fonds der Chemischen Industrie is thankfully acknowledged.

Notes and References

† E-mail: F.Gabbai@lrz.tu-muenchen.de

‡ *^{1}H NMR titration experiment*: incremental addition of pyrazine or pyrimidine (2 × 4 mg, 2 × 50 μmol) to a [$^2H_8$]THF solution (0.5 ml) of **1** (34 mg of **1**·2THF,[7] 50 μmol) did not result in any change of the chemical shift of the aromatic proton signals of either **2** and pyrazine or pyrimidine. The titration curves of **1** by pyridazine and phthalazine were obtained by adding incremental amounts of the 1,2-diazines to a [$^2H_8$]THF (0.45 ml) solution of **1** (14 mg, 20 μmol). After each addition, all solids were brought into solution by gentle heating. Following cooling and before formation of any precipitate, the ^{1}H NMR spectrum of the resulting solution was measured. The stability constant K is defined by K = [Host–Guest]/{[**2**][1,2-diazine]}. The THF concentration is considered as constant and it is therefore not taken into account in the expression of K. *^{1}H NMR data* for **3**: ^{1}H NMR (400 MHz, [$^2H_8$]THF): δ 1.77 (br, 8 H, OCH_2CH_2), 3.61 (br, 8 H, OCH_2), 7.00 (m, 4 H, $H^{2,3,6,7}$), 7.49 (m, 4 H, $H^{1,4,5,8}$), 7.97 (m, 4 H, $H^{5,6}$, phtha), 8.08 (m, 4 H, $H^{8,5}$, phtha), 9.64 (m, 4 H, $H^{1,4}$, phtha).

§ *Synthesis of* **3**: compound **1**·2THF[7] (34 mg, 50 μmol) was dissolved in THF (1 ml) and added to a THF (0.5 ml) solution of phthalazine (6.5 mg, 50 μmol). Crystals of **3** spontaneously precipitated in a 63% yield (15 mg) based on phthalazine [mp 215–255, (decomp)]. Elemental analysis. Calc. for $C_{36}H_{36}Br_2In_2N_4O_2$: C, 45.66; H, 3.80; N, 5.91. Found: C, 45.71; H, 3.83; N, 6.04%.

¶ *Crystal and structure determination data* for **3**: $C_{36}H_{36}Br_2In_2N_4O_2$, M = 946.15, monoclinic, space group $P2_1/n$, a = 10.252(1), b = 18.535(1), c = 19.140(2) Å, β = 99.76(1)°, U = 3584.4(5) Å^3, Z = 4, D_c = 1.753 g cm^{-3}, F(000) = 1856, Enraf-Nonius CAD4 diffractometer, Mo-Kα radiation (λ = 0.710 69 Å), T = 21 °C. Data were corrected for Lorentz, polarization, and absorption effects (ψ-scans, $T_{min/max}$ = 83/99%). The structure was solved by direct methods and refined by full-matrix least squares against F^2 (SHELXTL-PLUS, SHELXL-93). Of 6980 measured reflections [$(\sin\theta/\lambda)_{max}$ = 0.62 Å^{-1}], 6902 were used for refinement. The thermal motion of all non-hydrogen atoms was treated anisotropically. All H atoms were calculated in idealized geometry and allowed to ride on their corresponding C atom with U_{iso} = 1.5U_{eq} of the attached C-atom. The structure converged for 415 refined parameters to R_1 = 0.0498 and wR_2 = 0.0930. Residual electron densities: +1.607 and −0.463 e Å^{-3}. CCDC 182/800.

1 W. Uhl and M. Layh, *Z. Anorg. Allg. Chem.*, 1994, **620**, 856; H. E. Katz, *J. Am. Chem. Soc.*, 1985, **107**, 1420.
2 H. E. Katz, *Organometallics*, 1987, **6**, 1987.
3 T. Ooi, M. Takahashi and K. Maruoka, *J. Am. Chem. Soc.*, 1996, **118**, 11 307.
4 M. Reilly and T. Oh, *Tetrahedron Lett.*, 1995, **36**, 217.
5 V. Sharma, M. Simard and J. D. Wuest, *J. Am. Chem. Soc.*, 1992, **114**, 7931.
6 H. E. Katz, *J. Org. Chem.*, 1985, **50**, 1987.
7 F. P. Gabbaï, A. Schier, J. Riede and D. Schichl, *Organometallics*, 1996, **15**, 4119.
8 M. J. Hynes, *J. Chem. Soc., Dalton Trans.*, 1993, 311.
9 Y. Kuroda, A. Kawashima, Y. Hayashi and H. Ogoshi, *J. Am. Chem. Soc.*, 1997, **119**, 4929.
10 A. M. Maverick, M. L. Ivie, J. H. Waggenspack and F. R. Fronczek, *Inorg. Chem.*, 1990, **29**, 2403.
11 L. Pauling, *The Nature of the Chemical Bond*, Cornell University Press, Ithaca, NY, 1960.
12 A. Bondi, *J. Phys. Chem.*, 1964, **68**, 441.
13 D. C. Bradley, D. M. Frigo, I. S. Harding, M. B. Hursthouse and M. Motevalli, *J. Chem. Soc., Chem. Commun.*, 1992, 577.
14 A. Albert, R. Goldacre and J. Phillips, *J. Chem. Soc.*, 1948, 2240.
15 J. Reedijk, in *Comprehensive Coordination Chemistry*, ed. G. Wilkinson, R. D. Gillard and J. A. McCleverty, Pergamon, Oxford, 1987, vol. 2, ch. 13.2, p. 80.

Received in Basel, Switzerland, 15th January 1998; 8/00413G

On the origin of 1,5-induction in tin(IV) halide-promoted reactions of 4-alkoxyalk-2-enylstannanes with aldehydes

Lindsay A. Hobson, Mark A. Vincent, Eric J. Thomas*† and Ian H. Hillier*

The Department of Chemistry, The University of Manchester, Manchester, UK M13 9PL

A combination of experiment and theory has identified both the allyltin trichlorides 3 (R^2 = Bn, H) as key intermediates in tin(IV) chloride-promoted reactions of allylstannanes 1 (R^2 = Bn, H) and the transition structures that are involved in their reactions with aldehydes.

Useful levels of 1,5-, 1,6- and 1,7-asymmetric induction are obtained in tin(IV) halide-promoted reactions of 4-, 5- and 6-alkoxyalk-2-enylstannanes and aldehydes.[1] For example, tin(IV) chloride-promoted reactions betweeen aldehydes and the (4-benzyloxypent-2-enyl)stannane **1** (R^2 = Bn) (Scheme 1) give the 1,5-*syn*(*Z*)-alkenols **2** with excellent stereoselectivity (*syn*:*anti* ⩾ 97:3).[2] Similar results are obtained using the 4-hydroxypent-2-enylstannane **1** (R^2 = H).[3]

This stereoselectivity is consistent with generation of the allyltin trichlorides **3**, which react with the aldehydes *via* the chair-like transition structures **4**.[2] However, alternative explanations are possible, notwithstanding the results from trapping the allyltin trichlorides generated from the 5-alkoxypent-2-enylstannanes **5**.[4,5] For example, participation of the C(3)-epimers of the allyltin trichlorides **3** and boat-like transition structures for the reactions with aldehydes, would account for the overall 1,5-*syn* (*Z*)-stereoselectivity. We now report confirmation of the involvement of the allyltin trichlorides **3** in these reactions, together with high level modelling of the transition structure **4**.

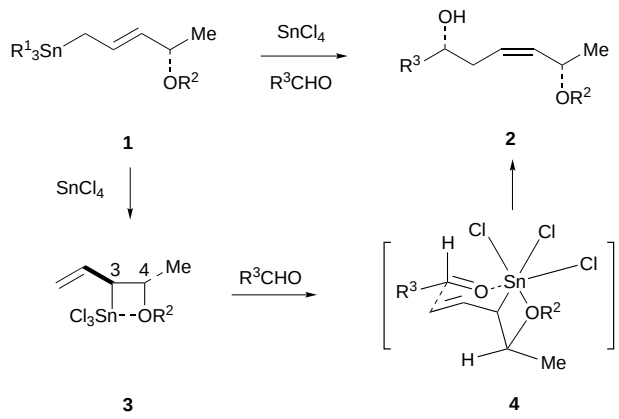

Scheme 1

Tin(IV) chloride was added to a solution of the 4-benzyloxypent-2-enylstannane **1** (R^2 = Bn) at −78 °C followed by an excess of PhLi. From this mixture the *syn*-4-benzyloxypent-1-en-3-yl(triphenyl)stannane **6**, containing less than 5% of its *anti* diastereoisomer, was isolated (see Scheme 2.) To avoid 1,3-migration of the triphenyltin moiety,[6] the alkenylstannane **6** was reduced using diimide to give (2*S*,3*S*)-2-benzyloxypent-3-yl(triphenyl)stannane **7**. The same sequence of reactions starting with the 4-hydroxypent-2-enylstannane **1** (R^2 = H) gave the 3-triphenylstannylpentan-2-ol **9** which was benzylated to give the *syn*-benzyl ether **7**.

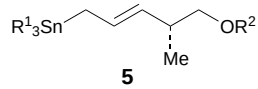

5

The hydroxyalkylstannane **9** could not be converted into a crystalline material suitable for X-ray diffraction and so its structure was confirmed by comparison with an authentic sample (see Scheme 3.) The racemic (*E*)- and (*Z*)-epoxides **10** and **14** were obtained from the corresponding alkenes using NBS and KOH.[7] Ring-opening using triphenylstannyllithium then gave the regioisomeric hydroxystannanes **11**/**12** and **15**/**9** which were separated and characterised spectroscopically. The configurations of these products were assigned on the basis that analogous epoxide ring-openings are known to proceed with inversion of configuration.[8] The *syn*-hydroxyalkylstannane **9** obtained from the *cis*-epoxide **14** was spectroscopically and chromatographically identical to that obtained from the trapping reaction of the hydroxystannane **1** (R^2 = H). Moreover, *O*-benzylation gave a benzyl ether which was identical to that prepared by reduction of the alkenylstannane **6**. The *anti*-hydroxyalkylstannane **12** obtained from the *trans*-epoxide **10** was distinctly different from that obtained from the trapping reaction of the hydroxystannane **1** (R^2 = H), and benzylation gave the *anti*-benzyloxystannane **13** which was clearly distinguishable from its *syn*-diastereoisomer **7** by ^{1}H and ^{13}C NMR spectroscopy.

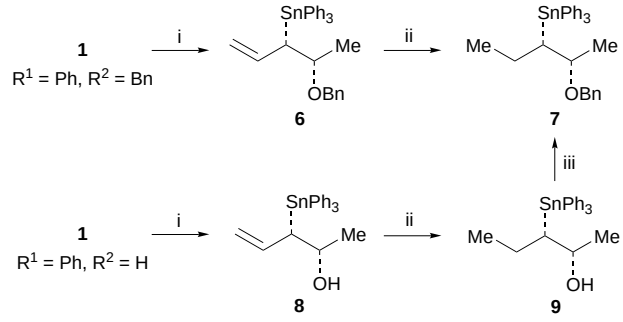

Scheme 2 *Reagents and conditions*: i, $SnCl_4$, −78 °C, 5 min, then PhLi (**6**, 54%; **8**, 35%); ii, diimide (**7**, 68%; **9**, 69%); iii, NaH, BnBr (68%)

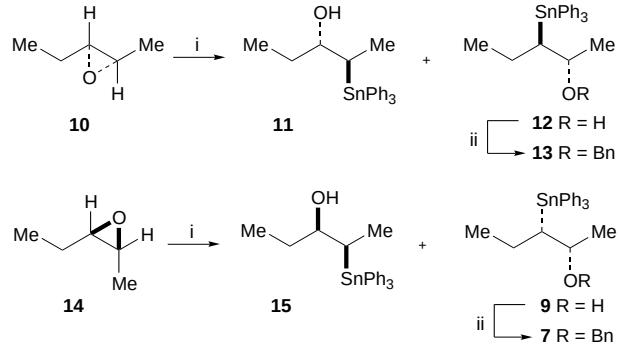

Scheme 3 *Reagents and conditions*: i, Ph_3SnLi (**11**, 30%; **12**, 20%; **15**, 20%; **9**, 20%); ii, NaH, BnBr (**13**, 61%; **7**, 72%)

It would appear that transmetallation of the 4-benzyloxy- and 4-hydroxy-pent-2-enylstannanes **1** (R^2 = Bn, H) with tin(IV) chloride gives the (3*S*,4*S*)-4-benzyloxy- and (3*S*,4*S*)-4-hydroxy-pent-1-en-3-yl)tin trichlorides **3** (R^2 = Bn, H) as originally postulated. By analogy with the transmetallation of the 5-alkoxypent-2-enylstannanes **5**,[5] it is likely that this transmetallation is due to kinetic control. However only low yields of products were obtained on attempted transmetallation of the pent-1-en-3-ylstannane **6** using either tin(IV) chloride or bromide, and so the interconversion of regioisomeric allyltin trihalides could not be investigated in this case.

The formation of the 1,5-*syn* (*Z*)-products from the reactions between the tin trichlorides **3** and aldehydes is consistent with participation of chair-like transition structures akin to **4**. However, why does the C(3)–C(4) bond prefer to be axial rather than equatorial, *i.e.* why are (*Z*)-alkenes obtained as the dominant products from these reactions rather than their (*E*)-isomers? To probe the factors involved in this stereoselectivity, high level electronic structure calculations have been carried out on the allyltin trichloride **16** and the transition structures for its reactions with formaldehyde which would lead to (*E*)- and (*Z*)-alkenols. A split valence basis was employed,[9] with electron correlation included at the density functional theory level (B3LYP), using GAUSSIAN94.[10] Stationary structures were identified as minima or saddle points by the calculation of harmonic frequencies.

We find two conformations of the allyltin trichloride **16**, corresponding to rotamers about the C(2)–C(3) bond, to be energy minima with Sn–O bond lengths of 2.457 and 2.531 A. Transition states for reactions of **16** with formaldehyde leading

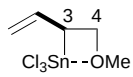

16

to both *cis*- and *trans*-double-bonded products have been located and identified as saddle points on the potential energy surfaces. These are summarised in Fig. 1.

There are considerable differences in the transition state structures and energy barriers leading to the two different stereoisomers. The transition structure leading to the *cis*-double-bonded product [Fig. 1(*a*)] has a considerably lower barrier (1.9 kcal mol^{-1}) and different structure, particularly about the tin atom, than the transition structure leading to the *trans*-isomer [Fig. 1(*b*)], which has a barrier of 12.0 kcal mol^{-1}. The favoured structure has a six-coordinated tin atom, with Sn–C and Sn–O bond lengths in the range 2.2–2.4 Å. The transition structure leading to the unfavoured *trans*-isomer has one of its Sn–O bond lengths considerably longer than normal (3.3 Å), so that the tin is effectively five-coordinated.

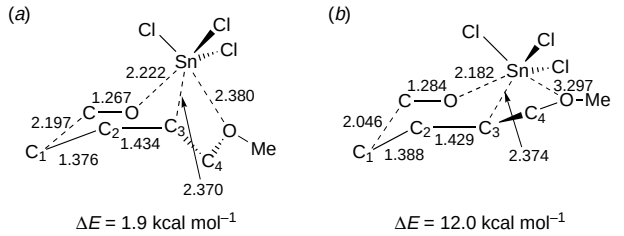

Fig. 1 Transition structures leading to (*a*) *cis* and (*b*) *trans* products. Bond lengths are in Å.

Two factors favour the transition structure shown in Fig. 1(*a*). Firstly, there is greater steric repulsion between the C(3)–C(4)–OMe entity and the chlorine atoms in the transition structure for formation of the unfavoured *trans*-isomer. Secondly, the different orientations of the C(3)–C(4) bond in the two transition structures leads to the long Sn–O bond in the disfavoured transition structure.

This work confirms the participation of the allyltin trichlorides **3** in tin(IV) chloride-promoted reactions of the allylstannanes **1**. The theoretical studies provide an insight into the factors which favour the formation of *cis*-alkenes in reactions of these allyltin trichlorides with aldehydes and complement recently reported computational studies into reactions between allylsilanes and aldehydes.[11,12]

We thank the University of Manchester and SmithKline Beecham for support (to L. A. H.) under the CASE Scheme, Dr M. Fedouloff of SmithKline Beecham for helpful discussions, and the EPSRC for support.

Notes and References

† E-mail: e.j.thomas@man.ac.uk

1 E. J. Thomas, *Chem. Commun.*, 1997, 411.
2 A. H. McNeill and E. J. Thomas, *Synthesis*, 1994, 322.
3 G. W. Bradley, D. J. Hallett and E. J. Thomas, *Tetrahedron: Asymmetry*, 1995, **6**, 2579.
4 J. S. Carey and E. J. Thomas, *Synlett*, 1992, 585.
5 R. L. Beddoes, L. A. Hobson and E. J. Thomas, *Chem. Commun.*, 1997, 1929.
6 V. J. Jephcote and E. J. Thomas, *J. Chem. Soc., Perkin Trans. 1*, 1991, 429.
7 A. T. Bottini, R. L. VanEtten and A. J. Davidson, *J. Am. Chem. Soc.*, 1965, **87**, 755.
8 L. D. Hall, P. R. Steiner and D. C. Miller, *Can. J. Chem.*, 1979, **57**, 38.
9 W. J. Hehre, R. Ditchfield and J. A. Pople, *J. Chem. Phys.*, 1972, **56**, 2257; R. Ditchfield, W. J. Hehre and J. A. Pople, *J. Chem. Phys.*, 1971, **54**, 724; M. S. Gordon, *Chem. Phys. Lett.*, 1980, **76**, 163; P. C. Hariharan and J. A. Pople, *Theor. Chim. Acta*, 1973, **28**, 213; A. Stromberg, O. Gropen and U. Wahlgren, *J. Comput. Chem.*, 1983, **4**, 181; an additional d-function with exponent 0.27 was used on tin.
10 M. J. Frisch, G. W. Trucks, H. B. Schlegel, P. M. W. Gill, B. G. Johnson, M. A. Robb, J. R. Cheeseman, T. A. Keith, G. A. Petersson, J. A. Montgomery, K. Raghavachari, M. A. Al-Laham, V. G. Zakrzewski, J. V. Ortiz, J. B. Foresman, J. Cioslowski, B. B. Stefanov, A. Nanayakkara, M. Challacombe, C. Y. Peng, P. Y. Ayala, W. Chen, M. W. Wong, J. L. Andres, E. S. Replogle, R. Gomperts, R. L. Martin, D. J. Fox, J. S. Binkley, D. J. Defrees, J. Baker, J. J. P. Stewart, M. Head-Gordon, C. Gonzalez and J. A. Pople, *GAUSSIAN 94*, Revision A.1, Gaussian, Inc., Pittsburgh, PA, 1995.
11 A. Bottoni, A. L. Costa, D. Di Tommaso, I. Rossi and E. Tagliavini, *J. Am. Chem. Soc.*, 1997, **119**, 121131.
12 K. Omoto, Y. Sawada and H. Fujimoto, *J. Am. Chem. Soc.*, 1996, **118**, 1750.

Received in Liverpool, UK, 28th January 1998; 8/00781K

Synthesis and X-ray crystal structure of the first tetrathiafulvalene-based acceptor–donor–acceptor sandwich

Klaus B. Simonsen,[a] Niels Thorup,[b] Michael P. Cava[c] and Jan Becher*[a]†

[a] *Department of Chemistry, Odense University, Campusvej 55, DK-5230 Odense M. Denmark*
[b] *Department of Chemistry, Technical University of Denmark, Building 207, DK-2800 Lyngby, Denmark*
[c] *Department of Chemistry, University of Alabama, Box 870336, Tuscaloosa, Alabama 35487 USA*

The synthesis and characterization of the bis-macrocyclic A–D–A sandwich 4·4PF_6 produced in a simple one-pot reaction is reported; only one acceptor unit participates in charge-transfer interactions with the TTF unit in the solid state of 4·4PF_6.

Since Stoddart reported the self-assembly of cyclobis(paraquat-*p*-phenylene) in the presence of electron-donating systems[1] and demonstrated the strong effect of noncovalent interactions, a remarkable number of related catenanes and rotaxanes have been prepared and studied.[2] These assemblies rely upon molecular recognition based on hydrogen bonding, donor–acceptor and π–π stacking interactions.[3] It is known that TTF forms a 1:1 electron-transfer complex with the π-electron deficient, tetracationic cyclobis(paraquat-*p*- phenylene).[4]

We were therefore interested in exploring the possibility of synthesizing a related acceptor–donor–acceptor (A–D–A) system in which the electroactive moieties were covalently fixed within the same molecule. Although, Staab and co-workers have reported a large series of elegant donor–acceptor cyclophanes, and modelled the orientation and distance dependence of charge-transfer (CT) interactions,[5] the alternative bis-macrocyclic A–D–A systems with TTF have not been reported. We have recently demonstrated the facile preparation of macrocyclic donor–acceptor systems based on TTF and the bipyridinium acceptor.[6] The relatively simple synthesis of this macrocycle may rely upon a templating effect due to the formation of a CT complex, which appears to be optimal when butane-1,4-diyl linkers were employed. Here we describe the efficient preparation of the first TTF-containing bis-macrocyclic A–D–A complex **4**·4PF_6, in which the π-electron donor TTF is sandwiched between two moderate π-electron acceptors. This unique structure was characterized *via* X-ray structure analysis.

The TTF thiolate protection protocol[7] developed in our group has made it possible to construct a variety of TTF-containing macrocycles[7b,8] and TTF-based catenanes.[9] Compound **4**·4PF_6 was prepared by treatment of **3** [prepared in two steps from tetrakis(2-cyanoethylthio)-TTF[7a] as outlined in Scheme 1] with 2 equiv. of 4,4′-bipyridine in refluxing MeCN. The macrocycle **4**·4PF_6 was isolated in 32% yield as the *trans* isomer, as a crystalline green solid, after chromatography[10] and anion exchange (NH_4PF_6).‡ This yield is quite acceptable, considering the formation of two macrocyclic rings in a one-pot reaction. The formation of a donor–acceptor complex during the reaction probably assists the ring-forming processes.[6]

The crystal structure of **4**·4PF_6MeCN was determined by X-ray diffraction,§ and the structure of the tetracation with atomic numbering is shown in Fig. 1 (anions and solvent molecules have been omitted for clarity). The unit cell contains two formula units, *i.e.*, two complex cations, eight PF_6 anions and six molecules of MeCN. The TTF part of the complex has a boat-like conformation. The dihedral angles between the least-squares planes A [S(1), S(2), C(3), C(42)] and B [S(1), S(2), S(3), S(4), C(1), C(2)] and between B and C [S(3), S(4), C(22), C(23)] are 6.5(1) and 21.3(1)°, respectively. Somewhat similar

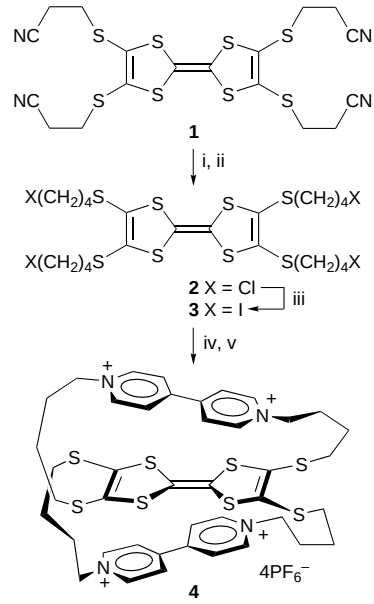

Scheme 1 *Reagents and conditions*: i, N_2, $CsOH·H_2O$ (6 equiv.), MeOH, DMF, room temp., N_2, 1 h, 79%; ii, 1-bromo-4-chlorobutane (6 equiv.), DMF, room temp., N_2 2 h, 89%; iii, NaI (40 equiv.), acetone, reflux, N_2, 48 h; iv, 4,4′-bipyridine (2 equiv.), MeCN, reflux, N_2, 4 d; v, NH_4PF_6, 32%

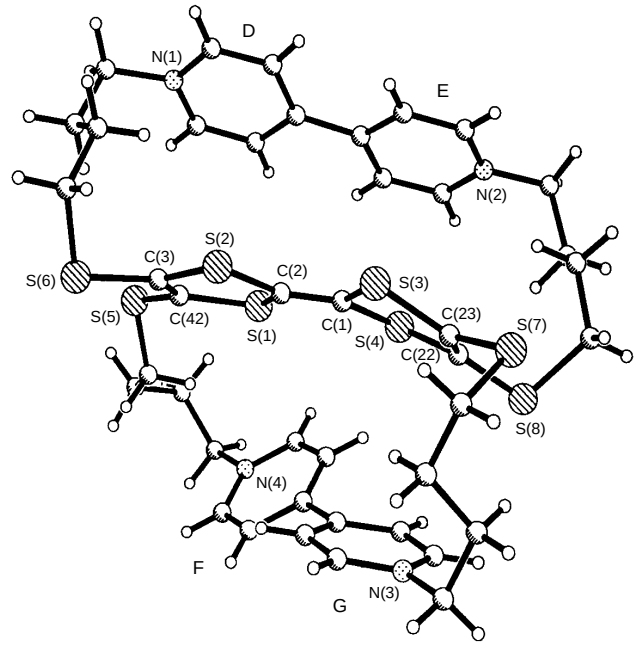

Fig. 1 Structure of **4**·4PF_6·3MeCN

Table 1 Cyclic voltammetry data: oxidation peak potentials

Compound	$E_{1/2}^1$/V	$E_{1/2}^2$/V
2	0.58	0.86
3	0.57	0.85
4	0.64	0.94

distortions have been observed in other TTF systems.[11] The bipyridinium units differ in conformation. The dihedral angle between the pyridine rings D(N1) and E(N2) is 7.3(2)°, whereas the angle between F(N4) and G(N3) is 39.3(2)°. The four pyridine rings D, E, F and G make angles of 25.1(1), 17.8(1), 24.1(2) and 55.0(2)° with the central part of TTF (plane B). Thus, the corresponding interplanar distances are not well defined. However, inspection of **4**·4PF_6 in Fig. 1 suggests a stronger interaction between the TTF part and the bipyridine part involving N(1) and N(2) than between TTF and the other bipyridine part, although no short S···N contacts are observed. The displacement parameters for the F atoms of the anions are rather high, indicating orientational disorder. Likewise, the solvent molecules appear to be somewhat disordered. Compound **4**·4PF_6 is prevented from stacking in homologous columnar stacks.[12] The shortest intermolecular S···S distance is 3.744(3) Å [between S(5) and S(7) (x − 1, y, z)], likewise indicating a weak interaction. Several C–H···F hydrogen bonds appears to be present, but the disorder of the F positions prevents a detailed description.

The simple ^{1}H NMR spectrum of **4**·4PF_6 indicates that the system must be flexible in solution as, due to high symmetry, all the butane-1,4-diyl linkers are equivalent in solution. Furthermore the ^{1}H NMR spectrum of **4**·4PF_6 is independent of temperature in the range 238–303 K.

The redox behavior of the precursors **2** and **3** and the donor acceptor complex **4**·4PF_6 were investigated by cyclic voltammetry (CV) (Table 1). The positive changes in the redox pattern are significant when going from the isolated TTF systems (**2** and **3**) to **4**·4PF_6. The change for the first potential (ΔE^1 = 70 mV) are a consequence of two factors. First, the charge transfer interactions are comparable with systems containing only one acceptor unit,[6] as evidenced by the UV–VIS (MeCN) spectrum, where **4**·4PF_6 showed a broad charge-transfer absorption band centered at 645 nm (470 M^{-1} cm^{-1}), similar to the one reported for the simpler systems.[6] Because of conformational restrictions the TTF unit is unable to interact with both of the acceptor units at the same time and therefore only a part of the change (*ca*. 30–40 mV) can be attributed to the charge transfer interactions. The rest is due to electrostatic repulsion, because the proximity of four positive charges on nitrogen makes it less favorable for the TTF moiety to generate the radical cation. The significant positive change for the second potential (ΔE^2 = 90 mV) can only be explained by electrostatic repulsion from the four pyridinium cations and the TTF radical cation, making the second oxidation less favorable, as no effect was observed in the parent system.[6]

The template-directed synthesis of the bismacrocyclic A–D–A sandwich **4**·4PF_6 shows the effect of charge-transfer interaction upon macrocyclization. The crystal structure of **4**·4PF_6 revealed two different bipyridinium units in the solid state, while NMR, UV–VIS and CV analyses illustrate that the system is very flexible in solution.

Notes and References

† E-mail: jbe@chem.ou.dk

‡ All new compounds were characterized using NMR spectroscopy (^{1}H and ^{13}C), plasma desorption mass spectrometry, CV and elemental analysis. CV: counter and working electrode, platinum; reference electrode, Ag/AgCl; supporting electrolyte, Bu_4NPF_6. Measurement carried out in MeCN at room temperature with scan speed = 100 mV s^{-1}. *Selected data* for **4**·4PF_6: mp 175 °C (decomp.); δ_H([$^2H_6$]DMSO) 9.37 (d, *J* 6.6, 8 H), 8.79 (d, *J* 6.6, 8 H), 4.80 (br s, 8 H), 2.85 (m, 8 H), 2.2–1.9 (br m, 8 H), 1.3–1.0 (br m, 8 H); δ_C ([$^2H_6$]DMSO) 147.55, 145.92, 125.99, 125.76, 105.79, 60.26, 33.27, 27.80, 23.91; *m/z* (PDMS) 1445 (M^+), 1300 (M − PF_6^-), 1155 (M − 2PF_6^-), 1010 (M − 3PF_6^-) (Calc. for $C_{42}H_{48}F_{24}N_4P_4S_8$: C, 34.91; H, 3.35; N, 3.88. Found: C, 34.91; H, 3.55; N, 3.98%.

§ *Crystal data* for **4**·4PF_6^-: the growth of single crystals of **4**·4PF_6·3MeCN was achieved by solvent diffusion of Et_2O into a solution of **4**·4PF_6 in MeCN: $C_{48}H_{57}F_{24}N_7P_4S_8$, M = 1568.37, triclinic, a = 13.1042(5), b = 16.2627(6), c = 17.1183(7) Å, α = 72.114(1), β = 81.395(1), γ = 73.180(1)°, V = 3315.8(2) Å^3, space group $P\bar{1}$, Z = 2, D_c = 1.571 g cm^{-3}, $F(000)$ = 1596, graphite monochromated Mo-Kα radiation, λ = 0.71073 Å, μ = 0.47 mm^{-1}, T = 294(1) K. Crystal size: 0.50 × 0.50 × 0.20 mm. The intensities of 28 724 reflections were measured on a Siemens SMART CCD diffractometer covering 99.3% of a complete hemisphere with θ_{max} = 26.37°, R_{int} = 0.0247. Structure solution, refinement of the structure and production of crystallographic illustrations were carried out using the Siemens SHELXTL package (ref. 13) and SHELX-97 (ref. 14). The refinement of 821 parameters on $F2$ using all 12 477 unique reflections converged at R_1 = 0.0757 [for $F_o > 4\sigma(F_o)$] and wR_2 = 0.21 for all reflections. CCDC 182/797.

1 D. Philp and J. F. Stoddart, *Synlett*, 1991, 445.
2 D. B. Amabilino, P. -L. Anelli, P. R. Ashton, G. R. Brown, E. Córdova, L. A. Godínes, W. Hayes, A. E. Kaifer, D. Philp, A. M. Z. Slawin, N. Spencer, J. F. Stoddart, M. S. Tolley and D. J. Williams, *J. Am. Chem. Soc.*, 1995, **117**, 11 142 and references cited therein; D. B. Amabilino and J. F. Stoddart, *Chem. Rev.*, 1995, **95**, 2725 and references cited therein.
3 P. R. Ashton, L. Pérez-García, J. F. Stoddart, A. J. P. White and D. J. Williams, *Angew. Chem., Int. Ed. Engl.*, 1995, **34**, 571 and references cited therein.
4 D. Philp, A. M. Z. Slawin, N. Spencer, J. F. Stoddard and D. J. Williams, *J. Chem. Soc., Chem. Commum.*, 1991, 1584; W. Devonport, M. A. Blower, M. R. Bryce and L. M. Goldenberg, *J. Org. Chem.*, 1997, **62**, 885; P.-L. Anelli, M. Asakawa, P. R. Ashton, R. A. Bissell, G. Clavier. R. Górski, A. E. Kaifer, S. F. Langford, G. Mattersteig, S. Menzer, P. Philp, A. M. Z. Slawin, N. Spencer, J. F. Stoddart, M. S. Tolley and D. J. Williams, *Chem. Eur. J.*, 1997, **3**, 1113.
5 H. A. Staab, G. H. Knaus, H.-E. Henke and C. Krieger, *Chem. Ber.*, 1983, **116**, 2785; H. A. Staab, R. Riemann-Hass, P. Ulrich and C. Krieger, *Chem. Rev.*, 1983, **116**, 2808; H. A. Staab, G. Gabel and C. Krieger, *Chem. Rev.*, 1983, **116**, 2827; H. A. Staab, R. Hinz, G. H. Knaus and C. Krieger, *Chem. Rev.*, 1983, **116**, 2835; H. A. Staab, C. P. Herz, C. Krieger and M. Rentea, *Chem. Rev.*, 1983, **116**, 3813; H. A. Staab, B. Starker and C. Krieger, *Chem. Rev.*, 1983, **116**, 3831.
6 K. B. Simonsen, K. Zong, R. D. Rogers, M. P. Cava and J. Becher, *J. Org. Chem.*, 1997, **62**, 679.
7 (*a*) N. Svenstrup, K. M. Rasmussen, T. K. Hansen and J. Becher, *Synthesis*, 1994, 809; (*b*) J. Becher, J. Lau., P. Leriche, P. Mørk and N. Svenstrup, *J. Chem. Soc., Chem. Commun.*, 1994, 2715; (*c*) K. B. Simonsen, N. Svenstrup, J. Lau, O. Simonsen, P. Mørk, G. J. Kristensen and J. Becher, *Synthesis*, 1996, 407.
8 P. Blanchard, N. Svenstrup and J. Becher, *Chem. Commun.*, 1996, 615; J. Lau, P. Blanchard, A. Riou, M. Jubault, M. P. Cava and J. Becher, *J. Org. Chem.*, 1997, **62**, 4936; K. B. Simonsen, N. Thorup and J. Becher, *Synthesis*, 1997, 1399.
9 Z.-T. Li, P. C. Stein, N. Svenstrup, K. H. Lund and J. Becher, *Angew. Chem., Int. Ed. Engl.*, 1995, **34**, 2524; Z.-T. Li, P. C. Stein, J. Becher, D. Jensen, P. Mørk and N. Svenstrup, *Chem. Eur. J.*, 1996, **2**, 624.
10 For chromatographic purification, see ref. 6.
11 F. Bertho-Thoraval, A. Robert, A. Souzu, K. Boubekeur and P. Bertail, *J. Chem. Soc., Chem. Commun.*, 1991, 843; T. K. Hansen, T. Jørgensen, F. Jensen, P. H. Thygesen, K. Christiansen, M. B. Hursthouse, M. A. Harman, B. G. Girmary, A. E. Underhill, J. D. Kilburn, K. Belmore, P. Roepstorff and J. Becher, *J. Org. Chem.*, 1993, **58**, 1359.
12 T. J. Kistenmacher, T. E. Phillips and D. O. Cowan, *Acta Crystallogr.*, 1974, **B30**, 763.
13 G. M. Sheldrick, *SHELXTL Users Manual*, Version 5.0, Siemens Analytical X-ray Instruments Inc., Madison, Wisconsin, USA, 1994.
14 G. M. Sheldrick, SHELX-97, University of Göttingen, Germany, 1997.

Received in Liverpool, UK, 9th December 1997; 7/08871J

A new cascade ring enlargement of isoxazolidines formed from 2-chloro-2-cyclopropylideneacetates

Chiara Zorn,[a] Andrea Goti,[a] Alberto Brandi,*[a]† Keyji Johnsen,[b] Sergei I. Kozhushkov[c] and Armin de Meijere*[c]‡

[a] *Dipartimento di Chimica Organica 'U. Schiff', and Centro di Studio sulla Chimica e la Struttura dei Composti Eterociclici e loro Applicazioni, C.N.R., Università di Firenze, Via G. Capponi 9, I-50121 Firenze, Italy*
[b] *Institut für Anorganische Chemie der Georg-August, Universität Göttingen, Tammannstrasse 4, D-37077 Göttingen, Germany*
[c] *Institut für Organische Chemie der Georg-August Universität Göttingen, Tammannstrasse 2, D-37077 Göttingen, Germany*

2-Chloro-2-cyclopropylideneacetate 1 and spiropentane analog 2 cycloadd pyrroline *N*-oxide 3 to give spiro[cyclopropane-1,5′-isoxazolidine]s 4 and 5 in good yields; due to the presence of a chlorine substituent on the carbon α to the spirocyclopropane ring, which facilitates a cyclopropyl to cyclobutyl ring enlargement, these compounds undergo a cascade rearrangement to yield indolizinone derivatives 8 and 9 cleanly (70–73% yield), offering a new method for the synthesis of the indolizine skeleton.

The strain energy incorporated in a cyclopropane ring is an extremely useful handle for molecular transformations in organic synthesis.[1] The selectivity of such a transformation and the operational conditions strongly depend on the molecular surroundings of the cyclopropane ring in a given skeleton.

It has already been demonstrated that isoxazolidines or isoxazolines with a spirocyclopropane ring at the 5-position are capable of undergoing a selective rearrangement affording 2-substituted tetrahydro- or dihydro-4-pyridones, respectively.[2] This process has been applied to the synthesis of natural and non-natural heterocyclic compounds and it has proved particularly useful for the synthesis of heterocycles with nitrogen at the bridgehead.[3] We now report a new selective thermal cascade ring enlargement process of 4-chloro substituted spiro[cyclopropane-1,5′-isoxazolidine]s, obtained by nitrone cycloaddition to methyl 2-chloro-2-cyclopropylideneacetate **1**[4,5] and to methyl (*Z*)-2-chloro-2-spiropentanylideneacetate **2**[6] which further expands the synthetic utility of this class of compounds.

Compounds **1** and **2** smoothly react with pyrroline *N*-oxide **3** at room temperature to give cycloadducts **4** and **5**, respectively, as single regioisomers (Scheme 1).

The regioselectivity of these cycloadditions is in accord with the one previously observed for electron-acceptor substituted methylenecyclopropanes.[3b,7] Compounds **4** and **5** are obtained as single diastereoisomers, the configuration of which has tentatively been assigned on the basis of the known preference of the methoxycarbonyl group to be placed *endo* with respect to the nitrone in the cycloaddition process.[7,8]

When the isoxazolidines **4** and **5** were submitted to the usual conditions for thermal rearrangement (toluene, 110 °C),[2] a complex mixture of products was obtained. However, by replacing toluene with the more polar DMSO a clean reaction occurred at 100 °C to give the hexahydroindolizin-5-ones **8**[9] and **9** in 70 and 73% yield, respectively (Scheme 1). These compounds were present only in minute amounts in the heated toluene solution. Spectroscopic data were consistent with the proposed structures **8** and **9**. The regioselective formation of compound **9**, the structure of which was assigned on the basis of the long-range coupling (^5J = 1.8 Hz) between the two groups of allylic protons observed in the ^{1}H NMR spectrum, is quite remarkable. This unexpected result was finally confirmed by an X-ray crystal structure analysis of compound **8** (Fig. 1).§

The fact that a polar solvent is essential for the success of this rearrangement suggests that it occurs *via* a highly polar transition structure. The polar solvent would certainly favour the cyclopropyl to cyclobutyl ring enlargement leading from **4**/**5** to **6**/**7**.[10] This might occur as an intramolecular S_N2 displacement or *via* tight ion-pair intermediates. The further ring-enlargement could be initiated by abstraction of the bridgehead proton in **6**/**7**, followed by N–O bond cleavage and reclosure to the indolizidin-5-ones **8**/**9**.

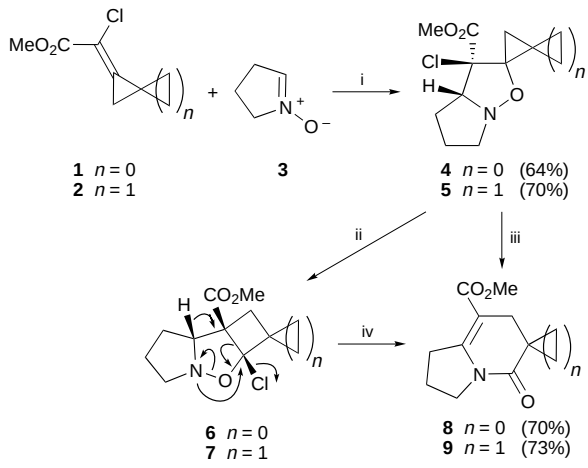

Scheme 1 *Reagents and conditions*: i, CH_2Cl_2, room temp., 5 d; ii, Al_2O_3, CH_2Cl_2, room temp.; iii, DMSO, 100 °C, 3 h; iv, DMSO, 100 °C

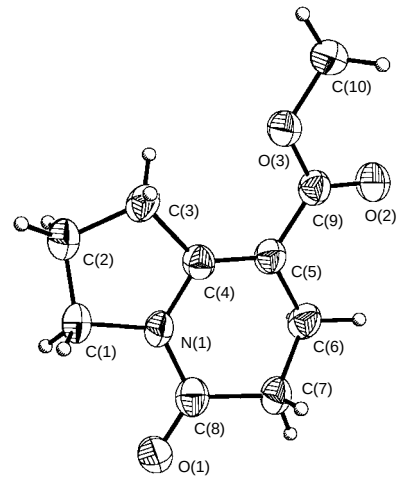

Fig. 1 Structure of 8-methoxycarbonyl-5-oxo-2,3,6,7-tetrahydro-1*H*-indolizine **8** in the crystal.

The intermediacy of the cyclobutyl derivatives **6**/**7** is probable, since these compounds could actually be isolated after stirring the isoxazolidines **4** and **5** in CH_2Cl_2 in the presence of Al_2O_3 at room temperature. Isoxazolidine **5** rearranged completely to **7** in 4 h, whereas **4** under the same conditions remained as a 6 : 1 mixture of **6** and **4** after 3 days.

The structural assignment of **6** and **7** was based on the presence of chlorine as proved by the mass spectrum, and the observation of diagnostic signals for the cyclobutane ring in the ^{13}C NMR spectrum (δ_C 102.1, 72.9, 27.7 and 25.8 in **6**; 107.5, 70.5, 28.5 and 25.5 in **7**). The *cis* relationship of the methoxycarbonyl group and the chlorine in **6**/**7** was tentatively assigned on the assumption that the displacement of chloride in **4** and **5** occurs *via* an S_N2 process, which fixes the relative configuration of the bridgehead proton and the CO_2Me group in any potential intermediate *en route* to **6**/**7**. The chloride then can enter only from the convex face of the molecule. When heated to 100 °C in DMSO, compounds **6** and **7** gave the same indolizidinones **8** and **9** as obtained directly from **4** and **5**.

In conclusion, a new domino rearrangement of spiro[cyclopropane-1,5′-isoxazolidine]s has been discovered. This process is made possible by the presence of a chlorine substituent on the carbon α to the spirocyclopropane ring, which facilitates a cyclopropyl to cyclobutyl ring enlargement mediated by a polar solvent. At higher temperature a further ring enlargement ensues with elimination of hydrogen chloride to produce hexahydroindolizidin-5-ones.

The generalization of this new process and its synthetic application are now being studied in our laboratories.

This work was supported on the Italian side by research funds from the University of Florence and, in part, CSCEA (CNR). On the German side this work was supported by the Deutsche Forschungsgemeinschaft (SFB 416, Project A) and the Fonds der Chemischen Industrie; generous gifts of chemicals by the BASF, Bayer, Hoechst, Degussa AG, and Hüls companies are gratefully acknowledged. C. Z. is grateful for financial support for the period in Göttingen by the ERASMUS Exchange Program.

Notes and References

† E-mail: brandi@chimorg.unifi.it
‡ E-mail: ameijer1@uni-goettigen.de

§ *Crystal data* for **8**: $C_{10}H_{13}NO_3$; crystal size 0.6 × 0.3 × 0.1 mm, monoclinic, $P2_1/c$, a = 13.787(11), b = 8.296(6), c = 8.264(5) Å, β = 91.582(19), γ = 90°, V = 944.9(12) Å^3, Z = 4, D_c = 1.372 Mg m^{-3}, 2.87 < θ < 23.16°, Mo-Kα radiation, λ = 0.71073, T = 133(2) K; 8957 measured reflections, 1328 independent reflections, empirical absorption correction, structure solution with direct methods with SHELXLS-86, refinement with SHELXL-93, 129 free parameters, R_1 = 0.0772 [$I > 2\sigma(I)$], wR_2 = 0.1999, refinement *via* full-matrix least-squares on F^2, largest diff. peak and hole 0.508 and −0.341 e Å^{-3}. CCDC 182/802.

1 *Carbocyclic Three-Membered Ring Compounds, Houben-Weyl Vol. E17*, ed. A. de Meijere, Thieme, Stuttgart 1997; J. Salaün, *Rearrangements involving the cyclopropyl group*, in *The Chemistry of the cyclopropyl group*, ed. S. Patai and Z. Rappoport, Wiley, New York 1987, pp. 809–878; P. Binger and H. M. Büch, *Top. Curr. Chem.*, 1987, **135**, 77; P. Binger and T. Schmidt, in *Houben-Weyl Vol. E17c*, ed. A. de Meijere, Thieme, Stuttgart 1997, pp. 2217–2294; A. Goti, F. M. Cordero and A. Brandi, *Top. Curr. Chem.*, 1996, **178**; A. Brandi and A. Goti, *Chem. Rev.*, 1998, **98**, 589.

2 A. Brandi, F. M. Cordero, F. De Sarlo, A. Goti and A. Guarna, *Synlett*, 1993, 1; A. Brandi, Y. Dürüst, F. M. Cordero and F. De Sarlo, *J. Org. Chem.*, 1992, **57**, 5666; A. Goti, B. Anichini, A. Brandi, S. I. Kozhushkov, C. Gratkowski and A. de Meijere, *J. Org. Chem.*, 1996, **61**, 1665.

3 (*a*) A. Brandi, S. Cicchi, F. M. Cordero, R. Frignoli, A. Goti, S. Picasso and P. Vogel, *J. Org. Chem.*, 1995, **60**, 6806; (*b*) A. Brandi, F. M. Cordero, A. Goti and A. Guarna, *Tetrahedron Lett.*, 1992, **33**, 6697; (*c*) F. M. Cordero, A. Brandi, C. Querci, A. Goti, F. De Sarlo and A. Guarna, *J. Org. Chem.*, 1990, **55**, 1762; (*d*) A. Brandi, S. Garro, A. Guarna, A. Goti, F. M. Cordero and F. De Sarlo, *J. Org. Chem.*, 1988, **53**, 2430.

4 T. Liese, G. Splettstösser and A. de Meijere, *Angew. Chem. Int. Ed. Engl.*, 1982, **21**, 790; T. Liese, S. Teichmann and A. de Meijere, *Synthesis*, 1988, 25; T. Liese, F. Seyed-Mahdavi and A. de Meijere, *Org. Synth.*, 1990, **69**, 148.

5 For reviews illustrating the synthetic applications of compound **1**, see: A. de Meijere, in *New Aspects of Organic Chemistry II*, ed. Y. Ohshiro, Proceedings of the Fifth International Kyoto Conference on New Aspects of Organic Chemistry - IKCOC 5, Kyoto Nov. 11–15, 1991, Kodansha, Tokyo, 1992, pp. 181–213; A. de Meijere and L. Wessjohann, *Synlett*, 1990, 20.

6 L. Wessjohann, K. Giller, B. Zuck, L. Skattebøl and A. de Meijere, *J. Org. Chem.*, 1993, **58**, 6442.

7 A. Brandi, F. M. Cordero, F. De Sarlo, R. Gandolfi, A. Rastelli and M. Bagatti, *Tetrahedron*, 1992, **48**, 3323.

8 J. J. Tufariello, in *1,3-Dipolar Cycloaddition Chemistry*, ed. A. Padwa, Wiley, New York, 1984, vol. 2, pp. 83–168.

9 J.-P. Célérier, C. Eskenazi, G. Lhommet and P. Maitte, *J. Heterocyclic Chem.*, 1979, **16**, 953; P. Brunerie, J.-P. Célérier, M. Huché and G. Lhommet, *Synthesis*, 1985, 735; K. Paulvannan and J. R. Stille, *Tetrahedron Lett.*, 1993, **34**, 8197; K. Paulvannan and J. R. Stille, *J. Org. Chem.*, 1994, **59**, 1613.

10 M. C. Caserio, W. M. Graham and J. D. Roberts, *Tetrahedron*, 1960, **11**, 171; J. D. Roberts and R. H. Mazur, *J. Am. Chem Soc.*, 1951, **73**, 2509; E. Renk and J. D. Roberts, *J. Am. Chem. Soc.*, 1961, **83**, 878.

Received in Cambridge, UK, 10th February 1998; 8/01168K

Ylide-like addition complexes in insertion reactions of CH with PH_3 and H_2S

Z.-X. Wang and M.-B. Huang*†

Graduate School at Beijing, University of Science and Technology of China, Academia Sinica, PO Box 3908, Beijing 100039, China

The intermediate addition complexes HC–PH_3 and HC–SH_2 formed in the CH insertion reactions with PH_3 and H_2S have large binding energies and short central bond lengths, exhibiting 'ylidic' features in their molecular and electronic structures.

We previously studied the CH insertion reactions with NH_3, H_2O and HF by means of *ab initio* calculations[1] and found intermediate addition complexes existing prior to the transition states in the reaction paths. The reaction paths for these reactions are illustrated by eqns. (4)–(6) where the reactants,

$$\underset{\textbf{ma}}{CH + XH_n} \rightarrow \underset{\textbf{mb}}{HC{-}XH_n} \rightarrow \underset{\textbf{mc}}{TS} \rightarrow \underset{\textbf{md}}{H_2CXH_{n-1}}$$

(1) X = P, n = 3; (2) X = S, n = 2; (3) X = Cl, n = 1

(4) X = N, n = 3; (5) X = O, n = 2; (6) X = F, n = 1

intermediate complexes (HC–XH_n), transition states (TS), and insertion products (H_2CXH_{n-1}) are denoted as **ma**, **mb**, **mc** and **md** (m = 4, 5 or 6), respectively, and the energy profiles have the following skeletons: E (**ma**) > E (**mb**) < E (**mc**) ⩾ E (**md**).

Recently we performed *ab initio* calculations for the CH insertion reactions with PH_3, H_2S and HCl. These reactions have similar reaction paths [illustrated by eqns. (1)–(3), respectively] and similar skeletons of the energy profiles to those for reactions (4)–(6). However, we have found that the intermediate addition complexes HC–PH_3 **1b** and HC–SH_2 **2b** initially formed in reactions (1) and (2) are not the simple complexes,[1] but are similar in nature to the phosphonium and sulfonium ylides (P- and S-ylides).

Standard *ab initio* molecular calculations were performed by using the Gaussian 94 W suite of programs.[2] The structures of reactants, intermediate complexes, transition states, and products were optimized at the (U)MP2(FC)/6-31G(d) and (U)MP2(FC)/6-311++G(d,p) levels. Frequency calculations were carried out at the (U)MP2(FC)/6-31G(d) level to characterize stationary points and to evaluate zero-point energies (ZPEs). Finally single-point (U)MP4SDTQ(FC)/6-311++G(2d,p)//(U)MP2(FC)/6-311++G(d,p) calculations were performed. For open-shell systems the $< S^2 >$ values are all < 0.8. We recalculated the insertion paths for reactions (4)–(6) at these levels and obtained similar results to those reported in ref. 1. The MP4SDTQ/6-311++G(2d,p)//MP2/6-311++G(d,p) energetic results (the spin-projected ones for the open-shell systems) corrected with the (MP2/6-31G(d)) ZPEs and the MP2/6-311++G(d,p) geometrical results are used unless otherwise noted.

The potential energy curves in Fig. 1 represent the calculated insertion reaction paths for reactions (1)–(3). The relative energies of **mb**, **mc** and **md** and the structures of **mb** (m = 1–3) are shown in Fig. 1. The term 'relative energy' (of a species) in the present article means the energy of a species relative to the reactants in the same reaction.

The binding energies of the intermediate addition complexes **1b**, **2b** and **3b** in reactions (1)–(3) are 43.4, 22.1 and 3.8 kcal mol^{-1} (1 cal = 4.184 J) respectively. The negative relative

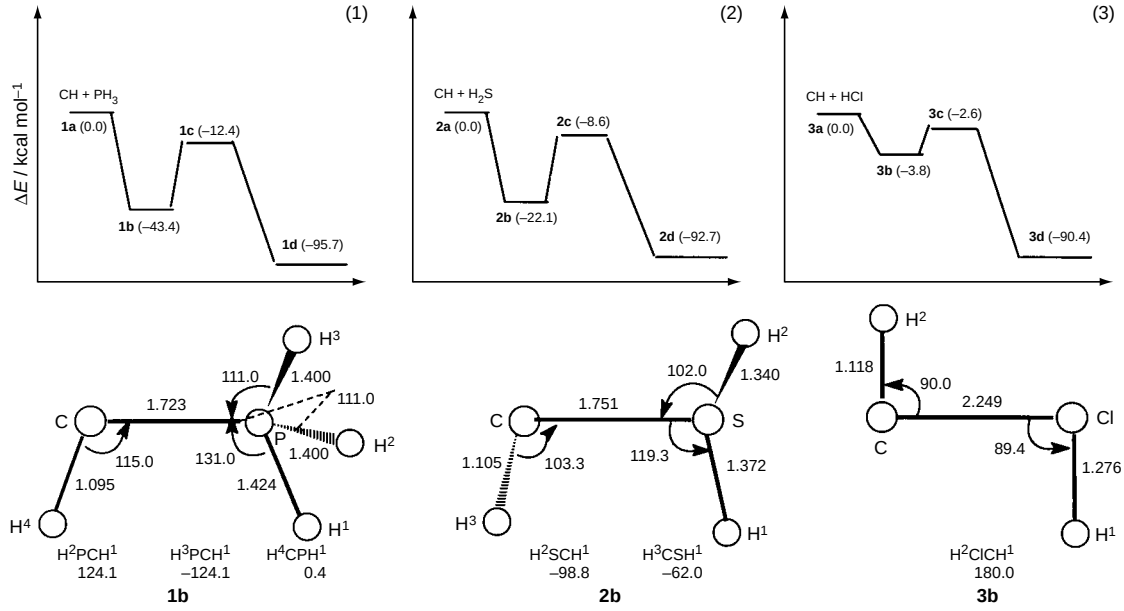

Fig. 1 A schematic diagram of the potential energy curves of the CH insertion reactions with PH_3 (1), H_2S (2) and HCl (3) with the MP4SDTQ/6-311++G(2d,p)//MP2/6-311++G(d,p) relative energies in kcal mol^{-1} [corrected with the MP2/6-31G(d) ZPEs] in parentheses. In the lower part of the figure are the MP2/6-311++G(d,p) structures of the intermediate addition complexes **mb** (m = 1–3) formed in the three insertion reactions (bond lengths in Å and angles in °).

Table 1 Binding energies (E_b) and the C–X bond distances (R) of the addition complexes HC–XH_n

	HC–PH_3 **1b**	HC–SH_2 **2b**	HC–ClH **3b**	HC–NH_3 **4b**	HC–OH_2 **5b**	HC–FH **6b**
E_b[a]/kcal mol^{-1}	43.4[b]	22.1[b]	3.8	24.9	7.9	1.5
R(C–X)[c]/Å	1.723	1.751	2.249	1.588	1.801	2.173
	(1.787)[d]	(1.724)	(1.700)	(1.398)	(1.368)	(1.344)

[a] The MP4SDTQ/6-311++G(2d,p)//MP2/6-311++G(d,p) + ZPE energetic results. [b] After the (MP4) BSSE corrections, these two values (the E_b values for **1b** and **2b**) are reduced by 3.4 and 3.4 kcal mol^{-1}, respectively. [c] Optimized at the MP2/6-311++G(d,p) level. [d] Values in parentheses are the C–X bond lengths in the respective insertion products.

Table 2 Calculated properties of HC–PH_3 and HC–SH_2

	E_{pt}[a]/ kcal mol^{-1}	ΔE[a]/ kcal mol^{-1}	H–C–X[b]/°	Q(C)[b]/e	Q(X)[b]/e
HC–PH_3 **1b**	52.3	0.2	115.0	−0.620	0.691
HC–SH_2 **2b**	70.6	7.1	103.3	−0.660	0.513

[a] E_{pt} and ΔE denote the proton-transfer energy and internal rotation barrier, respectively, calculated at the MP4SDTQ/6-311++G(2d,p)//MP2/6-311++G(d,p) + ZPE level. [b] H–C–X and Q (the charge on atomic centers) are predicted at the MP2/6-311++G(d,p) level.

energy values of the transition states **1c**, **2c** and **3c** (−12.4, −8.6 and −2.6 kcal mol^{-1}, respectively) and the large negative relative energy values of the insertion products **1d**, **2d** and **3d** (−95.7, −92.7 and −90.4 kcal mol^{-1}, respectively) indicate that the CH insertion reactions with PH_3, H_2S and HCl are all feasible and strongly exothermic.

In the following we focus on the addition complexes. Table 1 lists the binding energies and the C–X bond distances of the intermediate addition complexes **mb** (m = 1–6), together with the C–X bond lengths of the insertion products (**md**). As shown in Table 1, **1b** (HC–PH_3) and **2b** (HC–SH_2) have very large binding energies and very short C–X bond distances (1.723 and 1.751 Å, respectively) which are shorter than or comparable with the C–X bond lengths (1.787 and 1.724 Å) in **1d** and **2d**, respectively. The binding energies for **3b**, **5b** and **6b** are all very small (< 10 kcal mol^{-1}), and they all have very long C–X bond distances compared with those in their respective insertion products. Although the binding energy for **4b** is quite large (about half the value for its analogue **1b**), the C–N bond distance (1.588 Å) in **4b** is significantly longer than that (1.398 Å) in **4d**. It is also noted that the HCX angles in **1b** and **2b** (115.0 and 103.3°, respectively) are significantly larger than 90° while the HCX angles in the other complexes (also see ref. 1) are close to 90°. It is concluded that **1b** and **2b** are different from the other complexes which are the loosely bound lone-pair (of the X-atom) donor–acceptor complexes.[1]

The P- and S-ylides (H_2CPH_3 and H_2CSH_2) are important reactants in synthetic organic chemistry. In our previous studies,[1,3] we already noticed that the $^1CH_2$ insertion reactions into hydrides have similar reaction paths and similar energy profile skeletons to those for the CH insertion reactions. The P- and S-ylides could be considered as the intermediate addition complexes in the $^1CH_2$ insertion reactions with PH_3 and H_2S, respectively (see ref. 7), and it is natural to infer that the CH addition complexes **1b** and **2b** are similar to the P- and S-ylides (although **1b** and **2b** are radicals). As a prototype of ylides the P-ylide has been extensively investigated by quantum chemists[4–8] (its bonding nature is still being explored[4]), and the following features are known. The P-ylide has a short C–P bond length[4–6] (shorter than the length in H_3C–PH_2) and very large binding energy towards $^1CH_2$ + PH_3. There is a large charge separation at its C^-P^+ bond[4,6,8] and the rotational barrier about this bond is extremely low.[4,5,8] These features are considered as general features in the molecular and electronic structures of ylides.

Table 2 lists the calculated properties of **1b** and **2b**. The proton-transfer energy[8] (E_{pt}) is defined as a criterion of 'hypervalency' in ylides, and we have defined the E_{pt} values for **mb** as the energy differences between **mb** and **md**. The binding energies and E_{pt} values for the P- and S-ylides can be evaluated based on the energetic results reported in ref. 7 which were calculated at the MP levels comparable to those in the present study. The large binding energies for **1b** and **2b** (43.4 and 22.1 kcal mol^{-1}, respectively) are somewhat smaller than those for the P- and S-ylides (54–74 and 27–48 kcal mol^{-1}, respectively). The E_{pt} values for **1b** and **2b** are 52.3 and 70.6 kcal mol^{-1}, respectively, which are comparable with those for the P- and S-ylides (53–59 and 73–81 kcal mol^{-1}, respectively). The C–P bond length in **1b** is only 0.046 Å longer than the length of 1.677 Å[4,5] [at the MP2/6-311+G(d,p) level] in the P-ylide, and the C–S bond length in **2b** is about 0.1 Å longer than the length [1.635 Å[7] at the MP2/6-31G(d) level] in the S-ylide. The MP2 Mulliken charges on the C and P atoms in **1b** are −0.620 and +0.691, respectively (the MP2 charges of −0.76 and +0.55 for the P-ylide were reported in ref. 4) and the charges on the C and S atoms in **2b** are −0.660 and +0.513, respectively, which implies considerable charge separations in **1b** and **2b**. The rotational barrier in **1b** is extremely low (0.2 kcal mol^{-1}) as in the P-ylide (*ca*. 1 kcal mol^{-1} or less[4,5]), and the barrier in **2b** is 7.1 kcal mol^{-1} (no reported post-SCF results for the barrier in the S-ylide are available).

1b and **2b** are not loosely bound complexes and they have ylidic features in their molecular and electronic structures. Since **1b** and **2b** exist in deep minima in the potential energy surfaces (Fig. 1), they might be observed in some experiments (spectroscopy, EPR, *etc*). We would expect the ylide-like radicals **1b** and **2b** to be useful in synthetic chemistry as are the P- and S-ylides.

We thank the NNSFC for the financial support.

Notes and References

† E-mail: huaugmb@es1.gsbustc.ac.cn

1 Z.-X. Wang, R.-Z. Liu, M.-B. Huang and Z. H. Yu, *Can. J. Chem.*, 1996, **74**, 910.
2 Gaussian 94, Revision E.1, M. J. Frisch, G. W. Trucks, H. B. Schlegel, P. M. W. Gill, B. G. Johnson, M. A. Robb, J. R. Cheeseman, T. Keith, G. A. Petersson, J. A. Montgomery, K. Raghavachari, M. A. Al-Laham, V. G. Zakrzewski, J. V. Ortiz, J. B. Foresman, J. Cioslowski, R. B. Stefanov, A. Nanayakkara, M. Challacombe, G. Y. Peng, P. Y. Ayala, W. Chen, M. W. Wong, J. L. Andres, E. S. Replogle, R. Gomperts, R. L. Martin, D. J. Fox, J. S. Binkley, D. J. Defrees, J. Baker, J. P. Stewart, M. Head-Gordon, C. Gonzalez and J. A. Pople, Gaussian, Inc., Pittsburgh, PA, 1995.
3 Z.-X. Wang and M.-B. Huang, *Can. J. Chem.*, 1997, **75**, 996.
4 N. Laszlo, V. Tamas and R. Jozsef, *J. Phys. Chem.*, 1995, **99**, 10 142.
5 S. Bachrach, *J. Org. Chem.*, 1992, **57**, 4367.
6 T. Naito, S. Nagase and H. Yamataka, *J. Am. Chem. Soc.*, 1994, **116**, 10080.
7 B. F. Yates, W. J. Bouma and L. Radom, *J. Am. Chem. Soc.*, 1989, **109**, 2250.
8 R. A. Eades, P. C. Cassman and D. A. Dixon, *J. Am. Chem. Soc.*, 1981, **103**, 1066.

Received in Cambridge, UK, 20th February 1998; 8/01491D

Sugar-integrated gelators of organic fluids: on their versatility as building-blocks and diversity in superstructures

Kenji Yoza,[a] Yoshiyuki Ono,[a] Kanami Yoshihara,[a] Tetsuyuki Akao,[b] Hideyuki Shinmori,[c] Masayuki Takeuchi,[c] Seiji Shinkai*[c]† and David N. Reinhoudt[d]

[a] *Chemotransfiguration Project, Japan Science and Technology Corporation, Aikawa, Kurume, Fukuoka 839, Japan*
[b] *Biotechnology and Food Research Institute, Fukuoka Industrial Technology Center, Aikawa, Kurume, Fukuoka 839, Japan*
[c] *Department of Chemistry and Biochemistry, Graduate School of Engineering, Kyushu University, Hakozaki, Higashi-ku, Fukuoka, 812-81, Japan*
[d] *Chemotransfiguration Project, Faculty of Chemical Technology, University of Twente, 7500 AE Enschede, The Netherlands*

Three 1-*O*-methyl-4, 6-*O*-benzylidene derivatives of monosaccharides (D-glucose, D-galactose and D-mannose) were synthesised: they acted as versatile gelators of various organic fluids, indicating that saccharides are useful as potential building-blocks for molecular design of chiral gelators.

The development of new gelators of organic fluids has recently received much attention. They not only gelatinise various organic fluids but also create novel networks with fibrous superstructures which can be characterised by SEM pictures of the xerogels.[1–11] The gelators can be classified into two categories according to the difference in the driving force for the molecular aggregation, *viz*. hydrogen-bond-based gelators and nonhydrogen-bond-based gelators. Typical examples of the former group are the aliphatic amide derivatives,[1–4] whereas those of the latter group are cholesterol derivatives.[6–9] The superstructures of the organic gels of aliphatic amide derivatives show that they satisfy the complementarity of the intermolecular hydrogen-bonding interactions.[5–9] This observation stimulated us to use saccharides as a hydrogen-bond-forming segment in the gelators, because one can easily introduce a variety of hydrogen-bond-forming, chiral segments into gelators by selection from a saccharide library. In the literature examples of saccharide-containing gelators are very limited in spite of their high potential.[8,12] We synthesised glucose-based **1**, galactose-based **2** and mannose-based **3** and studied their gelation abilities. We found that the gelation properties, such as gel stability, superstructure and solvent-dependence, were profoundly related to the saccharide structure.

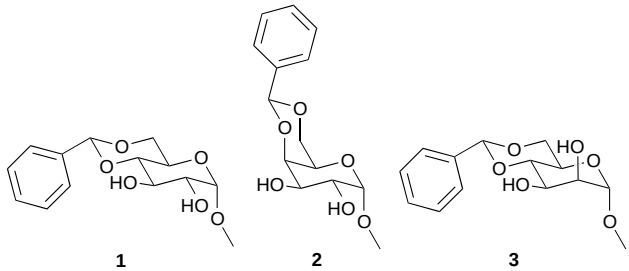

The synthesis of **1** has already been reported.[13] Gelators **2** and **3** were synthesised in a similar manner by treatment of the saccharide with benzaldehyde and $ZnCl_2$. The products were identified by ^{1}H NMR and IR spectroscopy and elemental analyses.

The gelation test was carried out as follows: the gelator (**1**–**3**: 3.0 mg) was mixed with solvent (0.10 ml) in a septum-capped test tube and the mixture was heated until the solid dissolved. The solution was cooled to room temperature and left for 1 h (G in Table 1 denotes that a gel was formed at this stage). Some solutions gelatinised at a gelator concentration below 1.0 wt% (SG or super-gelator; Table 1). Solvents in Table 1 are those which were gelatinised by either **1**, **2** or **3**.[14] Table 1 reveals that, in general, **2** acts as an excellent gelator of many organic fluids. In contrast, comparison of the gelation ability for *n*-heptane and cyclohexane reveals that **1** is more cohesive and tends to form a precipitate, whereas **3** is more soluble than the other two gelators and is frequently unable to coagulate in solution.

What is the origin of the difference in their gelation ability? The sole structural difference among **1**, **2** and **3** is the absolute configuration of C-2 and C-4. It is reasonable to assume that **1**, **2** and **3** show a different ability to form a gel network because of the different intermolecular hydrogen-bonding interactions. In the FT-IR spectra, the gel solutions gave two peaks (3473–3240 and 3576–3659 cm^{-1}) in the ν_{OH} region which could be assigned to hydrogen-bonded OH and free OH groups, respectively. As shown in Fig. 1, the peak intensity ratio (R) of hydrogen-bonded OH *vs*. free OH abruptly increased at the sol-gel phase-transition concentration. Furthermore, the largest R value was observed for **2**, which also features the greatest gelation ability. In contrast, the peak arising from hydrogen-bonded OH groups was hardly observed for **3** up to 0.5 wt%, indicating that **3** is too soluble to use as a good gelator. These FT-IR spectral data consistently indicate that the gel network in the present system is primarily constructed by intermolecular hydrogen-bonding interactions. A computational study (MOPAC 93 included in CS CHEM3D) indicated that the

Table 1 Organic fluids tested for gelation by **1**–**3**[a]

Organic fluid	**1**	**2**	**3**
n-Hexane	SG	SG	SG
n-Heptane	P	SG	SG
n-Octane	SG	SG	SG
Cyclohexane	P	SG	SG
Methylcyclohexane	SG	SG	SG
Benzene	G	SG	P
Toluene	SG	SG	SG
p-Xylene	SG	SG	SG
CCl_4	SG	SG	P
CS_2	P	SG	SG
Et_2O	G	SG	P
Ph_2O	SG	SG	G
n-Octanol	S	G	S
Et_3N	S	G	S
Et_3SiH	P	Gp	SG
$(EtO)_4Si$	P	SG	P
H_2O	P	S	G

[a] G = gel; SG = supergel; Gp = partial gel; P = precipitation; S = solution.

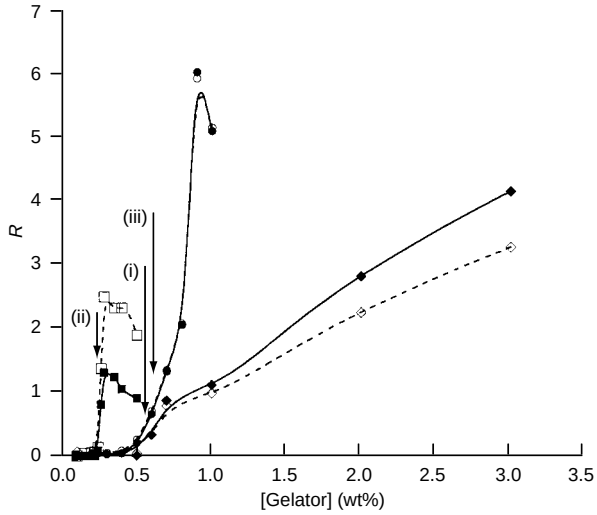

Fig. 1 Plot of the peak intensity ratio (R) of hydrogen-bonded OH groups *vs.* free OH groups as a function of [gelator] in toluene at 20 °C. There are two major peaks for hydrogen-bonded OH groups: the filled points were obtained from the intensities at ν_{OH} 3312–3240 cm^{-1}, whereas the open points are obtained from those at ν_{OH} 3473–3350 cm^{-1}; (○,●) **1**, (□,■) **2** and (◇,◆) **3**. The arrows indicate the sol-gel transition temperatures of (i) **1**, (ii), **2** and (iii) **3**.

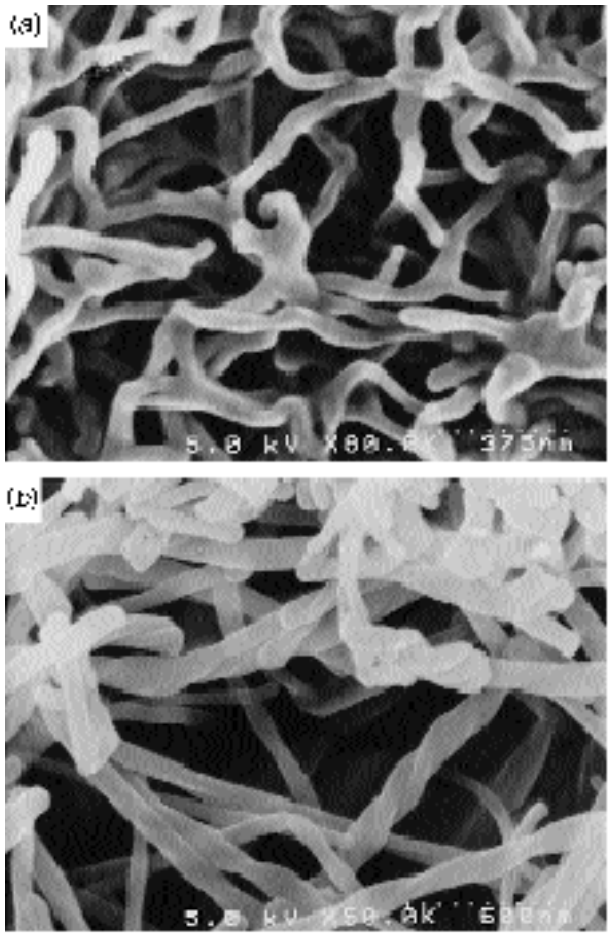

Fig. 2 SEM pictures of (*a*) the **1**/CCl_4 system and (*b*) the **3**/water system

intramolecular hydrogen-bonding distance (H···O) between 3-OH and 4-OR of the saccharides is not significantly different (*e.g.* 2.5 Å for **1** and 2.38 Å for **2**). This suggests that the differences in gelation ability are not due to the presence of a special OH group useful for intermolecular hydrogen-bonding, but rather is due to a structural preference in the molecular aggregation. We now consider that **2**, which has the benzylidene group and the pyranose ring arranged at almost a right angle, is able to enjoy both a benzene–benzene π–π stacking interaction and an OH–OH intermolecular hydrogen bonding interaction, whereas **1** and **3**, which are flatter than **2**, cannot enjoy both interactions simultaneously.

To obtain visual insights into the aggregation mode, we prepared a dry sample for SEM studies.[15] Fig. 2(*a*) shows a typical picture obtained from the xerogels of **1** or **2**. It is clear that the gelator forms a three-dimensional network with 50–200 nm frizzled fibrils. On the other hand, the fibrils obtained from the toluene gel of **3** are more linear (the picture is not shown here). Very interestingly, the fibrils obtained from the aqueous gel of **3** show a regular left-handed helical structure [Fig. 2(*b*)]. Presumably, in an aqueous system the balance between the hydrogen-bonding interaction and the hydrophobic interaction is different from that in other, organic media.

In conclusion, the present study has demonstrated for the first time that saccharides are promising building-blocks for new gelators with different gelation abilities and different three-dimensional network structures. We believe that such versatility of synthesis and diversity of products (including the creation of the helical structure) cannot be attained in a more simple fashion than with saccharides as building-blocks.

Notes and References

† E-mail: seijitcm@mbox.nc.kyushu-u.ac.jp

1 K. Hanabusa, K. Okui, K. Karaki, T. Koyama and H. Shirai, *J. Chem. Soc., Chem. Commun.*, 1992, 1371 and references cited therein; K. Hanabusa, M. Yamada, M. Kimura and H. Shirai, *Angew. Chem., Int. Ed. Engl.*, 1996, **35**, 1949; K. Hanabusa, K. Shimura, K. Hirose, M. Kimura and H. Shirai, *Chem. Lett.*, 1996, 885; K. Hanabusa, A. Kawakami, M. Kimura and H. Shirai, *Chem. Lett.*, 1997, 191.
2 E. J. de Vries and R. M. Kellogg, *J. Chem. Soc., Chem. Commun.*, 1993, 238.
3 M. Takafuki, H. Ihara, C. Hirayama, H. Hachisako and K. Yamada, *Liq. Cryst.*, 1995, **18**, 97.
4 J.-E. S. Sobna and F. Fages, *Chem. Commun.*, 1997, 327.
5 E. Otsumi, P. Kamaras and R. G. Weiss, *Angew. Chem., Int. Ed. Engl.*, 1996, **35**, 1324 and references cited therein.
6 P. Terech, I. Furman and R. G. Weiss, *J. Phys. Chem.*, 1995, **99**, 9558 and references cited therein.
7 K. Murata, M. Aoki, T. Suzuki, T. Hanada, H. Kawabata, T. Komori, F. Ohseto, K. Ueda and S. Shinkai, *J. Am. Chem. Soc.*, 1994, **116**, 6664 and references cited therein.
8 T. D. James, K. Murata, T. Harada, K. Ueda and S. Shinkai, *Chem. Lett.*, 1994, 273.
9 S. W. Jeong, K. Murata and S. Shinkai, *Supramol. Sci.*, 1996, **3**, 83.
10 T. Brotin, R. Utermöhlen, F. Fagles, H. Bouas-Laurent and J.-P. Desvergne, *J. Chem. Soc., Chem. Commun.*, 1991, 416.
11 J. van Esch, S. De Feyter, R. M. Kellogg, F. De Schryver and B. L. Feringa, *Chem. Eur. J.*, 1997, **3**, 1238.
12 S. Yamasaki and H. Tsutsumi, *Bull. Chem. Soc. Jpn.*, 1996, **69**, 561 and references cited therein.
13 M. Svaan and T. Anthonsen, *Acta Chem. Scand.*, 1986, **B40**, 119.
14 The following solvents were also tested, but **1**–**3** were soluble in these solvents and gels were not formed: nitrobenzene, *m*-cresol, 1,2-dichloroethane, CH_2Cl_2, $CHCl_3$, THF, dioxane, MeOAc, diethyl malonate, acetone, ethyl methyl ketone, DMA, DMF, DMSO, NMP, MeCN, MeOH, EtOH, BnOH, AcOH, Ac_2O, $PrNH_2$, Et_2NH, $PhNH_2$, pyridine, 2,2,2-trifluoroethanol and glycerol.
15 For the preparation of dry samples for SEM observations, see ref. 7 and S. W. Jeong and S. Shinkai, *Nanotechnology*, 1997, **8**, 179.

Received in Cambridge, UK, 30th January 1998; 8/00825F

Conjugated porphyrin oligomers from monomer to hexamer

Peter N. Taylor,[a] Juhani Huuskonen,[a] Garry Rumbles,[b] Robin T. Aplin,[a] Erik Williams[c] and Harry L. Anderson*[a]

[a] *Department of Chemistry, University of Oxford, Dyson Perrins Laboratory, South Parks Road, Oxford, UK OX1 3QY*
[b] *Department of Chemistry, Imperial College of Science, Technology and Medicine, London, UK SW7 2AY*
[c] *Micromass UK Ltd., Floats Road, Wythenshawe, Manchester, UK M23 9LZ*

A series of conjugated porphyrin oligomers have been prepared and the evolution in their electronic properties is discussed; the crystal structure of the dimer is presented, as well as the MALDI TOF mass spectrum of the hexamer.

Conjugated organic polymers are interesting because of their versatile opto-electronic properties and processability.[1] Recently many groups have focused on the synthesis of homologous series of precisely defined conjugated oligomers because the evolution in electronic properties with chain-length reveals the extent of π-conjugation.[2] Pure monodisperse oligomers also have the advantage that they can be characterised more fully, *e.g.* by single crystal X-ray diffraction, than polydisperse materials. Here we present the synthesis and electronic spectra of a series of conjugated porphyrin oligomers from monomer to hexamer, as well as the crystal structure of the dimer.

Many types of aromatic units have been used to synthesise conjugated polymers. The polarisability, optical oscillator strength and extensive coordination chemistry of the porphyrin macrocycle make it an ideal unit from which to build low band-gap materials. Most porphyrin oligomers are not conjugated because non-planarity leads to poor π-overlap, for example in *meso*-aryl porphyrins there is generally a twist of about 70° between the plane of the aryl ring and that of the porphyrin. Two strategies have been devised to overcome this problem: conjugated porphyrin oligomers have been synthesised by linking porphyrins with edge-fused aromatic units[3] or by linking them with acetylenes[4–7] (as the acetylene is linear it cannot twist out of conjugation with the porphyrin). The first soluble conjugated porphyrin polymer to be prepared had *iso*decylpropanoate sidechains[5b] which provide excellent solubility, but make short oligomers difficult to purify and have undesirable reactivity towards nucleophiles. In this work we chose to study oligomers derived from 5,15-bis(3,5-di-*tert*-butylphenyl)-10,20-bis(trihexylsilylethynyl)porphyrin **1a** because of their greater accessibility, stability and crystallinity.[8]

A stepwise approach was used to synthesise oligomers **1b**–**f** from the monomer **1a**, using just two reactions: (i) protodesilylation with TBAF and (ii) Glaser–Hay coupling with CuCl·TMEDA in CH_2Cl_2 under air.[5] The trihexylsilyl end-group was chosen because it facilitates chromatographic separation of unprotected, mono-protected and bis-protected oligomers generated by partial protodesilylation. Like all other types of conjugated oligomers, the solubility of these compounds decreases with increasing chain length; all the oligomers were characterised by ^{1}H NMR spectroscopy, but only the monomer, dimer, trimer and tetramer are soluble enough for ^{13}C NMR analysis. Attempts to prepare the octamer of this series, by coupling mono-protected tetramers, gave a totally insoluble material. FAB mass spectrometry does not work well with these compounds; a weak molecular ion peak was observed for the monomer, but no signals could be obtained for any of the oligomers. Fortunately, reflectron MALDI TOF MS using a anthracene-1,8,9-triol matrix, gave excellent spectra for all five oligomers, with the expected $M^{+\cdot}$ signals as the dominant species in each spectrum. Isotope resolved spectra were

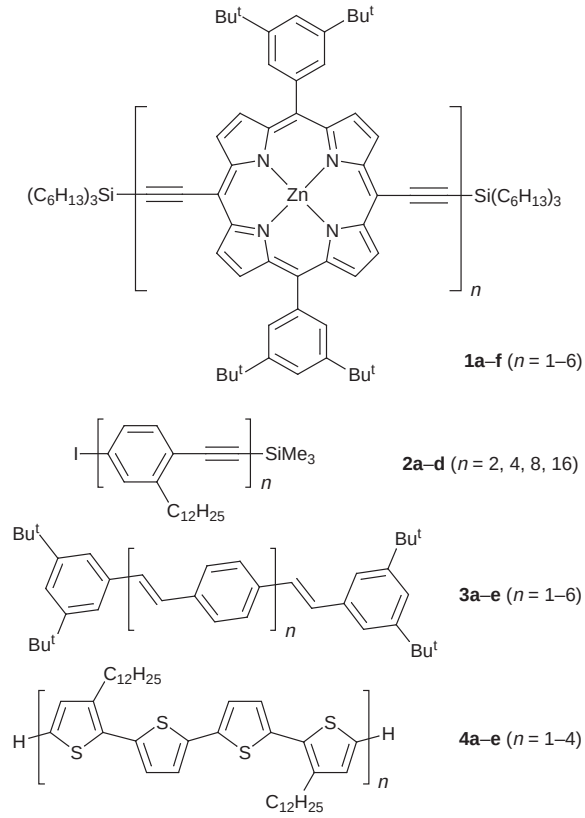

obtained for **1b**–**f** by tuning the time-lag focusing pulse voltage for each sample.[9] The observed and calculated isotopomer patterns for the hexamer **1f** are shown in Fig. 1. The crystal structure of the dimer **1b**,‡ illustrated in Fig. 2, shows that the entire 56-atom π-system is remarkably planar (to ±0.391 Å). The torsional angle between the porphyrins is zero in the solid

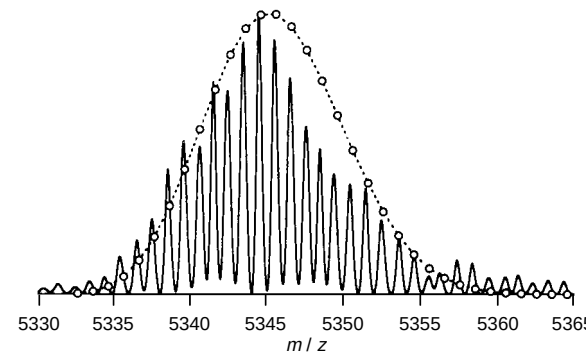

Fig. 1 Reflectron MALDI TOF mass spectrum of **1f**, using an anthracane-1,8,9-triol matrix. The calculated isotopomer pattern for $C_{348}H_{378}N_{24}Si_2Zn_6$ is marked by circles.

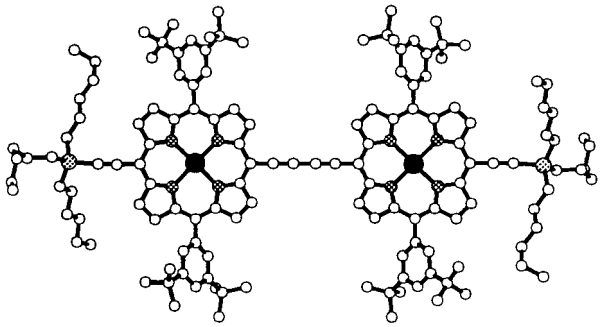

Fig. 2 Molecular structure of the dimer **1b** (pyridine ligands omitted for clarity). The bond lengths in the central butadiyne unit are 1.429(4) (*meso*-C–C), 1.210(4) (C≡C) and 1.368(5) Å (central C–C).

state, due to a crystallographic inversion centre at the centre of the molecule, although rotation about the butadiyne link may occur freely in solution. The crystal structures of several *meso*-ethynyl porphyrins have been reported,[4b,10] but this is the first structure of a *meso*-butadiyne-linked porphyrin dimer.

The electronic absorption spectra of **1a**–**f** in 1% pyridine–CH_2Cl_2 are shown in Fig. 3. As expected, the Q-band is red-shifted and intensified with increasing chain-length. A similar trend is seen in the fluorescence spectra; compounds **1a**–**f** each give a single emission peak at 650, 749, 810, 830, 850 and 858 nm respectively.§ Estimates for the optical HOMO–LUMO energy gap E_g were obtained from these fluorescence maxima, and also from the centres of gravity of the Q absorption bands. The values of E_g are plotted against reciprocal chain-length ($1/L$, where L is the length of the π-system in Å) in Fig. 4. The curves are linear, particularly for the longer oligomers, with no sign of saturation. The intercept at $L = \infty$ gives a predicted band gap for the polymer of 1.55 eV from absorption and 1.34 eV from emission; the absorption maximum of the *iso*decylpropanoate-substituted polymer in the same solvent is at 1.42 eV.[5b] We chose to plot reciprocal chain length, $1/L$, rather than $1/N$, where N is the degree of polymerisation, to facilitate comparison with other conjugated polymers. Fig. 4 includes data for oligomers of poly(*p*-phenyleneethynylene) **2a**–**d**,[2b] poly(*p*-phenylenevinylene) **3a**–**e**[2c] and poly(α-thiophene) **4a**–**d**.[2d] The gradient of these curves is a measure of the π-conjugation efficiency between neighbouring units. We conclude that the poly(porphyrinbutadiynylene) system (**1a**–**f**) has a similar conjugation efficiency to other, more conventional, conjugated polymers and yet it reaches a lower limiting π–π* gap because the porphyrin monomer unit starts at a lower HOMO–LUMO separation.

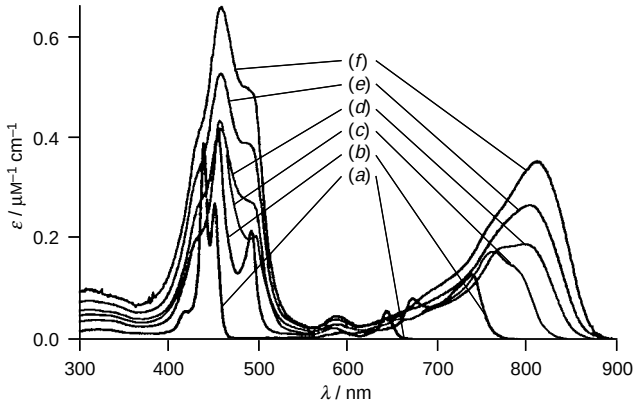

Fig. 3 Electronic absorption spectra of **1a**–**f** in 1% C_5H_5N–CH_2Cl_2: (*a*) **1a**, (*b*) **1b**, (*c*) **1c**, (*d*) **1d**, (*e*) **1e** and (*f*) **1f**

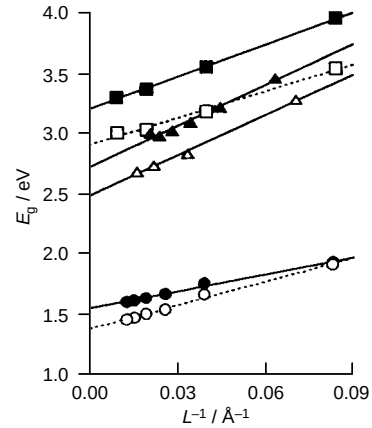

Fig. 4 Plot of optical band gap energy E_g against reciprocal chain length $1/L$ for (●) **1a**–**f** (absorption), (○) **1a**–**f** (emission), (■) **2a**–**d** (absorption), (□) **2a**–**d** (emission), (△) **3a**–**e** (absorption) and (▲) **4a**–**e** (absorption)

We thank the EPSRC (Polymer Synthesis Initiative), the Finnish Academy and the Emil Aaltonen Foundation for financial support, and the EPSRC mass spectrometry service (Swansea) for FAB mass spectra. Crystallographic work was done at Chemical Crystallography, University of Oxford, with generous assistance from Dr D. J. Watkin. We are grateful to Julia A. Elliott and Philip D. Siverns (Imperial College, London) for recording emission spectra.

Notes and References

† E-mail: harry.anderson@chem.ox.ac.uk

‡ *Crystal data* for **1b**·$2C_5H_5N$: monoclinic, space group $P2_1/n$ (no. 14), a = 14.299(3), b = 29.955(8), c = 16.232(4) Å, β = 105.07(2)°, U = 6714(3) Å^3, Z = 2, μ = 1.009 mm^{-1}, D_c = 1.147 g cm^{-3}, T = 180(2) K, $R(F^2)$ = 0.0617, $R_w(F^2)$ = 0.1784 for 11662 reflections with $I > 2\sigma(I)$. CCDC 182/798.

§ Near-IR emission spectra were measured both using a CCD camera and an S1-photocathode photomultiplier tube.

1 W. J. Feast, J. Tsibouklis, K. L. Pouwer, L. Groenendaal and E. W. Meijer, *Polymer*, 1996, **37**, 5017.
2 (*a*) J. M. Tour, *Chem. Rev.*, 1996, **96**, 537; (*b*) L. Jones, J. S. Schumm and J. M. Tour, *J. Org. Chem.*, 1997, **62**, 1388; (*c*) R. Schenk, H. Gregorious, K. Meerholz, J. Heinze and K. Müllen, *J. Am. Chem. Soc.*, 1991, **113**, 2634; (*d*) P. Bäuerle, T. Fischer, B. Bidlingmeir, A. Stabel and J. P. Rabe, *Angew. Chem., Int. Ed. Engl.*, 1995, **34**, 303; (*e*) R. E. Martin, U. Gubler, C. Boudon, V. Gramlich, C. Bosshard, J.-P. Gisselbrecht, P. Günter, M. Gross and F. Diederich, *Chem. Eur. J.*, 1997, **3**, 1505.
3 M. J. Crossley and P. L. Burn, *J. Chem. Soc., Chem. Commun.*, 1991, 1569.
4 (*a*) D. P. Arnold and D. A. James, *J. Org. Chem.*, 1997, **62**, 3460; (*b*) D. P. Arnold, D. A. James, C. H. L. Kennard and G. Smith, *J. Chem. Soc., Chem. Commun.*, 1994, 2131.
5 (*a*) H. L. Anderson, *Inorg. Chem.*, 1994, **33**, 972; (*b*) H. L. Anderson, S. J. Martin and D. D. C. Bradley, *Angew. Chem., Int. Ed. Engl.*, 1994, **33**, 655.
6 V. S.-Y. Lin and M. J. Therien, *Chem. Eur. J.*, 1995, **1**, 645; V. S.-Y. Lin, S. G. DiMagno and M. J. Therien, *Science*, 1994, **264**, 1105.
7 B. Jiang, S. W. Yang, D. C. Barbini and W. E. Jones Jr, *Chem. Commun.*, 1998, 213.
8 G. S. Wilson and H. L. Anderson, *Synlett.*, 1996, 1039.
9 R. D. Edmondson and D. H. Russell, *J. Am. Soc. Mass. Spectrom.*, 1996, **7**, 995; W. C. Wiley and I. H. McLaren, *Rev. Sci. Instrum.*, 1955, **26**, 1150.
10 S. M. LeCours, S. G. DiMagno and M. J. Therien, *J. Am. Chem. Soc.*, 1996, **118**, 11 854.

Received in Liverpool, UK, 4th February 1998; 8/01031E

Driving crystal construction *via* stoichiometry: π–π stacks in squaric acid organometallic salts

Dario Braga*† and Fabrizia Grepioni*‡

Dipartimento di Chimica G. Ciamician, Università di Bologna, Via Selmi 2, 40126 Bologna, Italy

Depending on the stoichiometric ratio, squaric acid (H_2SQA) reacts with $[Co(\eta^5\text{-}C_5H_5)_2][OH]$ to form crystalline materials based on anion–cation π–π stacks and/or squarate ion ribbons held together by O–H···O hydrogen bonds between squarate anions and by charge-assisted $C–H^{\delta+}\cdots O^{\delta-}$ hydrogen bonds between organometallic and organic components.

Organometallic crystal engineering is an almost uncharted territory. Work in this field promises a great deal of new discoveries because of the possibility of combining physical and chemical features of organic and organometallic molecules and ions in the solid state.[1] This may lead to the isolation of materials with novel conducting, magnetic or optoelectronic properties.

We have demonstrated that a great variety of new architectures can be obtained by combining organic moieties held together by strong O–H···O hydrogen bonds with non coordinating organometallic cations, such as $[Co(\eta^5\text{-}C_5H_5)_2]^+$ and $[Cr(\eta^6\text{-}C_6H_6)_2]^+$.[2] Chiral organic frameworks have also been obtained when enantiomerically pure chiral acids, such as L-tartaric and L-bisbenzoyltartaric acids have been used.[3]

We are now able to report that the reaction of the hydroxide $[Co(\eta^5\text{-}C_5H_5)_2][OH]$ with squaric acid (3,4-dihydroxy cyclobut-3-ene-1,2-dione, H_2SQA) in water (or THF) yields two different crystalline materials, namely $[Co(\eta^5\text{-}C_5H_5)_2]^+$-$[(HSQA)]^-$ **1** and $[Co(\eta^5\text{-}C_5H_5)_2]^+[(HSQA)(H_2SQA)]^-$ **2**, depending on the stoichiometric ratio between cobaltocenium hydroxide and squaric acid.§ The different stoichiometry is associated with a dramatic change in crystal structure, which is also reflected in a different colour of the crystalline materials. Squaric acid has been widely investigated for its electronic and physical properties.[4]

When the stoichiometric ratio between cobaltocenium hydroxide and squaric acid is 1 : 1, crystalline **1** is obtained. Contrary to what is usually observed with cobaltocenium salts, which are yellow, crystals of **1** are orange. Indeed, the structure of **1** presents some unique features that may account for this physical difference. The crystal is constituted of ribbons of $[(HSQA)]^-$ monoanions (Scheme 1) bonded *via* negatively charged O–H···O hydrogen bonds [O···O 2.446 Å] and of ribbons of cobaltocenium cations, Fig. 1. The 1 : 1 stoichiometry, combined with a good matching in size and shape between the cyclopentadienyl ligands and the $[(HSQA)]^-$ ions, leads to a superstructure in which the hydrogen bonded squarate ribbons intercalate between cobaltocenium cations (Fig. 1). The π–π distance is *ca*. 3.35 Å. The oxygen atoms form the outer rims of the $\{[(HSQA)]^-\}_n$ ribbons and interact with the $[Co(\eta^5\text{-}C_5H_5)_2]^+$ cations on both sides *via* charge assisted $C–H^{\delta+}\cdots O^{\delta-}$ hydrogen bonds (five H···O distances in the range 2.272–2.500 Å). What is more, the packing arrangement is chiral in space group $P2_1$. The unusual orange colour suggests formation of a charge transfer complex and prompts for further investigations in due course.[5]

On changing the stoichiometry to 1 : 2, the yellow crystalline **2** is obtained. It is constituted of supramolecular monoanions $[(HSQA)(H_2SQA)]^-$ resulting from the loss of one proton every two squaric acid molecules and arranged in ribbons bonded *via* negatively charged O–H···O hydrogen bonds (O···O 2.440, 2.436 Å).[6] The bonding within the superanions is provided by

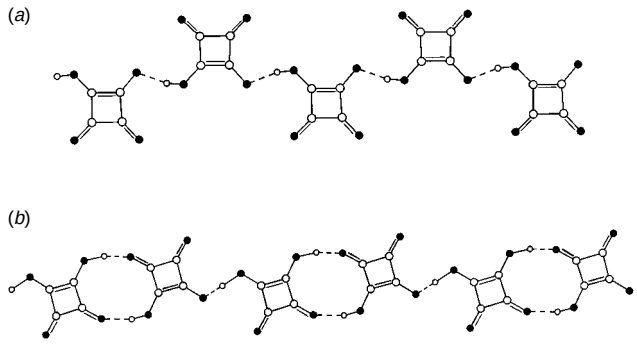

Scheme 1 (*a*) The $\{[(HSQA)]^-\}_n$ ribbon in crystalline **1** and (*b*) the $\{[(HSQA)(H_2SQA)]^-\}_n$ ribbon in crystalline **2**

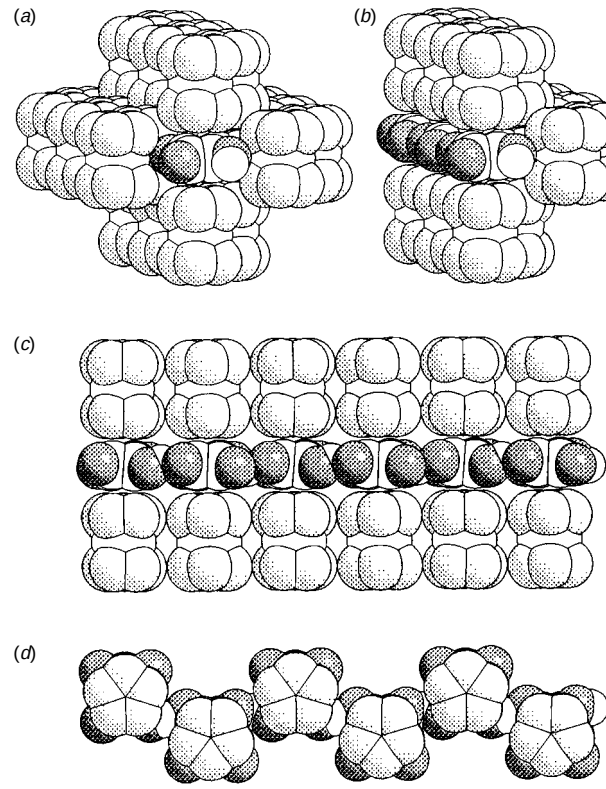

Fig. 1 'Dissection' of the packing arrangement in crystalline **1**: space filling representation of the $\{[(HSQA)]^-\}_n$ ribbon encapsulated within four (*a*), three (*b*) and two (*c*) rows of $[Co(\eta^5\text{-}C_5H_5)_2]^+$ cations. Note the good match in size and shape of the squaric acid moieties and of the cyclopentadienyl ligands (*d*). H atoms of the cations omitted for clarity. Relevant hydrogen bonding parameters (in Å, C–H···O < 2.5 Å): $O^-\cdots Q_{OH}$ 2.446; $C–H_{Cp}\cdots O$ 2.272, 2.339, 2.455, 2.455, 2.467.¶

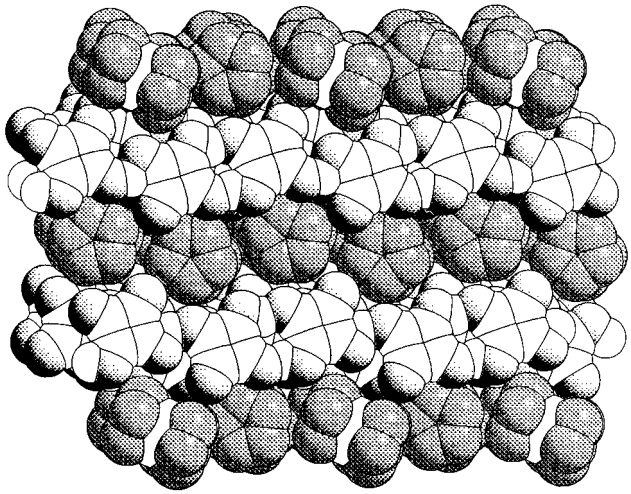

Fig. 2 Space filling representation of the stacking sequence of $\{[Co(\eta^5\text{-}C_5H_5)_2]^+\}_n/\{[(HSQA)(H_2SQA)]^-\}_n$ in crystalline **2**. H atoms of the cations omitted for clarity. Relevant hydrogen bonding parameters (in Å, C–H···O < 2.5 Å): $O_{OH}\cdots O_{CO}$ 2.550, 2.550, 2.574, 2.539; $O^-\cdots O_{OH}$ 2.436, 2.440; $C\text{–}H_{Cp}\cdots O$ 2.192, 2.213, 2.314, 2.328, 2.343, 2.401, 2.407, 2.408, 2.414, 2.437, 2.453, 2.465, 2.499, 2.500.¶

O–H···O hydrogen bonds, with formation of ten-membered ring systems (O···O distances in the range 2.539–2.574 Å) reminiscent of the carboxylic rings (Scheme 1). The ribbons are stacked in such a way that squarate moieties overlap hydrogen bonded rings, resulting in layers with oxygen atoms protruding above and below the layer surface. The cobaltocenium cations lie side-on the layer and interact *via* charge-assisted $C\text{–}H^{\delta+}\cdots O^{\delta-}$ hydrogen bonds (14 distances in the range 2.191–2.500 Å). Hence crystalline **2** can be described as a stacking sequence $\{[Co(\eta^5\text{-}C_5H_5)_2]^+\}_n/\{[(HSQA)(H_2SQA)]^-\}_n$ along the *c*-axis in the $P\bar{1}$ crystal (Fig. 2).

$C\text{–}H^{\delta+}\cdots O^{\delta}$ distances in both **1** and **2** fall towards the lower limit for interactions of this type, clearly indicating that the electrostatic interaction is reinforced by the difference in charge between organic anionic ribbons and organometallic cations.[7]

We have previously shown that self-aggregation of organic molecules into robust supramolecular frameworks can be controlled by reacting common organic acids with metallocene or metalloarene hydroxides. Since the organometallic cations possess only C–H donors they do not compete in the formation of strong hydrogen bonds. We have now shown that the same strategy can be used to obtain different structures starting from the same acid by changing the stoichiometry ratio. Though simple it may appear, this allows us to control the number of strong hydrogen bonding donor and acceptor sites, therefore the resulting crystal architectures. Analogous reactions involving the bis-benzene chromium cation are under investigation.

The help of Elise Champeil (visiting Erasmus student) and of the students attending the 1997/98 Inorganic Chemistry Laboratory Course is gratefully acknowledged. Financial support by MURST and by the University of Bologna (projects: Intelligent Molecules and Molecular Aggregates 1995–1997, and Innovative Materials, 1997–1999) is acknowledged.

Notes and References

† E-mail: dbraga@ciam.unibo.it
‡ E-mail: grepioni@ciam.unibo.it

§ Brown powder of $[Co(C_5H_5)_2]$ (4.73 mg, 0.025 mmol) was added to 10 ml of bidistilled water at room temperature. Oxygen was bubbled to completely oxidize cobaltocene to bright yellow $[Co(C_5H_5)_2]^+$. The resulting solution of $[Co(C_5H_5)_2][OH]$ is strongly basic (pH > 10). White powder of squaric acid (2.8 mg, 0.025 mmol for **1**, 5.6 mg, 0.050 mmol for **2**) was then added. **1** and **2** were crystallized by evaporation at room temperature in the air. The same materials can be obtained by oxidizing cobaltocene in THF at room temperature in the presence of the appropriate stoichiometric amount of solid squaric acid. The reaction in THF very likely proceeds *via* formation of the peroxide anion ($CoCp_2 + O_2 \rightarrow CoCp_2^+ + O_2^{\cdot-}$) which deprotonates the acid as in the case of the reaction between $[Cr(C_6H_6)_2]$ and cyclohexane-1,3-dione.[2] Compounds **1** and **2** separate out as orange and yellow solids, respectively, which are filtered and dissolved in a minimum quantity of water for recrystallization.

¶ *Crystal data*: $[Co(\eta^5\text{-}C_5H_5)_2]^+[HSQA]^-$ **1**: $C_{14}H_{11}CoO_4$, T = 150(2) K, M = 302.16, monoclinic, space group $P2_1$, a = 7.368(3), b = 11.017(6), c = 7.368(2) Å, β = 94.66(2), U = 596.1(4) Å^3, Z = 2, D_c = 1.683 g cm^{-3}, $F(000)$ = 308, μ = 1.445 mm^{-1}, θ-range 3.0–28°, 1626 reflections measured, 1512 of which independent, refinement on F^2 for 154 parameters, wR (F^2, all reflections) = 0.1624, R_1 [1196 reflections with $I > 2\sigma(I)$] = 0.0402. $[Co(\eta^5\text{-}C_5H_5)_2]^+[(HSQA)(H_2SQA)]^-$ **2**: $C_{18}H_{13}CoO_8$, T = 223(2) K, M = 416.21, triclinic, space group $P\bar{1}$, a = 6.732(3), b = 11.582(11), c = 21.033(7) Å, α = 92.99(6), β = 92.43(3), γ = 96.34(6)°, U = 1626(2) Å^3, Z = 4, D_c = 1.700 g cm^{-3}, $F(000)$ = 848, μ = 1.103 mm^{-1}, θ-range 3.0–25°, 6315 reflections measured, 4984 of which independent, refinement on F^2 for 454 parameters, wR (F^2, all reflections) = 0.2092, R_1 [3229 reflections with $I > 2\sigma(I)$] = 0.0662. Three cobaltocenium cations were found, one in general position and two lying on two independent inversion centres, while two squaric acid and two squarate moieties were found in general positions. Common to both compounds: Mo-Kα radiation, λ = 0.710 69 Å, monochromator graphite, ψ-scan absorption correction. All non-H atoms were refined anisotropically. (O)H atoms directly located from Fourier maps and not refined. H atoms bound to C atoms were added in calculated positions. The computer programs SHELX86[8a] and SHELXL92[8b] were used for structure solution and refinement. The computer program SCHAKAL92 was used for all graphical representations.[8c] In order to evaluate the C–H···O bonds the C–H distances were normalized to the neutron derived value of 1.08 Å and the program PLATON was used.[8d] CCDC 182/808.

1 D. Braga and F. Grepioni, *Chem. Commun.*, 1996, 571; *Coord. Chem. Rev.*, in press; D. Braga, F. Grepioni and G. R. Desiraju, *Chem. Rev.*, in press.
2 D. Braga, F. Grepioni, J. J. Byrne and A. Wolf, *J. Chem. Soc., Chem. Commun.*, 1995, 1023; D. Braga, A. Angeloni, F. Grepioni and E. Tagliavini, *Chem. Commun.*, 1997, 1447.
3 D. Braga, A. L. Costa, F. Grepioni, L. Scaccianoce and E. Tagliavini, *Organometallics*, 1996, **15**, 1084; D. Braga, A. Angeloni, F. Grepioni and E. Tagliavini, *Organometallics*, 1997, **16**, 5478.
4 Some neutron studies: Y. Wang, G. D. Stucky and J. M. Williams, *J. Chem. Soc., Perkin Trans. 2*, 1974, **35**; D. Semmigsen, F. J. Hollander and T. F. Koetzle, *J. Chem. Phys.*, 1977, **66**, 4405; D. Semmigsen, Z. Tun, J. Nelmes, R. K. McMullan and T. F. Koetzle, *Z. Crystallogr.*, 1995, **210**, 934 and references therein.
5 Most charge transfer complexes of substituted metallocenes or metalloarene complexes so far obtained have been prepared by ion exchange or electrocrystallization. See, for example: J. S. Miller, M. D. Ward, J. H. Zhang and W. M. Reiff, *Inorg. Chem.*, 1990, **29**, 4063; M. D. Ward, *Organometallics*, 1987, **6**, 754; M. D. Ward and J. C. Calabrese, *Organometallics*, 1989, **8**, 593.
6 M. Meot-Ner (Mautner), *J. Am. Chem. Soc.*, 1984, **106**, 1257; M. Meot-Ner (Mautner) and L. W. Sieck, *J. Am. Chem. Soc.*, 1986, **108**, 7525.
7 G. R. Desiraju, *Acc. Chem. Res.*, 1996, **29**, 441; T. Steiner, *Cryst. Rev.*, 1996, **6**, 1.
8 (*a*) G. M. Sheldrick, *Acta Crystallogr., Sect. A*, 1990, **46**, 467; (*b*) G. M. Sheldrick, SHELXL92, *Program for Crystal Structure Determination*, University of Göttingen, Göttingen, Germany, 1992; (*c*) E. Keller, SCHAKAL92 *Graphical Representation of Molecular Models*, University of Freiburg, Germany, 1992; (*d*) A. L. Spek, *Acta Crystallogr., Sect. A*, 1990, **46**, C31.

Received in Basel, Switzerland, 24th November 1997; 7/08438B

New cluster condensation modes in early transition metal thiophosphates: synthesis, structure and properties of $CsTa_4P_3S_{19}$, a novel layered material

Volkmar Derstroff and Wolfgang Tremel*†

Institut für Anorganische Chemie und Analytische Chemie, Universität Mainz, Becherweg 24, D-55099 Mainz, Germany

The new layer compound $CsTa_4S_5(S_2)(PS_4)_3$ was synthesized by the reaction of Ta metal in polythiophosphate melts. Its structure is based on $Ta_4S_5(S_2)$ clusters which are condensed by PS_4^{3-} groups.

In the past 20 years, lamellar transition metal chalcogenophosphates have been studied extensively because of their potential as cathodic materials and their intriguing structural, chemical and physical properties.[1–3] Among the group 5 derivatives, the structural dimensionality can vary from one- to three-dimensional as exemplified by V_2PS_{10},[4] Nb_2PS_{10}[5] and $Ta_4P_4S_{29}$.[6] This can be attributed to the variability in the metal coordination for the group 5 metals as well as the fascinating flexibility in the coordination of the chalcogen ligands.[7] The structures of typical group 5 thiophosphates are based on bicapped M_2S_{12} biprismatic units with a metal–metal bond inside. These biprisms are bonded together to form infinite M_2S_9 chains. In contrast to the 3d transition metal thiophosphates of the MPS_3 series, no intercalation behavior has been reported for group 5 thiophosphates.[8] This is surprising in view of their low-dimensional structures, but may be due to the fact that the complex host structures are not stable during the intercalation process.

In the quest for new intercalated early transition metal thiophosphates we have investigated reactions in $M–P_2Q_5–A_2Q–Q$ melts (M = Nb, Ta; Q = S, Se; A = alkali metal). The most significant results of these studies are that (*i*) a 'quasi-topotactic' cation insertion in porous host structures may be achieved[9] and (*ii*) that low-dimensional compounds with structures that exhibit novel unexpected cluster condensation modes can be obtained from reactions in thiophosphate melts as demonstrated by the first quaternary tantalum thiophosphate $CsTa_4(S_2)S_5(PS_4)_3$ whose synthesis, structure, and properties are reported here.

Single phase samples of the title compound were prepared by reacting the starting materials Ta, P_2S_5, Cs_2S and S in a 8 : 3 : 1 : 11 ratio at 600 °C.‡ The product was isolated in yields > 85% based on Ta. The crystal structure§ of this compound was determined by single-crystal X-ray diffraction. A view of a single anionic layer and the unit cell of $CsTa_4P_3S_{19}$ is given in Fig. 1(*a*). The Cs^+ cations are situated between the layers. The characteristic structural feature is a $(S_4P)_2TaS_2(S_4P)$-$TaS(S_2)Ta(PS_4)_2S_2Ta(PS_4)_2$ fragment with a $Ta_4S_5(S_2)$ core, which is shown in Fig. 1(*b*). The central Ta_2S_{11} unit is located on a crystallographic mirror plane; it is derived from the distorted bicapped biprismatic M_2Q_{12} units encountered in the structures of group 5 thiophosphates by replacing a bridging S_2^{2-} disulfide group by a S^{2-} anion. This leads to a seven-fold coordination for the central Ta atoms. The S–S distance of the S_2^{2-} pair is 2.046(10) Å, whereas the remaining S···S separations span the range from *ca.* 3.2 to 3.8 Å and must be considered non-bonding. Similarly, the Ta···Ta distance of 3.386(1) Å within the Ta_2S_{11} units is outside the metal–metal bonding range. The Ta_2S_{11} groups are not tied to each other through their own edges as is observed for Nb_2PS_{10},[5] but are interconnected by two each of their surrounding sulfur atoms through phosphorus atoms which are located at the center of adjacent tetrahedral PS_4 units and octahedrally coordinated tantalum atoms which share the remaining four S atoms of their coordination sphere with two adjacent PS_4 groups. Thus, each Ta_2S_{11} unit is fused in a *cis*-orientation with two PS_4 and two TaS_6 groups and may be viewed as a four-fold connecting element of the Ta–P–S network. The PS_4 groups act as chelating ligands for two adjacent tantalum atoms and serve as linear spacer units. The TaS_6 groups in turn are linked with two PS_4 groups and one Ta_2S_{11} unit. Thus, they act as centers with threefold connectivity. Combining these three structure elements in a 1 : 3 : 2 ratio {as indicated by the formulation $Cs[Ta_2S_5(S_2)Ta_2(PS_4)_3]$} leads to a network with two different hollows; the larger one (smallest diameter *ca.* 7 Å) takes up the

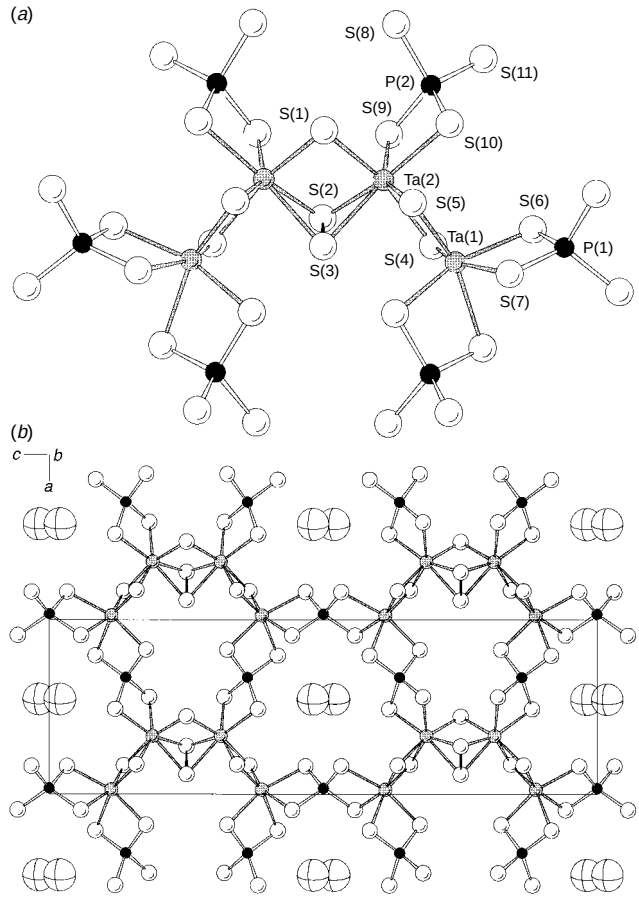

Fig. 1(*a*) Structure of the unit cell and a single $Ta_4P_4S_{19}$ layer (P, small black circles; Ta, large gray circles; S, large open circles) with Cs^+ cations above and below. (*b*) View of the central $(S_4P)_2TaS_2(S_4P)$-$TaS(S_2)Ta(PS_4)_2S_2Ta(PS_4)_2$ unit with atomic labeling scheme. Selected distances (Å): Ta(1)–Ta(2) 3.371(1), Ta(2)–Ta(2) 3.386(1), S(2)–S(3) 2.045(10), Ta(1)–S(4) 2.317(5), Ta(1)–S(5) 2.274(5), Ta(1)–S(6) 2.497(4), Ta(1)–S(7) 2.548(5), Ta(1)–S(8) 2.460(4), Ta(1)–S(11) 2.626(5), Ta(2)–S(1) 2.373(5), Ta(2)–S(3) 2.556(5), Ta(2)–S(4) 2.459(4), Ta(2)–S(5) 2.534(5), Ta(2)–S(9) 2.474(5), Ta(2)–S(10) 2.495(4), P(1)–S(7) 2.020(6), P(1)–S(6) 2.034(6), P(2)–S(11) 2.014(6), P(2)–S(10) 2.053(7), P(2)–S(8) 2.044(7), P(2)–S(9) 2.023(7).

Cs^+ cations whereas the smaller one (smallest diameter *ca.* 3 Å) remains empty.

The most significant structural feature of $CsTa_4P_3S_{19}$ that makes it unique compared to the known ternary group 5 thiophosphates is that the familiar bonding mode of a M_2Q_{11} or M_2Q_{12} cluster which is linked through its four outer coordination sites to four neighboring PS_4 groups is not observed and an additional structural motif, the TaS_6 group, is found instead. This may be caused by the size requirements of the counter cations which are located between layers or in channels of the anion framework. Since the TaS_6 fragment has a connectivity of three in these network structures, a more versatile structural chemistry may be envisaged.

The electronic structure of $CsTa_4P_3S_{19}$ may be approached in a zeroth order approximation by assigning formal charges according to $[Cs^+][(Ta^{5+})_4(S^{2-})_5(S_2^{2-})(PS_4^{3-})_3]$; the oxidation state of 5+ has been observed in other thiophosphates such as $Ta_4P_4S_{29}$;[6] this is in harmony with the observed non-bonding Ta···Ta distances; thus diamagnetic and semiconducting behavior are expected. Consequently, the optical spectrum of $CsTa_4P_3S_{19}$ (diffuse reflectance measurement) exhibits a sharp optical gap which is consistent with semiconducting behavior. The experimentally determined value is E_g = 1.65 eV.

From a synthetic point of view, $CsTa_4P_3S_{19}$ is the first group 5 compound that has been synthesized from a reactive chalcogenophosphate flux system.[11] Finally, the alkali ion-filled tunnels in the two-dimensional structure of $CsTa_4P_3S_{19}$, the three-dimensional structure of $CsNb_2P_2S_{12}$,[9] in which Cs^+ cations replace an isolated S_{10} ring from the $Ta_4P_4S_{29}$ structure,[6] as well as the observed ion conductivity in $LiTi_2(PS_4)_3$[12] suggest the possibility of ion exchange reactions.

This work was supported by the Deutsche Forschungsgemeinschaft and the Fonds der Chemischen Industrie. We are indebted to Heraeus Quarzschmelze Hanau (Dr. Höfer) for a generous gift of silica tubes.

Notes and References

† E-mail: tremel@indigotreml.chemie.uni-mainz.de

‡ Ta metal (Starck, 99.999%, 0.724 g, 4 mmol), P_2S_5 (Merck, 99.5%, 0.111 g, 1.5 mmol), Cs_2S (0.149 g, 0.125 mmol) and S (Aldrich, 99.99%, 0.176 g, 5.5 mmol) were sealed under vacuum (10^{-4} Torr) in a quartz tube, heated slowly to 200 °C and prereacted overnight. Subsequently the samples were heated to 600 °C at a rate of 1 °C min^{-1} and kept at this temperature for 7 days. Afterwards the samples were cooled to room temperature at a rate of 1 °C min^{-1}. The product can be separated from admixed polychalcogenides by washing with ethanol in *ca.* 85% yield. Sample homogeneity was checked by X-ray powder diffraction and electron microprobe analysis.

§ *Crystal data* for $CsTa_4P_3S_{19}$ at 25 °C: orthorhombic, space group *Pbcm* (no. 57), a = 8.637(2), b = 11.940(2), c = 27.202(5) Å, U = 2805.2(10) Å^3, Z = 4, λ = 0.710 73 Å, D_c = 3.691 g cm^{-3}, μ(Mo-Kα) = 18.411 mm^{-1}, crystal platelike, dimensions 0.1 × 0.15 × 0.15 mm, θ_{max} = 54°, data collected at 25° on a Nicolet $P2_1$ four circle diffractometer, 5794; unique data, 3081; data with $F_o^2 > 4\sigma(F_o^2)$, 2340; number of variables, 134. Structure solved and refined using SHELXS86 and SHELXL93, An empirical absorption correction based on ψ scans was applied to the data. Final R, R_w = 0.062, 0.134 (0.093, 0.147 for all data). CCDC 182/786.

1 R. Brec, *Solid State Ionics*, 1986, **22**, 3; *Progress in Intercalation Research*, ed. W. Müller-Warmuth and R. Schöllhorn, Kluwer Academic, 1995 and references therein.
2 G. A. Fatseas, M. Evain, G. Ouvard and M.-H. Whangbo, *Phys. Rev. B*, 1987, **35**, 3082; P. Colombet, G. Ouvrard, O. Antson and R. Brec, *J. Magn. Magn. Mater.*, 1987, **11**, 100; G. Ouvard, E. Prouzet, R. Brec, S. Benazeth and H. Dexpert, *J. Solid State Chem.*, 1990, **86**, 238; P. A. Joy and S. Vasudevan, *J. Am. Chem. Soc.*, 1992, **114**, 7792; P. A. Joy and S. Vasudevan, *Chem. Mater.*, 1993, **5**, 1182.
3 S. Lee, *J. Am. Chem. Soc.*, 1988, **110**, 8000 and references therein; V. Maisonneuve, V. B. Cajipe and C. Payen, *Chem. Mater.*, 1993, **5**, 758; A. Simon, J. Ravez, V. Maisonneuve, C. Payen and V. B. Cajipe, *Chem. Mater.*, 1994, **6**, 1575.
4 R. Brec, G. Ouvard, M. Evain, P. Grenouilleau and J. Rouxel, *J. Solid State Chem.*, 1983, **47**, 174.
5 R. Brec, P. Grenouilleau, M. Evain and J. Rouxel, *Rev. Chim. Miner.*, 1983, **20**, 295.
6 M. Evain, M. Queignec, R. Brec and J. Rouxel, *J. Solid State Chem.*, 1985, **56**, 148.
7 B. Krebs and G. Henkel, *Angew. Chem.*, 1991, **103**, 785; *Angew. Chem., Int. Ed. Engl.*, 1991, **30**, 769; L. C. Roof and J. C. Kolis, *Chem. Rev.*, 1993, **93**, 1037.
8 Interestingly, a quaternary niobium thiophosphate KNb_2PS_{10} has been prepared from eutectic NaCl–KCl fluxes: J. Do and H. Yun, *Inorg. Chem.*, 1996, **35**, 3729.
9 $CsNb_2(S_2)_2(PS_4)_2$, the first semimetallic thiophosphate[9] crystallizes with a 'stuffed' $TaPS_6$ structure:[10] V. Derstroff, G. Regelsky, H. Eckert and W. Tremel, in preparation.
10 S. Fiechter, W. F. Kuhs and R. Nitzsche, *Acta Crystallogr., Sect. B*, 1980, **36**, 2217; $Ta_4P_4S_{29}$, a derivative filled with an S_{10} ring, has been described by Rouxel and coworkers in ref. 6.
11 T. McCarthy and M. G. Kanatzidis, *Chem. Mater.*, 1993, **5**, 1061; T. McCarthy and M. G. Kanatzidis, *J. Chem. Soc., Chem. Commun.*, 1994, 1089; W. Tremel, H. Kleinke, C. Reisner and V. Derstroff, *J. Alloys Compd.*, 1995, **21**, 73.
12 V. Derstroff, G. Regelsky, H. Eckert and W. Tremel, to be published.

Received in Basel, Switzerland, 26th August 1997; revised manuscript received 31st January 1998; 8/01155I

A novel test system for *in situ* catalytic and electrochemical measurements on fuel processing anodes in working solid oxide fuel cells

Caine M. Finnerty, Robert H. Cunningham, Kevin Kendall and R. Mark Ormerod*†

Birchall Centre for Inorganic Chemistry and Materials Science, Department of Chemistry, Keele University, Keele, Staffordshire, UK ST5 5BG

A novel test system based around an extruded solid electrolyte tube enables the study of both the catalytic chemistry of fuel processing anodes in working solid oxide fuel cells and the electrochemical performance of the cell under the same conditions, allowing a direct correlation to be made between the fuel cell performance and the reforming characteristics of the anode.

Fuel cells are currently attracting a great deal of interest because they offer the possibility of more efficient and cleaner power generation. Solid oxide fuel cells (SOFCs) offer potential advantages over other fuel cell types because the high operating temperatures allow the possibility of running the cell directly on natural gas and other hydrocarbon fuels, internally reforming the fuel.[1–3] When a natural gas/steam mixture is passed over an SOFC anode at operating temperature, steam reforming (2) occurs, in addition to the methane decomposition (1) which results in carbon deposition. The CO produced by steam reforming may then undergo further reaction *via* the Water Gas shift reaction (3) and the Boudouard reaction (4).

$$CH_4 \rightarrow C_{(ads)} + 2H_2 \quad (1)$$

$$CH_4 + H_2O \rightarrow CO + 3H_2 \quad (2)$$

$$CO + H_2O \rightarrow CO_2 + H_2 \quad (3)$$

$$2CO \rightarrow C_{(ads)} + CO_2 \quad (4)$$

The CO and H_2 produced at the anode *via* internal reforming can then react with the oxygen ions [reactions (5) and (6)] that are formed at the cathode [reaction (7)] and pass through the solid electrolyte to the anode.

Anode cell reactions

$$H_2 + O^{2-} \rightarrow H_2O + 2e^- \quad (5)$$

$$CO + O^{2-} \rightarrow CO_2 + 2e^- \quad (6)$$

Cathode cell reactions

$$O_2 + 4e^- \rightarrow 2O^{2-} \quad (7)$$

However, several major problems of internal reforming remain to be solved, including the problem of carbon deposition on the anode and its subsequent deactivation which leads to poor durability,[3] obtaining the optimum anode formulation and the design of a suitable test system. Consequently, many SOFC studies use hydrogen as a fuel, and there is a lack of studies using hydrocarbons, whilst other studies have focused on important aspects of materials development.

In terms of obtaining the optimum anode formulation and cell operating conditions, one of the key problems is the design of a suitable test system to study the catalytic chemistry occurring at the anode and to evaluate the cell performance. The design and construction of such a system is not straightforward. In particular the problems of rapid heating of the cell to operating temperature, thermal cycling, sealing, obtaining gas tight connections and being able to make both electrochemical and gas analysis measurements all have to be overcome; a particular difficulty with planar-type devices.

Nickel/zirconia cermet anodes can be considered to be somewhat analogous to supported nickel steam reforming catalysts, which have been studied extensively.[4–6] It is therefore possible to study the catalytic behaviour of nickel-based anodes in powder form inside a conventional catalytic reactor; this approach has been demonstrated by several research groups.[2,7] In many other studies the primary focus is the electrochemical performance of the cell, and the influence of electrode composition or structure and other experimental parameters are monitored by measuring current or power densities.[8–10] There are a lack of studies in which the catalytic chemistry of the fuel reforming anode is studied when the anode is part of an actual SOFC.

Here, we report the development of a test system based on a small diameter, thin-walled extruded yttria-stabilised zirconia tubular reactor which can be used to study the catalytic activity of the fuel reforming anode, the chemistry occurring at the anode surface and the electrochemical performance of the fuel cell. This allows a direct correlation between the cell performance and the reforming characteristics of the anode. In addition the test cell can be readily used to study the problems of carbon deposition and poor durability in operation. The particular benefits of this test cell are that it can be rapidly assembled, heated and cooled, and it has no sealing or leakage problems, which many test devices suffer from. The zirconia reactor is housed in a furnace operated by a temperature controller which allows linear control up to 1373 K. As yttria-stabilised zirconia is a good thermal insulator, the ends of the electrolyte tube which project beyond the outer walls of the furnace remain sufficiently cool for a gas tight seal to be made, even when the furnace is at 1373 K. The test cell inlet is linked to a stainless-steel gas manifold which allows complete flexibility in the choice of fuel and fuel/steam ratio. The gas feed can be instantly switched between H_2, O_2, inert gas and fuel and gas mixtures of any combination can be achieved, enabling evaluation over a wide range of operating conditions and fuel compositions. The reactor outlet is linked to an on-line mass spectrometer which permits the fuel processing reactions at the anode to be directly studied in the actual SOFC under operating conditions, and allows the chemistry occurring at the anode surface to be investigated using temperature programmed measurements.

The anodes were prepared from a slurry of nickel oxide and 8 mol% yttria-stabilised zirconia which was milled for 3 h, with a small quantity of binding agent added at the end of the milling period. The anode can then be studied as a powder in a conventional reactor following firing. However, in this case the anode slurry is applied to the inside of the electrolyte tube prior to firing as in an actual SOFC. Following drying, the coated zirconia tubes were fired to 1573 K. Strontium-doped lanthanum manganite was used as the cathode. Nickel wire was used for current collection from the anode and silver wire from the cathode. A specially designed potentiostat was used for the electrochemical measurements. Following firing the anodes were reduced in the reactor at 1173 K for 30 min in H_2. Reforming reactions were carried out by passing the fuel mixture over the reduced anode at reaction temperature.

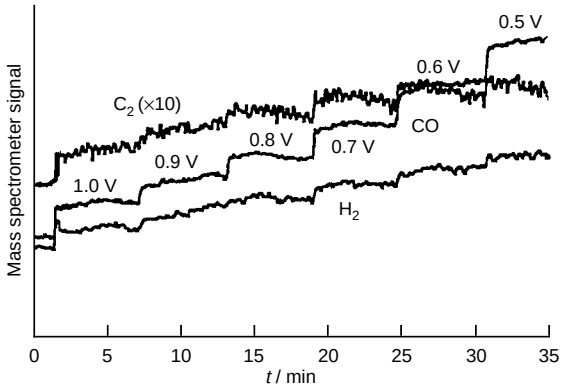

Fig. 1 The effect of drawing current on the reforming activity of a tubular SOFC with a nickel/zirconia anode running on a 19 : 1 methane–steam mixture at 1123 K

Thus the system allows the catalytic performance of the fuel reforming anode of an SOFC to be continuously monitored and can be used to study the reforming characteristics of different anode formulations over the full range of fuel cell operating conditions of temperature, gas flow rate and fuel composition. Importantly the anode is tested in an identical form and under the same conditions as in a working SOFC. The continuous real-time sampling of the on-line mass spectrometer enables any transient phenomena to be observed; such phenomena cannot be detected using a gas chromatograph. In combination with the linear temperature controller this also permits temperature programmed measurements to be carried out on the cells; temperature programmed reduction (TPR), oxidation (TPO) and reaction spectroscopy (TPRS). These have been used to study the firing and reduction characteristics (TPR, TPO), methane activation, methane steam reforming and the reaction pathways occurring at the anode surface (TPRS) and the nature and extent of carbon deposition following reforming (TPO). The detailed interpretation of these results will be reported elsewhere.[11] The same system and identical experimental arrangement can be used to carry out electrochemical measurements on the same cell, allowing a direct correlation to be made between the reforming characteristics of the anode and the fuel cell performance.

Furthermore, the system allows the chemistry occurring at the fuel reforming anode and the electrochemical performance of the SOFC to be simultaneously monitored under actual operating conditions. Fig. 1 shows the effect of drawing current from an SOFC with a nickel/zirconia anode, operating at 1123 K in a 19 : 1 methane–steam mixture, on the reforming reaction. It can clearly be seen that as the current drawn increases, *i.e.* as the cell potential decreases, there is increased methane conversion, stepwise increased production of hydrogen, and significantly increased formation of CO and C_2 species which parallel the increase in H_2 formation. Table 1 shows the corresponding cell performance. This demonstrates that we can directly correlate changes in the catalytic behaviour of the anode with the fuel cell performance.

Table 1 Electrochemical performance of a tubular SOFC running on a 19 : 1 methane/steam mixture at 1123 K

Cell potential/V	Current density/ mA cm^{-2}
1.0	93
0.9	117
0.8	146
0.7	160
0.6	197
0.5	232

In summary, we have developed an SOFC test system, based on an extruded zirconia tubular reactor, which can be used to investigate the catalytic behaviour of the fuel reforming anode, the anode surface chemistry and the electrochemical performance of the fuel cell, under genuine operating conditions. Catalytic measurements can be made on a working SOFC. Temperature programmed measurements can be carried out on anodes in an actual SOFC, and have been used to characterise different anode formulations, to study methane activation and reforming, and to evaluate the nature and level of carbon deposition on the anode during operation.

We thank the EPSRC for support under grant GR/K58647 and the award of a studentship to C. M. F.

Notes and References

† E-mail: r.m.ormerod@keele.ac.uk

1 N. Q. Minh and T. Takahashi, in *Science and Technology of Ceramic Fuel Cells*, Elsevier, Amsterdam, 1995, and references therein.
2 E. Achenbach and E. Rienche, *J. Power Sources*, 1994, **52**, 283.
3 A. L. Dicks, *J. Power Sources*, 1996, **61**, 113.
4 S. C. Tsang, J. B. Claridge and M. L. H. Green, *Catal. Today*, 1994, **23**, 3.
5 D. Qin and J. Lapszewicz, *Catal. Today*, 1994, **21**, 551.
6 O. Yamazaki, K. Tomishige and K. Fujimoto, *Appl. Catal. A: General*, 1996, **136**, 49.
7 R. T. Baker and I. S. Metcalfe, *Appl. Catal. A: General*, 1995, **126**, 297.
8 I. P. Kilbride, *J. Power Sources*, 1996, **61**, 167.
9 T. Tsai and S. A. Barnett, *Proc. 5th Int. Symp. on SOFCs*, The Electrochemical Soc., 1997, p. 274.
10 K. Eguchi, H. Mitsuyasu, Y. Mishima, M. Ohtaki and H. Arai, *Proc. 5th Int. Symp. on SOFCs*, The Electrochemical Soc., 1997, p. 358.
11 C. M. Finnerty, R. H. Cunningham and R. M. Ormerod, in preparation.

Received in Exeter, UK, 13th January 1998; 8/00345I

Cleavage of an aryl–CF_3 C–C bond with a transition metal in solution

Milko E. van der Boom, Yehoshoa Ben-David and David Milstein*†

The Weizmann Institute of Science, Department of Organic Chemistry, Rehovot 76100, Israel

Unprecedented oxidative addition of a strong, unstrained Ar–CF_3 bond to a metal complex in solution yields the new aryl–Rh^{III}–CF_3 complex 2.

Activation of strong C–C and C–F bonds by soluble metal complexes are topics of much current interest.[1–5] Recently, we reported homogeneous cleavage of a strong C–C bond and catalytic C–F activation by transition metal complexes.[2,5] Here we report the first metal insertion into an unstrained C–C single bond of a fluorocarbon in solution. The Ar–CF_3 bond cleaved is among the strongest known C–C bonds.

The new phosphine $C_6H_3CF_3$-1-$(CH_2PBu^t)_2$-2,6 **1** was prepared from 2-bromo-*m*-xylene by trifluoromethylation,[6] bromination and phosphination with $HPBu^t_2$.[7a] Compound **1** was obtained as a white powder and fully characterized by various NMR techniques and MS.‡ Reaction of $[RhCl(L)_2]_2$ (L = C_2H_4 or C_8H_{14}) with 2 equiv. of **1** (0.040 mmol) in a dioxane or toluene solution (10 ml) at 180 °C for 9 h in a sealed vessel affords exclusively the new rhodium complex $[Rh(CF_3)Cl\{C_6H_3(CH_2PBu^t)_2$-2,6$\}]$ **2**,§ which was characterized by ^1H, $^{31}P\{^1H\}$, $^{19}F\{^1H\}$ NMR and FDMS (Scheme 1).‡ The reaction can be run at lower temperatures when an excess of **1** is used, leading to quantitative formation of **2** after heating at 120 °C overnight. No other complexes were found. It is noteworthy that the cleaved bond is among the strongest C–C bonds known (compare BDE: Ph–CF_3 = 108.9 kcal mol^{-1}).[8a,b]

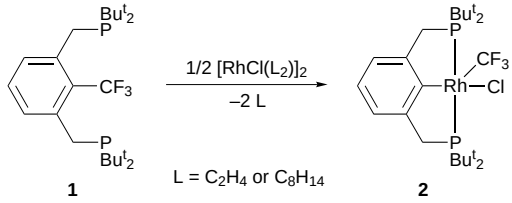

Scheme 1

In order to confirm the identity of complex **2**, we prepared the iodide analog $[Rh(CF_3)I\{C_6H_3(CH_2PBu^t)_2$-2,6$\}]$ **3** by dehydrochlorination of the known rhodium complex $[Rh(H)Cl\{C_6H_3(CH_2PBu^t)$-2,6$\}]$[7] (**4**; 0.080 mmol) with excess KH (40 equiv.) in THF (5 ml) followed by oxidative addition of CF_3I (5 psi) in a pressure vessel at room temperature (Scheme 2).¶

Complexes **2** and **3** exhibit similar spectroscopic properties.‡ The $^{31}P\{^1H\}$ NMR spectrum of **2** displayed a doublet of quartets at δ 62.6 ($^1J_{RhP}$ 116.7 Hz, $^3J_{PF}$ 16.3 Hz) for the two magnetically equivalent phosphorus nuclei which are coupled to rhodium and to three fluoride nuclei. The Rh–CF_3 moiety is clearly observed by $^{19}F\{^1H\}$ NMR as a doublet of triplets at δ 9.0 ($^2J_{RhF}$ 21.3 Hz, $^3J_{PF}$ 16.5 Hz). The ^1H NMR shows two 1 : 2 :1 triplets for the inequivalent Bu^t groups at δ 1.42 and 1.05 ($^3J_{PH}$ 7.0, 6.0 Hz), respectively, which collapse to singlets upon phosphorus decoupling. The four benzylic protons (CH_2P) appear as a typical AB pattern at δ 3.10 (ΔABq = 138 Hz, $^2J_{HH}$ 17.0, $^2J_{PH}$ 4.4 Hz), confirming the C_1 symmetry. The FDMS spectrum shows the M^+ (600) and a correct isotope pattern. Recently, two isostructural pentacoordinated rhodium-methyl complexes have been fully characterized by X-ray analysis.[2f,g]

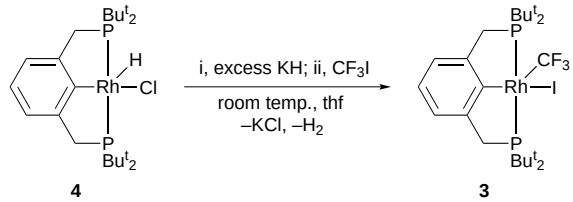

Scheme 2

Mechanistically, coordination of **1** to the metal centre is likely to precede the C–C bond activation step (Scheme 1). Coordination of both phosphine arms to the metal centre was postulated for the Me (instead of CF_3) analog of **1** with rhodium and iridium and was observed for similar substrates with platinum and ruthenium.[2,9] Performing the reaction at room temperature results in the formation of oligomers as indicated by NMR spectroscopy, which probably collapse to monomeric species upon heating. Formation of the oligomeric species is retarded when excess of **1** is used, enabling the C–C activation reaction at lower temperatures.

Interestingly, the expected product of $ArCF_2$–F bond cleavage **A** was not observed during the reactions, indicating a significantly lower activation barrier of the C–C *vs.* C–F oxidative addition. While the C–F bond is slightly stronger than C–CF_3 (BDE: $PhCF_2$–F = 112 kcal mol^{-1}),[8c] three C–F bonds are accessible for activation *vs.* one C–C bond. The formation of two strong aryl– and fluoroalkyl–M σ bonds and two five-membered rings at the expense of an unstrained sp^2–sp^3 C–C bond provides a substantial thermodynamic driving force for the oxidative addition process. There is an increased thermodynamic stability of M–C σ bonds with increasing fluorination of the alkyl group.[10]

This unique bond activation process may proceed *via* a concerted three-centered transition state **B** as recently elucidated for oxidative addition of rhodium and iridium to an Ar–CH_3 bond,[2f] which can be thermodynamically and even kinetically more favorable than the competing C–H activation process. However, the strongly electron withdrawing nature of the CF_3 group may make a nucleophilic attack on the arene by the electron-rich metal centre possible. Formation of an intermediate hexadienyl anion **C** followed by a 1,2-migration of the trifluoroalkyl group would give complex **2**. Further studies are required in order to clarify the mechanism of this unique oxidative addition process.

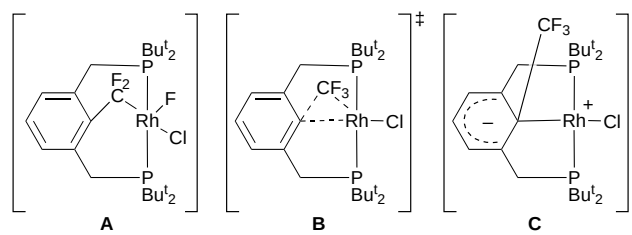

In conclusion, an unprecedented activation of a strong C–C single bond of a fluorinated organic substrate was achieved using a soluble transition metal complex. No $ArCF_2$–F bond cleavage was observed in parallel to the Ar–CF_3 oxidative addition process, although low-valent metal complexes are capable of activating C–F bonds,[3–5] indicating that nucleophilic rhodium complexes might be designed to selectively activate C–C bonds of fluorocarbons.

This research was supported by the US–Israel Binational Science Foundation, Jerusalem, Israel and by the MINERVA Foundation, Munich, Germany. D. M. is the holder of the Israel Matz Professorial Chair of Organic Chemistry.

Notes and References

† E-mail: comilst@wiccmail.weizmann.ac.il

‡ *Spectral data*: for **1** ^{1}H NMR ($CDCl_3$) δ 7.61 (d, 2 H, $^3J_{HH}$ 7.8 Hz, ArH), 7.20 (t, 1 H, $^3J_{HH}$ 7.8 Hz, ArH), 3.01 (s, 4 H, CH_2P), 1.02 [d, 36 H, $^3J_{PH}$ 10.9 Hz, $C(CH_3)_3$]. $^{31}P\{^1H\}$ NMR ($CDCl_3$) δ 38.9 (q, $^5J_{PF}$ 7.3 Hz). $^{19}F\{^1H\}$ NMR ($CDCl_3$) δ −49.8 (t, $^5J_{PF}$ 7.4 Hz, $ArCF_3$). MS: 463 (M^+ + 1).

For **2**: ^{1}H NMR (C_6D_6) δ 7.0 (m, 3 H, ArH), 3.37 (dvt, 2 H left part of ABq, $^2J_{HH}$ 17.0, $^2J_{PH}$ 4.2 Hz, CH_2P), 2.82 (dvt, 2 H right part of ABq, $^2J_{HH}$ 17.0, $^2J_{PH}$ 4.4 Hz, CH_2P), 1.42 [vt, 18 H, $^3J_{PH}$ 7.0 Hz, $C(CH_3)_3$], 1.05 [vt, 18 H, $^3J_{PH}$ 6.0 Hz, $C(CH_3)_3$]. $^{31}P\{^1H\}$ NMR (C_6D_6) δ 62.6 (dq, $^1J_{RhP}$ 116.7, $^3J_{PF}$ 16.3 Hz). $^{19}F\{^1H\}$ NMR (C_6D_6) δ 9.0 (dt, $^2J_{RhF}$ 21.3, $^3J_{PF}$ 16.5 Hz, $RhCF_3$). FDMS: M^+ 600 (correct isotope pattern).

For **3**: ^{1}H NMR (C_6D_6) δ 7.0 (m, 3 H, ArH), 3.42 (dvt, 2 H left part of ABq, $^2J_{HH}$ 17.0, $^2J_{PH}$ 4.8 Hz, CH_2P), 2.99 (dvt, 2 H right part of ABq, $^2J_{HH}$ 17.0, $^2J_{PH}$ 4.4 Hz, CH_2P), 1.49 [vt, 18 H, $^3J_{PH}$ 6.9 Hz, $C(CH_3)_3$], 1.03 [vt, 18 H, $^3J_{PH}$ 6.1 Hz, $C(CH_3)_3$]. $^{31}P\{^1H\}$ NMR (C_6D_6) δ 62.4 (dq, $^1J_{RhP}$ 115.6, $^3J_{PF}$ 15.7 Hz). $^{19}F\{^1H\}$ NMR (C_6D_6) δ 10.9 (dt, $^2J_{RhF}$ 21.5, $^3J_{PF}$ 15.6 Hz, $RhCF_3$).

§ Reaction of [{$IrCl(C_8H_{14})_2$}$_2$] with 2 equiv. of **1**, applying similar reaction conditions, resulted in a mixture of unidentified products. No C–C or C–F activation was indicated by NMR spectroscopy.

¶ 80% yield by $^{31}P\{^1H\}$ NMR, the other only product formed was the iodide analog of complex **4**.

1 J. W. Suggs and C.-H. Jun, *J. Am. Chem. Soc.*, 1984, **106**, 3054; R. A. Periana and R. G. Bergman, *J. Am. Chem. Soc.*, 1986, **108**, 7346; M. Murakami, H. Amii and Y. Ito, *Nature*, 1994, **370**, 540; J. C. Nicholls and J. L. Spencer, *Organometallics*, 1994, **13**, 1781; R. T. Li, S. T. Nguyen, R. H. Grubbs and J. W. Ziller, *J. Am. Chem. Soc.*, 1994, **116**, 10 032; C. Perthuisot, B. L. Edelbach, D. L. Zubris and W. D. Jones, *Organometallics*, 1997, **16**, 2016; K. McNeill, R. A. Andersen and R. G. Bergman, *J. Am. Chem. Soc.*, 1997, **119**, 11 244.

2 (*a*) M. Gozin, A. Weisman, Y. Ben-David and D. Milstein, *Nature*, 1993, **364**, 699; (*b*) M. Gozin, M. Aizenberg, S. Y. Liou, A. Weisman, Y. Ben-David and D. Milstein, *Nature*, 1994, **370**, 42; (*c*) S. Y. Liou, M. Gozin and D. Milstein, *J. Am. Chem. Soc.*, 1995, **117**, 9774; (*d*) S. Y. Liou, M. Gozin and D. Milstein, *J. Chem. Soc., Chem. Commun.*, 1995, 1965; (*e*) M. E. van der Boom, H.-B. Kraatz, Y. Ben-David and D. Milstein, *Chem. Commun.*, 1996, 2167; (*f*) B. Rybtchinski, A. Vigalok, Y. Ben-David and D. Milstein, *J. Am. Chem. Soc.*, 1996, **118**, 12 406; (*g*) M. Gandelman, A. Vigalok, L. J. W. Shimon and D. Milstein, *Organometallics*, 1997, **16**, 3981.

3 M. K. Whittlesy, R. N. Perutz, B. Greener and M. H. Moore, *Chem. Commun.*, 1997, 187; O. Blum, F. Frolow and D. Milstein, *J. Chem. Soc., Chem. Commun.*, 1991, 258; J. L. Kiplinger and T. G. Richmond, *Chem. Commun.*, 1996, 1115; J. Burdeniuc and R. H. Crabtree, *Science*, 1996, **271**, 340; B. L. Edelbach and W. D. Jones, *J. Am. Chem. Soc.*, 1997, **119**, 7734; M. J. Burk, D. L. Staley and W. Tumas, *J. Chem. Soc., Chem. Commun.*, 1990, 809.

4 For reviews on C–C and C–F activation: R. H. Crabtree, *Chem. Rev.*, 1985, **85**, 245; W. A. Herrmann and B. Cornils, *Angew. Chem., Int. Ed. Engl.*, 1997, **36**, 1048; G. C. Saunders, *Angew. Chem., Int. Ed. Engl.*, 1996, **35**, 2615; J. Burdeniuc, B. Jedlicka and R. H. Crabtree, *Chem. Ber./Recueil*, 1997, **130**, 145; J. L. Kiplinger, T. G. Richmond and C. E. Osterberg, *Chem. Rev.*, 1994, 373.

5 M. Aizenberg and D. Milstein, *Science*, 1994, **265**, 359; *J. Am. Chem. Soc.*, 1995, **117**, 8674.

6 G. E. Carr, R. D. Chambers, T. F. Holmes and D. G. Parker, *J. Chem. Soc., Perkin Trans. 1*, 1988, 921.

7 (*a*) C. J. Moulton and B. L. Shaw, *J. Chem. Soc., Dalton Trans.*, 1976, 1020; (*b*) S. Nemeh, C. Jensen, E. Binamira-Soriaga and W. C. Kaska, *Organometallics*, 1983, **2**, 1442.

8 (*a*) J. A. Kerr, *Handbook of Chemistry and Physics*, ed. R. C. Weast, CRC Press, Cleveland, OH, 65th edn., 1984; F-181–F-189; (*b*) J. B. Pedley, R. D. Naylor and S. P. Kirby, *Thermochemical Data of Organic Compounds*, Chapman and Hall, London, 2nd edn., 1986; (*c*) W. L. Dilling, *J. Org. Chem.*, 1990, **55**, 3286.

9 M. E. van der Boom, M. Gozin, Y. Ben-David, L. J. W. Shimon, F. Frolow, H.-B. Kraatz and D. Milstein, *Inorg. Chem.*, 1996, **35**, 7068; P. Dani, T. Karlen, R. A. Gossage, W. J. J. Smeets, A. L. Smeets, A. L. Spek and G. van Koten, *J. Am. Chem. Soc.*, 1997, **119**, 11 317.

10 R. B. King, *Acc. Chem. Res.*, 1970, **3**, 417.

Received in Cambridge, UK, 20th February 1998; 8/01457D

^{1}H NMR study of the hydrolysis of *N*-acylhydroxy[^{2}H]methylpyrroles

Andrew D. Abell,*† J. Christopher Litten‡ and Brent K. Nabbs

Department of Chemistry, University of Canterbury, Christchurch, New Zealand

KOH catalysed hydrolysis of the (*S*)- and (*R*)-*N*-(*N*-phthalylleucinyl)hydroxy[^{2}H]methylpyrroles 6b and 6c, in CD_3CN containing 1 equiv. of (+)-*sec*-butylamine, proceeds by an initial *N*- to *O*-acyl transfer with retention of configuration at the labelled centre, followed by trapping of an azafulvene to give (*S*)- and (*R*)-*sec*-butylamino[^{2}H]methylpyrroles 9b.

An electron-withdrawing group (EWG) on the nitrogen of a pyrrole of the type **5** is thought to suppress the formation of a highly electrophilic azafulvenium species **4** in nucleophilic substitution reactions (Scheme 1). In the absence of such deactivation, the analogous pyrroles **1** readily react with a nucleophile, *via* the postulated azafulvene intermediate **2**, to give products of the type **3a**.[1,2] Such a sequence is thought to be involved in the biosynthesis of uroporphyrinogen III, an important intermediate in the biosynthesis of vitamin B_{12} and related pigments.[3]

Pyrroles substituted with an EWG are found in natural products,[4] and they are also useful intermediates in organic synthesis[2,5] (*e.g.* in the synthesis deuterium-labelled porphobilinogen[2,6]—an important probe for studying the biosynthesis of vitamin B_{12}). The idea of suppressing azafulvene formation, with the introduction of an EWG on nitrogen, has also been used to develop latent reactive inhibitors of serine proteases.[7] Here, a hydroxymethylpyrrole derivative such as **6a** (a peptidic example of the general compound **5**) is stabilised by *N*-acylation with an amino acid—chosen to be recognised by the target enzyme. Enzyme catalysed deacylation yields a reactive azafulvene **2** which is then thought to lead to covalent inactivation of the enzyme by alkylation (see Scheme 1 where Nu^- is an amino acid in the enzyme's active site).

Removal of an EWG from a pyrrole nitrogen, by chemical or enzymatic hydrolysis, represents a key step in all the above applications of compounds of the type **5**. Here we report the stereochemical fate of the deuterium label of (*S*)- and (*R*)-*N*-(*N*-phthalylleucinyl)hydroxy[^{2}H]methylpyrroles **6b** and **6c** upon KOH catalysed hydrolysis in the presence of an external nucleophile [(+)-*sec*-butylamine]. This study provides evidence for (i) an intramolecular acyl transfer to give an *O*-acylpyrrole **8** [pathway (*a*), Scheme 2] as an intermediate in the deacylation sequence, and (ii) the facile formation of an azafulvene **2** on deacylation as evidenced by its trapping with an external nucleophile to give equal amounts of the (*S*)- and (*R*)-amino[^{2}H]methylpyrroles **9**. This sequence also serves to model the proposed mechanism of action of **6a** as a latent reactive inhibitor of serine proteases—the KOH mimics the protease catalysed deacylation and the external nucleophile mimics the final inactivation step. It should also be noted that the *O*-acyl intermediate **8** bears a strong resemblence to **10** which is also an inhibitor of serine proteases.[7]

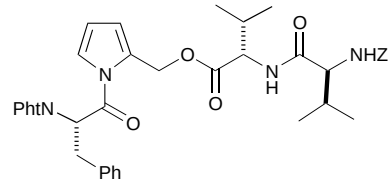

10

The key deuterium labelled hydroxymethylpyroles **6b** and **6c** were prepared from pyrrole-2-[^{2}H]carbaldehyde[2] by acylation with *N*-phthalylleucine acid fluoride according to the literature method,[8] followed by reduction with *R*- and *S*- Alpine-borane®, respectively.[2] The unlabelled analogue **6a** was similarly prepared by acylation of pyrrole-2-carbaldehyde followed by $Zn(BH_4)_2$ reduction of the formyl group. The epimeric purity at the deuterated centres of **6b** and **6c** was determined to be $> 9:1$ (see first column, Table 1) by integration of the pyrrole–CHD

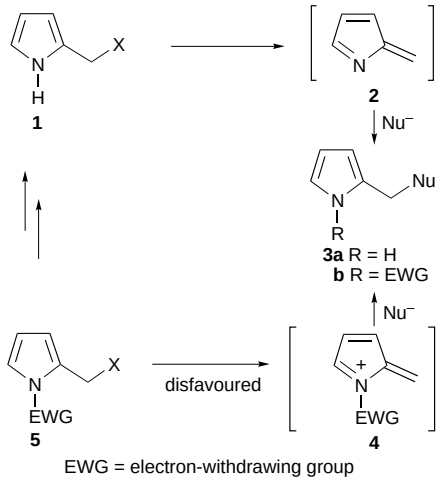

Scheme 1

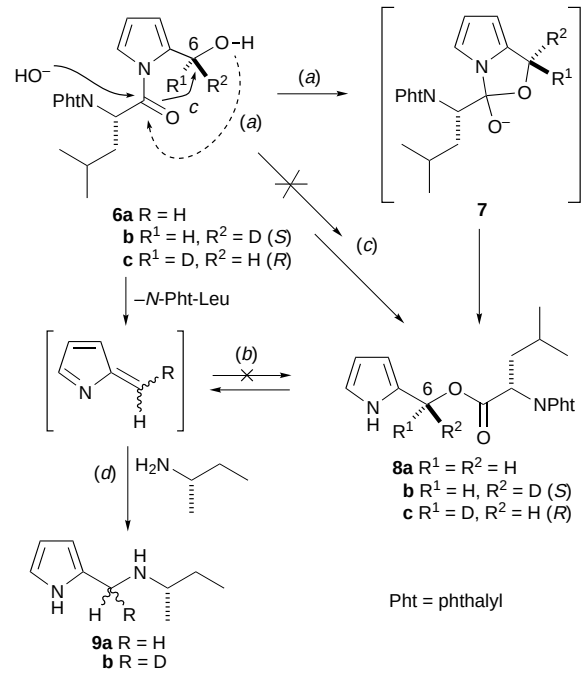

Scheme 2

Table 1 ^{1}H NMR resonances§ [CD_3CN, $CHCl_3$ internal standard (δ 7.25)] for the pyrrolemethylene group of **6** and the hydrolysis products **8** and **9** [KOH and (*S*)-(+)-*sec*-butylamine added]. In the spectra of **6a**–**c**, coupling of the signals with the OH proton were removed by homonuclear decoupling

	6a	**8a**	**9a**
	6c : **6b**	**8b** : **8c**	**9b**

singlet resonances at δ 4.21 and 4.24 respectively. The assigned configurations were consistent with related examples in which the absolute configuration has been determined by chemical conversion to the *O*-camphanate of [2-^{2}H] glycolic acid, a known literature reference compound.[2]

The mechanism of hydrolysis of compounds **6** was then studied.[7] In a typical experiment, an equivalent of KOH in D_2O (approx 10 μl) was added to a solution of either **6a**,**b** or **c** (3 mg) in CD_3CN (150 μl) containing $CHCl_3$ as an internal standard, and 1 equiv. of (+)-*sec*-butylamine (external nucleophile). The ratio of **6**, **8** and **9** was then monitored by ^{1}H NMR spectroscopy (the *exo*-methylene proton resonances of these compounds are shown in Table 1). The spectum taken immediately after mixing contained starting material **6**, *O*-acyl intermediate **8** and pyrrole amine **9** in a typical ratio of 1 : 1 : 1. ^{1}H NMR spectra of the mixtures after 18 h revealed that **6** and **8** had been completely converted to the pyrrole amine **9**.

The key points to note from the results shown in Table 1 are that the configurational purity (> 9 : 1) and absolute configurations§ of the starting materials **6b** and **c** are retained in the corresponding *O*- acyl intermediates **8b** and **c** (rows 2 and 3, Table 1). In theory, the formation of the *O*-acylpyrrole **8** could occur by either an intramolecular acyl transfer *via* the tetrahedral intermediate **7** [Scheme 2, pathway (*a*), retention of configuration], trapping of the azafulvene **2** with released *N*-phthalylleucine [Scheme 2, pathway (*b*), epimerisation at the methylene] or by an S_N2 like displacement [Scheme 2, pathway (*c*), inversion of configuration). The fact that the configurational purity at the [^{2}H]methylene centre of **8b** and **c** is intact, and also did not change with time, implies that these species are not in equlibrium with the azafulvene **2b**, hence pathway (*b*) is not operating. In addition, an S_N2 displacement at the methylene position of a hydroxymethylpyrrole has only been reported in extreme examples using a combination of Mitsunobu reaction conditions and an *N*-triflyl substituent to strongly deactivate the pyrrole ring and hence suppress azafulvene formation.[2] An *N*-acyl group is not sufficiently deactivating to promote S_N2 like displacement,[2] and hence a reaction of the type shown in pathway (*c*) is chemically unlikely under the conditions of the hydrolysis experiment. Pathway (*a*) is, however, consistent with both the literature and the observed results, *i.e*. the formation of **8** occurs with retention of configuration at the deuterated methylene centre. A second point to note is that equal mixtures of the (*S*) and (*R*) deuterium-labelled amines **9b** were produced as the end product in the reactions of **6b** and **c**, a result clearly consistent with the intermediacy of the azafulvene **2** [Scheme 2, pathway (*d*)]. Finally, as expected, the two oppositely labelled series **6b** and **c** gave complimentary results (rows 2 and 3, Table 1).

In summary, the above observations suggest that the *O*-acylpyrrole **8** is most likely formed *via* an intramolecular acyl transfer on hydrolysis of the *N*-(*N*-phthalylleucinyl)hydroxymethylpyrroles **6**. Evidence for the subsequent release of an azafulvene **2** is gained from the observed scrambling of the deuterium label at the [^{2}H]methylene position of **9** on trapping with (+)-*sec*-butylamine. Ongoing work is centred on the further development of these compounds as useful synthetic intermediates and inhibitors of serine proteases.

Notes and References

† E-mail: a.abell@chem.canterbury.ac.nz
‡ Present address: Karo Bio AB, Novum, S-14157 Huddinge, Sweden.
§ In the case of *N*-acylhydroxy[^{2}H]methylpyrroles, the methylene resonance is upfield for the (*S*)-isomer (*e.g.* **6b**) relative to the (*R*)-isomer (*e.g.* **6c**). This observation is reversed for *O*-acylpyrroles (*e.g.* **8b** and **8c**) (see ref. 2).

1 *The Chemistry of Pyrroles*, ed. A. R. Jones and G. P. Bean, Academic Press, London, 1977; *Comprehensive Heterocyclic Chemistry*, ed. A. R. Katritzky and C. W. Rees, Pergamon, Oxford, vol. 4, 1984; R. A. Barcock, N. A. Moorcroft and R. C. Storr, *Tetrahedron Lett.*, 1993, **34**, 1187.
2 A. D. Abell, B. K. Nabbs and A. R. Battersby, *J. Am. Chem Soc*., 1998, **120**, 1741.
3 A. R. Battersby, C. J. R. Fookes, K. E. Gustafson-Potter, E. McDonald and G. W. T. Matcham, *J. Chem. Soc., Perkin Trans. 1*, 1982, 2427.
4 M. J. Ortega, E. Zubia, J. L. Carballo and J. Salva, *Tetrahedron Lett.*, 1997, **38**, 331.
5 S. Singh and G. P. Basmadjian, *Tetrahedron Lett*., 1997, **38**, 6829.
6 J.-R. Schauder, S. Jendrezejewski, A. D. Abell, G. J. Hart and A. R. Battersby, *J. Chem. Soc., Chem. Commun*., 1987, 436.
7 A. D. Abell and J. C. Litten, *Tetrahedron Lett.*, 1992, **33**, 3005; A. D. Abell and J. C. Litten, *Aust. J. Chem.*, 1993, **46**, 1473.
8 J. Savrda, L. Chertanova and M. Wakselman, *Tetrahedron*, 1992, **33**, 3005.

Received in Cambridge, UK, 13th February 1998; 8/01276H

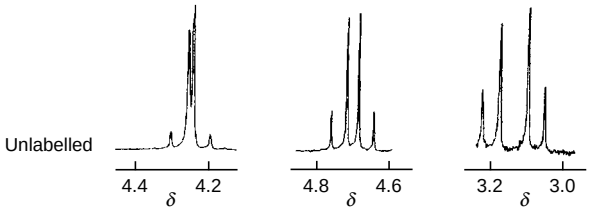

1276H/T1a/MTS/SS

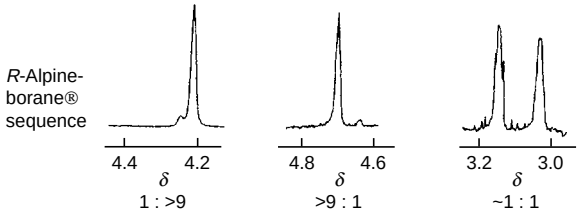

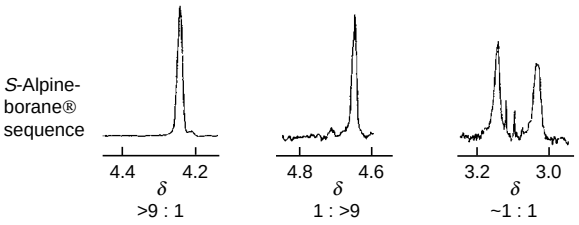

1276H/T1b/MTS/SS

Structural dependence of the reagent Ph_3PCl_2 on the nature of the solvent, both in the solid state and in solution; X-ray crystal structure of trigonal bipyramidal Ph_3PCl_2, the first structurally characterised five-coordinate R_3PCl_2 compound

Stephen M. Godfrey,† Charles A. McAuliffe, Robin G. Pritchard and Joanne M. Sheffield

Department of Chemistry, University of Manchester Institute of Science and Technology, Manchester, UK M60 1QD

The very delicate structural balance of Ph_3PCl_2 when prepared in diethyl ether solution is illustrated by its X-ray crystallographic study; unlike the ionic species, $[Ph_3PCl^+\cdots Cl^-\cdots{}^+ClPPh_3]Cl$, which prevails in dichloromethane solution, the non-solvated molecular species Ph_3PCl_2 is formed in diethyl ether which is the first example of a trigonal bipyramidal R_3PCl_2 compound to be structurally characterised, and this may have an effect on the chlorinating ability of the reagent.

Although there are a number of previous reports concerning compounds of stoichiometry R_3PCl_2, which are mainly focused on Ph_3PCl_2, they are predominantly concerned with the nature of such species in solution, using ^{31}P NMR spectroscopy.[1–9] All such studies, performed in acetonitrile or dichloromethane solution, concluded that the compounds are ionic, $[R_3PCl]Cl$. Similarly, conductivity studies of Ph_3PCl_2 in acetonitrile solution led Harris and coworkers[10,11] to conclude that the compound is ionic, $[Ph_3PCl]Cl$, since values close to those expected for a 1:1 electrolyte were recorded. However, Arzoumandis[13] investigated the structural nature of Ph_3PCl_2 in haloform solvents and concluded, from cryostatic and vibrational spectroscopic studies, that 1:1 $Ph_3PCl_2{\cdot}YCX_3$ (Y = H, D; X = Cl, Br) adducts were formed. It was reasoned that these species were molecular dimeric entities which contain six-coordinate phosphorus atoms.

Studies concerning the solid-state structure of R_3PCl_2 compounds are rare, and studies concerning R_3PCl_2 (R = Me, Ph) again concluded an ionic structure, $[R_3PCl]Cl$.[13–15]

There is renewed interest in the structural nature of compounds of stoichiometry, R_3EX_2 (E = P, As, Sb). We have established the solid-state molecular charge transfer 'spoke' structure for Ph_3PX_2, *viz*. $Ph_3P–X–X$, (X_2 = Br_2,[16] I_2,[17–19] IBr[20]), whereas other workers have shown that Ph_3PF_2 is trigonal bipyramidal[21,22] A Raman spectroscopic study[23] of Ph_3PCl_2 prepared in toluene solution suggested that two structural modifications could exist, an ionic form, $[Ph_3PCl]Cl$, prepared by bubbling dichlorine gas through a toluene solution of PPh_3 and, possibly, a trigonal bipyramidal form, prepared by passing a stream of dichlorine over the surface of a toluene solution of PPh_3.

Until very recently, no single crystal X-ray crystallographic data was available for any compound of stoichiometry R_3PCl_2. However, a crystallographic study[24] of the compound prepared from the reaction of PPh_3 and dichlorine in dichloromethane solution revealed an unusual dinuclear ionic compound, $[Ph_3PCl\cdots Cl\cdots ClPPh_3]Cl{\cdot}CH_2Cl_2$. The long Cl···Cl contacts are 3.279(6) Å (van der Waals radius for dichlorine is 3.6 Å). The solution $^{31}P\{H\}$ NMR of this species, recorded in $CDCl_3$ and CD_3CN gave single resonances at δ 65.5 and 66.5, respectively, these values being very similar to the values quoted by previous workers and indicating that the simple ionic species $[Ph_3PCl]Cl$ prevails in solution for these solvents, and the long range Cl···Cl contacts are broken, as expected.

It therefore occurred to us that a different structural modification of Ph_3PCl_2 could be exhibited in solvents of low relative permittivity (low polarity). One reason for this was the fact that $[Ph_3PCl\cdots Cl\cdots ClPPh_3]Cl{\cdot}2CH_2Cl_2$ contains a dichloromethane solvent molecule in the structure,[24] suggesting non-innocent behaviour, and although no bonding interactions between the solvent and the compound are observed, there nevertheless remains the fact that δ^+ hydrogens on the dichloromethane point towards the Cl^- ions giving a suspicion of long range electrostatic interaction, and, therefore, an implied influence on the structure adopted. Considering the widespread use of Ph_3PCl_2 as a chlorinating agent, the structural nature of the reagent is of great importance since the structure may influence its efficacy as a chlorinating agent and, possibly, the mechanism of chlorination. Consequently, the choice of solvent employed for a given chlorination reaction utilising Ph_3PCl_2 may be of fundamental importance.

Triphenylphosphine dichloride was prepared by us from the direct reaction of triphenylphosphine with dichlorine in diethyl ether in a 1:1 stoichiometric ratio [eqn. (1)].

$$PPh_3 + Cl_2 \xrightarrow[N_2, Et_2O]{\text{room temp.}} Ph_3PCl_2 \qquad (1)$$

The resultant white powder, which formed almost immediately upon addition of the dichlorine, was recrystallised from diethyl ether solution to produce a large quantity of colourless crystals on standing at room temperature for *ca*. 1 week. The melting point of the crystals was determined to be 118–119 °C {*cf*. 160–161 °C for $[Ph_3PCl\cdots Cl\cdots ClPPh_3]Cl{\cdot}2CH_2Cl_2$}. A crystal was chosen for analysis by single crystal X-ray diffraction. Interestingly, the structure‡ of Ph_3PCl_2 is shown to be the sole example of a molecular trigonal bipyramidal R_3PCl_2 compound, Fig. 1, and not the ionic structure, $[Ph_3PCl\cdots Cl\cdots ClPPh_3]Cl{\cdot}2CH_2Cl_2$ which prevails in dichloromethane solution. This result is important for two reasons: firstly, the very delicate balance between ionic and covalent forms for Ph_3PCl_2 is clearly illustrated, in the more polar CH_2Cl_2 an ionic structure is adopted whereas in diethyl ether a molecular form is revealed. Secondly, the acute solvent dependency of the structure of this reagent is clearly shown, and other workers utilising the reagent for chlorination reactions may find different rates and/or products which are dependent solely on the polarity of the solvent chosen. The structure of Ph_3PCl_2 contains two crystallographically independent molecules in the asymmetric unit which exhibit quite different P–Cl bond lengths. In one molecule, *d*(P–Cl) are quite similar, being 2.252(2) and 2.262(2) Å, however differences are observed in the other, 2.280(2) and 2.225(1) Å. Both molecules also exhibit slight distortions from regular trigonal bipyramidal geometry. These distortions and the asymmetry of the *d*(P–Cl) may arise from the ease of ionisation of the molecule. However, asymmetric bonds in multiple halide systems are not un-

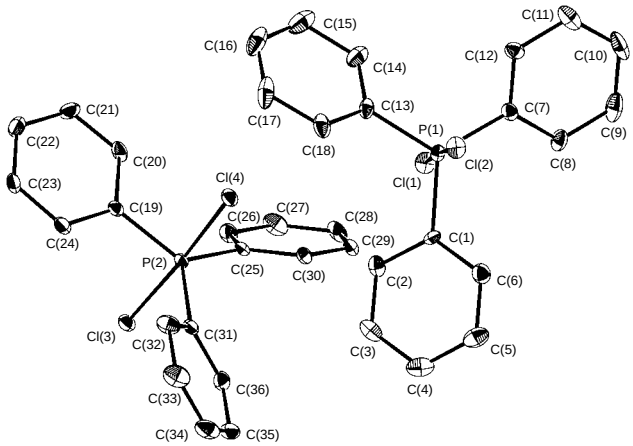

Fig. 1 X-Ray crystal structure of trigonal bipyramidal Ph_3PCl_2 (two crystallographically independent molecules are present in the asymmetric unit). Selected bond lengths (Å) and angles (°): P(1)–Cl(1) 2.280(2), P(1)–Cl(2) 2.225(1), P(2)–Cl(3) 2.262(2), P(2)–Cl(4) 2.252(2), C(7)–P(1)–C(1) 123.5(2), C(7)–P(1)–C(13) 118.2(2), C(1)–P(1)–C(13) 118.2(2) Cl(2)1–P(1)–Cl(1) 176.09(6), C(19)–C(25) 120.0(2), C(19)–P(1)–C(31) 123.6(2), C(25)–P(2)–C(31) 116.42, CI(4)–P(2)–Cl(3) 176.20(6).

common. The classic example is I_3^-, where asymmetric I–I bonds are ascribed to the influence of surrounding molecules or ions. Our recent work has shown even more dramatic examples of autosolvation in R_3PCl_2 systems.[25] In the case of Ph_3PCl_2 described here, comparison of the four Cl environments shows that the closest approaches between Cl and H in adjacent molecules are 2.92, 3.05, 2.83 and 2.82 for Cl(1), Cl(2), Cl(3) and Cl(4), respectively. As P–Cl(4) is the shortest P–Cl bond, it would appear that phenyl rings are exerting their influence on *d*(P–Cl). We have previously observed this phenomenon with interaction of Cl with δ^+ hydrogens on propyl chains.[25] Caution must be exercised when discussing E–X (E = P, As, Sb, Bi; X = Br, Cl) bond lengths however, since considerable asymmetry has already been illustrated from crystallographic studies *e.g.* Ph_3BiCl_2[26] [*d*(Bi–Cl) 2.529–2.615 Å], $[Me_3CH\text{-}CH_2]_3AsBr_2$,[27] [*d*(As–Br) 2.530–2.596 Å], Ph_3SbCl_2 [*d*(Sb–Cl) 2.382–2.490 Å].[28]

The solution structure of Ph_3PCl_2 in low-polarity solvents is also of importance since the trigonal bipyramidal structure of Ph_3PCl_2 could simply be a solid-state phenomenon, *i.e.* the molecule could auto-ionise in any given solvent, which has already been illustrated[25] when Ph_3PCl_2 is dissolved in CH_2Cl_2. Deuterated ether, C_2D_6O is not really available; however, we dissolved a sample of crystalline Ph_3PCl_2 prepared in Et_2O in deuterated benzene, C_6D_6, *i.e.* a non-polar solvent. A single resonance was observed in the NMR spectrum at δ −47, very different to that observed for the ionic $[Ph_3PCl\cdots Cl\cdots ClPPh_3]Cl\cdot CH_2Cl_2$ which exhibited resonances at δ 65.5 or 66.5 (recorded in CH_2Cl_2 and CH_3CN, respectively). This value of δ −47 is also completely different to any previously reported value for a sample of Ph_3PCl_2 which, prior to this work, has only been studied by $^{31}P\{H\}$ NMR spectroscopy in solvents of quite high polarity. This value of δ −47 is however comparable to analogous difluorophosphoranes, R_3PF_2, which are known to retain a molecular five-coordinate geometry in solution, *e.g.* $MePh_2PF_2$ (δ −43.2) and Ph_3PF_2 (δ −58.1).

The only $^{31}P\{H\}$ NMR study of a compound of stoichiometry R_3PCl_2,[27] which was claimed to be trigonal bipyramidal is $(C_6F_5)_3PCl_2$, which gave a single resonance at δ −110.[29]

Clearly, therefore, Ph_3PCl_2 retains a molecular trigonal bipyramidal structure in solvents of low polarity. Addition of CH_2Cl_2 to the C_6D_6 solution of Ph_3PCl_2 ionises the molecule to produce $[Ph_3PCl\cdots Cl\cdots ClPPh_3]Cl\cdot 2CH_2Cl_2$, since a resonance at δ 65.5 is observed and the former resonance at δ −47.0 disappears.

In conclusion, the solvent of preparation is critical in determining the structure of Ph_3PCl_2. A molecular form persists in solvents of low polarity which is converted into an ionic form in solvents of higher polarity. Which structure is adopted will almost certainly have an effect on the chlorinating ability of the reagent, and, possibly, the nature of any products formed.

We are grateful to the EPSRC for a research studentship (to J. M. S.).

Notes and References

† E-mail: Stephen.M.Godfrey@umist.ac.uk

‡ *Crystal data*: Triclinic, space group $P\bar{1}$ (no. 2) a = 9.408(2), b = 11.579(6), c = 16.203(2) Å, α = 95.23(3), β = 103.09(2), γ = 111.10(3)°, U = 1574.7(1) Å^3, Z = 4, D_c = 1.405 g cm^{-3}, μ = 5.04 cm^{-1}, $F(000)$ = 688. The structure analysis is based on 5280 reflections (Mo-Kα $2\theta_{max}$ = 49.9), 5222 observed [$I > 2\sigma(I)$], 379 parameters Absorption correction (min., max. transmission 0.81, 1.00). The structure was solved by direct methods and refined by full-matrix least squares. Final residual R_1 = 0.0762, wR_2 = 0.2137. Final residuals (all data) R_1 = 0.0941, wR_2 = 0.2681. CCDC 182/773.

1 G. A. Wiley and W. R. Stine, *Tetrahedron, Lett.*, 1967, 2321.
2 D. B. Denney, D. Z. Denney and B. C. Chang, *J. Chem. Soc., Dalton Trans.*, 1976, 1243.
3 K. B. Dillon, R. J. Lynch, R. N. Reeve and T. C. Waddington, *J. Chem. Soc., Dalton Trans.*, 1976, 1243.
4 C. Brown, M. Murrany and R. Schmutzler, *J. Chem. Soc. C*, 1970, 876.
5 E. L. Muetterties and W. Mahler, *Inorg. Chem.*, 1965, **4**, 119.
6 E. G. Schnell and E. G. Rochow, *J. Am. Chem. Soc.*, 1956, **78**, 1084.
7 F. Seel, K. Rudolph and R. Budenz, *Z. Anorg. Allg. Chem.*, 1965, **341**, 196.
8 R. Bartsh, O. Stelzer and R. Schmuttzler, *Z. Naturforsch., Teil B*, 1981, **36**, 1349.
9 R. Appel and H. Scholer, *Chem. Ber.*, 1977, **110**, 2382.
10 A. D. Beveridge and G. S. Harris, *J. Chem. Soc.*, 1966, 520.
11 G. S. Harris and M. F. Ali, *Tetrahedron Lett.*, 1968, 37.
12 G. G. Arzoumandis, *Chem. Commun.*, 1969, 520.
13 K. B. Dillon and T. C. Waddington, *Spectrochim. Acta, Part A*, 1971, **27**, 2381.
14 A. Finch, P. N. Gates and A. S. Muir, *J. Raman Spectrosc.*, 1988, **19**, 91.
15 J. Goubeau and R. Baumgartner, *Z. Electrochem.*, 1960, **64**, 598.
16 N. Bricklebank, S. M. Godfrey, A. G. Mackie, C. A. McAuliffe and R. G. Pritchard, *J. Chem. Soc., Chem. Commun.*, 1992, 355.
17 S. M. Godfrey, D. J. Kelly, A. G. Mackie, C. A. McAuliffe, R. G. Pritchard and S. M. Watson, *J. Chem. Soc., Chem. Commun.*, 1991, 1163.
18 N. Bricklebank, S. M. Godfrey, A. G. Mackie, C. A. McAuliffe, R. G. Pritchard and P. J. Kobryn, *J. Chem. Soc., Dalton Trans*, 1993, 101.
19 N. Bricklebank, S. M. Godfrey, H. P. Lane, C. A. McAuliffe, R. G. Pritchard and J. M. Moreno, *J. Chem. Soc., Dalton Trans.*, 1995, 2421.
20 N. Bricklebank, S. M. Godfrey, C. A. McAuliffe and R. G. Pritchard, *J. Chem. Soc., Dalton Trans.*, 1993, 2261.
21 F. Weller, D. Nuszhar, K. Dehncke, F. Gingl and J. Strahle, *Z. Anorg. Allg. Chem.*, 1991, **602**, 7.
22 K. M. Doxsee, E. M. Hannawait and T. J. R. Weakley, *Acta Crystallogr., Sect. C*, 1992, **48**, 1288.
23 M. A. H. A. Al-Juboori, P. N. Gates and A. S. Muir, *J. Chem. Soc., Chem. Commun.*, 1991, 1270.
24 S. M. Godfrey, C. A. McAuliffe, R. G. Pritchard and J. M. Sheffield, *Chem. Commun.*, 1996, 2521.
25 S. M. Godfrey, C. A. McAuliffe, R. G. Pritchard, J. M. Sheffield and G. M. Thompson, *J. Chem. Soc., Dalton Trans.*, 1997, 4823.
26 D. M. Hawley and G. Ferguson, *J. Chem. Soc. A*, 1968, 2539.
27 J. C. Pazic and C. George, *Organometallics*, 1989, **8**, 482.
28 S. P. Bone, M. J. Begley and D. B. Sowerby, *J. Chem. Soc., Dalton Trans.*, 1992, 2085.
29 H. J. Emeleus and J. M. Miller, *J. Inorg. Nucl. Chem.*, 1966, **28**, 622.

Received in Basel, Switzerland, 23rd July 1997; Revised manuscript received 30th January 1998; 8/00820E

Parahydrogen enhanced NMR studies on thermally and photochemically generated products from $[IrH_3(CO)(PPh_3)_2]$

Sarah Hasnip,[a] Simon B. Duckett,*[a]† Diana R. Taylor[b] and Mike J. Taylor[b]

[a] *Department of Chemistry, University of York, Heslington, York, YO1 5DD*
[b] *BP Chemicals, BP Chemicals Limited, Saltend, Hull, UK HU12 8DS*

Parahydrogen induced polarisation is used to enable the rapid NMR characterisation of thermally and photochemically generated complexes of general formula $[IrH_3(CO)_{3-x}(PPh_3)_x]$ (x = 1–3).

It has been shown that parahydrogen (p-H_2) increases the size of detectable signals in NMR spectroscopy by enabling access to non-Boltzmann spin populations.[1,2] This phenomenon has facilitated the observation of materials found in low concentrations, such as intermediates in catalytic hydrogenation reactions, species in minor reaction pathways such as $[RhH_2(PPh_3)_2Cl_2Rh(PPh_3)(CO)]$ and minor constituents in equilibria, for example *all-cis*-$[Ru(PMe_3)_2(CO)_2(H)_2]$.[3]

The reaction chemistry presented here relates primarily to hydrogen exchange reactions of $[IrH_3(CO)(PPh_3)_2]$. This complex has been shown by Harrod and Yorke[4] to exist in solution in two isomeric forms, **1a** with *trans* phosphines and *mer*-hydrides and **1b** with *cis* phosphines and *fac*-hydrides (Scheme 1). We describe how the sensitivity gain provided by p-H_2 allows the rapid characterisation of these, and related trihydride complexes of iridium, and enables the examination of their thermal and photochemical reactivity. We use pulsed field gradient-assisted 2D homo- and hetero-nuclear NMR methods to monitor these reactions.

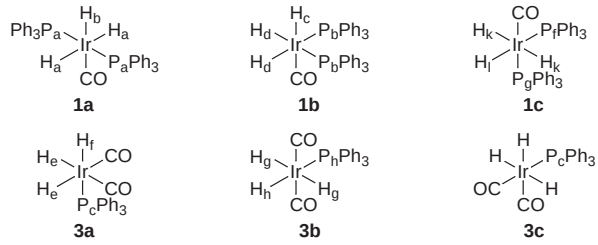

Scheme 1 Structural isomers of the trihydrides $[IrH_3(CO)(PPh_3)_2]$ and $[IrH_3(CO)_2(PPh_3)]$

When a 0.1 mM solution containing equal amounts of **1a** and **1b**, in [$^2H_6$]benzene under 3 atm of p-H_2, is monitored between 303 K and 343 K by ^1H NMR spectroscopy, enhanced resonances are detected in the hydride region of the spectrum. The $^1H\{^{31}P\}$ NMR spectrum shown in Fig. 1(*a*) was recorded at 343 K and shows two pairs of anti-phase multiplets that can be assigned to the hydride ligands of **1a** and **1b**.‡ These results confirm that the hydride ligands in **1a** and **1b** undergo exchange with free H_2. We note that under these conditions, even with the p-H_2 derived signal amplification, no resonances are detected that can be attributed to isomer **1c** (Scheme 1). The spectral features of the p-H_2 enhanced trihydrides, illustrated in Fig. 1, are surprising.[5] The two polarised hydride resonances at δ −9.29 and −10.02 are assigned to the hydride ligands H_a and H_b of **1a**, respectively.[4] In a regular $^1H\{^{31}P\}$ spectrum these signals would appear as doublets and triplets respectively with peak separation J_{HH}. The observed signals have relative intensities of 2 : 1 and their anti-phase line separation (4.4 and 8.8 Hz) indicates that the central feature of the triplet is no longer visible. This can be understood by examining the p-H_2 controlled populations of the eight spin wavefunctions of the trihydride (AX_2). While four wavefunctions are simple products of the form ααα, **αββ**, **βαα** and βββ, four belong to combinations of the form **α(αβ − βα)**, **α(αβ + βα)**, **β(αβ − βα)** and **β(αβ + βα)**. Exchange with p-H_2 (αβ − βα spin state) at **1a** involves the A and one X nucleus, with the result that the six product states indicated, **in bold**, become equally populated while the ααα and βββ states are unpopulated. Consequently, the only visible transitions for nucleus A, spin flips ααα↔**βαα** and **αββ**↔βββ, correspond to the outer lines of the triplet and are seen in emission and absorption. The emission–absorption phase profile reveals that J_{HH} is negative.[2] The central line, corresponding to spin flips **α(αβ − βα)**↔**β(αβ − βα)** and **α(αβ + βα)**↔**β(αβ + βα)**, vanishes because the associated levels have identical populations. In a similar way, examination of the symmetry allowed transitions for H_a (X_2) reveals that observable spin flips connect ααα↔α(αβ + βα), and β(αβ + βα)↔βββ. These transitions are separated by J_{AX} (J_{HH}) and are

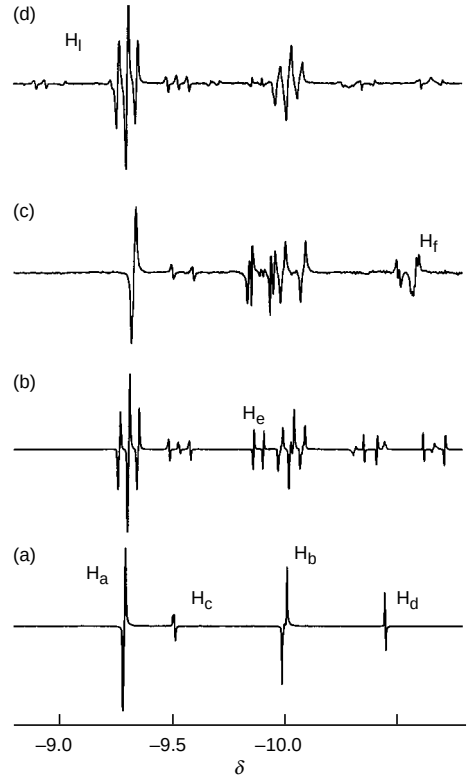

Fig. 1 NMR spectra (400 MHz) of $[IrH_3(CO)_{3-x}(PPh_3)_x]$ (x = 1–3) obtained with p-H_2 in C_6D_6 showing the hydride region only. The anti-phase components arise in transitions involving protons that originate from p-H_2. (*a*) $^1H\{^{31}P\}$ spectrum of **1a** and **1b** at 343 K; (*b*) ^1H spectrum of **1a** **1b** and **3a** generated *in situ* from $[IrH(CO)_2(PPh_3)_2]$; (*c*) $^1H\{^{31}P\}$ spectrum of a ^{13}CO labeled sample of **1a**, **1b** and **3a**; (*d*) $^1H\{^{31}P\}$ spectrum recorded at 313 K immediately after UV photolysis of a sample of **1a** and **1b**.

visible as emission and absorption signals, with twice the overall intensity seen for signal A (H_b).

Interestingly, isomer **1b** reveals a different pattern; the two hydride resonances at $\delta -9.53$ and -10.48, assigned to H_c and H_d respectively, appear as absorption and emission signals because J_{HH} is now positive. Because both hydride resonances are enhanced we can confirm that the dominant dihydrogen exchange pathway involves reductive elimination of H_cH_d rather than H_dH_d in **1b**. At 333 K the hydride resonance enhancements, 30-fold for **1a** and 5-fold for **1b**, are consistent with faster dihydrogen exchange at **1a**.

A modified heteronuclear multiple quantum correlation experiment (HMQC) using gradients and ^{31}P decoupling was used to measure the chemical shifts of the phosphorus nuclei of **1a** and **1b**.[6] In the two-dimensional map cross-peaks connect the hydrides to the corresponding phosphorus nuclei; P_a [$\delta(^{31}P)$ 18.0] connects to H_a and H_b whilst P_b [$\delta(^{31}P)$ 8.8] connects to H_c and H_d. Spectra recorded on this sample at 333 K using a ^{31}P decoupled gradient-assisted EXSY sequence (mixing time of 300 ms) contain cross-peaks that connect the two hydride resonances of **1a**. This indicates that the hydride ligands of **1a** are able to interchange identities *via* a process which is intramolecular with respect to the hydrides. This spectrum also contains nOe-derived cross-peaks that connect the hydrides to the *ortho*-phenyl protons of the phosphine ligand.[7] Under these conditions no cross-peaks connect the hydride resonances of **1a** to those of **1b**. However, with a mixing time of 500 ms cross-peaks connect the hydrides resonances of **1a** to free H_2.

When a frozen C_6D_6 solution of $[IrH(CO)_2(PPh_3)_2]$ **2**, under an atmosphere of *p*-H_2, is thawed and rapidly introduced into the NMR spectrometer for monitoring by ^1H spectroscopy at between 313 and 333 K, three hydride containing species are detectable [Fig. 1(*b*)]. Two of these species can be assigned to the previously described **1a** and **1b**, produced by CO loss from **2** and subsequent H_2 addition. The two new sets of anti-phase multiplets at $\delta -9.86$ and -10.54, are assigned to the hydride ligands H_e and H_f of the new product **3a** (Scheme 1) with $J_{HH} = -1.8$ Hz.‡ The H_e resonance of **3a** shows one additional *cis* phosphorus splitting [$J(P_cH)$ 17.24 Hz] while the resonance due to H_f shows a larger *trans* phosphorus splitting [$J(P_cH)$ 121.6 Hz]. Interestingly, if the sample is monitored after degassing and refilling with fresh *p*-H_2 then the observed resonances for **3a** are weaker than those seen initially. Repeating this process reduces their signal intensity still further, until eventually they are no longer visible.[8] The ^1H NMR spectrum of this sample, collected 48 h after filling the NMR tube with 50 Torr of ^{13}CO, revealed that $[IrH(^{13}CO)_2(PPh_3)_2]$ was formed, as evidence by the ^{13}C coupled hydride resonance at $\delta -10.3$ (J_{CH} 6.4 Hz). This sample was then refilled with *p*-H_2 and monitored by NMR spectroscopy as before. The fully carbon decoupled ^1H–^{13}C HMQC spectrum of this sample located a single carbonyl resonance for **3a**, while the corresponding ^1H–^{31}P spectrum reveals that the hydride resonance for H_e possesses additional ^{13}C couplings which are indicative of a planar $(H)_2Ir(^{13}CO)_2$ core [Fig. 1(*c*)]. These additional data indicate that **3a** has *fac*-hydrogen atoms (Scheme 1).[9] When a sample of the related complex $[IrH(CO)(PPh_3)_3]$ was examined with *p*-H_2 only **1a** and **1b** were detectable as *p*-H_2 enhanced products. These reactions are illustrated in Scheme 2.

$^1H\{^{31}P\}$ NMR spectra were obtained for C_6D_6 solutions under 3 atm of *p*-H_2 containing < 1 mg of $[IrH_3(CO)(PPh_3)_2]$, with normal and enriched levels of ^{13}CO, after 5 min UV irradiation.[10] These spectra contain enhanced hydride resonances for several new species in addition to those already described for **1a**, **1b** and **3a**. In order to characterise these new species gradient-assisted COSY{^{31}P} and HMQC experiments were recorded. Signals due to the remaining isomer of the bis-phosphine trihydride **1c** were assigned. Additional resonances assigned to the mono-triphenylphosphine complex **3b** are also present. For example, the hydride H_h at $\delta -9.08$ [J(HH) −4.6, J(PH) 136.4, J(PH) 17.6 Hz] seen in Fig. 1(*d*) connects with a hydride resonance at $\delta -10.10$ in the COSY spectrum and to two phosphorus nuclei [$\delta(^{31}P)$ 5.1 and 20.5] in the HMQC. These new isomers have short lifetimes with the result that after several minutes at 313 K the only species seen are **1a** and **1b**. They can be regenerated by repeating the photolysis step, however, when the sample is irradiated in the presence of benzaldehyde, a good CO source, resonances for **3a** are visible for much longer.

Here, we have shown that *p*-H_2 derived spectral amplification can be used to examine trihydride systems, and view species that are normally only readily visible under high pressures of H_2.[11] *In situ* ^{13}CO labelling of 1 mg samples proved to be a viable and cost-effective way of fully characterising the ligand sphere of these species. In addition, we have demonstrated that UV irradiation may be employed to generate normally unstable structural isomers for characterisation with *p*-H_2.[12]

Financial support from the EPSRC (Spectrometer and S. H.), BP Chemicals (CASE award S. H.), the Royal Society, NATO and Bruker Spectrospin, and discussions with Mr C. Sleigh, Professor R. Eisenberg, Professor R. N. Perutz and Dr R. J. Mawby are gratefully acknowledged.

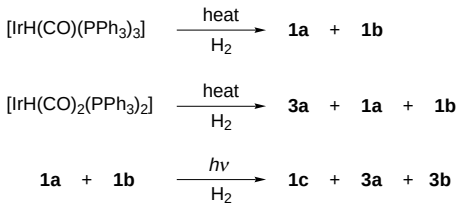

Scheme 2 *p*-H_2 enhanced trihydride products

Notes and References

† E-mail: sbd3@york.ac.uk

‡ *Selected spectroscopic data* at 333 K in C_6D_6 at 400.13 MHz (^1H), 161.45 MHz (^{31}P) and 100.2 MHz (^{13}C). **1a**: ^1H δ, 7.91 (*o*-phenyl H of P_a), −9.29 [H_a, J(HH) −4.4, $J(P_aH)$ 16.9 Hz], −10.02 [H_b, $J(P_aH)$ 19.7, J(HH) −4.4, $J(H^{13}CO)$ −36 Hz], ^{31}P, δ 18.0 (P_a, s), ^{13}C δ 179.6 [CO, t, J(PC) 10.3 Hz]. **1b**: ^1H, δ 7.9 (*o*-phenyl H of P_b), −9.51 [H_c, $J(P_bH)$ 17.1, $J(^{13}COH)$ 37.7, J(HH) + 2.4 Hz], −10.47 [H_d, $J(P_bH)$ + $J(P_b'H)$ 122, J(HH) + 2.4 Hz], ^{31}P, δ 8.8 (P_b, s), ^{13}C, δ 179.3 [CO, t J(PC) 10.8]. **1c**: ^1H, $\delta -9.08$ [H_l, $J(P_fH)$ 136.4, $J(P_gH)$ 17.6, J(HH) −4.6 Hz], −10.10 [H_k, $J(P_fH)$ = $J(P_gH)$ = J(HH) −4.4, Hz], ^{31}P, δ 20.5 (P_f), 5.1 (P_g). **3a**: ^1H, δ 7.9 (*o*-phenyl H or P_c), −9.86 [H_e, $J(P_cH)$ 17.2, $J(H^{13}CO_{trans})$ + $J(H^{13}CO_{cis})$ 40.6, J(HH) −2.4 Hz], −10.54 [H_f, $J(P_bH)$ 121.6, $J(^{13}COH)$ 4.7, J(HH) −2 Hz]. ^{31}P, δ 3.29 (P_c, s). ^{13}C, δ 172.15 [CO, d, J(PC) 6 Hz]. **3b**: ^1H, $\delta -8.8$ [H_h, $J(P_hH)$ 136.9, J(HH) −2.7 Hz], −9.7 [H_g, $J(P_hH)$ 121.6, J(HH) −2.4 Hz], ^{31}P, δ 43.2 (P_h, s).

1 C. R. Bowers and D. P. Weitekamp, *J. Am. Chem. Soc.*, 1987, **109**, 5541; J. Natterer and J. Bargon, *Proc. Nucl. Magn. Res. Spectrosc.*, 1997, **31** 293.
2 R. Eisenberg, *Acc. Chem. Res.*, 1991, **24**, 110.
3 S. B. Duckett, C. L. Newell and R. Eisenberg, *J. Am. Chem. Soc.*, 1994, **116**, 10548; S. B. Duckett and R. Eisenberg, *ibid.*, 1993, **115**, 5292; S. B. Duckett, R. J. Mawby and M. G. Partridge, *Chem. Commun.*, 1996, 383.
4 J. F. Harrod and W. J. Yorke, *Inorg. Chem.*, 1981, **20**, 1156.
5 Professor R. Eisenberg has seen similar effects with a tantalum complex, personal communication.
6 S. B. Duckett, G. K. Barlow, M. G. Partridge and B. A. Messerle, *J. Chem. Soc., Dalton Trans.*, 1995, **20**, 1427.
7 The starting anti-phase magnetisation must be refocussed; this requires two delays, $\frac{1}{2}J_{HH}$ for H_a and $\frac{1}{4}J_{HH}$ for H_b.
8 When a sapphire NMR tube filled with a toluene solution of **1** was warmed to 80 °C, first under 40 atm of CO and then under 40 atm of normal H_2, the resonances of **3a** are visible in the ^1H spectrum.
9 L. Malatesta, M. Angoletta and F. Conti, *J. Organomet. Chem.*, 1971, **33**, C43.
10 The labelled sample was prepared *in situ* by taking an NMR sample containing $[IrH_3(CO)(PPh_3)_2]$ and adding ^{13}CO.
11 R. Whyman, *J. Organomet. Chem.*, 1971, **29**, C36.
12 When $[IrH_2(Cl)(CO)(PPh_3)_2]$ is photolysed with *p*-H_2 the trihydrides **1a** and **1b** are detected.

Received in Cambridge, UK, 12th February 1998; 8/01224E

Carbohydrates to carbocycles: an expedient synthesis of pseudo-sugars

A. V. R. L. Sudha and M. Nagarajan*†

[a] *School of Chemistry, University of Hyderabad, Hyderabad-500 046, India*

A short and versatile synthesis of pseudo-sugars from sugars utilizing the Claisen rearrangement as the key step is described.

Conversion of sugars into carbocycles is an area which has attracted considerable attention in recent times.[1] Some important methodologies for achieving this are (i) Ferrier's mercuric ion mediated conversion of 6-deoxyhex-5-enopyranosyl compounds to deoxyinososе derivatives,[2] (ii) the radical cyclization approach of RajanBabu[3] and (iii) the zirconium mediated ring contraction of carbohydrate derivates to carbocycles by Taguchi.[4]

Pseudo-sugars are 2,3,4,5-tetrahydroxy-1-(hydroxymethyl)cyclohexanes, in which the ring oxygen atom of a sugar has been replaced by a methylene group. Pseudo-D-glucose, pseudo-D-galactose and pseudo-D-fructose have been suggested as replacements for their sugar counterparts as non-nutritive sweeteners.[5] Amino pseudo-sugars, which form the aglycon part of many aminoglycoside antibiotics, have chemotherapeutic potential as glycosidase inhibitors.[6] Pseudo-sugars and some related carbocyclic compounds are components of some antibiotics (validamycins) and enzyme inhibitors (adiposins).[7]

The biological significance of pseudo-sugars has led to the development of several approaches for their synthesis in optically pure form from various chiral sources. A comprehensive review on pseudo-sugars has been published.[8] Pseudo-β-D-altro-, pseudo-α-L-manno- and pseudo-β-D-gluco-pyranoses have been synthesized by Hudlicky[9] from homochiral microbial metabolites. Vandewalle[10] prepared eight pseudo-sugars belonging to the allo, gulo, manno and talo series which possess 2,3-*cis*-diol units from (1*R*,2*S*,3*R*,4*S*)-4-butyryloxy-2,3-(propane-2,2-diyldioxy)cyclohex-5-en-1-ol. The synthetic versatility of quinic acid was demonstrated by Shing in his synthesis of pseudo-β-D-manno-,[11] pseudo-β-D-fructo-,[11] pseudo-α-D-gluco-[12] and pseudo-α-D-manno-pyranoses.[12] Ferrier prepared crystalline pseudo-α-D-glucopyranose[13] from 2-deoxyinososе.

It occurred to us (as shown in the retrosynthesis in Scheme 1), that controlled hydroxylation of cyclohexene **1** should lead to the four pseudo-sugars, pseudo-α-D-glucopyranose, pseudo-α-D-mannopyranose, pseudo-β-D-glucopyranose and pseudo-β-D-mannopyranose. The conversion of **2** to **1** involves transformation of a glycal derivative into a cyclohexene, prototypes of which have been reported earlier by Büchi.[14] Compound **1** in turn can be readily derived from D-glucose *via* **2** and **3**. We describe here the successful realization of this strategy.

The primary hydroxy group in **4** was oxidized using pyridinium dichromate (PDC) to the aldehyde **5**, which was used without purification.[15] In order to introduce the C6–C7 double bond in **2**, methylenation of **5** was investigated under various conditions. Treatment of **5** with methyltriphenylphosphonium iodide and Bu^{n}Li led to a complex mixture. Wittig olefination of **5** with formylmethylene(triphenyl)-phosphorane and decarbonylation of the resultant unsaturated aldehyde with Wilkinson's catalyst gave **2** in very low yield. Finally, a combination of methyltriphenylphosphonium iodide and sodamide gave **2** in 40% overall yield from **4**.

Heating **2** in a sealed tube in *o*-dichlorobenzene at 240 °C afforded the rearranged chiral carbocycle **6** in 84% yield, based on recovered starting material (4%). The product **6**, being unstable, was subjected to $NaBH_4$ reduction without purification to give **1**.‡ The IR spectrum of **1** showed an olefin band at 1643 cm^{-1} and the presence of a hydroxy absorption at 3445 cm^{-1}. Unlike **2**,§ which showed the presence of five olefinic protons in its ^{1}H NMR spectrum, the rearranged carbocycle **1** exhibited only two olefinic protons as a multiplet at δ 5.74–5.78. The presence of the double bond in **1** was further confirmed from its ^{13}C NMR spectrum, which displayed resonances at δ 125.95 and 138.42 (Scheme 2).

Having synthesized the highly functionalized chiral synthon **1**, attempts were made to prepare the four pseudo-sugars, namely, pseudo-α-D-glucopyranose, pseudo-α-D-mannopyranose, pseudo-β-D-glucopyranose and pseudo-β-D-mannopyranose.

Catalytic OsO_4 dihydroxylation[16] of the double bond in **1** from the less hindered β-face gave the triol **7** in quantitative yield, which on debenzylation with 20% $Pd(OH)_2/C/H_2$ yielded pseudo-α-D-glucopyranose **8**, $[\alpha]_D$ +57.0 (*c* 0.65, H_2O) [lit.,[12] + 63.0 (*c* 0.6, H_2O)].

The primary hydroxy group in **1** was protected as the benzyl ether to yield **9**.¶ A mixture of partially benzylated pseudo-α-D-mannopyranose **10** and pseudo-β-D-glucopyranose **11** was obtained in one step from **9** involving a sequence of epoxidation and ring opening using MCPBA, water and 10% H_2SO_4.[17] Purification and separation by preparative TLC of the partially benzylated mixture gave **10** and **11** in 34 and 26% yields, respectively. Deprotection under similar conditions as those for

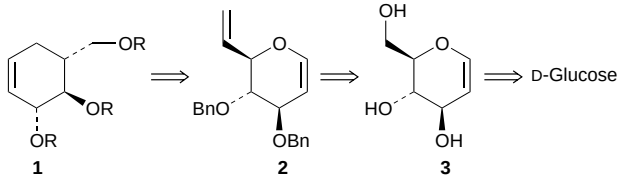

Scheme 1

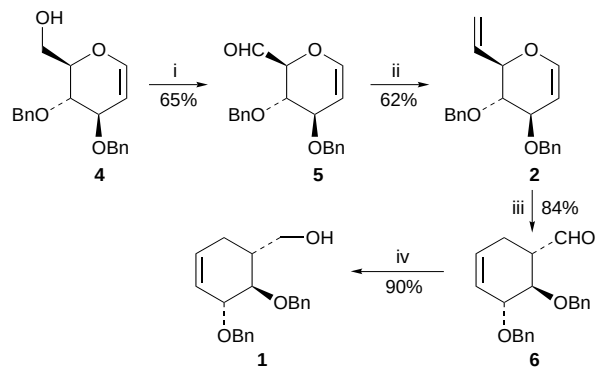

Scheme 2 *Reagents and conditions*: i, PDC, 4 Å molecular sieves, CH_2Cl_2, room temp., 10 h; ii, Ph_3MePI, $NaNH_2$, Et_2O, room temp., 30 min; iii, *o*-dichlorobenzene, 240 °C (sealed tube), 1 h; iv, $NaBH_4$, THF, room temp., 10 min

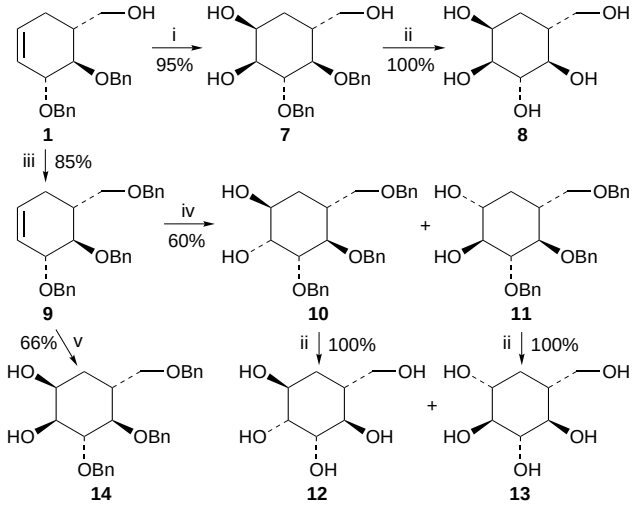

Scheme 3 *Reagents and conditions*: i, OsO_4, $K_3Fe(CN)_6$, K_2CO_3, Bu^{t}OH, H_2O, 24 h; ii, 20% $Pd(OH)_2/C/H_2$, 55 psi, 2 h; iii, NaH, DMF, BnBr, room temp., 10 h; iv, MCPBA, H_2O, 10% H_2SO_4, 48 h; v, aq. AcOH, AgOAc, I_2, Na (cat.), MeOH, 15 h

7 gave pseudo-α-mannopyranose **12**, $[\alpha]_D$ +1.5 (*c* 0.4, MeOH) [lit.,[12] $[\alpha]_D$ +1.9 (*c* 1.0, MeOH)], and pseudo-β-D-glucopyranose **13**, $[\alpha]_D$ +10.0 (*c* 0.3, H_2O) [lit.,[18] $[\alpha]_D$ +10.9 (*c* 0.83, H_2O)], from **10** and **11**, respectively, in quantitative yields (Scheme 3).

cis-Hydroxylation[19] of the alkene **9** under Woodward's conditions gave in 66% yield the tribenzyl diol **14** which on debenzylation afforded only pseudo-α-D-glucopyranose instead of the anticipated pseudo-β-D-mannopyranose, in quantitative yield. This is surprising as Woodward's hydroxylation is expected to give overall *syn*-hydroxylation from the more hindered face, in contrast to the osmium tetroxide hydroxylation.

The ^{1}H NMR spectra of all the pseudo-sugars were in consonance with the data reported in the literature. The structures of all new compounds were unambiguously established from their spectral and analytical data wherever appropriate.

A. V. R. L. thanks the CSIR (New Delhi) for providing financial assistance in the form of a research fellowship. We acknowledge the COSIST programme in chemistry for instrumental facilities.

Notes and References

† E-mail: mnsc@uohyd.ernet.in

‡ *Selected data* for **1**: ν_{max}(neat)/cm^{-1} 3445, 2924, 1454, 1093, 1028, 698; δ_H($CDCl_3$) (200 MHz) 1.81–2.21 (m, 3 H), 2.52–2.66 (br s, 1 H), 3.57–3.71 (m, 3 H), 4.20–4.27 (m, 1 H), 4.67–5.03 (m, 4 H), 5.74–5.78 (m, 2 H), 7.30–7.48 (m, 10 H); δ_C($CDCl_3$; 50 MHz) 138.42, 128.57, 128.48, 128.21, 127.87, 127.72, 125.95, 82.00, 81.15, 74.30, 71.30, 65.53, 40.62, 28.05 (Found: C, 77.80; H, 7.46. Calc. for $C_{21}H_{24}O_3$. C, 77.74; H, 7.46%).

§ *Selected data* for **2**: ν_{max}(neat)/cm^{-1} 3065, 2862, 1643, 1238, 1095, 696; δ_H($CDCl_3$; 200 MHz) 3.58–3.65 (dd, 1 H), 4.21–4.26 (dd, 1 H), 4.30–4.40 (t, 1 H), 4.61–4.92 (m, 4 H), 5.29–5.48 (m, 3 H), 5.94–6.14 (m, 1 H), 6.40–6.45 (d, 1 H), 7.20–7.33 (m, 10 H); δ_C($CDCl_3$; 50 MHz) 144.63, 139.90, 139.82, 134.54, 128.47, 128.02, 127.81, 127.71, 118.23, 100.48, 78.50, 78.11, 75.63, 73.87, 70.74 (Found: C, 78.28; H, 6.85. Calc. for $C_{21}H_{22}O_3$; C, 78.23; H, 6.88%).

¶ *Selected data* for **9**: ν_{max}(neat)/cm^{-1} 3030, 1496, 1454, 1155, 1097, 696; δ_H($CDCl_3$; 200 MHz) 2.02–2.30 (m, 3 H), 3.54–3.75 (m, 3 H), 4.12–4.24 (m, 1 H), 4.50–4.92 (m, 6 H), 5.66–5.85 (m, 2 H), 7.24–7.40 (m, 15 H); δ_C($CDCl_3$; 50 MHz) 139.14, 138.76, 128.52, 128.34, 127.91, 127.78, 127.51, 126.17, 81.11, 79.62, 74.29, 73.17, 71.44, 70.64, 39.47, 28.80 (Found: C, 81.18; H, 7.31. Calc. for $C_{28}H_{30}O_3$: C, 81.12; H, 7.29%).

1 R. J. Ferrier and S. Middleton, *Chem. Rev.*, 1993, **93**, 2779.
2 R. J. Ferrier, *J. Chem. Soc., Perkin Trans. 1*, 1979, 1455.
3 T. V. RajanBabu, *Acc. Chem. Res.*, 1991, **24**, 139.
4 T. Taguchi, H. Ito, Y. Motoki and Y. Hanzawa, *J. Am. Chem. Soc.*, 1993, **115**, 8835.
5 S. Ogawa, Y. Uematsu, S. Yoshida, N. Sesaki and T. Suami, *J. Carbohydr. Chem.*, 1987, **6**, 471.
6 T. K. M. Shing and L. H. Wan, *Angew. Chem., Int. Ed. Engl.*, 1995, **34**, 1643.
7 S. Ogawa, *Yuki. Gosei Kagaku Kyokai Shi*, 1985, **43**, 26.
8 T. Suami and S. Ogawa, *Adv. Carbohydr. Chem. Biochem.*, 1990, **28**, 41.
9 D. A. Entwistle and M. Hudlicky, *Tetrahedron Lett.*, 1995, **36**, 2591.
10 L. Pingli and M. Vandewalle, *Synlett*, 1994, 228.
11 T. K. M. Shing and Y. Tang, *Tetrahedron*, 1991, **47**, 4571.
12 T. K. M. Shing, Y. Cui and Y. Tang, *J. Chem. Soc., Chem. Commun.*, 1991, 756.
13 R. J. Ferrier and R. Blattner, *J. Chem. Soc., Chem. Commun.*, 1987, 1008.
14 G. Büchi and J. E. Powell Jr., *J. Am. Chem. Soc.*, 1967, **89**, 4559.
15 B. Fraser-Reid, R. A. Alonso, G. D. Vite and R. E. McDevitt, *J. Org. Chem.*, 1992, **57**, 573.
16 K. Yamamoto, M. Minato and J. Tsuji, *J. Org. Chem.*, 1990, **55**, 766.
17 F. Fringuelli, R. Germani, F. Pizzo and G. Savelli, *Synth Commun.*, 1989, **19**, 1939.
18 H. Paulsen and W. von Deyn, *Justus Liebigs. Ann. Chem.*, 1987, 125.
19 R. B. Woodward and F. V. Brutcher Jr., *J. Am. Chem. Soc.*, 1958, **80**, 209.

Received in Cambridge, UK, 24th December 1997; Revised manuscript received 5th March 1998; 8/01989D

X-Ray structure of bridged 2,2′-bi(adamant-2-ylidene) chloronium cation and comparison of its reactivity with a singly-bonded chloroarenium cation

T. Mori, R. Rathore, S. V. Lindeman and J. K. Kochi†

Department of Chemistry, University of Houston, Houston, Texas 77204-5641, USA

The unsymmetrically bridged 2,2′-bi(adamant-2-ylidene) chloronium hexachloroantimonate shows distinctive electrophilic (transfer) chlorination reactivity in comparison with the singly-bonded chloroarenium cation.

We recently reported[1] the isolation and structural characterization of a novel cationic chlorine–aromatic complex in which the chlorine atom is directly bonded to a single aromatic carbon atom in a manner similar to that qualitatively described for Wheland intermediates in electrophilic aromatic chlorinations.[2] The lability of the C–Cl bond in the highly colored (red) chloroarenium cation (**1**–Cl^+) is demonstrated by its ready

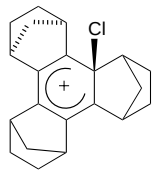

1–Cl^+

ability to transfer the positive chlorine (Cl^+) to a variety of aromatic and olefinic donors.[1] For example, an ice-cold solution of 2,2′-bi(adamant-2-ylidene)[3] (**2**) reacts with an equimolar amount of **1**–Cl^+ $SbCl_6^-$ in CH_2Cl_2 and immediately leads to the bleaching of the red color. The addition of cold hexane affords a colorless microcrystalline precipitate of **2**–Cl^+ $SbCl_6^-$ in quantitative yield [eqn. (1)]. The identity of **2**–Cl^+ $SbCl_6^-$ is

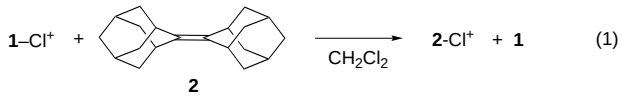

(1)

confirmed by spectral (IR and NMR) comparison with an authentic sample prepared from olefin **2** and $SbCl_5$ according to the procedure of Nugent.[4] Note that the chloronium salt **2**–Cl^+ $SbCl_6^-$ is extremely robust (if protected from moisture), and it may be stored at room temperature for several days without any decomposition. However despite its remarkable stability,[4] the structural proof for the nature of bonding in the olefin–chloronium complex **2**–Cl^+ has not been forthcoming. Accordingly, we now report (a) the single-crystal structure analysis of **2**–Cl^+ $SbCl_6^-$ and (b) its reactivity with various aromatic and olefinic donors in comparison with that of the chloroarenium cation **1**–Cl^+ $SbCl_6^-$.

A colorless crystal suitable for X-ray crystallography was grown by slow diffusion of hexane into a CH_2Cl_2 solution of **2**–Cl^+ $SbCl_6^-$ at −23 °C. Single crystal analysis‡ by X-ray crystallography established its molecular structure, and the ORTEP diagram in Fig. 1 shows that the chlorine atom is bonded to both olefinic carbon atoms, resulting in a bridged structure akin to that of the corresponding bromonium cation reported previously by Brown and co-workers.[5] The attachment of a positive chlorine (Cl^+) to the olefinic bond [C(1)–C(11)] in **2** generates an unsymmetrical cyclopropane ring system in which the C(1)–C(11) bond (2.08 Å) is significantly longer than the C(1)–C(17) bond (1.92 Å); the C(1)–C(11) bond (1.49 Å) is close to a normal single C–C bond. [Note that the hexachloroantimonate anion is only weakly coordinated to C(l7).][6]

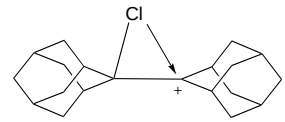

We ascribe the unique features of **2**–Cl^+ to an unsymmetrical structure in which chlorine is σ bonded to a single carbon center [C(11)], and the cationic charge on the adjacent center (C1) is stabilized (solvated) by the chlorine lone pair (acting as an n-donor). The bridged structure of **2**–Cl^+ is reminiscent of that described for the stabilization of carbocations by neighboring group participation.[7] Such a 'non-classical' structure of **2**–Cl^+ leads to a highly stabilized chloronium cation in comparison to the singly-bonded chloroarenium cation **1**–Cl^+ that readily transfers its positive chlorine to a variety of aromatic and olefinic donors [eqn. (1) and Table 1].

The electrophilic (transfer) chlorination of various aromatic donors with **2**–Cl^+ $SbCl_6^-$ was carried out as follows. A solution of **2**–Cl^+ $SbCl_6^-$ (0.02 M) in CH_2Cl_2 was treated with pentamethylbenzene (3 equiv.) at room temperature under an argon atmosphere. The colorless reaction mixture was stirred for 3 h, during which the solution took on a pale brown coloration. Aqueous workup of the reaction mixture and GC and GC–MS analysis indicated that only a trace amount of chloropentamethylbenzene (< 1%) was formed. The decom-

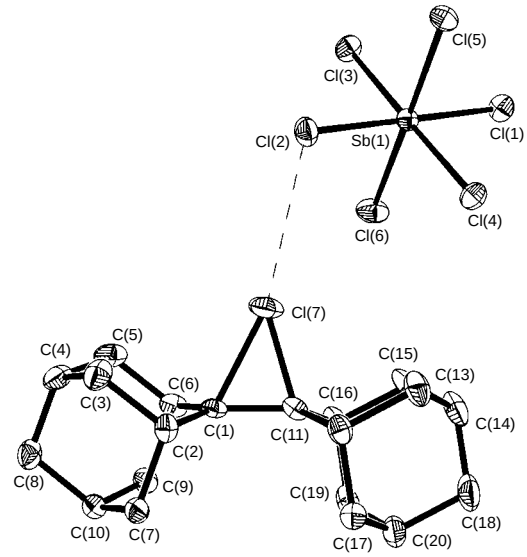

Fig. 1 ORTEP diagram of chloronium cation **2**–Cl^+ $SbCl_6^-$

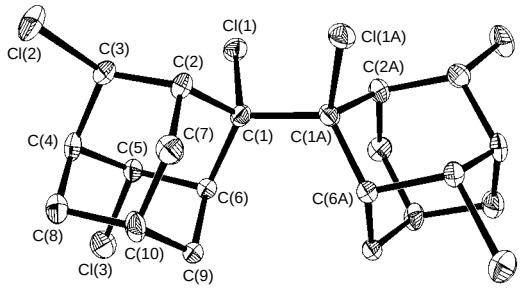

Fig. 2 ORTEP diagram of 2,2′,4,4′,9,9′-hexachloro-2,2′-biadamantane

position products of **2**–Cl^+ $SbCl_6^-$ were identified as the recovered olefin **2** (27%), the rearranged spiroketone (58%) and several unidentified products.[8] Similarly, the reaction of **2**–Cl^+ $SbCl_6^-$ with various other aromatic donors listed in Table 1 yielded mainly the decomposition products of **2**–Cl^+.[8] Furthermore, the treatment of excess cyclohexene (3 equiv.) with **2**–Cl^+ $SbCl_6^-$ in CH_2Cl_2 afforded only the decomposition products of **2**–Cl^+, and no chlorinated product derived form cyclohexene was detected. This remarkable absence of transfer chlorination toward various aromatic and olefinic donors by **2**–Cl^+ is in sharp contrast to the corresponding bromonium (or iodonium) cation which readily transfers its positive halogen (Br^+ or I^+) to a variety of olefinic donors.[9] The insufficient reactivity of **2**–Cl^+ towards various electron donors is consistent with our proposal of rather tight σ-bonded character to the bridged chloronium cation (*vide supra*). On the other hand, the enhanced reactivity of the corresponding **2**–Br^+ (or **2**–I^+) may be attributed to a more loose bromonium–olefin complex with predominant π-character.[10]

Although **2**–Cl^+ is an ineffective Cl^+-transfer agent, it readily oxidizes electron-rich aromatic donors to the corresponding cation radicals in its capacity as a one-electron oxidant. For example, treatment of a hexasubstituted aromatic donor (CRET)[11] with a solution of **2**–Cl^+ in CH_2Cl_2 at 25 °C yields the orange cation radical [$CRET^{\cdot+}$, λ_{max} = 518, 486 (sh) nm][11] in close to quantitative yield during the course of a 3 h period.

To further examine the differences in reactivities of **2**–Cl^+ and **2**–Br^+, we carried out the reaction of olefin **2** with dichlorine in CH_2Cl_2.[12] Thus, the addition of a cooled (−30 °C) solution of **2** to a yellow solution of chlorine in CH_2Cl_2 rapidly led to bleaching; and the careful subsequent addition of hexane led to colorless crystals during the course of a three day period. The crystalline material was filtered, and X-ray structure determination§ of a colorless single crystal revealed the molecular structure of the chlorinated product to be 2,2′,4,4′,9,9′-hexachloro-2,2′-biadamantane **3** as illustrated in Fig. 2. Removal of solvent from the filtrate revealed the presence of several other unidentified (chlorinated) products. The irreversible reaction of gaseous chlorine with **2** is to be constrasted with the corresponding reaction with bromine, in which **2** reacts reversibly with Br_2 resulting in a variety of intermediates together with **2**–Br^+. However, removal of the solvent and gaseous bromine *in vacuo* led to the quantitative recovery of olefin **2**.[13]

Further experiments are underway to determine the electron-density distribution in various aromatic and olefinic halonium complexes,[10] in order to more precisely characterize the nature of the bonding in these complexes.

We thank the National Science Foundation, Robert A. Welch Foundation for financial support and S. H. Loyd for preliminary experiments and T. Mori thanks the Japan Society for the Promotion of Science for a fellowship (No. 5026).

Notes and References

† E-mail: cjulian@popiuh.edu

‡ *Crystal data* for 2,2′-bi(adamant-2-ylidene) chloronium hexachloroantimonate [$(C_{20}H_{28}Cl)^+$ $SbCl_6^-\cdot CH_2Cl_2$]. X-Ray quality crystal (0.40 × 0.15 × 0.04 mm) was obtained from a CH_2Cl_2–C_6H_{14} mixture at −23 °C. M = 723.25, orthorhombic, space group $P2_12_12_1$, a = 10.3394(1), b = 16.0104(1) and c = 16.0930(1) Å, D_c = 1.803 mg m^{-3}, V = 2664 $Å^3$, Z = 4. Data collection was carried out on a Siemens SMART diffractometer equipped with a CCD detector, using Mo-Kα radiation (λ = 0.71073 Å), at −150 °C. The total number of reflections measured was 34 182, of which 12 224 reflections were symmetrically non-equivalent. The structure was solved by direct methods and refined by full-matrix least-squares procedure. Final residuals were $R1$ = 0.054 and $wR2$ = 0.103 for 8640 reflections with $I > 2\sigma(I)$.

§ *Crystal data* for 2,2′,4,4′,9,9′-hexachloro-2,2′-biadamantane [$(C_{20}H_{24}Cl_6)$]. Bi(adamantylidene) was added to a solution of chlorine in CH_2Cl_2 at −30 °C and the resulting pale yellow solution was layered with prechilled (−30 °C) hexane. A well-formed crop of crystals was obtained after a three day period at −23 °C. A colorless crystal with dimensions (0.1 × 0.1 × 0.15 mm) was used for X-ray structural study. M = 477.09, monoclinic, space group $C2/c$, a = 14.116(2), b = 6.8734(8) and c = 19.537(3) Å, D_c = 1.686 mg m^{-3}, V = 1879.4 $Å^3$, Z = 4. Data collection was carried out as described above and the total number of reflections measured was 4085, of which 2679 reflections were symmetrically non-equivalent. The structure was solved by direct methods and refined by full-matrix least-squares procedure. Final residuals were $R1$ = 0.074 and $wR2$ = 0.136 for 1727 reflections with $I > 2\sigma(I)$. (Note that this crystal also contained ~8% of 2,2′,9,9′,10,10′-hexachloro-2,2′-biadamantane as an isomeric impurity.)

1 R. Rathore, S. H. Loyd and J. K. Kochi, *J. Am. Chem. Soc.*, 1994, **116**, 8414.
2 R. Taylor, *Electrophilic Aromatic Substitutions*, Wiley, New York, 1990.
3 E. W. Meijer and H. Wynberg, *J. Chem. Ed.*, 1982, **59**, 1071.
4 W. A. Nugent, *J. Org. Chem.*, 1980, **45**, 4534. Also see, G. A. Olah, P. Schilling, W. Westerman and H. C. Lin, *J. Am. Chem. Soc.*, 1974, **96**, 4533.
5 (*a*) H. Slebocka-Tilk, R. G. Ball and R. S. Brown, *J. Am. Chem. Soc.*, 1985, **107**, 4504; (*b*) R. S. Brown, R. W. Nagorski, R. E. D. McClung, G. H. M. Aarts, M. Klobukowski, R. McDonald and B. D. Santarsiero, *J. Am. Chem. Soc.*, 1994, **116**, 2448 and references therein.
6 In various **2**–X^+ cations, the disposition of counteranion with respect to X^+ may be viewed as an indicator of the degree of the positive charge on the halogen atom. Thus the hexachloroantimonate anion in **2**–Cl^+ is only weakly coordinated (Cl^+–$ClSbCl_5^-$ = 3.51 Å) whereas the tribromide in **2**–Br^+ (Br^+–Br_3^- = 3.10 Å) and a water molecule in **2**–I^+ (I^+–OH_2 = 2.63 Å) are strongly coordinated to the halonium cation.
7 J. March, *Advanced Organic Chemistry*, 4th edn., Wiley, New York, 1992, pp. 308.
8 In order to determine the decomposition products from **2**–Cl^+, a 0.02 M solution of **2**–Cl^+ $SbCl_6^-$ in CH_2Cl_2 was stirred at 25 °C and aqueous sodium hydrogen carbonate (~5%) was added. The mixture was further stirred for 10 min and the CH_2Cl_2 layer was separated. Analysis by GC and GC–MS indicated the presence of **2** (10%), spiroketone (60%) and several unidentified products.
9 A. A. Neverov and R. S. Brown, *Can. J. Chem.*, 1994, **72**, 2540; R. S. Brown, *Acc. Chem. Res.*, 1997, **30**, 131 and references therein.
10 The possible π-character of both **2**–Br^+ and **2**–I^+ is indicated by the rather symmetrical bridging, with C–X bond lengths of ±0.03 Å in **2**–Br^+ Br_3^- [5*a*] and **2**–Br^+ $CF_3SO_3^-$ [5*b*] as well as ±0.01 Å in **2**–I^+ $CF_3SO_3^-$.[5*b*] Moreover, the 'olefinic' bond length in **2**–I^+ is shortened to 1.45 Å.
11 R. Rathore and J. K. Kochi, *J. Org. Chem.*, 1995, **60**, 4399.
12 Compare: J. H. Wieringa, J. Strating and H. Wynberg, *Tetrahedron Lett.*, 1970, 4579.
13 J. Strating, J. H. Wieringa and H. Wynberg, *J. Chem. Soc., Chem. Commun.*, 1969, 907. Also see, A. J. Bennet, R. S. Brown, R. E. D. McClung, M. Klobukowski and G. H. M. Aarts, *J. Am. Chem. Soc.*, 1991, **113**, 8532.

Received in Columbia, MO, USA, 15th December 1997; 7/09063C

Asymmetric intercalation of N^1-(acridin-9-ylcarbonyl)spermine at homopurine sites of duplex DNA

Ian S. Blagbrough,[a] Steven Taylor,[a] Mark L. Carpenter,[b] Vyacheslav Novoselskiy,[c] Tatyana Shamma[c] and Ian S. Haworth*[c]†

[a] *Department of Pharmacy and Pharmacology, University of Bath, Claverton Down, Bath, UK BA2 7AY*
[b] *Sir William Dunn School of Pathology, Oxford University, South Parks Road, Oxford, UK OX1 3RE*
[c] *Department of Pharmaceutical Sciences, University of Southern California, 1985Zonal Avenue, Los Angeles, CA 90033, USA*

N^1-(Acridin-9-ylcarbonyl)spermine binds at 5′-pu-p-pu..5′-py-p-py sites of DNA with the acridine moiety asymmetrically intercalated, stacked between the two purine bases; the spermine moiety interacts with the homopyrimidine phosphodiester backbone of the intercalation site and protects against DNase I cleavage of this backbone, but does not protect against cleavage of the homopurine backbone at the same intercalation site.

Acridine, a common DNA intercalator, has been used extensively to modulate the DNA binding properties of many ligands through covalent attachment of the acridine moiety. Examples include acridine conjugates with peptides,[1] oligodeoxynucleotides,[2] minor-groove DNA binders such as netropsin and distamycin[3] and the DNA alkylating agent cisplatin.[4,5] The binding selectivity of these conjugates generally reflects that of the non-acridine part of the molecule, although acridine conjugation seems to redirect the alkylation selectivity of some aniline mustards.[6] The site-specific photocleavage of DNA by acridine- 9-carboxamide–imidazole conjugates, in association with Co^{III}, may be a result of an acridine preference for intercalation at a 5′-GpG..5′-CpC site.[7]

Polyamines, such as spermine and spermidine, are polycationic molecules that have limited DNA-sequence selectivity, but may preferentially bind to GC-rich major grooves,[8] and AT-rich minor grooves.[9] Amongst many examples of polyamine conjugates[10] are those having polyamines covalently bound to long-chain lipids,[11] anthracene[12] and mustard alkylating agents such as chlorambucil.[13] There is no apparent evidence of the polyamine introducing a sequence-selective binding effect into any of these molecules, but in each it is believed that the polyamine enhances the binding affinity through electrostatic interactions with DNA.

To combine the intercalating effects of acridine and the high affinity polyamine binding to DNA, we have synthesized N^1-(acridin-9-ylcarbonyl)spermine **1**.‡ To investigate any possible sequence selectivity of **1**, we then used a DNase I protection assay with the Hind III/Nhe I restriction fragment of pBR322 plasmid duplex DNA.§ The protection from DNase I cleavage by **1** was pronounced at eight sites within the readable window of the gel (approximately from base-pair 81 to 150, Fig. 1). Of these, seven are homopyrimidine tracts of two or more bases. The remaining site corresponds to a 5′-CpG..5′-CpG sequence (site 5) and was only weakly protected. Of the pyrimidine tract sites, five span only two pyrimidine bases, with both 5′-CpC (sites 1 and 3, with weak protection at site 4) and 5′-TpT (sites 6 and 7) equally protected. Sites 2 and 8 contain longer 5′-CpCpT and 5′-CpTpTpT tracts, respectively, both of which are fully protected. Hence, the nature of the pyrimidine (C or T) seems to be unimportant in establishing protection against DNase I by polyamine amide **1**. In addition to the pyrimidine protection sites, some enhancement of cleavage is observed adjacent to several protection sites (for example, to the 3′ side of site 7). Such enhancement has been observed previously in this assay,[3] and could be the result of a DNA conformational change brought about by the binding of **1**.

1

In the DNase I assay we found no protection of purine tracts on the bottom strand (italicised in Fig. 1). This is an interesting result, given that such tracts have corresponding complementary pyrimidine tracts in the top strand. One might anticipate that the ligand binding causing the protection described above would also occur in these regions of the DNA, and would offer similar protection to the homopurine regions of the bottom strand. We conclude from this that there is an asymmetric binding of polyamine amide **1** to the homopurine..homopyrimidine DNA, such that only the pyrimidine backbone is protected from DNase I.

To investigate further this unusual experimental result, computer simulations were performed using 18-mer duplexes containing intercalation sites[12] corresponding to two protection sites. These were site 3 (intercalation site between base pairs

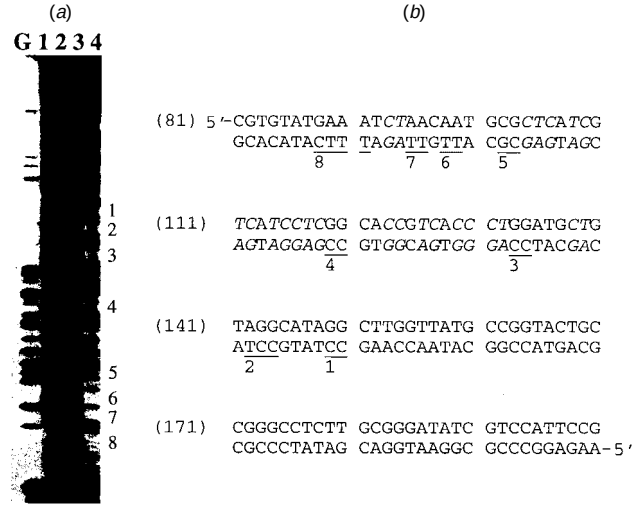

Fig. 1 Sites of DNase I protection by N^1-(acridin-9-ylcarbonyl) spermine **1** in a 3′-end [^{32}P]-bottom strand labelled Hind III/Nhe I restriction fragment of pBR322. (*a*) Autoradiogram showing Maxam–Gilbert dimethyl sulfate–piperidine mediated guanine specific cleavage (lane G), and DNase I cleavage in the presence of no polyamine amide **1** (lane 1), 0.2 μM **1** (lane 2), 1.0 μM **1** (lane 3) and 5.0 μM **1** (lane 4). Protection sites are numbered 1 to 8 in the 5′ to 3′ direction of the bottom strand. (*b*) Sequence of restriction fragment corresponding to the autoradiogram. Numbered and underlined sequences show protection sites; note that no protection was observed at italicised sequences.

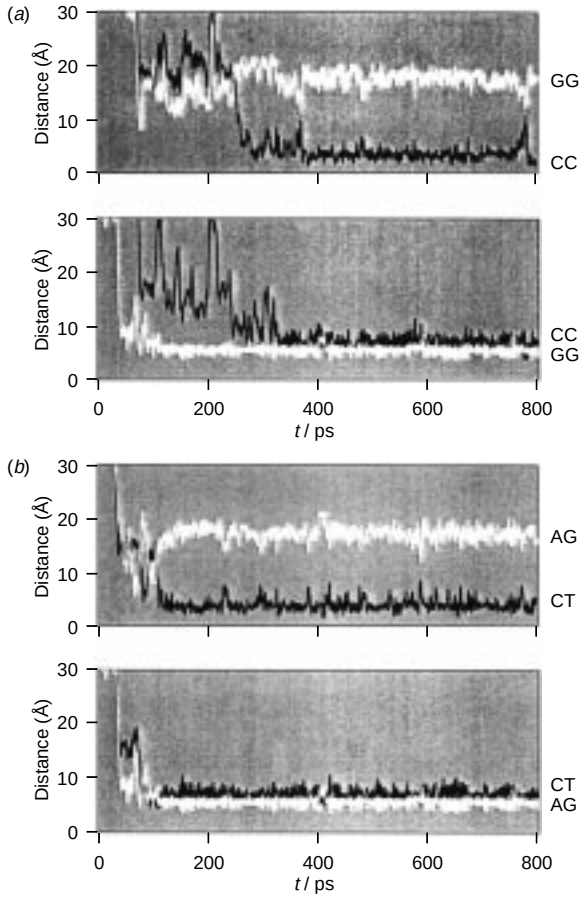

Fig. 2 Simulations of polyamine amide **1** with 18-mer DNA molecules having (a) a central 5′-GpG..5′-CpC intercalation site (site 3) and (*b*) a central 5′-ApG..5′-CpT intercalation site (site 2), showing in the upper panels of (*a*) and (*b*) the polyamine contact distances to the phosphates of the respective homopyrimidine and homopurine backbones, and in the lower panels the acridine contact distances to the C1′ atoms of the same backbones

133 and 134, 5′-GpG..5′-CpC in a sequence corresponding to base pairs 125 to 142) and site 2 (intercalation site between base pairs 142 and 143, 5′-ApG..5′-CpT, in a sequence corresponding to base pairs 134 to 151). Molecular dynamics simulations of the interactions of **1** with each site were performed in the AMBER4.1 forcefield using similar conditions to those described elsewhere.[12] Simulations were performed for 800 ps and the DNA motion was frozen throughout the calculations.[12] The ligand was initially positioned about 20 Å from the DNA, allowing it to move to the DNA, bind and then intercalate from either groove with a random orientation of the polyamine moiety.[12]

In Fig. 2 we show the results of these simulations. The data shown in the upper panels of Fig. 2(*a*) and (*b*) are the distances of the polyamine moiety to the phosphodiesters of each intercalation site, using, at each time point, the phosphate in each strand closest to the 'centre' of the polyamine (defined as the midpoint of the two secondary amines). In the lower panels, the distance from the centre of the acridine (pyridine) ring to the C1′ atoms of the deoxyriboses of each intercalation site, using, at each time point, the C1′ atom of each strand closest to the acridine centre. Following intercalation (after 300 ps for site 3 and 100 ps for site 2, from the major groove for each site), the acridine moiety remains closer to the homopurine strand for both sites. Conversely, whilst the acridine moiety is intercalated, the polyamine interacts only with the homopyrimidine strand for both sites.

This asymmetric intercalation binding geometry of the acridine moiety, stacked between two purine bases, and the concurrent polyamine location on the homopyrimidine phosphodiester backbone, provides a clear explanation of our DNase I protection data. Acridine and spermine show but small DNA sequence selective binding (see above), and neither molecule alone apparently exhibits the kind of sequence specificity shown by polyamine amide **1**. Based on computer simulation, this specificity seems to arise from acridine binding, and the polyamine plays the role of 'reporting' the specificity by binding to the homopyrimidine backbone and blocking DNase I cleavage. However, it is possible that the polyamine moiety plays a more direct role in determining the sequence selectivity of **1**, and we are currently synthesizing analogues of **1** to investigate this possibility further.

We thank the NIH (CA64299-01 to I. S. H.), the MRC (G9219146N to I. S. B.), and the Wellcome Trust (039750/A/93/A to I. S. B. and 035312/Z/92/Z to P. R. C. and M. L. C.) for financial support. We thank S. Carrington (University of Bath), Dr A. Rodger (University of Warwick), and Dr P. R. Cook (University of Oxford) for their interest and for generous advice. I. S. B. holds a Nuffield Foundation Science Lecturer's award (SCI/180/91/15/G). I. S. H. and I. S. B. are joint holders of a NATO grant (CRG 970290).

Notes and References

† E-mail: ihaworth@hsc.usc.edu

‡ Polyamine amide **1** was synthesized using N^1-mono-Boc-spermine[14] starting with spermine (free base) and Boc_2O (THF, 0–25 °C, 14 h, 54% after flash silica gel chromatography). Acylation with acridine-9-carboxylic acid [DCC (1.5 equiv.), cat. HOBt (0.05 equiv.), 48 h, DMF, 25 °C] afforded the desired mono-Boc protected conjugate as a viscous yellow oil (48% after flash silica gel chromatography). Deportection (TFA, 0 °C, 1 h) of the primary amine gave **1** as its poly-TFA salt, a yellow solid (100%) after lyophilisation.

§ The 197 base pair Hind III / Nhe I restriction fragment of pBR322 was labelled on the 3′-end of the bottom strand at the Hind III site (making base 34 the 3′-end of the bottom strand) with α-[^{32}P]dATP and reverse transcriptase (ref. 15). The labelled fragment was isolated, purified (PAGE, 6% non-denaturing gel), eluted from the gel with Tris–EDTA (TE) buffer (10 mM Tris, 0.1 mM EDTA, pH 8.0), precipitated with EtOH and redissolved in TE buffer. DNA footprinting with polyamine amide **1** (0.2–25.0 μM) was performed using DNase I (0.01 units ml^{-1}) at 25 °C (4 min, 2 mM $MgCl_2$, 2 mM $MnCl_2$, 20 mM NaCl, pH 7.5). The reaction was stopped using 80% formamide (5 μl) and cleavage products identified by co-electrophoresis with Maxam–Gilbert G-specific cleavage products on a denaturing gel (6% acrylamide, 8 M urea, 1500 V, 2 h).

1 F. Bailly, C. Bailly, N. Helbecque, N. Pommery, P. Colson, C. Houssier and J. P. Henichart, *Anti-Cancer Drug Des.*, 1992, **7**, 83.
2 E. Washbrook and K. R. Fox, *Biochem. J.*, 1994, 569.
3 A. Eliadis, D. R. Phillips, J. A. Reiss and A. Skorobogaty, *J. Chem. Soc., Chem. Commun.*, 1988, 1049.
4 C. Cullinane, G. Wickham, W. D. McFadyen, W. A. Denny, B. D. Palmer and D. R. Phillips, *Nucleic Acids Res.*, 1993, **21**, 393.
5 V. Murray, H. Motyka, P. R. England, G. Wickham, H. H. Lee, W. A. Denny, and W. D. McFadyen, *J. Biol. Chem.*, 1992, **267**, 18 805.
6 A. S. Prakash, W. A. Denny, T. A. Gourdie, K. K. Valu, P. D. Woodgate and L. P. Wakelin, *Biochemistry*, 1990, **29**, 9799.
7 J. D. Tan, E. T. Farinas, S. S. David and P. K. Mascharak, *Inorg. Chem.*, 1994, **33**, 4295.
8 M. Yuki, V. Grukhin, C.-S. Lee and I. S. Haworth, *Arch. Biochem. Biophys.*, 1996, **325**, 39.
9 N. Schmid and J.-P. Behr, *Biochemistry*, 1991, **30**, 4357.
10 I. S. Blagbrough, S. Carrington and A. J. Geall, *Pharm. Sci.*, 1997, **3**, 223 and references cited therein.
11 A. J. Geall and I. S. Blagbrough, *Tetrahedron Lett.*, 1998, **39**, 443.
12 A. Rodger, S. Taylor, G. Adlam, I. S. Blagbrough and I. S. Haworth, *Bioorg. Med. Chem.*, 1995, **3**, 861.
13 P. M. Cullis, L. Merson-Davies and R. Weaver, *J. Am. Chem. Soc.*, 1995, **117**, 8033.
14 I. S. Blagbrough and A. J. Geall, *Tetrahedron Lett.*, 1998, **39**, 439.
15 C. A. Laughton, T. C. Jenkins, K. R.. Fox and S. Neidle, *Nucleic Acids Res.*, 1990, **18**, 4479 and references cited therein.

Received in Corvallis, OR, USA, 22nd December 1997; 7/09193A

Routine determination of molecular crystal structures from powder diffraction data

William I. F. David,*[a]† Kenneth Shankland[a] and Norman Shankland[b]

[a] *ISIS Facility, Rutherford Appleton Laboratory, Chilton, Didcot, Oxon, UK OX11 0QX*
[b] *Department of Pharmaceutical Sciences, University of Strathclyde, Glasgow, UK G1 1XW*

The state of the art in determining molecular crystal structures from powder diffraction data using a global optimisation method is illustrated with a fast, automated simulated annealing approach to solving the previously unknown crystal structures of capsaicin, thiothixene and promazine hydrochloride.

The routine structure determination of molecular materials from single-crystal diffraction data is one of the principal triumphs of crystallography. In contrast, structure determination from powder diffraction data is problematic, hampered as it is by the severe loss of information arising from Bragg peak overlap. Here, we present a fast, automated, simulated annealing approach to the problem that provides a significant alternative to direct methods usually employed in attempts to solve structures from powder diffraction data.[1]

X-Ray diffraction data were collected for the compounds illustrated in Fig. 1 at 100 K on BM16 of the European Synchrotron Radiation Facility[2] (λ = 0.6528 Å), and the structures solved as follows. The position, orientation and conformation of an entire molecule in the refined unit cell were postulated and the level of agreement between the trial structure and the experimental diffraction data quantified by:[3]

$$\chi^2 = \sum_h \sum_k [(I_h - c\,|F_h|^2)(V^{-1})_{hk}(I_k - c\,|F_k|^2)]$$

where I_h and I_k are Lorentz-polarisation corrected, extracted integrated intensities from a Pawley refinement[4] of the diffraction pattern, V_{hk} is the covariance matrix from the Pawley refinement, c is a scale factor, and $|F_h|$ and $|F_k|$ are the structure factor magnitudes calculated from the trial structure.

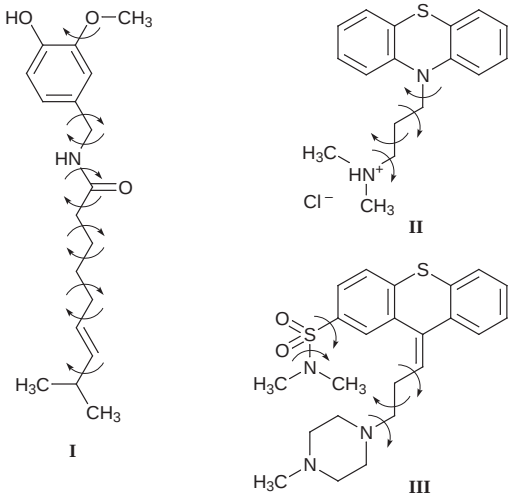

Fig. 1 Capsaicin **I** is the 'hot' component of chilli peppers. Promazine hydrochloride **II** and thiothixene **III** are tranquillisers. Internal degrees of freedom (indicated by the arrows) are 0–360° in every case, except for H–N–C=O in capsaicin, where the range 160–200° was sampled. The configurations around the C=C bonds in capsaicin and thiothixene were fixed as shown, in accordance with prior chemical knowledge, and the piperazine ring fixed in a chair conformation. The molecules have six, nine and five external degrees of freedom respectively.

The trial structure was subjected to a global optimisation in which torsion angles were the only internal degrees of freedom (Fig. 1) and bounds on the external degrees of freedom (three fractional coordinates for position and four quaternions for orientation[5]) were derived from the Euclidean normalisers of the relevant space groups.[6] Finally, the structure solutions obtained at the end of the simulated annealing runs were verified by Rietveld refinements[7] in which only scale and overall temperature factors were refined.

The method presented here has two distinctive elements. Firstly, the correlated integrated intensities figure-of-merit is formally equivalent to, but calculated typically two orders of magnitude faster than, the agreement factors used by others[8–10] that operate *via* a point-by-point comparison with the measured diffraction pattern. Secondly, the simulated annealing protocol contains a novel combination of elements that facilitate global searching of the complex multi-dimensional parameter space. These include a temperature reduction that cools more slowly if the χ^2 fluctuations (*cf.* heat capacity) are large, the capacity to generate random mutations (*cf.* a genetic algorithm approach[3]) and an algorithm to generate new parameter sets that samples the neighbouring parameter space efficiently whilst allowing large perturbations with an exponentially decreasing probability.

High quality solutions were obtained with ease for all three structures (Table 1), with remarkably good agreement between the observed and calculated diffraction patterns (Fig. 2). This close agreement arises from the ability of the simulated annealing algorithm to 'fine tune' both the internal and external

Table 1 Refined unit cells, extracted intensity information and final χ^2 for the compounds shown in Fig. 1[a]

	Compound		
	Capsaicin **I**	Promazine HCl **II**	Thiothixene **III**
Space group	$P2_1/c$	$P2_1/c$	$P2_1$
a/Å	12.2234(1)	11.8081(2)	10.1471(4)
b/Å	14.7900(1)	11.4895(3)	8.6883(1)
c/Å	9.4691(1)	13.4270(2)	13.6806(3)
β/°	93.9754(3)	111.722(1)	110.650(1)
2θ Data/°	2.7–22.5	3.0–20.0	2.5–20.4
Res./Å	1.67	1.88	1.84
N_{ref}	379	271	216
t_d/min	40	8	9
χ^2_{Paw}	13.05	3.70	9.43
χ^2_{Riet}	51.19	5.03	63.74
t_s/min	1860	112	205

[a] N_{ref} = Number of reflections in the data range shown. χ^2_{Paw} = Chi-squared for the Pawley type fit to the data range shown. χ^2_{Riet} = Chi-squared for the Rietveld fit of the output simulated annealing model to the data range shown, with only scale and overall temperature factor refined. Res = Maximum spatial resolution of data. t_d = Data collection time over the specified range. t_s = Time to simulated annealing solution (DEC Alphastation 500/500).

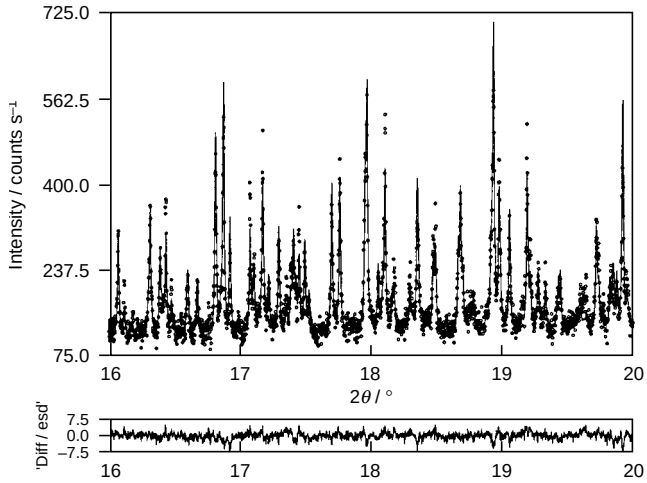

Fig. 2 Calculated (—) and observed (·) diffraction data for promazine hydrochloride **II**, with the crucial higher angle (*i.e.* higher spatial resolution) region shown. The calculated pattern is the result of a Rietveld refinement of the simulated annealing solution in which only the scale factor and overall temperature factor were refined. The atomic coordinates obtained from the simulated annealing algorithm were not refined.

degrees of freedom. Equally remarkable, given the limited spatial resolution of the data, is the agreement between the simulated annealing solution for capsaicin and a 0.7 Å resolution single-crystal structure determined subsequently in order to validate the simulated annealing approach (Fig. 3).

A combination of factors make the simulated annealing approach attractive as a method for structure determination: (*a*) the method works well on relatively low spatial resolution data, opening the way to rapid data collections (Table 1), (*b*) input models are easily constructed in internal coordinates using standard bond lengths and angles, (*c*) the process is entirely structure factor driven and thus no intra- or inter-molecular distance or energy checks are needed, and (*d*) the agreement factor is quick to calculate, leading to the rapid evaluation of the correct solution. In the case of capsaicin, structures were evaluated at a rate of *ca*. 150 per second. On smaller molecules, rates in excess of 1000 structure evaluations per second have been achieved. Ongoing optimisation of the goodness-of-fit χ^2 evaluation code promises to increase this rate still further.

In conclusion, we have demonstrated a very powerful method for solving molecular crystal structures from powder diffraction data. Although the experimental data were collected at a synchrotron source, the ability to solve structures reliably with data extending to resolutions of only $\approx$1.8 Å means that the approach will also be applicable to data collected on laboratory-based X-ray diffractometers. Approximately 77% of organic structures reported in the Cambridge Structural Database[11] have fewer atoms than thiothixene. It follows that the approach should have broad applicability in molecular crystal structure analysis.

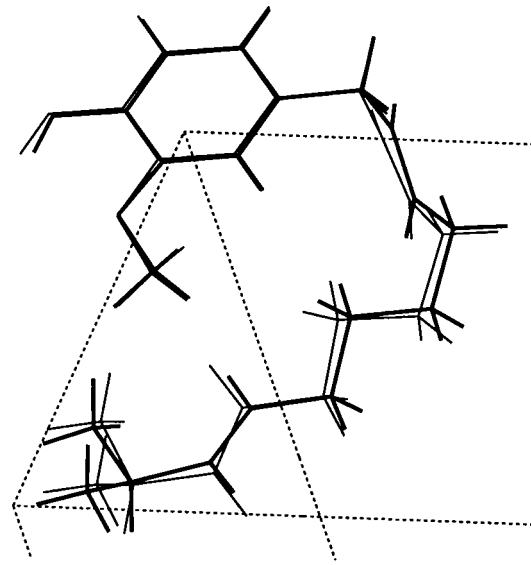

Fig. 3 The solved crystal structure of capsaicin **I** output directly from the simulated annealing algorithm, with the single-crystal solution shown overlaid in bold. The minimum, maximum and mean distances between pairs of corresponding capsaicin atoms are 0.045, 0.418 and 0.150 Å, respectively.

We thank Dr Andy Fitch of the ESRF for setting up BM16, Dr Chris Frampton of Roche Drug Discovery for determining the single-crystal structure of capsaicin, and Dr Joel Oliver of Procter and Gamble for helpful discussions regarding the structure of capsaicin.

Notes and References

† E-mail: wifd@isise.rl.ac.uk

1 D. M. Poojary and A. Clearfield, *Acc. Chem. Res.*, 1997, **30**, 414.
2 A. N. Fitch, *Nucl. Instrum. Methods Phys. Res. B*, 1995, **97**, 63.
3 K. Shankland, W. I. F. David and T. Csoka, *Z. Kristallogr.*, 1997, **212**, 550.
4 G. S. Pawley, *J. Appl. Crystallogr.*, 1981, **14**, 357.
5 J. Foley, A. Van Dam, S. Feiner and J. Hughes, *Computer Graphics, Principles and Practice*, Addison Wesley, Reading, MA, 2nd edn., 1993, ch. 21.
6 *International Tables for X-ray Crystallography Vol. A* (*Space Group Symmetry*), ed. T. Hahn, Kluwer Academic Publishers, Dordrecht, 1989.
7 H. M. Rietveld, *J. Appl. Crystallogr.*, 1969, **2**, 65.
8 K. D. M. Harris and M. Tremayne, *Chem. Mater.*, 1996, **8**, 2554.
9 Y. G. Andreev, P. Lightfoot and P. G. Bruce, *J. Appl. Crystallogr.*, 1997, **30**, 294.
10 B. M. Kariuki, H. Serrano-Gonzalez, R. L. Johnson and K. D. M. Harris, *Chem. Phys. Lett.*, 1997, **280**, 189.
11 F. H. Allen and O. Kennard, *Chem. Des. Automat. News*, 1993, **8**, 1.

Received in Cambridge, UK, 2nd February 1998; 8/00855H

Diastereoselective intramolecular nitroaldol entry to lycoricidine alkaloids

James McNulty*† and Ruowei Mo

Department of Chemistry, Brock University, St. Catharines, Ontario, Canada L2S 3A1

The alumina promoted 6-*exo*-*trig* intramolecular nitroaldol cyclization described proceeds in a highly diastereoselective manner *via* a proposed chelation controlled chair-like transition state, the major diastereomer having the correct relative configuration at three stereocentres as observed in the pancratistatin series of antitumor agents, in contrast to prior literature cyclization methods.

Nitroalkenes are valuable synthetic intermediates by virtue of their high reactivity and *umpolung* nature compared to carbonyl and amino substrates, to which they may be subsequently converted. They are highly reactive as Michael acceptors in conjugate addition processes[1] and dienophiles in Diels–Alder cycloadditions,[2] in addition to undergoing other valuable transformations.[3] Nitroalkenes are therefore valuable intermediates for the preparation of compounds of biological interest. Seebach has made extensive use of their high reactivity as Michael acceptors[1] and described applications towards the synthesis of alkaloids.[4] One attractive annulation strategy (Scheme 1) involves a combination Michael addition of a dianion onto the nitroalkene followed by subsequent intramolecular nitroaldol cyclization onto an appropriately functionalized carbonyl-containing side chain. This methodology has been applied towards the preparation of deoxylycorinone derivatives.[4] Other routes to lycoricidine-type alkaloids utilizing nitroalkenes have also been reported.[5]

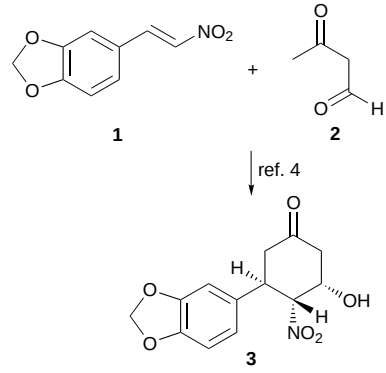

Scheme 1

In consideration of the structure of the valuable anticancer alkaloids pancratistatin **4** and *trans*-dihydrolycoricidine **5**,[6] the development of an intramolecular nitroaldol cyclization exhibiting alternative diastereoselectivity to that of the base promoted example described above would be of great value. We are currently addressing the issue of the nature of the C-ring hydroxy substituents of compounds **4** and **5** with respect to the anticancer pharmacophore and require a means of access to deoxy derivatives of **5**. The observation that the three substituents on the cyclohexane C-ring at positions 4, 4a and 10b‡ in the desired natural diastereomeric series lie in *equatorial* positions led us to consider the possibility of a chelation controlled intramolecular nitroaldol cyclization as a means of controlling the relative stereochemistry. We now report a neutral alumina promoted nitroaldol cyclization that provides the desired diastereoselectivity.

Michael addition of the copper–zinc reagent[7] derived from ethyl 4-bromobutyrate **6** (Scheme 2) to the piperonal derived nitroalkene **1** proceeded cleanly to give the ester **7**. Selective reduction of the ester with DIBAL-H gave aldehyde **8**, the key substrate for the intramolecular nitroaldol. Our analysis of the possibility of a chelation controlled chair-like transition state

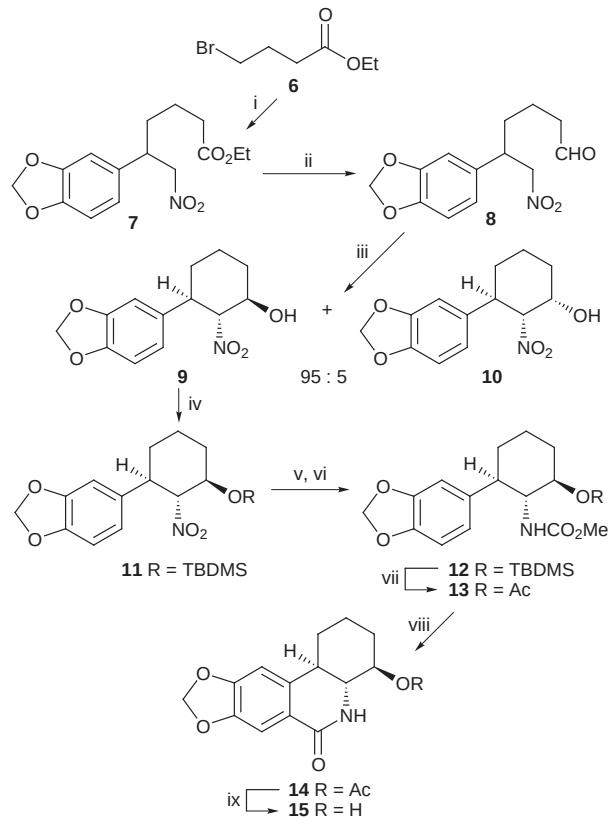

Scheme 2 *Reagents and conditions*: i, Zn, LiI (0.25 equiv.), DMF, 75 °C, 5 h; then CuCN (1 equiv.), LiCl (2 equiv.), THF, 0 °C, 5 min; cool to −78 °C, then **1**, −78 to 0 °C, 5 h, 81%; ii, DIBAL-H (1.3 equiv.), CH_2Cl_2, −78 °C, 5 h; iii, Activity 1 (Brockmann) alumina, 20 °C, 48 h, 71% from **7**; iv, TBDMSCl (1.3 equiv.), imidazole (2.5 equiv.), DMF, 20 °C, 24 h, 96%; v, Raney Ni, 650 psi H_2, MeOH, 20 °C, 4 h, 100%; vi, $ClCO_2Me$ (1.5 equiv.), 0 °C, CH_2Cl_2, Et_3N, 5 h, 96%; vii, Ac_2O, $FeCl_3$ (0.2 equiv.), 0 °C , 10 min, 85%; viii, Tf_2O (5.0 equiv.), DMAP (3.0 equiv.), CH_2Cl_2, 0–15 °C, 15 h; then 2 M HCl (aq.), THF, 18 °C, 14 h, then Ac_2O, DMAP, Et_3N, 0–18 °C, 12 h, 85%; ix, NaOMe (1.1 equiv.), THF–MeOH, 0–18 °C, 12 h, 96%

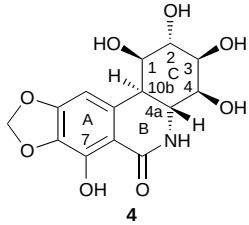

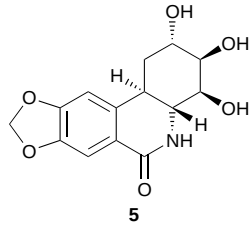

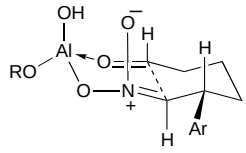

Fig. 1

(Fig. 1) for the intramolecular cyclization in conjunction with earlier reports[8a,b] on basic alumina promoted *inter*molecular nitroaldol reactions led to the following procedure. Aldehyde **8** was dissolved in CH_2Cl_2 and treated with *neutral* alumina at ambient temperature while solvent was removed under a nitrogen flow. Clean cyclization slowly occurred giving two diastereomers, **9** and **10**, in the ratio of 95 : 5. Importantly, no dehydration is observed when neutral alumina is employed at room temperature; however simply warming to 40 °C can result in the formation of nitroalkenes.[8a] Separation of the compounds was readily achieved (neutral alumina, CH_2Cl_2–MeOH, 95 : 5) and to our delight the *major* isomer proved to be **9**, as evidenced by ^{1}H NMR analysis (H-4a δ 4.45, dd, J = 11.2, 9.8 Hz). The high diastereoselectivity observed is consistent with the transition state model we propose in which an alumina–nitronate bischelated intermediate undergoes intramolecular cyclization *via* a late, chair-like transition state in which all developing substituents occupy equatorial-like positions. This model should prove useful in the prediction of diastereoselectivity in related 6-*exo*-*trig* nitroaldol reactions.

The utility of this diastereoselective cyclization was demonstrated by elaboration of the nitroaldol product **9** (Scheme 2) to lycoricidine analogue **15** retaining the desired natural stereochemistry. The alcohol of **9** was first protected§ to give the silyl ether **11**, which was quantitatively reduced over Raney Ni and protected to give the carbamate **12**. Attempts to cyclize this silyl protected carbamate by the method of Banwell[9] failed due to the instability of the TBDMS group under the cyclization conditions. The protecting group was therefore changed using the one-pot procedure of Ganem[10] providing the acetate **13**, which was cyclized[9] to give the tetracycle **14**. The yield on the Bischler–Napieralski cyclization was optimized by extending the hydrolysis time to 14 h, and employing an aqueous HCl–THF mixture instead of the reported aqueous AcOH. This also resulted in a small amount of acetate hydrolysis, as was observed under Banwell's conditions.[9] An overall yield of 85% of **14** could be realized from **13** when a final re-acetylation step was employed. Banwell's cyclization protocol is clearly more efficient than earlier methods in effecting this key transformation.[9] Finally, clean removal of the acetate protecting group provided us with the desired analogue 2,3-dideoxy-*trans*-dihydrolycoricidine **15**.

The diastereoselective nitroaldol cyclization described above provides a valuable access to deoxy derivatives of alkaloids **4** and **5**, both of which exhibit a high degree of anticancer activity,[6] having the correct relative stereochemistry at key positions C-4, C-4a and C-10b. Alkaloid **5** is currently the simplest known derivative that exhibits the full spectrum of anticancer activity.[6] The chemistry reported allows access to the simplified C-ring analogue **15**, lacking two hydroxy groups from **5**, which will provide valuable information concerning the pharmacophore of these alkaloids.

Further modifications of the C-ring based on the proposed transition state model and anticancer evaluation is currently in progress and will be reported shortly.

Financial support of this work by the National Science and Engineering Research Council of Canada, by a Cottrell Scholar award from Research Corporation (to J. McN) and by a Brock University SEED grant is gratefully acknowledged. We thank Mr Tim Jones for conducting mass spectral and 2D NMR analyses and the referees for valuable comments.

Notes and References

† E-mail: jmcnulty@chemiris.labs.brocku.ca

‡ The pancratistatin ring numbering system (ref. 6) is used throughout.

§ Compound **9** could be protected as the acetate, however intramolecular acyl transfer occurred when the nitro substituent was reduced, giving the acetamide.

1 H. Schafer and D. Seebach, *Tetrahedron*, 1995, **51**, 2305.
2 M. Node, K. Nishide, H. Imazato, R. Kurosaki, T. Inoue and T. Ikariya, *Chem. Commun.*, 1996, 2559.
3 S. E. Denmark, A. Thorarensen and D. S. Middleton, *J. Am. Chem. Soc.*, 1996, **118**, 8266; E. J. Corey and H. Estreicher, *J. Am. Chem. Soc*., 1978, **100**, 6294.
4 T. Weller and D. Seebach, *Tetrahedron Lett.*, 1982, **23**, 935; V. Ehrig and D. Seebach, *Chem. Ber.*, 1975, **108**, 1961.
5 For other approaches to lycoricidine alkaloids employing nitroalkenes, see H. Paulsen and M. Stubbe, *Tetrahedron Lett.*, 1982, **23**, 3171; R.S.C. Lopes, C.C. Lopes and C.H. Heathcock, *Tetrahedron Lett.*, 1992, **33**, 6775.
6 G. R. Pettit, G. R. Pettit III, R. A. Backhaus, M. R. Boyd and A. W. Meerow, *J. Nat. Prod.*, 1993, **56**, 1682.
7 C. Jubert and P. Knochel, *J. Org. Chem.*, 1992, **57**, 5431; C. Retherford, M. C. P. Yeh, I. Schipor, H. G. Chen and P. Knochel, *J. Org. Chem.*, 1989, **54**, 5200.
8 (*a*) R. Ballini, R. Castagnani and M. Petrini, *J. Org. Chem.*, 1992, **57**, 2160; (*b*) G. Rosini, R. Ballini and P. Sorrenti, *Synthesis*, 1983, 1014.
9 M. G. Banwell, B. D. Bissett, S. Busato, C. J. Cowden, D. C. R. Hockless, J. W. Holman, R. W. Read and A. W. Wu, *J. Chem. Soc., Chem. Commun.*, 1995, 2551.
10 B. Ganem and V. R. Small Jr., *J. Org. Chem.*, 1974, **39**, 3728.

Received in Corvallis, OR, USA, 5th January 1998; 8/00097B

Chiral diiminophosphoranes: a new class of ligands for enantioselective transition metal catalysis

Manfred T. Reetz,*† Edward Bohres and Richard Goddard

Max-Planck-Institut für Kohlenforschung, Kaiser-Wilhelm-Platz 1, D-45470 Mülheim/Ruhr, Germany

Chiral diamines such as (1*R*,2*R*)-1,2-diaminocyclohexane or *R*-2,2′-diamino-1,1′-binaphthalene can be converted into the corresponding diimino(triphenyl)phosphoranes, which serve as C_2-symmetric ligands for enantioselective transition metal catalyzed reactions such as copper-mediated cyclopropanations.

Chiral nitrogen-containing compounds are gaining increasing importance as ligands in enantioselective transition metal catalyzed reactions.[1] Although iminophosphoranes[2] of the general structure $R_3P{=}NR'$ possess a donor position at the nitrogen function capable of metal complexation,[3] chiral versions have not been prepared to date. Since iminophosphoranes are readily available from the corresponding primary amines $R'NH_2$, we envisioned a simple route to chiral chelating diiminophosphoranes and their possible use as ligands in enantioselective transition metal catalyzed reactions. Here we report the first examples of this concept.

Upon reacting the commercially available diamines **1** and **3** with Ph_3PBr_2 followed by base treatment according to a literature procedure (modified by working in the presence of molecular sieves),[4] compounds **2** and **4** were obtained in yields of 82 and 75%, respectively.

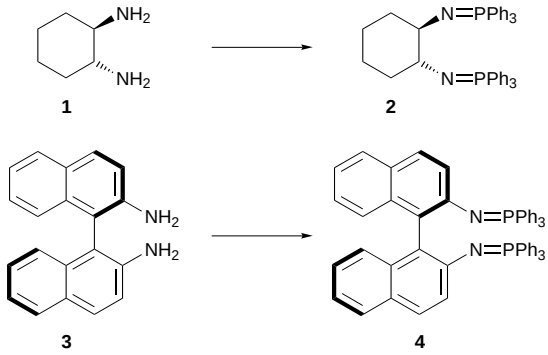

Scheme 1

Ligands **2** and **4** are crystalline compounds, which were characterized by standard methods, including ^{31}P NMR spectroscopy (δ −0.5 and −4.6, respectively, in CD_2Cl_2) and X-ray crystallography‡ (Fig. 1). The effect of the crystal environment appears to have a more significant effect on **2** than **4**, since whereas **4** exhibits exact C_2 symmetry in the crystal [N···N* 3.617(8) Å], even in spite of the presence of solvent of crystallization, in **2** the local C_2 symmetry is restricted to the cyclohexane ring and the two nitrogen atoms [N(1)···N(2) 3.770(2) Å].

These two chiral ligands are suitable for preparing a wide variety of new types of transition metal complexes. Indeed, the complexes **2**·Rh(cod)BF_4, **2**·$CoCl_2$ and **4**·CuOTf were readily synthesized in yields of *ca*. 80% by reacting the corresponding ligands with $[RhCl_2(cod)]_2$ (followed by $NaBF_4$), $CoCl_2(thf)_x$ or CuOTf, as appropriate. The crystal structures of **2**·Rh(cod)BF_4 and **2**·$CoCl_2$ confirm the flexibility of the diimino(triphenyl)-phosphorane ligand (Fig. 2). Thus, whereas the iminophosphor-

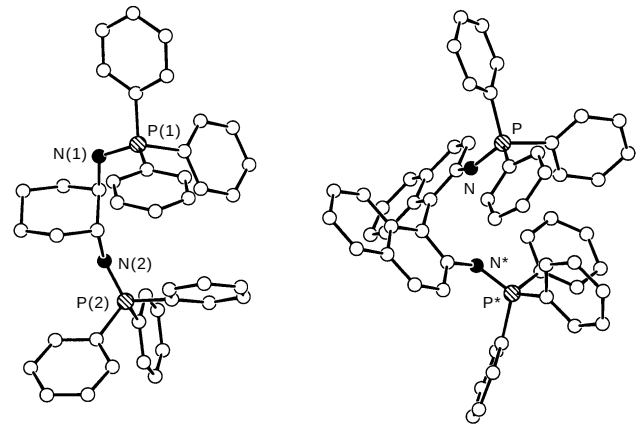

Fig. 1 Molecular structures of **2** (left) and **4** (in **4** the CD_2Cl_2 solvent of crystallization has been removed for clarity)

ane groups in the free ligand (**2**) occupy diaxial positions, in the complexed ligand both groups are equatorial, presumably enabling the N atoms to accommodate the metals [**2**·Rh(cod)BF_4 N···N 2.665(6) Å, N–Rh–N 77.3(3)°; **2**·$CoCl_2$ N···N 2.75(2) Å, N–Co–N 85.6(6)°]. In addition, the extent of the C_2 symmetry induced by the ligand strongly depends on the coordination sphere of the metal. In **2**·Rh(cod)BF_4 the approximately square-planar coordinated Rh atom deviates strongly (2.818 Å) from the local C_2 symmetry of the iminocyclohexane ring (dashed line, Fig. 2, left). In **2**·$CoCl_2$, on the other hand, the loss of symmetry is much smaller and distorted tetrahedral Co lies approximately (±0.2 Å) on the local C_2 axis of symmetry (dashed line, Fig. 2, right).

Preliminary studies using these chiral metal complexes for enantioselective catalysis have also been undertaken. Particularly worthy of note is the copper catalyzed cyclopropanation[5] of styrene **5** by ethyl diazoacetate **6** using the complex **4**·CuOTf (1.5 mol%) as the catalyst (Scheme 2). Adducts **7** and **8** were

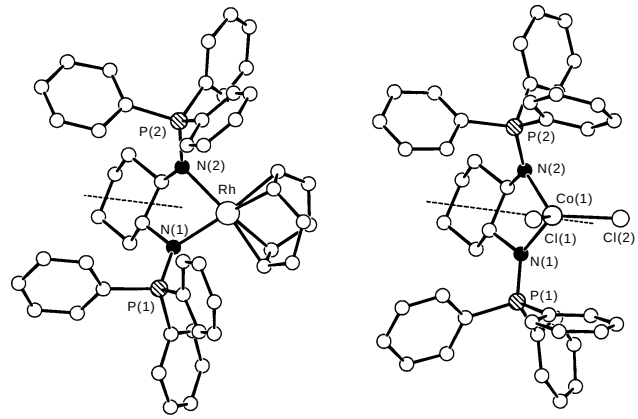

Fig. 2 Molecular structures of the [**2**·Rh(cod)]$^+$ cation in **2**·Rh(cod)BF_4 (left) and **2**·$CoCl_2$. Dashed lines indicate local C_2 symmetry.

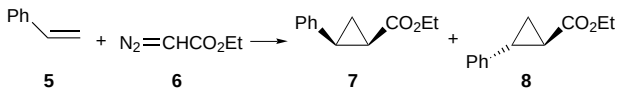

Scheme 2

formed in equal amounts, each having an enantiomeric excess (ee) of 90 and 74% in favour of the absolute configurations (*S*,*R*) and (*R*,*R*), respectively.§

In summary, we have developed a new and readily accessible class of chiral nitrogen containing ligands for asymmetric transition metal catalysis. The possibility of varying the substituents of phosphorus and/or utilizing other chiral diamines or functionalized amines is currently being explored.

Notes and References

† E-mail: reetz@mpi-muelheim.mpg.de

‡ *Crystal data*: **2**: $C_{42}H_{40}N_2P_2$, M_r = 634.7, colourless plate, crystal size 0.32 × 0.60 × 0.88 mm, a = 11.3778(2), b = 8.7847(2), c = 17.5062(3) Å, β = 103.296(1)°, U = 1702.85(6) Å^3, T = 100 K, monoclinic, space group $P2_1$ (no. 4), Z = 2, D_c = 1.24 g cm^{-3}, μ = 0.16 mm^{-1}. Siemens SMART diffractometer, Mo-Kα X-radiation, λ = 0.710 73 Å. 19 124 measured reflections, 9573 unique, 9288 observed [$I > 2.0\sigma(F_o^2)$]. The structure was solved by direct methods (SHELXS-86) and refined by full-matrix least squares (SHELXL-97) on F^2 for all data with Chebyshev weights to R = 0.059 (obs.), wR = 0.160 (all data), S = 1.05, H atoms riding, max. shift/error 0.001, residual ρ_{max} = 0.968 e Å^{-3}.

4·CD_2Cl_2: $C_{57}H_{42}Cl_2D_2N_2P_2$: M_r = 889.8, yellow prism, crystal size 0.28 × 0.39 × 0.46 mm, a = 10.703(1), b = 18.868(2), c = 22.522(2) Å, U = 4547.9(8) Å^3, T = 100 K, orthorhombic, space group $C222_1$ (no. 20), Z = 4, D_c = 1.30 g cm^{-3}, μ = 0.26 mm^{-1}. Enraf-Nonius CAD4 diffractometer, Mo-Kα X-radiation, λ = 0.710 69 Å. 2568 measured reflections, 2051 observed [$I > 2.0\sigma(F_o^2)$]. The structure was solved by direct methods (SHELXS-86) and refined by full-matrix least squares (SHELXL-97) on F^2 for all data with Chebyshev weights to R = 0.074 (obs.), wR = 0.231 (all data), S = 1.04, H atoms riding, solvent CD_2Cl_2 disordered over two positions, max. shift/error 0.001, residual ρ_{max} = 0.633 e Å^{-3}.

2·Rh(cod)BF_4: $C_{50}H_{52}BF_4N_2P_2Rh$, M_r = 932.6, orange prism, crystal size 0.35 × 0.52 × 0.59 mm, a = 13.732(2), b = 16.915(2), c = 19.222(3) Å, U = 4465(1) Å^3, T = 293 K, orthorhombic, space group $P2_12_12_1$ (no. 19), Z = 4, D_c = 1.39 g cm^{-3}, μ = 0.51 mm^{-1}. Enraf-Nonius CAD4 diffractometer, Mo-Kα X-radiation, λ = 0.710 69 Å. 5746 measured reflections, 5619 unique, 5114 observed [$I > 2.0\sigma(F_o^2)$]. Analytical absorption correction (T_{min} 0.7769, T_{max} 0.9805). The structure was solved by direct methods (SHELXS-86) and refined by full-matrix least squares (SHELXL-97) on F^2 for all data with Chebyshev weights to R = 0.059 (obs.), wR = 0.151 (all data), S = 1.03, H atoms riding, max shift/error 0.001, residual ρ_{max} = 1.681 e Å^{-3}.

2·$CoCl_2$·$3CH_2Cl_2$: $C_{45}H_{46}Cl_8CoN_2P_2$, M_r = 1019.3, blue prism, crystal size 0.35 × 0.42 × 0.62 mm, a = 24.447(1), b = 9.8142(4), c = 40.257(2) Å, β = 99.710(2)°, U = 9520.1(8) Å^3, T = 100 K, monoclinic, space group $C2$ (no. 5), Z = 8, D_c = 1.42 g cm^{-3}, μ = 0.91 mm^{-1}. Siemens SMART diffractometer, Mo-Kα X-radiation, λ = 0.710 73 Å. 48 840 measured reflections, spherical absorption correction, 20 400 unique, 13 253 observed [$I > 2.0\sigma(F_o^2)$]. The structure was solved by direct methods (SHELXS-86) and refined by full-matrix least squares (SHELXL-97) on F^2 for all data (Co, Cl, P anisotropic) with Chebyshev weights to R = 0.086 (obs.), wR = 0.199 (all data), S = 1.07, H atoms riding, max. shift/error 0.001, residual ρ_{max} = 0.998 e Å^{-3}. CCDC 182/796.

§ *Procedure*: a catalyst solution of **4**·CuOTf was prepared by mixing 1 equiv. of a copper(I) triflate benzene complex with 1.2 equiv. of ligand **4** in dry CH_2Cl_2 under an atmosphere of argon. A Schlenk tube was charged with 1.0 ml of a 0.015 M catalyst solution, freed from the solvent *in vacuo* and charged with styrene (1.0 ml of a 1.0 M solution in 1,2-dichloroethane). The mixture was cooled to −20 °C and treated with **6** (3 mmol in 3 ml of 1,2-dichloroethane) within 3 h using a syringe pump. The mixture was analyzed by GC (80% conversion).

1 A. Togni and L. M. Venanzi, *Angew. Chem.*, 1994, **106**, 517; *Angew. Chem., Int. Ed. Engl.*, 1994, **33**, 497; A. Pfaltz, *Acc. Chem. Res.*, 1993, **26**, 339.
2 A. W. Johnson and W. C. Kaska, *Ylides and Imines of Phosphorus*, Wiley, New York, 1993.
3 E. W. Abel and S. A. Mucklejohn, *Inorg. Chim. Acta*, 1979, **37**, 107; P. Imhoff, C. J. Elsevier and C. H. Stam, *Inorg. Chim. Acta*, 1990, **175**, 209; R. W. Reed, B. Santarsiero and R. G. Cavell, *Inorg. Chem.*, 1996, **35**, 4292; R. Appel and P. Volz, *Z. Anorg. Allg. Chem.*, 1975, **413**, 45.
4 K.-W. Lee and L. A. Singer, *J. Org. Chem.*, 1974, **39**, 3780.
5 Recent review: V. K. Singh, A. DattaGupta and G. Sekar, *Synthesis*, 1997, 137.

Received in Cambridge, UK, 16th December 1997; 7/09023D

Synthesis of characteristic lipopeptides of lipid modified proteins employing the allyl ester as protecting group

Thierry Schmittberger, Alain Cotté and Herbert Waldmann*†

Universität Karlsruhe, Institut für Organische Chemie, Richard-Willstätter-Allee 2, D-76128 Karlsruhe, Germany

Lipidated peptides which represent characteristic lipid modified substructures of lipidated human $G_{\alpha O}$ protein and the human N- and R-*Ras* proteins were built up efficiently by employing the selective Pd^0-mediated removal of allyl esters under very mild conditions as the key step.

Lipid modified proteins are critically involved in biological signal transduction.[1] Thus, the transmembrane G protein coupled receptors are *S*-palmitoylated, their downstream effectors, the heterotrimeric G proteins are *N*-myristoylated, *S*-palmitoylated and *S*-farnesylated, the H- and the N-*Ras* proteins carry palmitoyl and farnesyl groups and the R-*Ras* protein is palmitoylated and geranylgeranylated. For the proper execution of their biological functions the correct lipidation of these classes of proteins is paramount.[2–4]

For the study of the biological significance of lipidated proteins, in particular their possible roles in signal transduction processes, lipidated peptides that contain the characteristic structural elements of their parent proteins are very useful reagents.[5,6] Therefore, the development of efficient methods for the construction of lipidated peptides is of particular interest. However, the thioesters present in these peptide conjugates are readily hydrolyzed at pH > 7 and may be lost *via* base-mediated β-elimination; also the double bonds present in farnesyl and geranylgeranyl groups are attacked under acidic conditions.[7,8] Consequently, protecting groups have to be employed that can be removed under neutral conditions.[5,8] We now report that characteristic lipidated peptides which represent lipid modified substructures of lipidated proteins can efficiently be built up by employing the allyl ester[9] as a protecting group.

In order to construct the *N*-myristoylated and *S*-palmitoylated *N*-terminus **7** of a human $G_{\alpha O}$ protein which embodies the characteristic Myr-Gly-Cys(Pal)-AA-AA-Ser/Thr-AA motif found in many G proteins,[10] cystine bisallyl ester **1** was coupled with *N*-myristoylglycine and after reductive cleavage of the disulfide bond the liberated mercapto groups were *S*-palmitoylated to give the protected thioester **2** (Scheme 1). From **2** the allyl ester was removed with complete selectivity in high yield by Pd^0-mediated transfer of the allyl group to morpholine as the accepting nucleophile. Subsequent elongation of the peptide chain by the dipeptide **4** yielded a lipidated tetrapeptide allyl ester from which the allyl group was also cleaved to give the selectively unmasked lipotetrapeptide **5** in high yield.‡ Further extension of the peptide chain by the dipeptide allyl ester **6** and final Pd^0-mediated removal of the allyl group delivered the desired myristoylated and palmitoylated *N*-terminal G protein fragment **7**. The three allyl ester cleavages performed in this sequence proceeded with complete selectivity and without any undesired side reactions. The conditions of the noble-metal complex mediated allyl transfer are so mild that neither an attack on the base-sensitive thioester nor a base-induced β-elimination of the palmitoyl group occurred.

By means of this advantageous technique also the *S*-palmitoylated and *S*-geranylgeranylated *C*-terminus **14** of the human R-*Ras* protein[11] was efficiently built up (Scheme 2). To this end, the *S*-palmitoylated cysteinyl tripeptide allyl ester **8** was synthesized from $(BocGlyGlyCysOAll\text{-}S)_2$ by reductive cleavage of the disulfide and *S*-acylation, as described for **2** in Scheme 1 [the cystinyl precursor was built up from BocGly-GlyOH and cystine bis(allyl ester) by peptide coupling]. In this case 1,3-dimethylpyrimidine-2,4,6-trione (*N*,*N*′-dimethylbarbituric acid) **9**[12] was employed as accepting C-nucleophile in the Pd^0-mediated reaction. The C-terminal deprotection proceeded smoothly to give the desired carboxylic acid **10** in high yield. Elongation of the peptide chain by proline allyl ester **11** and a further Pd^0-mediated allyl ester cleavage in the presence of **9** delivered the *S*-palmitoylated tetrapeptide carboxylic acid **12** in high yield.‡ Finally, the synthesis was completed by coupling of **12** with *S*-geranylgeranylated cysteine methyl ester **13** to give the desired R-*Ras* peptide **14**.

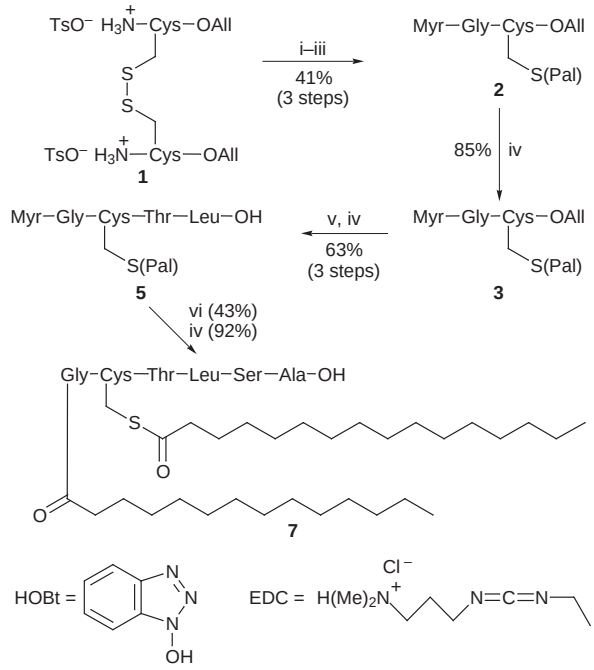

Scheme 1 *Reagents and conditions*: i, Myr-Gly-OH, EEDQ, NEt_3, CH_2Cl_2, Pr^iOH; ii, DTT, NEt_3, CH_2Cl_2; iii, palmitoyl chloride, DMAP, NEt_3, CH_2Cl_2; iv, $Pd(PPh_3)_4$, morpholine, THF; v, H-Thr-Leu-OAll **4**, EDC, HOBt, CH_2Cl_2; vi, H-Ser-Ala-OAll **6**, EDC, HOBt, CH_2Cl_2

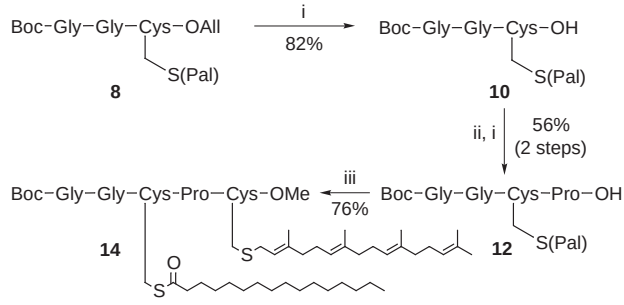

Scheme 2 *Reagents and conditions*: i, $Pd(PPh_3)_4$, **9**, THF; ii, ProOAll **11**, EDC, HOBt, CH_2Cl_2; iii, Cys(GerGer)OMe **13**, EDC, HOBt, CH_2Cl_2

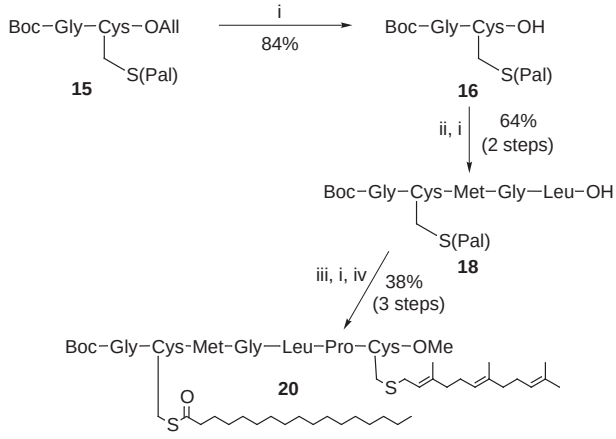

Scheme 3 *Reagents and conditions*: i, $[Pd(PPh_3)_4]$, **9**, THF; ii, MetGly-LeuOAll **17**, EDC, HOBt, CH_2Cl_2; iii, **11**, EDC, HOBt, CH_2Cl_2; iv, Cys(Far)OMe **19**, EDC, HOBt, CH_2Cl_2

In a third application the *S*-palmitoylated and *S*-farnesylated C-terminus **20** of the human N-*Ras* protein[11] was built up by employing the Pd^0 mediated cleavage of allyl esters as the key step (Scheme 3). In order to construct this molecule, the *S*-palmitoylated allyl ester **15** was deprotected in high yield to give the selectively unmasked *S*-palmitoylated dipeptide **16**. Coupling with the tripeptide **17** and subsequent allyl transfer to **9** yielded the pentapeptide carboxylic acid **18** in an efficient manner.‡ A chain elongation with proline allyl ester **11**, a further allyl removal and subsequent coupling with *S*-farnesylated cysteine methyl ester **19** delivered the N-*Ras* peptide **20**.

All Pd^0-catalyzed allyl ester cleavage reactions proceeded without any undesired side reaction. In no case could a β-elimination or a nucleophilic attack on the activated thioesters be observed.

The use of the allyl ester blocking function thus makes sensitive lipidated peptides available in an efficient manner which up to now has only been matched by enzymatic protecting techniques proceeding under extremely mild conditions.[8] This useful strategy readily gives access to further functionalized lipidated peptides.

This work was supported by the Deutsche Forschungsgemeinschaft and the Fonds der Chemischen Industrie.

Notes and References

† E-mail: waldmann@ochhades.chemie.uni-karlsruhe.de

‡ *General procedure*. To a solution of the peptide allyl ester (1 mmol) in THF or CH_2Cl_2 (30 ml) under Ar was added $Pd(PPh_3)_4$ (0.01 equiv.) and morpholine or **9** (1.2 equiv.). The solution was stirred at room temperature for 30–60 min. If morpholine was used as the nucleophile the solution was extracted with 10 ml of 1 M HCl and 10 ml of brine. The organic layer was dried with $MgSO_4$, the solvent was evaporated *in vacuo* and the product was isolated from the residue by flash chromatography on silica gel.

According to this procedure **5**, **12** and **18** were obtained.

Selected data for **5**: 84%; mp 127–131 °C; R_f 0.56 [CH_2Cl_2–MeOH–AcOH 90 : 10 : 1 (v/v/v)]; $[\alpha]_D^{25}$ −6 (*c* 0.5, DMF); δ_H(400 MHz, CD_3OD) 0.86 (t, *J* 7, 6 H, Me Pal, Me Myr), 0.90 (d, *J* 5.5, 3 H, Me Leu), 0.94 (d, *J* 5.5, 3 H, Me Leu), 1.17 (d, *J* 6.3, 3 H, Me Thr), 1.23 (s, 44 H, 12 CH_2 Pal, 10 CH_2 Myr), 1.40–1.51 (m, 7 H, β-CH_2 Pal, β-CH_2 Myr, β-CH_2 Leu, γ-CH Leu), 2.27 (t, *J* 8, 2 H, α-CH_2 Myr), 2.55 (t, *J* 8, 2 H, α-CH_2 Pal), 3.13 (dd, *J* 14, *J* 8, 1 H, α-CH Cys), 3.23 (dd, *J* 14, 4, 1 H, β-CH Cys), 3.75 (d, *J* 17, 1 H, α-CH Gly), 3.95 (d, *J* 17, 1 H, β-CH Gly), 4.21 (t, *J* 5.8, 1 H, α-CH Leu), 4.33 (d, *J* 3.5, α-CH Thr), 4.40 (dd, *J* 8, 4, 1 H, α-CH Cys), 4.40–4.47 (m, 1 H, β-CH Thr); δ_C(100.6 MHz, CD_3OD) 14.15 (Me Pal, Me Myr), 18.79 (Me Thr), 21.65 (Me Leu), 22.79 (CH_2 Pal, CH_2 Myr), 23.00 (Me Leu), 24.97 (γ-CH Leu), 25.61 (CH_2 Cys), 29.00–30.00 (12 CH_2 Pal, 10 CH_2 Myr), 32.04 (α-CH_2 Pal), 36.22 (α-CH_2 Myr), 40.71 (CH_2 Leu), 44.10 (CH_2 Cly), 51.67 (α-CH Leu), 54.45 (α-CH Cys), 58.53 (α-CH Thr), 67.25 (β-CH Thr), 170.53 (C=O), 170.79 (C=O), 175.41 (3 C=O), 201.22 (C=O, thioester); *m/z* [FABMS (glycerol)] 842.1 $[M + H]^+$. For **12**: 70%; R_f 0.20 [EtOAc–MeOH: 7 : 3 (v/v)]; $[\alpha]_D^{25}$ −29 (*c* 1.65, MeOH), mp 110–113 °C; δ_H(400 MHz, $CDCl_3$) 0.84 (t, *J* 6.7, 3 H, Me Pal), 1.19 (s, 24 H, 12 CH_2 Pal), 1.41 (s, 9 H, 3 CH_3 Boc), 1.52–1.64 (m, 3 H, β-CH_2 Pal), 1.89–2.23 (m, 2 H, 2 CH_2 Pro, CH_2Me Pal), 2.51 (t, *J* 7.1, 2 H, α-CH_2 Pal), 2.71–2.84 (m, 1 H, β-CH_2 Cys), 3.32–3.48 (m, 1 H, β-CH_2 Cys), 3.57–3.72 (m, 2 H, CH_2N Pro), 3.78–4.04 (m, 4 H, 2 CH_2 Gly), 4.30–4.40 (m, 1 H, α-CH Cys), 5.05–5.12 (m, 2 H, NH urethane, α-CH Pro), 8.35–8.46 (m, 2 H, 2 NH). For **18**: 79%; R_f 0.18 [EtOAc–MeOH 7 : 3 (v/v)]; $[\alpha]_D^{25}$ −33 (*c* 1.25, CH_3OH); δ_H(400 MHz, CD_3OD) 0.86 (t, *J* 6.6, 3 H, Me Pal), 0.94 (d, *J* 4.9, 6 H, Me Leu), 1.23 (s, 24 H, 12 CH_2 Pal), 1.44 (s, 9 H, 3 Me Boc), 1.51–1.76 (m, 3 H, β-CH_2 Pal, γ-CH Leu), 2.00–2.12 (m, 2 H, CH_2Me Pal), 2.08 (s, 3 H, Me Met), 2.17–2.25 (m, 2 H, γ-CH_2 Met), 2.50–2.57 (m, 4 H, α-CH_2 Pal, β-CH_2 Met), 3.25–3.34 (m, 2 H, β-CH_2 Cys), 3.85–3.98 (m, 2 H, CH_2 Gly), 4.05–4.22 (m, 2 H, CH_2 Gly), 4.62–4.74 (m, 3 H, α-CH Cys, α-CH Leu, α-CH Met); δ_C(100.6 MHz, CD_3OD) 14.13 (Me Pal), 15.24 (Me Met), 21.89 (Me Leu), 22.69 (CH_2 Pal), 22.90 (Me Leu), 24.80 (γ-CH Leu), 25.60 (CH_2 Pal), 28.42 (Me Boc), 29.29–31.40 (12 CH_2 Pal), 31.91 (β-CH_2 Cys), 41.21 (β-CH_2 Leu), 43.15 (β-CH_2 Cys), 44.04 (CH_2 Gly), 44.32 (CH_2 Gly), 79.99 (Cq Boc), 156.45 (C=O, urethane), 168.80 (C=O), 169.77 (C=O), 170.41 (C=O), 171.26 (C=O), 172.71 (C=O), 199.57 (C=O, thioester) (Calc. for $C_{39}H_{71}N_5O_9S_2$: C, 57.25; H, 8.75; N, 8.56. Found: C, 57.28; H, 8.97; N, 8.79%.)

1 P. J. Casey, *Science*, 1995, **268**, 221; G. Milligan, M. Parenti and A. J. Magee, *TIBS*, 1995, 181.
2 The H-, R- and K-*Ras* proteins can only transduce signals being passed on to them from growth factor receptors when they are lipid modified: S. E. Egan, R. A. Weinberg, *Nature*, 1993, **365**, 781; M. S. Boguski and F. McCormick, *Nature*, 1993, **366**, 643.
3 The signalling *via* GPCRs (S. Moffet, B. Mouillac, H. Bonin and M. Bouvier, *EMBO J.*, 1993, **12**, 349) and their corresponding downstream G proteins (P. B. Wedegaertner and H. R. Bourne, *Cell*, 1994, **77**, 1063) may be accompanied by the dynamic modification of their palmitoyl thioesters.
4 The lipidated C-terminus of R-*Ras* was shown to associate with the apoptosis suppressing proto-oncogene product Bcl-2, suggesting a role for R-*Ras* in the regulation of programmed cell death (apoptosis): M. J. Fernandez-Sarabia and J. P. Bischoff, *Nature*, 1993, **366**, 274.
5 For a review, see K. Hingerding, D. Alonso-Díaz and H. Waldmann, *Angew. Chem.*, 1998, **110**, 716; *Angew. Chem., Int. Ed. Engl.*, 1998, **37**, 688.
6 H. Waldmann, M. Schelhaas, E. Nägele, J. Kuhlmann, A. Wittinghofer and H. Schroeder, *Angew. Chem.*, 1997, **109**, 2334; *Angew. Chem., Int. Ed. Engl.*, 1997, **36**, 2238.
7 P. Stöber, M. Schelhaas, E. Nägele, P. Hagenbuch, J. Retey and H. Waldmann, *Bioorg. Med. Chem.*, 1997, **5**, 75.
8 For the synthesis of N-*Ras* lipopeptides by means of enzymatic protecting group techniques, see M. Schelhaas, S. Glomsda, M. Hänsler, H.-D. Jakubke and H. Waldmann, *Angew. Chem.*, 1996, **108**, 82; *Angew. Chem., Int. Ed. Engl.*, 1996, **25**, 106; H. Waldmann and E. Nägele, *Angew. Chem.*, 1995, **107**, 2425; *Angew. Chem., Int. Ed. Engl.*, 1995, **34**, 2259.
9 S. Friedrich-Bochnitschek, H. Waldmann and H. Kunz, *J. Org. Chem.*, 1989, **54**, 751.
10 S. M. Mumby, C. Kleuss and A. G. Gilman, *Proc. Natl. Acad. Sci. USA*, 1994, **91**, 2800.
11 J. F. Hancock, A. I. Magee, J. E. Childs and C. J. Marshall, *Cell.*, 1989, **57**, 1167.
12 H. Kunz and J. März, *Angew. Chem.*, 1988, **100**, 1424; *Angew. Chem., Int. Ed. Engl.*, 1988, **27**, 1375.

Received in Glasgow, UK, 4th December 1997; 7/08749G

Synthesis and crystal structures of low-valent binuclear vanadium complexes using the tethering ligand *m*-xylylenebis(acetylacetonate) (*m*-xba^{2-})

Peter J. Bonitatebus, Jr., Sanjay K. Mandal and William H. Armstrong*†

Department of Chemistry, Eugene F. Merkert Chemistry Center, Boston College, Chestnut Hill, MA 02167-3860, USA

An intriguing structural type new to low-valent vanadium chemistry and the binucleating ligand *m*-H_2xba is exhibited by the reported V^{III} dimers and the first structurally characterized bis(acetylacetonate) ligated complex of V^{II}.

Our interest in small molecule and organic functional group reduction using low-valent vanadium species featured in an anionic oxygen donor environment, as in the cases of carboxylate[1a] and aryloxide,[1b,c] has prompted us to investigate bis(acetylacetonates) as ligands in an attempt to synthesize binuclear complexes capable of intramolecular substrate binding and activation. Di- and tri-valent vanadium acetylacetonates are involved as undefined *in situ* intermediates in reactions ranging from epoxide deoxygenations[2] to dinitrogen uptake,[3] yet curiously very few structurally defined examples of bis(acetylacetonate) ligated V^{III} species have been reported.[4] Structurally characterized complexes with acetylacetonate bonded exclusively to V^{II} remain unknown,[4e] although they have been studied spectroscopically in solution.[5] The flexible *m*-xba^{2-} limits intermetallic distances acting as a tether, and should allow for a face-to-face approach of vanadia as observed in the chemistry of Cu^{II} where a discrete cofacial binuclear complex has been synthesized providing a cavity of well defined size and shape [Cu···Cu, 4.908(2) Å] appropriate for diatomic guest molecule incorporation (Fig. 1). Complexes of this type potentially will serve to promote and catalyze multielectron redox reactions, a strategy conceptually reminiscent of Collman's cofacial dimetalloporphyrin approach.[7]

We sought to prepare binuclear vanadium assemblies envisioning a target structure analogous to the Cu^{II} example, whereby reducible small molecules could be intramolecularly bound and activated. One obstacle in discrete dimer synthesis expected was oligomerization for these six-coordinate metal centers, yet here we report on the self-assembly and structures of novel discrete binuclear paramagnetic V^{II} and V^{III} complexes exhibiting an intriguing 'cage-like' structural type new to low-valent vanadium chemistry and the *m*-xba^{2-} ligand system. These compounds represent an important advance toward our target structure.

The reaction of $[VX_3(thf)_3]$[8] (X = Cl, Br) with 1 equiv. of the disodium salt of *m*-H_2xba,[9] generated in thf using 2 equiv. of NaH, proceeds at room temperature to produce complexes of the general formula $[V_2X_2(thf)_2(m\text{-xba})_2]$ (X = Cl, **1**, Br **2**) in 65% yield for both cases.‡ These compounds do not oligomerize upon standing in dichloromethane or thf solution over time, yet in the preparation of **1** and **2** insoluble precipitates thought to be oligomeric in nature along with NaX are removed by filtration. Complexes **1** and **2** were isolated as golden yellow–brown crystalline materials from concentrated thf solutions stored at 0 °C and were characterized by X-ray crystallography. The IR spectra§ of **1** and **2** show a strong band at 1559 cm^{-1} indicative of β-diketonate moieties chelated to the vanadia, along with two sets of doublets positioned at 867, 1020 and 918, 1065 cm^{-1}, assignable to ν_{C-O-C} stretching modes of coordinated and free thf molecules respectively.[10] The structure of **1** is shown in Fig. 2.¶

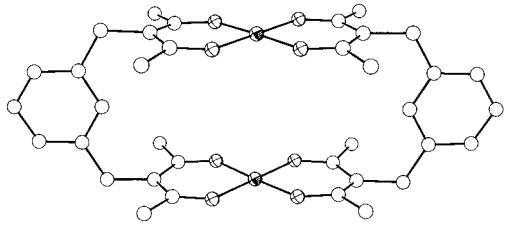

Fig. 1. Structure of $[Cu_2(m\text{-xba})_2]$[6]

The crystal structures of **1** and **2** revealed binuclear molecules with crystallographically imposed inversion symmetry. Compounds **1** and **2** are structurally analogous. The average V–O(acac) bond length of **1** [1.961(3) Å] is in good agreement with corresponding lengths of other rare acetylacetonates of V^{III} [av. 1.964(3) Å[4a] and 1.989(4) Å[4e]]. Considering the conformation of *m*-xba^{2-} in this structure, spanning the two vanadium atoms with a V···V distance of just over 11.66 Å and an aromatic ring-plane (centroids) separation of 5.366 Å, a structural rearrangement will be required to obtain the optimal distance for dual binding and activation of a small molecule. It is anticipated that dimers **1** and **2** will serve as useful precursors in establishing the desired *strati* conformation (see Fig. 1). Upon reduction of **1** or **2** in solution to reactive (II,II) species a structural change will be permitted to occur owing to rotational freedom about the C_{phenyl}–C_{benzyl} bond of the xylylene unit.

Our success with the synthesis of a discrete $V^{II,II}_2$ dimer compound $[V_2(tmeda)_2(m\text{-xba})_2]$ **3** is very encouraging considering the intention of generating a lower-valent species from a tethered $V^{III,III}_2$ assembly (**1** or **2**). Compound **3** was prepared in a similar manner (53% yield) to **1** and **2** using instead $[VCl_2(tmeda)_2]$[11] as a starting material.‡ Intensely colored midnight-blue X-ray quality crystals were isolated from concentrated thf solutions after removal of insoluble precipitates and NaCl by filtration, and cooling to 0 °C. The molecular structure and selected dimensions for **3** are shown in Fig. 3.¶ A structure similar to **1** and **2** was revealed with a V···V distance of 11.444(1) Å and an aromatic ring-plane (centroids) separation of 5.426 Å, as dictated by the *m*-xba^{2-} ligand orientation which again is in an extended conformation. The remaining sites are occupied by tmeda molecules. In comparing the changes in the vanadium coordination sphere, a subtle lengthen-

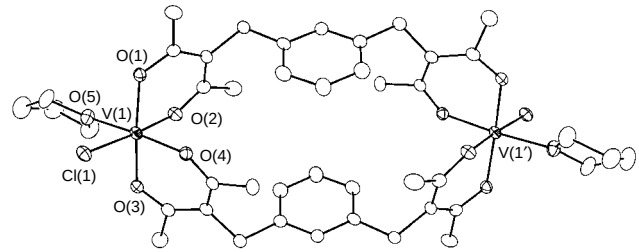

Fig. 2. Structure of **1** showing 30% probability thermal ellipsoids and atom-labeling scheme (hydrogen atoms are omitted for clarity). Selected bond distances (Å) and angles (°): V(1)–O(1) 1.941(2), V(1)–O(2) 1.962(2), V(1)–O(3) 1.985(2), V(1)–O(4) 1.955(2), V(1)–O(5) 2.097(2), V(1)–Cl(1) 2.366(1); O(1)–V(1)–O(2) 87.1(1), O(3)–V(1)–O(4) 85.4(1).

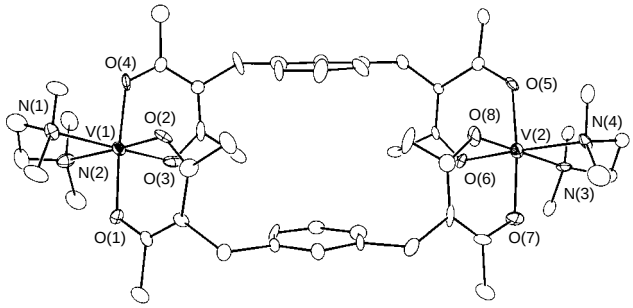

Fig. 3. Structure of **3** showing 30% probability thermal ellipsoids and atom-labeling scheme (hydrogen atoms are omitted for clarity). Selected bond distances (Å) and angles (°): V(1)–O(2) 2.035(9), V(1)–N(1) 2.23(1), V(1)–O(4) 2.04(1), V(1)–N(2) 2.26(1), V(1)–O(1) 2.03(1), V(1)–O(3) 2.00(1), V(2)–O(6) 2.020(9), V(2)–N(3) 2.20(2), V(2)–O(5) 2.06(1), V(2)–N(4) 2.22(1), V(2)–O(7) 2.02(1), V(2)–O(8) 2.05(1); O(5)–V(2)–O(6) 85.9(4), O(7)–V(2)–O(8) 86.8(5), O(1)–V(1)–O(2) 87.0(4), O(3)–V(1)–O(4) 86.8(5).

ing of the V–O(acac) bonds is observed [V–$O_{av.}$: **1** 1.961(3) Å, **3** 2.033(9) Å] consistent with a decrease in oxidation state. Compound **3** is, to our knowledge, the first example of a structurally characterized bis(acetylacetonate) ligated complex of V^{II}. An X-band EPR spectrum§ in frozen (77 K) thf solution displays an intense broad signal at $g = 4$ with no higher-field absorbances detected under these conditions. The successful preparation of a (II,II) dimer is of great interest considering the application of precursors **1** and **2** toward *strati* target structure synthesis *via* reduction and terminal halide removal.

Ongoing studies focus on testing the rearrangement proposition described above in working toward a cofacial conformation. We are also interested in extending our investigations to include bis(β-diketonates) with bridging groups other than the *m*-xylylene framework.

Notes and References

† E-mail: william.armstrong@bc.edu

‡ Complexes **1**–**3** analyzed satisfactorily. The scale of a typical reaction was on the order of 0.54 mmol in *m*-H_2xba ligand and vanadium-containing starting materials.

§ *Selected spectroscopic data*: **1**; UV–VIS (CH_2Cl_2): λ_{max}/nm (ε/dm^3 mol^{-1} cm^{-1}) = 304 (31 900), 359 (16 600); IR (Nujol, cm^{-1}) 1559vs, 1288s, 1207m, 1173m, 1065w, 1020s, 948s, 918w, 867s, 742m. **3**; EPR (thf 77 K, X-band) $g = 4$ (br); UV–VIS (thf): λ_{max}/nm (ε/dm^3 mol^{-1} cm^{-1}) = 288 (49 800), 343 (9110), 484 (2040), 592 (3380), 684 (2580); IR (Nujol, cm^{-1}) 1558vs, 1286s, 1201m, 1165w, 1127w, 1029s, 949s, 796s, 743m, 693w.

¶ *Crystal data*: **1**·thf; $C_{44}H_{56}Cl_2O_{11}V_2$, M = 989.763, monoclinic, space group $C2/c$, a = 20.2285(4), b = 13.0235(2), c = 20.2383(4) Å, β = 94.395(1)°, U = 5316.0(2) Å^3, Z = 4, D_c = 1.347 g cm^{-3}, F(000) = 2240, μ = 0.515 mm^{-1}, T = 183 K, λ = 0.710 73 Å, $2\theta_{max}$ = 56.58°, 15 553 measured reflections on a Siemens SMART CCD area-detector diffractometer, 6099 unique (R_{int} = 0.0376, no absorption correction). The structure was solved by direct methods and refined by FMLS methods on F^2 with statistical weighting, anisotropic displacement parameters for all non-hydrogen atoms (except those of the disordered thf solvent molecule), constrained isotropic H atoms to give $R' = \{\Sigma[w(F_o^2 - F_c^2)^2]/\Sigma[w(F_o^2)^2]\}^{1/2}$ = 0.0771 on all data, conventional R_1 = 0.0604 on F values of 4997 reflections having $F_o^2 > 4\sigma F_o^2$, goodness of fit S = 1.087 for all F^2 values and 300 refined parameters. Final difference map features were within ±0.920 e Å^{-3}. Programs: Siemens SMART and SAINT control and integration software, Siemens SHELXTL Version 5.

2·thf; $C_{44}H_{56}Br_2O_{11}V_2$, M = 1078.675, monoclinic, space group $C2/c$, a = 20.081(6), b = 13.264(6), c = 20.670(4) Å, β = 95.75(2)°, U = 5478.0(3) Å^3, Z = 4, D_c = 1.395 g cm^{-3}, F(000) = 2384, μ = 1.857 mm^{-1}, λ = 0.71073 Å, T = 183 K. 6944 reflections measured, 3894 unique data ($2\theta_{max}$ = 56.44°, R_{int} = 0.0917, no absorption correction). Structure solution and refinement were as for **1** including a disordered thf molecule to give 2698 reflections having $F_o^2 > 4\sigma F_o^2$ with conventional R_1 = 0.0968 (wR_2 = 0.1709) and goodness of fit S = 1.260 (307 parameters). Final difference map features were within 0.680 and −0.780 e Å^{-3}.

3·2thf; $C_{52}H_{80}N_4O_{10}V_2$, M = 934.943, monoclinic, space group Pn, a = 13.7459(8), b = 11.1388(6), c = 18.6718(5) Å, β = 90.816(2)°, U = 2858.6(2) Å^3, Z = 2, D_c = 1.249 g cm^{-3}, F(000) = 1148, μ = 0.385 mm^{-1}, λ = 0.710 73 Å, T = 183 K. 7530 reflections measured, 6244 unique data ($2\theta_{max}$ = 56.42°, R_{int} = 0.0658, semi-empirical absorption corrections). Structure solution and refinement performed as above including a partially disordered thf molecule to give 4173 reflections having $F_o^2 > 4\sigma F_o^2$ with conventional R_1 = 0.0655 (wR_2 = 0.1223) and goodness of fit S = 1.092 (644 parameters). Final difference map features were within 0.309 and −0.283 e Å^{-3}. CCDC 182/763.

1 (*a*) L. Gelmini and W. H. Armstrong, *J. Chem. Soc., Chem. Commun.*, 1989, 1904; (*b*) M. J. Scott, W. C. A. Wilisch and W. H. Armstrong, *J. Am. Chem. Soc.*, 1990, **112**, 2429; (*c*) W. C. A. Wilisch, M. J. Scott and W. H. Armstrong, *Inorg. Chem.*, 1988, **27**, 4333. Our interest in low-valent vanadium syntheses and reactivity appears elsewhere: (*d*) C. R. Randall and W. H. Armstrong, *J. Chem. Soc., Chem. Commun.*, 1988, 986; (*e*) D. B. Sable and W. H. Armstrong, *Inorg. Chem.*, 1992, **31**, 161; (*f*) H. H. Murray, S. G. Novick, W. H. Armstrong and C. S. Day, *J. Cluster Sci.*, 1993, **4**, 439; (*g*) J. A. Davis, C. P. Davie, D. P. Sable and W. H. Armstrong, *Chem. Commun.*, 1998, in press.

2 Y. Hayasi and J. Schwartz, *Inorg. Chem.*, 1981, **20**, 3473.

3 M. E. Vol'pin, M. A. Ilatovskaya, E. I. Larikov, M. L. Khidekel', Y. A. Shvetsov and V. B. Shur, *Dokl. Akad. Nauk SSSR*, 1965, **164**, 331.

4 (*a*) M. Doring, H. Gorls, E. Uhlig, K. Brodersen, L. Dahlenburg and A. Wolski, *Z. Anorg. Allg. Chem.*, 1992, **614**, 65; (*b*) P. Knopp, K. Wieghardt, B. Nuber, J. Weiss and W. S. Sheldrick, *Inorg. Chem.*, 1990, **29**, 363; (*c*) S. Lee, K. Nakanishi, M. Y. Chiang, R. B. Frankel and K. Spartalian, *J. Chem. Soc., Chem. Commun.*, 1988, 785; (*d*) V. I. Lisoivan and S. A. Gromilov, *Zh. Neorg. Khim.*, 1986, **31**, 2539; (*e*) E. Solari, S. De Angelis, C. Floriani, A. Chiesi-Villa and C. Guastini, *Inorg. Chem.*, 1992, **31**, 141. Also reported, [$(thf)_3$V(μ-acac)(μ-Cl)$ZnCl_2$], a dimeric structure of acetylacetonate bonded to V^{II} and Zn^{II} *via* one of its bridging oxygen atoms; (*f*) V. A. Grillo, E. J. Seddon, C. M. Grant, G. Aromi, J. C. Bollinger, K. Folting and G. Christou, *Chem. Commun.*, 1997, 1561.

5 J. M. Crabtree, D. W. Marsh, J. C. Tomkinson, R. J. P. Williams and W. C. Fernelius, *Proc. Chem. Soc.*, 1961, 336; W. P. Schaefer, *Inorg. Chem.*, 1965, **4**, 642;Y. Torii, H. Iwaki and Y. Inamura, *Bull. Chem. Soc. Jpn.*, 1967, **40**, 1550; V. A. Alekseevskii and T. A. Grabovskaya, *Russ. J. Inorg. Chem.*, 1985, **30**, 1739.

6 A. W. Maverick and F. E. Klavetter, *Inorg. Chem.*, 1984, **23**, 4129.

7 J. P. Collman, J. E. Hutchison, M. A. Lopez, R. Guilard and R. R. Reed, *J. Am. Chem. Soc.*, 1991, **113**, 2794; J. P. Collman, J. E. Hutchison, M. A. Lopez and R. Guilard, *J. Am. Chem. Soc.*, 1992, **114**, 8066; J. P. Collman, J. E. Hutchison, M. S. Ennis, M. A. Lopez and R. Guilard, *J. Am. Chem. Soc.*, 1992, **114**, 8074; J. P. Collman, J. E. Hutchison and P. S. Wagenknecht, *Angew. Chem., Int. Ed. Engl.*, 1994, **33**, 1537; R. Guilard, S. Brandes, C. Tardieux, A. Tabard, M. L'Her, C. Miry, P. Gouerec, Y. Knop and J. P. Collman, *J. Am. Chem. Soc.*, 1995, **117**, 11 721; J. P. Collman, M. S. Ennis, D. A. Oxford, L. L. Chng and J. H. Griffin, *Inorg. Chem.*, 1996, **35**, 1751.

8 L. E. Manzer, *Inorg. Synth.*, 1982, **21**, 135. The bromide derivative was prepared similarly and purified by Soxhlet extraction using thf.

9 The synthesis of *m*-H_2xba has been described previously: A. W. Maverick, D. P. Martone, J. R. Bradbury and J. E. Nelson, *Poyhedron*, 1989, **8**, 1549.

10 F. L. Bowden and D. Ferguson, *Inorg. Chim. Acta*, 1978, **26**, 251.

11 J. J. H. Edema, W. Stauthamer, S. Gambarotta, F. van Bolhuis, W. J. J. Smeets and A. L. Spek, *Inorg. Chem.*, 1990, **29**, 1302.

Received in Bloomington, IN, USA, 2nd December 1997; 7/08693H

Synthesis and characterization of poly(butyl acrylate-co-styrene)–silver nanocomposites by γ radiation in W/O microemulsions

Yadong Yin, Xiangling Xu,*† Chuanjun Xia, Xuewu Ge and Zhicheng Zhang

Department of Applied Chemistry, University of Science and Technology of China, Hefei 230026, PR China

Poly(butyl acrylate-co-styrene)–silver nanocomposites were prepared by γ-irradiation of microemulsions and metallic silver nanoparticles of near uniform size were found to be well dispersed in the polymer matrix.

Much attention has been paid to the synthesis and characterization of nanometer metal particle–organic polymer composites, owing to their intriguing optical, electrical and mechanical properties.[1–3] These composites are considered to be highly functional materials, with wide potential application in electromagnetic inference shielding films, non-linear optical materials and the like.

Several methods have been developed to synthesis the composites.[4–6] In general, two steps were needed: firstly, monomer was polymerized in the solutions, with metal ions introduced before or after the polymerization. Secondly, metal ions in the polymer matrix were reduced by a reducing agent or by calcining. Since polymerization and reduction were performed separately metal nanoparticles were not well dispersed in the polymer matrix.

Recently, Zhu *et al.*[7] developed a γ radiation method to prepare polyacrylamide–silver nanocomposites at room temperature. In this method, aqueous soluble monomer and metal salt were mixed homogeneously in aqueous solution. When the system was γ-irradiated, polymerization and reduction took place simultaneously, leading to a homogeneous dispersion of nanocrystalline metal particles in a polymer matrix.

However, in the above method, the compatibility of monomer and metal salt or metal salt aqueous solution was of importance. The application of the method was restricted when the metal salt was insoluble in the monomer or monomer solutions. In addition, the dimension of the metallic nanoparticles was not uniform, and size control was difficult. Furthermore, the polymer–metal nanocomposites were water absorptive, limiting their practical applications.

Here we report a novel method for preparing polymer–metal nanocomposites in microemulsions using γ radiation at room temperature. It was found that products formed by this method contained not only well dispersed but also monodisperse metal nanoparticles.

A W/O microemulsion was produced with Span 80 (sorbitanol monooleate) and SDS (sodium dodecyl sulfate) as emulsifier. The metal salt was dissolved in water before producing the microemulsion, and monomers (styrene or butyl acrylate) were dissolved in toluene. In order to reduce the emulsifier content in the microemulsion, 2-hydroxy-α-methacrylate (HEMA) was used as coemulsifier and comonomer simultaneously.

An aqueous solution containing 8.5 mass% $AgNO_3$ was prepared in advance. 10 g of the solution was then added to a mixture of 48 g toluene, 19 g butylacrylate (BA), 10 g styrene (St), 3 g SDS and 5 g HEMA. Span 80 was titrated into the mixture under stirring until a transparent microemulsion suddenly formed. After bubbling with N_2, the microemulsion was irradiated in the field of a ^{60}Co γ-ray source for 6 h with a radiation dosage of 1.8×10^4 Gy. After irradiation, the brown, semi-transparent microemulsion was de-emulsified by acetone and distilled water. The products were washed with distilled water, dried and ground into powder for further analysis.

The size and morphology of the P(BA-co-St)–silver nanocomposites were investigated by transmission electron microscopy (TEM) (Fig. 1) and X-ray diffraction (XRD) analysis. TEM images were conducted using a Hitachi Model H-800 transmission electron microscope and XRD patterns were recorded by a D_{max} γ_A X-ray diffractometer with graphite-monochromated Cu-Kα radiation (λ = 0.154 178 nm), using an accelerating voltage of 200 kV.

Fig. 2 shows the XRD pattern of the same sample as Fig. 1. The broad peak at $2\theta \approx 19.8°$ is attributed to the diffraction of non-crystalline co-polymer. The other three peaks with 2θ values of 38, 44.5 and 64° correspond to three crystal faces of 111, 200 and 220 of metallic crystalline silver, respectively (cubic system, a = 4.101 Å). The broadening in diffraction peaks shows that the product consisted of small metallic particles. The average size of silver particles estimated by Scherrer's equation[8] is 8.5 nm, which is in good agreement with the TEM result.

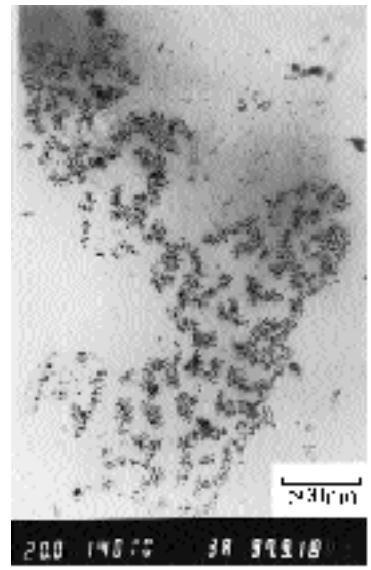

Fig. 1 TEM image of a poly(BA-co-St)–silver nanocomposite prepared by γ-irradiation of a microemulsion. Details in text.

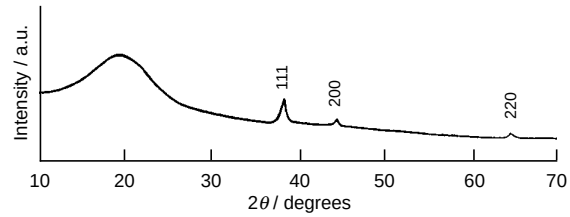

Fig. 2 XRD pattern of the same sample as in Fig. 1

In the conventional microemulsion method,[9,10] the metal salt was dissolved in one microemulsion system, and the reducing agent dissolved in another, in advance. When these two microemulsions were mixed together, only through interaction of two types of droplets could the metal ions be reduced to form metal clusters. However, control of particle size and distribution was difficult.

Another advantage of the new method is that polymerization of monomer and reduction of metal ions are both achieved by γ-irradiation. Radiolysis of the microemulsion system may produce radicals in the oil and aqueous phase. These radicals may effectively initiate the monomer in oil polymerization. Since the polymerization is a chain process it will be faster than the reduction process. With polymerization, the microemulsion system changes from liquid to viscous liquid, rubber or solid material, depending on the monomer type and the monomer content in the oil phase. The increase of the system's viscosity will certainly restrict water droplet aggregation and favour the synthesis of well-dispersed polymer–metal nanocomposites.

In summary, this novel method not only has all the advantages of the microemulsion and irradiation methods to produce metal nanoparticles, but also makes the process easier to control and gives near monodispersed nanoparticles. Furthermore, it makes it possible to synthesize versatile metal particles–polymer nanocomposites. It has advantages over the method developed in ref. 7, in which the monomer has to be soluble in water, because many more monomers are oil soluble than are water soluble. Moreover the composites prepared using oil soluble monomers have wider application.

Notes and References

† E-mail: xlxu@mail.ach.ustc.edu.cn

1 D. M. Bigg, *Polym. Composites*, 1996, **7**, 125.
2 L. T. Chang and C. C. Yen, *J. Appl. Polym. Sci.*, 1995, **55**, 371.
3 K. Ghosh and S. N. Maiti, *J. Appl. Polym. Sci.*, 1996, **60**, 323.
4 H. Tamai, S. Hamamoto, F. Nishiyama and Hajmeyasuda, *J. Colloid Interface Sci.*, 1995, **171**, 250.
5 C. C. Yen, *J. Appl. Polym. Sci.*, 1996, **60**, 693.
6 Y. Nakao, *J. Colloid Interface Sci.*, 1995, **171**, 386.
7 Y. J. Zhu, Y. T. Qian, X. J. Li and M. W. Zhang, *Chem. Commun.*, 1997, 1081.
8 C. N. J. Wagner and E. N. Aqua, *Adv. X-Ray Anal.*, 1964, **7**, 46.
9 P. Barnickel, A. Wokaum, W. Sager and H. F. Eicke, *J. Colloid Interface Sci.*, 1992, **148**, 80.
10 I. Lisiecki and M. P. Pileni, *J. Am. Chem. Soc.*, 1993, **115**, 3887.

Received in Cambridge, UK, 26th January 1998; 8/00676H

STM observation of *N*-octadecylacrylamide and *N*-octadecylcinnamoylamide monolayers self-assembled on a graphite surface

Pu Qian,*[a]† § Hiroshi Nanjo,[a] Toshiro Yokoyama,[a] Tokuji Miyashita[b] and Toshishige M. Suzuki*[a]‡

[a] *Tohoku National Industrial Research Institute, 4-2-1 Nigatake, Miyagino-ku, Sendai, 983-8551 Japan*
[b] *Institute for Chemical Reaction Science, Tohoku University, 2-1-1 Katahira, Aoba-ku, Sendai, 980-8577 Japan*

The STM observation of self-assembled *N*-octadecylacrylamide (ODA) and *N*-octadecylcinnamoylamide (ODC) on a graphite substrate clarified the head to tail alignment of the molecules and *s-trans* geometry of the alkene double bond and carbonyl group.

We have attempted to fabricate uniform Langmuir–Blodgett (LB) films having a well defined molecular orientation. In our previous study, we found that *N*-octadecylacrylamide (ODA) can form stable Langmuir monolayer and LB films on a solid substrate.[1–4] The X-ray diffraction study revealed that ODA forms two dimensional crystals in LB films.[5,6] Recently, we have observed the molecular arrangement of an ODA based LB film on a mica surface by atomic force microscopy (AFM) and obtained a molecular resolution image in which *N*-octyl chains are highly ordered to form two dimensional crystals.[7] The analysis of the AFM image and linear dichroism in polarized FTIR of the LB film[5,6] suggested that *N*-alkyl chains are tilted by *ca.* 28° against the film plane. Hydrogen bonding between ODA molecules was considered to be very important to stabilize the monolayer and the LB film. However direct evidence of intermolecular interaction between ODA molecules has not been clarified.

The scanning tunneling microscope (STM) is a powerful tool to image molecules at atomic resolution. Monolayers of physisorbed *n*-alkane and substituted alkanes on a flat substrate have been observed and the topological features of self-assembled two dimensional crystals discussed.[8–11] Different from LB films on mica, the molecules are aligned parallel to the graphite surface. This allows one to directly observe the molecular orientation and geometrical arrangement of monolayer. In the present study we applied the STM method to observe the molecular alignment of ODA molecules on the basal plane surface of highly oriented pyrolytic graphite (HOPG) to study their ordered structure and intermolecular interaction *in situ*. In addition, the molecular alignment of an ODA analogue *N*-octadecylcinnamoylamide (ODC) was also imaged.

ODA or ODC was dissolved in phenyloctane to near saturation and a drop of the solution was applied on the surface of freshly cleaved HOPG. The STM images were obtained in both constant current mode and constant height mode using Nano-Scope IIIa STM (Digital Instruments). The tunneling tip was a Pt–Ir tip purchased from Digital Instruments or a tungsten wire which was sharpened by electrolytical etching prior to use.

Fig. 1 shows the STM image of monolayer of ODA physisorbed on the HOPG surface (constant height mode). The two dimensional array of ODA molecules is clearly visible as stripes. The size of two dimensional crystals varies from a few 100 nm^2 to > 10 000 nm^2. Domain boundaries of adjacent crystals are observed with a rotation angle of 60°. This result suggests that ODA molecules are aligned by the influence of the graphite surface where the C–C–C atomic angle is 60°. Well ordered ODA molecules form stripe shaped lamella bands of *ca.* 2.7 nm width. A high resolution image of the monolayer is shown in Fig. 2 over a scan area of 8 × 8 nm (constant height mode). Increased brightness of the image corresponds to areas of higher electric conductance. Therefore the brighter parts can be attributed to the head groups containing conjugated π-electron systems and darker moieties to the alkyl chains. The molecular alignment is obviously in the head to tail structure. The alkene double bond appears to be downward to the molecular axis of ODA. The length of ODA observed along the molecular axis is roughly 2.7 nm which is consistent with that estimated by a CPK model. The separation of alkyl chains is *ca.* 0.47 nm. This value is slightly longer than that of two dimensional crystals of *n*-alkanes[8,9] presumably due to the presence of the bulky head group. The molecular axis of ODA

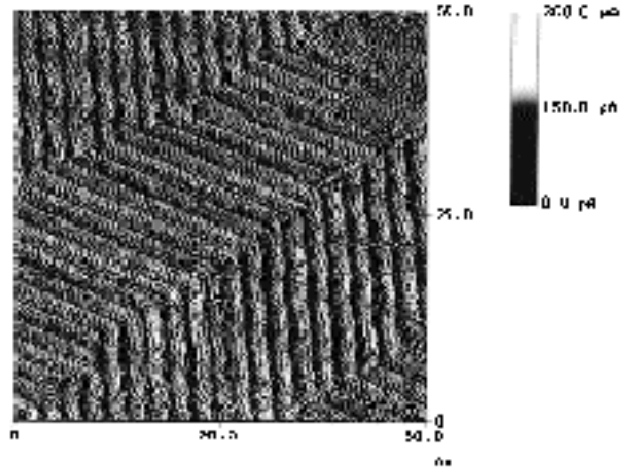

Fig. 1 STM image of a monolayer of ODA molecules self-assembled on a graphite surface. Image was taken in constant height mode. The area is 50 × 50 nm. Bias voltage is 1.1 V (tip positive) and current is 72 pA.

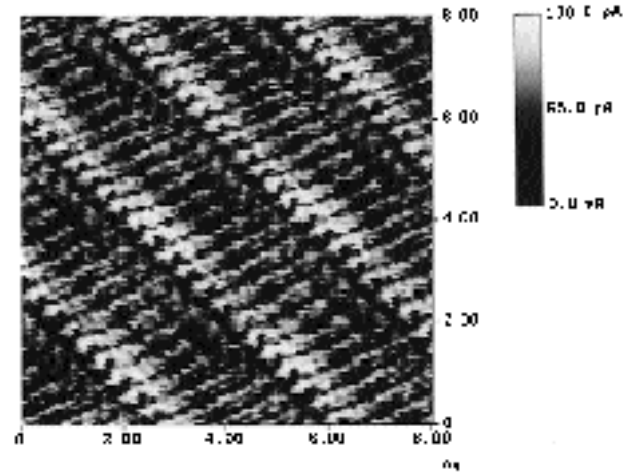

Fig. 2 STM image of a monolayer of ODA molecules self-assembled on a graphite surface. Image was taken in constant height mode. The scan area is 8 × 8 nm. Bias voltage is 1.0 V (tip positive) and current is 292 pA.

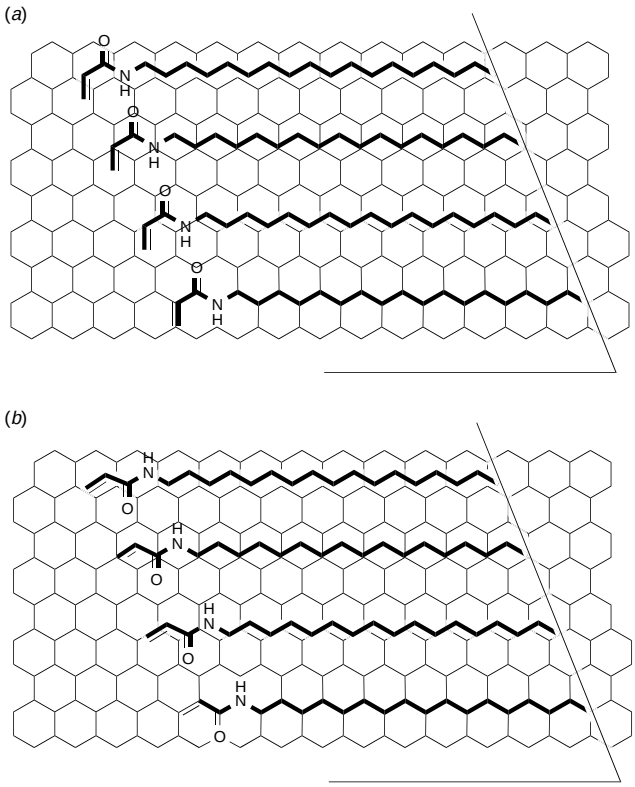

Fig. 3 Possible molecular arrangements of ODA with (*a*) an *s-trans* geometry and (*b*) an *s-cis* geometry, on a graphite surface. There are 18 carbon atoms in the alkyl chain of an ODA molecule.

appears to be inclined with an angle of *ca.* 70° *vs*. the orientation of the lamella band.

Possible molecular alignments of ODA on the graphite surface are schematically represented in Fig. 3(*a*) and 3(*b*) by which the observed inclination between the molecular axis of ODA and lamella band can be reproduced. Those two models are rotational isomers of ODA with respect to the amide group. The *s-trans* geometry [Fig. 3(*a*)] can consistently explain the observed alignment of ODA molecules where the intermolecular hydrogen bonds effectively link ODA molecules to form a molecular network. Such hydrogen bonds are unlikely to take place in *s-cis* geometry because the amide proton is then spatially remote from the carbonyl oxygen of an adjacent ODA molecule. The imaged morphology of the monolayer provides structural information of the constituent molecule and the observed inclination is very similar to that of the LB film deduced by FTIR and X-ray diffraction studies.[5,6]

Fig. 4 shows the high resolution STM image of ODC (scan area 8 × 8 nm, constant current mode) where a phenyl group is attached to an alkenic terminal of ODA. We can clearly distinguish the benzene rings and alkyl chains. The molecular ordering is again of head to tail structure as found in ODA. The head to tail distance is *ca.* 3.1 nm which agrees with the

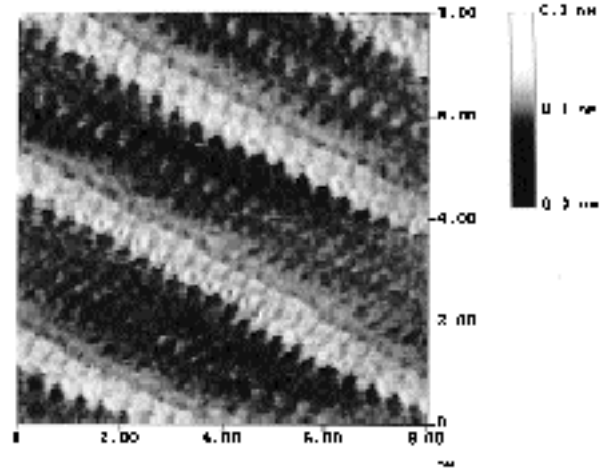

Fig. 4 STM image of a monolayer of ODC molecules self-assembled on a graphite surface. Image was taken in constant current mode. The scan area is 8 × 8 nm. Bias voltage is 0.85 V (tip positive) and current is 340 pA.

molecular length of ODC. Here also an inclination of ODA is observed against the lamella bands and the *s-trans* geometry around the amide group can explain the observed molecular arrangement.

The present STM observations have clarified the geometrical configuration of self-assembled ODA and ODC molecules where the intermolecular hydrogen bond in the amide group plays an important role in controlling the morphology of the molecular alignment.

Notes and References

† E-mail: B.Sen@tniri.go.jp
‡ E-mail: suzuki@tniri.go.jp
§ National Institute Post Doctoral Fellow of Japan Science and Technology Corporation.

1 T. Miyashita, H. Yoshida, T. Murakata and M. Matsuda, *Polymer*, 1987, **28**, 311.
2 T. Miyashita, K. Sakaguchi and M. Matsuda, *Polym. Commun.*, 1990, **31**, 461.
3 T. Miyashita, H. Yoshida and M. Matsuda, *Thin Solid Films*, 1987, **155**, L11.
4 T. Miyashita and M. Matsuda, *Thin Solid Films*, 1989, **168**, L47.
5 T. Miyashita and T. Suwa, *Langmuir*, 1994, **10**, 3387.
6 T. Miyashita and T. Suwa, *Thin Solid Films*, 1996, **284**, 330.
7 P. Qian, H. Nanjo, T. Yokoyama, T. Miyashita and T. M. Suzuki, *Thin Solid Films*, submitted.
8 J. P. Rabe and S. Buchholz, *Science*, 1991, **253**, 442.
9 A. Stabel, R. Heinz, J. P. Rabe, G. Wegner, F. C. De Schryver, D. Corens, W. Dehaen and C. Süling, *J. Phys. Chem.*, 1995, **99**, 8690.
10 M. Hibino, A. Sumi and I. Hatta, *Jpn. J. Appl. Phys.*, 1995, **34**, 3354.
11 H. Takeuchi, S. Kawauchi and A. Ikai, *Jpn. J. Appl. Phys.*, 1996, **35**, 3754.

Received in Cambridge, UK, 6th January 1998; 8/00194D

Typeset and printed by Black Bear Press Limited, Cambridge, England

ChemComm
FEATURE ARTICLE

Macromolecular tetrathiafulvalene chemistry

Martin R. Bryce,*† Wayne Devonport, Leonid M. Goldenberg and Changsheng Wang

Department of Chemistry, University of Durham, Durham, UK DH1 3LE

Recent developments in the functionalisation of tetrathiafulvalene (TTF) have enabled TTF units to be covalently linked into macromolecular systems. Convergent syntheses of dendrimers containing TTF units are presented, including a $(TTF)_{13}$ system in which TTF units are emplaced at all layers of the structural hierarchy. Thin layer cyclic voltammetry has established that the redox activity of TTF is retained in these macromolecules: sequential oxidation to the radical cation and dication occurs for all the TTF units, yielding highly-charged species in solution. Macromolecules comprising four and eight TTF units built around a phthalocyanine core are also described. These materials present novel architectures with the key property of multi-electron redox activity.

Tetrathiafulvalene—its molecular properties and functionalisation

Tetrathiafulvalene (TTF)[1,2] is famous as a π-electron donor in the field of organic molecular metals,[3] *e.g.* the complex TTF–TCNQ (TCNQ = 7,7,8,8-tetracyano-*p*-quinodimethane),[4] where the delocalised electrons responsible for conduction are derived from intermolecular charge transfer from TTF to the acceptor species. A few derivatives of TTF, notably bis(ethylenedithio)TTF (BEDT-TTF) form superconducting radical cation salts with closed shell anions,[5] *e.g.* the salt κ-(BEDT-TTF)$_2$Cu[N(CN)$_2$]Br which superconducts at temperatures below a T_c value of 11.5 K.[6] BEDT-TTF is also a component of interesting magnetic materials.[7]

In view of the unabated interest during the past 25 years in the molecular chemistry of TTF derivatives,[2,5] it is striking that TTF has rarely been incorporated into polymeric systems.[8] In this context, the key properties of TTF which make it an interesting building block are these: (i) oxidation of the TTF ring system to the radical cation and dication species occurs sequentially and reversibly at a very accessible potential window in a range of organic solvents (for unsubstituted TTF, $E_1^{\frac{1}{2}}$ = +0.34 and $E_2^{\frac{1}{2}}$ = +0.78 V *vs*. Ag/AgCl in MeCN); (ii) the oxidation potentials can be finely tuned by the attachment of appropriate substituents; (iii) the TTF radical cation is thermodynamically very stable (due to 6π-electron heteroaromaticity of the 1,3-dithiolium cation); (iv) TTF derivatives and their derived cation radicals readily form dimers, highly-ordered stacks, or two-dimensional sheets, which are stabilised by intermolecular π–π interactions and non-bonded sulfur ···sulfur interactions; and (v) TTF is stable to many synthetic transformations, although it is important to avoid strongly acidic conditions and oxidising agents.

Macromolecular aspects of TTF chemistry have been neglected primarily because of the synthetic challenge of obtaining suitably functionalised TTF derivatives in reasonable quantities. This barrier has recently been overcome with major progress in three important branches of synthetic TTF chemistry: (i) TTF can now be readily synthesised in 20 g batches;[9] (ii) methodology involving electrophilic substitution of lithiated TTF has been optimised to afford facile entry into a wide range of mono-substituted derivatives in high yield;[10] and (iii) selective protection/deprotection chemistry of the thiolate groups of the 1,3-dithiole-2-thione-4,5-dithiolate (dmit) system (and derived TTFs) has been developed, primarily by Becher and co-workers,[11] to provide multi-gram quantities of versatile building blocks for highly-functionalised TTF systems, including supramolecular architectures.[12]

Our work breaks new ground in the synthesis and redox properties of monodisperse macromolecules containing multi-TTF functionality, and this short review article will highlight progress in this area. At the outset our aim was to synthesise structurally well-defined multi-electron redox systems, exploiting the known solubility enhancement in highly-branched macromolecules (compared to their linear counterparts). A longer term aim is to combine the properties of TTF, which have been stated above, with the beneficial properties of polymers, such as film formation and processability. It should be noted that from a similar viewpoint other polymeric TTFs have been synthesised.[8] In earlier work, disubstituted TTFs were condensed to form polyamides,[8*a*] polyesters[8*b*] and polyurethanes,[8*c*] some of which were oxidised to radical cation systems. More recently, some well-defined main chain and side chain polymeric TTFs have been obtained,[8*d–g*] including some electrochemically polymerised systems.[8*g*]

Constructing TTF dendrimers

The study of dendrimers, cascade molecules and related hyperbranched systems is a rapidly-expanding topic in macromolecular science.[13] These materials comprise a multifunctionalised core, from which radiate repeating layers of monomers with a branch occurring at each monomer unit. They possess well-defined, three-dimensional structural order, and their size and architecture is precisely regulated in their synthesis, providing unique molecular frameworks for the disposition of functional groups in predetermined spatial arrangements. Initial research into dendrimers focused on obtaining higher generation systems with large molecular weights, whereas nowadays the emphasis is mainly on systems which incorporate functional groups at the exterior surface of, or embedded within, the dendrimer framework.[14] In the context of functional dendrimers, a variety of redox-active substituents have been built into the structures.[15,16] These materials are relevant to the development of: (i) new electron-transfer catalysts; (ii) studies on the dynamics of electron transport at surfaces and within restricted reaction spaces; (iii) new materials for energy conversion (iv) electronic and photo-optical materials; (v) organic magnets; and (vi) mimics of biological redox processes. The redox groups may behave independently in multi-electron processes (*n* identical non-interacting electroactive centres giving rise to a single *n*-electron wave) or they may interact intra- or inter-molecularly, in which case overlapping or closely-spaced redox waves are observed at different potentials.

Synthesis of arylester TTF dendrimers

In the first phase of our work on multi-TTF macromolecules, we synthesised aryl ester dendrimers functionalised with peripheral TTF groups.[17] 4-(Hydroxymethyl)-TTF **1**, which is readily available in multi-gram quantities,[10*a*] served as a convenient

starting material. A convergent strategy, based on a repetitive coupling/deprotection sequence, furnished dendrimer **8** comprising a 1,3,5-benzene triester core (derived from reagent **2**) and surface-functionalised with 12 TTF units. (In a convergent synthesis,[18] dendrimer construction begins at what will become the surface of the molecule, and progresses inwards *via* a series of dendron wedges of increasing size, several of which are attached to the core unit in the final step.) We used 5-(*tert*-butyldimethylsiloxy)isophthaloyl chloride **3**[19] as the functionalised reagent for the esterification reactions to build up successive generations.

The synthesis of the $(TTF)_{12}$ dendrimer **8** is shown in Scheme 1. The reaction of **1** with reagent **3** gave compound **4** (83% yield), deprotection of which (TBAF in THF at room temperature) afforded the bis(TTF) derivative **5** (85% yield) as a dendron wedge carrying the phenolic group as a reactive handle for further reactions. Following the same procedures that gave compounds **4** and **5**, reaction of 2 equiv. of alcohol **5** with reagent **3** yielded **6** (76% yield) and then $(TTF)_4$ dendron wedge **7** in 95% yield. Compound **7** reacted with the core reagent **2** to give the target dendrimer **8** in 48% yield.

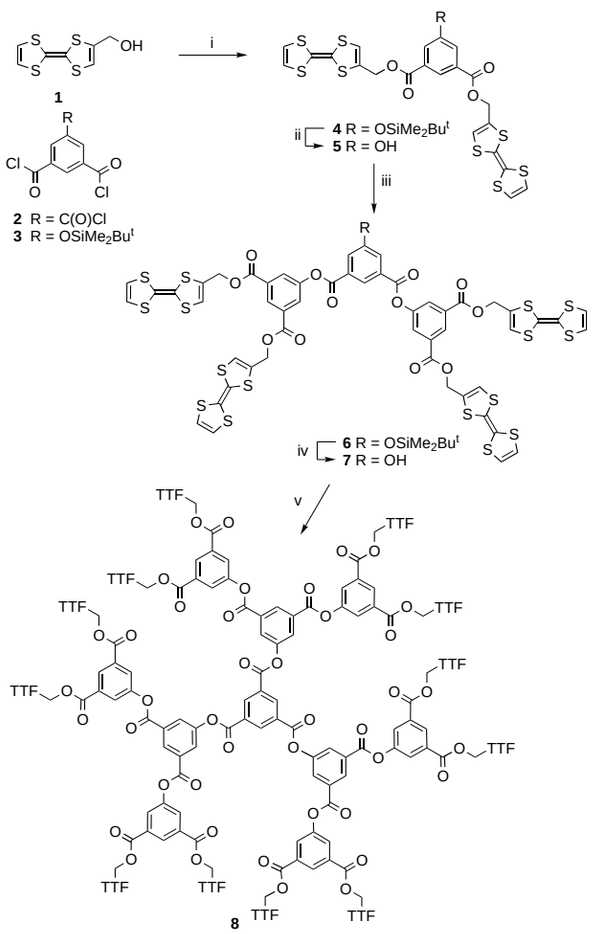

Scheme 1 *Reagents and conditions*: i, NEt_3, **3**, CH_2Cl_2, 20 °C; ii, TBAF, THF, 20 °C; iii, DMAP, **3**, CH_2Cl_2, 20 °C; iv, TBAF, THF, 20 °C; v, DMAP–$PhNMe_2$, **2**, CH_2Cl_2, 35 °C

Within this series of macromolecules, stability decreased with increasing generation, so no attempts were made to assemble molecules of higher molecular weight than **8**. Macromolecule **8** is an oil which is readily soluble in polar organic solvents. It is reasonably stable to storage at < 0 °C; however, when stored at room temperature, even in the dark and under an argon atmosphere, it decomposed after a few days. ^{1}H NMR spectroscopy and plasma desorption mass spectra (PDMS) were entirely consistent with structure **8**. The energy-minimised conformation of compound **8** is shown in Fig. 1: it is notable that all the TTF groups are exposed and, therefore, are available to participate in redox processes. (The proviso must be made that the conformation may be very solvent dependent.) The instability of **8** is possibly due to the high density of ester groups in the interior of the molecule.

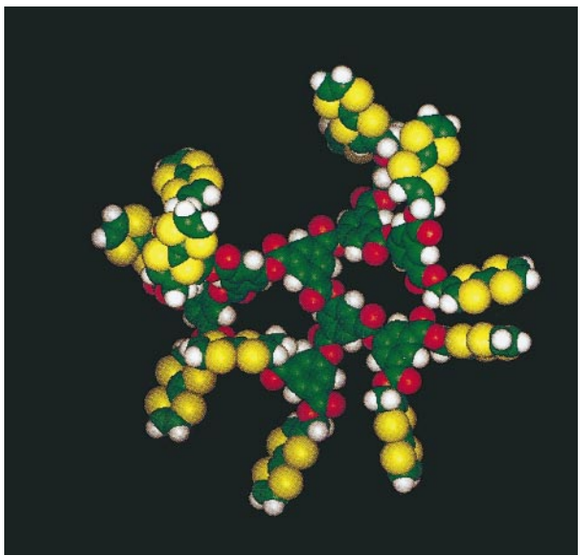

Fig. 1 Energy minimised conformation of **8**. Green = carbon; white = hydrogen; red = oxygen; yellow = sulfur.

With a view to improving the stability of the $(TTF)_x$ aryl ester dendrimers, we changed from trifunctional to bifunctional core units, to obtain more 'open' structures. Thus, using terephthaloyl chloride, biphenyl-4,4′-dicarbonyl dichloride and 4,4′-oxydibenzoyl dichloride as core reagents, the series of $(TTF)_8$ systems **9a–c** was constructed.[17b,20] These three compounds were all stable upon storage at room temperature in air and daylight for at least one year. However, the compounds containing the benzene and biphenyl cores, *viz*. **9a** and **9b**, were only sparingly soluble in organic solvents, whereas analogue **9c**, with the more flexible biphenyl ether core unit, showed good solubility in polar organic solvents (*e.g*. acetone and CH_2Cl_2).

Synthesis of *p*-xylyl TTF dendrimers

The use of entirely different building blocks afforded a second genre of TTF dendrimers, culminating in the synthesis of the macromolecule **21** comprising thirteen TTF units.[21] The special features of this work are that: (i) TTF units are emplaced at all layers of the structural hierarchy (unlike compounds **8** and **9**); and (ii) compound **14** was introduced as a new, readily-accessible (in multi-gram quantities) building block for TTF chemistry. The synthesis of **14** is shown in Scheme 3.

Zincate salt **10**,[22] which is a well-known precursor to the 1,3-dithiole-4,5-dithiolate dianion,[11b] reacted with α,α′-dichloro-*p*-xylene **11** to yield 4,5-disubstituted 1,3-dithiole-2-thione derivative **12** (60% yield) which was converted into the ketone **13** (84% yield) using mercuric acetate. Compound **14** was then synthesised in 78% yield by self-coupling of **13** in the presence of $P(OEt)_3$ under standard conditions,[23] and isolated as orange crystals. Compound **14** is our four-directional core reagent, and displacement of the benzylic chlorines of **14** by thiolate anions proved to be a facile process. For this purpose, we identified **20** as a suitable wedge from which a reactive thiolate anion could be generated, following the protocol developed by Becher *et al*. for related cyanoethyl-protected TTF-thiolate systems.[11]

Compound **16** was prepared in high yield by the literature route from **15**,[11a] and converted into ketone **17** (98% yield) using $Hg(OAc)_2$ (Scheme 4). Cross-coupling of equimolar

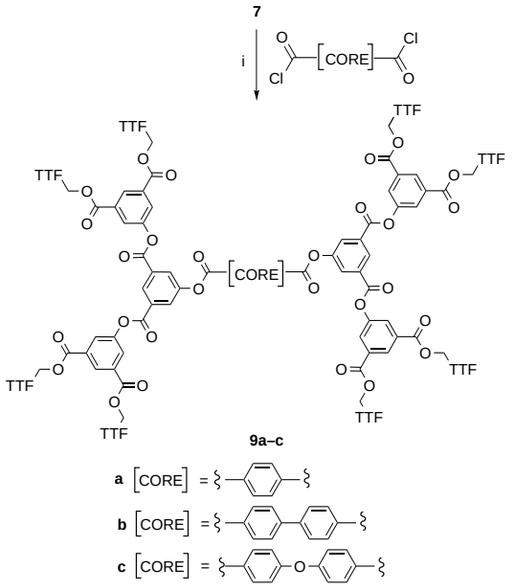

Scheme 2 *Reagents and conditions*: i, DMAP–PhNMe$_2$, **3**, CH_2Cl_2, 35 °C

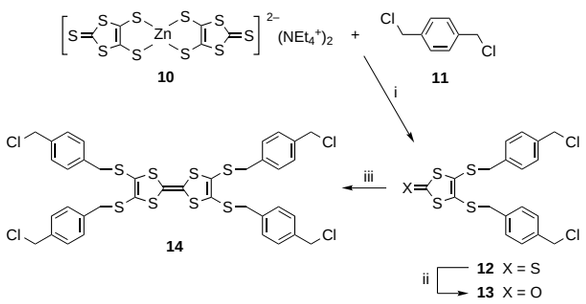

Scheme 3 *Reagents and conditions*: i, acetone reflux; ii, $Hg(OAc)_2$, $CHCl_3$–AcOH, 20 °C; iii, $P(OEt)_3$, 120 °C

amounts of thione **12** and ketone **17**, in the presence of $P(OEt)_3$, gave compound **18** in an optimised yield of 45%. The benzylic chlorides of compound **18** were then displaced by the thiolate derived from compound **19** (prepared by direct analogy with **18**) to afford **20** in 74% yield. The caesium thiolate salt of **20** (4 equiv.) reacted cleanly with compound **14** to furnish the $(TTF)_{13}$ macromolecule **21** in 66% yield, as an air-stable yellow–brown solid, which was soluble in polar organic solvents. Compound **21** was characterised unambiguously by a combination of elemental analysis, MALDI TOF mass spectrometry [which showed the parent ion peak at *m/z* 7377 (M^+: calc. for $C_{314}H_{276}S_{104}$ = 7372)] and ^{1}H NMR spectroscopy.

Redox properties of $(TTF)_x$ dendrimers

An important aspect of this work was to evaluate the solution redox properties of these macromolecules, for which we have used a variety of electrochemical techniques, *viz.* cyclic voltammetry (CV) using conventional disc platinum electrodes, CV using platinum ultra-microelectrodes (UME CV), chronoamperometry (CA) and thin layer cyclic voltammetry (TLCV). CV data are collated in Table 1 for a selection of the new compounds, together with TTF and the model TTF phenyl ester derivative **22** for comparison.

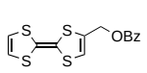

22

Table 1 Solution electrochemical data obtained by CV[a]

Compound	Solvent	$E_1^{\frac{1}{2}}$/V	$E_2^{\frac{1}{2}}$/V
TTF	MeCN–CH_2Cl_2 (1 : 1)	0.34	0.71
TTF	PhCN	0.34	0.78
5	MeCN–CH_2Cl_2 (1 : 1)	0.42	0.81
7	MeCN–CH_2Cl_2 (1 : 1)	0.42	0.81
8	MeCN–CH_2Cl_2 (1 : 1)	0.43	0.86
9c	MeCN–CH_2Cl_2 (1 : 1)	0.41	0.83
14	PhCN	0.58	0.92
20	PhCN	0.57	0.90
21	PhCN	0.57	0.90
22	MeCN–CH_2Cl_2 (1 : 1)	0.41	0.83

[a] Data were obtained at 20 °C under argon using a platinum working electrode (1.6 mm diameter) and a platinum wire counter electrode, compound (*ca.* 5×10^{-4} M), electrolyte = Bu_4N^+ PF_6^- (0.1 M); scan rate = 100 mV s^{-1} *vs.* Ag/AgCl.

These experiments established that all the compounds exhibited two redox couples typical of the TTF system (*i.e.* the sequential formation of the TTF radical cation and the dication).[24] The direct attachment of an ester substituent to TTF (*i.e.* TTF-CO_2R) is known to raise both the first and second oxidation potentials:[10c,25] surprisingly, a quantitatively similar effect is observed for compound **22**. This substituent effect accounts for the increased oxidation potentials of multi-TTF systems **5**, **7**, **8** and **9c**, compared to TTF. The attachment of alkylsulfanyl substituents to TTF also raises the oxidation potential[24] (an additive effect has been noted for one, two and four alkylsulfanyl substituents)[26] and this gives rise to the consistent anodic shift in the values of E_1 and E_2 for compounds **14**, **20**, **21**, in which each TTF unit contains four alkylsulfanyl groups, relative to TTF under the same conditions. For the *p*-xylyl TTF systems **14**, **20** and **21**, the redox waves were reversible. Within the aryl ester series, reversibility was observed only with the mono- and bis-(TTF) derivatives **22** and **5**, respectively: for the higher oligomers **7**, **8** and **9c**, slightly increased peak separations at higher scan rates were observed, consistent with quasi-reversible behaviour.

A general trend with our aryl ester TTF macromolecules is that as the number of TTF units increases, the first redox wave broadens slightly and the second wave sharpens.[17b] Similar behaviour has been reported previously for TTF amides immobilised on RuO_2 or PtO_2 surfaces,[27] and the data can be explained by adsorption or precipitation on the electrode surface. The CV and UME CV of $(TTF)_{12}$ system **8**, which are representative, are shown in Figs. 2(*a*) and (*b*), respectively.

The electrochemistry of the stable macromolecules **9c** and **21** has been studied using TLCV techniques.[28] In contrast to conventional CV, in TLCV the current is not limited by the mass transport to the electrode. Integrating the voltammetric waves against the one-electron reduction peak of the internal standard 2,3-dichloronaphthoquinone (DCNQ) provides convincing evidence that complete oxidation occurs for all the TTF units in these compounds. We note that the second TTF oxidation wave is slightly narrower than the first wave, which could be due to adsorption phenomena. Fig. 2(*c*) shows the TLCV of compound **9c** in the presence of DCNQ. We have established that TLCV is the most reliable method for assessing the extent of oxidation of multi-TTF derivatives in solution.[17b,21] These macromolecules provide some of the first all-organic dendritic poly(radical cations) and poly(dications). Almost all other workers in the field decided to include metal centres as redox active species,[15] although naphthalene diimides have been attached to PAMAM dendrimers to form poly(radical anions),[29] and interior anthraquinone units have been studied.[30]

We have also studied the chemical oxidation of the stable $(TTF)_8$ macromolecule **9c**.[17b] UV–VIS Spectroscopy is a convenient method for monitoring the formation of TTF radical

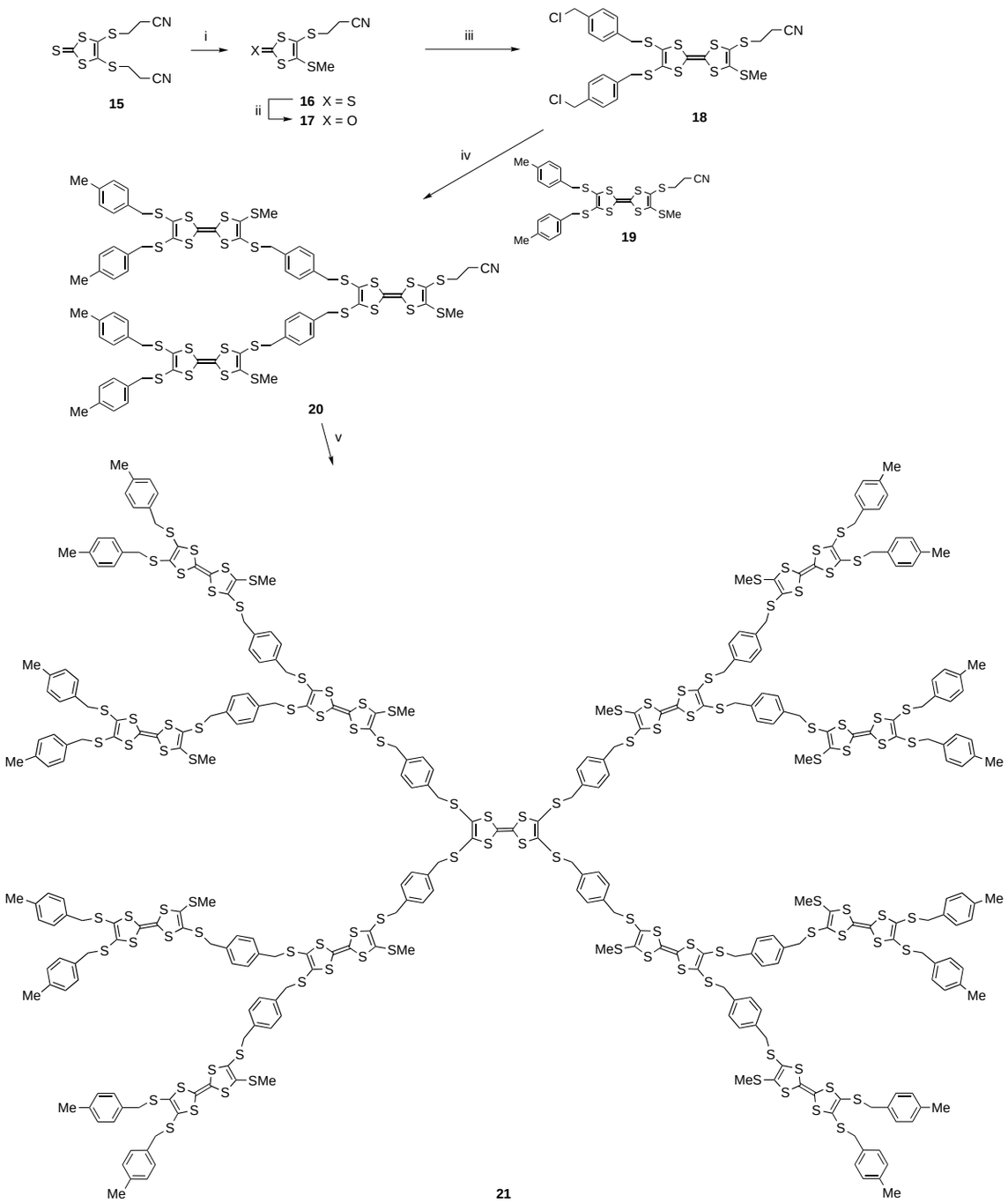

Scheme 4 *Reagents and conditions*: i, $CsOH.H_2O$ (1 equiv.), DMF–MeOH, 20 °C, followed by MeI; ii, $Hg(OAc)_2$, $CHCl_3$–AcOH, 20 °C; iii, **12**, $P(OEt)_3$, 125 °C; iv, **19**, $CsOH·H_2O$ (1 equiv.), DMF–MeOH, then **18**, 20 °C; v, $CsOH·H_2O$, DMF–MeOH, then **14**, 20–80 °C

cations, which have a characteristic absorption band at λ_{max} 580 nm for unsubstituted TTF.[31] As mentioned earlier, oxidised TTF units can form dimers or stacks, and they display lower energy absorptions, *e.g.* 830 nm for $(TTF^{+\cdot})_2$ dimers.[31b] The UV–VIS spectrum for **9c** in CH_2Cl_2 showed significant changes upon addition of I_2 to the solution: new broad absorption bands appeared at λ_{max} 525 and 830 nm. The higher energy band is consistent with the formation of isolated (non-interacting) TTF radical cations, while the lower energy band suggests the existence of interacting dimers. Dilution studies established that the absorption coefficient of the latter band decreased with increasing dilution; it is, therefore, assigned to an intermolecular dimer band. These data provide evidence that the oxidised macromolecules self-associate in solution, by virtue of intermolecular interactions of their peripheral TTF radical cations. The relatively rigid and short aryl ester branching units in **9c** presumably disfavour intramolecular dimerisation.[32] Intermolecular self-association of dendrimers by hydrogen-bonding[33] or coordinative bonds[34] has also been reported recently.

A phthalocyanine core with pendant multi-TTF functionality

Prompted by our increasing knowledge of the synthesis and redox properties of TTF dendrimers possessing aryl ester and TTF cores, reported above, we have investigated closely related macromolecules with core units of increased complexity, *e.g.*

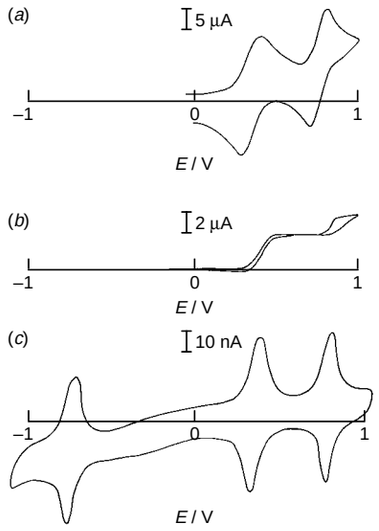

Fig. 2 Solution electrochemistry: (*a*) CV of **8** (solvent = MeCN, electrolyte = $Bu_4N^+PF_6^-$, Pt electrode, *vs*. Ag/AgCl, scan rate = 100 mV s^{-1}); (*b*) UME CV of **8** [solvent = MeCN–CH_2Cl_2 (1 : 1 v/v) electrolyte = $Bu_4N^+PF_6^-$, Pt electrode, *vs*. Ag/AgCl, scan rate = 20 mV s^{-1}]; (*c*) TLCV of **9c** (0.5×10^{-4} M) and 2,3-dichloronaphthoquinone (4.0×10^{-4} M) as internal reference (which gives rise to the wave at negative potential) in 1 M $Bu_4N^+PF_6^-$, solvent = CH_2Cl_2, *vs*. Ag/Ag^+, scan rate = 10 mV s^{-1}

phthalocyanines. It is envisaged that combining the versatile electrochemical, optical and coordination properties of phthalocyanines,[35] with the redox properties of pendant multi-TTF functionality should provide novel optoelectronic materials. In the longer term, the tendency of both phthalocyanines and TTFs to self-assemble by face-to-face π–π stacking, and the potential for coordinatively linking metallophthalocyanines to form stable polymers, might be harnessed to afford nanometer-sized molecular wires and cables, which could be electronically and/or ionically conducting.[36]

Synthesis of prototype Pc-$(TTF)_8$ and Pc-$(TTF)_4$ systems

The simplest methodology to symmetrically substituted phthalocyanines involves tetramerisation of a phthalonitrile precursor.[37] We, therefore, targeted compound **28**, with peripheral hexylsulfanyl substituents to impart solubility.[38] The synthesis is shown in Scheme 5.[39] TTF derivative **23** was obtained in 63% yield from readily available 1,3-dithiole half-units by cross-coupling methodology. One of the ester substituents on **23** was removed by treatment with LiBr in HMPA at 80 °C,[40] to afford monoester derivative **24** (88% yield) which was reduced with DIBAL-H to yield the alcohol derivative **25** (86% yield). The alkoxide ion of **25** (2 equiv.) reacted with 2,3-dibromo-4,5-di(bromomethyl)benzene **26** to yield the bis(TTF) system **27** (64% yield) which upon reaction with CuCN in DMF at 140 °C produced phthalonitrile derivative **28** (28% yield), this being the most problematical step in the whole Scheme. Tetramerisation of **28** to furnish the Pc-$(TTF)_8$ derivative **29** (56% yield) was achieved upon reaction with lithium pentanolate in pentanol at 125 °C. Analogous chemistry gave the Pc-$(TTF)_4$ system **30**.[39]

Compounds **29** and **30** were both isolated as dark green solids, which were soluble in a range of organic solvents (*e.g.* $CHCl_3$, CS_2, CH_2Cl_2 and toluene) but insoluble in alcohols, MeCN and DMF. Spectroscopic data, elemental analysis and MALDI TOF mass spectra were entirely consistent with the proposed structures.

Spectroscopic and electrochemical studies

Evidence for supramolecular aggregation of **29** and **30** was obtained from ^{1}H NMR and UV–VIS spectroscopic studies.[39] The ^{1}H NMR spectra of **29** and **30** at 20 °C in $CDCl_3$ gave broad

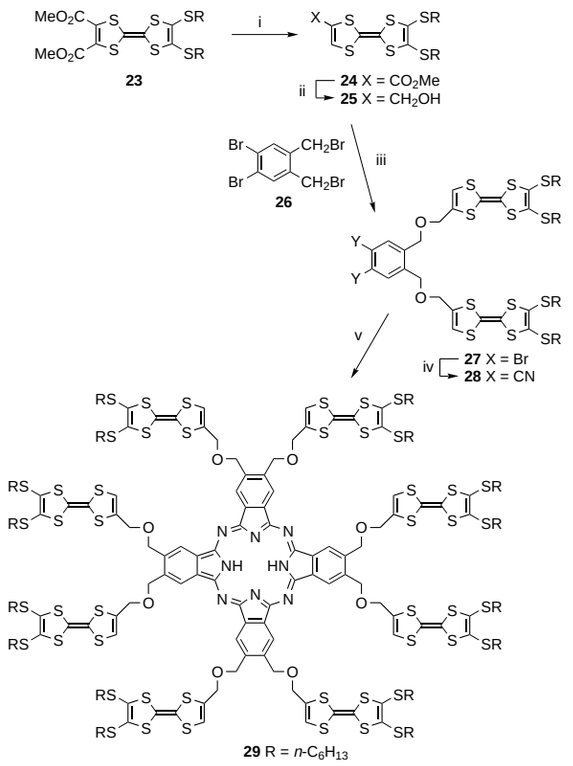

Scheme 5 *Reagents and conditions*: i, LiBr, HMPA, 80 °C; ii, DIBAL-H, THF, −78 to 20 °C; iii, NaH, THF, 40 °C, then **26**, 20 °C; iv, CuCN, DMF, 140 °C; v, lithium pentanolate, pentanol, 125 °C

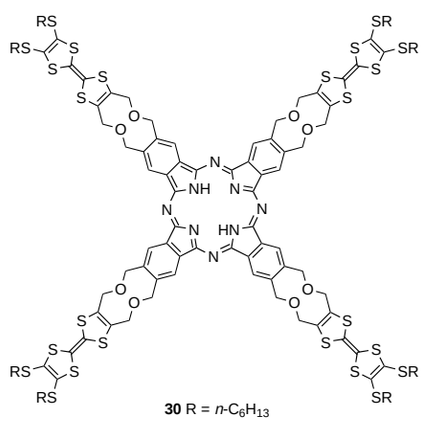

signals with no fine structure: ^{13}C NMR spectra were obtained at 50 °C in $CDCl_3$ and the signals for compound **29** were much sharper than those for compound **30**, suggesting that the latter compound is more aggregated in this solvent at the relatively high concentration of the NMR sample. No ESR signals were observed for either compound, suggesting that the broad NMR spectra were not due to radical impurities.

UV–VIS spectra of compounds **29** and **30** dissolved in a mixture of toluene and pyridine (99 : 1 v/v) at 20 °C are shown in Fig. 3. The split Q-band, which is characteristic of a metal-free phthalocyanine, is observed at λ_{max} 665 and 700 nm (for compound **29**) and at λ_{max} 674 and 709 nm (for compound **30**). The additional broader hypsochromically-shifted band at λ_{max} 636 (for **29**) and 648 (for **30**) is indicative of aggregated species.[36*a*]

The luminescence emission from compounds **29** and **30** was found to be of very low intensity and fell in the same spectral region as that of unsubstituted metal-free phthalocyanines.

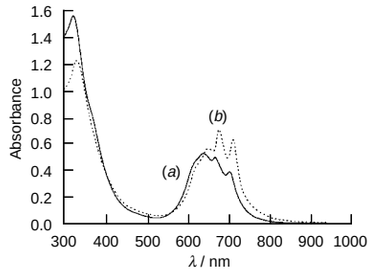

Fig. 3 UV–VIS spectra of (*a*) **29** (1.18×10^{-5} M) and (*b*) **30** (1.44×10^{-5} M) in toluene–pyridine (99 : 1 v/v)

Fluorescence quantum yields were $< 10^{-4}$ and $1.7 \pm 0.3 \times 10^{-4}$ for **29** and **30**, respectively. These values are very much lower than that obtained for a metal-free Pc lacking the TTF moieties, *cf.* Bu_4PcH_2 ($\Phi = 0.50$). We demonstrated that the fluorescence from Bu_4PcH_2 is efficiently quenched by the addition of TTF to the solution: in toluene the rate constant for this process was found to be diffusion controlled, $k_Q(1.1 \pm 0.1) \times 10^{10}$ $dm^3\ mol^{-1}\ s^{-1}$. Quenching in the tethered compounds **29** and **30** is, therefore, ascribed to rapid intramolecular electron transfer between the excited singlet state of the Pc core and a peripheral (neutral) TTF acting as an electron donor group. It will be interesting to explore if the fluorescence can be switched on when the TTF units are oxidised.

Solvent-dependent CV data were obtained for systems **29** and **30**. In PhCN, compound **29** exhibits the expected two TTF redox waves at $E_1^{\frac{1}{2}}$ +0.50 and $E_2^{\frac{1}{2}}$ +0.87 V (*vs.* Ag/AgCl) together with a third irreversible oxidation peak at +1.18 V (the corresponding reduction is not seen on the reverse sweep), and on the cathodic sweep a reduction peak is observed at $E^{\frac{1}{2}}$ −0.51 V. Based on literature precedents,[41] we assign these additional redox waves to a single-electron oxidation and reduction, respectively, of the phthalocyanine core unit. The electrochemistry of **30** was qualitatively similar to **29**, although the redox waves of the Pc unit were more discernable in CH_2Cl_2 than in PhCN, and they are clearly seen in the differential pulse voltammogram (DPV). The CV and DPV for **30** in CH_2Cl_2 are shown in Figs. 4(*a*) and (*b*), respectively.

Based on the CV peak current for compounds **29** and **30**, we suggest that all the TTF units are oxidised, although for compound **29** especially, the second TTF wave was less intense than the first wave. The solvent dependency of the electrochemistry and the UV–VIS spectra of these compounds suggests that the conformation and/or extent of aggregation vary considerably with the solvent. We have obtained qualitatively similar data for a pyrazinoporphyrazine system with eight appended TTF groups.[42]

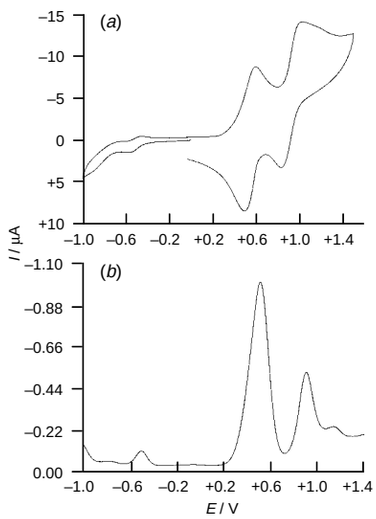

Fig. 4 (*a*) Cyclic voltammogram of **30** in CH_2Cl_2. Pt disc working electrode, 1.6 mm diameter; Pt wire counter electrode, *vs.* Ag/AgCl. Supporting electrolyte = 0.1 M $Bu_4N^+PF_6^-$; scan rate = 100 mV s^{-1}. (*b*) Differential pulse voltammogram of **30** in CH_2Cl_2: sample width = 8 ms; pulse amplitude = 50 mV; pulse width = 10 ms; pulse period = 200 ms; electrodes as Fig. 4(*a*).

Conclusions and future prospects

It is intended that this article will reinforce the fact that TTF is an interesting building block for covalent attachment into a variety of macromolecular assemblies. The synthesis of these multi-TTF systems would have been virtually impossible prior to the recent developments in synthetic methodology which have made available the functionalised TTF starting materials in multi-gram quantities. The materials described herein are tractable and amenable to unambiguous characterisation by standard spectroscopic, mass spectrometric and analytical techniques: they also possess aesthetically pleasing structures. If insolubility of the TTF system is a problem, this can be readily overcome by attachment of alkylsulfanyl chains (*e.g.* compound **29**). This substitution slightly raises the oxidation potential, which for our compounds generally has the added benefit of increased stability to acids and oxidising agents.

These materials present novel macromolecular architectures, with controlled emplacement of TTF groups, and our attention has focused on establishing their multi-electron redox activity. This work paves the way for combining the unique properties of the TTF molecule, which have fascinated scientists in the field of molecular solid state chemistry for over 25 years, with the beneficial properties of polymers, such as film formation and processability, to provide new optoelectronic materials.

Our results suggest interesting targets for future synthetic studies. Unsymmetrical systems, *i.e.* macromolecules constructed by the attachment of different wedges to the core units, are unexplored: in particular, combinations of different substituted TTF units with a strong gradient of redox properties, or π-donor and π-acceptor wedges within the same dendrimer structure, could lead to vectoral electron transport. The study of intra- and inter-dendrimer π–π stacking interactions of oxidised TTF units also promises to be a fruitful line of research.

We thank the EPSRC for funding (W. D. and C. W.) and the Royal Society for financial support (L. M. G.).

Martin Bryce was born in Sutton Coldfield, UK in 1953. He obtained a BSc from Wolverhampton Polytechnic and a DPhil from York University, under the supervision of Drs P. Hansen and J. M. Vernon. He was a postdoctoral fellow with Professor L. Weiler (University of British Columbia) and Professor R. W. Alder (University of Bristol). He was appointed as a Senior Demonstrator at Durham University in 1981, and subsequently as a Lecturer, Senior Lecturer, Reader and Professor of Chemistry (in 1995). In 1988 he was a Visiting Scientist at the Univesity of California, Santa Barbara, working in Professor Wudl's group. He has received the Bader Award and the Interdisciplinary Award from the Royal Society of Chemistry, and a Nuffield Foundation Research Fellowship. His research interests embrace the synthesis of new organic materials with unconventional electrical, optical and magnetic properties, supramolecular chemistry and new synthetic methodology.

Wayne Devonport was born in Barnsley, UK in 1970. He obtained his BSc from Bradford University, and a PhD from Durham University for work on the synthesis of TTF dendrimers. He then held a postdoctoral post at IBM, San Jose, and is currently employed as a research chemist at the Cabot Corporation, near Boston, USA. His research interests focus on well-defined surface modifications by organic and polymeric substrates.

Leonid Goldenberg was born in Zaporozh'e, Ukraine in 1957. He obtained his PhD for work on TTF salts at the Institute of

Chemical Physics of the USSR Academy of Sciences in Chernogolovka, where he is currently a Senior Research Fellow. He has recently been a visiting scientist at Durham University, working on organic thin films and the electrochemistry of charge-transfer materials.

Changsheng Wang was born in Hebei, China in 1963. He obtained his PhD for work on heterocyclic synthesis at Nankai University, China. He joined the faculty of Tsinghua University in 1988 and is currently working at Durham University with Professor Bryce on dendrimer and polymer synthesis.

Notes and References

† E-mail: m.r.bryce@durham.ac.uk

1 For initial references to TTF see: F. Wudl, G. M. Smith and E. J. Hufnage., *J. Chem. Soc., Chem. Commun.*, 1970, 1453; S. Hünig, G. Kiesslich, D. Scheutzow, R. Zahradnik and P. Carsky *Int. J. Sulfur Chem. Part C*, 1971, **6**, 109.

2 Reviews: G. Schukat and E. Fanghänel, *Sulfur Rep.*, 1993, **13**, 254; M. R. Bryce, *J. Mater. Chem.*, 1995, **5**, 1481.

3 Reviews: F. Wudl, *Acc. Chem. Res.*, 1984, **17**, 227; A. E. Underhill, *J. Mater. Chem.*, 1992, **2**, 1.

4 J. Ferraris, D. O. Cowan, V. V. Walatka and J. H. Perlstein, *J. Am. Chem. Soc.*, 1973, **95**, 948.

5 J. M. Williams, J. R. Ferraro, R. J. Thorn, K. D. Carlson, U. Geiser, H. H. Wang, A. M. Kini and M.-H. Whangbo, *Organic Superconductors (Including Fullerenes)*, Prentice Hall, Englewood Cliffs, 1992.

6 A. M. Kini, U. Geiser, H. H. Wang, K. D. Carlson, J. M. Williams, W. K. Kwok, K. G. Vandervoot, J. E. Thompson, D. L. Stupka, D. Jung and M.-H. Whangbo, *Inorg. Chem.*, 1990, **29**, 2555.

7 Reviews: P. Day and M. Kurmoo, *J. Mater. Chem.*, 1997, **7**, 1291; E. Coronado and C. J. Gómez-García, *Chem. Rev.*, 1988, in the press.

8 (*a*) C. U. Pittman, Jr., M. Narita and Y. F. Liang, *Macromolecules*, 1976, **9**, 360; (*b*) C. U. Pittman, Jr., Y. F. Liang and M. Ueda, *Macromolecules*, 1979, **12**, 355; (*c*) C. U. Pittman, Jr., Y. F. Liang and M. Ueda, *Macromolecules*, 1979, **12**, 541; (*d*) S. Frenzel, S. Arndt, R. M. Gregorious and K. Müllen, *J. Mater. Chem.*, 1995, **5**, 1529 and references cited therein; (*e*) S. Shimada, A. Masaki, K. Hayamizu, H. Matsuda, S. Okada and H. Nakaniashi, *Chem. Commun.*, 1997, 1421; (*f*) T. Yamamoto and T. Shimizu, *J. Mater. Chem.*, 1997, **7**, 1967; (*g*) J. Roncali, *J. Mater. Chem.*, 1997, **7**, 2307 and references cited therein.

9 A. J. Moore and M. R. Bryce, *Synthesis*, 1997, 407.

10 (*a*) J. Garín, J. Orduna, J. Uriel, A. J. Moore, M. R. Bryce, S. Wegener, D. S. Yufit and J. A. K. Howard, *Synthesis*, 1994, 489; (*b*) Review: J. Garín, *Adv. Heterocycl. Chem.*, 1995, **62**, 249; (*c*) For pioneering studies on TTF functionalisation using this methodology see: D. C. Green, *J. Org. Chem.*, 1979, **44**, 1476.

11 (*a*) J. Becher, J. Lau, P. Leriche, P. Mork and N. Svenstrup, *J. Chem. Soc., Chem. Commun.*, 1994, 2715; (*b*) N. Svenstrup and J. Becher, *Synthesis*, 1995, 215.

12 M. B. Nielsen, Z.-T. Li and J. Becher, *J. Mater. Chem.*, 1997, **7**, 1175; J. Becher, Z.-T. Li, P. Blanchard, N. Svenstrup, J. Lau, M. B. Nielsen and P. Leriche, *Pure Appl. Chem.*, 1997, **69**, 465; K. B. Simonsen and J. Becher, *Synlett.*, 1997, 1211; M. B. Nielsen and J. Becher, *Liebigs Ann. Recl.*, 1997, 2177.

13 G. R. Newkome, C. N. Moorefield and F. Vögtle, *Dendritic Molecules: Concepts, Synthesis, Perspectives*, VCH, Weinheim, 1996.

14 For reviews which emphasise the functional properties of dendrimers see: J. Issberner, R. Moors and F. Vögtle, *Angew. Chem., Int. Ed. Engl.*, 1994, **33**, 2413; R. Moors and F. Vögtle, in *Advances in Dendritic Macromolecules*, ed. G. R. Newkome, JAI Press, London, 1996, vol. 2, p. 41.

15 For a review of redox-active dendrimers, see: M. R. Bryce and W. Devonport, in *Advances in Dendritic Macromolecules*, ed. G. R. Newkome, JAI Press, London, 1996, vol. 3, p. 115.

16 C. B. Gorman, B. L. Parkhurst, K.-Y. Chen and W. Y. Shu, *J. Am. Chem. Soc.*, 1997, **119**, 1141.

17 (*a*) M. R. Bryce, W. Devonport and A. J. Moore, *Angew. Chem., Int. Ed. Engl.*, 1994, **33**, 1761; (*b*) W. Devonport, M. R. Bryce, G. J. Marshallsay, A. J. Moore and L. M. Goldenberg, *J. Mater. Chem.*, 1998, accepted for publication.

18 C. J. Hawker and J. M. J. Fréchet, *J. Am. Chem. Soc.*, 1990, **112**, 7638.

19 T. M. Miller, E. W. Kwock and T. X. Neenan, *Macromolecules*, 1992, **25**, 3143.

20 M. R. Bryce and W. Devonport, *Synth. Met.*, 1996, **76**, 305.

21 C. Wang, M. R. Bryce, A. S. Batsanov, L. M. Goldenberg and J. A. K. Howard, *J. Mater. Chem.*, 1997, **7**, 1189.

22 G. Steimecke, H.-J. Sieler, R. Kirmse and E. Hoyer, *Phosphorus Sulfur*, 1979, **7**, 49.

23 A. Krief, *Tetrahedron*, 1986, **42**, 1209.

24 S. L. Lichtenberger, R. L. Johnston, K. Hinkelmann, T. Suzuki and F. Wudl, *J. Am. Chem. Soc.*, 1990, **112**, 3302 and references cited therein.

25 A. S. Batsanov, M. R. Bryce, J. N. Heaton, A. J. Moore, P. J. Skabara, J. A. k. Howard, E. Ortí, P. M. Viruela and R. Viruela, *J. Mater. Chem.*, 1995, **5**, 1689.

26 A. J. Moore and M. R. Bryce, *J. Chem. Soc., Chem. Commun.*, 1991, 1638.

27 K. Kuo, P. R. Moses, J. R. Lenhard, D. C. Green and R. W. Murray, *Anal. Chem.*, 1979, **51**, 745.

28 A. T. Hubbard and F. C. Anson, in *Electroanalytical Chemistry*, ed. A. J. Bard, Marcel Dekker, New York, 1970, vol. 4, pp. 129–210; R. Carlier and J. Simonet, *Bull. Soc. Chim. Fr.*, 1988, 831.

29 I. Tobakovic, L. L. Miller, R. G. Duan, D. C. Tully and D. A. Tomalia, *Chem. Mater.*, 1997, **9**, 736.

30 V. V. Narayanan, G. R. Newkome, L. A. Echgoyen and E. Pérez-Coredo, *Polym. Prepr.*, 1996, **37**, 419.

31 (*a*) S. Hünig, G. Kiesslich, H. Quast and D. Scheutzow, *Liebigs Ann. Chem.*, 1973, 310; (*b*) J. B. Torrance, B. A. Scott, B. Welber, F. B. Kaufman and P. E. Seiden, *Phys. Rev. B*, 1979, **19**, 730.

32 In our latest development, we have observed intradendrimer interactions of peripheral TTF cation radicals in spectroelectrochemical studies of TTF dendrimers containing flexible glycol chains within their structures: C. A. Christensen, L. M. Goldenberg, M. R. Bryce and J. Becher, *Chem. Commun.*, 1998, 509.

33 F. Osterod and A. Kraft, *Chem. Commun.*, 1997, 1435; P. Thiyagarajan, F. Zeng, C. Y. Ku and S. C. Zimmerman, *J. Mater. Chem.*, 1997, **7**, 1221.

34 W. T. S. Huck, F. C. J. M. van Veggel and D. N. Reinhoudt, *J. Mater. Chem.*, 1997, **7**, 1213.

35 For monographs and reviews see: *Phthalocyanines, Properties and Applications*, ed. C. C. Leznoff and A. B. P. Lever, VCH, New York, 1989–1996, vols. 1–4; M. Hanack and M. Lang, *Adv. Mater.*, 1994, **6**, 819; M. J. Cook, *J. Mater. Chem.*, 1996, **6**, 677.

36 *Cf.* (*a*) C. F. van Nostrum, S. J. Picken and R. J. M. Nolte, *Angew. Chem., Int. Ed. Engl.*, 1994, **33**, 2173; (*b*) C. F. van Nostrum and R. J. M. Nolte, *Chem. Commun.*, 1996, 2385.

37 Review: C. C. Leznoff, in *Phthalocyanines, Properties and Applications*, ed. C. C. Leznoff and A. B. P. Lever, VCH, New York, 1989, vol. 1, p. 1.

38 The unsubstituted analogue of **29** (SR = H) was initially synthesised and found to be extremely insoluble in almost all organic solvents: M. A. Blower, M. R. Bryce and W. Devonport, *Adv. Mater.*, 1996, **8**, 63.

39 C. Wang, M. R. Bryce, A. S. Batsanov, C. F. Stanley, A. Beeby and J. A. K. Howard, *J. Chem. Soc., Perkin Trans. 2*, 1997, 1671.

40 For related reactions with TTF derivatives, see: P. Blanchard, M. Sallé, G. Duguay, M. Jubault and A. Gorgues, *Tetrahedron Lett.*, 1992, **33**, 2685; R. P. Parg, J. D. Kilburn, M. C. Petty, C. Pearson and T. G. Ryan, *J. Mater. Chem.*, 1995, **5**, 1609.

41 Review: A. B. P. Lever, E. R. Milaeva and G. Speier, in *Phthalocyanines, Properties and Applications*, ed. C. C. Leznoff and A. B. P. Lever, VCH, New York, 1993, vol. 3, p. 1.

42 C. Wang, M. R. Bryce, A. S. Batsanov and J. A. K. Howard, *Chem. Eur. J.*, 1997, **3**, 1679.

8/00536B

Crystal structure, ferromagnetic ordering and magnetic anisotropy for two cyano-bridged bimetallic compounds of formula $Mn_2(H_2O)_5Mo(CN)_7 \cdot nH_2O$

Joulia Larionova,[a] Joaquin Sanchiz,[a] Stéphane Gohlen,[b] Lahcène Ouahab[b] and Olivier Kahn*[a]†

[a] *Laboratoire des Sciences Moleculaires, Institut de Chimie de la Matière Condensée de Bordeaux, UPR CNRS no 9048, 33608 Pessac, France*

[b] *Laboratoire de Chimie du Solide et Inorganique Moléculaire, UMR CNRS no 6511, Université de Rennes 1, 35042 Rennes, France*

Slow diffusion of aqueous solutions containing $K_4[Mo^{III}(CN)_7]\cdot 2H_2O$ and a Mn^{II} salt, respectively, affords well shaped single crystals of two cyano-bridged bimetallic phases ordering ferromagnetically with a pronounced magnetic anisotropy in the magnetically-ordered phase.

Bimetallic hexacyanometallate compounds involving 3d metal ions, of the Prussian Blue type, are interesting materials at the frontier between solid state and molecular chemistry.[1–6] As a matter of fact, all their magnetic characteristics (nature of the interaction between nearest neighbors, saturation magnetization, coercivity) are nicely in line with the theoretical models developed in molecular magnetism,[7,8] in particular as far as the symmetry rules involving the magnetic orbitals are concerned.[9] However, these compounds have some drawbacks. First, nobody, as yet, has succeeded in growing single crystals suitable for thorough physical measurements; secondly, their crystal structure as deduced from X-ray powder patterns is cubic, so that they exhibit no magnetic anisotropy. Here, we report on two new cyano-bridged bimetallic species obtained as well shaped single crystals, exhibiting long-range ferromagnetic ordering along with pronounced magnetic anisotropy.

Slow diffusion in a H-shaped tube under nitrogen of two deoxygenated aqueous solutions containing $K_4[Mo(CN)_7]\cdot 2H_2O$[10] and $Mn(NO_3)_2\cdot 6H_2O$, respectively, afforded two kinds of single crystals, with elongated plate (α phase) and prism (β phase) shapes, respectively. Both phases are air sensitive, and all the magnetic investigations were carried out with either single crystals protected by a grease envelop or powder samples placed in quartz tubes sealed under vacuum.

The crystal structures of both phases were solved.‡ The local environments of the metal sites are similar, but the three-dimensional organizations are different. There is one molybdenum and two manganese sites. The molybdenum atom is surrounded by seven C–N–Mn linkages. All the cyano groups are bridging. The coordination polyhedron may be viewed as a distorted pentagonal bipyramid.[11,12] The two manganese sites are in distorted octahedral surroundings. The manganese atom Mn1 is surrounded by four N–C–Mn linkages and two water

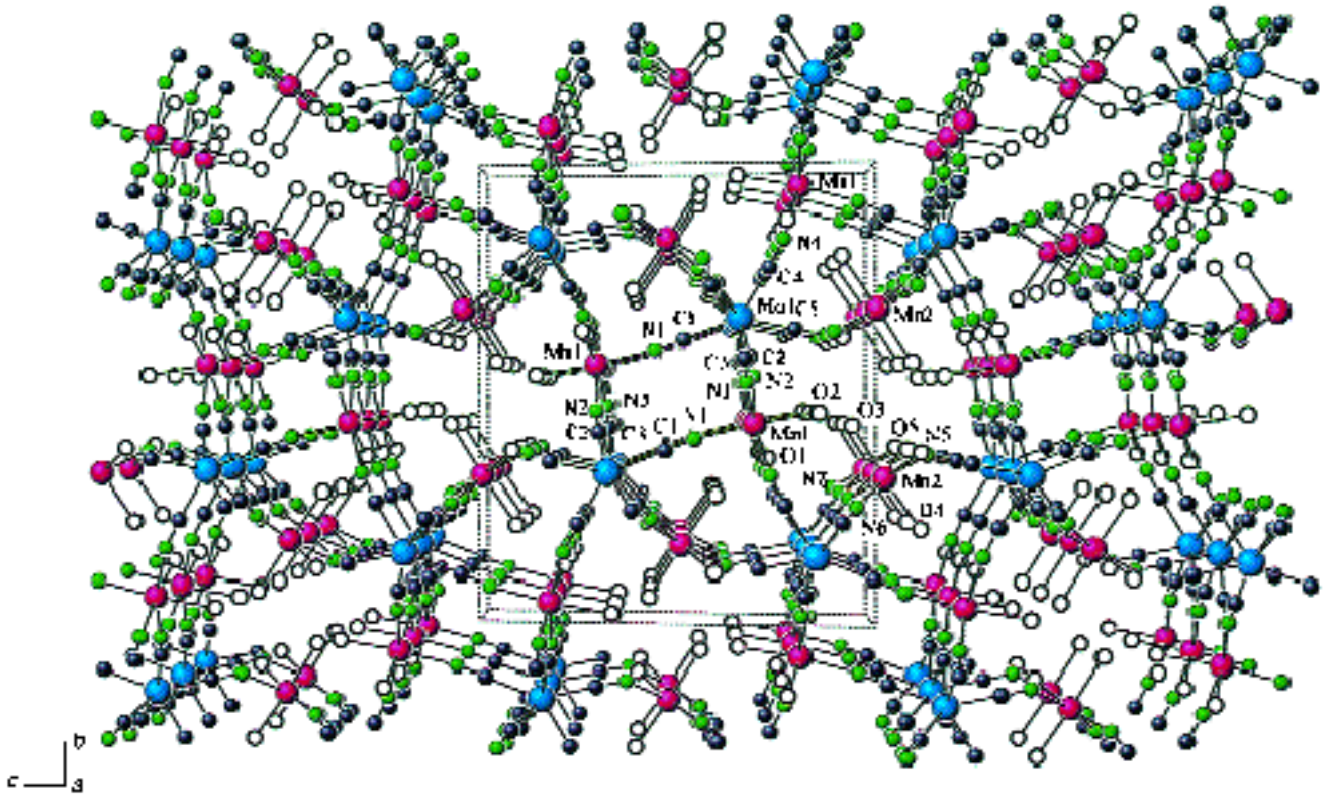

Fig. 1 Crystal structure of $Mn(H_2O)_5Mo(CN)_7\cdot 4H_2O$ (α phase). The manganese atoms are in red, the molybdenum atoms in blue, the oxygen atoms in white, the nitrogen atoms in green, and the carbon atoms in black. The non-coordinated water molecules are omitted for clarity. The Mo–C bond lengths range from 2.127(4) to 2.174(4) Å, the Mn–N bond lengths from 2.181(4) to 2.242(3) Å and the Mn–O bond lengths from 2.195(4) to 2.308(4) Å.

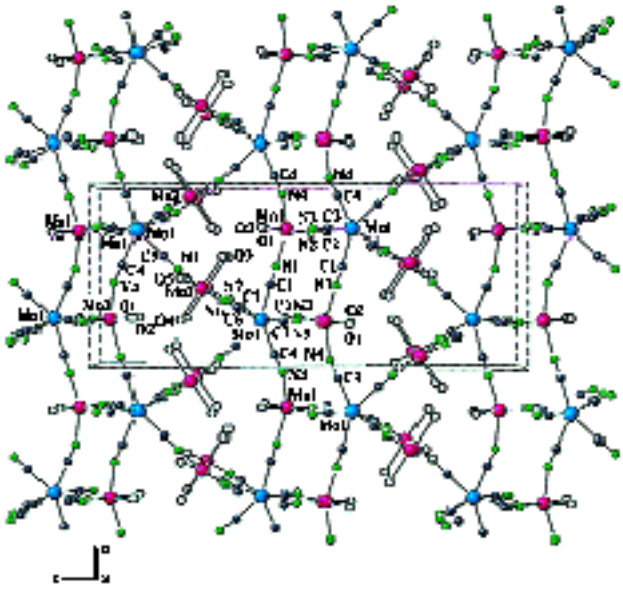

Fig. 2 Crystal structure of $Mn(H_2O)_5Mo(CN)_7{\cdot}4.75H_2O$ (β phase). The color codes are the same as in Fig. 1. The non-coordinated water molecules are omitted for clarity. The Mo–C bond lengths range from 2.110(7) to 2.191(7) Å, the Mn–N bond lengths from 2.158(5) to 2.190(6) Å and the Mn–O bond lengths from 2.223(6) to 2.350(5) Å.

molecules, and the manganese atom Mn2 is surrounded by three N–C–Mo linkages and three water molecules. The structural arrangements may be described as cyano-bridged $Mo1_2Mn1_2$ lozenge motifs linked to each other through two cyano bridges along the *a* axis direction to form a sort of accordion. The Mn2 atoms, located between the accordions, are linked to two molybdenum atoms of one of the accordions and one molybdenum atom of an adjacent accordion. In the α phase each lozenge is linked to four other lozenges through a cyano bridge in the *bc* plane along the [011] and [01$\bar{1}$] directions (Fig. 1). In the β phase each lozenge is linked to only two other lozenges through two cyano bridges in the *bc* plane along the [011] direction (Fig. 2).

Both phases exhibit a long-range magnetic ordering at T_c = 51 K. The field-cooled magnetization curves obtained in cooling a single crystal of the α phase within a magnetic field of 100 Oe aligned along the *a*, *b* and *c** axis directions, successively, are shown in Fig. 3. These curves display a characteristic break at T_c, then the magnetization remains constant as the temperature is lowered further. The strong magnetic anisotropy which is observed is probably of dipolar origin,[13] and reflects the low crystal symmetry which contrasts with the perovskite-like structure of the Prussian Blue phases. The field dependences of the magnetization below T_c reveal a saturation magnetization very close to 11 μ_B. This value corresponds to what is expected for a ferromagnetic state in which the S_{Mo} = 1/2 and S_{Mn} = 5/2 local spins are aligned along the field direction. The overall ferromagnetic nature of the interactions between the spin carriers is supported further by the profile of the $\chi_M T$ *vs.* *T* curves of polycrystalline samples, χ_M being the magnetic susceptibility per repeat unit and *T* the temperature. At room temperature, $\chi_M T$ is equal to 9.1(1) emu K mol^{-1} for both phases, which corresponds to what is expected for non-interacting Mo^{3+} and Mn^{2+} ions, and increases continuously and more and more rapidly as *T* is lowered.

Several factors confer a great interest on the compounds described in this paper, namely: (*i*) the beauty of the crystal

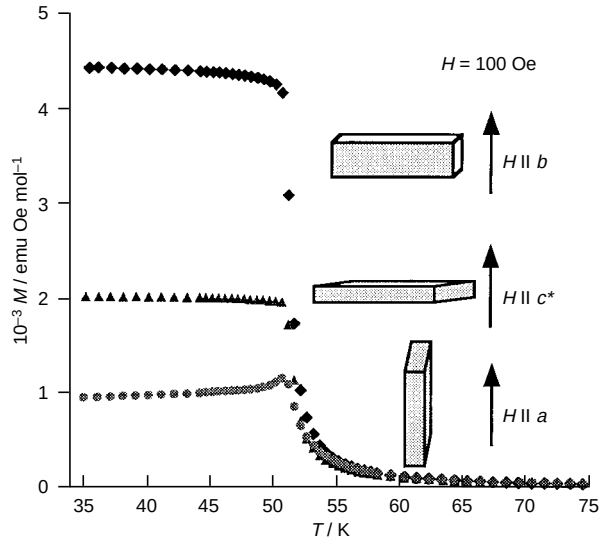

Fig 3 Field-cooled magnetization curves along the *a*, *b* and *c** axis directions of a single crystal of the α phase. The applied magnetic field is 100 Oe.

structures; (*ii*) the possibility of growing rather large single crystals suitable for anisotropy measurements; (*iii*) the presence of high-spin 3d and low-spin 4d spin carriers;[14] (*iv*) finally, the originality of the physical properties in the magnetically ordered state. These properties will be detailed in a subsequent paper.

Notes and References

† E-mail: kahn@icmcb.u-bordeaux.fr

‡ *Crystal data*: α phase: $C_7H_{18}N_7O_9Mn_2Mo$, *M* = 550.10, monoclinic, space group $P2_1/c$ (no. 14), *a* = 7.951(5), *b* = 16.819(3), *c* = 15.189(6) Å, *β* = 104.29(2)°, *U* = 1969(2) Å^3; *Z* = 4, D_c = 1.856, 3292 observations [$I \geqslant 2\sigma(I)$], 287 variables, *R* = 0.0351, wR_2 = 0.0690, GOF = 1.027.

β Phase: $C_7H_{19.5}N_7O_{9.75}Mn_2Mo$, *M* = 563.62, monoclinic, space group $P2_1/c$ (no. 14), *a* = 7.885(3), *b* = 10.406(7), *c* = 25.233(11) Å, *β* = 98.11(2)°, *U* = 2050(2) Å^3, *Z* = 4, D_c = 1.826, 2923 observations [$I \geqslant 2\sigma(I)$], 244 variables, *R* = 0.0475, wR_2 = 0.1025, GOF = 1.090. All data were collected at room temperature on an Enraf-Nonius CAD4 diffractometer with use of Mo-Kα radiation. CCDC 182/823.

1 D. Babel, *Comments Inorg. Chem.*, 1986, **5**, 285.
2 V. Gadet, T. Mallah, I. Castro and M. Verdaguer, *J. Am. Chem. Soc.*, 1992, **114**, 9213.
3 T. Mallah, S. Thiébaut, M. Verdaguer and P. Veillet, *Science*, 1993, **262**, 1554.
4 W. R. Entley and G. S. Girolami, *Inorg. Chem.*, 1994, **33**, 5165.
5 W. R. Entley and G. S. Girolami, *Science*, 1995, **268**, 397.
6 S. Ferlay, T. Mallah, R. Ouahès, P. Veillet and M. Verdaguer, *Nature* (*London*), 1995, **378**, 701.
7 O. Kahn, *Nature* (*London*), 1995, **378**, 667.
8 O. Kahn, *Adv. Inorg. Chem.*, 1996, **43**, 179.
9 O. Kahn, *Molecular Magnetism*, VCH, New York, 1993.
10 R. C. Young, *J. Am. Chem. Soc.*, 1932, **54**, 1402.
11 G. R. Rossman, F. D. Tsay and H. B. Gray, *Inorg. Chem.*, 1973, **12**, 824.
12 M. B. Hursthouse, K. M. A. Malik, A. M. Soares, J. F. Gibson and W. P. Griffith, *Inorg. Chim. Acta*, 1980, **45**, L81.
13 H. Iwamura, K. Inoue, N. Koga and T. Hayamizu, in *Magnetism: a Supramolecular Function*, ed. O. Kahn, NATO ASI Series, Kluwer, Dordrecht, 1996, p. 157.
14 J. Larionova, J. Sanchiz, B. Mombelli and O. Kahn, *Inorg. Chem.*, 1998, **37**, 679.

Received in Cambridge, UK, 26th February 1998; 8/01644E

First synthesis of a *C*-glycoside anologue of a tumor-associated carbohydrate antigen employing samarium diiodide promoted *C*-glycosylation

Dominique Urban,[a] Troels Skrydstrup*[a,b]† and Jean-Marie Beau*[a]

[a] *Université Paris-Sud, Laboratoire de Synthèse de Biomolécules, URA CNRS 462, Institut de Chimie Moléculaire, F-91405 Orsay Cédex, France*

[b] *Department of Chemistry, Aarhus University, Langelandsgade 140, 8000 Aarhus C, Denmark*

A hydrolytically stable analogue of the Tn antigen has been efficiently synthesized for the first time employing a SmI_2-promoted coupling of the pyridyl sulfone of *N*-acetylgalactosamine with an aldehydoamino acid derivative.

The Tn (GalNAcα1→*O*-Ser/Thr) and sialyl Tn (NeuAcα-2→6GalNAcα1→*O*-Ser/Thr) epitopes are major tumor-associated *O*-linked glycopeptide motifs of cell surface glycoproteins which are expressed in over 70% of human epithelial cancers such as lung, colon, stomach and breast carcinomas.[1] In normal cells, however, the Tn antigen is cryptic, where it is further glycosylated giving rise to complex carbohydrates of the mucin-type glycoproteins.[2] This antigen has also been identified as a partial structure of the HIV envelope glycoprotein gp120.[3] We are particularly interested in preparing analogues of these epitopes as molecular components of potential small molecular weight synthetic vaccines,[4] with high immunogenicity and *in vivo* stability against various carcinoma. A *C*-glycoside analogue in which the interglycosidic oxygen is replaced with a methylene group[5] may well conform to such desired properties. Here we present for the first time the synthesis of one such mimic of these tumor-associated antigens, namely that of *O*-(2-acetamido-2-deoxy-α-D-galactopyranosyl)-L-serine (Scheme 1).

Several recent syntheses of *C*-glycosidic amino acids have now appeared in the literature, although only one has been directly applied to 2-hexosamine derivatives. In this approach, Kessler reported the stereoselective synthesis of a *C*-glycoside mimic of N^4-(2-acetamido-2-deoxy-β-D-glucopyranosyl)-L-asparagine, an important constituent of *N*-glycopeptides, *via* the coupling of a glycosyl dianion with a modified asparatic acid derivative as the key step.[6,7]

We have recently shown that reductive samariation of glycosyl pyridyl sulfones in the presence of carbonyl substrates leads to a viable and rapid route to *C*-glycosides.[8] In particular, we have demonstrated that the anomeric organosamarium of *N*-acetylgalactosamine affords predominantly α-*C*-glycosides upon condensation with simple aldehydes and ketones.[8c,f] We hypothesized that with a suitable aldehyde precursor of an amino acid derivative, its coupling with **1** could lead to the required *C*-glycosidic amino acid after a subsequent deoxygenation step (Scheme 1). Preliminary results in this direction showed that the carbon chain of the aldehyde precursor was of ideal length for the coupled product to undergo *in situ* lactonization upon addition of the C^1-glycosyl anion to the aldehyde C=O bond, thus complicating the following deoxygenation.[8f] To prevent this event, we decided to employ the cyclic carbamate derivates of the type **2**, the synthesis of which is outlined in Scheme 2.

L-Aspartic acid was easily converted to alcohol **4** in four steps adopting the protocol described by McKillop for the conversion of amino acids to their corresponding cyclic carbamates.[9] Hence, esterification in acidic MeOH and treatment with $ClCO_2Et$ led to the dimethyl ester **3**. Subsequent reduction to the diol and cyclisation upon treatment with 2 equiv. of NaH afforded the cyclic carbamate **4** in an overall yield of 81%. Bis(silylation) was accomplished upon treatment of **4** with TBDMSOTf in collidine, after which the primary alcohol could be selectively liberated with HF in MeCN.[10] Oxidation employing the Swern conditions then gave crystalline aldehyde **2** in high yield.

The key coupling step, outlined in Scheme 3, was performed by adding a THF solution of SmI_2 (2 equiv.) to the previously described glycosyl pyridyl sulfone **5**[8c,f] and aldehyde (1.2 equiv.) at room temperature. An immediate reaction ensued, as monitored by the instantaneous consumption of the one-electron reducing agent, leading after work up to the isolation of the desired *C*-glycosides in high yield (82%) in favor of the α-anomers **6**‡ (α : β, 3.3 : 1). We note again the success of this anionic *C*-glycosylation reaction even though pyridyl sulfone **5** possesses an acidic NH proton. It was necessary to install a protecting group at the carbamate nitrogen in **2** for the coupling reaction to succeed. In its absence (*e.g.* replacing the TBDMS group by H), protonation at C1 of the sugar unit was the sole product observed.§

Whereas treatment of **6** (major isomer) with thiocarbonyl diimidazole¶ surprisingly led to the formation of a cyclic oxazoline involving the C2 acetamido group, use of the traditional Barton deoxygenation method proved effective for the removal of the newly created C7 hydroxy group. Thus

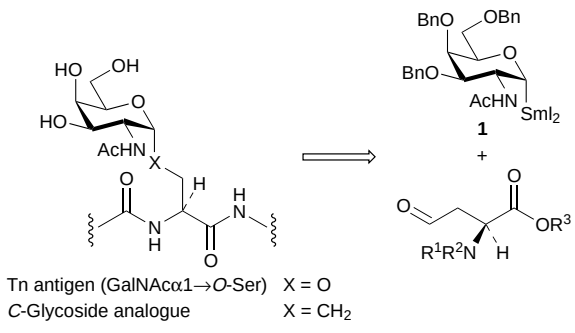

Scheme 1

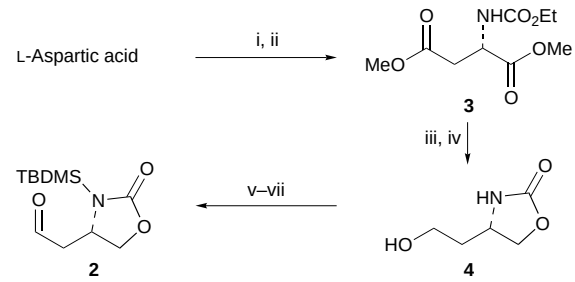

Scheme 2 *Reagents and conditions*: i, AcCl, MeOH; ii, $ClCO_2Et$, $NaHCO_3$, 93% (2 steps); iii, $NaBH_4$, $CaCl_2$, EtOH–THF (2 : 1); iv, NaH, THF, 87% (2 steps); v, TBDMSOTf, collidine; vi, HF, MeCN, 71% (2 steps); vii, $(COCl)_2$, Et_3N, DMSO, 99%

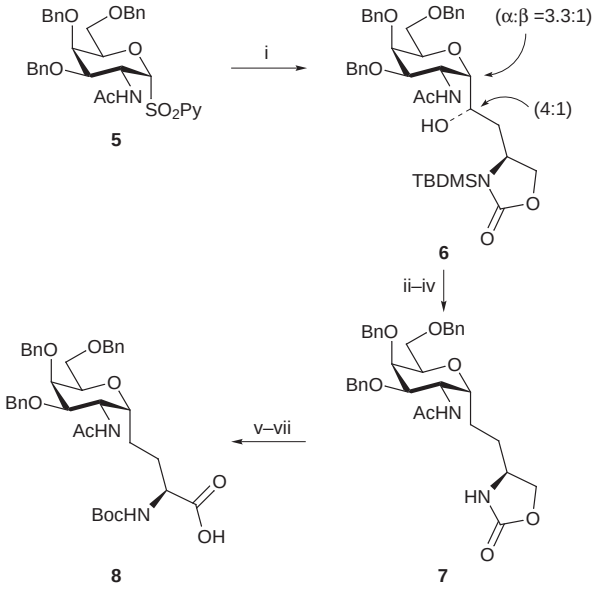

Scheme 3 *Reagents and conditions*: i, **2** (1.2 equiv.), SmI_2 (2.2 equiv.) THF, 20 °C, 82%; ii, NaH, CS_2, MeI, THF, 83%; iii, $HSnBu_3$ (1.5 equiv.), AIBN (0.05 equiv.), toluene, 110 °C; iv, TBAF (3.5 equiv.), THF, 95% (2 steps); v, $(Boc)_2O$ (1.5 equiv.), Et_3N (2.0 equiv.), DMAP (cat.), THF; vi, Cs_2CO_3 (cat.), MeOH, 83% (2 steps); vii, Jones oxidation, 70%

formation of the methyl xanthate from alcohol **6**, followed by tin hydride promoted radical deoxygenation, afforded **7** after desilylation in 79% (three steps). A three-step procedure involving introduction of a Boc group, selective hydrolysis of the cyclic carbamate[11] and oxidation of the primary alcohol to its corresponding carboxylic acid **8** then completed the synthesis of the desired *C*-glycosyl amino acid.‖

In conclusion, we have successfully prepared a hydrolytically stable Tn antigen mimic *via* a SmI_2-promoted *C*-glycosylation protocol. This important amino acid building block is now ready to be incorporated into small peptide chains in order to test them as potentially viable synthetic peptide vaccines against various human epithelial cancers, the results of which will be reported in due course.

Notes and References

† E-mail: ts@kemi.aau.dk

‡ *Selected data*: for **6** δ_H(250 MHz, $CDCl_3$) (major isomer) 6.18 (d, 1 H, *J* 8.4, NH), 4.37 (ddd, 1 H, *J* 9.4, 6.5, 2.9, H_5), 4.18 (dd, 1 H, *J* 11.2, 9.4, H_{6a}), 4.16 (ddd, 1 H, *J* 8.4, 3.1, 2.2, H_2), 3.88 (dd, 1 H, *J* 3.1, 3.1, H_3), 3.76 (dd, 1 H, *J* 6.5, 3.1, H_4), 3.74 (dd, 1 H, *J* 3.5, 2.2, H_1), 3.69 (dd, 1 H, *J* 11.2, 2.9, H_{6b}).

§ The protecting group on the carbamate nitrogen also plays a pivotal role for obtaining high coupling yields of the *C*-glycoside as exemplified by the use of the Boc group, where the *C*-glycosylation yield was reduced by one half. Another advantage is that it provides easily separable isomers.

¶ We have recently applied this reagent successfully for the deoxygenation of a *C*-disaccharide prepared *via* the SmI_2 route [see ref. 8(*b*)].

‖ It is interesting to note that *C*-glycoside **8** does not occupy the normally expected $^4C_1$ chair conformation, as is seen from the coupling constants ($J_{2,3}$ = 4.0, $J_{3,4}$ = 2.9, $J_{4,5}$ = 5.6 Hz). This has also been observed for other *N*-acetyl-α-*C*-galactosamines (ref. 12) and monosaccharides (ref. 13) derivatives possessing benzyl protecting groups at the C3, C4 and C6 hydroxy groups. However, the corresponding deprotected or peracetylated *C*-glycosides were found to possess the normal chair conformation.

1 G. F. Springer, *Science*, 1984, **224**, 1198; S. Sell, *Hum. Pathol.*, 1990, **21**, 1003; S. H. Itzkowitz, M. Yuan, C. K. Montgomery, J. Kjeldsen, H. K. Takahashi, W. L. Bigbee and Y. S. Kim, *Cancer Res.*, 1989, **49**, 197; S. Hakomori, *Curr. Opin. Immunol.*, 1991, **3**, 646.
2 K. L. Carraway and S. R. Hull, *Glycobiology*, 1991, **1**, 131; A. A. Gooley, A. Pisano and K. L. Williams, *Trends Glycosci. Glycotechnol.*, 1994, **6**, 328.
3 J.-E. S. Hansen, H. Clausen, C. Nielsen, L. S. Teglbjaerg, L. H. Hansen, C. M. Nielsen, E. Dabelsteen, L. Mathiesen, S. Hakomori and J. O. Nielsen, *J. Virol.*, 1990, **64**, 2833.
4 For previous work on the use of the Tn antigen as a potential vaccine against epithelial cancers, see: G. D. McLean and B. M. Longenecker, *Can. J. Oncol.*, 1994, **4**, 249; T. Toyokuni, B. Dean, S. Cai, D. Boisin, S. Hakamori and A. K. Singhal, *J. Am. Chem. Soc.*, 1994, **116**, 395; T. Toyokuni and A. K. Singhal, *Chem. Soc. Rev.*, 1995, **24**, 231; B. Liebe and H. Kunz, *Angew. Chem., Int. Ed. Engl.*, 1997, **36**, 618 and references cited therein.
5 M. H. D. Postema, *C-Glycoside Synthesis*, CRC Press, Boca Raton, FL, 1995; D. E. Levy and C. Tang, *The Chemistry of C-Glycosides*, Pergamon, Exeter, 1995; G. Casiraghi, F. Zanardi, G. Rassu and P. Spanu, *Chem. Rev.*, 1995, **95**, 1677; for a review on nucleophilic *C*-glycosyl donors, see J.-M. Beau and T. Gallagher, *Top. Curr. Chem.*, 1997, **187**, 1.
6 F. Burkhart, M. Hoffmann and H. Kessler, *Angew. Chem., Int. Ed. Engl.*, 1997, **36**, 1191 and references cited therein.
7 For other syntheses of *C*-glycosyl amino acids not discussed in ref. 6, see L. Lay, M. Meldal, F. Nicotra, L. Panza and G. Russo, *Chem. Commun.*, 1997, 1469; S. D. Debenham, J. S. Debenham, M. J. Burk and E. J. Toone, *J. Am. Chem. Soc.*, 1997, **119**, 9897.
8 (*a*) D. Mazéas, T. Skrydstrup and J.-M. Beau, *Angew. Chem., Int. Ed. Engl.*, 1995, **34**, 909; (*b*) O. Jarreton, T. Skrydstrup and J.-M. Beau, *Chem. Commun.*, 1996, 1661; (*c*) D. Urban, T. Skrydstrup, C. Riche, A. Chiaroni and J.-M. Beau, *Chem. Commun.*, 1996, 1883; (*d*) O. Jarreton, T. Skrydstrup and J.-M. Beau, *Tetrahedron Lett.*, 1997, **36**, 303; (*e*) T. Skrydstrup, O. Jarreton, D. Mazéas, D. Urban and J.-M. Beau, *Chem. Eur. J.*, 1998, **4**, 655; (*f*) D. Urban, T. Skrydstrup and J.-M. Beau, *J. Org. Chem.*, in the press.
9 N. Lewis, A. McKillop, R. J. K. Taylor and R. J. Watson, *Synth. Commun.*, 1995, **25**, 561.
10 D. E. Ward and B. F. Kaller, *Tetrahedron Lett.*, 1993, **34**, 407.
11 T. Ishizuka and T. Kunieda, *Tetrahedron Lett.*, 1987, **28**, 4185.
12 G. Rubinstenn, J. Esnault, J.-M. Mallet and P. Sinaÿ, *Tetrahedron: Asymmetry*, 1997, **8**, 1327.
13 T. Skrydstrup, D. Mazéas, M. Elmouchir, G. Doisneau, C. Riche, A. Chiaroni and J.-M. Beau, *Chem. Eur. J.*, 1997, **8**, 1342.

Received in Glasgow, UK, 11th February 1998; 8/01196F

Induced separation of a binate vesicle into two independent entities

Fredric M. Menger,*† Stephen J. Lee and Jason S. Keiper

Department of Chemistry, Emory University, Atlanta, Georgia 30322, USA

Two lipid vesicles, one residing in the aqueous interior of the other, separate into independent vesicles upon increasing the temperature or osmotic pressure; phase-contrast microscopy provides the details of the process.

Giant vesicles are spherical lamellar structures having diameters greater than one micrometer. Single giant vesicles can be isolated, manipulated and observed in real time by light microscopy. By contrast, small vesicles (so-called 'SUVs'), used conventionally in most vesicle research, are sub-microscopic and thus evaluatable in solution only by indirect spectroscopic means. Capitalizing upon this size advantage of giant vesicles, researchers have recently reported diverse membrane events ranging from cytomimetic phenomena[1] to surface reactions.[2]

Giant vesicles undergo a variety of morphological changes brought about by mechanical,[1] thermal,[3–5] chemical,[6–8] electrical[9] and pressure[10] alterations in the environment. Thermally-induced shape changes have, perhaps, garnered the most attention from the scientific community. For example, it was shown[5] that temperature affects the vesicle area-to-volume ratio, leading to budding and other shape transitions. Mathematical models explaining the various membrane phenomena are also available.[11,12]

Both natural phospholipids and synthetic lipids can self-asemble into giant vesicles. Didodecyldimethylammonium bromide (DDAB) is a good example of the latter. Use of 'unnatural' lipids is important because it provides a large array of compounds with which to relate membrane properties to molecular structure. We ourselves have employed DDAB, among various synthetic lipids, to observe vesicle aggregation, fusion, endocytosis and birthing.[1]

On occasion, a population of DDAB giant vesicles will contain a 'binate' vesicle that consists of one sphere within another of slighly larger size. Usually the components of the binate vesicle have a common area of contact as portrayed in Fig. 1.

When the system is subjected to heat or osmotic pressure, the binate vesicle separates into two independent vesicles. Since the initial and final surface areas and volumes of the vesicles can be quantified, one has a prime opportunity to monitor the translocation of lipid and vesicular water during the morphological change. Tracking the fate of components in model membrane systems is relevant to cell biology where membrane reorganization occurs in a controlled but poorly understood manner.

A few experimental details will clarify the procedure. DDAB and cholesterol were mixed by dissolving the solids in $CHCl_3$–MeOH and removing the solvent under reduced pressure. The resulting film was sonicated in deionized water and lyophilized to yield a white powder of intimately mixed lipids. Less than 0.1 mg of lipid mixture was smeared onto a glass microscope slide within the confines of a cemented 14 mm i.d. O-ring. Approximately 0.5 ml of deionized water was added to the sample, a glass coverslip applied, and the excess water drained. About 3 h of incubation at 20 °C produced a colony of giant vesicles.

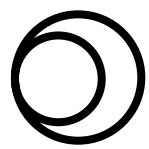

Fig. 1 Schematic representation of a binate vesicle

For heating experiments, the microscope slide was mounted on a hollow brass plate through which flowed water from a constant temperature bath. Temperatures were read from a thermocouple residing directly in the vesicle medium. Dilution experiments, in which the osmotic pressure was altered, were performed by taking up to 25–75 μl of vesicle suspension into a micropipet and gently releasing it into 0.5 ml of deionized water.

Vesicle transformations were observed with phase-contrast optics using a Nikon Diaphot-TMD inverted microscope. Images were recorded with the aid of a Dage-MTI CCD-72 solid-state camera connected in series to a Panasonic AG-1960 SVHS, a Hamamatsu Argus-10 image procesor, and a Sony black and white monitor. Image processing and radii determination from calibrated distances were accomplished using Image-Pro Plus software on a Micron Millenia workstation, while images were printed using a Tektronix Phaser 440 dye sublimation printer.

Fig. 2 shows the effect of heating a 95% DDAB–5% cholesterol vesicle from 20 to 29 °C. In Fig. 2(A), one sees a binate vesicle (adhered to a smaller single vesicle) with considerable apparent contact between the inner and outer bilayers (arrows). The outer vesicle seemingly 'peels' away from the inner vesicle [Fig. 2(B)–(E)] while assuming various non-spherical shapes in the process. In less than 1 min, two unattached spherical vesicles are formed [Fig. 2(F)].

Table 1 records the volumes and surface areas for vesicles in Figs. 2(A) and 2(F). Since the total volume of the two vesicles in Fig. 2(F) is 15.3 pl [compared to only 13.9 pl for the outer vesicle in Fig. 2(A)], 1.4 pl of water were incorporated into the system during the separation process. External water must have

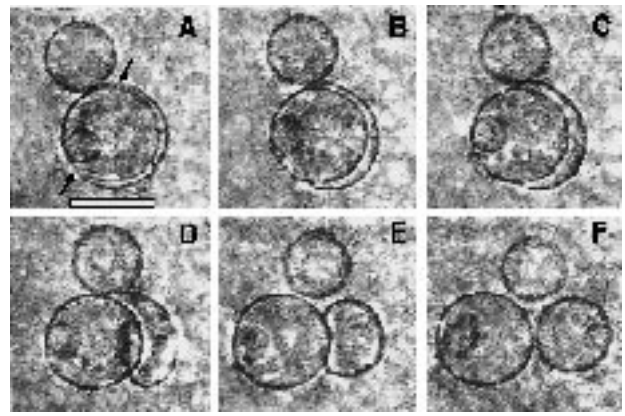

Fig. 2 Progressive separation of the outer shell of a binate vesicle induced by a temperature increase. Arrows in micrograph (A) define the region of membrane contact between the inner and outer vesicle before separation became evident. T = 29 °C raised from 20 °C; time from (A) to (F) = 1 min; bar = 25 μm.

Table 1 Vesicle radii, internal volumes and surface areas in Figs. 2 and 3[a]

	Before separation		After separation	
	Vesicle-1	Vesicle-2	Vesicle-1	Vesicle-2
Fig. 2				
Radius/μm	13.7	14.9	13.7	10.3
Volume/pl	10.7	13.9	10.7	4.6
Surface area/μm²	2360	2790	2360	1330
Fig. 3				
Radius/μm	24.4	27.8	23.5	24.1
Volume/pl	60.8	90.0	54.3	58.6
Surface Area/μm²	7450	9680	6940	7300

[a] Vesicle-1 represents the inner 'static' vesicle and vesicle-2 represents the outer 'active' vesicle.

entered the 'active' vesicle-2 exclusively because the volume of the 'static' vesicle-1 remained constant at 10.7 pl. Since the permeation rate of water through bilayers is generally much too slow to explain the observed influx,[13] it is likely that water enters vesicle-2 *via* an intervesicular gap as was observed previously in a laser-induced vesicle expulsion.[14]

Vesicle separation in Fig. 2 also led to a sizable decrease in the total surface area (from 5150 to 3690 μm² based on the assumption that the 'active' vesicle was originally an intact sphere). Even if the 'active' vesicle is taken to be an incomplete sphere [terminating at the arrows in Fig. 2(A)], there is a net decrease in lipid surface area of about 570 μm² as the new vesicle in Fig. 2(F) (of area 1330 μm²) is formed. One possible explanation is that lipid is deposited upon the 'static' inner vesicle by the 'active' outer vesicle. If this is true, then the deposited lipid must exist as a 'patch' on the surface of the 'static' vesicle because insufficient lipid was made available to coat the receptor vesicle entirely. Formation of bilayer patches residing on intact vesicles has been observed previously.[15]

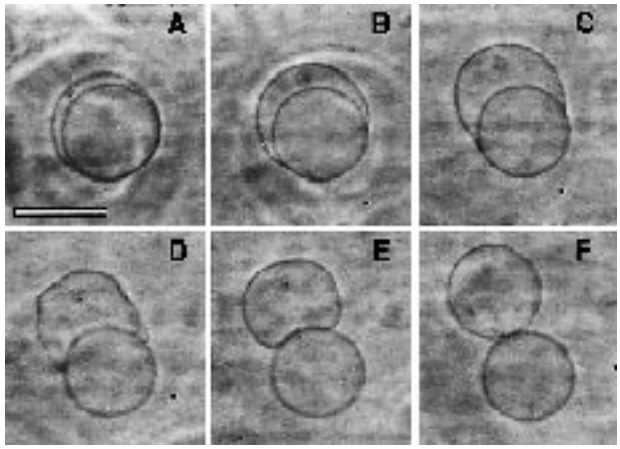

Fig. 3 Separation of a binate vesicle caused by dilution. Note the extreme undulation depicted in micrograph (D). T = 20 °C; time from (A) to (F) = 3 min; bar = 50 μm.

Lipid material could also have been lost to the bulk medium as sub-microscopic vesicles.[14]

An osmotic pressure change at constant temperature, created by dilution with deionized water, also induces vesicle separation (Fig. 3). Once again Table 1 reveals a volume increase requiring the input of external water. Thus, the total volume in Fig. 3(F) (112.9 pl) exceeds that of the outer periphery in Fig. 3(A) (90.0 pl). The need to supply external water is evident in Fig. 3(D) showing a flaccid and strongly undulating intermediate. Entry of water at narrow juncture gaps must be osmotically driven by monomeric DDAB and impurities that invariably exist in the inner vesicular regions.

Within the limits of uncertainty in the measurements, it appears that the surface area data are adequately explained by the two vesicles in Fig. 3 sharing a common membrane (*i.e.* the 'active' vesicle consisting of an incomplete sphere attached to an intact inner vesicle). Two-thirds of 9680 μm² plus a small osmotic swelling gives a value close of 7300 μm², the surface area found for the newly formed vesicle. The 7% volume decrease seen with the 'static' vesicle may reflect a compaction of bilayer lipid upon departure of the attached membrane.

Control experiments showed that vesicles composed of DDAB without cholesterol also manifested the separation phenomenon upon exposure to elevated temperatures and osmotic pressures. Thus, cholesterol-rich domains, if they exist at all, do not seem to play a role here in the observed membrane reorganization.

We thank the National Institutes of Health for supporting this work.

Notes and References

† E-mail: menger@emory.edu

1 F. M. Menger and K. D. Gabrielson, *Angew, Chem., Int. Ed. Engl.*, 1995, **34**, 2091.
2 R. Wick, M. I. Angelova, P. Walde and P. L. Luisi, *Chem. Biol.*, 1996, **3**, 105.
3 K. Berndl, J. Käs, R. Lipowsky, E. Sackmann and U. Seifert, *Europhys. Lett.*, 1990, **13**, 659.
4 J. Käs and E. Sackmann, *Biophys. J.*, 1991, **60**, 825.
5 H.-G. Döbereiner, J. Käs, D. Noppl, I. Sprenger and E. Sackmann, *Biophys. J.*, 1993, **65**, 1396.
6 E. Farge and P. F. Devaux, *Biophys. J.*, 1992, **61**, 347.
7 F. M. Menger and K. Gabrielson, *J. Am. Chem. Soc.*, 1994, **116**, 1567.
8 F. M. Menger and S. J. Lee, *Langmuir*, 1995, **11**, 3685.
9 J.-C. Bradley, M.-A. Guedeau-Boudeville, G. Jandeau and J.-M. Lehn, *Langmuir*, 1997, **13**, 2457.
10 L. Beney, J.-M. Perrier-Cornet, M. Hayert and P. Gervais, *Biophys. J.*, 1997, **72**, 1258.
11 H.-G. Döbereiner, E. Evans, M. Kraus, U. Seifert and M. Wortis, *Phys. Rev. E.*, 1997, **55**, 4458.
12 U. Seifert, *Adv. Phys.*, 1997, **46**, 13.
13 D. Needham, *Permeability and Stability of Lipid Bilayers*, ed. E. Disalvo and S. Simon, CRC Press, Boca Raton, 1995, pp. 49–76.
14 J. D. Moroz, P. Nelson, R. Bar-Ziv and E. Moses, *Phys. Rev. Lett.*, 1997, **78**, 386.
15 F. M. Menger and J. S. Keiper, *Angew. Chem., Int. Ed. Engl.*, 1997, **36**, 248.

Received in Columbia, MO, USA, 3rd October 1997; 7/07263E

Synthesis and characterization of $Co_3(O_2CCH_2CH_2PO_3)_2 \cdot 6H_2O$, a metal carboxylate–phosphonate with a framework structure

Anne Distler and Slavi C. Sevov*†

Department of Chemistry and Biochemistry, University of Notre Dame, Notre Dame, IN 46556, USA

The title compound is the first carboxylate–phosphonate with an extended three-dimensional structure, a framework of trimers of edge-sharing CoO_6-octahedra and organic species with two different functional groups, carboxylic and phosphonic, both coordinated to the metal atoms.

The use of multifunctional ligands for building infinite frameworks by coordination to metal centers has become an area gaining much interest in recent years.[1] Many such crystalline coordination polymers with two- and three-dimensional structures are already known for polynitrilies and polyamines coordinated to noble metals.[2] Similarly, polycarboxylic acids,[3] polyalcohols and polyethers,[4] and polyphosphonic acids,[5] have been used for the construction of such solid-state architectures through coordination to a variety of transition metals. Compounds utilizing organic species with two different functional groups, both coordinated to metal atoms, are very rare. Known are an aminophosphonate with an open-framework type structure,[6] and two layered compounds based on carboxylate–phosphonates.[7] Owing to the directionality of the coordination bond, most of these structures have relatively large voids, and are of potential interest for a variety of guest–host interactions and molecular recognition. A common problem for many of them, especially those with long bridging ligands, is the interpenetration of the frameworks which essentially results in blocking the otherwise available large openings. As far as thermal stability is concerned the phosphonates tend to be the more stable group. We are interested in combining two or more different functionalities in a single compound with a three-dimensional open-framework structure. Here we report on a carboxylate–phosphonate compound with such an extended framework built of transition metals coordinated by a bridging ligand with two different functional groups.

The title compound was initially made in an autoclave at 110 °C from $CoCO_3$ and 2-carboxyethylphosphonic acid, $HO_2CCH_2CH_2P(O)(OH)_2$, mixed in a molar ratio of 2 : 1. The synthesis can be also carried out in an open system as low as 80 °C. The compound crystallizes as spherical aggregates of red-purple crystals. A single crystal structure determination‡ revealed a three-dimensional network of linear trimers of edge-sharing CoO_6-octahedra with the organic molecules coordinated to the cobalt atoms by both functional ends (Fig. 1). The cobalt atoms are of two types, Co2 at an inversion center at the center of the trimer, and Co1 inside the other two octahedra (Fig. 2). The Co2-octahedron shares the two opposite parallel edges, O1 and O6, with the Co1-octahedra. The latter are rotated in opposite directions around the common edges keeping the three cobalt atoms in a straight line. This leads to shorter distances between some of the apical oxygen atoms, O2 and O3. These and one of the shared oxygens, O1 from an adjacent trimer, are bonded to a single phosphorus atom.

The acidic oxygens of both functional groups are fully deprotonated. The carboxy group is coordinated to Co1 as a monodentate ligand through its deprotonated oxygen atom leaving the 'double'-bonded oxygen, O5, as non-bonding (Fig. 2). Thus an extended structure of covalently bonded network –Co–O–P–C–C–C–O–Co– is formed. This network has one-dimensional, S-shaped voids filled with the water molecules, O6, 7 and 8 (Figs. 1 and 3). The latter complete the octahedral coordination sphere around the cobalt atoms by

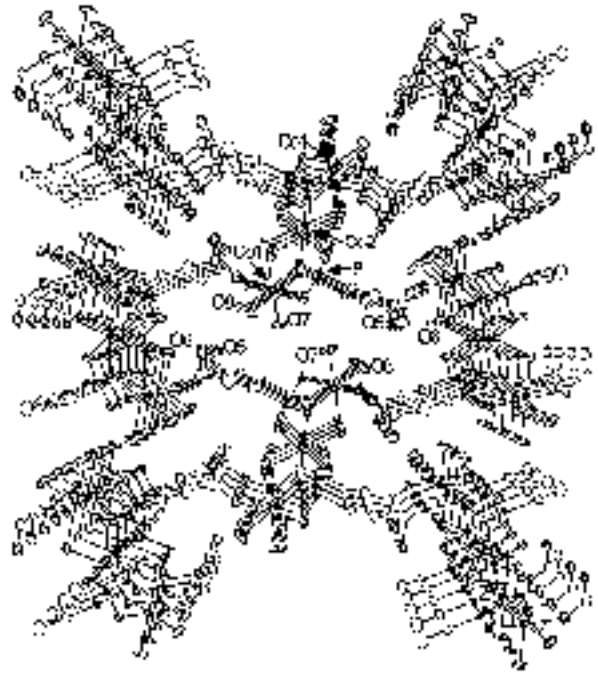

Fig. 1 A general view of $Co_3(O_2CCH_2CH_2PO_3)_2 \cdot 6H_2O$ along the *a* axis (*c* is horizontal) drawn with thermal ellipsoids with 50% probability. The atoms are shown with ellipsoids that are: open for C, cross- hatched for O, and shaded for Co and P. The water oxygens (O6, 7 and 8), the double bonded oxygen (O5), and cobalt and phosphorus of one trimer are labeled.

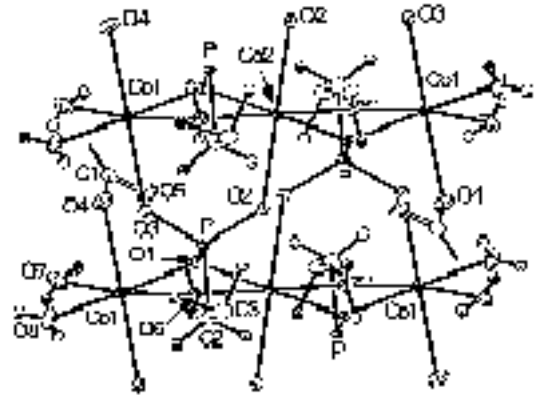

Fig. 2 A closer view of the bonding within and between the trimers of edge-sharing octahedra. Selected distances (Å): Co1–O1 2.066(4), Co1–O3 2.057(3), Co1–O4 2.105(4), Co1–O6 2.215(4), Co1–O7 2.098(4), Co1–O8 2.052(5), Co2–O1 2.098(3), Co2–O2 2.059(3), Co2–O6 2.168(4), P–O1 1.545(4), P–O2 1.517(4), P–O3 1.525(4), P–C2 1.807(6), C1–C2 1.509(8), C2–C3 1.516(9), C1–O5 1.260(7), C1–O4 1.267(7).

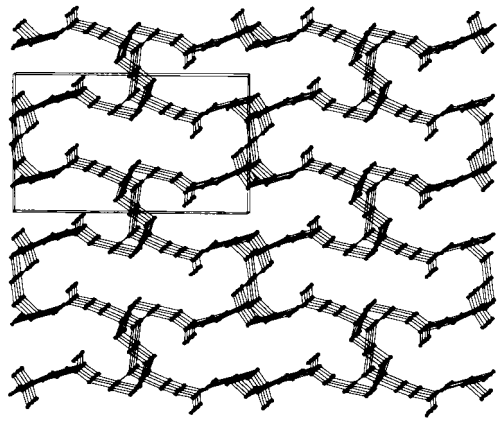

Fig. 3 A view along *a* (as in Fig. 1) of the compound with the water molecules omitted for clarity. The S-shaped one-dimensional openings are easier to see. This is what the dehydrated compound may look like.

coordinating to either one (O7 and O8 to Co1) or two (O6 to both Co1 and Co2) of them.

The IR spectrum of the compound shows the asymmetric and symmetric vibrations of the carboxy group at 1541 and 1419 cm^{-1}, respectively, the vibrations of the phosphonic group in the region 900–1100 cm^{-1}, and the typical bands of the coordinated water (broad at 3369 and sharp at 1646 cm^{-1}). The absence of a band in the region 1690–1730 cm^{-1} (the O–H vibration of a CO_2H group) is in agreement with a deprotonated carboxy group. Magnetic susceptibility measurements in the range 10–300 K show a Curie-type paramagnetism consistent with the structure of 'isolated' islands of cobalt trimers (μ = 9 μ_B). A mass loss of 17.5% was measured by TG at *ca.* 150 °C, and this is consistent with six molecules of water (also confirmed by IR after the dehydration). At that temperature the sample changes color from purple to an intense blue, and this confirms the lowering of the cobalt coordination number. Fig. 3 depicts the structure of the compound without the water molecules. Based on the van der Waals radii, the calculated free volume per unit cell of the treated compound is *ca.* 190 $Å^3$, or 23% of the total volume.§

This new compound provides potential for further explorations. For example, it may be possible to replace the water molecules with different amines. Also, the fact that the C=O part of the carboxylic acid is 'intact' can eventually be used for reactions with different organic molecules with catalytic, photoelectric, or other useful properties in order to 'anchor' them to the solid.

We thank the National Science Foundation (DMR-9701550) for the financial support.

Notes and References

† E-mail: ssevov@nd.edu

‡ *Crystal data* for $Co_3(O_2CCH_2CH_2PO_3)_2 \cdot 6H_2O$: M_w = 586.95, monoclinic, space group $P2_1/c$, Z = 2, a = 4.6086(9), b = 10.278(3), c = 17.504(3) Å, β = 95.74(1)°, U = 825.0(3) $Å^3$, μ = 32.61 cm^{-1}. A hemisphere of data was collected on a CAD4 single crystal diffractometer with graphite-monochromated Mo-Kα radiation at room temperature (crystal size 0.04 × 0.08 × 0.10 mm, ω–2θ scans, 2998 and 1455 collected and independent reflections (R_{int} = 7.87%), respectively). The structure was solved by direct methods and refined with the aid of the SHELXTL-V5.0 package. All lighter atoms, including hydrogen, were located from difference Fourier maps, and refined without constraints. XABS empirical absorption correction was applied to the data after the structure was refined with isotropic thermal parameters. Final residual values: R_1/wR_2 = 0.0498/0.1036 for 1185 observed reflections ($I \geqslant 2\sigma_I$) and 163 refined parameters (R_1/wR_2 = 0.0634/0.1114 for all data). CCDC 182/825.

§ While the manuscript was being reviewed we made and characterized two more metal carboxylate–phosphonates, an isostructural magnesium analog [a = 4.598(2), b = 10.278(4), c = 17.628(7) Å, β = 96.28(3)°, U = 828.1(4) $Å^3$] and a calcium carboxylate–phosphonate with a different structure. According to the structure determined from single crystal X-ray diffraction and IR spectra of the latter, the calcium is seven-coordinate, and the carboxylic group is not deprotonated but rather coordinated to the calcium *via* the carbonyl oxygen.

1 *Comprehensive Supramolecular Chemistry*, ed. J. L. Atwood, J. E. D. Davies, D. D. MacNicol and F. Vogtle, Pergamon, New York, 1996, vol. 6 (*Solid-state supramolecular chemistry: crystal engineering*) and vol. 7 (*Solid-state supramolecular chemistry: two- and three-dimensional inorganic networks*).

2 D. Venkataraman, S. Lee, J. S. Moore, P. Zhang, K. A. Hirsch, G. B. Gardner, A. C. Covey and C. L. Prentice, *Chem. Mater.*, 1996, **8**, 2030; R. Robson, B. F. Abrahams, S. R. Batten, R. W. Gable, B. F. Hoskins and J. Liu, *Supramolecular Architecture*, ed. T. Bein, ACS Symp. Ser. 499, ACS, Washington, DC, 1992, ch. 19; A. J. Blake, N. R. Champness, S. S. M. Chung, W. S. Li and M. Schröder, *Chem. Commun.*, 1997, 1005; P. Losier and M. J. Zaworotko, *Angew. Chem., Int. Ed. Engl.*, 1996, **35**, 2779.

3 O. M. Yaghi, C. E. Davis, G. Li and H. Li, *J. Am. Chem. Soc.*, 1997, **119**, 2861; O. M. Yaghi, H. Li and T. L. Groy, *J. Am. Chem. Soc.*, 1996, **118**, 9096; S. O. H. Gutschke, M. Molinier, A. K. Powell and P. T. Wood, *Angew. Chem., Int. Ed. Engl.*, 1997, **36**, 991; K. J. Lin and K. H. Lii, *Angew. Chem., Int. Ed. Engl.*, 1997, **36**, 2076.

4 J. R. Black, N. R. Champness, W. Levason and G. Reid, *Inorg. Chem.*, 1996, **35**, 4432; J. R. Black, N. R. Champness, W. Levason and G. Reid, *J. Chem. Soc., Chem. Commun.*, 1995, 1277; J. R. Black, N. R. Champness, W. Levason and G. Reid, *J. Chem. Soc., Dalton Trans.*, 1995, 3439.

5 D. M. Poojary, B. Zhang, P. Bellinghausen and A. Clearfield, *Inorg. Chem.*, 1996, **35**, 4942; G. Bonavia, R. C. Haushalter, C. J. O'Connor and J. Zubieta, *Inorg. Chem.*, 1996, **35**, 5603; R. LaDuca, D. Rose, J. R. D. DeBord, R. C. Haushalter, C. J. O'Connor and Jon Zubieta, *J. Solid State Chem.*, 1996, **123**, 408; G. Alberti, U. Costantino, F. Marmottini, R. Vivani and P. Zappelli, *Angew. Chem., Int. Ed. Engl.*, 1993, **32**, 1357; V. Soghomonian, R. Diaz, R. C. Haushalter, C. J. O'Connor and J. Zubieta, *Inorg. Chem.*, 1995, **34**, 4460; D. Lohse and S. C. Sevov, *Angew. Chem., Int. Ed. Engl.*, 1997, **36**, 1619.

6 S. Drumel, P. Janvier, D. Deniaud and B. Bujoli, *J. Chem. Soc., Chem. Commun.*, 1995, 1051.

7 S. Drumel, P. Janvier, P. Barboux, M. Bujoli-Doeuff and B. Bujoli, *Inorg. Chem.*, 1995, **34**, 148; S. Drumel, P. Janvier, M. Bujoli-Doeuff and B. Bujoli, *New J. Chem.*, 1995, **19**, 239.

Received in Bloomington, IN, USA, 10th February 1998; 8/01964I

Remarkable helix stabilization *via* edge-to-face tryptophan–porphyrin interactions in a peptide-sandwiched mesoheme

David A. Williamson and David R. Benson*†

Department of Chemistry, University of Kansas, Lawrence, KS 66045-0046, USA

Tryptophan residues in a peptide-sandwiched mesoheme provide helix stabilization *via* edge-to-face interactions between the Trp indole side-chains and the porphyrin ring.

Binding of heme by apomyoglobin and cytochrome b_5 is driven to a large extent by interactions between apolar amino acid side-chains and the porphyrin ring. This was convincingly demonstrated by an experiment in which the proximal histidine (His) ligand of myoglobin (Mb) was mutated to glycine without greatly diminishing the apoprotein's affinity for heme.[1] Furthermore, removal of heme from Mb[2] and from cytochrome b_5[3] leads to reduced protein helix content and decreased protein stability as interactions between the heme and amino acid side-chains in the heme binding pocket are lost.

The F-helix of *Aplysia limacina* Mb provides the proximal ligand (His-95) to the heme iron (Fig. 1).[4] A phenylalanine residue (Phe-91), which is also within the F-helix, is located at position $i - 4$ relative to His-95 (in mammalian Mbs, this position is usually occupied by leucine). The phenyl ring of Phe-91 is nearly perpendicular to the heme plane, and the hydrogen atoms in the 3- and 4-positions of the phenyl side-chain make van der Waals contact with the heme.[4] Similar interactions between heme and Phe residues are observed in cytochrome b_5.[5] An edge-to-face orientation between two aromatic groups is energetically favorable.[6] Stabilization arises from electrostatic interactions between hydrogen atoms on one ring, which bear a partial positive charge, and the π-electrons of the second ring.[7]

We have developed a class of hemoprotein models that we call peptide-sandwiched mesohemes (*e.g.* **1**).[8–11] His-to-iron

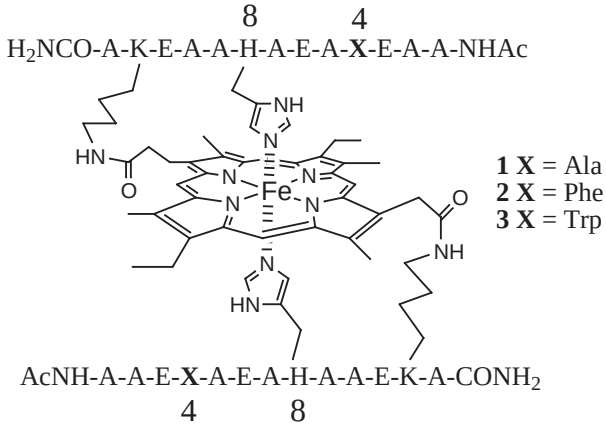

coordination in **1** induces the covalently attached peptides to adopt conformations with *ca.* 50% helix content, in aqueous solution at 8 °C.[10] Helix content can be increased to > 90% by addition of propan-1-ol (PrOH). From molecular modelling studies we have predicted that in **1** the angle between the peptide helix axis and the porphyrin plane will be about 30°.[12] When His ligands to heme iron in natural hemoproteins reside within helices, this angle is usually closer to 0°. The different

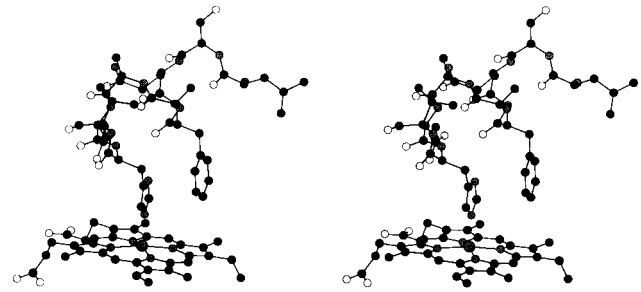

Fig. 1 Heme and F-helix of *Aplysia Limocina* Mb.[4] Atom colors: carbon (black); nitrogen (grey); oxygen (white).

orientations result from alternate combinations of His side-chain torsional angles χ_1 and χ_2. In **1** we predict that $\chi_1/\chi_2 \approx 180°/-90°$,[9,12] whereas in most hemoproteins utilizing His residues that reside in α-helices (including *Aplysia limacina* Mb), these values are closer to $-60°/90°$.[8]

In **1**, Ala-4 is at position $i - 4$ relative to the His ligand (His-8). Using the structure of **1** predicted from molecular modeling studies,[12] we replaced Ala-4 by Phe and by tryptophan (Trp) to investigate whether edge-to-face interactions between either aromatic amino acid side-chain and the heme was possible. From these studies we found that the indole side-chain of Trp can make such interactions if its side-chain torsional angles χ_1 and χ_2 are limited to *ca.* 180 and 90°, respectively. An energy minimized structure predicted for **3** is shown in Fig. 2. In contrast, the side-chain of Phe appears to be too small to permit contact with the heme in **2**.

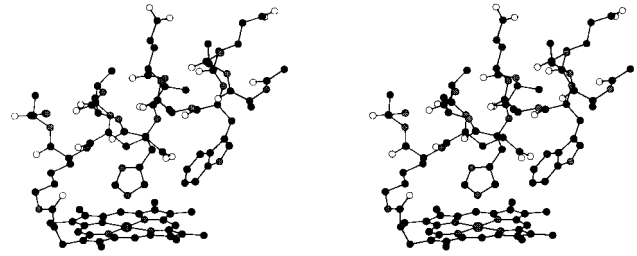

Fig. 2 Structure of **3** predicted by molecular modelling. Only one peptide is shown. Atom colors as in Fig. 1.

We have prepared **2** and **3** using our previously reported synthetic method.[8,9] CD spectra of **1** and **3** in neutral aqueous solution at 8 °C are shown in Fig. 3. The spectrum of **2** (not shown) is nearly identical to that of **1**. Using the mean residue ellipticity at 220 nm (θ_{220}) as a measure of peptide helix content,[8] we estimate that changing Ala-4 to Trp increases peptide helix content from *ca.* 50 to *ca.* 90% (maximum θ_{220} for **1**–**3** is calculated to be $-27\,700$ deg cm^2 dmol^{-1}). In contrast, changing Ala-4 to Phe leaves the peptide conformation unaltered. Both results are consistent with predictions from molecular modelling.

Aromatic amino acid side-chains,[13] as well as heme itself,[8,14] can contribute to CD spectra in the wavelength range normally

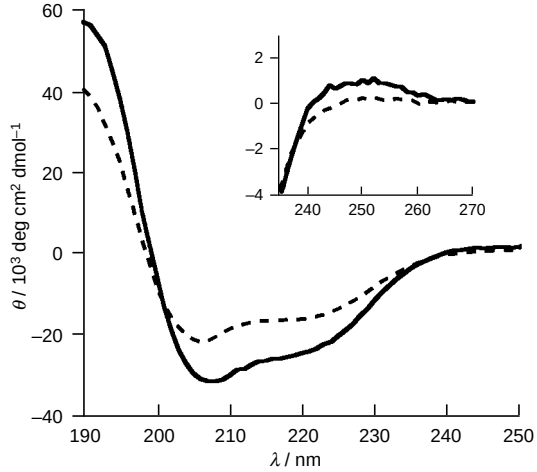

Fig. 3 CD spectra of **1** (- - -) and **3** (——) in 2 mM pH 7 potassium phosphate buffer at 8 °C

employed to determine peptide helix content. In fact, we observe a positive contribution in the CD spectrum of **3** near 250 nm that is absent in the spectra of **1** and **2** (Fig. 3, inset). This positive ellipticity probably arises *via* exciton coupling of the Trp side-chain with the peptide backbone amides and/or with the heme. Such contributions can lead to errors in peptide helix content determined by CD.[13] The amount of organic solvent required to achieve the maximum value of θ_{220} provides additional information about relative helix content in pure aqueous solution when comparing similar systems such as **1**–**3**. Fig. 4 shows θ_{220} plotted *vs.* volume percent of PrOH for **1** and **3** (the plot for **2** is identical to that for **1**, and thus is not shown). Whereas **1** and **2** require more than 30% (v/v) PrOH to reach maximal helix content, **3** reaches maximal helix content with only about 5% PrOH. This is consistent with **3** having much higher helix content than **1** and **2** in aqueous solution.

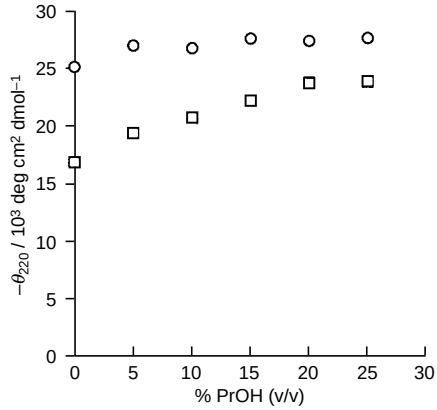

Fig. 4 θ_{220} as a function of PrOH concentration for **1** (□) and **3** (○). The plot for **2** is identical to that for **1**.

Aromatic amino acids are considered to be helix breakers[15] because their side-chain torsional angle χ_1 is restricted to the g^+ (300°) and t (180°) regions when they are forced to reside within a helix.[16] However, when the amino acid is within the first (*N*-terminal) turn of a helix, $\chi_1 = g^-$ (60°) is also accessible.[16] Because Phe-4 is within the first helical turn of **2**, it is not surprising that **1** and **2** exhibit similar conformational properties. In order for Trp to make edge-to-face contact with the heme in **3**, however, we predict that its side-chain must be restricted to $\chi_1 \approx 180°$ and $\chi_2 \approx 90°$. Our CD data indicate that the indole–heme interactions are sufficiently stabilizing to overcome the large entropy loss associated with such conformational restrictions. This is in keeping with the importance of such interactions in maintaining the structural integrity of natural hemoproteins.[2,3]

This work was supported by National Institutes of Health grant R29-GM52431-01A1.

Notes and References

† E-mail: benson@kuhub.cc.ukans.edu

1 D. Barrick, *Biochemistry*, 1994, **33**, 6546.
2 F. M. Hughson and R. L. Baldwin, *Biochemistry*, 1989, **28**, 4415.
3 T. E. Huntley and P. Strittmatter, *J. Biol. Chem.*, 1972, **247**, 4641.
4 M. Bolognesi, S. Onesti, G. Gatti, A. Coda, P. Ascenzi and M. Brunori, *J. Mol. Biol.*, 1989, **205**, 529. PDB accession code 1mba.
5 F. S. Mathews, P. Argos and M. Levine, *Cold Spring Harb. Symp. Quant. Biol.*, 1972, **36**, 387. PDB accession code 3b5c.
6 W. L. Jorgensen and D. L. Severance, *J. Am. Chem. Soc.*, 1990, **112**, 4768.
7 C. A. Hunter and J. K. M. Sanders, *J. Am. Chem. Soc.*, 1990, **112**, 5525.
8 D. R. Benson, B. R. Hart, X. Zhu and M. B. Doughty, *J. Am. Chem. Soc.*, 1995, **117**, 8502.
9 P. A. Arnold, D. R. Benson, D. J. Brink, M. P. Hendrich, G. S. Jas, M. L. Kennedy, D. T. Petasis and M. Wang, *Inorg. Chem.*, 1997, **36**, 5306.
10 M. Wang, M. L. Kennedy, B. R. Hart and D. R. Benson, *Chem. Commun.*, 1997, 883.
11 For a related system, see F. Nastri, A. Lombardi, G. Morelli, O. Maglio, G. D'Auria, C. Pedone and V. Pavone, *Chem. Eur. J.*, 1997, **3**, 340, and the subsequent paper in that issue.
12 SYBYL molecular modeling software, version 6.01, Tripos Associates, Inc., St. Louis, MO. We have recently reported detailed molecular modeling studies for an analogue of **1** constructed from mesoporphyrin IX (ref. 9, supporting information). The structure of **1** was generated from the analogue by altering the point of attachment between one propionate group and the heme ring followed by energy minimization.
13 A. Chakrabartty, T. Kortemme, S. Padmanabhan and R. L. Baldwin, *Biochemistry*, 1993, **32**, 5560.
14 G. Blauer, N. Sreerama and R. W. Woody, *Biochemistry*, 1993, **32**, 6674.
15 G. Merutka, W. Lipton, W. Shalongo, S.-H. Park and E. Stellwagen, *Biochemistry*, 1990, **29**, 7511.
16 M. J. McGregor, S. A. Islam and M. J. E. Sternberg, *J. Mol. Biol.*, 1987, **198**, 295.

Received in Columbia, MO, UK, 18th November 1997; 7/08368H

Unsaturated polymers containing boron and thiophene units in the backbone

Robert J.-P. Corriu,*[a] Thomas Deforth,[a] William E. Douglas,*[a]† Gilles Guerrero[a] and Walter S. Siebert*[b]

[a] *CNRS UMR 5637, Université Montpellier II, 34095 Montpellier cedex 5, France*
[b] *Anorganisch-Chemisches Institut der Universität, 69120 Heidelberg, Germany*

2,5-Dialkynylthiophenes $(RC{\equiv}C)_2C_4H_2S$ (R = Ph, Me_3Si or Bu^t) treated successively with $HBCl_2$ and Et_3SiH in CH_2Cl_2 undergo hydroboration polymerization to give intensely-coloured polymers of general structure $–[CH{=}CR–BCl–CR{=}CH–C_4H_2S]_n–$ for which the ^{11}B NMR resonances occur *ca*. 50 ppm upfield of those for analogous monomers.

Polythiophenes are important conjugated electroactive polymers. They possess interesting optical and electrical properties, and have many potential applications, for example in energy storage, electrochromic devices and electrochemical sensors.[1] Several of these effects depend on the nature and extent of doping of the polythiophene, usually with electron acceptors. We report here the synthesis by hydroboration polymerization of unsaturated polymers containing both thiophene and boron units. It was expected that such polymers possessing both electron-donor (sulfur) and electron-acceptor (boron) sites would show interesting properties, the boron with a vacant 2p orbital being available to act as an *in situ* electron-acceptor dopant.

Hydroboration polymerization has been previously described for polyaddition betwen thexylborane–dimethyl sulfide complex and either dienes[2] (affording saturated organoboron polymers) or diynes[3] (giving unconjugated unsaturated organoboron polymers). The hydroboration polymerization of dienes has also been performed with monobromoborane–dimethyl sulfide complex to give functional organoboron polymers.[4] However, for all these polymers the boron 2p orbitals are occupied because of the presence of the dimethyl sulfide donor ligand. We describe here the preparation of analogous polymers containing thiophene and alkene units in which the boron 2p orbital remains vacant.

The starting diynes **1a**,[5] **1b**[6][ν (C≡C) 2146 cm^{-1} (CCl_4)] and **1c** [ν (C≡C) 2220 cm^{-1} (CCl_4)], which were synthesized from 2,5-dibromothiophene and the corresponding alkynylzinc reagent RC≡CZnCl, undergo hydroboration with $HBCl_2$ (formed *in situ* from BCl_3 and Et_3SiH[7]) at −80 °C to give the bis(dichloroborane) derivatives **2** in 60–70% yield (Scheme 1). Subsequent reduction of **2** with Et_3SiH in the presence of additional diyne **1** gives the corresponding polymers **4**, most probably by hydroboration polymerization of intermediate bis(monochloroborane) derivatives **3** (Scheme 1).‡ The polymers are highly sensitive to oxygen and water and so far it has not been possible to obtain either satisfactory UV–VIS spectra or consistent molecular weight data by size exclusion chromatography (SEC) because of the very dilute nature of the solutions required in both cases. However, the SEC chromatograms show a component of molecular weight in excess of 100 000, which is possibly an overestimate since it was determined using polystyrene calibrants. The polymer colour is strongly dependent on the substituent R groups, being turquoise in the case of phenyl substituents (**4a**), red for trimethylsilyl groups (**4b**), and green for the homologue containing both phenyl and trimethylsilyl substituents.

The ^{11}B NMR resonance for the polymers in $CDCl_3$ solution occurs at δ_B 6–7 (*e.g.* **4a**: δ_B 6.5), about 50 ppm upfield of the resonance for **2** (δ_B 53) or chlorodivinylborane (δ_B 56).[8] These remarkable properties suggest the existence of electronic interactions between the boron and thiophene groups along the polymer chain. Further support for this interpretation is provided by the contrasting properties of model monomers **5a** and **5b** prepared by hydroboration of **1a** and **1b**, respectively, with 9-borabicyclo[3.3.1]nonane (9-BBN) in THF solution (Scheme 1). The model monomers are pale-coloured solids exhibiting ^{11}B NMR resonances around δ_B 58 as expected.[8] The formation of all three structural isomers for each model monomer **5** is to be expected since the reaction of 9-BBN with alkynes is known to be of low regioselectivity.[9]

The polymers **4** can be stabilized by transformation of the boron chloro functional group. Thus, treatment of **4b** with 3-dimethylaminopropan-1-ol in toluene under reflux afforded **6** as a red paste in 80% yield. SEC indicates that **6** is an oligomer of about 8 units and therefore polymer degradation has occurred during the synthesis. The ^{11}B NMR resonance at δ_B 2.8 lies in the region expected for amine adducts,[8] the boron 2p orbital being occupied.

Treatment of **1a**–**c** with thexylborane–dimethyl sulfide complex in CH_2Cl_2 in the presence of $(PPh_3)_2PdCl_2$ affords, respectively, polymers **7a**–**c** (Scheme 1), this borane reagent being known to give linear polymers with internal diynes.[3] The ^{11}B NMR resonances (δ_B 18–19) lie in the region expected for dimethyl sulfide adducts.[8] The boron 2p orbital is occupied and the colours are less intense than those of **4**. SEC showed that **7b** is an oligomer of 25 units with a polydispersity index of 3.7 (polystyrene calibrants). For comparison, the analogous model

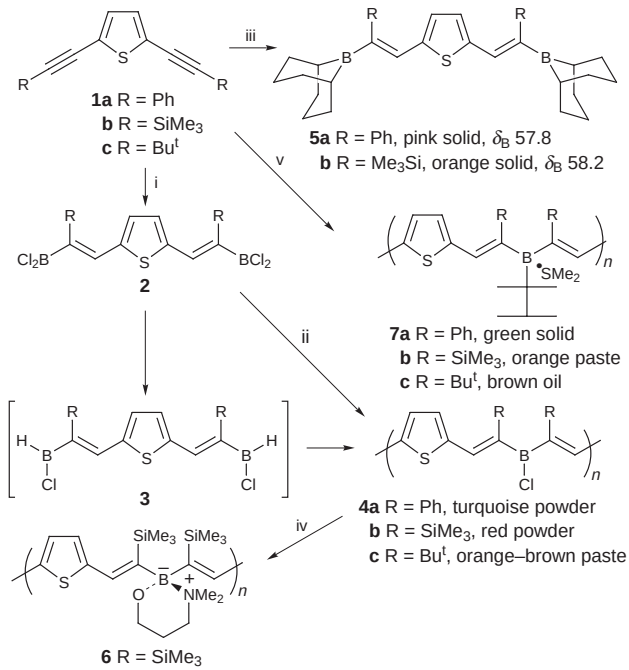

Scheme 1 *Reagents and conditions:* i, BCl_3, Et_3SiH, CH_2Cl_2, −78 to −40 °C; ii, **1**, Et_3SiH, −50 °C to room temp.; iii, 9-BBN, $Pt(PPh_3)_4$, THF, −78 to 65 °C; iv, $Me_2N(CH_2)_3OH$, PhMe, 110 °C; v, thexylborane–Me_2S, $(PPh_3)_2PdCl_2$, CH_2Cl_2, −78 °C to room temp. Only one of the various possible structural isomers is shown in each case.

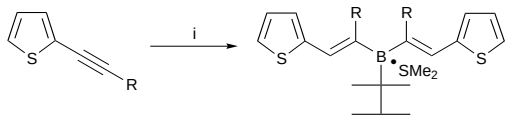

8a R = Ph, pink paste
b R = Me_3Si, red–orange oil
c R = Bu^t, brown oil

Scheme 2 *Reagents and conditions:* i, thexylborane–Me_2S, CH_2Cl_2, −78 °C to room temp. Only one of the three possible structural isomers is shown.

monomers **8a–c** were made starting from the corresponding monoalkynylthiophene (Scheme 2). The change in colour, corresponding to an absorption red-shift, on going from the model monomers **8a** and **8b** to the polymers **7a** and **7b** indicates the presence of some additional electron delocalization in the polymers. However, the extent must be slight since the ^{11}B NMR chemical shifts for the model monomers are essentially the same as those for the polymers. This is in contrast to the case of the intensely-coloured polymers **4** with an empty boron 2p orbital, for which an ^{11}B NMR upfield shift of *ca*. 50 ppm is observed (*vide supra*). Work is in progress on the synthesis by hydroboration polymerization of more stable analogues of **4**.

The European Commission is thanked for a fellowship awarded to T. D. under contract no. ERBCHBGCT940539 of the Human Capital and Mobility (Institutional Fellowships) Programme. Financial support from the Deutsche Forschungsgemeinschaft (SFB 247) and the Alexander von Humboldt Stiftung (to R. J.-P. C.) is gratefully acknowledged.

Notes and References

† E-mail: douglas@crit.univ-montp2.fr

‡ Polymers **4a–c** were prepared using the following one-pot procedure. A solution of BCl_3 in CH_2Cl_2 at −78 °C was treated dropwise with a CH_2Cl_2 solution containing Et_3SiH (2 equiv.) and the starting diyne **1** (0.5 equiv.). Addition of 50% of the latter Et_3SiH/diyne solution resulted in formation of the bis(dichloroborane) intermediate **2**. At this stage excess BCl_3 was removed from the reaction mixture *in vacuo* (5 min at −78 °C followed by 5 min at −40 °C) and addition of the Et_3SiH/diyne solution was then resumed at −50 °C. After addition was complete the reaction mixture was allowed to warm to room temperature overnight, becoming intensely coloured, and the polymers were isolated by removal of the solvent.

1 J. Roncali, *Chem. Rev*., 1992, **92**, 711.
2 Y. Chujo, I. Tomita, Y. Hashiguchi, H. Tanigawa, E. Ihara and T. Saegusa, *Macromolecules*, 1991, **24**, 345.
3 Y. Chujo, I. Tomita, Y. Hashiguchi and T. Saegusa, *Macromolecules*, 1992, **25**, 33.
4 Y. Chujo, N. Takizawa and T. Sakurai, *J. Chem. Soc., Chem. Commun*., 1994, 227.
5 F. Freeman and D. S. H. L. Kim, *J. Org. Chem*., 1992, **57**, 1722.
6 D. R. Rutherford, J. K. Stille, C. M. Elliott and V. R. Reichert, *Macromolecules*, 1992, **25**, 2294.
7 R. Soundarajan and D. S. Matteson, *Organometallics*, 1995, **14**, 4157.
8 H. Nöth and B. Wrackmeyer, in *NMR Basic Principles and Progress; Vol. 14, Nuclear Magnetic Resonance Spectroscopy of Boron Compounds*, ed. P. Diehl, E. Fluck and R. Kosfeld, Springer-Verlag, Berlin, 1978.
9 A. Pelter, K. Smith, D. Buss and A. Norbury, *Tetrahedron Lett*., 1991, **32**, 6239.

Received in Liverpool, UK, 26th January 1998; 8/00690C

Stereo- and regio-selective addition of iodotoluene difluoride to alk-1-ynes. Selective synthesis of 2-fluoro-1-iodoalk-1-enes

Shoji Hara,*† Masaki Yoshida, Tsuyoshi Fukuhara and Norihiko Yoneda*

Division of Molecular Chemistry, Graduate School of Engineering, Hokkaido University, Sapporo 060, Japan

***p*-Iodotoluene difluoride reacted with 1-alkynes to give *trans* adducts which could be converted to 2-fluoro-1-iodoalk-1-enes without isolation.**

The introduction of a fluorine atom into the double bond of natural products, such as terpenes,[1] nucleosides,[2] retinal,[3] fatty acids,[4] prostaglandins[5] and peptides[6] has been of great interest because the fluorinated analogues of natural compounds are expected to have different pharmacological properties from the original ones. The fluoroalkenyl parts of such compounds have been synthesized by the condensation of α-fluorocarbanions with carbonyl compounds[3,5,6*a*,*b*,7] or the β-elimination reaction from fluorohaloalkanes[2,4*b*,6*c*] but the stereoselectivities are generally low. A cross-coupling reaction using fluoroalkenyl halides or fluoroalkenylmetals would be a versatile method for the stereoselective synthesis of fluoroalkenes.[8] However, the cross-coupling method has not been adequately developed for fluoroalkene synthesis because stereoselective synthesis of the fluoroalkenyl halides is difficult. Recently, we reported that *p*-iodotoluene difluoride (**1**) can be directly prepared from *p*-iodotoluene by an electrochemical method and used for the fluorination of β-dicarbonyl compounds.[9] During our continuing study of the organic synthesis using **1**, we found that **1** adds to alk-1-ynes to give (*E*)-(2-fluoroalk-1-enyl)(4-methylphenyl)iodonium fluorides (**2**)[10,11] which could be converted to (*E*)-2-fluoro-1-iodoalk-1-enes stereo- and regio-selectively (Scheme 1).

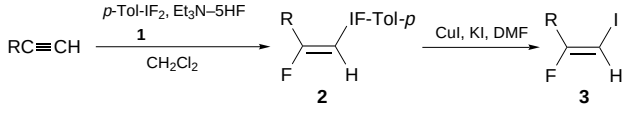

Scheme 1

p-Iodotoluene difluoride **1** was electrochemically prepared from *p*-iodototoluene in Et_3N–5HF[9] and used for further reaction without isolation. (*E*)-(2-Fluoroalk-1-enyl)(4-methylphenyl)iodonium fluoride (**2**), which was stable and could be isolated and characterized, was used for the further transformation without isolation. The iodonation of **2** by modification of the reported procedure[12] provided (*E*)-2-fluoro-1-iodoalk-1-enes (**3**) in good yields (Table 1).‡ The reaction can be carried out without the protection of functionalities such as ketones, esters, and even hydroxy groups in alkynes. Further application of this method to the stereoselective synthesis of fluoroalkenes is under investigation.

Table 1 Synthesis of (*E*)-1-iodo-2-fluoroalk-1-enes[a]

	Alkyne R	Yield of **3** (%)[b]
a	$Me(CH_2)_9$–	80[c]
b	$HO(CH_2)_9$–	65[d]
c	$Cl(CH_2)_9$–	77[d]
d	$MeO_2C(CH_2)_8$–	80
e	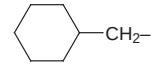	65
f	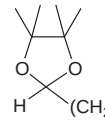	55
g	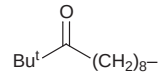	72

[a] If not mentioned elsewhere, the reaction was carried out as described in the notes. [b] Isolated yields based on alkynes used. [c] After the reaction of alkyne with **1**, 1 equiv. of CuI and KI in DMF (2 ml) was added. [d] After the reaction of alkynes with **1**, the reaction mixture was added to 10 equiv. of CuI and KI in CH_2Cl_2 (30 ml).

Notes and References

† E-mail: Hara@org-mc.eng.hokudai.ac.jp

‡ *Typical experimental procedure*: *p*-iodotoluene difluoride was electrochemically prepared in a divided cell made of Teflon™ PFA with a Nafion™ 117 film using two smooth Pt Sheets (20 × 20 mm) for the anode and cathode. *p*-Iodotoluene (3 mmol) and Et_3N–5HF (22 ml) were introduced into the anodic cell and Et_3N–5HF (22 ml) was introduced into the cathodic cell. The electrolysis was carried out under constant electricity (50 mA h^{-1}) until 2 F mol^{-1} of electricity was passed. The resulting Et_3N–5HF solution of *p*-iodotoluene difluoride in the anodic cell was used for further reaction. Methyl undec-10-ynoate (293 mg, 2 mmol) and CH_2Cl_2 (6 ml) were introduced into a reaction vessel made of Teflon™ PFA and *p*-iodotoluene difluoride (3 mmol) in Et_3N–5HF (22 ml) was added at 0 °C. After stirring for 1 h, the mixture was extracted with CH_2Cl_2, dried over $MgSO_4$, and concentrated under reduced pressure. The residue was dissolved in CH_2Cl_2 (5 ml) and added to CuI (3.8 g, 20 mmol) and KI (3.32 g, 20 mmol) in CH_2Cl_2 (25 ml). The reaction mixture was stirred at room temperature for 3 h and extracted with CH_2Cl_2. The product was isolated by column chromatography (silica gel/hexane–diethyl ether) in 80% yield. C=C Stereochemistry of **3a**–**g** was determined from $^3J_{H-F}$ data. Stereospecificities of >98% are indicated by GC, and ^1H and ^{19}F NMR spectroscopy. *Spectral data* for **2a**: δ_H(400 MHz, $CDCl_3$) 7.866 (d, *J* 8.3, 2 H), 7.2015 (d, *J* 8.3, 2 H), 6.725 (d, *J* 15.125, 1 H), 2.662–2.754 (m, 2 H), 2.361 (s, 3 H). 1.167–1.576 (m, 14 H), 0.881 (t, 7.1, 3 H); δ_F(84.67 MHz, $CDCl_3$)(C_6F_6 as an internal standard) −69.131 to −69.834 (m, 1 F). For **3d**: δ_H(400 MHz, $CDCl_3$) 5.67 (d, *J* 17.81, 1 H), 3.67 (s, 3 H), 2.50 (dt, *J* 7.32, 22.4 Hz, 2 H), 2.31 (t, *J* 7.56, 2 H), 1.64–1.51 (m, 4 H), 1.35–1.31 (m, 8 H); δ_F(84.67 MHz, $CDCl_3$)(C_6F_6 as an internal standard) −81.969 to −82.721 (m, 1 F); ν(neat)/cm^{-1} 1735 and 1650.

1 M. Schlosser, *Tetrahedron*, 1978, **34**, 3 and references cited therein.
2 J. R. McCarthy, E. T. Jarvi, D. P. Matthews, M. L. Edwards, N. J. Prakash, T. L. Bowlin, S. Mehdi, P. S. Sunkara and P. Bey, *J. Am. Chem. Soc.*, 1989, **111**, 1127.
3 A. Francesch, R. Alvarez, S. López and A. R. de Lera, *J. Org. Chem.*, 1997, **62**, 310.
4 (*a*) P.-Y. Kwork, F. W. Muellner and J. Fried, *J. Am. Chem. Soc.*, 1987, **109**, 3692; (*b*) D. Michel and M. Schlosser, *Synthesis*, 1996, 1007; (*c*) P. H. Buist, B. Behrouzian, K. A. Alexopoulos, B. Dawson and B. Black, *Chem. Commun.*, 1996, 2671.
5 M. L. Boys, E. W. Collington, H. Finch, S. Swanson and J. F. Whitehead, *Tetrahedron Lett.*, 1988, **29**, 3365; H. Nakai, N. Hamanaka, H. Miyake and M. Hayashi, *Chem. Lett.*, 1979, 1499.

6 (*a*) P. A. Bartlett and A. Otake, *J. Org. Chem.*, 1995, **60**, 3107; (*b*) L. G. Boros, B. De Corte, R. H. Gimi, J. T. Welch, Y. Wu and R. E. Handschumacher, *Tetrahedron Lett.*, 1994, **35**, 6033; (*c*) T. Allmendinger, E. Felder and E. Hungerbühler, *Tetrahedron Lett.*, 1990, **31**, 7301.
7 D. J. Burton, Z.-Y., Yang and W. Qiu, *Chem. Rev.*, 1996, **96**, 1641 and references cited therein.
8 P. L. Heinze and D. J. Burton, *J. Org. Chem.*, 1988, **53**, 2714; L. Xue, L. Lu, S. D. Pedersen, Q. Liu, R. M. Narske and D. J. Burton, *J. Org. Chem.*, 1997, **62**, 1064; B. V. Nguyen and D. J. Burton, *J. Org. Chem.*, 1997, **62**, 7758.
9 S. Hara, T. Hatakeyama, S.-Q. Chen, K. Ishi-i, M. Yoshida, M. Sawaguchi, T. Fukuhara and N. Yoneda, *J. Fluorine Chem.*, 1998, **87**, 189.
10 T. Kitamura, R. Furuki, H. Taniguchi and P. J. Stang, *Tetrahedron*, 1992, **48**, 7149; T. Kitamura, R. Furuki, H. Taniguchi and P. J. Stang, *Tetrahedron Lett.*, 1990, **31**, 703.
11 (*Z*)-(2-Fluoroalk-1-enyl)(aryl)iodonium salts were previously prepared from (alk-1-ynyl)(aryl)iodonium salts in low yields. However, (*E*)-isomers cannot be prepared by this method: M. Ochiai, Y. Kitagawa, M. Toyonari, K. Uemura, K. Oshima and M. Shiro, *J. Org. Chem.*, 1997, **62**, 8001.
12 M. Ochiai, K. Sumi, Y. Takaoka, M. Kunishima, Y. Nagao, M. Shiro and E. Jujita, *Tetrahedron*, 1988, **44**, 4905; M. Ochiai, K. Oshima and Y. Masaki, *Chem. Lett.*, 1994, 871.

Received in Cambridge, UK, 13th February 1998; 8/01273C

Synthesis of (±)-2′,3′-dideoxy-3′-fluoroapiosylpyrimidine nucleosides

Soon Kil Ahn,*[a,b]† Deukjoon Kim,[a] Hoe Joo Son,[b] Byeong Seon Jeong,[b] Ryung Kee Hong,[b] Bok Young Kim,[b] Eung Nam Kim,[b] Ku Hun Chung[b] and Jung Woo Kim[b]

[a] *College of Pharmacy, Seoul National University, San 56-1, Shinrim-dong, Kwanak-gu, Seoul, South Korea*
[a] *Chong Kun Dang Research Institute, 410 Shindorim-dong, Guro-gu, Seoul, South Korea*

Various (±)-2′,3′-dideoxy-3′-fluoroapiosylpyrimidine nucleoside analogs have been prepared.

Since the discovery and synthesis of nucleocidin,[1] which has a unique 4′-fluorosugar, a number of 4′-substituted nucleosides[2] and 4′-substituted carbocyclic nucleosides[3] have been synthesized and their biological activities evaluated. Among them, 4′-azidothymidine exhibited potent anti-HIV activity.

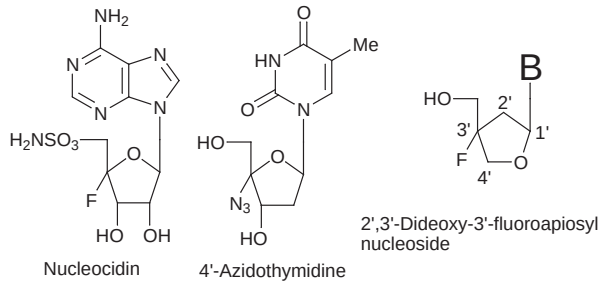

In our effort to synthesize novel 4′-substituted nucleoside derivatives with biological activity, we envisioned 2′,3′-dideoxy-3′-substituted apiosyl nucleosides to be one of these 4′-substituted nucleosides. While the synthesis and biological activities of a great many structurally modified nucleoside analogs have been reported, relatively little work has been done on the synthesis and biological activities of nucleoside analogs which contain apiose as the sugar moiety.[4] Here we report on the synthesis of (±)-2′,3′-dideoxy-3′-fluoroapiosylpyrimidine nucleosides.

The synthesis of the key intermediate, 2,3-dideoxy-3-fluoroapiofuranosyl acetate **6**, is shown in Scheme 1. Reformatsky reaction[5] of bis-silyl protected dihydroxyacetone **1**[6] with ethyl bromoacetate in the presence of activated zinc gave a β-hydroxy ester **2**. This was then treated with a 12% methanolic HCl solution at room temperature to afford hydroxy lactone **3** in 77% yield over two steps. The primary hydroxy group of **3** was selectively protected with a *tert*-butyldiphenylsilyl group to give **4** in 93% yield.[7] Fluorination of the tertiary alcohol of **4** with DAST in CH_2Cl_2 at room temperature gave fluoro lactone **5** in 32% yield. In this reaction the α,β-unsaturated lactone was obtained by elimination reaction in 27% yield. Reduction of fluoro lactone **5** to lactol with DIBAL-H at −78 °C followed by acetylation with Ac_2O gave the key intermediate, 2,3-dideoxy-3-fluoroapiofuranosyl acetate **6**, in 70% yield over two steps.

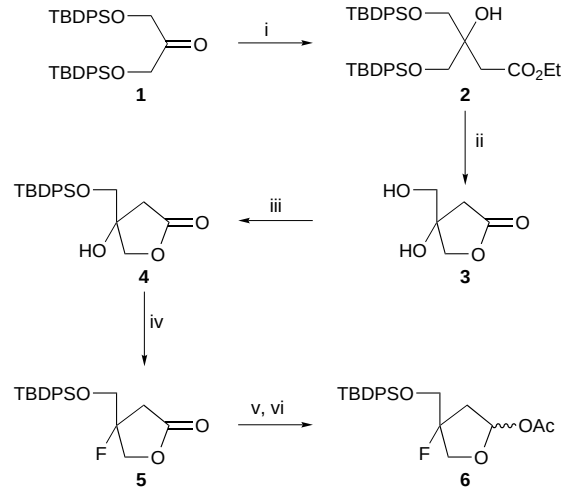

Scheme 1 *Reagents and conditions*: i, $BrCH_2CO_2Et$, activated Zn, benzene–toluene (2 : 1), reflux, 4 h; ii, 12% HCl in MeOH, room temp., 20 h, 77% (2 steps); iii, TBDPSCl, DMAP, Et_3N, CH_2Cl_2, room temp. overnight, 93%; iv, DAST, CH_2Cl_2, room temp. 1 h, 32%; v, DIBAL-H, CH_2Cl_2, −78 °C, 0.5 h; vi, Ac_2O, Et_3N, DMAP, CH_2Cl_2, room temp. 0.5 h, 70% (2 steps)

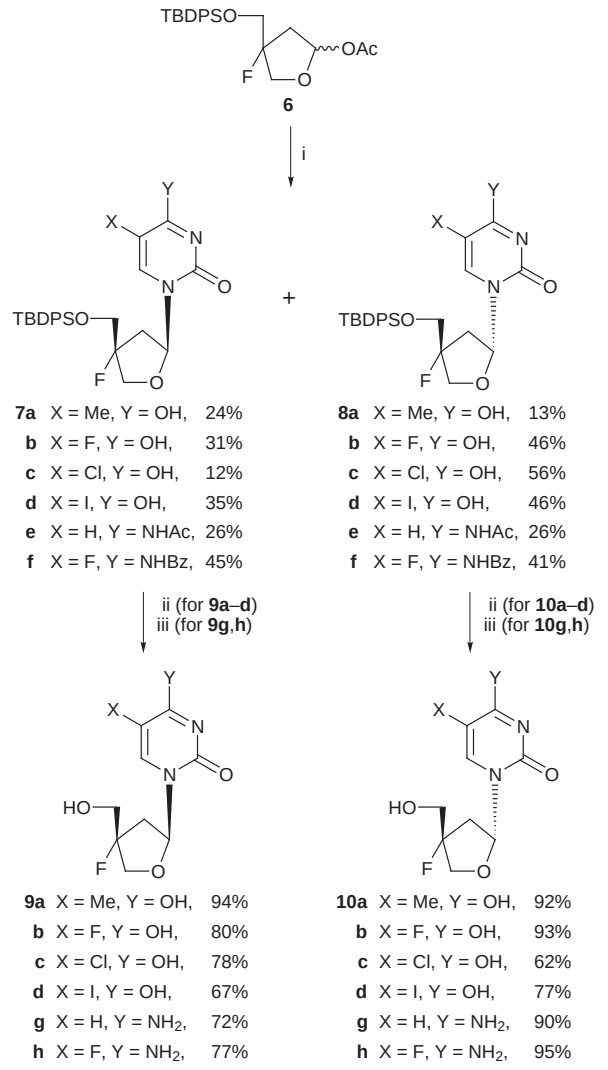

Scheme 2 *Reagents and conditions*: i, bis-silylated base, TMSOTf, $ClCH_2CH_2Cl$, 0 °C, 0.5 h; ii, TBAF, THF, room temp.; iii, methanolic NH_3, room temp. then TBAF, THF, room temp.

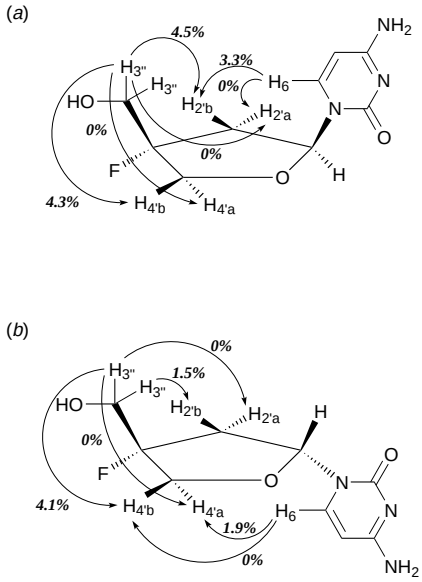

Fig. 1 NOE experiments of compounds (*a*) **9g** and (*b*) **10g**

The coupling of acetate **6** with bis-silylated pyrimidine derivatives under Vorbrüggen conditions is depicted in Scheme 2.[8] Bis-silylated pyrimidine derivatives were condensed with fluorosugar **6** in the presence of TMSOTf in 1,2-dichloroethane to give an α:β mixture of **7** and **8** in moderate yield. The mixtures were separated by silica gel column chromatography to give the individual isomers **7** and **8**. Deprotection of **7** and **8** afforded the pyrimidine nucleosides **9** and **10**, respectively.‡

The structural assignment of the uracil and cytosine analogs was made on the basis of ^{1}H NMR studies. For example, upon irradiation of the H-3″ protons in compound **9g**, nuclear Overhauser effects (NOEs) were observed for the H-2′$_b$ (4.5%) and H-4′$_b$ (4.3%) protons, while no NOEs were detected for the H-2′$_a$ and H-4′$_a$ protons. Irradiation of the H-6 proton resulted in an NOE for the H-2′$_b$ (3.3%) proton, while no NOE was observed for the H-2′$_a$ proton. In compound **10g**, upon irradiation of the H-3″ proton, NOEs were detected for the H-2′$_b$ (1.5%) and H-4′$_b$ (4.1%) protons, while no NOEs were observed for the H-2′$_a$ and H-4′$_a$ protons. Irradiation of the H-6 proton resulted in an NOE for the H-4′$_a$ (1.9%) proton, while no NOE was detected for the H-4′$_b$ proton (Fig. 1). The above results showed **9g** was the β-isomer and **10g** was the α-isomer. The relative configuration of the rest of the compounds in this report was assigned using the results of the same NOE experiments. The β-configuration of cytosine analog **9g** was determined conclusively on the basis of X-ray crystallography (Fig. 2).§ Compound **9g** assumes the 4′-*endo* conformation, in which the fluorine at C-4′ is approximately in a *gauche* disposition relative to the furan oxygen.

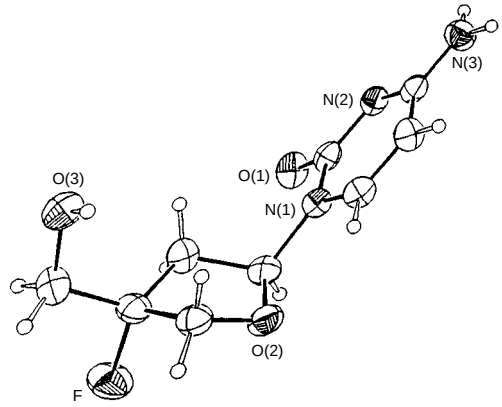

Fig. 2 ORTEP drawing of (±)-1-(2,3-dideoxy-3-fluoroapio-β-furanosyl)cytosine **9g**

Evaluation of antiviral activities and asymmetric synthesis of 2′,3′-dideoxy-3′-fluoroapiosyl nucleosides are in progress.

We are grateful to Drs C. I. Hong and S. J. Lee for helpful discussions. Special thanks are due to Mr W. K. Choi for ^{1}H NMR studies and Dr S. H. Kim for X-ray crystallography. One of us (D. Kim) acknowledges financial support from the KOSEF and Ministry of Health and Welfare (HMP-96-D-1017).

Notes and References

† E-mail: hck@bora.dacom.co.kr

‡ All new compounds gave satisfactory analytical and spectral data. *Selected data* for **9g**: mp 179–181 °C; δ_H([^{2}H$_6$]DMSO)2.21 (ddd, $J_{2'b,F}$ 35.5 $J_{2'b,2'a}$ 14.6, $J_{2'b,1'}$ 7.7, 1 H, H$_b$-2′), 2.44 (m, 1 H, H$_a$-2′), 3.66 (m, 2 H, H-3″), 3.94 (dd, $J_{4'a,F}$ 21.5, $J_{4'a,4'b}$10.8, 1 H, H$_a$-4′), 4.19 (dd, $J_{4'b,F}$ 35.1, $J_{4'b,4'a}$ 10.8, 1 H, H$_b$-4′), 6.10 (dd, $J_{1',2'b}$ 7.7, $J_{1',2'a}$ 6.6, 1 H, H-1′);δ_C(CD$_3$OD) 166.78, 157.14, 141.54, 105.40, 103.62, 95.14, 88.68, 75.33, 75.07, 63.00, 62.73, 40.67, 40.44; λ_{max}(H$_2$O)/nm 269.4, 229.0 (sh) (pH 7), 278.0, 209.3 (sh) (pH 2), 268.0 (pH 11) (Calc. for C$_9$H$_{12}$N$_3$O$_3$F; C, 47.16; H, 5.28; N, 18.33. Found: C, 47.21; H, 5.36; N, 18.22%). For **10g**: mp 219–220 °C; δ_H([^{2}H$_6$]DMSO) 2.08 (dddd, $J_{2'a,F}$ 21.9, $J_{2'a,2'b}$ 15.2, $J_{2'a,1}$ 2.5, $J_{2'a,4'b}$ 1.5, 1 H, H$_a$-2′), 2.56 (ddd, $J_{2'b,F}$ 35.7, $J_{2'b,2'a}$ 15.2, $J_{2'b,1'}$ 7.6,1 H, H$_b$-2′), 3.59 (dd, $J_{3'',F}$ 20.7, $J_{3'',3''}$ 12.1, 1 H, H-3″), 3.65(dd, $J_{3'',F}$ 16.7, $J_{3'',3''}$ 12.1, 1 H, H-3″), 3.96 (dd, $J_{4'b,F}$ 34.5, $J_{4'b,4'a}$ 10.9, 1 H, H$_b$-4′), 4.26 (ddd, $J_{4'a,F}$ 20.5, $J_{4'a4'b}$ 10.9, $J_{4'a,2'a}$ 1.5, 1 H, H$_a$-4′), 6.02 (dd, $J_{1',2'b}$ 7.6, $J_{1',2'a}$ 2.5, 1 H, H-1′), 7.54 (d, $J_{6,5}$ 7.4, 1 H, H-6); δ_C(CD$_3$OD) 166.81, 157.20, 141.15, 141.10, 104.64, 102.87, 94.45, 87.87, 76.15, 75.91, 62.81, 62.53, 40.93, 40.71; λ_{max}(H$_2$O)/nm 269.8, 229.2 (sh) (pH 7), 278.6, 219.6 (sh) (pH 2), 270.2 (pH 11) (Calc. for C$_9$H$_{12}$N$_3$O$_3$F; C, 47.16; H, 5.28; N, 18.33. Found: C, 47.09; H, 5.18; N, 18.48%).

§ *Crystal data* for **9g**: C$_9$H$_{12}$FN$_3$O$_3$, M = 229.22, monoclinic, space group $P2_1/c$ (No. 14), unit cell dimensions a = 5.1519 (10), b = 10.7326 (13), c = 17.756 (2) Å, β = 92.39 (2)°, V 981.0 (3) Å^3, T = 293 (2) K, Z = 4, μ = 0.130 mm^{-1}, F(000) = 480, 1580 reflections were measured and 1409 independent reflections were used for the structure solution. Final R values are as follows: $wR2$ = 0.0970 {R_1 = 0.0373 [I = 2σ(I)]}. CCDC 182/821.

1 I. D. Jenkins, J. P. H. Verheyden and J. G. Moffatt, *J. Am. Chem. Soc.*, 1976, **98**, 3346.
2 J. P. H. Verheyden and J. G. Moffatt, *J. Am. Chem. Soc.*, 1975, **97**, 4386; G. R. Owen, J. P. H. Verheyden and J. G. Moffatt, *J. Org. Chem.*, 1976, **41**, 3010; C. O. Yang, W. Kurz, E. M. Eugui, M. J. McRoberts, J. P. H. Verheyden, L. J. Kurz and K. A. M. Walker, *Tetrahedron Lett.*, 1992, **33**, 41; B. H. Lipshutz, S. Sharma, S. H. Dimock and J. R. Behling, *Synthesis*, 1992, 191; H. Maag, R. M. Rydzewski, M. J. McRoberts, D. Crawford-Ruth, J. P. H. Verheyden and E. J. Prisbe, *J. Med. Chem.*, 1992, **35**, 1440.
3 J. Beres, G. Sagi, E. Baitz-Gacs, I. Tomoskozi, L. Gruber and L. Otvos, *Tetrahedron*, 1989, **45**, 6271; K. Biggadike and A. D. Borthwick, *J. Chem. Soc., Chem. Commun.*, 1990, 1380; H. Maag and R. M. Rydzewski, *J. Org. Chem.*, 1992, **57**, 5823.
4 F. Perini, F. A. Carey and L. Jr. Long, *Carbohydr. Res.*, 1969, **11**, 159; J. M. J. Tronchet and J. Tronchet, *Carbohydr. Res.*, 1974, **34**, 263; J. M. J. Tronchet, J. Tronchet and R. Graf, *J. Med. Chem.*, 1974, **17**, 1055; D. K. Parikh and R. R. Watson, *J. Med. Chem.*, 1978, **21**, 706; M. J. Bamford, D. C. Humber and R. Storer, *Tetrahedron Lett.*, 1991, **32**, 271; Y. Terao, M. Akamatsu and K. Achiwa, *Chem. Pharm. Bull.*, 1991, **39**, 823; T. B. Sells and V. Nair, *Tetrahedron*, 1994, **50**, 117; F. Hammerschmidt, E. Öhler, J. Polsterer, E. Zbiral, J. Balzarini and E. DeClercq, *Liebigs Ann.*, 1995, 551; F. Hammerschmidt, J. Polsterer and E. Zbiral, *Synthesis*, 1995, 415.
5 M. W. Rathke, *Org. React.*, 1975, **22**, 423.
6 R. Sharma, J. Lee, S. Wang, G. W. A. Milne, N. E. Lewin, P. M. Blumberg and V. E. Marquez, *J. Med. Chem.*, 1996, **39**, 19.
7 S. K. Chaudhary and O. Hernandez, *Tetrahedron Lett.*, 1979, 99.
8 H. Vorbrüggen, K. Krolikiewicz and B. Bennua, *Chem. Ber.*, 1981, **114**, 1234.

Received in Cambridge, UK, 26th January 1998; 8/00665B

Phthalocyanines substituted with dendritic wedges: glass-forming columnar mesogens

Matthew Brewis, Guy J. Clarkson, Andrea M. Holder and Neil B. McKeown*†

Department of Chemistry, University of Manchester, Manchester, UK M13 9PL

Peripheral substitution of the phthalocyanine macrocycle with poly(aryl ether) dendritic wedges produces materials whose properties are dominated both by the columnar self-association of the phthalocyanine core and by the glass-forming character of the dendritic substituents.

Dendrimers are currently the focus of much attention due to their compact hierarchical structures. Although research into the synthesis of novel dendrimers continues at a rapid pace,[1] there is also considerable interest in the functionalisation of existing systems. For example, the versatile, convergent synthetic route to the poly(aryl ether) dendrimers of Fréchet[2] has allowed the incorporation of functional groups based on fullerene,[3] prophyrin[4] and ferrocene[5] moieties.

Our interests lie in the preparation of novel phthalocyanine (Pc) derivatives in which control over the structure of the bulk material is achieved by the attachment of suitable substituents to the Pc core.[6] This will help exploit the exciting electro-optical properties displayed by Pcs, *e.g.* photoconductivity and third-order harmonic generation. We describe here the synthesis of some phthalocyanine (Pc) derivatives which are substituted by poly(aryl ether) wedges and reveal the interesting properties of these novel materials which are dominated both by the self-association of the Pc subunit and by the glass forming character of the dendritic substituents. The preparation of these phthalocyanine-centred dendrimers involves a novel modification of the convergent route to dendrimer synthesis in which the formation of the core is used for dendrimer assembly, rather than the attachment of the dendritic wedges to a pre-existing core.

Phthalocyanine derivatives are best prepared from substituted phthalonitrile precursors. The aromatic nucleophilic substitution reaction between 4-nitrophthalonitrile and the benzylic alcohol group of the first, second and third generation

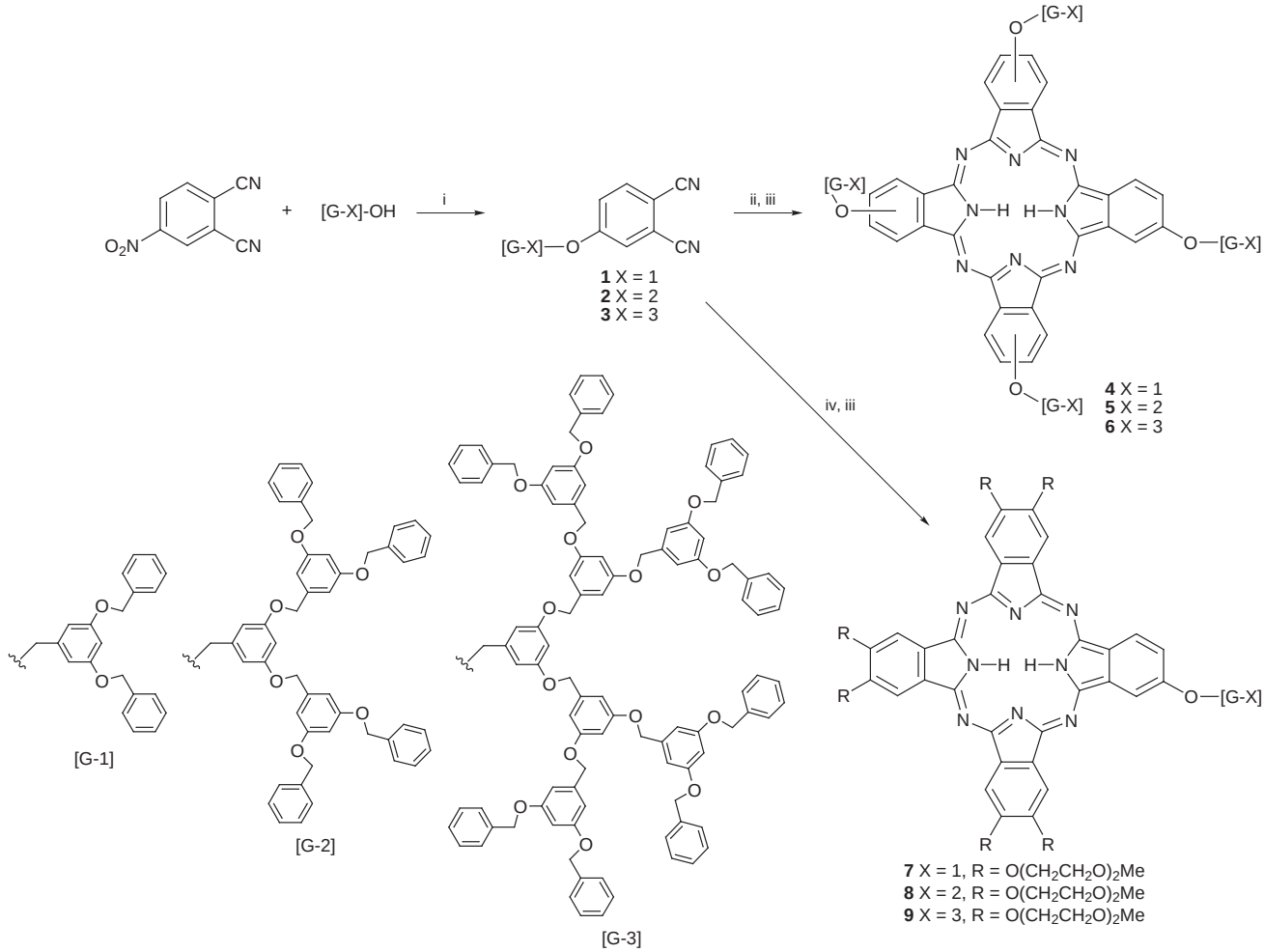

Scheme 1 *Reagents and conditions*: i, anhydrous K_2CO_3, DMF, 50 °C; ii, $C_5H_{11}OLi$, $C_5H_{11}OH$, 135 °C; iii, AcOH; iv, 4,5-bis(1,4,7-trioxaoctyl)-phthalonitrile, $C_5H_{11}OLi$, $C_5H_{11}OH$, 135 °C

Table 1 Transition temperatures of dendrimer-substituted Pcs[a]

Compound	Transition/°C			*D*/Å
	Glass → I	Glass → φ_h	φ_h → I	
4	—	115[b]	270[b]	31.2
5	112	—	—	—
6	71	—	—	
7	—	< −20[b]	> 320[b]	28.9
8	—	115	250–255	30.0
9	—	94	108–112	35.0

[a] I = isotropic liquid, φ_h = hexagonal columnar mesophase, *D* = intercolumnar distance calculated from 1,0 diffraction ring. [b] Transition not observed by DSC.

poly(aryl ether) wedges ([G-1]-OH, [G-2]-OH, [G-3]-OH)[2] gives the required phthalonitriles **1**–**3**, respectively, in 75–90% yield (Scheme 1). Cyclotetramerisation of **1**–**3** using lithium pentanolate in refluxing pentanol gives **4**–**6** in 10–20% yield, respectively, as a mixture of four inseparable isomers. Alternatively, a mixed cyclotetramerisation between each of the phthalonitriles **1**–**3** and a ten-fold excess of 4,5-bis(1,4,7-trioxaoctyl)phthalonitrile[7] produces unsymmetrical Pcs **7**–**9**, respectively. Each of these compounds is readily separated from octakis(1,4,7-trioxaoctyl)phthalocyanine and other Pc by-products by column chromatography. The structures of **1**–**9** were confirmed by ^{1}H NMR, UV–VIS absorption and IR spectroscopy.‡ All compounds gave satisfactory elemental analyses and all, except Pc **6**, exhibited a parent mass ion using fast atom bombardment (FAB) mass spectrometry.

Despite the steric bulk of the dendritic substituents, there is evidence of self-association of the Pc cores of **4**, **5** and **6** in dilute solution. For example, the ^{1}H NMR resonances corresponding to the twelve protons attached to the Pc core of **4**–**6** are broadened considerably even at a concentration of 1×10^{-4} mol dm^{-3} in $CDCl_3$. Aggregation is also apparent in the UV–VIS spectra of **4**–**6** in chloroform solution (1×10^{-5} mol dm^{-3}) by the presence of a broad peak centred at 630 nm. Aggregation is more evident in toluene at similar concentrations. The solution behaviour of these materials is analogous to that of 1,3,4-oxadiazole-based dendrimers which were specifically designed to produce columnar supramolecular structures.[8] There is much less evidence of broadening due to aggregation in the ^{1}H NMR spectra of **7**–**9**.

The thermal behaviour of **4**–**9**, as measured by optical polarising microscopy and differential scanning calorimetry (DSC), is reported in Table 1. On cooling from the isotropic melt, **4**, **7**, **8** and **9** display optical textures characteristic of a hexagonal columnar mesophase, although the initially observed 'sandy texture' exhibited by **9** requires annealing at 105 °C for several hours in order to obtain a recognisable texture. The hexagonal columnar mesophase is commonly encountered in Pc derivatives.[9] It is remarkable that the presence of the large dendritic wedge on Pc **9** does not prohibit columnar mesophase formation but merely limits the thermal range over which the mesophase is stable. A small angle X-ray diffraction analysis (powder) of the mesophase of **4** and **7**–**9** reveals in each case a single strong, sharp band which we believe originates from the (1, 0) plane of the hexagonal lattice. Based on this assumption, the calculated intercolumnar spacings are given in Table 1.

A potentially useful aspect of the thermal behaviour of these materials is their tendency to form a glassy rather than a crystalline solid phase, as indicated by DSC studies which show distinct second-order glass transitions both on heating and cooling. Thus, the non-mesogenic **5** and **6** produce clear, crack-free solid films by cooling from the melt or by spin-coating onto a glass substrate. UV–VIS absorption spectra of these non-birefringent films (λ_{max} = 620 nm) indicates strong cofacial interactions of the Pc cores. The absence of light scattering from domain boundaries is an attractive feature for optical studies.[10]

DSC analysis of **8** and **9** also shows a distinct reversible glass transition. No change in the optical texture is observed on cooling the mesophase below the glass transition temperature and it is concluded that an anisotropic glassy state is obtained in which the columnar structure is 'frozen'.[11] Small angle X-ray diffraction studies of the resulting brittle solids are also consistent with the retention of the columnar structure. Materials such as **8** and **9** which display both an anisotropic glassy phase and a readily aligned mesophase could be used to fabricate monodomainal films suitable for optical or electronic studies.

Notes and References

† E-mail: neil.mckeown@man.ac.uk

‡ *Selected data* for **1**: ν(KBr)/cm^{-1} 2229 (CN); δ_H($CDCl_3$, 500 MHz) 5.05 (4 H, s), 5.10 (2 H, s), 6.58 (1 H, t), 6.60 (2 H, d), 7.15 (1 H, dd), 7.25 (1 H, d), 7.29–7.45 (10 H, m), 7.65 (1 H, d); *m/z* (EI) 446 (M^+). For **2**: ν(KBr)/cm^{-1} 2230 (CN); δ_H($CDCl_3$, 500 MHz) 4.97 (4 H, s), 5.02 (8 H, s), 5.08 (2 H, s), 6.52 (1 H, t), 6.57 (2 H, t), 6.59 (2 H, d), 6.67 (4 H, d), 7.14 (1 H, dd), 7.23 (1 H, d), 7.29–7.42 (20 H, m), 7.65 (1 H, d); *m/z* (EI) 871 (M^+. For **3**: ν(KBr)/cm^{-1} 2232 (CN); δ_H($CDCl_3$, 500 MHz) 4.97 (8 H, s), 5.03 (16 H, s), 5.05 (2 H, s), 6.60–6.63 (7 H, m), 6.69–6.74 (14 H, m), 7.10 (1 H, dd), 7.23 (1 H, d), 7.29–7.46 (40 H, m), 7.64 (1 H, d); *m/z* (EI) 871 (M^+). For **4**: λ(CH_2Cl_2)/nm 718, 682, 654, 620, 422, 346; ν(KBr)/cm^{-1} 3275 (NH); δ_H($CDCl_3$, 500 MHz, 50 °C) −3.2 (2 H, br s), 5.06 (16 H, br s), 5.26 (8 H, br s), 6.65 (4 H, br s), 6.80 (8 H, brs), 7.29–7.45 (40 H, m), 7.7–9.1 (12 H, br M); *m/z* (FAB) 1788, (M^+). For **5**: λ(CH_2Cl_2/nm 716, 680, 654, 620, 422, 346; ν(KBr)/cm^{-1} 3276 (NH); δ_H($CDCl_3$, 500 MHz, 50 °C) −3.5 (2 H, br s), 4.75–5.05 (48 H, br m), 5.26 (8 H, br s), 6.40–6.75 (28 H, br m), 6.90 (8 H, br s), 7.29–7.45 (80 H, m), 7.7–9.1 (12 H, br m); *m/z* (FAB) 3488, (M^+). For **6**: λ(CH_2Cl_2)/nm 715, 680, 654, 620, 422, 346; ν(KBr)/cm^{-1} 3277 (NH); δ_H($CDCl_3$, 500 MHz, 50 °C −3.4 (2 H, br s), 4.66–5.05 (96 H, br m), 5.28 (8 H, br s), 6.30–6.70 (76 H, br m), 6.90 (8 H, br s), 7.29–7.45 (160 H, m), 7.7–9.1 (12 H, br m). For **7**: λ(CH_2Cl_2)/nm 700, 664, 646, 398, 342; ν(KBr)/cm^{-1} 3433 (NH); δ_H($CDCl_3$, 500 MHz, 50 °C) −2.14 (2 H, br s), 3.47 (18 H, s), 3.70 (12 H, t), 3.95 (12 H, t), 4.20 (12 H, t), 4.74 (12 H, t), 5.18 (4 H, s), 5.33 (2 H, s), 6.69 (1 H, t), 7.05 (2 H, d), 7.22–7.50 (10 H, br m), 8.55–8.70 (8 H, brm), 9.05 (1 H, d); *m/z* (FAB) 1542 (M^+). For **8**: λ(CH_2Cl_2)/nm 700, 664, 646, 398, 342; ν(KBr)/cm^{-1} 3422 (NH); δ_H($CDCl_3$, 500 MHz, 50 °C) −2.00 (2 H, br s), 3.46 (18 H, s), 3.70 (12 H, t), 3.95 (12 H, t), 4.20 (12 H, t), 4.74 (12 H, t), 4.98 (8 H, s), 5.10 (4 H, s), 5.53 (2 H, s), 6.52 (2 H, t), 6.65 (1 H, t), 6.73 (4 H, d), 7.03 (2 H, d), 7.18–7.32 (20 H, br m), 8.52–8.70 (8 H, br m), 9.02 (1 H, d); *m/z* (FAB) 1989 (M^+ + Na^+). For **9**: λ(CH_2Cl_2)/nm 702, 664, 640, 400, 340; ν(KBr)/cm^{-1} 3429 (NH); δ_H($CDCl_3$, 500 MHz, 50 °C) −1.70 (2 H, br s), 3.42 (18 H, s), 3.70 (12 H, t), 3.95 (12 H, t), 4.20 (12 H, t), 4.74 (12 H, t), 4.88 (16 H, s), 4.98 (8 H, s), 5.06 (4 H, s), 5.50 (2 H, s), 6.48 (2 H, t), 6.49 (1 H, t), 6.52 (4 H, t), 6.69 (8 H, d), 6.72 (4 H, d), 7.00 (2 H, d), 7.15–7.35 (40 H, br m), 8.62–8.75 (8 H, br m), 9.10 (1 H, d); *m/z* (FAB) 1989 (M^+ + Na^+).

1 For a recent review see: G. R. Newcombe, C. N. Moorefield and F. Vögtle, *Dendritic Molecules: Concepts, Syntheses and Perspectives*, VCH, Weinheim, 1996.
2 C. J. Hawker and J. M. J. Fréchet, *J. Am. Chem. Soc.*, 1990, **112**, 7638; K. L. Wooley, C. J. Hawker and J. M. J. Fréchet, *J. Am. Chem. Soc.*, 1991, **113**, 4252.
3 K. L. Wooley, C. J. Hawker, J. M. J. Fréchet, F. Wudl, G. Srdanov, S. Shi, C. Li and M. Kao, *J. Am. Chem. Soc.*, 1993, **115**, 9836.
4 R.-H. Jin, T. Aida and S. Inoue, *J. Chem. Soc., Chem. Commun.*, 1993, 1260.
5 C.-F. Shu and H.-M. Shen, *J. Mater. Chem.*, 1997, **7**, 47.
6 N. B. McKeown, *Phthalocyanine Materials: Synthesis, Structure and Function*, Cambridge University Press, Cambridge, 1998.
7 G. J. Clarkson, N. B. McKeown and K. E. Treacher, *J. Chem. Soc., Perkin Trans. 1*, 1995, 1817.
8 A. Kraft *Chem. Commun.*, 1996, 77.
9 J. Simon and C. Piechocki, *J. Am. Chem. Soc.*, 1982, **104**, 5245; K. Ohta, L. Jacquemin, C. Sirlin, L. Bosio and J. Simon, *New J. Chem.*, 1988, **12**, 751.
10 R. D. George and A. W. Snow, *Chem. Mater.*, 1994, **4**, 209; M. Brewis, G. J. Clarkson, V. Goddard, M. Helliwell, A. M. Holder and N. B. McKeown, *Angew. Chem., Int. Ed. Engl.*, in the press.
11 K. E. Treacher, G. J. Clarkson and N. B. McKeown, *Liq. Cryst.*, 1995, **19**, 887.

Received in Liverpool, UK, 4th March 1998; 8/01799I

A fluorescent cage for anion sensing in aqueous solution

Luigi Fabbrizzi,*† Ilaria Faravelli, Giancarlo Francese, Maurizio Licchelli, Angelo Perotti and Angelo Taglietti

Dipartimento di Chimica Generale, Università di Pavia, I-27100 Pavia, Italy

The dizinc(II) complex of the bistren cage 2 selectively includes the isostructural N_3^- and NCO^- ions in aqueous solution, but only N_3^- inclusion is signalled through the quenching of the fluorescent emission of the anthracene spacer.

Molecular recognition of anions is in most cases based on electrostatic interactions (which include hydrogen bonding). Typically, the receptor offers a concave array of sites suitable for anion binding: ammonium or guanidium groups, amide hydrogen atoms.[1] In general, the intrinsically low energy of the electrostatic interaction does not compete successfully with the anion hydration energy and recognition studies have to be carried out in non-aqueous and poorly polar solvents. Efficient binding of anions in water would require the use of stronger host–guest interactions. This may be the case of the metal–ligand interactions. In fact, metal containing receptors perform efficient anion recognition in aqueous solution. As an example, the dicopper(II) complex of the bistren cage **1** selectively includes polyatomic anions, *e.g.* N_3^-, NCO^-, HCO_3^-. While anion inclusion is demonstrated by X-ray diffraction studies on the solid complexes,[2] recognition in aqueous solution can be monitored spectrophotometrically and is characterised by values of the association constant, K_{assn}, as high as 10^5 dm^3 mol^{-1}.[3] Each of the two donor atoms of the included ambidentate anion occupies a vacant coordination site of each Cu^{II} centre (the axial position of a trigonal bipyramid) and selectivity derives from the matching between the anion 'bite' (*i.e.* the distance between the two donor atoms) and the distance between the two vacant axial positions.

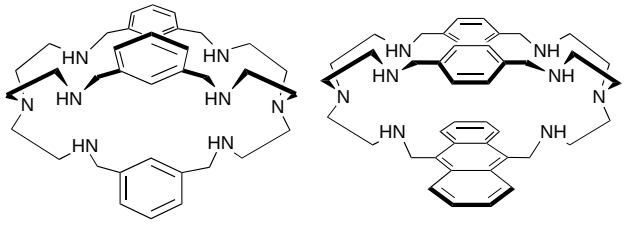

1 **2**

The function of recognition can be implemented to sensing if the receptor system contains a reporter subunit capable of signalling substrate binding through the variation of a chosen well detectable property. Fluorescence seems a particularly convenient property since it can be monitored in real time, even at very low concentration levels, by using a rather simple instrumentation. Fluorosensors for a large number of biotic and abiotic analytes have been designed during the past decade by appending a fluorescent fragment to the envisaged receptor framework:[4] in all cases, an efficient mechanism has to be provided for either quenching or reviving fluorescence, following substrate recognition. In contrast to the many efficient fluorosensors reported for cations to date, fluorescent sensors for anions are still rare.[4]

We have now synthesised the cage **2**, in which one of the spacers connecting the two tren compartments is the strongly fluorescent 9,10-anthracenyl fragment. The synthetic procedure, first involved the appending of two tren subunits to a 9,10-anthracenyl fragment; then, the terminal amine groups of each subunit were connected by 1,4-xylyl spacers.‡ Cage **2** incorporates pairs of metal ions, *e.g.* two Cu^{II}, and, following a cascade mechanism, can include ambidentate anions like N_3^- and NCO^-. However, we could not use the dicopper(II) complex as a fluorosensor, since Cu^{II} itself quenches the fluorescence of any proximate fluorophore through either an electron transfer (eT) or an energy transfer (ET) mechanism.[5] Therefore, we switched to Zn^{II}, which still forms stable complexes with amine ligands and, being redox inactive and having a filled 3d level, cannot be involved in either an eT or an ET process. Polyamine systems containing two Zn^{II} ions have been used to sense the imidazolate anion.[6]

The emitting behaviour of **2** (= L) in the pH range 2–12 was investigated by titrating with standard base a solution containing its octahydrochloride, $[H_8L]Cl_8$, plus excess acid, in the spectrofluorimetric cuvette. The corresponding fluorescence intensity, I_F, *vs.* pH profile, is shown in Fig. 1 (circles). At low pH values full anthracene fluorescence is observed. Then, I_F decreases in the pH range 4–6 following a sigmoidal pattern. Noticeably, the plot of I_F *vs.* the equiv. of added OH^- shows that fluorescence quenching takes place during the addition of the third equivalent of base (after that the excess acid had been neutralised). Amine groups display reducing properties and can transfer an electron to the proximate excited anthracenyl fragment, *An, quenching its fluorescence. It is possible that, after the neutralisation of the two protons released from the apical ammonium groups, the third proton leaves one of the ammonium groups adjacent to the An fragment allowing an eT process to take place. Then, a similar titration experiment was carried out on a solution containing also 2 equiv. of Zn^{II}. The corresponding I_F *vs.* pH profile (triangles) superimposes well on that observed for the titration of the cage alone until pH = 7. Here, I_F stops decreasing and increases again to reach a maximum at pH = 8.5. We ascribe this behaviour to the fact that from pH = 7 Zn^{II} ions enter the two tren compartments engaging all the amine nitrogen atoms in the coordinative bonds and preventing the electron transfer to *An. The maximum

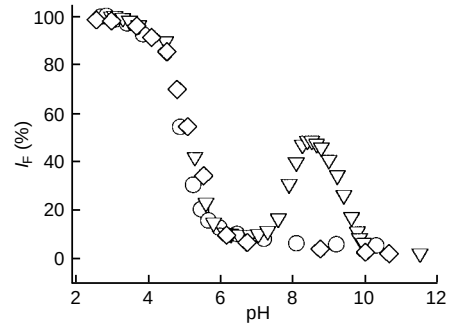

Fig. 1 pH dependence of the fluorescence intensity (I_F) for aqueous solutions containing: (○) **2** (10^{-4} M) plus excess acid; (▽) **2**, 2 equiv. of Zn^{II}, plus excess acid; (◇) **2**, 2 equiv. of Zn^{II}, 1 equiv. of N_3^-, plus excess acid.

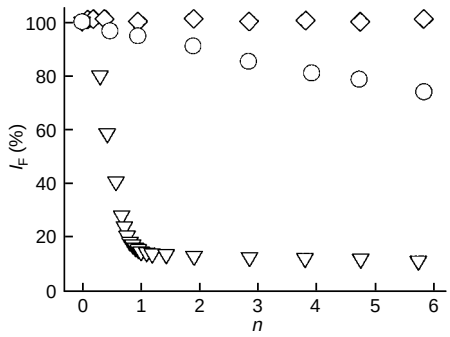

Fig. 2 Spectrofluorimetric titrations of aqueous solutions containing $[Zn^{II}(\mathbf{2})]^{2+}$ (10^{-4} M) and buffered to pH = 8.5: (▽) addition of N_3^-; (◇) addition of NO_3^- (no modification of I_F was observed also on addition of HCO_3^-, SO_4^{2-}, Cl^-, Br^-, NCO^-); (○) addition of N_3^- to a solution containing also 5 equiv. of NCO^-. *n* = Number of added equivalents of anion.

fluorescence should correspond to the maximum concentration of the $[Zn^{II}_2L_2]^{4+}$ complex. A further pH increase makes I_F decrease again. This may be due to the formation of a species in which an OH^- ion is coordinated to each metal centre. In particular, in the $[Zn^{II}_2L_2]^{4+}$ complex a water molecule is expected to occupy the axial position of each metal centre, completing five-coordination. Therefore, hydroxide containing species result from the deprotonation of the Zn^{II} bound water molecules.§ The OH^- anion can undergo an eT process and quench the proximate *An fragment. Intramolecular fluorescence quenching by coordinated OH^- ions is typically observed in Zn^{II} anthrylpolyamine complexes. Finally, in order to test the sensing behaviour of the dizinc(II) cage towards polyatomic anions, a titration with standard NaOH was carried out on a solution containing **2**, 2 equiv. of Zn^{II}, 1 equiv. of N_3^-, plus excess acid. In the corresponding profile (diamonds in Fig. 1) no fluorescence revival is observed above pH = 7, but I_F keeps decreasing until complete quenching. We ascribe this behaviour to the formation of a $[Zn^{II}_2L(N_3)]^{3+}$ inclusion complex.¶ Quenching may be due to an eT process from the electron rich N_3^- ion to the close *An fragment.

From molecular modelling, distances as short as 3 Å can be calculated between the closest nitrogen atoms of N_3^- and carbon atoms of the anthracene fragment, which may allow a fast through-space eT process to occur. Intermolecular quenching of anthracene by the N_3^- ion has been previously observed in aqueous ethanol and has been ascribed to an eT mechanism.[7] Comparison of the I_F *vs*. pH profiles of Figs. 1 and 2 indicates that at pH ≈ 8 the dizinc(II) cage could behave as a fluorescent sensor for the N_3^- ion: in particular, azide inclusion should be signalled through a substantial quenching of the anthracene fluorescence. Indeed, by titrating with a standard N_3^- solution an aqueous solution 10^{-4} M in **2**, containing 2 equiv. of Zn^{II} and buffered to pH = 8.0, a linear decrease of fluorescence was observed until the addition of 1 equiv. of azide (Fig. 2).

Least-squares analysis of the titration profile gave a value of $\log K_{assn}$ of 5.8 ± 0.1. Then, the receptor solution (1 equiv. of **2**, 2 equiv. of Zn^{II}, adjusted to pH = 8) was titrated with a series of anions: NO_3^-, HCO_3^-, SO_4^{2-}, Cl^-, Br^-. In all cases, no I_F decrease was observed even after the addition of 10 equiv. Moreover, the N_3^- titration profile as shown in Fig. 2 was not altered when the receptor solution contained also 10 equiv. of each one of the above anions. This indicates that these anions do not compete with N_3^- for inclusion: in particular, the corresponding K_{assn} values should be lower than $10^{3.6}$. The case of NCO^- is unique. On addition of NCO^- to the receptor solution, no I_F decrease was observed. However, the titration profile of N_3^- was remarkably affected by the presence of NCO^-: the greater the NCO^- concentration, the less steep the I_F decrease, indicating severe competition for inclusion within the cage. The profile reported in Fig. 2 refers to a solution containing 5 equiv. of NCO^-. From this a $\log K_{assn}$ of 6.5 can be calculated for NCO^-. Thus, NCO^- has a slightly greater affinity for **2** than N_3^-, but, due to its less pronounced reducing tendencies, when included in the cage, it is unable transfer an electron to the nearby *An fragment. N_3^- and NCO^- anions have a similar bite length (2.34 and 2.42 Å, respectively) and the rather high values of K_{assn} should reflect the favourable matching with the distance between the two vacant axial positions of the two Zn^{II} centres. The other linear triatomic anion, NCS^-, quenches fluorescence, but according to a much less steep profile, to which a much lower value of $\log K_{assn}$ corresponds: 2.45 ± 0.05. NCS^- is a one-electron reducing agent of strength comparable to that of N_3^- ($NCS^{\cdot}/NCS^-$ potential: 1.62 V *vs*. NHE; $N_3^{\cdot}/N_3^-$: 1.33),[8] which accounts for the occurrence of an intracomplex photoinduced eT process and fluorescence quenching. However, the much greater bite length (2.75 Å) should induce an endothermic rearrangement of the cage framework, making inclusion 2200 times much less favourable than for N_3^-.

This study demonstrates that the zinc(II) containing cage **2** is an efficient and selective receptor for ambidentate anions. First, it discriminates polyatomic anions from monoatomic anions, which have a less pronounced tendency to bridge two metal centres and whose inclusion is then disfavoured. Then, it recognises polyatomic anions on the basis of their bite length. Finally, the presence of the 9,10-anthracenyl spacer permits the inclusion of anions prone to a photo-induced eT process being signalled through fluorescence quenching.

Notes and References

† E-mail: fabbrizz@ipv36.unipv.it

‡ A solution of terephthalaldehyde (4.0 mmol in 250 ml of MeOH) was added dropwise over 2 h under magnetic stirring to a solution of the bistren derivative of the 9,10-anthracenyl fragment[6] (2.0 mmol in 750 ml of MeOH). The stirred solution was then heated to 50 °C and 2.5 g of $NaBH_4$ were added in small portions over 3 h. The solution was then stirred overnight at room temperature. MeOH was distilled off under reduced pressure, and the residue was dissolved in 100 ml of water. The aqueous solution was extracted with CH_2Cl_2 (3 × 50 ml). The organic phase was dried over Na_2SO_4 and the solvent was removed under reduced pressure to give a gold–yellow solid (yield: 55%). FAB MS *m/z* (%): 699 (100) M − H^+. **2** was used in solution studies as its hydrochloride, **2**·8HCl, which was satisfactorily analysed.

§ The following species were found to be present at equilibrium, in the 2–12 pH range, in a dioxane–water mixture (4 : 1, v/v), as ascertained through non-linear least-squares analysis of potentiometric titration data: $[Zn^{II}(H_3L)]^{5+}$, $[Zn^{II}_2L]^{4+}$, $[Zn^{II}_2L(OH)]^{3+}$, $[Zn^{II}_2L(OH)_2]^{2+}$. The dioxane–water medium was used to ensure a concentration of **2** ⩾ 10^{-3} M, as required, for potentiometric studies. A potentiometric titration study in pure water could not be carried out owing to the poor solubility of **2** (≈ 10^{-4} M).

¶ Potentiometric titration experiments in dioxane–water (4 : 1 v/v) indicated that the $[Zn^{II}_2L(N_3)]^{3+}$ complex is present as a major species in the pH range 6.5–9.0.

1 F. P. Schmidtchen and M. Berger, *Chem. Rev.*, 1997, **97**, 1609.
2 C. J. Harding, F. E. Mabbs, E. J. L. MacInnes, V. McKee and J. Nelson, *J. Chem. Soc., Dalton Trans.*, 1996, 3227.
3 L. Fabbrizzi, P. Pallavicini, A. Perotti, L. Parodi and A. Taglietti, *Inorg. Chim. Acta*, 1995, **238**, 5.
4 A. P. de Silva, H. Q. N. Gunaratne, T. Gunnlaugsson, A. J. M. Huxley, C. P. McCoy, J. T. Rademacher and T. E. Rice, *Chem. Rev.*, 1997, **97**, 1515.
5 V. Balzani and F. Scandola, *Supramolecular Photochemistry*, Ellis Horwood, Chichester, 1991, pp. 65–73.
6 L. Fabbrizzi, G. Francese, M. Licchelli, A. Perotti and A. Taglietti, *Chem. Commun.*, 1997, 581.
7 H. Shizuka, M. Nakamura and T. Morita, *J. Phys. Chem.*, 1980, **84**, 989.
8 P. Wardman, *J. Phys. Chem. Ref. Data*, 1989, **18**, 1710.

Received in Basel, Switzerland, 2nd February 1998; 8/00851E

14e η^1-Hydrocarbyliron complexes supported by hydrotris(3,5-diisopropylpyrazolyl)borate: the allyl complex prefers a highly coordinatively unsaturated 14e η^1-structure to a 16e η^3-structure‡

Munetaka Akita,*† Nobuhiko Shirasawa, Shiro Hikichi and Yoshihiko Moro-oka*

Research Laboratory of Resources Utilization, Tokyo Institute of Technology, 4259 Nagatsuta, Midori-ku, Yokohama 226-8503, Japan

Coordinatively unsaturated allyl and benzyl complexes with the hydrotris(3,5-diisopropylpyrazolyl)borate ligand (Tp^{iPr}), $Tp^{iPr}M$–allyl (M = Ni, Co, Fe) and $Tp^{iPr}Fe$–*p*-methylbenzyl, are prepared and characterized by X-ray crystallography, and the allyl ligand is coordinated to the Fe center in a η^1-fashion to form a 14e species in contrast to the η^3-coordination found for the Ni and Co complexes.

Coordinatively unsaturated organo-transition metal species have attracted much attention, in particular, in connection with catalytic transformations, which require open coordination sites for substrates (*e.g.* 14e species as polymerization catalysts),[1] and electron transfer processes.[2] Although many coordinatively unsaturated early transition metal complexes have been studied, few isolated examples of late transition metal complexes are known.[3] During the course of our study on organometallic complexes supported by the hydrotris(3,5-diisopropylpyrazolyl)borate ligand (Tp^{iPr}),[4]‡ we have found that coordinatively unsaturated hydrocarbyl complexes of the first row, late transition metals are obtained by using the Tp^{iPr} auxiliary. Herein we wish to report synthesis and structural characterization of coordinatively unsaturated hydrocarbyl complexes including a series of allyl complexes, $Tp^{iPr}M(allyl)$ (M = Ni, Co, Fe), and a η^1-*p*-methylbenzyliron complex, $Tp^{iPr}Fe$–$CH_2C_6H_4Me$-*p*.[5]

As the first attempts, we examined syntheses of complexes with the allyl ligand, which might stabilize a coordinatively unsaturated species through η^3-coordination. Treatment of the chloride precursors, $Tp^{iPr}MCl$ (M = Ni, Co, Fe), with allylmagnesium chloride in THF afforded the allyl complexes, $Tp^{iPr}M(allyl)$ (M = Ni **1**, Co **2**, Fe **3**), after extraction with pentane followed by crystallization (Scheme 1). The diamagnetic Ni complex **1** was stable in the air, whereas the other paramagnetic complexes **2** and **3** should be kept under an inert atmosphere.

The deep red Ni complex **1** was readily assigned to the structure with a η^3-allyl ligand on the basis of its ^1H NMR data similar to that of the structurally characterized analogue with the non-substituted Tp ligand,[6]‡ which also indicated occurrence of a dynamic process averaging the three pyrazolyl rings. X-Ray crystallography of **1**§¶ revealed the apparently C_s-symmetrical, square-pyramidal structure with the apical N(31) atom. The structure is similar to those of the Tp derivative[6] and the Co complex (Fig. 1), and distortion toward a square-planar structure is evident from the dissimilar Ni–N distances [Ni–N(11) 1.962(6), Ni–N(21) 1.962(5), Ni–N(31) 2.220(6) Å (difference: 0.26 Å)]. The allyl ligand is coordinated to the Ni center in a η^3-fashion as indicated by the very similar Ni–C distances [Ni–C(1) 1.991(9), Ni–C(2) 2.032(6), Ni(1)–C(3) 2.00(1) Å (difference: 0.04 Å)]. The deep green Co complex **2**§ with similar Co–η^3-allyl-carbon distances [Co–C(1) 2.066(6), Co–C(2) 2.056(4), Co–C(3) 2.077(8) Å] is isostructural with **1** (Fig. 1), though the square-pyramidal character is more evident compared to **1** judging from the smaller difference in the Co–N distances [Co–N(11) 1.983(4), Co–N(21) 1.995(4), Co–N(31) 2.153(4) Å (difference: 0.17 Å)]. Thus the Ni and Co allyl complexes are characterized as square-pyramidal η^3-allyl complexes with 18e- and 17e-configuration, respectively.

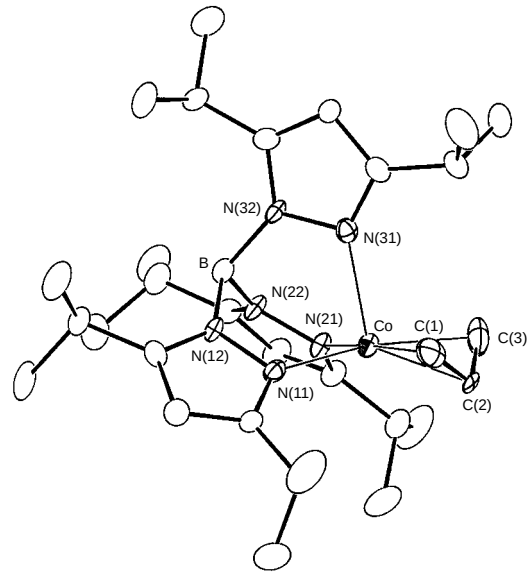

Fig. 1 Molecular structure of **2** drawn at the 30% probability level

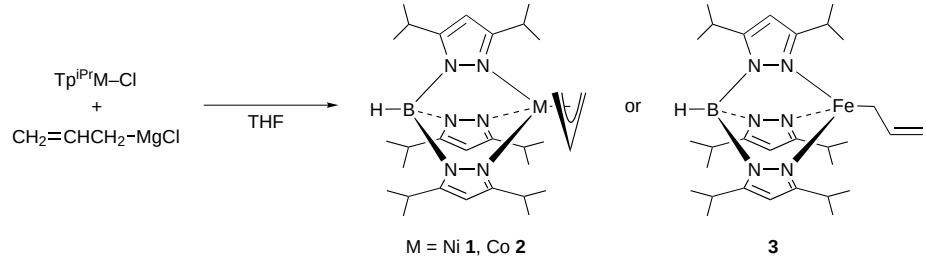

Scheme 1

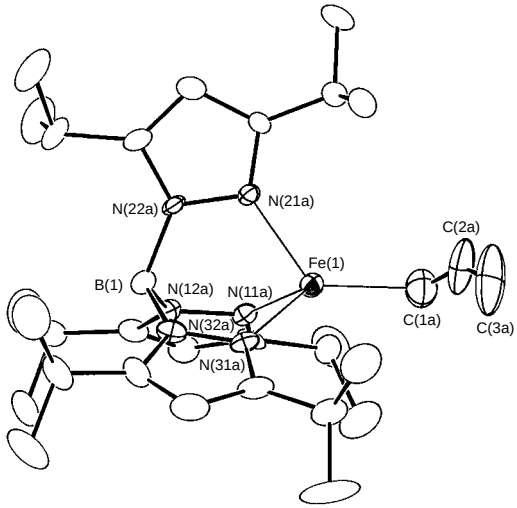

Fig. 2 Molecular structure of **3** drawn at the 30% probability level

The structure of the yellow Fe complex **3** (Fig. 2: two independent molecules)§ is in sharp contrast to those of the Ni and Co complexes. The Fe(1)–C(2a) [2.87(1) Å] and Fe(1)–C(3a) distances [3.75(2) Å] are non-bonding [*cf.* Fe–C(1a) 2.04(1) Å] and, therefore, the allyl ligand is coordinated to the iron center in a η^1-fashion. The iron center adopts a tetrahedral coordination geometry [Fe(1)–N(11a) 2.069(7), Fe(1)–N(21a) 2.071(8), Fe(1)–N(31a) 2.099(9) Å (difference: 0.03 Å)], although a slight deviation from an ideal C_3-symmetrical structure is indicated by the N–Fe(1)–C(1) angles [C(1a)–Fe(1)–N(11a) 119.2(4), C(1a)–Fe(1)–N(21a) 126.5(5); C(1a)–Fe(1)–N(31a) 130.8(6)°]. These structural features lead to the characterization of **3** as a 14e tetrahedral η^1-allyliron complex. Let us point out the curious electronic structure of **3**. If the allyl ligand is coordinated to the iron center in a η^3-fashion (4e-donor), the iron center can receive two more electrons to attain a 16e-configuration closer to coordinative saturation. Such structures are observed for the Ni (**1**) and Co complexes (**2**) with more metal d electrons as mentioned above. Despite this advantage of a η^3-structure, the iron complex with a lower number of d electrons does not adopt the η^3-structure (16e) but the η^1-structure (14e). According to our previous results, the monomeric Tp^RM–X type complexes‡ favor a tetrahedral structure,[7] although X is coordinated through a heteroatom (*e.g.* O, S) with lone-pair electrons, which may stabilize the coordinatively unsaturated metal center through π donation. For **3**, however, such stabilization is not available, and some intrinsic property of the Tp^RM-system may contribute to stabilization of the tetrahedral structures.

The successful isolation of the coordinatively unsaturated hydrocarbyl complex **3** prompted us to examine syntheses of other η^1-hydrocarbyl complexes.[5] As a typical example, the *p*-methylbenzyliron complex, $Tp^{iPr}Fe$–$CH_2C_6H_4Me$-*p* **4**, was prepared by the Grignard method analogous to Scheme 1, and X-ray crystallography§ revealed a tetrahedral coordination geometry of iron. The structural parameters around the iron center are essentially the same as those of the allyl complex **3** {Fe–C(1) 2.05(1) Å [C(1) is the α-carbon atom of the *p*-methylbenzyl group]; N–Fe–C(1) 116.9(4), 122.7(4), 136.5(4)°}, and slight distortion from a C_3-symmetrical structure is also noted.

In conclusion, coordinatively unsaturated 14e-organoiron complexes including allyl- (**3**) and benzyl-type complexes (**4**) have been synthesized and characterized. Further studies on molecular orbital analysis of the allyl complexes **1**–**3**, synthesis of other hydrocarbyl complexes and reactivity of the obtained hydrocarbyl complexes are now in progress. Preliminary experiments revealed that the η^1-hydrocarbyl complex **4** was readily carbonylated under a CO atmosphere (1 atm) to give the coordinatively saturated dicarbonyl–acyl complex, Tp^{iPr}-$Fe(CO)_2C(=O)CH_2C_6H_4Me$-*p* **5**. It is also found that **4** shows reactivity toward unsaturated hydrocarbons, and the results will be reported in due course.

We are grateful to the Ministry of Education, Science, Sports, and Culture of the Japanese Government for financial support of this research (Grant-in-Aid for Specially Promoted Research: 08102006).

Notes and References

† E-mail: makita@res.titech.ac.jp

‡ Abbreviations used: Tp^{iPr} = hydrotris(3,5-diisopropylpyrazolyl)borate; Tp = hydrotrispyrazolylborate; Tp^R = substituted Tp derivatives.

§ X-Ray diffraction measurements were made on a Rigaku RAXIS IV imaging plate area detector with graphite-monochromated Mo-Kα radiation. The refinements were made on F^2 with SHELXL-93 linked to teXsan. *Crystal data*: **1**: $C_{30}H_{51}BN_6Ni$, M_w = 565.3, T = −60 °C, triclinic, space group $P\bar{1}$, a = 9.778(3), b = 16.76(1), c = 9.720(8) Å, α = 90.348(4), β = 102.87(7), γ = 90.96(7)°, U = 1552(1) Å^3, Z = 2, D_c = 1.21 g cm^{-3}, μ = 6.54 cm^{-1}, $R(R_w)$ = 0.099 (0.121) for the 3648 unique data [$I > 3\sigma(I)$] and 355 parameters. **2**: $C_{30}H_{51}BCoN_6$, M_w = 565.5, T = −60 °C, triclinic, space group $P\bar{1}$, a = 9.733(8), b = 16.818(8), c = 9.718(9) Å, α = 90.88(6), β = 101.59(5), γ = 92.20(5)°, U = 1557(2) Å^3, Z = 2, D_c = 1.21 g cm^{-3}, μ = 5.80 cm^{-1}, $R(R_w)$ = 0.089 (0.107) for the 4644 unique data [$I > 3\sigma(I)$] and 343 parameters. **3** (two independent molecules): $C_{30}H_{51}BFeN_6$, M_w = 562.4, T = −60 °C, orthorhombic, space group $P2_12_12_1$, a = 18.796(2), b = 16.319(2), c = 21.653(4) Å, U = 6642(1) Å^3, Z = 8, D_c = 1.13 g cm^{-3}, μ = 4.80 cm^{-1}, $R(R_w)$ = 0.084 (0.101) for the 4988 unique data [$I > 3\sigma(I)$] and 709 parameters. **4**: $C_{35}H_{55}BFeN_6$, M_w = 626.5, T = −60 °C, triclinic, space group $P\bar{1}$, a = 11.818(9), b = 16.39(1), c = 9.408(4) Å, α = 90.56(4), β = 101.29(4), γ = 91.46(5)°, U = 1786(2) Å^3, Z = 2, D_c = 1.17 g cm^{-3}, μ = 4.53 cm^{-1}, $R(R_w)$ = 0.108 (0.117) for the 2812 unique data [$I > 3\sigma(I)$] and 401 parameters. ORTEP drawings of **1** and **4** are included in supplementary material available upon request from the authors. CCDC 182/804.

¶ The atomic numbering scheme for **1** is the same as that for **2** (Fig. 1) except the metal center.

1 G. W. Coates and R. M. Waymouth, *Comprehensive Organometallic Chemistry II*, ed. E. W. Abel, F. G. A. Stone and G. Wilkinson, Pergamon, Oxford, 1995, vol. 12, ch. 12.1; R. F. Jordan, *Adv. Organomet. Chem.*. 1991, **32**, 325; P. W. Dyer, V. C. Gibson, J. A. K. Howard, B. Whittle and C. Wilson, *J. Chem. Soc., Chem. Commun.*, 1992, 1666; K. Mashima, S. Fujikawa, Y. Tanaka, H. Urata, T. Oshiki, E. Tanaka and A. Nakamura, *Organometallics*, 1995, **14**, 2633. See also references cited therein.

2 A leading reference: D. Astruc, *Acc. Chem. Res.*, 1997, **30**, 383.

3 Homoleptic hydrocarbyliron complexes: B. K. Bower and H. G. Tennent, *J. Am. Chem. Soc.*, 1972, **94**, 2512; A. Klose, E. Solari, C. Floriani, A. Chiesi-Villa, C. Rizzoli and N. Re, *J. Am. Chem. Soc.*, 1994, **116**, 9123; R. C. Kerber, *Comprehensive Organometallic Chemistry II*, ed. E. W. Abel, F. G. A. Stone and G. Wilkinson, Pergamon, Oxford, 1995, vol. 7, ch. 2.3.1.

4 M. Aktia, K. Ohta, Y. Takahashi, S. Hikichi and Y. Moro-oka, *Organometallics*, 1997, **16**, 4121; Y. Takahashi, M. Akita, S. Hikichi and Y. Moro-oka, *Inorg. Chem.*, in press.

5 Very recently, analogous four-coordinated alkylchromium complexes were reported, though their structures were characterized as *cis*-divacant octahedra in contrast to the tetrahedral structures of the iron complexes **3** and **4**. J. L. Kersten, R. R. Kucharczyk, G. P. A. Yap, A. L. Rheingold and K. H. Theopold, *Chem. Eur. J.*, 1997, **3**, 1668.

6 H. Lehmkuhl, J. Näser, G. Mehler, T. Keil, F. Danowski, R. Benn, R. Mynott, G. Schroth, B. Gabor, C. Kruger and P. Betz, *Chem. Ber.*, 1991, **124**, 441.

7 S. Hikichi, T. Ogihara, K. Fujisawa, N. Kitajima, M. Akita and Y. Moro-oka, *Inorg. Chem.*, 1997, **36**, 4539; M. Ito, H. Amagai, H. Fukui, N. Kitajima and Y. Moro-oka, *Bull. Chem. Soc. Jpn.*, 1996, **69**, 1937; N. Kitajima, T. Katayama, K. Fujisawa, Y. Iwata and Y. Moro-oka, *J. Am. Chem. Soc.*, 1993, **115**, 7872; N. Kitajima and W. B. Tolman, *Prog. Inorg. Chem.*, 1995, **43**, 419.

Received in Cambridge, UK, 20th February 1998; 8/01460D

Face selectivity in electrophilic additions to methylenenorsnoutanes: relative importance of through-space, through-bond and electrostatic interactions

Goverdhan Mehta,*[a]† Chebolu Ravikrishna,[a] Shridhar R. Gadre,*[b] C. H. Suresh,[b] P. Kalyanaraman[c] and Jayaraman Chandrasekhar*[c]

[a] *School of Chemistry, University of Hyderabad, Hyderabad 500 046, India*
[b] *Department of Chemistry, University of Pune, Pune 411 007, India*
[c] *Department of Organic Chemistry, Indian Institute of Science, Bangalore 560 012, India*

4-Substituted 9-methylenenorsnoutanes undergo a variety of electrophilic additions with a small but consistent *syn* preference; *ab initio* MESP maps indicate that electrostatic factors and through-space interaction between the double bond and cyclopropane Walsh orbitals are unimportant in determining the face selectivity, while AM1 transition state energetics suggest that the observed preferences are determined primarily by through-bond interactions.

The origin of π-face selectivity in sterically unbiased substrates continues to be a challenging problem in spite of many innovative experimental[1a–d] and theoretical investigations.[1c–e] While the importance of hyperconjugative interactions has been clearly demonstrated in electrophilic additions in several olefinic substrates,[2a–c] the competing role of electrostatic effects has been equally well established in nucleophilic additions to related carbonyl derivatives.[1d–e,2d] However, the mode by which some substituents, like the vinyl and aryl groups, induce face selectivity is often complex.[1a,2d] Recently, the cyclopropyl ring has also been shown to exhibit unusual trends in selectivity. Three-membered ring fusion causes *anti* selectivity in electrophilic additions to 7-methylenenorbornanes, but a *syn* preference in isomeric bicyclo[2.2.2]octenes.[3] This reversal is especially surprising because through-space interaction between the olefinic bond and a cyclopropane Walsh orbital is strong in both substrates on the basis of photoelectron spectral studies.[4] In order to critically evaluate the relevance of such orbital interactions in the context of alternative models, we now report the results of a combined experimental and computational examination of face selectivity in electrophilic additions to 4-substituted 9-methylenenorsnoutanes **1**. These substrates enable a comparison of the effect of two subtly different cyclopropyl units in a truly sterically unbiased environment. This study complements our earlier investigation of nucleophilic additions to the corresponding ketones,[5] in which significant face selectivity was observed and attributed to effective transmittal of orbital and electrostatic effects through three-membered rings.

The 9-methylenenorsnoutanes **1b**–**d**, readily synthesized from the corresponding ketones[5] *via* Wittig olefination ($Ph_3P^+MeBr^-$, Bu^tOK, 80%), were subjected to dichlorocarbene addition, oxymercuration, epoxidation and hydroboration reactions (Scheme 1). The structures of the *E,Z*-diastereomers were deduced on the basis of ^1H and ^{13}C NMR data, but more specifically from (i) the greater deshielding of H-5 in the *E*-series compared to *Z*-series, (ii) the relative deshielding of H-2 and H-3 in the *Z*-series compared to the *E*- series and (iii) the deshielding of the quaternary C-4 carbon resonances in the *Z*-series compared to *E*-series. These observations could be further confirmed through selected lanthanide-induced shift (LIS) studies.

All the derivatives **1b**–**d** show a consistent preference for *syn* face addition. As noted in earlier studies[1,2] on remotely substituted 7-methylenenorbornanes and 2-methyleneadamantanes, oxymercuration shows the highest facial preference. Neutral electrophiles exhibit modest selectivity.

In order to interpret the above results, the topographical features of the molecular electrostatic potentials (MESP) of methylenenorsnoutane **1a** and its cyano analog **1b** were examined at the *ab initio* HF/6-31G(d,p)//HF/3-21G level using the program INDMOL.[6] Typically, a $R_2C{=}CH_2$ unit has MESP minima above and below the π cloud, shifted towards the methylene group, while a cyclopropyl ring has three minima in the CCC plane about 1.4 Å away from each C–C bond.[7] In **1a**,

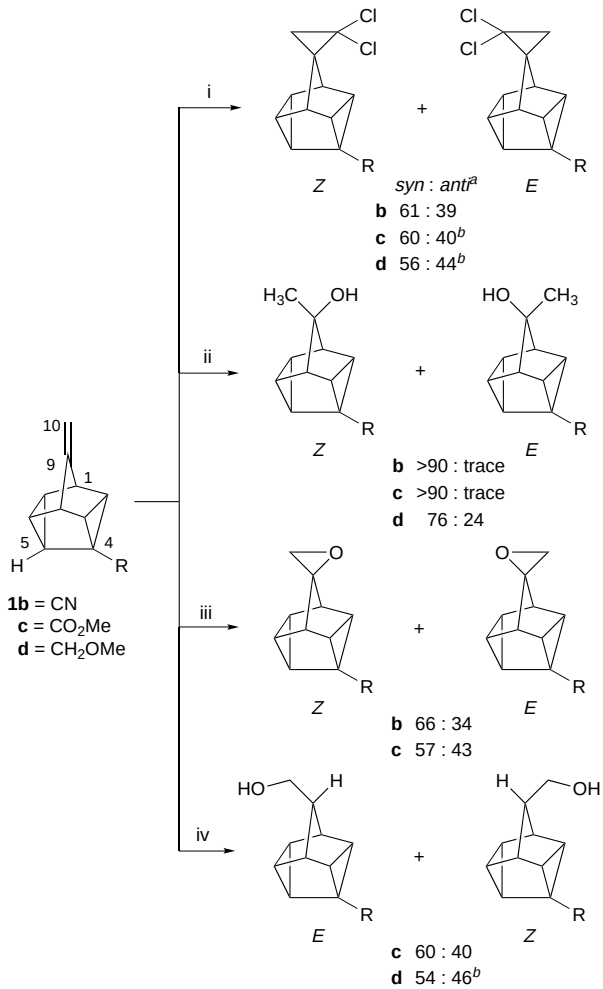

Scheme 1 *Reagents and conditions*: i, $CHCl_3$, 50% *aq.* NaOH, Et_3BnNCl, room temp., 75–80%; ii, $Hg(OAc)_2$, aq. THF, $NaBH_4$–NaOH, 80%; iii, MCPBA, CH_2Cl_2, Na_2CO_3, 5–10 °C, 75%; iv, B_2H_6–THF, H_2O_2–aq. NaOH, 80%. [a] Ratios based on ^1H NMR integration of crude reaction mixture (±5%). [b] *E* : *Z* mixture could not be separated. However, ^1H NMR data enabled identification of each isomer.

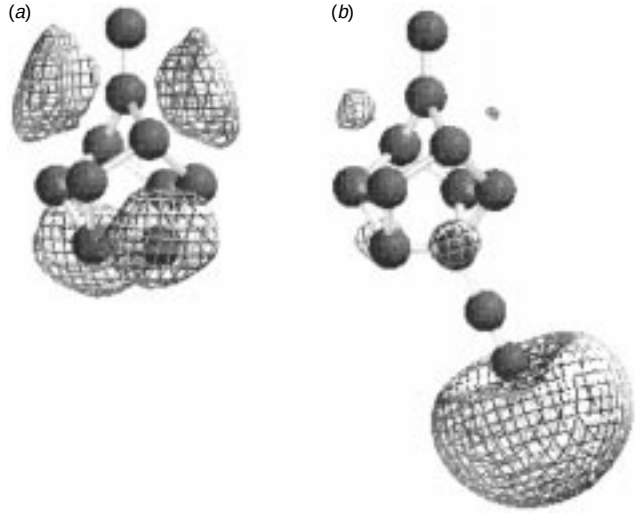

Fig. 1 MESP isopotential surfaces (contour level = −0.024 au) of (*a*) **1a** and (*b*) the cyano analogue **1b**

all the (3, +3) critical points (CPs at which the gradient of the potential vanishes and all the three eigen values of the Hessian are positive)[8] expected for the double bond and cyclopropyl rings are found. The pairs of CPs which share large negative regions [and are linked through (3, +1) saddle points] offer graphic proof of strong interactions between each of the cyclopropyl units and the olefinic π-bond as well as between the two cyclopropyl rings (see Fig. 1). These interactions were quantified earlier using photoelectron (PE) spectroscopy. In particular, σ–π interactions raise the π MO energy to 9.0 eV, compared to the value of 9.4 eV found in 7-methylenenorbornane.[4a]

The above interactions are substantially reduced by the introduction of a cyano group. The MESP minima due to the π-bond become shallow (−0.029 au compared to −0.047 au in the parent), while the CPs due to the cyclopropyl bonds are all virtually eliminated. There are no common negative regions indicative of σ–π interactions (see Fig. 1). These results are consistent with the PE spectrum of **1b**.[9] The first ionization potential, assigned to the π-bond, corresponds to 9.53 eV, fairly close to that of 7-methylenenorbornane.[4a] In the absence of electrostatic bias as well as through-space σ–π interactions in the substrate, the observed face-selectivities must have a different origin.

The activation energies for singlet : CCl_2 addition to substrates **1b**–**d** computed at the AM1 level with a modified version of MOPAC[10] provide further insights. As pointed out earlier,[2a,b] transition state geometries for carbene addition to olefins are unsymmetrical, with one C–C bond being formed to a greater extent. Hence, four sets of transition states were computed for each substrate, with facial approach being *syn* or *anti*, and the initial site of attack being C-9 or C-10.

As expected, no facial preference is computed for the transition states corresponding to initial approach towards the distal carbon (Table 1). However, in the higher energy structures in which the carbene attacks at the C-9 center, the substituents are computed to exert a small face selectivity. Consistent with the experimental data, both cyano and ester groups lead to a *syn* preference. The prediction for the methoxymethyl derivative is ambiguous since the relative activation energies are sensitive to the conformation of the

Table 1 AM1 activation energies for :CCl_2 addition to **1b**–**d**

Site of attack	Activation energy/kcal mol^{-1}							
	1b		**1c**		**1d** (C_s)		**1d** (C_1)	
	syn	*anti*	*syn*	*anti*	*syn*	*anti*	*syn*	*anti*
C-9	13.59	13.90	13.55	13.85	13.61	13.22	13.19	13.48
C-10	7.02	7.02	6.92	6.92	6.56	6.39	6.41	6.52

substituent. These results, especially the absence of selectivity for initial approach at C-10 and *syn* selectivity for approach at C-9 for strongly electron-withdrawing groups, suggest the operation of a relay of hyperconjugative interactions, which makes the *syn* face C–C bonds relatively electron deficient. Stabilization due to interactions between electron-rich C–C bonds and the σ*-orbital of the newly formed bond with the electrophile is greater for *syn* face approach.[11]

In summary, 4-substituted 9-methylenenorsnoutanes show *syn* selectivity in a variety of electrophilic additions. Electrostatic effects and through-space σ-π mixing are both unimportant in these substrates, as confirmed through MESP topographical analyses. The observed selectivities are primarily due to Cieplak-type hyperconjugative interactions[11] in the transition states, whose energetics are fairly correctly reproduced using AM1 calculations.

Notes and References

† E-mail: gmchem@uohyd.ernet.in

1 (*a*) G. Mehta and F. A. Khan, *J. Am. Chem. Soc.*, 1990, **112**, 6140; (*b*) H. Li and W. J. le Noble, *Recl. Trav. Chim. Pays-Bas*, 1992, **111**, 199; (*c*) B. W. Gung, *Tetrahedron*, 1996, **52**, 5263; (*d*) B. Ganguly, J. Chandrasekhar, F. A. Khan and G. Mehta, *J. Org. Chem.*, 1993, **58**, 1734; (*e*) M. N. Paddon-Row, Y.-D. Wu and K. N. Houk, *J. Am. Chem. Soc.*, 1992, **114**, 10 638.

2 (*a*) G. Mehta, G. Gunasekaran, S. R. Gadre, R. N. Shirsat, B. Ganguly and J. Chandrasekhar, *J. Org. Chem.*, 1994, **59**, 1953; (*b*) G. Mehta, F. A. Khan, S. R. Gadre, R. N. Shirsat, B. Ganguly and J. Chandrasekhar, *Angew. Chem., Int. Ed. Engl.*, 1994, **33**, 1390; (*c*) G. Mehta, F. A. Khan, B. Ganguly and J. Chandrasekhar, *J. Chem. Soc., Chem. Commun.*, 1992, 1711; (*d*) G. Mehta, F. A. Khan, N. Mohal, I. N. N. Namboothiri, P. Kalyanaraman and J. Chandrasekhar, *J. Chem. Soc., Perkin Trans. 1*, 1996, 2665.

3 M. Tsuji, T. Ohwada and K. Shudo, *Tetrahedron Lett.*, 1997, **38**, 6693. See also: R. W. Hoffmann, N. Hauel and B. Landmann, *Chem. Ber.*, 1983, **116**, 389.

4 (*a*) H. D. Martin, C. Heller, R. Haider, R. W. Hoffmann, J. Becherer and H. R. Kurz, *Chem. Ber.*, 1977, **110**, 3010; (*b*) R. W. Hoffmann, H. R. Kurz, J. Becherer and H. D. Martin, *Chem. Ber.*, 1978, **111**, 1275; (*c*) P. Bruckmann and M. Klessinger, *Angew. Chem., Int. Ed. Engl.*, 1972, **11**, 524.

5 G. Mehta, C. Ravikrishna, B. Ganguly and J. Chandrasekhar, *Chem. Commun.*, 1997, 75.

6 R. N. Shrisat, A. C. Limaye and S. R. Gadre, *J. Comput. Chem.*, 1993, **14**, 445. The MESP plots were generated using the program SPARTAN, Version 4.0, Wavefunction Inc., Irvine, CA, USA at the HF/6-31G(d)//HF/3-21G level.

7 S. R. Gadre and S. S. Pundlik, *J. Am. Chem. Soc.*, 1995, **117**, 9559.

8 R. F. W. Bader, *Atoms in Molecules, a Quantum Theory*, Clarendon, Oxford, 1990.

9 We thank Professor R. Gleiter for the PE Spectrum of **1b**.

10 J. J. P. Stewart, *J. Comput.-Aided Mol. Des.*, 1990, **4**, 1.

11 A. S. Cieplak, B. D. Tait and C. R. Johnson, *J. Am. Chem. Soc.*, 1989, **111**, 8447.

Received in Cambridge, UK, 5th January 1998; Revised manuscript received, 3rd March 1998; 8/02089B

Synthesis and dioxygenation of [5,10,15,20-tetrakis(α,α,α,α-*o*-pivaloyloxynaphthyl)porphinato]iron(II) with a covalently bound imidazolylalkyl group

Teruyuki Komatsu, Kaoru Sano and Eishun Tsuchida*†‡

Department of Polymer Chemistry, Advanced Research Institute for Science and Engineering, Waseda University, Tokyo 169-8555, Japan

Intramolecular *N*-imidazole coordinated [5,10,15,20-tetrakis(α,α,α,α-*o*-pivaloyloxynaphthyl)porphinato]iron(II) forms a stable dioxygen adduct in toluene at 25 °C; the sterically regulated coordination of the axial base leads to the low electron donation from the central iron to the bound O_2.

Synthetic tetraphenylporphinatoiron (FeTPP) derivatives have been extensively used for the study of hemoprotein analogs, because of their stability and advantage of covalent modification.[1] In particular, the design of both-faces encumbered models has been a topic of great interest for the preparation of stable O_2 carrying hemes.[2–5] The double-sided hindered porphyrins have actually prevented the undesired μ-oxo dimer formation. Symmetric 2,6-disubstituted TPPs are useful precursors, but the total synthetic yields to construct different structures on each side of the porphyrin plane are rather low.[6,7] In order to simply provide a second cavity under the porphyrin macrocycle, we have introduced *o*-substituted α-naphthyl groups to the four *meso*-positions. Non-substituted (tetranaphthylporphinato)iron(II) or (tetraanthracenylporphinato)iron(II) itself, however, cannot form a stable O_2 adduct at ambient temperature.[8,9] Basolo and coworkers only reported the dioxygenation of the single-face capped (naphthylporphinato)iron(II) at 0 °C.[10] Herein, we report for the first time, the synthesis, characterization and reversible O_2 coordination of [tetrakis(α,α,α,α-*o*-substituted-naphthyl)porphinato]iron(II) with covalently bound imidazolylalkyl chains at 25 °C.

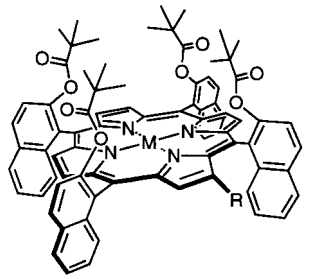

The precursor porphyrin, tetrakis(β-naphthol)porphine, was prepared by Lindsey's procedure from pyrrole and 2-methoxy-1-naphthaldehyde followed by removal of the methyl groups with BBr_3.[11,12] The α,α,α,α-isomer separated by column chromatography was condensed with pivaloyl chloride in THF at 65 °C, giving 5,10,15,20-tetrakis(α,α,α,α-*o*-pivaloyloxynaphthyl)porphine **1a** (71%). Introduction of imidazolylalkyl chains to the β-pyrrolic position of the porphyrin was performed according to our previously reported procedure with 8-imidazolyl-1-yl-octanoic acid.[13] For initial formylation, the copper(II) complex **1b** gave a high yield in the Vilsmeir reaction (97%). The obtained 2-formyl–**1b** was, however, rapidly decomposed in H_2SO_4/CH_2Cl_2, which is a typical copper removal condition. All attempts for demetallation of the 2-formyl-**1b** failed. These are in sharp contrast to the 2-formyl–[tetrakis(pivalamidophenyl)porphinato]copper(II) result.[13] Fortunately, we found that the direct Vilsmeir reaction with free base **1a** yielded 2-formyl–**1a** in 21% yield. Iron insertion was carried out using $FeBr_2$ in dry THF affording **2c′**, which is now available in gram quantities. The analytical data of all compounds described above were satisfactory obtained.

2c′ was converted to the iron(II) complex **2c** by reduction in a heterogeneous two-phase system (toluene/aqueous $Na_2S_2O_4$) under an N_2 atmosphere.[7] The UV–VIS absorption spectrum of the orange solution showed five-N-coordinated iron(II) species (λ_{max} = 439, 541, 562 nm, Fig. 1), which was constant in the range of 10 μmol dm^{-3}–3 mmol dm^{-3} at 10–70 °C. The paramagnetic S = 2 state of **2c** was evidenced by the β-pyrrolic proton signals at δ 46.8–59.4 downfield to TMS (25 °C).[14] No peaks were seen between δ −5 and −15, showing that a square planar iron(II) porphyrin (S = 1) did not exist. Consequently, we can conclude that **2c** is a five-coordinated complex *via* intramolecular imidazole binding under an N_2 atmosphere.

When O_2 or CO binds to **2c**, the resulting complexes are diamagnetic and the ^{1}H NMR spectra represented characteristics of S = 0. Its UV–VIS absorption also changed to those of the O_2 or CO adduct immediately upon exposure to O_2 or CO (Fig. 1). The dioxygenation was kinetically sufficiently stable and reversible at 25 °C depending on the O_2 partial pressure. Oxidation to iron(III) porphyrin, however, took place slowly (half-life ≈ 22 h at 25 °C). The final product was the Fe^{III}(OH)

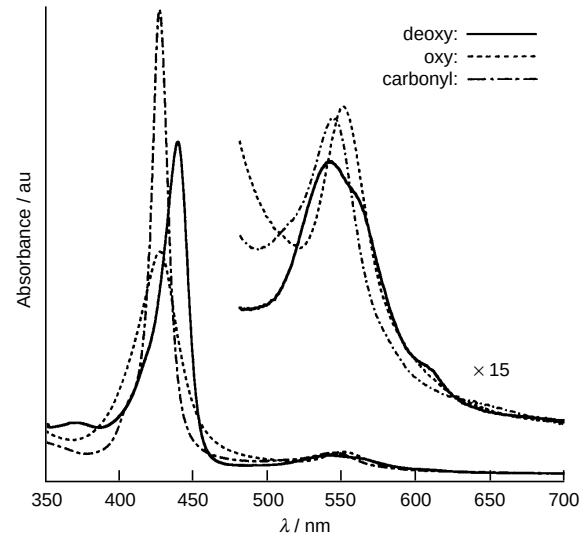

Fig. 1 Visible absorption spectral changes of **2c** in toluene at 25 °C

Table 1 O_2 and CO binding parameters for **2c** in toluene at 25 °C

	O_2			CO	
	$P_{1/2}$/ Torr	$10^{-7}k_{on}$/ dm^3 mol^{-1} s^{-1}	$10^{-3}k_{off}$/ s^{-1}	$10^4P_{1/2}$/ Torr	$10^{-6}k_{on}$/ dm^3 mol^{-1} s^{-1}
2c	18	2.4	5.0	1.5	3.3
Fe^{II}(TpivPPIm)[a]	0.29	64	1.4	—	31

[a] Ref. 13.

complex with λ_{max} at 420 and 567 nm.[15] The α-naphthalene rings obviously prevent μ-oxo porphyrin dimer formation. The rates of oxidation are strongly sensitive to water content, which is present in organic solvents when the two-phase preparation is used. From the results of the molecular simulation, the total energy of the **2c** μ-oxo-dimer was also extremely high and unlikely to be produced.

The O_2 and CO binding affinities [$P_{1/2}(O_2)$, $P_{1/2}$(CO)] were determined based on the UV–VIS absorption spectral changes (Table 1). The $P_{1/2}(O_2)$ value was 18 Torr at 25 °C, which is 60 times larger than that of [2-imidazolyloctanoyloxymethyl-5,10,15,20-tetrakis(α,α,α,α-*o*-pivalamidophenyl)porphinato]-iron(II) [Fe^{II}(TpivPPIm), $P_{1/2}(O_2)$ = 0.29 Torr].[13] The thermodynamic parameters of the dioxygenation of **2c** were also measured; $\Delta H°$ = −68 kJ mol^{-1} and $\Delta S°$ = −136 J K^{-1} mol^{-1}. Laser flash photolysis gave the association and dissociation rate constants (k_{on}, k_{off}) of these gaseous molecules.[13,16c,17] We considered that the low O_2 and CO binding affinities are mainly caused by two reasons, (*i*) the sterically regulated imidazole coordination by α-naphthyl groups and (*ii*) the relatively crowded pivaloyloxy cavity around the O_2 binding site. The following results clearly support these assumptions. (*i*) The equilibrium constant for 1,2-dimethylimidazole binding to **1c** (3×10^3 dm^3 mol^{-1}) was sterically hindered and one order of magnitude lower than those of the non-substituted Fe^{II}(TPP) or Fe^{II}(TpivPP).[10,16a] (*ii*) In the IR spectra, the coordinated CO or O_2 to **2c** showed a ν_{CO} at 1976 cm^{-1} ($\Delta\nu_{1/2}$ = 12 cm^{-1}) and a $\nu_{16_{O_2}}$ at 1169 cm^{-1} ($\Delta\nu_{1/2}$ = 11 cm^{-1}); the shifts in the stretching frequencies of $^{16}O_2$ and $^{18}O_2$ adducts (70 cm^{-1}) were in good agreement with Hooke's law. These values are significantly higher than other model hemes.[16b] The differences are probably due to the low π-back donation from the central iron, indicating weak coordination of the *trans* imidazole in **2c**. (*iii*) Kinetically, the low $k_{on}(O_2)$ leads to the low binding affinities of O_2. Based on the earlier important studies,[16c,17] the distal steric hindrance only reduces the association constant for O_2. The pivaloyloxy groups of **2c** are therefore more tilted in comparison to the pivalamide residues of Fe^{II}(TpivPPIm).

The structure of the dioxygenated **2c** complex was then simulated.[18] The dihedral angles of the four α-naphthyl groups with respect to the porphyrin plane are 75–83°, indicating the presence of an apolar space with a depth of *ca*. 4.5 Å under the porphyrin macrocycle. The imidazole coordination to the central iron is definitely oriented to avoid the four bulky naphthalene walls. It is also remarkable that the imidazole plane is unusually tilted from the Fe–N(Im) vector (ψ) with an angle of *ca*. 150°, which can not be seen in the same calculation of any other dioxygenated Fe^{II}(TPP) compounds [*e.g.* Fe^{II}(TpivPPIm)]. We considered that the unique tilting geometry of the imidazole ring may be related to the low electron donation from the central iron to the bound O_2 or CO.

This work was partially supported by the Core Research for Evolutional Science and Technology, JST.

Notes and References

† E-mail: eishun@mn.waseda.ac.jp
‡ CREST investigator, Japan Science and Technology Corporation.

1 For a review, see: for example, M. Momenteau and C. A. Reed, *Chem. Rev.*, 1994, **94**, 659.
2 A. R. Battesrby and A. D. Hamilton, *J. Chem. Soc., Chem. Commun.*, 1980, 117.
3 J. E. Baldwin, J. H. Cameron, M. J. Crossley, I. J. Dagley, S. R. Hall and T. Klose, *J. Chem. Soc., Dalton Trans.*, 1984, 1739.
4 K. S. Suslick and M. M. Fox, *J. Am. Chem. Soc.*, 1983, **105**, 1739.
5 M. M. Momenteau and D. Lavalette, *J. Chem. Soc., Chem. Commun.*, 1982, 341; P. Maillard, C. Schaeffer, C. Huel, J.-M. Lhoste and M. Momenteau, *J. Chem. Soc., Perkin Trans. 1*, 1988, 3285.
6 E. Rose, A. Kossanyi, M. Quelquejeu, M. Soleilhavoup, F. Duwavran, N. Bernard and A. Lecas, *J. Am. Chem. Soc.*, 1996, **118**, 1567.
7 E. Tsuchida, T. Komatsu, K. Arai and H. Nishide, *J. Chem. Soc., Dalton Trans.*, 1993, 2465.
8 J. P. Collman, R. R. Gagne, C. A. Reed, T. R. Halbert, G. Lange and W. T. Robinson, *J. Am. Chem. Soc.*, 1975, **97**, 1427.
9 J.-M. Cense and R.-M. Le Quan, *Tetrahedron Lett.*, 1979, 3725.
10 T. Hashimoto, R. L. Dyer, M. J. Crossley, J. E. Baldwin and F. Basolo, *J. Am. Chem. Soc.*, 1982, **104**, 2101.
11 J. S.Lindsey and R. W. Wagner, *J. Org. Chem.*, 1989, **54**, 828.
12 T. Hayashi, T. Miyahara, N. Hashizume and H. Ogoshi, *J. Am. Chem. Soc.*, 1993, **115**, 2049.
13 E. Tsuchida, T. Komatsu, S. Kumamoto, K. Ando and H. Nishide, *J. Chem. Soc., Perkin Trans. 2*, 1995, 747.
14 J. P. Collman, J. I. Brauman, K. M. Doxsee, T. R. Halbert, E. Bunnenberg, R. E. Linder, G. N. LaMar, J. D. Gaudio, G. Lang and K. Spartalian, *J. Am. Chem. Soc.*, 1980, **102**, 4182.
15 D. Lexa, M. Momenteau, J.-M. Saveant and F. Xu, *Inorg. Chem.*, 1985, **24**, 122.
16 (*a*) J. P. Collman, J. I. Brauman, T. J. Collins, B. L. Iverson, R. B. Pettman, J. L. Sessler and M. A. Walters, *J. Am. Chem. Soc.*, 1983, **105**, 3038; (*b*) J. P. Collman, J. I. Brauman, T. R. Halbert and K. S. Suslick, *Proc. Natl. Acad. Sci. USA*, 1976, **73**, 3333; (*c*) J. P. Collman, J. I. Brauman, B. L. Iverson, J. L. Sessler, R. M. Morris and Q. H. Gibson, *J. Am. Chem. Soc.*, 1983, **105**, 3052.
17 T. G. Traylor, S. Tsuchiya, D. Campbell, M. Mitchell, D. Stynes and N. Koga, *J. Am. Chem. Soc.*, 1985, **107**, 604.
18 The esff forcefield simulation was performed using an Insight II system (Molecular Simulations Inc.). The structure was generated by alternative minimizations and annealing dynamic calculations.

Received in Cambridge, UK, 27th January 1998; 8/00724A

Shish kebab-like chirality

Hans Engelkamp,[a] Cornelis F. van Nostrum,[a] Stephen J. Picken[b] and Roeland J. M. Nolte*[a]†

[a] *Department of Organic Chemistry, NSR Center, University of Nijmegen, 6525 ED Nijmegen, The Netherlands*
[b] *Akzo-Nobel Central Research Laboratories, Velperweg 76, 6800 SB Arnhem, The Netherlands*

The phthalocyanine units in a new optically active phthalocyaninatopolysiloxane are arranged in a rigid helical structure, providing a new kind of main-chain chirality in polymers.

In an earlier paper, we reported on the structure and properties of a chiral phthalocyanine with branched aliphatic tails derived from (*S*)-citronellol **1a**. This compound was shown to form a novel chiral columnar mesophase at room temperature, and an achiral D_r mesophase at elevated temperatures.[1] The helical structure that was proposed for the chiral mesophase is shown in Fig. 1(*c*). It represents one of the three possible arrangements of the phthalocyanine rings. In the first, these rings are arranged in a 'spiral staircase-like' manner [Fig. 1(*a*)]. In the second [Fig. 1(*b*)], the rings are positioned on top of each other, but the staggering angle between neighbouring phthalocyanines is nearly constant and always in the same direction. In the third, the normal of the plane of each phthalocyanine ring is tilted and gradually rotating along the stacking axis. The latter case was more fully in agreement with our X-ray diffraction and circular dichroism results. We denoted this new mesophase by D_h*. The second arrangement, however, could not be completely ruled out. To resolve this problem we recently synthesised a phthalocyaninatopolysiloxane **2a** with the same chiral side chains as **1a**. We present evidence here that in this polymer the phthalocyanine rings are arranged as depicted in Fig. 1(*b*), which confirms that in the mesophase of **1a** the rings have the previously proposed arrangement [Fig. 1(*c*)]. To the best of our knowledge, polymer **2a** is the first example of an optically active phthalocyaninatopolysiloxane. It displays what we would like to call 'Shish kebab-like chirality'[2] which is a new type of main chain chirality in polymers.

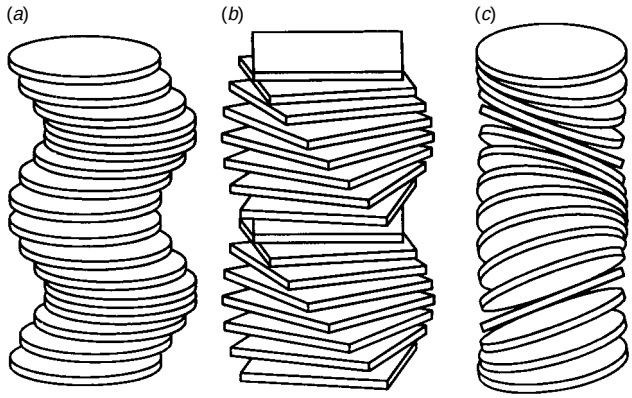

Fig. 1 Schematic representation of three possible helical arrangements of phthalocyanine molecules. The phthalocyanine rings are represented as discs in (*a*) and (*c*) and as squares in (*b*) to show more clearly the helical packing arrangement of the building blocks.

Dihydroxy(phthalocyaninato)silicon **1b** was synthesised following procedures previously developed for other octaalkoxyphthalocyanines.[3] This monomer was polymerised by heating *in vacuo* at 200 °C to give polymer **2a** as a dark blue solid, which was soluble in organic solvents.‡ From the exciton shift of the Q-band, from 680 nm in monomer **1b** to 550 nm in the polymer, the degree of polymerisation (DP) was roughly estimated to be 27.[4] In order to increase the molecular weight of polymer **2a**, we tried to polymerise dimers of the type HO(SiPC)O(SiPC)OH which were synthesised and purified separately. This method has been successfully used by Wegner to prepare high molecular weight phthalocyaninatopolysiloxanes.[3b] We were not able, however, to increase the molecular weight of **2a** by this procedure. We believe that the bulkiness of the aliphatic tails is the reason for this behaviour. In order to be able to compare the optical properties of **2a** with those of a reference compound we synthesised dimer **2b** from hydroxy(methyl)phthalocyaninatosilicon **1c**, which was prepared in an analogous manner to **1b**.‡

The circular dichroism and electronic absorption spectra of **1a**, **1b**, **2a** and **2b** in $CHCl_3$ are presented in Fig. 2. As can be seen, monomer **1b** [Fig. 2(*d*)] does not display any CD effect,

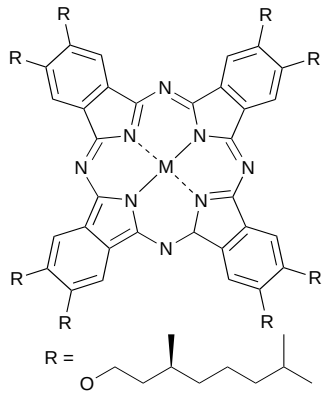

1a M = 2H
b M = $Si(OH)_2$
c M = Si(Me)OH

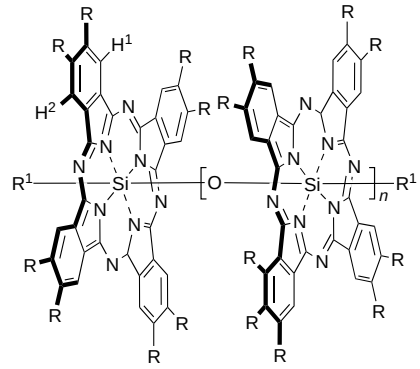

2a R^1 = OH, $n \approx 26$
b R^1 = Me, n = 1

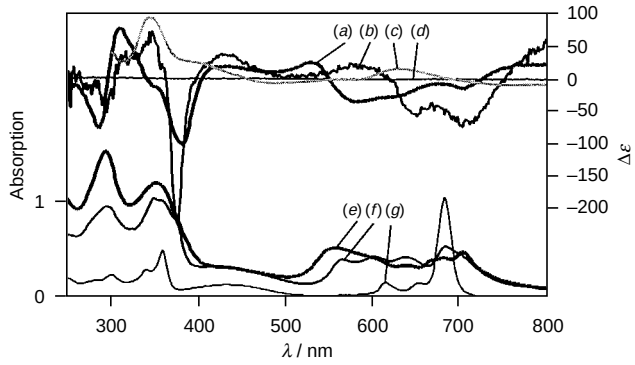

Fig. 2 Circular dichroism spectra of (*a*) **2a**, (*b*) **2b**, (*c*) **1a** and (*d*) **1b**, and electronic absorption spectra of (*e*) **2a**, (*f*) **2b** and (*g*) **1b**. All spectra are in $CHCl_3$ (10 μM) except for the mesophase of **1a**. In the latter case, the spectrum is of a film of 20 bilayers on a quartz plate; the scale is arbitrary.

indicating that its tails do not have a chiral influence on the electronic transitions of the aromatic core of this compound. The polymer **2a** [Fig. 2(*a*)] however, is strongly CD active. The negative couplet at 550 nm corresponds to the Q-band of the polymerised species, suggesting that its phthalocyanine rings are arranged in a left-handed helix.[5] This helicity is caused by the chiral side chains. Again, one could propose for the helical structure the three arrangements that are shown in Fig. 1. However, the silicon–silicon distance in phthalocyaninato-polysiloxanes is 3.3 Å (*vide infra*),[3] which is too short for the structures in Fig. 1(*a*) and 1(*c*) to be formed. This leaves only the structure of Fig. 1(*b*) as the possible helical arrangement for polymer **2a**. In the spectrum of **2a** recorded in dodecane at 120 °C (not shown), the intensity of the CD effect was only slightly decreased (by about 25%) suggesting that even at high temperatures the helical structure of **2a** is retained. The CD spectrum of dimer **2b** [Fig. 2(*b*)] shows the same features as that of polymer **2a**, but the couplet corresponding to the Q-band in the dimer is red-shifted with respect to the polymer. In the ^{1}H NMR spectrum of dimer **2b**, two resonances were present for the phthalocyanine protons (shown as H^1 and H^2 in the structure of **2**, confirming the asymmetry of the molecule. Increasing the temperature caused broadening of these resonances, but no coalescence could be observed below 120 °C. This result shows that the structure is very rigid. The CD spectrum of the mesophase of **1a** is also presented in Fig. 2(*c*). This spectrum is completely different from that of the polymer, eliminating the structure in Fig. 1(*b*) and therefore confirming the previous structural model for this mesophase [Fig. 1(*c*)]. If the polymer and the columnar mesophase had the same helical arrangement of molecular units, the CD spectra should be similar. The spectrum of an LB multilayer of **2a** (not shown) was very similar to the solution spectrum, which implies that effects due to orientational order or intercolumnar effects cannot explain the differences between the spectra of **1a** and **2a**.

X-Ray diffraction experiments were carried out, but did not provide any information about the periodicity or the pitch of the helix in **2a**. This negative result may be due to the rather low degree of polymerisation of **2a**. For such a pitch to be visible by X-ray, it should persist over extended length, *i.e.* several helical turns. This is easily accomplished in a liquid crystalline phase, *e.g.* in that of **1a**,[1] but probably not in a polymer with a degree of polymerisation of 25–30. In the X-ray diffraction pattern, the reflection corresponding to the intracolumnar Pc–Pc spacing was rather broad, probably as a result of the limited degree of polymerisation. A value of 3.3 Å could be calculated, which is in line with literature values.[3]

In summary, we have provided evidence that the stacked phthalocyanine molecules in the mesophase of **1a** and in polymer **2a** have a different helical arrangement. Current studies are aimed at the use of polymers of type **2a** as nonlinear optical materials and as optical switches.

Notes and References

† E-mail: tijdink@sci.kun.nl

‡ Polymer **2a** was synthesised starting from (*S*,*S*)-1,2-dicyano-4,5-bis(3,7-dimethyloctoxy)benzene (ref. 1). The latter compound was converted quantitatively into the diiminoisoindoline derivative with NH_3 and NaOMe in MeOH [ref. 3(*a*)]. After subsequent reaction with $SiCl_4$ in quinoline at 190 °C, followed by hydrolysis with water, a dark green crude product was formed. After repeated precipitation in MeOH and acetone, the dihydroxy-(phthalocyaninato)silicon **1b** was obtained (40%), which was polymerised *in vacuo* at 200 °C to give the violet–blue polymer **2a**. *Selected data* for **1b**: δ_H($CDCl_3$, 300 MHz) 0.7–2.8 (br, 152 H, aliph. H), 3.8–5.0 (m, 16 H, OCH_2), 6.5–9.0 (br, 8 H, ArH) ($C_{112}H_{176}N_8O_9Si$): Found (%) (Calc.): C, 74.45 (74.46). H, 9.86 (9.82); N, 6.16 (6.20).

Dimer **2b** was synthesised from hydroxy(methyl)phthalocyaninatosilicon **1c**, which was synthesised in a similar manner to **1b** using $MeSiCl_3$ instead of $SiCl_4$ as the silylating agent (yield 60%). Dimerisation with TlOTf in pyridine gave **2b** in 75% yield. *Selected data* for **1c**: δ_H($CDCl_3$, 300 MHz) −6.3 (s, 3 H, $SiCH_3$), 0.7–2.5 (m, 152 H, aliph. H), 4.0–4.8 (br, 16 H, OCH_2), 9.0 (s, 8 H, ArH). For **2b**: δ_H($CDCl_3$, 300 MHz) −8.35 (s, 6 H, $SiCH_3$) 0.8–2.5 (m, 304 H, aliph. H), 4.1–4.9 (br, 32 H, OCH_2), 8.26 (s, 8 H, ArH), 8.64 (s, 8 H, ArH).

1 C. F. van Nostrum, A. W. Bosman, G. H. Gelinck, P. G. Schouten, J. H. Warman, A. P. M. Kentgens, M. A. C. Devillers, A. Meijerink, S. J. Picken, U. Sohling, A.-J. Schouten and R. J. M. Nolte, *Chem. Eur. J.*, 1995, **1**, 171.

2 The term 'shish kebab polymer' has been used before in relation to phthalocyaninatopolysiloxanes: U. Drechsler and M. Hanack in *Comprehensive Supramolecular Chemistry, Vol. 9*, ed. J. L. Atwood, J. E. D. Davies, D. D. Macnicol and F. Vogtle, Pergamon, Oxford, 1996, pp. 283–311.

3 (*a*) W. Caseri, T. Sauer and G. Wegner, *Makromol. Chem., Rapid Commun.*, 1988, **9**, 651; (*b*) A. Ferencz, D. Neher, M. Schulze, G. Wegner, L. Viaene and F. C. De Schryver, *Chem. Phys. Lett.*, 1995, **245**, 23.

4 M. Fujiki, H. Tabei and T. Kurihara, *J. Phys. Chem.*, 1988, **92**, 1281.

5 N. Harada and K. Nakanishi, *Circular Dichroic Spectroscopy—Exciton Coupling in Organic Chemistry*, Oxford University Press, Oxford, 1983, pp. 6–9.

Received in Cambridge, UK, 12th February 1998; 8/01246F

Scandium triflate-catalyzed Strecker-type reactions of aldehydes, amines and tributyltin cyanide in both organic and aqueous solutions. Achievement of complete recovery of the tin compounds toward environmentally-friendly chemical processes

Shū Kobayashi,* Tsuyoshi Busujima and Satoshi Nagayama

Department of Applied Chemistry, Faculty of Science, Science University of Tokyo (SUT), and CREST, Japan Science and Technology Corporation (JST), Kagurazaka, Shinjuku-ku, Tokyo 162-0825, Japan

Scandium triflate ($CF_3SO_3^-$)-catalyzed Strecker-type reactions were successfully carried out by simply mixing aldehydes, amines and tributyltin cyanide at room temperature, to afford α-amino nitriles in high yields. The reactions proceeded smoothly in both organic and aqueous solutions, and complete recovery of the tin materials has been achieved.

The Strecker reaction provides one of the most efficient methods for the synthesis of α-amino nitriles, which are useful intermediates in the synthesis of amino acids[1] and nitrogen-containing heterocycles such as thiadiazoles, imidazoles, *etc*.[2] Although classical Strecker reactions have some limitations, use of trimethylsilylcyanide (TMSCN) as a cyano anion source provides promising and safer routes to these compounds.[1b,3] However, TMSCN is easily hydrolyzed in the presence of water, and it is necessary to perform the reactions under strict anhydrous conditions. In the course of our program to develop new synthetic reactions in aqueous media,[4] we have focused on tributyltin cyanide (Bu_3SnCN).[5] Bu_3SnCN is stable in water and a potential cyanate source, albeit there have been no reports of Strecker-type reactons using Bu_3SnCN to the best of our knowledge. Here we report scandium triflate ($CF_3SO_3^-$)-catalyzed Strecker-type reactions of aldehydes, amines and Bu_3SnCN in both organic and aqueous solutions. Complete recovery of the toxic tin compounds is also described.

We chose valeraldehyde, diphenylmethylamine and Bu_3SnCN as models, and the Strecker-type reaction was first performed in the presence of 10 mol% of $Sc(OTf)_3$ in organic solvents. The reactions proceeded smoothly at room temperature in acetonitrile, benzene, dichloromethane and toluene to afford the corresponding α-amino nitrile in high yields. Among these solvents tested, acetonitrile–toluene (1 : 1) gave the best yield (84%). It was found that no dehydration reagents such as molecular sieves, $MgSO_4$, drierite, *etc.* were needed in these reactions. We then performed the reaction in water. It was found that the model Strecker-type reaction also proceeded smoothly in the presence of a catalytic amount of $Sc(OTf)_3$‡ to give the corresponding α-amino nitrile in a 94% yield. No surfactant was needed in this reaction.[4a–c] The reaction is assumed to proceed *via* imine formation and successive cyanation,§ and it is noted that the dehydration process (imine formation) proceeded smoothly in water. Moreover, it was found that the reaction rate in water was almost the same as those in organic solvents.

While the desired reaction proceeded smoothly, it was thought that use of the toxic tin reagent might restrict the application of the reaction.[6] We then tried to recover the tin materials after the reaction (Scheme 1). The Strecker-type reaction was performed using an equimolar amount of an aldehyde and an amine, and a slight excess of Bu_3SnCN. After the reaction was completed, excess Bu_3SnCN was treated with a weak acid to form bis(tributyltin) oxide.[7] On the other hand, the adduct, α-(tributylstannylamino) amino nitrile (**1**), was hydrolyzed by adding water to produce α-amino nitrile **2** and tributyltin hydroxide, which was readily converted to bis(tributyltin) oxide.[7] Thus, all tin sources were converted to bis(tributyltin) oxide, which could be recovered quantitatively (*vide infra*). It has already been reported that bis(tributyltin) oxide can be converted to tributyltin chloride[8] and then to Bu_3SnCN.[5] Since the catalyst, $Sc(OTf)_3$, is also recoverable and reusable,[9] the present Strecker-type reactions represent a completely recyclable system.

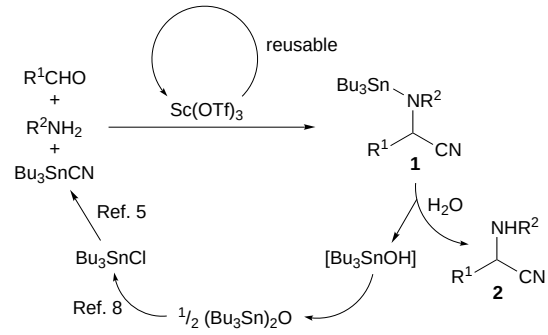

Scheme 1 Recycle system of the novel Strecker-type reactions

Several examples of the Strecker-type reaction are shown in Table 1. In all cases, including aromatic, aliphatic, heterocyclic, as well as α,β-unsaturated aldehydes, the reactions proceeded smoothly to afford the corresponding α-amino nitriles in high yields. While the adducts, α-(*N*-benzhydryl)amino nitriles, were readily converted to α-amino acids,[10] the present Strecker-type reactions using other amines such as aniline and benzylamine also proceeded smoothly to afford the corresponding adducts in high yields.

A typical experimental procedure is as follows. To a solution (3 ml) of aq. $Sc(OTf)_3$ (0.05 mmol, 10 mol%) were added an amine (0.5 mmol), Bu_3SnCN (0.75 mmol) and an aldehyde (0.5

Table 1 $Sc(OTf)_3$-catalyzed Strecker-type reactions

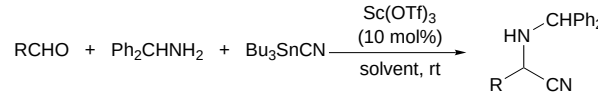

R	Yield (%) [in MeCN–toluene (1 : 1)]	Yield (%) (in H_2O)
Ph	88	88
PhCH=CH	83	84
2-Furyl	88	89
$Ph(CH_2)_2$	94	79
Bu	84	94
c-C_6H_{11}	86	94

mmol) successively, and the mixture was stirred at room temperature. After 20 h, the mixture was diluted with water, and the aqueous layer was extracted with ethyl acetate. $Sc(OTf)_3$ was recovered from the aqueous layer quantitatively and reused.[9] The combined organic layers were dried, filtered, and concentrated. The crude materials were treated with THF–1 M HCl (4 : 1, 3 ml) at room temperature for 1 h. Hexane and aq. saturated $NaHCO_3$ were added and the aqueous layers were extracted with ethyl acetate. The combined organic layers were dried, filtered and concentrated. The adduct was purified by column chromatography on alumina to afford the pure desired α-amino nitrile. Bis(tributyltin) oxide was recovered quantitatively (> 98%) by eluting with MeOH.

In summary, we have developed Strecker-type reactions of aldehydes, amines and Bu_3SnCN using $Sc(OTf)_3$ as a catalyst. The reactions proceeded smoothly in both organic and aqueous solutions to afford α-amino nitriles in high yields. Note that the experimental procedure is very simple; just mixing the three components and $Sc(OTf)_3$ in an appropriate solvent at room temperature. Moreover, complete recovery of the tin materials in these reactions has been achieved. While many useful tin reagents have been developed, their toxicity has sometimes limited their use in organic synthesis. This report provides a solution to this problem, and moves us further toward environmentally-friendly chemical processes.

This work was partially supported by a Grant-in-Aid for Scientific Research from the Ministry of Education, Science, Sports, and Culture, Japan, and an SUT Special Grant for Research Promotion. S. N. thanks the JSPS fellowship for Japanese Junior Scientists.

Notes and References

† E-mail: skobayas@ch.kagu.sut.ac.jp

‡ We found that rare earth triflates are stable Lewis acids in water.[9] Other rare earth triflates are also available in the present Strecker-type reactions.

§ It was confirmed that imine formation was much faster than cyanohydrin ether formation under these reaction conditions.

1 (*a*) A. Strecker, *Ann. Chem. Pharm.*, 1850, **75**, 27; (*b*) Y. M. Shafran, V. A. Bakulev and V. S. Mokrushin, *Russ. Chem. Rev.*, 1989, **58**, 148.
2 L. M. Weinstock, P. Davis, B. Handelsman and R. Tull, *J. Org. Chem.*, 1967, **32**, 2823; W. L. Matier, D. A. Owens, W. T. Comer, D. Deitchman, H. C. Ferguson, R. J. Seidehamel and J. R. Young, *J. Med. Chem.*, 1973, **16**, 901.
3 I. Ojima, S. Inaba and K. Nakatsugawa, *Chem. Lett.*, 1975, 331; K. Mai and G. Patil, *Tetrahedron Lett.*, 1984, **25**, 4583; S. Kobayashi, H. Ishitani and M. Ueno, *Synlett*, 1997, 115.
4 (*a*) S. Kobayashi, T. Wakabayashi, S. Nagayama and H. Oyamada, *Tetrahedron Lett.*, 1997, **38**, 4559; (*b*) S. Kobayashi, T. Wakabayashi and H. Oyamada, *Chem. Lett.*, 1997, 831; (*c*) S. Kobayashi, T. Busujima and S. Nagayama, *Chem. Commun.*, 1998, 19; (*d*) S. Kobayashi, in *Organic Reactions in Water*, ed. P. Grieco, Chapman and Hall, London, 1997.
5 J. G. A. Luijten and G. J. M. van der Kerk, *Investigations in the Field of Organotin Chemistry*, Tin Research Institute, Greenford, 1955, p. 106; M. Tanaka, *Tetrahedron Lett.*, 1980, **21**, 2959; S. Harusawa, R. Yoneda, Y. Omori and T. Kurihara, *Tetrahedron Lett.*, 1987, **28**, 4189.
6 A. G. Davies, *Organotin Chemistry*, VCH, Weinheim, 1997.
7 J. M. Brown, A. C. Chapman, R. Harper, D. J. Mowthorpe, A. G. Davies and P. J. Smith, *J. Chem. Soc., Dalton Trans.*, 1972, 338.
8 A. G. Davies, D. C. Kleinschmidt, P. R. Palan and S. C. Vasishtha, *J. Chem. Soc.* (*C*), 1971, 3972.
9 S. Kobayashi, *Synlett*, 1994, 689; S. Kobayashi, I. Hachiya, M. Araki and H. Ishitani, *Tetrahedron Lett.*, 1993, **34**, 3755.
10 M. S. Iyer, K. M. Gigstad, N. D. Namdev and M. Lipton, *J. Am. Chem. Soc.*, 1996, **118**, 4910.

Received in Cambridge, UK, 20th February 1998; 8/01464G

An unusual by-product from a non-synchronous reaction between ethyl 1,2,4-triazine-3-carboxylate and an enamine

John E. Macor,*[a]† William Kuipers[a] and Rene J. Lachicotte[b]

[a] *Department of Medicinal Chemistry, Astra Arcus USA, PO Box 20890, Rochester, NY 14602, USA*
[b] *Department of Chemistry, University of Rochester, Rochester NA 14627, USA*

The main product from the reaction of ethyl 1,2,4-triazine-3-carboxylate 3 and the pyrrolidine enamine of *N-tert*-butoxycarbonylpiperidone 2 was an azabicyclo[3.2.1]octane 4 which resulted not from a Diels–Alder reaction, but from a series of non-synchronous steps, demonstrating a heretofore unknown reaction pathway for the electron-deficient diene 3 and electron-rich dienophile 2.

Utilization of 1,2,4-triazines as electron-deficient dienes in inverse electron demand Diels–Alder reactions with enamines has found extensive use for the synthesis of substituted pyridine derivatives. The work of Boger,[1] Taylor,[2] Snyder[3] and others have demonstrated the generality and utility of this approach to functionalized pyridines.

In a series of studies,[4] Boger and Panek examined the reaction of ethyl 1,2,4-triazine-3-carboxylate **3**[5] with a variety of enamines, and found those reactions to be relatively low yielding and complicated by uncharacterized side products. However, we desired the tetrahydronaphthyridine **1** (Scheme 1) for a medicinal chemistry study and believed that the inverse electron demand Diels–Alder reaction between **3**[5] and the enamine derived from *N-tert*-butoxycarbonyl-4-piperidone **2** would provide rapid access to the desired heterocycle **1** (Scheme 1). The necessary enamine **2** was directly available from the reaction of pyrrolidine and *N-tert*-butoxycarbonyl-4-piperidone in anhydrous Et_2O in the presence of anhydrous $MgSO_4$, and the 1,2,4-triazine **3** was available from previous studies.[5] Reaction of **2** and **3** in $CHCl_3$ at room temperature provided only a trace (8%) of the desired tetrahydronaphthyridine **1** (Scheme 1).[6] The major component of the reaction mixture (26%) was an unidentified product whose preliminary spectral data suggested the incorporation of both components **2** and **3** from the reaction without the elimination of nitrogen as would be seen in a Diels–Alder adduct. Extensive NMR studies and mass spectral data suggested that the compound was a tetrahydro-1,2,4-triazine fused to an azabicyclo[3.2.1]octane core (**4**, Scheme 1).[7] Crystals were prepared of this compound (ethyl acetate–benzene) of sufficient quality that X-ray diffraction studies could be performed, and this experiment confirmed the structure of the by-product as that depicted by **4** (Fig. 1).[8]

The azabicyclo[3.2.1]octane clearly was not the result of a Diels–Alder reaction. A likely mechanism for its formation is shown in Scheme 1. The electron-rich β-position on enamine **2** attacked the electron-deficient C6 position of 1,2,4-triazine **3** in a vinylogous Michael reaction fashion. The negative charge introduced into the 1,2,4-triazine ring was stabilized by the electron-delocalizing carboxylate located at C3 of the heterocycle. Probably because of this stabilized zwitterionic species **5**, the ammonium moiety that resulted from the vinylogous Michael attack of the enamine underwent a proton transfer reaction which protonated the enolate and reformed the enamine, leading to **6**. The enamine **6** then attacked the proximate imine (Scheme 1) forming intermediate ammonium species **7** which yielded **4** upon hydrolysis.

These results, coupled with evidence from the literature,[4,9,10] suggest that the presence of an electron-delocalizing substituent at C3 of the 1,2,4-triazine can shift the balance of reactivity from a concerted Diels–Alder reaction to a stepwise, non-synchronous reaction which gives rise to the observed by-

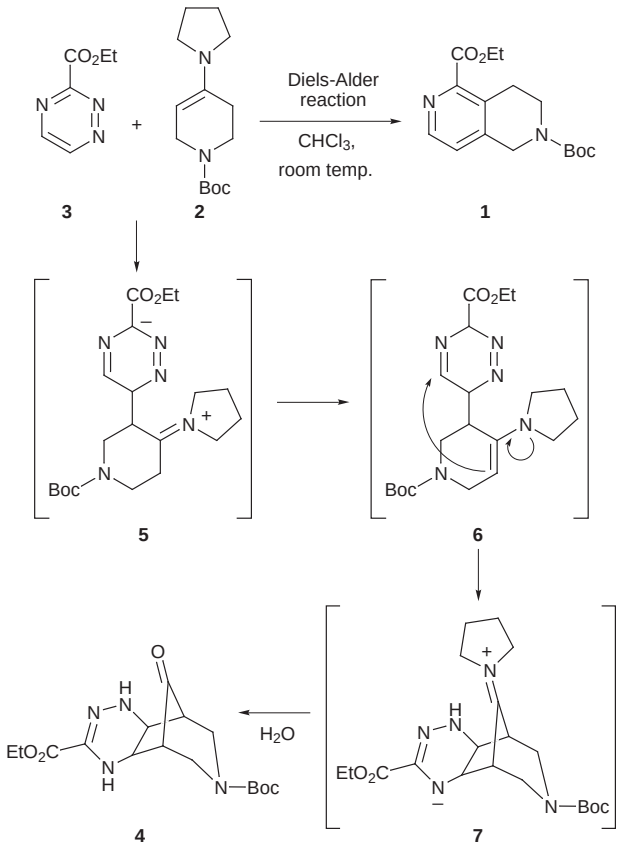

Scheme 1

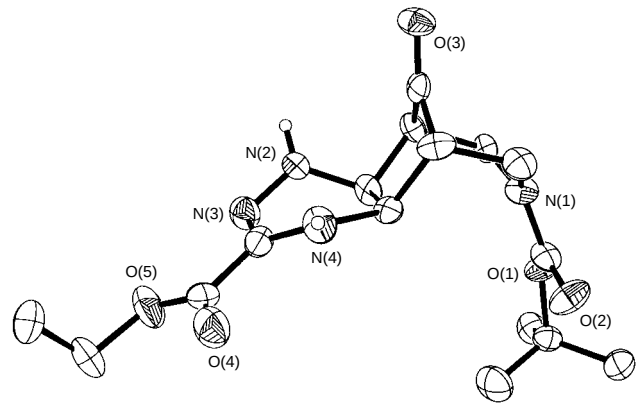

Fig. 1 Crystal structure of **4**

product **4**, especially if the C6 position is unsubstituted. The presence of the ethoxycarbonyl group provided resonance stabilization of the negative charge introduced into the 1,2,4-triazine ring from the attack of the enamine. This and possibly the steric hindrance of the ethoxycarbonyl group discouraged further reaction of C3 of the 1,2,4-triazine with the electrophilic iminium species in **5**, leading to the creation of the second enamine moiety. This newly formed enamine could then react in a relatively unhindered fashion, leading to the 7-azabicyclo[3.2.1]octane moiety found in **4**.

The result of this reaction might have general implications for the reactions of enamines (and other electron-rich dienophiles) with 1,2,4-triazines (or other electron-poor dienes) in attempted inverse electron demand Diels–Alder reactions. Previous examples of enamines reacting with azadienes with electron-delocalizing substituents on *both* carbon atoms involved with the Diels–Alder reaction (*i.e*. diethyl 1,2,4,5-tetrazine-3,6-dicarboxylate[9] and triethyl 1,2,4-triazine-3,5,6-tricarboxylate[4b]) are generally high yielding, suggesting that non-synchronous side reactions are either minimal or nonexistent. For example, triethyl 1,2,4-triazine- 3,5,6-tricarboxylate reacted with the pyrrolidine enamine derived from phenyl *n*-propyl ketone to afford the expected pyridine in 73% yield, whereas ethyl 1,2,4-triazine-3-carboxylate afforded only 10% of its expected pyridine when reacted with the same enamine.[4b] Also, when 3-(dimethoxymethyl)-1,2,4-triazine was used in place of ethyl 1,2,4-triazine-3-carboxylate, the Diels–Alder reactions of the acetal with enamines proceeded in higher yield.[4a] Therefore, it would appear that only in those cases where a resonance delocalizing group exists on one of the carbon atoms involved with the Diels–Alder reaction and the other, *para* carbon atom on the azadiene is unsubstituted, the balance of reactivity may be sufficiently altered to allow for, or favor, non-synchronous reactions such as vinylogous Michael reactions which would limit the amount of Diels–Alder product seen from these reactions. The result of these reactions would be products analogous to **4**. We are presently attempting to examine the generality of this hypothesis, and the implications for inverse electron demand Diels–Alder reactions.

The authors wish to thank Dr Paul Rosenberg for his efforts in establishing the collaboration for X-ray diffraction experiments between Astra Arcus and the University of Rochester.

Notes and References

† E-mail: macor_john.privlms3@msmail.bms.com
‡ *Present address*: Bristol-Myers Squibb Pharmaceutical Research Institute, Mail Stop H12-02, PO Box 4000, Princeton, NJ 08543-4000.

1 D. L. Boger and M. Patel, *Prog. Heterocycl. Chem.*, 1989, **1**, 30 and references cited therein.
2 E. C. Taylor, *Bull. Soc. Chim. Belg.*, 1988, **97**, 599 and references cited therein.
3 S. C. Benson, L. Lee and J. K. Snyder, *Tetrahedron Lett.*, 1996, **37**, 5061 and references cited therein; W.-H. Fan, M. Parikh and J. K. Snyder, *Tetrahedron Lett*., 1995, **36**, 6591 and references cited therein.
4 (*a*) D. L. Boger, J. S. Panek and M. M. Meier, *J. Org. Chem.*, 1982, **47**, 895; (*b*) D. L. Boger and J. S. Panek, *J. Am. Chem. Soc.*, 1985, **107**, 5745.
5 W. Paudler and K. Kraus, *Synthesis*, 1974, 351 and references cited therein.
6 *Selected data* for **1**: δ_H($CDCl_3$, 200 MHz) 8.50 (d, *J* 4.9, 1 H), 7.19 (d, *J* 4.9, 1 H), 4.63 (s, 2 H), 4.46 (q, *J* 7.1, 2 H), 3.66 (br t, *J* 5.9, 2 H), 3.17 (br t, *J* 5.9, 2 H), 1.50 (s, 9 H), 1.44 (t, *J* 7.1, 3 H); *m*/*z* (FAB LRMS) 308 (18%), 307 ([MH]$^+$, 96), 251 (100), 207 (8), 57 (71).
7 *Selected data* for **4**: white solid; mp 187.5–189.5 °C with effervescence; ν_{max}(KBr)/cm^{-1} 3359 (br), 1759, 1701, 1640; δ_H(DMSO, 500 MHz, 340 K) 6.66 (br m, NH), 6.48 (d, *J* 4.0, NH), 4.27 (br dd, *J* 12.7 and 12.9, 2 H), 4.19 (q, *J* 7.0, 2 H), 3.85 (t, *J* 5.0, 1 H), 3.39 (d, *J* 5.6, 1 H), 3.28 (d, *J* 12.7, 1 H), 3.19 (d, *J* 12.9, 1 H), 2.33 (s, 1 H), 2.26 (s, 1 H), 1.43 (s, 9 H), 1.24 (t, *J* 7.0, 3 H); δ_C(DMSO, 500 MHz, 340 K) 215.1, 161.3, 154.1, 137.4, 79.8, 60.7, 53.8, 53.2, 52.6, 52.4, 51.8, 50.3, 28.0, 14.0; *m*/*z* (FAB LRMS) 354 (19%), 353 ([MH]$^+$, 100), 297 (27). Calc. for $C_{16}H_{24}N_4O_5$: C 54.54; H, 6.87; N, 15.90. Found: C, 54.29; H, 6.93; N, 15.73%).
8 Crystals of **4** were grown in a concentrated EtOAc–benzene solution, and benzene was incorporated into the crystalline lattice in a ratio of 1 : 1 with **4**. A small single crystal was mounted on glass fiber under Paratone-8277 and placed on the X-ray diffractometer in a cold N_2ogen stream supplied by a Siemens LT-2A low temperature device. The X-ray intensity data were collected on a standard Siemens SMART CCD Area Detector System equipped with a normal focus molybdenum target X-ray tube operated at 2.0 kW (50 kV, 40 mA). A quadrant of data were collected using a narrow frame method with scan widths of 0.3° in *w*, and an exposure time of 30 s per frame. Frames were integrated to 40° with the Siemens SAINT program yielding a total of 3416 reflections, of which 1832 were independent reflections [*R*(int) = 0.0700]. The unit cell parameters were based upon the least-squares refinement of three dimensional centroids of 857 reflections at −80 °C, giving a monoclinic cell with *a* = 15.038(1), *b* = 13.967(1), *c* = 10.777(1) Å, β = 99.594(4)°, *V* = 2232.0(2) Å^3. The space group was assigned as $P2_1/c$ (*Z* = 4 and D_c = 1.281 g cm^{-3}) on the basis of systematic absences using the XPREP program (Siemens, SHELXTL 5.04). The absorption coefficient was 0.092 mm^{-1}. The structure was solved by direct methods and refined by full-matrix least-squares on F^2. All non-hydrogen atoms were refined with anisotropic thermal parameters, with H atoms included in idealized positions. The empirical formula is $C_{16}H_{24}N_4O_5{\cdot}C_6H_6$ giving a formula weight of 430.50 g mol^{-1}. Final *R* indices [1143 data having $I > 2\sigma(I)$]; R_1 (%) = 7.90 [R_1 = 0.0790; wR_2 = 0.1481]. CCDC 182/810.
9 D. L. Boger, R. S. Coleman, J. S. Panek and D. Yohannes, *J. Org. Chem.*, 1984, **49**, 4405.
10 J. E. Macor, PhD Thesis, Princeton University, 1986, pp. 21–23 and 66–68.

Received in Corvallis, OR, USA, 16th January 1998; 8/00563J

Regioselectivity in nucleophilic ring-opening of aziridinones

Erach R. Talaty*† and Mashitah M. Yusoff

Department of Chemistry, Wichita State University, Wichita, Kansas 67260-0051, USA

The proportions of products derived from competing modes of ring-opening of 1,3-di-*tert*-butylaziridinone and similar aziridinones by a variety of nitrogen, oxygen, sulfur and halogen nucleophiles do not agree with simple guidelines postulated in the literature for these types of aziridinones.

An important aspect of the chemistry of aziridinones is their mode of ring-opening by nucleophiles and the factors that

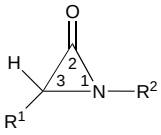

1 $R^1 = R^2 = Bu^t$
2 $R^1 = R^2$ = 1-adamantyl
3 R^1 = 1-adamantyl, $R^2 = Bu^t$
4 $R^1 = Bu^t$, R^2 = 1-adamantyl

govern the outcome. It has been reported[1,2] that ionic, aprotic nucleophiles (Z^-) cause rupture exclusively of the acyl–nitrogen bond (1,2-bond), whereas non-ionic protic nucleophiles (HZ) afford products derived solely or mainly from scission of the alkyl–nitrogen bond (1,3-bond). Our previous publications[3,4] clearly contradict this sample rule, albeit with a limited set of nucleophiles. We have embarked on a broader study of nucleophilic ring-opening of aziridinones.

An examination of the nitrogen nucleophiles (aprotic) in Table 1 reveals immediately that all of them do not cleave solely the alkyl–nitrogen bond of **1** as alleged in the literature.[1,2] In fact, the only ones that exhibit this pattern are all of the aromatic amines (entries 10–17), none of which was used previously in conjunction with aziridinones **1**–**4**. On the other hand, the simple aliphatic primary amines rupture exclusively the acyl–nitrogen bond of **1**. The secondary amines exhibit varying degrees of ring-opening (entries 3 and 5 giving exactly opposite results) that also seem to depend on the nature of the aziridinone (*e.g.* compare entries 2 and 32), indicating a subtle dependence on steric factors. Roughly speaking, stronger, unhindered nitrogen nucleophiles tend to cleave the acyl–nitrogen bond, whereas sterically hindered, weaker ones favor scission of the alkyl–nitrogen bond. However, there are exceptions to even this rough rule (entries 5, 18 and 19). The aprotic oxygen and sulfur nucleophiles also exhibit considerable variation in their selectivity, the alcohols being most consistent in favoring cleavage of the alkyl–nitrogen bond. The protic ionic nucleophiles also do not all afford products derived from acyl–nitrogen cleavage, as suggested in the literature.[1,2] In fact, the sharp difference between bromides and iodides on one hand and alkoxides on the other hand suggests the intervention of yet another factor, namely, hardness or softness of the nucleophile. Iodide, a soft nucleophile, attacks the soft alkyl carbon of **1**, whereas alkoxide, a hard nucleophile, prefers to attack the harder acyl carbon.

A priori, one can envisage the following two schemes that may determine the selectivity in ring-opening of the aziridinones. Scheme 1 resembles the S_N1/S_N2 type dichotomy encountered in nucleophilic aliphatic substitution [path (*a*) being unimolecular and path (*b*) being bimolecular], whereas Scheme 2 (competing bimolecular pathways) was apparently the basis of the guidelines given in the literature.[1,2] If Scheme 1 were to be the exclusive one prevailing, then the selectivity could be altered proportionately by changing the concentration of a nucleophile that tends to give both types of products. In our case, no such alteration or, at best, minor alterations could be effected in some cases that we examined. Scheme 1 would also indicate a strong dependence on nucleophilicity, path (*b*) being favored by powerful nucleophiles. However, as observed above, an excellent nucleophile such as iodide affords just the opposite type of product. It thus appears that, at least in the case of aziridinones **1**–**4**, no one scheme can satisfactorily explain the competing modes of ring-opening by nucleophiles, a conclusion that does not follow from a study of other types of aziridinones.[9]

We have extended the study of nitrogen nucleophiles to include those that might be synthetically useful as a route to larger heterocycles, as illustrated by the three new examples shown in Scheme 3.[10]

Note that (i) these are the only heterocyclic products isolated in each case; (ii) PhNHCN and $PhNH_2$ (mentioned in Table 1) give products derived from opposite modes of cleavage; (iii) specificity in the substitution pattern of these five-membered heterocyclic compounds can be controlled by the method of synthesis; and (iv) the structures of these three heterocyclic compounds could not have been predicted by previous guidelines.

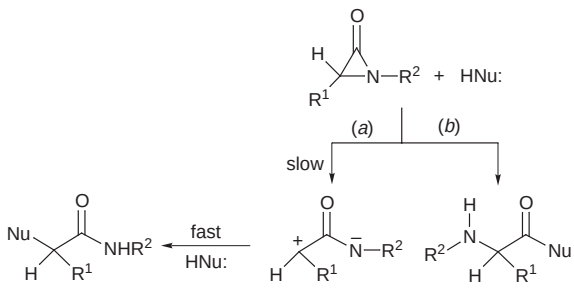

Scheme 1

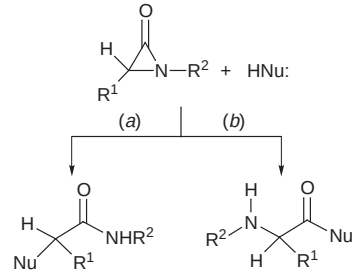

Scheme 2

Table 1 Relative modes of ring opening of aziridinones by various nucleophiles (0.06 mM each) in boiling toluene

					Major product			
						$\delta_H(CDCl_3)$		
Entry	Nucleophile	Aziridinone	Yield[a] (%)	1,2 : 1,3 cleavage (%)	Mp/°C	*C*-Bu^t	*N*-Bu^t	α-CH
1	$PrNH_2$	**1**	88	100 : 0	76–77	0.97	1.04	2.89
2	$BnNH_2$	**1**	92	100 : 0	81.5–82.5	0.97	0.99	2.92
3	Et_2NH	**1**	32	14 : 86	oil	1.02	1.35	2.51
4	Bu_2NH	**1**	54	< 22 : > 78	58–59	1.03	1.35	2.51
5	BnNHMe	**1**	54	86 : 14	oil	0.95	0.99	3.27
6	Pyrrolidine	**1**	65	6 : 94	106–107	1.02	1.33	2.36
7	Morpholine	**1**	48	< 2 : > 98	129–131	1.03	1.37	2.27
8	Piperidine	**1**	52	16 : 84	94–95	1.03	1.36	2.34
9	Piperazine	**1**	42	9 : 91	227	1.02	1.35	2.32
10	$PhNH_2$[b]	**1**	95	0 : 100	172–173	1.09	1.29	3.22
11	*p*-$MeC_6H_4NH_2$	**1**	94	0 : 100	157–157.5	1.08	1.29	3.17
12	*p*-$BrC_6H_4NH_2$	**1**	90	0 : 100	191–192	1.08	1.29	3.18
13	*p*-$MeOC_6H_4NH_2$	**1**	96	0 : 100	146–147	1.09	1.29	3.15
14	1-Aminonaphthalene	**1**	74	0 : 100	105–106	0.98	1.28	2.74
15	4-Aminoazobenzene	**1**	85	0 : 100	212–214	1.12	1.31	3.40
16	4-Aminobiphenyl	**1**	89	0 : 100	229–230	1.11	1.31	3.28
17	Ph_2NH	**1**	12	0 : 100	oil	1.10	1.24	4.23
18	H_2NCN[c]	**1**	94	100 : 0	258 (decomp.)	1.03	1.41	3.54
19	BnNHCN[c]	**1**	65	100 : 0	85–86	0.95	1.26	3.48
20	MeOH	**1**	84	< 7 : > 93	57–58	0.96	1.37	3.08
21	MeONa[d]	**1**	80	100 : 0	oil	0.89	1.00	2.80
22	PhOH	**1**	62	71 : 29	oil	1.04	1.12	3.17
23	Bu^tCH_2OH	**1**	71	5 : 95	oil	0.96	1.36	3.13
24	PhSH	**1**	72	55 : 45	52–53	1.02	1.13	3.20
25	PhSLi	**1**	80	86 : 14	52–53	1.02	1.13	3.20
26	$HSCH_2CO_2Et$	**1**	68	> 93 : < 7	52–53	0.98	1.06	3.12
27	H_2NCSNH_2[e]	**1**	93	55 : 45	258 (decomp.)	1.03	1.41	3.54
28	NaI/acetone	**1**	86	0 : 100	168–169	1.17	1.35	4.05
29	MgI_2 (anhydrous)[f]	**1**	86	0 : 100	168–169	1.17	1.35	4.05
30	$MgBr_2{\cdot}OEt_2$	**1**	87	0 : 100	157–158	1.14	1.36	4.00
31	$Mg(OEt)_2$	**1**	87	100 : 0	oil	0.91	1.01	2.90
32	$BnNH_2$	**3**	89	83 : 17	120–121	—	0.99	2.80
33	Morpholine	**3**	42	8 : 92	171–172	—	1.37	2.05
34	1-Aminonaphthalene	**3**	68	12 : 88	204–205	—	1.26	3.37
35	Morpholine	**2**	40	11 : 89	215–216			
36	1-Aminonaphthalene	**2**	70	7 : 93	121–122			

[a] Combined yield of the two cleavage products after purification. [b] Structure confirmed by using ^{15}N-labelled aniline, which exhibited a doublet (J = 8.05 Hz) at δ 69.22 in its ^{13}C (proton-decoupled) NMR spectrum (Ph^{15}NH*C*HBu^{t}CO). [c] The products are imidazolidinones, obtained by initial acyl–nitrogen cleavage followed by cyclization involving intramolecular nucleophilic attack on the nitrile (ref. 5). [d] See also ref. 6, where reaction was conducted in methanolic solution. [e] The major product is identical with that from entry 18 (net loss of H_2S) (ref. 7). [f] Ref. 8.

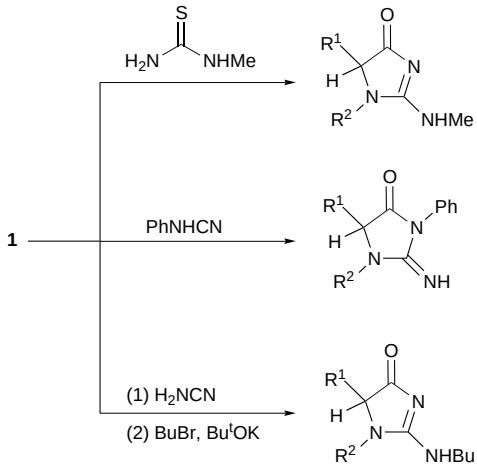

Scheme 3

Notes and References

† E-mail: talaty@twsuvm.uc.twsu.edu

1 I. Lengyel and J. C. Sheehan, *Angew. Chem., Int. Ed. Engl.*, 1968, 25.
2 G. L'abbe, *Angew. Chem., Int. Ed. Engl.*, 1980, 276.
3 E. R. Talaty, A. E. Dupuy, Jr. and C. M. Utermohlen, *J. Chem. Soc., Chem. Commun.*, 1971, 16.
4 M. M. Yusoff and E. R. Talaty, *Tetrahedron Lett.*, 1996, **48**, 8695.
5 E. R. Talaty, M. M. Yusoff, S. A. Ismail, J. A. Gomez, C. E. Keller and J. M. Younger, *Synlett*, 1997, **6**, 683.
6 J. C. Sheehan and J. H. Beeson, *J. Am. Chem. Soc.*, 1967, **89**, 362.
7 E. R. Talaty, J. A. Gomez, J. A. Dillon, E. Palomino, M. O. Agho, B. C. Batt, K. J. Gleason, S. Park, J. R. Hernandez, M. M. Yusoff, G. A. Rupp, F. C. Malone, M. F. Brummett, C. L. Finch, S. A. Ismail, N. Williams and M. Aghakhani, *Synth. Commun.*, 1987, 1063.
8 H. Quast and H. Leybach, *Chem. Ber.*, 1991, **124**, 2105, also studied this reaction.
9 R. V. Hoffman, N. K. Nayyar and W. Chen, *J. Org. Chem.*, 1995, **60**, 4121, have relied exclusively on Scheme 1 to explain products arising from an aziridinone involved as an intermediate (R^1 = Ph or CO_2Et, R^2 = Me) and have correlated products with nucleophilic constants. However, in no case was the aziridinone actually isolated. H. E. Baumgarten, J. F. Fuerholzer, R. D. Clark and R. D. Thompson, *J. Am. Chem. Soc.*, 1963, **85**, 3303; S. Sarel, B. A. Weissman and Y. Stein, *Tetrahedron Lett.*, 1971, 373, studied the reaction of KOBu^t, MeOH or Bu^{t}OH with 1-*tert*-butyl-3-phenylaziridinone and 1-*tert*-butyl-3-bis-norcholanylaziridinone, respectively, the results being in accord with the simple guidelines (refs. 1 and 2).
10 Second and third reactions: work done by S.A. Ismail in our laboratory.

Received in Corvallis, OR, USA, 20th January 1998; 8/00564H

Magnetoresistance in high oxidation state iron oxides

P. D. Battle,*[a]† M. A. Green,[a] J. Lago.[a] A. Mihut,[b] M. J. Rosseinsky,*[a]† L. E. Spring,[a,b] J. Singleton*[b] and J. F. Vente[a]

[a]*Inorganic Chemistry Laboratory, Department of Chemistry, University of Oxford, South Parks Road, Oxford , UK OX1 3QR*
[b]*Clarendon Laboratory, Department of Physics, University of Oxford, Parks Road, Oxford, UK OX1 3PU*

Magnetoresistance is observed in non-ferromagnetic oxides containing Fe^{IV} which have magnetic behaviour characteristic of small magnetic clusters.

Much attention has recently been focused on the observation of colossal magnetoresistance (CMR, *i.e.* almost 100% suppression of the zero-field resistance upon application of a magnetic field) near the coincident Curie and metal–insulator transition temperatures of ferromagnetic manganese oxides.[1] Investigation of oxides of metals other than manganese has shown CMR $\{\Delta\rho/\rho = [\rho(0) - \rho(B)]/\rho(0) < 72\%$ in 10 T$\}$ in ferromagnetic $La_{1-x}Sr_xCoO_3$[2] with a similar mechanism to that of the manganites being invoked, and $\Delta\rho/\rho = 4\%$ in a 7 T field at 150 K in the metallic ferromagnet $SrRuO_3$.[3] $\Delta\rho/\rho = 20\%$ at 6 T in Cr-based chalcogenide spinels has recently been reported.[4] We have been engaged in a search for magnetoresistance in first-row transition metal oxides,[5,6] and report here the first observation of significant magnetoresistance ($\Delta\rho/\rho \leqslant 19\%$ in 12 T at 4.2 K) in iron-based oxides with significant cooperative magnetic interactions but no long-range ferromagnetic order. The systems were chosen as dilute solid solutions between the itinerant helical antiferromagnet $SrFeO_3$, the ferromagnetic metal $SrCoO_3$ and the valence-unstable $CaFeO_3$, which undergoes disproportionation into Fe^{III} and Fe^{V}.[7]

Perovskite oxides of composition $SrFe_{0.9}Co_{0.1}O_3$ and $Sr_{0.9}Ca_{0.1}FeO_3$ were prepared by solid state reaction of the starting oxides plus strontium carbonate in air at 1100 °C followed by annealing under 800 bar O_2 at 400 °C for three days to maximise the metal oxidation states.‡ Rietveld refinement of powder neutron and X-ray (from both laboratory and high resolution synchrotron sources) diffraction data showed that both products were undistorted pure cubic perovskites, with an oxygen content corresponding to a mean cation oxidation state of +IV. This was confirmed by TGA reduction under hydrogen. Magnetic measurements over a range of fields and temperatures indicate the presence of strong and competing exchange interactions, consistent with the strong covalency produced by the high metal oxidation states. The Curie–Weiss law is obeyed above 260 K with moments of 7.9 (Ca) and 9(Co) μ_B, significantly enhanced over the high-spin Fe^{IV} spin-only value of 4.9 μ_B in both cases, in agreement with previous work on $SrFeO_{3.00}$[8] and $SrFe_{0.9}Co_{0.1}O_3$.[9] The Weiss constant was significantly more positive for the Co doped phase (210 K *cf.* 10 K).

History-dependent measurements on $SrFe_{0.9}Co_{0.1}O_3$ at 100 G show a maximum in both field-cooled (FC) and zero-field cooled (ZFC) magnetisations at 85 K (Fig. 1). $M(H)$ is linear at 300 K but becomes sigmoidal in shape (without hysteresis) below 170 K and shows no sign of saturation in a 50 kG measuring field (Fig. 1 inset). These observations are consistent with the existence of cooperative magnetic interactions without long-range magnetic order, resulting in the formation of small magnetic domains often characterised as cluster glass behaviour.[10] Mössbauer spectroscopy has previously suggested that the distribution of Co at low (< 0.2) doping levels in $SrFe_{1-x}Co_xO_3$ is inhomogeneous, with Co-rich regions being ferromagnetic in a non-ferromagnetic matrix.[11,12]

The magnetic behaviour of $Sr_{0.9}Ca_{0.1}FeO_3$ differs. The magnetisation is smaller than that of the Co-doped sample and decreases after a sharp maximum at 120 K. Neutron powder diffraction measurements (Fig. 2 inset) show that this coincides with the onset of antiferromagnetic long-range order with the

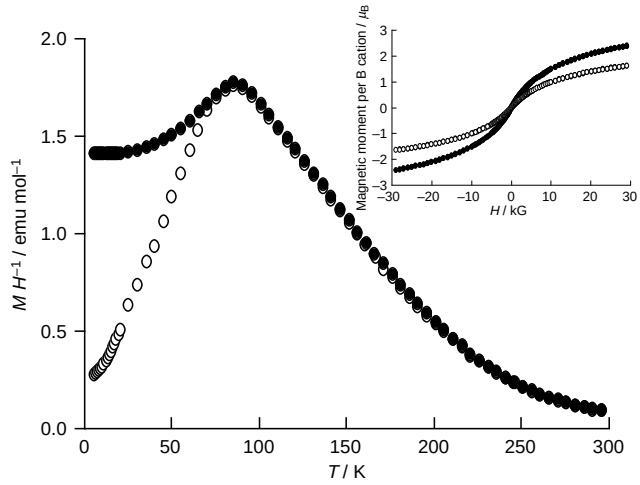

Fig. 1 Temperature dependence of M/H for $SrFe_{0.9}Co_{0.1}O_{3.00}$ in a measuring field of 100 G. Field-cooled (FC) data are shown as filled circles, zero-field-cooled (ZFC) as empty circles. Inset: ZFC $M(H)$ isotherm of $SrFe_{0.9}Co_{0.1}O_{3.00}$ at 45 K (filled circles) and 170 K. The sigmoidal shape indicates the existent of magnetic domains within the sample. $M(H)$ isotherms at different temperatures do not fall on a universal curve when plotted as a function of H/T, indicating the compound is not a classical superparamagnet.

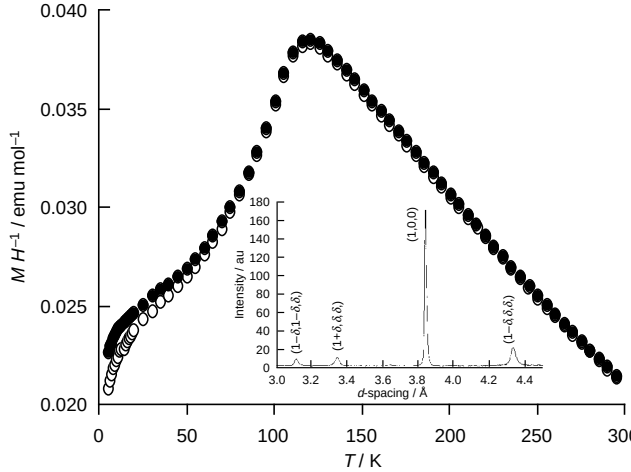

Fig. 2 Temperature dependence of M/H for $Sr_{0.9}Ca_{0.1}FeO_{3.00}$ in a 100 G measuring field. Field-cooled (FC) data are shown as filled circles, zero-field-cooled (ZFC) as empty circles. Inset: incommensurate magnetic Bragg peaks for the helical magnetic structure observed at 5 K (the nuclear (1 0 0) reflection is also shown.)

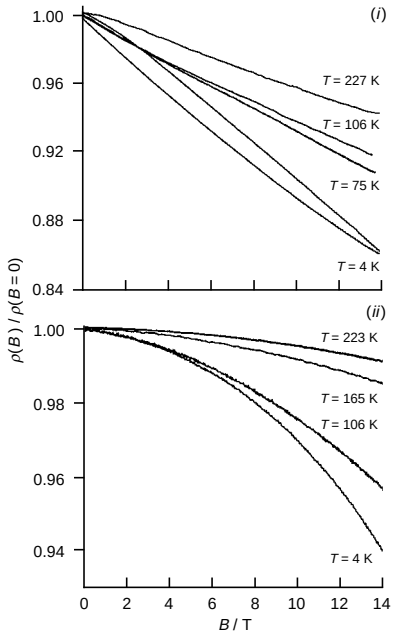

Fig. 3 Magnetoresistance isotherms of (*i*) $SrFe_{0.9}Co_{0.1}O_3$ and (*ii*) $Sr_{0.9}Ca_{0.1}FeO_3$

helical antiferromagnetic structure found for $SrFeO_3$.[13] There is, however, significant divergence between FC and ZFC data below 100 K (Fig. 2) suggesting the development of magnetic disorder at low temperatures. The adoption of a helical magnetic structure by $SrFeO_3$ in preference to one of the collinear structures common amongst perovskites,[14] demonstrates that the competing interactions necessary to cause spin-glass behaviour are present in this system. Furthermore, the presence of a disordered Ca/Sr distribution will introduce an element of randomness into the superexchange interactions; this effect is likely to be relatively large, given the sharp contrast in the properties of $SrFeO_3$ and $CaFeO_3$.

Despite the clear absence of a transition to a three-dimensionally ordered ferromagnetic state in the magnetisation measurements on either compound, significant magnetoresistance is observed for temperatures below 250K (Fig. 3), with values of the conservative figure-of-merit $[\rho(B = 12\ T) - \rho(B = 0)]/\rho(B = 0)$ of 9% at 50 K for $Sr_{0.9}Ca_{0.1}FeO_3$ and 18% at 4 K for $SrFe_{0.9}Co_{0.1}O_3$ (11% at 100 K).

Powder neutron diffraction indicates a smooth structural evolution with temperature. The absence of a localised to itinerant electron transition signalled by ferromagnetism produced by double exchange and of structural features associated with strong Jahn–Teller electron–phonon coupling provides a clear distinction from the behaviour of mixed-valence manganates. The observation of both magnetic behaviour suggestive of ferromagnetically correlated inhomogeneities and magnetoresistance appears to be analogous to the behaviour of the heterogeneous, ferromagnetic Cu–Co and Ag–Co alloys which are some of the best 'giant' magnetoresistance (GMR) materials.[15] In the alloys, the scattering of electrons at the grain boundaries between the ferromagnetic regions embedded in a conducting matrix is strongly reduced by the application of a magnetic field, which reduces the angle between the moments of the magnetic regions and suppresses spin-dependent scattering. The presence of ferromagnetic regions in the Co-doped system, seen by magnetisation isotherms to be present at temperatures where significant magnetoresistance is observed, may indicate that a similar mechanism operates in the present materials.

The magnetisation of both phases reported here suggests the presence of competing interactions and non-equilibrium behaviour due to cluster formation and blocking. The presence of competing ferro- and antiferro-magnetic interactions is a common feature of the two ternary iron oxides presented here, and suggests that this recipe for significant, albeit not colossal, magnetoresistance in oxides deserves further exploration, a suitable starting point being the optimisation of the effect in the current system.

We thank the EPSRC for support including a studentship for L. E. S. and access to station 2.3 at Daresbury Laboratory, where C. C. Tang assisted us, and to the HRPD and IRIS instruments at ISIS. We are particularly indebted to R. M. Ibberson for his assistance at the ISIS facility. J. L. thanks the Basque Government ('Gobierno Vasco-Eusko Jaurlarita') for a studentship and M. J. R. thanks the Royal Society for a grant towards the cost of developing the high pressure oxygen apparatus.

Notes and References

† E-mail: matthew.rosseinsky@chem.ox.ac.uk; peter.battle@chem.ox.ac.uk

‡ The high oxygen pressure was generated by diaphragm compression of 200 bar oxygen using a Fluitron compressor. The reaction mixture was contained in gold foil within an externally heated Rene 41 cold-seal vessel. X-Ray powder diffraction data were recorded using a Siemens D5000 diffractometer (Cu-Kα_1 radiation) in Bragg–Brentano geometry and also on station 2.3 of the Synchrotron Radiation Source, Daresbury Laboratory. Neutron powder diffraction data were recorded for $4 \leqslant T/K \leqslant 300$ on the high resolution diffractometer HRPD and on the long-wavelength IRIS instrument at the ISIS pulsed neutron source, Rutherford Appleton Laboratory. Rietveld refinement was carried out with the GSAS suite of programs. The refined compositions from the neutron data were $SrFe_{0.9}Co_{0.1}O_{3.00(1)}$ [a = 3.846 25(6) Å] and $Sr_{0.9}Ca_{0.1}FeO_{2.99(1)}$ (a = 3.846 21(5) Å], consistent with the observation that the cubic perovskite is only stable for oxygen content $2.97 \leqslant y \leqslant 3.00$[16] and TG estimates of $y = 3.00 \pm 0.05$. Our synthetic method for $SrFeO_3$ gives a = 3.85097(3) Å. Magnetic measurements were made with a Quantum Design MPMS5 SQUID magnetometer. Magnetoresistance measurements were made using standard, low-frequency (31 Hz), four-wire ac techniques in fields of up to 14 T with the current (0.2 mA) perpendicular to the magnetic field.

1 A. P. Ramirez, *J. Phys.: Condens. Matter*, 1997, **9**, 8171.
2 G. Briceno, H. Chang, X. Sun, P. G. Schultz and X.-D. Xiang, *Science*, 1995, **270**, 273.
3 S. C. Gausepohl, M. Lee, K. Char, R. A. Rao and C. B. Eom, *Phys. Rev. B*, 1995, **52**, 3459.
4 A. P. Ramirez, R. J. Cava and J. Krajewski, *Nature*, 1997, **386**, 156.
5 P. D. Battle, S. J. Blundell, M. A. Green, W. Hayes, M. Honold, A. K. Klehe, N. S. Laskey, J. E. Millburn, L. Murphy, M. J. Rosseinsky, N. A. Samarin, J. Singleton, N. E. Sluchanko, S. P. Sullivan and J. F. Vente, *J. Phys. Condens. Matter*, 1996, **8**, L427.
6 P. D. Battle, M. A. Green, N. S. Laskey, J. E. Millburn, M. J. Rosseinsky, S. P. Sullivan and J. F. Vente, *Chem. Commun.*, 1996, 767.
7 T. Takeda, S. Naka, M. Takano, T. Shinjo, T. Takada and M. Shimada, *Mater. Res. Bull.*, 1978, **13**, 61.
8 J. B. MacChesney, R. C. Sherwood and J. F. Potter, *J. Chem. Phys.*, 1965, **43**, 1907.
9 S. Kawasaki, M. Takano and Y. Takeda, *J. Solid State Chem.*, 1996, **121**, 174.
10 K. Eftimova, R. Laiho, K. G. Lisunov and E. Lahderanta, *J. Magn. Magn. Mater.*, 1996, **154**, 193.
11 T. Takeda, T. Watanabe and S. Komura, *J. Phys. Soc. Jpn.*, 1987, **56**, 336.
12 T. Takeda, T. Watanabe, S. Komura and H. Fuji, *J. Phys. Soc. Jpn.*, 1987, **56**, 731.
13 T. Takeda, Y. Yamaguchi and H. Watanabe, *J. Phys. Soc. Jpn*, 1972, **33**, 967.
14 E. O. Wollan and W. C. Koehler, *Phys. Rev.*, 1955, **100**, 545.
15 A. E. Berkowitz, J. R. Mitchell, M. J. Carey, A. P. Young, D. Rao, A. Starr, S. Zhang, F. E. Spada, F. T. Parker, A. Hutten and G. Thomas, *J. Appl. Phys.*, 1993, **73**, 5320.
16 Y. Takeda, K.Kanno, T. Takada, O. Yamamoto, M. Takano, N. Nakayama and Y. Bando, *J. Solid State Chem.*, 1986, **63**, 237.

Received in Cambridge, UK, 12th February 1998; 8/01220B

Manganese(IV) oxamato-catalyzed oxidation of secondary alcohols to ketones by dioxygen and pivalaldehyde

Rafael Ruiz,[a] Ally Aukauloo,[a] Yves Journaux,*[a]† Isabel Fernández,[b] José R. Pedro,*[b] Antonio L. Roselló,[b] Beatriz Cervera,[c] Isabel Castro[c] and M. Carmen Muñoz[d]

[a] *Laboratoire de Chimie Inorganique, URA 420, CNRS, Université de Paris-Sud, 91405 Orsay, France*
[b] *Departament de Química Orgànica, Facultat de Química, Universitat de València, 46100 Burjassot, València, Spain*
[c] *Departament de Química Inorgànica, Facultat de Química, Universitat de València, 46100 Burjassot, València, Spain*
[d] *Departamento de Física Aplicada, Universidad Politécnica de València, 46071 València, Spain*

A new manganese(IV) oxamato complex possessing a bis(μ-oxo)dimanganese core has been synthesized, magnetically and structurally characterized, and found to catalyze the aerobic oxidation of secondary alcohols to ketones with co-oxidation of pivalaldehyde to pivalic acid with good yields and high selectivities.

Interest in high valent manganese coordination chemistry stems largely from the fundamental role that manganese ion in relatively high oxidation states plays in biological dioxygen activation.[1] Manganese interacts with dioxygen and its reduced derivatives in a variety of enzymes from mononuclear (manganese superoxide dismutase) and dinuclear (manganese catalase or manganese ribonucleotide reductase) to tetranuclear (water-oxidizing complex in photosystem II), making use of the Mn^{II}, Mn^{III}, Mn^{IV} and, probably, Mn^{V} oxidation states. Once it was recognized that the active site in catalase and the water-oxidizing complex contains oxo-bridged dimanganese cores, considerable effort was devoted to obtaining dimeric manganese complexes which could be structural as well as functional models for this class of metalloproteins.[2] During the last two decades several bis(μ-oxo)dimanganese complexes with different ligand types have been reported, but comparatively scarce are the studies concerning their reactivities and, particularly, their use as oxidation catalysts.[3,4] In fact, the manganese complex in the water-oxidizing center also exhibits oxidation chemistry in its lower oxidation states.[5] Here we report the synthesis and physical characterization,‡ and the crystal and molecular structure§ of the manganese complex $[PPh_4]_4[Mn(opba)(O)]_2\cdot 4H_2O$ **1**, where opba = *o*-phenylenebis(oxamato) ligand, as well as a preliminary investigation of its catalytic oxidation properties with dioxygen.

The structure of **1** consists of centrosymmetric bis(μ-oxo)dimanganese(IV) complex anions, $[Mn_2(opba)_2(O)_2]^{4-}$ (Fig. 1), tetraphenylphosphonium cations and crystallization water molecules. The two crystallographically equivalent manganese atoms adopt a distorted octahedral geometry formed by two amide nitrogen and two carboxylate oxygen atoms from two symmetric related opba ligands (I = $-x$, $-y$, $-z$), each donating one of its NO donor set from oxamato to each of the manganese atom at *cis* sites; the coordination sphere of the manganese atoms being completed by two oxygen atoms from the two *cis*-bridging oxo groups. The short Mn–O(1) and Mn–O(1^{I}) bonds of 1.799(4) and 1.797(4) Å, respectively, and the acute O(1)–Mn–O(1^{I}) angle of 85.9(2)°, are entirely consistent with a di(μ-oxo)-bridged manganese(IV) complex.[2b] Within the planar Mn_2O_2 rhomb, the Mn···Mn^{I} and O···O distances are equal to 2.631(2) and 2.453(3) Å, respectively. The most interesting structural feature of **1** is, however, the bis-bidentate dinucleating coordination mode of the opba ligand. In fact, the oxamato groups of each opba ligand clamp the two manganese atoms, which are in turn tethered by the phenylene backbone between the amide nitrogen donor set. The phenylene linker forces a twist of the N(1)–C(5) and N(2)–C(10) bonds by 125.1(5) and 127.0(5)°, respectively, resulting in a dihedral angle between the mean planes of the oxamato groups of the opba ligand of 71.7(2)°. This distortion is also reflected in the Mn–N(amide) bond distances [1.986(5) and 2.006(5) Å] which are slightly longer than the Mn–O(carboxylate) ones [1.970(4) and 1.965(4) Å]. This unprecedent situation contrasts with that found for the related mononuclear manganese(III) complex with the 4,5-dichloro-opba derivative where the Mn–N(amide) and Mn–O(carboxylate) bond distances average 1.95 and 1.98 Å, respectively.[6] Within this complex the oxamato ligand adopts an almost planar configuration, and the coordination scheme is the familiar tetradentate N_2O_2 one with the ligand occupying the equatorial plane about the manganese atom (*trans* isomer).

We have investigated the capability of this novel dinuclear manganese(IV) complex towards oxidative catalytic transformations of various organic substrates by the combined use of dioxygen and an aldehyde as oxidant.[7] The results obtained for some representative primary and secondary alcohols, both aromatic and aliphatics, are detailed in Table 1. Complex **1** selectively catalyzes the oxidation of 1-phenylethanol to the corresponding ketone, acetophenone, by dioxygen plus pivalaldehyde in dichloromethane solution with good yields, *i.e.*

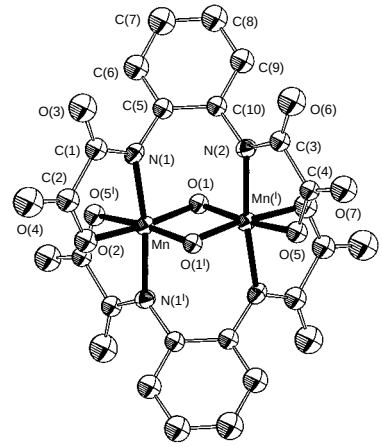

Fig. 1 Perspective view of the anionic dinuclear unit of **1** with the atom-numbering scheme (thermal ellipsoids are at the 30% probability level and hydrogen atoms have been omitted for clarity). Selected bond distances (Å) and angles (°) with standard deviations in parentheses: Mn–O(1) 1.799(4), Mn–O(1^{I}) 1.797(4), Mn–O(2) 1.970(4), Mn–O(5^{I}) 1.965(4), Mn–N(1) 1.986(5), Mn–N(2^{I}) 2.006(5), Mn–Mn^{I} 2.631(2); O(1)–Mn–O(1^{I}) 85.9(2), O(1)–Mn–O(2) 173.0(2), O(1)–Mn–O(5^{I}) 93.6(2), O(1)–Mn–N(1) 91.1(2), O(1)–Mn–N(2^{I}) 94.9(2), O(1^{I})–Mn–O(2) 93.8(2), O(1^{I})–Mn–O(5^{I}) 172.8(2), O(1^{I})–Mn–N(1) 94.5(2), O(1^{I})–Mn–N(2^{I}) 91.1(2), O(2)–Mn–O(5^{I}) 87.6(2), O(2)–Mn–N(1) 81.9(2), O(2)–Mn–N(2^{I}) 92.2(2), O(5^{I})–Mn–N(1) 92.7(2), O(5^{I})–Mn–N(2^{I}) 81.8(2), N(1)–Mn–N(2^{I}) 172.1(2), Mn–O(1)–Mn^{I} 94.1(2) (symmetry code: I = $-x$, $-y$, $-z$).

Table 1 Results for the oxidation of alcohols by dioxygen and pivalaldehyde catalyzed by **1**[a]

Entry	Alcohol	*t*/h	Yield (%)[b,c]
1	1-Phenylethanol	24	70
2	1-(*p*-Methoxyphenyl)ethanol	24	75
3	1-(*p*-Bromophenyl)ethanol	24	68
4	1-(*p*-Trifluoromethylphenyl)ethanol	24	65
5	1-(*p*-Nitrophenyl)ethanol	24	60
6	4-(*tert*-Butyl)cyclohexanol	48	50
7	*p*-Methoxybenzyl alcohol	12	95[d]

[a] Reactions were carried out at room temp. by adding a CH_2Cl_2 solution (0.2 cm^3) of alcohol (0.11 mmol) to a stirred mixture of metal catalyst (6.5×10^{-3} mmol) and pivalaldehyde (0.33 mmol) in CH_2Cl_2 (0.2 cm^3) under O_2 atmosphere. Consumption of alcohol and formation of ketone during the reaction were monitored by TLC. Obtained ketone and unreacted alcohol were separated by flash column chromatography on silica gel. [b] Yields refer to isolated and pure compounds (column chromatography on silica gel). All compounds exhibited spectral data consistent with their structures. [c] In the absence of metal catalyst some extension of oxidation was observed. [d] Reaction product was exclusively *p*-methoxybenzoic acid.

70% after 24 h (entry 1), with formation of pivalic acid as a coproduct. Moreover, for the series of *para*-substituted phenyl derivatives a small but non-negligible electronic effect is observed, as the substrate with the electron-donating methoxy substituent gives a somewhat higher yield of ketone than that with electron-withdrawing substituents such as trifluoromethyl or nitro groups, *e.g.* 75 *vs.* 60% after 24 h (entries 2 and 5, respectively). For all secondary benzyl alcohols, however, ketones were the only oxidation products as confirmed by ^1H NMR spectroscopy. Notably, for the oxidation of 4-(*tert*-butyl)cyclohexanol only 4-(*tert*-butyl)cyclohexanone was obtained, and no traces were detected of the corresponding Baeyer–Villiger oxidation product, 4-(*tert*-butyl)caprolactone (entry 6).[8] This observation suggests that the acylperoxy radicals generated *in situ* from the auto-oxidation of the aldehyde are not directly involved as potential oxidizing agents. As expected, under the same reaction conditions used for the oxidation of secondary alcohols to ketones, the primary alcohols give mixtures of both the aldehyde and the acid oxidation products in variable amounts depending on the reaction time, as exemplified by *p*-methoxybenzyl alcohol which leads to almost quantitative formation of *p*-methoxybenzoic acid, *i.e.* 95% after 12 h (entry 7).

Although it is premature to discuss the precise role of the metal complex in the catalytic mechanism at the present stage, it is noteworthy that **1** alone does not lead to alcohol oxidation under stoichiometric conditions and, consequently, involvement of a bis(μ-oxo)dimanganese(IV) species as the active oxidizing agent can also be ruled out. In a typical experiment, complex **1** (0.11 mmol) in dichloromethane (20 cm^3) does not react with the more reactive substrate 1-(*p*-methoxyphenyl)ethanol (0.11 mmol) even after a period of three days under stirring at room temperature with or without oxygen atmosphere conditions. That being so, manganese(IV)–acylperoxo or higher valent metal intermediate species, such as manganese(V)–oxo, derived from the oxidation of the bis(μ-oxo)manganese(IV) dimer by the combination of dioxygen and pivalaldehyde, are considered more likely to be responsible for the oxidation in our system. More interestingly, stable manganese(V)–oxo monomeric complexes with amido-containing ligands analogous to that used herein have been isolated and structurally characterized.[9] Attempts to isolate these reactive intermediate species using transition metal ions with more accessible high-valent oxidation states such as chromium are in progress.

This work was supported by the DGICYT, Ministerio de Educación y Ciencia (Spain) through projects PB94-0985 and PB94-1002. R. R. and B. C. thank the Ministerio de Educación y Ciencia (Spain) and the Conselleria de Educació i Ciència de la Generalitat Valenciana (Spain) for grants. We would also like to express our gratitude to Professor J. J. Girerd and Dr G. Blondin for fruitful discussions and continuous interest in this work.

Notes and References

† E-mail: jour@icmo.u-psud.fr

‡ *Synthesis and selected data for* **1**: the diethyl ester derivative of the opba ligand (1.54 g, 5 mmol) was dissolved in deoxygenated MeOH (100 cm^3), NMe_4OH at 25% in MeOH (8 cm^3, 20 mmol) was added to the solution and the resulting mixture was stirred at 60 °C for 15 min under N_2. A deoxygenated MeOH solution (50 cm^3) of $Mn(ClO_4)_2 \cdot 6H_2O$ (1.79 g, 5 mmol) was then added dropwise *via* a dropping funnel under N_2, and a gelatinous light yellow precipitate [presumably a Mn^{II} complex] rapidly formed, together with the crystalline white precipitate of NMe_4ClO_4. Addition of 33% aq. H_2O_2 (1 cm^3, 10 mmol) caused immediate darkening of the solution with concomitant disappearance of the yellow precipitate. The reaction mixture was further stirred at 60 °C for 30 min under N_2. The dark-brown solution was filtered to eliminate the solid NMe_4ClO_4, and reduced to a final volume of 10 cm^3 on a rotatory evaporator. The concentrated solution was treated successively with diethyl ether and acetone to give a black solid which was recuperated in warm water (50 cm^3). The resulting mixture was filtered to eliminate solid particles (mainly MnO_2), and an excess of PPh_4Cl (3.75 g, 10 mmol) dissolved in the minimum amount of water was then added dropwise to the dark-brown solution under gentle warming. Slow evaporation of the filtered solution in air afforded, after a few days, well shaped large prismatic dark-brown crystals of **1** suitable for X-ray analysis which were filtered on paper and air-dried (60%). Satisfactory chemical analyses obtained (C, H, N, P, Mn). ν_{max}/cm^{-1} (KBr) 3477vs (O–H) from H_2O, 1672 (sh), 1647vs, 1617vs (C=O) and 1403s, 1306s (C–O) from opba ligand, and 643m (Mn–O) from Mn_2O_2 ring. λ_{max}/nm 390 ($\varepsilon/dm^3\ mol^{-1}\ cm^{-1}$ 10800), 440 (sh) (7080) and 605 (1170) (MeCN). Variable-temperature magnetic susceptibility (Faraday balance, 80–300 K): $J = -158.0\ cm^{-1}$ ($H = -J\ S_1 \cdot S_2$, $S_1 = S_2 = 3/2$).

§ *X-Ray crystal structure analysis*: Enraf-Nonius CAD-4 diffractometer, Mo-Kα, $\lambda = 0.710\,73$ Å, graphite monochromator, 293 K. Lorentz and polarization effects but not absorption correction ($\mu = 3.78\ cm^{-1}$). *Data collection, solution and refinement*: *ω–θ*, standard Patterson methods with subsequent full-matrix least-squares refinement. SHELX86, SHELX93.[10] $C_{116}H_{96}Mn_2N_4O_{18}P_4$, triclinic, space group $P\bar{1}$, $a = 13.245(3)$, $b = 13.964(3)$, $c = 14.835(3)$ Å, $\alpha = 73.59(2)$, $\beta = 77.98(2)$, $\gamma = 84.60(2)°$, $U = 2572.6(10)$ Å^3, $Z = 2$, $D_c = 1.33\ g\ cm^{-3}$, $1 \leqslant \theta \leqslant 25°$, crystal $0.15 \times 0.15 \times 0.10$ mm. 6681 reflections measured, 4485 assumed as observed with $I \geqslant 2\sigma(I)$. Refinement on F^2 of 651 variables with anisotropic thermal parameters for all non-H atoms gave $R = 0.060$ and $R_w = 0.150$ with $S = 0.936$ (obs. data). CCDC 182/809.

1 V. L. Pecoraro, M. J. Baldwin and A. Gelasco, *Chem. Rev.*, 1994, **94**, 807.
2 (*a*) K. Wieghardt, *Angew. Chem., Int. Ed. Engl.*, 1989, **28**, 1153; (*b*) J. E. McGrady and R. Stranger, *J. Am. Chem. Soc.*, 1997, **119**, 8512 and references therein.
3 R. Hage, *Recl. Trav. Chim. Pays-Bas*, 1996, **115**, 385 and references therein; W. Ruttinger and G. C. Dismukes, *Chem. Rev.*, 1997, **97**, 1.
4 R. Hage, J. E. Iburg, J. Kerschner, J. H. Koek, E. L. M. Lempers, R. J. Martens, U. S. Racherla, S. W. Russell, T. Swarthoff, M. R. P. Van Vliet, J. B. Warnaar, L. Van der Wolf and B. Krijnen, *Nature*, 1994, **369**, 637; C. Zondervan, R. Hage and B. L. Feringa, *Chem. Commun.*, 1997, 419.
5 W. F. Beck, J. Sears, G. W. Brudvig, R. J. Kulawiec and R. H. Crabtree, *Tetrahedron*, 1989, **45**, 4903.
6 M. Fettouhi, L. Ouahab, A. Boukhari, O. Cador, C. Mathoniere and O. Kahn, *Inorg. Chem.*, 1996, **35**, 4932.
7 R. Ruiz, M. Triannidis, A. Aukauloo, Y. Journaux, I. Fernández, J. R. Pedro, B. Cervera, I. Castro and M. C. Muñoz, *Chem. Commun.*, 1997, 2283.
8 K. Kaneda, S. Ueno, T. Imanaka, E. Shimotsuma, Y. Nishiyama and Y. Ishii, *J. Org. Chem.*, 1994, **59**, 2915.
9 T. J. Collins, R. D. Powell, C. Slebodnick and E. S. Uffelman, *J. Am. Chem. Soc.*, 1990, **112**, 899; F. M. McDonnell, N. L. P. Fackler, C. Stern and T. V. O'Halloran, *J. Am. Chem. Soc.*, 1994, **116**, 7431.
10 G. M. Sheldrick, SHELX. A Program for Crystal Structure Determination, University of Göttingen, Germany, 1990; G. M. Sheldrick, SHELXL93. Program for the Refinement of Crystal Structures, University of Göttingen, Germany, 1993.

Received in Basel, Switzerland, 3rd February 1998; 8/00930I

Arylsulfurdiimides: a new class of sulfur–nitrogen anion

Andrey V. Zibarev,[a] Enno Lork[b] and Rüdiger Mews*[b]†

[a] *Institute of Organic Chemistry, Russian Academy of Sciences, Siberian Division, 630090 Novosibirsk, Russia*
[b] *Institut für Anorganische und Physikalische Chemie der Universität Bremen, Leobener Straße NW2, Postfach 330440, D-28334 Bremen, Germany*

***N*-Aryl-*N′*-trimethylsulfurdiimides (aryl = 2,6-$F_2C_6H_3$, 2-FC_6H_4) react with TASF to give quantitatively the corresponding TAS salts with the $ArNSN^-$ anions (2a, 2b), isoelectronic with arylthionylimides 3; because of the short terminal SN bond the anions should be regarded as thiazylamide rather than sulfurdiimide anions.**

Sulfurdiimide salts K^+RNSN^- [R = Me_3C,[1] Me_3Si,[1] $(Me_3C)_2P$,[2] $(Me_3C)_2As$,[2] $PhSO_2$[3]] have been prepared from the appropriate silyl derivatives $RNSNSiMe_3$ and KNH_2 or $KOCMe_3$ while $Li^+Me_3NSN^-$ was obtained from $Me_3SnNSNSnMe_3$ and LiMe.[4] The reaction of $Me_3SiNSNSiMe_3$ and $KOCMe_3$ under more drastic conditions leads to the cleavage of the second Si–N bond with formation of K_2N_2S,[5] which has been used, particularly by the research groups of Herberhold and Chivers as reagents in the chemistries of groups 14 and 15.[6] Protonation with CF_3CO_2H leads to unstable RNSNH (R = Me_3C, Me_3Si) and HNSNH, respectively.[7] Titanosulfurdiimides are obtained from $K^+Me_3CNSN^-$ and Cp_2TiCl_2.[8] Strong covalent metal–nitrogen interaction is expected for these complexes as Woollins and coworkers have shown for *cis*-$[Pt(NSNSiMe_3)_2(PPh_3)_2]$[9] and $[Pt(NSNSC_6H_4NO_2\text{-}4)_2(Ph_2PCH_2CH_2PPh_2)]$.[10]

Arylsulfurdiimide anions are unknown, fluoroarylsulfur diimide anions are likely intermediates in the CsF promoted cyclisation of *N*-fluoroaryl-*N′*-silylsulfurdiimides $Ar_FNSNSiMe_3$ under elimination of Me_3SiF to give benzothiadiazoles.[11,12] Even spectroscopic evidence for these intermediates is lacking.

Upon cleavage of the SiN bond in $Ar_FNSNSiMe_3$ with TASF $\{[(Me_2N)_3S]^+[Me_3SiF_2]^-\}$[13] the sulfurdiimide salts **2** are readily available (Scheme 1).

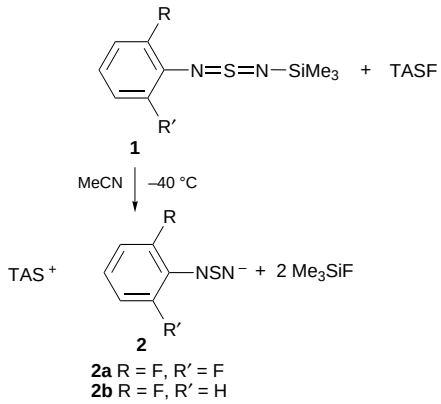

Scheme 1

After removal of all volatiles at −30 to −20 °C, salts **2** are isolated in quantitative yield as orange–yellow solids.‡ On warming to room temperature these highly reactive salts decompose immediately to give brown tars. With MeI they react even at −35 °C to give Ar_FNSNMe.

Single crystals of salts **2** were obtained from MeCN–diethyl ether solutions at −40 °C and X-ray data were collected at −110 °C. Figs. 1 and 2 show the anions of salts **2a** and **2b**; for comparison the structure of 2,6-difluorophenylthionylimide $C_6H_3F_2NSO$ **3a** (Fig. 3), isoelectronic with **2a**, was also determined.§ All three compounds adopt the *Z*-conformation and the torsion angle between the aryl plane and the NSA group

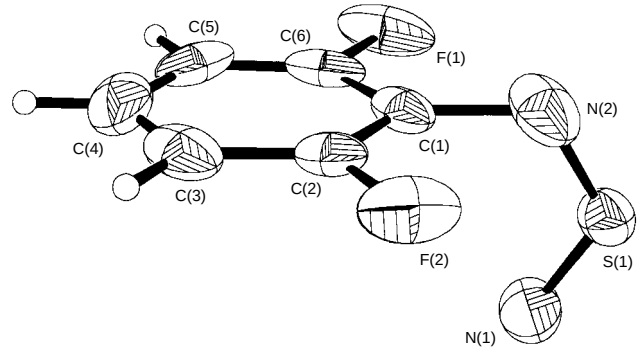

Fig. 1 Structure of the anion of **2a** with selected bond distances (pm) and angles (°) (average of three independent anions): S(1)–N(1) 144.2, S(1)–N(2) 158.9, N(2)–C(1) 140.7; N(1)–S(1)–N(2) 122.3, S(1)–N(2)–C(1) 119.0; τ = 77.7

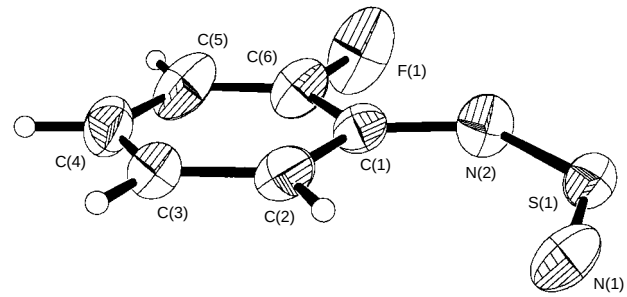

Fig. 2 Structure of the anion of **2b** with selected bond distances (pm) and angles (°): S(1)–N(1) 145.8(4), S(1)–N(2) 159.9(4), N(2)–C(1) 139.0(6), N(1)–S(1)–N(2) 124.8(2), C(1)–N(2)–S(1) 126.5(3); τ = 6.8(5)

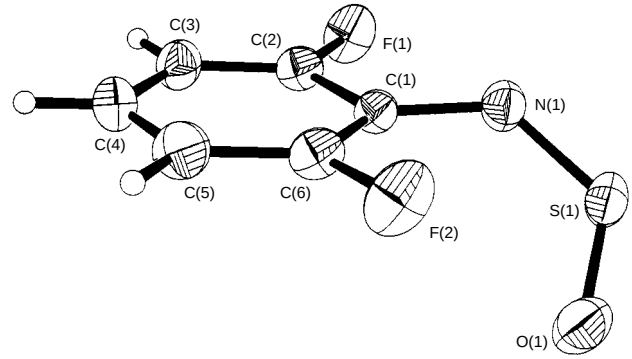

Fig. 3 Structure of **3a** with selected bond distances (pm) and angles (°): S–O 144.8(1), S–N 151.5(1), N–C 140.4(2), N–S–O 120.7(1), C–N–S 130.1(1); τ = 43.6(1)

(A = O,N) seems to be determined by the electronic repulsion between the *ortho* substituents and these groups. In the thionylimide **3a** this angle is 43.6°, in the corresponding negatively charged sulfurdiimide anions these angles are between 75.6 and 79.0° (three independent molecules). In **2b** this repulsion forces the NSN group almost into the aryl plane (τ = 6.8°).

According to the bond lengths in the –NSN– fragment the anions of salts **2** should be regarded as thiazylamides **A** rather than sulfurdiimides **B** (Scheme 2).

A **B**

Scheme 2

The terminal SN bond distances in **2a** (144.2 pm) and **2b** (145.8 pm) correspond to the $S^{IV}{\equiv}N$ triple bond in thiazylhalides (NSF 144.6 pm,[14] NSCl 145.0 pm[15]) and $(CF_3)_2NO(SN)$ (142.3 pm)[16] and also agree well with the SO bond in the isoelectronic thionylimide 2,6-$C_6H_3F_2NSO$ **3a** (144.8 pm). In thiazyl derivatives the XSN angle is 117–119°, in **3a** 120.7° and in the anions of **2** 122–125°. For the bridging SN bonds of **2** the distances 158.9 pm for **2a** and 159.9 pm for **2b** are between double and single bond lengths.

A. Z. is grateful to Deutsche Forschungsgemeinschaft and to Russian Foundation for Basic Research (project 96-03-33276) for financial support.

Notes and References

† E-mail: mews@chemie.uni-bremen.de

‡ *Preparation of* ***2***: TASF[13] (1.37 g, 5 mmol) was placed into one side of a two-armed lambda-shaped glass vessel fitted with a Teflon valve, 5 mmol of the corresponding $ArNSNSiMe_3$ **1**[17] was placed into the other side. In a vacuum line 20 ml of MeCN was distilled onto TASF, this solution was mixed with **1** at −40 °C and stirred at this temperature for 2 h. Then 30 ml of Et_2O was condensed onto the reaction mixture at −196 °C, the λ-tube was placed into a cryostat at −40 °C for crystal growth and **2a** and **2b** were obtained as orange–yellow crystalline solids after removal of the solvents. Because of their thermal instability the compounds were characterised only by low temperature X-ray crystallography.

§ *Crystal data*: $C_{12}H_{21}F_2N_5S_2$ **2a**, monoclinic, space group $P2_1/c$, a = 1666.7(6), b = 1159.4(4), c = 2549.0(11) pm; β = 92.42(3)°, U = 4.921(3) nm³, Z = 12, D_c = 1.366 g cm^{-3}, μ = 0.345 mm^{-1}, F(000) 2136, crystal dimensions 1.1 × 0.4 × 0.2 mm, 12 180 reflections collected with 2.64 < θ < 27.52°, 9824 used in structural analysis. The data for **2a**, **2b** and **3a** were collected on a Siemens P4 diffractometer using Mo-Kα radiation (λ = 71.073 pm) at 173 K. The structures were solved by direct methods.[18] All non-hydrogen atoms were refined anisotropically. The refinement (597 parameters) converged with wR_2 = 0.2521 (R_1 = 0.0867) and final difference electron density maxima and minima of 1510 and −840 e nm^{-3}.

$C_{12}H_{22}FN_5S_2$ **2b**: monoclinic, space group $C2/c$, a = 2685.2(6), b = 898.8(2), c = 1505.1(5) pm, β = 115.54(2)°, U = 3.278(2) nm³, Z = 8, D_c = 1.295 g cm^{-3}, μ = 0.333 mm^{-1}, F(000) 1360, crystal dimensions 0.5 × 0.4 × 0.1 mm. 4477 reflections collected with 2.65 < θ < 22.50°, 2147 used in structural analysis. The refinement (189 parameters) converged with wR_2 = 0.1381 (R_1 = 0.0555) and final difference electron maxima and minima of 493 and −383 e nm^{-3}.

$C_6H_3F_2NOS$ **3a**: monoclinic, space group $C2_1/c$, a = 374.37(4), b = 2106.4(3), c = 873.7(2) pm, β = 100.95(1)°, U = 0.6765(2) nm³, Z = 4, D_c = 1.720 g cm^{-3}, μ = 0.448 mm^{-1}, F(000) 352, crystal dimensions 0.8×0.6×0.5 mm. 2041 reflections collected with 2.56 < θ < 27.49°, 1402 used in structural analysis. The refinement (102 parameters) converged with wR_2 = 0.0809 (R_1 = 0.0297) and final difference electron maxima and minima of 337 and −229 e nm^{-3}. CCDC 182/817.

1 D. Hänssgen and B. Ross, *Z. Anorg. Allg. Chem.*, 1981, **473**, 80.
2 M. Herberhold, W. Ehrenreich, W. Bühlmeyer and K. Guldner, *Chem. Ber.*, 1986, **119,** 1424.
3 H. W. Roesky, W. Schmieder and W. S. Sheldrick, *Chem. Commun.*, 1981, 1013; H. W. Roesky, W. Schmieder, W. Isenberg, W. S. Sheldrick and G. M. Sheldrick, *Chem. Ber.*, 1982, **115**, 2714.
4 D. Hänssgen and R. Steffens, *J. Organomet. Chem.*, 1982, **236**, 53.
5 M. Herberhold and W. Ehrenreich, *Angew. Chem., Int. Ed. Engl.*, 1986, **21**, 633.
6 *Gmelin Handbook of Inorganic and Organometallic Chemistry*, *Sulfur Nitrogen Compounds*, Part 7, Springer, Berlin, 1991, p.10 ff.
7 M. Herberhold, W. Jellen, W. Bühlmeyer, W. Ehrenreich and J. Reiner, *Z. Naturforsch., Teil B*, 1985, **40**, 1229.
8 M. Herberhold, F. Neumann, G. Süss-Fink and U. Thewalt, *Inorg. Chem.*, 1987, **26**, 3612.
9 N. P. C. Walker, M. B. Hursthouse, C. P. Warrens and J. D. Woollins, *J. Chem. Soc., Chem. Commun.*, 1985, 227.
10 R. Jones, D. J. Williams, P. T. Wood and J. D. Woollins, *Polyhedron*, 1989, **8**, 91.
11 A. V. Zibarev and A. O. Miller, *J. Fluorine Chem.*, 1990, **50**, 359.
12 I. Yu. Bagryanskaya, Yu. V. Gatilov, A. O. Miller, M. M. Shakirov and A. V. Zibarev, *Heteroatom Chem.*, 1994, **5**, 561.
13 W. J. Middleton, *Org. Synth.*, 1985, **64**, 221.
14 R. L. Cook and W. H. Kirchhoff, *J. Chem. Phys.*, 1967, **47**, 4521.
15 T. Beppo, E. Hirota and Y. Morino, *J. Mol. Spectrosc.*, 1970, **36**, 386; W. C. Emken and K. Hedberg, *J. Chem. Phys.*, 1973, **58**, 2195.
16 G. Hartmann, R. Mews, G. M. Sheldrick, R. Anderskewitz, M. Niemeyer and H. J. Emeleus, *J. Fluorine Chem.*, 1986, **34**, 46.
17 A. V. Zibarev and R. Mews, unpublished work.
18 Structure solution and graphics, Siemens SHELXTL-Plus: G. M. Sheldrick, Release 4.0 for Siemens R3 Crystallographic Research Systems, Siemens Analytical X-Ray Instruments Inc., Madison, WI, 1989; Structure refinement, SHELXL-93, G. M. Sheldrick, University of Göttingen.

Received in Cambridge, UK, 13th February 1998; 8/01262H

Stereoselective synthesis of linear bipyridyl–phenylene based ruthenium rods from enantiopure building blocks

Kenneth Wärnmark,[a] Paul N. W. Baxter[b] and Jean-Marie Lehn*[b]†

[a] *Organic Chemistry 1, Department of Chemistry, Lund University, PO Box 124, SE-221 00 Lund, Sweden*
[b] *Laboratoire de Chimie Supramoléculaire, ISIS, Institut Le Bel, Université Louis Pasteur, 4 rue Blaise Pascal, F-67000 Strasbourg, France*

Extended stereochemically pure C_2-symmetric diruthenium rods, Λ,Λ-1, Δ,Δ-1, Λ,Λ-2 and Δ,Δ-2, have been synthesized from enantiomerically pure building blocks.

The synthesis of nanosize-components for potential applications in electronic or optical systems is a central theme in current material science.[1] The design of molecular counterparts to macroscopic electronic components has largely focussed on molecular wires.[2]

In a molecular approach to microscopic semiconductor technology, we are interested in finding molecular counterparts to doped material. Conjugated π-systems such as rods consisting of linear phenylene chains could function as molecular wires. In principle, electronic conductivity along the axis of the rods in the form of photo- or electro-chemically generated positive hole doping may be achieved by incorporation of photo- and redox-active metal centres, such as Ru^{II}, into the periphery of the rods. The ruthenium doping would be expected to change the conductivity and optical properties of the phenylene chain and add signal reading abilities to it.

Directly connected or phenylene bridged 2,2′-bipyridyl (bpy) units may be regarded as phenylene chains that contain sites for metal coordination. The 4′,4″-linkage between two 2,2′-bipyridyl (bpy) units in $[\{(bpy)_2Ru\}_2(LL)][PF_6]_4$ (LL = 2,2′:4,′4″:2″,2‴-quaterpyridine) gives the complex a transoid overall conformation and mediates a weak metal-to-metal interaction.[3] However, to construct a linear molecular wire containing ruthenium centres, the bpy units must be linked in the 5-position either directly or by a linker such as phenylene. In addition, the electronic transitions that are the most intense in the bpy and phen (phen = 1,10-phenanthroline) rings take place along the longer axis of these ligands making linkages of bpy or phen units in the 5,5′- and 3,8-positions, respectively, attractive.[4]

We herein present the synthesis of the shortest constituents of a series of linear π-conjugated phenylene type ruthenium rods **1** and **2** (Fig. 1) in which bpy units are linked directly, dmqtby‡ (**3**), or *via* a *para*-phenylene bridge, bmbpyb‡ (**4**), to each other in the 5-position.§

The incorporation of more than one $[(phen)_2Ru]^{2+}$ unit into the molecular wire of bpy-type will give rise to diastereoisomers since each unit may have Λ- or Δ-configuration at the ruthenium centre. Enantiomerically pure (ep) and diastereomerically pure (dp) syntheses of various polypyridine ruthenium complexes using the appealing concept of ep building blocks have been successfully pursued by several groups.[5]

Ligands **3** and **4**, respectively, were reacted with 2.2 equiv. of ep Λ-**5** and Δ-**5**,¶ respectively, giving Λ,Λ-**1**, Δ,Δ-**1**, Λ,Λ-**2** and Δ,Δ-**2**, respectively [58% yield of **1** and 49% yield of **2** after purification on a Bio-Beads S-X1 (Bio-Rad laboratories) size-exclusion column, MeCN–toluene (1:1)].‖ Ligands **3** and **4**, respectively, were also reacted with 2.2 equiv. of racemic **5**, giving the mixture of all stereoisomers Λ,Λ-**1**, Δ,Δ-**1**, Δ,Λ-**1** (mix-**1**) and Λ,Λ-**2**, Δ,Δ-**2**, Δ,Λ-**2** (mix-**2**), respectively.

The ligand **3** and the phenylene-bridged homologue **4** were synthesized by a $Pd(PPh_3)_4$ catalysed Stille cross-coupling protocol[6] between respectively, the dibrominated bridging units 6,6′-dibromo-3,3′-bipyridyl and 1,4-bis[5-(2-bromopyridyl)]benzene and two equiv. each of 2-trimethylstannyl-5-methylpyridine.

The ^{1}H NMR spectrum of Λ,Λ-**1** (and Δ,Δ-**1**) is much less complicated than the ^{1}H NMR spectrum of mix-**1**. Obviously, the short distance between the asymmetric ruthenium centres in **1** leads to large enough differences in ^{1}H NMR shifts for the diastereoisomers Λ,Λ-**1** (Δ,Δ-**1**) and Δ,Λ-**1** to be observable. For **2** in contrast, where the asymmetric ruthenium centres are further apart (by a *para*-phenylene unit), the ^{1}H NMR spectrum of Λ,Λ-**2** (and Δ,Δ-**2**) is identical to the ^{1}H NMR spectrum of mix-**2**.

That Λ,Λ-**1**, Δ,Δ-**1**, Λ,Λ-**2** and Δ,Δ-**2** are essentially ep and dp as demonstrated by the fact that in the circular dichroism spectra, Λ,Λ-**1** and Δ,Δ-**1** as well as Λ,Λ-**2** and Δ,Δ-**2**, respectively, are almost perfect mirror images (Fig. 2). For Λ,Λ-**1** and Δ,Δ-**1** the diastereomeric excess could be determined to > 98.5% by ^{1}H NMR spectroscopy because of the differences in ^{1}H NMR chemical shifts between Λ,Λ-**1** (Δ,Δ-**1**) and mix-**1**.

One measure of the degree of electronic communication between metal centres in symmetrical dimers is the separation of the oxidation potential between the two centres. The results from cyclic voltammetry (CV) of the linear complexes **1** show only one reversible oxidative wave at 1.31 V *vs.* SCE in MeCN, indicating no communication between the ruthenium centres.** Furthermore, one reversible reductive wave at −1.11 V *vs.* SCE in DMF and two reductive cathodic waves at −1.32 and −1.49 V appeared (the corresponding anodic waves could not be detected because of extensive adsorption). The first reductive wave is assigned to ligand **3** and the two others most likely to the phenanthroline ligand in analogy with the assignments of the

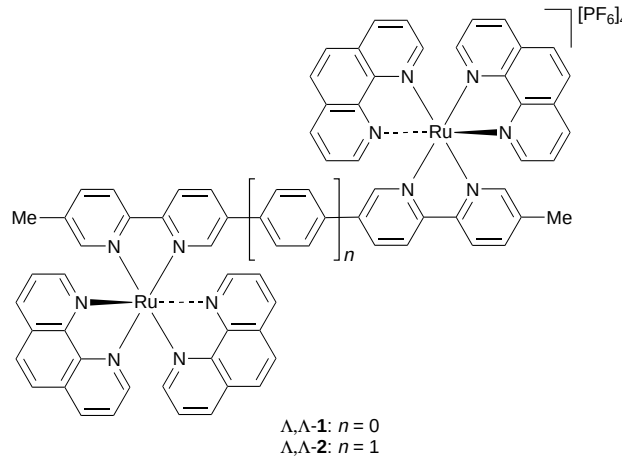

Λ,Λ-**1**: $n = 0$
Λ,Λ-**2**: $n = 1$

Fig. 1

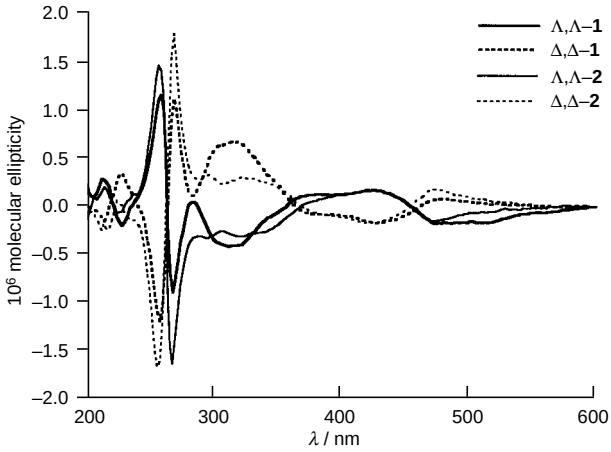

Fig. 2 Circular dichroism spectra of Λ,Λ-**1**, Δ,Δ-**1**, Λ,Λ-**2** and Δ,Δ-**2** in MeCN

CV of the analogue $[\{(bpy)_2Ru\}_2(LL)][PF_6]_4$, bridged in the 4′,4″-position (reversible reductive waves at −1.10, −1.44, −1.57 V *vs*. SCE in MeCN).[3] The CV of the phenylene-bridged linear complexes **2** shows also only one reversible 2e oxidative wave at 1.29 V *vs*. SCE in MeCN, one reversible reductive wave at −1.19 and one reductive cathodic wave at −1.36 V *vs*. SCE in DMF (a third reductive wave could not be observed). The reductive waves in complex **2** are assigned in analogy with complex **1** to ligands **4** and phen, respectively.

The complexes **1** and **2** have almost identical electronic spectra in MeCN. Only one flat MLCT band could be detected [λ = 450 (ε = 2.54 × 10^4), 448 nm (2.98 × 10^4 dm^3 mol^{-1} cm^{-1}), respectively] demonstrating that the Ru–dmqtpy and Ru–bmbpyb transitions are of similar energy as for Ru–phen and being almost identical to the monoruthenium complex $[Ru(bpy)_3]^{2+}$ [λ = 452 nm (ε = 1.45 × 10^4 dm^3 mol^{-1} cm^{-1})].[7] Thus the red-shift for the Ru–(bridging ligand) MLCT band, observed in the analogue $[\{(bpy)_2Ru\}_2(LL)][PF_6]_4$ and indicating a weak metal–metal interaction,[3] seems to be absent in complexes **1** and **2**. The π–π* transitions for compounds **1** [λ = 265 (ε = 1.52 × 10^5), 224 nm, (1.13 × 10^5 dm^3 mol^{-1} cm^{-1})] and **2** [λ = 263 (ε = 1.69 × 10^5), 223 nm, (1.22 × 10^5 dm^3 mol^{-1} cm^{-1})] are located almost at the same wavelength as for $[Ru(phen)_3]^{2+}$ [λ = 263 (ε = 1.13 × 10^5), 224 nm (8.03 × 10^4 dm^3 mol^{-1} cm^{-1})].[8] The values of the absorption coefficients indicate that these π–π* transitions in complexes **1** and **2** are phenanthroline based. More difficult is the assignment of Ru–(bridging ligand) π–π* transitions.

The excitations of compounds **1** and **2** in the MLCT band resulted in intense emission at 639 and 613 nm, respectively, being somewhat red-shifted compared to $[\{(bpy)_2Ru\}_2(LL)][PF_6]_4$. Excitation in the phenanthroline π–π* bands leads to an intense emission at 735 and 417 nm for each of the two complexes **1** and **2**.

In conclusion stereoisomerically pure linear bipyridyl–phenylene based ruthenium rods, **1** and **2**, have been synthesized from ep building blocks. By the methods used in this work no electronic communication between the two halves of the rods could be detected. Oxidation or reduction at a given centre may however be expected to delocalize over the whole system and provides means for p and n doping of such types of inorganic molecular rods.

We thank Emmanuelle Leize and Alain Van Dorsselaer, Laboratoire de Spectrométrie de Masse Bio-Organique, for electrospray-MS measurements as well as the University of Lund and the Collège de France (P. N. W. B.) for financial support.

Notes and References

† E-mail: lehn@chimie.u-strasbg.fr

‡ dmqtpy = 5,5‴-dimethyl-2,2′:5′,5″:2″,2‴-quaterpyridine and bmbpyb = 1,4-bis[5-(5′-methyl)-2,2′-bipyridyl)]benzene.

§ Linear oligoruthenium rods have also been constructed with ethynyl linkers between phen or bpy.[5h,9]

¶ Prepared by several resolutions following a literature procedure;[10] ep **5** reacts with bidentate ligands with retention of configuration.[5a,b]

‖ Complexes **1** and **2** were characterised by ^{1}H NMR spectroscopy, elemental analysis and electrospray MS {**1**: *m/z* 315.9 [**1** − $4PF_6$]$^{4+}$, 469.5 [**1** − $3PF_6$]$^{3+}$, 776.4 [**1** − $2PF_6$]$^{2+}$ and 1696.1 [**1** − PF_6]$^+$ and **2**: *m/z* 333.9 [**2** − $4PF_6$]$^{4+}$, 493.9 [**2** − $3PF_6$]$^{3+}$ and 813.7 [**2** − $2PF_6$]$^{2+}$}.

** Cyclic voltammetry was performed with 0.1 M Bu_4PF_6 as electrolyte and Ag/AgCl as reference electrode. The Ag/AgCl electrode is −50 mV *vs*. SCE.

1 J.-M. Lehn, *Supramolecular Chemistry: Concepts and Perspectives*, VCH, Weinheim, 1995.
2 J. S. Miller, *Adv. Mater.*, 1990, **2**, 378, 495, 601; ref. 1, ch. 8.
3 A. J. Downard, G. E. Honey, L. F. Phillips and P. J. Steel, *Inorg. Chem.*, 1991, **30**, 2259.
4 B. Bosnich, *Acc. Chem. Res.*, 1969, **2**, 266; J. Hidaka and B. E. Douglas, *Inorg. Chem.*, 1964, **3**, 1180.
5 (*a*) X. Hua and A. Von Zelewsky, *Inorg. Chem.*, 1991, **30**, 3796; (*b*) X. Hua and A. Von Zelewsky, *Inorg. Chem.*, 1991, **34**, 5791; (*c*) L. S. Kelso, D. A. Reitsma and F. R. Keene, *Inorg. Chem.*, 1996, **35**, 5144; (*d*) T. J. Rutherford, M. G. Quagliotto and F. R. Keene, *Inorg. Chem.*, 1995, **34**, 3857; (*e*) K. Wärnmark, J. A. Thomas, O. Heyke and J.-M. Lehn, *Chem. Commun.*, 1996, 701; (*f*) K. Wärnmark, O. Heyke, J. A. Thomas and J.-M. Lehn, *Chem. Commun.*, 1996, 2603; (*g*) F. M. MacDonnell and S. Bodige, *Inorg. Chem.*, 1996, **35**, 5758; (*h*) D. Tzalis and Y. Tor, *J. Am. Chem. Soc.*, 1997, **119**, 852; (*i*) S. Bodige, A. S. Torres, D. J. Maloney, D. Tate, G. R. Kinsel, A. K. Walker and F. MacDonnell, *J. Am. Chem. Soc.*, 1997, **119**, 10 364; (*j*) T. J. Rutherford and F. R. Keene, *Inorg. Chem.*, 1997, **36**, 3580; (*k*) T. J. Rutherford, O. Van Gitje, A. Kirsch-De Mesmaeker and F. R. Keene, *Inorg. Chem.*, 1997, **36**, 4465.
6 P. Baxter, J.-M. Lehn, A. DeCian and J. Fischer, *Angew. Chem., Int. Ed. Engl.*, 1993, **32**, 69.
7 E. Amouyal, A. Homsi, J.-C. Chambron and J.-P. Sauvage, *J. Chem. Soc., Dalton Trans.*, 1990, 1841.
8 R. H. Fabian, D. M. Klassen and R. W. Sonntag, *Inorg. Chem.*, 1980, **19**, 1977.
9 R. W. Romero and R. Ziessel, *Tetrahedron Lett.*, 1994, **35**, 9203; D. Tzalis and Y. Tor, *Tetrahedron Lett.*, 1995, **36**, 6017; *Chem. Commun.*, 1996, 1043.
10 B. Bosnich and F. P. Dwyer, *Aust. J. Chem.*, 1966, **19**, 2229.

Received in Cambridge, UK, 24th February 1998; 8/01551A

Ruthenium-catalysed synthesis of indoles from anilines and trialkanolamines in the presence of tin(II) chloride dihydrate

Chan Sik Cho, Hyo Kyun Lim, Sang Chul Shim,*† Tae Jeong Kim and Heung-Jin Choi

Department of Industrial Chemistry, College of Engineering, Kyungpook National University, Taegu 702-701, Korea

Anilines react with trialkanolamines in dioxane in the presence of a catalytic amount of a ruthenium catalyst together with tin(II) chloride dihydrate to give the corresponding indoles in moderate to good yields.

Transition metal-catalysed cyclisation reactions have been a useful and convenient method for the formation of a wide variety of heterocycles. Thus, the formation of the structural core of indoles has also been attempted using transition metal catalysts[1] since several naturally occurring indoles exert a broad spectrum of physiological activities.[2] As part of our continuing studies on transition metal-catalysed synthesis of *N*-heterocyclic compounds,[3] we have recently developed and reported a novel ruthenium-catalysed synthesis of *N*-alkylindoles from *N*-alkylated anilines and triethanolamine as the C_2-fragment.[4] However, aniline did not act as a cyclisation counterpart in the formation of indole itself under the ruthenium-catalysed system. After numerous attempts were made to achieve the formation of indoles from the primary aromatic amines under the reaction system used, eventually, it was found that the addition of tin(II) chloride dihydrate allows the formation of indoles. We now report a facile synthesis of indoles from readily available primary aromatic amines and triethanolamine in the presence of a ruthenium catalyst together with $SnCl_2{\cdot}2H_2O$.

We examined the cyclisation between aniline (**1**) and triethanolamine (**2**) in the presence of $SnCl_2{\cdot}2H_2O$ to optimise the reaction conditions using similar catalytic systems which we employed for the synthesis of *N*-alkylindoles. The yield of indole (**3**) was considerably affected by the molar ratio of **1** to **2** as has been observed in our recent report (Scheme 1).[4] Table 1 shows that the highest yield of **3** was obtained at the molar ratio of 10. The reaction was also affected by the amount of $SnCl_2{\cdot}2H_2O$. The use of equimolar amounts of **2** and $SnCl_2{\cdot}2H_2O$ resulted in the best yield of **3**. A decrease in the amount of $SnCl_2{\cdot}2H_2O$ afforded **3** in a lower yield, but the yield of **3** did not change with an increase in the amount of $SnCl_2{\cdot}2H_2O$ employed. However, the reaction did not proceed at all without $SnCl_2{\cdot}2H_2O$. The effect of several metallic halides other than $SnCl_2{\cdot}2H_2O$ upon this cyclisation was examined. As shown in Table 1, all the salts except for iron(III) chloride examined were moderately effective in the formation of **3**, but $FeCl_3$ exhibited nearly the same activity as $SnCl_2{\cdot}H_2O$ under the reaction conditions employed.

The present cyclisation could also be applied to many primary aromatic amines, several representative results being summarised in Table 2.‡ The product yield was dependent on the electronic nature of the substituent on anilines. With anilines such as toluidine and anisidine, having electron-donating

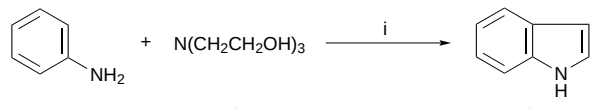

1 **2** **3**

Scheme 1 *Reagents and conditions*: i, $RuCl_3{\cdot}nH_2O$, PPh_3, $SnCl_2{\cdot}2H_2O$, dioxane, 180 °C, 20 h

Table 1 Ruthenium-catalysed synthesis of indole (**3**) under various conditions[a]

Molar ratio (**1** : **2**)	Metallic halides (mmol)	GLC yield (%)[b]
4	$SnCl{\cdot}2H_2O$ (1)	30
6	$SnCl{\cdot}2H_2O$ (1)	29
8	$SnCl{\cdot}2H_2O$ (1)	30
10	$SnCl{\cdot}2H_2O$ (1)	52
10	$SnCl{\cdot}2H_2O$ (0.5)	25
10	$SnCl{\cdot}2H_2O$ (2.0)	51
10	—	Trace
10	$AlCl_3$ (1)	20
10	$SbCl_3$ (1)	16
10	$BiCl_3$ (1)	7
10	$LaCl_3$ (1)	7
10	$FeCl_3$ (1)	52
10	$ZnCl_2$ (1)	15

[a] All reactions were carried out with **2** (1 mmol), $RuCl_3{\cdot}nH_2O$ (7 mol% based on **2**), and PPh_3 (2 mol% based on **2**) in dioxane (10 ml) at 180 °C for 20 h. [b] Based on **2**.

character, the product yield was generally higher than that when chloroanilines having electron-withdrawing Cl substituent were used (runs 2–8). In the cases of *meta*-substituted anilines such as *m*-toluidine and *m*-anisidine, the corresponding indoles were obtained as a regioisomeric mixture in good yields (runs 3 and 5). The enhancement of reactivity of the two-methyl substituted anilines is interesting when compared to the reactivity of the mono-substituted anilines (runs 10–12). However, in the case of 2,5-dimethoxyaniline, the corresponding indole was obtained only in 15% yield (run 13).

Similar treatment of anilines **4** with tri(propan-2-ol)amine (**5**) under the above reaction system afforded two regioisomeric

Table 2 Ruthenium-catalysed synthesis of various indoles[a]

Run	Anilines	Indoles	Isolated yield (%)[b]
1	Aniline	Indole	46
2	*o*-Toluidine	7-Methylindole	66
3	*m*-Toluidine	4- and 6-Methylindole	65[c]
4	*p*-Toluidine	5-Methylindole	38
5	*m*-Anisidine	4- and 6-Methoxyindole	47[c]
6	*p*-Anisidine	5-Methoxyindole	33
7	*o*-Chloroaniline	7-Chloroindole	9
8	*p*-Chloroaniline	5-Chloroindole	21
9	*p*-Isopropylaniline	5-Isopropylindole	56
10	2,3-Dimethylaniline	6,7-Dimethylindole	99
11	2,5-Dimethylaniline	4,7-Dimethylindole	86
12	3,5-Dimethylaniline	4,6-Dimethylindole	90
13	2,5-Dimethoxyaniline	4,7-Dimethoxyindole	15

[a] All reactions were carried out with anilines (10 mmol), **2** (1 mmol), $RuCl_3{\cdot}nH_2O$ (7 mol% based on **2**), PPh_3 (2 mol% based on **2**), and $SnCl_2{\cdot}2H_2O$ (1 mmol) in dioxane (10 ml) at 180 °C for 20 h. [b] Based on **2**. [c] Isomeric molar distributions were determined by ^1H NMR spectroscopy (300 MHz): 4-methylindole : 6-methylindole = 1 : 1; 4-methoxyindole : 6-methoxyindole = 1 : 2.8.

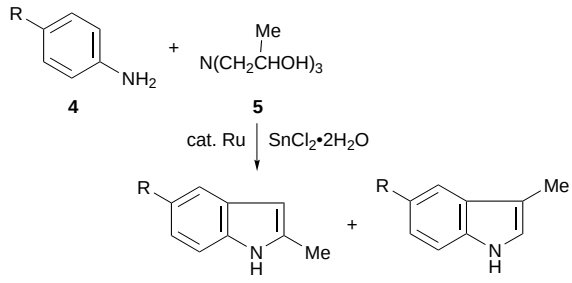

	6 + 7	6:7
R = Me	99%	4:1
R = OMe	96%	5:1
R = Cl	66%	5:1
R = Bu^{i}	99%	5:1

Scheme 2

indoles, **6** and **7**, in quantitative isolated yields, favoring the formation of 2-methylindoles **6** (Scheme 2). In a separate experiment, we observed that a similar reaction of *p*-toluidine with **5** gave two isomeric indoles in 118% GLC yield based on **5**. This result indicates that at least two propan-2-ol groups out of three in **5** are available for the C_2-fragment counterpart.

Although the exact role of $SnCl_2{\cdot}2H_2O$ in the present reaction is still obscure, the reaction pathway seems to be the initial formation of 2-anilinoethanols§ by amine exchange reactions[4b,5] between anilines and trialkanolamines followed by a similar catalytic cycle to that which has already been proposed in ruthenium-catalysed synthesis of indoles from anilines and ethylene glycols.[6]

The authors are grateful to KOSEF (97-05-01-05-01-3)-OCRC and the Non-directed Research Fund of Korea Research Foundation (1997-001-D00294) for financial support of this work.

Notes and References

† E-mail: scshim@kyungpook.ac.kr

‡ General experimental procedure: a mixture of aniline (10 mmol), alkanolamine (1 mmol), $RuCl_3{\cdot}nH_2O$ (0.07 mmol), $SnCl_2{\cdot}2H_2O$ (1 mmol) and PPh_3 (0.21 mmol) in dioxane (10 ml) was placed in a stainless steel autoclave. After the system was flushed with nitrogen gas, the mixture was stirred at 180 °C for 20 h. The reaction mixture was filtered through a short column (silica gel, CH_2Cl_2) and evaporated under reduced pressure. To the residual oily material was added 30 ml of CH_2Cl_2 and the mixture was washed twice with 50 ml of aq. 5% HCl solution to remove excess aniline. The organic layer was dried over anhydrous NA_2SO_4. Removal of the solvent left an oil which was separated by column chromatography (ethyl acetate–hexane) to give indoles.

§ In a separate experiment, we observed that a similar ruthenium-catalysed reaction between *N*-benzyl-*p*-toluidine and triethanolamine resulted in the formation of a small amount of 2-(*N*-benzyl-*p*-tolylamino)ethanol by GC–MS analysis.

1 J. Tsuji, *Palladium Reagents and Catalysis*, Wiley, Chichester, 1995; B. C. Söderberg and J. A. Shriver, *J. Org. Chem*., 1997, **62**, 5838 and references cited therein.
2 G. W. Gribble, in *Comprehensive Heterocyclic Chemistry II*, ed. C. W. Bird, Pergamon Press, Oxford, 1996, vol. 2, pp. 207–257.
3 C. S. Cho, J. W. Lee, D. Y. Lee, S. C. Shim and T. J. Kim, *Chem. Commun*., 1996, 2115; C. S. Cho, L. H. Jiang, D. Y. Lee, S. C. Shim, H. S. Lee and S.-D. Cho, *J. Heterocycl. Chem*., 1997, **34**, 1371; C. S. Cho, D. Y. Chu, D. Y. Lee, S. C. Shim, T. J. Kim, W. T. Lim and N. H. Heo, *Synth. Commun*., 1997, **34**, 4141.
4 (*a*) S. C. Shim, Y. Z. Youn, D. Y. Lee, T. J. Kim, C. S. Cho, S. Uemura and Y. Watanabe, *Synth. Commun*., 1996, **26**, 1349; (*b*) D. Y. Lee, C. S. Cho, J. H. Kim, Y. Z. Youn, S. C. Shim and H. Song, *Bull. Korean Chem. Soc*., 1996, **17**, 1132.
5 S.-I. Murahashi, T. Hirano and T. Yano, *J. Am. Chem. Soc*., 1978, **100**, 348; S.-I. Murahashi, K. Kondo and T. Hakata, *Tetrahedron Lett*., 1982, **23**, 229.
6 Y. Tsuji, K.-T. Huh and Y. Watanabe, *J. Org. Chem*., 1987, **59**, 1673.

Received in Cambridge, UK, 6th February 1998; 8/01090K

Unexpected enhancement of the photonuclease activity of $Ru(bpz)_3^{2+}$ by Cu/Zn superoxide dismutase

Etienne Gicquel, Nicole Paillous*† and Patricia Vicendo

Laboratoire IMRCP, UMR 5623, Université Paul Sabatier, 118 route de Narbonne, 31062 Toulouse Cedex 4, France

Cu/Zn SOD led to an unexpected enhancement of the photonuclease activity of $Ru(bpz)_3^{2+}$ *via* an increase in the production of singlet oxygen.

The ruthenium complexes possess versatile photoredox properties, which are exploited in a wide variety of applications including the photolysis of water,[1–3] development of novel photonucleases[4–8] and more recently for modelling chemical photolyases.[9] The photonuclease[4] activity of these complexes stems in part from their redox potential in the excited state. If this is above that of guanine,[10] the nucleobase with the lowest oxidation potential, under irradiation the polypyridyl ruthenium complexes may induce an electron transfer from DNA to the dye in the excited state, giving rise to single strand breaks in the double helix of DNA.[11,12] The efficiency of this type I mechanism for producing single strand breaks is higher than that of the type II mechanism.[13] Furthermore, it has been shown that electron transfer leads to formation of covalent photoadducts between ruthenium complexes such as tris(1,4,5,8-tetraazaphenanthrene)ruthenium(II) [$Ru(tap)_3^{2+}$][14] and tris(2,2′-bipyrazyl)ruthenium(II) [$Ru(bpz)_3^{2+}$][15] and DNA.

In the case of $Ru(bpz)_3^{2+}$, the mechanism of single strand breaking is complex, involving electron transfer, formation of singlet oxygen and radical species.[15] In order to identify the various oxygenated species involved in the photonuclease activity of $Ru(bpz)_3^{2+}$, and the superoxide anion in particular, we used the Cu/Zn superoxide dismutase (Cu/Zn SOD). While this enzyme should give rise to a reduction in efficiency of the DNA cleavage by $Ru(bpz)_3^{2+}$, *via* a dismutation of $O_2^{\cdot -}$, an unexpected increase in photonuclease activity of this complex was observed. Here, we report the main characteristics of this unexpected effect.

As shown in a previous study,[15] $Ru(bpz)_3^{2+}$ (1.8 μM) in solution [5 mM phosphate buffer (pH 7.4), 10 mM NaCl] and irradiated at 436 nm in the presence of supercoiled phage φX174 DNA (18 μM) induced single strand breaks with a quantum yield of 10^{-5} (Fig. 1). In the presence of Cu/Zn SOD (Cu/Zn SOD from human erythrocytes, 22 U ml^{-1}, 0.299 μM), the number of single strand breaks was 2.4-fold higher at 60 s. This enzyme is not able to induce alone DNA breakage upon irradiation at 436 nm. The same finding was obtained, under similar experimental conditions, with Cu/Zn from bovine erythrocytes. Furthermore, the plot of the number of photoinduced DNA single strand breaks against time in the presence of SOD was not linear. There was an increase in rate with duration of irradiation. After 90 s irradiation, nearly all the supercoiled form of the plasmid had been transformed into the relaxed circular form. This was not observed in the absence of SOD even after 30 min of irradiation.

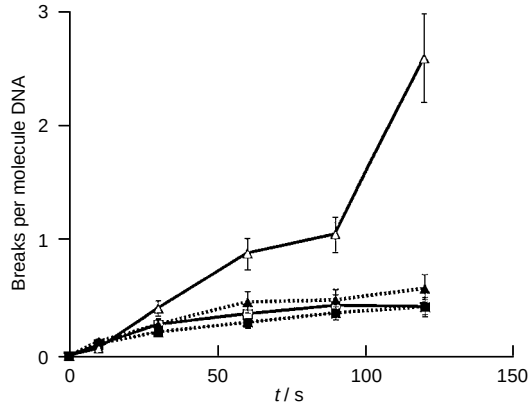

Fig. 1 Plot of number of DNA single strand breaks per molecule of φX174 plasmid DNA photoinduced by $Ru(bpz)_3^{2+}$ at 436 nm against irradiation time: (□) $Ru(bpz)_3^{2+}$, (■) $Ru(bpz)_3^{2+}$ in the absence of oxygen, (△) $Ru(bpz)_3^{2+}$ with Cu/Zn SOD and (▲) $Ru(bpz)_3^{2+}$ with Cu/Zn SOD in the absence of oxygen

In the absence of oxygen, SOD had no significant effect on the DNA single strand breaks induced by $Ru(bpz)_3^{2+}$ (Fig. 1). This indicated that the action of SOD depended on the presence of oxygen, and was mediated by the production of oxygenated species. Catalase (22 U ml^{-1}) and desferioxamine (17 mM) were not found to modify the number of DNA single strand breaks induced by $Ru(bpz)_3^{2+}$ in the presence of Cu/Zn SOD. This observation indicates that the effect of Cu/Zn SOD did not result from the formation of $OH^{\cdot}$ *via* a Fenton reaction. Furthermore, the photonuclease activity of $Ru(bpz)_3^{2+}$ was not augmented in the presence of iron SOD (from *Escherichia coli*). It thus appeared that the action of Cu/Zn SOD was specific to this particular enzyme.

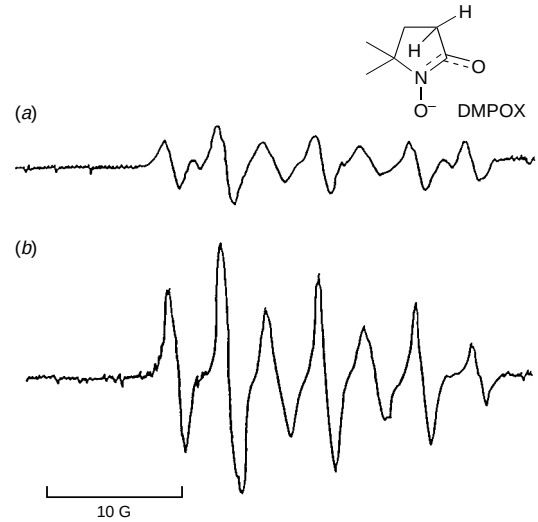

Fig. 2 EPR spectra of UV irradiated (λ > 400 nm) solutions containing DMPO and ruthenium complexes: (*a*) $Ru(bpz)_3^{2+}$ and (*b*) $Ru(bpz)_3^{2+}$ with Cu/Zn SOD

In order to better understand the function of oxygenated radical species in the photoactivation of $Ru(bpz)_3^{2+}$ by Cu/Zn SOD, EPR studies have been performed. EPR studies on $Ru(bpz)_3^{2+}$ (10^{-3} M) irradiated (λ > 400 nm) in the presence of 5,5-dimethyl-2-pyrolidine 1-oxide (DMPO) (150 mM) failed to detect $OH^{\cdot}$ radicals, and indicated the presence of 5,5-dimethyl-2-pyrolidone 1-oxyl radicals (DMPOX) (a_N = 4.1, a_H = 7.2) derived from the oxidation of DMPO by singlet oxygen[16]

(Fig. 2). The formation of this radical was increased almost three-fold by addition of Cu/Zn SOD (22 U ml^{-1}) (Fig. 2). EPR studies of irradiated Cu/Zn SOD in the presence of DMPO did not show the formation of radicals. It thus appeared that the action of Cu/Zn SOD on $Ru(bpz)_3^{2+}$ was mediated by an increase in the production of singlet oxygen, which is responsible for the enhanced photonuclease activity of this complex. This hypothesis was supported by the results obtained on addition of *N*-acetylhistidine (50 mM) and DABCO (20 mM), singlet oxygen scavengers. They led to a 100% inhibition in production of DMPOX radicals in the presence or absence of Cu/Zn SOD. Moreover, *N*-acetylhistidine abolished totally the increase in DNA single strand breaks obtained after photosensitization of DNA by $Ru(bpz)_3^{2+}$ in the presence of this enzyme (Fig. 3).

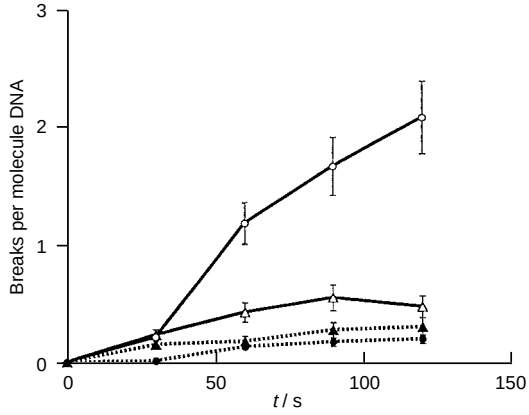

Fig. 3 Plot of number of DNA single strand breaks per molecule of ϕX174 plasmid DNA photoinduced by $Ru(bpz)_3^{2+}$ at 436 nm against irradiation time: (△) $Ru(bpz)_3^{2+}$, (▲) $Ru(bpz)_3^{2+}$ with *N*-acetylhistidine, (○) $Ru(bpz)_3^{2+}$ with Cu/Zn SOD and (●) $Ru(bpz)_3^{2+}$ with Cu/Zn SOD and *N*-acetylhistidine

The action of Cu/Zn SOD (22 U ml^{-1}) on the electron transfer process was investigated by determining the efficiency of $Ru(bpz)_3^{2+}$ (1.5×10^{-4} M) covalent addition to calf thymus DNA (1.5×10^{-3} M in nucleotides) upon irradiation at 436 nm in the presence or absence of this enzyme. Quantification of ruthenium bound to DNA by ICP[15] analysis failed to identify any difference in the kinetics or equilibrium of the addition of $Ru(bpz)_3^{2+}$ to DNA. After 2 h of irradiation at 436 nm in the presence or absence of SOD, the photoadditions reached a plateau corresponding to 1.4×10^{-7} mol of $Ru(bpz)_3^{2+}$ per mg of calf thymus DNA or one molecule of complex for 11 ± 1 nucleotides. SOD thus did not appear to alter the photoreactivity of $Ru(bpz)_3^{2+}$ mediated by electron transfer.

Analysis by UV–VIS spectroscopy of the photochemical behavior of $Ru(bpz)_3^{2+}$ (10^{-5} M) in 5 mM phosphate buffer (pH 7.4) and 10 mM NaCl irradiated at 436 nm showed that SOD did not affect the rate of photodecomposition of $Ru(bpz)_3^{2+}$ (Fig. 4). This observation suggested that the increase in production of singlet oxygen by $Ru(bpz)_3^{2+}$ in the presence of SOD was not due to enhanced photostability of the complex. EPR studies on solutions of complexes of ruthenium of various redox potentials such as tris(2,2′-bipyridyl)ruthenium(II) [$Ru(bipy)_3^{2+}$] [$E(Ru^{2+*}/Ru^{+})$ = 0.77 V *vs*. SCE in MeCN][17] (10^{-3} M) and tris(2,2′-bipyrazyl)(dipyrido[3,2-*a*:2′3′-*c*]phenazine-N^4,N^5)ruthenium(II) [$Ru(bpz)_2dppz^{2+}$] [$E(Ru^{2+*}/Ru^{+})$ = 1.21 V *vs*. SCE in MeCN[13] (10^{-3} M) revealed that, in the absence of SOD, these two compounds generated under irradiation the same radical DMPOX as $Ru(bpz)_3^{2+}$ [$E(Ru^{2+*}/Ru^{+})$ = 1.45 V *vs*. SCE in MeCN].[17] In the presence of Cu/ZnSOD, the increase in production of this radical was, with $Ru(bipy)_3^{2+}$ and $Ru(bpz)_2dppz^{2+}$, 1.4- and 2.6-fold higher, respectively, than in the absence of Cu/Zn SOD. These results show that the increase in production of the DMPOX radical generated by these

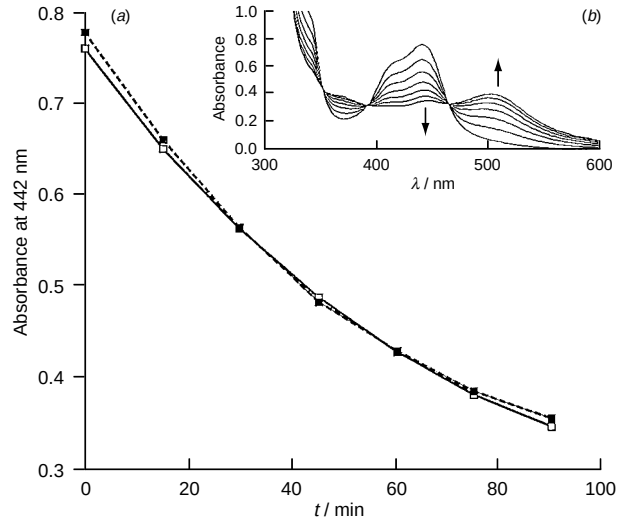

Fig. 4 (*a*) Absorbance at 442 nm of UV irradiated (λ = 436 nm) solutions of $Ru(bpz)_3^{2+}$ (□) without additive and (■) with SOD. (*b*) Variation in absorption spectra of $Ru(bpz)_3^{2+}$ in 5 mM phosphate buffer (pH 7.4) and 10 mM NaCl upon irradiation at 436 nm.

ruthenium complexes in the presence of Cu/Zn SOD partly depends on the redox potential of their excited state.

In conclusion, Cu/Zn SOD led to an unexpected enhancement of the photonuclease activity of $Ru(bpz)_3^{2+}$, which may result from an increase in singlet oxygen production. This unusual phenomenon may be correlated to the strongly oxidizing nature of this dye.

We thank Mr Alain Mari for his technical assistance with the EPR studies.

Notes and References

† E-mail: paillous@ramses.ups-tlse.fr

1 K. Kalyanasundaram, *Coord. Chem. Rev.*, 1982, **46**, 159.
2 J. M. Lehn, J. P. Sauvage and R. Ziessel, *Nouv. J. Chim.*, 1980, **4**, 355.
3 R. J. Crutchley and A. B. P. Lever, *J. Am. Chem. Soc.*, 1980, **102**, 7128.
4 J. M. Kelly, A. B. Tossi, D. J. McConnell and C. OhUigin, *Nucleic Acids Res.*, 1985, **13**, 6017.
5 H. Y. Mei and J. K. Barton, *Proc. Natl. Acad. Sci. USA*, 1988, **85**, 13 395.
6 M. B. Fleisher, K. C. Waterman, N. J. Turro and J. K. Barton, *Inorg. Chem.*, 1986, **25**, 3549.
7 J. M. Kelly, D. J. McConnell, C. OhUigin, A. B. Tossi, A. Kirsch-De Mesmaeker, A. Masschelein and J. Nasielski, *J. Chem. Soc., Chem. Commun.*, 1987, **24**, 1821.
8 A. B. Tossi and J. M. Kelly, *Photochem. Photobiol.*, 1989, **49**, 54.
9 P. J. Dandliker, R. E. Holmlin and J. K. Barton, *Science*, 1997, **275**, 1465.
10 P. Subramanian and G. J. Dryhurst, *J. Electroanal. Chem. Interfac. Electrochem.*, 1987, **224**, 137.
11 A. Kirsch De Mesmaeker, A. G. Orellana, J. K. Barton and N. J. Turro, *Photochem. Photobiol.*, 1990, **52**, 461.
12 J. P. Lecomte, A. Kirsch De Mesmaeker, J. M. Kelly, A. B. Tossi and H. Görner, *Photochem. Photobiol.*, 1992, **55**, 681.
13 C. Sentagne, J. C. Chambron, J. P. Sauvage and N. Paillous, *J. Photochem. Photobiol. B: Biol.*, 1994, **26**, 165.
14 L. Jacquet, J. M. Kelly and A. Kirsch-De Mesmaeker, *J. Chem. Soc., Chem. Commun.*, 1995, 913.
15 P. Vicendo, S. Mouysset and N. Paillous, *Photochem. Photobiol.*, 1997, **65**, 647.
16 M. M. Mossoba, Ionel Rosenthal, A. J. Carmichel and P. Riesz, *Photochem. Photobiol.*, 1984, **39**, 731.
17 M. A. Haga, E. S. Dodsworth, G. Eryavec, P. Seymour and A. B. P. Lever, *Inorg. Chem.*, 1985, **24**, 1091.

Received in Cambridge, UK, 20th January 1998; 8/00545A

Novel mechanistic proposal for the Dötz reaction derived from a density functional study: the chromahexatriene route

Maricel Torrent, Miquel Duran and Miquel Solà*

Department of Chemistry and Institute of Computational Chemistry, University of Girona, E-17071 Girona, Spain

A new mechanism for the Dötz reaction of vinylcarbene complexes with ethyne proceeds through a chromahexatriene intermediate instead of a vinylketene with smooth energy changes and low energy barriers.

One of the most important synthetic transformations leading to C–C bond formation involves the reaction of chromium carbenes with alkynes. This process, a formal [3 + 2 + 1] cycloaddition known as the benzannulation or Dötz reaction,[1] generates substituted phenols by sequential coupling of the alkyne, the carbene and one carbonyl ligand at a $[Cr(CO)_3]$ template. The major interest in this reaction is its utility in organic and organometallic synthesis.

The most widely accepted mechanism[2] assumes that the reaction starts with a reversible decarbonylation followed by alkyne coordination, yielding η^3-vinylallylidene complexes **1** (Scheme 1). Two diverging routes have been postulated from this point. According to Dötz,[2] complexes **1** form η^4-vinylketenes **2** by CO insertion into the chromium–carbene bond, followed by electrocyclic ring closure to yield η^4-cyclohexadienones **3**, which can finally turn into the direct precursor of the phenol derivative **4** after enolization and aromatization. As suggested by Casey,[3] an alternative possibility is that metallation of the arene ring occurs in complex **1** to form **5**, which subsequently undergoes carbonylation to yield **6**. Reductive elimination from **6** gives intermediate **3**, where both scenarios merge again.

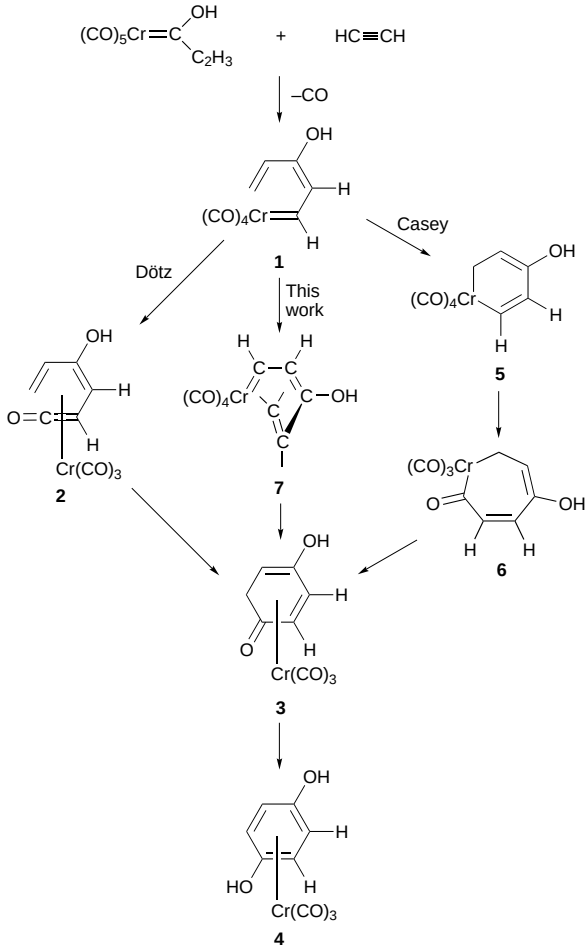

Scheme 1 Postulated routes for the benzannulation reaction

It has proven difficult to validate these mechanistic suggestions since the rate-limiting step typically involves CO ligand loss to open a coordination site for the alkyne to bind. Once bound, rapid ring closure occurs to give the observed products. No single reaction has been followed completely through the individual steps illustrated in Scheme 1, although there are now several examples of isolation and structural characterization of presumed intermediates relevant to η^3-allylidene complexes[4] and η^4-vinylketene complexes.[5] Additional support for the Dötz route has also been provided by extended Hückel molecular orbital[6] and recent quantum chemical calculations.[7] However, most steps are still only postulated. Thus, although kinetic investigations[8] strongly support the assumption for the CO loss as one of the first reaction steps, most of the subsequent intermediates have so far escaped experimental observation.

According to our calculations,[9–14]‡ vinylallylidene complex **1** is a branching point from which the reaction may go on through a third energy path, different from the ones mentioned above. The new proposed pathway also leads to η^4-cyclohexadienone **3**, but, instead of inserting a CO ligand into the Cr–carbene bond, complex **1** can better create first a π-interaction with the terminal C–C double bond yielding a chromahexatriene complex, which undergoes CO insertion in the next step.

The advantage of such a structural arrangement taking place before CO insertion can be seen from Fig. 1. Complex **1** (usually described as an η^3-vinylallylidene[2]) is found to be more favorable in an η^1-coordination (as depicted in Fig. 1) by 11.8 kcal mol^{-1}. The most outstanding feature of η^1-vinylallylidene complex **1** is the agostic interaction between chromium and one of the C_5–H bonds of the terminal alkenyl ligand. The length of the C_5–H bond is *ca.* 0.05 Å larger than the usual distance for a C(sp^2)–H bond, and clearly corresponds to the ones observed for this kind of interactions.[15] The vacant coordination site in complex **1** created after release of a CO ligand *cis* to the carbene fragment remains temporarily blocked by the C_5–H group, and the reaction is prevented from going backwards to the reactants. Once **1** is formed, the ring chain evolves to a more stable conformation through a dπ interaction between chromium and the C_4–C_5 olefinic bond, the release of energy being 11.2 kcal mol^{-1} (Fig. 1). An early, small energy barrier in the path from **1** to **7** (1.8 kcal mol^{-1}) arises from the loss of the agostic interaction while C_4 has not approached the metal center enough (Cr–C_4 = 3.248 Å in **1**, 3.055 Å in TS1, and 2.272 Å in **7**). A crucial feature of complex **7** as compared to complex **1** is the shortening of the distance between C_5 and the CO ligand to be transferred to the Cr–C_5 bond (C_5–CO = 3.517 Å in **1**, and 2.559 Å in **7**), which facilitates CO insertion in the subsequent step (C_5–CO = 2.262 Å in TS2, and 1.533 Å in **3**). Intermediate **7** is directly comparable to η^2-alkenylamino(aryl)carbene complexes of W[16] and Mn,[17] as well as to the more recently

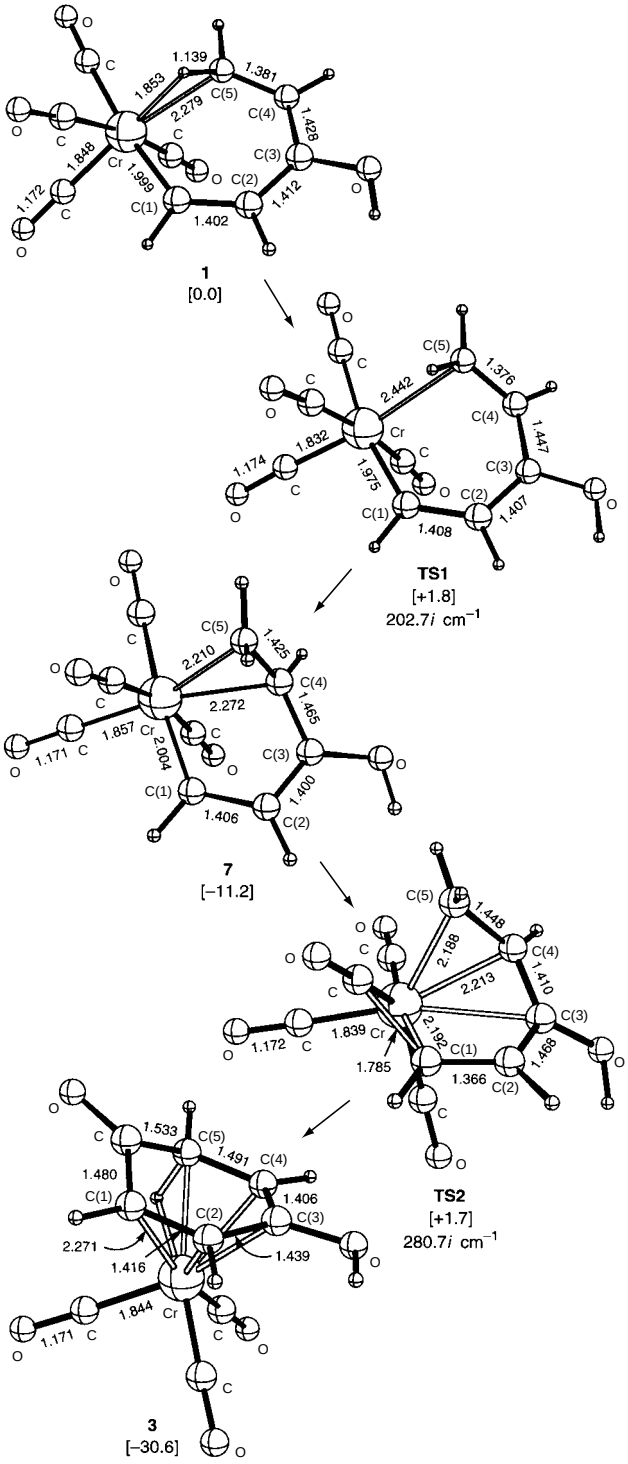

Fig. 1 Geometries of all stationary points and energies relative to complex **1**. Selected bond distances are given in Å, and energies (in square brackets) in kcal mol^{-1}. Compounds **1**, **7** and **3** correspond to minimum energy structures; their absolute energies are −1767.313742, −1767.331596 and −1767.362571 au, respectively. **TS1** (−1767.310883 au) and **TS2** (−1767.310945 au) are first-order saddle points.

reported structure of an alkynylarylcarbene complex of tungsten.[18] In the field of organochromium chemistry, a similar olefin coordination has been also observed for an alkene-[19] and some alkyne-carbenechromium[20] complexes. The strongest support for the existence of **7**, however, probably comes from a recent investigation by Barluenga *et al*.,[4] where a chromahexatriene similar to **7** has been isolated and characterised by ^{1}H and ^{13}C NMR spectroscopy. Experimental data from this study demonstrate that the alkenyl ligand is attached to the metal center through the C_4–C_5 double bond.

Interestingly, chromahexatriene **7** is not an endpoint of the reaction because it connects to a more stable intermediate, as shown in Fig. 1. Distortion of the $Cr(CO)_4$ umbrella mainly accounts for the energy required to reach **TS2** (12.9 kcal mol^{-1}). This is largely compensated by the formation of an agostic interaction in **3**, together with the new Cr–C coordinated bonds in the formed ring. Species **3** with such an agostic interaction has a known precedent in related cationic manganese cyclohexenyl complexes.[21] The fact that the reaction does not end at **7** is consistent again with the experimental results reported by Barluenga *et al*.[4] These authors found that the synthesised chromahexatriene was not stable in solution at room temperature, and decomposed to yield the most common final product in the Dötz reaction with aminocarbenes.[4]

Additional theoretical work on the routes proposed by Dötz and Casey is presently in progress in our laboratory. Preliminary results indicate that the chromahexatriene mechanism presented here seems to be the most favorable of the three proposed routes. Whether this conclusion can be generalised to substrates other than vinyl carbene complexes is the subject of further research.§

Notes and References

† E-mail: miquel@stark.udg.es

‡ Calculations have been carried out with the GAUSSIAN 94 series of programs[9] using the DFT methodology with the non-local BP86 functional.[10] All geometries have been fully optimised. We have also verified that the imaginary frequency for each transition state exhibits the expected motion.

§ Financial support is acknowledged from the Spanish DGES under project PB95-0762. M. T. thanks the Direcció General de Recerca de la Generalitat de Catalunya for a fellowship. We thank the CESCA for a generous allocation of computing time.

1 K. H. Dötz, *Angew. Chem., Int. Ed. Engl.*, 1975, **14**, 644.
2 K. H. Dötz, *Angew. Chem., Int. Ed. Engl.*, 1984, **23**, 587.
3 C. P. Casey in *Reactive Intermediates*, ed. M. Jones, Jr., and R. A. Moss, Wiley, New York, 1981, vol. 2, p. 155.
4 J. Barluenga, F. Aznar, A. Martín, S. García-Granda and E. Pérez-Carreño, *J. Am. Chem. Soc.*, 1994, **116**, 11 191.
5 E. Chelain, R. Goumont, L. Hamon, A. Parlier, M. Rudler, H. Rudler, J. C. Daran and J. Vaissermann, *J. Am. Chem. Soc.*, 1992, **114**, 8088; B. A. Anderson, J. Bao, T. A. Brandvold, C. A. Challener, W. D. Wulff, Y.-C. Xu and A. L. Rheingold, *J. Am. Chem. Soc.*, 1993, **115**, 10 671.
6 P. Hofmann and M. Hämmerle, *Angew. Chem., Int. Ed. Engl.*, 1989, **28**, 908; P. Hofmann, M. Hämmerle and G. Unfried, *New J. Chem.*, 1991, **15**, 769.
7 M. M. Gleichmann, K. H. Dötz and B. A. Hess, *J. Am. Chem. Soc.*, 1996, **118**, 10 551.
8 H. Fischer, J. Mühlemeier, R. Märkl and K. H. Dötz, *Chem. Ber.*, 1982, **115**, 1355.
9 GAUSSIAN 94, Gaussian, Inc. Pittsburg PA, 1995.
10 A. D. Becke, *Phys. Rev.*, 1988, **A38**, 3098; J. P. Perdew, *Phys. Rev.*, 1986, **B33**, 8822; *ibid*., 1986, **B34**, 7406E.
11 H. B. Schlegel, *J. Comput. Chem.*, 1982, **3**, 214.
12 The 6-31G** basis set[13] was employed for C, O and H atoms. For the chromium atom we used a basis set as described by Wachters[14] in a (62111111/3312/311) contraction scheme.
13 J. S. Binkley, J. A. Pople and W. J. Hehre, *J. Am. Chem. Soc.*, 1980, **102**, 939.
14 A. J. H. Wachters, *J. Chem. Phys.*, 1970, **52**, 1033.
15 F. Zaera, *Chem. Rev.*, 1995, **95**, 2651.
16 C. P. Casey, A. J. Shusterman, N. W. Vollendorf and K. J. Haller, *J. Am. Chem. Soc.*, 1982, **104**, 2417.
17 M. J. McGeary, T. L. Tonker and J. L. Templeton, *Organometallics*, 1985, **4**, 2102.
18 K. H. Dötz, T. Schäfer, F. Kroll and K. Harms, *Angew. Chem., Int. Ed. Engl.*, 1992, **31**, 1236.
19 K. H. Dötz, M. Popall and G. Müller, *J. Org. Chem.*, 1987, **334**, 57.
20 F. Hohmann, S. Siemoneit, M. Nieger, S. Kotila and K. H. Dötz, *Chem. Eur. J.*, 1997, **3**, 853.
21 T. R. Tritcak, J. B. Sheridan, M. L. Cote, R. A. Lalancette and J. P. Rose, *J. Chem. Soc., Dalton Trans.*, 1995, **6**, 931.

Received in Cambridge, UK, 22nd December 1997; 7/09126E

Synthesis, structure and cationic ring-opening polymerization (ROP) of a strained [2]carbathioferrocenophane

Rui Resendes, Paul Nguyen, Alan J. Lough and Ian Manners*†

Department of Chemistry, University of Toronto, 80 St. George Street, Toronto, Ontario, Canada M5S 3H6

The synthesis and cationic ring-opening polymerization of a novel [2]carbothiaferrocenophane is reported; the polymerization represents the first cationic ring-opening polymerization of a metal-containing ring.

Macromolecules containing transition metal atoms in the main chain are attracting growing attention as a result of their combination of processability and interesting physical properties.[1–3] Until recently, the development of this area has been hindered by the lack of viable synthetic routes to these materials.[2] The recent discovery of a thermal ring-opening polymerization (ROP) route to poly(ferrocenes) from strained [1]- and [2]-metallocenophanes **1** provided facile access to high molecular mass metallocene-based polymers **2** with interacting metal atoms.[4–6] Subsequently, examples of anionic and transition metal-catalyzed ROP of [1]ferrocenophanes have also been reported which afford routes to polymers with controlled architectures including block and graft copolymers.[7–10] Recent attention has focused on detailed studies of the interesting properties of the resulting poly(metallocenes) including their electrochemical, charge transport, electrochromic and morphological (*e.g.* liquid crystalline) properties and their potential function as precursors to spin-aligned magnetic materials *via* oxidation or pyrolysis.[5,11–15]

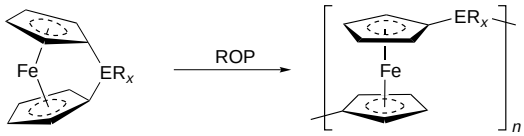

1 **2**

Cationic polymerization provides an important, well established methodology for the preparation of organic polymers which complements other synthetic routes.[16,17] However, to date, cationic ROP of a metal-containing ring has not been reported. In this paper we report the synthesis of a novel [2]ferrocenophane which undergoes the first example of such a cationic ROP process.

Few examples of unsymmetrically bridged [2]ferrocenophanes have been reported.[18] We found that the reaction of the pmdeta (pmdeta = 1,1,4,7,7-pentamethyldiethylenetriamine) adduct of ($C_5Me_4CH_2Li$)(C_5H_4Li)Fe in Et_2O at −78 °C with 1 equiv. of $S(SO_2Ph)_2$ afforded **3** in 30% yield as deep red crystals after purification by vacuum sublimation. The identity of **3** was confirmed by ^{1}H and ^{13}C NMR and GC–MS.[19] The ^{1}H NMR spectrum revealed the α and β protons of the Cp ring at δ 4.69 and 3.64, respectively. The large separation of the Cp proton resonances is indicative of the ring strain present in **3**. Of note, is the bridging CH_2 resonance which occurs quite downfield at δ 4.17, indicating a deshielded environment. The ^{13}C NMR shows the C_{ipso} resonances of the Cp′ (tetramethyl-Cp) and Cp rings occurring at δ 83.8 and 93.7, respectively. This is, again, consistent with the proposed structure of **3**. An X-ray diffraction analysis of a suitable single crystal was also performed.[20] The molecular structure of **3** is shown in Fig. 1; of note is the 18.5(1)° angle between the planes of the Cp′ and Cp rings. This

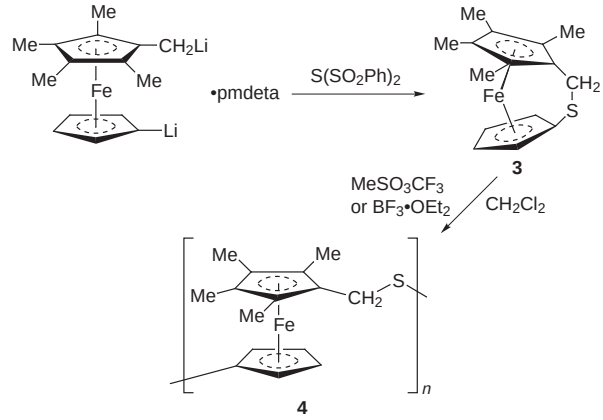

3

4

Scheme 1

suggests that **3** possesses significant ring strain and may be a suitable candidate for ROP.

DSC analysis of **3** revealed an endotherm associated with the melting point at 68 °C and an exotherm due to ROP at 210 °C. When a sample of **3** was heated at 215 °C in a sealed, evacuated Pyrex tube, a yellow fibrous material which was insoluble in common organic solvents was obtained. A small fraction, which was soluble in C_6D_6, was shown to be the ring-opened poly(carbothiaferrocene) **4** by ^{1}H NMR (see below). GPC analysis of this soluble fraction (in THF) revealed a M_w of *ca.* 6000 with a PDI value of 1.1.

Samples of **3** in C_6D_6 did not undergo ROP under the influence of anionic initiators such as Bu^{n}Li. However, treatment of both CH_2Cl_2 and C_6D_6 solutions of **3** with methyl triflate, $MeSO_3CF_3$, resulted in a color change from bright red to light orange, followed by the precipitation of a fine yellow powder. ^{1}H NMR analysis of the soluble fraction demonstrated

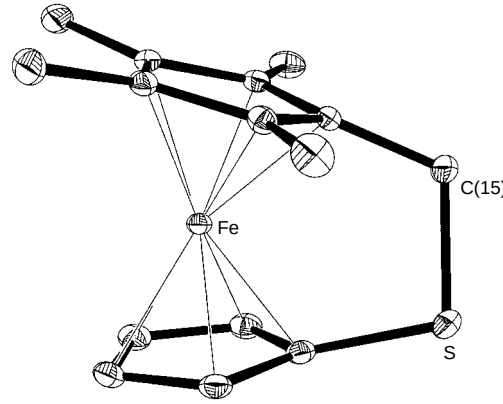

Fig. 1 X-Ray crystal structure of **3**, showing 30% thermal ellipsoids. Hydrogen atoms have been omitted for clarity. Selected bond lengths (Å) and angles (°): Fe–Cp$_{centroid}$ 1.82(2), C(15)–S 1.844(2), Cp$_{ipso}$–S 1.783(2), Cp′$_{ipso}$–C(15) 1.513(3); α (angle between Cp planes) 18.51(14), β_1 [angle between Cp plane and Cp$_{ipso}$–S bond) 10.9(2), β_2 [angle between Cp′ plane and Cp′$_{ipso}$–C(15) bond] 9.5(2).

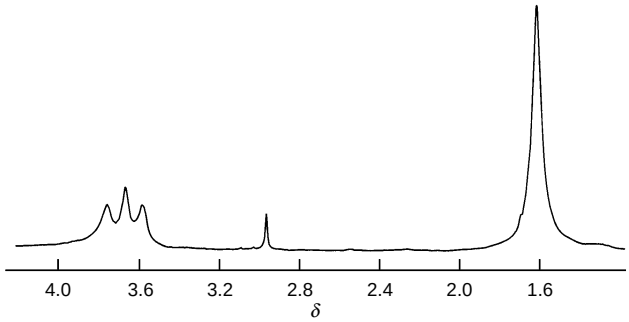

Fig. 2 400 MHz ^{1}H NMR (C_6D_6) of **4** (soluble fraction)

that ROP to yield **4** had indeed occurred (Fig. 2).[21] Of note in the ^{1}H NMR spectrum of **4** is the broad multiplet centered at δ 3.65 which arises from both the Cp and bridging methylene protons as well as the broad resonance centered at δ 1.61 corresponding to the Cp′ methyl protons.

A side reaction of the MeOTf initiated polymerization involved oxidation of the resulting material. In an attempt to circumvent this, initiation of ROP was attempted with the alternative Lewis acid, $BF_3{\cdot}OEt_2$. Indeed, when a toluene solution of **3** was treated with 0.02 equiv. of $BF_3{\cdot}OEt_2$, ROP did occur, as evidenced by ^{1}H NMR, the immediate color change of the solution, and the precipitation of **4**. However, unlike the MeOTf initiated polymerization, no oxidation of the polymer was apparent. ^{1}H NMR analysis of the soluble fraction and CP MAS ^{13}C NMR[22] analysis of the bulk material confirmed the presence of **4** and is consistent with the proposed structure. In addition, analysis by mass spectrometry revealed peaks which could be assigned to species possessing oligomeric $[(\eta\text{-}C_5Me_4)Fe(\eta\text{-}C_5H_4)CH_2S]_x$ units where x = 1–3. This again is consistent with the proposed polymeric structure of **4**.

In summary, we have shown that the novel [2]ferrocenophane **3** successfully undergoes both thermal and cationic initiated ROP to afford the polymer **4**, the high molecular mass fraction of which is insoluble in common organic solvents. Future work in this area will involve studies of the ROP mechanism and copolymerization of **4** with other heterocycles in an effort to obtain soluble, high molecular mass materials.

We would like to thank the Petroleum Research Fund (PRF) administered by the American Chemical Society for funding of this research. R. R. thanks the University of Toronto for an Open Scholarship (1997–98) and P. N. thanks the Natural Science and Engineering Research Council of Canada (NSERC) for a postdoctoral fellowship. I. M. is grateful to the Alfred P. Sloan Foundation for a Research Fellowship (1994–98), NSERC for an E. W. R. Steacie Fellowship (1997–1998), and the University of Toronto for a McLean Fellowship (1997).

Notes and References

† E-mail: imanners@alchemy.chem.utoronto.ca

‡ *Crystallographic data* for **3**: $C_{15}H_{18}FeS$, M_w = 286.2, monoclinic, space group $P2_1/c$, a = 8.0787(6), b = 24.179(3), c = 7.5462(10) Å, β = 117.553(7)°, U = 1306.9(2) Å^3, Z = 4, D_c = 1.455 g cm^{-3}, μ = 12.87 cm^{-1}, R_1 (wR_2) = 0.0365(0.975). CCDC 182/807

1 See, for example: C. U. Pittman, Jr., C. E. Carraher, M. Zeldin, J. E. Sheats and B. M. Culbertson, *Metal-Containing Polymeric Materials*, Plenum, New York, 1996; M. H. Chisholm, *Angew. Chem., Int. Ed. Engl.*, 1991, **30**, 673; M. Rosenblum, *Adv. Mater.*, 1994, **6**, 159.
2 I. Manners, *Angew. Chem., Int. Ed. Engl.*, 1996, **35**, 1602.
3 P. F. Brandt and T. B. Rauchfuss, *J. Am. Chem. Soc.*, 1992, **114**, 1926; D. L. Compton, P. F. Brandt, T. B. Rauchfuss, D. F. Rosenbaum and C. F. Zukoski, *Chem. Mater.*, 1995, **7**, 2342.
4 D. A. Foucher, B.-Z. Tang and I. Manners, *J. Am. Chem. Soc.*, 1992, **114**, 6246.
5 I. Manners, *Adv. Organomet. Chem.*, 1995, **37**, 131.
6 J. M. Nelson, H. Rengel and I. Manners, *J. Am. Chem. Soc.*, 1993, **115**, 7035.
7 Y. Ni, R. Rulkens and I. Manners, *J. Am. Chem. Soc.*, 1996, **118**, 4102.
8 Y. Ni, R. Rulkens, J. K. Pudelski and I. Manners, *Macromol. Rap. Commun.*, 1995, **16**, 637.
9 N. P. Reddy, H. Yamashita and M. Tanaka, *J. Chem. Soc., Chem. Commun.*, 1995, 2263.
10 P. Gómez-Elipe, P.M. Macdonald and I. Manners, *Angew. Chem., Int. Ed. Engl.*, 1997, **36**, 762.
11 R. Rulkens, A. J. Lough, I. Manners, S. R. Lovelace, C. Grant and W. E. Geiger, *J. Am. Chem. Soc.*, 1996, **118**, 12 683; X.-H. Liu, D. W. Bruce and I. Manners, *Chem. Commun.*, 1997, 289; R. Petersen, D. A. Foucher, B.-Z. Tang, A. J. Lough, N. P. Raju, J. E. Greedan and I. Manners, *Chem. Mater.*, 1995, **7**, 2045.
12 S. Barlow, L. Rohl, S. Shi, C. M. Freeman and D. O'Hare, *J. Am. Chem. Soc.*, 1996, **118**, 7578.
13 M. T. Nguyen, A. F. Diaz, V. V. Dementev and K. H. Pannell, *Chem. Mater.*, 1994, **6**, 952.
14 M. Hmyene, A. Yasser, M. Escorne, A. Percheron-Guegan and F. Garnier, *Adv. Mater.*, 1994, **6**, 564.
15 J. M. Nelson, P. Nguyen, R. Petersen, H. Rengel, P. M. Macdonald, A. J. Lough, I. Manners, N. P. Raju, J. E. Greedan, S. Barlow and D. O'Hare, *Chem. Eur. J.*, 1997, **3**, 573; R. Rulkens, R. Resendes, A. Verma, I. Manners, K. Murti, E. Fossum, P. Miller and K. Matyjaszewski, *Macromolecules*, 1997, **30**, 8165.
16 J. S. Hrkach and K. Matyjaszewski, *J. Inorg. Organomet. Polym.*, 1995, **5**, 183; K. Matyjaszewski, *J. Phys. Org. Chem.*, 1995, **8**, 197.
17 P. A. Wagner and J. H. Benson, in *Encyclopedia of Polymer Science and Engineering*, ed. H. F. Mark, N. M. Bikales, C. G. Overberger and G. Menges, Wiley, New York, 1989, vol. 16, p. 246; S. Penczek, P. Kubisa and K. Matyjaszewski, *Adv. Polym. Sci.*, 1980, **37**, 1; 1985, **68**/**69**, 186.
18 (*a*) S. Chao, J. L. Robbins and M. S. Wrighton, *J. Am. Chem. Soc.*, 1983, **105**, 181; (*b*) R. B. Abramovitch, J. J. Atwood, M. L. Good and B. A. Lampert, *Inorg. Chem.*, 1975, **14**, 3085.
19 For **3**: ^{1}H NMR (400 MHz, C_6D_6): δ 4.69 (m, 2 H, η-C_5H_4), 4.17 (s, 2 H, CH_2S), 3.64 (m, 2 H, η-C_5H_4), 2.41 (s, 6 H, η-C_5Me_4), 1.65 (s, 6 H, η-C_5Me_4); ^{13}C NMR (400 MHz, C_6D_6, room temp.): δ 93.7 (Cp_{ipso}), 84.7 (η-C_5Me_4), 84.6 (η-C_5H_4), 83.8 (Cp'_{ipso}), 81.2 (η-C_5Me_4), 71.2 (η-C_5H_4), 42.6 (CH_2S), 12.3 (η-C_5Me_4), 11.2 (η-C_5Me_4); GC–MS (70 eV): *m/z* (%) 286 (100) [M$^+$], 194 (8) [M$^+$ − 4CH$_3$ − S], 126 (11) [M$^+$ − 4CH$_3$ − CH$_2$ − S − Fe].
20 A crystal of **3** suitable for X-ray diffraction analysis was obtained from a recrystallization in minimal hexanes at −30 °C.
21 For **4**: ^{1}H NMR (400 MHz, C_6D_6): δ 3.65 (br, m, 6 H, η-C_5H_4, CH_2S), 2.95 (br, s, CH_3OTf), 1.61 (br, s, 12 H η-C_5Me_4).
22 For **4**: ^{13}C CP MAS NMR (400 MHz, 8 kHz spin rate): δ 83.6–72.1 (br, m, η-C_5Me_4, η-C_5H_4), 35.9 (br, s, CH_2), 10.4 (br, s, C_5Me_4).

Received in Bath, UK, 13th January, 1998; 8/00378E

Sulfur dioxide gas detection by reversible η^1-SO_2–Pt bond formation as a novel application for periphery functionalised metallo-dendrimers‡

Martin Albrecht,[a] Robert A. Gossage,[a] Anthony L. Spek[b] and Gerard van Koten*[a]†

[a] *Debye Institute, Department of Metal-Mediated Synthesis, Utrecht University, Padualaan 8, 3584 CH Utrecht, The Netherlands*
[b] *Bijvoet Centre for Biomolecular Research, Crystal and Structural Chemistry, Utrecht University, Padualaan 8, 3584 CH Utrecht, The Netherlands*

Multimetallics such as dendrimer 3 which are functionalised at their periphery with platinum(II) metal centres reversibly absorb SO_2 to yield macromolecules with significantly enhanced solubility characteristics and drastic colour changes; properties which make these compounds highly active sensors for milligram quantities of toxic SO_2 gas.

Since the first reports of synthetic dendrimers in the late 1970s, these compounds have been of widespread interest.[1] Several applications for this type of macromolecule have been realised owing to their unique properties, *e.g.* homogeneous catalysis,[2] as receptors for bioactive molecules[3] or in photophysical applications.[4] Herein we report the first example of transition-metal modified dendrimers which reversibly bind SO_2 and therefore have potential for use as molecular sensors for this toxic gas.

Platinum(II) complexes of type **1** (Scheme 1) have been shown to be suitable precursors for the synthesis of multimetallic systems. Using the methodology developed by Miller *et al.*[5] trimetallic compound **2** and dendrimer **3** containing platinum(II) functional units have been prepared from **1** (Scheme 1).[6,7] The characterisation of these materials, however, is hampered by their low solubility properties. In contrast to their carbosilane analogues,[2] dendrimers which contain aryl-ester core units have been calculated to be planar molecules.[6] This molecular geometry may be the reason for the low solubility of **2** and **3** in common organic solvents. From earlier experiments however, it has been shown that mononuclear platinum and nickel complexes containing the terdentate monoanionic diaminoaryl ligand [NCN$^-$ = {C_6H_2-(CH_2NMe_2)$_2$-2,6-R-4}$^-$] reversibly bind SO_2[8–10] and coordination of this ligand is known to greatly increase the solubility of the resulting five-coordinate platinum(II) compounds.[11] All these SO_2 adducts possess a generalised square pyramidal geometry around the metal centre.[12] A crystal structure determination of the SO_2 adduct of **1c** (**4**; Fig. 1) confirms that SO_2 is bound to Pt in a η^1-binding mode through sulfur and is positioned at the apex of a distorted square-pyramid, which best describes the geometry around the metal centre.§ No disorder arising from interactions with iodide have been found. It is noteworthy that in earlier studies,[13] SO_2 has been found to be bound to iodide, which is competitive to platinum in size and electronegativity.

Thus, we have studied the effect of the presence of SO_2 on dendrimers which are functionalised with square planar platinum(II) metal centres. Compounds **2** and **3** react instantaneously when exposed to SO_2 (g) to form the corresponding SO_2 adducts **5** and **6**,¶ respectively (Scheme 2), both in the solid state and in solution (*e.g.* $CHCl_3$, toluene; max. solubility of **6** in $CHCl_3$: 2.5 mass%). Adduct formation is suggested by ^{1}H NMR spectroscopy, since the resonance signals of protons in close proximity to Pt undergo a characteristic down field shift [0.23 ppm for the CH_2N methylene protons and 0.16 ppm for the $N(CH_3)_2$ groups].[8] Owing to the change of the coordination number around the metal centre, the electronic spectrum shows two new absorption bands at *ca.* 350 and 400 nm (CH_2Cl_2 solution). The exact wavelengths of these bands depend on the metal-bound halogen atom, but are not significantly changed by different substituents on the aryl ring of the NCN ligand.[14] The band at higher frequency is quite strong with absorption coefficients > 20 000 dm^3 mol^{-1} cm^{-1}. In an atmosphere of SO_2, adduct formation of these new materials occurs quantita-

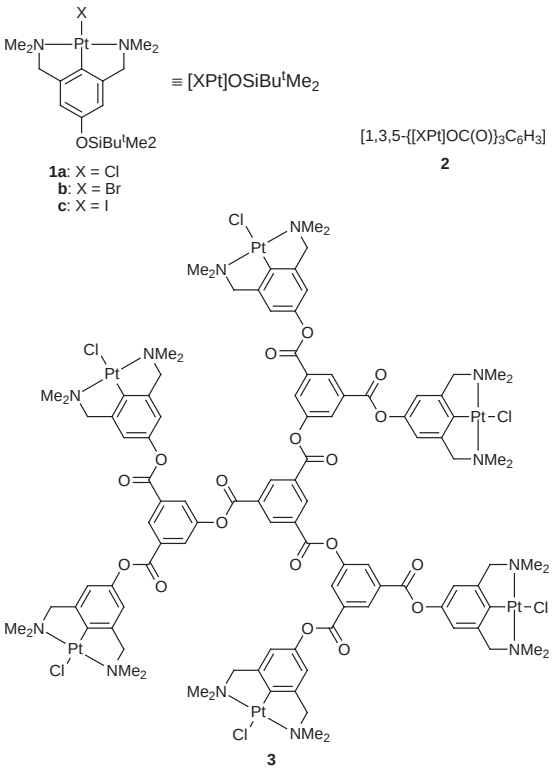

Scheme 1 Mono- and multi-metallic platinum(II) complexes containing aryldiamine ligands

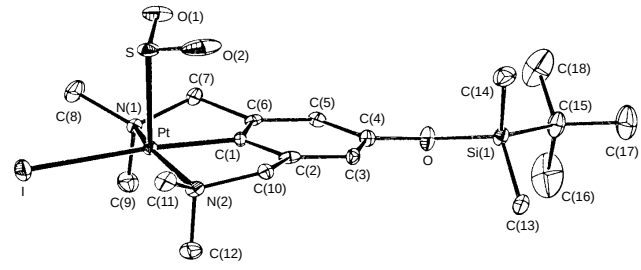

Fig. 1 ORTEP plot (50% probability level) of **4**. Hydrogen atoms have been omitted for clarity. Selected bond lengths (Å) and angles (°), Pt–I 2.7175(7), Pt–N(1) 2.112(4), Pt–N(2) 2.113(5), Pt–C(1) 1.946(6), Pt–S 2.4792(15), S–O(1) 1.443(4), S–O(2) 1.433(6); I–Pt–S 94.14(4), C(1)–Pt–S 91.44(18).

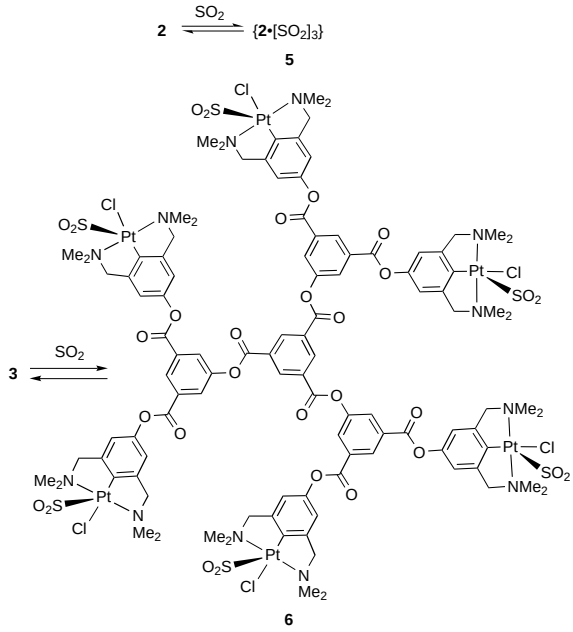

Scheme 2 Formation of the SO_2 adducts **5** and **6** from the corresponding multimetallic precursors upon addition of sulfur dioxide

tively both when the compounds are in the solid state or in solution. The reaction process can be followed visually and/or by UV–VIS spectroscopy, as a characteristic change from colourless to bright orange is noted. Traces of SO_2 are sufficient to observe this change. For example, with a CH_2Cl_2 solution of **2** which is exposed to SO_2, concentrations as low as 10 mg dm^{-3} (at a platinum/SO_2 molar ratio of 0.2) can be detected using UV–VIS spectroscopy. Similarly, when the atmosphere contains SO_2 (3 ± 0.5%), coating of a filter paper with **2** by 10 nmol mm^{-2} is already sufficient to detect a significant colour change. Obviously, higher sensitivity towards SO_2 can be achieved by increasing the concentration of the adsorbed dendrimer.‖

Desorption of SO_2 from adducts **5** and **6** can be achieved by a number of mild procedures, such as heating to 40 °C for several minutes or reducing the pressure to *ca.* 2.7 kPa (20 mm Hg). Both methods quantitatively regenerate **2** or **3**, respectively. Repetitive adsorption/desorption cycles have been performed without significant loss of material or activity.

In contrast to monomeric analogues or dendrimers containing flexible cores (*e.g.* carbosilanes or aminoalkanes), the organometallic trimer and dendrimer presented here possess a rigid disc-like molecular structure and therefore are probably better candidates for recovery *via* ultrafiltration technology.[15,**] Owing to the electronic characteristics of the NCN–metal unit,[16] the Pt–C bond in monomeric and dendritic compounds is resistant to insertion reactions of SO_2. In addition, this stability allows the construction of macromolecules starting from simple organometallic building blocks rather than from metal-free ligand precursors.[1,2] Such a methodology reduces the difficulties associated with quantitative end-group substitution.[6]

The organometallic compounds presented here are characterised by their high reactivity towards sulfur dioxide and even submillimolar quantities of this gas are indicated by a drastic colour change. Moreover, mild and selective methods are available to recycle the adducts to the SO_2 free compounds in order to regenerate the 'detector'. In addition, these materials can be used in the solid state (pure or adsorbed onto an inert surface) or in dilute solution, a property which greatly broadens their potential application. An increase in sensitivity and/or efficiency may be possible with dendrimers of higher generation or by adjustment of the ligand array around the Pt metal centre, *e.g.* by changing the metal-bound halogen atom. Optimization of the properties of these dendrimers is a subject of current investigation in our laboratories.

We thank Huub Kooijman for crystal data collection and Utrecht University for financial assistance. This work was supported in part (A. L. S.) by the Netherlands Foundation for Chemical Research (S. O. N.) with financial aid from the Netherlands Organisation for Scientific Research (N. W. O.).

Notes and References

† E-mail: g.vankoten@chem.ruu.nl

‡ Part of this report was presented at the 4th European Conference on Molecular Electronics (ECME), University of Cambridge, UK, September 1997.

§ *Crystal data* for **4**: $C_{18}H_{33}IN_2O_3PtSSi$, M_r = 707.61, orange, cut to shape crystal (0.15 × 0.30 × 0.30 mm), orthorhombic, space group $Pna2_1$ (no. 33), a = 11.7451(8), b = 17.3316(12), c = 11.8018(12) Å, U = 2402.4(3) Å^3, Z = 4, D_c = 1.9564(2) g cm^{-3}, $F(000)$ = 1360, μ(Mo-Kα) = 72.8 cm^{-1}, 8751 reflections measured, 4177 independent, R_{int} = 0.0274, (2.10 < θ < 27.50°, ω scan, T = 150 K, Mo-Kα radiation, graphite monochromator, λ = 0.710 73 Å) on an Enraf-Nonius CAD4-T diffractometer on rotating anode. CCDC 182/779.

¶ *Selected data* for **6**: ^{1}H NMR ($CDCl_3$–SO_2), δ 9.26 (s, 3 H), 8.81 (s, 3 H), 8.32 (s, 6 H), 6.79 (s, 12 H), 4.24 (s, 24 H) 3.20 (s, 72 H); λ_{max} (ε/dm^3 mol^{-1} cm^{-1}) (CH_2Cl_2–SO_2): 405 nm (sh, 11 000), 354 nm (42 000). According to stopped-flow measurements, the equilibrium between **3** and **6** is reached in less than 5 ms (UV–VIS) after addition of SO_2.

‖ Compare the threshold values which are presently in use: Central Europe (Zürich): 100 ng dm^{-3}; North America (Los Angeles): 520 ng dm^{-3}.

** Successful application of ultrafiltration techniques in membrane reactors has been demonstrated recently for the first generation dendrimers: A. W. Kleij, R. A. Gossage, N. Brinkmann, U. Kragl and G. van Koten, manuscript in preparation. N. Brinkmann, Diploma Thesis, Forschungszentrum Jülich, Germany, 1997. A. W. Kleij, R. A. Gossage, H. Kleijn, G. van Koten, U. Kragl and N. Brinkmann, *2nd Anglo–Dutch Symposium on Catalysis and Organometallic Chemistry*, Amsterdam, 1997, poster 09.

1 G. R. Newkome, C. N. Morefield and F. Vögtle, *Dendritic Molecules, Concepts, Syntheses, Perspectives*, VCH, Weinheim, 1996; J. M. J. Fréchet, *Science*, 1994, **263**, 1710; J. Issberner, R. Moors and F. Vögtle, *Angew. Chem.*, 1994, **106**, 2507; *Angew. Chem., Int. Ed. Engl.*, 1994, **33**, 2413.
2 J. W. J. Knapen, A. W. van der Made, J. C. de Wilde, P. W. M. N. van Leeuwen, P. Wijkens, D. M. Grove and G. van Koten, *Nature*, 1994, **372**, 659.
3 P. Wallimann, P. Seiler and F. Diederich, *Helv. Chim. Acta*, 1996, **79**, 779.
4 C. J. Hawker, K. L. Wooley and J. M. J. Fréchet, *J. Am. Chem. Soc.*, 1993, **115**, 4375; E. C. Constable, *Chem. Commun.*, 1997, 1073.
5 T. M. Miller, E. W. Kwock and T. X. Neenan, *Macromolecules*, 1992, **25**, 3143.
6 P. J. Davies, D. M. Grove and G. van Koten, *Organometallics*, 1997, **16**, 800.
7 The synthesis of **3** will be reported separately: M. Albrecht, R. A. Gossage and G. van Koten, manuscript in preparation.
8 J. Terheijden, G. van Koten, P. Mul, D. J. Stufkens, F. Muller and C. H. Stam, *Organometallics*, 1986, **5**, 519.
9 M. Albrecht, R. A. Gossage, A. L. Spek and G. van Koten, manuscript in preparation.
10 U. Schimmelpfennig, R. Zimmering, K. D. Schleinitz, R. Stösser, E. Wenschuh, U. Baumeister and H. Hartung, *Z. Anorg. Allg. Chem.*, 1993, **619**, 1931.
11 P. Steenwinkel, H. Kooijman, A. L. Spek, D. M. Grove and G. van Koten, *Organometallics*, submitted.
12 D. M. P. Mingos, *Transition Met. Chem.*, 1978, **3**, 1; R. R. Ryan, G. J. Kubas, D. C. Moody and P. G. Eller, *Struct. Bonding* (*Berlin*), 1981, **46**, 47; G. J. Kubas, *Acc. Chem. Res.*, 1994, **27**, 183.
13 M. R. Snow and J. A. Ibers, *Inorg. Chem.*, 1973, **12**, 224.
14 L. A. van de Kuil, H. Luitjes, D. M. Grove, J. W. Zwikker, J. G. M. van der Linden, A. M. Roelofsen, L. W. Jenneskens, W. Drenth and G. van Koten, *Organometallics*, 1994, **13**, 468.
15 U. Kragl, C. Dreisbach and C. Wandrey, in *Applied Homogeneous Catalysis with Organometallic Compounds*, ed. B. Cornils and W. A. Herrmann, VCH, Weinheim, 1996, vol. 2, p. 832.
16 G. van Koten, *Pure Appl. Chem.*, 1989, **61**, 1681; M. H. P. Rietveld, D. M. Grove and G. van Koten, *New J. Chem.*, 1997, **21**, 751.

Received in Cambridge, UK, 1st December 1997; 7/08630J

Systematic synthesis of a series of hydroperoxo-, alkylperoxo- and μ-peroxo-palladium complexes supported by the hydrotris(3,5-diisopropylpyrazolyl)borate ligand (Tp^{iPr}), $Tp^{iPr}Pd(py)–OOX$ [X = $PdTp^{iPr}(py)$, H, Bu^t], *via* dehydrative condensation of a hydroxo complex, $Tp^{iPr}Pd(py)–OH$

Munetaka Akita,*† Taichi Miyaji, Shiro Hikichi and Yoshihiko Moro-oka*

Research Laboratory of Resources Utilization, Tokyo Institute of Technology, 4259 Nagatsuta, Midori-ku, Yokohama 226-8503, Japan

A series of hydroperoxo, *tert*-butylperoxo and μ-peroxo complexes of palladium, $Tp^{iPr}Pd(py)(OOX)$ [X = H, Bu^t, $PdTp^{iPr}(py)$; Tp^{iPr}: hydrotris(3,5-diisopropylpyrazolyl)borate] is prepared by dehydrative condensation of a hydroxo complex, $Tp^{iPr}Pd(py)(OH)$, with HOOX.

Transition metal peroxo, hydroperoxo and alkylperoxo species are postulated as key intermediates of catalytic oxygenations such as transition metal catalyzed oxidation of organic compounds and physiological metabolic reactions.[1] For investigation of the reaction mechanisms it is essential to characterize the structure and chemical properties of possible intermediates but well-characterized examples of peroxo complexes‡ are still rare. In our laboratory first row transition metal peroxo complexes supported by hydrotris(pyrazolyl)borate ligands (Tp^R) have been studied from the bioinorganic viewpoint.[2] As for their synthetic methods, we have established that transition metal hydroxo complexes are versatile precursors for peroxo complexes *via* dehydrative condensation with ROOH. Recently our research target is extended to peroxo complexes not related to metalloproteins (Co, Ni, and the second row metals)[3] for comprehensive understanding of chemistry of transition metal dioxygen complexes based on the Tp^R ligand system. Herein we report synthesis and characterization of a series of peroxo palladium complexes, $Tp^{iPr}Pd(py)–OO–X$ [X = H, Bu^t, $PdTp^{iPr}(py)$; Tp^{iPr}: hydrotris(3,5-diisopropylpyrazolyl)borate].§

The starting hydroxo complex, (κ^2-Tp^{iPr})Pd(py)–OH **1**,¶ was prepared by hydrolysis of the corresponding chloro complex, (κ^2-Tp^{iPr})Pd(py)–Cl,‖ with aqueous NaOH solution. Complex **1** turned out to be basic enough to be condensed with various protic substrates including acetic acid, phenol, methanol and hydroperoxides (Scheme 1). Reaction with a slight excess amount of H_2O_2 (30% aqueous solution) in THF gave the hydroperoxo complex **2** as yellow solids, and the yellow *tert*-butylperoxo complex **3** was obtained *via* condensation with *tert*-butylhydroperoxide (70%; the remaining part was Bu^t–OO–Bu^t) in benzene. The condensation products **2** and **3** were characterized as square-planar 16e Pd^{II}-complexes on the basis of their spectroscopic features [(*i*) the three non-equivalent pyrazolyl rings; (*ii*) the incorporation of py; (*iii*) the B–H stretching vibration appearing below 2500 cm^{-1} indicating κ^2-coordination of the Tp^{iPr} ligand[3b]]. Characterization of the hydroperoxo complex **2** was based on the OOH signal (^{1}H NMR) observed at δ 6.86 (*cf.* the OH signal of **1**: δ −1.79), which disappeared upon addition of a drop of D_2O, but neither ν(O–O) nor ν(O–H) stretching vibration was detected. The molecular structure of *tert*-butylperoxo complex **3** was confirmed by X-ray crystallography** (Fig. 1.)

The successful condensation reactions of **1** prompted us to examine synthesis of a dinuclear μ-peroxo complex *via* reaction

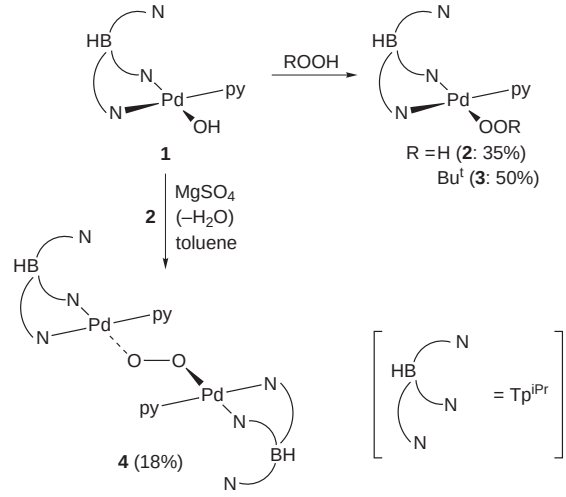

Scheme 1

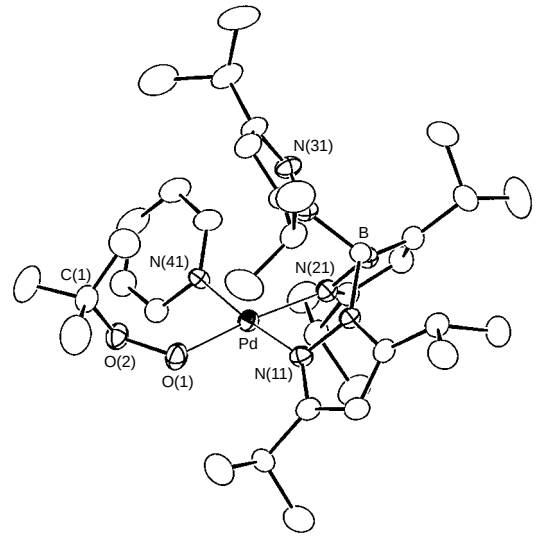

Fig. 1 Molecular structure of the *tert*-butylperoxo complex **3**. Selected interatomic distances (Å) and angles (°): O(1)–O(2) 1.440(5), O(2)–C(1) 1.439(6), Pd(1)–O(1) 1.981(4), Pd–N(11) 1.983(4), Pd–N(21) 2.021(4), Pd(1)···N(31) 3.582(5), Pd–N(41) 2.010(4); Pd–O(1)–O(2) 114.2(3), O(1)–O(2)–C(1) 109.5(4), N(21)–Pd–O(1) 174.4(1).

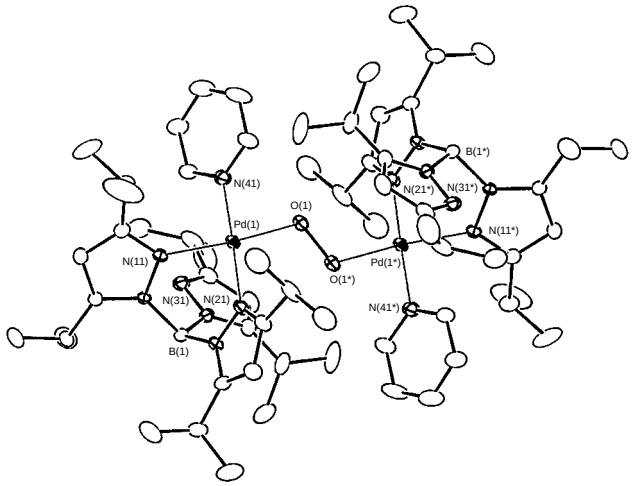

Fig. 2 Molecular structure of the μ-peroxo complex **4** drawn at the 30% probability level. Selected interatomic distances (Å) and bond angles (°). O(1)–O(1*) 1.445(5), Pd(1)–O(1) 1.971(3), Pd(1)–N(11) 2.056(3), Pd(1)–N(21) 2.020(3), Pd(1)···N(31) 3.486(3), Pd(1)–N(41) 2.035(3); Pd(1)–O(1)–O(1*) 111.8(2), N(11)–Pd(1)–O(1) 174.2(1).

with the hydroperoxo complex **2**. As was expected, stirring a mixture of **1** and **2** in toluene in the presence of $MgSO_4$ (a dehydrating reagent) gave the μ-peroxodipalladium complex **4** after crystallization from pentane–ether (Scheme 1). Because **4** was sensitive to moisture, addition of $MgSO_4$ was essential to remove water formed by the condensation. Otherwise the condensation was reversed and an equilibrated mixture of **1**, **2** and **4** was obtained. The μ-peroxo complex **4** could be also formed by condensation of **1** with 0.5 equiv. of H_2O_2, but a mixture of products containing **4** was obtained. The spectroscopic features of **4** were similar to those of **1**–**3** mentioned above, and its molecular structure was determined by X-ray crystallography** (Fig. 2).

According to the CSD database, **3** and **4** are the first examples of structurally characterized η^1-alkylperoxo and μ-peroxo complexes of palladium, respectively.[5] The four-coordinated square-planar geometry around the palladium centers is evident from the interligand N–Pd–N (or O) angles close to right angles [87.2–96.0(2)° **3**, 85.0–96.9(1)° **4**] as well as the Pd(1)···N(31) separations [3.582(5) Å **3**, 3.486(3) Å **4**] non-bonding interaction. The lone pair electrons of the N(31) atoms do not project toward the vacant axial site of the palladium centers. The O–O distances of **3** [1.440(5) Å] and **4** [1.445(5) Å] fall in the typical range of the O–O distances of organic and inorganic peroxo compounds.[1,4] Because no interaction is observed between Pd(1) and O(1*) [2.845(3) Å] in **4**, the bridging O_2 part is described as a μ-η^1 : η^1-peroxo ligand. It is notable that the Pd–O distances of the peroxo complexes **3** [1.981(4) Å] and **4** [1.971(3) Å] are slightly shorter than that of the hydroxo complex **1′** [2.021(7) Å]. Although two diastereomeric structures are possible for the dinuclear complex **4** due to the (κ^2-Tp^{iPr})Pd(py) fragment being chiral, only one isomerically pure species (X-ray structure: *meso* form lying on a crystallographic inversion center) is present as indicated by the observation of only one set of the three CH signals for the three pyrazolyl rings in Tp^{iPr}.‖

The stability and reactivity of the square-planar peroxo complexes were considerably different from those of the first row metal complexes with tetrahedral or trigonal-bipyramidal geometry.[2–4] The peroxopalladium complexes **2**–**4** were thermally stable. The *tert*-butylperoxo complex **3** decomposed when heated at 85 °C for 3 h (in C_6D_6) in the absence of an external substrate, and the hydroperoxo (**2**) and μ-peroxo complexes (**4**) slowly (1–3 days) decomposed at ambient temperature. Addition of PPh_3, however, caused their decomposition giving the phosphine oxide (O=PPh_3) in 43% (from **2**), 71% (from **3**) and 45% yields (from **4**), although the fate of the Tp^{iPr}Pd-moieties was not clear. A complicated mixture of coordination products was merely obtained as observed by ^{1}H NMR monitoring of reaction mixtures. Preliminary experiments on reactivity of the peroxo complexes **2**–**4** toward hydrocarbons revealed that vinyl ethyl ether was converted to ethyl acetate by the action of **2**–**4** but no reaction was observed with simple alkene such as hex-1-ene.

We are grateful to the Ministry of Education, Science, Sports, and Culture of the Japanese Government for financial support of this research (Grant-in-Aid for Specially Promoted Research: 08102006).

Notes and References

† E-mail: makita@res.titech.ac.jp

‡ In this paper, 'peroxo complex' stands for a complex containing an M–OO fragment such as peroxo, hydroperoxo and alkylperoxo complexes.

§ Abbreviations used in this paper: Tp^{iPr} = hydrotris(3,5-diisopropylpyrazolyl)borate; py = pyridine.

¶ The monomeric structure of the hydroxo complex was confirmed by X-ray crystallography of a derivative of **1** with the hydrotris(4-bromo-3,5-diisopropylpyrazolyl)borate ligand (**1′**).**

‖ Tp^{iPr}Pd(py)–Cl was synthesized by successive treatment of $PdCl_2(PhCN)_2$ with KTp^{iPr} and pyridine. M. Akita, T. Miyaji, N. Muroga, S. Hikichi and Y. Moro-oka, to be submitted.

** X-Ray diffraction measurements were made on a Rigaku RAXIS IV imaging plate area detector with graphite-monochromated Mo-Kα radiation (λ = 0.710 69 Å) at −60 °C. The refinements were made on *F* based on the observed reflections [$I > 3\sigma(I)$]. *Crystal data*: **1′**·H_2O: $C_{32}H_{51}BBr_3N_7O_2Pd$, M_w = 922.7, triclinic, space group $P\bar{1}$, a = 11.624(5), b = 18.367(9), c = 10.057(2) Å, α = 102.47(3), β = 106.46(3), γ = 75.59(4), U = 1970(1) Å^3, Z = 2, D_c = 1.57 g cm^{-3}, μ = 36.0 cm^{-1}, $R(R_w)$ = 0.082 (0.101) for the 6091 independent reflections (of 7037 measured reflections) and 410 parameters. An ORTEP drawing is available as supplementary material. **3**: $C_{36}H_{60}BN_7O_2Pd$, M_w = 740.1, triclinic, space group $P\bar{1}$, a = 13.002(7), b = 14.580(7), c = 11.29(1) Å, α = 109.69(6), β = 92.41(7), γ = 88.66(5)°, U = 2014(3) Å^3, Z = 2, D_c = 1.22 g cm^{-3}, μ = 5.0 cm^{-1}, $R(R_w)$ = 0.079 (0.089) for the 7254 independent reflections (of 7854 measured reflections) and 424 parameters. **4**·2C_5H_{12}: $C_{74}H_{126}B_2N_{14}O_2Pd_2$, M_w = 1478.3, orthorhombic, space group *Pbca*, a = 18.791(3), b = 22.280(3), c = 19.158(4) Å, U = 8020(2) Å^3, Z = 4, D_c = 1.22 g cm^{-3}, μ = 5.0 cm^{-1}, $R(R_w)$ = 0.051 (0.056) for the 7015 independent reflections (of 8202 measured reflections) and 424 parameters. CCDC 182/805.

1 R. A. Sheldon and J. K. Kochi, *Metal-Catalyzed Oxidations of Organic Compounds*, Academic Press, New York, 1981; S. Patai, *The chemistry of Peroxides*, Wiley, Chichester, 1983; *Oxygen Complexes and Oxygen Activation by Transition Metals*, ed. A. E. Martel and D. T. Sawyer, Plenum, New York, 1988; *Organic Peroxides*, ed. W. Ando, Wiley, Chichester, 1992; *Metal–Dioxygen Complexes*, *Chem. Rev.*, 1994, **94**, 567.

2 N. Kitajima and Y. Moro-oka, *Chem. Rev.*, 1994, **94**, 737; N. Kitajima and W. B. Tolman, *Prog. Inorg. Chem.*, 1995, **43**, 419; see also, S. Trofimenko, *Chem. Rev.*, 1993, **93**, 943.

3 (*a*) Co: S. Hikichi, H. Komatsuzaki, N. Kitajima, M. Akita, M. Mukai, T. Kitagawa and Y. Moro-oka, *Inorg. Chem.*, 1997, **36**, 266; (*b*) Rh: M. Akita, K. Ohta, Y. Takahashi, S. Hikichi and Y. Moro-oka, *Organometallics*, 1997, **16**, 4121; (*c*) Y. Takahashi, M. Hashimoto, S. Hikichi, M. Akita and Y. Moro-oka, unpublished work; (*d*) Ru: Y. Takahashi, M. Akita, S. Hikichi and Y. Moro-oka, *Inorg. Chem.*, in press.

4 N. Kitajima, T. Katayama, K. Fujisawa, Y. Iwata and Y. Moro-oka, *J. Am. Chem. Soc.*, 1993, **115**, 7872; N. Kitajima, H. Komatsuzaki, S. Hikichi, M. Osawa and Y. Moro-oka, *J. Am. Chem. Soc.*, 1994, **116**, 11596; S. Hikichi, H. Komatsuzaki, M. Akita and Y. Moro-oka, *J. Am. Chem. Soc.*, in press.

5 A tetrameric μ-*tert*-butylperoxopalladium complex [Pd(μ-O_2CCl_3)(μ-OOBu^t)]$_4$ [O–O 1.49 Å; mean Pd–O 1.994(3) Å], was reported: H. Mimoun, R. Charpentier, A. Mitschler, J. Fischer and R. Weiss, *J. Am. Chem. Soc.*, 1980, **102**, 1047. A monomeric η^2-peroxo complex, (η^2-O_2)Pd(PBu$^t_2$Ph)$_2$ [O–O 1.37(2) Å, Pd–O 2.051(14), 2.057(12) Å] was also reported: T. Yoshida, K. Tatsumi, M. Matsumoto, K. Nakatsu, A. Nakamura, T. Fueno and S. Otsuka, *Nouv. J. Chim.*, 1979, **3**, 761.

Received in Cambridge, UK, 9th February 1998; 8/01111G

Syntheses and structures of a new class of aza- and thio-ether macrocyclic d^0 imido complexes

Paul J. Wilson, Alexander J. Blake, Philip Mountford*† and Martin Schröder*†

Department of Chemistry, University of Nottingham, Nottingham, UK NG7 2RD

The synthesis and structures of a family of macrocyclic, d^0 titanium imido complexes $[Ti(NBu^t)(L)Cl_2]$ (L = $[9]aneN_3$, $Me_3[9]aneN_3$, $[9]aneS_3$ or $Me_2[9]aneN_2S$) are reported; the new compounds are isolobal analogues of group 4 metallocene dichlorides.

The triaza macrocycle $R_3[9]aneN_3$ (R = H or alkyl) and its thioether analogue, $[9]aneS_3$, are effective six-electron capping ligands for a range of transition metal centres.[1] As part of a study of early transition metal imido chemistry,[2] we were interested to determine whether these ligands might support imido chemistry at d^0 centres. No $R_3[9]aneN_3$- or $[9]aneS_3$-supported imido complexes have been reported previously,[3] and none of $[9]aneS_3$ with any group 4 element. Indeed, previous

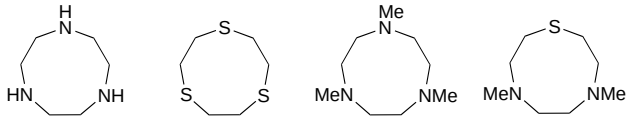

$[9]aneN_3$ $[9]aneS_3$ $Me_3[9]aneN_3$ $Me_2[9]aneN_2S$

examples of $[9]aneS_3$ transition metal complexes have been almost entirely restricted to later, low to mid-oxidation state transition metals,[1b] presumably due to hard–soft acid–base considerations;[4] the two exceptions are the d^1 V^{IV} vanadyl complex $[V(O)([9]aneS_3)Cl_2]$[5a] and the trioxorhenium species $[R(O)_3([9]aneS_3)]^+$.[5b] The $[9]aneN_3$ or $[9]aneS_3$ macrocycle–metal–imide fragment (Scheme 1) is isolobal and valence isoelectronic[6] with the ubiquitous bis(η^5-cyclopentadienyl)metal moiety. Consequently complexes containing this ligand set would clearly promise an interesting and extensive reaction chemistry that may have applications in alkene polymerisation and related catalysis.[7] Additionally, both the ring and/or the imido ligand N-substituents in such complexes may be readily varied so as to control solubility and electronic and steric properties. We report herein a new class of macrocyclic, d^0 imido complexes containing $[9]aneN_3$, $[9]aneS_3$, $Me_3[9]aneN_3$, and $Me_2[9]aneN_2S$.

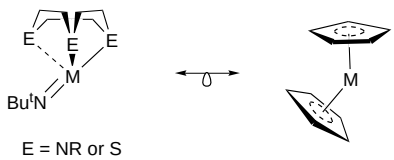

E = NR or S

Scheme 1

The syntheses and structures of the new compounds are shown in Scheme 2.‡ Addition of $[9]aneN_3$ or $[9]aneS_3$ to a dichloromethane solution of $[Ti(NBu^t)Cl_2(py)_3]$[2d] results in displacement of the pyridine ligands and formation of $[Ti(NBu^t)([9]aneN_3)Cl_2]$ **1** and $[Ti(NBu^t)([9]aneS_3)Cl_2]$ **2**, respectively. For comparative purposes and to establish the scope of the reactions, we also prepared the related complex $[Ti(NBu^t)(Me_3[9]aneN_3)Cl_2]$ **3** and its mixed N_2S-donor homologue $[Ti(NBu^t)(Me_2[9]aneN_2S)Cl_2]$ **4** in an analogous fashion.

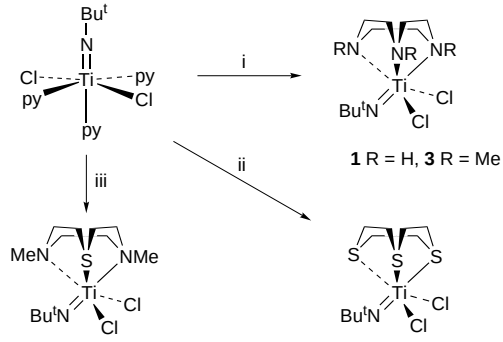

Scheme 2 *Reagents and conditions*: i, $R_3[9]aneN_3$, CH_2Cl_2, room temp., 2 h, 71% (for **1**) or 92% (for **3**); ii, $[9]aneS_3$, CH_2Cl_2, room temp., 2 h, 21%; iii, $Me_2[9]aneN_2S$, CH_2Cl_2, room temp., 24 h, 68%

Compound **4** crystallises exclusively as the isomer shown in Scheme 2 (*i.e.* with S *cis* to the *tert*-butylimido group). The yellow–orange compounds **1**–**4** are all mildly air- and moisture-sensitive.

Recrystallisation from cold dichloromethane solutions yielded crystals suitable for X-ray diffraction analysis.§ The molecular structures of **1** and **2** are shown in Figs. 1 and 2 respectively, and selected bond lengths and angles for all four compounds **1**–**4** are summarised in Table 1 for ease of comparison. The solid state structures are fully consistent with solution ^1H and ^{13}C NMR data in $CDCl_3$.

All four monomeric complexes feature an approximately octahedral titanium(IV) coordination sphere that is comprised of a *fac*-coordinated macrocycle, a multiply-bonded *tert*-butylimido ligand and two mutually *cis* chloride ligands. The Ti–$N_{macrocycle}$ or Ti–S bonds *trans* to NBu^t are significantly lengthened relative to their *cis* Ti–$N_{macrocycle}$ or Ti–S counterparts, reflecting the well known *trans* influence of the imido ligand.[3b] The angles subtended at the imido nitrogen lie in the

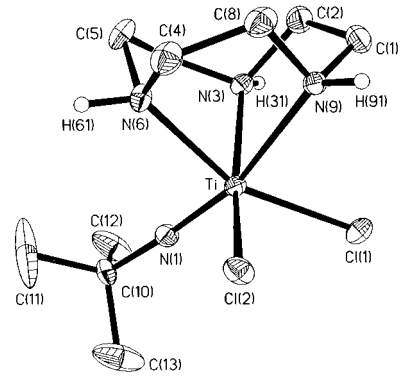

Fig. 1 Displacement ellipsoid (40% probability) plot for $[Ti(NBu^t)([9]aneN_3)Cl_2]$ **1**. Hydrogen atoms are excluded except for those bonded to N; these are drawn as spheres of arbitrary radius. The CH_2Cl_2 solvent molecule is also excluded.

Table 1 Comparison of selected distances (Å) and angles (°) for **1**–**4**; *cis* and *trans* refer to coordination sites with respect to NBu^t

Compound	Ti–N_{cis}	Ti–N_{trans}	Ti–S_{cis}	Ti–S_{trans}	Ti–Cl	Ti–N_{imide}	Cl–Ti–Cl	C–N_{imide}–Ti
1	2.213(3) 2.227(3)	2.359(3)	—	—	2.407(1) 2.403(1)	1.703(3)	97.23(4)	174.3(2)
2	—	—	2.575(1) 2.591(1)	2.750(1)	2.370(1) 2.379(1)	1.694(3)	103.02(4)	178.3(3)
3	2.265(3) 2.270(3)	2.437(3)	—	—	2.394(1) 2.392(1)	1.694(2)	95.75(4)	171.0(2)
4	2.285(9)	2.498(8)	2.561(4)	—	2.379(4)[a] 2.397(4)[b]	1.708(8)	98.0(2)	166.4(6)

[a] *Trans* to S_{cis}. [b] *Trans* to N_{cis}.

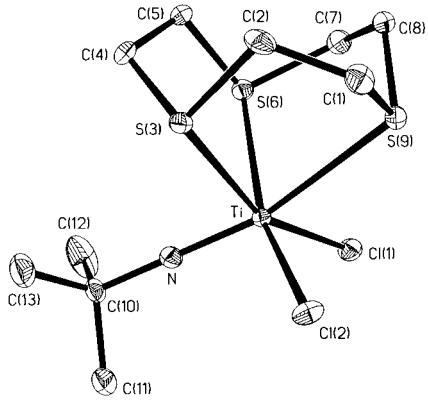

Fig. 2 Displacement ellipsoid (40% probability) plot for [Ti(NBu^t)([9]aneS$_3$)Cl$_2$] **2**. Hydrogen atoms and the CH_2Cl_2 solvent molecule are excluded.

range 166.4(6)–178.3(3)°, consistent with the NBu^t ligand acting as four-electron donor to Ti^{IV} and forming a Ti≡N_{imide} triple bond (pseudo-$\sigma^2\pi^4$ configuration).[3a] Table 1 shows that the Ti–Cl bond lengths in **1** and **3** (*i.e.* both *trans* to N) are significantly longer than those in **2** (*i.e. trans* to S). Consistent with these observations, compound **4** has a Ti–Cl bond *trans* to N [2.397(4) Å] that is significantly longer than that *trans* to S [2.379(4) Å]. In addition, the ligand R_3[9]aneN$_3$ in **1** and **3** produces Cl–Ti–Cl angles of 97.23(4) and 95.75(4)°, respectively, while [9]aneS$_3$ gives a substantially increased angle of 103.02(4)° in **2**. These data demonstrate clearly the importance of the different macrocycles in tuning and varying structural parameters of **1**–**4**, which, in other systems, have been shown[7] to be important features in catalyst design.

The complexes [Ti(NBu^t)([9]aneS$_3$)Cl$_2$] **2** and [Ti(NBu^t)(Me$_2$[9]aneN$_2$S)Cl$_2$] **4** are the first group 4 derivatives of [9]aneS$_3$ or R_2[9]aneN$_2$S.[8] Furthermore, the four complexes **1**–**4** represent the first such macrocycle–imido derivatives, and are related to oxo complexes of Me$_3$[9]aneN$_3$.[9] Preliminary studies have demonstrated that the chloride ligands in **3** may be substituted to give [Ti(NBu^t)(Me$_3$[9]aneN$_3$)(R)$_2$] (R = CH_2SiMe_3 or CH_2Ph), and we have also prepared the cationic group 5 complexes [Nb(NBu^t)(Me$_3$[9]aneN$_3$)Cl$_2$]X (X = Cl or PF_6) which are valence isoelectronic with **1**–**4**. Reactivity studies of all the new complexes are underway.

We thank the EPSRC, Leverhulme Trust, Royal Society and University of Nottingham for support. P. M. is the Royal Society of Chemistry Sir Edward Frankland Fellow.

Notes and References

† E-mail: Philip.Mountford@Nottingham.ac.uk or Martin.Schroder@Nottingham.ac.uk

‡ Satisfactory spectroscopic and analytical data for **1**–**4** have been obtained.

§ *Crystal data* for **1**–**4**. Crystals were mounted in a film of RS3000 perfluoropolyether oil (Hoechst) on a glass fibre and transferred to a Stoë Stadi-4 four-circle diffractometer and data were collected at 150(2) [220(2) for **4**] K. **1**: $C_{10}H_{24}Cl_2N_4Ti\cdot CH_2Cl_2$, M = 404.07, monoclinic, space group $P2_1/c$, a = 10.677(3), b = 11.371(3), c = 15.752(3) Å, β = 104.20(3)°, U = 1854.1(7) Å^3, Z = 4, μ = 1.04 mm^{-1}, all 3096 independent reflections (R_{merge} = 0.03) used in refinement, no. of parameters refined 182, final R indices: R = 0.039, wR_2 = 0.059. **2**: $C_{10}H_{21}Cl_2NS_3Ti\cdot CH_2Cl_2$, M = 455.20, monoclinic, space group $P2_1/n$, a = 12.035(3), b = 12.368(3), c = 13.925(3) Å; β = 108.47(2)°, U = 1965.9(6) Å^3, Z = 4, μ = 1.28 mm^{-1}, 3471 independent reflections (R_{merge} = 0.03), no. of parameters refined 182, final R indices: R = 0.039, R_w = 0.040. **3**: $C_{13}H_{30}Cl_2N_4Ti\cdot CH_2Cl_2$, M = 446.15, orthorhombic, space group *Pbca*, a = 15.104(6), b = 14.515(6), c = 19.933(7) Å, U = 4370(3) Å^3, Z = 8, μ = 0.88 mm^{-1}, 3597 independent reflections (R_{merge} = 0.02) used in refinement, no. of parameters refined 209, final R indices: R = 0.047, wR_2 = 0.0584. **4**: $C_{12}H_{27}Cl_2N_3STi\cdot CH_2Cl_2$, M = 449.17, monoclinic, space group $P2_1/n$, a = 10.114(3), b = 14.445(6), c = 15.207(4) Å, β = 107.24(3)°, U = 2121.8(10) Å^3, Z = 4, μ = 1.00 mm^{-1}, 2759 independent reflections (R_{merge} = 0.12), 2152 reflections with $I > 0$ used in refinement, no. of parameters refined 200, final R indices: R = 0.102, wR_2 = 0.130. CCDC 182/820.

1 P. Chaudhuri and K. Weighardt, *Prog. Inorg. Chem.*, 1987, **25**, 329; K. Wieghardt, *Pure Appl. Chem.*, 1988, **60**, 509; A. J. Blake and M. Schröder, *Adv. Inorg. Chem.*, 1990, **35**, 1; S. C. Rawle and S. R. Cooper, *Struct. Bonding* (*Berlin*), 1990, **72**, 1; N. R. Champness, J. P. Danks and M. Schröder, *Coord. Chem. Rev.*, 1998, in press.

2 (*a*) P. Mountford, *Chem. Commun.*, 1997, 2127 (Feature Article); (*b*) G. I. Nikonov, A. J. Blake and P. Mountford, *Inorg. Chem.*, 1997, **36**, 1107; (*c*) P. J. Stewart, A. J. Blake and P. Mountford, *Inorg. Chem.*, 1997, **36**, 1982; (*d*) A. J. Blake, P. E. Collier, S. C. Dunn, W.-S. Li, P. Mountford and O. V. Shishkin, *J. Chem. Soc., Dalton Trans.*, 1997, 1549.

3 See the following and references therein: (*a*) D. E. Wigley, *Prog. Inorg. Chem.*, 1994, **42**, 239; (*b*) W. A. Nugent and J. M. Mayer, *Metal–Ligand Multiple Bonds*, Wiley-Interscience, New York, 1988.

4 For a discussion and leading references see S. J. A. Pope, N. R. Champness and G. Reid, *J. Chem. Soc., Dalton Trans.*, 1997, 1639.

5 (*a*) G. R. Willey, M. T. Lakin and N. W. Alcock, *J. Chem. Soc., Chem. Commun.*, 1991, 1414; (*b*) H.-J. Kuppers, B. Nuber, J. Weiss and S. R. Cooper, *J. Chem. Soc., Chem. Commun.*, 1990, 979.

6 D. N. Williams, J. P. Mitchell, A. D. Poole, U. Siemeling, W. Clegg, D. C. R. Hockless, P. A. O'Neil and V. C. Gibson, *J. Chem. Soc., Dalton Trans.*, 1992, 739; T. A. Albright, J. K. Burdett and M.-H. Whangbo, *Orbital Interactions in Chemistry*, Wiley-Interscience, New York, 1985.

7 *Applied Homogeneous Catalysis with Organometallic Compounds*, ed. B. Cornils and W. A. Herrmann, VCH, Weinheim, 1996.

8 For recent examples see: V. A. Grillo, G. R. Hanson, T. W. Hambley, L. R. Gahan, K. S. Murray and B. Moubaraki, *J. Chem. Soc., Dalton Trans.*, 1997, 305; U. Heinzel, A. Henke and R. Mattes, *J. Chem. Soc., Dalton Trans.*, 1997, 501 and references therein.

9 P. Jeske, G. Haselhorst, T. Weyhermüller, K. Wieghardt and B. Nuber, *Inorg. Chem.*, 1994, **33**, 2462.

Received in Cambridge, UK, 3rd March 1998; 8/01753K

Electrochemical–hydrothermal synthesis and structure determination of a novel layered mixed-valence oxide: $BaV_7O_{16}{\cdot}nH_2O$

Xiqu Wang, Lumei Liu, Ranko Bontchev and Allan J. Jacobson*†

Department of Chemistry, University of Houston, Houston, Texas 77204, USA

The electrochemical–hydrothermal synthesis of a new mixed-valence oxide $BaV_7O_{16}{\cdot}nH_2O$ ($n \approx 4.4$) with $[V_7O_{16}]$ layers containing both vanadium oxygen tetrahedra and distorted octahedra is reported.

Vanadium oxide bronzes have been the focus of many studies because of their complex structural, physical and chemical properties. Compounds formed by high temperature synthesis and by intercalation reactions of V_2O_5 have been reported.[1–3] Most recently, hydrothermal methods have been shown to be an effective approach for the synthesis of new layered vanadium oxide bronzes containing either inorganic or organic interlayer cations.[3–12] Such materials have been of interest because of their potential application as cathode materials in secondary lithium batteries.[12] The structures of the vanadium bronzes are based on distorted vanadium–oxygen octahedra or square pyramids and VO_4 tetrahedra. The layered structures contain either single layers of corner and edge-shared polyhedra[3–8] or double layers that also contain face-shared units.[9–12] Examples of single layer structures recently reported are $(C_3N_2H_{12})_{0.5}V_2O_5$[3] and $(C_6H_{14}N_2)V_6O_{14}{\cdot}H_2O$[5,6] while the compounds δ-$M_{0.25}V_2O_5{\cdot}H_2O$ (M = Ni, Ca)[10] and $NMe_4V_8O_{20}$[12] have double layers.

Hydrothermal reactions can lead to high yields of well developed single crystal products but are known to be very sensitive to the specific reaction conditions used. For example, the pH has been shown to play a critical role in determining the final products of hydrothermal synthesis of vanadium oxides in reactions containing tetramethylammonium cations.[13] At present, we are investigating whether a modification of conventional hydrothermal synthesis in which one of the metal ion reactants is electrochemically introduced can provide better control over product formation. Previous studies of the hydrothermal electrosynthesis of thin films of $BaTiO_3$ and $SrTiO_3$ have been reported but the technique has not been used specifically for the synthesis of new compounds.[14] Here, we report the synthesis and structure of the new layered vanadium oxide bronze $BaV_7O_{16}{\cdot}nH_2O$ using the electrochemical–hydrothermal method. Other barium vanadium oxide bronzes have been synthesized hydrothermally.[15–17]

The synthesis experiments were performed using a Teflon-lined autoclave fitted with feedthroughs for electrical connections between the electrodes inside the reaction chamber and the external circuit. In a typical experiment, 40 ml of 0.01 M $Ba(NO_3)_2$ solution (pH = 1.2) was sealed in the autoclave. The anode (working electrode) was a vanadium metal plate (20 × 10 × 0.254 mm). A gold foil was used as cathode (counter electrode) and a Pt wire as a pseudo-reference electrode. The experiment was conducted with current densities in the range 0.1–1 mA generated by a commercial power source (MacPile, Biologic Scientific Instruments) at 170 ± 2 °C for 100 h. Black shiny plates of $BaV_7O_{16}{\cdot}nH_2O$ coprecipitated together with black needles of the known compound BaV_3O_8[15] and an unidentified minor phase.

The tetragonal structure of $BaV_7O_{16}{\cdot}nH_2O$ is a new structure type in which $[V_7O_{16}]$ double layers are stacked along the [001] unit cell direction with Ba^{2+} ions and H_2O molecules located between the layers (Figs. 1 and 2).‡ There are three different vanadium atom positions in the layers. V(1) and V(2) atoms are coordinated by oxygen atoms to form distorted octahedra while V(3) has tetrahedral coordination. The $V(2)O_6$ distorted octahedra share *trans* edges with two $V(1)O_6$ units to form trimers which in turn are connected by edge sharing $V(1)O_6$ octahedra to form zigzag chains. The chains are interconnected into single layers by sharing one oxygen atom. The layers are stacked along [001] with all of the short V=O oxygen atoms on the same side of the layer. The two octahedral layers are directly connected by sharing common edges to form a double layer of composition $[V_7O_{16}]$. The tetrahedra are located between the distinctive 1 × 2 windows of both octahedral layers.

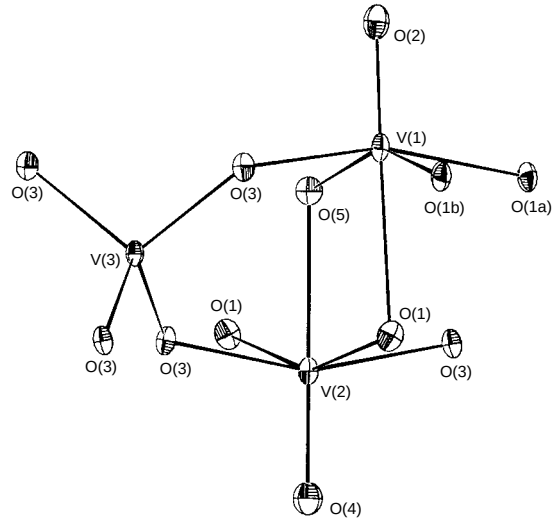

Fig. 1 Coordination environments of the vanadium atoms. Thermal ellipsoids are drawn with 50% probability. Bond lengths (Å): V(1)–O(2) 1.600(5); V(1)–O(5) 1.843(2), V(1)–O(1a) 1.941(4), V(1)–O(1b) 2.006(4), V(1)–O(3) 2.020(4), V(1)–O(1) 2.390(4), V(2)–O(4) 1.611(7), V(2)–O(1) (×2) 1.976(4), V(2)–O(3) (×2) 1.995(4), V(2)–O(5) 2.273(6), V(3)–O(3) (×4), 1.790(4).

The $V(1)O_6$ and $V(2)O_6$ octahedra show distortions typical of V_2O_5 related oxides. The vanadium atoms are displaced from the center of each octahedron along a local [001] direction to give short 'vanadyl' distances of 1.600 and 1.611 Å for V(1) and V(2), respectively. The corresponding distances *trans* to the vanadyl oxygen atoms are 2.390 and 2.273 Å. The $V(1)O_6$ $V(2)O_6$ octahedra are comparably distorted with O···O distances in the range 2.57–2.95 Å [V(1)] and 2.58–2.91 Å [V(2)]. The $V(2)O_6$ octahedron is noticeably elongated in the basal plane along the axis of the trimeric edge-shared unit (2.91 *cf.* 2.58 Å). Bond valence sums were calculated using the parameters for V^{IV}–O.[18] The values calculated are 4.42, 4.18 and 3.94 v.u. for V(1), V(2) and V(3) respectively and are consistent with mixed valence vanadium ions with an average oxidation state of 4.29. The bond valence sums suggest that V(3) which is tetrahedrally coordinated by oxygen atoms [d(V–O) = 1.790 Å] is tetravalent. This unusual V^{IV}–O coordination is found only in rare cases such as in the structure of Ba_2VO_4 [average d(V–O) = 1.76 Å].[19] The V(1) and V(2) positions are occupied both

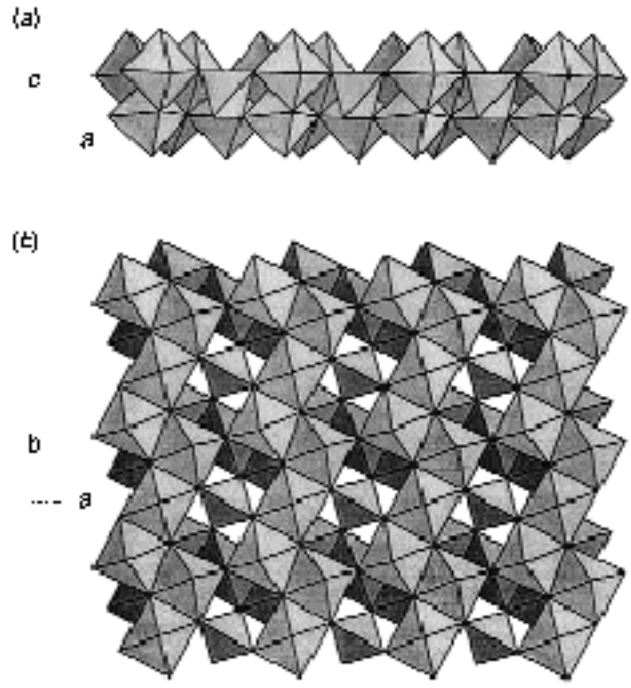

Fig. 2 Projections of the $[V_7O_{16}]$ layer along (*a*) [010] and (*b*) along [001]

by V^{IV} and V^{V}, with some preference for V^{V} at the V(1) position where symmetry is lower.

The barium cations occupy two different interlayer positions both with an occupancy of about one third. The two Ba positions are only 2.61 Å apart and cannot be occupied simultaneously. Both barium atoms are coordinated by vanadyl oxygen atoms from the layers above and below and by interlayer H_2O molecules. One water molecule is located between the Ba cation layer and the vanadate layer and is well ordered. The water molecules located in the same layer as the barium cations are highly disordered. Four distinct partially occupied sites were located and refined to give a total water content $n \approx 4.4$ in $BaV_7O_{16}{\cdot}nH_2O$. Refinement of the barium occupancies gave a Ba : V atomic ratio of 1.04(1) : 7, in good agreement with a ratio of 0.98 : 7 determined by electron microprobe analysis.§

The structure of the $BaV_7O_{16}{\cdot}nH_2O$ layers is an example of a new layer topology but is related to other double layer vanadate structures, for example, δ-$Ca_{0.25}V_2O_5{\cdot}H_2O$[10] and σ-$Zn_{0.25}V_2O_5{\cdot}H_2O$.[11] In the δ phase, all of the vanadium atoms have distorted octahedral environments. In the layer structure of the σ phase the vanadium atoms are found in distorted octahedral, square pyramidal and tetrahedral coordinations. One of the oxygen atoms in the tetrahedron is not coordinated to other vanadium atoms in the layer, an arrangement observed in several single layer structures.[3–6] In contrast, in the title compound all oxygen atoms in the $V(3)O_4$ tetrahedra are shared with V(1) and V(2) atoms.

In summary, a new layered mixed-valence barium vanadium oxide $BaV_7O_{16}{\cdot}nH_2O$ with vanadium ions present in both distorted octahedral and tetrahedral coordination environments was synthesized by electrochemical–hydrothermal synthesis. This result together with preliminary data on other vanadium systems suggest that the combination of electrocrystallization under hydrothermal conditions is a generally useful synthetic method.

This work was supported in part by the National Science Foundation under Grant DMR-9214804 and by the Robert A. Welch Foundation.

Notes and References

† E-mail: ajjacob@uh.edu

‡ *Crystal data* for $BaV_7O_{16}{\cdot}nH_2O$, M = 829.1, space group $P4_2/m$, a = 6.1598(4), c = 21.522(2) Å, Z = 4, D_c = 3.38 g cm^{-3}, black thin plate, crystal size 0.15 × 0.15 × 0.01 mm, Mo-Kα radiation (λ = 0.710 73 Å), μ = 6.30 mm^{-1}, $2\theta_{max}$ = 57°, $R(F)$ = 0.0517, $wR(F^2)$ = 0.112, GOF = 1.245 for 89 parameters and 819 unique reflections with $I > 2\sigma(I)$.

Intensities were measured on a SMART platform diffractometer equipped with a 1 K CCD area detector using graphite-monochromatized Mo-Kα radiation at −50 °C. A hemisphere of data (1271 frames at 5 cm detector distance) was collected using a narrow-frame method with scan widths of 0.30° in ω and an exposure time of 30 s per frame. The first 50 frames were remeasured at the end of data collection to monitor instrument and crystal stability, and the maximum correction applied on the intensities was *ca.* 1%. The data were integrated using the Siemens SAINT program, with the intensities corrected for Lorentz factor, polarization, air absorption, and absorption due to variation in the path length through the detector faceplate. Final cell constants were refined using 2547 reflections having $I > 10\sigma(I)$. An absorption correction was first made using the program SADABS based on equivalent reflections. The structure was solved with direct methods and refined using SHELXTL. All atom positions except the disordered water oxygen atoms were derived by direct methods and refined anisotropically in the final refinements. The disordered water oxygen atoms were located from difference maps and refined isotropically with the same thermal parameter and free occupancies. CCDC 182/816.

§ Electron microprobe analysis was carried out with a JEOL JXA-8600 instrument operating at 15 keV with a 10 μm beam diameter and a beam current of 30 nA. Counting times in the range of 40–100 s were used for both peaks and background.

1 J. Galy, *J. Solid State Chem.*, 1992, **100**, 229.
2 H. T. Evans, Jr. and J. M. Hughes, *Am. Mineral.*, 1990, **75**, 508.
3 D. Riou and G. Férey, *J. Solid State Chem.*, 1995, **120**, 137.
4 Y. Zhang, C. J. O'Connor, A. Clearfield and R. C. Haushalter, *Chem. Mater.*, 1996, **8**, 595.
5 L. F. Nazar, B. E. Koene and J. Britten, *Chem. Mater.*, 1996, **8**, 327.
6 Y. Zhang, R. C. Haushalter and A. Clearfield, *Chem. Commun.*, 1996, 1055.
7 P. Y. Zavalij, M. S. Whittingham, E. A. Boylan, V. K. Pecharsky and R. A. Jacobson, *Z. Kristallogr.*, 1996, **211**, 464.
8 T. G. Chirayil, E. A. Boylan, M. Mamak, P. Y. Zavalij and M. S. Whittingham, *Chem. Commun.*, 1997, 33.
9 F. Zhang, P. Y. Zavalij and M. S. Whittingham, *Mater. Res. Bull.*, 1997, **32**, 701.
10 Y. Oka, T. Yao and N. Yamamoto, *J. Solid State Chem.*, 1997, **132**, 323.
11 Y. Oka, O. Tamada, T. Yao and N. Yamamoto, *J. Solid State Chem.*, 1996, **126**, 65.
12 T. G. Chirayil, P. Y. Zavalij and M. S. Whittingham, *J. Mater. Chem.*, 1997, **7**, 2193.
13 M. S. Whittingham, E. Boylan, R. Chen, T. Chirayil, F. Zhang and P. Y. Zavalij, *Mater. Res. Soc. Symp. Proc.*, 1997, **453**, 115.
14 M. Yoshimura, S.-E. Yoo, M. Hayashi and N. Ishizawa, *Jpn. J. Appl. Phys.*, 1989, **28**, L2007.
15 Y. Oka, T. Yao and N. Yamamoto, *J. Solid State Chem.*, 1995, **117**, 407.
16 Y. Oka, O. Tamada, T. Yao and N. Yamamoto, *J. Solid State Chem.*, 1995, **114**, 359.
17 Y. Oka, T. Yao, N. Yamamoto and O. Tamada, *Mater. Res. Bull.*, 1997, **32**, 59.
18 N. E. Brese and M. O'Keeffe, *Acta Crystallogr., Sect. B*, 1991, **47**, 192.
19 G. Liu and J. E. Greedan, *J. Solid State Chem.*, 1993, **103**, 228.

Received in Bloomington, IN, USA, 14th January 1998; revised manuscript received 2nd March 1998; 8/02059K

First structurally characterised lithium hexafluorophosphate complexes with acyclic Lewis bases: ion-separated $[Li_2(hmpa)_5]^{2+}\cdot 2(PF_6^-)$ and ion-contacted $[(pmdeta)LiPF_6]_2$ [hmpa = $(Me_2N)_3PO$; pmdeta = $MeN(CH_2CH_2NMe_2)_2$]

David R. Armstrong,[a] Amit H. Khandelwal,[b] Lesley C. Kerr,[c] Sonja Peasey,[c] Paul R. Raithby,[c] Gregory P. Shields,[c] Ronald Snaith*[c]† and Dominic S. Wright[c]

[a] *Department of Pure and Applied Chemistry, University of Strathclyde, 295 Cathedral Street, Glasgow, UK G1 1XL*
[b] *Defence Evaluation and Research Agency, Structural Materials Centre, Farnborough, Hampshire, UK GU14 0LX*
[c] *Department of Chemistry, University of Cambridge, Lensfield Road, Cambridge, UK CB2 1EW*

Reactions of NH_4PF_6 with Bu^nLi in toluene containing hmpa or pmdeta afford the complexes $[Li_2(hmpa)_5]^{2+}\cdot 2(PF_6)^-$ 1, an ion-separated species containing an unusual dinuclear dication, and $[(pmdeta)LiPF_6]_2$ 2 in which PF_6^- anions bridge (pmdeta)Li^+ units *via* Li···F interactions, this being the first observation of a bridging mode for this anion; *ab initio* MO calculations help explain the very different structures of 1 and 2.

Lithium salts are favoured electrolytes in medium-sized rechargeable batteries[1] which have military use as well as use in laptops/personal computers and mobile phones. Anions stable at the voltages generated (typically, 4.2 V) are required for these applications. Hence, $LiPF_6$ dissolved in organic carbonates such as ethylene or dimethyl carbonate has attracted much interest. However, there are practical problems: commercially supplied $LiPF_6$ is expensive and often impure, it is difficult to handle owing to its sensitivity to air, moisture and light, and it releases toxic hydrogen fluoride upon hydrolysis. Further, and surprisingly, there are no published structural data on complexes of $LiPF_6$ with other than macrocyclic ligands (which lead to ion-separated species).[2] Given these deficiencies, we have investigated and now report a synthetic method for assembling $LiPF_6$ complexes *in situ* and the solid-state structures of two of them: $[Li_2(hmpa)_5]^{2+}\cdot 2(PF_6^-)$ **1** an ion-separated species containing a previously unknown dinuclear dication, and $[(pmdeta)LiPF_6]_2$ **2** an ion-contacted species in which PF_6^- anions bond in an unprecedented way, bridging metal centres *via* Li···F contacts. We report also the results of *ab initio* MO calculations on $LiPF_6$ and its complexes with selected acyclic Lewis bases.

Complexes **1** and **2** were synthesised by the 'ammonium salt' route whereby ammonium salts are reacted with metal sources in toluene containing stoichiometric amounts of a Lewis base.[3] Here, NH_4PF_6 suspended in toluene containing hmpa or pmdeta was treated with Bu^nLi solution, cooling of the resulting solutions affording high yields of crystalline materials, identified as **1** and **2**. The advantages of this *in situ* route are clear: $LiPF_6$ units are assembled from very pure precursors prior to being captured by Lewis bases present, and these steps occur quickly and under mild and anhydrous conditions. In contrast, the direct route to these complexes is ineffective: solid $(LiPF_6)_\infty$ dissolves in hmpa or pmdeta (neat or with non-polar solvents present also) to give oils, from which crystalline materials are unobtainable.

The solid-state structures of **1** and **2** have been determined by X-ray crystallography.‡ Complex **1** crystallises in the trigonal space group $P6_3/m$ and consists of dications $[Li_2(hmpa)_5]^{2+}$ and separate PF_6^- anions. The former (Fig. 1) are each made up of two terminal (hmpa)Li^+ units [Li(1)–O(1) 1.83(2) Å] linked by three μ-hmpa molecules [Li(1)–O(2) 1.992(12) Å]. Such triple μ-O bridges are extremely rare although they occur in the acetamide complex $(LiClO_4)_2\cdot(\mu\text{-}MeCONH_2)_3\cdot(MeCONHCOMe)_2$[4] and, in the closest analogy, in $[BrLi(\mu\text{-}hmpa)_3LiBr]$.[5]

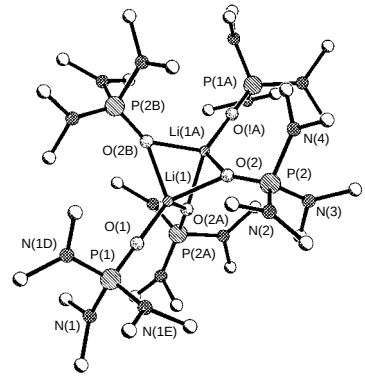

Fig. 1 Molecular structure of the cation of $[Li_2(hmpa)_5]^{2+}\cdot 2(PF_6^-)$ **1**; hydrogen atoms omitted for clarity

Rarity notwithstanding, the dication of **1** appears to represent something of a 'thermodynamic sink'. It forms irrespective of the stoichiometric amounts of hmpa provided during the synthesis of **1**. Further we have observed the same dication in the structures of $[Li_2(hmpa)_5]^{2+}\cdot(GeBr_3^-)_2$ and $[Li_2(hmpa)_5]^{2+}\cdot(SnPh_3^-)_2$.[6]

The solid-state structure of **2** also contains dinuclear units although here the ions are contacted (Fig. 2). Two (pmdeta)Li^+ units [Li–N 2.181(6), 2.189(6), 2.207(6) Å; mean 2.192 Å] are joined *via* two PF_6^- anions each of which provides two bridging fluorine atoms, one to each cation [Li(1)–F(1) 2.140(5), Li(1)–F(3A) 1.914(6) Å]. These bridges, which are almost linear (mean Li–F–P, 175.5°), result in formation of a central $(LiFPF)_2$ eight-membered ring. So far as we can ascertain, **2** is the first ion-contacted $LiPF_6$ complex. More widely, a bridging mode for the PF_6^- anion is seemingly unprecedented. Hitherto, whenever this anion has been found coordinating (in itself, a rare occurrence) it has done so to just one metal centre using one, two or three of its F atoms, *e.g.* η^1 in $(Me_3P)(NO)(CO)_3W(F)PF_5$,[7a] η^2 in $F_4P(F)_2Na\cdot$dibenzo-36-crown-

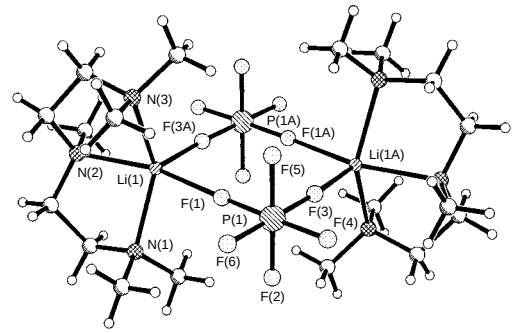

Fig. 2 Molecular structure of $[(pmdeta)LiPF_6]_2$ **2**

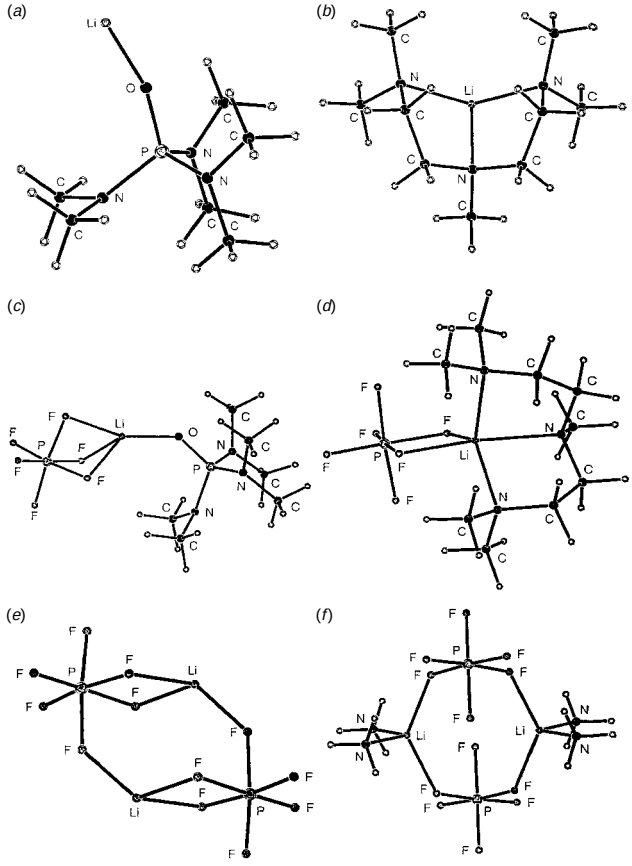

Fig. 3 Optimised structures (6-31G** basis set) of (*a*) Li^+·hmpa, (*b*) Li^+·pmdeta, (*c*) $LiPF_6$·hmpa, (*d*) $LiPF_6$·pmdeta, (*e*) $(LiPF_6)_2$, (*f*) $(LiPF_6·2NH_3)_2$

$12·Na(F)_2PF_4$,[7b] and η^3 in $F_3P(F)_3Na$·ferrocene benzo-15-crown-5.[7c]

Finally, we have employed *ab initio* MO calculations (6-31G** basis set[8] and using the program GAMESS[9]) to probe the reasons behind the very different molecular structures of **1** and **2** and to examine the energetics of $LiPF_6$ complexation. Species were optimised without constraint and confirmed as true minima by positive frequency tests. Monomeric, uncomplexed $LiPF_6$ itself favours an η^3-structure $F_3P(F)_3Li$; an η^2 arrangement is almost as stable (relative energy, +0.7 kcal mol^{-1}) but an η^1 one is of much higher energy (+13.2 kcal mol^{-1}). Calculations on pmdeta and hmpa show that the charges on the N centres of the former are −0.59 (two NMe_2) and −0.62 (NMe), and that the charge on the O centre of the latter is −0.75. In purely electrostatic terms, both of these molecules are more attractive to Li^+ than is anionic PF_6^-, for which the charge on each F centre is −0.49. This is especially so for hmpa, a point borne out by the complexation energy of Li^+ by a single hmpa ligand [Fig. 3(*a*)] being a massive −69.3 kcal mol^{-1}; the enthalpy of formation of Li^+·pmdeta, with all three N atoms coordinated [Fig. 3(*b*)] is −94.5 kcal mol^{-1}. From such data one can see why highly polar hmpa ligands will likely exclude PF_6^- anions from Li^+ coordination spheres, especially so since it is feasible stereochemically to place four hmpa ligands around each Li^+, in a $Li(hmpa)_4^+$ cation or in a dinuclear species $[Li_2(hmpa)_5]^{2+}$, as found in **1**. In contrast, the optimised structure of Li^+·pmdeta shows clearly that it would not be possible to place even two (less polar) pmdeta ligands around a Li^+ cation; hence the appearance of Li–F contacts in **2**.

The monomeric complexes $LiPF_6$·hmpa and $LiPF_6$·pmdeta were also calculated. The lowest energy structure of the former [Fig. 3(*c*)] shows the PF_6^- anion η^3-bonded to Li^+ [Li–F distances, 1.983 Å (twice) and 1.938 Å] and the complexation energy of $LiPF_6$ by hmpa is −39.7 kcal mol^{-1}. For the latter [Fig. 3(*d*)], the asymmetry imposed by the pmdeta ligand (and seen in the structure of **2**) is reflected in two different Li–F bond lengths (1.917, 1.988 Å) and in three different Li–N bond lengths (2.142, 2.194, 2.251 Å); the complexation energy is −49.0 kcal mol^{-1}. Finally, we optimised the structures of some dimeric species. For $(LiPF_6)_2$ itself [Fig. 3(*e*)], each Li^+ has three Li–F contacts, two provided by one PF_6^- anion (Li–F 1.877 Å) and one by the other (1.663 Å). This basic structure is retained when each Li^+ is complexed by a single monodentate Lewis base, as in the structure found for $(LiPF_6·NH_3)_2$. However, bis(complexation), as in $(LiPF_6·2NH_3)_2$ [Fig. 3(*f*)], reproduces the key structural features found in **2**, each Li^+ centre now contacting two F atoms (Li–F, 1.972, 1.973 Å) provided by two PF_6^- anions.

Notes and References

† E-mail: rs10003@cus.cam.ac.uk

‡ *Crystal structure determinations*: **1**: $C_{30}H_{90}F_{12}Li_2N_{15}O_5P_7$, M_r = 1199.4, trigonal, space group $P6_3/m$, a = 12.931(7), c = 20.62(2) Å, U = 2986(4) Å^3, T = 150(2) K, Z = 2, D_c = 1.335 g cm^{-3}, μ(Mo-Kα) = 2.91 cm^{-1}, $F(000)$ = 1268, λ = 0.710 73 Å, 4253 reflections, 1338 unique. Final $R(F)$ = 0.0798 for 712 reflections with $[I > 2\sigma(I)]$ and $wR(F^2)$ = 0.203 on all data, 138 parameters, GOF = 1.059. **2**: $C_9H_{23}F_6LiN_3P$, M_r = 325.21, monoclinic, space group $P2_1/c$, a = 9.025(6), b = 9.829(9), c = 18.199(6) Å, β = 103.92(4)°, U = 1567(2) Å^3, T = 150(2) K, Z = 4, D_c = 1.379 g cm^{-3}, μ(Mo-Kα) = 2.29 cm^{-1}, $F(000)$ = 680, λ = 0.710 69 Å, 2941 reflections, 2757 unique. Final $R(F)$ = 0.0466 for 1769 reflections with $[I > 2\sigma(I)]$ and $wR(F^2)$ = 0.258 on all data, 186 parameters, GOF = 1.056; CCDC 182/791.

1 G. Pistoia, *Lithium batteries: new materials, developments and perspectives*, Industrial Chemistry Library, Elsevier, Amsterdam, 1994, vol. 5; A. G. Ritchie, *Philos. Trans. R. Soc. London A*, 1996, **354**, 1643.

2 Four solid-state structures of $LiPF_6$ complexes are known, all containing cyclic ligands and all being ion-separated: R. Schwesinger, K. Piontek, W. Littke and H. Prinzbach, *Tetrahedron Lett.*, 1985, **26**, 1201; E. C. Constable, L.-Y. Chung, J. Lewis and P. R. Raithby, *J. Chem. Soc., Chem. Commun.*, 1986, 1719; E. C. Constable, M. J. Doyle, J. Healy and P. R. Raithby, *ibid.*, 1988, 1262; C. G. Choo, S. D. Rychnovsky and M. C. Etter, *Chem. Mater.*, 1994, **6**, 1200.

3 R. Snaith and D. S. Wright, in *Lithium Chemistry: A Theoretical and Experimental Overview*, eds. A.-M. Sapse and P. v. R. Schleyer, Wiley, New York, 1995, ch. 8.

4 P. S. Gentile, J. G. White and D. D. Cavalluzzo, *Inorg. Chim. Acta*, 1976, **20**, 37.

5 D. Barr, M. J. Doyle, R. E. Mulvey, P. R. Raithby, D. Reed, R. Snaith and D. S. Wright, *J. Chem. Soc., Chem. Commun.*, 1989, 318.

6 D. Stalke and D. S. Wright, unpublished work.

7 (*a*) R. V. Honeychuck and W. W. Hersh, *Inorg. Chem.*, 1989, **28**, 2869; (*b*) J. M. Maud, J. F. Stoddart, H. M. Colquhoun and D. J. Williams, *Polyhedron*, 1984, **3**, 675; (*c*) P. D. Beer, H. Sikanyika, C. Blackburn, J. F. McAleer and M. G. B. Drew, *J. Chem. Soc., Dalton Trans.*, 1990, 3295.

8 W. J. Hehre, R. Ditchfield and J. A. Pople, *J. Chem. Phys.*, 1972, **56**, 2257; P. C. Hariharan and J. A. Pople, *Theor. Chim. Acta*, 1973, **28**, 213; J. D. Dill and J. A. Pople, *J. Chem. Phys.*, 1975, **62**, 2921.

9 M. Dupuis, D. Spangler and J. J. Wendoloski, GAMESS NRCC Software Catalogue, Program No. 2 GOI, vol. 1, 1980; M. F. Guest, J. Kendrick and S. A. Pope, GAMESS Documentation, Daresbury Laboratory, Warrington, UK, 1983; M. F. Guest, P. Fantucci, R. J. Harrison, J. Kendrick, J. H. van Lenthe, K. Schoeffel and P. Sherwood, GAMESS-UK Daresbury (CFS Ltd., 1993).

Received in Cambridge, UK, 19th December 1997; revised manuscript received 13th February 1998; 8/01280F

Dendritic rods with a poly(triacetylene) backbone: insulated molecular wires

Albertus P. H. J. Schenning,[a] Rainer E. Martin,[a] Masato Ito,[a] François Diederich,*[a]† Corinne Boudon,[b] Jean-Paul Gisselbrecht[b] and Maurice Gross[b]

[a] *Laboratorium für Organische Chemie, ETH-Zentrum, Universitätstrasse 16, CH-8092 Zürich, Switzerland*
[b] *Laboratoire d'Electrochimie et de Chimie Physique du Corps Solide, U.R.A. au C.N.R.S. no 405, Faculté de Chimie, Université Louis Pasteur, 1 et 4, rue Blaise Pascal, F-67008 Strasbourg Cedex, France*

Multinanometer long phenylacetylene-end-capped poly(triacetylene) (PTA) oligomers with dendritic side chains of generation one to three have been prepared; UV–VIS measurements indicate that there is no loss of π-electron conjugation along the PTA backbone in the higher generation compounds despite distortion from planarity due to the bulky dendritic wedges.

Rigid, linearly-conjugated rod-like oligomers and polymers with the poly(triacetylene) (PTA) backbone feature interesting electronic, nonlinear optical and mesomorphic properties.[1,2] We now describe the merger of dendrimer chemistry[3] with our ongoing development of functionalized PTAs to generate insulated molecular wires. Encapsulation of the linear π-conjugated backbone by laterally attached, sterically shielding dendritic wedges should enhance the processability and stability of PTA oligomers and polymers. At the same time, steric hindrance between adjacent dendritic wedges of higher generation could possibly cause nonplanarity and deconjugation of the backbone. Here, we report the synthesis of monodisperse multinanometer long dendritic PTA rods of first, second and third generation and show that π-electron conjugation in these tubular macromolecules is fully maintained at all generation levels. Previously, Schlüter and co-workers had described the preparation of cylindrical dendrimers with a poly(*p*-phenylene) backbone as the core.[4]

The convergent synthesis of the different dendritic rods is described in Scheme 1. Different generations (**G1**, **G2** and **G3**) of Fréchet-type dendrons[5] were attached to (*E*)-2,3-bis[(triisopropylsilyl)ethynyl]but-2-ene-1,4-diol **1**[1a] using the Mitsunobu reaction[6] to give the dendritic silyl-protected monomers **2**–**4**. The yield of the third generation compound **4** was very low (4%), possibly due to steric shielding of the carboxylic acid reaction centres by the bulky dendritic wedges in the molecule. After deprotection with TBAF in wet THF, the free *trans*-enediynes **5**–**7** were obtained. The dendritic wedges substantially stabilise the usually rather unstable free *trans*-enediynes, and compounds **5**–**7** can be stored in the air at ambient temperature for months without decomposition. Oxidative Hay coupling[7] of **5**–**7** in the presence of phenylacetylene as an end-capping reagent[1a] provided the oligomeric PTAs as solids. The first generation compound **5** afforded separable oligomers up to the pentamer (**8a**–**e**) which were isolated by size-exclusion chromatography (SEC), whereas, for steric reasons, the second generation derivative **6** only yielded isolable oligomers up to the trimer (**9a**–**c**).‡ Finally, due to severe steric overcrowding, conversion of the third generation enediyne **7** only gave end-capped monomer and dimer (**10a**,**b**) in pure form and sufficient yields.§

In the ^{1}H NMR spectra of the different generation oligomers, with averaged C_{2h}-symmetry, the number of *tert*-butyl resonances is equal to the number of monomeric sub-units. The ^{13}C NMR spectra did not display a significant difference in chemical shift between the clearly discernible acetylenic C-atom resonances in oligomers of same length but different dendritic generation. Force-field calculations of the third generation dimer **10b** showed clearly that the conformation of the PTA backbone, including the two end-capping phenyl groups, is not planar due to the steric hindrance of the bulky dendritic wedges. On the other hand, the first generation derivatives **8a**–**e**, similar to previous PTA oligomers,[1] should have a planar conjugated backbone. Such nonplanarity may be achieved by rotating around C(sp)–C(sp^2) and C(sp)–C(sp) single bonds in the backbone. This, in return, suggested that a decrease or even complete loss of the π-electron conjugation along the PTA backbone could occur in the higher generation compounds, which should be observable by means of spectroscopic measurements.[8]

In the electronic absorption spectra of all three oligomeric series ($CHCl_3$, Fig. 1), the longest-wavelength absorption maximum (λ_{max}) is bathochromically shifted with increasing rod length and evidently no saturation in either case was observed, confirming recent findings.[1b,2] A comparison of the spectra of dimers **8b**, **9b** and **10b** revealed that, independent of the dendritic generation number, the longer-wavelength absorptions, which originate from electronic transitions within the conjugated PTA backbone, appear at almost the same positions (around λ = 400 nm) with nearly identical fine structure and molar extinction coefficients [Fig. 1(*a*)]. Similarly, position, fine structure and molar extinction coefficients of the longer wavelength absorption bands in the spectra of trimers **8c** (first generation) and **9c** (second generation) are nearly identical [Fig. 1(*b*)]. A precise determination of λ_{max} required deconvolution of the UV–VIS spectra.¶ The obtained values for the dimers [Fig. 1(*a*)] showed a minimal bathochromic shift in changing from generation one to three: λ_{max} = 428.0 ± 0.2 (**8b**), 430.0 ± 0.3 (**9b**) and 431.1 ± 0.2 nm (**10b**). For all dendritic rods, the λ_{max} values were converted into energies (E_{max}/eV) which were then plotted against the reciprocal number of monomer units (1/*n*). These plots revealed for all three oligomeric series straight lines intersecting the ordinate at nearly identical E_{max} (2.57 ± 0.06 eV).[1b,2] All these data provide impressive support that π-electron delocalisation and effective conjugation length[1b] of the PTA backbone are not affected by distortions out of planarity due to steric compression of the bulky dendritic wedges at higher generations. Apparently, π-electron conjugation involving the acetylenic fragments in the PTA backbone is best described as being cylindrical rather than resulting from orbital overlap within a distinct plane and is therefore fully maintained upon rotation about C(sp)–C(sp^2) and C(sp)–C(sp) single bonds.[8–10]

The electrochemical properties of the dendritic rods **8a**–**e** and **9a**–**c** were studied by steady-state voltammetry and cyclic voltammetry in CH_2Cl_2 (+0.1 M Bu_4NPF_6).‖ All oligomers could not be oxidised in the accessible potential range but were reduced in several irreversible steps, with the electrons being transferred to the conjugated PTA backbone.[1a,b] The irreversibility increases with the dendritic generation due probably to steric hindrance.[11] As the oligomeric length increased, the first reduction step occurred at increasingly less negative potential. Plots of $E_{1/2}$ *vs.* 1/*n* (*n* = oligomeric length) gave a straight line in both series.

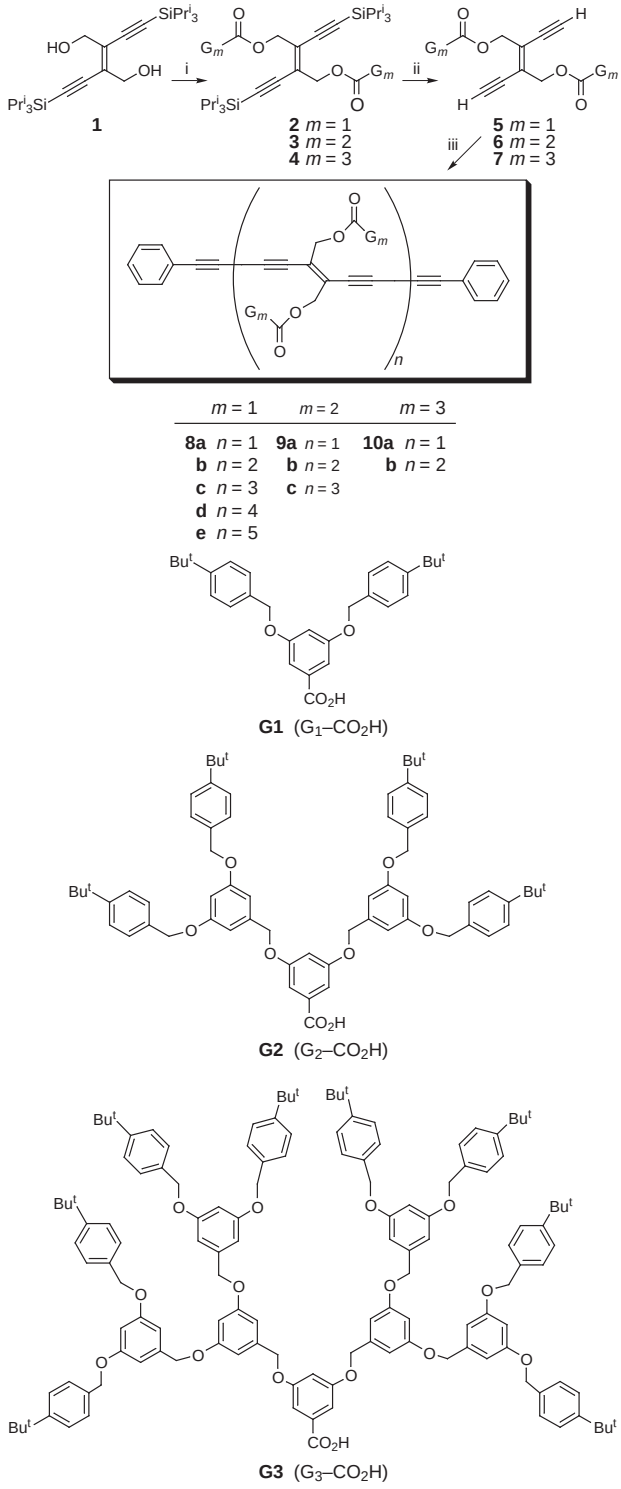

Scheme 1 *Reagents and conditions*: i, **G1**, **G2** or **G3**, *N*,*N*,*N*′,*N*′-tetramethylazodicarboxamide (TMAD), PBu_3, THF, 60 °C, 24 h, 81% (**2**), 61% (**3**), 4% (**4**); ii, TBAF, wet THF, 1 h, 99% (**5**), 99% (**6**), 99% (**7**); iii, **5**, **6** or **7**, CuCl, TMEDA, PhC≡CH, CH_2Cl_2, air, 25 °C, 2 h, 17% (**8a**, MW = 1193 D), 6% (**8b**, MW = 2185 D), 3% (**8c**, MW = 3176 D), 1% (**8d**, MW = 4167 D), 0.4% (**8e**, MW = 5159 D), or 9% (**9a**, MW = 2267 D), 6% (**9b**, MW = 4332 D), 2% (**9c**, MW = 6396 D), or 13% (**10a**, MW = 4414 D), 3% (**10b**, MW = 8626 D)

In the dendritic PTA rods described here, the insulating layer created by the dendritic wedges protects and stabilises the central conjugated backbone but does not alter its electronic characteristics. Efforts are now under way to prepare insulated molecular wires with the novel poly(pentaacetylene) backbone

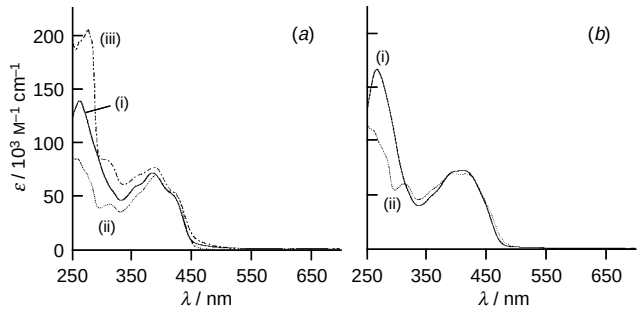

Fig. 1 Electronic absorption spectra of (*a*) (i) **8b**, (ii) **9b** and (iii) **10b** and (*b*) (i) **8c** and (ii) **9c** in $CHCl_3$ at 298 K

[–(C≡C–C≡C–CR=CR–C≡C–C≡C)$_n$–] which, thus far, has proven quite unstable in the absence of dendritic encapsulation.[12]

Support from the ETH Research Council (TEMA grant) and a JSPS fellowship (M. I.) is gratefully acknowledged.

Notes and References

† E-mail: diederich@org.chem.ethz.ch

‡ The dendritic rods extend in length from 19.4 (monomer) to 49.4 Å (pentamer).[1a]

§ The separation of the oligomers was achieved by preparative size-exclusion chromatography (SEC) on Bio-Beads S-X1 (Bio-Rad) with CH_2Cl_2 as eluent, and the purity of the fractions was checked by analytical SEC. All new compounds were fully characterised by ^{1}H and ^{13}C NMR, FT-IR, UV–VIS and elemental analyses (except **10b**) and MALDI-TOF-MS (matrix: 9-nitroanthracene), which depicted either the $[M + Na]^+$ or $[M + K]^+$ ions as base peaks.

¶ The UV–VIS spectra were deconvoluted using software programme PRO FIT, ver. 5.0.0 for Power Macintosh, Quantum Soft, Zürich, 1990–1996, with a self-written plug-in module.

‖ *Electrochemical data* in CH_2Cl_2 (+0.1 M Bu_4NPF_6, glassy carbon electrode). Half-wave potentials $E_{1/2}$ (V *vs.* Fc/Fc$^+$) and slopes (mV) in parenthesis: **8a**: −1.79 (98), −2.30 (120). **8b**: −1.60 (90), −1.76 (90). **8c**: −1.54 (140), −1.76 (110), −2.21 (100). **9a**: −1.84 (135), −2.35 (114). **9b**: −1.62 (105), −1.82 (110), −2.30 (75). **9c**: −1.56 (145), −1.78 (100), −2.22 (105).

1 (*a*) J. Anthony, C. Boudon, F. Diederich, J.-P. Gisselbrecht, V. Gramlich, M. Gross, M. Hobi and P. Seiler, *Angew. Chem., Int. Ed. Engl.*, 1994, **33**, 763; (*b*) R. E. Martin, U. Gubler, C. Boudon, V. Gramlich, C. Bosshard, J.-P. Gisselbrecht, P. Günter, M. Gross and F. Diederich, *Chem. Eur. J.*, 1997, **3**, 1505.
2 J.-F. Nierengarten, D. Guillon, B. Heinrich and J.-F. Nicoud, *Chem. Commun.*, 1997, 1233.
3 G. R. Newkome, C. N. Moorefield and F. Vögtle, *Dendritic Molecules: Concepts, Synthesis, Perspectives*, VCH, Weinheim, New York, 1996; D. A. Tomalia, A. M. Naylor and W. A. Goddard, *Angew. Chem., Int. Ed. Engl.*, 1990, **29**, 138; J. M. J. Fréchet, *Science*, 1994, **263**, 1710.
4 R. Klopsch, P. Franke and A.-D. Schlüter, *Chem. Eur. J.*, 1996, **2**, 1330; B. Karakaya, W. Claussen, K. Gessler, W. Saenger and A.-D. Schlüter, *J. Am. Chem. Soc.*, 1997, **119**, 3296.
5 C. J. Hawker and J. M. J. Fréchet, *J. Chem. Soc., Chem. Commun.*, 1990, 1010; C. J. Hawker and J. M. J. Fréchet, *J. Am. Chem. Soc.*, 1990, **112**, 7638.
6 T. Tsunoda, Y. Yamamiya, Y. Kawamura and S. Ito, *Tetrahedron Lett.*, 1995, **36**, 2529; O. Mitsunobu, *Synthesis*, 1981, 1.
7 A. S. Hay, *J. Org. Chem.*, 1962, **27**, 3320.
8 H. Tanaka, M. Thakur, M. A. Gomez and A. E. Tonelli, *Polymer*, 1991, **32**, 1834.
9 K. P. C. Vollhardt, *Organic Chemistry*, Freeman, New York, 1987, p. 519.
10 For a discussion of the bonding in buta-1,3-diyne, see: D. A. Plattner, Y. Li and K. N. Houk, in *Modern Acetylene Chemistry*, ed. P. J. Stang and F. Diederich, VCH, Weinheim, 1995, p. 1.
11 C. B. Gorman, *Adv. Mater.*, 1997, **9**, 1117; P. J. Dandliker, F. Diederich, A. Zingg, J.-P. Gisselbrecht, M. Gross, A. Louati and E. Sanford, *Helv. Chim. Acta*, 1997, **80**, 1773.
12 M. Schreiber, Doctoral Dissertation, ETH Zürich, No. 11904, 1996.

Received in Cambridge, UK, 13th February 1998; 8/01269E

Selective epoxidation in dense phase carbon dioxide

David R. Pesiri,[a] David K. Morita,[b] William Glaze[c] and William Tumas*[b]†

[a] *Department of Environmental Sciences and Engineering, University of North Carolina, Chapel Hill, NC 27599, USA*
[b] *Chemical Science and Technology Division, Los Alamos National Laboratory, Los Alamos, NM 87545, USA*
[c] *Carolina Environmental Program, University of North Carolina, Chapel Hill, NC 27599, USA*

Selective epoxidations with transition metal catalysts (V, Ti, Mo) and Bu^{t}OOH proceed with high conversions and high selectivity in dense phase carbon dioxide.

The selective catalytic oxidation of olefins constitutes one of the most fundamentally important classes of synthetically useful reactions and is typically carried out in aromatic or chlorinated hydrocarbon solvents.[1,2] We report here the first demonstration that dense phase carbon dioxide‡ is an effective solvent for the selective oxidation of activated alkenes using Bu^{t}OOH and a number of transition metal catalysts. High valent oxovanadium(V) tri(isopropoxide) [VO(OPr^i)$_3$] with Bu^{t}OOH catalyzes the epoxidation of a wide range of allylic and homoallylic alcohols with high selectivities and catalytic turnovers in CO_2. We have also investigated other known catalysts such as VO(acac)$_2$ and Mo(CO)$_6$ for oxidations in dense phase CO_2. In the presence of chiral ancillary tartrate ligands, titanium isopropoxide catalysts lead to epoxides with high enantioselectivity in this medium in what is believed to be the first example of stereoselective oxidation in a supercritical fluid. We have found that the VO(OPr^i)$_3$-catalyzed epoxidation of allylic and homoallylic alcohols proceeds three times faster in CO_2 than in hexane, a solvent to which CO_2 solubility and reactivity have been compared.[3]

Several recent publications have demonstrated the potential of supercritical CO_2 as an alternative reaction medium for synthetic transformations.[4] Although there are several descriptions of mostly non-selective, low conversion, heterogeneous oxidations,[5] there have been no reports on selective homogeneous metal-catalyzed oxidations in dense phase carbon dioxide despite the fact that CO_2 is oxidatively stable and therefore should be an ideal solvent for this chemistry. Table 1 contains our results from a wide range of allylic and homoallylic alcohols which were oxidized with high conversions and selectivities to the corresponding epoxides using VO(OPr^i)$_3$ and Bu^{t}OOH in liquid CO_2 at 25 °C. We could find no inherent advantage of operating above the critical point of CO_2 since these reactions are often carried out at or below room temperature in conventional solvents. Therefore, the majority of our studies focused on liquid carbon dioxide. Under the anhydrous conditions of our experiments the reactions were visibly homogeneous and the product epoxides were found to be stable and could be isolated in high yields as their acetate derivatives (up to 91%).[6]

We have found that the reactivity of olefins with Bu^{t}OOH and VO(OPr^i)$_3$ as a catalyst parallels that reported in conventional solvents; activated olefins react faster than simple olefins[7] and allylic alcohols react faster than homoallylics.[8] At 25 °C most homoallylic and allylic alcohols reacted completely within 24 h with VO(OPr^i)$_3$, while no detectable reaction was observed for oct-1-ene and cyclohexene under the same reaction conditions. Allylic alcohols were found to react about four times faster than homoallylics.

We studied the kinetics of the VO(OPr^i)$_3$-catalyzed epoxidation of olefins to benchmark the reactivity in CO_2 relative to that in organic solvents since no rate data in any solvent have been reported for epoxidation reactions with this catalyst to date. The rate law was found to be first order in olefin, oxidant and catalyst with an inverse, non-integral dependence on Bu^{t}OH. Table 2 summarizes our kinetic data and shows the overall solvent effect on the epoxidation reaction is not great, as expected for such a non-polar (and non-ionic) reaction. At low constant catalyst concentrations, and during initial conditions (low [Bu^{t}OH]), we can consider the observed rate constant to be pseudo-second order. The rate constant, k', for (*Z*)-non-3-en-1-ol in CO_2 was determined to be 9 M^{-1} s^{-1} at 25 °C. Rates for epoxidations using VO(OPr^i)$_3$ are slower than those observed in CH_2Cl_2 by a third and are roughly equal to those observed in toluene and acetonitrile. The rate constant is about three times larger in CO_2 than in hexane, suggesting that aromatic solvents may be better models than alkanes for solubility in dense phase carbon dioxide.§ The rate of the epoxidation reaction using VO(OPr^i)$_3$ was found to be at least 20-fold slower when run with 90% Bu^{t}OOH in water rather than anhydrous Bu^{t}OOH–decane.¶ VO(OPr^i)$_3$ is a moisture sensitive catalyst and is subject to hydrolysis of the V–OR bonds to form stable, and apparently CO_2-insoluble, complexes in the presence of H_2O thus limiting its activity.

VO(acac)$_2$ is an effective epoxidation catalyst in organic solvents but we have been unable to obtain significant

Table 1 Epoxidation of allylic and homoallylic alcohols with VO(OPr^i)$_3$ in liquid CO_2[a]

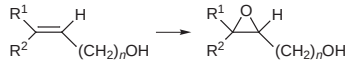

R^1	R^2	*n*	Conversion %	Selectivity (%)	
				Epoxide	Aldehyde
Me	H	1	> 99	85	15
Me(CH$_2$)$_2$	H	1	> 99	> 99	—
Me	Me	1	> 96	86	—
Me$_2$C=CH(CH$_2$)$_2$	Me	1	> 99	> 95	—
Me	Me$_2$C=CH(CH$_2$)$_2$	1	> 99	> 99	—
H	Et	2	> 99	89	—
Et	H	2	> 99	89	—
H	Me(CH$_2$)$_4$	2	> 99	99	—

[a] 24 h reaction in liquid CO_2 (10.3 bar), 1.47 mM VO(OPr^i)$_3$ (3.5 mol%), 0.42 mM substrate, 100 mM ROOH, magnetically stirred and analyzed by GC.

Table 2 Rate of epoxidation of (*Z*)-non-3-en-1-ol with $VO(OPr^i)_3$ in serveral solvents[a]

Solvent	k'/M^{-1} s^{-1}	Relative rate
CH_2Cl_2	30	3.3
MeCN	18	2.0
PhMe	17	1.9
CO_2	9	1.0
CCl_4	5	0.6
n-C_6H_{14}	3	0.3

[a] $[VO(OPr^i)_3]$ = 1.47 mM (3.5 mol%), $[Bu^tOOH]$ = 100 mM, [olefin] = 42 mM, T = 24 °C, CO_2 reactions run at 29 bar. $k' = k_{\text{initial,pseudo second order}}$ $[VO(OPr^i)_3]$. Rates reported in this work are accurate to within 10%.

conversions in dense phase CO_2 under similar conditions, presumably due to the limited solubility of $VO(acac)_2$ in CO_2. We are in the process of examining other, more 'CO_2-philic', acetylacetonate-based ligands including highly fluorinated systems. We have also examined the Mo(CO)–Bu^tOOH oxidation system and found that unactivated alkenes such as cyclohexene can be oxidized to their corresponding diols in CO_2 at elevated temperatures [95 °C, eqn. (1)].[9] We were surprised

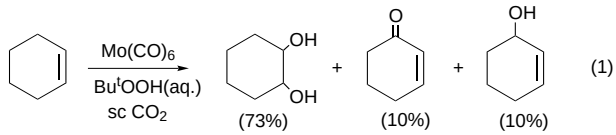

(1)

to find that oxidations utilizing aqueous Bu^tOOH (*e.g.* 90% Bu^tOOH–H_2O) gave significantly higher conversions than those run with dry Bu^tOOH (*e.g.* Bu^tOOH–decane) for the $Mo(CO)_6$ system suggesting an interesting effect of water.‖ High concentrations of Mo catalysts (200 mg, 12.5 mol%) were necessary for this reaction. The oxidation of cyclohexene resulted in a 73% selectivity to cyclohexene-1,2-diol at 74% conversion (presumably from the hydrolysis of cyclohexene oxide) during a 12 h reaction using aqueous Bu^tOOH with additional products derived from allylic oxidation [eqn. (1)]. Using anhydrous Bu^tOOH resulted in only 15% conversion of cyclohexene to oxidized products.

We have found that $Ti(OPr^i)_4$, in the presence of chiral tartrate ligands, results in enantioselective epoxidation catalysis in CO_2 [eqn. (2)]. Although the limited solubility of diethyl

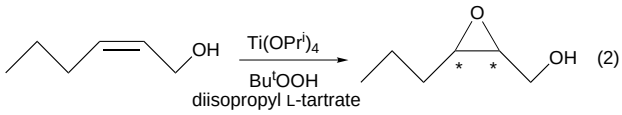

(2)

tartrate in liquid CO_2 limits the activity of this system, the use of diisopropyl tartrate in its place resulted in high conversions to epoxide. Only 16% enantiomeric excess (ee) was obtained for the epoxidation of(*E*)-hex-2-en-1-ol with the titanium–diisopropyl tartrate (0.322 mmol $Ti(OPr^i)_4$, 0.389 mmol diisopropyl tartrate) catalyst at 25 °C (93% conversion). At 0 °C the enantioselectivity increased to 87% with the same substrate during a 72 h reaction (> 99% conversion). This unoptimized result approaches the 94% ee reported by Katsuki and Sharpless.[10]

It is clear that dense phase CO_2 is an effective solvent for these olefin epoxidation reactions, with rates and selectivities similar to those observed in organic solvents. Given its oxidative stability, CO_2 shows promise as an environmentally benign solvent alternative for chemical oxidation. We are currently exploring a number of other catalytic reactions, including heterogeneous catalytic oxidation, in this important medium.**

This work was supported as part of the Los Alamos Catalysis Initiative by The Department of Energy through a Laboratory Directed Research and Development (LDRD) grant. We would like to acknowledge many helpful discussions with Dr Tom Baker and Dr Steve Buelow.

Notes and References

† E-mail: tumas@lanl.gov

‡ Dense phase fluids refer to systems that would be considered gases at their temperature of use, but are compressed to the point that they have liquid-like densities (ρ = 0.3 - 1.0 g cm^{-3}) including systems above their critical point (*e.g.* supercritical fluids).

§ The solubility and reactivity of dense phase CO_2 has been compared to hydrocarbons, aromatics and fluorocarbons.

¶ It is important to note that the use of decane to introduce the alkyl hydroperoxide to sc CO_2 reactions constituted less than 1% of the solvent volume (600 μl of 5.6 M Bu^tOOH in decane, or 265 μl decane in 33 ml of solvent).

‖ Preliminary results on the $Mo(CO)_6$-catalyzed oxidation of cyclic olefins with Bu^tOOH (aqueous and anhydrous in decane) yielded $k' = 5 \times 10^{-5}$ s^{-1} for anhydrous ROOH, $k' = 1 \times 10^{-3}$ s^{-1} for aqueous ROOH.

** The overall experimental setup and the general experimental procedures including sampling and product recovery have been described in detail elsewhere.[4,11] All high pressure reactions were carried out in custom-built stainless steel high pressure cells (33 ml volume) with sapphire view windows which enabled the direct visual observation of reactions. Proper safety precautions were taken for these high pressure reactions. An homogeneous solution was observable and complete conversion to the corresponding epoxide was detected, usually within 2 h. Yields were determined by gas chromatography of letdown solutions using authentic standards when available. GC–MS and ^{1}H NMR analysis were also used to confirm product identification.

1 *Organic Syntheses by Oxidation with Metal compounds*, ed. W. J. Mijs, and C. R. H. I. de Jonge, Plenum Press, New York, 1986; R. A. Sheldon and J. K. Kochi, *Metal Catalyzed Oxidation of Organic Compounds*, Academic Press, New York, 1981.
2 K. B. Sharpless, *Chemtech.*, 1985, 692; E. D. Mihelich, K. Daniels and D. J. Eickhoff, *J. Am. Chem. Soc.*, 1981, **103**, 7690; D. J. Berrisford, C. Bolm and K. B. Sharpless, *Angew. Chem., Int. Ed. Engl.*,1995, **34**, 1059; K. A. Jorgensen, *Chem Rev.*, 1989, **89**, 431.
3 J. A. Hyatt, *J. Org. Chem.*, 1984, **49**, 5097.
4 A number of reactions have been carried out in dense phase CO_2, for example see: P. G. Jessop, T. Ikariya and R. Noyori, *Science*, 1995, **269**, 1065; D. A. Morgenstern, R. M. LeLacheur, D. K. Morita, S. L. Borkowski, S. Feng, G. H. Brown, L. Luan, M. F. Burk and W. Tumas, in *Green Chemistry, Designing Chemistry for the Environment*, ed. P. T. Anastas and T. C. Williamson, American Chemical Society Symposium, 1996, No. 626, p. 132; P. G. Jessop, T. Ikariya, and R. Noyori, *Chem. Rev.*, 1995, **95**, 259; J. W. Rathke, R. J. Klingler and T. B. Krause, *Organometallics*, 1991, **10**, 1350; J. B. McClain, D. E. Betts, D. A. Canelas, E. T. Samulski, J.M. DeSimone, J. D. London, H. D. Cochran, G. D. Wignall, D. Chillura-Martino and R. Triolo, *Science*, 1996, **274**, 2049.
5 L. Zhou and A. Akgerman, *Ind. Eng. Chem. Res.*, 1995, **34**, 1588; L. Zhou, C. Erkey and A. Akgerman, *Ind. Eng. Chem. Res.*, 1995, **41**, 2122; K. M. Dooley and F. C. Knopf, *Ind. Eng. Chem. Res.*, 1987, **26**, 1910; P. Srinivas and M. Mukhopadhyay, *Ind. Eng. Chem. Res.*, 1997, **36**, 2066; R. N. Occhiogrosso and M. A. McHugh, *Chem. Eng. Sci.*, 1987, **42**, 2481; G. Suppes, R. N. Occhiogrosso and M. A. McHugh, *Ind. Eng. Chem. Res.*, 1997, **36**, 2066.
6 T. Itoh, K. Jitsukawa, K. Kaneda and S. Teranishi, *J. Am. Chem. Soc.*, 1979, **101**, 159.
7 K. Takai, K. Oshima and H. Nozaki, *Bull. Chem. Soc. Jpn.*, 1983, **56**, 3791.
8 R. B. Dehnel and G. H. Whitman, *J. Chem. Soc., Perkin Trans. 1*, 1979, **4**, 953.
9 J. Kolis, *et al.*, Mo catalyzed oxidations in dense phase CO_2 (personal communication).
10 T. Katsuki and K. B. Sharpless, *J. Am. Chem. Soc.*, 1980, **102**, 5976.
11 S. Buelow, P. Dell'Orco, D. K. Morita, D. R. Pesiri, E. Birnbaum, S. Borkowski, G. Brown, S. Feng, L. Luan, D. A. Morgenstern and W. Tumas, in *Frontiers in Benign Chemical Synthesis and Processing*, ed. P. T. Anastas and T. C. Williamson, Oxford University Press, in the press.

Received in Cambridge, UK, 27th February 1998; 8/01655K

Novel change in rate-determining step within an E1cB mechanism during aminolysis of a sulfamate ester in acetonitrile

William J. Spillane,*† Paul McGrath, Chris Brack and Keith Barry (in part)

Chemistry Department, National University of Ireland, Galway, Ireland

The observation of biphasic Brønsted plots (β_1 *ca.* 0.7 and β_2 *ca.* 0) in the aminolysis (alicyclic amines, pyridines) of 4-nitrophenyl *N*-benzylsulfamate 1a in MeCN is interpreted as being due to a mechanistic change from $(ElcB)_{irrev}$ to $(ElcB)_{rev}$; the change in rate-determining step occurs at approximately the pK_a of 1a and other more basic substrates give straight line plots; an entropy study supports the change from a bimolecular to a unimolecular mechanism.

Recently in our laboratory we have been studying the elimination-addition reactions of sulfamoyl chlorides with anilines[1] and of sulfamate esters with a series of amines[2] (pyridines, alicyclic amines and quinuclidines) in $CHCl_3$ and MeCN. The mechanism was seen as being E2 with ElcB-like character. UV kinetics fitted the rate law $k_{RR'NH}$[RR′NH][ester], and good straight line Brønsted type plots were obtained in this work. In particular, the aminolysis of the 4-nitrophenyl *N*-benzyl ester **1a** in $CHCl_3$ at 37 °C gave straight line Brønsted plots.[2] However, we have now found that this ester in MeCN at 37 °C gives curved plots with similar series of amines (Fig. 1). These plots are essentially biphasic with slopes β_1 *ca.* 0.7 at lower pK_as and β_2 *ca.* 0 at higher pK_as and are best interpreted in terms of a mechanistic change within the ElcB mechanism from $(ElcB)_{irrev}$ (amines of lower pK_a) to $(ElcB)_{rev}$ (amines of higher pK_a). The change from general to specific base catalysis expected for such a mechanistic change[3] is clearly evident in Fig. 1. The situation may be represented by Scheme 1. At lower amine pK_as the rate-determining step is the bimolecular formation of the conjugate base of the substrate **2** and the second step is relatively rapid departure of the leaving groups and formation of products *p*-nitrophenol and sulfamide ($k_2 >> k_{-1}$[RR′NH_2^+]). The reaction path from **2** to products may involve an *N*-sulfonylamine ($BnN{=}SO_2$)[1,2,4]

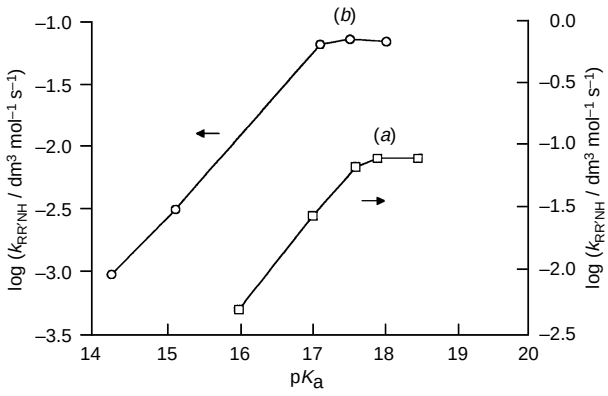

Fig. 1 Biphasic Brønsted plots for the aminolysis of **1a** in MeCN 37 °C: (*a*) alicyclic amines from left to right: morpholine, 1-formylpiperazine, 1-(2-hydroxyethyl)piperazine, 1-(2-aminoethyl)piperazine and piperazine; (*b*) pyridines from left to right: 2-aminopyridine, 2-amino-4-methylpyridine, 4-aminopyridine, DMAP and 4-pyrrolylpyridine

Further support for this mechanistic change comes from an activation study using morpholine, 1-(2-aminoethyl)piperazine and piperazine [Fig. 1(*a*)] and DMAP and 4-pyrrolylpyridine [Fig. 1(*b*)] with the ester **1a** in MeCN. The observed entropy changes ($\Delta S^{\pm}$, J K^{-1} mol^{-1}) are (temperature range in parenthesis): morpholine −262 (17–47 °C), 1-(2-aminoethyl)piperazine −59 (17–47 °C), piperazine −11 (17–47 °C), DMAP −124 (15–43 °C) and 4-pyrrolylpyridine −32 (15–46 °C). These entropy changes support the onset of a unimolecular $(ElcB)_{rev}$ mechanism as the basicity of the catalytic amine is increased, and with piperazine and 4-pyrrolylpyridine the reaction should proceed substantially *via* this mechanism. Typical values of $\Delta S^{\pm}$ for the $(ElcB)_{rev}$ mechanism lie[5] in the range of *ca.* +150 to − 40 J K^{-1} mol^{-1} and these authors also report much more negative entropies (−55 to −170 J K^{-1} mol^{-1}) for studies on related substrates undergoing $B_{AC}2$, S_N2 and E2 mechanisms. $\Delta S^{\pm}$ values of −163 to −130 J K^{-1} mol^{-1} have been reported for the $(ElcB)_{irrev}$ mechanism.[6]

When the substrate was **1b** using the same set of alicyclic amines in MeCN, surprisingly a straight line Brønsted plot was obtained (β = 0.19) [Fig. 2(*b*)]. Again with a slightly less basic ester **1c** no curvature was seen in the Brønsted plot (β = 0.35) using a set of pyridine bases [Fig. 2(*a*)]. The reason for this behaviour became apparent when we measured[7] and calculated[8] pK_as in MeCN for the esters **1**. The values obtained (calculated in parenthesis) were: **1a** 17.68 ± 0.5 (~ 16.5 ± 0.5),[9] **1b** 19.1 ± 0.1 (19.5 ± 0.5) and **1c** 18.56 ± 0.3 (~ 18.87 ± 0.5).[9] The ester **1a** showed curvature because the catalytic bases used are sufficiently strong to remove the substrate proton, the k_1 step becomes unimportant kinetically and k_2 dominates giving the observed $(ElcB)_{rev}$ mechanism. A referee has pointed out that the plots in Fig.1 are analogous to classical Eigen plots, and in keeping with this the changeover in rate-determining step occurs at about the pK_a of **1a**, i.e. ΔpK = 0; in the case of the other two esters studied the available amines are all less basic than the substrate, and the NH proton is not extensively removed and a change in rate determining step is therefore not observed with these esters.

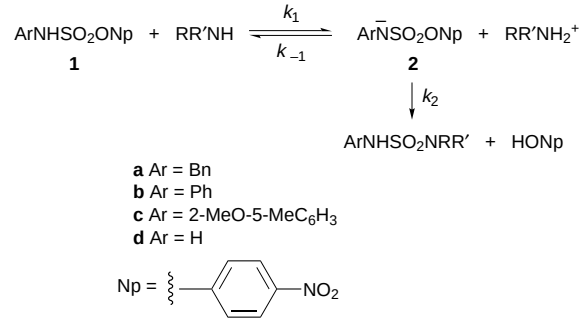

Scheme 1

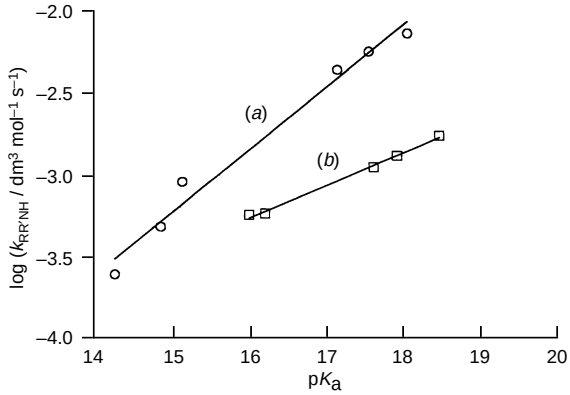

Fig. 2 Brønsted plots for the aminolysis of sulfamate esters in MeCN at 37 °C: (*a*) pyridines from left to right: 2-aminopyridine, 2,4,6-trimethylpyridine, 2-amino-4-methylpyridine, 4-aminopyridine, DMAP and 4-pyrrolylpyridine using **1c**; (*b*) alicyclic amines from left to right: morpholine, thiomorpholine, 1-(2-hydroxyethyl)piperazine, 1-(2-aminoethyl)piperazine and piperazine using **1b**

In $CHCl_3$ we have never observed curvature in Brønsted plots with **1a**, **1b** or with 4-nitrophenylsulfamate **1d** and various series of amines. This may be due to a more substantial difference in basicity between the substrates and the catalytic amines in this medium compared to MeCN. This view can be at least qualitatively supported by considering the Gibbs energy differences ($\Delta\Delta G$) for the ionization of the substrates and the conjugate bases $RR'NH_2^+$ in solvents of differing relative permittivity.[10]

Change in rate-determining step within an ElcB reaction path involving carbanions has been demonstrated by a number of groups.[11–15] However such a change involving nitrogen acids has not been clearly demonstrated previously; Caplow[16] has obtained a very similar plot (β_1 *ca.* 0.77 and β_2 *ca.* 0) to those in Fig.1 for the decomposition of carbamates in water in the presence of various amines, but has interpreted it differently. Hence the present work is the first clear-cut example of this ElcB mechanistic change not involving a carbon acid.

Notes and References

† E-mail: William.Spillane@UCG.ie

1 W. J. Spillane, F. A. McHugh and P. O. Burke, *J. Chem. Soc., Perkin Trans. 2*, 1998, 13.
2 W. J. Spillane, G. Hogan, P. McGrath, J. King and C. Brack, *J. Chem. Soc., Perkin Trans. 2*, 1996, 2099.
3 A. F. Cockerill and R. G. Harrison, *Mechanisms of elimination and addition reactions involving the X = Y groups*, in *Chemistry of double-bonded functional groups*, ed. S. Patai, Part 1, Supplement A, Wiley, London, 1977.
4 A. Williams and K. T. Douglas, *J. Chem. Soc., Perkin Trans. 2*, 1974, 1727.
5 A. Vigroux, M. Bergon, C. Bergonzi and P. Tisnes, *J. Am. Chem. Soc.*, 1994, **116**, 11787 and earlier papers; M. Mowafak Al Sabbagh, M. Calman and J.-P. Calman, *J. Chem. Soc., Perkin Trans. 2*, 1984, 1233 and earlier papers; G. Cevasco and S. Thea, *J. Org. Chem.*, 1995, **60**, 70 and earlier papers; F. Nome, W. Erbs and V. R. Correia, *J. Org. Chem.*, 1981, **46**, 3802; T. J. Broxton, *Aust. J. Chem.*, 1985, **38**, 77; K. T. Leffek and G. Schroeder, *Can. J. Chem.*, 1982, **60**, 3077.
6 A. Jarczewski and G. Schroeder, *Polish J. Chem.*, 1978, **52**, 1985.
7 B. R. Cho, S. J. Lee and Y. K. Kim, *J. Org. Chem.*, 1995, **60**, 2072. The method described was employed to measure the pK_as of some of the amines used and was adapted to measure the substrate pK_as.
8 Using the Advanced Chemistry Development (ACD) Inc., Canada, pK_a program, which calculates pK_a in water, 8.0 was added to the values obtained since this was the approximate difference between calculated (for H_2O) and experimental values (in MeCN) for the various series of amines studied.
9 These are approximate values since the calculations had to be performed without the *p*-nitro group. The program cannot calculate pK_a for compounds with > 20 atoms other than hydrogen.
10 C. Reichardt, in *Solvents and Solvent Effects in Organic Chemistry*, 2nd edn., VCH, Weinheim, 1988, section 4.2.
11 J. C. Fishbein and W. P. Jencks, *J. Am. Chem. Soc.*, 1988, **110**, 5075 and earlier papers.
12 C. K. M. Heo and J. W. Bunting, *J. Org. Chem.*, 1992, **57**, 3570 and earlier papers.
13 S. Thea, N. Kashefi-Naini and A. Williams, *J. Chem. Soc., Perkin Trans. 2*, 1981, 65 and earlier papers.
14 J. F. King and R. P. Beatson, *Tetrahedron Lett.*, 1975, 973.
15 J. L. Kice and L. Weclas, *J. Org. Chem.*, 1985, **50**, 32.
16 M. Caplow, *J. Am. Chem. Soc.*, 1968, **90**, 6795.

Received in Cambridge, UK, 23 February 1998; 8/01505H

Facial selectivity in the cycloaddition of heterodienes to carbohydrate cyclic ketene acetals. A novel synthesis of disaccharide derivatives

Stephen C. Johnson, Curtis Crasto and Sidney M. Hecht*

Departments of Chemistry and Biology, University of Virginia, Charlottesville, Virginia 22901, USA

Carbohydrate ketene acetals derived from mannopyranose and glucopyranose are shown to serve as electron-rich dienophiles in facially selective, Lewis acid-catalyzed inverse electron demand hetero-Diels–Alder reactions.

The inverse electron demand hetero-Diels–Alder reaction of electron-rich dienophiles with electron-poor enones and enals has been established as a useful method for the stereospecific construction of 3,4-dihydro-2*H*-pyran analogues.[1,2] These intermediates have been transformed easily into synthetically useful carbohydrates, and their structural components have been found to be present in a host of natural products.[2–4]

We recently reported the synthesis of carbohydrate cyclic ketene acetals.[5] Herein, we describe studies that demonstrate the ability of this intrinsically asymmetric class of compounds to serve as electron-rich dienophiles in facially selective, Lewis acid-catalyzed inverse electron demand hetero-Diels–Alder reactions.

To establish the use of carbohydrate cyclic ketene acetals as dienophiles in hetero-Diels–Alder reactions, the mannopyranose (**1**) and glucopyranose (**2**) derivatives[5] were each treated with acrolein (1.2 equiv.) in CH_2Cl_2 at ambient temperature. No reaction occurred in the absence of a Lewis acid, even at 220 °C. However, after 19 h in the presence of Yb(fod)$_3$[6] (0.05 equiv.), the crude product derived from **1** was obtained as a *ca.* 5 : 1 mixture of diastereomers (**3a** and **3b**), as judged by integration of the vinylic proton resonances (Scheme 1). The cycloadduct **3a** was isolated after silica gel chromatography as a single regio- and stereo-isomer in *ca.* 80–85% yield.‡ Analogously, after 72 h the cycloadduct **4** was isolated as a single regio- and stereo-isomer (**4a** or **4b**), albeit in much lower yield (24%), from the glucopyranose derivative **2**. The specific orthoester isomer obtained must reflect both the intrinsic *endo : exo* Diels–Alder selectivity, with the obvious exception of products derived from acrolein, as well as the facial selectivity of addition to the asymmetric dienophile.[7]

Extensive studies have been conducted to demonstrate the high degree of asymmetric induction in Diels–Alder reactions of 1-oxabuta-1,3-diene analogues with electron-rich dienophiles.[8,9] Boger and Robarge have reported on the pressure-promoted reaction of methyl (*E*)-4-phenyl-2-oxobut-3-enoate (**5a**, Table 1) with a wide range of electron-rich dienophiles to provide cycloadducts that exhibit *endo : exo* Diels–Alder selectivities of 4–9 : 1.[8] Similarly, Tietze has recently utilized several asymmetric 1-oxabuta-1,3-dienes derived from chiral oxazolidinones in which large *endo* Diels–Alder selectivities have been obtained.[9] *exo* Diels–Alder selectivities can be achieved by a judicious choice of Lewis acid catalyst.

In an attempt to provide insight into the stereoselectivity of [4+2] cycloadditions with carbohydrate cyclic ketene acetals, mannopyranose derivative **1** was treated with 1-oxabuta-1,3-diene analogues **5a**–**5d** in the presence of Yb(fod)$_3$ (Table 1).§ Achiral heterodienes **5a** and **5b** exhibited excellent reactivity with **1** in CH_2Cl_2 at ambient temperature, cleanly providing the [4 + 2] cycloadducts **6a**/**7a** and **6b**/**7b** in 97 and 80% yields, respectively.¶ Each analogue was isolated as an *ca.* 1 : 1 mixture of diastereomers; similar results were obtained with Eu(hfc)$_3$. Compounds **6a**/**7a** (as a 1.2 : 1 mixture; *cf.* Table 1) were converted to (*R*)-phenylsuccinic acid *via* a two step procedure to establish the (*S*)-phenyl configuration of the cycloadduct.‖ Therefore, **6a**/**7a**, being a diastereomeric mixture of cyclic *endo*- and *exo*-orthoesters, but having the phenyl substituents with the same absolute configuration, must be derived from a facially controlled orientation of the diene **5a**. Specifically, the cycloaddition of a **5a** with **1** proceeds *via* an *exo* Diels–Alder selective process with attack of the diene onto the back face of the dienophile and an *endo* Diels–Alder selective process with attack onto the front face (*cf.* Table 1).[13]

To further enhance the stereoselectivity of the cycloaddition, **1** was treated with **5c** and **5d** in the presence of Yb(fod)$_3$. The use of asymmetric dienes **5c** and **5d** did provide a more diastereoselective route to [4 + 2] cycloadducts (Table 1). The crude cycloadducts **6c**/**7c** were obtained in 81% yield as a 5.3 : 1 mixture of diastereomers. Likewise, cycloadducts **6d**/**7d** were obtained as a 32 : 1 mixture of diastereomers. Cycloadducts **6c**/**7c** and **6d**/**7d** were determined to be cyclic *endo*-orthoesters by NOESY experiments, thereby establishing the (*R*)-orientation of the spiro-linkage (*i.e.* the same as in **3a**). Presumably this reflects addition of the heterodienes to the ketene acetal from the more hindered face.

The ability of [4 + 2] cycloadducts derived from carbohydrate cyclic ketene acetals to provide uniquely substituted *O*-glycosides was assessed using cycloadducts **6a**/**7a** and **6d**/**7d**. Treatment with $BF_3{\cdot}OEt_2$ (1.0 equiv.) and Et_3SiH (1.0 equiv.) in dry benzene provided the corresponding β-D-mannopyranosides **9**/**10** and **11**, respectively. Compounds **9**/**10** derived from a 1 : 1 mixture of cyclic *endo*- and *exo*-orthoesters, were also obtained as a diastereomeric mixture of acetals in 54% yield. Compound **11** was obtained as a pure regio- and stereo-isomer in 40% yield; the absolute stereochemistry of the stereocenter produced in the Et_3SiH reduction was defined by the known[14] stereoselective hydride transfer.

The facially and *exo* selective hetero-Diels–Alder reaction described herein constitutes the novel use of a carbohydrate as a scaffold to direct the stereochemistry of formation of a second carbohydrate (precursor).

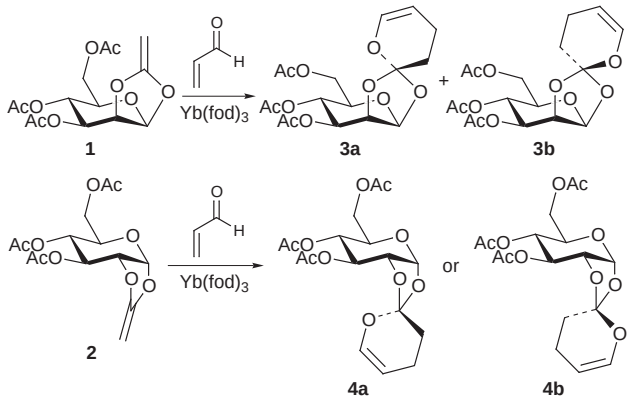

Scheme 1

Table 1 Results of Diels–Alder reactions

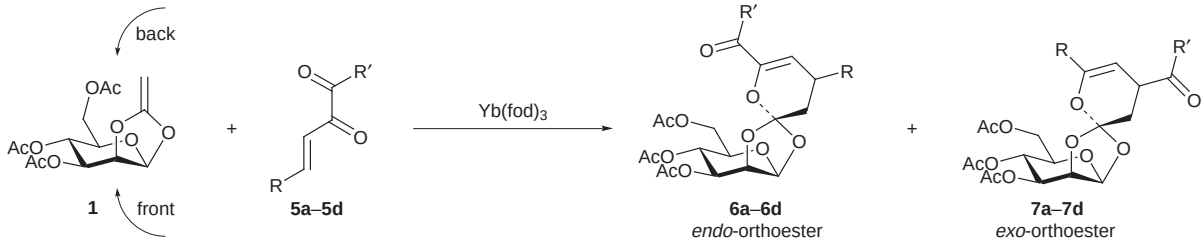

Series	R	R′	Solvent	*T*/°C	Diastereoselectivity[a]	Yield (%)[b]
a	Ph	OMe	CH_2Cl_2	25	1.2:1	97
b	OEt	OEt	CH_2Cl_2	25	1:1	80
c	Ph	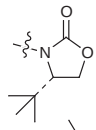	Benzene	Reflux	5.3:1[c,d]	81
d	Ph	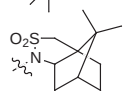	Benzene	Reflux	32:1[d]	50

[a] Determined by ^{1}H NMR spectroscopy by integration of the vinyl proton resonances. The absolute stereochemistry at the allylic carbon was established explicitly for **6a**/**7a** and **6c**/**7c**. [b] Isolated yields of purified cycloadduct after chromatography on SiO_2. [c] After extensive chromatography on SiO_2, the product was obtained as an almost pure compound, albeit in low yield (13%) from **1**. [d] The *endo*-orthoester is the major product.

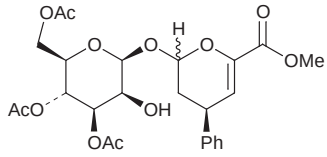
9/10

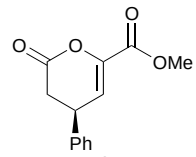
8

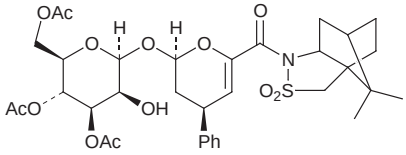
11

This study was supported by Research Grant CA53913 from the National Cancer Institute.

Notes and References

† E-mail: sidhecht@virginia.edu

‡ Cycloadducts **3a** and **4** were each isolated as oils and characterized by ^{1}H NMR spectroscopy. Each analogue exhibited resonances in the range δ 4.81–4.87 (m) and 6.16–6.19 (d, *J* 6). Additionally, the regioisomers indicated in the scheme were identified by analysis of the allylic resonances (δ 2.25–2.30).

§ The β,γ-unsaturated α-keto esters **5a** (M. Reimer, *J. Am. Chem. Soc.*, 1924, 46, 783) and **5b** (W. Trowitzsch, *Z. Naturforsch., Teil B*, 1977, **32**, 1068) were prepared as described. Heterodiene **5c** was prepared by acylation of lithiated 4-*tert*-butyloxazolidin-2-one[10] with the appropriate α-keto acid chloride by a standard procedure in 43% yield. Analogously, heterodiene **5d** was prepared from lithiated (1*S*)-(−)-camphor-2,10-sultam in 81% yield.[11]

¶ Compounds **6a**/**7a**–**6d**/**7d** were characterized by ^{1}H NMR spectroscopy; especially diagnostic was the resonance in the range δ 5.88–6.24.

‖ Compounds **6a**/**7a** were treated with $BF_3{\cdot}OEt_2$ (2.0 equiv.) and Et_3SiH (1.0 equiv.) in benzene[12] to provide the lactone **8** in 61% yield. Optical rotation for **8**: $[\alpha]_D^{22}$ −47.2 (*c* 1.0, CH_2Cl_2). The enantiopurity of **8** was established by ^{1}H NMR studies conducted with Eu(hfc)$_3$; the enantiopurity exceeded 95%. Ozonolysis of **8**, followed by acid hydrolysis, provided (*R*)-phenylsuccinic acid which was confirmed by comparison with a commercial sample.

1 G. Desimoni and G. Tacconi, *Chem. Rev.*, 1975, 75, 651. For applications to carbohydrates, see S. David, A. Lubineau and A. Thieffry, *Tetrahedron*, 1978, **34**, 299 and S. David, J. Eustache and A. Lubineau, *J. Chem. Soc., Perkin Trans. I*, 1979, 1795.

2 D. L. Boger and S. M. Weinreb, *Hetero-Diels–Alder Methodology in Organic Synthesis*, Academic Press, San Diego, 1987.

3 See, *e.g.* R. R. Schmidt, *Acc. Chem. Res.*, 1986, **19**, 250 and references cited therein.

4 L. F. Tietze and E. Voss, *Tetrahedron Lett.*, 1986, **27**, 6181.

5 M. L. Sznaidman, S. C. Johnson, C. Crasto and S. M. Hecht, *J. Org. Chem.*, 1995, **60**, 3942.

6 For examples of the use of lanthanide catalysts in Diels–Alder reactions, see M. Bednarski and S. Danishefsky, *J. Am. Chem. Soc.*, 1983, **105**, 3716.

7 The enhanced reactivity of **1** *vs.* **2** with acrolein could involve better coordination of the oxyphilic Yb^{3+} catalyst with the dienophile, thereby allowing for better stabilization of the $HOMO_{dienophile}$ and a lower energy transition state. See J. Sauer and R. Sustmann, *Angew. Chem., Int. Ed. Engl.*, 1980, **19**, 779.

8 D. L. Boger and K. D. Robarge, *J. Org. Chem.*, 1988, **53**, 3373.

9 L. F. Tietze, C. Schneider and A. Montenbruck, *Angew. Chem., Int. Ed. Engl.*, 1994, **33**, 980.

10 D. A. Evans, M. D. Ennis and D. J. Mathre, *J. Am. Chem. Soc.*, 1982, **104**, 1737.

11 W. Oppolzer, C. Chapuis and G. Bernardinelli, *Helv. Chim. Acta*, 1984, **67**, 1397.

12 W.-C. Chou, L. Chen, J.-M. Fang and C.-H. Wong, *J. Am. Chem. Soc.*, 1994, **116**, 6191.

13 For reference to the use of chiral dienophiles in diastereofacially selective [4 + 2] cycloadditions, see W. Choy, L. A. Reed, III and S. Masamune, *J. Org. Chem.*, 1983, **48**, 1139.

14 For examples of the regio- and stereo-selective reduction of orthoesters with hydrides, see E. Eliel and F. W. Nader, *J. Am. Chem. Soc.*, 1970, **92**, 3045; G. Stork and S. D. Rychnovsky, *J. Am. Chem. Soc.*, 1987, **109**, 1565.

Received in Corvallis, OR, USA, 5th January 1998; 8/00103K

Libraries of non-covalent hydrogen-bonded assemblies; combinatorial synthesis of supramolecular systems

Mercedes Crego Calama,[a] Ron Hulst,[b] Roel Fokkens,[c] Nico M. M. Nibbering,[c] Peter Timmerman,*[a]† and David N. Reinhoudt*[a]†

[a] *Laboratory of Supramolecular Chemistry and Technology, University of Twente, PO Box 217, 7500 AE, Enschede, The Netherlands*
[b] *Laboratory of Chemical Analysis, University of Twente, PO Box 217, 2700 AE, Enschede, The Netherlands*
[c] *Institute of Mass Spectrometry, University of Amsterdam, Nieuwe Achtergracht 129, 1018 WS Amsterdam, The Netherlands*

Libraries of hydrogen-bonded assemblies formed by mixing the individual components under thermodynamically controlled conditions are characterized by ^{1}H NMR spectroscopy and Ag$^+$ assisted MALDI-TOF mass spectrometry.

The combinatorial strategy to create structural diversity has revolutionized the field of chemistry over the past decade.[1] Instead of synthesizing a single molecule, combinatorial chemistry allows the simultaneous synthesis of large libraries of structurally well-defined molecules.[2] For this purpose combinatorial methodologies have been developed for a variety of synthetic transformations (*e.g.* peptide,[3] oligonucleotide,[4] heterocycle[5] and carbohydrate[6] synthesis) either on solid supports[7,8] or in solution.[9,10] Recently, libraries of synthetic receptor molecules, *e.g.* for sequence-selective peptide binding, were reported using a similar combinatorial strategy.[11,12]

Libraries of organic molecules are prepared by statistical combination of reactive molecular fragments *via* the irreversible formation of covalent bonds. In principle, one could also use non-covalent interactions, like hydrogen bonding, to build in a reversible way libraries of assemblies of small complementary molecules. Non-covalent synthesis is a valuable alternative to the classical covalent synthesis of complex supramolecular systems.[13] Recently, Lehn,[14] Sanders[15] and others[16] reported libraries that were obtained *via* reversible formation of covalent (imines, esters) or coordinative (Zn- or Fe-complexes) bonds under conditions of thermodynamic equilibrium.

Here we describe the first example of a non-covalent synthesis of combinatorial libraries of hydrogen bonded assemblies under thermodynamically controlled conditions. *N* different assemblies [**1x**]$_3$ (**x** = **a,b,c**, . . .,*N*; Fig. 1) were mixed in solution under conditions that allow the reversible exchange of the components **1x** to give *M* heteromeric assemblies in addition to the *N* homomeric assemblies (see Fig. 2). The total number of assemblies *P* (*i.e.* $N + M$) present in such a library rapidly increases with increasing *N* [eqn. (1)].

$$P = N + N(N-1) + [N(N-1)(N-2)]/6 \qquad (1)$$

For the smallest possible library ($N = 2$, $P = 4$) we have studied the combination of calix[4]arene bismelamines **1a**,**b** with 5,5-diethyl barbiturate. The individual homomeric assemblies [**1a**]$_3$ and [**1b**]$_3$ form spontaneously in apolar solvents by mixing 3 equiv. of **1a** (or **1b**) with 6 equiv. of 5,5-diethyl barbiturate and are stable down to submillimolar concentrations.[17] The assembly process is driven by the formation of 36 cooperative hydrogen bonds, resulting in significant downfield shifts for the various NH protons [Fig. 3(*a*) and (*b*)].

Mixing of 5 mM solutions of [**1a**]$_3$ and [**1b**]$_3$ at 0 °C (ratio 2 : 1) in [$^2H_8$]toluene gave only a mixture of the two separate homomeric assemblies [Fig. 3(*c*)]. Exchange of the components **1a** and **1b** between the two assemblies is extremely slow at this temperature and, as a consequence, formation of the heteromeric assemblies [**1a**]$_2$[**1b**] and [**1a**][**1b**]$_2$ is not observed.‡ Only at ⩾15 °C do the heteromeric assemblies start to form slowly. This reflects the relatively high kinetic stability of the separate assemblies in this apolar solvent. After 2.5 h at 25 °C the system has reached the thermodynamic equilibrium [Fig. 3(*d*)]. In the more polar solvent $CDCl_3$ the exchange of components **1a** and **1b** is much faster. The [**1a**]$_3$ and [**1b**]$_3$ mixture equilibrates within seconds at 25 °C. Only below −50 °C are the homomeric assemblies [**1a**]$_3$ and [**1b**]$_3$ kinetically inert.

The low-field region of the ^{1}H NMR spectrum is particularly diagnostic as it exclusively displays the hydrogen bonded NH_{barb} protons (δ 13–15) and NH_{arom} protons (δ 8–9). The [$^2H_8$]toluene ^{1}H NMR spectrum of the four component library shows 12 of the 16 NH_{barb} proton signals as separate peaks and 7 of the 8 NH_{arom} proton signals [Fig. 3(*d*)]. The four different assemblies were identified by means of 2D NOESY, ROESY, COSY and TOCSY analysis.§ The relative concentration of the four different assemblies in the mixture was subsequently determined as 1.0 ([**1a**]$_3$) : 3.0 ([**1a**]$_2$[**1b**]) : 3.0 ([**1a**][**1b**]$_2$) : 1.0 ([**1b**]$_3$) (±10%), in agreement with the statistical distribution of

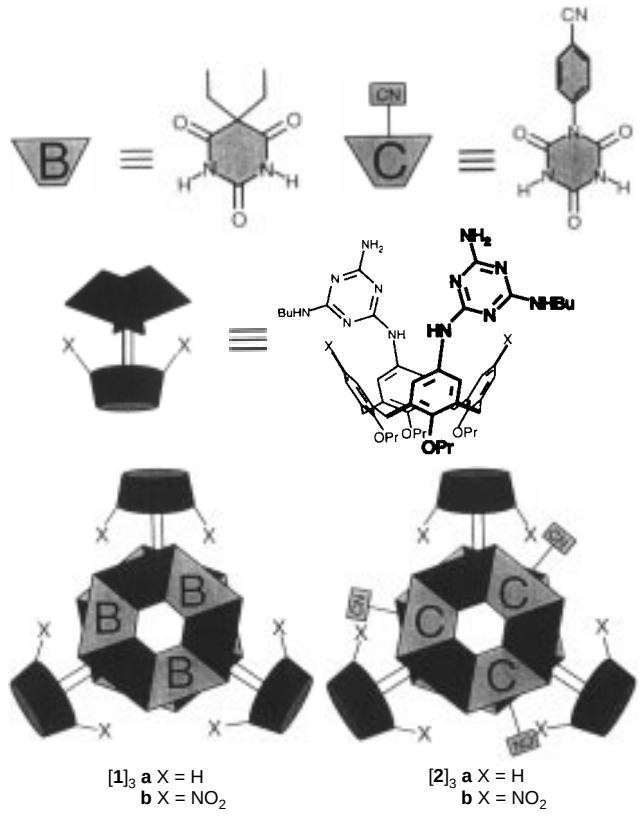

Fig. 1 Schematic representation of hydrogen bonded assemblies [**1**]$_3$ and [**2**]$_3$

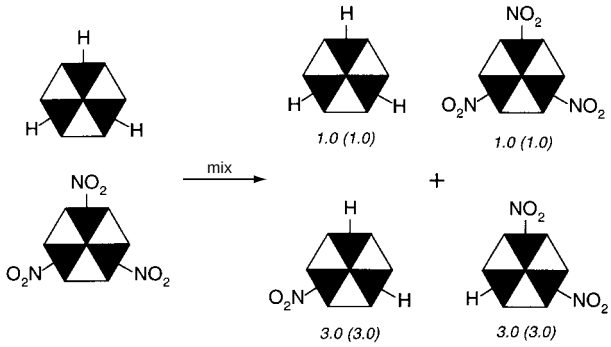

Fig. 2 Non-covalent synthesis of library of assemblies [**1a**]$_3$, [**1a**]$_2$[**1b**], [**1a**][**1b**]$_2$, and [**1b**]$_3$; experimentally determined ratio is given with statistical ratio in parentheses

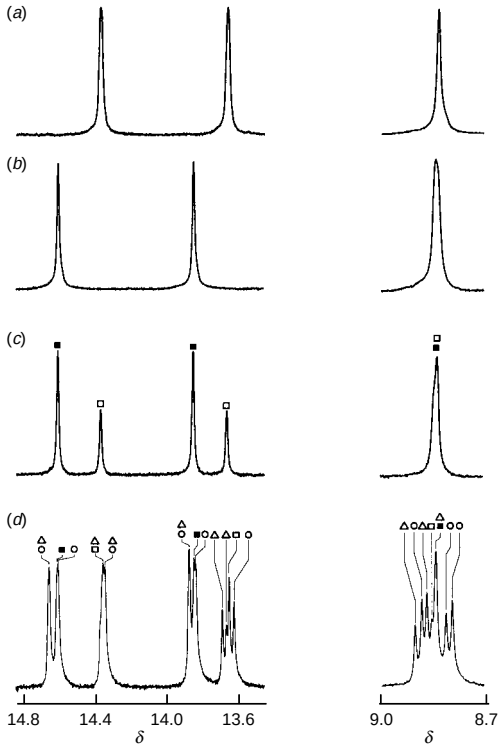

Fig. 3 Low field regions of the ^{1}H NMR spectra of (*a*) homomeric assembly [**1a**]$_3$; (*b*) homomeric assembly [**1b**]$_3$; (*c*) 2 : 1 mixture of homomeric assemblies [**1a**]$_3$ (■) and [**1b**]$_3$ (□) at 0 °C; (*d*) library of assemblies [**1a**]$_3$ (■), [**1a**]$_2$[**1b**] (○), [**1a**][**1b**]$_2$ (△), [**1b**]$_3$ (□) 2.5 h after mixing homomeric assemblies [**1a**]$_3$ and [**1b**]$_3$ at 25 °C (ratio 6 : 4). All spectra were recorded at 400 MHz in [^{2}H$_8$]toluene.

components **1a** and **1b** over the various assemblies. Unfortunately, the $CDCl_3$ spectrum displayed insufficient resolution to determine the relative composition of the mixture.

Characterization of the library was also performed by mass spectrometry using Ag^+ assisted MALDI-TOF MS technique.[18] For this purpose we studied the assemblies [**2a**]$_3$ and [**2b**]$_3$, which contain cyano substituents to coordinate to the Ag^+ labels (Fig. 1). Individual solutions of the assemblies, pretreated with 1.5–2.0 equiv. of CF_3CO_2Ag in $CHCl_3$ for at least 24 h, give intense signals in the MALDI-TOF spectra at *m/z* 4348.1 (calc. for $C_{222}H_{252}N_{60}O_{30}{\cdot}^{107}Ag^+$: 4347.9) and 4620.4 (calc. for $C_{222}H_{246}N_{66}O_{42}{\cdot}^{107}Ag^+$: 4618.8), respectively, for the monovalent Ag^+ complexes. As expected the MALDI-TOF spectrum of a mixture of the CF_3CO_2Ag pretreated $CHCl_3$ solutions (5 mM each) of assemblies [**2a**]$_3$ and [**2b**]$_3$ clearly shows two additional signals for both the monovalent Ag^+ complexes of the heteromeric assemblies [**2a**]$_2$[**2b**] and [**2a**][**2b**]$_2$ at *m/z* 4438.3 (calc. for $C_{222}H_{250}N_{62}O_{34}{\cdot}^{107}Ag^+$: 4437.9) and 4527.7 (calc. for $C_{222}H_{248}N_{64}O_{38}{\cdot}^{107}Ag^+$: 4528.9), respectively.¶ Especially for the characterization of libraries with more components, mass spectrometry will be an important tool.

The reversible library concept presented here can in principle be extended to libraries of any desirable size. For example, by mixing 10 different assemblies [**1x**]$_3$ a library of 220 different hydrogen-bonded assemblies is created. Subsequently, the information in the different assemblies can be stored by a covalent post-modification step, *e.g. via* a metathesis reaction.[19] Covalent post-modification of hydrogen-bonded assemblies is currently under active investigation in our group.

Notes and References

† E-mail: p.timmerman@ct.utwente.nl; d.n.reinhoudt@ct.utwente.nl

‡ Two different types of kinetic processes characterize the hydrogen bonded assemblies, *i.e.* (*i*) exchange of 5,5-diethyl barbiturate and (*ii*) exchange of components **1**. The rate constant for the former process is in the order of 0.5–3.0 s^{-1} in [^{2}H$_8$]toluene at 303 K as determined by 2D EXSY NMR. The latter process is much slower and can only be measured at the 'laboratory timescale'.

§ The chemical shifts of the NH protons are strongly influenced ($\Delta\delta_{max}$ = 0.15) by the starting concentrations of **1a** and **1b**.

¶ The peak intensity of assembly [**2b**]$_3$ in the MALDI-TOF spectrum of the mixture is significantly lower than that for assembly [**2a**]$_3$ most probably due to the strongly decreased affinity of this assembly for Ag^+ ions as a result of the electron-withdrawing effect of the six NO_2 groups. Evidence comes from the low mass region of the spectrum, which exclusively displays a signal for the [**2a**]$\cdot^{107}Ag^+$ complex and not the [**2b**]$\cdot^{107}Ag^+$ complex even when [**2b**] is present in four-fold excess.

1 L. C. Hsieh-Wilson, X.-D. Xiang and P. G. Schultz, *Acc. Chem. Res.*, 1996, **29**, 164.
2 For recent reviews, see *Combinatorial Chemistry, Chem. Rev.*, 1997, **97**, (special issue); S. H. DeWitt and A. W. Czarnik, *Acc. Chem. Res.*, 1996, **29**, 114; F. Balkenhohl, Von dem Bussche-Hünnefeld, A. Lansky and C. Zechel, *Angew. Chem.*, 1996, **108**, 2436; L. A. Thompson and J. A. Ellman, *Chem. Rev.*, 1996, **96**, 555.
3 A. Borchardt and W. C. Still, *J. Am. Chem. Soc.*, 1994, **116**, 373.
4 D. P. Bartel and J. W. Szostak, *Science*, 1993, **261**, 1411.
5 B. A. Bunin and J. A. Ellman, *J. Am. Chem. Soc.*, 1992, **114**, 10 977.
6 R. Liang, L. Yan, J. Loebach, M. Ge, Y. Uozomi, K. Sekanina, N. Horan, J. Gildersleeve, C. Thompson, A. Smith, K. Biswas, W. C. Still and D. Kahne, *Science*, 1996, **274**, 1520.
7 R. B. Merrifield, *J. Am. Chem. Soc.*, 1963, **85**, 2149.
8 P. P. Hermkens, H. C. J. Ottenheijm and D. Rees, *Tetrahedron*, 1996, **52**, 4527.
9 D. L. Boger, C. M. Tarby, P. L. Myers and L. H. Caporale, *J. Am. Chem. Soc.*, 1996, **118**, 2109 and references cited therein.
10 D. P. Curran and S. Hadida, *J. Am. Chem. Soc.*, 1996, **118**, 2531.
11 R. Boyce, G. Li, H. P. Nestler, T. Suenaga and W. C. Still, *J. Am. Chem. Soc.*, 1994, **116**, 7955; Y. Cheng, T. Suenaga and W. C. Still, *J. Am. Chem. Soc.*, 1996, **118**, 1813; M. T. Burger and W. C. Still, *J. Org. Chem.*, 1995, **60**, 7382.
12 M. Scott Goodman, V. Jubian, B. Linton and A. D. Hamilton, *J. Am. Chem. Soc.*, 1995, **117**, 11 610.
13 G. M. Whitesides, E. E. Simanek, J. P. Mathias, C. T. Seto, D. N. Chin, M. Mammen and D. M. Gordon, *Acc. Chem. Res.*, 1995, **28**, 37.
14 I. Huc and J.-M. Lehn, *Proc. Natl. Acad. Sci. USA*, 1997, **94**, 2106.
15 S. J. Rowan and J. K. M. Sanders, *Chem. Commun.*, 1997, 1407; S. J. Rowan, P. A. Brady and J. K. M. Sanders, *J. Am. Chem. Soc.*, 1997, **119**, 2578; S. J. Rowan, P. A. Brady and J. K. M. Sanders, *Angew. Chem., Int. Ed. Engl.*, 1996, **35**, 2143.
16 S. Sakai, Y. Shigemasa and T. Sasaki, *Tetrahedron Lett.*, 1997, **38**, 8145; B. Klekota, M. H. Hammond and B. L. Miller, *Tetrahedron Lett.*, 1997, **38**, 8639.
17 P. Timmerman, R. H. Vreekamp, H. Hulst, W. Verboom, D. N. Reinhoudt, K. Rissanen, K. A. Udachin and J. Ripmeester, *Chem. Eur. J.*, 1997, **3**, 1823; R. H. Vreekamp, H. Hubert, J. P. M. Van Duynhoven, W. Verboom and D. N. Reinhoudt, *Angew. Chem., Int. Ed. Engl.*, 1996, **35**, 1215.
18 K. A. Jolliffe, M. Crego Calama, R. Fokkens, N. M. M. Nibbering, P. Timmerman and D. N. Reinhoudt, *Angew. Chem.*, in the press.
19 J.-L. Weidmann, P. Timmerman and D. N. Reinhoudt, unpublished results.

Received in Liverpool, UK, 4th February 1998; 8/01028E

Spectroscopic identification and reactivity of $[Ir(CO)_3I_2Me]$, a key reactive intermediate in iridium catalysed methanol carbonylation

Talit Ghaffar,[a] Harry Adams,[a] Peter M. Maitlis,[a] Glenn J. Sunley,[b] Michael J. Baker[b] and Anthony Haynes*[a]

[a] *Department of Chemistry, University of Sheffield, Sheffield, UK S3 7HF*
[b] *BP Chemicals Ltd, Hull Research and Technology Centre, Saltend, Hull, UK HU12 8DS*

The dimer $[Ir(CO)_2I(\mu\text{-}I)Me]_2$ 2 reacts with CO to give the tricarbonyl $[Ir(CO)_3I_2Me]$ 3 identified by high pressure IR and NMR spectroscopy and isotopic labelling; kinetic data for the migratory CO insertion reaction of 3 support its role as a key intermediate in iridium catalysed methanol carbonylation.

A new homogeneous catalytic process for the carbonylation of methanol to acetic acid has recently been commercialised by BP Chemicals.[1,2] The *Cativa* process is based on a promoted iridium/iodide catalyst system, and shows enhancements in rate, selectivity and stability compared with the established rhodium-based technology. The catalytic cycles for the two metals are similar, but show some important differences.[3–6] Forster's original kinetic and spectroscopic studies of the iridium system led to the proposal of catalytic cycles involving both anionic and neutral complexes. At moderate iodide concentrations, the resting state of the catalyst is the anionic methyl complex, $[Ir(CO)_2I_3Me]^-$ **1** and the rate determining step is thought to be carbonylation of this species [eqn. (1)]

$$\underset{\mathbf{1}}{[Ir(CO)_2I_3Me]^-} + CO \rightarrow [Ir(CO)_2I_3(COMe)]^- \qquad (1)$$

Both the catalytic reaction and the carbonylation of **1** were found to be inhibited at high $[I^-]$, suggesting a mechanism involving neutral intermediates formed by iodide dissociation from **1**.[6] We recently reported that the carbonylation of **1** is promoted substantially by protic solvents which can aid the dissociation of an iodide ligand.[7] Here, we report the synthesis and characterisation of $[Ir(CO)_2I(\mu\text{-}I)Me]_2$ and its reaction with carbon monoxide to give $[Ir(CO)_3I_2Me]$. This tricarbonyl species, a key intermediate in the proposed carbonylation mechanism, was never detected in Forster's original studies. Its observation has now allowed us to compare the rate of migratory CO insertion in neutral and anionic species.

In our initial attempts to synthesise and isolate a neutral iridium methyl complex we used silver salts (*e.g.* $AgBF_4$) to abstract iodide from the anionic precursor, **1**. Although IR spectroscopy indicated the formation of a product with ν(CO) bands (2119 and 2074 cm^{-1}) similar to those reported by Forster for $[Ir(CO)_2I_2Me]_n$, we were not able to isolate a pure product from these reactions. Treatment of **1** with indium triiodide in CH_2Cl_2 gave a species with identical IR absorptions to those found in the reactions with silver salts. In this case the product was isolated in good yield by extraction into hot cyclohexane and characterised as an iodide-bridged dimer, $[Ir(CO)_2I(\mu\text{-}I)Me]_2$ **2** [eqn. (2)], by spectroscopy‡ and X-ray crystallography.§ Addition of 2 equiv. of I^- to **2** quickly regenerates the anion, **1**, indicating that the iodide bridges are broken quite easily.

$$\underset{\mathbf{2}}{NBu_4[Ir(CO)_2I_3Me]} + InI_3 \rightarrow 0.5\,[Ir(CO)_2I_2Me]_2 + NBu_4[InI_4] \qquad (2)$$

Isolation of **2** has allowed us to investigate its reaction with CO. Brief bubbling of CO through a solution of **2** in CH_2Cl_2 resulted in the formation of small amounts of a species, **3**, with ν(CO) bands at 2156 and 2096 cm^{-1}. A third absorption, at 2116 cm^{-1} of similar intensity to the other two, was revealed by computer subtraction of the bands of unreacted **2**. The number and relative intensities of these bands are consistent with a *fac*-tricarbonyl complex [symmetry C_s, ν(CO) modes 2A′ + A″].[9] Under an inert atmosphere, **3** was found to revert to **2** over several minutes.

The reaction stereochemistry was probed by using isotopic labelling. The IR spectrum of the product obtained from the reaction of **2** with ^{13}CO (1 atm) in CH_2Cl_2 displayed three ν(CO) bands, one of which (2096 cm^{-1}) was at identical frequency to a band of unlabelled **3**, whereas the other two absorptions (2142 and 2081 cm^{-1}) were shifted to low frequency. This behaviour is exactly as expected if the incoming ^{13}CO ligand coordinates *trans* to the methyl group to give **3*** (Scheme 1), which retains C_s symmetry. The two A′ ν(CO) modes of **3*** involve vibration of all three carbonyl ligands, explaining the observed shift of two of the ν(CO) bands. The A″ mode involves only the two equivalent carbonyls, and is unaffected by labelling of the CO *trans* to methyl. All the observed ν(CO) frequencies for **3** and **3*** can be modelled accurately by a CO factored force field.¶ When the ^{13}CO atmosphere was removed, **3*** was found to revert cleanly to **2**, with no detectable retention of isotopic label. The reversible reaction of **2** with CO is therefore stereospecific, with the ligand entering and leaving from the site *trans* to methyl. The C–O stretching force constant for the carbonyl ligand *trans* to methyl is calculated to be *ca.* 30 N m^{-1} larger than that for the two carbonyls *trans* to iodides. The unique carbonyl therefore experiences less π back donation from the iridium centre, consistent with the higher lability at this site.

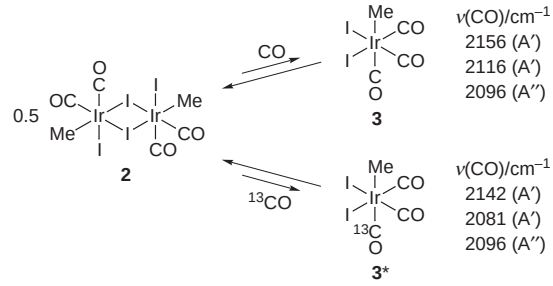

Scheme 1

Less than 10% conversion of **2** into **3** was achieved using CO at atmospheric pressure. Larger quantities of **3** were observed using a high pressure infrared cell to monitor the reaction *in situ*.[5] At 400 psi, essentially complete conversion of **2** into **3** was achieved, using CH_2Cl_2 or chlorobenzene as solvent. By contrast, in acetonitrile formation of **3** was suppressed even at high CO pressures, presumably due to cleavage of the dimer and occupation of the vacant site by a solvent molecule. This was confirmed by the observation of ν(CN) for $[Ir(CO)_2(NC\text{-}Me)I_2Me]$ at 2341 cm^{-1} and osmometry measurements (observed molecular weight 538) for solutions of **2** in MeCN.

Evidence for **3** was also obtained by high pressure NMR spectroscopy using a sample of **2** isotopically enriched with ^{13}C

in both methyl (> 99%) and carbonyl (70–80%) positions. When a solution of this sample in CD_2Cl_2 was placed under 415 psi ^{13}CO (> 99% enriched), new doublets were observed in the ^{13}C NMR spectrum at δ −21.7 and 148.7 ($^2J_{CC}$ 27 Hz) which are assigned to mutually *trans* methyl and carbonyl ligands in **3**. The carbonyls *trans* to iodide gave a singlet at δ 146.1 with no coupling to the *cis* ligands resolved. The methyl group of **3** was also detected by ^1H NMR spectroscopy at δ 2.14 (d, J_{CH} 139 Hz).

It has been proposed previously by Forster[6] and ourselves[7] that **3** is a reactive intermediate in the carbonylation of **1**, and that the tricarbonyl is activated towards migratory CO insertion compared with the anionic precursor. We have therefore studied the reaction of **3** with CO to investigate the validity of this proposal. Below 40 °C, complex **3** was found to be stable indefinitely in chlorobenzene under 400 psi CO. Above this temperature, a reaction was observed in which the ν(CO) bands of **3** were replaced by new absorptions at 2176w, 2115s and 1708m cm^{-1}. These bands correspond well with those assigned by Forster[6] to a neutral acetyl complex, $[Ir(CO)_3I_2(COMe)]$, the relative intensities suggesting a *mer*-tricarbonyl configuration, **4** (Scheme 2). An iridium acetyl species was also observed in the high-pressure NMR experiment after heating to 70 °C [^{13}C, δ 52.4 (CH_3CO), 186.4 (CH_3CO), $^1J_{CC}$ 35 Hz; ^1H, δ 3.04, $^1J_{CH}$ 131, $^2J_{CH}$ 5.5 Hz].

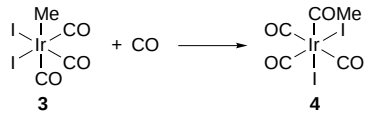

3 **4**

Scheme 2

Pseudo-first order rate constants, k_{obs}, for this reaction were obtained by monitoring the exponential decay of the high frequency ν(CO) band of **3** at 2156 cm^{-1}. Values of k_{obs} measured in chlorobenzene over the temperature range 44–85 °C are shown in Table 1. An Eyring plot of these data yields activation parameters $\Delta H^{\ddagger}$ 89±3 kJ mol^{-1} and $\Delta S^{\ddagger}$ −36 ±8 J mol^{-1} K^{-1}. Carbonylation of complex **3** is more than 800 times faster than for the anion, **1** at 85 °C in chlorobenzene,[7] representing a lowering of the observed $\Delta G^{\ddagger}$ by 20 kJ mol^{-1} on replacing an iodide ligand by CO. Extrapolation to higher temperatures reduces the difference in rates, but even at 180 °C, the neutral complex is predicted to react *ca*. 9 times faster than the anion. These new kinetic data validate the proposal that migratory insertion occurs in a neutral complex after dissociation of iodide from **1**. Addition of small amounts of methanol was found to accelerate the carbonylation of **3** (see Table 1) but not to the dramatic extent found previously for **1**.[7] Activation parameters calculated for the reaction in 1% methanol–chlorobenzene are $\Delta H^{\ddagger}$ 73±2 kJ mol^{-1} and $\Delta S^{\ddagger}$ −79±6 J mol^{-1} K^{-1}.

An explanation for the acceleration of migratory insertion in **3** relative to **1** may reside in the increased competition for π-backbonding in the tricarbonyl complex, **3**. Theoretical calculations on similar systems have suggested that increasing the number of π acceptor ligands lowers the energy of the LUMO (an out of phase combination of π^*_{CO} with d_π) and facilitates methyl migration.[10] Acceleration of migratory CO insertion by coordination of a π acceptor ligand has also been reported for $[Ir(CO)(PPh_3)_2Cl(Me)]^+$.[11]

Table 1 First order rate constants for the carbonylation of **3** in chlorobenzene and in chlorobenzene containing 1% (v/v) methanol (p_{CO} = 400 psi).

T/ °C	10^4 k_{obs}/s^{-1} (PhCl)	*T*/ °C	10^4 k_{obs}/s^{-1} (PhCl–1% MeOH)
44	1.64	44	5.10
		47	6.75
52	3.73	52	10.6
59	9.47	59	17.6
67	19.7	68	39.5
76	41.1		
85	87.6		

To summarise we have confirmed Forster's original suggestion that neutral intermediates play a key role in the migratory insertion step for the iridium catalysed carbonylation of methanol. We have obtained spectroscopic evidence for the previously undetected species, $[Ir(CO)_3I_2Me]$ **3** which undergoes CO insertion at a rate substantially faster than its anionic precursor, **1**.

We thank BP Chemicals, The Royal Society, and the University of Sheffield for supporting this research. We thank Cambridge Isotope Laboratories for an award of ^{13}C labelled carbon monoxide, Dr Mike Taylor (BP, Sunbury, UK) for carrying out high pressure NMR experiments and Dr George Morris for helpful discussions.

Notes and References

† E-mail: a.haynes@sheffield.ac.uk

‡ Analytical and spectroscopic data for $[Ir(CO)_2I(\mu\text{-}I)Me]_2$ **2**. Analysis. Found: C, 7.0; H, 0.4; I, 49.1. Calc for $C_6H_6Ir_2I_4O_4$: C, 7.0; H, 0.6; I, 49.1%. *M* (PhCl). Found: 1001. Calc. 1034; IR (CH_2Cl_2), ν(CO)/cm^{-1}: 2119, 2074. NMR (CD_2Cl_2): δ_H 1.94, 1.88; δ_C 152.4, 150.3 (CO), −5.30, −8.76 (CH_3). The NMR data suggest the existence of isomeric forms of the dimer in solution.

§ An X-ray crystal structure of **2** shows it be a centrosymmetric dimer, very similar to the chloride analogue.[8] Of particular note is the asymmetry in the Ir–(μ-I)–Ir bridges with a significantly longer Ir–(μ-I) bond *trans* to methyl [2.799(2) Å] than *trans* to CO [2.716(2) Å], attributable to the high *trans* influence of the methyl ligand. Full details of the structure will be reported in a full paper.

¶ The stretching (*k*) and interaction (*i*) force constants used to fit the observed ν(CO) frequencies of **3** and **3*** were: k_1 = 1810 N m^{-1}, k_2 = 1840 N m^{-1}, i_{11} = 35.5 N m^{-1}, i_{12} = 24.6 N m^{-1} where $CO_{(1)}$ is *trans* to I and $CO_{(2)}$ is *trans* to Me.

1 *Chem. Br.*, 1996, **32**, 7.
2 *Chem. Ind.* (*London*), 1996, 483.
3 D. Forster, *Adv. Organomet. Chem.*, 1979, **17**, 255.
4 T. W. Dekleva and D. Forster, *Adv. Catal.*, 1986, **34**, 81.
5 P. M. Maitlis, A. Haynes, G. J. Sunley and M. J. Howard, *J. Chem. Soc., Dalton Trans.*, 1996, 2187.
6 D. Forster, *J. Chem. Soc., Dalton Trans.*, 1979, 1639.
7 J. M. Pearson, A. Haynes, G. E. Morris, G. J. Sunley and P. M. Maitlis, *J. Chem. Soc., Chem. Commun.*, 1995, 1045.
8 N. A. Bailey, C. J. Jones, B. Shaw and E. Singleton, *J. Chem. Soc., Chem. Commun.*, 1967, 1051.
9 P. S. Braterman, *Metal Carbonyl Spectra*, Academic Press, 1975.
10 P. Margl, T. Ziegler and P. E. Blöchl, *J. Am. Chem. Soc.*, 1996, **118**, 5412.
11 M. Kubota, T. M. McClesky, R. K. Hayashi and C. G. Webb, *J. Am. Chem. Soc.*, 1987, **109**, 7569.

Received in Cambridge, UK, 26th January 1998; 8/00659H

Dehydrogenation of ethane over gallium oxide in the presence of carbon dioxide

Kiyoharu Nakagawa,[a,b] Masato Okamura,[a] Naoki Ikenaga,[a] Toshimitsu Suzuki*[a,b]† and Tetsuhiko Kobayashi[c]

[a] *Department of Chemical Engineering, Faculty of Engineering, and*
[b] *High Technology Research Center, Kansai University, Suita, Osaka, 564-8680, Japan*
[c] *Osaka National Research Institute, AIST, MITI, Ikeda, Osaka 563-8577, Japan*

Gallium oxide is found to be an effective catalyst for the dehydrogenation of ethane to ethene in the presence of carbon dioxide at 650 °C, giving 18.6% ethene yield with a selectivity of 94.5%.

Ethene is predominantly produced by steam cracking of naphtha, ethane or liquid petroleum gas at high temperatures at short residence time.

In order to reduce energy consumption of ethene production, oxidative dehydrogenation of ethane is proposed [eqn. (1)].

$$C_2H_6 + 1/2O_2 \rightarrow C_2H_4 + H_2O \quad (1)$$

The reaction becomes exothermic and thermodynamically could be possible at relatively low temperatures. However, it is necessary to remove heat from the reaction and to avoid over oxidation to CO_2 to give high selectivity towards ethene. Recently, a great variety of catalysts have been developed and tested for this reaction.[1–3] In the oxidative dehydrogenation of propane, Burch and Crabb[4] pointed out that thermal non-catalytic oxidative cracking of propane proceeded to give propene in the same yield as compared to catalyzed runs which were operated about 50 °C lower than that of non-catalyzed runs. This suggests that catalyzed oxidative dehydrogenation of lower alkanes is not highly superior to thermal oxidative pyrolysis.

Recently, several attempts have been made to use carbon dioxide as an oxidant for coupling of methane,[5] dehydrogenation of ethylbenzene[6] or propane.[7] However, the role of CO_2 in these reactions is still not clear. In addition, the effects of CO_2 on the conversion and yield of the product are not significant.

Here, we study the dehydrogenation of ethane to ethene over several metal oxide catalysts, and we have found that CO_2 markedly promoted dehydrogenation of ethane over Ga_2O_3 catalyst.

The catalysts used were commercially available MgO, Al_2O_3, SiO_2, CaO, TiO_2, V_2O_5, Cr_2O_3, Mn_3O_4, Fe_3O_4, ZnO, Ga_2O_3, Y_2O_3, ZrO_2, Nb_2O_5, MoO_3, In_2O_3, SnO_2, La_2O_3, CeO_2, Ta_2O_5 and Tl_2O_3. The reaction was carried out with a fixed-bed flow type quartz reactor (i.d. 10 × 350 mm) at atmospheric pressure. Using 200 mg of a catalyst, 5 ml min^{-1} of C_2H_6 and 25 ml min^{-1} of CO_2 were introduced. The runs were conducted for 30 min and products were analyzed by gas chromatography.

Fig. 1 shows ethene yields on the various metal oxide catalysts. Thermal dehydrogenation occurred to give only 2.3% of ethene yield. Equilibrium conversion of ethane to ethene is *ca.* 50% at 650 °C at a C_2H_6–Ar (or CO_2) ratio of 1 : 5. MgO, CaO, SiO_2, Ta_2O_5, Al_2O_3, SnO_2, MoO_3, and Tl_2O_3 did not show any catalytic activity while CeO_2, Nb_2O_5, Fe_3O_4, and ZrO_2 exhibited only slight catalytic activity. The order of the activity of oxides at the reaction temperature of 650 °C was as follows: Ga_2O_3 > Cr_2O_3 > V_2O_5 > TiO_2 > Mn_3O_4 > In_2O_3 > ZnO > La_2O_3. The C_2H_4 selectivities in all the metal oxide catalysts were > 85% in the dehydrogenation of ethane in the presence of CO_2. As expected, Cr_2O_3 and V_2O_5 exhibited high activities. These catalysts are known to be active catalysts for dehydrogenation of alkanes. Ga_2O_3 afforded the highest yield of ethene

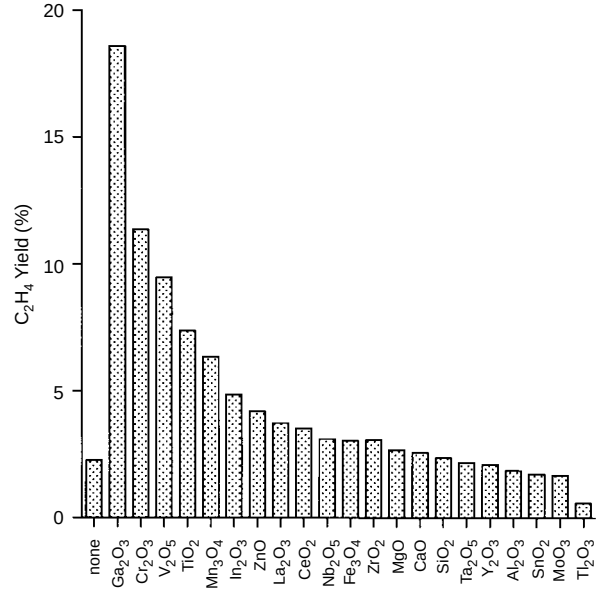

Fig. 1 Dehydrogenation of C_2H_6 in the presence of CO_2. Catalyst 200 mg; temperature: 650 °C; C_2H_6 : CO_2 = 5 : 25 ml min^{-1}; SV = 9000 h^{-1} ml (g cat)$^{-1}$.

(18.6%) amongst the various metal oxide catalysts. However, little work has dealt with Ga_2O_3 catalyst in the dehydrogenation of propane.[8]

Table 1 lists ethene yields on Ga_2O_3, Cr_2O_3, and V_2O_5 catalysts in the presence and absence of CO_2. The activity of the Ga_2O_3 catalyst in the presence of CO_2 was twice that in the absence of CO_2. Dehydrogenation of C_2H_6 in the presence of CO_2 over Ga_2O_3 catalyst produced mainly C_2H_4, CO, H_2 and H_2O. The yield of ethene with the Cr_2O_3 catalyst in the presence of CO_2 was slightly higher as compared to the run in Ar. The promoting effect of CO_2 in the dehydrogenation of C_3H_8 on Cr_2O_3/SiO_2 has been reported,[5] but the increase in the propene yield was only 2.6% at 550 °C. On the other hand, the effect of

Table 1 Dehydrogenation of ethane in the presence of carbon dioxide[a]

Catalyst	Surface area/ m^2 g^{-1}	Conv. (%) C_2H_6	Yield (%) C_2H_4	Selectivity (%) C_2H_4	CH_4	C_3H_8
$Ga_2O_3(CO_2)$	9.8	19.6	18.6	95.0	3.8	1.0
Ga_2O_3(Ar)	9.8	9.6	9.0	94.0	5.0	0.7
$Cr_2O_3(CO_2)$	2.8	12.1	11.4	93.8	5.8	0.4
Cr_2O_3(Ar)	2.8	10.4	10.2	97.6	1.8	0.6
$V_2O_5(CO_2)$	3.5	9.8	9.5	97.1	2.9	—
V_2O_5(Ar)	3.5	12.5	11.5	91.7	7.4	0.9

[a] Reaction conditions: 650 °C, SV = 9000 h^{-1} ml (g cat)$^{-1}$. Composition of the feed gas; C_2H_6 : CO_2(Ar) = 5 : 25 ml min^{-1}.

CO_2 on the yield of ethane with V_2O_5 in the presence of CO_2 was slightly detrimental. CO_2 promoted dehydrogenation of ethane exclusively over Ga_2O_3 catalyst. To our knowledge, such a marked promotion effect of CO_2 in a hydrocarbon conversion process has never been previously observed. The role of CO_2 in dehydrogenation of C_2H_6 over Ga_2O_3 catalyst is, as yet, unclear. With CO_2 considerable amounts of CO and H_2O were formed during the reaction, indicating reaction of CO_2 with H_2. The amount of H_2O was 1.09 mmol and that of CO was 1.07 mmol at 650 °C after 0.5 h. Dehydrogenation of C_2H_6 was strongly inhibited when Ga_2O_3 was impregnated onto a basic oxide such as MgO or La_2O_3. Another characteristic feature in the reaction in CO_2 is the increase in the yield of CH_4. From these findings the role of CO_2 may be as follows: slightly acidic CO_2 may strongly adsorb onto basic sites of gallium oxide, and as a result, the acidity of Ga_2O_3 would be enhanced. This possibility is reinforced by the fact that after dehydrogenation a certain amount of carbon was formed on the catalyst (Ga_2O_3, Cr_2O_3, and V_2O_5). Dehydrogenation of ethane would be catalyzed by acid sites on Ga_2O_3.

This work was supported by the Grant-in Aid for Scientific Research (C) No.09650864 from the Ministry of Education, Science and Culture Japan. K. N. is grateful for his research assistantship from the High Technology Research Center, Kansai University.

Notes and References

† E-mail: tsuzuki@ipcku.kansai-u.ac.jp

1 F. Cavani and F. Trifirò, *Catal. Today*, 1995, **24**, 307.
2 H. H. Kung, *Adv. Catal.*, 1994, **40**, 1.
3 W. Ueda, S. W. Lin and I. Tohmoto, *Catal. Lett.*, 1997, **44**, 241
4 R. Burch and E. M. Crabb, *Appl. Catal. A*, 1993, **100**, 111.
5 T. Nishiyama and K. Aika, *J. Catal*, 1990, **122**, 346.
6 M. Sugino, H. Shimada, T. Turuda, H. Miura, N. Ikenaga and T. Suzuki, *Appl. Catal. A*, 1995, **121**, 125.
7 I. Takahara and M. Saito, *Chem. Lett.*, 1996, 973.
8 T. Hattori, M. Komai, A. Satsuma and Y. Murakami, *Nippon Kagaku Kaishi*, 1991, **5**, 648.

Received in Cambridge, UK, 6th January 1998; 8/00184G

Four-electron electrocatalytic reduction of dioxygen to water by an ion-pair cobalt porphyrin dimer adsorbed on a glassy carbon electrode

Francis D'Souza,*† Yi-Ying Hsieh and Gollapalli R. Deviprasad

Department of Chemistry, Wichita State Unviersity, Wichita, KS 6720-0051, USA

An ion-pair porphyrin dimer, formed by reacting the tetrachloro salt of [tetrakis(*N*-methylpyridyl)porphyrinato]-cobalt and the tetrasodium salt of [tetrakis(4-sulfonatophenyl)porphyrinato]cobalt, adsorbed electrochemically on a glassy carbon electrode is shown to catalytically reduce O_2 to water by four electrons.

Mimicking enzymatic catalytic reactions using metalloporphyrin dimers is an area of active research. Towards this, covalently linked porphyrin dimers are most widely used and by employing such dimers, four-electron reduction of O_2 to H_2O has been demonstrated.[1,2] That is, either Co or Fe porphyrin dimers, with closely spaced porphyrin rings (inter-ring distance *ca.* 3.5 Å), adsorbed on a glassy carbon (GC) electrode, catalyze the reduction of O_2 to H_2O at low pH. The postulated mechanism involves formation of a μ-ligated O_2 complex, followed by electrochemical reduction and protonation to produce H_2O. The inter-ring distance and the rigidity of the dimer are believed to be important factors governing the formation of the μ-ligated O_2 complex for the overall catalytic process.[1*a*]

Water soluble monomeric Co porphyrins, bearing either positive charges on the ring periphery, such as the tetrachloro salt of [tetrakis(*N*-methylpyridyl)porphyrinato]cobalt, [Co(TMPyP)]Cl_4 or negative charges on the ring periphery, such as the tetrasodium salt of [tetrakis(4-sulfonatophenyl)-porphyrinato]cobalt, Na_4[Co(TPPS)] (Fig. 1), are known to adsorb irreversibly on a GC electrode and catalytically reduce O_2 by two electrons to produce H_2O_2.[3] It is also known that these oppositely charged porphyrins form stable face-to-face bound porphyrin dimers with 1 : 1 molecular stoichiometry when they are mixed together in solution.[3,4] Spectroscopic investigations have shown[4] that the inter-ring distance between the porphyrin rings of these dimers is *ca.* 3.1 Å. This distance is shorter by 0.4 Å than that of a closely spaced covalently linked porphyrin dimer known to reduce O_2 directly to water.[1*a*] These results suggest that the ion-pair dimers should also be utilized as electrode materials for catalytic reduction of O_2. Sawaguchi *et al.*[1*i*] initially examined the catalytic behaviour for O_2 reduction by using electrodes coated with ion-pair Fe–Fe porphyrin dimer and reported a 12% catalytic efficiency towards four-electron reduction of O_2 to H_2O. In the present study, we have observed a catlaytic efficiency up to 98% when an ion-pair Co–Co porphyrin dimer, adsorbed electrochemically on a glassy carbon electrode, under elevated pH conditions is used.

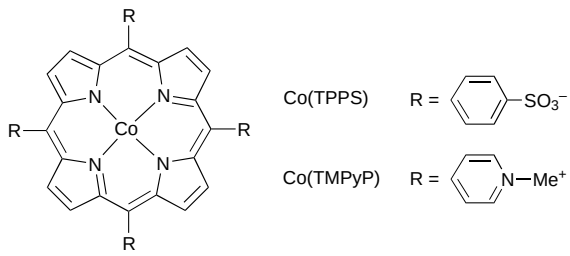

Fig. 1 The structural formulae of the water-soluble Co porphyrins used to form ion-pair dimer

Fig. 2 shows the cyclic voltammograms‡ (CVs) for O_2 reduction on the dimer, [Co(TMPyP)][Co(TPPS)]§ adsorbed GC electrode¶ (curve 1), a monomer, Co(TMPyP)Cl_4 adsorbed GC electrode (curve 2) and a bare GC (curve 3) in O_2 saturated 0.05 M NH_4Cl.‖ Curve 4 shows the CV for the dimer adsorbed electrode in the absence of O_2. Two irreversible peaks located at E_{pc} = −0.49 V and E_{pc} = −0.76 V *vs.* Ag/AgCl, are observed for the dimer adsorbed electrode. There is a positive shift of peak potential by 360 mV for O_2 reduction for the monomer adsorbed GC electrode as compared to that observed for the bare GC electrode (Curves 2 and 3). Similar voltammetric behavior is also seen for the monomer, Co(TPPS) adsorbed electrode and a dimer, [Co(TMPyP)][(H_2TPPS)], in which only one of the porphyrins has a Co metal ion and the other is a free-base porphyrin, adsorbed electrode. These results are similar to that reported for the catalytic two-electron reduction of O_2 to peroxide.[5]

The peak potential for O_2 reduction on the dimer adsorbed electrode is located at E_{pc} = −0.22 V *vs.* Ag/AgCl (curve 1). This peak potential is positively shifted by 120 mV when compared to the peak potential for O_2 reduction on the monomer adsorbed electrode (curve 2). Additionally, larger, peak currents, proportional to (scan rate)$^{1/2}$, are obtained for the dimer adsorbed electrode. The positive shift of the peak potential and the larger catalytic currents for O_2 reduction on the dimer adsorbed electrode suggest the occurrence of four-electron reduction of O_2 to H_2O.[1*a*] In order to quantify these results, voltammetry at a rotating disk-ring electrode has been performed.

Fig. 3(*a*) shows voltammetric curves, recorded with the use of a rotating (Pt ring)–(GC disk) electrode,** for O_2 reduction at various rotation rates. The catalyst was adsorbed on the disk.¶ Disk potential was scanned from 0.1 to −0.5 V while ring

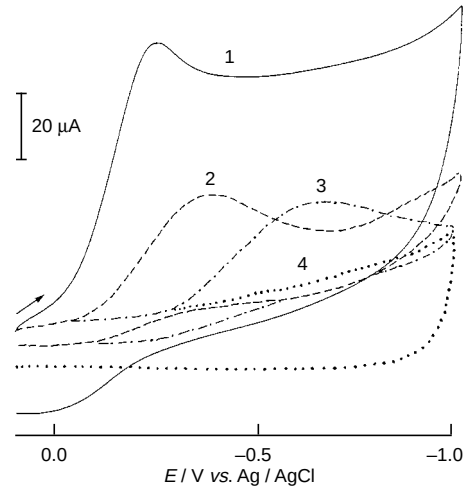

Fig. 2 Cyclic voltammograms for dioxygen reduction at [Co(TPP-S)][Co(TMPyP)]/GC electrode (curve 1), Co(TMPyP)/GC electrode (curve 2) and bare glassy carbon electrode (curve 3) in O_2 saturated 0.05 M NH_4Cl. Curve 4 represents the CV of [Co(TPPS)][Co(TMPyP)] adsorbed electrode in the absence of O_2. Scan rate = 100 mV s^{-1}.

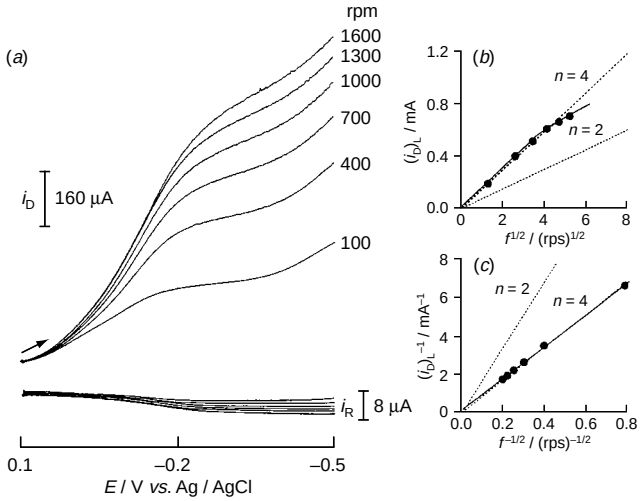

Fig. 3 (*a*) Rotating (platinum ring)–(glassy carbon disk) electrode voltammetry for the [Co(TMPyP)][Co(TPPS)] adsorbed on the disk and the O_2 saturated 0.05 M NH_4Cl aqueous solution. Ring potential, E_R = 1.0 V. Disk potential scan rate, 20 mV s^{-1}. (*b*) and (*c*) are the Levich and Koutecky–Levich plots for the plateau currents from Fig. 3(*a*). Dashed lines are calculated for the O_2 reduction by two and four electrons. Area of the electrode = 0.164 cm^2, concentration of O_2 = 0.5 mM, diffusion coefficient of O_2 = 2.6 × 10^{-5} cm^2 s^{-1}, kinematic viscosity = 0.01 cm s^{-1}.

potential was kept at E_R = 1.0 V in order to detect any H_2O_2 generated by a two-electron reduction process of O_2 at the disk.[1a] Larger disk currents have been obtained for the dimer than for the monomer adsorbed on the graphite electrodes. Levich and Koutecky–Levich plots[6] of the plateau currents from Fig. 3(*a*) are shown in Fig. 3(*b*) and (*c*). The calculated number of electrons involved in the reduction of O_2 from the slope of Fig. 3(*c*) is found to be 3.8 ± 0.2 electrons per O_2 molecule while this value for Co(TMPyP), Co(TPPS) and the Co–H_2 dimer adsorbed electrodes is found to be 2.0 ± 0.2 electrons. It is observed that the occurrence of four-electron reduction for the dimer adsorbed electrode is dependent on the positive switching potential, E_λ during the adsorption of the dimer onto the electrode surface. When E_λ was < 1.2 V, the number of electrons in the process was between 3 and 4.

As expected, negligent amounts of ring currents are observed for the Co–Co dimer adsorbed electrode when the ring potential is held at +1.0 V, *i.e.*, a potential where oxidation of H_2O_2, a two-electron reduction product of O_2 generated at the disk occurs. The ratio of the ring to disk current, i_R/i_D, is 0.01 for the adsorbed dimer which is much smaller than the collection efficiency of 0.36 determined with the use of the $[Fe(CN)_6]^{3-/2-}$ redox couple under the same solution conditions. The i_R/i_D ratio for the adsorbed dimer does not change appreciably with the rotation rate and amounts to 98% of the disk current resulting from four-electron reduction of O_2 to H_2O.[7]

For the electrode coated with the covalently linked Co porphyrin dimer, the catalytic activity towards four-electron reduction of O_2 depends strongly on pH.[1a] For pH > 4.5, only H_2O_2, *i.e.*, a two-electron product is formed.[1a] For the presently investigated ion-pair Co–Co dimer, the calculated 3.8 ± 0.2 number of electrons, at a relatively high pH (5.3) and low ionic strength (0.05 M), indicates its greater ability to catalyze reduction of O_2 by four electrons. This ability of the easy to prepare 'ion-pair' dimer to catalyze, by four-electron reduction of O_2 to H_2O at elevated solution pH is commendable. Further studies to understand the role of E_λ during the process of surface adsorption and the mechanistic details of four-electron reduction of O_2 using different ion-pair porphyrin dimers are in progress.

The authors are thankful to Professor W. Kutner for helpful discussions. This work is supported by NSF (Grant No. EPS-9550487) and matching support from the State of Kansas. The authors are also thankful to the donors of the Petroleum Research Fund, administered by the American Chemical Society for support of this work.

Notes and References

† E-mail: dsouza@wsuhub.uc.twsu.edu

‡ Cyclic voltammetry was performed on a model 263 A potentiostat/galvanostat of EG & G (Princeton, NJ) by using a typical three-electrode cell arrangement. A glassy carbon electrode (0.3 cm diameter) of BAS was used as the working electrode. A Pt wire served as the counter electrode and an Ag/AgCl electrode was used as the reference one.

§ The dimer, [Co(TMPyP)][Co(TPPS)], was synthesized by a stoichiometric reaction of $[Co(TMPyP)]Cl_4$ (100 mg) (Mid-Century Chemicals Co., Posen, IL) in 20 ml of MeOH–EtOH (1 : 1 v/v) and $Na_4[Co(TPPS)]$ (117 mg) (Mid-Century Chemicals Co.) in 10 ml of MeOH–EtOH (1 : 1 v/v) at room temp. The resulting solid which precipitated was centrifuged, filtered, washed repeatedly with MeOH to yield (71%) pure dimer. UV–VIS in water, λ_{max} (log ε), 322 (4.52), 427 (5.16), 543 (0.16). Elemental analysis of the synthesized dimer revealed the presence of a large number (12 to 16) of water molecules.

¶ The GC working electrode prior to the experiments was initially cleaned with alumina powder and was further treated with 2 M H_2SO_4. The surface of the electrode was roughened by using fine quality sand paper. The porphyrin (dimer or monomer) was adsorbed on the glassy carbon electrode under multicyclic voltammetry conditions. For this, a slurry of porphyrin (*ca.* 1 mM) in 0.025 M NaCl solution was used. The potential was scanned for the range 1.2 to −0.1 V (nearly 30 cycles), until a scan-number-independent voltammogram was obtained. The electrode was then removed from the solution, rinsed thoroughly with distilled water and then immersed in the blank supporting electrolyte solution. The electrochemical measurements were performed at room temperature in 0.05 M NH_4Cl (pH 5.3).

‖ A 0.05 M NH_4Cl solution of low ionic strength (μ = 0.05) was used to avoid possible decomposition of the adsorbed ion-pair porphyrin dimer on the electrode surface.

** The rotating ring-disk electrode (RRDE) voltammetry, was performed by using a Model AFCB1 bipotentiostat, MSRX Speed Control Unit and AFMSRX Modulated Speed Rotator of Pine Instrument Co. (Grove City, PA). A model BD-95 dual channel recorder of Kipp and Zonen (Bohemia, NY) was used to record the voltammograms. Radius of the disk, gap and ring of the platinum-(glassy carbon) ring-disk electrode was 0.23, 0.25 and 0.27 cm, respectively. an Ag/AgCl and Pt wire served as the reference and auxiliary electrodes, respectively.

1 (*a*) J. P. Collman, P. S. Wagenknecht and J. E. Hutchison, *Angew. Chem., Int. Ed. Engl.*, 1994, **33**, 1537; (*b*) J. P. Collman, P. Denisevich, Y. Konai, M. Marrocco, C. Doval and F. C. Anson, *J. Am. Chem. Soc.*, 1980, **102**, 6027; (*c*) R. R. Durand, C. S. Benscome, J. P. Collman and F. C. Anson, *J. Am. Chem. Soc.*, 1983, **105**, 2710; (*d*) J. P. Collman, N. H. Hendricks, K. Kim and C. J. Bencosme, *J. Chem. Soc., Chem. Commun.*, 1987, 1537; (*e*) C. K. Chang, J. Y. Liu and I. Abdalmuhdi, *J. Am. Chem. Soc.*, 1984, **106**, 2725; (*f*) H. Y. Liu, M. J. Weaver, C. B. Wang and C. K. Chang, *J. Electroanal. Chem., Interfacial Electrochem.*, 1983, **145**, 439; (*g*) H. Y. Liu, I. Abdalmuhdi, C. K. Chang and F. C. Anson, *J. Phys. Chem.*, 1985, **89**, 665; (*h*) R. Karaman, S. Jeon, O. Almarsson and T. C. Bruice, *J. Am. Chem. Soc.*, 1992, **114**, 4899; (*i*) T. Sawaguchi, T. Matsue, K. Itaya and I. Uchida, *Electrochim. Acta.*, 1991, **36**, 703.

2 For other monomeric metalloporphyrins known to catalyze the reduction of dioxygen to water, see: F. C. Anson, C. Shi and B. Steiger, *Acc. Chem. Res.*, 1997, **30**, 437.

3 E. Ojadi, R. Selzer and H. Linschitz, *J. Am. Chem. Soc.*, 1985, **107**, 7783; H. van Willigen, U. Das, E. Ojadi and H. Linschitz, *J. Am. Chem. Soc.*, 1985, **107**, 7784; U. Hofstra, K. B. M. Koehorst and T. J. Schaafsma, *Chem. Phys. Lett.*, 1986, **130**, 555; D. K. Geiger and C. A. Kelly, *Inorg. Chim. Acta.*, 1988, **154**, 137.

4 U. Hofstra, R. B. M. Koehorst and T. J. Schaafsma, *Magn. Reson. Chem.*, 1987, **25**, 1069.

5 F. D'Souza, G. R. Deviprasad and Y.-Y. Hsieh, *J. Electroanal. Chem.*, 1996, **411**, 167; F. D'Souza, Y.-Y. Hsieh and G. R. Deviprasad, *J. Electroanal. Chem.*, 1997, **426**, 17.

6 V. G. Levich, *Physicochemical Hydrodynamics*, Prentice-Hall, Englewood Cliff, NJ, 1962; J. Koutecky and V. G. Levich, *Zh. Fiz. Khim.*, 1956, **32**, 1565; N. Oyama and F. C. Anson, *Anal. Chem.*, 1980, **52**, 1192.

7 A. Bettelheim and T. Kuwana, *Anal. Chem.*, 1979, **51**, 2257.

Received in Bloomington, IN, USA, 5th December 1997; 7/08768C

Lithium fluoride formed *in situ* is trapped by $[TiF_3(C_5Me_5)]_2$: an equilibrium with cleavage of a Ti–F–Ti bond and a model compound for molecular lithium fluoride

Alojz Demsar,*[a]† Andrej Pevec,[a] Ljubo Golič,[a] Saša Petriček,[a] Andrej Petrič[a] and Herbert W. Roesky*[b]

[a] *Faculty of Chemistry and Chemical Technology, University of Ljubljana, Aškerčeva 5, SLO-1000, Ljubljana, Slovenia*
[b] *Institut für Anorganische Chemie der Universität, Tammannstrasse 4, D-37077 Göttingen, Germany*

Synthesis and structure of $[\{(C_5Me_5)TiF_3\}_4(LiF)]$ and its solution equilibrium involving cleavage of a titanium–fluorine–titanium bond is reported.

Fluorine bridging accounts for structural diversity of fluorides of main group elements and transition metals and for formation of reaction intermediates.[1] The reactivity of a Ti–F–Ti unit in fluorotitanium compounds is of particular interest since the cleavage of this unit would leave the titanium centre with high electrophilicity due to polar Ti–F bonds.[2] The catalytic activity of the fluorotitanium binaphthol complex used in the enantioselective addition of allylsilanes to aldehydes[3] was explained by cleavage of two Ti–F–Ti bonds during the catalytic cycle.[2] Here, we report on the equilibrium of cleavage and reformation of two Ti–F–Ti bonds in a solution of $[\{(C_5Me_5)TiF_3\}_4(LiF)]$ **1** observed by ^{19}F NMR spectroscopy.

The high lattice energy of lithium fluoride explains the absence of its solid complexes.[4] Lithium fluoride, prepared *in situ* from lithium chloride and trimethyltin fluoride, has now been successfully trapped by $[TiF_3(C_5Me_5)]_2$ to yield **1**. The reaction of $[TiF_3(C_5Me_5)]_2$, Me_3SnF and LiCl in a molar ratio of 2 : 1 : 1 in THF followed by evaporation of Me_3SnCl and solvent and recrystallization from pentane afforded red crystals of **1**.‡ The molecule of **1** in the solid state§ consists of two $[Ti_2F_6(C_5Me_5)_2]$ units connected by a lithium atom and a bridging fluorine atom (Fig. 1). Each titanium atom is coordinated by five fluorines and a C_5Me_5 ligand. The lithium atom is coordinated by four fluorines arranged in a distorted tetrahedron. The Li–F distances are similar to those in $Li[\{(Me_3Si)_3C\}AlF_3]\cdot THF$[5] with fourfold coordinated lithium, however shorter than those in lithium fluoride (2.009 Å).[6] Bonding to lithium as well as *trans*-positioned C_5Me_5 ligand causes elongation of the Ti–F bonds. The Ti–F–Ti bonds not affected by the *trans*-C_5Me_5 ligand are on average 10% longer than the terminal Ti–F bonds.

A color change from orange to red is observed when cooling toluene or chloroform solutions of **1** from 322 to 272 K. Two temperature dependent sets of resonances are found in variable temperature (VT) ^{19}F NMR spectra of $CDCl_3$ or $[^2H_8]$toluene solutions of **1**. The high temperature set of five resonances reversibly converts to a low temperature set of seven resonances on cooling as shown in Fig. 2 in $[^2H_8]$toluene solution. The changes in spectra are in agreement with the equilibrium shown in Scheme 1. Four sharp resonances in the high temperature set (intensity ratio of 2 : 2 : 1 : 2) are assigned to $[\{(C_5Me_5)_2Ti_2F_7\}Li]$ **1a** by comparison with the ^{19}F NMR spectrum of $[\{(C_5Me_5)_2Ti_2F_7\}_2Ca]$.[7] The assignment is consistent with

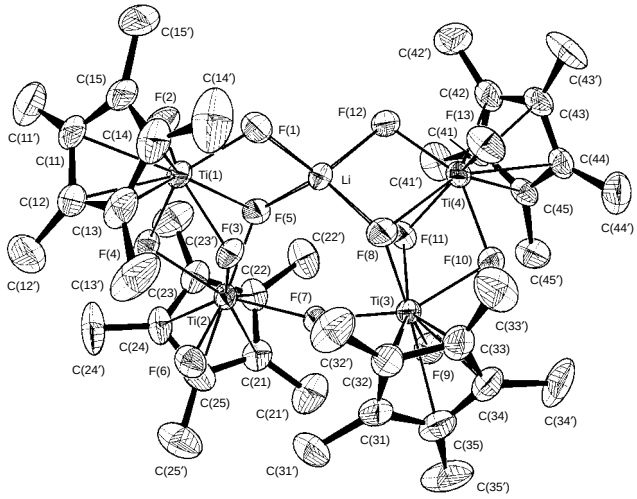

Fig. 1 Crystal structure of **1**. Hydrogen atoms are not shown. Selected bond lengths (Å) and angles (°): Ti(1)–F(1) 1.873(4), Ti(1)–F(2) 1.822(6), Ti(1)–F(3) 1.978(4), Ti(1)–F(4) 1.999(4), Ti(1)–F(5) 2.421(5), Ti(2)–F(6) 1.826(5), Ti(2)–F(5) 1.966(4), Ti(2)–F(7) 2.007(3), Ti(2)–F(4) 2.024(4), Ti(2)–F(3) 2.136(5), Li–F(1) 1.864(13), Li–F(5) 1.926(13), Li–F(8) 1.932(12), Li–F(12) 1.866(12); F(1)–Ti(1)–F(2) 93.0(2), F(1)–Ti(1)–F(5) 75.3(2), F(1)–Ti(1)–F(3) 85.0(2), F(1)–Ti(1)–F(4) 142.9(2), Ti(2)–F(8)–Ti(3) 161.1(2), F(1)–Li–F(12) 110.1(7), F(1)–Li–F(5) 89.1(4), F(5)–Li–F(8) 121.0(7).

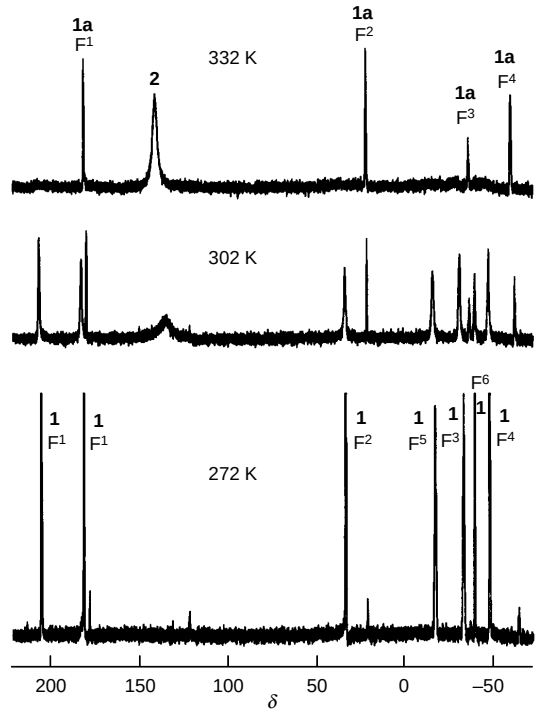

Fig. 2 ^{19}F NMR spectra of **1** ($[^2H_8]$toluene solution) at 332, 302 and 272 K. See Scheme 1 for labels. The area of the signal at δ −38.8 (F^6) in 272 K trace is one half of the respective areas of the other signals.

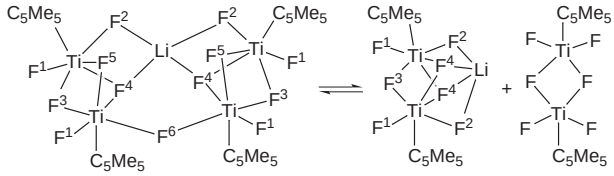

Scheme 1 Equilibrium in solution of **1**

lithium symmetrically bonded to two terminal and to two bridging fluorines from the $[Ti_2F_7(C_5Me_5)_2]^-$ moiety. The bonding of fluorines to quadrupolar lithium causes decoupling of fluorine resonances and a high field shift as already observed in the calcium compound.[7] The resonance of terminal fluorines appears as a quintet due to coupling to four fluorine atoms. The remaining, fifth, broad line of the high temperature set is attributed to the resonance of $[(C_5Me_5)TiF_3]_2$.¶ The low temperature set has six resonances of equal intensities and one with half of the intensity that could be assigned to **1** having six pairs of equivalent fluorine atoms and a single fluorine atom bridging two $[Ti_2F_6(C_5Me_5)_2]$ units. The ^{7}Li NMR signal of **1** appears as a singlet at 302 K, and as a quintet at 272 K, showing coupling to four fluorine atoms.

The equilibrium shown in Scheme 1 was studied by VT ^{19}F NMR of a [$^2H_8$]toluene solution of **1** in the temperature range 272–312 K, and resulted in $\Delta H = 75 \pm 3$ kJ mol^{-1} and $\Delta S = 197 \pm 2$ J mol^{-1} K^{-1}.‖ The large positive ΔS value supports an entropy driven dissociation equilibrium. Moreover, a shift of the equilibrium to dissociation was observed in ^{19}F NMR spectra after diluting the solution of **1**. The dissociation involves cleavage of two titanium–fluorine–titanium bonds and changes in the lithium coordination sphere. The determined enthalpy could be therefore only a crude estimate of the binding energy of the titanium–fluorine bond.

In conclusion, *in situ* prepared lithium fluoride was trapped with $[TiF_3(C_5Me_5)]_2$ giving **1**. Dissociation of **1** to **1a** and $[TiF_3(C_5Me_5)]_2$ is accompanied by a cleavage of Ti–F–Ti bonds. In solution observed **1a** could serve as a model compound for studying the reactivity of 'lithium fluoride' since the lithium atom is in a rather distorted coordination sphere. Its reactivity is already demonstrated by reforming **1** at low temperatures.

This work was supported by the Ministry of Science and Technology of the Republic of Slovenia and the Deutsche Forschungsgemeinschaft.

Notes and References

† E-mail: alojz.demsar@uni-lj.si

‡ Lithium fluoride in bulk is unreactive towards $[TiF_3(C_5Me_5)]_2$.[8] *Data for* **1**. Decomposition 100–110 °C. Anal. Calc. for $C_{40}H_{60}F_{13}LiTi_4$: C, 48.71; H, 6.13. Found: C, 47.86; H, 6.22%. ^{1}H NMR (300 MHz, $CDCl_3$, 302 K) δ 2.10 (s) and 2.14 (s). ^{19}F NMR (282 MHz, $CDCl_3$, 302 K), resonances of **1a**: δ 148.4 (qnt, 2 F, $^2J_{FF}$ 40 Hz), 25.0 (s, 2 F), −32.4 (m, 1 F), −62.1 (s, 2 F); resonances of **1**: δ 183.6 (s, 2 F), 149.5 (s, 2 F), 32.0 (s, 2 F), −10.4 (s, 2 F), −30.8 (s, 2 F), −36.8 (s, 1 F), −43.2 (s, 2 F); resonance of **2**: δ 121 (br s). ^{7}Li NMR (116 MHz, $CDCl_3$, 302 K): δ −1.64 (s); 272 K: δ −1.63 (qnt, $^1J_{LiF}$ 49 Hz). IR (Nujol) (cm^{-1}): 630s, 615vs, 522m, 494s.

§ *X-Ray crystallography. Crystal data for* **1**: $C_{40}H_{60}F_{13}LiTi_4$, M = 986.36, red parallelepiped crystal of dimensions 0.4 × 0.4 × 0.2 mm, triclinic, space group $P\bar{1}$, a = 11.144(2), b = 11.660(1), c = 20.730(3) Å, α = 96.609(9), β = 99.970(9), γ = 112.746(8)°, U = 2397.0(6) Å^3, Z = 2, D_c = 1.367 g cm^{-3}, T = 293 K, Enraf-Nonius CAD-4 diffractometer using Mo-Kα radiation (λ = 0.710 73 Å) in the 2θ range 2–56°, 12 080 reflections total, 11 483 unique. The structure was solved by direct methods and refined using Xtal 3.2.[9] Full matrix, least squares refinement on F of 523 parameters converged at R = 0.065 and wR = 0.059 using 3867 reflections with $I > 2.5\sigma(I)$. CCDC 182/814.

¶ Dimeric $[TiF_3(C_5Me_5)]_2$ exists in the solid state.[10] The ^{19}F NMR spectrum of $[TiF_3(C_5Me_5)]_2$ at 248 K in $CDCl_3$ has resonances of terminal (δ 158.7, s, 4 F) and bridging (δ −40.6, s, 2 F) fluorine atoms that coalesce at 273 K to a broad singlet (δ 114).

‖ By integrating the ^{19}F NMR resonances of terminal fluorines bound to lithium (F^2) in **1** and **1a**, respectively, (0.02 M [$^2H_8$]toluene solution) the following C_1/C_{1a} concentration ratios were found: 1.54 (312 K), 2.18 (302 K), 3.38 (297 K), 4.62 (292 K), 6.26 (287 K), 7.87 (282 K), 15.04 (272 K).). The equilibrium constants were calculated using equation: $K = C_{1a}C_2/C_1 = C^2_{1a}/C_1$.

1 A. F. Janzen, *Coord. Chem. Rev.*, 1994, **130**, 355.
2 R. O. Duthaler and A. Hafner, *Angew. Chem.*, 1997, **109**, 43; *Angew. Chem., Int. Ed. Engl.*, 1997, **36**, 43.
3 D. R. Gauthier, Jr. and E. M. Carreira, *Angew. Chem.*, 1996, **108**, 2521; *Angew. Chem., Int. Ed. Engl.*, 1996, **35**, 2363.
4 F. S. Mair and R. Snaith, in *Encyclopaedia of Inorganic Chemistry*, ed. R. B. King, Wiley, Chichester, UK, 1994, vol. 1, p. 35.
5 A. G. Avent, W.-Y. Chen, C. Eaborn, I. B. Gorell, B. B. Hitchcock and J. D. Smith, *Organometallics*, 1996, **15**, 4343.
6 A. F. Wells, *Structural Inorganic Chemistry*, Clarendon Press, Oxford, UK, 4th edn., 1975, p. 375.
7 A. Pevec, A. Demsar, V. Gramlich, S. Petricek and H. W. Roesky, *J. Chem. Soc., Dalton Trans.*, 1997, 2215.
8 H. W. Roesky, M. Sotoodeh and M. Noltemeyer, *Angew. Chem.*, 1992 **104**, 869; *Angew. Chem., Int. Ed. Engl.*, 1992, **31**, 864.
9 *Xtal3.2 Reference Manual*, ed. S. R. Hall, H. D. Flack and J. M. Steward, Universities of Western Australia, Geneva and Maryland, 1992.
10 M. Sootodeh, I. Leichtweis, H. W. Roesky, M. Noltemeyer and H.-G. Schmidt, *Chem. Ber.*, 1993, **126**, 913.

Received in Basel, Switzerland, 8th January 1998; 8/00245B

Elucidation of the mechanism of alkene epoxidation by hydrogen peroxide catalysed by titanosilicates: a computational study

Duangkamol Tantanak, Mark A. Vincent and Ian H. Hillier*†

Department of Chemistry, University of Manchester, Manchester, UK M13 9PL

Calculated transition states for alkene epoxidation by hydrogen peroxide, catalysed by titanosilicates, predict that it is the oxygen atom of the titanium(IV)–hydroperoxide intermediate closer to the metal centre which attacks the alkene.

Zeolite-based metal oxide systems are effective catalysts for a variety of oxidation reactions, many of considerable industrial importance.[1] Of particular interest are titanium containing zeolites such as TS-1, TS-2 and Ti-MCM-41, which involve framework Ti^{IV} species, and which catalyse, under mild conditions, many useful oxidations with hydrogen peroxide, such as alkene epoxidation.[2] EXAFS studies[3] suggest that in these catalysts the titanium is 4-coordinate, but may expand its coordination sphere on interaction with adsorbates. The active species for oxidation *via* hydrogen peroxide is generally considered to be a hydroperoxide species accommodated in the titanium coordination sphere, and possibly hydrogen bonded to a water or alcohol molecule, as in structure **I**.[1]

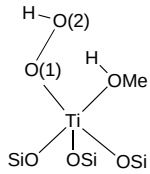

I

The mechanism of the subsequent epoxidation reaction involving structure **I** is far from clear at present, particularly with regards to which oxygen atom [O(1) or O(2)] attacks the carbon–carbon double bond of the alkene. On the basis of stereoselectivity Adam *et al.*[4] propose a mechanism for the epoxidation of chiral allylic alcohols involving attack of O(2), the oxygen atom closer to the hydrogen atom. Using steric arguments, Clerici and Ingallina[5] also suggest that it is this oxygen atom [O(2)] that attacks the alkene. However, there is no real evidence that rules out attack of the oxygen atom [O(1)] directly bonded to the titanium centre. There is thus a need for a more complete understanding of the catalytic mechanism, which will be aided by an investigation of the potential energy surface, particularly of the structure and energetics of the transition states corresponding to attack by either O(1) or O(2). We here describe high level *ab initio* calculations which address this question.

As is common practice,[6] we have used a finite molecular cluster to model the active site of **I**, in which the silicon atoms are terminated by hydrogen atoms. A more complete treatment would naturally take proper account of the effect of the infinite lattice,[7] but finite clusters are taken to be a good initial approximation. Stationary structures on the potential energy surface involving the interaction of the cluster with ethene were located using a 3-21G* basis, electron correlation being included using density functional theory employing a B3LYP functional. The calculations were carried out using GAUSSIAN94.[8]

The minimum energy structures of the cluster with ethene close by are shown in Fig. 1. The structures shown in Fig. 1(*a*) and (*b*), which are close in energy, are on the reaction pathway leading to the two transition states involving attack on ethene by O(1) and O(2), respectively. Of particular note is the sideways coordination of the peroxy group, with both Ti–O distances [1.95 and 2.23 Å in the lowest energy structure, Fig. 1(*a*)] being significantly longer compared to the three Ti–O(Si) distances. Of these two distances, one is considerably shorter, implying preferential interaction of O(1) with the Ti^{IV} centre, and a corresponding weaker interaction of O(2). A previous calculation[9] of the related system, $Ti(OH)_3OOH$, gave one longer (2.59 Å) and one shorter (1.87 Å) Ti–O length, compared to our structure, suggesting a somewhat different coordination mode. Our reactant structures are however similar to that found in the crystal structure of {[(η^2-*tert*-butylperoxo)titanatrane]$_2$·3 dichloromethane},[10] when Ti–O lengths of 1.91 and 2.27 Å were found, although the O–O distance (1.47 Å) is a little shorter than our calculated value (1.54 Å). We have located a third minimum energy structure [Fig. 1(*c*)] with a considerably longer Ti–O(2) length, which is best described as having the O_2H group bonded end-on. We find this structure, which resembles the one calculated by Neurock and Manzer,[11] to be 2.6 kcal mol^{-1} higher in energy than our lower energy structure.

Two transition structures, both leading to the formation of the epoxide, were located (Fig. 2). The lower energy one involves attack on the ethene π-bond by the oxygen atom, O(1) [Fig. 2(*a*)], closest to the titanium centre, with a lengthening of the Ti–O(1) bond compared to the reactant, and an associated shortening of the Ti–O(2) bond. The developing negative charge on the O(2)–H group leads to the formation of a Ti–OH

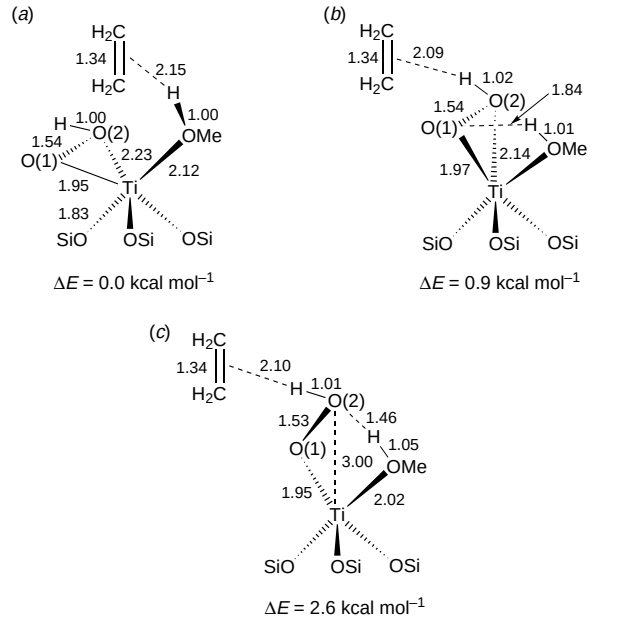

Fig. 1 Structures of ethene-cluster reactants

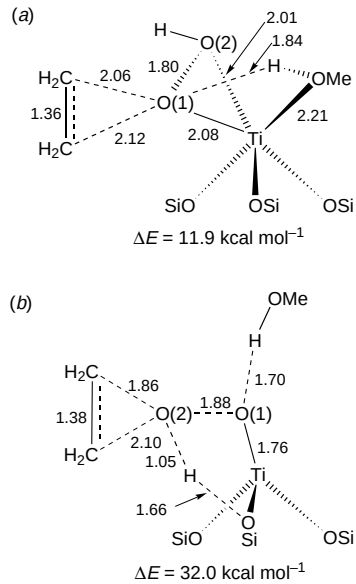

Fig. 2 Transition structures for attack of each hydroperoxide oxygen atom on ethene. ΔE is the calculated barrier.

bond in the product. When compared to this transition state, the second one involving the attack by O(2) [Fig. 2(*b*)] is of higher energy and has both O–C distances shorter and the O–O distance longer, so that the second mechanism, attack by O(2), proceeds *via* a later transition state. This second mechanism is significantly different from the first, involving a developing Ti–O double bond [Fig. 2(*b*)] (of length 1.76 Å in the transition state) and proton transfer to a siloxy group. Such a product involving a Ti–O double bond has been found to be less stable than the corresponding species with Ti–O single bonds.[12]

The two transition states that we have identified correspond to barriers that differ in energy by 20.1 kcal mol^{-1}. The relative ordering of these barriers is unlikely to change if more accurate calculations employing a larger basis and a better treatment of electron correlation were to be carried out. We have also used a continuum treatment[13] to estimate the effect of a polar solvent on the calculated barriers. We find that using a relative permittivity of 78.3 to model solvation by water, the barrier for attack of O(1) is unaltered, whilst the barrier for attack of O(2) is reduced to 25.8 kcal mol^{-1}. We are thus confident that the preferred route for attack involves O(1), and that inclusion of solvent does not affect this conclusion.

We have thus identified the mechanism of the epoxidation reaction, and obtained a transition state structure that may be of value in designing related enantioselective catalysts.[14]

This work was supported by the EPSRC and by a Royal Thai Government Scholarship to Duangkamol Tantanak.

Notes and References

† E-mail: ian.hillier@man.ac.uk

1 C. B. Khouw, C. B. Dartt, J. A. Labinger and M. E. Davis, *J. Catal.*, 1994, **149**, 195.
2 R. Murugavel and H. W. Roesky, *Angew. Chem., Int. Ed. Engl.*, 1997, **36**, 477.
3 S. Bordiga, S. Coluccia, C. Lamberti, L. Marchese, A. Zecchina, F. Boscherini, F. Buffa, F. Genoni, G. Leofanti, G. Petrini and G. Vlaic, *J. Phys. Chem.*, 1994, **98**, 4125.
4 W. Adam, A. Corma, T. I. Reddy and M. Renz, *J. Org. Chem.*, 1997, **62**, 3631.
5 M. G. Clerici and P. Ingallina, *J. Catal.*, 1993, **140**, 71.
6 F. Haase and J. Sauer, *J. Am. Chem. Soc.*, 1995, **117**, 3780.
7 S. P. Greatbanks, I. H. Hillier, N. A. Burton and P. Sherwood, *J. Chem. Phys.*, 1996, **105**, 3770.
8 M. J. Frisch, G. W. Trucks, H. B. Schlegel, P. M. W. Gill, B. G. Johnson, M. A. Robb, J. R. Cheeseman, T. A. Keith, G. A. Petersson, J. A. Montgomery, K. Raghavachari, M. A. Al-Laham, V. G. Zakrzewski, J. V. Ortiz, J. B. Foresman, J. Cioslowski, B. B. Stefanov, A. Nanayakkara, M. Challacombe, C. Y. Peng, P. Y. Ayala, W. Chen, M. W. Wong, J. L. Andres, E. S. Replogle, R. Gomperts, R. L. Martin, D. J. Fox, J. S. Binkley, D. J. Defrees, J. Baker, J. P. Stewart, M. Head-Gordon, C. Gonzalez and J. A. Pople, GAUSSIAN94, Gaussian Inc., Pittsburgh PA, 1995.
9 Y.-D. Wu and D. K. W. Lai, *J. Org. Chem.*, 1995, **60**, 673.
10 G. Boche, K. Möbus, K. Harms and M. Marsch, *J. Am. Chem. Soc.*, 1996, **118**, 2770.
11 M. Neurock and L. E. Manzer, *Chem. Commun.*, 1996, 1133.
12 P. E. Sinclair and C. R. A. Catlow, *Chem. Commun.*, 1997, 1881.
13 J. B. Foresman, T. A. Keith, K. B. Wiberg, J. Snoonian and M. J. Frisch, *J. Phys. Chem.*, 1996, **100**, 16 098.
14 S. Feast, D. Bethell, P. C. B. Page, F. King, C. H. Rochester, M. R. H. Siddiqui, D. J. Willock and G. J. Hutchings, *J. Mol. Catal. A*, 1996, **107**, 291.

Received in Exeter, UK, 7th February 1998; 8/01164H

Aldol and Knoevenagel condensations catalysed by modified Mg–Al hydrotalcite: a solid base as catalyst useful in synthetic organic chemistry

M. Lakshmi Kantam,*[a] B. M. Choudary,*[a]† Ch. Venkat Reddy,[a] K. Koteswara Rao[a] and F. Figueras[b]

[a] *Indian Institute of Chemical Technology, Hyderabad 500007 India*
[b] *Institut De Recherches Sur La Catalyse, 2 Avenue Albert Einstein, 69626 Villeurbanne cedex, France*

Aldol and Knoevenagel condensations were performed with suitably activated Mg–Al hydrotalcite as catalyst in quantitative yields in the liquid phase under mild reaction conditions at a faster rate for the first time.

In recent years, there has been increasing emphasis on the use and design of environment-friendly solid acid–base catalysts to reduce the amount of toxic waste and by-products arising from the chemical processes prompted by stringent environment protection laws. The challenge is to perform heterogeneous catalysis reactions leading to C–C bond formation which are widely employed in organic synthesis.[1] The versatile Knoevenagel and aldol condensations have numerous applications in the elegant synthesis of fine chemicals[2] and are classically catalysed by bases[3,4] in the liquid phase system. On the laboratory scale, many catalysts have been known to effect the Knoevenagel and aldol condensations and include alumina,[5] sepeolite,[6] zeolites,[7] clays,[8] hydrotalcites[9–11] and anionic resins.[12]

Table 1 Aldol condensation between acetone and substituted benzaldehydes catalysed by MHT catalyst at 60 °C[a]

Entry	R^1	*t*/h	Yields (%)[b]
1	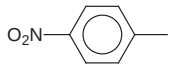	1	97[c]
2	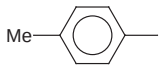	1	96
3	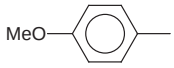	1.5	95
4	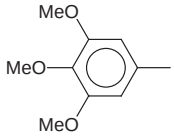	0.5	98
5	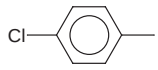	1.5	94
6	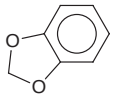	1	96[d]
7	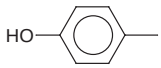	14	8[c]
8	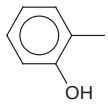	15	No reaction

[a] All reactions were performed on 2 mmol substrate in 10.3 ml (140 mmol) acetone using 0.2 g of MHT. [b] ^{1}H NMR yields based on aldehyde. [c] Aldol to dehydrated product (1 : 1). [d] Isolated yield.

Layered double hydroxides (LDHs) or hydrotalcite-like compounds (HTLCs) have recently received much attention[13] in view of their potential usefulness as adsorbents, anion exchangers and most importantly as basic catalysts.[14] LDHs upon thermal decomposition at about 450 °C give a highly active homogeneous mixed oxide which is a potential basic catalyst used for a variety of organic transformations such as aldol condensation,[15] nucleophilic halide exchange,[16] alkylation of diketones,[17] epoxidation of activated olefins with hydrogen peroxide[18] or Claisen–Schmidt condensation.[19]

The previous work[10,15,17,19] on aldolisations using HTLCs was performed generally at higher temperatures. Recently, we reported[20] a modified method for the activation of the hydrotalcite catalyst whose basicity was tuned for base catalysed condensation reactions in the liquid phase under very mild reaction conditions. Herein, we report Knoevenagel and aldol condensations catalysed by this modified hydrotalcite (MHT) with quantitative yields at a faster rate of reaction under very mild liquid phase conditions (Tables 1 and 2) for the first time as part of our investigation into the scope and applicability of MHT for a variety of organic reactions.

In the case of aldol reactions, the aldol was the major product when the reaction was conducted at room temperature but the yields were poor except in the case of benzaldehyde.[20] When the reaction was conducted at 60 °C, yields were improved drastically but the reaction proceeded to give the dehydrated product (entries 2–6) predominantly except in the case of *p*-nitrobenzaldehyde (entry 1) where the ratio of aldol to α,β-unsaturated product was 1 : 1. In the case of *o*-hydroxybenzaldehyde (entry 8) there was no reaction, while the *p*-hydroxybenzaldehyde (entry 7) showed little activity (< 10%) with the formation of both the aldol and the dehydrated product (1 : 1) (Scheme 1). The inactivity of these compounds may be attributed to the fact that the basic sites present on the

Table 2 Knoevenagel condensation catalysed by MHT[a]

Entry	R^1	R^2	Y	Solvent	*t*/h	Yields (%)[b]
1	Ph	H	CN	Toluene	1	100
2	Ph	H	CO_2Et	Toluene	2	50
3	PhCH=CH	H	CN	Toluene	2	87
4	PhCH=CH	H	CO_2Et	DMF	1	61
5	3-$MeOC_6H_4$	Me	CN	Toluene	1	100
6	3-$MeOC_6H_4$	Me	CO_2Et	Toluene	4	61
7	2-Furyl	H	CN	Toluene	0.5	100
8	2-Furyl	H	CO_2Et	Toluene	2	100
9	4-$NO_2C_6H_4$	H	CN	Toluene	1	100
10	4-$NO_2C_6H_4$	H	CO_2Et	Toluene	2	100
11	2-$MeOC_6H_4$	H	CN	Toluene	1	96.0[c]
12	2-$MeOC_6H_4$	H	CO_2Et	Toluene	4	83.0
13	$-cC_5H_{10}-$		CN	Toluene	0.5	100
14	$-cC_5H_{10}-$		CO_2Et	DMF	1	33.3

[a] All reactions were performed on 2 mmol substrate and 2 mmol active methylene compound using 0.05 g of MHT in 10 ml dry toluene at room temperature. [b] ^{1}H NMR yields based on aldehyde. [c] Isolated yield.

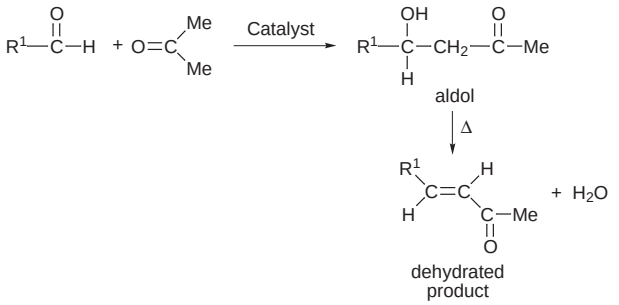

Scheme 1 Aldol condensation between acetone and substituted benzaldehydes

catalyst surface were neutralised by the adsorption of the phenolic moiety which is acidic in nature. All other substrates irrespective of the nature of the substituent present on the phenyl ring shown in Table 1 resulted in good yields in shorter reaction times.

Knoevenagel condensations (Scheme 2) involving various aromatic carbonyl compounds and aliphatic ketone, cyclohexanone with (a) malononitrile and (b) ethyl cyanoacetate as the active methylene compounds were carried out with MHT at room temperature (Table 2). The results are quite impressive, when compared with results reported for solid catalysts requiring vapour phase conditions and longer reaction times, and this present modified hydrotalcite is the first heterogeneous catalyst reported in the literature which perform the reactions at room temperatures in excellent yields. All the reactions proceeded smoothly in toluene with the exception of cinnamaldehyde and cyclohexanone with ethyl cyanoacetate. However, when DMF was used as the solvent, cinnamaldehyde and cyclohexanone condensed affording the corresponding product. The solvent effect established here is in consonance with the results reported by others.[21]

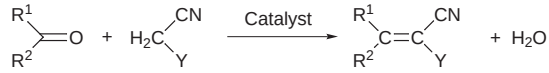

Scheme 2 Knoevenagel condensation of different carbonyl compounds with malononitrile or ethyl cyano acetate

Thus, good yields of aldol and Knoevenagel products can be obtained in heterogeneous catalysis using hydrotalcites provided that the solid is suitably activated. This new solid base catalyst is a practical alternative to soluble bases both in Knoevenagel and aldol reactions in view of the following advantages: (a) high catalytic activity under very mild liquid phase conditions in general for both the reactions described above and specifically at room temperature for the accomplishment of Knoevenagel reactions, (b) easy separation of the catalyst by simple filtration, (c) waste minimisation and (d) possibility of reuse.

This work was realised in the frame of an Indo-French co-operative programme, funded by IFCPAR (project No. IFC/1106-2/96/2460).

Notes and References

† E-mail: iict@ap.nic.in

1 *Comprehensive Organic Synthesis*, ed. B. M. Trost, Pergamon Press, Oxford, 1991, vol. 2, p. 133–340.
2 G. Marciniak, A. Delgado, G. Leelere, J. Velly, N. Decken and J. Schwartz, *J. Med. Chem.*, 1989, **32**, 1402; D. Enders, S. Muller, A. S. Demir, *Tetrahedron Lett.*, 1988, **29**, 6437.
3 E. Knoevenagel, *Chem. Ber.*, 1894, **27**, 2345; G. Jones, *Org. React.*, 1967, **15**, 204.
4 J. March, *Advanced Organic Chemistry*, Wiley, 4th edn., 1992; C. H. Heathcock, In *Comprehensive Organic Synthesis*, ed. B. M. Trost, Pergamon Press, Oxford, 1991, vol. 2, pp. 341–394.
5 J. Muzart, *Synth. Commun.*, 1985, **15**, 285; J. Muzart, *Synthesis*, 1982, **60**, 1.
6 A. Corma and R. M. Martin-Aranda, *J. Catal.*, 1991, **130**, 130.
7 A. Corma, V. Fornes, R. M. Martin-Aranda, H. Garcia and J. Primo, *Appl. Catal.*, 1990, **59**, 237.
8 Y. V. Subba Rao and B. M. Choudary, *Synth. Commun.*, 1991, **21**, 1163.
9 M. J. Climent, A. Corma, S. Iborra and J. Primo, *J. Catal.*, 1995, **151**, 60.
10 D. Tichit, M. H. Lhouty, A. Guida, B. H. Chiche, F. Figueras, A. Auroux, D. Bartalini and E. Garronne, *J. Catal.*, 1995, **151**, 50.
11 A. Corma, V. Fornes, R. M. Martin-Aranda and F. Rey, *J. Catal.*, 1992, **134**, 58.
12 W. Richardhein and J. Melvin, *J. Org. Chem.*, 1961, **26**, 4874.
13 F. Cavani, F. Trifiro and A. Vaccari, *Catal. Today*, 1991, **11**, 173.
14 W. T. Reichle, *J. Catal.*, 1985, **94**, 547; J. G. Nunan, P. B. Himelfarb, R. G. Herman, K. Klier, C. E. Bogdan and G. W. Simmons, *Inorg. Chem.*, 1989, **28**, 3868; C. Busetto, G. Delpiero, G. Manara, F. Trifiro and A. Vaccari, *J. Catal.*, 1984, **85**, 260.
15 E. Suzuki and Y. Ono, *Bull. Chem. Soc. Jpn.*, 1988, **61**, 1008.
16 E. Suzuki, M. Okamoto and Y. Ono, *J. Mol. Catal.*, 1990, **61**, 283.
17 C. Cativiela, F. Figueras, J. I. Garcia, J. A. Mayoral and M. Zurbano, *Synth. Commun.*, 1995, **25**, 1745.
18 C. Cativiela, F. Figueras, J. M. Fraile, J. I. Garcia and J. A. Mayoral, *Tetrahedron Lett.*, 1995, **36**, 4125.
19 W. T. Reichle, USP 4, 458, 026, 1984 to Union Carbide.
20 K. Koteswara Rao, M. Gravelle, J. Sanchez and F. Figueras, *J. Catal.*, 1998, **173**, 115; Mg–Al hydrotalcite synthesised with Mg : Al in a ratio of 2.5 was first calcined at 450 °C in a flow of air at the rate of 10 °C min^{-1} to reach 450 °C and maintained for 8 h. The solid was then rehydrated at room temperature under flow of nitrogen gas (6 l h^{-1}), saturated with water vapour for about 6 h and used for the reactions. Reusability of the catalyst: after completion of the reaction, the catalyst was filtered off and then activated in a similar way as fresh catalyst and found to be active for both aldol and Knoevenagel reactions.
21 P. Laszlo, *Acc. Chem. Res.*, 1986, **19**, 121; P. W. Lednor and R. deRuiter, *J. Chem. Soc., Chem. Commun.*, 1991, 1625.

Received in Cambridge, UK, 3rd November 1997; 7/07874I

Synthesis of double-mesopore silica using aqueous ammonia as catalyst

Xiaozhong Wang,*† Tao Dou and Yongzhuang Xiao

Institute of Special Chemicals, Taiyuan University of Technology, Taiyuan, 030024, China

Double-mesopore silica with a characteristic N_2 adsorption isotherm and narrow bimodal mesopore distribution is synthesized rapidly at room temperature by using aqueous ammonia as the catalyst.

The synthesis of inorganic frameworks with specific and organized pore networks is of potential importance in catalysis,[1,2] separation technology[3] and biomaterials engineering.[4,5] Since the first synthesis of mesoporous MCM-41 materials,[6,7] there has been intense activity in the design and synthesis of a variety of mesoporous solids. Generally, the typical N_2 adsorption isotherm, which plays a significant role in characterization of the new mesoporous materials, of MCM-41 materials shows type IV behavior with a sharp inflection characteristic of capillary condensation within uniform mesopores at P/P_0 *ca.* 0.3–0.4[8] and with an additional hysteresis loop following in the P/P_0 region of 0.8–1.0.[1,7] The hysteresis loop at $P/P_0 > 0.8$ is now acknowledged to arise from interparticle capillary condensation[1,9] or from the structure collapse of portions of the MCM-41 structure during the hydrothermal treatment or calcination.[10,11] However, if this hysteresis loop lifts up sharply, this may imply that a change in the texture has occurred on the mesoporous frameworks of the product. Pang and coworkers[12] recently presented a report on the synthesis of bimodal mesopore distribution silica with a sharp lefting-up hysteresis loop at $P/P_0 > 0.8$ on its N_2 adsorption isotherm by calcining a wet surfactant-containing silicate gel. However, there is no discernable inflection in the vicinity of $P/P_0 = 0.35$ on the N_2 adsorption–desorption isotherms to indicate the existence of smaller mesopores. Kloetstra *et al.*[13] also succeeded in synthesizing a bimodal pore size distribution molecular sieve by overgrowing mesoporous MCM-41 on a faujasite. Unfortunately, they have not provided any information on the detailed analysis of the N_2 adsorption isotherm and the corresponding pore size distribution curve. Double-mesopore molecular sieves of narrow pore distribution may find broad potential applications in electronic, optical or sensing devices.[14,15] Here, we present a synthesis of a double-mesopore silica mesostructure which has a typical mesopore X-ray diffraction pattern but narrow bimodal mesopore distribution. In the synthesis the process was completed in a relatively short time at room temperature by using aqueous ammonia as the catalyst.

The preparation procedure is as follows: stoichiometric surfactant cetyltrimethylammonium bromide (CTAB) was added to deionized water with stirring at room temperature until the solution became clear. The silica source tetraethylorthosilicate (TEOS) was then added to the solution with stirring. Finally, aqueous ammonia was slowly added until the pH of the solution was *ca.* 9.5. The molar composition of final gel mixtures was $2.0TEOS : 0.68–2.0NH_3{\cdot}H_2O : 0.4CTAB : 230H_2O$. The mixtures were stirred continuously for *ca.* 7 min. During this short time the fluid mixture became progressively more viscous, and eventually set into jelly-like monoliths that assumed the shape of the container. Then the jelly-like solid product was washed repeatedly with distilled water in a centrifuge, dried in air at 353 K and finally calcined in air at 2 K min^{-1} to 823 K for 6 h to remove the template.

Powder X-ray diffraction (XRD) patterns (recorded on a D/max-rA diffractometer with Cu-Kα radiation, 40 kV, 20 mA) of the as-synthesized and calcined silica products are shown in Fig. 1. Different from the results of Pang and coworkers[12] that the gel precursor dried at room temperature is amorphous according to XRD, the pattern for the as-synthesized silica product exhibits a broad, yet clear, diffraction peak with a *d*-spacing of 5.2 nm. The appearance of a diffraction peak at this low angle suggests that after a short time of stirring mesostructure has been formed in the jelly-like solid product with a pore system lacking long-range order. Upon removal of the template by calcination, the basal spacing decreases to 4.4 nm and the scattering intensity increases substantially, suggesting that the calcination process may promote siloxane cross-linking and thereby improve the ordering of the oxide framework. The XRD patterns are reminiscent of HMS[11] and MSU[9] mesoporous materials.

Important trends are revealed in Fig. 2 by the N_2 adsorption–desorption isotherms and the corresponding BJH[16] pore size distribution based on the desorption branch (obtained on an ASAP 2000 analyser) for the calcined product. This is a typical irreversible type IV adsorption isotherm with two separate, well expressed H1 hysteresis loops as defined by IUPAC[17] at relative pressures P/P_0 of 0.24–0.45 and 0.8–1.0. Nevertheless, the pore size distribution reveals that there are two mesopore sizes in the material, *i.e.* a bimodal distribution. The first condensation step on the isotherm at $P/P_0 = 0.24–0.45$ is similar to that for usual MCM-41 materials with markedly higher saturation sorption capacity, though not very steep. This was attributed to a slight pore size heterogeneity of the sample with a pore size of *ca.* 2.6–3.0 nm as seen in Fig. 2(*b*), but an exceptionally high mesopore surface area of 1064.6 $m^2\ g^{-1}$, corresponding to a total pore volume of 0.66 $cm^3\ g^{-1}$. This is in agreement with the XRD results, *i.e.* broad lines are observed. However, the second condensation step on the isotherm at $P/P_0 > 0.8$ is much steeper than the first. This indicates the presence of a significant amount of secondary mesopores with a remarkably narrow pore size distribution centred at *ca.* 19 nm. The total pore volume for the larger mesopores is 1.18 $cm^3\ g^{-1}$ with a total surface area of 243.1 $m^2\ g^{-1}$. This inflection at higher relative pressures differs completely from that of previously-synthesized mesoporous materials. In addition, the broad hysteresis loops in the isotherms reflect its long mesopores with no pore-blocking effects, which limit the emptying and filling of the accessible

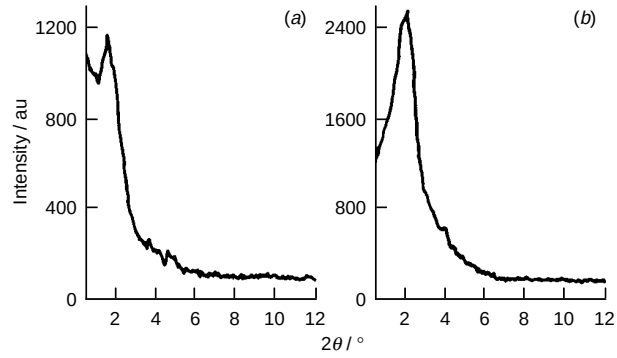

Fig. 1 Powder X-ray diffraction patterns of (*a*) as-synthesized sample and (*b*) calcined sample

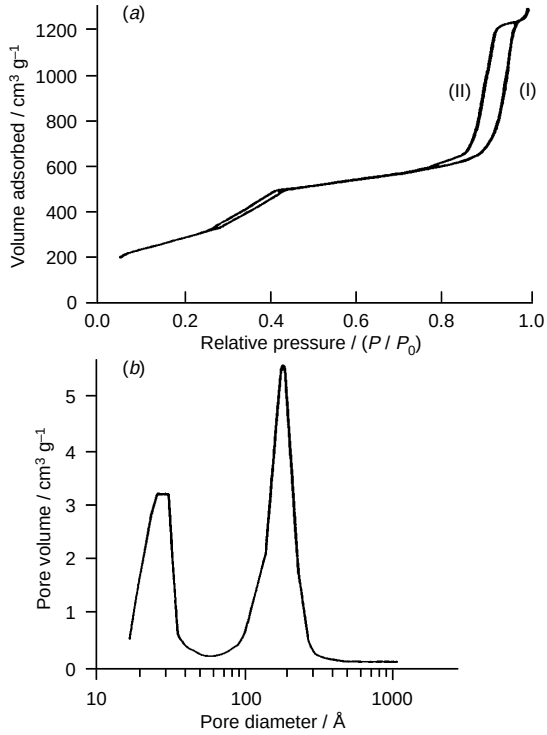

Fig. 2 (*a*) N_2 adsorption (I)–desorption (II) isotherms on the calcined sample and (*b*) the pore size distribution of the material

volume. Fig. 3 is a TEM image of the calcined sample (recorded on a JEOL 200CX microscope). It is evident that, different from most crystalline mesoporous sieves such as MCM-41 which has a well organized hexagonal pore structure, the present material contains a large number of randomly distributed channels with both smaller cylindrical- to hexagonal-shaped channels and larger stripe-like channels lacking long-range packing order. As can be seen from the TEM image, both sets of mesopores are present as a 'homogeneous' mixture throughout the entire sample. The formation of larger stripe-like mesopores may be due to the incomplete condensation of SiO_2 species between adjacent surfactant micelles.

In summary, we have discovered a simple and novel synthesis of a double-mesopore silica with a characteristic N_2 adsorption isotherm and narrow bimodal mesopore distribution. The synthesis process is completed in a relatively short time at room temperature by using aqueous ammonia as the catalyst. This may imply that surfactant micelles in the initial reaction mixtures are of different size or shape, and the hydrolysis of TEOS and the following cooperative condensation of SiO_2 species with surfactant micelles was incomplete over the short time of reaction. Further experimental results show that the similar double-mesopore silicas can also be synthesized by substituting tetraethylammonium hydroxide or NaOH for aqueous ammonia as the catalyst and that pH adjustment of the reaction mixtures plays a critical role in the synthesis. However, if the pH in the reaction mixtures increases beyond a certain degree, the double-mesopore silica will change into considerably ordered single-peaked mesoporous silica. These results provide us with a new angle for a further understanding of the formation mechanism of mesoporous silica materials. More detailed synthetic investigations and studies of the mechanism of formation of double-mesopore silica are in progress.

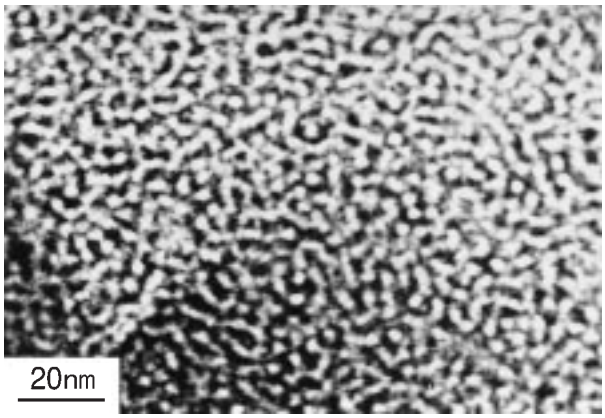

Fig. 3 Transmission electron micrograph of the calcined sample

We would like to thank Dr Guoyi T. and Xihua C. at the Tsinghua University for the TEM data, Dong W. and Yanzheng F. at the Institute of Coal Chemistry, the Chinese Academy of Sciences for the XRD data and N_2 adsorption measurements respectively, and we are also grateful to the National Natural Science Foundation of China, the Oversea-Returned Personnel Foundation of Shanxi Province and the Natural Science Foundation of Shanxi Youth for financial support.

Notes and References

† E-mail: mailbox@tyut.edu.cn

1 P. T. Tanev, M. Chibeve and T. J. Pinnavaia, *Nature*, 1994, **368**, 321.
2 R. Burch, N. Cruise, D. Gleeson and S. C. Tsang, *Chem. Commun.*, 1996, 951.
3 R. M. Barrer, *Hydrothermal Chemistry of Zeolites*, Academic Press, London, 1982.
4 G. Guillemin, J. L. Patat, S. Fournie and M. Chetail, *J. Biomed. Mater. Res.*, 1989, **21**, 557.
5 J. L. Casci, *Stud. Surf. Sci. Catal.*, 1994, **85**, 329.
6 J. S. Beck, J. C. Vartuli, W. J. Roth, M. E. Leonowicz, C. T. Kresge, K. D. Schnitt, C.-T. W. Chu, D. H. Olson, E. W. Sheppard, S. B. McCullen, J. B. Higgins and J. L. Schlenkere, *J. Am. Chem. Soc.*, 1992, **114**, 10834.
7 C. T. Kresge, M. E. Leonowicz, W. J. Roth, J. C. Vartuli and J. S. Beck, *Nature*, 1992, **359**, 710.
8 P. J. Branton, P. G. Hall and K. S. W. Sing, *J. Chem. Soc., Chem. Commun.*, 1993, 1257.
9 S. A. Bagshaw, E. Prouzet and T. J. Pinnavaia, *Science*, 1995, **269**, 1242.
10 Z. Luan, H. He, W. Zhou, C. Cheng and J. Klinowski, *J. Chem. Soc., Faraday Trans.*, 1995, **91**, 2955.
11 P. T. Tanev and T. J. Pinnavaia, *Science*, 1995, **267**, 865.
12 W. Lin, J. Chen, Y. Sun and W. Pang, *J. Chem. Soc., Chem. Commun.*, 1995, 2367.
13 K. R. Kloetstra, H. W. Zandbergen, J. C. Jansen and H. Van Bekkum, *Microporous Mater.*, 1996, **6**, 287.
14 G. D. Stucky, *Mater. Res. Soc. Symp. Proc.*, 1991, **206**, 507.
15 A. Stein, G. A. Ozin and G. D. Stucky, *J. Soc. Photogr. Sci. Technol. Jpn.*, 1990, **53**, 322.
16 E. P. Barrett, L. G. Joyner and P. P. Halenda, *J. Am. Chem. Soc.*, 1951, **73**, 373.
17 K. S. W. Sing, D. H. Everett, R. A. W. Haul, L. Moscow, R. A. Pieroffl, J. Rouquerol and T. Siemieni-ewska, *Pure Appl. Chem.*, 1985, **57**, 603.

Received in Cambridge, UK, 5th January 1998; 8/00113H

An intramolecular H_3O_2 bridge as the resting form of an active metal-bound hydroxide in a dinuclear zinc(II) complex

Franc Meyer*† and Peter Rutsch

Anorganisch-Chemisches Institut der Universität Heidelberg, Im Neuenheimer Feld 270, D-69120 Heidelberg, Germany

An intramolecular Zn–O_2H_3–Zn bridge as a complexed form of metal-bound hydroxide exhibits enhanced reactivity compared to the related Zn–OH–Zn unit, illustrated by the reaction with CO_2.

Various hydrolytic metalloenzymes are known to contain two or more divalent metal ions in close proximity within their active site,[1] and in particular the coordinatively flexible Zn^{II} is found in several native systems like alkaline phosphatase (AP),[2a] P1 nuclease[2b] and phospholipase C (PLC).[2c] Although different and specific mechanisms for the individual catalytic processes are most probably involved, it is believed to be a dominant feature that a metal hydroxide intermediate produced by the deprotonation of zinc-bound water hydrolytically attacks the substrate which itself might be activated by coordination to an adjacent metal ion.[1] Consequently there is considerable interest in the design of polynuclear metal complexes containing Zn–OH_2 or Zn–OH functions to serve as models for these hydrolytic zinc enzymes,[3,4] however hydrolytically active systems with a di- or tri-nuclear zinc core have still remained rare.[5] Recently a combination of both Zn–OH_2 and Zn–OH has been reported in the form of an intermolecular Zn–O_2H_3–Zn bridge and suggested to represent a new structural and possibly functional motif in oligozinc enzyme chemistry.[6] Here we report the synthesis and structural characterisation of a discrete dinuclear zinc(II) complex incorporating an intramolecular $H_3O_2^-$ bridge as well as evidence for its enhanced reactivity compared to the frequently observed Zn–OH–Zn function.[4]

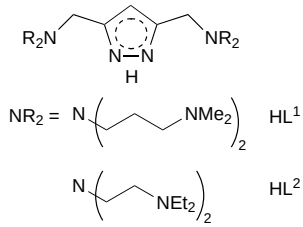

Ligands L^1 and L^2 are employed, which have been shown to predominantly form dinuclear complexes with five-coordinate N_4X ligation for divalent 3d transition metal ions.[7–9] Thereby the range of accessible metal–metal separations can be selectively tuned by altering the chain length of the chelating side arms attached to the pyrazolate heterocycle,[9] *i.e.* the choice of either L^1 or L^2. Deprotonation of HL^1 by means of BuLi and subsequent reaction with 2 equiv. of $Zn(ClO_4)_2·6H_2O$ and $NaBPh_4$ affords the dinuclear zinc(II) complex **1**‡ whose molecular structure has been determined by X-ray diffraction§ (Fig. 1), thereby confirming that a monoatomic oxygen bridge spans two five-coordinate zinc atoms with a metal–metal separation of d(Zn···Zn) = 3.613 Å. Although its proton could not be located in the crystallographic analysis, a sharp IR absorption at 3618 cm^{-1} clearly identifies this secondary bridge as a discrete metal-bound hydroxide.

In contrast, a similar synthetic procedure starting from HL^2 yields a bimetallic complex **2** with an intramolecular $H_3O_2^-$ bridging moiety as revealed by a single crystal X-ray crystallographic analysis (Fig. 2). Obviously the shorter side arms of L^2 pull the two metal centres back and apart [d(Zn···Zn) = 4.374 Å] and thus prevent a bridging position for the small hydroxide ion. Incorporation of an additional water molecule then establishes the $H_3O_2^-$ unit with a very strong intramolecular hydrogen bridge {d[O(1)···O(2)] = 2.462 Å},[10] where the remaining H atoms are involved in weak hydrogen bonding to two acetone solvent molecules incorporated in the crystal lattice {d[O(1)···O(4)] = 2.875 Å; d[O(1)···O(5)] = 3.050 Å}. The $H_3O_2^-$ entity in **2** might be viewed as a hydrated and thereby protected form of a Zn-bound OH^-. For a related FHO(H)-bridged dicobalt complex[9] evidence could be obtained for the reversible extrusion of the incorporated water molecule, which in **2** would generate an active Zn–OH function in close vicinity

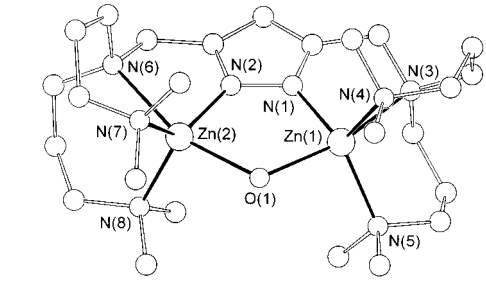

Fig. 1 Molecular structure of the cation of **1**. Selected atomic distances (Å) and bond angles (°): Zn(1)–O(1) 2.132(2), Zn(1)–N(1) 1.969(3), Zn(1)–N(3) 2.480(3), Zn(1)–N(4) 2.089(3), Zn(1)–N(5) 2.101(3), Zn(2)–O(1) 2.149(2), Zn(2)–N(2) 1.959(3), Zn(2)–N(6) 2.437(3), Zn(2)–N(7) 2.099(3), Zn(2)–N(8) 2.101(3), Zn(1)···Zn(2) 3.613; O(1)–Zn(1)–N(3) 159.2(1), O(2)–Zn(2)–N(6) 160.7(1), Zn(1)–O(1)–Zn(2) 115.1(1).

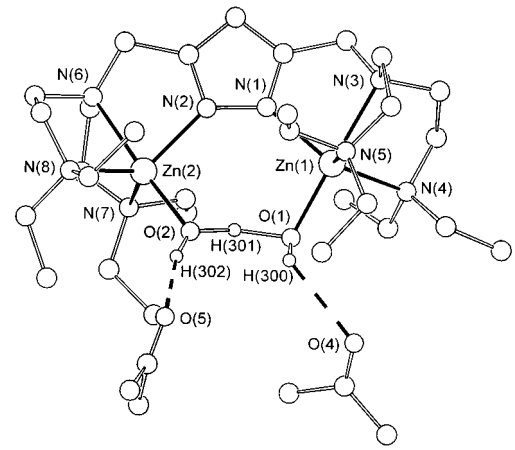

Fig. 2 Molecular structure of the cation of **2**. Selected atomic distances (Å) and bond angles (°): Zn(1)–O(1) 1.961(5), Zn(1)–N(1) 2.057(6), Zn(1)–N(3) 2.231(6), Zn(1)–N(4) 2.224(6), Zn(1)–N(5) 2.199(6), Zn(2)–O(2) 1.969(5), Zn(2)–N(2) 2.070(6), Zn(2)–N(6) 2.248(6), Zn(2)–N(7) 2.208(7), Zn(2)–N(8) 2.199(7), Zn(1)···Zn(2) 4.374, O(1)···O(2) 2.462, O(1)···O(4) 2.875, O(2)···O(5) 3.050; O(1)–Zn(1)–N(3) 171.1(2), O(2)–Zn(2)–N(6) 174.3(3).

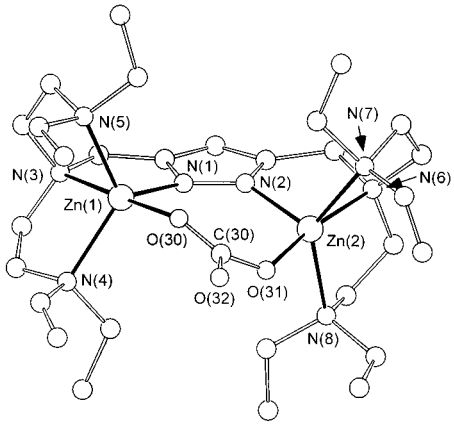

Fig. 3 Molecular structure of the cation of **3**. Selected atomic distances (Å) and bond angles (°): Zn(1)–O(30) 2.009(5), Zn(1)–N(1) 2.028(8), Zn(1)–N(3) 2.255(7), Zn(1)–N(4) 2.155(6), Zn(1)–N(5) 2.113(9), Zn(2)–O(31) 2.027(5), Zn(2)–N(2) 1.987(7), Zn(2)–N(6) 2.253(8), Zn(2)–N(7) 2.153(8), Zn(2)–N(8) 2.185(7), Zn(1)···Zn(2) 4.180; O(30)–Zn(1)–N(3) 177.1(3), O(31)–Zn(2)–N(6) 171.4(3), O(30)–C(31)–O(31) 132.5(8).

to a second Lewis-acidic Zn centre. In order to test the expected higher reactivity of **2** compared to **1**, CO_2 was bubbled into solutions of the complexes in acetone. While no reaction was detected for **1**, the appearance of strong IR bands at 1618 and 1401 cm^{-1} for **2** indicates the readily occurring absorption of CO_2 with formation of the bicarbonate complex **3**, whose crystal structure is presented in Fig. 3.

In conclusion the reactivity of these dinuclear complexes is drastically varied by appropriate changes of the ligand matrix, *i.e.* of the chelating side arms attached to the pyrazolate. The intramolecular Zn–O_2H_3–Zn bridge as characterised structurally for **2** can be viewed as a hydrated and thus resting form of an active Zn–OH function in close proximity to a second zinc ion capable of binding potential substrate molecules. It thus resembles the oligonuclear array of zinc ions with intermetallic distances larger than 4 Å found in the active sites of metalloenzymes like PLC and P1 nuclease. As evidenced by the reaction with CO_2, **2** exhibits enhanced reactivity compared to the corresponding OH-bridged complex and should thus be a promising candidate for inducing the hydrolytic cleavage of various substrates, which is presently under investigation.

Acknowledgement is made to Professor Dr G. Huttner for his generous and continuous support of our work as well as to the Deutsche Forschungsgemeinschaft (Habilitandenstipendium for F. M.) and the Fonds der Chemischen Industrie. We thank Dr F. Rominger and Professor Dr P. Hofmann for collecting the X-ray data of complex **3**.

Notes and References

† E-mail: Franc@sun0.urz.uni-heidelberg.de

‡ Satisfactory elemental analyses were obtained for all new complexes.

§ *Crystal data*: for **1**: $C_{73}H_{94}B_2N_8OZn_2$, M = 1252.0, triclinic, space group $P\bar{1}$, a = 11.793(2), b = 14.705(3), c = 20.064(4) Å, α = 100.29(2), β = 99.64(1), γ = 101.06°, U = 3286(1) Å^3, Z = 2, D_c = 1.264 g cm^{-3}, μ(Mo-Kα) = 0.780 mm^{-1}, 8905 reflections observed [$I > 2\sigma(I)$], 828 parameters, largest difference peak 1.010 e Å^{-3}, final R, R_w on [$I > 2\sigma(I)$] data were 0.049, 0.1140, goodness of fit on F^2 = 1.111. For **2**: $C_{77}H_{104}B_2N_8O_2Zn_2\cdot 2.5C_3H_6O$, M = 1471.3, monoclinic, space group $P2_1/c$, a = 17.974(5), b = 26.809(6), c = 17.543(4) Å, β = 92.11(1)°, U = 8448(4) Å^3, Z = 4, D_c = 1.183 g cm^{-3}, μ(Mo-Kα) = 0.621 mm^{-1}, 6527 reflections observed [$I > 2\sigma(I)$], 831 parameters, largest difference peak 1.008 e Å^{-3}, final R, R_w on [$I > 2\sigma(I)$] data were 0.078, 0.1816, goodness of fit on F^2 = 1.036. For **3**: $C_{78}H_{102}B_2N_8O_3Zn_2\cdot C_3H_6O$, M = 1410.2, monoclinic, space group $P2_1/c$, a = 17.5944(2), b = 12.9761(2), c = 48.2254(1) Å, β = 90.530(1)°, U = 7880.1(2) Å^3, Z = 4, D_c = 1.188 g cm^{-3}, μ(Mo-Kα) = 0.661 mm^{-1}, 8889 reflections observed [$I > 2\sigma(I)$], 801 parameters, largest difference peak 1.501 e Å^{-3}, final R, R_w on [$I > 2\sigma(I)$] data were 0.115, 0.322, goodness of fit on F^2 = 1.061. All structures were solved by direct methods with the SHELXS-97 and refined with the SHELXL-97 programs.[11] CCDC 182/815.

1 N. Sträter, W. N. Lipscomb, T. Klabunde and B. Krebs, *Angew. Chem., Int. Ed. Engl.*, 1996, **35**, 2024.
2 (*a*) E. E. Kim and H. W. Wyckoff, *J. Mol. Biol.*, 1991, **218**, 449; (*b*) A. Volbeda, A. Lahm, F. Sakiyama and D. Suck, *EMBO J.*, 1991, **10**, 1607; (*c*) E. Hough, L. K. Hansen, B. Birknes, K. Jynge, S. Hansen, A. Hordvik, C. Little, E. Dodson and Z. Derewenda, *Nature*, 1989, **338**, 357.
3 R. Alsfasser, S. Trofimenko, A. Looney, G. Parkin and H. Vahrenkamp, *Inorg. Chem.*, 1991, **30**, 4098; S. Uhlenbrock and B. Krebs, *Angew. Chem., Int. Ed. Engl.*, 1992, **31**, 1647; M. Ruf, K. Weis and H. Vahrenkamp, *J. Chem. Soc., Chem. Commun.*, 1994, 135.
4 C. Flassbeck, K. Wieghardt, E. Bill, C. Butzlaff, A. X. Trautwein, B. Nuber and J. Weiss, *Inorg. Chem.*, 1992, **31**, 21; P. Chaudhuri, C. Stockheim, K. Wieghardt, W. Deck, R. Gregorzik, H. Vahrenkamp, B. Nuber and J. Weiss, *Inorg. Chem.*, 1992, **31**, 1451; R. Alsfasser and H. Vahrenkamp, *Chem. Ber.*, 1993, **126**, 695; C. Bazzicalupi, A. Bencini, A. Bianchi, V. Fusi, L. Mazzanti, P. Paoletti and B. Valtancoli, *Inorg. Chem.*, 1995, **34**, 3003.
5 H. Adams, N. A. Bailey, D. E. Fenton and Q.-Y. He, *J. Chem. Soc., Dalton Trans.*, 1995, 697; W. H. Chapman, Jr. and R. Breslow, *J. Am. Chem. Soc.*, 1995, **117**, 5462; M. Yashiro, A. Ishikubo and M. Komiyama, *J. Chem. Soc., Chem. Commun.*, 1995, 1793; C. Wendelsdorf, S. Warzeska, E. Kövári and R. Krämer, *J. Chem. Soc., Dalton Trans.*, 1996, 3087; T. Koike, M. Inoue, E. Kimura and M. Shiro, *J. Am. Chem. Soc.*, 1996, **118**, 3091; M. Yashiro, A. Ishikubo and M. Komiyama, *Chem. Commun.*, 1997, 83.
6 M. Ruf, K. Weis and H. Vahrenkamp, *J. Am. Chem. Soc.*, 1996, **118**, 9288.
7 M. Itoh, K. Motoda, K. Shindo, T. Kamiusuki, H. Sakiyama, N. Matsumoto and H. Okawa, *J. Chem. Soc., Dalton Trans.*, 1995, 3635.
8 F. Meyer, S. Beyreuther, K. Heinze and L. Zsolnai, *Chem. Ber./Recueil*, 1997, **130**, 605; F. Meyer, A. Jacobi, B. Nuber, P. Rutsch and L. Zsolnai, *Inorg. Chem.*, 1998, **37**, 1213.
9 F. Meyer, K. Heinze, B. Nuber and L. Zsolnai, *J. Chem. Soc., Dalton Trans.*, 1998, 207.
10 M. Ardon and A.Bino, *Structure Bonding* (*Berlin*), 1987, **65**, 1.
11 G. M. Sheldrick, SHELXL-97, Program for Crystal Structure Refinement, Universität Göttingen, 1997; G. M. Sheldrick, SHELXS-97, Program for Crystal Structure Solution, Universität Göttingen, 1997.

Received in Basel, Switzerland, 15th January 1998; 8/00412I

1,1′,2,2′,3,3′-Tetrathiadiazafulvalenes; preparation and characterisation of *trans*-[ClCNS$_2$C=CS$_2$NCCl]

Tosha M. Barclay,[a] A. Wallace Cordes,[a] Richard T. Oakley,*[b]† Kathryn E. Preuss[b] and Robert W. Reed[b]

[a] *Department of Chemistry and Biochemsitry, University of Arkansas, Fayetteville, Arkansas 72071, USA*
[b] *Department of Chemistry and Biochemistry, University of Guelph, Guelph, Ontario N1G 2W1, Canada*

Reduction of 4,5-dichloro-1,2,3-dithiazolylium chloride with two equivalents of triphenylantimony in liquid SO_2 affords the 1,1′,2,2′,3,3′-tetrathiadiazafulvalene *trans*-[ClCNS$_2$C=CS$_2$NCCl]; the structural features and redox chemistry of this novel ring system are described.

A wide range of 1,2,3-dithiazolyl radicals **1** have been characterized in solution by EPR spectroscopy.[1,2] Little, however, is known of the structural fate of such species. Do they associate weakly into S-bonded dimers, as do many 1,2,3,5-dithiadiazolyls **2**[3] and 1,3,2-dithiazolyls **3**,[4–6] or might they bond

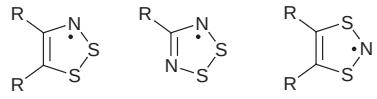

1 **2** **3**

through carbon, thereby giving access to fulvalene derivatives? In order to investigate this possibility, we have examined the redox chemistry of 4,5-dichloro-1,2,3-dithiazolylium chloride **4** (Appel's salt[7]), and have discovered that double reduction of this material affords **5** [eqn. (1)], the first example of a 1,1′,2,2′,3,3′-tetrathiadiazafulvalene.

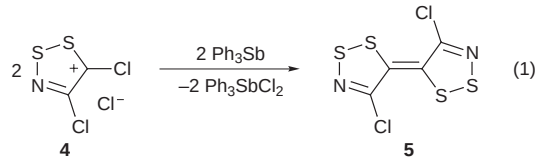

4 **5** (1)

The yield of **5** from **4** is very sensitive to the reaction conditions. We have explored the use of a variety of reducing agents and solvents, and to date the most effective combination utilizes triphenylantimony in liquid sulfur dioxide. Accordingly, when 50 ml of SO_2 was condensed at 77 K onto solid **4** (2.08 g, 10.0 mmol) and triphenylantimony (3.88 g, 11.0 mmol) in an H-cell, and the mixture allowed to warm slowly (2 h) to room temperature, a dark brown precipitate was produced. This solid was filtered off and back-washed twice with liquid SO_2. The solvent was removed from the reactor, and the residual solid washed sequentially with 50 ml MeCN, 50 ml aq. EtOH and 50 ml CH_2Cl_2. The solid was then extracted with 4 × 80 ml hot carbon disulfide, the deep purple extracts combined and the solvent removed to leave crude **5**, which was recrystallized from toluene as dark black–purple needles (0.42 g, 1.5 mmol, 30%), mp 120–121 °C, λ_{max} (CH_2Cl_2) 565 nm ($\varepsilon = 1.3 \times 10^4$ l mol^{-1} cm^{-1}).‡

The crystal stucture§ of **5** consists of discrete molecular units. The molecules, which lie on a crystallographic inversion centre, are planar to within 0.011 Å, and adopt a slipped π-stack structure running along the *x* direction. Fig. 1 illustrates the packing of a coplanar array of molecules, and provides a summary of both inter- and intra-molecular contacts. The pattern of intramolecular distances is consistent with the valence bond representation shown. Taken collectively, the S–S, S–N and S–C distances are all slightly longer than those observed in 1,2,3-dithiazolylium salts,[8] as expected from the lower oxidation state.

Previous investigations of the chemistry of Appel's salt have focussed on its reactions with nucleophiles.[9] Its reduction, as described here, parallels the behavior of 3-chloro-1,2-dithiolylium salts, which can be reduced to 1,1′,2,2′-tetrathiafulvalenes.[10] In the present case we have no evidence for a *cis*-isomer, presumably because of prohibitive steric interactions between the two chlorines. We have been unable to detect (by EPR spectroscopy) any signal attributable to **1** (R = Cl), a presumed intermediate in the reaction; its association (and subsequent reduction) are extremely rapid. Cyclic voltammetry on solutions of **5** in CH_2Cl_2 ($NBu^n_4PF_6$ supporting electrolyte, ref. SCE) reveals a reversible oxidation wave to the radical cation [**5**]$^+$ at $E_{\frac{1}{2}}$ = 0.80 V, with a second reversible oxidation wave at $E_{\frac{1}{2}}$ = 1.25 V, corresponding to formation of the closed shell dication [**5**]$^{2+}$. There is also an irreversible reduction process near −1.10 V. Similar behaviour has been observed for benzo-bis-1,2,3-dithiazoles.[11] Chemical oxidation to the radical cation can be effected by bromine. When dissolved in liquid SO_2 in the presence of $AlCl_3$, the radical cation salt [**5**]Br exhibits a strong and persistent EPR signal (g = 2.015) consisting of a 1:2:3:2:1 quintet arising from hyperfine coupling (a_N = 0.096 mT) to two equivalent nitrogen nuclei. Given the many advances in molecular conductor design that have arisen from the classical tetrathiafulvalene framework,[12] we believe this new system also holds rich potential as a molecular building block. To this end we are currently investigating the charge transfer chemistry of **5** and related compounds.

We thank the NSERC, the NSF/EPSCOR program and the State of Arkansas for financial support. We also acknowledge the NSERC for a post-graduate scholarship to K. E. P. and the US Department of Education for a doctoral fellowship to T. M. B.

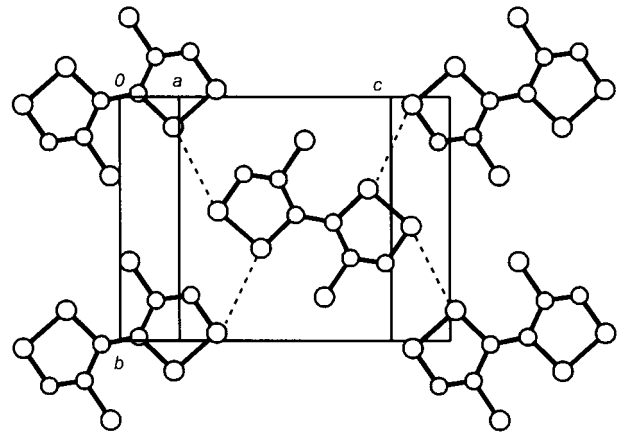

Fig. 1 Crystal packing in **5**. Selected bond lengths (Å): S–S 2.0759(15), S–N 1.657(4), S–C 1.768(4), N–C 1.276(6), N(C–C) 1.458(5), C–C 1.383(7), C–Cl 1.719(4). The intermolecular S···S distance (dashed line) is 3.4929(16) Å.

Notes and References

† E-mail: oakley@chembio.uoguelph.ca

‡ Satisfactory elemental (C and N) analyses have been obtained for **5**.

§ *Crystal data* for **5**: data were collected (at 293 K) on an Enraf-Nonius CAD-4 automated diffractometer with graphite-monochromated Mo-Kα radiation (λ = 0.710 73 Å) using θ–2θ scans to $2\theta_{max}$ = 52°. The structure was solved by direct methods and refined by full-matrix least-squares analysis which minimized $\Sigma w(\Delta F)^2$. $C_4Cl_2N_2S_4$, M = 275.20, monoclinic, space group $P2_1/c$, a = 3.9795(10), b = 8.9447(14), c = 11.973(2) Å, β = 92.537(17)°, U = 425.76(14) Å^3, Z = 2, D_c = 2.15 g cm^{-3}, μ = 1.64 mm^{-1}. 55 Parameters were refined using 827 unique observed reflections [$I > 1.0\sigma(I)$] to give R = 0.046 and R_w = 0.048. CCDC 182/838.

1 R. Mayer, G. Domschke, S. Bleisch and A. Bartl, *Z. Chem.*, 1981, **21**, 326.

2 R. Mayer, G. Domschke and S. Bleisch, *Tetrahedron Lett.*, 1978, 4003; R. Mayer, G. Domschke, S. Bleisch, A. Bartl and A. Stăsko, *Z. Chem.*, 1981, **21**, 146, 264; R. Mayer, G. Domschke, S. Bleisch, J. Fabian, A. Bartl and A. Stăsko, *Collect. Czech. Chem. Commun.*, 1984, **49**, 684; R. Mayer, S. Bleisch, G. Domschke, A. Tkáč and A. Stăsko, *Org. Magn. Reson.*, 1979, **12**, 532; S. R. Harrison, R. S. Pilkington and L. H. Sutcliffe, *J. Chem. Soc., Faraday Trans. 1*, 1984, **80**, 669.

3 A. W. Cordes, R. C. Haddon and R. T. Oakley, in *The Chemistry of Inorganic Ring Systems*, ed. R. Steudel, Elsevier, Amsterdam, 1992, p. 295.

4 G. Wolmershäuser and G. Kraft, *Chem. Ber.*, 1990, **123**, 881.

5 G. Heckmann, R. Johann, G. Kraft and G. Wolmershäuser, *Synth. Met.*, 1991, **41**–**43**, 3287.

6 E. G. Awere, N. Burford, R. C. Haddon, S. Parsons, J. Passmore, J. V. Waszczak and P. S. White, *Inorg. Chem.*, 1990, **29**, 4821; G. Wolmershäuser, M. Schnauber and T. Wilhelm, *J. Chem. Soc., Chem. Commun.*, 1984, 573.

7 R. Appel, H. Janssen, M. Siray and F. Knoch, *Chem. Ber.*, 1985, **118**, 1632.

8 J. W. Bats, H. Fuess, K. L. Weber and H. W. Roesky, *Chem. Ber.*, 1983, **116**, 1751.

9 T. Beson, K. Emayan and C. W. Rees, *J. Chem. Soc., Perkin Trans. 1*, 1995, 2097; O. A. Rakitin, C. W. Rees and O. G. Vaslova, *Chem. Commun.*, 1996, 1273; G. L'abbé, B. D'hooge and W. Dehaen, *J. Chem. Soc., Perkin Trans. 1*, 1995, 2379.

10 H. Behringer and E. Meinetsberger, *Liebigs Ann. Chem.*, 1981, 1928.

11 T. M. Barclay, A. W. Cordes, J. D. Goddar, R. C. Mawhinney, R. T. Oakley, K. E. Preuss and R. W. Reed, *J. Am. Chem. Soc.*, 1997, **119**, 12 136.

12 For recent reviews, see: M. R. Bryce, *Chem. Soc. Rev.*, 1991, **20**, 355; R. Gomper and H. W. Wagner, *Angew. Chem. Int. Ed. Engl.*, 1988, **27**, 1437; M. C. Grossel and S. C. Weston, *Contemp. Org. Synth.*, 1994, **1**, 317.

Received in Columbia, MO, USA, 2nd October 1997; 7/07143D

Convergent synthesis of the *trans*-fused 6-*n*-6-6 (*n* = 7–10) tetracyclic ether system based on a ring-closing metathesis reaction

Tohru Oishi,[a,b] Yoko Nagumo[a] and Masahiro Hirama*[a,b]†

[a] *Department of Chemistry, Graduate School of Science, Tohoku University, Sendai 980-8578, Japan*
[b] *CREST, Japan Science and Technology Corporation (JST), Japan*

A convergent synthesis of the *trans*-fused 6-*n*-6-6 (*n* = 7–10) tetracyclic ether system was achieved *via* stereoselective alkylation and ring-closing metathesis reaction.

The synthesis of ciguatoxin[1] has received considerable attention because of its striking structure and biological activity. Although numerous techniques have been developed for the synthesis of medium ring ethers,[2] efficient methods for assembling fragments are still needed. In the course of our synthetic study of ciguatoxin,[3] we developed a convergent route to the *trans*-fused 6-7-6 tricyclic ether system *via* formation of the central oxepene ring by alkene metathesis.[4–6] Here we describe a new technique for synthesizing *trans*-fused 6-*n*-6-6 (*n* = 7–10) tetracyclic polyether systems (**1a**–**e**) from glycolate **3** (Scheme 1). The central *n*-6 bicyclic rings of these systems are efficiently constructed by stereoselective alkylation and the subsequent ring-closing metathesis reaction of dienes (**2**).

Syntheses of the dienes **2a** and **2b**, precursors for 6-7-6-6 systems (**1a** and **1b**), are shown in Scheme 2. Coupling of *tert*-butyl ester **3** with iodide **4**‡ using LDA in the presence of HMPA gave **5** and the diastereomer **6** in a 3 : 1 ratio. These compounds were separated using silica gel column chromatography. Removal of the TIPS group of **5** using TBAF followed by treatment with $TsOH{\cdot}H_2O$ in toluene at 90 °C gave lactone **7**. The addition of vinylmagnesium bromide to **7** gave hemiacetal **8**, and reduction of **8** with Et_3SiH in the presence of $BF_3{\cdot}OEt_2$[7] proceeded stereoselectively, giving **10** as a single isomer. Methylation of the hemiacetal **8** using Me_3Al and $BF_3{\cdot}OEt_2$[8] gave **11** only in low yield (~4%); however, the alkylation of the corresponding methyl acetal **9** under the same reaction conditions gave **11** in good yield (72%) as a single isomer. Reductive removal of the benzyl groups of **10** and **11** using lithium naphthalenide[9] followed by Swern oxidation and subsequent Wittig olefination gave dienes **2a** and **2b**, respectively.

Syntheses of dienes **2c**–**e**, precursors for **1c**–**e**, respectively, are also shown in Scheme 2. Treatment of **7** with allylmagnesium bromide followed by reduction of the resulting hemiacetal (Et_3SiH, $BF_3{\cdot}OEt_2$) gave **12** as a single isomer. The olefin **12** was converted to **2c** in the same manner as **2a** and **2b**. Syntheses of **2d** and **2e** were performed using triflate chemistry.[10] Treatment of the triflate derived from alcohol **13** using lithium acetylide in the presence of 1,3-dimethyl-3,4,5,6-tetrahydro-2(1*H*)-pyrimidone (DMPU) followed by partial hydrogenation gave **2d**, whereas treatment of the same triflate using allylmagnesium bromide in the presence of CuBr gave **2e**.

Ring-closing metathesis reactions of dienes **2a**–**e** using Grubbs' catalyst ($(PCy_3)_2Cl_2Ru{=}CHPh$ (**14**) were examined (Table 1). The reactions of **2a** and **2b** in benzene gave 6-**7**-6-6 tetracyclic ethers **1a**, and **1b** having an angular methyl group in

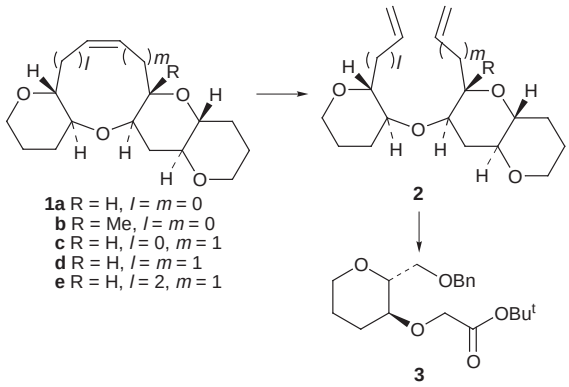

Scheme 1

Table 1 Ring-closing metathesis reaction of **2a**–**e**[a]

Diene	Product	*J*/Hz[b]	Yield (%)
2a	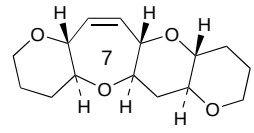 **1a**	12.9	81[d]
2b	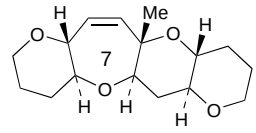 **1b**	12.8	94[d] 82[e]
2c	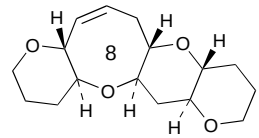 **1c**	11.0	94[e]
2d	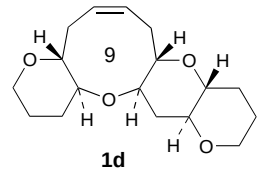 **1d**	10.5[c]	87[e]
2e	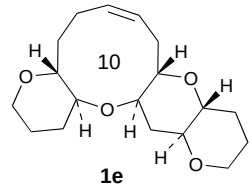 **1e**	10.9	68[e]

[a] Reactions were carried out in the presence of 12–21 mol% of catalyst **14**. [b] Coupling constants between the olefin protons. [c] The value at −40 °C. [d] In benzene at 50–60 °C for 5–7 days (0.04 M). [e] In CH_2Cl_2 at 35 °C for 1–2 days (0.004–0.04 M).

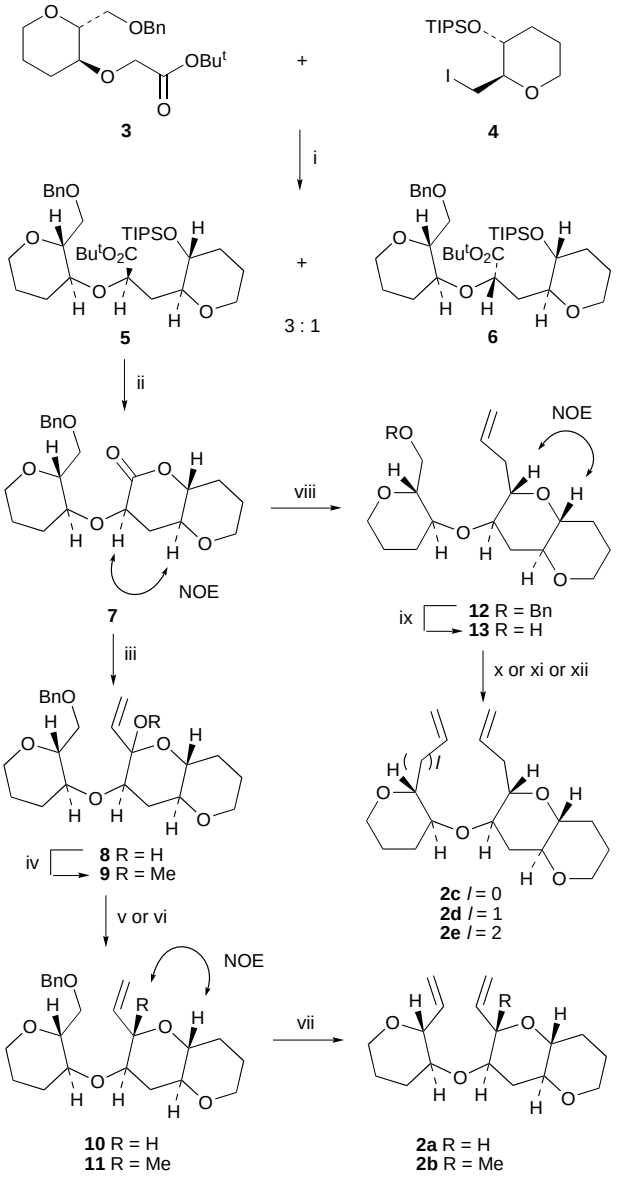

Scheme 2 *Reagents and conditions*: i, LDA, HMPA, THF, −78 to 0 °C, 61%; ii, Bu_4NF, THF, $TsOH·H_2O$ (cat.), toluene, 90 °C, 84%; iii, H_2C=CHMgBr, THF, −78 °C, 80%; iv, $CH(OMe)_3$, CSA, CH_2Cl_2, 80; v, Et_3SiH, $BF_3·OEt_2$, MeCN, −20 °C, 71%; vi, Me_3Al, $BF_3·OEt_2$, CH_2Cl_2, 0 °C to room temp., 72%; vii, Li, $C_{10}H_8$, THF; $(COCl)_2$, Et_3N, DMSO, CH_2Cl_2, −78 to −40 °C; $Ph_3P^+MeBr^-$ $NaN(SiMe_3)_2$, THF, 0 °C to room temp., 72% (for **2a**), 64% (for **2b**); viii, H_2C=$CHCH_2MgBr$, THF, Et_2O, −78 °C; Et_3SiH, $BF_3·OEt_2$, MeCN, −20 °C to room temp., 90%; ix, Li, $C_{10}H_8$, THF, 91%; x, $(COCl)_2$, Et_3N, DMSO, CH_2Cl_2, −78 to 0 °C; $Ph_3P^+MeBr^-$, $NaN(SiMe_3)_2$, THF, 0 °C to room temp., 83%; xi, Tf_2O, Py, CH_2Cl_2, −15 °C; LiC≡CH, DMPU, THF, −78 to 0 °C; H_2, Lindlar cat. AcOEt, 47%; xii, Tf_2O, Py, CH_2Cl_2, −15 °C; H_2C=$CHCH_2MgBr$, CuBr, Et_2O, 0 to 10 °C, 84%

81 and 94% yield, respectively. These reactions required five to seven days. However, we found a remarkable solvent effect because the reaction of **2b** in CH_2Cl_2 proceeded smoothly and was completed within two days. This method was also quite effective in the construction of the larger rings. Cyclic polyethers **1c** (6-**8**-6-6), **1d** (6-**9**-6-6) and **1e** (6-**10**-6-6 system) were synthesized from **2c**–**e**, respectively, in good yields. The structures of these products were unambiguously determined by NMR and mass spectroscopy.

The present technique will serve as a versatile synthetic tool for the synthesis of polyether marine toxins. Further synthetic studies of ciguatoxin are presently being conducted in our laboratory.

This work was supported in part by a Grant-in-aid for Scientific Research from the Ministry of Education, Science, Sports, and Culture of Japan, the Naito Foundation and the Uehara Memorial Foundation. We also wish to thank Dr M. Ueno and Mr T. Sato, Instrumental Analysis Center for Chemistry, Faculty of Science, Tohoku University for the measurement of NMR and mass spectra.

Notes and References

† E-mail: hirama@ykbsc.chem.tohoku.ac.jp

‡ Compounds **3** and **4** were prepared from (*2R*,*3S*)- and (*2S*,*3R*)-2-(benzyloxymethyl)tetrahydropyran-3-ol, respectively, by standard procedures.[4]

1 M. Murata, A. M. Legrand, Y. Ishibashi, M. Fukui and T. Yasumoto, *J. Am. Chem. Soc.*, 1990, **112**, 4380; M. Satake, A. Morohashi, H. Oguri, T. Oishi, M. Hirama, N. Harada and T. Yasumoto, *J. Am. Chem. Soc.*, 1997, **119**, 11 325.

2 E. Alvarez, M. T. Díaz, L. Hanxing and J. D. Martín, *J. Am. Chem. Soc.*, 1995, **117**, 1437; S. Hosokawa and M. Isobe, *Synlett*, 1995, 1179; M. Inoue, M. Sasaki and K. Tachibana, *Tetrahedron Lett.*, 1997, **38**, 1611.

3 T. Suzuki, O. Sato, M. Hirama, Y. Yamamoto, M. Murata, T. Yasumoto and N. Harada, *Tetrahedron Lett.*, 1991, **32**, 4505; O. Sato and M. Hirama, *Synlett*, 1992, 705; H. Oguri, S. Hishiyama, T. Oishi and M. Hirama, *Synlett*, 1995, 1252; T. Oishi, M. Shoji, K. Maeda, N. Kumahara and M. Hirama, *Synlett*, 1996, 1165; H. Oguri, S. Hishiyama, O. Sato, T. Oishi, M. Hirama, M. Murata, T. Yasumoto and N. Harada, *Tetrahedron*, 1997, **53**, 3057; T. Oishi, K. Maeda and M. Hirama, *Chem. Commun.*, 1997, 1289; T. Oishi, M. Shoji, N. Kumahara and M. Hirama, *Chem. Lett.*, 1997, 845.

4 T. Oishi, Y. Nagumo and M. Hirama, *Synlett*, 1997, 980.

5 W. J. Zuercher, M. Hashimoto and R. H. Grubbs, *J. Am. Chem. Soc.*, 1996, **118**, 6634 and references cited therein.

6 For recent applications of the metathesis reactions to the synthesis of monocyclic and terminal cyclic ether systems, see: K. C. Nicolaou, M. H. D. Postema and C. F. Claiborne, *J. Am. Chem. Soc.*, 1996, **118**, 1565; K. C. Nicolaou, M. H. D. Postema, E. W. Yue and A. Nadin, *J. Am. Chem. Soc.*, 1996, **118**, 10335; J. S. Clark and J. G. Kettle, *Tetrahedron Lett.*, 1997, **38**, 123; J. S. Clark and J. G. Kettle, *Tetrahedron Lett.*, 1997, **38**, 127; M. Delgado and J. D. Martín, *Tetrahedron Lett.*, 1997, **38**, 6299; M. T. Crimmins and A. L. Choy, *J. Org. Chem.*, 1997, **62**, 7548.

7 D. L. Lewis, J. K. Cha and Y. Kishi, *J. Am. Chem. Soc.*, 1982, **104**, 4976.

8 K. Tomooka, K. Matsuzawa and K. Suzuki, *Tetrahedron Lett.*, 1987, **28**, 6339.

9 H.-J. Liu, J. Yip and K.-S. Shia, *Tetrahedron Lett.*, 1997, **38**, 2253.

10 H. Kotsuki, I. Kadota and M. Ochi, *Tetrahedron Lett.*, 1989, **30**, 1281; H. Kotsuki, I. Kadota and M. Ochi, *Tetrahedron Lett.*, 1990, **31**, 4609.

Received in Cambridge, UK, 2nd March 1998; 8/01678J

Probabilities of formation of bimolecular cyclic hydrogen-bonded motifs in organic crystal structures: a systematic database analysis

Frank H. Allen,*[a] Paul R. Raithby,*[b] Gregory P. Shields[a,b] and Robin Taylor[a]

[a] *Cambridge Crystallographic Data Centre, 12 Union Road, Cambridge, UK CB2 1EZ*
[b] *Department of Chemistry, Lensfield Road, Cambridge, UK CB2 1EW*

A database methodology has been developed to locate all possible occurrences of bimolecular cyclic hydrogen-bonded motifs in the Cambridge Structural Database and to calculate their probabilities of formation; the top 24 motifs involving D–H···A (D, A = N or O) are identified.

The design process in crystal engineering depends crucially on the high probabilities of formation of a limited number of strong intermolecular interactions.[1,2] These non-covalent motifs, termed bimolecular couplings[3] or supramolecular synthons[2] by analogy with molecular synthesis, often involve strong hydrogen bonds. Despite their successes[1,2] crystal structure prediction and retrosynthesis depend heavily on evidence gleaned from visual surveys of limited subsets of existing crystal structures.[4] To extend the list of potential H–bonded synthons, we must identify and categorise the diversity of motifs that occurs, *e.g.* in the > 170 000 crystal structures recorded in the Cambridge Structural Database (CSD).[5] This data driven approach establishes the topologies, chemical constitutions and probabilities of formation of all H-bonded motifs in an objective manner.

Here we report probabilities of formation for cyclic bimolecular motifs that incorporate D–H···A (D, A = N or O) bonds. Our procedure identifies the important structure-determining H-bonded motifs that link pairs of molecules in crystal structures, *i.e.* we are interested in the immediate non-covalently bonded environment(s) of the molecule(s) that comprise the crystal chemical unit (CCU)‡. Once identified, we envisage that extension of a structure using each of these primary links can be visualised in a manner that mimics crystal growth, and that we can then generate and describe complete networks for structure classification and comparison purposes.[6]

The CSD System program Quest3D,[5] which can locate general non-bonded contacts according to pre-defined geometrical criteria, has been modified to investigate H–bonded motifs. For each target molecule in the CCU, the modifications are (a) identify potential donors (D–H) and acceptors (A), (b) locate bonds D–H···A involving the target molecule according to preset geometrical constraints, (c) establish whether pairs of H-bonds between the target and a neighbouring molecule form a cyclic motif, classify other H-bonds as isolated, (d) establish motif ring sizes (using shortest intramolecular bond paths), their symmetry (both topological and crystallographic), and their chemical constitutions and (e) provide interactive graphical display of each cyclic motif.

Despite the generality of our modifications to Quest3D, the initial analysis specifically addresses cyclic systems: it provides probability statistics for bimolecular cyclic motifs involving N–H or O–H donors and N or O acceptors, *i.e.* motifs that incorporate the strongest H-bonds and, hence, can be regarded as structure determining. In our automated procedure, all D–H bond lengths were normalised to mean values from neutron diffraction,[7] and H···A distance limits were established from histograms generated using the October 1996 release of the CSD: 2.30 Å in N–H···N, 2.25 Å in N–H···O, and 2.20 Å in O–H···N and O–H···O. Additionally, the D–H···A angle was required to be > 90°. CSD entries were accepted for analysis if they were classified as error-free, organic, and had $R < 0.10$.

The size, symmetries and chemical constitution of each cyclic motif were combined into a chemical topology record and these were sorted to yield raw occurrence values (N_{occ}). While these figures are interesting, their interpretation is complicated by the fact that they depend on the number of times that the various donor and acceptor groups occur in the CSD. For example, the carboxylic acid ring motif might have a high N_{occ} value simply because carboxylic acids are common in the CSD. To correct for this effect, we determined a probability of occurrence (expressed as a percentage), Prob = $100\,N_{occ}/N_{poss}$, for each of the 75 most common motifs. Here, N_{poss} is the number of times that the motif could possibly occur, given: (a) the number of structures in the CSD that contain the required functional group(s), and (b) the number of times that the groups(s) occur in the CCU of each structure. The automatic generation of N_{poss} is complicated, *inter alia*, by the need to consider: (a) the presence or absence of topological symmetry, (b) which overlapping fragments can be used simultaneously in forming motifs, (c) the three-dimensional geometry of certain fragments, (d) the effects of bifurcation and other multi-centre bonds and (e) the sharing of H-bonds between two rings. We have generated a set of logical rules§ which take account of these considerations; the effects of (c) are not straightforward to assess, and no account has been taken of competition for donor-

Table 1 Probability-ordered statistics for the 24 motifs in the CSD having $N_{occ} > 25$ and Prob > 20%

Motif No.	N_{occ}	N_{poss}	Prob (%)	Symm[a] (%)
1	93	96	97	—
2	199	218	91	—
3	36	40	90	—
4	36	44	82	—
5	62	82	76	—
6	206	354	58	—
7	158	290	55	—
8	79	154	51	—
9	86	192	45	—
10	38	92	41	68
11	45	114	40	—
12	47	120	39	—
13	44	118	37	—
14	204	556	37	75
15	58	159	37	62
16	39	111	35	64
17	29	83	35	79
18	847	2541	33	65
19	99	306	32	—
20	93	341	27	76
21	172	660	26	64
22	50	206	24	—
23	876	3687	24	62
24	84	404	21	64

[a] Motif possess crystallographic symmetry; other motifs are topologically (hence crystallographically) asymmetric.

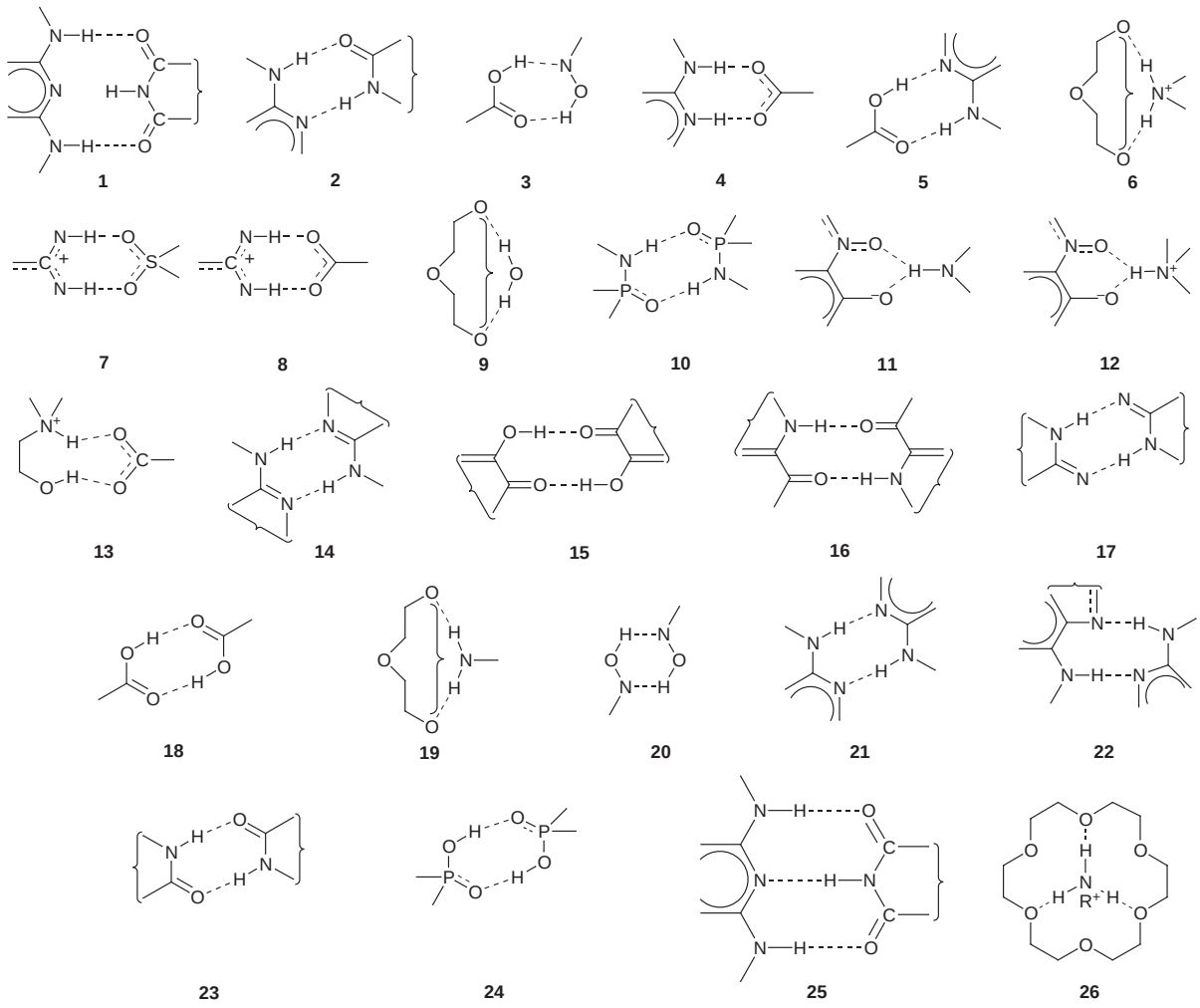

Fig. 1 Probability-ordered H-bonded motifs **1**–**24** and recognition motifs **25** and **26** (see text)

H between different acceptors or *vice versa*. Although the rules are capable of further refinement, principally for rarer situations, we believe that the relative probabilities for the most common motifs presented in Table 1 are reliable.

The probability-ordered Fig. 1 and Table 1 include the 24 motifs that have $N_{occ} > 25$ and Prob > 20%. Motifs **1** and **2** are part of the triply H-bonded motif **25** (**1** is the envelope ring), having some analogies with nucleotide recognition in DNA, and a potent supramolecular synthon.[2,8] The other very high probability motifs, **3**–**5**, all occur in relatively few individual structures (12, 17 and 20 respectively), but **5** is noted by Desiraju.[2] Motif **6** represents a portion of an 18-crown-6 ether–ammonium complex. Here, three N-H donors from $[RNH_3]^+$ normally lie above the ring and the complete pattern, **26**, is best regarded as the recognition motif. Analogous complexes of 18-crown-6 with water (**9**) or RNH_2 (**19**) have lower but still appreciable probabilities.

The low probabilities of formation of the carboxylic acid **18** and cyclic amide **23** motifs might be considered surprising. However, they reflect chemical environments that contain many competing acceptors and donors, together with steric influences, particularly in the amide case. If the analysis is restricted to mono- and di-carboxylic acids without other functional groups, then Prob for motifs **18** and **23** rises to 95.5 and 84.8% respectively. The cyclic amides of motif **23** have their H-donors constrained to be *cis* to the =O acceptor. In flexible acyclic amides, which are usually *anti*, the overall probability of forming a cyclic motif is only 8.4%. However, if the analysis is restricted to structures having only primary or secondary amide functions, then the probability rises to 44.1% for the cyclic case and to 15.7% for the acyclic case. Using these statistics we are now analysing why particular motifs do not occur with greater frequency, and what alternative interactions are possible.

Notes and References

† E-mail: allen@ccdc.cam.ac.uk

‡ The crystal chemical unit (CCU) contains the complete unique molecule(s) that comprise the crystal structure. Where molecular and crystallographic symmetry coincide the fractional molecules are expanded by symmetry to form the CCU prior to the investigation of H-bonded motifs.

§ A brief description of these rules is provided as Supplementary material which is available on the World Wide Web: http://www.rsc.org/suppdata/cc/1998/1043.

1 C. B. Aakeröy and K. R. Seddon, *Chem. Soc. Rev.*, 1993, **22**, 397.
2 G. R. Desiraju, *Angew. Chem., Int. Ed. Engl.*, 1995, **34**, 2311.
3 W. Jones, V. R. Pedireddi, A. P. Chorlton and R. Docherty, *Chem. Commun.*, 1996, 997.
4 G. A. Jeffrey and S. Takagi, *Acc. Chem. Res*., 1978, **11**, 264; L. Leiserowitz and A. T. Hagler, *Proc. R. Soc. London, Ser. A*, 1983, **338**, 133.
5 F. H. Allen and O. Kennard, *Chem. Des. Autom. News*, 1993, **8**, 1; 31.
6 M. C. Etter, *Acc. Chem. Res*., 1990, **23**, 120; J. Bernstein, R. E. Davis, L. Shimoni and N.-L. Chang, *Angew. Chem., Int. Ed. Engl*., 1995, **34**, 1555.
7 F. H. Allen, O. Kennard, D. G. Watson, L. Brammer, A. G. Orpen and R. Taylor, *J. Chem. Soc., Perkin Trans. 2*, 1987, S1.
8 W. Saenger, *Principles of Nucleic Acid Structure*, Springer-Verlag, New York, 1984, ch. 6; J.-M. Lehn, M. Mascal, A. DeCian and J. Fischer, *J. Chem. Soc., Chem. Commun*., 1990, 479; G. M. Whitesides, E. E. Simanek, J. P. Mathais, C. T. Seto, D. N. Chin, M. Mammen and D. M. Gordon, *Acc. Chem. Res.*, 1995, **28**, 37.

Received in Cambridge, UK, 19th February 1998; 8/01424H

Tropic acid biosynthesis: the incorporation of (*RS*)-phenyl[2-^{18}O,2-^{2}H]lactate into littorine and hyoscyamine in *Datura stramonium*

Chi W. Wong,[a] John T. G. Hamilton,[b] David O'Hagan*[a]† and Richard J. Robins[c]

[a] *Department of Chemistry, University of Durham, Science Laboratories, South Road, Durham, UK DH1 3LE*
[b] *Microbial Biochemistry Section, Department of Food Science, The Queen's University of Belfast, Newforge Lane, Belfast, UK BT9 5PX*
[c] *Laboratoire d'Analyse Isotopique et Electrochimique de Metabolismes, CNRS UPRES-A 6006, Université de Nantes, Departement de Chimie, 2 rue de la Houssinière, 44072, Nantes cedex 03, France*

The incorporation of oxygen-18 from (*RS*)-phenyl-[2-^{18}O,2-^{2}H]lactate into the tropane alkaloids littorine 1 and hyoscyamine 2 in *Datura stramonium* reveals that up to 29% of the oxygen-18 is lost during the transformation of 1 to 2.

The biosynthetic origin of the tropate ester moiety of the alkaloid hyoscyamine **2** has been the subject of attention for many years.[1,2] It was shown in 1972 that this ester arises as a consequence of a carbon skeleton rearrangement of a phenylpropanoid metabolite derived from L-phenylalanine.[3]

We were able to show in 1995[4] that (*R*)-phenyllactate was the relevant phenylpropanoid metabolite, and in a notable development Robins *et al.* demonstrated[5] that the tropate ester moiety is derived after a *direct isomerisation* of littorine **1**, the (*R*)-phenyllactate ester of tropine, to hyoscyamine **2**, the tropine ester of (*S*)-tropic acid, as represented in Scheme 1. Although the substrate for the isomerisation is now established, the nature of the enzyme and the mechanism of the process remains unknown. There is a superficial similarity of the rearrangement to some coenzyme-B_{12} mediated isomerisations which has led to speculation that this is a coenzyme-B_{12} process,[6,7] however the characteristic vicinal interchange process common to carbon skeleton coenzyme-B_{12} mediated isomerisations[8] *does not occur*[9] in the littorine **1** to hyoscyamine **2** rearrangement.

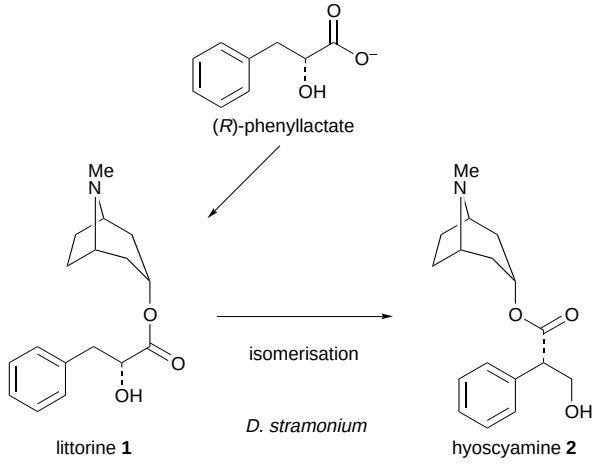

Scheme 1

In order to explore this process further we have studied the incorporation of sodium (*RS*)-phenyl[2-^{18}O,2-^{2}H]lactate into both of the alkaloids **1** and **2** in transformed root cultures of *Datura stamonium*.[10] The requisite (*RS*)-phenyl[2-^{18}O,2-^{2}H]lactate was prepared as shown in Scheme 2. In the event only *ca.* 50% of the oxygen-18 isotope from $H_2{}^{18}O$ was introduced by exchange into phenyl[1-^{2}H]acetaldehyde, presumably as the hydrate is stable to dehydration under the reaction conditions. This route provided a sample of (*RS*)-phenyl[2-^{18}O,2-^{2}H]lactate which had an M + 1/M + 3 ratio of 1.10 as determined by GC–MS analysis. The material was pulse fed (days 5, 7 and 9) to transformed root cultures[10] of *D. stramonium* at a final concentration of 0.64 mM, and the alkaloids were extracted from the root tissue on days 11, 13, 15 and 17 as previously described. GC–MS analysis of the alkaloid extracts allowed determination of isotope content from the relative abundances of the M + 1 (^{2}H only) and M + 3 (^{2}H + ^{18}O)

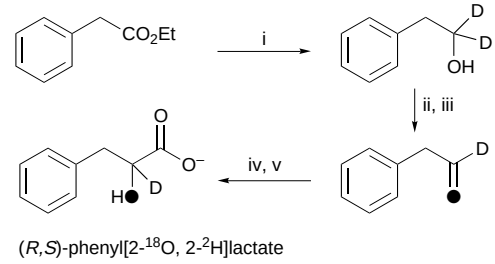

Scheme 2 *Reagents and conditions*: i, $LiAlD_4$, Et_2O, 2 h, 73%; ii, PCC, CH_2Cl_2, 2 h, 83%; iii, $H_2{}^{18}O$ (97 atom%), THF, HCl, 120 °C, 5 h; iv, TMSCN, Et_3N, CH_2Cl_2, 2 h, then aq. HCl, 24 h, 69%; v, aq. NaOH, 46%

Table 1 GC–MS derived data for the alkaloids **1** and **2** on four different days after supplementation of *D. stammonium* root cultures with (*RS*)-phenyl[2-^{18}O,2-^{2}H]lactate. For these studies the mass spectrometer was operated in the selected ion monitoring mode (SIM) measuring ion currents at *m*/*z* 289 (M), 290 (M + 1), 291 (M + 2) and 292 (M + 3). The data are presented after natural abundance levels have been subtracted. The corrections made to each of the ion peak areas for natural isotope abundances were determined experimentally using authentic standard compounds

	Day 11		Day 13		Day 15		Day 17	
	1	**2**	**1**	**2**	**1**	**2**	**1**	**2**
M	83.39	90.58	86.49	90.73	84.39	89.00	87.93	90.01
M + 1	9.19	6.48	7.48	6.53	8.50	7.58	6.74	6.78
M + 3	7.24	3.15	5.88	2.95	6.92	3.61	5.24	3.35
M + 1/M + 3 ratio	**1.27**	**2.06**	**1.27**	**2.21**	**1.23**	**2.10**	**1.29**	**2.02**
^{18}O loss from **1** to **2** (%)	25		29		28		25	

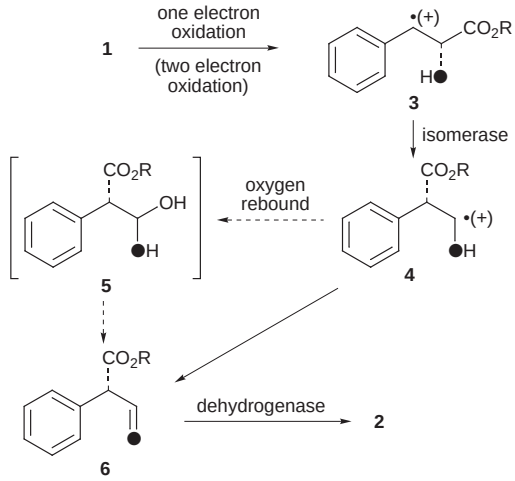

Scheme 3

ions. The levels of incorporation were determined by selective ion monitoring (SIM) and the values in Table 1 are corrected for natural isotope abundances. There was no significant incorporation (M + 2 = 0 ± 0.3) into the M + 2 ions and these are not included in Table 1. Of particular significance for this study is the M + 1/M + 3 ratio in the molecular ions of both **1** and **2**, which is independent of total incorporation (12–17%). The extracted littorine **1** on each of the four days had an M + 1/M + 3 = 1.26 ± 0.02, whereas the hyoscyamine had a value of M + 1/M + 3 = 2.1 ± 0.07. This change of ratio represents a loss of *ca.* 25–29% of the M + 3 abundance in hyoscyamine relative to littorine **1** and a corresponding enrichment of the M + 1 abundance of hyoscyamine **2** relative to littorine in going from **1** to **2**. Thus there is an exchange of *ca.* 25–29% of oxygen-18 for oxygen-16 in going from littorine **1** to hyoscyamine **2**.

Our working hypothesis for the rearrangement of **1** and **2** involves two enzymatic activities, an iron–oxo isomerase and a dehydrogenase, as illustrated in Scheme 3. This hypothesis developed from ideas of Sankawa,[11,12] who rationalised a number of isomerisation reactions in terms of iron–oxo enzyme processes. Three mechanistic scenarios emerge in the light of this result. In general, iron–oxo processes are considered to involve radicals and it can be envisaged that a Fe^{IV}–O· species abstracts hydrogen (the 3′-*pro-R* hydrogen)[9] to generate a substrate radical **3**. After rearrangement, the product radical **4** is quenched in a classical manner by delivery of an hydroxyl radical from Fe^{IV}–OH (oxygen rebound) to generate hydrate **5** followed by collapse of the hydrate to give aldehyde **6**. The high retention of oxygen-18 found experimentally is compatible with this process if (i), a partially stereospecific collapse of the hydrate occurs under enzymatic control, or (ii) a fully stereospecific process removes the unlabelled oxygen, but there is some exchange at the aldehyde prior to reduction by a dehydrogenase. A non-stereospecific process would of course result in 50% loss of oxygen-18 and this is not observed.

A similarly high retention of oxygen (80%) was observed previously[13] in the oxidation of **7** to **8** in a P-450 mediated process operating during oestrogen biosynthesis. It was concluded[13,14] in that case that the observation is most consistent with a disproportionation process [Scheme 4(*a*)] involving $Fe^{IV}OH$ and the product radical, rather than the more common oxygen rebound [Scheme 4(*b*)] process. It is poignant that a similar level of oxygen-18 retention is found in this study and such a disproportionation must remain under consideration. The partial loss of isotope can then be attributed to some exchange of the carbonyl oxygen of aldehyde **6** with the aqueous medium

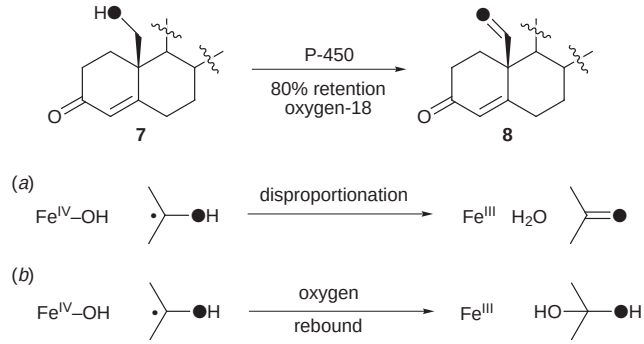

Scheme 4

prior to reduction by a dehydrogenase. Finally, an additional mechanism would involve a two-electron oxidation of **1** to generate carbocation **3**, as illustrated in the brackets in Scheme 3. Such a process has some precedent with the accepted mechanisms of thromboxane and prostacyclin synthases,[15] where carbocation intermediates are implied, and in some recent mechanistic studies[16] on P-450 systems, where carbocations gave rise to side products during the hydroxylation of cyclopropane substrates. As illustrated in Scheme 3, rearrangement to carbocation **4** followed by a direct collapse to aldehyde **6** prior to reduction would not require any loss of oxygen-18. Some exchange then at the aldehyde level is also consistent with the experimental result. A fuller discussion of the various mechanistic possibilities is given elsewhere.[17]

We thank the CIBA foundation for an ACE award and the EPSRC for a Studentship (C. W. W.).

Notes and References

† E-mail: david.o'hagan@durham.ac.uk

1 R. Robinson, *Proceedings of the University of Durham Philosophical Society*, 1927–1932, **8**, 14.
2 R. Robinson, *Structural Relations of Natural Products*, Clarendon Press, Oxford, 1955.
3 E. Leete, N. Kowanko and R. A. Newmark, *J. Am. Chem. Soc.*, 1975, **97**, 6826.
4 N. C. J. Chesters, D. O'Hagan and R. J. Robins, *J. Chem. Soc., Chem. Commun.*, 1995, 127.
5 R. J. Robins, P. Bachmann and J. G. Woolley, *J. Chem. Soc., Perkin Trans. 1*, 1994, 615.
6 E. Leete, *Can. J. Chem.*, 1987, **65**, 226; E. Leete, *J. Am. Chem. Soc.*, 1984, **106**, 7271.
7 M. Ansarin and J. G. Woolley, *J. Chem. Soc., Perkin Trans. 1*, 1995, 487.
8 J. Rétey and D. Arigoni, *Experientia*, 1966, **22**, 783.
9 N. C. J. E. Chesters, K. Walker, D. O'Hagan and H. G. Floss, *J. Am. Chem. Soc.*, 1996, **118**, 925.
10 R. J. Robins, N. C. J. E. Chestrs, D. O'Hagan, A. J. Parr, N. J. Walton and J. G. Woolley, *J. Chem. Soc., Perkin Trans. 1*, 1995, 481.
11 M. F. Hashim, T. Hakamatsuka, Y. Ebizuka and U. Sankawa, *FEBS Lett.*, 1990, **271**, 219.
12 T. Hakamatsuka, M. F. Hashim, Y. Ebizuka and U. Sankawa, *Tetrahedron*, 1991, **47**, 5969.
13 M. Akhtar, M. R. Calder, D. L. Corina and J. N. Wright, *Biochem. J.*, 1982, **201**, 569.
14 M. Akhtar and J. N. Wright, *Nat. Prod. Rep.*, 1981, **8**, 527.
15 V. Ullrich and R. Brugger, *Angew. Chem., Int. Ed., Engl.*, 1994, **33**, 1911.
16 M. Newcomb, M.-H. Le Tadic-Biadatti, D. L. Chestney, E. S. Roberts and P. F. Hollenberg, *J. Chem. Soc.*, 1995, **117**, 12 091.
17 D. O'Hagan and R. J. Robins, *Chem. Soc. Rev.*, 1998, in the press.

Received in Cambridge, UK, 2nd February, 1998; Revised manuscript received 2nd March 1998; 8/01722K

Regioselective introduction of two boronic acid groups into [60]fullerene using saccharides as imprinting templates

Tsutomu Ishi-i, Kazuaki Nakashima and Seiji Shinkai*†

Chemotransfiguration Project, Japan Science and Technology Corporation (JST), 2432 Aikawa, Kurume, Fukuoka 839, Japan

Two boronic acid groups were introduced into [60]fullerene using saccharides as template molecules: it was found that the regioselectivity changes depending on the saccharide structure.

The molecular imprinting technique attracted considerable attention in the 1970s, but recently has been revived as an active research area.[1–3] The principle involves copolymerisation of vinyl monomers with divinyl monomers in the presence of guest metals or molecules to produce three-dimensional network polymers.[1–3] Although this technique has achieved some degree of success, two complex problems have been left unresolved, *i.e.* the evaluation of the imprinting effect is difficult because it can be performed only in a heterogeneous system, and the storage capacity is small because only the particle surface is useful for the re-binding of guests. Is there an alternate method in which both the imprinting process and the estimation process can be carried out in a more reliable homogeneous system? [60]Fullerene and its homologues are moderately soluble in organic solvents and have plenty of reactive C=C double bonds which are useful for the immobilisation of functional groups. It thus occurred to us that they would be useful as a base for the imprinting of functional groups and for use in a homogeneous system. There are a limited number of precedents for regioselective introduction of substituents into [60]fullerene.[4–6] In order to apply [60]fullerene to the memory storage, we here chose saccharides as the template and guest molecules and boronic acids as the functional groups. Saccharides have several specific advantages for the present purpose which other template molecules do not have, *i.e.* (i) they can arrange two boronic acid groups in a variety of spatial positions, (ii) removal and re-binding can occur reversibly, and (iii) because of their inherent chirality, chiroselective introduction of two boronic acid groups is possible.[7] We here report the fact that, using saccharides as template molecules, two boronic acid groups can be regioselectively introduced into [60]fullerene; the regiospectrum is closely related to the structure of saccharides used as template molecules.

In order to access saccharide–boronic acid 1 : 2 complexes **6**–**9**, we first synthesised **5** from 4-bromo-*o*-xylene **1** (Scheme 1). Compound **5**, which was isolated as a cyclic trimer,[7,8] was identified by ^{1}H NMR, IR (KBr) and mass (negative SIMS) spectral evidence and elemental analysis. Complexes **6**–**9** were synthesised from **5** and the corresponding saccharides in refluxing toluene with azeotropic removal of water under a nitrogen atmosphere. The products were identified by ^{1}H and ^{11}B NMR and IR (KBr) spectral evidence and elemental analyses.[9] The reaction of **6**–**9** with [60]fullerene was carried out in refluxing toluene for 40 h in the presence of 18-crown-6 and KI under a nitrogen atmosphere. To simplify the product analysis, the saccharides were removed by the treatment with aqueous 1.2 mol dm^{-3} HCl solution and then the boronic acid groups in the product **11** were protected using 2,2-dimethylpropane-1,3-diol[10] (Scheme 2). The product was purified by column chromatography. We thus isolated a regioisomeric mixture of **12** in 49–58% yield. This mixture was subjected to HPLC analysis [COSMOSIL 5 PBB, *n*-hexane–toluene (3 : 7 v/v)]. The results are summarised in Table 1.

In the HPLC analysis, 7–8 peaks were always observable and the relative intensity changed depending on the saccharide used as the template molecule. Compounds **6**, **7** and **8** with D-threitol, D-mannito 3,4-carbonate and 3-*O*-methyl-D-glucofuranose as template molecules, respectively, afforded major peaks for Peak 7 (47.3%), Peak 8 (55.7%) and Peak 6 (72.5%), respectively, whereas compound **9** with 1-*O*-methyl-α-D-mannopyranoside as a template molecule featured a rather nonselective product distribution. The results imply that the saccharide changes the distance between two *o*-xylenyl dibromide groups in **6**–**9** and the addition reaction occurs at different C=C double bonds on the [60]fullerene surface.

It is difficult to isolate the eight different isomers of disubstituted **12** and thus identify the structure of each isomer. We decided to attempt the isolation of Peak 6 [with the highest (72.5%) yield] in the mixture obtained from **8** and [60]fullerene. Through trial and error it was found that Peak 6 can be isolated by recrystallisation from *n*-hexane–CH_2Cl_2: the HPLC analysis showed a single peak for Peak 6. In the ^{1}H NMR spectrum (300 MHz, [$^2H_8$]toluene, 90 °C) of this compound (**12a**) one could observe one CH_3 proton peak (δ 0.71, 12 H) and one CH_2 proton peak (δ 3.50, 8 H) for the protective groups and four CH_2 proton peaks (δ 4.04, 4.04, 4.12 and 4.19, 2 H each) and three ArH proton peaks (δ 7.42, 8.13 and 8.17, 2 H each) for the *o*-xylenyl groups. This splitting pattern is commensurate with either C_2 symmetry (*cis*-3, *trans*-2 or *trans*-3) or C_s symmetry (*cis*-1, *cis*-2,

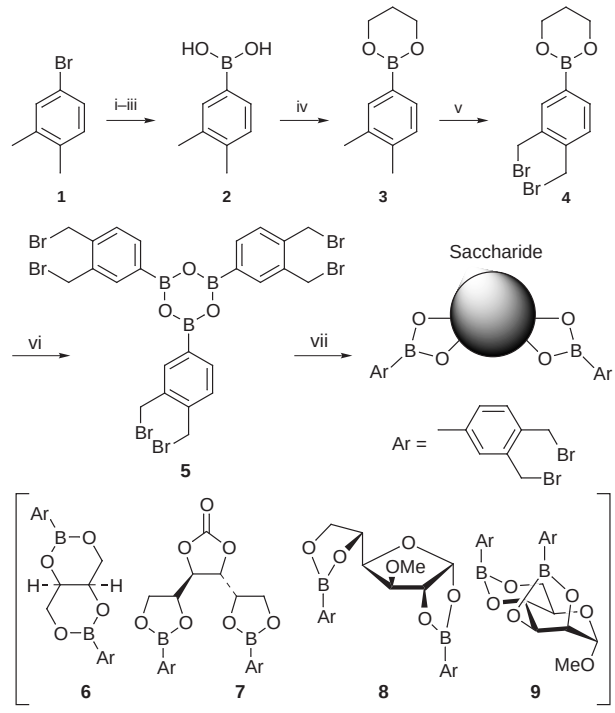

Scheme 1 *Reagent and conditions*: i, Mg, THF; ii, $B(OMe)_3$, −60 °C; iii, H_2SO_4, 69% from **1**; iv, propane-1,3-diol, toluene, reflux, 71%; v, NBS, CCl_4, reflux, 50%; vi, HCl, THF, 90%; vii, saccharide, toluene, reflux, 82% for **6**, 95% for **7**, 76% for **8** and 60% for **9**

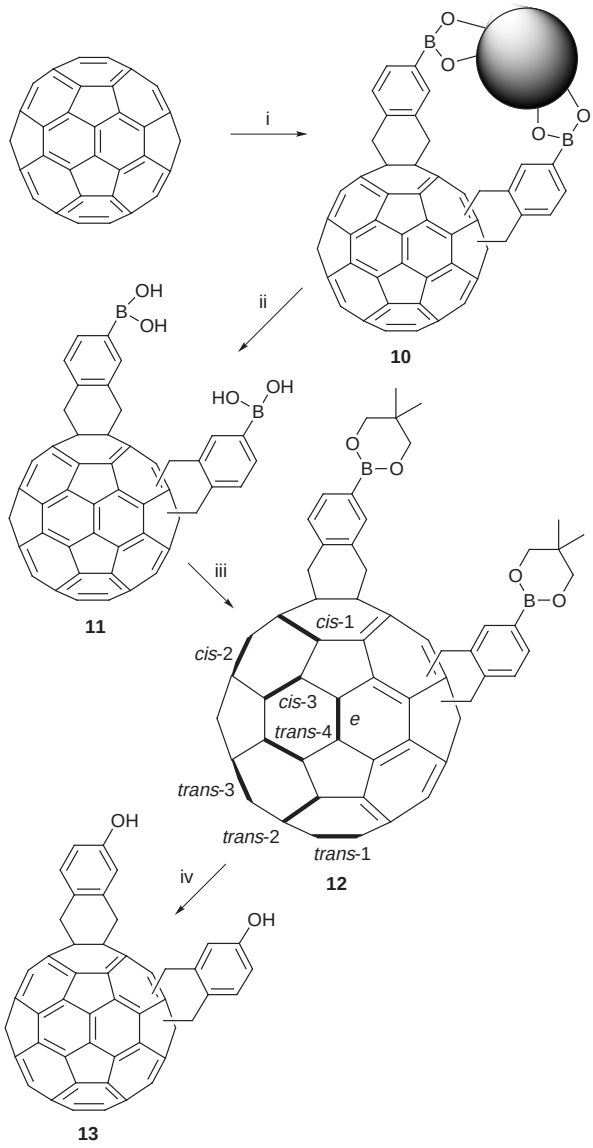

Scheme 2 *Reagent and conditions*: i, **6**–**9**, KI, 18-crown-6, toluene, reflux; ii, HCl, THF: iii, 2,2-dimethylpropane-1,3-diol, toluene, reflux, 49% from **6**, 53% from **7**, 58% from **8** and 52% from **9**; iv, 30% H_2O_2, AcOH, THF, 56%

Table 1 Results of HPLC analysis of **12**

Peak number	Retention time/min	Product (%)[a]			
		6	**7**	**8**	**9**
1	39.6	1.5	4.2	0.2	5.6
2	41.5	2.3	4.3	1.5	7.5
3	43.0	5.4	3.4	3.0	11.4
4	46.5	7.8	10.5	3.7	15.2
5	49.7	12.3	7.7	3.6	23.7
6	51.2	11.3	14.2	72.5	15.6
7	52.9	47.3	0	0	0
8	54.1	12.1	55.7	15.5	21.0

[a] Computed from the peak area obtained by the chromatogram followed at 350 nm.

trans-1 or *trans*-4).[4–6,11] Among them, the size of the saccharide used as the template molecule is too small or too large to give *cis*-1, *trans*-1, *trans*-2 and *trans*-3: therefore, these isomers can be excluded. The residual, possible isomers are *cis*-2, *cis*-3 and *trans*-4.

In absorption spectroscopy (CH_2Cl_2, 25 °C) compound **12a** gave two absorption maxima at 643 and 708 nm. Since these absorption maxima are observable only for *cis*-3 and *trans*-4,[11,12] *cis*-2 can be excluded. The solubility of **12a** into deuterated NMR solvents was not high enough to obtain a satisfactory ^{13}C NMR spectrum, so we converted **12a** to **13a** (Nishimura's phenol adduct[6]) *via* treatment with H_2O_2 (56% yield). Compound **13a** did not coincide either with *cis*-2 or with *cis*-3, as reported by Nishimura.[6] Furthermore, the ^{13}C NMR spectrum (75.5 MHz, [$^2H_6$]DMSO, 120 °C) gave 30 sp^2 carbon peaks and 2 sp^3 carbon peaks for the [60]fullerene moiety. This splitting pattern is commensurate with C_s-symmetrical *cis*-2 and *trans*-4.[11,12] Thus **12a** can be identified as *trans*-4.[13]

As a preliminary study to test whether **11a** retains the memory for 3-*O*-methyl-D-glucose, we carried out solid (excess 3-*O*-methyl-D-glucose)–liquid ([$^2H_8$]THF) extraction with **11a**. Judging from the fact that the ratio of the integral intensity between 1-H in the complexed 3-*O*-methyl-D-glucose and ArH in the complexed **11a** is 1 : 6, one can conclude that **11a** can quantitatively bind the templated saccharide.

In conclusion, the present study has demonstrated that saccharides are useful as potential templates to regioselectively introduce two boronic acid groups into [60]fullerene.

Notes and References

† E-mail: seijitcm@mbox.nc.kyushu-u.ac.jp

1 For a comprehensive review, see G. Wulff, *Angew. Chem., Int. Ed. Engl.*, 1995, **34**, 1812.
2 G. Wulff and S. Schauhoff, *J. Org. Chem.*, 1991, **56**, 395 and references cited therein.
3 C. Yu and K. Mosbach, *J. Org. Chem.*, 1997, **62**, 4057 and references cited therein.
4 E. Nakamura, H. Isobe, H. Tokuyama and M. Sawamura, *Chem. Commun.*, 1996, 1747; H. Isobe, H. Tokuyama, M. Sawamura and E. Nakamura, *J. Org. Chem.*, 1997, **62**, 5034.
5 J.-F. Nierengarten, V. Gramlich, F. Cardullo and F. Diederich, *Angew. Chem., Int. Ed. Engl.*, 1996, **35**, 2101; J.-F. Nierengarten, T. Habicher, R. Kessinger, F. Cardullo, F. Diederich and V. Gramlich, *Helv. Chim. Acta*, 1997, **80**, 2238.
6 M. Taki, S. Sugita, Y. Nakamura, E. Kasashima, E. Yashima, Y. Okamoto and J. Nishimura, *J. Am. Chem. Soc.*, 1997, **119**, 926.
7 For comprehensive reviews of saccharide–boronic acid interactions, see T. D. James, K. R. A. S. Sandanayake and S. Shinkai, *Angew. Chem., Int. Ed. Engl.*, 1996, **35**, 1910; T. D. James, P. Linnane and S. Shinkai, *Chem. Commun.*, 1996, 281.
8 T. D. James, H. Shinmori and S. Shinkai, *Chem. Commun.*, 1997, 71.
9 From extensive ^1H and ^{11}B NMR spectroscopic and X-ray crystallographic studies it was found that in **6** boronic acids react with 1,3-diols to form two six-membered rings, and in **8** the saccharide moiety adopts the furanose form. These results will be discussed in detail elsewhere.
10 M. Takeuchi, Y. Chin, T. Imada and S. Shinkai, *Chem. Commun.*, 1996, 1867.
11 A. Hirsch, I. Lamparth and H. R. Karfunkel, *Angew. Chem., Int. Ed. Engl.*, 1994, **33**, 437.
12 G. Schick, A. Hirsch, H. Mauser and T. Clark, *Chem. Eur. J.*, 1996, **2**, 935; F. Djojo, A. Herzog, I. Lamparth, F. Hampel and A. Hirsch, *Chem. Eur. J.*, 1996, **2**, 1537.
13 In **12a**, three isomers (in–in, out–in and out–out) are available, in principle, owing to the direction of the $B(OCH_2CMe_2CH_2O)$ group in the benzene ring. Judging from the size of the template saccharide and the splitting pattern of the ^1H NMR spectrum, the out–in and out–out isomers can be excluded. Thus, **12a** isolated here is the in–in isomer. For an explanation of the concept of in–in, out–in and out–out isomers, see refs. 4–6.

Received in Cambridge, UK, 27th February 1998; 8/01648H

Circular polarization of photochemiluminescence from the photoisomer of a conformationally fixed 2,11-diaza[3.3](9,10)anthracenoparacyclophane derivative‡

Hideki Okamoto,*[a]† Harry P. J. M. Dekkers,[b] Kyosuke Satake[a] and Masaru Kimura[a]

[a] *Department of Chemistry, Faculty of Science, Okayama University, Tsushima-Naka 3-1-1, Okayama, 700-8530, Japan*
[b] *Leiden Institute of Chemistry, Gorlaeus Laboratories, Leiden University, PO Box 9502, 2300, RA Leiden, The Netherlands*

The conformation of 2,11-diaza[3.3](9,10)anthracenoparacyclophane 1, which underwent photointerconversion with isomer 2, was fixed with the aid of a chiral camphanic auxiliary to have molecular chirality, and the photochemiluminescence from the modified 2a was circularly polarized reflecting the chirality of the emitting state.

2,11-Diaza[3.3](9,10)anthracenoparacyclophane **1** has been developed as a photochromic material which undergoes photointerconversion with isomer **2**.[1] In the photochromic reaction, we recently found that photocycloreversion of **2** to **1** was chemiluminescent, attributable to the formation of excited **1*** as in the case of non-bridged cycloadducts between benzene and anthracene (Scheme 1).[2,3] Such chemiluminescent photoreactions are attractive as a probe to analyze the potential surface of excited states and as an optical data storage system of read-out by fluorescence.[2–4] We have attempted to introduce a chiral source into the cyclophane system since the chirality may cause circular polarization of both the fluorescence of **1** and the photochemiluminescence of **2** as well as photocontrol of chiroptical properties. Circular polarization of luminescence (CPL) is a useful probe to obtain structural and electronic information in an excited state,[5] and steric and electronic features of the emitting state of the photochemiluminescence may be analyzed by CPL. Here, we report a simple method to introduce molecular chirality into the cyclophane system **1** by modification with a chiral auxiliary, and CPL from the modified **1a** and **2a**.

The cyclophanes **1a** and **1b** were prepared by acylation of the amino derivative **1d** with commercially available (1*S*)-(−)-camphanic chloride and (1*S*)-(+)-10-camphorsulfonyl chloride, respectively. The modified cyclophane **1a** showed circular dichromism (CD) in its absorption bands suggesting the side-chains were fixed in a special conformation inducing molecular chirality (Fig. 1) while **1b** indicated CD only arising from the carbonyl chromophore in the auxiliary camphorsulfonyl groups. As the chiral center in **1b** was separated by one extra methylene group than in **1a**, the camphorsulfonyl group may not restrict the side-chain conformation in **1b**. The conformation of **1a** was analyzed by NOESY spectroscopy. Fig. 2 shows the

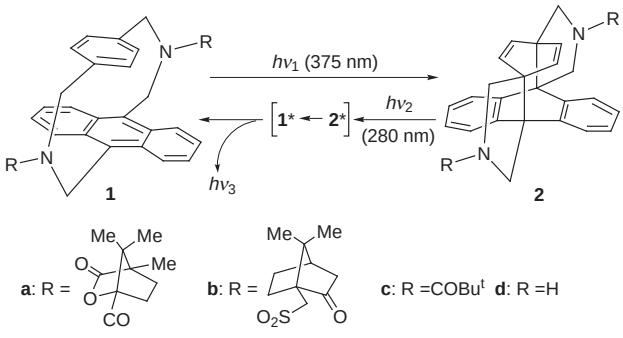

Scheme 1

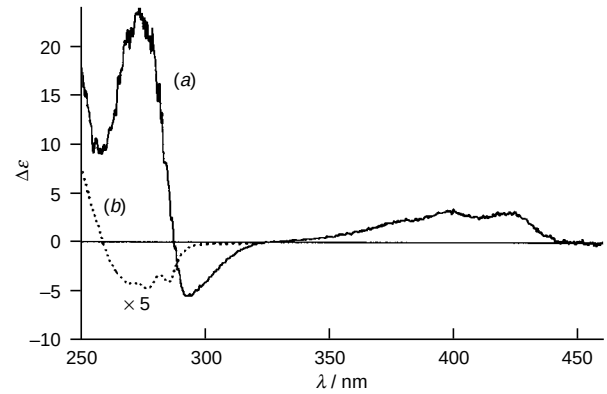

Fig. 1 CD spectra of (*a*) **1a** and (*b*) **2a** in CH_2Cl_2

NOESY spectrum of **1a** in which four cross-peaks important in determining the conformation of **1a** appeared and are correlated by dotted lines. From the spectrum, it is evident that the 7′-Me[1] proton was located close to aromatic protons H_e, H_g and H_j, and

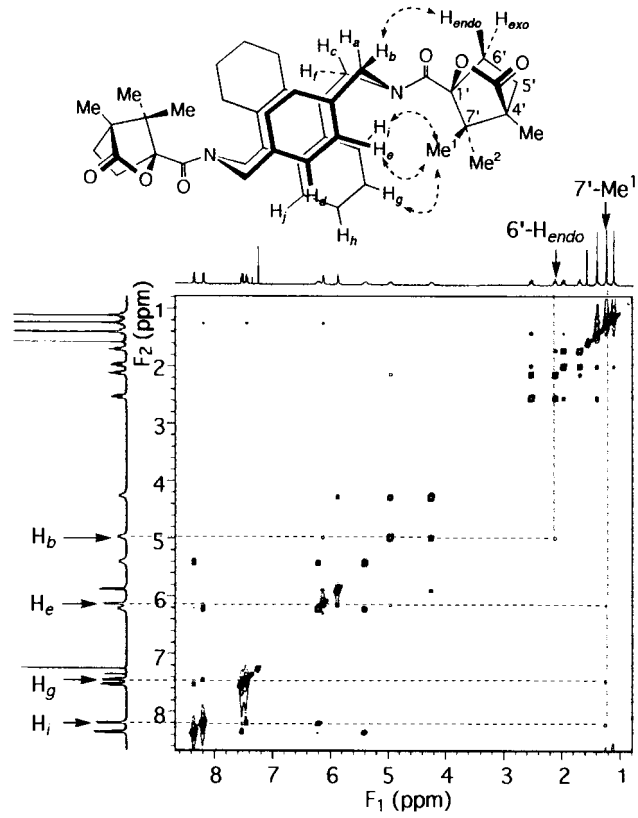

Fig. 2 NOESY spectrum of **1a** in $CDCl_3$ (500 MHz)

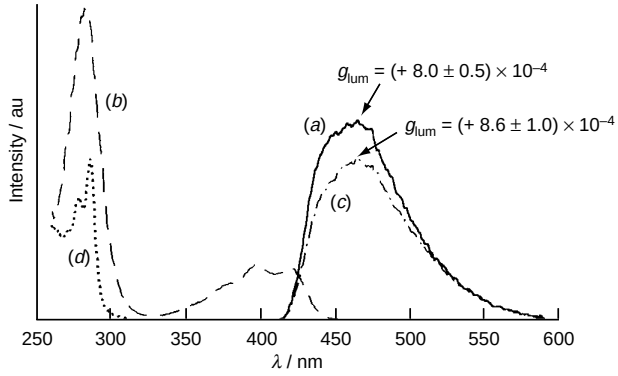

Fig. 3. Fluorescence spectra of **1a** and **2a** (in CH_2Cl_2); (*a*) Emission and (*b*) the excitation spectra of **1a**; (*c*) Photochemiluminescence and (*d*) the action spectra of **2a**. The observed g_{lum} values are shown at the detection wavelength (460 nm).

that 6′-H_{endo} was fixed near by one of the bridge methylene protons H_b. Empirical force field (MM2)[6] calculation showed that **1a** adopted the most stable C_2-symmetrical conformer consistent with the NOESY results .

The cyclophane **1a** underwent photointerconversion with **2a** and a change in CD was detected (Fig. 1). Cyclophane **1a** showed a positive Cotton effect in the longer wavelength absorption band, while **2a** showed a negative Cotton effect in its absorption band centered at 280 nm. The specific rotation of **1a** was $[\alpha]_D^{23}$ ($CHCl_3$) +192° and that of **2a** was $[\alpha]_D^{23}$ ($CHCl_3$) −1.4°.

Compound **2a** underwent chemiluminescent photocycloreversion providing excited **1a*** as in the case of **2** which underwent no conformational restriction such as **2c**.[2] The photochemiluminescence spectrum was the same in profile with that of fluorescence of **1a** (Fig. 3). Fluorescence assignable to **2a** itself was not detected.[3] The action spectrum for the emission of **2a** was identical with the absorption of **2a** showing no contamination with **1a** during the measurement. The quantum yields of fluorescence of **1a** and the photochemiluminescence of **2a** were 0.33 and 0.23, respectively. The decay of both emissions was analyzed as a dual exponential curve and the lifetimes were 7.8 ns (26%) and 18.4 ns (74%) for **1a**, and 6.9 ns (28%) and 16.6 ns (72%) for **2a**.

The fluorescence of **1a** was circular polarized as expected from its structural features. The dissymmetry factor for the fluorescence [$g_{lum} = 2(I_L - I_R)/(I_L + I_R)$; I_L and I_R are intensity of left and right circularly polarized emission, respectively] of **1a** was g_{lum} (+8.0 ± 0.5) × 10^{-4} (λ_{em} = 460 nm, λ_{ex} = 375 nm, in CH_2Cl_2). The CPL for the photochemiluminescence of **2a** was also detected and its g_{lum} value was the same as that of fluorescence of **1a** within experimental error, g_{lum} = (+8.6 ± 1.0) × 10^{-4}(λ_{em} = 460 nm, λ_{ex} = 280 nm in CH_2Cl_2).§ This is the first observation of circular polarization of photochemiluminescence which may enable examination of structural change in an excited state during an adiabatic reaction. The dissymmetry factor for the absorption [$g_{abs} = 2(\varepsilon_L - \varepsilon_R)/(\varepsilon_L + \varepsilon_R)$; ε_L and ε_R are molar absorptivity for left and right circular polarized light, respectively] of **1a** was +6.4× 10^{-4} at 375 nm (in CH_2Cl_2). In the case of **1a**, overlap between fluorescence and long wavelength absorption bands suggested that the fluorescent process was the reverse transition of the absorption [*cf.* Fig. 3, curves (a) and (b)], and the g_{abs} was almost same as g_{lum}. These suggest that the structure of **1a** did not differ largely between the ground and the emitting states. Differently, for **2a**, g_{abs} was −6.3 × 10^{-4} at 280 nm (in CH_2Cl_2) showing opposite sign compared with the g_{lum} of the photochemiluminescence. In the case of **2a**, as the structures of the light absorbing and the emitting species were quite different from each other, the changes of electronic and steric properties during the photoreaction caused inversion of sign between g_{abs} and g_{lum}.

In summary, modification with a chiral camphanic auxiliary induced molecular chirality of the cyclophane **1a** and the photoisomer **2a**. The photoexcited **2a*** rapidly reverted to **1a*** and recalled the electronic and steric features of **1a*** which was the same as those generated on excitation of **1a**.

The authors are grateful to Professor E. W. Meijer of Eindhoven University of Technology for correspondence about CPL and encouragement. The present work was partly supported by the Okayama Foundation for Science and Technology.

Notes and References

†E-mail: hokamoto@cc.okayama-u.ac.jp

‡ Here photochemiluminescence denotes luminescence which is emitted from an electronically excited product formed by an adiabatic reaction of an excited starting molecule ($h\nu_3$ in Scheme 1).

§ In the CPL measurement on **2a**, both the starting **2a** and the photoproduct **1a** were capable of absorbing the excitation light (280 nm), however after the measurement only **2a** was detected in the sample. Thus in the photostationary state **2a** existed preferentially to **1a** and the present CPL observed in photochemiluminescence of **2a** was regarded as that responsible mainly to **2a**.

1 M. Usui, T. Nishiwaki, K. Anda and M. Hida, *Chem. Lett.*, **1984**, 1561; M. Usui, T. Nishikawa, K. Anda and M. Hida, *Nippon Kagaku.*, **1988**, 273.
2 H. Okamoto, K. Satake and M. Kimura, *Chem. Lett.*, **1997**, 873.
3 N. C. Yang, M. J. Chen and P. Chen, *J. Am. Chem. Soc.*, 1984, **106,** 7310; N. C. Yang, M. J. Chen and K. T. Mak, *J. Am. Chem. Soc.*, 1982, **104**, 853; M. Kimura, H. Okamoto, H. Kura, A. Okazaki, E. Nagayasu, K. Satake, S. Morosawa, M. Fukazawa, H. Abdel-Halim and D. O. Cowan, *J. Org. Chem.*, 1988, **53**, 3908; M. Kimura, H. Okamoto and S. Kashino, *Bull. Chem. Soc. Jpn.*, 1994, **67**, 2203; H. Okamoto, M. Kimura, K. Satake and S. Morosawa, *Bull. Chem. Soc. Jpn.*, 1993, **66**, 2436; A. Albini and E. Fasani, *J. Am. Chem. Soc.*, 1988, **110**, 7760.
4 T. Okada, K. Kida and N. Mataga, *Chem. Phys. Lett.*, 1982, **88**, 157.
5 H. P. J. M. Dekkers, in *Circular Dichromism: Principles and Applications*, eds. K. Nakanishi, N. Berova and R. W. Woody, VCH, New York, 1994, p. 121.
6 N. L. Allinger, *J. Am. Chem. Soc.*, 1977, **99**, 8127.

Received in Cambridge, UK, 16th February 1998; 8/01296B

Reaction behaviour of a complex containing a tungsten phosphorus triple bond with σ-acceptor compounds of group 13

Manfred Scheer,*[a]† Jan Müller,[a] Gerhard Baum[a] and Marco Häser[b]

[a] *Institute of Inorganic Chemistry, University of Karlsruhe, D-76128 Karlsruhe, Germany*
[b] *Institute of Physical Chemistry, University of Karlsruhe, D-76128 Karlsruhe, Germany*

[LW≡P→$GaCl_3$] 5 [L = $N(CH_2CH_2NSiMe_3)_3$] is prepared by treatment of [LW≡P] with $(GaCl_3)_2$; decomposition of 5 in CH_2Cl_2 affords dimerisation under Me_3SiCl elimination to give a cationic W_2P_2 tetrahedral complex 6; both complexes are structurally characterised.

In 1995 Cummins[1] and Schrock[2] and their coworkers succeeded in the synthesis and the first structural characterisation of complexes **1** and **2**, respectively, containing a metal phosphorus triple bond. Our synthetic goal, however, has been directed towards the alkoxide substituted complexes **3** where the phosphido ligand coordinates additionally to a metal pentacarbonyl fragment.[3] The $^1J_{WP}$ coupling constant was observed to be 554 (**3a**) and 536 Hz (**3b**) for the triple bond and appeared to be in contradiction with the 138 Hz found for the W complex **2a**. To shed light onto this problem we decided to synthesise **2a** (M′ = W) *via* the reaction of [WCl(L)] [L = $N(CH_2CH_2NSiMe_3)_3$] with $Li[P(SiMe_3)_2]$. Subsequent reaction with $[M'(CO)_5(thf)]$ leads to the *trans*-substituted complexes **4**.[4] ^{31}P NMR data (**4a**: δ 679.8, $^1J_{WP}$ 426 Hz; **4b**: δ 728.1, $^1J_{WP}$ 413 Hz) combined with theoretical calculations reveal that the linear coordination of a complex fragment to the phosphido atom is responsible for a dramatic increase of the s character of the triple bond and consequently for the increase of the coupling constant. In further studies it was of interest how coupling constant and triple bond length behave by coordination of a simple σ-acceptor group. Herein we report our results of the reaction of **2a** with group 13 Lewis acids.

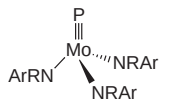

R = $C(CD_3)_2CH_3$
Ar = $C_6H_3Me_2$-3,5
1

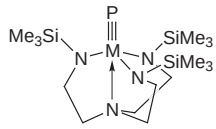

M = W(**a**), Mo(**b**)
2

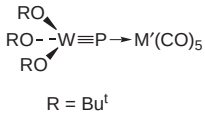

R = Bu^t
M′ = W(**a**), Cr(**b**)
3

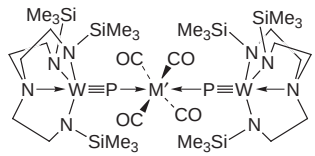

M′ = W(**a**), Cr(**b**)
4

The reaction of **2a** with $BH_3{\cdot}SMe_2$ only led to an insoluble solid. Elemental analysis did not indicate the formation of the expected adduct [LW≡P→BH_3]. Even following the reaction by ^{31}P NMR only showed that the starting material disappeared but no new signal could be detected. In the reaction of **2a** with $BF_3{\cdot}OEt_2$ in CH_2Cl_2, however, a ^{31}P NMR signal at δ 607 ($^1J_{WP}$ 478 Hz) could be observed for a short time. Then the reaction mixture became black and insoluble black material precipitated.

Reaction of **2a** with the dimer $[GaCl_3]_2$ in a 2 : 1 ratio in toluene led to the isolation of a yellow crystalline compound **5**, which is sparingly soluble in toluene, thf and CH_2Cl_2.‡ The $^{31}P\{^1H\}$ NMR spectrum of **5** reveals one signal at δ 366 bearing one pair of satellites with $^1J_{WP}$ = 712 Hz. The high field shift as well as the considerable increase of the coupling constant is consistent with those found in **4.** However, the observed coupling constant is one of the largest for these triple bond systems. Almost identical NMR data were detected in the structurally uncharacterised complex $[LW{=}PMe]^+$-$[OTf]^-$ (δ 339, $^1J_{WP}$ = 748 Hz) synthesised by Schrock and coworkers.[5]

The molecular structure of **5** was established by a single-crystal X-ray diffraction study.§ The main feature of the molecular structure of **5** is the entirely linear arrangement of the N_{ax}–W–P–Ga axis (Fig. 1). The Cl atoms of the $GaCl_3$ group are slightly disordered. The orientations of the Cl atoms are slightly eclipsed to the W–N(2) bonds, but staggered to the N(1)–C(1) bond. The W≡P bonding distance is 2.168(4) Å which is only slightly longer than the bond length found in **2a** (2.162 Å). This indicates the replacement of almost the same amount of phosphorus 3p σ-contribution to the W≡P bond in **2a** by 3s-orbital contribution of the former lone pair of the phosphorus, produced through the coordination to a σ-acceptor such as $GaCl_3$. This finds further support from the dramatic increase of $^1J_{WP}$. Owing to the remarkable backbonding ability of the W≡P moiety to the W^0 centre the triple bond length increases from 2.162(4) in **2a** to 2.202(2) Å in **4a**.[4] The most significant difference in bonding distances in comparison to **2a** occurs for the N_{ax}–W bond which is shortened by 0.10 Å. This is probably

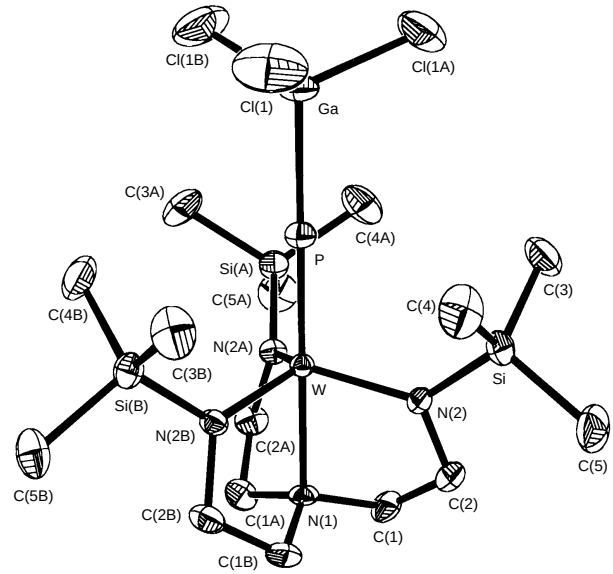

Fig. 1 Molecular structure of **5** (only one position of the Cl atoms is drawn for clarity). Selected bond lengths (Å) and angles (°): W–P 2.168(4), P–Ga 2.335(4), W–N(1) 2.248(10), W–N(2) 1.967(3), Ga–Cl(1) 2.159(11), Ga–Cl(2) 2.186(12), N(1)–W–P 180.0, W–P–Ga 180.0, N(1)–W–N(2) 77.52(8).

due to a reduced electron density at the metal core which results in a higher acceptor ability of the W atom. The Ga–P distance is 2.335(4) Å. This is consistent for Ga–P single bonds as found in *e.g.* $GaCl_3(PMe_3)$ (2.353 Å).[6]

The structural features of **5** were modelled using the B-P86/SVP density functional approximation.[7] The structural optimisation resulted in a molecular shape best described in terms of C_3 symmetry. There is good agreement between the calculated and experimentally observed structural parameters [calc.: d(W≡P) = 2.186 Å, d(W–N_{eq}) = 2.007 Å; exptl.: d(P–Ga) = 2.335(4) Å, d(W≡P) = 2.168(4) Å, d(W–N_{eq}) = 1.967(3) Å]. The only exceptions are the calculated distances for P–Ga and W–N_{ax}, which are longer by 0.1 and 0.2 Å, respectively. For the latter bond, the same effect was found in the calculated and experimental structures of **2a** and **4a**.[4]

Electronic energies, calculated with the B-P86/SVP (B3-LYP/ SVP) approximation, show reaction of **2a** with 0.5 $(GaCl_3)_2$ to be exothermic at −68 (−61) kJ mol^{-1}. The same methods calculated the energies for the reaction of **2a** with BH_3·thf to be −22 (−2) kJ mol^{-1}.[4] In accordance with the experimental observation the formation of a BH_3 adduct seems to be less favoured in comparison with the preferred formation of the $GaCl_3$ adduct **5**.¶

However, a solution of **5** in CH_2Cl_2 appears to be unstable. After a few days the yellow–brown colour of the solution disappears. Red, star shaped crystals of **6** and an amorphous solid precipitated. According to a $^{31}P\{^1H\}$ NMR study the CH_2Cl_2 solution contains no detectable amounts of phosphorus. The red crystalline compound was examined by X-ray diffraction,§ but only a weak data set was obtained. However, it was possible to solve the structure to a reasonable degree. The structure revealed a tetrahedral $[W_2P_2]^+$ moiety, where the W atoms are coordinated by two tren type ligands (Fig. 2). These are linked together by two $GaCl_2$ groups which are in the former position of the $SiMe_3$ moieties. Furthermore, all $SiMe_3$ groups are removed and $[GaCl_4]^-$ and Cl^- occur as counter ions. The W–P bonds are now 2.462(12) and 2.473(10) Å and the W–W bond is 2.585(2) Å. A related nitrido bridged tungsten dimer is $[W_2(\eta^5\text{-}C_5H_4Pr^i)Cl_2(\mu\text{-}NR)(\mu\text{-}C_2Et_2)]$ with an analogous W–W distance of 2.5923(5) Å.[8] Obviously, in the first step of the conversion of **5** the Si–N bond is cleaved to form the thermodynamically stable $SiClMe_3$. The replacement by $GaCl_2$ moieties leads to a rearrangement resulting in the formation of the W_2P_2 complex **6**.

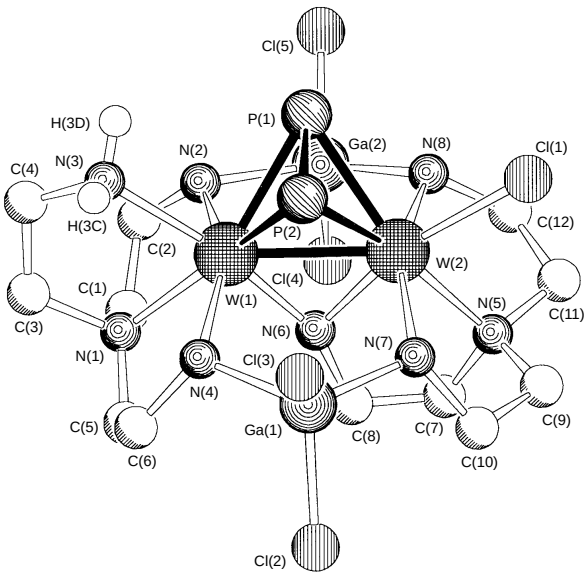

Fig. 2 Molecular structure of **6**. Selected bond lengths (Å): P(1)–P(2) 2.07(2), W(1)–P(1) 2.461(12), W(1)–P(2) 2.473(10), W(2)–P(1) 2.483(11), W(2)–P(2) 2.498(9); Cl(1)–W(2) 2.464(12), W(1)–W(2) 2.585(2), W(1)–N(6) 1.97(3), W(2)–N(6) 2.00(3).

The transformation of **5** into **6** could explain the instability of complexes of the type $[LW{\equiv}P{\rightarrow}EX_3]$ (E = B, Ga; X = H, F, Cl). Loss of $SiClMe_3$ or $SiHMe_3$ decreases the steric protection of the W≡P triple bond which results in arbitrary formation of higher aggregates of unknown composition. Deliberate attempts to remove $SiMe_3$ groups may activate the [LW≡P] complex with their preferred end-on reactivity to undergo side-on reactions. This is a goal for further investigations.

The authors thank the Deutsche Forschungsgemeinschaft and the Fonds der Chemischen Industrie for financial support.

Notes and References

† E-mail: mascheer@achibm6.chemie.uni-karlsruhe.de

‡ *Spectroscopic data* for **5** ([$^2H_8$]thf): $^{31}P\{^1H\}$ NMR, δ 366, J_{WP} 712; ^1H NMR, δ 3.91 (t, 6 H, CH_2), 2.46 (t, 6 H, CH_2), 0.45 (s, 27 H, CH_3); $^{13}C\{^1H\}$ NMR, δ 55.16 (s, CH_2), 52.36 (s, CH_2), 5.38 (s, CH_3); correct elemental analysis.

§ *Crystal structure analysis*: **5**: $C_{15}H_{39}Cl_3GaN_4PSi_3W$, M = 750.66, trigonal, space group $P31c$, $a = b$ = 11.867(2), c = 12.207(2) Å, Z = 2, U = 1488.7(4) Å^3, D_c = 1.675 Mg m^{-3}, μ(Mo-Kα) = 52.9 cm^{-1}, F(000) = 740, T = 200(2) K. A total of 4631 reflections with $7.76 \leqslant 2\theta \leqslant 51.42°$ were collected on a STOE IPDS (image plate detector system) with Mo-Kα radiation (0.710 69 Å), of which 1811 were independent (R_{int} = 0.0364). The 1749 reflections with $I \geqslant 2\sigma(I)$ were used in the full least squares refinement. The structure was solved by direct methods (SHELXS-86) and standard Fourier techniques (SHELXL-93). Full matrix least squares refinement of the thermal parameters (anisotropic for all atoms except hydrogen) led to convergence with final residuals of R_1 = 0.0189 and wR_2 = 0.0461 and GOF = 1.078 for 110 variables. Residual electron density was found to be between 0.925 and −0.441 e Å^{-3}. **6**: $4[C_{45}H_{95}Cl_5Ga_2N_8P_2W_2][GaCl_4]Cl_3{\cdot}3CH_2Cl_2$, M = 4681.56, tetragonal, space group $I\bar{4}$, $a = b$ = 22.059(3), c = 13.185(3) Å, U = 6416(2) Å^3, Z = 2 (for four molecules of the W_2P_2 complex), D_c = 2.421 Mg m^{-3}, F(000) = 4364, μ(Mo-Kα) = 98.24 cm^{-1}, 225 parameters, crystal size 0.08×0.04×0.02 mm, T = 200(2) K. A total of 6756 reflections with $3.7 < \theta < 45°$ were collected on a STOE IPDS with Mo-Kα radiation (0.710 69 Å), 3757 of them were independent (R_{int} = 0.1825). 2867 reflections with $I \geqslant 2\sigma(I)$ were used in the full least squares refinement. The structure was solved as above. Full matrix least squares refinement of the thermal parameters (anisotropic for all W, Ga, P and Cl atoms except those of the solvent CH_2Cl_2) led to convergence with final residuals of wR_2 = 0.2245 for all reflections, corresponding to a conventional R_1 = 0.0952 for the observed F_o data. Residual electron density was found to be between 2.839 and −1.718 e Å^{-3}. CCDC 182/813.

¶ The reaction between **2a** and BH_3·thf presumably leads to elimination of $HSiMe_3$.

1 C. E. Laplaza, W. M. Davis and C. C. Cummins, *Angew. Chem.*, 1995, **107**, 2181; *Angew. Chem., Int. Ed. Engl.*, 1995, **34**, 2042.
2 N. C. Zanetti, R. R. Schrock and W. M. Davis, *Angew. Chem.*, 1995, **107**, 2184; *Angew. Chem., Int. Ed. Engl.*, 1995, **34**, 2044.
3 M. Scheer, K. Schuster, T. A. Budzichowski and M. H. Chisholm, W. E. Streib, *J. Chem. Soc., Chem. Commun.*, 1995, 1671.
4 M. Scheer, J. Müller and M. Häser, *Angew. Chem.*, 1996, **108**, 2637; *Angew. Chem., Int. Ed. Engl.*, 1996, **35**, 2492.
5 N. C. Mösch-Zanetti, R. R. Schrock, W. M. Davis, K. Wanninger, S. W. Seidel and M. B. O'Donoghue, *J. Am. Chem. Soc.*, 1997, **119**, 11037.
6 J. C. Charter, G. Jugie, R. Enjalbert and J. Galy, *Inorg. Chem.*, 1978, **7**, 1248.
7 Structure optimizations were performed using the TURBOMOLE set of programs with the RI-*J* approximation (K. Eichkorn, O. Treutler, H. Öhm, M. Häser and R. Ahlrichs, *Chem. Phys. Lett.*, 1995, **242**, 652). For definition of the B-P86 density functional, see: A. D. Becke, *Phys. Rev. A*, 1988, 38, 3098; J. P. Perdew, *Phys. Rev. B*, 1986, **33**, 8822; 1986, **34**, 7046. The acronym SVP refers to TURBOMOLE split valence basis sets, augmented by a shell of polarization functions, see: A. Schäfer, H. Horn and R. Ahlrichs, *J. Chem. Phys.*, 1992, **97**, 2571. Quasi-relativistic pseudopotentials were used for tungsten (D. Andrae, U. Häußermann, M. Dolg, H. Stoll and H. Preuß, *Theor. Chim. Acta*, 1990, **77**, 123; A. Bergner, M. Dolg, W. Küchle, H. Stoll and H. Preuß, *Mol. Phys.*, 1993, **80**, 1431). The corresponding SVP basis sets optimized for W by F. Weigend, K. Eichkorn and R. Ahlrichs are unpublished.
8 M. L. Green, P. C. McGowan and P. Mountford, *J. Chem. Soc., Dalton Trans.*, 1995, 1207.

Received in Cambridge, UK, 9th February 1998; 8/01136B

Hydrogenation of butane-2,3-dione with heterogeneous cinchona modified platinum catalysts: a combination of an enantioselective reaction and kinetic resolution

Martin Studer,*[a]† Victor Okafor[b] and Hans-Ulrich Blaser[a]

[a] *Scientific Services, Novartis Services AG, CH-4002 Basel, Switzerland*
[b] *University of the Witwatersrand, Department of Chemistry, Johannesburg, South Africa*

(*R*)-3-Hydroxybutan-2-one was obtained with 85–90% ee albeit in low yield by the Pt/Al_2O_3 cinchona catalyzed hydrogenation of butane-2,3-dione by a combination of enantioselective hydrogenation and kinetic resolution.

Modified heterogeneous catalysts for enantioselective hydrogenation are of interest, both from a theoretical and practical point of view.[1] Up to now only two efficient catalyst systems are known and only a few substrate types can be hydrogenated with enantioselectivities of 90% or higher. Most notable is the tartrate modified Raney-nickel catalyst with an ee of up to 98% for β-keto esters and β-diketones,[2–4] and the cinchona modified Pt catalysts for the hydrogenation of α-keto esters with 95% ee.[5] Even though some progress in expanding the scope of the latter was reported recently,[6–8] none of the new systems had an ee > 60%. Here we describe the enantioselective hydrogenation of butane-2,3-dione **1**, where we obtained (*R*)-3-hydroxybutan-2-one (*R*)-**2** in up to 90% ee by a combination of enantioselective hydrogenation and kinetic resolution using a Pt/Al_2O_3 catalyst modified with 10,11-dihydrocinchonidine (HCd).

Vermeer *et al.*[6] investigated the enantioselective hydrogenation of **1** to **2** and found an ee of 38% when using a 6.3% Pt/silica catalyst modified with cinchonidine in CH_2Cl_2 at 0 °C. We decided to re-investigate this substrate using a catalyst that gave the highest enantioselectivities so far reported for several α-keto esters (5% Pt/Al_2O_3, JMC type 94, pretreated for 2 h at 400 °C with H_2).[5] First, we investigated the effect of several reaction parameters.[9] Modifier type and concentration, as well as the solvent, had a very strong effect on the enantioselectivity, while the influence of H_2 pressure (25–135 bar) and temperature (0–25 °C) were found to be negligible. The best results were obtained with HCd in toluene (ee ≈ 50%). During the course of this investigation we noticed that at conversions > 80% the ee started to rise and the reaction did not stop at **2** but slowly continued to give the corresponding diols **3** (Scheme 1), a fact not described by Vermeer *et al.*[6]

These findings prompted us to investigate the two consecutive hydrogenation steps in more detail. The first step was carried out by hydrogenating 5 ml **1** with 50 mg catalyst, 10 mg HCd and 20 ml toluene in a 50 ml autoclave at 107 bar, stopping the reaction at the time given in Table 1. Because the reaction of **2** to **3** was considerably slower, the second step was carried out by hydrogenating the filtrate of the above described reaction mixture (after 15 min reaction time) with 125 mg catalyst and 25 mg HCd at 107 bar. Again, the reaction was stopped after the time given in Table 2, Figs. 1 and 2.

These results show that as the concentration of **2** declined, the ee of **2** increased from 50 to 85–90%, albeit with a rather low chemical yield of < 30%. We analyzed our data on the basis of the reaction network shown in Scheme 1. For the calculations we assumed that the reactions of **1** or **2** were first order in substrate and in catalyst, leading to equations of the type d[(*R*)-**2**]/dt = [cat]{k_R'[**1**] − (k_{RR}' + k_{RS}')[(*R*)-**2**]} at constant hydrogen pressure. The time dependent concentration of all species was calculated by numerically integrating these equations. The apparent rate constants k_i' at 107 bar H_2 were obtained by minimizing the difference between measured and calculated data points (least-squares, MS EXCEL 7.0 Solver subroutine). The reported k_i values are $k_i = k_i'$/[cat]. In the absence of modifier, the following values were found: $k_R = k_S = 17\ h^{-1}\ g^{-1}$, $k_{SR} = k_{RS} = 3\ h^{-1}\ g^{-1}$, $k_{RR} = k_{SS} = 4$

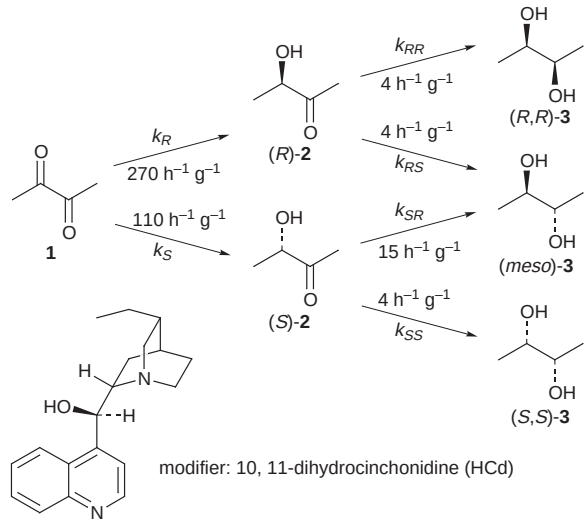

Scheme 1 Reaction scheme, modifier structure and calculated apparent rate constants

Table 1 Analytical results of the first step (**1** → **2**) [GLC area%, β-Dex 100 (Supelco 2-4301), l = 30 m, ø = 0.25 mm, 50 °C]

t/min	[**1**] (%)	[**2**] (%)	Ee of [**2**] (%)	[**3**][a] (%)
1	85	13	44	0
2	69	29	47	0
3	19	75	46	1
10	3	85	47	7
15	3	81	50	10

[a] All isomers.

Table 2 Analytical results of the second step (**2** → **3**) (GLC, as above)

t/ min	[**2**] (%)	Ee of **2** (%)	(Chiral)-[**3**] (%)	Ee [**3**] (%)	(*meso*)-[**3**] (%)	[**3**] total (%)	(chiral)-**3**: (*meso*)-**3**
0	82	50	3	29	6	9	0.5
30	45	74	16	43	31	47	0.5
60	27	85	23	54	41	64	0.6
75	20	85	28	63	44	71	0.6
90	13	86	30	60	49	79	0.6
100	9	90	33	65	50	83	0.7

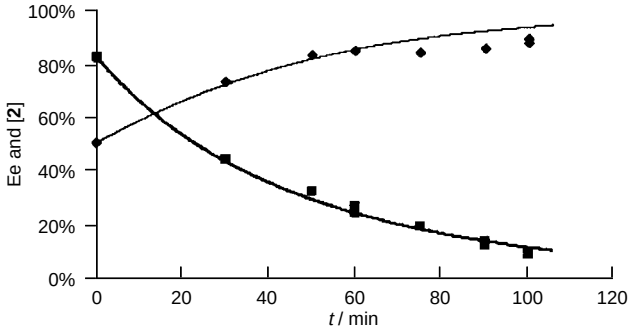

Fig. 1 Concentration and ee of **2** during step 2. (◆) ee **2** measured; (—) ee **2** calc.; (■) [**2**] measured; [**2**] calc.

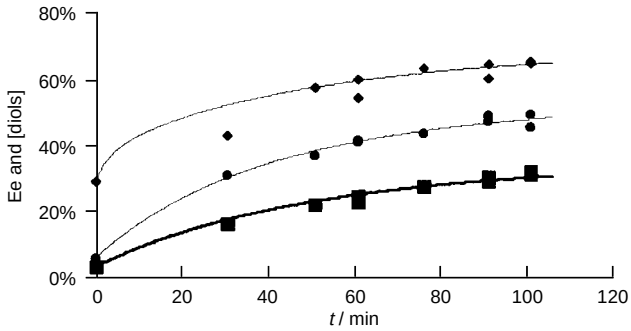

Fig. 2 Concentration and ee of **3** during step 2. (◆) ee chiral **3** measured; (—) ee chiral **3** calc.; (●) [*meso*-**3**] measured; (—) [*meso*-**3**] calc.; (■) [chiral **3**] measured; (—) [chiral **3**] calc.

h^{-1} g^{-1}. For the modified system, we obtained: k_R = 270 h^{-1} g^{-1}, k_S = 110 h^{-1} g^{-1}, k_{SR} = 15 h^{-1} g^{-1}, k_{RS} = k_{RR} = k_{SS} = 4 h^{-1} g^{-1}. Three points are important. First, our model describes the measured data well. Secondly, we confirmed the observation of Vermeer *et al.*[6] that the hydrogenation of **1** is a 'ligand accelerated' reaction as observed for several α-keto acid derivatives.[1] Unfortunately, the enantiodiscrimination is modest, leading to only 50% ee. Thirdly, the increase in the ee of **2** during the second step is due to kinetic resolution because k_{RS} is significantly larger for the modified than for unmodified catalyst, while k_{RS}, k_{RR} and k_{SS} remain virtually unchanged. This leads to a fast disappearance of (*S*)-**2**, and to a predominance of the *meso*-diol **3**. Another consequence is a gradual increase in the ee of the two chiral **3** molecules in favor of the (*R*,*R*)-**3**.

To the best of our knowledge, only two analogous investigations of the enantioselective reduction of diketones were reported. Kitamura *et al.*[10] and Fan *et al.*[11] investigated the hydrogenation of **1** using a homogeneous Ru^{II}–(*S*)-BINAP catalyst. Tai *et al.*[3] and Brunner *et al.*[12] reported results on the hydrogenation of acetylacetone, a 1,3-dione, with a heterogeneous tartrate modified nickel catalyst. The results for both systems are quite different from ours: in both cases, enrichment was found for the diols but not for the intermediate hydroxy ketone. Unfortunately, no enantioselectivities were reported for **2** in refs. 10 and 11. For (*R*,*R*)- and (*S*,*S*)-**3**, both found an ee approaching 100% in favor of (*S*,*S*)-**3**, but a rather high *meso*:chiral ratio of 3. This can be explained assuming a very high enantioselectivity for the first step ($k_S \gg k_R$), and $k_{SR} \cong 3k_{SS}$. Similar to our results, Tai *et al.* found a modest ee of 74% in the first step with acetylacetone as substrate.[3] However, when 70% of the corresponding hydroxy ketone was converted, they obtained an ee of 98% for the chiral diols with the (*R*,*R*)-diol in excess (and only 8% of the *meso* form). They showed that this was due to a high k_{RR} value. The major difference between the two heterogeneous systems is that in the case of the 1,3-dione, the diastereoselective reaction of the major intermediate is faster, leading to enriched diol, whereas in our case the minor intermediate reacts preferentially, leading to an enriched hydroxyketone.

V. O. thanks the Foundation for Research Development, South Africa, and Andrew W. Mellon Foundation, USA, for financial support.

Notes and References

† E-mail: martin.studer@sn.novartis.com

1 H. U. Blaser, H. P. Jalett, M. Müller and M. Studer, *Catal. Today*, 1997, **37**, 441.
2 S. Nakagawa, T. Sugimura and A. Tai, *Chem. Lett.*, 1997, 589.
3 A. Tai, K. Ito and T. Harada, *Bull. Chem. Soc. Jpn.*, 1981, **54**, 223.
4 A. Tai, T. Kikukawa, T. Sugimura, Y. Inoue, S. Abe, T. Osawa, S. Fujii and T. Harada, *Bull. Chem. Soc. Jpn.*, 1994, **67**, 2473.
5 H. U. Blaser, H. P. Jalett and J. Wiehl, *J. Mol. Catal.*, 1991, **68**, 215.
6 W. A. H. Vermeer, A. Fulford, P. Johnston and P. B. Wells, *J. Chem. Soc., Chem. Commun.*, 1993, 1053.
7 T. Mallat, M. Bodmer and A. Baiker, *Catal. Lett.*, 1997, **44**, 95.
8 G. Z. Wang, T. Mallat and A. Baiker, *Tetrahedron: Asymmetry*, 1997, **8**, 2133.
9 V. Okafor, H.-U. Blaser and M. Studer, unpublished results.
10 M. Kitamura, T. Ohkuma, S.Inoue, N. Sayo, H. Kumobayashi, S. Akutagawa, T. Ohta, H. Takaya and R. Noyori, *J. Am. Chem. Soc.*, 1988, **110**, 629.
11 Q.-h. Fan, C.-h. Yeung and A. S. C. Chan, *Tetrahedron: Asymmetry*, 1997, **8**, 4041.
12 H. Brunner, T. Amberger and J. Wiehl, *Bull. Soc. Chem. Belg.*, 1991, **100**, 571.

Received in Cambridge, UK, 18th February 1998; 8/01390J

Typeset and printed by Black Bear Press Limited, Cambridge, England

ChemComm
FEATURE ARTICLE

Precious metal polymers: platinum or gold atoms in the backbone

R. J. Puddephatt

Department of Chemistry, The University of Western Ontario, London, Canada N6A 5B7

The synthesis and characterisation of oligomers and polymers containing gold or platinum atoms in the backbone are reported. The polymers range in structure from the conjugated, rigid-rod type containing linear gold(I) centres to hyperbranched or dendrimeric materials containing octahedral platinum(IV) centres.

Introduction

This article gives a personal account of the synthesis and characterization of some new types of oligomers and polymers with either platinum or gold atoms in the chain backbone. These form a small part of the more general field of metal-containing polymers, which are of interest since they might have unusual optical or electrical properties or they might be useful as precursors to other materials or as catalyst precursors. There are several known types of linear-chain polynuclear coordination complexes containing platinum or gold, including the stacked, one dimensional conductors or semiconductors $K_2Pt(CN)_4Br_{0.30}\cdot 3H_2O$,[1] $[Pt(NH_2Et)_4][PtCl_2(NH_2Et)_4]Cl_4\cdot 4H_2O$ and $K_4[Pt_2(P_2O_5H_2)_4X]\cdot nH_2O$ (X = Cl, Br, I),[2] and the simple halogen-bridged gold(I) halides.[3] More recently, rigid rod polymers such as $[Pt(PBu_3)_2(\mu\text{-}C{\equiv}C{-}R{-}C{\equiv}C{-})_n$ **1** (R = aryl spacer group) have been reported.[4] The dialkynyl ligands, and related but neutral diisocyanide ligands, are particularly well suited to the design of rigid-rod polymers and examples are now known with Pt–Pt bonds and even Pt_3 cluster units in the backbone as illustrated by **2** and **3**, PP = $Ph_2PCH_2PPh_2$.[5,6] The first part of this article will describe the further development of this field to include gold-containing rigid-rod polymers.

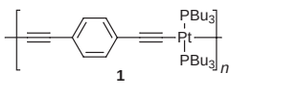

1

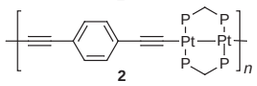

2

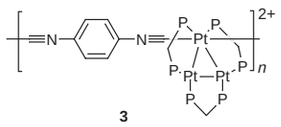

3

Gold-containing oligomers and polymers

Gold(I) tends to have a coordination number of two with linear stereochemistry,[3] so it is well suited to form linear rigid-rod polymers. If neutral polymers are to be formed, one neutral ligand L and one anionic ligand X^- are required for each gold(I) centre. Suitable ligands might then include L–R–X^-, where R is a linear spacer group, and L might be an isocyanide and X^- an acetylide. Alternatively, one ligand L–R–L and $^-$X–R–X^- could be used for each two gold(I) centres. The general types of polymers targetted are then shown as **4**–**6**. Since many of these polymers proved to be insoluble, it has been important to prepare model compounds containing only two gold(I) atoms, by using capping monodentate ligands in combination with one bridging ligand, in order to optimise the synthetic methods and to facilitate characterization of the polymers.

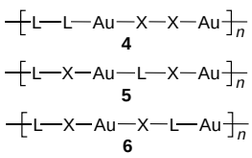

Diisocyanides, diacetylides and isocyanoacetylides

Since the isocyanide functionality is sensitive to bases, the most successful synthetic route to isocyanide(alkynyl)gold(I) complexes is by reaction of oligomeric or polymeric compounds $(AuC{\equiv}CR)_n$, in which the alkynyl ligand bridges by bonding to one gold atom through the σ donor and to a second gold atom using its π electrons,[7] with an isocyanide ligand. Although the explosive Au_2C_2 has been known for many years, the more stable (**CAUTION**: but still potentially explosive) digold diacetylides $(AuC{\equiv}C{-}Ar{-}C{\equiv}CAu)_n$ **7** needed for this work were unknown and were prepared according to eqn. (1), B = base, in which the aryl spacer group Ar = 1,4-C_6H_4, 4,4′-$C_6H_4C_6H_4$ or 1,4-(2,5-$Me_2C_6H_2$).[8]

$$2[Me_2SAuCl] + HCC\text{-}Ar\text{-}CCH + 2\ B \rightarrow 2\ Me_2S + 2\ BH^+Cl^- + \{Au\text{-}C{\equiv}C\text{-}Ar\text{-}C{\equiv}C\text{-}Au\}_n \quad (1)$$

Suitable binuclear gold(I) model compounds [RN≡CAuC≡C–Ar–C≡CAuC≡NR] **8** (R = Bu^t or Xy = 2,6-dimethylphenyl) and [RC≡CAuC≡N–Ar–N≡CAuC≡CR] **9** [R = Bu^t or Ph, Ar = 1,4-C_6H_4, 1,4-(2-MeC_6H_3), 1,4-(2,6-$Bu^t_2C_6H_2$), 1,4-(C_6Me_4), 1,4′-(2,6-$Me_2C_6H_2)_2$], were then prepared as shown in eqns. (2) and (3).[8]

$$1/n\ \{AuCC\text{-}Ar\text{-}CCAu\}_n + 2\ RNC \rightarrow \underset{\mathbf{8}}{[RN{\equiv}C\text{-}Au\text{-}C{\equiv}C\text{-}Ar\text{-}C{\equiv}C\text{-}Au\text{-}C{\equiv}NR]} \quad (2)$$

$$2/n\ \{AuCCR\}_n + CN\text{-}Ar'\text{-}NC \rightarrow \underset{\mathbf{9}}{[RC{\equiv}C\text{-}Au\text{-}C{\equiv}N\text{-}Ar'\text{-}N{\equiv}C\text{-}Au\text{-}C{\equiv}CR]} \quad (3)$$

While eqns. (2) and (3) indicate that the products are molecular in nature, and this is the case in solution, the compounds associate in the solid state either through π stacking between aryl groups of neighbouring molecules[9] or, more commonly, through intermolecular Au···Au bonding.[8] These weak Au···Au interactions, which are known in several other classes of gold(I) complexes, are thought to have strengths of 5–10 kcal mol^{-1}, similar to the strength of hydrogen bonds, and are thought to arise from relativistic London forces.[10] The association present in crystals of [PhC≡C–Au–C≡N$Bu^t_2C_6H_2$N≡C–Au–C≡CPh] comprises both aryl π stacking and Au···Au bonding and is shown in Fig. 1.

It was then possible to prepare polymers **10** containing alternating diacetylide and diisocyanide ligands according to

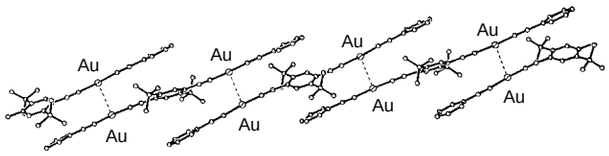

Fig. 1 The intermolecular association present in the solid state structure of [PhC≡CAuC≡NBu^t$_2$C$_6$H$_2$N≡CAuC≡CPh] due to (*a*) π-stacking and (*b*) Au···Au bonding. The Au···Au distance is 3.174(1) Å.

eqn. (4) (Ar and Ar′ are as defined earlier). The polymers are

$$1/n\ \{AuCC\text{-}Ar\text{-}CCAu\}_n + CN\text{-}Ar'\text{-}NC \rightarrow \{\text{-}Au\text{-}C{\equiv}C\text{-}Ar\text{-}C{\equiv}C\text{-}Au\text{-}C{\equiv}N\text{-}Ar'\text{-}N{\equiv}C\text{-}\}_n \quad (4)$$

10

insoluble, which might have been predicted since intermolecular association through π stacking and/or Au···Au bonding will lead to effective crosslinking of the linear rigid-rods into a three-dimensional network. Though each individual interaction is likely to be weak, the combination of many interactions for each polymer chain is likely to give strong crosslinking leading to insolubility. The polymers are therefore characterised only in the solid state by elemental analysis and by comparison of spectroscopic data with those of the well characterised model compounds.[8]

One interesting property of these gold(I) complexes is that they are emissive at room temperature either in the solid state or in solution.[9,11] The emission is strongly red shifted in the solid compared to solution state as illustrated in Fig. 2, particularly

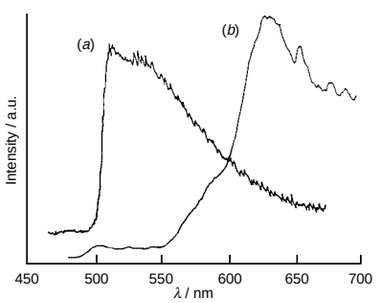

Fig. 2 The emission spectra of XyNC–Au–CCC$_6$H$_4$NO$_2$-4, (*a*) in solution in CH_2Cl_2 and (*b*) in the solid state, showing the red shift in the solid state. In this case the association in the solid state is due to π-stacking.

when Au···Au bonding orπ stacking is present in the solid state structures. In addition, there is a red shift in the emission and a decrease in emission intensity as the molecules increase in size, as illustrated for the solid state spectra shown in Fig. 3, and this

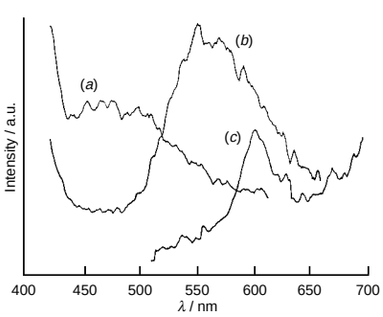

Fig. 3 The solidstate emission spectra of gold(I) complexes showing the red shift with increasing molecular size: (*a*) [Bu^{t}N≡C–Au–C≡CPh], (*b*) XyN≡C–Au–CCC$_6$H$_4$–C$_6$H$_4$CC–Au–C≡NXy] and (*c*) {Au–C≡C–C$_6$H$_2$Me$_2$C≡C–Au–C≡NC$_6$H$_2$Bu^t$_2$)N≡C}$_n$

provides evidence for at least some π conjugation in the rigid-rod chains.[9]

The new ligands 4-HC≡CC$_6$H$_4$N≡C and 4-HC≡C–2-MeC$_6$H$_3$N≡C bind readily to gold(I) in forming the complexes such as [4-HC≡CC$_6$H$_4$N≡C–Au–Cl] **11** and [4-HC≡C–2-MeC$_6$H$_3$N≡C–Au–C≡CBu^t] **12**. The acetylide derivatives such as **12** give weak Au···Au bonded association in the solid state [Au···Au 3.479(2) Å] and form oligomeric complexes H–(C≡C–Ar–N≡C–Au–)$_n$–C≡CBu^t **13** by elimination of Bu^{t}CCH on heating as illustrated in Scheme 1.[12] The oligomers tend to precipitate from solution when n = 4–6 and then no further chain growth occurs.

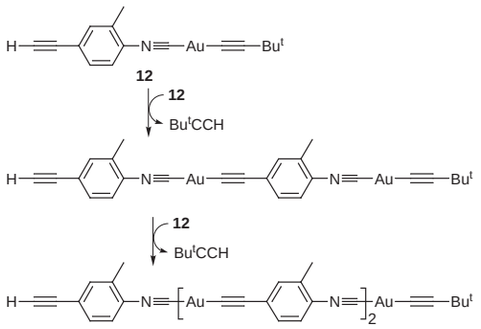

Scheme 1

Diphosphines, diacetylides and phosphinoacetylides

Diphosphines cannot give strictly linear rigid-rod compounds since there will be a tetrahedral angle at each phosphorus atom. The question then arises as to whether these ligands will give polymers at all, since ring formation is also possible.

The digold(I) diacetylides described above can be capped with monodentate phosphine ligands such as PMe_3 to give binuclear model complexes such as [(Me$_3$P)Au–C≡C–C$_6$H$_2$Me$_2$–C≡C–Au(PMe$_3$)] **14** and this forms loose polymers in the solid state by intermolecular Au···Au bonding (Fig. 4).[9,13]

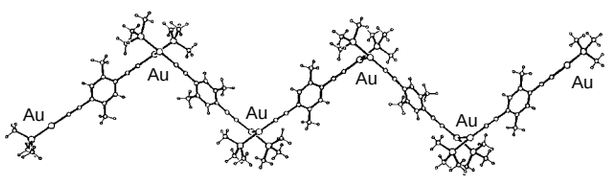

Fig. 4 The intermolecular association through Au···Au bonding in the complex [(Me$_3$P)Au–C≡C–C$_6$H$_2$Me$_2$–C≡C–Au(PMe$_3$)]

The diphosphines Ph$_2$PC$_6$H$_4$PPh$_2$ or Pr^i$_2$PC$_6$H$_4$C$_6$H$_4$PPr^i$_2$ can also give binuclear model complexes such as PhC≡C–Au-Pr^i$_2$PC$_6$H$_4$C$_6$H$_4$PPr^i$_2$–Au–C≡CPh **15** which has the *anti* conformation with respect to the two P–Au vectors as shown in Fig. 5; the bulky Pr^i groups prevent the formation of

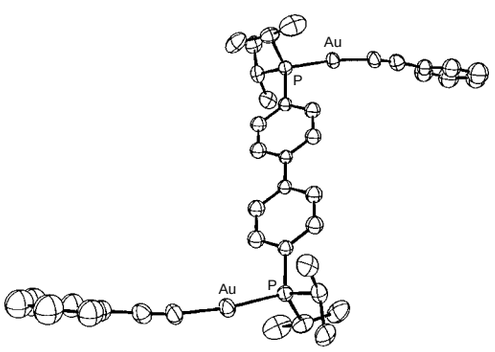

Fig. 5 The *anti* conformation of the two P–Au vectors in [PhC≡C–Au-Pr^i$_2$PC$_6$H$_4$C$_6$H$_4$PPr^i$_2$–Au–C≡CPh] **15**

intermolecular Au···Au bonding in**15**. It is then straightforward to prepare polymers (Au–C≡C–Ar–C≡C–Au–PR$_2$–Ar′–PR$_2$–)$_n$ **16** incorporating both diphosphine and diacetylide bridges. It is likely that the *anti* conformation of the P–Au vectors in **15** is

maintained in these polymers, which are sufficiently soluble when R = Pr^i to allow molecular mass determination by GPC. The improved solubility probably arises because the bulky Pr^i groups prevent crosslinking by intermolecular Au···Au bonding.

It is possible to tailor the system to give rings instead of polymers. Thus, ligands $R_2PCH_2PR_2$ give digold complexes in which the *syn* conformation of the two P–Au vectors is preferred so as to allow intramolecular Au···Au bonding, as for example in $CH_2(PCy_2–Au–O_2CCF_3)_2$ **17** or $CH_2(PPh_2–Au–C{\equiv}CBu^t)_2$ **18** shown in Fig. 6.[14,15] This conformation is

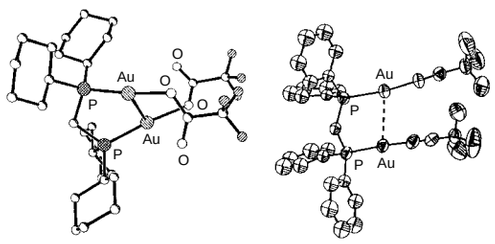

Fig. 6 The *syn* conformation of the two P–Au vectors in $[CH_2(PCy_2–Au–O_2CCF_3)_2]$ **17** and $[CH_2(PPh_2–Au–C{\equiv}CBu^t)_2]$ **18**

maintained on reaction of **17** with rigid-rod bridging ligands and so large rings are formed in $[CH_2(PR_2–Au–C{\equiv}C–Ar–C{\equiv}C–Au–PR_2)_2CH_2]$ **19** or $[CH_2(PR_2–Au–C{\equiv}N–Ar–N{\equiv}C–Au–PR_2)_2CH_2]^{4+}$ **20**. The structure of the complex **20** with R = cyclohexyl and the bridging ligand 1,4-$C{\equiv}NC_6H_4N{\equiv}C$ is shown in Fig. 7.

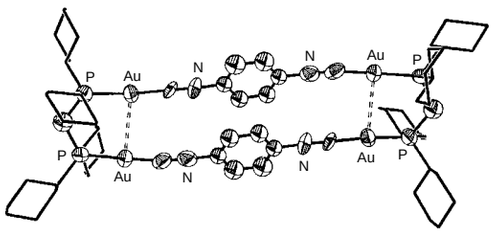

Fig. 7 The structure of the cationic ring complex **20** (R = Cy and Ar = 1,4-C_6H_4)

It is also possible to use mixed phosphine–acetylide donors in forming polymers of gold(I). Thus the ligands $Ph_2PC{\equiv}CH$ and $Pr^i_2PC{\equiv}CH$ form model complexes $HC{\equiv}CPR_2–Au–Cl$ which, on treatment with base, can eliminate HCl to give the polymers $\{R_2PC{\equiv}C–Au–\}_n$ **21**.[16]

Angular diacetylides and triacetylides

In the complexes with diphosphines or phosphinoacetylides, the chains are not strictly linear because of the tetrahedral angle at phosphorus, yet polymers can still be formed in preference to the alternative ring structures. What will happen if an angle is introduced in the diacetylide bridge? The dialkyne 1,3-$(HC{\equiv}C)_2C_6H_3$Me-5 yields digold(I) model complexes 1,3-$(L–Au–C{\equiv}C)_2C_6H_3$Me-5 **22** (L = phosphine, phosphite or isocyanide ligand) which form ribbon structures in the solid state through Au···Au bonding as seen in Fig. 8.[17]

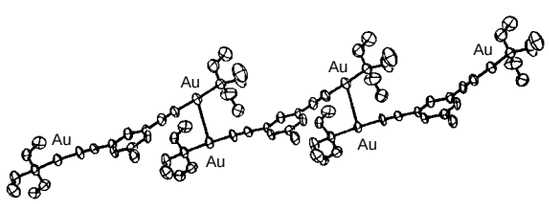

Fig. 8 The intermolecular association through Au···Au bonding in the complex $[1,3\text{-}(L–Au–C{\equiv}C)_2C_6H_3Me\text{-}5]$ [L = $P(OMe)_3$]

Kinked polymers such as **23** are formed when linear diisocyanide ligands are used but, if the neutral bridging ligand is also non-linear, then ring structures such as **24** are formed instead (Scheme 2).[17]

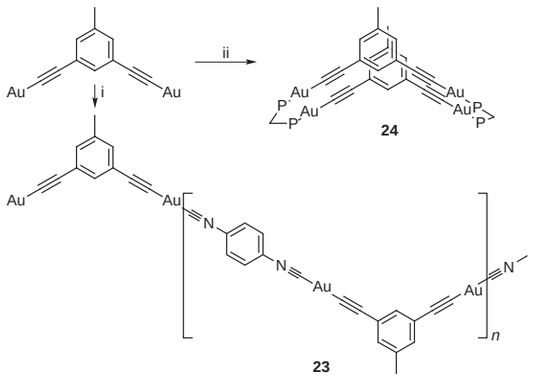

Scheme 2 *Reagents*: i, $C_6H_4(CN)_2$; ii, $Ph_2PCH_2PPh_2$

If a third acetylide link is added as in 1,3,5-$(HC{\equiv}C)_3C_6H_3$, the gold derivatives can in principle form more complex network polymers either through intermolecular Au···Au bonding or through the use of bridging ligands. The capped complexes 1,3,5-$(L–Au–C{\equiv}C)_3C_6H_3$ **25** are found to form one-dimensional ribbon structures in the solid state with one gold atom not taking part in Au···Au bonding (Fig. 9). With all bridging ligands,

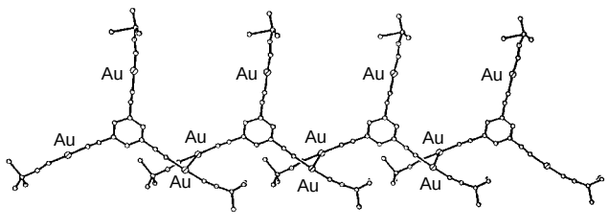

Fig. 9 The intermolecular association through Au···Au bonding in the complex $[1,3,5\text{-}(L–Au–C{\equiv}C)_3C_6H_3]$ (L = $Bu^tN{\equiv}C$)

whether the strictly linear diisocyanides or angular diphosphines, insoluble polymers **26** are formed (Scheme 3).[18]

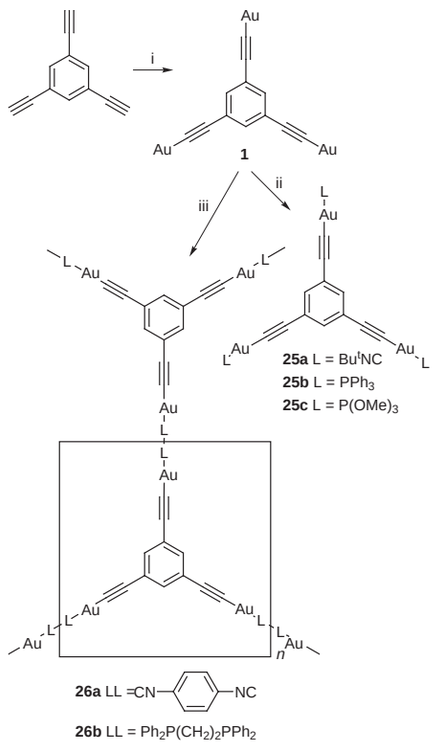

Scheme 3 *Reagents*: i, $[AuCl(SMe_2)]$, NaOAc; ii, 3L; iii, 1.5 L–L

Rings and polymers with diphosphine and bis(pyridyl) ligands

The principles determining if rings or polymers would be formed were now understood in general terms but the detailed structures of the polymers could not be determined since they could not be crystallised. A series of experiments was carried out next using flexible diphosphine ligands $(CH_2)_n(PPh_2)_2$ and a more labile linear bridging ligand *trans*-1,4-bis(pyridyl)-ethene. It was argued that the intramolecular Au···Au bonding interactions would decrease progressively with increasing *n* and so the preferred structure would switch from the large rings to polymers at some point in the series (Scheme 4). Further, the polymers could reversibly cleave to smaller fragments in solution owing the lability of the pyridine donors and this might allow crystallisation and so to full structural characterisation of the polymers.[19]

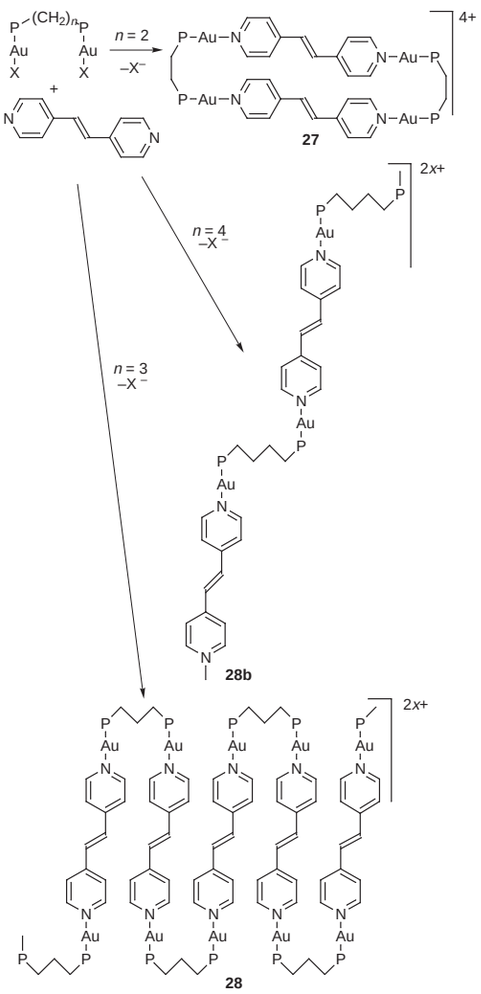

Scheme 4 X = CF_3CO_2, P = PPh_2

With $(CH_2)_2(PPh_2)_2$, the ring structure $[Au_4(\mu\text{-}Ph_2PCH_2CH_2PPh_2)_2(\mu\text{-}NC_5H_4CH{=}CHC_5H_4N)_2]^{4+}$ **27** is preferred as shown in Fig. 10 but the Au···Au distance of 3.625(3) Å indicates very weak Au···Au bonding and no significant Au···Au attraction is expected for higher values of *n*.[19]

The switch to a polymeric structure $[\{Au_2[\mu\text{-}Ph_2P(CH_2)_nPPh_2](\mu\text{-}NC_5H_4CH{=}CHC_5H_4N)\}_n]^{2n+}$ **28** occurs when $n = 3$ and the polymer **28a** has an interesting sinusoidal conformation as shown in Fig. 11(*a*), since the conformation of adjacent P–Au vectors is *syn*. There is then a switch to the *anti* conformation of P–Au vectors when $n = 4$, such that a more stretched polymer chain is formed in **28b** [Fig. 11(*b*)].[19]

An interesting case occurs when $n = 5$, since three different structural forms have been crystallised (Fig. 12). Two of these

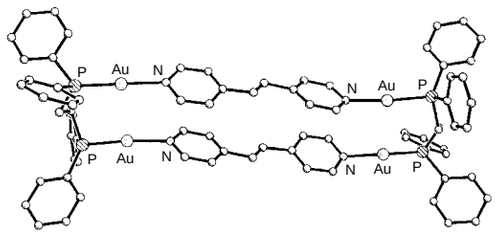

Fig. 10 The structure of the cationic ring complex $[Au_4(\mu\text{-}Ph_2PCH_2CH_2PPh_2)_2(\mu\text{-}NC_5H_4CH{=}CHC_5H_4N)_2]^{4+}$

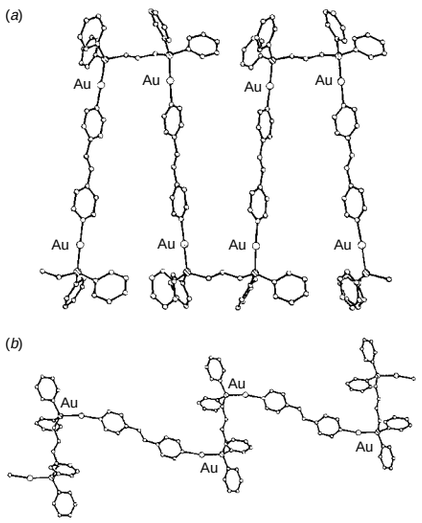

Fig. 11 The structures of the cationic polymer chains $[\{Au_2[\mu\text{-}Ph_2P(CH_2)_nPPh_2](\mu\text{-}NC_5H_4CH{=}CHC_5H_4N)\}_n]^{2n+}$; (*a*) $n = 3$; (*b*) $n = 4$

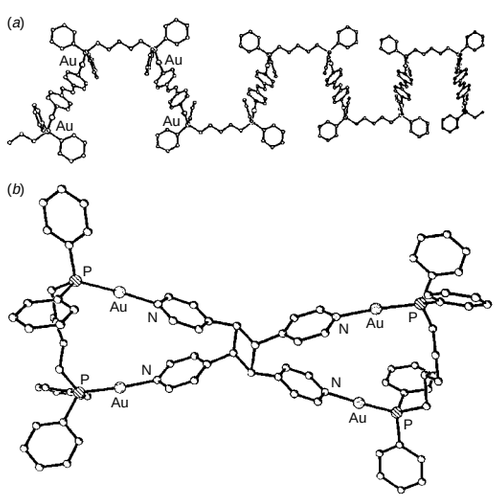

Fig. 12 The structures of the helical (*a*) cationic polymer chains $[\{Au_2[\mu\text{-}Ph_2P(CH_2)_5PPh_2](\mu\text{-}NC_5H_4CH{=}CHC_5H_4N)\}_n]^{2n+}$, and of the cyclobutane ring form (*b*)

are polymers **28c**, one of which has the sinusoidal conformation as in **28a** but the other has a conformation intermediate between *syn* and *anti* and the resulting chain adopts a helical structure [Fig. 12(*a*)]. In most of the structurally characterised polymers, the chains pack parallel to one another but the helical polymer has chains that cross over one another while running in mutually perpendicular directions. The third structural form with $n = 5$ proved to be a novel ring structure with a central cyclobutane ring formed by a 2 + 2 cycloaddition reaction of two bis(pyridyl)ethylene ligands [Fig. 12(*b*)]. Further study showed

that this form was only obtained when crystallisation was carried out in the open laboratory and it is thought to be formed by a photochemical cyclisation of small amounts of ring structure present in equilibrium with the chain forms as shown in Scheme 5.[16]

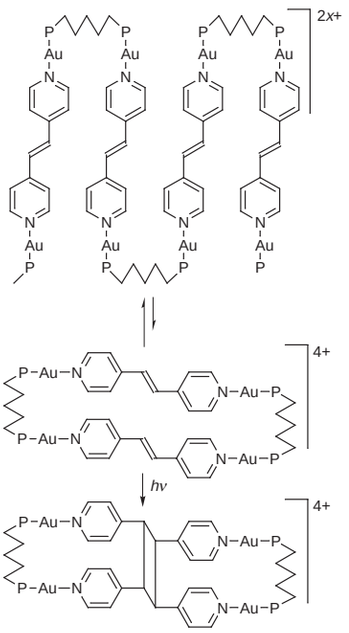

Scheme 5 P = PPh_2

The complex with $n = 6$ proved to be a stretched polymer **28d** (Fig. 13) whose structure is similar to that of **28b**, having *anti* conformation of adjacent P–Au vectors but with the long $(CH_2)_6$ chain partly folded back on itself.[16]

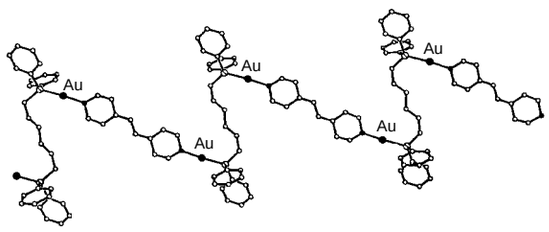

Fig. 13 The structure of the cationic polymer chain $[\{Au_2[\mu\text{-}Ph_2P(CH_2)_6PPh_2](\mu\text{-}NC_5H_4CH{=}CHC_5H_4N)\}_n]^{2n+}$

The polymers **28** are not conjugated since there is a saturated carbon chain in the diphosphine ligands. However, conjugated polymers can be prepared by using the diphosphine ligands *trans*-$Ph_2PCH{=}CHPPh_2$ or $[Fe(\eta^5\text{-}C_5H_4PPh_2)_2]$; the structure of the polymer **29** prepared from the latter ligand is shown in Fig. 14 and has the stretched polymer form with *anti*

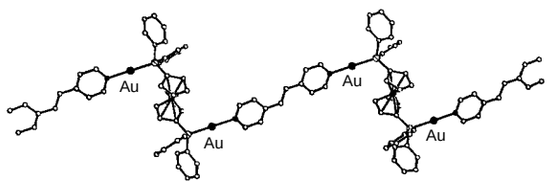

Fig. 14 The structure of the cationic polymer chain $[\{Au_2[\mu\text{-}Fe(C_5H_4PPh_2)_2](\mu\text{-}NC_5H_4CH{=}CHC_5H_4N)\}_n]^{2n+}$

conformation of adjacent P–Au vectors. This polymer, as a pressed disc, converts from being an insulator to a semiconductor when doped with iodine, partial oxidation of ferrocene to ferricenium centres is thought to be a likely rationalisation of this observation.[16]

In conclusion, it is now possible to tailor the structures of gold(I) compounds with bridging ligands to give either rings or polymers. The polymers have interesting structures and preliminary studies indicate the possibility of optical and electronic properties based on the conjugation along the chains.

Platinum-containing oligomers and polymers

The synthesis of oligomers or polymers with platinum atoms in the backbone is based on the two simple reactions shown in eqns. (5) and (6). The first is a ligand substitution of a diimine

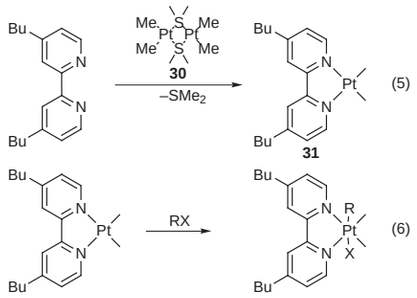

ligand such as 4,4′-di-*tert*-butyl-2,2′-bipyridine onto a dimethylplatinum(II) centre by displacement of weakly bound Me_2S ligands from $[Pt_2Me_4(\mu\text{-}SMe_2)_2]$ **30** to give **31**,[20] while the second involves oxidative addition of an alkyl halide to the platinum(II) centre of **31**, a reaction which occurs easily for primary alkyl halides and is tolerant to a wide range of functional groups.[21] Both reactions occur in almost quantitative yield and so are ideal for multistep syntheses as described below.

Linear chain platinum polymers

The oxidative addition to platinum(II) of alkyl halides containing polymerisable substituents can lead to polymers with organoplatinum(IV) substituents as side chains,[22] but the key to making polymers with platinum atoms in the backbone is to use alkyl halides with a bipyridine substituent. Thus, the oxidative addition of a bromomethyl derivative of 2,2′-bipyridine, 4-$BrCH_2$-4′-Me-2,2′-$(C_5H_4N)_2$ **32**, to **31** gives a platinum(IV) complex with a free bipyridine group, which can then coordinate to a second dimethylplatinum unit, and repetition of the sequence can give oligomers with platinum atoms in the backbone as shown in Scheme 6.[23]

A simple self-assembly of a platinum containing polymer occurs on reaction of **32** with **30** as shown in Scheme 7. Displacement of the Me_2S ligands from **30** gives the platinum(II) monomer **33** which undergoes polymerisation by intermolecular oxidative addition.[23]

Dendrimeric platinum polymers

To make a dendrimer, it is necessary to introduce a branch in each generational growth step.[24] This requires at least a trifunctional reagent having two alkyl halide and one bipyridine or one alkyl halide and two bipyridine units as present in **34** and **35** respectively. The first successful synthesis is a convergent

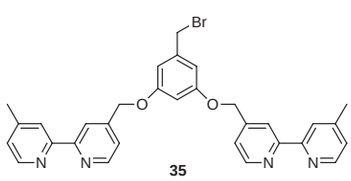

method based on the reagent **34** (Scheme 8). Reagent **34** can add to 2 equiv. of **31** to give the diplatinum(IV) complex **36**, which

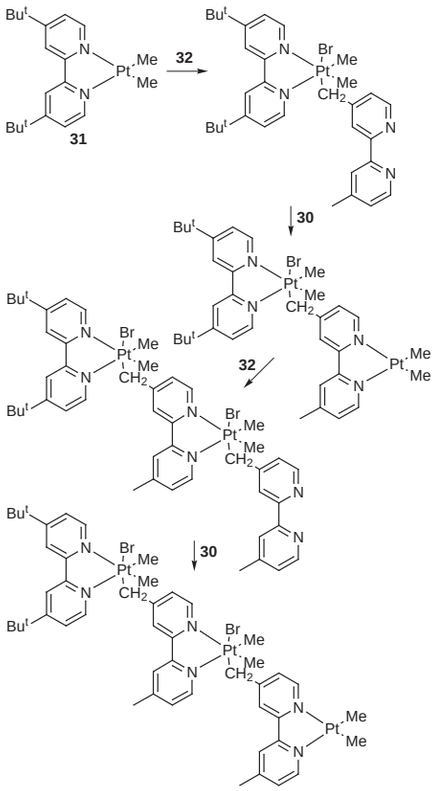

Scheme 6

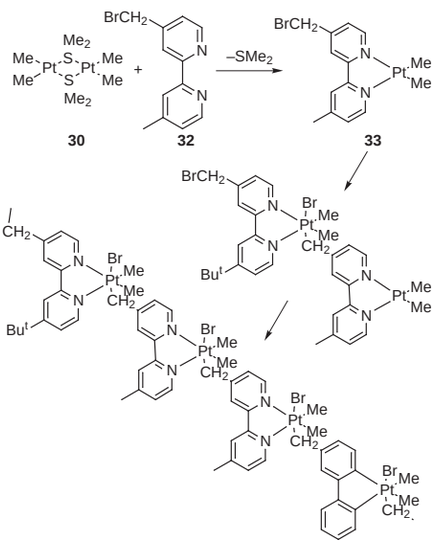

Scheme 7

can then add a dimethylplatinum(II) group to the free bipyridine to regenerate a reactive platinum(II) centre in **37**, whose structure is shown in Fig. 15.[25]

Now repetition of the cycle using **37** and **34** gives a Pt_7 dendrimer **38** (Scheme 9). One more generation can be grown, but the reactive platinum(II) centre, which is formed at the centre of the molecule in a convergent synthesis, becomes increasingly sterically congested with each generation and eventually the oxidative addition step fails.[25]

The self-assembly of a hyperbranched polymer with platinum atoms in the backbone is readily achieved by reaction of **34** with **30**. The first step is ligand substitution to give the platinum(II) complex, which then undergoes polymerisation by intermolecular oxidative addition (Scheme 10).[25]

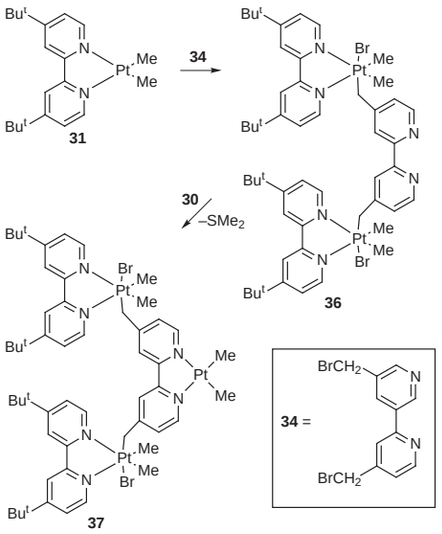

Scheme 8

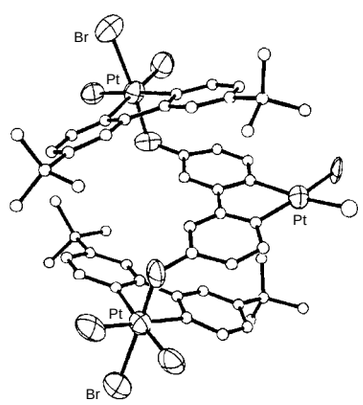

Fig. 15 The structure of the $Pt^{IV}_2Pt^{II}$ complex **37**

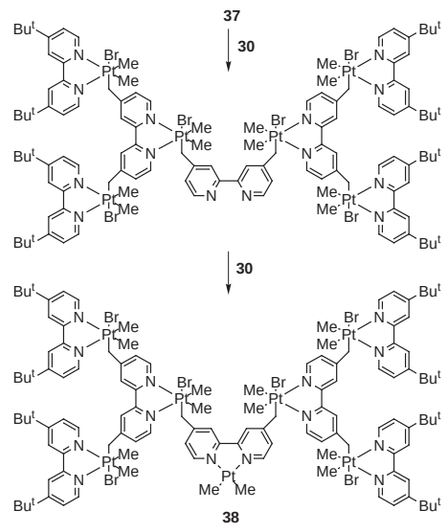

Scheme 9

A divergent method for dendrimer growth is based on the reagent **35**, which contains one bromomethyl group and two bipyridine groups. With this system, the reactive platinum(II)

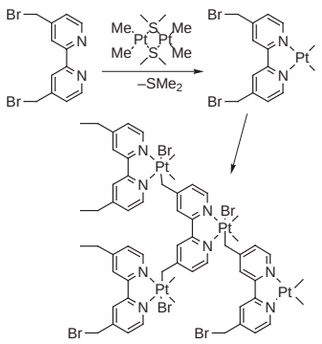

Scheme 10

centres are formed at the periphery of the dendrimer and it is easy to introduce a different metal in the outer generation as shown in Scheme 11, using as a source of dimethylpalladium units the complex $[Pd_2Me_4(\mu\text{-pyridazine})_2]$ **39**.[26]

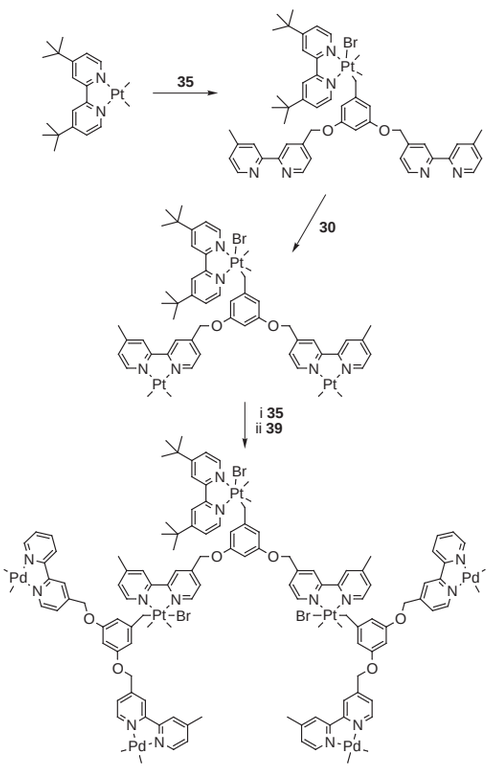

Scheme 11

Stars and exotic molecules based on polyfunctional cores

Polyfunctional cores are useful for facilitating the rapid growth of complex molecules. Two useful core molecules for platinum oligomers are **40** and **41**. The synthesis of a Pt_9 dendrimer by

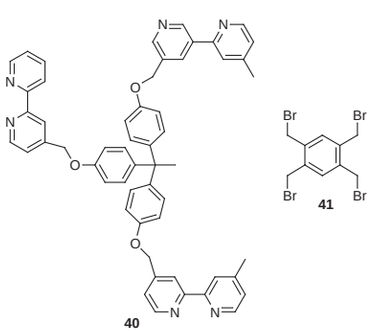

40 **41**

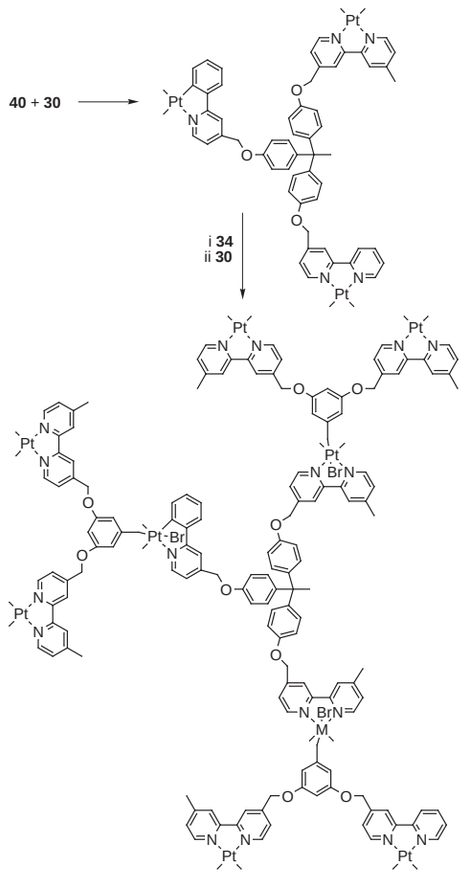

Scheme 12

use of the core reagent **40** and the dendrimer reagent **34** is shown in Scheme 12.[26]

The core reagent **41** is useful for assembling four molecules which contain one platinum(II) centre each, including simple molecules like **31** or the more complex linear or dendrimeric molecules prepared in Schemes 6, 8 and 9.[23,25,27] An example is shown in Scheme 13 and the most complex example so far prepared is the Pt_{28} dendrimer shown in Fig. 16 and formed by coupling four Pt_7 dendrimer units **38** to the tetrafunctional core.

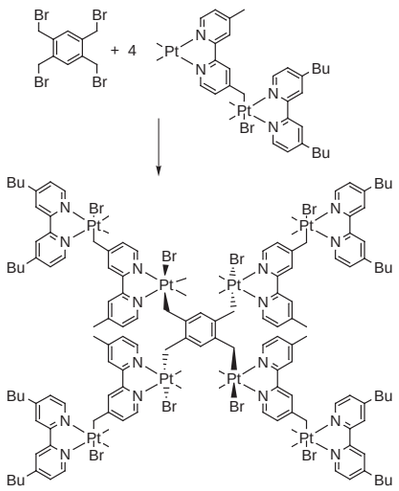

Scheme 13

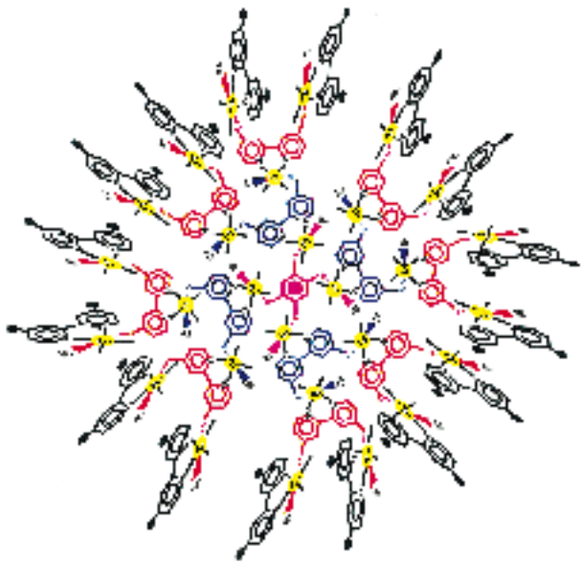

Fig. 16 Proposed structure of the Pt_{28} dendrimer

Acknowledgements

I thank the NSERC (Canada) and 3M (Canada) for financial support of this work and the excellent students and coworkers, whose names are listed in the references, who made major contributions to this chemistry. Collaborations with crystallographers, H. A. Jenkins, Lj. Manojlovic-Muir, K. W. Muir, N. C. Payne, J. J. Vittal and G. P. A. Yap have been invaluable. This article is based on the Nyholm Award lecture delivered in London in October 1997, and is dedicated with gratitude to my PhD mentors at University College London, Professors A. G. Davies and R. J. H. Clark.

Dick Puddephatt was educated at University College, London, graduating with a PhD in 1968 for research in synthetic and mechanistic organometallic chemistry with A. G. Davies and in spectroscopic studies with R. J. H. Clark. After a postdoctoral fellowship in Canada with H. C. Clark, he held a faculty position at the University of Liverpool from 1970–1978 before moving to a position as Professor of Chemistry at the University of Western Ontario. He has received the Alcan and Steacie awards of the Canadian Society of Chemistry, The CIC Medal of the Canadian Institute of Chemistry, and the Chemistry of the Noble Metals and Nyholm Lecture awards of the Royal Society of Chemistry and is a Fellow of the Royal Society of Canada.

Notes and References

1 J. R. Ferraro and J. M. Williams, in *Introduction to Synthetic Electrical Conductors*, Academic Press, New York, 1987, p. 139.
2 R. J. H. Clark, in *Lower-Demensional Systems and Molecular Electronics*, ed. R. M. Metzger, P. Day and G. C. Papavassilion, Plenum, New York, 1991, p. 263.
3 R. J. Puddephatt, *The Chemistry of Gold*, Elsevier, Amsterdam, 1978.
4 (*a*) J. Lewis, M. S. Khan, A. K. Kakkar, B. F. G. Johnson, T. B. Marder, H. B. Fyfe, F. Wittman, R. H. Friend and A. E. Dray, *J. Organomet. Chem.*, 1992, **425**, 165; (*b*) S. J. Davies, B. F. G. Johnson, M. S. Khan and J. Lewis, *J. Chem. Soc., Chem. Commun.*, 1991, 187.
5 M. J. Irwin, G. Jia, J. J. Vittal and R. J. Puddephatt, *Organometallics*, 1996, **15**, 5321.
6 A. M. Bradford, E. Kristof, M. Rashidi, D.-S. Yang, N. C. Payne and R. J. Puddephatt, *Inorg. Chem.*, 1994, **33**, 2355.
7 D. M. P. Mingos, J. Yau, S. Menzer and D. J. Williams, *Angew. Chem., Int. Ed. Engl.*, 1995, **34**, 1894.
8 M. J. Irwin, G. Jia, N. C. Payne and R. J. Puddephatt, *Organometallics*, 1996, **15**, 51.
9 M. J. Irwin, J. J. Vittal and R. J. Puddephatt, *Organometallics*, 1997, **16**, 3541.
10 J. Li and P. Pyykko, *Chem. Phys. Lett.*, 1992, **197**, 586.
11 (*a*) C.-M. Che, H.-K. Yip, W.-C. Lo and S.-M. Peng, *Polyhedron*, 1994, **13**, 887; (*b*) V. W.-W. Yam and S. W.-K. Choi, *J. Chem. Soc., Dalton Trans.*, 1996, 4227.
12 G. Jia, N. C. Payne, J. J. Vittal and R. J. Puddephatt, *Organometallics*, 1993, **12**, 4771.
13 G. Jia, R. J. Puddephatt, J. D. Scott and J. J. Vittal, *Organometallics*, 1993, **12**, 3565.
14 G. Jia, R. J. Puddephatt and J. J. Vittal, *J. Organomet. Chem.*, 1993, **449**, 211.
15 N. C. Payne, R. Ramachandran and R. J. Puddephatt, *Can. J. Chem.*, 1995, **73**, 6.
16 M. J. Irwin, L. M. Rendina, J. J. Vittal and R. J. Puddephatt, *Chem. Commun.*, 1996, 1281; M. J. Irwin, PhD thesis, University of Western Ontario, 1997.
17 M.-A. McDonald, H. A. Jenkins and R. J. Puddephatt, unpublished work; M.-A. McDonald, MSc Thesis, University of Western Ontario, Canada, 1997.
18 M. J. Irwin, Lj. Manojlovic-Muir, K. W. Muir, R. J. Puddephatt and D. S. Yufit, *Chem. Commun.*, 1997, 219.
19 M. J. Irwin, J. J. Vittal, G. P. A. Yap and R. J. Puddephatt, *J. Am. Chem. Soc.*, 1996, **118**, 13101.
20 J. D. Scott and R. J. Puddephatt, *Organometallics*, 1983, **2**, 1643.
21 L. M. Rendina and R. J. Puddephatt, *Chem. Rev.*, 1997, **97**, 1735.
22 S. Achar, R. J. Puddephatt and J. D. Scott, *Polyhedron*, 1996, **15**, 2363; *Can. J. Chem.*, 1996, **74**, 1983; S. Achar, J. D. Scott, J. J. Vittal and R. J. Puddephatt, *Organometallics*, 1993, **12**, 4592; S. Achar, J. D. Scott and R. J. Puddephatt, *Organometallics*, 1992, **11**, 2325.
23 S. Achar and R. J. Puddephatt, *Organometallics*, 1995, **14**, 1681.
24 N. Ardoin and D. Astruc, *Bull. Soc. Chim. Fr.*, 1995, **132**, 875.
25 S. Achar, J. J. Vittal and R. J. Puddephatt, *Organometallics*, 1996, **15**, 43; S. Achar and R. J. Puddephatt, *Angew. Chem., Int. Ed. Engl.*, 1994, **33**, 847.
26 G.-X. Liu and R. J. Puddephatt, *Organometallics*, 1996, **15**, 5257.
27 S. Achar and R. J. Puddephatt, *J. Chem. Soc., Chem. Commun.*, 1994, 1895.

8/00244D

The X-ray crystal structures of perdeuteriated and protiated enzyme elongation factor Tu are very similar

Serena J. Cooper,[a] David Brockwell,[b] James Raftery,[a] David Attwood,[b] Jill Barber[b] and John R. Helliwell*[a]†

[a] *Department of Chemistry, University of Manchester, Manchester, UK M13 9PL*
[b] *School of Pharmacy and Pharmaceutical Science, University of Manchester, Manchester, UK M13 9PL*

X-Ray structural comparisons show that perdeuteriation does not affect the overall fold or domain arrangement of elongation factor Tu.

Perdeuteriation involves replacing all the non-exchangeable hydrogens in a molecule with deuterium. For proteins this can be achieved by growing a bacterial expression system on a fully deuteriated medium, which is a technique used for protein NMR[1] and has potential for protein neutron scattering studies.[2,3] Whilst the effects of D_2O on proteins are well documented and indeed is a method used in the study of enzyme mechanisms,[4] there is a paucity of structural information on the impact of perdeuteriation. Most of the published information on perdeuteriation derives from the elegant work of the groups of Crespi and Berns in the 1960s.[5,6] Their experiments, as well as more recent data, indicate that perdeuteriation has a destabilising effect on proteins. Conversely biological properties such as ligand binding do not appear to be drastically changed.[7–9] This leads to the possibility of preparing perdeuteriated proteins with similar activities but with modified physical properties relative to the parent protiated protein. As part of a larger study on the effects of perdeuteriation on proteins we compare the X-ray crystal structure of perdeuteriated with that of native *i.e.* protiated, elongation factor Tu (EFTu) from *Escherichia coli*.

Both forms of the enzyme were prepared using an *E. coli* over-expression system, with the perdeuteriated form utilising a deuterium adapted *E. coli* strain, MRE600D.[10] Once cells were grown all further processes were carried out in an aqueous (H_2O) environment, so only the deuterons unable to exchange with the solvent remained attached to the protein. The native and perdeuteriated enzymes were purified identically. Analysis by electrospray mass spectrometry showed that the protein was 95% deuteriated on carbon, and that 78 of the 668 non carbon bound deuterons did not exchange with protium during isolation (*ca.* 24 h).

Crystals of both native and perdeuteriated EFTu were obtained by utilising conditions similar to those of Kjeldgaard and Nyborg.[11]‡ Both forms of the enzyme were subjected to limited cleavage with 1% trypsin for 1 h on ice. In this period a 14 peptide fragment, between Ala45 and Arg58, is excised and no further proteolysis occurs. Cleavage does not affect enzyme activity, as assessed by GDP binding assays. Crystals grew within a few days, to a typical size of $0.3 \times 0.3 \times 0.5$ mm but deteriorated after approximately one week, as determined by visual examination. Within each droplet the crystals displayed a range of (roughly) bipyramidal habits. Protiated crystals were found to diffract to *ca.* 3.5 Å using Cu-Kα radiation from a rotating anode with an R-AXIS IIc area detector. The diffraction resolution was extended to 2.5 Å at station PX7.2 SRS Daresbury.§ Many of the crystals were found to diffract poorly or were twinned. A 4.0 Å data set of a perdeuteriated EFTu crystal was measured on the R-AXIS IIc area detector using rotating anode Cu-Kα radiation.¶ A second perdeuteriated crystal was measured at station PX7.2 SRS Daresbury and although it diffracted to 2.8 Å was subsequently found to be adversely affected by twinning. All the crystals were of space group $P4_32_12$ with small but significant variation in the unit cell dimensions. We are not certain whether this variation is the result of perdeuteriation, but it is most probably simply due to the variety of crystal morphologies, as also observed previously.[11]

We have solved both the 2.5 Å protiated and 4.0 Å perdeuteriated structures by molecular replacement using GDP-EFTu coordinates based on a 2.6 Å analysis, kindly given to us by Professor M. Kjeldgaard of Aarhus University.[11]‖ The native and perdeuteriated models have been refined to *R* factors of 0.230 and 0.217 respectively.** The lower resolution of the perdeuteriated structure deems it unrealistic to draw any very detailed comparisons between the two structures, *i.e.* particularly with reference to differences in bonding distances. However it does readily allow a comparison between the overall domain to domain arrangement, as well as secondary structure. EFTu is an ideal candidate to examine the importance of perdeuteriation on proteins as it is a large (393 amino acid) multiple domain protein, the only other perdeuteriated X-ray structure available to date being a small (149 amino acids) single domain protein.[3] EFTu comprises three domains, and therefore has a large potential for conformational flexibility. The two refined X-ray models were aligned with respect to each other and also to the original Aarhus model,[11] using the program LSQMAN.[12] The rms distance deviations between protein C_α atoms of these alignments are, in ascending order of disagreement: 0.56 Å Aarhus protiated to our protiated; 0.79 Å Aarhus protiated to perdeuteriated and 0.83 Å perdeuteriated to our protiated. The protiated to protiated value of 0.56 Å represents the 'control' rms against which the other two should be compared. The rms overlap value of 0.56 Å between protiated and protiated EFTu models corresponds well with the Luzzati (0.55 Å) and Cruickshank (0.29 Å) estimates for the errors in our protiated model.†† Thus subtle structural differences between perdeuteriated and protiated EFTu cannot be ruled out yet and clearly requires confirmation.

To examine possible structural differences in more detail we also aligned each domain individually, *i.e.* our protiated EFTu domains 1, 2 and 3 with perdeuteriated EFTu domains 1, 2 and 3 in turn, and thereby accentuate any domain shifts. The rms distance deviations (for only the C_α atoms within the relevant domains) are; domain 1, 0.76 Å; domain 2, 0.99 Å and domain 3, 0.80 Å. The rms distance deviations for all C_α atoms in the above alignments are; 0.96 Å based on domain 1; 1.15 Å based on domain 2 and 0.99 Å based on domain 3. The greatest deviation is within the loop or turn regions, as can be seen in Fig. 1. However, considering typical temperature factors of $\geqslant$40 for these regions, a coordinate displacement of *ca.* 0.7 Å[2] would be expected in any case. Overall it appears that there are no major domain shifts (*i.e.* none $>$1.5 Å) and both structures have the same fold and global arrangement of domains. Thus the X-ray crystal structure analyses clearly show that perdeuteriation has no effect on the tertiary structure of EFTu. This is a significant finding for structural techniques that utilise perdeuteriated proteins such as NMR and neutron diffraction. It appears that the observed physiochemical differences[7] between protiated and perdeuteriated EFTu are not of an overall structural nature. X-Ray studies are underway on a number of

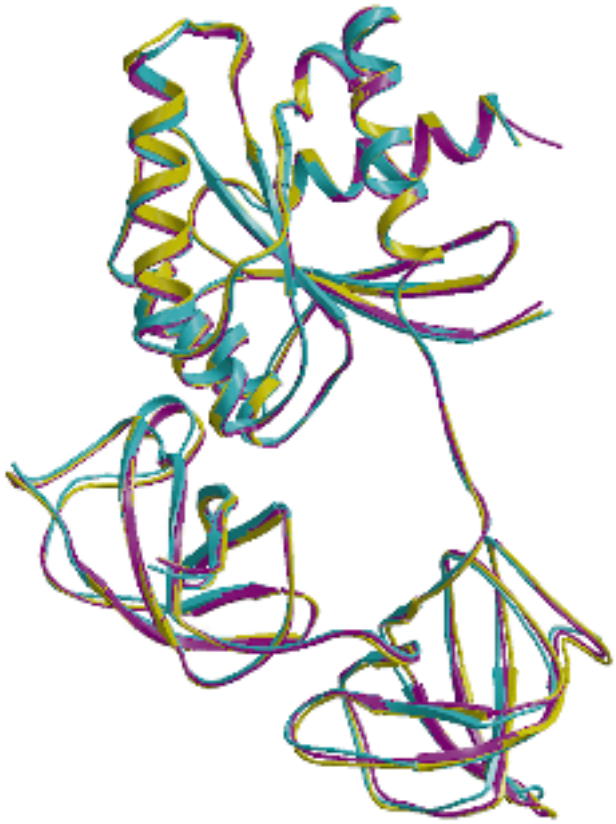

Fig. 1 Overlay of perdeuteriated and protiated EFTus indicating the similarity of the domain domain arrangements. Key: yellow, our protiated structure; magenta, Aarhus protiated structure, reproduced with permission;[11] cyan, perdeuteriated structure. Figure created using MOLSCRIPT.[13]

other proteins and will allow further analysis of the potential structural changes due to perdeuteriation to compare with the EFTu results presented here.

We thank The Wellcome Trust for a Sir Henry Wellcome Commemorative Award for Innovative Research and Ms Lu Yu and Professor Simon Gaskell (UMIST) for collaboration with the electrospray mass spectrometry work. We thank Professor M. Kjeldgaard of Aarhus University for the 2.6 Å GDP-EFTu coordinates. We thank Professor D. W. J. Cruickshank for discussion on coordinate precision based on his Data Precision Indicator (DPI). J. R. H. thanks the BBSRC who funded molecular graphics and computer workstations and partial (33%) salary support for J. R. and The Wellcome Trust who funded the R-AXIS and SERC who funded the rotating anode generator.

Notes and References

† E-mail: john.helliwell@man.ac.uk

‡ Crystals were grown by vapour diffusion in 20 μl sitting drops, determined by screening as: 10 mM $MgCl_2$, 50 mM Tris-HCl at pH7, 0.5 mM dithiothreitol (DTT), 1 mM NaN_3, 10 mM phenylmethylsulfonyl fluoride (PMSF), 10 mM guanosine diphosphate (GDP) and either 4.7 mg ml^{-1} protiated EFTu with 3.5–4.25% PEG (6000 Da) or 1.9 mg ml^{-1} perdeuteriated EFTu with 3–4.5% PEG (6000 Da). All drops were equilibrated with a reservoir of 200 μl 10% (6000 Da).

§ 2.5 Å data were collected at station PX7.2 Daresbury from a single protiated crystal. A total of 27° of data yielded an R_{merge} of 0.078 for 14 002 reflections with a completeness of 89%, whereby 63% of the reflections have $I \geqslant 3\sigma(I)$. Unit cell dimensions are $a = b = 70.8$ $c = 163.4$ Å.

¶ 60° of 4.0 Å resolution data from a single perdeuteriated EFTu crystal were collected on the Manchester R-AXIS IIc, which yielded an R_{merge} of 0.22 for 5230 reflections, 60% of which have $I \geqslant 3\sigma(I)$, for the strong reflections the merging R is 0.05 and the overall R_{merge} only increases above 0.25 for data higher than 4.2 Å resolution. The data are 97% complete. The unit cell dimensions are $a = b = 69.8$ $c = 160.5$ Å.

‖ Molecular replacements were carried out using AMORE.[14] Both using the 2.6 Å resolution Aarhus coordinates with our X-ray data to 4 Å. The R factors at this stage for the protiated and perdeuteriated are 0.345 and 0.348 respectively.

** Subsequent to molecular replacement both structures were subjected to further rigid body refinement and simulated annealing followed by positional and B-factor refinement using XPLOR.[15] After inspection on the graphics and insertion of the Mg^{2++} and GDP co-factors into the protiated model it was put through further rounds of positional and B-factor refinement using the maximum likelihood method in REFMAC.[14] A round of refinement is defined as positional and B-factor refinement followed by model inspection/rebuilding. The perdeuteriated model was also further refined using REFMAC.[14] A bulk solvent correction was applied. The GDP and Mg^{2++} co-factors were added in the second round of refinement. R_{free}[15] was used as a guide for both protiated and perdeuteriated refinements, final values are 0.341 and 0.335, respectively.

†† The precision of protein model coordinates can be estimated using the Luzzati approach[16–18] and more recently that of Cruickshank,[19] who has considered the various protein cases in detail, including a medium resolution refined model based on initial better resolution coordinates. The Luzzati coordinate error estimates for the protiated and perdeuteriated EFTu models are 0.55 Å (5–2.45 Å) and 0.51 Å (8–4 Å) respectively. Likewise the Cruickshank estimates are 0.29 and 0.72 Å, respectively, with due account taken of the use of restraints in these refinements.

1 L. E. Kay and K. H. Gardner, *Curr. Opin. Struct. Biol.*, 1997, **7**, 722.
2 A. Wlodawer, *Prog. Biophys. Mol. Biol.*, 1982, **40**, 1.
3 T. R. Gamble, K. R. Clauser and A. A. Kossiakoff, *Biophys. Chem.*, 1994, **53**, 15.
4 K. B. Schowen and R. L. Schowen, *Methods Enzymol.*, 1982, **87**, 551.
5 D. S. Berns, *Biochemistry*, 1963, **6**, 1377.
6 A. Hattori, H. L. Crespi and J. J. Katz, *Biochemistry*, 1965, **4**, 1213.
7 D. J. Brockwell, *The Inhibition of Elongation Factor Tu by Kirromycin*, PhD Thesis, University of Manchester, 1996.
8 J. P. Derrick, L. Y. Lian, G. C. K. Roberts and W. V. Shaw, *Biochemistry*, 1992, **31**, 8191.
9 R. J. Brennan, A. Awan, J. Barber, E. Hunt, K. L. Kennedy and S. Sadegholnejat, *J. Chem. Soc., Chem. Commun.*, 1994, 1615.
10 D. Bloor, *Production of Deuteriated Elongation Factor Tu for Use in NMR Studies*, PhD Thesis, University of Manchester, 1992.
11 M. Kjeldgaard and J. Nyborg, *J. Mol. Biol.*, 1992, **223**, 724.
12 G. J. Kleywegt and T. A. Jones, *Joint CCP4 and ESF-EACBM Newsletter on Protein Crystallography*, 1994, **31**, 9.
13 P. J. Kraulis, *J. Appl. Crystallogr.*, 1991, **24**, 946.
14 Collaborative Computational Project, Number 4, S. Bailey, *Acta Crystallogr., Sect. D*, 1994, **50**, 760.
15 A. T. Brünger, *X-PLOR v3.1 Manual—A System for Crystallography and NMR*, Yale University Press, New Haven, CT, USA, 1992.
16 P. V. Luzzati, *Acta Crystallogr.*, 1952, **5**, 802.
17 G. J. Kleywegt and A. T. Brunger, *Structure*, 1996, **4**, 897.
18 G. Kleywegt, T. Bergfors, H. Senn, L. P. B. Gsell, K. Shudo and T. A. Jones, *Structure*, 1994, **2**, 1241.
19 D. W. J. Cruickshank, in *Macromolecular refinement, Proceedings of the Daresbury Study Weekend*, Daresbury Laboratory, Warrington W4A 4AD, 1996, pp. 11–22.

Received in Cambridge, UK, 9th February 1998; 8/01152D

Expected and unexpected outcomes of a heteroborane isomerisation

Shirley Dunn, Georgina M. Rosair, Andrew S. Weller and Alan J. Welch*

Department of Chemistry, Heriot-Watt University, Edinburgh, UK EH14 4AS

Gentle thermolysis of compound 1, an intermediate in the isomerisation of an overcrowded icosahedral carbametallaborane, surprisingly yields two rearranged products, compound 2 (expected from theory) and compound 3 (unexpected).

There is a substantial and continuing interest in the isomerisations of heteroboranes and the mechanisms by which such isomerisations occur.[1] Recently[2] we reported the first experimental isolation of an intermediate in the isomerisation of an overcrowded, notional C_{cage}-adjacent icosahedral metallacarborane. We showed that this species has a closed, non-icosahedral structure which previously had been recognised only theoretically,[3] and we demonstrated that it was a true intermediate by effecting its conversion to a C_{cage}-separated icosahedron on gentle warming.

We now report the results of initial experiments with a system where one boron vertex is tagged with an SMe_2 group, which allows significant new insight into the precise isomerisation mechanism.

Deprotonation of the recently reported carbaborane 7,8-Ph_2-9-SMe_2-7,8-*nido*-$C_2B_9H_9$[4,5] with NaH in thf, followed by reaction with $[MoBr(MeCN)_2(\eta^3\text{-}C_3H_5)(CO)_2]$ at 0 °C, yields the neutral, charge-compensated species **1** in good yield.‡ Compound **1** displays carbonyl stretching bands in the IR spectrum at relatively high frequency (1971 and 1917 cm^{-1}, CH_2Cl_2) which identify it as a potential non-icosahedron. This was confirmed by a crystallographic study§ which revealed the structure shown in Fig. 1. Thus compound **1** constitutes only the second example of a derivative of Wales' hypothetical '1,2-C_2' intermediate[3] in the isomerisation of 1,2-*closo*-$C_2B_{10}H_{12}$ to 1,7-*closo*-$C_2B_{10}H_{12}$. However, the presence of the SMe_2 function attached to B(3) affords the possibility of mapping the movement of that boron atom when **1** is converted to the appropriate analogue of 1,7-*closo*-$C_2B_{10}H_{12}$, thus yielding valuable additional mechanistic information.

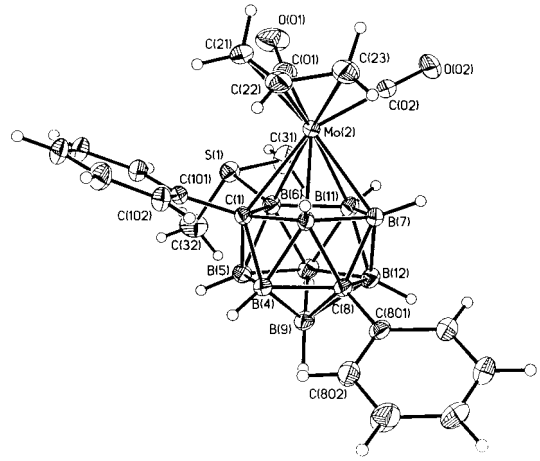

Fig. 2 Perspective view of **2**. Selected bond distances (Å) and angles (°): Mo(2)–C(01) 1.947(3), Mo(2)–C(02) 1.931(3), Mo(2)–C(21) 2.360(3), Mo(2)–C(22) 2.236(3), Mo(2)–C(23) 2.355(3), C(01)–O(01) 1.159(4), C(02)–O(02) 1.155(3), C(1)–C(101) 1.521(3), C(8)–C(801) 1.512(4), B(6)–S(1) 1.937(3); C(01)–Mo(2)–C(02) 77.73(13).

To our considerable surprise, gentle thermolysis (thf reflux) of **1** affords two new carbametallaboranes, compounds **2** and **3**, isolated by thin layer chromatography in reasonable yields.‡ Both display carbonyl stretching IR bands at low frequencies relative to those in **1** (1936 and 1853 cm^{-1} in **2**; 1931 and 1840 cm^{-1} in **3**) as expected for icosahedral compounds. Structural study of **2** and of **3**§ confirmed this prediction. Compound **2** (Fig. 2) has a 1,8-Ph_2-2-(η^3-C_3H_5)-2,2-$(CO)_2$-6-SMe_2-2,1,8-*closo*-$MoC_2B_9H_8$ architecture whereas in compound **3** (Fig. 3) the SMe_2 group is bound to B(7), *i.e.* **3** is 1,8-Ph_2-2-(η^3-C_3H_5)-2,2-$(CO)_2$-7-SMe_2-2,1,8-*closo*-$MoC_2B_9H_8$. The overall reaction scheme is shown in Scheme 1, compound **4**

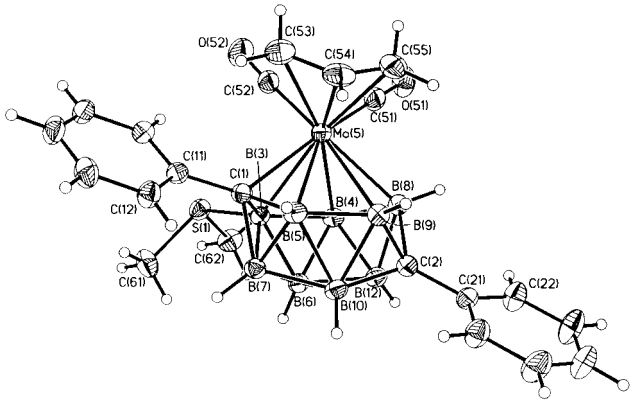

Fig. 1 Perspective view of **1** (numbered as in ref. 3). Selected bond distances (Å) and angles (°): Mo(5)–C(51) 1.973(4), Mo(5)–C(52) 1.989(4), Mo(5)–C(53) 2.374(4), Mo(5)–C(54) 2.243(4), Mo(5)–C(55) 2.362(4), C(51)–O(51) 1.152(4), C(52)–O(52) 1.153(4), C(1)–C(11) 1.506(4), C(2)–C(21) 1.493(3), B(3)–S(1) 1.934(3); C(51)–Mo(5)–C(52) 76.57(14).

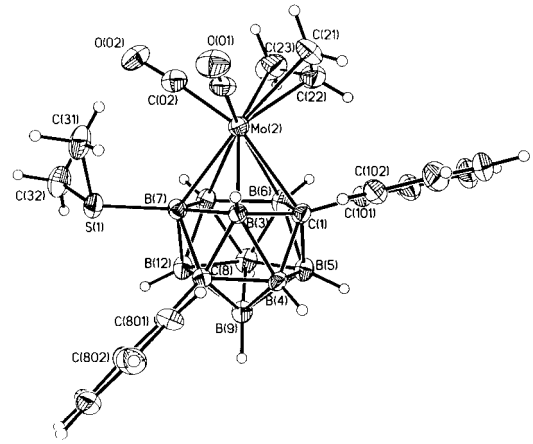

Fig. 3 Perspective view of **3**. Selected bond distances (Å) and angles (°): Mo(2)–C(01) 1.974(8), Mo(2)–C(02) 1.929(9), Mo(2)–C(21) 2.368(9), Mo(2)–C(22) 2.201(9), Mo(2)–C(23) 2.370(9), C(01)–O(01) 1.152(10), C(02)–O(02) 1.170(10), C(1)–C(101) 1.513(9), C(8)–C(801) 1.509(9), B(7)–S(1) 1.936(7); C(01)–Mo(2)–C(02) 85.1(3).

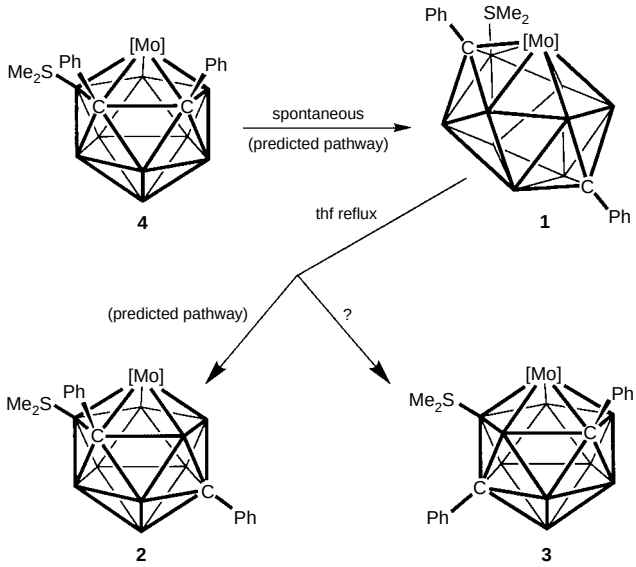

Scheme 1 Reaction scheme for formation of compound **1** from the notional overcrowded precursor **4**, and subsequent tranformation of **1** into both **2** and **3**. The pathways identified as 'predicted' are those which are in agreement with the predictions of ref. 3. [Mo] = $Mo(\eta^3\text{-}C_3H_5)(CO)_2$.

representing the likely non-isolable (overcrowded) initial reaction product. To support the assumption that the B–S bond remains intact under the conditions of gentle thermolysis employed, a sample of 7,8-Ph_2-9-SMe_2-7,8-*nido*-$C_2B_9H_9$ was heated to reflux in thf for 1 h and was recovered unchanged (^{1}H NMR spectroscopy).

As far as the relative positions of the cage carbon atoms is concerned both **2** and **3** are examples of '1,7-I_h' species. According to Wales[3] 1,2-I_h $C_2B_{10}H_{12}$ is predicted to transform to the 1,2-C_2 $C_2B_{10}H_{12}$ intermediate *via* a single route, whereas 1,2-C_2 $C_2B_{10}H_{12}$ can rearrange to 1,7-I_h $C_2B_{10}H_{12}$ *via* two possible routes, all pathways involving low symmetry transition states. We have successfully tracked the transformation of **4** into the isolated intermediate **1**, and one pathway for the subsequent transformation of **1** into **2**, thus providing experimental support for these theoretical predictions. However, the conversion of **1** into the unexpected product **3** must occur *via a* pathway not currently articulated, and clearly demonstrates that further experimental and theoretical work in this fascinating area is warranted.

We thank the EPSRC and the Callery Chemical Co. for support.

Notes and References

† E-mail: a.j.welch@hw.ac.uk

‡ *Syntheses and selected data*: **1**: 7,8-Ph_2-9-SMe_2-7,8-*nido*-$C_2B_9H_9$[4,5] (1.73 mmol) in thf (30 ml) was deprotonated with an excess of NaH, then added to a stirring solution of $[MoBr(MeCN)_2(\eta^3\text{-}C_3H_5)(CO)_2]$ (1.73 mmol) in thf (10 ml) at 0 °C. The solution was allowed to warm to room temp. and stirred for a total of 2 h. Removal of solvent *in vacuo* and work up by column chromatography [silica, CH_2Cl_2–light petroleum (7 : 3)] afforded a single orange band. Recrystallisation from CH_2Cl_2–light petroleum at 4 °C afforded diffraction-quality crystals of compound **1** (65% yield). IR (CH_2Cl_2) ν/cm^{-1}: 2554 (br, B–H), 1971 (vs, CO), 1917 (m, CO). ^{1}H NMR (200 MHz, $CDCl_3$), δ 7.85 (m, 2 H, Ph), 7.72 (m, 2 H, Ph), 7.38–7.19 (m, 6 H, Ph), 3.81 (m, 1 H, $allyl_{centre}$), 2.68 (dd, 1 H, $allyl_{syn}$), 2.55 (s, 3 H, SMe), 2.46 (dd, 1 H, $allyl_{syn}$), 2.15 (s, 3 H, SMe), 1.90 (d, 1 H, $allyl_{anti}$), 1.18 (d br, 1 H, $allyl_{anti}$); ^{11}B{^{1}H} NMR (124.8 MHz, $CDCl_3$), δ 15.1 (1 B), 6.8 (2 B), 1.9 (2 B), −3.8 (1 B), −15.0 (1 B), −24.1 (2 B).

2 and **3**: compound **1** (0.41 mmol) was dissolved in thf (15 ml) and heated to reflux for 1 h. Solvent was removed *in vacuo* and the residue applied as a concentrated CH_2Cl_2 solution to a TLC plate. Elution with CH_2Cl_2–light petroleum (2 : 3) (under a nitrogen atmosphere) afforded two mobile bands, compounds **2** (R_f *ca.* 0.30) and **3** (R_f *ca.* 0.35). Both bands were recovered and recrystallised from CH_2Cl_2–light petroleum at 4 °C to afford diffraction-quality crystals in 54 and 31% yield, respectively. **2**: IR (CH_2Cl_2) ν/cm^{-1}: 2569 (br, B–H), 1936 (vs, CO), 1853: (s, CO). ^{1}H NMR (200 MHz, $CDCl_3$), δ 7.43 (m, 2 H, Ph), 7.29–7.10 (m, 8 H, Ph), 4.19 (m, 1 H, $allyl_{centre}$), 3.32 (dd, 1 H, $allyl_{syn}$), 2.93 (s, SMe), 2.21 (s, SMe), 2.39 (dd, 1 H, $allyl_{syn}$), 1.42 (d, 1 H, $allyl_{anti}$), 1.32 (d, 1 H, $allyl_{anti}$); ^{11}B{^{1}H} NMR (128.4 MHz, $CDCl_3$), δ 2.7 (1 B), −1.4 (1 B), −3.4 (1 B), −4.3 (1 B), −7.4 (2 B), −12.1 (2 B), −14.5 (1 B). **3**: IR (CH_2Cl_2) ν/cm^{-1}: 2559 (m br, B–H), 1931 (vs, CO), 1840 (vs, CO). ^{1}H NMR (200 MHz, $CDCl_3$), δ 7.57 (m, 2 H, Ph), 7.38–6.87 (m, 8 H, Ph), 3.71 (dd, 1 H, $allyl_{syn}$), 3.18 (m, 1 H, $allyl_{centre}$), 2.59 (apparent s, 6 H, 2 × SMe), 1.80 (d, 1 H, $allyl_{syn}$), 1.62 (dd, 1 H, $allyl_{anti}$), 1.22 (d, 1 H, $allyl_{anti}$); ^{11}B{^{1}H} NMR (128.4 MHz, $CDCl_3$), δ 4.4 (1 B), 0.8 (1 B), −5.5 (3 B), −9.2 (1 B), −11.1 (sh, 1 B), −11.6 (1 B), −13.2 (1 B).

§ *Crystallographic data*: **1**: $C_{21}H_{29}B_9MoO_2S$, M_r = 538.7, crystal size 0.4 × 0.4 × 0.8 mm, monoclinic, space group $P2_1/n$, a = 13.4348(9), b = 10.7968(8), c = 19.0756(13) Å, β = 110.320(7)°, U = 2594.8(3) Å^3, Z = 4, D_c = 1.379 g cm^{-3}, F(000) = 1096, μ = 0.60 mm^{-1}. Siemens P4 diffractometer, 293(2) K, Mo-Kα radiation, λ = 0.710 73 Å, $2\theta_{max}$ = 50 °, 4567 unique reflections, 3456 observed [$F_o > 4\sigma(F_o)$], corrections for absorption (ψ-scans), Lorentz and polarisation effects. Structure solved by direct methods and refined (on F^2) by full-matrix least squares (339 variables) to R_1 = 0.0337, wR_2 = 0.0680 (for observed data), S = 1063. Max., min. residual electron density 0.25, −0.30 e Å^{-3}.

2: $C_{21}H_{29}B_9MoO_2S$, M_r = 538.7, crystal size 0.4 × 0.4 × 0.8 mm, monoclinic, space group $P2_1/n$, a = 11.8254(10), b = 11.5468(7), c = 19.7695(11) Å, β = 107.277(5)°, U = 2577.6(3) Å^3, Z = 4, D_c = 1.388 g cm^{-3}, F(000) = 1096, μ = 0.61 mm^{-1}. Siemens P4 diffractometer, 293(2) K, Mo-Kα radiation, λ = 0.710 73 Å, $2\theta_{max}$ = 50 °, 4539 unique reflections, 3639 observed [$F_o > 4\sigma(F_o)$], corrections for absorption (ψ-scans), Lorentz and polarisation effects. Structure solved by direct methods and refined (on F^2) by full-matrix least squares (307 variables) to R_1 = 0.0298, wR_2 = 0.0666 (for observed data), S = 1094. Max., min. residual electron density 0.29, −0.40 e Å^{-3}.

3: $C_{21}H_{29}B_9MoO_2S$, M_r = 538.7, crystal size 0.1 × 0.3 × 0.4 mm, monoclinic, space group $P2_1/n$, a = 12.8226(12), b = 13.840(2), c = 15.3573(14) Å, β = 109.733(7)°, U = 2565.4(5) Å^3, Z = 4, D_c = 1.395 g cm^{-3}, F(000) = 1096, μ = 0.61 mm^{-1}. Siemens P4 diffractometer, 293(2) K, Mo-Kα radiation, λ = 0.710 73 Å, $2\theta_{max}$ = 50°, 4475 unique reflections, 2881 observed [$F_o > 4\sigma(F_o)$], corrections for absorption (ψ-scans), Lorentz and polarisation effects. Structure solved by direct methods and refined (on F^2) by full-matrix least squares (307 variables) to R_1 = 0.0622, wR_2 = 0.1420 (for observed data), S = 1.047. Max., min. residual electron density 1.78, −0.75 e Å^{-3}. CCDC 182/819.

1 A. J. Welch and A. S. Weller, *J. Chem. Soc., Dalton Trans.*, 1997, 1205 and references therein.
2 S. Dunn, G. M. Rosair, Rh. Ll. Thomas, A. S. Weller and A. J. Welch, *Angew. Chem., Int. Ed. Engl.*, 1997, **36**, 645.
3 D. J. Wales, *J. Am. Chem. Soc.*, 1993, **115**, 1557. A most helpful animation of the isomerisation processes considered in this paper is available on the World Wide Web (http://brian.ch.cam.ac.uk/publications.html).
4 G. M. Rosair, A. J. Welch, A. S. Weller and S. K. Zahn, *J. Organomet. Chem.*, 1997, **536**, 299.
5 G. M. Rosair, A. J. Welch and A. S. Weller, *Organometallics* 1998, in press.

Received in Cambridge, UK, 18th December 1997; 7/09061G

Supramolecular assembly of low-dimensional silver(I) architectures *via* amide–amide hydrogen bonds

Christer B. Aakeröy*† and Alicia M. Beatty

Department of Chemistry, Kansas State University, Manhattan, Kansas, 66506, USA

The ligand nicotinamide (L) is used to propagate the linear coordination geometry of AgL_2 into 1-D and 2-D assemblies *via* a combination of coordinate covalent bonds and specific intermolecular hydrogen-bond interactions; the precise nature of the resulting lamellar structures are also influenced by the nature of the counterion.

Some recent efforts in the field of crystal engineering have focused on the predictable assembly of organic molecular solids *via* intermolecular interactions,[1] and it has become clear that certain functional groups *e.g.* carboxylic acids and amides, are reliable, robust connectors for the formation of hydrogen-bonded organic networks.[2] However, relatively little work has been done in constructing predictable assemblies of coordination compounds *via* directional intermolecular interactions.[3] Ordered assemblies of transition metal complexes (*e.g.* 'coordination polymers'[4]) are being studied for their potential as useful conductive, porous and magnetic materials.[5] From a crystal engineering standpoint, the advantage of using transition metals is that the shape of the main building unit can be controlled by using a metal–ligand system that is known to exhibit a desired coordination geometry. A specific geometry can then be propagated throughout the crystal structure by attaching substituents (intermolecular connectors) to the ligands. In order to probe the strength and reliability of various intermolecular connectors, a low-dimensional metal–ligand system is a convenient starting point, as this may allow us to drive the assembly of linear coordination complexes into one or two dimensions in the crystal lattice *via* specific intermolecular interactions. Silver(I) is one of the few metal ions that commonly displays linear coordination, thus AgL_2 complexes of silver(I) with pyridine derivatives provide the required low-dimensional building blocks.[6] The amide functionality is an appropriate intermolecular connector for this study,[7] in part due to its well known ability to form hydrogen-bonding networks in organic molecular solids,[8] and also because it is unlikely that silver(I) ions will coordinate to either the amide carbonyl oxygen or amine nitrogen atoms in the presence of a pyridine nitrogen. In order to also investigate the influence of the steric requirements and hydrogen-bonding ability of the counter ion on the supramolecular assembly, we have initiated a systematic structural study of a family of silver complexes. We now report the X-ray single crystal structures of three new compounds,[9] $[Ag(C_5H_4NCONH_2)_2][O_3SCF_3]$ **1**, $[Ag(C_5H_4NCONH_2)_2][BF_4]$ **2** and $[Ag(C_5H_4NCONH_2)_2][PF_6]$ **3**, which contain infinite low-dimensional architectures, assembled through intermolecular hydrogen bonds.‡

The reaction of silver(I) triflate with nicotinamide leads to the formation of dinicotinamidesilver(I) triflate **1** (mp 183–185 °C), where the cationic complex contains a silver ion coordination to two nicotinamide ligands in a near-linear fashion, L–Ag–L 174.29(8)°. As expected, the coordination to the silver ion is through the ring nitrogen atoms. The 1-D geometry of the complex cation is propagated in the solid state through amide–amide hydrogen bonds [N···O 2.920(3) Å], leading to infinite $C_1^1(12)$ chains.[10] Neighbouring chains are linked through symmetry related hydrogen bonds, r(N···O) = 2.898(3) Å, forming a 'head-to-head' $R_2^2(8)$ motif. These two intermolecular interactions create an infinite ladder-like arrangement (Fig. 1). There are no further hydrogen-bond interactions between adjacent cationic ladders. The anion acts as a cross-link between two cationic ladders *via* weak hydrogen bonds to the two remaining amide hydrogen atoms, r(N···O) = 3.094(3) and 3.179(3) Å. Thus the presence of a triflate ion, which has oxygen atoms readily available as hydrogen-bond acceptors, does not disrupt the formation of the intended ligand–ligand hydrogen bonds, and the amide functionalities propagate a linear assembly of the silver complexes.

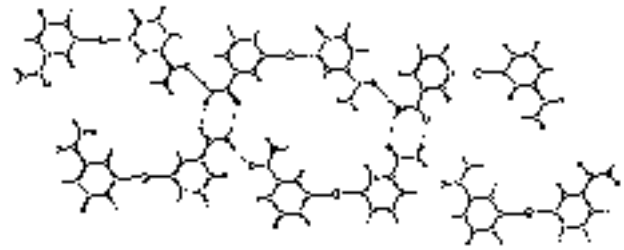

Fig. 1 Infinite 1D ladder motif in **1**, constructed *via* $C_1^1(12)$ and $R_2^2(8)$ hydrogen bonds between linear cationic moieties

Reaction of silver(I) tetrafluoroborate with nicotinamide yields the linear complex, dinicotinamidesilver(I) tetrafluoroborate **2** (mp 217–220 °C), where again the silver ion is coordinated to two ligands in a linear fashion, N–Ag–N [177.3(2)°]. However, in this structure, two unique amide–amide hydrogen bonds, r(N···O) = 2.966(7) and 2.863(7) Å, form two $C_1^1(4)$ chains, which generate infinite two-dimensional sheets (Fig. 2). The anions are sandwiched between cationic sheets, held there by two N–H···F; r(N···F) = 2.979(7) and 3.082(8) Å, and one C–H···F;r(C···F) = 3.138(7) Å, hydrogen bonds. The overall crystal packing displays an ...ABAABA...

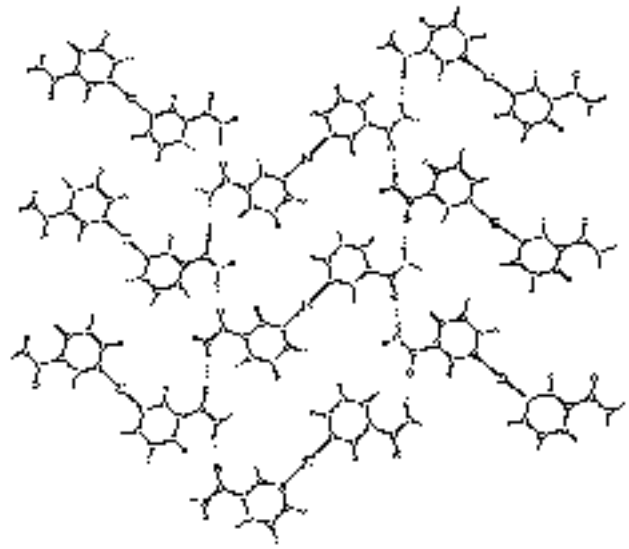

Fig. 2 2D cationic network in **2**, formed by $C_1^1(4)$ hydrogen bonds (the same 2D motif is found in the crystal structure of **3**

Fig. 3 Edge-on view of the lamellar crystal packing in **3**; hexafluorophosphate counter ions are positioned between silver-containing cationic sheets

arrangement, where A is a cationic sheet and B is an anionic layer (Fig. 3). Within ABA units the distance between cationic sheets is *ca.* 3.6 Å, while the separation between ABA units is *ca.* 3.2 Å, with no hydrogen bonds between cationic layers.

The reaction of silver(I) hexafluorophosphate with nicotinamide yields dinicotinamidesilver(I) hexafluorophosphate **3** (mp 234–238 °C), which again contains the expected linear cationic complex, N–Ag–N 173.4(1)°. Neighboring cations are linked *via* two unique amide–amide hydrogen bonds, r(N···O) = 2.943(4) and 2.870(4) Å, leading to a 2D network that is virtually identical to the cationic sheet observed in **2** (Fig. 2). The anions are positioned between sheets through two N–H···F hydrogen bonding interactions, r(N···F) = 3.033(4) and 3.058(4) Å. The crystal structure displays an ...ABAABA... packing (Fig. 3), with cationic sheets separated by *ca.* 3.8 Å within ABA units and *ca.* 3.4 Å between ABA units.

The structures of **1**, **2** and **3** demonstrate that the silver ion provides the desired linear AgL_2 building unit, and neighboring amide functionalities assemble these complexes into either 1-D or 2-D supramolecular architectures *via* intermolecular hydrogen bonds. Although the precise geometries of the hydrogen-bond networks change in this series, amide–amide interactions persist in the presence of anions with widely differing geometries and coordinating abilities. Consequently, we have gained a level of control over the way in which adjacent linear silver(I) complexes are arranged within the 3-D lattice. However, a detailed comparison of the crystal structures of **1** *vs.* **2** and **3** indicates that the counter ion does play an important role in the assembly of these complexes, resulting in the formation of either 1-D or 2-D cationic motifs based on prevailing amide–amide interactions. For example, 2-D cationic sheets are observed in structures where the anion is approximately spherical and with relatively low-coordinating ability ($[BF_4]^-$ and $[PF_6]^-$), whereas cationic ladders arise in the presence of a more anisotropic counter ion with stronger hydrogen-bond acceptors. In the case of the lamellar 2-D assemblies displayed by **2** and **3**, we hope to specifically control inter-layer separations by altering the characteristics of the counterion. Moreover, we are also examining how changes to the position of the amide functionality (*e.g.* 4-carboxamidepyridine *vs.* 3-carboxamidepyridine) and the presence of other substituents on the ligand, influence the nature of the hydrogen-bond networks and the resulting 3-D packing.

The work presented here illustrates that directional hydrogen bonds can be used in assembly of transition-metal complexes even in competition with potentially disruptive counterion interactions. Consequently, we can expect that many principles of crystal engineering that have been developed and tested in organic solid-state chemistry will assume further relevance in supramolecular aspects of coordination chemistry.

We acknowledge financial support from Kansas State University, NSF-EPSCoR (OSR-9550487) and DuPont.

Notes and References

† E-mail: aakeroy@ksu.edu

‡ *Crystal data*: **1**: $C_{13}H_{12}AgF_3N_4O_5S$, triclinic, space group $P\bar{1}$, a = 7.4761(5), b = 108812(7), c = 11.1832(9) Å, α = 98.898(6), β = 106.639(6), γ = 99.406(5)°, U = 845.2(1) Å^3, Z = 2, D_c = 1.969 g cm^{-3}, μ = 1.383 mm^{-1}, R_1 (all data) = 0.0191, R^2 (all data) = 0.0460.

2: $C_{12}H_{12}AgBF_4N_4O_2$, monoclinic, space group $P2_1/c$, a = 9.9693(7), b = 9.7488(6), c = 15.5105(10) Å, β = 97.971(4)°, U = 1492.9(2) Å^3, Z = 4, D_c = 1.953 g cm^{-3}, μ = 1.410 mm^{-1}, R_1 (all data) = 0.0591, R_2 (all data) = 0.1185.

3: $C_{12}H_{12}AgF_6N_4O_2P$ monoclinic, space group $P2_1/c$, a = 8.1458(7), b = 9.9241(10), c = 20.000(2) Å, β = 98.387(7)°, U = 1559.5(3) Å^3, Z = 4, D_c = 2.064 g cm^{-3}, μ = 1.442 mm^{-1}, R_1 (all data) = 0.0346, R_2 (all data) = 0.0566. CCDC 182/831.

1 G. R. Desiraju, *Crystal Engineering: The Design of Organic Solids*, Elsevier, Amsterdam, 1989; *Angew. Chem., Int. Ed. Engl.*, 1995, **34**, 2311; C. B. Aakeröy, *Acta Crystallogr., Sect. B*, 1997, **53**, 569; M. J. Zaworotko, *Nature*, 1997, **386**, 220; M. M. Conn and J. Rebek, Jr., *Chem. Rev.*, 1997, **97**, 1647.

2 S. Coe, J. J. Kane, T. L. Nguyen, L. M. Toledo, E. Wininger, F. W. Fowler and J. W. Lauher, *J. Am. Chem. Soc.*, 1997, **119**, 86; C. B. Aakeröy and M. Nieuwenhuyzen, *J. Am. Chem. Soc.*, 1994, **116**, 10 983; K. E. Schwiebert, D. N. Chin, J. C. MacDonald and G. M. Whitesides, *J. Am. Chem. Soc.*, 1996, **118**, 4018; R. E. Melendez, C. V. Krishnamohan, M. J. Zaworotko, C. Bauer and R. D. Rogers, *Angew. Chem., Int. Ed. Engl.*, 1996, **35**, 2213; O. Felix, M. W. Hosseini, A. de Cian and J. Fischer, *Angew. Chem., Int. Ed. Engl.*, 1997, **36**, 102; P. Brunet, M. Simard and J. D. Wuest, *J. Am. Chem. Soc.*, 1997, **119**, 2737; A. Marsh, M. Silvestri and J.-M. Lehn, *Chem. Commun.*, 1996, 1527; W. T. S. Huck, R. Hulst, P. Timmerman, F. C. J. M. van Eggel and D. N. Reinhoudt, *Angew. Chem., Int. Ed. Engl.*, 1997, **36**, 1006.

3 A. D. Burrows, C.-W. Chan, M. M. Chowdhry, J. E. McGrady and D. M. P. Mingos, *Chem. Soc. Rev.*, 1995, 329; A. D. Burrows, D. M. P. Mingos, A. J. P. White and D. J. Williams, *Chem. Commun.*, 1996, 97; L. Carlucci, G. Ciani, D. M. Proserpio and A. Sironi, *J. Chem. Soc., Dalton Trans.*, 1997, 1801; A. Hassan and S. Wang, *J. Chem. Soc., Dalton Trans.*, 1997, 2009; C. M. Drain, K. C. Russel and J.-M. Lehn, *Chem. Commun.*, 1996, 337;

4 O. M. Yaghi, G. Li and H. Li, *Nature*, 1995, **378**, 703; A. J. Blake, N. R. Champness, S. S. M. Chung, W.-S. Li and M. Schröder, *Chem. Commun.*, 1997, 1005; S. Subramanian and M. J. Zaworotko, *Angew. Chem., Int. Ed. Engl.*, 1995, **34**, 2127; E. C. Constable, *Chem. Commun.*, 1997, 1073; M. Fujita, Y. J. Kwon, S. Washizu and K. Ogura, *J. Am. Chem. Soc.*, 1994, **116**, 1151.

5 J.-M. Lehn, *Angew. Chem., Int. Ed. Engl.*, 1990, **29**, 1342; J. S. Miller, A. J. Epstein and W. M. Reiff, *Acc. Chem. Res.*, 1988, **21**, 114; S. Subramanian and M. J. Zaworotko, *Coord. Chem. Rev.*, 1994, **137**, 357.

6 D. Venkataraman, S. Lee, J. S. Moore, P. Zhang, K. A. Hirsch, G. B. Gardner, A. C. Covey and C. L. Prentice, *Chem. Mater.*, 1996, **8**, 2030; L. Carlucci, G. Ciani, D. M. Proserpio and A. Sironi, *J. Am. Chem. Soc.*, 1995, **117**, 4562.

7 Hydrogen bonding in transition metal complexes containing nicotinamide has been noted previously, however not in the context of supramolecular design: B. L. Kindberg, E. H. Griffith and E. L. Amma, *Chem. Commun.*, 1977, 461; A. Vegas, A. Pérez-Salazar and F. Silió, *Acta Crystallogr., Sect. B*, 1981, **37**, 1916; J. Emsley, N. M. Reza, H. M. Dawes and M. B. Hursthouse, *J. Chem. Soc., Dalton Trans.*, 1986, 313; J. Skorsepa, K. Györyovà, M. Melník, K. Smolander and M. Ahlgrèn, *Acta Crystallogr., Sect. C*, 1995, **51**, 1069.

8 Amide–amide interactions in organic molecular solids involve 'head-to-head' $R_2^2(8)$ or cetemer $C_1^1(4)$ hydrogen bonds: L. Leiserowitz and M. Tuval, *Acta Crystallogr., Sect. B*, 1978, **34**, 1230.

9 Suitable crystals of all compounds were grown from aqueous solutions containing 1 : 2 mixtures of the appropriate silver(I) salt and nicotinamide (3-pyridine carboxamide).

10 For information about graph-set notation, see: J. Bernstein, R. E. Davis, L. Shimoni and N.-L. Chang, *Angew. Chem., Int. Ed. Engl.*, 1995, **34**, 1555; M. C. Etter, J. C. MacDonald and J. Bernstein, *Acta Crystallogr., Sect. B*, 1990, **46**, 356.

Received in Cambridge, UK, 4th November 1997; 7/07919B

$NH_4V_3O_8$: a novel sinusoidal layered compound formed by the cation templating effect

Songping D. Huang*† and Yongkui Shan

Department of Chemistry and Center for Materials Research and Characterization, PO Box 23346, University of Puerto Rico, San Juan, PR 00931, USA

V_2O_5 reacts with aqueous NH_3 under hydrothermal conditions to give a novel sinusoidal layered compound $NH_4V_3O_8$; the structure features weak hydrogen bonds between the $V_3O_8^-$ layers and the NH_4^+ cations that occupy the interlayer space.

There has been renewed interest in alkali-metal vanadium oxide bronzes owing to their applications as cathode materials in rechargeable high-energy-density lithium batteries[1] and to their diverse structural chemistry.[2] The common synthetic schemes to produce such compounds include high temperature solid state reactions,[3] redox intercalations[4] or electrochemical methods.[5] Recently, hydrothermal techniques have been demonstrated to facilitate the synthesis and crystal growth of organic-based vanadium oxide bronzes such as α-, β-$(H_2en)_{0.5}V_2O_5$ (en = ethylenediamine)[6] and $(DABCOH_2)V_6O_{14}$ (DABCO = 1,4-diazabicyclo[2.2.2]octane),[7] to name but a few. To a lesser extent, hydrothermal methods are used in the synthesis of alkali-metal vanadium oxide bronzes.[8] We are interested in the chemistry of metastable layered alkali-metal vanadates that can be used as suitable starting materials for *in situ* hydrothermal intercalation/liquid crystal templating reactions that may produce microporous–mesoporous composite materials.[9] Our entry to this chemistry capitalizes on both the unique chemical properties of V_2O_5 and the hydrothermal method. Vanadium pentoxide is slightly soluble in water and forms a pale yellow solution containing dispersed V_2O_5 layers. Such exfoliated layers can react with acids to give the discrete cationic VO_2^+ species as well as react with bases to give a variety of mono-, di- and polyoxometallate anions.[10] By controlling the basicity of the reaction media and by judicious selection of suitable template cations, we have been able to direct the reaction of V_2O_5 with inorganic bases to form new solid state vanadate compounds rather than discrete isopolyvanadate anions. In this report, we wish to describe the synthesis and structural characterization of a novel layered vanadium oxide compound, $NH_4V_3O_8$ **1**, formed by a mild hydrothermal reaction. Compound **1** is distinct from the many layered compounds in the alkali-metal vanadium oxide family in that it contains highly corrugated layers, and all the vanadium ions in the structure are in the +5 oxidation state.

Pure $NH_4V_3O_8$ can be conveniently prepared from the base-induced polymerization/condensation reaction of V_2O_5 with aqueous NH_3 under hydrothermal conditions. Thus, when a sealed thick-walled Pyrex tube containing 100 mg (0.55 mmol) V_2O_5, 30 mg (0.56 mmol) NH_4Cl, 0.1 ml (0.37 mmol) 28% aqueous NH_3 and 0.5 ml of a mixed solvent composed of H_2O–MeOH (1 : 1, v/v) was heated at 110 °C for 4 days, analytically pure orange–brown single crystals of $NH_4V_3O_8$ were obtained in *ca.* 52% yield.‡ It is important to control the molar ratio of V_2O_5 : NH_3 to *ca.* 3 : 2 as excess NH_3 will lead to the formation of NH_4VO_3 as a by-product. However, addition of NH_4Cl to the reaction can increase the yield while suppressing the formation of the by-product. Eqn. (1) is the mass-balanced reaction that describes the formation of **1**:

$$3V_2O_5 + 2NH_3(aq) + H_2O \xrightarrow{\text{hydrothermal reaction}} 2NH_4V_3O_8 \quad (1)$$

The structure of **1** was determined by X-ray single crystal analysis.§¶ The asymmetric unit contains one N, three H, two V and five O atoms. Six atoms, including N, H(1), H(2), V(2), O(2) and O(5), are situated on the crystallographic mirror planes perpendicular to the [010] direction. The $V_3O_8^-$ layer is formed parallel to the *ab* plane, consisting of highly distorted VO_5 square pyramids around V(1) and VO_6 octahedra around V(2). First, every two square pyramids share a common edge. Such two edge-sharing square pyramid units are then linked with one another to form one-dimensional chains along the *b*-direction. Between these chains reside the VO_6 octahedra which share two edges with two neighboring, edge-sharing square-pyramidal units from one chain and two corners with two different square-pyramidal units from the adjacent chain in an alternating fashion. Fig. 1 shows the interconnection of the VO_5 square pyramids and VO_6 octahedra within one $V_3O_8^-$ layer. Five oxygen atoms are engaged in terminal, *i.e.* O(1) and O(2), doubly bridging, *i.e.* O(3) and triply bridging, *i.e.* O(4) and O(5) coordination, respectively. The layers are stacked along the *c*-direction with the NH_4^+ cations occupying the interlayer space. Because of the weak hydrogen bonding between the terminal oxygen atoms in the vanadium oxide layers and the H atoms from the NH_4^+ cations [*i.e.* O(1)–N 3.16 and O(2)–N 2.92 Å], the structure consists of highly corrugated $V_3O_8^-$ sheets arranged as if the layers intended to bend over in order to maximize the hydrogen bonding. As a result, each individual layer appears to have the sinusoid shape, shown in Fig. 2, so that two protons from a NH_4^+ cation can each form hydrogen bonds with two terminal O atoms on the same layer. Otherwise, a flat layer can only allow for a single hydrogen bond between the tetrahedral NH_4^+ ion and a terminal O atom from one layer.

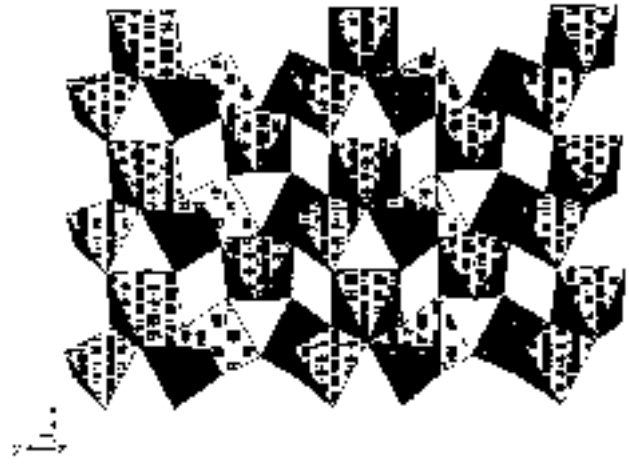

Fig. 1 The structure of one $V_3O_8^-$ layer, showing the interconnection of the VO_5 square pyramids and VO_6 octahedra

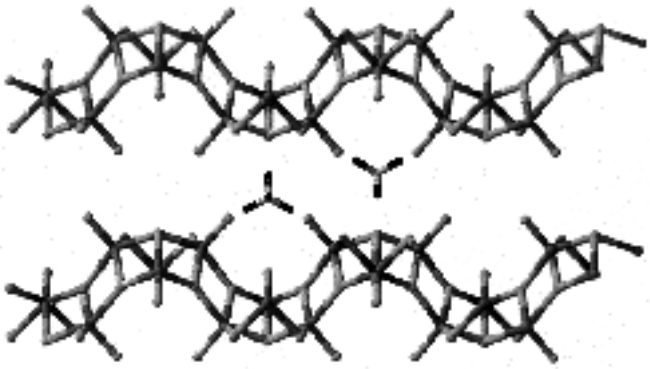

Fig. 2 The structure of layered $NH_4V_3O_8$, viewed down the *a*-direction

Both vanadium ions are in the +5 formal oxidation state as confirmed by the ESCA study.‖ The V–O bond distances within the layer range from 1.605(4) Å, involving the terminal oxygen atoms, to 2.281(6) Å, involving the triply bridging oxygen atoms.

In conclusion, a novel sinusoidal layered compound $NH_4V_3O_8$ has been synthesized and structurally characterized. Recently, Whittingham and coworkers showed that $(NMe_4)V_3O_8$ can be obtained by heating $(NMe_4)V_3O_7$ in air to *ca.* 200 °C.[11] However, the structure of $(NMe_4)V_3O_8$ has remained unknown, and is possibly related to **1**. In the current synthesis, **1** can best be thought of as being formed by reconstructing V_2O_5 layers through a base-induced polymerization/condensation reaction in the presence of the NH_4^+ cation template. To the best of our knowledge, **1** is the first example of a ternary layered vanadium oxide obtained by such a route. This method may open up a new avenue to a potentially large number of novel layered or open-framework materials with the use of other suitable templates.

This work was supported by the US National Science Foundation and the Department of Energy Through the EPSCoR Programs (OSR-9452893 and DE-FC02-91ER75674). We thank the National Institutes of Health for a grant in support of the purchase of a Siemens CCD SMART diffractometer (3S06GM08102-25S1/M1HREV).

Notes and References

† E-mail: huang@zintl.chem.uprr.pr

‡ The product was isolated by water and acetone washing and separated by hand from a small amount of colorless NH_4VO_3 (*ca.* 5–10%) crystals and black $V_3O_{7+\delta}$ (*ca.* 2%) crystals. The unit cell parameters for $V_3O_{7+\delta}$ are: tetragonal, space group *P*4/*mbm* (no. 127), a = 8.9065(6), c = 5.5823(1) Å, U = 442.82(3) Å^3, Z = 2. We have not been able to refine the structure satisfactorily because of severe disorder at two oxygen sites.

§ *Crystallographic data* for **1**: $V_3O_8H_4N$, monoclinic, space group $P2_1/m$ (no. 11), a = 4.993(7), b = 8.423(1), c = 7.849(1) Å, β = 96.426(3)°, U = 328.45(7) Å^3, Z = 2, D_c = 3.022 g cm^{-3}, μ = 4.189 mm^{-1}, T = 295 K, structure solution and refinement based on 480 reflections with $I_o \geqslant 3.0\sigma(I_0)$ converged at R = 0.036, R_w = 0.044 and goodness-of-fit = 1.15. Data were collected on a Siemens SMART diffractometer using Mo-Kα radiation (λ = 0.710 73 Å). An empirical absorption correction based on simulated ψ-scans was applied to the data set. All hydrogen atoms were located from the difference Fourier maps, and were included in the structure but not refined. Further details of the crystal structure investigations of **1** are available from the Fachinformationszentrum Karlsruhe, D-76344 Eggenstein-Leopoldshafen (Germany), on quoting the depository number CSD-407899. CCDC 182/829.

¶ The phase identity and homogeneity of **1** were confirmed by comparing the experimental X-ray powder diffrction patterns of the bulk material with those calculated from the single crystal X-ray data.

‖ Electron spectroscopy chemical analysis (ESCA) gave two overlapping peaks for V2p$_{3/2}$ at 515.37 and 516.68 eV, which is consistent with V^{5+} ions in two different coordination environments. In addition, the binding energies for O 1s are 533.77, 531.95 and 530.21 eV, confirming three different bonding modes of the oxygen atoms in $NH_4V_3O_8$.

1 M. S. Whittingham, *Prog. Solid State Chem.*, 1978, **12**, 41; *Solid State Ionics*, 1994, 69.
2 P. Hagenmuller, in *Non-Stoichiometric Compounds, Tungsten Bronzes, Vanadium Bronzes and Related Compounds*, ed. D. J. Bevan and P. Hagenmuller, Pergamon, Oxford, 1973, vol. 1.
3 P. Hagenmuller and A. Lesaicherre, *C. R. C. Hebd. Seances Acad. Sci.*, 1963, **256**, 170; H. Kessler and M. J. Sienko, *J. Solid State Chem.*, 1970, **1**, 152.
4 D. W. Murphy, P. A. Christian, F. J. Disalvo and J. V. Waszczak, *Inorg. Chem.*, 1979, **18**, 2800.
5 M. S. Whittingham, *J. Electrochem. Soc.*, 1976, **123**, 315.
6 D. Riou and G. Férey, *J. Solid State Chem.*, 1995, **120**, 137; D. Riou and G. Férey, *Inorg. Chem.*, 1995, **34**, 6520; Y. Zhang, R. C. Haushalter and A. Clearfield, *Inorg. Chem.*, 1996, **35**, 4950.
7 L. F. Nazar, B. E. Coene and J. F. Britten, *Chem. Mater.*, 1996, **8**, 327; Y. Zhang, R. C. Haushalter and A. Clearfield, *Chem. Commun.*, 1996, 1055.
8 Y. Oka, T. Yao and N. Yamamoto, *Nippon Seramikkusu Kyokai Gakujutsu Ronbunshi*, 1990, **98**, 1366.
9 Special Section, in *Science*, 1991, **254**, 1300; C. T. Kresge, M. E. Leonowicz, W. J. Roth, J. C. Vartuli and J. S. Beck, *Nature*, 1992, **359**, 710; J. S. Beck, J. C. Vartuli, W. J. Roth, M. E. Leonowicz, C. T. Kresge, K. D. Schmitt, C. T.-W. Chu, D. H. Olson, E. W. Sheppard, S. B. McCullen, J. B. Higgins and J. L. Schlenker, *J. Am. Chem. Soc.*, 1992, **114**, 10 834.
10 F. A. Cotton and G. Wilkinson, *Advanced Inorganic Chemistry*, Wiley, New York, 5th edn., 1988, pp. 668–669.
11 T. G. Chirayil, E. A. Boylan, M. Mamak, P. Y. Zavalij and M. S. Whittingham, *Chem. Commun.*, 1997, 33.

Received in Bloomington, IN, USA, 27th January 1998; 8/00743H

A cyano bridged iron(III) linear chain with alternating $Fe(CN)_6$–Fe(cyclam) (cyclam = 1,4,8,11-tetraazacyclodecane) units and unexpected ferromagnetic behaviour

Enrique Colacio,*† José M. Domínguez-Vera,[a] Mustapha Ghazi,[a] Raikko Kivekäs,[b] Martti Klinga[b] and José M. Moreno[a]

[a] *Departamento de Química Inorgánica de la Universidad de Granada, Facultad de Ciencias, Universidad de Granada, 18071 Granada, Spain*
[b] *Department of Chemistry, Laboratory of Inorganic Chemistry, University of Helsinki, Finland*

The X-ray crystal structure and magnetic properties of a cyano-bridged iron(III) linear chain containing alternating iron sites and unexpected ferromagnetic behaviour, justified on the basis of the axial distortion from regular octahedral geometry of one of the iron(III) ions, are reported.

The design and elaboration of new systems with original magnetic, optical and/or electrical properties is at the heart of molecular magnetism.[1] In the last few years, there has been a considerable interest in the preparation and properties of molecular magnets.[2] One potential general route to the synthesis of molecular magnets is to make analogues of Prussian blue, in which all the centres are paramagnetic.[3] Following this route, several Prussian analogues have been prepared with the aim of enhancing the ordering temperature by changing the nature of the interaction between the paramagnetic ions through the cyanide bridge. Recently, the room temperature barrier was overcome at 315 K with a $Cr^{III}/[V^{II}–V^{III}]$ compound.[4] Even though these materials can be synthesized by applying the techniques of molecular chemistry and then considered as molecular-based magnets, however, because their magnetic properties can only be tuned by changing the pair of interacting paramagnetic ions, they are close to the ionic magnets. Lately, a hybrid approach has been used in order to obtain molecular-based magnets. It consists of combining $[M(CN)_6]^{n-}$ building blocks with transition metal ion complexes. Following this approach several cyano-bridged bimetallic complexes with 2D[5] and 3D[6] structures have been prepared, which undergo magnetic phase transitions at lower temperature than the Prussian blue analogues. Because they are molecular systems their magnetic properties can be chemically tuned by not only varying the metal ions but also the ligands. By using the same synthetic strategy it is possible to design MM'_6 cyano bridged heptanuclear entities (M = Fe^{III} or Cr^{III}; M′ = Cu^{II} or Ni^{II} and Mn^{II}, respectively).[7] Among them, the $CrNi_6$ and $CrMn_6$ species exhibit high-spin ground states of S = 15/2 and 27/2, respectively. We have now found that from the building blocks $[Ni(cyclam)]^{2+}$ and $[Fe(CN)_6]^{3-}$, two different cyano-bridged complexes can be obtained, depending on the stoichiometric ratio of the reactants. Thus, by dropwise addition of an aqueous solution of $K_3[Fe(CN)_6]$ (1 mmol, 20 ml) to an aqueous solution of $[Ni(cyclam)][ClO_4]_2$ (1 mmol, 50 ml) a brown precipitate is immediately obtained, whose analytical data point to the formula $[Ni(cyclam)]_3[Fe(CN)_6]_2\cdot 6H_2O$. Preliminary magnetic measurements suggest that this compound orders ferromagnetically below 8 K. It is noteworthy that the precipitate dissolves upon addition of a large excess of $[Fe(CN)_6]^{3-}$ (10 : 1 molar ratio), leading to a dark green solution, from which prismatic dark brown crystals of $[Fe(cyclam)][Fe(CN)_6]\cdot 6H_2O$ **1** appear within one week.‡ It is noteworthy that the presence of a large excess of $[Fe(CN)_6]^{3-}$ promotes the substitution of Ni^{II} from $[Ni(cyclam)]^{2+}$ by Fe^{III}. Consequently, complex **1** can also be prepared from cyclam and $K_3[Fe(CN)_6]$. The structure§ of **1** was determined by X-ray analysis (Fig. 1) and it consists of polymeric chains of alternating $[Fe(CN)_6]^{3-}$ and $[Fe(cyclam)]^{3+}$ ions running along the *a* axis, and crystal water molecules. In the chain two CN^- groups of each $[Fe(CN)_6]^{3-}$ unit bridge two iron(III) atoms with Fe···Fe distances of 5.129(1) Å. Both types of iron atoms are located on symmetry elements 2/*m*, and the bridging CN^- ions as well as the C(6) atom of the cyclam ligand lie on the mirror plane. The chains are almost linear as the bond angles for the bridging CN^- group are *ca.* 175°. The Fe–C–N angles for terminal CN^- groups in $[Fe(CN)_6]^{3-}$ do not deviate significantly from linearity. The iron centre in the $[Fe(CN)_6]^{3-}$ unit adopts a minimally distorted octahedral environment, where the *cis*-C–Fe–C angles are close to 90° and Fe–C distances equal for bridging [1.925(8) Å] and terminal [1.936(6) Å] CN^- groups. Owing to coordination of the CN^- groups, the iron centre of the $[Fe(cyclam)]^{3+}$ unit assumes an axially distorted octahedral FeN_6 chromophore. The two axial positions are occupied by the nitrogen atoms of the bridging CN^- groups with Fe–N distances of 2.069(6) Å and the equatorial positions by the N_4 set of donor atoms from the cyclam ligand with Fe–N distances of 1.963(5) Å. The equatorial coordination planes of Fe(1) and Fe(2) are not parallel but form a dihedral angle of 10.7(1)°. In the crystal, the chains are linked by hydrogen bonds involving the lattice water molecules and the N(2) and N(4) nitrogen atoms of the $[Fe(CN)_6]^{3-}$ and $[Fe(cyclam)]^{3+}$ units, respectively, thus leading to a two dimensional layer structure. The donor–acceptor distances range from 2.738(8) to 2.836(7) Å, whereas the nearest Fe···Fe interchain separation is 8.101(1)

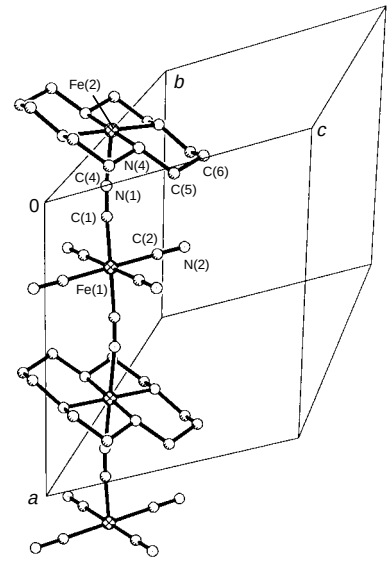

Fig. 1 A perspective view of the chain complex **1**

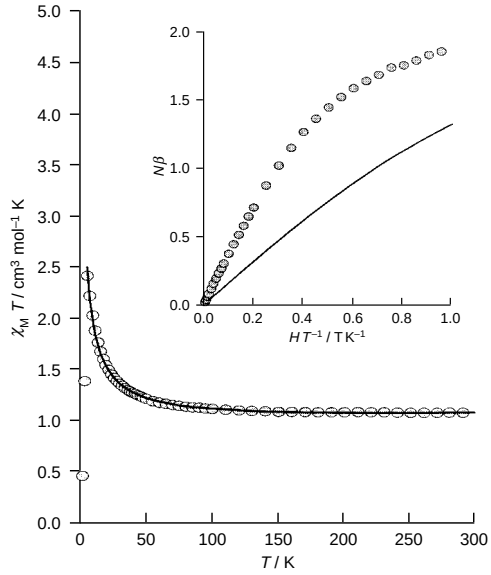

Fig. 2 Magnetic data ($\chi_M T$ *vs.* T) of **1**. Inset: magnetization data ($N\beta$ *vs.* H/T) of **1** (solid line represents the theoretical value of the Brillouin function for $S = \frac{1}{2}$).

Å. It should be noted that, among Fe^{III} polymers, structurally characterized chain complexes are rare and those with alternating iron sites are rarer still,[8] compound **1** being the first example of an iron(III) chain containing alternating iron sites but not alternating bridging ligands.

The temperature dependence of the $\chi_M T$ product per Fe_2 unit in the range 2–295 K is shown in Fig. 2. The $\chi_M T$ product at room temperature, 1.06 cm^3 mol^{-1} K, is significantly larger than the spin-only value of 0.75 cm^3 mol^{-1} K expected for two isolated low spin iron(III) ions ($S = \frac{1}{2}$), assuming $g = 2.00$, probably because of an orbital contribution to the magnetic moment of the low-spin Fe^{III} ions. As the temperature is lowered, $\chi_M T$ remains almost constant until around 100 K, then increases smoothly to reach a maximum of 2.41 cm^3 mol^{-1} K at 6 K and finally decreases sharply to 0.45 cm^3 mol^{-1} K upon cooling to 2 K. Such magnetic behaviour is characteristic of a dominant ferromagnetic coupling within the chain and interchain antiferromagnetic interactions, which are responsible for the decrease of $\chi_M T$ at very low temperature. The experimental magnetization values per Fe_2 unit as a function of the applied field at 5 K (Fig. 2) are greater than those predicted by the Brillouin function for two magnetically isolated iron(III) with $S = \frac{1}{2}$, thus confirming the existence of a ferromagnetic interaction between iron(III) ions. Apparently, **1** is the first example of an iron(III) chain exhibiting ferromagnetic intrachain exchange interactions. For estimating the magnitude of the ferromagnetic coupling, first, the magnetic susceptibility data ($T > 6$ K) were fitted to the Baker's expression[9] for a $S = \frac{1}{2}$ uniformly spaced ferromagnetic chain with the Hamiltonian in the form $H = -J \sum_i^{n-1} S_i \cdot S_{i+1}$.

The best fit parameters were $J = 8.6$ cm^{-1} and $g = 2.27$. The polycrystalline powder EPR spectrum at 100 K seems to be axial with $g_\perp = 2.21$ and $g_\parallel = 2.03$. At first glance, the ferromagnetic behaviour observed for **1** is rather unexpected taking into account the magnetic orbitals involved in the exchange interaction. Low-spin iron(III) ion in octahedral surroundings (t_{2g}^5) has the unpaired electron density on *xy*, *xz* and *yz* d orbitals, which are degenerate. If the Fe(1)–CN–Fe(2) bond is considered to lie along the *z* axis, with the *x* and *y* axes pointing toward the equatorial CN$^-$ groups for Fe(1) and toward the nitrogen atoms of the macrocycle for Fe(2), the *xz* and *yz* orbitals on both iron(III) ions would overlap through the π orbitals of the CN$^-$ group to give rise to antiferromagnetic contributions. A closer examination of the structure of **1**, however, reveals that while the coordination polyhedron of Fe(1) is almost perfectly octahedral (O_h point symmetry), that of Fe(2) is axially elongated along the CN–Fe(2)–NC direction (D_{4h}). For this tetragonal distortion the ground state configuration becomes $(xz, yz)^4(xy)^1$. Then, the ferromagnetic interaction might be the result of the orthogonality between the $(xy)^1$ orbital (b_{2g}) on Fe(2) and the *xz* and *yz* (t_{2g}) orbitals on Fe(1). It is of note that a similar unexpected ferromagnetic coupling has been also observed between two cyano-bridged Cr^{III}[d^3, $(t_{2g})^3$], in the compound *catena*-cyano(phthalocyaninato)chromium(III).[10] Even though no crystal structure determination has been reported for this compound, the Cr^{III} ions in the chain should be in a distorted octahedral surrounding. If so, a similar orbital explanation to that for **1** can be applied to the Cr^{III} compound in order to justify the observed ferromagnetic interaction. In view of these results, more examples are needed of cyano-bridged chain Cr^{III} and Fe^{III} complexes in order to definitively clarify the origin of the ferromagnetic exchange interaction. In this sense, the reaction of $[M(CN)_6]^{3-}$ (M = Cr^{III} and Fe^{III}) toward metal–macrocycle complexes is currently under examination.

This work was supported by the Dirección General de Investigación Científica y Técnica (project PB94-0764) and by the Junta of Andalucía.

Notes and References

† E-mail: ecolacio@goliat.ugr.es

‡ IR (cm^{-1}): ν(OH) 3583, 3480; ν(NH) 3349, 3100; ν(CN) 2151, 2125. Anal. Calc. for $C_{16}H_{36}Fe_2N_{10}O_6$: C, 33.32; H, 6.30; N, 24.30; Found: C, 33.29; H, 6.38; N, 24.04%.

§ *Crystal structure analysis* for **1**: Rigaku AFC7S diffractometer, graphite monochromatized Mo-Kα radiation, $\lambda = 0.71073$ Å, 298 K. Lorentz-polarisation and absorption corrections (ψ scan). $C_{16}H_{36}Fe_2N_{10}O_6$, monoclinic, space group *C*2/*m*, $a = 10.259(2)$, $b = 16.201(3)$, $c = 8.892(2)$ Å, $\beta = 110.99(3)°$, $U = 1379.8(5)$ Å^3, $Z = 2$, $D_c = 1.387$ Mg m^{-3}, $F(000) = 604$. $\mu = 1098$ mm^{-1}, crystal dimensions $0.22 \times 0.10 \times 0.09$ mm. 1335 Reflections were collected with 932 considered as observed [$I > 2\sigma(I_o)$]. Structure was solved by direct methods (SHELX-86) and refined on F^2 by full-matrix least squares to $R_1 = 0.0568$ ($wR_2 = 0.1124$). CCDC 182/827.

1 *Magnetism: a Supramolecular Function*, ed. O. Kahn, Kluwer Academic, NATO-ASI Series C-484, Dordrecht, 1996; *Molecular Magnetism: from Molecular Assemblies to Devices*, ed. E. Coronado, P. Delhaes, D. Gatteschi and J. S. Miller, Kluwer Academic, NATO-ASI Series E-321, Dordrecht, 1996.
2 *Magnetic Molecular Materials*, ed. D. Gatteschi, O. Kahn, J. S. Miller and F. Palacios, Kluwer Academic Publisher, NATO-ASI Series E-198, Dordrecht, 1991; O. Kahn, *Molecular Magnetism*, VCH, New York, 1993.
3 M. Verdaguer, *Science*, 1996, **272**, 698; W. Entley and G. S. Girolami, *Science*, 1995, **268**, 397; O. Kahn, *Nature*, 1995, **378**, 667.
4 S. Ferlay, T. Mallah, R. Ouahes, P. Veillet and M. Verdaguer, *Nature*, 1995, **378**, 701.
5 M. Ohba, N. Maruoono, E. Okawa, T. Enoki and J. M. Latour, *J. Am. Chem. Soc.*, 1994, **116**, 11566; M. Ohba, E. Okawa, T. Ito and A. Ohto, *J. Chem. Soc., Chem. Commun.*, 1995, 1545; H. Miyasaka, N. Matsumoto, N. Re, E. Gallo and C. Floriani, *Inorg. Chem.*, 1997, **36**, 670; H. Miyasaka, N. Matsumoto, H. Okawa, N. Re, E. Gallo and C. Floriani, *J. Am. Chem. Soc.*, 1996, **118**, 981; H.-Z. Kou, D.-Z. Liao, P. Cheng, Z.-H. Jiang, S.-P. Yan, G. L. Wang, X.-K. Yao and H.-G. Wang, *J. Chem. Soc., Dalton Trans.*, 1997, 1503.
6 M. Salah El Fallah, E. Rentschler, A. Caneschi, R. Sessoli and D. Gatteschi, *Angew. Chem., Int. Ed. Engl.*, 1996, **35**, 9047.
7 R. J. Parker, D. C. R. Hockless, B. Moubaraki, K. J. S. Murray and L. Spiccia, *Chem. Commun.*, 1996, 2789; T. Mallah, C. Auberger, M. Verdaguer and P. Veillet, *J. Chem. Soc., Chem. Commun.*, 1995, 61; A. Scuiller, T. Mallah, M. Verdaguer, A. Nivorozkhin, J. Tholence and P. Veillet, *New J. Chem.*, 1996, **20**, 1.
8 C. S. Hong, J. Kim, N. H. Hue and Y. Do, *Inorg. Chem.*, 1996, **35**, 5110.
9 G. A. Baker Jr., G. S. Rushbruke and H. E. Gilbert, *Phys. Rev. A*, 1964, **135**, 1272.
10 M. Schwartz, W. E. Hatfield, M. D. Joesten, M. Hanack and A. Datz, *Inorg. Chem.*, 1985, **24**, 4198.

Received in Basel, Switzerland, 6th January 1998; 8/00188J

Molecular assembly of two-α-helix peptide induced by haem binding

Seiji Sakamoto, Akihiko Ueno and Hisakazu Mihara*†

Department of Bioengineering, Faculty of Bioscience and Biotechnology, Tokyo Institute of Technology, Nagatsuta, Yokohama 226-8501, Japan

A designed two-α-helix peptide H2α-17 bound effectively Fe^{III}–mesoporphyrin (haem), and the haem binding simultaneously induced the molecular assembly of the peptide from a monomeric to a tetrameric form.

The self-assembly of polypeptides and functional chromophores, such as chlorophyll and haem, has a significant role in nature, the assembled species displaying highly efficient functions. For example, in the bacterial light-harvesting complex LH2, nine identical units, each consisting of two kinds of α-helical polypeptides and three bacteriochlorophyll *a* (Bchl*a*) units, are combined into a ring-shaped assembly.[1] In the LH2 protein, the orientation and assembly of a large number of Bchl*a* units are regulated by the polypeptide three-dimensional structure in membranes and effective energy-transfer is accomplished. So far, in the field of *de novo* protein design, considerable effort has been devoted to construction of polypeptide three-dimensional structure and conjugation of porphyrin molecules *via* chelation[2–4] or covalent linkage[5–8] with peptides. However, to develop a larger supramolecular system, such as LH2, it will be necessary to construct and regulate self-assembling systems composed of multiple polypeptide units and porphyrin molecules. In line with this aim, we have designed and synthesized a two-α-helix peptide which binds Fe^{III}–mesoporphyrin (haem). Furthermore, we found that the haem-binding simultaneously induced the self-association of the peptide, and that the haem groups were highly oriented in the self-assembled peptides.

17-peptide segment was designed to take an amphiphilic α-helix structure, which was stabilized by two sets of E–K salt bridges (Fig. 1). The two segments were dimerized *via* the disulfide linkage of the Cys^{21} residues. As axial ligands of haem, His was introduced at the ninth position to deploy a haem parallel to the helix. Four Leu residues per helix were arranged around the His to construct a hydrophobic haem-binding site. Even though the hydrophobicity of the sequence may be low, it is expected that the haem binding increases the overall hydrophobicity of the peptide and induces molecular association through hydrophobic interactions. The peptide was synthesized *via* solid-phase methodology using the Fmoc strategy and purified with HPLC to high purity (> 98%). The peptide gave a molecular ion peak at *m*/*z* 4012.2 [(M + H)$^+$] (calc. 4011.7) *via* matrix assisted laser desorption ionization time-of-flight mass spectrometry.

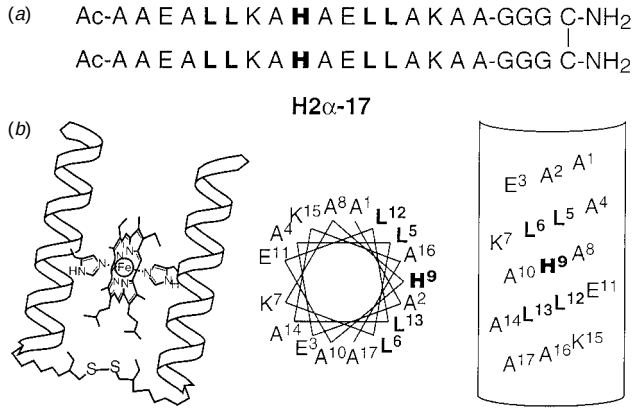

Fig. 1 Structure of the designed peptide, H2α-17. (*a*) Amino acid sequence of H2α-17; (*b*) illustration of the two-α-helix peptide structure bound to the haem, and helix wheel and net drawings of the 17-peptide.

Circular dichroism (CD) studies revealed that the peptide H2α-17 showed a typical α-helical pattern in buffer (pH 7.4) [Fig. 2(*a*)]. From the ellipticity at 222 nm ($[\theta]_{222}$ = −17 100 deg cm^2 dmol^{-1}), the α-helicity was estimated as 54%.[9] Since the monomeric peptide (H1α-17) showed a lower α-helix content ($[\theta]_{222}$ = −6800 deg cm^2 dmol^{-1}, 20%), the two α-helix segments in H2α-17 gathered together by orienting the hydrophobic side-chains inside, resulting in stabilization of the three-dimensional structure. Interestingly, the α-helicity of H2α-17 was increased by the addition of haem ($[\theta]_{222}$ = −26 800 deg cm^2 dmol^{-1}, 85%) [Fig. 2(*a*)]. The addition of an excess amount of cyanide ion (2.5×10^{-2} mol dm^{-3}, 2.5×10^3 equiv.) inhibited the coordination of H2α-17, resulting in a decrease in the α-helicity to the level observed without the haem. Additionally, there was no significant change in the CD spectra by the addition of haem at acidic pH (2.0–6.0). Because the pK_a of imidazole is *ca.* 6.0, the pH effect is attributed to the protonation of the His side chains such that they cannot act as a ligand. Therefore, we concluded that the increase in α-helicity of H2α-17 took place *via* the haem-binding by ligation with His residues. The thermal stability of the peptide in the presence or absence of haem was also examined by CD measurements. H2α-17 showed a midpoint of thermal transition (T_m) at 35 °C [Fig. 2(*b*)]. Similar to the α-helicity, haem binding increased remarkably the T_m value of the peptide to 62 °C. This result indicates that the haem binding increases the stability of the 2α-helix structure.

To further characterize the haem-binding with the peptide, UV–VIS titration of the haem with H2α-17 was carried out in buffer. With increasing peptide concentration, an increase of the Soret band at 405 nm and a decrease of the band at 355 nm of haem were observed (Fig. 3). That is, the UV–VIS spectrum of haem was converted from that of the high spin to the low spin form with an isosbestic point at 390 nm.[8] The UV–VIS spectrum of the haem in the presence of peptide resembles those

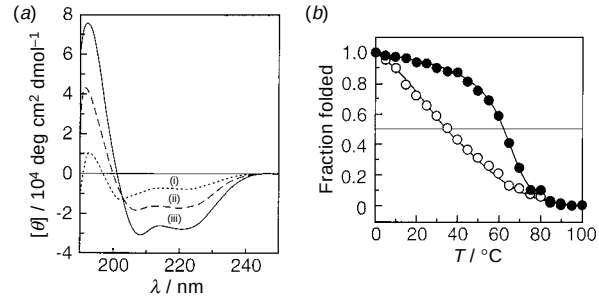

Fig. 2 (*a*) CD spectra of (i) H1α-17 and H2α-17 in the (ii) absence and (iii) presence of haem (1.0 equiv.) in 2.0×10^{-2} mol dm^{-3} Tris·HCl buffer (pH 7.4) at 25 °C. [H2α-17] = 1.0×10^{-5} mol dm^{-3} and [H1α-17] = 2.0×10^{-5} mol dm^{-3}. (*b*) Temperature denaturation profiles of H2α-17 in the (○) absence and (●) presence of haem (1.0 equiv.) in the buffer.

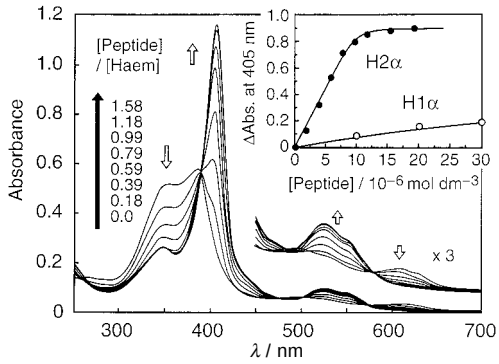

Fig. 3 UV–VIS spectra of haem with increasing H2α-17 concentration in the buffer (pH 7.4) at 25 °C. [haem] = 1.0×10^{-5} mol dm^{-3}. Inset: plots of absorbance at the Soret band of haem as a function of concentration.

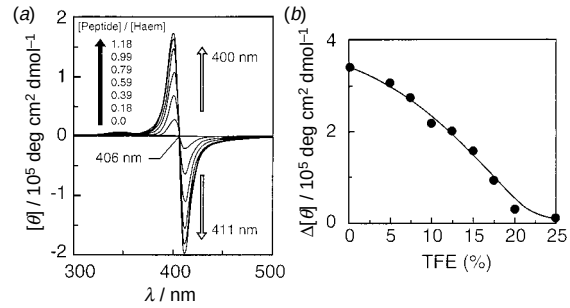

Fig. 5 (*a*) CD spectra of haem with increasing H2α-17 concentration in the buffer (pH 7.4) at 25 °C. [haem] = 1.0×10^{-5} mol dm^{-3}. (*b*) Effect of TFE content on the Soret CD intensity of haem bound to the peptide. $\Delta[\theta] = [\theta]_{max} - [\theta]_{min}$.

of natural cytochromes with six-coordinate iron. The binding constant (K_a) determined from the absorbance change at the Soret band using a single site binding equation,[4] was 1.1×10^7 mol^{-1} dm^3 (Fig. 3, inset). On the other hand, addition of H1α-17 caused little increase of the Soret band, suggesting that the monomeric peptide could not bind the haem effectively in this concentration range. This result implies that the 2α-helix structure and the consequent formation of the hydrophobic pocket are essential for the haem-binding.[4]

To examine the molecular assembly of the peptide in aqueous solution, the peptide samples were passed through a size-exclusion column. In the absence of haem, the peptide showed a sharp single peak [Fig. 4(*a*)]. It is reasonable to conclude that the peptide is in the monomeric form in the buffer, because sedimentation equilibrium studies demonstrated that the peptide existed as the monomeric form [MW_{obs} = 3600 (MW_{calc} = 4010)] under the same conditions. Furthermore, the peptide did not show any concentration dependence of the α-helicity at (0.1–2.0) $\times$ 10^{-5} mol dm^{-3}. When the peptide solution containing the haem (1.0 equiv.) was chromatographed, the haem was co-eluted with the peptide in a sharp peak at a higher molecular weight, suggesting that the haem was tightly bound to the peptide and that the haem-binding gave rise to the formation of a higher self-association state of the peptide [Fig. 4(*b*),(*c*)]. The sedimentation equilibrium studies revealed that the peptide was in a tetrameric form (MW_{obs} = 19 300, 4.2-mer) after haem-binding [Fig. 4(*d*)]. As further evidence supporting the self-association of peptide–haem conjugates, the haem bound to the peptide showed a strong induced CD peak in the Soret region, which was split into a negative peak at a longer wavelength and a positive peak at a shorter wavelength (Fig. 5). The split Cotton effect, *i.e.* exciton-coupling, indicates that the haem groups are highly oriented with respect to each other in close positions in the self-assembled peptides. With increasing percentage volume of trifluoroethanol (TFE), the ellipticity gradually decreased [Fig. 5(*b*)]. Dissociation of the haem from the peptide cannot explain the reduced Soret CD, because the UV–VIS study indicated that the peptide bound the haem with the six-coordinate form below 25% TFE (K_a = *ca.* x 10^7 mol^{-1} dm^3). Thus, the decrease of the Soret CD seems to be attributed to a change of association state of the peptide–haem conjugate from a tetrameric to a monomeric form. This TFE titration study implies that the hydrophobic interaction is important for the self-association of the peptide–haem conjugates. That is, the haem-binding increases the overall hydrophobicity of the amphiphilic 2α-helix peptide and induces the molecular assembly of the peptide–haem conjugates.

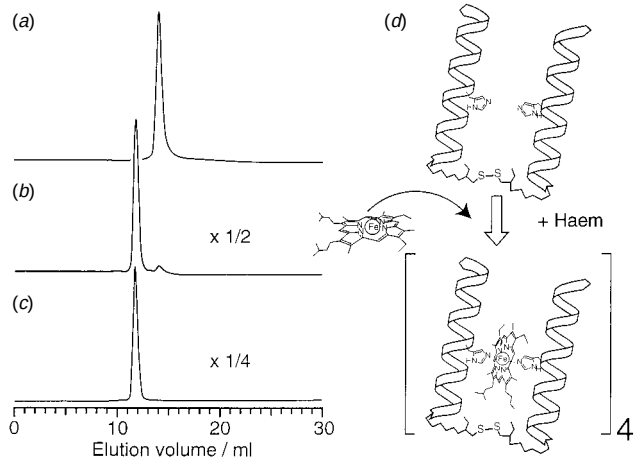

Fig. 4 Size-exclusion chromatograms of H2α-17 (*a*)–(*c*) and the schematic representation of self-assembly of two-α-helix peptide induced by the haem binding (*d*). (*a*) H2α-17 (1.0×10^{-5} mol dm^{-3}) in the absence of haem, detection at 220 nm. (*b*) H2α-17 (1.0×10^{-5} mol dm^{-3}) in the presence of haem 1.0 equiv.), detection at 220 nm. (*c*) H2α-17 (1.0×10^{-5} mol dm^{-3}) in the presence of haem (1.0 equiv.), detection at 405 nm. Column, Superdex 75 HR 10/30 (10 $\times$ 300 mm), 0.1 mol dm^{-3} NaCl/5.0 $\times$ 10^{-2} mol dm^{-3} Tris·HCl buffer (pH 7.4) at 25 °C; flow rate, 0.5 ml min^{-1}.

In conclusion, the association and orientation of functional chromophores can be accomplished using an artificially designed polypeptide. These findings could lead to studies applicable to the regulation of haem functions by polypeptide three-dimensional structures and to the development of peptidyl devices with haem functions.

We are grateful to Professor F. Arisaka, Tokyo Institute of Technology, for ultracentrifugation analyses.

Notes and References

† E-mail: hmihara@bio.titech.ac.jp

1 G. McDermott, S. M. Prince, A. A. Freer, A. M. Hawthornthwaite-Lawless, M. Z. Papiz, R. J. Cogdell and N. W. Isaacs, *Nature*, 1995, **374**, 517.
2 F. Rabanal, W. F. DeGrado and P. L. Dutton, *J. Am. Chem. Soc.*, 1996, **118**, 473.
3 H. K. Rau and W. Haehnel, *J. Am. Chem. Soc.*, 1998, **120**, 468.
4 S. Sakamoto, S. Sakurai, A. Ueno and H. Mihara, *Chem. Commun*., 1997, 1221.
5 T. Sasaki and E. T. Kaiser, *J. Am. Chem. Soc*., 1989, **111**, 380.
6 H. Mihara, Y. Haruta, S. Sakamoto, N. Nishino and H. Aoyagi, *Chem. Lett*., 1996, 1; H. Mihara, K. Tomizaki, T. Fujimoto, S. Sakamoto, H. Aoyagi and N. Nishino, *Chem. Lett*., 1996, 187.
7 F. Nastri, A. Lombardi, G. Morelli, O. Maglio, G. D'Auria, C. Pedone and V. Pavone, *Chem. Eur. J.*, 1997, **3**, 340; G. D'Auria, O. Maglio, F. Nastri, A. Lombardi, M. Mazzeo, G. Morelli, L. Paolillo, C. Pedone and V. Pavone, *Chem. Eur. J.*, 1997, **3**, 350.
8 P. A. Arnold, D. R. Benson, D. J. Brink, M. P. Hendrich, G. S. Jas, M. L. Kennedy, D. T. Petasis and M. Wang, *Inorg. Chem.*, 1997, **36**, 5306.
9 J. M. Scholtz, H. Qian, E. J. York, J. M. Stewart and R. L. Baldwin, *Biopolymers*, 1991, **31**, 1463.

Received in Cambridge, UK, 9th March 1998; 8/01900B

An antibody transesterase derived from reactive immunization that utilizes a wide variety of alcohol substrates

Chao-Hsiung Lin, Timothy Z. Hoffman, Yiling Xie, Peter Wirsching* and Kim D. Janda*†

Departments of Chemistry and Molecular Biology, The Scripps Research Institute and the Skaggs Institute for Chemical Biology, 10550 N. Torrey Pines Road, La Jolla, California 92037, USA

A monoclonal antibody obtained from reactive immunization catalyzes transesterifications of alcohol substrates with both broad and unusual specificity.

Reactive immunization has emerged as a new tool for the study of catalysis at the interface of chemistry and biology.[1] Unlike traditional immunization methods that invoke noncovalent interactions to elicit an antibody repertoire, reactive immunization makes use of a chemical reaction to direct the course of the immune response. Powerful applications have resulted in catalytic antibodies that use an enamine mechanism for myriad aldol reactions,[2,3] an alternative pathway for the allylic rearrangement exemplified by Δ^5-3-ketosteroid isomerase,[4] and the enantioselective hydrolysis of a naproxen ester.[5] A tenet which has emerged is that broad substrate specificities, ascribed to the special ontogeny of antibodies induced by immunogens that form covalent bonds within the binding pocket during induction, may be a feature in catalysts derived from reactive immunization.

We discovered that one of our earlier antibodies[1] SPO50C1, derived from immunization with a reactive bis(4-methylsulfonylphenyl) phosphonate, catalyzed the transesterification of *p*-sulfonylphenyl ester **1** by a large number of different alcohols **2** under aqueous conditions (Fig. 1). Therein, our results required the elaboration of the above hypothesis to include not only broad specificity, but also unanticipated or unusual characteristics with regard to substrate tolerance. Notably, alkyl alcohols as substrates in antibody catalysis have not been previously reported. The binding of these alcohols was unexpected, in light of the aromatic and immunogenic nature of the phenolic leaving group, as was their associated reactivities.

The mechanism of the SPO50C1 reaction to yield esters **3** proceeded by way of a covalent acyl–antibody intermediate (species F in the ping-pong notation of Cleland[6]) as substantiated quantitatively by pre-steady-state kinetic analysis of the observed stoichiometric 'burst' formation of phenol **4** upon antibody acylation (k_{obs} = 1.8 s^{-1}).‡ Therefore, as judged from rates of product ester formation (second product Q), deacylation was entirely the rate-determining step. In that SPO50C1 was also a relatively fast esterase with **1** (k_{cat} = 0.56 min^{-1}), alcohols competed effectively with water to partition the acyl intermediate.

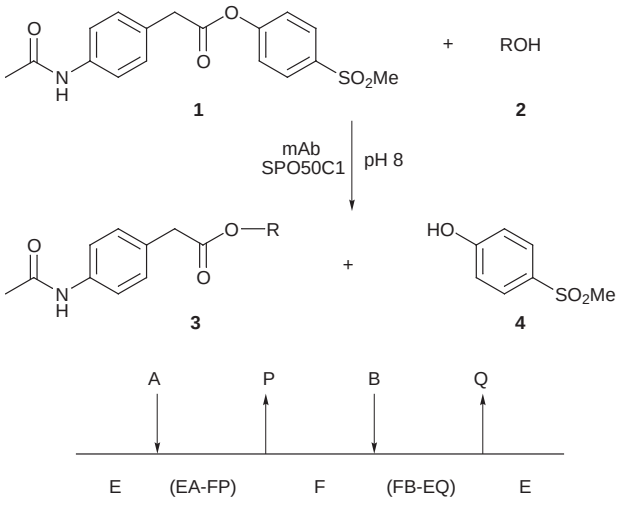

Fig. 1 Reaction catalyzed by SPO50C1

All alcohols were true substrates for the antibody and afforded observed saturation kinetics (Table 1). Significantly, it was shown that even at very high concentrations of some alcohols (*i.e.* 2.43 M for MeOH) the plateau in maximum rates resulted from saturation and not a detrimental 'organic solvent effect' on antibody activity.§ The trend in kinetic data cannot be explained merely in terms of the chemical reactivity of the alcohols, but most likely by a subtle interplay of nucleophilicity, hydrophobic effects and steric interactions.

Correlation analyses[7] of catalysis with Hansch hydrophobicity constants (π), Taft steric constants (E_s) or a multiparameter equation were nonlinear. While decreased K_m values roughly paralleled increased hydrophobicity [$\Delta\log(1/K_m)/\Delta\pi \sim 1$], k_{cat} showed the opposite bias together with breaks and plateaus. The specificity (k_{cat}/K_m) across the entire series of primary alcohols was remarkably similar with K_m becoming dominant and elevating k_{cat}/K_m about 10-fold only at high π values (π = 3.0, 3.5) (entries 10, 11) or with aromatic structures (entries 12, 13). MeOH, as might be predicted due to a low π (0.5), had the highest K_m, and perhaps because of its high nucleophilicity also gave the best turnover. The secondary alcohols were expectedly slower substrates than their primary congeners, however the differences did not reflect the solution reactivities of these alcohols (compare ratios of entries 3 and 4; k_{cat} = 4.4, k_{uncat} = 78.6). Although Bu^nOH (entry 5) and the other primary alcohols could be considered more efficient substrates (k_{cat}/K_m) than Pr^iOH, the latter was comparable or faster under saturating conditions [*i.e.* k_{cat} (entry 4)/k_{cat} (entry 5) = 5.6]. The k_{cat} for Pr^iOH even approached that of BnOH which was 128 times more reactive in solution. Furthermore, Pr^iOH was 10-fold and 100-fold faster than the other secondary alcohols (entries 7, 14), respectively; in addition cyclohexanol (not depicted) showed no detectable activity. Clearly, there was unique behavior associated with Pr^iOH as a substrate for SPO50C1.

The catalysis by SPO50C1 contrasts with the transesterification of some acyl trypsins[8] and esterases[9] where the more hydrophobic alcohols are often better substrates than lower homologs, except MeOH, and secondary alcohols show little or no activity. Also, Bu^nOH (entry 5) was particularly unusual and showed a tangible downward break in both k_{cat} and K_m. It is possible that nonproductive binding modes, as proposed for special substrates of chymotrypsin,[10] were operative. Aromaticity and steric constraints were contributing factors in the SPO50C1 reactions evidenced by the surprising lack of reactivity of cyclohexylmethanol (not depicted) (compare entries 6, 12). Interestingly, phenethyl alcohol was the most specific substrate which might reflect a favorable combination of hydrophobic and/or aromatic interactions and flexibility of the side-chain hydroxy functionality.

Table 1 Kinetic constants[a] for catalytic antibody SPO50Cl transesterification experiments

Entry	Substrate	k_{cat}/min^{-1}	K_m/mM	(k_{cat}/K_m)/ M^{-1} min^{-1}	k_{uncat}/ M^{-1} min^{-1}	Effective molarity/M
1	MeOH	1.4	8.7×10^2	1.7	2.9×10^{-3}	4.8×10^2
2	EtOH	0.19	3.1×10^2	0.60	2.8×10^{-4}	6.8×10^2
3	Pr^{n}OH	0.22	1.2×10^2	1.8	1.1×10^{-3}	2.0×10^2
4	Pr^{i}OH	0.050	5.1×10^2	0.090	1.4×10^{-5}	3.6×10^3
5	Bu^{n}OH	9.0×10^{-3}	19	0.48	1.5×10^{-4}	60
6	Bu^{i}OH	0.050	48	1.1	2.8×10^{-5}	1.8×10^3
7	Bu^{s}OH	1.4×10^{-3}	65	0.022	nd	nd
8	$C_5H_{11}OH$	0.020	7.3	2.9	3.7×10^{-5}	5.4×10^2
9	PrCH(Me)OH	2.0×10^{-3}	9.1	0.22	1.9×10^{-5}	1.1×10^2
10	$C_6H_{13}OH$	0.020	1.1	19	nd	nd
11	$C_7H_{15}OH$	0.020	1.2	17	nd	nd
12	BnOH	0.060	3.9	15	1.8×10^{-3}	33
13	$PhCH_2CH_2OH$	0.13	5.0	26	2.0×10^{-3}	65
14	MeCH(Ph)OH	4.0×10^{-4}	18	0.023	3.7×10^{-6}	1.1×10^2

[a] Determined at 22 °C in 100 mM bicine, pH 8.0 with 2% MeCN as cosolvent in the presence or absence of antibody. Antibody-catalyzed reactions used 10 μM SPO50Cl and varying concentrations of alcohol in the presence of substrate **1** fixed at 200 μM (close to both the solubility limit and saturation). The mAb has one functional active site (ref. 1). Assays were conducted using reverse-phase (C-18) HPLC (MeCN–H_2O–0.1% TFA eluent) by observing the formation of the ester product at 254 nm. The background rates for entries 4, 6, 8, 9 and 14 were determined at 60 °C and extrapolated to 22 °C by assuming an activation energy of 25 kcal mol^{-1}. The half-life for the spontaneous hydrolysis of **1** at 22 °C under the reaction conditions was 99 min. nd = Not determined (no ester formation was observed at 60 °C). All values have an estimated experimental error of ±10%.

The parameter of 'effective molarity'[11] was used as a measure of the catalytic power of SPO50C1. Although the mechanisms of the antibody-catalyzed and the one-step, base-catalyzed background transesterifications are different, an operational estimate can be made by comparing k_{cat} (min^{-1}) (k_{cat} represents the number of moles of ester product produced per mole of antibody per minute) to k_{uncat} (M^{-1} min^{-1}), the second-order rate constant for alcoholysis. Thus, for example, to achieve the same rate of product synthesis in the uncatalyzed transesterification of **1** by Pr^{i}OH, the concentration of Pr^{i}OH must approach 3600 M (0.050 min^{-1}/1.4×10^{-5} M^{-1} min^{-1}) (Table 1, entry 4). While our previous antibody transesterase, PCP21H3, derived from a transition-state analogue, attained rate enhancements of $>10^6$ M, the alcohol acceptors were restricted to a class structurally congruent to the hapten wherein small changes in binding energy were important.[12]

Our findings here indicated that the influence of structural and electronic factors upon catalysis were not overwhelming. The results refine our view that traditional, inert haptens program complementary binding pockets of somewhat limited scope, whereas reactive immunogens lead to active sites that are more unusual in their substrate tolerance and reactivity. This approach potentially allows one to procure antibodies with the intricate mechanisms of enzymes along with other features useful for biologcal and chemical applications.

This research was supported by NIH Grant GM43858 and The Skaggs Institute for Chemical Biology.

Notes and References

† E-mail: kdjanda@scripps.edu

‡ Reactions were performed in a Hi-Tech stopped-flow spectrophotometer by observing the increase in absorbance due to the formation of **4** (ε_{266} = 13 360 M^{-1} cm^{-1}); 0.2 ml cell, 1 cm path length, 0.2 ml stop volume, 33 ms filter time. The conditions were as described in Table 1 using 1.0 μM antibody.

§ None of the alcohols had any detrimental effect on activity as judged from time-dependent assays of free antibody incubated with alcohols at concentrations above the observed saturation limit.

1 P. Wirsching, J. A. Ashley, C.-H. L. Lo, K. D. Janda and R. A. Lerner, *Science*, 1995, **270**, 1775.
2 J. Wagner, R. A. Lerner and C. F. Barbas III, *Science*, 1995, **270**, 1797.
3 C. F. Barbas III, A. Heine, G. Zhong, T. Hoffmann, S. Gramatikova, R. Björnestedt, B. List, J. Anderson, E. A. Stura, I. A. Wilson and R. A. Lerner, *Science*, 1997, **278**, 2085.
4 C.-H. Lin, T. Z. Hoffman, P. Wirsching, C. F. Barbas III, K. D. Janda and R. A. Lerner, *Proc. Natl. Acad. Sci. USA*, 1997, **94**, 11 773.
5 C.-H. L. Lo, P. Wentworth Jr., K. W. Jung, J. Yoon, J. A. Ashley and K. D. Janda, *J. Am. Chem. Soc*., 1997, **119**, 10 251.
6 W. W. Cleland, *Biochim. Biophys. Acta*, 1963, **67**, 104.
7 C. Hansch and A. Leo, *Substituent Constants for Correlation Analysis in Chemistry and Biology*, Wiley, New York, 1979.
8 F. Seydoux, J. Yon and G. Némethy, *Biochim. Biophys. Acta*, 1969, **171**, 145.
9 P. Barton, A. P. Laws and M. I. Page, *J. Chem. Soc., Perkin Trans. 2*, 1994, 2021; D. Wynne and Y. Shalitin, *Eur. J. Biochem*., 1972, **31**, 554; P. Greenzaid and W. P. Jencks, *Biochemistry*, 1971, **10**, 1210.
10 M. I. Page, *Chem. Soc. Rev*., 1973, **2**, 295; M. I. Page and W. P. Jencks, *Proc. Natl. Acad. Sci. USA*, 1971, **68**, 1678.
11 W. P. Jencks, *Catalysis in Chemistry and Enzymology*, Dover, New York, 1969, ch. 5.
12 P. Wirsching, J. A. Ashley, S. J. Benkovic, K. D. Janda and R. A. Lerner, *Science*, 1991, **252**, 680.

Received in Glasgow, UK, 24th February 1998; 8/01569D

Precise control of RNA cleavage by ribozyme mimics

Andrew T. Daniher and James K. Bashkin*†

Department of Chemistry, Washington University, St. Louis, MO 63130-4899, USA

A highly-modified DNA building block, lacking both sugar and base moieties, is synthesized and incorporated into oligonucleotides to form functional mimics of ribozymes.

We demonstrate here that second-generation ribozyme mimics based on a serinol–terpyridine reagent, when incorporated into a DNA oligonucleotide, cleave their target RNA in a sequence-specific manner. Furthermore, the position of cleavage within the target sequence was precisely controlled by the location of the terpyridine within the oligonucleotide. These second-generation mimics function with greatly improved efficiency over our previous terpyridine reagents.[1,2] We attribute the improved cleavage to increased flexibility of the target RNA strand that results when serinol replaces a nucleotide in the DNA sequence: this eliminates a DNA/RNA base-pair near the cleavage site and may lower the barrier for phosphorane formation.

Functional ribozyme mimics consist of an oligonucleotide for molecular recognition and an attached RNA cleavage (transesterification) agent.[3,4] These ribozyme mimics are designed to extend the antisense approach to translation arrest by creating a catalytic cycle independent of any enzyme-mediated RNA cleavage. The antisense method is a gene-specific technique for blocking protein synthesis that inhibits the translation of mRNA into proteins.[5]

Our group previously reported the first wholly synthetic ribozyme mimic,[1] which was comprised of a 17-mer DNA probe with a pendant terpyridyl (terpy) complex of Cu^{II} incorporated in DNA *via* a thymidine derivative.[2] Aqueous (terpy)Cu^{II} is a known RNA transesterification and hydrolysis agent.[6–8]

We wished to improve cleavage efficiency and the ease of preparation of ribozyme mimics. Here we report greatly improved RNA cleavage and much simpler synthetic routes. The new reagents (Scheme 1) are conjugates of serinol and terpyridine. Serinol, a reduced form of serine, mimics the spacing of the sugar backbone of DNA; it and related compounds have previously been used as building blocks for abasic DNA sites.[9,10] An abasic DNA site eliminates one Watson–Crick base pair in a duplex and increases the conformational flexibility of the double-stranded region. The RNA in an RNA/DNA duplex is relatively inert towards cleavage when compared to its single-stranded form, perhaps because the duplex is a more conformationally rigid structure than the single strand.[11,12] Incorporation of the serinol residue into a DNA sequence allows formation of a duplex with the complementary RNA strand, and increases the flexibility of the RNA in the region opposite the serinol. This flexible RNA region should more readily form the pentacoordinate phosphorane required for transesterification, and should therefore undergo enhanced cleavage compared to a perfectly base-paired sequence.[9]

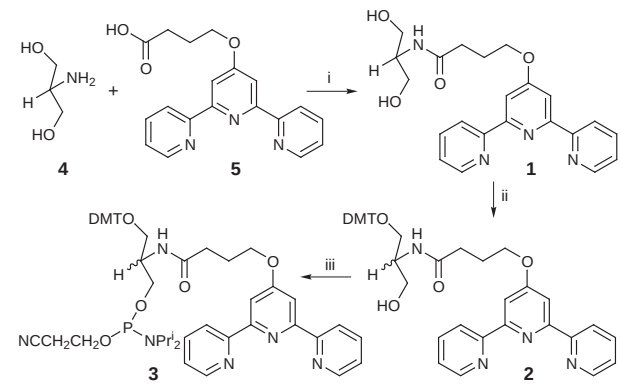

Scheme 1 *Reagents and conditions*: i, EDC, DMF, room temp., 30 h, 45.5%; ii, Py, Et_3N, DMT-Cl, 30%; iii, Et_3N, CH_2Cl_2, 2-cyanoethyl *N*,*N*-diisopropylchlorophosphoramidite, room temp. 20 min, 47%

Derivatizing serinol in an unsymmetrical fashion gave stereoisomers **A** and **B**. Fukui suggested that related compounds, derivatives of the 2*R*,3*R* isomer of L-threoninol, preferentially target the major groove upon incorporation into DNA.[13] Since free rotation can occur in the serinol backbone, both **A** and **B** should be able to reach either groove. This paper describes work on a mixture of stereoisomers **A** and **B**.

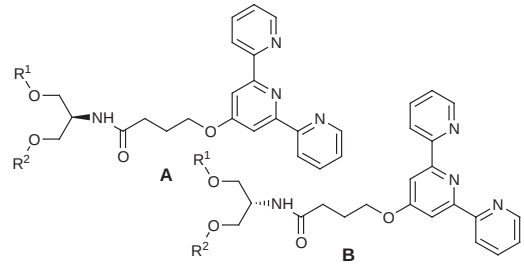

The synthesis of **3** is shown in Scheme 1. Serinol, a *meso* compound, possesses the same spacing between alcohols (three carbons) as a normal deoxynucleoside. Serinol **4** was coupled to the terpyridine (terpy) acid **5** with 1-(3-dimethylaminopropyl)-3-ethylcarbodiimide hydrochloride (EDC), giving **1** (45.5%). Subsequent 4,4′-dimethoxytrilyl (DMT) protection of one of the primary alcohols of **1** gave **2** in 30% yield. Phosphitylation of **2** resulted in the desired phosphoramidite **3** as a mixture of stereoisomers (47%).

Several 17-mer probes designed to target a 159-mer fragment of the HIV *gag* gene mRNA were prepared *via* automated DNA synthesis, using **3** and/or standard nucleoside phosphoramidites. The RNA sequence is shown below, with the 17-mer recognition region underlined.

5′-$^{1(775)}$GGAGAA^{6} AUUUAUAAAA^{16} GAUGGAUAAU^{26} CCUGGGAUUA^{36}
AAUAAAAUAG^{46} UAAGAAUGUA^{56} UAGCCCUACC^{66} CAGCAUUCUG^{76}
GACAUAAGAC^{86} AAGGACCAAA^{96} GGAAC<u>CUUUA</u>^{106} <u>GAGACUAUGU</u>^{116}
<u>AGA</u>CCGGUUC^{126} UAUAAAACUC^{136} UAAGAGCCGA^{146} GCAAGCUUCA^{156}
CAG$^{159(933)}$-3′

The 17-mer DNA probe sequences, in 5′ to 3′ orientations with **X** indicating the serinol–terpy residue, are:

1a 5′-CTACATAGTCTCTAAAG-3′ **1b** **X**TACATAGTCTCTAAAG
1c CTACA**X**AGTCTCTAAAG **1d** CTACATAG**X**CTCTAAAG
1e CTACATAGTC**X**CTAAAG

Derivatives **1b**–**e** of probe **1** differ in the location of the serinol–terpy residue, but all bind to the same region of the RNA target. Control probes for **1b**–**e** [named **1(b**–**e)-ctrl**] were also prepared using **6** (Glen Research) in place of serinol–terpy reagent **3**.

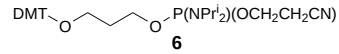

6

These probes explicitly test for any enhanced cleavage activity that flexible, abasic reagents might confer on the target RNA.

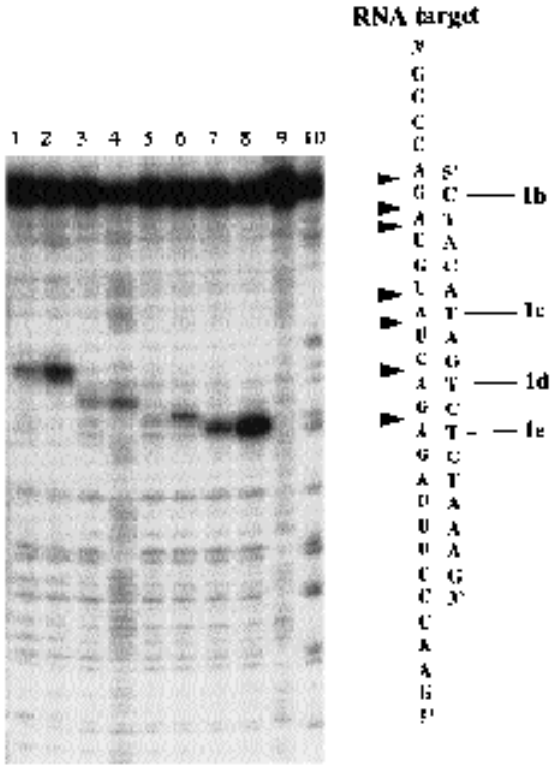

Fig. 1 Site-specific RNA cleavage with serinol–terpyridine probes. Lane 1: **1b**. Lane 2: **1b** + $CuCl_2$. Lane 3: **1c**. Lane 4: **1c** + $CuCl_2$. Lane 5: **1d**. Lane 6: **1d** + $CuCl_2$. Lane 7: **1e**. Lane 8: **1e** + $CuCl_2$. Lane 9: base. Lane 10: RNase T1. Reactions were carried out at 45 °C in a total volume of 10 μl containing the following: 0.1 M $NaClO_4$, 10 mM HEPES (pH 7.5), *ca* 10^{-9} M RNA target, 5 μM probe and 10 μM $CuCl_2$. The probes and $CuCl_2$ were premixed. The reactions were stopped after 24 h with EDTA.

Having prepared the serinol–terpy probes and appropriate controls, we investigated their inherent RNA cleavage abilities. Fig. 1 shows representative results from one set of experiments in which the cleavage of the target RNA was carried out by **1b–e**. To perform these reactions, a solution of a probe (5 μM) was combined with 5′-end labelled RNA (*ca*. 10^{-3} μM) in 10 mM HEPES buffer (pH 7.5), with 0.1 M $NaClO_4$ to control ionic strength. As indicated in Fig. 1, each experiment was done both with and without added 10 μM $CuCl_2$. Reactions were incubated at 45 °C and analyzed by electrophoresis on a denaturing 6% polyacrylamide gel.

Cleavage resulting from the various serinol–terpy-containing probes occurred at the RNA nucleotides opposite the serinol–terpy groups. As the terpy was moved from one internal position to the next, the cleavage followed in a precise manner (Fig. 1). Cleavage occurred whether the terpy was at an internal or external position of the RNA/DNA duplex. No specific cleavage occurred for the unmodified DNA control probe **1a** or the controls **1(b–e)-ctrl** (data not shown). Thus, the flexible, abasic site generated by **6** did not promote cleavage of the RNA target.

The amount and the location of cleavage depended on the serinol–terpy probe used and the temperature. However, the major determining factor was the primary sequence and location of the catalyst. Cleavage sites were identified by comparison with RNase Tl and base hydrolysis lanes (Fig. 1 and Table 1). Generally, cleavage occurred to the 3′- and 5′-sides of the RNA nucleotide opposite serinol, and spanned from one to three positions. Apparent background cleavage is seen in Fig. 1 in those lanes (1,3,5 and 7) corresponding to reactions with no added Cu^{II}. Additional experiments showed that this background cleavage derives from Cu^{II} ion that is scavenged by the terpy-containing DNA probes during synthesis and purification (data not shown). Treating the probes with EDTA prior to reaction eliminated the background cleavage. Adding Cu^{II} (but not divalent Fe, Mg, Pb or Zn) recovered the cleavage activity of the EDTA-treated ribozyme mimics (data not shown).

Table 1 Cleavage results from sequence-specific reactions of ribozyme mimics with the 159-mer target RNA, in the presence of Cu^{II} ion

		% Total cleavage	
Probe	Cleavage Sites	24 h	72 h
1b	G^{118}, A^{117}, U^{116}	18	48
1c	A^{113}, U^{112}	10	35
1d	A^{110}	10	40
1e	A^{108}	48	84

The synthesis of the serinol–terpyridine building block allows the introduction of cleaving agents anywhere within a DNA probe. This approach provides a much more efficient synthetic means of incorporating terpy into oligonucleotides than the preparation of intact nucleoside derivatives. We observed a marked increase in cleavage efficiency compared to our first-generation ribozyme mimics. Our first mimic cleaved 28% of its target after 3 days at 45 °C. Our best second-generation mimic cleaved 84% of its target after 3 days at 45 °C. The serinol backbone may enhance transesterification because it creates an artificial abasic site when incorporated into an oligonucleotide and duplexed to RNA. The RNA site opposite this modified monomer is not base-paired, so it has greater flexibility. This flexibility should allow the terpy ligand to span both the major and minor grooves in the RNA/DNA duplex, and should allow the RNA to adopt reactive conformations. The serinol–terpyridine ribozyme mimics are consistent with our belief that cleavage must occur within the duplex region in order to free the mimic for catalytic turnover.

This work was supported in part by NSF Grant CHE-9318581. Acknowledgment is also made to the donors of The Petroleum Research Fund, administered by the ACS, for partial support of this research.

Notes and References

† E-mail: Bashkin@wuchem.wustl.edu

1 J. K. Bashkin, E. I. Frolova and U. S. Sampath, *J. Am. Chem. Soc.*, 1994, **116**, 5981.
2 J. K. Bashkin, J. Xie, A. T. Daniher, U. Sampath and J. L.-F. Kao, *J. Org. Chem.*, 1996, **61**, 2314.
3 B. N. Trawick, A. T. Daniher and J. K. Bashkin, *Chem. Rev.*, 1998, in the press.
4 D. Magda, M. Wright, S. Crofts, A. Lin and J. L. Sessler, *J. Am. Chem. Soc.*, 1997, **119**, 6947.
5 A. D. Mesmaeker, R. Haener, P. Martin and H. E. Moser, *Acc. Chem. Res.*, 1995, **28**, 366.
6 L. A. Jenkins, J. K. Bashkin and M. E. Autry, *J. Am. Chem. Soc.*, 1996, **118**, 6822.
7 S. Liu and A. D. Hamilton, *Tetrahedron Lett.*, 1997, **38**, 1107.
8 B. Linkletter and J. Chin, *Angew. Chem., Int. Ed. Engl.*, 1995, **34**, 472.
9 M. A. Reynolds, T. A. Beck, P. B. Say, D. A. Schwartz, B. P. Dwyer, W. J. Daily, M. M. Vaghefi, M. D. Metzler, R. E. Klem and L. J. Arnold, Jr., *Nucleic Acids Res.*, 1996, **24**, 760.
10 K. Fukui, K. Iwane, T. Shimidzu and K. Tanaka, *Tetrahedron Lett.*, 1996, **37**, 4983.
11 K. A. Kolasa, J. R. Morrow and A. P. Sharma, *Inorg. Chem.*, 1993, **32**, 3983.
12 D. Huesken, G. Goodall, M. J. J. Blommers, W. Jahnke, J. Hall, R. Haener and H. Moser, *Biochemistry*, 1996, **35**, 16 591.
13 K. Fukui, M. Morimoto, H. Segawa, K. Tanaka and T. Shimidzu, *Bioconjugate Chem.*, 1996, **7**, 349.

Received in Bloomington, IN, USA, 30th January 1998; 8/00818C

A pyridazine Schiff-base macrocycle hosts a dicobalt centre in five different redox states: evidence for a mixed valent $Co^{I}Co^{II}$ species

Sally Brooker,*† Robert J. Kelly and Paul G. Plieger

Department of Chemistry, University of Otago, PO Box 56, Dunedin, New Zealand

Electrochemical studies of $[Co^{II}_2L(MeCN)_4][ClO_4]_4$ 1, the first structurally characterised dicobalt complex to be bridged by pyridazine units, reveal two one-electron reductions as well as two one-electron oxidations at high potentials; one-electron reduction generates a mixed valent $Co^{I}Co^{II}$ species which exhibits an intervalence charge transfer band at 965 nm.

Despite intense interest in cobalt(I) complexes as reactive centres for catalytic processes, such as CO_2 fixation and the reduction of water to dihydrogen or as models for vitamin B_{12}, there are relatively few examples of the isolation of such complexes in the absence of the stabilising effects of phosphines or phosphites.[1–4] Notable exceptions to this generalisation include structurally characterised complexes by Creutz *et al.*[3] and by Floriani and coworkers.[4]

We are studying complexes of chelating ligands based on 3,6-diformylpyridazine[5–8] and have found that the resulting dicopper(II) complexes exhibit positive reduction potentials (two well separated one-electron reductions),[7,8] and that dimanganese(II) complexes can be formed and are air stable.[6] These observations clearly indicate that our pyridazine-containing ligands are, as one might expect on the basis of their π-acceptor properties, good at stabilising low oxidation states of transition metal ions. Of these ligands, the macrocyclic ligands are expected to be particularly effective because strong chelation to the metal centres should hinder any subsequent decomposition reactions. Hence we have extended our studies to include a wide range of transition metal ions, with a view to stabilising and isolating unusually low oxidation state complexes.[6–8] Pyridazine- or phthalazine-bridged dicobalt(II) complexes are rare and, to our knowledge, no electrochemical studies have been reported for such complexes.[9] To date, there are no known examples with pyridazine-containing macrocyclic ligands. We report here on an air stable dicobalt(II) complex of the Schiff-base macrocyclic ligand L.

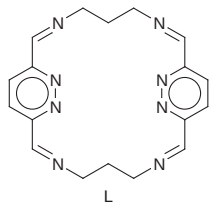

L

Transmetallation of the macrocyclic complex $[Pb_2L'][ClO_4]_4$ {L′ is the (4 + 4) analogue of L}[5,6] with cobalt(II) perchlorate in MeCN yields, after vapour diffusion of diethyl ether into the air stable solution, dark red crystals of $[Co_2L(MeCN)_4][ClO_4]_4$ **1**, in 57% yield.‡ The IR spectrum of **1** shows the presence of an imine absorption and the absence of absorptions due to either amine or carbonyl bonds. The FAB mass spectrum has a cluster of peaks consistent with the presence of $[Co_2L(ClO_4)_3]^+$, thus indicating that the original (4 + 4) Schiff-base macrocycle L′ had ring contracted to the (2 + 2) macrocycle L. This ring contraction, also observed in the case of the dicopper(II) and dimanganese(II) complexes,[6–8] was subsequently confirmed by single crystal X-ray structure analysis of a crystal obtained by slow evaporation of an acetonitrile solution of **1** to which an excess of sodium perchlorate had been added (Fig. 1).§

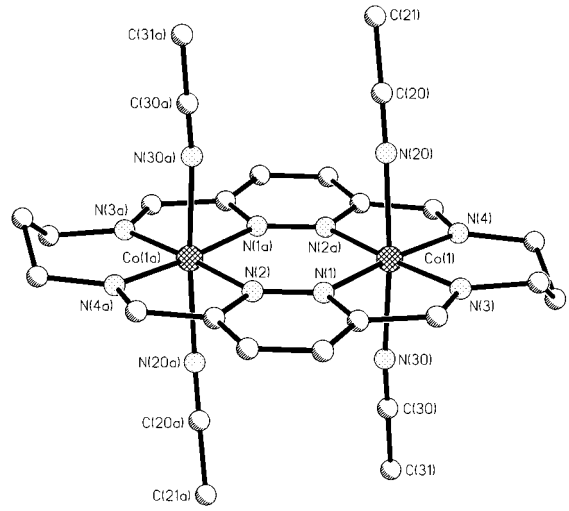

Fig. 1 Perspective view of one of the two independent cations of **1**, $[Co_2L(MeCN)_4]^{4+}$. Selected interatomic distances (Å) and angles (°): Co(1)–N(3) 1.984(4), Co(1)–N(4) 1.964(4), Co(1)–N(2a) 2.005(4), Co(1)–N(1) 2.013(4), Co(1)–N(30) 2.127(4), Co(1)–N(20) 2.135(4), Co(1)···Co(1a) 3.809(1); N(3)–Co(1)–N(4) 94.3(2), N(3)–Co(1)–N(2a) 175.5(2), N(4)–Co(1)–N(2a) 81.2(2), N(3)–Co(1)–N(1) 80.8(2), N(4)–Co(1)–N(1) 174.7(2), N(2a)–Co(1)–N(1) 103.7(2), N(3)–Co(1)–N(30) 92.8(2), N(4)–Co(1)–N(30) 88.8(2), N(2a)–Co(1)–N(30) 87.6(2), N(1)–Co(1)–N(30) 89.4(2), N(3)–Co(1)–N(20) 93.7(2), N(4)–Co(1)–N(20) 90.3(2), N(2a)–C0(1)–N(20) 85.9(2), N(1)–Co(1)–N(20) 92.1(2), N(30)–Co(1)–N(20) 173.5(2).

Cyclic voltammetry was carried out on $[Co_2L][ClO_4]_4$ in dry MeCN and revealed two one-electron reduction waves at remarkably high potentials ($E_{\frac{1}{2}}$ = −0.11 V and $E_{\frac{1}{2}}$ = −0.33 V, *vs.* Ag/0.01 M $AgNO_3$, Fig. 2) plus two one-electron oxidation waves at positive potentials ($E_{\frac{1}{2}}$ = +0.87 V and $E_{\frac{1}{2}}$ = +1.06 V, *vs* Ag/0.01 M $AgNO_3$, Fig. 2). The two reduction waves are tentatively assigned to $Co^{II}Co^{II} \rightarrow Co^{II}Co^{I}$ and $Co^{II}Co^{I} \rightarrow$

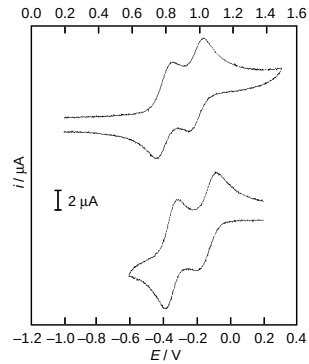

Fig. 2 Cyclic voltammogram of **1** in MeCN (1×10^{-3} M, 0.1 M NEt_4ClO_4, platinum counter electrode *vs.* Ag/0.01 M $AgNO_3$, 200 mV s^{-1}, in this system $Fc–Fc^+$ = +0.09 V).

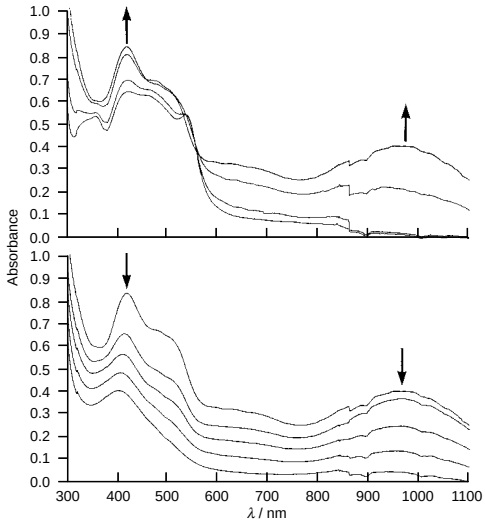

Fig. 3 Spectral changes during two step bulk electrolysis of **1** in MeCN. Top: first one-electron reduction (E = −0.29 V, 0.92 electron equivalents transferred). Bottom: second one-electron reduction (E = −0.60 V, 0.94 electron equivalents transferred).

$Co^{I}Co^{I}$ reductions and the two oxidation waves to be $Co^{II}Co^{II} \rightarrow Co^{II}Co^{III}$ and $Co^{II}Co^{III} \rightarrow Co^{III}Co^{III}$ oxidations.¶

As no electrochemical studies have been reported on the handful of other known 1,2-diazine bridged cobalt complexes, it is not possible to make comparisons with these.[9] However, comparison with the redox properties of other related cobalt complexes, such as those provided by the systematic study of monocobalt complexes of a series of N_4-macrocycles by Busch and coworkers [$-2.21 < E_{\frac{1}{2}}(Co^{II} \rightarrow Co^{I}) < -0.72$ V *vs.* Ag/Ag^+ (0.1 M) in MeCN],[10] confirms that the reductions of **1** are, indeed, occurring at relatively high potentials. In that study the presence of an N_3 pyridine diimine or of two N_2 conjugated diimine groups in the N_4-macrocycle was found to greatly stabilise Co^{I} [$E_{\frac{1}{2}}(Co^{II} \rightarrow Co^{I})$ = − 0.72 V and −0.86 V *vs.* Ag/Ag^+ (0.1 M) in MeCN, respectively].[10] Similarly, as the pyridazine macrocycle L incorporates imine bonds conjugated with pyridazine units an even greater enhancement of stability of Co^{I} results. In fact the observed potentials for **1** fall close to the range normally observed for oxidation of Co^{II} to Co^{III}.[11] For example, in the Busch complexes mentioned earlier the potentials for this oxidation process fall in the range −0.09 to +0.17 V *vs.* Ag/Ag^+ (0.1 M).[10] Again this is in clear contrast with the substantially more positive potentials observed for the oxidation processes of **1**, which presumably result from the build up of positive charge on the complex (+6 on the fully oxidised complex).

It is important to note that in our dicobalt(II) complex the two reductions and the two oxidations all occur in separate one electron steps: in the case of the reductions they are separated by 220 mV ($K_c = 5.24 \times 10^3$) whereas the oxidations are separated by 190 mV ($K_c = 1.63 \times 10^3$). Hence the mixed valent redox products are moderately stable. Preliminary spectroelectrochemical studies of the reduction processes indicate the existence of an intervalence charge transfer band in the mixed valent $Co^{I}Co^{II}$ complex, with the growth of a broad band centred at 965 nm (2790 $dm^3\ mol^{-1}\ cm^{-1}$) as the first electron is added to **1**, followed by bleaching of this band as the second electron is added (Fig. 3).‖ Further work, including solvent and temperature dependence studies, is necessary to confirm this. In contrast, oxidation of **1** does not result in a long wavelength absorption so in this case the mixed valent state appears to be valence localised.

The redox chemistry of the complexes derived from the macrocyclic ligand L is clearly rich: the ability of this ligand to stabilise dinuclear complexes in low oxidation states is very exciting and the reactivity of these complexes is being explored. Further characterisation of all of the redox states by, as appropriate, EPR or NMR spectroscopy, is underway, along with attempts to isolate each species. Finally, these ligands allow us to systematically study the magnetic exchange properties of unique pyridazine-bridged complexes and this feature of **1** is also under investigation.[8]

This work was supported by grants from the University of Otago. We thank Professor W. T. Robinson (University of Canterbury) for the X-ray data collection and B. M. Clark (University of Canterbury) for the FAB mass spectrum. S. B. thanks the University of Otago for the granting of study leave which facilitated the drafting of this paper, Dr E. Bothe and Professor K. Wieghardt (MPI für Strahlenchemie) for stimulating discussions, and also gratefully acknowledges the financial support of the Alexander von Humboldt Stiftung.

Notes and References

† E-mail: sbrooker@alkali.otago.ac.nz

‡ Satisfactory C, H, N, analysis was obtained for acetonitrile-free **1** (the coordinated acetonitrile molecules are lost on drying *in vacuo*).

§ *Crystal data* for **1**: $C_{26}H_{32}Cl_4N_{12}O_{16}$, dark red block, 0.80 × 0.46 × 0.10 mm, triclinic, space group $P\bar{1}$, a = 10.993(2), b = 11.768(2), c = 17.008(3) Å, α = 86.952(10), β = 87.634(11), γ = 64.321(14)°, U = 1979.6(5) Å^3, Z = 2, μ = 1.19 mm^{-1}. Data were collected at 170 K on a Siemens P4 four-circle diffractometer using graphite-monochromated Mo-Kα radiation. 8997 Reflections were collected in the range $4 < 2\theta < 54°$ and the 8495 independent reflections were used in the structural analysis after a semi-empirical absorption correction had been applied. The structure was solved by direct methods (SHELXS-86)[12] and refined against all F^2 data (SHELXL-93)[13] to $R1$ = 0.0596 [for 5483 $F > 4\sigma(F)$; $wR2$ = 0.53 and goodness of fit = 1.04 for all 8495 F^2; 554 parameters; all non-hydrogen atoms anisotropic]. CCDC 182/833.

¶ The analogous dizinc complex shows no redox activity in the range − 0.4 to +1.5 V, *vs.* Ag/0.01 M $AgNO_3$, under the same conditions.

‖ The cyclic voltammogram is unchanged after the two-electron reduction of **1** is complete.

1 D. G. Brown, *Prog. Inorg. Chem.*, 1973, **18**, 177; F. R. Keene, C. Creutz and N. Sutin, *Coord. Chem. Rev.*, 1985, **64**, 247; C. Creutz and N. Sutin, *ibid.*, 321; M. B. Davies, *ibid.*, 1994, **134**, 195; K. Tanaka, *Adv. Inorg. Chem.*, 1995, **43**, 409.
2 See, for example: R. J. Fitzgerald, B. B. Hutchinson and K. Nakamoto, *Inorg. Chem.*, 1970, **9**, 2618; V. L. Goedken and S.-M. Peng, *J. Chem. Soc., Chem. Commun.*, 1974, 914; E. J. Corey, N. J. Cooper, W. M. Canning, W. N. Lipscomb and T. F. Koetzle, *Inorg. Chem.*, 1982, **21**, 192; K. V. Katti, P. R. Singh and C. L. Barnes, *Inorg. Chem.*, 1992, **31**, 4588.
3 C. Creutz, H. A. Schwarz, J. F. Wishart, E. Fujita and N. Sutin, *J. Am. Chem. Soc.*, 1991, **113**, 3361 and references therein.
4 S. De Angelis, E. Solari, E. Gallo, C. Floriani, A. Chiesi-Villa and C. Rizzoli, *Inorg. Chem.*, 1996, **35**, 5995; F. Arena, C. Floriani and P. F. Zanazzi, *J. Chem. Soc., Chem. Commun.*, 1987, 183 and references therein.
5 S. Brooker, R. J. Kelly and G. M. Sheldrick, *J. Chem. Soc., Chem. Commun.*, 1994, 487.
6 S. Brooker and R. J. Kelly, *J. Chem. Soc., Dalton Trans.*, 1996, 2117 and references therein.
7 S. Brooker, R. J. Kelly, B. Moubaraki and K. S. Murray, *Chem. Commun.*, 1996, 2579 and references therein.
8 S. Brooker, R. J. Kelly, P. G. Plieger, B. Moubaraki and K. S. Murray, unpublished work.
9 J. E. Andrew, P. W. Ball and A. B. Blake, *Chem. Commun.*, 1969, 143; P. W. Ball and A. B. Blake, *J. Chem. Soc., Dalton Trans.*, 1974, 852; A. van der Putten, A. Elzing, W. Visscher and E. Barendrecht, *J. Chem. Soc., Chem. Commun.*, 1986, 477; T. Wen, L. K. Thompson, F. L. Lee and E. J. Gabe, *Inorg. Chem.*, 1988, **27**, 4190.
10 A. M. Tait, F. V. Lovecchio and D. H. Busch, *Inorg. Chem.*, 1977, **16**, 2206.
11 P. Comba and A. F. Sickmüller, *Inorg. Chem.*, 1997, **36**, 4500.
12 G. M. Sheldrick, *Acta Crystallogr., Sect. A*, 1990, 467.
13 G. M. Sheldrick, SHELXL 93, University of Göttingen, 1993.

Received in Cambridge, UK, 9th March 1998; 8/01891J

[{(dppe)Pt}$_2$B$_7$H$_{11}$]: An *arachno*-bimetallanonaborane based on the uncommon *n*-B$_9$H$_{15}$ cluster framework

Ramón Macías, Nigam P. Rath and Lawrence Barton*†

Department of Chemistry, University of Missouri-St. Louis, St. Louis, MO 63121, USA

The first bimetallanonaborane, [{(dppe)Pt}$_2$B$_7$B$_{11}$], based on the uncommon *n*-B$_9$H$_{15}$ cluster framework, is prepared and characterized as a final product from the reaction of pentaborane (9) with [PtCl$_2$(dppe)].

The coordination number pattern recognition theory for boranes and carbaboranes, as described by Williams in 1976,[1] requires that in order to generate *arachno*-clusters from *nido* systems, a highest connectivity vertex, adjacent to the open face, is removed. The predicted cluster framework for an *arachno* 9-vertex system is illustrated by structure **I** and recognized as

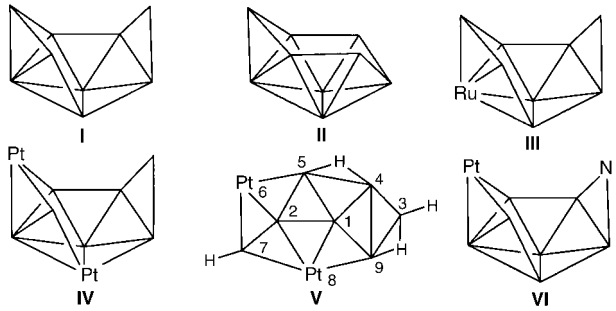

n-*arachno* B$_9$H$_{15}$. In contrast, the more commonly encountered 9-vertex *arachno*-species are derived by removal of a low connectivity vertex from *nido*-B$_{10}$H$_{14}$ to generate derivatives of what are referred to as *i*-B$_9$H$_{15}$ (structure **II**) and *i*-C$_2$B$_7$H$_{13}$.[2] With the exception of the ruthenanonaborane, [2-(η^6-C$_6$Me$_6$)-2-RuB$_8$H$_{14}$], (structure **III**)[3] reported in trace yields in a preliminary communication in 1986, all the known nine-vertex *arachno*-metallaboranes have structures based on the *i*-B$_9$H$_{15}$ framework.[4] This article describes the synthesis and complete characterization of a diplatinanonaborane whose structure is based on a polyhedral nine-vertex *n*-B$_9$H$_{15}$ *arachno*-cluster type and for which the application of electron-counting rules suggest that the species is another example of the growing list of 'rule-breakers'.

Derivatives of B$_5$H$_9$, in which an electrophilic group has replaced a bridging H atom, are well known.[5] Group 10 derivatives, [2,3-μ-{ML$_n$(X)}B$_5$H$_8$], where M = Ni, Pd, Pt, L$_n$ = (PR$_3$)$_2$, dppe [dppe = (Ph$_2$PCH$_2$)$_2$], X = Cl, Br, are isolated if the reaction between [B$_5$H$_8$]$^-$ and ML$_n$X$_2$ is carried out and worked up at low temperatures.[6] Such species are generally unstable at room temperature in solution, usually resulting in decomposition involving reduction of the metal moiety to elemental metal by the borane moiety. Herein, we describe the results when the reaction mixture, Li[B$_5$H$_8$] and PtCl$_2$(dppe), is allowed to warm to room temperature, dried *in vacuo* for 2 days, exposed to air and separated using TLC on silica gel following filtration through silica gel.[8] Thus [{(dppe)Pt}$_2$B$_7$H$_{11}$] is prepared from [2,3-μ-{(dppe)Pt(Cl)}B$_5$H$_8$], in *ca*. 10% yield as a yellow air-stable crystalline solid, along with [(dppe)PtB$_3$H$_7$],[8a] [(dppe)(BH$_3$)$_2$],[8b] and what appear to be Pt chloride salts. NMR and mass spectral data identified the yellow solid as [{(dppe)Pt}$_2$B$_7$H$_{11}$].[9] This was confirmed by a single crystal structure determination of the diethyl ether sesquisolvate.[10]

The structure of [{(dppe)Pt}$_2$B$_7$H$_{11}$], given in Fig. 1, consists of a nine-vertex *n*-*arachno* framework, obtained by removal of two adjacent vertices of connectivity six and four respectively, from an 11-vertex *closo*-octadecahedron. The {(dppe)Pt} moieties are located at the 6 and 8 positions in the *n*-*arachno* B$_9$H$_{15}$ framework, each replacing a BH group and a bridging H atom. There are bridging H atoms at the B(4)–B(5) and B(3)–B(9) edges and *endo*-H atoms on B(3) and B(7). Only the latter *endo*-H atom is observed from the X-ray structure determination but the presence is clearly confirmed from NMR spectral data. [{(dppe)Pt}$_2$B$_7$H$_{11}$] is shown as structure **IV** and a topological representation, showing the numbering scheme and the *endo*-hydrogens, is given as structure **V**. Bond distances are within the normal ranges for Pt–B, Pt–P and B–B bonding connections. The B(4)–B(9) edge bridged by a BH$_2$ group, at 1.739(13) Å, is similar to that observed for the same cluster interboron connection in *n*-B$_9$H$_{15}$[2,11] and in the ruthenaborane,[3] but it is much shorter than the corresponding B–B interaction in the recently discovered azaplatinaborane, [3,3-(PMe$_2$Ph)$_2$-3-PtB$_7$H$_{10}$-μ-5,6-(NHR)], 1.92(2) Å,[12] in which the B–B edge is bridged by a NHEt group (structure **VI**). NMR data conform to the observed molecular structure for this new biplatinaborane. The ^{11}B spectrum exhibits four resonances of relative

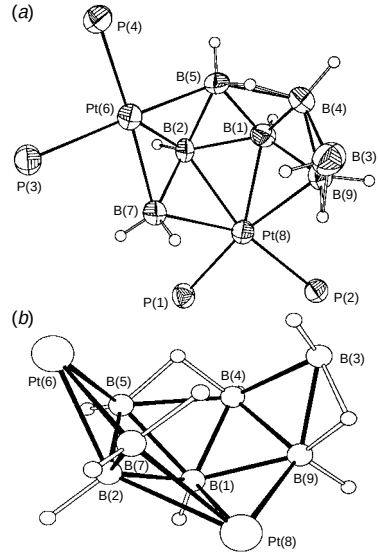

Fig. 1 (*a*) Projection of [{(dppe)Pt}$_2$B$_7$H$_{11}$]], showing only the P atoms of the chelating ligand on Pt. Ellipsoids are drawn at the 50% probability level. In addition to a terminal H atom on each B there is an *exo*-terminal H at position 3, indicated by ^{1}H NMR spectra. (*b*) Alternative representation with the ligands omitted for clarity. Selected interatomic distances (Å): from Pt(6) to P(3) 2.285(2), to P(4) 2.278(2), to B(2) 2.190(9), to B(5) 2.192(0), to B(7) 2.208(9); from Pt(8) to P(1) 2.289(2), to P(2) 2.295(2), to B(1) 2.227(9), to B(2) 2.267(9), to B(7) 2.328(9), to B(9) 2.302(9); interboron values: B(4)–B(9) 1.739(13), B(3)–B(9) 1.80(2), B(3)–B(4) 1.82(2), the other B–B distances are in the range 1.765(13)–1.883(13). Selected angles (°) P(3)–Pt(6)–P(4) 85.83(8), P(1)–Pt(8)–P(2) 84.97(7), P(3)–Pt(6)–B(5) 174.5(2), P(4)–Pt(6)–B(7) 167.6(3), P(1)–Pt(8)–B(9) 170.3(2), P(2)–Pt(8)–B(7) 152.1(2), B(4)–B(3)–B(9) 57.5(5).

intensity 1 : 4 : 1 : 1 and ^{1}H-{^{11}B(selective)} experiments reveal eleven different cage H atoms of which two are bridging and two are *endo*-hydrogen atoms. In addition, ^{31}P NMR spectra exhibit four different resonances of equal intensity; two doublets, an overlapped doublet of doublets that is seen as an apparent triplet, and a singlet. Each signal shows additional coupling to ^{195}Pt. Since P atoms in the same chelating dppe ligand effectively do not couple, we must be observing four-bond $^4J(^{31}P–^{31}P)$ coupling constants. From Fig. 1(*a*), it appears that P(3) and P(4) are effectively *trans* to P(2) whereas P(1) is directed towards the cluster B(1)–B(9) connection. This conformation suggests that the P atoms involved in ^{31}P–^{31}P coupling are P(3), P(4) and P(2). Thus we assign P(2) to the observed apparent triplet, P(3) and P(4) to the doublets and P(1) to the singlet. The cage connectivities of the Pt atoms are different; that for Pt(6) is three whereas that for Pt(8) is four and this appears to be reflected in the differences in ^{195}Pt–^{31}P coupling constants listed in ref. 9. Characterization of [{(dppe)Pt}$_2$B$_7$H$_{11}$] is completed by mass spectral data. The most intense envelope is that for the $[M - BH_3]^+$ ion, suggesting that the connection of the μ-H-BH$_2$ group is quite fragile, perhaps accounting for the preference of *i*-B$_9$H$_{15}$ isomers for nonaboranes and their derivatives.

A final point of note concerning [{(dppe)Pt}$_2$B$_7$H$_{11}$] is that it appears not to conform to the polyhedral skeletal electron pair theory (PSEPT) counting rules.[13] An *arachno* nine-vertex cluster requires $n + 3$ skeletal electron pairs, which for this cluster would be 12 electron pairs. Using the conventional electron-counting methods devised by Wade,[14] [{(dppe)Pt}$_2$B$_7$H$_{11}$] possesses 11 skeletal electron pairs. Such ambiguity has been observed for essentially all clusters containing three-connectivity group 10 metal moieties.[15] Some examples of such systems include [(PPh$_3$)$_2$(CO)Os(PPhMe$_2$)Cl(μ-H)PtB$_5$H$_7$],[15*a*] [(PEt$_3$)$_2$Pt(CMe)$_2$B$_4$H$_4$][15*b*] and [(PPhMe$_2$)$_2$PtB$_8$H$_{12}$].[15*c*] In these systems, the organometallic Pt fragment is best regarded as a square planar 16-electron center that contributes two orbitals and two electrons to the cluster framework. Under this scenario, the metal moiety is not isolobal with a conventional three orbital, two electron conical vertex and the skeletal electron count is two electrons short of the number required for compliance with the PSEPT. In [{(dppe)Pt}$_2$B$_7$H$_{11}$] this feature may be ascribed to the vertex unit [(dppe)Pt] at the 6-position. Apparently in [{(dppe)Pt}$_2$B$_7$H$_{11}$], the two Pt vertices, with different connectivity, contribute differently to the total skeletal electron count for the cluster. The vertex Pt(8), which has connectivity 4 may be considered to be a 'normal' conical vertex conforming to the PSEPT, although in a formal sense each [(dppe)Pt] vertex subrogates a BH(μ-H) moiety. This appears to represent a new example of the so-called rule breakers, and such phenomena warrant further investigation.

We acknowledge support by the Missouri Research Board and the ACS-PRF (grant 31001-AC3). We also acknowledge instrumentation grants from the NSF (No. CHE-9309690 and CHE-9318696), the DOE (Grant No. DE-FG02-92CH10499) and the UM-St. Louis Center for Molecular Electronics. We thank Professor Michael Gross of the Washington University Mass Spectrometry NIH Research Resource (Grant. No. P41RR094) for the mass spectra. Experimental details for the preparation and spectral characterization of [{(dppe)Pt}$_2$B$_7$H$_{11}$], [(dppe)PtB$_3$H$_7$] and [(dppe)(BH$_3$)$_2$] are available upon request from the authors.

Notes and References

† E-mail: lbarton@umsl.edu

1 R. E. Williams, *Adv. Inorg. Chem. Radiochem.*, 1976, **18**, 66.
2 L. Barton, *Top. Cur.. Chem.*, 1982, **100**, 169.
3 M. Bown, X. L. R. Fontaine, N. N. Greenwood, J. D. Kennedy and M. Thornton-Pett, *J. Organomet. Chem.*, 1986, **315**, C1.
4 J. D. Kennedy, *Prog. Inorg. Chem.*, 1986, **36**, 211; K. B. Gilbert, S. K. Boocock and S. G. Shore, in *Comprehensive Organometallic Chemistry*, ed. G. Wilkinson, E. W. Abel and F. G. A. Stone, Pergamon, Oxford, 1982, part 6, ch. 41, pp. 879–945; L. Barton and D. K. Srivastava, *Comprehensive Organometallic Chemistry, II*, ed. G. Wilkinson, E. W. Abel and F. G. A. Stone, Pergamon, Oxford, 1995, vol. 1, ch. 8, pp. 275–373.
5 T. Onak, G. B. Dunks, I. W. Searcy and J. Spielman, *Inorg. Chem.*, 1967, **6**, 1465; D. F. Gaines and T. V. Iorns, *J. Am. Chem. Soc.*, 1967, **89**, 3375; R. A. Geanangel and S. G. Shore, *J. Am. Chem. Soc.*, 1967, **89**, 6771.
6 N. N. Greenwood and J. Staves, *J. Chem. Soc., Dalton Trans.*, 1977, 1788; N. N. Greenwood, J. D. Kennedy and J. Staves, *J. Chem. Soc., Dalton Trans.*, 1978, 1146.
7 Full experimental details available as supplementary material upon request from the authors.
8 (*a*) NMR data for [(dppe)PtB$_3$H$_7$], (CDCl$_3$, 294–297 K) {ordered as: relative intensity δ(^{11}B) (rel. to BF$_3$·OEt$_2$) [δ(^{1}H)]} 1BH 19.8 [3.28]; 2BH$_2$ 4.1 [4.20 (2 H); 2.80 (2 H), $^1J(^{195}Pt–^1H)$ *ca*. 63 Hz]; additional cage δ(^{1}H) −2.64 (2μ-H). δ(H)(dppe) 7.69–7.41 (4C$_6$H$_5$), 2.37 (m 2CH$_2$). δ(^{31}P) (CDCl$_3$, 294–297 K, rel. 85% H$_3$PO$_4$) 55.4, $^1J(^{195}Pt–^{31}P)$ 2541 Hz. Data compare very well with those for [(PPh$_3$)$_2$PtB$_3$H$_7$], in J. Bould, J. D. Kennedy and W. S. McDonald, *Inorg. Chim. Acta.*, 1992, **196**, 201; (*b*) [(dppe)(BH$_3$)$_2$], (CDCl$_3$, 294–297 K): 2BH$_3$ −39.9 [1.02; AA′XX′ spin system, N = 15.77 Hz]; $^1J(^{11}B–^1H)$ coupling constants not resolved due to the broadness of the boron resonances. δ(^{31}P) (CDCl$_3$, 294–297 K, rel. 85% H$_3$PO$_4$) 18.9 (br).
9 Selected NMR data for [{(dppe)Pt}$_2$B$_7$H$_{11}$], (CDCl$_3$, 294–297 K) {ordered as: relative intensity δ(^{11}B) (rel. to BF$_3$·OEt$_2$) [δ(^{1}H)]} 1BH 39.2 [3.98], 4B 15.2 [4.98, 4.80, 4.22, 4.12, 2.82 (*endo*) [$^2J(^{195}Pt–^1H)$ *ca*. 67 Hz], 1BH$_2$ −4.7 [2.07 (m, J 5.1 Hz; *endo*/*exo*)], 1BH −24.6 [1.34]; additional cage δ(^{1}H) −0.23 (bridging), −1.74 (bridging). δ(^{1}H)(dppe) 8.0–6.9 (4C$_6$H$_5$), 2.31 (m, CH$_2$), 1.87 (m, CH$_2$). The ^{11}B spectra were too broad to observe coupling constants. δ(^{31}P) (CDCl$_3$, 228 K, rel. 85% H$_3$PO$_4$) 55.7 [d, P(3 or 4)], 53.1 [d of d, P(2)], 49.4 [s, P(1) and 45.3 d, P(4 or 3)]; $^4J[^{31}P(4\text{ or }3)–^{31}P(2)]$ 12.2 Hz, $^1J[^{195}Pt–^{31}P(4\text{ or }3)]$ 2658 Hz; $^4J[^{31}P(4\text{ or }3)–^{31}P(2)] + {}^4J[^{31}P(3\text{ or }4)–^{31}P(2)]$ 19.0 Hz, $^1J[^{195}Pt–^{31}P(2)]$ 2534 Hz; $^1J[^{195}Pt–^{31}P(1)]$ 2419 Hz; $^4J[^{31}P(2)–^{31}P(3\text{ or }4)]$ 22.6 Hz, $^1J[^{195}Pt–^{31}P(3\text{ or }4)]$ 2609 Hz. Low resolution MS (VG, ZAB-E: FAB in CH$_2$Cl$_2$, 3-nitrobenzyl alcohol matrix) overlapped with the $M - H_2$ ion, gave an apparent cutoff at *m/z* 1280 (calc. for $^{12}C_{52}{}^1H_{59}{}^{11}B_7{}^{31}P_4{}^{198}Pt_2$ 1280). Observed and calculated mass spectral parent profiles showing isotopic distribution for the $[M - BH_3]$ ion, with *m/z* (max.) = 1259, compare very well.
10 *Crystal data* for $C_{58}H_{74}B_7O_{1.5}P_4Pt_2$, [(dppe)$_2Pt_2B_7H_{11}$], M = 1384.90 (includes 1.5 molecules of Et$_2$O), triclinic, space group $P\bar{1}$, a = 12.8918(1), b = 13.7153(1), c = 17.8679(2) Å, α = 97.118(1), β = 94.409(2), γ = 108.92(1)°, U = 2942.44(5) Å^3, D_c = 1.563 Mg m^{-3}, Z = 2, F(000) = 1370, μ(Mo-Kα) = 4.897 mm^{-1}, T = 223(2) K. A total of 11 509 (R_{int} = 0.07) independent reflections, $2\theta_{max}$ = 52.0° on a Siemens CCD single-crystal X-ray diffractometer using ω scans. The final $wR(F^2)$ for all unique reflections was 0.119 with a conventional $R(F)$ of 0.049 [for 8526 reflections with $I > 2\sigma(I)$] for 677 parameters. CCDC 182/824.
11 J. C. Huffman, PhD Thesis, Indiana University, 1974, p. 771; R. A. Beaudet, *Mol. Struct. Energ.*, 1986, **5**, 417.
12 U. Dörfler, P. A. Salter, X. L. R. Fontaine, N. N. Greenwood, J. D. Kennedy and M. Thornton-Pett, *J. Chem. Soc., Dalton Trans.*, (7/08097B). We thank the authors for providing us with a copy of this manuscript prior to publication.
13 K. Wade, *Adv. Inorg. Chem. Radiochem.*, 1976, **18**, 60; R. W. Rudolph, *Acc. Chem. Res.*, 1976, **9**, 446; D. M. Mingos, *Acc. Chem. Res.*, 1984, **17**, 311.
14 J. D. Kennedy, *Main Group Metal Chem.*, 1989, **12**, 149.
15 (*a*) J. Bould, J. E. Crook, N. N. Greenwood and J. D. Kennedy, *J. Chem. Soc., Dalton Trans.*, 1991, 185; (*b*) G. B. Barker, M. Green, T. P. Onak, F. G. A. Stone, C. B. Ungermann and A. J. Welch, *J. Chem. Soc., Chem. Commun.*, 1980, 1186; (*c*) S. K. Boocock, N. N. Greenwood, M. J. Hails, J. D. Kennedy and W. S. McDonald, *J. Chem. Soc., Dalton Trans.*, 1981, 1415.

Received in Bloomington, IN, USA, 6th February 1998; 8/01093E

Synthesis of verdinochlorins: a new class of long-wavelength absorbing photosensitizers

Andrei N. Kozyrev,[a] James L. Alderfer,[b] Thomas J. Dougherty[a] and Ravindra K. Pandey*[a]

[a] *Chemistry Section, Department of Radiation Biology, Division of Radiation Medicine, Roswell Park Cancer Institute, Buffalo, NY 14263, USA*

[b] *The Department of Biophysics, Roswell Park Cancer Institute, Buffalo, NY 14263, USA*

Reaction of 13²-oxopyropheophorbide *a* with CH_2N_2 produced three isomeric methoxyverdinochlorins *via* expansion of the cyclopentanedione ring E; these long-wavelength absorbing verdinochlorins represent the first example of verdins with a reduced pyrrolic ring system, and their structural assignments have been made on the basis of ^{1}H NMR studies; a mechanism of verdinochlorin formation is discussed.

Verdins are a special class of green porphyrins **1** with a fused

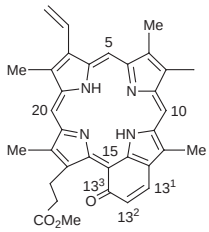

1

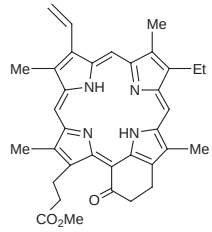

2

cyclohexenone ring system, which are obtained by the oxidation of the cyclohexanoneporphyrins or rhodins **2** under acidic reaction conditions.[1] Verdin's conjugated exocyclic ring has a strong electron-withdrawing effect and causes a dramatic change in the electronic spectrum, with a prominent absorption near 690 nm.[2] Due to their intense green color, Fischer named this class of compounds as 'verdins' (from Latin *verdo* = green).[1] The chemistry of rhodins and verdins was further explored by Clezy, who prepared a variety of porphyrins with fused exocyclic rings.[3] The utility of this class of compounds as photosensitizers for the treatment of cancer by photodynamic therapy (PDT) was demonstrated by Morgan *et al*.[4]

Recently, we have discovered a new and simple method for the preparation of 13²-oxopyropheophorbide *a* **3** by LiOH-promoted allomerization of pyropheophorbide *a*.[5] The oxopyropheophorbide *a* initially obtained as the carboxylic acid was readily converted into the corresponding methyl ester **3** by treating briefly with CH_2N_2. However, if a large excess of CH_2N_2 was used and the reaction mixture was left at room temperature for 4–6 h, a mixture of three main compounds was obtained. These were separated into individual components by preparative TLC. The most mobile orange band had a long-wavelength absorption at λ_{max} 777 nm (29% yield), the second band was red in color (λ_{max} 747 nm, yield: 26%) and the most polar compound was isolated as a green band with λ_{max} 739 nm (yield: 15%) (Scheme 1). Significant bathochromic shifts in the electronic absorption spectra indicated the presence of a conjugated electron-withdrawing exocyclic ring system. Mass spectral analyses of all three products gave the same molecular ion at *m/z* 590. Thus, compared to chlorin **3** an increase in mass by 28 daltons is observed.

It has been shown that CH_2N_2 reacts with cyclic α-diketones,[6] *e.g*. croconic acid, to produce trimethoxy-*p*-benzoquinone by an unusual ring expansion. Under these reaction conditions, we anticipated the possibility of CH_2 insertion into the diketocyclopentane ring of chlorin **3**, which would yield the product(s) with fused cyclohexenone rings, named here as verdinochlorins (*i.e*. verdin with a reduced pyrrole ring).

The structural assignments of the predicted reaction products were confirmed by extensive ^{1}H NMR studies (Fig. 1). The ^{1}H NMR spectra revealed that, compared to starting diketochlorin **3**, all these compounds had an additional signal at δ 4.2, integrating for three protons, along with an additional singlet at δ 6.1 (for the chlorins having absorptions at 738 and 747 nm), and δ 6.85 (for the chlorin absorbing at λ_{max} 777 nm) for the olefinic proton of the cyclohexenone ring, suggesting that all three products were structural isomers. The 2D ROESY NMR data further provided valuable information for the final structural identification. In the NMR spectrum, the orange band (λ_{max} 777 nm) showed the most lowfield shifted signal of the proton at position 13¹ of the cyclohexenone ring, suggesting a closer proximity to the chlorin macrocycle. This was further confirmed by ROESY experiments which clearly showed the through-space interaction of the 13¹-olefinic proton with the resonances of the 13²-methoxy group and the 12-methyl substituent. Upfield shifted resonances for the 17-H proton (δ 5.1) indicated the presence of the neighboring keto group at the 13³-position.[7] Based on these results, the structure for the fast moving band (λ_{max} 777 nm) was assigned as 13²-methoxy-13³-oxoverdinochlorin **9**.

Both the red (λ_{max} 747 nm) and green (λ_{max} 739 nm) verdinochlorin isomers had resonances at δ 6.1 for the protons at the 13²-position. On the basis of the chemical shift of the 17-H, observed at δ 5.3 (similar to **9**), the structure of the red verdinochlorin was assigned as the 13¹-methoxy-13³-keto-isomer **10**. However, for the green isomer, the 17-H resonance was observed at δ 4.7, which suggested the structure to be that of 13³-methoxy-13¹-ketochlorin **11**. In contrast to chlorins **9** and **10**, compound **11** is not a 'true' verdinochlorin, based on the position of the oxo group, and is named as 'isoverdinochlorin'.

The mechanism of the formation of the verdinochlorin isomers seems to be similar to that of the ring enlarged diketone obtained by CH_2N_2 treatment of croconic acid.[8] The insertion of the CH_2 fragment into the cyclopentane dione ring (between the 13/13¹ and 13¹/13² carbon atoms) will produce diketocyclohexane intermediates **4** and **5** (Scheme 1). The enolization of the acidic hydrogens adjacent to the keto function will generate the isomeric hydroxyverdinochlorins **6**–**8**. The hydroxy functions can then react with a second molecule of CH_2N_2 to give the resulting methoxyverdinochlorions **9**–**11**. From the reaction mixture, we did not isolate the cyclohexanone analog in which the keto groups were present at positions 13² and 13³. This indicates that the reactivity of the 13²-keto group in diketochlorin **3** is diminished due to the steric hindrance caused by the substituents attached to the adjacent reduced pyrrolic ring. Thus, CH_2N_2 as nucleophile preferentially attacks the keto group present at the 13¹-position.

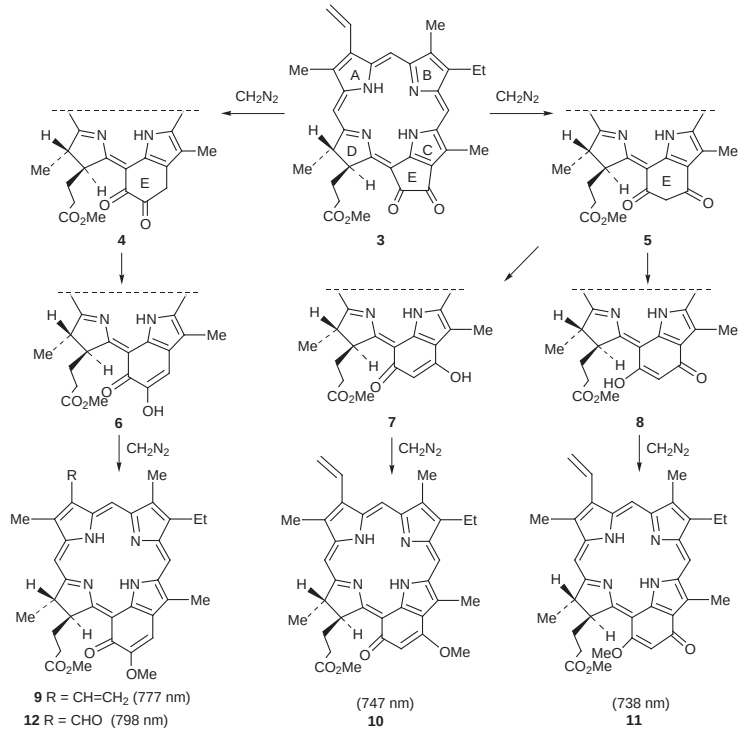

Scheme 1

Compared to most of the chlorins, all verdinochlorin isomers **9**–**11** showed a significant red shift of the long-wavelength absorption (Qy-band) in their UV–VIS spectra, which makes them attractive candidates as photosensitizers for photodynamic therapy. It was interesting to observe that the position of the methoxy group in the cyclohexenone ring of verdinochlorins **9** and **10** plays an important role in the shift of the Q_y-band. Thus, compared to chlorin **3**, 13^3-methoxyverdinochlorin **10** gave a red shift of 69 nm, while an even greater shift (99 nm) was observed for the 13^2-methoxy isomer **9**. Both verdinochlorins **9** and **10** had Q_x-bands around 560 nm, while isoverdinochlorin **11** on the other hand showed Q_x-absorption at 600 nm. These absorptions are obviously responsible for their red and green color respectively.

In order to achieve a further bathochromic shift, the vinyl group in chlorin **9** (λ_{max} 777 nm) was replaced with a formyl substituent. The corresponding formyl analog **12** showed an unusually large red-shifted long-wavelength Q_y-band in the near-IR region (λ_{max} 798 nm). Owing to their long wavelength absorptions in the red region, these compounds will have definite advantages over Photofrin® (a porphyrin derivative) for treating tumors which are deeply seated.

In conclusion, the new class of chlorins discussed here are the first examples of chlorins with a fused cyclohexenone rings. These compounds are obtained by the ring expansion of the fused cyclopetanedione ring attached to the chlorin system. This methodology has great potential in designing long-wavelength absorbing photosensitizers for PDT, and is currently being explored in our laboratory. The reactions discussed above might also be useful for the preparation of petroporphyrins with cyclohexane/phenyl ring systems. Biological *in vivo* PDT experiments with these compounds are currently in progress and will be published elsewhere.

We thank Professor Kevin M. Smith, University of California, Davis for helpful discussions. This work was supported by grants from Mallinckrodt Medical Inc., St. Louis, the National Institutes of Health (CA 55791), and the Oncologic Foundation of Buffalo. Partial support of the NMR facility by an RPCI Center Support Grant (CA 16056) is also acknowledged.

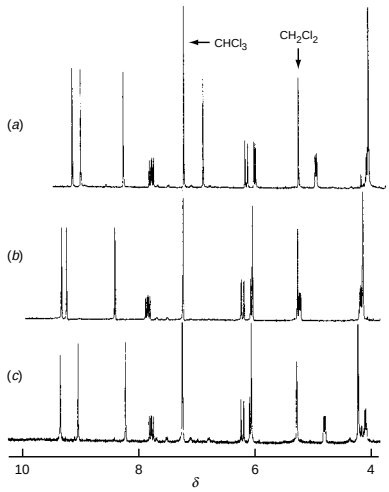

Fig. 1 ^{1}H NMR spectra (400 MHz) of (*a*) verdinochlorin **9**, (*b*) verdinochlorin **10** and (*c*) verdinochlorin **11**

Notes and References

† E-mail: pdtctr@sc3101med.buffalo.edu

1 H. Fisher and J. Ebersberger, *Justus Liebigs Ann. Chem.*, 1934, **509**, 19.
2 J. H. Fuhrhop, in *The Porphyrins*, ed. D. Dolphin, Elsevier, 1978, vol. 2.
3 P. S. Clezy, *Aust. J. Chem.*, 1991, **44**, 1163 and references cited therein.
4 A. R. Morgan, A. Rampersaud, R. W. Keck, and S. H. Selmam, *Photochem. Photobiol.*, 1987, **46**, 441.
5 A. N. Kozyrev, T. J. Dougherty and R. K. Pandey, *Chem. Commun.*, 1998, 481.
6 J. S. Pizey, *Synthetic Reagents*, Wiley, 1972, vol. 2.
7 A. N. Kozyrev, G. Zheng, C. Zhu, T. J. Dougherty, K. M. Smith and R. K. Pandey, *Tetrahedron Lett.*, 1996, **37**, 6431.
8 R. West and J. Niu, in *The Chemistry of the Carbonyl Group*, ed. J. Zabicky, Interscience, New York, 1970, vol. 2, p. 262.

Received in Corvallis, OR, USA, 12th February 1998; 8/01367E

Star-branched non-covalent complexes between carboxylic acids and a tris(imidazoline) base

Arno Kraft*[a]† and Roland Fröhlich[b]

[a] *Institut für Organische Chemie und Makromolekulare Chemie II, Heinrich-Heine-Universität Düsseldorf, Universitätsstr. 1, D-40225 Düsseldorf, Federal Republic of Germany*

[b] *Institut für Organische Chemie, Westfälische Wilhelms-Universität Münster, Corrensstr. 40, D-48149 Münster, Federal Republic of Germany*

Simple dissolution of 3 : 1 mixtures of aromatic carboxylic acids with suitable solubilising groups and tris(4,5-dihydroimidazol-2-yl)benzene 6 gave branched hydrogen-bonded assemblies 7 that were soluble in chlorinated and aromatic solvents.

Although Nature has perfected the controlled formation of stable hydrogen-bonded aggregates in water, self-assembly of well-defined, non-covalently bonded, high-molar-mass complexes in solution still remains a challenge for chemists.[1] Self-assembly by non-covalent interactions is an elegant approach to many kinds of large defined molecules, circumventing time-consuming chemical syntheses that are often accompanied by enormous purification problems. This can also become crucial in the design of new materials. For example, diaryl-substituted 1,3,4-oxadiazoles have lately received considerable interest as potential electron-transporting materials in electroluminescent devices based on fluorescent dyes and polymers.[2,3] Amongst these, branched structures such as **1** and dendrimers with $\geqslant 3$ oxadiazoles per molecule have the particular attraction of being highly soluble in organic solvents and of forming stable, amorphous, thin films.[3,4] It would be much simpler if such compounds were obtained through an assembly process from smaller components. For this, the non-covalent interaction between carboxylic acids and amidine bases looked very attractive.[5] We decided to use cyclic amidine derivatives which are easier to prepare than unsubstituted amidines and which were already the subject of X-ray crystal structure studies by Hosseini and co-workers who showed that dicarboxylic acids and bis(tetrahydropyrimidine)s or bis(imidazoline)s self-assemble to hydrogen-bonded sheets and networks in the solid state.[6]

A three-star branched structure would result when acids such as **2** or **3** (readily obtained by palladium-catalysed carbonylation of the corresponding aryl iodides)[4] were combined with, *e.g.* a 1,3,5-trisubstituted benzene containing three amidine substituents such as tris(imidazoline) **6**. Although melt condensation of benzene-1,3,5-tricarboxylic acid (**4**) and imidazolidin-2-one was reported to give **6** in modest yield,[7] a modified imidazoline synthesis[8] in solution proved to be more reliable. Hydrochloride **5** was prepared analogously in a single step from **4** and ethylenediamine in boiling ethylene glycol under acid catalysis (Scheme 1). Treatment with aqueous NaOH and sublimation gave the free base **6** in high purity.‡

Salt formation resulted from simple dissolution of a 1 : 3 mixture of **6** and various carboxylic acids in warm $CHCl_3$–EtOH.[9] Upon standing, the salts **7** crystallised from concentrated solutions (usually after evaporation of some of the $CHCl_3$), and one recrystallisation provided analytically pure samples.‡ It was surprising to note that salts obtained from acids with solubilising groups (such as *tert*-butyl derivatives of benzoic acid, **2** or **3**, but not benzoic acid or acetic acid) and **6** are remarkably soluble in non-polar organic solvents, *viz* $CHCl_3$ (**7b**: 40–50 mg cm^{-3}, **7a,c**: >100 mg cm^{-3}) or toluene, although **6** is insoluble in all common non-acidic organic solvents and, for example, acid **2** dissolves only sparingly in $CHCl_3$ (< 1 mg cm^{-3}) or EtOH.

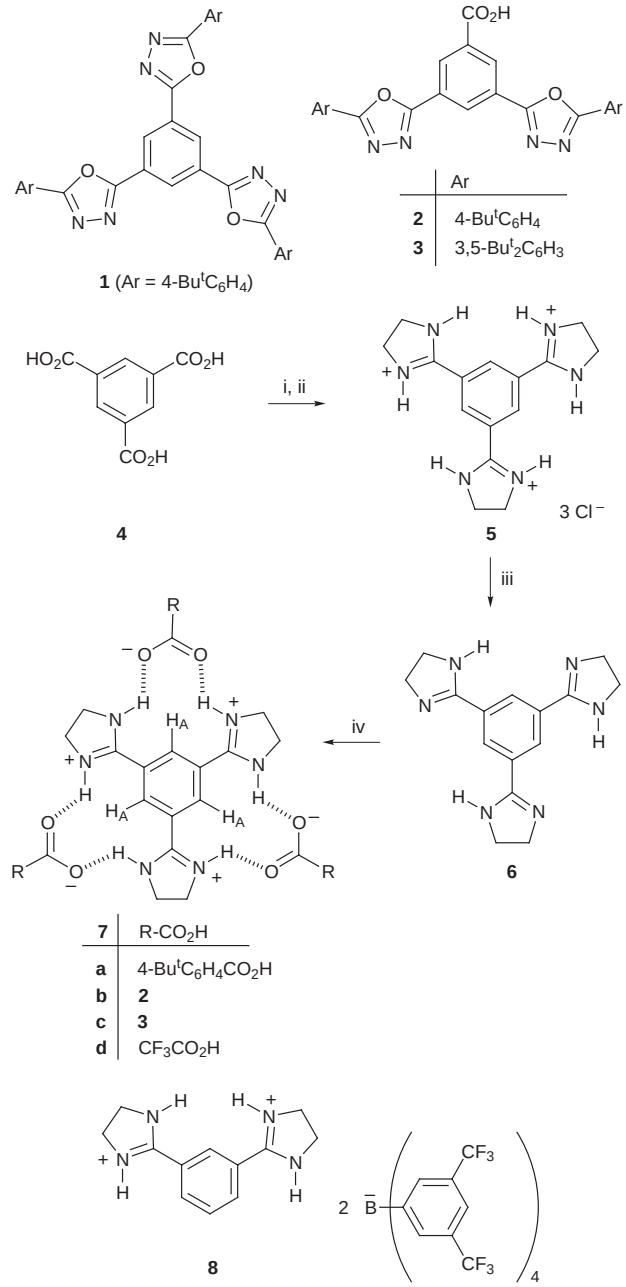

Scheme 1 *Reagents and conditions*: i, $H_2NCH_2CH_2NH_2$, $H_2NCH_2CH_2NH_2 \cdot 2HCl$, TsOH, ethylene glycol, reflux, 3 h; ii, HCl; iii, NaOH, 64%; iv, RCO_2H (3 equiv.), EtOH–$CHCl_3$, reflux, 56–87%

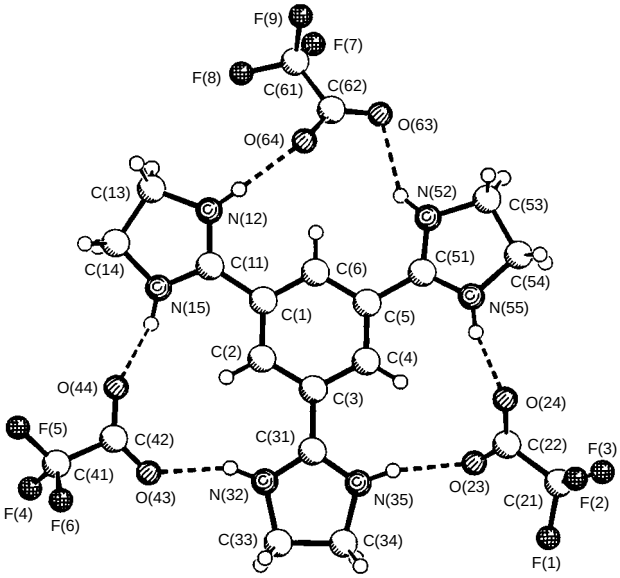

Fig. 1 Crystal structure of **7d**

The ^{1}H NMR spectra of **7a**–**c** in $CDCl_3$ show a broad singlet for the hydrogen-bonded imidazoline NH at δ *ca.* 13. The core's aromatic protons H_A give rise to a diagnostic singlet at an unusual chemical shift of δ *ca.* 10.1. Addition of a polar cosolvent shifts the H_A signal up-field, and in neat [$^2H_6$]DMSO the corresponding resonance is observed at δ *ca.* 8.5. Such a difference of $\Delta\delta$ *ca.* 1.6 for an aromatic proton signal cannot be explained by protonation of **6** alone or simple solvent effects, and must be attributed to the fact that, in the complex, H_A experiences considerable steric pressure. Polar solvents (DMSO, MeOH) cause the complexes to dissociate, whereas in a non-polar solvent each carboxylate forms hydrogen-bonds to two imidazoline NH units, with all non-polar groups facing the outside, probably similar to Hosseini's self-assembled structures.[6] This is further illustrated by the crystal structure of model complex **7d** for which the deviation from C_3-symmetry may be either a consequence of crystal packing effects or an indication that the third carboxylate is less strongly bound than the remaining two (Fig. 1).§

A 1 : 3 stoichiometry of the **6**–carboxylic acid complexes was supported by Job's method of continuous variation. Dilution experiments showed that the ^{1}H NMR chemical shifts of complexes **7a**–**c** in $CDCl_3$ remain unchanged over a concentration range of 10^{-1} to 3×10^{-5} mol dm^{-3} ($\Delta\delta < 0.1$) although the core signals show some line-broadening below 10^{-3} mol dm^{-3}. ^{1}H NMR dilution studies of **8** and tetrabutylammonium benzoate in $CDCl_3$–CD_3OD (97 : 3) gave an association constant of 990 ± 230 dm^3 mol^{-1} for the formation of a simple 1 : 1 complex. Self-association can be excluded unless, as initial experiments have shown, the acid component contains additional functional groups capable of hydrogen bonding, *e.g.* amide groups. Although complexes **7a**–**c** dissociated during column or gel-permeation chromatography (with CH_2Cl_2 as eluent) and mass spectrometry (chemical ionization, fast atom bombardment or matrix-assisted laser desorption/ionisation), vapour-pressure osmometry allowed us to determine the number-average molar mass M_n in solution at concentrations > 5 mmol dm^{-3}: 830 g mol^{-1} (against benzil or **1** as standard) for **7a**, 1810 g mol^{-1} for **7b**, both in $CHCl_3$ at 30 °C, and 2400 g mol^{-1} (against benzil or polystyrene 2000 as standard) for **7c** in toluene at 50 °C. All M_n values are close to the calculated values of 817, 1850 and 2187 g mol^{-1}, respectively, and provide evidence that the complexes are not dissociated under these conditions.

Further investigations towards the use of this simple self-assembly process for the preparation of larger assemblies and ordered supramolecular stacks, and their applicability in electroluminescent devices are in progress.

The Fonds der Chemischen Industrie, the Deutsche Forschungsgemeinschaft and Professor G. Wulff are gratefully acknowledged for financial support as well as Ms H. Fürtges for assistance in the preparation of starting materials.

Notes and References

† E-mail: kraft@iris-oc2.oc2.uni-duesseldorf.de

‡ All compounds were characterised by microanalysis, IR and NMR spectroscopy. *Selected data* for **5**: δ_H(300 MHz, D_2O) 4.23 (s, CH_2), 8.58 (s, C_6H_3). For **6**: mp 383–385 °C (lit.[7] 340 °C); *m/z* (CI-MS, NH_3) 283, 282, 381 (53, 100, 83%, M^+), 254, 253 (58, 99), 240 (56), 224 (55). For **7a**: mp 389–390 °C (decomp.); δ_H(300 MHz, $CDCl_3$) 1.34 (s, CH_3), 4.14 (s, NCH_2), 7.41, 8.01 (AA′XX′, C_6H_4), 10.12 (s, H_A), 13.0 (br s, NH); δ_H(500 MHz, [$^2H_6$]DMSO) 1.30 (s, CH_3), 3.68 (s, NCH_2), 7.49, 7.87 (AA′XX′, C_6H_4), 8.45 (s, H_A). For **7b**: mp 235–240 °C/lc/283–285 °C/i (decomp.); δ_H(500 MHz, $CDCl_3$) 1.38 (s, CH_3), 4.36 (s, NCH_2), 7.56, 8.10 (AA′XX′, C_6H_4), 8.90 (3 H, t, *J* 1.6), 8.97 (6 H, d, $C_6H_3CO_2^-$), 10.10 (s, H_A), 12.9 (br s, NH); δ_H(500 MHz, [$^2H_6$]DMSO) 1.36 (s, CH_3), 3.80 (s, NCH_2), 7.69, 8.13 (AA′XX′, C_6H_4), 8.55 (s, H_A), 8.78 (6 H, d, *J* 1.6), 8.85 (3 H, t, $C_6H_3CO_2^-$). For **7c**: mp 328–329 °C (decomp.); δ_H(300 MHz, $CDCl_3$) 1.42 (s, CH_3), 4.38 (s, CH_2), 7.66 (6 H, t, *J* 1.7), 8.03 (12 H, d, C_6H_3), 8.97 (3 H, t, *J* 1.6), 9.06 (6 H, d, $C_6H_3CO_2^-$), 10.16 (s, H_A), 13.0 (br s, NH). For **7d**: mp 240–242 °C (decomp.); δ_H(300 MHz, D_2O) 4.18 (s, CH_2), 8.50 (s, H_A).

§ X-Ray crystal structure analysis of **7d**: $C_{21}H_{21}N_6O_6F_9$, M = 624.44, 0.5 × 0.3 × 0.2 mm (from MeOH), a = 12.464(1), b = 22.884(2), c = 9.122(1) Å, V = 2601.8(4) Å^3, ρ_{calc} = 1.594 g cm^{-3}, μ = 14.21 cm^{-1}, Z = 4, orthorhombic, space group P$na2_1$ (No. 33), λ = 1.54178 Å, T = 223 K, $\omega/2\theta$ scans, 2834 reflections collected (+*h*, −*k*, +*l*), [(sin θ/λ] = 0.62 Å^{-1}, 2834 independent and 2525 observed reflections [$I \geqslant 2\ \sigma(I)$], 380 refined parameters, R = 0.064, wR^2 = 0.179, max. residual electron density 0.57 (−0.36) e Å^{-3}, Flack parameter −0.1(3), hydrogens calculated and riding. Data set were collected with an Enraf–Nonius CAD4 diffractometer. Programs used: data reduction MolEN, structure solution SHELXS-86, structure refinement SHELXL-93, graphics SCHAKAL-92. CCDC 182/822.

1 Some recent examples include: J. Yang, J.-L. Marendaz, S. J. Geib and A. D. Hamilton, *Tetrahedron Lett.*, 1994, **35**, 3665; G. M. Whitesides, E. E. Simanek, J. P. Mathias, C. T. Seto, D. N. Chin, M. Mammen and D. M. Gordon, *Acc. Chem. Res.*, 1995, **28**, 37; A. Marsh, M. Silvestri and J.-M. Lehn, *Chem. Commun.*, 1996, 1527; W. T. S. Huck, R. Hulst, P. Timmerman, F. C. J. M. van Veggel and D. N. Reinhoudt, *Angew. Chem., Int. Ed. Engl.*, 1997, **36**, 1006; D. J. Pesak and J. S. Moore, *Angew. Chem., Int. Ed. Engl.*, 1997, **36**, 1633; Y. Wang, F. Zeng and S. C. Zimmerman, *Tetrahedron Lett.*, 1997, **38**, 5459; F. Zeng and S. C. Zimmerman, *Chem. Rev.*, 1997, **97**, 1681.

2 For example: Y. Hamada, C. Adachi, T. Tsutsui and S. Saito, *Jpn. J. Appl. Phys.*, 1992, **31**, 1812; A. R. Brown, D. D. C. Bradley, J. H. Burroughes, R. H. Friend, N. C. Greenham, P. L. Burn, A. B. Holmes and A. Kraft, *Appl. Phys. Lett.*, 1992, **61**, 2793; K. Naito, M. Sakurai and S. Egusa, *J. Phys. Chem. A*, 1997, **101**, 2350.

3 J. Bettenhausen and P. Strohriegl, *Adv. Mater.*, 1996, **8**, 507; J. Bettenhausen and P. Strohriegl, *Macromol. Rapid Commun.*, 1996, **17**, 623.

4 A. Kraft, *Liebigs Ann. Chem.*, 1997, 1463.

5 For a recent example of an amidine complex see: J. P. Kirby, J. A. Roberts and D. G. Nocera, *J. Am. Chem. Soc.*, 1997, **119**, 9230; for a complex with substituted guanidines see: A. Metzger, V. M. Lynch and E. V. Anslyn, *Angew. Chem., Int. Ed. Engl.*, 1997, **36**, 862.

6 M. W. Hosseini, R. Ruppert, P. Schaeffer, A. De Cian, N. Kyritsakas and J. Fischer, *J. Chem. Soc., Chem. Commun.*, 1994, 2135; O. Félix, M. W. Hosseini, A. De Cian and J. Fischer, *Angew. Chem., Int. Ed. Engl.*, 1997, **36**, 102; O. Félix, M. W. Hosseini, A. De Cian and J. Fischer, *Tetrahedron Lett.*, 1997, **38**, 1933.

7 G. Kränzlein and H. Bastian (IG Farben), DRP 695473, 1937; *Chem. Abstr.*, 1941, **35**, 141b.

8 V. B. Piskov, V. P. Kasperovich and L. M. Yakovleva, *Chem. Heterocycl. Compd. (Engl. Transl.)*, 1976, **12**, 917.

9 Since the pK_a of protonated 2-phenylimidazoline and benzoic acid is 9.88 and 4.25, respectively, it is expected that the imidazolines in **7** are completely protonated: B. Fernández, I. Perillo and S. Lamdan, *J. Chem. Soc., Perkin Trans. 2*, 1973, 1371.

Received in Cambridge, UK, 17th March 1998; 8/02111B

Synthesis of a potent inhibitor of HIV reverse transcriptase

Chris J. Hamilton,[a] Stanley M. Roberts[b]† and Alexander Shipitsin[c]

[a] *Department of Chemistry, Exeter University, Stocker Road, Exeter, Devon, UK EX4 4QD*
[b] *Robert Robinson Laboratories, Department of Chemistry, Liverpool University, Liverpool, UK L69 3BX*
[c] *Engelhardt Institute of Molecular Biology, Russian Academy of Sciences, 32 Vavilov Street, Moscow 117984, Russia*

The newly synthesised P_β,–P_γ-difluoromethylenebisphosphonate analogue 2 of *nor*-carbovir triphosphate is a potent inhibitor of HIV reverse transcriptase; it also exhibits a greatly enhanced stability to dephosphorylation, in foetal blood serum, relative to AZTTP and other nucleoside triphosphates.

The *in vivo* lability of the P–O–P phosphate ester bonds in nucleoside triphosphates (NTPs) possessing interesting biological activity *in vitro* has prompted the search for more stable analogues. A great deal of effort has centred on the substitution of the phosphate ester oxygen atoms with carbon to give the corresponding phosphonates. These phosphonates are generally more stable to hydrolytic cleavage whilst being isosteric with their parent phosphates. The lower electronegativity of the methylene group, compared to oxygen, leads to a significant decrease in the acid dissociation constants of these phosphonic acids, which is often reflected in a reduction of biological activity. Through the seminal work of Blackburn and co-workers, halogenoalkylphosphonates have been shown to have improved potential as phosphate mimetics, as they more closely resemble the steric and electronic features of their parent units.[1]

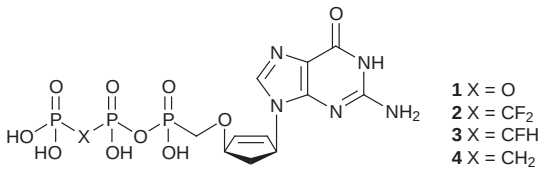

We have previously shown that the pyrophosphoryl phosphonate **1** shows potent inhibition of HIV reverse transcriptase (HIV-rt), comparable to that of both AZT and carbovir triphosphates.[2] It is noteworthy that the active compound **1** has an absolute configuration that is the mirror image of that expected for a natural nucleotide.[3] Previous assessments of other such 'unnatural' nucleosides have shown them to exhibit reduced cytoxicity relative to their natural enantiomers.[4]

Further progress in this area would result from structural modifications of the diphosphate unit in **1** to further enhance its stability *in vivo* whilst still retaining good biological activity. To these ends we have prepared a series of bisphosphonates **2**–**4** with progressive fluoro-substitution within the P_β,P_γ-methylene linker group, as described in Scheme 1.

Noteworthy features of the chemical syntheses include the preparation of the tetraethyl difluoromethylenebisphosphonate **5** by coupling diethyl difluoromethylphosphonate with diethyl chlorophosphate,[5] and the preparation of tetraethyl fluoromethylenebisphosphonate **7** using the easy to handle and readily available fluorinating reagent *N*-fluorodibenzenesulfonimide.[6] The tetraesters were hydrolysed using bromotrimethylsilane and subsequently converted into their respective tributylammonium salts **6**, **8** and **9**. The bisphosphonates were coupled to the nucleoside monophosphonate **10** *via* the activated morpholidate **11**.[2,7] Products were purified by anion

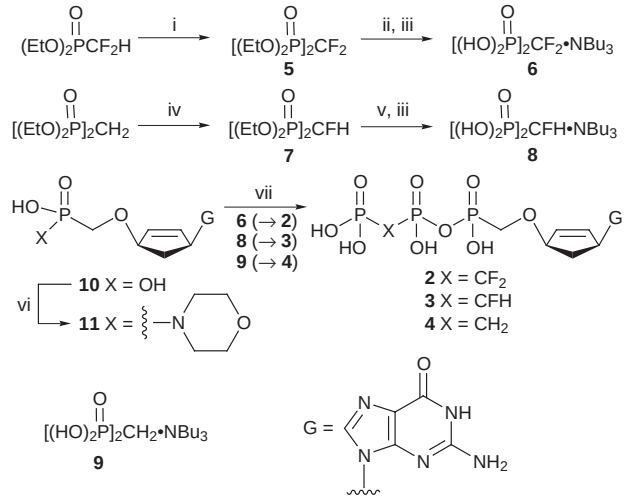

Scheme 1 *Reagents and conditions*: i, LDA, THF, −70 °C, 1 h, then $ClP(O)(OEt)_2$, −70 °C, 1 h (34%); ii, Me_3SiBr, room temp., 18 h (83%); iii, NBu_3, EtOH, H_2O, room temp., 90 min; iv, KHMDS, THF, −78 °C, 1 h, then *N*-fluorodibenzenesulfonimide, THF–toluene, −78 °C, 90 min (26%); v, Me_3SiBr, room temp., 72 h (98%); vi, morpholine, DCC, Bu^tOH, H_2O, reflux, 5 h; vii, DMSO, room temp., 0.5–7 days (24–32%)

exchange, followed by reverse phase chromatography, and isolated as their ammonium salts.[8]

The efficacies of **2**–**4** as inhibitors of recombinant HIV-1-rt (Du Pont cat. No. NEI-490) were examined using the Du Pont RT-Detect™ Reverse Transcriptase Assay (cat. No. NEK-070) and the results are shown in Table 1.

Compounds **2**–**4** showed an expected correlation of increased activity with an increase in fluoro-substitution, culminating in the CF_2 analogue **2** being just an order of magnitude less active than the parent compound **1**.

The stability of the CF_2 compound **2** in human foetal blood serum was assessed and compared with AZTTP, some natural nucleoside triphosphates, and the pyrophosphoryl phosphonates' natural enantiomer, **1**-ent (Table 2). Blood serum is an appropriate medium in which to perform this assay as it contains numerous dephosphorylating enzymes and so provides a good model system of the extracellular environment *in vivo*. The half-

Table 1 Relative efficacy of substrates **1**–**4** as inhibitors of HIV-rt[a]

Compound	IC_{50}[b]/μM
1	0.5
2	5.8
3	34.8
4	> 100
AZTTP	1.0

[a] The IC_{50} values shown are the results from enzyme assays carried out in reaction mixtures containing 0.1 units ml^{-1} of HIV-rt, which were incubated at 37 °C for 110 min. [b] IC_{50} = substrate concentration required to inhibit to HIV-rt by 50%.

Table 2 Half-life time in fetal blood serum at 37 °C

Compound	$t_{1/2}$
1-ent	65 min[a]
2	45 h[a]
dGTP	< 30 min[b]
dATP	< 30 min[b]
AZTTP	5 min[b]

[a] As determined by the appearance of the phosphonate **10**. [b] As determined by the disappearance of the nucleoside triphosphate.

life of compound **2** was found to be 90 times greater than those of the natural purine NTPs, dGTP and dATP and also significantly greater than that of the pyrophosphoryl phosphonate **1**-ent. Evidently, the P_β,P_γ-difluoromethylene group greatly enhances the stability of compound **2** towards enzymatic dephosphorylation of the terminal phosphate group. Cleavage of the phosphate ester linkage at the P_α,P_β position could also be reduced as a result of the CF_2 analogue **2** being a poorer substrate for those dephosphorylating enzymes which function to hydrolyse NTPs at this position.

In conclusion, we have shown that it is possible to incorporate two stabilising phosphonate linkages in the 5′-side chain of the 'unnatural' enantiomer of carbovir triphosphate with only a modest compromise in biological activity whilst significantly enhancing biological stability. The use of more lipophilic derivatives of compound **2**, in order to facilitate drug delivery into whole cells, is currently under investigation and will be reported in due course.

We thank the MRC for a research studentship (to C. J. H.) and Wellcome Research Laboratories for the generous donation of AZT, made available through the MRC AIDS Reagent Project.

Notes and References

† E-mail: sj11@liverpool.ac.uk

1 G. M. Blackburn, D. Kent, F. Eckstein and T. Perée, *Nucleosides Nucleotides*, 1985, **4**, 165; G. M. Blackburn and D. Kent, *J. Chem. Soc., Perkin Trans. 1*, 1986, 913; G. M. Blackburn and D. Kent, *J. Chem. Soc., Chem. Commun.*, 1981, 930.

2 D. Coe, S. M. Roberts and R. Storer, *J. Chem. Soc., Perkin Trans. 1*, 1992, 2695; V. Merlo, S. M. Roberts, R. Storer and R. Bethell, *J. Chem. Soc., Perkin Trans. 1*, 1994, 1477.

3 Both enantiomers of carbovir triphosphate are equally effective as inhibitors of HIV-rt; W. Miller, S. Daluge, E. Garvey, S. Hopkins, J. Reardon, F. Boyd and F. Miller, *J. Biol. Chem.*, 1992, **267**, 21220.

4 T. Lin, M. Luo, M. Liu, Y. Zhu, E. Gullen, G. Dutschman and Y. Cheng, *J. Med. Chem.*, 1996, **39**, 1757.

5 M. Obayashi, E. Ito, K. Matsui and K. Kondo, *Tetrahedron Lett.*, 1982, **23**, 2323.

6 E. Differding, R. Duthaler, A. Krieger, R. Rüegg and C. Schmit, *Synlett*, 1991, 395; previous methodology employed perchloryl fluoride (C. McKenna and P. Shen, *J. Org. Chem.*, 1981, **46**, 4573) or acetyl hypofluorite (D. Hebel, K. Kirk, J. Kinjo, T. Kovács, L. Lesiak, J. Balzarini, E. De Clercq and P. Torrence, *Bioorg. Med. Chem. Lett.*, 1991, **7**, 357).

7 J. Moffatt and H. Khorana, *J. Am. Chem. Soc.*, 1961, **83**, 649; J. Moffatt, *Can. J. Chem.*, 1964, **42**, 599.

8 *Selected data* for **2**: ν_{max}(KBr)/cm^{-1} 1269 (P=O); λ_{max}(H_2O)/nm 252.0; δ_H(400 MHz, D_2O) 1.89 (1 H, dt, *J* 15.6, 4.4, 5′-βH), 2.97 (1 H, dt, *J* 14.0, 7.2, 5′-αH), 3.84 (2 H, d, *J* 9.2, PCH_2), 4.76–4.81 (1 H, br, 4′-H), 5.28–5.0 (1 H, br, 1′-H), 6.07–6.11 (1 H, m, 2′-H), 6.33–6.38 (1 H, m, 3′-H), 7.75–7.87 (1 H, br, 8-H); δ_F(376 MHz, D_2O) 42.40–42.90 (br, CF_2); δ_P(162 MHz, D_2O) −1.69 (br, P_β), 3.90 (br, P_γ), 11.44 (d, *J* 31.0, P_α); *m/z* (ES) 522 (6%, MH^+), 328 (15, M − $CH_2F_2O_4P_2$). For **3**: ν_{max}(KBr)/cm^{-1} 1236 (P=O); δ_P(162 MHz, D_2O) 2.44 (br, P_β), 9.61 (br, P_γ), 10.34 (d, *J* 29.0, P_α); *m/z* (ES) 504 (57%, MH^+), 328 (100, M − $CFH_3O_4P_2$). For **4**: ν_{max}(KBr)/cm^{-1} 1216 (P=O); δ_P(162 MHz, D_2O) 15.97 (1P, br, P_β), 10.08 (2P, br, P_α and P_γ); *m/z* (ES) 486 (35%, MH^+), 328 (100, M − $CH_4O_4P_2$).

Received in Cambridge, UK, 9th February 1998; 8/01127C

Synthesis and structural characterization of $Cp_2Ti(SiH_3)(PMe_3)$

Leijun Hao, Anne-Marie Lebuis and John F. Harrod*†

Department of Chemistry, McGill University, Montreal, Canada H3A 2K6

The title compound, the first example of a structurally fully characterized, unsubstituted silyl complex of a group 4 element, has been synthesized and showed unusual thermal stability compared to its analog $Cp_2Ti(SiH_2Me)(PMe_3)$.

Very few reports of reactions of SiH_4 with transition metal compounds have appeared, presumably because of the hazards associated with its use.[1]‡ There are also very few examples of structurally well characterised transition metal complexes with SiH_3 ligands.[2] We recently reported the synthesis of compounds **1** and **2** by reaction of SiH_4 with Cp_2TiMe_2.[3] This reaction can

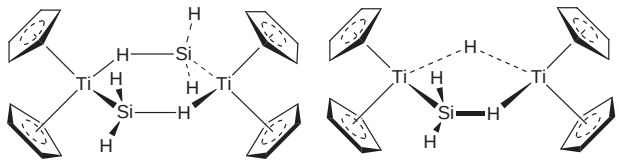

be carried out either with SiH_4 from a cylinder, or with SiH_4 generated *in situ* by catalytic redistribution of $SiH(EtO)_3$. The latter reaction is a convenient procedure for the safe generation of small amounts of SiH_4.[3] Although the structures of **1** and **2** were confidently assigned on the basis of their NMR spectra, we have not been able to obtain either of them in the form of crystals suitable for structure determination by X-ray diffraction. We now report the preparation and structure determination of the related phosphine complex, $Cp_2Ti(SiH_3)(PMe_3)$ **3**, an analog of the organosilyl complexes reported earlier,[4,5] and the first structurally fully characterized, unsubstituted silyl complex of a group 4 metal.

Reaction of Cp_2TiMe_2 with SiH_4 in the presence of PMe_3 in diethyl ether–toluene solution proceeds smoothly to give **3** in 76% yield as square purple plates. Solutions of **3** in toluene or benzene are relatively thermally stable and so could be fully characterized both in solution and in solid state. The structure of **3**, together with some bond parameters, is shown in Fig. 1.§ Of the bond parameters, only the Ti–Si bond length falls outside the range previously determined for $Cp_2Ti(SiHRR')(PMe_3)$ complexes (R = H, R′ = Ph **4**; R = Ph, R′ = Ph **5** or Me **6**).[4] The relevant values are: 2.594(2) **3**, 2.650(1) **4**, 2.652(1) **5** and 2.646(2) Å **6**, indicative of a stronger Ti–Si bond in **3**. The Ti–Si bond distance in **3** is essentially identical to those observed in the phenylsilyl analogue of **1** and in $(Bu^tCH_2)_3TiSi(SiMe_3)_3$.¶ The perspective of **3** shown in Fig. 1 is chosen to show the perfect *gauche* arrangements of the SiH_3 and PMe_3 ligands with respect to the Cp_2Ti unit and the mirror plane symmetry of the molecule. These features are not exhibited by the other organosilyl complexes where the local symmetry of the silyl ligand is lower than C_{3v}.

The spectroscopic data are consistent with the structure revealed by the X-ray analysis. The ^1H NMR spectrum of **1** is consistent with it being a paramagnetic species since only broad resonances were observed and no resonance was observed in the $^{31}P\{^1H\}$ spectrum. Solutions of **3** in toluene give the characteristic EPR spectrum shown in Fig. 2. The doublet of quartets (g = 1.9956) is accounted for by the coupling of the single unpaired electron of Ti^{III} to a single ^{31}P nucleus (a_P = 28.6 G) and to the three Si–H protons (a_H = 4.3 G). Satellites due to coupling to the Ti isotopes [I = 7/2, ^{49}Ti (5.5%); I = 5/2, ^{47}Ti (7.75%)] with a_{Ti} = 7.8 G are also observable. The values for a_P and a_{Ti} are in, or very close to, the ranges observed for **4**, **5** and **6** (28.8–29.9 G and 7.7 to 8.7 G respectively), as is the g value (1.9944–1.9976).[4,5] The value for a_H is somewhat larger than the values for the organosilyl complexes (2.6–3.2 G) which may be a result of the slightly shorter Ti–Si bond in **3**.[4,5]

Solutions of **3** in toluene are stable for several days at room temperature in an argon atmosphere. This stability is unusual and unexpected, given the fact that the compound is a primary silane.[4–6] The closest analog $Cp_2Ti(SiH_2Me)(PMe_3)$ **7**, synthesized from the reaction of Cp_2TiMe_2 and SiH_3Me, generated *in situ* by catalytic redistribution of $SiHMe(EtO)_2$,[3] in the presence of PMe_3 in hexane solution, was stable only for several hours and decomposed to the titanocene(III) hydride **8** and the titanocene(III) silyl compound **9**, as shown in Scheme 1.‖ Similar dehydrocoupling reactions were also observed for other analogous $Cp_2Ti(SiHRR')(PMe_3)$ compounds.[5] We attribute the greater stability of **3** to stronger Ti–Si and Ti–P bonds and a resulting high formation constant for the phosphine complex.

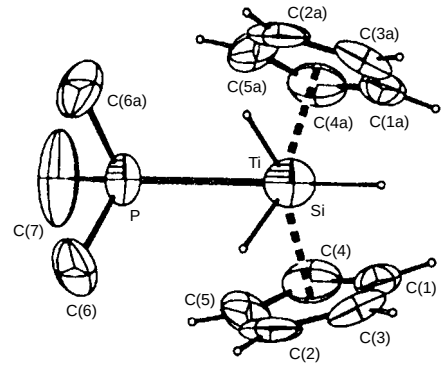

Fig. 1 A view of the structure of **3** down the Si–Ti bond (30% probability ellipsoids). Selected bond lengths (Å) and bond angles (°): Ti–P 2.559(2), Ti–Si 2.594(2), Si–H(av.) 1.53(7); P–Ti–Si 83.91(6), Cp(cent)–Ti = 2.031(3), Cp(cent)–Ti–Cp(cent) 134.2(4).

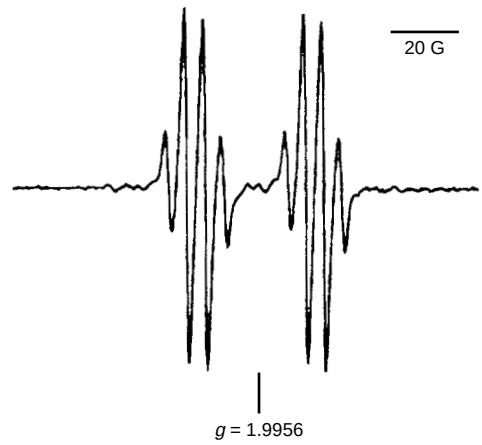

Fig. 2 EPR spectrum of **3** in toluene at room temperature

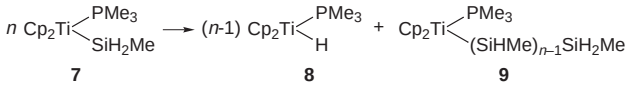

7 **8** **9**

Scheme 1

The consequent suppression of phosphine dissociation to give the coordinatively unsaturated intermediate necessary for reaction of the titanium with Si–H bonds prevents the hydrogen transfer reaction depicted in Scheme 1. In the absence of PMe_3, Cp_2TiMe_2 catalyses the rapid dehydrocoupling of SiH_4 to an insoluble, pyrophoric polymer.

Studies of reactions of SiH_4 with other group 4 compounds are in progress.

We thank NSERC (Canada) and the Fonds FCAR de Québec for financial support, Professor Don Berry for useful discussions, and the Laboratoire de Crystallographie par Rayons X de l'Université de Montréal for access to a diffractometer.

Notes and References

† E-mail: harrod@omc.lan.mcgill.ca

‡ SiH_4 spontaneously explodes and burns immediately on exposure to air.

§ *Crystal data*: **3**: $C_{13}H_{22}PSiTi$, M = 285.26, orthorhombic, space group *Pcmn*, a = 8.661(4), b = 12.516(4), c = 14.330(4) Å, V = 1553(1) Å^3, Z = 4, Z' = ½, D_c = 1.220 g cm^{-1}, F(000) = 604, crystal size: 0.78 × 0.60 × 0.26 mm. Data were collected at 220 K on a Enraf-Nonius CAD4 diffractometer using Cu-Kα radiation (λ = 1.540 56 Å) in the ω–2θ scan mode. A total of 22400 reflections were measured in the range 5.96° < θ < 69.83° giving 1553 unique reflections, of which 1500 with $I > 2\sigma(I)$ were considered observed. Analytical absorption correction (μ = 62.37 cm^{-1}; range 0.03–0.29). The structure was solved by direct method using SHELXS96 and refined by full-matrix least squares on F^2. Hydrogens on Si were located on the difference map and refined successfully. R = 0.062 [for $I > 2\sigma(I)$] and wR_2 = 0.1703 (for all data). CCDC 182/828.

¶ Ti–Si bond distances in $[Cp_2Ti(\mu\text{-}HSiHPh)]_2$ and in $(Bu^tCH_2)_3Ti\text{-}Si(SiMe_3)_3$ are 2.594(2) Å (average) and 2.594(7) Å respectively.[6]

‖ *EPR data in toluene*: **7**: g = 1.9941, a_{Ti} = 7.0 G, a_P = 28.97 G, a_H = 3.35 G. **8**: g = 1.9929, a_{Ti} = 6.8 G, a_P = 28.2 G, a_H = 10.6 G. **9**: g = 1.9933, a_P = 28.74 G, a_H = 3.37 G. Bercaw and Brintzinger also reported the generation of a titanocene hydride phosphine compound $Cp_2TiH(PPh_3)$ which gave a similar EPR spectrum to **8**.[7]

1 J. J. Schneider, *Angew. Chem., Int. Ed. Engl.*, 1996, **35**, 1068; U. Schubert, *Adv. Organomet. Chem.*, 1990, **30**, 151; J. L. Speier, *Adv. Organomet. Chem.*, 1979, **17**, 407.

2 B. J. Aylett and J. M. Campbell, *J. Chem. Soc. A*, 1969, 1910; B. J. Aylett, J. M. Campbell and A. Walton, *J. Chem. Soc. A*, 1969, 2110; E. A. V. Ebsworth, V. M. Marganian, F. J. S. Reed and R. O. Gould, *J. Chem. Soc., Dalton Trans.*, 1978, 1167; H.-G. Woo, R. H. Heyn and T. D. Tilley, *J. Am. Chem. Soc.*, 1992, **114**, 5698; S. Schmitzer, U. Weis, H. Kab, W. Buchner, W. Malisch, T. Polzer, U. Posset and W. Kiefer, *Inorg. Chem.*, 1993, **32**, 30; X.-L. Luo, G. J. Kubas, C. J. Burns, J. C. Bryan and C. J. Unkefer, *J. Am. Chem. Soc.*, 1995, **117**, 1159; W. Malisch, S. Moller, O. Fey, R. Pikl, U. Posset and W. Kiefer, *J. Organomet. Chem.*, 1996, **507**, 117.

3 L. Hao, A.-M. Lebuis, J. F. Harrod and E. Samuel, *Chem. Commun.*, 1997, 2193.

4 E. Samuel, Y. Mu, J. F. Harrod, Y. Dromzee and Y. Jeannin, *J. Am. Chem. Soc.*, 1990, **112**, 3435; J. Britten, Y. Mu, J. F. Harrod, J. Polowin, M. C. Baird and E. Samuel, *Organometallics*, 1993, **12**, 2672.

5 H. G. Woo, J. F. Harrod, J. Hénique and E. Samuel, *Organometallics*., 1993, **12**, 2883.

6 C. Aitken, J. F. Harrod and E. Samuel, *J. Am. Chem. Soc.*, 1986, **108**, 4059; L. H. McAlexander, M. Hung, L. Li, J. B. Diminnie, Z. Xue, G. P. A. Yap and A. L. Rheingold, *Organometallics*., 1996, **15**, 2883.

7 J. E. Bercaw and H. H. Brintzinger, *J. Am. Chem. Soc.*, 1969, **91**, 7301.

Received in Bloomington, IN, USA, 4th February 1998; 8/00967H

Modified Mg–Al hydrotalcite: a highly active heterogeneous base catalyst for cyanoethylation of alcohols

Pramod S. Kumbhar,† Jaime Sanchez-Valente and François Figueras*‡

Institut de Recherches sur la Catalyse, 2 Av. A. Einstein, 69626 Villeurbanne, France

Modified Mg–Al hydrotalcite (Mg : Al = 3 : 1) prepared by thermal decarbonation followed by rehydration of a conventional Mg–Al hydrotalcite is found to be a highly active, reusable and air stable catalyst for cyanoethylation of alcohols.

Cyanoethylation of alcohols is a widely used reaction for the synthesis of drug intermediates and organic compounds of industrial interest.[1] Acrylonitrile undergoes cyanoethylation with a number of monohydric alcohols to give alkoxypropionitriles which, after hydrogenation, give industrially important amines. The reaction is catalysed by homogeneous base catalysts such as alkali hydroxides[2] and alkoxides[3] and tetraalkyl ammonium hydroxide. However, these catalysts need to be neutralised before purification of the product, resulting in the generation of waste, loss of catalyst and reduced product yields. Alternatively, use of anion exchange resins as heterogeneous catalyst have also been reported.[4,5] Recently, Hattori and Kabashima[6] reported use of alkaline earth oxides, hydroxides and alumina supported KF and potassium hydroxide supported on alumina as heterogeneous catalysts for this reaction. High activities were reported for high temperature activated MgO catalyst (800 °C *in vacuo*). The general reaction scheme for cyanoethylation of alcohols is shown in Scheme 1.

Previously we had reported that modified hydrotalcite, prepared by thermally decarbonating the conventional Mg–Al hydrotalcite followed by controlled rehydration, is highly active for aldol and Knoevenagel condensation reactions.[7,8] The high activity of this catalyst is attributed to the presence of a large number of OH^- groups, generated during rehydration of the thermally activated hydrotalcite, which act as Brönsted basic sites. The use of modified hydrotalcites as heterogeneous Brönsted basic catalysts instead of homogeneous catalysts such as alkali hydroxides and alkoxides has a number of advantages, *viz*. ease of separation, reusability, no waste, and higher activities and selectivities (depending on the reaction).

In continuation of our above mentioned work here we report that the modified hydrotalcites having formula $[Mg_{(1-x)}Al_x(OH)_2](OH)_x{\cdot}yH_2O$ show unprecedented high activity for the cyanoethylation of alcohols with acrylonitrile. The activity of this catalyst is the highest so far reported in the literature for any heterogeneous catalyst. The catalysts were found to be reusable without significant loss in activity. The other interesting aspect of this work is that these catalysts were found to be active even after exposure to air in this reaction, a rare phenomena for a solid basic catalyst.

Mg–Al hydrotalcites having Mg : Al = 3 : 1 was synthesised using the procedure reported by Miyata *et al*.[9] The presence of pure hydrotalcite structure was confirmed by powder X-ray diffraction. The preparation of modified hydrotalcite includes activation of the hydrotalcite in carbon dioxide free N_2 at 450 °C, followed by cooling and hydrating the material in a flow of nitrogen saturated with water at room temperature in a controlled fashion.

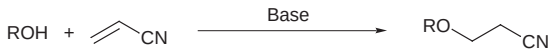

Scheme 1

The catalytic reactions were carried out using 10 ml of alcohol and 4 mmol of acrylonitrile. The catalyst after rehydration was transferred to the reactor containing the alcohol followed by addition of acrylonitrile. The samples were analysed by gas-liquid chromatography.

Table 1 shows a comparison of the modified hydrotalcites rehydrated for different periods of time with fresh and calcined hydrotalcites and MgO (from the results of Hattori[6]) for the reaction of acrylonitrile with MeOH in which methoxypropionitrile is the only product. The modified hydrotalcites are much more active than MgO, which also needs a very high activation temperature (800 °C *in vacuo*). The hydrotalcite as such shows only marginal activity as it contains very few basic sites. It is interesting to note that even though the calcined hydrotalcite has a high Lewis basicity, it is only marginally active. This shows that this reaction is catalysed by weak Brönsted basic sites (OH^- sites).

Similar to our earlier results for the aldol condensation reaction,[7] for cyanoethylation the catalytic activity also depends upon the rehydration time. In the present case optimum activity is observed for the catalyst rehydrated for 6 h (catalyst = 0.1 g, water saturated N_2 flow = 80 ml min^{-1}).

The reusability of the catalyst was studied by using the same catalyst after allowing the catalyst to settle, decanting the supernatanat reaction mixture and continuing the reaction by introducing fresh reactants (acrylonitrile and MeOH). The results are sumarised in Table 2. The catalyst was found to be reusable without appreciable loss in activity.

The study was further extended to other monohydric alcohols such as EtOH, Pr^iOH, BuOH and Bu^tOH. The results are summarised in Table 3. Except for Bu^tOH, the catalysts are found to be highly active for all the alcohols, which is in agreement with the results for the homogeneous catalyst. The selectivity for the corresponding alkoxypropionitrile was 100%,

Table 1 Comparison of various catalysts for cyanoethylation of acrylonitrile with MeOH[a]

Catalyst	Conditions for activation of the catalyst	*t*/min	Conversion of acrylonitrile (%)
Mg–Al Hydrotalcite	used as was	120	2.5
Mg–Al Hydrotalcite	N_2 flow at 450 °C	120	20
Modified Mg–Al Hydrotalcite	N_2 at 450 °C rehydration for 3 h in wet N_2 at room temp.	90	98
Modified Mg–Al Hydrotalcite	N_2 at 450 °C rehydration for 6 h in wet N_2 at room temp.	45	99.8
Modified Mg–Al Hydrotalcite	N_2 at 450 °C rehydration for 12 h in wet N_2 at room temp.	45	100
MgO[b]	800 °C *in vacuo*	120	98.7

[a] Reaction conditions: acrylonitrile (0.04 mol), MeOH (10 ml), 50 °C, Catalyst (0.1 g). [b] Results from ref. 6.

Table 2 Reusability of modified Mg Al hydrotalcite catalyst (rehydrated for 6 h) for cyanoethylation of acrylonitrile with MeOH[a]

Cycle	Conversion (%)
1	99.8
2	98.0
3	96.0

[a] Reaction conditions as in Table 1.

except for Pr^{i}OH, in which case the selectivity for β-isopropoxypropionitrile was 80%.

Normally, solid basic catalysts are highly sensitive to air and loose their activity due to carbonation when exposed, preventing them from being used industrially. To check this an experiment was carried out to see if the catalyst remained active when exposed to air. To our surprise we found that the modified hydrotalcite catalyst, even after exposure to air (1 h), showed the same activity as a sample not exposed (100% conversion in 45 min). This result makes this catalyst attractive for practical use.

Table 3 Cyanoethylation of various monohydric alcohols with acrylonitrile over modified Mg–Al hydrotalcite (rehydrated for 6 h)[a]

Alcohol	*t*/min	Conversion of acrylonitrile (%)
EtOH	25	100
Pr^{i}OH	90	95.6
BuOH	20	100
Bu^{t}OH	120	10

[a] Reaction conditions as in Table 1.

In summary we have shown that modified Mg–Al hydrotalcite is a highly active, reusable and air stable catalyst for cyanoethylation of monohydric alcohols.

We thank the Indo-French Centre for Promotion of Advanced Research (IFCPAR project no. IFC/1106-2696-2460) for financial support. J. S. V. thanks Conacyt de Mexico for a PhD grant.

Notes and References

† On leave from Herdillia Chemicals Ltd., Navi Mumbai, India.
‡ E-mail: figueras@catalyse.univ-lyon1.fr

1 H. A. Bruson, in *Organic Reactions*, ed. R. Adams, Wiley, London, 1949, vol. 5, p. 79.
2 J. H. MacGregor and C. Pugh, *J. Chem. Soc.*, 1945, 535.
3 W. P. Unlermoheln, *J. Am. Chem. Soc.*, 1945, **67**, 1505.
4 C. J. Schmidle and R. C. Mansfield, *Ind. Eng. Chem.*, 1952, **44**, 2867.
5 M. J. Astle and J. A. Zaslowsky, *Ind. Eng. Chem.*, 1952, **44**, 2867.
6 H. Hattori and K. Kabashima, *Appl. Catal. A: Gen. Lett.*, 1997, **161**, L33.
7 K. Rao, F. Figueras, J. Sanchez and M. Gravelle, *J. Catal.*, 1998, **173**, 115.
8 M. Lakshmi Kantam, K. Rao, B. M. Choudary, C. Venkat Reddy and F. Figueras, *Chem. Commun.*, in the press.
9 S. Miyata, T. Kumura and M. Shimada, *U.S. Pat.*, 1975, 3 879 523.

Received in Liverpool, UK, 6th March 1998; 8/01872C

Germyl anion species-promoted formation of cyanofluoromethylene compounds: first and efficient synthesis of fluorinated homoallylic and homoprop-2-ynylic cyanides

Yasuo Yokoyama*† and Kunio Mochida‡

Department of Chemistry, Faculty of Science, Gakushuin University, 1-5-1 Mejiro, Toshima-ku, Tokyo 171-8588, Japan

Various fluorinated homoallylic and homoprop-2-ynylic cyanides could be synthesized from 2-fluoro-2-phenylthio-2-phenylacetonitrile and some allylic or prop-2-ynylic chlorides in excellent yields by use of a germyl anion species.

Recently, fluorine-contained organic compounds have attracted wide attention among scientists in the fields of agrochemicals, pharmaceuticals and material sciences. Various antiviral, antitumor and antifungal agents and advanced materials have been synthesized in which fluorine substitution plays a significant role in their biological activities and physical properties.[1] Thus, the formation of an organofluorine compound is a most important reaction in organic synthesis. Particularly, synthetic methodology for a monofluorinated compound ($R^1R^2R^3CF$)[2] is a very attractive target of study, because it is difficult due to the chemical lability of the foregoing compound in some cases. Concerning this problem, we focused on the synthesis of the cyanofluoromethylene compound [$R^1R^2C(CN)F$] as an easy and effective formation of a monofluorinated product. This compound has cyano and fluoro substituents on the same carbon, and could be employed as a useful fluorine-containing building block, because the cyano group is easily transformed to other substituents.[3] Moreover, this molecule is important from the viewpoint of the multifunctional carbon structure.[4] There are two strategies which give the foregoing molecule. One is a stepwise introduction of cyano and fluoro groups,[5] and the other is introduction of a cyanofluoromethylene unit to a substrate. In particular, the latter method is suitable for the synthesis of cyanofluoromethylene compounds because the target molecule can be formed more straightforwardly. However, only a few synthetic examples have been reported at the present time.[6] In this regard, we have developed the germyl anion species-promoted synthesis of a cyanofluoromethylene compound by use of 2-fluoro-2-phenylthio-2-phenylacetonitrile as the cyanofluoromethylene source. Herein we report the first and efficient syntheses of fluorinated homoallylic and homoprop-2-ynylic cyanides.

Some selected data of reactions of 2-fluoro-2-phenylthio-2-phenylacetonitrile with (*E*)-3-chloro-1-phenylprop-1-ene (cinnamyl chloride) in the presence of various activators are summarized in Table 1.

As expected, some germyl anion species were found to give fluorinated homoallylic cyanides (entries 1–3). The yield of the desired compound was affected by the nature of the counter cation. When germyl anions having Li^+ and K^+ were used, the yield of the target product was low. Many unidentified by-products were obtained, whereas the starting cyanide was consumed completely (entries 1 and 3). On the other hand, 2-fluoro-2-phenylthio-2-phenylacetonitrile could be activated effectively by Et_3GeNa to give the active intermediate. This species reacted with cinnamyl chloride to give the corresponding compound quantitatively (entry 2). Other group 14 element-containing anions, such as Me_3SiNa,[7] Et_3SnNa§ and Bu^nLi were not useful for this type of reaction (entries 4–6). In addition, the starting cyanide was transformed to the desired homoallylic cyanide in low yield when lithium naphthalenide (LN), which is well known as a strong one-electron reducing agent,[9] was applied (entry 7). These facts suggested that only Et_3GeNa was suitable for the synthesis of the fluorinated homoallylic cyanide. The reason why Et_3GeNa was favorable for the activation and the cleavage of a sulfur–carbon bond¶ is unclear, but this phenomenon is probably due to the thiophilicity of the germanium atom and the stability of the active intermediate.

Various allylic and prop-2-ynylic chlorides could be also used as substrates instead of cinnamyl chloride under the same reaction conditions (Table 1, entry 2). In Table 2, the results of application of this reaction for some substrates are presented. When 3-chloroprop-1-ene was used as an electrophile, the desired simple homoallylic cyanide was obtained in excellent yield (entry 1). When 1-chlorobut-2-ene (*E*:*Z* = 73:27) was employed, the *E*-isomer of the target compound was obtained predominantly (entry 2, *E*:*Z* = 73:27). Some *E*-allylic chlorides, such as (*E*)-1-chlorohex-2-ene, (*E*)-1-chlorooct-2-ene, (*E*)-1-chlorononon-2-ene and (*E*)-1-chloro-3,5-dimethylocta-2,6-diene could be transformed to the desired products having *E*-configuration in excellent yields (entries 3–6). These results suggested that no isomerization of the olefin occurred under these reaction conditions. Other primary allylic chlorides were also employed as electrophiles (entries 7 and 8). On the other hand, when secondary allylic chloride (3-chlorobut-1-ene) was used, the desired compound was obtained in moderate yield (76%, *syn*:*anti* = 64:36, entry 9). An *E*-isomer of entry 2 was obtained which was formed by the attack of a nucleophile at the γ-carbon as a by-product (24%), because the intermediate was sterically hindered. Furthermore, 1-chlorohexa-2,4-diene and some prop-2-ynylic chlorides could react with the active intermediate to give the corresponding fluorinated cyanides in excellent yields without decomposition of the starting chlorides (entries 10–12). In these cases, products formed by attack of the nucleophile to the γ-position (or ε-position) of chlorides could not be detected at all, except in the case of entry 9. These results revealed that the presented method was applicable to the

Table 1 Synthesis of fluorinated cyanides by use of various activators

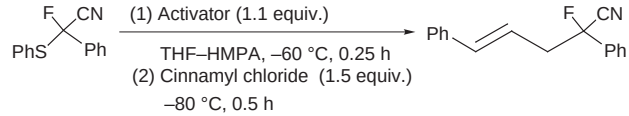

Entry	Activator	Yield[a] (%)
1	Et_3GeLi	35
2	Et_3GeNa	98
3	Et_3GeK	5.6
4	Me_3SiNa	NR[b]
5	Et_3SnNa	2.8
6	Bu^nLi	36
7	LN[c]	36

[a] Isolated yield. Identified by ^1H, ^{19}F and ^{13}C NMR analysis. [b] Starting cyanide was recovered (98%). [c] Lithium naphthalenide.

Table 2 Synthesis of various fluorinated homoallylic and homoprop-2-ynylic cyanides

Entry	Product[a]	Yield[b] (%)
1	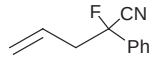	96
2	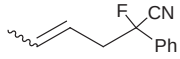	99
3	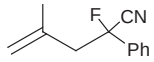	95
4	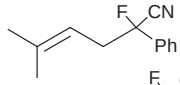	97
5	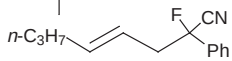	96
6	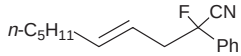	96
7	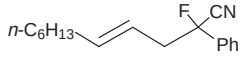	96
8	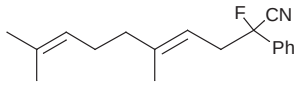	95
9[c]	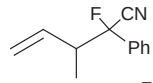	76
10	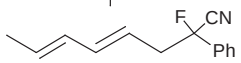	96
11	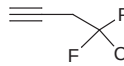	97
12	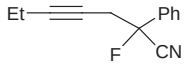	95

[a] All compounds were identified by ^{1}H, ^{19}F and ^{13}C NMR analysis. [b] Isolated yield. [c] The second operation was carried out for 3 h.

synthesis of many types of fluorinated homoallylic and homoprop-2-ynylic cyanides.

A typical procedure is as follows. To a THF solution (20 ml) of 2-fluoro-2-phenylthio-2-phenylacetonitrile (377 mg, 1.55 mmol) was added an HMPA solution of Et_3GeNa[11] (4 ml, 0.42 M) slowly at −60 °C. After stirring for 0.25 h at −60 °C, the temperature was lowered to −80 °C, and cinnamyl chloride (355 mg, 2.32 mmol) was added. The mixture was stirred for 0.5 h at −80 °C and then was passed through a short column of silica gel and eluted with Et_2O. Concentration of this eluate followed by column chromatographic purification afforded 380 mg (98%) of the corresponding compound (Table 1, entry 2).

In conclusion, we have developed the first syntheses of fluorinated homoallylic and homoprop-2-ynylic cyanides. This reaction proceeded smoothly to give the corresponding product in excellent yield under mild reaction conditions. The efficient synthesis presented here can presumably be employed in fluorine chemistry as a useful method for monofluorinated compounds. Further investigation of applications of this reaction and a mechanistic study are now in progress.

Notes and references

† E-mail: 940429@gakushuin.ac.jp
‡ E-mail: kunio.mochida@gakushuin.ac.jp
§ A stannyl anion (Bu_3SnLi)-promoted reductive lithiation of a phenyl sulfide and an ethyl sulfide was reported by T. Takeda and co-workers (ref. 8).
¶ Effective activation of a carbon–sulfur bond using germyl anion species has already been presented in our previous work (ref. 10).

1 For selected reviews, see *Organofluorine Chemicals and Their Industrial Applications*, ed. R. E. Banks, Soc. Chem. Ind., London, 1979; *Biomedical Aspects of Fluorine Chemistry*, ed. R. Filler and Y. Kobayashi, Kodansha Ltd., Tokyo, 1982; *Fluorine-containing Molecules, Structure, Reactivity, Synthesis*, ed. J. K. Liebman, A. Greenberg, and W. R. Dolbier Jr., VCH, New York, 1988; *Fluorine in Bioorganic Chemistry*, ed. J. T. Welch and S. Eshwarakrishman, Wiley, New York, 1991.
2 Y. Takeuchi, *J. Synth. Org. Chem. Jpn.*, 1988, **46**, 145 and ref. 1.
3 For examples, see E. D. Bergmann, S. Cohen, E. Hoffman and Z. Rand-Meir, *J. Chem. Soc.*, 1961, 3452; H. Gershon, S. G. Shuman and A. D. Spevack, *J. Med. Chem.*, 1967, **10**, 536; P. Bey, F. Gerhart, V. V. Dorsselaer and C. Danzin, *J. Med. Chem.*, 1983, **26**, 1551.
4 For a review and some papers, see Y. Takeuchi, *J. Synth. Org. Chem. Jpn.*, 1997, **55**, 886; Y. Takeuchi, K. Takagi, T. Yamada, M. Nabetani and T. Koizumi, *J. Fluorine Chem.*, 1994, **68**, 149; Y. Takeuchi, S. Kawahara, S. Suzuki and T. Koizumi, *J. Org. Chem.*, 1996, **61**, 301.
5 For example, Y. Takeuchi, N. Itoh, T. Satoh, T. Koizumi and K. Yamaguchi, *J. Org. Chem.*, 1993, **58**, 1812 and references cited therein.
6 R. G. Pews and Z. Lysenko, *J. Org. Chem.*, 1985, **50**, 5115.
7 H. Sakurai, A. Okada, M. Kira and K. Yonezawa, *Tetrahedron Lett.*, 1971, 1511.
8 T. Takeda, K. Ando and T. Fujiwara, *Chem. Lett.*, 1985, 1149.
9 T. Cohen, W. M. Daniewski and R. B. Weisenfeld, *Tetrahedron Lett.*, 1978, 4665; C. G. Screttas and M. M. Screttas, *J. Org. Chem.*, 1978, **43**, 1064; C. G. Screttas and M. M. Screttas, *J. Org. Chem.*, 1979, **44**, 713; T. Cohen and R. B. Weisenfeld, *J. Org. Chem.*, 1979, **44**, 3601; D. J. Ager, *Tetrahedron Lett.*, 1981, **22**, 2923; C. Rücker, *Tetrahedron Lett.*, 1984, **25**, 4349; T. Cohen and B.-S. Guo, *Tetrahedron*, 1986, **42**, 2803.
10 Y. Yokoyama and K. Mochida, *Synlett*, 1996, 1991; Y. Yokoyama and K. Mochida, *Tetrahedron Lett.*, 1997, **38**, 3443; Y. Yokoyama and K. Mochida, *Synlett*, 1997, 907; Y. Yokoyama and K. Mochida, *Synlett*, 1998, 37.
11 E. J. Bulten and J. G. Noltes, *Tetrahedron Lett.*, 1966, 4389; E. J. Bulten and J. G. Noltes, *Tetrahedron Lett.* 1967, 1443.

Received in Cambridge, UK, 12th March 1998; 8/02005A

Stereoselective Michael/aldol tandem reaction triggered by thiolate anion or analogues

Akio Kamimura,*[a]† Hiromasa Mitsudera,[a] Shigeru Asano,[a] Akikazu Kakehi[b] and Michihiko Noguchi[a]

[a] *Department of Applied Chemistry, Faculty of Engineering, Yamaguchi University, Ube 755-8611, Japan*
[b] *Department of Material Engineering, Faculty of Engineering, Shinshu University, Nagano 380-8553, Japan*

A combination of a *tert*-butyl α,β-unsaturated ester, an aldehyde and lithium thiophenolate in CH_2Cl_2 undergoes a one-pot Michael/aldol tandem reaction to give a condensation adduct of the three components, an α-phenylthiomethyl-β-hydroxy ester, in good yield with high *syn*-selectivity.

The Michael addition is one of the most powerful methodologies in organic synthesis.[1] Thiols are frequently used as good nucleophiles for the reaction with α,β-unsaturated esters, ketones or nitriles to give the corresponding Michael adducts quantitatively. The reaction is regarded as generating a β-thioenolate intermediate as a result of nucleophilic attack of the thiolate at the β-carbon of the Michael acceptor;[2] the intermediate is then protonated to give the Michael adduct. If the β-thioenolate intermediate was able to be used for the aldol reaction, a new Michael/aldol tandem reaction[3] could be developed and might provide a useful methodology for the construction of carbon skeleton since sulfur functionality is convenient for further transformation to other functional groups. There have been several similar examples of this type of reaction with carbon,[4] nitrogen[5] and silicon nucleophiles.[6] Although thiolate and its analogues have also been used in a similar way, good examples are limited to α,β-unsaturated ketones,[7] and the same sequence for α,β-unsaturated esters contains many problems.[7a,d,8] Additionally, the stereochemical outcome of the reaction with esters has not been clear so far. Here, we report a novel one-pot three-component condensation of thiolate, an α,β-unsaturated ester and an aldehyde with high *syn*-stereoselectivity.

The reaction procedure was quite simple; lithium thiophenolate was generated from thiophenol on treatment with butyllithium at −78 °C in CH_2Cl_2 to give a white precipitate, most of which remained undissolved following addition of acryrate esters at −78 °C. To the heterogeneous mixture, aldehyde was added at the same temperature; the reaction mixture then became a homogeneous pale yellow solution. The solution was maintained at −50 °C for 7 h and the three-component condensation adducts **3** were obtained (Scheme 1). To our surprise, no S_N2 product from CH_2Cl_2 and lithium thiolate was observed. The results are summarised in Table 1.‡

The reaction exhibited several interesting features. Firstly, choice of reaction solvent was quite important; CH_2Cl_2 or Et_2O were the only suitable solvents to perform the reaction. Other coordinative solvents such as THF or propiononitrile were not useful; only the simple Michael adduct of thiol and acrylate was formed. The counter cation was also important; use of lithium thiophenolate was essential. The reaction of methyl or ethyl acrylate gave the three component adducts **3a** or **3b** in 62 or 64% yield, respectively, but neither of their diastereomeric ratios were satisfactory (entries 1 and 2). The stereoselectivity was significantly improved when *tert*-butyl acrylate was used instead; the tandem adduct **3c** was obtained in 80% with 92 : 8 *syn*-selectivity (entry 3). The present stereoselectivity is much higher than the analogous aldol reaction of ester enolates generated from *tert*-butyl propionate with LDA, in which the reported *syn* : *anti* ratio was almost 1 : 1.[9] The tandem adducts **3**, starting from other aromatic and α,β-unsaturated aldehydes, were prepared in similar yields with high *syn*-selectivity (entries 4–6). Aliphatic aldehydes also gave the adduct in moderate yield, along with formation of the self-aldol product of the aldehyde (entry 7).

We also examined analogues of thiolate for the reaction. Lithium phenylselenolate,[10] which was generated from diphenyl diselenide and methyllithium,§ was found to be effective for the reaction; again the *syn*-enriched adduct **4a** was isolated in 63% (entry 8). The diastereoselectivity and yield of **4** for the reaction with aromatic aldehydes were slightly less than those for the reactions promoted by thiolate in CH_2Cl_2 (entries 8–10). The reaction with an aliphatic aldehyde, however, gave **4d** in only poor yield (entry 11). Phenoxide was too unreactive to promote the reaction (entry 12). We also tried to apply the present sequence to methyl vinyl ketone with thiolate and benzaldehyde, but only trace amounts of the corresponding tandem adduct were formed.

The stereochemistries of **3** and **4** were determined in the following way (Scheme 2); the phenylseleno group in compound **4a** was replaced by hydrogen on treatment with Bu_3SnH. Diastereomeric ratios of **4a** (85 : 15) and **6** (82 : 18) were almost the same within experimental error. The NMR spectrum of the

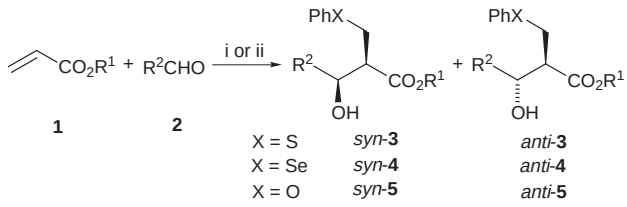

Scheme 1 *Reagents and conditions*: i, PhSLi, CH_2Cl_2, −78 °C, then −50 °C; ii, PhSeSePh, MeLi·LiBr, Et_2O, −78 °C, then room temp.

Table 1 The three-component condensation of thiolate, acrylate and aldehyde

Entry	R^1	R^2	X	Product	Yield (%)[a]	*syn* : *anti*[b]
1	Me	Ph	S	**3a**	62	71 : 29
2	Et	Ph	S	**3b**	64	66 : 34
3	Bu^t	Ph	S	**3c**	80	92 : 8
4	Bu^t	*p*-ClC_6H_4	S	**3d**	71	89 : 11
5	Bu^t	1-naphthyl	S	**3e**	92	88 : 12
6	Bu^t	PhCH=CH	S	**3f**	52	81 : 19
7	Bu^t	C_5H_{11}	S	**3g**	65	73 : 27
8	Bu^t	Ph	Se	**4a**	63	85 : 15
9	Bu^t	*p*-ClC_6H_4	Se	**4b**	52	81 : 19
10	Bu^t	2-naphthyl	Se	**4c**	64	84 : 16
11	Bu^t	C_9H_{19}	Se	**4d**	23	nd[c]
12	Bu^t	Ph	O	**5a**	0	—

[a] Isolated yield. [b] Determined by reversed phase HPLC analyses. [c] nd = not determined.

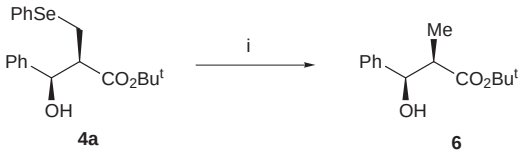

4a **6**

Scheme 2 *Reagents and conditions*: i, Bu_3SnH, AlBN, toluene, 110 °C (75%)

minor isomer of **6** was found to be identical to the known *anti*-diastereomer,[11] and we concluded that the major isomers of **4a** and **6** had *syn*-configuration. The stereochemistries of the other thio analogues **3** were determined on the basis of comparison of their ^{1}H NMR spectra and HPLC patterns.

The present methodology is useful for the preparation of γ-butyrolactone from lithium thiophenolate, fumarate ester and aldehyde. For example, reaction of the three components in CH_2Cl_2 at −50 °C for 5 h resulted in the formation of γ-butyrolactone **7** along with the β-hydroxy ester. The mixture was then treated with PPTS in refluxing toluene to give lactone **7** in 64% yield (Scheme 3). NOE measurements and HPLC analysis revealed that the 4,5-*cis* isomer was formed as the major isomer in an 80 : 20 ratio.

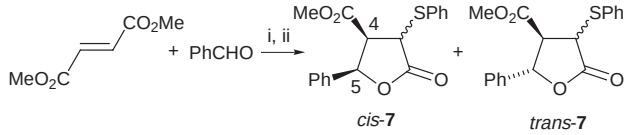

cis-**7** *trans*-**7**

64%; 4,5-*cis*:4,5-*trans* = 80:20

Scheme 3 *Reagents and conditions*: i, PhSLi, CH_2Cl_2, −78 °C, then −50 °C, 7 h; ii, PPTS, toluene, 110 °C, 2 h

Due to the heterogeneity of the mixture of acryrate and thiolate, the mechanism of the reaction and origin of the stereoselectivity are not clear; attempts to trap the β-thioenolate intermediate have so far been unsuccessful. Indeed, since most of the white precipitate of lithium thiophenolate in CH_2Cl_2 is undissolved in the presence of the acrylate esters, the concentration of the β-thioenolate intermediate in the absence of aldehyde should be very low. We assume that the active intermediate is formed with assistance due to coordination of the aldehyde to the lithium cation. Further investigation and application of the reaction will be reported in due course.

We thank Ube Industries Ltd. and Sumitomo Chemical Industry Ltd. for their financial support.

Notes and References

† E-mail: ak10@po.cc.yamaguchi-u.ac.jp

‡ All new compounds were fully characterised by spectroscopic analysis and microanalysis or HRMS.

§ Although lithium phenylselenolate should be generated from selenol and butyl lithium, we wished to avoid using the selenol formed from diselenide due to its toxicity and evil odour. After exploring several potential routes to lithium selenolate, we found that it was generated directly from a solution of diselenide *via* addition of methyl- or butyl-lithium. Although half of the selenium source is wasted as alkyl phenyl selenide, the present method was advantageous because anhydrous selenolate anion with no proton source was generated directly from commercially available diphenyl diselenide; the yellow colour of the diselenide disappeared when an equimolar amount of alkyllithium had been added.

1 M. E. Jung, in *Comprehensive Organic Synthesis*, ed. B. M. Trost, Pargamon, Oxford, 1991, vol. 4, pp. 1–67.
2 O. Miyata, T. Shinada, I. Ninomiya, T. Naito, T. Date, K. Okamura and S. Inagaki, *J. Org. Chem.*, 1991, **56**, 6556; R. Clauss, W. Hinz and R Hunter, *Synlett*, 1997, 57.
3 For review for tandem reaction, see R. A. Bunce, *Tetrahedron*, 1995, **48**, 13 103.
4 J. F. G. A. Jansen and B. K. Feringa, *Tetrahedron Lett.*, 1991, **32**, 3239.
5 S. G. Davies and O. Ichihara, *J. Synth. Org. Chem. Jpn.*, 1997, **55**, 26 and references cited therein; S. G. Davies and D. R. Fenwick, *Chem. Commun.*, 1997, 565; N. Tsukada, T. Shimada, Y. S. Gyoung, N. Asao and Y. Yamamoto, *J. Org. Chem.*, 1995, **60**, 143; Y. Yamamoto, N. Asao and T. Yuehara, *J. Am. Chem. Soc.*, 1992, **114**, 5427; A. Hosomi, T. Yanagi and M. Hojo, *Tetrahedron Lett.*, 1991, **32**, 2371; N. Asao, T. Uyehara and Y. Yamamoto, *Tetrahedron*, 1990, **46**, 4563.
6 I. Fleming and J. D. Kilburn, *J. Chem. Soc., Chem. Commun.*, 1986, **305**; 1198; I. Fleming and A. K. Sarkar, *J. Chem. Soc., Chem. Commun.*, 1986, 1199.
7 (*a*) A. G. M. Barrett and A. Kamimura, *J. Chem. Soc., Chem. Commun.*, 1995, 1755; (*b*) T. Yura, N. Iwasawa and T. Mukaiyama, *Chem. Lett.*, 1986, 187; (*c*) M. Suzuki, T. Kawagishi and R. Noyori, *Tetrahedron Lett.*, 1981, **22**, 1809; (*d*) A. Itoh, S. Ozawa, K. Oshima and H. Nozaki, *Tetrahedron Lett.*, 1980, **21**, 361.
8 J. I. Levin, *Synth. Commun*., 1992, 961.
9 C. H. Heathcock, C. T. Buse, W. A. Kleschick, M. C. Pirrung, J. E. Sohn and J. Lampe, *J. Org. Chem*., 1980, **45**, 1066.
10 For generation of selenolate anion, see: C. Paulmier, *Selenium Reagents and Intermediates in Organic Synthesis*, Pergamon, Oxford, 1986, pp. 25–27 and references cited therein; D. Liotta, *Acc. Chem. Res.*, 1984, **17**, 28; D. L. J. Clive, *Tetrahedron*, 1978, **34**, 1049; H. Reich, *Acc. Chem. Res.*, 1979, **12**, 22.
11 E. J. Corey and S. S. Kim, *J. Am. Chem. Soc.*, 1990, **112**, 4976.

Received in Cambridge, UK, 2nd February 1998; 8/00870A

Total synthesis of (±)-aglaiastatin, a novel bioactive alkaloid

Takumi Watanabe,[a] Shiho Kohzuma,[b] Tomio Takeuchi,[a], Masami Otsuka[c] and Kazuo Umezawa*[b]†

[a]*Institute of Microbial Chemistry, 3-14-23 Kamiosaki, Shinagawa-ku, Tokyo 141, Japan*
[b] *Department of Applied Chemistry, Faculty of Science and Technology, Keio University, 3-14-1 Hiyoshi, Kohoku-ku, Yokohama 223, Japan*
[c] *Faculty of Pharmaceutical Sciences, Kumamoto University, 5-1 Oe-Honmachi, Kumamoto 862, Japan*

The first total synthesis of aglaiastatin has been accomplished using pyrrolopyrimidinone construction by simultaneous nucleophilic attack of a nitrogen unit at the carbonyl group and the acyl iminium ion.

We recently isolated aglaiastatin **1**, a novel alkaloid, from the leaves of the tropical plant *Aglaia odorata*; it acts as an agent that induces normal morphology in K-*ras*-transformed fibroblasts.[1] It was shown to be a specific inhibitor of protein synthesis, and the alkaloid displayed potent growth inhibition against various tumor cell lines (*e.g.* IC_{50} value for K-*ras*-NRK cells: 1.67 ng ml^{-1}).

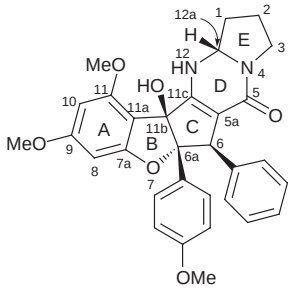

aglaiastatin **1**

Aglaiastatin consists of five fused rings (indicated as A, B, C, D, and E rings for convenience). Related benzofurocyclopentane systems (rings ABC) can be seen in the structures of other natural products such as rocaglamide,[2] and rocaglaol,[3] however, the five-ring system in **1** is rare and has not been reported, except in the case of an unnamed alkaloid.[4] Rocaglamide has been synthesized,[5] but aglaiastatin and the unnamed compound containing the pyrrolopyrimidinone system have never been synthesized.

Since construction of the ABC ring system had already been reported by several groups, development of methodology to construct the CDE ring system was the most challenging task. For the synthesis of aglaiastatin, an ABC ring system with a side chain at the C-5a position as a DE ring precursor was expected to be a promising intermediate for this synthesis. Starting from this substance, E ring formation and subsequent closure of the D ring could afford aglaiastatin. We anticipated that these reaction steps to form the DE ring system could be performed in one synthetic operation. Scheme 1 shows our strategy for the synthesis. At first, we planned to introduce a protected aminobutyraldehyde into the ABC ring prepared according to the reported procedure.[5b] Hydrolysis of the acetal should cause nucleophilic addition of the amide nitrogen to the aldehyde to afford the desired five-membered ring corresponding to the E ring. We anticipated that an acyl iminium ion should be generated by dehydration under acidic conditions. With this compound thus accessible, simultaneous nucleophilic addition of one nitrogen unit to two electrophilic groups, the ketone on the C ring and the acyl iminium moiety on the E ring, would form the D ring. Use of an ammonium salt as the one nitrogen unit for double nucleophilic reaction has been reported in some synthetic studies.[6]

Scheme 2 shows the protocol for the synthesis, which was begun by a coupling between commercially available 4-aminobutyraldehyde diethyl acetal and carboxylic acid **2** by use of the BOP [benzotriazol-1-yloxytris(dimethylamino)phosphonium hexafluorophosphate] reagent[7] to give amide **3** in excellent yield. Starting material **2** (racemic form) is an intermediate formed in Taylor's procedure for the total synthesis of rocaglamide[5b] and was prepared as an epimeric mixture at the C-2 carboxy group ($\alpha:\beta$ = 55:45). The subsequent oxidation step was unexpectedly problematic. Swern oxidation and Dess–Martin oxidation of **3** could not afford the desired ketone **4** reproducibly. Then, we turned our attention to SO_3·pyridine oxidation.[8] However, the reaction rate under the standard procedure was very sluggish. After optimization of the reaction

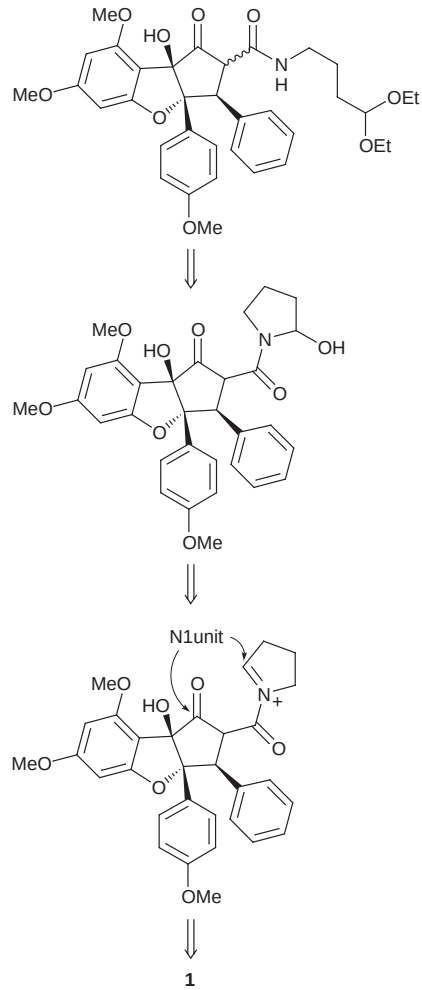

1

Scheme 1

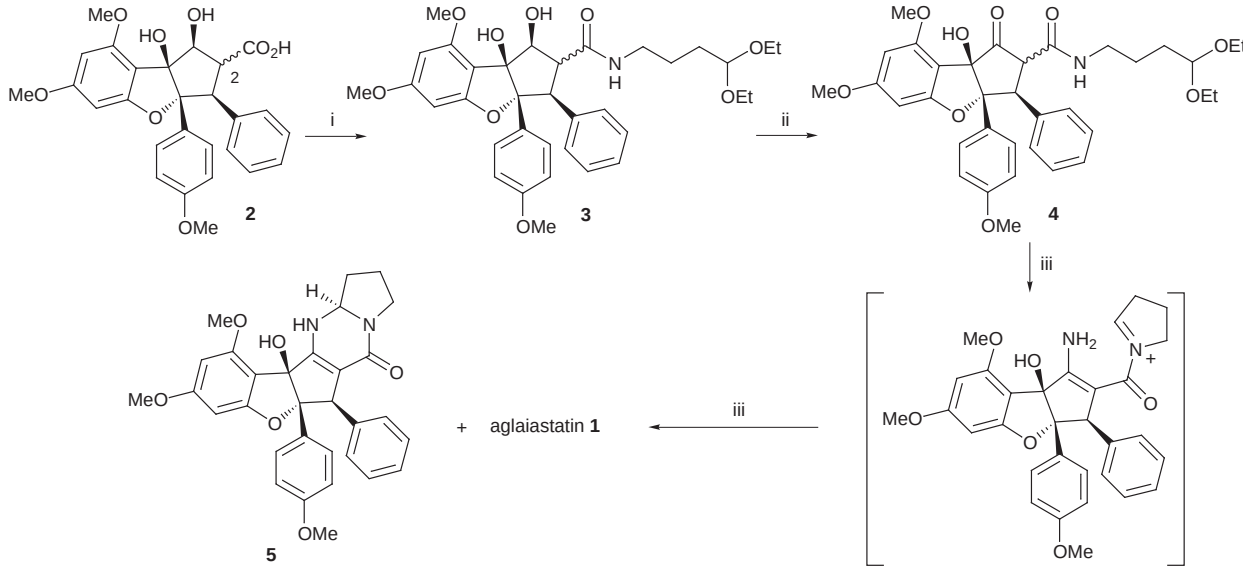

Scheme 2 *Reagents and conditions*: i, $H_2N(CH_2)_3CH(OEt)_2$, BOP reagent, Et_3N, room temp., CH_2Cl_2, 95%; ii, SO_3·pyridine, Et_3N, room temp., DMSO, 97%; iii, 1 M HCl, THF, then HCO_2H, HCO_2NH_4, room temp., MeOH, 70% for two steps (**1** : **5** = 2 : 1). The yield of **1** and **5** after chromatographic separation was 40 and 19%, respectively.

conditions, the use of a large excess of reagent finally gave satisfactory results. When the reaction was conducted for 1 h using 30 equiv. of SO_3·pyridine, the required ketone **4** was obtained in 97% yield. Prolonged reaction time or heating resulted in contaminating by-products. Although the α : β distribution about the amide group at C-2 varied in every trial, the β isomer was obtained predominantly. For the final pyrrolopyrimidinone formation, hydrolysis of the acetal with HCl and concomitant cyclization would have given the *N*-acyl hydroxypyrrolidine intermediate (not isolated) depicted in Scheme 1. After the usual workup, the crude material was treated with 99% formic acid in the presence of a large excess of ammonium formate (*ca.* 100 equiv.) in MeOH for 4 days. As a consequence, the desired (±)-aglaiastatin was obtained as a mixture of diastereomers at C-12a in high combined yield (70%). Fortunately, aglaiastatin was the predominant product [aglaiastatin (**1**) : diastereomer (**5**) = 2 : 1 determined by ^{1}H NMR]. Selectivity in the formation of **1** *versus* **5** would be explained by nucleophilic attack of the NH_2 group in the convex structure of ABC ring at the downward facing surface of the E ring. The iminium ion would probably be facing upwards due to steric hindrance. These stereoisomers could be easily separated by silica gel column chromatography to give pure **1** and **5** in 40 and 19% yield, respectively. Thus, we accomplished the first total synthesis of (±)-aglaiastatin.

The spectral properties (^{1}H and ^{13}C NMR, FABMS, IR) of the synthetic aglaiastatin, were indistinguishable from those of the natural aglaiastatin, except for optical rotation. Further, optically active aglaiastatin was obtained by separation with semi-preparative scale chiral HPLC (Daicel Chiralpak AD). One of the separated samples of synthetic aglaiastatin showed nearly the same value {$[\alpha]_D^{23}$ + 148.1 (*c* 0.1, MeOH)} as natural aglaiastatin [+151.2 (*c* 0.1, MeOH)]. It also displayed identical growth-inhibitory activity toward K-*ras*-NRK cells (IC_{50} value: 1.49 ng ml^{-1}) to that of the authentic sample (IC_{50} value: 1.67 ng ml^{-1}).

In conclusion, we have accomplished the first total synthesis of the novel protein synthesis inhibitor aglaiastatin. In the process, we developed a new methodology for pyrrolopyrimidinone construction using one nitrogen unit for the ring closure. Attempts to utilize this synthetic scheme for the synthesis of structurally related analogs and enantiomeric synthesis of aglaiastatin are under way.

The authors thank Dr Y. Nishimura and Mr N. Matsumoto, Institute of Microbial Chemistry, for valuable suggestions, and Dr H. Naganawa, Dr R. Sawa and Mr I. Momose, Institute of Microbial Chemistry, for spectroscopic analysis.

Notes and References

† E-mail: umezawa@applc.keio.ac.jp

1 T. Ohse, S. Ohba, T. Yamamoto, T. Koyano and K. Umezawa, *J. Nat. Prod.*, 1996, **59**, 650.
2 M. L. King, C-C. Chiang, H-C. Ling, E. Fujita, M. Ochiai and A. T. McPhail, *J. Chem. Soc., Chem. Commun*., 1982, 1150.
3 F. Ishibashi, C. Satasook, M. B. Isman and G. H. N. Towers, *Phytochemistry*, 1993, **32**, 307.
4 U. Kokpol, B. Venaskulchai, J. Simpson and R. T. Weavers, *J. Chem. Soc., Chem. Commun*., 1994, 773; V. Dumontet, O. Thoison, O. R. O. Omobuwajo, M-T. Martin, G. Perromat, A. Chiaroni, C. Riche, M. Païs, T. Sévenet and A. H. A. Hadi, *Tetrahedron*, 1996, **52**, 6931.
5 B. M. Trost, P. D. Greenspan, B. V. Yang and M. G. Saulnier, *J. Am. Chem. Soc*., 1990, **112**, 9022; (*b*) A. E. Davey, M. J. Schaeffer and R. J. K. Taylor, *J. Chem. Soc., Perkin Trans. 1*, 1992, 2657 and references cited therein; (*c*) G. A. Kraus and J. O. Sy, *J. Org. Chem.*, 1989, **54,** 77; (*d*) K. S. Feldman and C. J. Burns, *J. Org. Chem.*, 1991, **56,** 4601.
6 For example; T. H. Jones, J. B. Franko and M. S. Blum, *Tetrahedron Lett.*, 1980, **21**, 789; K. Abe, T. Tsugoshi and N. Nakamura, *Bull. Chem. Soc. Jpn.*, 1984, **57**, 3351; K. Abe, H. Okumura, T. Tsugoshi and N. Nakamura, *Synthesis*, 1984, 597; R. Bossino, S. Marcaccini, P. Paoli, R. Pepino and C. Polo, *Synthesis*, 1991, 999.
7 B. Castro, J. R. Dormoy, G. Evin and C. Selve, *Tetrahedron Lett.*, 1975, 1219.
8 J. R. Parikh and W. J. von E. Doering, *J. Am. Chem. Soc.*, 1967, **89**, 5505.

Received in Cambridge, UK, 23rd February 1998; 8/01502C

Heats of Lewis base complexation, deaggregation and stabilization by α-silicon in a family of primary alkyllithiums

Robert F. Schmitz, Marius Schakel, Marcel Vos and Gerhard W. Klumpp*†

Scheikundig Laboratorium Vrije Universiteit, De Boelelaan 1083, 1081 HV Amsterdam, The Netherlands

For primary alkyllithiums, enthalpies of Lewis base induced tetramer → dimer and dimer → monomer conversion, intramolecular Li–NMe_2R complexation and stabilization by α-$SiMe_2R$ are given.

Any understanding and control of σ-organolithium (RLi) reactivity requires extensive knowledge of each of the various forms in which RLis occur: aggregates R_mLi_m (m = 2,4,6), complexes of aggregates with Lewis bases [LB (R_2O, R_3N)] $R_mLi_m{\cdot}n$LB (m, n = 2,4; 4, 1–4) and, in relatively rare cases, monomer complexes RLi·nLB (n = 2,3).[1] Nevertheless, fundamental data, such as enthalpies of transfer of RLi from one aggregation state into another, are scarce: BuLi/THF, ΔH(complexed tetramer → complexed dimer) ≈ −2 kJ (mol RLi)$^{-1}$;[2] Bu^tLi/cyclopentane–Et_2O, ΔH(uncomplexed tetramer → complexed dimer) ≈ −38 kJ (mol RLi)$^{-1}$;[3] neopentyllithium/Et_2O, ΔH(complexed dimer → complexed monomer) ≈ −3 kJ (mol RLi)$^{-1}$.[1] For a family of intramolecularly amine-complexed (trimethylsilyl)methyllithium derivatives $LiCH_2Si(Me)_2CH_2$–Z (**1**–**3**, Z = $N(CH_2X)CH_2Y$, see Fig. 1)[4] and for the parent (trimethylsilyl)methyllithium (**4**, Z = H),[5] we now present relative stabilities of exhaustively complexed monomer, dimer and tetramer, respectively, as well as uncomplexed tetramer. Inclusion in our study of 3-(dimethylamino)propyllithium (**5**),[6] the analogue of **3** in which $SiMe_2$ is replaced by CH_2, provided a measure of RLi stabilization by α-silicon.

In Fig. 1, heats of protonation of **1**–**5** by Bu^sOH [ΔH, kJ (mol RLi)$^{-1}$, benzene, 25 °C]‡ are given together with the monomer (**1**), dimer ($\mathbf{2_2}$) and tetramer [$\mathbf{3_4}$, $\mathbf{4_4}$, $\mathbf{5_4}$ (**a** : **b** = 6 : 4)] structures in which **1**–**5** prevail under the conditions of experiment.

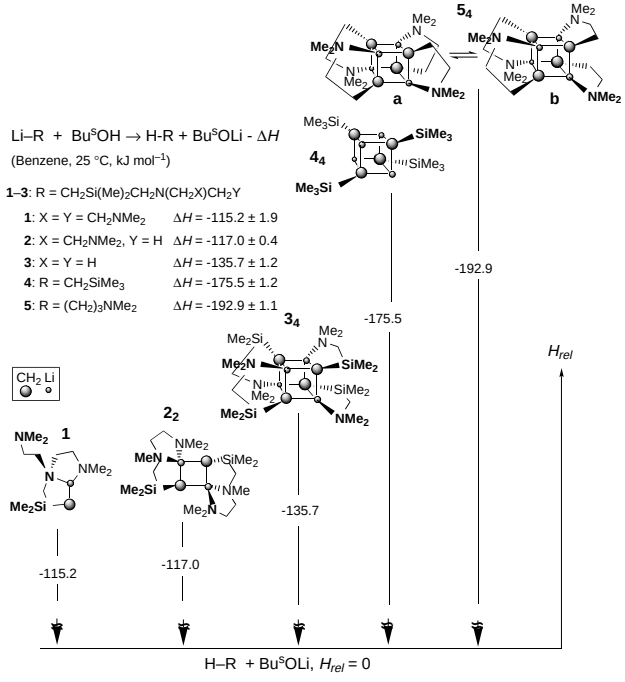

Fig. 1 Heats of protonation by Bu^sOH [ΔH/kJ (mol RLi)$^{-1}$, vertical arrows)] and relative stabilities [H_{rel}/kJ (mol RLi)$^{-1}$]

The protonation products (H–R, Fig. 1) of **1**–**5** are assigned equal *relative* enthalpies since they are devoid of special interactions.§ On this basis, negative differences of heats of protonation equal differences of relative enthalpies (stabilities) of RLi species. We also assume that in **1**–**4**, variation of Z is of minor influence, if at all, on the nature of C–Li.¶ Thus, $\Delta H(\mathbf{3_4}) - \Delta H(\mathbf{2_2}) \approx -19$ kJ (mol RLi)$^{-1}$ indicates that for type-**4** RLi species, amine complexation induced deaggregation of complexed tetramer into dimer is of considerable exothermicity. Further deaggregation of complexed dimer into monomer is nearly thermoneutral: $\Delta H(\mathbf{2_2}) - \Delta H(\mathbf{1}) \approx -2$ kJ (mol RLi)$^{-1}$. $\Delta H(\mathbf{4_4}) - \Delta H(\mathbf{3_4}) \approx -40$ kJ (mol RLi)$^{-1}$ gives the average strength of an N–Li bond in a tetrameric type-**4** RLi complexed by four NMe_3-type nitrogens.‖ $\Delta H(\mathbf{5_4}) - \Delta H(\mathbf{3_4}) \approx -57$ kJ (mol RLi)$^{-1}$ provides an experimental measure of the practically[8] and theoretically[9] important carbanion stabilization by silicon. Parenthetically, the close similarity of $\Delta H(\mathbf{5_4})$, −193 kJ (mol RLi)$^{-1}$, and ΔH of tetrameric 3-methoxypropyllithium under the same conditions [−190 kJ (mol RLi)$^{-1}$][10] testifies to the very similar lithium complexation propensities of –OMe and –NMe_2.

The energetics found in this study for LB induced tetramer → dimer and dimer → monomer conversion, respectively, are in accord with the results of quantum mechanical calculations on MeLi which indicate the latter to be rather more difficult,[11] although, as the present and the previous experiments show, actual values depend on the nature of R and LB (*cf.* ref. 1). Likewise, as expected,[9] the value found for the energy of stabilization of tetrameric primary RLi by α-$SiMe_2R$ [57 kJ (mol RLi)$^{-1}$] is in between those calculated[9] for $LiCH_2SiH_3$ (39 kJ mol^{-1}) and for $^-CH_2SiH_3$ (104 kJ mol^{-1}). The similarity found for –OMe and –NMe_2 as complexing groups of RLi agrees with the very similar capacities of R_2O and R_3N for acceleration of RLi reactions[12] and suggests that the above amine data also approximate those for ethers.

Notes and References

† E-mail: klumpp@chem.vu.nl

‡ *Ca.* 8 × 10^{-4} mol dm^{-3}; 3–5 measurements per compound; calorimeter: ref. 7.

§ ^{29}Si NMR of **1** and **2** (H instead of Li) did not indicate N–Si bonding.

¶ This assumption is based on our finding[6] that the C_4Li_4 cores of $\mathbf{5_4}$**a** and Et_4Li_4 are practically the same, *i.e.* introduction of and intramolecular complexation by γ-NMe_2 does not affect C–Li.

‖ The first LB unit is bonded more strongly to lithium than the following ones.[5,11]

1 G. Fraenkel, A. Chow and W. R. Winchester, *J. Am. Chem. Soc.*, 1990, **112**, 6190 and references cited therein.
2 J. Heinzer, J. F. M. Oth and D. Seebach, *Helv. Chim. Acta*, 1985, **68**, 1848; J. F. McGarrity and C. A. Ogle, *J. Am. Chem. Soc.*, 1985, **107**, 1805.
3 T. F. Bates, M. T. Clarke and R. D. Thomas, *J. Am. Chem. Soc.*, 1988, **110**, 5109.
4 H. Luitjes, F. J. J. de Kanter, M. Schakel, R. F. Schmitz and G. W. Klumpp, *J. Am. Chem. Soc.*, 1995, **117**, 4179.

5 H. L. Lewis and T. L. Brown, *J. Am. Chem. Soc.*, 1970, **92**, 4664.
6 G. W. Klumpp, M. Vos, F. J. J. de Kanter, C. Slob, H. Krabbendam and A. L. Spek, *J. Am. Chem. Soc.*, 1985, **107**, 8292.
7 F. J. M. Freijee, G. van der Wal, G. Schat, O. S. Akkerman and F. Bickelhaupt, *J. Organomet. Chem*., 1982, **240**, 229.
8 P. Magnus, *Aldrichim. Acta*, 1980, **13**, 43.
9 P. v. R. Schleyer, T. Clark, A. J. Kos, G. W. Spitznagel, C. Rohde, D. Arat, K. N. Houk and N. G. Rondan, *J. Am. Chem. Soc.*, 1984, **106**, 6467.
10 P. J. A. Geurink and G. W. Klumpp, *J. Am. Chem. Soc.*, 1986, **108**, 538.
11 E. Kaufmann, K. Raghavachari, A. E. Reed and P. v. R. Schleyer, *Organometallics*, 1988, **7**, 1597.
12 *E.g.*, P. Bartlett, C. V. Goebel and W. P. Weber, *J. Am. Chem. Soc.*, 1969, **91**, 7425.

Received in Liverpool, UK, 9th February 1998; 8/01157E

Preparation of vicinal diimines: a new dehydrogenative coupling reaction of aldimines mediated by ytterbium metal

Wu-Song Jin, Yoshikazu Makioka, Yuki Taniguchi, Tsugio Kitamura and Yuzo Fujiwara*†

Department of Chemistry and Biochemistry, Graduate School of Engineering, Kyushu University, 6-10-1 Hakozaki, Higashiku, Fukuoka 812-8581, Japan

Dehydrogenative coupling takes place to give vicinal diimine compounds in the reaction of aromatic aldimines with ytterbium metal followed by treatment with aromatic aldehydes such as 1-naphthaldehyde (1-NpCHO) as a hydrogen acceptor.

Lanthanide metals have been utilized for various transformations of organic functional groups or C–C bond formations *via* coupling reactions.[1] Previously, we have demonstrated that ytterbium metal causes the coupling reaction of carbonyl and thiocarbonyl compounds,[2] and that imines undergo a similar reaction to give 1,2-diamines or α-amino acids.[3] Imamoto and Nishimura and others reported that samarium(II) compounds are also capable of the coupling of imines to give 1,2-diamines.[4] Recently, a triphenylimine dianion complex [Yb(η^2-Ph_2CNPh)$(HMPA)_3$] has been successfully isolated from the direct reaction of ytterbium metal and triphenylimine and characterized by X-ray analysis.[5] In a continuing study of the reactions of aldimines and ytterbium metal, we have found that the reaction of aromatic aldimines and ytterbium metal followed by addition of oxidants produces the corresponding vicinal diimine compounds [eqn. (1)]. Here we report these new results.

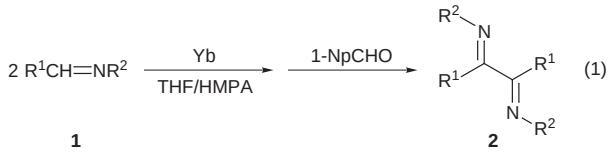

First, *N*-benzylideneaniline (**1a**) was reacted with 0.5 equiv. of ytterbium metal at room temperature then an oxidant was added and the mixture was stirred for 2 h to give the dehydrogenative coupling product, *N*,*N*′-diphenyl-1,2-diphenylethane-1,2-diimine (**2a**) in 81% yield [eqn. (2)].‡ The effects

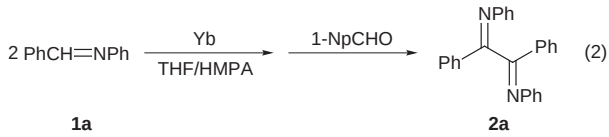

of various oxidants toward the dehydrogenative coupling reaction of **1a** are summarized in Table 1. From the data in Table 1 one can see that aromatic aldehydes (entries 1–4) are the best compared with others. In particular when 1-NpCHO is used, the best result is obtained, whereas the yield of the product is only 7% when an aliphatic aldehyde is used (entry 5). In addition, it is apparent that $CuCl_2$, peroxides and Bu^tNO_2 give inferior results (entries 6–9) and that only 17% yield is obtained in the case of O_2 (entry 10). The presence of HMPA as an additive is necessary in this reaction since the reaction of **1a** and ytterbium metal cannot proceed in THF alone.

The reaction also occurred with various aromatic aldimines as well as **1a**. The representative results for the dehydrogenative coupling reaction of other aldimines **1** are listed in Table 2. When the substrates are non-substituted, *p*-methyl- and *p*-methoxy-substituted aromatic aldimines **1a**–**d**,**f**,**g**, the reactions proceed smoothly to afford **2a**–**d**,**f**,**g** (entries 1–4 and 6, 7) in good to high yields. On the other hand, the yields of **2** were low in the reactions of *p*-cyano- and *p*-chloro-substituted aldimines **1e** and **1h** (entries 5 and 8). Thus, the electron-donating substituent on the benzene ring is profitable to the reaction. In the reaction of the *o*-methyl-substituted aldimine **1i** at room temperature, only small amounts of **2i** were formed, and the hydrogenation product (o-$MeC_6H_4CHNHPh)_2$ was formed as the main product. This is due to the steric hinderence of the diazametallacyclopentane intermediate toward dehydrogenation with 1-NpCHO (*vide infra*). However, **2i** could be obtained in a moderate yield at reflux temperature (entry 9). The reaction did not occur in the case of C_6H_5CH=$NCMe_3$ (**1j**), and **1j** was recovered (entry 10), due to it's lower reactivity towards ytterbium metal.

Table 1 Effect of various oxidants on the dehydrogenative coupling reaction of aldimine **1a**[a]

Entry	Oxidant	mmol	Yield of **2a**[b] (%)
1	1-NpCHO	2	60
2	1-NpCHO	1	81
3	o-$MeOC_6H_4CHO$	2	49
4	p-MeC_6H_4CHO	2	31
5	Pr^iCHO	2	7
6	$CuCl_2$	2	—
7	m-$ClC_6H_4CO_3H$	2	6
8	$K_2S_2O_8$	2	—
9	Bu^tONO	2	1
10	O_2[c]	2	17

[a] Reaction conditions: 1.0 mmol **1a**, 0.5 mmol Yb, 2 ml THF, 0.5 ml HMPA, 2 μl MeI. [b] GC yield based on **1a**. [c] One atm., 24 h.

Table 2 Dehydrogenative coupling reaction of aldimines **1** mediated by ytterbium metal[a]

Entry	Substrate	R^1	R^2	Product	Yield (%)[b]
1	**1a**	Ph	Ph	**2a**	81
2	**1b**	p-MeC_6H_4	Ph	**2b**	90
3	**1c**	p-$MeOC_6H_4$	Ph	**2c**	86
4	**1d**	p-$MeOC_6H_4$	p-MeC_6H_4	**2d**	58[c]
5	**1e**	p-NCC_6H_4	Ph	**2e**	5[c]
6	**1f**	Ph	p-MeC_6H_4	**2f**	74
7	**1g**	Ph	p-$MeOC_6H_4$	**2g**	73
8	**1h**	Ph	p-ClC_6H_4	**2h**	55
9	**1i**	o-MeC_6H_4	Ph	**2i**	50[d]
10	**1j**	Ph	Bu^t	No reaction	

[a] See footnote ‡ for the reaction conditions. [b] GC yield based on **1**. Considerable amounts of 1-$NpCH_2OH$ were also formed. [c] Isolated yield. [d] At reflux temperature.

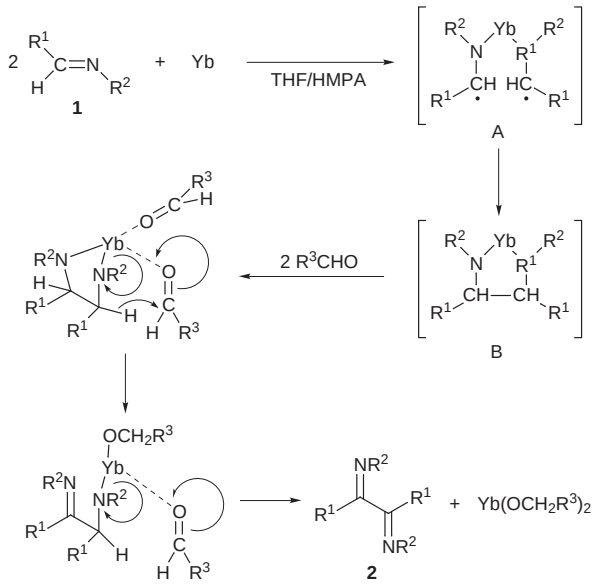

Scheme 1

Although the reaction mechanism is not yet clear, a possible reaction mechanism is shown in Scheme 1. First, one atom of ytterbium metal reacts with two molecules of aldimine **1** *via* two-electron transfer from ytterbium to give a diazametallacyclopentane intermediate B, probably *via* formation of an intermediate A.[6] Subsequent treatment with an aldehyde would cause the coordination and double hydrogen transfer, as in a similar manner to the Meerwin–Pondorf–Varley reduction/Oppenauer oxidation,[7] to give **2** and ytterbium alkoxides, which gives an alcohol R^3CH_2OH after hydrolysis.

In summary, ethane-1,2-diimines **2** can be prepared from the reaction of aromatic aldimines **1** with ytterbium metal followed by treatment with aromatic aldehydes. To the best of our knowledge, this is the first example of metal mediated dehydrogenative coupling of aldimines. Further mechanistic investigation and extension of this reaction are in progress.

The present work was supported in part by a Grant-in-Aid for Scientific Research on Priority Areas No. 283, 'Innovative Synthetic Reactions' from Monbusho. Y. M. gratefully acknowleges the financial support of this research by the Japan Society for the Promotion of Science in the form of Research Fellowships for Young Scientists.

Notes and References

† E-mail: yfujitcf@mbox.nc.kyushu-u.ac.jp

‡ Typical procedure for the dehydrogenative coupling of **1** with Yb metal: THF (2 ml), HMPA (0.5 ml) and methyl iodide (2 μl) were successively added to a mixture of **1c** (211 mg, 1.0 mmol) and ytterbium (87 mg, 0.5 mmol) under argon, which was stirred for 2 h at room temperature. Then, 1-NpCHO (156 mg, 1.0 mmol) was added to the mixture. The resulting mixture was stirred for an additional 2 h at room temperature. Usual work-up followed by a silica gel column chromatography (*n*-hexane–ethyl acetate) gave 119 mg (57%) of the desired compound **2c**.

1 T. Imamoto, *Lanthanides in Organic Synthesis*, Academic Press, London, 1994, pp. 7–19; Y. Fujiwara, K. Takaki and Y. Taniguchi, *J. Alloys Compd.*, 1993, **192**, 200.

2 For example, Z. Hou, K. Takamine, K. Aoki, O. Shiraishi, Y. Fujiwara and H. Taniguchi, *J. Org. Chem.*, 1988, **53**, 6077; Z. Hou, H. Yamazaki, K. Kobayashi, Y. Fujiwara and H. Taniguchi, *J. Chem. Soc., Chem. Commun.*, 1992, 722; K. Takaki, F. Beppu, S. Tanaka, Y. Tsubaki, T. Jintoku and Y. Fujiwara, *J. Chem. Soc., Chem. Commun.*, 1990, 516; Y. Makioka, S. Uebori, M. Tsuno, Y. Taniguchi, K. Takaki and Y. Fujiwara, *Chem. Lett.*, 1994, 611; Y. Makioka, M. Tsuno, S. Ueboki, Y. Taniguchi, K. Takaki and Y. Fujiwara, *J. Org. Chem.*, 1996, **61**, 372.

3 K. Takaki, Y. Tsubaki, S. Tanaka, F. Beppu and Y. Fujiwara, *Chem. Lett.*, 1990, 203; K. Takaki, S. Tanaka and Y. Fujiwara, *Chem. Lett.*, 1991, 493; Y. Taniguchi, T. Kuno, M. Nakahashi, K. Takaki and Y. Fujiwara, *J. Alloys Compd.*, 1994, **216**, L9-12; Y. Taniguchi, T. Kuno, M. Nakahashi, K. Takaki and Y. Fujiwara, *Appl. Organomet. Chem.*, 1995, **9**, 491.

4 T. Imamoto and S. Nishimura, *Chem. Lett.*, 1990, 1141; E. J. Enholm, D. C. Forbes and D. P. Holub, *Synth. Commum.*, 1990, **20**, 981; A. Lebrun, E. Rantze, J.-L. Namy and H. B. Kagan, *New J. Chem.*, 1995, **19**, 699.

5 Y. Makioka, Y. Taniguchi, Y. Fujiwara, K. Takaki, Z. Hou and Y. Wakatsuki, *Organometallics*, 1996, **15**, 5476.

6 J. G. Smith and I. Ho, *J. Org. Chem.*, 1972, **37**, 653.

7 C. Djerassi, *Org. React.*, 1951, **6**, 207.

Received in Cambridge, UK, 23rd February 1998; 8/01514G

Discovery that quinoline and triphenylphosphine alter the electronic properties of hydrogenation catalysts

Jinquan Yu and Jonathan B. Spencer*†

University Chemical Laboratory, Lensfield Road, Cambridge, UK CB2 1EW

Quinoline and triphenylphosphine are found to influence the polarisation of the palladium–hydrogen bond in heterogeneous hydrogenation; this provides a possible explanation for why the addition of these compounds increases the selectivity of the semi- reduction of alkynes.

The selective reduction of alkynes to *cis*-alkenes using heterogeneous catalysts, such as palladium on carbon, is a key reaction in organic chemistry.[1,2] Quinoline and triphenylphosphine have been widely used as additives in heterogeneous hydrogenation to improve the selectivity of this reaction.[3] There has been great interest in rationalising how these compounds alter the properties of the palladium to achieve superior selectivity. Several theories have been put forward, including the selective blocking of sites that cause the side reactions and promoting the rearrangement of the surface structure.[4–6] It has not been possible, however, to probe whether quinoline and triphenylphosphine, both potentially strong ligands, could alter the electronic properties of the metal catalyst. Recently we have devised an approach to achieve this by determining which electronic mode [mode (*a*) $M^{\delta+}$–$H^{\delta-}$ or (*b*) $M^{\delta-}$–$H^{\delta+}$, Scheme 1] of hydrometalation is promoted by the catalyst.[7,8]

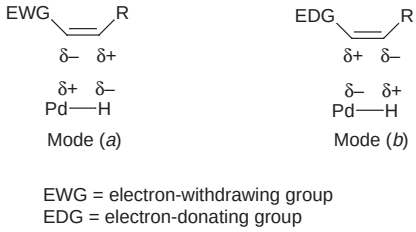

Scheme 1

When *cis*-enol ether **1** is isomerised to the *trans*-isomer **2** using deuterium and palladium on carbon the location of the deuterium on the double bond reports which mode of hydrometalation takes place (Scheme 2). The result with unmodified palladium on carbon (Fig. 1) is that the deuterium is incorporated almost entirely at position I, which shows that mode (*b*) ($M^{\delta-}$–$H^{\delta+}$) is dominant; this is a consequence of the polarisation of the palladium–hydrogen bond being induced by the electronic dipole of the substrate.[7,8] Remarkably, when this reaction is carried out in the presence of quinoline, mode (*a*) ($M^{\delta+}$–$H^{\delta-}$) is significantly enhanced (Fig. 1). This suggests that the quinoline, being a strong electron-donating ligand, is capable of stabilising the electron-deficient metal centre in mode (*a*) ($M^{\delta+}$–$H^{\delta-}$). The enhancement of mode (*a*) is found to be dependent on the concentration of quinoline (Table 1). No further enhancement of mode (*a*) occurs when the quinoline concentration is increased above 100 mM, suggesting saturation of the surface by quinoline at this concentration.

The same experiment has been carried out with triphenylphosphine, another electron-donating ligand, and this is found also to promote mode (*a*) ($M^{\delta+}$–$H^{\delta-}$) to a similar extent (Table 1). These results prompted us to propose an explanation for origin of the selectivity of these catalysts for triple bonds over

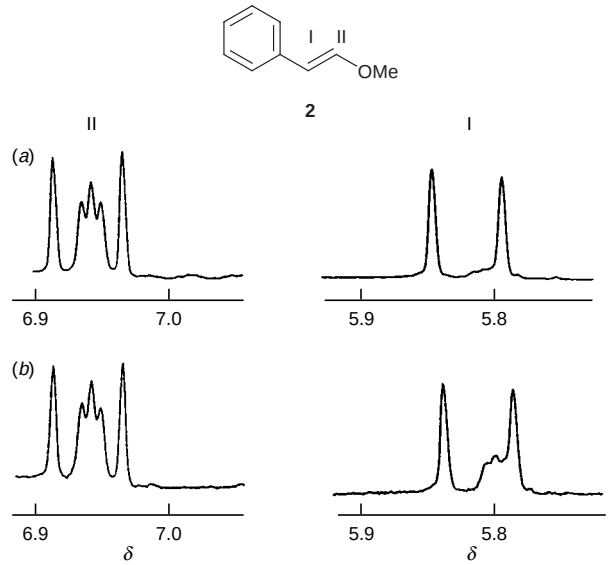

Fig. 1 Part of the ^{1}H NMR spectrum (250 MHz) (double bond region) for compound **2** (in $CDCl_3$) formed by the isomerization of the corresponding *cis*-isomer using D_2 and (*a*) Pd/C or (*b*) Pd/C with 50 mM quinoline. The triplets observed inside the doublets arise from deuterium hydrogen coupling in the labelled compound.

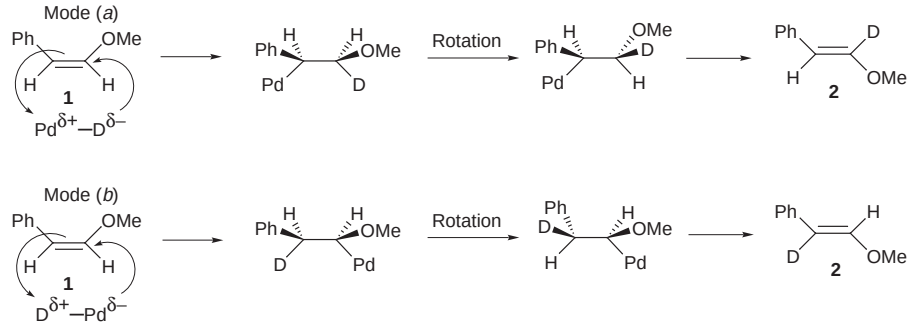

Scheme 2

Table 1 Dependance of reaction mode on ligand[a]

Ligand	Concentration (mM)	Deuterium distribution[b] (%)		Relative ratio of deuterium (%)	
		I	II	I	II
Quinoline	0	56	1	98	2
Quinoline	50	50	19	72	28
Quinoline	100	36	27	57	43
Quinoline	150	36	27	57	43
PPh_3	25	30	22	58	42

[a] A typical example of the procedure: to a solution of *cis*-β-methoxystyrene (134 mg, 1 mmol) in 3 ml of benzene was added 20 mg 10% Pd/C and 39 mg of quinoline (0.3 mmol). The mixture was degassed and refilled with D_2 through a balloon. The reaction mixture was stirred for 2 h at room temperature under 1 atm of D_2 followed by removal of the catalyst by filtration. The filtrate was evaporated to give a mixture of quinoline and the product (162 mg) which was determined by ^{1}H NMR spectroscopy to consist of 40% reduced product, 48% *cis*-isomer and 12% *trans*-isomer. The pure form of the *trans*-isomer was obtained by column chromatography eluting with hexane, and the incorporation of the deuterium at each position on the double bond was determined by integration of the respective ^{1}H NMR signals, using the methyl group as an internal standard. For the experiment performed using 100 mM quinoline samples were taken over the whole course of the reaction. The deuterium distribution across the double bond was found not to vary with reaction time. [b] Errors for the data are ±5%.

double bonds. The main side reactions in the reduction of alkynes to *cis*-alkenes are the further reduction and isomerisation of this product. It is well-documented that a triple bond is more vulnerable to nucleophillic attack than a double bond,[9] therefore, an increase in nucleophility of the metal hydrogen species should improve the selectivity for reduction of the triple bond. The shift from purely mode (*b*) ($M^{\delta-}$–$H^{\delta+}$) towards mode (*a*) ($M^{\delta+}$–$H^{\delta-}$), brought about by the modification of the catalyst with electron-rich ligands, clearly indicates that the metal hydrogen species is made more nucleophilic and hence provides a clue to the origin of the improved selectivity.

Interestingly, promotion of mode (*a*) ($M^{\delta+}$–$H^{\delta-}$) was previously found for the Lindlar catalyst (palladium modified with lead acetate) when it was compared to palladium on carbon.[8] The Lindlar catalyst also gives better selectivity for the reduction of alkynes to *cis*-alkenes, again suggesting that it is the change in the electronic properties of the palladium that is responsible for its improved reactivity.

This study establishes that quinoline and triphenylphosphine act as ligands for heterogeneous palladium and alter the electronic properties of the metal. This provides a new insight into how quinoline and triphenylphosphine may improve the selectivity of palladium catalysts for the semi-reduction of alkynes.

We thank the Royal Society for the award of a Royal Society University Research Fellowship (J.B.S.) and the British Council and the Chinese Government for the award of Sino-British Friendship Scholarship (J. Y.).

Notes and References

† E-mail: jbs20@cam.ac.uk

1 M. Friefelder, *Practical Catalytic Hydrogenation*, Wiley- Interscience, New York, 1971; P. Rylander, *Hydrogenation Methods*, Academic Press, New York, 1985.
2 K. Mori, *The Total Synthesis of Natural Products*, ed. J. ApSimon, Wiley-Interscience, New York, 1981, vol. 4; P. A. Bartlett, *Tetrahedron*, 1980, **36**, 3.
3 S. Siegel, in *Comprehensive Organic Synthesis*, ed. B. M. Trost and I. Fleming, Pergamon, 1991, vol. 8, pp. 418–440, and references cited therein.
4 A. B. McEwen, M. J. Guttieri, W. F. Maier, R. M. Laine and Y. Shvo, *J. Org. Chem*., 1983, **48**, 4436.
5 S. Siegel and J. A. Hawkins, *J. Org. Chem*., 1986, **51**, 1638.
6 J. A. Ulan, E. Kuo and W. F. Maier, *J. Org. Chem*., 1987, **52**, 3126.
7 J. Yu and J. B. Spencer, *J. Am. Chem. Soc*., 1997, **119**, 5257.
8 J. Yu and J. B. Spencer, *J. Org. Chem.*, 1997, **62**, 8618.
9 R. W. Strozier, P. Caramella and K. N. Houk, *J. Am. Chem. Soc*., 1979, **101**, 1340.

Received in Liverpool, UK, 22nd January 1998; 8/00629F

Halogen to metal π-donation in metalloporphyrins

Zeev Gross,* Atif Mahammed and Claudia M. Barzilay

Department of Chemistry, Technion-Israel Institute of Technology, Haifa 32000, Israel

The ^{1}H NMR analysis of the paramagnetic *trans*-dihalogeno-ruthenium(IV) and osmium(IV) porphyrins reveals that the halides have a pronounced effect on both the magnitude and the direction of charge transfer between the metal and the porphyrin, that the degree of covalency of metal–halide bonds increases in the order of Mn^{III} < Ru^{IV} < Os^{IV}, and that the relative strength of halogen-to-metal π-donation is Cl < Br < I.

The relative π-donation strength of halides has become a matter of dispute in recent years. While both early and recent *ab initio* calculations suggested that π-donation increases down the group, F < Cl < Br < I,[1] the conclusions from NMR chemical shift analysis of halomethyl cations (^{13}C) and boron halides (^{11}B) are opposite.[2] A similar conflict seems to exist for halogeno-coordinated metalloporphyrins. The ^{1}H NMR spectra of halogeno-coordinated manganese(III) porphyrins were originally analyzed in terms of competition for π-donation to the metal by the halide (X → M CT) and the porphyrin (P → M CT), and the π-donation ability was proposed to decrease in the order of I < Br < Cl < F.[3] But, much more recent investigations of Mn^{III} and Fe^{III} porphyrins have shown that their metal–ligand bonds are predominantly charge rather than orbital controlled.[4,5] For (*trans*-dihalogeno)ruthenium(IV) tetraphenylporphyrins, the monotonic trend of decreasing upfield isotropic shifts of pyrrole-H down the halide group,[6] opposite to that in (halogeno)manganese(III) porphyrins, led to the conclusion that the order of π-donation ability is Cl < Br < I.[7] But, while Ke *et al*. analyzed the isotropic shifts in terms of P → M CT, M → P CT was indicated by investigation of a (*trans*-dibromo)ruthenium(IV) porphyrin.[8] Obviously, without a definite conclusion about the direction of the CT process in these complexes, the relative π-donation ability of the halides cannot be determined.

The contradictory NMR analyses of the *trans*-dihalogeno-ruthenium(IV) tetraphenylporphyrins calls for the examination of a larger range of porphyrin structures, as well as of the analogous osmium(IV) complexes.[9] These tetragonally distorted octahedral complexes are exceptionally well suited for the current investigation owing to their stability, high symmetry, well resolved NMR spectra, and because the metal ion is confined to the porphyrin's plane and only the d_π orbitals are singly occupied.[10] Accordingly, we have prepared a large series of dihalogeno-ruthenium(IV) and -osmium(IV) complexes with both pyrrole-unsubstituted and *meso*-unsubstituted porphyrins (Scheme 1),[11] taking advantage of our recently introduced synthetic method for their preparation.[12] The detailed ^{1}H NMR analysis leads to the conclusion that the relative π-donation ability of the halides is Cl < Br < I for all metalloporphyrins, and that the main difference between the metal complexes is an icnrease of σ-covalency of their bonds with axial ligands in the order of Mn^{III} < Ru^{IV} < Os^{IV}.

The first concern in the NMR analysis is the separation of the isotropic shifts into contributions from dipolar (pseudocontact, through field) and contact (through σ and/or π orbitals) shifts.[3b] Examination of Table 1 clearly shows that the *meso*-aryls of the (por)$Os^{IV}X_2$ complexes experience only dipolar shifts, as all isotropic shifts are shifted downfield and they decrease as a function of their distance from the metal exactly as predicted by eqn. (1), which is relevant for purely dipolar shifts.[3b]

$$(\Delta H/H)_i^{dip} : (\Delta H/H)_j^{dip} = [(3\cos^2\theta - 1)/r_i^3] : [3\cos^2\theta - 1)/r_j^3] \quad (1)$$

$$(\Delta H/H)_i^{iso} = (\Delta H/H)_i^{dip} + (\Delta H/H)_i^{con} \quad (2)$$

The results of eqn. (1) were also used in eqn. (2), which allows the calculation of the contact shifts at the pyrrole protons,

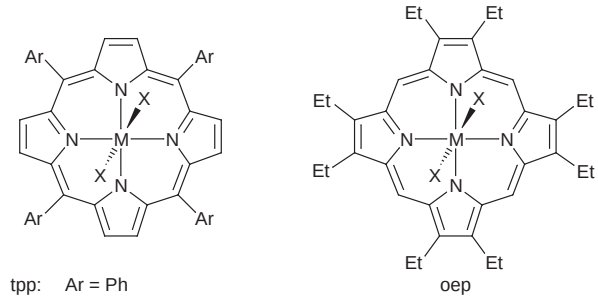

tpp: Ar = Ph
ttp: Ar = C_6H_4Me-4
tdmp: Ar = $C_6H_3Me_2$-2,6
tmp: Ar = $C_6H_2Me_3$-2,4,6

oep

M = Ru, Os; X = Cl, Br, I

Scheme 1

Table 1 ^{1}H NMR isotropic shifts (ppm, $CDCl_3$, 23 °C) of the (por)OsX_2 complexes, and their separation into contributions from dipolar and contact shifts[a]

	Phenyl				Pyrrole			
	o-H	*m*-H	*o*-Me	*p*-Me	H	α-CH_2	β-Me	*meso*-H
Geometric factor[b]	10.0	4.63	3.90	3.01	20.10	10.5	6.40	30.00
$(\Delta H/H)_{iso}$, X = Cl	2.66	0.90	0.79	0.67	−13.99	15.18	2.27	11.73
X = Br	2.42	0.90	0.81	0.64	−13.30	15.08	2.21	11.22
X = I	2.07	0.94	0.91	0.60	−12.02	14.55	2.05	10.40
$(\Delta H/H)_{dip}$, X = I[c]	2.07	−0.96	0.81	0.62	4.16	2.17	1.32	6.21
$(\Delta H/H)_{con}$, X = I[d]	0.00	−0.02	0.10	0.02	−16.8	12.38	0.73	4.19

[a] $(\Delta H/H)_{iso}$, the difference in chemical shifts between identical protons in the paramagnetic osmium(IV) and diamagnetic *trans*-dioxo osmium(VI) complexes. [b] Calculated from the crystal structure of (tmp)OsI_2 and normalized to *o*-H = 10. [c] Calculated by eqn. (1), starting with the isotropic shift of *o*-H in (ttp)OsI_2. [d] Calculated by eqn. (2). The pyrrole-H contact shifts for X = Cl and X = Br are −19.3 and −18.6 ppm, respectively.

Table 2 ^{1}H NMR isotropic shifts (ppm, $CDCl_3$, 23 °C) of the (por)RuX_2 complexes[a]

	Phenyl					Pyrrole			
	o-H	*o*-Me	*m*-H	*p*-H	*p*-Me	H	α-CH_2	β-Me	*meso*-H
X = Cl	−1.6	2.33	5.27	−1.5	1.49	−63.8	55.46	4.66	−2.41
X = Br	−3.49	2.74	7.75	−2.28	1.61	−53.75	55.85	5.05	−7.08
X = I	−4.06	2.64	10.33	−1.96	1.53	−32.55	54.12	5.18	−28.61

[a] Referenced against the diamagnetic dioxoruthenium(VI) complexes. An isotropic shift of −0.95 ppm was reported for *meso*-H of (oep)RuF_2: C. Sishta, M. Ke, B. R. James and D. Dolphin, *J. Chem. Soc., Chem. Commun.*, 1986, 787.

and a fair estimate of its contribution to the *meso*-H and pyrrole-CH_2CH_3 isotropic shifts in the (oep)$Os^{IV}X_2$ complexes. Large and alternating contact shifts of protons (−16.18 ppm) and methylene groups (+12.38 ppm) attached to the β-pyrrole carbons together with the relatively small downfield shifts at *meso*-H (+4.19 ppm) are clearly evident from Table 1. This pattern is fully consistent with π-contact shifts due to P (3e, filled) → M (d_π, singly occupied) CT, but not with M → P (4e, LUMO) CT.[3b] We may safely conclude that the decrease of P → M CT in the order of I < Br < Cl, as reflected by the pyrrole-H contact shifts of δ −16.8, −18.6, and −19.4, respectively, is a result of an increase in X → M CT, *i.e.* the relative π-donation ability in the (por)$Os^{IV}X_2$ complexes is I > Br > Cl.

The spectral analysis of the ruthenium(IV) complexes is less straightforward, since large contact shifts mask any possible contribution by the dipolar shift, even at the aryl protons. This is evident from the alternation of the isotropic shifts for the *meso*-aryl substituents (*ortho- vs. meta- vs. para*-H, as well as *ortho*-H *vs. ortho*-Me, and *para*-H *vs. para*-Me) and the exceptionally large pyrrole-H and *meso*-H shifts (Table 2). The large upfield shifts of both pyrrole-H and *meso*-H are consistent only with a simultaneous action of P → M (upfield pyrrole-H) and M → P (upfield *meso*-H) π charge transfer mechanisms. This explains the earlier mentioned contradictory analyses about the direction of the CT process in the *meso*-substituted (tpp)$Ru^{IV}X_2$ complexes. The most illuminating observation is that the relative importance of M → P CT clearly changes from very low in the dichloro complexes (small shifts of the *meso*-H and *meso*-aryls) to highly significant in the diiodo complexes [$\Delta\delta$(*meso*-H) ≈ $\Delta\delta$(pyrrole-H)]. This phenomenon suggests a π-donation strength series in the order of I > Br > Cl, since as more electron density is transferred from the axial ligand to the metal, M → P CT should indeed increase at the expense of P → M CT.

Finally, we suggest that the relatively small isotropic shifts and the lack of M → P CT in the osmium(IV) porphyrins reflect the well known phenomenon of increased σ-covalency of metal–ligand bonds in post-lanthanide transition metals relative to their 4d analogs.[13] This proposal is supported by the exceptionally large substitution inertness of the (por)OsX_2 complexes.[14] An additional consequence is that halogeno–metal bonds in osmium(IV) porphyrins are not expected to be unusually short, in contrast to the analogous ruthenium complexes with their very strong π-bonding component.[7] Comparison of the bond lengths in (tmp)OsI_2 (Os–I 2.655 Å, this study)[11] and (ttp)Os(Cl_2 (Os–Cl 2.294 Å)[9c] with EXAFS data for *trans*-dihalogeno osmium(IV) complexes of a non-porphyrinic ligand (Os–I 2.627 Å, Os–Cl 2.227 Å),[15] clearly supports this prediction. We conclude that the binding of axial ligands to d^4-metalloporphyrins changes from predominantly covalent for Os^{IV} through intermediate in Ru^{IV} to predominantly ionic in Mn^{III}.[4] In all cases, the extent of P → M CT is a sensitive probe of the energy difference between the singly occupied d_π orbitals and the low-energy 3e orbitals of the porphyrin. In the ionic halogeno–Mn^{III} bonds, the energy of the d_π orbitals is reduced as the bond lengths increase (Mn–I > Mn–Br > Mn–Cl).[16,17] However, the decrease of P → M CT in the order of I < Br < Cl for the osmium(IV) and ruthenium(IV) porphyrin clearly reflects an increase in the energy of the d_π orbitals due to X → M CT, *i.e.* the relative π-donation ability is I > Br > Cl.

We thank Dr S. Cohen from the Hebrew University of Jerusalem for the determination of the X-ray crystal structure of (tmp)OsI_2. This research was supported by the United States–Israel Binational Science Foundation.

Notes and References

† E-mail: chrlOzg@tx.technion.ac.il

1 F. Bernardi, A. Bottoni and A. Venturini, *J. Am. Chem. Soc.*, 1986, **108**, 5395; J. Kapp, C. Schade, A. M. El-Nahasa and P. von R. Schleyer, *Angew. Chem., Int. Ed. Engl.*, 1996, **35**, 2236; G. Frenking, S. Fau, C. M. Marchand and H. Grützmacher, *J. Am. Chem. Soc.*, 1997, **119**, 6648.
2 G. A. Olah, G. Rasul, L. Heiliger and G. K. S. Prakash, *J. Am. Chem. Soc.*, 1996, **118**, 3580.
3 (*a*) G. N. La Mar and F. A. Walker, *J. Am. Chem. Soc.*, 1975, **97**, 5103; (*b*) G. N. La Mar and F. A. Walker, in *The Porphyrins*, ed. D. Dolphin, Academic Press, New York, 1979, vol. IV, ch. 2, pp. 61–157.
4 P. Turner and M. J. Gunter, *Inorg. Chem.*, 1994, **33**, 1406.
5 T. Ohya and M. Sato, *J. Chem. Soc., Dalton Trans.*, 1996, 1519.
6 For the determination and definition of isotropic shifts, see Table 1 and ref. 3(*b*).
7 M. Ke, C. Sishta, B. R. James, D. Dolphin, J. W. Sparapany and J. A. Ibers, *Inorg. Chem.*, 1991, **30**, 4766.
8 K. Rachlewicz and L. Latos-Grazynski, *Inorg. Chim. Acta*, 1988, **144**, 123.
9 Only (oep)$OsBr_2$ and (ttp)Os(Cl_2 were previously reported: (*a*) C.-M. Che, W.-H. Leung and W.-C. Chung, *Inorg. Chem.*, 1990, **29**, 1841; (*b*) W.-H. Leung, T. S. M. Hun, K.-Y. Wong and W.-T. Wong, *J. Chem. Soc., Dalton Trans.*, 1994, 2713; (*c*) J. A. Smieja, K. M. Ormberg, L. N. Busuego and G. L. Breneman, *Polyhedron*, 1994, **13**, 339.
10 For establishment of the $S = 1$ ground state of these derivatives by magnetic susceptibility studies, and for the temperature dependence of their NMR spectra, see refs. 7–9 and 12.
11 Supplementary material: synthetic procedures for all complexes, Tables S1–S4 with the full NMR data, on ORTEP drawing of (tmp)OsI_2, and Tables C1–C5 with the full data of its X-ray crystal structure (CCDC 182/830) (13 pp.). See http://www.rsc.org./suppdata/cc/1998/1105.
12 Z. Gross and C. M. Barzilay, *J. Chem. Soc., Chem. Commun.*, 1995, 1287; Z. Gross and A. Mahammed, *Inorg. Chem.*, 1996, **35**, 7260.
13 N. Kaltsoyannis, *J. Chem. Soc., Dalton Trans.*, 1997, 1; P. Pyykkö, *Chem. Rev.*, 1988, **88**, 563.
14 In contrast to the (por)$Ru(X)_2$ complexes, the osmium(IV) analogs were found to be perfectly stable toward silica and alumina (synthetic section of supplementary material); the reaction time for preparation of (tpp)MPh_2 from (tpp)MCl_2 and PhLi is 24 h for M = Os,[9b] but only 30 min for M = Ru.[7]
15 N. R. Champness, C. S. Frampton, W. Levason and S. R. Preece, *Inorg. Chim. Acta*, 1995, **233**, 43.
16 B. Cheng, F. Cukiernik, P. H. Fries, J.-C. Marchon and W. R. Scheidt, *Inorg. Chem.*, 1995, **34**, 4627 and references therein.
17 Also, the pyrrole-H isotropic shift of the (perchlorato)manganese(III) porphyrin is much lartger than in the halogeno-coordinated derivatives.[4]

Received in Cambridge, UK, 9th December 1997; 8/02315H

Formation and X-ray structure of a novel water-soluble tertiary–secondary phosphine complex of ruthenium(II): $[Ru\{P(CH_2OH)_3\}_2\{P(CH_2OH)_2H\}_2Cl_2]$

Lee Higham, Annie K. Powell, Michael K. Whittlesey,*† Sigrid Wocadlo and Paul T. Wood*

School of Chemical Sciences, University of East Anglia, Norwich, UK NR4 7TJ

The novel secondary–tertiary hydroxymethylphosphine complex, all-*trans* $[Ru\{P(CH_2OH)_3\}_2\{P(CH_2OH)_2H\}_2Cl_2]$, is formed by the room temperature reaction of excess tris(hydroxymethyl)phosphine, $P(CH_2OH)_3$, with either $RuCl_3\cdot H_2O$ or $[Ru(PPh_3)_3Cl_2]$; the X-ray crystal structure of the complex shows extensive intra- and inter-molecular hydrogen bonding consistent with the high water solubility of the complex.

The need for separation and recovery of expensive transition metal catalysts from organic products has led to the well known concept of aqueous/organic biphasic catalysis in which a catalyst that is selectively soluble in the aqueous phase is used to effect the transformation of reactants to products that are themselves selectively soluble in the organic phase.[1] Aqueous transition metal phosphine catalysts have largely been based on di or tri-sulfonated arylphosphines, such as $P(m\text{-}C_6H_4SO_3Na)_3$ (TPPTS). While highly active water-soluble analogues of triphenylphosphine complexes are known, many useful catalysts incorporate alkylphosphines and hydrophilic analogues of these are highly sought after. Tris(hydroxymethyl)phosphine (THMP), $P(CH_2OH)_3$, was initially studied by Chatt *et al.*, but after the disappointing results on the catalytic activity of rhodium complexes, this ligand was largely ignored.[2] There has recently been an upsurge of interest in THMP[3] (and related bi- and tri-dentate alkyl phosphines[4]) with the preparation of a range of complexes with applications in medicinal chemistry as well as catalysis.[5] The report that ruthenium complexes bearing the related water-soluble 1,3,5-triaza-7-phosphaadamantane (PTA) derivative[6] catalysed the reduction of aldehydes to alcohols in a biphasic organic/aqueous medium in the presence of sodium formate prompted us to synthesize tris(hydroxymethyl)phosphine complexes of ruthenium to look for similar properties. We report here that the reaction of $RuCl_3$ with excess THMP does not lead to straightforward coordination of the ligand, but rather results in the formation of a novel tertiary–secondary hydroxymethylphosphine metal complex resulting from the elimination of formaldehyde from THMP.

Addition of a fourfold excess of $P(CH_2OH)_3$ in ethanol to an ethanolic solution of $RuCl_3\cdot H_2O$ at room temperature results in the immediate formation of a green solution. The $^{31}P\{^1H\}$ NMR spectrum shows no remaining free phosphine (δ −24), but does show signals corresponding to THMP oxide (δ 45)[7] and the cation, $[P(CH_2OH)_4]^+$, at δ 24. There is a single ruthenium containing compound, **1**, which gives rise to two triplets in an A_2B_2 pattern at δ 13.5 and 9.7. The same products may be obtained upon stirring an aqueous solution of THMP with a dichloromethane solution of $[Ru(PPh_3)_3Cl_2]$ in a biphasic reaction. Removal of the solvent and recrystallisation of the resulting oil from methanol–hexane yielded yellow crystals of **1** suitable for X-ray crystallography.

The crystal structure shows that **1** is the octahedral ruthenium complex, $[Ru\{P(CH_2OH)_3\}_2\{P(CH_2OH)_2H\}_2Cl_2]$, (Fig. 1)‡ in which two of the tris(hydroxymethyl)phosphine groups have eliminated formaldehyde to give the secondary phosphine ligand $P(CH_2OH)_2H$. The asymmetric unit of the crystal structure corresponds to half a complex molecule with the ruthenium atom positioned on an inversion centre in space group $P2_1/c$. This gives rise to the all-*trans* stereochemistry for the three different ligand types. The phosphorus atom of the tertiary phosphine, P(2), is bonded to ruthenium and the carbon atoms of three hydroxymethyl groups with bond angles in the range 99.2(3)–119.2(2)°. The atom P(1) of the secondary phosphine is bonded to ruthenium, two hydroxymethyl groups and a hydrogen atom and shows a greater degree of distortion from tetrahedral geometry with bond angles in the range 105.7(3)–122.0(2)°. There is a significant difference between the two Ru–P lengths with the distance to the secondary phosphine being about 0.1 Å longer [2.414(2) *cf.* 2.318(2) Å]. The X-ray structure also shows the presence of extensive intra- and inter-molecular hydrogen bonding interactions with a total of 14 contacts per molecule in the range 2.75–3.25 Å (Fig. 2). This has also been observed for other crystallographically characterised complexes containing hydroxymethyl phosphine ligands, notably $[Pd(THMP)_4]\cdot MeOH$,[5a] which has a number of hydrogen bonds shorter than 2.8 Å.

The spectroscopic data for **1** in solution are consistent with the solid state structure.§ The higher field triplet resonance in the $^{31}P\{^1H\}$ NMR spectrum is assigned to the secondary phosphine ligand because of the large P–H coupling (J = 253 Hz) observed in the proton-coupled spectrum. The ^1H NMR spectrum shows two broad singlet resonances (δ 4.53 and 4.48) in a ratio of 1 : 0.6 due to the methylene groups in the tertiary and secondary phosphine ligands. The IR spectrum of **1**

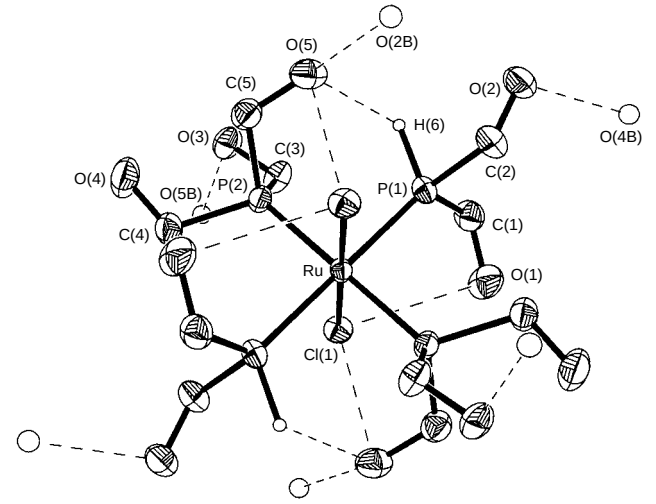

Fig. 1 View of **1** showing the atom numbering scheme and the intra- and inter-molecular hydrogen bonds (30% probability ellipsoids). Hydrogen atoms with the exception of H(6) have been omitted for clarity. Selected bond distances (Å) and angles (°): Ru–P(1) 2.414(2), Ru–P(2) 2.318(2), Ru–Cl(1) 2.450(1), P(1)–C(1) 1.813(6), P(1)–C(2) 1.898(7), P(2)–C(3) 1.856(6), P(2)–C(4) 1.890(6), P(2)–C(5) 1.832(6), C(1)–O(1) 1.407(7), C(2)–O(2) 1.427(7), C(3)–O(3) 1.387(6), C(4)–O(4) 1.389(7), C(5)–O(5) 1.443(8); P(1)–Ru–P(1A) = P(2)–Ru–P(2A) = Cl(1)–Ru–Cl(1A) 180.0, P(1)–Ru–P(2) 85.58(6), P(1)–Ru–Cl(1) 93.12(5), P(2)–Ru–Cl(1) 86.68(5)°. Selected hydrogen bonding distances (Å): O(1)···Cl(1) 3.142(8), O(2)···O(4B) 2.709(8), O(3)···O(5B) 2.777(8), O(5)···Cl(1A) 3.226(7), O(5)···O(2B) 3.067(8).

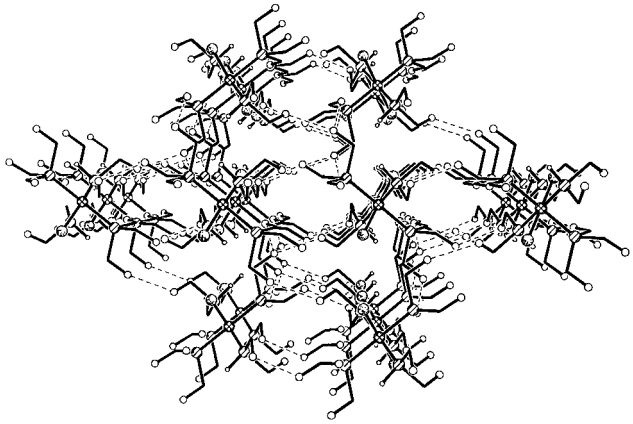

Fig. 2 View of the packing in **1** down the crystallographic *c* axis showing the hydrogen bonding

recorded in KBr shows a band at 2374 cm^{-1} which is assigned to ν(P–H).

The mechanism by which **1** is generated is not clear at present. There is no evidence for formation of the THMP complex $[Ru\{P(CH_2OH)_3\}_4Cl_2]$ nor for free secondary phosphine $P(CH_2OH)_2H$, although the elimination of formaldehyde accounts for the formation of the phosphonium cation observed by ^{31}P NMR.[8] There have been two reports of deprotonation of THMP to give metal alkoxide complexes,[9] but we can find no precedence for the formation of the secondary phosphine. This present facile route into water soluble metal complexes containing a reactive P–H bond offers great scope for further ligand functionalization.

We thank EPSRC for a studentship (L. H.), Johnson Matthey plc for the loan of ruthenium trichloride and Albright and Wilson Ltd. for a gift of $[P(CH_2OH)_4]Cl$. M. K. W. thanks UEA for financial support.

Notes and References

† E-mail: m.whittlesey@uea.ac.uk

‡ *Crystal data* for $[Ru\{P(CH_2OH)_3\}_2\{P(CH_2OH)_2H\}_2Cl_2]$ **1**: $C_{10}H_{32}Cl_2O_{10}P_4Ru$, M = 608.20, monoclinic, a = 9.367(5), b = 13.623(2), c = 9.650(1) Å, U = 1102.8(6) Å^3, T = 293 K, space group $P2_1/c$, Z = 2, μ(Mo-Kα) = 1.287 mm^{-1}. 3193 reflections collected on a Rigaku RAXIS II image plate of which 1847 were unique (R_{int} = 0.0548), 1421 had $F_o > 4\sigma(F_o)$, 5.7 < 2θ < 50.60, no absorption correction was applied. Structure solved by direct methods using SHELXS and all non-hydrogen atoms refined anisotropically using full matrix least squares (SHELXL-93).[10] $R1$ = 0.0423 (for 4σ data), $wR2$ = 0.1204, S = 1.005 (for all data). CCDC 182/861.

§ *Spectroscopic data* for $[Ru\{P(CH_2OH)_3\}_2\{P(CH_2OH)_2H\}_2Cl_2]$ **1**: NMR {270 MHz, CD_3OD, 298 K}: ^1H, δ 4.48 (br s, 8 H), 4.53 (br s, 12 H); $^{31}P\{^1H\}$, δ 9.7 (t, $^2J_{PP}$ 37.5 Hz), 13.5 (t, $^2J_{PP}$ 37.5); $^{13}C\{^1H\}$, 57.4 (vt, $|^1J_{PC} + {}^3J_{PC}|$ 27.2 Hz), 57.9 (vt, $|^1J_{PC} + {}^3J_{PC}|$ 26.8 Hz); IR (KBr, cm^{-1}), 3345s, 2966s, 2923s, 2854s, 2374m, 1627m, 1459m, 1376s, 1180m, 1023vs, 961m, 861m, 718m, 579m. Satisfactory elemental analysis (C, H) was obtained.

1 W. A. Herrmann and C. W. Kohlpainter, *Angew. Chem., Int. Ed. Engl.*, 1993, **32**, 1524; G. Papadogiankis and R. A. Sheldon, *New. J. Chem.*, 1996, **20**, 175; F. Joó and A. Kathó, *J. Mol. Catal.*, 1997, **116**, 3.
2 J. Chatt, G. L. Leigh and R. M. Slade, *J. Chem. Soc., Dalton Trans.*, 1973, 2021.
3 N. J. Goodwin, W. Henderson and J. K. Sarfo, *Chem. Commun.*, 1996, 1551; N. J. Goodwin, W. Henderson, B. K. Nicholson, J. K. Sarfo, J. Fawcett and D. R. Russell, *J. Chem. Soc., Dalton Trans.*, 1997, 4377.
4 G. T. Baxley, W. K. Miller, D. K. Lyon, B. E. Miller, G. F. Nieckarz, T. J. R. Weakley and D. R. Tyler, *Inorg. Chem.*, 1996, **35**, 6688; V. S. Reddy, K. V. Katti and C. L. Barnes, *J. Chem. Soc., Dalton Trans.*, 1996, 1301; V. S. Reddy, D. E. Berning, K. V. Katti, C. L. Barnes, W. A. Volkert and A. R. Ketring, *Inorg. Chem.*, 1996, **35**, 1753; C. J. Smith, V. S. Reddy and K. V. Katti, *Chem. Commun.*, 1996, 2557; D. E. Berning, K. V. Katti, C. L. Barnes and W. A. Volkert, *Chem. Ber.*, 1997, **130**, 907.
5 (*a*) J. W. Ellis, K. N. Harrison, P. A. T. Hoye, A. G. Orpen, P. G. Pringle and M. B. Smith, *Inorg. Chem.*, 1992, **31**, 3026; (*b*) G. T. Baxley, T. J. R. Weakley, W. K. Miller, D. K. Lyon and D. R. Tyler, *J. Mol. Catal.*, 1997, **116**, 191; (*c*) D. E. Berning, K. V. Katti, P. R. Singh, C. Higginbothom, V. S. Reddy and W. A. Volkert, *Nucl. Med. Biol.*, 1996, **23**, 617.
6 D. J. Darensbourg, F. Joó, M. Kannisto, A. Kathó and J. Reibenspies, *Organometallics*, 1992, **11**, 1990; D. J. Darensbourg, F. Joó, M. Kannisto, A. Kathó, J. Reibenspies and D. J. Daigle, *Inorg. Chem.*, 1994, **33**, 200.
7 A. W. Frank, D. J. Daigle and S. L. Vail, *Textile Res. J.*, 1982, 738.
8 A. W. Frank, D. J. Daigle and S. L. Vail, *Textile Res. J.*, 1982, 678.
9 P. A. T. Hoye, P. G. Pringle, M. B. Smith and K. Worboys, *J. Chem. Soc., Dalton Trans.*, 1993, 269; D. E. Berning, K. V. Katti, L. J. Barbour and W. A. Volkert, *Inorg. Chem.*, 1998, **37**, 334.
10 G. M. Sheldrick, University of Göttingen, 1993.

Received in Cambridge, UK, 24th February 1998; 8/01546E

Diastereoselective asymmetric cyclopropanation of (*S*)-(+)-α-(diethoxyphosphoryl)vinyl *p*-tolyl sulfoxide

Wanda H. Midura,[a] Jerzy A. Krysiak,[a] Michał W. Wieczorek,[b] Wiesław R. Majzner[b] and Marian Mikołajczyk*[a]†

[a] *Centre of Molecular and Macromolecular Studies, Polish Academy of Sciences, Department of Organic Sulfur Compounds, 90-363 Łódź, Sienkiewicza 112, Poland*

[b] *Institute of General Food Chemistry, Technical University of Łódź, 90-924 Łódź, Stefanowskiego 4/10, Poland*

The title sulfoxide 1 reacts with fully deuterated dimethylsulfoxonium methylide, diphenylsulfonium isopropylide and diphenyldiazomethane to form the corresponding cyclopropanes 4 as single diastereoisomers; the chirality of the cyclopropane (+)-4c obtained from 1 and diphenyldiazomethane is (S_S,S_C) as determined by X-ray diffraction analysis; based on experimental data, the steric course of the asymmetric cyclopropanation is proposed.

α,β-Unsaturated sulfoxides have been widely used in asymmetric synthesis as versatile chiral reagents with the sulfinyl group playing the role of a chiral auxiliary.[1,2] Since α,β-unsaturated sulfoxides having no additional electron-withdrawing substituents on the double bond exhibit low reactivity, we recently designed a new type of activated chiral vinyl sulfoxides, namely α-phosphorylvinyl *p*-tolyl sulfoxide **1** and its β-substituted (Me, Ph, Bu^n) analogues.[3,4] The phosphoryl group in **1** activates not only the C=C bond but also makes possible further reactions such as, for instance, the Horner–Wittig reaction. The chiral sulfoxides **1** were found to be good Michael acceptors as well as Diels–Alder dienophiles. They were also used as key reagents for the construction of monocyclic- and condensed carbo- and hetero-cycles *via* tandem Michael addition/intramolecular Horner–Wittig reaction. However, the asymmetric induction in these reactions was not very high.

Now we extend our work in this area by reporting a fully diastereoselective, asymmetric cyclopropanation of the sulfoxide (*S*)-(+)-**1**. The present study on asymmetric cyclopropanation was stimulated by the fact that a wide variety of natural products and currently-used insecticides contain the cyclopropane ring in a chiral environment.[5] Moreover, to the best of our knowledge, there are only two reports describing asymmetric cyclopropanation using enantiopure vinylic sulfoxides as chiral reagents.[6,7] Thus, Hamdouchi[6] reacted the sulfoxide (*S*)-(+)-**2** with dimethyl(oxo)sulfonium methylide and obtained a mixture of two diastereoisomeric cyclopropanation products in a 5.9 : 1 ratio. On the other hand, the reaction of the cyclic vinylic sulfoxide **3** with allylmagnesium bromide was found by Iwata[7] to give the corresponding cyclopropane as a single diastereoisomer, however, accompanied by the side coupling product.

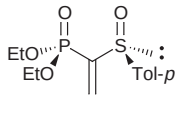

1

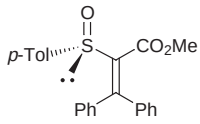

2

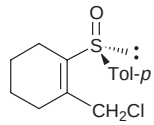

3

In our preliminary experiment (*S*)-(+)-α-(diethoxyphosphoryl)vinyl *p*-tolyl sulfoxide **1** was treated with an excess of dimethyl(oxo)sulfonium methylide in DMSO at room temperature and gave the expected cyclopropane (*S*)-(+)-**4a** as the only product [eqn. (1)], isolated by flash chromatography on silica gel in 90% yield. The asymmetric version of the reaction was realized by using fully deuterated dimethyl(oxo)sulfonium methylide as the CD_2 transfer agent (Scheme 1). Although the chirality at the newly formed quaternary α-carbon atom is due to isotopic substitution (CH_2 *vs.* CD_2), the ^{31}P NMR spectrum of the crude cyclopropane [$^2H_2$]-**4a** formed revealed only one sharp signal at δ_P 22.3, strongly suggesting that only one diastereoisomer was formed. The deuterium decoupled ^{1}H NMR spectra (500 MHz) of the pure product isolated in 92% yield confirmed its full diastereoisomeric purity (the cyclopropane methylene protons appeared in the spectrum as doublets of doublets at δ 1.26 and 1.38 with $^2J_{H–H}$ = 4.8 and $^3J_{H–H}$ = 9.8 and 14.0 Hz).

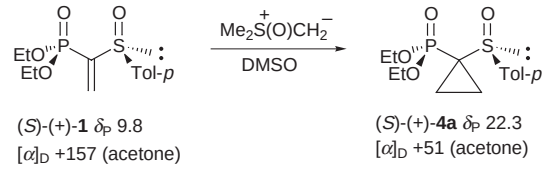

(1)

Similarly, treatment of (*S*)-(+)-**1** with diphenylsulfonium isopropylide (prepared according to the procedure described by Corey[8]) in THF at room temperature yielded the corresponding cyclopropane (+)-**4b** which was isolated in a pure state by flash chromatography in 65% yield. To our delight, also in this case the cyclopropanation reaction resulted in the formation of a single diastereoisomer, as evidenced by the ^{1}H and ^{31}P NMR spectra of the product.

In addition to sulfur ylides, in the course of these studies the behaviour of the vinylic sulfoxide (*S*)-(+)-**1** towards diazomethane and diphenyldiazomethane was investigated. Whereas the reaction of the former dipole was found to give rise to 3-diethoxyphosphorylpyrazole *via* transient formation of the corresponding 1,3-cycloadduct, elimination of toluene-*p*-sulfenic acid and tautomerization,‡ the latter reacted with (*S*)-(+)-**1** affording a single diastereoisomeric cyclopropane (+)-**4c** as indicated by the ^{1}H and ^{31}P NMR spectral analysis of the crude product.§ After flash chromatography, pure (+)-**4c** (mp 89–91 °C) was obtained in 86% yield. To provide an unequivocal proof of the full asymmetric induction occuring in this reaction, the cyclopropane (+)-**4c** was oxidized by MCPBA to the

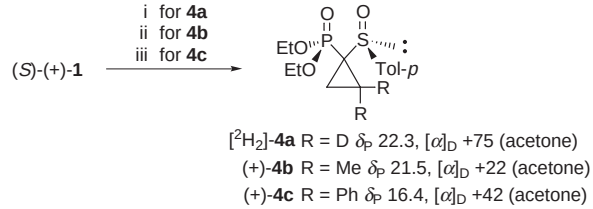

Scheme 1 *Reagents and conditions*: i, $(CD_3)_2S(O)CD_2$, [$^2H_6$]DMSO; ii, Ph_2SCMe_2, THF; iii, Ph_2CN_2, Et_2O

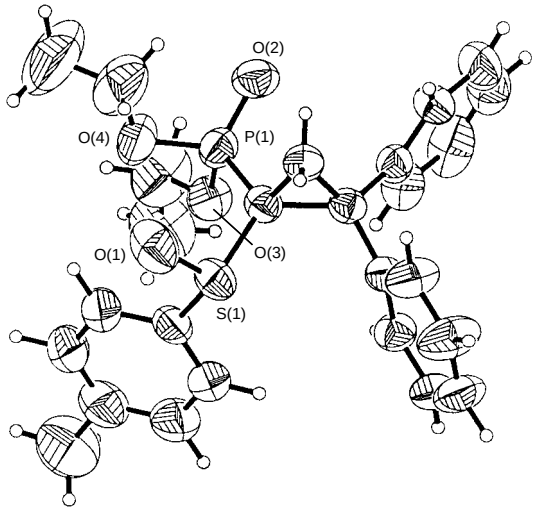

Fig. 1 X-Ray structure of (+)-**4c**. Ellipsoids are shown at the 50% probability level

optically active sulfone (+)-**5c**. Its ^{1}H NMR spectrum recorded in the absence and in the presence of (*R*)-(+)-*tert*-butylphenylphosphinothioic acid as a chiral solvating agent[9] showed only two doublets of doublets for the cyclopropyl methylene protons (δ 2.67 and 2.83; $^2J_{H–H}$ = 6 and $^3J_{P–H}$ = 7.1 and 8.4 Hz, respectively), while in the spectrum of the racemic sulfone (±)-**5c** prepared in an independent way in the presence of a

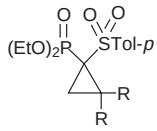

(+)-**5b** R = Me δ_P 21.7, $[\alpha]_D$ 8.5 (acetone)
(+)-**5c** R = Ph δ_P 15.1, $[\alpha]_D$ 25.0 (acetone)

chiral phosphinothioic acid, all the signals of the appropriate protons were doubled. In a similar way, the full enantiomeric purity of the sulfone (+)-**5b** obtained from (+)-**4b** was also confirmed.

In order to rationalize the steric course of the above described fully diastereoselective cyclopropanations of the sulfoxide (*S*)-(+)-**1**, we determined the crystal and molecular structure of the cyclopropane (+)-**4c** by X-ray diffraction (Fig. 1).¶ It turned out that the absolute configuration of the newly formed chiral centre at the α-carbon atom is *S*. Moreover, both polar sulfinyl

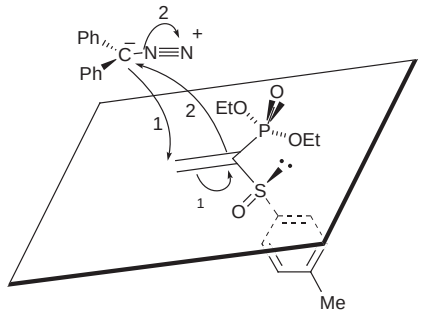

Fig. 2 The proposed steric course of the reaction of Ph_2CN_2 with the sulfoxide (*S*)-(+)-**1**

and phosphoryl groups in **4c** are in *anti*-like orientation [the torsional angle S(1)–O(1)···P(1)–O(2) is equal to 93.3 (±0.1)°]. Therefore, it is reasonable to assume that (*S*)-(+)-**1** adopts a similar conformation, and nucleophilic addition of diphenyldiazomethane to the vinylic β-carbon atom of **1** (step 1) and subsequent ring closure (step 2) occur exclusively from the less-hindered diastereotopic face occupied by the electron lone pair at sulfur, as schematically depicted in Fig. 2.

A two-step mechanism for cyclopropanation was supported by isolation of the intermediate adduct **6** which was formed together with the cyclopropane (+)-**4c** when the reaction was carried out in the presence of LiCl [eqn. (2)]. Its subsequent

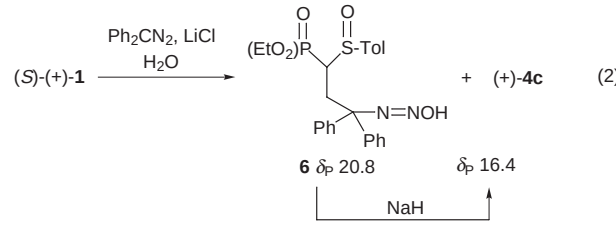

cyclization to (+)-**4c** was found to occur in the presence of NaH.

In summary, we have described the fully diastereoselective asymmetric synthesis of a new type of optically active cyclopropane **4** which is geminally substituted with two different heteroatoms. The specific reactivity of each heteroatomic centre provides interesting possibilities for further transformations of the cyclopropane **4** into optically active cyclic and acyclic derivatives.

Notes and References

† E-mail: marmikol@bilbo.cbmm.lodz.pl

‡ The results of the reaction of diazomethane with sulfoxide **1** and its β-substituted analogues will be published elswhere.

§ The formation (10%) of the corresponding 3-phosphorylpyrazoline (δ_P 19.3) was observed.

¶ *Crystal data* for (+)-**4c**; $C_{26}H_{29}O_4PS$, M = 468.52, orthorhombic, space group $P2_12_12_1$; a = 9.301 (7), b = 16.209 (7), c = 16.755 (6) Å; V = 2526 (2) Å^3; Z = 4; D_C = 1.232 g cm^{-3}; μ = 19.67 cm^{-1} (Cu-Kα). A total of 5042 unique reflections were collected in the conventional $\omega/2\theta$ scan mode, of which 4817 observed reflections [$I > 2\sigma(I)$] were used in the structure solution (direct methods) and refinement (full-matrix least-squares) to give final R = 0.0429 for 339 refined parameters and ωR = 0.1107. The absolute configuration was established by the Flack parameter, 0.001 (16). CCDC 182/835.

1 M. Mikołajczyk, J. Drabowicz and P. Kiełbasiński, *Chiral Sulfur Reagents: Applications in Asymmetric and Stereoselective Synthesis*, CRC Press, Boca Raton, 1997.
2 A.-H. Li, L.-X. Dai and V. K. Aggarwal, *Chem. Rev.*, 1997, **97**, 2341.
3 M. Mikołajczyk and W. H. Midura, *Tetrahedron: Asymmetry*, 1992, **3**, 1515.
4 W. H. Midura and M. Mikołajczyk, *Phosphorus, Sulfur, Silicon*, 1994, **95**–**96**, 397.
5 H. U. Reissig, in *The Chemistry of Cyclopropyl Group*, ed. S. Patai and Z. Rappoport, Wiley, New York, 1987, ch. 8; H. W. Liu and C. T. Walsh, *idem*, ch. 16; J. Salaün, M. S. Baird, *Curr. Med. Chem.*, 1995, **2**, 511.
6 Ch. Hamdouchi, *Tetrahedron Lett.*, 1992, **33**, 1701.
7 T. Imanishi, T. Ohara, K. Sugiyama, Y. Ueda, Y. Takemoto and C. Iwata, *J. Chem. Soc., Chem. Commun.*, 1992, 296.
8 E. J. Corey and M. Jautelat, *J. Am. Chem. Soc.*, 1967, **89**, 3912.
9 J. Drabowicz, B. Dudziński, M. Mikołajczyk, S. Colonna and N. Gaggero, *Tetrahedron: Asymmetry*, 1997, **13**, 2267 and references cited therein.

Received in Cambridge, UK, 16th February 1998; 8/01299G

Electrochemically active threading intercalator with high double stranded DNA selectivity

Shigeori Takenaka,*[a]† Yoshihiro Uto,[b]‡ Hideki Saita,[b] Makoto Yokoyama,[b] Hiroki Kondo[b] and W. David Wilson[c]

[a] *Department of Chemical Systems and Engineering, Kyushu University, Fukuoka, 812-8581, Japan*
[b] *Department of Biochemical Engineering and Science, Kyushu Institute of Technology, Iizuka 820-8502, Japan*
[c] *Department of Chemistry, Georgia State University, Atlanta, Georgia 30303, USA*

A naphthalene diimide threading intercalator carrying ferrocenyl moieties as its termini can discriminate double stranded DNA from single stranded counterparts owing to a difference in their dissociation rates.

Discrimination of double stranded nucleic acids from single stranded ones is of utmost importance in basic and applied molecular biology. Hybridization of DNA with its complementary DNA or RNA is based on this discrimination and one has to discriminate single stranded RNA of such viruses as HIV from double stranded human chromosomal DNA when targeting the former. Single and double stranded nucleic acids may be discriminated by intercalators but none is known to achieve this feat with a high margin. Recently, threading intercalators were developed in which their substituents can penetrate between the base pairs of double stranded DNA when bound to it.[1,2] This type of intercalator, *e.g.* naphthalene diimides, forms a very stable complex with double stranded DNA, and they dissociate much more slowly from double stranded DNA than do classical intercalators.[1–3] When electrochemically active groups are attached to a threading intercalator, the resulting molecule will serve as a double stranded DNA selective electrochemical probe.[4,5] This idea was substantiated with a naphthalene diimide **1** carrying two ferrocenyl moieties at its ends.

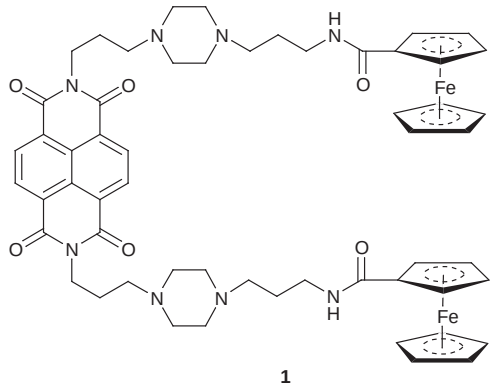

1

Naphthalene diimide **1** was prepared by a reaction of the corresponding amino derivative with *N*-hydroxysuccinimide ester of ferrocenecarboxylic acid and purified by silica gel chromatography (MeOH) followed by recrystallization from water (yield, 25%).

Compound **1** undergoes hypochromic and bathochromic shifts of the absorption band of the naphthalene diimide chromophore upon binding to sonicated calf thymus DNA, which is indicative of DNA intercalation. Sodium dodecyl sulfate-driven dissociation experiments[3] carried out with the complex of **1** and intact or denatured calf thymus DNA§ showed that the dissociation rate constant (k_d) of **1** from the intact DNA was 0.06 s^{-1} at 20 °C, whereas that of **1** from the denatured DNA was 4.2 s^{-1}. These magnitudes of dissociation rate constant are one of the smallest for synthetic intercalators. The ratio of 70 in k_d suggests that single and double stranded DNA can be discriminated kinetically by **1**. Note that these magnitudes are minimal estimates, since 'the denatured' DNA is not necessarily composed of single stranded DNA alone. To test whether compound **1** can discriminate single and double stranded DNA on the electrode surface, the following experiments were carried out.

A DNA-immobilized electrode was prepared by a reaction of mercaptohexyl dT_{20} oligonucleotide on a gold electrode with an area of 2.0 mm^2.[7] HPLC experiments revealed that 64 pmol of mercaptohexyl oligonucleotide was immobilized on this electrode. Then 2 μl of a solution containing appropriate amounts (0–70 pmol) of target dA_{20} oligonucleotide were placed on this modified electrode and kept at 25 °C for 20 min to allow hybridization with the immobilized probe dT_{20}. After this reaction, 2 μl of a 1 mM solution of **1** were placed on the

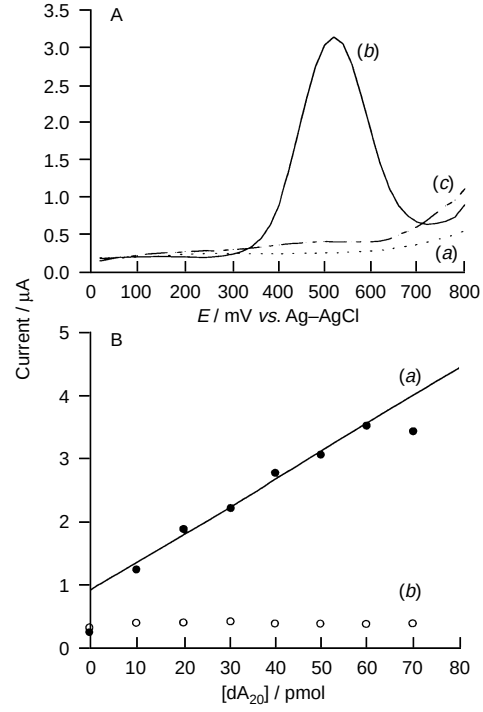

Fig 1 (A) Differential pulse voltammograms (DPVs) of **1** bound to the dT_{20}-immobilized electrode before (*a*) and after hybridization with 60 pmol of dA_{20} (*b*) or dT_{20} (*c*). Differential pulse voltammograms were measured in 50 mM AcOK–AcOH buffer (pH 5.2) with Ag–AgCl and Pt wire as reference and counter electrodes, respectively. Pulse period 200 ms; scan rate 100 mV s^{-1}; pulse amplitude 50 mV; pulse width 50 ms. (B) Correlation of the current response at 521 mV for **1** with the amount of dA_{20} (*a*) and dT_{20} (*b*).

electrode for 5 min. Following washing with 50 mM AcOK–AcOH buffer (pH 5.2) by vortexing for 5 s at 20 °C, cyclic voltammograms (CVs) and differential pulse voltammograms (DPVs) of the complex were measured in the same buffer. Fig. 1(A) shows examples of DPVs for this electrode treated with dA_{20} (target DNA) or dT_{20} (non-target DNA). It is clear that the electrochemical signal is generated only in the presence of complementary oligonucleotide dA_{20} [trace (*b*)] and the current response obtained for dT_{20}, non-complementary to the sequence of dT_{20}, was barely above background [trace (*c*)]. A current response due to the ferrocenyl moieties of **1** increased linearly up to 60 pmol with an increase in the amount of dA_{20} (correlation coefficient 0.990) and then levelled off as shown in Fig. 1(B) [trace (*a*)]. The amount of dA_{20} at the break point (60 pmol) was in agreement with the amount of the probe dT_{20} immobilized on the electrode (64 pmol). The estimated detection limit was 1.0 fmol of target oligonucleotide. This procedure could be repeated several times and the current response per immobilized oligonucleotide was reproducible even with electrodes of different lot samples.

We estimated the amount of the ligand **1** bound on this electrode to be 13 pmol from the area under the CV peak after hybridizing with 60 pmol of dA_{20}. This value is about 30 times smaller than that expected from Scatchard analysis, which revealed that three base pairs of double stranded DNA are required to accommodate a single molecule of **1**. Therefore, *ca*. 400 pmol of **1** ought to be bound to 60 pmol of $dA_{20}dT_{20}$. This discrepancy can arise from several reasons. First, intercalation and redox reaction of **1** on the electrode surface could be less efficient than those in solution. Alternatively, part of **1** could undergo dissociation from DNA during washing of the complexed and intercalated electrode. Despite this low efficiency, the electrochemical responses of the active electrode were stable during the experiment (*ca*. 2 min).

In conclusion, the electrochemically active threading intercalator **1**, coupled with a DNA-carrying electrode, enabled the sensitive detection of target DNA fragments. The whole manipulation was carried out over a short period of time as long as the sensor is prepared and yet the sensitivity of detection is ultra-high, making this sensing system most feasible for practical use in DNA analysis and gene diagnosis.

This work was supported in part by Grants-in-Aid for Scientific Research from the Ministry of Education, Science, Sports and Culture, Japan, and from the Japan Society for the Promotion of Science.

Notes and References

† E-mail: staketcm@mbox.nc.kyushu-u.ac.jp
‡ Research fellow of the Japan Society for the Promotion of Science.
§ Denaturation of DNA was carried out by heating at 100 °C for 10 min and then immediately cooling on ice.

1 S.-F. Yen, E. J. Gabbay and W. D. Wilson, *Biochemistry*, 1982, **21**, 2070.
2 F. A. Tanious, S.-F. Yen and W. D. Wilson *Biochemistry*, 1991, **30**, 1813.
3 W. D. Wilson and F. A. Tanious, in *Molecular Aspects of Anticancer Drug–DNA Interactions*, ed. S. Neidle and M. J. Waring, Macmillan Press, Riverside, NJ, 1994, p. 243.
4 S. Takenaka, Y. Uto, H. Kondo,T. Ihara and M. Takagi, *Anal. Biochem.*, 1994, **218**, 436.
5 Y. Uto, H. Kondo, M. Abe, T. Suzuki and S. Takenaka, *Anal. Biochem.*, 1997, **250**, 122.
6 J. D. McGhee and P. H. von Hippel, *J. Mol. Biol.*, 1974, **86**, 469.
7 M. Maeda, Y. Mitsuhashi, K. Nakano and M. Takagi, *Anal. Sci.*, 1992, **8**, 82.

Received in Cambridge, UK, 23rd February 1998; 8/01539B

Quantitative formation of the intermediate of alkene insertion in the copolymerization of *p*-methylstyrene and carbon monoxide catalyzed by [(Pr^{i}DAB)Pd(Me)(NCMe)]$^+$BAr$_4^-$

Carla Carfagna,*† Mauro Formica, Giuseppe Gatti, Alfredo Musco and Annarita Pierleoni

Università degli Studi di Urbino, Istituto di Scienze Chimiche, Piazza Rinascimento, 6-61029 Urbino (PS), Italy

The intermediate after the first CO and *p*-methylstyrene insertion in the chain growth process of the copolymerization of these monomers has been quantitatively obtained from [(Pr^{i}DAB)Pd(Me)(NCMe)]$^+$[{3,5-(CF$_3$)$_2$C$_6$H$_3$}$_4$B]$^-$ in CHCl$_3$ at 20 °C.

In recent years there has been increasing interest in carbon monoxide olefin copolymerization.[1] We and others have found that ionic Pd complexes with non-coordinating anions and chiral nitrogen ligands, such as bioxazolines, are active precatalysts for the copolymerization of styrene and carbon monoxide, to yield isotactic optically active polymers.[2,3] The use of achiral nitrogen ligands, however, leads to syndiotactic copolymers.[4]

From our recent study, the objective of which was to test the catalytic properties of various nitrogen ligands with different π-acceptor capacity,[5] the complex [Pr^{i}DABPd(Me)(NCMe)]$^+$[{3,5-(CF$_3$)$_2$C$_6$H$_3$}$_4$B]$^-$ **1** (Pr^{i}DAB = 1,4-di-isopropyl-1,4-diaza-buta-1,3-diene) proved to be a very active precatalyst in the copolymerization of styrene and 4-methylstyrene with carbon monoxide, giving alternating syndiotactic polyketones under very mild conditions (1 bar CO and 0 °C). In addition, the complex **1** is a convenient starting point for modelling the first steps of the polymer chain growth, as described here.

By exposure of the precatalyst solution **1** to a CO atmosphere, under conditions used for the copolymerization reaction, the corresponding acetyl carbonyl complex **2**‡ was obtained, which reversibly releases one CO group; bubbling nitrogen through a CH_2Cl_2 solution at −15 °C resulted in the formation of **3**, and exposure of the solution of **3** to CO atmosphere led to the regeneration of **2**[1j] (Scheme 1). The structure of **3**§ was confirmed by the presence, in the ^{13}C NMR spectrum, of the Pd–CO resonance at δ 174.8 and by the absence of the acetyl signals.

We then focused our attention on the next step, the olefin insertion, to see whether our catalytic system would allow quantitative insertion and isolation of the reaction product. We performed the reaction using directly the more reactive compound **3** which was isolated as a white powder from **2**. By adding an equimolecular amount of *p*-methylstyrene at −10 °C to a slightly yellow $CHCl_3$ solution of **3** and heating gently to 20 °C, a colour change to dark orange occurred. The new compound formed in 100% yield corresponds to the 5-membered palladacycle **4**, in agreement with the NMR evidence.¶ In particular, in the carbonyl region of the ^{13}C NMR spectrum, the resonance of a typical acetyl group at δ 224.9 is present, while the Pd–CO signal has disappeared. This result is confirmed by the IR spectrum, which shows an absorption at 1721 cm^{-1} for the acetyl CO coordinated to Pd.[1j,6f] Moreover, the CH_2 and CH signals are detected in the DEPT ^{13}C NMR spectrum. The CH–CH_2 fragment is confirmed by the corresponding three-spin pattern observed in the ^{1}H NMR spectrum, where the relatively high value of the geminal coupling J_{ab} = −19.7 Hz is typical of a CH_2 linked to a CO group, while the values of the two vicinal couplings, J = 8.3 and 3.5 Hz, are representative of two

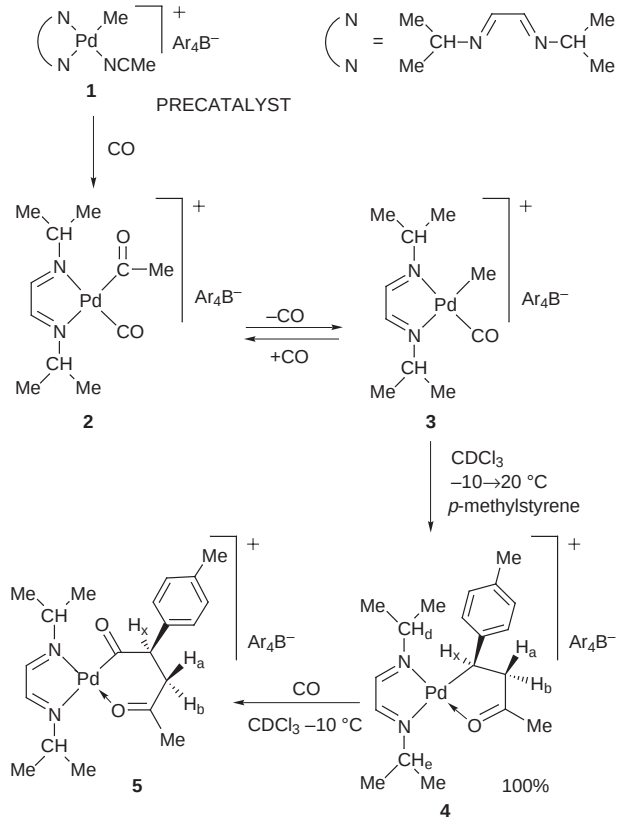

Scheme 1

substantially different dihedral angles. Evidence for two non-equivalent isopropyl groups is given by the two different CH chemical shifts observed in both the ^{1}H and ^{13}C NMR spectra. Moreover, the two methyl groups, within each isopropyl group, are non-equivalent due to the dissymmetry introduced by the styrene monomeric unity. The signals of the two *meta* aromatic hydrogens are assigned on the basis of NOEs with the adjacent methyl, while the remaining *ortho* aromatic hydrogens show NOEs with CH_x. The *ortho* hydrogens also show NOEs with CH_d, thus allowing the assignment of the latter. Moreover the NOE observed between the *ortho* hydrogens and CH_a but not CH_b is in agreement with an orientation of the phenyl group closer to CH_a. Therefore the conformation across the CH–CH_2 bond is as depicted in the Newmann projection in Fig. 1, in agreement also with the values of J_{ax} = 8.3 and J_{bx} = 3.5 Hz,

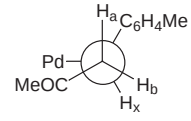

Fig. 1

due to nearly *anti* and *gauche* relationships, respectively. This suggests that the conformation of the pentatomic ring is slightly folded.

Insertions of different alkenes into metal–acyl bonds have already been reported[6,1*j*] but to the best of our knowledge there are in the literature only two examples of reaction of styrene with a palladium–acyl complex. After insertion, the reaction products have been described either as a mixture of allylic and chelate structures in very rapid equilibrium[1*c*] or as an allylic intermediate.[7] Therefore it appears that the quantitative formation of 5-membered palladacyle **4** as the only observable species is unprecedented. Compound **4** can be isolated as a relatively stable dark red oil by removing the solvent under reduced pressure; in $CHCl_3$ solution it proved to be stable up to 50 °C.

In the next step, CO was bubbled through a solution of **4** in $CHCl_3$ at −10 °C for 15 min, yielding the six-membered chelate complex **5** in solution.‖ Evidence for the insertion of CO comes from the doubling of the CO signals in the ^{13}C NMR spectrum and in the IR spectrum. The deshielding observed for both the proton and carbon resonances of the CH group of the CH–CH_2 fragment shows that the CO has inserted into the Pd–CH bond, as expected.[1*j*]

In conclusion, the results of this work show that by using the proper ligand it has been possible for the first time to quantitatively obtain and determine the conformation of the first intermediate in the syndiotactic copolymerization of CO and styrene derivatives, *i.e.* the 5-membered palladacyle **4**; it results from the insertion of *p*-methylstyrene into the Pd–acyl bond formed in **3** as a result of α-methyl migration. Furthermore, it has been possible to obtain the new complex **5** which represents the second step of the copolymerization reaction.

We are currently exploring the use of the isolable complex **4**, as a preformed catalyst, for the synthesis of syndiotactic copolymers.

We thank Professor C. J. Elsevier (University of Amsterdam) for helpful discussions. This work was supported by Ministero dell'Università e della Ricerca Scientifica e Tecnologica and Consiglio Nazionale delle Ricerche.

Notes and References

† E-mail: schim@fis.uniurb.it

‡ *Selected data* for **2**: $\delta_H(CD_2Cl_2, -75\ °C)$ 7.98 and 7.92 (s, 1 H each, C*H*=N), 7.65 (s, 8 H, Ar-H_o), 7.47 (s, 4 H, Ar-H_p), 3.72 [m, 2 H, C*H*$(CH_3)_2$], 2.67 (s, 3 H, COCH_3), 1.10 [d, J_{HH} 6.1, 12 H, CH(CH_3)$_2$]; $\delta_C(CD_2Cl_2, -75\ °C)$ 214.5 (*C*OCH$_3$), 172.9 (Pd–*C*O), 164.1 and 160.5 (*C*=N), 162.1 (q, $^1J_{CB}$ 49.4, Ar-C_i), 134.9 (Ar-C_o), 128.9 (q, $^2J_{CF}$ 31.4, Ar-C_m), 124.7 (q, $^1J_{CF}$ 272.6, *C*F$_3$), 117.9 (Ar-C_p), 63.8 and 59.5 [*C*H$(CH_3)_2$], 41.6 (CO*C*H$_3$), 23.2 and 22.0 [CH(*C*H$_3$)$_2$]; ν_{max}(Nujol)/cm^{-1} 2137 (Pd–CO), 1750 (COCH$_3$), 1611 (C=N). Compound **2** can also be synthesized directly by reaction of Pr^{i}DABPdMeCl and $Na^+BAr_4^-$ in the presence of CO.

§ *Selected data* for **3**: $\delta_H(CDCl_3, -20\ °C)$ 7.96 and 7.92 (s, 1 H each, C*H*=N), 7.69 (s, 8 H, Ar-H_o), 7.54 (s, 4 H, Ar-H_p), 4.13 and 3.77 [sept, 1 H each, C*H*$(CH_3)_2$], 1.36 (s, 3 H, Pd–CH_3), 1.25 [d, J_{HH} 6.7, 12 H, CH(CH_3)$_2$]; $\delta_C(CD_2Cl_2, 0\ °C)$ 174.8 (Pd–*C*O), 165.8 and 160.1 (*C*=N), 161.5 (q, $^1J_{CB}$ 49.6, Ar-C_i), 134.6 (Ar-C_o), 128.7 (q, $^2J_{CF}$ 30.0, Ar-C_m), 124.3 (q, $^1J_{CF}$ 272.5, *C*F$_3$), 117.5 (Ar-C_p), 63.4 and 56.3 [*C*H$(Me)_2$], 22.7 and 21.8 [CH(*C*H$_3$)$_2$], 5.7 (Pd–*C*H$_3$); ν_{max}(Nujol)/cm^{-1} 2130 (Pd–CO), 1610 (C=N). Compound **3** was isolated as a white powder.

¶ *Selected data* for **4**: $\delta_H(CDCl_3, -3\ °C)$ 7.80 and 7.78 (s, 1 H each, C*H*=N), 7.71 (s, 8 H, Ar-H_o), 7.54 (s, 4 H, Ar-H_p), 7.20 and 7.00 (d, 2 H each, Ph-H_o, Ph-H_m), 3.88 [sept, 1 H, C$H_d$$(CH_3)_2$], 3.68 [sept, 1 H, C$H_e$$(CH_3)_2$], 3.76 (dd, J_{HH} 8.3 and 3.5, 1 H, CH_x–CH_2), 3.04 (dd, J_{HH} 19.7 and 8.3, 1 H, CH–CH_a), 2.70 (dd, J_{HH} 19.4 and 3.5, 1 H, CH–CH_b), 2.39 (s, 3 H, CO–CH_3), 2.19 (Ph–CH_3), 1.29, 1.17 and 1.09 [d, J_{HH} 6.4, 12 H, CH(CH_3)$_2$]; $\delta_C(CDCl_3, -20\ °C)$ 224.9 (*C*OCH$_3$), 161.7 (q, $^1J_{CB}$ 49.2, Ar-C_i), 161.2 and 157.1 (*C*=N), 139.9 (Ph-C_i), 134.8 (Ar-C_o), 132.1 (Ph-C_o), 130.8 (Ph-C_p), 128.8 (q, $^2J_{CF}$ 31.5, Ar-C_m), 124.5 (q, $^1J_{CF}$ 272.4, *C*F$_3$), 119.9 (Ph-C_m), 117.6 (Ar-C_p), 62.1 and 59.5 [*C*H$(Me)_2$], 52.0 (CH–*C*H$_2$), 47.0 (*C*H–CH$_2$), 29.2 (CO*C*H$_3$), 22.8, 22.0, 21.4 and 21.3 [CH(*C*H$_3$)$_2$], 21.9 (Ph-*C*H$_3$); ν_{max}(film)/cm^{-1} 1721 (CO), 1610 (C=N).

‖ *Selected data* for **5**: $\delta_H(CDCl_3, -20\ °C)$ 7.80 (s, 2 H, C*H*=N), 7.73 (s, 8 H, Ar-H_o), 7.58 (s, 4 H, Ar–H_p), 7.22 (s, 4 H, Ph-H_o, Ph-H_m), 4.65 (dd, J_{HH} 10.6 and 2.0, 1 H, C*H*–CH$_2$), 3.79 [br s, 2 H, C*H*$(CH_3)_2$], 3.60 (dd, J_{HH} 18.7 and 11.3, 1 H, CH–CH_2), 2.80 (d, J_{HH} 18.7, 1 H, CH–CH_2), 2.33 (s, 3 H, Ph–CH_3), 2.29 (s, 3 H, CO–CH_3), 1.21 and 1.10 [d, J_{HH} 6.1, 12 H, CH(CH_3)$_2$]; $\delta_C(CDCl_3, -20\ °C)$ 211.7 and 207.1 (*C*O–CH$_3$, *C*O–CH), 161.7 (q, $^1J_{CB}$ 49.6, Ar-C_i), 140.4 (Ph-C_i), 134.8 (Ar-C_o), 130.9 (Ph–C_o), 129.5 (Ph-C_m), 128.8 (q, $^2J_{CF}$ 30.5, Ar-C_m), 124.5 (q, $^1J_{CF}$ 272.7, *C*F$_3$), 117.8 (Ar-C_p), 61.9 (*C*H–CH$_2$), 46.2 (CH–*C*H$_2$), 30.1 (CO–*C*H$_3$), 22.5 [CH(CH$_3$)$_2$], 21.2 (Ph-*C*H$_3$); ν_{max}(film)/cm^{-1} 1722 (br, CO), 1610 (C=N).

1 (*a*) Eur. Pat. Appl. 229408 (1986): E. Drent, *Chem. Abstr.*, 1988, **108**, 6617b; (*b*) M. Barasacchi, G. Consiglio, L. Medici, G. Petrucci and U. W. Suter, *Angew. Chem., Int. Ed. Engl.*, 1991, **30**, 989; (*c*) M. Brookhart, F. C. Rix, J. M. DeSimone and J. C. Barborak, *J. Am. Chem. Soc.*, 1992, **114**, 5894; (*d*) A. Batistini, G. Consiglio and U. W. Suter, *Angew. Chem., Int. Ed. Engl.*, 1992, **31**, 303; (*e*) A. Sen and Z. Jiang, *Macromolecules*, 1993, **26**, 911; (*f*) V. Busico, P. Corradini, L. Landriani and M. Trifuoggi, *Makromol. Chem. Rapid. Commun.*, 1993, **14**, 261; (*g*) A. Sen, *Acc. Chem. Res.*, 1993, **26**, 303; (*h*) Z. Jiang, S. E. Adams and A. Sen, *Macromolecules*, 1994, **27**, 2694; (*i*) E. Drent and P. H. M. Budzelaar, *Chem. Rev.*, 1996, **96**, 663; (*j*) F. C. Rix, M. Brookhart and P. S. White, *J. Am. Chem. Soc.*, 1996, **118**, 4746; (*k*) M. Brookhart and M. L. Wagner, *J. Am. Chem. Soc.*, 1996, **118**, 7219; (*l*) M. Sperrle, A. Aeby, G. Consiglio and A. Pfaltz, *Helv. Chim. Acta*, 1996, **79**, 1387.

2 S. Bartolini, C. Carfagna and A. Musco, *Macromol. Chem. Rapid. Commun.*, 1995, **16**, 9; S. Brückner, C. De Rosa, P. Corradini, W. Porzio and A. Musco, *Macromolecules*, 1996, **29**, 1535.

3 M. Brookhart, M. I. Wagner, G. G. A. Bolavoine and H. A. Haddou, *J. Am. Chem. Soc.*, 1994, **116**, 3641.

4 P. Corradini, C. De Rosa, A. Panunzi, G. Petrucci and P. Pino, *Chimia*, 1990, **44**, 52; M. Barsacchi, A. Batistini, G. Consiglio and U. W. Suter, *Macromolecules*, 1992, **25**, 3604; B. Milani, E. Alessio, G. Mestroni, A. Sommazzi, F. Garbassi, E. Zangrando, N. Bresciani-Pahor and L. Randaccio, *J. Chem. Soc., Dalton Trans.*, 1994, 1903; B. Milani, A. Anzilutti, L. Vicentini, A. Sessanta o Santi, E. Zangrando, S. Geremia and G. Mestroni, *Organometallics*, 1997, **16**, 5064.

5 Experimental details and full spectroscopic characterization will be given in a forthcoming publication.

6 (*a*) J. S. Brumbaugh, R. R. Whittle, M. Parvez and A. Sen, *Organometallics*, 1990, **9**, 1735; (*b*) F. Ozawa, T. Hayashi, H. Koide and A. Yamamoto, *J. Chem. Soc., Chem. Commun.*, 1991, 1469; (*c*) R. van Asselt, E. E. C. G. Gielens, R. E. Rülke and C. J. Elsevier, *J. Chem. Soc., Chem. Commun.*, 1993, 1203; (*d*) B. A. Markies, K. A. N. Verkerk, M. H. P. Rietveld, J. Boersma, H. Kooijman, A. L. Spek and G. van Koten, *J. Chem. Soc., Chem. Commun.*, 1993, 1317; (*e*) A. Sen, *Acc. Chem. Res.*, 1993, **26**, 303; (*f*) R. van Asselt, E. E. C. G. Gielens, R. E. Rülke, K. Vrieze and C. J. Elsevier, *J. Am. Chem. Soc.*, 1994, **116**, 977; (*g*) R. E. Rülke, V. E. Kaasjager, D. Kliphuis, C. J. Elsevier, P. W. N. M. van Leeuwen and K. Vrieze, *Organometallics*, 1996, **15**, 668.

7 G. P. C. M. Dekker, C. J. Elsevier, K. Vrieze, P. W. N. M. van Leeuwen and C. F. Roobeek, *J. Organomet. Chem.*, 1992, **430**, 357.

Received in Liverpool, UK, 9th February 1998; 8/01158C

Triplet state photophysics in an aryleneethynylene π-conjugated polymer

Keith A. Walters, Kevin D. Ley and Kirk S. Schanze*†

Department of Chemistry, University of Florida, Gainesville, FL 32611-7200, USA

The triplet state photophysics of a polyaryleneethynylene π-conjugated polymer and a related model compound are investigated with various techniques, including laser flash photolysis and time-resolved thermal lensing (TRTL).

The photophysical and photochemical properties of π-conjugated polymers have been of significant recent interest.[1] Although most work on the photophysics of π-conjugated polymers has focused on the $^1\pi,\pi^*$ manifold, considerable evidence suggests that $^3\pi,\pi^*$ excitons are also involved in their rich photochemistry.[2–5] Unfortunately, owing to the absence of phosphorescence in most π-conjugated polymers[2] little is known about the absolute energies and yields of the triplets produced by direct excitation.

We recently initiated a photophysical study of aryleneethynylene-based π-conjugated polymers that contain a photoactive transition metal chromophore in the π-conjugated backbone.[6,7] A primary objective of this work is to understand the interaction between backbone-based $^1\pi,\pi^*$ and $^3\pi,\pi^*$ excited states and metal complex-based $d \rightarrow \pi^*$ charge transfer excitations. However, in order to pursue this line of investigation in the metal–organic polymers, it is necessary to have a firm understanding of the properties of the $^1\pi,\pi^*$ and $^3\pi,\pi^*$ excited states of the all-organic polymers. Here, we report the results of a detailed photophysical study which compares the photophysical properties of the singlet and triplet manifolds of aryleneethynylene polymer **P0** and model compound **1** in dilute THF solution (Scheme 1).‡

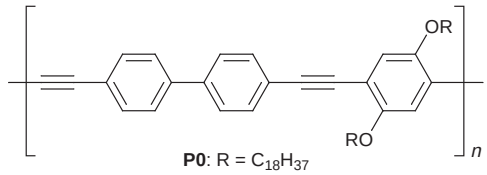

P0: R = $C_{18}H_{37}$

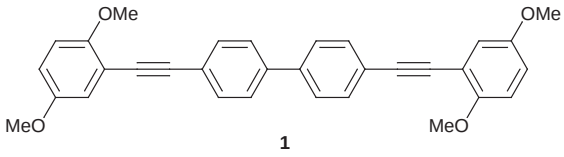

1

Scheme 1

Pulsed laser excitation (355 nm, 10 ns FWHM, 4 mJ pulse^{-1}) of **1** and **P0** affords a long lived transient [τ(**1**) = 142 μs, τ(**P0**) = 169 μs§], which is assigned to a $^3\pi,\pi^*$ state. The triplet state difference absorption spectra of **1** and **P0** (Fig. 1) are characterized by bleaching of the ground state π,π^* absorption band [λ_{max}(**1**) = 360 nm, λ_{max}(**P0**) = 410 nm] and a broad (triplet–triplet) absorption band that extends to longer wavelengths. Interestingly, the difference spectra of **1** and **P0** are remarkably similar, except that the bleach and absorption bands are red-shifted in the polymer. The qualitative similarity in the triplet–triplet absorption spectra implies that the electronic structure of the triplet state is similar in the model and polymer.

In order to determine the triplet energies of **1** and **P0** (E_T), Stern–Volmer quenching studies were carried out with a series

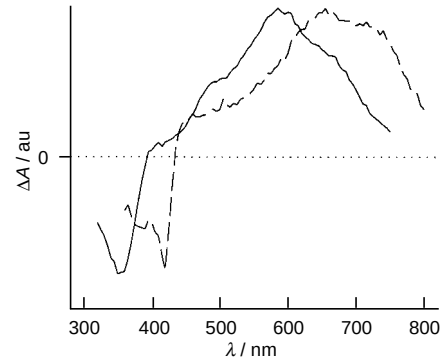

Fig. 1 Triplet state difference absorption spectra of (solid line) **1** and (dashed line) **P0** in degassed THF solution

of triplet acceptors of varying energy.[8,9]¶ Triplet quenching rate constants (k_q) were obtained from Stern–Volmer analysis of the observed triplet decay lifetimes in vacuum degassed THF solutions as a function of quencher concentration. The triplet energies were then estimated by fitting the experimental Sandros plots (Fig. 2)[10] with a Marcus equation that is appropriate for bimolecular reactions which occur at or near diffusion control,[11,12]

$$k_q = \frac{k_d}{1 + \exp(\Delta G/RT) + (k_{-d}/k_{en}^0)\exp(\Delta G^{\ddagger})} \quad (1a)$$

$$\Delta G^{\ddagger} = \Delta G + \frac{\lambda}{\ln 2}\ln\left\{1 + \exp[-(\Delta G \ln 2)/\lambda]\right\} \quad (1b)$$

where k_d and k_{-d} are the rate constants for forward and reverse diffusion in solution, k_{en}^0 is a pre-exponential factor, λ is the reorganizational energy and $\Delta G = (E^{00}_{Acceptor} - E_T)$. By using parameters derived from a previous study[13] ($k_d = 1.0 \times 10^{10}$

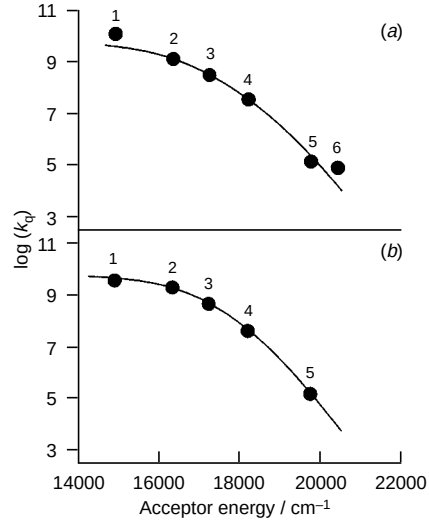

Fig. 2 Sandros plots for (*a*) **P0** and (*b*) **1**. Points are experimentally determined rate constants with various triplet energy acceptors,¶ and fitted lines are calculated as explained in the text.

Table 1 Photophysical properties of model compound **1** and polymer **P0**[a]

Compound	τ_{fl}/ns	Φ_{fl}[b]	E_S/cm^{-1} (kcal mol^{-1})	λ[c]/cm^{-1}	E_T[c]/cm^{-1} (kcal mol^{-1})	Φ_T	10^{-8} k_r/s^{-1}	10^{-8} k_{nr}/s^{-1}	10^{-8} k_{isc}/s^{-1}
1	1.15	0.90	24 200 (69.2)	1000	17 700 (50.6)	$\leqslant$0.10[d,e]	7.8	$\leqslant$0.87	$\leqslant$0.87
P0	0.53	0.60[f]	23 100 (66.0)	1200	17 500 (51.2)	0.12[e]	11	5.7	2.3

[a] THF solutions at 298 K. [b] Fluorescence quantum yields determined using 9,10-dicyanoanthracene (DCA) and perylene as actinometers (Φ_{DCA}^{EtOH} = 0.89, $\Phi_{Perylene}^{EtOH}$ = 0.89). [c] Values based on a Marcus fit to quenching data as described in text. [d] Upper limit. [e] See footnote §. [f] See foonote **.

M^{-1} s^{-1}, k'_{-d} = 2.0 × 10^{10} M^{-1} s^{-1}, k_{en}^0 = 5 × 10^{10} s^{-1}), best fits of the Sandros plots for **1** and **P0** were attained by varying λ and E_T in eqn. (1). These values are listed in Table 1, and plots of the fitted quenching data are shown in Fig. 2. Surprisingly, E_T for the model compound and the polymer is the same within experimental error (±5%).

A second objective of the present study was to determine the triplet yields (Φ_T) for **1** and **P0**. However, in order to determine this parameter it is necessary to know the fluorescence quantum yields (Φ_{fl}). Therefore, fluorescence spectra of **1** and **P0** were obtained [λ_{max}(**1**) = 413 nm, λ_{max}(**P0**) = 433 nm], and Φ_{fl} values were determined from the integrated fluorescence spectra (Table 1).[14]‖ Fluorescence lifetimes (τ_{fl}) for **1** and **P0** are also listed in Table 1. Next, the triplet yield (Φ_T) for **P0** was determined by time-resolved thermal lensing (TRTL).[15,16] In this method, Φ_T is derived from the ratio of the 'slow' and 'total' heat deposition signals (U_{slow} and U_{total}, respectively) after correcting for the energy of the pump laser ($E_{h\nu}$) and the fluorescence quantum yield,

$$U_{slow}/U_{total} = E_T\Phi_T/(E_{h\nu} - E_S\Phi_{fl}) \quad (2)$$

where E_S is the energy of the singlet state (Table 1). The U_{slow}/U_{total} ratio of a vacuum degassed THF solution of **P0** was determined to be 0.15, and the triplet yield calculated with eqn. (2) is listed in Table 1.** Unfortunately, Φ_T for **1** could not be measured with TRTL owing to strong triplet–triplet absorption at the thermal lensing probe wavelength (633 nm). However, the experimentally derived Φ_{fl} for **1** (0.90) provides an upper limit for Φ_T ($\leqslant$0.1).**

The photophysical characterization of the singlet and triplet states of **1** and **P0** allows us to assess the effect that the extended π-conjugation in the polymer has on its triplet state properties. It is surprising that E_T is the same for the polymer and model compound. However, the more important parameter is the singlet–triplet splitting energy (E_{ST}), which is defined as $E_S - E_T$. Interestingly, E_{ST} is lower by almost 1000 cm^{-1} in **P0** compared to **1** (5600 *vs.* 6500 cm^{-1}). The lower E_{ST} indicates that the electron exchange energy is smaller in the polymer,[17] which presumably is due to the fact that the delocalization of the LUMO (and/or the HOMO) for the $\pi \rightarrow \pi^*$ transition is greater in **P0** than in **1**. Moreover, it is of interest that the experimentally determined E_{ST} for **P0** is comparable to values calculated using semi-empirical MO theory.[18,19]

The rates of radiative decay, non-radiative decay and intersystem crossing (k_r, k_{nr} and k_{isc}, respectively) for the $^1\pi,\pi^*$ state of **1** and **P0** have been determined by using the experimental Φ_{fl}, τ_{fl} and Φ_T values (Table 1). First, note that k_r is comparable in **1** and **P0**. This is not surprising given that the orbital basis and transition dipole for radiative transitions are similar in the model and the polymer. By contrast, k_{nr} and k_{isc} are significantly larger in **P0** than in **1**. The larger non-radiative decay rate in the polymer may arise from 'defect sites' (*e.g.* unreacted end groups and/or defects in the polymer backbone) that quench the $^1\pi,\pi^*$ exciton. The larger (effective) intersystem crossing rate in **P0** may arise from the smaller E_{ST} value.

We gratefully acknowledge the National Science Foundation (Grant No. CHE-9401620) for support of this work.

Notes and References

† E-mail: kschanze@chem.ufl.edu

‡ **P0** was synthesized *via* a Pd-mediated cross-coupling reaction of the polymer subunits (see ref. 7 for complete synthetic details). *Selected characterization*: **P0**: GPC ($CHCl_3$, polystyrene standards) M_n = 65.2 kD, M_w = 209.2 kD (PDI = 3.2). ^{1}H NMR ($CDCl_3$) δ 0.87 (bt, t), 1.24 (br, s), 1.56 (br, m), 1.84 (br, m), 4.04 (br, t), 6.92 (br, s), 7.0 (br, s), 7.62 (br, s). ^{13}C NMR ($CDCl_3$) δ 14.1, 22.7, 26.1, 29.4, 29.7, 32.0, 69.7, 87.0, 94.8, 114.0, 116.9, 122.8, 126.8, 132.1, 140.0, 153.7. **1**: ^{1}H NMR ($CDCl_3$) δ 3.79 (s, 6 H, OCH_3), 3.89 (s, 6 H, OCH_3), 6.86 (m, 4 H, phenyl), 7.08 (d, 2 H, phenyl), 7.63 (d, 8 H, biphenyl). ^{13}C NMR ($CDCl_3$) δ 55.8, 56.5, 86.7, 93.2, 112.2, 112.9, 115.8, 118.0, 122.7, 126.7, 132.1, 139.9, 153.2, 154.5.

§ In ref. 6 we reported the triplet lifetime for a sample of **P0** in Ar-purged THF (τ_T = 4 μs). In that study the lifetime was suppressed due to quenching by residual oxygen. The triplet lifetimes reported herein are for samples that were freeze–pump–thaw degassed five times and sealed at 10^{-5} Torr. It is conceivable that even under these conditions the triplet lifetime is suppressed by oxygen quenching.

¶ Triplet acceptors (see Fig. 2): 1, anthracene; 2, [4,4′-bis(carboethoxy)-2,2′-bipyridyl]Re(CO)$_3$Cl; 3, *trans*-stilbene: 4, (2,2′-bipyridyl)Re(CO)$_3$Cl; 5, biacetyl; 6, *p*-terphenyl.

‖ In ref. 6 we reported the fluorescence quantum yield for **P0** in Ar-purged THF (Φ_{fl} = 0.28). The sample of **P0** used in that study was structurally equivalent to that used in the present study, but it had a substantially lower molecular weight (M_n = 13.5 kD, M_w = 37.4 kD). The higher molecular weight of the sample of **P0** used in the present study accounts for the larger fluorescence yield reported herein.

** The Φ_T values for **P0** and **1** were confirmed using photoacoustic calorimetry [Φ_T (**P0**) = 0.12, Φ_T (**1**) = 0.05].

1 L. J. Rothberg, M. Yan, F. Papadimitrakopoulos, M. E. Galvin, E. W. Kwock and T. M. Mille, *Synth. Met.*, 1996, **80**, 41 and references therein.
2 B. Xu and S. Holdcroft, *Adv. Mater.*, 1994, **6**, 325.
3 M. S. A. Abdou, F. P. Orfino, Y. Son and S. Holdcroft, *J. Am. Chem. Soc.*, 1997, **119**, 4518.
4 R. D. Scurlock, B. Wang, P. R. Ogilby, J. R. Sheats and R. L. Clough, *J. Am. Chem. Soc.*, 1995, **117**, 10 194.
5 H. F. Wittman, R. H. Friend, M. S. Khan and J. Lewis, *J. Chem. Phys.*, 1994, **101**, 2693.
6 K. D. Ley, C. E. Whittle, M. D. Bartberger and K. S. Schanze, *J. Am. Chem. Soc.*, 1997, **119**, 3423.
7 K. D. Ley and K. S. Schanze, *Coord. Chem. Rev.*, in press.
8 S. L. Murov, I. Carmichael and G. L. Hug, *Handbook of Photochemistry*, Marcel Dekker, New York, 1993, p. 54.
9 L. A. Worl, R. Duesing, P. Chen, L. D. Ciana and T. J. Meyer, *J. Chem. Soc., Dalton Trans.*, 1991, 849.
10 K. Sandros, *Acta Chem. Scand.*, 1964, **18**, 2355.
11 V. Balzani and F. Bolletta, *J. Am. Chem. Soc.*, 1978, **100**, 7404.
12 V. Balzani, F. Bolletta and F. Scandola, *J. Am. Chem. Soc.*, 1980, **102**, 2152.
13 Y. Wang and K. S. Schanze, *Inorg. Chem.*, 1994, **33**, 1354.
14 G. A. Crosby and J. N. Demas, *J. Phys. Chem.*, 1971, **75**, 991.
15 S. E. Braslavsky and G. E. Heibel, *Chem. Rev.*, 1992, **92**, 1381.
16 R. T. Cambron and J. M. Harris, *J. Phys. Chem.*, 1993, **97**, 13 598.
17 S. P. McGlynn, F. J. Smith and G. Cilento, *Photochem. Photobiol.*, 1964, **3**, 269.
18 J. W. Blatchford, T. L. Gustafson and A. J. Epstein, *J. Chem. Phys.*, 1996, **105**, 9214.
19 D. Beljonne, H. F. Wittmann, A. Köhler, S. Graham, M. Yonnus, J. Lewis, P. R. Raithby, M. S. Khan, R. H. Friend and J. L. Brédas, *J. Chem. Phys.*, 1996, **105**, 3868.

Received in Columbia, MO, USA, 15th December 1997; 7/09064A

Stereoselective conversion of 2′,3′-dideoxydidehydro carbocyclic nucleosides into 2′-deoxy carbocyclic nucleosides

James V. Barkley,[a] Anupma Dhanda,[a] Lars J. S. Knutsen,[b]†‡ May-Britt Nielsen,[a] Stanley M. Roberts*[a]§ and David R. Varley[c]

[a] *Department of Chemistry, Liverpool University, Liverpool, UK L69 7ZD*
[b] *Novo-Nordisk A/S, Novo Nordisk Park, DK-2760, Malov, Denmark*
[c] *Department of Chemistry, Exeter University, Exeter, Devon, UK EX4 4QD*

Treatment of 2′,3′-dideoxydidehydro carbocyclic nucleosides 5–9 with *N*-bromoacetamide in AcOH gives bromoesters 10–14 with good stereocontrol: debromination and hydrolysis furnishes 2′-deoxy carbocyclic nucleosides, *e.g.* 22.

The preparation of 2′,3′-dideoxydidehydro carbocyclic nucleosides **1** (Scheme 1) has been the subject of a great deal of attention, owing to the biological activity of carbovir and related compounds.[1] The conversion of the readily-available alkenes of general stucture **1** into structurally more complex carbocyclic nucleosides **2** and 2′-deoxy carbocyclic nucleosides **4** has been fraught with difficulty. For example, bis-hydroxylation of compounds **1** tends to give an equimolar mixture of isomers corresponding to *ribo*- and *lyxo*-sugars **2** and **3**.[2] The preference for the formation of the carbocyclic *ribo*nucleoside on steric grounds is countered by a stabilizing Cieplak effect which favours formation of the *lyxo* analogues.[3]

Conversion of *ribo*-carbocyclic nucleosides **2** into 2′-deoxy *ribo*-carbocyclic nucleosides **4** [path (*b*)] through reaction of the diol with AcBr in MeCN and subsequent hydrodehalogenation is marred by the formation of the desired bromohyrins corresponding to the *ara*- and isomeric *xylo*-bromohydrins in an unfavourable 1 : 5 ratio.[4]

Direct conversion of carbocyclic nucleosides of type **1** into deoxy *ribo* systems of type **4** [path (*c*)] by hydroboration was investigated by Deardorff *et al.*;[5] unfortunately the 3′-hydroxy and the 2′-hydroxy compounds were both obtained, in a 2 : 1 ratio.

Herein we report a novel stereoselective method for the transformation of alkenes **1** into the corresponding alcohols **4**.

Most of the starting materials for this study (**5**, **6**, **8** and **9**) were prepared from (±)-*cis*-1-acetoxy-2-(acetoxymethyl)-cyclopent-4-ene; a typical procedure is described below. Compound **7** was prepared from compound **5**.¶

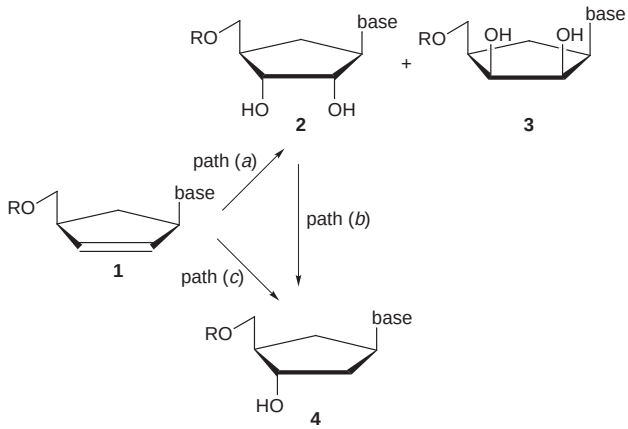

Scheme 1

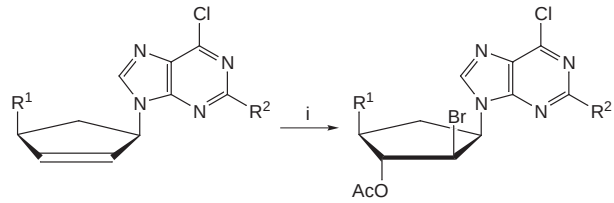

5	$R^1 = CH_2OAc$, $R^2 = NH_2$	**10**
6	$R^1 = CH_2OAc$, $R^2 = H$	**11**
7	$R^1 = CH_2OAc$, $R^2 = Cl$	**12**
8	$R^1 = CH_2OCPh_3$, $R^2 = NH_2$	**13**
9	$R^1 = CH(OAc)CH_2OAc$, $R^2 = NH_2$	**14**

Scheme 2 *Reagents and conditions*: i, NBS or *N*-bromoacetamide, AgOAc, AcOH, 18 h, room temp.

Treatment of the cyclopentene derivative **5** with NBS or *N*-bromoacetamide and AgOAc in AcOH afforded bromoacetate **10** as the sole product in 68% yield (Scheme 2). This bromoester was recrystallized and the stereochemistry confirmed by X-ray crystallography (Fig. 1).‖

Similarly, compounds **6**–**8** produced the corresponding haloesters **11**–**13** in 47–69% yield.** In the latter case the NMR spectrum of the crude product, besides the major product **13**, gave evidence of a few percent of an isomeric product, in too small an amount to isolate. Treatment of the diester **9** under the standard reaction conditions afforded the expected product **14** (49%) [with spectroscopic properties in accord with the assignments for compounds **10**–**13** and an isomeric substance (13%)]. We tentatively assign a 2′-acetoxy-3′-bromo structure to the minor product on the basis of NMR spectroscopy.

The conversion of the alkenes **5**–**9** into the bromoesters **10**–**14** is reminiscent of the conversion of the cyclopentene

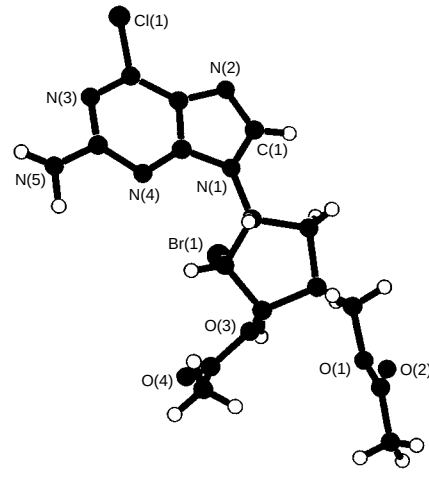

Fig. 1 X-Ray structure of compound **10**

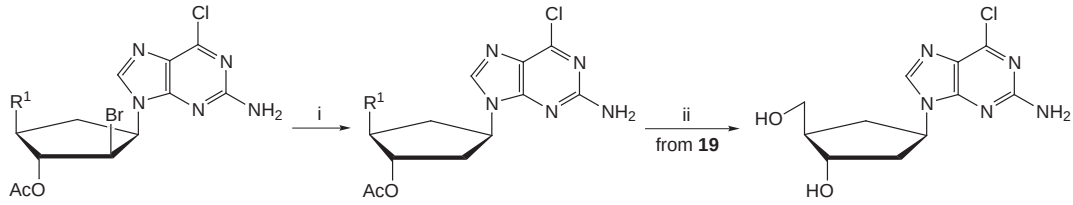

10 $R^1 = CH_2OAc$ **19**
14 $R^1 = CH(OAc)CH_2OAc$ **20**
18 $R^1 = CH_2OH$ **21**

22

Scheme 4 *Reagents and conditions*: i, Bu^n_3SnH, AIBN, THF, heat, 3–7 h (68–92%); ii, K_2CO_3, MeOH, 2 h (96%)

derivative **15** into the dihalides **16** and **17** (ratio 8 : 1) (Scheme 3), in that in both cases the major product is formed *via* the intermediacy of a *syn*-halonium ion.[6] However, the preferential formation of compound **16** was explained by a proposed stabilisation of the *syn*-iodonium ion by the adjacent hydroxy group, a phenomenon which is clearly impossible in our cases. Instead we believe that the formation of the *syn*- and *anti*-bromonium ions are reversible processes and only on formation of the *syn*-bromonium ion is attack by the nucleophile possible, from the more exposed face and distant from the heteroatom bonded to C-1′.

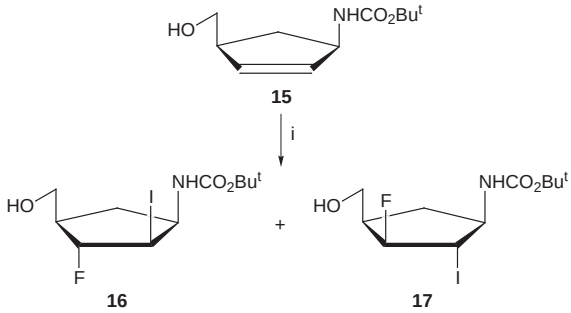

Scheme 3 *Reagents and conditions*: i, *N*-iodosuccinimide, tetrabutylammonium dihydrogen trifluoride, CH_2Cl_2

Detritylation of bromoester **13** was accomplished using aq. AcOH to furnish the alcohol **18** in 66% yield. Treatment of compounds **10**, **14** and **18** with tri-*n*-butyltin hydride in hot THF furnished the nucleoside analogues **19**–**21** (Scheme 4).‡‡ Methanolysis of the diester **19** provided the 2′-deoxycarbocyclic nucleoside in almost quantitative yield.

In summary, the stereocontrolled addition of Br/OAc to dideoxydidehydro carbocyclic nucleosides give facile access to 2′-bromo-2′-deoxyribo carbocyclic nucleosides.[7]

Novo-Nordisk A/S provided studentships for A. D., M.-B. N. and D. V. R. and this financial support is gratefully acknowledged.

Notes and References

† Present address, Cerebrus Ltd., Oakdene Court, 613 Reading Road, Winnersh, Wokingham, UK RG41 5UA.
‡ E-mail: l.knutsen@cerebrus.ltd.uk
§ E-mail: sj11@liverpool.ac.uk

¶ *Synthesis* of **5**. 2-Amino-6-chloro-9*H*-purine (264 mg, 1.56 mmol) and NaH (60% dispersed in mineral oil, 68 mg, 1.71 mmol) were dissolved in anhydrous DMF (7.0 ml) and stirred for 10 min at room temperature and at 50 °C for 10 min. The reaction mixture was added to a suspension of (±)-(1*R*,2*R*)-1-acetoxy-2-(acetoxymethyl)cyclopent-4-ene (339 mg, 1.71 mmol) and tetrakis(triphenylphosphine)palladium (180 mg, 0.156 mmol) in DMF (7.0 ml) using a cannula, rinsing with anhydrous THF (3 × 2.0 ml). The reaction was excluded from light and stirred for 3 h at 50 °C. The reaction mixture was then cooled to room temperature. Water (25 ml) was added and the mixture was extracted wtih CH_2Cl_2 (4 × 50 ml). The combined organic layers were dried with $MgSO_4$ and the solvent was evaporated *in vacuo* to give a crude yellow oil. The oil was purified by column chromatography on silica gel eluting with CH_2Cl_2–EtOH (19 : 1) giving **5** (50% yield) as a clear oil.

Synthesis of **7**. Compound **5** (224 mg, 0.728 mmol) was dissolved in CH_2Cl_2 (8 ml) and the solution was cooled to 0 °C. Me_3SiCl (276 μl, 2.184 mmol) was added followed by isopentyl nitrite (292 μl, 2.184 mmol) which was added slowly to maintain the temperature at 0 °C. The reaction mixture was stirred for 2 h at 0 °C and for 5 h at room temperature. Water (5 ml) was added and the mixture was extracted with CH_2Cl_2 (3 × 10 ml). The combined organic layers were concentrated *in vacuo* to give a crude yellow oil. The oil was purified by column chromatography on silica gel eluting with EtOAc–light petroleum (2 : 1) giving **7** (60% yield) as a clear oil.

‖ *Crystal data* for **10**: $C_{15}H_{17}BrClN_5O_4$, M = 446.69, colourless prism, monoclinic, $P2_1/n$, 0.15 × 0.20 × 0.25 mm, a = 15.597(5), b = 7.077(2), c = 17.178(2) Å, β = 96.13(2)°, V = 1885.4 Å^3, T = −120 °C, Z = 4, μ(Mo-Kα) = 23.29 cm^{-1}; 3769 reflections measured, 3630 unique, R = 0.055, R_w = 0.080. CCDC 182/834.

** *Selected data* for **11**: δ_H(300 MHz; $CDCl_3$) 2.08 (s, 3 H, C*H*$_3$ of Ac), 2.17 (s, 3 H, C*H*$_3$ of Ac), 2.55 (m, 3 H, 2 × H-6′ and H-4′), 4.35 (m, 2 H, 2 × H-5′), 4.79 (m, 1 H, H-2′), 5.13 (m, 1 H, H-1′), 5.40 (m, 1 H, H-3′), 8.26 (s, 1 H, H-2), 8.70 (s, 1 H, H-8); δ_c(75 MHz; $CDCl_3$) 20.8 (CH_3, *C*H$_3$ of Ac), 20.9 (CH_3, *C*H$_3$ of Ac), 30.1 (CH_2, C-6′), 42.5 (CH, C-4′), 55.1 (CH, C-2′), 56.2 (CH, C-1′), 64.9 (CH_2, C-5′), 80.5 (CH, C-3′), 143.6 (CH), 150.8 (C), 151.6 (C), 152.0 (CH), 169.5 (C, C=O) and 170.7 (C, C=O).

†† *Selected data* for **19**: δ_H(400 MHz; $CDCl_3$) 1.98 (m, 1 H, H-6′), 2.08 (s, 3 H, C*H*$_3$ of Ac), 2.09 (s, 3 H, C*H*$_3$ of Ac), 2.30 (dd, 1 H, *J* 13 and 8, H-6′), 2.52–2.62 (m, 3 H, H-1′ and H-2′), 4.30 (m, 2 H, H-5′), 4.90 (m, 1 H, H-1′), 5.22 (m, 3 H, H-3′ and NH_2), 7.78 (s, 1 H, H-1′); δ_c(100 MHz; $CDCl_3$) 20.8 (CH_3, *C*H$_3$ of Ac), 21.1 (CH_3, *C*H$_3$ of Ac), 33.0 (CH_2, C-6′), 37.3 (CH, C-2′), 43.6 (CH, C-4′), 54.1 (CH, C-1′), 64.8 (CH, C-5′), 75.4 (CH, C-4′), 126.0 (CH, C-5), 140.9 (C, C-8), 151.6 (C, C-4), 153.4 (C, C-6), 158.7 (C, C-2), 170.3 (C, C=O) and 171.0 (C, C=O).

1 V. E. Marquez, *Adv. Antiviral Drug Dev.*, 1996, **2**, 89; H. F. Olivo and J. Yu, *Tetrahedron: Asymmetry*, 1997, **8**, 3785; *J. Chem. Soc., Perkin Trans. 1*, 1998, 391 and references therein.
2 S. M. Roberts and K. A. Shoberu, *J. Chem. Soc., Perkin Trans. 1*, 1991, 2605; E. A. Saville-Jones, S. D. Lindell, N. S. Jennings, J. C. Head and M. J. Ford, *J. Chem. Soc., Perkin Trans. 1*, 1991, 2603; C. G. Palmer, R. McCague, G. Ruecroft, S. Savage, S. J. C. Taylor and C. Ries, *Tetrahedron Lett.*, 1996, **37**, 4601; see also V. K. Aggarwal and N. Monteiro, *J. Chem. Soc., Perkin Trans. 1*, 1997, 2531; S. E. Ward, A. B. Holmes and R. McCague, *Chem. Commun.*, 1997, 2085; B. M. Trost, R. Marsden and S. D. Guile, *Tetrahedron Lett.*, 1997, **38**, 1707.
3 N. Katagiri, Y. Ito, K. Kitano, A. Toyota and C. Kaneko, *Chem. Pharm. Bull.*, 1994, **42**, 2653; see also G. Poli, *Tetrahedron Lett.*, 1989, **30**, 7385.
4 R. Marumoto, Y. Yoshioka, Y. Furukawa and M. Honjo, *Chem. Pharm. Bull.*, 1976, **24**, 2624.
5 D. R. Deardorff, R. G. Linde, A. M. Martin and M. J. Shulman, *J. Org. Chem.*, 1989, **54**, 2759.
6 A. Toyota, Y. Ono and C. Kaneko, *Tetrahedron Lett.*, 1995, **36**, 6123.
7 The corresponding nucleosides have been prepared; see L. J. S. Knutsen, *Nucleosides Nucleotides*, 1992, **11**, 961; it has been reported that 2′-bromo-2′-deoxynucleosides show enhanced stability to 3′-exonucleases: M. Aoyagi, Y. Ueno, A. Ono and A. Matsuda, *Bioorg. Med. Chem. Lett.*, 1996, **6**, 1573.

Received in Cambridge, UK, 3rd March 1998; 8/01759J

Phosphorus complex of corrole

Roberto Paolesse,*[a] Tristano Boschi,[a] Silvia Licoccia,[a] Richard G. Khoury[b] and Kevin M. Smith[b]†

[a] *Dipartimento di Scienze e Tecnologie Chimiche, Università di Roma Tor Vergata, Roma, 00133, Italy*
[b] *Department of Chemistry, University of California, Davis, CA 95616, USA*

Reaction of 8,12-diethyl-2,3,7,13,17,18-hexamethylcorrole (1) with $POCl_3$ in pyridine affords the first non-metal derivative of corrole; in this compound, 2, the phosphorus is in a pentavalent state and is different from analogous complexes of porphyrins.

Non-porphyrin polypyrrolic macrocycles represent a novel field of research which has experienced impressive expansion in the last few years.[1] These compounds are particularly intriguing for both theoretical and experimental reasons. For example, they can enable studies of the way in which skeletal variations influence the aromaticity and the chemical properties of the macrocycles, thereby opening potential applications of these molecules in different fields, ranging from catalysis to biomedical sciences.

Among porphyrin analogues, corrole (*e.g.* **1**) was one of the first examples to be reported in the literature; it was synthesized

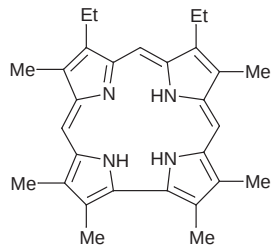

1

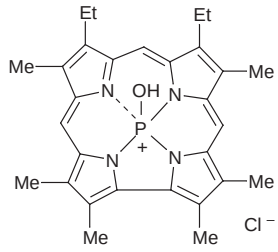

2

more than 30 years ago by Johnson and Kay during their attempts to approach the corrin nucleus of vitamin B_{12}.[2] But recent investigations using the corrole macrocycle have revealed interesting differences in its coordination behavior compared with the analogous porphyrin complexes. Corrole, for example, is able to stabilize high oxidation states for coordinated metals, and to retain a planar conformation even when the peripheral positions are fully substituted.[1a,b] Despite these interesting properties, the coordination chemistry of corrole is substantially limited to the first row transition metals; expansion of the so-called 'periodic table' of metallocorrolates should allow researchers to study, in more detail, the coordination behavior of this macrocycle. In particular, coordination of phosphorus can be intriguing due to the non-metal character of this element and because it is, in its pentavalent state, the smallest ion so far coordinated to a porphyrin.[3] Herein we report the synthesis and characterization of the first example of a phosphorus corrole derivative.

Reaction of 8,12-diethyl-2,3,7,13,17,18-hexamethylcorrole (**1**; H_3EMC)[2] with $POCl_3$ in pyridine at room temperature showed an immediate spectrophotometric change, with the formation of the spectrum of the characteristic corrole monocation.[4] When the mixture was heated at reflux the optical spectrum quickly changed (indicating the formation of a complex), with the complete disappearance of the absorbance characteristic of the corrole; Fig. 1 shows the optical spectra of the corrole monocation and the phosphorus complex. Evaporation of the solvent and recrystallization from CH_2Cl_2–hexane afforded a purple powder. In complexes with porphyrins, phosphorus has been reported to be hexacoordinated in a +V oxidation state;[3] in the case of octaethylporphyrin a transient +III state has been reported to be an intermediate during the metallation reaction.[3] In the present case of corrole, the electronic absorption spectrum is similar to those of other main group metallocorrolates.[5] By analogy with porphyrins it can be classified as 'normal',[6] thereby indicating the presence of the +V oxidation state for the coordinated phosphorus.

The ^1H NMR spectrum of the phosphorus corrole was also typical of a metallocorrolate, with the absence of internal NH resonances and the expected pattern for peripheral substituents. ^{31}P NMR spectroscopy showed a resonance for coordinated phosphorus at −102.5 ppm (relative to external H_3PO_4), which is significantly different from phosphorus complexes of porphyrins in which the phosphorus signal is at *ca.* −200 ppm.[7] This feature indicated that the diamagnetic ring current effect is less influential in determining the phosphorus resonance in the corrole derivative compared with porphyrin complexes. This difference can be attributed to two major factors: (i) the diminished aromatic character of corrole relative to porphyrin, and/or (ii) a different coordination geometry of phosphorus in the corrole complex. Both ^1H and ^{13}C NMR spectra ruled out the first hypothesis because resonances of the corrole derivative have almost the same chemical shifts as do the analogous porphyrinates.[8] A different coordination geometry seems more likely because the EI mass spectrum of the corrole complex showed a molecular peak at *m/z* 483, indicating the presence of only one ligand at an axial position. Analogous phosphorus porphyrinates are hexacoordinated.[3]

X-Ray characterization‡ performed on a single crystal of the phosphorus corrolate **2** allowed its unambiguous structural identification. The molecular structure is shown in Fig. 2. The phosphorus atom exhibits pentacoordinated geometry, lying more than 0.4 Å out of the mean corrole plane toward the oxygen atom of the axial hydroxy group. The P–O bond distance of 1.531 Å can be attributed to a single bond and is similar to the observed P–O distance in an analogous porphyrin complex.[3] The P–N bond lengths average 1.80 Å. These lengths

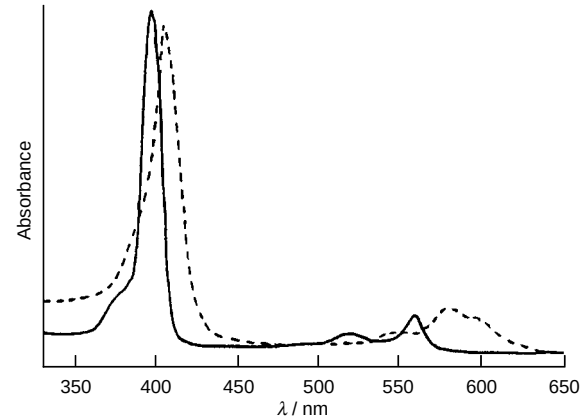

Fig. 1 Optical spectra, in CH_2Cl_2, of $[H_4EMC]^+$ (– – –), and [(EMC)-P(OH)]Cl (**2**), (——)

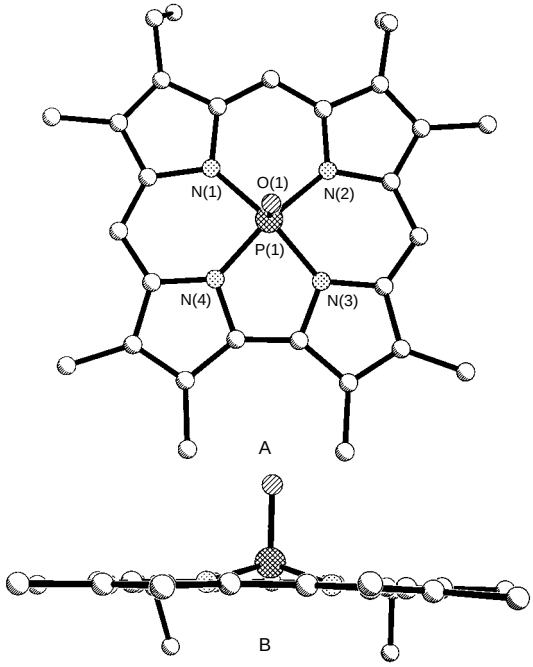

Fig. 2 Molecular structure‡ of [(EMC)P(OH)]Cl (**2**). A, top view; B, edge on view. The chloride counterion is omitted.

are shorter than those measured in any other metal complexes of this macrocycle[1a,b] and are not equivalent, as usual for metallocorrolates. Contrary to the situation in porphyrin derivatives the phosphorus corrolate macrocycle is almost planar, the mean plane deviation of the 23 core atoms being 0.0245 Å. The cationic nature of the macrocycle is confirmed by the presence of a chloride counterion.

The phosphorus complex reported herein is the first non-metal derivative of corrole; moreover, it represents a further example of different coordinative behavior of this macrocycle compared with the analogous and more ubiquitous porphyrin macrocycle. We are presently investigating the axial chemistry of this complex, and these studies will be the subject of a full paper.

This work was supported by Murst and CNR (Italy/USA Bilateral Project No. 95.01178) and by the National Science Foundation (CHE-96-23117).

Notes and References

† E-mail: kmsmith@ucdavis.edu

‡ *Crystal Data* for **2** ($C_{29}H_{32}N_4PO)(H_2O)(Cl)$: Crystals of **2** were grown from a mixture of CH_2Cl_2 and *c*-C_6H_6. A single parallel-piped crystal was selected with dimensions 0.20 × 0.14 × 0.10 mm. The unit cell was triclinic, space group $P\bar{1}$ with cell dimensions a = 11.038(3), b = 11.749(3), c = 12.031(3) Å, α = 96.50(2), β = 101.77(2), γ = 116.40(2)°, V = 1330.7(6) Å^3 and Z = 2 (M = 537.02, ρ_{calc} = 1.340 g cm^{-3}, μ = 2.112 mm^{-1}). Of 3778 reflections measured, 3513 were independent and 3054 had $I > 2\sigma$ (R_{int} = 0.044); number of parameters = 343. Final R factors were $R1$ = 0.0543 (based on observed data) and w$R2$ = 0.1957 (based on all data). CCDC 182/832.

1 For recent reviews, see: (*a*) S. Licoccia and R. Paolesse, in *Metal Complexes with Tetrapyrrole Ligands III*, ed. J. W. Buchler, Springer-Verlag, Berlin, 1995; (*b*) J. L. Sessler and S. J. Weghorn, in *Expanded, Contracted & Isomeric Porphyrins*, Pergamon Press, Oxford, 1997; (*c*) A. Jasat and D. Dolphin, *Chem. Rev.*, 1997, **97**, 2267; (*d*) E. Vogel, *Pure Appl. Chem.*, 1996, **68**, 1355; (*e*) E. Vogel, *J. Heterocycl. Chem.*, 1996, **33**, 1461.

2 A. W. Johnson and I. T. Kay, *J. Chem. Soc.*, 1965, 1620.

3 P. Sayer, M. Gouterman and C. R. Connell, *J. Am. Chem. Soc.*, 1977, **99**, 1082; C. J. Carrano and M. Tsutsui, *J. Coord. Chem.*, 1977, **7**, 79; S. Mangani, E. F. Meyer, D. L. Cullen, M. Tsutsui and C. J. Carrano, *Inorg. Chem.*, 1983, **22**, 1858.

4 R. Grigg, in *The Porphyrins*, ed. D. Dolphin, Academic Press, New York, 1978, vol. II, p. 327.

5 R. Paolesse, S. Licoccia and T. Boschi, *Inorg. Chim. Acta*, 1990, **178**, 9.

6 M. Gouterman, in *The Porphyrins*, ed. D. Dolphin, Academic Press, New York, 1978, vol. III , p. 1.

7 T. Barbour, W. J. Belcher, P. J. Brothers, C. E. F. Rickard and D. C. Ware, *Inorg. Chem.*, 1992, **31**, 746.

8 T. R. Janson and J. J. Katz, in *The Porphyrins*, ed. D. Dolphin, Academic Press, New York, 1978, vol IV, p. 1.

Received in Corvallis, OR, USA, 23rd February 1998; 8/01544I

Rotational oscillation of two interlocked porphyrins in cerium bis(5,15-diarylporphyrinate) double-deckers

Kentaro Tashiro, Takashi Fujiwara, Katsuaki Konishi and Takuzo Aida*†

Department of Chemistry and Biotechnology, Graduate School of Engineering, The University of Tokyo, 7-3-1 Hongo, Bunkyo-ku, Tokyo 113-8656, Japan

Dynamic NMR coupled with racemization studies on chiral cerium bis(5,15-diarylporphyrinate) double-deckers demonstrate that the two interlocked porphyrin ligands oscillate rotationally around the metal center.

Oscillating molecules are interesting in their potential utilities for sensors, information transfer/storage devices and molecular machines, and several examples of molecular and supramolecular oscillating systems have been reported to date.[1,2] Particularly interesting are oscillators consisting of chromophoric units because of a possible switching of their oscillation characteristics by light and/or redox. Metal bis(porphyrinate)s are double-decker complexes, in which a metal atom is sandwiched by two chromophoric porphyrin ligands.[3] Recently, we have found that the porphyrin ligands in cerium bis(porphyrinate)s rotate thermally around the metal center, through studies on optical resolution and racemization behavior of a chiral cerium bis(tetraarylporphyrinate) with a symmetry group D_2.[4] The chirality of the complex originates from the staggered geometry of the two facing porphyrin ligands, where the relative rotation of the ligands leads to racemization. Herein we report that cerium bis(5,15-diarylporphyrinate)s are potential molecular oscillators, in which the two interlocked porphyrin ligands rotationally oscillate back and forth around the metal center.

We have already reported that the D_2-symmetric, chiral cerium complex **1a**, in contrast to a zirconium analogue of the same porphyrin ligands, shows no sign of optical resolution in chiral HPLC, as a result of racemization *via* a fast rotation of the porphyrin ligands.[4] Our motivation to the present study arose from a preliminary observation that enantiomeric separation of **2a**‡ by chiral HPLC was also unsuccessful in spite of the presence of interferant bulky *meta*-substituents (Bu^t) on the *meso*-phenyl groups perpendicular to the porphyrin plane. In order to compare the rotatability of the porphyrin ligands in **2a** with that of **1a**, temperature-dependent NMR signal coalescence profile was investigated for exchangeable proton signals *via* ligand rotation. At a low temperature such as −20 °C in $CDCl_3$, **2a** showed four doublet signals at δ 8.48 (*a*), 8.58 (*a*′), 8.76 (*b*) and 8.84 (*b*′) [Scheme 1(*a*)] owing to nonequivalent pyrrole-β protons,§ where the exchangeable pairs are signals *a*/*a*′ and *b*/*b*′. Upon elevating the temperature, the paired signals *a* and *a*′, for example, coalesced completely at 0 °C. From this coalescence profile, the rate constant for the rotation of the porphyrin ligands in **2a** was evaluated at 0 °C to be 0.52×10^2 s^{-1},¶ which is almost comparable to that of **1a** (0.63×10^2 s^{-1}) at 1 °C.[4]

Here one should note two possible rotating paths, I and II, for the complex to racemize (Scheme 2), where path II is sterically more demanding than path I, since the former path must transiently involve an energetically disfavored 'eclipsed conformation' with respect to the two facing porphyrin ligands. In order to evaluate the rotating rate *via* path II, we synthesized two new chiral double-decker complexes **1b** and **2b**, which bear a flexible oligoether strap between the two porphyrin ligands.‡ Their CPK models suggested that path I is unlikely to occur even when the oligoether strap adopts the most extended

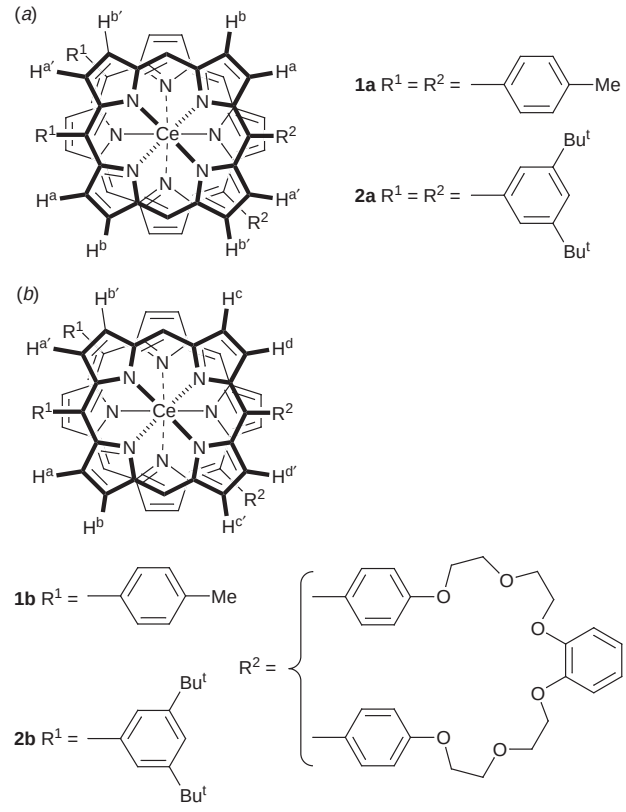

Scheme 1

conformation, thereby allowing selective evaluation of the rotating rate *via* path II. Prior to dynamic NMR studies, we investigated the possibility of optical resolution of these two strapped complexes by chiral HPLC,‖ where **2b** was successfully separated into enantiomers. The enantiomers exhibited clear mirror-image circular dichroism (CD) spectra to each other (Fig. 1), but the spectral intensity at 10 °C gradually decreased with time, where the rotating rate constant *via* path II was evaluated to be 0.39×10^{-3} s^{-1}.¶ In sharp contrast,

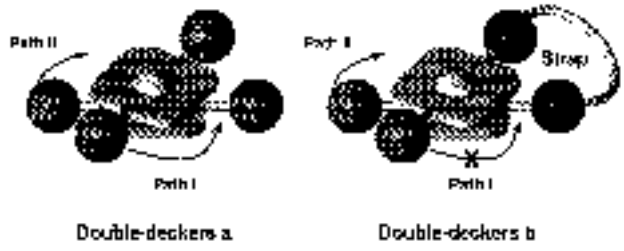

Scheme 2

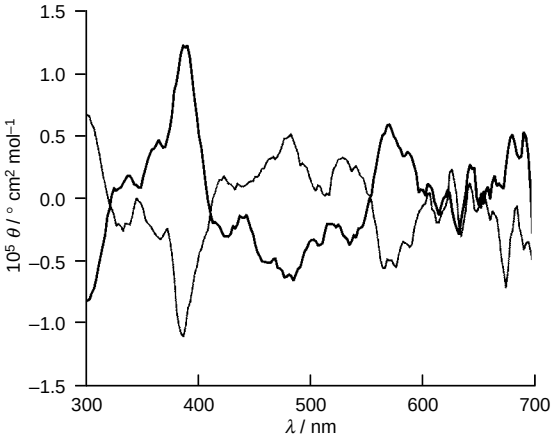

Fig. 1 Circular dichroism (CD) spectra of the enantiomers of **2b** in hexane–EtOH (1/1) at 10 °C

complex **1b** showed no sign of optical resolution, indicating that **1b** is more subject than **2b** to the ligand rotation *via* path II.

In order to evaluate the rotation rate of **1b**, we conducted ^{1}H NMR spectroscopy in $CDCl_3$ at varying temperatures. If the relative rotation of the porphyrin ligands is slower than the NMR chemical shift timescale, **1b** should display eight non-equivalent pyrrole-β signals because of the low symmetry of the molecular structure. In fact, we observed at 0 °C eight doublets at δ 8.30 (*a*), 8.38 (*d*), 8.54 (*d*′), 8.60 (*a*′), 8.68 (*b*), 8.72 (*c*), 8.81 (*b*′) and 8.82 (*c*′) [Scheme 1(*b*)]§, where exchangeable pairs *via* ligand rotation are *a*/*a*′, *b*/*b*′, *c*/*c*′ and *d*/*d*′, as determined from the cross-peaks in the EXSY spectra. However, even upon elevating the temperature to 55 °C, none of the paired signals coalesced, indicating that the site exchange in **1b** is much slower than that in the non-strapped analogue **1a**. Thus, the saturation transfer method[5,6] was applied, which is informative of exchange phenomena much slower than the NMR chemical shift timescale: When the pyrrole-β signal *d*′ was irradiated at, *e.g.*, 25 °C (δ 8.50), the paired signal *d* (δ 8.35) decreased to one-third in intensity. As the temperature was lowered, the saturation transfer was less pronounced, and virtually disappeared at 0 °C. From the degree of saturation transfer from the signals *d*′ to *d* at 10 °C, the rate constant for the rotation of the porphyrin ligands (path II) in **1b** was evaluated to be 0.37 s^{-1},** which is almost three orders of magnitude larger than that of **2b**.

The observed rotation rates for the strapped complexes (**1b** and **2b**), compared with those for non-strapped **1a** and **2a**, allow us to estimate that the rotation *via* sterically more demanding path II takes place much less frequently at every 10^2 to 10^5 times the rotation *via* path I occurs. Therefore, cerium bis(5,15-diarylporphyrinate) double-deckers may be regarded as molecular oscillators, where the two facing porphyrin ligands rotationally oscillate around the metal center, because of the interlocking by the *meso*-aryl groups. Studies on stimuli-responsive oscillations of metal bis(porphyrinate) double-deckers are the subject worthy of further investigation.

We thank Dr N. Morisaki for HRMS measurement, and K. T. thanks JSPS Research Fellowships for Young Scientists.

Notes and References

† E-mail: aida@macro.t.u-tokyo.ac.jp

‡ According to the method reported in ref. 4, **2a** was obtained as brown powder in 11% yield. ^{1}H NMR (270 MHz, $CDCl_3$, −20 °C) δ 9.57 (s, 4 H, *o-endo*-H), 9.14 (s, 4 H, *meso*), 8.84, 8.76, 8.58, 8.48 (d × 4, *J* 4 Hz, 16 H, pyrrole-β), 7.78 (s, 4 H, *p*-H), 6.34 (s, 4 H, *o-exo*-H), 2.06 (s, 36 H, *endo*-Bu^t), 1.14 (s, 36 H, *exo*-Bu^t). FAB-HRMS (*m*/*z*); calc. for M + H$^+$ ($C_{96}H_{105}CeN_8$): 1509.7517, found: 1509.7510. For the synthesis of **1b** and **2b**, the ether linkages of 5-(4′-methoxyphenyl)-15-(4′-tolyl)porphine and 5-(4′-methoxyphenyl)-15-(3′,5′-di-*tert*-butylphenyl)porphine were cleaved, respectively, by BR_3 and the products were reacted with the corresponding α,ω-tosylated oligoether in the presence of Cs_2CO_3 to give bridged free bases, which were metallated with $Ce(acac)_3{\cdot}nH_2O$ in refluxing 1,2,4-trichlorobenzene for 3 h under Ar. The crude products were chromatographed on alumina and recrystallized from CH_2Cl_2–hexane. The isolated yields were 5.6 (**1b**) and 17 (**2b**) %, respectively. **1b**: ^{1}H NMR (270 MHz, $CDCl_3$, 0 °C) δ 9.68 (d × 2, 4 H, *o-endo*-H in C_6H_4Me and C_6H_4O), 9.09, 9.08 (s × 2, 4 H, *meso*), 8.82, 8.81, 8.72, 8.68, 8.60, 8.54, 8.38, 8.30 (d × 8, *J* 4 Hz, 16 H, pyrrole-β), 8.12 (d, *J* 7 Hz, 2 H, *m-endo*-H in C_6H_4Me), 7.89 (br s, 2 H, *m-endo*-H in C_6H_4O), 7.17–7.08 (m, 6 H, *m-exo*-H in C_6H_4Me and $C_6H_4O_2$), 6.98 (br s, 2 H, *m-exo*-H in C_6H_4O), 6.61 (br s, 2 H, *o-exo*-H in C_6H_4O), 6.35 (d, *J* 7 Hz, 2 H, *o-exo*-H in C_6H_4Me), 4.80–4.26 (m, 16 H, CH_2), 2.80 (s, 6 H, CH_3). FAB-HRMS calc. (*m*/*z*): for M$^+$ ($C_{80}H_{62}CeN_8O_6$): 1370.3847, found: 1370.3876. **2b**: ^{1}H NMR (270 MHz, $CDCl_3$, 21 °C) δ 9.64 (br s, 2 H, *o-endo*-H in C_6H_4O), 9.52 (t, *J* 2 Hz, 2 H, *o-endo*-H in C_6H_3), 9.06, 9.02 (s × 2, 4 H, *meso*), 8.81, 8.80, 8.76, 8.65, 8.64, 8.56, 8.51, 8.28 (d × 8, *J* 4 Hz, 16 H, pyrrole-β), 7.85 (br s, 2 H, *m-endo*-H in C_6H_4O), 7.76 (t, *J* 2 Hz, 2 H, *p*-H in C_6H_3), 7.14–7.03 (m, 4 H, $C_6H_4O_2$), 6.95 (br s, 2 H, *m-exo*-H in C_6H_4O), 6.59 (br s, 2 H, *o-exo*-H in C_6H_4O), 6.31 (t, *J* 2 Hz, 2 H, *o-exo*-H in C_6H_3), 4.76–4.22 (m, 16 Hz, CH_2), 2.01 (s, 18 H, *endo*-Bu^t), 1.11 (s, 18 H, *exo*-Bu^t). FAB-HRMS (*m*/*z*): calc. for M + H$^+$ ($C_{94}H_{91}CeN_8O_6$): 1567.6117, found: 1567.6068.

§ Assignments were made by ^{1}H–^{1}H COSY and EXSY spectroscopies upon consideration of magnetic effects of proximate *meso*-aryl substituents.

¶ Calculated by the method reported in ref. 4.

‖ With a Chiralcel OD-H (Daicel) column using hexane–EtOH (1/1) as eluent at a flow rate of 0.5 ml min^{-1}; retention times: 35.9 and 85.8 min.

** According to the method described in ref. 6, the rate constant of exchange (*k*) was calculated by the equation: $k = (I_0 - I_{irrad})/I_{irrad}\ T_1^{-1}$, where I_0 and I_{irrad} represent intensity of the pyrrole-β signal *d* and that upon irradiation to saturate the exchangeable proton singal *d*′, respectively, and T_1 represents the spin–lattice relaxation time for the signal *d*′.

1 M. Postel, M. Pfeffer and J. G. Riess, *J. Am. Chem. Soc.*, 1977, **99**, 5623; J. T. B. H. Jastrzebski, G. van Koten, M. Konijn and C. H. Stam, *J. Am. Chem. Soc.*, 1982, **104**, 5490; E. W. Abel, N. J. Long, K. G. Orrell, A. G. Osborne, H. M. Pain and V. Sik, *J. Chem. Soc., Chem. Commun.*, 1992, 303; H. Görls, B. Neumüller, A. Scholz and J. Scholz, *Angew. Chem., Int. Ed. Engl.*, 1995, **34**, 673.

2 D. B. Amabilino and J. F. Stoddart, *Chem. Rev.*, 1995, **95**, 2725.

3 J. W. Buchler, K. Elsässer, M. Kihn-Botulinsky and B. Scharbert, *Angew. Chem., Int. Ed. Engl.*, 1986, **25**, 286; J. W. Buchler and B. Scharbert, *J. Am. Chem. Soc.*, 1988, **110**, 4272; G. S. Girolami, S. N. Milam and K. S. Suslik, *J. Am. Chem. Soc.*, 1988, **110**, 2011; K. M. Kadish, G. Moninot, Y. Hu, D. Dubois, A. Ibnfassi, J.-M. Barbe and R. Guilard, *J. Am. Chem. Soc.*, 1993, **115**, 8153; D. Y. Dawson, H. Brand and J. Arnold, *J. Am. Chem. Soc.*, 1994, **116**, 9797; G. S. Girolami, C. L. Hein and K. S. Suslik, *Angew. Chem., Int. Ed. Engl.*, 1996, **35**, 1223; D. K. P. Ng and J. Jiang, *Chem. Soc. Rev.*, 1997, **26**, 433.

4 K. Tashiro, K. Konishi and T. Aida, *Angew. Chem. Int. Ed. Engl.*, 1997, **36**, 856.

5 C. L. Perrin and T. J. Dwyer, *Chem. Rev.*, 1990, **90**, 935.

6 J. K. M. Sanders and B. K. Hunter, *Modern NMR Spectroscopy*, Oxford University, Oxford, 1987.

Received in Cambridge, UK, 17th February 1998; 8/01350K

Metal silicates by a molecular route as catalysts for epoxidation of alkenes with *tert*-butyl hydroperoxide

David Juwiler,[a] Jochanan Blum[b] and Ronny Neumann*[a]†

[a] *Casali Institute of Applied Chemistry, Graduate School of Applied Science, The Hebrew University of Jerusalem, Jerusalem, Israel 91904*

[b] *Department of Organic Chemistry, The Hebrew University of Jerusalem, Jerusalem, Israel 91904*

Macroporous, site isolated metal silicates are synthesized by a molecular route; the molybdenum silicate is especially active for the selective epoxidation of alkenes with *tert*-butyl hydroperoxide.

The epoxidation of alkenes with 'redox molecular sieves' has been studied intensively during the last decade.[1] The titanium-substituted silicalite of the MFI structure, TS-1, has been the flagship of this effort. The small pored TS-1 is remarkably effective for epoxidation of small linear olefins due to the isomorphous distribution of titanium in the silicalite framework leading to isolated Ti–$(OSi)_4$ active centers held responsible for its unique activity. In the quest to develop similar catalysts viable for larger substrates, most attention has been directed towards mesoporous catalysts such as Ti–MCM-41.[2] A much less studied approach has been to use amorphous metallosilicate aerogels[3] and xerogels[4] prepared by sol–gel synthesis. The use of the sol–gel technique has limited the possibility of obtaining only M–O–Si connectivities (M = Ti, V, Mo and W) because the rate of reaction of the metal alkoxides in the sol–gel method is much faster than that of the silicon alkoxide.[5] Reduced metal site isolation considerably reduces the catalytic effectiveness of amorphous metallosilicates. Recently, a non-aqueous molecular route has been described for the preparation of metal silicates[6] [eqn. (1)] (M = Ti, Zr, Hf, Cu) which by design leads to metal site isolation within the silicate.

$$MCl_4 + HOSi(OBu^t)_3 \longrightarrow M[OSi(OBu^t)_3]_4 \xrightarrow{\Delta} M[O(SiO)_3]_4 + CH_2CMe_2 + H_2O \quad (1)$$

The molecular route procedure is based on the synthesis of an alkoxy intermediate which forms a metal silicate polymer by thermal elimination of isobutene and water rather than by hydrolysis and condensation as in the sol–gel technique. We have now utilized this technique to prepare macroporous titanium, vanadium, molybdenum and tungsten silicate. The molybdenum analog was especially active towards the selective epoxidation of bulky alkenes with *tert*-butyl hydroperoxide (TBHP).

The metal silicates described in this paper were prepared by adapting the method reported for the titanium silicate.[7] Thus, 40 mmol tri-*tert*-butoxysilanol[7,8] in 100 ml toluene was reacted with 10 mmol of metal chloride, $TiCl_4$, $V(O)Cl_3$, $Mo(O)Cl_4$ and $W(O)Cl_4$, respectively, in the presence of 40 mmol Et_3N at room temperature for 2 h. The precipitates were filtered and then calcinated for 12 h at ~250 °C to yield TiO_2–$4SiO_2$, $VO_{2.5}$–$3SiO_2$, MoO_3–$4SiO_2$ and WO_3–$4SiO_2$, respectively. The calcination temperature was chosen after thermogravimetric measurements showed clean peaks for isobutene and water elimination at this temperature.‡ N_2—physisorption measurements using the BET method showed that the metal silicates were macroporous with large pore sizes of 130 ± 20 Å and relatively low surface areas of 25 ± 5 $m^2\ g^{-1}$. The IR spectra showed the expected peak[9] at 950–960 cm^{-1} attributable to the Si–O stretching vibration polarized by the metal atom.§

The catalytic activity of the four metallosilicates was first compared using the reactive but bulky cyclooctene as the model substrate (Table 1). Using 30% hydrogen peroxide as oxidant, reactivity was very low and the metal silicate was dissolved into the homogeneous phase, presumably by aqueous hydrolysis. On the other hand, using 6 M *tert*-butyl hydroperoxide in *n*-decane as oxidant, a high yield of cyclooctene oxide was observed for the molybdenum silicate, MoO_3–$4SiO_2$. The vanadium silicate showed intermediate activity, whereas TiO_2–$4SiO_2$ and WO_3–$4SiO_2$ were only slightly active. With both oxidants there was no cyclooctene conversion without metal silicate. The stability of MoO_3–$4SiO_2$ was tested by filtering the reaction mixture at reaction temperature. There was no discernible loss in activity when the heterogeneous silicate was recycled in three consecutive runs. No metal leaching into the organic phase was measurable.¶

Table 1 Epoxidation of cyclooctene catalysed by metal silicates[a]

Metal silicate	Conversion (mol%) (Oxidant 30% H_2O_2)	Conversion (mol%) (Oxidant 6 M TBHP)
TiO_2–$4SiO_2$	0	5
$VO_{2.5}$–$3SiO_2$	0	40
MoO_3–$4SiO_2$	5	90
WO_3–$4SiO_2$	15	7

[a] Reaction conditions: 1.5 mmol cyclooctene, 1.5 μmol metal silicate (according to formula in table above), 0.1 ml 30% H_2O_2 + 1 ml acetone or 0.25 ml 6 M TBHP in *n*-decane, 60 °C, 12 h. Analysis was carried out by GLC (HP-5890) using a dimethyl polysiloxane column (RTX-1, 30 m, 0.32 mm id, 0.25 μm coating).

A more complete examination of the activity of MoO_3–$4SiO_2$ was carried out using different alkene substrates. First, the effect of the TBHP:alkene ratio was studied in the epoxidation of linear alkenes (Fig. 1). In general, doubling the amount of

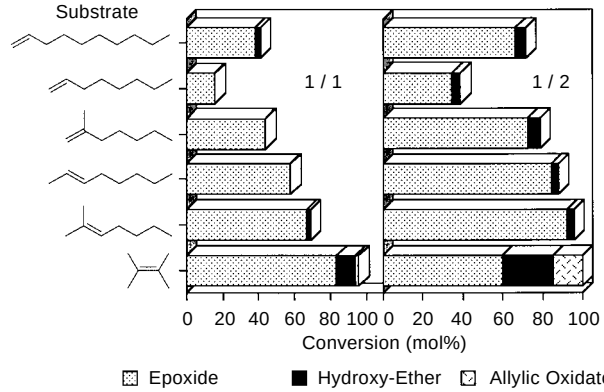

Fig. 1 Epoxidation of linear alkenes catalysed by MoO_3–$4SiO_2$ as a function of the oxidant : substrate ratio. Reaction conditions: 1.5 mmol substrate, 7.5 μmol (0.5 mol%) metal silicate, 1.5 mmol 6 M TBHP in *n*-decane (left panel), 3.0 mmol 6 M TBHP in *n*-decane (right panel), 50 °C, for dec-1-ene 80 °C, 12 h. Analysis was carried out by GLC (HP-5890) using a dimethyl polysiloxane column (RTX-1, 30 m, 0.32 mm id, 0.25 μm coating). Unknown products were identified by GC–MSD (HP-GCD) under similar conditions.

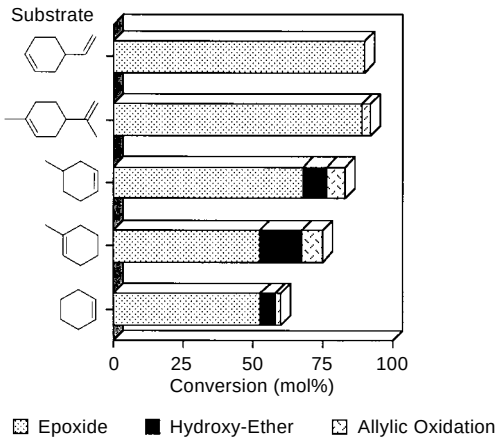

Fig. 2 Epoxidation of cyclic alkenes catalysed by MoO_3–$4SiO_2$. Reaction conditions: 1.5 mmol substrate 7.5 μmol (0.5 mol%) metal silicate, 1.5 mmol 6 M TBHP in *n*-decane, 50 °C, 12 h. For limonene and 4-vinylcyclohexene 0.15 μmol (0.1 mol%) metal silicate was used. Analysis was as described for Fig. 1.

TBHP increases the conversion and yield to epoxide, but the selectivity is somewhat lowered due to formation of α,β-hydroxy *tert*-butyl ethers by ring opening of the epoxide formed. In very reactive (nucleophilic) compounds such as 2,3-dimethylbut-2-ene excess oxidant also brought on formation of allylic oxidation products. An increase in the reaction temperature was also beneficial for the epoxidation reaction. For example, in the opoxidation of dec-1-ene, the conversions under conditions given in Fig. 2 (TBHP:1-decene = 2 : 1) were 37, 72 and 96 mol% for 50, 80 and 110 °C, respectively, with some decrease in selectivity to epoxide from 93% (50 and 80 °C) to 85% at 110 °C. The reactivity of bulkier cyclic alkenes has also been investigated (Fig. 2). In contrast to the microporous TS-1, there was no sieving effect and all substrates tested were reactive. For the monofunctional cyclic alkenes moderate selectivity was observed with some epoxide ring opening to the α,β-hydroxy *tert*-butyl ethers and the formation of a mixture of allylic oxidation products. 4-Vinylcyclohexene reacted quite selectively to form epoxide at the ring double bond (10 : 1 ratio). In addition, a small amount of diepoxide was formed (ratio monoepoxides : diepoxide = 13.3). The reaction of limonene was considerably less selective. Both epoxides were formed in similar amounts. There was a considerable amount of diepoxide formed as well (ratio monoepoxides : diepoxide = 5.5) as well as a small amount of allylic oxidation products. It is notable that the decrease in the amount of catalyst has a positive effect on reaction selectivity coupled with only a small decrease in conversion. The MoO_3–$4SiO_2$ prepared by the molecular route is a new heterogeneous catalyst for effective epoxidation of alkenes with anhydrous TBHP and compares well with 'redox molecular sieves'[1] and amorphous aerogels.[3]

This research was supported by the United States–Israel Binational Science Foundation (BSF), Jerusalem, Israel (grant no. 95–00076).

Notes and References

† E-mail: ronny@vms.huji.ac.il

‡ The thermogravimetric analysis showed weight loss (sharp peaks) at 250, 260 and 270 °C for TiO_2–$4SiO_2$, WO_3–$4SiO_2$ and MoO_3–$4SiO_2$, respectively, which was ±2% of the loss expected upon elimination of isobutene and water according to eqn. (1).

§ IR spectra: TiO_2–$4SiO_2$ 1084, 959, 800 (sh), 461 cm^{-1}; $V_2O_{2.5}$–$3SiO_2$ 1169, 1080, 990, 804, 749, 675, 505 cm^{-1}; MoO_3–$4SiO_2$ 1092, 951, 903, 855, 588, 465 cm^{-1}; WO_3–$4SiO_2$ 1078, 961, 924, 803, 586, 465 cm^{-1}.

¶ Leaching for MoO_3–$4SiO_2$ was tested according to the method suggested by Lempers and Sheldon (ref. 10) by heating 39 mg (0.1 mmol) MoO_3–$4SiO_2$ with 20 mmol 6 M TBHP in *n*-decane for 24 h at 60 °C, and filtering the solution while 'hot'.

1 I. W. C. E. Arends, R. A. Sheldon, M. Wallau and U. Schuchardt, *Angew. Chem., Int. Ed. Engl*., 1997, **36**, 1143.
2 A. Corma, M. T. Navarro and J. Pérez-Pariente, *J. Chem. Soc., Chem. Commun*., 1994, 147.
3 R. Hutter, T. Mallat, D. Dutoit and A. Baiker, *Top. Catal*., 1996, **3**, 421; R. Hutter, T. Mallat and A. Baiker, *J. Catal*., 1995, **153**, 165 and 177.
4 R. Neumann and M. Levin-Elad, *Appl. Catal. A*, 1995, **122**, 85; R. Neumann and M. Levin–Elad, *J. Catal*., 1997, **166**, 206.
5 J. Livage, M. Henry and C. Sanchez, *Inorg. Solid State Chem*., 1988, **18**, 259.
6 K. W. Terry, and T. D. Tilley, *Chem. Mater*., 1991, **3**, 1001; K. W. Terry, C. G., Lugmair, P. K. Gantzel and T. D. Tilley, *Chem. Mater*., 1996, **8**, 274.
7 M. G. Voronkov, A. N. Lazarev and A. K. Baigozhin, *J. Gen. Chem. (USSR)*, 1956, **26**, 3421.
8 Y. Abe and I. Kijima, *Bull. Chem. Soc. Jpn*., 1969, **42**, 1118.
9 M. A. Camblor, A. Corma and J. Pérez-Pariente, *J. Chem. Soc., Chem. Commun*., 1993, 557.
10 H. E. B. Lempers and R. A. Sheldon, *Stud. Surf. Sci. Catal*., 1996, **105**, 1061.

Received in Liverpool, UK, 20th February 1998; 8/01492B

Photocurrent responses associated with heterogeneous electron transfer at liquid/liquid interfaces

David J. Fermín, Zhifeng Ding, H. Dung Duong, Pierre F. Brevet and Hubert H. Girault*†

Laboratoire d'Electrochimie, Departement de Chimie, Ecole Polytechnique Fédérale de Lausanne, CH-1015 Lausanne, Switzerland

Photocurrent measurements originating from the electron transfer between photoexcited water soluble porphyrins and hydrophobic redox species are studied at the polarised water/1,2-dichloroethane (DCE) interface.

Artifical photosynthesis still remains a formidable technological challenge and a focal point for scientists well into the next century. Apart from solar cells based on dye sensitised colloidal semiconducting films,[1,2] no major breakthrough has been achieved in the field of solar energy conversion since the solid state photovoltaic cell.[3] A novel approach may rely on interfaces between two immiscible electrolyte solutions (ITIES), in which electron exchange involves redox centres separated by a defect-free junction. Despite recent advances in photochemistry[4] and electrochemistry at ITIES,[5,6] very few works have dealt with photocurrent measurements associated with heterogeneous electron transfer processes.[7–9] The present report describes photocurrent responses corresponding to the oxidation/reduction of a photoexcited water soluble porphyrin by hydrophobic redox centres such as TCNQ and 1,2-diferrocenylethane (DFCET) at the water/DCE interface.

One of the major obstacles for studying electron transfer at ITIES are the interferences introduced by ion transfer reactions.[5] Therefore, it is critical that charged species remain in their respective phases over a certain potential range. This condition was achieved by cell 1, where $Zn(TPPC)^{4-}$ denotes zinc tetrakis(carboxyphenyl)porphyrin and BTPPATPBCl is the organic electrolyte bis(triphenylphosphoranylidene)ammonium tetrakis(4-chlorophenyl)borate. Under the cell 1 arrangement, a potential window of *ca.* 0.8 V can be obtained without any significant faradaic response in the dark. The polarisation of the liquid/liquid interfaces (1.54 cm^2 surface area) was performed by a custom built four-electrode potentiostat.

Photocurrent measurements were also obtained with low frequency chopped light and lock-in detection (Stanford Research SR830).

Photocurrent transient responses associated with the heterogeneous quenching of $Zn(TPPC)^{4-}$ by TCNQ and DFCET are displayed in Fig. 1. The Galvani potential difference was determined from the formal transfer potential of tetramethylammonium ion (TMA), $\Delta^{w_o}\phi^{0'}_{TMA} = 0.160$ V.[10] Wavelengths < 450 nm were cut off by a Schott filter in order to avoid the absorption region of the ferrocene derivative. By convention, a positive current corresponds to a negative charge crossing from the organic to the aqueous phase. It is observed that the current is positive in the presence of the electron donor, and negative for the case of the electron acceptor. In the absence of either quencher or sensitiser, no photocurrent responses are obtained within the potential window.

The fact that neither reactants nor products transfer across the interface indicate that photocurrent responses are associated with heterogeneous electron transfer phenomena. Kotov and Kuzmin[11–13] have studied the case where a homogeneous photoreaction is followed by transfer of the charge products across the water/DCE interface. The shapes of the transient responses reported by these authors are essentially different to those observed in Fig. 1, and an order of magnitude slower. The heterogeneous nature of the electron transfer process is further confirmed by the dependence of the photocurrent sign on whether the excited state of the porphyrin is reduced or oxidised.

The transient photocurrent in Fig. 1 depends on the applied Galvani potential difference across the interface. For TCNQ, the photocurrent is rather small at positive potentials and increases toward negative potentials. The photocurrent exhibits an in-phase response followed by a slow decay upon illumination. When the illumination is interrupted, a positive overshoot is observed before the photocurrent relaxes to zero. These

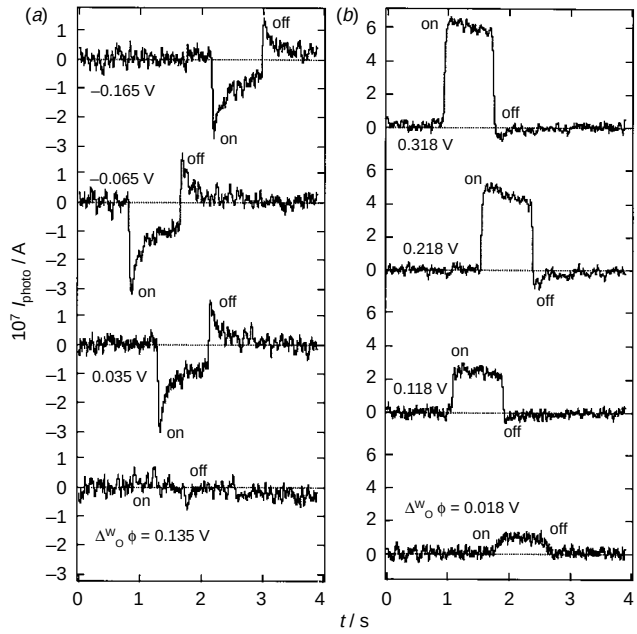

Fig. 1 Photocurrent transient measurements at various Galvani potential differences obtained from cell 1 and employing as quenchers TCNQ (*a*) and DFCET (*b*). Illumination was provided by a 450 W Arc-Xe lamp. λ < 450 nm were cut by a Schott filter. It is observed that the photocurrent is negative (electron transfer from water to DCE) in the presence of TCNQ and positive for DFCET.

Ag	Ag_2SO_4	10^{-4} M $Zn(TPPC)^{4-}$ (aq) 0.01 M Li_2SO_4	0.01 M BTPPATPBCl 10^{-3} M quencher (DCE)	0.001 M BTPPATPBCl 0.01 M LiCl (aq)	Ag'Cl	Ag'

Cell 1

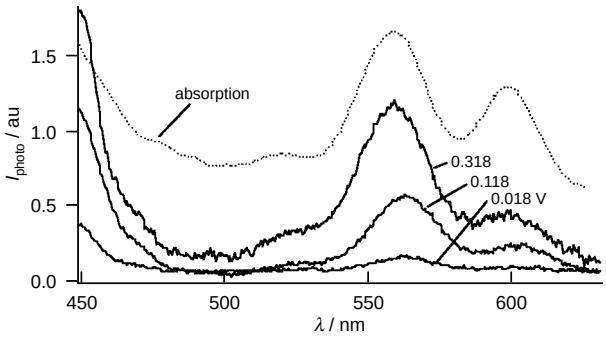

Fig. 2 Photocurrent spectra of cell 1 at various potentials in the presence of DFCET. The transmission absorption spectrum of $Zn(TPPC)^{4-}$ is also superimposed for qualitative comparison.

transients resemble the behaviour observed for interfacial electron–hole recombination at p-type semiconductor/electrolyte junctions.[14] For DFCET, the recombination features are not so evident, but the photocurrent increases progressively as the potential is increased.

Photocurrent action spectra obtained at various Galvani potential differences are contrasted with the transmission absorption spectrum of the system in Fig. 2. The similar features in both spectra confirm the relation between electron transfer and the excited state of the porphyrin. It is observed the onset of the Soret band, which corresponds to the second singlet excited state S_2 located at *ca.* 430 nm. The photocurrent spectra also show three Q band transitions in the region 500–630 nm, which are associated with the first singlet excited state S_1 (560 nm) and its vibrational overtones. Although the wavelength of the photocurrent responses coincides with the absorption bands, the relative intensities are somehow different. The origin of this effect is still unclear, but it could indicate that the porphyrin involved in the electron exchange process have a different environment in comparison to the bulk porphyrin, probably due to adsorption.

Some of the features observed in the photocurrent transients in Fig. 1 can be explained in terms of a competition between product separation following the electron transfer step and the return electron transfer (recombination). In analogy with homogeneous photochemistry, the complex formed during the electron transfer phenomena can be denominated ion pair.[4,15] In the present case, this intermediate has an essentially heterogeneous stucture, therefore the forward electron transfer as well as the recombination reaction involve faradaic responses. In general, the photoelectrochemical reduction of a sensitiser S by an electron donor Q can be represented by Scheme 1 where $[S^{-}\cdots Q^{+}]$ represents the intermediate ion pair, and the subindexes w, o and int stand for aqueous, organic and interfacial region respectively. According to this mechanism, the initial photocurrent will be determined by the competition between electron transfer [eqn. (3)] and the decay of the excited state [eqn. (2)]. The subsequent decay of the photocurrent will be an effect of the recombination reaction [eqn. (5)], and the steady state photocurrent will be a function of the rate constants k_1–k_4. A quantitative analysis of the transient responses is currently in preparation.

$$S_w \xrightarrow{h\nu} S_w^* \qquad \text{Photoexcitation} \qquad (1)$$

$$S_w^* \xrightarrow{k_1} S_w \qquad \text{Decay of the excited state} \qquad (2)$$

$$S_w^* + Q_o \xrightarrow{k_2} [S^{-}\cdots Q^{+}]_{int} \qquad \text{Electron transfer} \qquad (3)$$

$$[S^{-}\cdots Q^{+}]_{int} \xrightarrow{k_3} S_w^{-} + Q_o^{+} \qquad \text{Product separation} \qquad (4)$$

$$[S^{-}\cdots Q^{+}]_{int} \xrightarrow{k_4} S_w + Q_o \qquad \text{Recombination} \qquad (5)$$

Recent results reveal that the photocurrent density is independent of the angle of illumination and linearly dependent on the light intensity.[16] This behaviour further suggests that the porphyrin molecules involved in the photocurrent responses are effectively confined to the liquid/liquid contact surface. It has also been found that diffusion effects become significant at high photocurrent levels ($> 10^{-5}$ A cm^{-}).[16]

Several other quenchers have been studied, showing different kinetics of electron transfer and recombination. In general, recombination features are dependent on the applied potential, indicating that the competition between recombination and product separation is affected by the Galvani potential difference. Moreover, the initial photocurrent is also dependent on the applied potential, reflecting a change in the electron transfer rate constant. The fact that the photocurrent increases as the potential becomes more negative in the case of TCNQ, and with increasing potentials for DFCET, suggests that these effects are not related to changes in the interfacial concentration of the porphyrin.[5,17,18] In contrast to the behaviour at semiconductor/electrolyte interfaces, the experimental evidence indicates that the activation energy for the electron transfer is affected by the applied potential.

The results presented in this report indicate that $Zn(TPPC)^{4-}$ is an ideal sensitiser for the study of heterogeneous electron transfer across the water/DCE interface. Both positive and negative photocurrents can be obtained upon replacing an electron donor for an electron acceptor in the organic phase. The photocurrent responses exhibit the same feature of the absorption spectra of the porphyrin. Evidence of back electron transfer appears in a similar fashion to electron–hole interfacial recombination at the semiconductor/electrolyte junctions.

We are grateful to the financial support of the Fonds National Suisse de la Recherche Scientifique (Project 2000-043381-95/1). We are also indebted to Valérie Devaud for the technical assistance. The Laboratoire d'Electrochimie is part of the European Network ODRELLI (Organisation, Dynamics and Reactivity at Electrified Liquid/Liquid interfaces).

Notes and References

† E-mail: Hubert.Girault@epfl.ch

1 B. O'Reagan and M. Grätzel, *Nature*, 1991, **353**, 737.
2 M. Grätzel, *Platinum Met. Rev.*, 1994, **38**, 151.
3 A. L. Fahrenbruch and R. H. Bube, *Fundamentals of Solar Cells*, Academic Press, 1983.
4 G. J. Kavarnos, *Fundamentals of Photoinduced Electron Transfer*, VCH Publishers, Inc., 1993.
5 H. H. Girault, *Mod. Aspects Electrochem.*, 1993, **25**, 1.
6 I. Benjamin, *Annu. Rev. Phys. Chem.*, 1997, **48**, 407.
7 A. R. Brown, L. J. Yellowlees and H. H. Girault, *J. Chem. Soc., Faraday Trans.*, 1993, **89**, 207.
8 F. L. Thomson, L. J. Yellowlees and H. H. Girault, *J. Chem. Soc., Chem. Commun.*, 1988, 1547.
9 V. Marecek, A. H. De Armond and M. K. De Armond, *J. Am. Chem. Soc.*, 1989, **111**, 2561.
10 For a comprehensive list of free energy of ion transfer at various liquid/liquid interfaces see the web site dcwww.epfl.ch.
11 N. A. Kotov and M. G. Kuzmin, *J. Electroanal. Chem.*, 1990, **285**, 223.
12 N. A. Kotov and M. G. Kuzmin, *J. Electroanal. Chem.*, 1992, **341**, 47.
13 N. A. Kotov and M. G. Kuzmin, *J. Electroanal. Chem.*, 1992, **338**, 99.
14 L. M. Peter, *Chem. Rev.*, 1990, **90**, 753.
15 I. R. Gould, J. E. Moser, B. Armitage and S. Farid, *Res. Chem. Intermed.*, 1995, **21**, 793.
16 D. J. Fermin, Z. Ding, H. Duong, P.-F. Brevet and H. H. Girault, in preparation.
17 W. Schmickler, *J. Electroanal. Chem.*, 1997, **429**, 123.
18 Z. Ding, D. J. Fermin, P.-F. Brevet and H. H. Girault, in preparation.

Received in Exeter, UK, 18th February 1998; 8/01444B

Dinuclear cyclometallated platinum(II) complex as a sensitive luminescent probe for SDS micelles

Li-Zhu Wu,[a] Tsz-Chun Cheung,[a,b] Chi-Ming Che,[a]*† Kung-Kai Cheung[a] and Michael H. W. Lam[b]

[a] *Department of Chemistry, The University of Hong Kong, Pokfulam Road, Hong Kong, PR China*
[b] *Department of Biology and Chemistry, City University of Hong Kong, Tat Chee Ave., Hong Kong, PR China*

The photoluminescent properties of two dinuclear cyclometallated Pt^{II} complexes, $[Pt_2L^1{}_2(\mu\text{-dppm})]^{2+}$ 1 and $[Pt_2L^2{}_2(\mu\text{-dppm})]^{2+}$ 2, in SDS micellar solution are studied and 1 is found to undergo enhancement of luminescence as well as switching of emissive states upon incorporation into SDS micelle.

Metal–metal to ligand charge transfer (MMLCT) emission has been receiving growing interest in the photophysics and photochemistry of dinuclear Pt^{II} diimine complexes.[1] Such emission depends on the extent of Pt^{II}–Pt^{II} and/or ligand–ligand interactions. These interactions are weak under normal circumstances, but are sensitive to the surrounding environment. Thus, with suitable molecular design, such MMLCT emission of dinuclear Pt^{II} systems may serve as a means to probe the chemical environment in which the Pt^{II} complex is presented. One potentially important application is the probing of transformations in micellar microheterogenerous environments.[2] Here, we highlight a conformational non-rigid dinuclear cyclometallated Pt complex $[Pt_2L^1{}_2(\mu\text{-dppm})]^{2+}$ **1** (dppm = $Ph_2PCH_2PPH_2$) (Fig. 1) as a new spectroscopic probe for SDS micelles.[3] The flexible conformation of the Pt^{II} complex prompts the intramolecular metal–metal and/or ligand–ligand interactions, and hence its MMLCT emission, to be sensitive to the microheterogenerous environments of the SDS micelles (Scheme 1).

The ligand L^1 [4-(*p*-diethylphosphonophenyl)-6-phenyl-2,2′-bipyridine] was obtained from the reaction between 4-(*p*-bromophenyl)-6-phenyl-2,2′-bipyridine and diethyl phosphite in the presence of a Pd^0 catalyst.[4] The dinuclear Pt^{II} complex **1** was prepared by stirring $[PtL^1Cl]$ and 1,2-bis(diphenylphosphino)methane in MeCN–EtOH. It was isolated as a PF_6^- salt. For comparison, an analogous complex, $[Pt_2L^2{}_2(\mu\text{-dppm})]^{2+}$ **2** [L^2 = 4-(4-chlorophenyl)-6-phenyl-2,2′-bipyridine] (Fig. 1), without $PO(OC_2H_5)_2$ groups was also prepared.‡ The structure of **2**$[PF_6]_2$ has been characterized by X-ray crystallography (Fig. 2).§ The two planar $[PtL^2]$ units are nearly parallel to each other with a dihedral angle of 4.6°, and staggered with a torsion angle of 27.2°. The configurations of the two $[PtL^2]$ units are identical and are related by a C_2 axis passing through the $–CH_2–$ unit of the dppm ligand. The intramolecular Pt–Pt distance is 3.150(1) Å. This is shorter than the intramolecular Pt–Pt distance of $[Pt_2L^3{}_2(\mu\text{-dppm})]^{2+}$ (L^3 = 6-phenyl-2,2′-bipyridine) (3.301 Å)[5] but is comparable to that in $[Pt_2(NH_3)_4(\mu\text{-}C_4H_5N_2O_2)_2]^{2+}$ (3.131 Å).[6] The structure of **1** is expected to resemble that of **2** as the spectroscopic properties of **1**$[PF_6]_2$ and **2**$[PF_6]_2$ are similar,¶ we envisage that there is also weak metal–metal and/or ligand–ligand interactions in the former complex.

Emission spectra of **1**$[PF_6]_2$ in CH_2Cl_2 and **2**$[PF_6]_2$ in MeCN show low energy bands at 648 nm and 661 nm, respectively, which are both attributable to the MMLCT $\{^3[(d\sigma^*)\sigma(\pi^*)]\}$ transitions.[1] However, in MeOH, no emission from **1** can be observed. This is most probably due to quenching by solvent molecules at the open coordination sites. As shown in Fig. 3(*a*), addition of SDS micelles to an aqueous solution of **1** leads to an emission with λ_{max} at 530 nm (τ = 1.4 μs), which is similar to the MLCT emissions of related mononuclear cyclometallated Pt^{II} complexes.[7] Interestingly, no MMLCT emission can be observed. We attribute that the SDS micelle creates a protecting environment for the Pt^{II} complex so that enhancement of emission is recorded upon incorporation of the dinuclear Pt^{II} complex. The fact that the emission of **1**–SDS micelle is very different from those observed in CH_2Cl_2 solution and solid state suggests no intramolecular and/or intermolecular Pt^{II}–Pt^{II} interaction between the two cyclometallated Pt^{II} units upon incorporation of the complex in the SDS micelle.

It is well established that with increasing ionic strength, micelles will undergo substantial transformations in size and shape to create cylindrical micelles with large aggregation number and SDS head groups will be brought closer in proximity.[8] We found that the emission properties of **1** in the SDS micelle are dramatically altered by the addition of counter cations. Fig. 3 shows the emission spectra of **1** in the SDS micellar solution recorded at different NaCl concentrations. Initial addition of NaCl slightly enhances the intensity and

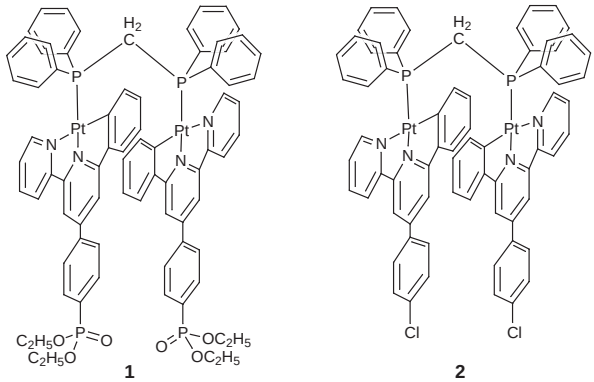

Fig. 1 Complexes **1** and **2**

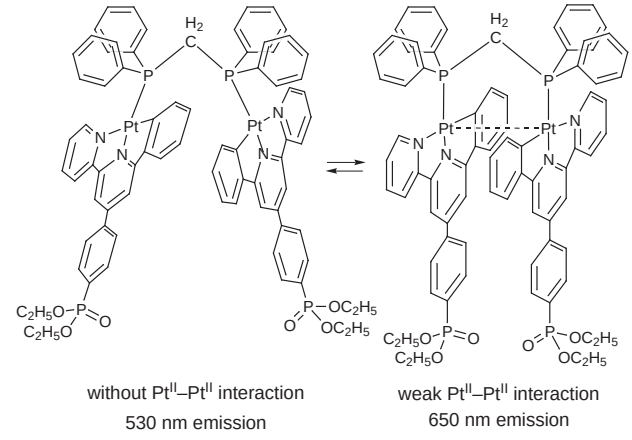

Scheme 1

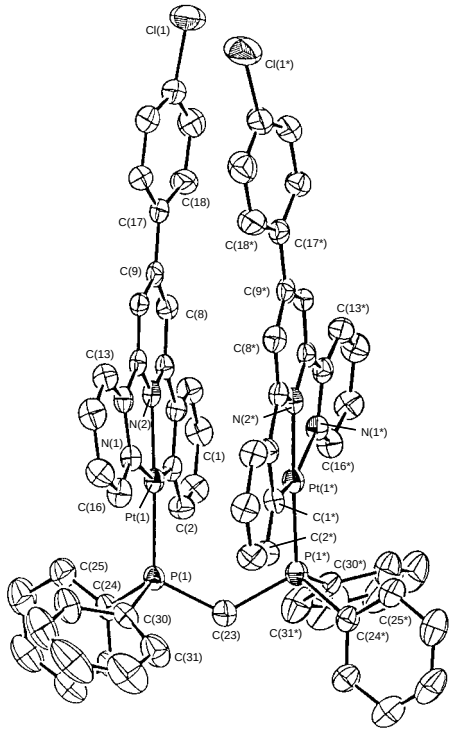

Fig. 2 Perspective view of **2**. Selected bond lengths (Å) and angles (°): Pt–Pt 3.150(1), Pt(1)–N(1) 2.15(1), Pt(1)–C(29) 2.02(1), P(1)–C(2) 1.84(1), N(1)–C(14) 1.34(1), N(2)–C(19) 1.35(1), Pt(1)–P(1) 2.25(1), Pt(1)–N(2) 2.00(1), P(1)–C(1) 1.82(1), P(1)–C(8) 1.82(1), N(1)–C(18) 1.37(1), N(2)–C(23) 1.36(1); P(1)–Pt(1)–N(1) 106.1(2), P(1)–Pt(1)–C(29) 95.5(2), N(1)–Pt(1)–C(29) 104.0(5), Pt(1)–P(1)–C(1) 115.4(3), Pt(1)–P(1)–C(8) 116.2(3), P(1)–Pt(1)–C(29) 95.5(2), N(1)–Pt(1)–N(2) 77.3(2), N(2)–Pt(1)–C(29) 80.9(3), Pt(1)–P(1)–C(2) 113.4(3), C(1)–P(1)–C(2) 105.6(4).

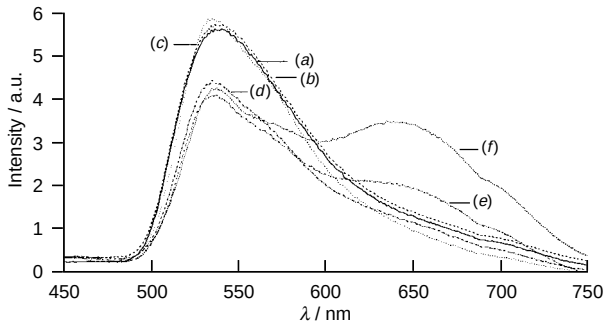

Fig. 3 Emission spectra of **1** at various [NaCl] in SDS micellar solution. [SDS] = 1.52×10^{-2} mol dm^{-3}, [**1**] = 3.46×10^{-6} mol dm^{-3}, [NaCl] mol dm^{-3}: (*a*) 0, (*b*) 0.06, (*c*) 0.2, (*d*) 0.3, (*e*) 0.4, (*f*) 0.5.

lifetime of the 530 nm emission. An additional emission maximum at 650 nm gradually develops as [NaCl] increases. The 650 nm emission corresponds well to the ^{3}MMLCT emission of **1** recorded in CH_2Cl_2 solution and in solid state. Time resolved emission spectra of **1** in SDS micellar solution recorded at [NaCl] = 0.5 M show different decay rates for the 530 and 650 nm emission maxima. This indicated that the two emissions are coming from two different excited states. Presumably they are the MLCT excited states of the two non-interacting cyclometallated Pt^{II} units and the MMLCT excited states of two interacting ones (Scheme 1), respectively. The sensitive responses of the luminescent properties of **1** to [NaCl] can be rationalized as follows. The cyclometallated Pt^{II} molecules may not reside too deep in the SDS micellar cores and are still subjected to quenching by the solvent molecules. Addition of Na^+ brings the SDS head groups closer in proximity through a reduction in electrostatic repulsion. This would reduce water penetration at the micellar surface and enhance the hydrophobicity of the medium so that solvent induced non-radiative decay at the open coordination sites is prohibited. Thus, the intensity and lifetime of the 530 nm emission are both enhanced upon initial addition of NaCl. Importantly, the alignment of the SDS head group with Na^+ cations would also force two cyclometallated Pt^{II} units close enough for intramolecular metal–metal and/or ligand–ligand interaction (Scheme 1). This ultimately leads to an accessible MMLCT excited state and accounts for the 650 nm emission at high NaCl concentration. The alignment of the SDS head groups in the micellar solution would be expected to depend on the size of the counter cations. We found that addition of K^+ or NH_4^+ gave a similar effect on the photoluminescence of the micellar solution of **1**. However, the bulky NMe_4^+ cation did not give rise to any low energy emission with $\lambda_{max} \geqslant 600$ nm.

The above data show that the emission properties of a cyclometallated dinuclear Pt^{II} complex are sensitive to the micelle environment. Switching from MLCT to MMLCT emission is observed upon micellar transformation. This reveals the potential application of weak metal–metal interaction present in a conformational non-rigid molecule as a sensitive probe for micellar microheterogeneous environments.

We acknowledge support from Hong Kong Research Grant Council and the University of Hong Kong.

Notes and References

† E-mail: cmche@hkucc.hku.hk

‡ *NMR data*: **1**$[PF_6]_2$: ^{1}H NMR (CD_3CN, 270 MHz), δ 1.40 (t, CH_2CH_3, 12 H), 4.29 (q, CH_2CH_3, 8 H), 4.88 [t, PCH_2P, ^3J(PtPCH$_2$) 13 Hz]. ^{31}P{^{1}H} NMR (MeCN), δ 19.46 [PCH_2P, ^1J(PtP) 2037 Hz], 16.75 [(EtO)OP]. **2**$[PF_6]_2$: ^{1}H NMR (CD_3CN, 270 MHz), δ 5.23 [t, PCH_2P, ^3J(PtPCH$_2$) 13 Hz]. ^{31}P{^{1}H} NMR (MeCN), δ 19.16, ^1J(PtP) 2060 Hz.

§ *Crystal data* for **2**$[PF_6]_2$; $C_{69}H_{52}Cl_2F_{12}N_4Pt_2P_4 \cdot 2C_3H_7NO$, M = 1893.33, monoclinic, space group $C2/c$ (no. 15), T = 301 K, a = 13.099(2), b = 38.901(4), c = 14.259(5) Å, β = 90.98(2)°, U = 7264(2) Å^3, Z = 4, D_c = 1.732 g cm^{-3}, μ(Mo-Kα) = 40.75 cm^{-1}, F(000) = 3720, an orange crystal of dimensions 0.50 × 0.07 × 0.05 mm, data collected by an Enraf-Nonius CAD4 diffractometer with graphite monochromated Mo-Kα radiation (λ = 0.710 73 Å), intensity data were corrected for Lorentz and polarization effects and empirial absorption corrections based on the ψ-scan of four strong reflections. Convergence for 3551 reflections with $I > 3\sigma(I)$ was reached at R = 0.029, wR = 0.032, goodness-of-fit = 1.48, $(\Delta/\sigma)_{max}$ = 0.03, the final difference Fourier map was featureless with maximum positive and negative peaks of 0.91 and 0.60 e Å^{-3} respectively. CCDC 182/806.

¶ *Spectroscopic data*: **1**$[PF_6]_2$: UV–VIS (CH_2Cl_2) [λ/nm, (ε/dm^3 mol^{-1} cm^{-1})]: 290 (6.58×10^4), 320 (4.30×10^4). Emission spectrum (CH_2Cl_2, 298 K) (λ_{max}/nm, τ/μs): 648 (2.30). **2**$[PF_6]_2$: UV–VIS (MeCN) [λ/nm, (ε/dm^3 mol^{-1} cm^{-1})]: 293 (4.79×10^4), 320 (4.12×10^4), 400–526 (3.90×10^3–1.00×10^3), 532–561 (9.70×10^2–2.00×10^2). Emission spectrum (MeCN, 298 K) (λ_{max}/nm, τ/μs): 661 (0.19).

1 V. H. Holding and V. M. Miskowski, *Coord. Chem. Rev.*, 1991, **111**, 145; J. A. Bailey, V. M. Miskowski and H. B. Gray, *Inorg. Chem.*, 1993, **32**, 369; H. K. Yip, C. M. Che, Z. Y. Zhou and T. C. W. Mak, *J. Chem. Soc., Chem. Commun.*, 1992, 1369.
2 J. H. Fendler, *Membrane Mimetic Chemistry*, Wiley-Interscience, New York, 1982.
3 H. Q. Liu, T. C. Cheung and C. M. Che, *Chem. Commun.*, 1996, 1039.
4 T. Hirao, T. Masunaga, Y. Ohshiro and T. Agawa, *Synthesis*, 1981, 56.
5 T. C. Cheung, K. K. Cheung, S. M. Peng and C. M. Che, *J. Chem. Soc., Dalton Trans.*, 1996, 1645.
6 J. P. Laurent, P. Lepage and F. Dahan, *J. Am. Chem. Soc.*, 1982, **104**, 7335.
7 C. W. Chan, T. F. Lai, C. M. Che and S. M. Peng, *J. Am. Chem. Soc.*, 1993, **115**, 11 245; M. Maestri, V. Sandrini, A. von Zelewsky and P. Jolliet, *Helv. Chim. Acta*, 1988, **71**, 134.
8 J. P. Krathovil, *J. Colloid Interface Sci.*, 1980, **75**, 271.

Received in Cambridge, UK, 3rd March 1998; 8/01754I

A novel, internally-solvated phosphinomethanide; crystal structure of $Li[C(SiMe_3)_2\{P(C_6H_4CH_2NMe_2\text{-}2)_2\}]$

William Clegg, Simon Doherty,*† Keith Izod*† and Paul O'Shaughnessy

Department of Chemistry, University of Newcastle upon Tyne, Newcastle upon Tyne, UK NE1 7RU

Metallation of $P\{CH(SiMe_3)_2\}(C_6H_4CH_2NMe_2\text{-}2)_2$ with Bu^nLi yields a novel lithium phosphinomethanide in which the ligand exhibits an unprecedented tridentate PN_2 coordination mode and in which there are no short contacts between lithium and the planar carbanion centre.

Over the last decade an extensive chemistry has emerged for phosphorus-stabilised carbanionic ligands such as the phosphinomethanides, R_2PCR_2, and diphosphinomethanides, $(R_2P)_2CR$. Interest in these ligands arises from their ability to bind to metal centres in a variety of coordination modes, providing varying degrees of steric hindrance and electron donation. Mono-, di- and tri-phosphinomethanides are known to coordinate as monodentate C-donors,[1] η^2-CP-donors,[2] bidentate PP-donors,[3] heteroallyl ligands,[4] and bridging ligands.[5] We now describe a unique coordination mode for such a ligand in a lithium derivative of an amino-functionalised phosphinomethanide.

Treatment of the tertiary phosphine $P\{CH(SiMe_3)_2\}(C_6H_4CH_2NMe_2\text{-}2)_2$ **1** with 1 equiv. of Bu^nLi in diethyl ether yields the novel phosphinomethanide $Li[C(SiMe_3)_2\{P(C_6H_4CH_2NMe_2\text{-}2)_2\}]$ **2**, isolated in high yield as yellow, air-sensitive plates (Scheme 1).‡ Whilst metallation of the related ligand $HC(PMe_2)(SiMe_3)_2$ requires heating under reflux with Bu^nLi for three weeks in hexane,[1] metallation of **1** was complete within 12 h at room temperature. It is reasonable to attribute the enhanced susceptibility of **1** towards deprotonation to chelation assistance, *i.e.* the coordination of an amino-group to lithium prior to the deprotonation step.

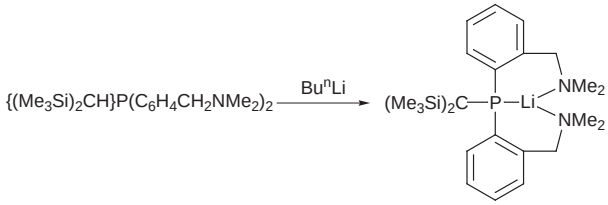

Scheme 1

The room temperature ^1H NMR spectrum of **2** exhibits two $SiMe_3$ signals, together with extremely broad resonances due to the benzylic and NMe_2 protons. These latter signals sharpen considerably at 60 °C, which suggests a dynamic process, possibly involving changes in chelate ring conformation or dissociation of the NMe_2-groups, in solution. In contrast, the ^{31}P and ^7Li NMR spectra of **2** consist of a sharp quartet and doublet respectively [$^1J(^{31}P–^7Li)$ 88.9 Hz], suggesting that a Li–P interaction is maintained in solution.

Since the addition of polydentate amines to lithium phosphinomethanides favours the formation of C-bonded species,[1] we were interested to observe the influence of intramolecular coordination of the dimethylamino groups on the structure of **2**. Unexpectedly, an X-ray diffraction study of **2** revealed an unprecedented tridentate PN_2 coordination mode for the phosphinomethanide ligand (Fig. 1).§ The lithium lies in a trigonal pyramidal environment (sum of angles at Li = 326.1°), coordinated solely by the phosphorus and nitrogen atoms of the ligand, forming two puckered, six-membered chelate rings, each with a bite angle of *ca.* 98°. The carbanion centre C(1) is perfectly planar [sum of angles at C(1) = 359.4°] and has no significant intra- or inter-molecular contacts to Li. Few examples of planar, isolated carbanions have been reported and the majority of these contain highly delocalised polyarylmethanide derivatives.[6]

As is common in phosphinomethanide species, the P–C(1) distance in **2** [1.735(3) Å] is substantially shorter than that expected for a P–C single bond, suggesting significant P–C multiple bond character. Indeed the P–C(1) distance in the tertiary phosphine $\{(Me_3Si)_2CH\}P(CH_2C_6H_4\text{-}2\text{-}NMe_2)_2$ **3**, which is isomeric with **1**, is 1.865(2) Å.[7] The P–C(1) distance in **2** is considerably longer than both the P–CH_2 distance of 1.702(2) Å in $[(PhCH_2)_2NLi\cdot CH_2PPh_3]_n$, a Li complex of a neutral P^V ylide,[8] and the P–C bond length range of 1.64(1) to 1.690(5) Å in a series of lithiated phosphine oxide compounds.[9] Such a difference is to be expected since these latter compounds are P^V derivatives with substantial ylidic character. The Si–C(1) distances of 1.818(3) and 1.826(3) Å are similar to previously reported Si–C distances in other silicon-stabilised carbanions.[10]

The Li–P distance of 2.427(6) Å is short in comparison to analogous distances in lithium phosphinomethanides where the ligand binds in its more usual coordination modes. For example, the Li–P distances in $[Li\{C(PMe_2)(SiMe_3)_2\}]_2$[1] and (tmen)-$Li\{C(PPh_2)_2(SiMe_3)\}$[3] are 2.519(4) and 2.530(7) Å, respectively. This may reflect the increased ionic contribution to the Li–P interaction associated with the delocalisation of charge from the carbanion centre to phosphorus.

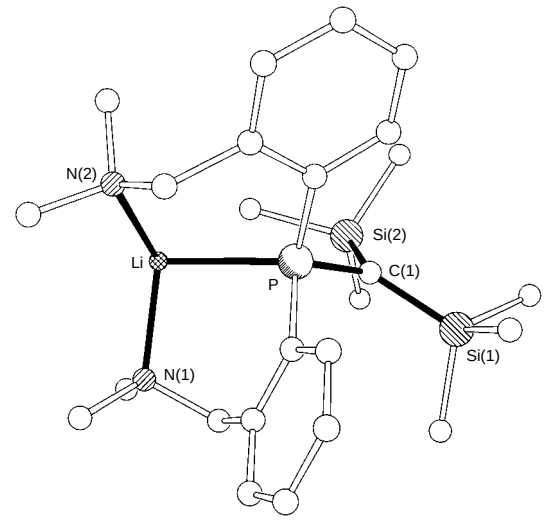

Fig. 1 Molecular structure of **2** (H atoms omitted for clarity). Selected bond lengths (Å) and angles (°): Li–P 2.427(6), Li–N(1) 2.096(6), Li–N(2) 2.083(6), C(1)–P 1.735(3), C(1)–Si(1) 1.818(3), C(1)–Si(2) 1.826(3), P–Li–N(1) 98.4(2), P–Li–N(2) 97.4(2), N(1)–Li–N(2) 130.3(3), Li–P–C(1) 126.31(16), P–C(1)–Si(1) 126.26(18), P–C(1)–Si(2) 113.61(17), Si(1)–C(1)–Si(2) 119.49(16).

Investigations into the coordination behaviour of this and related amino-functionalised phosphinomethanides are currently in progress.

Notes and References

† E-mail: k.j.izod@ncl.ac.uk; simon.doherty@ncl.ac.uk

‡ *Characterisation* of **2**: ^{1}H NMR (C_6D_6, 343K), δ 0.39 (s, $SiMe_3$), 0.62 (s, $SiMe_3$), 1.75 (br s, NMe_2), 3.10 (br s, CH_2NMe_2), 6.91–7.16 (m, ArH); ^{31}P NMR (C_6D_6), δ −18.2 [q, $^1J(^{31}P–^7Li)$ 88.9 Hz]; ^{7}Li NMR (C_6D_6), δ 1.25 (d).

§ *Crystal data* for **2**: $C_{25}H_{42}LiN_2PSi_2$, M = 464.7, triclinic, space group $P\bar{1}$, a = 9.1358(12), b = 9.3158(13), c = 17.369(2) Å, α = 86.816(3), β = 98.275(3), γ = 68.972(4)°, U = 1378.1(3) Å^3, Z = 2, D_c = 1.120 g cm^{-3}, μ = 0.20 mm^{-1} (Mo-Kα radiation, λ = 0.710 73 Å), T = 160 K, crystal size 0.28 × 0.18 × 0.02 mm. The structure was solved by direct methods and refined on F^2 values of all 4816 unique data (8451 data measured on Bruker AXS SMART diffractometer, $2\theta_{max}$ = 50°, R_{int} = 0.0501) with anistropic displacement parameters and riding isotropic hydrogen atoms; $wR2$ = 0.1161 for all F^2 values, conventional R = 0.0539 for F values of 2925 reflections having $F_o^2 > 2\sigma(F_o^2)$, goodness of fit = 0.985, for all F^2 values and 291 refined parameters. A final difference map was essentially featureless. Programs were standard Bruker AXS SMART, SAINT and SHELXTL together with local programs. CCDC 182/837.

1 H. H. Karsch, K. Zellner, P. Mikulcik, J. Lachmann and G. Muller, *Organometallics*, 1990, **9**, 190.
2 H. H. Karsch, B. Deubelly, J. Hofmann, U. Pieper and G. Muller, *J. Am. Chem. Soc.*, 1988, **110**, 3654.
3 H. H. Karsch, G. Grauvogl, P. Mikulcik, P. Bissinger and G. Muller, *J. Organomet. Chem.*, 1994, **465**, 65.
4 H. H. Karsch, A. Appelt and G. Muller, *Angew. Chem., Int. Ed. Engl.*, 1986, **25**, 823.
5 H. H. Karsch, G. Ferazin and P. Bissinger, *J. Chem. Soc., Chem. Commun.*, 1994, 505.
6 U. Pieper and D. Stalke, *Organometallics*, 1993, **12**, 1201 and references therein; T. Kottke and D. Stalke, *Chem. Ber./Recueil*, 1997, **130**, 1365; N. Wiberg, G. Wagner, G. Reber, J. Riede and G. Muller, *Organometallics*, 1987, **6**, 35; F. Adam, C. Eaborn, P. B. Hitchcock and J. D. Smith, *Chem. Commun.*, 1996, 741.
7 W. Clegg, S. Doherty, K. Izod and P. O'Shaughnessy, unpublished work.
8 D. R. Armstrong, M. G. Davidson and D. Moncrieff, *Angew. Chem., Int. Ed., Engl.* 1995, **34**, 478.
9 W. Zarges, M. Marsch, K. Harms, F. Haller, G. Frenking and G. Boche, *Chem. Ber.*, 1991, **124**, 861; S. E. Denmark, K. A. Swiss and S. R. Wilson, *Angew. Chem., Int. Ed. Engl.*, 1996, **35**, 2515; C. J. Cramer, S. E. Denmark, P. C. Miller, R. L. Dorow, K. A. Swiss and S. R. Wilson, *J. Am. Chem. Soc.*, 1994, **116**, 2437.
10 C. Eaborn, K. Izod and J. D. Smith, *J. Organomet. Chem.*, 1995, **500**, 89 and references therein.

Received in Basel, Switzerland, 16th February 1998; 8/01342J

Synthesis of polystyrene and silica gel polymer hybrids *via* π–π interactions

Ryo Tamaki, Ken Samura and Yoshiki Chujo*

Department of Polymer Chemistry, Graduate School of Engineering, Kyoto University, Yoshida, Sakyo-ku,Kyoto, 606-8501, Japan

Homogeneous polystyrene and silica gel polymer hybrids have been prepared utilizing the sol–gel reaction of phenyltrimethoxysilane; π–π interactions between phenyl groups of the organic polymer and those of silica gel were found to play a critical role for the homogeneity.

In recent years a large variety of organic and inorganic polymer hybrids have been synthesized by the sol–gel technique utilizing alkoxysilanes.[1–4] A most noticeable characteristic of these hybrid materials is the molecular-level integration of organic and inorganic elements. The interactions that have been utilized to integrate organic and inorganic phases are generally classified into two groups; covalent bonding and hydrogen bonding interactions.[2] The former interaction is attained by the incorporation of silane coupling groups into organic segments.[5] The latter interaction is effective when organic segments have polar functional groups such as amide and urethane groups. The interaction acts between these functional groups and residual silanol groups of silica gel.[1] On the other hand, π–π interactions are known as one of the types of attractive non-covalent bonding interactions which play a critical role in, for example, the stabilization of the double helical structure of DNA and complexation in host–guest systems.[6] Here we introduce a new approach to synthesize homogeneous polymer hybrids utilizing π–π interactions. Homogeneous polymer hybrids of polystyrene and silica gel were successfully prepared by this method.

Polystyrene and silica gel polymer hybrids were prepared by utilizing a sol–gel reaction of phenyltrimethoxysilane (PhTMOS). The sol–gel reaction proceeds *via* hydrolysis and subsequent condensation of alkoxysilanes. When an alkyl-substituted alkoxysilane is used as a starting material, the alkyl group is introduced into silica gel since the Si–C bond does not undergo hydrolysis reaction. Thus, phenyl groups would be introduced into the silica gel by the sol–gel reaction of PhTMOS.

As shown in Scheme 1, the alkoxysilane was added to a THF solution of polystyrene (M_w = 24 500, M_n = 17 700, M_w/M_n = 1.39) followed by an addition of 0.1 M HCl as catalyst. The mixture was then heated at 30 °C and the temperature was gradually raised to 80 °C and the sample kept at this temperature for a week. For comparison, other alkoxysilanes such as tetramethoxysilane (TMOS) methyltrimethoxysilane (MTMOS) and isobutyltrimethoxysilane (Bu^{i}TMOS) were also used as starting materials. The mass ratio of alkoxysilane to polystyrene was 0.1 or 1.0. Homogeneity of the obtained polymer hybrids was evaluated optically. Transparency of the polymer hybrids is attained only when silica gel particles embedded within polystyrene are smaller than the wavelength of light.[2] As shown in Table 1, transparent polymer hybrids were obtained for both mass contents when PhTMOS was used as a starting material for the sol–gel reaction. In contrast, polymer hybrids became translucent or turbid when TMOS, MTMOS or Bu^{i}TMOS were used. Other alkoxysilanes containing a phenyl ring were also employed for the synthesis of the polymer hybrids. Mesityltrimethoxysilane (MesTMOS) gave homogeneous polymer hybrids when the mass ratio was 0.1. However, the homogeneity deteriorated as the mass ratio was increased to 1.0. The result might be attributed to methyl groups on the phenyl ring of MesTMOS, which are suspected to interrupt the π–π interaction. When phenethyltrimethoxysilane (PhenethylTMOS) was used as the starting material homogeneous polymer hybrids were obtained for both mass contents. These results demonstrate that a phenyl ring is necessary for the homogeneous dispersion of polystyrene and silica gel. In addition, as was observed for MesTMOS, spatial bulkiness on

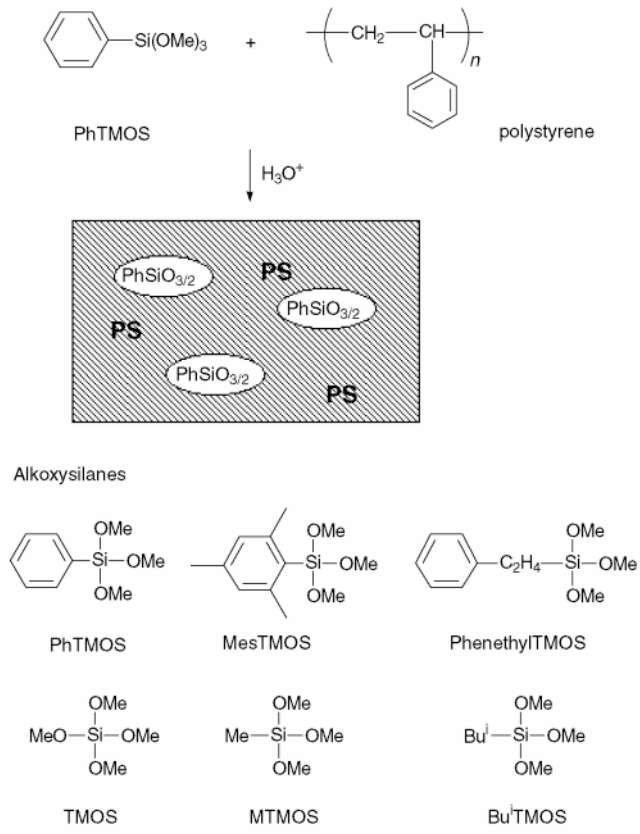

Scheme 1

Table 1 Effect of alkyl groups on homogeneity of silica gel hybrids

Run	$RSi(OMe)_3$[a]	$RSi(OMe)_3$ /PS[a]	0.1 M HCl/ml	Appearance
1	Ph	0.1	0.045	Transparent
2	Ph	1	0.045	Transparent
3	OMe	0.1	0.059	Turbid
4	OMe	1	0.059	Turbid
5	Me	0.1	0.078	Turbid
6	Me	1	0.078	Turbid
7	Bu^i	0.1	0.052	Turbid
8	Bu^i	1	0.052	Turbid
9	Mesityl	0.1	0.037	Transparent
10	Mesityl	1	0.037	Turbid
11	Phenethyl	0.1	0.040	Transparent
12	Phenethyl	1	0.040	Transparent

[a] 0.5 g of PS was dissolved in 5 ml of THF with $RSi(OR)_3$ and acid catalyst. The mixture was heated at 30–80 °C in an oven.

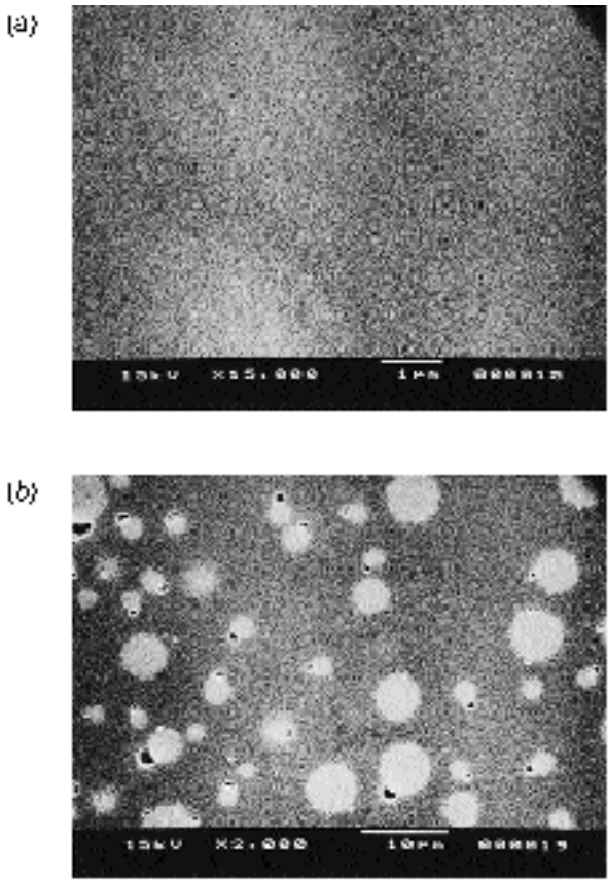

Fig. 1 Scanning electron micrographs of (*a*) a polymer hybrid prepared from PhTMOS and PS (*b*) a polymer hybrid prepared from MTMOS and PS

the phenyl rings was found to lead to deterioration of the homogeneity. Considering these results, it is expected that the stacking between phenyl rings of polystyrene and silica gel, rather than hydrophobic interactions, is critical for the homogeneous dispersion of the polymer and silica gel. Clear differences were observed in SEM measurements. As shown in Fig. 1, phase separation appeared in the polymer hybrid prepared from MTMOS with a mass ratio of 0.1 and silica gel domains of $\geqslant 5$ μm were observed. On the other hand, a polymer hybrid prepared from PhTMOS showed no recognizable segregation at this level. As the mass ratio of alkoxysilanes was increased to 1.0, the size of silica gel domains increased to 50 μm in the polymer hybrid prepared from MTMOS, while the polymer hybrid prepared from PhTMOS still showed a uniform image.

We also carried out the synthesis of polymer hybrids starting from poly(diallylphthalate) and polycarbonate as organic components which also have phenyl rings as repeating units. As observed in the case of polystyrene, transparent polymer hybrids were obtained when PhTMOS or PhenethylTMOS was used as a starting reagent for the inorganic part, while other alkoxysilanes such as TMOS, MTMOS or Bu^{i}TMOS gave only inhomogeneous polymer hybrids.[7] These results indicate that π–π interactions are quite effective for the synthesis of homogeneous polymer hybrids of aromatic polymers and silica gel.

Notes and References

† E-mail: tama@chujo.synchem.kyoto-u.ac.jp

1 Y. Chujo and T. Saegusa, *Adv. Polym. Sci.*, 1992, **100**, 11.
2 B. M. Novak, *Adv. Mater.*, 1993, **5**, 422.
3 U. Schubert, N, Husing and A. Lorenz, *Chem. Mater.*, 1995, **7**, 2010.
4 J. Wen and G. L. Wilkes, *Chem. Mater.*, 1996, **8**, 1667.
5 Y. Chujo, E. Ihara, S. Kure and T. Saegusa, *Macromolecules*, 1993, **26**, 5681.
6 C. A. Hunter and J. K. M. Sanders, *J. Am. Chem. Soc.*, 1990, **112**, 5525 and references therein.
7 R. Tamaki and Y. Chujo, unpublished work.

Received in Cambridge, UK, 12th December 1997; 7/08948A

Reductive elimination of α-alkynyl substituted zirconacyclopentenes: formation of cyclobutene derivatives

Yuanhong Liu,[a] Wen-Hua Sun,[a] Kiyohiko Nakajima[b] and Tamotsu Takahashi*[a]†

[a] *Catalysis Research Center and Graduate School of Pharmaceutical Sciences, Hokkaido University, Sapporo 060, Japan*
[b] *Department of Chemistry, Aichi University of Education, Igaya, Kariya 448, Japan*

Reductive elimination of α-alkynyl substituted zirconacyclopentenes, prepared from diaryldiynes and Cp_2ZrEt_2, proceeded upon heating or in the presence of dimethyl acetylenedicarboxylate to give alkynylcyclobutene derivatives.

Reductive elimination of two organic groups on metals is a basic reaction step for making new C–C bonds.[1] Although this step has been intensively investigated for late transition metal compounds, it has not been well studied for early transition metal compounds such as zirconium. To the best of our knowledge, only a few reductive couplings of two organic groups of organozirconium compounds have been reported, such as photolysis or oxidation of diphenylzirconocene producing biphenyl,[2] CO insertion into organozirconocenes or zirconacycles followed by migration giving ketone derivatives,[3] or an alkynyl–phenyl coupling *via* ate-complexation.[4] Here we report that the reductive coupling of α-alkynyl substituted zirconacyclopentenes, prepared by the reaction of diaryldiynes with Cp_2ZrEt_2, proceeded upon heating or in the presence of additives such as dimethyl acetylenedicarboxylate to give alkynylcyclobutene derivatives.

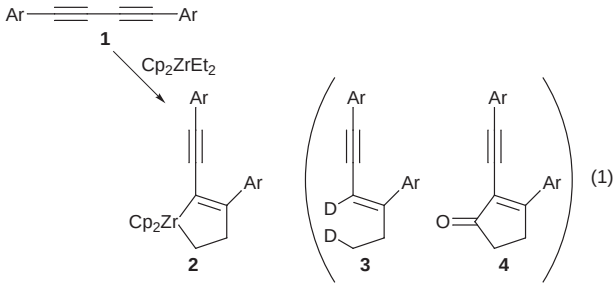

We have already reported that a reaction of diynes with $Cp_2Zr(CH_2{=}CH_2)$ *in situ* prepared from Cp_2ZrEt_2 afforded α-alkynylzirconacyclopentenes (**2**) which gave a dideuterated enyne **3** after deuterolysis [5] and α-alkynylcyclopentenones **4** by treatment with CO/I_2 [reaction (1)].[6] Here we find that, upon heating **2a**–**c** in THF at 50 °C for 9 h in the presence of 2 equiv. of PMe_3, a reductive elimination reaction of **2a**–**c** proceeds to afford the complexes **5a**–**c** in 61–86% NMR yields. Treatment of **5a**–**c** with an excess of I_2 produced alkynylcyclobutenes **6a**–**c** in 70–84% NMR yields based on diynes [reaction (2)]. This indicates that reductive elimination of **2a**–**c** took place to give cyclobutene derivatives. The Cp_2Zr^{II} species formed by the reductive elimination were trapped as alkyne complexes stabilized by PMe_3 and **6a**–**c** to give **5a**–**c**.[7]‡ This is the first example of the direct formation of cyclobutene derivatives from zirconacyclopentenes, to the best of our knowledge.[8]

In the presence of 1 equiv. of hex-3-yne instead of PMe_3, zirconacyclopentadienes **7a**–**d** were formed.[9] After hydrolysis of **7a**–**d**, cyclobutenyldienes **8a**–**d** were obtained in 74–85% yields as mixtures of two regioisomers in a ratio of 3 : 1 as expected (Scheme 1). Deuterolysis of **7a** instead of hydrolysis

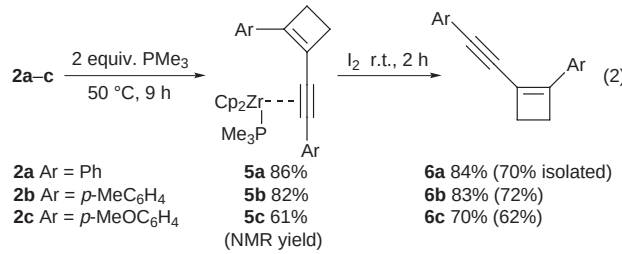

afforded a dideuterated product with > 98% deuterium incorporation. The zirconacyclopentadiene **7a** was further converted into benzene derivatives **9** as a mixture of two

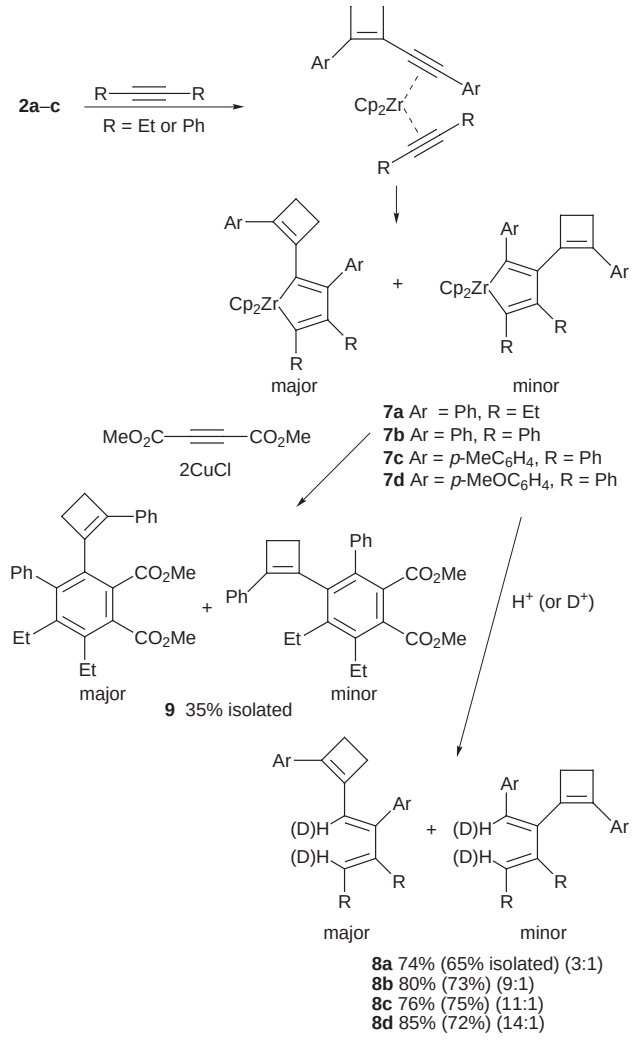

Scheme 1

regioisomers by the reaction with dimethyl acetylenedicarboxylate by our method.[10] The structure of minor isomer **9** was determined by X-ray analysis.§

Addition of dimethyl acetylenedicarboxylate to **2a**–**d** induced the direct formation of free **6a**–**d** in 64, 63, 62 and 69% NMR yields, respectively [reaction (3)]. Although the zirconium species trapped by dimethyl acetylenedicarboxylate was not clearly detected in this reaction, NMR study of this reaction revealed that the cyclobutene formation from **2a** at 50 °C obeys the first order rule and the reaction rate was 1.6×10^{-2} min^{-1}. This indicates that the presence of dimethyl acetylenedicarboxylate does not cause the reductive elimination. Dimethyl acetylenecarboxylate liberates **6** from zirconium.

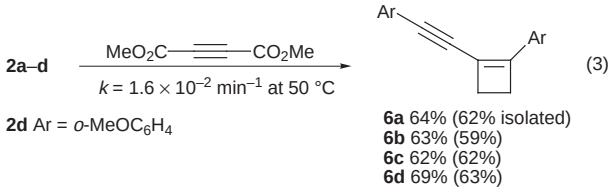

(3)

Note that the cyclobutene formation was also induced by the reaction of **2a** with allyl chloride,[11] vinyl butyl ether,[12] and a homoallyl bromide[13] as shown in Scheme 2. Hydrolysis of these reaction mixtures gave the corresponding products **10**–**12** in 70, 53 and 60% yields, respectively.

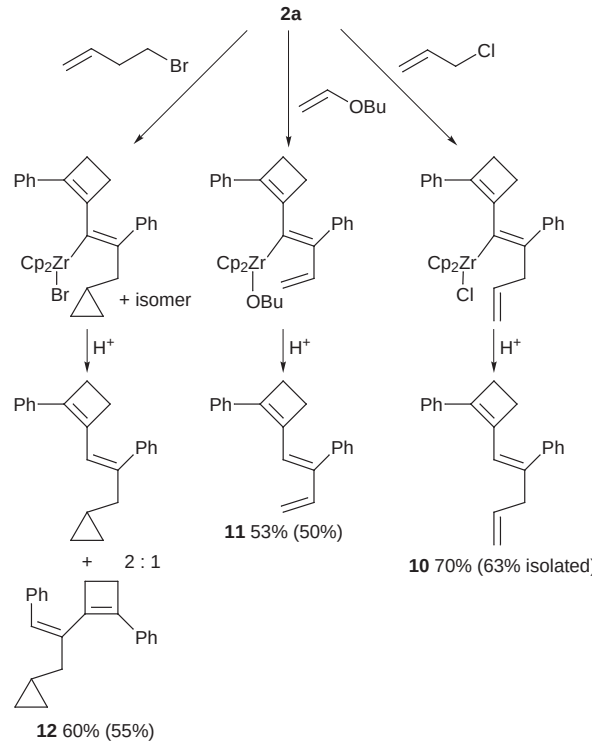

Scheme 2

Notes and References

† E-mail: tamotsu@cat.hokudai.ac.jp

‡ *NMR data* for **5a**: $\delta_H(C_6D_6)$ 1.18 (d, *J* 6.2, 9 H), 2.65 (br, 2 H), 2.79 (br, 2 H), 5.54 (br, 10 H), 6.92–7.66 (m, 10 H); $\delta_C(C_6D_6)$ 17.12(d), 25.89, 29.97, 102.91, 124.46, 124.74, 125.83, 126.08, 128.08, 128.50, 129.79, 138.62, 142.68, 154.39, 156.04(d), 178.77(d).

§ *Crystal data* for **9** (minor isomer): $C_{30}H_{30}O_4$, M = 454.57, monoclinic, space group $P2_1/n$ (no. 14), a = 7.0458(3), b = 20.7179(6), c = 17.3291(8) Å, β = 94.627(6)°, U = 2521.4(2) Å^3, Z = 4, D_c = 1.20 g cm^{-3}, μ(Cu-Kα) = 5.9 cm^{-1}, 5565 measured reflections, 3950 reflections with $I > 3\sigma(I)$, R = 0.046. CCDC 182/826.

1 J. P. Collman, L. S. Hegedus, *Principles and Applications of Organotransition Metal Chemistry*, University Science Books, Mill Valley, CA, 1980.

2 V. Skibbe and G. Erker, *J. Organomet. Chem.*, 1983, **241**, 15; M. J. Burk, W. Tumas, M. S. Ward and D. R. Wheeler, *J. Am. Chem. Soc.*, 1990, **112**, 6133.

3 F. Rosenfeldt and G. Erker, *Tetrahedron Lett.*, 1980, **21**, 1637; C. J. Rousset, D. R. Swanson, F. Lamaty and E. Negishi, *Tetrahedron Lett.*, 1989, **30**, 5105; E. Negishi, *Comprehensive Organic Synthesis*, ed. L. A. Paquette, Pergamon, 1991, vol. 5, 1163.

4 K. Takagi, C. J. Rousset and E. Negishi, *J. Am. Chem. Soc.*, 1991, **113**, 1440.

5 T. Takahashi, K. Aoyagi, V. Denisov, N. Suzuki, D. Choueiri and E. Negishi, *Tetrahedron Lett.*, 1993, **34**, 8301.

6 T. Takahashi, Z. Xi, Y. Nishihara, K. Kasai, S. Huo and E. Negishi, *Tetrahedron*, 1997, **53**, 9123.

7 T. Takahashi, D. R. Swanson and E. Negishi, *Chem. Lett.*, 1987, 623; S. L. Buchwald, B. T. Watson and J. C. Huffman, *J. Am. Chem. Soc.*, 1987, **109**, 2544.

8 Recently Negishi *et al*. reported the cyclobutene formation from 1,4-diiodobutene derivatives which were prepared from zirconacyclopentenes. See E. Negishi, F. Liu, D. Choueiry, M. M. Mohamud, A. Silveira, Jr. and M. Reeves, *J. Org. Chem.*, 1996, **61**, 8325.

9 E. Negishi, S. J. Holms, J. M. Tour, J. A. Miller, F. E. Cederbaum, D. R. Swanson and T. Takahashi, *J. Am. Chem. Soc.*, 1989, **111**, 3336; S. L. Buchwald and R. B. Nielsen, *J. Am. Chem. Soc.*, 1989, **111**, 2870; Z. Xi, R. Hara and T. Takahashi, *J. Org. Chem.*, 1995, **60**, 4444.

10 T. Takahashi and M. Kotora, Z. Xi, *J. Chem. Soc., Chem. Commun.*, 1995, 361.

11 T. Takahashi, N. Suzuki, M. Kageyama, D. Y. Kondakov and R. Hara, *Tetrahedron Lett.*, 1993, **34**, 4811; N. Suzuki, D. Y. Kondakov, R. Hara, M. Kageyama, M. Kotora and T. Takahashi, *Tetrahedron*, 1995, **51**, 4519.

12 T. Takahashi, D. Y. Kondakov, Z. Xi and N. Suzuki, *J. Am. Chem. Soc.*, 1995, **117**, 5871.

13 T. Takahashi, D. Y. Kondakov and N. Suzuki, *Tetrahedron Lett.*, 1993, **34**, 6571.

Received in Cambridge, UK, 10th February 1998; 8/01163J

An efficient chemical method for removing N-terminal extra methionine from recombinant methionylated human growth hormone

Osamu Nishimura,*[a]† Masato Suenaga,[a] Hiroaki Ohmae,[a] Shinji Tsuji[a] and Masahiko Fujino[b]

[a] *Biotechnology Laboratories, Pharmaceutical Research Division, Takeda Chemical Industries, Ltd., Yodogawa-ku, Osaka 532, Japan*

[b] *Takeda Chemical Industries, Ltd., Chuou-ku, Osaka 541, Japan*

Conversion of recombinant methionylated human growth hormone (Met-hGH) into its non-methionylated form (hGH) has been successfully achieved by a chemical process, which consists of a transamination reaction and phenylene-1,2-diamine treatment.

Production of recombinant proteins for clinical use has been increasing with the advent of genetic engineering technology. However, there are still numerous problems in the production of recombinant proteins. Typically, difficulties remain in the addition of methionine at the N-terminus corresponding to the initiation cordon (ATG),[1] refolding from inactive inclusion bodies,[2–4] post-translational modification[5–7] and heterogeneity[8,9] caused by endogenous proteases. We have encountered and given some answers to these problems during the production of various kinds of recombinant proteins in our laboratories, such as interferon-α,[5] interferon-γ,[6,8] interleukin-2[10] and the basic fibroblast growth factor mutein.[7]

Recombinant proteins are often produced with an additional methionine at the N-terminus because methionine aminopeptidase is strongly influenced by the kind of amino acid residue.[11] Thus, the N-terminal methionine is hard to cleave when the side chain of the adjacent amino acid is bulky or charged. Recombinant human growth hormone(hGH) produced in *Escherichia coli* is fully methionylated[1] because the N-terminal amino acid is phenylalanine. The removal of the additional N-terminal methionine is a great concern in the production of recombinant hGH for therapeutic applications since physiological features, such as biological activity, stability *in vivo* and antigenicity of methionylated derivatives, may be different from those of the natural species. In this regard, we have previously reported a procedure for cleavage by aminopeptidase M.[12]

Dixon and co-workers removed the N-terminal residue of *Pseudomonas* cytochrome c-551 after transamination[13,14] in order to study whether the N-terminal residue is essential for the function of the protein or not. However, this method has never been used to remove an additional methionine at the N-terminus of recombinant proteins. We took advantage of this method for the production of hGH from Met-hGH[12] produced in *E. coli*, and found it to be of great value as a versatile procedure for the preparation of non-methionylated hGH, as well as other non-methionylated recombinant proteins.

Here we describe our chemical procedure for removing extra-methionine at the N-terminus and show the first example of removing an additional methionine at the N-terminus of a recombinant protein using a chemical method.

To obtain hGH, we optimized both the transamination and the scission reaction and found that the best conditions were: 8 mM $CuSO_4$, 0.5 M glyoxylic acid and 10% pyridine for the former and 40 mM phenylene-1,2-diamine, 2 M NaOAc and 2 M AcOH for the latter. As shown in Scheme 1, Met-hGH[12] was converted into the oxo-acyl form‡ and then passed through a column of Sephadex G-25.§ The resulting product was cleaved with phenylene-1,2-diamine¶ to give crude hGH, in *ca.* 70% conversion yield, which was then purified by chromatography on Sephadex G-25, followed by DEAE-5PW.‖ Thus, about 60 mg of the purified hGH was obtained from 100 mg of Met-hGH. To confirm the structural identity of the purified hGH, protein chemical analysis was performed. The N-terminal amino acid sequence, the C-terminal amino acid and the amino acid analysis were all in good agreement with those predicted from the corresponding cDNA sequence. The purified hGH was migrated as a single band on SDS-PAGE and showed the electrophoretic mobility of a *ca.* 22 kDa species under reducing conditions (Fig. 1). Copper ions were not detected in the

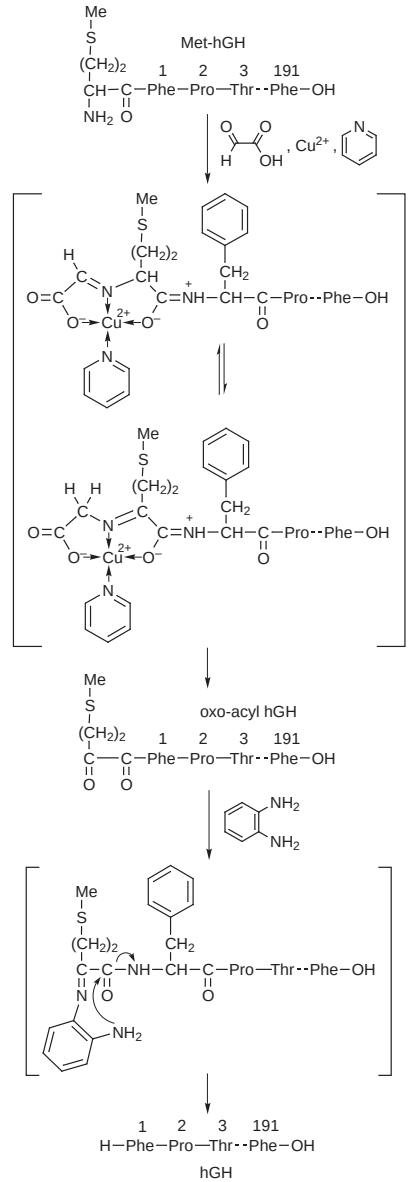

Scheme 1

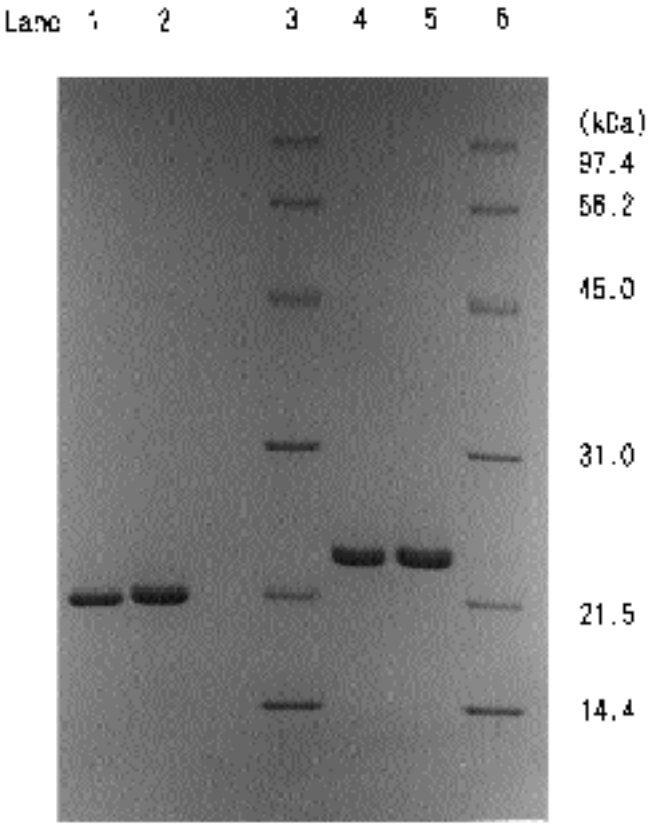

Fig. 1 SDS-PAGE of Met-hGH and hGH obtained from Met-hGH after transamination. Lanes 1 and 2: nonreducing conditions. Lanes 4 and 5: reducing conditions. Lanes 1 and 4: hGH. Lanes 2 and 5: Met-hGH. Lanes 3 and 6, marker proteins.

purified hGH when checked by AAS. To obtain further structural information, the purified hGH was subjected to mapping analysis.** As shown in Fig. 2, the peptide map obtained was identical to that of authentic hGH.†† The purified hGH also had the same order of activity as that of authentic hGH,†† when assayed using Nb2 Node lymphoma cells,[15] indicating that hGH obtained from Met-hGH has essentially the same chemical and biological identity as that of authentic hGH.††

In conclusion, we could obtain hGH from Met-hGH by a chemical method, and we could also apply the same procedure to other methionylated recombinant proteins including neurotrophin-3,[4] interleukin-2[10] and betacellulin,[16] to give the corresponding desired proteins having no methionine at the N-terminus. These results suggest that the present method might be widely applicable to the preparation of non-methionylated recombinant proteins for clinical use and show a new way for the production of recombinant proteins.

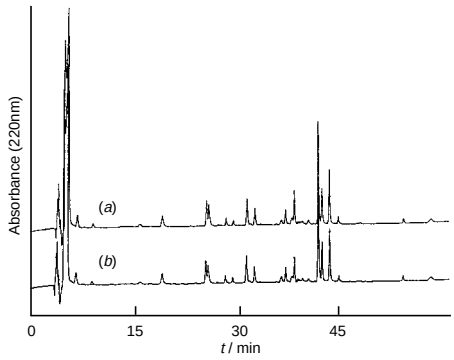

Fig. 2 Peptide maps of (*a*) authentic hGH and (*b*) hGH obtained from Met-hGH after transamination

We express our appreciation to Dr K. Meguro and Dr Y. Sumino for their encouragement and helpful discussion throughout this study. We are also grateful to Dr S. Iwasa and Dr T. Kurokawa for determining the biological activity and Dr H. Sawada for culturing the recombinant *E. coli*. Thanks are also due to Dr D. G. Cork for proofreading the manuscripts.

Notes and References

† E-mail: nishimura_osamu@takeda.co.jp

‡ To 3.75 g of glyoxylic acid monohydrate were added 1.2 ml of 0.5 M $CuSO_4$ and 7.5 ml of pyridine and the total volume was adjusted to 15 ml. Then 60 ml of Met-hGH (protein content 1.67 mg ml^{-1}) solution containing 3 M urea was added and incubated for 1 h at 25 °C.

§ The reaction mixture was applied at a flow rate of 0.5 l h^{-1} to a Sephadex G-25 (Pharmacia Biotech, Sweden) column (4.6 × 60 cm) equilibrated with 20 mM Tris-HCl buffer (pH 8.0) containing 2.5 M urea, and the sample was eluted with the same buffer. The main fraction (200 ml) was pooled.

¶ 200 ml of the protein solution, 200 ml of 4 M NaOAc, 4 M AcOH, 3 M urea and 1.73 g of phenylene-1,2-diamine were mixed and incubated for 3 days at 4 °C. In order to minimize oxidation, nitrogen was bubbled through the solutions to remove as much oxygen as possible and the incubations were carried out under nitrogen.

‖ The reaction mixture was applied at a flow rate of 2 l h^{-1} to a Sephadex G-25 (Pharmacia Biotech, Sweden) column (11.3 × 80 cm) equilibrated with 20 mM Tris-HCl buffer (pH 8.0) containing 2.5 M urea and the sample was eluted with the same buffer. The pooled fraction (1000 ml) was applied at a flow rate of 1 l h^{-1} to a DEAE-5PW (Tosoh Corporation, Japan) column (5.53 × 20 cm) equilibrated with 50 mM Tris-HCl buffer (pH 8.0) containing 2.5 M urea. After adsorption, the protein was eluted with a linear gradient of pH (8–4) between 50 mM Tris-HCl buffer (pH 8.0) containing 2.5 M urea and 50 mM MES buffer (pH 4.0) containing 2.5 M urea. The main fraction (150 ml) (protein content 0.4 mg ml^{-1}) was pooled.

** hGH was dissolved in 0.2 M Tris-HCl buffer (pH 8.0). The solution was incubated with TPCK-treated-trypsin (Worthington Biochemical Corp.) at a substrate-enzyme ratio of 25 : 1 (w/w) at 37 °C for 18 h, followed by a second enzyme addition to give a final concentration of 12.5 : 1 (w/w). At the end of the digest (6 h), the pH was lowered to 3 with 1 M HCl. The tryptic peptides were analyzed by reversed-phase HPLC (RP-HPLC) using a C8P-50 (Showa Denko, Japan) column (4.6 × 300 mm) and eluted at a flow rate of 0.8 ml min^{-1} with a linear gradient of 8–56% MeCN in the presence of 0.1% TFA.

†† The hGH standard was obtained from the National Institute of Health Sciences (Japan).

1 K. C. Olson, J. Fenno, N. Lin, R. N. Harkins, C. Snider, W. H. Kohr, M. J. Ross, D. Fodge, G. Prender and N. Stebbing, *Nature (London)*, 1981, **293**, 408.
2 S. Honda, H. Sugino, K. Nishi, K. Nara and A. Kakinuma, *J. Biotechnol.*, 1987, **5**, 39.
3 T. Yamada, A. Fujishima, K. Kawahara, K. Kato and O. Nishimura, *Arch. Biochem. Biophys.*, 1987, **257**, 194.
4 M. Suenaga, H. Ohmae, S. Tsuji, T. Itoh and O. Nishimura, *Biotechnol. Appl. Biochem.*, in the press.
5 T. Takao, M. Kobayashi, O. Nishimura and Y. Shimonishi, *J. Biol. Chem.*, 1987, **262**, 3541.
6 S. Honda, T. Asano, T. Kajio and O. Nishimura, *Arch. Biochem. Biophys.*, 1989, **69**, 612.
7 M. Suenaga, H. Ohmae, S. Tsuji, Y. Tanaka, N. Koyama and O. Nishimura, *Prep. Biochem. Biotechnol.*, 1996, **26**, 259.
8 S. Honda, T. Asano, T. Kajio, S. Nakagawa, S. Ikeyama, Y. Ichimori, H. Sugino, K. Nara, A. Kakinuma and H. Kung, *J. Interferon Res.*, 1987, **7**, 145.
9 M. Kobayashi, T. Asano, M. Utsunomiya, Y. Itoh, Y. Fujisawa, O. Nishimura, K. Kato and A. Kakinuma, *J. Biotechnol.*, 1988, **8**, 1.
10 T. Yamada, K. Kato, K. Kawahara and O. Nishimura, *Biochem. Biophys. Res. Commun.*, 1986, **135**, 837.
11 A. Ben-Bassat, K. Bauer, S. Y. Chang, K. Myambo, A. Boosman and S. Chang, *J. Bacteriol.*, 1987, **169**, 751.
12 S. Nakagawa, T. Yamada, K. Kato and O. Nishimura, *Biotechnology*, 1987, **5**, 824.
13 H. B. F. Dixon and V. Moret, *Biochem. J.*, 1965, **94**, 463.
14 H. B. F. Dixon, *Biochem. J.*, 1964, **92**, 661.
15 T. Tanaka, R. P. C. Shiu, P. W. Gout, C. T. Beer, R. L. Noble and H. G. Friesen, *J. Clin. Endocrinol. Metab.*, 1980, **51**, 1058.
16 M. Seno, H. Tada, M. Kosaka, R. Sasada, K. Igarashi, Y. Shing, J. Folkman, M. Ueda and H. Yamada, *Growth Factors*, 1996, **13**, 181.

Received in Cambridge, UK, 16th February 1998; 8/01297K

X-Ray crystal and *ab initio* structure of 3-ethynylcyclopropene: a curiously short carbon–carbon double bond

Kim K. Baldridge,[a] Bluegrass Biggs,[b] Dieter Bläser,[c] Roland Boese,*[c]† Robert D. Gilbertson,[b] Michael M. Haley,*[b]‡ Andreas H. Maulitz[c] and Jay S. Siegel*[d]§

[a] *San Diego Supercomputer Center, PO Box 85608, San Diego, CA 92186-9784, USA*
[b] *Department of Chemistry, University of Oregon, Eugene, OR 97403-1253, USA*
[c] *Institut für Anorganische Chemie, Universität-GH Essen, Universitätsstrasse 5-7, D-45117 Essen, Germany*
[d] *Department of Chemistry, University of California, San Diego, La Jolla, CA 92093-0358, USA*

The X-ray crystal structure of 3-ethynylcyclopropene shows that the carbon–carbon double bond of the molecule is unusually short [1.255(2) Å], whereas theoretical calculations suggest a relative insensitivity of the bond length to adjacent orbital interactions.

Recent crystallographic studies of lightly-substituted cyclopropenes have illustrated the uncommon bonding modes in these small-ring hydrocarbons, such as formation of bent, banana-like bonds.[1,2] One of our groups recently reported the preparation of highly unsaturated analogs, such as 3-ethynylcyclopropene **1**,[3]

1

and sought to investigate the solid-state structures of these compounds. In keeping with the extraordinary geometrical results, we report herein the X-ray crystal structure of **1** as well as model calculations to explain the experimental atomic distances for **1**.

Molecule **1** was prepared according to the literature method.[3] A single crystal (mp −94 °C) was grown using the low-temperature techniques described previously.[4,5] The structure analysis was performed at 120 K.¶ With intermolecular H···H separations of 2.73 Å or greater, the crystal packing of **1** is assumed not to cause significant distortions. The molecular structure and bond distances and angles are presented in Fig. 1 and Table 1, respectively. As expected, the sp^3 bond angle about C(1)–C(3)–C(2) is highly constrained, being only 49.4°. The most striking feature of the bond lengths found for **1** is the amazingly short C=C bond. At 1.255 Å, this value is midway between the accepted values of a typical double and triple bond.[6] The analogous bond length in structurally related 3-ethenylcyclopropene **2** is somewhat longer at 1.279 Å.[2b] All of the other bond lengths and bond angles of **1** are typical of their respective structural subunits. A systematic error in the measurement of the C(1)–C(2) bond distance is rather unlikely since the ellipsoids of the anisotropic displacement parameters

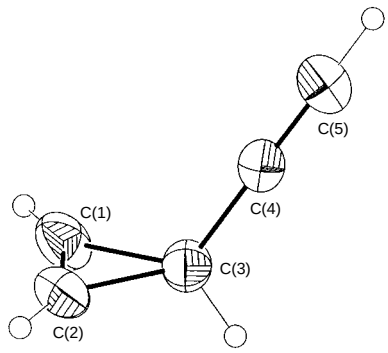

Fig. 1 Molecular structure of **1** with the ellipsoids drawn at the 50% level

Table 1 Interatomic distances and angles for **1**

Atoms	Distance/Å	Atoms	Angle (°)
C(1)–C(2)	1.255(2)	C(1)–C(2)–C(3)	65.2(1)
C(1)–C(3)	1.500(2)	C(2)–C(1)–C(3)	65.4(1)
C(2)–C(3)	1.502(2)	C(1)–C(3)–C(2)	49.4(1)
C(3)–C(4)	1.448(2)	C(1)–C(3)–C(4)	121.4(1)
C(4)–C(5)	1.184(2)	C(2)–C(3)–C(4)	121.4(1)
		C(3)–C(4)–C(5)	179.0(1)

are not elongated in the direction of the double bond.[7] In any case, the C(1)–C(2) bond length in **1** is the shortest crystallographically observed carbon–carbon double bond known in any hydrocarbon.[8]

2 R = $CH{=}CH_2$ **6** R = Me
3 R = NO_2 **7** R = H
4 R = CHO **8** R = F
5 R = C≡N **9** R = NH_2

In order to gain some insight into the nature of the cyclopropene structural fragment, a series of 3-monosubstituted cyclopropenes **2**–**9** was calculated in addition to **1**.[9] We first surveyed the variation in length of the C=C bond with regard to computational method (Table 2). Convergence in RHF methods is around a value of 1.27 Å; the effects of increasing basis set size was minimal. The effects of dynamic correlation were tested using a variety of techniques, including density functional techniques, Moller–Plesset theory of order 2 and the coupled cluster doubles method. The effect of each technique can be identified by focusing on the different dynamic correlation methods using the same basis set [DZ(2df,2p)]. Dynamic correlation of any type tends to increase the predicted bond length from the restricted Hartree–Fock method. Centering on the hybrid method of including dynamical correlation, and further increasing basis set size, one arrives at a convergent value for the double bond length around 1.28 Å, 0.03 Å longer than experiment. We feel it is unlikely that higher level calculations will decrease the bond length any nearer to the experimental value; thus, our best estimate of equilibrium bond length is 1.28 Å.

Given the result of the basis set analysis on **1**, we opted for a highly polarized basis set available in CADPAC, and performed computations on **1**–**9** using RHF/8s6p3d and B3PW91/8s6p3d methods (Table 3). The range of computed double bond lengths is only 0.02 Å, indicating a weak sensitivity of C(1)–C(2) length with regard to the C(3) substituent. The addition of dynamic electron correlation increases the predicted bond lengths uniformly by *ca*. 0.015 Å across the series, and makes no change in the trend. The experimentally measured value for **2** (1.279 Å) is well-bracketed by the computational predictions, but the values predicted for **1** are 0.01–0.02 Å longer than that

Table 2 The double bond length in **1** as a function of computational method

Method	Bond length/Å
RHF/6-31G(d,p)	1.2722
RHF/6-31GE	1.2749
RHF/DZ(2df,p)	1.2749
RHF/DZ(2df,2p)	1.2740
RHF/DZ(3df,3pd)	1.2704
RHF/8s6p3d	1.2710
BPW91/6-31GE	1.3022
BPW91/DZ(2df,2p)	1.3036
B3PW91/6-31G	1.3015
B3PW91/DZP	1.3003
B3PW91/6-31GE	1.2923
B3PW91/DZ(2df,2p)	1.2930
B3PW91/8s6p3d	1.2838
B3LYP/8s6p3d	1.2833
MP2/6-31G(2d,p)	1.3029
MP2/DZ(2df,2p)	1.3016
CCD/DZ(2df,2p)	1.2951
Experiment	1.2550

Table 3 C(1)–C(2) distance calculated for **1**–**9**

		Distance/Å	
Compound	R	RHF/8s6p3d	B3PW91/8s6p3d
3	NO_2	1.279	1.295
4	CHO[a]	1.265	1.279
	CHO[b]	1.263	1.278
5	C=N	1.267	1.283
1	C=CH	1.268	1.284
2	$CHCH_2$[a]	1.270	1.285
	$CHCH_2$[b]	1.270	1.286
6	Me	1.273	1.289
7	H	1.271	1.287
8	F	1.283	1.300
9	NH_2[c]	1.273	1.289
	NH_2[d]	1.274	1.290
average		1.271	1.287
standard deviation		0.006	0.006
range		0.020	0.022

[a] *anti* conformer (C_s symmetry). [b] *gauche* conformer (C_1 symmetry). [c] Lone pair *syn* (C_s symmetry). [d] Lone pair *anti* (C_s symmetry).

observed experimentally. This deviation could come from difficulties in approximating the orbital arrangement in **1**, even by the extreme basis sets we are using.

We acknowledge the National Science Foundation (CHE-9502588, CHE-9628565 and ACS-8902827) and the Fonds der Chemischen Industrie for support of this research. A grant for supercomputing time was provided by the San Diego Supercomputer Center.

Notes and References

† E-mail: boese@structchem.uni-essen.de (X-ray)
‡ E-mail: haley@oregon.uoregon.edu (synthesis)
§ E-mail: jss@chem.ucsd.edu (calculations)

¶ *Crystal data* for **1**: C_5H_4, M = 64.0876, cylindric single crystal of 0.3 mm diameter, a = 8.731(3), b = 6.169(3), c = 7.981(3) Å, β = 110.13(3)°, V = 403.6(3) Å^3 (from 30 refined reflections in the range of 20 < 2θ < 25°), 120 K, monoclinic, space group $P2_1/c$, Z = 4, ρ_{calc} = 1.055 g cm^{-3}, Mo-Kα radiation, μ = 0.06 mm^{-1}, 1164 data collected (2θ_{max} = 60°), 952 unique reflections (R_{merg} = 0.011), 718 observed [$F_o \geq 4\sigma(F)$], correction for a cylindrical crystal, structure refinement (C atoms anisotropic, H atoms isotropic without constraints, no extinction correction) with Siemens SHELXTL-PLUS (Ver. 4.2), 63 parameters, R = 0.0399, R_w = 0.0412, $w^{-1} = \sigma^2(F_o) + 0.0003F_o^2$, maximum residual electron density of 0.17 e Å^{-3}. CCDC 182/864.

1 R. Boese, in *Advances in Strain in Organic Chemistry*, ed. B. Halton, JAI Press, London, 1992, vol. 2, p. 191.
2 (*a*) R. Boese, D. Bläser, R. Gleiter, K.-H. Pfeifer, W. E. Billups and M. M. Haley, *J. Am. Chem. Soc.*, 1993, **115**, 743; (*b*) R. Boese, D. Bläser, W. E. Billups, M. M. Haley, W. Luo and B. E. Arney, Jr., *J. Org. Chem.*, 1994, **59**, 8125.
3 M. M. Haley, B. Biggs, W. A. Looney and R. D. Gilbertson, *Tetrahedron Lett.*, 1995, **36**, 3457.
4 R. Boese and M. Nussbaumer, in *Organic Crystal Chemistry, IUCr Crystallographic Symposia*, ed. D. W. Jones and A. Katrusiak, Oxford University Press, Oxford, England, 1994, vol. 7, p. 20.
5 R. Boese, D. Osswald, D. Brodalla and D. Mootz, *J. Appl. Crystallogr.*, 1985, **18**, 316.
6 F. Allen, O. Kennard, D. G. Watson, L. Brammer, A. G. Orpen and R. Taylor, *J. Chem. Soc., Perkin Trans 2*, 1987, S1.
7 With high bond orders, *e.g.* triple bonds, X-ray methods tend to determine bond distances too short because in the refinement procedure the atom positions are shifted towards the bonding electrons. In such cases the ellipsoids are streched in the bonding direction; however, this is not the case with **1** (Fig. 1). This effect can be reduced by high angle refinements or applying a weighted scheme which increases the weights for high angle data. In our case this had only a very small effect.
8 A search of the Cambridge crystallographic data base revealed the previous record holder of shortest C=C bond in a hydrocarbon to be 3-ethenylcyclopropene **2** [ref. 2(*b*)].
9 Reported here are Restricted Hartree–Fock (RHF), density functional (DFT), hybrid density functional (HDFT), Moller–Plesset perturbation theory (MP2) (ref. 10) and coupled cluster doubles (CCD) (ref. 11) theories. These calculations were performed using CADPAC (ref. 12) and GAUSSIAN94 (ref. 13) programs. Basis sets are reported including 6-31G(ndqf,mp) (ref. 14), 6-31GE, DZ(nd,mp), (ref. 15) and the 8s6p3d basis set, where the number of f functions (q = 0–1), d functions (n = 0–3) and p functions (m = 0–3). The 6-31GE and 8s6p3d basis sets are special to CADPAC. The former basis is obtained from the 6-31G basis by (i) adding diffuse s and p functions with exponents 1/3 that of the lowest exponent in the parent basis, and (ii) using two sets of polarization functions, which are slightly on the diffuse side. The result is a basis set between DZP and TZ + 2P type basis sets in quality which is biased towards property calculations. The latter basis is one of the largest polarized double-z sets used in this study. The DFT method employed was Beck's 1988 functional (ref. 16) along with Perdew and Wang's 1991 gradient-corrected correlation functional (ref. 17), denoted BPW91. The HDFT method includes a mixture of Hartree–Fock exchange with DFT exchange-correlation, denoted B3PW91. This is Becke's 3 parameter functional (ref. 18) where the nonlocal correction is provided by the Perdew 91 expression (ref. 17). A B3LYP [correlation functional including both local and nonlocal terms provided by Lee, Yang and Parr (refs. 18, 19)] calculation is done for comparison purposes. The nature of each stationary point was uniquely characterized by analytically calculating and diagonalizing the matrix of energy second derivatives (Hessian) to determine the number of imaginary frequencies.
10 B. I. Dunlap, J. W. D. Connolly and J. R. Sabin, *J. Chem. Phys.*, 1979, **71**, 3396.
11 J. A. Pople, R. Krishnan, H. B. Schlegel and J. S. Binkley, *Int. J. Quant. Chem., XIV*, 1978, 545.
12 R. D. Amos and J. E. Rice, 'CADPAC: The Cambridge Analytic Derivatives Package', issue 5.2, Cambridge, 1987.
13 M. J. Frisch, G. W. Trucks, H. B. Schlegel, P. M. W. Gill, B. G. Johnson, M. A. Robb, J. R. Cheeseman, T. A. Keith, G. A. Petersson, J. A. Montgomery, K. Raghavachari, M. A. Al-Laham, V. G. Zakrzewski, J. V. Ortiz, J. B. Foresman, J. Cioslowski, B. B. Stefanov, A. Nanayakkara, M. Challacombe, C. Y. Peng, P. Y Ayala, W. Chen, M. W. Wong, J. L. Andres, E. S. Replogle, R. Gomperts, R. L. Martin, D. J. Fox, J. S. Binkley, D. J. DeFrees, J. Baker, J. P. Stewart, M. Head-Gordon, C. Gonzalez and J. A. Pople, Gaussian, Inc., Pittsburgh, PA, 1994.
14 R. Ditchfield, W. J. Hehre and J. A. Pople, *J. Chem. Phys.*, 1971, **54**, 724; W. J. Hehre, R. Ditchfield and J. A. Pople, *J. Chem. Phys.*, 1972, **56**, 2257.
15 T. H. Dunning, Jr. and P. J. Hay, *Modern Theoretical Chemistry*, Plenum, New York, 1976, p. 1.
16 A. D. Becke, *Phys. Rev. A.*, 1988, **38**, 3098.
17 J. P. Perdew and Y. Wang, *Phys. Rev. B*, 1992, **45**, 13244.
18 A. D. Becke, *J. Chem. Phys.*, 1993, **98**, 5648.
19 C. Lee, W. Yang and R. G. Parr, *Phys. Rev. B*, 1988, **37**, 785.

Received in Corvallis, OR, USA, 9th February 1998; 8/01217B

Spherical polyphenylene dendrimers *via* Diels–Alder reactions: the first example of an A_4B building block in dendrimer chemistry

Frank Morgenroth, Alexander J. Berresheim, Manfred Wagner and Klaus Müllen*†

Max-Planck-Institut für Polymerforschung, Ackermannweg 10, 55128 Mainz, Germany

The [2+4]cycloaddition of the novel A_4B building block 2,3,4,5-tetrakis(4-triisopropylsilylethynylphenyl)cyclopenta-2,4-dienone 3 with 3,3',5,5'-tetraethynylbiphenyl 1 allows the rapid synthesis of a spherical polyphenylene nanoparticle with 102 benzene rings.

Dendrimers form highly symmetric layered molecules that adopt a spherical shape at higher generations.[1,2] The three-dimensional form of dendrimers is determined by the core, the interior building blocks and the surface groups. Our synthetic approach towards polyphenylene dendrimers is based on the selective Diels–Alder cycloaddition of 3,4-bis(4-triisopropylsilylethynylphenyl)-2,5-diphenylcyclopenta-2,4-dienone **2** with the four dienophile functions of 3,3',5,5'-tetraethynylbiphenyl **1**.[3,4] Compound **2** reacts only as diene since the triisopropylsilyl (TIPS) groups make the ethynyl functions inaccessible for dienophiles (see Scheme 1). The TIPS groups of the first dendrimer generation **4a** can be removed quantitatively using Bu_4NF and the resulting **4b** can undergo another [2+4]cycloaddition with **2**. This cycloaddition-deprotection sequence allows the synthesis of a third generation dendrimer, consisting of pentaphenylbenzene units, which has a diameter of about 5 nm according to computer generated ball-and-stick models.[4] As revealed by molecular dynamics simulations on the second

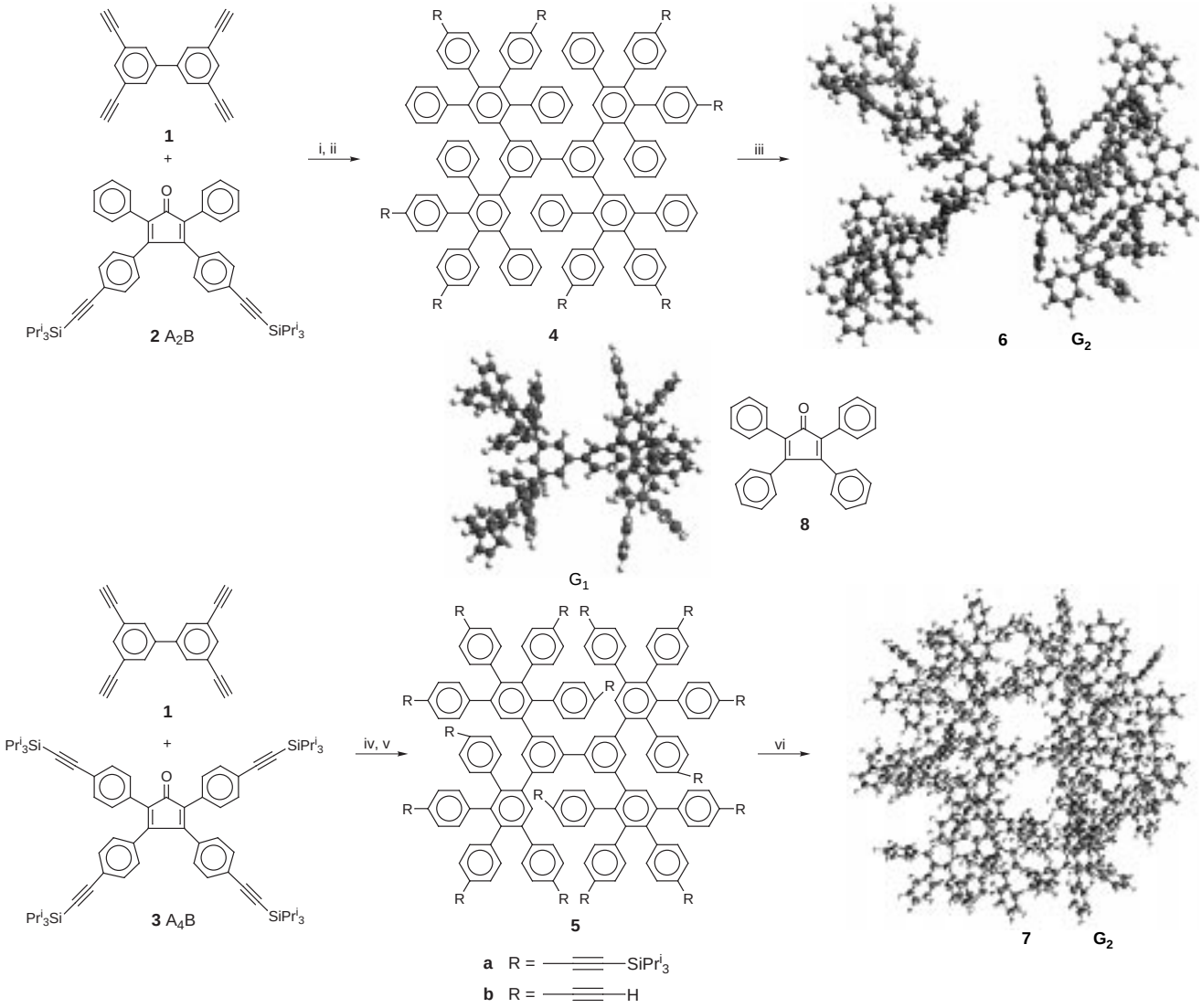

Scheme 1 *Reagents and conditions:* i, Ph_2O–α-methylnaphthalene (1 : 1), 180–200 °C, 14 h, 89%; ii, Bu_4NF, THF, 25 °C, 5 h, > 98%; iii, **8**, Ph_2O–α-methylnaphthalene (1 : 1), 180–200 °C, 15 h, 86%; iv, Ph_2O–α-methylnaphthalene (1 : 1), 180–200 °C, 14 h, 77%; v, Bu_4NF, THF, 25 °C, 5 h, 87%; vi, Ph_2O–Bu^tOMe (8 : 11), 190 °C, 44 h, 62%

generation dendrimer **6**, the higher dendrimer generations represent shape-persistent nanoparticles.

Here we investigate the influence of the branching unit on the shape of the dendrimer employing **1** as core and a four-directional A_4B building block **3** rather than the A_2B building block **2**. Thereby, we introduce 2,3,4,5-tetrakis[4-triisopropylsilylethynylphenyl)cyclopenta-2,4-dienone **3** as a powerful multifunctional reagent that allows the rapid construction of a spherical polyphenylene architecture.

Cyclopentadienone **3** contains four dienophile units and one diene function and can thus be regarded as an A_4B building block which represents, to the best of our knowledge, the first example of a dendrimer branching element possessing a multiplicity higher than 3.[5] Compound **3** was prepared by the base-catalyzed condensation of 4,4'-bis(triisopropylsilyl)benzil and 1,3-bis(4-triisopropylsilylethynyl)acetone (83%, red crystals).[6] The acetone was obtained *via* the Sonogashira coupling[7] of triisopropylsilylacetylene and 1,3-di(4-bromophenyl)acetone (82%). The latter was synthesized by converting 4-bromobenzyl bromide with $Fe(CO)_5$ in the presence of NaOH under phase transfer conditions (CH_2Cl_2–H_2O; 43%).

The four-fold Diels–Alder reaction of the A_4B building block **3** with the tetraethynylbiphenyl **1** led to the first dendrimer generation **5a** (77%, white solid). After cleaving the TIPS groups (**5b**), further reaction with **3** provided a mixture of products, determined by mass spectrometry, consisting of the desired sixteen-fold Diels–Alder product, and mainly of the fourteen-fold [2+4]cycloaddition product.† In contrast, addition of tetraphenylcyclopentadienone **8** to **5b** led smoothly to the desired sixteen-fold Diels–Alder product **7** exclusively, which was isolated as a white solid in 62% yield (see Scheme 1).

The different results obtained by the reaction of **5b** with **2** or **3** can be easily rationalized by looking at ball-and-stick models, which were generated using the MM2 (85) force field with the CERIUS 2 program package and applying the Conjugate Gradient 200 algorithm (compare Scheme 1):[8] As expected, the appearances of the corresponding first generations **4** and **5** are very similar, as both dendrimers contain 22 benzene rings and differ only in the number of substituents, while having the same spatial extension. The corresponding second generations already exhibit clearly dissimilar shapes. The dendrimer **6**, with 62 benzene rings, synthesized using the A_2B building block **2**, possesses a dumb-bell like structure, whereas the use of the A_4B building block **3** leads to 'nanoball' architecture **7**, which possesses 102 benzene rings. As the second generations of both dendrimers have a maximum extension of about 4 nm, the density of benzene rings is dramatically increased in **7**. In the case of the more strongly branched dendrimer **7** the space available for a new dendrimer shell is sufficient to accommodate the incoming eighty unsubstituted benzene rings spherically around the dendrimer core. The fact that the 64 sterically demanding TIPS groups of the A_4B building blocks cannot be accommodated, proves the concept of densest packing.[9,10] The preferred formation of the fourteen-fold cycloaddition product can be understood according to Tomalia as a sterically induced stoichiometry.[11]

The obtained dendrimers exhibit unexpectedly good solubility in common organic solvents such as toluene and CH_2Cl_2. Therefore, they can be fully characterized by matrix-assisted laser desorption ionization time of flight mass spectrometry (MALDI-TOF-MS) as well as ^1H and ^{13}C NMR spectroscopy. The perfect agreement between calculated and experimentally determined *m*/*z* ratios for the dendrimers as well as GPC analysis confirm their monodispersity.§ With respect to the physical properties of the dendrimers their thermal stability is noteworthy. The thermogravimetric analysis yielded decomposition temperatures well above 450 °C for the TIPS substituted and 580 °C for the unsubstituted dendrimers under air.

The special features of the results presented above can be summarized as follows: (i) in contrast to the established concept based on metallo-organic coupling reactions for the construction of polyphenylene dendrimers[12] (as well as the closely related hyperbranched polyphenylenes),[13] the growth of the dendrimers presented here is achieved *via* [2+4]cycloaddition followed by a desilylation; (ii) using the A_4B building block **3** and the core **1** the second dendrimer generation exhibits properties such as spherical shape in spite of the core's D_{2h} symmetry and the densest packing of benzene rings which one would generally expect only for higher generation numbers; (iii) using a defined dendrimer core, the shape of the dendrimer formed depends on the cyclopentadienone used.

Our current investigations involve light scattering experiments on higher dendrimer generations as well as microscopic visualization after adsorption on substrate surfaces.

Notes and References

† E-mail: muellen@mpip-mainz.mpg.de

‡ The amount of higher Diels–Alder cycloaddition products can be increased by repeated treatment with cyclopentadienone **2b**.

§ *Selected data* for **3**: FD-MS: *m*/*z* 1105, calc. for $C_{73}H_{100}OSi_4$: 1106; δ_H (200 MHz, CD_2Cl_2, 303 K) 7.37–7.28 (m, 8H), 7.17 (d, ^3J 8.0, 4H, H_{Aryl}), 6.89 (d, ^3J 8.0, 4H, H_{Aryl}), 1.13 (s, 84H, H_{TIPS}); δ_C(75 MHz, CD_2Cl_2, 303 K) 199.7 (**C**=O), 154.8, 133.5, 132.5, 132.4, 131.4, 130.8, 130.1, 126.2, 124.8, 123.5, 107.7 [Ar*C*≡CSi(Pr^i)$_3$], 107.3 [Ar*C*≡CSi(Pr^i)$_3$], 93.4 [ArC≡*C*Si(Pr^i)$_3$], 92.7 [ArC≡*C*Si(Pr^i)$_3$], 19.2 [CH(*C*H$_3$)$_2$], 12.1 [*C*H(CH$_3$)$_2$]; mp 296 °C (decomp.). For **7**: MALDI-TOF-MS: *m*/*z* 7762, calc. for $C_{612}H_{410}$: 7764; δ_H(500 MHz, THF, 303 K) 7.70–7.34 (br, 24H), 7.25–6.03 (br, 386H); δ_C(125 MHz, THF, 303 K) 145.55, 145.45, 145.36, 144.60, 144.54, 144.43, 144.22, 144.18, 144.05, 144.03, 143.99, 143.91, 143.87, 143.80, 143.73, 143.69, 143.62, 143.58, 143.45, 142.99, 142.86, 142.80, 142.69, 142.64, 142.56, 135.60, 135.50, 135.45, 135.38, 135.33, 135.29, 135.16, 135.09, 135.02, 134.95, 134.87, 134.76, 134.70, 134.65, 134.57, 133.49, 133.38, 133.34, 130.92, 130.29, 130.24, 130.18, 129.95, 129.86, 129.55, 129.49, 129.04, 128.87, 128.72, 128.60, 109.67; GPC analysis (polystyrene as standard): M_w/M_n = 1.04; mp > 300 °C.

1 G. R. Newkome, C. N. Moorefield and F. Vögtle, *Dendritic Molecules*, VCH Verlag, Weinheim, 1996

2 J. M. J. Fréchet and C. J. Hawker, in *Comprehensive Polymer Science, 2. Supl.*, ed. G. Allen, S. L. Aggarwal and S. Russo, Elsevier, Oxford, 1996, S. 70–129.

3 F. Morgenroth, E. Reuther and K. Müllen, *Angew. Chem.*, 1997, **109**, 647; *Angew. Chem., Int. Ed. Engl*., 1997, **36**, 631.

4 F. Morgenroth, C. Kübel and K. Müllen, *J. Mater. Chem.*, 1997, **7**, 1207.

5 It ought to be mentioned in this context that Fréchet and Otha have recently described the synthesis of an end-reactive AB_4 dendron (made from two different AB_2 building blocks) for the accelerated synthesis of dendritic polymers: M. Ohta and J. M. J. Fréchet, *J. Macromol. Sci., Pure Appl. Chem.*, 1997, **A34**, 2025.

6 F. Morgenroth and K. Müllen, *Tetrahedron*, 1997, **53**, 15349 and references cited therein.

7 S. Takahashi, Y. Kuroyama, K. Sonogashira and N. Hagihara, *Synthesis*, 1980, 627.

8 CERIUS^2, Molecular Simulations Inc., Waltham, MA, USA. For more details see ref. 4. Additional data are to be published.

9 M. Maciejewski, *J. Macromol. Sci. Chem.*, 1982, **A17**, 689.

10 P.-G. de Gennes and H. Hervet, *J. Phys. Lett.*, 1983, **44**, L-351.

11 D. A. Tomalia and H. D. Durst, *Top. Curr. Chem.* 1993, **165**, 193.

12 T. M. Miller, T. X. Neenan, R. Zayas and H. E. Bair, *J. Am. Chem. Soc.*, 1992, **114**, 1018.

13 Y. H. Kim and O. W. Webster, *J. Am. Chem. Soc.* 1990, **112**, 4592.

Received in Cambridge, UK, 18th February 1998; 8/01395K

Self-assembly of (*P*)-heterohelicenediol into a four-leaf clover motif

Kazuhiko Tanaka*† and Yoshinori Kitahara

Department of Chemistry, Graduate School of Science, Kyoto University, Kyoto 606-8224, Japan

(*P*)-2,13-Bis(hydroxymethyl)heterohelicenediol [(*P*)-1] self-assembles through a right-handed helical network of hydrogen bonds to form a four-leaf clover motif; a full turn of the helix comprises four chiral subunits which associate in a *left-handed* helical manner with a 4_3 screw axis.

The construction of highly ordered supramolecular structures has important implications not only for the developement of new materials such as nanoscale molecular devices,[1–4] but also for the synthesis of artificial systems that can mimic biological functions.[5] Among the self-assembled supramolecular architectures, such as tapes,[6] capsules,[7] spheres,[8] squares,[9] cylinders[5] and helices,[10,11] helical arrangements[12,13] are characterized by chirality based on the screw sense [right-handed (*P*) or left-handed (*M*) helicity], and hence the helicoselective (or enantioselective) synthesis of helical motifs is an active field of research in supramolecular chemistry.[14] Here we report the first example of construction of a four-leaf clover motif from optically active (*P*)-2,13-bis(hydroxymethyl)dithieno[3,2-*e*:3′,2′-*e*′]benzo[1,2-*b*:4,3-*b*′]bis[1]benzothiophene [(*P*)-**1**] (Fig. 1).[15]

Crystals suitable for X-ray crystallographic analysis were grown from a solution of (*P*)-**1** in CH_2Cl_2–acetone.‡ The stereoview of the crystal structure (Fig. 2) clearly shows that (*P*)-**1** self-assembles through a right-handed helical network of hydrogen bonds. A full turn of the helix comprises four chiral helicenediols and the pitch of the helix is 15.49 Å. The most remarkable feature of (*P*)-**1** is that the right-handed helicenediols arrange in a *left-handed* helical manner and the cloverleaf motif repeats by the 4_3 screw axis. In the supramolecular structure, one of the hydroxy functionalities of (*P*)-**1** forms an intramolecular bridge to the other hydroxy group of the same molecule and also forms an intermolecular hydrogen bond to one of the hydroxy groups of an adjacent molecule (Fig. 3). The

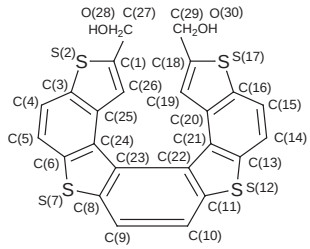

Fig. 1 Numbering scheme of heterohelicenediol

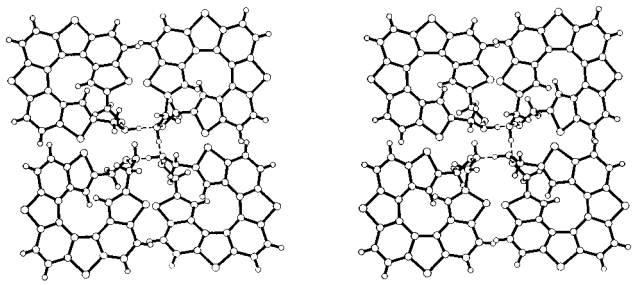

Fig. 2 A stereoview of the four-leaf clover motif of (*P*)-heterohelicenediol assembled along the *c* axis

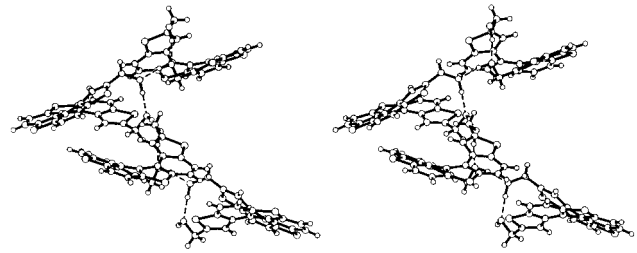

Fig. 3 Stereoview of (*P*)-heterohelicenediol from the crystallographic *b* axis

interplanar angle between the terminal thiophene rings of (*P*)-**1** is 33.83° (Table 1). This is in contrast with the guest-free racemic heterohelicenediol (*PM*)-**1** which self-assembles to form an alternate-leaf motif (Fig. 4).§ In the crystal of (*PM*)-**1**, the two stacking columns, consisting of helicenediols of the same helicity, are aligned along the *c* axis. Since each hydroxy group of (*PM*)-**1** interacts with one of the hydroxy functions of an adjacent molecule *via* an intermolecular hydrogen bond, the interplanar angle between the terminal thiophene rings increases to 44.70° (Table 1). This represents an increase of

Table 1 Interplanar angles between the adjacent rings and the terminal thiophene rings (°)

	(*P*)-**1**	(*PM*)-**1**	(*PM*)-**1**·EtOH[a]
ring(1)–ring(2)	8.40	5.82	8.29
ring(2)–ring(3)	6.92	7.70	8.29
ring(3)–ring(4)	9.73	10.46	11.63
ring(4)–ring(5)	9.35	12.72	9.33
ring(5)–ring(6)	8.73	9.84	7.10
ring(6)–ring(7)	6.33	6.61	7.30
ring(1)–ring(7)	33.83	44.70	37.96

[a] Ref. 16.

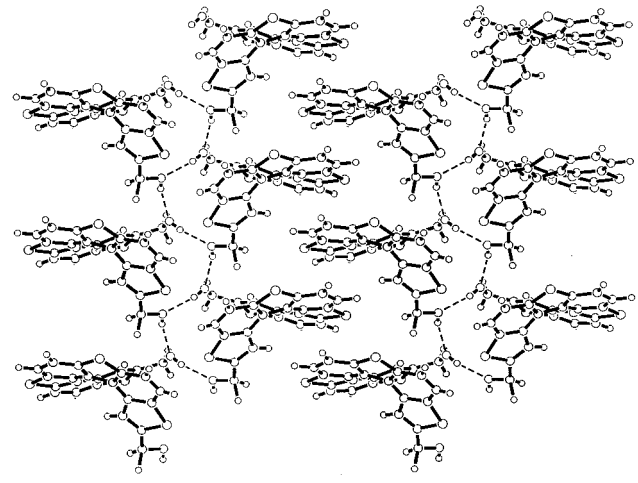

Fig. 4 Side view of the hydrogen-bonding network showing an alternate-leaf motif of racemic heterohelicenediol

10.87° or 32.1%. When the racemic heterohelicenediol (*PM*)-**1** forms an inclusion complex with EtOH through helical hydrogen-bonding, the interplanar angle decreases to 37.96°.[16] These results clearly indicate that the helicene framework exhibits significant elasticity by changing its dihedral angle. The distortion from planarity locates on the central aromatic rings of the helical framework, and therefore the dihedral angles between two adjacent rings range from 8.73 to 9.73 for (*P*)-**1** and from 9.84 to 12.72° for (*PM*)-**1**. However, the double bond character of two helicenediols are unchanged. Thus, the carbon–carbon bond distances of the outer rings range from 1.33 to 1.36 Å in the case of (*P*)-**1** and from 1.33 to 1.37 Å in (*PM*)-**1**, and the inner carbon–carbon bond distances [C(20)–C(21), C(22)–C(23) and C(24)–C(25)] are 1.42 Å for (*P*)-**1**, and in a range of 1.41 to 1.43 Å for (*PM*)-**1**. The inner carbon–carbon bond lengths in the thiophene rings [C(19)–C(20), C(21)–C(22) and C(25)–C(26)] range from 1.43 to 1.47 Å for both (*P*)-**1** and (*PM*)-**1**. The common feature of these helical geometry is that the carbon–sulfur bond distances in the thiophene rings of (*P*)-**1**, (*PM*)-**1** and (*PM*)- **1**·EtOH are uniformly lengthened from 1.71 to 1.73 Å.

The present results reveal for the first time that the helical conjugated π-electron framework of helicenediol **1** acts as a helical spring due to the pattern of hydrogen bonds.

This work was supported by a Grant-in-Aid for Scientific Research on Priority Areas 'Organic Nonlinear Optics' (No. 09222212) from the Japanese Ministry of Education, Science, Culture and Sports.

Notes and References

† E-mail: tanaka@kuchem.kyoto-u.ac.jp

‡ *Crystal data* for (*P*)-**1**: $C_{24}H_{14}O_2S_4$, M = 462.61, crystal size 0.40 × 0.26 × 0.40 mm, crystal system, tetragonal, space group $P4_3$, a = 11.4866(9), c = 15.493(3) Å, V = 2044.1(4) Å^3, Z = 4, D_c = 1.503 g cm^{-3}. The final cycle of full-matrix least-squares refinement was based on 1538 observed reflections and 271 variable parameters and converged with unweighted and weighted agreement factors of R = 0.032 and R_w = 0.050, respectively.

§ *Crystal data* for (*PM*)-**1**: $C_{24}H_{14}O_2S_4$, M = 462.61, crystal 0.25 × 0.75 × 0.01 mm, crystal system, orthorhombic, space group *Pccn*, a = 15.217(6), b = 33.919(9), c = 7.85(1) Å, V = 4051(7) Å^3, Z = 8, D_c = 1.517 g cm^{-3}. The final cycle of full-matrix least-squares refinement was based on 1588 observed reflections and 328 variable parameters and converged with unweighted and weighted agreement factors of R = 0.069 and R_w = 0.077, respectively. The crystal data were collected on a Rigaku AFC7R diffractometer using Cu-Kα radiation and a 12 kW rotating anode generator at a temperature of 20 °C using the ω–2θ scan technique. CCDC 182/860.

1 J.-M. Lehn, *Angew. Chem., Int. Ed. Engl.*, 1990, **29**, 1304.
2 G. R. Desiraju, *Angew. Chem., Int. Ed. Engl.*, 1995, **34**, 2311.
3 C. Piguet, J.-C. Bünzli, G. Bernardinelli, G. Hopfgartner, S. Petoud and O. Schaad, *J. Am. Chem. Soc.*, 1996, **118**, 6681.
4 D. B. Amabilino and J. F. Soddart, *Chem. Ber.*, 1995, **95**, 2725.
5 M. R. Ghadiri, J. R. Granja and L. K. Buehler, *Nature*, 1994, **369**, 301.
6 J. C. MacDonald and G. M. Whitesides, *Chem. Rev.*, 1994, **94**, 2383.
7 M. M. Conn and J. Rebeck, Jr., *Chem. Ber.*, 1997, **97**, 1647.
8 M. Fugita, D. Oguro, M. Miyazawa, H. Oka, K. Yamaguchi and K. Ogura, *Nature*, 1995, **378**, 469.
9 J. Manna, J. C. Kuel, J. A. Whiteford, P. J. Stang, D. C. Muddiman, S. A. Hofstadler and R. D. Smith, *J. Am. Chem. Soc.*, 1997, **119**, 11 611.
10 D. M. Bassani, J.-M. Lehn, G. Baum and D. Fenske, *Angew. Chem., Int. Ed. Engl.*, 1997, **36**, 1845.
11 P. N. W. Baxter, H. Sleiman, J.-M. Lehn and K. Rissanen, *Angew. Chem., Int. Ed. Engl.*, 1997, **36**, 1297.
12 Y. Hamuro, S. J. Geib and A. D. Hamilton, *J. Am. Chem. Soc.*, 1997, **119**, 10 587.
13 A. Williams, *Chem. Eur. J.*, 1997, **3**, 15.
14 C. Piguet, G. Bernardinelli and G. Hopfgartner, *Chem. Rev.*, 1997, **97**, 2005.
15 K. Tanaka, H. Osuga, H. Suzuki, Y. Shogase and Y. Kitahara, *J. Chem. Soc., Perkin Trans. 1*, 1998, 935.
16 K. Tanaka, Y. Shogase, H. Osuga, H. Suzuki, W. Nakanishi, N. Nakamura and Y. Kawai, *J. Chem. Soc., Chem. Commun.*, 1995, 1873.

Received in Cambridge, UK, 27th February 1998; 8/01650J

Relative β-elimination rates of heteroatoms from alkyl and aminyl radicals

Sunggak Kim*† and Jae Ho Cheong

Department of Chemistry, Korea Advanced Institute of Science and Technology, Taejon, 305-701, Korea

The relative β-elimination rates of heteroatoms from alkyl radicals are in the order of Br≥PhSe > PhS > $PhSO_2$ > Cl, whereas the order of PhSe > $PhSO_2$ > PhS ~ Br is observed for β-eliminations from aminyl radicals, indicating a dependence on the nature of radicals.

The β-elimination reaction of heteroatoms is one of characteristic properties of radical reactions [eqn. (1)][1] and its driving

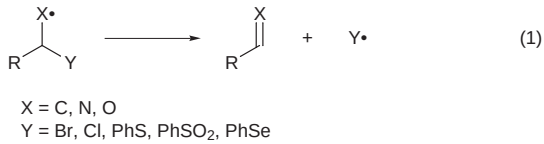

force is known to be relief of ring strain,[2] the evolution of CO_2 and SO_2,[3] or the generation of a π-bond along with the cleavage of a weaker σ-bond. The ease of β-fragmentation depends on (i) the strength of the σ-bond broken (C–Y) and also (ii) the nature of π-bonds formed (C=X).[4] In the former case, it is expected that the weaker the breaking bond is, the faster the β-fragmentation would be. As far as we are aware, there are no reports of the β-elimination of heteroatoms from aminyl radicals. We conceived that it could be possible that the relative β-elimination rates of heteroatoms from alkyl and aminyl radicals would depend on the nature of π-bonds formed and we investigated this intriguing possibility.

Although relative β-elimination rates of heteroatoms from alkyl radicals were reported previously,[6] we briefly examined the β-elimination rates using *N*-hydroxypyridine-2-thione ester **2** [eqn. (2)][7] and experimental results are shown in Table 1.

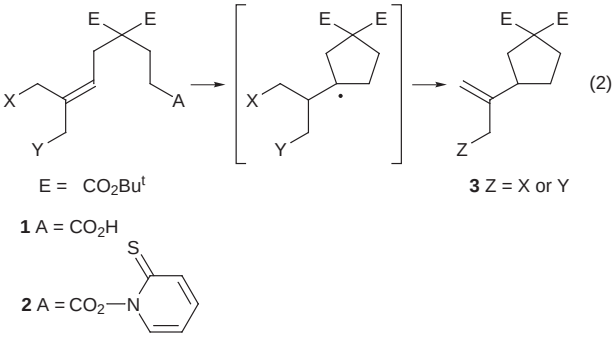

Treatment of acid **1** with *N*-hydroxypyridine-2-thione (1.2 equiv.), DCC (1.2 equiv.) and DMAP (0.1 equiv.) in CH_2Cl_2 at room temperature for 2 h afforded the thiohydroxamate **2**, which decomposed to some extent during isolation. Thus, the reaction was carried out in CH_2Cl_2 at 50 °C without isolation of **2**. To examine the relative β-elimination rates of the bromo and the phenylthio groups, when **2a** was heated at 50 °C for 5 h, the bromide was preferentially eliminated (entry 1). A same result was obtained with **2b** for the competition between the bromide and the phenylsulfonyl groups (entry 2). However, the elimination of the bromide competed more equally with that of the phenylseleno group, although the former was favored over the latter to some extent (entry 5). Furthermore, the phenylsulfonyl group underwent preferential elimination in the presence of the chloride (entry 4) and the elimination of the phenylthio group was much faster than that of the phenylsulfonyl group, although the phenylsulfonyl group underwent elimination to a small extent (3%) (entry 3).[8] When the present reactions were monitored in $CDCl_3$ by ^1H NMR spectroscopy, the allyl species **3** turned out not to be susceptible to radical addition-elimination by the radical species ejected in the elimination step. Thus, the relative rates of β-eliminations of heteroatoms from alkyl radicals are in the order of Br≥PhSe > PhS > $PhSO_2$ > Cl.

To study the effect of aminyl radicals on the β-eliminations of heteroatoms, we utilized the radical reaction of phenylsulfonyl substituted oxime ethers [eqn. (3)]. Recently, we reported free

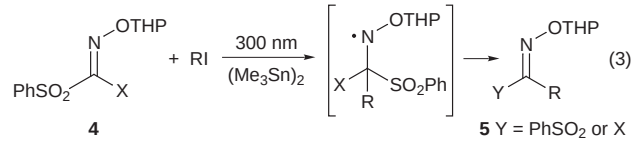

radical acylation approaches involving alkyl radical additions to sulfonyl substituted oxime ethers as acylating agents.[9] Phenylsulfonyl bromo oxime ether **4a** was prepared by the known procedure using (phenylsulfonyl)nitromethane **6** by three-step sequence involving bromination, *O*-methylation with CH_2N_2 and the subsequent protection as a THP ether.[10] The bromide group in **4a** was further displaced by sodium thiophenoxide, sodium thiomethoxide and sodium benzeneselenoate in THF to afford **4b** (85%), **4c** (78%) and **4d** (68%) [eqn. (4)]. As shown

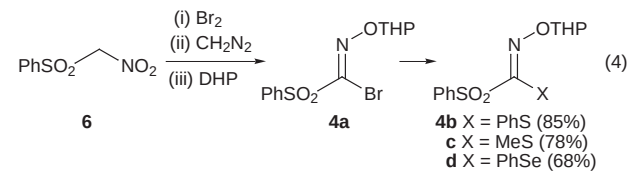

in Table 2, when a solution of 4-phenoxybutyl iodide, **4a** and hexamethylditin in benzene was irradiated at 300 nm for 16 h, somewhat surprisingly the bromo oxime ether was obtained in 78% yield (entry 1), indicating that the phenylsulfonyl group

Table 1 β-Eliminations of heteroatoms from carbon-centered radicals[a]

		Substrate **2**[b]		Product **3**	
Entry		X	Y	Z	Yield[c] (%)
1	**a**	Br	PhS	PhS	87
2	**b**	Br	$PhSO_2$	$PhSO_2$	79
3	**c**	PhS	$PhSO_2$	$PhSO_2$	89
				PhS	3
4	**d**	Cl	$PhSO_2$	Cl	80
5	**e**	Br	PhSe	PhSe : Br[d]	76

[a] Reaction time: 5–7 h. [b] *E*/*Z* ratio: **2a** (1.4 : 1), **2b** (5.4 : 1), **2c** (10.8 : 1), **2d** (6.7 : 1), **2e** (3.1 : 1). [c] Isolated yield. [d] Ratio = 76 : 24. The ratio was determined by ^1H NMR spectroscopy.

Table 2 β-Eliminations of heteroatoms from nitrogen-centered radicals

Entry		Substrate **4**[b] X	Substrate **4**[b] Y	Product **5** Z	Yield (%)
1	**a**	$PhSO_2$	Br	Br	78
2	**b**	$PhSO_2$	PhS	PhS	58
3	**c**	$PhSO_2$	MeS	MeS	74
4	**d**	$PhSO_2$	PhSe	$PhSO_2$	65
5	**e**	PhS	Br	messy	

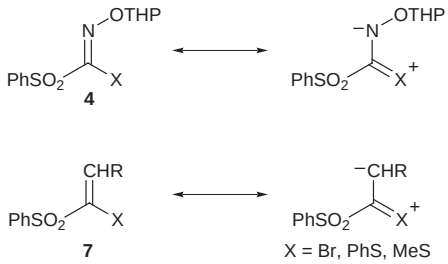

Fig. 1

was preferentially eliminated over the bromide group. This result is in sharp contrast with the above results obtained for alkyl radicals (Table 1). Similar results were also obtained with **4b** and **4c** (entries 2 and 3), showing the preferential elimination of the phenylsulfonyl group over the phenylthio and methylthio groups. However, competition between the phenylsulfonyl and the phenylseleno groups showed that the phenylseleno group was eliminated preferentially (entry 4). Attempts to study the relative β-elimination rate between the phenylthio group and bromide[10,11] were unsuccessful because the intermolecular addition of an alkyl radical onto the phenylsulfenyl bromo oxime ether (entry 5) turned out to be inefficient.

The results obtained in this study are rather interesting and indicate that phenylsulfonyl groups on aminyl radicals undergo facile elimination relative to the bromide, methylthio, and phenylthio groups. We have no clear answer why the relative rates of β-elimination of heteroatoms, particularly the phenylsulfonyl group, from alkyl and aminyl radicals are so different. When the contributing resonance structures of **7** and **4** were compared (Fig. 1), we suggest that resonance in **4** is much more important than resonance in **7**, thereby giving unusually strong carbon–bromine and carbon–sulfur bonds in **4** due to the contribution of significant double bond character. Apparently, resonance contribution from the phenylsulfonyl group is not possible.

We thank the Korea Research Foundation and OCRC for financial support, and Dr C. Schiesser, University of Melbourne, for helpful suggestions.

Notes and References

† E-mail: skim@sorak.kaist.ac.kr

1 D. P. Curran, *Synthesis*, 1988, 489; C. P. Jasperse, D. P. Curran and T. L. Fevig, *Chem. Rev.*, 1991, **91**, 1237; P. Dowd and W. Zhang, *Chem. Rev.*, 1993, **93**, 2091.
2 S. Kim, S. Lee and J. S. Koh, *J. Am. Chem. Soc.*, 1991, **113**, 5106; S. Kim, I. S. Kee and S. Lee, *J. Am. Chem. Soc.*, 1991, **113**, 9882; W. R. Bowman, D. N. Clark and R. J. Marmon, *Tetrahedron Lett.*, 1991, **32**, 6441; M. Newcomb, *Tetrahedron*, 1993, **49**, 1151.
3 M. Feldhues and H. J. Schafer, *Tetrahedron*, 1985, **41**, 4213; F. L. Guyader, B. Quiclet-Sire, S. Seguin and S. Z. Zard, *J. Am. Chem. Soc.*, 1997, **119**, 7410; J. Xiang, W. Jiang, J. Gong and P. L. Fuchs, *J. Am. Chem. Soc.*, 1997, **119**, 4123.
4 P. Dowd and S.-C. Choi, *J. Am. Chem. Soc.*, 1987, **109**, 6548; J. E. Baldwin, R. M. Adlington and J. Robertson, *Tetrahedron*, 1989, **45**, 909; S. Kim, G. H. Joe and J. Y. Do, *J. Am. Chem. Soc.*, 1993, **115**, 3328; S. Kim, K. H. Kim and J. R. Cho, *Tetrahedron Lett.*, 1997, **38**, 3915.
5 D. H. R. Barton, D. Crich and W. B. Motherwell, *J. Chem. Soc., Chem. Commun.*, 1983, 939; D. H. R. Barton, D. Crich and G. Kretzschmar, *J. Chem. Soc., Perkin Trans. 1*, 1986, 39.
6 P. J. Wagner, J. H. Sedon and M. J. Lindstrom, *J. Am. Chem. Soc.*, 1978, **100**, 2579; T. E. Boothe, J. L. Greene, Jr. and P. B. Shevlin, *J. Am. Chem. Soc.*., 1976, **98**, 951.; T. E. Boothe, J. L. Greene, Jr. and P. B. Shevlin, *J. Org. Chem.*, 1980, **45**, 794.
7 D. H. R. Barton, D. Crich and W. B. Motherwell, *Tetrahedron*, 1985, **41**, 3901; D. H. R. Barton, C.-Y. Chern and J. C. Jaszberenyi, *Tetrahedron Lett.*, 1992, **33**, 5013.
8 Y. Ueno, T. Miyano and M. Okawara, *Tetrahedron Lett.*, 1982, **23**, 443.
9 S. Kim, I. Y. Lee, J.-Y. Yoon and D. H. Oh, *J. Am. Chem. Soc.*, 1996, **118**, 5138; S. Kim and J.-Y. Yoon, *J. Am. Chem. Soc.*, 1997, **119**, 5982; S. Kim, J.-Y. Yoon and I. Y. Lee, *Synlett*, 1997, 475.
10 P. A. Wade and H. R. Hinney, *J. Am. Chem. Soc.*, 1979, **101**, 1319.
11 F. G. Bordwell and J. E. Bartmess, *J. Org. Chem.*, 1978, **43**, 3101.

Received in Cambridge, UK, 2nd April 1998; 8/02507J

Radical-chain racemisation of tetrahydrofurfuryl acetate under conditions of polarity-reversal catalysis: possible implications for the radical-induced strand cleavage of DNA

Yudong Cai and Brian P Roberts*†

Christopher Ingold Laboratories, Department of Chemistry, University College London, 20 Gordon Street, London, UK WC1H 0AJ

Alkanethiols with electron-withdrawing *S*-alkyl groups and silanethiols act as polarity-reversal catalysts to promote the radical-chain racemisation of (*R*)-tetrahydrofurfuryl acetate at 60 °C, while simple alkanethiols are ineffective.

There is now good evidence that, at least under anaerobic conditions, strand cleavage of DNA which involves the 4′-radical **1** proceeds as shown in Scheme 1, *via* an intermediate radical cation **2** which can subsequently trap a nucleophile to give an α- alkoxyalkyl radical of the type **3**.[1] In principle, if the radical **3** (or a similar oligonucleotide-derived α-oxyalkyl radical) were to abstract hydrogen from an undamaged strand to regenerate the 4′-radical **1**, a homolytic *chain* process for the cleavage of DNA could be established. If such a radical-chain mechanism for the destruction of DNA could be promoted when desirable in a therapeutic context (*e.g.* to amplify the effects of radiation damage to a tumour or to increase the effectiveness of the various antineoplastic agents that operate *via* radical pathways[2]), the biological implications would be of considerable importance.

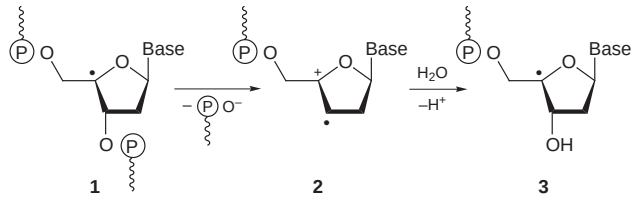

1 **2** **3**

Scheme 1

However, hydrogen-atom abstraction by **3** from the 4′-position in DNA is an (essentially) thermoneutral process that involves two radicals of almost identical electronegativity, and such reactions would be expected to be very slow at moderate temperatures.[3] The radicals **1** and **3** should be nucleophilic species, with relatively low ionisation energies, and it occurred to us that the overall transfer of hydrogen from DNA to **3** (or to another α-oxyalkyl radical) might be promoted by a suitable polarity-reversal catalyst[4,5] of the type El–H, where El• is an electrophilic radical. Here we report the results of experiments designed to investigate this general possibility, by examining the effects of polarity-reversal catalysts on the identity reaction [eqn. (1)] of tetrahydrofurfuryl acetate **4**.

The extent to which the overall reaction [eqn. (1)] takes place was judged by starting with (*R*)-tetrahydrofurfuryl acetate[6] and monitoring the enantiomeric excess (ee) of the remaining ester as a function of time, using chiral-stationary-phase GLC (Supelco β-DEX 120, 30 m × 0.25 mm bore capillary column; 0.25 μm coating containing permethylated β-cyclodextrin). When a benzene solution containing (*R*)-**4** (99.4% ee, 0.50 mol dm^{-3}), *tert*-butylbenzene or methyl benzoate (0.30 mol dm^{-3}, as an internal concentration standard for GLC analysis) and di-*tert*-butyl hyponitrite[7] (TBHN, 0.025 mol dm^{-3}) was heated at 60 °C under argon for 3 h, *ca.* 10% of **4** was consumed and the ee of the remaining (*R*)-ester was undiminished. The TBHN acts

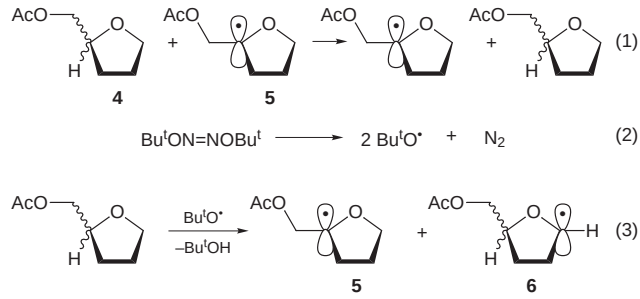

4 **5** **6**

as a thermal source of *tert*-butoxyl radicals [eqn. (2)]‡ which, in the absence of other reagents, will abstract hydrogen from **4** to give mainly the α-alkoxyalkyl radicals **5** and **6** [eqn. (3)].§ We conclude that neither **5** nor **6** abstracts hydrogen directly from **4** to give **5** at a significant rate under the reaction conditions. The experiment was then repeated in the presence of small amounts (usually 5 mol% based on **4**) of various thiols as potential polarity-reversal catalysts, and the results are presented graphically in Fig. 1. Under these conditions, only a trace of tetrahydrofurfuryl acetate was consumed during the first 90 min, although a small amount (⩽5%) of the ester was consumed subsequently when the thiol concentration had become very low. It can be seen that while 5 mol% of a simple alkanethiol such as *tert*-dodecanethiol (mixture of isomers) or dodecane-1-thiol causes only a very small amount of racemisation of (*R*)-**4**, thiols with electron-withdrawing groups attached to sulfur bring about a significant increase in the rate of racemisation and evidently act as polarity-reversal catalysts for the overall reaction [eqn. (1)], according to the chain propagation cycle shown in Scheme 2. Thus, 1-thio-β-D-glucopyranose tetraacetate, 2,2,2-trifluoroethanethiol¶ and, in particular, triphenylsilanethiol are efficient catalysts. The more sterically-demanding triisopropylsilanethiol and the less acidic methyl thioglycolate (MeO_2CCH_2SH) were less effective while, as expected, L-cysteine ethyl ester (a model for glutathione) was totally ineffective. Of course, hydrogen-atom abstraction by XS• to form **6** followed by 'repair' to regenerate **4** is an unobservable process in the present system.‖ Abstraction of hydrogen from **4** by XS• is evidently more efficient when the substituent X is an electron-withdrawing group, probably

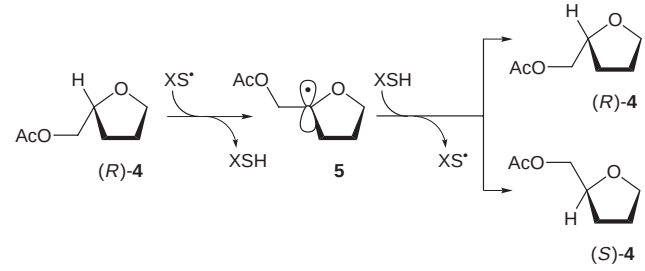

Scheme 2

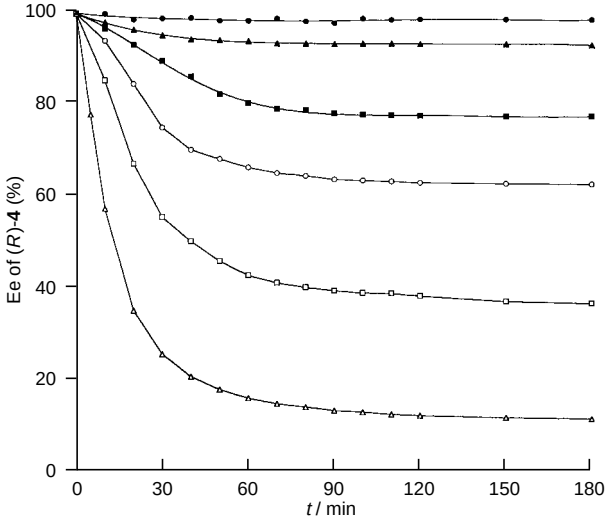

Fig. 1 The racemisation of (*R*)-tetrahydrofurfuryl acetate in benzene at 60 °C in the presence of various thiols (5 mol% based on the acetate): (●) *tert*-dodecanethiol, (▲) dodecane-1-thiol, (■) methyl thioglycolate, (○) 2,2,2-trifluoroethanethiol, (□) 1-thio-β-D-glucopyranose tetraacetate and (△) triphenylsilanethiol (in order of increasing efficiency as catalysts)

because the S–H bond is stronger and the thiyl radical is more electrophilic when the sulfur atom is relatively electron deficient.[3b,5c] The silyl group acts as a π-electron-pair acceptor.

Triisopropylsilanethiol is a less effective catalyst than triphenylsilanethiol, which may be a consequence of relatively slow transfer of a hydrogen atom from and to a tertiary site when the XS group is bulky. With 5 mol% TBHN and 5 mol% thiol catalyst, racemisation does not go to completion (see Fig. 1). Apart from depletion of the initiator, this is presumably a result of removal of thiyl radicals by self-coupling to give disulfide and, especially in the later stages of the reaction when the thiol concentration is reduced, by combination of XS$^{\bullet}$ with the radicals **5** or **6**. When the initial amount of Ph_3SiSH was increased to 10 mol%, under otherwise identical conditions, the rate of racemisation of (*R*)-**4** *decreased*, while with 2.5 mol% Ph_3SiSH the initial rate of racemisation was slightly greater than that achieved with 5 mol% catalyst, although the final ee after 3 h (33%) was appreciably larger. We interpret these results as indicating that at high thiol concentrations rotational exchange between the enantiomeric conformations of **5** becomes competitive with trapping of this radical by thiol to regenerate **4**, so that **5** begins to retain a memory of the absolute configuration of the molecule of **4** from which it was derived. It follows that the rate of racemisation provides a lower limit for the rate of the overall reaction [eqn. (1)] under conditions of polarity-reversal catalysis.

We conclude that the thermoneutral reaction shown in eqn. (1) is subject to polarity-reversal catalysis by appropriately substituted thiols. Provided that the possible protective effect of glutathione can be overcome (perhaps by reversible binding of the polarity-reversal catalyst to DNA), it may be possible to apply this principle to amplify radical-induced damage to DNA *in vivo*, especially in the oxygen-deficient environment present in many types of tumour cell.[9] Encouragingly, racemisation of (*R*)-**4** still takes place in the presence of *both* Ph_3SiSH (5 mol%) and *tert*-dodecanethiol (5 mol%), albeit at an initial rate about six times slower than that observed in the presence of the silanethiol alone.

These results will also have implications for the design of enantioselective radical-chain reactions based on the use of homochiral thiols as polarity-reversal catalysts,[5e] when it is obviously important to *suppress* racemisation of the product.

We are very grateful to Drs D. J. Madge and A. B. Tabor for useful discussions and to Dr P. Anastasis (Kiralchem Ltd.) for all his help in supplying the enantiopure tetrahydrofurfuryl alcohol from which (*R*)-**4** was prepared.

Notes and References

† E-mail: b.p.roberts@ucl.ac.uk

‡ The half-life of TBHN at 60 °C is *ca*. 55 min [ref. 7(*a*)].

§ When a cyclopropane solution containing **4** and di-*tert*-butyl peroxide was irradiated with UV light while the sample was in the microwave cavity of an EPR spectrometer (ref. 8), overlapping EPR spectra of **5** and **6** were observed between 180 and 280 K; at 270 K the value of [**5**]/[**6**] was *ca*. 0.7. At 270 K, the radical **5** showed $a(2\ H_{\beta}^{exocyclic})$ 8.60, $a(2\ H_{\beta})$ 26.14, $a(2\ H_{\gamma})$ 0.75 and $a(2\ H_{\delta})$ 2.08 G, and g 2.0030; the radical **6** showed $a(1\ H_{\alpha})$ 13.50, $a(1\ H_{\beta})$ 30.89, $a(1\ H_{\beta}')$ 25.26, $a(2\ H_{\gamma})$ 0.75 and $a(1\ H_{\delta})$ 2.25 G, and g 2.0032. The hyperfine splitting constants confirm that the radical **5** preferentially adopts the conformation shown, in which the exocyclic C_{β}-O bond eclipses the formal C_{α}–$2p_{\pi}$ SOMO, although two-fold rotation about the C_{α}–C_{β} bond is evidently sufficiently fast at 270 K to render the two faces of the ring magnetically-equivalent. However, below *ca.* 260 K, selective line-broadening was observed in the spectrum of **5**, indicating that rotational exchange between the two enantiomeric conformations is no longer fast on the EPR timescale.

¶ This thiol is volatile (bp 36 °C) and some could have been lost by evaporation during the reaction.

‖ While the *tert*-butoxyl radical abstracts hydrogen at comparable rates from the two carbon atoms adjacent to the ring-oxygen in **4**, it is likely that thiyl radicals (especially the less bulky ones) will be more selective and give mainly **5** by attack at the tertiary CH group.

1 For recent relevant papers, see B. Giese, X. Beyrich-Graf, P. Erdmann, M. Petretta and U. Schwitter, *Chem. Biol.*, 1995, **2**, 367; A. Gugger, R. Batra, P. Rzadek, G. Rist and B. Giese, *J. Am. Chem. Soc.*, 1997, **119**, 8740; B. Giese, A. Dussy, E. Meggers, M. Petretta and U. Schwitter, *J. Am. Chem. Soc.*, 1997, **119**, 11 130; S. Peukert, R. Batra and B. Giese, *Tetrahedron Lett.*, 1997, **38**, 3507; D. Crich and X.-S. Mo, *Tetrahedron Lett.*, 1997, **38**, 8169; D. Crich and Q. Yao, *Tetrahedron*, 1998, **54**, 305.

2 J. Stubbe and J. W. Kozarich, *Chem Rev.*, 1987, **87**, 1107; J. Stubbe, J. W. Kozarich, W. Wu and D. E. Vanderwall, *Acc. Chem. Res.*, 1996, **29**, 322; A. P. Breen and J. A. Murphy, *J. Chem. Soc., Perkin Trans. 1*, 1993, 2979.

3 (*a*) B. P. Roberts and A. J. Steel, *J. Chem. Soc., Perkin Trans. 2*, 1994, 2155; (*b*) B. P. Roberts, *J. Chem. Soc., Perkin Trans. 2*, 1996, 2719.

4 (*a*) V. Paul and B. P. Roberts, *J. Chem. Soc., Chem. Commun.*, 1987, 1322; (*b*) V. Paul and B. P. Roberts, *J. Chem. Soc., Perkin Trans. 2*, 1988, 1183; (*c*) H.-S. Dang and B. P. Roberts, *J. Chem. Soc., Perkin Trans. 1*, 1993, 891; (*d*) P. L. H. Mok, B. P. Roberts and P. T. McKetty, *J. Chem. Soc., Perkin Trans. 2*, 1993, 665; (*e*) H.-S. Dang, V. Diart, B. P. Roberts and D. A. Tocher, *J. Chem. Soc., Perkin Trans. 2*, 1994, 1039.

5 (*a*) R. P. Allen, B. P. Roberts and C. R. Willis, *J. Chem. Soc., Chem. Commun.*, 1989, 1387; (*b*) J. N. Kirwan, B. P. Roberts and C. R. Willis, *Tetrahedron Lett.*, 1990, **31**, 5093; (*c*) S. J. Cole, J. N. Kirwan, B. P. Roberts and C. R. Willis, *J. Chem. Soc., Perkin Trans. 1*, 1991, 103; (*d*) H.-S. Dang and B. P. Roberts, *Tetrahedron Lett.*, 1995, **36**, 2875; (*e*) M. B. Haque and B. P. Roberts, *Tetrahedron Lett.*, 1996, **37**, 9123; (*f*) H.-S. Dang and B. P. Roberts, *J. Chem. Soc., Perkin Trans. 1*, 1998, 67.

6 M. P. Balfe, M. Irwin and J. Kenyon, *J. Chem. Soc.*, 1941, 312. (*R*)-(−)-Tetrahydrofurfuryl alcohol, which showed $[\alpha]_D^{20}$ −2.3 (neat, d = 1.054), was obtained from Kiralchem Ltd., 17 Canalside, 2-4 Orsman Road, London N1 5QJ. It was converted to the acetate by treatment with Ac_2O in the presence of NEt_3.

7 (*a*) H. Kiefer and T. G. Traylor, *Tetrahedron Lett.*, 1966, 6163; (*b*) G. D. Mendenhall, *Tetrahedron Lett.*, 1983, **24**, 451.

8 J. A. Baban and B. P. Roberts, *J. Chem. Soc., Perkin Trans. 2*, 1981, 161; V. Diart and B. P. Roberts, *J. Chem. Soc., Perkin Trans. 2*, 1992, 1761; B. P. Roberts and A. J. Steel, *J. Chem. Soc., Perkin Trans. 2*, 1992, 2025.

9 S. Rockwell, *Oncol. Res.*, 1997, **9**, 383.

Received in Liverpool, UK, 11th February 1998; 8/01381K

X-Ray crystal structure of 1,6-diacetyl-3,4,7,8-tetramethyl-2,5-dithioglycoluril, a highly twisted acetamide

Christopher N. Cow, James F. Britten and Paul H. M. Harrison*†

Department of Chemistry, McMaster University, 1280 Main Street West, Hamilton, Ontario, Canada L8S 4M1

In the structure of 1,6-diacetyl-3,4,7,8-tetramethyl-2,5-dithioglycoluril, as determined by X-ray crystallography, one acetyl group lies essentially coplanar with the attached thioureido ring (τ = 2.6°), while the plane through the other acetyl group is highly twisted (τ = 55.0°) relative to the corresponding thiourea moiety to which it is appended.

Twisted amides, in which interaction between the nitrogen lone pair and the carbonyl π system is diminished or prevented, have attracted considerable interest, since they display unusually high reactivity towards nucleophiles, and have thus been proposed to act as models for the enzymic activation of peptide units.[1,2] In many cases, the amide bond is forced into a twisted conformation as a result of the covalent chemical bonding within the molecule,[2,3] while in others, the twist results either from enforced pyramidalization of nitrogen,[4] or else from steric effects.[1,5,6] In the latter regard, for example, Yamada[6] reported that 3-pivaloyl-1,3-thiazolidine-2-thione **1** has a twist angle τ =

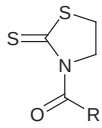

1 R = Bu^t
2 R = Me

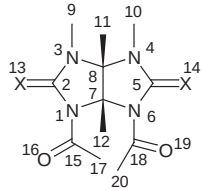

3 X = S
4 X = O

74.3°, where τ is defined as 1/2 (ω_1 + ω_2), and ω_1 and ω_2 are the O=C–N–C and C–C(O)–N–C′ dihedral angles, as defined by Winkler and Dunitz,[7] with the alteration suggested by Yamada.[6] The N–C(O) bond in **1** is long (1.448 Å) when compared to 3-acetyl-1,3-thiazolidine-2-thione **2**, (1.413 Å), which also possesses a much smaller twist angle (τ = 20.1°). Compound **1** is highly reactive towards nucleophiles, even at neutral pH.[1,6,8] In contrast, 3-pivaloyl-1,3-oxazolidine-2-one is unreactive;[1] the presence of the thione moiety thus contributes to the twisting of the amide bond in **1**.

We have shown that glycoluril derivatives can act as templates to facilitate a rapid, intramolecular Claisen-like condensation reaction between acyl groups attached to N(1) and N(6).[9] We have proposed that this process is facilitated in part by the comparatively high electrophilicity of the acyl groups attached to the glycoluril moiety, as has been observed for tetraacetylglycoluril by Hase and Kuhling as well as by Tice and Ganem.[10] In view of the steric strain between the two *N*-acyl groups attached to the same side of a glycoluril system, and the close structural relationship between glycolurils and oxazolidinones,[9] we reasoned that this electrophilic character might result from twisting around the bond between the glycoluril and the attached acyl groups. To test this hypothesis, we examined the X-ray crystal structures of several acylglycolurils. Herein, the X-ray crystal structure of 1,6-diacetyl-3,4,7,8-tetramethyl-2,5-dithioglycoluril‡ **3** is described. The results show that steric crowding in this derivative enforces a highly twisted conformation in *one* of the two acetyl groups in **3**.

The preparation of diacetyl dithioglycoluril **3** has been reported previously.[11] Crystals of **3** were obtained by slow evaporation of a solution in CH_2Cl_2.§ ORTEP drawings of two orthogonal views of the molecule are given in Fig. 1, along with selected bond lengths. In this structure, one acetyl group is held close to coplanar with the thioureido ring of the glycoluril (τ = 2.6°), while the other is twisted significantly out of the ureido ring plane, with τ = 55.0°. This out of plane twist is accompanied by a significant lengthening of the N–C(O) bond, from 1.397(3) Å for the coplanar acetyl group [N(1)–C(15)] to 1.447(3) Å for the twisted amide [N(6)–C(18)]. Careful examination of the crystal packing in **3** showed no close non-bonded interactions around the twisted acetyl group.¶ Although the protons of both acetyl groups appeared at the same chemical shift by NMR analysis, at least down to −60 °C, IR spectroscopy of **3** confirmed the presence of one twisted amide bond in solution. Thus, the spectrum‖ exhibits two distinct C=O stretching absorptions, at 1738 and 1680 cm^{-1}. In contrast, monoacetyl dithioglycoluril[11] exhibits a single stretch at 1681

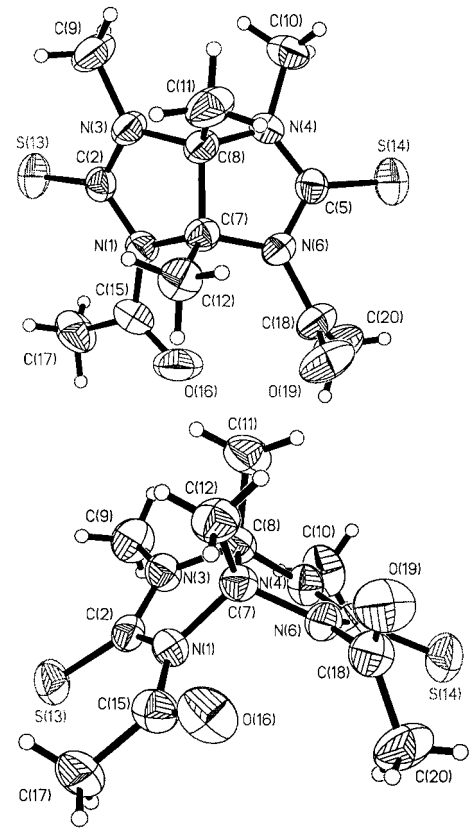

Fig. 1 Two approximately orthogonal ORTEP diagrams of the X-ray crystallographic structure of glycoluril **3**. Selected bond lengths (Å) and angles (°): N(1)–C(2): 1.394(3), N(1)–C(15) 1.397(3), N(1)–C(7) 1.505(3), C(2)–S(13) 1.650(2), C(5)–N(6) 1.367(3), C(5)–S(14) 1.660(2), N(6)–C(18) 1.447(3), N(6)–C(7) 1.461(3), C(15)–O(16) 1.211(3), C(18)–O(19) 1.190(3), C(5)–N(6)–C(18) 122.6(2), C(2)–N(1)–C(15) 129.9(2).

cm^{-1}. This shift to higher frequency with increasing τ is analogous to that reported by Yamada.[6] Thus, the twisted and untwisted acetyl groups apparently interconvert on a time scale between that of NMR and IR analysis.

The observed twist angle is unique to the best of our knowledge for any acetamide: **3** is much more twisted than **2**, and approaches the value for the far more hindered pivaloyl derivative **1**, without requiring the presence of the *tert*-butyl group for steric interaction. The presence of sulfur plays an important role in this effect, since the oxygen analog **4** has τ = 1.5 and 21.6° for the untwisted and twisted acetyl groups respectively, but otherwise resembles **3** in geometry.[12] The twist in glycolurils **3** and **4** is probably the result of unfavourable electrostatic interactions between the two acyl oxygen atoms, which would be forced into close proximity if both acetyl groups were to remain coplanar with their respective attached ureido rings. The larger twist in **3** could result from further steric interactions between the acyl methyl group and the thione (*cf.* **2**); however, the lack of twisting of one acetyl group in **3** suggests that this effect is not major. Rather, we prefer to explain the twist as being due to electron density on nitrogen being pushed into the thione in **3** to a greater extent than into the corresponding carbonyl group in **4**.[14] This effect results in less overlap of the nitrogen lone pairs with the carbonyl groups of the twisted acetyl moieties. The unfavourable interaction of the two acyl oxygen atoms can thus more readily be mitigated in **3** by twisting one acetyl group into the observed twisted conformation. The distances between the two acyl oxygen atoms are 3.03 Å in **3** and 2.84 Å in **4**. One amide resonance interaction in **3** is thus almost fully maintained, while that in the twisted acetyl group is severely compromised. This explanation is consistent with greater electron density on N(6) than on N(1) which results in an increased bond length for N(1)–C(2) compared to N(6)–C(5). Also, shortening of the N(6)–C(7) and concomitant lengthening of the C(7)–N(1) bonds, as well as the tilt of the C(12) methyl group towards the N(1) side of the molecule, and other distances and angles on the acyl-substituted side of **3** are fully in agreement with our interpretation.

Whether activation of the acyl carbon of **3** as a result of this twist enhances the intramolecular Claisen-like condensation of diacylglycolurils is under investigation. It is interesting to speculate that similar unfavourable interactions between a substrate amide carbonyl oxygen atom and another negatively polarized oxygen functionality in a protease could provide a mechanism for twisting of the substrate amide bond prior to nucleophilic attack by water.

This work was financially supported by the Natural Sciences and Engineering Research Council of Canada.

Notes and References

† E-mail: pharriso@mcmail.cis.mcmaster.ca

‡ For nomenclature and numbering system for **3**, see ref. 11.

§ *Crystal data* for **3**: $C_{12}H_{18}N_4O_2S_2$, M = 314.42, T = 300 K, monoclinic, space group $P2_1/n$ (no. 14), a = 10.1648(1), b = 14.4512(3), c = 10.2116(2) Å, β = 99.881(1)°, V = 1477.77(4) Å^3, Z = 4, D_x = 1.413 Mg m^{-3}, graphite monochromated Mo-Kα rotating anode radiation, λ = 0.71073 Å, μ = 3.67 cm^{-1}, crystal size 0.3 × 0.2 × 0.1 mm, 12 100 reflections (3035 unique) with θ > 26.5° measured using a Siemens SMART CCD area detector; R_{int} = 0.040 after SADABS absorption correction ($T_{min,max}$ = 0.684, 0.940); full-matrix least-squares refinement on F^2 using SHELXTL software, $wR2$ = 0.123 for all data, $R1$ = 0.047 for 2150 reflections with $I > 2\sigma$, 254 parameters, S = 1.071, non-hydrogen atoms anisotropic, hydrogens isotropic; residual $\Delta\rho_{min,max}$ = −0.195, 0.226 e Å^{-3}. CCDC 182/840.

¶ There appears to be only one other reported crystal structure for an acylglycoluril, that of 1,4-dinitro-3,6-diacetylglycoluril (ref. 13), which is described as having only a small twist angle. In this case, similar arguments were made in relation to the crystal packing not influencing the twist of the acyl groups.

‖ The FT-IR spectrum of **3** was recorded in $CHCl_3$, on a Bio-Rad SPC 3200 spectrophotometer.

1 S. Yamada, T. Sugaki and K. Matsuzaki, *J. Org. Chem.*, 1996, **61**, 5932.
2 Q. P. Wang, A. J. Bennet, R. S. Brown and B. D. Santarsiero, *J. Am. Chem. Soc.*, 1991, **113**, 5757; V. Somayaji, K. I. Skorey, R. S. Brown and R. G. Ball, *J. Org. Chem.*, 1986, **51**, 4866; V. Somayaji and R. S. Brown, *J. Org. Chem.*, 1986, **51**, 2676; T. G. Lease and K. J. Shea, *J. Am. Chem. Soc.*, 1993, **115**, 2248.
3 For reviews, see: T. G. Lease and K. J. Shea, in *Advances in Theoretically Interesting Molecules*, R. P. Thummel, JAI Press, Greenwich, 1992, vol. 2, pp. 79–112; A. Greenberg, in *Structure and Reactivity*, ed. J. F. Liebman and A. Greenberg, VCH, New York, 1988, vol. 7, ch. 4; H. K. Hall, Jr. and A. El-Shekeil, *Chem. Rev.*, 1983, **83**, 549. For other examples, see: K. J. Shea, T. G. Lease and J. W. Ziller, *J. Am. Chem. Soc.*, 1990, **112**, 8627; A. J. Bennet, Q. P. Wang, H. Ślebocka-Tilk, V. Somayaji and R. S. Brown, *J. Am. Chem. Soc.*, 1990, **112**, 6383.
4 H. Ślebocka-Tilk and R. S. Brown, *J. Org. Chem.*, 1987, **52**, 805.
5 A. Mühlebach, G. P. Lorenzi and V. Gramlich, *Helv. Chim. Acta*, 1986, **69**, 389.
6 S. Yamada, *Angew. Chem., Int. Ed. Engl.*, 1993, **32**, 1083.
7 F. K. Winkler and J. D. Dunitz, *J. Mol. Biol.*, 1971, **59**, 169.
8 S. Yamada, *J. Org. Chem.*, 1992, **57**, 1591; S. Yamada, M. Nakamura and I. Kawauchi, *Chem. Commun.*, 1997, 8857.
9 S. Sun and P. Harrison, *Tetrahedron Lett.*, 1992, **33**, 7715; S. Sun and P. Harrison, *J. Chem. Soc., Chem. Commun.*, 1994, 2235; C. Cow, D. Valentini and P. Harrison, *Can. J. Chem.*, 1997, **75**, 884; S. Sun, L. Edwards and P. Harrison, *J. Chem. Soc., Perkin Trans. 1*, 1998, 437.
10 C. Hase and D. Kuhling, *Liebigs Ann. Chem.*, 1975, 95; C. M. Tice and B. Ganem, *J. Org. Chem.*, 1983, **48**, 2106.
11 C. N. Cow and P. H. M. Harrison, *J. Org. Chem.*, 1997, **62**, 8834.
12 S. Sun, C. Cow and P. Harrison, unpublished results.
13 P. J. Boileau, E. Wimmer, M. Pierrot, A. Baldy and R. Gallo, *Acta Crystallogr.*, 1985, **C41**, 1680.
14 W. Walter and J. Voss, *The Chemistry of Thioamides*, in *The Chemistry of Amides*, ed. J. Zabicky, Series ed. S. Patai, Wiley, Chichester, 1970, pp. 383–475.

Received in Corvallis, OR, USA, 24th February 1998; 8/01580E

Association of two-coordinate copper(I) complexes: switching on and off Cu···Cu, ligand···ligand and Cu–ligand interactions

Xiang-Yang Liu, Fernando Mota, Pere Alemany, Juan J. Novoa* and Santiago Alvarez*†

Departament de Química Inorgànica and Departament de Química Física Universitat de Barcelona, Diagonal 647, 08028 Barcelona, Spain

A combined theoretical *ab initio* and structural database study is presented of the different interactions that allow two-coordinate copper(I) molecules to associate, from weak interactions to chemical bonds, giving rise to different structures.

Copper(I) complexes[1,2] with stoichiometry CuXL appear as bimolecular aggregates with Cu···Cu (**1**, with the two monomers in an eclipsed or a rotated conformation) or Cu···X (**2**) contacts, or forming dimers with a cyclic Cu_2X_2 core as in **3**, or

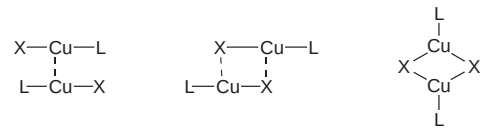

1 **2** **3**

intermediate geometries. Also binuclear complexes with bidentate ligands bridging two copper atoms present molecular structures topologically equivalent to **1**. The Cu···Cu distances in these compounds span a large range (from 2.6 to 3.5 Å), suggesting the existence of weakly bonding interactions between the d^{10} ions, similar to those extensively studied for the related silver(I) compounds.[3–6]

The first semiempirical studies of bimolecular copper(I) aggregates,[7] based on extended Hückel calculations, proposed that mixing of the occupied d_{z^2} with the empty p_z atomic orbitals would convert the repulsion between the closed d shells into a weak bonding interaction. *Ab initio* studies have been reported for copper(I) complexes with monoatomic bridges,[8,9] and for the association between rigid monomers in $[Cu(PH_3)Cl]_2$ or in the interpenetrated networks of Cu_2O.[10,11] However, the rich structural chemistry of the [CuLX] groups outlined above has not been analyzed in detail and an explanation for the factors that determine the choice between structures **1**–**3** is still needed. For this reason, we present here the results of a theoretical *ab initio* MP2 (triple-ζ + polarisation basis set) study of the intermolecular interactions between two-coordinate copper(I) complexes in the model compounds $[Cu(NH_3)Cl]_2$, $[Cu(N_2)Cl]_2$ and $[Cu(PH_3)Cl]_2$, combined with a structural database analysis.‡ The structural parameters that describe the geometry of a bimolecular aggregate **4** are the bond angle β, the

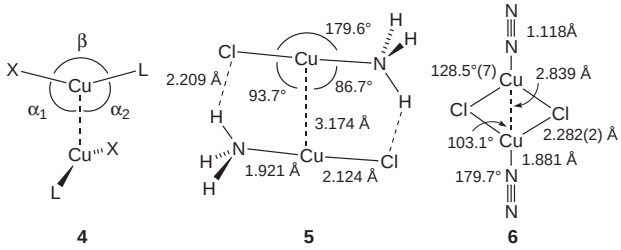

4 **5** **6**

intermolecular angles Cu–Cu–Cl (α_1) and Cu–Cu–E (α_2, E = N, P), and the torsion angle Cl–Cu–Cu–Cl (τ).

The most remarkable features of the optimized structure of $[Cu(NH_3)Cl]_2$ **5** are its eclipsed conformation, a relatively long Cu···Cu distance and the existence of short intermolecular N–H···Cl contacts. A dimer of type **3** with bridging chloro ligands was explored for $[Cu(NH_3)Cl]_2$, but no minimum was found for such a structure or for the alternative **2**, and the hydrogen-bonded structure **5** was always obtained in the optimization procedure. Nevertheless, a strong bonding interaction exists between the two bent monomers in a rhombic structure **3** of $[Cu(NH_3)Cl]_2$ [−40 kcal mol^{-1}] although the energy required to bend the monomers (17 kcal mol^{-1} per monomer) makes the bonding energy relatively small (−7 kcal mol^{-1}). Hence, the intermolecular aggregate of type **5** with two hydrogen bonds is more stable (bonding energy −22 kcal mol^{-1}) than the rhombic form at the present level of computation. The choice of a ligand with weaker or no hydrogen bonding capabilities, such as PH_3 or N_2 in $[Cu_2L_2Cl_2]$ (L = PH_3 or N_2), makes a structure of type **1** less favorable, with only a weak Cu···Cu interaction left. Therefore, structure **3** becomes the most stable one in these cases, with dissociation energies of 17 and 18 kcal mol^{-1} for L = PH_3 and N_2, respectively (optimized structural parameters for the latter shown in **6**). Notice that the halophosphine complexes of stoichiometry $Cu(PR_3)X$ crystallize with structure **3** (13 structures) predicted to be more stable by our calculations, except for those with the bulkiest phosphines which give isolated monomers (four structures).

We analyzed in some detail the potential energy surface of $[Cu(NH_3)Cl]$ in its staggered conformation (τ = 90°), in which both ligand···ligand and ligand···metal interactions are minimized. The interaction between two linear $[Cu(NH_3)Cl]$ monomers (with $\alpha_1 = \alpha_2$ = 90°) is found to be attractive by 1–3 kcal mol^{-1} for all the range of distances between 2.5 and 5.0 Å. The bonding energy presents a maximum (−3.2 kcal mol^{-1}) at Cu···Cu 3.004 Å, similar to the values reported by Pyykkö *et al*. for $[Cu(PH_3)Cl]_2$ with a similar geometry,[10] and to that found for the interaction between rigid networks in Cu_2O.[11] They probably indicate the existence of a weakly bonding Cu···Cu interaction in the staggered form, which should coexist with the stronger ligand···ligand hydrogen bonding in the most stable eclipsed structure **5**. Bending the monomers does not improve the intermolecular interaction, although aggregates in which β is as small as 165° are still stable toward dissociation into linear monomers. Interestingly, the Cu···Cu distance is predicted to shorten for smaller bond angles (Fig. 1, triangles), a behavior that can be also found for the experimental data (Fig. 1, squares and circles for inter- and intra-molecular contacts, respectively).The aggregate in the eclipsed conformation is stabilized by slipping the two monomers (*i.e.* α_1 = 87°, α_2 = 93° and β = 177°), while the Cu···Cu distance (2.694 Å) is significantly shortened.

Further support for the bonding nature of the Cu···Cu contact in both its eclipsed and staggered forms has been obtained from a topological analysis[12] of the calculated electron density of $[Cu(NH_3)Cl]_2$. A bond critical point was found between the two Cu atoms in $[Cu(NH_3)Cl]_2$, with electron densities of 0.017 and 0.028 for the eclipsed and staggered structures, respectively, consistent with a weak bonding interaction. The values found for all characteristic parameters of the critical points are similar to those for closed shell interactions such as the O–H···O

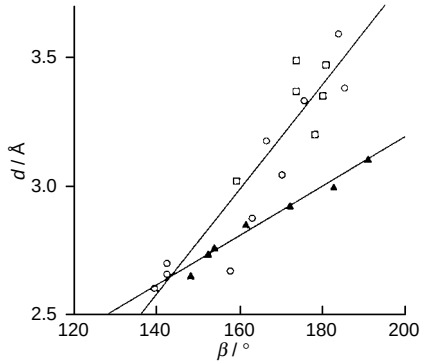

Fig. 1 Optimized Cu···Cu distance as a function of the bond angle β for the dimer $[Cu(NH_3)Cl]_2$ (triangles). Structural data for intermolecular (squares) and intramolecular (circles) contacts with flexible bridging ligands in an eclipsed conformation also plotted for comparison.

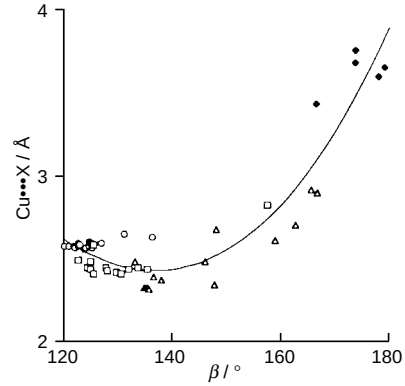

Fig. 2 Longest Cu···X distance as a function of the bond angle β for bimolecular aggregates $[CuLX]_2$ of types **1** and **2**, and for dimers **3**, where X = Cl (triangles, 13 structures), Br (squares, 14 structures), I (circles, 21 structures) or N (diamonds, 5 structures)

hydrogen bonds (see ref. 12, p. 292). In addition, bond critical points between the hydrogen and chlorine atoms in the eclipsed conformer confirm the existence of inter-ligand hydrogen bonds. A previous study of the electron density in a bridged silver(I) binuclear complex also showed the bonding nature of the Ag···Ag interaction.[13] It is interesting to stress that in $[Cu(NH_3)Cl]_2$ there is Cu···Cu bonding even if the copper atoms are 3.174 Å apart. In contrast, a similar analysis of the electron density of the rhombic structure of $[Cu(N_2)Cl]_2$, with a shorter Cu···Cu distance (2.839 Å), shows no bond critical point between the copper atoms. These results clearly show that it is the molecular topology, not the distance, that determines the existence of a Cu···Cu bonding interaction. Such results are consistent with the importance of the d_{z^2}–p_z hybridization[4,7] for the Cu···Cu interaction (possibly a part of the important correlation effects in post Hartree–Fock calculations[5]): in the intermolecular aggregate $[Cu(NH_3)Cl]_2$ the empty p_z orbital of Cu can participate in the Cu···Cu interaction, and a bond critical point is found between the copper atoms. In contrast, in the optimized structure of $[Cu(N_2)Cl]_2$, the p_z orbital is involved in metal–ligand bonding (corresponding to a formal sp^2 hybridization at Cu), the d_{z^2}–p_z donor–acceptor interaction should be quenched, and no Cu···Cu bond critical point is found.

The variety of structures found for the bimolecular aggregates of the [CuLX] compounds can be explained taking into account the reluctance of the monomers to bend, together with the variety of intermolecular interactions available to them: (*i*) weak Cu···Cu bonding interaction, (*ii*) intermolecular hydrogen bonds between ligands, (*iii*) new Cu–X bonds (when the X ligands have unshared electron pairs), and (*iv*) steric hindrance imposed by highly bulky ligands L that may prevent two monomers from approaching close enough to allow bonding interactions. For instance, a Cu···Cu contact at 2.810 Å is found in a staggered conformation with no supporting metal–ligand or hydrogen-bonding interactions in $[Cu(pyFc)_2][CuCl_2]$ [pyFc = 1,1′-bis(2-pyridyl)octamethylferrocene].[14] On the other hand, the hydrogen-bonded structure **5** found for our model compound has an experimental counterpart in $[Cu(Me_4pip)Br]$[15] (Me_4pip = 2,2,6,6-tetramethylpiperidine), which presents a N–H···Br distance of 2.653Å and a Cu···Cu distance of 3.362 Å.

The attractive Cu···X interaction predicted in our calculations for $[Cu(L_2)Cl]_2$ (L = PH_3, N_2) that may result in the formation of a rhombic dimer of type **3** is in keeping with the coordinative unsaturation of Cu^I in two-coordinate complexes, manifested in their well known tendency to form three- or four-coordinate compounds.[1,2] In fact, one can view the different structures experimentally found as snapshots along the pathway that takes one from bimolecular aggregates of type **1** to dimers of type **3**, along which the Cu···X distance and the bond angle β are expected to decrease in a concerted way. This is precisely what is found (Fig. 2) for the structurally characterized dimers of type **3** and those weakly bound aggregates of type **1** or **2** (with X = Cl, Br, I or N). Alternatively, the [CuLX] monomers associate through Cu···X contacts forming chains of trigonally coordinated Cu atoms, that have been structurally characterized for X = L = Br.[15] When the two ligands have an unshared electron pair as in the $[CuX_2]^-$ monomers, two Cu···X contacts per molecule can be formed, thus giving chains of tetrahedrally coordinated Cu atoms, as frequently found in the salts of the $[CuX_2]^-$ anions (X = Cl, Br, or I).

Work supported by DGES, project PB95-0848 and by CIRIT, grant 1995SGR-00421. The allocation of computing resources at the Centre de Supercomputació de Catalunya (CESCA) was funded in part through a grant of Fundació Catalana per a la Recerca and Universitat de Barcelona.

Notes and References

† E-mail: salvarez@kripto.qui.ub.es

‡ Details of the *ab initio* calculations[16] and of the structural database search[17] can be obtained from the authors.

1 B. J. Hathaway, in *Comprehensive Coordination Chemistry*, ed. G. Wilkinson, Pergamon, Oxford, 1987.
2 S. Jagner and G. Helgesson, *Adv. Inorg. Chem.*, 1991, **37**, 1.
3 P. Pyykkö, *Chem. Rev.*, 1997, **97**, 597 and references therein.
4 Y. Jiang, S. Alvarez and R. Hoffmann, *Inorg. Chem.*, 1985, **24**, 749.
5 P. Pyykkö and Y. Shao, *Angew. Chem., Int. Ed. Engl.*, 1991, **30**, 604.
6 J. Li and P. Pyykkö, *Chem. Phys. Lett.*, 1992, **197**, 586.
7 P. K. Mehrotra and R. Hoffmann, *Inorg. Chem.*, 1978, **17**, 2187.
8 A. Schäfer and R. Ahlrichs, *J. Am. Chem. Soc.*, 1994, **116**, 10 692.
9 A. Schäfer, C. Huber, J. Gaus and R. Ahlrichs, *Theor. Chim. Acta*, 1993, **87**, 29.
10 P. Pyykkö, N. Runeberg and F. Mendizabal, *Chem. Eur. J.*, 1997, **3**, 1451.
11 E. Ruiz, S. Alvarez, P. Alemany and R. A. Evarestov, *Phys. Rev. B*, 1997, **56**, 7189.
12 R. F. W. Bader, *Atoms In Molecules. A Quantum Theory*, Clarendon Press, Oxford, 1990.
13 M. A. Romero, J. M. Salas, M. Quirós, M. P. Sánchez, J. Molina, J. El Bahraoui and R. Faure, *J. Mol. Struct.*, 1995, **354**, 189.
14 U. Siemeling, U. Vorfeld, B. Neumann and H.-G. Stammler, *Chem. Commun.*, 1997, 1723.
15 R. P. Shibaeva, V. F. Kaminskii, E. B. Yagubskii and L. A. Kushch, *Kristallografiya*, 1983, **28**, 92.
16 M. J. Frisch *et al.*, GAUSSIAN 94 (Revision E.1), Gaussian, Inc., Pittsburgh, PA, 1995.
17 F. H. Allen and O. Kennard, *Chem. Des. Automat. News*, 1993, **8**, 31.

Received in Basel, Switzerland, 16th February 1998; 8/01343H

Parallel synthesis of alkyl methacrylate latexes for use as catalytic media

Paul D. Miller and Warren T. Ford*†

Department of Chemistry, Oklahoma State University, Stillwater, OK 74078, USA

Among thirty-two anion exchange latexes prepared by parallel synthesis, those containing 2-ethylhexyl methacrylate units are the most active as catalytic media for alkaline hydrolysis of *p*-nitrophenyl alkanecarboxylates.

Cationic polymers and colloids, such as soluble polyelectrolytes,[1] macroscopic anion exchange resins,[2] surfactant micelles,[1,3] and 0.2 μm diameter latex particles[4] in aqueous media catalyze reactions of anions with uncharged organic compounds. The catalytic activities are due primarily to high local concentrations of the anionic and uncharged reactants in the small volume fraction of the polymer or colloid phase or pseudophase in the aqueous mixture, although enhanced intrinsic rate constants sometimes contribute. Amounts of less than 1 mg ml^{-1} of polystyrene latexes containing quaternary ammonium anion exchange sites increase the rate of *o*-iodosobenzoate-catalyzed hydrolysis of *p*-nitrophenyl diphenyl phosphate up to 6300 times faster than in water alone.[4] These rate enhancements in anion exchange latexes are as high or higher than those in cationic micelles,[5] and the activity persists at very low particle concentrations, whereas surfactants have high catalytic activity only above the critical micelle concentration.

An important potential application of colloidal catalysts is hydrolytic decontamination of toxic organophosphates, phosphonates and fluorophosphonates which are widely used as insecticides and are stockpiled as chemical warfare agents.[6] However, these polystyrene latex particles failed to promote the hydolysis of diisopropyl fluorophosphate (DFP) in pH 11 aqueous media,[7] probably due to an unfavorable partition coefficient of the aliphatic DFP into the aromatic polystyrene latex particles. Reasoning that aliphatic polymers would absorb larger amounts of aliphatic reactants, we synthesized a family of cationic latexes from copolymers of alkyl methacrylates and vinylbenzyl chloride and tested their activities for basic hydrolysis of active esters.

Diversity strategies for the synthesis of biologically active compounds are employed at all major pharmaceutical companies, have been used in search of superconductive, magnetic, and phosphorescent materials,[8] and have been used to prepare polymer catalysts.[9] One widespread method is the combinatorial synthesis of different compounds in polymer beads that can be separated and tested individually. Since latex particles are too small to be separated as single beads, we employed a parallel method to prepare a diverse series of alkyl methacrylate-based catalysts.

Twenty-nine latex copolymers of 25 mass% vinylbenzyl chloride (VBC, 70 : 30 *m* : *p*) and 73 mass% aliphatic methacrylates were prepared on a 500 mg scale using 1% divinylbenzene to cross-link the particles, 1% (*m*,*p*-vinylbenzyl)-trimethylammonium chloride to stabilize the particles during growth, and 2,2′-azobis(*N*,*N*′-dimethyleneisobutyramidine) dihydrochloride as a water-soluble radical initiator. The latexes differed in the number and combination of aliphatic monomers present. Polymerizations were carried out using sets of 12 test tubes, each containing a different mixture of monomers and a 7 mm stirring bar. The test tubes were supported in a 60 °C water bath on a multiplate magnetic stirrer. Anion exchange sites in the form of quaternary ammonium groups were introduced to six latexes at one time in separate vials in a sealed pressure reactor by reaction of the vinylbenzyl chloride component with either trimethylamine (TMA) at 60 °C or tributylamine (TBA) at 95 °C. Methanol was added to the vials and to the reactor to promote permeation of the polymers by the amines and to equalize pressure inside and outside the vials. Each quaternized latex was purified by repeated washing and ultrafiltration through a 0.1 μm membrane filter on a syringe. The resulting anion exchange particles contained 19–20 mol% of quaternary ammonium units (Fig. 1). Representative samples were 130–140 nm in diameter by TEM measurements.

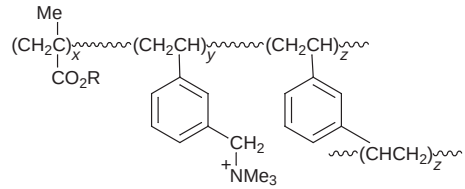

Fig. 1 Structure of TMA-quaternized latexes

Table 1 presents the results of screening the catalytic activities of 0.6 mg ml^{-1} alkyl methacrylate latexes for hydrolysis of *p*-nitrophenyl (PNP) hexanoate (Scheme 1) in pH 9.4 borate buffer solution.

Rate enhancements relative to rates in the absence of latex ranged from 2.3 for the polystyrene–TMA latex (15 in Table 1)

Table 1 Observed rate constants for hydrolysis of PNP–hexanoate in latex dispersions

Latex	Methacrylate[a,b]	$10^3\ k_{obs}/s^{-1}$
1	Butyl	2.0
2	Isobutyl	2.1
3	2-Chloroethyl	1.8
4	Tetrahydrofurfuryl	2.3
5	2-Ethylhexyl	4.1
6	Butoxyethoxyethyl	1.9
7	Ethoxyethoxyethyl	1.8
8	2-Ethylbutyl	2.0
9	*n*-Hexyl	2.1
10	*n*-Octyl	3.1
11	*n*-Decyl	3.3
12	*n*-Dodecyl	3.5
13	Tetrahydropyranyl	1.8
14	Furfuryl	1.9
15	Polystyrene	0.8
16	Butyl (TBA)	5.1
17	Polystyrene (TBA)	3.9
18	2-Ethylhexyl (TBA)	5.4

[a] All latexes were quaternized with trimethylamine except 16, 17 and 18 which were quaternized with tributylamine. [b] Latex concentration was 0.6 mg ml^{-1}, quaternary ammonium ion concentration $[N^+]$ = 62 μM, and substrate concentration 2.5 μM in 0.02 M borate buffer (pH 9.4) at 30.0 °C. Psuedo-first-order rate constants were calculated for formation of *p*-nitrophenoxide measured by increase of absorbance at 410 nm over the first 20% conversion. The k_{obs} values were reproducible to within 5% from triplicate measurements with each latex, and from triplicate preparations of latexes 1, 5 and 15–18. k_w for the reaction in the absence of latex was $3.26 \times 10^{-4}\ s^{-1}$.

Table 2 Intraparticle rate constants and equilibrium constants

	Styrene		Butyl MA		2-Ethylhexyl MA	
PNP ester	$10^3\ k_L/s^{-1}$	$10^{-3}\ K$/ dm^3 mol^{-1}	$10^3\ k_L/s^{-1}$	$10^{-3}\ K$/ dm^3 mol^{-1}	$10^3\ k_L/s^{-1}$	$10^{-3}\ K$/ dm^3 mol^{-1}
TMA-quaternized						
Acetate	1.3	2.0	9.3	2.3	7.4	2.3
Hexanoate	5.7	2.1	5.9	11.8	4.7	21
Octanoate	4.7	12.7	5.3	46	4.9	70
TBA-quaternized						
Acetate	11.9	3.1	9.5	4.1	9.0	5.0
Hexanoate	5.8	15.1	5.8	25	5.8	31
Octanoate	5.7	69	5.3	74	5.1	88

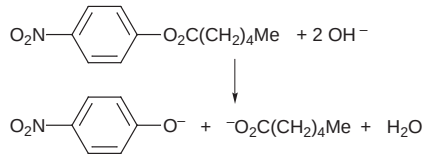

Scheme 1

to 16.5 for the 2-ethylhexyl methacrylate–TBA latex (18), and all alkyl methacrylate–TMA latexes were more active than the polystyrene–TMA latex. There was a sizable increase of activity on increase of the alkyl chain length from hexyl (9) to octyl (10) but only smaller increases between other pairs of C_{2n}-alkyl methacrylate latexes (1, 9–12). The branched 2-ethylhexyl methacrylate latex (5) was more active than the linear octyl methacrylate latex (10) having the same number of carbon atoms. Fourteen more TMA-quaternized latexes (not shown) containing mixtures of two methacrylate monomers and VBC gave rate constants between those of the latexes in Table 1 containing the same individual monomers. Finally Table 1 indicates that particles containing TBA sites (16–18) are more active than those containing TMA sites (1,5,15).

Activities of the styrene, butyl methacrylate and 2-ethylhexyl methacrylate-based latexes were measured at 5–6 different particle concentrations. Pseudo-first order intraparticle rate constants (k_L) for the hydrolysis of PNP-acetate, hexanoate, and octanoate and equilibrium binding constants (K) of the PNP ester to quaternary ammonium ion sites in the latex were calculated from double reciprocal plots of duplicate measurements of each rate constant using eqn. (1), where k_w is the rate

$$1/(k_{obs}-k_w)=1/(k_L-k_w)K[N^+] + 1/(k_L-k_w) \quad (1)$$

constant in the absence of latex.[10] (A 'binding constant' of the nonionic PNP ester to the ion exchange sites is a misnomer. 'Partition coefficient' would be better, but the binding constant formalism[10] is easy to apply.) The results are reported in Table 2.

The major differences in the activities are due to the binding constants: the longer the aliphatic chain of the PNP ester, and the more lipophilic the quaternary ammonium ion, the greater the binding constant. The much larger increases in the binding constants from polystyrene–TMA to polystyrene–TBA than with the corresponding methacrylate latexes is due to the TBA increasing the aliphatic character of aromatic latexes more than of aliphatic latexes.

Parallel synthesis has enabled rapid evaluation of 32 latex catalysts and selection of the most informative ones for analysis of intraparticle rate constants and binding constants. This diversity approach can be used to identify active polymer catalysts for many other important chemical reactions.

This research was supported by the U.S. Army Research Office.

Notes and References

† E-mail: wtford@osuunx.ucc.okstate.edu

1 W. K. Fife, *Trends Polym. Sci.*, 1995, **3**, 214; J. H. Fendler and E. H. Fendler, *Catalysis in Micellar and Macromolecular Systems*, Academic, New York, 1975.
2 W. T. Ford and M. Tomoi, *Adv. Polym. Sci.*, 1984, **55**, 49; M. Tomoi and W. T. Ford, in *Synthesis and Separations Using Functional Polymers*, ed. D. C. Sherrington and P. Hodge, Wiley, Chichester, 1988, pp. 181–207.
3 C. A. Bunton and G. Savelli, *Adv. Phys. Org. Chem.*, 1986, **22**, 213.
4 J. J. Lee and W. T. Ford, *J. Am. Chem. Soc.*, 1994, **116**, 3753; W. T. Ford and H. Yu, *Langmuir*, 1993, **9**, 1999.
5 R. A. Moss, K. W. Alwis and G. O. Bizzigotti, *J. Am. Chem. Soc.*, 1983, **105**, 681; R. A. Moss, A. T. Kotchevar, B. D. Park and P. Scrimin, *Langmuir*, 1996, **12**, 2200.
6 Y.-C. Yang, J. A. Baker and J. R. Ward, *Chem. Rev.*, 1992, **92**, 1729.
7 J. Walker and F. Hoskins, US Army Natick RDEC, personal communication.
8 X.-D. Xiang, X. Sun, G. Briceno, Y. Lou, K.-A. Wang, H. Chang, W. G. Wallace-Freedman, S.-W. Chen and P. G. Schultz, *Science*, 1995, **268**, 1738; G. Briceno, H. Chang, X. Sun, P. G. Schultz and X.-D. Xiang, *Science*, 1995, **270**, 273; X.-D. Sun, C. Gao, J. Wang and X.-D. Xiang, *Appl. Phys. Lett.*, 1997, **70**, 3353.
9 F. M. Menger, A. V. Eliseev and V. A. Migulin, *J. Org. Chem.*, 1995, **60**, 6666; K. D. Shimizu, B. M. Cole, C. A. Krueger, K. W. Kuntz, M. L. Snapper and A. Hoveyda, *Angew. Chem., Int. Ed. Engl.*, 1997, **36**, 1704.
10 F. M. Menger and C. E. Portnoy, *J. Am. Chem. Soc.*, 1967, **89**, 4698.

Received in Columbia, MO, USA, 9th January 1998; 8/00383A

From helicate to infinite coordination polymer: crystal and molecular structures of silver(I) complexes of readily prepared di-Schiff bases

Paul K. Bowyer, Keith A. Porter, A. David Rae, Anthony C. Willis and S. Bruce Wild*†

Research School of Chemistry, Institute of Advanced Studies, Australian National University, Canberra, ACT 0200, Australia

The readily prepared di-Schiff base of pyridine-2-aldehyde and ethane-1,2-diamine 1 reacts with silver(I) tetrafluoroborate to form by self-assembly the double-stranded D_2-helicate (±)-$[Ag_2\mathbf{1}_2](BF_4)_2$; the corresponding Schiff base of (1*R*,2*R*)-cyclohexane-1,2-diamine [(*R*,*R*)-2] reacts with silver(I) nitrate to produce the homochiral single-stranded C_2-coordination polymer *M*-$\{[Ag\{(R,R)\text{-}\mathbf{2}\}]NO_3{\cdot}2H_2O\}_\infty$.

Double- and triple-stranded helicates are generated when metals combine with ligands containing appropriate metallophilic and helicating elements. Thus, the bis(methylene)oxy group inserted between a pair of semi-rigid 2,2′-bipyridines destabilises single-stranded mononuclear metal chelates of univalent Group 11 ions, but facilitates the self-assembly of double-stranded dinuclear metal helicates.[1,2] Moreover, a homochiral helicating element in the ligand can induce considerable stereoselectivity in the product.[3] There is now available a wide variety of structural motifs for the self-assembly of double- and triple-stranded helicates, many of which are derived from ligands having as their metallophilic elements familiar chelating entities, including 2,2′-bi- and oligo-pyridines and related compounds,[4] and a tetra(tertiary phosphine).[5] Herein we report the syntheses and crystal and molecular structures of silver(I) complexes of the readily prepared di-Schiff bases **1**[6] and (*R*,*R*)-**2**,[7] *viz*. the double-stranded helicate (±)-$[Ag_2\mathbf{1}_2](BF_4)_2$ and the

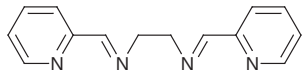

1

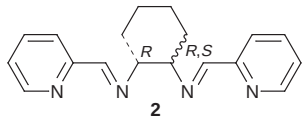

2

infinite single-stranded coordination polymer *M*-$\{[Ag\{(R,R)\text{-}\mathbf{2}\}]NO_3{\cdot}2H_2O\}_\infty$. The crystal and molecular structures of the related double-stranded helicate (±)-$[Ag_2\{(R,S)\text{-}\mathbf{2}\}_2](CF_3SO_3)_2$ have been determined previously[8] and detailed NMR spectroscopic investigations of this compound and the parent (±)-$[Ag_2\mathbf{1}_2](CF_3SO_3)_2$ have indicated that both helicates have two-fold symmetry in solution.[8,9] In other work, it has been shown that silver(I) combines with a single enantiomer of a bis(pyridyl) ligand derived from L- or D-tartaric acid to give an extended single- stranded helicate, whereas the corresponding racemic form of the ligand produces a disilver(I) complex incorporating both enantiomers in a *meso* arrangement.[10]

The complex (±)-$[Ag_2\mathbf{1}_2](BF_4)_2$ was isolated as pale-yellow prisms from acetonitrile–diethyl ether, mp 221–221.5 °C (decomp.).‡ The ^{1}H NMR spectrum of the complex in [$^2H_3$]acetonitrile is consistent with the presence of a pair of homotopic ligands[2] and the electrospray MS of the complex at a cone potential of 25 V displays a pattern of peaks in the range *m*/*z* 776–783 due to $[Ag_2\mathbf{1}_2{\cdot}BF_4]^+$. The salt crystallises as a racemic compound in the orthorhombic space group $C222_1$ (no. 20) with four pseudo inversion related pairs of cations and associated anions in the unit cell [Fig. 1(*a*)].§ Each disilver(I) cation has D_2 symmetry with the two homotopic ligands spanning both silver(I) ions. The Ag···Ag distance in the cation is 3.024 Å (av.). The overall structure can be described as a modulation of an idealised *Fddd* parent structure in which true inversion relates two substructures of *F*222 symmetry with *C*-centred layers of the different substructures interleaved perpendicular to ***c***. Within a layer, the dimeric cation occupies a site of 222 symmetry with the anions located on two-fold rotation axes parallel to ***b*** at 1/2, ± 0.15, 0 from the cation. The modulation lowers the symmetry of the structure from *Fddd* to $C222_1$ (a subgroup of *Fddd*) and destroys the crystallographic symmetry relationships between the substructures, which now also have $C222_1$ symmetry. The modulation displaces layers of one substructure along ***a*** and displaces layers of the other substructure along ***b***, while retaining a pseudo inversion between adjacent layers. Layers of the first substructure contain two-fold rotation axes parallel to ***a*** that relate adjacent layers of the second substructure and layers of the second substructure contain two-fold rotations parallel to ***b*** that relate adjacent layers of the first substructure. The asymmetric unit for the space group $C222_1$ contains two quarters of a dimeric cation and one anion from the first substructure and two quarters of a dimeric cation and two half anions from the second sub-

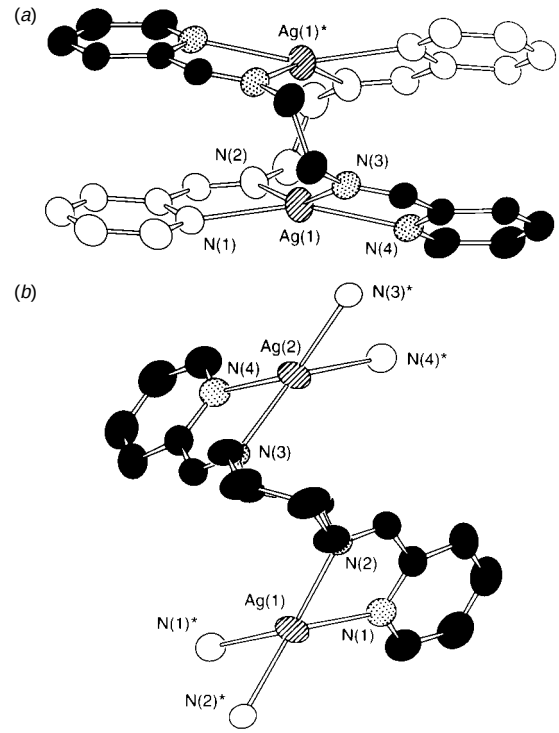

Fig. 1 Molecular structures of double-stranded helical cation of (±)-$[Ag_2\mathbf{1}_2](BF_4)_2$ (*a*) and of repeating unit of cation of single-stranded *M*-$\{[Ag\{(R,R)\text{-}\mathbf{2}\}]NO_3{\cdot}2H_2O\}_\infty$ (*b*)

structure. It was not necessary to invoke disorder in the structure.

The complex *M*-{[Ag{(*R*,*R*)-**2**}]NO_3·$2H_2O$}$_\infty$ crystallises as amber plates from acetonitrile–diethyl ether in the hexagonal space group $P6_522$. The polynuclear metal cation of the complex is an infinite helical polymer of C_2 symmetry with each interlocking Ag_2N_4 unit completing 0.73 turns of a left-handed (*M*) helix [Fig. 1(*b*)]. The pitch of the single-stranded palindromic helix is 6.5 Å and the Ag···Ag distances are 5.42 Å (av.). Each tetrahedral silver ion in the helix has the *S* configuration. Parallel helical chains form layers perpendicular to ***c*** with the 6_5 screw axis of $P6_522$ relating adjacent layers to give an overall structure of *M* helicity. The reference layer at z = 1/4 propogates parallel to ***a***, inducing pseudorotation axes midway between the real rotation axes (Fig. 2). The pseudosymmetry of the structure allows the possibility of homometric solutions, a translation of 1/2 ***b*** relating alternative positions for the polymer chain that produces the same intensities should the 1/2 ***a*** translation hold exactly. The ligands enclose N(terminal)–Ag–Ag–N(terminal) angles of 190.5° (av.), implying an average pitch of 7.3 Å for the Ag_2N_4 helical core. Comparative refinement allowed the absolute structure to be determined. The ^{1}H NMR spectrum in [$^2H_3$]acetonitrile and the electrospray MS of the complex are consistent with disproportionation of the polymer into dinuclear metal helicates in solution. The helical displacements in the helicate and the helicalpolymer are evident in the space-filling diagram given in Fig. 3. Fig. 1 shows the *ob* and *lel* arrangements of the central carbon–carbon bonds in the two structures. The crystal molecular structures of two other single-stranded helicate polymers derived from achiral ligands have been described previously.[11,12] To our knowledge, however, the only other homochiral coordination polymer to be structurally characterised is the complex *P*-{Ag[(*R*,*R*)-DIOP]NO_3}$_n$ {DIOP = (4*R*,5*R*)-*trans*-4,5-bis[(diphenylphosphino)methyl]-2,3-dimethyl-1,3-dioxalane} in which each silver ion in the polymer is coordinated by two phosphorus atoms of adjacent (*R*,*R*)-DIOP ligands and a nitrate-*O* atom.[13]

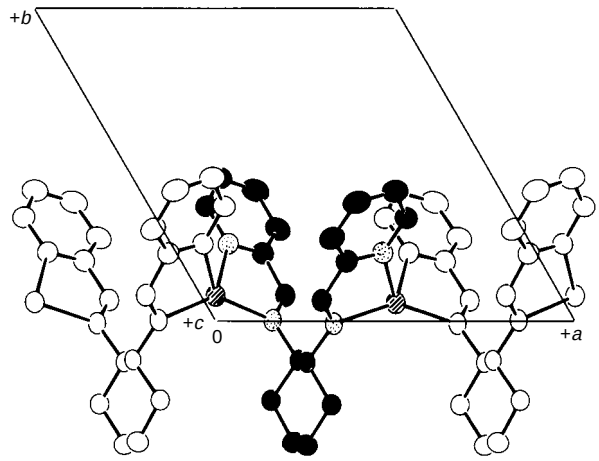

Fig. 2 Cation of *M*-{[Ag{(*R*,*R*)-**2**}]NO_3·$2H_2O$}∞ at z = 1/4

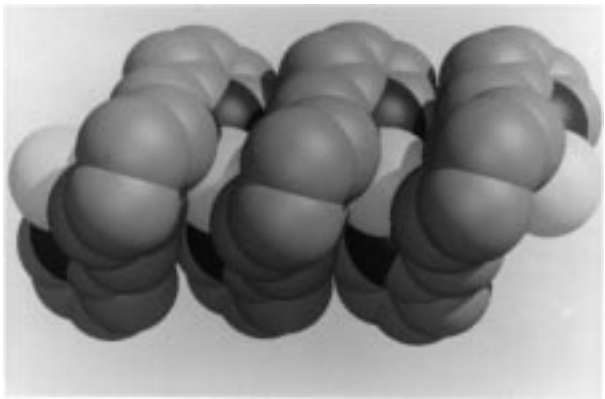

Fig. 3 Space-filling diagram of cation of *M*-{[Ag{(*R*,*R*)-**2**}]NO_3·$2H_2O$}$_\infty$ with hydrogen atoms omitted

We should like to thank Professor P. A. Williams of the University of Western Sydney for a sample of (*R*,*R*)-**2**.

Notes and References

† E-mail: sbw@rsc.anu.edu.au

‡ Satisfactory elemental analyses were obtained.

§ *Crystal data* for (±)-[Ag_2**1**$_2$](BF_4)$_2$: $C_{28}H_{28}Ag_2B_2F_8N_8$, M_r 865.93, pale yellow block, space group $C222_1$ (no. 20), a = 10.420(2), b = 25.036(7), c = 25.202(7) Å, U = 6573(3) Å^3, Z = 8; D_c = 1.749 g cm^{-3}, μ(Mo-Kα) = 12.67 cm^{-1}. Philips PW1100/ 20 diffractometer; T = 293 K, ω–2θ scan method. A total of 4176 unique data were collected in the range 5 ⩽ 2θ ⩽ 55° of which 1650 [$I > 3\sigma(I)$] were used for the refinement. Initial unconstrained refinement of the data gave an R value of 0.060, but spreads in equivalent bond lengths were as high as 0.2 Å, which indicated refinement difficulties associated with the pseudo-inversion centre relating adjacent layers of the structure. Subsequent constrained refinement using the program RAELS96 (A. D. Rae, Australian National University, Canberra, Australia) with use of 176 independent parameters to describe the 53 anisotropic non-hydrogen atoms in the structure gave R and R_w values of 0.048 and 0.059, respectively, with a uniform distribution of error over all data classes. *M*-{[Ag{(*R*,*R*)-**2**}]NO_3·$2H_2O$}$_\infty$: $C_{18}H_{28}AgN_5O_7$, M_r 498.29, pale yellow hexagonal plate, space group $P6_522$ (no. 179), $a = b$ = 10.876(4), c = 63.522(8) Å, U = 6507(4) Å^3, Z = 12; D_c = 1.526 g cm^{-3}, μ(Cu-Kα) = 77.78 cm^{-1}. Rigaku AFC6R diffractometer; T = 296 K, ω scan method. A total of 2067 independent reflections having 2θ ⩽ 120° were measured. Constrained refinement (RAELS96) with use of 109 variables to describe the 31 non-hydrogen atoms in the asymmetric unit and their anisotropic thermal motion gave R and R_w values of 0.072 and 0.101, respectively, for 1026 reflections with [$I > 3\sigma(I)$] for a poorly diffracting thin plate. The homometrically related structure refined to an R value of 0.15. Refinement in $P6_122$ gives the incorrect helicity for the ligand and produces worse refinement statistics. CCDC 182/843.

1 J.-M. Lehn, A. Rigault, J. Siegel, J. Harrowfield, B. Chevrier and D. Moras, *Proc. Natl. Acad. Sci. USA*, 1987, **84**, 2565.
2 C. Piguet, G.Bernardinelli and G. Hopfgartner, *Chem. Rev.*, 1997, **97**, 2005.
3 W. Zarges, J. Hall, J.-M. Lehn and C. Bolm, *Helv. Chim. Acta*, 1991, **74**, 1843; E. C. Constable, T. Kulke, M. Neuburger and M. Zehnder, *Chem. Commun.*, 1997, 489; G. Baum, E. C. Constable, D. Fenske and T. Kulke, *Chem. Commun.*, 1997, 2043; C. Provent, S. Hewage, G. Brand, G. Bernardinelli, L. J. Charbonniere and A. F. Williams, *Angew. Chem., Int. Ed. Engl.*, 1997, **36**, 1287.
4 E. C. Constable, *Prog. Inorg. Chem.*, 1994, **42**, 67; J.-M. Lehn, *Supramolecular Chemistry*, VCH, Weinheim, 1995; A. F. Williams, *Chem. Eur. J.*, 1997, **3**, 15.
5 A. L. Airey, G. F. Swiegers, A. C. Willis and S. B. Wild, *Inorg. Chem.*, 1997, **36**, 1588.
6 D. H. Busch and J. C. Bailar, *J. Am. Chem. Soc.*, 1956, **78**, 1137.
7 T. J. Goodwin, R. S. Vagg and P. A. Williams, *Proc. R. Soc. NSW*, 1984, **117**, 1.
8 G. C. van Stein, G. van Koten, K. Vrieze and A. L. Spek, *J. Am. Chem. Soc.*, 1984, **106**, 4486.
9 G. C. van Stein, G. van Koten, K. Vrieze, A. L. Spek, E. A. Klop and C. Brevard, *Inorg. Chem.*, 1985, **24**, 1367.
10 T. Suzuki, H. Kitsuki, K. Isobe, N. Moriya, Y. Nakagawa and M. Ochi, *Inorg. Chem.*, 1995, **34**, 530.
11 O. J. Gelling, F. van Bothius and B. L. Feringa, *J. Chem. Soc., Chem. Commun.*, 1991, 917.
12 M. Withersby, A. J. Blake, N. R. Champness, P. Hubberstey, W.- S. Li and M. Schröder, *Angew. Chem., Int. Ed. Engl.*, 1997, **36**, 2327.
13 B. Wu, W.-J. Zhang, S.-Y. Yu and X.-T. Wu, *J. Chem. Soc., Dalton Trans.*, 1997, 1795.

Received in Columbia, MO, USA, 20th December 1997; revised manuscript received 2nd January 1998; 8/00083B

Michael addition to α,β-unsaturated arene ruthenium(II) cyclopentadiene complexes: *endo* nucleophilic addition

Robert M. Moriarty,*[a]† Livia A. Enache,[a] Richard Gilardi,[b] George L. Gould[a] and Donald J. Wink[a]

[a] *Department of Chemistry, University of Illinois at Chicago, Chicago, IL 60607-7061, USA*
[b] *Laboratory for the Structure of Matter, Naval Research Laboratory, Washington, DC 20375-5341, USA*

Certain carbon and sulfur nucleophiles add to the β-terminus of the styrene system in α,β-unsaturated arene ruthenium(II) cyclopentadiene complexes, and unexpected *endo* addition occurs preferentially in some cases.

Metals in either their neutral (Cr^0, Fe^0, Mo^0) or charged state (Fe^{II}, Ru^{II}, Pd^{II}, Os^{II}, Co^{II}) activate complexed unsaturated ligands towards nucleophilic addition.[1] This behaviour is due to net inductive withdrawal of electron density from the ligand and stabilization of the anionic charge resulting from addition of the nucleophile. The addition of the nucleophile occurs on the *exo* face of the ligand, distal to the metal.[2] Within the context of this direct nucleophilic addition to the complexed ligand, one might anticipate that conjugate addition could likewise occur in α,β-unsaturated ligated systems such as styryl or 1,2-dihydronaphthalene, and indeed this has been observed; in both cases η^6-chromium(0) complexes of the aromatic ring were used. In the simplest case, tricarbonyl(η^6-styrene)chromium,[3] this type of reaction occurred in 7–30% yield, but with a discouraging mixture of side-products. Better synthetic results were obtained by Semmelhack and in the case of addition of $LiCMe_2CN$ upon tricarbonyl(η^6-1,2-dihydronaphthalene)chromium.[3b,4] The stereochemistry of the product was proposed to correspond to *exo* addition, on the basis of a ^1H NMR spectrum of the decomplexed ligand.[4a] Two other examples of conjugate addition to arene-$Cr(CO)_3$ complexes were reported.[5]

Because of our interest in nucleophilic displacement reactions upon (η^6-arene)(η^5-cyclopentadienyl)ruthenium(II) complexes,[6] we studied the Michael addition in this series with α,β-unsaturated arene ligands. The objectives were to make the reaction more synthetically useful, partly as the rate of the nucleophilic displacement, *via* addition-elimination, on aryl halides increases in the order $Cr^0(CO)_3 < Mo^0(CO)_3 \ll CpFe^+ < Mn^+(CO)_3$,[7] and also to establish the stereochemistry of the addition relative to the result observed with the $Cr(CO)_3$ group. The substrates and transformations are shown in Scheme 1.[8]

Pure *endo* forms of products **2b** and **2c**, and the *exo* form of **4** could be separated *via* fractional recrystallization from acetone–water and the X-ray structures of the major isomers could be determined.‡

The X-ray structure of the major product from reaction of **1c** with KCN is in Fig. 1. The Cl Me and C2 CN are *syn* and on the same face as the metal. This highly strained array corresponds

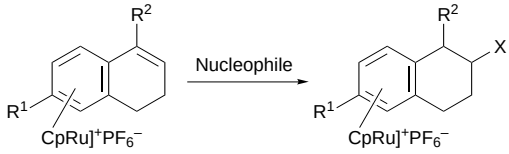

1a $R^1 = R^2 = H$
b R^1 = OMe, $R^2 = H$
c R^1 = OMe, R^2 = Me

2a $R^1 = R^2 = H$, X = CN — *endo*:*exo* 1:1
b R^1 = OMe, $R^2 = H$, X = CN — *endo*:*exo* 2:1
c R^1 = OMe, R^2 = Me, X = CN — *endo*:*exo* 3:1
3a $R^1 = R^2 = H$, X = SPh — *endo*:*exo* 3:1
b R^1 = OMe, $R^2 = H$, X = SPh — *endo*:*exo* 5:4
c R^1 = OMe, R^2 = Me, X = SPh — *endo* only

Scheme 1

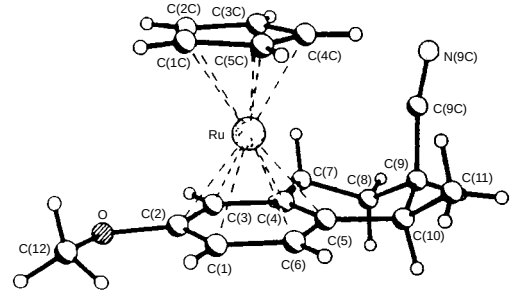

Fig. 1 X-Ray structure of compound **2c**

to *endo* addition and *exo* protonation and differs from the result observed for conjugate addition in two cases in which the stereochemistry was determined.[3b,5b] A similar preference for the *endo* addition was determined from combined NMR and X-ray studies of other products in our study (Scheme 1). An X-ray of the major component of product **2b** also shows *endo* selectivity. The major component of product **4** was the 'expected' *exo*.

How is one to explain *endo* nucleophilic addition? In a direct displacement upon a metal-complexed aromatic ring, basically an S_N2 type mechanism, the nucleophile attacks at the carbon atom undergoing displacement forming a new bond to that center (with inversion) with concomitant cleavage of a bond to the metal, *i.e.* the ligated metal is the 'leaving group'.[10] This description requires *exo* attack. Conjugate addition of the type studied here is controlled by the stereoelectronic effects of the S_N2' reaction.[11] This process occurs with *syn* stereochemistry, although it has not been recognized that the carbon–metal bond could constitute the leaving group [Fig. 2(*a*)]. Fig. 2(*b*) shows the orbital representation which reveals the LUMO of the complex and the preference for *syn* addition.

The reactions were generally slower for **1b** as compared to **1a** (rate retarding effect of OMe) and slower still for **1c** (steric effect of Cl methyl group). With KCN (5 equiv.) in DMF–H_2O in the presence of NH_4Cl (3 equiv.), the conditions required for the complete disappearance of the starting material for 70 °C overnight for **1a** → **2a** and 90 °C overnight for **1b** → **2b** and **1c** → **2c**. The yields of *endo*/*exo* mixtures of isomers after chromatographic separation on silica gel (acetone–CH_2Cl_2 1:4) were 86 (*endo*:*exo* 1:1), 85 (*endo*:*exo* 2:1) and 82% (*endo*:*exo* 3:1) respectively. The reactions with thiophenol

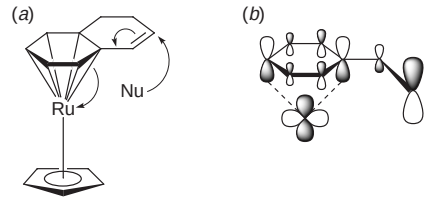

Fig. 2 (*a*) The S_N2' type mechanism illustrating *endo* conjugate nucleophilic addition to styrene-type substrates complexed to Ru^{II}. (*b*) Simple orbital diagram which represents LUMO calculated from ZINDO for the $CpRu(C_{10}H_{10})^+$ model.

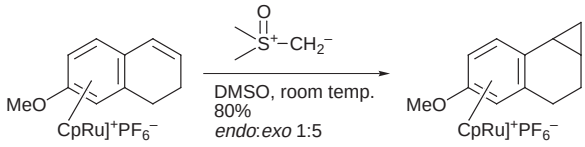

1b **4**

Scheme 2

(1.5 equiv.) were carried out in NMR tubes in CD_3CN in the presence of Hunig's base (Pr^i_2NEt). Judging by the disappearance of the signals of the starting material in the NMR spectrum, substrate **1a** reacted completely in 30–45 min when 2 equiv. of base was used at 45 °C, and overnight with only 0.5 equiv. of Hunig's base at 25 °C. Substrate **1b** reacted completely at 45 °C overnight in the presence of Hunig's base (0.5 equiv.), and substrate **1c** reacted in only *ca.* 80% when treated with Hunig's base (0.5 equiv.) at 60 °C for 36 h. The observed *endo : exo* ratios were: **3a** (3 : 1), **3b** (5 : 4) and **3c** (*endo* only).

A more advanced example is the Corey–Chaykovsky cyclopropanation in which dimethyloxosulfonium methylide[9] is used in a reaction which occurs at room temp. within minutes (**1b** → **4**) (complete disappearance of the starting material, 80% isolated yield after chromatography, *endo : exo* 1 : 5, Scheme 2).

How does one reconcile *endo* addition with the observed *exo* addition of Semmelhack and others?[3b,5a] These workers used Li carbon anions and the conjugate addition in these cases is reversible.[12] Accordingly, the least hindered *exo* (*cis*-1,2) product perdominates. In contrast, our cyanide addition method involving *in situ* NH_4Cl/H_2O insures formation of the kinetic product, by immediate protonation at the benzylic position. Kinetic control is also possible in the addition of PhSH in the presence of less than 1 equiv. of base. In agreement with the interpretation, cyclopropanation (**1b** → **4**) yields the *exo* product in 5 : 1 ratio because of the reversibility associated with carbanion addition in the absence of a protic acid.[9,13] Semi-empirical quantum calculations (ZINDO, INDO1 level basis set)[14] on a (η^5-cyclopentadienyl)(η^6-1,2-dihydronaphthalene)-Ru cation model complex, as well as its Fe substituted analog, indicate that a nucleophilic attack at the *endo* face of the conjugated π-system is slightly preferred over the *exo* face. Furthermore, the model calculations indicate that an *anti* stereochemistry of protonation to the resulting η^5-pentadienyl form of the intermediate [Fig. 2(*a*)] as the α-styryl C would be expected, consistent with the major selectivity observed in the Ru system reported here. Interpreting these predictive models in the context of the stereochemistries reported for S_N2' addition[11] indicate that a general model in which attack of the nucleophile *syn* to the leaving group (Ru–C bond) in π-complexed styryl or dihydronaphthyl complexes is reasonable. Further theoretical and experimental studies are in progress to test this hypothesis.

This work was supported through NSF grant CHE-9520157.

Notes and References

† E-mail: moriarty@uic.edu

‡ *Crystal* data for **2b** (major): $C_{17}H_{18}F_6NOPRu$, M = 498.367, monoclinic, $P2_1/c$, a = 7.5734(11), b = 16.771(2), c = 14.6457(12) Å, U = 857.3(4) Å^3, T = 294(2) K, Z = 4, μ = 0.996 mm^{-1}, 4264 reflections measured (θ_{max} = 27.50°), 3878 independent (R_{int} = 0.0124) with 3182 observed [$I > 2\sigma(I)$]. For **2c** (major): $C_{18}H_{20}F_6NOPRu$, M = 512.394, orthorhombic, $P2_1P2_1P2_1$, a = 28.326(3), b = 7.1095(6), c = 9.7180(7) Å, U = 1957.1(3) Å^3, T = 294(2) K, Z = 4, μ = 0.946 mm^{-1}, 2917 reflections measured (θ_{max} = 21.96°), 2395 independent (R_{int} = 0.0106) with 1727 observed [$I > 2\sigma(I)$]. For **4** (major): $C_{17}H_{19}F_6OPRu$, M = 485.3681, monochlinc, $P2_1$, a = 8.921(3), b = 25.389(7), c = 9.037(3) Å, U = 1805.0(10) Å^3, T = 294(2) K, Z = 4, μ = 1.019 mm^{-1}, 2675 reflections measured (θ_{max} = 23.47°), 2413 independent (R_{int} = 0.0144) with 1921 observed [$I > 2\sigma(I)$]. CCDC 182/811.

1 S. G. Davies, *Organotransition Metal Chemistry: Applications to Organic Synthesis*, Pergamon Press, New York, 1986, pp. 116–155; A. G. Pearson, *Metallo-Organic Chemistry*, Wiley, New York, 1988, pp. 163–389.

2 M. R. Churchill and R. Mason, *Proc. R. Soc. Lond., A*, 1964, **279**, 191; A. N. Nesmeyanov, N. A. Vol'kenau, L. S. Shilovtseva and V. A. Petrakova, *Izv. Akad. Nauk., Ser. Khim.*, 1975, 1151; M. F. Semmelhack, H. T. Hall, Jr., R. Farina, M. Yoshifuji, G. Clark, T. Bargar, K. Hirotsu and J. Clardy, *J. Am. Chem. Soc.*, 1979, **101**, 3535; in a study involving benzylic substitution and nucleophilic addition to the benzene ring in cyclopentadienyl(η^6-tetrahydronaphthalene)iron(II) complexes, Grundy and collaborators were led to believe that "the Fe(Cp) group may be less effective in 'face blocking' of arene nuclei than is the $Cr(CO)_3$ fragment and is unlikely to be able to exert sufficient influence to direct a first methyl group stereospecifically *exo*" (S. L. Grundy, A. R. H. Sam and S. R. Stobart, *J. Chem. Soc., Perkin Trans. 1*, 1989, 1663).

3 (*a*) G. R. Knox, D. G. Leppard, P. L. Pauson and W. E. Watts, *J. Organomet. Chem.*, 1972, **34**, 347; (*b*) M. F. Semmelhack, W. Seufert and L. Keller, *J. Am. Chem. Soc.*, 1980, **102**, 6584.

4 (*a*) M. F. Semmelhack, *Organic Synthesis Today and Tomorrow*, Proceedings of the 3rd IUPAC Symposium on Organic Synthesis, Madison, Wisconsin, U.S.A., 15–20 June 1980, pp. 63–69; (*b*) M. F. Semmelhack, *Ann. N.Y. Acad. Sci.*, 1977, **295**, 36.

5 (*a*) M. Uemura, T. Minami and Y. Hayashi, *J. Chem. Soc., Chem. Commun.*, 1984, 1193. This paper reported the Michael addition of LiC(CN)MeCOCHMeOEt to tricarbonyl(5-methoxy-1,2-dihydronaphthalene)chromium. *Exo* addition was assumed. (*b*) P. Bloem, D. M. David, L. A. P. Kane-Maguire, S. G. Pyne, B. W. Skelton and A. H. White, *J. Organomet. Chem.*, 1991, **407**, C19 and references cited therein. These workers studied the addition of MeLi to tricarbonyl(*N*-benzylidene-1-methylaniline)chromium. *Exo* addition was determined by X-ray analysis.

6 R. M. Moriarty, Y.-Y. Ku and L. Guo, *J. Chem. Soc., Chem. Commun.*, 1988, 1621; R. M. Moriarty, Y.-Y. Ku and U. S. Gill, *J. Chem. Soc., Chem. Commun.*, 1987, 1493; R. M. Moriarty, Y.-Y. Ku and U. S. Gill, *Organometallics*, 1988, **7**, 660; R. M. Moriarty and U. S. Gill, *organometallics*, 1985, **5**, 253; U. S. Gill and R. M. Moriarty, *Synth. React. Inorg. Met.-Org. Chem.*, 1986, **16**, 485; U. S. Gill and R. M. Moriarty, *Synth. React. Inorg. Met.-Org. Chem.*, 1986, **16**, 1103; R. M. Moriarty, Y.-Y. Ku and U. S. Gill, *J. Chem. Soc., Chem. Commun.*, 1987, 1837.

7 A. C. Knipe, S. J. McGuinness and W. E. Watts, *J. Chem. Soc., Perkin Trans. 2*, 1981, 193.

8 Various nitrogen nucleophiles (hydrazine, methylhydrazine, *gem*-dimethylhydrazine, 1,2-dimethylhydrazine, 1,2-ethylenediamine, ethylamine, ethanolamine) were also studied. Oxygen nucleophiles did not undergo addition to **1a**–**c** under our conditions. Since no stereochemical *endo : exo* assignments could be reliably made from the available data, the nitrogen nucleophiles (NMR tube experiments, [$^2H_6$]DMSO) were not extensively included in the present study. Still, they displayed extremely interesting reactivity patterns worth noting (data from ^{1}H NMR, ^{13}C NMR, HRMS + FAB analysis). With H_2NNH_2, H_2NEt and $H_2NCH_2CH_2NH_2$, **1**–**c** reacted completely in 30 min at rt (*ca.* 80% conversion of **1a** in the first 5 min). H_2NNHMe adds slower than hydrazine itself, and H_2NNMe_2, adds even slower. $H_2NCH_2CH_2OH$ reacted very slowly, with < 30% conversion, when heated up to 100 °C. Pr^iNH_2 and MeNHNHMe did not react even after 48 h at rt or 60 °C overnight.

9 E. J. Corey and M. Chaykovsky, *J. Am. Chem. Soc.*, 1965, **87**, 1353.

10 B. E. R. Schilling, R. Hoffmann and J. W. Faller, *J. Am. Chem. Soc.*, 1979, **101**, 592.

11 G. Stork and W. N. White, *J. Am. Chem. Soc.*, 1956, **78**, 4604; G. Stork and W. N. White, *J. Am. Chem. Soc.*, 1956, **78**, 4609. For a very comprehensive review of the S_N2' reaction, see R. M. Magid, Tetrahedron Report Number 87, *Tetrahedron*, 1980, **36**, 1901.

12 Semmelhack presents evidence of a mobile equilibrium between I and II. The example of ref. 5(*b*) is complicated by the α,β-unsaturation being –N=CHPh.

13 An X-ray structure of the major component of product **4** has been obtained.

14 Molecular orbital and predictive results were obtained using M. C. Zerner's ZINDO program (version 3.0) from CAChe Scientific. Atomic coordinates were first optimized using molecular mechanics (augmented CAChe MM2 force field), and orbital energies calculated directly using the INDO 1 basis set. Self-consistent field molecular orbital energies were obtained in the restricted Hartree–Fock level within 4 Å self-consistent reaction field (SCRF) cavity with the relative permittivity and refractive index of water.

Received in Corvallis, OR, USA, 10th October 1997; 7/07386K

The first synthesis of the *Streptomyces* derived antibiotic U-62162

Lilian Alcaraz and Richard J. K. Taylor†

Department of Chemistry, University of York, Heslington, York, UK YO1 5DD

U-62162, a member of the manumycin family of antibiotics, has been prepared as a mixture of diastereoisomers and shown to contain a *syn*-hydroxy epoxide nucleus and a 1,3-*syn*-disposed dimethyl unit in the upper side chain; the cornerstone of the synthetic route utilises organometallic addition to a monoprotected quinone epoxide—the first time this approach has been successfully employed to prepare a manumycin antibiotic.

The manumycin group of natural products, which includes manumycin A **1**[1] and alisamycin **2**,[2] have attracted a great deal of attention due to their antibiotic, antitumour and enzyme inhibitory properties.[1–4] With two exceptions, all members of this family have a 2-amino-3-hydroxycyclopentenone polyenamide lower side chain. The exceptions are nisamycin **3**,[3] which is the carboxylic acid corresponding to alisamycin, and U-62162 **4**.[4] U-62162, an antibiotic isolated from *Streptomyces verdensis* (UC-8157), was reported by researchers from the Upjohn Company in 1982, and has a unique five-carbon saturated lower side chain terminating in a carboxylic acid. Extensive NMR experiments were carried out to assign structure **4**, but the only stereochemical information revealed was the *E*-orientation of the alkene in the top side chain.

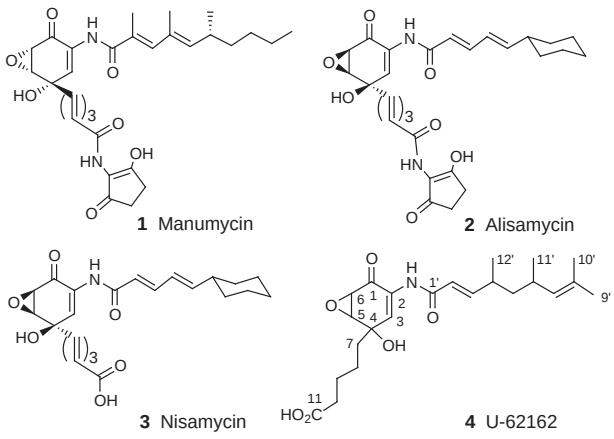

We recently reported[5] the first total synthesis of alisamycin **2** and nisamycin **3**. The initial synthetic approach investigated for these compounds involved organometallic elaboration of the monoprotected quinone epoxide **5**, as summarised in Scheme 1.

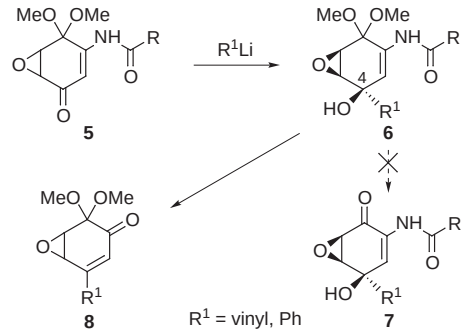

Scheme 1

This approach was ultimately unsuccessful because of the lability of the C-4 hydroxy group, which is tertiary and doubly allylic in adduct **6** when R^1 is an unsaturated lower side chain; attempted hydrolysis of the acetal moiety to give **7** resulted, under a wide range of conditions, in the formation of degradation products, one of which was tentatively identified as enone **8**. A successful alternative approach to alisamycin and nisamycin was eventually designed,[5] but we were intrigued by the possibility that the original methodology, shown in Scheme 1, might be applicable to the synthesis of related compounds in which the hydroxy group is less labile, *i.e.* where R^1 is not alkenyl. Here we describe the successful implementation of this approach for the synthesis of U-62162.‡

Model studies (Scheme 2) were carried out to assess the viability of this approach. Compound **9**, prepared using similar procedures to those described later, was treated with TsOH in aqueous acetone, giving a reasonable yield of the required alcohols **10** and **11**. The fact that the two epimers were formed during the reaction indicates that some carbocation formation is still occurring, but as the enamide unit remained intact, and hydrolysis products of type **8** were not observed, this route was thus adopted for the synthesis of U-62162.

The first objective in the natural product synthesis was to elucidate the relative stereochemistry of the side chain methyl substituents in the upper side chain (Scheme 3). The readily available[7] *syn*- and *anti*-dimethylvalerolactones **12** were therefore converted into the isomeric alcohols **13** and on to the acids **14** using the straightforward sequence illustrated. Treatment of acids **14** with oxalyl chloride in CH_2Cl_2 gave the corresponding acid chlorides which were used to acylate amine **15**.[5] The resulting adducts **16**, as diastereomeric mixtures, were then converted into quinone epoxides **17** *via* the three-step sequence shown.

The high-field NMR spectra of the *syn*- and *anti*-diastereomers of **16**, **17** and the other acylated intermediates, were compared to the data published for U-62162.[4] Significant differences were observed, which indicated that the natural product contained the *syn*-dimethyl arrangement [*e.g. syn*-**17**: δ_H 0.91 (3 H, d, *J* 6.5, H-11′); *anti*-**17**: δ_H 0.89 (3 H, d, *J* 6.5, H-11′); U-62162:[4] δ_H 0.91 (3 H, d, *J* 6.6, H-11′). We therefore set out to convert *syn*-**16** into U-62162 (Scheme 4).

5-*tert*-Butyldimethylsilyloxy-1-iodopentane[8] was transmetallated (Bu^tLi, Et_2O) and then treated with *syn*-**16**; as

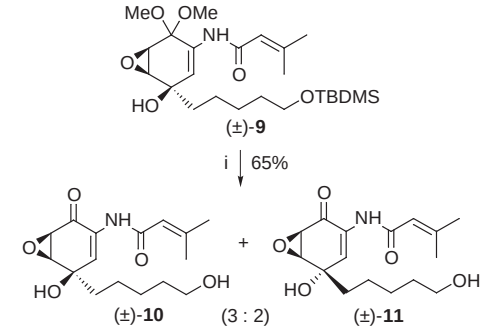

Scheme 2 *Reagents and conditions*: i, TsOH, aq. acetone

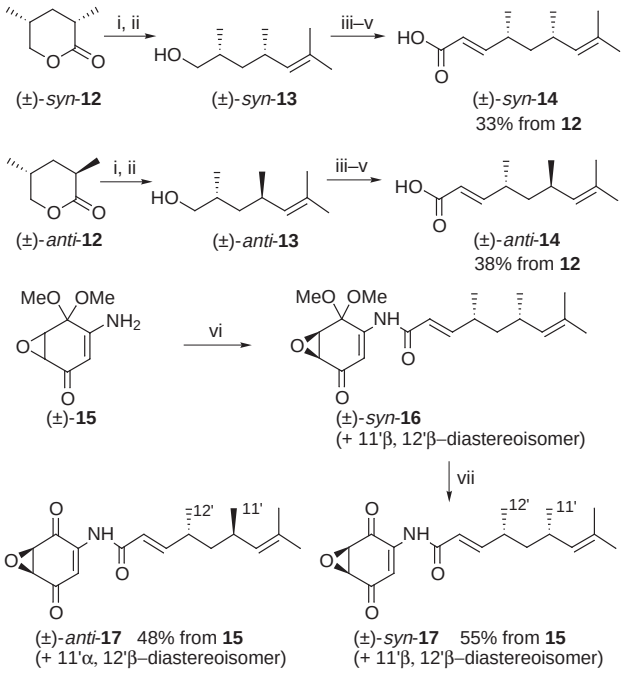

Scheme 3 *Reagents and conditions*: i, DIBAL-H, THF, −78 °C (ref. 7); ii, $Ph_3P{=}CMe_2$, THF, 0 °C; iii, DMSO, $(COCl)_2$, −60 °C, then Et_3N, CH_2Cl_2, room temp.; iv, $Ph_3P{=}CHCO_2Et$, CH_2Cl_2, room temp.; v, LiOH, aq. MeOH–THF; vi, acid chloride from **14**, LiOBu^t, THF, 0 °C; vii, $LiHBEt_3$, THF, −78 °C, then K10, CH_2Cl_2, room temp., then PDC, CH_2Cl_2, room temp.

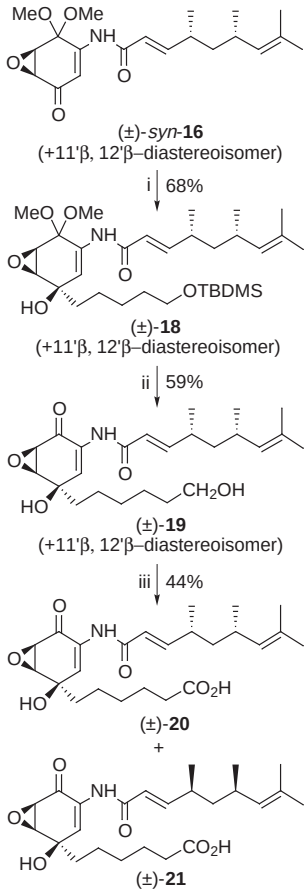

Scheme 4 *Reagents and conditions*: i, $Li(CH_2)_5OTBDMS$, Et_2O, −78 °C; ii, TBAF, THF, room temp., then TsOH, aq. acetone; iii, PCC, NaOAc, CH_2Cl_2, room temp., then $NaClO_2$, KH_2PO_4, 2-methylbutene, aq. Bu^{t}OH, room temp.

expected,[5] addition occurred with total stereoselectivity from the face opposite the epoxide. The deprotection of adduct **18** could be carried out directly using TsOH in aqueous acetone but the process was rather slow and inefficient. The preferred method involved fluoride-induced desilylation followed by acetal hydrolysis using TsOH. This sequence gave diol **19** (accompanied by a small amount of the *anti*-hydroxy epoxide§ which was easily removed by chromatography). Oxidation of **19** to an inseparable mixture of the corresponding acids **20**/**21** was achieved by a two-step procedure (PCC, then sodium chlorite). Compounds **20**/**21,** although a diastereomeric mixture, showed data consistent with that published for U-62162 [*e.g.* δ_H (synthetic) 7.42 (d, *J* 2.5, H-3) 3.68 (dd, *J* 4.0, 2.5, H-5), 3.55 (d, *J* 4.0, H-6); δ_H (published[4]) 7.43 (d, *J* 2.7, H-3) 3.69 (dd, *J* 4.0, 2.7, H-5), 3.56 (d, *J* 4.0, H-6); δ_C (synthetic) 190.2 (C-1), 130.6 (C-2), 130.3 (C-3), 71.2 (C-4), 58.6 (C-5), 53.7, C-6); δ_C (published[4]) 189.6 (C-1), 130.0 (C-2), 129.8 (C-3), 70.6 (C-4), 57.9 (C-5), 53.0, C-6)].§ The *syn*-hydroxy epoxide arrangement, now confirmed for U-62162, is in accord with the biosynthetic rationale recently proposed by Gould and Floss.[9]

This research establishes an efficient route to the antibiotic U-62162 and also provides further stereochemical information. We are now working to assign U-62162 as **20** or **21** and to complete an enantioselective synthesis.

We thank the European Community for a Marie-Curie Fellowship (L. A.), and Professor P. Kocienski for helpful advice concerning the preparation of compounds **12.**

Notes and References

† E-mail: rjkt1@york.ac.uk

‡All new compounds were fully characterised by high field ^1H and ^{13}C NMR spectroscopy and by high resolution mass spectrometry, with the exception of those in Scheme 2 (NMR characterisation only). All compounds are racemic and **16**–**19** are mixtures of diastereoisomers.

§ The *anti*-hydroxy epoxide isomer of **19** was also converted into the corresponding diastereomeric U-62162 analogues. The NMR spectrum of this mixture showed significant differences to **20**/**21** [*e.g.* δ_H 7.55 (d, *J* 3.0, H-3); δ_C 128.9 (C-3), 60.2 (C-5)], providing further evidence that the natural product possesses the *syn*-hydroxy epoxide stereochemistry.

1 F. Buzzetti, E. Gaumann, R. Hutter, W. Keller-Schierlein, L. Neipp, V. Prelog and H. Zaher, *Pharm. Acta Helv.*, 1963, **38**, 871; A. Zeeck, K. Schroder, K. Frobel, R. Grote and R. Thiericke, *J. Antibiot.*, 1987, **40**, 1530; A. Zeeck, K. Frobel, C. Heusel, K. Schroder and R. Thiericke, *J. Antibiot.*, 1987, **40**, 1541. We have recently completed a total synthesis of manumycin A and revised its structure to **1** (L. Alcaraz, G. Macdonald, J. P. Ragot, N. J. Lewis and R. J. K. Taylor, *J. Org. Chem*., in the press).

2 S. Chatterjee, E. K. S. Vijayakumar, C. M. M. Franco, J. Blumbach, B. N. J. Ganguli, H. W. Fehlhaber and H. Kogler, *J. Antibiot.*, 1993, **46**, 1027; K.-I. Hayashi, M. Nakagawa, T. Fujita and M. Nakayama, *Biosci. Biotechnol. Biochem.*, 1994, **58**, 1332.

3 K.-I. Hayashi, M. Nakagawa and M. Nakayama, *J. Antibiot.*, 1994, **47**, 1104; K.-I. Hayashi, M. Nakagawa, T. Fujita, S. Tanimori and M. Nakayama, *J. Antibiot.*, 1994, **47**, 1110.

4 L. Slechta, J. I. Cialdella, S. A. Mizsak and H. Hoeksema, *J. Antibiot.*, 1982, **35**, 556.

5 L. Alcaraz, G. Macdonald, I. Kapfer, N. J. Lewis and R. J. K. Taylor, *Tetrahedron Lett.*, 1996, **37**, 6619; R. J. K. Taylor, L. Alcaraz, I. Kapfer-Eyer, G. Macdonald, X. Wei and N. J. Lewis, *Synthesis*, in the press.

6 E. C. L. Gautier, A. E. Graham, A. McKillop, S. P. Standen and R. J. K. Taylor, *Tetrahedron Lett*., 1997, **38**, 1881.

7 C. Schregenberger and D. Seebach, *Liebigs Ann. Chem.*, 1986, 2081.

8 J. Saunders, D. C. Tipney and P. Robins, *Tetrahedron Lett.*, 1982, **23**, 2045; E. A. Mash, S. B. Hemperly, K. A. Nelson, P. C. Heidt and S. Van Deusen, *J. Org. Chem.*, 1990, **55**, 2045.

9 Y. Hu, C. R. Melville, S. J. Gould and H. G. Floss, *J. Am. Chem. Soc.*, 1997, **119**, 4301 and references therein; for a recent review of biosynthetic discoveries in this area, see H. G. Floss, *Nat. Prod. Rep.*, 1997, **14**, 433 (Section 3.4.2).

Received in Glasgow, UK, 12th February 1998; 8/01265B

New procedures for the Juliá–Colonna asymmetric epoxidation: synthesis of (+)-clausenamide

Michael W. Cappi,[a] Wei-Ping Chen,[b]† Robert W. Flood,[a] Yong-Wei Liao,[b] Stanley M. Roberts,*[a]‡ John Skidmore,[a] John A. Smith[c] and Natalie M. Williamson[a]

[a] *Department of Chemistry, Liverpool University, Liverpool, UK L69 7ZD*
[b] *College of Pharmacy, Second Military Medical University, Shanghai 200433, PR China*
[c] *School of Biological Sciences, Liverpool University, Liverpool, UK L69 7ZB*

The oxidation of chalcone 1 to optically active epoxide 2 [a precursor of (+)-clausenamide (+)-3] may be effected using a 15-mer or 20-mer of L-leucine bound to a PEG based support; poly-L-leucines of this type may be used as immobilised catalysts in a fixed-bed reactor.

The polyamino acid catalysed asymmetric epoxidation of α,β-unsaturated ketones was discovered by Juliá and Colonna.[1] The reaction entailed taking a polyamino acid, such as poly-L-leucine, and allowing it to swell to form a gel in the presence of an organic solvent, 4 M aq. NaOH and H_2O_2. After several hours, the substrate was added to the three-phase system (insoluble polyamino acid, organic solvent–substrate, and water–H_2O_2–NaOH). This system was used by Lantos[2] and Ferreira[3] in the synthesis of selected target molecules.

Recently, it has been shown that the original three-phase system used by Juliá and Colonna can be replaced by a non-aqueous two-phase system[4] and this modified procedure has been used to prepare diltiazem, Taxol™ side-chain[5] and other interesting structures.[6]

These recent advances in the utilisation of the Juliá–Colonna oxidation focused our attention on three issues: (i) understanding the mechanism of the reaction; (ii) finding a suitable methodology for conducting the reaction on a large scale; and (iii) broadening the range of target molecules that can be made by using the Juliá–Colonna technique as the key step. Some progress has been made in each of these areas, as detailed below.

Understanding the mechanism of the Juliá–Colonna oxidation is the key to the application of the methodology to a broader range of substrates. Typically the polyamino acid catalyst is prepared by synthesis of the appropriate amino acid *N*-carboxy anhydride (NCA) and then initiating polymerisation using a nucleophile (water, an alcohol or an amine). Using L-leucine and 1,3-diaminopropane this procedure gives a polymer with a molecular weight range of 1500–3000;[7] it was of interest to determine whether the heterogeneous nature of the polymer and/or the method of preparation[8] were important with regard to the intriguing catalytic properties of the system.

Thus, L-leucine NCA was polymerised using a polyethylene glycol polystyrene based[9] amino nucleophile as the initiator to give CAT 1. At the same time a PEG-polystyrene supported 15-mer of L-leucine (CAT 2) and a PEG-polystyrene supported 20-mer of L-leucine (CAT 3) were prepared using a peptide synthesiser. The effectiveness of these catalysts for the conversion of chalcone **1** into the corresponding epoxide **2** (Scheme 1) is detailed in Table 1.

It is clear that the homogeneous polymers of leucine behave in a very similar manner to the material prepared in the usual way from the *N*-carboxy anhydride. This is the first time that a simple polyamino acid, prepared using a peptide synthesiser, has been shown to catalyse the Juliá–Colonna asymmetric epoxidation reaction. Variation in the amino acid content of the homogeneous peptide chain (*i.e.* 'point mutation' of the 'synthetic enzyme'[10]) is currently under way to help to elucidate the mechanism of this fascinating reaction.

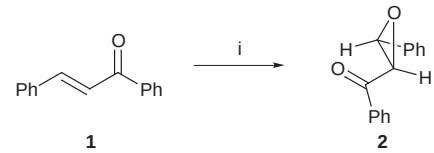

1 **2**

Scheme 1 *Reagents and conditions:* i, biphasic conditions: base, oxidant, *e.g.* urea–H_2O_2, solvent, *e.g.* THF, room temp.

Under the biphasic reaction conditions the polypeptide does not swell to any appreciable extent. This suggested that the substrate in a suitable solvent might be passed through a column of the catalyst mixed with the oxidant to furnish a fixed-bed reactor convenient for a large scale continuous flow synthesis of optically active epoxides. A miniature system was studied.

Poly-L-leucine, immobilised on cross-linked aminomethyl-polystyrene[11] (CLAMPS), was slurry packed into a Pasteur pipette together with oxidant. A solution of chalcone **1** dissolved in a solvent containing DBU (0.5% v/v) was passed through the column. Gratifyingly, good conversions of **1** to epoxide **2** of good to excellent optical purity was observed. A comparison of two oxidants and five solvents (Table 2) suggested that DABCO–H_2O_2[12] and *tert*-butyl methyl ether are the components of choice for further study.

The epoxide **2** was utilised to prepare (+)-clausenamide **3**, an antiamnaesic agent with potent hepatoprotective activity[13] (Scheme 2). Oxidation of ketone **2** under the conditions recommended by Flisak[14] afforded the ester **4**, which was converted into the amide **5** using (±)-2-methylamino-1-phenylethanol. Oxidation of the hydroxy amide **5** and subsequent base-catalysed cyclisation under prescribed conditions[15] furnished a 1 : 1 mixture of diastereomeric lactams (+)-**7** and (−)-**8** [epimerisation of (−)-**8** to provide further quantities of (+)-**7** may be effected by base[16]]. Diastereoselective reduction of (+)-**7** with $NaBH_4$ generated (+)-clausenamide (+)-**3** in 89% yield; the synthetic material had physical properties in accord with those documented previously.[17] This naturally occurring compound is now available from chalcone **1** in six steps and 40% overall yield.

Table 1 Oxidation of chalcone **1** using polyleucine catalysts[a]

Catalyst	*t*/h	Conversion (%)	Ee[b] (%)
CAT 1	1.5	78	83
CAT 2	1.5	89	87
CAT 3	1.5	66	89

[a] Typical reaction conditions: chalcone (25 mg) in THF (0.75 cm^3) with catalyst (50 mg), DBU (6 equiv.) and urea–H_2O_2 (4.8 equiv.). [b] Ees determined by chiral HPLC.

Table 2 Oxidation of chalcone **1** using a fixed-bed of poly-L-leucine[a]

Oxidant	Solvent	Residence time/min	Conversion (%)	Ee[b](%)
Urea–H_2O_2	THF	15	63	94
Urea–H_2O_2	EtOAc	20	87	96
Urea–H_2O_2	Bu^{t}OMe	20	93	96
DABCO–H_2O_2	THF	15	80	98
DABCO–H_2O_2	CH_2Cl_2	15	74	84
DABCO–H_2O_2	EtOAc	15	57	92
DABCO–H_2O_2	Bu^{t}OMe	20	> 97	> 98
DABCO–H_2O_2	MeCN	25	87	86

[a] *Reagents and conditions*: immobilised poly-L-leucine (300 mg) was packed in a column with oxidant (30 mg). Chalcone **1** (50 mg) in solvent (0.5 cm^3) was added and the column was eluted with the same solvent. [b] Ees determined by chiral HPLC.

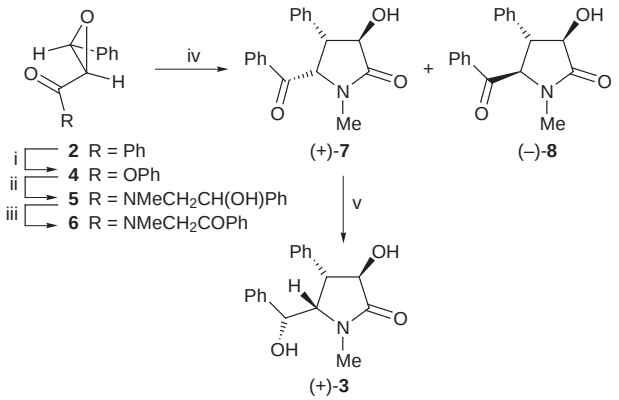

Scheme 2 *Reagents and conditions*: i, MCPBA, CH_2Cl_2, reflux, 78%; ii, (±)-2-methylamino-1-phenylethanol, CH_2Cl_2, 0 °C to room temp., 93%; iii, $KMnO_4$–$CuSO_4$, CH_2Cl_2, room temp., 76%; iv, aq. LiOH, Et_2O–THF, room temp., 93%; v, $NaBH_4$, MeOH, 0 °C to room temp., 83%

We thank the BBSRC for Fellowships (to W.-P. C. and N. M. W.), the EPSRC (Studentship to R. W. F., Fellowship to J. S.) and the Leverhulme Centre for Innovative Catalysis (Fellowship to M. W. C.).

Notes and References

† Present address: Department of Chemistry, Liverpool University, Liverpool, UK L69 7ZD.
‡ E-mail: sj11@liv.ac.uk

1 S. Banfi, S. Colonna, H. Molinari, S. Juliá and J. Guixer, *Tetrahedron*, 1984, **40**, 5207 and references cited therein. For recent reviews, see M. E. Lasterra-Sánchez and S. M. Roberts, *Curr. Org. Chem.*, 1997, 187; S. Ebrahim and M. Wills, *Tetrahedron: Asymmetry*, 1997, **8**, 3163.
2 J. R. Flisak, K. J. Gombatz, M. M. Holmes, A. A. Jarmas, I. Lantos, W. L. Mendelson, V. J. Novack, J. J. Remich and L. Snyder, *J. Org. Chem.*, 1993, **58**, 6247.
3 J. A. N. Augustyn, B. C. B. Bezuidenhoudt, A. Swanepoel and D. Ferreira, *Tetrahedron*, 1990, **46**, 4429; H. van Rensburg, P. S. van Heerden, B. C. B. Bezuidenhoudt and D. Ferreira, *Chem. Commun.*, 1996, 2747.
4 P. A. Bentley, S. Bergeron, M. W. Cappi, D. E. Hibbs, M. B. Hursthouse, T. C. Nugent, R. Pulido, S. M. Roberts and L. E. Wu, *Chem. Commun.*, 1997, 739.
5 B. M. Adger, J. V. Barkley, S. Bergeron, M. W. Cappi, B. E. Flowerdew, M. P. Jackson, R. McCague, T. C. Nugent and S. M. Roberts, *J. Chem. Soc., Perkin Trans. 1*, 1997, 3501.
6 J. V. Allen, M. W. Cappi, P. D. Kary, S. M. Roberts, N. M. Williamson and L. E. Wu, *J. Chem. Soc., Perkin Trans. 1*, 1997, 3297.
7 P. A. Bentley, W. Kroutil, J. A. Littlechild and S. M. Roberts, *Chirality*, 1997, **9**, 198.
8 H. R. Kricheldorf, *Comp. Polym. Sci.*, 1989, **3**, 531.
9 The peptide chain is linked *via* a hydroxymethylphenoxyacetic acid linker and *via* a polyethylene glycol graft to polystyrene particles of 75–150 μm in diameter. The density of attachment was 0.17 mmol peptide per gram of starting resin.
10 S. Juliá, J. Masana and J. C. Vega, *Angew. Chem., Int. Ed. Engl.*, 1980, **19**, 929.
11 S. Itsuno, M. Sakakura and K. Ito, *J. Org. Chem.*, 1990, **55**, 6047.
12 A. A. Oswald and D. L. Guertin, *J. Org. Chem.*, 1963, **28**, 651.
13 Y. Liu, C. Z. Shi and J. T. Zhang, *Yaoxue Xuebao*, 1991, **26**, 166; T. G. Lin, G. T. Liu, K. J. Li, B. L. Zhao and W. J. Xin, *Zhongguo Yaolixue Yu Dulixue Zhazhi*, 1992, **16**, 97.
14 P. W. Baures, D. S. Eggleston, J. R. Flisak, K. Gombatz, I. Lantos, W. Mendelson and J. J. Remich, *Tetrahedron Lett.*, 1990, **31**, 6501.
15 D. F. Huang and L. Huang, *Tetrahedron*, 1990, **46**, 3135; J. Q. Wang and W. S. Tian, *J. Chem. Soc., Perkin Trans. 1*, 1996, 209.
16 M. H. Yang, Y. Y. Chen and H. Liang, *Huaxue Xuebao*, 1987, **45**, 1170.
17 W. Hartwig and L. Born, *J. Org. Chem.*, 1987, **52**, 4352; M. H. Yang, Y. Y. Chen and L. Huang, *Phytochemistry*, 1988, **27**, 445.

Received in Cambridge, UK, 20th February 1998; 8/01450G

Typeset and printed by Black Bear Press Limited, Cambridge, England

ChemComm
FEATURE ARTICLE

Mechanism-based inhibition of carbohydrate-mediated biological recognitions

Pamela Sears† and Chi-Huey Wong

Department of Chemistry and the Skaggs Institute for Chemical Biology, The Scripps Research Institute, 10550 North Torrey Pines Road, La Jolla, CA 92037, USA

Carbohydrates are often associated with specific biological recognition, targeting and signalling processes that play important roles in both normal and disease states. The efforts of many groups have been directed toward the synthesis of complex saccharides and saccharide mimics in the hope of understanding these recognition processes and developing effective agents for their intervention. As compared to research with other classes of biomolecules, however, the pace of major advances in glycobiology and development of carbohydrate-based therapeutics has been relatively slow, due to a combination of factors including the complexity of glycans in natural systems and a lack of facile synthetic techniques and analytical methods available for carbohydrate-related research. This review discusses some of the most recent developments in the field, with particular emphasis on the use of combined chemical and enzymatic approaches for the synthesis of saccharides and mimetics. Some of the highlights include the studies of selectin–carbohydrate and aminoglycoside–RNA interactions, and the synthesis and evaluation of inhibitors of glycoprocessing enzymes.

Although ubiquitous in nature, carbohydrates represent one of the least exploited classes of biomolecules. It is now known that carbohydrates are key elements in various molecular recognition processes. Carbohydrates play a role in infection by a variety of pathogens; they are important for cellular trafficking in acute and chronic inflammation and metastasis; and they play key roles in differentiation, development, regulation and many other intercellular communication and signal transduction events.[1] At the molecular level, carbohydrate-mediated recognition processes are not well understood, however. Although several potential targets for therapeutic intervention have been recognized, the rate of development of saccharide-based pharmaceuticals has been slower than that of the other classes of biomolecules. This is due to a number of factors. First, there are still some extremely difficult technical problems faced by glycobiologists and glycochemists. There is no replication system available for the amplification of minute amounts of carbohydrates to facilitate structure analysis and synthesis, nor is there a machine available for the solid-phase synthesis of oligosaccharides to facilitate the study of their functions. Because cells glycosylate lipids and proteins in a very heterogeneous fashion, it is not feasible to simply grow cells and purify the glycoproteins and glycolipids to homogeneity in large quantity. The heterogeneity of natural glycoconjugates also makes characterization difficult, although recent advances in mass spectral analysis have facilitated structural identification of oligosaccharides with picomoles of material. In addition, the synthesis of free oligosaccharides—not to mention glycoconjugates—in large quantities for research and therapeutic purposes is very difficult and expensive. Secondly, carbohydrates generally possess poor properties for drug development. The affinity of carbohydrates for their protein receptors is almost inevitably weak,[2–6] with dissociation constants in the millimolar range, and carbohydrates are generally orally inactive and sensitive to glycosidases *in vivo*. As a result, carbohydrates may only be used in injectable form for the treatment of acute symptoms.

It is clear, however, that these recognition processes are of fundamental importance in organism development, cell–cell communication, and cell and protein targeting. They are involved in the progression of a variety of diseases, such as invasion and metastasis of tumors. Likewise, many disease states are associated with changes in glycosylation at the cellular level. Pharmaceutical control of such recognition processes may therefore be beneficial. Furthermore, understanding the mechanism of carbohydrate recognition may lead to the development of new concepts and new strategies to tackle the problems of carbohydrate-based drug development. This

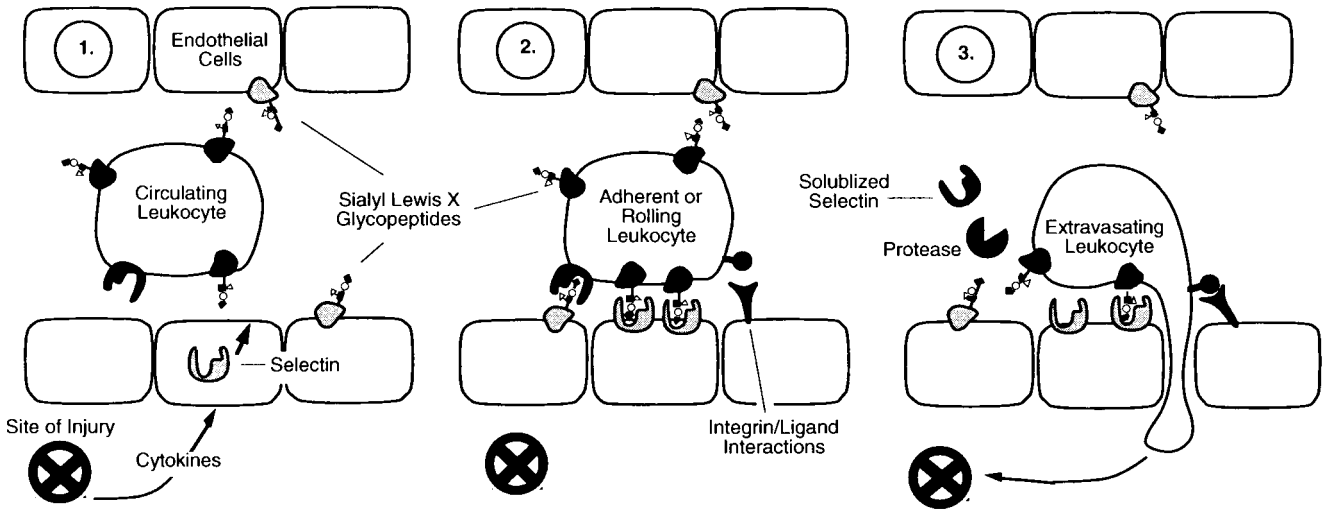

Fig. 1 Sialyl Lewis X-mediated cell adhesion in inflammatory reaction

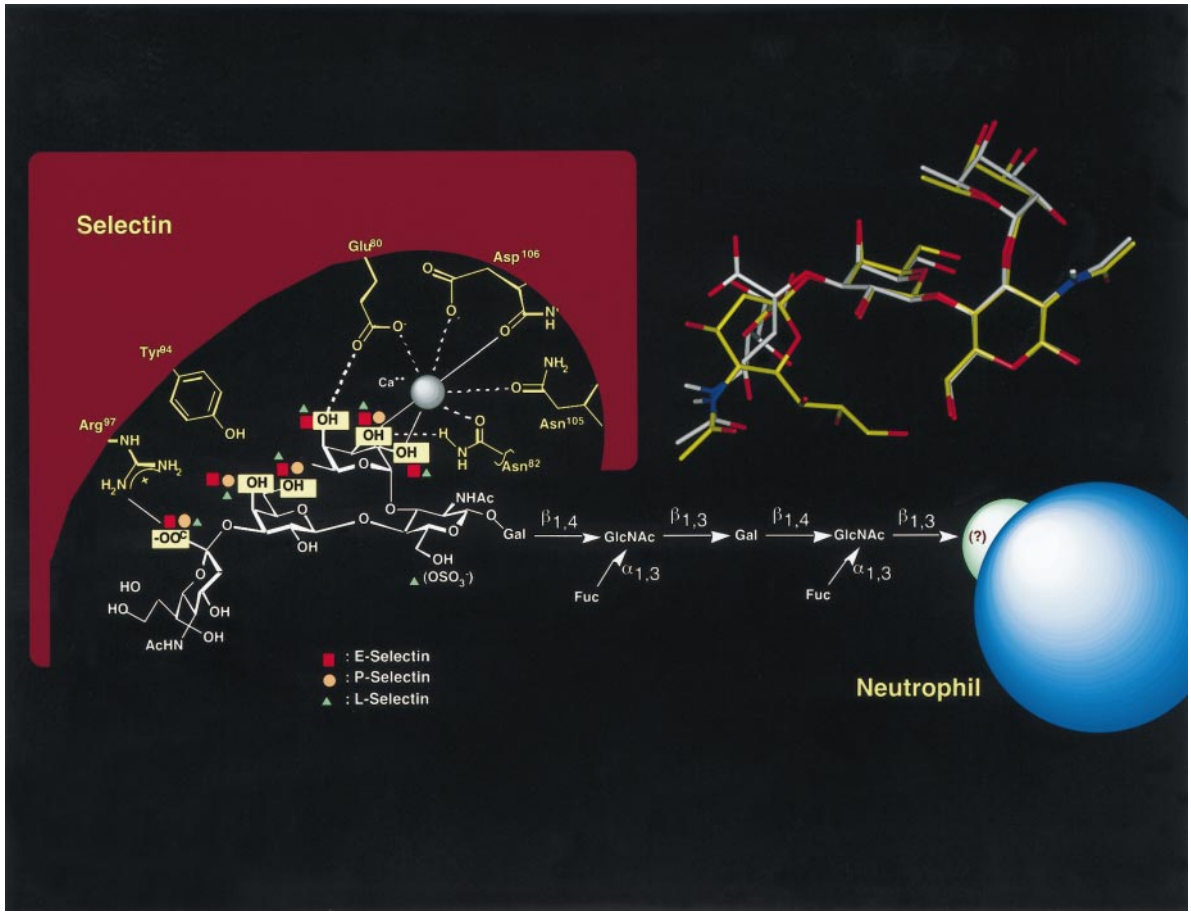

Fig. 2 Overlay of the conformation of sialyl Lewis X bound to E- or P-Selectin (yellow) with that bound to the L-selectin (white), and the functional groups essential for selectin recognition

review focuses on some of the most recent efforts toward the synthesis of complex carbohydrates, carbohydrate mimetics and inhibitors of glycoprocessing enzymes. It concentrates on the development of molecules that inhibit the natural functions of selectins, RNA, glycosidases and glycosyltransferases.

Cellular trafficking *via* selectin–carbohydrate interactions

A new class of carbohydrate-binding glycoproteins called selectins have recently been identified on the surface of specific cell types. These glycoproteins have been named E-,[7] P-[8] and L-selectins[9,10] according to the cell type on which each was initially found (*i.e.* endothelium, platelets and lymphocytes, respectively). The selectins are all homologous and have similar tertiary structures. The *N*-terminal region is made up of a calcium-dependent lectin-like domain and an epidermal growth factor-like (EGF) domain, which are necessary for carbohydrate binding. Following these are a number of modules (~ 60 amino acids) similar to those found in certain complement binding proteins. The exact number of modules depends on the selectin, though their function is, as yet, unknown. The X-ray crystal structure of the lectin and EGF domains of human E-selectin was determined[11] and its amino acid sequence is homologous to another mammalian lectin, the mannose binding protein,[12] for which the structure has also been solved. Carbohydrate ligands that are recognized by the selectins have been identified. E-Selectin recognizes sialyl Lewis X (SLe^x) on the surface of neutrophils.[13–15] P-Selectin also binds sialyl Lewis X on neutrophils or leukocytes with a lower affinity.[16,17] L-Selectin weakly recognizes sialyl Lewis X on endothelial cells but the affinity is higher with a sulfate group on the 6-position of Gal[18,19] or perhaps more likely on the 6-position of the GlcNAc residue.[17,20] Some sulfated Le^x also bind to E- and P-selectin[21] and questions regarding the true physiological ligands for these selectins still exist, particularly since the specificity of the selectins towards these ligands is by no means absolute.

The selectin–carbohydrate interaction is initiated at an early stage of the inflammatory reaction[22,23] or metastasis.[24–26] As illustrated in Fig. 1, when tissue injury occurs, cytokines are released to signal endothelial cells to display P- and then E-selectins to recruit neutrophils to the site of injury. Recruitment is mediated by the adhesion of neutrophils to endothelial cells through the multivalent interaction of SLe^x and P- or E-selectin on the respective cell surfaces, followed by a more tight interaction between integrins on neutrophils and the intercellular adhesion molecule (ICAM-1) on endothelial cells, resulting in the extravasation of neutrophils at the site of injury. Over recruitment of neutrophils can be deleterious, causing damage to normal cells and leading to inflammation. Intervention of this process by partially inhibiting the adhesion step has thus been considered to be a new strategy for creating anti-inflammatory agents, and it is expected that many acute symptoms such as reperfusion injury, stroke, asthma and arthritis may be treated with this approach. In support of this idea, the carbohydrate ligands of these selectins, especially those of E- and P-selectin, have been shown to be potentially useful for the treatment of these acute symptoms.[27,28]

Chemoenzymatic synthesis of oligosaccharides and glycoproteins

The syntheses of SLe^x and related structures[29–34] have played a very important role in defining the structure–function relationship. Studies with these molecules have not only provided confirmation of the function of the ligand but have also unravelled the essential groups involved in ligand recognition (Fig. 2). For SLe^x interaction with E- and L-selectins, it has

been shown that the three hydroxy groups of fucose,[35,36] the 2- and 6-hydroxy groups of galactose[37] and the carboxylate of neuraminic acid[35] are essential for binding and that the GlcNAc residue is not critical.[38] For P-selectin, the essential functional groups are generally the same, but the 2- or 4-hydroxy group of fucose seems not to be critical.[35] These discoveries together with the conformations of SLe^x determined by NMR spectroscopy[39–43] provide a basis for the design of new structures to mimic the active conformation of SLe^x, which may lead to the discovery of new and better anti-inflammatory agents.

The conformation of SLe^x in solution[39] is different from that bound to E- and P-selectin,[42] especially in the orientation of the neuraminic acid residue, though similar to that bound to L-selectin.[43] The conformational and structure–function relationship studies suggest it should be possible to design small molecules that are constrained to resemble the active form of SLe^x and thus improve the inhibition potency (Fig. 2).

Regarding the preparation of SLe^x, enzymatic techniques have been developed for its large-scale synthesis,[39] and the use of glycosyltransferases coupled with regeneration of sugar nucleotide substrates, first illustrated in the synthesis of *N*-acetyl lactosamine,[44] has proven to be useful for the large-scale process. SLe^x has been prepared on kilogram scales based on this strategy. This multienzyme system not only eliminates the problem of product inhibition caused by the released nucleoside (di)phosphates, but also reduces the cost of the expensive sugar nucleotide. This method has been extended to the synthesis of hyaluronic acid,[45] and we believe that, once the appropriate glycosyltransferases are available, it should be possible to produce any biologically known oligosaccharide in large quantities based on this methodology, since methods for the regeneration of all sugar nucleotides have been developed.[46] To date, a wide variety of glycosyltransferases have been cloned. An up-to-date listing can be found in our recent review.[47] Many of the enzymes are inactive when produced in bacterial expression systems, but the development of new high-level eukaryotic expression systems (especially using yeast,[48] baculovirus,[39] and *Aspergillus*[49]) for the preparation of glycosyltransferases has made possible the large-scale enzymatic synthesis of oligosaccharides.

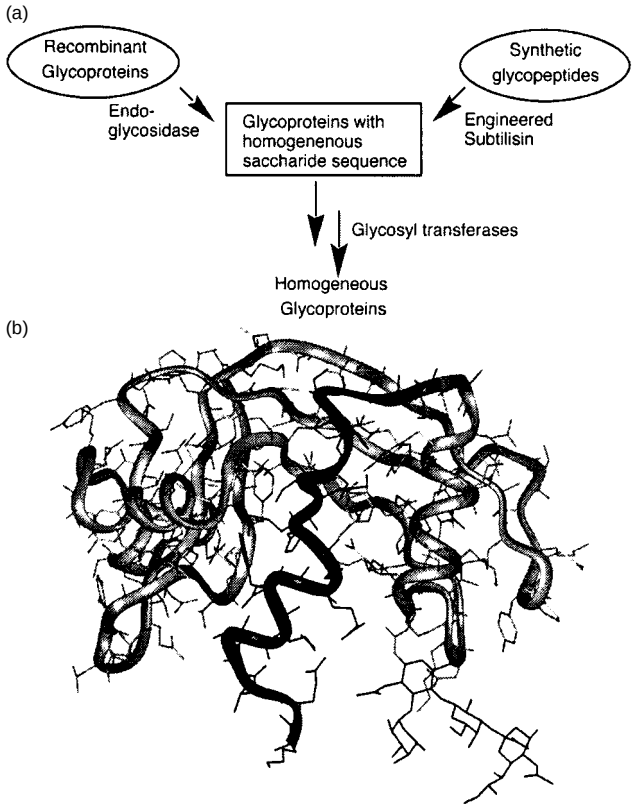

Fig. 3 (a) Strategies for enzymatic synthesis of glycoproteins containing well-defined oligosaccharides; (b) sialyl Lewis X-Ribonuclease A glycoform

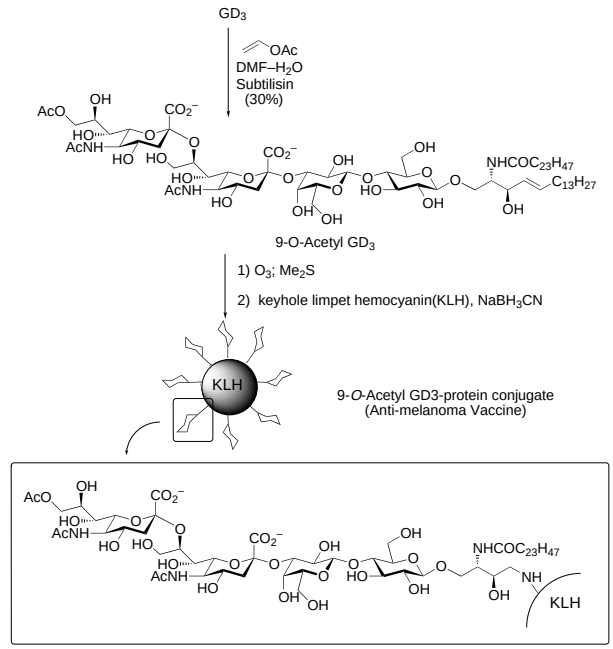

Fig. 4 Enzymatic synthesis of the melanoma antigen 9-*O*-acetyl-GD_3 for the preparation of vaccines

Sulfation of saccharides, too, can be accomplished enzymatically, and can be coupled with regeneration of PAPS for the large-scale synthesis of oligosaccharide sulfates.[50] *N*-Acetyllactosamine-6-sulfate, for example, has been prepared from *N*-acetyllactosamine, and this disaccharide can be easily converted to SLe^x-6-sulfate with commercially available α-1,3-fucosyltransferase and α-2,3-sialyltransferase.

Glycosyltransferases can be applied to solid-phase synthesis[51,52] and coupled with other enzymatic reactions to expand the scope of their synthetic application. As an alternative approach, the normally hydrolytic glycosidases can be forced into the synthetic direction by addition of large amounts of acceptor, or by sequestering the product. A glycosidase-catalyzed synthesis of disaccharides, for example, can be coupled *in situ* with a glycosyltransferase reaction to improve the overall yield.[53] Complex glycopeptides and glycoproteins, while not easily accessible by normal solid-phase synthesis, can be synthesized chemoenzymatically as well. A (short) monoglycosylated peptide ester may be ligated to another peptide in aqueous solution *via* subtilisin-catalyzed aminolysis, and the resulting glycopeptide may then be further elaborated with glycosyltransferases.[54–56] Several engineered thermostable thiosubtilisins have proven to be quite useful for glycopeptide synthesis, and the mechanisms of increased aminolysis to hydrolysis and stabilization have been elucidated.[54,57,58] Recently, subtilisin has been applied to the synthesis of new ribonuclease glycoforms, as illustrated in Fig. 3.[55] Other engineered subtilisins useful for peptide ligation have been developed by Wells and co-workers for the total synthesis of ribonuclease A and its analogs.[59] The enzymatic synthesis of glycoproteins is useful as currently there is no method available for the preparation of homogenous glycoproteins. The strategy illustrated in Fig. 3 may be useful in this regard. Glycoproteins produced by fermentation, which are inevitably heterogeneous in their carbohydrate composition, may be remodelled to a homogeneous species *via* enzymatic (endoglycosidase) removal of the heterogeneous saccharide units, followed by addition of new sugars with glycosyltransferases. The enzymatic method for glycopeptide synthesis is complementary to the solution- and solid-phase chemical approaches,[60–62] but may be more suitable for the synthesis of large glycopeptides.

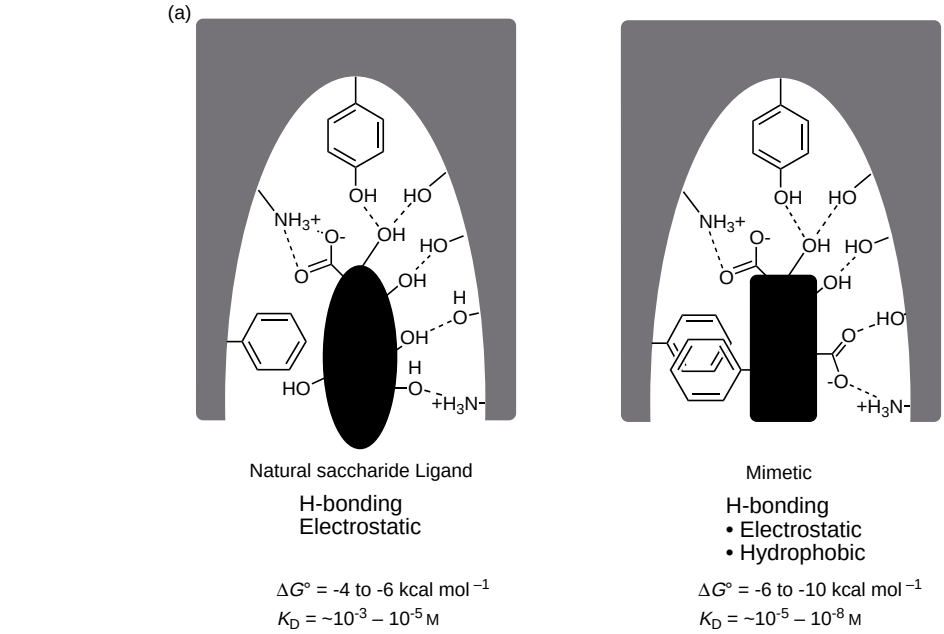

(b)

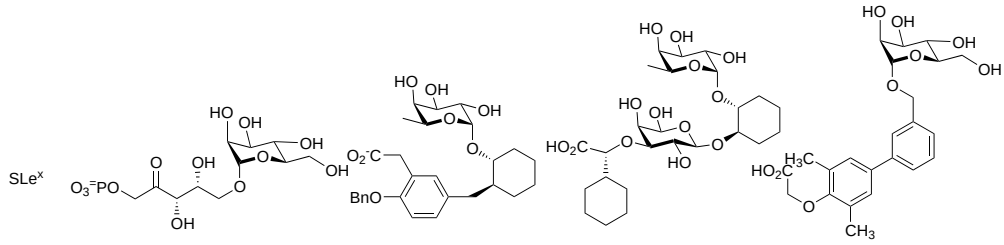

E-Selectin	0.7 mM	100 μM	0.63 mM	80 μM	50 μM
P-Selectin	8 mM	0.6 μM	—	—	—
L-Selectin	4 mM	95 μM	—	—	—

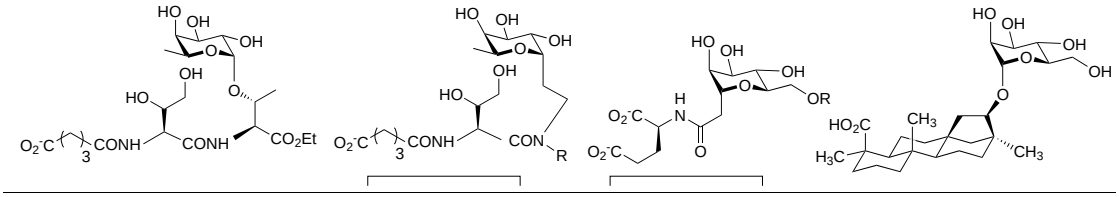

		R=$CH_2CONH(CH_2)_{13}CH_3$	R=H	R=$(CH_2)_{15}CH_3$	R=H	
E-Selectin	0.5 mM	37 μM	0.3 mM	53 μM	0.1 mM	>3 mM
P-Selectin	1 mM	7 μM	4 mM	2.2 μM	>3 mM	80 μM
L-Selectin	5 mM	190 mM	>5 mM	7.6 μM	2.7 mM	>3 mM

Fig. 5 (a) Strategy for the development of carbohydrate mimetics. (b) Representative sialyl Lewis X (SLe^x) mimetics and their relative activities against selectins as compared to SLe^x. (For a review on SLe^x mimetics, see Simanek *et al.*[100]).

Enzymatic elaboration can be extended to lipids, as well. The ganglioside GM_3 may be converted to GD_3 with α-2,8-sialyltransferase (GD_3 synthase), and the melanoma antigen 9-*O*-acetyl-GD_3 can be prepared from GD_3 *via* subtilisin-catalyzed acetylation in DMF using vinyl acetate[63] (Fig. 4).

Rational design and synthesis of sialyl Lewis X mimetics

As mentioned previously, complex carbohydrates may not be ideal candidates for drug development, and so the development of carbohydrate mimetics which contain additional recognition groups (hydrophobic or charged) and are simpler, more stable, more active than the parent structure, and perhaps orally active has become an interesting subject for research [see Fig. 5(a) for an overall strategy]. In the case of the SLe^x–selectin interaction, the structure–function relationship study and conformational analysis have led to the rational development of SLe^x mimetics which may be comparable to or even better than the natural ligand as inhibitors of selectins. Several groups have been actively engaged in this effort, and several SLe^x mimetics developed [see Fig. 5(b) and relative activity][64–72] have been shown to have IC_{50} values for the selectins decreased from the millimolar range for SLe^x to the low micromolar range for the mimetics.

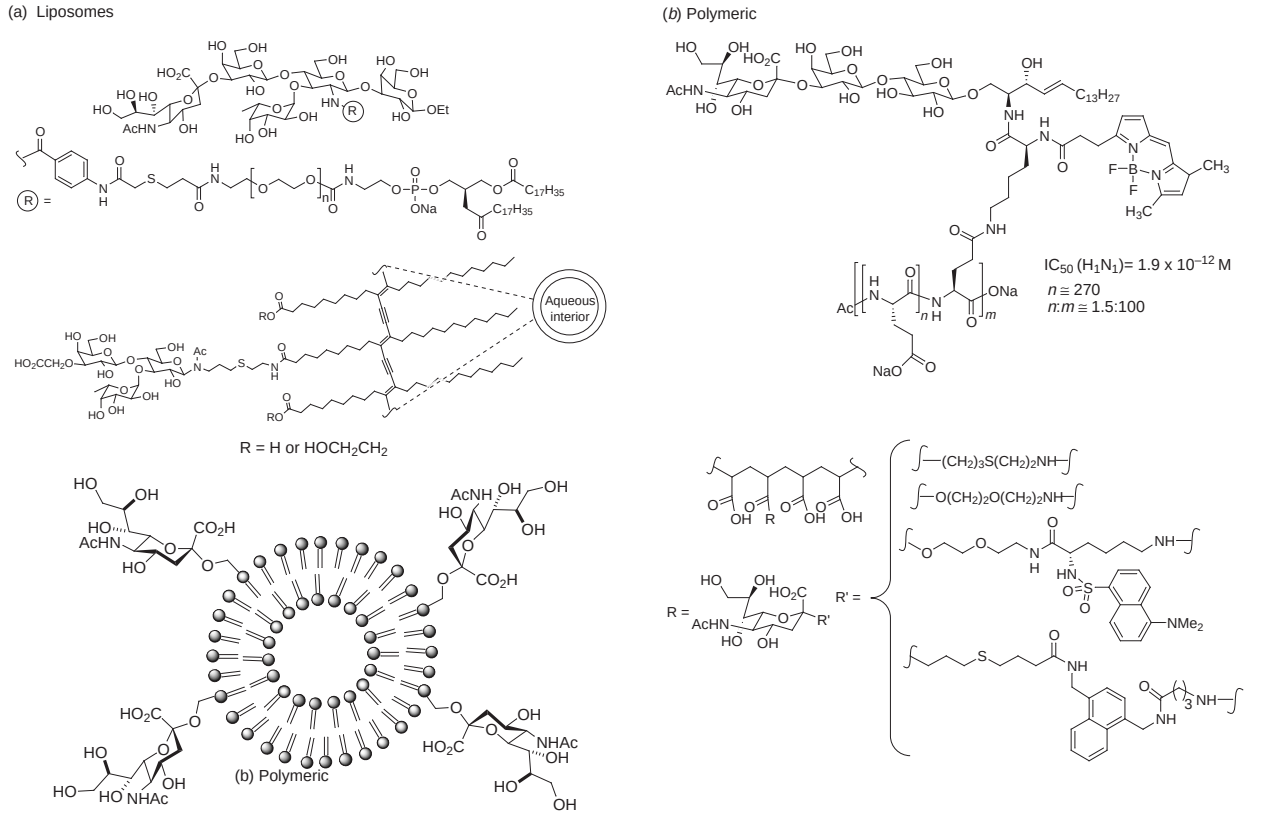

Fig. 6 Representative carbohydrate-based multivalent inhibitors of selectins and influenza haemagglutinin, both (a) liposome-based and (b) polymer-based

Polyvalent inhibitors of receptor–ligand interaction

Cell-surface receptor–ligand interactions, such as selectin–ligand interaction, are often multivalent, and so the inhibitor prepared in a multivalent form is expected to increase the inhibition potency. Indeed, both polymeric and liposome-like SLe^x derivatives have been shown to be much more active (by a factor of ~70–5000 depending on the structure and formulation) than the monomeric species as inhibitors of E- and P-selectin.[73,74] One should be careful, however, in extrapolating *in vitro* binding constants to *in vivo* activities. Polyvalent structures composed of ligands that are expected to show moderate non-specific binding in their monomeric form may show not only an increase in the strength of specific binding, but an increase in the strength of non-specific binding as well. For example, a polymer composed of repeating units of a ligand with a single cationic group will bind strongly to a polyanionic species, even though the monomer binds the polyanionic species only weakly. This is the principle of ion exchange

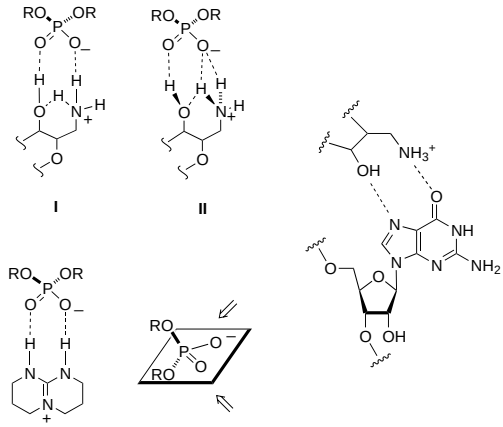

Fig. 7 Interactions of hydroxamic acids with nucleic acids, showing the binding to the phosphodiester backbone as compared to a guanidino group, and binding to the Hoogsten face of guanine

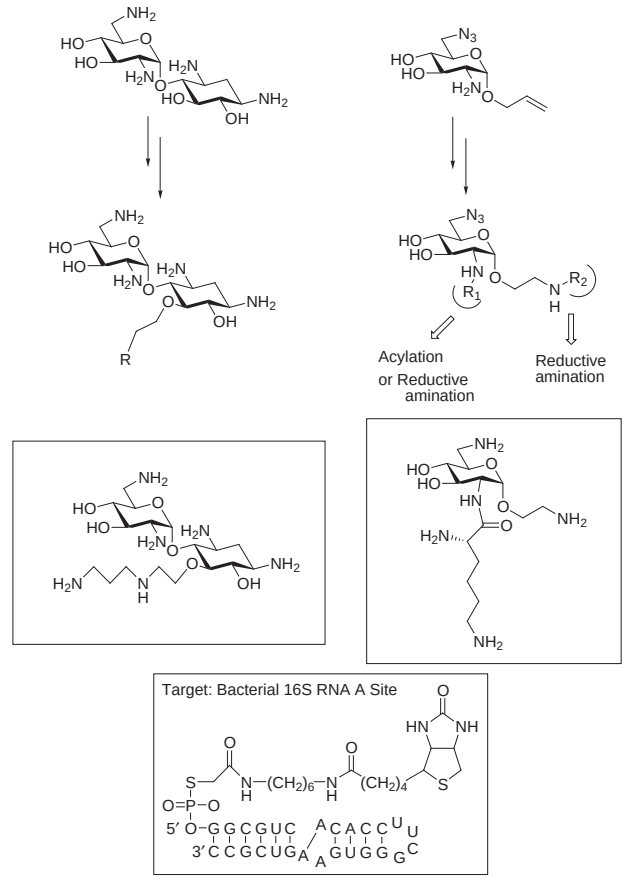

Fig. 8 Library approach for discovering new aminoglycosides with antibiotic activity. Synthetic route to 2,6-dideoxy-2,6-diaminoglucose and neamine-based libraries.

resins, after all. One should therefore begin with a molecule that has good specificity for the target of interest. In the future, perhaps the SLe^x mimetics described above, which already have better affinities for the selectins than SLe^x itself, can be converted to a multivalent form to increase the activity and specificity.

Previous work on the inhibition of the influenza virus haemagglutinin interactions with the host cell-surface sialoglycoproteins has also demonstrated the effectiveness of polyvalent inhibitors, and highly effective inhibitors with IC_{50} values ranging from 10^{-11}–10^{-12} M have been developed.[75,76] Some representative carbohydrate-based polyvalent systems are shown in Fig. 6.

Combinatorial approaches for discovering carbohydrate mimetics

The combinatorial approach has also been used in finding peptides that bind to E-selectin.[77] In many cases, the carbohydrate–receptor interaction is not well understood, so the aforementioned rational design of carbohydrate mimetics becomes difficult. In such cases, the combinatorial synthesis approach is perhaps the most effective way of finding lead inhibitors. Alternatively, the combinatorial approach can be useful for lead optimization. For example, the aminoglycoside antibiotic Neomycin B has recently been found as inhibitor of the Rev response element (RRE),[78] but the inhibition has not been well studied with regard to the origin of the selectivity. This is true with respect to the interaction of many other aminoglycoside antibiotics with certain sequences of RNA, including ribozymes.[79] However, one interesting common feature of these antibiotics is that most of them contain a *trans*-1,3-hydroxylamine or *trans*-1,3-diamine motif. Our recent model study also indicates that phosphodiesters complex the gluco-type 1,3-hydroxylamine more strongly than a bicyclic guanidine, and may also interact with the Hoogsten face of guanine[80] (see Fig. 7). This finding has led us to use a combinatorial approach to rapidly synthesize a library of

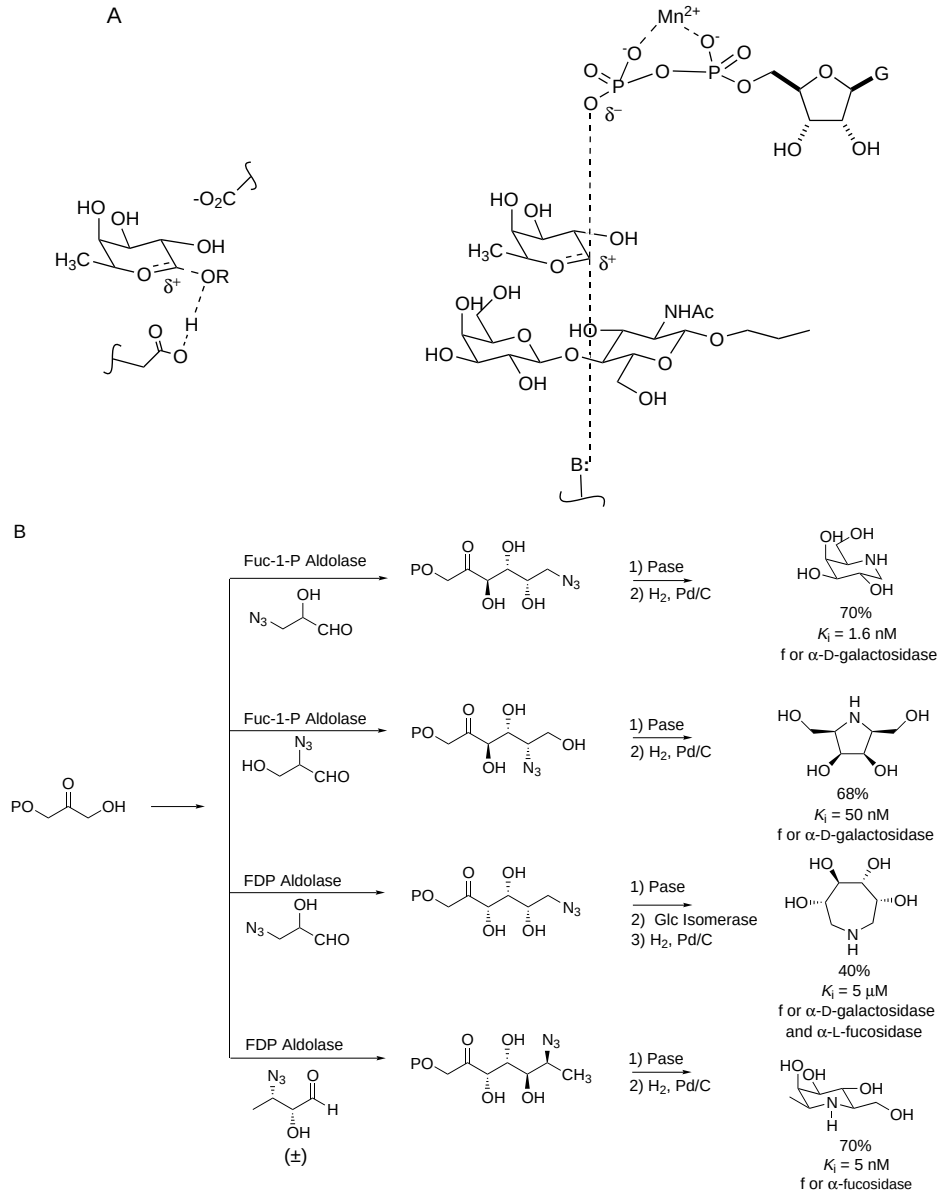

Fig. 9 (A) Postulated transition-state structure of α-fucosidase and human α-1,3-fucosyltransferase and a designed synergistic inhibitor complex; (B) aldolase reactions for production of iminocyclitol inhibitors; (following pages) (C) representative inhibitors of glycosidases and glycosyltransferases: a, Heifetz, *et al.*;[101] b, Palcic, *et al.*;[99] c, Murray, *et al.*;[94] d, Lu, *et al.*;[97] e, Hashimoto, *et al.*;[98] f, Schmidt and Frische;[102] g, Tropea, *et al.*;[103] h, Wong, *et al.*;[89] i, Elbein, *et al.*;[104] j, Pan, *et al.*;[105] k, Dorling, *et al.*;[106] l, Cottaz, *et al.*;[107] m, Tsuji, *et al.*;[108] n, Asano, *et al.*;[109] o, Dong, *et al.*;[110] p, Bernotas, *et al.*;[111] q, Wong, *et al.*;[112] r, Moris-Varas, *et al.*;[95] s, Jeong, *et al.*;[90] t, Ichikawa and Igarashi;[92] u, Schedler, *et al.*;[113] v, Takayama, *et al.*;[114] w, Knapp, *et al.*;[115] x, Sollis, *et al.*;[116] y, Kim, *et al.*[117]

C

(a)

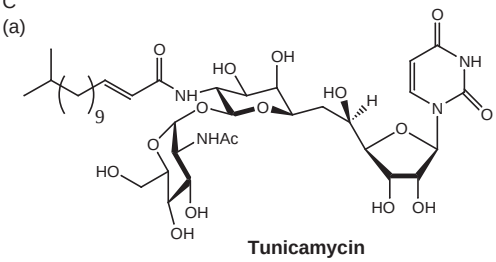

Tunicamycin

UDP-GlcNAc:Dolichol phosphate
GlcNAc Phosphotransferase
IC_{50} = 7 nM

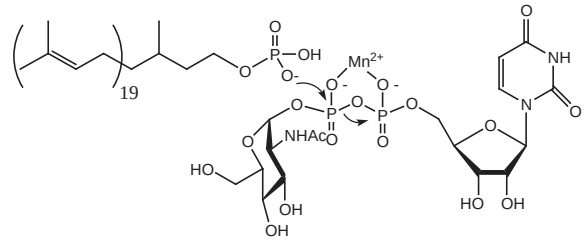

GlcNAc phosphotransferase reaction

(b)

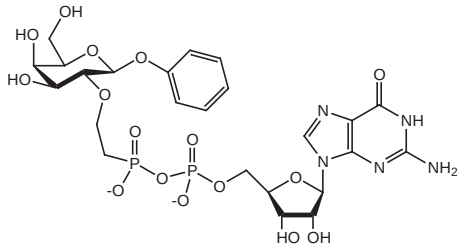

α-1,2-Fucosyltransferase
K_i = 2–16 μM

(c)

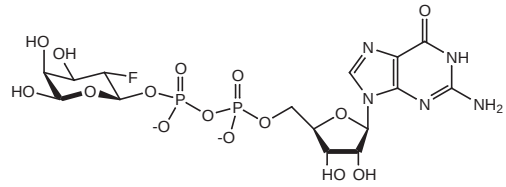

α-1,3-Fucosyltransferase
K_i = 4 μM

(d)

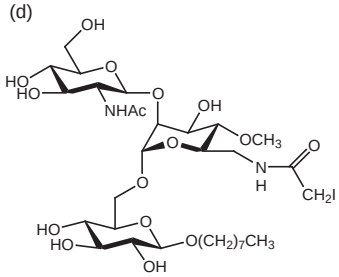

N-Acetylglucosaminyltransferase V
K_i = 21 μM

(e)

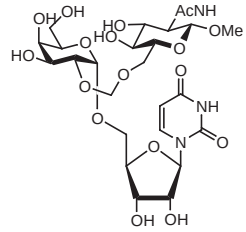

β-1,4-Galactosyltransferase
K_i = 1.35 μM

(f)

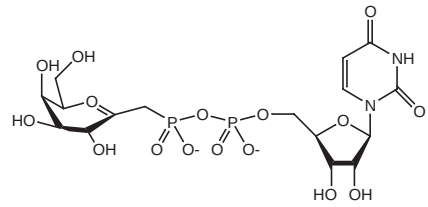

β-1,4-Galactosyltransferase
K_i = 62 μM

(g)

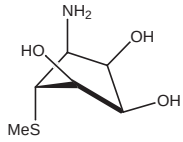

Mannostatin A
α-Mannosidase I I
IC_{50} = 10–15 nM

(h)

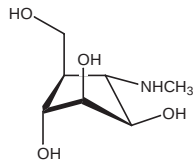

α-D-Mannosidase
(Jack Bean)
IC_{50} = 62 nM

(i)

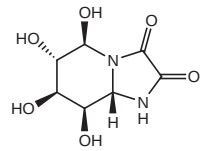

Kifunensine
α-Mannosidase I
(Mung Bean)
IC_{50} = 20-50 nM

(j)

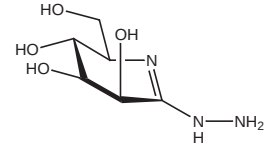

Bovine a-mannosidase I
IC_{50} = 4 μM

(k)

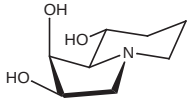

Swainsonine
Lysosomal mannosidase
IC_{50} = 100 nM

(l)

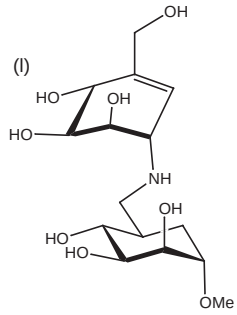

α-D-Mannosidase
K_i = 30 μM[I]

(m)

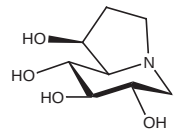

Castanospermine
α-Glucosidase I
IC_{50} = 1.2 μM

(n)

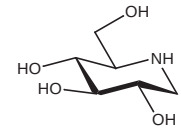

1-deoxynojirimycin
α-Glucosidase II
(rat liver)
K_i = 4.6 μM

Fig. 9 continued

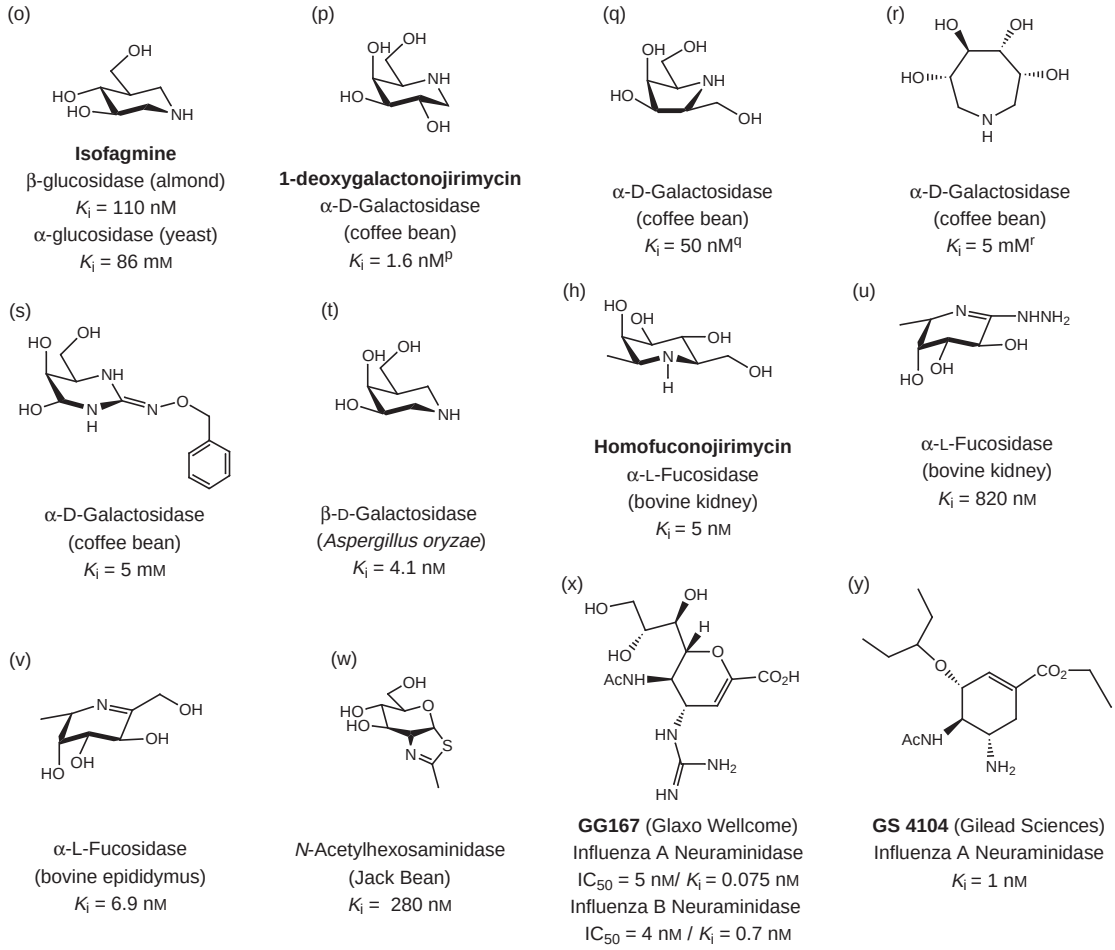

Fig. 9 continued

aminoglycoside mimetics containing either the neamine core or the 2,6-dideoxy-2,6-diaminoglucose (Fig. 8) and screen the library for new compounds that bind to RRE[81] or other RNA sequences, especially the bacterial 16S rRNA A site, a useful target for preventing bacterial infection.[82] As a result, several Neomycin B mimetics have been found to be more active than Neomycin B itself.[81] The combinatorial synthesis is facilitated by the use of the polyethylene glycol ether as the carrier. The product can be easily isolated by precipitation with ether, so that chromatography is not necessary.[83] Both rational and library approaches have also been used to develop new aminoglycoside antibiotic mimetics to target the bacterial 16S rRNA A site and some potent new antibiotics have been discovered.[82]

Inhibition of glycosidases and glycosyltransferases

Another strategy for the intervention of carbohydrate recognition processes is to inhibit the enzymes associated with oligosaccharide biosynthesis. Both glycosidases and glycosyltransferases are important enzymes involved in the processing and synthesis of oligosaccharides and are therefore obvious targets for intervention. The mechanisms of glycosidases have been well studied[84–86] and means for inhibition of these enzymes have been developed.[87–92] Glycosyltransferase reactions are thought to proceed through transition states similar to those of the glycosidase reactions, which are believed to proceed through a half-chair transition state with a substantial sp^2 character developed at the anomeric center [Fig. 9(A)].[49,93,94] Based on this mechanistic rationale, many transition-state analog inhibitors of glycosidases, especially iminocyclitols, have been developed [Fig. 9(B),(C)]. The five-, six- and seven-membered iminocyclitols have been synthesized based on the sequence of aldolase reaction and Pd-mediated reductive amination.[89,95] These nitrogen-containing heterocycles have also been used as key components in the synthesis of glycosyltransferase inhibitors.[89] In addition, both bisubstrate and trisubstrate analogs and fluorinated sugar nucleotides have been developed as glycosyltransferase inhibitors.[94,96–99]

Conclusions and future prospects

Molecular recognition of carbohydrates and related structures in biological systems represents a new frontier of research. Many of these recognition events occur at the very early stage of disease development and other signalling processes and new strategies and techniques are needed to study the recognition events in detail. Chemistry will continue to play a key role in uncovering the molecular mechanism of carbohydrate recognition and in development of novel structures to control the recognition process and combat disease. As the principles of carbohydrate recognition become well understood, carbohydrate mimetics will be developed to overcome some of the undesirable properties of parent structures, and additional groups (such as hydrophobic groups) complementary to the receptor can be further incorporated to the mimetics to enhance binding and to improve the activity. Finally, the multivalency strategy can then be utilized to further increase the activity and to control *in vivo* the function of carbohydrates.

Acknowledgements

We thank many of our co-workers, whose names are listed in the references, for their contributions to this research. Our work

was financially supported by the National Institutes of Health, the National Science Foundation and Novartis Pharma.

Chi-Huey Wong received his BS and MS degrees from the National Taiwan University and a PhD in Chemistry from the Massachusetts Institute of Technology under George M. Whitesides in 1982. After a year of postdoctoral research at Harvard University, he taught at Texas A&M University for six years, after which he moved to The Scripps Research Institute where he became the Ernest W. Hahn Professor of Chemistry in 1989. He is also head of the Frontier Research Program on Glycotechnology at RIKEN, Japan. His research interests are in the fields of bioorganic chemistry and biocatalysis.

Pamela Sears received her BS and MS degrees from University of California at Berkeley, and her PhD in Macromolecular Structure and Chemistry from the Scripps Research Institute in 1996 with Chi-Huey Wong. After a year of postdoctoral research, she became an Assistant Professor of Chemistry in 1997 at the Scripps Research Institute. Her research interests include enzymatic synthesis of biomolecules and evolution of enzymes for saccharide biosynthesis.

Notes and References

† E-mail: psears@scripps.edu

1 A. Varki, *Glycobiology*, 1993, **3**, 97.
2 R. U. Lemieux, *Acc. Chem. Res.*, 1996, **29**, 373.
3 C. P. J. Glaudemans, *Chem. Rev.*, 1991, **91**, 25.
4 F. A. Quiocho, *Pure Appl. Chem.*, 1989, **61**, 1293.
5 E. J. Toone, *Curr. Opin. Struct. Biol.*, 1994, **4**, 719.
6 T. C. Lee and R. T. Lee, *Acc. Chem. Res.*, 1995, **28**, 321.
7 M. P. Bevilacqua, S. Stengelin, M. A. Gimbrone, Jr. and B. Seed, *Science*, 1989, **243**, 1160.
8 G. I. Johnston, R. G. Cook and R. P. McEver, *Cell*, 1989, **56**, 1045.
9 M. H. Siegelman, M. Van de Rijn and I. L. Weissman, *Science*, 1989, **243**, 1165.
10 L. A. Lasky, M. S. Singer, T. A. Yednock, D. Dowbenko, C. Fennie, H. Rodriguez, T. Nguyen, S. Stachel and S. D. Rosen, *Cell*, 1989, **56**, 1045.
11 B. J. Graves, R. L. Crowther, C. Chandran, J. M. Rumberger, S. Li, K.-S. Huang, D. H. Presky, P. C. Familletti, B. A. Wolitzky and D. K. Burns, *Nature*, 1994, **367**, 532.
12 W. I. Weis, K. Drickamer and W. A. Hendrickson, *Nature*, 1992, **360**, 127.
13 M. L. Philips, E. Nudelman, F. C. A. Gaeta, M. Perez, A. K. Singhal, S.-I. Hakomori and J. C. Paulson, *Science*, 1990, **250**, 1130.
14 J. B. Lowe, L. M. Stoolman, R. P. Nair, R. D. Larsen, T. L. Berhend and R. M. Marks, *Cell*, 1990, **63**, 475.
15 G. Walz, A. Aruffo, W. Kolanus, M. Bevilacqua and B. Seed, *Science*, 1990, **250**, 1132.
16 M. J. M. Polley, M. L. Phillips, E. Wayner, E. Nudelman, A. K. Singhal, S.-I. Hakomori and J. C. Paulson, *Proc. Natl. Acad. Sci. USA*, 1991, **88**, 6224.
17 Q. Zhou, K. L. Moore, D. F. Smith, A. Varki, R. McEver and R. D. Cummings, *J. Cell Biol.*, 1991, **115**, 557.
18 S. Hemmerich, C. R. Bertozzi, H. Leffler and S. D. Rosen, *Biochemistry*, 1994, **33**, 4820.
19 S. Hemmerich and S. D. Rosen, *Biochemistry*, 1994, **33**, 4839.
20 E. V. Chandrasekaran, R. K. Jain, R. D. Larsen, K. Wlasichuk and K. L. Matta, *Biochemistry*, 1995, **34**, 2925.
21 T. Feizi, *Curr. Opin. Struct. Biol.*, 1993, **3**, 701.
22 R. P. McEver, K. L. Moore and R. D. Cummings, *J. Biol. Chem.*, 1995, **270**, 11 025.
23 T. A. Springer, *Nature*, 1990, **346**, 425.
24 J. Sakamoto, K. Furukawa, C. Cordon-Cardo, B. W. T. Yin, W. J. Rettig, H. F. Oettgen, L. J. Old and K. O. Lioyd, *Cancer Res.*, 1986, **46**, 1553.
25 S. H. Itzkowitz, M. Yuan, Y. Fukushi, A. Palekar, P. C. Phelps, A. M. Shamsuddin, B. F. Trump, S.-I. Hakomori and Y. S. Kim, *Cancer Res.*, 1986, **46**, 2627.
26 T. Muramatsu, *Glycobiology*, 1993, **3**, 294.
27 M. S. Mulligan, J. C. Paulson, S. DeFrees, Z.-L. Zheng, J. Lowe and P. A. Ward, *Nature*, 1993, **364**, 149.
28 T. Murohara, J. Marigiotta, L. M. Phillips, J. C. Paulson, S. DeFrees, S. Zalipsky, L. S. S. Guo and A. M. Lefer, *Cardiovas. Res.*, 1995, **30**, 965.
29 A. Kameyama, H. Ishida, M. Kiso and A. Hasegawa, *Carbohydr. Res.*, 1991, **209**, C1.
30 K. C. Nicolaou, C. W. Hummel, N. J. Bockovich and C.-H. Wong, *J. Chem. Soc., Chem. Commun.*, 1991, **13**, 870.
31 U. Sprengard, G. Kretschmar, E. Bartnik, C. Huls and H. Kunz, *Angew. Chem., Int. Ed. Engl.*, 1995, **34**, 990.
32 S. J. Danishefsky, J. Gervay, J. M. Peterson, F. E. McDonald, K. Koseki, D. A. Griffith, T. Oriyama and S. Marsden, *J. Am. Chem. Soc.*, 1995, **117**, 1940.
33 T. J. Martin and R. R. Schmidt, *Tetrahedron Lett.*, 1992, **33**, 6123.
34 H. Kondo, Y. Ichikawa and C.-H. Wong, *J. Am. Chem. Soc.*, 1992, **114**, 8748.
35 N. K. Brandley, M. Kiso, S. Abbas, P. Nikrad, O. Srivastava, C. Foxall, Y. Oda and A. Hasegawa, *Glycobiology*, 1993, **3**, 663.
36 J. Y. Ramphal, Z.-L. Zheng, C. Perez, L. Walker, S. A. DeFrees and F. C. A. Gaeta, *J. Med. Chem.*, 1994, **37**, 3459.
37 W. Stahl, U. Sprengard, G. Kretschmar and H. Kunz, *Angew. Chem., Int. Ed. Engl.*, 1994, **33**, 2096.
38 S. A. DeFrees, F. C. A. Gaeta, Y. C. Lin, Y. Ichikawa and C.-H. Wong, *J. Am. Chem. Soc.*, 1993, **115**, 7549.
39 Y. Ichikawa, Y.-C. Lin, D. P. Dumas, G.-J. Shen, E. Garcia-Junceda, M. A. Williams, R. Bayer, C. Ketcham, L. E. Walker, J. C. Paulson and C.-H. Wong, *J. Am. Chem. Soc.*, 1992, **114**, 9283.
40 R. M. Cooke, R. S. Hale, S. G. Lister, G. Shah and M. P. Weir, *Biochemistry*, 1994, **33**, 10 591.
41 P. Hensley, P. J. McDevitt, I. Brooks, J. J. Trill, J. A. Feild, D. E. McNulty, J. R. Connor, D. E. Griswold, N. V. Kumar, K. D. Kopple, S. A. Carr, B. J. Dalton and K. Johanson, *J. Biol. Chem.*, 1994, **269**, 23 949.
42 K. Scheffler, B. Ernst, A. Katopodis, J. L. Magnani, W. T. Wang, R. Weisemann and T. Peters, *Angew. Chem., Int. Ed. Engl.*, 1995, **34**, 1841.
43 L. Poppe, G. S. Brown, J. S. Philo, P. V. Nikrad and B. H. Shah, *J. Am. Chem. Soc.*, 1997, **119**, 1727.
44 C.-H. Wong, S. L. Haynie and G. M. Whitesides, *J.Org. Chem.*, 1982, **47**, 5416.
45 C. DeLuca, M. Lansing, I. Martin, F. Crescenzi, G.-J. Shen, M. O'Regan and C.-H. Wong, *J. Am. Chem. Soc.*, 1995, **117**, 5869.
46 Y. Ichikawa, R. Wang and C.-H. Wong, *Methods Enzymol.*, 1994, **247**, 193.
47 P. Sears and C.-H. Wong, *Cell. Mol. Life Sci.*, 1998, **54**, 223.
48 C. H. Krezdorn, G. Watsele, R. B. Kleene, S. X. Ivanov and E. G. Berger, *Eur. J. Biochem.*, 1993, **212**, 113.
49 B. W. Murray, S. Takayama, J. Schultz and C.-H. Wong, *Biochemistry*, 1996, **35**, 11 183.
50 C.-C. Lin, G.-J. Shen and C.-H. Wong, *J. Am. Chem. Soc.*, 1995, **117**, 8031.
51 M. Schuster, P. Wang, J. C. Paulson and C.-H. Wong, *J. Am. Chem. Soc.*, 1994, **116**, 1135.
52 R. L. Halcomb, H. Huang and C.-H. Wong, *J. Am. Chem. Soc.*, 1994, **116**, 11 315.
53 G. F. Herrmann, Y. Ichikawa, C. Wandrey, F. C. A. Gaeta, J. C. Paulson and C.-H. Wong, *Tetrahedron Lett.*, 1993, **19**, 3091.
54 P. Sears, P. Wang, K. Witte, M. Schuster and C.-H. Wong, *J. Am. Chem. Soc.*, 1994, **116**, 6521.
55 K. Witte, P. Sears, R. Martin and C.-H. Wong, *J. Am. Chem. Soc.*, 1997, **119**, 2114.
56 C.-H. Wong, M. Schuster, P. Wang and P. Sears, *J. Am. Chem. Soc.*, 1993, **115**, 5893.
57 P. Sears and C.-H. Wong, *Biotechnol. Prog.*, 1996, **12**, 423.
58 R. D. Kidd, H. P. Yennawar, P. Sears, C.-H. Wong and G. K. Farber, *J. Am. Chem. Soc.*, 1996, **118**, 1645.
59 D. Y. Jackson, J. Burnier, C. Quan, M. Stanley, J. Tom and J. A. Wells, *Science*, 1994, **266**, 243.
60 H. Kunz, *Pure Appl. Chem.*, 1993, **65**, 1223.
61 T. Bielfeldt, S. Peters, M. Meldal, K. Bock and H. Paulsen, *Angew. Chem., Int. Ed. Engl.*, 1992, **31**, 857.
62 S. J. Danishefsky and M. T. Bilodeau, *Angew. Chem., Int. Ed. Engl.*, 1996, **35**, 1381.
63 S. Takayama and C.-H. Wong, *Tetrahedron Lett.*, 1996, **37**, 9271.
64 B. N. N. Rao, M. B. Anderson, J. H. Musser, J. H. Gilbert, M. E. Schaefer, C. Foxall and B. K. Brandley, *J. Biol. Chem.*, 1994, **269**, 19 663.
65 T. Uchiyama, V. P. Vassilev, T. Kajimoto, W. Wong, H. Huang, C.-C. Lin and C.-H. Wong, *J. Am. Chem. Soc.*, 1995, **117**, 5395.

66 S.-H. Wu, M. Shimazaki, C.-C. Lin, L. Qiao, W. J. Moree and C.-H. Wong, *Angew. Chem., Int. Ed. Engl.*, 1996, **35**, 88.
67 D. Dupre, H. Bui, I. L. Scott, R. V. Market, K. M. Keller, P. J. Beck and T. P. Kogan, *Bioorg. Med. Chem. Lett.*, 1996, **6**, 569.
68 A. Liu, K. Dillon, R. M. Campbell, D. C. Cox and D. M. Huryn, *Tetrahedron Lett.*, 1996, **37**, 3785.
69 M. J.Bamford, M. Bird, P. M. Gore, D. S. Holmes, R. Priest, J. C. Prodger and V. Saez, *Bioorg. Med. Chem. Lett.*, 1996, **6**, 239.
70 C.-C. Lin, M. Shimazaki, M.-P. Heck, S. Aoki, R. Wang, T. Kimura, H. Ritzen, S. Takayama, S.-H. Wu, G. Weitz-Schmidt and C.-H. Wong, *J. Am. Chem. Soc.*, 1996, **118**, 6826.
71 C.-H. Wong, F. Moris-Varas, C.-C. Lin and G. Weitz-Schmidt, *J. Am. Chem. Soc.*, 1997, **119**, 8152.
72 H. C. Kolb and B. Ernst, *Chem. Eur. J.*, 1997, **3**, 1571.
73 S. A. DeFrees, L. Philips, L. Guo and S. Zalipsky, *J. Am. Chem. Soc.*, 1996, **118**, 1601.
74 W. Spevak, C. Foxall, D. H. Charych, F. Dasgupta and J. O. Nagy, *J. Med. Chem.*, 1996, **39**, 1018.
75 G. B. Sigal, M. Mammen, G. Dahmann and G. M. Whitesides, *J. Am. Chem. Soc.*, 1996, **118**, 3789.
76 H. Kamitakahara, T. Suzuki, N. Nishigori, Y. Suzuki, O. Kanie and C.-H. Wong, *Angew. Chem., Int. Ed. Engl.*, 1998, in the press.
77 C. L. Martens, S. E. Cwirla, R. Y. W. Lee, E. Whitehorn, E. Y. F. Chen, A. Bakker, E. L. Martin, C. Wagstrom, P. Goplain, C. W. Smith, E. Tate, K. H. Koller, P. J. Schatz, W. J. Dower and R. W. Barett, *J. Biol. Chem.*, 1995, **270**, 21 129.
78 M. L. Zapp, S. Stern and M. R. Green, *Cell*, 1993, **74**, 969.
79 U. Von Ahsen and H. F. Noller, *Science*, 1993, **260**, 1500.
80 M. Hendrix, P. B. Alper, E. S. Priestley and C.-H. Wong, *Angew. Chem., Int. Ed. Engl.*, 1997, **36**, 95.
81 W. K. C. Park, M. Auer, H. Jaksche and C.-H. Wong, *J. Am. Chem. Soc.*, 1996, **118**, 10 150.
82 P. B. Alper, M. Hendrix, P. Sears and C.-H. Wong, *J. Am. Chem. Soc.*, 1997, in the press.
83 H. Han, M. M. Wolfe, S. Brenner and K. D. Janda, *Proc. Natl. Acad. Sci. USA*, 1995, **92**, 6419.
84 M. L. Sinnott, *Chem. Rev.*, 1990, **90**, 1171.
85 A. J. Kirby, *Nature*, 1996, **3**, 107.
86 S. G. Withers and I. P. Street, *J. Am. Chem. Soc.*, 1988, **110**, 8551.
87 B. Winchester and G. W. Fleet, *Glycobiology*, 1992, **2**, 199.
88 B. Ganem, *Acc. Chem. Res.*, 1996, **29**, 340.
89 C.-H. Wong, R. L. Halcomb, Y. Ichikawa and T. Kajimoto, *Angew. Chem., Int. Ed. Engl.*, 1995, **34**, 521.
90 J.-H. Heong, B. W. Murray, S. Takayama and C.-H. Wong, *J. Am. Chem. Soc.*, 1996, **118**, 4227.
91 S. Knapp, A. Purandara, K. Rupitz and S. G. Withers, *J. Am. Chem. Soc.*, 1994, **116**, 7461.
92 Y. Ichikawa and Y. Igarashi, *Tetrahedron Lett.*, 1995, **36**, 4585.
93 S. C. Kim, A. N. Singh and F. M. Raushel, *Arch. Biochem. Biophys.*, 1988, **267**, 54.
94 B. W. Murray, V. Wittmann, M. Burkart, S.-C. Hung and C.-H. Wong, *Biochemistry*, 1997, **36**, 823.
95 F. Moris-Varas, X. H. Qian and C.-H. Wong, *J. Am. Chem. Soc.*, 1996, **118**, 7647.
96 L. Qiao, B. W. Murray, M. Shimazaki, J. Schultz and C.-H. Wong, *J. Am. Chem. Soc.*, 1996, **118**, 7653.
97 P.-P. Lu, O. Hindsgaul, C. A. Compston and M. M. Palcic, *Bioorg. Med. Chem.*, 1996, **4**, 2011.
98 H. Hashimoto, T. Endo and Y. Kajihara, *J. Org. Chem.*, 1997, **62**, 1914.
99 M. M. Palcic, L. D. Heerze, O. P. Srivastava and O. Hindsgaul, *J. Biol. Chem.*, 1989, **264**, 17 174.
100 E. E. Simanek, G. J. McGarvey, J. A. Jablonski and C.-H. Wong, *Chem. Rev.*, 1998, in the press.
101 A. Heifetz, R. W. Kennan and A. D. Elbein, *Biochemistry*, 1979, **18**, 2186.
102 R. R. Schmidt and K. Frische, *Bioorg. Med. Chem. Lett.*, 1993, **3**, 1747.
103 J. E. Tropea, G. P. Kaushal, I. Pastuszak, M. Mitchell, T. Aoyagi, R. J. Molyneux and A. D. Elbein, *Biochemistry*, 1990, **29**, 10 062.
104 A. D. Elbein, J. E. Tropea, M. Mitchell and G. P. Kaushel, *J. Biol. Chem.*, 1990, **265**, 15 599.
105 Y. T. Pan, G. P. Kaushel, G. Panadreaou, B. Ganem and A. D. Elbein, *J. Biol. Chem.*, 1991, **267**, 8313.
106 P. R. Dorling, C. R. Huxtable and S. M. Colegate, *Biochem. J.*, 1980, **191**, 649.
107 S. Cottaz, J. S. Brimacombe and M. A. J. Ferguson, *Carbohydr. Res.*, 1993, **247**, 341.
108 E. Tsuji, M. Muroi, N. Shiragami and A. Takatsuki, *Biochem. Biophys. Res. Commun.*, 1996, **220**, 459.
109 N. Asano, K. Oseki, E. Kaneko and K. Matsui, *Carbohydr. Res.*, 1994, **258**, 243.
110 W. Dong, T. Jespersen, M. Bols, T. Skrydstrup and M. R. Sierks, *Biochemistry*, 1996, **35**, 2788.
111 R. C. Bernotas, M. A. Pezzone and B. Ganem, *Carbohydr. Res.*, 1987, **167**, 305.
112 C.-H. Wong, L. Provencher, J. A. J. Porco, S.-H. Jung, Y.-F. Wang, L. Chen, R. Wang and D. H. Steensma, *J. Org. Chem.*, 1995, **60**, 1492.
113 D. J. A. Schedler, B. R. Bowen and B. Ganem, *Tetrahedron Lett.*, 1994, **35**, 3845.
114 S. Takayama, R. Martin, J. Wu, K. Laslo, G. Siuzdak and C.-H. Wong, *J. Am. Chem. Soc.*, 1997, **119**, 8146.
115 S. Knapp, D. Vocadlo, Z. Gao, B. Kirk, J. Lou and S. G. Withers, *J. Am. Chem. Soc.*, 1996, **118**, 6804.
116 S. L. Sollis, P. W. Smith, P. D. Howes, P. C. Cherry and R. C. Bethell, *Biorg. Med. Chem. Lett.*, 1996, **6**, 1805.
117 C. U. Kim, W. Lew, M. A. Williams, H. Liu, L. Zhang, S. Swaminathan, N. Bischofberger, M. S. Chen, D. B. Mendel, C. Y. Tai, W. G. Laver and R. C. Stevens, *J. Am. Chem. Soc.*, 1997, **119**, 681.

8/00838H

Binding of D-serine-terminating cell-wall analogues to glycopeptide antibiotics

André M. A. van Wageningen, Thomas Staroske and Dudley H. Williams*†

Cambridge Centre for Molecular Recognition, University Chemical Laboratory, Lensfield Road, Cambridge, UK CB2 1EW

Binding studies of –L-Lys-D-Ala-D-Ser-terminating ligands, used as model systems for cell-wall precursors found in VanC resistant bacteria, with vancomycin, chloroeremomycin and teicoplanin show that they bind to these glycopeptides in a similar manner as –L-Lys-D-Ala-D-Ala-terminating ligands, but that the binding constants are one to two orders of magnitude lower.

The glycopeptide antibiotics vancomycin and teicoplanin are well-known for their theurapeutic use as antibiotics of last resort against methicillin-resistant *Staphylococcus aureus* (MRSA).[1] The antibacterial activity of the glycopeptides results from interference of the synthesis of the growing bacterial cell wall by binding to the precursor peptide sequence terminating in –L-Lys-D-Ala-D-Ala.[2,3] The molecular features responsible for the antibacterial activity of these antibiotics are well understood. Important features promoting activity include dimerisation of the antibiotics, in the cases of vancomycin and chloroeremomycin (also known as A82846B and LY264826), and the presence of a membrane anchor (a C_{11} alkyl chain) in the case of teicoplanin.[2,3]

Recently there has been a rise in the number of cases of vancomycin-resistant enterococcal infections in hospitals.[4] In most cases this resistance is caused by the presence of peptidoglycan precursors terminating in –D-Ala-D-Lac rather than –D-Ala-D-Ala; so-called VanA and VanB resistance.[5] It has been demonstrated that the glycopeptides bind –D-Ala-D-Lac-terminating cell-wall analogues in a similar way[6] to the corresponding –D-Ala-D-Ala-terminating ones but considerably weaker.[6,7] A different form of vancomycin resistance seems to be specifically found in *E. gallinarum* and *E. casseliflavus*.[8–10] In these bacteria cell-wall precursors terminating in –D-Ala-D-Ser have been found.[11] Vancomycin shows reduced activity against these VanC resistant bacteria (MIC 2–32 μg ml^{-1}), whereas teicoplanin remains more or less active (MIC ⩽ 0.5 μg ml^{-1}).[12,13]

Although binding constants for *N*-acetyl-D-Ala-D-Ser towards vancomycin and teicoplanin have been determined,[14] no evidence is provided that these ligands bind in a similar way to the –D-Ala- and –D-Lac-terminating peptides. Therefore, we decided to investigate the molecular details of the binding of –D-Ser-terminating cell-wall analogues using di-*N*-acetyl-L-Lys-D-Ala-D-Ser (synthesised in our laboratory by solid phase peptide synthesis). The tripeptide was used as we believe that this tripeptide is a better model system for the cell-wall precursors than the dipeptide. Her we report our initial results on the binding of –D-Ser-terminating peptides to vancomycin, chloroeremomycin and teicoplanin.

UV difference spectrophotometry was used to determine the binding constants of the different antibiotics to di-*N*-acetyl-L-Lys-D-Ala-D-Ser.‡ The results are summarised in Table 1.

It is clear that vancomycin and chloroeremomycin show reduced binding to the –D-Ser-terminating tripeptide compared to binding the –D-Ala-terminating cell-wall analogue. Significantly, vancomycin binds more weakly to the tripeptide terminating in –D-Ser relative to that terminating in –D-Ala by a factor of 20; this difference is larger than that between the corresponding dipeptides (a factor of 7 difference).[14] The decrease is, however, not as dramatic as that observed for the –D-Lac-terminating cell-wall analogue. This may explain the increased activity of vancomycin against bacteria showing VanC resistance compared to bacteria with VanA or VanB resistance. Furthermore, the results indicate that the difference in activity of vancomycin and teicoplanin against VanC resistant bacteria may be caused by the difference in binding strength to the –D-Ser-terminating peptide, which is about one order of magnitude greater for teicoplanin. In general, the results indicate that the introduction of a hydroxymethyl group, present on the serine residue, compared to the methyl group on the alanine residue does not result in as large a change in binding energy as to the change of the amide group to an ester group (as found in lactate-terminating peptides).

In complexes with ligands terminating in –D-Ala[15] and –D-Lac[6] a large downfield shift occurs in NMR spectra of the signal corresponding to the amide proton of residue 2 (w_2), due to the formation of a hydrogen bond between the ligand carboxylate and the amide proton. In case of the –D-Ser-terminating ligand the chemical shift of w_2 of chloroeremomycin moves from δ 8.48 (free antibiotic) to *ca.* 11.2 in the fully bound complex.§ This clearly indicates the formation of hydrogen bond from the amide hydrogen to the carboxylate of the D-Ser residue.

To gain evidence that not only was the carboxylate anion of the –D-Ser tripeptide bound in the manner typical of a cell-wall analogue to a glycopeptide antibiotic, but also that the whole peptide was anchored in the usual way, two-dimensional NOESY and TOCSY spectra were obtained.¶ The experiments establish that the serine sidechain is buried against ring 4, that the alanine methyl group points towards proton 7d (see Fig. 1), that the lysine sidechain is situated over ring 7 of the antibiotic, and that the lysine backbone Ac group is adjacent to the *epi*-vancosamine sugar attached to residue 6 (Table 2). A schematic representation of the inferred binding of the serine tripeptide to the glycopeptide antibiotics is represented in Fig. 1.

In conclusion, we have demonstrated that glycopeptides bind –D-Ala-D-Ser-terminating cell-wall analogues, found in bacteria with VanC resistance, in a similar way as –D-Ala-D-Ala- and –D-Ala-D-Lac-terminating cell-wall analogues. The binding strength of the –D-serine-terminating tripeptides is lower than the corresponding alanine ones, but not as low as the –D-lactate-terminating peptides, which can account for the less severe nature of the resistance observed in bacteria exhibiting VanC resistance.

Table 1 Summary of binding constants (K_{ass}) to glycopeptide antibiotics with tripeptide cell-wall analogues, di-*N*-acetyl-L-Lys-D-Ala-X, determined by UV difference spectrophotometry

	K_{ass}/dm^3 mol^{-1}		
Antibiotic	X = D-Ala	X = D-Lac	X = D-Ser
Vancomycin	1.5×10^6 [a]	410[b]	$(7 \pm 2) \times 10^4$
Chloroeremomycin	1.3×10^6 [c]	245,[d] 1.6×10^3 [b]	$(8 \pm 1) \times 10^4$
Teicoplanin	1.6×10^6 [e]	n.d.[f]	$(5 \pm 1) \times 10^5$

[a] Ref. 17. [b] Ref. 7. [c] Ref. 16. [d] Ref. 6. [e] Ref. 18. [f] n.d. = not determined.

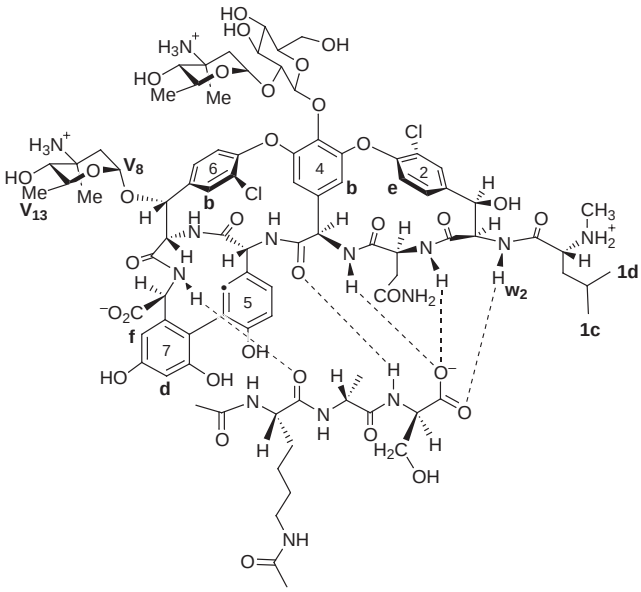

Fig. 1 Exploded view of the binding of di-*N*-acetyl-L-Lys-D-Ala-D-Ser to chloroeremomycin. Dashed lines indicate hydrogen bonds.

Table 2 Observed NOEs between di-*N*-acetyl-L-Lys-D-Ala-D-Ser and chloroeremomycin

Assignment	δ (ppm)	Observed NOEs
D-Ser-α	4.33, 4.45[a]	1c, d
D-Ser-β	2.53, 2.54[a]	2e, 4b
	3.38, 3.65[a]	2e
D-Ala-α	4.84	6b
D-Ala-β	1.15	7d
Lys-α-Ac	2.06	6b, V_8, V_{13}
Lys-β	1.66	7f
Lys-γ	1.48	7f

[a] Two chemical shifts observed due to the different environments in each half of the asymmetric antibiotic dimer.

We thank the Dutch Technology Foundation STW (A. M. A. v. W.) and the EPSRC (T. S.) for financial support, Eli Lilly for the gift of chloroeremomycin, and Lepetit for the gift of teicoplanin.

Notes and References

† E-mail: dhw1@cam.ac.uk

‡ UV spectrophotometry was carried out on a UVIKON 940 dual beam spectrophotometer. Both the reference and sample cells contained 50 μM antibiotic in 0.1 mol dm^{-3} phosphate buffer (pH 4.5, 298 K). Aliquots of a ligand solution containing 50 μM antibiotic were added to the sample cell. The solution was stirred after each addition, and the absorbance at both *ca.* 240 and *ca.* 280 nm was measured repeatedly until stable. The data at *ca.* 240 nm were subtracted from those at *ca.* 280 nm and analysed as previously described (ref. 16).

§ The limiting chemical shift of w_2 for the vancomycin complex could not be determined due to low solubility of the complex.

¶ The spectra were obtained from samples containing chloroeremomycin (15 mmol dm^{-3}) and di-*N*-acetyl-L-Lys-D-Ala-D-Ser (15 mmol dm^{-3}) in D_2O and 10% D_2O–H_2O at 290 K (pH 4.5). The NOESY and TOCSY spectra were recorded on a Bruker DRX 500 spectrometer in phase-sensitive mode using Time Proportional Phase Increment (TPPI) to give quadrature detection in f_1. 2048 complex data points were recorded in f_2 and 512 real points in f_1 using mixing times of 100–150 ms. Zero filling was used to give a final transformed matrix of 2048 × 2048 real points.

1 M. Foldes, R. Munro, T. C. Sorrell, S. Shankar and M. Toohey, *J. Antimicrob. Chemother.*, 1983, **11**, 21.
2 D. H. Williams, *Nat. Prod. Rep.*, 1996, **13**, 469.
3 D. H. Williams, M. S. Searle, M. S. Westwell, J. P. Mackay, P. Groves and D. A. Beauregard, *Chemtracts*, 1994, **7**, 133.
4 H. C. Neu, *Science*, 1992, **257**, 1064.
5 C. T. Walsh, S. L. Fisher, I.-S. Park, M. Prahalad and Z. Wu, *Chem. Biol.*, 1996, **3**, 21.
6 R. J. Dancer, A. C. Try, G. J. Sharman and D. H. Williams, *Chem. Commun.*, 1996, 1445.
7 N. E. Allen, D. L. LeTourneau and J. N. Hobbs, *J. Antibiot.*, 1997, **50**, 677.
8 S. Dutka-Malen, C. Molinas, M. Arthur and P. Courvalin, *Gene*, 1992, **112**, 53.
9 F. Navarro and P. Courvalin, *Antimicrob. Agents Chemother.*, 1994, **38**, 1788.
10 R. Leclercq, S. Dutka-Malen, J. Duval and P. Courvalin, *Antimicrob. Agents Chemother.*, 1992, **36**, 2005.
11 P. E. Reynolds, H. A. Snaith, A. J. Maguire, S. Dutka-Malen and P. Courvalin, *Biochem. J.*, 1994, **301**, 5.
12 M. Arthur and P. Courvalin, *Antimicrob. Agents Chemother.*, 1993, **37**, 1563.
13 H. S. Gold and R. C. Moellering, *N. Engl. J. Med.*, 1996, **335**, 1445.
14 D. Billot-Klein, D. Blanot, L. Gutmann and J. v. Heijenoort, *Biochem. J.*, 1994, **304**, 1021.
15 P. Groves, M. S. Searle, M. S. Westwell and D. H. Williams, *Chem. Commun.*, 1994, 1519.
16 J. P. Mackay, U. Gerhard, D. A. Beauregard, R. A. Maplestone and D. H. Williams, *J. Am. Chem. Soc.*, 1994, **116**, 4573.
17 M. Nieto and H. R. Perkins, *Biochem. J.*, 1971, **123**, 789.
18 A. Malabarba, A. Trani, G. Tarzia, P. Ferrari, R. Pallanza and M. Berti, *J. Med. Chem.*, 1989, **32**, 783.

Received in Liverpool, UK, 4th February 1998; 8/01030G

Iron(II)-mediated fragmentation of unsaturated hydroperoxy acetals: a rapid synthetic route to 13-membered macrolides

Kevin J. McCullough,*[a]† Yuji Motomura,[b] Araki Masuyama[b] and Masatomo Nojima*[b]

[a] *Department of Chemistry, Heriot-Watt University, Edinburgh, UK EH14 4AS*
[b] *Department of Materials Chemistry, Faculty of Engineering, Osaka University, Suita, Osaka 565-0871, Japan*

Treatment of (1-hydroperoxy)cyclohexyloxyethyl acrylate with either iron(II) sulfate or iron(II) sulfate/copper(II) chloride affords novel 13-membered macrolides *via* tandem radical scission-cyclisation reactions.

The development of synthetic strategies to macrocyclic compounds has attracted considerable attention because many of them are naturally occurring and several possess important biological properties.[1,2] In this respect, intramolecular radical addition to α,β-unsaturated ketones has been found to provide convenient access to a variety of macrocycles.[3] This method is generally based on the intramolecular cyclisation of the long-chain unsaturated radicals generated by the reaction of the corresponding iodo enones and their homologues with tributyltin hydride.[4] We report herein that the iron(II)-mediated fragmentation of the readily prepared 1-(hydroperoxy)-cycloalkyloxyethyl acrylates provides an alternative approach to the synthesis of novel macrolides.[5,6]

The key to our approach is the ease of preparation of the desired intermediate unsaturated hydroperoxy acetals **4**. Thus, treatment of a solution of vinyl ether **1** and unsaturated alcohol **3** (3 equiv.) in CH_2Cl_2 with ozone (1 equiv.) at −70 °C resulted in the selective ozonolysis of the electron rich vinyl ether **1** to give carbonyl oxide **2** which was subsequently captured by **3** affording the corresponding hydroperoxide **4** in moderate yield (**3a**, 27%; **3b**, 40%) (Scheme 1).[7] Subsequent treatment of a solution of the hydroperoxide **4a** in MeCN with a solution of iron(II) sulfate (1 equiv.) and copper(II) chloride (3 equiv.) in water at room temperature gave the macrolide **8a** (49%) and the acyclic diketone **9a** (17%) (Scheme 2).‡ Compound **8a** was shown to be the structurally novel 13-membered bislactone by X-ray crystallographic analysis (Fig. 1).§ From hydroperoxide **3b**, the corresponding chloro-substituted macrolide **8b** was obtained in 35% yield, along with the unidentified acyclic products.¶

These results indicate that the acyclic radical **6**, generated by sequential fragmentation of the O–O bond to give oxy radical **5** followed by β-scission of the cyclohexylidene ring, had undergone a very efficient intramolecular cyclisation to give **7**, which in turn reacted with copper(II) chloride to provide the chlorinated macrolide **8**.[8]

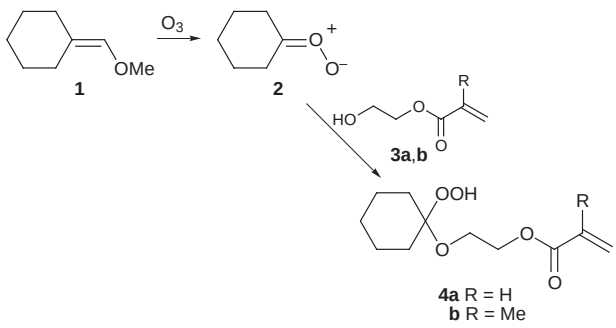

Scheme 1

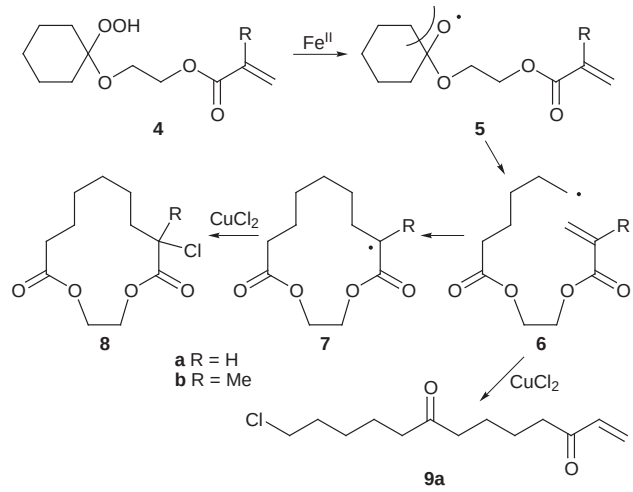

Scheme 2

In the absence of copper(II) chloride, the reaction of the hydroperoxide **4a** with iron(II) sulfate (2 equiv.) yielded three new crystalline products: the monomeric bislactone **10a** (18%) and two dimeric isomers **11a** (Scheme 3). X-Ray crystallographic analysis of the higher melting dimer (mp 168 °C; 25%) demonstrated unambiguously that this was the *meso*-isomer (Fig. 2).‖ Thus, the other dimeric isomer **11a** (mp 140.5–141.5 °C; 25%) was assigned as the *dl* form. From the hydroperoxide **4b**, the monocyclic macrolide **10b** was obtained in 25% yield along with unidentified acyclic products. Since the corresponding dimeric compounds were not observed in significant quantities, it appears that the sterically more hindered radical **7b** does not undergo dimerisation as readily as **7a**.

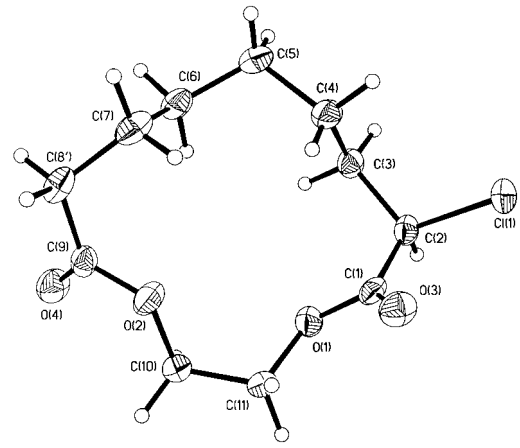

Fig. 1 The molecular structure of macrolide **8a** as determined by X-ray crystallography (ORTEP, 50% probability ellipsoids for non-hydrogen atoms) (ref. 10)

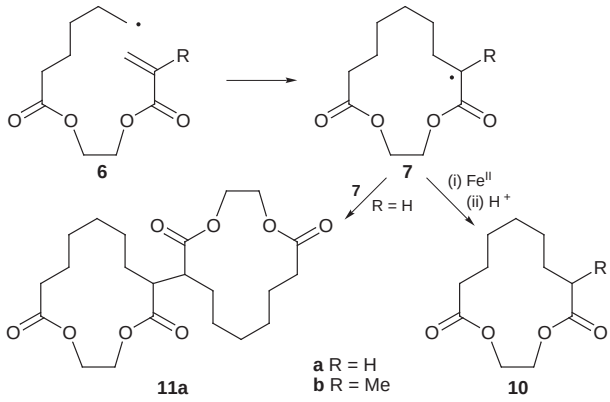

Scheme 3

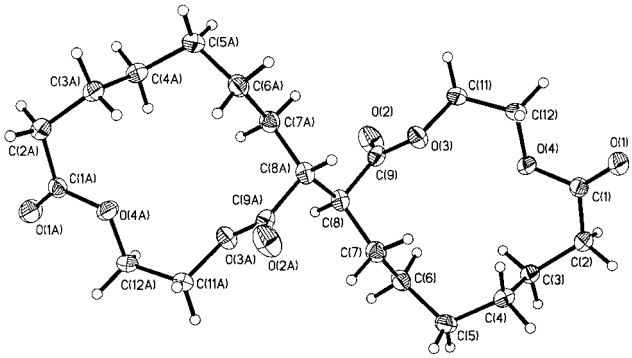

Fig. 2 The molecular structure of the dimeric macrolide **11a** as determined by X-ray crystallography (ORTEP, 50% probability ellipsoids for non-hydrogen atoms) (ref. 10)

The iron(II) catalysed decomposition of the methyl-substituted hydroperoxide **12** results in the formation of the monomeric chloromacrolide **15** as the sole isolable product (54%, a mixture of two isomers in the ratio *ca*. 2 : 1). Thus, intermediate **13** had undergone a selective β-scission of the cyclohexylidene ring *via* the more highly substituted radical **14** as outlined in Scheme 4. Similar selectivity has been observed previously in the thermal rearrangements of α-substituted 1,2,4-trioxanes.[9]

In summary, the readily available unsaturated hydroperoxy acetals such as **4** offer considerable potential as precursors of novel macrolides. The fragmentation-cyclisation reactions take place under relatively mild conditions and do not require high

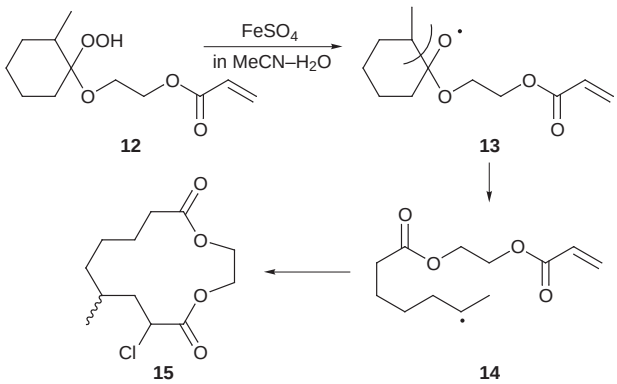

Scheme 4

dilution techniques (0.01–0.05 M). Moreover, the mode of termination can be controlled by the judicious choice of reaction conditions.

This work was supported in part by a Grant-in Aid for Scientific Research on Priority Areas (09270212) from the Ministry of Education, Science, Culture and Sports of Japan. We thank the British Council (Tokyo) for the award of travel grant to K. J. McC., M. N. and A. M.

Notes and References

† E-mail: k.j.mccullough@hw.ac.uk

‡ All new compounds gave satisfactory microanalytical and spectroscopic data.

§ *Crystal data* for **8a**: $C_{11}H_{17}ClO_4$, M = 248.70, colourless needles, monoclinic, space group $P2_1/c$ (No. 14), a = 15.1404 (12), b = 5.0426 (4), c = 16.1490 (11) Å, β = 100.550 (5)°, U = 1212.12 (2) Å^3, Z = 4, D_c = 1.363 g cm^{-3}, $F(000)$ = 528, μ(Mo-Kα) = 0.312 cm^{-1}. The intensity data were collected on a Siemens P4 diffractometer at 160 (2) K using graphite monochromated Mo-Kα radiation (λ = 0.710693 Å). The structure was solved by direct methods and refined by full-matrix least-squares methods on F^2 using anisotropic temperature factors for the non-hydrogen atoms (SHELXTL[10]). At convergence, the discrepancy indices R_1 and wR_2 were 0.032 [for 1942 data with $F_o > 4\sigma(F_o)$] and 0.0878 (all 2111 unique data) respectively. The final difference Fourier map contained no feature greater than ±0.31 e Å^{-3}.

¶ Since the separation of **8b** from other acyclic products was difficult, the reaction mixture was ozonised further to break down the latter. Thus, **8b** could be cleanly isolated by column chromatography on silica gel.

‖ *Crystal data* for **11a** (higher mp dimer): $C_{22}H_{34}O_8$, M = 426.49, colourless prisms, triclinic, space group $P\bar{1}$ (No. 2), a = 5.0600 (10), b = 8.512 (2), c = 13.090 (2) Å, α = 88.800 (10), β = 83.78 (2), γ = 77.010 (10)°, U = 546.1 (2) Å^3, Z = 1 (molecule on an inversion centre), T = 160(2) K, D_c = 1.297 g cm^{-3}, $F(000)$ = 230, μ(Mo-Kα) = 0.098 cm^{-1}. The final discrepancy indices R_1 and wR_2 were 0.0341 [for 1595 data with $F_o > 4\sigma(F_o)$] and 0.0883 (all 1907 unique data) respectively. The final difference Fourier map contained no feature greater than ±0.20 e Å^{-3}. CCDC 182/842.

1 K. C. Nicolaou, *Tetrahedron*, 1977, **33**, 683; C. J. Roxburgh, *Tetrahedron*, 1995, **51**, 9676.
2 For some recent examples see: M. P. Doyle, C. S. Peterson, M. N. Protopopova, A. B. Marnett, D. L. Parker, Jr., D. G. Ene and V. Lynch, *J. Am. Chem. Soc.*, 1997, **119**, 8826; D. Meng, P. Bertinato, A. Balog, D.-S. Su, T. Kamenecka, E. J. Sorense and S. J. Danishefski, *J. Am. Chem. Soc.*, 1997, **119**, 10 073; A. B. Smith, III and G. R. Ott, *J. Am. Chem. Soc.*, 1996, **118**, 13 095.
3 C. Thebtaranonth and Y. Thebtaranonth, in *Cyclization Reactions*, CRC Press, Boca Raton, 1994.
4 N. A. Porter, B. Lacher, V. H.-T. Chang and D. R. Magnin, *J. Am. Chem. Soc.*, 1989, **111**, 8309; S. A. Hitchock and G. Pattenden, *Tetrahedron Lett.*, 1990, **31**, 3641; J. E. Baldwin, R. M. Adlington, M. B. Mitchell and J. Robertson, *Tetrahedron*, 1991, **47**, 5901; I. Ryu, K. Nagahara, S. Tsunoi and N. Sonoda, *Synlett*, 1994, 643; A. L. J. Beckwith, K. Drok, B. Maillard,M. Degueol-Castaing and A. Philippon, *Chem. Commun.*, 1997, 499.
5 For the metal ion promoted ring-opening of α-siloxy-, α-hydroxy- and α-alkoxy-substituted cycloalkyl hydroperoxides, see: I. Saito, R. Nagata, K. Yuba and T. Matuura, *Tetrahedrol Lett.*, 1983 **24**, 4439 and references cited therein.
6 S. L. Schreiber, B. Hulin and W.-F. Liew, *Tetrahedron*, 1986, **42**, 2945 and references cited therein.
7 Y. Ushigoe, Y. Torao, A. Masuyama and M. Nojima, *J. Org. Chem.*, 1997, **62**, 4949.
8 J. K. Kochi, in *Free Radicals*, ed. J. K. Kochi, Wiley, New York, 1973, vol. 1, ch. 11.
9 A. Haq, B. Kerr and K. J. McCullough, *J. Chem. Soc., Chem. Commun.*, 1993, 1076.
10 SHELXTL/PC (Ver. 5.03), G. M. Sheldrick, Siemens Analytical X-ray Instruments Inc., Madison, WI, USA.

Received in Liverpool, UK, 4th March 1998; 8/01802B

Merrifield chemistry on electropolymers: protection/(photo)deprotection of amine functions

Sandrine Morlat-Therias,[a] Mario S. Passos,[a,b] Saad K. Ibrahim,[a] Thierry Le Gall,[a] M. Arlete Queiros[b] and Christopher J. Pickett*[a]†

[a] *The Nitrogen Fixation Laboratory, John Innes Centre, Norwich Research Park, Norwich, UK NR4 7UH*
[b] *Departamento de Química, Escola de Ciências, Universidade do Minho, Campus de Gualtar, 4700 Braga, Portugal*

Amine protection/(photo)deprotection strategies allow functionalisation of electrode bound poly(pyrrole) films *via* reactions with active esters.

Polymers with substituent groups covalently anchored along the conjugated backbone of poly(pyrrole) or poly(thiophene) constitute a class of hybrid materials possessing potentially interactive electrical and molecular domains. They are consequently receiving considerable attention for sensing, electrocatalysis and other applications.[1–3] For example, a change in the redox response of an oligonucleotide functionalised pyrrole occurs upon recognition (binding) of a strand of complementary DNA.[3] The range of materials that can be made, and also aspects of their microfabrication, have been somewhat circumscribed by the need to synthesise and electropolymerise the appropriately substituted pyrrole or thiophene *monomer*.[4] This is problematic in cases where the desired substituent group is sensitive to the oxidative conditions of electropolymerisation or where the substituent is an inhibitor of this process. We have shown that one way in which such problems can be overcome is by *post-polymerisational modification* of pre-formed electropolymers which possess active ester groups.[4] The desired substituent groups are covalently attached to the polymer by amide or ester bond formation, and this general approach has been successfully adapted by others.[5] The converse derivatisation, reaction of *amine functionalised electropolymers* with active esters, could provide a complementary strategy for electropolymer functionalisation. This has the attraction that well-established protocols for solid-phase amine chemistry that have been developed on Merrifield resins might be adapted to electropolymers.[6] Herein we describe some first steps in this direction (Scheme 1).

Anodic oxidation of 3-pyrrol-1-ylpropylammonium cation **AH**$^+$ (Pt or vitreous carbon, 0.2 M $[NBu_4][BF_4]$–MeCN) gives the electroactive polymeric film poly(**AH**$^+$). The electropolymer can be (reversibly) deprotonated to give the free amine form, poly(**A**) but is otherwise quite unreactive: pentafluorophenolate active esters fail to modify bulk films of poly(**A**). Penetration of the film by the reagent is presumably prevented by close-packing of the polymer chains.

The problem is overcome by generating amine groups within the polymer from *N*-protected precursors. Fluoren-9-ylmethoxycarbonyl (Fmoc) and 6-nitroveratryloxycarbonyl (Nvoc) derivatised monomers **B** and **C** were synthesised from **A** (Scheme 1). Both of the *N*-protected monomers undergo facile electropolymerisation, as typified by the potentiodynamic growth of poly(**C**) (Fig. 1). Base deprotection of poly(**B**) or photodeprotection of poly(**C**) gives poly(**A**) (Scheme 1), as illustrated by the FTIR spectra shown in Fig. 2.

In contrast with the inertness of poly(**A**) produced directly by electrooxidation of **A**, the amino polymer generated by *either* deprotection route readily forms amide derivatives upon reaction with pentafluorophenolate active esters. For example, diffuse reflectance FTIR spectroscopy shows that poly(**A**) formed by photolysis reacts with Fmoc-glycine pentafluoro-

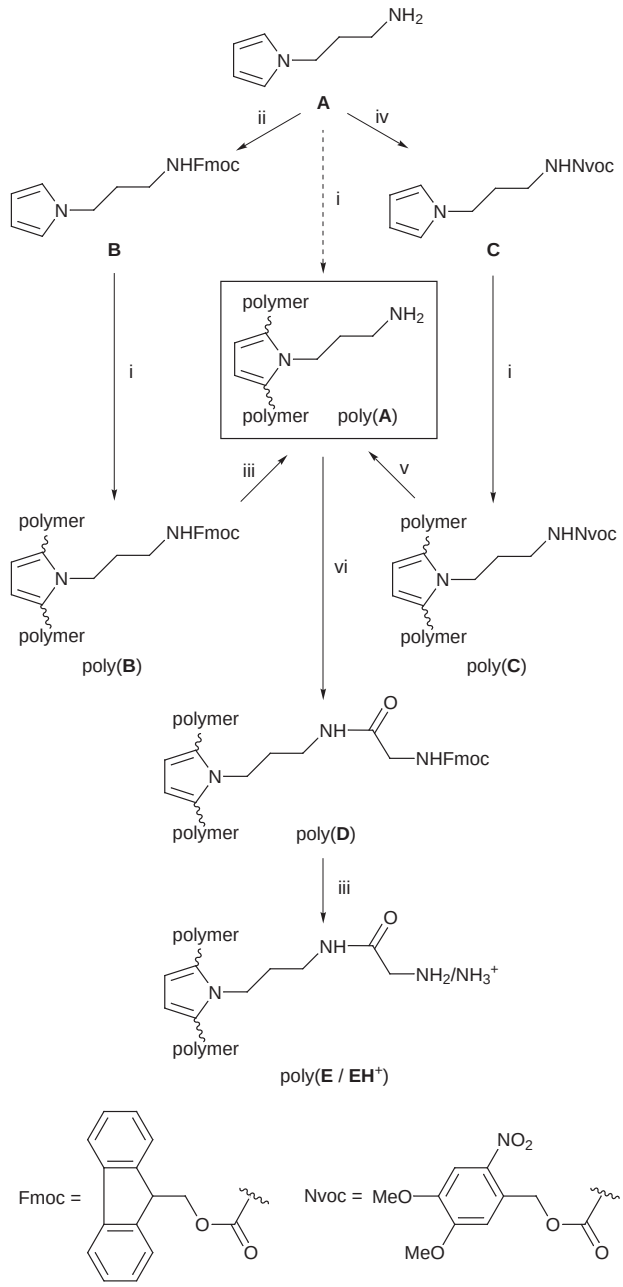

Scheme 1 *Reagents and conditions*: i, MeCN, 0.2 M $[NBu_4][BF_4]$, 5 mM **AH**$^+$; ii, FmocCl, Na_2CO_3, dioxane–water (1 : 1), 12 h, 22 °C; iii, 30% piperidine–MeCN, 1 h, room temp.; iv, NvocCl, Na_2CO_3, dioxane–water (1 : 1), 12 h, 22 °C; v, irradiation of 1 μm film for 4 h in 1% $HBF_4 \cdot 2Et_2O$–MeCN using 30 W mercury UV/pyrex filter transmitting through 1 cm of solvent under nitrogen; vi, 25 mM Fmoc-glycine pentafluorophenolate ester in 12% Et_3N–MeCN, room temp., 4 h

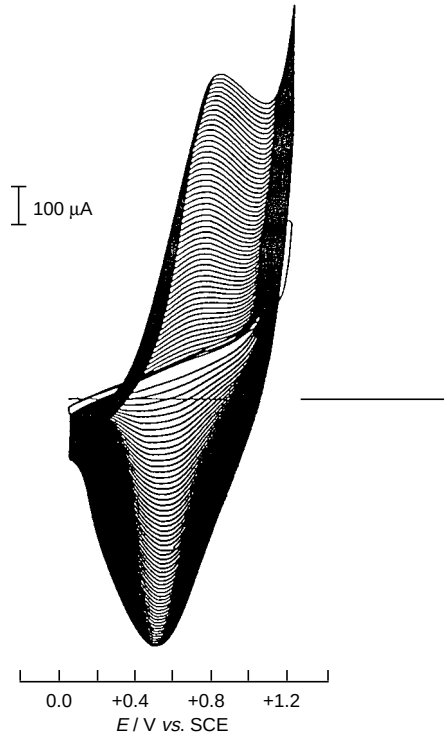

Fig. 1 Potentiodynamic growth of the Nvoc protected polymer, poly (**C**). The polymer was grown on a polished Pt disc electrode of radius 0.32 cm by cycling the potential between 0.0 and 1.20 V *vs.* SCE at 50 m V s^{-1} in 0.2 M $[NBu_4][BF_4]$–MeCN–5 mM **C**.

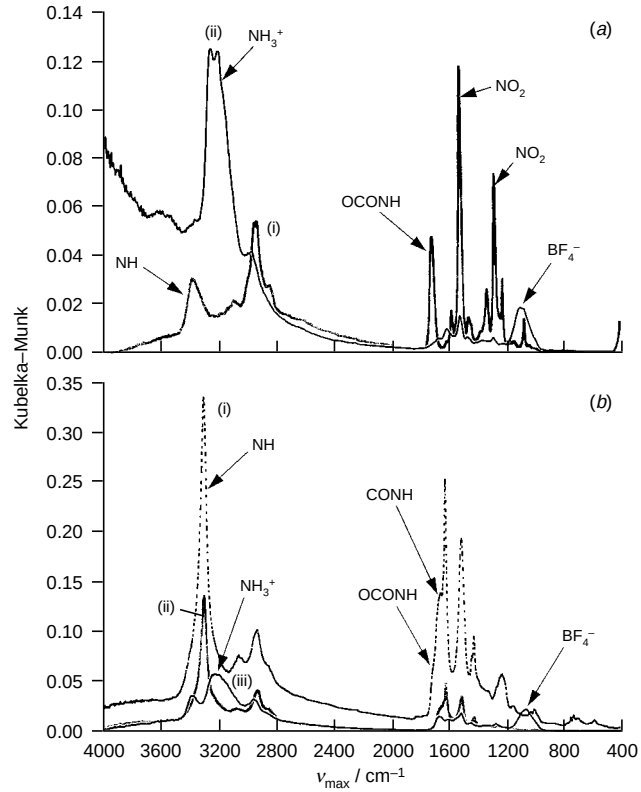

Fig. 2 (*a*) Diffuse reflectance FTIR spectra of (i) the Nvoc protected poly(**C**) and (ii) deprotected alkylammonium poly(**AH**$^+$) produced by photolysis of poly(**C**). (*b*) Diffuse reflectance FTIR spectra of (i) the Fmoc-glycine derivative, poly(**D**), formed by treating the poly(**A**) modified electrode with Fmoc-glycine pentafluorophenolate ester, (ii) the deprotected poly(**D**), which gives the amine film poly(**E**) by removal of Fmoc with piperidine, and (iii) the alkylammonium film poly(**EH**$^+$) formed by protonation of poly(**E**) (1% v/v $HBF_4 \cdot 2Et_2O$ in MeCN). Modifying the groups within the polymer changes the diffuse reflectivity characteristics of the film and thus relative band intensity *between* spectra.

phenolate (Fig. 2). Moreover, this Fmoc-glycine-derivatised film, poly(**D**), can in turn be chemically deprotected with piperidine to unmask the fresh terminal amine groups of poly(**E**).

The difference in polymer reactivity clearly lies with access to the amine groups and is explained by deprotection affording molecular cavities around these groups and/or the relatively bulky Fmoc and Nvoc groups producing a more open polymer network.

Although the deprotection pathways lead to a decrease in conductivity, as judged from the redox response of the polymer backbone, optimisation of the deprotection conditions and/or the use of protected 3-substituted pyrroles may be expected to lead to enhanced conductivity.

In conclusion, we have shown that an amine-functionalised electropolymer based on an N-substituted poly(pyrrole) can be made either directly or by chemical or photochemical deprotection routes. The deprotection routes afford polymers which react with active esters to form amides, whereas the directly synthesised amino polymer is unreactive under the same conditions. Finally, we note that (i) the chemical and photolytic deprotection strategies offer a means of *patterning* electropolymers with arrays possessing differing molecular functions,[7] (ii) 'cavity formation' by amine deprotection/photodeprotection might provide a means for molecular *imprinting* of an electropolymer,[8] and (iii) successive protection/deprotection/peptide bond formation cycles (Merrifield chemistry) can be performed on electropolymers.

We thank the Royal Society for providing a Fellowship (to S. M.-T.), the John Innes Foundation for providing a Studentship (to T. Le G.), the 'Comissao INVOTAN' for providing travel and subsistence funds (to M. P.) and the BBSRC for supporting this work.

Notes and References

† E-mail: chris.pickett@bbsrc.ac.uk

1 T. Livache, A. Roget, E. Dejean, C. Barthet, G. Bidan and R. Téoule, *Nucleic Acids Res.*, 1994, **22**, 2915.
2 S. K. Ibrahim, C. J. Pickett and C. Sudbrake, *J. Electroanal. Chem.*, 1995, **387**, 139.
3 H. Korri-Youssoufi, F. Garnier, P. Srivastava, P. Godillot and A. Yassar, *J. Am. Chem. Soc.*, 1997, **119**, 7388.
4 C. J. Pickett and K. S. Ryder, *J. Chem. Soc., Dalton Trans.*, 1994, 2181; M. S. Passos, M. A. Queiros, T. Le Gall, S. K. Ibrahim and C. J. Pickett, *J. Electroanal. Chem.*, 1997, **435**, 189.
5 K. S. Ryder, D. G. Morris and J. M. Cooper, *J. Chem. Soc., Chem. Commun.*, 1995, 1471; H. Korri-Youssoufi, P. Godillot, P. Srivastava, A. El Kassmi and F. Garnier, *Synth. Met.*, 1996, **83**, 117; H. Korri-Youssoufi, P. Godillot, P. Srivastava, A. El Kassmi and F. Garnier, *Synth. Met.*, 1997, **84**, 169.
6 M. C. Pirrung, *Chem. Rev.*, 1997, **97**, 473.
7 T. Livache, B. Fouque, A. Roget, J. Marchand, G. Bidan, R. Téoule and G. Mathis, *Anal. Biochem.*, 1998, **255**, 188.
8 G. Wulff, *Angew. Chem., Int. Ed. Engl.*, 1995, **34**, 1812.

Received in Cambridge, UK, 24th March 1998; 8/02292E

One pot synthesis of mono- or bi-cyclic phosphiranes and phosphirenes

Maria Zablocka,[b] Yannick Miquel,[a] Alain Igau,[a] Jean-Pierre Majoral*[a]† and Aleksandra Skowronska*[b]

[a] *Laboratoire de Chimie de Coordination du CNRS, 205 route de Narbonne, 31077 Toulouse Cedex, France*
[b] *Polish Academy of Sciences, Centre of Molecular and Macromolecular Studies, Sienkiewicza 112, 90-363 Lodz, Poland*

Treatment of phospholene oxide 1, vinylphosphine oxide 11 or alkynylphosphine oxide 14 with [Cp_2Zr] 2 followed by addition of a chlorophosphine leads to various phosphiranes and phosphirenes.

The heterocyclic chemistry of phosphorus is underdeveloped in comparison with its oxygen, nitrogen and sulfur counterparts in spite of the fact that a number of phosphorus rings appear to be useful reagents and ligands. Indeed, a recent review covers the rich and versatile chemistry of three-membered carbon–phosphorus heterocycles.[1] Several routes for the preparation of these derivatives, namely phosphiranes, phosphirenes, diphosphiranes, diphosphirenes and related species, have been reported. In contrast only a few syntheses of fused ring systems incorporating at least one phosphirane ring and another phosphorus containing heterocycle are known.

In the course of our studies devoted to the use of zirconium derivatives as tools in organic, organometallic and main group element chemistry,[2] we developed a new method for the preparation of fused ring systems involving phospholene oxide **1**, zirconocene [Cp_2Zr] **2** and dichlorophosphines $RPCl_2$ **3**. Such a methodology can be extended to the synthesis of various substituted phosphiranes and phosphirenes. We report here the general one pot preparation of some of these new compounds.

Treatment of phospholene oxide **1** with [Cp_2Zr] **2**[3]—prepared *via* the reaction of Cp_2ZrCl_2 with 2 equiv. of Bu^nLi at −78 °C in THF—leads to the formation of the zirconacyclopropaphospholane oxide **4** (Scheme 1). The ^{31}P NMR spectrum of **4** exhibits a resonance at δ 81.5 (compared with **1**, δ = 62.0). Such a significant deshielding effect suggests the participation of the phosphoryl group to the stabilization of the resulting zirconium complex **4**.[4] This assumption is corroborated by IR spectroscopy: the ν(PO) band is shifted from 1193 (**1**) to 1162 cm^{-1} (**4**).[5] Compound **4** is further characterized by ^1H NMR as well as by ^{13}C NMR spectroscopy, which shows, for example, the expected deshielded signals for the carbon atoms directly linked to zirconium.[6] Addition of phenyl(dichloro)phosphine to **4** in THF at −78 °C proceeds with removal of Cp_2ZrCl_2 and formation of the phosphiranophospholane oxide **5a** [δ_P 60.6 and −177.4 (d, J_{PP} 8.3 Hz)]. The shielded signal at δ −177.4 is typical for a phosphirane structure,[1,7] while the resonance at δ 60.6 fits well with the phospholane part of **5a**. Such a bicyclic structure is corroborated by ^{13}C NMR analysis.[6]

A similar exchange reaction involving **4** and either methyl- or *tert*-butyl-(dichloro)phosphine affords the fused bicyclic systems **5b** or **5c**, respectively [**5b**: δ_P 63.6 and −191.1 (d, J_{PP} 7.1 Hz); **5c**: δ_P 55.0 and −174.8 (d, J_{PP} 30.1 Hz)] (Scheme 1).

It should be emphasized that, in marked contrast to the behaviour of **1** towards **2**, the phospholene **6** does not give the

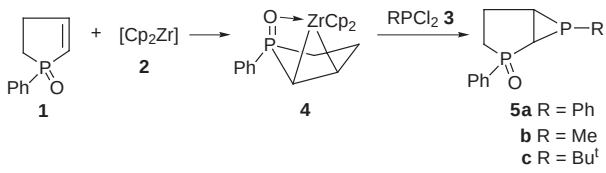

Scheme 1

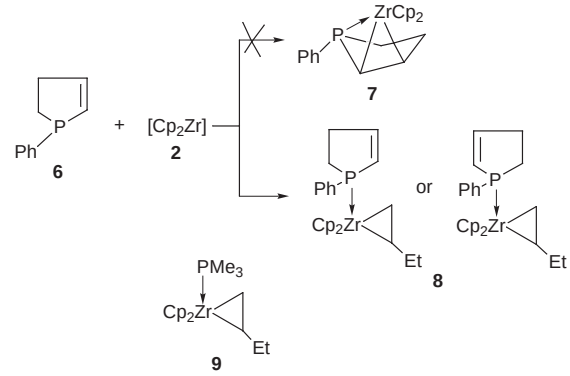

Scheme 2

expected zirconacyclopropaphospholane derivative **7**, but instead the zirconocene complex **8** (Scheme 2) is characterized. The structure of **8** can be unambiguously established by NMR analysis.[6] Investigation of the [Cp_2ZrCl_2 + 2Bu^nLi] reaction has been found to give $Cp_2Zr(nBu)_2$ at −78 °C, which then decomposes to give $Cp_2Zr(CH_2{=}CHEt)$ (the effective source of **2**) identified as its PMe_3 complex **9**.[8] Therefore compound **6** plays the role of PMe_3 and the olefinic part of **6** is not involved in the reaction. Addition of phenyl(dichloro)phosphine to **8** gives **6** and the products of the reaction of zirconocene **2** with phenyl(dichloro)phosphine, *i.e.* $(PhP)_4$ and $(PhP)_5$.

It should also be noted that the reaction of the phospholene sulfide **10** with **2** proceeds quite differently: only desulfurization occurs with the formation of **6**[9] (Scheme 3).

This demonstrates clearly, for the first time, the key role played by a phosphoryl group for the stabilization of intermediates and for the orientation of reactions involving phosphorus derivatives and zirconium species. Up to now only the dramatic influence of the phosphorus lone pair of phosphines has been pointed out.[10]

The same remarkable behaviour is found when the linear vinylphosphine oxide **11** is treated with **2** and then with phenyl(dichloro)phosphine. The reaction proceeds *via* the formation of the zirconium complex **12** (δ_P 47)[4] to give the phosphirane **13** [δ_P 31.3 and −178.3 (d, J_{PP} 30 Hz)][6] (Scheme 4). Such a reaction is not limited to olefinic systems. Indeed addition of the acetylenic phosphine oxide **14** to a THF solution of **2** at −78 °C leads to the fully characterized zirconacyclopropene species **15**.[4,6] Further addition of phenyl- or methyl-(dichloro)phosphine to **15** gives new phosphirene derivatives **16a** or **16b**, respectively (Scheme 4). No traces of phosphirane or phosphirene is detected when the same reactions are conducted with the corresponding linear vinyl or acetylenic phosphines instead of the phosphine oxides **11** or **14**.

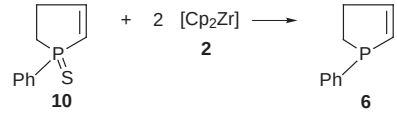

Scheme 3

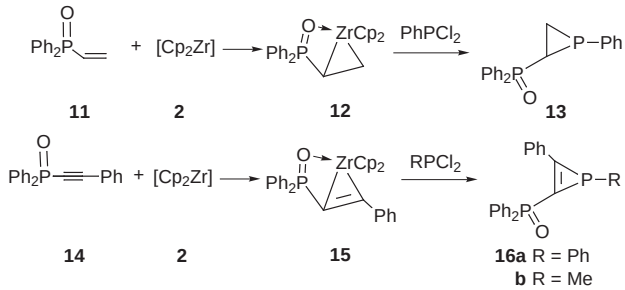

Scheme 4

Mechanistic studies and extension of these reactions to other substrates are underway.

Thanks are due to CNRS (France) and KBN (Poland) for financial support.

Notes and References

† E-mail: majoral@lcctoul.lcc-toulouse.fr

1 F. Mathey, *Chem. Rev.*, 1990, **90**, 997.
2 N. Cénac, A. Chrostowska, J.-M. Sotiropoulos, B. Donnadieu, A. Igau, G. Pfister-Guillouzo and J.-P. Majoral, *Organometallics* 1997, **16**, 4551; L. Dupuis, N. Pirio, P. Meunier, A. Igau, B. Donnadieu and J.-P. Majoral, *Angew. Chem., Int. Ed. Engl.*, 1997, **36**, 987; M. Zablocka, A. Igau, B. Donnadieu, J.-P. Majoral and A. Skowronska, *Chem. Commun.*, 1997, 1239 and references cited therein.
3 For recent reviews on zirconocene, see for example: Y. Hanzawa, H. Ito and T. Taguchi, *Synlett*, 1995, 299; A. Ohff, S. Pulst, C. Lefeber, N. Peulecke, P. Arndt, V. V. Burkalov and U. Rosenthal, *Synlett*, 1996, 111 references cited therein.
4 A dimeric form cannot be totally ruled out for **4**, **12** and **15**.
5 M. Zablocka, A. Igau, J.-P. Majoral and K. M. Pietrusiewicz, *Organometallics*, 1993, **12**, 603.
6 Selected data for **4**: δ_C($CDCl_3$) 41.0 (d, J_{PC} 96.0, PCHZr), 58.1 (d, J_{PC} 13.5, CHZr), 33.2 (d, J_{PC} 19.2, CH_2), 29.0 (d, J_{PC} 73.6, PCH_2). For **5a**: δ_C 26.3 [dd, $J_{P(O)C}$ 16.5, J_{PC} 38.0, P(O)CHP], 24.7 (d, J_{PC} 51.0, CHP), 24.3 [d, J_{PC} 71.8, P(O)CH_2], 22.5 (d, J_{PC} 7.5, CH_2). For **8**: δ_C 21.6 (s, CH_3), 22.4 (d, J_{PC} 12.2, ZrCH_2), 35.6 (s, ZrCHCH_2), 39.4 (d, J_{PC} 18.2, PCH_2CH_2), 40.0 (d, J_{PC} 18.7, PCH_2), 41.8 (d, J_{PC} 3.3, ZrCH). For **13**: δ_C 28.2 (dd, J_{PC} 29.0, J_{PC} = 13.0, CH), 25.5 (dd, J_{PC} 13.5, J_{PC} 2.9, CH_2). For **15**: δ_C 153.5 [d, $^1J_{PC}$ 59.7, P(O)CZr], 148.3 (d, J_{PC} 6.1, ZrCPh). For **16a**: δ_C 145.0 [dd, J_{PC} 53.2, $J_{P(O)C}$ 10.2, P(O)C=], 139.6 (dd, J_{PC} 62.6, $J_{P(O)C}$ 2.7, PCPh).
7 A. Mahieu, Y. Miquel, A. Igau, B. Donnadieu and J.-P. Majoral, *Organometallics*, 1997, **16**, 3086.
8 Compound **9** was isolated as two isomers (PMe_3/Et *cis* or *trans*) (refs. 11, 12). According to NMR spectroscopy only the *trans* isomer for **8** was formed. However, these data do not allow the determination of the position of the C=C π-system in the phospholane ring with respect to the zirconacyclopropane fragment.
9 Full desulfurisation occurs when 1 equiv. of **1b** is treated with 2 equiv. of **2**.
10 See for example: M. Zablocka, F. Boutonnet, A. Igau, F. Dahan, J.-P. Majoral and K. M. Pietrusiewicz, *Angew. Chem., Int. Ed. Engl.*, 1993, **32**, 1735; M. Zablocka, A. Igau, N. Cénac, B. Donnadieu, F. Dahan, J.-P. Majoral and K. M. Pietrusiewicz, *J. Am. Chem. Soc.*, 1995, **117**, 8083.
11 S. L. Buchwald, B. T. Watson and J. C. Huffman. *J. Am. Chem. Soc.*, 1987, **109**, 2544.
12 E. I. Negishi, S. J. Holmes, J. M. Tour, J. A. Miller, F. E. Cederbaum, D. R. Swanson and T. Takahashi, *J. Am. Chem. Soc.*, 1989, **111**, 3336; P. Binger, P. Müller, R. Benn, A. Rufinska, B. Gabor, C. Krüger and P. Betz, *Chem. Ber.*, 1989, **122**, 1035.

Received in Cambridge, UK, 19th March 1998; 8/02173B

Cuprophilicity, a still elusive concept: a theoretical analysis of the ligand-unsupported Cu^{I}–Cu^{I} interaction in two recently reported complexes

Josep-M. Poblet[a] and Marc Bénard*[b]†

[a] *Departament de Quimica, Universitat Rovira i Virgili, Pc. Imperial Tarraco 1, E-43005-Tarragona, Spain*
[b] *Laboratoire de Chimie Quantique, UMR 7551, CNRS et Université Louis Pasteur, 4 rue B. Pascal, F-67000 Strasbourg, France*

Density functional theory (DFT) calculations explain the short ligand-unsupported Cu^{I}–Cu^{I} contact recently reported for the $[CuL]^{+}[CuCl_2]^{-}$ complex [L = 1,1′-bis(2-pyridyl)octamethylferrocene] by a strong electrostatic attraction (−64 kcal mol^{-1}) between the two moieties and rule out the initially suggested metallophilic interaction, but cuprophilicity might account for the dimerization occurring in a family of trimetallic complexes.

Weak attraction between transition metal atoms with closed-shell electronic configuration was first evidenced by Schmidbaur *et al*. in the cases of intra- and intermolecular Au^{I}–Au^{I} contacts.[1] The term aurophilicity was coined to describe these interactions, but it soon became clear that similar aggregation processes could also involve metal atoms other than gold, such as Tl^{I} or Hg^{II}.[2] These closed-shell interactions in inorganic chemistry have been reviewed by Pyykkö.[2] The occurrence of analogous metallophilic[3] effects involving lighter metal atoms and more specifically Cu^{I} has been the subject of a long debate due to the intramolecular character of the reported interactions.[2,4] Recently, two examples of unsupported Cu^{I}–Cu^{I} contacts with metal–metal distances of 2.905 Å[5] and 2.810 Å[6] have been tentatively assigned to cuprophilic interactions. On the theoretical side, recent studies by Pyykkö *et al*. suggest that the stabilization of the $ClCuPH_3$ model dimer due to the metallophilic interaction between the Cu^{I} atoms does not exceed −1.5 kcal mol^{-1} when extrapolated to the best level of theory, and is associated with a rather long metal–metal distance of 3.143 Å.[7] The goal of this study was to investigate by means of DFT and extended Hückel calculations other possible origins for the unsupported Cu^{I}–Cu^{I} interactions in the two complexes for which cuprophilicity has been addressed.

Metallophilic interactions are not easy to characterize from quantum chemical calculations. Pyykkö *et al.*[2,3] have demonstrated that metallophilicity is due to attractive dispersion forces that should overcome the Pauli repulsion between the d^{10} or the d^{10} s^2 closed shells. For metals of the third transition row, the attractive forces are greatly enhanced by relativistic effects.[2,7] Since neither *ab initio* Hartree–Fock nor DFT calculations account for dispersion-type R^{-6} terms these levels of theory unavoidably predict repulsive behaviour between unsupported metallophilic fragments.[2,3] Conversely, if these methods are able to account for an attractive interaction, it should be clear that it is not of the metallophilic type.

This is the principle of the investigations performed on $[CuL]^{+}[CuCl_2]^{-}$ [L = 1,1′-bis(2-pyridyl)octamethylferrocene] **1** for which a cuprophilic interaction had been tentatively suggested to explain the short Cu^{I}–Cu^{I} contact (2.810 Å) observed between the two copper subsystems.[6] Complex **1** has been slightly modeled by replacing octamethylferrocene with ferrocene (**1′**) and by assuming perfect C_{2v} symmetry, which implies that the coordination axes of the anion and the cation are perpendicular (Fig. 1). We then carried out a full geometry optimization of **1′** by means of gradient-corrected DFT calculations.‡ Selected geometrical parameters obtained from the calculation are reported in the caption of Fig. 1 and compared to experiment. The observed environment of the copper atoms is reproduced by the calculation with great accuracy, including the Cu–Cu bond length (calc. 2.822 Å, exptl. 2.810 Å). The interaction energy between the two fragments is calculated to be −64.1 kcal mol^{-1}, after BSSE correction. The presence of a bonding interaction at this level of theory and its order of magnitude clearly show that the attraction between the $[CuL]^{+}$ and the $[CuCl_2]^{-}$ subunits should not be assigned to cuprophilicity. Since the interaction involves charged moieties, the bonding may instead be due to Coulombic forces. Mulliken population analyses, carried out either from the extended Hückel (EHT) or from the DFT orbitals, indicate that the charge transfer between the two moieties is negligible (Table 1). The negative charge in the $(CuCl_2)^{-}$ fragment is distributed between the chlorine atoms while the Cu atom remains either neutral (+0.04e, DFT), or significantly positive (+0,24e, EHT). Even though the point charge distributions in the cationic fragment is noticeably different for EHT and DFT (Table 1), the $(CuCl_2)^{-}/(CuL)^{+}$ electrostatic attraction computed from the point charge model are similar (62.0 kcal mol^{-1} with EHT, −67.9 kcal mol^{-1} with DFT) and practically reproduce the fragment interaction energy obtained from DFT calculations. Other models of space partitioning[8,9] applied to the DFT wave function, however, predict some charge transfer toward the $(CuL)^{+}$ moiety and the fragment electrostatic energies computed from those models are scaled accordingly (Table 1).

In order to obtain an estimate of the fragment/fragment Coulombic interaction independent of space partitioning, we relied on standard energy decomposition analysis[10,11] and computed the total energy starting from the wave functions computed for the $(CuCl_2)^{-}$ and $(CuL)^{+}$ fragments assumed isolated, but occupying their geometrical positions in the complex. The interaction energy is now −69.4 kcal mol^{-1}. The difference with respect to the value of −64.1 kcal mol^{-1} reported above corresponds to the fragment relaxation energy. The fragment interaction energy is made up of: (i) the Pauli

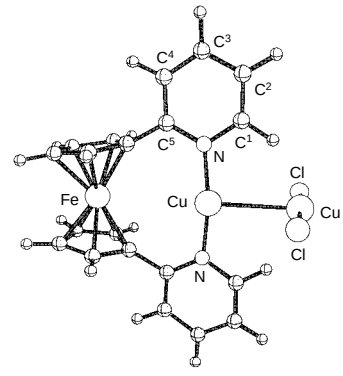

Fig. 1 Molecular structure of **1′** optimized from gradient corrected DFT calculations (C_{2v} symmetry assumed). Selected bond lengths (Å) and angles (°): Cu–Cu 2.822 (2.810); Cu–Cl 2.119 (2.095); Cu–N 1.895 (1.925); Cu···Fe 3.74; Fe-Ω 1.668 (Ω centroid of a Cp ring); N–Cu–Cu 95.0 (94.3); Cl–Cu–Cu 88.8 (89.1). Numbers in parentheses are the averaged experimental values.

Table 1 Point charge distributions (electrons) computed for **1′** using (i) the Mulliken space partitioning applied to the EHT and to the DFT wave functions, and (ii) the Hirshfeld[8] and the Voronoi[9] space partitionings, both applied to the DFT wave function. The electrostatic interaction energy between the two fragments is calculated from those point charges

Atoms	Mulliken (EHT)	Mulliken (DFT)	Hirshfeld (DFT)	Voronoi (DFT)
Fragment $(CuL)^+$:				
Cu	+0.032	+0.482	+0.247	+0.240
N	−0.336	−0.461	−0.086	−0.100
Cl + H1	+0.333	+0.352	+0.058	+0.148
C2 + H2	−0.037	+0.005	+0.034	+0.175
C3 + H3	+0.115	+0.034	+0.044	+0.052
C4 + H4	−0.038	+0.019	+0.023	−0.091
C5	+0.433	+0.178	+0.076	+0.020
Fe	−0.243	−0.012	+0.048	−0.036
Cp	+0.134	+0.119	+0.027	+0.060
Total $(CuL)^+$	+0.997	+0.962	+0.647	+0.732
Fragment $(CuCl_2)^-$:				
Cu	+0.239	+0.037	+0.111	+0.088
Cl	−0.618	−0.499	−0.379	−0.410
Total $(CuCl_2)^-$	−0.997	−0.961	−0.647	−0.732
Electrostatic interaction energy/kcal mol^{-1}				
	−62.0	−67.9	−28.9	−41.6

repulsion, +38.8 kcal mol^{-1}; (ii) the Coulombic attraction, −86.4 kcal mol^{-1}, and (iii) the energy associated with electron reorganization in the complex, which is also attractive and reaches −21.8 kcal mol^{-1}. This latter term includes the stabilization due to the mutual polarization of the two fragments which is a purely electrostatic effect that can be distinguished from charge transfer and orbital interaction.[11] This energy decomposition analysis stresses the importance of the Pauli repulsion which should not be exclusively assigned to the Cu^I–Cu^I contact, but also to the two short Cu···H1 distances (2.28 Å). It also proves, without assuming any space partitioning, the prominent influence of the Coulombic interaction.

Siemeling and colleagues[6] noted that a complex closely related to **1**, $[Cu(C_5H_3NMe_3\text{-}2,4,6)_2][CuCl_2]$ **2**,[12] does not display a similar Cu–Cu interaction. The structure of **2** is characterized by the stacking of planar $[Cu(C_5H_3NMe_3\text{-}2,4,6)_2]^+$ fragments separated by $(CuCl_2)^-$ moieties perpendicular to the N–Cu–N axis, but the Cu···Cu distance is now 3.61 Å.[12] This increase of the interfragment separation may be tentatively assigned to steric crowding induced by the presence of four Me substituents. However, providing a final answer to this problem will require the geometry optimization of models of **2**, with and without the Me substituents.

The case of $[Cu_3L'_3]_2$ {L′ = 2-[3(5)-pyrazolyl]pyridine} **3**[5] and related dimers of Cu^I_3 and Ag^I_3 complexes[13] seems more relevant to metallophilic interactions. Preliminary calculations of the extended Hückel type carried out on these molecules indicate that the Mulliken charge of the copper atoms is close to zero and confirm that no significant orbital interaction is at work between the two monomers. However, a conclusive argument proving the existence of metallophilic interactions on such large systems is at present impossible to obtain from quantum chemical calculations. It is however of interest to extrapolate from Pyykkö's calculations on $[ClMPH_3]_2$[7] the order of magnitude of the metallophilic stabilization in **3** and in its silver counterpart.

Pyykkö's potential energy curves were obtained at the *ab initio* MP2 level of calculation with very large basis sets.[7] They display energy minima at 3.208 Å for Au, 3.113 Å for Ag and 3.137 Å for Cu. The curves are however extremely shallow, especially for copper. The stabilization energy computed at the minimum is −3.07 kcal mol^{-1} but a separation of 4.5 Å still provides a favourable interaction which amounts to −1.2 kcal mol^{-1}. The crystal structure of **3** displays two short-range Cu–Cu interactions (2.905 Å) between the two monomers, but also six Cu···Cu distances between 4.44 Å and 4.75 Å.[5] Most of the metallophilic stabilization (*ca*. 60%) might then originate in these long distance interactions. However, providing a quantitative estimate for the overall stabilization energy requires caution. A comparison between MP2 calculations and more elaborate methods carried out for $[XAuPH_3]_2$ (X = H, Cl) indicates that MP2 overestimates the real stabilization energy by a factor of 2.[2,7] Scaling down accordingly the value deduced from Pyykkö's potential energy curves provides an overall stabilization of *ca*. −6 kcal mol^{-1} due to the cuprophilic effect between the two monomers, 60% of which is assigned to the intermediate range Cu···Cu interactions. A similar reasoning applied to the silver equivalent of **3** yields an estimate of *ca*. −7.5 kcal mol^{-1} for the metallophilic interaction, but in this case the intermediate range interactions account for no more than one third of the global stabilization.

All calculations were carried out on workstations purchased with funds provided by the DGICYT of the Government of Spain and by the CIRIT of Generalitat of Catalunya (Grants no. PB95-0639-C02-02 and SGR95-426). We are pleased to thank Dr Pierre Braunstein for stimulating discussions.

Notes and References

† E-mail: benard@quantix.u-strasbg.fr

‡ *Computation*: gradient-corrected DFT calculations on complex **1** have been carried out by means of the ADF program.[14] We used the local spin density approximation characterized by the electron gas exchange ($X\alpha$ with α = 2/3) together with Vosko–Wilk–Nusair[15] parametrization for correlation. Becke's nonlocal corrections to the exchange energy[16] and Perdew's nonlocal corrections to the correlation energy[17] were added. Slater basis sets of triple-ζ+ polarization quality were used to describe the valence electrons of C, N, O and H. For first-row atoms, a 1s frozen core was described by means of a single Slater function. For copper, the frozen core composed of the 1s to 2sp shells was also modelled by a minimal Slater basis; 3sp electrons were described by double-ζ Slater functions, 3d and 4s by triple-ζ functions and 4p by a single orbital.[18]

1 (*a*) H. Schmidbaur, W. Graf and G. Müller, *Angew. Chem., Int. Ed. Engl.*, 1988, **27**, 417; (*b*) H. Schmidbaur, *Gold Bull.*, 1990, **23**, 11.
2 P. Pyykkö, *Chem. Rev.*, 1997, **97**, 597.
3 P. Pyykkö, J. Li and N. Runeberg, *Chem. Phys. Lett.*, 1994, **218**, 133.
4 See, for example: S. P. Abraham, A. G. Samuelson and J. Chandrasekhar, *Inorg. Chem.*, 1993, **32**, 6107 and references therein.
5 K. Singh, J. R. Long and P. Stavropoulos, *J. Am. Chem. Soc.*, 1997, **119**, 2942.
6 U. Siemeling, U. Vorfeld, B. Neumann and H.-G. Stammler, *Chem. Commun.*, 1997, 1723.
7 P. Pyykkö, N. Runeberg and F. Mendizabal, *Chem. Eur. J.*, 1997, **3**, 1451.
8 F. L. Hirshfeld, *Theor. Chim. Acta*, 1977, **44**, 129.
9 G. Voronoï, *Journal für die reine und angewandte Mathematik*, 1908, **134**, 198.
10 K. Kitaura and K. Morokuma, *Int. J. Quantum Chem.*, 1976, **10**, 325.
11 P. S. Bagus, K. Herrmann and C. W. Bauschlicher, Jr., *J. Chem. Phys.*, 1984, **80**, 4378; 1984, **81**, 1966.
12 P. C. Healy, J. D. Kildea, B. W. Skelton and A. H. White, *Aust. J. Chem.*, 1989, **42**, 115.
13 (*a*) M. K. Ehlert, S. J. Rettig, A. Storr, R. C. Thompson and J. Trotter, *Can. J. Chem.*, 1990, **68**, 1444; 1992, **70**, 2161; (*b*) N. Masciocchi, M. Moret, P. Cairati, A. Sironi, G. Ardizzoia and G. L. Monica, *J. Am. Chem. Soc.*, 1994, **116**, 7668.
14 (*a*) ADF 2.3 User's Guide, Chemistry Department, Vrije Universiteit, Amsterdam, The Netherlands, 1997; (*b*) E. J. Baerends, D. E. Ellis and P. Ros, *Chem. Phys.*, 1973, **2**, 41; (*c*) G. te Velde and E. J. Barrends, *J. Comput. Phys.*, 1992, **99**, 84.
15 S. H. Vosko, L. Wilk and M. Nusair, *Can. J. Phys.*, 1980, **58**, 1200.
16 (*a*) A. D. Becke, *J. Chem. Phys.*, 1986, **84**, 4524; (*b*) A. D. Becke, *Phys. Rev. A*, 1988, **38**, 3098.
17 J. P. Perdew, *Phys. Rev. B*, 1986, **33**, 8882; 1986, **34**, 7406.
18 J. G. Snijders, E. J. Baerends and P. Vernooijs, *At. Nucl. Data Tables*, 1982, **26**, 483.

Received in Basel, Switzerland, 24th February 1998; 8/01560K

Crystal engineering through charge transfer interactions; assisted formation of a layered coordination polymer (4-cyanopyridine)cadmium(II) iodide·diiodine

Rosa D. Bailey, Laura L. Hook and William T. Pennington*†

Department of Chemistry, Clemson University, Clemson, South Carolina 29634-1905, USA

Formation of a layered coordination polymer (4-cyanopyridine)cadmium(II) iodide is assisted by n–σ* donor–acceptor interactions between coordinated iodine atoms of the layers and iodine molecules which bridge adjacent layers.

We are very interested in the role that (n–σ*) charge transfer interactions might play in the design of functional solids. We have utilized this interaction to prepare a variety of diazine·I_2 complexes in which N···I charge-transfer interactions at either end of both the donor and acceptor molecules result in the formation of extended chains.[1] More recently we have reported on the utility of N···I based charge transfer complexes for the interconversion of polymorphic forms of a donor molecule, tetrapyridylpyrazine,[2,3] and have begun a systematic investigation of complexes of iodine with a variety of nitrogen-based donors.[4]

We are also interested in the role that coordination polymers might play in structure design. Group 12 (IIB) metal halides are particularly promising, owing to the variety of coordination numbers and geometries provided by the d^{10} configuration of the metal center. This structural diversity is closely dependent on factors such as the dimensions of the metal ions and halides, nature of other ligands, and the availability of other structure controlling interactions, such as hydrogen-bonding and charge transfer.[5–7] If this diversity can be controlled, group 12 metal halides offer an ideal system for structural engineering and design.

We have found that pyrazine forms 1 : 1 complexes with cadmium(II) halides, CdX_2·pyrazine (X = Cl **1**, Br **2**, I **3**).[8] All of the complexes crystallize as infinite CdX_2 chains in which cadmium atoms are doubly bridged by pairs of halide atoms; pyrazine ligands complete the pseudo-octahedral coordination of the cadmium atoms and link the CdX_2 chains to form extended two-dimensional layers. Numerous attempts to form a similar architecture with the bridging ligand, 4-cyanopyridine, were unsuccessful; however, an interesting bis-pyridyl complex, bis(4-cyanopyridine)cadmium(II) iodide **4**, was formed.[9] This complex crystallizes as infinite CdI_2 chains, in which cadmium atoms are doubly bridged by pairs of iodine atoms; 4-cyanopyridine ligands coordinated through the pyridyl nitrogen atom occupy *trans* positions to complete an octahedral coordination about the cadmium. The chains are associated into layers through self-association of the cyano groups. When co-crystallized with mercury(II) iodide (1 : 2 ratio) bis(4-cyanopyridine)cadmium(II) iodide·$2HgI_2$ **5** is formed. The layer structure of **4** is essentially unchanged in **5**, as the mercury(II) iodide molecules are intercalated between the layers.

Based on the donor–acceptor interactions between coordinated iodine atoms and the mercury center observed in **5**, it was anticipated that a similar interaction might occur with molecular iodine serving as the acceptor. Here, we report the construction‡ of a layered structure, (4-cyanopyridine)cadmium(II) iodide which was the unattainable target of our previous efforts. It is particularly significant that the formation of this structure is made possible by the assistance of n → σ* charge transfer interactions between the coordinated iodides and a complexed neutral iodine molecule.

Similar to the (pyrazine)CdX_2 complexes, 4-(cyanopyridine)cadmium(II) iodide I_2 **6** (Fig. 1) crystallizes as infinite CdI_2 chains in which cadmium atoms are doubly bridged by pairs of iodide atoms; adjacent cadmium atoms in the chain are related by mirror symmetry perpendicular to the ***a***-axis at (0 *y z*).§ The 4-cyanopyridine ligand is bonded through both the pyridyl and nitrile groups to complete a pseudo-octahedral coordination of the cadmium atoms and acts as a bridging ligand to link the CdI_2 chains related by a 2_1 operation parallel to ***b*** at (1/4 *y* 1/4), to form extended two-dimensional layers (Fig. 2). The layers are bisected by a mirror plane perpendicular to the ***c***-axis at (*x y* 1/4). The layers are joined in the stacking direction (the ***c***-axis) through an n → σ* charge transfer interaction from the

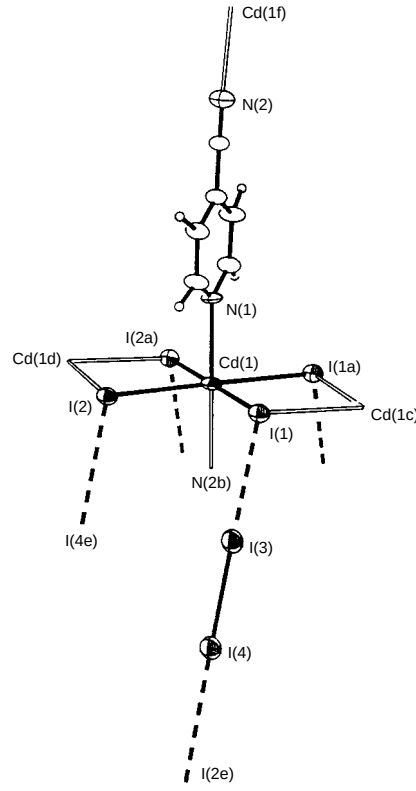

Fig. 1 Thermal ellipsoid plot (50% probability) of **6**; selected distances (Å) and angles (°): Cd(1)–I(1) 2.949(1), Cd(1)–I(2) 2.942(1), I(1)–I(3) 3.367(1), I(2)–I(4e) 3.436(1), I(3)–I(4) 2.757(1), Cd(1)–N(1) 2.391(9), Cd(1)–N(2b) 2.403(10); I(1)–Cd(1)–I(2) 91.2(1), I(1)–Cd(1)–N(1) 90.2()2, I(2)–Cd(1)–N(1) 90.6(2), I(1)–Cd(1)–I(1a) 88.1(1), I(2)–Cd(1)–I(1a) 179.0(1), I(2)–Cd(1)–I(2a) 89.4(1), I(1)–Cd(1)–N(2b) 89.6(2), I(2)–Cd(1)–N(2b) 89.7(2), N(1)–Cd(1)–N(2b) 179.7(4), Cd(1)–I(1)–Cd(1c) 91.9(1), Cd(1)–I(2)–Cd(1d) 90.4(1), Cd(1)–I(1)–I(3) 105.9(1), Cd(1)–I(2)–I(4e) 107.6(1), I(1)–I(3)–I(4) 178.8(1), I(3)–I(4)–I(2e) 177.8(1). (Atoms labelled with a lower-case character were generated by the following symmetry operation: a *x*, *y*, 1/2 − *z*; b 1/2 − *x*, −1/2 + *y*, 1/2 − *z*; c 1 − *x*, *y*, *z*; d − *x*, *y*, *z*; e 1/2 − *x*, 1/2 − *y*, 1 − *z*; f 1/2 − *x*, 1/2 − *y*, −*z*.)

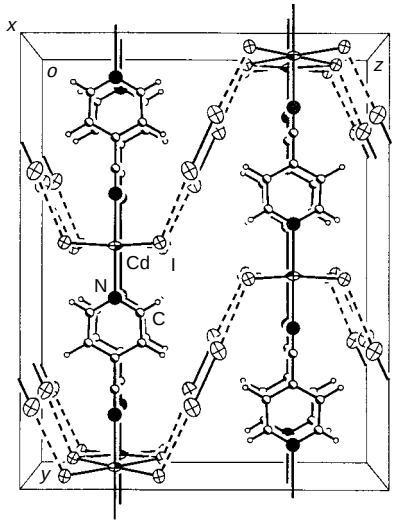

Fig. 2 Crystal packing of **6**, viewed down the ***a***-axis, parallel to the CdI_2 chains

coordinated iodine atoms as donors to either end of a bridging I_2 molecule.

The Cd–I···I donor–acceptor (n → σ* charge transfer) interactions are present at either end of the I_2 molecule and involve both of the coordinated iodine atoms. The interactions occur at approximately tetrahedral angles at the coordinated iodide and are oriented in a linear fashion to the I–I σ-bond. The I···I distances are well within the sum of van der Waals radii for iodine (1.98 Å),[10] and are similar to those seen in the related compounds, $Cd(NH_3)_4I_2{\cdot}I_2$ [3.386(2) Å] and $Cd(NH_3)_4(I{\cdot}I_2)_2$ [3.3780(9) Å].[11]

That these interactions occur only to the cyano-coordinated side of the CdI_2 plane is a result of the smaller size of the cyano-group; unfavorable steric interactions involving the pyridine rings prevent interaction on the other side of the CdI_2 plane.¶ When 4-cyanopyridine and cadmium(II) iodide are combined in a variety of stoichiometric ratios (1 : 1, 1 : 2, 2 : 1) in the absence of I_2, compound **4** is the only product formed. The considerably weaker donor strength of the nitrile group relative to the pyridyl group is presumably the reason for preferred formation of **4**. When I_2 is present, however, combination of cadmium(II) iodide and 4-cyanopyridine in the same stoichiometric ratios yields **6** as the only product. Formation of **6** and the fact that 4-cyanopyridine does serve as a bridge in this compound appears to be a result of the structural support provided by the charge transfer complexed iodine molecules which link adjacent groups in a zigzag fashion to form a reinforced three-dimensional network.

Thermal analysis of **6** by TGA‖ showed an initial mass loss of *ca.* 42% with an onset temperature of 83 °C. A second mass loss of 11% occurred at 163 °C, and the remainder of the mass was lost at 408 °C. These data suggest that **6** thermally decomposes by initial loss of the bridging I_2 molecule (35% by mass) coupled with a small amount of the ligand, the remainder of the ligand is lost in the second event, followed by sublimation of cadmium iodide at high temperature. The initial process is probably more complicated than simple diffusion of I_2 out of the solid. Powder diffraction on a sample of **6** heated to 120 °C for approximately 20 h revealed CdI_2 as the only crystalline product. This result coupled with our observation that recrystallization of **6** from ethanol gives **4** and CdI_2, and that leaching of **6** with boiling hexane leaves behind only solid CdI_2 suggests that the layered structure of **6** is tenuous. Removal of the supporting I_2 molecules leads to total collapse of the two-dimensional architecture and of the compound itself.

Continuing efforts to find gentler methods to remove or perhaps to exchange the I_2 supports through a diffusion process are underway. The stabilization of **6** by charge transfer interactions suggests the utility of these highly directional and attractive forces for isolating other metastable structures, and we are actively pursuing additional examples of this interesting phenomenon.

We thank the National Science Foundation for funds to purchase the Rigaku and Scintag diffractometers used in this work. We also thank Dr T. W. Hanks of Furman University for assistance with thermal analysis and for helpful discussion.

Notes and References

† E-mail: billp@clemson.edu

‡ *Synthesis* of $(C_6H_4N_2)CdI_2{\cdot}I_2$ **6**: 4-Cyanopyridine (0.0618 g, 0.594 mmol) was dissolved in a solution of cadmium(II) iodide (0.224 g, 0.613 mmol) and iodine (0.195 g, 0.770 mmol) in 95% ethanol. Slow evaporation of solvent yielded 0.279 g of red crystals of **6** (65% yield based on the ligand); mp 154–155 °C. IR(Nujol) (cm^{-1}): 2280, 1617, 1413, 1225, 826, 557, 207, 188. Elemental analyses calc. (obs.): C 9.95 (10.31), H 0.56 (0.58), N 3.87 (3.80)%.

§ *Crystal data* for $(C_6H_4N_2)CdI_2{\cdot}I_2$ **6**: orthorhombic, space group *Cmcm* (no. 63); a = 8.411(2), b = 20.277(4), c = 15.986(3) Å, U = 2726(1) $Å^3$ (based on 25 reflections; 20.35 < 2θ < 39.48°), Z = 8 [atoms Cd(1), N(1), C(3), C(4) and N(2) lie on mirror perpendicular to ***c*** (z = 1/4); atoms I(1) and I(2) lie on mirrors perpendicular to ***a*** (x = 0) and 1/2, respectively)], D_c = 3.53 g cm^{-3}, μ(Mo-Kα) = 10.63 mm^{-1}, empirical absorption correction, transmission coefficients: 0.77–1.00, 1370 unique data measured, 973 observed [$I > 2\sigma(I)$], $R(F)$ = 0.028, $R_w(F)$ = 0.035. Data were collected on a reddish-brown platelet (0.02 × 0.15 × 0.15 mm) at −110 ± 1 °C by using a Rigaku AFC7R (18 kW) diffractometer with graphite-monochromated Mo-Kα radiation (λ = 0.710 73 Å) to $2\theta_{max}$ of 50.0°. Non-hydrogen atoms were refined anisotropically and hydrogen atoms were refined isotropically. CCDC 182/863.

¶ All attempts to prepare similar compounds with ligands possessing only larger pyridyl donors (such as pyrazine and 4,4′-bipyridine) have been unsuccessful, presumably due to steric protection of the metal halide donor sites.

‖ Thermal gravimetric analysis of **6** was performed on a Perkin-Elmer Series 7 analyzer with the TGA7 software package (version 2.20). For onset calculations, the samples were heated at a constant rate of 5 °C min^{-1} from 25 °C until all of the material had evaporated.

1 R. D. Bailey, M. L. Buchanan and W. T. Pennington, *Acta Crystallogr., Sect. C*, 1992, **48**, 2259.
2 R. D. Bailey, M. Grabarczyk, T. W. Hanks, E. M. Newton and W. T. Pennington, *Electronic Conference on Trends in Organic Chemistry* (*ECTOC-1*), ed. H. S. Rzepa and J. M. Goodman (CD-ROM), 1995, Royal Society of Chemistry publications. See also http://www.ch.ic.ac.uk/ectoc/papers
3 R. D. Bailey, M. Grabarczyk, T. W. Hanks and W. T. Pennington, *J. Chem. Soc., Perkin Trans. 2*, 1997, 2773.
4 R. D. Bailey, G. W. Drake, M. Grabarczyk, T. W. Hanks, L. L. Hook and W. T. Pennington, *J. Chem. Soc., Perkin Trans. 2*, 1997, 2781.
5 P. A. W. Dean, *Prog. Inorg. Chem.*, 1978, **24**, 109 and references therein.
6 D. G. Tuck, *Rev. Inorg. Chem.*, 1979, **1**, 209 and references therein.
7 Some examples of the structural diversity of cadmium include: B. F. Abrahams, M. J. Hardie, B. F. Hoskins, R. Robson and E. E. Sutherland, *J. Chem. Soc., Chem. Commun.*, 1994, 1049; T. Soma, H. Yuge and T. Iwamoto, *Angew. Chem., Int. Ed. Engl.*, 1994, **33**, 1665; M. Fujita, Y. J. Kwon, M. Miyazawa and K. Ogura, *J. Chem. Soc., Chem. Commun.*, 1994, 1977; H. Yuge and T. Iwamoto, *Acta Crystallogr., Sect. C*, 1995, **51**, 374; M. Hashimoto and T. Iwamoto, *Acta Crystallogr., Sect. C*, 1994, **50**, 496; C.. K. Schauer and O. P. Anderson, *J. Am. Chem. Soc.*, 1987, **109**, 3646; M. Nieuwenhuyzen, W. T. Robinson and C. J. Wilkins, *Polyhedron*, 1991, **10**, 2111; R. D. Rogers and A. H. Bond, *Inorg. Chim. Acta*, 1996, **250**, 105.
8 R. D. Bailey and W. T. Pennington, *Polyhedron*, 1997, **16**, 417.
9 R. D. Bailey, L. L. Hook, A. K. Powers, T. W. Hanks and W. T. Pennington, *Mater. Res. Bull. Suppl: Crystal Eng.*, in press.
10 A. Bondi, *J. Phys. Chem.*, 1964, **68**, 441.
11 K.-F. Tebbe and M. Plewa, *Z. Anorg. Allg. Chem.*, 1982, **489**, 111.

Received in Columbia, MO, USA, 13th November 1997; 7/08225H

Asymmetric Diels–Alder reaction *via* enzymatic kinetic resolution using ethoxyvinyl methyl fumarate

Yasuyuki Kita,*† Tadaatsu Naka, Masashi Imanishi, Shuji Akai, Yasushi Takebe and Masato Matsugi

Graduate School of Pharmaceutical Sciences, Osaka University, 1-6, Yamada-oka, Suita, Osaka 565 Japan

A domino-type asymmetric [4 + 2] cycloaddition reaction following enzymatic kinetic resolution using ethoxyvinyl methyl fumarate is described.

We have already reported that ethoxyvinyl esters are better acylating reagents for enzymatic kinetic resolution of alcohols than the generally used vinyl esters.[1] One of the remarkable features of these acylating reagents is the facile preparation of esters bearing various acyl moieties.[2] Therefore, we planned a novel reaction system based on the idea that the acyl moiety inserted by enzymatic kinetic resolution is used in the subsequent reaction stage. Here we report a convenient asymmetric one-pot [4 + 2] cycloaddition reaction following an enzymatic kinetic resolution using readily-prepared ethoxyvinyl methyl fumarate.

The enatiomerically pure 7-oxabicyclo[2.2.1]heptene derivative **2** is a useful compound in the syntheses of many natural products.[3] Many synthetic approaches to **2** have been reported to date,[4] and the intramolecular Diels–Alder reaction of the enantiomerically pure furfuryl fumarate derivative **1** is one of the most effective methods (Scheme 1).[5]

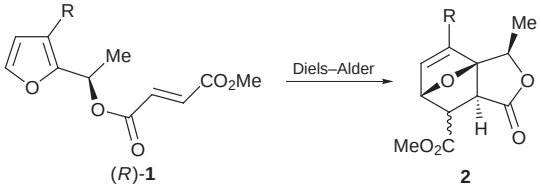

Scheme 1

We anticipated an easy and highly stereoselective synthesis of optically active **2** *via* the enzymatic acylation of (±)-furfuryl alcohol **4** using ethoxyvinyl methyl fumarate **3**, followed by rapid intramolecular Diels–Alder reaction between the inserted fumarate moiety and the diene moiety on the furan ring. In the reactions related to the kinetic resolution by enzymatic acylation, use of the acylating reagent not only as an acyl donor but also as a component of the next reaction stage has rarely been reported.‡ The unknown ethoxyvinyl methyl fumarate **3** was prepared by the reported[6] method shown in Scheme 2 and used as an acetone solution without further purification.§

First, we examined which enzyme was suitable for kinetic resolution of (±)-**4a** using **3** as the acylating reagent. We checked the optical purity of the acylated product **1a** prior to the

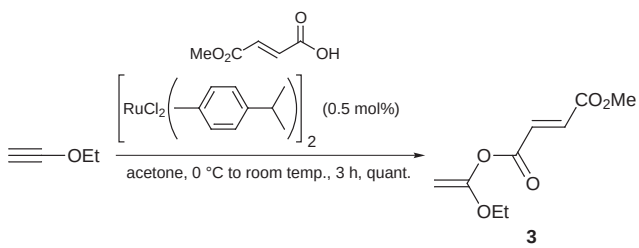

Scheme 2

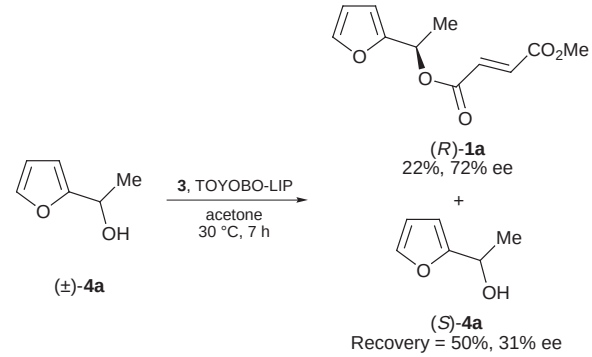

Scheme 3

formation of cycloadduct **2**. After screening a number of enzymes (amano AK, AY, PS, PPL, PLE, A-6, meito-MY, OF, chirazyme L3, TOYOBO-LIP)¶ we found that only TOYOBO-LIP gave an optically active furfuryl methyl fumarate (*R*)-**1a** (22% yield, 72% ee) (Scheme 3). The absolute configuration of the product **1a** was determined by converting the unreacted **4a** to the known nitrobenzoate derivative.[7]

Next, we studied the influence of enzyme TOYOBO-LIP on the intramolecular Diels–Alder reaction of (±)-**1a**.[8] Consequently, we found that the cycloadduct product, *syn*-**2a** (4% ee), was obtained with 24% de in preference to *anti*-**2a** (23% ee).‖ Thus it is apparent that enzyme TOYOBO-LIP played an important role in the diastereo- and enantio-facial selectivity of this intramolecular cycloaddition process (Scheme 4).[9]

Although it can be assumed that the enzymatic hydrolysis, which utilizes the small amount of water in the solvent, depends on the asymmetric environment produced by TOYOBO-LIP,[10] how the enzyme participates in the face-selectivity of the cycloaddition remains to be elucidated at the present time. This result suggests that the possibility exists of increasing the enantioselectivity observed at the enzymatic kinetic resolution stage (72% ee) by carrying out the cycloaddition reaction in the same pot. In practice, we succeeded in the highly stereoselective

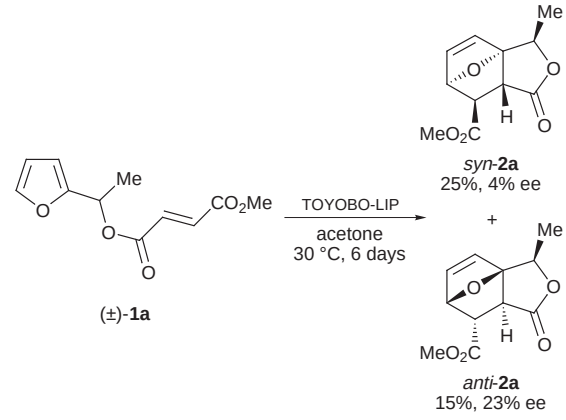

Scheme 4

Table 1 Asymmetric Diels–Alder reaction following kinetic resolution using enzyme

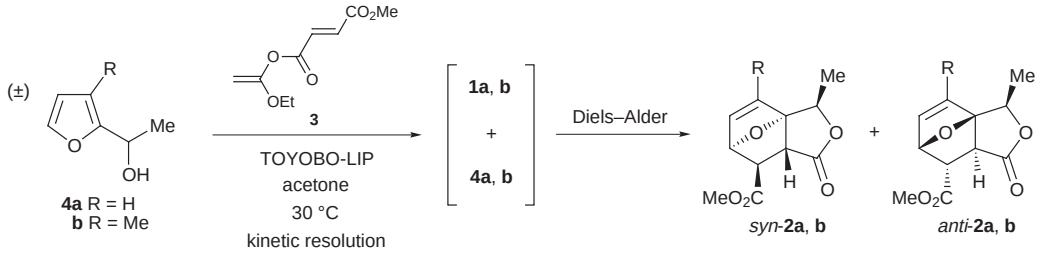

Entry	Substrate	Solvent	*t*/days	Total yield of **2** (%) (% de)[a]	Ee (%)[b] *syn*-**2**	Ee (%)[b] *anti*-**2**	Recovery of **1** (%)	Recovery of **4** (%) (absolute config. of major **4**)
1	**4a**	Acetone	6	18 (26)	86	93	21	56 (*S*)
2	**4a**	Acetone	8	32 (24)	79	81	20	18 (*S*)
3	**4a**	THF	8	28 (24)	81	48	5	38 (*S*)
4	**4b**	Acetone	1	43 (100)	84	N.D.[c]	N.D.[d]	39 (*S*)
5	**4b**	THF	1	37 (100)	84	N.D.[c]	N.D.[d]	33 (*S*)

[a] Diastereomeric excess was determined *via* ^{1}H NMR analysis of the crude product. [b] Enantiomeric excess was determined by HPLC (Chiralcel OJ). [c] *anti*-**2b** was not detected *via* ^{1}H NMR analysis. [d] **1b** was not detected by thin layer chromatography.

synthesis of **2** (*syn*-**2**: 84–86% ee, *anti*-**2a**: 93% ee) as a result of carrying out the enzymatic kinetic resolution and cycloaddition in one pot in acetone (Table 1, entry 1). The success of this one-pot reaction is mainly due to the acylating reagent **3**, which could be used without a work-up procedure, since compound **3** is not stable and cannot usually be isolated.

In conclusion, we developed a novel methodology such that the acyl moiety inserted during an enzymatic kinetic resolution was used as part of the constituent structure during the next reaction stage.** In this one-pot reaction, an interesting phenomenon was observed, *i.e.* the optical purity of the enzymatic acylated product was increased during the cycloaddition stage. Consequently, we achieved the convenient synthesis of optically active **2**. This one-pot asymmetric synthesis might be applied to the syntheses of other useful biologically-active compounds, and other applications are now being developed.

Notes and References

† E-mail: kita@em.phs.osaka-u.ac.jp

‡ Only one example of an enzymatically acrylated product being utilized in the synthesis of chiral polymers has been reported; A. Ghogana and S. Kumar, *J. Chem. Soc., Chem. Commun.*, 1990, 134.

§ Ethoxyvinyl methyl fumarate was used as an acetone solution, since it could not be purified due to its instability. Although the solution contained a catalytic amount of the ruthenium complex, it has already been confirmed that enzymatic kinetic resolution of various alcohols is not affected by the ruthenium complex. Details of these results will be reported in the near future.

¶ LIP is *Pseudomonas aeruginosa* on Hyflo Super-Cel and is commercially available from TOYOBO.

‖ In the absence of an enzyme, the diastereomeric excess was 10% de in this cycloaddition reaction using (*R*)-**1**; B. Thomas and S. Jürgen, *Tetrahedron: Asymmetry*, 1997, **8**, 703.

** *Typical procedure*: a mixture of (±)-furfuryl alcohol **4a** (0.5 mmol), LIP (100 mg) and ethoxyvinyl methyl fumarate (0.5 mmol) (see footnote §) was stirred at 30 °C. After 6 days, the reaction mixture was filtered through a Celite pad and the filtrate was concentrated *in vacuo*. The residue was purified by column chromatography over silica (hexane–EtOAc) to give cycloadduct **2a** (40 mg, 18%), furfuryl methyl fumarate (*R*)-**1a** (46 mg, 21%) and furfuryl alcohol (*S*)-**4a** (73 mg, 56%).

1 Y. Kita, Y. Takebe, K. Murata, T. Naka and S. Akai, *Tetrahedron Lett.*, 1996, **37**, 7369; S. Akai, T. Naka, Y. Takebe and Y. Kita, *Tetrahedron Lett.*, 1997, **38**, 4243.
2 N. Shibata, M. Matsugi, S. Fukui, C. Fujimori, K. Gotanda, K. Murata and Y. Kita, *Tetrahedron: Asymmetry*, 1997, **8**, 703; Y. Kita, Y. Takeda, M. Matsugi, K. Iio, K. Gotanda, K. Murata and S. Akai, *Angew. Chem., Int. Ed. Engl.*, 1997, **36**, 1529.
3 R. H. Schlessinger, X. H. Wu and T. R. Pettus, *Synlett*, 1995, 536; M. E. Jung and V. C. True, *Tetrahedron Lett.*, 1988, **29**, 6059; L. M. Harwood, T. Ishikawa, H. Phillips and D. J. Watkin, *J. Chem. Soc., Chem. Commun.*, 1990, 605.
4 Y. N. Yamakoshi, W.-Y. Ge, K. Okayama, T. Takahashi and T. Koizumi, *Heterocycles*, 1996, **42**, 129; R. H. Schlessinger, T. R. R. Pettus, J. P. Springer and K. Hoogsteen, *J. Org. Chem.*, 1994, **59**, 3246; E. J. Corey and T.-P. Loh, *Tetrahedron Lett.*, 1993, **34**, 2979.
5 J. Zylber, A. Tubul and P. Brun, *Tetrahedron: Asymmetry*, 1995, **6**, 377.
6 Y. Kita, H. Maeda, K. Omori, T. Okuno and Y. Tamura, *J. Chem. Soc., Perkin Trans. 1*, 1993, 2999.
7 J. Kamiñska, I. Górnicka, M. Sikora and J. Góra, *Tetrahedron: Asymmetry*, 1996, **7**, 907.
8 H. Oikawa, K. Katayama, Y. Suzuki and A. Ichihara, *J. Chem. Soc., Chem. Commun.*, 1995, 1321.
9 S. Laschat, *Angew. Chem., Int. Ed. Engl.*, 1996, **35**, 289.
10 T. S. Cload, R. D. Liu, M. R. Pastor and G. P. Schultz, *J. Am. Chem. Soc.*, 1996, **118**, 1787; 1996, **118**, 1789.

Received in Cambridge, UK, 23rd February 1998; 8/01496E

Rare earth stabilization of mesoporous alumina molecular sieves assembled through an N°I° pathway

Wenzhong Zhang and Thomas J. Pinnavaia*†

Department of Chemistry and Center for Fundamental Materials Research, Michigan State University, East Lansing, MI 48824-1322, USA

The incorporation of 1.0–5.0 mol% Ce^{3+} or La^{3+} ions in MSU-X alumina molecular sieves, prepared through an N°I° assembly pathway, dramatically improves their thermal stability without altering the mesopore size or the wormhole channel motif.

Following the supramolecular assembly of M41S mesoporous molecular sieves in 1992,[1] there have been relatively few reports of mesostructured aluminas. Davis and coworkers[2] have prepared porous aluminas (*ca*. 20 Å pore diameters) by the hydrolysis of aluminium alkoxides in the presence of a carboxylate surfactant as the structure director. The assembly pathway involved S–I complexation reaction between the surfactant (S) and the inorganic reagent (I), as judged by the presence of IR bands characteristic of chelating carboxylate groups. Yada *et al*.[3] reported the preparation of hexagonal alumina mesostructures by electrostatic S^-I^+ assembly of dodecyl sulfate surfactants and aluminium nitrate. However, the mesostructures were not stable to surfactant removal. In contrast, we have obtained mesoporous alumina molecular sieves, denoted MSU-X, by N°I° assembly of electrically neutral polyethylene oxide surfactants (N°) and an aluminium alkoxide as the inorganic precursor (I°).[4,5] These materials exhibited wormhole channel motifs and BJH pore diameters that can be extended beyond 100 Å, depending on the surfactant size.

One limitation of MSU-X alumina molecular sieves is the loss of surface area and porosity when they are heated above 500 °C. The potential applications of these materials in catalysis and other materials areas could be greatly extended by improving their thermal stability. One possible approach to improving the thermal stability of a metastable alumina is to dope the oxide framework with rare earth cations. For instance, the incorporation of rare earths into γ-alumina (pseudoboehmite) and other transition aluminas is known to stabilize these metastable phases against sintering and conversion to α-alumina (corundum). Two stabilization mechanisms have been proposed, namely, the formation of a surface rare earth aluminate phase[6] and the simple replacement of Al^{3+} by rare earth ions in the pseudoboemite structure, which reduces the lability of the oxide matrix.[7] Analogous mechanisms might also be effective in stabilizing the non-crystalline (amorphous) framework walls of MSU-X alumina molecular sieves against collapse at elevated temperatures. In the present work, we demonstrate that MSU-X aluminas indeed are stabilized by doping with rare earth metal ions.

The incorporation of Ce^{3+} or La^{3+} into MSU-X aluminas was accomplished by first dissolving the corresponding rare earth nitrate in a solution of the non-ionic surfactant in warm butanol. The solution was cooled to room temperature and then aluminium *sec*-butoxide was added with stirring. After an additional 1 h of stirring at ambient temperature, a dilute solution of water in *sec*-butanol was added dropwise. The reaction vessel was then placed in a reciprocating shaker bath at 45 °C for a period of 40 h. Recovery of the as-synthesized reaction products was achieved by filtration and air drying.

The molar compositions of the above reaction mixtures were as follows:

$$0.05\ Ce^{3+}\ (\text{or } 0.01\ La^{3+}) : 1.0\ Al(Bu^sO)_3 : 0.40\ \text{Tergitol}\ (\text{or } 0.20\ \text{Pluronic}) : 3.0\ H_2O : 15.5\ Bu^sOH$$

where the non-ionic surfactants are Tergitol® 15-S-12 (Union Carbide) with the formula $C_{15}H_{33}E_{12}OH$ (E is a polyethylene oxide segment) and Pluronic® P65 or P123 (BASF) block copolymers with the respective compositions $E_{19}P_{30}E_{19}$ and $E_{20}P_{69}E_{20}$ (P is a isopropylene oxide segment).

Essentially all of the N° surfactant could be removed from the alumina mesostructures by extraction with hot ethanol. For convenience, however, the as-synthesized products were freed of surfactant and prepared directly for N_2 adsorption studies in one step by calcining at 500 °C for 6.0 h. Under the calcination conditions the pure alumina mesostructures assembled from the three N° surfactants begin to collapse, as evidenced by a broadening of the one-line diffraction pattern and a decrease in the surface area and pore volume. Upon the introduction of 1–5 mol% rare earth ions, however, the thermal stability of the framework is greatly improved, as judged by substantial increases in surface areas and liquid pore volume (see below).

N_2 adsorption–desorption isotherms for alumina molecular sieves doped with 5.0% Ce^{3+} and 1.0% La^{3+} are shown in Fig. 1. The positions of the pore filling steps in the adsorption curves shift to higher P/P_0 values with increasing surfactant size, as expected for pore structures formed by a supramolecular assembly process. The desorption hystereses signify some

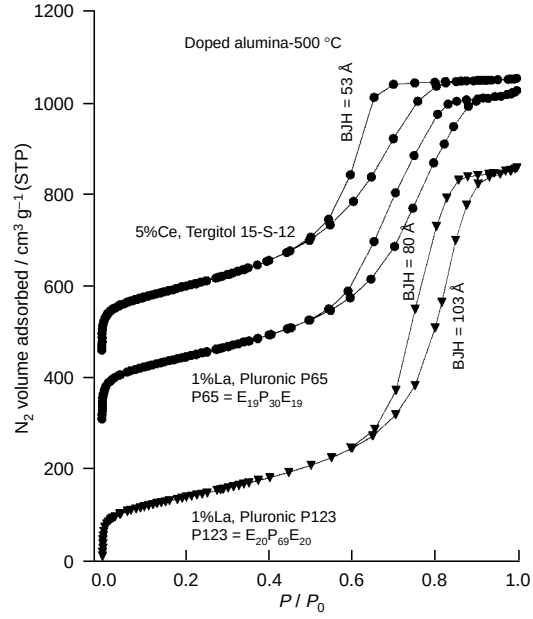

Fig. 1 N_2 adsorption–desorption isotherms of rare earth-stabilized MSU-X alumina molecular sieves assembled in the presence of the non-ionic surfactants Tergitol 15-S-12, Pluronic P65, and Pluronic P123 as structure directors and calcined at 500 °C. The BJH pore sizes obtained from the desorption isotherms are included for comparison.

Table 1 Physical properties of mesoporous MSU-X alumina molecular sieves prepared by N°I° assembly

Surfactant	Rare earth (mol%)	Calcination temp.[a]/ °C	S_{BET}/ $m^2\ g^{-1}$	BJH pore size/Å	Liquid pore volume/$cm^3\ g^{-1}$	XRD, *d*/nm
15-S-12	0	500	391	50	0.48	7.8
15-S-12	0	600	267	55	0.31	8.0
15-S-12	5 (Ce)	500	530	53	0.92	8.0
15-S-12	5 (Ce)	600	357	54	0.65	8.0
P65	1 (La)	500	517	80	1.11	> 8.3
P123	1 (La)	500	487	108	1.31	> 10.0

[a] All the samples were calcined in air for 6 h.

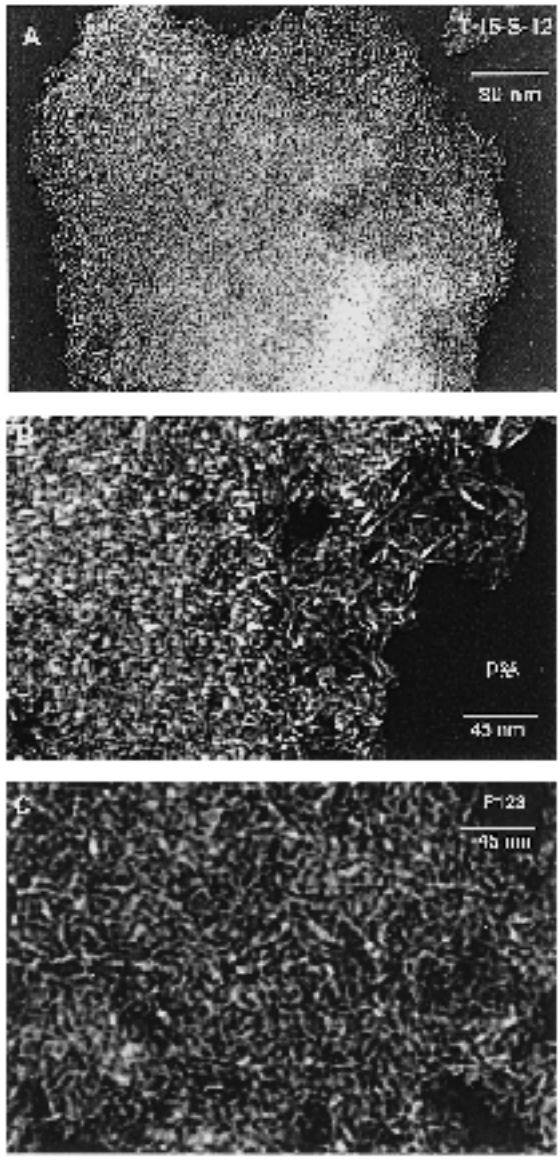

Fig. 2 TEM images of rare earth-stabilized MSU-X alumina molecular sieves assembled from non-ionic surfactants and calcined at 500 °C: (A) 5.0% Ce^{3+}, Tergitol 15-S-12; (B) 1.0% La^{3+}, Pluronic P65; (C) 1.0% La^{3+}, Pluronic P123

degree of pore blocking. These qualitative features of the isotherms also are observed for the pure alumina mesostructures. Furthermore, the doped mesostructures exhibit XRD basal spacings and wormhole TEM images (*cf*., Fig. 2) equivalent to those observed for the pure alumina phases. Therefore, the introduction of the rare earth cations at the 1.0–5.0 mol% level does not alter the N°I° assembly of MSU-X aluminas.

As can be seen from the results provided in Table 1, the incorporation of 5.0 mol% Ce^{3+} in the alumina framework assembled from Tergitol® 15-S-12 results in a 35% increase in the surface area after calcination at 500 or 600 °C. Moreover, the presence of the rare earth nearly doubles the pore volume without changing the average BJH pore size. Thus, the thermal stability of the amorphous framework walls clearly is enhanced without sacrificing the channel size or packing motif. Improved thermal stability also is realized for the La^{3+}-doped mesostructures assembled from Pluronic surfactants, even at the 1 mol% doping levels.

We conclude from the above results that the framework walls of mesoporous MSU-X molecular sieve aluminas are stabilized by the incorporation of rare earth cations. This stabilization effect is general in scope and can be applied over a range of rare earth metal ion loadings to structures assembled from different families of non-ionic polyethylene oxide surfactants. Although the framework walls in MSU-X alumina molecular sieves are amorphous and lack the quasi-crystalline order of transition aluminas, the stabilization mechanisms most likely are related. Thus, rare earth doping also should be effective in stabilizing the amorphous walls of alumina mesostructures assembled through S–I and S^-I^+ pathways.[2,3]

Based in part on the absence of XRD evidence for the formation of rare earth aluminates upon calcination, we favor a stabilization mechanism in which the lability of the oxide framework is reduced through site substitution of aluminium by rare earth cations. The incorporation of the rare earth cations into the oxide framework occurs during the mesostructure assembly process. We may rule out a doping process in which the rare earth is first incorporated into the mesostructure by complexation to the polar ethylene oxide head groups of the surfactant phase and then subsequently transferred into the framework upon calcination. Rare earth incorporation into the framework occurs even when the surfactant is removed from the mesostructure by solvent extraction under ambient conditions. Thus, the direct incorporation of the rare earth cations into the framework structure is a general feature of the assembly pathway.

The partial support of this research by the National Science Foundation through CRG grant CHE-9633798 is gratefully acknowledged.

Notes and References

† E-mail: pinnavaia@cem.msu.edu

1 C. T. Kresge, M. E. Leonowicz, W. J. Roth, J. C. Vartuli and J. S. Beck, *Nature*, 1992, **359**, 710.
2 F. Vaudry, S. Khodabandeh and M. E. Davis, *Chem. Mater*., 1996, **8**, 1451.
3 M. Yada, M. Machida and T. Kijima, *Chem. Commun*., 1996, 769.
4 S. A. Bagshaw, E. Prouzet and T. J. Pinnavaia, *Science*, 1995, **269**, 1242.
5 S. A. Bagshaw and T. J. Pinnavaia, *Angew. Chem., Int. Ed. Engl*., 1996, **35**, 1102.
6 S. Matsuda, A. Kato, M. Mizumoto and H. Yamashita, *Proc. Int. Congr. Catal., Berlin*, 1984, **4**, P879; L. P. Haack, J. E. de Vries, K. Otto and M. S. Chattha, *Appl. Catal. A*, 1992, **82**, 199.
7 F. Mizukami, K. Maeda, M. Watanabe, K. Masuda, T. Sano and K. Kuno, *Stud. Surf. Sci. Catal*., 1991, **71**, 557; J. S. Church, N. W. Cant and D. L. Trimm, *Appl. Catal*., 1993, **101**, 105.

Received in Columbia, MO, USA, 12 November 1997; 7/08178B

Synthesis of novel monoazo benzotriazole dyes specifically for surface enhanced resonance Raman scattering‡

Duncan Graham,*† Clare McLaughlin, Gerard McAnally, Joanna C. Jones, Peter C. White and W. Ewen Smith

Department of Pure and Applied Chemistry, University of Strathclyde, Glasgow, UK G1 1XL

Surface enhanced resonance Raman scattering (SERRS) has considerable potential as an ultra-sensitive analytical technique; for the first time the synthesis of specific dye ligands designed to overcome major problems in obtaining reliable SERRS is described.

Surface enhanced resonance Raman scattering (SERRS) has recently proven to be an extremely sensitive and selective technique for the detection and identification of suitable molecules.[1–4] It has significant advantages, being applicable to a wide range of chromophores and provides molecularly informative analysis with minimal separation procedures at attomolar concentrations or below. The main problem for analysis by SERRS is that the technique lacks reliability and reproducibility. We report for the first time the synthesis of four dyes specifically designed to provide effective and reliable SERRS. They are based on simple azo structures and utilise a surface complexing group to release the advantages of SERRS for accurate and reliable analysis.

The technique requires the adsorption of a suitable analyte onto an appropriate metal surface, excitation of the surface with light and collection of the scattered radiation. The Raman component of scattering, enhanced by contributions from molecular resonance and surface enhancement can rival fluorescence in efficiency and provide molecularly specific signals. In this study silver colloid is used to provide the metal surface[5] and 457.9 nm excitation was provided by an argon ion laser. The main problem is to produce a chromophore for both resonance and surface attachment which will withstand changes in conditions of the analyte solution and will not desorb from the silver.

The dyes synthesised use benzotriazole as a surface attachment group. Benzotriazole dyes have been synthesised before but only as dyes and not metal complexing agents for improved spectroscopy.[6] Benzotriazole is commonly used as an anti-tarnish agent on silver and is believed to adhere by complexing to more than one silver ion to form a polymeric species coated on the surface.[7–9] Thus covalent attachment to the surface is possible and the orientation of the dye will be fixed. This eliminates changes in peak wavenumber owing to orientational changes or desorption from the surface commonly observed below monolayer coverage.[10] The colloid used is stable for three to six months due to the high negative charge on the surface and has been routinely used for analysis previously.[3,5] The main advantage of covalent attachment through benzotriazole is that the process is essentially irreversible and can displace surface charged species. Thus, once attached the dye remains in position over a wide range of experimental conditions and concentrations to provide reproducible analysis.

Four monoazo dyes containing benzotriazole were synthesised by diazotising 5-aminobenzotriazole§ and coupling¶ to phenylamine analogues (Fig. 1). The analogues used were aniline, anisidine, dimethoxyaniline and naphthalamine to produce the dyes 4-(5′-azobenzotriazolyl)phenylamine **1**, 3-methoxy-4-(5′-azobenzotriazolyl)phenylamine **2**, 3,5-dimethoxy-4-(5′-azobenzotriazolyl)phenylamine **3** and 4-(5′-azobenzotriazolyl)naphthalen-1-ylamine **4**.‖ The amino derivatised aromatics were chosen for two reasons. Firstly the amine group provides a suitable point for derivatisation once the dye has been synthesised and secondly the aromatic ring is highly activated towards electrophilic attack of the diazonium. The diazotised aminobenzotriazole is not a strong electrophile and requires an activated aromatic ring, *i.e.* aniline and the presence of a buffer. In this case sodium acetate buffered to a pH of 6.0 by the addition of glacial acetic acid was used. The buffer ensured the aromatic amine was not protonated thus maintaining the reactivity. Acetone was added to aid solubility and allow the reaction to proceed smoothly. The products precipitated and were purified by trituration using methanol and diethyl ether.

Each of the dyes produced distinct, strong SERRS at 1×10^{-7} M except 4-(5′-azobenzotriazolyl)phenylamine **1** which was used at a concentration of 1×10^{-5} M (Fig. 2). The enhancement obtained depends on the separation between the electronic maximum and the laser frequency. In the case of dye **1**, the spectrum is weak because the absorbance maximum is well away from the excitation frequency and hence from resonance. Major peaks which appear in all four are the quadrant stretch of the phenyl ring just above 1600 cm^{-1}, the azo stretch above 1400 cm^{-1}, and bands at around 1150 and 950 cm^{-1} which correspond to more complex phenyl and bridge stretching modes.

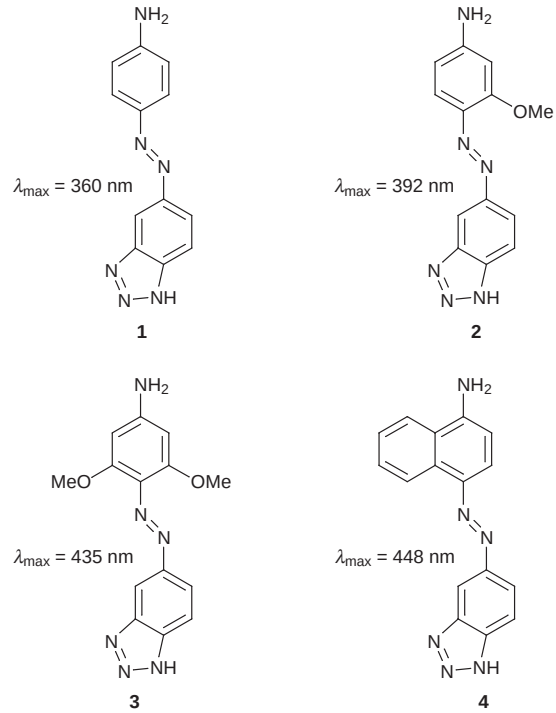

Fig. 1 The four benzotriazole dyes synthesised and their corresponding λ_{max} in methanol

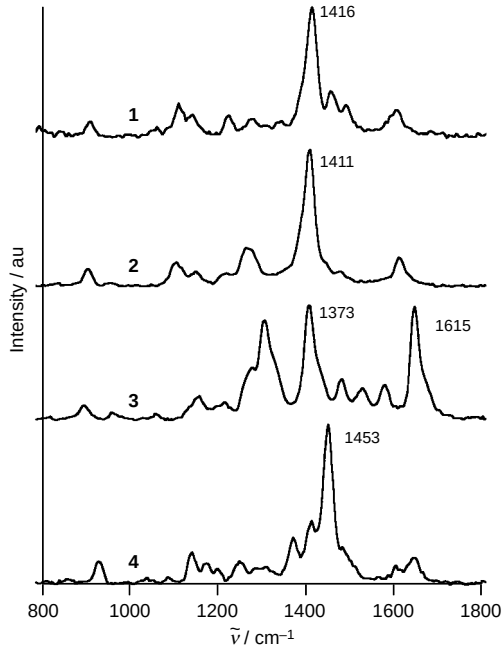

Fig. 2 SERRS spectra of the dyes at 457.9 nm at 1×10^{-7} M except for **1** which was at 1×10^{-5} M

Three dyes produce similar spectra and exact peak positions can be used to discriminate between them. However, when a second methoxy group is added to anisidine analogue, the resulting dye produces a spectrum which is quite different. The extra electron donation of the methoxy group has probably twisted the ring and also created sufficient electron donation to produce partial bonding to the C–N and N=N bonds.

Surface enhancement of vibrations is dependent upon the orientation of the molecule on the surface.[10] Hence different vibrations are enhanced as the molecular orientation changes producing a variation in spectra. Changes in surface orientation are related to the concentration of the analyte on the surface. However by making use of the strong complexing nature of benzotriazole on the silver a structure locked in one conformation can be obtained. The vibrations enhanced will always be the same at any concentration therefore increasing reliability. Dye **3** was studied in more detail between 5×10^{-9} and 1×10^{-6} M and unlike previous studies the relative intensities and position of the signals remained constant. The signal intensity obtained was proportional to concentration which will allow development of quantitative analysis by SERRS.

The technique has now been shown to be reliable and since it is sensitive to changes in the environment and structure of the chromophore, there is considerable scope for the synthesis of designed dyes to permit specific analytical procedures to be developed for ultra-sensitive analysis. For example the ligands require chemical functionalisation to allow addition of groups such as metal complexing functions or attachment to target analyte molecules such as DNA. This is a significant breakthrough which demonstrates that with the correct attention to surface chemistry SERRS can be used as a reliable analytical method.

Notes and References

† E-mail: duncan.graham@strath.ac.uk

‡ This work arose from initial studies with a different focus by Heather Wilson, PhD, University of Strathclyde, 1994.

§ *Diazotisation*: 5-aminobenzotriazole (1.0 g, 1.1 equiv., 7.63 mmol) was dissolved in HCl (5 ml, 50% v/v) and diazotised by dropwise addition of sodium nitrite (0.578 g, 1.2 equiv., in 5 ml H_2O) at 0 °C. An excess of sodium nitrite was detected using starch iodide paper. A dark blue colour indicated excess nitrous acid which inferred the formation of the diazonium salt.

¶ *Coupling*: the amine (1 equiv.) was dissolved in sodium acetate buffer (1.0 M, 5 ml, pH 6.0) and acetone (5 ml). Diazotised aminobenzotriazole (1.1 equiv.) was added to this solution dropwise at 0 °C with stirring over 1 h after which the solution was neutralised by addition of sodium hydroxide (2 M). The solid produced was isolated by filtration and washed with saturated KCl (3×50 ml) prior to purification by trituration using metahnol and diethyl ether.

‖ All novel compounds were characterized by UV spectrometry, proton NMR and FAB mass spectrometry. The purity of the compounds was confirmed by HPLC [retention time for **2** = 4.9 min at 430 nm from methanol–water (60 : 40)] owing to the difficulty in crystallisation. **2**: 40%, R_f [CH_2Cl_2–CH_3OH (9/1)] 0.34; δ_H[400 MHz, $(CD_3)_2SO$] 3.96 (3 H, s, OCH_3), 6.46 (1 H, s, H-2), 6.61 (1 H, d, *J* 8.8, H-5), 7.10 (2 H, br s, NH_2), 7.85 (1 H, dd, *J* 6.0 H-6), 7.98 (2 H, d, *J* 10.2, H-6′,7′), 8.18 (1 H, s, H-4′); λ_{max}(MeOH) 392 nm; FAB MS: *m*/*z* 269.1144 [$C_{13}H_{12}ON_6$ (*M* + 1) < 0.1 ppm].

1 K. Kneipp, Y. Wang, H. Kneipp, L. T. Perelman, I. Itzkah, R. Dasari and M. S. Feld, *Phys. Rev. Lett.*, 1997, **78**, 1667; S. Nie and S. R. Emory, *Science*, 1997, **275**, 1102; K. Kneipp, Y. Wang, R. R. Dasari and M. S. Feld, *Appl. Spectrosc.*, 1995, **49**, 780.
2 C. Rodger, W. E. Smith, G. Dent and M. Edmondson, *J. Chem. Soc., Dalton Trans.*, 1996, **5**, 791.
3 C. H. Munro, W. E. Smith and P. C. White, *Analyst*, 1995, **120**, 993.
4 C. H. Munro, W. E. Smith, D. R. Armstrong and P. C. White, *J. Phys. Chem.*, 1995, **99**, 879.
5 C. H. Munro, W. E. Smith, M. Garner, J. Clarkson and P. C. White, *Langmuir*, 1995, **11**, 3712.
6 J. Daud and S. B. Saxena, *J. Soc. Dyers Colour.*, 1994, **110**, 154.
7 H. Wilson and W. E. Smith, *J. Raman Spectrosc.*, 1994, **25**, 899.
8 J. C. Rubin, *Chem. Phys. Lett.*, 1990, **167**, 209.
9 Y. Ling, Y. Guan and K. N. Han, *Corrosion Sci.*, 1995, **51**, 367.
10 D. A. Weitz, M. Moskovits and J. A. Creighton, *Chemistry and Structure at Interfaces*, ed. R. B. Hall and A. B. Ellis, VCH, Deerfield Beach, FL, 1986.

Received in Exeter, UK, 13th February 1998; 8/01289J

First total synthesis of (+)-3-deoxy-D-*glycero*-D-*galacto*-2-nonulosonic acid (KDN) from a non-carbohydrate source

Martin Banwell,*[a]† Chris De Savi[a] and Keith Watson[b]

[a] *Research School of Chemistry, Institute of Advanced Studies, The Australian National University, Canberra, ACT 0200, Australia*

[b] *Biota Chemistry Laboratory, Chemistry Department, Monash University, Clayton, Victoria 3168, Australia*

Enantiopure *cis*-1,2-dihydrocatechol 2, a product obtained by microbial oxidation of chlorobenzene, has been converted into KDN 1 *via* a ten step reaction sequence.

In 1986 Inoue isolated the deaminated sialic acid (+)-3-deoxy-D-*glycero*-D-*galacto*-2-nonulosonic acid (KDN, **1**) from the

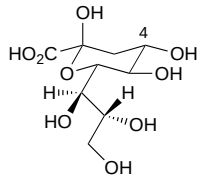

1

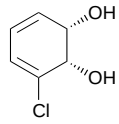

2

membrane polysialoglycoproteins of rainbow trout eggs.[1] Since KDN is likely responsible for protection of the egg membrane from attack by bacterial sialidases,[2] this compound is of interest as a sialic acid analogue that could be incorporated into other biologically relevant glycoproteins in order to protect them against sialidase activation by certain bacteria.[3] Such possibilities have sparked considerable interest in KDN glycoscience with the result that several syntheses of the title compound have now been reported.[1,4] All of these involve elaboration of carbohydrate-based starting materials. We now describe the first total synthesis of KDN from a non-carbohydrate source. The reaction sequence used will enable the preparation of novel analogues including those which incorporate ^{17}O-, ^{13}C- and/or ^{2}H-labels in various combinations. Such analogues[5] should be useful for probing the biological role(s) of KDN and related carbohydrate natural products.

The reaction sequence leading to compound **1** was inspired by the seminal work of Hudlicky and co-workers who have demonstrated the value of *cis*-1,2-dihydrocatechols as starting materials for the synthesis of various pentoses and hexoses.[6,7] In the present work (Scheme 1) the *cis*-1,2-dihydrocatechol **2**, which is obtained in >99% ee *via* microbial oxidation of chlorobenzene, was used. Thus, the acetonide derivative, **3**,[8] of compound **2** underwent regioselective and diastereofacially-selective *cis*-dihydroxylation on reaction with osmium tetraoxide and the resulting diol **4**[8] was reacted with 2,2-dimethoxypropane in the presence of toluene-*p*-sulfonic acid (TsOH) to give the *bis*-acetonide **5**‡ {99%, $[\alpha]_D$ + 68 (*c* 3.4)§}. Surprisingly, this last compound failed to react with ozone, perhaps because both faces of the π-bond are hindered by the *endo*-methyl groups associated with the adjacent 1,3-dioxolane rings. To circumvent such difficulties, diol **4** was converted into the corresponding bis(*tert*-butyldimethylsilyl ether) **6**[9] {83%, mp <25 °C, $[\alpha]_D$ − 56 (*c* 6.4)} which underwent smooth ozonolytic cleavage to give, after a reductive work-up with $NaBH_4$, the ester alcohol **7** {99%, $[\alpha]_D$ + 12 (*c* 6.8)}. The *tert*-butyldimethylsilyl ether derivative, **8** {100%, $[\alpha]_D$ + 2 (*c* 1.5)}, of the latter compound was then prepared in quantitative yield by standard methods. This compound was converted, over two conventional steps, into the unstable D-mannose derivative **9** {87% from **8**, $[\alpha]_D$ + 14 (*c* 5.8)}. Reaction of compound **9** with Vasella's pyruvate anion equivalent **10**,[10,11] under conditions we have used previously,[12] gave a *ca.* 2 : 3 mixture of the *syn*- and *anti*-addition products, **11** {37%, $[\alpha]_D$ + 10 (*c* 1.9)} and **12**

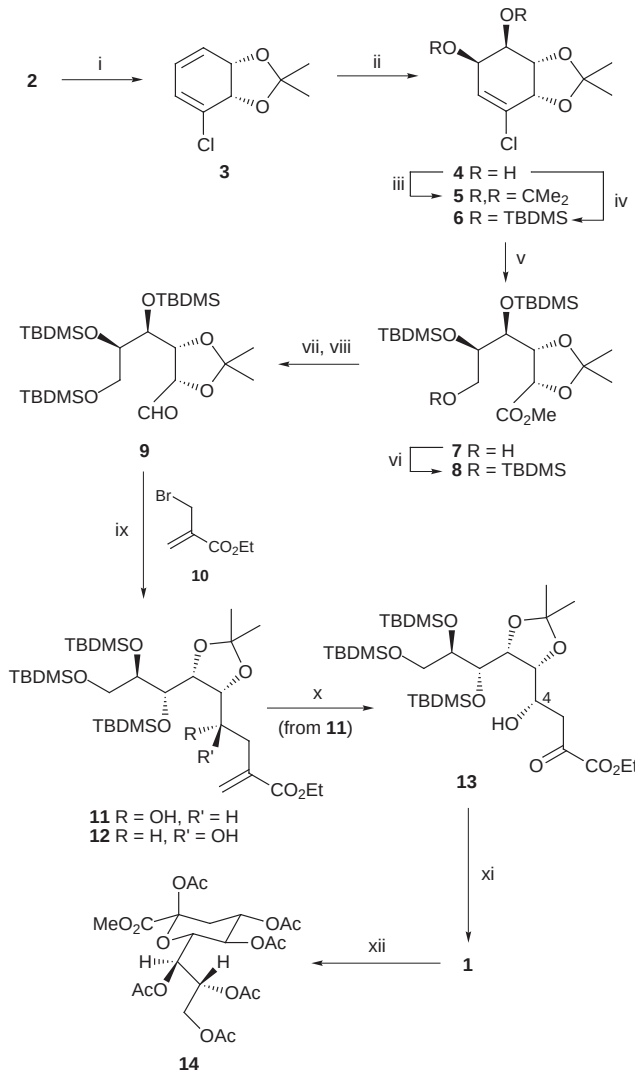

Scheme 1 *Reagents and conditions*: i, see ref. 8; ii, see ref. 8; iii, $Me_2C(OMe)_2$, TsOH (cat.), 18 °C, 1.0 h; iv, TBDMSCl (4 equiv.), imidazole (5 equiv.), DMF, 18 °C, 16 h; v, O_3, MeOH, −78 to 0 °C, 0.1 h, then $NaBH_4$ (4 equiv.), 18 °C, 2 h; vi, TBDMSOTf (1.5 equiv.), 2,6-lutidine (3 equiv.), CH_2Cl_2, 0 to 18 °C, 16 h; vii, LAH (1.5 equiv.), THF, −10 °C, 2 h; viii, $(COCl)_2$ (1.2 equiv.), DMSO, CH_2Cl_2, −78 to 0 °C, 1 h, then Et_3N (2.6 equiv.); ix, Zn dust (4.0 equiv.), sat. aq. NH_4Cl, THF, 0 to 18 °C, 1.5 h; x, O_3, MeOH, −78 °C, 0.033 h, then Me_2S (5 equiv.), −78 to 18 °C, 2 h; xi, 4 : 1 TFA–H_2O, 18 °C, 18 h; xii, Dowex 50W resin (H^+ form), MeOH, 6 h, 18 °C, then Ac_2O (10 equiv.), DMAP (trace), pyridine, 18 °C, 20 h

{52%, $[\alpha]_D$ + 16 (*c* 1.6)}, respectively. The components of this mixture were readily separated from one another by semi-preparative HPLC and compound **11** was then subjected to reaction with ozone. In this way the α-keto ester **13** {98%, $[\alpha]_D$ + 5 (*c* 2.2)} was obtained. Treatment of compound **13** with 4 : 1 TFA–water at 18 °C for 16 h resulted in deprotection of all the hydroxy groups as well as cyclisation to give KDN which was identical, as judged by ^{1}H NMR analysis, with an authentic sample prepared by enzymatic methods.[4g] For the purposes of further spectroscopic characterisation, KDN was esterified using MeOH and the intermediate methyl ester subjected to exhaustive acetylation. In this way the KDN derivative **14**[13] {68% from **13**, mp 100–104 °C; lit.,[13] 104–105 °C; $[\alpha]_D$ − 17 (*c* 1.9); lit.,[13] − 20 (*c* 0.7)} was obtained and the structure of this compound follows from spectroscopic data.¶ In addition, this material proved identical with a sample {$[\alpha]_D$ − 17 (*c* 1.2)} prepared from authentic KDN. Interestingly, while ozonylitic cleavage of compound **12** gave 4-*epi*-**13** {98%, $[\alpha]_D$ + 17 (*c* 5.0)}, sequential treatment of the latter compound with TFA–water, acidic MeOH then Ac_2O–pyridine only gave a complex mixture of uncharacterisable products.

We thank the Institute of Advanced Studies for financial support and the ARC for the provision of an APA (Industry) Scholarship to C. D. S. Dr Gregg Whited (Genencor International Inc.) is thanked for providing generous quantities of diol **2**.

Notes and References

† E-mail: mgb@rsc.anu.edu.au

‡ All new and stable compounds had spectroscopic data [IR, UV, NMR, mass spectrum] consistent with the assigned structure. Satisfactory combustion and/or high resolution mass spectral analytical data were obtained for new compounds and/or suitable derivatives.

§ All optical rotations were determined in $CHCl_3$ at 20 °C.

¶ *Selected data* for **14**: δ_H(300 MHz, $CDCl_3$) 5.40 (dd, *J* 6.4 and 2.3, 1 H), 5.27 (m, 1 H), 5.15 (dt, *J* 6.0 and 2.5, 1 H), 4.97 (t, *J* 9.7, 1 H), 4.43 (dd, *J* 12.2 and 2.2, 1 H), 4.19 (dd, *J* 10.1 and 2.4 Hz, 1 H), 4.14 (dd, *J* 12.2 and 5.8, 1 H), 3.78 (s, 3 H), 2.63 (dd, *J* 13.7 and 5.3, 1 H), 2.08 (obscured multiplet, 1 H), 2.16 (s, 3 H), 2.12 (s, 3 H), 2.07 (s, 3 H), 2.04 (s, 3 H), 2.02 (s, 3 H), 2.01 (s, 3 H); δ_C (75 MHz, $CDCl_3$) 170.6, 170.1, 170.0, 169.7, 169.6, 168.2, 166.0, 97.2, 71.4, 70.1, 68.7, 67.3, 66.8, 61.8, 53.2, 35.4, 20.8, 20.7, 20.6 (3 methyl carbon resonances obscured or overlapping); ν_{max}(KBr)/cm^{-1} 2961, 1750, 1437, 1372, 1233, 1169, 1114, 1055, 1013, 946; *m/z* (EI, 70 eV) 534 ($M^{+\cdot}$, < 1%), 433 (100), 373 (100) [HRMS: Calc. for $C_{22}H_{30}O_{15}$ ($M^{+\cdot}$), 534.1585. Found: 534.1583].

1 D. Nadano, M. Iwasaki, S. Endo, K. Kitajima, S. Inoue and Y. Inoue, *J. Biol. Chem*., 1986, **261**, 11 550.
2 E. Schreiner and E. Zbiral, *Liebigs Ann. Chem*., 1990, 581.
3 K. Kitajima, *Bio. Ind*., 1997, **14**, 11 and references cited therein.
4 (*a*) H. Tsukamoto and T. Takahashi, *Tetrahedron Lett*., 1997, **38**, 6415; (*b*) T.-H. Chan and M.-C. Lee, *J. Org. Chem*., 1995, **60**, 4228; (*c*) A. Dondoni, A. Marra and P. Merino, *J. Am. Chem. Soc*., 1994, **116**, 3324; (*d*) K. Sato, T. Miyata, I. Tanai and Y. Yonezawa, *Chem. Lett*., 1994, 129; (*e*) M. Nakamura, K. Furuhata and H. Ogura, *Chem. Pharm. Bull*., 1988, **36**, 4807; (*f*) R. Shirai, M. Nakamura, S. Hara, H. Takayanagi and H. Ogura, *Tetrahedron Lett*., 1988, **29**, 4449. Various enzymatic methods for the preparation of KDN have been reported: see (*g*) T. Sugai, A. Kuboki, S. Hiramatsu, H. Okazaki and H. Ohta, *Bull. Chem. Soc. Jpn.*, 1995, **68**, 3581 and references cited therein.
5 For recent work concerned with the synthesis of KDN analogues, see: G. B. Kok, A. K. Norton and M. von Itzstein, *Synthesis*, 1997, 1185; G. B. Kok and M. von Itzstein, *Synthesis*, 1997, 769; X.-L. Sun, T. Kai, H. Takayanagi and K. Furuhata, *J. Carbohydr. Chem*., 1997, **16**, 541; T. Kai, X.-L. Sun, H. Takayanagi and K. Furuhata, *J. Carbohydr. Chem*., 1997, **16**, 521; T.-H. Chan, Y.-C. Xin and M. von Itzstein, *J. Org. Chem*., 1997, **62**, 3500; G. B. Kok, B. L. Mackey and M. von Itzstein, *Carbohydr. Res*., 1996, **289**, 67; A. Hasegawa, N. Suzuki, F. Kozawa, H. Ishida and M. Kiso, *J. Carbohydr. Chem*., 1996, **15**, 639.
6 For two excellent reviews, see T. Hudlicky, D. A. Entwistle, K. K. Pitzer and A. J. Thorpe, *Chem. Rev*., 1996, **96**, 1195; T. Hudlicky, K. A. Abboud, D. A. Entwistle, R. Fan, R. Maurya, A. J. Thorpe, J. Bolonick and B. Myers, *Synthesis*, 1996, 897. See, also, F. Yan, B. V. Nguyen, C. York and T. Hudlicky, *Tetrahedron*, 1997, **53**, 11 541; T. Hudlicky, K. K. Pitzer, M. R. Stabile, A. J. Thorpe and G. M. Whited, *J. Org. Chem*., 1996, **61**, 4151.
7 For reviews on the applications of *cis*-1,2-dihydrocatechols in synthesis, see ref. 6 and T. Hudlicky and A. J. Thorpe, *Chem. Commun*, 1996, 1993; T. Hudlicky and J. W. Reed, in *Advances in Asymmetric Synthesis*, ed. A. Hassner, JAI, Greenwich, CT, 1995, vol. 1, p. 271; S. M. Brown, and T. Hudlicky, in *Organic Synthesis: Theory and Applications*, ed. T. Hudlicky, JAI, Greenwich, CT, 1993, vol. 2, p. 113; H. A. J. Carless, *Tetrahedron: Asymmetry*, 1992, **3**, 795; D. A. Widdowson, D. W. Ribbons and S. D. Thomas, *Janssen Chimica Acta*, 1990, 3.
8 T. Hudlicky, M. Mandel, J. Rouden, R. S. Lee, B. Bachmann, T. Dudding, K. J. Yost and J. S. Merola, *J. Chem. Soc., Perkin Trans. 1*, 1994, 1553.
9 T. Hudlicky, F. Rulin, T. Tsunoda, H. Luna, C. Andersen and J. D. Price, *Isr. J. Chem*., 1991, **31**, 229.
10 F. Baumberger and A. Vasella, *Helv. Chim. Acta*, 1986, **69**, 1205. For a review on, *inter alia*, pyruvate anion equivalents, see L. Kovács, *Recl. Trav. Chim. Pays-Bas*, 1993, **112**, 471.
11 Chan and Lee [ref. 4(*b*)] have used a closely related nucleophilic addition reaction in their synthesis of KDN.
12 M. Banwell, C. De Savi, D. Hockless and K. Watson, *Chem. Commun*, 1998, 645.
13 M. Nakamura, H. Takayanagi, K. Furuhata and H. Ogura, *Chem. Pharm Bull*., 1992, **40**, 879; M. Nakamura, K. Furuhata, T. Yamasaki and H. Ogura, *Chem. Pharm. Bull*., 1991, **39**, 3140; M. Nakamura, K. Furuhata, K. Yamazaki, H. Ogura, H. Kamiya and H. Ida, *Chem. Pharm Bull*., 1989, **37**, 2204.

Received in Cambridge, UK, 9th March 1998; 8/01889H

N-Nitrosated *N*-hydroxyguanidines are nitric oxide-releasing diazeniumdiolates

Garry J. Southan,*[a]†‡ Aloka Srinivasan,[b] Clifford George,[c] Henry M. Fales[d] and Larry K. Keefer[b]

[a] *Intramural Research Support Program, SAIC Frederick, NCI-FCRDC, Frederick, MD 21702, USA*
[b] *Chemistry Section, Laboratory of Comparative Carcinogenesis, National Cancer Institute, Frederick Cancer Research and Development Center, Frederick, MD 21702, USA*
[c] *Laboratory for the Structure of Matter, Naval Research Laboratory, Washington, DC 20375, USA*
[d] *Laboratory of Chemistry, National Heart, Lung and Blood Institute, Bethesda, MD 20892, USA*

***N*-Hydroxyguanidines can be nitrosatively converted to zwitterionic diazeniumdiolates of crystallographically-confirmed structure H_2N^+=C[NHR][N(O)NO]$^-$, whose hydrolytic dissociation at physiological pH leads to both NO and N_2O; the results appear to account for the formation of the 'potential intercellular nitric oxide carrier' produced on exposing N^G- hydroxy-L-arginine (a metabolic intermediate in mammalian NO biosynthesis) to aerobic NO.**

Nitric oxide (NO) is a recently discovered bioeffector molecule that is critically involved in regulation of blood pressure, neurotransmission, sexual function, immunity and an array of other physiological phenomena.[1] It is rapidly destroyed by biochemical oxidants such as oxyhemoglobin, superoxide and oxygen,[2] leading to speculation that its regulatory properties might depend, in part, on conversion to a biochemical storage form[3] that protects it from oxidation while in transit from the site of biosynthesis in one cell to the target of its required signalling action in another.

Recently, the formation of such a 'potential intercellular nitric oxide carrier' was reported to occur on exposing N^G-hydroxy-L-arginine **1a**, an intermediate in NO biosynthesis, to aerobic nitric oxide solutions.[4] The product was ultraviolet-active and longer lived as a vasodilator than molecular NO,[5] but its structure has yet to be elucidated.

We present evidence here based on work with model *N*′-substituted *N*-hydroxyguanidines that this bioactive compound may be a naturally occurring diazeniumdiolate (Scheme 1, structure **2a**). While there was no observable reaction when NO was bubbled into degassed solutions of *N*′-(*p*-methoxybenzyl)-*N*-hydroxyguanidine **1b** in water, subsequent introduction of air led to appearance of an ultraviolet maximum at 322 nm, a result reminiscent of that seen with both *N*-hydroxyguanidine **1c**[5] and **1a** itself.[6] A similar outcome was observed when NO_2 was introduced instead of air into anaerobic solutions of **1b** and NO, suggesting that N_2O_3, formed either on autoxidation of NO or on radical coupling of NO with NO_2, had reacted nitrosatively[7] with **1b**. When alternate nitrosation conditions were effected by dissolving 0.1 g of **1b**·HCl in 2 ml of 0.1 M aqueous AcOH and adding 1 equiv. of sodium nitrite as a saturated aqueous solution at 0 °C, a crystalline precipitate began to form that, when collected after 20 min of total reaction time (yield of **2b** 95%, mp 136–147 °C with gradual decomposition), was suitable for X-ray diffractometric investigation without further purification. (Indeed, attempts to recrystallize this relatively unstable substance have thus far led to partial decomposition.) The molecular structure,§ refined to an *R* value of 0.034, is shown in Fig. 1.

The crystallographic data show that nitrosation of **1b** occurred at the nitrogen bound to the oxygen atom to give a diazeniumdiolate product **2b**, as shown in Scheme 1. Noteworthy structural features include the cisoid oxygens in the

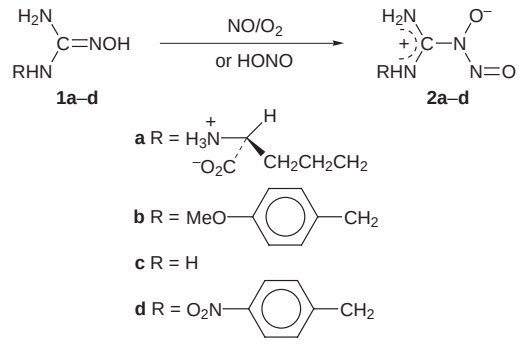

Scheme 1

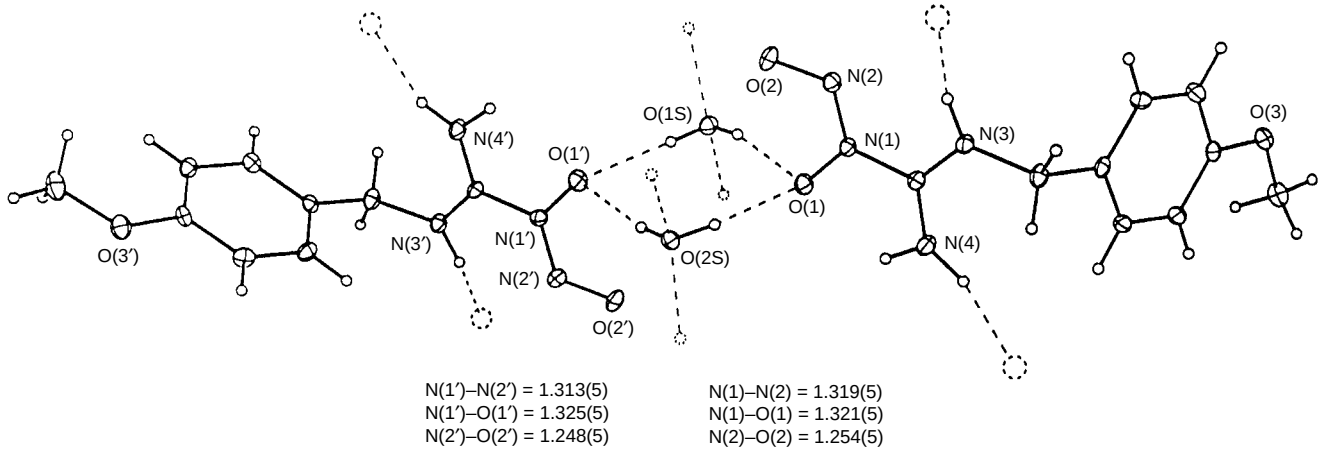

N(1′)–N(2′) = 1.313(5)
N(1′)–O(1′) = 1.325(5)
N(2′)–O(2′) = 1.248(5)

N(1)–N(2) = 1.319(5)
N(1)–O(1) = 1.321(5)
N(2)–O(2) = 1.254(5)

Fig 1 Molecular structure of the asymmetric unit of **2b** summarizing bond lengths within the diazeniumdiolate (ONNO) groups. Dotted atoms are symmetry related. Dotted bonds are hydrogen bonds.

$N_2O_2^-$ group and the presence of two different conformers of **2b** along with two water molecules in the asymmetric unit that forms a hydrogen bonded helix (Fig. 1). Similar results were obtained on nitrosation of the *p*-nitrophenyl analogue **1d**; although the structure of the diazeniumdiolate product **2d** did not refine well (R = 0.125), this was due to disorder in the crystal which could not be modelled in the refinement. The atomic connectivity and atom assignments are, however, well defined.¶

Rapid measurement of the ultraviolet spectrum on dissolution of **2b** in water permitted quantitative determination of the characteristic chromophore's extinction coefficient (2.5 mM^{-1} cm^{-1} at λ_{max} = 322 nm). The NMR spectrum, run at −50 °C in CD_3OD–tetramethylsilane to minimize the rapid decomposition observed at room temperature, consisted of singlets for the CH_3O and CH_2 protons at δ 3.77 and 4.57, respectively, and an aryl AA′BB′ pattern with shifts of δ 6.93 and 7.30 (*ortho* and *meta* to OCH_3, respectively) and J = 8.6, 2.7, and 0.4 Hz for the *ortho*, *meta* and *para* couplings, respectively. The mass spectra of **2b** and **2d** were unusual (but not unprecedented) in their failure to produce an observable MH^+ ion in either the electrospray or fast atom bombardment modes; strong peaks due to the respective benzyl cations were seen in both cases, but ^{15}N-labelling indicated that the terminal NO was rapidly lost even under the mildest possible electrospray conditions.

Compound **2b** was found to decompose with gas evolution on dissolution in aqueous media. At pH 10, *N*-(*p*-methoxybenzyl)cyanamide **3b** and N_2O were each produced in ⩾95% yield in a relatively slow reaction (half-life at 37 °C variable but estimated as 15–25 min) that is presumably initiated by deprotonation of the NH_2 group followed by loss of *cis*-hyponitrite (⁻O–N=N–O⁻), a known progenitor of N_2O.[8] Compound **2b** tended to disappear more rapidly as pH was lowered, with a half-life at pH 3 of about 5 min; some denitrosation was observed at very low pH, **1b** being the most abundant of the organic products seen in 0.1 M HCl. The major gaseous product at low pH proved to be NO, reaching yields of 0.9 moles per mole of **2b** at pH 3 compared with 0.25 moles of N_2O. While the mechanism of NO formation is not clear at this time, there can be little doubt about its production; its identity was confirmed both by the presence of its aqueous autoxidation product, nitrite ion,[9] in the reaction mixture and by a well-established, highly selective chemiluminescence method.[10] In physiological buffer (10 mM phosphate, pH 7.4), *N*-(*p*-methoxybenzyl)urea **4b** was produced in 90% yield, with 8% conversion to **3b** and a small amount of an unidentified product also detected by HPLC. At pH 7.4, 0.5 moles of N_2O were produced along with 0.3 moles of NO per mole of **2b** dissociated. These reactions are summarized in Scheme 2. Comparable results were observed on hydrolysis of **2c** and **2d**.

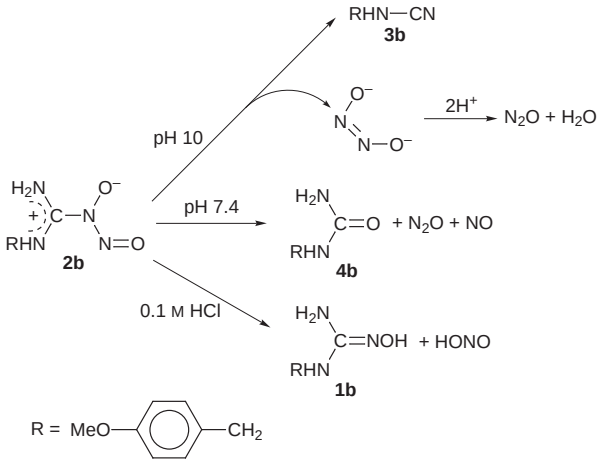

Scheme 2

Since nitrosation of all four *N*-hydroxyguanidines **1a**–**d** yields hydrolytically unstable products with ultraviolet maxima near 320 nm that generate significant quantities of NO in neutral buffer, the crystallographic data for products **2b** and **2d** strongly suggest that the 'nitric oxide carrier' seen by Hecker *et al.*[4] on exposing **1a** to aerobic NO was diazeniumdiolate **2a**.

We postulate that our data may be of two-fold biological significance. First, if free **1a** can be shown to encounter suitably nitrosating conditions *in vivo*, the product **2a** would constitute a naturally occurring diazeniumdiolate that spontaneously releases NO at physiological pH; two other natural products containing the diazeniumdiolate functional group, dopastin and alanosine, have been reported to release NO only on one-electron oxidation.[11] Second, the NO-generating properties of compounds **2** may render them useful as prodrugs for treating clinical disorders arising from deficiencies of biosynthetic NO.[1] The possible medicinal value of **2** and analogous structures will be investigated.

Notes and References

† Present address: Inotek Inc., 3rd Floor, 3130 Highland Avenue, Cincinnati, OH 45219-2374, USA.
‡ E-mail: gjsouthan@aol.com

§ *Crystal data* for **2b**. $C_9H_{12}N_4O_3{\cdot}H_2O$, M_r = 242.24, monoclinic space group $P2_1$, a = 12.452(2), b = 7.156(1), c = 12.887(2) Å, β = 97.74(1)°, V = 1137.8(3) Å^3, Z = 4, D_c = 1.414 Mg m^{-3}, λ(Mo-Kα) = 0.71073 Å, μ = 0.113 mm^{-1}, F(000) = 512, T = 223 K. A set of 1773 reflections was collected, and 1388 were observed with $F_o > 4\sigma(F_o)$, $R1$ = 0.034 and $wR2$ = 0.083.

¶ Crystals were triclinic, space group $P\bar{1}$, a = 6.256(1), b = 7.120(3), c = 13.180(2) Å, α = 95.11(1), β = 92.33(1), γ = 106.01(1)°. CCDC 182/839.

1 L. K. Keefer, C .F. Nathan and W. J. Payne, in *Encyclopedia of Molecular Biology and Molecular Medicine*, ed. R .A. Meyers, VCH, Weinheim, 1996, vol. 4, p. 200.
2 D. A. Wink, M. B. Grisham, J. B. Mitchell and P. C. Ford, *Methods Enzymol*., 1996, **268**, 12.
3 D. I. Simon, M. E. Mullins, L. Jia, B. Gaston, D. J. Singel and J. S. Stamler, *Proc. Natl. Acad. Sci. USA*, 1996, **93**, 4736.
4 M. Hecker, H. Macarthur, W. C. Sessa, G. J. Southan, T. A. Swierkosz, D. T. Walsh, A. Zembowicz and J. R. Vane, in *The Biology of Nitric Oxide. 2. Enzymology, Biochemistry and Immunology*, ed. S. Moncada, M. A. Marletta, J. B. Hibbs, Jr. and E. A. Higgs, Portland Press, London, 1992, p. 128.
5 A. Zembowicz, T. A. Swierkosz, G. J. Southan, M. Hecker and J. R. Vane, *Br. J. Pharmacol*., 1992, **107**, 1001.
6 M. Hecker, M. Boese, V. B. Schini-Kerth, A. Mülsch and R. Busse, *Proc. Natl. Acad. Sci. USA*, 1995, **92**, 4671.
7 D. L. H. Williams, *Nitrosation*, Cambridge University Press, Cambridge, 1988.
8 J. Yoo and J. M. Fukuto, *Biochem. Pharmacol*., 1995, **50**, 1995. These authors have proposed **2** as a possible intermediate (postulated to form on coupling of an oxidatively generated *N*-hydroxyguanidine radical cation with NO) in the slow reaction of hydroxyguanidines with anaerobic NO.
9 L. J. Ignarro, J. M. Fukuto, J. M. Griscavage, N. E. Rogers and R. E. Byrns, *Proc. Natl. Acad. Sci. USA*, 1993, **90**, 8103.
10 M. Feelisch and E. A. Noack, *Eur. J. Pharmacol*., 1987, **142**, 465; C. M. Maragos, D. Morley, D. A. Wink, T. M. Dunams, J. E. Saavedra, A. Hoffman, A. A. Bove, L. Isaac, J. A. Hrabie and L. K. Keefer, *J. Med. Chem.*, 1991, **34**, 3242.
11 T. A. Alston, D. J. T. Porter and H. J. Bright, *J. Biol. Chem*., 1985, **260**, 4069.

Received in Corvallis, OR, USA, 23rd February 1998; 8/01543K

Synthesis and application in asymmetric synthesis of azacrown ethers derived from D-glucose

Péter Bakó,[a]† Kristóf Vizvárdi,[a] Zoltán Bajor[a] and László Tõke*[b]

[a] *Department of Organic Chemical Technology, Technical University of Budapest, H-1521 Budapest, Hungary*
[b] *Organic Chemical Technology Research Group of the Hungarian Acadamy of Sciences at the Technical University of Budapest, H-1521 Budapest, Hungary*

New chiral monoaza-15-crown-5 derivatives and lariat ethers anellated to phenyl β-D-glucoside have been synthesized which show significant asymmetric induction as phase transfer catalysts in the Michael addition of 2-nitropropane to chalcone (84% ee) and in the Darzens condensation of phenacyl chloride with benzaldehyde (74% ee).

One of the most attractive types of asymmetric synthesis is that in which chiral products are generated under the influence of chiral crown ether catalysts. Although many optically active crown ethers have been prepared, only a few have been used successfully as catalysts in asymmetric reactions.[1] Previously, we reported the asymmetric Michael addition of phenyl acetate to acrylate catalyzed by chiral crown ethers composed of two glucose units (85% ee).[1,2] The substituents on the sugar unit of the macrocycle[1,2] and the side arms at the nitrogen atom in the crown ring[3] play an important role in the catalytic activity of the crown ethers. The latter compounds with heteroatoms in the side arm, named lariat ethers or armed crown ethers, are known to display special complexation, high lipophilic character and unique guest specificity *via* macroring–side arm cooperativity.[4] It is therefore reasonable to study the effect of using different pendant arms on the chiral crown ether catalyst in asymmetric reactions.

We now report on the synthesis and application of new monoaza-15-crown-5 compounds **4**–**12**.

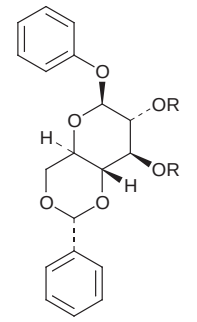

1 R = H
2 R = $(CH_2)_2O(CH_2)_2Cl$
3 R = $(CH_2)_2O(CH_2)_2I$

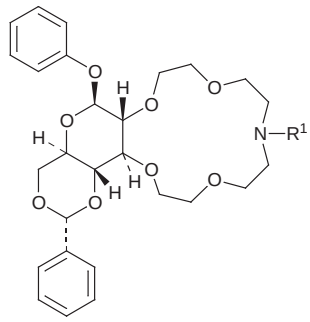

4 R^1 = Bu
5 R^1 = $Pr^i{}_2CH$
6 R^1 = C_6H_{11}
7 R^1 = $C_6H_{11}CH_2$
8 R^1 = Bn
9 R^1 = $Ph(CH_2)_2$
10 R^1 = $HO(CH_2)_2$
11 R^1 = $MeO(CH_2)_2$
12 R^1 = $HO(CH_2)_3$

Their synthesis starts from phenyl 4,6-*O*-benzylidene-β-D-glucopyranoside **1**. The vicinal free hydroxy groups in compound **1** were alkylated using the method of Di Cesare and Gross,[5] with bis(2-chloroethyl) ether acting as solvent and reagent, under liquid–liquid (LL) two-phase reaction conditions, in the presence of tetrabutylammonium hydrogen sulfate (as a phase transfer catalyst) and 50% aq. NaOH to give compound **2** (room temperature, 8 h, column chromatography). The exchange of chlorine for iodine in **2** was carried out using NaI in acetone (reflux, 24 h), resulting in the bis(iodide) derivative **3**. Compound **3** was cyclized with various primary amines: *n*-butylamine, 2,4-dimethylpentan-3-ylamine, cyclohexylamine, cyclohexylmethylamine, benzylamine, 2-phenylethylamine, ethanolamine, 2-methoxyethylamine and propanolamine, respectively, according to the method described previously,[6] which requires dry Na_2CO_3 in MeCN as solvent (reflux, 32–40 h, column chromatography). We thus obtained the corresponding 15-membered macrocycles **4**–**12**, the yields of the ring closure steps after chromatography being in the range 32–54% (Table 1). All structures were ascertained by ^{1}H NMR, ^{13}C NMR, COSY, mass and elemental analysis.‡

Table 1 Yield and characterisation data of compounds **2**–**12**

Compound	Yield (%)[a]	$[\alpha]^{20}$ (c 1, $CHCl_3$)	Mp/°C
2	29	−35.5	74–75
3	95	−28.6	58–59
4	44	−43.0	105–106
5	32	−35.4	58–60
6	39	−39.2	oil
7	32	−41.1	107–108
8	42	−34.9	oil
9	48	−44.3	153–55
10	48	−35.2	oil
11	54	−40.1	oil
12	45	−44.9	oil

[a] After column chromatography.

Compounds **4**–**12** were then used as phase transfer catalysts in different reactions in which enantiomeric mixtures can be formed. These catalysts proved to be effective in two reactions: the Michael addition of 2-nitropropane to chalcone (Scheme 1),

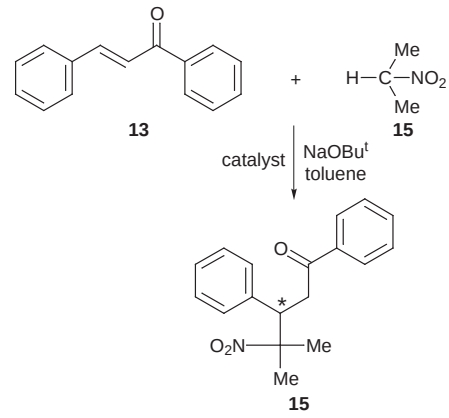

Scheme 1

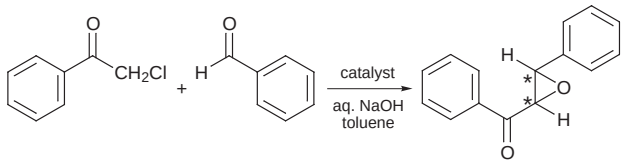

16 17 18

Scheme 2

and the Darzens condensation of phenacyl chloride with benzaldehyde (Scheme 2).

The Michael addition was carried out in a solid–liquid (SL) system; in toluene, employing solid NaOBu^t as base (35 mol%) and chiral catalyst (7 mol%) at room temperature.§ After the usual work-up procedure the adduct was isolated by preparative TLC, and the asymmetric induction, expressed in terms of the enantiomeric excess (ee), was monitored by measuring the optical rotation of the product **15** and comparing it with literature values[3] and by ^{1}H NMR analysis using (+)-Eu(hfc)$_3$ as a chiral shift reagent. The results are shown in Table 2.

As can be seen, the substituents at the N-atom of the catalyst have a significant influence on both the chemical yield and the enentioselectivity. In all cases the (*S*)-(+)-adducts **15** were found to be in excess. The catalyst having the bulky 2,4-dimethylpentan-3-yl group at the N-atom gave the lowest chemical yield and chiral induction (entry 2), and the crown ether having a phenylethyl group (**9**) proved to be the best (entry 6). The methyl ether **11** showed a higher ee value than its free hydroxy analogue **10** (entry 8 and 7). The length of the side arm is decisive: catalyst **8** having a benzyl group shows poor chiral induction (6% ee), while compound **9** containing a phenylethyl group gives high enantioselectivity (84% ee).

The Darzens condensation (Scheme 2) was performed in a binary LL system, using a toluene–30% aq. NaOH (5 : 1) mixture.¶ The work-up procedure and determination of ee was carried out in a similar manner to that mentioned for the Michael addition. In all cases the epoxy ketone product **18** with a negative optical rotation was found to be in excess, which on the basis of the optical rotation of the pure enantiomer, corresponds to an absolute configuration of (2*R*,3*S*).[7] Low enantioselectivities were obtained using catalysts **4**–**8** (entries 1–5). The macrocycle **10** [R = $(CH_2)_2$OH] having the hydrophilic hydroxyethyl group at the N-atom gave 52% ee (entry 7) but this value was dramatically reduced (13% ee) for its methyl ether **11** (entry 8). It is interesting to note that the effect of the compound containing a free hydroxy group on the magnitude of the enantioselectivity for the Darzens condensation is the reverse of that for the Michael reactions (entries 7 and 8). The importance of the chain-length at the N-atom in the catalytic activity is reflected particularly in the experiment shown in entry 9: catalyst **12** [R = $(CH_2)_3$OH] proved to be the most effective, resulting in 74% ee at room temperature. With regard to the effectiveness of the crown ether structure for enantiomeric induction, we suppose that the substituent at the nitrogen atom of the catalyst takes part in the complexation of the salt of the anion by complexation of the cation in the third dimension, working as a pseudo-lariat ether, and as a consequence increases the effectiveness of the phase transfer process. Reactions running in the absence of chiral catalyst give only racemic products.

Table 2 Effect of chiral crown catalysts **4**–**12** on the asymmetric Michael addition and Darzens condensation

		Michael addition		Darzens condensation	
Entry	Catalyst	Yield (%)[a]	Ee (%)[b]	Yield (%)	Ee (%)[b]
1	**4**	61	27	92	4
2	**5**	15	4	33	3
3	**6**	50	23	94	4
4	**7**	53	24	70	8
5	**8**	56	6	88	4
6	**9**	78	82 (84)[c]	72	30
7	**10**	71	45	86	52 (53)[c]
8	**11**	65	60	72	13
9	**12**	42	6	68	74

[a] Based on isolation by preparative TLC. [b] Determined by optical rotation. [c] Determined by ^{1}H NMR spectroscopy in the presence of Eu(hfc)$_3$ as chiral shift reagent.

The authors gratefully acknowledge Professor Dr Suzanne Toppet for NMR spectroscopic identification of the compounds, Dr Erik Van der Eycken and Professor Dr Georges J. Hoornaert for useful discussions (Laboratorium voor Organische Synthese, K. U. Leuven). This work was partly supported by the Hungarian Academy of Sciences and the National Science Foundation (OTKA T015677) and the Soros Foundation.

Notes and References

† E-mail: p-bako@chem.bme.hu

‡ *Selected data* for **2**: δ_H(250 MHz, $CDCl_3$, $SiMe_4$) 7.50–7.06 (m, 10 H, ArH), 5.56 (s, 1 H, Benzylidene-CH), 5.06 (d, *J* 7.6, 1 H, anomer-H), 4.36 (dd, *J* 10.5, 4.3, 1 H, H-6), 4.09–3.53 (m, 21 H, 8 CH_2O, 5 CH). For **3**: 7.50–7.05 (m, 10 H, ArH), 5.56 (s, 1 H, benzylidene-CH), 5.06 (d, *J* 7.6, 1 H, anomer-H), 4.38–4.36 (dd, *J* 10.5, 4.3, 1 H, H-6), 4.02–3.52 (m, 18 H, 8 CH_2O, 2 CH), 3.21–3.18 (m, 3 H, H-2, H-3, H-5). For **9**: 7.37–7.02 (m, 15 H, ArH), 5.54 (s, 1 H, benzylidene-CH), 5.06 (d, *J* 7.6, 1 H, anomer-H), 4.36 (dd, *J* 10.5, 4.3, 1 H, H-6), 4.10–3.57 (m, 15 H, 6 CH_2O and 3 CH), 3.54–3.47 (m, 2 H, H-2, H-5), 2.89–2.76 (m, 8 H, 3 NCH_2, CH_2Ph).

§ The Michael addition was performed as follows: 1.44 mmol of chalcone and 3.36 mmol of 2-nitropropane were dissolved in 3 ml of anhydrous toluene, and then 0.1 mmol of crown ether and 0.5 mmol of base were added. The mixture was stirred under an Ar atmosphere. After completing the reaction (8–40 h) a mixture of 7 ml of toluene and 10 ml of water was added. The organic phase was processed in the usual manner. The product was purified on silica gel by preparative TLC with hexane–ethyl acetate (10 : 1) as eluent; mp 146–148 °C, $[\alpha]_D^{20}$ + 68 (*c* 1, CH_2Cl_2) (84% ee) (lit.,[3] +80.8, for pure enantiomer), δ_H 7.85 (m, 2 H, Ph), 7.52 (m, 3 H, Ph), 7.25 (m, 5 H, Ph), 4.18–3.25 (m, 3 H, CH_2, CH), 1.62 (s, 3 H, CH_3), 1.54 (s, 3 H, CH_3).

¶ Typical experimental procedure for the asymmetric Darzens condensation: a toluene solution of 1.3 mmol of phenacyl chloride (3 ml) was treated with 1.9 mmol of benzaldehyde and 0.1 mmol of catalyst in 0.6 ml of 30% NaOH solution. The mixture was stirred under Ar atmosphere. After completing the reaction 7 ml of toluene were added, the organic phase washed with water, dried over $MgSO_4$ and the solvent evaporated. The residue was chromatographed on preparative silica gel of 2 mm thickness (Kieselgel 60 GF_{254}), using CH_2Cl_2 as eluent; $(\alpha)_{578}^{20}$ −111 (*c* 1, CH_2Cl_2) (52% ee) (lit.,[7] −214, for pure enantiomer); δ_H 8.01 (m, 2 H, Ph), 7.60 (t, 1 H, Ph), 7.48 (t, 2 H, Ph), 7.40–7.30 (m, 5 H, Ph), 4.29 (d, *J* 2, 1 H), 4.08 (d, *J*, 1 H).

1 L. Tõke, P. Bakó, Gy. M. Keserû, M. Albert and L. Fenichel, *Tetrahedron*, 1998, **54**, 213 and references cited therein.
2 L. Tõke, L. Fenichel and M. Albert, *Tetrahedron Lett.*, 1995, **36**, 5951.
3 P. Bakó, Á. Szöllõsy, P. Bombicz and L. Tõke, *Heteroatom Chem.*, 1997, **8**, 333.
4 G. W. Gokel, *Chem. Soc. Rev.*, 1992, **21**, 39.
5 P. Di Cesare and B. Gross, *Synth. Commun.*, 1979, 4581.
6 P. Bakó and L. Tõke, *J. Inclusion Phenom.*, 1995, **23**, 195.
7 B. Marsman and H. Wynberg, *J. Org. Chem.*, 1979, **44**, 2312.

Received in Liverpool, UK, 16th March 1998; 8/02098A

Photochemical reduction of nitrite to ammonia at a solid phase photoredox system

J. Rajan Premkumar and Ramasamy Ramaraj*

School of Chemistry, Madurai Kamaraj University, Madurai-625 021, India

The photoassisted reduction of the nitrite anion to ammonia in alkaline aqueous solution was achieved by illumination with visible light in the presence of $[Ni(teta)]^{2+}$ and $[Ru(bpy)_3]^{2+}$ adsorbed Nafion membrane.

The reduction of nitrogen oxyanions has been one of the most interesting aspects in recent chemistry concerned with the development of new methods for artificial nitrogen fixation and the conversion of pollutants such as NO_x into useful chemicals, and also in bioinorganic chemistry in comparing enzymatic reactions with their model ones.[1–7] In artificial photosynthesis, the aim is to mimic the ability of green plants and other photosynthetic organisms in their use of sunlight to make high energy chemicals.[8] In homogeneous solution, the photoredox products recombine in the dark to regenerate the starting materials or undergo side reactions to deplete the concentration of the high energy products.[8] Attempts to construct artificial solar energy conversion systems have been made in terms of the use of micro- and macro-heterogeneous reaction environments such as micelles, bilayers, *etc.*[8–10] However, the utilization of the solid–solution interface has not been studied extensively except in the context of photogalavanic cells. Tris(2,2′-bipyridine)ruthenium(II), ($[Ru(bpy)_3]^{2+}$) has been established as the best photosensitizer for photoredox reactions both in homogeneous and in microheterogeneous media.[8,11,12] Here we describe the utilization of $[Ru(bpy)_3]^{2+}$ and the macrocyclic nickel(II) complex $[Ni(teta)]^{2+}$, (teta = 5,5,7,12,12,14-hexamethyl-1,4,8,11,-tetraazacyclotetradecane) in the solid phase which can be used efficiently to realize a multistep photoreduction of nitrite to ammonia.

The $[Ru(bpy)_3]^{2+}$ and the macrocyclic $[Ni(teta)]^{2+}$ complex ions were prepared according to literature procedures.[13,14] $[Ni(teta)]^{2+}$ was adsorbed into Nafion membrane (1 cm^2 area, Aldrich) by dipping the membrane into an aqueous solution containing a known concentration of $[Ni(teta)]^{2+}$. The membrane Nf/$[Ni(teta)]^{2+}$ was then washed and dipped in distilled water. The $[Ni(teta)]^{2+}$ complex was adsorbed irreversibly and the amount of $[Ni(teta)]^{2+}$ adsorbed into the Nafion membrane was determined by measuring the decrease in the absorbance of $[Ni(teta)]^{2+}$ (λ_{max} = 460 nm, ε_{460} = 40 $dm^3\ mol^{-1}\ cm^{-1}$) in solution after dipping. The $[Ni(teta)]^{2+}$ adsorbed Nafion membrane was then dipped in an aqueous solution containing a known concentration of $[Ru(bpy)_3]^{2+}$ and then washed with distilled water to give the membrane Nf/$[Ni(teta)]^{2+}$/$[Ru(bpy)_3]^{2+}$. $[Ru(bpy)_3]^{2+}$ was also adsorbed irreversibly and the amount of $[Ru(bpy)_3]^{2+}$ adsorbed in the Nf/$[Ni(teta)]^{2+}$/$Ru(bpy)_3]^{2+}$ membrane was determined by measuring the decrease in the absorbance of $[Ru(bpy)_3]^{2+}$ (λ_{max} = 452 nm, ε_{452} = 14 600 $dm^3\ mol^{-1}\ cm^{-1}$) in solution after dipping. The Nf/$[Ni(teta)]^{2+}$ and Nf/$[Ni(teta)]^{2+}$/$[Ru(bpy)_3]^{2+}$ membranes were characterized by absorption and emission spectra. Fig. 1 shows the absorption spectra of $[Ni(teta)]^{2+}$ in Nafion membrane recorded using JASCO 7800 spectrophotometer. [Ni-(teta)]$^{2+}$ adsorbed into Nafion membrane is evident [Fig. 1(*b*)] when compared to $[Ni(teta)]^{2+}$ in water [Fig. 1(*a*)]. A similar result was also obtained for the Nf/$[Ni(teta)]^{2+}$/$[Ru(bpy)_3]^{2+}$ membrane.

The Nf/$[Ni(teta)]^{2+}$/$[Ru(bpy)_3]^{2+}$ membrane was dipped into a photolysis cell containing deaerated aqueous 1 mol dm^{-3} sodium nitrite–1 mol dm^{-3} sodium hydroxide and then irradiated with visible light. A 500 W tungsten–halogen lamp was used as the light source with a water filter cell (6 cm pathlength with Pyrex glass windows) and a Pyrex-glass filter to cut off IR and UV radiations. The distance between the light source and the Nafion membrane was 40 cm. After 30 min irradiation, the cell solution was tested for ammonia, hydroxylamine and hydrazine.[15] Only ammonia was identified as the sole nitrite reduction product. The ammonia concentration was determined using Nessler's reagent and careful spectroscopic analysis in the 400–430 nm wavelength range.[16] The samples for analysis were obtained by interrupting the photochemical process at intervals for several seconds and transferring 1 ml of the solution to a 5 ml standard measuring flask (smf). Then 0.5 ml of freshly prepared Nessler's reagent[17] was added to the smf and the solution was made up to a volume of 5 ml with water. A calibration curve was obtained by dissolving a standard amount of ammonium chloride in water and using Nessler's reagent as described above.[16]

The yield of NH_3(aq) formed after 30 min irradiation using samples containing different amounts of $[Ru(bpy)_3]^{2+}$ in Nf/$[Ni(teta)]^{2+}$ matrix was determined [Fig. 2(*b*)] and the corresponding turnover numbers (TON) of the adsorbed $[Ru(bpy)_3]^{2+}$ complex based on yields of NH_3(aq) are shown in Fig. 2(*a*). The TON for $[Ru(bpy)_3{}^{2+}$ was obtained from the relation: 6 × mol of NH_3(aq) produced/mol of $[Ru(bpy)_3]^{2+}$ adsorbed.

The results were reproducible and the Nafion membrane was stable over months and could be reused in repeated experiments. The absence of any one reaction component (visible light, $[Ni(teta)]^{2+}$, $[Ru(bpy)_3]^{2+}$ or $NaNO_2$) in the solid–solution photoredox system led to no formation of NH_3(aq). When the homogeneous solution containing the photoredox system [Ni-(teta)]$^{2+}$–$[Ru(bpy)_3]^{2+}$ was irradiated (*i.e.* in the absence of

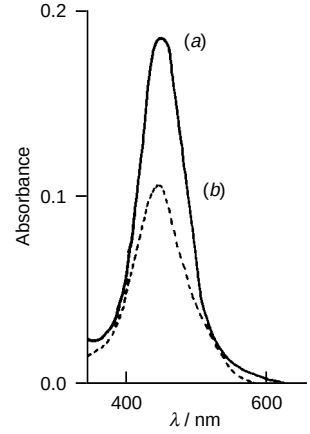

Fig. 1 Absorption spectra of (*a*) $[Ni(teta)]^{2+}$ in water and (*b*) $[Ni(teta)]^{2+}$ adsorbed in Nafion membrane

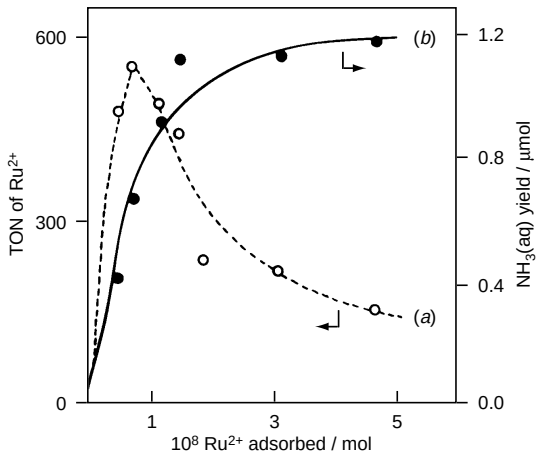

Fig. 2 (*a*) Turnover numbers (TONs) of $[Ru(bpy)_3]^{2+}$ and (*b*) yields of NH_3(aq) observed for the Nf/$[Ni(teta)]^{2+}$/$[Ru(bpy)_3]^{2+}$ matrix (1 cm²) dipped in deaerated aqueous 1 mol dm^{-3} $NaNO_2$–1 mol dm^{-3} NaOH. Irradiation time 30 min; 3.75×10^{-6} mol of $[Ni(teta)]^{2+}$ was adsorbed.

Nafion) negligible amounts of NH_3(aq) were produced compared with Nf/$[Ni(teta)]^{2+}$/$[Ru)bpy)_3]^{2+}$.

The amount of $[Ru(bpy)_3]^{2+}$ adsorbed into the Nafion matrix was found to influence the yield of NH_3(aq) produced [Fig. 2(*b*)]. An increase of concentration of $[Ru(bpy)_3]^{2+}$ in the Nafion increased the yield of NH_3(aq) and the TON of $[Ru(bpy)_3]^{2+}$ up to a limiting value, above which a decrease in the TON was observed [Fig. 2(*a*)], at higher local concentrations, the self quenching of the excited state $[Ru(bpy)_3]^{2+}$ complex and a light filtering effect were predominent.

In the solid-phase photoredox system, the excited-state electron-transfer quenching between $*[Ru(bpy)_3]^{2+}$ and $[Ni(teta)]^{2+}$ (Ni^{II}) complex produces $[Ru(bpy)_3]^{3+}$ and $[Ni(teta)]^{+}$ (Ni^{I}) complex. The latter (Ni^{I}) reacts[18] with NO_2^- to produce $[Ni(O^-–N^-–O^-)]$ (Ni^{III}). This species undergoes successive reductions and finally produces $[Ni(teta)]^{2+}$ and NH_3(aq) (Scheme 1). The overall reaction is given by eqn. (1). The role

$$NO_2^- + 6e^- + 5H_2O \rightarrow NH_3(aq) + 7OH^- \qquad (1)$$

of Nafion matrix in the photo-induced electron transfer reaction between $[Ru(bpy)_3]^{2+}$ and the $[Ni(teta)]^{2+}$ complexes is (*i*) immobilization of positively charged metal complexes in a dispersed state and (*ii*) provision of a microheterogeneous environment for the reacting molecules.

The present work demonstrates the importance of the immobilization of photoredox molecules in a solid matrix to realize the multistep one-electron transfer process by a series of one-electron transfer reaction (Scheme 1). Investigations into the role of the $[Ru(bpy)_3]^{2+}$ and $[Ni(teta)]^{2+}$ catalyst in Nafion membrane in the production of ammonia by nitrite reduction are under way.

We acknowledge the Department of Science and Technology for providing financial assistance. J. P. acknowledges the Council of Scientific and Industrial Research for the Research Associateship. We also thank Professor S. Rajagopal for his valuable suggestions.

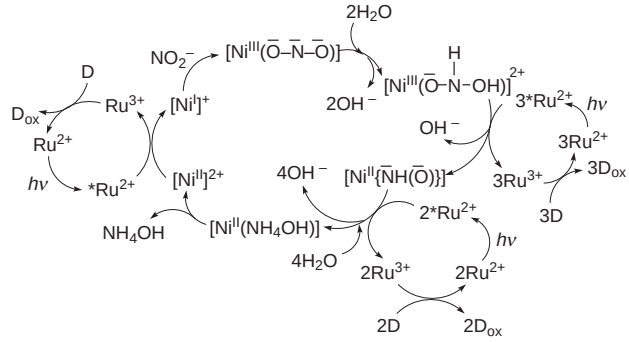

Scheme 1 Schematic illustration of photocatalytic reduction of nitrite at a Nafion matrix containing $[Ni(teta)]^{2+}$ and $[Ru(bpy)_3]^{2+}$. $[Ni^{II}]^{2+}$ = $[Ni(teta)]^{2+}$, Ru^{2+} = $[Ru(bpy)_3]^{2+}$. D = electron donor (H_2O), and D_{ox} = oxidized species of electron donor.

Notes and References

† E-mail: socmku@pronet.xlweb.com

1 J. Chatt, J. R. Dilworth and R. L. Richards, *Chem. Rev.*, 1978, **78**, 589.
2 J. Y. Becker and S. Avrahm, *J. Electroanal. Chem.*, 1990, **280**, 119.
3 M. W. W. Adams and L. E. Mortenston, in *Molybdenum Enzymes*, ed. T. S. Spiro, Wiley, New York, 1985.
4 J. N. Younathan, K. S. Wood and T. J. Meyer, *Inorg. Chem.*, 1992, **31**, 3280.
5 C. Reuben, E. Galun, H. Cohen, R. Tenne, R. Kalish, Y. Muraki, K. Hashimoto, A. Fujishima, J. M. Butler and C. L. Clement, *J. Electroanal. Chem.*, 1995, **396**, 233 and references therein.
6 A. Kudo, K. Domen, K. Maruya and T. Onishi, *Chem. Lett.*, 1987, 1019.
7 I. Willner, N. Lapidot and A. Riklin, *J. Am. Chem. Soc.*, 1989, **111**, 1883.
8 *Energy Resources Through Photochemistry and Catalysis*, ed. M. Graetzel, Academic Press, London, 1993.
9 D. Meisel, M. S. Matheson and J. Rabani, *J. Am. Chem. Soc.*, 1978, **180**, 117.
10 W. E. Ford, J. W. Otvos and M. Calvin, *Nature*, 1978, **274**, 507.
11 *Heterogeneous Photochemical Electron Transfer*, ed. M. Graetzel, CRC Press, Boca Raton, FL, 1989.
12 K. Kalyanasundaram, *Coord. Chem. Rev.*, 1982, **46**, 159.
13 G. Sprintschnik, H. W. Sprintschnik, P. P. Kirsch and D. G. Whitten, *J. Am. Chem. Soc.*, 1976, **98**, 2337.
14 N. F. Curtis, *J. Chem. Soc.*, 1964, 2644.
15 F. Feigl, *Spot Tests in Inorganic Analysis*, Elsevier, New York, 1958, p. 235.
16 R. Tenne, K. Patel, K. Hashimoto and A. Fujishima, *J. Electroanal. Chem.*, 1993, **347**, 409.
17 A. I. Vogel, *A Text Book of Quantitative Inorganic Analysis*, Longman, 3rd edn., 1975, p. 783.
18 I. Taniguchi, N. Nakashima, K. Matsushita and K. Yasukouchi, *J. Electroanal Chem.*, 1987, **224**, 199.

Received in Cambridge, UK, 2nd February 1998; 8/00852C

Novel approaches towards the generation of excited triplets of organic guest molecules with zeolites

Kasi Pitchumani,[a] Manoj Warrier,[a] John R. Scheffer*[b] and V. Ramamurthy*[a]†

[a] *Department of Chemistry, Tulane University, New Orleans, LA 70118, USA*
[b] *Department of Chemistry, University of British Columbia, Vancouver, Canada V6T 1Z1*

Alkali metal cation-exchanged zeolites (M^+X or M^+Y) can be used as 'microreactors' in which to carry out photochemical rearrangement reactions of organic guests.

Considering that a number of reactions originate from excited states that are not efficiently reached by direct excitation, it is important to establish strategies that generate molecules in their excited triplet states within zeolites.[1] We show below that three approaches can be used to generate triplets of organic molecules within zeolites. The 'heavy and light atom effects' employ the cations present within zeolites to perturb the excited state dynamics of the guest molecules; the sensitization technique utilizes a second guest molecule (a sensitizer) to turn on triplet reactivity.

Dibenzobarrelene **1a** and benzobarrelene **1b** and enones **1c** and **1d** were chosen as probe molecules for the present study because their photochemical behavior is known to be multiplicity-dependent and relatively simple (Scheme 1).[2] As shown in Fig. 1, molecules such as **1a** can easily be accommodated within the supercages of a zeolite.

To conduct cation-dependent photochemistry, **1a**–**d** were introduced into the cavities of zeolites M^+X by adsorption from hexane solution and irradiated either as powders or as hexane slurries. Experiments were also carried out with M^+Y zeolites. The approach involving the use of a triplet sensitizer employed acetophenone, *p*-methoxyacetophenone, α-aminoacetophenone hydrochloride and xanthone as the second component. These were introduced into zeolite K^+Y by adsorption from hexane solution. The resulting vacuum-dried, sensitizer-containing zeolite complexes were then transferred to hexane solutions of **1a**–**d** to produce a series of 'double-loaded' complexes. The mole ratio of sensitizer to reactant was maintained at 1 : 1 in every case, but the amount of material loaded onto the zeolite, the loading level, was varied from 13 to 85, a loading level of 13 referring to an average of one molecule of sensitizer and one reactant molecule for every 13 zeolite supercages. The double loaded zeolite complexes were photolyzed as hexane slurries or as powders at $\lambda > 290$ nm (Pyrex), where reactants do not absorb significantly. Following photolysis, the organic materials were extracted from the zeolites with diethyl ether or tetrahydrofuran and analyzed by capillary gas chromatography. Mass balances were excellent (> 85%), indicating that the photoproduct ratios were not skewed by selective inclusion of one of the products. The results for cation dependent chemistry are summarized in Table 1. Results from sensitization studies (only a few sensitizers) are compiled in Table 2. Since the behavior of enones **1c** and **1d** was identical to that of **1a** and **1b** upon sensitization results are not shown.

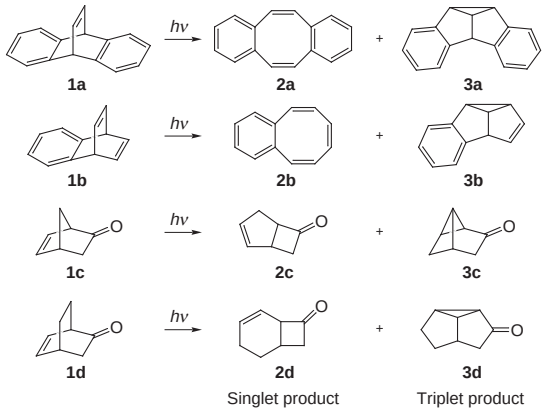

Scheme 1

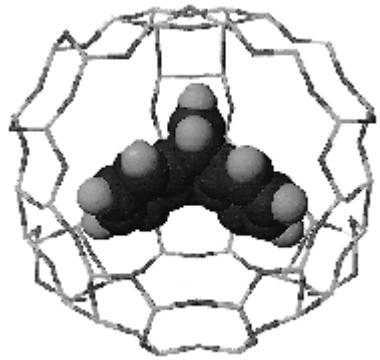

Fig. 1 Dibenzobarrelene included within a supercage; drawing generated by Chem X program

Table 1 Photoproduct distribution from irradiation of compounds **1a** and **1b** in M^+X and M^+Y zeolites[a]

			Slurry[b]	
Medium	Compound	Conv. (%)	% COT **2**	% SBV **3**
MeCN	**1a**		77	23
Acetone	**1a**		0	100
LiX	**1a**	4 (23)[c]	33 [80][d]	67 [20]
NaX	**1a**	6 (20)	38 [72]	62 [28]
KX	**1a**	17 (30)	53 [57]	47 [43]
RbX	**1a**	16 (26)	25 [31]	75 [69]
CsX	**1a**	24 (41)	13 [17]	87 [83]
TlX	**1a**	98 (88)	< 1 [+]	> 99 [> 99]
Hexane	**1b**		96	4
Sens.[e]	**1b**		0	100
NaX	**1b**	77	95	5
KX	**1b**	59	92	8
RbX	**1b**	63	86	14
CaX	**1b**	84	88	12
TlX	**1b**	90	8	92

[a] The product ratios were independent of % conversion within the estimated error limits of ±2% and represent an average of at least 5 independent runs. [b] Slurry irradiations were conducted in hexane for 2 h. Solid state irradiations were carried out for 20 h. Conversions are comparable, since all irradiations were conducted under identical conditions. [c] Numbers in parentheses are for solid state irradiations. [d] Numbers in brackets are for zeolites saturated with water. [e] Acetophenone sensitization in hexane solution.

Table 2 Photoproduct distribution from irradiation of compounds **1a** and **1b** in K^+Y zeolite containing various triplet energy sensitizers[a]

Compound (Sensitizer)	Loading level[b]	Slurry[c] % COT **2**	Slurry[c] % SBV **3**	Solid[c] % COT **2**	Solid[c] % SBV **3**
(4-Methoxyacetophenone)					
1a	25	< 1	> 99	< 1	> 99
1a	40	4	96	< 1	> 99
1a	85	13	87	< 1	> 99
(α-Aminoacetophenone HCl)					
1a	25	8	92	5	95
1a	40	16	84	10	90
(4-Methoxyacetophenone)					
1b	13	10	90	1	99
1b	25	34	66	2	98
1b	40	51	49	20	80
(α-Aminoacetophenone HCl[d])					
1b	13	39	61	18	82
1b	25	54	46	63	37

[a] The product ratios were independent of % conversion within the estimated error limits of ±2% and represent an average of at least 5 independent runs. [b] Loading level refers to the average number of supercages per guest molecule. For example, a value of 25 indicates one probe molecule and one sensitizer molecule per 25 supercages. [c] Slurry irradiations were conducted in hexane for 2 h. Solid state irradiations were carried out for 20 h. Conversions are comparable since all irradiations were conducted under identical conditions. [d] In this case, the sensitizer is anchored to the zeolite *via* an ionic bond, which allows the photoproducts to be removed selectively and the complex reused. No decrease in zeolite efficiency was seen after as many as 6 runs.

Of the three techniques, the sensitization method was found to be general. Triplet–triplet energy transfer occurred in every case (**1a**–**d**) in the doubly loaded K^+Y zeolites. In the presence of an equimolar amount of sensitizer, triplet yields of well over 90% are readily attainable. *p*-Methoxyacetophenone is the sensitizer of choice among those tested. Sensitization works well even when there is only one sensitizer and one acceptor molecule present in 40 or more zeolite cages.

The heavy atom response of compounds **1a** and **1b** is stronger than that observed in the oxadi-π-methane rearrangement of **1c** and **1d**. Essentially 100% triplet state behavior is observed with **1a** and **1b**. The triplet state product observed with **1c** and **1d** never exceeded more than 30% even with Tl^+ as the cation.[3,4] Based on the observations made with the above four systems we conclude that 'El Sayed's rule' holds good within zeolites as well: the degree of heavy atom effect on mixing the states of different multiplicity depends on the electronic configuration ($n\pi^*$ and $\pi\pi^*$).[5]

An unusual observation was made with light cations in the case of **1a**. For **1a**, the Li^+ and Na^+ exchanged zeolites lead to surprisingly large amounts of triplet photoproduct **3a** (67 and 62%, respectively), but the reaction is relatively slow. This 'light atom' effect disappears, however, when the complexes are equilibrated with water before use. The exact mechanism by which Li^+ and Na^+ bring about triplet chemistry in the case of **1a** is not clear. We speculate that by binding strongly to the guest molecule, the light atoms perturb its symmetry characteristics and thus influence the intersystem crossing rates relative to an unperturbed molecule. Consistent with this suggestion, the effect falls off with N^+ (62%) and K^+ (47%), which are expected to bind less strongly. Further where solvation of the cations by water disrupts their strong binding to dibenzobarrelene, the 'light atom' effect of Li^+ is completely eliminated (20% triplet), and there is a normal progressive increase in perturbing power for the others (Na^+, 28%; K^+, 43%; Rb^+, 69%; Cs^+, 83%; Tl^+, > 99%); the classical heavy atom effect becomes increasingly important as the atomic number of the perturbing ion increases.

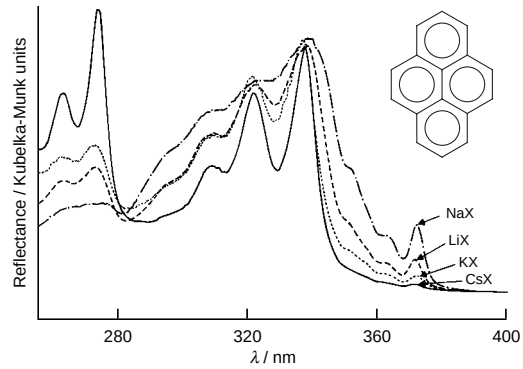

Fig. 2 Diffuse reflectance spectra of pyrene within 'dry' M^+Y zeolites. The intensity of the S_0 to S_1 band is dependent on the cation.

Interactions between light cations and included guest molecules such as benzene and anthracene adsorbed on zeolites were noted as early as 1963.[6] The perturbations of electronic states as well as the modifications of the vibrational modes are explained by a lowering of the symmetry of aromatic molecules in the adsorbed state. Our own observations with pyrene are consistent with the above suggestions.[7] Diffuse reflectance spectra recorded for pyrene, at a low loading level (Fig. 2), within a number of cation exchanged X and Y zeolites suggest that the interaction between the cation and pyrene is strong and that the strength of interaction depends on the polarizability of the cation. In Fig. 2, the intensity of the 0–0 transition of the S_0 to S_1 band is dependent on the charge density of the cation present within supercages. Our working model is that the symmetry reduction of the aromatic molecule occurs due to strong interaction between the cation and the aromatic along the π face resulting in slight bending of the aromatic plane. The example provided here indicates that such symmetry reductions also may influence the S_1 to T_n intersystem crossing process as well.

The authors thank the donors of the Petroleum Research Fund, administered by the American Chemical Society, for partial support of this research (V. R. and J. R. S.). Financial support by the Natural Sciences and Engineering Research Council of Canada (J. R. S.) and Chemical Sciences Program, The US Department of Energy (V. R.) is also gratefully acknowledged. J. R. S. thanks M. D. Fryzuk for helpful discussions.

Notes and References

† E-mail: murthy@mailhost.tcs.tulane.edu

1 D. W. Breck, *Zeolite Molecular Sieves: Structure, Chemistry and Use*, Wiley, New York, 1974; H. van Bekkum, E. M. Flanigen and J. C. Jansen, *Introduction to Zeolite Science and Practice*, Elsevier, Amsterdam, 1991; A. Dyer, *An Introduction to Zeolite Molecular Sieves*, Wiley, Chichester, 1988.
2 Dibenzobarrelene **1a**: E. Ciganek, *J. Am. Chem. Soc.*, 1966, **88**, 2882; Benzobarrelene **1b**: H. E. Zimmerman, R. S. Givens and R. M. Pagni, *J. Am. Chem. Soc.*, 1968, **90**, 6096.
3 B. Borecka, A. D. Gudmundsdottir, G. Olovsson, V. Ramamurthy, J. R. Scheffer and J. Trotter, *J. Am. Chem. Soc.*, 1994, **116**, 10 322.
4 A recent report that appeared after submission of this manuscript claims that oxa-di-π-methane products alone were obtained when **1c** and **1d** were included within Tl^+ and Cs^+ Y. But in our hands, triplet product was obtained in < 30% yield and the major products were the singlet derived products **2c** and **2d**. R. Sadeghpoor, M. Gandhi, H. M. Najafi and F. Farzaneh, *Chem. Commun.*, 1998, 329.
5 M. El Sayed, *Chem. Rev.*, 1977, **77**, 793.
6 C. L. Angell and M. V. Howell, *J. Colloid. Surf. Sci.*, 1968, **28**, 279; B. Coughlan, W. M. Carroll, P. O.'Malley and J. Nunan, *J. Chem. Soc., Faraday Trans. 1*, 1981, **77**, 3037.
7 V. Ramamurthy, D. R. Sanderson and D. F. Eaton, *J. Phys. Chem.*, 1993, **97**, 13 380.

Received in Columbia, MO, 6th November 1997; 7/08013A

Synthesis of an oxorhenium(v) corrolate from porphyrin with detrifluoromethylation and ring contraction

Man Kin Tse, Zeying Zhang, Thomas C. W. Mak and Kin Shing Chan*†

Department of Chemistry, The Chinese University of Hong Kong, Shatin, New Territories, Hong Kong

Metallation of highly electron deficient 5,10,15,20-tetrakis(trifluoromethyl)porphyrin 1 with [$Re_2(CO)_{10}$] in refluxing PhCN resulted in a novel synthesis of oxorhenium(v) 5,10,15-tris(trifluoromethyl)corrolate 2 characterized by single crystal X-ray crystallography.

A new family of porphyrins having highly electron deficient perfluoroalkyl groups in the *meso*-positions has been efficiently synthesized recently by the acid-catalyzed condensation of perfluoro-1-(2′-pyrrolyl)alkan-1-ols.[1] Metallo-perfluoroalkylporphyrins have attracted considerable interest owing to their special non-planar conformation,[1] unusual electronic features,[2] and catalytic properties.[3] In order to explore the chemistry of these electron deficient metalloporphyrins, we have prepared the metal complexes of the porphyrin 5,10,15,20-tetrakis(trifluoromethyl)porphyrin (H_2TCF_3P, **1**). In the course of metallation of **1** with [$Re_2(CO)_{10}$], we have discovered a novel oxorhenium(v) corrolate **2**, [Re(TCF_3C)(O)], with concomitant detrifluoromethylation and ring contraction of the porphyrin **1** (Scheme 1).

When **1** was refluxed with [$Re_2(CO)_{10}$] in benzonitrile in N_2 for 1 h, the brown solution changed to pink. After cooling in air for 1 h, the solution turned to a muddy green suspension. A diamagnetic red product **2** was obtained in *ca.* 9% yield after chromatographic separation in air, together with other uncharacterized side products. The diamagnetic ^{1}H NMR spectrum of **2** showed a doublet at δ 9.88 (J 4.8 Hz) and a multiplet at δ 10.09 with integration ratio of 1 to 3, respectively. The β-pyrrolic protons were therefore non-equivalent. Moreover, the molecular ion appeared at 702 in the mass spectrum and was too low for any expected carbonyl or oxorhenium porphyrin.‡

The structure of **2** was obtained from a single crystal X-ray study.§ The structure was shown to be an oxorhenium corrolate **2** [Fig. 1(*a*)] with detrifluoromethylation and ring contraction having taken place at one of the *meso*-carbons of **1**. C(1) and C(19) of **1** were bonded together with a distance of 1.417(4) Å to form a corrole skeleton. The distances between the opposite nitrogens N(1)···N(3) and N(2)···N(4) were 3.751 and 3.754 Å, respectively, and were shorter than that of the free base porphyrin **1** by *ca.* 30%.¶ The central rhenium lay in a square pyramidal environment in which the corrolate trianion constructed the basal square and the oxygen acted as the axial ligand with Re=O bond length of 1.662(2) Å.[4] The characteristic Re=O stretching frequency appeared at about 994 cm^{-1} in the IR spectrum.[5] Owing to the contraction of the porphyrin to corrole, the large central rhenium deviated from the mean plane of the nitrogens by 0.701 Å [Fig. 1(*b*)] toward the oxygen to accommodate the typical Re–N bond distance of 2 Å.[5] To the best of our knowledge, it is the first oxorhenium porphyrin like macrocycle to be characterized by X-ray crystallography.

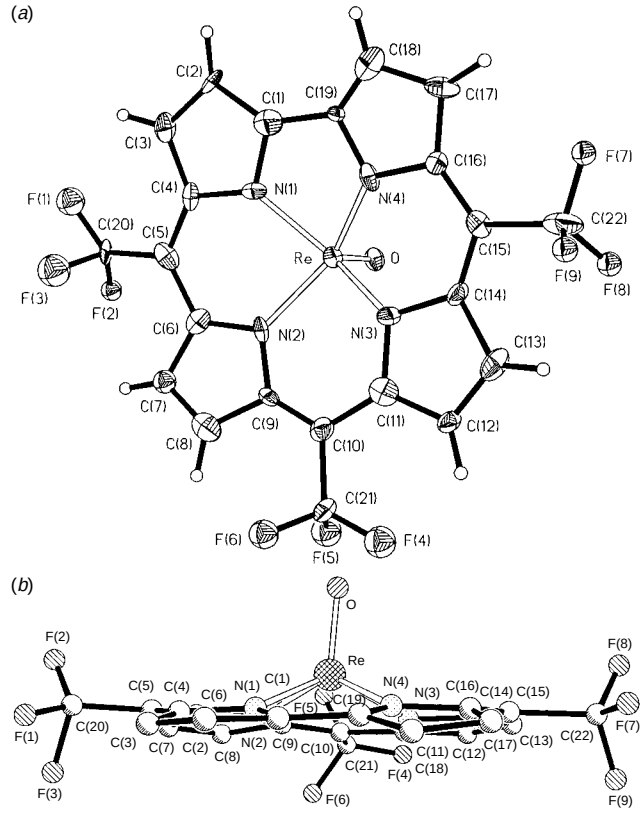

Fig. 1 (*a*) ORTEP view of [Re(TCF_3C)(O)] showing the atom labelling. The thermal ellipsoids are drawn at a 35% probability level and hydrogen atoms have been omitted for clarity. (*b*) Simplified diagram of the side view of [Re(TCF_3C)(O)].

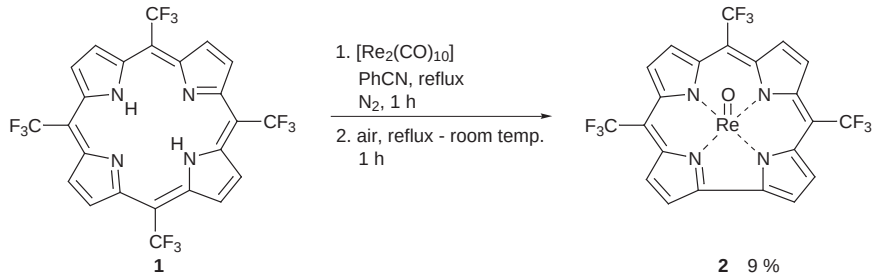

1 **2** 9 %

Scheme 1

The novel oxorhenium corrolate likely arose from the reduction of **1** by $[Re_2(CO)_{10}]$ *via* a cyclopropane intermediate. The formation of cyclopropane product has been reported in the reaction of octaethylporphyrinogen with transition metals.[6] The driving force for corrole formation is probably due to the release of steric hindrance in this and other non-planar porphyrin-like macrocycles.[7] However, the mechanism of novel detrifluoromethylation and ring contraction to form a corrole from a porphyrin remains unclear. Further studies of the electron deficient corrole are in progress.

We thank Direct Grant of the Chinese University of Hong Kong and Shell Chemical Company of Hong Kong for financial support.

Notes and References

† E-mail: ksc@cuhk.edu.hk

‡ The molecular ion of [*meso*-tetrakis(trifluoromethyl)porphyrinato] rhenium, $[ReTCF_3P]^+$ occurs at *m/z* 767. UV–VIS (CH_2Cl_2): λ_{max}/nm (log ε) 429 (4.64), 549 (3.71), 589 (3.87).

§ Single crystals suitable for X-ray crystallographic studies were obtained by slow evaporation of a $CHCl_3$–MeOH solution of **2**. *Crystal data* for oxorhenium(v) 5,10,15-tris(trifluoromethyl)corrolate **2**, $C_{22}H_8F_9N_4ReO$: red prism, monoclinic, space group C_2, a = 19.219(4), b = 13.798(3), c = 8.112(2) Å, β = 111.59(3)°, Z = 4, μ = 6.186 mm^{-1}, 2465 reflections collected [T = 293(2) K], 2396 independent reflections (R_{int} = 0.0315) observed. The structure was solved by direct methods and refinement was by full-matrix least squares. In the final refinement, calculated H atom positions were included using a riding model with fixed isotropic U. R_1 [$I > 2\sigma(I)$] = 0.0388, wR_2 = 0.1101. Programs used: Siemens SHELXTL PLUS (PC Version). CCDC 182/857.

¶ The distances between opposite nitrogens of **1** were found to be 4.159 and 4.180 Å. The crystal structure of **1** will be published elsewhere.

1 H. Ogose, H. Kuroda and H. Murase, *Jpn. Pat.*, Kokai Tokkyo Koho JP 02 311 478 [90 311 478] (Cl. C07D487/22), 27 Dec. 1990, Appl. 89/133,037, 26 May 1989; T. P. Wijeseera and R. W. Wagner, *US Pat.*, 5 241 062 (Cl. 540–145 C07d487/22), 31 Aug. 1993, Appl. 5,702, 19 Jan. 1993; S. G. Dimagno, M. J. Therien and R. A. Williams, *J. Org. Chem.*, 1994, **59**, 6943.

2 S. G. Dimagno, A. K. Wertsching and C. R. Ross, *J. Am. Chem. Soc.*, 1995, **117**, 8279; J. G. Goll, K. T. Moore, A. Ghosh and M. J. Therien, *J. Am. Chem. Soc.*, 1996, **118**, 8344.

3 In *Metalloporphyrins in Catalytic Oxidations*, ed. R. A. Sheldon, Marcel Dekker, New York, 1994; B. Meunier, *Chem. Rev.*, 1992, **92**, 1411; P. E. Ellis Jr. and J. E. Lyons, *Coord. Chem. Rev.*, 1990, **105**, 181; T. P. Wijesekera, J. E. Lyons and P. E. Ellis Jr. *Catal. Lett.*, 1996, **36**, 69.

4 M. Tsutsui, C. P. Hrung, D. Ostfeld, T. S. Srivastava, D. L. Cullen and E. F. Meyer Jr., *J. Am. Chem. Soc.*, 1975, **97**, 1975; A.-M. Lebuis and A. L. Beauchamp, *Can. J. Chem.*, 1993, **71**, 2060; C. Bolzati, F. Tisato, F. Refosco, G. Bandoli and A. Dolmella, *Inorg. Chem.*, 1996, **35**, 6221; B. Noll, S. Noll, P. Leibnitz, H. Spies, P. E. Schulze, W. Semmler and B. Johannsen, *Inorg. Chim. Acta*, 1997, **255**, 399; S. Bélanger, S. Fortin and A. L. Beauchamp, *Can. J. Chem.*, 1997, **75**, 37; B. Dirghangi, K. Menon, M. A. Pramanik and A. Chakravorty, *Inorg. Chem.*, 1997, **36**, 1095.

5 For the diphosphine rhenium porphyrin, average Re–N bond length was 2.059(5) Å; J. P. Collman, J. M. Garner, K. Kim and J. A. Ibers, *Inorg. Chem.*, 1988, **27**, 4513; for the nitridorhenium(v) porphyrins, Re–N bond lengths range from 2.074(4) to 2.086(4) Å; J. W. Buchler, A. D. Cian, J. Fischer, S. B. Kruppa and R. Weiss, *Chem. Ber.*, 1990, **123**, 2247.

6 J. Jubb, C. Floriani, A. Chiesi-Villa and C. Rizzoli, *J. Am. Chem. Soc.*, 1992, **114**, 6571; U. Piarulli, C. Floriani, A. Chiesi-Villa and C. Rizzoli, *J. Chem. Soc., Chem. Commun.*, 1994, 895.

7 R. Paolesse, S. Licoccia, G. Bandoli, A. Dolmella and T. Boschi, *Inorg. Chem.*, 1994, **33**, 1171; S. Licoccia, E. Tassoni, R. Paolesse and T. Boschi, *Inorg. Chim. Acta*, 1995, **235**, 15.

Received in Cambridge, UK, 13th March 1998; 8/02033G

Regio- and stereo-specific addition of chlorodibutyltin hydride to prop-2-ynylic ethers

Terence N. Mitchell*† and Said-Nadjib Moschref

Fachbereich Chemie, Universität Dortmund, D-44221 Dortmund, Germany

A number of prop-2-ynylic ethers smoothly undergo regio- and stereo-specific hydrostannation with chlorodibutyltin hydride in good to nearly quantitative yield at room temperature in benzene.

The importance of vinyltins in cross-couplings of the Stille–Migita type[1] has recently led to efforts to find new approaches to their preparation. A very useful approach has recently been designed by Yamamoto and co-workers,[2] who used zirconium and hafnium tetrachlorides as Lewis acid catalysts in the hydrostannation of alkynes; a refinement of this procedure[3] involves the *in situ* preparation of the tin hydride from the corresponding chloride and triethylsilane. In all cases reported, the procedure gave single isomers derived from *trans* attack of the tin hydride.

The disadvantage of this methodology is that the Lewis acid centre is blocked when the alkyne contains substituents bearing a lone pair; thus we have found that prop-2-ynylic ethers or amines, which are synthetically much more important than simple alkynes, do not react satisfactorily.

In an attempt to circumvent this problem we had recourse to the long-known but relatively little used chlorodibutyltin hydride,[4] which is readily prepared by mixing the dihydride[5] and dichloride. A hint of the potential of this reagent had been provided relatively recently by Davies,[6] who observed a rapid hydrostannation of a prop-2-ynylic alcohol (2-methylprop-3-yn-2-ol, 2 h at room temperature in toluene), though with the formation of a *Z*/*E* isomer mixture. An exothermic reaction occurs when the hydride chloride is mixed with prop-2-ynylic ethers [reaction (1)], but when the two reagents are mixed slowly at room temperature and stirred for 4 h in benzene the hydrostannation occurs in yields which are good to virtually quantitative (63–99%), only one single isomer being detected.

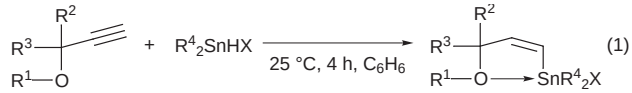

(1)

This is in clear contrast to the behaviour of tributyltin hydride, which gives product mixtures containing predominantly either the *E*- or the *Z*-isomer (depending on the amount of tin hydride used) when allowed to react under free radical conditions with unsubstituted prop-2-ynylic alcohols and ethers;[7] in contrast, a clean reaction does occur (*via* regiospecific *trans* addition) with substituted prop-2-ynylic residues attached to either oxygen[8] or nitrogen,[9] though yields are variable. Table 1 gives details of the ethers used in this work and the respective yields. The reactions are carried out as follows: the dialkyltin dihydride[5] (2.5 mmol) is added at 0 °C during 10 min to the dichloride (2.5 mmol) with constant stirring. The mixture is stirred for 0.5 h at room temperature and a solution of the prop-2-ynyl ether[10] (5 mmol) in benzene (5 ml) is added during 10 min with stirring. The reaction mixture is stirred for 4 h at room temperature, the volatiles removed at the oil pump, and the colourless oil (which solidifies on storing at 5 °C) obtained is characterised by multinuclear NMR spectroscopy.

Table 1 Addition of halodialkyltin hydrides to prop-2-ynyl ethers

Prop-2-ynyl ether				Halodialkyltin hydride		
	R^1	R^2	R^3	R^4	X	Yield (%)[a]
1a	Allyl	Pr	H	Bu	Cl	93
1b	2-Methylallyl	H	H	Bu	Cl	71
1c	Cyclohex-2-enyl	H	H	Bu	Cl	> 91
1d	But-2-enyl	H	H	Bu	Cl	63
1e	Et	Me	Me	Bu	Cl	> 98
1f	2-Furyl	H	H	Bu	Br	97
1g	2-Methylallyl	H	H	Bu	Br	> 98
1h	2-Furyl	H	H	Et	Cl	> 98
1i	2-Furyl	H	H	Me	Cl	> 98
1j	Et	Me	Me	Me	Cl	97

[a] From integration of ^{1}H NMR spectra.

The ^{1}H NMR spectra confirm that the reaction has occurred in a *trans* manner with attack of the tin at the terminal carbon [^3J(H,H) = 12–13 Hz]. In a control experiment with hex-1-yne a mixture of *E* (^3J = 18 Hz) and *Z* (^3J = 12.5 Hz) isomers is observed, clearly demonstrating that the ether oxygen determines the reaction course. The tin resonance occurs at relatively high field [1 to 13 ppm compared with 56 (*E*) and 67 ppm (*Z*) in the isomers derived from hex-1-yne], suggesting intramolecular coordination between oxygen and tin in the product. This is confirmed by the carbon-13 data: one-bond tin–carbon coupling constants are of a magnitude expected for pentacoordination at tin (540–664 Hz). Analogous results are obtained using other compounds R_2SnHX (R = Me, Et; X = Cl, Br). Treatment of the vinyltins (**1**) with Grignard reagents lead to the corresponding trialkyltin species: thus, for example, treatment of (**1f**) with EtMgBr leads to a product showing the expected NMR spectroscopic data [δ(^{119}Sn) −40.5 ppm, vinyl ^{1}H–^{1}H coupling constant 10.4 Hz].

Notes and References

† E-mail: mitchell@citrin.chemie.uni-dortmund.de

1 T. N. Mitchell, in *Metal-catalysed Cross-coupling Reactions*, ed. F. Diederich and P. J. Stang, Wiley-VCH, Weinheim, Berlin, New York, Chichester, Brisbane, Singapore, Toronto, 1998, p. 167.
2 N. Asao, J.-X. Liu, T. Sudoh and Y. Yamamoto, *J. Org. Chem.*, 1996, **61**, 4568; N. Asao, J.-X. Liu, T. Sudoh and Y. Yamamoto, *J. Chem. Soc., Chem. Commun.*, 1995, 2405.
3 V. Gevorgyan, J.-X. Liu and Y. Yamamoto, *Chem. Commun.*, 1998, 37.
4 W. P. Neumann and J. Pedain, *Tetrahedron Lett.*, 1964, 2461; A. K. Sawyer and J. E. Brown, *J. Organomet. Chem.*, 1966, **5**, 438; A. K. Sawyer, J. E. Brown and G. S. May, *J. Organomet. Chem.*, 1968, **11**, 192.
5 G. J. M. Van der Kerk, J. G. Noltes and J. G. A. Luijten, *J. Appl. Chem.*, 1957, **7**, 366.
6 A. G. Davies, W. J. Kinart and D. K. Ossei-Kissi, *J. Organomet. Chem.*, 1994, **474**, C11.

7 M. E. Jung and L. A. Light, *Tetrahedron Lett.*, 1982, **23**, 3851.
8 M. Lautens and A. H. Huboux, *Tetrahedron Lett*., 1990, **31**, 3105; T. Konoike and Y. Araki, *Tetrahedron Lett*., 1992, **33**, 5093.
9 J. L. Anderson and C. A. Roberts, *Tetrahedron Lett*., 1998, **39**, 159.
10 L. Brandsma, *Preparative Acetylenic Chemistry*, Elsevier, Amsterdam, 2nd edn., 1988.

Received in Liverpool, UK, 18th March 1998; 8/02160K

An unusual reaction of hexafluoroacetone with methylenediphosphines. Facile synthesis of carbodiphosphoranes

Igor Shevchenko†

Institute of Bioorganic Chemistry, Murmanskaya Street 1, 252660 Kiev, Ukraine

The oxidation of bis[bis(dialkylamino)phosphinyl]methanes with hexafluoroacetone does not lead to the expected dioxaphospholane heterocycles, but yields quantitatively carbodiphosphoranes.

It is well known that phosphines react with 2 equiv. of hexafluoroacetone (HFA) to give phosphoranes in which the phosphorus atom is part of a dioxaphospholane heterocycle.[1–4] It turns out that this is not the only possible pathway for this reaction. Here we report on an unusual reaction of HFA with bis[bis(dialkylamino)phosphinyl]methanes **1a,b** which gives quantitatively carbodiphosphoranes **3a,b** (Scheme 1). Formally this reaction can be considered to be an addition of the tautomeric P–H ylide form of **1** to the carbonyl function of HFA. The presence of a methylene group between the two phosphorus atoms is thus a necessary condition for this reaction.

After slow bubbling of gaseous HFA through a solution of **1a** or **1b** in hexane at 20 °C, NMR spectra of the reaction mixtures show the presence of only compound **3a** or **3b**, respectively; the ^{31}P NMR spectra of the reaction mixtures display one singlet at δ 33–37. Carbodiphosphorane **3a** is stable in hexane solution at room temperature for several hours, whereas **3b** containing the more bulky diethylamino substituents is respectively more stable and its hexane solution can be stored without decomposition for two days. Evaporation of the solvent causes decomposition of the molecule.

The choice of hexane as a solvent is very important for this reaction. In other solvents carbodiphosphoranes **3a,b** are less stable and their synthesis may be accompanied by the formation of byproducts. The ^{1}H NMR spectra of **3a** and **3b** were recorded immediately after HFA had been added to a solution of **1a** or **1b** in [$^2H_8$]toluene.‡ They show a characteristic low field septet at δ 6.2, confirming the location of the two equivalent protons α to the CF_3 groups. It is interesting that the dimethylamino groups of **3a** appear in the ^{1}H NMR spectrum, not as a doublet, but as a pseudo-triplet at δ 2.59 with a broadened central line, which is consistent with the NMR data of known compounds. The analogous carbodiphosphorane having chlorine atoms instead of HFA units at the two phosphorus atoms shows the same pattern for the Me_2N groups in its ^{1}H NMR spectrum.[5]

The mechanism of this reaction probably includes the intermediate formation of monoylides **2a** or **2b**. However, we could not detect these compounds *via* NMR spectroscopy. Even if only 1 equiv. of HFA was added to the methylenediphosphines **1a,b** the ^{31}P NMR spectrum of the reaction mixture displayed only two equal signals, for the starting compound **1** and the reaction product **3**.

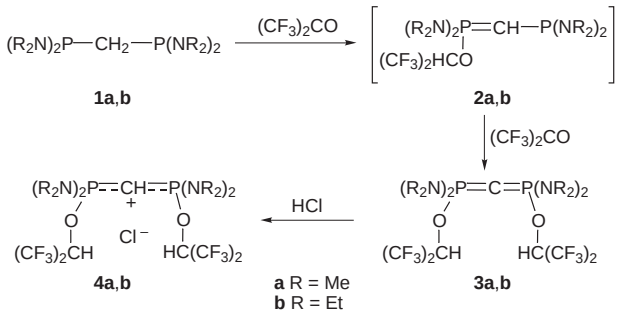

Scheme 1

The ylidic structure of carbodiphosphoranes **3a,b** is confirmed by their reaction with HCl, which gives the stable salts **4a,b**. As a strong base, **3a,b** reacts with ammonium hydrochlorides. That is why **4a,b** can also be formed in small quantities together with **3a,b**, if starting methylenediphosphines **1a,b** are contaminated with dialkylammonium chlorides. However, **4a,b** are not soluble in hexane and can be easily separated. The structures of **4a,b** are entirely consistent with the NMR data obtained.§ In contrast to most carbodiphosphoranes described previously,[6–10] compounds **3a,b** are easily obtainable and can be used in further reactions without isolation from the reaction mixture. The possible application of **3a,b** in Wittig reactions and the presence of hydrogen atoms α to the CF_3 groups make these compounds interesting synthons for organic and elementoorganic synthesis. We are currently investigating their chemical properties.

Dedicated to Doctor Hans-Martin Schiebel on the occasion of his 65th birthday.

Notes and References

† E-mail: ishev@bioorg.kiev.ua

‡ *Selected data* for **3a**: δ_P(80 MHz, C_6H_{14}) 36.7; δ_H(200 MHz, [$^2H_8$]toluene) 2.59 (pseudo t, $^3J_{PH}$ 11.6, 24 H, NCH_3), 6.25 (sept, $^3J_{FH}$ 6.8, 2 H, CHCF$_3$); δ_F(188.3 MHz, C_6H_{14}) −73.0 (d, $^3J_{HF}$ 6.8, 12F). For **3b**: δ_P(80 MHz, C_6H_{14}) 33.6; δ_H(200 MHz, [$^2H_8$]toluene) 0.98 (t, $^3J_{HH}$ 7.1, 24 H, NCH$_2$CH_3), 3.00 (m, 16 H, NCH_2CH$_3$), 6.09 (sept, $^3J_{FH}$ 6.8, 2 H, CHCF$_3$); δ_F(188.3 MHz, C_6H_{14}) −72.9 (d, $^3J_{HF}$ 6.8, 12F).

§ To a solution of **3a** or **3b** in hexane, 1 equiv. of HCl in Et_2O was added at 20 °C. The precipitated **4a** or **4b** was separated and recrystallized from CH_2Cl_2–Et_2O at −15 °C. *Selected data* for **4a**: 63%, mp 183–185 °C (decomp.); δ_P(80 MHz, $CDCl_3$) 58.6; δ_H(200 MHz, $CDCl_3$) 2.71 (pseudo t, $^3J_{PH}$ 10.7, 24 H, NCH_3), 3.67 (t, $^2J_{PH}$ 10.0, 1 H, PCHP), 6.71 (sept, $^3J_{FH}$ 5.9, 2 H, CHCF$_3$); δ_C(50.3 MHz, $CDCl_3$) 7.4 (t, $^1J_{PC}$ 209, PCP), 37.3 (pseudo t, $^2J_{PC}$ 4.9, 8C, NCH_3), 70.3 (sept, $^2J_{FC}$ 34, 2 C, CHCF$_3$), 120.8 (q, $^1J_{FC}$ 285, 4CF$_3$); δ_F(188.3 MHz, $CDCl_3$) −73.9 (d, $^3J_{HF}$ 5.9, 12F). (Calc. for $C_{15}H_{27}ClF_{12}N_4O_2P_2$: C, 29.02; H, 4.38. Found: C, 28.77; H, 4.32%). For **4b**: 52%, mp 151–153 °C; δ_P(80 MHz, $CDCl_3$) 59.1; δ_H(200 MHz, $CDCl_3$) 1.06 (t, $^3J_{HH}$ 6.8, 24 H,NCH$_2$CH_3), 3.05 (m, 16 H, NCH_2CH$_3$), 3.23 (t, $^2J_{PH}$ 13.7, 1 H, PCHP), 6.75 (sept, $^3J_{FH}$ 5.9, 2 H, CHCF$_3$); δ_C(50.3 MHz, $CDCl_3$) 7.3 (t, $^1J_{PC}$ 209, PCP), 13.7 (s, 8C, NCH$_2$CH_3), 40.6 (s, 8C, NCH_2CH$_3$), 70.4 (spet, $^2J_{FC}$ 34, 2C, CHCF$_3$), 120.8 (q, $^1J_{FC}$ 285, 4CF$_3$); δ_F(188.3 MHz, $CDCl_3$) −73.0 (d, $^3J_{HF}$ 5.9, 12F) (Calc. for $C_{23}H_{43}ClF_{12}N_4O_2P_2$: C, 37.69; H, 5.91. Found: C, 37.12; H, 5.79%).

1 M. Witt, K. S. Dathathreyan and H. W. Roesky, *Adv. Inorg. Chem. Radiochem.*, 1986, **30**, 223.
2 R. Burgada and R. Setton, 'Preparation, Properties and Reactions of Phosphoranes', in *The Chemistry of Organophosphorus Compounds*, ed. F. R. Hartley, in *The Chemistry of Functional Groups*, Series ed. S. Patai, Wiley, Chichester, New York, Brisbane, Toronto, Singapore, 1994, vol. 3, ch. 3, pp. 185–272.
3 F. U. Seifert and G.-V. Röschenthaler, *J. Fluorine Chem.*, 1995, **70**, 171.
4 I. Neda, C. Melnicky, A. Vollbrecht, A. Fischer, P. G. Jones and R. Schmutzler, *Z. Anorg. Allg. Chem.*, 1996, **622**, 1047.

5 A. P. Marchenko, G. N. Koydan, N. A. Oleynik, I. S. Zal'tsman and A. M. Pinchuk, *Zh. Obshch. Khim.*, 1988, **58**, 1665.
6 A. W. Johnson, *Ylides and Imines of Phosphorus*, Wiley, New York, Chichester, Brisbane, Toronto, Singapore, 1993, ch. 3, pp. 64–68.
7 O. I. Kolodiazhniy, *The Chemistry of Phosphorus Ylids*, N. Dumka, Kiev, 1994, ch. 5, pp. 330–338.
8 P. Dyer, O. Guerret, F. Dahan, A. Baceiredo and G. Bertrand, *J. Chem. Soc., Chem. Commun.*, 1995, **22**, 2339.
9 H. Schmidbaur and S. Schnatterer, *Chem. Ber.*, 1983, **116**, 1947.
10 R. Appel, U. Baumeister and F. Knoch, *Chem. Ber.*, 1983, **116**, 2275.

Received in Liverpool, UK, 5th March 1998; 8/01805G

Synthesis of $[Ni(NH_3)_6]C_{60}\cdot 6NH_3$ *via* ion exchange in liquid ammonia—a new, versatile access to ionic fullerides

Klaus Himmel and Martin Jansen*†

Institut für Anorganische Chemie der Rheinischen Friedrich-Wilhelms-Universität Bonn, Gerhard-Domagk-Str. 1, 53121 Bonn, Germany

The ammoniate $[Ni(NH_3)_6]C_{60}\cdot 6NH_3$ is prepared from K_2C_{60} *via* cation exchange in liquid ammonia; the structure of the compound is determined by X-ray crystal structure analysis.

Since the discovery of superconductivity in K_3C_{60},[1] ionic fullerides have been in the focus of scientific interest. However, up to now research has been restricted to fullerides of alkali (including the analogous Tl^+), alkaline earth and some rare earth metals,[2] which form directly from the respective metal and fullerene during solid state reactions. Several attempts have been made to introduce other metals.[3] In most cases, however, the composition and constitution of the products could not be determined conclusively. To our knowledge, only the compounds $Na_{2+x}Hg_yC_{60}$[4] and $[Ni(C_5Me_5)_2]C_{60}\cdot CS_2$[5] have been fully characterized.

As the alkali fullerides readily dissolve in liquid ammonia,[6,7] ion exchange in this solvent using a thoroughly dried macroreticular exchange resin could offer a general approach to the synthesis of fullerides with any counterion that can be loaded onto the resin and is soluble in liquid ammonia, at the same time. Recently, we have shown this route to be suitable for the synthesis of fullerides with organic cations.[8] The preparation of the novel fulleride $[Ni(NH_3)_6]C_{60}\cdot 6NH_3$ reported here, and of isostructural $[Mn(NH_3)_6]C_{60}\cdot 6NH_3$ and $[Cd(NH_3)_6]C_{60}\cdot 6NH_3$,[9] extends the applicability of the exchange route to transition metals, and thus broadens its scope significantly.

Reacting a solution of K_2C_{60} in ammonia with an ion exchange resin loaded with Ni^{2+} yielded $[Ni(NH_3)_6]C_{60}\cdot 6NH_3$ in black shiny crystals.‡ Suitable crystals were selected in an inert oil matrix under a microscope and were used for an X-ray single crystal structure analysis.§

$[Ni(NH_3)_6]C_{60}\cdot 6NH_3$ crystallises in a distorted rock salt type of structure (Fig. 1). Nickel hexaammine complexes occupy the octahedral sites in a fcc fulleride sublattice. Each molecule of ammonia of solvation is coordinated *via* a hydrogen bond to one ammonia in the ligand sphere of the ammine complex. This extended coordination sphere of Ni^{2+} can fit its shape flexibly to the needs of the octahedral site of the C_{60}^{2-} sublattice, at the same time fixing the fulleride anion orientationally. The thermal parameters of the fulleride (Fig. 2) are reasonable and do not indicate any disorder. The shortest intermolecular carbon to carbon distance is 3.36 Å (3.11 Å in neutral C_{60}). By comparing the shortest Ni–C distance (4.62 Å) with the distance between the centre of the octahedral site and the nearest carbon atom in fcc C_{60} (3.65 Å) it becomes evident that the accommodation of the hexaammine complex and the extra six solvent molecules per formula unit leads to a considerable expansion of the C_{60} sublattice. The quite strong deviation of the crystal structure from the ideal cubic symmetry of rock salt indicates that packing requirements more strongly determine the structure than do electrostatic interactions. Hydrogen atoms of the solvent ammonia show the shortest intermolecular distances to the fulleride. This fact suggests an interaction of N–H dipoles with electron density on the fulleride surface that could be responsible for the localisation of the anion in a fixed orientation. Similar interactions of C–H dipoles have been discussed previously.[10]

Dianions C_{60}^{2-} should be subject to Jahn–Teller distortion due to the asymmetric occupation of the degenerate t_{1u} orbital of neutral C_{60}. The nature and the degree of this distortion, however, have been discussed controversially.[11] In particular, it can be very difficult to separate distortions caused by an intrinsic Jahn–Teller effect from those due to a low site symmetry of the unit under discussion. The fulleride dianion in the present structure is somewhat distorted from the ideal I_h symmetry. The mean distance of the carbon atoms from the centre of the fulleride is 3.541(2) Å with a spread from 3.555(2) Å (C13) to 3.520(3) Å (C16). Though the range is larger than in neutral C_{60} (0.012 Å),[12] it could well be a result of the interactions with the low symmetrical environment established by the hydrogen atoms. Actually, we have shown that in an environment of higher symmetry the point symmetry I_h of a divalent fulleride can be retained.[13]

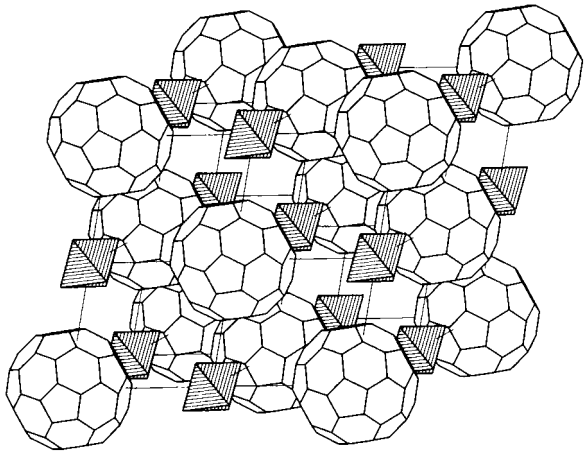

Fig. 1 Distorted rock salt type arrangement of fulleride dianions and nickel hexaammine cations (octahedra)

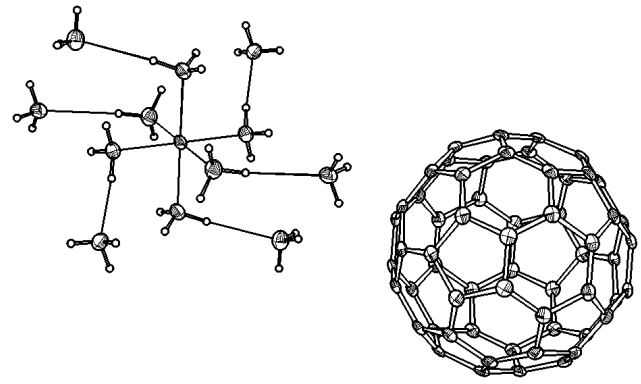

Fig. 2 ORTEP plot[15] (50% probability ellipsoids) of the cationic and anionic units in $[Ni(NH_3)_6]C_{60}\cdot 6NH_3$

Apart from the Ni compound presented in this paper we have been able to synthesise $(BnNMe_3)_2C_{60}\cdot 3NH_3$;[8] $(PhNMe_3)_2C_{60}\cdot 4NH_3$, $[Mn(NH_3)_6]C_{60}\cdot 6NH_3$ and $[Cd(NH_3)_6]C_{60}\cdot 6NH_3$[9] *via* ion exchange in liquid ammonia, which demonstrates the wide, general applicability of the procedure developed. As an attractive option, these ammoniates offer access to fullerides of transition metals by removing ammonia *in vacuo* and/or at elevated temperatures.

We wish to thank Hoechst AG, Frankfurt, for providing C_{60}.

Notes and References

† E-mail: mjansen@snchemie2.chemie.uni-bonn.de

‡ Preparation of nickel hexaammine fulleride ammoniate: 1 g of exchange resin (Amberlyst 15, Fluka) loaded with Ni^{2+} was thoroughly dried and placed on one side of a H-type glass vessel equipped with a glass sieve (porosity 3). 80 mg (1.0×10^{-4} mol) K_2C_{60} were placed on the other side of the sieve. After cooling (ethanol–dry ice slush) ammonia was condensed into the vessel until the glass sieve was completely covered. The reaction mixture was stored at 230 K for about 3 weeks. In this time K_2C_{60} slowly diffused onto the ion exchange resin where $[Ni(NH_3)_6]C_{60}\cdot 6NH_3$ precipitated as shiny black platelets that are sensitive to air, moisture and elevated temperature. The crystals were removed from liquid ammonia, transferred into an inert oil mixture (1 : 1 Perfluorpolyether 216, Riedel-de Haën/ Perfluorpolyether Fomblin Y HVAC 40/11, Aldrich) which was cooled with a nitrogen stream to 230 K, and picked up on the tip of a glass capillary mounted on a goniometer head.

§ *Crystal data* for $[Ni(NH_3)_6]C_{60}\cdot 6NH_3$: $C_{60}H_{36}N_{12}Ni$, M = 938.72, black platelets, triclinic, space group $P\bar{1}$ (no. 2), a = 988.3(2), b = 1021.1(2), c = 1050.2(2) pm, α = 77.79(2), β = 80.04(2), γ = 79.64(2)°, V = 1.0089(3) nm^3, Z = 1, D_c = 1.619 g cm^{-3}, μ(Mo-Kα) = 0.55 mm^{-1}. 4611 reflections measured, 3959 independent, 3653 reflections observed with $I > 2\sigma(I)$, 361 parameters, no restraints. Diffraction data were collected with an Enraf-Nonius CAD4 diffractometer (Mo-Kα, λ = 71.069 pm) at 113(2) K to θ_{max} = 26°. The structure was solved by the Patterson method and refined on F^2 using all independent reflections.[14] Hydrogen atoms of the ammonia molecules were located by difference Fourier synthesis. The final wR_2 value was 0.099 [corresponding to a conventional R value of 0.037 by using only reflections with $I > 2\sigma(I)$]. CCDC 182/844.

1 (*a*) A. F. Hebard, M. J. Rosseinsky, R. C. Haddon, D. W. Murphy, S. H. Glarum, T. T. M. Palstra, A. P. Ramirez and A. R. Kortan, *Nature*, 1991, **350**, 600; (*b*) K. Holczer, O. Klein, S.-M. Huang, R. B. Kaner, K.-J. Fu, R. L. Whetten and F. Diederich, *Science*, 1991, **252**, 1154.

2 (*a*) A. C. Duggan, J. M. Fox, P. F. Henry, S. J. Heyes, D. E. Laurie and M. J. Rosseinsky, *Chem. Commun.*, 1996, 1191; (*b*) A. R. Kortan, N. Kopylov, E. Özdas, A. P. Ramirez, R. M. Fleming and R. C. Haddon, *Chem. Phys. Lett.*, 1994, **223**, 501; (*c*) E. Özdas, A. R. Kortan, N. Kopylov, A. P. Ramirez, T. Siegrist, K. M. Rabe, H. E. Bair, S. Schuppler and P. H. Citrin, *Nature*, 1995, **375**, 126; (*d*) A. S. Ginwalla, A. L. Balch, S. M. Kauzlarich, S. H. Irons, P. Klavins and R. N. Shelton, *Chem. Mater.*, 1997, **9**, 279.

3 (*a*) Z. Gu, J. Qian, Z. Jin, X. Zhou, S. Feng, W. Zhou and X. Zhu, *Solid State Commun.*, 1992, **82**, 167; (*b*) D. K. Patel, D. M. Thompson, M. C. Baird, L. K. Thompson and K. F. Preston, *J. Organomet. Chem.*, 1997, **545**–**546**, 607.

4 J. M. Fox, P. F. Henry and M. J. Rosseinsky, *Chem. Commun.*, 1996, 2299.

5 W. C. Wan, X. Liu, G. M. Sweeney and W. E. Broderick, *J. Am. Chem. Soc.*, 1995, **117**, 9580.

6 D. W. Murphy, M. J. Rosseinsky, R. M. Fleming, R. Tycko, A. P. Ramirez, R. C. Haddon, T. Siegrist, G. Dabbagh, J. C. Tully and R. E. Walstedt, *J. Phys. Chem. Solids*, 1992, **53**, 1321

7 W. K. Fullagar, P. A. Reynolds and J. W. White, *Solid State Commun.*, 1997, **104**, 23.

8 K. Himmel and M. Jansen, *Z. Anorg. Allg. Chem.*, 1998, **624**, 1.

9 K. Himmel and M. Jansen, unpublished results. The crystal structures have been determined by single crystal X-ray diffraction.

10 P. Paul, Z. Xie, R. Bau, P. D. W. Boyd and C. A. Reed, *J. Am. Chem. Soc.*, 1994, **116**, 4145.

11 (*a*) N. Koga and K. Morokuma, *Chem. Phys. Lett.*, 1992, **196**, 191; (*b*) P. Bhyrappa, P. Paul, J. Stinchcombe, P. W. D. Boyd and C. A. Reed, *J. Am. Chem. Soc.*, 1993, **115**, 11 004; (*c*) M. M. Khaled, R. T. Carlin, P. C. Trulove, G. R. Eaton and S. Eaton, *J. Am. Chem. Soc.*, 1994, **116**, 3465; (*d*) P. W. D. Boyd, P. Bhyrappa, P. Paul, J. Stinchcombe, R. D. Bolskar, Y. Sun and C. A. Reed, *J. Am. Chem. Soc.*, 1995, **117**, 2907; (*e*) P. C. Trulove, R. T. Carlin, G. R. Eaton and S. Eaton, *J. Am. Chem. Soc.*, 1995, **117**, 6265.

12 H. B. Bürgi, E. Blanc, D. Schwarzenbach, S. Liu, Y.-J. Lu, M. M. Kappes and J. A. Ibers, *Angew. Chem., Int. Ed. Engl.*, 1992, **31**, 640.

13 K. Himmel and M. Jansen, *Inorg. Chem.*, in press.

14 G. M. Sheldrick, SHELXS 86/SHELXL 93, Programs for Crystal Structure Determination and the Refinement of Structures, University of Göttingen, 1986 and 1993.

15 C. K. Johnson, ORTEP, *A Fortran Thermal Ellipsoids Program for Structure Illustrations*, Oak Ridge, Tennessee, 1965 (modified by R. Hundt, Bonn University, 1970).

Received in Basel, Switzerland, 6th March 1998; 8/01862F

Simultaneous 1,2-, 1,3- and 1,4-addition of trithiazyl trichloride to a conjugated diene

Charles W. Rees* and Tai-Yuen Yue

Department of Chemistry, Imperial College of Science, Technology and Medicine, London, UK SW7 2AY

1,4-Diphenylbuta-1,3-diene and trithiazyl trichloride 1 react to give a bi(thiadiazole) 2, an isothiazoloisothiazole 3, a dithiazolothiazine 4 and the thiazinodithiatriazepines 5 and 6, all of which could arise from initial addition of the trimer 1, or its monomer, to the conjugated diene by 1,2-,1,4- and, for the first time to an all-carbon diene, 1,3-('criss-cross') cycloaddition reactions.

We have shown that trithiazyl trichloride $(NSCl)_3$ **1**, in thermal equilibrium with its monomer N≡SCl,[1] converts monoenes and monoynes directly into 1,2,5-thiadiazoles.[2] Furthermore, 1-alkyl-2,5-diphenylpyrroles are similarly converted into the bi(1,2,5-thiadiazole) **2**, thus reacting as masked 1,3-dienes.[3] It would be interesting therefore to explore the reaction of the reagent **1** with acyclic conjugated dienes where 1,3- and 1,4-cycloaddition, as well as 1,2-cycloaddition, can be envisaged, as shown in Scheme 1.

When (*E,E*)-1,4-diphenylbuta-1,3-diene was treated with a deficiency of **1** (1 mol) in refluxing CCl_4 for 30 min a rapid and complex reaction ensued, from which five crystalline organic compounds **2**–**6** were isolated in low yields† by careful chromatography and shown to be derivatives of five different, rare or new heterocyclic ring systems (Scheme 2). The same five products were obtained in higher yields,† shown in brackets in Scheme 2, when the diene was treated with **1** (1 mol) in refluxing toluene for 1 h. With more trimer (3 mol) in refluxing toluene for 16 h, the reaction was less complex and **2** was the major product (60%). In spite of their very different structures, the carbon connectivity of the starting diene is retained in all of these products.

The bi(1,2,5-thiadiazole) **2** was identical with that formed from *N*-alkyl-2,5-diphenylpyrroles.[3]

The isothiazolo[5,4-*d*]isothiazole structure **3** was suggested by its high stability and symmetry (^{1}H and ^{13}C NMR) and its mass spectrum, which gave fragments for PhCN and C_2S_2. This product was synthesised independently from the oxime of 5-benzoyl-3-phenylisothiazole[4] and disulfur dichloride in DMF at 100 °C, providing another approach to this rare ring system.

The new dithiazolo[4,5-*d*]thiazine *S*-oxide structure **4** was based on its spectroscopic properties and confirmed by X-ray crystallography.[5] The sulfoxide group suggested that formation of **4** had involved oxidation, possibly during isolation; an examination of the five products **2**–**6** showed that all were stable to air except for the brown compound **5** which was oxidised to **4** when adsorbed on silica. Compound **5** was rapidly and cleanly converted into **4** by MCPBA in CH_2Cl_2 at room temperature. Link scan mass spectrometry showed that **4** and **5** gave the same pattern of daughter ions, the same species ($C_{16}H_{10}N_2S_3$) being

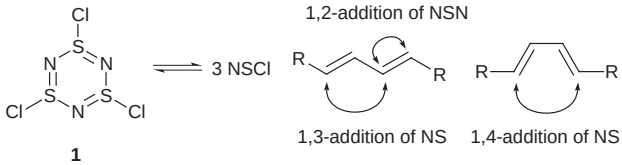

1

Scheme 1

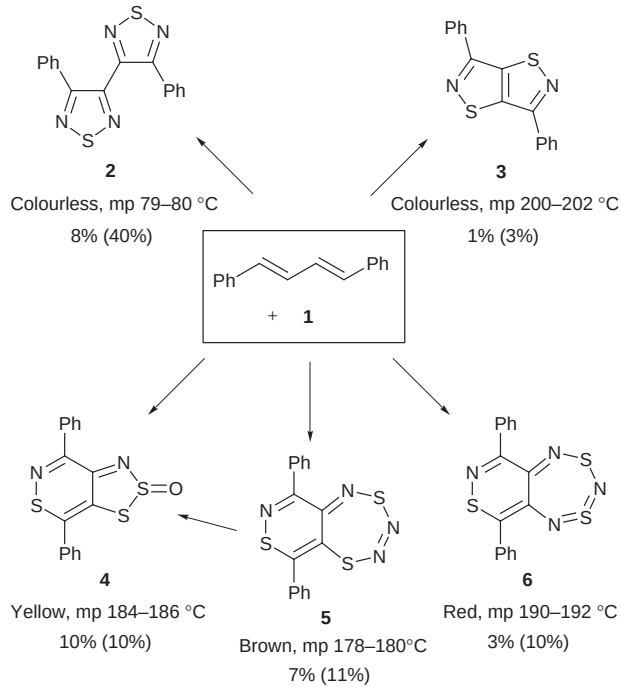

Scheme 2

formed from **4** by loss of O and from **5** by loss of N_2. This suggested the new thiazinodithiatriazepine structure **5** for the brown product, which agreed with all its spectroscopic properties, including the dominant loss of N_2 in the mass spectrum. Conversion of **5** into **4** could result from oxidation at the least hindered sulfur atom, to give **7**, followed by extrusion of N_2.

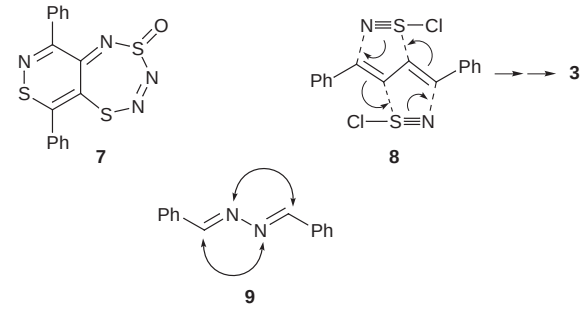

The structure of the final product **6**, which is isomeric with **5**, was assigned on the basis of spectroscopic properties and a chemical degradation. Its molecular ion was much stronger than that of **5** and showed no loss of N_2.

The formation of all five products can be explained by initial 1,2-, 1,3- and 1,4-cycloaddition processes (Scheme 1). The bi(thiadiazole) **2** is probably formed by addition of the trimer, as

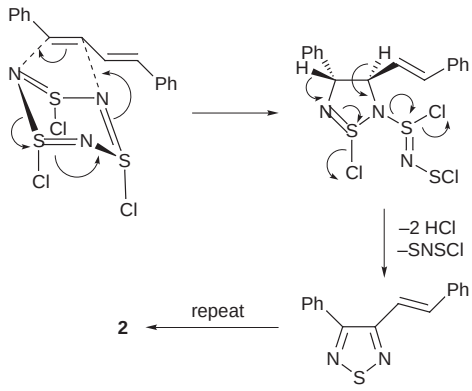

Scheme 3

an N–S–N unit, across C_1–C_2 and C_3–C_4, exactly as for monoenes[2] and pyrroles,[3] as shown in Scheme 3.

The structure of the isothiazoloisothiazole **3** suggests the addition of S–N units, possibly the monomeric species N≡SCl, across C_1–C_3 and C_2–C_4, as shown in **8**. Subsequent elimination of HCl and oxidation, possibly *via* chlorination, would give the stable aromatic system **3**. Such 'criss-cross' cycloadditions[6] have been reported for azabutadienes, particularly for azines such as 1,4-diphenyl-2,3-diazabuta-1,3-diene **9**,[7] but the present reaction is, we believe, the first example of a criss-cross cycloaddition to an all-carbon diene.

The 1,2-thiazine ring common to the remaining products suggests the 1,4-addition of an N–S unit, probably the monomer, to the diene. Since at least four molecules of monomer are required to form compounds **5** and **6**, it is possible that the Diels–Alder process is followed by reaction with a molecule of trimer, with overall elimination of 4 HCl units to give the intermediate **11** (Scheme 4). Initial Diels–Alder reaction, elimination of HCl and a hydrogen shift would give 3,6-diphenyl-1,2-thiazine **10**, which is nucleophilic at C_4. Attack on the trimer **1** at nitrogen, followed by a second nucleophilic attack by C_5 at sulfur and elimination of the remaining HCl, could give the key intermediate **11**. This is formally a 16π antiaromatic system which could become 14π by extrusion of any one of the sulfur atoms. Extrusion of S_3 or S_1 would then lead to the observed products **5** and **6**, respectively, and **4** has been shown to arise by oxidation and N_2 extrusion from **5**.

Thus the initially puzzling array of products from this one diene can be explained by invoking all three cycloaddition modes of the diene with the reactive trimer **1** and its more reactive monomer. At present the only product produced in high yield is the bi(1,2,5-thiadiazole) **2**, under more vigorous conditions; the analogous di-*p*-tolyl compound was also the main product from the same reaction of the corresponding butadiene.

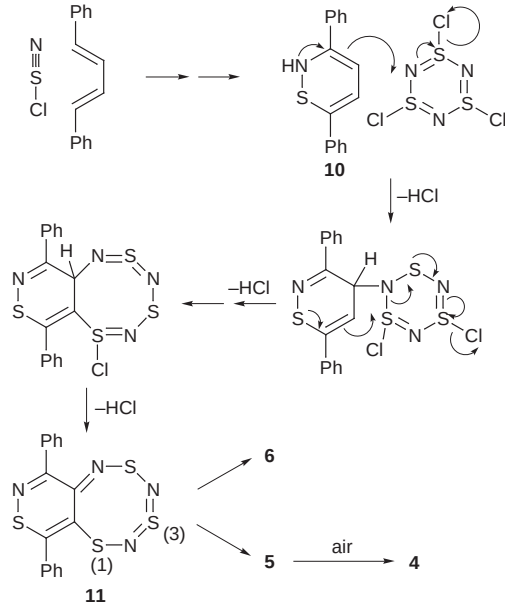

Scheme 4

It is hoped that similar reactions of unsymmetrical and functionalised conjugated dienes will prove to be more selective and hence of synthetic as well as mechanistic value.

We gratefully acknowledge financial support from the Commonwealth Scholarship Commission and the British Council (T-Y. Y.) and from MDL Information Systems (UK) Ltd, Professor D. J. Williams for the X-ray structure determination, the Wolfson Foundation for establishing the Wolfson Centre for Organic Chemistry in Medical Science at Imperial College, and a referee for valuable comments.

Notes and References

† Yields are based on the minimum amount of trimer **1**, which is in deficiency, required to give each product.

1 *Gmelin Handbook of Inorganic Chemistry*, ed. B. Heibel, *Sulfur-Nitrogen Compounds*, Part 2, Springer-Verlag, Berlin, 8th edn., 1985, p. 92.
2 X.-G. Duan, X.-L. Duan, C. W. Rees and T.-Y. Yue, *J. Chem. Soc., Perkin Trans. 1*, 1997, 2597.
3 X.-G. Duan and C. W. Rees, *J. Chem. Soc., Perkin Trans. 1*, 1997, 3189.
4 X.-L. Duan, R. Perrins and C. W. Rees, *J. Chem. Soc., Perkin Trans. 1*, 1997, 1617.
5 D. J. Williams, Imperial College, unpublished results.
6 *1,3-Dipolar Cycloaddition Chemistry*, ed. A. Padwa, Wiley, Chichester, 1984, vol. 1.
7 T. Wagner-Jauregg, *Synthesis*, 1976, 349; S. Rádl, *Aldrichim. Acta*, 1997, **30**, 97.

Received in Liverpool, UK, 18th March 1998; 8/02159G

Highly selective coupling of organoboron compounds *via* oxovanadium(v)-induced oxidation

Takuji Ishikawa, Suguru Nonaka, Akiya Ogawa and Toshikazu Hirao*†

Department of Applied Chemistry, Faculty of Engineering, Osaka University, Yamada-oka, Suita, Osaka 565-0871, Japan

Reaction of organoboranes or organoborane ate complexes (obtained by treatment with Bu^{n}Li or CsF) with oxovanadium(v) compounds results in the intramolecular oxidative coupling of organic groups on the boranes or borates.

One-electron oxidation of organometallics with metallic oxidants is expected to offer synthetically useful transformations *via* intermediates with a higher oxidation state involving organometallic radical cation species.[1] An oxovanadium(v) compound, $VO(OR)X_2$, has been revealed to be an efficient one-electron oxidant,[1a,2] as exemplified by oxidative desilylation of organosilicon compounds.[3] The reaction path is explained by the intermediacy of radical cations and radicals *via* desilylation, which provides a versatile route to electrophilic synthetic equivalents. Carbon–carbon bond forming reactions *via* oxidation of organoboranes using metallic oxidants have not been investigated except for a few transformations of functional groups.[4] We herein report a novel ligand coupling of organoboron compounds induced by an oxovanadium(v) compound.

When organoborane compound **1a**, derived from phenylacetylene and dicyclohexylborane,[5] was treated with 3 equiv.[6] of $VO(OEt)Cl_2$ at room temperature in CH_2Cl_2, [(*E*)-2-phenylethenyl]cyclohexane **2a** was selectively produced without the formation of bi(cyclohexyl) **3a** and 1,4-diphenylbutadiene **4a**, as shown in Scheme 1. It should be noted that the coupling reaction occurs selectively.

To gain insight into the reaction pathway, the following crossover reaction was examined (Scheme 2). When an equimolar mixture of bis(2-methylcyclohexyl)[(*E*)-2-phenylethenyl]borane **1b** and dicyclohexyl[(*E*)-2-(4-methylphenyl)ethenyl]borane **1c** was treated with $VO(OEt)Cl_2$, 1-methyl-2-(2-phenylethenyl)cyclohexane **2b** and [2-(4-methylphenyl)ethenyl]cyclohexane **2c** were produced, with only trace amounts of crossover products **2b′** and **2c′**. Although trace amounts of crossover products were obtained, the result may imply that the coupling reaction proceeds intramolecularly.

The corresponding ate complexes of the organoboranes are expected to undergo more facile oxidation. A higher yield was attained in the reaction of the borate **5a** generated from **1a** and Bu^{n}Li (Scheme 3).[7] No butylated product was detected in the reaction mixture, indicating that the organic groups are effectively differentiated in the coupling reaction. The stereoisomer was, however, obtained in a small amount. Use of $VO(OPr^i)_2Cl$, which has a lower oxidation capability, decreased the yield. CH_2Cl_2 was found to be superior to Et_2O as a solvent.

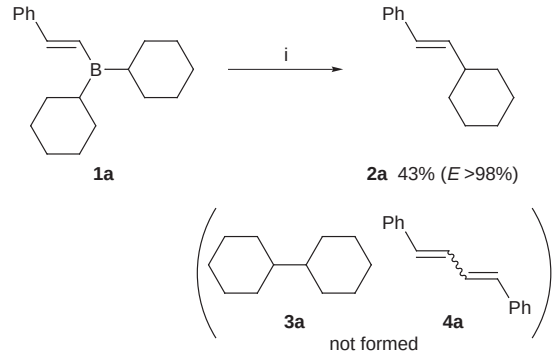

Scheme 1 *Reagents and conditions*: i, $VO(OEt)Cl_2$ (3 equiv.), CH_2Cl_2, room temp., 2 h

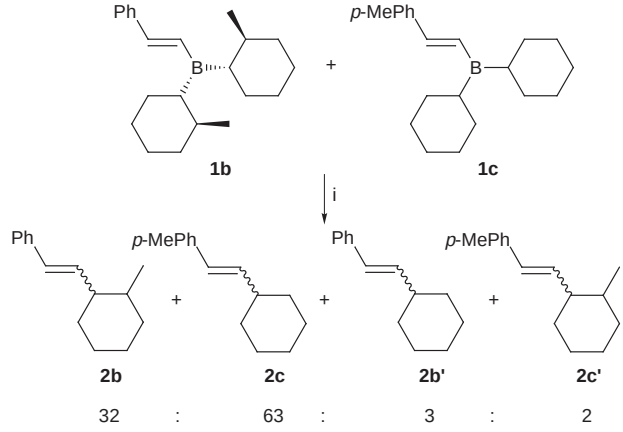

Scheme 2 *Reagents and conditions*: i, $VO(OEt)Cl_2$ (3 equiv.), CH_2Cl_2, −78 °C, 4 h

Representative results for the borate **5** are summarized in Table 1. A distinct substituent effect was observed with R^1. Starting from the 2-(4-methylphenyl)ethenyl- and 2-(ethoxycarbonyl)ethenyl-substituted boranes **1c** and **1e**, highly stereoselective coupling reactions were performed, but the organoborate derived from **1f** did not couple under the reaction conditions. These findings suggest that the coupling reaction is controlled by the electronic nature of the substituents in **5**. The reaction of the ate complex **5d** with $VO(OEt)Cl_2$ afforded 1-phenylhex-1-ene **2g** as the main product, in sharp contrast to the above-mentioned observation. The cyclopentyl group was found to scarcely participate in the coupling reaction under the conditions described, but oxidation with $VO(OPr^i)_2Cl$ led to the incorporation of the cyclopentyl group together with **2g**.

Use of CsF or TBAF to form organoborate **6a**[7] improved the stereoselectivity, giving the *E* isomer exclusively (Scheme 4).

Although the reaction path is ambiguous, the intramolecular ligand coupling is achieved *via* oxidation with the oxovanadium(v) compound. The oxidation of alkenylborates with iodine is known to give the corresponding coupling products as a single stereoisomer, in which an ionic mechanism is proposed generally.[5a,8] On the other hand, the present oxovanadium-

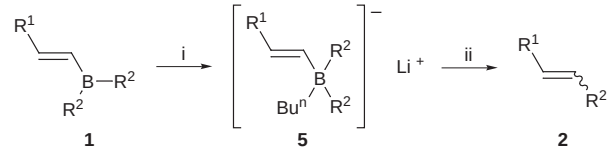

Scheme 3 *Reagents and conditions*: i, Bu^{n}Li (1 equiv.), −78 °C, 1 h; ii, $VO(OEt)Cl_2$ (3 equiv.)

Table 1 Oxidative cross-coupling reaction of borate **5**[a]

1							
	R^1	R^2	Oxovanadium	Solvent	Product	Yield (%)[b]	$E:Z$[c]
1a	Ph	cyclohexyl	$VO(OEt)Cl_2$	CH_2Cl_2	**2a**	82 (70)	92 : 8
1a	Ph	cyclohexyl	$VO(OPr^i)_2Cl$	CH_2Cl_2	**2a**	69	92 : 8
1a	Ph	cyclohexyl	$VO(OEt)Cl_2$	Et_2O	**2a**	52	69 : 31
1b	Ph	2-methylcyclohexyl	$VO(OEt)Cl_2$	CH_2Cl_2	**2b**	47 (30)[d]	92 : 8
1c	4-MeC_6H_4	cyclohexyl	$VO(OEt)Cl_2$	CH_2Cl_2	**2c**	65 (55)	96 : 4
1d	4-MeC_6H_4	cyclopentyl	$VO(OEt)Cl_2$	CH_2Cl_2	**2d**	trace[e]	—
1d	4-MeC_6H_4	cyclopentyl	$VO(OPr^i)_2Cl$	CH_2Cl_2	**2d**	(21)[f]	93 : 7
1e	EtO_2C	cyclohexyl	$VO(OEt)Cl_2$	CH_2Cl_2	**2e**	95 (60)	97 : 3
1f	*n*-hexyl	cyclohexyl	$VO(OEt)Cl_2$	CH_2Cl_2	**2f**	not detected	

[a] All reactions were performed at room temperature for 2 h unless otherwise stated. [b] Determined by ^1H NMR spectroscopy based on the alkyne. Isolated yield is shown in a parentheses. [c] The olefinic geometry. [d] Reaction temperature is −78 °C, *syn* : *anti* = 50 : 50. PhCH=CHBu **2g** was isolated in 10% yield ($E:Z$ = 93 : 7). [e] **2g** was isolated in 40% yield ($E:Z$ = 85 : 15). [f] **2g** was isolated in 20% yield ($E:Z$ = 95 : 5).

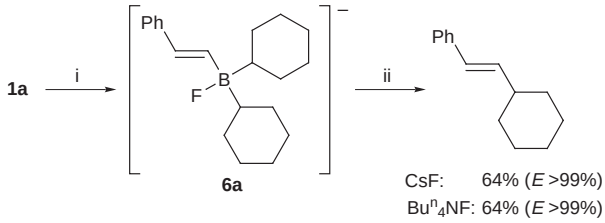

Scheme 4 *Reagents and conditions:* i, CsF or TBAF (1 equiv.), CH_2Cl_2, room temp., 1 h; ii, $VO(OEt)Cl_2$ (3 equiv.), CH_2Cl_2, room temp., 2 h

induced reaction of **5** provides the coupling products with *E* configuration preferentially. Taking this stereochemical observation into account in the oxidation of **5**, a radical-like species is assumed to be involved as an intermediate in the intramolecular coupling step, since a radical species is generated by aerobic oxidation of triethylborane[9] and electrochemical oxidation of borates.[10] Further investigations are now in progress.

The use of the facilities of the Analytical Center, Faculty of Engineering, Osaka University, is acknowledged. This work was partly supported by a Grant-in-Aid for Scientific Research on Priority Areas from the Ministry of Education, Science, and Culture, Japan.

Notes and References

† E-mail: hirao@ap.chem.eng.osaka-u.ac.jp

1 Recent reviews of radical generation using metallic reagents: (*a*) J. Iqbal, B. Bhatia and N. K. Nayyar, *Chem. Rev.*, 1994, **94**, 519; (*b*) P. I. Dalko, *Tetrahedron*, 1995, **51**, 7579; (*c*) N. Arai and K. Narasaka, *Yuki Gousei Kagaku Kyoukaishi*, 1996, **54**, 964; (*d*) T. Hirao, *Chem. Rev.*, 1997, **97**, 2707; for oxidation of organometallics: (*e*) R. F. Jordan, R. F. LaPointe, C. S. Bajgur, S. F. Echols and R. Willett, *J. Am. Chem. Soc.*, 1987, **109**, 4111; (*f*) M. J. Burk, W. Tumas, M. D. Ward and D. R. Wheeler, *J. Am. Chem. Soc.*, 1990, **112**, 6133.

2 F. Freeman, in *Organic Synthesis by Oxidation with Metal Compounds*, ed. W. J. Mijs and C. R. H. de Jonge, Plenum, New York, 1986, p. 1; Decarboxylation-deoxygenation: I. K. Meier and J. Schwartz, *J. Am. Chem. Soc.*, 1989, **111**, 3069; Phenolic coupling: M. A. Schwartz, R. A. Holton and S. W. Scott, *J. Am. Chem. Soc.*, 1969, **91**, 2800; S. M. Kupchan, V. Kameswaran, J. T. Lynn, D. K. Williams and A. J. Liepa, *J. Am. Chem. Soc.*, 1975, **97**, 5622.

3 T. Fujii, T. Hirao and Y. Ohshiro, *Tetrahedron Lett.*, 1992, **33**, 5823; 1993, **34**, 5601; T. Hirao, T. Fujii and Y. Ohshiro, *Tetrahedron Lett.*, 1994, **35**, 8005; *Tetrahedron*, 1994, **50**, 10 207.

4 N. Miyaura, M. Itoh and A. Suzuki, *Synthesis*, 1976, 618; *Tetrahedron Lett.*, 1976, 255; 1977, 173; 1977, 3369.

5 (*a*) A. Pelter, K. Smith and H. C. Brown, in *Borane Reagents*, Academic Press, London, 1988; (*b*) E. Negishi, in *Organometallics in Organic Synthesis*, Wiley, New York, vol. 1, 1980.

6 A decrease (2 equiv.) in the amount of $VO(OEt)Cl_2$ lowered the yield.

7 The formation of the ate complexes has been reported with Bu^{n}Li: ref. 5(*a*) and E. Negishi, M. J. Idacavage, K.-W. Chiu, T. Yoshida, A. Abramovitch, M. E. Goettel, A. Silveira and H. D. Bretherick, *J. Chem. Soc., Perkin Trans. 2*, 1978, 1225. With CsF: L. Garnier, B. Plunian, J. Morter and M. Vaultier, *Tetrahedron Lett.*, 1996, **37**, 6699; M. Reetz, T. C. M. Niemeyer and K. Harms, *Angew. Chem., Int. Ed. Engl.*, 1991, **30**, 1472 and 1474.

8 N. J. LaLima and A. B. Levy, *J. Org. Chem.*, 1978, **43**, 1279 and references cited therein.

9 K. Nozaki, K. Wakamatsu, T. Nonaka, W. Tückmantel, K. Oshima and K. Utimoto, *Tetrahedron Lett.*, 1986, **27**, 2007; K. Nozaki, K. Oshima and K. Utimoto, *J. Am. Chem. Soc.*, 1987, **109**, 2547.

10 T. Taguchi, M. Itoh and A. Suzuki, *Chem. Lett.*, 1973, 719; T. Taguchi, Y. Takahashi, M. Itoh and A. Suzuki, *Chem. Lett.*, 1974, 1021.

Received in Cambridge, UK, 6th March 1998; 8/01844H

Palladium-mediated intramolecular acylation reaction in the attempted phosphinylation of a sterically hindered trifluoromethylsulfonyloxybiaryl carboxylic ester†

Gerhard Bringmann,*[a]‡ Andreas Wuzik,[a] Christoph Vedder,[a] Matthias Pfeiffer[b] and Dietmar Stalke[b]

[a] *Institut für Organische Chemie der Universität Würzburg, Am Hubland, 97074 Würzburg, Germany*
[b] *Institut für Anorganische Chemie der Universität Würzburg, Am Hubland, 97074 Würzburg, Germany*

The unexpected palladium-assisted cyclization reaction of a sterically hindered *o*-methoxycarbonyl-*o′*-trifluoromethylsulfonyloxybiaryl gives fluorenone 4, *via* intramolecular acylation instead of the attempted phosphinylation.

Chiral phosphine ligands, mostly bisphosphines, constitute versatile tools for efficient transition metal catalyzed asymmetric reactions.[1] For some types of reactions, however, the use of bisphosphine transition metal complexes is hampered by their lack of reactivity and selectivity towards the desired reaction pathway. These problems can be overcome by the use of monodentate phosphine ligands ('MOP' ligands) introduced by Hayashi *et al*., who have demonstrated the efficiency of such ligands in enantioselective hydrosilylation and allylic alkylations.[2,3]

A promising novel MOP ligand with a biaryl backbone would be **3**, which, in contrast to related axially chiral binaphthyl derivatives previously prepared,[2,3] should exhibit a distinctly higher steric hindrance—and thus stereo-differentiation—in the proximity of the phosphorous part. Its *O*-trifluromethylsulfonyl activated synthetic precursor **2** should easily be synthesized in an enantiomerically pure form, with either configuration at the biaryl axis, by atropisomer-selective ring cleavage[4] of the configuratively unstable[5] lactone-bridged biaryl **1**. Here we report on the preparation and attempted phosphinylation of **2** (here still in racemic form), leading to a novel palladium-mediated ring closure to give fluorenone **4**.

Triflate **2**§ was synthesized from lactone **1**¶ by ring cleavage with $MeOH–K_2CO_3$ and esterification of the resulting free phenolic oxygen function with Tf_2O (Scheme 1). Reaction of **2** with $HP(O)Ph_2$ in the presence of $Pd(OAc)_2$ (10 mol%) and Hünig's base ($EtNPr^i_2$) according to Hayashi's method[6] gave no detectable amount of the anticipated phosphine oxide **3**, the most conspicuous product being a yellow nonpolar compound (28% isolated yield‖), which turned out to be the unexpected fluorenone **4**.**

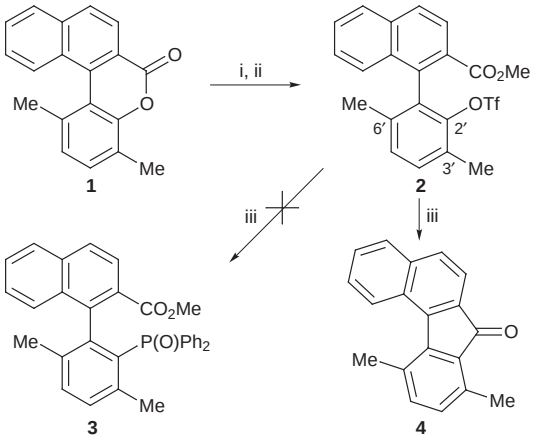

Scheme 1 *Reagents and conditions*: i, MeOH, K_2CO_3, THF, room temp., 1 h; ii, Tf_2O, DABCO, CH_2Cl_2, 0 °C, 12 h; iii, $Pd(OAc)_2$, dppp, $HP(O)Ph_2$, $EtNPr^i_2$, Me_2SO, 100 °C, 6 d

Its structure was elucidated mainly *via* NMR, mass and combustion analytical data and confirmed by an X-ray structure analysis of single crystals obtained from light petroleum–Et_2O (2 : 1) (see Fig. 1), which unambiguously proves the unexpected tetracyclic constitution.†† Due to the steric hindrance in the C(5)–C(4c)– C(4b)–C(4a))–C(4) 'bay' with the adjacent methyl group at C(4), the molecule is not flat, but helically twisted, giving rise to two enantiomers. These are both found in the crystal, Fig. 1 arbitrarily showing the *M*-helical enantiomer. The overall molecular distortion of the 'inner spiral loop',[7] *i.e.* the sum of the dihedral angles α [C(13)– C(4)–C(4a)–C(4b), 5.6(9)°], β [C(4)–C(4a)–C(4b)–C(4c), 23.7(9)°] and γ [C(4a)–C(4b)–C(4c)–C(5), 10.4(8)°], is distinctly smaller (39.7°) than for comparably substituted lactones related to **1** (> 60°).[7]

The reason why no phosphine oxide **3** was formed must be seen in the unusually high steric hindrance at the substitution site, C-2′, which is bounded (as in other cases) by the bulky

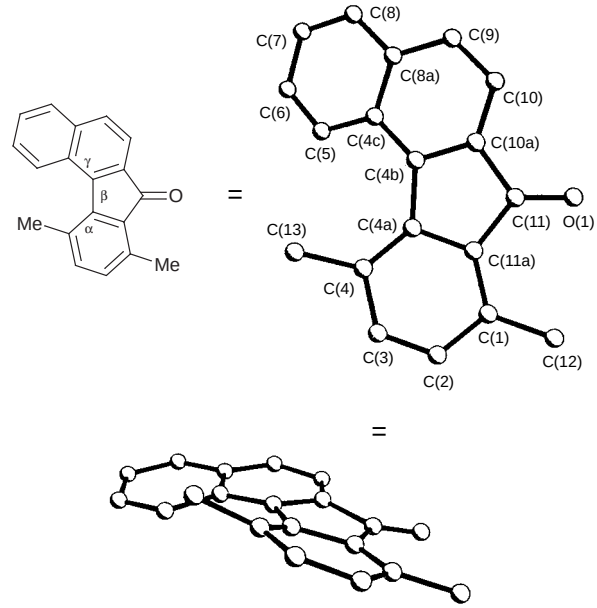

Fig. 1 Molecular structure of fluorenone **4** in the crystal. All hydrogen atoms are omitted for clarity. Selected bond length (Å) and angles (°): O(1)–C(11) 1.238(6), C(11)–C(11a) 1.470(7), C(10a)–C(4b) 1.390(7), C(10)–C(9) 1.372(6), C(9)–C(8a) 1.410(7), C(4c)–C(4b) 1.431(6), C(11)–C(10a) 1.479(6), C(8a)–C(4c) 1.426(6), C(4b)–C(4a) 1.501(6), C(4a)–C(11a) 1.427(6), C(4)–C(13) 1.514(7), C(1)–C(12) 1.495(7); O(1)–C(11)–C(10a) 124.9(5), O(1)–C(11)–C(11a) 128.2(4), C(4b)–C(10a)–C(10) 123.6(4), C(9)– C(8a)–C(8) 120.8(5), C(5)–C(4c)–C(4b) 123.8(5), C(4c)–C(4b)–C(4a) 133.8(5), C(4)–C(4a)–C(4b) 132.5(5), C(4a)–C(4)–C(13) 127.1(4), C(11a)–C(1)–C(12) 123.0(5), C(4a)–C(11a)–C(11) 107.6(4), C(4b)–C(10a)–C(11) 109.1(5), C(11a)–C(11)–C(10a) 106.9(5), C(11a)–C(4a)–C(4b) 107.9(4).

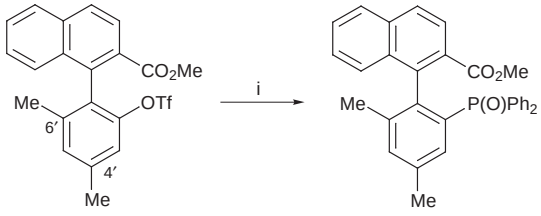

5 **6**

Scheme 2 *Reagents and conditions*: i, $Pd(OAc)_2$, dppp, $HP(O)Ph_2$, $EtNPr^i_2$, Me_2SO, 100 °C, 6 d

substituted naphthyl residue at C-1′ *and* by the unprecedented additional methyl group at C-3′ (Scheme 1). That this extra steric hindrance is responsible for the failure of the introduction of the sterically demanding phosphorus substituent was demonstrated by successfully performing the desired substitution on the regioisomeric compound **5**,‡‡ in which the methyl group is located at C-4′ (Scheme 2). Under the same reaction conditions as applied above, this triflate smoothly gave the desired phosphine oxide **6**,§ in high yields (74% of isolated pure material) and within the 'normal'[6] reaction time of about 12 h. The much slower fluorenone formation from the 3′-methyl isomer **2**, apparently by C–C bond formation of the presumed 2′-palladated intermediate§§ with the methoxycarbonyl substituent on the naphthalene part, took about a week.

To the best of our knowledge, the ring closure reaction of **2** to give **4** is the first intramolecular acylation mediated by $Pd(OAc)_2$ to give substituted fluorenone systems. Initial attempts to enhance the yield of **4** and decrease the reaction times, *e.g.* by using larger amounts of the palladium catalyst, gave improved yields of up to 42%, while in the absence of either $Pd(OAc)_2$, $EtNPr^i_2$ or $HP(O)Ph_2$, no reaction took place. Investigations to further optimize this new reaction, also with respect to the suppression of the likewise observed deoxygenation, and to investigate its possible application to natural product synthesis, are in progress.

This work was supported by the Deutsche Forschungsgemeinschaft (SFB 347 'Selektive Reaktionen Metall-aktivierter Moleküle') and by the Fonds der Chemischen Industrie.

Notes and References

† Part 69 in the series 'Novel Concepts in Directed Biaryl Synthesis'; for Part 68, see W. A. Schenk, J. Kümmel, I. Reuther, N. Burzlaff, A. Wuzik, O. Schupp, G. Bringmann, submitted for publication in *Eur. J. Inorg. Chem.*

‡ E-mail: bringman@chemie.uni-wuerzburg.de

§ All new compounds were fully characterized by spectroscopic and analytic methods.

¶ Prepared from the corresponding bromonaphthoic aryl ester, in analogy to ref. 7.

‖ In this reaction, likewise 25% of starting material **2** was recovered, along with its deoxygenation product (H instead of OTf, 29%).

** *Selected data* for **4**: ν_{max}(KBr)/cm^{-1} 1690 (CO); δ_H($CDCl_3$, 25 °C) 2.64 (s, 3 H, Me), 2.68 (s, 3 H, Me), 6.99, 7.20 (d × 2, 2 H, 2-H, 3-H, $^2J_{HH}$ 7.9), 7.47–7.57 (m, 2 H, Ph), 7.70–7.77 (m, 2 H, Ph), 7.81–7.88 (m, 1 H, Ph), 8.31–8.37 (m, 1 H, Ph); δ_C 194.8 (C=O), 145.5–119.3 (Ph), 23.7, 17.6 (Ph*Me*); *m/z* 258 (100%) $[M]^+$, 243 (10) $[M - CH_3]^+$, 230 (15) $[M - CO]^+$, 228 (18) $[243 - CH_3]^+$.

†† *Crystal data* for **4**: $C_{19}H_{14}O$, orange needles, crystal dimensions 0.3 × 0.3 × 0.3, M = 258.30, monoclinic, space group $P2_1/c$, a = 11.602(3), b = 14.641(2), c = 7.7016(14) Å, β = 102.914(8)°, V = 1275.1(4) Å^3, Z = 4, D_c = 1.345 g cm^{-3}, μ = 0.081 mm^{-1}, F(000) = 544, 2810 reflections collected ($3 \leqslant \theta \leqslant 23°$) at 173(2) K, 1664 independent (R_{int} = 0.1079), 1663 used in the structure refinement, $R1$ = 0.0652 [$I \geqslant 2\sigma(I)$], $wR2$ = 0.1665 [all data], gof = 0.974 for 184 parameters, largest difference peak/hole = 0.233/−0.307 e Å^{-3}. Data were collected from a shock-cooled crystal on an Enraf-Nonius CAD4 four circle diffractometer (graphite-monochromated Mo-Kα radiation, λ = 0.71073 Å) equipped with low temperature devices (ref. 8). The structure was solved by direct methods (SHELXS-96 (ref. 9) and refined by full-matrix least-squares methods against F^2 (SHELXL-96) (ref. 10). Anisotropic refinement of all non-H atoms. R values: $wR2 = [[w(F_o^2 - F_c^2)^2]/[w(F_o^2)^2]]^{1/2}$, $R1 = ||F_o| - |F_c||/|F_o|$. CCDC 182/859.

‡‡ The triflate **5** was synthesized analogously to compound **2**, starting from the corresponding *o*-methoxycarbonyl-*o*′-hydroxybiaryl, which had been prepared earlier (ref. 11).

§§ We suspect that the oxidative addition of the aryl triflate to the Pd reagent, comparable to the first reaction step of a Heck reaction, is the initiating step, leading to an Ar–Pd–OTf species, for which the deoxygenation product (see note ‖) constitutes a significant hint. This Pd intermediate should then further react with the ester functionality.

1 R. Noyori, *Chem. Soc. Rev.*, 1989, **18**, 187 and references cited therein.
2 T. Hayashi, *Acta Chem. Scand.*, 1996, **50**, 259.
3 T. Hayashi, M. Kawatsutra and Y. Uozumi, *Chem. Commun.*, 1997, 551.
4 G. Bringmann, R. Walter and R. Weirich, *Methods of Organic Chemistry* (*Houben Weyl*), ed. G. Helmchen, R. W. Hoffmann, J. Mulzer and E. Schaumann, Thieme, Stuttgart, 1995, vol. E21a, pp. 567–587; G. Bringmann and T. Hartung, *Tetrahedron*, 1993, **49**, 7891; G. Bringmann, T. Pabst, S. Busemann, K. Peters and E.-M. Peters, *Tetrahedron*, 1998, **54**, 1425.
5 G. Bringmann, H. Busse, U. Dauer, S. Güssregen and M. Stahl, *Tetrahedron*, 1995, **51**, 3149; G. Bringmann and O. Schupp, *S. Afr. J. Chem.*, 1994, **47**, 83.
6 Y. Uozumi, N. Suzuki, A. Ogiwara and T. Hayashi, *Tetrahedron*, 1994, **50**, 4293.
7 G. Bringmann, T. Hartung, L. Göbel, O. Schupp, C. L. J. Ewers, B. Schöner, R. Zagst, K. Peters, H. G. von Schnering and C. Burschka, *Liebigs Ann. Chem.*, 1992, 225.
8 T. Kottke and D. Stalke, *J. Appl. Crystallogr.*, 1993, **26**, 616; T. Kottke, R. Lagow and D. Stalke, *J. Appl. Crystallogr.*, 1996, **29**, 465.
9 G. M. Sheldrick, SHELXS-96, *Acta Crystallogr., Sect. A*, 1990, **46**, 467.
10 G. M. Sheldrick, SHELXL-96, Program for crystal structure refinement, Universität Göttingen, 1996.
11 G. Bringmann, M. Breuning, A. Wuzik, K. Peters and E.-M. Peters, *Z. Kristallogr.*, 1998, 213, 339.

Received in Liverpool, UK, 27th February 1998; 8/01674G

Rearrangement of *o*-(chloromethyldimethylsilyl)phenylmethoxide: evidence for an apical position of the migrating group in a trigonal bipyramid intermediate

Yousef M. Hijji,† Paul F. Hudrlik*‡ and Anne M. Hudrlik

Department of Chemistry, Howard University, Washington, DC 20059, USA

Chloromethylsilane 5a undergoes a rearrangement reaction to give oxasilacyclopentane 9 rather than oxasilacyclohexane 10, indicating that the methyl group migrates in preference to the aryl group.

Rearrangements of α-substituted organosilanes, with migration of an organic group from silicon to carbon, have been found to take place under acidic,[1] basic[1–4] or thermal[1] conditions. Little is known about the stereochemistry of the migration reaction, although migration from the apical position of a trigonal bipyramid has been suggested.[4] In contrast, the stereochemistry of nucleophilic substitutions at silicon has been extensively studied, and is generally interpreted as proceeding through pentacoordinate trigonal bipyramid intermediates, usually with entering and leaving groups in the apical positions.[5] With the increasing use of carbon-functional organosilicon compounds in organic synthesis, it is important to establish the stereochemistry of the fundamental reactions in organosilicon chemistry.[6] We report the first evidence for the stereochemistry of the base-induced rearrangement.

We have previously found the γ-oxidopropyl group on silicon to be effective as an internal nucleophile, and reported the cleavage reactions of γ-hydroxysilanes **1** (for generation of benzyl and allyl anion equivalents) (Scheme 1),[7] and the rearrangement reactions of γ-hydroxysilanes **2** (forming carbon–carbon bonds *via* a silicon template) (Scheme 2).[2]

More rigid γ-hydroxysilanes would be expected to be more efficient for this purpose, and we have therefore been studying the use of *o*-silylbenzyl alcohols **6** in the cleavage and rearrangement reactions. In the course of this work, we have found that *o*-silyl benzyl alcohols **6** can be easily prepared by rearrangement of silyl ethers **5** of *o*-bromobenzyl alcohol with Li or Bu^{t}Li in Et_2O (Scheme 3).[8]

Silyl ether **5a** provides an opportunity to study the relative importance of migratory aptitude (aryl *vs.* methyl) compared to stereochemical preference of the migrating group (apical *vs.* equatorial). Compound **5a**§ was prepared in 78% yield by treatment of *o*-bromobenzyl alcohol with 1.3 equiv. of $ClSiMe_2CH_2Cl$ in Et_2O–NEt_3 for 1 h at room temperature. [An impurity (*ca.* 6% by GC), believed to be $(ClCH_2Si)_2O$ was present: GC–MS *m/z* 181 (40%, $M^+ - CH_2Cl$), 153 (100); additional peaks at δ 2.76 (s) and 0.24 (s) in the ^{1}H NMR spectrum.] Treatment of **5a** with Bu^{t}Li in THF (30 min at −78 °C, then removal of the cold bath for 5 min, and workup by addition of saturated $NaHCO_3$) led to disappearance of **5a** with appearance of one product, assigned as oxasilacyclopentane **9**. [Some $(ClCH_2Si)_2O$ (*ca.* 7% by GC) was also observed in the GC and GC–MS.] Compound **9** is believed to arise *via* rearrangement (see Scheme 3) to γ-oxidosilane **7**, followed by methyl migration (presumably *via* trigonal bipyramid intermediate **8**, see Scheme 4). Aryl migration would have given oxasilacyclohexane **10**.

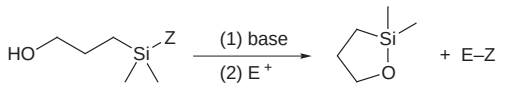

1 Z = Bn, allyl

Scheme 1

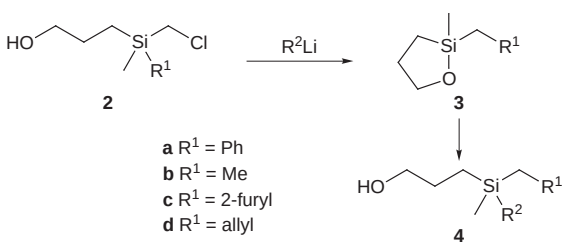

Scheme 2

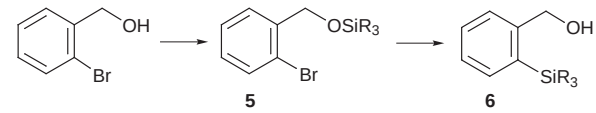

Scheme 3

The structure of **9** was supported by the spectra, in particular the mass spectrum, which showed the base peak at 149 ($M^+ -$ Et), and the ^{1}H NMR spectrum, which was different from that reported for oxasilacyclohexane **10**.[9] The ^{1}H NMR spectrum of the crude product included δ 7.2–7.6 (m, ArH) 5.16 (s, CH_2O) and 0.39 (s, MeSi), as well as peaks due to $(ClCH_2Si)_2O$ (singlets at δ 2.76 and 0.24) and a small amount of THF. [Comparison with the reported ^{1}H NMR spectrum of compound **10**[9] suggested that **10**, if present, was less than 10%.] The ^{13}C NMR spectrum showed δ 6.30 ($SiCH_2CH_3$), 8.83 ($SiCH_2CH_3$), 71.72 (CH_2O), 121.55, 126.73, 129.49, 131.21, 134.14 (small), 150.07 (small), as well as 30.72 (small, $SiCH_2Cl$), peaks for THF, and three peaks in the SiMe region. The GC–MS showed *m/z* 178 (15%, M^+), 163 (8, $M^+ -$ Me), 149 (100, $M^+ -$ Et), 135 (8) and 105 (11). The structure of **9** was further confirmed by

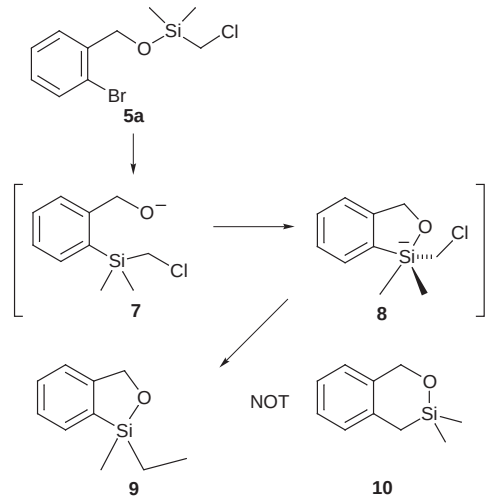

Scheme 4

treatment (in THF) with excess MeLi (−78 °C, 1 h) which gave a mixture of *o*-(ethyldimethylsilyl)benzyl alcohol[8] (major) and *o*-(trimethylsilyl)benzyl alcohol[8] (minor).[10]

Migratory aptitudes in rearrangements of halomethylsilanes under basic conditions have been correlated with the ability of the migrating group to stabilize a negative charge.[3,4] In our studies of the rearrangement reactions of γ-hydroxysilanes **2**, we found that the phenyl group had a greater migratory aptitude than the methyl group, as expected.[2] Treatment of γ-hydroxysilane **2a** with several bases resulted in oxasilacyclopentane **3a**, the product of phenyl migration; in some cases, a small amount (< 5%) of 2-phenyl- 2-ethyl-1-oxa-2-silacyclopentane, the product of methyl migration, was also observed. (Treatment of γ-hydroxysilane **2a** with 2 equiv. of MeLi in Et_2O gave product **4a**, presumably by trapping of **3a** with MeLi.)[2]

The comparison of the migratory aptitudes in the acyclic system **2a** (phenyl migration) with those in the cyclic system **5a** (methyl migration) is very interesting. Perhaps the cyclic system **8a** has geometrical constraints which disfavor aryl migration. To the extent oxygen would prefer the apical position in a trigonal bipyramid intermediate (apical entry, electronegativity, see **8**),[11] the Si–Ar bond in the *o*-benzyl alcohol system would have to be equatorial. The preference for methyl migration in **5a** suggests that *migration is favored by an apical position of the migrating group in a trigonal bipyramid intermediate.* This work also suggests that *o*-silylbenzyl alcohol substrates should be useful for carbon–carbon bond forming reactions *via* rearrangements without interference from the aryl group.

Financial support from the National Science Foundation (CHE-9505465 and CHE9007879) is gratefully acknowledged.

Notes and References

† Present address: Morgan State University, Baltimore, MD 21251, USA.
‡ E-mail: phudrlik@fac.howard.edu
§ The IR, ^1H NMR and mass spectra were in agreement with the structure.

1 For leading references, see P. F. Hudrlik, Y. M. Abdallah, A. K. Kulkarni and A. M. Hudrlik, *J. Org. Chem*., 1992, **57**, 6552.
2 P. F. Hudrlik, Y. M. Abdallah and A. M. Hudrlik, *Tetrahedron Lett*., 1992, **33**, 6743 and references cited therein.
3 R. Damrauer, V. E. Yost, S. E. Danahey and B. K. O′Connell, *Organometallics*, 1985, **4**, 1779.
4 S. L. Aprahamian and H. Shechter, *Tetrahedron Lett*., 1990, **31**, 1089.
5 Although not simultaneously for reactions proceeding with retention of stereochemistry: R. R. Holmes, *Chem. Rev*., 1990, **90**, 17; A. R. Bassindale and P. G. Taylor, in *The Chemistry of Organic Silicon Compounds*, ed. S. Patai and Z. Rappoport, Wiley, New York, 1989, part 1, pp. 839–892.
6 I. Fleming, A. Barbero and D. Walter, *Chem. Rev*., 1997, **97**, 2063.
7 P. F. Hudrlik, Y. M. Abdallah and A. M. Hudrlik, *Tetrahedron Lett*., 1992, **33**, 6747.
8 Y. M. Hijji, P. F. Hudrlik, C. O. Okoro and A. M. Hudrlik, *Synth. Commun*., 1997, **27**, 4297.
9 E. Baciocchi, R. Bernini and O. Lanzalunga, *J. Chem. Soc., Chem. Commun*., 1993, 1691.
10 For other examples of cleavage at silicon by intramolecular alkoxide, see: C. Rücker, *Tetrahedron Lett*., 1984, **25**, 4349; W. Kirmse and F. Söllenböhmer, *J. Chem. Soc., Chem. Commun*., 1989, 774.
11 Nucleophilic substitution reactions at silicon are felt to occur *via* apical entry, and although pseudorotation of the pentacoordinate intermediate is possible, oxygen is more apicophilic than carbon. See ref. 5 and C. Chuit, R. J. P. Corriu, C. Reye and J. C. Young, *Chem. Rev*., 1993, **93**, 1371; R. R. Holmes, *Chem. Rev*., 1996, **96**, 927.

Received in Corvallis, OR, USA, 16th February 1998; 8/01377B

A new probe of superconductivity: quantitative measurements on defined electron transfer with solute at the interface between liquid electrolyte and oxocuprate electrode in the superconducting state

Stephen J. Green,[a] David R. Rosseinsky,*[a]† Andrei L. Kharlanov[b] and J. Paul Attfield[b]

[a] *Department of Chemistry, The University, Exeter, UK EX4 4QD*
[b] *IRC in Superconductivity, University of Cambridge, Cambridge, UK CB3 0HE*

The rate of electron transfer, between dissolved decamethylferrocene molecules and an oxocuprate high temperature superconductor [Tl 1223] electrode, represented in impedance spectroscopy by an electrical resistance term R_{CT}, is shown to be measurable (R_{CT} tending to dip around the superconducting transition temperature), so opening up the prospect of a new, controllably variable, probe of superconductivity.

There are now oxocuprate high-temperature superconductors (HTSCs) having superconducting transition temperatures T_c of 135 K.[1] Superconductivity at even higher temperatures would significantly enhance technological applicability. The resistanceless current in a superconductor is carried by paired charge carriers which form below T_c, usually together with an energy gap around the Fermi level in the density of states. Despite protracted efforts, the mechanism of oxocuprate HTSC superconductivity is not well understood.[2] Linking an understanding of the pairing mechanism to the oxocuprate structure clearly presents the most promising route to maximizing T_c by design; here we suggest a novel probe towards that goal, monitoring the rates of electron transfer directly to or from the HTSC at and about its T_c.

A liquid electrolyte (chloroethane with tetrahydrofuran and 2-methyltetrahydrofuran, plus a lithium salt electrolyte) is now available[3–6] in which the electron-transfer reactions of freely diffusing electroactive species, here ferrocene or decamethylferrocene, at macrosized Pt electrodes could be followed by cyclic voltammetry at temperatures as low as 99.5 K.[5] Next, at specially designed cryorobust HTSC electrodes[6] (including leads for the *in situ* determination, by a four-point resistivity measurement[6] on the electrode in use, of its superconducting transition temperature), charge transfer between freely diffusing ferrocene and a demonstrably superconducting HTSC microelectrode at 102 K could be clearly detected by cyclic voltammetry.[5] Now we have studied by impedance spectroscopy the temperature dependence of the charge-transfer rate (proportional to the charge-transfer conductance R_{CT}^{-1}), and report here our observations on electron transfer between decamethylferrocene and the HTSC Tl 1223 electrode comprising the recently synthesized[7] $(Tl_{0.5}Pb_{0.5})(Sr_{1.6}Ca_{0.4})Ca_2Cu_3O_9$.‡

The equipment has been described in detail.[6] The precise value of T_c for the Tl 1223 was determined by magnetic susceptibility (Fig. 1). The behaviour of an electrode/electrolyte interface can be represented§ by R_{CT} (inversely proportional to charge-transfer rate), and (in parallel) the parameter C_{eff} which approximates to the double layer capacitance; it can thus be examined by electrochemical impedance studies together with standard procedures§ for fitting the equivalent circuit elements. The variation of R_{CT} and C_{eff} with temperature, through T_c, is shown in Fig. 2 (together with a notional time-constant $R_{CT} \times C_{eff}$, and the parameter§ Φ) where increases or decreases from otherwise smooth curvature occur when the sample traverses T_c. Excursions from smooth curves in the temperature range about T_c have been repeatedly observed[8] for these parameters in solid-state electrochemical reductions of Ag^+ with an electrolyte of solid Rb_4AgI_5, and also for an oxocuprate electrode immersed in liquid electrolyte when the solvent itself has been reduced,[9] though a decrease rather than an increase in their capacitance parameters has been observed in these related systems. The limited amount of experimental data available has left interpretation of the HTSC transitions speculative apart from Kuznetzov's theory[2,10] and a recent primitive elaboration[11] of the Ginsburg–Landau SC model which effects a decrease in double-layer capacitance on temperature increase up to T_c. Gluzman and Kuznetzov[2] were able to account for the generally observed[8,9] 'hump' in the charge transfer rate around T_c without the participation of paired carriers (disfavoured by increased reorganisation energy of electrolyte[10]),¶ in contradiction of Lorenz *et al.*[8] who assign the increase in the Faradaic current around T_c to paired charge carriers. Lorenz *et al.*[8] do point out that the smaller electrolyte reorganisation energy in solids *cf.* liquids makes pair transfer more likely in their systems than in liquids, with the implication that no excursions from smooth curvature, or 'humps', should occur with liquid electrolytes. Without inflicting excessive violence on our results, excising extreme data points could just accommodate nil excursions from smooth curves (points × in Fig. 2), but such a conclusion can be settled only by further, improved, experiments. However, the major advance represented by our preliminary observations lies in demonstrating the accessibility of choice of

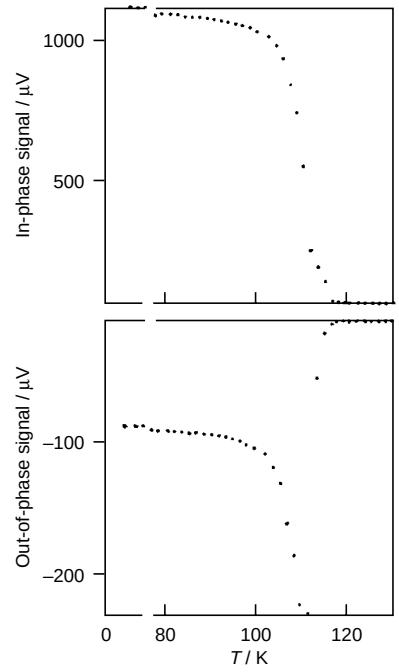

Fig. 1 Magnetic susceptibility measurements on Tl 1223 as in-phase and out-of-phase magnetometer signals showing T_c at 116 K

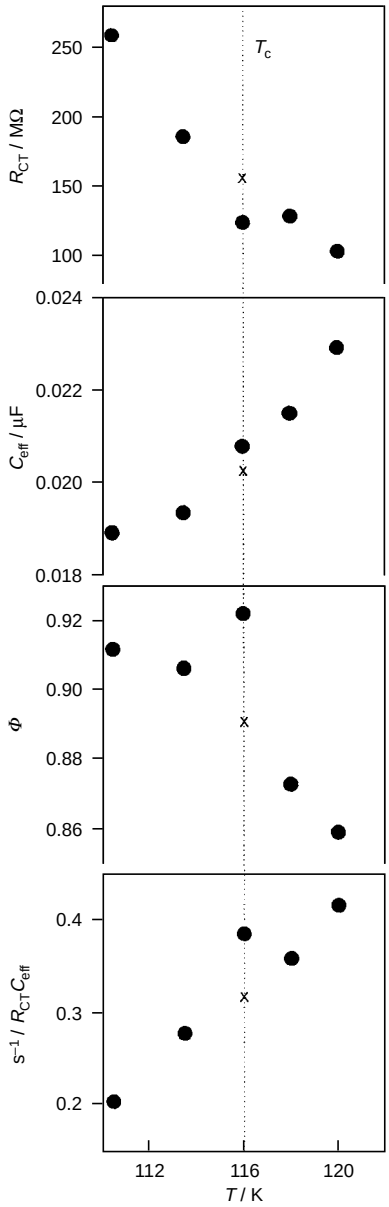

Fig. 2 Top to bottom: charge-transfer resistance R_{CT}, effective double-layer capacitance C_{eff}, phase parameter Φ and (inverse) effective time-constant $1/R_{CT}C_{eff}$ observed for DMFc/Tl 1223 at the electrolyte/electrode interface

solute electroactives, which here is a redox species rather than the electrolyte itself[8] or the actual solvent.[9] Neither of the previous studies[8,9] allows of control of the redox potential of the electroactive species, nor the use of electroactives with two linked redox sites¶ which offer the prospect of probing the transfer of paired charge carriers from within the superconductor. Such innovations should provide new insights into the superconductivity mechanism.[2] This creation of a new probe of superconductivity is clearly notable.

We thank the EPSRC for a grant.

Notes and References

† E-mail: D.R.Rosseinsky@exeter.ac.uk

‡ The electroactive species was 5 mM decamethylferrocene (DMFc) with 0.2 M $LiBF_4$ in solvent comprising 16 : 7 : 1 by volume chloroethane–tetrahydrofuran–2-methyltetrahydrofuran. The apparatus[3–6] with the addition of a Solartron 1286 frequency response analyser monitored the electrode response over the frequency range 10–10^5 Hz to a perturbation of ±100 mV superimposed on the HTSC electrode, about the approximate electrode potential for DMFc–$DMFc^+$ of 0 V with respect to the commonly used Ag-wire quasi-reference electrode.

§ Solartron programmes ZPLOT and ZVIEW allow simulation of the observed electrochemical impedance *via* a model circuit consisting of resistance and capacitance-like ($\Phi \neq 1$) circuit elements. The phase-related quantity Φ, unity for a true capacitance, is often fitted as < 1 (*i.e.* $< 90°$ for the current : potential phase difference) for electrochemical processes.

¶ From electrostatic considerations Kuznetzov[10] predicts a disfavouring fourfold increase in the solvent reorganisation barrier for the transfer of paired charge carriers *cf.* transfer of single electrons, to a single acceptor site. However, for transfer to two separate acceptors, the reorganisation energy will increase only twofold, and the transfer should be best favoured if the spacial separation of the acceptors is commensurate with the coherence length of the superconductor. Such a condition will hold for an electroactive species with two appropriately spaced redox centres.

1 G. B. Peacock, I. Gameson, M. Slaski, W. Z. Zhou, J. R. Cooper and P. P. Edwards, *Adv. Mater.*, 1995, **7**, 925.
2 S. Gluzman and A. M. Kuznetsov, *Phys. Rev. B*, 1995, **52**, 9190.
3 S. J. Green, D. R. Rosseinsky and M. J. Toohey, *J. Am. Chem. Soc.*, 1992, **114**, 9702.
4 S. J. Green, D. R. Rosseinsky and M. J. Toohey, *J. Chem. Soc., Chem. Commun.*, 1994, 325.
5 S. J. Green, D. R. Rosseinsky and D. C. Sinclair, *J. Chem. Soc., Chem. Commun.*, 1994, 1421.
6 S. J. Green, D. R. Rosseinsky and M. J. Toohey, *J. Electrochem. Soc.*, 1995, **142**, 22 725.
7 M. A. G. Aranda, D. C. Sinclair and J. P. Attfield, *Physica C*, 1994, **221**, 304.
8 W. J. Lorenz, G. Saemann-Ischenko and M. W. Breiter, in *Modern Aspects of Electrochemistry*, Number 28, ed. B. E. Conway, Plenum Press, New York, 1995.
9 S. R. Peck, L. S. Curtin, J. T. McDevitt, R. W. Murray, J. P. Collman, W. A. Little, T. Zetterer, H. M. Duan, C. Dong and A. M. Hermann, *J. Am. Chem. Soc.*, 1992, **114**, 6771.
10 A. M. Kuznetsov, *J. Electroanal. Chem.*, 1990, **278**, 1.
11 L. D. Zusman and D. N. Beratan, *J. Phys. Chem.*, 1997, **101**, 7095.

Received in Cambridge, UK, 1st April 1998; 8/02475H

Unique promotion effect of CO and CO_2 on the catalytic stability for benzene and naphthalene production from methane on Mo/HZSM-5 catalysts

Shetian Liu, Qun Dong, Ryuichiro Ohnishi and Masaru Ichikawa*†

Catalysis Research Center, Hokkaido University, Sapporo 060, Japan

The addition of CO and CO_2 to the methane feed results in a remarkable promotion of catalyst stability for direct benzene and naphthalene production from methane on Mo/HZSM-5 and Co modified Mo/HZSM-5 catalysts at 973 K owing to the efficient suppression of coke formation.

The catalytic conversion of methane to petrochemical feedstocks such as ethylene and benzene is of current importance and industrial interest in the effective utilization of carbon resources of natural gas. During the past five years, the non-oxidative conversion of methane to benzene has been studied on zeolite-supported Mo catalysts in terms of the reaction mechanism and catalyst characterization.[1–6] Our recent works demonstrate the methane is effectively dehydrocondensed into various aromatics such as benzene and naphthalene on Mo/HZSM-5 and modified Mo/HZSM-5 at high temperatures of 873–1073 K.[7] Nevertheless, methane conversion decreased drastically after a few hours owing to serious coke deposition on the catalysts. To reduce coke formation, some preliminary efforts have been reported using selected oxidative reagents such as oxygen[2] and carbon dioxide (10% or higher in the methane gas feed),[6] but aromatic product formation was completely inhibited on Mo/HZSM-5 catalysts. Here we describe that the inclusion of CO and/or CO_2 in the methane flow results in the promotion of aromatic product formation and a remarkable improvement of the catalyst stability in the prolonged dehydrocondensation reaction of methane at 973 K on Mo/HZSM-5 and CoMo/HZSM-5 catalysts owing to the substantial suppression of coke formation on the catalysts. Furthermore, ^{13}CO isotopic labeling and temperature programmed oxidation (TPO) experiments demonstrate that the CO added to the methane feed, as a carbon and oxygen donor when it is dissociated on the catalysts, not only is efficiently incorporated into aromatics such as benzene, but also results in removal of the surface coke.

Mo/HZSM-5 and Co modified Mo/HZSM-5 catalysts with 3 wt.% Mo loading were prepared by impregnation (incipient wetness) of NH_4ZSM-5 (SiO_2/Al_2O_3 = 20–1900; surface area, 780–925 $m^2\ g^{-1}$, Toso Co. and CRI Zeolyst, Inc.) with $(NH_4)_6Mo_7O_{24}\cdot 4H_2O$ and $Co(NO_3)_2$ aqueous solutions. After the impregnated samples were dried at 393 K and calcined at 773 K in air, catalytic tests were carried out under methane (1 atm), both with and without CO or CO_2, in a continuous microreactor system equipped with a quartz tube (8 mm id) packed with 0.3 g of catalyst pellets of 20–24 mesh, as reported previoulsy.[7] After flushing with He at 973 K, a feed gas mixture of 98% CH_4 with 2% Ar as internal standard for analysis both with and without CO or CO_2 was introduced into the fixed bed reactor at a flow rate of 7.5 ml min^{-1} [space velocity = 1500 ml h^{-1} (g cat)$^{-1}$] through a mass flow controller (Brooks 5850E). Using an internal standard analyzing method, conversion of methane, CO and CO_2, selectivities of hydrocarbon products and coke formed on the catalyst were evaluated to the mass balance for carbon and hydrogen.[7] The reaction between CO and CH_4 on Mo/HZSM-5 was studied by using the isotopic labeling (^{13}CO, 99% enriched) technique in a closed circulating reaction system, and both the gas phase mixture (containing mainly methane, carbon monoxide, ethane and ethylene) and the condensed products (mainly benzene collected using an ethanol–dry ice trap) were analyzed by GC-MS (Perkin-Elmer, Auto System GC, 910 Q-Mass). The coke deposited on the catalyst surface after reaction was evaluated by a TPO technique using 20% O_2 + 80% N_2 as the oxidant, and the tail gas was intermittently analyzed by on-line GC.

The addition of CO to the methane feed gas exerts a significant effect on the catalytic performances of Mo/HZSM-5 and CoMo/HZSM-5 for methane dehydrocondensation to promote the formation of benzene and naphthalene, and on the catalyst stability, as shown in Figs. 1 and 2. Using pure methane as the feed gas the methane conversion and benzene formation rates decreased greatly (less than 1/4–1/5 of the initial activities during 24 h reaction time on stream). By contrast, for methane with 1.8–12% CO in the feed gas, the decrease in methane conversion was much lower, regardless of the partial pressure of CO, as shown in Fig. 1. After attaining a moderate increase of benzene and naphthalene formation rates, compared with those achieved using pure methane in the early stage of the reaction, their formation rates were almost constant during prolonged reaction of more than 50 h. In the steady reaction stage, the amount of CO is almost constant before and after reaction

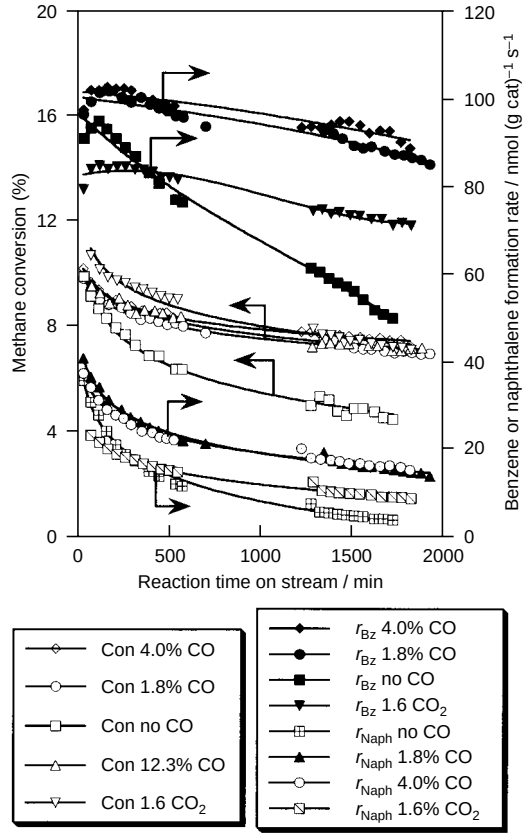

Fig. 1 Catalytic performances of 3% Mo/HZSM-5 for methane aromatization with the addition of CO and CO_2 to the methane feed gas at 973 K [Open symbols represent methane conversion and solid symbols the formation rates of benzene (r_{Bz}) and naphthalene (r_{Naph}), respectively]

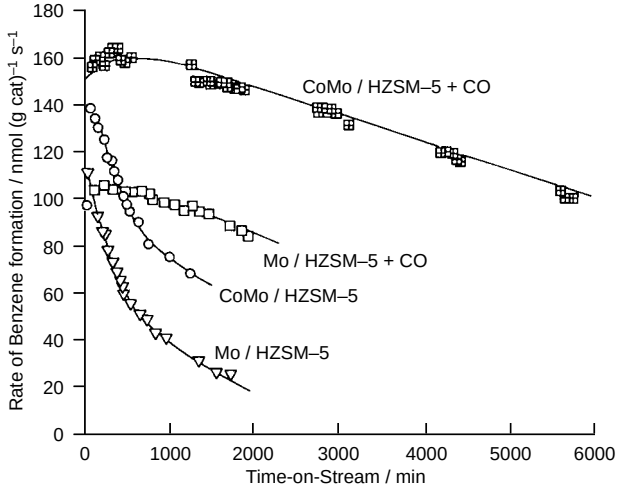

Fig. 2 Rates of benzene formation in methane aromatization reaction on 3% Mo/HZSM-5 (▽) and 1% Co, 3% Mo/HZSM-5 (○) catalysts using pure methane and (□) on 3% Mo/HZSM-5 and (⊞) on 1% Co, 3% Mo/HZSM-5 using methane + 4% CO at 973 K and 1 atm

through the catalyst beds in all cases of CO addition. The results imply that CO is regenerated, possibly due to the reaction of the surface carbon with the active oxygen species derived from CO dissociation as shown in Scheme 1.

These remarkable effects (improved catalytic stability, increased promotion of benzene formation) caused by the inclusion of CO have also been observed for modified catalysts such as CoMo/HZSM-5, as is shown in Fig. 2. The benzene formation rates are above 100 nmol (g cat)$^{-1}$ s^{-1} even after 100 h on the CoMo/HZSM-5 in the reaction of CH_4 + 3.5% CO, while the activity decreased greatly [less than 10 nmol (g cat)$^{-1}$ s^{-1}] using pure methane under the same reaction conditions.

Similarly, the stability of the catalyst was also improved by adding a few per cent CO_2 into the feed gas, as shown in Fig. 1. The addition of 1.6% CO_2 yielded higher methane conversion and hydrogen formation rate. Benzene formation was suppressed in comparison with that achieved with CO addition, but it was stable during the prolonged reaction time. Nevertheless, it was found that the addition of larger amounts of CO_2 (> 10%) in the methane feed gas largely inhibited the formation of aromatic products such as benzene. When the partial pressure of CO_2 was low (< 4%) in the feed gas, twice the amount of CO was detected compared with when CO_2 was added to the feed gas on the basis of the carbon content, while no CO_2 was observed in the outlet gas of the reaction. It is suggested that CO_2 is converted with CH_4 to produce twice the amount of CO under these reaction conditions by a reforming process (CO_2 + $CH_4 \rightarrow 2CO + 2H_2$). The formed CO may cause a similar promotion of product formation and improvement of catalytic stability.

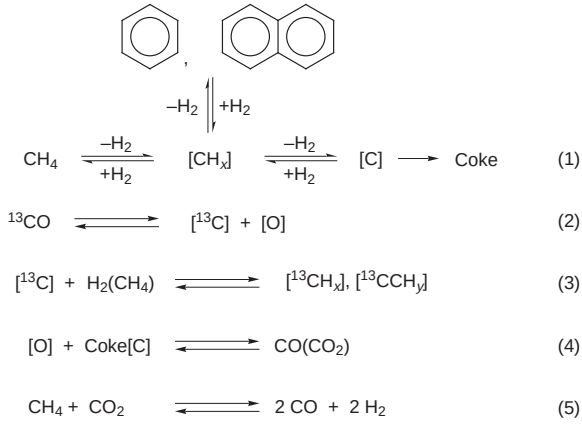

Scheme 1

The different effects of CO and CO_2 on methane aromatization may be associated with their different chemical properties: CO is dissociated on the Mo/HZSM-5 catalyst to form the common active CH_x surface species, similar to methane, which is converted to aromatics, and the dissociated [O] may react with surface coke to regenerate CO. However, CO_2 is more active towards reaction with surface CH_x derived from methane dissociation, yielding 2 mol of CO and H_2. Such effective consumption of surface intermediates with CO_2 causes the marked suppression of methane aromatization towards benzene. It is conceivable that benzene formation is a structure sensitive reaction, which requires a large concentration of active CH_x species on the catalysts. No appreciable differences in product selectivities for benzene and naphthalene were found, whether pure methane, or methane plus CO or CO_2 on the Mo/HZSM-5 and Co modified Mo/HZSM-5 catalysts, were used.

It was demonstrated by the TPO experiments that the amount of coke formed on the catalyst surface was greatly reduced by adding various amounts of CO or CO_2 to the methane feed gas. Increasing the CO concentration from 1.7% to 12.0% resulted in suppression of coke formation on the catalyst surface, particularly the irreversible or inert coke which was oxidized to CO_2 at temperatures above 773 K. Increasing the CO_2 partial pressure in the methane feed gas decreased the coke formation to a much lower level; this may be related to its weak oxidizing property (mentioned above).

To understand the role of CO in the methane aromatization reaction, the $^{13}CO + CH_4$ reaction was conducted. The starting composition of the reactant mixture was 8% ^{13}CO + 92% CH_4 with a total pressure around 220 Torr. Even after 5 min at 973 K, the level of ^{13}C incorporation in methane ($^{13}CH_4$) reached 8%. The isotopic abundance of ^{13}C incorporated in the benzene molecules was detected by GC-MS analysis as a random distribution ($^{13}CC_5H_6$ 47.6%, $^{13}C_2C_4H_6$ 36.7%, $^{13}C_3C_3H_6$ 13.0%, $^{13}C_4C_2H_6$ 2.4%, $^{13}C_5CH_6$ 0.3%) regardless of the reaction time of methane on Mo/HZSM-5. These results suggest that the carbon derived from CO dissociation is efficiently incorporated into the benzene formation and the isotopic scrambling reaction between ^{13}CO and $^{12}CH_4$ proceeds rapidly under these reaction conditions at 973 K.

Based on the above results we suggest a unique role of CO in the methane aromatization reaction, resulting in stabilization of catalyst performance and promotion of benzene formation, as shown in Scheme 1. Firstly, CO and CH_4 may dissociate on the catalyst surface, mostly on the Mo sites, to form active species such as [C], [O] and [CH_x] through reactions (1) and (2); the active carbon species [C] from CO is hydrogenated to [CH_x] fragments as illustrated in reaction (3), followed by the oligomerization with [CH_x] derived from CH_4 to form higher hydrocarbons such as benzene and naphthalene in reaction (1) on the catalyst; the dissociated oxygen species [O] from CO may react with the surface inert carbon species (coke) to regenerate CO, resulting in the suppression of coke formation on the catalyst through reaction (4).

Notes and References

† E-mail: michi@cat.hokudai.ac.jp

1 L. Wang, L. Tao, M. Xie, G. Xu, J. Huang and Y. Xu, *Catal. Lett.*, 1993, **21**, 35.
2 Y. Xu, S. Liu, L. Wang, M. Xie and X. Guo, *Catal. Lett.*, 1995, **30**, 135.
3 A. Szöke and F. Solymosi, *Appl. Catal. A: General*, 1996, **142**, 361.
4 S.-T. Wong, Y. Xu, L. Wang, S. Liu, G. Li, M. Xie and X. Guo, *Catal. Lett.*, 1996, **38**, 39.
5 Y. Xu, Y. Shu, S. Liu, J. Huang and X. Guo, *Catal. Lett.*, 1995, **35**, 233.
6 D. Wang, J. H. Lunsford and M. P. Rosynek, *J. Catal.*, 1997, **169**, 347.
7 S. Liu, Q. Dong, R. Ohnishi and M. Ichikawa, *Chem. Commun.*, 1997, 1455.

Received in Cambridge, UK, 25th February 1998; 8/01582A

Facilitation of the copper(II)-promoted dephosphorylation of adenosine 5′-triphosphate (ATP^{4-}) by the antiviral nucleotide analogue, 9-[2-(phosphonomethoxy)ethyl]adenine (PMEA)‡

Helmut Sigel,*[a]† Claudia A. Blindauer,[a] Antonín Holý[b] and Hana Dvořáková[b]

[a] *Institute of Inorganic Chemistry, University of Basel, Spitalstrasse 51, CH-4056 Basel, Switzerland*
[b] *Institute of Organic Chemistry and Biochemistry, Academy of Sciences, CZ-16610 Prague, Czech Republic*

The antiviral PMEA is able to mimic the structuring adenosine 5′-monophosphate (AMP^{2-}) in the reactive intermediate, $[Cu_3(ATP)(AMP)(OH)]^-$, and to promote the dephosphorylation of ATP; PMEA is about twice as effective as (the ultimate product of this hydrolysis) AMP.

Mechanistic studies on the metal ion-promoted hydrolysis of nucleoside 5′-triphosphates (NTP^{4-}) to nucleoside 5′-diphosphates (NDP^{3-}) and inorganic phosphate (P_i) revealed for this most simple transphosphorylation reaction, which consists of the transfer of a phosphoryl group to water, that the most reactive species contain two metal ions per NTP^{4-}.[1,2] This reflects the known 'general need' for two metal ions in enzymatic phosphoryl transfer reactions.[3] The *in vitro* dephosphorylation of ATP^{4-} in the presence of divalent metal ions (M^{2+}) proceeds *via* dimers of composition $[M_2(ATP)]_2$.[2] Depending on the kind of metal ion involved, hydrolysis occurs either *via* intermolecular H_2O attack or *via* intramolecular hydroxide attack of a phosphate-coordinated $M(OH)^+$ unit,[1b] as is the case with Cu^{2+}. Hence, $[Cu_2(ATP)]_2(OH)^-$ is the most reactive species for Cu^{2+}-promoted dephosphorylation.[1b,2] Such studies with copper are of general interest due to the evidence that there is an ATP-dependent Cu^{II} transporter in the Golgi apparatus[4] and the observation that the Menkes P-type ATPase is a transmembrane copper-translocating pump, which is defective in the human disorder called Menkes disease.[5] There is also a somewhat older suspicion that $Cu(ATP)^{2-}$ is involved in the inhibition of human erythrocyte ($Ca^{2+} + Mg^{2+}$)-ATPase.[6] Mixed Cu(ATP)(L) complexes (L = tryptophanate, *etc*. see also below) protect ATP against hydrolysis.[2]

In the reactive dimeric $[M_2(ATP)]_2$ complexes, which occur in low concentration and involve purine stacking[7] and N^7-M^{2+} coordination, one of the two ATPs takes over a structuring role and thus acts as its own hydrolytic 'enzyme'.§ This role cannot be taken over by adenosine, D-ribose 5-monophosphate or by tubercidin 5′-monophosphate ($TuMP^{2-}$, 7-deaza-AMP^{2-}) because these ligands are unable to form the required bridge in the reactive species, but it can be taken over by adenosine 5′-monophosphate (AMP^{2-}). In the presence of Cu^{2+}, this then leads, by promoting further the reactivity of the Cu^{2+}/ATP system, to the reactive $[Cu_3(ATP)(AMP)(OH)]^-$ species shown in Fig. 1.[8a] How does the related antiviral PMEA behave in this reaction? This adenine-nucleotide analogue (see Fig. 2) is active against various viruses, including hepatitis B (HBV) and human immunodeficiency viruses (HIV-1 and HIV-2).[9,10] After its twofold phosphorylation by cellular nucleotide kinases,[11] the resulting triphosphate analogue can serve as a substrate for the viral DNA polymerase or reverse transcriptase and subsequently terminates the growing nucleic acid chain.[12] Thus it was interesting to see whether $PMEA^{2-}$ would be able to mimic AMP^{2-} in the reactive intermediate (Fig. 1) and to facilitate thus also the Cu^{2+}-promoted dephosphorylation of ATP^{4-}.

The results of our experiments¶ are shown in Fig. 3 in parallel with the data obtained with AMP under identical conditions. These latter data agree (within the error limits) with those obtained previously.[1b] The addition of an approximately sevenfold excess of AMP to the Cu^{2+}/ATP 2:1 system facilitates the dephosphorylation reaction by a factor of about three (Fig. 3).‖ Indeed, $PMEA^{2-}$ can take over the structuring role of AMP^{2-} (or ATP^{4-}) in the reactive species (Fig. 1) and, astonishingly, it is twice as effective!** This is possibly due to the somewhat increased flexibility of $PMEA^{2-}$ compared with AMP^{2-} as a result of the replacement of the ribose residue by the open chain (see Fig. 2).†† To our knowledge, this is the first example demonstrating in a 'simple' reaction a close relationship between PMEA and its parent nucleotide AMP.

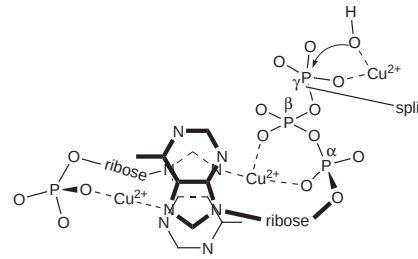

Fig. 1 Probable structure of the reactive $[Cu_3(ATP)(AMP)(OH)]^-$ species. The intramolecular attack of OH^- is indicated on the right-hand side, while the left-hand side shows the metal ion bridging which stabilizes the purine stack by coordination to the phosphate group of AMP^{2-} and to N^7 of ATP^{4-}. In the reactive $[M_2(ATP)]_2(OH)^-$ dimer the structuring ATP^{4-} occupies formally the left side in the above structure.

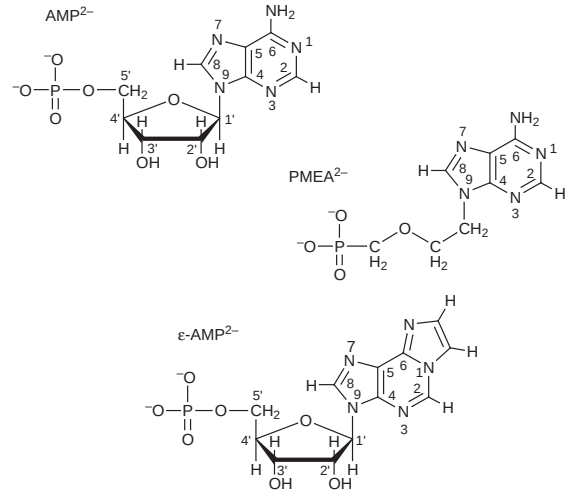

Fig. 2 Structure of the dianion of 9-[2-(phosphonomethoxy)-ethyl]adenine ($PMEA^{2-}$) in comparison with those of adenosine 5′-monophosphate (AMP^{2-}) and 1,N^6-ethenoadenosine 5′-monophosphate (ε-AMP^{2-})

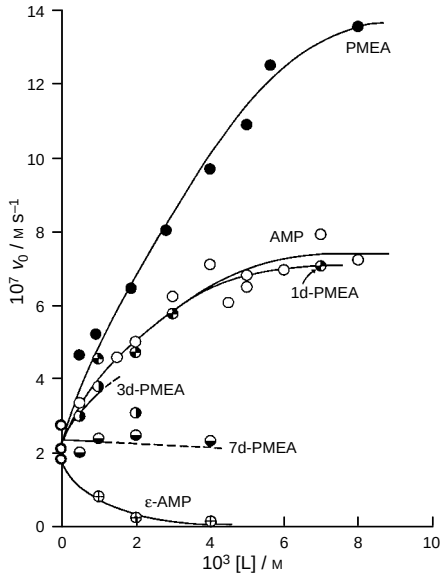

Fig. 3 Influence of PMEA (●) and AMP (○) as well as of some related derivatives (L) on the initial rate v_o (м s^{-1}) of dephosphorylation of the Cu^{2+}/ATP 2 : 1 system ($[Cu^{2+}]_{tot} = 2 \times 10^{-3}$ м and $[ATP]_{tot} = 10^{-3}$ м) in aqueous solution at pH_o 6.70 (I = 0.1 м, $NaClO_4$; 50 °C).¶ The broken lines indicate uncertainty due to precipitation.

These observations initiated further experiments with the deaza derivatives of PMEA, in which the three aromatic nitrogens, N^1, N^3, and N^7 (see Fig. 2), are systematically replaced by a CH unit. Fig. 3 shows that 1-deaza-$PMEA^{2-}$ facilitates the Cu^{2+}-promoted ATP^{4-} dephosphorylation at pH 6.7 about as well as AMP^{2-}.‡‡ Unfortunately, addition of 3-deaza-PMEA and 7-deaza-PMEA to a Cu^{2+}/ATP 2 : 1 system leads, even at relatively low concentrations, to turbidity of the reaction solution and finally to a precipitate. Nevertheless it is evident that 3-deaza-$PMEA^{2-}$ can also facilitate the reaction while some inhibition of the system occurs on addition of 7-deaza-$PMEA^{2-}$. This agrees with previous observations made with $TuMP^{2-}$ (7-deaza-AMP^{2-})[1b] which had confirmed the earlier suggestion[1a] regarding the importance of N^7 for the structure of the reactive intermediate.[2,8a]

To demonstrate how delicate the structure of the reactive intermediate (Fig. 1) is, we repeated a previous Cu^{2+}/ATP 1 : 1 experiment[1b] with 1,N^6-ethenoadenosine 5′-monophosphate (ε-AMP^{2-}; Fig. 2) under the present Cu^{2+}/ATP 2 : 1 conditions. The inhibition of the reaction is dramatic (Fig. 3); a fourfold excess of ε-AMP prevents the dephosphorylation of ATP^{4-} almost completely. The stacking properties of ε-AMP^{2-} are very similar to those of AMP^{2-};[13] however, in Cu(ε-AMP) the metal ion is bound to the phosphate group and the '1,10-phenanthroline'-like N^6, N^7 site[13] which leads to a different orientation of the metal ion in space. Consequently, this AMP derivative cannot take over the structuring role needed in the reactive species (Fig. 1), but it strongly inhibits, as is usual for ternary Cu(ATP)(L) complexes,[1b] the dephosphorylation reaction of the Cu^{2+}/ATP system. This inhibition re-emphasizes how well $PMEA^{2-}$ is suited to mimic AMP^{2-} in certain reactions.

This study was supported by the Swiss National Science Foundation (H.S.) and within the COST D8 programme by the Swiss Federal Office for Education and Science (H. S.) and the Ministry of Education of the Czech Republic (A. H.).

Notes and References

† E-mail: sigel@ubaclu.unibas.ch

‡ This is part 12 of 'Hydrolysis of Nucleoside Phosphates'; for part 11 see ref. 14.

§ In the presence of metal ions these adenine-nucleotide systems[8a] show thus related properties to ribozymes;[8b] their possible role in early evolution has been discussed.[8a]

¶ The disodium salt of ATP (> 98%; p.a.) was obtained from Serva Feinbiochemica GmbH, Heidelberg, Germany. The other reagents were the same as used previously.[15] The liberated P_i was determined by the molybdate method;[1,14] a critical summary of the methodology is given in ref. 2. No buffers were used to adjust the pH of the solutions because they inhibit metal ion-promoted dephosphorylation reactions.[2] Instead, the pH was adjusted with conc. NaOH or $HClO_4$ using a glass rod ('dotting'; volume changes negligible).[1,2] To obtain the initial pH, *i.e.* pH_o = 6.70, and the corresponding initial rate for the dephosphorylation, $v_o = d[P_i]/dt$ (м s^{-1}), at least two experiments were carried out in this pH range; these results were then interpolated to the desired pH_o as shown, *e.g.* in Figs. 1 and 3 of ref. 1*a* and 2, respectively. Usually v_o is reproducible to ±10%, but for a very rapid reaction and/or an unstable pH the error limit may increase to ±25%. Attempts to carry out the analogous experiments with Zn^{2+} failed due to precipitation; the very low solubility of Zn(PMEA) is known.[16a]

‖ ATP^{4-} hydrolyzes in a 10^{-3} м solution at pH_o 9.5 (I = 0.1 м, $NaClO_4$; 50 °C) with $v_o = 0.015 \times 10^{-8}$ м s^{-1}, whereas in a solution of the same ATP concentration and under the same conditions but in the presence of a twofold excess of Cu^{2+} at pH_o 5.5, where the reaction proceeds *via* $[Cu_2(ATP)]_2(OH)^-$, $v_o = 30 \times 10^{-8}$ м s^{-1};[2] *i.e.* Cu^{2+} promotes the hydrolysis of ATP^{4-} by a moderate factor of 2000. For solutions with [ATP] = 0.1 м the corresponding rates are: ATP alone, $v_o = 1.5 \times 10^{-8}$ м s^{-1}; with Cu^{2+}/ATP = 2 : 1 $v_o = 3 \times 10^{-3}$ м s^{-1}; hence, one obtains a large promotion factor of 2×10^5.[2] At pH_o 6.70 (Fig. 3) the corresponding promotion factors due to Cu^{2+} are only slightly smaller.[2] The pitfalls connected with comparisons of the indicated kind have been discussed in ref. 2 (pp. 515–519). Therefore, conclusions regarding nonenzymatic reactions (*e.g.* ref. 3,17), that divalent metal ions have little effect on the rate of ATP hydrolysis, have to be considered with care; much depends on the metal ion and the conditions (pH, *etc.*) involved.

** This is despite the higher basicity of the phosphonate group in $PMEA^{2-}$ (pK_a = 6.90)[15] compared to that of the phosphate group in AMP^{2-} (pK_a = 6.21)[18] which disfavours Cu^{2+} binding of $PMEA^{2-}$ (due to the competition with H^+) by a factor of about 0.5.

†† For the M^{2+}-binding properties of PMEA see ref. 16.

‡‡ Hence, N^1 has no significant role in the Cu^{2+}-promoted hydrolysis of ATP which contrasts with a recent claim[19] made for the Zn^{2+}/ATP system.

1 (*a*) H. Sigel and P. Amsler, *J. Am. Chem. Soc.*, 1976, **98**, 7390; (*b*) H. Sigel, F. Hofstetter, R. B. Martin, R. M. Milburn, V. Scheller-Krattiger and K. H. Scheller, *J. Am. Chem. Soc.*, 1984, **106**, 7935.
2 Comprehensive review: H. Sigel, *Coord. Chem. Rev.*, 1990, **100**, 453.
3 N. Sträter, W. N. Lipscomb, T. Klabunde and B. Krebs, *Angew. Chem., Int. Ed. Engl.*, 1996, **35**, 2024.
4 M. J. Bingham, T. J. Ong, W. J. Ingledew and H. J. McArdle, *Am. J. Physiol.-Gastrointest. & Liver Physiol.*, 1996, **34**, G741.
5 M. J. Petris, J. F. B. Mercer, J. G. Culvenor, P. Lockhart, P. A. Gleeson and J. Camakaris, *EMBO J.*, 1996, **15**, 6084.
6 C. Tallineau, M. Barriere, M. Boulard, P. Boulard-Heitzmann, R. Pontcharraud, D. Reiss and O. Guillard, *Biochim. Biophys. Acta*, 1984, **775**, 51.
7 H. Sigel, *Pure Appl. Chem.*, 1998, in press.
8 (*a*) H. Sigel, *Inorg. Chim. Acta*, 1992, **198**–**200**, 1; (*b*) A. M. Pyle, *Met. Ions Biol. Syst.*, 1996, **32**, 479.
9 E. De Clercq, A. Holý and I. Rosenberg, *Antimicrob. Agents Chemother.*, 1989, **33**, 185.
10 L. Naesens, R. Snoeck, G. Andrei, J. Balzarini, J. Neyts and E. De Clercq, *Antivir. Chem. Chemother.*, 1997, **8**, 1.
11 (*a*) A. Merta, I. Votruba, J. Jindřich, A. Holý, T. Cihlář, I. Rosenberg, M. Otmar and T. Y. Herve, *Biochem. Pharmacol.*, 1992, **44,** 2067; (*b*) S. A. Foster, J. Černý, Y.-c. Cheng, *J. Biol. Chem.*, 1991, **266**, 238.
12 J. Neyts and E. De Clercq, *Biochem. Pharmacol.*, 1994, **47**, 39.
13 1,N^6-ethenoadenosine derivatives: H. Sigel, *Chimia*, 1987, **41**, 11.
14 H. Sigel and R. Tribolet, *J. Inorg. Biochem.*, 1990, **40**, 163.
15 C. A. Blindauer, A. H. Emwas, A. Holý, H. Dvořáková, E. Sletten and H. Sigel, *Chem. Eur. J.*, 1997, **3**, 1526.
16 Reviews: (*a*) H. Sigel, *Coord. Chem. Rev.*, 1995, **144**, 287; (*b*) H. Sigel, *J. Indian Chem. Soc.*, 1997, **74**, 261 (P. Ray Award Lecture).
17 S. J. Admiraal and D. Herschlag, *Chem. Biol.*, 1995, **2**, 729.
18 H. Sigel, S. S. Massoud and N. A. Corfù, *J. Am. Chem. Soc.*, 1994, **116**, 2958.
19 E. Z. Utyanskaya, M. G. Neihaus, B. V. Lidskii and A. E. Shilov, *React. Kinet. Catal. Lett.*, 1995, **54,** 431; E. Utyanskaya, T. V. Mikhailova, A. O. Pavlov and A. E. Shilov, *ACH–Models Chemistry*, 1996, **133**, 65.

Received in Basel, Switzerland, 26th February 1998; 8/01615A

Ion flux and deposition rate measurements in the RF continuous wave plasma polymerisation of acrylic acid

A. J. Beck,[a] R. M. France,[a] A. M. Leeson,[a] R. D. Short,*[a]† A. Goodyear[b] and N. St. J. Braithwaite[b]

[a] *Department of Engineering Materials, Laboratory for Surface and Interface Analysis, University of Sheffield, Sheffield, UK S1 3JD*

[b] *The Open University, Oxford Research Unit, Foxcombe Hall, Berkeley Road, Boars Hill, Oxford, UK OX1 5HR*

Ion flux and deposition rate measurements made in plasmas of acrylic acid support the view that at low plasma power ions are primarily responsible for deposit growth.

In general, the mechanisms that lead to the deposition of plasma polymers are poorly understood. Yasuda[1] has described plasma polymerisation as proceeding through a rapid step-growth polymerisation (RSGP) mechanism. The RSGP mechanism is very general and was probably not intended to cover the entire range of conditions under which plasma polymer deposits form. However, in the absence of other schemes, it is widely quoted.[2] The nature of the reactive species in the RSGP mechanism is not made clear, but the orthodox view is that they are radicals.

This paper is concerned with the plasma polymerisation of acrylic (propenoic) acid in RF sustained glow-discharges of low input powers, *P*. Previously, functional group retention has been reported in the deposits from plasmas of carboxylic acids[3,4] and unsaturated alcohols.[5] Based on plasma-phase mass spectral measurements of ions and neutrals, we have proposed that functional group retention arises from oligomerisation (ion–molecule) reactions in the plasma.[3–5] At low *P*, dimeric[3–5] and trimeric[3,4] cations have been detected by mass spectrometry and under these same conditions functional group retention was highest.[3–5] The degree of dimer and trimer formation and functional group retention decreased with increased *P*. Deposition of polymer has been attributed to the ion flux arriving at a surface, but this has not been proven.[6]

Ion flux measurements are particularly difficult to make in plasmas used for the deposition of polymers. The problem arises from the build-up of an insulating layer on the active area of the probe used to measure the ion flux. Braithwaite *et al.*[7] have described a novel electrostatic probe that allows ion flux measurements to be made even when the surface of the probe is coated with an insulating material. The principles of operation are described in ref. 7.

To the best of our knowledge, ion flux measurements have not been made before in plasmas of C-, H- and O-containing monomers. The plasma polymerisation of these compounds has received considerable attention, as deposits from these compounds are used to control processes that depend upon surface chemistry. The effect of *P* on ion flux and deposition rate has been investigated. XPS analysis of the solid-phase plasma polymers is undertaken. We correlate changes in ion flux, deposition rate and surface chemistry with those previously reported in the plasma-phase.[4]

The apparatus (described more fully in ref. 8) consisted of a tubular glass reactor which was pumped by means of a rotary pump. The plasma was sustained by an RF generator (13.56 MHz) and amplifier inductively coupled to the plasma reactor. The *P* used was in the range 0.5–15 W and flow rate (ϕ) was fixed at 0.8 cm^3 (STP) min^{-1}. Acrylic acid (Aldrich > 99% purity) was pumped through a needle valve at a pressure of 2.5 $\times$ 10^{-2} mbar. Deposition rate measurements were made using a quartz crystal microbalance (Leybold, Manchester, UK), which was inserted into the plasma region, using a solid support to ensure consistent positioning of the crystal. In a separate series of experiments, the ion flux probe was placed in the plasma, close to where the quartz crystal had been, to determine the relationship between RF power and ion flux to this region. The presence of this probe is no more perturbing than the crystal balance, merely providing a loss surface for ions. The probe is biased negatively by RF pulses and the transient current used to determine ion flux. Changes in the probe voltage are limited to ensure the sheath potential changes at a much slower rate compared to the transit time of the ions crossing the sheath, this having a square-root dependence on ion mass and plasma density. This ensures the measured current is due to the particle fluxes only and not a redistribution of charge in the sheath.[7] This mode of operation makes the probe insensitive to ion mass.

Fig. 1 shows how the deposition rate varies with *P*. It clearly show two regimes: at *P* of < 4 W, the deposition rate increased with *P*; the deposition rate increased three-fold from *P* = 0.5 $\rightarrow$ 3 W. Above *P* = 4 W, the deposition rate remained essentially constant. These regimes are consistent with those previously described in the plasma-phase mass spectrometry of acrylic acid.[4] Over the range *P* = 1–4 W, the ion signal from the dimer of acrylic acid, expressed as the ratio of the intensity of the dimer signal to monomer signal, decreased smoothly by over 90% with *P*. By *P* = 5 W, the dimer signal had effectively fallen to zero.

Fig. 2 shows that the ion flux increased at a constant rate between *P* = 1–3 W (0.1 ± 0.1 $\times$ 10^{18} ions m^{-2} s^{-1}). Just above *P* = 4 W there was a marked jump in ion flux. Ion flux then continued to rise steadily with *P*, up to *P* = 14 W (1 ± 0.1 $\times$ 10^{18} ions m^{-2} s^{-1}).

It is between *P* = 0.5–4 W that the most significant change in the retention of carboxylic acid from the acrylic acid occurred. At *P* = 0.5 W, 80.5% retention of carboxylic acid was achieved, but at *P* = 1 W this was down to 58% retention. Retention continued to decline further with increased *P*, and a wider range of oxygen–carbon functional groups were incorporated into the plasma deposit.

The correlation between ion flux and deposition rate is not a simple one. In the plasma there is both deposition and ablation

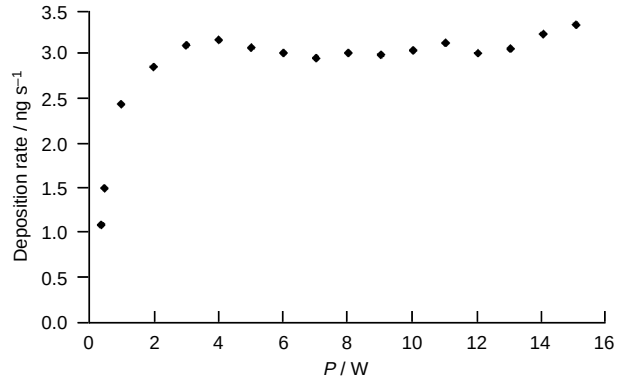

Fig. 1 Measured deposition rates *vs. P*

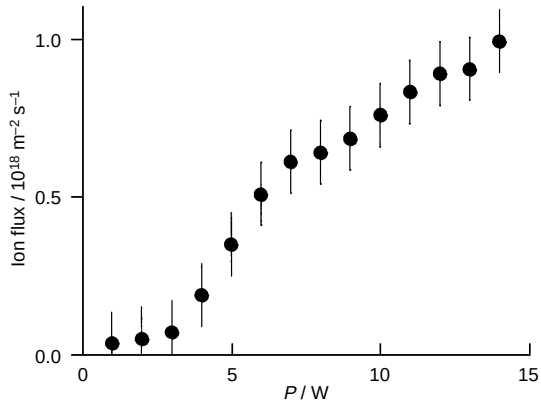

Fig. 2 Measured ion flux *vs. P*

of material. Ablation becomes more important at higher *P*. When this is taken into account, the different trends in ion flux and deposition rate data can be accommodated and fit with our understanding of plasma polymerisation.

In the acrylic acid system, at low *P* (0.5 W) there is extensive oligomerisation in the plasma-gas phase and these oligomers deposit to give a highly functionalised, low molecular weight film. These oligomers make up the bulk of the ion flux, which was too low to measure, with confidence, below $P = 1$ W. The deposition rate was correspondingly low.

The ion flux and deposition rate increased steadily with *P*, but at $P = 4$ W, their behaviour diverges. The deposition rate did not increase further with *P*. The constant deposition rate above $P = 4$ W represents a balance between deposition and ablation, with the increased ion flux being responsible for ablation.

Increased *P* had a dramatic effect on the extent of gas-phase oligomerisation. Above $P = 4$ W, oligomeric species from the plasma do not appreciably contribute to the deposit growth, which may now be explained by the flux of smaller ionic fragments and possibly radical grafting. Incorporation of carboxylic acid functional groups may have occurred by reaction of the surface with 'intact' monomer in the plasma, or other fragments containing carboxylic acid. Oxidation of the surface by the plasma can not be ruled out. At high *P*, the surface chemistry becomes closer to that of a plasma oxidised polymer surface.

This interpretation challenges the more orthodox view that neutral and free radical chemistry are solely responsible for deposit growth. The ability to make ion flux measurements in depositing plasmas is an important advance. The measurements themselves further point to the importance of the ionic component of these plasmas. Ion flux measurements help explain the effect *P* has upon surface chemistry and deposition rates.

We acknowledge the Leverhulme Trust for support of A. J. B. (Award F118AK).

Notes and References

† E-mail: r.short@shef.ac.uk

1 H. Yasuda, *Plasma Polymerisation*, Academic Press, London, 1985.
2 A. Grill *Cold Plasmas in Materials Fabrication*, IEEE Press, Piscataway, 1993, pp. 186–187.
3 A. J. Beck, L. O'Toole, R. D. Short, A. P. Ameen and F. R. Jones, *J. Chem. Soc., Chem. Commun*., 1995, 1053.
4 L. O'Toole, A. J. Beck, A. P. Ameen, F. R. Jones and R. D. Short, *J. Chem. Soc., Faraday Trans.*, 1995, **91**, 3907.
5 L. O'Toole and R. D. Short, *J. Chem. Soc., Faraday Trans.*, 1997, **93**, 11 141.
6 M. R. Alexander, F. R. Jones and R. D. Short, *J. Phys. Chem. B.*, 1997, **101**, 3619.
7 N St. Braithwaite, J. P. Booth and G. Cunge, *Plasma Sources Sci. Technol.*, 1996, **5**, 677.
8 L. O'Toole, R. D. Short, A. P. Ameen and F. R. Jones, *J. Chem. Soc., Faraday Trans*., 1995, **91**, 1363

Received in Cambridge, UK, 4th March 1998; 8/01778F

The first enantioselective syntheses of vicinal difluoropyrrolidines and the first catalytic asymmetric synthesis mediated by the C_2 symmetry of a –CHFCHF– unit

Charles M. Marson*† and Robert C. Melling

Department of Chemistry, Queen Mary and Westfield College, University of London, London, UK E1 4NS

The first enantiopure vicinal difluorides of C_2 symmetry have been prepared by the introduction of fluorine at both centres in a single operation; the first asymmetric synthesis using a catalyst whose chirality depends on organofluorine asymmetry is described.

The stereoselective synthesis of organofluorine compounds[1,2] is of major importance in many fields, including pharmaceuticals,[1–3] nucleoside and carbohydrate chemistry,[1b] biochemistry,[4,5] liquid crystals[6] and polymers.[7] Many fluorinated α-amino acids are potent antitumour and antiviral agents.[1a,4a] The importance of monofluoro analogues as antimetabolites is illustrated by (2*R*,3*R*)-fluorocitric acid, an aconitase inhibitor that blocks the citric acid cycle.[2,5] Additionally, organofluoro ligands can be more powerful than oxygen ligands in coordinating metals.[8]

Whereas enantiocontrolled syntheses of monofluoroorganic compounds are well established, synthesis of an enantiopure vicinal difluoro compound, especially of C_2 symmetry, has not to the best of our knowledge been reported prior to this communication.[9,10] Generally, molecular fluorine adds to alkenes with *syn*-stereoselection, thereby precluding the formation of C_2 symmetric difluorides;[11] where *trans*-addition is observed yields are usually low.[12] For example diethylaminosulfur trifluoride (DAST),[13] one of the most commonly used reagents for the conversion of alcohols into fluorides, gives merely a trace of 1,2-difluorocyclohexanes, and with loss of stereointegrity compared with the initial cyclohexane-1,2-diol.[14] SF_4 acts on (+)- or (−)-tartaric acid, exchanging both hydroxy groups for fluorine, but with complete loss of optical activity, by formation of only the *meso*-difluoroacid.[15a] With tartrate esters, XeF_2 was similarly unsuccessful.[10c] Despite those previous accounts, we here report the enantiocontrolled introduction of fluorine at two adjacent carbon stereocentres in a single operation, and describe syntheses of enantiopure vicinal difluorides **5**, and an asymmetric process using some of those difluorides as catalysts.

In view of reports[15] that double vicinal displacements of tartaric acid derivatives by fluoride do not proceed with enantiocontrol, displacements on cyclic systems were investigated. (3*R*,4*R*)-Diacetoxysuccinic anhydride **1**[16] was reacted with a primary amine (1 equiv., 12 h, 20 °C), and the intermediate amido acid treated directly with $SOCl_2$ (2 equiv., 24 h, 20 °C) to give the diacetoxypyrrolidin-2,5-dione **2** (**2a**, R = Ph; **2b**, R = *n*-C_8H_{17}; **2c**, R = cyclohexyl) (Scheme 1). The pyrrolidin-2,5-diones **2** were reduced with $NaBH_4$–I_2 in THF (12 h) and the diols **3** liberated by a two-stage work-up involving stirring with 1:1 AcOH–HCl (10 M) for 10 h, followed by washing with methanolic KOH (2 M). Reaction of the diols **3** with Tf_2O (2 equiv., 4 h, −80 °C) in the presence of pyridine (2 equiv.) afforded the bis(trifluoromethanesulfonates) **4**. These were isolable in the cases of **4a** (R = Ph) and **4b** (R = *n*-octyl) but **4c** (R = cyclohexyl) decomposed rapidly during column chromatography. The bis(trifluoromethanesulfonates) **4** were reacted with Bu_4NF (3 equiv., 16 h, −80 to 20 °C) in THF, resulting in stereoselective introduction of fluorine with clean inversion at both centres to give the difluoropyrrolidines **5a**–**c**, in respective yields of 76, 83 and 40%.‡ To the best of our knowledge, 3,4-difluoropyrrolidines have not been previously prepared, either in racemic or enantiopure form.

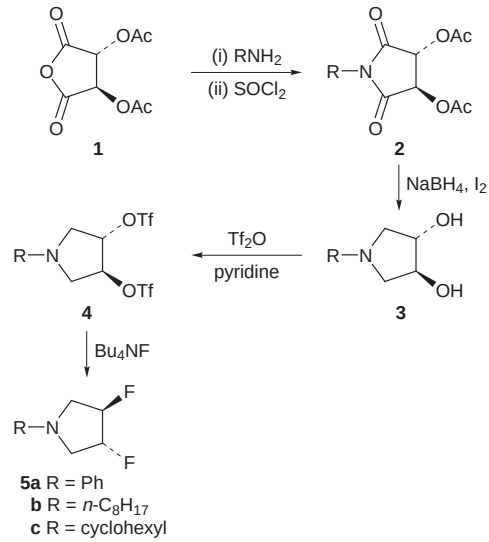

Scheme 1

Catalysis of the epoxidation of allylic alcohols by difluorides **5** was investigated; reactions were conducted in CH_2Cl_2 using 15 mol% of $Ti(OPr^i)_4$ and 10 mol% of catalyst (Scheme 2, Table 1, entries 2–7). In the absence of a catalyst, racemic **7** was obtained in 81% yield. Diol **3a** afforded 2,3-epoxygeraniol **7** (97%) in 25% ee in favour of the (2*S*,3*S*)-enantiomer (entry 2).

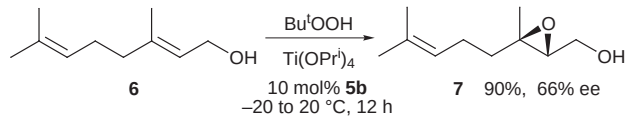

Scheme 2

Table 1 Asymmetric epoxidation of geraniol (1.6 mmol) with *tert*-butyl hydroperoxide, titanium tetraisopropoxide (15 mol%) and the difluorinated catalyst **5b** (10 mol%)

Entry	Catalyst	*T*/°C	*t*/h	Yield (%)	Ee (%)	Configuration
1	—	−20 to 20	12	81	—	racemic
2	**3a**	−20 to −10	0.67	97	25	(*S*,*S*)
3	**5b**	−20 to 20	1	68	50	(*R*,*R*)
4	**5b**	0	1	74	51	(*R*,*R*)
5	**5b**	**−20 to 20**	**12**	**90**	**66**	(***R*,*R***)
6	**5b**	−80	3	23	27	(*R*,*R*)
7	**5c**	−20 to 20	12	87	10	(*R*,*R*)

The use of **5c** (−20 to 20 °C over 12 h) afforded 2,3-epoxygeraniol (87%) in 10% ee in favour of the (2*R*,3*R*)-enantiomer (entry 7). However, **5b** afforded a 90% yield of 2,3-epoxygeraniol **7** in 66% ee in favour of the (2*R*,3*R*)-enantiomer (entry 5). Entries 3–5 suggest that fluoro groups may provide greater enantioselection than hydroxy groups (entry 2), at least in the case of a C_2 vicinal unit which is part of a heterocyclic ring. The reversal of the major enantiomer of 2,3-epoxygeraniol when using catalyst **3** compared with catalyst **5** would be expected if the modes of binding of the hydroxy and fluoro catalysts had important features in common. Samples of alcohol **7** were converted into the acetate (1 equiv. Ac_2O, 1 equiv. pyridine, 10 mol% DMAP in CH_2Cl_2 at 0 to 20 °C over 2 h), and the ee determined by observation of ^{1}H NMR peak of the acetate methyl group upon treatment with Eu(hfc)$_3$;[17] the acetate (10 mg in 0.5 ml of C_6D_6) was treated with consecutive portions of 10–20 ml of a filtered solution of 35 mg of Eu(hfc)$_3$ in 0.5 ml of C_6D_6.

The presence of fluorine ligands in organic reactions mediated by catalysis is an emerging area of importance.[18] To date, however, the chirality has not been a consequence of the spatial arrangement of the fluorine atoms, but of the asymmetry of an unrelated organic ligand (*e.g.* BINOL).[18] Consequently, the present examples are, to the best of our knowledge, the first examples of asymmetric synthesis catalyzed by a compound whose chirality depends upon organofluorine asymmetry.

In the catalytic asymmetric Sharpless epoxidation,[19] free hydroxy groups on the catalyst (dialkyl tartrate) are a prerequisite for enantioselectivity. In marked contrast to such Sharpless catalysts, the difluorides **5** lack hydroxy groups and are incapable of deprotonation that could lead to ligand exchange, and yet **5a–c** are viable catalysts for asymmetric epoxidation.

Compounds **5a** and **5c** are particularly suitable substructures for liquid crystal applications, and difluoropyrrolidines **5** and their derivatives are currently being evaluated for use as liquid crystals and other new materials; additional catalytic processes are also under investigation.

Support from the EPSRC for a studentship (to R. C. M.) under the ROPA initiative is gratefully acknowledged.

Notes and References

† E-mail: c.m.marson@qmw.ac.uk.

‡ All compounds gave satisfactory spectral data (NMR, IR, MS), and all new compounds gave satisfactory elemental analyses or HRMS. *Selected data* for **4a**: prisms, mp 126.5–127 °C (hexane), $[\alpha]_D$ +46.2 (*c* 1, $CHCl_3$); δ_H(250 MHz, $CDCl_3$) 7.30 (m, 2 H), 6.88 (t, *J* 9.0, 1 H), 6.60 (d, *J* 9.0 2 H), 5.52 (t, *J* 2.5, 2 H) 3.95 (dd, *J* 11.0, 5.0, 2 H), 3.65 (dd, *J* 11.0, 3.0, 2 H); δ_C (62.2 MHz, $CDCl_3$) 145.5 (d), 129.7 (d), 118.9 (s), 118.5 (q), 112.6 (d), 85.4 (d), 51.3 (t). For **5a**: needles, mp 89.5 °C (hexane), $[\alpha]_D$ −40.6 (*c* 3.5, $CHCl_3$); δ_H(600 MHz, $CDCl_3$) 7.30 (m, 2 H), 6.76 (t, *J* 7.0, 1 H), 6.60 (d, *J* 7.0, 2 H), 5.30 (dm, $^2J_{HF}$ 49.3, $^3J_{HF}$ 12.6, 2 H), 3.70 (m, 4 H); δ_C(150.9 MHz, $CDCl_3$) 146.6 (s), 129.4 (d), 117.1 (d), 112.0 (d), 92.8 (ddd, $^1J_{CF}$ 180, $^2J_{CF}$ 33), 51.6 (m); δ_F(564.8 MHz, $CDCl_3$, internal $CFCl_3$) −190.3 (m).

1 (*a*) V. Aoloshonok, in *Biomedical Frontiers of Fluorine Chemistry*, ed. I. Ojima, J. R. McCarthy and J. T. Welch, American Chemical Society Symposium Series, Washington, DC, 1996, vol. 639, pp. 26–41; (*b*) J. R. McCarthy, P. S. Sunkasa, D. P. Matthews, A. J. Bitonti, E. T. Jarvi, J. S. Sabol, R. J. Resvick, E. W. Huber, W. A. van der Donk, G. Yu and J. Stubbe, *ibid.*, pp. 246–264; (*c*) M. Namchuk, C. Braun, J. D. McCarter, and S. G. Withers, *ibid.*, pp. 265–278; M. Namchuk, C. Braun, J. D. McCarter and S. G. Withers, *ibid.*, pp. 279–293.

2 P. Bravo and G. Resnati, *Tetrahedron Asymmetry*, 1990, **1**, 661.

3 D. Bouzard, P. Dicesare, M. Essiz, J. P. Jacquet, J. R. Kiechel, P. Remuzon, A. Weber, T. Oki, M. Masuyoshi, R. E. Kessler, J. Fungtomc and J. Desiderio, *J. Med. Chem.*, 1990, **33**, 1344.

4 (*a*) J. T. Welch and S. Eswarakrishnan, *Fluorine in Bio-organic Chemistry*, Wiley, New York, 1991; (*b*) J. A. Wilkinson, *Chem. Rev.*, 1992, **92**, 505.

5 E. Kun, E. Kirsten and M. L. Sharma, *Proc. Natl. Acad. Sci. USA*, 1977, **74**, 4942.

6 H. Liu and H. Nohira, *Liq. Crystal.*, 1996, 581.

7 C. K. Chen, Y. L. Hu, M. Spears, J. W. Hodby, B. M. Wanklyn, A. V. Narlikar and S. B. Samanta, *J. Mater. Sci. Lett.*, 1996, **15**, 886.

8 H. Plenio, R. Diodone and D. Badura, *Angew. Chem., Int. Ed. Engl.*, 1997, **36**, 156.

9 For a single example of a racemic *vic*-difluoro-2,3-dihydrobenzo[*b*] furan, see: R. Ruzziconi and G. V. Sebastiani, *J. Heterocycl. Chem.*, 1980, **17**, 1147.

10 For *meso*-difluorides see: (*a*) M. Hudlicky, *J. Fluorine Chem.*, 1987, **36**, 373; (*b*) A. Baklouti and R. El Gharbi, *J. Fluorine Chem.*, 1979, **13**, 297; (*c*) T. B. Patrick, S. Khazaeli, S. Nadji, K. Hering-Smith and D. Reif, *J. Org. Chem.*, 1993, **58**, 705; (*d*) G. A. Olah, J. T. Welch, Y. D. Vankar, M. Nojima, I. Kerekes and J. A. Olah, *J. Org. Chem.*, 1979, **44**, 3872.

11 S. Rozen and M. Brand, *J. Org. Chem.*, 1986, **51**, 3607.

12 M. Sato, T. Hirokawa, A. Hattori, A. Toyota and C. Kaneko, *Tetrahedron: Asymmetry*, 1994, **5**, 975.

13 W. J. Middleton, *J. Org. Chem.*, 1975, **40**, 574; M. Hudlicky, *Org. React.*, 1988, **35**, 513.

14 D. F. Shellhamer, D. T. Austine, K. M. Gallego, B. R. Ganesh, A. A. Hanson, K. A. Hanson, R. D. Henderson, J. M. Prince and V. L. Heasley, *J. Chem. Soc., Perkins Trans. 2*, 1995, 861.

15 (*a*) A. I. Burmakov, L. A. Motnyak, B. V. Kunshenko, L. A. Alexeva and L. M. Yagupolskii, *J. Fluorine Chem.*, 1981, **19**, 151; (*b*) for a racemic route to mixtures of difluorosuccinic acid derivatives from maleic anhydride and F_2, see: R. G. Syvret, D. L. Vassilaros, D. M. Parees and G. P. Pez, *J. Fluorine Chem.*, 1994, **67**, 277.

16 R. L. Shriner and C. L. Furrow, *Org. Synth.*, 1963, **Coll. Vol. IV,** 242.

17 Y. Gao, R. M. Hanson, J. M. Klunder, S. Y. Ko, H. Masamune and K. B. Sharpless, *J. Am. Chem. Soc.*, 1987, **109**, 5765.

18 R. O. Duthaler and A. Hafner, *Angew. Chem., Int. Ed. Engl.*, 1997, **36**, 43.

19 T. Katsuki and K. B. Sharpless, *J. Am. Chem. Soc.*, 1980, **102**, 5974.

Received in Liverpool, UK, 2nd March 1998; 8/01718B

Transfer of alk-1-enyl group from boron to boron: preparation of *B*-[(*E*)-alk-1-enyl]-9-borabicyclo[3.3.1]nonane

Masayuki Hoshi,*† Kazuya Shirakawa and Akira Arase

Department of Applied and Environmental Chemistry, Kitami Institute of Technology, 165 Koen-cho, Kitami 090-8507, Japan

Treatment of (*E*)-alk-1-enyldicyclohexylborane 1 with *B*-methoxy-9-borabicyclo[3.3.1]nonane (*B*-MeO-9-BBN) at 0 °C results in transfer of alk-1-enyl group from boron to boron to give *B*-[(*E*)-alk-1-enyl]-9-BBN 2 with retention of configuration.

Alkenylboranes have been widely used as one of the most important intermediates in organic synthesis, and generally they are prepared by hydroboration of alkynes with borane derivatives.[1] In some cases, however, hydroboration is not necessarily the most reliable route. For example, a stoichiometric hydroboration of alk-1-yne with 9-BBN is not efficient because it causes dihydroboration to give a significant amount of 1,1-diboryl adduct.[2,3] In order to suppress the dihydroboration, the reaction requires a 100% excess of alk-1-yne and must be carried out at 0 °C for 18 h.[2]

We recently reported that hydroboration of alk-1-ynes with 1,3,2-benzodioxaborole (catecholborane) and hydroboration of 1-haloalk-1-ynes with 9-BBN, both of which are sluggish at room temperature in THF,[4] are accelerated by addition of a catalytic amount (5 mol%) of dicyclohexylborane in THF to afford *B*-[(*E*)-alk-1-enyl]catecholborane and *B*-[(*Z*)-1-haloalk-1-enyl]-9-BBN in high yields, respectively.[5] Dicyclohexylborane probably plays a critical role in a catalytic cycle. In the former reaction, it is presumed that dicyclohexylborane would hydroborate the alk-1-yne and the resulting (*E*)-alk-1-enyldicyclohexylborane would undergo exchange of the alk-1-enyl group for a hydrogen atom of catecholborane to give *B*-[(*E*)-alk-1-enyl]catecholborane with retention of configuration and regeneration dicyclohexylborane. The latter dicyclohexylborane-promoted hydroboration appears to include a similar catalytic cycle. These exchange reactions may belong to the category of not hydroboration but transfer reaction. It seems probable that such transfer reactions provide a method for the preparation of some alkyl- or alkenyl-boranes whose formation is very difficult or inefficient *via* hydroboration. We report here an efficient and stereoselective preparation of *B*-[(*E*)-alk-1-enyl]-9-BBN **2** *via* treatment of (*E*)-alk-1-enyldicyclohexylborane **1** with a slightly excess of *B*-MeO-9-BBN at 0 °C [eqn. (1)].

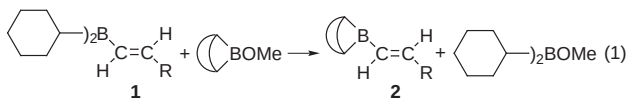

1 **2** (1)

The reaction of (*E*)-hex-1-enyldicyclohexylborane **1a** in THF with an equimolar amount of *B*-MeO-9-BBN in hexanes was carried out at 0 °C for 1 h, and the reaction mixture, after removal of solvents, was analysed by ^{1}H NMR spectroscopy. In the alkenyl region, the two double triplets at δ 6.20 and 6.73 arising from **1a** decreased considerably while two double triplets appeared at δ 6.23 and 6.83 (*J* 17.3 Hz, *trans* alkenyl protons), indicating that *B*-[(*E*)-hex-1-enyl]-9-BBN **2a**[2,6] had been formed in a stereoselective manner, the ratio of **1a** : **2a** being 20 : 80. In the same spectrum we also observed two singlets, one at δ 3.76 arising from the methyl protons of unreacted *B*-MeO-9-BBN and the other at δ 3.69 arising from those of dicyclohexylmethoxyborane. These results suggest that the (*E*)-hex-1-enyl group transferred from the boron atom of **1a** to the boron atom of *B*-MeO-9-BBN with complete retention of the stereochemistry. The reaction at 0 °C for 2 h improved the ratio of **1a** : **2a** to 8 : 92. The reaction with 1.2 equiv. of *B*-MeO-9-BBN under otherwise identical conditions resulted in a slight increase for **2a**; the **1a** : **2a** ratio was 6 : 94 (entry 1, Table 1). However, no further improvement in the ratio was achieved by increasing the amount of *B*-MeO-9-BBN to 1.5 equiv.

The reaction of various compounds **1** with 1.2 equiv. of *B*-MeO-9-BBN was carried out at 0 °C for 2 h. These results including NMR data for **1** are summarised in Table 1. The reaction of (*E*)-3,3-dimethylbut-1-enyldicyclohexylborane **1b** proceeded smoothly and stereoselectively to give *B*-[(*E*)-3,3-dimethylbut-1-enyl]-9-BBN **2b**; the **1b** : **2b** ratio was 5 : 95 (entry 2). In the reaction of (*E*)-2-phenylethenyldicyclohexylborane **1c** the reaction mixture was analysed by ^{11}B NMR spectroscopy, since the alkenyl protons of *B*-[(*E*)-2-phenylethenyl]-9-BBN **2c** were indistinguishable from those of **1c**. From the ^{11}B NMR spectrum of the reaction mixture in THF–hexanes‡ **1c** was found to be converted to **2c** with a high ratio (**1c** : **2c** = 1 : 99) (entry 3). 3-Substituted *B*-[(*E*)-alk-1-enyl]-9-BBN, having a functionality at a position very close to the alkenyl moiety, may be a potential intermediate because of its poly-functional properties. The present transfer reaction is applicable to such functionalised (*E*)-prop-1-enyldicyclohexylboranes without any difficulties. Thus, (*E*)-3-chloroprop-1-enyldicyclohexylborane **1d** and (*E*)-3-methoxyprop-1-enyldicyclohexylborane **1e** were converted to the corresponding compounds **2** stereoselectively (entries 4 and 5). 3-Substituted (*E*)-prop-1-enyldicyclohexylboranes **1f**–**h** having an oxygen protected with Ac, THP and TMS groups were also converted to *B*-[(*E*)-3-acetoxyprop-1-enyl]-9-BBN **2f**, *B*-[(*E*)-3-(tetrahydro-2*H*-pyran-2-yloxy)prop-1-enyl]-9-BBN **2g** and *B*-[(*E*)-3-(trimethylsiloxy)prop-1-enyl]-9-BBN **2h**, respectively (entries 6–8).

Previously Brown and Gupta reported that boron–carbon bond formation *via* redistribution between trialkylborane and borate required temperatures above 100 °C.[7] It should be noted that the present reaction proceeds smoothly at 0 °C despite the redistribution reaction involving boron–oxygen bond cleavage, and thus appears to be applicable to transfer of alkenyl groups containing a thermally unstable functionality.

One of the characteristic reactions of *B*-alkenyl-9-BBN is the 1,4-addition reaction with but-3-en-2-one.[8] *In situ* addition of **2** to but-3-en-2-one under conditions identical to those described in the literature gave the corresponding 4-(alk-1-enyl)butan-2-one, while the yields were a little lower than those reported. Thus, the present reaction is expected to be synthetically useful, although there may still be room for improvement.

In conclusion, *B*-[(*E*)-alk-1-enyl]-9-BBN **2** can be produced efficiently *via* the reaction of (*E*)-alk-1-enyldicyclohexylborane **1** with *B*-MeO-9-BBN. This transfer of an alk-1-enyl group is performed with complete retention of configuration under very mild conditions. We note that this study provides, to the best of our knowledge, the first example of the transfer of an alk-1-enyl group from boron to boron in stoichiometric amounts. The

Table 1 Reaction of (*E*)-alk-1-enyldicyclohexylborane **1** with *B*-MeO-9-BBN[a]

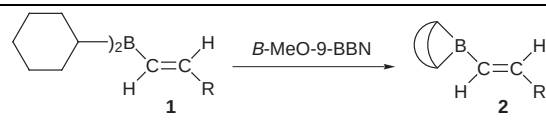

Entry	R	Alkenyl protons (δ)[b]	Alkenyl protons (δ)[b]	Ratio[c] **1**:**2**
1	Bu^n	**1a** 6.20 (1-H, dt, *J* 17.6 and 1.3 Hz); 6.73 (2-H, dt, *J* 17.6 and 6.5 Hz)	**2a** 6.23 (1-H, dt, *J* 17.3 and 1.3 Hz); 6.83 (2-H, dt, *J* 17.3 and 6.5 Hz)	6:94
2	Bu^t	**1b** 6.11 (1-H, d, *J* 18.1 Hz); 6.88 (2-H, d, *J* 18.1 Hz)	**2b** 6.14 (1-H, d, *J* 17.6 Hz); 6.79 (2-H, d, *J* 17.6 Hz)	5:95
3	Ph	**1c** 7.01 (1-H, d, *J* 18.3 Hz)[d]; [^{11}B NMR δ 72][e]	**2c** 7.00 (1-H, d, *J* 17.8 Hz)[d]; [^{11}B NMR δ 44][e]	1:99[f]
4	CH_2Cl	**1d** 6.45 (1-H, d, *J* 17.6 Hz); 6.56 (2-H, dt, *J* 17.6 and 5.6 Hz)	**2d** 6.49 (1-H, dt, *J* 17.1 and 1.1 Hz); 6.71 (2-H, dt, *J* 17.1 and 5.9 Hz)	7:93
5	CH_2OMe	**1e** 6.42 (1-H, dt, *J* 18.1 and 1.2 Hz); 6.62 (2-H, dt, *J* 18.1 and 4.6 Hz)	**2e** 6.47 (1-H, dt, *J* 17.8 and 1.5 Hz); 6.77 (2-H, dt, *J* 17.8 and 4.5 Hz)	7:93
6	CH_2OAc	**1f** 6.42 (1-H, dt, *J* 18.1 and 1.2 Hz); 6.56 (2-H, dt, *J* 18.1 and 4.6 Hz)	**2f** 6.44 (1-H, dt, *J* 17.6 and 1.5 Hz); 6.71 (2-H, dt, *J* 17.6 and 4.5 Hz)	1:99
7	CH_2OTHP	**1g** 6.44 (1-H, dt, *J* 17.8 and 1.3 Hz); 6.68 (2-H, dt, *J* 17.8 and 4.7 Hz)	**2g** 6.49 (1-H, dt, *J* 17.6 and 1.5 Hz); 6.82 (2-H, dt, *J* 17.6 and 4.4 Hz)	1:99
8	CH_2OTMS	**1h** 6.42 (1-H, dt, *J* 17.8 and 1.6 Hz); 6.68 (2-H, dt, *J* 17.8 and 4.2 Hz)	**2h** 6.47 (1-H, dt, *J* 17.6 and 1.7 Hz); 6.81 (2-H, dt, *J* 17.6 and 4.1 Hz)	5:95

[a] Conditions: **1** (1 equiv.), *B*-MeO-9-BBN (1.2 equiv.), at 0 °C for 2 h. [b] ^{1}H NMR spectra, after removal of solvent(s), were obtained in $CDCl_3$ solutions containing TMS. [c] Determined by ^{1}H NMR spectroscopy. [d] The signal of the other alkenyl proton overlapped that of the phenyl protons. [e] ^{11}B NMR spectra (δ relative to $BF_3{\cdot}OEt_2$) were obtained in THF or THF–hexanes solutions. [f] Determined by ^{11}B NMR spectroscopy.

scope and limitations of this reaction are now under investigation.

Notes and References

† E-mail: HOSHI-Masayuki/chem@king.cc.kitami-it.ac.jp

‡ The spectrum exhibited an additional two singlets, one of which was *B*-MeO-9-BBN (δ 56.5) and the other was dicyclohexylmethoxyborane (δ 52). In the ^{11}B NMR analysis using $CDCl_3$ solutions, the signal of **2c** was indistinguishable from that of **1c**.

1 For example, see A. Pelter, K. Smith and H. C. Brown, *Borane Reagents*, Academic Press, London, 1988; M. Vaultier and B. Carboni, in *Comprehensive Organometallic Chemistry II*, ed. E. W. Abel, F. G. A. Stone and G. Wilkinson, Pergamon, New York, 1995, vol. 11, ch. 5, p. 191.

2 H. C. Brown, C. G. Scouten and R. Liotta, *J. Am. Chem. Soc.*, 1979, **101**, 96.

3 K. K. Wang, C. G. Scouten and H. C. Brown, *J. Am. Chem. Soc.*, 1982, **104**, 531.

4 H. C. Brown and S. K. Gupta, *J. Am. Chem. Soc.*, 1975, **97**, 5249; H. C. Brown, C. D. Blue, D. J. Nelson and N. G. Bhat, *J. Org. Chem.*, 1989, **54**, 6064.

5 A. Arase, M. Hoshi, A. Mijin and K. Nishi, *Synth. Commun.*, 1995, **25**, 1957; M. Hoshi and A. Arase, *Synth. Commun.*, 1997, **27**, 567.

6 J. C. Colberg, A. Rane, J. Vaquer and J. A. Soderquist, *J. Am. Chem. Soc.*, 1993, **115**, 6065.

7 H. C. Brown and S. K. Gupta, *J. Am. Chem. Soc.*, 1970, **92**, 6983; 1971, **93**, 2802.

8 P. Jacob and H. C. Brown, *J. Am. Chem. Soc.*, 1976, **98**, 7832.

Received in Cambridge, UK, 10th March 1998; 8/01939H

First lanthanide complexes and unusual coordination behavior of hexakis(3,5-dimethylpyrazolyl)cyclotriphosphazene

Bo Hwan Koo, Younghun Byun, Eunkee Hong, Youngjo Kim and Youngkyu Do*†

Department of Chemistry and Center for Molecular Science, Korea Advanced Institute of Science and Technology, Taejon 305-701, Korea

Reaction of hexakis(3,5-dimethylpyrazolyl)cyclotriphosphazene (L) with $LnCl_3$ (Ln = La, Ce, Nd, Sm) affords new mononuclear lanthanophosphazenes [L·$LnCl_3$] with hendecahedral coordination polyhedron in which the ligand L employs an unprecedented κ⁵N binding core consisting of one cyclotriphosphazene ring nitrogen atom and four pyridinic nitrogen atoms of two sets of geminal pyrazolyl groups.

The use[1–6] of exocyclic donor groups attached to phosphazene skeletal phosphorus appears to be the most versatile method of preparing metallophosphazene complexes, the chemistry of which has been the subject of increasing research interest in conjunction with the potential opportunities for discovering new materials.[7] Successful applications of exocyclic donors such as pyrazolyl[1–4] and cyclopentadienyl[5] groups are cases in point. However, the scope of the coordination chemistry of hexakis(3,5-dimethylpyrazolyl)cyclotriphosphazene (L), a potential multidentate ligand due to its multiple chelate sites,[8] has only been examined with d^{10} metal halides[1] and d^9 Cu^{II} ion,[2] revealing the limited coordination behavior with the binding cores of (κ³N) for mononuclear species and (κ³N–κ²N) and (κ³N–κ³N) for dinuclear complexes. Here, we present the first examples of lanthanophosphazenes [L·$LnCl_3$] (Ln = La, Ce, Nd, Sm) where the ligand L acts as an unprecedented κ⁵N binding core donor for a metal center to form a hendecahedral coordination sphere.

A solid mixture of anhydrous $LnCl_3$ (0.3–0.6 mmol) and L (0.2 mmol) was allowed to react in 20 ml of CH_2Cl_2 under N_2 atmosphere. After being stirred at room temperature for 12 h, the reaction mixture was filtered. The volume of the filtrate was reduced *in vacuo*, and *ca*. 30 ml of Et_2O added. The resulting crystalline solid‡ was collected and recrystallized from CH_2Cl_2–Et_2O, affording the extremely air sensitive analytically pure§ product [L·$LnCl_3$] (Ln = La **1**, Ce **2**, Nd **3**, Sm **4**) in a yield of 50–55%.

In contrast to the single phosphazene ring P–N stretching band at 1226 cm^{-1} for free L, the appearance of two ν_{PN} peaks at *ca*. 1235 and 1210 cm^{-1} for [L·$LnCl_3$] indicates that the phosphazene ring nitrogen atom is involved in coordination to the metal center. In addition, the comparison of the IR spectra suggests that all four lanthanophosphazenes have the same structural core. Single crystal X-ray analysis,¶ performed on **4**, revealed unprecedented κ⁵N pentadentate coordination behavior of L as displayed in Fig. 1. One cyclophosphazene ring nitrogen atom N(1) and four pyridinic nitrogen atoms N(12), N(22), N(32) and N(42) from two sets of geminal pyrazole substituents on P(1) and P(2) constitute the κ⁵N binding core to coordinate $SmCl_3$, forming an eight-coordinate complex. The analysis of the shape parameters[11] indicates that the coordination sphere of **4** can be best described as a distorted hendecahedron illustrated in Fig. 2. The complexation caused P_3N_3 ring puckering the extent of which can be measured from the displacement of the N(1) atom (0.305 Å) from the plane defined by P(1), P(2), P(3), N(2) and N(3) and the dihedral angle of 22.1° between the P(1)N(1)P(2) plane and the P(1)N(3)P(3)N(2)P(2) plane. The overall molecular symmetry approaches *pseudo*-C_s. The Sm atom interacts more strongly with L *via* the phosphazene ring nitrogen atom N(1) than *via* the pyridinic nitrogen atoms: the $Sm–N_{ring}$ bond distance of 2.499 Å is shorter than the average $Sm–N_{pyz}$ distance of 2.832 Å. It is noteworthy that the reversed pattern in interaction between metal centers and the ligand L was observed in previously reported transition metal phosphazene complexes.[1,2]

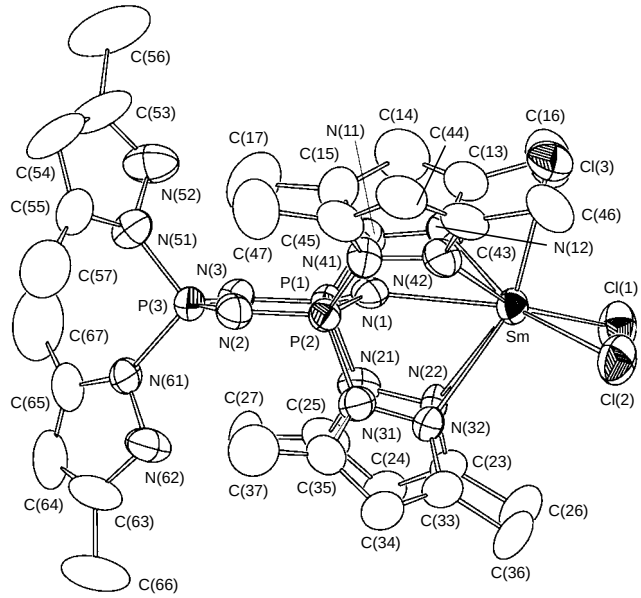

Fig. 1 Molecular structure of **4** showing the atom numbering scheme. Selected bond distances (Å) and angles (°): Sm–Cl(1) 2.659(3), Sm–Cl(2) 2.632(3), Sm–Cl(3) 2.628(2), Sm–N(1) 2.499(8), Sm–N(12) 2.859(10), Sm–N(22) 2.771(8), Sm–N(32) 2.860(8), Sm–N(42) 2.839(10), P(1)–N(1) 1.592(9), P(1)–N(3) 1.564(10), P(2)–N(1) 1.593(9), P(2)–N(2) 1.574(9), P(3)–N(2) 1.577(9); Cl(1)–Sm–N(1) 135.1(2), Cl(1)–Sm–N(12) 78.3(2), Cl(1)–Sm–N(22) 79.8(2), Cl(1)–Sm–N(32) 126.1(2), Cl(1)–Sm–N(42) 160.2(2), Cl(3)–Sm–N(32) 140.2(2).

In solution at room temperature, the compounds [L·$LnCl_3$] lose their solid state symmetry and undergo a new type of fluxional motion (Fig. 3) not seen in d^{10} metal complexes of L.[1]

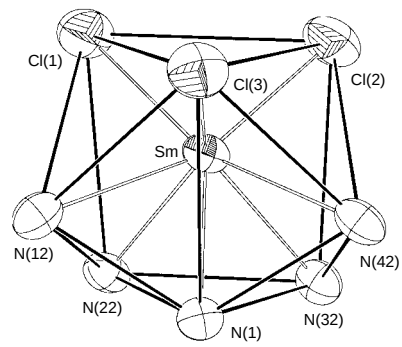

Fig. 2 Hendecahedral coordination geometry of **4**

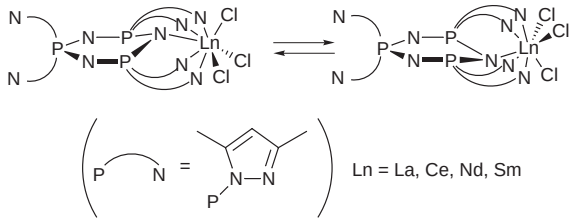

Fig. 3 Solution fluxional motion of $[L{\cdot}LnCl_3]$ in $CDCl_3$

The $^{31}P\{^1H\}$ NMR spectra§ of $[L{\cdot}LnCl_3]$ complexes are of A_2X type, invoking only the rotational motion of geminal pyrazolyl groups at P(3) around P–N bonds. However ^1H-NMR spectra§ in $CDCl_3$ show two pyrazolyl ring proton signals of ratio 2 : 4 and four methyl peaks with 12 : 6 : 6 : 12 ratio and thus indicate the presence of two types of magnetically different pyrazolyl rings in 1 : 2 ratio. Two pyrazolyl rings at P(3) and four pyrazolyl rings involved in coordination are respectively magnetically identical, requiring the presence of a fluxional motion such as the movement of the N(1)–$LnCl_3$ unit as illustrated in Fig. 3. The assignment of the most upfield peak as 3-methyl protons of pyrazolyl groups coordinated to metal was made based on the observation of the upfield shift and simultaneous broadening of the peak upon cooling to 218 K for **4**.

The use of 3,5-dimethyl substituted pyrazole seems critical in preparing compounds of the type $[L{\cdot}LnCl_3]$ since analogous reactions with cyclotriphosphazene ligand containing unsubstituted or mono 3-methyl substituted pyrazoles do not proceed as monitored by *in situ* NMR spectroscopy. Efforts to establish the reactivity scope of $[L{\cdot}LnCl_3]$ toward various reagents including d^{10} metal halides are in progress.

We gratefully acknowledge financial support provided by the Korea Science and Engineering Foundation.

Notes and References

† E-mail: ykdo@single.kaist.ac.kr

‡ Color of products: white for **1**, **2**, **4** and sky blue for **3**.

§ *Selected data*: **1**, IR (Nujol), ν_{PN}/cm^{-1} 1237, 1210; $^{31}P\{^1H\}$ NMR ($CDCl_3$), δ 0.8 (1 P, t, *J* 45 Hz) and −1.3 (2 P, d, *J* 48 Hz); ^1H NMR ($CDCl_3$), δ 6.07 (2 H, d, $^4J_{PH}$ 3.5 Hz), 5.84 (4 H, s), 2.63 (12 H, s), 2.41 (12 H, s), 2.19 (6 H, s), 2.00 (6 H, s). **2**, IR, ν_{PN}/cm^{-1} 1235, 1210; $^{31}P\{^1H\}$ NMR, δ 7.8 (1 P, t, *J* 45 Hz) and 1.3 (2 P, d, *J* 37 Hz); ^1H NMR, δ 7.04 (2 H, s), 4.95 (4 H, s), 3.89 (12 H, s), 3.57 (6 H, s), 2.80 (6 H, s), −4.23 (12 H, s). **3**, IR, ν_{PN}/cm^{-1} 1236, 1213; $^{31}P\{^1H\}$ NMR, δ 13.0 (1 P, t, *J* 44 Hz) and −39.7 (2 P, d, *J* 47 Hz); ^1H NMR, δ 6.75 (2 H, s), 5.57 (4 H, s), 3.39 (12 H, s), 3.22 (6 H, s), 2.61 (6 H, s), −3.42 (12 H, s). **4**, IR, ν_{PN}/cm^{-1} 1233, 1209; $^{31}P\{^1H\}$ NMR, δ 5.4 (2 P, d, *J* 48 Hz) and 1.0 (1 P, t, *J* 49 Hz); ^1H NMR, δ 6.14 (2 H, d, $^4J_{PH}$ 3.7 Hz), 5.67 (4 H, s), 2.56 (12 H, s), 2.25 (6 H, s), 2.19 (6 H, s), 1.73 (12 H, s). Satisfactory elemental analyses were obtained for all four compounds by Oneida Research Services, USA.

¶ *Crystallographic data* for **4**·$2CH_2Cl_2$: $C_{32}H_{46}Cl_7N_{15}P_3Sm$, M_r = 1132.25, monoclinic, space group $P2_1/c$, a = 16.860(3), b = 17.330(12), c = 18.289(5) Å, β = 113.669(14)°, U = 4894.2(16) Å^3, Z = 4, D_c = 1.537 g cm^{-3}, $F(000)$ = 2276, μ(Mo-Kα) = 1.722 mm^{-1}, R_1 = 0.0552, wR_2 = 0.1412 for 3899 observed reflections [$|F_o| > 4.0\sigma(F_o)$]. Reflection data were collected on an Enraf-Nonius CAD4TSB diffractometer with graphite-monochromated Mo-Kα radiation at 293 K. A total of 4926 data were collected in the range 4° < 2θ < 50°. Two oil-coated crystals were used to collect reflection data due to their rapid decaying nature. All data were collected with the ω–2θ scan mode and corrected for L_p effects. The decay correction of each crystal was applied to the data set. The structure was solved by Patterson's heavy atom methods (SHELXS-86).[9] Non-hydrogen atoms except solvate atoms were refined by full-matrix least-squares techniques (SHELXL-93)[10] with anisotropic displacement parameters. The solvate CH_2Cl_2 molecules exhibited positional disorder and the Cl atoms were each assigned an occupancy factor of 0.4 and 0.6. All hydrogens except disordered CH_2Cl_2 hydrogens were placed at their geometrically calculated positions [$d_{C–H}$ = 0.93(pyrazolyl), $d_{C–H}$ = 0.96(methyl)] and refined riding on the corresponding carbon atoms with isotropic thermal parameters [(1.2U(pyrazolyl), 1.5U(methyl)]. CCDC 182/858.

1 Y. Byun, D. Min, J. Do, H. Yun and Y. Do, *Inorg. Chem.*, 1996, **35**, 3981; D. Min and Y. Do, *Chem. Lett.*, 1994, 1989.
2 K. R. J. Thomas, V. Chandrasekhar, P. Pal, S. R. Scott, R. Hallford and A. W. Cordes, *Inorg. Chem.*, 1993, **32**, 606; K. R. J. Thomas, V. Chandrasekhar, S. R. Scott, R. Hallford and A. W. Cordes, *J. Chem. Soc., Dalton Trans.*, 1993, 2589.
3 K. R. J. Thomas, P. Tharmaraj, V. Chandrasekhar, C. D. Bryan and A. W. Cordes, *Inorg. Chem.*, 1994, **33**, 5382; K. R. J. Thomas, P. Tharmaraj, V. Chandrasekhar and E. R. T. Tiekink, *J. Chem. Soc., Dalton Trans.*, 1994, 1301.
4 A. Chandrasekaran, S. S. Krishnamurthy and M. Nethaji, *J. Chem. Soc., Dalton Trans.*, 1994, 63; A. Chandrasekaran, S. S. Krishnamurthy and M. Nethaji, *Inorg. Chem.*, 1994, **33**, 3085; 1993, **32**, 6102.
5 H. R. Allcock and M. L. Turner, *Macromolecules*, 1993, **26**, 3; H. R. Allcock, J. A. Dodge, I. Manners, M. Parvez, G. H. Riding and K. B. Visscher, *Organometallics*, 1991, **10**, 3098; H. R. Allcock, J. A. Dodge, I. Manners and G. H. Riding, *J. Am. Chem. Soc.*, 1991, **113**, 9596; I. Manners, G. H. Riding, J. A. Dodge and H. R. Allcock, *J. Am. Chem. Soc.*, 1989, **111**, 3067; I. Manners, W. D. Coggio, M. N. Mang, M. Parvez and H. R. Allcock, *J. Am. Chem. Soc.*, 1989, **111**, 3481.
6 H. R. Allcock, R. A. Nissan, P. J. Harris and R. R. Whittle, *Organometallics*, 1984, **3**, 432; H. R. Allcock, K. D. Lavin, N. M. Tollefson and T. L. Evans, *Organometallics*, 1983, **2**, 432; H. R. Allcock, A. G. Scopelianos, R. R. Whittle and N. M. Tollefson, *J. Am. Chem. Soc.*, 1983, **105**, 1316.
7 J. E. Mark, H. R. Allcock and R. West, *Inorganic Polymers*, Prentice-Hall Inc., New York, 1992, ch. 3; V. Chandrasekhar and K. R. J. Thomas, *Appl. Organomet. Chem.*, 1993, **7**, 1.
8 K. D. Gallicano, N. L. Paddock, S. J. Rettig and J. Trotter, *Inorg. Nucl. Chem. Lett.*, 1979, **15**, 417; K. D. Gallicano and N. L. Paddock, *Can. J. Chem.*, 1982, **60**, 521.
9 G. M. Sheldrick, SHELXS-86 User Guides, Crystallographic Department, University of Göttingen, Germany, 1985.
10 G. M. Sheldrick, SHELXL-93 User Guides, Crystallographic Department, University of Göttingen, Germany, 1993.
11 C. W. Haigh, *Polyhedron*, 1996, **15**, 605; S. J. Lippard, *Prog. Inorg. Chem.*, 1967, **8**, 109.

Received in Cambridge, UK, 11th March 1998; 8/01988F

High-speed multilayer film assembly by alternate adsorption of silica nanoparticles and linear polycation

Yuri M. Lvov,[a] James F. Rusling,*[a]† D. Laurence Thomsen,[a,b] Fotios Papadimitrakopoulos,[a,b] Takeshi Kawakami[c] and Toyoki Kunitake[c]

[a] *Department of Chemistry, U-60, University of Connecticut, Storrs, CT, 06269-4060, USA*
[b] *Institute of Materials Science, U-136, University of Connecticut, Storrs, CT, 06269-4060, USA*
[c] *Faculty of Engineering, Kyushu University, Fukuoka 812, Japan*

QCM showed that SiO_2/poly(diallyldimethylammonium chloride) (PDDA) film assembly could be achieved in 2 s for 45 nm silica nanoparticle monolayers and 20 s for PDDA monolayers, with film integrity demonstrated by SEM and spectroscopic ellipsometry.

Layer-by-layer assembly of films containing nanoparticles and oppositely charged polyions provides a viable approach to advanced materials or devices with molecularly engineered properties.[1] Building on pioneering work of Iler,[2] who used oppositely charged colloidal particles to make films, linear polyions[3–6] have permitted materials such as dendrimers,[7] proteins,[8] latex[9] and inorganic nanoparticles to be incorporated.[10–14] For most materials used in layer-by-layer electrostatic film assembly, 6–15 min are required for every step of monolayer formation.[2–14] Here we show that time to assemble nanoparticle/linear polyion films can be decreased 100-fold.

Films were assembled with colloidal 45 nm diameter SiO_2 and linear quaternary ammonium polymer poly(diallyldimethyl-ammonium chloride) (PDDA, MW = 70 000) in 0.01 M NaCl at pH 9.5. Silica is negatively charged and PDDA is positively charged at this pH.[14] We monitored assembly with a quartz crystal microbalance (QCM, USI System, Japan)[14,15] in two modes. For stepwise measurement, a Ag- or Au-coated resonator was immersed alternately in polycation or silica solutions for a given period, dried, and the QCM frequency change measured. For *in situ* monitoring, only one side of the resonator was in permanent contact with the surface of the solution and the frequency change was recorded continuously. Films were assembled on electrodes of the QCM resonator by repeating alternate adsorption of PDDA and silica. From the Sauerbrey equation, taking into account characteristics of the quartz resonators (F_o = 9 MHz), the following relation holds between adsorbed dry mass ΔM (ng) on the electrode of area S = 0.16 cm^2 and frequency shift ΔF (Hz):[8,15]

$$-\Delta F = -1.83 \times 10^8 \, \Delta M/S$$

For scanning electron microscopy (SEM, Hitachi S-900), a resonator with an assembled film was cross-sectioned and coated with a 20 Å Pt film. Film thicknesses were measured from cross-sectional images.[14]

Spectroscopic ellipsometry[16] at incidence angles of 70, 72, 76 and 78° and wavelengths of 300–1000 nm was done on films deposited on silicon (100) with native oxide to determine thickness and optical constants using a variable angle spectroscopic ellipsometer (Woollman Co.)

Fig. 1 shows *in situ* QCM of alternate PDDA and SiO_2 adsorption without intermediate sample drying. In the first step, PDDA was adsorbed onto a Ag electrode. QCM frequency decreased during the first 60 s, after which a slower change was observed as adsorption saturation set in. Then, the resonator was immersed in pure water (black dots) for washing. Next, the film was immersed in a SiO_2 dispersion and silica adsorption saturation occurred in several seconds. After subsequent water washing, the film was immersed again in PDDA solution, and so on. Each step was reproducible and the adsorption process reached 90% saturation in 10 s for SiO_2 and 40 s for PDDA.

To find the minimum time for producing good quality films, we tested adsorption times from 15 min to 2 s, drying the films after every other deposition step. Linear growth of film mass and thickness with adsorption cycle number was observed in most cases. The QCM frequency shift was $-\Delta F = 1200 \pm 60$ Hz for SiO_2 and 100 ± 10 Hz for PDDA for 15 min adsorption. A minimal time for the process was found for assembled multilayers by decreasing time and monitoring ΔF corresponding to each layer. For 15 min, 10 min, 5 min, 1 min and 20 s PDDA adsorption gave $-\Delta F = 100$ Hz. For SiO_2 minimal adsorption time was 2 s, with $-\Delta F = 1200$ Hz. SiO_2/PDDA assembly with less than 2 s/20 s adsorption times deteriorated the film growth process. Sample drying after every PDDA deposition was necessary for regular multilayer growth.

We also analyzed the structures of $(SiO_2/PDDA)_{6-24}$ films assembled with 2 s/20 s adsorption times with drying after every deposition step (Table 1). Fig. 2 gives a typical SEM image of such a SiO_2/PDDA film. The image shows densely packed silica spheres and its surface is smooth on the level of one silica sphere (*ca.* ±40 nm). SiO_2/PDDA bilayer thickness was estimated from total film thickness and number of adsorption cycles. For six films assembled with 2 s/20 s times $\langle d \rangle$ = 24.6 ± 0.4 nm, the same as for SiO_2/PDDA assembled with 'traditional' 15 min adsorption steps. This corresponds to mean thickness of closely packed spheres of 45 nm diameter and indicates complete surface filling.

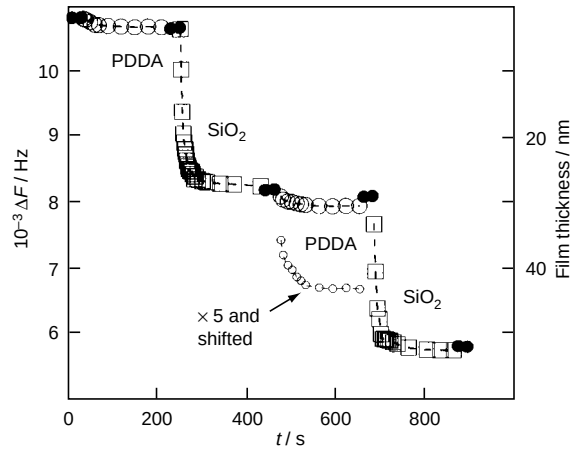

Fig. 1 QCM monitoring of PDDA and SiO_2 sequential adsorption on a silver electrode: PDDA (○), intermediate water-washing (●) and SiO_2 (□). The third step PDDA curve drawn with 5× amplification. 45 nm diameter SiO_2 was used at 10 mg ml^{-1} (Nissan Kagaku, Japan) and 3 mg ml^{-1} linear poly(diallyldimethylammonium chloride) (PDDA, MW = 70 000, Aldrich) were used in 0.01 M NaCl at pH 9.5.

Table 1 Structural parameters of 45 nm SiO_2/PDDA films assembled with 2 s/20 s adsorption

No. of bilayers/ substrate	Total QCM ΔF/Hz	Mass from QCM/ 10^6 g cm^{-2}	Thickness/nm (SEM)	Thickness/nm Ellipsometry	Film density/ g cm^{-3}
4/Si				99	
6/Si				149	
7/Si or Ag	8400	23.0		173	1.38
8/Au	11200	30.6	210		1.45
20/Ag	24500	67.0	480		1.40
24/Ag	33000	90.2	610		1.48

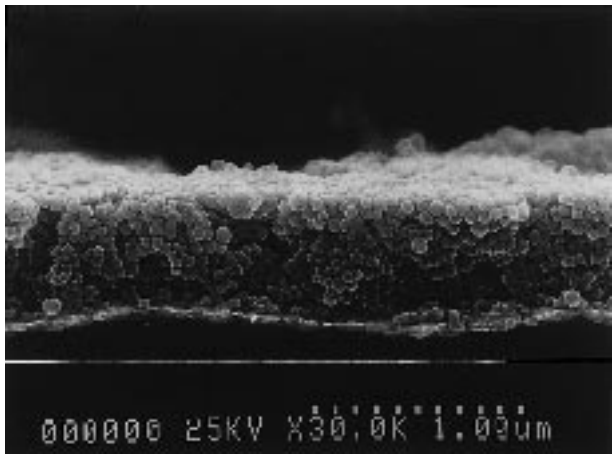

Fig. 2 SEM cross-sectional view of {PDDA+ (45 nm SiO_2/PDDA)$_{24}$} film deposited using the 2 s/20 s monolayer adsorption on silver electrode

Ellipsometric data were modeled with a Lorentz oscillator for an effective medium approximation,[16] to take into account the film's surface inhomogeneities and voids (*cf.* Fig. 2). A graph of ψ and θ values of the seven-bilayer film is given in Fig. 3. The film refractive index at 633 nm was estimated at 1.25, *i.e.* < 1.48 for pure silica.

Bilayer thicknesses from QCM, SEM and ellipsometry for films assembled on different substrates agree very well (Table 1). Average density of SiO_2/PDDA multilayers is $<\rho>$ = 1.43 ± 0.05 g cm^{-3}. To calculate the silica packing coefficient in the

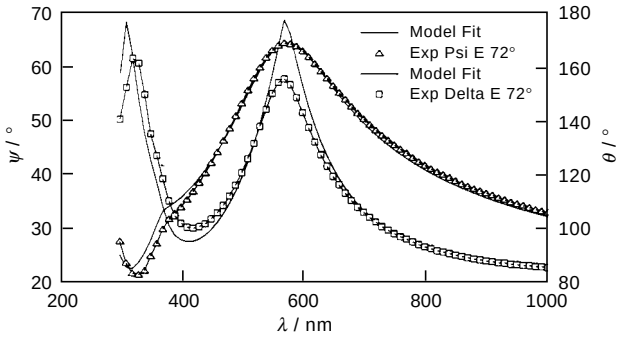

Fig. 3 Ellipsometric measurements of {PDDA + (45 nm SiO_2/PDDA)$_7$} film thickness on silicon wafer: ψ and θ values of the film at 72° incidence and the model fit (see text). Lorentz oscillator constants were determined simultaneously with thicknesses (Table 1) as Am 1.2 = 240 ± 6, Br1.2 = 1.9 ± 0.2, En1.2 = 20.5 ± 0.3.

films, we assumed that the dry film consists of SiO_2, PDDA and air-filled pores. The mass ratio for PDDA to PDDA/SiO_2 is 100 Hz/1300 Hz = 0.077. Taking into account component densities[14] ($<\rho>$ = 1.43, ρ_{SiO_2} = 2.2 and ρ_{PDDA} = 1.1 g cm^{-3}) we obtain the volume ratio $V_{PDDA}/V_{bilayer}$ = 0.1. From the equation $\rho_{PDDA}\,V_{PDDA} + \rho_{SiO_2}\,V_{SiO_2} + \rho_{air}\,V_{air} = <\rho>\,V$, where the air-term is very small, V_{SiO_2}/V = 0.6. This is very close to the theoretical dense-packing coefficient for spheres (0.63), and corresponds to details in the SEM micrographs. SiO_2/PDDA film volume composition is: 60% SiO_2 + 10% polycation + 30% air-filled pores. These pores are formed by closely packed 45 nm SiO_2 and have a typical dimension of 20 nm. The films have controlled pores which could be varied by the choice of nanoparticle diameter.

We estimate the diffusion limitation for surface coverage $A(t)$ by adsorption from solution of particles with diffusion coefficient D[4,17] from $A(t) = 2/\pi C(Dt)^{1/2}$. For t = 2 s, C = 10 mg cm^{-3} and assuming for 45 nm silica $D = 1.1 \times 10^{-7}$ cm^2 s^{-1},[18] $A \approx 3 \times 10^{-6}$ g cm^{-2} and the layer thickness $L = A(t)/<\rho> \approx$ 21 nm. This is reasonably close to the experimental silica layer thickness of 24.6 nm. Thus, 2 s corresponds roughly to the diffusion limited time for SiO_2 monolayer adsorption.

Similar estimates for diffusion limits on PDDA show that in 20 s a hundred monolayers could be delivered to the surface. 20 s does not correspond to diffusion limited adsorption. Hence, conformational changes upon adsorption probably govern the time needed to make uniform monolayers. The mechanism of PDDA relaxation is not clear, but sample drying speeds the process. Relevant ideas about kinetics of polycation adsorption on a charged surface have been discussed.[19]

This work was supported by US PHS grant no. E503154 from the NIEHS, NIH. Its contents are solely the responsibility of the authors and do not necessarily represent the official views of NIEHS, NIH.

Notes and References

† E-mail: jrusling@nucleus.chem.uconn.edu

1 J. Fendler, in *Thin Films, vol. 20 Organic thin films and surfaces: directions for the nineties*, ed. A. Ulman, Academic Press, 1995, p. 11.
2 R. Iler, *J. Colloid Interface Sci.*, 1966, **21**, 569.
3 G. Decher and J.-D. Hong, *Ber. Bunsenges. Phys. Chem.*, 1991, **95**, 1430.
4 Y. Lvov, G. Decher and H. Möhwald, *Langmuir*, 1993, **9**, 481.
5 G. Decher, *Science*, 1997, **227**, 1232.
6 M. Ferreira and M. Rubner, *Macromolecules*, 1995, **28**, 7107.
7 V. Tsukruk, F. Rinderspacher and V. Bliznyuk, *Langmuir*, 1997, **13**, 2171.
8 Y. Lvov, K. Ariga, M. Onda, I. Ichinose and T. Kunitake, *J. Am. Chem. Soc.*, 1995, **117**, 6117.
9 V. Bliznyuk and V. Tsukruk, *Polymer Prepr.*, 1997, **38**, 963.
10 E. Kleinfeld and G. Ferguson, *Science*, 1994, **265**, 370.
11 N. Kotov, I. Dekany and J. Fendler, *J. Phys. Chem.*, 1995, **99**, 3312.
12 Y. Liu, A. Wang and R. Claus, *J. Phys. Chem. B*, 1997, **101**, 1385.
13 A. Krozer, S.-A. Nordin and B. Kasemo, *J. Colloid Interface Sci.*, 1995, **176**, 479.
14 Y. Lvov, K. Ariga, I. Ichinose and T. Kunitake, *Langmuir*, 1997, **13**, 6195.
15 G. Sauerbrey, *Z. Phys.*, 1959, **155**, 206.
16 D. Aspnes, J. Theeten and F. Hottier, *Phys. Rev. B*, 1979, **20**, 3292.
17 R. v. Klitzig and H. Möhwald, *Thin Solid Films*, 1996, **284**, 352.
18 R. Finsy, E. Moreels, A. Bottger and H. Lekkerkerker, *J. Chem. Phys.*, 1985, **82**, 3812.
19 V. Tsukruk, V. Blyznyuk, D. Visser, A. Campbell, T. Bunnig and W. Adams, *Macromolecules*, 1997, **30**, 6615.

Received in Columbia, MO, USA, 18th February 1998; 8/01456F

Molecular Prussian Blue analogues: synthesis and structure of cubic $Cr_4Co_4(CN)_{12}$ and $Co_8(CN)_{12}$ clusters

Julie L. Heinrich, Polly A. Berseth and Jeffrey R. Long*†

Department of Chemistry, University of California, Berkeley, CA 94720 USA

Reactions between $[M(H_2O)_3(tacn)]^{3+}$ (M = Cr, Co) and $[Co(CN)_3(tacn)]$ are demonstrated to produce the molecular box clusters $[Cr_4Co_4(CN)_{12}(tacn)_8]^{12+}$ and $[Co_8(CN)_{12}(tacn)_8]^{12+}$ with core structures consisting of a single cubic unit excised from the Prussian Blue type framework.

The venerable solid pigment Prussian Blue, $Fe^{III}_4[Fe^{II}(CN)_6]_3{\cdot}zH_2O$, is readily prepared by addition of iron(III) ions to an aqueous ferrocyanide solution. This reaction can be generalized to include a variety of octahedral hexaaquo and hexacyano transition metal complexes which combine under similar conditions to form an extensive family of Prussian Blue type compounds:[1,2]

$$x[M(H_2O)_6]^{y+} + y[M'(CN)_6]^{x-} \rightarrow M_x[M'(CN)_6]_y{\cdot}zH_2O \quad (1)$$

The three-dimensional structures adopted by these compounds are based on a simple cubic lattice of alternating metal atoms M and M′ connected *via* linear M′–CN–M linkages. Characteristic of the framework are the cubic cavities demarcated by $M_4M'_4(CN)_{12}$ cages and capable of lodging small neutral molecules or charge-compensating monovalent cations. Such resident species can ordinarily be displaced or exchanged without disrupting the metal–cyanide host framework, giving rise to a range of molecular sieve, ion exchange and catalytic properties.[2–5] In addition, the bridging cyanide ligand is capable of mediating magnetic exchange between neighboring metal centers, and recognition of how the choice of M and M′ can influence the strength of the exchange has enabled the design of bulk magnetic materials with increasingly higher ordering temperatures.[6–9] Recent work has shown how the magnetic properties of these materials can be adjusted electro- and photochemically.[10–11]

In an effort to extend this remarkably diverse chemistry to a molecular level, we have initiated experiments directed toward the preparation of discrete cluster analogues of the cubic cages inherent to the Prussian Blue type structure. Our synthetic approach closely parallels that employed in eqn. (1), relying upon M′–CN–M bridge formation *via* displacement of water by the nitrogen end of cyanide:

$$4[M(H_2O)_3(tacn)]^{y+} + 4[M'(CN)_3(tacn)]^{x-} \rightarrow [M_4M'_4(CN)_{12}(tacn)_8]^{4(y-x)+} \quad (2)$$

Now, however, the tridentate ligand 1,4,7-triazacyclononane (tacn) blocks a single face on each of the transition metal reactants, preventing growth of the three-dimensional framework. Rather, it is proposed that the molecules will assemble into a compact cluster, $[M_4M'_4(CN)_{12}(tacn)_8]^{4(y-x)+}$, consisting of a cube of metal atoms with each edge spanned by a cyanide bridge and each corner capped by a tacn ligand. Herein, we report the initial use of this strategy to construct two such molecular Prussian Blue analogues.

A pink equimolar solution of $[Cr(H_2O)_3(tacn)][CF_3SO_3]_3$[12] and $[Co(CN)_3(tacn)]$[13] in water was boiled to dryness to give an orange residue. The residue was dissolved in a 1 : 1 mixture of acetonitrile and ethyl acetate; careful addition of diethyl ether then permitted separation of a pale orange solid suspension from an orange oil. The solid was collected, washed with ether, and dried to give $[Cr_4Co_4(CN)_{12}(tacn)_8][CF_3SO_3]_{12}{\cdot}8H_2O$ **1** in 46% yield.‡ The IR spectrum of **1** exhibits a single sharp absorption at ν_{CN} = 2177 cm^{-1}, consistent with the symmetry (T_d, ignoring tacn ligand conformations) of the expected cubic cluster. Furthermore, the direction and magnitude of the shift in energy of this absorption relative to that of the $[Co(CN)_3(tacn)]$ precursor (ν_{CN} 2129 cm^{-1}) is characteristic of M′–CN–M bridge formation,[1] and correlates well with the analogous shift from $K_3[Co(CN)_6]$ (ν_{CN} 2126 cm^{-1}) to $Cr[Co(CN)_6]$ (ν_{CN} 2186 cm^{-1}).[14] The positive ion electrospray mass spectrum of **1** confirms the presence of the $[Cr_4Co_4(CN)_{12}(tacn)_8]^{12+}$ cluster, which displays a fragmentation pattern attributable to successive losses of $[Cr(tacn)]^{3+}$ and/or $[Co(CN)_3(tacn)]$ moieties. Crystals of **1** obtained by numerous different methods invariably produced only very broad X-ray diffraction peaks at low θ angles, indicative of poor long-range ordering (presumably due to the many possible similar-energy configurations for packing twelve triflate anions per cluster cation). In the course of these experiments, a solitary crystal of superior quality was encountered and determined by single crystal X-ray analysis to contain a square cluster of formula $[Cr_2Co_2(CN)_6(Me_2SO)_2(tacn)_4]^{6+}$. Apparently, in this particular preparation, a residual amount of dimethyl sulfoxide lingering from the synthesis of $[Cr(H_2O)_3(tacn)][CF_3SO_3]_3$ served to block two of the Cr sites from further reacting to produce a cube.

Cluster preparations involving anions other than triflate were undertaken in hope that an alternative anion shape might promote formation of more rigorously ordered crystals. The compound $[Co_8(CN)_{12}(tacn)_8][OTs]_{12}{\cdot}14H_2O$ **2** was synthesized in 86% yield§ using a procedure similar to that described above. Yellow rectangular plate crystals were grown by allowing a methanol solution of **2** to slowly evaporate. X-Ray analysis¶ revealed the structure of the anticipated cluster with a cubic $Co_8(CN)_{12}$ core (Fig. 1). This cluster, with its novel boxlike geometry,‖ may be regarded as a three-dimensional extension of the above square cluster, as well as previously reported square clusters, such as $[Au_4(CN)_4Pr^n_8]$[18] and the more recent 'supramolecular' squares constructed using a variety of neutral bridging ligands.[19] On average, the clusters measure 4.937(7) Å on a cube edge, slightly smaller than the corresponding cage dimensions of 5.083 and 5.105 Å observed in Prussian Blue[16] and $Co^{II}_3[Co^{III}(CN)_6]_2{\cdot}12H_2O$[17] (to our knowledge, there is no known Prussian Blue analogue containing exclusively Co^{III}), respectively, at ambient temperature. The cyanide ligands spanning each edge deviate slightly (but irregularly) from linearity, as reflected in the Co–C–N and Co–N–C angles, which fall within the range 175(1)–180(1)°. Oxygen atoms from a single tosylate anion are positioned over each of the six cube faces in the crystal. No appreciable build-up of electron density was observed inside the cluster cavity; however, in view of the poor quality of the diffraction data, this does not exclude the possibility that a solvent molecule is present. Square openings (Fig. 2) on the cube faces could potentially permit entry by a guest molecule or ion. Based on the van der Waals radii of carbon and nitrogen, the minimum width of these openings is 1.7 Å, and the minimum diameter of the internal cavity is 3.7 Å. The high positive charge associated with the cubic cage should impart a strong preference for anion

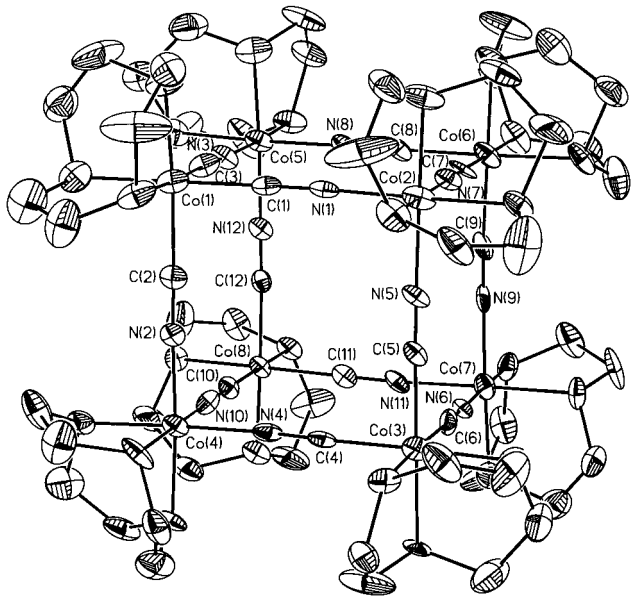

Fig. 1 Structure of the cubic $[Co_8(CN)_{12}(tacn)_8]^{12+}$ cluster in **2** showing 30% probability ellipsoids and the core atom labeling scheme. One orientation of the cyanide ligands is shown;¶ hydrogen atoms are omitted for clarity. Selected mean interatomic distances (Å) and angles (°) (X is a cyanide C or N atom): Co–X 1.89(2), Co–N 1.94(2), X–X 1.15(3), Co···Co 4.937(7); X–Co–X 89.9(7), Co–X–X 178(1), N–Co–X 92.0(9), N–Co–N 86.2(8).

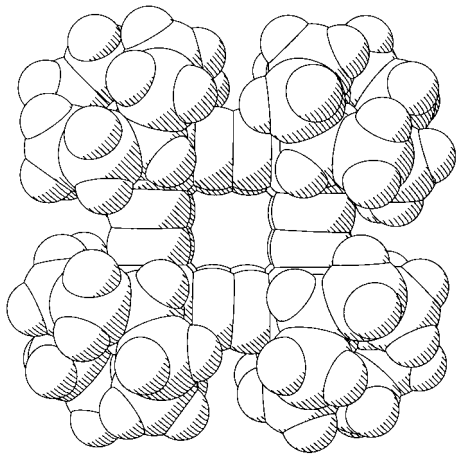

Fig. 2 Space filling model of the $[Co_8(CN)_{12}(tacn)_8]^{12+}$ cluster (including hydrogen atoms) viewed down a cube face

incorporation, as opposed to the cation affinity displayed by Prussian Blue type solids.[2–4]

By varying the metal atoms M and M′ employed in eqn. (2), we hope to produce an array of cubic cluster magnets with a variability in properties comparable to that which has evolved in Prussian Blue type materials.[6–11] The $[Cr_4Co_4(CN)_{12}(tacn)_8]^{12+}$ cluster represents an initial member in this array, possessing four Cr^{III} ions arranged in a tetrahedron over the cube vertices [replacing atoms Co(2), Co(4), Co(5) and Co(7) in Fig. 1] and separated by intervening diamagnetic Co^{III} ions. The temperature dependence of the magnetic susceptibility of **1** was measured using a SQUID magnetometer; a fit of the data to the Curie–Weiss law gives $C = 6.78$ emu K mol^{-1} and $\Theta = 1.21$ K. The effective magnetic moment of 7.5(1) μ_B and associated g value of 1.97 are reasonable for four isolated $S = 3/2$ Cr^{III} ions per cluster molecule.

Investigations further probing the magnetism, electrochemistry, and inclusion properties of these and related molecular Prussian Blue analogues are in progress.

This research was funded by the University of California and NSF Grant No. CHE 97-27410. We thank Dr R. Hage and Unilever for an initial donation of tacn ligand, N. Crawford, M. Shores, Dr J. P. Kirby, Professor J. Leary, Dr U. Andersen and Dr S. Koenig for experimental assistance, Professor J. McCusker for helpful discussions, Professor A. Stacy for use of the SQUID magnetometer and Professor T. D. Tilley for use of the IR spectrometer.

Notes and References

† E-mail: jlong@cchem.berkeley.edu

‡ Absorption spectrum (H_2O): λ_{max}/nm (ε_M/dm^3 mol^{-1} cm^{-1}) 291 (sh, 970), 367 (740), 476 (330). IR (KBr): ν_{CN} 2177 cm^{-1}. ES$^+$ MS: *m*/*z* 1640 ([**1** − 2CF_3SO_3 − 8H_2O]$^{2+}$), 1043 ([**1** − 3CF_3SO_3 − 8H_2O]$^{3+}$). Anal. Calc. for $C_{72}H_{136}Co_4Cr_4F_{36}N_{36}O_{44}S_{12}$: C, 23.23; H, 3.67; N, 13.55. Found: C, 23.16; H, 3.61; N, 13.05%.

§ Absorption spectrum (H_2O): λ_{max}/nm (ε_M/dm^3 mol^{-1} cm^{-1}) 364 (786), 469 (476). IR (KBr): ν_{CN} 2200 cm^{-1}. ES$^+$ MS: *m*/*z* 1118 ([**2** − 3OTs − 14H_2O]$^{3+}$), 796 ([**2** − 4OTs − 14H_2O]$^{4+}$). Anal. Calc. for $C_{144}H_{232}Co_8N_{36}O_{50}S_{12}$: C, 41.95; H, 5.67; N, 12.23. Found: C, 41.96; H, 5.63; N, 12.05%.

¶ *Crystal data*: $C_{144}H_{224}Co_8N_{36}O_{46}S_{12}$, $M = 4123.82$, monoclinic, space group $P2_1/n$, $Z = 4$, $a = 15.1773(2)$, $b = 36.0654(2)$, $c = 34.5918(4)$ Å, $\beta = 91.337(1)°$, $V = 18929.5(3)$ Å^3, $\mu = 0.900$ mm^{-1}. Data ($2 < 2\theta < 46°$) were collected at 135 K using a Siemens SMART diffractometer with graphite monochromated Mo-Kα radiation. The structure was solved by direct methods with the aid of successive difference Fourier maps, and was refined in three overlapping blocks against all data (26910 unique) using SHELXTL 5.0. The clusters are disordered over two externally indistinguishable orientations (one is shown in Fig. 1), in which only the positions of the cyanide C and N atoms are reversed; an occupancy factor of 0.5C + 0.5N was assigned to each of the cyanide atom sites. (In view of the substitutional inertness of Co^{III} and the sharpness of the ν_{CN} peak in the IR spectrum, it is unlikely that the cyanide bridges have reoriented in the individual cluster molecules.) Ten of the twelve tosylate anions are disordered over at least two positions, and were modeled accordingly. The final agreement factors $R_1 = 0.1476$ and $wR_2 = 0.3882$ are high due to the extensive anion disorder present in the crystal and the accompanying poor data quality. CCDC 182/855.

‖ An abstract reporting the synthesis of related $M_8(CN)_{12}$ (M = Co, Rh) clusters capped by cyclopentadienyl ligands recently appeared.[15]

1 D. F. Shriver, S. A. Shriver and S. E. Anderson, *Inorg. Chem.*, 1965, **4**, 725.
2 K. R. Dunbar and R. A. Heintz, *Prog. Inorg. Chem.*, 1997, **45**, 283 and references therein.
3 G. B. Seifer, *Russ. J. Inorg. Chem.*, 1959, **4**, 841.
4 C. Loos-Neskovic, M. Fedoroff and E. Garnier, *Talanta*, 1989, **36**, 749.
5 J. Kuyper and G. Boxhoorn, *J. Catal.*, 1987, **105**, 163.
6 V. Gadet, T. Mallah, I. Castro and M. Verdageur, *J. Am. Chem. Soc.*, 1992, **114**, 9213.
7 T. Mallah, S. Thiébaut, M. Verdaguer and P. Veillet, *Science*, 1993, **262**, 1554.
8 W. R. Entley and G. S. Girolami, *Science*, 1995, **268**, 397.
9 S. Ferlay, T. Mallah, R. Ouahès, P. Veillet and M. Verdaguer, *Nature*, 1995, **378**, 701.
10 O. Sato, T. Iyoda, A. Fujishima and K. Hashimoto, *Science*, 1996, **271**, 49.
11 O. Sato, T. Iyoda, A. Fujishima and K. Hashimoto, *Science*, 1996, **272**, 704.
12 C. K. Ryu, R. B. Lessard, D. Lynch and J. F. Endicott, *J. Phys. Chem.*, 1989, **93**, 1752.
13 F. Galsbøl, C. H. Petersen and K. Simonsen, *Acta Chem. Scand.*, 1996, **50**, 567.
14 J.-F. Bertrán, J. B. Pascual and E. R. Ruiz, *Spectrochim. Acta, Part A*, 1990, **46**, 685.
15 K. K. Klausmeyer and T. B. Rauchfuss, in *Abstracts from the 215th National Meeting of the American Chemical Society*: Division of Inorganic Chemistry, abstract no. 478.
16 H. J. Buser, D. Schwarzenbach, W. Petter and A. Ludi, *Inorg. Chem.*, 1977, **16**, 2704.
17 A. Ludi and H. U. Güdel, *Helv. Chim. Acta*, 1968, **51**, 2006.
18 R. F. Phillips and H. M. Powell, *Proc. R. Soc. London Ser. A*, 1939, **173**, 147.
19 P. J. Stang and B. Ogdan, *Acc. Chem. Res.*, 1997, **30**, 502 and references therein.

Received in Bloomington, IN, USA, 25th March 1998; 8/02351D

Crystal structures and electrical conducting properties of the first molecular metals based on a novel electron acceptor, 4-oxo-2,6-bis(dicyanomethylene)-2,6-dihydrocyclopentadithiophene (CPDT)

Kazuko Takahashi*† and Shinji Tarutani

Department of Chemistry, Graduate School of Science, Tohoku University, Sendai 980-8578, Japan

A novel electron acceptor CPDT has been synthesized; the Fermi surfaces of the metallic anion radical salts of CPDT are purely one-dimensional, while the acceptor molecules form rigid and tight two-dimensional networks in the crystal structures of the salts.

Electron-accepting molecules with three terminal electron-withdrawing groups appear to be promising components for organic conductors because they would have high electron accepting abilities as well as highly rigid and coplanar conformations, giving stable anion radicals and dianions owing to the effective conjugation of the three terminal groups.[1] We have now designed and successfully synthesized such a novel acceptor molecule, 4-oxo-2,6-bis(dicyanomethylene)-2,6-dihydrocyclopenta[2,1-*b*;3,4-*b*′]dithiophene (CPDT) **1**. Further-

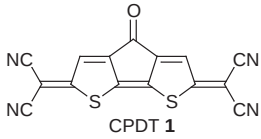

CPDT **1**

more, we have obtained metallic anion radical salts of **1** and have clarified the conducting properties and crystal structures of the metallic salts. These are the first examples of molecular metals of the heterophene–TCNQ family.[2]

CPDT was synthesized starting from the ketal **2**[3] (Scheme 1). CPDT‡ is reduced reversibly in three successive one-electron transfer reactions to give the stable anion radical, dianion and trianion radical species which demonstrate, by cyclic voltammetry, three pairs of single-electron redox waves with good reversibility at half-wave reduction potentials of +0.04, −0.27 and −1.43 V (*vs.* SCE in CH_2Cl_2 at 25 °C). The first reduction potential is more positive by 0.18 V than that of **4** (−0.14 V). The log K_{sem} value[4] of CPDT (5.26) is larger by 1.36 than that of **4** (3.90), indicating that the anion radical of CPDT is thermodynamically stabilized by delocalization of the unpaired electron over the three terminal electron-accepting groups.

Interestingly, the crystalline anion radical salts $(Me_4N)[CPDT]_2$, $(Et_4N)[CPDT]_2$, $(Me_4P)[CPDT]_2$ and $(Me_4As)[CPDT]_2$, prepared by electrochemical reduction, are metallic at room temperature and their conductivities reach maximum values (σ_{max}) of 170, 290, 55 and 55 S cm^{-1} at the $T_{\sigma max}$ values listed in Table 1. $T_{\sigma max}$ becomes lower as the size of the counter cation in these four salts is increased. Below $T_{\sigma max}$, the metallic states

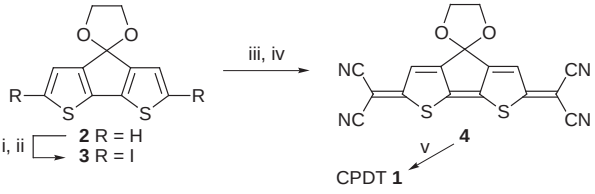

Scheme 1 *Reagents and conditions*: i, LiBu, THF, −40 °C, then 0 °C, 30 min; ii, I_2, Et_2O, −78 °C, then room temp., 30 min, 56%; iii, $NaCH(CN)_2$, THF, $Pd(PPh_3)_4$, THF, reflux, 4 h; iv, Br_2, H_2O, room temp., 74%; v, 70% aq. $HClO_4$, CH_2Cl_2, 0 °C, 3 h, 96%

Table 1 Properties of anion radical salts of CPDT

Cation	Ratio[a]	σ_{rt}[b]/S cm^{-1}	$T_{\sigma max}$/K	T_{MI}/K
Me_4N	1 : 2	160	250	130
Et_4N	1 : 2	260	220	150
Me_4P	1 : 2	47	215	165
Me_4As	1 : 2	42	173	173–185

[a] By elemental analysis. [b] Measured by four probe method on a single crystal.

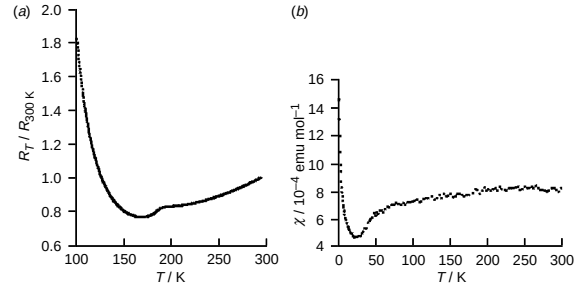

Fig. 1 Temperature dependence of (*a*) the resistivity and (*b*) the magnetic susceptibility of $(Me_4As)[CPDT]_2$

gradually become unstable, and drastic decreases in the conductivities with the transition to the semiconducting phases occurred at *ca.* 130 K for the Me_4N salt, 150 K for the Et_4N salt, 165 K for the Me_4P salt and 173–185 K for the Me_4As salt [Table 1 and Fig. 1(*a*)]. The metallic properties were also confirmed by the temperature dependence of the magnetic susceptibility measurement using a SQUID susceptometer [Fig. 1(*b*)]. The magnetic susceptibilities of the Me_4N and Me_4As salts are invariable from room temperature down to T_{DIA} = 135 and 50 K, respectively, which are regarded as Pauli-like, and decrease drastically at these temperatures with the transition to the diamagnetic phases. The phase transition mechanisms seem to be significantly different from each other, although the crystal structures are isomorphous, as described below. Occurrence of the Peierls type transition is suggested in the Me_4N salt, since T_{MI} is almost identical with T_{DIA}. However, in the Me_4As salt, the magnetic susceptibility does not decrease even after the M–I transition has occurred [Fig. 1(*b*)], and the magnitude of the magnetic susceptibility of the Me_4As salt (8×10^{-4} emu mol^{-1}) is significantly large when compared with those of ordinal molecular metals. These phenomena suggest the existence of a $4k_F$ charge density wave (CDW) growing phase[5] at the temperature region between 150 (T_{MI}) and 50 K (T_{DIA}) in the Me_4As salt.

The crystal structures of the metallic salts $(Me_4N)[CPDT]_2$, $(Me_4P)[CPDT]_2$ and $(Me_4As)[CPDT]_2$, which are isomorphous with each other, were determined by X-ray analysis.§ The unit cell contains four crystallographically equivalent acceptor molecules and two equivalent cations, giving a cation to acceptor ratio of 1 : 2. The formal charge on CPDT is −0.5. The unit cell contains two acceptor columns stacking along the *b*-axis and each column is separated by a cation layer [Fig. 2(*a*)].

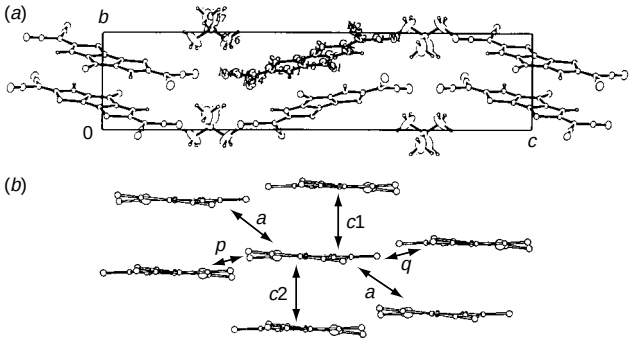

Fig. 2 Crystal structure of $Me_4N[CPDT]_2$: (*a*) projection onto the *bc*-plane and (*b*) overlap mode viewed along the acceptor short axis

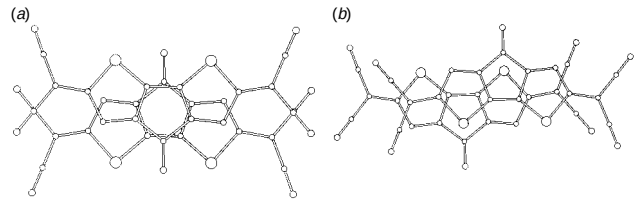

Fig. 3 Overlaping modes of CPDT molecules in $(Me_4N)[CPDT]_2$: (*a*) intra-dimer overlap, (*b*) inter-dimer overlap

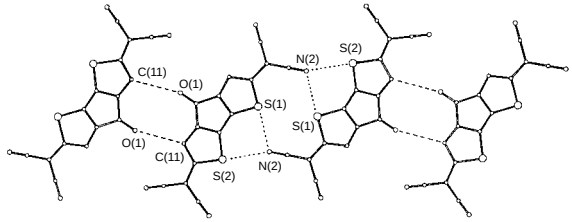

Fig. 4 Side-by-side interaction of CPDT in $(Me_4N)[CPDT]_2$

The acceptor column is constituted by weakly dimerised CPDT molecules with intra-dimer interplanar distances of 3.20–3.21 Å [*c*1 in Fig. 2(*b*)] and inter-dimer interplanar distances of 3.32–3.33 Å [*c*2 in Fig. 2(*b*)]. The overlapping mode is the so-called 'ring-over-ring' type in the intra-dimer overlap and the 'ring-over-bond' type in the inter-dimer overlap (Fig. 3). Interestingly, there are two S1–N2 (3.01–2.97 Å) and two S2–N2 (3.04–2.99 Å) contacts, and there are two short intermolecular hydrogen bonds between O1···H11 (3.25–3.28 Å) along the acceptor short axis in the crystal structures of these salts (Fig. 4). Thus rigid and tight two-dimensional layered intermolecular networks are constructed along the *ab*-plane.

The intermolecular overlap integrals of the metallic salts are summarized in Table 2. There is no significant difference between *c*1 and *c*2, which indicates that the degree of the dimerization is very weak in these salts. On the other hand, the overlap integrals along the acceptor shot axis are less than 1/300 of *c*1 or *c*2 (Table 2), in spite of the existence of the inter-column S–N and O–H contacts. This is ascribed to the extremely small π-atomic orbital coefficients of the O and the S

Table 2 Intermolecular overlap integrals (*S*) of the anion radical salts[a]

	$S/10^{-3}$		
Overlap direction[b]	Me_4N salt	Me_4P salt	Me_4As salt
*c*1 (intra-dimer)	−19.65	−18.83	−18.83
*c*2 (intra-dimer)	16.53	14.37	15.14
a (inter-column)	0.0744	0.0559	0.0713
p (S1–N2 contact)	0.00429	0.0913	0.00393
q (O1–H11 contact)	0.00672	0.0104	0.0260

[a] Calculated with π-atomic orbital coefficients obtained by the extended Hückel MO method using bond angles and bond lengths obtained from the X-ray analysis. [b] The overlap directions are indicated in Fig. 2(*b*).

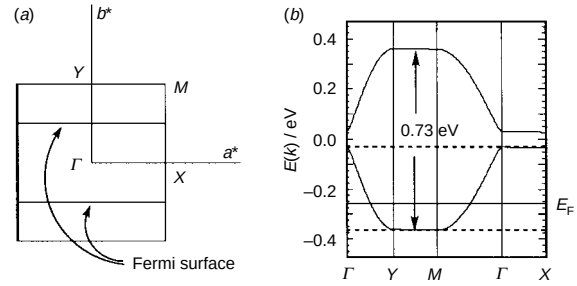

Fig. 5 (*a*) Fermi surface and (*b*) band structure of $(Me_4N)[CPDT]_2$, calculated by the tight binding approximation method

atoms in the LUMO of CPDT. From the tight-binding band calculations[6] using the overlap integrals shown in Table 2, it is demonstrated that these salts have highly one-dimensional Fermi surfaces opened along the *a**-axis [Fig. 5(*a*)]. These salts have a split band structure due to their dimerized crystal structures and the lower energy band is half filled [Fig. 5(*b*)]. The calculated band widths are 0.73, 0.67 and 0.68 eV in the Me_4N, Me_4P and Me_4As salts, respectively. The phase transition of the Me_4N salt at 130 K appears to be caused by a Peierls transition, since salts with a large band width can obtain a large energy benefit by forming the band gap.

This work was supported by the Ministry of Education, Science and Culture, Japan (Grant-in-Aid for Science Research on Priority Area of Molecular Conductors No. 06243105).

Notes and References

† E-mail: tkazuko@kiki.chem.tohoku.ac.jp

‡ *Selected data* for CPDT **1**, mp > 300 °C; ν_{max}(KBr)/cm^{-1} 3047, 2218, 1732, 1504, 1460, 1325, 1252, 1225, 957, 897, 760; $\lambda_{max}(CH_2Cl_2)$/nm (log ε) 553 (sh, 4.32), 520 (4.93), 489 (4.74), 458 (sh, 4.37), 360 (3.48), 341 (3.62), 323 (sh, 3.75), 314 (sh, 3.89), 297 (4.27), 286 (4.26), 274 (4.16); *m*/*z* (70 eV) 321 (M^+ + 3, 2.23%), 320 (M^+ + 2, 11.47), 319 (M^+ + 1, 19.38) and 318 (M^+, 100) [HRMS: 317.9673 (M^+]. Calc. 317.9670] (Calc. for $C_{15}H_2N_4OS_2$: C, 56.60; H, 0.63; N, 17.60. Found: C, 56.44; H, 0.78; N, 17.39%).

§ *Crystal data* for $(Me_4N)[CPDT]_2$: monoclinic, space group *P*2/n, *a* = 7.4763(7), *b* = 6.9411(7), *c* = 30.428(4) Å, β = 91.523(10)°, *V* = 1578.5(3) Å^3, *Z* = 4, $\rho_{calc.}$ = 1.495 g cm^{-1}, μ(Cu-Kα) = 31.81 cm^{-1}, *R* (R_w) = 0.062 (0.067) for independent 2129 reflections [$I > 5.00\sigma(I)$]. For $(Me_4P)[CPDT]_2$: monoclinic, space group *P*2/n, *a* = 7.446(2), *b* = 6.984(2), *c* = 31.596(2) Å, β = 92.33(2)°, *V* = 1641.7(6) Å^3, *Z* = 4, $\rho_{calc.}$ = 1.472 g cm^{-1}, μ(Cu-Kα) = 35.10 cm^{-1}, *R* (R_w) = 0.035 (0.038) for independent 2203 reflections [$I > 3.00\sigma(I)$]. For $(Me_4As)[CPDT]_2$: monoclinic, space group *P*2/n, *a* = 7.430(1), *b* = 6.994(2), *c* = 31.922(2) Å, β = 92.50(1)°, *V* = 1657.2(5) Å^3, *Z* = 4, $\rho_{calc.}$ = 1.546 g cm^{-1}, μ(Cu-Kα) = 41.30 cm^{-1}, *R* (R_w) = 0.034 (0.036) for independent 2446 reflections [$I > 3.00\sigma(I)$]. The data were collected on a Rigaku AFC-5R diffractometer with graphite monochromated Cu-Kα radiation (λ = 1.54178 Å, ω–2θ scan technique). After absorption correction, the structures were solved by direct methods (SIR92) and expanded using Fourier techniques. The non-hydrogen atoms were refined anisotopically. Some hydrogen atoms were refined isotopically, the others were included in fixed positions. CCDC 182/836.

1 K. Takahashi and S. Tarutani, *Adv. Mater*., 1995, **7**, 639; S. Tarutani, T. Mori, H. Mori, S. Tanaka and K. Takahashi, *Chem. Lett.*, 1997, 627.
2 K. Yui, Y. Aso, T. Otsubo and F. Ogura, *Bull. Chem. Soc. Jpn*., 1989, **62**, 1539; K. Yui, H. Ishida, Y. Aso, T. Otsubo, F. Ogura, A. Kawamoto and J. Tanaka, *Bull. Chem. Soc. Jpn*., 1989, **62**, 1547; S. Yoshida, M. Fujii, Y. Aso, T. Otsubo and F. Ogura, *J. Org. Chem*., 1994, **59**, 3077.
3 P. Jordens, G. Rawson and H. Wynberg, *J. Chem. Soc. C*., 1970, 273.
4 M. R. Bryce, E. Fleckenstein and S. Hünig, *J. Chem. Soc., Perkin Trans. 2*, 1990, 1777.
5 S. Kagoshima, H. Nagasawa and T. Sambongi, *One-Dimensional Conductors*, Springer-Verlag, 1982; S. Kagoshima, T. Ishiguro and H. Anzai, *J. Phys. Soc. Jpn.*, 1976, **41**, 2061.
6 T. Mori, A. Kobayashi, Y. Sasaki, H. Kobayashi, G. Saito and H. Inokuchi, *Bull. Chem. Soc. Jpn*., 1984, **57**, 627.

Received in Cambridge, UK, 23rd February 1998; 8/01500G

Synthesis and molecular and electronic structure of monomeric [Ti(η⁸-C_8H_8)(NBu^t)]

Alexander J. Blake,[a] Simon C. Dunn,[a] Jennifer C. Green,[b]† Nicholas M. Jones,[b] Aidan G. Moody[a] and Philip Mountford[a]*†

[a] *Department of Chemistry, University of Nottingham, Nottingham, UK NG7 2RD*
[b] *Inorganic Chemistry Laboratory, South Parks Road, Oxford, UK OX1 3QR*

Reaction of [Ti(NBu^t)Cl_2(py)$_3$] with $K_2[C_8H_8]$ gave the monomeric, pseudo-two-coordinate complex [Ti(η⁸-C_8H_8)(NBu^t)] 1 which has been crystallographically characterised; the electronic structure of 1 has been investigated using density functional theory calculations and gas phase photoelectron spectroscopy.

As part of an ongoing programme in titanium–imido chemistry we found that the compound [Ti(NBu^t)Cl_2(py)$_3$] provides a useful synthetic entry to a range of sandwich, half-sandwich and other new titanium imido compounds.[1] We noticed that although cyclopentadienyl and, to a lesser extent, arene coligands have been widely used in transition metal imido chemistry,[2] there has been only one report of imido complexes bearing cyclooctatetraenyl coligands, namely the dinuclear μ-arylimido derivatives [M_2(η⁸-C_8H_8)$_2$(μ-$NC_6H_3Pr^i_2$-2,6)$_2$] (M = Zr, Hf).[3] We were therefore interested to see if using the smaller titanium congener would lead to a mononuclear derivative. Here we describe the synthesis and molecular and electronic structure of the cyclooctatetraenyltitanium imido complex [Ti(η⁸-C_8H_8)(NBu^t)] **1**.

Addition of 1 equiv. of $K_2[C_8H_8]$ to [Ti(NBu^t)Cl_2(py)$_3$] in THF at −50 °C gave a dark red solution. Standard workup and crystallisation from pentane gave [Ti(η⁸-C_8H_8)(NBu^t)] **1** as a spectroscopically pure, dark yellow powder in 68% yield. Compound **1** is highly air- and moisture-sensitive, and its ^{1}H and ^{13}C NMR spectra contain signals attributable to a *tert*-butylimido ligand and an octahapto-coordinated C_8H_8 ring. Crystals of **1** suitable for X-ray diffraction analysis could be obtained by careful tube sublimation at 90–100 °C, 5×10^{-6} mbar.‡ The solid state structure of **1** is shown in Fig. 1. The Ti=NBu^t and Ti···C_8H_8 (ring centroid) distances of 1.699(6) and 1.369 Å are normal for terminal titanium-*tert*-butylimido and titanium(IV)-η⁸-cyclooctatetraenyl complexes, respectively.[4] The near-linearity of the Ti=N–Bu^t angle [Ti(1)–N(1)–C(1) 177.1(5)°] is consistent with the imido ligand acting as a four-electron donor to the titanium centre (*vide infra*), giving an overall metal valence-electron count of 16.

The pseudo-two-coordinate, 'one-legged piano stool' geometry for **1** is unique in early transition metal imido and cyclooctatetraenyl ligand chemistry.[2,5] A search of the Cambridge Structural Database[4] for complexes of the type [Ti(η⁸-C_8H_8)(L)$_n$] showed that the formal value of *n* is at least three. As mentioned, there has been only one report of imido complexes bearing cyclooctatetraenyl coligands, these being dinuclear.[3] The molecular structure of [Ti(η⁸-C_8H_8)(NBu^t)] is apparently related to those of the 18 valence electron, later transition metal compounds [Os(η⁶-C_6Me_6)(NBu^t)],[6a] [Ir(η⁵-C_5Me_5)(NBu^t)],[6b] and [Ni(η⁵-C_5H_5)(NO)].[6c] The bonding in these compounds is analagous to that of mixed ring sandwich compounds[7] as we[8,9] and others[10] have previously analysed.

The gas phase He photoelectron (PE) spectrum§ of [Ti(η⁸-C_8H_8)(NBu^t)] **1** is shown in Fig. 2, and numerical data are summarised in Table 1. Its assignment is made relatively straightforward by comparison with related imido and cyclooctatetraenyl compounds.[7b,8] The apparent paucity of low ionisation energy (IE) bands for **1** is explained by the fact that the e_2 ionisation of the Ti–C_8H_8 ring δ bonding orbitals overlaps with the e_1 ionisation of the Ti–N π bonds producing a complex band centred at 8 eV. Band C at 10.91 eV may be assigned to an e_1 ionisation of the C_8H_8 ring π orbitals. An increase in the intensity of bands A and B relative to C in the He II spectrum indicated that the e_2 and $2e_1$ orbitals that give rise to bands A and B have significant metal character.

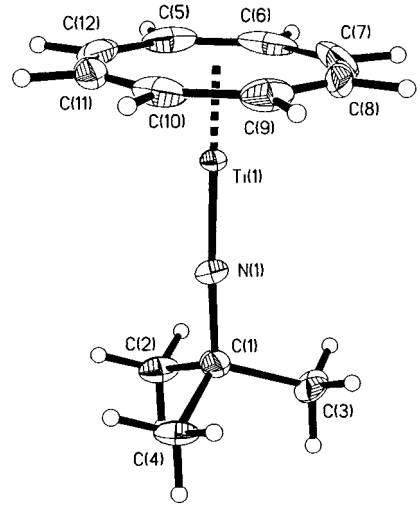

Fig. 1 Displacement ellipsoid plot of [Ti(η⁸-C_8H_8)(NBu^t)] **1**. Hydrogen atoms are drawn as spheres of arbitrary radius. Displacement ellipsoids are drawn at the 40% probability level. Selected bond lengths (Å) and angles (°): Ti(1)–N(1) 1.699(6), Ti(1)–$C_{average}$ 2.280 [range 2.267(8) to 2.290(8)], Ti(1)···C_8(centroid) 1.369; Ti(1)–N(1)–C(1) 177.1(5), C_8(centroid)–Ti(1)–N(1) 179.3.

An interesting comparison may be made with the 17 valence electron, d^1 compound [Ti(η⁸-C_8H_8)(η⁵-C_5Me_5)].[7b] In the PE spectrum of this compound there is an additional low-lying ionisation band of the extra d electron at 5.28 eV, but the e_2 and $2e_1$ bands are also found to be coincident with a maximum at

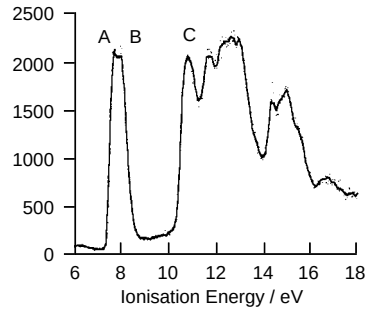

Fig. 2 He I full range PE spectrum of **1** [see http://www.rsc.org/suppdata/cc/1998/1235 for PE spectrum of **1**: (*a*) He I full range, (*b*) He I short range, (*c*) He II short range]

Table 1 Comparison of calculated ionisation energies (eV) and bond lengths (Å) for **1** and [Ti(η^8-C_8H_8)(NH)], **2**, with experimental values for **1**

	1 (exptl.)	**1** (calc.)	**2** (calc.)
Ionisation energies			
$1e_2$	7.78 (A)	7.70	8.16
$2e_1$	8.05 (B)	7.88	8.91
$1e_1$	10.91 (C)	[a]	10.83
Bond lengths			
Ti–C	2.267(8)–2.290(8)	2.282	2.275
Ti–N	1.699(6)	1.689	1.683
C–C ring	1.37(2)–1.44(2)	1.409	1.408
Bu^t	1.51(1)–1.52(1)	1.519	

[a] SCF convergence not achieved for this ion state.

7.54 eV. Furthermore, the $1e_1$ band lies at 10.5 eV, which is of a very similar energy to that for **1**. Thus we may conclude that the cyclopentadienyl–imido analogy[8] holds for these compounds and that *tert*-butylimido is electronically similar to the pentamethylcyclopentadienyl ligand though it provides one less electron.

Density functional calculations[11] were used to optimise the geometry of **1**.¶ C_s symmetry was assumed but in addition parameters were fixed so that the Ti-ring fragment had C_{8v} symmetry and the N–Bu^t fragment C_{3v} symmetry. Calculated bond lengths and angles are compared with the experimental ones in Table 1 which shows that the agreement is very good. Calculation of IEs‖ for **1** proved difficult because of the low symmetry and the proximity of ion states of identical symmetry. IE calculations were therefore also carried out on [Ti(η^8-C_8H_8)(NH)] **2** as a model for **1**. C_{8v} symmetry was assumed throughout these calculations. The calculated IEs for both **1** and **2** are given in Table 1 along with experimental values for **1**. The *tert*-butyl substituent has a bigger effect on the $2e_1$ IE than the e_2 EI. The closeness of the two ion states means that their exact assignment is uncertain.

Isosurfaces for these two orbitals (e_2 and $2e_1$) together with those for the $1e_1$ and the a_1 N–Ti σ-bonding orbital are shown in Fig. 3. Mulliken population analysis of the ground state structure of **1** gives the Ti contribution to the $2e_1$ and e_2 orbitals as 26% and 21%, while that of $1e_1$ is estimated as 8%. This is consistent with the intensity increase of bands A + B relative to C as the photon energy is increased. The most striking aspect of the metal ligand bonding orbitals is that binding to the imido group is through σ and π orbitals whereas that to the C_8H_8 ring is virtually exclusively through δ symmetry orbitals. This is in contrast to bis-cyclopentadienyl metal complexes where both rings compete for the metal π symmetry orbitals.

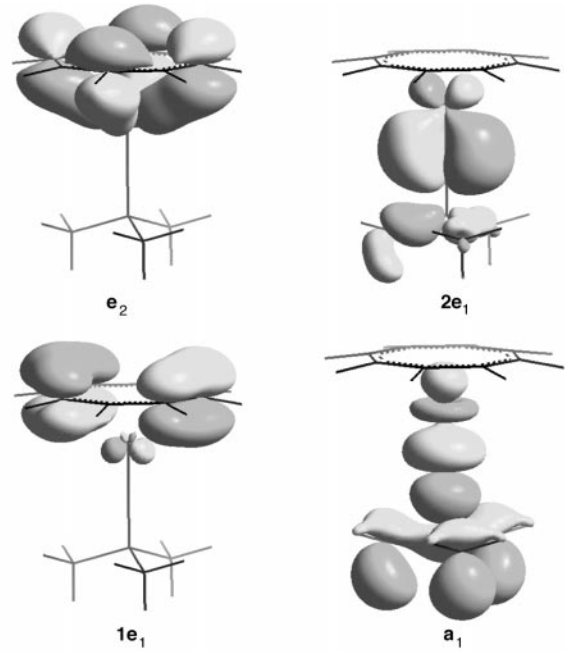

Fig. 3 Isosurfaces for the e_2, $2e_1$, $1e_1$ and M–N a_1 orbitals of **1** (see http://www.rsc.org/suppdata/cc/1998/1235 for a full colour version of this figure)

In conclusion, we have firmly established a new class of early transition metal cyclooctatetraenyl and imido complexes through structural, spectroscopic and theoretical studies. Recent preliminary studies suggest that the Ti=NBu^t linkage in **1** is reactive towards a range of organic substrates. Our work in this area and syntheses of other early transition metal cyclooctatetraenyl–imido complexes are continuing.

This work was supported by grants from the EPSRC, Leverhulme Trust and Royal Society. We thank Professor F. G. N. Cloke for valuable advice and discussions, and CCLRC Daresbury Laboratory for access to CSD.

Notes and References

† E-mail: Philip.Mountford@Nottingham.ac.uk (www:http://www.nottingham.ac.uk/~pczwww/Inorganic/PMount.html) or Jennifer.Green@chem.ox.ac.uk. Philip Mountford is The Royal Society of Chemistry Sir Edward Frankland Fellow.

‡ *Crystal data* for **1**: $C_{12}H_{17}NTi$, M = 223.17, triclinic, space group $P\bar{1}$ (no. 2), a = 6.255(3), b = 8.980(4), c = 11.144(6) Å, α = 82.58(6), β = 89.74(4), γ = 70.51(6)°, U = 584.7(8) Å^3, Z = 2, T = 150(2) K, μ = 0.69 mm^{-1}, no. of $I > 3\sigma(I)$ data used in refinement 1204, no. of parameters refined 129, full-matrix least squares on F with Chebychev polynomial weighting scheme, final R indices: R = 0.094, R_w = 0.097 for 4774 data, GOF = 1.14 (on F), final $(\Delta/\sigma)_{max}$ 0.001, largest residual peaks 1.12 and −1.09 e Å^{-3}. CCDC 182/841.

§ PE spectra were measured using a PES Laboratories 0078 spectrometer and were calibrated with N_2, Xe and He.

¶ Calculations were performed using the density functional methods of the Amsterdam Density Functional (ADF) code Version 2.3.0.[11] The basis set used triple-ζ accuracy sets of Slater orbitals with a single polarisation function added to main group atoms, 2p on H, 3p on C and N. Cores of the atoms were frozen, (C 1s, N 1s and Ti 3p). Vosko, Wilk and Nusair's local exchange correlation potential[12] was employed with non-local exchange corrections by Becke[13] and non-local correlation corrections by Perdew.[14] Vertical ionisation energies were estimated by calculating the energy of the molecular ion, with identical geometry to the optimised structure for the molecule, in its ground and low lying excited states and subtracting the energy of the molecular ground state.

1 P. Mountford, *Chem. Commun.*, 1997, 2127 (Feature Article).
2 D. E. Wigley, *Prog. Inorg. Chem.*, 1994, **42**, 239.
3 D. J. Arney, M. A. Bruck, S. R. Huber and D. E. Wigley, *Inorg. Chem.*, 1992, **31**, 3749.
4 The Cambridge Structural Database: D. A. Fletcher, R. F. McMeeking and D. Parkin, *J. Chem. Inf. Comput. Sci.*, 1996, **36**, 746; F. H. Allen and O. Kennard, *Chem. Des. Autom. News*, 1993, **8**, 1; 31.
5 F. G. N. Cloke in *Comprehensive Organometallic Chemistry II*, ed. E. W. Abel, F. G. A. Stone and G. Wilkinson, Elsevier, New York, 1995, vol. 4.
6 (*a*) R. I. Michelman, R. A. Andersen and R. G. Bergman, *J. Am. Chem. Soc.*, 1991, **113**, 5100; (*b*) D. S. Glueck, J. Wu, F. J. Hollander and R. G. Bergman, *J. Am. Chem. Soc.*, 1991, **113**, 2041; (*c*) I. A. Ronova, N. V. Alekseeva, N. N. Veniaminov and M. A. Kravers, *J. Struct. Chem.*, 1995, **16**, 441.
7 (*a*) S. Evans, J. C. Green, S. E. Jackson and B. Higginson, *J. Chem. Soc., Dalton Trans.*, 1974, 304; (*b*) R. R. Andréa, A. Terpstra, A. Oskam, P. Bruin and J. H. Teuben, *J. Organomet. Chem.*, 1986, **307**, 307.
8 D. S. Glueck, J. C. Green, R. I. Michelman and I. N. Wright, *Organometallics*, 1992, **11**, 4221.
9 C. N. Field, J. C. Green, M. Mayer, V. A. Nasluzov, N. Rösch and M. R. F. Siggel, *Inorg. Chem.*, 1996, **35**, 2504; J. C. Green and C. Underwood, *J. Organomet. Chem.*, 1997, **528**, 91.
10 X. Li, J. S. Tse, G. M. Bancroft, R. J. Puddephatt, Y. F. Hu and K. H. Tan, *Inorg. Chem.*, 1996, **35**, 2515.
11 ADF 2.3.0, E. J. Baerends and G. te Velde, Theoretical Chemistry, Vrije Universiteit, Amsterdam, 1997.
12 S. H. Vosko, L. Wilk and M. Nusair, *Can. J. Phys.*, 1980, **58**, 1200.
13 A. D. Becke, *Phys. Rev. A*, 1988, **38**, 2398.
14 J. P. Perdew, *Phys. Rev. B*, 1986, **33**, 8822; **34**, 7046.

Received in Cambridge, UK, 11th March 1998; 8/01968A

ChemComm
FEATURE ARTICLE

Linked arene clusters

Brian F. G. Johnson,* Caroline M. Martin and Paul Schooler

University Chemical Laboratory, Lensfield Road, Cambridge, UK CB2 1EW

The synthesis, isolation and characterisation of a number of [2$_n$]cyclophane transition metal clusters with nuclearities ranging from four to twelve atoms is described. The primary objective of this work has been to prepare molecules composed of alternating cyclophane and cluster subunits which may be considered as precursors to novel organometallic polymer chains and networks. This aim has been achieved to a certain degree using the [2.2.2]paracyclophane ligand, which has been shown to interact with metal clusters (*e.g.* tetracobalt nonacarbonyl) *via* all three of its aromatic rings. Also, the dimerisation of a hexaruthenium-[2.2.2]paracyclophane complex has yielded a remarkable dodecanuclear bis-arene cluster which may form the basis for a novel linear polymeric chain containing only metal atoms in the backbone. We have also been able to demonstrate that the coordinated [2.2.2]paracyclophane unit is able to embrace metal ions such as Ga^{I} and Ag^{I} giving rise to a concomitant change in the observed IR spectrum of the attached cluster. This perspective highlights these areas of research and also examines the factors controlling coordination mode preferences of the [2$_n$]cyclophane ligand and the central cluster nuclearity and geometry.

The interaction between both transition and main group metal ions with a variety of [2$_n$]cyclophane ligands has been of considerable interest to chemists for several decades.[1] These complexes were initially prepared in order to explore the unusual properties exhibited by the [2$_n$]cyclophane ligands which stem from the overlap of their π molecular orbitals and give rise to highly unique electronic and structural effects.[2] More recently, however, interest has been further stimulated by the potential for the [2$_n$]cyclophane ligands to serve as bridging units between redox-active metal centres in organometallic polymers and networks. Materials of this type are expected to exhibit a wide range of potentially interesting electrical and non-linear optical properties.[3]

The graphitic interaction

Over the past few years we have been actively involved in the study of organometallic cluster complexes, in particular, those containing coordinated arene ring systems.[4] The work described in this article was initially stimulated by the trends that emerged from a detailed examination of the solid-state structures of a number of bis-arene clusters of the type $[Ru_6C(CO)_{11}(arene)_2]$.[5] These investigations revealed an overwhelming tendency for the organic rings to become interlocked thus forming layers of organic substrate interspersed by layers of cluster units. Such layering was invariably found to be a result of the face-to-face (although typically off-centred) arrangement of aromatic ligands in adjacent molecules at distances comparable to that obeserved in graphite. It was also discovered that these packing interactions are propagated throughout the entire solid and result in the formation of supramolecular chains and stacks.[5]

This study revealed that it was primarily the difference in bonding mode adopted by the arene ligands (η^6 or μ_3) combined with their arrangement around the metallic core (*cis* or *trans*) that determined the packing motif within the crystal structure. For example, the two isomeric clusters *trans*-$[Ru_6C(CO)_{11}(\eta^6\text{-}C_6H_6)_2]$ **1** and $[Ru_6C(CO)_{11}(\eta^6\text{-}C_6H_6)(\mu_3\text{-}\eta^2:\eta^2\text{-}C_6H_6)]$ **2** adopt different packing regimes in the solid-state (Fig. 1). In **1**, the molecules are arranged in long columnar structures with an interarene separation of 3.52 Å [Fig. 1(*a*)].[6]

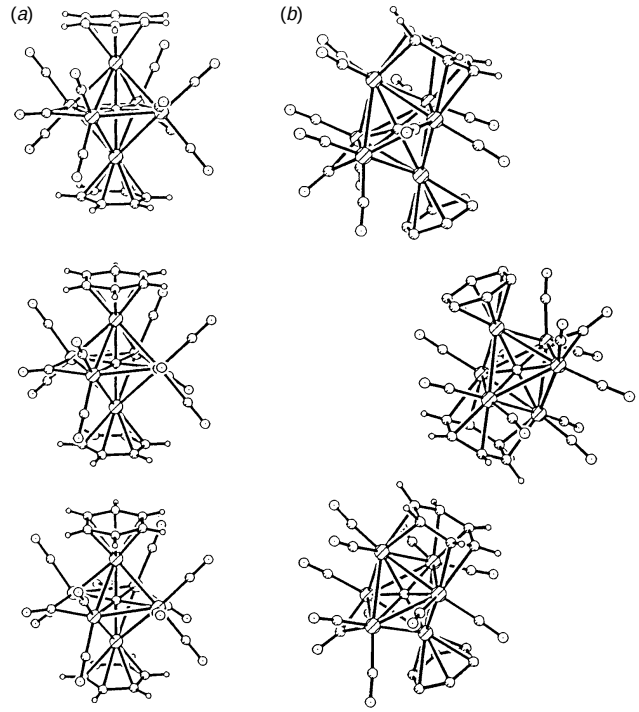

Fig. 1 Solid state packing of (*a*) $[Ru_6C(CO)_{11}(\eta^6\text{-}C_6H_6)_2]$ **1** as rods; and of (*b*) $[Ru_6C(CO)_{11}(\eta^6\text{-}C_6H_6)(\mu_3\text{-}\eta^2:\eta^2\text{-}C_6H_6)]$ **2** as snakes

Such a macromolecular structure arises from the arrangement of the arene rings which lie in parallel planes on the central cluster unit and permit the formation of a linear supramolecular rod. In **2**, however, the arene ligands are carried in planes which meet at a dihedral angle of 45°. As would be expected, this results in the introduction of kinks in the columnar structures producing supramolecular snakes instead [Fig. 1(*b*)].[7] In compound **2**, it should also be noted that the only close interactions observed between adjacent molecules in the crystal structure occur between η^6–η^6 bound rings and μ_3–μ_3 bound rings at distances of 3.29 and 3.56 Å, respectively. Although η^6–μ_3 interactions are known for other arene clusters, such as in the crystal structure of $[Os_3(CO)_6(C_6H_6)_2]$,[8] none are observed in that of compound **2**.

The study of these arene–arene interactions is of fundamental importance. This is because it is through such interactions that a mechanism in which charge transfer may occur throughout the crystalline lattice may be envisaged. Furthermore, one could speculate that it may be possible to create strong chemical bridges between adjacent arene clusters thus generating novel two-dimensional polymeric cluster chains and three-dimensional networks. It was with these ideas in mind that the class of ligands known as the cyclophanes, with their unique combina-

tion of strong chemical bridges linking aromatic rings and ability to transfer charge through space from one arene ring to the next within the same molecule, were considered as highly appropriate cluster linking groups.[9]

Linking arene clusters: the cyclophanes

There are two fundamentally different approaches which may be taken in order to produce linked arene clusters. The first involves the generation and subsequent coupling of activated arene clusters, while the second involves the addition of clusters to a pre-linked arene ligand (Scheme 1). The first approach has

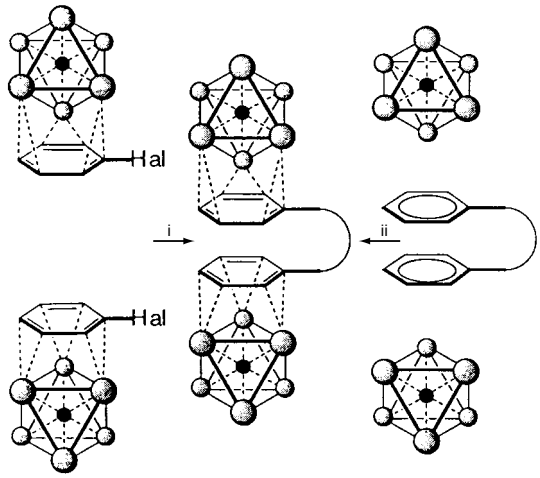

Scheme 1 The two principal routes to arene cluster linkage: i, cluster addition before coupling; ii, coupling before cluster addition

proved to be extremely difficult. In this case, the linkage of two arenes involves the initial preparation of halogenated arene cluster derivatives which are then coupled by the use of a reagent such as sodium metal. Such halogenated arene ligands are known to undergo C–halogen bond cleavage upon heating with transition metal carbonyls,[10] while attempting to halogenate the arene whilst coordinated to the cluster is difficult because transition metal carbonyl clusters are usually insufficiently robust to survive the harsh reaction conditions required. It should be noted, however, that the coupling of chromium tricarbonyl arene complexes has been successfully achieved and therefore the possiblity of linking arene clusters in an analogous manner cannot be entirely excluded. In these chromium compounds, the metal may be considered to remove π electron density from the bonded arene and thereby permit the face-to-face coupling of the fragments with enhanced yield.[11] In principle, these effects should be even greater if arene clusters can be coupled in the same way.

The more attractive approach is to use pre-linked arene ligands. Following a review of the literature, it was decided that the [2_n]cyclophanes would be an ideal class of ligand for our purpose.[12] These are a family of molecules whose structures generally consist of stacked aromatic rings held in close proximity by ethano bridges. They are rigid, well defined, and moderately accessible by relatively simple synthetic procedures. Typically, they possess strained molecular structures due to the strength of the electronic repulsions between the arene rings, and they have unusual electronic properties which stem from an 'end-on' overlap of π electron density giving essentially a single π-electron system. As mentioned earlier, this overlap should provide the additional possibility of electronic communication between bridged cluster units. Cyclophane linkages that may act as one, two or three-dimensional connectors such as [2.2]paracyclophane,[13] [2.2.2]paracyclophane,[14] and tetramesitylene[15] respectively, are currently available (Fig. 2). An example of how one can envisage such ligands being used in the construction of supramolecular networks is illustrated in Fig. 3 for the [2.2.2]paracyclophane

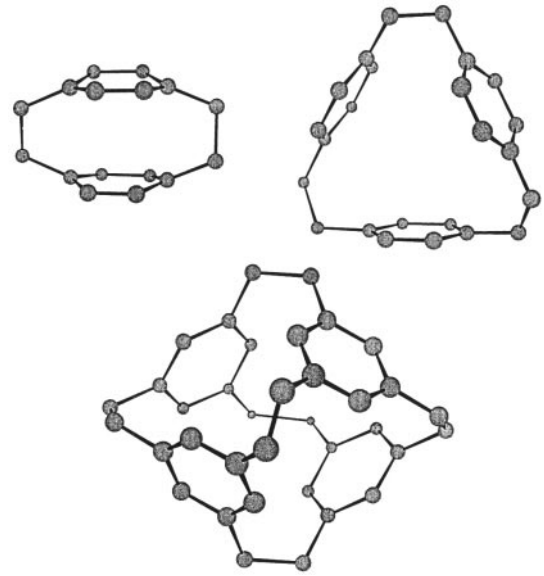

Fig. 2 The molecular structures of [2.2]paracyclophane (top left), [2.2.2]paracyclophane (top right) and tetramesitylene (bottom), respectively

ligand. In this case the triangular ligand can be seen to participate in the formation of hexagonal arrays in analogy to graphite with transition metal clusters forming the edges and cyclophane ligands the nodes.

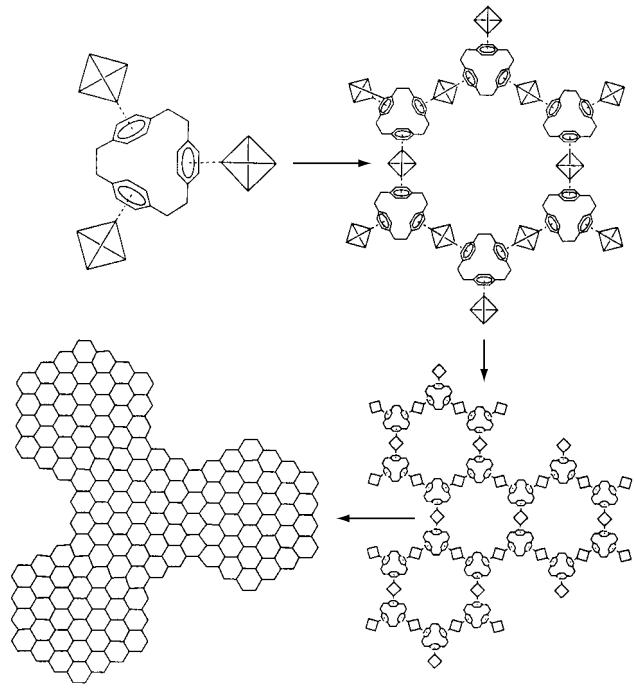

Fig. 3 The construction of a supramolecular hexagonal two-dimensional network using metal centres linked by the [2.2.2]paracyclophane ligand

[2.2]Paracyclophane clusters

Research in this area was initiated using the simplest of the [2_n]cyclophane ligands, [2.2]paracyclophane. The cluster chemistry of [2.2]paracyclophane has recently been reviewed,[16] and therefore only a short account will appear here. [2.2]Paracyclophane carbonyl clusters of ruthenium with nuclearities between two[17] and eight[18] have been structurally characterised and shown to display arene bonding modes ranging from η^6, to μ_2-η^3:η^3 and μ_3-η^2:η^2:η^2.[17–19] There is, however, a marked

tendency for the [2.2]paracyclophane to adopt the facial μ_3 coordination mode, and this is particularly apparent in the hexaruthenium carbido cluster $[Ru_6C(CO)_{14}(arene)]$ where the simpler arenes (benzene, toluene, xylene and mesitylene) tend to adopt the apical η^6 mode.[20] This effect is also apparent from work on the redox coupling reaction of $[Ru_5C(CO)_{14}]^{2-}$ and $[(C_{16}H_{16})Ru(NCMe)_3]^{2+}$ in which the cyclophane ligand, initially bound in an η^6 manner to a single metal atom, migrates during the course of the reaction to produce $[Ru_6C(CO)_{14}(\mu_3\text{-}\eta^2:\eta^2:\eta^2\text{-}C_{16}H_{16})]$ in which the ligand is bound to a triangular metal face.[21]

It is evident, however, that none of the [2.2]paracyclophane compounds observed to date contain separate cluster moieties linked through a cyclophane unit. The reason for this is believed to originate from the through-space resonance effect within the ligand, whereby the electron-withdrawing nature of the cluster attached to one ring deactivates the second uncoordinated ring toward further cluster association. This effect appears to be so large that even single metal fragments such as chromium tricarbonyl will not coordinate to the second ring, and instead, complete displacement of the cluster occurs with the formation of $[Cr(CO)_3(C_{16}H_{16})]$. Therefore, the aims of more recent work have been to achieve cluster linkage using substituted or alternative types of $[2_n]$cyclophane ligand.

Isomerisation and substitution effects

An important aspect of this work is to consider how the nature of the ligand influences the bonding mode adopted upon coordination to a metal cluster. Hence, an investigation into how different bridge substituted [2.2]cyclophanes effect cluster coordination patterns was undertaken. The molecular structures of two isomeric cluster species, $[Ru_6C(CO)_{14}(p\text{-}C_{16}H_{16})]$ **3** and $[Ru_6C(CO)_{14}(m\text{-}C_{16}H_{16})]$ **4**, have been determined by X-ray diffraction and a third, $[Ru_6C(CO)_{14}(o\text{-}C_{16}H_{16})]$ **5**, inferred by spectroscopy (Fig. 4).[20,22] The *para*-substituted ligand is found

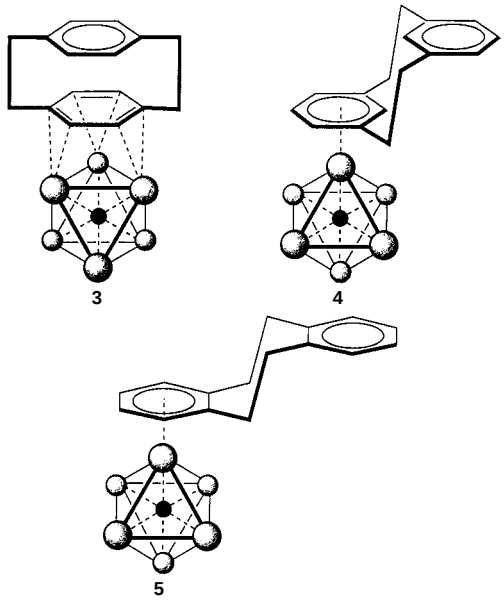

Fig. 4 The structures of three isomeric hexaruthenium [2.2]cyclophane clusters

to adopt a facial μ_3 coordination mode upon the hexaruthenium carbido core, while the *meta*- and *ortho*-isomers prefer to adopt the η^6 bonding mode, interacting with a single metal atom only. There are two possible explanations for this behaviour. Firstly, it may be due to the superior donor capability of [2.2]paracyclophane over [2.2]meta- and [2.2]orthocyclophane, whereby the extensive overlap of π molecular orbitals in the *para*-isomer allows for sufficient supply of electron density for the three metal atoms.[23] There is little, if any, overlap of π molecular orbitals in the *meta*- and *ortho*-isomers and hence, they can be envisaged as only being able to support a single metal atom. This effect has been demonstrated electrochemically for $[Ru_6C(CO)_{14}(C_{16}H_{16})]$, whereby the *para*-isomer is far more difficult to reduce than either the *meta*- or *ortho*-isomers (-0.937, -0.893 and -0.890 V, respectively). Alternatively, the difference in coordination mode may be explained by the inherent distortion of the aromatic rings within the cyclophanes themselves (Fig. 5).[24] In [2.2]paracyclophane, the aromatic

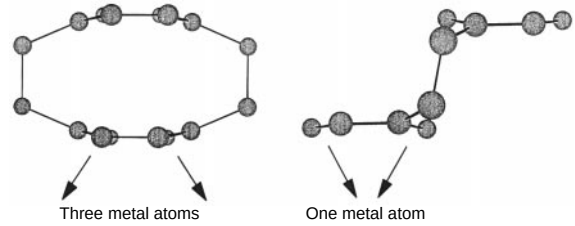

Fig. 5 The molecular structure of (left) [2.2]paracyclophane compared with (right) [2.2]metacyclophane.

rings are convex, bulging outwards from the centre of the molecule due to inter-arene repulsion. Thus, in [2.2]paracyclophane the π orbitals are oriented outwards in such a way that they would be expected to interact more effectively with a trimetallic face than a single metal atom. However, in the *meta*-isomer the aromatic rings are concave, with the π orbitals oriented towards a focal point and thus the ligand is predisposed to interact with only a single metal atom. Furthermore, the distortion of the rings in both [2.2]para- and [2.2]metacyclophanes cause the aromatic C–H bonds to bend out of the plane. In [2.2]paracyclophane this occurs such that the C–H bonds point toward the centre of the molecule and in [2.2]metacyclophane such that they point away. Since the C–H bonds bend away from the underlying metal triangle in, for example $[Os_3(CO)_9(\mu_3\text{-}C_6H_6)]$,[25] it is therefore unsurprising that [2.2]paracyclophane adopts the facial bonding mode on the hexaruthenium cluster. Similarly, since the C–H bonds point toward the metal atom in mononuclear arene complexes it is not surprising either that the [2.2]metacyclophane ligand adopts an apical bonding mode.[26] In [2.2]orthophane the aromatic rings are planar and therefore presumably the preference of this ligand for the apical η^6 mode is not as strong as that of the *meta*-isomer.[27]

Asymmetry

Since [2.2]paracyclophane interacts with metal clusters differently to its monoarene analogue, *para*-xylene,[20] it also seemed important to question whether [2.2]paracyclophane ligands bearing substituents upon their aromatic rings would interact differently from their monomeric analogues; and in cases where this substitution was not symmetrical, it would also be of interest to establish which ring the cluster unit would prefer to coordinate. In this regard, an investigation into the interaction of several ring-substituted [2.2]paracyclophane ligands with ruthenium carbonyl clusters has been carried out; the result of which is illustrated in Fig. 6.[28] It has been shown that the cluster unit always coordinates to the amine substituted ring of the 4-amino[2.2]paracyclophane ligand,[29] whereas it coordinates to the unsubstituted ring of 4-bromo[2.2]paracyclophane.[30] This behaviour may be explained in terms of the relative activating or deactivating effect of the substituents. The amino substituent is thought to push electron density onto the ring, thus making it more activated toward cluster association (as demonstrated by the planar geometry of the nitrogen). In fact, a closer analysis of the metal–ligand interface in $[Ru_6C(CO)_{14}(\mu_3\text{-}\eta^1:\eta^2:\eta^2\text{-}C_{16}H_{15}NH_2)]$ **6** suggests that the metal triangle interacts with only five aromatic carbon atoms (Fig. 7); the sixth (that attached to the nitrogen atom) remaining uncoordinated, possibly because it possesses insufficient electron density. The octahedral cluster retains the required electron count of 86 if the

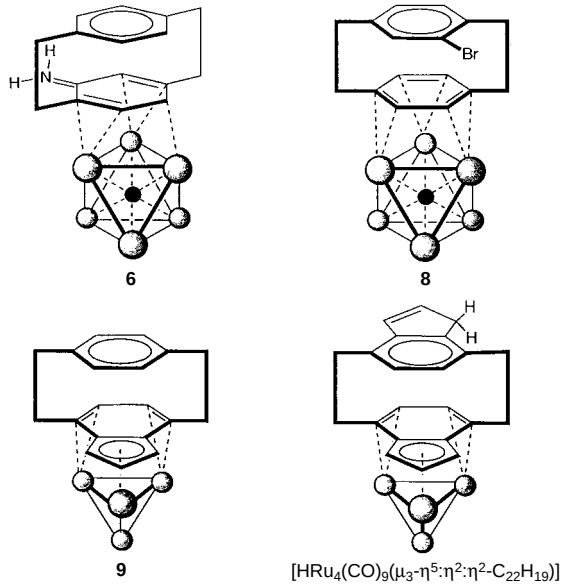

Fig. 6 The structures of some ring-substituted [2.2]paracyclophane ruthenium clusters: the 4-amino[2.2]paracyclophane cluster $[Ru_6C(CO)_{14}(\mu_3\text{-}\eta^1:\eta^2:\eta^2\text{-}C_{16}H_{15}NH_2)]$ **6**; the 4-bromo[2.2]paracyclophane cluster $[Ru_6C(CO)_{14}(\mu_3\text{-}\eta^2:\eta^2:\eta^2\text{-}C_{16}H_{15}Br)]$ **8**; the [2.2]parabenzoindenophane cluster $[HRu_4(CO)_9(\mu_3\text{-}\eta^5:\eta^2:\eta^2\text{-}C_{19}H_{17})]$ **9**; and the *anti*-[2,2]paraindenophane cluster $[HRu_4(CO)_9(\mu_3\text{-}\eta^5:\eta^2:\eta^2\text{-}C_{22}H_{19})]$

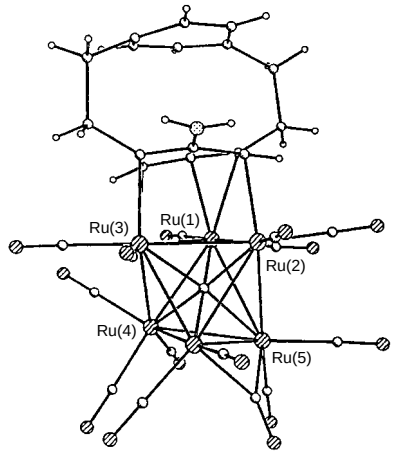

Fig. 7 The molecular structure of $[Ru_6C(CO)_{14}(\mu_3\text{-}\eta^1:\eta^2:\eta^2\text{-}C_{16}H_{15}NH_2)]$ **6**

substituted cyclophane is considered as a six electron donating dienyl ligand. It should be noted that this complex, to our knowledge, is the only example of an aniline ring coordinated to a cluster *via* its aromatic ring; other aromatic amine containing compounds such as 2,5-dimethylaniline yield N–H bond activated species only, *e.g.* as with the compound $[HRu_3(CO)_{10}(C_6H_3Me_2NH)]$ **7** (Fig. 8).[31] Presumably 4-amino-[2.2]paracyclophane cannot form such a compound because of the steric constraints imposed by the second aromatic ring.

In contrast, the bromo substituent in $[Ru_6C(CO)_{14}(\mu_3\text{-}\eta^2:\eta^2:\eta^2\text{-}C_{16}H_{15}Br)]$ **8**, is thought to deactivate the ring toward cluster coordination by pulling electron density away from it, and hence the cluster coordinates to the unsubstituted ring by default. Again this compound is unusual because contrary to the comments made above, the C–Br bond does not undergo oxidative-cleavage. In this example the resistance to C–Br cleavage is probably because the cyclophane unit blocks the path to an aryne or 'cyclophyne' type cluster.[32]

These results suggest that the cluster exerts a significant directing influence upon the substitution chemistry of a coordinated cyclophane ligand. From this, it may be further concluded that the coordinated ring, in for example $[Ru_6C(CO)_{14}(p\text{-}C_{16}H_{16})]$ **3**, should be activated towards nucleophilic attack in aromatic substitution reactions, whereas the uncoordinated ring should be more susceptible to electrophilic attack by default. Hence, in aromatic substitution reactions which employ mild conditions (that is conditions mild enough for the metal clusters to survive such as in the reaction of $[Ru_6C(CO)_{14}(C_6H_6)]$ with phenyllithium[33]), such clusters could be used to prepare unusually substituted [2.2]paracyclophane compounds not easily accessible *via* alternative routes.

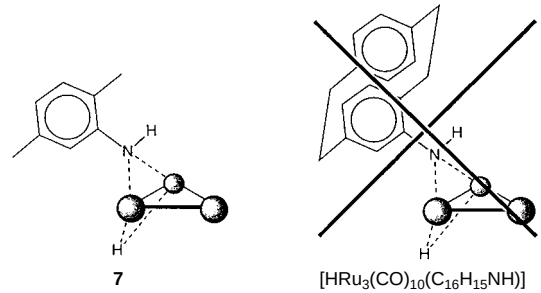

Fig. 8 The structure of the N–H activated cluster $[HRu_3(CO)_{10}(C_6H_3Me_2NH)]$ **7** formed from 2,5-dimethylaniline. 4-Amino-[2.2]paracyclophane does not form an analogous compound, probably due to steric reasons.

Finally, the interaction of the [2.2]parabenzoindenophane[34] and *anti*-[2.2]paraindenophane[35] ligands with transition metal clusters has been investigated in collaboration with Prof. Henning Hopf of Braunschweig, Germany (Fig. 6). Although the former ligand possesses both a benzene and an indene face, it has been found that cluster coordination occurs only *via* the condensed indene face as in, for example, the tetranuclear cluster $[HRu_4(CO)_9(C_{19}H_{17})]$ **9** (Fig. 9). Here the ligand

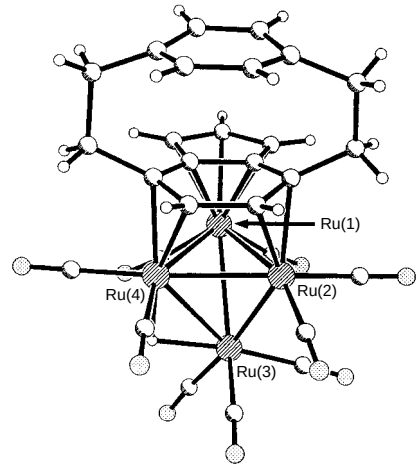

Fig. 9 The molecular structure of $[HRu_4(CO)_9(\mu_3\text{-}\eta^5:\eta^2:\eta^2\text{-}C_{19}H_{17})]$ **9**

undergoes C–H bond activation which converts the cyclopentadiene ring to a cyclopentadienyl system; as such the cluster coordinates to the ring that is richest in π electron density *via* an η^9-(cyclopentadienyl–diene) interaction. Despite this predisposition of the indene face in [2.2]parabenzoindenophane, *anti*-[2.2]paraindenophane has also been shown to bond to only one cluster unit even though it possesses two indene rings suitable for cluster coordination (Fig. 6). This again is probably due to through space deactivation effects. All attempts to add monometallic fragments such as $[Mo(CO)_4]^+$ and $[FeCp]^+$ to the second cyclopentadiene ring, or to link these *anti*-[2.2]indenophane ruthenium carbonyl clusters by reaction with $FeCl_2{\cdot}2thf$ have so far been unsuccessful.[36]

The interaction of [2.2.2]paracyclophane with ruthenium carbonyl clusters

[2.2.2]Paracyclophane does not yield the diverse range of products observed for [2.2]paracyclophane when reacted with

$[Ru_3(CO)_{12}]$ under similar reaction conditions.[16] Instead, the thermolysis of [2.2.2]paracyclophane with 3 molar equiv. of $[Ru_3(CO)_{12}]$ in octane under reflux over a 6 h period affords just three new complexes: $[Ru_6(CO)_{15}(\eta^6\text{-}C_{24}H_{24})]$ **10** (5%), $[Ru_{12}(CO)_{28}(\eta^6\text{-}C_{24}H_{24})_2]$ **11** ($\approx$0.1%) and $[Ru_6C(CO)_{14}(\eta^6\text{-}C_{24}H_{24})]$ **12** (30%) (Scheme 2).[37] These may be readily

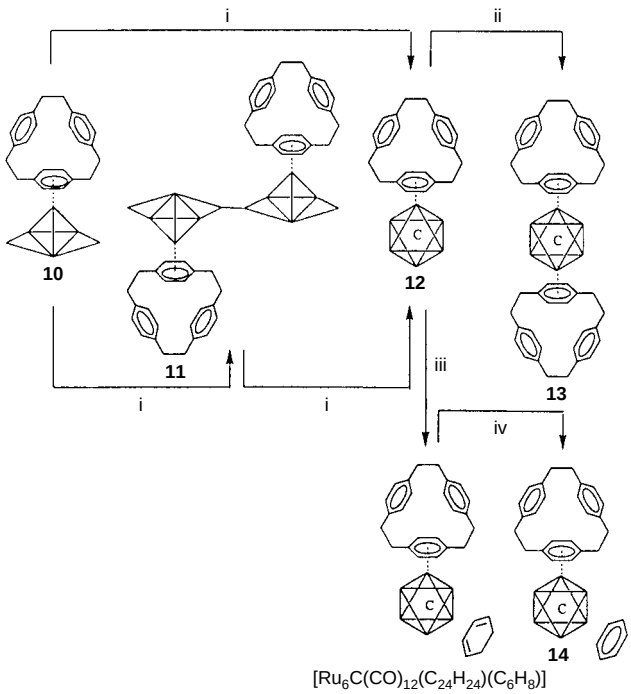

Scheme 2 Routes to some [2.2.2]paracyclophane ruthenium clusters. *Reagents and conditions*: i, $[Ru_3(CO)_{12}]$, heat in octane; ii, $C_{24}H_{24}$, heat in nonane; iii, cyclohexa-1,3-diene with 2.2 equiv. Me_3NO in CH_2Cl_2; and iv, heat in hexane or 1.1 equiv. Me_3NO in CH_2Cl_2.

separated by thin layer chromatography on silica using dichloromethane–hexane (1 : 2, v/v) as eluent. In each of these compounds the central cluster unit is based on a hexanuclear metal framework but of differing geometries. In compound **10**, the metal atoms are arranged as a doubly edge-bridged tetrahedron (an 88 valence electron cluster). By analogy to the mesitylene complex, $[Ru_6(CO)_{15}(\eta^6\text{-}C_6H_3Me_3)]$,[38] the arene ligand in compound **10** is coordinated in an η^6 manner to the apex of the central tetrahedron that is not involved in edge-bridging, and a dihapto (η^2-μ_4) carbonyl ligand is located in each of the butterfly sites. This compound may be converted by heating in octane to the octahedral hexaruthenium carbido cluster, $[Ru_6C(CO)_{14}(\eta^6\text{-}C_{24}H_{24})]$ **12**, in which the arene again coordinates to a single metal atom. An intermediate compound, $[Ru_{12}(CO)_{28}(\eta^6\text{-}C_{24}H_{24})_2]$ **11**, is also isolated in trace amounts during this conversion, and the molecular structure of this compound **11** is shown in Fig. 10. It is formally a dodeca-ruthenium bis-arene cluster, which makes it the largest arene cluster prepared by our group to date. This molecule contains a fused bis-(doubly edge-bridged tetrahedron) metallic framework in which ten of the metal atoms are essentially coplanar—all those except the two that carry the cyclophane ligands. It is easy to envisage the process by which compound **11** may be derived from **10** by the simple removal of a single carbonyl ligand from one of the edge-bridging metal atoms and the dimerisation of the resultant unsaturated species to produce the 174 valence electron cluster. The two hexaruthenium units of this cluster are related by an inversion centre and the linking metal–metal bond is located between two edge-bridging metal atoms. Two of the carbonyl ligands which were terminal at the edge-bridging metal atom in compound **10** migrate to a bridging position, possibly in order to stabilise the new linkage in compound **11**. Despite the change of the local arrangement of

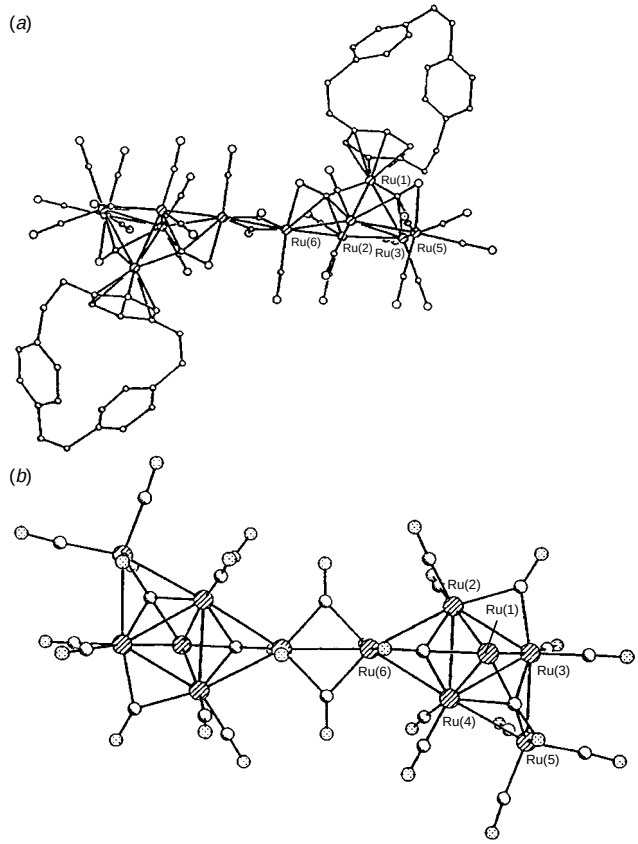

Fig. 10 The molecular structure of $[Ru_{12}(CO)_{28}(\eta^6\text{-}C_{24}H_{24})_2]$ **11**, with (*a*) and without (*b*) the [2.2.2]paracyclophane ligands, respectively

carbonyl ligands at the linkage, the η^2-μ_4-CO ligands are retained in the four butterfly sites of compound **11**.

Since compounds **10** and **11** both possess two edge bridging metal atoms, and compound **10** can dimerise to form compound **11** upon the loss of a carbonyl ligand, it should be possible, at least in principle, for further oligomerisation to occur such that a polymeric material based solely on a metal backbone could be prepared (Scheme 3). However, as yet all attempts to induce further oligomerisation by thermal, chemical or photolytic means have resulted in the now well established closure of the metallic core[39] to form the octahedral hexaruthenium carbido cyclophane cluster $[Ru_6C(CO)_{14}(\eta^6\text{-}C_{24}H_{24})]$ **12**. It should also be noted that the loss of a carbonyl ligand from the cluster, followed by dimerisation of the resulting unsaturated fragments, as observed in the conversion of **10** to **11**, also provides a mechanism to explain the unexpected and generally observed irreversibility of arene cluster reductions during cyclic voltammetry.

An additional arene ligand may also be introduced onto the monocyclophane hexaruthenium carbido cluster **12**. The reaction of compound **12** with an excess of [2.2.2]paracyclophane in refluxing nonane yields the *trans*-bis-arene derivative $[Ru_6C(CO)_{11}(\eta^6\text{-}C_{24}H_{24})_2]$ **13**, while a related mixed arene cluster, $[Ru_6C(CO)_{11}(\eta^6\text{-}C_{24}H_{24})(\mu_3\text{-}\eta^2 : \eta^2\text{-}C_6H_6)]$ **14**, in which the cyclophane ligand adopts an apical mode and the benzene ligand a facial bonding mode (Fig. 11 and Scheme 2), is obtained from the reaction of **12** with cyclohexadiene and trimethylamine *N*-oxide.[40] Compounds **13** and **14** are of particular relevance to our objective of preparing organometallic network precursors since the cluster acts as a bridge between two arene ligands here.

The [2.2.2]paracyclophane ligand has also been shown to undergo reaction with $[Ru_5C(CO)_{15}]$, and the cluster $[Ru_5C(CO)_{12}(\eta^6\text{-}C_{24}H_{24})]$ **15** is the sole product formed during thermolysis in heptane.[37] In this compound, the cyclophane replaces all three carbonyl ligands on one basal metal atom of

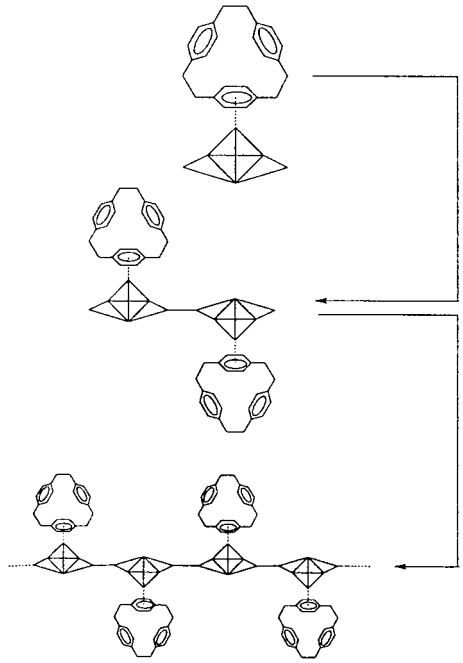

Scheme 3 The dimerisation of $[Ru_6(CO)_{15}(\eta^6\text{-}C_{24}H_{24})]$ **10** to $[Ru_{12}(CO)_{28}(\eta^6\text{-}C_{24}H_{24})_2]$ **11** and the hypothetical metal based polymer $[Ru_6(CO)_{14}(\eta^6\text{-}C_{24}H_{24})]_n$

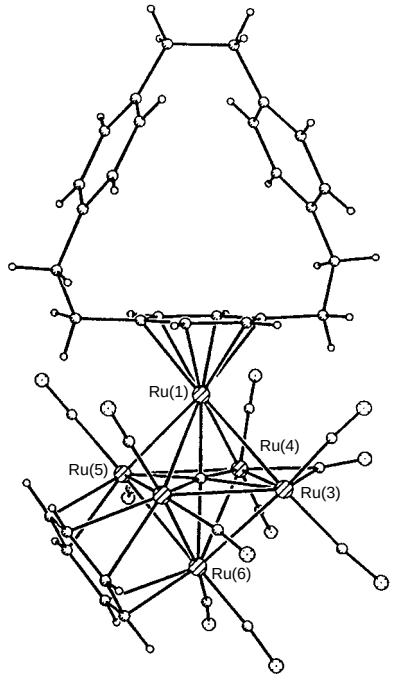

Fig. 11 The molecular structure of $[Ru_6C(CO)_{11}(\eta^6\text{-}C_{24}H_{24})(\mu_3\text{-}\eta^2:\eta^2:\eta^2\text{-}C_6H_6)]$ **14**

the parent square pyramidal cluster. Under an atmosphere of carbon monoxide, compound **15** undergoes the reversible addition of a carbonyl ligand to form the bridged butterfly complex, $[Ru_5C(CO)_{13}(\eta^6\text{-}C_{24}H_{24})]$ **16** (Scheme 4). This is thought to occur by a mechanism similar to that observed for the analogous benzene cluster, *i.e.* by the coordination of a carbonyl ligand at the metal carrying the arene (formally that richest in electron density) with the concomitant breakage of a base–apex metal–metal bond.[41] However, the unrivalled degree of isomerism displayed by the benzene analogue is not displayed by the [2.2.2]paracyclophane complex (benzene can not only adopt the basal-η^6 bonding mode upon the square pyramidal cluster $[Ru_5C(CO)_{12}]$, but also the apical-η^6 and facial μ_3 modes).[42] Instead, continuous exposure to a carbon monoxide atmosphere

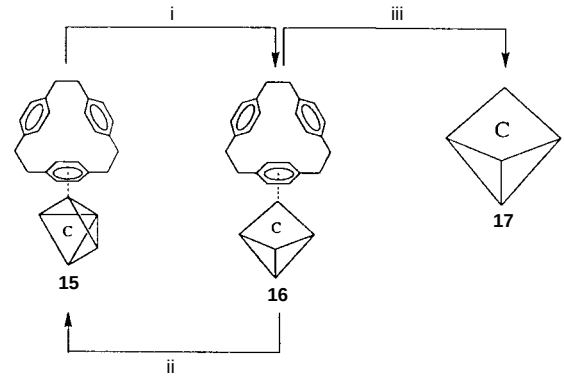

Scheme 4 The reactivity of $[Ru_5C(CO)_{12}(\eta^6\text{-}C_{24}H_{24})]$ **15**. *Reagents and conditions*: i, CO bubble in CH_2Cl_2 over 5 min; ii, N_2 bubble in CH_2Cl_2; iii, 1 atm CO over CH_2Cl_2 for 1 day.

causes compound **16** to release the cyclophane ligand and form the binary cluster, $[Ru_5C(CO)_{16}]$ **17**. Compound **17** possesses the same bridged butterfly metal geometry as the analogous osmium cluster.[43]

A correlation between the chemical shifts of coordinated and uncoordinated aromatic ring protons in ruthenium–[2.2]paracyclophane clusters of differing nuclearities and bonding modes has been discussed in detail elsewhere.[16] This family of ruthenium–[2.2.2]paracyclophane clusters also show marked trends in their ^{1}H NMR spectra as illustrated in Table 1. It

Table 1 ^{1}H NMR characteristics of several ruthenium [2.2.2)paracyclophane clusters

	Compound	M : CO ratio	Mean δ of bound aromatic protons	Mean δ of free aromatic protons
10	$[Ru_6(CO)_{15}(C_{24}H_{24})]$	2.50	5.82	6.82
15	$[Ru_5C(CO)_{12}(C_{24}H_{24})]$	2.40	5.54	6.83
12	$[Ru_6C(CO)_{14}(C_{24}H_{24})]$	2.33	5.25	6.74
14	$[Ru_6C(CO)_{11}(C_{24}H_{24})(C_6H_6)]$	1.83	5.26	6.76
13	$[Ru_6C(CO)_{11}(C_{24}H_{24})_2]$	1.83	5.01	6.69

appears that the magnitude of the chemical shift of both the coordinated and free cyclophane rings is somewhat dependent on both the metal to carbonyl ratio of the cluster and, if present, the coordination mode of the second arene ligand. For example, the mean chemical shift of the aromatic protons on the bound ring of the cyclophane moves to higher field as the metal to carbonyl ratio falls and the electron-withdrawing power of the cluster increases. The difference in the chemical shift of the aromatic protons between $[Ru_6C(CO)_{11}(\eta^6\text{-}C_{24}H_{24})_2]$ **13** and $[Ru_6C(CO)_{11}(\eta^6\text{-}C_{24}H_{24})(\eta_3\text{-}\eta^2:\eta^2:\eta^2\text{-}C_6H_6)]$ **14** may be related to the magnitude of interaction between the cyclophane and the cluster. This is weaker for compound **14** because of the influence of the second arene which being in the facial coordination mode is the more tightly bound of the two arene ligands.

The [2.2.2]paracyclophane ligand has been observed only in the apical η^6 bonding mode in ruthenium carbonyl clusters. This is in contrast to [2.2]paracyclophane which tends to adopt the facial μ_3-mode, and again this may possibly be attributed to the observation that the aromatic rings in [2.2.2]paracyclophane adopt a more planar configuration than those in [2.2]paracyclophane.

The interaction of [2.2.2]paracyclophane and cobalt carbonyl clusters

The reaction of [2.2.2]paracyclophane with an excess of $[Co_4(CO)_{12}]$ in hexane, affords three new cluster complexes:

$[Co_4(CO)_9(\eta\text{-}C_{24}H_{24})]$ **18** (20%), $[\{Co_4(CO)_9\}_2(\eta\text{-}C_{24}H_{24})]$ **19** (2%) and $[\{Co_4(CO)_9\}_3(\eta\text{-}C_{24}H_{24})]$ **20** ($\approx$ 0.1%). These may be readily separated by thin layer chromatography on silica using dichloromethane–hexane (1 : 3, v/v) as eluent (Scheme 5).[44]

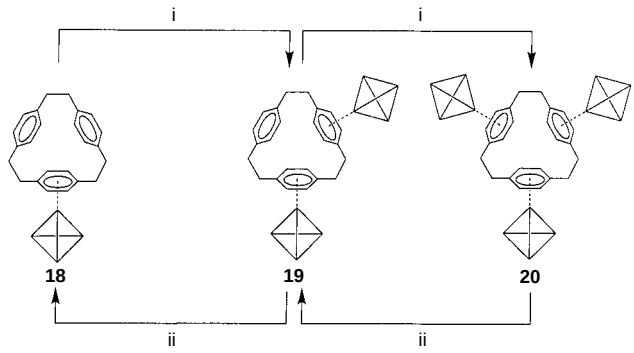

Scheme 5 The interconversion of compounds $[\{Co_4(CO)_9\}_n(\eta\text{-}C_{24}H_{24})]$ (n = 1, 2 and 3). *Conditions*: i, $[Co_4(CO)_{12}]$, heat in hexane; ii, heat in toluene {clusters removed from cyclophane as $[Co_4(CO)_9(toluene)]$}.

Complex **18** may be conveniently converted to **19** and in turn **19** to **20** by the progressive addition of $[Co_4(CO)_{12}]$ in hexane. Conversely, compound **20** ejects a cluster unit to form **19** and then another to form **18** when heated in toluene. This process occurs *via* arene exchange whereby the metal clusters are transferred from the cyclophane ligand to the toluene forming $[Co_4(CO)_9(\eta^6\text{-}C_6H_5Me)]$. The molecular structures of compounds **18** and **19** have been established by single crystal X-ray diffraction and are shown in Fig. 12(*a*) and (*b*), respectively. In

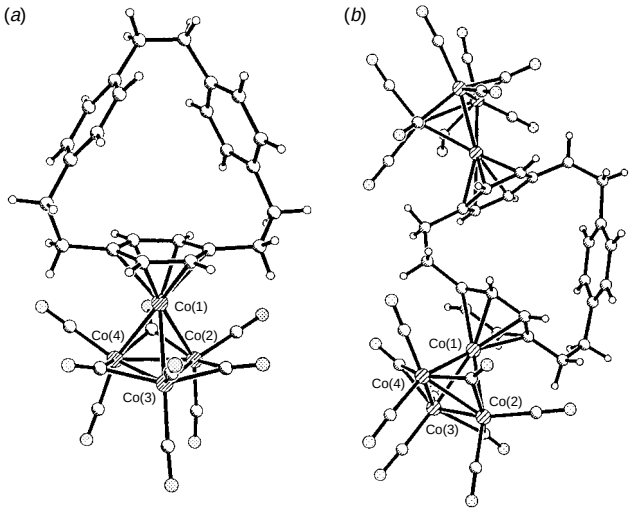

Fig. 12 The crystal structures of (*a*) $[Co_4(CO)_9(\eta\text{-}C_{24}H_{24})]$ **18**; and (*b*) $[\{Co_4(CO)_9\}_2(\eta\text{-}C_{24}H_{24})]$ **19**

both molecules the coordinated rings of the cyclophane ligands are bound to a single metal atom in an η^6-manner and lie parallel to, and staggered with respect to, the more distant underlying metal triangle. Compounds **19** and **20** are the first examples of metal clusters linked by a cyclophane ligand, and are of particular interest as potential precursor sub-units for the construction of one and two-dimensional organometallic networks and polymers discussed above. Furthermore, preliminary electrochemical analyses, although complex, suggest the existence of electronic communication between the metal clusters in compounds **19** and **20**.[44]

The binding of soft metal cations

It has been known for some time that metal atoms and ions may bond to [2.2.2]paracyclophane by *endo*-coordination as well as *exo*-coordination.[45] In *endo*-coordination the metal atom resides in or near the ligand cavity such as in the π cryptates formed with Ga^I and Ag^I salts.[46,47] It has also been possible to demonstrate this effect using the ruthenium [2.2.2]paracyclophane clusters described herein.[37] For example, the addition of either Ga^I or Ag^I salts brings about a considerable change in the IR (carbonyl) spectrum of the parent cluster. This effect may be considered to occur as a consequence of the reduction in the electron density available for carbonyl π back donation which in turn causes a shift of the spectrum to higher wavenumbers. Table 2 illustrates this point for the complexes

Table 2 IR characteristics (carbonyl region) of $[Ru_6C(CO)_{14}(C_{24}H_{24})]$ **12** in the presence and absence of soft metal cations

Compound	Formula	ν_{CO}/cm^{-1} CH_2Cl_2
12	$[Ru_6C(CO)_{14}(C_{24}H_{24})]$	2074, 2023 and 1813
21	$[Ru_6C(CO)_{14}(C_{24}H_{24})Ag][BF_4]$	2084, 2045 and 1878
22	$[Ru_6C(CO)_{14}(C_{24}H_{24})Ga][GaCl_4]$	2089, 2051 and 1894

$[Ru_6C(CO)_{14}(\eta^6\text{-}C_{24}H_{24}Ag)][BF_4]$ **21** and $[Ru_6C(CO)_{14}(\eta^6\text{-}C_{24}H_{24}Ga)][GaCl_4]$ **22**. A comparison of the IR values of these two compounds with those of the parent cluster $[Ru_6C(CO)_{14}(\eta^6\text{-}C_{24}H_{24})]$ **12** indicates a clear shift. The magnitude of this shift may be rationalised in terms of the strength of the cation–cyclophane interaction. This is greater for the gallium(I) ion which is thought to be located at the centre of the cyclophane cavity than for silver which only remains at the edge (Fig. 13).[14,46] This behaviour does not extend to the [2.2.2]paracyclophane complexes of cobalt (and even of chromium tricarbonyl) which undergo extensive decomposition on treatment with either Ga^I or Ag^I salts presumably by some redox reaction.

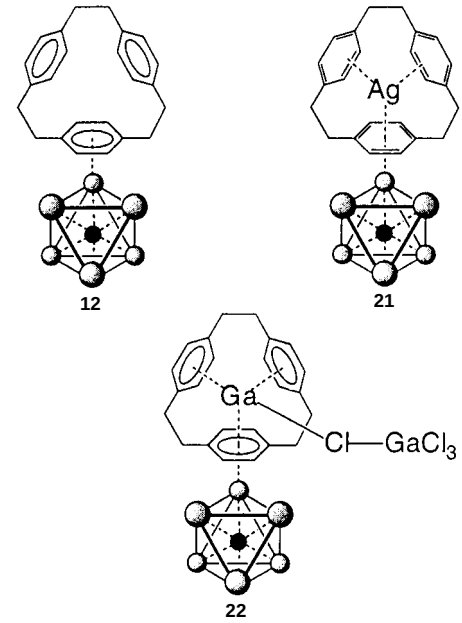

Fig. 13 The binding of Ga^I and Ag^I cations to $[Ru_6C(CO)_{14}(\eta^6\text{-}C_{24}H_{24})]$ **12**

Conclusions

Several novel compounds have been described which will, hopefully, in due course serve as potential building blocks for one- and two-dimensional cluster polymers and networks. These include $[Ru_{12}(CO)_{28}(\eta^6\text{-}C_{24}H_{24})_2]$ **11**, in which there is a metal containing back-bone; $[Ru_6C(CO)_{11}(\eta^6\text{-}C_{24}H_{24})_2]$ **13** and $[Ru_6C(CO)_{11}(\eta^6\text{-}C_{24}H_{24})(\mu_3\text{-}\eta^2 : \eta^2 : \eta^2\text{-}C_6H_6)]$ **14**, in which hexaruthenium clusters link two arene ligands together; and

$[\{Co_4(CO)_9\}_2(\eta\text{-}C_{24}H_{24})]$ **19** and $[\{Co_4(CO)_9\}_3(\eta\text{-}C_{24}H_{24})]$ **20**, in which a [2.2.2]paracyclophane bridges two and three tetracobalt clusters, respectively. It should be noted, however, that as yet we have been unable to sustain chain growth in any of these examples. In the case of compound] **11**, the induction of further oligomerisation instead results in conversion to monomeric closed octahedral hexaruthenium carbido clusters. Although it has been possible to prepare ruthenium carbonyl clusters containing two arene ligands it has, so far, proved difficult to introduce a second ruthenium cluster onto the cyclophane ligand. This is thought to be due to the interaction between the cyclophane molecule and the ruthenium cluster being too strong to permit the addition of further metallic units, and the cyclophane being unable to supply sufficient electron density to satisfy two cluster cores. For cobalt, however, each aromatic ring of the [2.2.2]paracyclophane ligand may be utilised in cluster coordination. So far, the introduction of a second cyclophane ligand onto the tetrahedral Co_4 core has been unsuccessful, which is possibly due to the weakness of the metal–arene interaction (as demonstrated by arene exchange reactions with toluene) which permits multiple complexation of clusters by a single ligand, but is too weak to allow the substitution of further carbonyl ligands by a poorer π-accepting cyclophane ligand.

Acknowledgements

We would like to thank the EPSRC, the University of Cambridge and the Newton Trust (P.S.) for financial support. We would also like to thank Prof. Henning Hopf (Technische Universität Braunschweig), Dr Paul J. Dyson (Imperial College, London) and Dr Simon Parsons (University of Edinburgh) for their involvement in this project.

Prof. Brian F. G. Johnson is Professor of Inorganic Chemistry in the Department of Chemistry, the University of Cambridge, Cambridge CB2 1EW. He obtained his PhD from the University of Nottingham (1963). He then spent postdoctoral positions at M.I.T. and the University of Manchester where he became a lecturer (1965). Lectureships were also held at University College London (1967–1970) and the University of Cambridge (1970–1990). He held the Crum Brown Chair of Inorganic Chemistry at the University of Edinburgh (1990–1995) before returning to Cambridge (1995). He was elected as a Fellow of the Royal Society (1991) and Fellow of the Royal Society of Edinburgh (1992).

Dr Caroline M. Martin is an associate lecturer in the Department of Chemistry, the University of Cambridge, Cambridge CB2 1EW. She obtained her PhD from the University of Edinburgh (1994) and she held a postdoctoral fellowship at University College London for one year before moving to her current post (1995).

Paul Schooler is a final year PhD student under the supervision of Prof. Brian F. G. Johnson in the Department of Chemistry, the University of Cambridge, Cambridge, UK CB2 1EW. He will soon take up a postdoctoral position at Texas A.&M. University (October 1998) under the supervision of Prof. F. Albert Cotton.

References

1 See for example: J. Schulz and F. Vogtle, *Top. Curr. Chem.*, 1994, **172**, 41.
2 D. J. Cram and D. I. Wilkinson, *J. Am. Chem. Soc.*, 1960, **82**, 5721.
3 E. D. Laganis, R. H. Voegeli, R. T. Swann, R. G. Finke, H. Hopf and V. Boekelheide, *Organometallics*, 1982, **1**, 1415.
4 D. Braga, P. J. Dyson, F. Grepioni and B. F. G. Johnson, *Chem. Rev.*, 1994, **94**, 1585.
5 B. F. G. Johnson, P. J. Dyson and C. M. Martin, *J. Chem. Soc., Dalton Trans.*, 1996, 2395.
6 D. Braga and F. Grepioni, *Acc. Chem. Res.*, 1994, **27**, 51.
7 D. Braga, F. Grepioni, P. J. Dyson and B. F. G. Johnson, *J. Cluster Sci.*, 1992, **3**, 297 and references cited therein.
8 S. L. Ingham, B. F. G. Johnson and J. M. G. Nairn, *J. Chem. Soc., Chem. Commun.*, 1995, 189.
9 M. Sheehan and D. J. Cram, *J. Am. Chem. Soc.*, 1969, 3553.
10 A. J. Deeming and D. M. Speel, *Organometallics*, 1997, **16**, 289.
11 P. J. Dyson, A. G. Hulkes and P. Suman, *Chem. Commun.*, 1996, 2223.
12 F. Vögtle, *Cyclophane Chemistry*, Wiley, New York, 1993.
13 C. J. Brown and A. C. Farthing, *Nature*, 1949, **164**, 915.
14 C. Cohen-Addad, P. Baret, P. Chautemps and J. L. Pierre, *Acta Crystallogr., Sect. C*, 1983, **39**, 1346.
15 F. Vögtle, J. Gross, C. Seel and M. Nieger, *Angew. Chem., Int. Ed. Engl.*, 1992, **31**, 1069.
16 P. J. Dyson, B. F. G. Johnson and C. M. Martin, *Trends Organomet. Chem.*, .
17 A. J. Blake, P. J. Dyson, B. F. G. Johnson and C. M. Martin, *J. Chem. Soc., Chem. Commun.*, 1994, 1471.
18 See for example: C. M. Martin, A. J. Blake, P. J. Dyson, S. L. Ingham and B. F. G. Johnson, *J. Chem. Soc., Chem. Commun.*, 1995, 555.
19 D. Braga, F. Grepioni, P. J. Dyson, B. F. G. Johnson and C. M. Martin, *J. Chem. Soc., Dalton Trans.*, 1995, 909.
20 D. Braga, F. Grepioni, E. Parisini, P. J. Dyson, A. J. Blake and B. F. G. Johnson, *J. Chem. Soc., Dalton Trans.*, 1993, 2951.
21 P. J. Dyson, B. F. G. Johnson, C. M. Martin and P. Schooler, unpublished work.
22 B. F. G. Johnson, C. M. Martin, P. Schooler and R. Tregonning, unpublished work, .
23 P. J. Dyson, D. G. Humphrey, J. E. McGrady, D. M. F. Mingos and D. J. Wilson, *J. Chem. Soc., Dalton Trans.*, 1995, 4039.
24 D. J. Cram and J. M. Cram, *Acc. Chem. Res.*, 1971, **4**, 205.
25 M. A. Gallop, M. P. Gomez-Sal, C. E. Housecroft, B. F. G. Johnson, J. Lewis, S. M. Owen, P. R. Raithby and A. H. Wright, *J. Am. Chem. Soc.*, 1992, **114**, 2502.
26 M. Elian, M. M. L. Chen, D. M. P. Mingos and R. Hoffmann, *Inorg. Chem.*, 1976, **15**, 114.
27 P. Domiano, P. Cozzini, R. M. Claramunt, J. L. Lavandera, D. Sanz and J. Elguero, *J. Chem. Soc., Perkin Trans.*, 1992, 1609.
28 H. Hopf, B. F. G. Johnson, C. M. Martin and P. Schooler, unpublished work .
29 D. J. Cram and N. L. Allinger, *J. Am. Chem. Soc.*, 1955, **77**, 6289.
30 D. J. Cram and A. C. Day, *J. Org. Chem.*, 1966, **31**, 1227.
31 E. Sappa and L. Milone, *J. Organomet. Chem.*, 1973, 383.
32 R. D. Adams and X. Qu, *Organometallics*, 1995, **14**, 2238.
33 T. Borchert, J. Lewis, H. Pritzkow, R. H. Raithby and H. Wadepohl, *J. Chem. Soc., Dalton Trans.*, 1995, 1061.
34 S. El-Tamany, F. W. Raulfs and H. Hopf, *Angew. Chem., Int. Ed. Engl.*, 1983, **22**, 633.
35 H. Hopf, F.-W. Raulfs and D. Schomburg, *Tetrahedron*, 1986, **42**, 1655.
36 H. Hopf and J. Dannheim, *Angew. Chem., Int. Ed. Engl.*, 1988, **27**, 701.
37 B. F. G. Johnson, C. M. Martin and P. Schooler, unpublished work.
38 C. E. Anson, P. J. Bailey, G. Conole, B. F. G. Johnson, J. Lewis, M. McPartlin and H. R. Powell, *J. Chem. Soc., Chem. Commun.*, 1989, 442.
39 C. M. Martin, P. J. Dyson, S. L. Ingham, B. F. G. Johnson and A. J. Blake, *J. Chem. Soc., Dalton Trans.*, 1995, 2741.
40 P. J. Dyson, B. F. G. Johnson, J. Lewis, M. Martinelli, D. Braga and F. Grepioni, *J. Am. Chem. Soc.*, 1993, **115**, 9062.
41 D. Braga, F. Grepioni, P. Sabatino, P. J. Dyson, B. F. G. Johnson, J. Lewis, P. J. Bailey, P. R. Raithby and D. Stalke, *J. Chem. Soc., Dalton Trans.*, 1993, 985.
42 P. J. Bailey, D. Braga, P. J. Dyson, F. Grepioni, B. F. G. Johnson, J. Lewis and P. Sabatino, *J. Chem. Soc., Chem. Commun.*, 1992, 177.
43 B. F. G. Johnson, J. Lewis, W. H. J. Nelson, J. N. Nicholls, J. Puga, P. R. Raithby, M. J. Rosales, M. Schröder and M. D. Vargas, *J. Chem. Soc., Dalton Trans.*, 1983, 2447.
44 P. Schooler, B. F. G. Johnson, C. M. Martin, P. J. Dyson and S. Parsons, *Chem. Commun.*, 1998, 791.
45 C. Elschenbroich, J. Schneider, M. Wunsch, J.-L. Pierre, P. Baret and P. Chautemps, *Chem. Ber.*, 1988, **121**, 177.
46 H. Schmidbaur, R. Hager, B. Huber and G. Müller, *Angew. Chem., Int. Ed. Engl.*, 1987, **26**, 338.

8/00147B

Universality of LNA-mediated high-affinity nucleic acid recognition

Sanjay K. Singh and Jesper Wengel*†

Department of Chemistry, University of Copenhagen Centre for Synthetic Bioorganic Chemistry, Universitetsparken 5, DK-2100 Copenhagen, Denmark

LNA (locked nucleic acid) is a novel class of nucleic acid mimic structurally closely resembling RNA; incorporation of three LNA monomers together with six ribonucleotide monomers afforded the first ribo-LNA sequence; unprecedented thermal stabilities of duplexes towards complementary DNA and RNA without compromising base-pairing selectivity were obtained for ribo-LNA, thus establishing the universality of LNA-mediated efficient targeting of natural nucleic acids.

LNA (Fig. 1) has been recently introduced as a novel nucleic acid mimic able to induce unprecedented increases in the thermal stability of duplexes towards both DNA and RNA in different 2′-deoxynucleotide sequence contexts.[1,2]‡ Other appealing characteristics of LNA include efficient automated oligomerization, satisfactory aqueous solubility and stability towards 3′-exonucleolytic degradation.[1,2] Further definitions and details are given in Fig. 1 and Table 1.

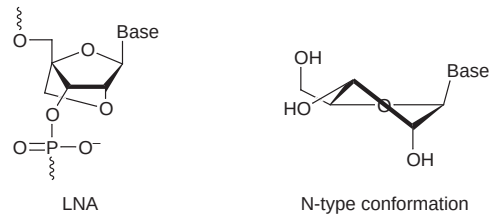

Fig. 1 Structure of the thymine LNA monomer $\mathbf{T^L}$ used in this study. LNA is defined as an oligonucleotide containing one or more LNA monomers. Deoxy-LNA is defined as an LNA consisting of LNA monomers and 2′-deoxynucleotide monomers. Ribo-LNA is defined as an LNA consisting of LNA monomers and ribonucleotide monomers. Also shown is the preferred monomer conformation in A-type duplexes (generally RNA/RNA and DNA/RNA, N-type conformation).

In entries 5–8 (Table 1) the hitherto reported LNA hybridization data (melting temperatures, T_m) for nonamer mixed sequences are summarized[1,2] and compared with the results for the corresponding unmodified reference duplexes. It should be noted that ΔT_m in Table 1 and in the text denotes increases in T_m per LNA monomer incorporated. In this comparative study, the thymine LNA monomer $\mathbf{T^L}$ is used as a representative example, but it is noteworthy that analogous results have been obtained for other pyrimidine and purine LNA monomers.[2] Incorporation of three $\mathbf{T^L}$ monomers together with six deoxynucleotides (to give a nonamer deoxy-LNA) induces remarkable increases in the thermal affinity towards both DNA and RNA (ΔT_m = +5.3 and +7.3 °C, respectively, entries 5 and 6). The fully modified LNA displayed yet higher thermal stabilities (entries 7 and 8). It has been clearly shown that LNA obeys the Watson–Crick base-pairing rules discriminating with excellent selectivity between fully matched and singly mis-matched complementary nucleic acids.[1,2]

Consequently, fully modified LNA as well as deoxy-LNA are able to sequence-selectively recognize complementary DNA/RNA with unprecedented thermal affinities. It is at this point important to note that comparable DNA and RNA recognition has so far only been demonstrated for 2′-fluoro N3′-P5′-phosphoramidates (ΔT_m = +3 to +5 °C).[3] We believe that the explanation offered by these authors, namely a strong pre-organization of the pentofuranose ring of the modified monomers into an N-type conformation[3] (Fig. 1), is viable also for LNA,[1,2] leading eventually to entropically favourable duplex formation.[4]

To explore the universality of LNA-mediated nucleic acid recognition, we decided to examine the properties of the ribo-LNA 5′-r(G$\mathbf{T^L}$GA$\mathbf{T^L}$A$\mathbf{T^L}$GC) (**LNA-1**) consisting of three thymine LNA monomers $\mathbf{T^L}$ and six ribonucleotide monomers. Synthesis of **LNA-1** was efficiently performed by the phosphor-

Table 1 Hybridization data of LNA and reference strands[a]

Entry	Duplex	T_m/°C	ΔT_m/°C
1	5′-d(GTGATATGC)/3′-d(CACTATACG)	28	—
2	5′-d(GTGATATGC)/3′-r(CACUAUACG)	28	—
3	5′-r(GUGAUAUGC)/3′-d(CACTATACG)	27	—
4	5′-r(GUGAUAUGC)/3′-r(CACUAUACG)	38	—
5[1]	5′-d(G$\mathbf{T^L}$GA$\mathbf{T^L}$A$\mathbf{T^L}$GC)/3′-d(CACTATACG)	44	+5.3[b]
6[1]	5′-d(G$\mathbf{T^L}$GA$\mathbf{T^L}$A$\mathbf{T^L}$GC)/3′-r(CACUAUACG)	50	+7.3[c]
7[2]	5′-(**G^{L}T^{L}G^{L}A^{L}T^{L}A^{L}T^{L}G^L ^{Me}C^L**)/3′-d(CACTATACG)	64	+4.0[b]/+4.1[d]
8[2]	5′-(**G^{L}T^{L}G^{L}A^{L}T^{L}A^{L}T^{L}G^L ^{Me}C^L**)/3′-r(CACUAUACG)	74	+5.1[c]/+4.0[c]
9	5′-r(G$\mathbf{T^L}$GA$\mathbf{T^L}$A$\mathbf{T^L}$GC)/3′-d(CACTATACG)	55	+9.3[d]
10	5′-r(G$\mathbf{T^L}$GA$\mathbf{T^L}$A$\mathbf{T^L}$GC)/3′-d(———T———)	38	—
11	5′-r(G$\mathbf{T^L}$GA$\mathbf{T^L}$A$\mathbf{T^L}$GC)/3′-d(———G———)	37	—
12	5′-r(G$\mathbf{T^L}$GA$\mathbf{T^L}$A$\mathbf{T^L}$GC)/3′-d(———C———)	34	—
13	5′-r(G$\mathbf{T^L}$GA$\mathbf{T^L}$A$\mathbf{T^L}$GC)/3′-r(CACUAUACG)	63	+8.3[e]
14	5′-r(G$\mathbf{T^L}$GA$\mathbf{T^L}$A$\mathbf{T^L}$GC)/3′- r(———C———)	45	—

[a] A = adenosine monomer, C = cytidine monomer, G = guanosine monomer, U = uridine monomer, T = thymidine monomer, ^{Me}C = 5-methylcytidine monomer, $\mathbf{X^L}$ = LNA monomer.[1,2] Oligo-2′-deoxynucleotide sequences are depicted as d(sequence) and oligoribonucleotide sequences as r(sequence). 5′-r(G$\mathbf{T^L}$GA$\mathbf{T^L}$A$\mathbf{T^L}$GC) = **LNA-1**. The melting temperatures (T_m values) were obtained as the maxima of the first derivatives of the melting curves (A_{260} *vs.* temperature) recorded as described earlier.[1,2] ΔT_m values are the increases in the thermal stability per LNA monomer incorporated compared to the corresponding reference duplex. [b] Compared to entry 1. [c] Compared to entry 2. [d] Compared to entry 3. [e] Compared to entry 4.

amidite approach[5] using ribonucleoside 3′-phosphoramidites and thymine LNA monomer 3′-phosphoramidite.[1,2]§

The results of thermal melting studies are shown in Table 1 (entries 9–14). Sharp monophasic transitions were obtained in all experiments. It is convincingly demonstrated that **LNA-1** displays hitherto unseen increases in thermal stability (towards DNA: ΔT_m = +9.3 °C, entry 9, compared to entry 3; towards RNA: ΔT_m = +8.3 °C, entry 13, compared to entry 4). From experiments targeting singly mis-matched complements (entries 10–12 and 14) it is revealed that recognition by **LNA-1** is sequence selective. These results indicate that the chimeric ribo-LNA oligomers (or possibly oligomers consisting of LNA monomers and 2′-*O*-alkylribonucleotide monomers[6]) could prove very useful, *e.g.* for optimizing the properties of antisense oligonucleotides.

Because of the known preference for ribonucleotide monomers in A-type duplexes to adopt an N-type conformation,[7] and the established preorganization of LNA monomers into an N-type conformation,[1,2]‡ we had anticipated an additive effect (though levelling off when increasing the number of LNA monomers) on the thermal stability of duplexes involving ribo-LNA. However, comparison of the T_m values obtained for the fully modified LNA (entries 7 and 8) with the T_m values obtained for **LNA-1** reveals an interesting point. Thus, while introduction of only three LNA monomers leads to increased T_m values of +28 °C (towards DNA, entry 9) and +25 °C (towards RNA, entry 13), the corresponding increases in T_m obtained for the fully modified LNA were comparatively lower, namely +37 and +36 °C, respectively. In other words, the effect of introducing six additional LNA monomers in the nonamer amounts to a total increase in T_m of only +9 and +11 °C, respectively. It seems from these results that an LNA monomer profoundly effects the neighbouring ribonucleotide monomers, probably by inducing an overall preorganization, *e.g.* through increased intra-strand base stacking. A similar trend, albeit less pronounced, can be observed from the data shown in entries 5 and 6 for the deoxy-LNA containing three $\mathbf{T^L}$ monomers. By comparing the T_m values of entries 5 and 9 it is revealed that the thermal affinity towards DNA is larger for **LNA-1** than for the corresponding deoxy-LNA. This fact cannot be explained by the shift from an RNA- to a DNA-like oligomer as the corresponding reference T_m values are similar (28 and 27 °C, entries 1 and 2). Instead, the above suggested effect of the LNA monomers on the surrounding ribonucleotide monomers could be an explanation.

Through the results reported herein and the results reported recently,[1,2] the compatibility of LNA monomers with both ribo- and deoxyribo-nucleotide monomers (as well as the effectiveness of fully modified LNA) for high-affinity recognition of both DNA and RNA targets has been established. The structural variants of LNA evaluated demonstrate the universality of LNA-mediated nucleic acid targeting and indicate superior nucleic acid recognition for ribo-LNA. In addition, the pivotal role of the pentofuranose-phosphate backbone in nucleic acid recognition processes has been stressed. Further studies on thermodynamics and the structure of the duplexes have been initiated in order to fully understand the remarkable properties of LNA.

The Danish Natural Science Research Council and Exiqon A/S, Denmark, are thanked for financial support. Ms Britta Dahl, Ms Jette Poulsen and Dr Carl Erik Olsen are thanked for oligonucleotide synthesis and analysis.

Notes and References

† E-mail: wengel@kiku.dk

‡ Synthesis of the uracil and cytosine LNA monomers has been independently published by another group (S. Obika, D. Nanbu, Y. Hari, K. Morio, Y. In, T. Ishida and T. Imanishi, *Tetrahedron Lett.*, 1997, **38**, 8735). Oligomerization of these monomers was not reported.

§ **LNA-1** was synthesized on a 0.2 μmol scale on a polystyrene solid support (Pharmacia) derivatized by a cytidine monomer using a Biosearch 8750 DNA Synthesizer. The stepwise coupling yield of the thymine LNA monomer 3′-phosphoramidite {(1*R*,3*R*,4*R*,7*S*)-7-[2-cyanoethoxy(diisopropylamino)phosphinoxy]-1-(4,4′-dimethoxytrityloxymethyl)-3-(thymin-1-yl)-2,5-dioxabicyclo[2.2.1]heptane} was >99% (20 min couplings) which was equivalent to the coupling yields obtained (6 min couplings) for commercial ribonucleoside 3′-phosphoramidites {2′-*O*-*tert*-butyldimethylsilyl-3′-*O*-[2-cyanoethoxy(diisopropylamino)phosphino]-5′-*O*-(4,4′-dimethoxytrityl)-2-*N*-(*tert*-butylphenoxyacetyl)guanosine (Perseptive Biosystems) and -6-*N*-(phenoxyacetyl)adenine (Biogenex)} as determined spectrophotometrically by the release of the DMT cation after each coupling step. After detritylation, the oligomer was cleaved from the solid support and partly deprotected using 40% aqueous methylamine (10 min, 55 °C). After cooling to −18 °C, the solid support was removed (centrifugation) and washed [2 × 0.25 cm^3; EtOH–MeCN–H_2O (3 : 1 : 1, v/v/v)]. The solvents were evaporated, and the residue was desilylated using a method described earlier.[8] Capillary gel electrophoresis[9] was used to document the purity of **LNA-1** (>90%). The composition of **LNA-1** [5′-r(G$\mathbf{T^L}$GA$\mathbf{T^L}$A$\mathbf{T^L}$GC)] was verified by MALDI-MS:[9] $[M - H]^-$ found 2932.9; calculated 2932.9.

1 S. K. Singh, P. Nielsen, A. A. Koshkin and J. Wengel, *Chem. Commun.*, 1998, 455.
2 A. A. Koshkin, S. K. Singh, P. Nielsen, V. K. Rajwanshi, R. Kumar, M. Meldgaard, C. E. Olsen and J. Wengel, *Tetrahedron*, 1998, **54**, 3607.
3 D. G. Schultz and S. M. Gryaznov, *Nucleic Acids Res.*, 1996, **24**, 2966.
4 E. T. Cool, *Chem. Rev.*, 1997, **97**, 1473.
5 M. H. Caruthers, *Acc. Chem. Res.*, 1991, **24**, 278.
6 L. L. Cummins, S. R. Owens, L. M. Risen, E. A. Lesnik, S. M. Freier, D. McGee, C. J. Guinosso and P. D. Cook, *Nucleic Acids Res.*, 1995, **23**, 2019.
7 P. Herdewijn, *Liebigs Ann.*, 1996, 1337.
8 F. Wincott, A. DiRenzo, C. Schaffer, S. Grimm, D. Tracz, C. Workman, D. Sweedler, C. Gonzalez, S. Scaringe and N. Usman, *Nucleic Acids Res.*, 1995, **23**, 2677.
9 M. Meldgaard, N. K. Nielsen, M. Bremner, O. S. Pedersen, C. E. Olsen and J. Wengel, *J. Chem. Soc., Perkin Trans. 1*, 1997, 1951.

Received in Glasgow, UK, 24th February 1998; 8/01571F

Fate of the C-1′ peroxyl radical in the 2′-deoxyuridine system

Chryssostomos Chatgilialoglu*† and Thanasis Gimisis*‡

I.Co.C.E.A., Consiglio Nazionale delle Ricerche, Via P. Gobetti 101, 1-40129 Bologna, Italy

The mechanism of 2-deoxyribonolactone formation from the reaction of photogenerated 2′-deoxyuridin-1′-yl radical with molecular oxygen in water has been investigated.

A number of agents are able to react with DNA to generate macromolecular radical species.[1] These processes are of considerable importance since they can lead to base modification or strand scissions. As research progresses in the area of the mechanism of attack of oxidative DNA cleavers, it becomes evident that hydrogen abstraction from the C-1′ position is involved in many cases.[2,3] Evidence for the existence of these radical species is mainly based on product studies,[4,5] although spectroscopic and theoretical studies have been reported.[6,7] Furthermore, based on the β-(acyloxy)alkyl radical rearrangement of a C-2′ radical, we have suggested that C-1′ radicals are stabilized substantially by the presence of the base and that the degree of stabilization is similar for purine and pyrimidine moieties.[8] Under aerobic conditions, however, C-1′ radicals **1** afford 2-deoxyribonolactone **2** [eqn. (1)] through a number of

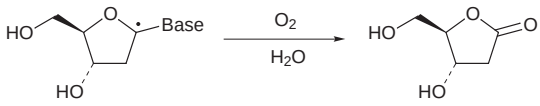

1 **2** (1)

currently disputed pathways.[1,2,5] We report herein an *ex novo* synthesis of *tert*-butyl ketone **6**[9] and the mechanism of the formation of **2** [eqn. (1)].

The recently reported synthesis of **6** has two major drawbacks:[9] (i) a known psiconucleoside triol, prepared by a low yielding, laborious procedure, is used as the precursor,[10] and (ii) a total lack of regioselectivity in the protection step of this triol is observed. For these reasons, we used as our precursor compound **3**, readily available in diastereomerically pure form from the corresponding protected 1′,2′-didehydro-2′-deoxyuridine by a literature procedure.[11] When **3** was treated with $(TMS)_3SiH$[12] under normal free radical conditions, the crystalline cyanide **4** was obtained in excellent yield (94%) (Scheme 1).[13] Short treatment of **4** with excess of Bu^tLi yielded, after silica gel purification, the protected *tert*-butyl ketone **5** as the major product (37% yield, 45% based on recovered starting material).§ Finally, deprotection (NH_4F, MeOH, 60 °C, 24 h, 90%) produced the water soluble adduct **6**.

A quartz tube containing ketone **6** (23 mg; 0.073 mmol) in H_2O (200 μl) was photolyzed with a 500 W high pressure mercury lamp at room temperature. During the photolysis, continuous bubbling of air through the sample ensured the presence of O_2 in the reaction mixture. After 6 h of photolysis, ^1H NMR analysis (CD_3CN) of the lyophilized sample indicated a product ratio of 1 : 0.15 : 0.15 for **6** : **2** : uracil.[14] The products were derivatized with Bu^tMe_2SiCl/imidazole/DMF and isolated by flash chromatography (hexane–ethyl acetate 9:1) to give **7**[14]

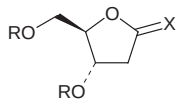

7 R = TBDMS, X = ^{16}O
8 R = TBDMS, X = ^{18}O

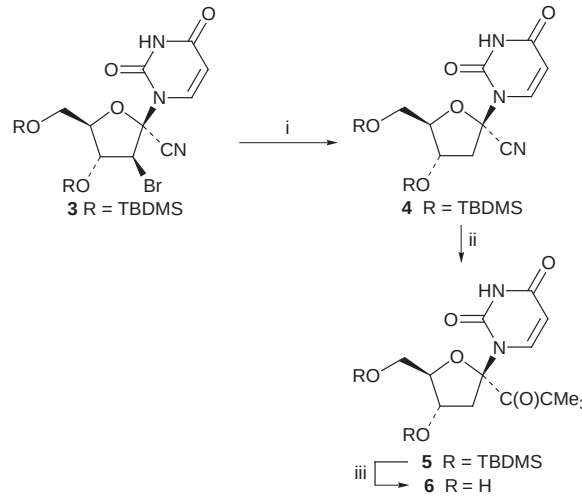

Scheme 1 *Reagents and conditions:* i, $(TMS)_3SiH$, AIBN, toluene, 80 °C, 2 h, 94%; ii, 3 equiv. Bu^tLi, THF, −78 °C, 5 min, 37%; iii, NH_4F, MeOH, 60 °C, 24 h, 90%

and **5** in 15 and 85% yield, respectively. GC–MS analysis of compound **7** showed an isotopic cluster of $[M - 57]^+$ as reported in Fig. 1(*a*). A control experiment showed that photolysis of the sample under anaerobic conditions gave neither compound **2** nor uracil among the products.

The oxygen source of the carbonyl in the lactone **2** was determined by photolysis of **6** in the presence of ^{16}O–^{16}O and

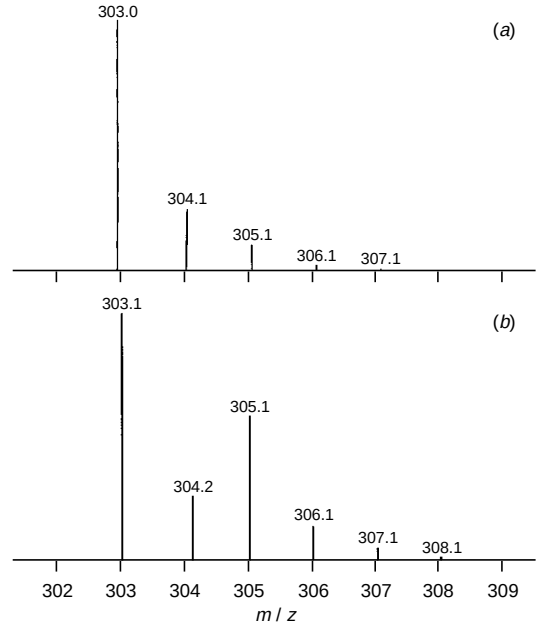

Fig. 1 Isotopic clusters of $[M - 57]^+$ from the electron impact mass spectra of protected 2-deoxyribonolactone obtained by GC–MS analysis. (*a*) Sample isolated from the reaction in $H_2{}^{16}O$ (of natural isotopic distribution). (*b*) Sample isolated from the reaction in $H_2{}^{18}O$ (95 atom% ^{18}O).

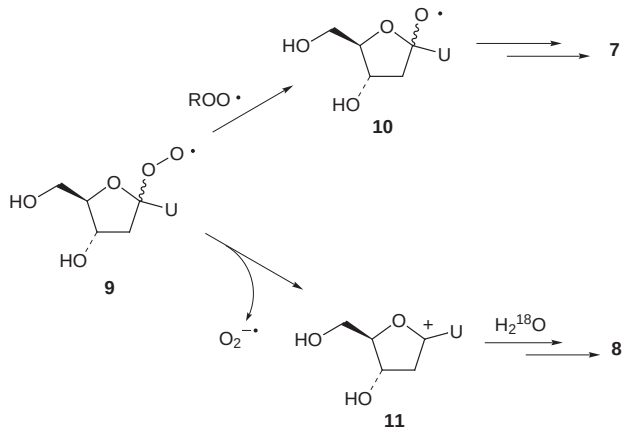

Scheme 2 Proposed mechanism for the formation of 2-deoxyribonolactone

$H_2{}^{18}O$. For this reason, the above experiment was performed in $H_2{}^{18}O$ (95 atom% ^{18}O) as solvent. After work-up, the protected 2-deoxyribonolactone was analyzed by GC–MS. Inspection of the mass spectrum of the isotopic cluster of $[M - 57]^+$, shown in Fig. 1(*b*), indicates the presence of coeluting isotopomers **7** and **8**. Analysis of this isotopic cluster revealed that the product of interest contains 65 and 35% oxygen-16 and oxygen-18, respectively. A control experiment showed that the product lactone **2** does not exchange oxygen with the solvent under the conditions employed.

The mechanism we envisage for the formation of the ^{18}O-labelled 2-deoxyribonolactone is outlined in Scheme 2. Reaction of C-1′ radical **1** with O_2 gives the peroxyl radical **9.** Laser flash photolysis studies showed that rate constant for oxygen trapping of the C-1′ radical is about 1×10^9 M^{-1} s^{-1}.[7] The peroxyl radical **9** decays either *via* a bimolecular reaction with another peroxyl radical to generate the alkoxyl radical **10** or *via* a unimolecular path (heterolytic cleavage) to generate the carbocation **11** and superoxide radical anion.[15a] The heterolytic cleavage of peroxides or alternatively the reaction of electron-rich carbon-centered radicals to give superoxide and carbocations is not without precedent.[15] The cationic intermediate **11** was trapped by $H_2{}^{18}O$, thus demonstrating the partition between the two channels.

An important consequence of the mechanism in Scheme 2 is that the C-1′ peroxyl radical generated on DNA, in the absence of good hydrogen donors, should mainly undergo heterolytic cleavage since the probability that two macromolecular peroxyl radicals meet is low. This finding accentuates the different chemical reactivity exhibited by the C-1′ radical species when compared with the one observed in the more studied C-5′ and C-4′ positions,[1] a reactivity which is mainly due to the presence of the two α-heteroatoms present in the anomeric position. Further work on the reactions of compounds **3** and **4** with a variety of electrophiles and on the kinetics of radical reactions associated with the C-1′ position is in progress.

We are grateful to the European Commission for a ‘Marie Curie’ post-doctoral fellowship to T. G., to NATO for a Collaborative Research Grant, and to Drs C. Ferreri and M. Lucarini for helpful discussions.

Notes and References

† E-mail: chrys@area.bo.cnr.it
‡ E-mail: gimisis@area.bo.cnr.it

§ *Selected data* for **5**: white solid, mp (pentane) 179–181 °C. δ_H(200 MHz; C_6D_6) −0.06, −0.04 (3 H each, s, SiMe), −0.01 (6 H, s, 2 × SiMe), 0.86, 0.91 (9 H each, s, SiBu^t), 1.27 (9 H, s, Bu^t), 2.26 (1 H, dd, *J* 13.8, 7.4, 2′α-H), 3.46 (1 H, dd, *J* 12.3, 2.4, 5′α-H), 3.62 (2 H, m, 4′, 5′β-H), 3.75 (1 H, dd, *J* 13.8, 8.8, 2′β-H), 4.41 (1 H, ddd, *J* 8.8, 7.4, 3′-H), 5.73 (1 H, d, *J* 8.2, 5-H), 8.15 (1 H, d, *J* 8.2, 6-H), 9.29 (1 H, bs, NH); δ_C(50 MHz; C_6D_6) −5.63, −5.57, −5.02, −4.42 (each CH_3), 18.0, 18.4 (each C), 25.78, 25.79, 29.0 (each 3 × CH_3), 42.5 (CH_2), 43.5 (C), 60.2 (CH_2), 68.5, 87.0 (each CH), 97.5 (C), 102.0, 139.0 (each CH), 150.5, 163.2, 201.2 (each C).

1 *DNA and RNA Cleavers and Chemotherapy of Cancer and Viral Diseases*, ed. B. Meunier, Kluwer, Dordrecht, 1996; for a review, see G. Pratviel, J. Bernadou and B. Meunier, *Angew. Chem., Int. Ed. Engl.*, 1995, **34**, 746.
2 For a recent review, see C. Chatgilialoglu and T. Gimisis, in *Free Radicals in Biology and Environment*, ed. F. Minisci, Kluwer, Dordrecht, 1997, pp. 281–292.
3 For some recent work, see X. Zeng, Z. Xi, L. S. Kappen, W. Tan and I. H. Goldberg, *Biochemistry*, 1995, **34**, 12 435; Y.-J. Xu, Z. Xi, Y.- S. Zhen and I. H. Goldberg, *Biochemistry*, 1995, **34**, 12 451; M. Pitié, J. Bernadou and B. Meunier, *J. Am. Chem. Soc.*, 1995, **117**, 2935; H. Sugiyama, K. Fujimoto and I. Saito, *J. Am. Chem. Soc.*, 1995, **117**, 2945; H. Sugiyama, K. Fujimoto, I. Saito, E. Kawashima, T. Sekine and Y. Ishido, *Tetrahedron Lett.*, 1996, **37**, 1805; G. P. Cook and M. M. Greenberg, *J. Am. Chem. Soc.*, 1996, **118**, 10 025; T. Melvin, S. W. Botchway, A. W. Parker and P. O'Neil, *J. Am. Chem. Soc.*, 1996, **118**, 10 031; M. M. Meijler, O. Zelenko and A. S. Sigman, *J. Am. Chem. Soc.*, 1997, **119**, 1135; H. Sugiyama, K. Fujimoto and I. Saito, *Tetrahedron Lett.*, 1997, **38**, 8057; O. Zelenko, J. Gallagher and A. S. Sigman, *Angew. Chem., Int. Ed. Engl*., 1997, **36**, 2776.
4 T. Gimisis and C. Chatgilialoglu, *J. Org. Chem.*, 1996, **61**, 1908; T. Gimisis, C. Castellari and C. Chatgilialoglu, *Chem. Commun*., 1997, 2089.
5 I. H. Goldberg, *Acc. Chem. Res.*, 1991, **24**, 191; B. K. Goodman and M. M. Greenberg, *J. Org. Chem.*, 1996, **61**, 2.
6 E. G. Hole, W. H. Nelson, E. Sagstuen and D. M. Close, *Radiat. Res.*, 1992, **129**, 119; D. M. Close, W. H. Nelson, E. Sagstuen and E. O. Hole, *Radiat. Res.*, 1994, **137**, 300; K. Miaskiewicz and R. Osman, *J. Am. Chem. Soc.*, 1994, **116**, 232; A.-O. Colson and M. D. Sevilla, *J. Phys. Chem.*, 1995, **99**, 3867.
7 C. Chatgilialoglu, T. Gimisis, M. Guerra, C. Ferreri, C. J. Emanuel, J. H. Horner, M. Newcomb, M. Lucarini and G. F. Pedulli, *Tetrahedron Lett.*, in the press.
8 T. Gimisis, G. Ialongo, M. Zamboni and C. Chatgilialoglu, *Tetrahedron Lett.*, 1995, **36**, 6781; T. Gimisis, G. Ialongo and C. Chatgilialoglu, *Tetrahedron*, 1998, **54**, 573.
9 M. M. Greenberg, D. J. Yoo and B. K. Goodman, *Nucleosides Nucleotides*, 1997, **16**, 33.
10 A. Holy, *Nucleic Acids Res.*, 1974, **1**, 289.
11 K. Haraguchi, Y. Itoh, H. Tanaka, K. Yamaguchi and T. Miyasaka, *Tetrahedron Lett.*, 1993, **34**, 6913; Y. Itoh, K. Haraguchi, H. Tanaka, E. Gen and T. Miyasaka, *J. Org. Chem.*, 1995, **60**, 656.
12 C. Chatgilialoglu, *Acc. Chem. Res*., 1992, **25**, 118; C. Chatgilialoglu, *Chem Rev*., 1995, **95**, 1229.
13 The reduction using Bu_3SnH was reported to give 77% yield, see Y. Yoshimura, F. Kano, S. Miyazaki, N. Ashida, S. Sakata, K. Haraguchi, Y. Itoh, H. Tanaka and T. Miyasaka, *Nucleosides Nucleotides*, 1996, **15**, 305.
14 For compounds **2** and **7**, see F. J. Lopez-Herrera, M. Valpuesta-Fernandez and S. Garcia-Claros, *Tetrahedron*, 1990, **46**, 7165; A. P. Kozikowski and A. K. Ghosh, *J. Org. Chem.*, 1984, **49**, 2762.
15 (*a*) C. von Sonntag and H.-P. Schuchmann, *Angew. Chem., Int. Ed. Engl.*, 1991, **30**, 1229; (*b*) K. U. Ingold, T. Paul, M. J. Young and L. Doiron, *J. Am. Chem. Soc.*, 1997, **119**, 12 364.

Received in Glasgow, UK, 25th March 1998; 8/02375A

Coupling of fluoroform with aldehydes using an electrogenerated base

Rachid Barhdadi, Michel Troupel*† and Jacques Périchon

Laboratoire d'Electrochimie, Catalyse et Synthèse Organique, (UMR7582) CNRS-Université Paris 12 Val-de-Marne. 2, rue H. Dunant, 94 320 Thiais, France

Trifluoromethylated alcohols are easily obtained in a one pot electroreaction in which cathodic reduction of iodobenzene generates a strong base which deprotonates fluoroform, inducing its coupling with aldehydes.

Fluorinated molecules and particularly trifluoromethylated compounds are widely used in the pharmaceutical or agrochemical fields, and much effort has been devoted to establishing improved methods for the introduction into organic substrates of fluoro or trifluoromethyl groups.

The most common reactants used to achieve trifluromethylation reactions[1] are organometallic compounds, *e.g.* CF_3Cu[2] and CF_3ZnX[3] (X = CF_3, Br, I *etc.*) or the Ruppert reactant CF_3SiMe_3.[4] These compounds are themselves generally prepared from CF_3I or CF_3Br. The electroreduction of CF_3Br is also a convenient method to obtain trifluoromethylated derivatives.[5]

Fluoroform CF_3H is a side product of fluoroorganic chemistry which is not utilised in organic synthesis. Compared to halofluorocarbons, this gas has low toxicity and is not an ozone depleting agent, although it is a powerful greenhouse gas and thus not a useful refrigerant. The use of CF_3H in organic chemistry is a real challenge which could turn an environmental liability into a commercial opportunity. One hindrance is the low reactivity of CF_3H, which is a very weak acid; its pK_a has been estimated to be in the range of 25–28.[6]

Concerning CF_3H as a source of trifluoromethyl anion, the only chemical method reported used strong bases such as Bu^tOK[7] or $MeSOCH_2K$.[8] An electrochemical procedure, which involves an electrogenerated base obtained by electroreduction of pyrrolidone, has also been described.[7] These reactions allow the synthesis of trifluoromethylated alcohols from aldehydes or ketones *via* a low temperature (−50 °C) two step procedure. The solvent DMF seems to play an important role, trapping the CF_3^- anion and giving a tetrahedral intermediate which is the actual trifluoromethylating agent.[8]

We have previously shown that the reduction of aromatic halides such as PhI or PhBr at a cathode covered with an electrolytic deposit of cadmium generates a strong base able to deprotonate weakly acidic molecules, inducing a coupling reaction with electrophilic compounds.[9] The present work is devoted to the extension of this technique to the case of fluoroform, which can then be coupled with aromatic aldehydes under very simple and mild conditions.

The experiments were conducted as a one-step procedure. To DMF was added Bu_4NBF_4 (4×10^{-2} mol l^{-1}) as a supporting electrolyte, an aromatic aldehyde ArCHO (0.5 mol l^{-1}) as the electrophile and iodobenzene (0.5–1.5 mol l^{-1}) as the probase. The solution, maintained at 5–10 °C, was supplied in CF_3H *via* slow bubbling at normal pressure.

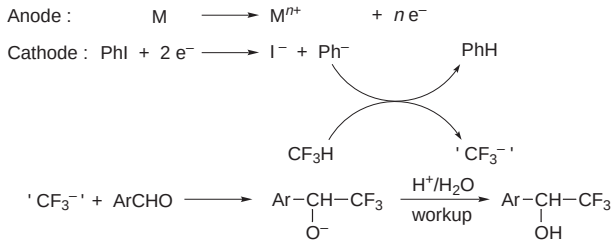

Scheme 1

The undivided electrochemical cell has been described elsewhere.[10] The electrolyses were carried out at constant current (1 A dm^{-2}) using a sacrificial magnesium or aluminium anode and a nickel grid cathode freshly coated with a small deposit of cadmium obtained by electroreduction of $CdBr_2$.[9]

We observed that the reaction required an excess of probase and electricity to achieve full conversion of ArCHO. For example, when the electrolysis was conducted in solutions containing PhCHO and PhI (1 : 1), there was 30–40% residual benzaldehyde after the iodobenzene had been consumed. This is probably due to side reactions involving Ph^- and/or CF_3^-, which were not identified. Consequently, all syntheses were performed in the presence of excess iodobenzene (2–3 equiv.) allowing complete transformation of the aromatic aldehyde. Trifluoromethylated alcohols were obtained upon standard workup (solvent evaporation and acidic hydrolysis) and re-

Table 1 Electrogenerated base mediated coupling of fluoroform with aldehydes

Aldehyde	Product	Yield (%)
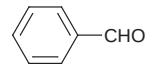	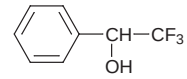	71
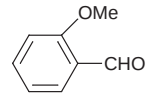	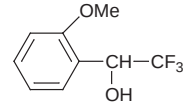	12
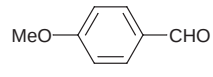	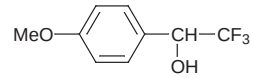	73
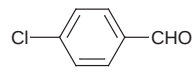	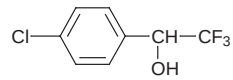	51
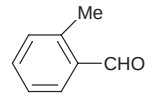	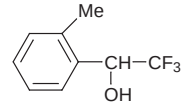	53
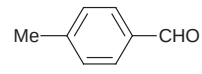	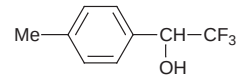	76
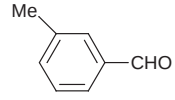	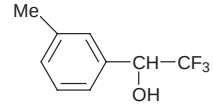	66
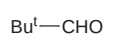	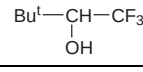	46

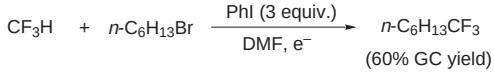

Scheme 2

covered in a pure form by suitable extraction and chromatography on silica gel, and characterised by mass, ^{1}H NMR and ^{19}F NMR analysis.

The reaction pathway corresponds to that shown in Scheme 1. Our results, presented in Table 1, show that various aromatic aldehydes yield the corresponding trifluoromethylated alcohols in moderate to good yields. A limitation of this one-pot reaction is that the aldehyde cannot be more easily reduced than the probase PhI. Indeed, when starting from easily reducible compounds, *e.g.* *o*-, *m*- or *p*-(α,α,α-trifluoromethyl)-benzaldehyde, the sole product recovered is the corresponding pinacol. This would also explain the low yield obtained from 2-methoxybenzaldehyde (see Table 1), for which a large amount of pinacol was detected. For aliphatic aldehydes, we achieved success only with pivalaldehyde, as enolizable compounds mainly gave aldolisation products.

Our method is also suitable for the trifluoromethylation of alkyl halides. (Scheme 2). Finally, we have also proved that

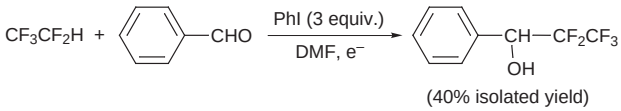

Scheme 3

fluorocarbons other than fluoroform can be used. One example is the coupling of pentafluoroethane with benzaldehyde (Scheme 3).

Notes and References

† E-mail: barhdadi@glut-cnrs.fr

1 D. J. Burton and Z. Y. Yan, *Tetrahedron*, 1992, 48, 189; M. A. McClinton and D. A. McClinton, *Tetrahedron*, 1992, **48**, 6555.
2 Y. Kobayashi, K. Yamamoto and I. Kumadai, *Tetrahedron Lett*., 1979, **42**, 4071; Y. Kobayashi, K. Yamamoto, T. Asai, M. Nakano and I. Kumadai, *J. Chem. Soc., Perkin Trans. 1*, 1980, 2755; Y. Kobayashi and I. Kumadai, *J. Chem. Soc., Perkin Trans. 1*, 1980, 661; J. M. Paratian, S. Sibille and J. Périchon, *J. Chem. Soc. Chem. Commun*., 1992, 53.
3 W. Tyrra and D. Nauman, *J. Prakt. Chem*., 1996, **338**, 283.
4 P. Ramaiah, R. Krishnamurti and G. K. S. Prakash, *Org. Synth.*, 1995, 232.
5 J. M. Paratian, E. Labbe, S. Sibille, J. Y. Nédélec and J. Périchon, *Denki Kagaku*, 1994, **62**, 1129.
6 K. J. Klabunde and D. J. Burton, *J. Am. Chem. Soc*., 1972, **94**, 5985.
7 T. Shono, M. Ishifune, T. Okada and S. Kashimura, *J. Org. Chem.*, 1991, **56**, 2.
8 B. Folléas I. Marek, J. F. Normant and L. S. Jalmes, *Tetrahedron Lett.*, 1998, **39**, 2973.
9 R. Barhdadi, J. Gal, M. Heintz and M. Troupel, *J. Chem. Soc., Chem. Commun.*, 1992, 50; R. Barhdadi, B. Simsen, M. Troupel and J. Y. Nédélec, *Tetrahedron*, 1997, **53**, 1721.
10 J. Chaussard, J. C. Folest, J. Y. Nédélec, S. Sibille, J. Périchon and M. Troupel, *Synthesis*, 1990, 2, 369.

Received in Liverpool, UK, 18th February 1998; 8/01406J

Nickel indenyl complexes as precatalysts for dehydropolymerization of phenylsilane

Frédéric-Georges Fontaine, Talin Kadkhodazadeh and Davit Zargarian*

Département de Chimie, Université de Montréal, Montréal, Québec, Canada H3C 3J7

The complex (1-MeInd)Ni(PPh_3)Cl reacts with $AgBF_4$, $AlCl_3$, methylaluminoxane, or $LiAlH_4$ to produce intermediates which catalyze the dehydropolymerization of $PhSiH_3$.

Polysilanes have attracted a great deal of interest in recent years primarily because of their potential applications in optoelectric devices and as precursors to silicon carbide ceramics.[1] The initial discovery of transition metal-catalyzed dehydropolymerization of silanes[2] and the subsequent development of a class of efficient catalysts for this reaction[3] have shown that this approach holds great promise as a viable method for preparing high molecular mass polysilanes. Some of the best systems reported to date are derivatives of group 4 metallocenes which polymerize primary aromatic silanes to yield linear polysilanes with M_n on the order of 7000 (about 100 monomers), in addition to cyclic oligomers.[4] Most late metal complexes, on the other hand, redistribute silanes or couple them to give oligomers only (dimers, trimers, *etc.*);[5] notable exceptions are some complexes of platinum metals which polymerize aliphatic silanes[6] and cyclic silanes such as silicon-bridged ferrocenophanes[7] and silafluorene.[6] In the course of our studies on the complexes (Ind)Ni(PPh_3)X (Ind = indenyl, 1-methylindenyl; X = Cl, Br, Me)[8] and [(Ind)Ni(PPh_3)L′]$^+$ (L′ = PPh_3, PMe_3, MeCN)[9] we have found the first example of a late metal compound capable of catalysing the polymerization of $PhSiH_3$ to linear chains containing about 30–80 monomeric units, as described below.

Although $PhSiH_3$ does not react with (1-MeInd)Ni(PPh_3)Cl, **1**, addition of $AgBF_4$ to their mixture caused an immediate colour change (wine-red to black) and a vigorous evolution of gas (presumably H_2). The work-up‡ of the reaction mixture after 24 h gave an oily white solid which showed a ^{1}H NMR spectrum typical§ of poly(phenylsilylene); GPC¶ analysis showed that this material contained $(PhHSi)_n$ with M_w = 2017 and M_n = 1469 (Table 1, run 1). Using $AlCl_3$ as initiator gave shorter oligomers‖ (run 2) while methylaluminoxane (MAO) gave comparable results to $AgBF_4$ (run 3). The higher solubility of MAO allows the reactions to be carried out at lower temperatures or in toluene, both of which give improved results (runs 4 and 5).

The formation of Si–Si bonds is rapid at the outset of the reaction but slows down considerably after about 30 min, such that the build-up of higher chains (M_n *ca.* 2000–3000) takes several hours. Extending the reaction time to 7 days results in significantly higher molecular mass polyphenylsilanes for reactions carried out in CH_2Cl_2 (run 3 *vs.* run 6), but is not advantageous for reactions carried out in toluene (run 5 *vs.* run 7). This difference may be related to the higher solubility and/or stability of the catalytically active species (presumably a cation) in CH_2Cl_2 as compared to toluene.** This feature differentiates the present nickel complexes from some of the group 4 metallocene-based catalysts which decompose in chlorinated solvents.[4b]

The amount of solvent is also an important factor in the dehydropolymerization of silanes: the best results are normally obtained with very little or no solvent at all, which favours linear chain growth over the formation of cyclic oligomers.[3b,4a] We found, however, that very concentrated solutions (about 4 M in silane) result in the formation of intractable polymers, implying perhaps a significant degree of cross-linking caused by the coupling of backbone Si–H groups. It appears, therefore, that dilute conditions are better for obtaining polysilanes in this Ni system.

The most likely candidates for the catalytically active species in our system are cationic Ni–H or Ni–SiR_3 species, but we have not succeeded in detecting or isolating any such intermediates. We have found, however, that complex **1** reacts with $LiAlH_4$ to give an intermediate (presumably a neutral Ni–H species)†† which can polymerize $PhSiH_3$ (run 8). These reactions are very sensitive to solvent polarity (run 9), temperature (run 10), and reaction time (run 11), probably reflecting the limited solubility of $LiAlH_4$. Since $LiAlH_4$ can initiate the polymerization of $PhSiH_3$ and is also used in its preparation from $PhSiCl_3$,[10] we decided to explore the possibility of conducting these two steps consecutively in one pot. Thus, reacting $PhSiCl_3$ with an excess of $LiAlH_4$ and adding this mixture to a dilute Et_2O solution of

Table 1 Dehydropolymerization of $PhSiH_3$ with (1-MeInd)Ni(PPh_3)Cl[a]

Run	Initiator	Solvent	[Ni] : init. : Si	*t*/d	10^{-3} M_w	10^{-3} M_n	M_w/M_n
1	$AgBF_4$	CH_2Cl_2	1 : 10 : 90	1	2.0	1.5	1.37
2	$AlCl_3$	CH_2Cl_2	1 : 9 : 90	1	1.3	0.6	2.13
3	MAO	CH_2Cl_2	1 : 9 : 100	1	1.8	1.1	1.69
4	MAO	CH_2Cl_2 (−40 °C)	1 : 9 : 100	1	4.4	2.5	1.80
5	MAO	Toluene	1 : 9 : 100	1	4.8	2.9	1.64
6	MAO	CH_2Cl_2	1 : 9 : 100	7	7.1	5.9	1.20
7	MAO	Toluene	1 : 9 : 100	7	5.0	3.2	1.57
8	$LiAlH_4$	CH_2Cl_2	1 : 4 : 94	1	2.0	1.6	1.21
9	$LiAlH_4$	Toluene	1 : 3 : 100	1	0.6	0.5	1.24
10	$LiAlH_4$	CH_2Cl_2 (−40 °C)	1 : 3 : 100	1	0.7	0.5	1.58
11	$LiAlH_4$	CH_2Cl_2	1 : 4 : 94	7	3.6	1.6	2.27

[a] The initial concentration of $PhSiH_3$ was 0.15 M in all experiments; the yields were > 90% in all cases except run 9 for which the yield *was* 35%.

1 produced the usual colour change accompanied by vigorous evolution of gas.‡‡ The mixture of $(PhHSi)_n$ obtained from this reaction was shown to have M_w = 7565 and M_n = 1541 (M_w/M_n = 4.9).

In conclusion, complex **1** reacts with cationic initiators or $LiAlH_4$ to form species which catalyze the dehydropolymerization of $(PhSiH)_n$ with molecular masses and polydispersities comparable to those obtained from the best early metal systems.[3,4] Some interesting features of this nickel system include no introduction period, good activity at ambient or lower temperatures, tolerance of chlorinated solvents, and relatively narrow polydispersities (*e.g.*, run 6). Studies aimed at elucidating the mechanism of this reaction are in progress.

The authors gratefully acknowledge NSERC (Canada) for financial support of this work, Professors T. D. Tilley and J. F. Harrod for valuable discussions, and Professor Bruce Arndtsen and Ngiap Lim for the use of their GPC.

Notes and References

† E-mail: zargarian.davit@umontreal.ca

‡ The work-up procedure consisted of passing a toluene solution of the reaction mixture, with or without pre-treatment with methanol, through a short column of Celite, followed by evaporation and analysis by ^{1}H NMR and GPC.

§ ^{1}H NMR spectra of $(PhSiH)_n$ ($CDCl_3$, 300 MHz) contain Si–H resonances at δ *ca.* 3.7 for cyclic oligomers and broad signals centred around δ 5 for the linear polysilanes. These resonances appear *ca.* 1 ppm more downfield in C_6D_6.[11]

¶ The molecular masses were determined with a Waters Associates 600E Chromatograph equipped with a refractive index detector (Waters 410 differential refractometer) and Styragel HR 0.5, HR 2, and HR 4 columns in THF calibrated against a polystyrene standard. The manipulation of the peaks was done using the Waters Millennium Chromatography Manager 2010 v2.15 software.

‖ We speculate that the lower molecular masses obtained from the $AlCl_3$-initiated reactions may be caused by secondary reactions promoted by $AlCl_3$ (*e.g.*, silane redistribution or Cl transfer to silane chains).

** A reviewer has suggested that higher molecular mass values in run 6 may arise instead from the conversion of some of the Si–H bonds in the polysilane to Si–Cl as a result of being in contact with CH_2Cl_2 for a few days; the Si–Cl bonds would then be converted to siloxanes during the work-up. Although free radical halogenation of $(PhSiH)_n$ has been observed[12] to occur in CCl_4 and CBr_4, it seems to us that such reactions should be less likely in CH_2Cl_2. Nevertheless, this possibility can not be ruled out, and we caution the reader that the polysilanes obtained in runs 6 may not be pure $(PhSiH)_n$.

†† In our attempts to isolate Ni–H species, we have noted that reacting complex **1** with H^- sources produces a black compound which shows a fleeting signal at δ *ca.* −24 in its ^{1}H NMR spectrum; the isolation of this compound, however, has eluded us so far.

‡‡ The ratio of $PhSiCl_3$: $LiAlH_4$ was *ca.* 1 : 1.3, the reaction was run for four days, and the yield was 80%.

1 R. West, *J. Organomet. Chem.*, 1986, **300**, 327; R. D. Miller and J. Michl, *Chem. Rev.*, 1989, **89**, 1359.
2 C. Aitken, J. F. Harrod and E. Samuel, *J. Organomet. Chem.*, 1985, **279**, C11.
3 For a few leading references see: (*a*) T. D. Tilley, *Acc. Chem. Res.*, 1993, **26**, 22; (*b*) J. F. Harrod, Y. Mu and E. Samuel, *Polyhedron*, 1991, **10**, 1239; (*c*) R. M. Shaltout and J. Y. Corey, *Organometallics*, 1996, **15**, 2866; (*d*) W. H. Campbell, T. K. Hilty and L. Yurga, *Organometallics*, 1989, **8**, 2615; (*e*) J. P. Banovetz, K. M. Stein and R. M. Waymouth, *Organometallics*, 1991, **10**, 3430; (*f*) E. Hengge, P. Gspaltl and E. Pinter, *J. Organomet. Chem.*, 1996, **521**, 145; (*g*) N. Choi, S. Onozawa, T. Sakakura and M. Tanaka, *Organometallics*, 1997, **16**, 2765.
4 (*a*) T. Imori and T. D. Tilley, *Polyhedron*, 1994, **13**, 2231 and references therein; (*b*) V. K. Dioumaev and J. F. Harrod, *J. Organomet. Chem.*, 1996, **521**, 133 and references therein.
5 K. Yamamoto, H. Okinoshima and M. Kumada, *J. Organomet.*, 1970, **23**, C7; I. Ojima, S.-I. Inaba and T. Kogure, *J. Organomet. Chem.*, 1973, **55**, C7; L. S. Chang and J. Y. Corey, *Organometallics*, 1989, **8**, 1885; M. F. Lappert and R. K. Maskell, *J. Organomet. Chem.*, 1984, **264**, 217; K. A. Brown-Wensley, *Organometallics*, 1987, **6**, 1590; M. Tanaka, T. Kobayashi, T. Hayashi and T. Sakakura, *Appl. Organomet. Chem.*, 1988, **2**, 91; P. Boudjouk, A. B. Rajkumar and W. L. Parker, *J. Chem. Soc., Chem. Commun.*, 1991, 245; B. Berris, *US Pat.*, 5 047 569, 1991; B. Berris and S. P. Diefenbach, *US Pat.* 5 003 100, 1991; K. Yokoyama, K. Taniguchi and Y. Kiso, *Eur. Pat. Appl.*, 0 314 327, 1989.
6 H. Yamashita, M. Tanaka and K. Honda, *J. Am. Chem. Soc.*, 1995, **117**, 8873; B. P. S. Chauhan, T. Shimizu and M. Tanaka, *Chem. Lett.*, 1997, 785.
7 Y. Ni, R. Rulkens, J. K. Pudelski and I. Manners, *Macromol. Rapid Commun.*, 1995, **16**, 637; N. P. Reddy, H. Yamashita and M. Tanaka, *J. Chem. Soc., Chem. Commun.*, 1995, 2263.
8 T. A. Huber, F. G.-Bélanger and D. Zargarian, *Organometallics*, 1995, **14**, 4997; T. A. Huber, M. Bayrakdarian, S. Dion, I. Dubuc, F. G.-Bélanger and D. Zargarian, *Organometallics*, 1997, **16**, 5811; M. Bayrakdarian, M. J. Davis, C. Reber and D. Zargarian, *Can. J. Chem.*, 1996, **74**, 2115.
9 R. Vollmerhaus, F. G.-Bélanger and D. Zargarian, *Organometallics*, 1997, **16**, 4762.
10 R. A. Benkeser, H. Landesman and D. J. Foster, *J. Am. Chem. Soc.*, 1952, **74**, 648.
11 H.-G. Woo, J. F. Walzer and T. D. Tilley, *J. Am. Chem. Soc.*, 1992, **114**, 7047.
12 J. P. Banovetz, Y.-L. Hsiao and R. M. Waymouth, *J. Am. Chem. Soc.*, 1993, **115**, 2540.

Received in Bloomington, IN, USA, 30th March 1998; 8/02428F

Crystallographic characterization of the helical diketone, $C_{36}H_{14}O_2$, a new product from the flash vacuum pyrolysis of decacyclene in the presence of oxygen

Saeed Attar, David M. Forkey,† Marilyn M. Olmstead and Alan L. Balch*‡

Department of Chemistry, University of California, Davis, California 95616, USA

The helical diketone, $C_{36}H_{14}O_2$, is formed during the flash vacuum pyrolysis of decacyclene in the presence of oxygen and has been characterized by X-ray crystallography.

The synthesis and properties of non-planar, polycyclic hydrocarbons that mimic structural motifs within the fullerenes have recently received considerable attention.[1] While the chemical reactivity of the fullerenes themselves is so far largely confined to reactions on the outer surface of the molecule,[2] the availability of fullerene-shaped hydrocarbons allows the exploration of the chemical behavior of not only the convex exterior but also the concave interior as well as the edges of these curved molecules. The high temperature (1250 °C) flash vacuum pyrolysis (FVP) of deacyclene **1**, as described by Scott and co-workers, produces the fullerene-shaped hydrocarbon $C_{36}H_{12}$ **2**, along with two related products, **3** and **4**, as shown in Scheme 1.[3] Crystallographic characterization of **2** reveals that its structure closely resembles that of C_{60}, with a degree of pyramidalization of the central carbon atoms at the base of the bowl that slightly exceeds that of the fullerene but with some outward splaying at the rim of hydrogenated carbon atoms.[4] Here we describe the identification of another product, the helical diketone **5**, that can form in this pyrolytic process through oxidation.

During several preparations of **2** by flash vacuum pyrolysis of decacyclene with subsequent chromatographic separation of the soluble products,[3] we noted that the contents of the second chromatographic band, the one that usually contained the doubly closed bowl **3**, changed when air leaked into the pyrolysis system. Further examination of this band revealed the presence of a new compound, the diketone **5**, (*Chem. Abstr.*, Index Name, cyclopenta[*pqr*]naphth[2′,1′,8′ : 5,6,7]-*as*-indaceno[1,2,3,4-*tuva*]picene-15,16-dione) which was produced in yields of *ca.* 0.3–0.5%.

The dione **5** has been fully characterized *via* both spectroscopic§ and X-ray crystallographic data. Because of the similarities in molecular symmetry and structure, the dione **5** and the doubly closed bowl **3** show comparable but different features in their ^{1}H NMR spectra. Orange crystals of $C_{36}H_{14}O_2 \cdot 1.125\ CH_2Cl_2 \cdot 0.75\ MeOH \cdot 0.25\ H_2O$ readily form through the diffusion of MeOH into CH_2Cl_2 solution of the compound.¶ Two views of the molecule are shown in Fig. 1. Bond distances within the molecule are given in Table 1.

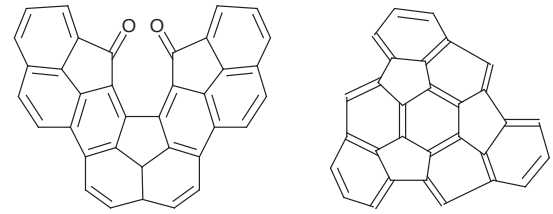

5 **6**

Although the molecule has no crystallographically imposed symmetry, it is divided into two nearly identical halves with an approximate two-fold axis that passes through the C(13)–C(33) bond. The two C–O distances are consistent with the diketone

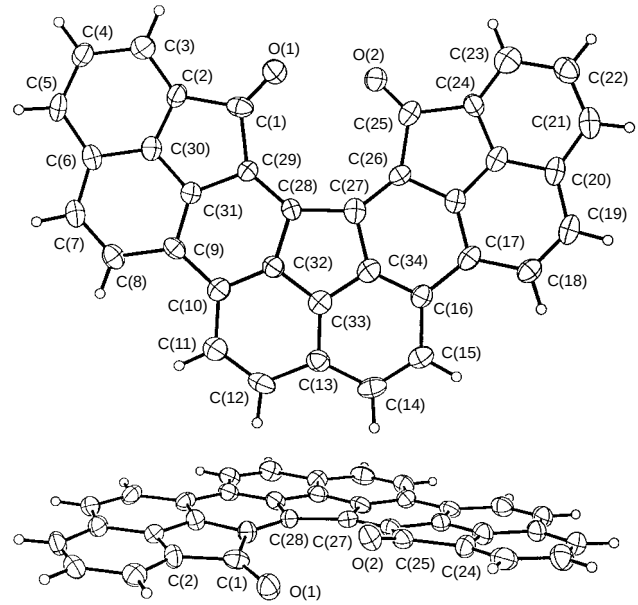

Fig. 1 A perspective view of an isolated molecule of $C_{36}H_{14}O_2$ with 50% thermal contours. The top view looks down on the nearly flat surface of the molecule while the lower view emphasizes the non-planarity and helicity of the region near the two oxygen atoms.

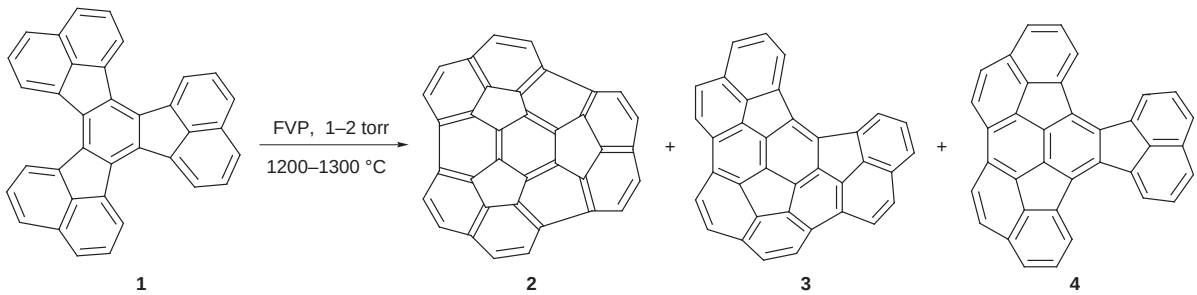

1 **2** **3** **4**

Scheme 1

Table 1 Bond lengths for $C_{36}H_{14}O_2$

Bond	Distance/Å	Bond	Distance/Å
O(1)–C(1)	1.205(7)	O–(2)–C(25)	1.204(7)
C(1)–C(2)	1.526(9)	C(24)–C(25)	1.528(8)
C(2)–C(3)	1.366(8)	C(23)–C(24)	1.354(9)
C(3)–C(4)	1.421(9)	C(22)–C(23)	1.422(9)
C(4)–C(5)	1.378(8)	C(21)–C(22)	1.371(9)
C(5)–C(6)	1.421(8)	C(20)–C(21)	1.419(9)
C(6)–C(7)	1.412(8)	C(19)–C(20)	1.428(9)
C(7)–C(8)	1.368(9)	C(18)–C(19)	1.363(9)
C(8)–C(9)	1.461(8)	C(17)–C(18)	1.452(8)
C(9)–C(10)	1.443(8)	C(16)–C(17)	1.441(8)
C(10)–C(11)	1.425(8)	C(15)–C(16)	1.441(8)
C(11)–C(12)	1.372(9)	C(14)–C(15)	1.366(9)
C(12)–C(13)	1.440(8)	C(13)–C(14)	1.436(9)
C(1)–C(29)	1.526(8)	C(25)–C(26)	1.516(8)
C(28)–C(29)	1.371(8)	C(26)–C(27)	1.375(8)
C(27)–C(28)	1.514(8)	C(24)–C(36)	1.396(9)
C(2)–C(30)	1.403(8)	C(20)–C(36)	1.411(8)
C(6)–C(30)	1,415(8)	C(26)–C(35)	1.436(8)
C(29)–C(31)	1.449(8)	C(17)–C(35)	1.399(8)
C(9)–C(31)	1.382(8)	C(35)–C(36)	1.406(9)
C(30)–C(31)	1.401(8)	C(27)–C(34)	1.460(9)
C(28)–C(32)	1.436(8)	C(16)–C(34)	1.385(8)
C(10)–C(32)	1.399(8)	C(33)–C(34)	1.392(8)
C(32)–C(33)	1.395(8)	C(13)–C(33)	1.390(8)

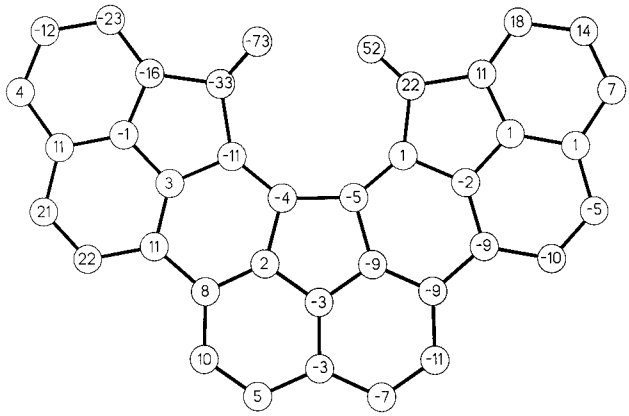

Fig. 2 Deviations (in 0.01 Å) of the atomic positions from the mean molecular plane for $C_{36}H_{14}O_2$

formulation, and the four immediately adjacent C–C bonds are the longest C–C bonds in the molecule. The dione **5** is not planar but has a slight helical twist, as shown in the lower part of Fig. 1. This helicity arises from the juxtaposition of the two oxygen atoms, which bend away from one another to avoid unduly close contact. The non-bonded O···O distance in **5** is 2.708 (6) Å. Fig. 2 shows the distances of the various carbon atoms from the mean plane of the carbon atoms in **5**. Although individual molecules of **5** are chiral, each crystal is a racemate of the two *M* and *P* enantiomers.

In the solid state, the individual molecules of **5** pack in columns along the *b* axis as shown in Fig. 3. Within each column, all molecules have like chirality. However, there are inversion centers between the columns, so that adjacent columns have opposite chiralities. The packing conforms to the β motif, which is one of the four packing arrangements found for polynuclear aromatic hydrocarbons.[5,6] The motif is characterized by a short *b* screw axis and graphitic planes. The β motif is the one utilized by polynuclear aromatic hydrocarbons that are, like the diketone **5**, non-planar.

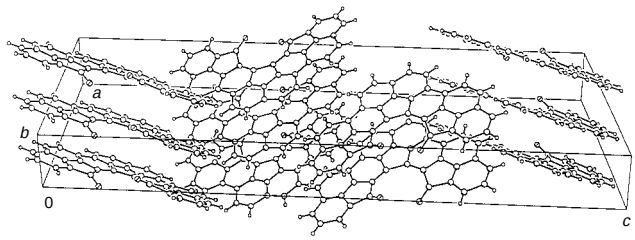

Fig. 3 A view of the solid state packing in $C_{36}H_{14}O_2$

The formation of the diketone **5** during our flash vacuum pyrolysis of decacyclene has been traced to a leak in the gas inlet system that allowed air to enter the gas stream during pyrolysis. It is likely that **5** formed from oxidation of the doubly closed bowl **3**, since **5** and **3** are related by cleavage of one of the C–C bonds on the periphery of the corannulene-like portion of **3**. However, as indicated by mass spectroscopic and NMR data, the doubly closed bowl **3** is not converted into **5** during the general workup of the pyrolysis products, nor does exposure of a solution of **3** to one atmosphere of O_2 in $CHCl_3$ solution for 30 min under room light lead to the formation of the dione **5**. Those pyrolysis reactions that produced **5** yielded little or none of the doubly closed bowl **3**, but did produce **2**. The C–C bonds on the edges of these non-planar hydrocarbons are subject to considerable strain, and as the present case reveals, cleavage of just one such bond in **3** can result in the formation the nearly planar dione **5**, with considerable release of strain. In a related study, cleavage of a carbon–carbon bond on the periphery of the semibuckminsterfullerene, $C_{30}H_{12}$ **6**, has been observed in its reaction with $(Ph_3P)_2Pt(C_2H_4)$.[7] Clearly the chemistry of these non-planar hydrocarbons that are related to fullerenes deserves continued attention,[8] and reactivity at the edges is likely to be a prominent feature.

We thank the National Science Foundation (Grant CHE 9610507) for financial support and Professor G. Stanley for a preprint of ref. 7.

Notes and References

† On leave from the Department of Chemistry, California State University, Sacramento, CA 95819, USA.
‡ E-mail: albalch@ucdavis.edu

§ *Selected data* for **5**: δ_H(300 MHz; $CDCl_3$) 7.98 (d, 2 H, *J* 9.0), 7.93 (d, 2 H, *J* 7.2), 7.74 (d, 2 H, *J* 8.7), 7.61 (d, 2 H, *J* 8.7), 7.59 (d, 2 H, *J* 8.1), 7.40 (d, 2 H, *J* 9.0), 7.39 (dd, 2 H, *J* 8.1 and 7.2); ν_{max}/cm^{-1} 1720 (C=O); *m*/*z* 478.5 (M^+).

¶ *Crystal data* for **5**: Orange needles of $C_{36}H_{14}O_2 \cdot 1.125\ CH_2Cl_2 \cdot 0.75\ MeOH \cdot 0.25\ H_2O$, clinic, space group $P2_1/c$, a = 17.469(4), b = 3.8213(8), c = 38.627(9) Å, β = 95.18(2)°, T = 130(2) K, Z = 4, Cu-Kα radiation (λ = 1.54178 Å). Refinement of 3372 reflections and 406 parameters yielded $wR2$ = 0.2138 for all data and a conventional R_1 = 0.071 based on 2120 reflections with $I > 2\sigma(I)$. The largest peak and hole in the final differnece map are 0.40 and −0.57 e Å^{-3}. CCDC 182/865.

In contrast, crystals of the doubly closed bowl, $C_{36}H_4$ **3**, precipitate as orange needles with a hexagonal form. A data set was collected with the crystal indexed in the trigonal *R* crystal system; $a = b$ = 20.076 (4), c = 4.2691 (8) Å. Attempts to solve the structure failed, probably because of twinning.

1 L. T. Scott, *Pure Appl. Chem.*, 1996, **68**, 291; P. W. Rabideau and A. Sygula, *Acc. Chem. Res.*, 1996, **29**, 235; R. Faust, *Angew. Chem., Int. Ed. Engl.*, 1995, **34**, 1429.
2 A. Hirsh, *The Chemistry of Fullerenes*, Thieme, Stuttgart, 1994; *The Chemistry of Fullerenes*, ed. R. Taylor, World Scientific, New Jersey, 1995.
3 L. T. Scott, M. S. Bratcher and S. Hagen, *J. Am. Chem. Soc.*, 1996, **118**, 8743.
4 D. M. Forkey, S. Attar, B. C. Noll, R. Koerner, M. M. Olmstead and A. L. Balch, *J. Am. Chem. Soc.*, 1997, **119**, 5766.
5 G. R. Desiraju and A. Gavezzotti, *J. Chem. Soc., Chem. Commun.*, 1989, 621.
6 G. R. Desiraju and A. Gavezzotti, *Acta Crystallogr., Sect. B*, 1989, **45**, 473.
7 R. M. Shaltout, R. Sygula, A. Sygula, F. Fronczek, G. G. Stanley and P. W. Rabideau, *J. Am. Chem. Soc.*, 1998, **120**, 835.
8 T. J. Seiders, K. K. Baldridge, J. M. O'Conner and J. S. Siegel, *J. Am. Chem. Soc.*, 1997, **119**, 4781.

Received in Columbia, MO, USA, 11th November 1997; 7/08149I

A starburst porphyrin polymer: a first generation dendrimer

Tyler Norsten and Neil Branda*†

Department of Chemistry, University of Alberta, Edmonton, AB, Canada T6G 2E1

Tetra(chlorobenzyl)porphyrin 3b reacts with 4 equiv. hydroxyphenylporphyrin 2 to give the first example of a pentaporphyrin that can be considered to be a first generation dendrimer.

Porphyrins and metalloporphyrins are fascinating chromophores due predominantly to the fact that their photophysical behaviour is sensitive to the type and position of substitution within or around the ring, as well as the presence of neighbouring porphyrins or other chromophore centres. To better understand the complexity of the electronic or photonic communication between porphyrins,[1] covalently linked conjugated[2] and non-conjugated[3] oligomeric porphyrin assemblies, as well as non-covalently linked supramolecular chromophoric assemblies[4] have been prepared and studied. These short, multiply linked chromophoric polymers are successfully paving the way to a better understanding of the fundamental interactions between neighbouring porphyrin centres.

Dendrimers are a specific class of compounds that comprise one of the fastest growing areas of polymer research.‡[5] These hyperbranched starburst polymers differ from their traditional linear counterparts in that the repeating units cascade outwardly from a central core rather than elongating in a linear fashion. The attraction here is that as successive generations are iterated, dendrimers become increasingly globular and exhibit intriguing structural properties such as internal voids and cavities created by the multiple branches folding back upon themselves. Knowing this, we were surprised when we could not find any examples of a fully porphyrinic dendrimer. There are several examples of the two extreme cases: (1) multiple porphyrins covalently linked onto a non-porphyrin core,[6] and (2) non-porphyrin dendrimer branches fused to a singular porphyrin core.[7] Here we report the first example of a dendrimer where the core and repeating polymeric unit are themselves both porphyrins. It is hoped that this new class of branched chromophores will combine the advantages of the hybrid properties of both porphyrins and dendrimers.

With a divergent§ synthetic approach in mind, the polymeric cycle leading to dendrimer **1** was designed to consist of ester-reduction, activation of the resulting alcohol and coupling to form an ether linkage. The ether linkage was chosen because of its chemical stability towards a wide range of synthetic conditions including those required for future iterations. Another attractive feature of this approach is that both the precursor to the active core **3b** [*meso*-tetrakis(4-methoxycarbonylphenyl)porphyrin **3a**] and the repeating unit [5,10,15-tris(methoxycarbonylphenyl)-20-(4-hydroxyphenyl)-porphyrin **2**] can be prepared in the same one-pot procedure as previously reported.[8] Porphyrins **2** and **3a** are easily separated and purified by trituration with acetone followed by column chromatography (SiO_2). Porphyrin **3a** was reduced[9] with $LiAlH_4$ and the resulting tetraalcohol chlorinated[10] to give the core **3b** following known procedures. The first generation dendrimer **1** was prepared from building blocks **2** and **3b** in one step as outlined in Scheme 1, by coupling 4 equiv. **2** to 1 equiv. **3b** in the presence of NaOH in DMF at 80–100 °C for 24 h. Pentaporphyrin **1** was isolated as a purple solid in 48% yield after purification by column chromatography (SiO_2, $CHCl_3$–2% CH_3CN) and by GPC.

Pentaporphyrin **1** was highly soluble in a wide range of organic solvents such as THF, $CHCl_3$ and CH_2Cl_2. It is

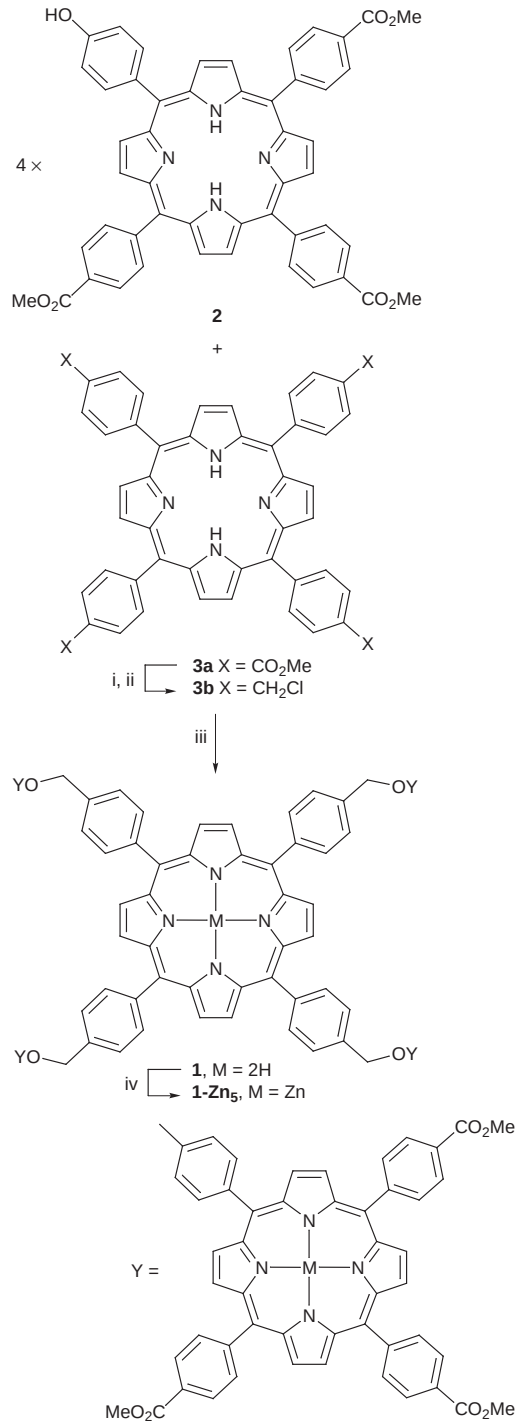

Scheme 1 *Reagents and conditions*: i, $LiAlH_4$, THF, reflux; ii, $SOCl_2$; iii, NaOH, DMF, 80–100 °C; iv, $Zn(OAc)_2{\cdot}2H_2O$, MeOH, $CHCl_3$

interesting to note that it is in fact significantly more soluble than either building blocks **2** or **3**. The pentaporphyrin **1** displays 12 divergent ester groups suitable for submission to future dendrimeric cycles.

The first generation dendrimer **1** was characterized by MALDI-TOF mass spectrometry and ^{1}H NMR and UV–VIS absorption spectroscopies. The ^{1}H NMR and COSY spectra of **1** in $CDCl_3$ are consistent with the assigned structure. A significant difference is observed for the resonances of the two core porphyrin N–H hydrogens (−2.61 ppm) and the eight porphyrin N–H hydrogens located within the peripheral porphyrins (−2.75 ppm) of the starburst. Molecular modeling suggests that the radial porphyrin arms are capable of folding back towards the core of the starburst molecule; however, ROSEY NMR studies show no long-range communication. Minimum energy calculations predict that the four radially linked porphyrins ideally exist in a propeller type arrangement around the core with an edge-to-edge distance of 61 Å. The dendrimer exists in the nanoscale range after only one generation!

The MALDI-TOF mass spectrum of **1** shows a peak at 3883.7 mass units (mu) corresponding to the parent ion [M + H], this is in accordance with the calculated value of 3883.3 mu for $C_{248}H_{174}N_{20}O_{28}$. Also evident are fragmentation peaks separated by 804 mu at 3079, 2275 and 1471 mu corresponding to the consecutive loss of a peripheral porphyrin from the central core (Fig. 1).

The UV–VIS spectrum of the porphyrin dendrimer in $CHCl_3$ shows absorption maxima at 424 (2 140 000),¶ 517 (74 200), 552 (38 200), 591 (23 700) and 647 (17 400) nm. The absorption spectrum of **1** appears to resemble the sum of appropriate model compounds.‖ Studies to quantify any subtle shifts in absorption and changes in molar extinction coefficients are currently under way.

The pentametallo zinc derivative **1**–$\mathbf{Zn_5}$ was cleanly prepared by treating a $CHCl_3$ solution of the free base dendrimer with an excess of a saturated MeOH solution of $Zn(OAc)_2{\cdot}2H_2O$. The MALDI-TOF mass spectrum of **1**–$\mathbf{Zn_5}$ is consistent with the replacement of the 10 porphyrin hydrogen atoms by five zinc atoms, as is the ^{1}H NMR spectrum with the disappearance of the eight peripheral porphyrin hydrogens at −2.75 ppm and the two core hydrogens at −2.61 ppm. As expected, the addition of five metals to the dendrimer greatly decreased its solubility in chlorinated solvents (CH_2Cl_2 and CH_3Cl), however **1**–$\mathbf{Zn_5}$ remained highly soluble in THF.

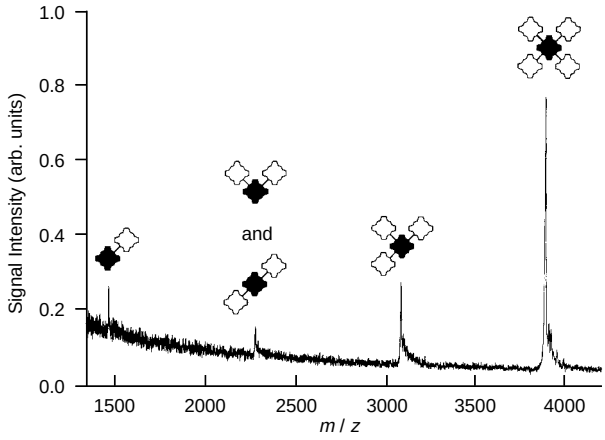

Fig. 1 MALDI-TOF mass spectrum of first generation porphyrin dendrimer **1** showing the parent mass peak [M + H] as well as peaks corresponding to the sequential loss of one peripheral porphyrin (unshaded polygons) from the central core porphyrin (shaded polygon). All-*trans*-retinoic acid was used as the matrix without added cation.[11] Synthetic peptides bracketing the mass of interest (4000 mu) were used as external standards for calibration.

The starbursts **1** and **1**–$\mathbf{Zn_5}$ represent the birth of a new type of dendrimeric framework. It will be interesting to see what electronic or photonic applications the future holds for the next generation.

We are grateful to Dr David Schriemer for his help with the MALDI-TOF mass spectrometry studies and to the Natural Sciences and Engineering Research Council of Canada for financial support.

Notes and References

† E-mail: neil.branda@ualberta.ca

‡ http://dendrimers.cas.usf.edu/links.html. This web site lists academic and commercial laboratories working on dendrimer research as well as an up to date list of publications on dendrimers.

§ In a divergent approach, dendrimers are constructed from a central core out to the periphery in an iterative fashion of repeating generations. In contrast, a convergent approach builds the dendrimer from the periphery towards the core.

¶ Molar extinction coefficient (ε/M^{-1} cm^{-1}).

‖ Benzyl and phenyl ethers of porphyrins **2** and **3b** respectively were prepared as model compounds for comparative photophysical studies by reacting the hydroxyphenylporphyrin **2** with benzylbromide and by reacting tetrachloroporphyrin **3b** with phenol.

1 M. R. Wasielewski, *Chem. Rev.*, 1992, **92**, 435.
2 R. W. Wagner, J. S. Lindsey, J. Seth, V. Palaniappan and D. F. Bocian, *J. Am. Chem. Soc.*, 1996, **118**, 3996; M. J. Crossley and P. L. Burn, *J. Chem. Soc., Chem. Commun.*, 1991, 1569; H. L. Anderson, *Inorg. Chem.*, 1994, **33**, 972; K. Ichihara and Y. Naruta, *Chem. Lett.*, 1995, 631; J. Seth, V. Palaniappan, T. E. Johnson, S. Prathapan, J. S. Lindsay and D. F. Bocian, *J. Am. Chem. Soc.*, 1994, **116**, 10 578; A. Osuka, T. Okada, S. Taniguchi, K. Nozaki, T. Ohno and N. Mataga, *Tetrahedron Lett.*, 1995, **36**, 5781.
3 O. Mongin and A. Gossauer, *Tetrahedron*, 1997, **53**, 6835; G. M. Dubowchik and A. D. Hamilton, *J. Chem. Soc., Chem. Commun.*, 1986, 1391; M. Takeuchi, Y. Chin, T. Imada and S. Shinkai, *Chem. Commun.*, 1996, 1867.
4 J. L. Sessler, B. Wang and A. Harriman, *J. Am. Chem. Soc.*, 1993, **115**, 10 418; T. Arimura, C. T. Brown, S. L. Springs and J. L. Sessler, *Chem. Commun.*, 1996, 2293; J.-P. Collin, A. Harriman, V. Heitz, F. Odobel and J.-P. Sauvage, *J. Am. Chem. Soc.*, 1994, **116**, 5679; C. A. Hunter and R. K. Hyde, *Angew. Chem., Int. Ed. Engl.*, 1996, **35**, 1936.
5 F. Zeng and S. C. Zimmerman, *Chem. Rev.*, 1997, **97**, 1681.
6 N. Maruo and N. Nishino, *Kobunshi-Ronbunshu*, 1997, **54**, 731.
7 P. J. Dandliker, F. Diederich, J.-P. Gisselbrecht, A. Louati and M. Gross, *Angew. Chem., Int. Ed. Engl.*, 1995, **34**, 2725; P. J. Dandliker, F. Diederich, A. Zingg, J.-P. Gisselbrecht, M. Gross, A. Louati and E. Sanford, *Helv. Chim. Acta.*, 1997, **80**, 1773; R. Sadamoto, N. Tomioko and T. Aida, *J. Am. Chem. Soc.*, 1996, **118**, 3978; P. Bhyrappa, J. K. Young, J. S. Moore and K. S. Suslick, *J. Am. Chem. Soc.*, 1996, **118**, 5708; Y. Tomoyose, D.-L. Jiang, R.-H. Jin, T. Aida, T. Yamashita, K. Horie, E. Yashima and Y. Okamoto, *Macromolecules*, 1996, **29**, 5236.
8 L. R. Milgrom and F. O'Neill, *Tetrahedron*, 1995, **51**, 2137.
9 N. Datta-Gupta and T. J. Bardos, *J. Heterocyc. Chem.*, 1966, **3**, 495.
10 N. Robic, C. Bied-Charreton, M. Perrée-Fauvet, C. Verchère-Béaur, L. Salmon and A. Gaudemer, *Tetrahedron Lett.*, 1990, **31**, 4739.
11 D. C. Schriemer and L. Liang, *Anal. Chem.*, 1996, **68**, 2721.

Received in Columbia, MO, USA, 22nd January 1998; 8/00636I

Nucleophilic substitution of optically active 1-alkoxypolyfluoroalkyl sulfonates

Hiroshi Matsutani,[a] Hervé Poras,[a] Tetsuo Kusumoto*[a]† and Tamejiro Hiyama[b]

[a] *Sagami Chemical Research Center, Nishiohnuma, Sagamihara, Kanagawa 229-0012, Japan*
[b] *Department of Material Chemistry, Graduate School of Engineering, Kyoto University, Yoshida, Kyoto 606-8501, Japan*

Reaction of 1-alkoxypolyfluoroalkyl sulfonates with lithium tetraalkylaluminates gives stereospecifically alkylated products with a high degree of inversion of configuration; in contrast, the ees of the resulting ethers are slightly reduced in the reaction with trialkylaluminium reagents.

Chiral acetals are versatile building blocks for the synthesis of biologically active agents and functional materials.[1] However, few optically pure compounds are known whose acetal carbon only is chiral.[2] We have recently reported that the Baeyer–Villiger reaction of optically active α-alkoxyalkyl ketones affords optically active 1-alkoxyalkyl carboxylates. The resulting acetals undergo the substitution reaction with lithium dialkylcuprates in the presence of $BF_3{\cdot}OEt_2$ to give optically active alkoxyalkanes with inversion of configuration.[3] We undertook to expand the concept to trifluoroacetaldehyde because fluorinated chiral compounds are receiving increasing attention in view of their remarkable biological and physical properties.[4] Furthermore, the nucleophilic C–C bond-forming substitution reaction at a carbon bearing a trifluoromethyl group with inversion of configuration is unprecedented.[5,6] We report herein a nucleophilic substitution of optically active 1-alkoxypolyfluoroalkyl sulfonates with an organoaluminium reagent[7] to give optically active alkoxypolyfluoroalkanes with a high degree of inversion of configuration.

Optically active 1-alkoxypolyfluoroalkyl sulfonates were prepared according to Scheme 1. Trifluoroacetaldehyde or heptafluorobutanal was liberated *in situ* from hemiacetal **1a** or hydrate **1b**, respectively, and allowed to react with benzyl alcohol to give racemic hemiacetal **2a** or **2b**, which was converted to the corresponding sulfonate with alkane- or arenesulfonyl chloride, triethylamine and DMAP.[5a,8] The resulting hemiacetal derivatives were resolved by HPLC (Daicel CHIRALPAK AD or CHIRALCEL OD) to afford (+)- and (−)-**3a**–**d**. Alternatively, (*S*)-(+)-**3a** (79% ee‡) was prepared by asymmetric addition of benzyl alcohol to trifluoroacetaldehyde using an (*R*)-binaphthol–titanium(IV) complex[9] followed by mesylation at 0 °C.[10]

With sulfonates **3a**–**d** in hand, we then studied C–C bond-forming reactions using various organometallic reagents. In contrast to the corresponding acetaldehyde acetals,[3,11] **3a** did not react with $Bu_2CuLi{\cdot}LiI/BF_3{\cdot}OEt_2$. However, treatment of (*R*)-(−)-**3a** (61% ee) with $AlEt_3$ in toluene at −20 °C gave (−)-2-benzyloxy-1,1,1-trifluorobutane **4a** in 66% yield with 46% ee [eqn. (1) and Table 1, entry 1]. Since the absolute

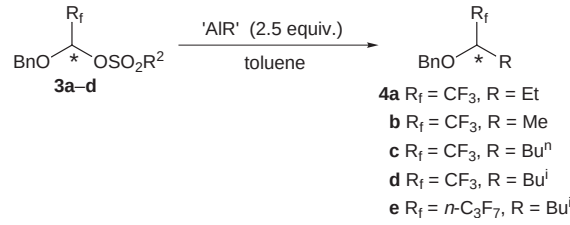

(1)

configuration of ether (−)-**4a** is *S* and that of mesylate (−)-**3a** is *R*,§ we conclude that the reaction has proceeded with inversion of configuration. This is the first observation of a stereospecific nucleophilic substitution reaction giving C–C bond formation at a CF_3-substituted carbon with inversion of configuration, although the enantiomeric excess (ee) of **3a** was slightly lost in **4a**. This observation suggests that Lewis acid $AlEt_3$ induced the formation of an oxocarbenium ion intermediate, which led to racemization to some extent.[3] After some trials, we were delighted to find that the use of $LiAlEt_4$[12] instead of $AlEt_3$ gave (*R*)-(+)-**4a** in 59% yield with 83% ee, starting from (*S*)-(+)-**3a** (83% ee).¶ It is noteworthy that the stereochemical integrity of the substrate was completely maintained (Table 1, entry 2). Thus, the Lewis acidity of the organometallic reagent affects significantly the stereochemical course of the reaction.

To demonstrate the generality of the substitution reaction, optically active sulfonates **3a**–**c** were allowed to react with various organoaluminium reagents. The results are summarized in Table 1. The chirality transfer, *i.e.* the ratio of (% ee of **4**)/(% ee of **3**), is shown also. Using $AlEt_3$, benzenesulfonate (*R*)-(−)-**3b**‖ gave ether (*S*)-(−)-**4a** with 76% chirality transfer (entry 3). On the other hand, the same substrate reacted stereospecifically with $LiAlEt_4$ with 97% chirality transfer (entry 4). Similar results were obtained with optically active tosylate **3c** (entry 5 and 6). Reaction of (*S*)-(+)-**3c**‖ (100% ee) with $LiAlEt_4$ gave (*R*)-(+)-**4a** with 98% ee. Similarly, $AlMe_3$, $AlBu^n_3$, and $AlBu^i_3$ reacted stereospecifically with optically active tosylate **3c**, while the corresponding aluminates ($LiAlMe_4$, $LiAlBu^n_4$ and $LiAlBu^i_4$) reacted with higher stereospecificity (entries 8, 10 and 12 *vs.* entries 7, 9 and 11). The low yield of ether **4b** may be attributed to the poor solubility of $LiAlMe_4$ in toluene (entry 8, Table 1).

Optically active 1-benzyloxy-2,2,3,3,4,4,4-heptafluorobutyl toluene-*p*-sulfonate **3d** derived from heptafluorobutanal also reacted with organoaluminium reagents stereospecifically (entries 12 and 13). Treatment of **3d** with $AlBu^i_3$ afforded optically active ether **4e** with 23% chirality transfer in low yield. In contrast, **3d** reacted with $LiAlBu^i_4$ with 84% chirality transfer. Although the absolute configurations of sulfonate **3d** and ether **4e** remain to be determined, the reaction may be assumed to have proceeded with inversion of configuration as in the cases of **3a**–**c**.

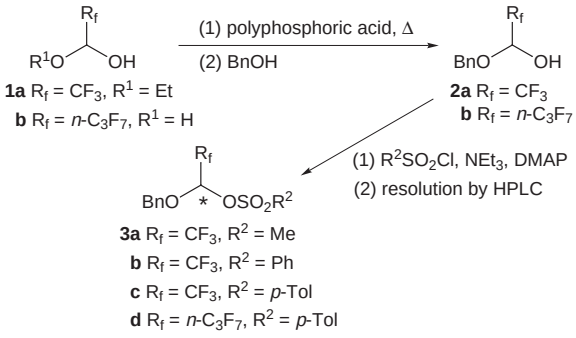

Scheme 1

Table 1 Nucleophilic substitution of optically active 1-alkoxypolyfluoroalkyl sulfonates using organoaluminium reagents

Entry	Substrate	Ee (%)	'AlR'	*T*/°C	*t*/h	Product	Yield (%)	Ee (%)	Chirality transfer (%)[a]
1	(*R*)-(−)-**3a**[b]	61	$AlEt_3$	−20	0.5	(*S*)-(−)-**4a**[d]	66	46	75
2	(*S*)-(+)-**3a**[b,c]	83	$LiAlEt_4$	0	1.5	(*R*)-(+)-**4a**[d,e]	59	83	100
3	(*R*)-(−)-**3b**[f]	93	$AlEt_3$	−20	0.5	(*S*)-(−)-**4a**[d]	57	71	76
4	(*R*)-(−)-**3b**[f]	98	$LiAlEt_4$	0	1.5	(*S*)-(−)-**4a**[d]	61	95	97
5	(*S*)-(+)-**3c**[f]	100	$AlEt_3$	−20	0.5	(*R*)-(+)-**4a**[d]	75	82	82
6	(*S*)-(+)-**3c**[f,g]	100	$LiAlEt_4$	0	1.5	(*R*)-(+)-**4a**[d,h]	69	98	98
7	(*R*)-(−)-**3c**[f]	91	$AlMe_3$	−20	0.5	(*S*)-(−)-**4b**[i]	66	69	76
8	(*R*)-(−)-**3c**[f]	90	$LiAlMe_4$	0–40	2.5	(*S*)-(−)-**4b**[i,j]	26	78	87
9	(*R*)-(−)-**3c**[f]	92	$AlBu^n_3$	−20	0.5	(*S*)-(−)-**4c**[k]	67	72	78
10	(*S*)-(+)-**3c**[f]	100	$LiAlBu^n_4$	r.t.	1.0	(*R*)-(+)-**4c**[k,l]	62	90	90
11	(*R*)-(−)-**3c**[f]	94	$AlBu^i_3$	−20	0.5	(*S*)-(−)-**4d**[m]	76	61	65
12	(*S*)-(+)-**3c**[f]	100	$LiAlBu^i_4$	0	1.5	(*R*)-(+)-**4d**[m,n]	46	93	93
13	(−)-**3d**	98	$AlBu^i_3$	−20	0.5	(−)-**4e**	17	23	23
14	(+)-**3d**[o]	100	$LiAlBu^i_4$	45	2.0	(+)-**4e**[p]	43	84	84

[a] See text. [b] The absolute configuration was assigned on the basis of the optical rotation of (*S*)-(+)-**3a** prepared using an (*R*)- binaphthol–titanium(IV) complex (ref. 9 and 10). [c] $[\alpha]_D^{20}$ +46 (*c* 1.0, $CHCl_3$). [d] The (*S*)-isomer prepared from (*S*)-3,3,3-trifluoro-1,2-epoxypropane **5** showed $[\alpha]_D^{20}$ −40 (*c* 1.0, $CHCl_3$). [e] $[\alpha]_D^{20}$ +41 (*c* 1.0, $CHCl_3$). [f] The absolute configuration was estimated by analogy with entries 1 and 2. [g] $[\alpha]_D^{20}$ +38 (*c* 1.0, $CHCl_3$). [h] $[\alpha]_D^{20}$ +51 (*c* 1.0, $CHCl_3$). [i] The (*S*)-isomer prepared from **5** showed $[\alpha]_D^{20}$ −15 (*c* 1.0, $CHCl_3$). [j] $[\alpha]_D^{20}$ −14 (*c* 1.0, $CHCl_3$). [k] The (*S*)-isomer prepared from **5** showed $[\alpha]_D^{20}$ −37 (*c* 1.1, $CHCl_3$). [l] $[\alpha]_D^{20}$ +43 (*c* 1.1, $CHCl_3$). [m] The (*S*)-isomer prepared from **5** showed $[\alpha]_D^{20}$ −39° (*c* 1.0, $CHCl_3$). [n] $[\alpha]_D^{20}$ +49 (*c* 1.0, $CHCl_3$). [o] $[\alpha]_D^{20}$ +33 (*c* 1.1, $CHCl_3$). [p] $[\alpha]_D^{20}$ +25 (*c* 1.0, $CHCl_3$).

The versatility of the present reaction is demonstrated by the transformation of the products to optically active 1,1,1-trifluoroalkan-2-ols [eqn. (2)]. Hydrogenolysis of benzyl ether

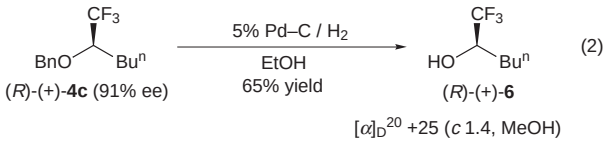

(2)

(*R*)-(+)-**4c** removed the benzyl moiety to furnish (*R*)-(+)-1,1,1-trifluorohexan-2-ol **6**[13] which is a key chiral building block of antiferroelectric liquid crystalline materials.[14]

Notes and References

† E-mail: kus-scrc@ppp.bekkoame.or.jp

‡ Enantiomeric excess (ee) was analyzed by HPLC with CHIRALCEL or CHIRALPAK (both available from Daicel).

§ The absolute configuration of ethers **4a**–**d** was assigned on the basis of the optical rotation of a corresponding authentic sample prepared from (*S*)-3,3,3-trifluoro-1,2-epoxypropane **5**.

¶ *Typical procedure*. A toluene (2.0 ml) solution of lithium tetraalkylaluminate prepared *in situ* from the corresponding alkyllithium (0.63 mmol) and trialkylaluminum (0.63 mmol) was added dropwise to a stirred solution of **3** (0.25 mmol) in toluene (2.5 ml). The reaction mixture was stirred for the indicated period and quenched with dilute HCl. The resulting mixture was extracted with Et_2O. The organic layer was washed with aq. NaCl, dried and concentrated. The residue was purified by silica gel column chromatography. All new compounds were fully characterized by IR, mass and NMR spectroscopy and elemental analysis.

‖ The absolute configurations of sulfonates **3b**,**c** were estimated on the basis of the configurations of products **4a**–**d** as well as the stereochemical course of the reaction.

1 H. Fujioka and Y. Kita, in *Studies in Natural Products Chemistry*, ed. A.-U. Rahman, Elsevier, Amsterdam, The Netherlands, 1994, vol. 14, pp. 469–516; R. J. Ferrier, R. Blattner, R. H. Furneaux, P. C. Tyler, R. H. Wightman and N. R. Williams, in *Carbohydrate Chemistry*, The Royal Society of Chemistry, Cambridge, 1991, vol. 23, ch. 7; D. Seebach, R. Imwinkelried and T. Weber, in *Modern Synthetic Methods 1986*, ed. R. Scheffold, Springer Verlag, Berlin, Heidelberg, 1986, vol. 4, pp. 125–259; J. K. Whitesell, *Chem. Rev*., 1989, **89**, 1581; T. Mukaiyama and M. Murakami, *Synthesis*, 1987, 1043.

2 Synthesis of an optically active 1-alkoxy-2,2,2-trichloroethyl ester has been achieved enzymatically: R. Chênevert, M. Desjardins and R. Gagnon, *Chem. Lett.*, 1990, 33.

3 H. Matsutani, S. Ichikawa, J. Yaruva, T. Kusumoto and T. Hiyama, *J. Am. Chem. Soc.*, 1997, **119**, 4541 and refs. therin.

4 See, for example: M. Hudlicky and A. E. Pavlath, ed., *Chemistry of Organic Fluorine Compounds II*, ACS Monograph 187, American Chemical Society, Washington, DC, 1995; *Organofluorine Chemicals and their Industrial Applications*, ed. R. E. Banks, Ellis Harwood, Chichester, 1979; B. E. Smart, *Chem. Rev.*, 1996, **96**, 1555.

5 For substitution at the carbon bearing a trifluoromethyl group by a heteroatom nucleophile, see: (*a*) P. J. Casara, M. T. Kenny and K. C. Jund, *Tetrahedron Lett.*, 1991, **32**, 3823; (*b*) T. Hagiwara, K. Tanaka and T. Fuchikami, *Tetrahedron Lett.*, 1996, **37**, 8187; (*c*) K. Mikami, T. Yajima, M. Terada, S. Kawauchi, Y. Suzuki and I. Kobayashi, *Chem. Lett.*, 1996, 861; (*d*) T. Katagiri, H. Thara, M. Takahashi, S. Kashino, K. Furuhashi and K. Uneyama, *Tetrahedron: Asymmetry*, 1997, **8**, 2933; (*e*) E. C. Tongco, G. K. S. Prakash and G. A. Olah, *Synlett*, 1997, 1193; (*f*) A. Ishii, F. Miyamoto, K. Higashiyama and K. Mikami, *Chem. Lett.*, 1998, 119.

6 A substitution reaction of a cyclic diastereomeric *O*,*N*-acetal having a trifluoromethyl group with organolithium reagents with retention of configurations been reported recently: A. Ishii, F. Miyamoto, K. Higashiyama and K. Mikami, *Tetrahedron Lett.*, 1998, **39**, 1199.

7 Organoaluminium reagents cleave acetals: A. Mori, J. Fujiwara, K. Maruoka and H. Yamamoto, *J. Organomet. Chem.*, 1985, **285**, 83.

8 J. Crank, D. R. K. Harding and S. S. Szinai, *J. Med. Chem.*, 1970, **13**, 1212.

9 Diastereo- and enantio-selective ene reaction and aldol reaction of trifluoroacetaldehyde using a chiral binaphthol–titanium(IV) complex: K. Mikami, T. Yajima, T. Takasaki, S. Matsukawa, M. Terada, T. Uchimaru and M. Maruta, *Tetrahedron*, 1996, **52**, 85.

10 H. Poras, H. Matsutani, J. Yaruva, T. Kusumoto and T. Hiyama, *Chem. Lett.*, in the press. Assignment of the absolute configuration of mesylate (*S*)-(+)-**3a** is also discussed.

11 Organocopper or cuprate reagents associated with BF_3 cleave acetals. See, for example: A. Ghribi, A. Alexakis and J. F. Normant, *Tetrahedron Lett.*, 1984, **25**, 3075.

12 E. B. Baker and H. H. Sisler, *J. Chem. Soc.*, 1953, 5193.

13 T. Yonezawa, Y. Sakamoto, K. Nogawa, T. Yamazaki and T. Kitazume, *Chem. Lett.*, 1996, 855.

14 For a review, see: A. Fukuda, Y. Takanishi, T. Isozaki, K. Ishikawa and H. Takezoe, *J. Mater. Chem.*, 1994, **4**, 997.

Received in Cambridge, UK, 6th March 1998; 8/01847B

Linear fused oligoporphyrins: potential molecular wires with enhanced electronic communication between bridged metal ions

Laurent Jaquinod, Olivier Siri, Richard G. Khoury and Kevin M. Smith*†

Department of Chemistry, University of California, Davis, CA 95616, USA

Syntheses of nanometer scale, directly beta-fused oligoporphyrins sharing an extended π-system are described.

One-dimensional oligomers containing photoactive and/or redox-active units allow the possibility of long distance delocalization of electron density and metal–metal interactions between multiple metal centres.[1] These appealing architectures may present a range of interesting opportunities based on energy- and electron-transfer processes involving communication along and between these units. Such 'photonic molecular wires' based on side-to-side oligomerization of *meso*-functionalized porphyrins have been studied and have been shown to absorb light at one end of an array of porphyrins and then emit a different photon at the other end.[2] Crossley and Burn outlined criteria which these molecular wires need to meet, and described a synthetic approach to rigid π conjugated porphyrin-based molecular wires.[3] These oligoporphyrins, in which individual porphyrin rings are bridged by coplanar aromatic systems, were synthesized by sequential condensation of porphyrin-2,3-diones and/or porphyrin-2,3,12,13-tetraones with aromatic *ortho*-diamines. The versatility of this methodology was further demonstrated in the recent synthesis of thiophene appended porphyrins[4] and donor bridge-acceptor systems involving porphyrin and phenanthroline.[5] However, the conjugation pathway through bridged oligoporphyrins does not exhibit a large fully-delocalized aromatic network which could possibly give rise to metallic type conduction, and could rather be described as a series of weakly-interacting chromophore conjugation loops.[6] Directly fused oligoporphyrins sharing a common extended π electron system have not been yet synthesized. We now describe their synthesis based on pyrrolo-fused porphyrin building blocks, readily available in three steps from Ni^{II} 5,10,15,20-tetraphenylporphyrin.[7]

Because of the instability of the metal-free fused pyrroloporphyrins,[7b] the oligomerization step was carried out on the more stable nickel or copper complexes, **1** and **2**. Under non-acidic conditions, quaternized 2,5-bis(*N*,*N*-dimethylaminomethyl)-3,4-diethylpyrrole **3**[8] reacted smoothly in refluxing MeOH–THF (1 : 1) with **1** in the presence of 10 equiv. of $K_3Fe(CN)_6$ to afford, after chromatography, an 18% yield of porphyrin trimer **4** [λ_{max} 405, 481 (Soret band), 557, 649, 681, 715 nm] (Scheme 1). Pre-quaternisation of the pyrrole with MeI was found to be necessary in order to enhance its reactivity toward the nucleophilic, but sterically congested, fused pyrroloporphyrin **1**. The formation of a new central free base porphyrin was revealed by the NH resonances (−2.55 ppm) in the ^1H NMR spectrum. The molecular structure of **4**·$(HCl)_2$ was further confirmed by X-ray crystallography. The central porphyrin appears to possess enhanced basicity since $CHCl_3$ readily caused protonation to give the dication (which was crystallized). This protonation phenomenon apparently facilitated the crystal packing by enabling π–π stacking to occur only between terminal porphyrins, thus giving rise to independent linear rods of fused porphyrins (Fig. 1). Attempts to grow suitable crystals of the non-protonated species failed, which was most likely caused by a random π–π stacking. The inner porphyrin dication adopts a saddle conformation with a mean plane deviation of the 24 core atoms of 0.376 Å. Both of the terminal nickel porphyrins adopt a ruffled conformation with a mean plane deviation of the 24 core atoms of 0.411 and 0.428 Å. The porphyrin trimer has an edge-to-edge span of 27.0 Å and the intermolecular distance between metals is 16.16 Å.

Mixed condensation of **2**, **3** and pyrrole [THF–MeOH/$K_3Fe(CN)_6$/reflux] gave the fused dimer **6** [λ_{max} 397, 468 (Soret band), 548, 590, 652 nm], as well as some fused trimer **5** in unoptimized yields of 6 and 5%, respectively (Scheme 1). MALDI-TOF mass spectroscopy confirmed dimer and trimer formation, with ions at *m/z* 1069.5 and 1716.8. Compared with pyrroloporphyrin **1**, the bathochromic shift and hyperchromic effect displayed by the fused porphyrins reflect their extended π-conjugation. The Soret bands of **4**–**6** are significantly red

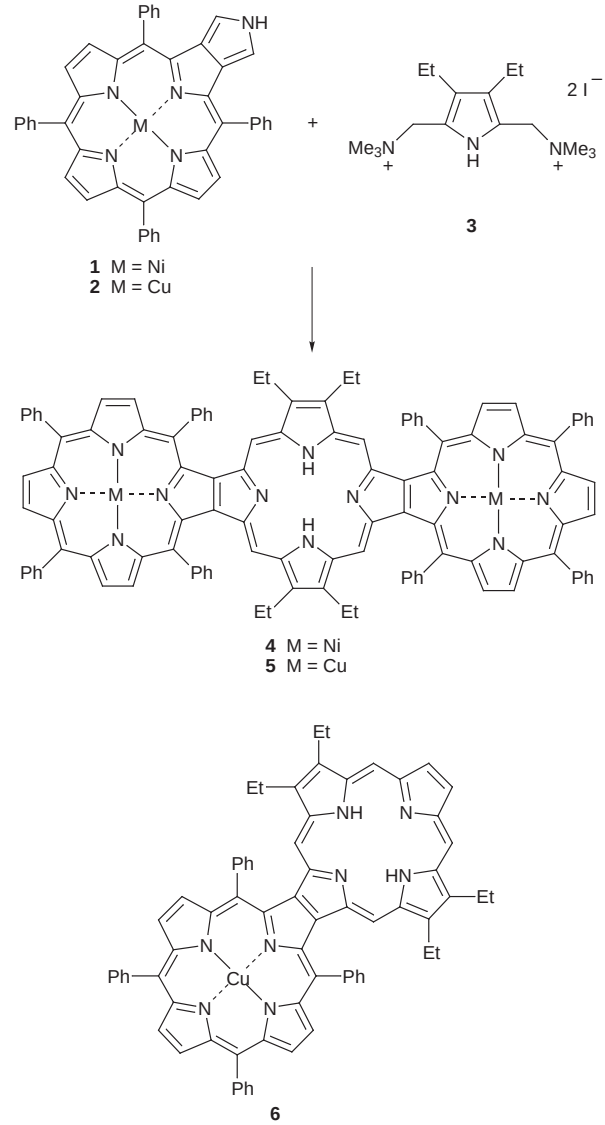

Scheme 1

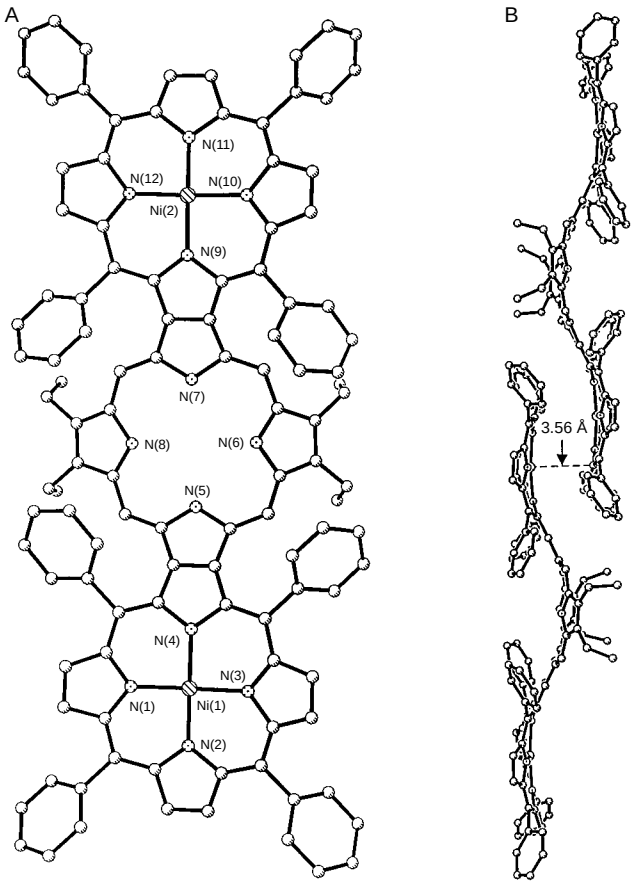

Fig. 1 Molecular structure of **4**. (A) Top view. (B) Side packing view of two trimer molecules. Hydrogen atoms have been omitted for clarity.

shifted from 430 nm (**1**) to 484 and 468 nm in **5** and **6**, respectively. The most notable feature in the absorption spectra is an intense Q band at 652 (dimer **6**) or 722 nm (trimer **5**), reminiscent of a chlorin or bacteriochlorin type visible spectrum. Metallation of **4** using an excess of $Zn(OAc)_2$ in MeOH–$CHCl_3$ gave quantitatively the Ni^{II}–Zn^{II}–Ni^{II} species, **7**. The Q band electronic absorption was found at 742 nm and was shifted to 752 nm upon addition of pyridine. Addition of TFA to a brown solution of free base **4** gave a red–pink dication species displaying three split Soret bands at 414, 455 and 516 nm, and a broad Q band at 838 nm. Surprisingly, these fused linear porphyrins are very soluble in a number of organic solvents, including chlorinated solvents; their protonation even enhances their solubilty.

Further synthetic work is aimed at the functionalization of these systems to generate higher fused oligomers, and at development of the chemistry of the dimer and trimer.

This work was supported by grants from the National Science Foundation (CHE-96-23117) and the National Institutes of Health (HL-22252).

Notes and References

† E-mail: kmsmith@ucdavis.edu

‡ *Crystal Data* for **4**, $C_{112}H_{80}N_{12}Ni_2 \cdot 7.33[CHCl_3] \cdot [CH_3OH] \cdot [2[Cl^-]$: X-ray diffraction data were collected on a Siemens P4 rotating anode diffractometer with a nickel filter monochromator [λ(Cu Kα) = 1.54178 Å] at 130(2) K in $\theta/2\theta$ scan mode to $2\theta_{max}$ = 113°. Crystals were grown from slow diffusion of heptane in a mixture of $CHCl_3$ and MeOH. A single parallelepiped crystal was selected with dimensions 0.16 × 0.08 × 0.04 mm. The crystal lattice was monoclinic with a space group of $P2_1/c$. Cell dimensions were a = 38.335(7), b = 16.994(3), c = 19.110(4) Å, α, γ = 90, β = 100.091(14), V = 12257(4) Å3 and Z = 4 (M = 2689.35, ρ_{calc} = 1.456 g cm^{-3}, μ = 5.628 mm^{-1}). Of 17 517 reflections measured, 16 228 were independent and 8884 had $I > 2\sigma$ (R_{int} = 0.068); number of parameters = 1455. Final R factors were R_1 = 0.1096 (based on observed data) and wR_2 = 0.345 (based on all data). The structure was solved by direct methods and refined (based on F^2 using all independent data) by full matrix least-squares methods (Siemens SHELXTL V. 5.03). Hydrogen atom positions were located by their idealized geometry and refined using a riding model. An absorption correction was applied using XABS2.[9] CCDC 184/848.

1 J. M. Tour, *Chem. Rev.*, 1996, **96**, 537; M. D. Ward, *Chem. Soc. Rev.*, 1995, 121.
2 R. W. Wagner and J. S. Lindsey, *J. Am. Chem. Soc.*, 1994, **116**, 9759; H. L. Anderson, S. J. Martin and D. D. C. Bradley, *Angew. Chem., Int. Ed. Engl.*, 1994, **33**, 655.
3 M. J. Crossley and P. L. Burn, *J. Chem. Soc., Chem. Commun.*, 1991, 1569.
4 M. J. Crossley and J. K. Prashar, *Tetrahedron Lett.*, 1997, 6751.
5 P. T. Gulyas, S. J. Langford, N. R. Lokan, M. G. Ranasinghe and M. N. Paddon-Row, *J. Org. Chem*., 1997, **62**, 3038.
6 T. X. Lu, J. R. Reimers, M. J. Crossley and N. S. Hush, *J. Phys. Chem*. 1994, **98**, 11 878.
7 (*a*) L. Jaquinod, C. Gros, M. M. Olmstead and K. M. Smith, *Chem. Commun.*, 1996, 1475; (*b*) C. P. Gros, L. Jaquinod, R. G. Khoury, M. M. Olmstead and K. M. Smith, *J. Porphyrins Phthalocyanines*, 1997, **1**, 201.
8 L. T. Nguyen, M. O. Senge and K. M. Smith, *J. Org. Chem*., 1996, **61**, 998.
9 S. R. Parkin, B. Moezzi and H. Hope, *J. Appl. Crystallogr*., 1995, **28**, 53.

Received in Corvallis, OR, USA, 2nd March 1998; 8/01676C

Total synthesis and absolute configuration of FR65814

Seiji Amano, Noriko Ogawa, Masami Ohtsuka, Seiichiro Ogawa and Noritaka Chida*†

Department of Applied Chemistry, Faculty of Science and Technology, Keio University, Hiyoshi, Kohoku-ku, Yokohama 223-8522, Japan

The chiral and highly stereoselective synthesis of FR65814 1, a novel immunosuppressant, starting from D-glucose is described; this first total synthesis fully confirms the proposed structure of 1.

FR65814 **1** is a sesquiterpene isolated from the culture broth of *Penicillium* and is reported to show potent immunosuppressive

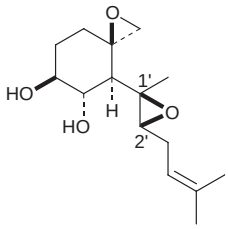

FR65814 **1**

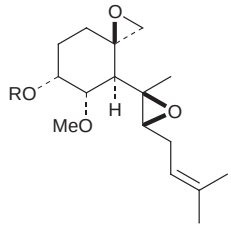

fumagillin **2** R = CO(CH=CH)$_4$CO$_2$H
E
fumagillol **3** R = H

activity.[1] The structure of **1** was tentatively assigned[1] on the basis of the spectral similarity to fumagillol **2**, a hydrolysis product of fumagillin **3**, which showed antiparasitic and carcinolytic activity.[2] The recent discovery of the inhibitory activity of fumagillin against endothelial cell proliferation and tumor-induced angiogenesis has attracted much biological attention,[3] and compounds related to fumagillin are expected to be anti-cancer drug candidates.[3] Such interesting biological activity as well as their challenging structures have stimulated synthetic efforts and the total syntheses of racemic fumagillin[4a] and optically active fumagillol[4b] have been reported. However, no report on the synthesis of **1** has appeared. Here, as a part of our continuous studies on the synthesis of biologically important compounds containing the cyclohexane unit, starting from aldohexoses and utilizing Ferrier's carbocyclization,[5,6] we report the first total synthesis of **1** from D-glucose.

Commercially available methyl 4,6-*O*-benzylidene-α-D-glucopyranoside **4** was transformed into 2,3-di-*O*-(4-methoxybenzyl)-6-deoxyhex-5-enopyranoside derivative **5** (Scheme 1) by essentially the same procedure as that reported for the preparation of the corresponding di-*O*-benzyl derivative[6a] (4-methoxybenzyl chloride was employed instead of benzyl bromide). Catalytic Ferrier's carbocyclization of **5** with Hg(OCOCF$_3$)$_2$ in aqueous acetone,[7] followed by β-elimination afforded cyclohexenone **6** in 84% yield. Reduction of the carbonyl group using Luche's conditions gave allyl alcohol **7** as the sole product in 90% yield. After protection of the alcohol function as a tetrahydropyranyl (THP) ether (99% yield), the acetoxy function in **8** was removed *via* a xanthate to provide **9** in 63% yield. Deprotection of the *O*-THP group afforded **10** in 96% yield. Claisen rearrangement of **10** with triethyl orthopropionate at 140 °C successfully introduced a carbon-side chain with the correct stereochemistry to provide **11** (74% yield).‡ Saponification of the ester group in **11** with Bu^{t}OK in DMSO[8] followed by iodolactonization gave **12** as the sole product,‡ whose iodo function was cleanly removed with Bu$^n_3$SnH to give **13** in 80% yield from **11**. DIBAL-H reduction of **13** afforded the corresponding lactol, whose Wittig reaction with $Ph_3P{=}CH_2$ gave **14** in 90% yield. After protection of the hydroxy group in **14**, the alkene portion was converted into primary alcohol by

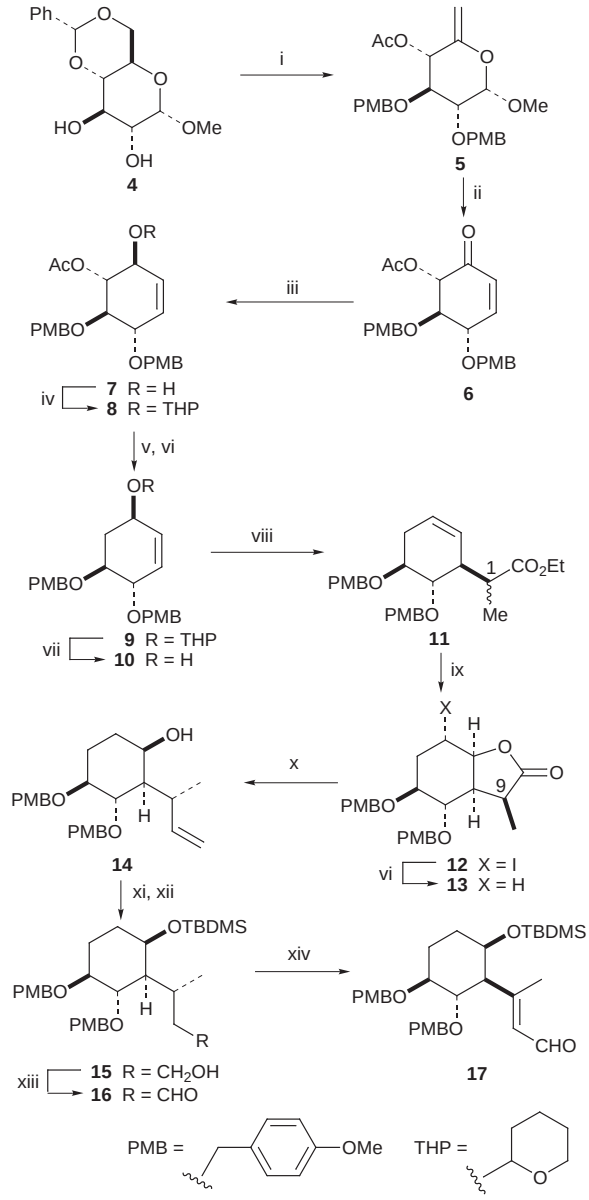

Scheme 1 *Reagents and conditions*: i, see ref. 6(*a*); ii, Hg(OCOCF$_3$)$_2$ (5 mol%), acetone–H$_2$O, then MsCl, Et$_3$N, CH$_2$Cl$_2$; iii, NaBH$_4$, CeCl$_3$·7H$_2$O, MeOH, 0 °C; iv, 3,4-dihydro-2*H*-pyran, PPTS, CH$_2$Cl$_2$; v, MeONa, MeOH, then NaH, imidazole, CS$_2$, MeI, THF; vi, AIBN, Bu$^n_3$SnH, toluene, reflux; vii, PPTS, EtOH, 50 °C; viii, EtC(OEt)$_3$, EtCO$_2$H, 140 °C; ix, Bu^{t}OK, DMSO, then I$_2$, KI, aq. NaHCO$_3$–THF; x, DIBAL-H, toluene, −78 °C, then Ph$_3$PMe$_3$Br, BuLi, THF; xi, TBDMSOTf, 2,6-lutidine, CH$_2$Cl$_2$, 0 °C; xii, BH$_3$·THF, THF, 0 °C, then H$_2$O$_2$, NaOH; xiii, Pr$^n_4$NRuO$_4$, NMO, CH$_2$Cl$_2$; xiv, KN(SiMe$_3$)$_2$, TMSCl–Et$_3$N, THF, 0 °C, then Pd(OAc)$_2$, MeCN, 0 °C

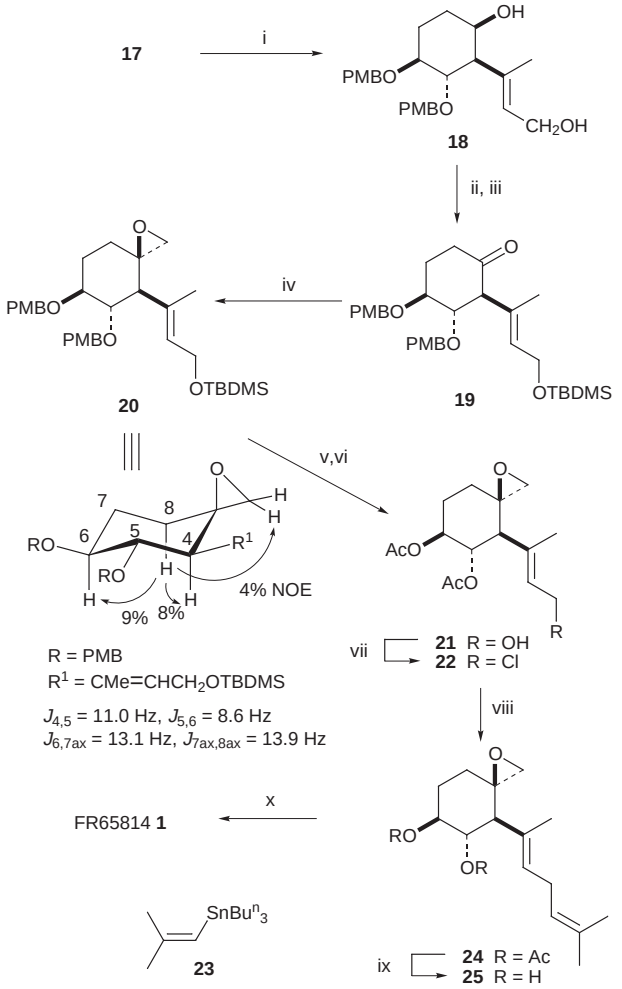

Scheme 2 *Reagents and conditions*: i, DIBAL-H, toluene, −78 °C, then Bu^n_4NF, THF; ii, TBDMSCl, imidazole, DMF; iii, DMSO, Ac_2O; iv, $Me_3S(O)I$, NaH, DMSO, room temp.; v, DDQ, CH_2Cl_2–H_2O; vi, Ac_2O, pyridine, then Bu^n_4NF, THF; vii, LiCl, $MeSO_2Cl$, collidine, DMF; viii, **23**, $Pd(PPh_3)_4$ (10 mol%), THF, 50 °C; ix, MeONa, MeOH; x, vanadyl acetylacetonate (5 mol%), Bu^tOOH, CH_2Cl_2, −18 °C

hydroboration-oxidation to provide **15** (85% yield). Perruthenate oxidation[9] of **15** gave aldehyde **16** in 81% yield, which was converted into α,β-unsaturated aldehyde with *E*-geometry§ **17** in 45% yield by silyl enol ether formation followed by treatment with stoichiometric amount of $Pd(OAc)_2$.[10] The *Z*-isomer of **17** was isolated as the minor product (4% yield).

Having finished the preparation of highly oxygenated cyclohexane ring with carbon side-chain, elongation of the carbon chain and introduction of the bis-epoxide functionality were explored. DIBAL-H reduction of **17** and subsequent deprotection of the *O*-silyl group afforded diol **18** (Scheme 2). Protection of the primary alcohol function followed by oxidation of the secondary alcohol with Ac_2O–DMSO generated ketone **19** in 82% yield from **17**. Reaction of **19** with stabilized sulfur ylide[11] proceeded stereoselectively and afforded spiro epoxide **20** as the sole product in 57% yield. The observed coupling constants and NOE of **20** supported the assigned structure. Treatment of **20** with DDQ followed by conventional acetylation afforded diacetate, whose *O*-silyl protecting group was removed to provide **21** in 90% yield. The allyl alcohol **21** was transformed into allylic chloride **22** quantitatively. Stille coupling[12] of **22** with isobutenyltributyltin[13] **23** in the presence of $Pd(PPh_3)_4$ successfully provided the coupling product, *E*-diene§ **24**, in 72% yield. Removal of the *O*-acetyl group gave diol **25** in 95% yield. The final transformation, introduction of the second epoxide functionality, was stereoselectively achieved by vanadium-catalyzed epoxidation[14] to give FR65814 **1** in 70% yield.¶ The spectroscopic (^{1}H and ^{13}C NMR) data for synthetic **1** were identical with those of natural FR65814, and the physical properties of **1** {mp 39–40 °C (from Et_2O–hexanes); $[\alpha]_D^{21}$ − 41 (*c* 0.25, MeOH)} showed good accord with those of the natural product {mp 39–40 °C (from Et_2O–hexanes); mixed mp, 39–40 °C; $[\alpha]_D^{23}$ − 38.4[1] (*c* 2.4, MeOH)}. This successful first total synthesis of **1** confirmed the assigned structure of FR65814, and provided a novel synthetic pathway from carbohydrates to highly oxygenated terpenes possessing a cyclohexane unit.

We thank Fujisawa Pharmaceutical Co., Ltd., (Osaka, Japan) for providing us with natural FR65814. Financial support in the form of a Grant-in-Aid for Scientific Research on Priority Areas from the Ministry of Education, Science, Sports and Culture, of the Japanese Government is gratefully acknowledged.

Notes and References

† E-mail: chida@applc.keio.ac.jp

‡ Compound **11** was obtained as an inseparable diastereomeric mixture at C-1 (1 : 1). Interestingly, epimerization at C-1 occurred during the saponification step and compound **12** was obtained as the single product. The stereochemistry at C-9 in **12** was confirmed by NOE experiments.

§ The NOE experiments clearly showed that the geometry of the double bond in both **17** and **24** should be *E*. No isomerization of the double bond was observed during the coupling reaction between **22** and **23**.

¶ A small amount (less than 5%) of diastereomeric epoxide (1′,2′-diepi-FR65814) was isolated. The chemical shifts and appearance of the hydrogen attached to the carbon bearing epoxide ring (H-2′) of **1** and its diastereomer in the ^{1}H NMR spectra ($CDCl_3$) are found to be characteristic: FR65814, fumagillol, δ 2.61 (dd, *J* 5.9, 7.1); 1′,2′-diepi-FR65814, δ 3.14 (br m); *cf.* δ 2.56 (dd, *J* 5.9, 7.1).

1 H. Hatanaka, T. Kino, M. Hashimoto, Y. Tsurumi, A. Kuroda, H. Tanaka, T. Goto and M. Okuhara, *J. Antibiot.*, 1988, **41**, 999.
2 J. A. DiPaolo, D. S. Tarbell and G. E. Moore, in *Antibiotics Annual 1958–1959*, ed. H. Welch and F. Marti-Ibanez, Medical Encyclopedia, Inc., New York, 1959, p. 541.
3 D. E. Ingber, T. Fujita, S. Kishimoto, K. Sudo, T. Kanamaru, H. Brem and J. Folkman, *Nature*, 1990, **348**, 555; D. E. Ingber, *Semin. Cancer Biol.*, 1992, **3**, 57; J. Folkman and D. E. Ingber, *Semin. Cancer Biol.*, 1992, **3**, 89; N. Sin, L. Meng, M. Q. W. Wang, J. J. Wen, W. G. Bornmann and C. M. Crews, *Proc. Natl. Acad. Sci. USA*, 1997, **94**, 6099; E. C. Griffith, Z. Su, B. E. Turk, S. Chen, Y.-H. Chang, Z. Wu, K. Biemann and J.O. Liu, *Chem. Biol.*, 1997, **4**, 461.
4 (*a*) E. J. Corey and B. B. Snider, *J. Am. Chem. Soc.*, 1972, **94**, 2549; (*b*) D. Kim, S. K. Ahn, H. Bae, W. J. Choi and H. S. Kim, *Tetrahedron Lett.*, 1997, **38**, 4437.
5 R. J. Ferrier and S. Middleton, *Chem. Rev.*, 1993, **93**, 2779.
6 (*a*) N. Chida, M. Ohtsuka, K. Nakazawa and S. Ogawa, *J. Org. Chem.*, 1991, **56**, 2976; (*b*) N. Chida, M. Ohtsuka and S. Ogawa, *J. Org. Chem.*, 1993, **58**, 4441; N. Chida, M. Jitsuoka, Y. Yamamoto, M. Ohtsuka and S. Ogawa, *Heterocycles*, 1996, **43**, 1385; N. Chida, K. Sugihara and S. Ogawa, *J. Chem. Soc., Perkin Trans. 1*, 1997, 275.
7 N. Chida, M. Ohtsuka, K. Ogura and S. Ogawa, *Bull. Chem. Soc. Jpn.*, 1991, **64**, 2118.
8 F. C. Chang and N. F. Wood, *Tetrahedron Lett.*, 1964, 2969.
9 S. V. Ley, J. Norman, W. P. Griffith and S. P. Marsden, *Synthesis*, 1994, 639.
10 Y. Ito, T. Hirao and T. Saegusa, *J. Org. Chem.*, 1978, **43**, 1011.
11 E. J. Corey and M. Chaykovsky, *J. Am. Chem. Soc.*, 1965, **87**, 1353.
12 F. K. Sheffy, J. P. Godschalx and J. K. Stille, *J. Am. Chem. Soc.*, 1984, **106**, 4833; J. K. Stille, *Angew. Chem., Int. Ed. Engl.*, 1986, **25**, 508.
13 M. L. Saihi and M. Pereyre, *Bull. Soc. Chim. Fr.*, 1977, 1251.
14 K. B. Sharpless and R. C. Michaelson, *J. Am. Chem. Soc.*, 1973, **95**, 6136.

Received in Cambridge, UK, 19th March 1998; 8/02169D

Synthesis of chiral carbohydrate-centered dendrimers

Michael Dubber and Thisbe K. Lindhorst*†

Institut für Organische Chemie der Universität Hamburg, Martin-Luther-King-Platz 6, D-20146 Hamburg, Germany

D-Glucose was converted into its per-*O*-(2-aminoethyl)-functionalized derivative 4, which served as initiator core for the construction of the chiral, monodisperse PAMAM-type carbohydrate-centered hybrid dendrimer 7.

Dendrimer chemistry is a rapidly developing field of research.[1] Dendrimers offer the prospect of novel materials with advantagous properties, allowing them to serve as soluble catalysts,[2] dendritic boxes[3] or other supramolecular dendritic arrangements. Furthermore, new applications such as enantioselective synthesis with chiral dendrimers, or favourable bioapplications such as in transfection[4] and glycobiology, are currently being explored. Dendrimer chemistry has been combined with carbohydrate chemistry in order to form multivalent glycomimetics[5] (glycodendrimers) with antiadhesive properties or other carbohydrate containing dendrimers.[6] Other than from the point of view of glycobiology, the combination of carbohydrates and dendrimers is attractive for the manipulation of dendritic structures leading to modified properties of, as yet, unestimated value. Carbohydrate cores are especially appealing for the design of dendrimers due to their easy availibility from the chiral pool and renewable resources, biocompatibility, low toxicity and natural polyfunctionality. In addition, intrinsic chirality may be introduced into dendrimers by using carbohydrate cores.[7] Furthermore, the stereochemical shape of dendrimers may be easily manipulated by choosing differently configurated monosaccharides, and the core multiplicity may be altered by utilizing mono-, di- or even oligosaccharides as carbohydrate cores, such as trehalose or raffinose. This is of special interest as the shape and composition of dendrimers may dramatically affect their host–guest relationships.[8]

Here we report the first synthesis of a carbohydrate-centered Starburst® PAMAM dendrimer based on a reaction sequence which is suited to converting reducing sugars into carbohydrate derivatives which can serve as initiator cores for the development of PAMAM generations. This was exemplified with D-glucose. First, allyl α-D-glucoside **1**, which was obtained by Fischer glycosylation, was perallylated to **2** under phase transfer catalysis (Scheme 1). Partially allylated products were not formed as the allylation rate increases with the extent of allylation of the starting material under these conditions.[9] Ozonolysis of the resulting allyl 2,3,4,6-tetra-*O*-allyl-α-D-glucoside (**2**) was performed in a $NaHCO_3$-buffered CH_2Cl_2–MeOH reaction mixture[10] to yield the desired penta-hemiacetal after reduction with PPh_3. This was characterized as the corresponding pentahydrate by NMR spectroscopy in D_2O. The penta-hemiacetal was submitted to a reductive amination reaction: application of $BnNH_2$ led to nearly inseparable mixtures comprised of cyclic amines, due to intramolecular reactions. However, the use of Bn_2NH and sodium acetoxyborohydride[11] as the reducing agent gave the desired benzyl cluster **3** at −10 °C in high yields without purification problems. Then **3** was converted into the pentaamine **4** by heterogeneous catalytic transfer hydrogenation reaction[12] with ammonium formate and Pd (10% on charcoal) in MeOH in a clean reaction. Thus the target compound **4** could be synthesized starting from allyl glucoside (**1**) in 43% overall yield.

The glucose derivative **4** represents a stereochemically well-defined, oligofunctional molecule with five uniformly functionalized spacers. It may serve as core molecule for the synthesis of carbohydrate-centered glycoclusters[13] or of carbohydrate-centered dendrimers. It was submitted to the reaction sequence leading to PAMAM dendrimer generations, consisting of the exhaustive Michael addition of the polyamine to methyl acrylate, followed by amidation of the resulting methyl esters with ethylenediamine.[14] Indeed reaction of **4** with methyl acrylate led to the decaester **5** in quantitative yield, which was quantitatively converted into the first generation hybrid PAMAM dendrimer **6** with ethylenediamine (Scheme 2). Further branching at the amino functions at the periphery of the molecule led to the eicosaester **7**, also in quantitative yield. The monodisperse structures of **5**–**7** could unequivocally be confirmed by NMR spectroscopy as ^1H–^{13}C HMBC NMR allowed the detection of each individual branch of every molecule.‡ All synthesized compounds are chiral.§ However, the specific rotation values of the carbohydrate-centered dendrimers decrease with increasing generation, according to observations made in the literature,[15] whereas the molar rotation values remain in the same range (*ca.* 400).

In conclusion, a reaction sequence has been elaborated which is generally applicable for the facile and uniform conversion of free saccharides into fully *O*-(2-aminoethyl)-functionalized derivatives such as **4**. These are suited for dendritic expansion, opening the door into a wide array of structurally diverse, but well-defined, carbohydrate-centered PAMAM dendrimers. The new hybrid dendrimers may be custom-designed by choice of the carbohydrate core giving rise to possible advantageous

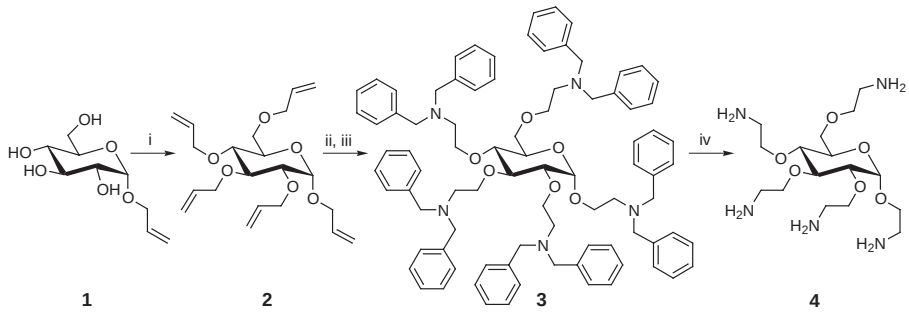

Scheme 1 *Reagents and conditions*: i, allyl chloride (5 equiv.), 40% aq. NaOH, Bu_4NBr (1 equiv.), 35 °C, 16 h, 76%; ii, O_3, $NaHCO_3$, CH_2Cl_2–MeOH 6 : 1, work-up with PPh_3; iii, $Na(AcO)_3BH$, AcOH, Bn_2NH, THF, work-up with 1 M NaOH, 74% (2 steps); iv, Pd–C (10%), NH_4HCO_2, MeOH, 76%

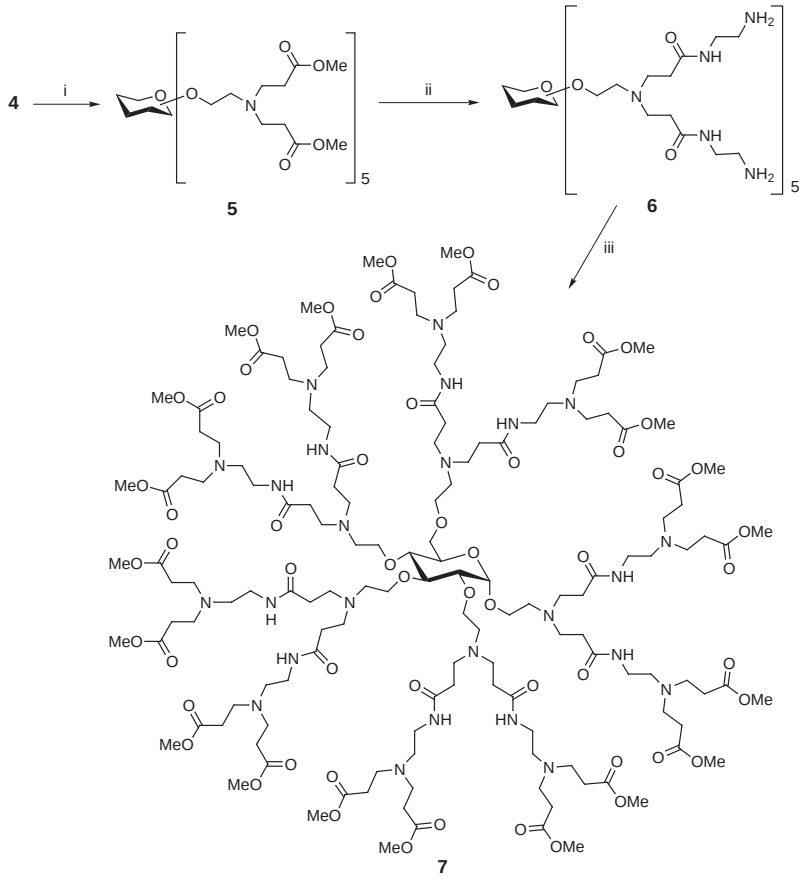

Scheme 2 *Reagents and conditions*: i, methyl acrylate (22 equivs.), MeOH, 3 d, room temp., quant.; ii, ethylendiamine (600 equivs.), MeOH, 5 d, +5 °C, quant. iii, methyl acrylate (60 equivs.), MeOH, 3 d, room temp., quant.

properties compared to classical PAMAMs, such as altered solubilities and overall shapes, better biodegradibility, lower toxicity and chirality.

The authors wish to thank Dr V. Sinnwell for NMR experiments, Professor Dr J. Thiem for his assistance and the Fonds der Chemischen Industrie (FCI) for financial support.

Notes and References

† E-mail: tklind@chemie.uni-hamburg.de

‡ All compounds showed consistent NMR and mass spectral data. *Selected data* for **7**: MALDI-TOF (positive) [Calc. for $C_{146}H_{257}N_{25}O_{56}$: 3258.8. Found 3261.0 (M + 1)]; δ_H(500 MHz, CD_3OD) 5.02 (d, 1 H, $J_{1,2}$ 3.2, H-1), 4.03–3.93 (m, 2 H, OCH_2CH_2N), 3.88–3.59 (m, 73 H, H-5, H-6, H-6′, 4 OCH_2CH_2N, 20 OCH_3), 3.54 (dd ≈ t, 1 H, $J_{2,3}$ 9.2, $J_{3,4}$ 9.2, H-3), 3.34–3.27 [m, 21 H, H-2, 10 $C(O)NCH_2CH_2N$], 3.26 (dd ≈ t, 1 H, $J_{4,5}$ 9.2, H-4), 3.0–2.89 [m, 20 H, 10 $NCH_2CH_2C(O)N$], 2.89–2.76 (dd ≈ t, 50 H, 5 OCH_2CH_2N, 20 $NCH_2CH_2CO_2Me$), 2.64–2.57 [dd ≈ t, 20 H, 10 $C(O)NCH_2CH_2N$], 2.54–2.49 (dd ≈ t, 40 H, 20 $NCH_2CH_2CO_2Me$), 2.49–2.41 [dd ≈ t, 20 H, 10 $NCH_2CH_2C(O)N$]; δ_C 175.9 (20 CO_2Me), 175.7–175.5 (10 CO_2N), 99.2 (C-1), 84.5 (C-3), 83.2 (C-2), 80.9 (C-4), 73.1 (C-5), 73.0, 72.9, 72.5, 71.8, 70.7, 68.3 (C-6, 5 OCH_2CH_2N), 55.7, 55.6, 55.5, 55.0, 54.7 (5 OCH_2CH_2N), 55.0 [20 $C(O)NCH_2CH_2N$], 53.4 (20 CO_2CH_3), 52.7, 52.6, 52.6, 52.5, 52.5 [10 $NCH_2CH_2C(O)N$], 51.7 (20 $NCH_2CH_2CO_2Me$), 39.7 [10 $C(O)NCH_2CH_2N$], 35.8, 35.7, 35.6, 35.6, 35.5 [10 $NCH_2CH_2C(O)N$], 34.8 (20 NCH_2CH_2 CO_2Me).

§ Selected specific optical rotations: **1** $[\alpha]_D^{20}$ +160.5 (*c* 1.09, MeOH); **3** $[\alpha]_D^{27}$ +35.2 (*c* 1.18, $CHCl_3$); **5** $[\alpha]_D^{27}$ +34.6 (*c* 0.96, MeOH); **7** $[\alpha]_D^{25}$ +13.1 (*c* 0.38, MeOH).

1 F. Zeng and S. C. Zimmerman, *Chem. Rev.*, 1997, **97**, 1681.
2 M. T. Reetz, G. Lohmer and R. Schwickardi, *Angew. Chem.*, 1997, **109**, 1559; *Angew. Chem., Int. Ed. Engl.*, 1997, **36**, 1526.
3 J. F. G. A. Jansen, E. M. M. de Brabander-van den Berg and E. W. Meijer, *Recl. Trav. Chim. Pays-Bas*, 1995, **114**, 225.
4 M. X. Tang, C. T. Redemann and F. C. Szoka, *Bioconjugate Chem.*, 1996, **7**, 703.
5 D. Zanini and R. R. Roy, *J. Am. Chem. Soc.*, 1997, **119**, 2088.
6 N. Jayaraman, S. A. Nepogodiev and J. F. Stoddart, *Chem. Eur. J.*, 1997, **3**, 1193.
7 H. W. I. Peerlings and E. W. Meijer, *Chem. Eur. J.*, 1997, **3**, 1563; P. K. Murer, J.-M. Lapierre, G. Greiveldinger and D. Seebach, *Helv. Chim. Acta*, 1997, **80**, 1648.
8 R. Esfand, A. E. Beezer, J. C. Mitchell and L. J. Twyman, *Pharm. Sci.*, 1996, **2**, 1; D. M. Watkins, Y. Sayed-Sweet, J. W. Klimash, N. J. Turro and D. A. Tomalia, *Langmuir*, 1997, **13**, 3136.
9 R. M. Nouguier and M. Mchich, *J. Org. Chem.*, 1985, **50**, 3296.
10 S. L. Schreiber, R. E. Claus and J. Reagan, *Tetrahedron Lett.*, 1982, **23**, 3867.
11 A. F. Abdel-Magid, K. G. Carson, B. D. Harris, C. A. Maryanoff and R. D. Shah, *J. Org. Chem.*, 1996, **61**, 3849.
12 S. Ram and L. D. Spicer, *Tetrahedron Lett.*, 1987, **28**, 515.
13 C. Kieburg, M. Dubber and T. K. Lindhorst, *Synlett*, 1997, 1447.
14 A. D. Miltzer, D. A. Tirrell, A. A. Jones, P. T. Inglefield, D. M. Hedstrand and D. A. Tomalia, *Macromolecules*, 1992, **25**, 4541.
15 D. Seebach, J.-M. Lapierre, G. Greiveldinger and K. Skobridis, *Helv. Chim. Acta*, 1994, **77**, 1673.

Received in Liverpool, UK, 20th January 1998; 8/00560E

New optically active hexaaza triphenolic macrocycles: synthesis, molecular structure and crystal packing features

Srinivas R. Korupoju and Panthapally S. Zacharias*†

School of Chemistry, University of Hyderabad, Hyderabad-500 046, India

3 + 3 Condensed optically active hexaaza triphenolic macrocyles 1 and 2 are synthesised and characterised; molecular and close packing structures of macrocycle 2 are discussed.

Synthesis and study of new ligands with phenolic groups is an area of active research interest because of their use as models for biological metal-binding sites, their ability to form metal complexes with interesting magnetic exchange, redox and catalytic properties.[1] 2,6-Diformyl-4-methylphenol[2] **A** is a useful source to synthesise such ligands and oxo-bridged macrocyclic complexes with diamines in the presence of template metal salts.[1] Although 2 + 2 condensed macrocyclic dinuclear complexes are the favoured products, a few 3 + 3 and 4 + 4 multinuclear macrocyclic complexes have been reported,[3] but the free ligands have not been isolated. Preformed ligands are required to investigate host–guest interactions, to synthesise complexes of metals inert to template reactions and complexes of heteronuclear metals. So far only 2 + 2 condensed metal-free macrocycles have been isolated (H^+ as a template ion) from **A**.[4] For the first time we report the synthesis and structural characterisation of a new template-free, 3 + 3 condensed and optically active hexaimine triphenolic Schiff base macrocycle **1** derived from **A** and *trans*-(*R*,*R*)-1,2-cyclohexyldiamine **B**,[5] and its reduced analogue hexaamine triphenolic macrocycle **2**. Macrocycles **1** and **2** have the potential to bind three metal ions through oxo-bridges.

The reaction of **A** and **B** in methanol in equimolar ratio using the high dilution technique affords a 3 + 3 Schiff-base macrocycle **1** as yellow solid in high yield. The molecular ion peak at *m/z* 727 of **1** indicates the condensation of three units of **A** and three units of **B**. The macrocycle **2**, the reduced analogue of macrocycle **1** was obtained by the reduction of **1** with $NaBH_4$ in methanol[6] and was identified by its molecular ion peak at *m/z* 739. Compounds **1** and **2** are also characterised by IR, NMR and CHN analysis.‡ The molecular structure of **2** was confirmed from its crystal structure (crystals of **1** were not suitable for X-ray structure determination).

The X-ray structure of **2**§ was performed on single crystals grown by slow evaporation from benzene. It crystallises in space group *R*3 (no.146) wherein the molecular three-fold symmetry coincides with the crystallographic three-fold axis. The macrocyclic cavity is defined by 27 atoms in which six N-atoms and 21 C-atoms are present. The three phenolic-OH groups projected inside the cavity generate three equivalent N_2O_2 sub-cavities. The geometry of these sub-cavities appears suitable for metal complexation as the two N and two O atoms provide appropriate coordination sites. The macrocycle is stabilised by intra-molecular (O–H···N, N–H···O, N–H···N) hydrogen bonding with H···acceptor distances lying in the range 2.02–2.29 Å. An ORTEP drawing of **2** with intramolecular hydrogen bonding is shown in Fig. 1.

The macrocycle has an internal hydrophilic cavity capable of forming hydrogen bonds and has an external hydrophobic periphery. The molecules are extended in the *ab* plane with the mean plane of the molecule perpendicular to the *c*-axis. It can be seen from the packing diagram (Fig. 2) that each molecule is surrounded by six molecules leading to a trigonal network structure. The organisation of the molecules in the *ab* plane is governed by the hydrophobic interaction between the methyl groups of moiety **A** and methylene groups of moiety **B** and is not assisted by any other observable interactions. The two $CH_3\cdots CH_3$ and cyclohexyl $CH_2\cdots CH_2$ close packing C–C distances are 3.96 and 4.00 Å, respectively. The stacking in the *c*-axis is maintained by inter-molecular N–H···N hydrogen bonding [N(2)–H(2)···N(1): D = 3.22 Å, d = 2.23 Å, θ =

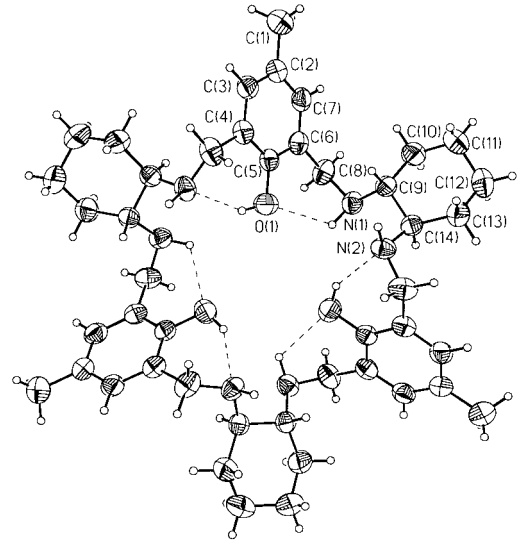

Fig. 1 An ORTEP diagram of macrocycle **2**; thermal ellipsoids are shown at the 50% probability level

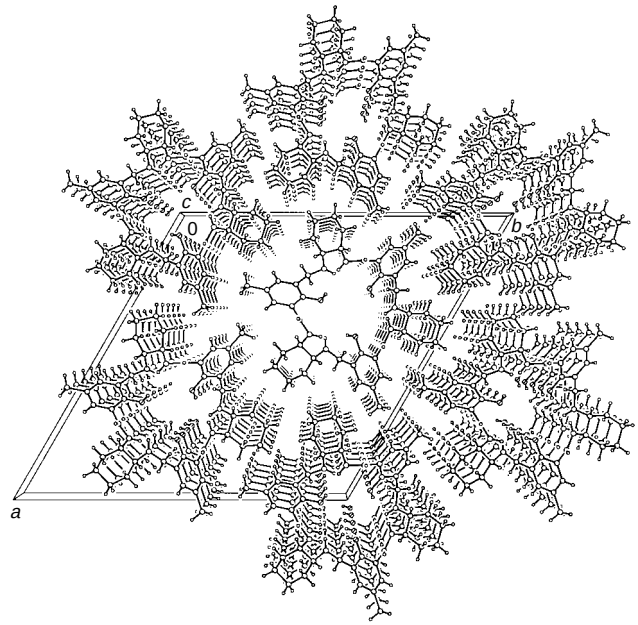

Fig. 2 Stacks viewed down the *c*-axis of macrocycle **2**

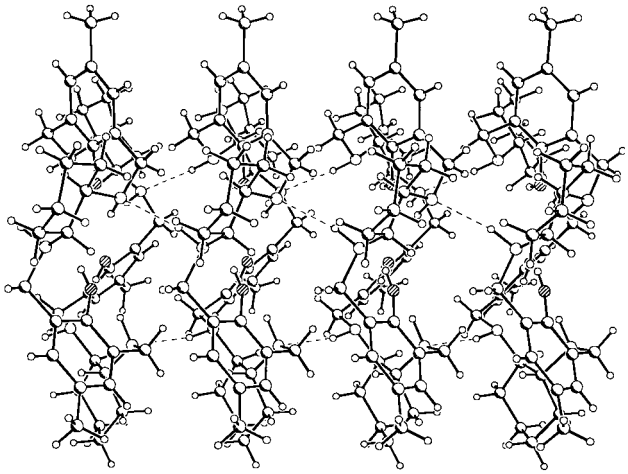

Fig. 3 The intermolecular hydrogen bonds between the molecules viewed down the *Y*-axis of macrocycle **2**

167.32°) and supported by weak C–H···O interactions (H···O, 2.9 Å) leading to a channel like structure. The aromatic rings of the moiety **A** in the stacks are separated by 5.143 Å as shown in Fig. 3. The three-dimensional trigonal assembly of the macrocycle is maintained by hydrophobic interactions in the *ab* plane and hydrogen bonding along the *c*-axis. Although carry-over of the molecular symmetry into the crystal is not very common, the non-centrosymmetric trigonal networking of molecules as shown in Fig. 3 is reported to have important applications in NLO and an example of such arrangements due to intermolecular hydrogen bonding has been reported recently.[7]

The X-ray structure of macrocycle **2** suggests an analogous structure for macrocycle **1**. The successful synthesis of **1** and **2** results from the stability of the 27-membered macrocycle possibly due to its optimum ring size and the intramolecular hydrogen bonding interactions.

Further studies on the host–guest properties of **1** and **2** with metal ions, solvent molecules, organic guest molecules and variations in crystal packing pattern by changing the substituents on the macrocycle in different solvents are in progress.

S. R. K. gratefully acknowledges the UGC, New Delhi for financial support and the National Single Crystal Diffractometer Facility of this department (DST) for crystallography.

Notes and References

† E-mail: pszsc@uohyd.ernet.in

‡ **1**: yield 80%. IR: ν/cm^{-1} 1639 (C=N); ^{1}H NMR ($CDCl_3$) δ 8.66 (s, HC=N), 8.2 (s, HC=N), 7.56 (s, Ar-H), 6.89 (s, Ar-H), 3.3 (m, =N–CH), 2.08 (s, Ar-CH_3), 1.86–1.46 (m, CH_2CH_2). ^{13}C NMR ($CDCl_3$) δ 19.92, 24.45, 33.26, 33.48, 73.49, 75.45, 118.78, 122.99, 126.89, 129.56, 134.20, 156.15, 159.32, 163.46; FABMS: Calc. for $C_{45}H_{54}N_6O_3$ *m/z* 727. Found 727 (M^+). Anal. Calc. C, 74.35; H, 7.49; N, 11.57. Found: C, 74.23; H, 7.46; N, 11.93%. $[\alpha]_D^{27}$ = −239 (*c* 1, CH_2Cl_2).

2: yield 70%. IR: ν/cm^{-1} 1612 (NH); ^{1}H NMR ($CDCl_3$) δ 6.8 (s, Ar-H), 5.00 (br, NH), 3.6–3.9 (q, $HNCH_2$), 2.1 (s, Ar-CH_3), 2.45–1.2 (m, CH_2CH_2); ^{13}C NMR ($CDCl_3$) δ 20.52, 25.00, 31.24, 47.74, 60.47, 125.17, 127.21, 128.24, 154.18; FABMS: Calc. for $C_{45}H_{66}N_6O_3$ *m/z* 739. Found: 739 (M^+). Anal. Calc. C, 73.13; H, 9.00; N, 11.38. Found: C, 73.44; H, 8.99; N, 11.30%. $[\alpha]_D^{27}$ = −189 (*c* 1, CH_2Cl_2).

§ *Crystal structure determination of* **2**: $C_{45}H_{66}N_6O_3$, M = 739, trigonal, space group $R\bar{3}$ (no.146), a = 26.499(4), b = 26.499(4), c = 5.1433(10) Å, α = β = 90°, γ = 120.0° U = 3127.7(9) Å^3, T = 293(2) K, Z = 3, μ = 0.07 mm^{-1}; 1367 independent reflections out of 3641 collected with 1.52 < θ < 24.94, 173 parameters one restraint, R_{int} = 0.0229. Refinement method: full-matrix least squares on F^2, Final R indices [$I > 2\sigma(I)$]: R_1(observed) = 0.0449, wR_2 = 0.1073. R(all data): R_1 = 0.0535, wR_2 = 0.1211. The absolute configuation of macrocycle **2** could not be determined from the X-ray data. CCDC 182/867.

1 N. H. Pilkington and R. Robson, *Aust. J. Chem*., 1970, **23**, 2225; P. A. Vigato, S. Tamburini and D. E. Fenton, *Coord. Chem. Rev*., 1990, **106**, 25; P. Guerriero, S. Tamburini and P. A. Vigato, *Coord. Chem. Rev*., 1995, **139**, 17; V. McKee and S. S. Tandon, *J. Chem. Soc., Dalton Trans*., 1991, 221; S. Brooker and T. C. Davidson, *Chem. Commun*., 1997, 2007; S. K. Dutta, J. Ensling, R. Werner, U. Florke, W. Haase, P. Gutlich and K. Nag, *Angew. Chem., Int. Ed. Engl*., 1997, **36**, 152.

2 R. R. Gagne, C. L. Spiro, T. J. Smith, C. A. Hamann, W. R. Thies and A. K. Shiemke, *J. Am. Chem. Soc*., 1981, **103**, 4073.

3 A. J. Downard, V. Mc Kee, and S. S. Tandon, *Inorg. Chim. Acta*., 1990, 173; D. E. Fenton, S. J. Kitchen, C. M. Spencer, S. Tamburini and P. A. Vigato, *J. Chem. Soc., Dalton Trans*., 1988, 685; H. C. Aspinall, J. Black, I. Dodd, M. M. Harding and S. J. Winkley, *J. Chem. Soc., Dalton Trans*., 1993, 709; B. F. Hoskins, R. Robson and P. Smith, *J. Chem. Soc., Chem. Commun*., 1990, 488; S. S. Tandon, L. K. Thompson, J. N. Bridson and C. Benelli, *Inorg. Chem*., 1995, **34**, 5507; S. Brooker, V. McKee, W. B. Shepard and L. K. Pannell, *J. Chem. Soc., Dalton Trans*., 1987, 2555; K. K. Nanda, K. Venkatsubramanian, D. Majumdar and K. Nag, *Inorg. Chem*., 1994, **33**, 1581.

4 A. J. Atkins, D. Black, A. J. Blake, A. Marin-Becerra, S. Parsons, L. Rez-Ramirez and M. Schroder, *Chem. Commun*., 1996, 457; Z. Wang, J. Reibenspies and A. E. Martell, *Inorg. Chem*., 1997, **36**, 629.

5 J. F. Larrow, E. C. Jacobson, Y. Gao, Y. Hong, X. Nie and C. M. Zepp, *J. Org. Chem*., 1994, **59**, 1939.

6 S. K. Mandal and K. Nag, *J. Org. Chem*., 1986, **51**, 3900.

7 V. R. Thalladi, S. Brasselet, D. Blaser, R. Boese, J. Zyss, A. Nangia and G. R. Desiraju, *Chem. Commun*., 1997, 1841 and references therein.

Received in Cambridge, UK, 20th March 1998; 8/02201A

Synthesis and characterisation of a microporous zirconium silicate with the structure of petarasite

J. Rocha,*[a]† P. Ferreira,[a] Z. Lin,[a] J. R. Agger[b] and M. W. Anderson[b]

[a] *Department of Chemistry, University of Aveiro, 3810 Aveiro, Portugal*
[b] *Department of Chemistry, UMIST, PO Box 88, Manchester, UK M60 1QD*

The synthesis and structural characterisation of AV-3, a microporous sodium zirconium silicate with the structure of the mineral petarasite, are reported.

Recently, the synthesis of inorganic microporous framework solids containing metal atoms in different coordination geometries has raised considerable interest. We have been particularly concerned with the chemistry of microporous titanium silicates containing tetracoordinated Si^{4+} and Ti^{4+} usually in octahedral coordination.[1–3] As a natural extension of this work, we are now engaged in a systematic study aimed at preparing novel microporous zirconium silicates. Although several mineral microporous zirconium silicates are known, so far, little has been done in order to synthesise such solids in the laboratory.[4] Here we wish to report the synthesis and structural characterisation of a synthetic analogue (denoted AV-3, Aveiro microporous solid no. 3) of the rare mineral petarasite (Mont St-Hilaire, Québec, Canada), $Na_5Zr_2Si_6O_{18}(Cl,OH)\cdot 2H_2O$.[5]

AV-3 was prepared in Teflon-lined autoclaves under hydrothermal conditions. An alkaline solution was made by mixing 5.35 g sodium silicate solution (27% m/m SiO_2, 8% m/m Na_2O, Merck), 7.21 g H_2O, 1.43 g NaOH (Merck), 2.00 g NaCl (Aldrich) and 1.00 KCl (Merck). 0.84 $ZrCl_4$ (Aldrich) were added to this solution and stirred thoroughly. The gel, with a composition 1.75 Na_2O : 0.28 K_2O : 1.0 SiO_2 : 0.15 ZrO_2 : 25 H_2O, was autoclaved for 10 days at 230 °C. The crystalline product was filtered, washed with distilled water and dried at ambient temperature, the final product being an off-white microcrystalline powder.

AV-3 samples were characterised by bulk chemical analysis (ICP), powder X-ray diffraction (XRD), scanning electron microscopy (SEM), ^{29}Si and ^{23}Na solid state NMR and FTIR spectroscopies and thermogravimetry (TG).

The crystal structure of petarasite (and AV-3) consists of an open three-dimensional framework built of corner-sharing six-membered silicate rings and [ZrO_6] octahedra (Fig. 1).[5]

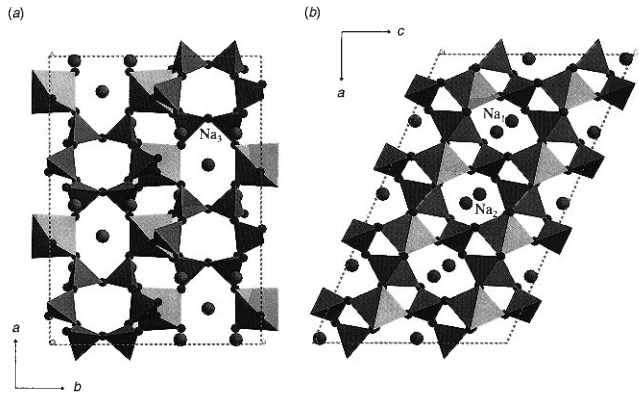

Fig. 1 Polyhedral representations of the petarasite (and AV-3) structure viewed along (*a*) [0 0 1] showing the corner-sharing, six-membered silicate rings and Zr octahedra; Na(3) and Cl ions reside in the elliptical channels; (*b*) [0 1 0] showing the elliptical channels which accommodate the Na(1) and Na(2) ions

Elliptical channels (3.5 × 5.5 Å) defined by mixed six-membered rings, consisting of pairs of [SiO_4] tetrahedra linked by Zr octahedra, run parallel to the *b* and *c* axes. Other channels limited by six-membered silicate rings run parallel to the *c* axis. The sodium, chloride and hydroxyl ions and the water molecules reside within the channels.

Fig. 2 shows the experimental and simulated powder XRD patterns of AV-3. The unit cell parameters have been calculated assuming a monoclinic unit cell, space group $P2_1/m$, and cell dimensions a = 10.771, b = 14.505, c = 6.575 Å, β = 112.664°, and are similar to those reported for petarasite (a = 10.795, b = 14.493, c = 6.623 Å, β = 113.214°).[5]

The AV-3 ^{29}Si solid-state NMR spectrum with magic-angle spinning (MAS) (not shown) displays three peaks at δ −86.6, −91.9 and −94.3 in 1 : 0.9 : 1 intensity ratio. In accord with this observation, the crystal structure of petarasite calls for the presence of three unique Si sites with equal populations.[5]

The sheared ^{23}Na triple-quantum (3Q) MAS NMR spectrum[6] of AV-3 [Fig. 3(*a*)] contains two resolved peaks at δ *ca.* 5.9 and 2.4 (F1) and, due to a distribution of isotropic chemical shifts, a relatively broad signal centred at δ *ca.* 9.6. From the centres of gravity δ_1 and δ_2 (F_1 and F_2 dimensions, respectively) of the two-dimensional spectrum it is possible to estimate the (average) isotropic chemical shift, δ_{iso}, and the second-order quadrupole effect parameters, SOQE, of the lines:[7] S1 (−3.9, 2.1 MHz), S2 (−1.9, 2.5 MHz) and S3 (−1.4, 3.1 MHz). Petarasite contains three crystallographically independent seven-coordinated sodium sites.[5] Na(1) and Na(2) reside in channels parallel to *b* and Na(3) is located in channels parallel to *c*. The [$Na(1)O_5(H_2O)Cl$] and [$Na(2)O_5(H_2O)Cl$] polyhedra are distorted monocapped octahedra, while the [$Na(3)O_6Cl$] polyhedron is a distorted hexagonal pyramid. A second Cl atom may be considered part of the Na(3) coordination and this is, hence, the most distorted sodium site. Accordingly, peak S3, which displays the largest SOQE, is attributed to site Na(3). This assignment is supported by ^1H–^{23}Na cross-polarisation (CP) MAS NMR spectroscopy [Fig. 3(*b*)]. Indeed, the broad low-frequency tail seen in the single-quantum ^{23}Na MAS NMR spectrum, which is due to peak S3 [see F2 projection in Fig. 3(*a*)], is hardly seen in the CP MAS NMR spectrum. Such a behaviour is expected for Na(3) because this site is not coordinated to any water molecules. The Cl and OH ions are disordered over the Na(3) sites and only those environments which contain OH will, in principle, cross-polarise. In contrast,

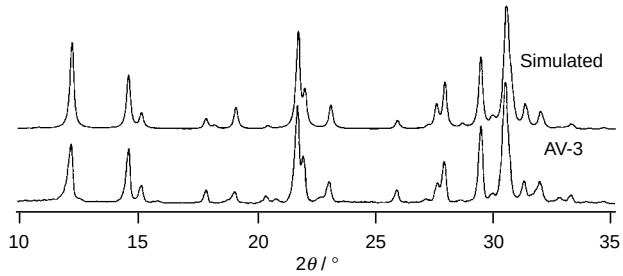

Fig. 2 Experimental and simulated powder XRD patterns of AV-3

sites Na(1) and Na(2), which have water molecules in their coordination spheres, cross-polarise relatively well. The quantification of multiple-quantum MAS NMR spectra is not a trivial problem. Indeed, the intensity of the resonances is not representative of the actual concentration of species because the excitation of the multiple-quantum coherences is strongly dependent on the NMR quadrupole frequency. However, since we have recorded the ^{23}Na 3Q MAS NMR spectrum of AV-3 with a strong (160 kHz) radiofrequency field we believe the measured peak intensities are approximately correct. These have been derived by both volume integration and deconvolution of the isotropic (F1) sum projection. These methods yield for S1, S2 and S3 intensity ratios of 1.0 : 1.0 : 0.8–0.9, respectively, in good agreement with the crystal structure of petarasite.

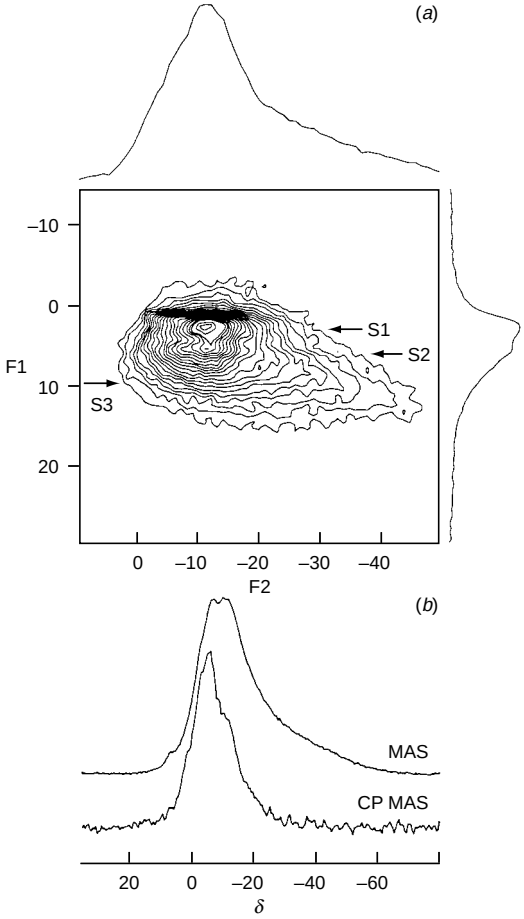

Fig. 3 (*a*) 3Q ^{23}Na MAS NMR spectrum of AV-3 recorded at 105.85 MHz on a Bruker MSL 400P with a rf field amplitude of *ca.* 160 kHz. 210 data points were acquired in the t_1 dimension in increments of 7.0 μs. To produce pure-absorption lineshapes a simple two-pulse sequence was used.[7,9] The ppm scale was referenced to ν_0 frequency in the ν_2 domain and to $3\nu_0$ in the ν_1 domain (reference 1 M aqueous NaCl). (*b*) Single-quantum ('conventional') ^{23}Na MAS and CP MAS NMR (0.5 ms contact time) spectra of AV-3.

TG provides further evidence that the structures of AV-3 and petarasite[8] are very similar. The total AV-3 mass loss between 30 and 830 °C is 5.34% and it is due to the release of molecular water, structural or adsorbed. This value corresponds to 2.4 water molecules and is in excess of the two water molecules revealed by the crystal-structure analysis. Thus, as petarasite,[8] the solid contains a considerable amount of adsorbed water. Between *ca.* 800 and 1100 °C a second stage of dehydration occurs with a mass loss of 3.14% {3.19% in petarasite corresponding to $[Cl_{0.67}(OH)_{0.33}]$}, probably due to the loss of Cl and OH. The parent AV-3 and the material calcined at 750 °C and rehydrated in air overnight at room temperature display similar TGA curves and powder XRD patterns. The fact that the framework does not collapse until the release of Cl indicates that this is an essential constituent of the structure.[8]

The FTIR spectrum of AV-3 (not shown) resembles the spectrum reported for petarasite,[8] and confirms the presence of strucutral and adsorbed water. In addition, the spectrum contains a ring-breathing band at *ca.* 775 cm^{-1} characteristic of ring silicates.

In conclusion, we report the successful synthesis and structural characterisation of a microporous framework zirconium silicate, AV-3, possessing the structure of the rare mineral petarasite.

This work was supported by PRAXIS XXI and FEDER.

Notes and References

† E-mail: rocha@dq.ua.pt

1 M. W. Anderson, O. Terasaki, T. Ohsuna, A. Philippou, S. P. Mackay, A. Ferreira, J. Rocha and S. Lidin, *Nature*, 1994, **367**, 347.
2 J. Rocha, P. Brandão, Z. Lin, A. Ferreira and M. W. Anderson, *J. Phys. Chem.*, 1996, **100**, 14 978.
3 M. S. Dadachov, J. Rocha, A. Ferreira, Z. Lin and M. W. Anderson, *Chem. Commun.*, 1997, 2371.
4 A. I. Bortun, L. N. Bortun and A. Clearfield, *Chem. Mater.*, 1997, **9**, 1854.
5 S. Ghose, C. Wan and G. Y. Chao, *Can. Mineral.*, 1980, **18**, 503.
6 A. Medek, J. S. Harwood and L. Frydman, *J. Am. Chem. Soc.*, 1995, **117**, 12 779.
7 C. Fernandez, J. P. Amoureux, J. M. Chezeau, L. Delmotte and H. Kessler, *Microporous Mater.*, 1996, **6**, 331.
8 G. Y. Chao, T. T. Chen and J. Baker, *Can. Mineral.*, 1980, **18**, 497.
9 J. Rocha, P. Ferreira, Z. Lin, P. Brandão, A. Ferreira and J. D. Pedrosa de Jesus, *J. Phys. Chem.*, in press.

Received in Cambridge, UK, 14th April 1998; 8/02737D

An enantioselective Baylis–Hillman reaction catalyzed by chiral phosphines under atmospheric pressure

Tadakatsu Hayase,[a] Takanori Shibata,[a] Kenso Soai*[a]† and Yasuo Wakatsuki[b]

[a] *Department of Applied Chemistry, Faculty of Science, Science University of Tokyo, Kagurazaka, Shinjuku-ku, Tokyo, 162-8601, Japan,*

[b] *The Institute of Physical and Chemical Research (RIKEN), Wako, Saitama, 351-0198, Japan,*

2,2'-Bis(diphenylphosphino)-1,1'-binaphthyl (BINAP) catalyzes the enantioselective Baylis–Hillman reaction between pyrimidine- 5-carbaldehydes and acrylates to provide chiral α-methylene β-hydroxy esters in up to 44% ee under atmospheric pressure.

The condensation of an aldehyde and acrylate is known as the Baylis–Hillman reaction, and increasing interest has been focused on this reaction.[1] It affords α-methylene β-hydroxy esters, which are furnished with functional groups for further transformations.[2] Therefore the development of an enantioselective Baylis–Hillman reaction would provide a useful synthetic tool for the preparation of chiral polyfunctionalized compounds. However, only very limited examples have been reported, such as an enantioselective Baylis–Hillman reaction between nitrobenzaldehyde[3] or aliphatic aldehydes[4] and methyl vinyl ketone catalyzed by chiral tertiary amines. Moreover, very high pressure is required to afford adducts with low to moderate enantiomeric excess (ee). Thus, exploration of enantioselective Baylis–Hillman reactions is a challenging problem.[5]

Here we report the first example, to the best of our knowledge, of a chiral phosphine-catalyzed intermolecular enantioselective Baylis–Hillman reaction under atmospheric pressure.[6,7]

In the presence of a catalytic amount (20 mol%) of various chiral phosphines, the enantioselective Baylis–Hillman reaction of pyrimidine-5-carbaldehyde **1a** with methyl acrylate was examined at 20 °C in $CHCl_3$ (Table 1, entries 1–6). By the use of bidentate chiral phosphines (DIOP, NORPHOS), a chiral phosphine possessing a hydroxy group (BPPFOH) or an axially chiral monodentate phosphine (MOP), Baylis–Hillman adduct **2a** was obtained; however, almost no or only slight asymmetric induction was observed (entries 1–4). On the other hand, we found that (*S*)-BINAP,[8] an axially chiral bidentate phosphine, catalyzes the enantioselective reaction to give chiral (−)-α-methylene β-hydroxy ester **2a** in 44% ee (entry 5). Adduct (+)-**2a** with 43% ee was obtained by the use of (*R*)-BINAP. These enantioselectivities are comparable with those of the reported enantioselective methods using chiral tertiary amines under high pressures.[3,4] (*S*)-Tol-BINAP is also an effective asymmetric catalyst and **2a** was provided in improved yield along with slightly decreased ee (entry 6).

Table 1 Chiral phosphine-catalyzed Baylis–Hillman reaction

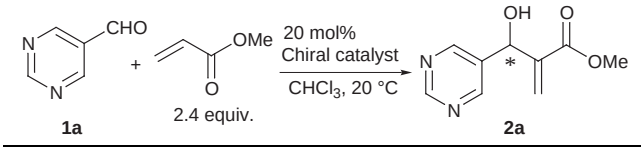

Entry	Chiral catalyst	*t*/h	Yield (%)	Ee (%)[a]
1	(2*R*,3*R*)-DIOP[b]	19	28	< 1
2	(2*R*,3*R*)-NORPHOS[c]	21	32	3
3	(*R*,*S*)-BPPFOH[d]	20	46	2
4	(*S*)-MOP[e]	66	53	< 1
5	(*S*)-BINAP	85	24	44
6	(*S*)-Tol-BINAP[f]	89	41	31

[a] Determined by HPLC analyses using a chiral column. [b] DIOP = 2,3-*O*-isopropylidine-2,3-dihydroxy-1,4-bis(diphenylphosphino)butane. [c] NORPHOS = 2,3-bis(diphenylphosphino)bicyclo[2.2.1]hept-5-ene. [d] BPPFOH = (*R*)-1-[(*S*)-1′,2-bis(diphenylphosphino)ferrocenyl]ethanol. [e] MOP = 2-(diphenylphosphino)-2′-methoxy-1,1′-binaphthyl. [f] Tol-BINAP = 2,2′-bis(di-*p*-tolylphosphino)-1,1′-binaphthyl.

Table 2 Effect of reaction temperature

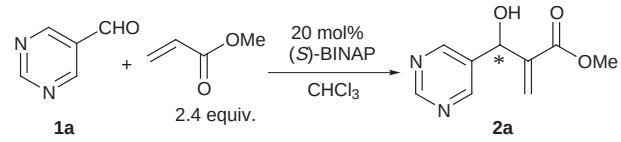

Entry	*T*/°C	*t*/h	Yield (%)	Ee (%)[a]
1	0	127	18	43
2	20	85	24	44
3	50	38	49	42
4	70	19	38	41

[a] Determined by HPLC analyses using a chiral column.

Next, the BINAP-catalyzed Baylis–Hillman reaction was performed at various temperatures (Table 2). In this reaction, the temperature did not significantly affect the enantioselectivities, however, **2a** was obtained in the highest yield (49%) at 50 °C (entry 3).‡

Various acrylates were submitted to this enantioselective Baylis–Hillman reaction (Table 3, entries 1–3). The yield and ee were dependent on the bulk of the acrylate: the less bulky acrylate gave the higher yield and ee. 2-Methylpyrimidine-5-carbaldehyde **1b** also reacts with methyl acrylate in the presence of BINAP. The reaction proceeded slowly but adduct

Table 3 Reaction of aldehydes **1a,b** with various active olefins

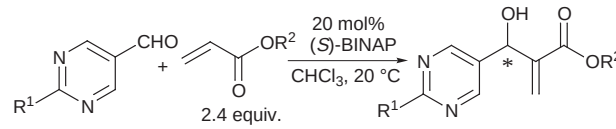

Entry	R^1	R^2	*t*/h	Yield (%)	Ee (%)[a]
1	H	Pr^i	95	8	9
2	H	Et	62	12	25
3	H	Me	85	24	44
4	Me	Me	329	18	37
5[b]	Me	Me	62	26	30

[a] Determined by HPLC analyses using a chiral column. [b] Tol-BINAP was used as a chiral catalyst.

2b was obtained in moderate ee (entry 4). Acceleration of the reaction was observed by the use of Tol-BINAP, and **2b** was provided in higher yield but with lower ee (entry 5).

As described, the present chiral phosphine-catalyzed reaction would provide a new method for enantioselective Baylis–Hillman reaction under atmospheric pressure.

Financial support by a Grant-in-Aid for Scientific Research from the Ministry of Education, Science, Sports and Culture, Japan, is gratefully acknowledged.

Notes and References

† E-mail: ksoai@ch.kagu.sut.ac.jp

‡ *General experimental procedure* (Table 2, entry 3): To a $CHCl_3$ solution (1.0 ml) of (*S*)-BINAP (62.3 mg) and pyrimidine-5-carbaldehyde **1a** (54.4 mg) was added methyl acrylate (0.11 ml) at ambient temperature. The reaction mixture was stirred for 38 h at 50 °C, then it was evaporated to dryness under reduced pressure. Purification of the crude product by TLC gave pure Baylis–Hillman adduct (–)-**2a** (47.8 mg, 49%). The ee was determined to be 42% by HPLC analysis (chiral column: Daicel Chiralcel OD-H, eluent: 3% Pr^iOH in hexane, flow rate: 1.0 ml min^{-1}, wavelength for UV detector: 254 nm, retention time: 36 min for the major isomer and 41 min for the minor isomer).

1 Reviews, see: D. Basavaiah, P. D. Rao and R. S. Hyma, *Tetrahedron*, 1996, **52**, 8001; S. E. Drewes and G. H. P. Roos, *ibid.*, 1988, **44**, 4653; H. M. R. Hoffmann and J. Rabe, *Angew. Chem., Int. Ed. Engl*., 1985, **24**, 4653.

2 For example, see: I. E. Marcó, P. R. Giles, Z. Janousek, H. J. Hindley, J.-P. Declercq, B. Tinant, J. F.-Dupont and J. S. Svensen, *Recl. Trav. Chim. Pays-Bas*, 1995, **114**, 239; M. Bailey, I. E. Marcó and W. D. Ollis, *Tetrahedron Lett*., 1991, **32**, 2687; J. M. Brown, *Angew. Chem., Int. Ed. Engl*., 1987, **26**, 190.

3 T. Oishi, H. Oguri and M. Hirama, *Tetrahedron: Asymmetry*, 1995, **6**, 1241.

4 I. E. Marcó, P. R. Giles and H. J. Hindley, *Tetrahedron*, 1997, **53**, 1015.

5 For diastereoselective Baylis–Hillman reactions, see: L. J. Brzezinski, S. Rafel and J. W. Leathy, *J. Am. Chem. Soc*., 1997, **119**, 4317 and ref. 1.

6 For the use of trialkylphosphines in non-asymmetric Baylis–Hillman reaction, see: S. Rafel and J. W. Leathy, *J. Org. Chem.*, 1997, **62**, 1521.

7 Bis(diphenylphosphino)butane (CHIRAPHOS) was utilized as a catalyst in the reaction of an *N*-tosyl imine with methyl acrylate but no asymmetric induction was reported to be observed: S. Bertenshaw and M. Kahn, *Tetrahedron Lett.*, 1989, **30**, 2731. Intramolecular enantioselective reaction using chiral phosphine was reported (14% ee): F. Roth, P. Crygak and G. Fráter, *Tetrahedron Lett.*, 1992, **33**, 1045.

8 For early examples of the use of BINAP in enantioselective hydrogenation: R. Noyori and H. Takaya, *Acc. Chem. Res*., 1990, **23**, 345.

Received in Cambridge, UK, 6th April 1998; 8/02594K

Phosphorus–carbon bond activation of PMe_3 at a dimolybdenum center: synthesis and structure of $[Cp^*Mo(\mu\text{-}O_2CMe)]_2(\mu\text{-}PMe_2)(\mu\text{-}Me)$

Jun Ho Shin and Gerard Parkin*

Department of Chemistry, Columbia University, New York, New York 10027, USA

The reaction of $Mo_2(\mu\text{-}O_2CMe)_4$ with KCp* in the presence of PMe_3 yields $[Cp^*Mo(\mu\text{-}O_2CMe)]_2(\mu\text{-}PMe_2)(\mu\text{-}Me)$ as a result of cleavage of the P–CH_3 bond.

The quadruply bonded dimolybdenum acetato complex $Mo_2(\mu\text{-}O_2CMe)_4$ has been shown to exhibit an extensive chemistry, allowing access to a large variety of mononuclear, dinuclear and polynuclear complexes.[1] In this paper, we report an unusual reaction of $Mo_2(\mu\text{-}O_2CMe)_4$ which results in P–C bond activation of PMe_3 at a dimolybdenum center.

As part of an effort to find new methods of synthesis for permethylcyclopentadienyl molybdenum complexes,[2] we have studied the reaction of $Mo_2(\mu\text{-}O_2CMe)_4$ with KCp* (Cp* = $\eta^5\text{-}C_5Me_5$) in the presence of PMe_3. Interestingly, rather than yielding a 'molybdenocene' derivative,[3] the bridging dimethylphosphido–methyl complex, $[Cp^*Mo(\mu\text{-}O_2CMe)]_2(\mu\text{-}PMe_2)(\mu\text{-}Me)$, is obtained in *ca*. 30% isolated yield over a period of 3 days at room temperature (Scheme 1). The molecular structure of $[Cp^*Mo(\mu\text{-}O_2CMe)]_2(\mu\text{-}PMe_2)(\mu\text{-}Me)$ has been determined by X-ray diffraction (Fig. 1 and Table 1),[4] thereby demonstrating that the P–CH_3 bond of PMe_3 has been cleaved. ^1H and ^{13}C NMR spectroscopic data also provide decisive evidence in accord with this formulation. For example, the ^1H NMR spectrum exhibits three doublets at δ 0.97 ($^2J_{PH}$ 10 Hz), 0.91 ($^2J_{PH}$ 9 Hz), and −5.25 ($^3J_{PH}$ 5 Hz) for the $[Mo_2(\mu\text{-}PMe_2)(\mu\text{-}Me)]$ moiety, with the lattermost resonance attributed to the molybdenum methyl group.

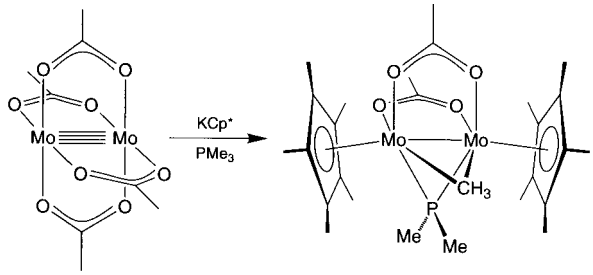

Scheme 1

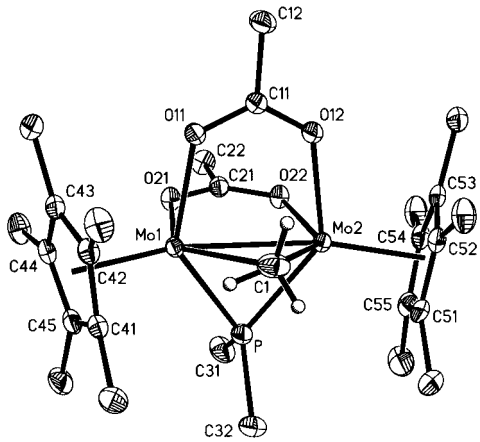

Fig. 1 Molecular structure of $[Cp^*Mo(\mu\text{-}O_2CMe)]_2(\mu\text{-}PMe_2)(\mu\text{-}Me)$

Table 1 Selected bond lengths for $[Cp^*Mo(\mu\text{-}O_2CMe)]_2(\mu\text{-}PMe_2)(\mu\text{-}Me)$

X	*d*[Mo(1)–X][a]/Å	*d*[Mo(2)–X][b]/Å
Mo(*x*)	2.8447(5)	2.8447(5)
C(1)	2.300(7)	2.301(7)
P	2.3883(13)	2.3853(13)
O(1*y*)	2.179(3)	2.161(3)
O(2*y*)	2.145(3)	2.152(3)
C(*z*1)	2.259(4)	2.251(5)
C(*z*2)	2.241(4)	2.253(4)
C(*z*3)	2.364(4)	2.371(4)
C(*z*4)	2.419(4)	2.421(5)
C(*z*5)	2.352(4)	2.327(5)

[a] $x = 2, y = 1, z = 4$. [b] $x = 1, y = 2, z = 5$.

The facile cleavage of the P–CH_3 bond in the formation of $[Cp^*Mo(\mu\text{-}O_2CMe)]_2(\mu\text{-}PMe_2)(\mu\text{-}Me)$ is of interest not only because such transformations are rare,[5,6] but also because the P–CH_3 bond cleavage in this system takes precedence over the much more ubiquitous C–H bond cleavage reactions of PMe_3.[7] Furthermore, the structure of $[Cp^*Mo(\mu\text{-}O_2CMe)]_2(\mu\text{-}PMe_2)(\mu\text{-}Me)$ is noteworthy because both $[PMe_2]$ and [Me] fragments remain coordinated to the metal centers after cleavage has taken place. We are aware of three other examples of P–CH_3 cleavage reactions of PMe_3,[8–10] only one of which yields a product that contains both $[PMe_2]$ and [Me] groups coordinated to a metal, namely the reaction of $CpNi(\mu\text{-}H)(\mu\text{-}CO)WCp_2$ with PMe_3 to give $CpNi(\mu\text{-}PMe_2)(\mu\text{-}CO)WCpMe(PMe_3)$.[8]

In addition to representing a noteworthy example of P–C bond cleavage, $[Cp^*Mo(\mu\text{-}O_2CMe)]_2(\mu\text{-}PMe_2)(\mu\text{-}Me)$ is also of interest from a structural perspective since there are no examples of dimolybdenum complexes with bridging methyl groups listed in the Cambridge Structural Database.[11,12] Bridging methyl groups have been proposed to adopt five different coordination modes (Scheme 2), which may be classified as (i) symmetric pyramidal,[13] (ii) symmetric planar,[14] (iii) monohapto agostic,[15] (iv) dihapto agostic,[16,17] and (v) trihapto agostic.[17,18] Of these modes, the bridging methyl group in $[Cp^*Mo(\mu\text{-}O_2CMe)]_2(\mu\text{-}PMe_2)(\mu\text{-}Me)$ is appropriately described as symmetric pyramidal, with chemically equivalent Mo–C bond lengths [2.300(7) and 2.301(7) Å][19] and an acute Mo–C–Mo bond angle [76.4(2)°].[20] The $^1J_{CH}$ coupling constant associated with this methyl group is 113 Hz, less than that for

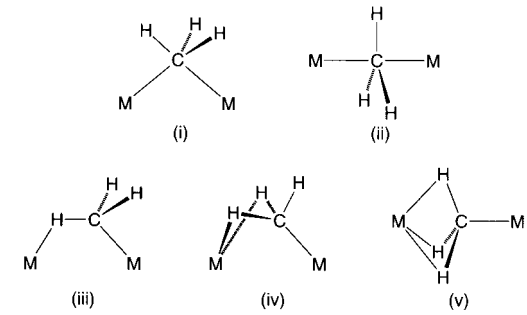

Scheme 2

typical terminal molybdenum methyl groups (*ca.* 127–136 Hz),[21] and possibly reflects a diminished s-contribution to the C–H bond,[22] rather than an agostic interaction.[20]

The Mo–Mo separation of 2.8447(5) Å in $[Cp^*Mo(\mu\text{-}O_2CMe)]_2(\mu\text{-}PMe_2)(\mu\text{-}Me)$ is consistent with the presence of a direct Mo–Mo interaction.[23] In this regard, the Mo–Mo separation is longer than the values in complexes with formal double bonds, *e.g.* $[CpMo]_2(\mu\text{-}S)_2(\mu\text{-}SPr^i)(\mu\text{-}PPh_2)$ [2.623(2) Å][24] and $[(C_5Me_4H)Mo(CO)](\mu\text{-}PPh_2)_2[Mo(CO)(C_5Me_4\text{-}P(O)Ph_2)]$ [2.744(1) Å],[25] and notably shorter than the values in other phosphido bridged complexes such as $[CpMo(CO)_2]_2(\mu\text{-}PMe_2)(\mu\text{-}H)$ [3.262(7) Å],[26] $[CpMo(CO)_2]_2(\mu\text{-}PBu^t_2)(\mu\text{-}H)$ [3.247(1) Å],[27] and $[CpMo(CO)_2]_2(\mu\text{-}PPh_2)(\mu\text{-}H)$ [3.244(1) Å].[28,29] Furthermore, the length of the Mo–Mo bond in $[Cp^*Mo(\mu\text{-}O_2CMe)]_2(\mu\text{-}PMe_2)(\mu\text{-}Me)$ is marginally longer than the W–W separation of 2.78 Å in Chisholm's closely related tungsten complex, $Cp_2W_2(\mu\text{-}\eta^2\text{-}O_2CEt)_2(\mu\text{-}\eta^1\text{-}O_2CEt)(\mu\text{-}NMe_2)$, which has been assigned to a single bond.[30]

In summary, the reaction of $Mo_2(\mu\text{-}O_2CMe)_4$ with KCp* in the presence of PMe_3 yields $[Cp^*Mo(\mu\text{-}O_2CMe)]_2(\mu\text{-}PMe_2)(\mu\text{-}Me)$, the formation of which involves a novel P–CH_3 cleavage reaction of PMe_3.

We thank the US Department of Energy, Office of Basic Energy Sciences (#DE-FG02-93ER14339) for support of this research. G. P. is the recipient of a Presidential Faculty Fellowship Award (1992–1997).

Notes and References

† E-mail: parkin@chem.columbia.edu

1 *Multiple Bonds Between Metal Atoms*, ed. F. A. Cotton and R. A. Walton, Clarendon Press, Oxford, 2nd edn., 1993.

2 See, for example: J. H. Shin and G. Parkin, *Polyhedron*, 1994, **13**, 1489.

3 For example, $Mo_2(\mu\text{-}O_2CMe)_4$ reacts with NaCp to yield 'molybdenocene' derivatives.[3a,b] Furthermore, a pentalene complex has been obtained from the reaction of $Mo_2(\mu\text{-}O_2CMe)_4$ with $K_2[C_8H_4(1,4\text{-}SiPr^i_3)_2]$.[3c] (*a*) J. C. Smart and C. J. Curtis, *Inorg. Chem.*, 1978, **17**, 3290; (*b*) J. Bashkin, M. L. H. Green, M. L. Poveda and K. Prout, *J. Chem. Soc., Dalton Trans.*, 1982, 2485; (*c*) M. C. Kuchta, F. G. N. Cloke and P. B. Hitchcock, *Organometallics*, 1998, **17**, 934.

4 $[Cp^*Mo(\mu\text{-}O_2CMe)]_2(\mu\text{-}PMe_2)(\mu\text{-}Me)$ is monoclinic, $P2_1/n$ (no. 14), a = 10.989(1), b = 14.0436(9), c = 18.844(2) Å, β = 90.353(9)°, U = 2908(1) Å^3, Z = 4, T = room temp., R_1 = 0.0404 [$I > 2\sigma(I)$]. The hydrogen atoms of the bridging methyl group were located and refined isotropically, giving the following bond lengths (Å): C1–H1a 0.86, C1–H1b 0.97, C1–H1c 0.84 Å. CCDC 182/868.

5 P. E. Garrou, *Chem. Rev.*, 1985, **85**, 171; M. Michman, *Isr. J. Chem.*, 1986, **27**, 241.

6 In contrast to P–C cleavage in alkylphosphines, the cleavage of P–C bonds in arylphosphines is common, with the ease of cleavage typically following the order $P–C_{sp3} < P–C_{sp2} < P–C_{sp}$.[5] The majority of examples of $P–C_{sp3}$ bond cleavage, however, involve degradation of bidentate phosphine ligands.[6a–e] (*a*) V. Riere, M. A. Ruiz, F. Villafañe, C. Bois and Y. Jeannin, *J. Organomet. Chem.*, 1989, **375**, C23; (*b*) I. J. B. Lin, J. S. Lai and C. W. Liu, *Organometallics*, 1990, **9**, 530; (*c*) K.-B. Shiu, S.-W. Jean, H.-J. Wang, S.-L. Wang, F.-L. Liao, J.-C. Wang and L.-S. Liou, *Organometallics*, 1997, **16**, 114 and references therein; (*d*) N. M. Doherty, G. Hogarth, S. A. R. Knox, K. A. Macpherson, F. Melchior, D. A. V. Morton and A. G. Orpen, *Inorg. Chim. Acta*, 1992, **198**–**200**, 257; (*e*) F. A. Cotton, J. A. M. Canich, R. L. Luck and K. Vidyasagar, *Organometallics*, 1991, **10**, 352.

7 See, for example: F. A. Cotton and G. Wilkinson, *Advanced Inorganic Chemistry*, Wiley, 1988, 5th edn., p. 1217; A. D. Ryabov, *Chem. Rev.*, 1990, **90**, 403; A. E. Shilov and G. B. Shul'pin, *Chem. Rev.*, 1997, **97**, 2879.

8 T. Nakajima, I. Shimizu, K. Kobayashi, H. Koshino and Y. Wakatsuki, *Inorg. Chem.*, 1997, **36**, 6440.

9 W. Lin, S. R. Wilson and G. S. Girolami, *Inorg. Chem.*, 1994, **33**, 2265.

10 J. F. Hartwig, R. G. Bergman and R. A. Andersen, *J. Organomet. Chem.*, 1990, **394**, 417.

11 CSD Version 5.14. *3D Search and Research Using the Cambridge Structural Database*, F. H. Allen and O. Kennard, *Chem. Des. Automat. News*, 1993, **8**(1), 1 and 31.

12 It is also noteworthy that the Cp* ligands of $[Cp^*Mo(\mu\text{-}O_2CMe)]_2(\mu\text{-}PMe_2)(\mu\text{-}Me)$ are not coordinated in a symmetric η^5-fashion, with Mo–C bond lengths that range from 2.24 to 2.42 Å (see Table 1).

13 Representative examples include $[Me_2Al(\mu\text{-}Me)]_2$,[13a] $[Cp^*CrMe(\mu\text{-}Me)]_2$,[13b] $\{[Cp^R]_2M(\mu\text{-}Me)\}_2$ (M = Ce, Yb, Y)[13c] and $\{Me_3Al\text{-}[(Me_3Si)_2N]Mn(\mu\text{-}Me)\}_2$.[13d] (*a*) J. C. Huffman and W. E. Streib, *Chem. Commun.*, 1971, 911; (*b*) S. K. Noh, S. C. Sendlinger, C. Janiak and K. H. Theopold, *J. Am. Chem. Soc.*, 1989, **111**, 9127; (*c*) S. D. Stults, R. A. Andersen and A. Zalkin, *J. Organomet. Chem.*, 1993, **462**, 175 and references therein; (*d*) M. Niemeyer and P. P. Power, *Chem. Commun.*, 1996, 1573.

14 For example, $[Cp_2Zr(\eta^2\text{-}OCMe_2)]_2(\mu\text{-}AlMe_2)(\mu\text{-}Me)$,[14a] $Cp^*_2Lu(\mu\text{-}Me)LuMeCp^*_2$,[14b] $Cp^*_2M[(\mu\text{-}Me)M'Me_2(\mu\text{-}Me)]_2MCp^*_2$ (M = Y, Lu; M′ = Al, Ga),[14c] $Cp^*_2Sm[(\mu\text{-}Me)AlMe_2(\mu\text{-}Me)]_2SmCp^*_2$[14d] and $[(Cp^{Me})_3U]_2(\mu\text{-}Me)$.[14e] (*a*) R. W. Waymouth, K. S. Potter, W. P. Schaefer and R. H. Grubbs, *Organometallics*, 1990, **9**, 2843 and references therein; (*b*) P. L. Watson, *J. Am. Chem. Soc.*, 1983, **105**, 6491; (*c*) M. A. Busch, R. Harlow and P. L. Watson, *Inorg. Chim. Acta*, 1987, **140**, 15; (*d*) W. J. Evans, L. R. Chamberlain, T. A. Ulibarri and J. W. Ziller, *J. Am. Chem. Soc.*, 1988, **110**, 6423; (*e*) S. D. Stults, R. A. Andersen and A. Zalkin, *J. Am. Chem. Soc.*, 1989, **111**, 4507 and references therein.

15 For examples, and for a discussion of the factors responsible for the bridging methyl group in $[\{Cp(CO)Fe\}_2(\mu\text{-}CO)(\mu\text{-}Me)]^+$ adopting a monohapto agostic interaction, see: B. E. Bursten and R. H. Cayton, *Organometallics*, 1986, **5**, 1051 and references therein.

16 For example, $Cp^*_2Yb(\mu\text{-}Me)_2Pt(dippe)$[16a] and $[CpV(NC_6H_3Pr^i_2)(\mu\text{-}Me)_2]_2(\mu\text{-}Mg)$.[16b] (*a*) D. J. Schwartz, G. E. Ball and R. A. Andersen, *J. Am. Chem. Soc.*, 1995, **117**, 6027; (*b*) M. C. W. Chan, J. M. Cole, V. C. Gibson and J. A. K. Howard, *Chem. Commun.*, 1997, 2345.

17 $[LiBMe_4]$ exhibits both dihapto and trihapto bridging methyl interactions. See: W. E. Rhine, G. Stucky and S. W. Peterson, *J. Am. Chem. Soc.*, 1975, **97**, 6401.

18 For example, $Cp^*_2Yb(\mu\text{-}Me)BeCp^*$. See: C. J. Burns and R. A. Andersen, *J. Am. Chem. Soc.*, 1987, **109**, 5853.

19 For comparison, the mean length for terminal Mo–CH_3 interactions listed in the Cambridge Structural Database is 2.23 Å, with a range of 2.03–2.40 Å.

20 Although a short Mo···H separation of 2.02 Å suggests that some monohapto agostic character to the interaction could be considered, we feel that the equivalence of the Mo–C bond lengths and the acute Mo–C–Mo bond angle is a more important indicator of the type of bridge [see, for example ref. 13(*c*)].

21 For example, $(Cp^{Bu^t})_2MoMe_2$ (128 Hz),[21a] $[(Cp^{Bu^t})_2Mo(CO)Me][I]$ (136 Hz),[21a] $[(Cp^{Bu^t})_2Mo(PMe_3)Me][I]$ (130 Hz),[21a] and $Cp^*Mo(NO)_2Me$ (127 Hz).[21b] (*a*) J. H. Shin and G. Parkin, unpublished work; (*b*) W. L. Elcesser, M. Sörlie and J. L. Hubbard, *Organometallics*, 1996, **15**, 2534.

22 $^1J_{CH}$ coupling constants for hydrocarbons correlate with the hybridization (sp^n) of the bonding orbital according to the relationship $^1J_{CH} = 500(1/1 + n)$. See: (*a*) H. S. Gutowsky and C. S. Juan, *J. Am. Chem. Soc.*, 1962, **84**, 307; (*b*) N. Muller and D. E. Pritchard, *J. Chem. Phys.*, 1959, **31**, 1471.

23 Considering a bridging methyl group as a L–μ-X ligand,[23a] the Mo–Mo interaction may be described as a formal single bond. Alternatively, the interaction may be described as a formal double bond if an electron counting procedure[23b] that does not explicitly consider the 3-center–2-electron nature of the Mo–Me–Mo fragment is used. (*a*) M. L. H. Green, *J. Organomet. Chem.*, 1995, **500**, 127; (*b*) J. P. Collman, L. S. Hegedus, J. R. Norton and R. G. Finke, *Principles and Applications of Organotransition Metal Chemistry*, University Science Books, Mill Valley, CA, 1987.

24 H. Adams, N. A. Bailey, A. P. Bisson and M. J. Morris, *J. Organomet. Chem.*, 1993, **444**, C34.

25 W.-K. Wong, F. L. Chow, H. Chen, B. W. Au-Yeung, R.-J. Wang and T. C. W. Mak, *Polyhedron*, 1990, **9**, 2901.

26 R. J. Doedens and L. F. Dahl, *J. Am. Chem. Soc.*, 1965, **87**, 2576.

27 R. A. Jones, S. T. Schwab, A. L. Stuart, B. R. Whittlesey and T. C. Wright, *Polyhedron*, 1985, **4**, 1689.

28 H. Hartung, B. Walther, U. Baumeister, H.-C. Böttcher, A. Krug, F. Rosche and P. G. Jones, *Polyhedron*, 1992, **11**, 1563.

29 For further comparison, the unbridged Mo–Mo single bond length in $[CpMo(CO)_3]_2$ is 3.235(1) Å. See: R. D. Adams, D. M. Collins and F. A. Cotton, *Inorg. Chem.*, 1974, **13**, 1086.

30 M. H. Chisholm, M. J. Hampden-Smith, J. C. Huffman, J. D. Martin, K. A. Stahl and K. G. Moodley, *Polyhedron*, 1988, **7**, 1991.

Received in Bloomington, IN, USA, 5th March 1998; 8/01835I

Direct synthesis of organochlorosilanes by the reaction of metallic silicon with hydrogen chloride and alkene/alkyne

Masaki Okamoto, Satoshi Onodera, Yuji Yamamoto, Eiichi Suzuki and Yoshio Ono*†

Department of Chemical Engineering, Tokyo Institute of Technology, Ookayama, Meguro-ku, Tokyo 152, Japan

Organosilicon compounds were directly synthesized from metallic silicon, alkene/alkyne and HCl, $EtHSiCl_2$ being obtained with 47% selectivity from Si, C_2H_4 and HCl at 513 K, and CH_2=$CHSiHCl_2$ and $EtHSiCl_2$ with 39 and 23% selectivity, respectively, when C_2H_2 was used in place of C_2H_4.

Methylchlorosilanes, especially dimethyldichlorosilane, are produced industrially by the reaction of metallic silicon with MeCl using a copper catalyst.[1] The direct synthesis of dimethyldichlorosilane is the key step for synthesizing silicone polymers. Various mechanisms have been proposed for this direct synthesis.[2] We carried out the reaction in the presence of butadiene as a silylene trapping agent and found that an appreciable amount of silacyclopent-3-enes was formed together with methylchlorosilanes.[3] This indicates the intermediacy of silylene-type species in this heterogeneous reaction. It was presumed that the silylene species are formed on the surface of a silicon–copper alloy, through which silicon atoms diffuse out to the surface from the phase of metallic silicon. The intermediacy of the silylene species has also been proposed for the selective formation of trialkoxysilanes in the direct reactions of metallic silicon with alcohols.[4]

HCl also reacts with metallic silicon to afford chlorosilanes, mainly trichlorosilane.[5] We presume that the surface silylene is also an intermediate for the selective formation of trichlorosilane.

It is well known that the addition of silylenes to alkenes gives vinylsilanes *via* silacyclopropane intermediates.[6,7] It is very plausible that silylene species at the surface also react with alkenes to form silacyclopropanes. In previous work, we have reported that ethylmethoxysilanes are obtained by the reaction of metallic silicon, MeOH and C_2H_4.[8] When allyl propyl ether was used instead of C_2H_4, allyldimethoxysilane was obtained in 38% selectivity.[9]

In this work, we report that alkylsilanes are directly prepared by the reaction of metallic silicon and HCl in the presence of C_2H_4 or propene. Organosilanes are also obtained by the reaction of metallic silicon, HCl and C_2H_2.

The reactions were carried out in a fixed-bed flow reactor. The mixture of metallic silicon (8.9 mmol) and copper(I) chloride (0.79 mmol) as a catalyst was placed in a quartz tube reactor (id 10 mm) and preheated at 723 K for 10 min. Then, HCl (3 mmol h^{-1}) and C_2H_4 (12 mmol h^{-1}) was fed to the reactor at 513 K. The reactor effluents were analyzed every 10 min by GC.

Fig. 1 shows the time courses of the rates of formation of products and cumulative conversion of silicon. Ethyldichlorosilane and trichlorosilane were obtained as the main products. The rates of formation of these products increased to the maximum with reaction time and then decreased. Small amounts of dichlorosilane and tetrachlorosilane were also formed. The cumulative conversion of silicon reached 36% in 12 h. Though the reaction was stopped at 12 h in the experiment in Fig. 1, further increases in silicon conversion would be attained on further extending reaction time. The overall selectivity for ethyldichlorosilane for 12 h was 47%. The selectivities for dichlorosilane, trichlorosilane and tetrachlorosilane were 6, 45 and 2%, respectively.

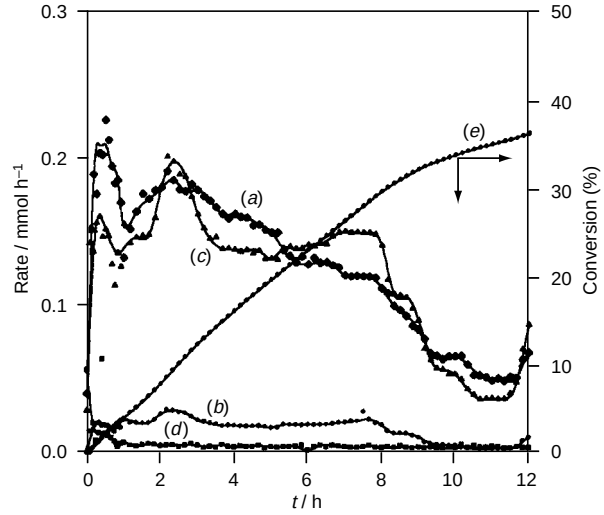

Fig. 1 Time courses of formation rates of the products and cumulative conversion of silicon in the reaction of silicon, HCl and C_2H_4. Preheating: 723 K for 10 min; reaction: 513 K, Si: 8.9 mmol, CuCl: 0.79 mmol. Feed: HCl (3 mmol h^{-1}) and C_2H_4 (12 mmol h^{-1}). Rates of formation of (*a*) ethyldichlorosilane, (*b*) dichlorosilane, (*c*) trichlorosilane, (*d*) tetrachlorosilane and (*e*) conversion of silicon.

Note that ethyldichlorosilane was the sole organosilane produced. To explain this fact, we propose the following reaction scheme involving surface silylene **1** as shown in Scheme 1. In the absence of C_2H_4, the surface silylene reacts with HCl. The subsequent reactions through surface species **2** and **3** lead to the formation of $HSiCl_3$ as the main product. The formation of $HSiCl_3$ by the addition of HCl to dichlorosilylene has been reported.[10] The silylene intermediate **1** reacts with C_2H_4 to form silacyclopropane species **4**. The species **4** is converted into the surface species **5** by attack of HCl. Finally attack of HCl on the species **5** leads to the cleavage of the two Si–Cu bonds to form ethyldichlorosilane.

Use of propene instead of C_2H_4 under similar conditions resulted in the formation of propyldichlorosilane and isopropyldichlorosilane with the selectivities of 10 and 24%, respectively, together with chlorosilanes.

When C_2H_2 was used instead of alkenes, vinyldichlorosilane and ethyldichlorosilane were produced. After preheating the

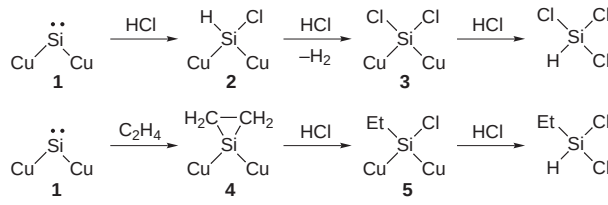

Scheme 1

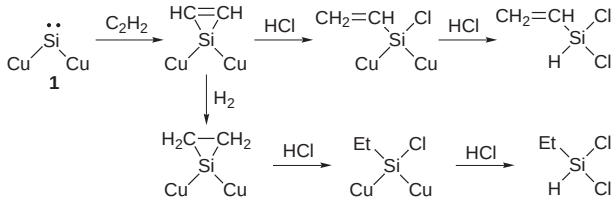

Scheme 2

Table 1 Effect of C_2H_2 : HCl ratio on the Si–HCl–C_2H_2 reaction[a]

C_2H_2 : HCl ratio	Si conversion (%)	(C_2H_3)-$HSiCl_2$ (%)	$EtHSiCl_2$ (%)	H_2SiCl_2 (%)	$HSiCl_3$ (%)	$SiCl_4$ (%)
0.33	15	27	15	4	53	1
0.26	16	34	21	0	45	0
0.2	31	23	11	4	61	1
0.13	37	22	11	5	62	1
0.07	67	10	3	11	76	1
0	85	—	—	6	93	1

[a] Preheating: 723 K for 10 min; reaction: 513 K for 5 h, Si: 8.9 mmol, Cu: 0.20 mmol, HCl: 15 mmol h^{-1}.

silicon–CuCl mixture at 723 K, only HCl (15 mmol h^{-1}) was fed at 513 K for 10 min. During this period, 1% of silicon charged in the reactor was consumed to form chlorosilanes, the main product being $HSiCl_3$. Then, the feed of HCl was changed to a mixture of HCl (15 mmol h^{-1}) and C_2H_2 (4 mmol h^{-1}). Vinyldichlorosilane and ethyldichlorosilane were produced together with chlorosilanes. The overall selectivities in the 5 h reaction for vinyldichlorosilane and ethyldichlorosilane were 39 and 23%, respectively, these two organosilanes accounting for 62% of the products. About 13% of silicon charged in the reactor was consumed in 5 h. A plausible mechanism for the formation of vinyl- and ethyl-dichlorosilane is shown in Scheme 2.

The silylene intermediate **1** reacts with C_2H_2 to form a silacyclopropene surface species, which is attacked by HCl to form a surface species containing a vinyl group. Silacyclopropene intermediates are often postulated in the reaction of silylenes with alkynes, though normally only dimeric products, 1,4-disilacyclohexa-2,5-dienes are obtained.[7,11] The exclusive formation of monomeric products indicates the silylene species do not exist in the vapor phase, but are located on the surface. Formation of ethyldichlorosilane indicates that the hydrogenation of the intermediate(s) occurs on the surface.

Table 1 shows the effect of the C_2H_2 : HCl molar ratio on the product distribution. Without C_2H_2, high conversion of metallic silicon is attained, giving trichlorosilane as a main product. As the C_2H_2 : HCl ratio increases, the reactivity of metallic silicon decreases. The selectivity for organosilanes was highest at a C_2H_2 : HCl ratio of 0.26.

The reactions of silicon, HCl and alkene/alkyne offer a new method for synthesizing organosilanes directly from metallic silicon.

Notes and References

† E-mail: yono@o.cc.titech.ac.jp

1 R. J. H. Voorhoeve, *Organohalosilanes: Precursors to Silicones*, Elsevier, Amsterdam, 1967.

2 D. H. Hurd and E. G. Rochow, *J. Am. Chem. Soc.*, 1945, **67**, 1057; A. L. Klebansky and V. S. Fikhtengolts, *J. Gen. Chem. USSR*, 1956, **26**, 2795; R.J. H. Voorhoeve and J. C. Vlugter, *J. Catal.*, 1965, **4**, 220; I. M. Podgornyi, S. A. Golubtsov, K. A. Andrianov and E. G. Mangalin, *J. Gen. Chem. USSR*, 1974, **44**, 739; M. P. Clarke, *J. Organomet. Chem.*, 1989, **376**, 165, and references therein; K. M. Lewis, D. McLeod, B. Kanner, J. L. Falconer and T. Frank, in *Catalyzed Direct Reactions of Silicon*, ed. K. M. Lewis and D. G. Rethwisch, Elsevier, Amsterdam, 1993, pp. 333–440, and references therein.

3 M. Okamoto, S. Onodera, T. Okano, E. Suzuki and Y. Ono, *J. Organomet. Chem.*, 1997, **531**, 67.

4 M. Okamoto, E. Suzuki and Y. Ono, *J. Catal.*, 1994, **145**, 537; M. Okamoto, K. Yamamoto, E. Suzuki and Y. Ono, *J. Catal.*, 1994, **147**, 15.

5 I. Shiihara and J. Iyoda, *Bull. Chem. Soc. Jpn.*, 1959, **32**, 636; B. Kanner and K. M. Lewis, in *Catalyzed Direct Reactions of Silicon*, ed. K. M. Lewis and D. G. Rethwisch, Elsevier, Amsterdam, 1993, pp. 1–66, and references therein; W. C. Breneman, in *Catalyzed Direct Reactions of Silicon*, ed. K. M. Lewis and D. G. Rethwisch, Elsevier, Amsterdam, 1993, pp. 441–457.

6 P. S. Skell and E. J. Goldstein, *J. Am. Chem. Soc.*, 1964, **86**, 1442; V. J. Tortorelli, M. Jones, Jr., S. Wu and Z. Li, *Organometallics*, 1983, **2**, 759; M. Ishikawa, K. Nakagawa and M. Kumada, *J. Organomet. Chem.*, 1979, **178**, 105.

7 P. P. Gaspar, in *Reactive Intermediates*, ed. M. Jones, Jr., and R. A. Moss, Wiley, New York, 1981, vol. 2, pp. 335–385, and references therein; Y.-N. Tang, in *Reactive Intermediates*, ed. R. A. Abramovitch, Plenum Press, New York, 1982, vol. 2, pp. 297–366, and references therein.

8 M. Okamoto, N. Watanabe, E. Suzuki and Y. Ono, *J. Organomet. Chem.*, 1995, **489**, C12.

9 M. Okamoto, E. Suzuki and Y. Ono, *J. Chem. Soc., Chem. Commun.*, 1994, 507.

10 R. C. Bracken, U.S. Patent 3 565 590, 1971.

11 T. J. Barton, J. A. Kilgour, *J. Am. Chem. Soc.*, 1974, **96**, 7150; E. A. Chernyshev, N. G. Komalenkova, S. A. Bashkirova and V. V. Sokolov, *Zh. Obshch. Khim.*, 1978, **48**, 830; E. A. Chernyshev, N. G. Komalenkova and S. A. Bashkirova, *Zh. Obshch.Khim.*, 1971, **41**, 1175; M. Ishikawa, K. Nakagawa and M. Kumada, *J. Organomet. Chem.*, 1977, **131**, C15; W. H. Atwell, D. R. Weyenberg, *J. Am. Chem. Soc.*, 1968, **90**, 3438.

Received in Cambridge, UK, 5th January 1998; 8/00121I

A novel molecular species incorporating a cyclic organolithate anion and a disiloxane-solvated lithium cation

Colin Eaborn,*† Salima M. El-Hamruni, Peter B. Hitchcock and J. David Smith*†

School of Chemistry, Physics and Environmental Sciences, University of Sussex, Brighton, UK BN1 9QJ

The disiloxane $O\{SiMe_2CH(SiMe_3)_2\}_2$ is readily metallated by LiMe in thf (thf = tetrahydrofuran) to give the compound $SiMe_2C(SiMe)_3LiC(SiMe_3)_2SiMe_2OLi(thf)_2$, the crystal structure of which is reported.

In 1983 we reported the first diorganolithate, $[Li(thf)_4][Li\{C(SiMe_3)_3\}_2]$ **1** (thf = tetrahydrofuran)[1] and more recently we described the related cyclic species **2**.[2] We have now obtained and structurally characterized the somewhat more distantly related cyclic lithate **3**, which has unprecedented features.

$[Li(thf)_4][CH_2SiMe_2C(SiMe_3)_2LiC(SiMe_3)_2SiMe_2CH_2]$

2

$[SiMe_2C(SiMe_3)_2LiC(SiMe_3)_2SiMe_2OLi(thf)_2]$

3

We have found that the disiloxane $O\{SiMe_2CH(SiMe_3)_2\}_2$[3] is metallated by LiMe in thf at room temperature, that is much more readily than $(Me_3Si)_3CH$,[4] probably because of initial interaction of the siloxane oxygen atom with the Li of the LiMe.‡ Recrystallization of the product, **3**, from heptane gave crystals suitable for an X-ray diffraction study, which yielded the structure shown in Fig. 1.§

The main novel features of **3** are as follows.

(*a*) In contrast to **1** and **2**, in each of which the lithate anion and the solvated lithium cation are well separated, compound **3** is a molecular dipolar species, the $Li(2)^+$ centre being attached to the lithate ion *via* the oxygen of the siloxane linkage. Both the O(1) and Li(2) atoms have essentially planar geometries [sum of angles 358.6(5) and 360.0(6)°, respectively]. The Si–O–Si angle is 138.5(3)°, a fairly normal value for a siloxane linkage.[5] The angle between the bonds to the thf molecules, O(3)–Li(2)–O(2) 101.2(6)°, is narrow, presumably to minimize steric interactions.

(*b*) As far as we can ascertain compound **3** is the first example of a structurally characterized disiloxane–metal complex in which the ligand is attached to the metal only through its oxygen atom. In all other examples of coordination of disiloxane oxygen to a metal this bonding is supported by bonding through another atom of the ligand; examples include systems of the types Me_3SiO–Pd–Si,[6] Me_3SiO–Zr–CH_2SiMe_2,[7] and Me_3SiO–Li–N–Si.[8] (A polysiloxane analogue of a crown ether complex, $[K(OSiMe_2)_7]^+$,[9] and siloxane-solvation of Na and K centres within complex polysiloxane frameworks[10] were recently reported.) Remarkably, since siloxanes are normally thought to be much weaker donors than organic ethers,[6,7,11] the Li–O bond to the siloxane oxygen in **3**, 1.917(12) Å, is not significantly longer than those to the thf molecules, mean 1.912(12) Å. [See also (*d*) below. In contrast, the O–M bonds in the Pd and Zr compounds mentioned above are rather long, and this was attributed to the poor donor ability of siloxanes.[6,7]] The interaction of the oxygen lone pair with Li leads to a large increase in the Si–O(1) bond length to a mean of 1.704(5) Å from the 1.63–1.64 Å usually found in disiloxanes.[5]

(*c*) The mean Li–C bond length in **3**, 2.12(2) Å, is not significantly different from that in **1**, 2.18(1) Å, or **2**, 2.156(4) Å. To accommodate the demands of the six-membered ring the C–Li–C angle is lowered to 144.2(7)°, compared with 180° in **1** and 171.4(7)° in **2**. The closest contacts between the Li atom and the methyl groups are to C(6) and C(18) [Li–C(6) 3.12, Li–C(18) 3.00 Å], there are corresponding contacts (3.04 Å) in **2**.

(*d*) In contrast to **2**, in which the exocyclic C–$SiMe_3$ bonds and endocyclic C–$SiMe_2CH_2$ bonds are all essentially of equal length, mean 1.829(4)°, in **3** the C–$SiMe_3$ bonds have a mean length of 1.835(4)°, effectively identical with those in **2**, but the endocyclic C–$SiMe_2O$ bonds have a mean length of only 1.806(6)°. This can be attributed to more effective delocalization of carbanionic charge by negative hyperconjugation[12] directed towards oxygen rather than towards carbon.[7] Such enhancement of the negative charge on the oxygen atom could strengthen the O(1)–Li(2) interaction. (Or, from an alternative viewpoint, this interaction could enhance the hyperconjugation.)

(*e*) The mean of the Si–C–Si angles in **3** is 117.3°, compared with 115.9° in **2**, but, the separate values, and those of the Li–C–Si angles, range more widely than in **2**. The Me_3Si–C–$SiMe_3$ angles, mean 114.0(2)°, are markedly smaller than the Me_3Si–C–$SiMe_2O$ angles, mean 119.6°, these latter angles varying

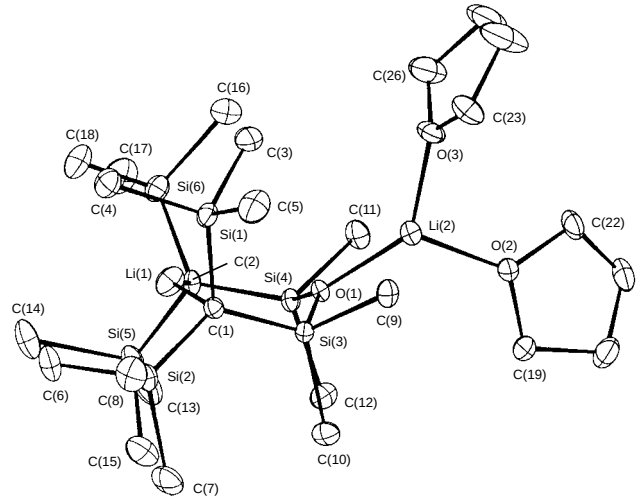

Fig. 1 Selected bond lengths (Å) and angles (°) for **3**: C(1)–Si(1) 1.843(7), C(1)–Si(2) 1.829(7), C(1)–Si(3) 1.809(6), C(2)–Si(4) 1.804(6), C(2)–Si(5) 1.834(7), C(2)–Si(6) 1.836(7), C(1)–Li(1) 2.105(14), C(2)–Li(1) 2.13(2), O(1)–Si(3) 1.706(5), O(1)–Si(4) 1.702(5), O(1)–Li(2) 1.917(12), O(2)–Li(2) 1.909(12), O(3)–Li(2) 1.914(13), Si–Me (mean) 1.886(6); Si(1)–C(1)–Si(2) 113.5(3), Si(1)–C(1)–Si(3) 115.5(3), Si(2)–C(1)–Si(3) 124.4(4), Si(4)–C(2)–Si(5) 117.8(4), Si(4)–C(2)–Si(6) 120.8(4), Si(5)–C(2)–Si(6) 114.6(3), C(1)–Li(1)–C(2) 144.2(7), Li(1)–C(1)–Si(3) 93.2(4), Li(1)–C(2)–Si(4) 94.8(4), Li(1)–C(1)–Si(1) 99.6(5), Li(1)–C(2)–Si(5) 104.5(5), Li(1)–C(2)–Si(6) 97.2(5), Si(3)–O(1)–Li(2) 109.1(5), Si(4)–O(1)–Li(2) 111.0(5) O(1)–Li(2)–O(2) 125.6(7), O(1)–Li(2)–O(3) 133.2(7), O(2)–Li(2)–O(3) 101.2(6), Si(3)–O(1)–Si(4) 138.5(3), O(1)–Si(3)–C(9) 100.3(3), O(1)–Si(3)–C(10) 104.3(3), O(1)–Si(4)–C(1) 99.4(3), O(1)–Si(4)–C(12) 106.1(3), Me–Si–Me (mean) 103.9(4).

from 115.5(3) to 124.4(4)°. As in **2** the two CSi_3 systems on either side of the molecule are distorted and tilted (with respect to the Li–C bonds) differently; presumably this is predominantly to maximize Me···Me distances, but it also accommodates the observed Me···Li interactions. In consequence the molecule as a whole has no symmetry.

Compound **3** can be expected to serve as a source of the dicarbanionic ligand $(Me_3Si)_2\bar{C}SiMe_2OSiMe_2\bar{C}(SiMe_3)_2$. This ligand should give novel cyclic and linear-polymeric derivatives of a range of metals, and may be especially effective in the case of cyclic derivatives of elements for which the dialkylmetals prefer a bent C–M–C framework, *e.g.* Ca,[13] Yb[14,15] and Eu.[15]

We thank the EPSRC for financial support and the Libyan Government for the award of a postgraduate scholarship to S. M. El-H.

Notes and References

† E-mail: c.eaborn@sussex.ac.uk; j.d.smith@sussex.ac.uk

‡ Water (0.3 cm^3) was added to a solution of $(Me_3Si)_2(ClMe_2Si)CH$[16] (4.74 g) in 1,4-dioxane (40 cm^3) and the mixture was stirred at room temperature overnight. The solvent was removed to leave $(Me_3Si)_2(HOMe_2Si)CH$[3] which was distilled under vacuum then left exposed to the air for 3 days to give $O\{SiMe_2CH(SiMe_3)_2\}_2$, with ^{1}H NMR data identical with those previously reported.[3] A solution of LiMe (1.20 mmol) in hexane (0.90 cm^3) was added dropwise at room temperature to a stirred solution of the $O\{SiMe_2CH(SiMe_3)_2\}_2$ (0.27 g, 0.60 mmol) in thf (10 cm^3). The mixture was stirred overnight at room temperature and the solvent then removed under vacuum to leave a sticky solid, which was crystallized from heptane at room temperature. ^{1}H NMR (C_6D_6): δ_H 0.43 (coincident s, 48 H, $SiMe_3$ and $SiMe_2$), 1.30 (s, 8 H, thf) and 3.30 (s, 8 H, thf). δ_C 7.7 ($SiMe_3$), 8.7 ($SiMe_2$), 25.1 (thf) and 68.8 (thf). δ_{Si} –10.8 ($SiMe_3$) and 2.2 ($SiMe_2$). δ_{Li} 0.63 and 0.78, overlapping. The yield of **3** as estimated from the ^{1}H NMR spectrum of the initial product solution was >90%.

§ *Crystal data* for **3**: M = 607.2; monoclinic, space group $P2_1/n$ (non-standard no. 14), a = 9.416(2), b = 16.959(2), c = 23.900(4) Å, β = 93.51(10), U = 3809(1) Å^3, D_c = 1.06 Mg m^{-3}, Z = 4, $F(000)$ = 1336, Mo-Kα radiation, λ = 0.710 73 Å, crystal size 0.2 × 0.2 × 0.1 mm, μ(Mo-Kα) = 0.24 mm^{-1}, T = 173(2) K. CAD4 diffractometer, θ–2θ scan mode, $2 < \theta < 25°$, 6677 independent reflections. Structure solution by direct methods (SHELXS-86) and full matrix least-squares refinement on F^2 (SHELX-93) with all non-hydrogen atoms anisotropic and H atoms in riding mode with $U_{iso} = 1.5U_{eq}$(C). Final R_1 = 0.089 for 4429 reflections with $I > 2\sigma(I)$, wR_2 0.253 (all data). CCDC 182/870.

1 C. Eaborn, P. B. Hitchcock, J. D. Smith and A. C. Sullivan, *J. Chem. Soc., Chem. Commun.*, 1983, 827.
2 C. Eaborn, Z.-R. Lu, P. B. Hitchcock and J. D. Smith, *Organometallics*, 1996, **15**, 1651.
3 N. Wiberg and H. Köpf, *J. Organomet. Chem.*, 1986, **315**, 9.
4 Z. H. Aiube and C. Eaborn, *J. Organomet. Chem.*, 1984, **269**, 217.
5 E. Lukevics, O. Pudova and R. Sturkovich, *Molecular Structure of Organosilicon Compounds*, Ellis Horwood, Chichester, 1989, pp. 175–208.
6 M. Knorr, P. Braunstein, A. Tiripicchio and F. Ugozzoli, *Organometallics*, 1995, **14**, 4910.
7 E. L. Lyszak, J. P. O'Brien, D. A. Kort, S. K. Hendges, R. N. Redding, T. L. Bush, M. S. Hermen, K. B. Renkema, M. E. Silver and J. C. Huffman, *Organometallics*, 1993, **12**, 338.
8 S. Walter, U. Klingebiel and M. Noltemeyer, *Chem. Ber.*, 1992, **125**, 783.
9 M. R. Churchill, C. H. Lake, S.-H. L. Chao and O. T. Beachley, *J. Chem. Soc., Chem. Commun.*, 1993, 1577; C. Eaborn, P. B. Hitchcock, K. Izod and J. D. Smith, *Angew. Chem., Int. Ed. Engl.*, 1995, **34**, 2679.
10 V. A. Igonin, S. V. Lindeman, Yu. Y. Struchkov, O. I. Shchegolikhina, A. A. Zhadanov, Yu. A. Moltsova and I. V. Razumovskaya, *Metalloorg. Khim.*, 1991, **4**, 1355.
11 A. R. Bassindale and P. G. Taylor, in *The Chemistry of Organic Silicon Compounds*, ed. S. Patai and Z. Rappoport, Wiley, Chichester, 1989, pp. 822–823.
12 P. v. R. Schleyer, T. Clark, A. J. Kos, G. W. Spitznagel, C. Rohde, D. Arad, K. N. Houk and N. G. Rondan, *J. Am. Chem. Soc.*, 1984, **106**, 6467.
13 C. Eaborn, S. A. Hawkes, P. B. Hitchcock and J. D. Smith, *Chem. Commun.*, 1997, 1961.
14 C. Eaborn, P. B. Hitchcock, K. Izod and J. D. Smith, *J. Am. Chem. Soc.*, 1994, **116**, 12071.
15 C. Eaborn, P. B. Hitchcock, K. Izod, Z.-R. Lu and J. D. Smith, *Organometallics*, 1996, **15**, 4783.
16 D. Seyferth and H. Lang, *Organometallics*, 1991, **10**, 551.

Received in Cambridge, UK, 3rd April 1998; 8/02553C

Practical methods for synthesizing four incompletely condensed silsesquioxanes from a single $R_8Si_8O_{12}$ framework

Frank J. Feher,*† Daravong Soulivong and Frank Nguyen

Department of Chemistry, University of California, Irvine, CA 92697-2025, USA

The reaction of (c-C_6H_{11})$_8Si_8O_{12}$ 1 with triflic acid (TfOH) can produce two different ditriflates with the formula (c-C_6H_{11})$_8Si_8O_{11}$(OTf)$_2$, which can be hydrolyzed selectively to four different incompletely condensed silsesquioxane frameworks with the formula (c-C_6H_{11})$_8Si_8O_{11}$(OH)$_2$ (2, 4, 7 and 8).

Incompletely condensed silsesquioxanes have attracted broad interest as models for silica surfaces,[1–3] ligands for main group, transition-metal and lanthanide elements,[4–6] building blocks for network solids,[7,8] and precursors to new families of silsesquioxane-containing polymers.[9,10] Our recent discovery that a single Si–O–Si linkage in a fully-condensed $R_8Si_8O_{12}$ framework (*i.e.* **1**) can be cleaved selectively by strong acids [*e.g.* HBF_4–BF_3 or

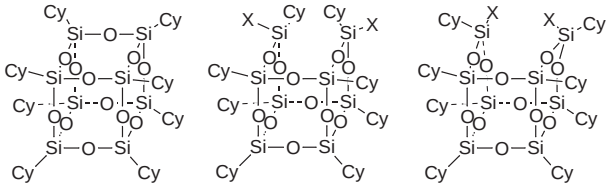

1 Cy = c-C_6H_{11} **2** X = OH **3** OTf **4** X = OH **5** NHPh

TfOH (triflic acid)] provides an important new method for preparing incompletely condensed frameworks (*e.g.* **2** and **4**),[11] but there are still strong incentives for devising practical routes to silsesquioxanes with reactive SiOH groups. Here, we report an improved method for synthesizing **2**, as well as the discovery of an interesting acid-induced rearrangement reaction of **1** that provides access to two other incompletely condensed frameworks (*i.e.* **7** and **8**).

The reaction of **1** with TfOH (5 equiv., 25 °C, C_6H_6, 30 min) occurs rapidly upon mixing to afford quantitative NMR yields of a C_{2v}-symmetric ditriflate derived from cleavage of a single Si–O–Si linkage (*e.g.* **3**).[11] This ditriflate reacts with a variety of nucleophiles to afford products resulting from substitution of triflate with complete inversion of stereochemistry at Si.[12] When water[11] or aniline[12] are used as nucleophiles in large excess, **4** or **5** can be obtained in high yield. Disilanol **4** is hydrolytically stable, but **5** reacts very slowly with water to afford several products resulting from hydrolysis of Si–N bonds, including disilanol **2**. Both the rate and selectivity of hydrolysis can be greatly increased by performing the reaction with 6 M HCl. Under these conditions, high yields of **2** are obtained within a few minutes of mixing.‡ This route to **2** is far superior to our previously reported method[11] based on Me_3Sn-OH-mediated hydrolysis of fluoride-substituted frameworks, and it allows both **2** and **4** to be prepared from a common intermediate (*i.e.* **3**) which can be obtained in high yield from a readily available $R_8Si_8O_{12}$ framework.

When **1** is reacted with a larger excess of TfOH (10 equiv., 25 °C, C_6H_6, 3 h), cleavage of additional Si–O–Si linkages is observed, but the major product is not a tetratriflate derived from cleavage of the second Si–O–Si linkage. Instead, this reaction produces large amounts (*ca.* 70%) of a new C_2-symmetric framework with two Si–OTf groups. If cleavage of the second Si–O–Si linkage by TfOH and intramolecular displacement of a triflate group both occur with complete inversion of stereochemistry at Si, the mechanism proposed in Scheme 1 predicts that this new ditriflate is **6**.§ This ditriflate reacts with H_2O or aqueous $NaHCO_3$ to afford **7**;¶ hydrolysis of the ditriflate *via* sequential reaction with excess aniline and 6 M HCl affords **8**. The structures of **7** and **8** were established by comparison to authentic samples prepared by alternative methods. Disilanol **8** is available in 15–20% yield *via* the slow (3–36 months) hydrolytic condensation of $CySiCl_3$.[3] Disilanol **7** can be independently synthesized *via* sequential reactions of **8** with HBF_4–BF_3, Me_3SnOH and aqueous HCl. The stereochemical consequences of these reactions are well established and known to invert the stereochemistry of SiOH groups on silsesquioxane frameworks.[11,13,14]

The formation of **6** during the reaction of **1** with TfOH is surprising because it requires formation of an Si_5O_5 ring under conditions where Si_4O_4 rings are cleaved selectively and Si–OH groups are quickly converted into Si–OTf groups by an excess of TfOH. It is difficult to rationalize the high selectivities observed in these reactions. Nevertheless, it is abundantly clear that Si–O–Si cleavage by strong acids can be extremely selective and that the formation of new Si–O–Si linkages can be competitive.

In conclusion, the reaction of **1** with TfOH can produce two different ditriflates (**3** and **6**), which can be hydrolyzed selectively to four different incompletely condensed silsesquioxane frameworks (**2**, **4**, **7** and **8**). These results represent an important advance in the chemistry of discrete silsesquioxanes

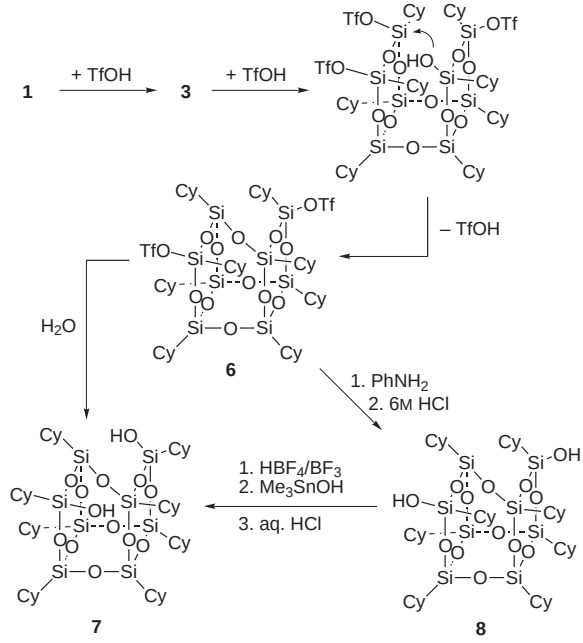

Scheme 1

because **1** is available in high yield *via* base-catalyzed hydrolytic condensation of $CySi(OMe)_3$[15] and catalytic hydrogenation of readily available $Ph_8Si_8O_{12}$.[16,17] Our efforts to expand the generality of these reactions, as well as the reaction chemistry of **3** and **6** will be reported in due course.

These studies were supported by the National Science Foundation and Phillips Laboratory (Edwards AFB).

Notes and References

† E-mail: fjfeher@uci.edu

‡ Disilanol **2** was prepared in quantitative yield by adding an excess of 6 M HCl to a solution of **5** in THF. The product obtained after evaporation of the THF and a standard aqueous work-up with Et_2O as an extraction solvent was identical in all respects to an authentic sample of **2** prepared according to ref. 11.

§ The ditriflate tentatively assigned as **6** was prepared by reacting **1** (102 mg, 0.094 mmol) and TfOH (83 μl, 0.943 mmol) at 25 °C for 3 h according to the procedure described for the synthesis of **3**.[11] Repeated attempts to crystallize the crude product were unsuccessful because the ditriflate is extremely water sensitive and highly soluble in all solvents with which it does not react. The crude product obtained after evaporation of the solvent is *ca.* 70% pure (by ^{13}C and ^{29}Si NMR spectroscopy) and should be used immediately to avoid decomposition. Selected characterization data: $^{13}C\{^1H\}$ NMR (125 MHz, $CDCl_3$, 25 °C), δ 27.35–25.26 (CH_2), 23.24, 23.00, 22.95, 22.66 (s CH, 1 : 1 : 1 : 1). $^{29}Si\{^1H\}$ NMR (99 MHz, $CDCl_3$, 25 °C), δ −62.82, −64.84, −67.25, −68.02 (1 : 1 : 1 : 1). A C_2-symmetric structure with the opposite orientation of Cy and OTf groups is equally consistent with all of our spectroscopic and analytical data. Although this structure it is considered unlikely on the basis of mechanistic considerations, it should not be ruled out until the structure of **6** is confirmed by a single-crystal X-ray diffraction study.

¶ For **7**: ^1H NMR (500 MHz, $CDCl_3$, 25 °C), δ 2.38 (br s, 2 H), 1.73 (br m, 40 H), 1.24 (br m, 40 H), 0.42 (br m, 8 H). $^{13}C\{^1H\}$ NMR (125 MHz, $CDCl_3$, 25 °C), δ 27.45, 27.40, 27.37, 26.76, 26.70, 26.60, 26.52, 26.45, 26.42 (for CH_2), 23.46, 23.29, 23.27, 22.15 (1 : 1 : 1 : 1 for CH). $^{29}Si\{^1H\}$ NMR (99 MHz, $CDCl_3$, 25 °C): δ −57.47, −66.18, −67.24, −67.76 (1 : 1 : 1 : 1). MS (70 eV, 200 °C, relative intensity): *m*/*z* 1015 ($[M - Cy]^+$, 100%), 932 ($[M - 2Cy]^+$, 15%), 466 ($[M - 2Cy]^{2+}$, 35%). Anal. Calc. for $C_{48}H_{90}O_{13}Si_8$ (found): C, 52.42 (52.40); H, 8.25 (8.05)%. Mp by DSC: 233.5 °C.

1 F. J. Feher, S. H. Phillips and J. W. Ziller, *Chem. Commun.*, 1997, 829.
2 F. J. Feher, T. A. Budzichowski, K. Rahimian and J. W. Ziller, *J. Am. Chem. Soc.*, 1992. **114**, 3859.
3 F. J. Feher, D. A. Newman and J. F. Walzer, *J. Am. Chem. Soc.*, 1989, **111**, 1741.
4 F. J. Feher and T. A. Budzichowski, *Polyhedron*, 1995, **14**, 3239.
5 R. Murugavel, V. Chandrasekhar and H. W. Roesky, *Acc. Chem. Res.*, 1996, **29**, 183.
6 W. A. Herrmann, R. Anwander, V. Dufaud and W. Scherer, *Angew. Chem., Int. Ed. Engl.*, 1994, **33**, 1285.
7 H. C. L. Abbenhuis, H. W. G. van Herwijnen and R. A. van Santen, *Chem. Commun.*, 1996, 1941.
8 H. C. L. Abbenhuis, S. Krijnen and R. A. van Santen, *Chem. Commun.*, 1997, 331.
9 J. D. Lichtenhan, *Comments Inorg. Chem.*, 1995, **17**, 115.
10 J. D. Lichtenhan, C. J. Noel, A. G. Bolf and P. N. Ruth, *Mater. Res. Soc. Symp. Proc.*, 1996, **435**, 3.
11 F. J. Feher, D. Soulivong and A. E. Eklund, *Chem. Commun.*, 1998, 399.
12 F. J. Feher, D. Soulivong and F. Nguyen, *Angew. Chem., Int. Ed. Engl.*, submitted.
13 F. J. Feher, D. Soulivong and G. T. Lewis, *J. Am. Chem. Soc.*, 1997, **119**, 11 323.
14 F. J. Feher, S. H. Phillips and J. W. Ziller, *J. Am. Chem. Soc.*, 1997, **119**, 3397.
15 J. F. Brown and L. H. Vogt, *J. Am. Chem. Soc.*, 1965, **87**, 4313.
16 F. J. Feher and T. A. Budzichowski, *J. Organomet. Chem.*, 1989, **373**, 153.
17 C. L. Frye, in *Ring-Ring Equilibration of Cyclosiloxanes*, ed. A. P. Hagen, Deerfield Beach, FL, 1986.

Received in Bloomington, IN, USA, 8th April 1998; 8/02670J

Synthesis, molecular structure, and reactivity of an Li_2Br_4 octahedrally stabilized organoaluminium bromide dimer

Xiao-Wang Li, Jianrui Su and Gregory H. Robinson*

Department of Chemistry, The University of Georgia, Athens, GA 30602-2556, USA

The synthesis, molecular structure, and reactivity of an unusual Li_2Br_4 octahedrally stabilized organoaluminium bromide dimer, $[(Mes_2C_6H_3)AlBr_3Li]_2$, is described.

Utilization of the sterically demanding 2,6-dimesitylphenyl ligand, ($Mes_2C_6H_3$), with group 13 elements has afforded a number of interesting compounds in recent years. Monomeric compounds of boron, $(Mes_2C_6H_3)BBr_2$,[1] gallium, $(Mes_2C_6H_3)_2GaX$ (X = Cl,[2] Br[3]), and indium ($(Mes_2C_6H_3)_2InBr$,[4] have been reported. Gallium and indium dimers such as $[(Mes_2C_6H_3)GaCl_2]_2$ and $[(Mes_2C_6H_3)InCl_2]_2$[5] have also been prepared. It is particularly significant that this ligand system has been shown to stabilize cyclogallenes, organometallic 2π-electron aromatic moieties, $M_2[(Mes_2C_6H_3)Ga]_3$[6–9] (M = Na, K). In notable contrast, the corresponding organoaluminium chemistry of this ligand has proven considerably less fruitful. Reaction of Me_3SiCl with $[(Mes_2C_6H_3)AlH_3{\cdot}LiOEt_2]_n$ gives $(Mes_2C_6H_3)AlCl_2{\cdot}OEt_2$.[10] Herein we report the synthesis,† molecular structure, and reactivity of the Li_2Br_4 octahedrally stabilized aluminium bromide dimer $[(Mes_2C_6H_3)AlBr_3Li]_2$ **1**. Reaction of **1** with lithium 2,6-diisopropylphenylamide, $Li[N(H)(Pr^i_2C_6H_3)]$, affords $(Mes_2C_6H_3)Al[N(H)(Pr^i_2C_6H_3)]_2$, **2**.

The structure of **1** (Fig. 1)‡ which resides about a center of symmetry, may be described as an Li_2Br_4 octahedrally stabilized aluminium bromide dimer. The Li_2Br_4 octahedron is facilitated by the displacement of the lithium atoms from the *ipso*-carbon atoms of the ligands by $AlBr_3$ moieties. **1** is easily compared with the unsolvated (2,6-dimesitylphenyl)lithium dimer, $[(Mes_2C_6H_3)Li]_2$.[11] Perhaps most interesting is the differences in lithium coordination of **1** compared to that of $[(Mes_2C_6H_3)Li]_2$. In $[Mes_2C_6H_3)Li]_2$ the primary interaction between the lithium and the ligand involves the *ipso*-carbon atoms. The Li–C_{ipso} bond distances are 2.17(1) and 2.16(1) Å while the secondary lithium–carbon interactions (with the *ipso*-carbon atoms of the *o*-mesityl substituents) range from 2.51(1) to 2.56 Å. In striking contrast from $[(Mes_2C_6H_3)Li]_2$, the lithium atoms in **1** only interact with the 2,6-dimesitylphenyl ligand in an η^6-aryl ring fashion with lithium–carbon contacts ranging from 2.38(4) to 2.70(4) Å. In addition to the Li–(η^6-aryl) ring interaction, and quite unlike other reported lithium aryls, the core **1** is further stabilized by weak lithium–bromine contacts: 2.52(2), 2.67(3) and 2.80(3) Å. These distances are considerably longer than the corresponding value reported for gaseous LiBr (2.35 Å).[12] Furthermore, the Li···Li separation in **1** of 3.45(6) Å is considerably longer than the values reported for $[(Mes_2C_6H_3)Li]_2$ (2.31, 2.27 Å). The environment about the aluminium atom may be described as distorted tetrahedral with bond angles ranging from 99.0(5) to 122.5(5)°. The Al–C bond distance in **1** of 1.96(2) Å compares well with other four-coordinate aluminium compounds. The Al–Br bond distances, 2.359(5), 2.285(6) and 2.398(5) Å, for Al–Br(1), Al–Br(2) and Al–Br(3), respectively, are comparable to other reported Al–Br distances.[13–15]

The unusual structure of **1** underscores the often substantial differences in chemical behavior of organoaluminium moieties relative to other group 13 congeners. However, it is interesting that reaction of **1** with $Li[N(H)(Pr^i_2C_6H_3)]$ proceeds in an expected manner affording **2**. The aluminium atom in **2** assumes a trigonal planar geometry [bond angles about Al: 127.3(5), 116.4(2) and 116.4(2)°] (Fig. 2) with generally unremarkable Al–Cl [1.978(11) Å] and Al–N [1.788(6) Å] bond distances. The Al–N bond distance in **2** is quite comparable to values reported for $[CpAl–N(Pr^i_2C_6H_3)]_2$ [1.796(2) and 1.811(3) Å][16] while these are much shorter than the distances reported for $[(Me_3CCH_2)_2Al–N(H)(Pr^i_2C_6H_3)]_2$ [2.013(5) and 2.007(5) Å].[17] **2** contains a mirror plane which bisects the N–Al–N bond

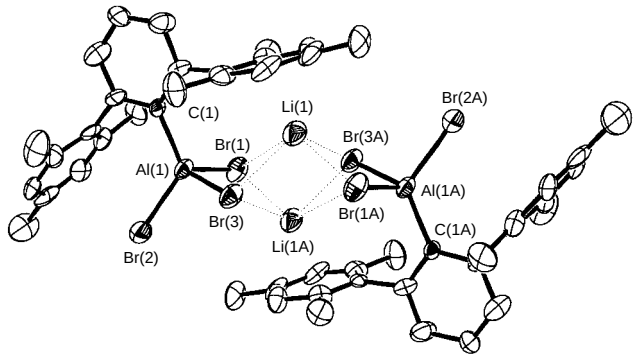

Fig. 1 Molecular structure of $[(Mes_2C_6H_3)AlBr_3Li]_2$ **1**. Selected bond distances (Å) and angles (°): Al(1)–C(1) 1.96(2), Al(1)–Br(1) 2.359(5), Al(1)–Br(2) 2.285(6), Al(1)–Br(3) 2.398(5), Br(1)–Li(1A) 2.67(3), Br(3)–Li(1) 2.52(3), Br(3)–Li(1A) 2.80(3), Li(1)–Li(1A) 3.41(5), Li(1)–C(7) 2.70(3), Li(1)–C(8) 2.70(3), Li(1)–C(9) 2.51(3), Li(1)–C(10) 2.43(3), Li(1)–C(11) 2.38(4), Li(1)–C(12) 2.55(4), C(1)–Al(1)–Br(1) 111.1(5), C(1)–Al(1)–Br(2) 122.2(5), C(1)–Al(1)–Br(3) 115.5(5), Br(2)–Al(1)–Br(1) 106.2(2), Br(2)–Al(1)–Br(3) 99.0(2), Br(1)–Al(1)–Br(3) 100.0(2), Al(1)–Br(1)–Li(1A) 88.5(7), Al(1)–Br(3)–Li(1) 106,1(8), Al(1)–Br(3)–Li(1A) 84.9(7), Li(1)–Br(3)–Li(1A) 79.6(9).

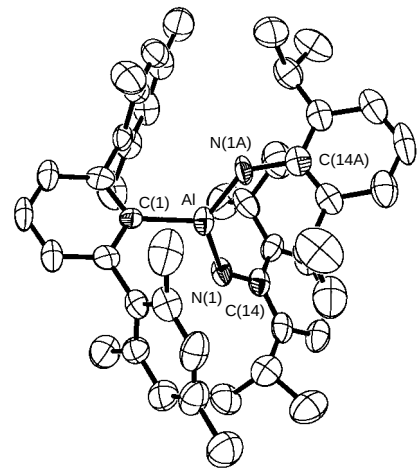

Fig. 2 Molecular structure of $(Mes_2C_6H_3)Al[N(H)(Pr^i_2C_6H_3)_3$ **2**. Selected bond distances (Å) and angles (°): Al(1)–C(1) 1.978(11), Al(1)–N(1) 1.788(6), N(1)–C(14) 1.436(10); N(1)–Al(1)–C(1) 116.4(2), N(1)–Al(1)–N(1A) 127.3(5), C(14)–N–Al(1) 138.1(6).

angle while containing atoms Al, C(1) and C(4). The central phenyl ring of the ligand resides at an angle of 63.2° relative to the aluminium trigonal plane [C–Al(N)–N]. Indeed, significant π-bonding would appear to be precluded in **2** by the fact that both nitrogen trigonals [C–N(H)–Al] are twisted at an angle of 23.1° relative to the aluminium trigonal plane.

The formation of **2** suggests that **1** may be utilized in a variety of reactions as a means to approach other interesting derivatives.

Notes and References

† *Synthesis*: **1** a solution of $(Mes_2C_6H_3)Li$ (0.80 g, 2.5 mmol) in diethyl ether (40 ml) was added over a period of 10 min to an ether (30 ml) solution of $AlBr_3$ (0.67 g, 2.5 mmol) at −78 °C. The reaction mixture was stirred for 3 h and allowed to warm to room temp. over a period of 2 h. The resulting solution became yellow and was stirred for additional 30 h. After filtration, the solution was concentrated. Cooling this solution to −25 °C for several days afforded **1** (0.78 g) as colorless crystals. Yield: 53%, mp 67 °C. ^{1}H NMR (300 MHz, 298 K, [$^2H_8$]THF): δ 1.92 (s, 12 H, *o*′-CH_3), 1.98, (s, 12 H, *o*′-CH_3), 2.13 (s, 6 H, *p*′-CH_3), 2.17, (s, 6 H, *p*′-CH_3), 6.65–6.73 [m, 6 H, CH(aromatic)], 6.76 [s, 8 H, *m*′-CH (aromatic)]. ^{13}C NMR (300 MHz, 298 K, [$^2H_8$]THF): δ 19.91, 20.06, 20.48, 20.62, 20.81 (methyl C); 125.90, 126.32, 126.68, 126.86–134.02, 139.23, 142.12, 145.98 (aromatic C).

2: an ether (50 ml) solution of $Li[N(H)(Pr^i_2C_6H_3)]$ (0.22 g, 1.5 mmol), prepared from $(Pr^i_2C_6H_3)NH_2$ and *n*-C_4H_9Li, at 0 °C in ether, was slowly added to an ether (30 ml) solution of **1** (0.42 g, 0.70 mmol) at −78 °C. The reaction mixture was stirred for 3 h and allowed to warm to room temp. over a period of 2 h, and stirred for additional 30 h. After filtration, the solvent of the yellow solution was evaporated *in vacuo*. The residue was extracted with hexane (50 ml). The volume of the solution was reduced *in vacuo* to *ca*. 15 ml. Cooling the concentrated solution at −25 °C for a week afforded colorless needle crystals of **2**. X-Ray quality crystals were grown from diethyl ether–hexane (1 : 1). Yield: 78%. mp. 154 °C. ^{1}H NMR (300 MHz, 298 K, C_6D_8): δ 1.07 [d, 12 H, $CH(CH_3)_2$], 1.2 [d, 12 H, $CH(CH_3)_2$], 1.90 (s, 6 H, *o*′-CH_3), 1.93 (s, 6 H, *o*′-CH_3), 2.04 (s, 3 H, *p*′-CH_3), 2.08 (s, 3 H, *p*′-CH_3), 3.24–3.29, [m, 4 H, $CH(CH_3)_2$], 4.39 (s, 2 H, NH), 6.63–6.69 [m, 12 H, CH (aromatic)], 6.71–6.73 [m, 4 H, *m*′-CH (aromatic)]. ^{13}C NMR (300 MHz, 298 K, C_6D_8): δ 8.18, 8.26, 16.38, 18.10, 18.38, 18.65, 19.91, 20.17 (alkyl C), 123.20, 123.42, 124.09, 124.75, 124.98–141.2, 142.87, 144.50, 145.96 (aromatic C).

‡ *Crystallographic data* for **1** and **2**: colorless cubic crystals of **1** (0.2 × 0.1 × 0.1 mm) and **2** (0.2 × 0.2 × 0.1 mm) were mounted in glass capillaries under an atmosphere of N_2 in a drybox. Single crystal X-ray intensity data were collected on a Siemens P4 diffractometer (50 kV/40 mA), with graphite-monochromated Mo-Kα radiation (λ = 0.710 73 Å) at 21 °C, using the ω scan technique to a maximum 2θ value of 45°. Cell parameters and an orientation matrix for data collection were obtained from a least-squares analysis of the setting of up to 30 carefully centered reflections in the range $15.0° < 2\theta < 30.0°$. Absorption corrections were carried out using the empirical ψ-scan method. The structures were solved by direct methods using the SHELXTL 5.0[18] software package. All non-hydrogen atoms were refined using anisotropic thermal parameters. Hydrogen atoms were placed at ideal positions riding on the attached carbon and nitrogen atoms without further refinement.

Crystal data: **1**: a = 9.982(8), b = 10.179(2), c = 12.948(3) Å, α = 95.30(2), β = 94.90(4), γ = 107.70(2)°, V = 1239.0(11) Å^3, D_c = 1.574 g cm^{-3}, Z = 1 for triclinic space group $P\bar{1}$. Refinement converged at $R1$ = 0.070, $wR2$ = 0.20 using the F^2 refinement for 2150 observed reflections. Data collection and refinement for **2** proceeded in a fashion similar to that described for **1**.

2: a = 24.604(14), b = 10.312(5), c = 18.173(8) Å, β = 115.50(5)°, V = 4161.8(34) Å^3, D_c = 1.106 g cm^{-3}, Z = 4 for monoclinic space group $C2/c$. Refinement converged at $R1$ = 0.097, $wR2$ = 0.23 using the F^2 refinement for 1449 observed reflections. CCDC 182/851.

1 W. J. Grigsby and P. P. Power, *J. Am. Chem. Soc*., 1996, **118**, 7981.
2 X.-W. Li, W. T. Pennington and G. H. Robinson, *Organometallics*, 1995, **14**, 2109.
3 R. C. Crittendon, X.-W. Li, J. Su and G. H. Robinson, *Organometallics*, 1997, **16**, 2443.
4 X.-W. Li, W. T. Pennington and G. H. Robinson, *Main Group Chem.*, 1995, **3**, 301.
5 G. H. Robinson, X.-W. Li and W. T. Pennington, *J. Organomet. Chem.*, 1995, **501**, 399.
6 X.-W. Li, W. T. Pennington and G. H. Robinson, *J. Am. Chem. Soc.*, 1995, **117**, 7578.
7 X.-W. Li, Y. Xie, P. R. Schreiner, K. D. Gripper, R. C. Crittendon, C. F. Campana, H. F. Schaefer III and G. H. Robinson, *Organometallics*, 1996, **15**, 3798.
8 Y. Xie, P. R. Schreiner, H. F. Schaefer III, X.-W. Li and G. H. Robinson, *J. Am. Chem. Soc.*, 1996, **118**, 10635.
9 Y. Xie, P. R. Schreiner, H. F. Schaefer III, X.-W. Li and G. H. Robinson, *Organometallics*, 1998, **17**, 114.
10 R. J. Wehmschulte, W. J. Grigsby, B. Schiemenz, R. A. Bartlett and P. P. Power, *Inorg. Chem.*, 1996, **35**, 6694.
11 K. Ruhlandt-Senge, J. J. Ellison, R. J. Wehmschulte, F. Pauer and P. P. Power, *J. Am. Chem. Soc*., 1993, **115**, 11353.
12 P. A. Akisin and N. G. Rambidi, *Z. Phys. Chem.*, 1960, **213**, 111; *Z. Neorg. Khim. SSSR*, 1960, **5**, 23.
13 M. Mocker, C. Robl and H. Schnöckel, *Angew. Chem., Int. Ed. Engl.*, 1994, **33**, 1754; P. A. Akisin, N. G. Rambidi and E. Z. Zasovin, *Sov. Phys. Crystallogr.* (*Engl. Transl.*), 1959, **4**, 167.
14 E. Rytter, B. E. D. Rytter, H. A. Øye and J. Krogh-Moe, *Acta Crystallogr., Sect. B*, 1975, **31**, 2177.
15 M. A. Petrie, P. P. Power, H. V. R. Dias, K. Ruhlandt-Senge, K. M. Waggoner and R. J. Wehmschulte, *Organometallics*, 1993, **12**, 1086.
16 J. D. Fisher, P. J. Shapiro, G. P. A. Yap and A. L. Rheingold, *Inorg. Chem.*, 1996, **35**, 271.
17 S. Schauer, W. T. Pennington and G. H. Robinson, *Organometallics*, 1992, **11**, 3287.
18 G. M. Sheldrick, SHELXTL 5.0, Crystallographic Computing System, Siemens Analytical X-ray Instruments, Madison, WI, 1995.

Received in Columbia, MO, USA, 30th January 1998; 8/00847G

A two-dimensional network constructed from hexamolybdate, octamolybdate and $[Cu_3(4,7\text{-phen})_3]^{3+}$ clusters: $[\{Cu_3(4,7\text{-phen})_3\}_2\{Mo_{14}O_{45}\}]$

Douglas Hagrman, Pamela J. Zapf and Jon Zubieta*†

Department of Chemistry, Syracuse University, Syracuse, NY 13244, USA

The hydrothermal reaction of $Cu(SO_4)\cdot H_2O$, MoO_3, 4,7-phenanthroline and water yields $[\{Cu_3(4,7\text{-phen})_3\}_2\{Mo_{14}O_{45}\}]$, a material exhibiting a two-dimensional network constructed from $(Mo_6O_{19})^{2-}$ and $(Mo_8O_{26})^{4-}$ clusters linked through planar cyclic $\{Cu_3(4,7\text{-phen})_3{}^3\}^+$ clusters.

Inorganic oxides are ubiquitous in the geosphere and the biosphere[1,2] and are represented not only by the complex aluminosilicates which make up vast proportions of igneous rocks,[3] by ores and gems but also by complex oxides fashioned by biomineralization, such as bones, shells, teeth and spicules.[4,5] The intense contemporary interest in solid state oxides reflects their properties, which endow these materials with applications ranging from heavy construction to microcircuitry.[5] Consequently, there has evolved a significant effort in the manipulation of inorganic oxide microstructures.

One synthetic approach is to mimic Nature's remarkable mixtures of inorganic oxides coexisting with organic molecules. In such materials, the inorganic oxide contributes to the increased complexity and hence functionality through incorporation as one component in a multilevel structured material where there is synergistic interaction between organic and inorganic components.[6] There are now four major classes of materials in which organic components exert a significant structural role in controlling the inorganic oxide microstructure: zeolites,[7,8] mesoporous oxides of the MCM-41 class,[9] biomineralized materials,[10] and microporous octahedral–tetrahedral or square-pyramidal–tetrahedral framework transition metal phosphates (TMPO) with entrained organic cations.[11,12] We have recently identified a fifth class of organic–inorganic oxide hybrid materials: ditopic organonitrogen-templated molybdenum oxides.[13] A common structural motif for this class of materials consists of a molybdate cluster entrained within a scaffolding provided by a coordination cation polymer; for example, $[\{Cu(4,4'\text{-bpy})_4\}Mo_8O_{26}]$ and $[\{Ni(H_2O)_2(4,4'\text{-bpy})_2\}_2Mo_8O_{26}]$ exhibit the δ- and ε- forms of the octamolybate cluster, respectively. As part of our continuing studies of this class of materials, we have sought to exploit rigid linkers other than the linear rod, such as 4,7-phenanthroline which has resulted in the isolation of an unusual two-dimensional array of clusters[14,15] in the material $[\{Cu(4,7\text{-phen})_3\}_2\{Mo_{14}O_{45}]\}\cdot 0.5H_2O$ (**1**).

The hydrothermal reaction of $Cu(SO_4)\cdot H_2O$, MoO_3, 4,7-phenanthroline and water in the mole ratio 1 : 1.8 : 1.7 : 1654 at 200 °C for 99.5 h yielded **1** in 90% yield as brown rhombs. The IR spectrum exhibited a complex pattern of bands in the range 700–950 cm^{-1}, ascribed to ν(Mo=O) and ν(Mo–O–Mo).

As shown in Fig. 1(*a*) and (*c*), the structure of **1**‡ is constructed from the linking of three independent molecular clusters: $\{Cu_3(4,7\text{-phen})_3\}^{3+}$, β-$(Mo_8O_{26})^{4-}$ and $(Mo_6O_{19})^{2-}$. While the hexa- and octa-molybdate clusters are well known aggregates,[16] the trinuclear copper(I) cluster cation provides a novel twenty-one membered cyclic structure. The extended structure is generated through the bonding of terminal and bridging oxo-groups of the clusters to the Cu^I sites of the rings. As shown in Fig. 1(*a*), one motif consists of linear chains of β-$(Mo_8O_{26})^{4-}$ clusters linked through $\{Cu_3(4,7\text{-phen})_3\}^{3+}$ rings into a one-dimensional ribbon. Adjacent parallel ribbons are linked through $\{Mo_6O_{19}\}^{2-}$ clusters into a two-dimensional sheet structure, as shown in Fig. 1(*a*). Each hexamolybdate

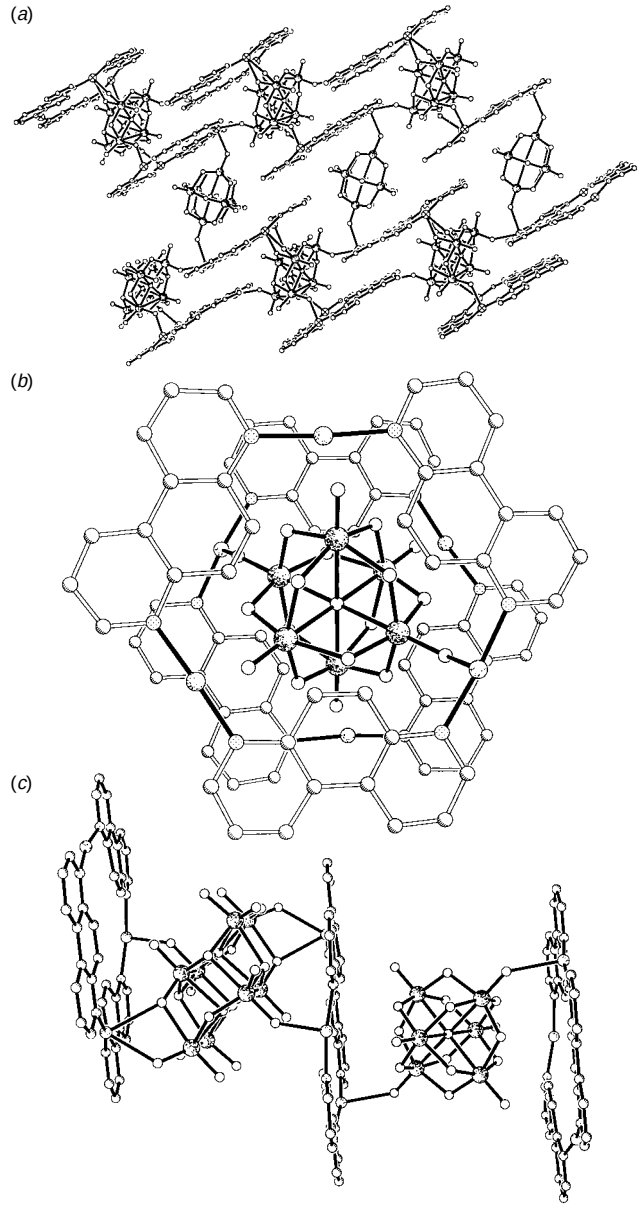

Fig. 1 (*a*) A view of the sheet structure of $[\{Cu_3(4,7\text{-phen})_3\}_2\{Mo_{14}O_{45}\}]\cdot 0.5H_2O$ **1** along the (112) plane, illustrating the linking of $[\{Cu_3(4,7\text{-phen})_3\}_2\{Mo_8O_{26}\}]_n^{2n+}$ chains by $(Mo_6O_{19})^{2-}$ clusters. (*b*) A view of the sandwiching of the $(Mo_6O_{19})^{2-}$ cluster between two nearly coplanar $\{Cu_3(4,7\text{-phen})_3\}^{3+}$ clusters. (*c*) A view of the crosslinking chain of alternating hexanuclear and octanuclear molybdate clusters, contrasting the alignment of the $(Mo_6O_{19})^{2-}$ cluster with the centroids of the $\{Cu_3(4,7\text{-phen})_3\}^{3+}$ rings and the displacement of the $(Mo_8O_{26})^{4-}$ cluster from the centroid causing a parallel shearing of the subsequent Cu_3 ring.

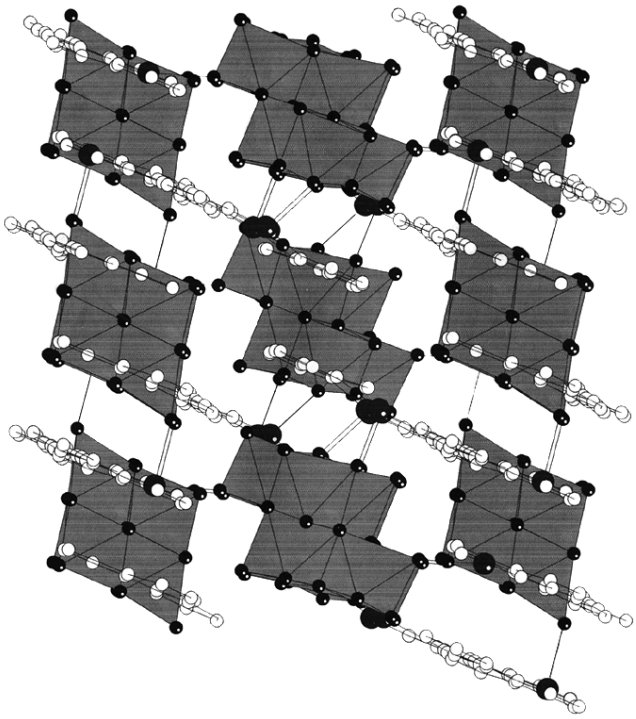

Fig. 2 A polyhedral representation of the cluster stacking parallel to the planes of the $\{Cu_3(4,7\text{-phen})_3\}^{3+}$ rings

cluster is sandwiched between two planar $\{Cu_3(4,7\text{-phen})_3\}^{3+}$ rings as shown in Fig. 1(*b*). The hexanuclear clusters are aligned with opposite Mo_3 triangular faces of the Mo_6 octahedron parallel to the Cu_3 rings. In contrast, the centroid of the β-$(Mo_8O_{26})^{4-}$ cluster does not align with the centroids of the sandwiching Cu_3 rings, which are displaced *ca.* 4.5 Å by parallel shearing with respect to each other. This allows the approach of two additional Cu_3 rings whose interactions with the oxo-groups of the octanuclear cluster propagate the chain. In this fashion, each octamolybdate cluster bonds to four Cu_3 rings, while each hexamolybdate cluster links only two such rings. Each Cu_3 ring bonds to one hexamolybdate and two octamolybdate clusters.

A curious feature of the structure is the presence of both $(Mo_6O_{19})^{2-}$ and β-$(Mo_8O_{26})^{4-}$ clusters as building blocks for the two-dimensional sheet, as shown in Fig. 2. However, this observation reflects the synthetic approach of exploiting hydrothermal conditions which requires a shift from the thermodynamic to the kinetic domain, such that equilibrium phases are replaced by structurally more complex metastable phases.[17] The structure-directing role of the copper coordination complex cluster is manifest in interactions whose geometric correspondence produces the architecture of the network. While it remains premature to classify such syntheses in terms of 'designed' routes, it should be noted that the very complexity of the hybrid material produces a limit on the degree of predictability. Moreover, design may not require total predictability, but rather a reciprocity of structure–function relationships for a class of materials which evolve as sufficient numbers of examples are characterised. Indeed, the chemistry of the Cu–organodiamine–molybdate system appears to be extraordinarily diverse, encompassing a variety of molybdate clusters, chains and sheets as building blocks. In the specific case of 4,7-phenanthroline as ligand, compound **1** was observed in a fairly narrow pH range (*ca.* 6–8), outside of which other as yet unidentified phases were observed.

Upon thermal treatment, **1** exhibits a 0.5 mass% loss at *ca.* 120 °C owing to the loss of the water of crystallization and a further 30 mass% loss between 310 and 350 °C, corresponding to the loss of the organic ligand. When carried out in oxygen, the product of thermolysis is a pale green material of approximate composition $Cu_6Mo_{14}O_{45}$, whose powder diffraction pattern is distinct from that of known copper molybdates. We are investigating the use of hybrid materials such as **1** in the preparation of novel heterometallic molybdate phases.

This work was supported by a grant from the National Science Foundation CHE9617232.

Notes and References

† E-mail: jazubiet@mailbox.syr.edu

‡ *Crystal data:* $C_{36}H_{25}Cu_3Mo_7N_6O_{23}$: triclinic, space group $P\bar{1}$; a = 12.7440(1), b = 13.0051(2), c = 14.0194(2) Å, α = 87.304(1), β = 87.596(1), γ = 70.315(1)°, U = 2198.02(5)Å^3, Z = 2, D_c = 2.678 g cm^{-3}; structure solution and refinement based on 9761 reflections converged at R_1 = 0.0491, wR_2 = 0.0952. CCDC 182/852.

1 N. N. Greenwood and A. Earnshaw, *Chemistry of the Elements*, Pergamom Press, New York, 1984
2 L. L. Hench, *Inorganic Biomaterials, in Materials Chemistry, An Emerging Discipline*, ed. L. V. Interrante, L. A. Casper and A.-B. Ellis, ACS Series 245, 1995, ch. 21, pp. 523–547.
3 B. Mason, *Principles of Geochemistry*, Wiley, New York, 3rd edn., 1966.
4 S. Mann, *J. Chem. Soc., Dalton Trans.*, 1993, 1.
5 S. Mann, S. L. Burkett, S. A. Davis, C. E. Fowler, N. H. Mendelson, S. D. Sims, D. Walsh and N. T. Whilton, *Chem. Mater.*, 1997, **9**, 2300.
6 S. I. Stupp and P. V. Braun, *Science*, 1997, **277**, 1242.
7 J. V. Smith, *Chem. Rev.*, 1998, **88**, 149.
8 M. L. Occelli and H. C. Robson, *Zeolite Synthesis*, American Chemical Society, Washington DC, 1989.
9 C. T. Kresge, M. E. Leonowicz, W. J. Roth, J. C. Vartuli and J. S. Beck, *Nature*, 1992, **359**, 710.
10 S. Mann, *Nature*, 1993, **365**, 499.
11 R. C. Haushalter and L. A. Mundi, *Chem. Mater.*, 1992, **4**, 31.
12 M. I. Khan, L. M. Meyer, R. C. Haushalter, C. L. Schweitzer, J. Zubieta and J. L. Dye, *Chem. Mater.*, 1996, **8**, 43.
13 D. Hagrman, C. Zubieta, D. J. Rose, J. Zubieta and R. C. Haushalter, *Angew. Chem., Int. Ed. Engl.*, 1997, **36**, 873.
14 For other examples of polyoxoanions linked into extended arrays see: I. Loose, M. Böing, R. Klein, B. Krebs, R. P. Schultz and B. Scharbert, *Inorg. Chim. Acta*, 1997, **263**, 99 and references therein; J. R. D. DeBord, R. C. Haushalter, L. M. Meyer, D. J. Rose, P. J. Zapf and J. Zubieta, *Inorg. Chim. Acta*, 1997, **256**, 165; J. R. Gálan-Mascaios, C. Giménez-Saig, S. Triki, C. J. Gómez-Garcia, E. Coronado and L. Ouahab, *Angew. Chem., Int. Ed. Engl.*, 1995, **34**, 1460.
15 Another manifestation of linked clusters is provided by solids constructed from bridged metal halide clusters. See, for example: N. Prokopuk and D. F. Shriver, *Inorg. Chem.*, 1997, **36**, 5609 and references therein; O. Reckeweg and H.-J. Meyer, *Z. Naturforsch., Teil B*, 1995, **50**, 1377.
16 M. T. Pope, *Heteropoly and Isopoly Oxometalates*, Springer, New York, 1983.
17 J. Gopalakrishnan, *Chem. Mater.*, 1995, **7**, 1265.

Received in Columbia, MO, USA, 2nd March 1998; 8/01742E

Synthesis of a highly strained permethylenated cycloocta-1,5-diyne derivative by acid-catalysed thermal rearrangement

Stefan Kammermeier,[a] Rik R. Tykwinski,[b] Peter Siemsen,[a] Paul Seiler[a] and François Diederich*[a]†

[a] *Laboratorium für Organische Chemie, ETH-Zentrum, Universitätstrasse 16, CH-8092 Zürich, Switzerland*
[b] *Department of Chemistry, University of Alberta, Edmonton, Alberta, T6G 2G2 Canada*

Preparation of a dimeric derivative of 1,1,2,2-tetraethynylethane (3,4-diethynylhexa-1,5-diyne) and its unexpected rearrangement to a permethylenated cycloocta-1,5-diyne, the structure of which was confirmed by X-ray crystallography, is reported.

Derivatives of tetraethynylethene (3,4-diethynylhex-3-ene-1,5-diyne) have already been used as building blocks for the preparation of expanded carbon-rich structures.[1] Thus, perethynylated octadehydro[12]annulenes were synthesized by oxidative Hay coupling[2] of *cis*-bis(trialkysilyl)-protected tetraethynylethenes.[3] The same reaction involving their non-planar analogues—derivatives of 1,1,2,2-tetraethynylethane (3,4-diethynylhexa-1,5-diyne)[4,5]—should lead to macrocyclic dimers such as isomeric *syn*-**1** and *anti*-**1**. Here we report the synthesis of these compounds as well as their unexpected, acid-catalysed thermal rearrangement to a permethylenated cycloocta-1,5-diyne, the structure of which was clarified by X-ray crystal structure analysis.

Starting from hexa-1,5-diyne-3,4-dione **2**,[6] the orthoesters **4** and **5** were prepared *via* the diol *meso*-**3** and isolated, in both cases, as an inseparable mixture of diastereoisomers. Subsequent oxidative dimerisation of **5** under Hay conditions gave diastereoisomeric mixtures of *syn*-**1** and *anti*-**1**, which could be separated from each other by column chromatography (Scheme 1). The *syn*-structure with the larger molecular dipole moment was assigned to the product with the longer retention time.

Both *syn*-**1** and *anti*-**1** seemed to be promising precursors to octadehydro[12]annulene **6** (Scheme 2), an interesting, hitherto scarcely available perethynylated antiaromatic annulene.[3] The essential elimination of the orthoester functionality[7] in *syn*-**1** or *anti*-**1**, however, could not be accomplished using the methods developed in our group for the conversion of orthoester derivatives of 1,1,2,2-tetraethynylethanes, such as **4**, into the corresponding tetraethynylethenes. Owing to the instability of *syn*-**1** and *anti*-**1**, both vacuum pyrolysis in the presence of camphorsulfonic acid at 150 °C[5] or heating in 1,2-dichlorobenzene to 170 °C in the presence of catalytic amounts of hydroiodic acid[8] failed to produce **6**. Instead, the latter reaction conditions produced at 120 °C, to our great surprise, exclusively the rearranged product **7**, which was isolated in 41% yield as an inseparable 2 : 1 mixture of diastereoisomers (NMR) featuring unexpectedly high kinetic and thermal stability (Scheme 2).‡

The structure of **7** as a highly strained permethylenated cycloocta-1,5-diyne could only be elucidated by X-ray analysis (Fig. 1).§ The cycloocta-1,5-diyne unit bearing four exocyclic double bonds is nearly planar; the C-atoms *C*H(OR)$_3$ of the two orthoester moieties are approximately 0.7 Å out of the plane. Two diastereoisomers of **7** were isolated from the acid-catalysed thermolysis, owing to the undefined configuration of these two C-atoms. The analysed crystal, however, contained only one diastereoisomer bearing an *anti* arrangement of the ethoxy groups. In the eight-membered ring, the transannular distance between the triple bonds is 2.59 Å, which is in good agreement with similar cycloocta-1,5-diyne derivatives.[9] The internal bond angles at the sp C-atoms (157.4°) differ considerably from the regular geometry. Furthermore, slight bending of the Pr$^i_3$Si groups at the sp centres is observed. This is probably a result of crystal packing effects.

The formation of **7** from **1** can be rationalised by assuming a cascade mechanism consisting of electrocyclic or radical reactions. In the first step, thermal cleavage of the C–C bonds in both dioxolane rings occurs by a conrotatory 12π-electrocyclic ring opening. The presence of HI is clearly important for this process since heating **1** in the absence of the acid catalyst only led to extensive decomposition. The formed intermediate contains two parallel-facing hexa-1,2,3,4,5-pentaene moieties. A formal intramolecular [4π + 4π]-cycloaddition between the central butatriene units finally results in the formation of the strained cycloocta-1,5-diyne system. The parent cycloocta-1,5-diyne system has also been obtained, but in poor yield only

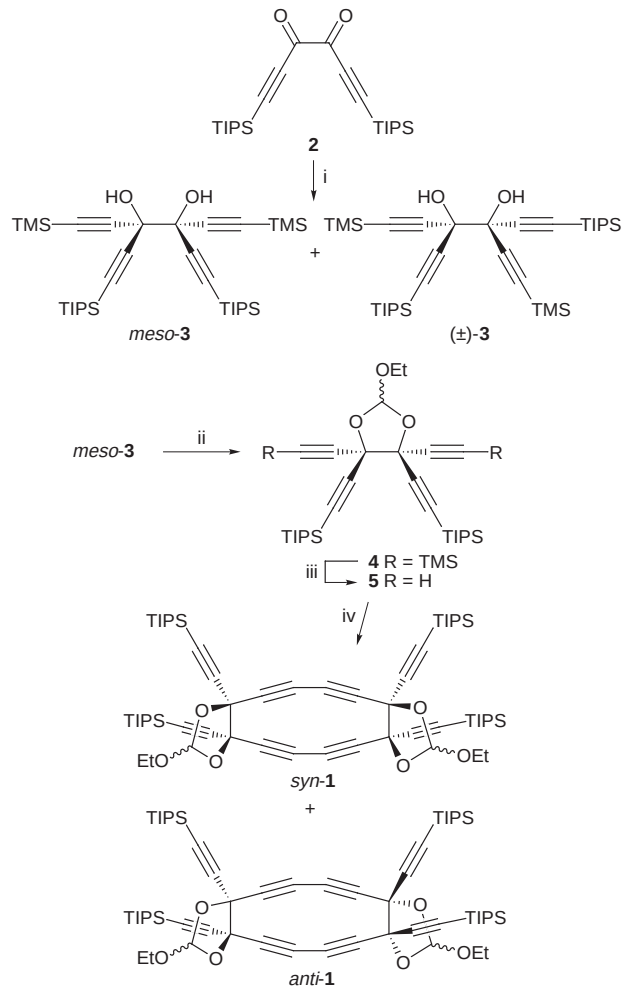

Scheme 1 *Reagents and conditions*: i, $Me_3Si–C\equiv C–MgBr$, THF, 20 °C, 48% (*meso*-**3**), 25% [(±)-**3**]; ii, $HC(OEt)_3$, CSA (cat.), CH_2Cl_2, 20 °C, 89%; iii, K_2CO_3, MeOH–THF, 95%; iv, CuCl, TMEDA, O_2, CH_2Cl_2, 20 °C, 27% (*syn*-**1**), 44% (*anti*-**1**)

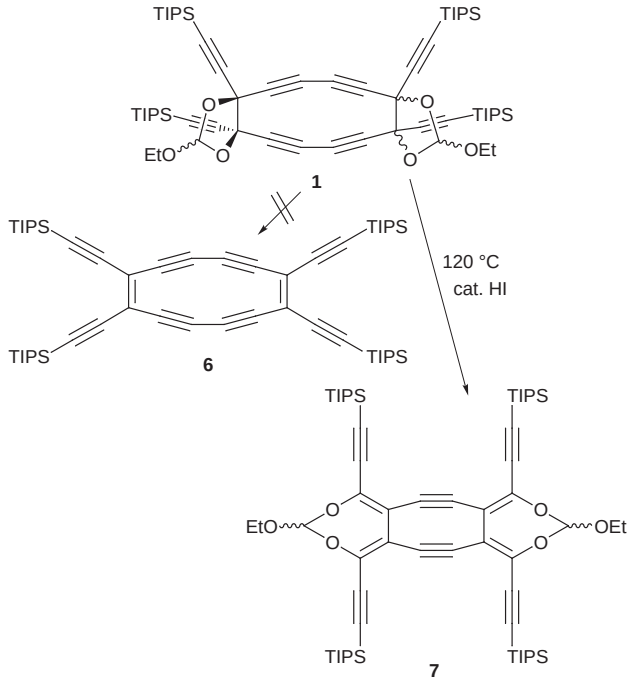

Scheme 2

(2%), by the dimerisation of buta-1,2,3-triene.[9] In both cases, this dimerisation is probably not concerted, but proceeds *via* a biradical mechanism. The higher yield in our system can be explained by the intramolecularity of the reaction in addition to the steric hindrance of the TIPS groups, which precludes intermolecular reactions.

The substitution of the orthoester groups in **1** by other thermally or photochemically removable protecting groups is now under way in order to prepare **6**. Furthermore, experiments with such compounds could clarify the mechanism of the acid required for the formation of **7**.

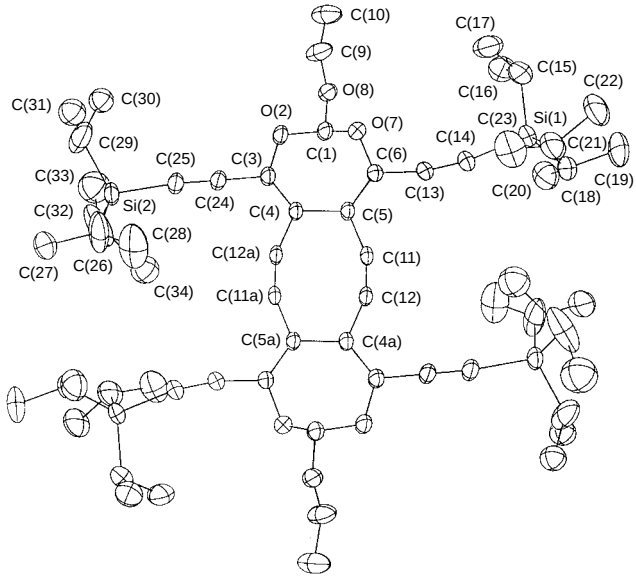

Fig. 1 Molecular structure of **7** in the crystal. The thermal ellipsoids are drawn at the 30% probability level. Selected bond lengths [Å] and angles [°]: C(1)–O(2) 1.420(3), C(1)–O(7) 1.408(3), C(6)–O(7) 1.377(3), C(5)–C(6) 1.353(4), C(4)–C(5) 1.502(3), C(5)–C(11) 1.423(3), C(11)–C(12) 1.206(4), C(6)–C(13) 1.419(3), O(8)–C(1)–O(7) 109.0(2), C(6)–O(7)–C(1) 116.1(2), C(5)–C(6)–C(7) 122.7(2), C(4)–C(5)–C(11) 112.9(2), C(4)–C(5)–C(6) 124.9(2), C(5)–C(11)–C(12) 156.3(2), C(11)–C(12)–C(4a) 158.6(2).

This work was supported by the Swiss National Science Foundation. S. K. thanks the German Fonds der Chemischen Industrie for a postdoctoral fellowship.

Notes and References

† E-mail: diederich@org.chem.ethz.ch

‡ *Selected data* for **7** (2 : 1 mixture of diastereoisomers): mp 188–191 °C (decomp.) [Found: C, 70.71; H, 9.49. Calc. For $C_{62}H_{96}O_6Si_4$ (1049.79): C, 70.94; H, 9.22]; λ_{max} ($CHCl_3$)/nm 321 (ε 61 100, sh), 337 (90 100), 351 (88 100), 400 (7500) and 432 (5500); ν($CHCl_3$)/cm^{-1} 2944 (s), 2856 (s), 2122 (w), 1550 (m), 1456 (m), 1217 (s), 878 (m), 722 (s) and 678 (s); δ_H(400 MHz, $CDCl_3$) [5.86 (1.33 H, s), 5.84 (0.67 H, s)], 3.85 (4 H, q, *J* 7.1), 1.30 (6 H, t, *J* 7.1) and 1.10 (84 H, s); δ_C(100.6 MHz, $CDCl_3$) [136.08 major, 135.86 minor (C = *C*–O)], [112.60 major, 112.53 minor (*C* = C–O)], [111.92 minor, 111.43 major (C≡C)], [107.53 minor, 107.43 major (CH, orthoester)], [102.88 major, 102.61 minor (C≡C)], 101.12 (C≡C), [62.76 major, 62.72 minor (CH_2, orthoester)], 18.67 (CH_3, Pr^i) 14.79 (CH_3, orthoester) and 11.29 (CH, Pr^i); *m/z* (MALDI-TOF-MS) 1049 (M^+, 100%).

§ *Crystal data* for **7**: $C_{62}H_{96}O_6Si_4$, M_r = 1049.75, triclinic, space group $P\bar{1}$, D_c = 1.07 g cm^{-3}, Z = 1, a = 9.374(1), b = 11.402(3), c = 15.399(4) Å, α = 97.42(2), β = 92.19(2), γ = 95.00(2)°, V = 1623.8(6) Å^3, T = 223 K, Nonius CAD4 diffractometer, λ(CuKα) = 1.5418 Å. Single crystals were obtained by slow diffusion of pentane into a $CHCl_3$ solution. The structure was solved by direct methods (SHELXS-86: E. Egert and G. M. Sheldrick, University of Göttingen) and refined by full-matrix least-squares analysis (SHELXL-93: G. M. Sheldrick, University of Göttingen), using an isotropic extinction correction and $w = 1/[\sigma^2(F_o^2) + (0.1648P)^2 + 0.84P]$, where $P = (F_o^2 + 2F_o^2)/3$. The Pr$^i_3$Si groups are statically disordered; for C(16), C(17), C(22) and C(23) two sets of atomic parameters were refined isotropically with weights of 0.7 and 0.3 respectively; for C(30), C(31), C(33) and C(34) three sets of atomic parameters were refined with weights of 0.33. All other heavy atoms were refined anisotropically (H-atoms of the ordered skeleton isotropically, whereby H-positions are based on stereochemical considerations). Final $R(F)$ = 0.070, $wR(F^2)$ = 0.218 for 411 variables and 4514 reflections with $I > 2\sigma(I)$ and $\theta < 65°$. For clarity, only one orientation of the disordered Pr$^i_3$Si groups is shown in Fig. 1. CCDC 182/874.

1 F. Diederich, *Nature*, 1994, **369**, 199; F. Diederich, in *Modern Acetylene Chemistry*, eds. P. J. Stang and F. Diederich, VCH, Weinheim, 1995, p. 443; R. R. Tykwinski and F. Diederich, *Liebigs Ann./Recueil*, 1997, 649.

2 A. S. Hay, *J. Org. Chem*., 1962, **27**, 3320.

3 J. Anthony, C. B. Knobler and F. Diederich, *Angew. Chem., Int. Ed. Engl*., 1993, **32**, 406; J. Anthony, A. M. Boldi, C. Boudon, J.-P. Gisselbrecht, M. Gross, P. Seiler, C. B. Knobler and F. Diederich, *Helv. Chim. Acta*, 1995, **78**, 797.

4 A. H. Alberts and H. Wynberg, *J. Chem. Soc., Chem. Commun*., 1988, 748; H. Hauptmann, *Angew. Chem., Int. Ed. Engl*., 1975, **14**, 498; H. Hauptmann, *Tetrahedron Lett.*, 1975, 1931; H. Hauptmann, *Tetrahedron Lett.*, 1974, 3587; K. G. Migliorese, Y. Tanaka and S. I. Miller, *J. Org. Chem*., 1974, **39**, 739; K. Sisido, N. Hirowatari, H. Tamura, H. Kobata, H. Takagisi and T. Isida, *J. Org. Chem*., 1970, 35, 350; F. J. Wilson and W. M. Hyslop, *J. Chem. Soc*., 1924, 1556.

5 R. R. Tykwinski, F. Diederich, V. Gramlich and P. Seiler, *Helv. Chim. Acta*, 1996, **79**, 634.

6 R. Faust and C. Weber, *Tetrahedron*, 1997, **53**, 14 655.

7 A. P. Marchand, V. Vidyasagar, W. H. Watson, A. Nagl and R. P. Kashyap, *J. Org. Chem*., 1991, **56**, 282; J. S. Josan and F. W. Eastwood, *Aust. J. Chem*., 1968, **21**, 2013; G. Crank and F. W. Eastwood, *Aust. J. Chem*., 1964, 17, 1392; M. Ando, H. Ohhara and K. Takase, *Chem. Lett*., 1986, 879; R. R. Sauers and P. A. Odorisio, *J. Org. Chem*., 1979, **44**, 2980; R. W. Hoffmann and M. Reiffen, *Chem. Ber*., 1977, **110**, 49.

8 Heating orthoesters of 1,1,2,2-tetraethynylethanes, such as **4**, in 1,2-dichlorobenzene to 170 °C in the presence of catalytic amounts of HI produces the corresponding tetraethynylethenes in around 50% yield; P. Siemsen, S. Kammermeier and F. Diederich, unpublished results; M. Konieczny and R. G. Harvey, *J. Org. Chem*., 1980, **45**, 1308.

9 E. Kloster-Jensen and J. Wirz, *Helv. Chim. Acta*, 1975, **58**, 162; E. Kloster-Jensen and J. Wirz, *Angew. Chem., Int. Ed. Engl*., 1973, **12**, 671; H. N. C. Wong. P. J. Garratt and F. Sondheimer, *J. Am. Chem. Soc*., 1974, **96**, 5604; R. Destro, T. Pilati and M. Simonetta, *Acta Crystallogr., Sect. B*, 1977, **33**, 447; R. Gleiter and R. Merger, in *Modern Acetylene Chemistry* ed. P. J. Stang and F. Diederich, VCH, Weinheim, 1995, p. 285.

Received in Cambridge, UK, 20th April 1998; 8/02927J

Synthesis and biological activity of an optically pure 10-spirocyclopropyl analog of huperzine A

Alan P. Kozikowski,*[a]† K. R. C. Prakash,[a] Ashima Saxena[b] and Bhupendra P. Doctor[b]

[a] *Georgetown University Medical Center, Drug Discovery Program, Institute for Cognitive and Computational Sciences, 3970 Reservoir Road, N.W., Washington, DC 20007-2197, USA*
[b] *Division of Biochemistry, Walter Reed Army Institute of Research, Washington, DC 20307, USA*

The synthesis of a spirocyclic analog of huperzine A that bears a cyclopropane ring at its 10-position has been carried out in an enantioselective manner using a diastereoselective Michael–aldol reaction; in assays of AChE inhibition, this compound was found to be nearly as active as huperzine A itself, with comparable on and off rates from the enzyme.

Huperzine A (HA), a potent reversible inhibitor of acetylcholinesterase (AChE), is an important psychotherapeutic agent for improving cognitive function in Alzheimer's patients by enhancement of central cholinergic tone.[1] Because of the tremendous promise this alkaloid holds for the palliative treatment of a disease that afflicts millions of individuals worldwide, we and others have been engaged in an intensive effort to explore the structure–activity relationships of this alkaloid.[2] From biological studies with mammalian AChE, Torpedo AChE, mammalian BChEs (butyrylcholinesterases) and mouse AChE mutants, together with molecular modeling studies, mammalian Tyr337(330) and Trp86(84) have been implicated in the binding of HA to AChE.[3] This particular interaction is of the cation (NH_3^+)–π type,[4] while other amino acid residues appear to participate in hydrogen bonding to the pyridone NH and the carbonyl group.[5] The superior inhibition properties of HA have been attributed to the very slow dissociation ($t_{0.5}$ = 35 min) of the AChE–huperzine A complex in solution.[6] To date, we have identified several analogs of HA that have comparable or better activity than the parent structure. In particular, the C-10 axial methyl analog of HA was found to be about 8-fold more potent than HA, whereas the 10,10-dimethyl analog was found to possess comparable activity. In exploring further modifications to this region of the molecule, we felt that it would be of interest to examine a spirocyclic analog bearing a cyclopropyl group at C-10. Such an analog can be viewed as a ring constrained version of the dimethyl derivative. The possibility exists, however, that its activity might be improved due both to the smaller size of the cyclopropyl group and possible electronic effects which may be capable of enhancing interactions with the enzyme.

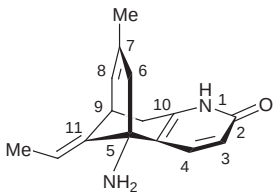

Huperzine A (HA) **1**

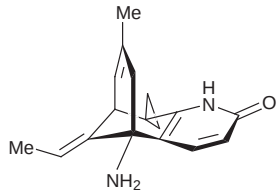

Spirocyclopropyl Analog **2**

The chemical pathway that was followed to assemble the cyclopropyl analog **2** is shown in Schemes 1 and 2. The key intermediate **7b** was obtained in good yield through a sequence of steps starting from the reaction of cyclohexanedione monoethylene ketal **3** with (2-chloroethyl)dimethylsulfonium iodide/Bu^{t}OK in Bu^{t}OH at room temperature to afford the spirocyclohexanone **4** in 60% yield (Scheme 1).[7] The spirocyclohexanone **4** was transformed to the β-keto ester **7a** employing conditions identical to those reported previously.[1,2] Transesterification of **7a** with (−)-8-phenylmenthol gave the desired ester derivative **7b** in 75% overall yield.[8] Next, a diastereoselective Michael–aldol reaction of **7b** with methacrolein was carried out. Under optimal conditions, the reaction was run at −20 °C over a two day period. The alcohol mixture **8a** that formed was converted to a 12.5 : 1 mixture (ratio from ^{1}H NMR analysis) of the olefins **9a** and **9b**, respectively, in 70% yield by NaOAc–HOAc induced elimination of the derived mesylate **8b**. These olefins were readily separable by column chromatography on silica gel using 1 : 9 ethyl acetate–hexanes as eluent. The major isomer **9a** was subjected to a Wittig olefination reaction to afford the *Z*-isomer **10a**. Isomerization of the double bond using thiophenol–AIBN gave a mixture of the *E*- and *Z*-isomers **10b** and **10a** in a 6 : 1 ratio, respectively. The ester group of this mixture was reduced to alcohols **11a** and **11b** by treatment with LAH in THF, and these isomers were separated by column chromatography. The enantiomeric purity of the major isomer **11b** was confirmed at this stage by transforming it to its Mosher ester derivative. ^{1}H and ^{19}F NMR spectroscopy revealed the compound to be of at least 98% optical purity. Jones oxidation of the alcohol **11b** afforded the acid **12**, which was converted to urethane **13** by Curtius rearrangement. Lastly, the required compound **2** was obtained in 75% yield by the removal of the protecting groups from **13** using TMSI in $CHCl_3$ at reflux. The optical rotation of crystalline **2** (mp 235 °C) was found to be −73 (*c* 0.83, $CHCl_3$). For purposes of biological comparison, we also prepared the spirocyclopropyl analog in racemic form, using basically the same approach as above but omitting the transesterification reaction with 8-phenylmenthol.

The biological activity of the analogs of huperzine A was evaluated using AChE purified from fetal bovine serum.[9] AChE

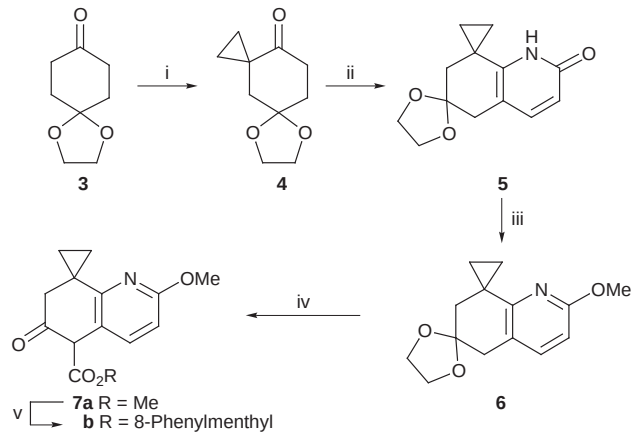

Scheme 1 *Reagents and conditions*: i, $Me_2S^+CH_2CH_2Cl$ I^-, KI, KOBu^t, Bu^{t}OH, room temp.; ii, ethyl propiolate, MeOH–NH_3, 100 °C, 300 psi; iii, MeI, Ag_2CO_3, $CHCl_3$, reflux; iv, MeOH–HCl, reflux, then $(MeO)_2CO$, NaH, THF, reflux; v, (−)-8-phenylmenthol, TsOH, benzene, reflux

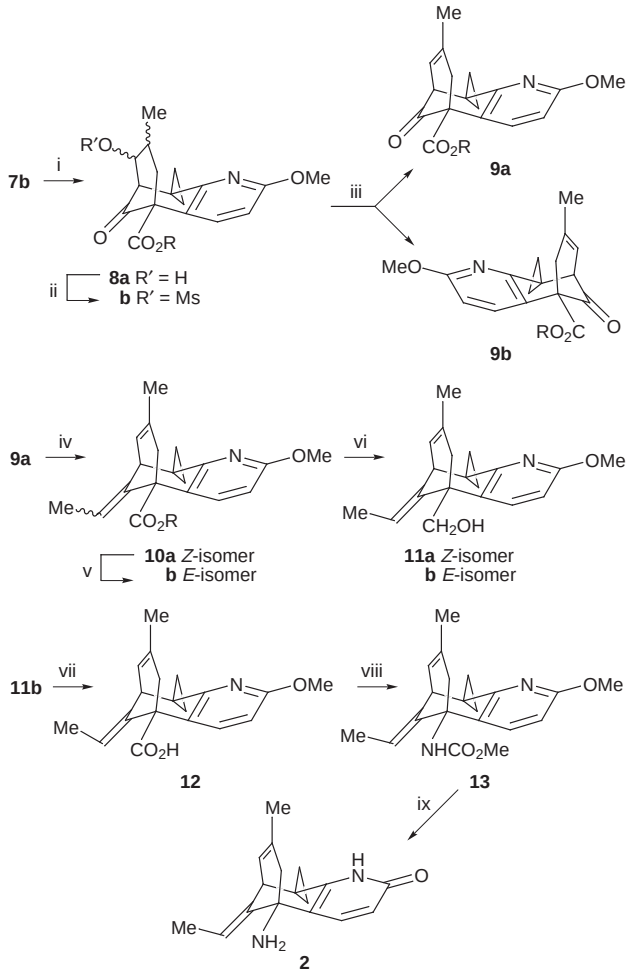

Scheme 2 *Reagents and conditions*: i, CH_2=CMeCHO, $(Me_2N)_2C$=NH, CH_2Cl_2, −20 °C; ii, $MeSO_2Cl$, Et_3N, DMAP, CH_2Cl_2, room temp.; iii, NaOAc, AcOH, reflux; iv, $Ph_3P^+Et\ Br^-$, KOBu^t, THF, room temp.; v, PhSH, AlBN, toluene, reflux; vi, LAH, THF, reflux; vii, Jones reagent, acetone, room temp.; viii, $(PhO)_2PON_3$, Et_3N, toluene, reflux, 2 h, then MeOH, reflux; ix, TMSI, $CHCl_3$, reflux, 6 h, then MeOH, reflux

activity was measured in 50 mM sodium phosphate, pH 8.0, at 22 °C as described previously using acetylthiocholine as the substrate.[10] The interaction of HA and its analogs with AChE can be described by eqn. (1):[6]

$$E + HUP\text{-}A \underset{k_{off}}{\overset{k_{on}}{\rightleftharpoons}} E \cdot HUP\text{-}A$$

The ratio k_{off}/k_{on} is the dissociation constant (K_I). The K_I values for the inhibition of FBS AChE with analogs of HA were determined by equilibrating a known amount of enzyme (1–2 units ml^{-1}) with various concentrations of the analog. Plots of percent residual activity *versus* [analog] were used to calculate K_I by the steady state method. The rate constant for the inhibition of AChE was determined by diluting an appropriate volume of stock solutions (1–2 μM) of each analog of huperzine A into the enzyme solution (5–10 units ml^{-1} in 50 mM sodium phosphate, pH 8.0, containing 0.05% BSA) and measuring the residual enzyme activity at various time intervals. Plots of percent residual activity *versus* time at each concentration were used to calculate the rate of inhibition (k_{on}). Direct measurement of the rate constant of regeneration of enzyme activity (k_{off}) was initiated by > 10 000-fold dilution of HA-inhibited AChE (2–4 μM) to ascertain that the rate of inhibition by residual inhibitor was negligible in the reactivation medium.

As is apparent from an examination of k_{on}, k_{off} and the K_Is reported in Table 1, the optically pure 10-spirocyclopropyl analog of HA is comparable in activity to HA itself in both its

Table 1 Kinetic and inhibition parameters for huperzine A, 10,10-dimethylhuperzine A and 10-spirocyclopropylhuperzine A

Inhibitor	$k_{on}/10^{-6}$ M^{-1} min^{-1}	k_{off}/ min^{-1}	K_I[a]/ nM	K_I[b]/ nM
(−)-Huperzine A	4.2	0.016	3.9	5.6
(±)-10,10-Dimethylhuperzine A	0.76	0.01	13.2	17.0
(±)-10-Spirocyclopropylhuperzine A	1.0	0.014	14.0	12.4
(−)-10-Spirocyclopropylhuperzine A	2.4	0.015	6.4	8.8

[a] $K_I = K_{off}/K_{on}$. [b] Determined by the steady state method.

inhibition constants and kinetic parameters, and as expected, it is slightly more active than the 10,10-dimethyl analog (comparison of racemic materials). Further studies are now underway to examine whether these 10-substituted analogs show greater elements of neuroprotection from glutamate toxicity than does HA itself. The neuroprotective aspect of HA represents a newly discovered property of this molecule.[11] This pharmacological property together with the AChE inhibitory activity further enhances the value of huperzine A and its analogs as therapeutic agents for the treatment of Alzheimer's disease.[11]

We are indebted to the Department of Defense (DMAD17-93-V-3018) for partial support of these studies.

Notes and References

† E-mail: kozikowa@giccs.georgetown.edu

1 J.-S. Liu, Y.-L. Zhu, C.-M. Yu, Y.-Z. Zhou, Y.-Y. Han, F.-W. Wu and B.-F. Qi, *Can. J. Chem.*, 1986, **64**, 837; Y. Xia and A. P. Kozikowski, *J. Am. Chem. Soc.*, 1989, **111**, 4116 and references cited therein; S.-S. Xu, Z.-X. Gao, Z. Weng, Z.-M. Du, W.-A. Xu, J.-S. Yang, M.-L. Zhang, Z.-H. Tong, Y. S. Fang, X.-S. Chai and S.-L. Li, *Acta Pharmacol. Sin.*, 1995, **16**, 391.

2 G. Campiani, L.-Q. Sun, A. P. Kozikowski, P. Aagaard and M. McKinney, *J. Org. Chem.*, 1993, **58**, 7660; A. P. Kozikowski, G. Campiani, V. Nacci, A. Sega, A. Saxena and B. P. Doctor, *J. Chem. Soc., Perkin Trans. 1*, 1996, 1287; A. P. Kozikowski, G. Campiani, L.-Q. Sun, S. Wang, A. Saxena and B. P. Doctor, *J. Am. Chem. Soc.*, 1996, **118**, 11 357.

3 A. Saxena, N. Qian, I. M. Kovach, A. P.Kozikowski, Y. P. Pang, D. C. Vellom, Z. Radic, D. Quinn, P. Taylor and B. P. Doctor, *Protein Sci.*, 1994, **3**, 1770. The dual numbering system provides the residue number in the species designated followed by the corresponding residue in *Torpedo* AChE.

4 D. A. Dougherty and D. A. Stauffer, *Science*, 1990, **253**, 872.

5 A. P. Kozikowski and Y. P. Pang, in *Trends in QSAR and Molecular Modeling '92*, Proceedings of the 9th European Symposium on Structure–Activity Relationships: QSAR and Molecular Modeling, ed. C. G. Wermuth, ESCOM Science Publishers, Leiden, The Netherlands, 1993; Y. P. Pang and A. P. Kozikowski, *J. Comput. Aided Mol. Design*, 1994, **8**, 669; M. Raves, M. Harel, Y. P. Pang, I. Silman, A. P. Kozikowski and J. L. Sussman, *Nature Struct. Biol.*, 1997, **4**, 57.

6 Y. Ashani, J. O. Peggins and B. P. Doctor, *Biochem. Biophys. Res. Commun.*, 1992, **184**, 719.

7 S. M. Ruder and R. C. Ronald, *Tetrahedron Lett.*, 1984, **25**, 5501.

8 F. Yamada, A. P. Kozikowski, E. R. Reddy, Y.-P. Pang, J. H. Miller and M. McKinney, *J. Am. Chem. Soc.*, 1991, **113**, 4695. *Selected data* for **2**: *m/z* (%) 268 (M^+, 10), 225 (100); $\delta_H(CDCl_3)$ 0.97 (2 H, br m), 1.25 (1 H, br s), 1.57 (3 H, s), 1.66 (3 H, d, *J* 6.6), 1.70 (1 H, m), 2.12 (1 H, d, *J* 16.5), 2.23 (1 H, d, *J* 16.8), 2.65 (1 H, d, *J* 4.5), 5.46 (1 H, br s), 5.54 (1 H, q, *J* 12.9, 6.6), 6.35 (1 H, d, *J* 9.6), 7.87 (1 H, d, *J* 9.3); $\delta_C(CDCl_3)$ 164.4, 146.3, 142.3, 139.8, 134.1, 122.9, 122.3, 116.6, 111.1, 77.4, 55.3, 49.7, 42.8, 29.6, 26.8, 22.6, 17.1, 12.8, 12.4.

9 D. De La Hoz, B. P. Doctor, J. S. Ralston, R. S. Rush and A. D. Wolfe, *Life Sci.*, 1986, **39**, 195.

10 G. L. Ellman, D. Courtney, V. Andres and R. M. Featherstone, *Biochem. Pharmacol.*, 1961, **1**, 88.

11 H. S. Ved, M. L. Koeinig, J. R. Dave and B. P. Doctor, *NeuroReport*, 1997, **8**, 963.

Received in Corvallis, OR, USA, 2nd March 1998; 8/01748D

Preparation, first X-ray structure analysis and reactivity of hexacoordinate silicon compounds with a tetradentate azomethine ligand

F. Mucha, U. Böhme and G. Roewer*†

Institut für Anorganische Chemie der Technischen, Universität Bergakademie Freiberg, Leipziger Str. 29, 09596 Freiberg, Germany

Hexacoordinate silicon compounds and polymers with the tetradentate azomethine ligand *N*,*N*′-ethylenebis(2-hydroxyacetophenoneiminate) (H_2salen*) have been prepared and characterized; the X-ray structure analysis of (salen*)SiF_2 clearly demonstrates the octahedral coordination of the silicon atom.

Hypervalent silicon compounds attract interest from both the structural and reactivity point of view.[1] The isolation of such compounds allows detailed insight into mechanistic pathways of nucleophilic substitution at silicon.[1e] On the other hand compounds based on such synthons should exhibit interesting properties as electronic materials. Different types of hypercoordinate silicon compounds have so far been reported: (*a*) the initial compounds were octahedral fluorosilicate $[SiF_6]^{2-}$ and derivatives thereof,[2] (*b*) derivatives of 2,2′-bipyridyl, (*c*) complexes with different bidentate ligands such as 1,3-diketonates, 2-dimethylaminomethylphenyl or 1,2-diolates, (*d*) phthalocyaninato derivatives.[1]

We set out to synthesize hexacoordinate silicon complexes containing the salen* ligand. This ligand is able to chelate to silicon atom through four donor atoms. There are some rare examples of salen silicon compounds known from the literature,[3] but characterization of these compounds seems doubtful.[4] Structural aspects are uncertain owing to the lack of crystal structure data.

Transition metal salen complexes have been investigated extensively.[5] Different types of salen ligands have been applied recently, mainly in transition metal complex catalysts, for the transformation of organic substrates.[6] We used a slightly modified salen ligand [*N*,*N*′-ethylenebis(2-oxyacetophenoneiminate) = salen*] with methyl groups at the azomethine carbon instead of hydrogen. This prevents unwanted side reactions caused by the azomethine protons. The key compound (salen*)$SiCl_2$ **1** can be prepared by two different routes (i and ii, Scheme 1).‡ Elemental analysis indicates the formation of a complex of the composition (salen*)$SiCl_2$. Preparation of **1** *via* reaction of H_2salen* with $SiCl_4$ (route i) yields a product with two ^{29}Si NMR signals and 18 signals in the ^{13}C NMR spectrum. This points to the formation of two different isomers **1a** and **1b** in a ratio of 1 : 1, according to the intensity of the signals. The same type of isomerism has been observed in tin salen compounds and confirmed by Mössbauer spectroscopy.[7]

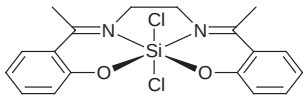

1a

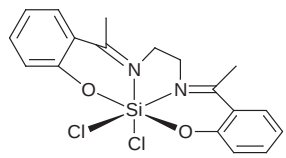

1b

The extremely high field shift of the ^{29}Si NMR signals for the isomers of **1** (δ −186.1, −188.0) indicates the presence of hexacoordinate silicon atoms. Reaction of Si_2Cl_6 with H_2salen* (ii in Scheme 1) gives only one isomer with nine signals in the ^{13}C NMR spectrum and one ^{29}Si NMR signal at δ −188. Hydrogenchloride and hydrogen are evolved in this reaction.

The chlorine atoms in **1** can be substituted for fluorine by treating **1** with ZnF_2 in THF. For the preparation of the fluoro derivative **2** the mixture of isomers **1a** and **1b** was used. The resulting product **2** represents only one isomer as concluded from NMR data. This information hints to a rearrangement of the coordination sites of the salen* ligand during nucleophilic substitution of the chlorine by fluorine. The mechanism of this reaction as well as the energy differences between the isomers **1a** and **1b** seem to be quite interesting and will be subject of further investigation. Complex **2** is more soluble in organic solvents than the chloro derivative and we were able to obtain single crystals of **2** by recrystallization from acetonitrile. The X-ray crystal structure analysis of **2** provides the molecular structure shown in Fig. 1.§ It was solved and refined in space group $P2_1/a$ with four molecules of **2** and four molecules of acetonitrile per unit cell. There is a distorted octahedral coordination geometry around silicon. The fluorine atoms are situated at axial positions (*trans* isomer), whereas the salen* ligand occupies the four equatorial positions.

There are a number of crystal structures of bis(chelate) compounds with hexacoordinate silicon. Most of these have essentially a tetrahedral arrangement around silicon with the coordinated nitrogen donor atoms 'capping' the tetrahedra at relatively large distances (N–Si between 2.5 and 3.0 Å).[8] The Si–F distance in **2** corresponds well with bond length found in other hypervalent silicon compounds (1.60–1.73 Å).[1d,9] The Si–O and Si–N distances are remarkably short compared to other hexacoordinate silicon compounds.[8] The distortion of the octahedral coordination environment around silicon probably originates from the conformation of the chelating salen* ligand.

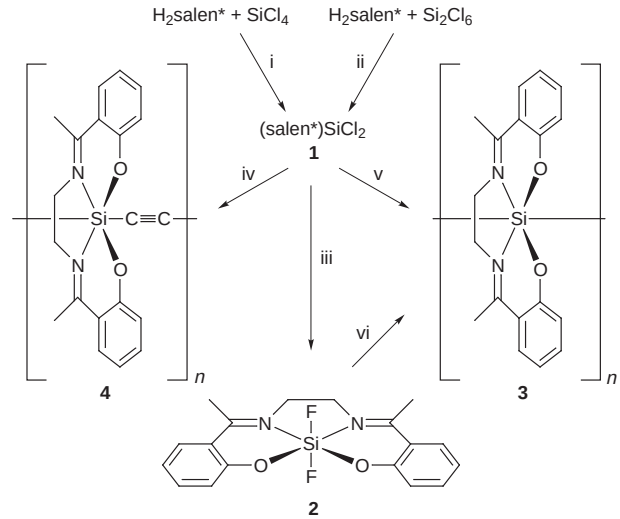

Scheme 1 *Reagents and conditions*: i and ii, THF, 2 h, reflux, 90%; iii, ZnF_2, THF, 1 h reflux, 20%, extraction with THF; iv, LiCCLi or BrMgCCMgBr, THF–*n*-hexane, 6 h reflux; v, (salen*)$SiCl_2$ and K in ratio 1 : 2, toluene, 6 h reflux; vi, (salen*)SiF_2 and Li, THF, 2 h room temp.

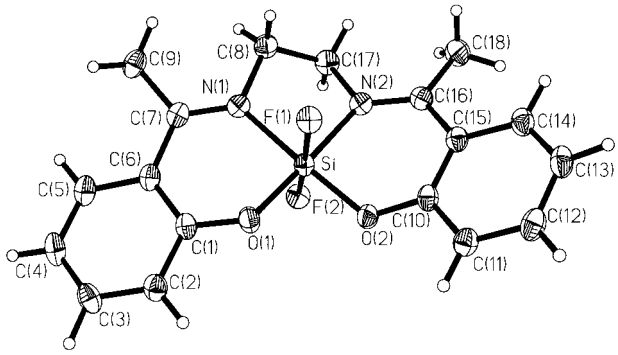

Fig. 1 Crystal structure of **2**. Selected bond distances (Å) and angles (°): Si–F(1) 1.677(1), Si–F(2) 1.670(1), Si–O(1) 1.721(1), Si–O(2) 1.724(1), Si–N(1) 1.931(2), Si–N(2) 1.937(2); F(1)–Si–F(2) 172.40(5), O(1)–Si–N(2) 178.00(6), O(2)–Si–N(1) 1.76.75(6), F(1)–Si–O(1) 91.68(6), F(1)–Si–O(2) 93.85, F(1)–Si–N(1) 86.93(5), F(1)–Si–N(2) 87.36(6), F(2)–Si–O(1) 93.17(6), F(2)–Si–O(2) 92.00(6), F(2)–Si–N(1) 86.96(5), F(2)–Si–N(2) 87.60(6).

There is a considerable torsion along the atoms N(1)–C(8)–C(17)–N(2) of *ca.* 46°. The result of this is that one azomethine unit is bended under and the other above the plane N(1)SiN(2).

Experiments to obtain stacked polymers **3** by reaction of **1** or **2** with alkaline metals or magnesium are very promising. These polymers are poorly soluble in organic solvents and more stable towards moisture than the monomers. They have been characterized by elemental analysis, IR and NMR spectroscopy. Furthermore it is possible to react **1** with dilithium acetylide or the corresponding Grignard reagent to obtain polymers of type **4** which are linked by Si–C≡C–Si units (Scheme 1). Polymers with similar backbone but different chelating ligands have been described recently.[10]

Complexes of the type (salen*)Si(Cl)R **5** and **6** are available by reaction of Na_2(salen*) with $RSiCl_3$ [R = Me, Ph; eqn. (1)]. Only one isomer is formed in both cases as revealed by NMR data. At present it is not possible to decide whether these are the *cis*- or *trans*-isomers. These organosilicon compounds are more soluble in organic solvents than **1**.

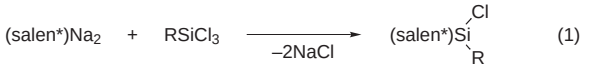

R = Me **5** or Ph **6**

Investigations relating to electric conductivity and optical properties of the new class of silicon polymers **3** and **4** will be carried out in the future. Further studies to explore the chemistry of these truly hexacoordinate silicon compounds are under way.

Notes and References

† E-mail: voewer@orion.hrz.tu-freiberg.de

‡ *Selected spectroscopic data*: All new compounds gave satisfactory analytical data.

(salen*)$SiCl_2$ **1a**/**1b**: [NMR, $(CD_3)_2SO$ δ] mixture of isomers ^{13}C, C^1 157.3/158.1, C^2 118.8/119.4, C^3 135.1/136.9, C^4 120.6/120.7, C^5 129.9/131.2, C^6 120.2/120.5, C^7 176.4/171.6, C^8 46.1/46.7, C^9 18.6/20.7; ^{29}Si, −186.1/−188.0; IR ν(C=N) 1630 cm^{-1}, ν(Si–Cl) 521 cm^{-1}, δ(Si–O–C) 1104 cm^{-1}.

(salen*)$SiCl_2$ **1a** from Si_2Cl_6: [NMR, $(CD_3)_2SO$ δ] ^{13}C, C^1 157.3, C^2 119.4, C^3 136.9, C^4 120.7, C^5 131.2, C^6 120.5, C^7 176.4, C^8 46.7, C^9 20.7; ^{1}H, δ C^2–C^5 6.8–8.1, C^8 4.2, C^9 1.5; ^{29}Si −188.0.

(salen*)SiF_2 **2**: (NMR, $CDCl_3$ δ) ^{13}C, C^1 160.3, C^6 121.9, C^7 170.7, C^8 46.4, C^9 18.2; ^{29}Si, 187.9 [t ^2J(SiF) 179.2 Hz]; IR ν(C=N) 1610 cm^{-1}, ν(Si–F) 954 cm^{-1}.

[(salen*)Si]$_n$ **3**: (NMR, solid state, δ) ^{29}Si, −130 (br); IR ν(C=N) 1613 cm^{-1}, δ(Si–O–C) 1100 cm^{-1}.

[(salen*)SiCC]$_n$ **4**: [NMR, $(CD_3)_2SO$ δ] ^{13}C, C^1 168.4, C^6 120.0 C^7 169.1, C^8 51.4, C^9 22.2; ^{29}Si −88 (br); IR ν(C=N) 1607 cm^{-1}, ν(Si–C) 840 cm^{-1}, Raman: ν(C≡C) 2260 cm^{-1}.

(salen*)MeSiCl **5**: [NMR, $(CD_3)_2SO$ δ] ^{13}C, C^1 158.4, C^6 120.9, C^7 175.9, C^8 45.3, C^9 19.2, C^{19} (Si–Me) 5.9; ^{29}Si, −150.7; IR ν(C=N) 1629 cm^{-1}, ν(Si–Cl) 509 cm^{-1}, ν(Si–C) 798 cm^{-1}.

(salen*)PhSiCl **6**: [NMR, $(CD_3)_2SO$, δ] ^{13}C, C^1 159.7, C^6 121.1, C^7 179.8, C^8 46.9, C^9 18.2; ^{29}Si, −173.1; IR ν(C=N) 1612 cm^{-1}, ν(Si–Cl) 488 cm^{-1}, ν(Si–C) 840 cm^{-1}.

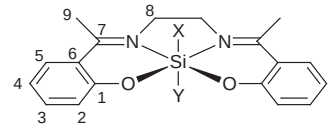

§ *Crystal data* for (salen*)SiF_2 **2** (white crystals from MeCN): $C_{20}H_{21}F_2N_3O_2Si{\cdot}CH_3CN$, monoclinic space group $P2_1/a$, a = 12.3826(5), b = 10.8405(5), c = 13.8507(5) Å, β = 98.800(5); U = 1837.3(1) Å^3, Z = 4, D_c = 1.451 g cm^{-3}, μ = 1.503 mm^{-1}, F(000) = 840. A single crystal of approximate dimensions 0.2 × 0.5 × 0.6 mm was mounted on a glass fibre under paraffin oil and transferred to the diffractometer. Data were collected at −10 °C on an Enraf-Nonius CAD-4 diffractometer using graphite-monochromated Cu-Kα radiation (λ = 1.5418 Å) with ω–2θ scans. The structure was solved by direct methods and refined by full matrix least squares on F^2 with anisotropic thermal parameters. Hydrogen atom positions were located and isotropically refined. R = 0.0431 for 3358 reflections ($F_o > 2\sigma F_o$) and 0.0482 for all 3784 reflections, GOF = S = 1.033. CCDC 182/854.

1 (*a*) R. J. P. Corriu and J. C. Young, in *The Chemistry of Organic Silicon Compounds*, ed. S. Patai and Z. Rappoport, Wiley, Chichester, 1989, p. 1241; (*b*) R. R. Holmes, *Chem. Rev.*, 1990, **90**, 17, 1996, **96**, 927; (*c*) R. J. P. Corriu, *J. Organomet. Chem.*, 1990, **400**, 81; (*d*) C. Chuit, R. J. P. Corriu, C. Reye and J. C. Young, *Chem. Rev.*, 1993, **93**, 1371; (*e*) A. R. Bassindale and P. G. Taylor, in *The Chemistry of Organic Silicon Compounds*, ed. S. Patai, Z. Rappoport, Wiley, Chichester, 1989, p. 839; (*f*) R. J. P. Corriu and J. C. Young, in *The Silicon–Heteroatom Bond*, ed. S. Patai, Z. Rappoport, Wiley, Chichester, 1991, p. 1 and 49.

2 J. A. A. Ketelaar, *Z. Kristallogr.*, 1935, **92**, 155.

3 (*a*) B. N. Ghose, *Acta Chim. Hungarica*, 1985, **118**, 191; (*b*) K. S. Siddiqi, F. M. A. M. Aqra, S. A. Shah and S. A. A. Zaidi, *Polyhedron*, 1993, **12**, 1967.

4 Compare for instance the wrong data of elemental analysis in ref. 3(*b*). The calculated sum formula was given with $C_{14}H_{14}Cl_2N_2Si$ and the found data fitted this formula well. The correct formula should be $C_{16}H_{14}Cl_2N_2O_2Si$!

5 M. D. Hobday and T. D. Smith, *Coord. Chem. Rev.*, 1972, **9**, 311 and references therein.

6 T. Linker, *Angew. Chem.*, 1997, **109**, 2150, *Angew. Chem., Int. Ed. Engl.*, 1997, **36**, 2060 and references therein; C.Bolm and F. Bienewald, *Angew. Chem.*, 1995, **107**, 2883, *Angew. Chem., Int. Ed. Engl.*, 1995, **34**, 2640.

7 J. N. R. Ruddick, J. R. Sams, *J. Inorg. Nucl. Chem.*, 1975, **37**, 564.

8 C. Breliere, F. Carre, R. J. P. Corriu, M. Poirier, G. Royo and J. Zwecker, *Organometallics*, 1989, **8**, 1831; F. Carre, G. Cerveau, C. Chuit, R. J. P. Corriu and C. Reye, *New J. Chem.*, 1992, **16**, 63; F. Carre, C. Chuit, R. J. P. Corriu, A.Mehdi and C. Reye, *Organometallics*, 1995, **14**, 2754.

9 I. Kalikhman, S. Krivonos, D. Stalke, T. Kottke and D. Kost, *Organometallics*, 1997, **16**, 3255.

10 K. Boyer-Elma, F. H. Carré, R. J. P. Corriu and W. E. Douglas, *J. Chem. Soc., Chem. Commun.*, 1995, 725; I. W. Shim and W. M. Risen, *J. Organomet. Chem.*, 1984, **260**, 171.

Received in Basel, Switzerland, 5th December 1997; revised manuscript received 9th April 1998; 8/03060J

Hepta-1,6-diene and diallyl ether complexes of palladium(0) and platinum(0): a route to L–M(alkene)$_2$ complexes containing non-activated alkenes

Jochen Krause, Karl-Josef Haack, Günter Cestaric, Richard Goddard and Klaus-Richard Pörschke*†

Max-Planck-Institut für Kohlenforschung, Postfach 10 13 53, D-45466 Mülheim an der Ruhr, Germany

With hepta-1,6-diene and diallyl ether, Pd^0 and Pt^0 form highly reactive homoleptic dinuclear M$_2$(1,6-diene)$_3$ complexes, which are cleaved by donors L (*e.g.* C$_2$H$_4$, phosphanes, phosphites, isonitriles) to afford mononuclear derivatives L–M(1,6-diene); the X-ray structure of (Me$_3$P)Pd{(η^2-CH$_2$=CHCH$_2$)$_2$O} has been determined.

Although d^{10} L–M(alkene)$_2$ complexes with non-activated alkenes are well known for M = Ni, Pt, they are scarce for M = Pd. Indeed, whereas the full series of phosphane derivatives with R = Me, Et, Pr^i, Ph, and Cy is known for the parent ethene complexes (R$_3$P)M(C$_2$H$_4$)$_2$ (M = Ni, Pt), (Cy$_3$P)Pd(C$_2$H$_4$)$_2$[1] is apparently the only reported Pd derivative. In view of their potential importance as a source of the [L–Pd^0] moiety for stoichiometric and catalytic reactions in homogeneous solutions under mild conditions,[2] it is clearly highly desirable to have a convenient route to reactive L–Pd(alkene)$_2$ complexes.

Following on from our synthesis of *rac*/*meso*-(μ-η^2,η^2-C$_7$H$_{12}$){Ni(η^2,η^2-C$_7$H$_{12}$)}$_2$,[3] we have reacted (cod)PdCl$_2$ with Li$_2$cot in hepta-1,6-diene and obtained a colorless precipitate of the Pd derivative **1** (61%). Analogously, reaction in diallyl ether yields complex **2** and in tetramethyldivinyldisiloxane complex **3** (Scheme 1). The latter corresponds to the already known {μ-(η^2-CH$_2$=CHSiMe$_2$)$_2$O}[M{(η^2-CH$_2$=CHSiMe$_2$)$_2$O}]$_2$ (M = Ni, Pt; the Pt *rac*-derivative is structurally characterized).[4] Although complexes **1** and **2** slowly decompose around 0 °C, they are significantly more stable and easier to handle than, *e.g.*, the comparable homoleptic Pd(cod)$_2$ or Pd(C$_2$H$_4$)$_3$.[1,5] In the case of Pt^0, we have prepared complex **4** (65%; mp 110 °C) by the same route as for **1**.

When **1**–**4** are reacted with π- or σ-donor molecules L, such as C$_2$H$_4$, PR$_3$ and P(OR)$_3$ (R = alkyl, aryl), and isonitriles,‡ the bridging 1,6-diene ligand is displaced and complexes of the type L–M(1,6-diene) are obtained in 80–95% yield (Table 1). The products have been characterized by elemental analyses, mass spectra, IR and NMR spectra. In addition, the crystal structure of **15** has been determined (see below). Displacement reactions show that the hepta-1,6-diene ligands are readily replaced by diallyl ether or diallylamine and the latter by the divinyldisiloxane (Scheme 2). The hepta-1,6-diene complexes are the most reactive and hence preferential starting materials. However, for many purposes the diallyl ether complexes are most convenient because of (*i*) good stability and easy isolation and handling, (*ii*) high reactivity, and (*iii*) low price of the ligand. A survey of the literature reveals that **18** has been previously obtained accidentally, but the excellent suitability of this class of complexes as starting materials for further reactions has apparently not been recognized.[6] ¶ L–Pd(1,6-diene) complexes are generally stable

Table 1 Pd^0 and Pt^0 1,6-diene complexes§

Complex	Formula[a]	Selected identifying data[b,c,d]
Pd$_2$(C$_7$H$_{12}$)$_3$ **1**	C$_{21}$H$_{36}$Pd$_2$ (501.4)	Voluminous precipitate, insoluble in thf; slowly decomp. ≈0 °C
Pd$_2$(C$_6$H$_{10}$O)$_3$ **2**	C$_{18}$H$_{30}$O$_3$Pd$_2$ (507.3)	Poorly soluble in thf (−30 °C); slowly decomp. >0 °C
Pd$_2${(CH$_2$=CHSiMe$_2$)$_2$O}$_3$ **3**	C$_{24}$H$_{54}$O$_3$Pd$_2$Si$_6$ (772.0)	Off-white crystals; mp 55 °C
(C$_2$H$_4$)Pd(C$_7$H$_{12}$) **5**	C$_9$H$_{16}$Pd (230.7)	Light yellow; extremely soluble; C$_2$H$_4$: δ(H) 3.39
(Me$_3$P)Pd(C$_7$H$_{12}$) **6**	C$_{10}$H$_{21}$PPd (278.7)	Mp ≈27 °C; δ(P) −22.3
(Pr$^i_3$P)Pd(C$_7$H$_{12}$) **7**	C$_{16}$H$_{33}$PPd (362.8)	Mp 52 °C; M$^+$ 362; δ(P) 53.6
(Cy$_3$P)Pd(C$_7$H$_{12}$) **8**	C$_{25}$H$_{45}$PPd (483.0)	Mp 131 °C; M$^+$ 482; δ(P) 40.3
(Bu$^t_3$P)Pd(C$_7$H$_{12}$) **9**	C$_{19}$H$_{39}$PPd (404.9)	Decomp. at 20 °C to give Pd(PBu$^t_3$)$_2$; δ(P) 88.4 (−80 °C)
(Ph$_3$P)Pd(C$_7$H$_{12}$) **10**	C$_{25}$H$_{27}$PPd (464.9)	Mp 87 °C decomp.; δ(P) 30.6
{(4-MeC$_6$H$_4$)$_3$P}Pd(C$_7$H$_{12}$) **11**	C$_{28}$H$_{33}$PPd (507.0)	Mp 114 °C; δ(P) 28.2
{(PhO)$_3$P}Pd(C$_7$H$_{12}$) **12**	C$_{25}$H$_{27}$O$_3$PPd (512.9)	Stable at 20 °C for several days; δ(P) 150.3
{(2,6-Me$_2$C$_6$H$_3$O)$_3$P}Pd(C$_7$H$_{12}$) **13**	C$_{31}$H$_{39}$O$_3$PPd (597.0)	Mp 131 °C decomp.; δ(P) 156.1
{(2,6-Pr$^i_2$C$_6$H$_3$O)$_3$P}Pd(C$_7$H$_{12}$) **14**	C$_{43}$H$_{63}$O$_3$PPd (765.4)	Mp 142 °C; δ(P) 155.9
(Me$_3$P)Pd(C$_6$H$_{10}$O) **15**	C$_9$H$_{19}$OPPd (280.6)	Mp 79 °C decomp.; δ(P) −21.8
(Pr$^i_3$P)Pd(C$_6$H$_{10}$O) **16**	C$_{15}$H$_{31}$OPPd (364.8)	Mp 63 °C; δ(P) 55.2
(Ph$_3$P)Pd(C$_6$H$_{10}$O) **17**	C$_{24}$H$_{25}$OPPd (466.9)	Mp 112 °C decomp.; δ(P) 31.3
(Cy$_3$P)Pd(C$_6$H$_{10}$O) **18**[6]	C$_{24}$H$_{43}$OPPd (485.0)	Mp 145 °C; M$^+$ 484; δ(P) 41.8
{(PhO)$_3$P}Pd(C$_6$H$_{10}$O) **19**	C$_{24}$H$_{25}$O$_4$PPd (514.9)	Mp 92 °C decomp.; δ(P) 151.4
(Bu^{t}NC)Pd(C$_6$H$_{10}$O) **20**	C$_{11}$H$_{19}$NOPd (287.7)	Tan; ν(N≡C) 2148 cm^{-1}
(Pr$^i_3$P)Pd(C$_6$H$_{10}$NH) **21**	C$_{15}$H$_{32}$NPPd (363.8)	M$^+$ 363; δ(P) 54.7
(Ph$_3$P)Pd(C$_6$H$_{10}$NH) **22**	C$_{24}$H$_{26}$NPPd (465.9)	δ(P) 31.2
(Pr$^i_3$P)Pd{(CH$_2$=CHSiMe$_2$)$_2$O} **23**	C$_{17}$H$_{39}$OPPdSi$_2$ (453.1)	Mp 75 °C decomp.; δ(P) 48.6
Pt$_2$(C$_7$H$_{12}$)$_3$ **4**	C$_{21}$H$_{36}$Pt$_2$ (678.7)	Voluminous precipitate, poorly soluble in thf; mp 110 °C decomp.
(C$_2$H$_4$)Pt(C$_7$H$_{12}$) **24**	C$_9$H$_{16}$Pt (319.3)	Light yellow; extremely soluble; C$_2$H$_4$: δ(H) 2.91, ^2J(PtH) 59 Hz
(Pr$^i_3$P)Pt(C$_7$H$_{12}$) **25**	C$_{16}$H$_{33}$PPt (451.5)	Orange; mp 75 °C; M$^+$ 451; δ(P) 46.5, ^1J(PtP) 3393 Hz
(Ph$_3$P)Pt(C$_7$H$_{12}$) **26**	C$_{25}$H$_{27}$PPt (553.5)	Yellow; mp 110 °C decomp.; M$^+$ 553; δ(P) 25.8, ^1J(PtP) 3513 Hz

[a] Satisfactory elemental analyses (C, H, P, Pd, Pt) were obtained for all compounds with the exception of non-isolated **5** and **24**. [b] All compounds are colorless, if not indicated otherwise. [c] EI mass spectra at 70 eV; the data refer to ^{106}Pd and ^{195}Pt. [d] ^{31}P NMR shifts (downfield positive) relative to external 85% aqueous H$_3$PO$_4$; solvent is [^{2}H$_8$]thf.

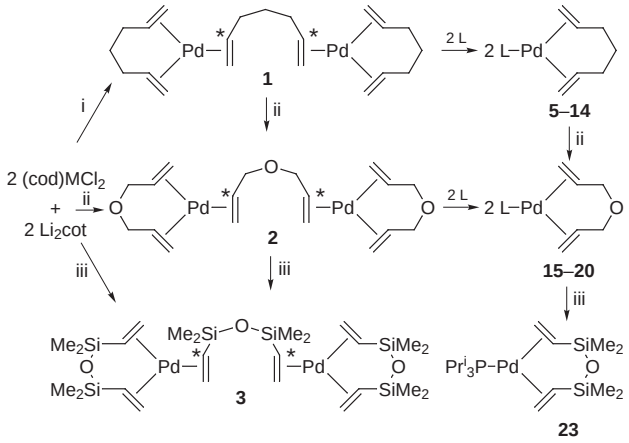

Scheme 1 *Reagents and conditions:* i, hepta-1,6-diene; ii, diallyl ether; iii, tetramethyldivinyldisiloxane

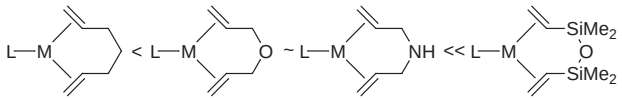

Scheme 2 Sequence of increasing stability (decreasing reactivity) of L–M(1,6-diene) complexes (M = Ni, Pd, Pt)

and we have found that other 1,6-dienes, such as diallylsilanes, are equally applicable. In contrast, L–M(1,6-enyne) complexes (M = Ni, Pd, Pt) are apparently not stable.

The X-ray structure determination of **15** (Fig. 1)‖ reveals a trigonal-planar (*TP*-3) coordination of the Pd atom by the phosphorus atom and the C=C bonds of the diallyl ether ligand. The geometry indicates that the 1,6-diene moiety is able to chelate two coordination sites at a d^{10} *TP*-3 M^0 center with little strain. Thus, the angles D1–Pd–D2, P–Pd–D1, and P–Pd–D2 (D1, D2 are the mid-points of the C=C bonds) are all very close to 120°, and the C=C carbon atoms lie exactly in the coordination plane. Moreover, the Pd^0(1,6-diene) moiety adopts the expected chair-like conformation, and the C=C bonds [mean 1.38(1) Å] are only slightly lengthened as compared with an uncoordinated C=C bond (1.34 Å), indicating that back-bonding is rather weak for Pd^0.

These complexes find application in homogeneous catalysis in those cases where an unsaturated complex fragment [L–Pd^0] (L *e.g.* PPh_3), rather than a coordinatively saturated complex like $Pd(PPh_3)_4$, is expected to catalyze the reaction. For example, we have observed that [L–Pd] complexes (*e.g.* **7** and **16**) catalyze regio- and stereo-selectively the linear trimerization of alk-1-ynes to 1,4,6-trisubstituted *cis*-hexa-1,3-dien-5-ynes between −30 and 20 °C (Scheme 3).[7]

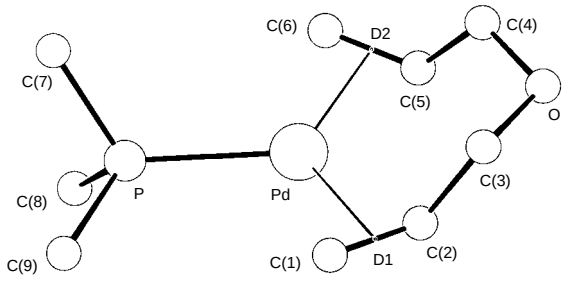

Fig. 1 Molecular structure of **15**. Selected bond lengths (Å): Pd–P 2.303(1), Pd–C(1) 2.151(5), Pd–C(2) 2.155(5), Pd–C(5) 2.157(5), Pd–C(6) 2.160(5), C(1)–C(2) 1.364(8), C(5)–C(6) 1.386(9), D1···D2 3.57(1). Selected bond angles (°): D1–Pd–D2 121.8(6), P–Pd–D1 119.4(3), P–Pd–D2 118.6(3).

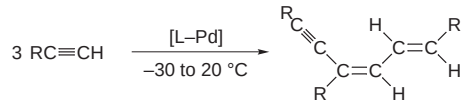

Scheme 3 R = Bu, CMe_2OH, Ph, Bu^t, $SiMe_3$

Notes and References

† E-mail: poerschke@mpi-muelheim.mpg.de

‡ It is expected that donors such as pyridines, phosphoranes, carbanions and heterocarbenes will coordinate together with 1,6-diene ligands on the Pd and Pt centers, as has already been shown for Ni.[3,8,9]

§ *Representative synthesis protocols:* **1**: a 0.2 M solution of Li_2cot (150 ml, 30 mmol) in diethyl ether was slowly added to a suspension of (cod)$PdCl_2$ (8.57 g, 30 mmol) in 40 ml of hepta-1,6-diene at −78 °C. When the temperature was raised to −40 °C a voluminous precipitate began to form, consisting of **1** and LiCl. At −20 °C the suspension was so dense that it could hardly be stirred. When diethyl ether was evaporated under vacuum at −10 °C, **1** dissolved again. LiCl was removed by filtration, and to the light green solution 50 ml of pentane was added (−30 °C), whereupon pure, colorless **1** precipitated. The product was isolated by filtration, washed with cold pentane, and dried under vacuum (−30 °C). Yield: 4.59 mg (61%).

7: a colorless solution of **1** (501 mg, 1.00 mmol) in 1 ml of hepta-1,6-diene was treated with a solution of PPr^i_3 (320 mg, 2.00 mmol) in 5 ml of pentane. When the mixture was cooled from −30 to −78 °C colorless crystals separated. After disposal of the mother liquor the product was washed with cold pentane and dried under vacuum (20 °C). Yield: 610 mg (84%).

16: a solution of **7** (363 mg, 1.00 mmol) in 5 ml of diethyl ether was treated with diallyl ether (0.13 ml, 1.05 mmol). After 1 h the colorless mixture was cooled to −78 °C, whereupon the crystalline product separated (isolation as described for **7**). Yield: 347 mg (95%). For identifying data see Table 1.

¶ Other Pd complexes with substituted diallyl ether[6] and hepta-1,6-diene-type ligands[10] have been reported previously.

‖ *Crystal data* for **15**: $C_9H_{19}OPPd$, M_r = 280.6, colorless prism, crystal size 0.28 × 0.42 × 0.46 mm, a = 10.050(2), b = 9.194(2), c = 13.053(1) Å, β = 101.866(10)°, V = 1180.2(4) Å^3, T 293 K, monoclinic, space group $P2_1/n$ (No. 14), Z = 4, D_c = 1.58 g cm^{-3}, μ = 1.67 mm^{-1}. Enraf-Nonius CAD4 diffractometer. Mo-Kα X-radiation, λ = 0.710 69 Å. 5598 measured reflections, 2688 unique, 2315 observed [$I > 2.0\sigma(F_o^2)$]. The structure was solved by direct methods (SHELXS-86) and refined by full-matrix least-squares on F^2 for all data with Chebyshev weights to R = 0.043 (obs.), wR = 0.118 (all data), S = 1.07, H atoms isotropic, max. shift/error 0.001, residual ρ_{max} = 1.95 e Å^{-3}, 0.8 Å from Pd. CCDC 182/845.

1 M. Green, J. A. K. Howard, J. L. Spencer and F. G. A. Stone, *J. Chem. Soc., Chem. Commun.*, 1975, 449.

2 J. Krause, Dissertation, Universität Düsseldorf, 1993; K.-J. Haack, Dissertation, Universität Düsseldorf, 1994; G. Cestaric, Planned Dissertation.

3 B. Proft, K.-R. Pörschke, F. Lutz and C. Krüger, *Chem. Ber.*, 1991, **124**, 2667.

4 P. B. Hitchcock, M. F. Lappert and N. J. W. Warhurst, *Angew. Chem.*, 1991, **103**, 439; *Angew. Chem., Int. Ed. Engl.*, 1991, **30**, 438; P. B. Hitchock, M. F. Lappert, C. MacBeath, F. P. E. Scott and N. J. W. Warhurst, *J. Organomet. Chem.*, 1997, **528**, 185.

5 M. Green, J. A. K. Howard, J. L. Spencer and F. G. A. Stone, *J. Chem. Soc., Dalton Trans.*, 1977, 271.

6 T. Yamamoto, M. Akimoto and A. Yamamoto, *Chem. Lett.*, 1983, 1725; T. Yamamoto, M. Akimoto, O. Saito and A. Yamamoto, *Organometallics*, 1986, **5**, 1559.

7 J. Krause, G. Cestaric and K.-R. Pörschke, manuscript in preparation.

8 U. Rosenthal, S. Pulst, R. Kempe, K.-R. Pörschke, R. Goddard and B. Proft, *Tetrahedron*, 1998, **54**, 1277.

9 C. Pluta, K.-R. Pörschke, B. Gabor and R. Mynott, *Chem. Ber.*, 1994, **127**, 489.

10 A. Döring, P. W. Jolly, R. Mynott, K.-P. Schick and G. Wilke, *Z. Naturforsch., Teil B*, 1981, **36**, 1198; P. W. Jolly, *Angew. Chem.*, 1985, **97**, 279; *Angew. Chem., Int. Ed. Engl.*, 1985, **24**, 283.

Received in Cambridge, UK, 27th March 1998; 8/02381F

Strong influence of the polyanion structure on the secondary structure of solid heteropolyacids and their catalytic activity; methyl *tert*-butyl ether synthesis in the pseudo-liquid phase of heteropolyacids

Sawami Shikata and Makoto Misono*†

Department of Applied Chemistry, Graduate School of Engineering, The University of Tokyo, Hongo, Bunkyo-ku, Tokyo 113-8656, Japan

It has been shown that the high catalytic activity of a Dawson-type heteropolyacid for gas-phase methyl *tert*-butyl ether synthesis at low temperatures is attributable to its amorphous secondary structure, which brings about a flexible pseudo-liquid phase and facilitates rapid absorption and desorption of molecules.

High catalytic activities of Keggin-type heteropolyacids for gas-phase synthesis of methyl *tert*-butyl ether (MTBE) have already been reported.[1] We recently found that a Dawson-type heteropolyacid ($H_6P_2W_{18}O_{62}$) was more than ten times more active than Keggin-type heteropolyacids ($H_nXW_{12}O_{40}$, X = P, Si, Ge, B, Co) at a low temperature that is favorable for the equilibrium of this reaction.[2,3] In the present study, it has been deduced that the high catalytic activity of $H_6P_2W_{18}O_{62}$ is due to its amorphous and flexible pseudo-liquid phase that is very probably brought about by the elliptical shape of the primary structure (polyanion) of $P_2W_{18}O_{62}^{6-}$. As described below, both heteropolyacids were nearly anhydrous, so that the water content was not regarded to be the main factor controlling the activities.

Pseudo-liquid phase behaviour is a unique phenomenon of heteropolyacids.[4] Polar and basic molecules are rapidly absorbed into the solid lattice and react there, the solid catalyst behaving in a sense like a concentrated solution.[5] This behaviour often brings about high catalytic activities and unique selectivities. MTBE synthesis catalyzed by the heteropolyacids has already been inferred to take place in the pseudo-liquid phase based on the following facts;[3] (*i*) the relative catalytic activities of various heteropolyacids can not be explained by the acidity, but are well correlated with the absorption behavior, (*ii*) the dependence of the rate on methanol pressure was very similar to that for the pseudo-liquid phase observed previously, and (*iii*) the catalytic activity of $Cs_{2.5}H_{0.5}PW_{12}O_{40}$ for which the reaction takes place on the surface was lower than that of $H_6P_2W_{18}O_{62}$, although the acid site concentration on the surface was more than ten times greater for $Cs_{2.5}H_{0.5}PW_{12}O_{40}$ than for $H_6P_2W_{18}O_{62}$.[6]

MTBE synthesis was carried out in a flow reactor at atmospheric pressure at 323 K as reported previously.[3] Prior to the reaction, catalysts were treated in a flow of N_2 at 423 or 523 K. In ordinary experiments, the feed gas was a mixture of methanol, isobutylene and N_2 with a volume ratio of 1 : 1 : 3 and the total flow rate was 90 cm^3 min^{-1}. In *ex situ* XRD measurements, the samples after pretreatment or reaction were quickly transferred onto a sample holder and sealed by polyethylene film to avoid contact with moisture. This was performed in an N_2 flow in the case of thermal pretreatment.

Fig. 1 shows the time courses of MTBE synthesis over $H_3PW_{12}O_{40}$ and $H_6P_2W_{18}O_{62}$, after pretreatments at 423 and 523 K. Just after the start of the reaction, rapid increases in the MTBE yields were observed (0–10 min). These are due to the rapid absorption of reactants and formation of MTBE in the solid bulk as discussed previously.[3] Here the MTBE yields at 10–15 min are regarded to relate to the initial activities. For $H_3PW_{12}O_{40}$, the initial activity was strongly influenced by the pretreatment temperature and the activities at the stationary stage (after 2 h) were very low because of excessive absorption, as reported previously.[3] On the other hand, for $H_6P_2W_{18}O_{62}$, irrespective of the pretreatment temperature, after the absorption progressed in the initial stage and MTBE yield increased rapidly, high stationary catalytic activities were maintained.

Powder XRD patterns for the two kinds of heteropolyacids just after two different pretreatments and after the stationary states of reaction are shown in Fig. 2. The peak intensities in Fig. 2 are normalized on the basis of the peak area of polyethylene film used to cover the samples (marked by solid circles). The Keggin-type heteropolyacid after pretreatment at 423 K [Fig. 2(*a*)(*i*)] showed an ordinary cubic bcc pattern. It was noted that the lattice constant was slightly smaller (d = 11.7 Å) than that of $H_3PW_{12}O_{40}\cdot 6H_2O$ (d = 12.1 Å).[7] After reaction [Fig. 2(*a*)(*ii*)], the cubic pattern was essentially retained, while the lines became broader with a small increase in the lattice constant (d = 12.1 Å) and additional weak lines appeared. After the Keggin-type heteropolyacid was treated at 523 K, the lines were much weaker [Fig. 2(*a*)(*iii*)], indicating that the secondary structure was almost amorphous. It is remarkable that after the reaction, the XRD pattern which was very like that after the reaction of the 423 K-treated sample, appeared again [Fig. 2(*a*)(*iv*)]. According to IR spectra, the primary structures were intact for all of these samples.[6,8]

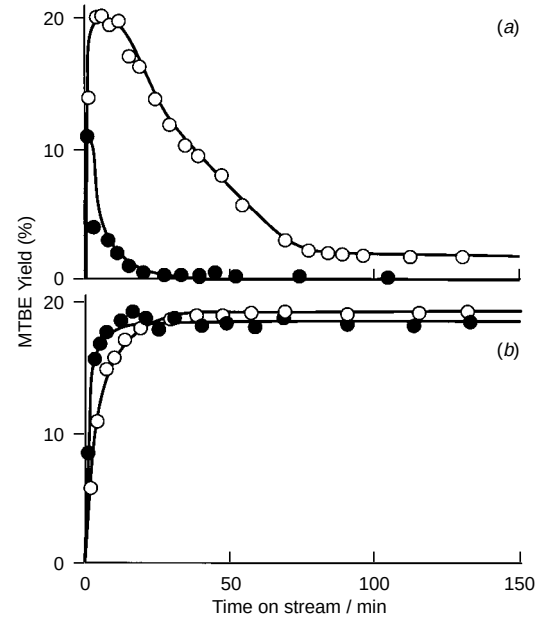

Fig. 1 Effects of pretreatment temperature on MTBE synthesis catalyzed by $H_3PW_{12}O_{40}$ (*a*) and $H_6P_2W_{18}O_{62}$ (*b*) pretreated at 423 K (●), 523 K (○) in an N_2 flow. Catalyst mass: 0.5 g, reaction temperature: 323 K, methanol : iso-C_4H_8 : N_2 = 1 : 1 : 3, flow rate: 90 cm^3 min^{-1}.

Table 1 The secondary structures and the catalytic activities of MTBE synthesis over $H_3PW_{12}O_{40}$ and $H_6P_2W_{18}O_{62}$

Primary structure	Pretreatment temperature/K	Secondary structure: Before reaction	Secondary structure: After reaction	Catalytic activity[a]: Initial	Catalytic activity[a]: Stationary
$H_3PW_{12}O_{40}$	423	Cubic	Cubic	2	> 0
(Keggin type)	523	Amorphous	Cubic	20	< 2
$H_6P_2W_{18}O_{62}$ (Dawson type)	423	Amorphous	Amorphous	17	18
	523	Amorphous	Amorphous	17	18

[a] MTBE yields (%) at the initial (10–15 min) and stationary (after 2 h) stages.

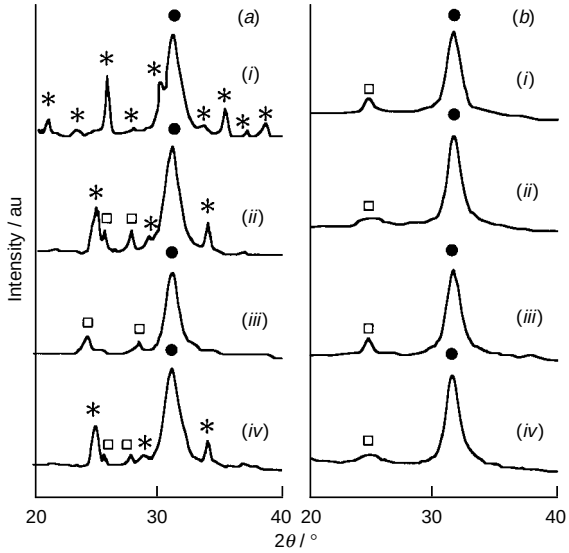

Fig. 2 Powder XRD patterns of $H_3PW_{12}O_{40}$ (*a*) and of $H_6P_2W_{18}O_{62}$ (*b*), before and after MTBE synthesis reaction. (*i*) After pretreatment at 423 K, (*ii*) after reaction at 323 K of the sample (*i*), (*iii*) after pretreatment at 523 K, and (*iv*) after reaction of the sample (*iii*). (●) Peaks of polyethylene film, (*) peaks due to cubic structure and (□) unknown structures.

In contrast, for the Dawson-type heteropolyacid, the XRD lines were weak and broad before and after the reaction for both treatments [Fig. 2(*b*)(*i*)–(*iv*)], indicating that the secondary structure was always mostly amorphous. IR spectra showed that the primary structure (heteropolyanion) was retained. Although there remain unidentified structures, it is evident that the samples of Fig. 2(*a*)(*i*), (*ii*) and (*iv*) are mostly crystalline and those of Fig. 2(*b*)(*i*)–(*iv*) and Fig. 2(*a*)(*iii*) are mostly amorphous.

These structural data are compared with the results of catalytic activity in Table 1. A close correspondence was noted in Table 1 between the secondary structures and the reaction rates observed for the eight cases; two heteropolyacids with two different pretreatments for the initial and stationary states. A high rate was always observed when the secondary structure was amorphous, and a low rate was observed for crystalline cubic structures. For example, $H_3PW_{12}O_{40}$ treated at 523 K showed high activity at first, but the activity declined to a very low level at the steady state, accompanying the change of the secondary structure from amorphous to crystalline (cubic), while $H_6P_2W_{18}O_{62}$ always showed a high activity and amorphous XRD pattern. It was confirmed experimentally that surface areas and pore volumes of the two heteropolyacids little changed with the change of the pretreatment temperature (423 or 523 K). The acid strength also remains constant.[9] According to the DTA–TG analyses, although the water desorbs more easily for the Dawson-type at low temperatures, both heteropolyacids were nearly anhydrous after treatment at 523 K. Moreover, the differences in the water content between the pretreatments at 423 and 523 K were smaller for $H_3PW_{12}O_{40}$ (0.3 H_2O/heteropolyanion) than for $H_6P_2W_{18}O_{62}$ (*ca.* 1 H_2O/heteropolyanion). This is in contrast to the fact that the catalytic behaviour differed more for the Keggin-type [Fig. 1(*a*)] than the Dawson-type [Fig. 1(*b*)] between the 423 and 523 K treatments. Hence, the water content is not the main factor controlling these activities.

We previously indicated[3] that the high catalytic activity of $H_6P_2W_{18}O_{62}$ is brought about by a high-activity state of the pseudo-liquid phase in which moderate amounts of molecules are absorbed and the absorption–desorption is rapid, while the pseudo-liquid phase of $H_3PW_{12}O_{40}$ is in a low-activity state where the absorption is excessive and slow. The transformation between active and less active pseudo-liquid phases with partial pressure was reported previously.[10] If this conclusion is combined with the present results summarized in Table 1, an interesting correlation is deduced between the nature of the pseudo-liquid phase (secondary structure) and the polyanion structure (primary structure). That is, the elliptical shape of the Dawson anion is not suitable for the formation of a stable crystalline structure and leads to an amorphous and flexible structure, the absorption–desorption being easier and catalytic activity high, while the spherical shape of the Keggin anion favors a crystalline cubic structure, where absorption–desorption is slow and catalytic activity is low.

A part of the present study was presented at the Symposium of Catalysis Society of Japan.[11]

Notes and References

† E-mail: tmisono@hongo.ecc.u-tokyo.ac.jp

1 A. Igarashi, T. Matsuda and Y. Ogino, *J. Jpn. Petrol. Inst.*, 1979, **22**, 331.
2 S. Shikata, T. Okuhara and M. Misono, *Sekiyu Gakkaishi*, 1994, **37**, 632.
3 S. Shikata, T. Okuhara and M. Misono, *J. Mol. Catal.*, 1995, **100**, 49.
4 M. Misono, *Catal. Rev., -Sci. Eng.*, 1987, **29**, 269; K. Y. Lee, T. Arai, S. Nakata, S. Asaoka, T. Okuhara and M. Misono, *J. Am. Chem. Soc.*, 1992, **114**, 2836.
5 T. Okuhara, T. Hashimoto, M. Misono, Y. Yoneda, H. Niiyama, Y. Saito and E. Echigoya, *Chem. Lett.*, 1983, 573.
6 S. Shikata, S. Nakata, T. Okuhara and M. Misono, *J. Catal.*, 1997, **166**, 263.
7 G. M. Brown, M.-R. Noe-Spirlet, W. R. Busing and H. A. Levy, *Acta Crystallogr., Sect. B*, 1977, **33**, 1038.
8 K. Na, T. Okuhara and M. Misono, *J. Chem. Soc., Faraday. Trans.*, 1995, **91**, 367.
9 F. Lefebvre, F. X. Liu-Cai and A. Auroux, *J. Mater. Chem.*, 1994, **4**, 125.
10 K. Takahashi, T. Okuhara and M. Misono, *Chem. Lett.*, 1985, 841.
11 S. Shikata and M. Misono, *Shokubai*, 1997, **39**, 174.

Received in Cambridge, UK, 18th March 1998; 8/02138D

Synthesis, structure and Co–C bond homolysis of an intramolecularly bridged (tetrahydrofurfuryl)cobalt(salen) complex: a simple model of enzyme-bound coenzyme B_{12}

Rolf Blaauw,[a] Juul L. van der Baan,*[a]† Sijbe Balt,[a] Martinus W. G. de Bolster,[a] Gerhard W. Klumpp,[a] Huub Kooijman[b] and Anthony L. Spek[b]

[a] *Scheikundig Laboratorium, Vrije Universiteit, De Boelelaan 1083, 1081 HV Amsterdam, The Netherlands*
[b] *Kristal-en Structuurchemie, Universiteit Utrecht, Padualaan 8, 3584 CH Utrecht, The Netherlands*

Air oxidation of a Co^{II}(salen) derivative, whose ethanediyl moiety carries a methylene-linked 4-hydroxypent-1-en-3-yl substituent, yields an intramolecularly bridged (tetrahydrofurfuryl)Co^{III}(salen) complex of which the crystal structure has been determined; this B_{12} model is very resistant to Co–C bond homolysis, even in the presence of a large excess of the radical trap TEMPO.

The bond dissociation energy of the Co–C bond of coenzyme B_{12} (5′-deoxyadenosylcobalamin) is estimated to be 31 kcal mol^{-1}. Despite the weakness of the Co–C bond, there is a high efficiency of radical recombination following Co–C bond homolysis,[1] a key step in coenzyme B_{12}-dependent enzymatic rearrangements. It has been suggested that one of the factors responsible for this apparent contradiction is the β-oxygen of the 5′-deoxyadenosyl ligand, which can stabilise the initial pyramidal geometry at the 5′-C of the adenosyl radical and/or impose a rotational barrier to the $C_{4'}$–$C_{5'}$-bond.[2] Radical pair recombination efficiency is expected to be even higher when the cofactor is bound to the active site of the enzyme, where the cobalamin and 5′-deoxyadenosyl moieties are kept close to each other until the substrate enters. Recently, we found that (organo)Co(salen) complexes containing a cobalt-to-salen polymethylene bridge show a much stronger resistance to thermal and photochemical decomposition than the non-bridged complex (*n*-butyl)Co(salen).[3] In order to study whether this resistance would be further enhanced by the introduction of a β-oxygen substituent, we have synthesised a (tetrahydrofurfuryl)Co(salen) complex in which the tetrahydrofurfuryl ligand (as a deoxyadenosyl mimic) is attached to the equatorial salen ligand by a methylene link. Here, we report on the synthesis and structure of this compound and present some preliminary results concerning the photolytic homolysis of its Co–C bond.

Our synthetic approach was based on our finding that (tetrahydrofurfuryl)Co^{III}(salen) **1** is formed in 78% yield when a *ca.* 3×10^{-2} M solution of Co^{II}(salen) in CH_2Cl_2 containing 20 equiv. of pent-4-en-1-ol is exposed to air for 20 h (Scheme 1).§ The formation of **1** may proceed by intramolecular nucleophilic attack by the hydroxy group on an intermediate cobalt(III)–alkene π-complex.[4,5] The reaction is regiospecific: (tetrahydropyran-3-yl)Co(salen) is not formed.

In order to prepare an intramolecularly bridged tetrahydrofurfurylcobalt complex in a way analogous to **1**, we synthesised Co^{II}(salen) derivative **5** according to Scheme 2. Bromide **2** (prepared from but-3-yn-1-ol *via C*-alkylation with $THPOCH_2CH_2Br$, reduction to *trans*-alkenol with LAH, *O*-alkylation with Bu_3SnCH_2I followed by Wittig–Still rearrangement, and bromination with Ph_3PBr_2) was reacted with methyl *N*-benzylideneglycinate to give a monoalkylation product which was then treated with tartaric acid in THF–H_2O at 0 °C to selectively deprotect the amino ester moiety while leaving the THP ether intact. Subsequent conversion of amino ester **3** to 1,2-diamine **4** (isolated as its dihydrochloride) was straightforward and analogous to our previously published procedure.[5] Addition of NaOAc to a solution of **4** and 2 equiv. salicylaldehyde in hot EtOH, followed by reaction of the resulting H_2salen ligand with $Co(OAc)_2$ in THF at 60 °C gave cobalt(II) complex **5** as an orange microcrystalline product. From the ^1H and ^{13}C NMR spectra of compounds **2**–**5** [paramagnetic **5** was characterised after oxidation with iodine to the corresponding iodocobalt(III) complex] it is evident that the alkylation step leading to glycine derivative **3** is diastereoselective, **4** being obtained as a mixture of two diastereomers in a ratio of *ca.* 3 : 1.

Upon exposure to air, a red solution of **5** in CH_2Cl_2 turned green in one day, indicating oxidation to a pentacoordinate organocobalt(III) complex. Concentration *in vacuo* and precipitation with Et_2O furnished a green solid, which was subjected to flash column chromatography (aluminium oxide, 10% MeOH in CH_2Cl_2) to remove traces of cobalt(II) material. The green product (80% yield) was shown by ^1H and ^{13}C NMR spectroscopy to consist of a 3 : 1 mixture of two diastereomers of **6**.¶ Thus, a reaction similar to that of Co^{II}(salen) with pent-4-en-1-ol had occurred, but now in an intramolecular fashion

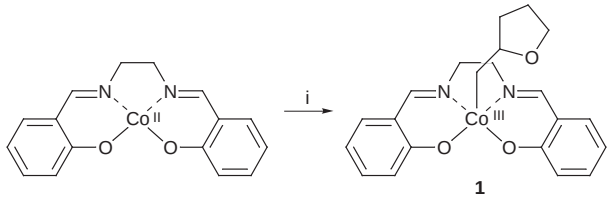

Scheme 1 *Reagents and conditions*: i, pent-4-en-1-ol (20 equiv.), CH_2Cl_2, O_2

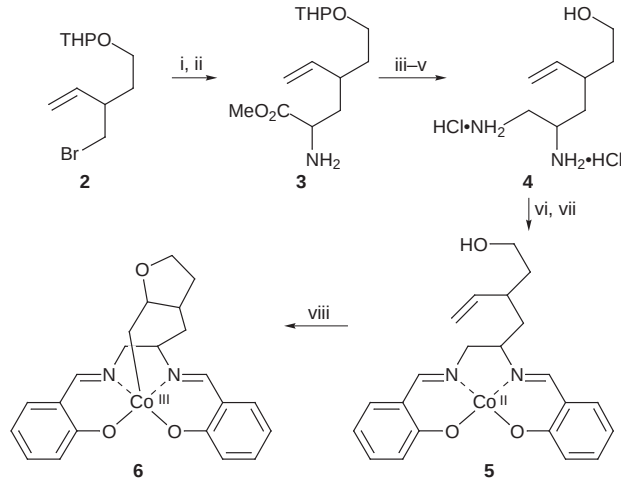

Scheme 2 *Reagents and conditions*: i, $MeO_2CCH_2N{=}CHPh$, LDA, DMPU,‡ THF; ii, tartaric acid, THF–H_2O, 0 °C; iii, NH_3, MeOH; iv, $LiAlH_4$, THF; v, 1 M HCl; vi, salicylaldehyde, $NaOAc{\cdot}3H_2O$, EtOH, 60 °C; vii, $Co(OAc)_2$, THF, 60 °C; viii, CH_2Cl_2 or MeOH, O_2

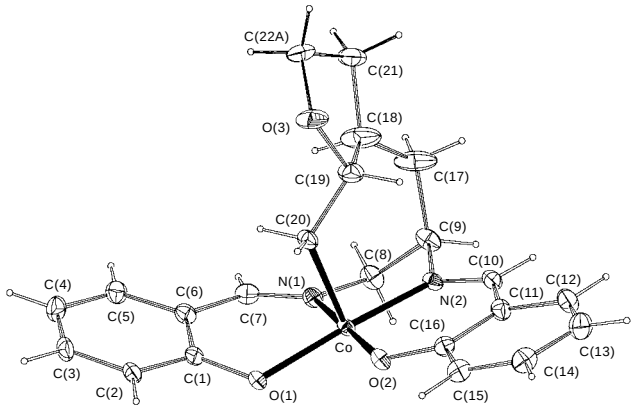

Fig. 1 ORTEP diagram drawn at the 30% probability level and atom numbering scheme of half a dimer of **6a**. The minor disorder component and solvent molecules have been omitted for clarity. Suffix A denotes the major disorder component. Selected distances (Å) and angles (°): Co–C(20) 1.960(6), Co–O(1) 1.932(3), Co–O(2) 1.882(4), Co–N(1) 1.864(5), Co–N(2) 1.886(4), C(19)–C(20) 1.476(9), C(18)–C(19) 1.534(10), C(17)–C(18) 1.422(10), N(1)–C(7) 1.276(8), N(2)–C(10) 1.287(8), C(19)–O(3) 1.456(8); Co–C(20)–C(19) 119.3(4), C(18)–C(19)–C(20) 115.5(6), C(17)–C(18)–C(19) 122.0(8), C(20)–Co–O(1) 91.8(2), C(20)–Co–O(2) 90.0(2), C(20)–Co–N(1) 91.5(2), C(20)–Co–N(2) 92.7(2).

(Scheme 2). The reaction was found to be much faster in MeOH (reaction time *ca*. 1 h), yet gave the two diastereomers of **6** in the same yield and ratio as in CH_2Cl_2.

The major diastereomer of **6** was selectively crystallised from CH_2Cl_2 and gave crystals suitable for X-ray structure analysis, establishing its structure as **6a** (Fig. 1).‖ The solid-state structure of **6a** is a centrosymmetric dimer. Hexacoordination of cobalt is established by the bonding of the cobalt atom of one molecule to a salen oxygen atom of its enantiomeric partner [Co–O = 2.259(3) Å]. Half of the dimeric structure is shown in Fig. 1, together with selected bond lengths and angles.** The Co–C bond length of 1.960(6) Å is comparable with the values found in related organocobalt Schiff base complexes.[6,7] In the crystal structure, the THF moiety is described with a disorder model consisting of two alternative positions for atom C(22). The bond lengths around C(18), the anisotropicity of C(17) and C(18) as well as the distribution of residual electron density around the furan moiety indicate the presence of additional, unresolved disorder, which is most probably conformational in nature. The twist-chair conformation of the carbon bridge and the anti-periplanar orientation of cobalt and oxygen in the *trans*-annulated THF ring are almost identical with those found in the crystal structures of other bridged organocobalt(salen) complexes.[5,6]

Preliminary laser photolysis experiments in toluene show that **6** is very resistant to Co–C bond homolysis. Even in the presence of a large excess of the radical trap TEMPO, the quantum yield Φ is only 0.03 ± 0.005.†† This value is much lower than the quantum yield determined under similar conditions for the (alkyl)Co(salen) complex with a cobalt-to-ligand four-methylene bridge (Φ = 0.25).[3] The quantum yield as a function of trap concentration has also been determined for non-bridged complex **1** and compared to that of (*n*-butyl)Co(salen).[3] The difference in Φ-values at high trap concentration is less pronounced than for the bridged complexes, but nevertheless significant; Φ-values are 0.19 and 0.28 for **1** and (*n*-butyl)Co(salen), respectively. These results support the suggestion that the β-oxygen substituent in (β-alkoxyalkyl)cobalt(III) complexes facilitates radical recombination of cobalt(II) and C· following Co–C bond homolysis.[2] Recombination efficiency is dramatically enhanced in complexes like **6**, whose β-alkoxy substituent is part of an intramolecular bridge which, like B_{12}-dependent enzymes, enforces a close proximity of the alkyl radical to cobalt(II). A detailed study of the homolysis of the Co–C bond of **6** and comparable complexes is in progress.

This work was supported in part (A. L. S.) by The Netherlands Foundation for Chemical Research (SON) with financial aid from the Netherlands Organisation for Scientific Research (NWO).

Notes and References

† E-mail: vdbaan@chem.vu.nl

‡ DMPU = *N*,*N*′-dimethylpropyleneurea.

§ *Selected data* for **1**: δ_H($CDCl_3$, 200 MHz) 7.81, 7.77 (2s, 2 H), 7.28 (m, 4 H), 6.92 (dd, 2 H), 6.50 (dd, 2 H), 4.1–3.7 (m, 5 H), 3.60 (m, 1 H), 3.33 (m, 1 H), 2.95–2.7 (m, 2 H), 1.95–1.5 (m, 4 H); δ_C($CDCl_3$, 400 MHz) 165.6 (qC), 165.5 (qC), 164.3 (CH), 163.9 (CH), 133.0 (CH), 132.9 (CH), 132.5 (CH), 123.8 (CH), 123.5 (CH), 119.7 (qC), 119.6 (qC), 115.0 (CH), 82.1 (CH), 67.4 (CH_2), 59.2 (CH_2), 58.9 (CH_2), 30.2 (CH_2), 25.7 (CH_2) (Calc. for $C_{21}H_{23}N_2O_3Co.CHCl_3$: C, 49.88; H, 4.57; N, 5.29; O, 9.06. Found: C, 49.90; H, 4.51; N, 5.75; O, 9.79%).

¶ *Analytical data* for **6**: (Calc. for $C_{22}H_{23}N_2O_3Co\cdot0.25H_2O$: C, 61.90; H, 5.55; O, 12.18. Found: C, 61.48; H, 5.48; O, 12.05%).

‖ *Selected data* for **6a**: δ_H(CD_3OD, 200 MHz) 8.11, 7.95 (2s, 2 H), 7.18 (m, 4 H), 7.02 (m, 2 H), 6.50 (2dd, 2 H), 4.20–3.95 (m, 3 H), 3.75–3.5 (m, 3 H), 3.40 (m, 1 H), 2.63 (dd, 1 H), 2.25–2.0 (m, 2 H), 1.65 (m, 2 H), 1.51 (m, 1 H); δ_C (CD_3OD, 200 MHz) 166.9 (C-7), 165.5 (C-10), 134.8, 134.5, 134.4, 134.2 (C-3/5/12/14), 123.7, 123.1 (C-2/5), 115.4, 115.0 (C-4/13), 88.5 (C-19), 67.5 (C-9), 66.5 (C-8), 64.5 (C-22), 43.2 (C-17), 42.4 (C-18), 37.0 (C-21). Quaternary carbons and C-20 not observed.

** *Crystal data* for **6a**: $C_{44}H_{46}Co_2N_4O_6\cdot4CH_2Cl_2$, M_r = 1184.47, red–brown, block-shaped crystal (0.1 × 0.2 × 0.2 mm), monoclinic, space group $P2_1/c$ (no. 14) with a = 11.0406(19), b = 11.0095(19), c = 20.838(4) Å, β = 103.209(14)°, V = 2465.9(8) Å^3, Z = 2, D_c = 1.595 g cm^{-3}, F(000) = 1216, μ(Mo-Kα) = 11.6 cm^{-1}, 15 569 reflections measured, 4341 independent, R_{int} = 0.1097, (1.0 < θ° < 27.5, ω scan, T = 150 K, Mo-Kα radiation, graphite monochromator, λ = 0.71073 Å) on an Enraf–Nonius CAD4 Turbo diffractometer on rotating anode. Data were corrected for Lp effects and for a linear instability of 3% of the reference reflections, but not for absorption. The structure was solved by automated direct methods (SHELXS96). Refinement on F^2 was carried out by full-matrix least-squares techniques (SHELXL96) for 311 parameters; no observance criterion was applied during refinement. A disorder model was introduced to describe the conformational disorder of the tetrahydrofuran moiety. Hydrogen atoms were included in the refinement on calculated positions riding on their carrier atoms. Refinement converged at a final *wR*2 value of 0.1796, *R*1 = 0.0655 [for 2936 reflections with $F_o > 4\sigma(F_o)$], S = 1.047. A final difference Fourier showed no residual density outside −1.00 and 1.28 e Å^{-3} (near CH_2Cl_2, indicating a slight disorder). CCDC 182/849.

†† Samples of **6** (1.0 × 10^{-4} M) and TEMPO (0–1.0 M) in toluene were irradiated with a 337 nm nitrogen laser at 295 ± 0.5 K. Decomposition was followed at the maximum absorbance of the Co^{III}–C band at 668 nm. Detailed experimental set-up and conditions are described in ref. 3.

1 C. D. Garr and R. G. Finke, *J. Am. Chem. Soc.*, 1992, **114**, 10 440; C. D. Garr and R. G. Finke, *Inorg. Chem.*, 1993, **32**, 4414.
2 W. B. Lott, A. M. Chagovetz and C. B. Grissom, *J. Am. Chem. Soc.*, 1995, **117**, 12 194.
3 R. Blaauw, I. E. Kingma, W. L. Werner, S. Wolowiec, J. L. van der Baan, S. Balt, M. W. G. de Bolster and G. W. Klumpp, *Inorg. Chim. Acta*, 1998, **269**, 203.
4 B. T. Golding, H. L. Holland, U. Horn and S. Sakrikar, *Angew. Chem., Int. Ed. Engl.*, 1970, **9**, 959.
5 I. E. Kingma, M. Wiersma, J. L. van der Baan, S. Balt, F. Bickelhaupt, M. W. G. de Bolster, G. W. Klumpp and A. L. Spek, *J. Chem. Soc., Chem. Commun.*, 1993, 832.
6 B. van Arkel, J. L. van der Baan, S. Balt, F. Bickelhaupt, M. W. G. de Bolster, I. E. Kingma, G. W. Klumpp, J. W. E. Moos and A. L. Spek, *J. Chem. Soc., Perkin Trans. 1*, 1993, 3023.
7 M. Calligaris, G. Nardin and L. Randaccio, *Coord. Chem. Rev.*, 1972, **7**, 385.

Received in Liverpool, UK, 24th February 1998; 8/01579A

Neutral isonitrile adducts of alkali and alkaline earth metals‡

Catherine F. Caro, Peter B. Hitchcock, Michael F. Lappert*† and Marcus Layh

The Chemistry Laboratory, University of Sussex, Brighton, UK BN1 9QJ

Isonitriles are shown to form stable neutral adducts with some group 1 and 2 metal complexes; the synthesis and structures of $[Li\{N(R)C(Ph)NC(Ph)=CR_2\}(CNPh)]_2$, $[LiNR_2(CNPh)]_2$, $[Mg(CHR_2)_2(CNC_6H_3Me_2\text{-}2,6)_2]$ and $[Mg(CHR_2)(\mu\text{-}Br)(CNBu^t)]_2$ are described (R = $SiMe_3$).

Nitriles and isonitriles are important in transition metal chemistry and nitriles also in the coordination chemistry of main group elements.[1] In contrast, isonitrile adducts of main group elements are rare. They include early reports on labile adducts of trialkyl- or triaryl-boranes,[2] $[AlPh_3\{CN(c\text{-}C_6H_{11})\}]$[3] and polyhedral boranes.[4] Recently, X-ray structures of $[Al(C_5H_5)_3(CNBu^t)]$,[5] the labile $[BPh_3\{CNC_6H_4(OSiMe_3)\text{-}4\}]$[6] and $[B(C_6F_5)(CNAr)\{N(Bu^t)B(C_6F_5)N(Bu^t)C{=}NAr\}]$[7] have been published; and spectroscopic evidence has been provided for the labile $[SiR^1R^2(CNR^3)]$ [R^1 = $C_6H_2\{CH(SiMe_3)_2\}_3$-2,4,6; R^2 = $C_6H_2Me_3$-2,4,6; and R^3 = R^2, Pr^i or $C_6H_2Bu^t_3$-2,4,6][8] and the 1 : 1 adducts of $LiCH(SiMe_3)_2$ and $[Li\{N(Bu^t)C(SiMe_3)C(H)C(SiMe_3)NBu^t\}(CNR')]$ (R′ = Bu^t or $C_6H_3Me_2$-2,6).[9] Boche and coworkers have described the anionic isonitrile complex $[Li(CNPh_2)\{(-)\text{-sparteine}\}(thf)_2]$ (thf = OC_4H_8).[10] We now report the first thermally stable and structurally authenticated complexes of lithium and magnesium in which an isonitrile acts as a neutral ligand.

Addition of an isonitrile R′NC to $Li\{N(R)C(Ph)=CR_2\}(thf)$ **A**[11] yielded (Scheme 1, step i) the enamide **1a** (R′ = *c*-C_6H_{11}) or **1b** (R′ = $C_6H_3Me_2$-2,6), while **A** with PhCN gave [eqn. (1)] the 1,3-diazaallyl **2** which with PhNC gave (Scheme 1, step ii) the dimeric 1 : 1 adduct **3** (R = $SiMe_3$).

Walborsky and Ronman have shown that treatment of an isonitrile R′NC with a lithium alkyl or a Grignard reagent derived from an alkyl halide R″Hal gave the metallo-aldimine, which was a convenient source of various organic compounds (*e.g.* see ref. 12). Surprisingly, we now find that the new Grignard reagent $[Mg(\mu\text{-}Br)(CHR_2)(OEt_2)]_2$ **4** with an isonitrile R′NC simply gave (Scheme 1, step iii) the 1 : 1 adduct $[Mg(\mu\text{-}Br)(CHR_2)(CNR')]_2$ (R′ = Bu^t **5a** or $C_6H_3Me_2$-2,6 **5b**). Even when heated, the latter did not undergo an isomerisation to yield the insertion product, a magnesio-aldimine. Likewise, $Mg(CHR_2)_2$[13] and R′NC gave (Scheme 1, step iv) the thermally stable adduct $[Mg(CHR_2)_2(CNR')_2]$ (R′ = Bu^t **6a** or $C_6H_3Me_2$-2,6 **6b**). These results are all the more unexpected since $LiCHR_2$ readily underwent insertion reactions with the same isonitriles.[9] On the other hand, we now show that the isoelectronic $LiNR_2$ and PhNC gave (Scheme 1, step v) the adduct $[LiNR_2(CNPh)]_2$ **7**, whereas[14] $LiNR_2$ + PhCN readily yielded the benzamidinate insertion product $[Li\{N(R)C(Ph)NR\}]_2$.

The new, pale yellow (**5**) or colourless, highly air-sensitive, readily hydrocarbon-soluble, crystalline solids **1**–**7** gave satisfactory analyses and NMR and IR spectra. Their formulation as isonitrile adducts (rather than insertion products) is consistent with the low frequency shift ($\Delta\delta$) of the $^{13}C\{^1H\}$ NMR spectral signal [δ(R′NC)] and the increase ($\Delta\nu$) in the NC stretching mode ν(R′N≡C) for each of **1**–**7** compared with the value in the free ligand R′NC, Table 1. The trends in $\Delta\delta[^{13}C\{^1H\}]$ and $\Delta\nu$(NC) for (R′NC)ML_n (**1**–**7**) indicate, in valence bond terms, that (*i*) the triply bonded canonical form is more significant in the complex ($R'N^+{\equiv}C^-ML_n \leftrightarrow R'N{=}C{=}ML_n$) than in the free ligand ($R'N^+{\equiv}C^- \leftrightarrow R'N{=}C$:), and (*ii*) the largest values for $\Delta\delta[^{13}C\{^1H\}]$ and $\Delta\nu$(NC) are found for the strongest Lewis acid ML_n in accord with the inequality sequence $Mg(Br)CHR_2$ > $Mg(CHR_2)_2$ > $Li(NR_2)$ > $Li[N(R)C(Ph)=CR_2]$. A cumulene-type canonical form for an isonitrile-transition metal complex is significant when M can participate in $d_\pi \rightarrow \pi^*$ bonding, as in the d^8 $[Ni(CNAr)_4]^{2+}$ [$\Delta\nu$(NC) negative], in contrast to, *e.g.* the d^2 $[Mo[CN)_4(CNMe)_4]$, having $\Delta\nu$(NC) positive.[1]

The X-ray molecular structures of complexes **3** and **6b** are shown in Figs. 1 and 2; those of **5a** and **7** will appear in a full paper.§ In each, the M–C–NR′ and C–N–R′ vectors are close to linear, and the short R′N–C distances are consistent with NC being a triple bond. The trends in the latter (d_{NC}, Table 1) are consistent with the above inequality sequence. The centrosym-

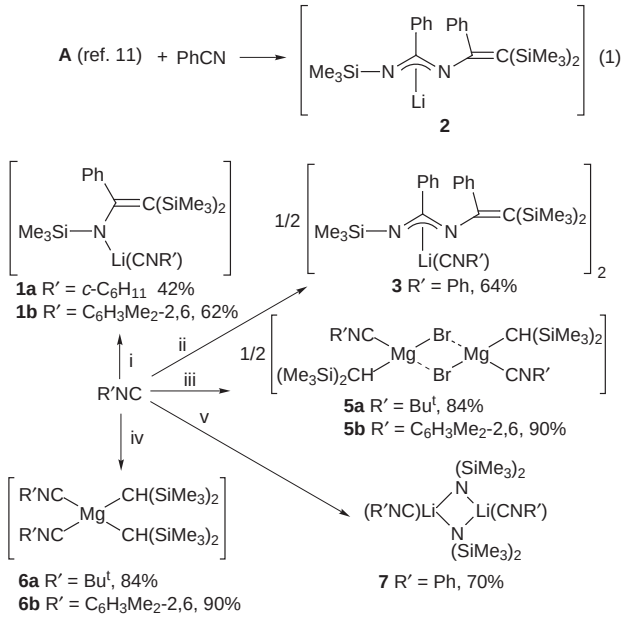

Scheme 1 Synthesis of the isonitrile adducts **1**–**7**. *Reagents and conditions*: i, **A**, Et_2O; ii, **2**, Et_2O; iii, $[Mg(\mu\text{-}Br)\{CH(SiMe_3)_2\}(OEt_2)]_2$ **4**, PhMe; iv, $Mg[CH(SiMe_3)_2]_2$, PhMe; v, $Li[N(SiMe_3)_2]$, C_5H_{12}. Reagents were mixed at −78 °C or −35 °C; the mixture was then brought to *ca.* 25 °C.

Table 1 Some important structural and spectroscopic data for compounds **1**–**7** and the isonitriles R′NC

	Property				
Compound	$\delta(^{13}C_{NC})$	$\Delta\delta(^{13}C)$	ν_{NC}/cm^{-1}	$\Delta\nu_{NC}$	d_{NC}/Å
7	156.4	10.7	2170	43	1.148(5) (av.)
3	166.3	0.8	2165	38	1.157(4)
PhNC	167.1		2127		—
5b	135.8	35.0	2191	76	—
6b	156.4	14.4	2173	58	1.14(1) (av.)
1b	163.6	7.2	—	—	—
2,6-$Me_2C_6H_3NC$	170.8		2115		—
5a	135.4	20.6	2216	76	1.07(2)
6a	141.8	14.2	2201	58	—
Bu^tNC	154.0		2136		—

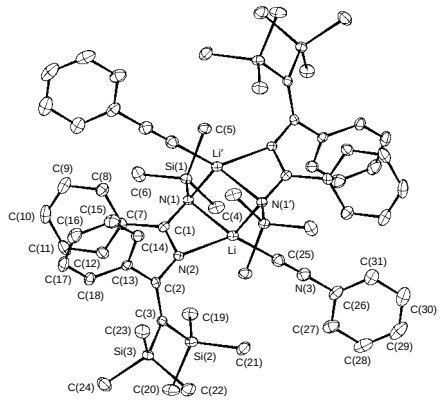

Fig. 1 Molecular structure of **3** with selected bond distances (Å) and angles (°): Li–N(1) 2.174(5), Li–N(2) 2.035(5), Li–N(1′) 2.115(5), Li–C(25) 2.178(6), N(3)–C(25) 1.157(4); N(3)–C(25)–Li 171.4(3), C(25)–N(3)–C(26) 176.0(3)

metric dimer **3** (Fig. 1), having a planar [LiN(1)Li′N(1)′] ring, has a ladder-like structure similar to that of [Li{N(R)C(C_6H_4Me-4)NR}(thf)]$_2$.[14] The shortest metal contact is to N(2) [2.035(5) Å] while the distances Li–N(1) 2.174(5), Li–N(1)′ 2.115(5) and Li–C(25) 2.178(6) Å are significantly longer. Compound **7** is also a dimer, but in contrast to **3**, the Li atoms are only three-coordinate with essentially symmetrical bridging NR_2 groups. The coordination sphere around Li is completed by the neutral isonitrile ligand with a slightly longer Li–C bond than in **3**. The overall geometry is therefore closely related to [{Li(μ-NR_2)L}$_2$] (*e.g.* L = OEt_2[15a] or NBu^t[15b]). Compound **6b** (Fig. 2) is monomeric with a distorted tetrahedral environment at Mg and fairly standard Mg–C σ-bond distances[13] of 2.148(7) and 2.138(9) Å, while the contacts to the neutral isonitrile ligands [2.31(1) Å] are much longer. The Grignard complex **5a** is unusual in that while it is a centrosymmetric dimer in the solid, the two monomeric MgBr(CHR_2) units are only weakly bound, the [Mg(μ-Br)]$_2$ moiety being unsymetrical: Mg–Br 2.561(5), Mg···Br 2.927(5) Å. The former distance is unexceptional, being close to those found (2.56–2.58 Å) in the symmetrical dimers [Mg(μ-Br)(Et)L]$_2$ (L = OEt_2[16a] or NEt_3[16b]) **B** and [Mg(μ-Br)(CHR_2)(OEt_2)]$_2$ **4** (details will be published in the full paper). This contrast between the structures of **4** and **5a** is consistent with the suggestion that the Mg–CNR′ bond is strong. This is further evident by the exceptionally short Mg–CHR_2 distance of 1.89(1) Å; *cf.* 2.114(7) and 2.125(6) Å in **4** or of 2.094(11)–2.18 Å in **B**,[16] which are close to the Mg–CNR′ bond lengths of 2.12(2) Å in **5a**. The angles at N [179(2)°] and C [174(2)°] of **5a** are close to linear.

It is noteworthy that in each of **1**–**7**, the isonitrile ligand is firmly bound to the metal as shown not only by the thermal stability but also that, in at least some of the cases, R′NC displaces Et_2O or thf from a precursor metal substrate (Scheme 1). Such complexes may have opened a new chapter in main group metal coordination chemistry.

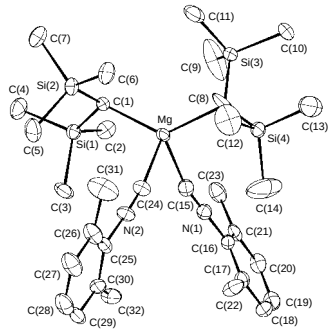

Fig. 2 Molecular structure of **6b** with selected bond distances (Å) and angles (°): Mg–C(1) 2.148(7), Mg–C(8) 2.138(9), Mg–C(15) 2.307(10), Mg–C(24) 2.306(9), N(1)–C(15) 1.140(10), N(1)–C(15)–Mg 168.02(7), C(15)–N(1)–C(16) 177.2(8)

We thank ESPRC and FMC Corporation (Bromsgrove and Dr F. Reed) for a CASE award for C. F. C. and EPSRC for a fellowship for M. L.

Notes and References

† E-mail: m.f.lappert@sussex.ac.uk

‡ No reprints available.

§ *Crystallographic data* for **3**/**7**/**6b**/**5a**: $C_{62}H_{84}Li_2N_6Si_6$/$C_{26}H_{46}Li_2N_4Si_4$/$C_{32}H_{56}MgN_2Si_4$/$C_{24}H_{56}Br_2MgN_2Si_4$, M = 1095.8/540.9/605.5/693.5 all monoclinic, space group $P2_1/n$/$C2/c$/$P2_1/P2_1/c$, a = 11.401(2)/12.991(7)/10.310(6)/11.053(3), b = 23.979(5)/12.508(4)/11.925(8)/15.155(4), c = 11.956(2)/21.727(3)/16.316(6)/13.144(5) Å, β = 90.18(1)/106.84(3)/104.25(4)/113.52(2), U = 3269(1)/3379(2)/1944(2)/2019(1) Å^3, Z = 2/4/2/2, D_c = 1.11/1.06/1.03/1.14 Mg m^{-3}, F(000) = 1176/1168/660/728, λ(Mo-Kα) = 0.710 73 Å, μ = 0.17/0.20/0.19/2.17 mm^{-1}. Data were collected at 173(2) K on a Enraf Nonius CAD4 diffractometer in the ω–2θ mode for the range of 2 < θ < 25° (**3**, **6b**) or 2 < θ < 30° (**7**, **5a**). The structure was solved by direct methods (SHELXS86) and refined with full matrix least squares on all F^2 (SHELXL93). All non-hydrogen atoms were anisotropic, and hydrogen atoms were included in the riding mode with U_{iso}(H) = 1.2 U_{eq}(C) or 1.5 U_{eq} for Me groups. Final residuals for 5748/5120/3593/3546 independent reflections were R_1 = 0.080/0.079/0.100/0.228, wR_2 = 0.142/0.121/0.195/0.289 and for the 4093/3391/2688/1565 with $I > 2\sigma(I)$, R_1 = 0.049/0.046/0.068/0.103, wR_2 = 0.116/0.106/0.168/0.226. **7** is disordered across a crystallographic twofold rotation axis with the N, Si and Li atoms ordered, but with two alternative positions for the PhNC groups and two slightly different positions for each of the methyl groups. CCDC 182/862.

1 E. Singleton and H. E. Oosthuizen, *Adv. Organomet. Chem.*, 1983, **22**, 209; B. N. Storhoff and H. C. Lewis, *Coord. Chem. Rev.*, 1977, **23**, 1; H. Endres, in *Comprehensive Coordination Chemistry*, ed. G. Wilkinson, R. D. Gillard and J. A. McCleverty, Pergamon, Oxford, 1987, vol. 2, p. 261.
2 J. Casanova and R. E. Schuster, *Tetrahedron Lett.*, 1964, 405; J. Casanova, H. R. Kiefer, D. Kuwada and A. H. Boulton, *ibid.*, 1965, 703; G. Hesse and H. Witte, *Liebigs Ann. Chem.*, 1965, **687**, 1; G. Hesse, H. Witte and G. Bittner, *ibid*, p. 9; W. P. Fehlhammer, H. Hoffmeister, H. Stolzenberg and B. Boyadjiev, *Z. Naturforsch., Teil B*, 1989, **44**, 419.
3 G. Hesse, H. Witte and P. Mischke, *Angew. Chem., Int. Ed. Engl.*, 1965, **4**, 355.
4 *E.g.* A. Arafat, J. Baer, J. C. Huffman and L. J. Todd, *Inorg. Chem.*, 1986, **25**, 3757.
5 J. D. Fisher, M.-Y. Wei, R. Willett and P. J. Shapiro, *Organometallics*, 1994, **13**, 3324.
6 M. Tamm, T. Lügger and F. E. Hahn, *Organometallics*, 1996, **15**, 1251.
7 C. Klöfkorn, M. Schmidt, T. Spaniol, T. Wagner, O. Costisor and P. Paetzold, *Chem. Ber.*, 1995, **128**, 1037.
8 N. Takeda, H. Suzuki, N. Tokitoh and R. Okazaki, *J. Am. Chem. Soc.*, 1997, **119**, 1456.
9 P. B. Hitchcock, M. F. Lappert and M. Layh, *Chem. Commun.*, 1998, 201.
10 B. Ledig, M. Marsch, K. Harms and G. Boche, *Angew. Chem., Int. Ed. Engl.*, 1992, **31**, 79.
11 P. B. Hitchcock, J. Hu, M. F. Lappert, M. Layh and J. Severn, *Chem. Commun.*, 1997, 1189; P. B. Hitchcock, M. F. Lappert and M. Layh, *Inorg. Chim. Acta*, 1998, **269**, 181.
12 H. M. Walborsky and P. Ronman, *J. Org. Chem.*, 1978, **43**, 731 and references therein.
13 P. B. Hitchcock, J. A. K. Howard, W.-P. Leung and S. F. Mason, *J. Chem. Soc., Chem. Commun.*, 1990, 847.
14 D. Stalke, M. Wedler and F. T. Edelmann, *J. Organomet. Chem.*, 1992, **431**, C1; and references therein.
15 (*a*) M. F. Lappert, M. J. Slade, A. Singh, J. L. Atwood, R. D. Rogers and A. Shakir, *J. Am. Chem. Soc.*, 1983, **105**, 302; (*b*) G. Boche, I. Langlotz, M. Marsch, K. Harms and G. Frenking, *Angew. Chem., Int. Ed. Engl.*, 1993, **32**, 1171.
16 (*a*) A. L. Spek, P. Voorbergen, G. Schat, C. Blomberg and F. Bickelhaupt, *J. Organomet. Chem.*, 1974, **77**, 147; (*b*) J. Toney and G. D. Stucky, *Chem. Commun.*, 1967, 1168.

Received in Basel, Switzerland, 15th December 1997; 7/08976G

$Ln_2\square Ti_2O_7$ (Ln = La, Nd, Sm, Gd): a novel series of defective Ruddlesden–Popper phases formed by topotactic dehydration of $HLnTiO_4$†‡

V. Thangadurai,[a] G. N. Subbanna[b] and J. Gopalakrishnan*[a]†

[a] *Solid State and Structural Chemistry Unit, Indian Institute of Science, Bangalore 560 012, India*
[b] *Materials Research Centre, Indian Institute of Science, Bangalore 560 012, India*

Topotactic dehydration of $HLnTiO_4$ (Ln = La, Nd, Sm or Gd) around 480–500 °C yields a new series of metastable layered perovskite oxides, $Ln_2\square Ti_2O_7$, that possess a defective $Sr_3Ti_2O_7$ structure, where the cubooctahedral sites within the double-perovskite layers are most likely vacant.

Several layered oxides consisting of metal–oxygen (MO_6) octahedra are regarded as derivatives of the three-dimensional perovskite ($CaTiO_3 \equiv ABO_3$) structure.[1] Of these, the Ruddlesden–Popper (R–P) phases, $A_2[A_{n-1}B_bO_{3n+1}]$, originally discovered in the Sr–Ti–O system,[2] are the most widely known, because members/derivatives of this family exhibit several important physical properties of current interest. Thus, La_2CuO_4, an $n = 1$ member of this family, is the parent material for the Bednorz–Müller discovery[3] of superconducting layered cuprates, $Sr_{2-x}Ln_{1+x}Mn_2O_7$ (Ln = La or rare earth), $n = 2$ members of this series, exhibit ferromagnetic and magnetoresistive properties[4] and $K_2La_2Ti_3O_{10}$, an $n = 3$ member,[5] exhibits ion-exchange and hydration behaviour appropriate for photocatalytic decomposition of water.[6]

Oxides of the formula $NaLnTiO_4$ (Ln = La, Nd, Sm, Gd), originally synthesized by Blasse,[7] are novel $n = 1$ members of the R–P family exhibiting a unique ordering of Na and La atoms at the alternate interlayer sites between the single perovskite sheets in the sequence $-Ln_2-TiO_{4/2}O_2-Na_2-TiO_{4/2}O_2-Ln_2-$ along the *c*-axis.[8] Clearly, the ordering seems to be dictated by the off-centre distortion of $3d^0$: TiO_6 octahedra[9] giving rise to short and long axial Ti–O bonds, the oxygen to the short Ti–O bonds pointing towards the Na layer. Recently, protonated derivatives, $HLnTiO_4$, have been prepared[10] from $NaLnTiO_4$ by Na^+/H^+ exchange in dilute HNO_3.

Considering the topotactic nature of this ion-exchange which preserves the structural features of the parent $NaLnTiO_4$, $HLnTiO_4$ would consist of the layer sequence $-Ln_2-OTiO_{4/2}(OH)-(OH)TiO_{4/2}O-Ln_2-$ along the *c*-direction (Fig. 1). Accordingly, we visualized that a topotactic dehydration would result in a condensation of the adjacent single-perovskite $TiO_{4/2}O(OH)$ sheets to give double-perovskite $Ti_2O_{10/2}O_2$ ($\equiv Ti_2O_7$) sheets on elimination of a water molecule (Fig. 1). The dehydration product, $Ln_2Ti_2O_7$, would be a novel $n = 2$ member of the R–P series similar to $Sr_3Ti_2O_7$,[2] where the interlayer cubooctahedral Sr-sites in the ($SrTi_2O_7$) perovskite sheets would be vacant. Here we show that indeed dehydration of $HLnTiO_4$ (Ln = La, Nd, Sm, Gd) proceeds by this mechanism yielding a new series of $Ln_2\square Ti_2O_7$ that are related to $Sr_3Ti_2O_7$. It must be mentioned that these layered titanates are truly metastable phases stabilized by the topotactic nature of the dehydration reaction under the mild conditions; the stable titanates of this composition adopt either the <110> terminated layered perovskite structure[11] for $La_2Ti_2O_7$ and $Nd_2Ti_2O_7$ or the pyrochlore structure[12] for the other titanates.

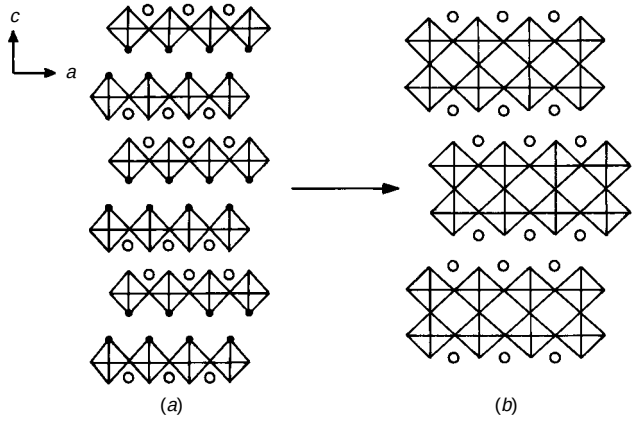

Fig. 1 Schematic representation of dehydration of (*a*) $HLnTiO_4$ to give (*b*) layered $Ln_2\square Ti_2O_7$. The open circles represent Ln atoms and the closed dots in (*a*) denote OH.

$NaLnTiO_4$ (Ln = La, Nd, Sm, Gd) were prepared as reported in the literature[8] by reacting Na_2CO_3, Ln_2O_3 and TiO_2 at 900 °C for 2 days with intermittent grinding. $HLnTiO_4$ were prepared by ion-exchange in 0.1 M HNO_3 as reported in the literature,[10] followed by drying in the air at ambient condition. Powder X-ray diffraction (XRD) patterns (JEOL JDX-8P X-ray powder diffractometer using Cu-Kα radiation) (Fig. 2) and the unit cell parameters (Table 1) obtained by least-squares refinement of the powder XRD data indicated the formation of $HLnTiO_4$.

We investigated the dehydration of $HLnTiO_4$ by thermogravimetry (TG) in air (Cahn TG-131 system, heating rate 1 °C min^{-1}). All the samples showed a single-step mass loss in the region 250–500 °C corresponding to the dehydration reaction

$$2\ HLnTiO_4 \rightarrow Ln_2Ti_2O_7 + H_2O \qquad (1)$$

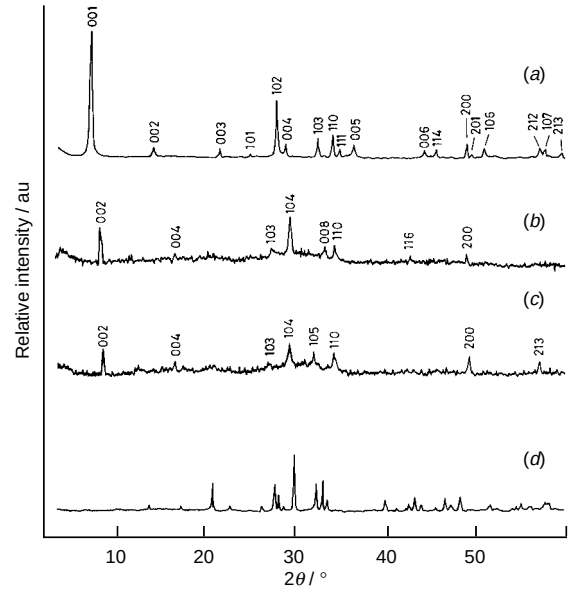

Fig. 2 Powder XRD patterns (Cu-Kα) of (*a*) $HLaTiO_4$, (*b*) $La_2\square Ti_2O_7$, (*c*) $Nd_2\square Ti_2O_7$ and (*d*) sample (*b*) heated at 900 °C; stable $La_2Ti_2O_7$

Table 1 Synthesis conditions and lattice parameters of the parent ($HLnTiO_4$) and product ($Ln_2\square Ti_2O_7$) oxides

Parent	Lattice parameters/Å		Synthesis conditions	Product	Lattice parameters/Å	
	a	*c*			*a*	*c*
$HLaTiO_4$	3.722(2)	12.303(6)	500 °C; 15 min	$La_2\square Ti_2O_7$	3.725(3)	21.68(5)
$HNdTiO_4$	3.694(2)	12.099(6)	500 °C; 15 min	$Nd_2\square Ti_2O_7$	3.705(6)	21.15(8)
$HSmTiO_4$	3.689(1)	11.995(5)	500 °C; 12 min	$Sm_2\square Ti_2O_7$	3.679(2)	21.14(6)
$HGdTiO_4$	3.698(3)	11.769(9)	480 °C; 15 min	$Gd_2\square Ti_2O_7$	3.679(3)	20.81(6)

The mass% losses observed in this temperature range are in agreement with the expected mass losses within ±0.1% error.

In an attempt to characterize the dehydration products, we recorded the powder XRD patterns of the TG residues. The patterns however did not show the characteristic features expected for the formation of a layered $Ln_2\square Ti_2O_7$; instead the patterns showed broad features corresponding to the stable $Ln_2Ti_2O_7$ phases. Heating $HLnTiO_4$ separately in air around 750 °C and above clearly showed the formation of stable $Ln_2Ti_2O_7$ (Fig. 2). We therefore believed that formation of layered $Ln_2\square Ti_2O_7$ would perhaps occur at lower temperatures, immediately after the dehydration. Accordingly, we investigated the dehydration of $HLnTiO_4$ around 450–500 °C for various durations, monitoring the samples by both mass loss and powder XRD. We found that samples (*ca*. 1 g) heated at 480–500 °C for about 15 min in air showed XRD patterns (Fig. 2) characteristic of the desired layered structure. The reflections at *ca*. 10.8, 5.4, 2.6, 1.85 Å (for $La_2\square Ti_2O_7$) clearly indicated the formation of a phase similar to $Sr_3Ti_2O_7$ with a tetragonal unit cell, $a \approx 3.725$ and $c \approx 21.68$ Å. The observation of a strong reflection at *ca.* 3.10 Å which could be indexed as (104) however indicated that the structure would not exactly be the same as $Sr_3Ti_2O_7$ with *I*4/*mmm* space group. Moreover, many of the reflections in the pattern are broad, suggesting poor crystallinity/disorder of the samples. In Fig. 2, we show powder XRD patterns of two of the members (Ln = La, Nd) and in Table 1, we list the lattice parameters of the parent ($HLnTiO_4$) and product ($Ln_2\square Ti_2O_7$) phases together with synthesis conditions.

In order to characterize the layered $Ln_2\square Ti_2O_7$ further, we recorded the electron diffraction (ED) patterns (JEOL JEM 200-CX transmission electron microscope). All the samples are quite crystalline showing typical perovskite like $\sqrt{2}a_c \times \sqrt{2}a_c$ patterns in the [001] direction. When the beam direction is along [010], we see clear evidence for a *ca.* 21 Å repeat in the *c** direction which is consistent with the *c* axis of the tetragonal cell found from XRD patterns (Table 1). We also see lattice fringes with a *ca*. 10 Å repeat (which would correspond to 0.5 *c*) in the lattice image (Fig. 3) recorded with the same [010] beam orientation. The ED patterns however show streaking both in the *a***b**-plane as well as along the *c**-direction, which indicate considerable disorder. Disorder in the *c** periodicity is also seen in the lattice images. The disorder could arise from a turbostratic stacking of the double-perovskite Ti_2O_7 sheets in the dehydrated samples. Despite the disorder, the presence of a tetragonal or pseudotetragonal cell with $\sqrt{2}(\approx 3.7) \times \sqrt{2}(\approx 3.7) \times \approx 21$ Å dimension is clear from the ED patterns for all the $Ln_2\square Ti_2O_7$ members studied, showing that gentle dehydration of $HLnTiO_4$ indeed yields a layered $Ln_2\square Ti_2O_7$ that is related to $Sr_3Ti_2O_7$.

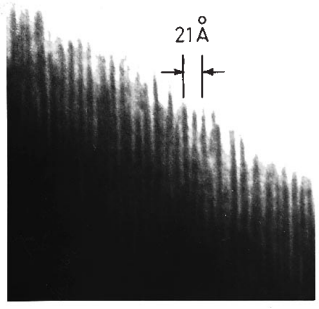

Fig. 3 Lattice image of $La_2\square Ti_2O_7$ corresponding to the electron diffraction pattern recorded with the [010] beam direction, revealing the presence of *ca*. 10 Å fringes in the *c*-direction.

We believe that the present work has shown for the first time the possibility of transforming $n = 1$ R–P members to $n = 2$ members (albeit defective) of the same series by a topotactic dehydration reaction. The key to the success of this $n = 1$ to $n = 2$ transformation lies in the 1 : 1 ordering of the Na and Ln atoms in the precursor $NaLnTiO_4$ oxides, which in turn is dictated by the distortion of d^0 : TiO_6 octahedra giving short and long axial Ti–O bonds.[9] We envisage that the method could be generalized and extended to the synthesis of metastable 2*n* R–P phases from appropriately tailored *n* R–P phases.

We thank the Indo–French Centre for the Promotion of Advanced Research, New Delhi for financial support. One of us (V. T.) thanks the Council of Scientific and Industrial Research, New Delhi for the award of a research fellowship.

Notes and References

† E-mail: gopal@sscu.iisc.ernet.in

‡ Contribution No. 1337 from the Solid State and Structural Chemistry Unit.

1 A. R. Wells, *Structural Inorganic Chemistry*, Clarendon Press, Oxford, 5th edn., 1984.
2 S. N. Ruddlesden and P. Popper, *Acta Crystallogr.*, 1957, **10**, 538; 1958, **11**, 54.
3 J. G. Bednorz and K. A. Müller, *Z. Phys. B*, 1986, **64**, 189.
4 Y. Moritomo, A. Asamitsu, H. Kuwahara and Y. Tokura, *Nature*, 1996, **380**, 141; R. Seshadri, C. Martin, M. Herien, B. Raveau and C. N. R. Rao, *Chem. Mater.*, 1997, **9**, 270; P. D. Battle, M. A. Green, N. S. Laskey, J. E. Millburn, L. Murphy, M. J. Rosseinsky, S. P. Sullivan and J. F. Vente, *Chem. Mater.*, 1997, **9**, 552.
5 J. Gopalakrishnan and V. Bhat, *Inorg. Chem.*, 1987, **26**, 4299.
6 T. Takata, Y. Furumi, K. Shinohara, A. Tanaka, M. Hara, J. N. Kondo and K. Domen, *Chem. Mater.*, 1997, **9**, 1063.
7 G. Blasse, *J. Inorg. Nucl. Chem.*, 1968, **30**, 656; G. Blasse and G. P. M. Van den Heuvel, *J. Solid State Chem.*, 1974, **10**, 206.
8 S. H. Byeon, K. Park and M. Itoh, *J. Solid State Chem.*, 1996, **121**, 430; K. Toda, Y. Kameo, S. Kurita and M. Sato, *J. Alloys Comp.*, 1996, **234**, 19.
9 N. S. P. Bhuvanesh and J. Gopalakrishnan, *J. Mater. Chem.*, 1997, **7**, 2297.
10 S. H. Byeon, J. J. Yoon and S. O. Lee, *J. Solid State Chem.*, 1996, **127**, 119.
11 P. M. Gasperin, *Acta Crystallogr., Sect. B*, 1975, **31**, 2129.
12 M. A. Subramaian, G. Aravamudan and G. V. Subba Rao, *Prog. Solid State Chem.*, 1983, **15**, 55.

Received in Cambridge, UK, 7th April 1998; 8/02644K

1,4,7-Triazacyclononane-1-succinic acid-4,7-diacetic acid (NODASA): a new bifunctional chelator for radio gallium-labelling of biomolecules

João P. André,[a,b] Helmut R. Maecke,*[a] Margareta Zehnder,[c] Ludwig Macko[c] and Kayhan G. Akyel[d]

[a] *Division of Radiological Chemistry, Institute of Nuclear Medicine, University Hospital, Petersgraben 4, 4031 Basel, Switzerland*
[b] *Department of Chemistry, University of Minho, Braga, Portugal*
[c] *Institute for Inorganic Chemistry, University of Basel, Basel, Switzerland*
[d] *Novartis Pharma AG, Basel, Switzerland*

A new bifunctional chelator NODASA (1,4,7-triazacyclononane-1-succinic acid-4,7-diacetic acid) has been synthesised, its kinetically inert gallium(III) complex was crystallographically characterized and conjugated to a model aminoacidamide showing the feasibility of a prelabelling approach with ^{68,67}Ga.

Over the past ten years a constant interest in the chemistry of bifunctional chelators useful in biomedical applications has been evident.[1,2] Many were designed for coupling to monoclonal antibodies[3,4] and other biomolecules.[5] Recently bioactive peptides were successfully introduced into the clinic for *in vivo* visualization of tumours.[6,7] As these peptides show very fast blood clearance and diffusion into tissues the use of short lived metallic positron emitters becomes possible. In this context ^{68}Ga ($t_{1/2}$ = 68 min) is of special interest because its half-life is compatible with the rate of localization of small targeting molecules. For our purpose a bifunctional chelator is needed which is comprised of a gallium immobilizing moiety and a short carboxylate arm for coupling to the N-terminal end of bioactive peptides. We aim at using this bifunctional chelator in a preconjugation ^{67,68}Ga-labelling approach of somatostatin analogues. This preconjugation allows the covalent coupling of a well defined radiometal complex of high specific activity; this will be very important with regard to most radiopeptides because of their potential pharmacological effects.

Therefore we synthesised a new N-functionalised 1,4,7-triazamacrocycle in three steps by alkylation of 1,4,7-triazacyclononane (Scheme 1): (i) with 1 equiv. of bis(diphenylmethyl) D,L-bromosuccinate in chloroform; (ii) with 2 equiv. of *tert*-butyl bromoacetate in acetonitrile in the presence of K_2CO_3 followed by deprotection with 6 M HCl (iii). The overall yield of the synthesis of 1,4,7-triazacyclononane-1-succinic acid-4,7-diacetic acid (NODASA) was slightly > 50%.‡

Crystals of Ga(NODASA) were obtained from an aqueous solution of the ligand and $Ga(NO_3)_3$ in equimolar amounts (pH 3, 70 °C, 1 h; Scheme 1 (iv), followed by slow evaporation. Characterization by X-ray diffraction§ showed that the complex is electrically neutral and the Ga^{III} ion is fully chelated in a slightly distorted octahedral environment (Fig. 1). The β-carboxylate remains protonated and does not participate in the complexation. The three nitrogen atoms of the triazacyclononane define a plane in a facial arrangement and three of the pendant carboxylate oxygens constitute another one. These planes are almost coplanar with a dihedral angle of 1.75°. The *trans* N–Ga–O bond angles average 165.4°. This leads to a relative twist of the N_3 and O_3 planes by 14.6° away from a symmetrically staggered conformation, similar to the parent complex Ga(NOTA)[8] and different previously synthesised nickel(II) and chromium(III) NOTA complexes.[9] The variation in the individual Ga–O and Ga–N bond lengths is very small showing overall high similarity to the parent complex Ga(NOTA).[10] Ga(NODASA) was also characterized by its ^{1}H, ^{13}C and ^{69}Ga NMR spectra.¶ A multiplet centered at δ 3.75 (Fig. 2) due to the magnetically non equivalent acetate hydrogens is the most dramatic effect in the ^{1}H NMR spectrum of the chelate in relation to the free ligand, which exhibits a singlet at δ 3.50. The sharp multiplets of the ethylenic protons might show the existence of slow intramolecular processes of interconversion

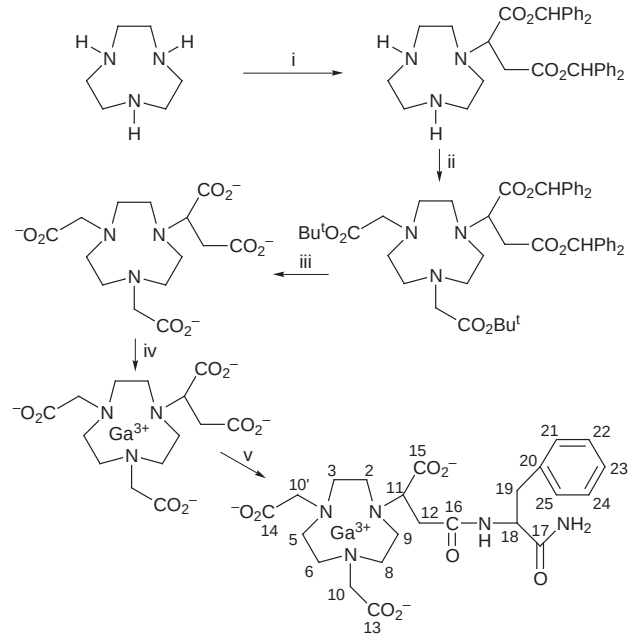

Scheme 1 Synthesis of the chelate Ga(NODASA) and coupling to D-phenylalanineamide

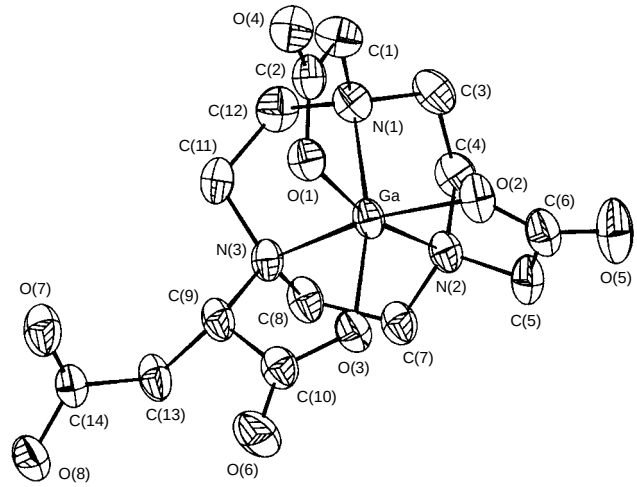

Fig. 1 ORTEP drawing of the Ga(NODASA) complex. Ga–N(1) 2.101(3), Ga–N(2) 2.098(3), Ga–O(1) 1.937(3), Ga–O(3) 1.942(3) Å; O(1)–Ga–O(3) 94.7(1), O(2)–Ga–N(3) 165.6(1), O(2)–Ga–N(2) 82.5(1), N(2)–Ga–N(3) 84.1(1)°.

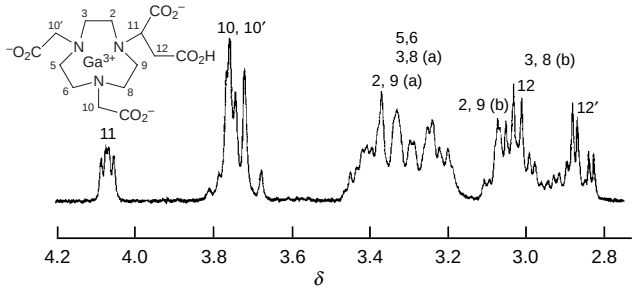

Fig. 2 ^{1}H NMR (400 MHz) spectrum of Ga(NODASA) in D_2O, 7 mM, pD = 3.6 and T = 22 °C

between the (λλλ) and (δδδ) conformations[11] of the ring backbone arising from the high rigidity of the system.

Although the structural results give some important indications about the binding of Ga^{III} to the macrocycle, the stability of this chelate is very important for successful applications *in vivo*. With a complexation competition method using ^{67}Ga as a radiotracer and NOTA‖ as an auxiliary competing ligand it has been possible to estimate the conditional stability constant for the complex at different pH values. The equilibration has been followed for nine days. The determination of the ligand protonation constants allows the calculation of the thermodynamic stability constant of Ga(NODASA) to $\log K_{Ga(NODASA)}$ = 30.9(0.2) compared to 30.98 of Ga(NOTA).[12]

An even more important indicator for *in vivo* applications is the measurement of the rate of exchange of Ga^{III} in blood serum under the physiological conditions.[14] For this experiment $^{67}Ga^{III}$ is first incubated with about 50 times excess of NODASA at pH 6.2 in 0.5 M ammonium acetate buffer (25 min, 90 °C) in order to incorporate the metal ion. Then the complex is mixed with blood serum and the exchange kinetics with transferrin are measured at 37 °C. This was done by taking aliquots of the serum, separating them by gel filtration, which allows the separation of ^{67}Ga(NODASA) from gallium(III)–transferrin ($\log K$ = 23.7),[13] and measuring the activity in both fractions with use of radiometric detection. The results clearly show that ^{67}Ga–NODASA virtually does not transfer any ^{67}Ga to transferrin over the observed period of 5 days, fulfilling the criterion of high kinetic stability.

The kinetic stability of Ga(NODASA) with respect to the acid-catalysed dissociation has been demonstrated with the aid of the ^{67}Ga complex, kept in 0.1 M glycine–HCl buffer, pH 2, at 37 °C. Aliquots of this solution were analysed by HPLC. After 5 days the complex was still 100% intact.

The fact that the β-carboxylate remains free while the other three carboxylates are involved in five-membered chelate rings, upon coordination to the metal ion, offers a very interesting possibility to couple the chelate to a biomolecule. As a model peptide we coupled D-phenylalanineamide to Ga(NODASA) [Scheme 1 (v), in DMSO–DMF (2 : 1)] using HATU** [15] as the coupling reagent with almost quantitative yield.†† HATU allows coupling of carboxylate functions to primary amines within minutes rendering even the coupling of ^{68}Ga(NODASA) to peptides feasible.

In summary, ^{67,68}Ga(NODASA) can be used in a pre-labelling approach followed by conjugation to a biomolecule. This approach is currently being followed using somatostatin analogues.

This work was supported by the Swiss National Science Foundation (No. 31-42516/94).

Notes and References

† E-mail: maecke@ubaclu.unibas.ch

‡ The ligand had satisfactory elemental analysis, ^{1}H, ^{13}C NMR and mass spectra. The pK_a values were determined by pH potentiometry: p$K_{HL^{3-}}$ = 11.71, p$K_{H_2L^{2-}}$ = 5.94, p$K_{H_3L^-}$ = 4.27, pK_{H_4L} = 3.22 and p$K_{H_5L^+}$ = 1.95 (0.50 M KNO_3).

§ *Crystal data*: $C_{14}H_{20}GaN_3O_8 \cdot 3H_2O$, monoclinic, space group $P2_1/n$ [a = 7.6077(6), b = 20.573(3), c = 12.186(2) Å, β = 97.726(9)°], Z = 4, F(000) = 1000, μ = 2.56 mm^{-1}, Cu-Kα = 1.54180 Å, T = 293 K, θ_{max} = 77.50°, ω–2θ scan technique, 3561 independent reflections, 3011 used in refinement, 284 parameters refined, final R = 5.08, final R_w = 0.0626, Chebychev polynomial weighting. CCDC 182/850.

¶ ^{13}C NMR 100 MHz (D_2O), δ 31.3 (C12), 44.9 (C2,9, 52.8–53.5 (C3,5,6,8), 61.9 and 62.0 (C10,10′), 65.8 (C11), 174.8 and 175.0 (C13,14,15,16). ^{69}Ga NMR 72.05 MHz (D_2O) shows a single resonance at δ + 165 ($w_{1/2}$ = 1000 Hz).

‖ 1,4,7-Triazacyclononane-1,4,7-triacetic acid.

** O-(7-Azabenzotriazol-1-yl)-1,1,3,3-tetramethyluronium hexafluorophosphate.

†† R_f[SiO_2, isopropyl alcohol–NH_3(aq) (7 : 3)] = 0.40; *m/z* (ESI^+) : 574.4(MH^+, 15), 594.1 (MNa^+, 100); ^{13}C NMR 100 MHz (D_2O), δ 32.0 (C12), 38.3 (C19), 44.0 (C2,9), 52.4–53.0 (C3,5,6,8) 54.4 and 54.8 (C18), 61.5 (C10,10′), 64.5 and 65.0 (C11), 128.4–128.9 (C21–25), 136.8 (C20), 169.4 (C17), 171.5 (C13,14), 172.4 (C15), 174.0 (C16).

1 M. K. Moi and C. F. Meares, *J. Am. Chem. Soc.*, 1988, **110**, 6267.
2 D. Parker, *Chem. Soc. Rev.*, 1990, **19**, 271.
3 T. A. Waldmann, *Science*, 1991, **252**, 1657.
4 R. P. Junghans, D. Dobbs, M. W. Brechbiel, S. Mirzadeh, A. A. Raubitschek, O. A. Gansow and T. A. Waldmann, *Cancer Res.*, 1993, **53**, 5683.
5 T. J. Norman, F. C. Smith, D. Parker, A. Harrison, L. Royle and C. A. Walker, *Supramol. Chem.*, 1995, **4**, 305.
6 S. W. J. Lamberts, W. H. Bakker, J.-C. Reubi and E. P. Krenning, *New Eng. J. Med.*, 1990, 1246.
7 A. Otte, E. Jermann, M. Behe, M. Goetze, H. C. Bucher, H. W. Roser, A. Heppeler, J. Mueller-Brand and H. R. Maecke, *Eur. J. Nucl. Med.*, 1997, **24**, 792.
8 A. S. Craig, D. Parker, H. Adams and N. A. Bailey, *J. Chem. Soc., Chem. Commun.*, 1989, 1793.
9 K. Wieghardt, U. Bossek, P. Chaudhuri, W. Herrmann, B. C. Menke and J. Weiss, *Inorg. Chem.*, 1982, **21**, 4308.
10 C. J. Broan, J. P. L. Cox, A. S. Craig, R. Kataly, D. Parker, A. Harrison, A. M. Randall and G. Ferguson, *J. Chem. Soc., Perkin Trans. 2*, 1991, 87.
11 D. A. Moore, P. E. Fanwick and M. J. Welch, *Inorg. Chem.*, 1990, **29**, 672.
12 E. T. Clarke and A. E. Martell, *Inorg. Chim. Acta*, 1991, **181**, 273.
13 S. Kulprathipanja, D. J. Hnatowich, R. Beh and D. Elmaleh, *Int. J. Nucl. Med. Biol.*, 1979, **6**, 138.
14 A. Riesen, T. A. Kaden, W. Ritter and H. R. Maecke, *J. Chem. Soc., Chem. Commun.*, 1989, 460.
15 L. A. Carpino, *J. Am. Chem. Soc.*, 1993, **115**, 4397.

Received in Basel, Switzerland, 16th February 1998; 8/01294F

Thermally responsive novel anion exchange membranes for electrodialysis

Toshikatsu Sata, Shin-ichiro Emori and Koji Matsusaki

Department of Applied Chemistry and Chemical Engineering, Faculty of Engineering, Yamaguchi University, Tokiwadai 2557, Ube City, Yamaguchi Prefecture, 755, Japan

Anion exchange membranes containing *N*-isopropylacrylamide as a component showed a decrease in osmotic flux through the membrane, and an increase and decrease respectively in the transport numbers of NO_3^- and SO_4^{2-} relative to Cl^- with increasing temperature.

The concentration of NO_3^- in groundwater has been greatly increasing because of excessive use of artificial fertilizers. The EC proposed that the concentration of NO_3^- in drinking water should be below 25 ppm, however, it exceeds this in many places in Europe and also in Japan. A high NO_3^- concentration in drinking water can endanger human health because this can lead to the formation of nitrosamines and nitriles which cause cell poisoning. Many methods to remove NO_3^- from groundwater have been proposed and tried: reverse osmosis, electrodialysis, ion exchange, *etc.* It is important to preserve the properties of natural water, and electrodialysis is the most suitable method for this purpose. Although it is desirable to perform electrodialysis at high temperature to save energy, using a NO_3^- permselective anion exchange membrane, osmotic flux of water through the ion exchange membranes increases with increasing temperature, and the amount of water processed therefore decreases.

Poly(*N*-isopropylacrylamide) is a well known heat-sensitive polymer.[1] It is soluble in water at room temperature but undergoes a phase separation at temperatures higher than its lower critical solution temperature (LCST, *ca.* 32 °C). At higher temperatures, the intrinsic affinity of *N*-isopropylacrylamide polymer chains for themselves is enhanced due to thermal dissociation of hydrating water molecules from the polymer chains. Hydrophobic interactions between isopropyl groups drastically increase and the polymers condense with each other, precipitating rapidly in the solution. Cross-linked copolymers containing *N*-isopropylacrylamide as a monomer have been also extensively studied as hydrogels used in solute separation,[2] immobilization of enzymes,[3] drug release regulating systems,[4] *etc.* Cross-linked copolymer gels containing ionic monomers such as acrylic acid, 2-methyl-2-acrylamidopropane sulfonic acid, *etc.*, were also reported to show similar swelling and deswelling properties with change in temperature. If ion exchange membranes contain *N*-isopropylacrylamide as a component, it is expected that the membranes will show a thermal response.

Two types of cross-linked anion exchange membranes containing *N*-isopropylacrylamide were prepared: (*i*) 1 part (part by mass) of acrylonitrile–butadiene rubber was dissolved in a mixture of 5 parts of *N*-isopropylacrylamide (supplied by Kojin Co., Ltd.), 10 parts of glycidyl methacrylate, 5 parts of ethylene glycol dimethacrylate and 0.24 parts of benzoyl peroxide (M-1 membrane), (*ii*) 1 part of acrylonitrile–butadiene rubber was dissolved in a mixture of 5 parts of *N*-isopropylacrylamide, 10 parts of dimethylaminoethyl methacrylate, 5 parts of ethylene glycol dimethacrylate and 0.24 parts of benzoyl peroxide (M-2 membrane). The two obtained pasty mixtures were coated on a woven fabric made of poly(vinyl chloride), and polymerized at 85 °C for 24 h under an N_2 atmosphere after covering with a polyester film on both sides. After polymerization, the copolymer membrane from the M-1 composition was immersed in a 1 M aqueous NMe_3 (75 mass%) and acetone (25 mass%) mixed solution for 48 h at room temperautre to introduce quaternary ammonium groups on the glycidyl groups. The M-2 copolymer membrane was immersed in a methyl iodide (60 mass%)–hexane (40 mass%) mixed solution for 24 h to quaternize the tertiary amino groups. A commercial anion exchange membrane, NEOSEPTA AM-1 (Tokuyama Corp.; benzyltrimethylammonium groups; cross-linkage, 10%) was used as a standard anion exchange membrane. Before use, the membranes were equilibrated with 1.0 M HCl and 0.5 M NH_3 alternately several times, and then equilibrated with solutions to be used in the measurements.

Reduced osmotic flux through anion exchange membranes was measured between pure water and 4.0 M NaCl at different temperatures with stirring according to the reported[5] methods. Transport numbers, calculated from a membrane potential, and electrical resistance of the membrane were measured at different temperatures. Water content and ion exchange capacity of the membranes were determined by conventional methods.[5] Electrodialysis was carried out in a four-compartment cell with Ag–AgCl electrodes (solution in each compartment, 100 cm^3; effective membrane area, 2×5 cm).[6] The two middle compartments were separated from the anolyte and catholyte, which consisted of NaCl solution of the same Na^+ concentration as that of the solution to be measured, by a cation exchange membrane (NEOSEPTA CM-2, Tokuyama Corp.; transport number of Na^+ was > 0.99 in the electrodialysis of 0.50 M NaCl solution at a current density of 20 mA cm^{-2}). The anion exchange membrane to be studied was placed at the center of the cell, and a 1 : 1 mixed salt solution, either 0.02 M $NaNO_3$–0.02 M NaCl ($[Na^+] = 0.04$ M) or 0.25 M Na_2SO_4–0.25 M NaCl ($[Na^+] = 0.50$ M) was electrodialyzed at a current density of 1 or 10 mA cm^{-2} for 60 min under vigorous agitation (stirring at 1500 ± 100 rpm). Studied temperatures for electrodialysis were 25.0, 30.0, 32.0, 35.0 and 40.0 °C. All measurements were performed after the membranes, solutions and the cell had been equilibrated at the respective temperature (immersed in a thermostat for > 24 h). After electrodialysis, the change in the concentrations of the anions in the middle compartments was determined by the Mohr method, and chelate back titration or ion chromatography (Hitachi Ion Chromatography L-6000). Then the transport number of anions A relative to chloride ions was calculated by following equation: $P_{Cl}^{A} = (t_A/t_{Cl})/(C_A/C_{Cl})$, where t_A and t_{Cl} are the transport numbers of anions A and Cl^- in the membrane, and C_A and C_{Cl} are the average concentrations of anions A and Cl^- ions in the desalting side solution during electrodialysis, respectively. P_{Cl}^{A} represents the permeated equivalent of anions A through the membrane when 1 equiv. of Cl^- is permeated through. The current efficiency was calculated from the amount of transported anions and electricity measured by coulometry.

Table 1 shows the characteristics of the prepared anion exchange membranes and the commercial membrane. The electrical resistances of the M-1 and M-2 membranes was high and their water content was low compared with those of the commercial membrane because of their low ion exchange capacity. Although transport numbers of the M-1 and M-2 membranes were lower than that of the commercial membrane

Table 1 Characteristics of anion exchange membranes

	NEOSEPTA AM-1	M-1	M-2
Electric resistance[a]	1.1	17.8	12.7
Transport number[b]	0.94	0.84	0.90
Ion exchange capacity[c]	2.25	1.18	0.92
Water content[d]	0.27	0.12	0.07
Thickness/mm	0.13	0.12	0.10
Reinforcing	PVC	PVC	PVC

[a] Ω cm^2; measured with 1000 Hz ac at 25.0 °C after equilibration with 0.5 M NaCl. [b] Calculated from a membrane potential generated from 0.50 M NaCl │Membrane│ 2.50 M NaCl at 25.0 °C. [c] Mequiv. per g (Cl^-) dry membrane at 25.0 °C. [d] g (H_2O) per g (Cl^-) dry membrane, measured at 25.0 °C after equilibration with pure water.

at 25.0 °C, they increased with increasing temperature and reached 0.89 (M-1) and 0.94 (M-2) at 35.0 °C (the transport number of the commercial membrane slightly decreased with increasing temperature: 0.94 at 25 °C, 0.93 at 35 °C). The electrical resistances of both M-1 and M-2 membranes were constant between 32 and 35 °C, while that of the commercial membrane decreased monotonously with increasing temperature.

Fig. 1 shows the change in the reduced osmotic flux through M-1 and commercial membrane. In general, the reduced osmotic flux of water through ion exchange membranes increases with increasing temperature as found for the commercial membrane. However, the M-1 membrane showed completely different behavior: the reduced osmotic flux decreased from 25 °C with increasing temperature and attained a constant value from 32 °C. This is thought to be due to the decrease in hydrophilicity of membrane originated from the aggregation of isopropyl groups in the membranes. In fact, water contents of both M-1 and M-2 membranes decreased with increasing temperature and attained a constant value from 32 °C (water content of the commercial membrane increased: 27% at 25.0 °C; 31% at 40 °C).

Fig. 2 shows the transport number of NO_3^- relative to Cl^-. Although $P_{Cl}^{NO_3}$ of the commercial membrane did not change with temperature, it should be noted that NO_3^- selectively permeate through the anion exchange membranes containing *N*-isopropylacrylamide with increasing temperature. It was reported that hydrophilicity of anion exchange membranes greatly affects the permselectivity between two anions: with decreasing hydrophilicity of the membranes, less hydrated anions such as NO_3^- and Br^- selectively permeate through the membrane, and the permeation of strongly hydrated anions, F^- and SO_4^{2-}, decreases.[6] Because the aggregation of isopropyl groups in the M-1 and M-2 membranes makes the membranes hydrophobic with increasing temperature, the permeation of NO_3^- is thought to be enhanced. Though the ratio of mobilities between NO_3^- and Cl^- in the membrane phase did not change in all membranes with temperature, the ion exchange equilibrium constant between NO_3^- and Cl^- of the M-1 membrane increased with increasing temperature: $K_{Cl}^{NO_3}$ = 1.5 at 25 °C and 2.2 at 35 °C (K_{Cl}^{NO3} of the commercial membrane was 1.95 and independent of temperature.) It is apparent that the decrease in hydrophilicity of the M-1 and M-2 membranes with increasing temperature caused selective uptake of the less hydrated anions NO_3^- (Gibbs hydration energies of NO_3^- and Cl^- are 270 and 317 kJ mol^{-1}, respectively).[7] The decrease in the hydrophilicity of the membranes also decreased permeation of SO_4^{2-} remarkably since SO_4^{2-} is strongly hydrated.[7] This is a desirable property for anion exchange membranes because precipitation of $CaSO_4$ in electrodialyzers and in membranes is a serious problem in electrodialysis. P_{Cl}^{SO4} of the commercial membrane increased slightly with increasing temperature. Finally, the current efficiencies of the M-1 (96%) and M-2 membranes (93%) were slightly lower than that of the commercial membrane (99%). Anion exchange membranes containing *N*-isopropylacrylamide are suitable in electrodialysis to remove NO_3^- from groundwater with low energy without precipitation of $CaSO_4$.

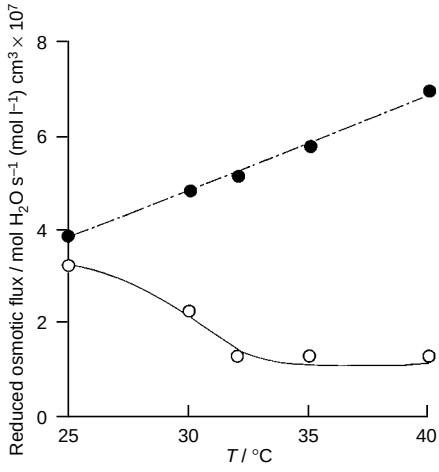

Fig. 1 Change in reduced osmotic flux with temperature. (●) Commercial anion exchange membrane (NEOSEPTA AM-1); ○: M-1 membrane. Measurements in 4.0 M NaCl│Membrane│pure water; effective membrane area = 10 cm^2.

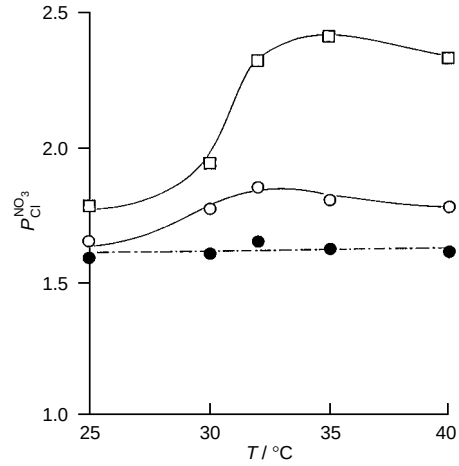

Fig. 2 Change in transport number of NO_3^- relative to Cl^- with temperature. (●) Commercial anion exchange membrane (NEOSEPTA AM-1); ○: M-1 membrane; □: M-2 membrane. A 0.02 M $NaNO_3$–0.02 M NaCl mixed solution was electrodialyzed at different temperatures (current density = 1 mA cm^{-2}).

Notes and References

† E-mail: HAG07574@niftyserve.or.jp

1 Y. Hirokawa, T. Tanaka and E. S. Matsuo, *J. Chem. Phys.*, 1984, **81**, 6379; M. Shibayama and T. Tanaka, *Adv. Polym. Sci.*, 1993, **1**, 109.
2 H. Feil, Y. H. Bae, J. Feijen and S. W. Kim, *J. Membrane Sci.*, 1991, **64**, 283.
3 L. C. Dong and A. S. Hoffman, *J. Controlled Release*, 1986, **4**, 223.
4 Y. H. Lim, D. Kim and D. S. Lee, *J. Appl. Polymer Sci.*, 1997, **64**, 2647; A. S. Hoffman, *J. Controlled Release*, 1987, **4**, 297.
5 Y. Kosaka and H. Shimizu, *Ion Exchange Membranes*, Kyoritsu Shuppan Co., Ltd., 1963, p. 123.
6 T. Sala, T. Yamaguchi and K. Malsusaki, *J. Phys. Chem.*, 1995, **99**, 12 875.
7 H. Oholaki, *Hydration of ions*, Kyoritsu Shuppan Co., Ltd., 1992, p. 30.

Received in Cambridge, UK, 9th February 1998; 8/01133H

Novel palladium complexes of Se,N,Se tridentate ligands derived from cycloalkeno-1,2,3-selenadiazoles

Susan Ford,[a] Christopher P. Morley*[a] and Massimo Di Vaira[b]

[a] *Department of Chemistry, University of Wales Swansea, Singleton Park, Swansea, UK SA2 8PP*
[b] *Dipartimento di Chimica, Università degli Studi di Firenze, Via Maragliano 75/77, 50144 Firenze, Italy*

The reaction between $[Pd_2(dba)_3]$ (dba = dibenzylideneacetone), a trialkylphosphine, and a cycloalkeno-1,2,3-selenadiazole in toluene under reflux leads in good yield to the complexes $[PdL(PR_3)]$ [L = $SeC(R^1)=C(R^2)N=NC(R^1)=C(R^2)Se$; $R^1–R^2 = (CH_2)_n$; R = Et, Bu^n] containing a novel Se,N,Se tridentate ligand formed by the coupling of two 1,2,3-selenadiazole molecules; the structure of the product with R = Bu^n and *n* = 4 has been determined by X-ray crystallography.

The chemistry of organoselenium ligands has attracted increased attention in the last few years, as a result of both their greater accessibility, and the realisation that they may display significantly different properties from their sulfur analogues.[1] We have previously demonstrated that 1,2,3-selenadiazoles may serve as the precursors to a range of selenium-containing ligands in cyclopentadienylcobalt complexes,[2] and recently reported on their reactions with $[Pt(PPh_3)_4]$.[3] The palladium compound $[Pd(PPh_3)_4]$ behaves quite differently from its platinum analogue, yielding novel dinuclear diselenolenes (Scheme 1).[4] We have now studied the reactivity of a range of cycloalkeno-1,2,3-selenadiazoles (**1a**–**c**) towards other palladium(0) phosphine complexes, generated *in situ* from $[Pd_2(dba)_3]$ **2** (dba = dibenzylideneacetone).

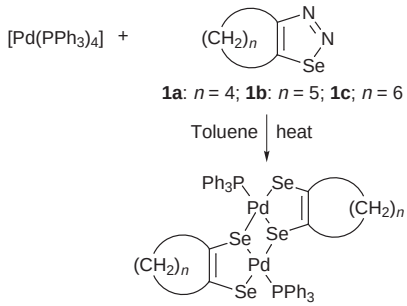

Scheme 1

Heating a mixture of 2 equiv. of one of the 1,2,3-selenadiazoles **1a**–**c** with **2**, in the presence of triethylphosphine or tri-*n*-butylphosphine, leads to the formation of a deep purple solution, from which the product **3a**–**c** or **4a**–**c** may be isolated in good yield by column chromatography (Scheme 2).‡ These intensely coloured compounds have the general formula $[PdL(PR_3)]$ and contain the first examples of a new type of ligand L = $SeC(R^1)=C(R^2)N=NC(R^1)=C(R^2)Se$, which may be considered as an alicyclic analogue of an azo-dye.

The detailed mechanism of the reaction remains unclear. In general, 1,2,3-selenadiazoles react *via* elimination of dinitrogen to yield a selenaketocarbene, the fate of which determines the outcome of the reaction.[5] Attack on another molecule of intact 1,2,3-selenadiazole is, to our knowledge, unprecedented. We therefore postulate initial insertion of palladium(0) into the selenium–nitrogen bond of a 1,2,3-selenadiazole molecule, followed by carbon–nitrogen bond formation by addition of a selenaketocarbene to this palladium(II) intermediate (Scheme 3). It is interesting that behaviour analogous to that of $[Pd(PPh_3)_4]$ is not observed. This we ascribe to the greater basicity of the phosphines used in this study, when compared with that of triphenylphosphine.

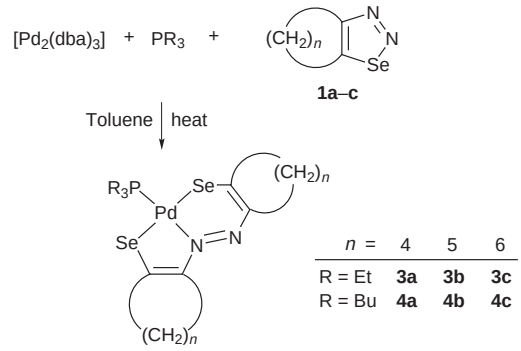

Scheme 2

The molecular structure of **4a** has been determined by X-ray crystallography§ and is shown in Fig. 1. The palladium atom is square-planar coordinated, with the phosphine *trans* to a nitrogen atom of the novel tridentate Se,N,Se ligand. The twelve atoms associated with the π-system of the ligand [Se–C(C)=C(C)–N=N–C(C)=C(C)–Se] are also coplanar, so that overall this part of the molecule is virtually flat. Only the three *n*-butyl groups on the phosphine protrude significantly from the coordination plane. There are relatively few examples of Pd–Se distances in the literature. The bond lengths in **4a** [2.370(1), 2.371(1) Å] are comparable with the shortest thus far reported. In the related complexes [Pd{PhSeNC(4-MeC_6H_4)NNC(4-MeC_6H_4)NSePh}(PPh_3)][6] **5** and [PdCl{5-MeC_6H_3-2-(N=N-4′-MeC_6H_3-2′-SePh)}][7] **6** the Pd–Se distances are 2.375(1) and 2.4495(4) Å, respectively. The Pd–P distance is typical for PBu^n_3 derivatives, and similar to that in [Pd{2-OC_8H_8N=N(-5′-$NO_2C_6H_3$-2′-O)}(PBu^n_3)] **7**[8] [**4a**, 2.264(2); **7**, 2.289(2) Å]. The Pd–N distance of 2.081(8) is rather long [*cf.* 2.024(2),

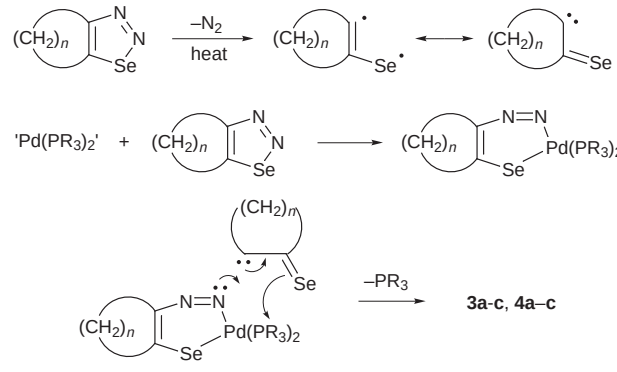

Scheme 3

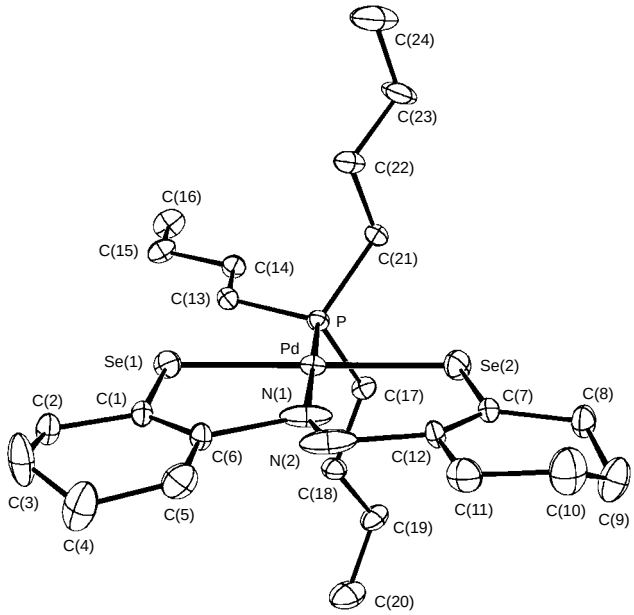

Fig. 1 Structure of **4a** with H atoms omitted for clarity. Selected bond lengths (Å) and angles (°): Pd–N(1) 2.081(8), Pd–P 2.264(2), Pd–Se(1) 2.370(2), Pd–Se(2) 2.371(1); P–Pd–Se(1) 91.72(6), Se(1)–Pd–N(1) 88.0(3), N(1)–Pd–Se(2) 93.1(3), Se(2)–Pd–P 87.23(6).

1.989(2) and 1.997(4) Å in **5**, **6** and **7**, respectively]. There is also considerable thermal motion associated with the nitrogen atoms, implying that the N(1)–Pd interaction is rather weak, and not strongly directional. Detailed discussion of bond angles and bond lengths in the azo-group is therefore not appropriate. The molecular formula is confirmed by the mass spectrum, where there is an intense cluster around m/z = 656 corresponding to the molecular ion, with the expected isotope distribution.

The NMR spectroscopic data show that this structure is maintained in solution for **4a**, and that the structures of **3a**–**c** and **4b**,**c** are similar. The selenium atoms are inequivalent and give rise to two signals in the ^{77}Se NMR spectrum, each of which shows a small splitting (J = 9 Hz) due to coupling to the phosphorus atom in the *cis* position. As expected, each atom in the two alicyclic rings gives a separate ^{13}C resonance.

The complexes **3a**–**c** and **4a**–**c** may be expected to resemble diselenolenes and dithiolenes in having delocalised metal–ligand bonding. We therefore anticipate rich and varied chemical and physical behaviour for these compounds and their derivatives.

We thank EPSRC for the provision of a studentship (to S. F.), Johnson Matthey plc for the loan of palladium salts, and the Ministero dell'Università e della Ricerca Scientifica e Tecnologica for financial support (to M. di V.).

Notes and References

† E-mail: c.p.morley@swan.ac.uk

‡ *Synthesis* of **4b**: a mixture of **1b** (0.19 g, 1.01 mmol), **2**·dba (0.28 g, 0.24 mmol) and PBu^n_3 (0.10 g, 0.50 mmol) in toluene (100 cm^3) was heated under reflux for 1 h under an N_2 atmosphere. The solvent was removed by evaporation under reduced pressure and the residue chromatographed on alumina. The product was eluted with a mixture of hexane and toluene (1 : 2) as a bright purple band. It was purified by recrystallization from hexane. Yield: 0.17 g (53%). Mp 146 °C. ^{1}H NMR (400 MHz, $CDCl_3$, $SiMe_4$), δ 3.13 (m, 2 H), 3.05 (m, 2 H), 2.88 (m, 2 H), 2.71 (m, 2 H), 1.93 (m, 8 H), 1.84 (m, 2 H), 1.72 (m, 4 H), 1.50 (m, 8 H), 1.43 (m, 6 H), 0.91 (t, 9 H); ^{13}C NMR (100 MHz, $CDCl_3$, $SiMe_4$), δ 157.3, 144.1, 141.9, 131.3, 36.9, 35.9, 34.7, 30.4, 26.3, 25.6, 25.2 [J(^{13}C–^{31}P) 29 Hz], 24.8, 24.2 [J(^{13}C–^{31}P) 14 Hz], 24.0, 22.7, 13.7; ^{31}P NMR (101 MHz, $CDCl_3$, external 85% H_3PO_4), δ 13.70; ^{77}Se NMR (47.7 MHz, $CDCl_3$, external $SeMe_2$), δ 548 [J(^{77}Se–^{31}P) 9 Hz], 366 [J(^{77}Se–^{31}P) 9 Hz]; IR (KBr disk), 2929vs, 2857s, 1578m, 1479m, 1450m, 1405m, 1359m, 1307w, 1262m, 1091vs, 1050s, 904m, 802s, 720w cm^{-1}; UV–VIS (hexane): λ_{max}/nm (ε/dm^3 mol^{-1} cm^{-1}) 570 (6000), 480 (5000), 295 (13 000), 250 (29 000), 220 (12 000); MS (FAB): m/z (%) 656 (74) [M$^+$], 203 (100) [PBu^n_3].

§ *Crystal data* for **4b**: $C_{24}H_{43}N_2PPdSe_2$; M = 654.90; crystal size 0.05 × 0.50 × 0.70 mm, triclinic, space group $P\bar{1}$ (no. 2); a = 9.930(2), b = 12.044(3), c = 13.277(3) Å, α = 63.43(2), β = 83.55(2), γ = 81.16(2)°, U = 1401.6(6) Å^3 (by least squares refinement on setting angles of 24 reflections, Z = 2), F(000) = 660, D_c = 1.552 g cm^{-3}, μ(Mo-Kα) = 3.33 mm^{-1}. Data collection (Enraf-Nonius CAD4, graphite-monochromated Mo-Kα radiation, λ = 0.71069 Å, T = 295 K), ω–2θ scans, 2.5 < θ < 25°. 4956 measured reflections (±h, ±k, +l), 4923 unique. Structure solution by direct methods, with SIR,[9] and heavy atom procedures with SHELXL-93.[10] Empirical absorption correction (ψ scan; min., max. correction factors 0.66, 1.00). Final refinement cycles performed against F^2 with all non-hydrogen atoms anisotropic and hydrogen atoms in calculated positions. Refinement on 274 variables converged at R_1 = 0.052 (based on 2936 reflections with F_o > 4σF_o), R_1 = 0.110 (on all reflections), wR_2 = 0.139, GOF = 1.021. Max., min. peaks in the final difference map = 0.54, −0.53 e Å^{-3}. CCDC 182/872.

1 E. G. Hope and W. Levason, *Coord. Chem. Rev.*, 1993, **122**, 109.
2 C. P. Morley, *Organometallics*, 1989, **8**, 800; M. R. J. Dorrity, A. Lavery, J. F. Malone, C. P. Morley and R. R. Vaughan, *Heteroatom Chem.*, 1992, **3**, 87; C. P. Morley and R. R. Vaughan, *J. Chem. Soc., Dalton Trans.*, 1993, 703; *J. Organomet. Chem.*, 1993, **444**, 219.
3 P. K. Khanna and C. P. Morley, *J. Chem. Res.* (*S*), 1995, 64.
4 S. Ford, P. K. Khanna and C. P. Morley, *J. Chem. Soc., Dalton Trans.*, submitted for publication.
5 H. Meier and E. Voigt, *Tetrahedron*, 1972, **28**, 187.
6 T. Chivers, K. McGregor and M. Parvez, *Inorg. Chem.*, 1994, **33**, 2364.
7 P. G. Jones and M. C. Ramirez de Arellano, *J. Chem. Soc., Dalton Trans.*, 1996, 2713.
8 F. Hintermaier, F. Kuhlwein, C. Robl and W. Beck, *Z. Anorg. Allg. Chem.*, 1995, **621**, 829.
9 A. Altomare, M. C. Burla, M. Camalli, G. Cascarano, C. Giacovazzo, A. Guagliardi and G. Polidori, *J. Appl. Crystallogr.*, 1994, **27**, 435.
10 G. M. Sheldrick, SHELXL-93, Program for Crystal Structure Refinement, University of Göttingen, 1993.

Received in Basel, Switzerland, 21st April 1998; 8/02956C

Regiospecific synthesis of 2,3-naphthylenebis(diphenylphosphines) by double insertion of alkynylphosphines into nickel(0)–benzyne complexes

Martin A. Bennett,*† Christopher J. Cobley, Eric Wenger and Anthony C. Willis

Research School of Chemistry, Australian National University, Canberra, ACT 0200, Australia

The double insertion of diphenylprop-1-ynylphosphine into the nickel(0)–benzyne bond of the complexes [Ni(1,2-η-4,5-$X_2C_6H_2$)(PEt_3)$_2$] (X = H, F) forms 2,3-naphthylenebis(diphenylphosphines) regiospecifically.

Small cycloalkynes or arynes, which are short-lived in the free state, are stabilised by coordination to d^{10} transition metal fragments such as ML_2 (M = Ni, L_2 = dcpe,‡ $2PEt_3$; M = Pt, L_2 = dcpe, $2PPh_3$).[1] Unsymmetrical acetylenes (RC≡CR′) undergo double insertion into nickel(0)–benzyne complexes of type **1** to give a mixture of isomeric naphthalenes (**2a**, **2b**), whose ratio is determined by the stereoelectronic properties of the inserted alkyne (Scheme 1).[2,3]

Recently we have been interested in extending this chemistry to alkynylphosphines, which could provide a novel route to functionalised naphthylenebis(tertiary phosphines), potential ligands that are not readily accessible by conventional syntheses.[4] Herein, we report the regiospecific reaction of diphenylprop-1-ynylphosphine[5] with the Ni^0–aryne complexes [Ni(1,2-η-4,5-$X_2C_6H_2$)(PEt_3)$_2$] (X = H **1a**, F **1b**) (Scheme 2).

Reduction of the appropriate (2-bromoaryl)nickel(II) complexes [NiBr(2-Br-4,5-$X_2C_6H_2$)(PEt_3)$_2$] (X = H, F) with lithium in diethyl ether at −40 °C, followed by evaporation of ether and extraction with hexane at −60 °C, yielded yellow solutions of the complexes **1a** and **1b** that were used *in situ* for all subsequent insertion reactions.[2,3] The addition of 2.5 equiv. of diphenylprop-1-ynylphosphine at −78 °C, followed by warming to room temperature, resulted in a dark red solution containing a complex mixture as shown by $^{31}P\{^1H\}$ NMR spectroscopy. However, by addition of bromine, orange nickel(II) complexes of type **3** were isolated and fully characterised.§¶ The high overall yields of **3a** and **3b** (up to 97%), together with the molecular structure determination of the chelate, planar-coordinated dibromonickel(II) complex [$NiBr_2\{C_{12}H_8F_2(PPh_2)\}$] **3b** (Fig. 1), confirmed that the reaction produced regiospecifically 2,3-naphthylenebis(diphenylphosphines) as the only observable insertion products.‖

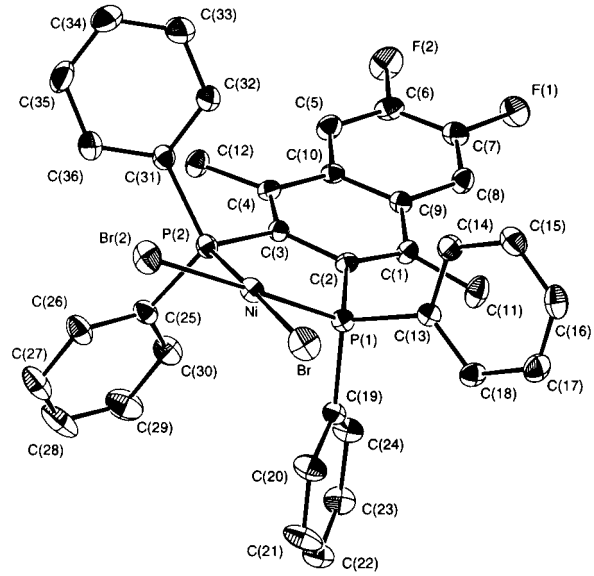

Fig. 1 ORTEP (25% probability) representation of **3b**. Hydrogen atoms have been omitted for clarity.

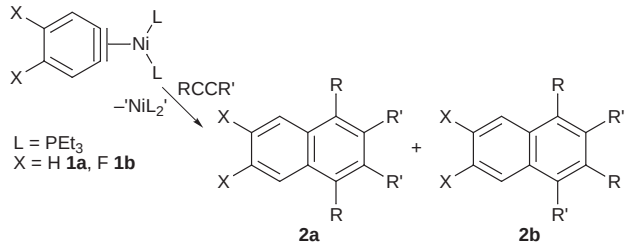

Scheme 1

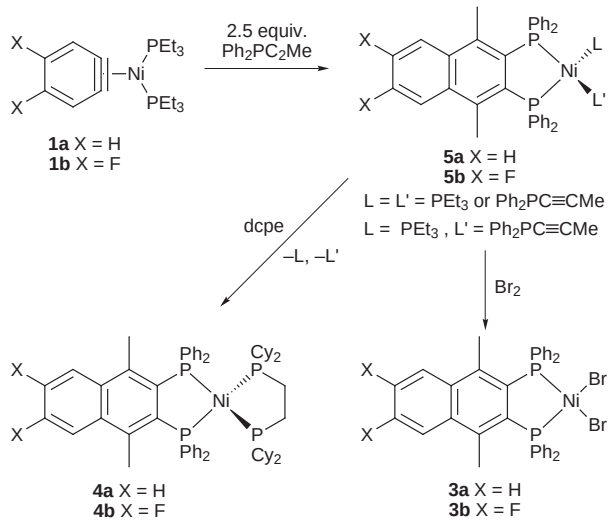

Scheme 2

Treatment of the initial dark red solutions with 1 equiv. of dcpe greatly simplified the $^{31}P\{^1H\}$NMR spectra, which showed in each case the presence of a single Ni^0 complex, [$Ni\{C_{12}H_8X_2(PPh_2)_2\}$dcpe)] (X = H **4a**, F **4b**), together with free PEt_3 and $Ph_2PC{\equiv}CMe$. On the basis of these results, the $^{31}P\{^1H\}$NMR spectrum (202.4 MHz) of the dark red solution could be assigned to a mixture of unsymmetrical nickel(0)–tertiary phosphine complexes of type **5**, all containing the newly formed naphthylenebis(diphenylphosphine) with a combination of PEt_3 or $Ph_2PC{\equiv}CMe$ as ancillary ligands (Scheme 2).

Reaction of **3a** or **3b** over 24 h at 50 °C with a large excess of NaCN in Me_2SO liberated quantitatively the pure 2,3-naphthylenebis(diphenylphosphines) **6a** and **6b** as white solids {overall yields based on [$Ni(cod)_2$] of up to 78%}.§¶

Exposure of **5a** or **5b** to air led to nickel–phosphine bond cleavage and only partial oxidation of the naphthylenebis(diphenyl)phosphines, forming the mono(phosphine oxides) $C_{12}H_8X_2(PPh_2)\{P(O)Ph_2\}$ **7a** and **7b**,[6] the structure of **7b** being

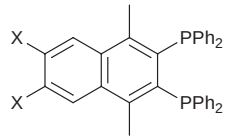

6a X = H
6b X = F

confirmed by X-ray diffraction.‖ The stronger oxidising agent, H_2O_2, was necessary to accomplish complete oxidation to the bis(phosphine oxides), $C_{12}H_8X_2\{P(O)Ph_2\}_2$ **8a** and **8b**.

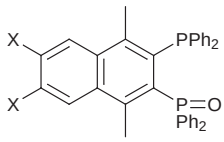

7a X = H
7b X = F

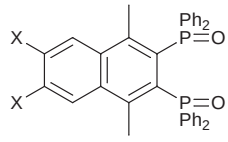

8a X = H
8b X = F

Theoretical calculations[7] suggest that the PPh_2 moiety, like CO_2Me, is electron withdrawing. The regiospecificities described above are indeed similar to those observed in the insertion of methyl 2-butynoate, $MeC{\equiv}CCO_2Me$, into complex **1b**, where the direction of insertion was believed to be electronically controlled and to require π-coordination of the alkyne.[1–3] In agreement, preferential side bonding of the C≡C bond of $Ph_2PC{\equiv}CMe$ to the Ni centre, as opposed to coordination *via* the phosphorus lone pair, has been observed. The reaction between equimolar quantities of $[Ni(cod)_2]$, dcpe and $Ph_2PC{\equiv}CMe$ gave the Ni^0–η^2-alkyne species, $[Ni(\eta^2\text{-}Ph_2PC{\equiv}CMe)(dcpe)]$ **9a**, as the main product; a small amount of the P-bonded isomer **9b**, was also formed (Scheme 3).

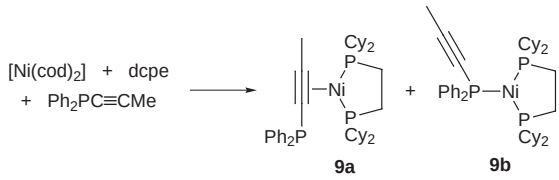

9a **9b**

Scheme 3

This chemistry is currently being investigated as a potential method for the synthesis of water-soluble diphosphines. We thank the Royal Society for the award of a Fellowship to C. J. C.

Notes and References

† E-mail: bennett@rsc.anu.edu.au
‡ dcpe = bis(dicyclohexylphosphino)ethane, $Cy_2PCH_2CH_2PCy_2$
§ Supplementary data describing full experimental details are available. (See http://www.rsc.org/suppdata/cc/1998/1307)
¶ *Selected NMR data* for compounds **3**, **4**, **6**–**9**: **3a**: $^{31}P\{^1H\}$ NMR ($CDCl_3$, 80.96 MHz) δ 65.5 (s). **3b**: $^{31}P\{^1H\}$ NMR ($CDCl_3$, 80.96 MHz) δ 65.8 (s); ^{19}F NMR ($CDCl_3$, 188.1 MHz) δ −132.6 [app. t, J(HF) 9.4 Hz]. **4a**: $^{31}P\{^1H\}$ NMR (C_6D_6, 80.96 MHz) δ 47.2 [t, ^2J(PP) 26.6 Hz], 52.1 [t, ^2J(PP) 26.6 Hz]; **4b**: $^{31}P\{^1H\}$ NMR (C_6D_6, 80.96 MHz) δ 47.4 [t, ^2J(PP) 27.4 Hz], 52.3 [t, ^2J(PP) 27.4 Hz]; ^{19}F NMR (C_6D_6, 188.1 MHz) δ −139.6 [app. t, J(HF) 10.2 Hz]. **6a**: $^{31}P\{^1H\}$ NMR (C_6D_6, 80.96 MHz) δ −6.2 (s). **6b**: $^{31}P\{^1H\}$ NMR (C_6D_6, 80.96 MHz) δ −5.6 (s); ^{19}F NMR (C_6D_6, 188.1 MHz) δ −138.5 [app. t, J(HF) 10.3 Hz]. **7a**: $^{31}P\{^1H\}$ NMR [$(CD_3)_2CO$, 80.96 MHz] δ −6.6 [d, ^3J(PP) 37.4 Hz], 31.0 [t, ^3J(PP) 37.4 Hz]. **7b**: $^{31}P\{^1H\}$ NMR [$(CD_3)_2CO$, 80.96 MHz] δ −6.3 [d, ^3J(PP) 36.7 Hz], 31.0 [t, ^3J(PP) 36.7 Hz]; ^{19}F NMR [$(CD_3)_2CO$, 188.1 MHz] δ −135.3 (m), −136.0 (m). **8a**: $^{31}P\{^1H\}$ NMR [$(CD_3)_2CO$, 80.96 MHz] δ 34.3 (br s); **8b**: $^{31}P\{^1H\}$ NMR [$(CD_3)_2CO$, 80.96 MHz] δ 33.4 (br s); ^{19}F NMR [$(CD_3)_2CO$] 188.1 MHz] δ −133.9 (br). **9a**: $^{31}P\{^1H\}$ NMR (C_6D_6, 80.96 MHz) δ −15.3 [dd, ^3J(PP) 24.0, ^3J(PP) 37.0 Hz], 67.7 [dd, ^2J(PP) 46.4, ^3J(PP) 24.0 Hz], 72.9 [dd, ^2J(PP) 46.4, ^3J(PP) 37.0 Hz].
‖ *Crystal data and data collection parameters*: **3b**: $C_{36}H_{28}Br_2F_2NiP_2$, M = 779.07, red–brown rod, crystal size 0.42 × 0.14 × 0.12 mm, monoclinic, space group $P2_1/c$ (no. 14), a = 8.633(2), b = 22.707(3), c = 16.237(3) Å, β = 97.49(2)°, U = 3155.8(9) Å^3, Z = 4, D_c = 1.640 g cm^{-3}, μ(Mo-Kα) = 32.94 cm^{-1}, F(000) = 1560, analytical absorption correction; 7474 unique data ($2\theta_{max}$ = 55.1°), 4594 with $I > 2\sigma(I)$; R = 0.046, wR = 0.036, GOF = 1.40.

7b: $C_{36}H_{28}F_2OP_2$, M = 576.56, colourless plates, crystal size 0.44 × 0.19 × 0.06 mm, monoclinic, space group Cc (no. 9), a = 9.541(3), b = 28.86(1), c = 11.187(4) Å, β = 106.87(3)°, U = 2948(2) Å^3, Z = 4, D_c = 1.229 g cm^{-3}, μ(Mo-Kα) = 1.88 cm^{-1}, F(000) = 1200, analytical absorption correction; 2667 unique data ($2\theta_{max}$ = 50.1°), 1415 with $I > 3\sigma(I)$; R = 0.043, wR = 0.035, GOF = 1.33. CCDC 182/847.

1 M. A. Bennett and E. Wenger, *Chem. Ber./Recueil*, 1997, **130**, 1029 and references therein.
2 M. A. Bennett and E. Wenger, *Organometallics*, 1995, **14**, 1267.
3 M. A. Bennett and E. Wenger, *Organometallics*, 1996, **15**, 5536.
4 A. J. Carty, N. J. Taylor and D. K. Johnson, *J. Am. Chem. Soc.*, 1979, **101**, 5422; D. K. Johnson, T. Rukachaisirikul, Y. Sun, N. J. Taylor, A. J. Canty and A. J. Carty, *Inorg. Chem.*, 1993, **32**, 5544.
5 A. J. Carty, N. K. Hota, T. W. Ng, H. A. Patel and T. J. O′Connor, *Can. J. Chem.*, 1971, **49**, 2706.
6 A. Avey, D. M. Schut, T. J. R. Weakley, and D. R. Tyler, *Inorg. Chem.*, 1993, **32**, 233; M. A. Bakar, A. Hills, D. L. Hughes and G. J. Leigh, *J. Chem. Soc., Dalton Trans.*, 1989, 1417.
7 E. Louattani, A. Lledós, J. Suades, A. Alvarez-Larena and J. F. Piniella, *Organometallics*, 1995, **14**, 1053.

Received in Cambridge, UK, 24th March 1998; 8/02291G

Remarkable effects of side-chain alkyl substituents on thermochromic behavior of peralkyldecasilanes

Kuninori Obata[a] and Mitsuo Kira*[a,b]†

[a] *Photodynamics Research Center, The Institute of Physical and Chemical Research (RIKEN), 19-1399, Koeji, Nagamachi, Aoba-ku, Sendai 980-0868, Japan*

[b] *Department of Chemistry, Graduate School of Science, Tohoku University, Aoba-ku, Sendai 980-8578, Japan*

The absorption spectrum of perhexyldecasilane shows marked temperature dependence; a two-site model, similar to the transition from a random coil to an all pseudo-*trans* rod conformation proposed for poly(dihexylsilylene), is proposed to explain this effect.

Much attention has been focused on the remarkable thermochromism and unusual emission spectra of linear peralkylpolysilanes.[1] Typically, while poly(dihexylsilylene) exhibits a broad absorption band at *ca*. 315 nm at room temperature, upon cooling below *ca.* −30 °C, the absorption band becomes much narrower and shifts significantly to higher wavelength; the difference of λ_{max} between the low and high temperature regions ($\Delta\lambda_{max}$) amounts 39 nm.[2a] The origin of the thermochromism is usually ascribed to the transition at low temperatures from a random coil to an all pseudo-*trans* rod conformation of the silicon backbone,[2] while Miller *et al.* have proposed that the red shift at low temperatures is caused by aggregation of polysilane chains.[3] In order to elucidate the origin of the thermochromism of the polysilanes, it is desirable to investigate peralkyloligosilanes with uniform Si chain lengths. However, there has been no study of peralkyloligosilanes other than permethyloligosilanes[4] reported until now, while we have recently reported circular dichroism (CD) spectral features of oligo(dipropylsilylene)s with terminal chiral aralkyl groups.[5] We report here that the absorption spectra of peralkyloligosilanes with ten or more Si atoms in a chain are remarkably temperature dependent, a feature which depends strongly on the side-chain alkyl substituents.

Wurtz coupling of a mixture of a dialkyldichlorosilane and a trialkylchlorosilane with lithium in THF gave a mixture of the corresponding peralkyloligosilanes, as shown in Scheme 1. Oligosilanes having 3–11 Si chains were separated as pure compounds *via* recycle HPLC from a mixture of peralkyloligosilanes. The structures were characterized by means of NMR spectroscopy, elemental analyses and mass spectrometry.‡

The absorption band maxima at 293 K and their dependence on the Si chain lengths of perpropyl- **2** and perhexyloligosilanes **3** were similar to those of permethyloligosilanes,[6] while small alkyl substituent effects were observed. These absorption bands are assigned to the σ→σ* electronic transitions of the Si main chains.[4,6]

Peralkyloligosilanes having more than five Si atoms in a chain showed significant red-shifts of the maxima with lowering temperatures. The most remarkable thermochromism was observed in perhexyloligosilanes with 10 and 11 Si atoms in the chain. Fig. 1 shows the temperature dependence of absorption spectra of peralkyldecasilanes **1a** (**1**, n = 10), **2a** (**2**, n = 10) and **3a** (**3**, n = 10). With lowering temperatures, the absorption maxima of these decasilanes shifted to longer wavelength, but the extent of the red-shift ($\Delta\lambda_{max}$) from 293 to 77 K was markedly dependent on the substituents; $\Delta\lambda_{max}$ values were < 10, 13 and 19 nm for **1a**, **2a** and **3a**, respectively; upon increasing the chain-length of the alkyl substituents, the thermochromic behavior of the decasilanes resembles more closely that of poly(dihexylsilylene). The temperature dependence of the absorption spectrum of **3a** was analyzed using a two-site model similar to the transition from random coil to the all pseudo-*trans* rod conformation model for poly(dihexylsilylene) (Scheme 2). Thus, a linear relationship was observed between $\log(A_1/A_2)$ and $1/T$, where A_1 and A_2 are the areas of the

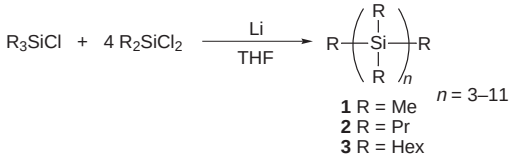

Scheme 1

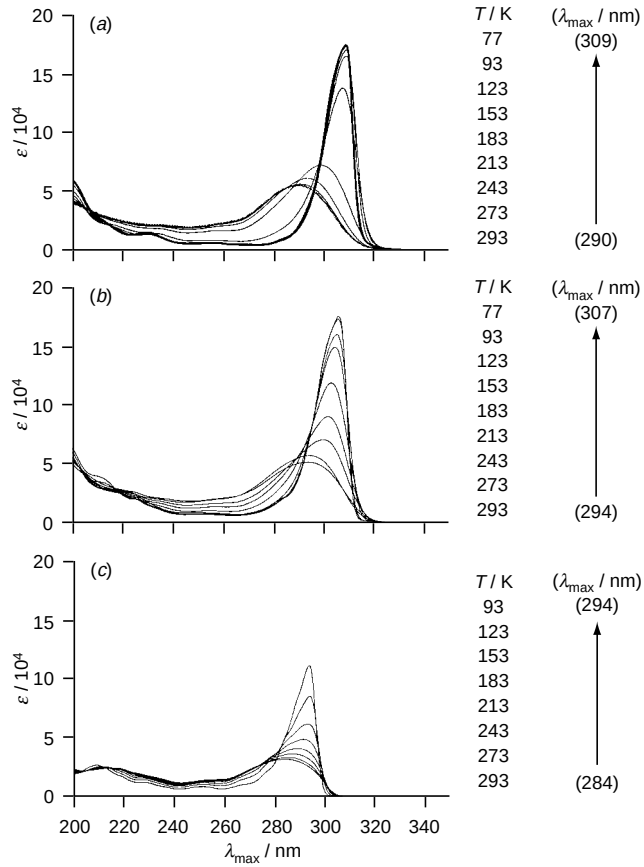

Fig. 1 Temperature dependence of absorption spectra of (*a*) docosahexyldecasilane **3a**, (*b*) docosapropyldecasilane **2a** and (*c*) docosamethyldecasilane **1a** in 3-methylpentane

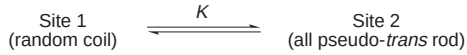

Scheme 2

absorptions bands at 290 and 310 nm for **3a**, respectively; the absorption spectra of **3a** were deconvoluted to the two bands by band-shape analysis. From the slope of the linear relationship, the enthalpy difference between the two sites was estimated to be 9 kcal mol^{-1}.

The remarkable effect of the substituents on the temperature dependence of the absorption spectrum of decasilane is ascribed to the importance of the steric energies between the side-chain alkyl substituents. MM2 force field calculations using standard parameters for organosilicon compounds proposed by Allinger[7] showed that the most stable conformation of **1a**–**3a** was as loose helical rods having a dihedral angle of *ca.* 170° for seven Si tetrads, irrespective to the alkyl substituents; the all-*trans* rod structure (the dihedral angle = 180°) showed much higher steric energy due to the severe steric repulsion between alkyl groups in 1,3-positions. The energy differences between the loose helical rod conformation and the other conformations with one *gauche* arrangement in the 7 Si tetrads of a decasilane are 5.3 and 8.9 kcal mol^{-1} for **2a** and **3a**, respectively; this value is much smaller for **1a** (0.5 kcal mol^{-1}). A one-*gauche* conformation in **3a** or **2a** causes severe steric repulsion between alkyl substituents, while the repulsion is less important in **1a**. The steric energy calculated by the MM2 method is in good agreement with the experimental ΔH values for the transition from Site 1 to Site 2, suggesting that the transition occurs between an assembly of conformations with one or more *gauche* Si tetrads to an assembly of all pseudo-*trans* rod conformations including a loose helical conformation.

Notes and References

† E-mail: mkira@kriso1.chem.tohoku.ac.jp

‡ *Selected data* for **2a**: 0.3% yield (based on Pr_2SiCl_2); a white powder; δ_H(300 MHz, C_6D_6) 0.65–1.05 (m, 44 H), 1.10–1.28 (m, 66 H), 1.60–1.80 (m, 44 H); δ_C(75 MHz, C_6D_6) 16.8, 17.4, 17.66, 17.67, 17.8, 18.8, 18.9, 18.97, 19.00, 19.04, 20.9, 21.0; several peaks overlap. The ^{29}Si NMR spectrum of **2a** was not measured due to poor sample solubility. For **3a**: 0.5% yield (based on Hex_2SiCl_2); a colorless viscous oil; δ_H($CDCl_3$) 0.63–0.75 (m, 32 H), 0.79–0.94 (m, 78 H), 1.20–1.44 (m, 176 H); δ_C($CDCl_3$) 13.79, 14.13, 14.44, 14.64, 14.91, 14.96, 22.74, 22.83, 22.87, 25.06, 27.16, 27.43, 27.51, 33.98, 34.17, 34.38, 34.40, 31.63, 31.82, 31.86; δ_{Si}($CDCl_3$) −33.82, −27.92, −26.18, −25.84, −10.12.

1 For reviews, see: R. D. Miller and J. Michl, *Chem. Rev.*, 1989, **89**, 1359; J. Michl, J. W. Downing, T. Karatsu, A. J. McKinley, G. Poggi, G. M. Wallraff, R. Sooriyakumaran and R. D. Miller, *Pure Appl. Chem.*, 1988, **60**, 959; J. M. Zeigler, *Synth. Met.*, 1989, **28**, C581; R. West, *J. Organomet. Chem.*, 1986, **300**, 327; R. West, in *The Chemistry of Organosilicon Compounds*, ed. S. Patai and Z. Rappoport, Wiley, Chichester, 1989, ch. 19, p. 1207.

2 (*a*) L. A. Harrah and J. M. Zeigler, *J. Poly. Sci., Polym. Lett. Ed.*, 1985, **23**, 209; (*b*) P. Trefonas, III, J. R. Damewood, Jr., R. West and R. D. Miller, *Organometallics*, 1985, **4**, 1318.

3 R. D. Miller, G. M. Wallraff, M. Baier, P. M. Cotts, P. Shukla, T. P. Russel, F. C. Schryver and D. Declercq, *J. Inorg. Organomet. Polym.*, 1991, **1**, 505; P. Hukla, P. M. Cotts, R. D. Miller, T. P. Russel, O. A. Smith, G. M. Wallraff, M. Baier and P. Thiyagarajan, *Macromolecules*, 1991, **24**, 5606.

4 (*a*) Y.-P. Sun and J. Michl, *J. Am. Chem. Soc.*, 1992, **114**, 8186 and references cited therein.

5 K. Obata, C. Kabuto and M. Kira, *J. Am. Chem. Soc.*, 1997, **119**, 11 345.

6 M. Kumada and K. Tamao, *Adv. Organomet. Chem.*, 1968, **6**, 19.

7 M. R. Frierson, M. R. Imam, V. B. Zalkow and N. L. Allinger, *J. Org. Chem.*, 1988, **53**, 5248.

Received in Cambridge, UK, 19th March 1998; 8/02171F

Homogeneous catalysis. Use of a ruthenium(II) complex for catalysing the ene reaction

William W. Ellis, W. Odenkirk and B. Bosnich*†

Department of Chemistry, The University of Chicago, 5735 S. Ellis Avenue, Chicago, IL 60637, USA

The complex *trans*-[Ru(salen)(NO)(H_2O)]$^+$ catalyses the ene reaction between activated enophiles and olefins to give homoallylic alcohols by a stepwise process.

The oxo-ene reaction, which usually involves the addition of alkenes to aldehydes to produce homoallylic alcohols [eqn. (1)],

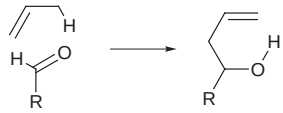

(1)

is potentially a useful method of carbon–carbon bond construction.[1] Its implementation, however, suffers from a number of difficiencies. Among these is the necessity of employing high temperatures for most reactions. The obvious method for promoting the reaction at lower temperatures by using conventional Lewis acids such as $AlCl_3$,[2] BF_3,[3] $SnCl_4$[4] or $TiCl_4$,[5] can lead to new problems.[1] Whereas these Lewis acids do indeed promote the reaction, they lead to the formation of Lewis acid alcohol intermediates which can release a proton. The released acid can itself act as a catalyst (Prins reaction) and can cause other reactions to occur with the substrates and product. Snider[1,6] has shown that the use of Me_2AlCl can promote the ene reaction without proton interference because the methyl groups are capable of rapidly scavenging the proton to give methane. The resultant formation of alkoxide adducts, however, consumes the Lewis acid promoter and, consequently, the Lewis acid is used in stoichiometric or greater quantities. In addition, alkylaluminium halides have been shown to transfer the alkyl group to the aldehyde[7] and to undergo the Oppenauer oxidation.[8] Milder Lewis acids such as those derived from Zn^{II}[9] and Ti^{IV}[10] have been shown to act as true catalysts for a limited number of intramolecular and intermolecular ene reactions, respectively.

Here we report the use of a new type of Lewis acid catalyst for the ene reaction. It is the d^6 ruthenium(II) complex, *trans*-[Ru(salen)(NO)(H_2O)] SbF_6 **1**, which we have employed for

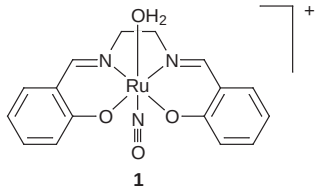

1

catalysing the Diels–Alder[11] and Mukaiyama reactions.[12] The air and moisture stable catalyst **1** is readily prepared in two steps from commercially available [Ru(NO)Cl_3] and the ligand.[11] Although Ru^{II} complexes are generally electron-rich and consequently do not act as Lewis acids, the incorporation of the electron-withdrawing NO^+ ligand, the coordination of hard ligands, namely N and O, and the presence of a positive charge all conspire to produce a Lewis acidic ruthenium centre. Further, because the water ligand *trans* to the NO^+ ligand is very labile,[11] this coordination site is readily available for binding the enophile (usually an aldehyde) to activate it for reaction and, after reaction, the homoallylic alcohol product is expected to be labile for efficient turnover.

Some of these results are collected in Table 1. As is commonly observed for Lewis acid promotion, only electron-difficient carbonyl-containing enophiles engage in the ene reaction at acceptable rates. Generally, ruthenium(II) aquo complexes are weak acids having a pK_a similar to AcOH acid (in water).[13] In order to determine the ability of acid to promote the reactions, 2 mol% TFA was used under the same conditions to promote the reaction shown in entry 1 (Table 1). It was found that < 1% conversion to the ene product occurred after 150 h, indicating that acid is neither responsible for, nor competitive with, the ruthenium catalysed process.

Although, like other promoters, the ruthenium catalyst has its limitations for the ene reaction, it serves to demonstrate that structurally defined transition metal complexes which are not normally oxophilic can be modified to act as genuine catalysts for the generally resistant ene reaction. It is probable, however, that the present catalyst will find practical applications in the intramolecular ene reaction. The conversion of (+)-citronellal to *l*-isopulegol [eqn. (2)] is an important step in the industrial

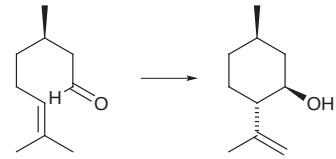

(2)

production of *l*-menthol[14] where $ZnBr_2$ in stoichiometric amounts at *ca.* 5 °C is used to give *l*-isopulegol in 95% yield over the other isomers. Using 1 mol% of the ruthenium catalyst in $MeNO_2$ at 25 °C, (+)-citronellal is converted to *l*-isopulegol after 6 h. An 80% yield of *l*-isopulegol was obtained, with the remaining product consisting of the other (three) isomers.[9,14,15] Given this efficient conversion, it is possible to entertain the prospect of using chiral analogues of the present catalyst for asymmetric catalytic intramolecular ene reactions.

In order to ascertain if the present catalysed ene reactions are concerted or stepwise processes we have investigated the products from a number of 1,3-dienes. A typical transformation is illustrated in eqn. (3), together with the putative inter-

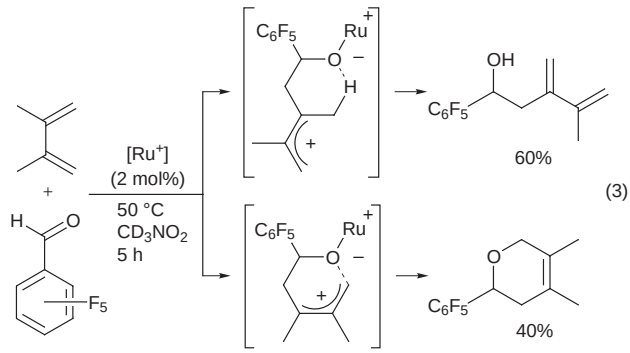

(3)

mediates. The two products are formed in constant kinetic proportions and are not interconverted in the presence of the

Table 1 Catalytic ene reaction using **1** (2 mol%) in $MeNO_2$ at 50 °C

Entry	Enophile (0.5 M)	Olefin (conc./M)	Product	Isomer ratio[a]	*t*/h[b]	Isolated yield (%)
1	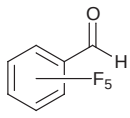	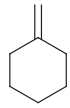 (1.5)	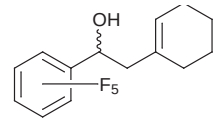	—	5	88[c]
2	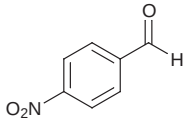	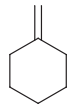 (0.75)	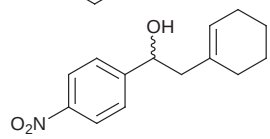	—	10	83[c]
3	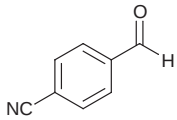	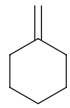 (0.75)	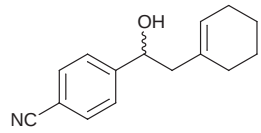	—	50	82[c]
4	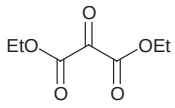	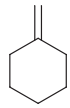 (1.5)	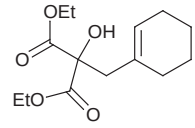	—	42	59
5	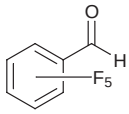	 (1.5)	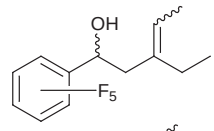	56:44	5	85[c]
6	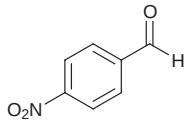	 (0.75)	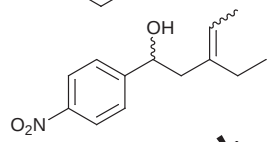	66:34	40	75[c]
7[d]	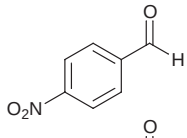	 (0.75)	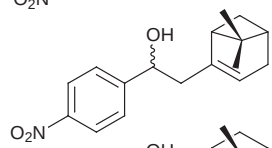	81:19	24	47
8[d]	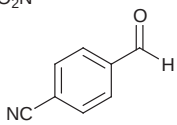	 (0.75)	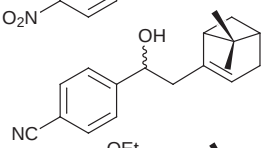	78:22	41	45
9[d]	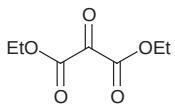	 (1.5)	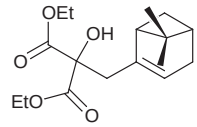	—	37	35

[a] Isomers not assigned. [b] Time required for >95% reaction of enophile. [c] Only the pure product is formed by ^1H NMR spectroscopy. [d] In [$^2H_6$]acetone.

catalyst. The formation of the two products [eqn. (3)] suggests that the ene reaction with the 1,3-diene may occur *via* a non-concerted process where the carbenium ion has sufficient lifetime to promote either the ene reaction or the hetero-Diels–Alder reaction. Although it is recognized that the allylic cation may have a greater stability than a localized carbenium ion formed by monoolefins, the formation of the two products when 1,3-dienes are used indicates that in the present systems the monoolefin ene reactions could proceed by carbenium ion intermediates.[16]

This work was supported by grants from the NIH.

Notes and References

† E-mail: bos@uchicago.edu

1 B. B. Snider, in *Comprehensive Organic Synthesis*, ed. B. M. Trost and I. Fleming, Pergamon, Oxford, 1991, vol. 2, p. 527 and refs. therein.
2 J. P. Benner, G. B. Gill, J. J. Parrott and B. Wallace, *J. Chem. Soc., Perkin Trans. 1*, 1984, 291.
3 P. M. Wovkulich and M. R. Uskokovich, *J. Org. Chem.*, 1982, **47**, 1600.
4 J. K. Whitesell, A. Bhattacharya, D. A. Aguilar and K. Henke, *J. Chem. Soc., Chem. Commun.*, 1982, 989; K. Mikami, T. P. Loh and T. Nakai, *Tetrahedron Lett.*, 1988, **48**, 6305.
5 J. K. Whitesell, K. Nabora and D. Deyo, *J. Org. Chem.*, 1989, **54**, 2258.
6 B. B. Snider and D. J. Rodini, *Tetrahedron Lett.*, 1980, 1815.
7 B. B. Snider and B. E. Goldman, *Tetrahedron Lett.*, 1986, **42**, 2951.
8 .M. Majewski and G. W. Bantle, *Synth Commun.*, 1990, **20**, 2549.
9 S. Sakane, K. Maruoka and H. Yamamoto, *Tetrahedron*, 1986, **42**, 2203.
10 K. Michami, M. Terada, E. Sawa and T. Nakai, *Tetrahedron Lett.*, 1991, **32**, 6571.
11 W. Odenkirk, A. L. Rheingold and B. Bosnich, *J. Am. Chem Soc.*, 1992, **114**, 6392.
12 W. Odenkirk, J. Whelan and B. Bosnich, *Tetrahedron Lett.*, 1992, **39**, 5729.
13 J. A. Broomhead, G. Basolo and R. G. Pearson, *Inorg. Chem.*, 1964, **3**, 826.
14 Y. Nakatani and K. Kawashima, *Synthesis* ,1978, 147.
15 W. Oppolzer and V. Snieckus, *Angew. Chem., Int. Ed. Engl.*, 1978, **17**, 476; K. Sakai and O. Oda, *Tetrahedron Lett.*, 1972, 4375.
16 B. B. Snider and E. Ron, *J. Am. Chem. Soc.*, 1985, **107**, 8160.

Received in Corvallis, OR, USA, 9th February 1998; 8/01215F

A modular approach to constructing multi-site receptors for isophthalic acid

Christopher Bielawski, Yuan-Shek Chen, Peng Zhang, Peggy-Jean Prest and Jeffrey S. Moore*†

Departments of Chemistry, Materials Science & Engineering, and the the Beckman Institute for Advanced Science and Technology, University of Illinois at Urbana-Champaign, Urbana, IL 61801, USA

New multi-topic receptors which may serve as building blocks for constructing receptor arrays form highly stable complexes with isophthalic acid.

We are interested in developing simple, modular systems of receptor arrays and multi-topic ligands for the purpose of constructing stable, self-assembled nanostructures through multiple non-covalent interactions. This requires that the associating systems be easily synthesized, show strong supramolecular affinity, and be general for implementation in a variety of molecular designs. While molecular self-assembly is recognized as a method to prepare nanostructures,[1] there exists the need for simple building blocks that can be linked to form arrays of receptors and complementary ligands. Herein we report the design and synthesis of the primary receptor unit **1a**, its heterocomplexation with isophthalic acid, and demonstration of its use in modular construction of multi-site receptors.

The primary receptor unit was designed to be incorporated within oligo(phenyleneethynylene) backbones that have been extensively employed by our group to construct a variety of molecular architectures.[2] 2-Aminopyridines are well-known[3] to associate strongly with carboxylic acids, and a pair of these groups positioned on alternating sites of a 1,3-connected phenyleneethynylene backbone provides excellent shape complementarity to isophthalic acid, as shown in eqn. (1). Molecular

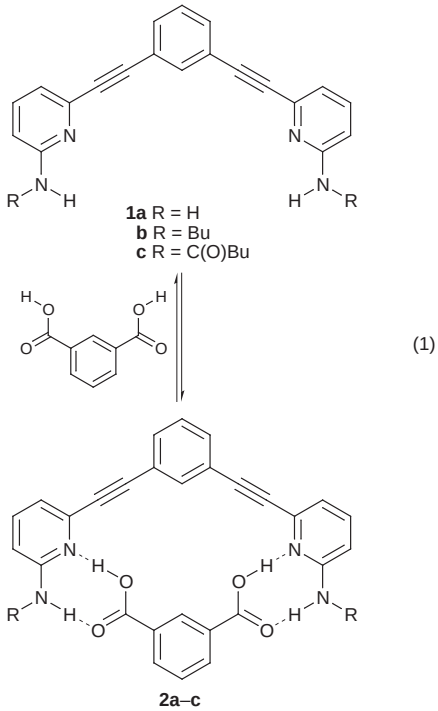

(1)

modeling‡ indicates that both **1a** and isophthalic acid can maintain favorable planar conformations with typical hydrogen bond distances, suggesting that tight binding should be realized. An important feature of this design is the torsional flexibility that exists between adjacent aromatic residues. The rotational barrier[4] about the sp–sp^2 bond is only *ca.* 600 cal mol^{-1}, which permits accessibility to favorable binding geometries. However, the most important aspect of **1a** is its ease of synthesis§ which was accomplished by coupling[5] 2 equiv. of the known[6] 2-amino-6-ethynylpyridine to 1,3-diiodobenzene in 78% yield.

Co-crystallization of **1a** and isophthalic acid from THF by slow evaporation resulted in single crystals suitable for X-ray structure determination.¶ The complex (Fig. 1) packs in 2D sheets with alternating hydrophobic and hydrophilic layers. All hydrogen bond donors and acceptors are fully saturated forming a set of six hydrogen bond interactions for each host and guest in the solid phase. The average dihedral angle between the heterocyclic residues and the phenyl ring is 12.5 ± 1.7°. Job's method[7] confirmed the stoichiometry of **1a** and isophthalic acid to be 1 : 1 in solution.

The binding characteristics of the receptor with 5-*tert*-butylisophthalic acid were determined in solvent systems with varying polarity at 20 °C using ^{1}H NMR titration and dilution methods.[8] As shown in Table 1, the association constant was found to be greater‖ than 10^6 M^{-1} in $CDCl_3$, reflecting a tight fit of the guest with the host. Due to increased solvation, the association constants in 1 : 9 and 1 : 4 [$^2H_6$]DMSO–$CDCl_3$ (v/v) solution were largely reduced to 320 and 80 M^{-1}, respectively.

While probing the potential of **1a** as a principle sub-unit in more complex systems, we anticipated encountering solubility problems. An obvious and synthetically simple solution was to transform the amine groups to more soluble derivatives. Therefore, a pair of analogues **1b** and **1c** were synthesized§ and studied. The association constants of receptors **1b** and **1c** with 5-*tert*-butylisophthalic acid were similar to that of receptor **1a**, all being greater‖ than 10^6 M^{-1} in $CDCl_3$. However, as shown in Table 1, the binding affinity in a 1 : 9 [$^2H_6$]DMSO–$CDCl_3$ (v/v)

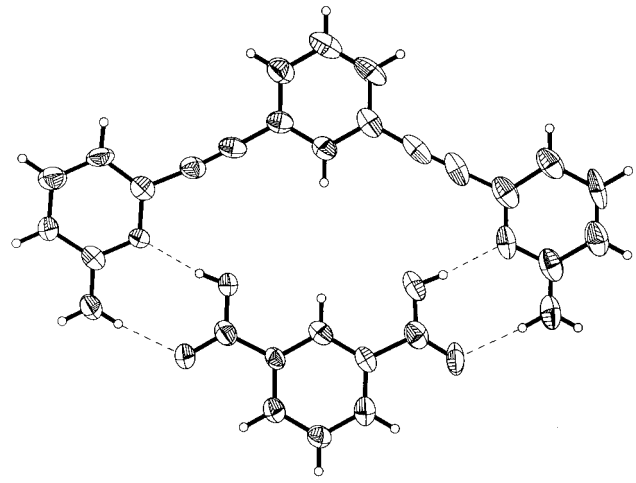

Fig. 1 ORTEP drawing at the 50% probability level of the complex formed between **1a** and isophthalic acid. Hydrogen bonding is indicated by thin dashed lines.

solution showed some noticeable differences. The association constants of **1b** and **1c** with 5-*tert*-butylisophthalic acid were 55 and 50 M^{-1} respectively. The reduction in affinity relative to receptor **1a** is believed to stem both from the increase in the extent of desolvation upon complexation and the greater entropic loss in rotational freedom about the aminopyridine bond. Our results showed that acylation or alkylation are synthetically simple ways to enhance the solubility of **1a** without significantly reducing the binding strength.

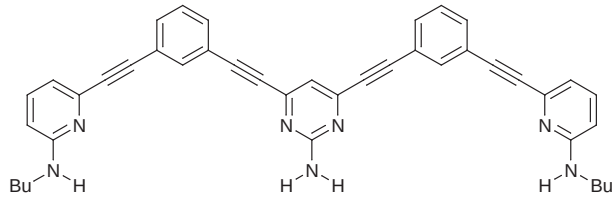

3

To demonstrate the modularity of this building block set, receptor **3**, which can potentially bind two units of isophthalic acid, was synthesized§ in a manner similar to that of **1a**. After several attempts at obtaining a crystal structure of receptor **3** and various derivatives of isophthalic acid, only crystals from a dioxane solution of 5-hydroxyisophthalic and **3** were suitable for X-ray diffraction. Although the quality of the crystal¶ was poor, the data set obtained was sufficient to confirm the dual binding of 5-hydroxyisophthalic acid (Fig. 2) and reveal the packing pattern as being similar to complex **2**. In solution, the stoichiometry of the complex was determined to be 2 : 1 by Job's method.[7]

Table 1 Association constants of receptors **1a**–**c** with 5-*tert*-butylisophthalic acid at 20 °C in a variety of solvent systems[a]

	Association constant/M^{-1}		
Receptor	in $CDCl_3$[b]	in 1 : 9 [$^2H_6$]DMSO–$CDCl_3$ (v/v)	in 1 : 4 [$^2H_6$]DMSO–$CDCl_3$ (v/v)
1a	$> 10^6$	320	80
1b	$> 10^6$	55	[c]
1c	$> 10^6$	50	[c]

[a] Association constants were determined by non-linear least-squares fitting of the experimental binding isotherm. The error is ±15%. [b] Estimated lower limit (see footnote ‖). [c] No observable binding affinity.

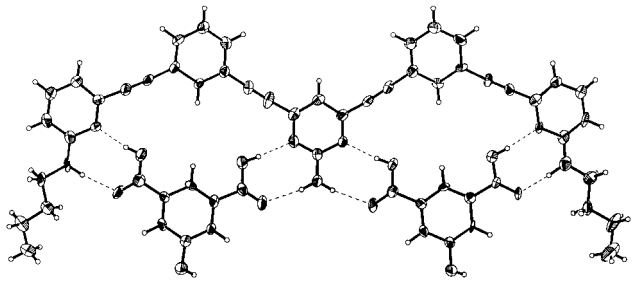

Fig. 2 ORTEP drawing at the 50% probability level of the complex formed between **3** and 5-hydroxyisophthalic acid. Hydrogen bondiong is indicated by thin dashed lines. The structure contains solvent molecules (dioxane) which have been removed for clarity.

In conclusion, we have shown that receptor **1a** possesses a high affinity towards isophthalic acid and can easily be modified to alleviate solubility difficulties. The synthesis of **3** demonstrates that **1a** can be implemented as a building block for the construction of arrays of multi-site receptors for isophthalic acid. By combining multi-topic ligands and multi-site receptors, it should be possible to form stable, self-assembled nanostructures. In addition, we are also working on linear (AB) and 2D (AB_2) supramolecular polymers based on host : guest complex **2**. Details of these studies will be reported in due course.

This work was supported by the NSF Young Investigator program (Grant CHE-94-96105). Additional support from the Camille Dreyfus Teacher-Scholar Awards Program is acknowledged. C. B. gratefully thanks Pfizer, Inc. for a summer undergraduate research followship (1996).

Notes and References

† E-mail: moore@aries.scs.uiuc.edu

‡ Molecular modeling was performed on a Silicon Graphics Indigo workstation using Cerius² and MacroModel software packages.

§ All new compounds gave satisfactory analytical and spectral data.

¶ *Crystal data* for **1a**-isophthalic acid: $C_{28}H_{20}N_4O_4$, M_r = 476.48 g mol^{-1}, colorless, columnar crystal (0.26 × 0.06 × 0.06 mm), triclinic, space group $P\bar{1}$, a = 7.6156(10), b = 11.493(2), c = 14.462(2) Å, α = 108.586(3), β = 96.039(3), γ = 101.298(3)°, V = 1157.3(3) Å^3, Z = 2, ρ_{calc} = 1.367 g cm^{-3}, μ = 0.094 mm^{-1}. Of 5147 reflections measured, 3165 were independent, and 1524 were used for refinement; wR_2 = 0.1597 and R_1 = 0.1077 for 301 parameters. For **3**·[5-hydroxyisophthalic acid]$_2$·[dioxane]$_3$: $C_{70}H_{73}N_7O_{16}$, M_r = 1268.35 g mol^{-1}, pale yellow, tabular crystal (0.18 × 0.10 × 0.04 mm), triclinic, space group $P\bar{1}$, a = 13.0983(11), b = 14.6384(13), c = 18.0368(15) Å, α = 106.833(2), β = 93.572(2), γ = 93.343 (2)°, V = 3293.2(5) Å^3, Z = 2, ρ_{calc} = 1.279 g cm^{-3}, μ = 0.092 mm^{-1}. Of 14 147 reflections measured, 8808 were independent, and 4059 were used for refinement; wR_2 = 0.3410 and R_1 = 0.2181 for 823 parameters. Data for both structures were collected on a Siemans CCD/platform diffractometer using graphite-monochromated Mo-Ka radiation (λ = 0.71073 Å, 0.3° ω scans, $2\theta_{max}$ = 46.0°) at 198(2) K. No absorption corrections were applied. Using SHELXTL, each structure was solved by direct methods and refined by full-matrix least-squares techniques on F^2 with anisotropic displacement parameters for the non-hydrogen atoms. Hydrogen atoms were included as fixed contributors in idealized positions. CCDC 182/866.

‖ Estimated by dilution to 50 μM.

1 S. C. Zimmerman, F. Zeng, D. E. C. Reichert and S. V. Kolotuchin, *Science*, 1996, **271**, 1095; J. S. Moore, *Curr. Opin. Solid State Mater. Sci.*, 1996, **1**, 777; G. M. Whitesides, J. P. Mathias and C. T. Seto, *Science*, 1991, **254**, 1312.

2 J. S. Moore, *Acc. Chem. Res.*, 1997, **30**, 402.

3 A. D. Hamilton, E. Fan, S. Van Arman, C. Vincent, F. Garcia-Tellado and S. J. Geib, *Supramol. Chem.*, 1993, **1**, 247; M. C. Etter and D. A. Adsmond, *J. Chem. Soc., Chem. Commun.*, 1990, 589; R. W. Gellert and I. N. Hsu, *Acta. Crystallogr., Sect. C*, 1988, **44**, 311.

4 K. Okuyama, T. Hasegawa, M. Ito and N. Mikami, *J. Phys. Chem.*, 1984, **88**, 1711.

5 K. Sonogashira, T. Tohda and N. Hagihara, *Tetrahedron Lett.*, 1975, **50**, 4467.

6 M. Inouye, T. Miyake, M. Furusyo and H. Nakazumi, *J. Am. Chem. Soc.*, 1995, **117**, 12 416.

7 P. Job, *Ann. Chim.* (*Paris*), 1928, **9**, 113; K. C. Ingham, *Anal. Biochem.*, 1975, **68**, 660.

8 C. S. Wilcox, in *Frontiers in Supramolecular Chemistry and Photochemistry*, ed. H. J. Schneider and H. Durr, VCH, New York, 1991, p. 123.

Received in Columbia, MO, USA, 3rd October 1997; 7/07262G

Cationic ruthenium allenylidene complexes as a new class of performing catalysts for ring closing metathesis

A. Fürstner,*[a]† M. Picquet,[b] C. Bruneau,[b] and P. H. Dixneuf*[b]‡

[a] *Max-Planck-Institut für Kohlenforschung, D-45470 Mülheim/ Ruhr, Germany*
[b] *UMR 6509: CNRS - Université de Rennes, Laboratoire de Chimie de Coordination et Catalyse, Campus de Beaulieu, F-35042, Rennes, France*

Cationic allenylidene ruthenium complexes [Ru=C=C=CR_2(L)(Cl)(arene)]PF_6 (L = PCy_3, PPr^i_3), easily prepared from $RuCl_2$(L)(*p*-cymene), prop-2-yn-1-ol and $NaPF_6$, are found to be excellent catalyst precursors for ring closing olefin metathesis.

The recent development of a new generation of well-defined catalysts precursors for olefin metathesis has had a tremendous impact on progress in this field.[1,2] Most popular among them are the *neutral 16-electron* ruthenium carbene complexes $Cl_2(PCy_3)_2$Ru=CHR (**1a**: R = Ph, **1b** R = −CH=CPh_2) described by Grubbs[3] which are distinguished by excellent activity as well as good compatibility with various functional groups in the substrates. Since these catalysts are fairly stable against oxygen and moisture, they represent a simple yet efficient tool for advanced organic synthesis and polymer chemistry. A major drawback, however, resides in the use of either diazoalkanes or diphenylcyclopropene for the preparation of these complexes, *i.e.* reagents which are hazardous or rather difficult to make, respectively. However, an improvement of the synthesis of complexes **1** synthesis has just been achieved starting from Ru(H)(H_2)Cl$(PCy_3)_2$.[4]

We now describe a new class of efficient single-component catalyst for ring closing olefin metathesis: the *cationic 18-electron* allenylidene ruthenium complexes [Ru=C=C=$CR_2(PR_3)$-(Cl)(arene)]PF_6 **5**, easily available in three steps from $RuCl_3.xH_2O$, which also provide an unprecedented example of the involvement of metal allenylidene complexes in catalysis.[5]

The 18-electron complexes of the general formula (η^6-arene)$RuCl_2(PR_3)$ such as **3**, which are readily obtained from commercially available [(η^6-arene)$RuCl_2]_2$ **2** upon addition of a phosphine,[6] are very active in catalytic transformations of alkynes,[7] but exhibit only very low catalytic activity for ring opening metathesis polymerization (ROMP) of strained cycloalkenes and ring closing metathesis (RCM). However, they can be activated either upon addition of diazoalkanes[8] or by *in situ* irradiation with UV light.[9] A route has been designed in order to straightforwardly introduce around a Ru(+2) site only *one* bulky phosphine, *one* cumulenylidene ligand attached to the metal *via* a Ru=C bond, and *one* easy to displace *p*-cymene group, three likely conditions to produce an active olefin metathesis catalyst precursor. As the activation of prop-2-yn-1-ols with selected ruthenium precursors has been shown to give the Ru=C=C=CR_2 moiety,[10] complexes **3** were reacted with a prop-2-ynyl alcohol such as **4** in the presence of $NaPF_6$ in MeOH at ambient temperature and cleanly led to the formation of the cationic allenylidene complexes **5a-c**, isolated in high yields as violet powders (Scheme 1). It is noteworthy that the corresponding salts with less bulky R_3P groups existed only as transient allenylidene intermediates *in situ* adding methanol to give methoxycarbene [Ru=C(OMe)CH=CR_2] complexes[11] which are inactive as olefin metathesis catalysts.

A preliminary assessment of the performance of these complexes in ring closing metathesis revealed a strong correlation with the nature of the chosen phosphine. In line with

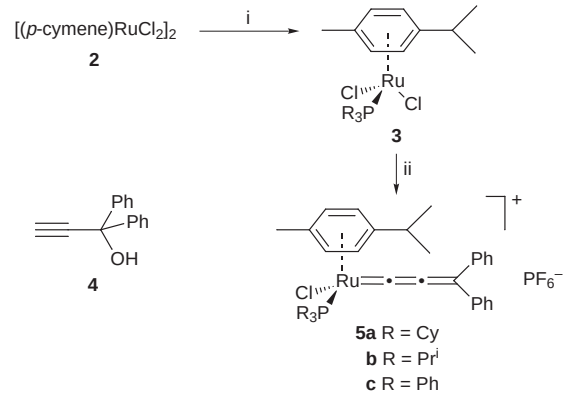

Scheme 1

Table 1 Screening of the catalytic activity of the allenylidene complexes **5**[a]

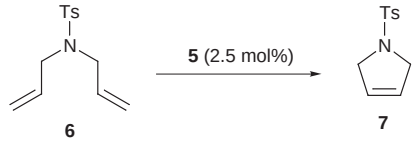

6 **7**

Entry	Catalyst	Solvent	Additive	*T*/°C	*t*/h	Yield (%)[b]
1	**5c**	toluene	—	80	3	2
2	**5b**	toluene	—	80	3	66
3	**5b**	CH_2Cl_2	—	40	26	95 (76)
4	**5a**	toluene	—	80	3	79
5	**5a**	toluene	—	80	4	100 (83)
6	**5a**	toluene	PCy_3 (5%)[c]	80	3	31

[a] General conditions: diene (1 mmol), catalyst (0.025 mmol), solvent (5 ml). [b] GC yield (isolated yield). [c] Based on the diene.

Table 2 Ring closing metathesis employing Ru-allenylidene catalyst **5a**[a]

Substrate	Product	Yield (%)
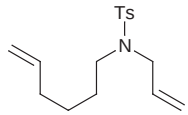 **8**	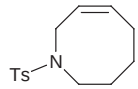 **9**	75
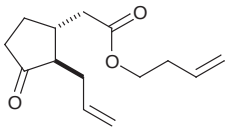 **10**	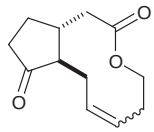 **11**	40
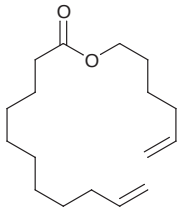 **12**	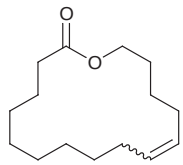 **13**	90
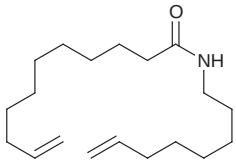 **14**	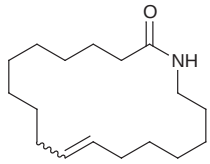 **15**	73
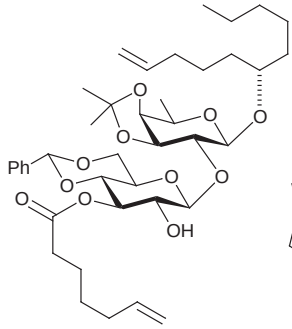 **16**	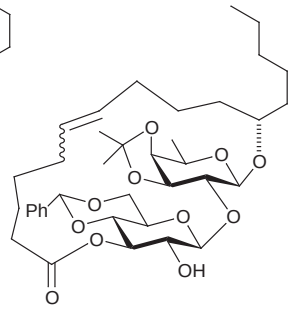 **17**	85

[a] All reactions using **5a** were carried out in toluene at 80 °C using a catalyst loading of 5 mol%.

previous observations with ruthenium-based initiators,[3,8,9] their catalytic activity decreases in the order PCy_3 > PPr^i_3 ≫ PPh_3 (Table 1). With **5a** (2.5 mol%) as the catalyst, diene **6** is quantitatively cyclized to dihydropyrrole **7** after 4 h in toluene at 80 °C (entry 5). Dichloromethane can also be used, although the turnover frequency of **5** is slightly lower in this particular reaction medium at 40 °C (*cf.* entries 2 and 3).

Having established the optimum reaction conditions, we applied catalyst **5a** to RCM of a set of representative diene substrates. As can be seen from the results compiled in Table 2, this catalyst nicely applies to the formation of essentially all ring sizes ≥ 5, including macrocyclic and medium sized products. The isolated yields obtained were found to be good to excellent and are comparable to those previously obtained using the Grubbs carbenes **1** [**9**: 75% *vs.* (68%);[12] **13**: 90% *vs.* (79%);[2c] **15**: 73% *vs.* 83%;[2a] **17**: 85% *vs.* 77%[2d]]. Only in the case of the 10-membered ring of jasmine ketolactone **11**, did the allenylidene complex **5a** turn out to be somewhat less efficient [**11**: 40% *vs.* (86%)[13]].

Particularly noteworthy are the smooth cyclizations of the conformationally flexible dienes **12** and **14** to 16- and 18-membered cycloalkenes **13** and **15**, respectively. The hydrogenation of compound **13** under standard conditions leads to the macrocyclic musk exaltolide,[14] which is used as a valuable perfume ingredient. Disaccharide **17** is an advanced intermediate *en route* to tricolorin A, a carcinostatic resin glycoside isolated from *Ipomoea tricolor*.[2d] The examples summarized in Table 2 clearly highlight the excellent compatibility of the allenylidene catalyst **5a** with various functional groups, including even unprotected secondary hydroxy groups.

Although the mode of action of these new metathesis catalysts and the nature of the actual intermediates involved in the catalytic cycle require further indepth studies, we have shown that the addition of an excess of PCy_3 strongly retards the metathetic conversion.

Current work in our laboratories is aiming at investigating the mechanism as well as to further explore the preparative scope of these readily accessible and highly promising metathesis catalysts, since they allow substantial possible variations of their basic structural motive.

The authors are grateful to Deutscher Akademischer Austauschdienst (DAAD) for a stipend to M. P., covering his stay in Mülheim for a three month period. We also thank K. Langemann and T. Müller, Mülheim, for providing various starting materials.

Notes and References

fuerstner@mpi-muelheim.mpg.de
† E-mail: pierre.dixneuf@univ-rennes1.fr

1 K. J. Ivin and J. C. Mol, *Olefin Metathesis and Metathesis Polymerization*, Academic Press, New York, 1997; R. H. Grubbs, S. J. Miller and G. C. Fu, *Acc. Chem. Res.*, 1995, **28**, 446; M. Schuster and S. Blechert, *Angew. Chem., Int. Ed. Engl.*, 1997, **36**, 2036; A. Fürstner, *Top. Catal.*, 1997, **4**, 285; S. K. Armstrong, *J. Chem. Soc., Perkin Trans. 1*, 1998, 371.
2 (*a*) A. Fürstner and K. Langemann, *Synthesis*, 1997, 792; (*b*) A. Fürstner and K. Langemann, *J. Org. Chem.* 1996, **61**, 8746; (*c*) A. Fürstner and K. Langemann, *J. Org. Chem.*, 1996, **61**, 3942; (*d*) A. Fürstner and T. Müller, *J. Org. Chem.*, 1998, **63**, 424.
3 S. T. Nguyen, R. H. Grubbs and J. W. Ziller, *J. Am. Chem. Soc*. 1993, **115**, 9858; P. Schwab, M. B. France, J. W. Ziller and R. H. Grubbs, *Angew. Chem., Int. Ed. Engl.* 1995, **34**, 2039; E. L. Dias, S. T. Nguyen and R. H. Grubbs, *J. Am. Chem. Soc.*, 1997, **119**, 3887.
4 T. E. Wilhelm, T. R. Belderrain, S. N. Brown and R. H. Grubbs, *Organometallics*, 1997, **16**, 3867.
5 A ruthenium allenylidene intermediate has been suggested in the catalytic coupling of propy-2-yn-1-ols with allylic alcohols, *cf* B. M. Trost and J. A. Flygare, *J. Am. Chem. Soc*., 1992, **114**, 5476.
6 M. A. Bennett and A. K. Smith, *J. Chem. Soc., Dalton Trans*., 1974, 233; R. A. Zelonka and M. C. Baird, *Can. J. Chem.* 1972, **50**, 3063.
7 C. Bruneau and P. H. Dixneuf, *Chem. Commun.*, 1997, 507.
8 A. W. Stumpf, E. Saive, A. Demonceau and A. F. Noels, *J. Chem., Soc. Chem. Commun.*, 1995, 1127; A. Demonceau, A. W. Stumpf, E. Saive and A. F. Noels, *Macromolecules*, 1997, **30**, 3127.
9 A. Hafner, A. Mühlebach and P. A. van der Schaaf, *Angew. Chem., Int. Ed. Engl.*, 1997, **36**, 2121.
10 P. H. Dixneuf and C. Bruneau, in *Organic Synthesis via Organometallics, OSM 5*, ed. G. Helmchen, Vieweg, Wiesbaden, 1997, p. 1; D. Péron, A. Romero and P. H. Dixneuf, *Organometallics*, 1995, **14**, 3319.
11 D. Pilette, L. Ouzzine, H. Le Bozec, P. H. Dixneuf, C. E. F. Rickard and W. R. Roper, *Organometallics*, 1992, **11**, 809.
12 M. S. Visser, N. M. Heron, M. T. Didiuk, J. F. Sagal and A. H. Hoveyda, *J. Am. Chem. Soc.*, 1996, **118**, 4291.
13 A. Fürstner and T. Müller, *Synlett*, 1997, 1010.
14 Exaltolide is a trademark of Firmenich SA, Geneva, Switzerland; for a general review see: G. Ohloff, *Riechstoffe und Geruchssinn*, Springer, Berlin, 1990.

Received in Cambridge, UK, 1st May 1998; 8/03286F

Palladium-catalyzed cross-coupling of organolead compounds with organostannanes

Suk-Ku Kang,*† Hyung-Chul Ryu and Sang-Chul Choi

Department of Chemistry, Sung Kyun Kwan University, Natural Science Campus, Suwon 400-746, Korea

The palladium-catalyzed cross-coupling of organolead triacetates with organostannanes has been accomplished in the presence of $Pd_2(dba)_3{\cdot}CHCl_3$ (5 mol%) and NaOMe (5 equiv.) in MeOH–MeCN (1 : 1) under mild conditions.

The palladium-catalyzed cross-coupling of organostannanes with aryl of vinyl halides and triflates, known as the Stille reaction,[1] has become a versatile tool in organic synthesis. Main group metals such as lead(IV),[2] bismuth[3] and thallium[4] have been of limited use in cross-coupling reactions. Recently, Pinhey[2] reported the arylation, alkenylation and alkynylation of organolead(IV) tricarboxylates with soft carbon nucleophiles. As an alternative to organic electrophiles, hypervalent iodonium compounds were employed in the cross-coupling with organostannanes.[5] However, the coupling reaction of organolead compounds as electrophiles with organostannanes is not known. Here we report the cross-coupling of organostannanes with organolead(IV) compounds.

Initially, we examined the cross-coupling of phenyllead triacetate **1a**[6] with vinyl tributylstannane **2a** to determine the optimum reaction conditions. After series of fruitless experiments, we found that the use of NaOMe as a base was crucial in this coupling. Of the catalysts $Pd_2(dba)_3{\cdot}CHCl_3$, $Pd(OAc)_2$ and $PdCl_2$ tested, $Pd_2(dba)_3{\cdot}CHCl_3$ was the best. Even though $CHCl_3$ was also effective, the solvent system MeOH–MeCN (1 : 1) was most suitable. To avoid homocoupling, CuI (10 mol%) was added as a cocatalyst (Scheme 1).[7]

Phenyllead triacetate **1a** was reacted with vinyl tributylstannane **2a** in the presence of NaOMe (5 equiv.) using $Pd_2(dba)_3{\cdot}CHCl_3$ (5 mol%) and CuI (10 mol%) as catalysts in MeOH–MeCN (1 : 1) at room temperature for 2 h to afford styrene **3a** as the sole product in 80% yield (entry 1, Table 1). Under the same conditions the reaction of **1a** with the β-styrylstannane **2b** gave the coupled product (*E*)-β-stilbene **3b** in 72% yield (entry 2). When phenyllead triacetate **1a** was treated with α-styrylstannane **2c**, (*E*)-β-stilbene **3b** was also obtained as the sole product *via* the mechanism of *cine* substitution[8] in 40% yield (entry 3). For the alkynylstannane **2d**, the reaction with **1a** gave the coupled product **3c** in 79% yield (entry 4). When the same reaction was conducted in $CHCl_3$ as the only solvent, the coupled product **3c** was obtained in 45% yield along with the homocoupled product (30%).[9] Treatment of 2-furyl(tributyl)stannane **2e**, 3-furyl(tributyl)stannane **2f**, and 3-thienyl-substituted stannane **2g** with *p*-methoxyphenyllead triacetate **1b**[10] afforded the substituted furans **3d**,[11] **3e**[12] and thiophene **3f**[13] in 73, 70 and 85% yields, respectively (entries 5–7).‡ For the coupling of **1b** with 2-furyl stannane **2e** under the same conditions without addition of CuI as catalyst, the coupled product **3e** was obtained in 60% yield after 7 h along with the homocoupled product (25%). However, the addition of CuI (10

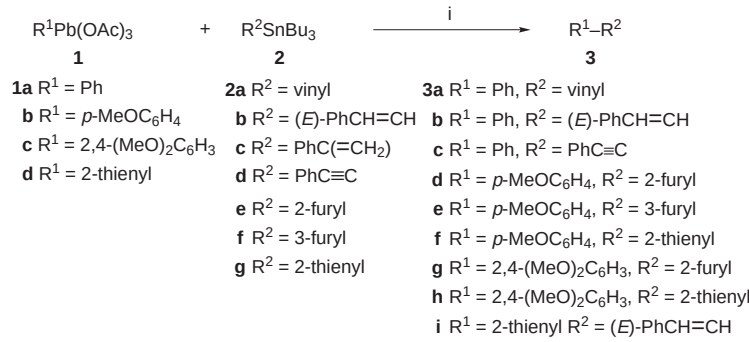

Scheme 1 *Reagents and conditions*: i, $Pd(dba)_3{\cdot}CHCl_3$ (5 mol%), CuI (10 mol%), NaOMe (5 equiv.), MeOH–MeCN (1 : 1)

Table 1 Palladium-catalyzed cross-coupling of organostannanes with organolead triacetates

Entry	Organolead compounds	Organostannanes	*T*/°C	*t*/h	Product	Isolated yield (%)[a]
1	**1a**	**2a**	room temp.	2	**3a**	80 (trace)
2	**1a**	**2b**	room temp.	2	**3b**	72 (trace)
3	**1a**	**2c**	60	3	**3b**	40
4	**1a**	**2d**	room temp.	2	**3c**	79 (10)
5	**1b**	**2e**	room temp.	2	**3d**	73 (10)
6	**1b**	**2f**	60	2	**3e**	70 (trace)
7	**1b**	**2g**	60	2	**3f**	85 (10)
8	**1c**	**2e**	room temp.	3	**3g**	72 (trace)
9	**1c**	**2g**	room temp.	3	**3h**	73 (trace)
10	**1d**	**2b**	60	2	**3i**	62 (10)

[a] The yields in parentheses are the yields of the homocoupling products, which are easily separated by column chromatography.

mol%) improved the yield to 73% yield with reduced reaction time (2 h) and reduced homocoupling (10%). The 2,4-dimethoxyphenyllead triacetate **1c**[14] was also coupled with 2-furyl and 2-thienyl substituted stannanes **2e** and **2g** at room temperature for 3 h to afford the coupled products **3g**§ and **3h**[15] in 72 and 73% yields, respectively (entries 8 and 9). Finally, 2-thienyllead triacetate **1d**[16] was reacted with (*E*)-β-styrylstannane **2b** to give the coupled product **3i**[17] in 62% yield (entry 10). The results are summarized in Scheme 1 and Table 1.

Although the detailed mechanism for the role of NaOMe remains to be elucidated, it is presumed that organolead trimethoxide $RPb(OMe)_3$ is formed[18] and drives facile oxidative addition[19] with Pd^0 to give polar reactive intermediate $RPdPb(OMe)_3$, which allows the transmetallation and coupling to proceed under mild conditions

A typical procedure is as follows: To a stirred solution of *p*-methoxylphenyllead triacetate **1b** (140 mg, 0.28 mmol) and NaOMe (77 mg, 1.42 mmol) in MeOH–MeCN (1 : 1, 3 ml) was added $Pd_2(dba)_3{\cdot}CHCl_3$ (14 mg, 5 mol%) and CuI (5 mg, 10 mol%), followed by 2-thienyl(tributyl)stannane **2g** (100 mg, 0.27 mmol) *via* syringe at room temperature under N_2, and the reaction mixture was stirred at 60 °C for 2 h and cooled to room temperature. The reaction mixture was extracted with Et_2O (20 ml), washed three times with water, dried over anhydrous $MgSO_4$ and evaporated *in vacuo*. The crude product was separated by SiO_2 column chromatography (hexanes, R_f = 0.28) to afford the coupled product **3f** (44 mg, 85%).

In conclusion, the palladium-catalyzed cross-coupling reaction of organolead triacetates with organostannanes was achieved under mild conditions.

The authors wish to acknowledge the financial support of the Korea Research Foundation in the Program Year 1997.

Notes and References

† E-mail: skkang@chem.skku.ac.kr

‡ *Selected data* for **3e**: TLC, SiO_2, hexanes, R_f = 0.36; δ_H(400 MHz, $CDCl_3$) 3.83 (s, 3 H), 6.65 (m, 1 H) 6.92 (m, 2 H), 7.42 (m, 3 H), 7.65 (s, 1 H); ν_{max} (neat)/cm^{-1} 3054, 2928, 1605, 1275; *m*/*e* (EI) 174 (100%), 159 (75), 131 (45), 77 (40).

§ *Selected data* for **3g**: TLC, SiO_2, EtOAc–hexanes (1 : 10), R_f = 0.37; δ_H(400 MHz, $CDCl_3$) 3.96 (s, 3 H), 4.04 (s, 3 H), 6.59 (m, 1 H), 6.68 (m, 1 H), 6.70 (m, 1 H), 6.91 (m, 1 H), 7.54 (dd, 1 H), 7.87 (d, 1 H); ν_{max}(neat)/cm^{-1} 3055, 2856, 1422, 1265, 896, 740; *m*/*z* (EI) 203 (100%), 188 (24), 161 (41), 102 (119).

1 J. K. Stille, *Angew. Chem., Int. Ed. Engl*., 1986, **25**, 508–524; T. N. Mitchell, *Synthesis*, 1992, 803; V. Farina, in *Comprehensive Organometallic Chemistry II*, ed. E. W. Abel, F. G. A. Stone and G. Wilkinson, Pergamon, New York, 1995, vol. 12, ch. 3, 4; V. Farina, *Pure Appl. Chem*., 1996, **68**, 73.

2 J. T. Pinhey, *Aust. J. Chem*., 1991, **44**, 1353; J. T. Pinhey, *Pure Appl. Chem*., 1996, **68**, 819; S. Hashimoto, Y. Miyazaki, T. Shinoda and S. Ikegami, *J. Chem. Soc., Chem. Commun*., 1990, 1100.

3 Y. Matano and H. Suzuki, *Bull. Chem. Soc. Jpn.*, 1996, **69**, 2673.

4 R. C. Larock and C. A. Fellows, *J. Am. Chem. Soc*., 1982, **104**, 1900; R. C. Larock, S. Varaprah, H. H. Lau and C. A. Fellows, *J. Am. Chem. Soc.*, 1984, **106**, 5274; E. C. Tayler and A. Mckillop, *Acc. Chem. Res*., 1970, **3**, 338; R. C. Larock and H. Yang, *Synlett*, 1994, 748.

5 R. M. Moriarty and W. R. Epa, *Tetrahedron Lett.*, 1992, **33**, 4095; R. J. Hinkle, G. T. Poulter and P. J. Stang, *J. Am. Chem. Soc*., 1993, **115**, 11 626; S-K. Kang, H-W. Lee, J-S. Kim and S-C. Choi, *Tetrahedron Lett*., 1996, **37**, 3723; S-K. Kang, H-W. Lee, S-B. Jang, T-H. Kim and J-S. Kim, S*ynth. Commun*., 1996, **26**, 4311.

6 J. Morgan and J. T. Pinhey, *J. Chem. Soc., Perkin Trans. 1*, 1990, 715.

7 The CuCl-catalyzed homocoupling of vinyl- and aryl-lead diacetates was reported by Pinhey see J. Morgan, C. J. Parkinson and J. T. Pinhey, *J. Chem. Soc., Perkin Trans. 1*, 1994, 3361.

8 K. Kikukawa, H. Umekawa and T. Matsuda, *J. Organomet. Chem.*, 1986, **311**, C44; G. Stork and R. C. A. Isaacs, *J. Am. Chem. Soc*., 1990, **112**, 7399; C. A. Busacca, J. Swestock, R. E. Johnson, T. R. Bailey, L. Musza and C. A. Rodger, *J. Org. Chem*., 1994, **59**, 7553; V. Farina and M. A. Hossain, *Tetrahedron Lett*., 1996, **37**, 6997.

9 The substituted lead(IV) triacetates undergo homocoupling in the presence of $Pd_2(dba)_3{\cdot}CHCl_3$ (5 mol%) in $CHCl_3$ at room temperature for 10 min. See, S-K. Kang, U. Shivkumar, C. Ahn, S-C. Choi and J-S. Kim, *Synth. Commun*., 1997, **27**, 1893.

10 *p*-Methoxyphenyllead triacetate **1b** was easily prepared from anisole by treatment with lead tetraacetate. See R. P. Kozyrod and J. T. Pinhey, *Org. Synth*., 1984, **62**, 24.

11 S. Pelter, M. Rowlands and G. Clements, *Synthesis*, 1987, 51.

12 R. H. Young, R. L. Martin, N. Chinh, C. Mallon and R. H. Kayser, *Can. J. Chem*., 1972, **50**, 932.

13 L. J. Baldwin, S. Pakray, R. N. Castle and M. L. Lee, *J. Heterocyclic Chem*., 1985, **22**, 1667.

14 L. C. Willemsens, D. de V. J. Spierenburg and J. Wolters, *J. Organomet. Chem*., 1972, **39**, C61.

15 T. Sone, R. Yokoyama, Y. Okuyama and K. Sato, *Bull. Chem. Soc. Jpn*., 1986, **59**, 83.

16 H. C. Bell, J. R. Kalman, J. T. Pinhey and S. Sternhell, *Aust. J. Chem*., 1979, **32**, 1521.

17 A. Kasahara, T. Izumi and T. Ogihara, *J. Heterocyclic Chem*., 1989, **26**, 597.

18 Recently, it was reported that the modification of ligands influences the efficiency of the metal–metal exchange: C. J. Parkinson, J. T. Pinhey and M. J. Stoermer, *J. Chem. Soc., Perkin Trans. I*, 1992, 1911.

19 The oxidative addition of organostannanes to a palladium(0) complex is known: E. Shirakawa, H. Yoshida and T. Hiyama, *Tetrahedron Lett*., 1997, **38**, 5177.

Received in Cambridge, UK, 14th April 1998; 8/02726I

Typeset and printed by Black Bear Press Limited, Cambridge, England

ChemComm
FEATURE ARTICLE

Tetracyanoethylene-based organic magnets

Joel S. Miller[a]† and Arthur J. Epstein[b]‡

[a] *Department of Chemistry, University of Utah, Salt Lake City, Utah 84112-0850, USA*
[b] *Department of Physics and Department of Chemistry, The Ohio State University, Columbus, Ohio 43210-1106, USA*

Several classes of organic magnets based upon the tetracyanoethenide radical anion, [TCNE]$^{\cdot-}$, either unbound, μ, and μ_4 bonded to zero, two and four metal sites have been reported. The putative μ_4 bonded V(TCNE)$_x$ room temperature magnet has been extended to include M(TCNE)$_x$ (M = Mn, Fe, Co, Ni) magnets. M for this class of magnets is assigned to be in the divalent oxidation state. A σ-[TCNE]$_2^{2-}$ dimer intermediate has been isolated. The intrachain magnetic coupling for the 1-D coordination polymers having [TCNE]$^{\cdot-}$ μ-bridge bonded to [Mn^{III}porphyrins]$^+$ is discussed in the context of a structure–function correlation arising from the dihedral angle between the [Mn^{III}TPP]$^+$'s MnN$_4$ and [TCNE]$^{\cdot-}$ mean planes and the magnitude of magnetic coupling. This correlation is ascribed to the increasing importance of the σ-Mn^{III} d_{z^2}/[TCNE]$^{\cdot-}$ p_z overlap with decreasing dihedral angle.

From time immemorial magnets comprised a few metals or their oxides with the key component of all magnets, the unpaired electron spins, solely residing in d- or f-orbitals. Extension to organic radicals was first discussed in 1963 from a conceptional point of view,[1] but their experimental realization was not achieved until 1985. At that time [Fe(C$_5$Me$_5$)$_2$]$^{\cdot+}$[TCNE]$^{\cdot-}$ (TCNE = tetracyanoethylene) with a magnetic ordering temperature, T_c, of 4.8 K was reported to be the first magnet with spin residing in a p-orbital[2] that (i) required spins in p-orbitals, (ii) exhibited magnetic hysteresis, (iii) did not have extended network bonding in 1, 2 or 3 dimensions, (iv) was soluble in conventional organic solvents, and (v) did not require metallurgical preparative methods. Today, molecule-based magnets include many diverse examples of materials exhibiting magnetic ordering including ferromagnets, ferrimagnets, canted/weak ferromagnets, metamagnets and spin glasses. Materials range from p-orbital-based organic nitroxides,[3,4] p/d-orbital-based mixed organic radicals/organometallic or inorganic coordination systems,[4–6] to the more classical d-orbital-based inorganic coordination compounds (*e.g.* mixed metal oxalates and cyanides),[4,5] with several classes of the organic/metal-ion-containing-ones possessing TCNE studied in our laboratory. As is the intent of feature articles in this journal, we provide a personal account of the results on two classes of TCNE-based magnets, namely, M[TCNE]$_x$ and [Mn(porphyrin)][TCNE] magnets. Broad reviews on molecule-based magnets, however, are available.[3–6]

M(TCNE)$_x$ Magnets

In 1991 V(TCNE)$_x$·y(CH$_2$Cl$_2$) ($x \sim 2$; $y \sim 1/2$) **1a**, prepared from the room temperature reaction of V^0(C$_6$H$_6$)$_2$ and TCNE, was reported to be a magnet below a critical temperature estimated to be ~400 K.[4,7] Owing to the structural disorder, variable composition and extreme oxygen/water sensitivity the structure and oxidation state assignment of this valence-ambiguous material has yet to be elucidated. Although the structure is as yet unknown, based upon the magnetic, IR, and elemental analyses data, **1a** is formulated as V^{II}(TCNE)$_2$·1/2(CH$_2$Cl$_2$) with S = 3/2 V^{II} and two S = 1/2 [TCNE]$^{\cdot-}$ systems. A 3-D network structure **2**, with each vanadium

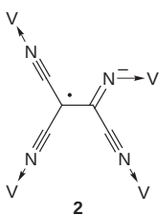

2

surrounded by up to six ligands which are primarily nitrogens from different [TCNE]$^{\cdot-}$ species, and the [TCNE]$^{\cdot-}$ species binding up to four different vanadiums *via* σ-N bonds, is proposed.

Compound **1a** exhibits a field-dependent magnetization, $M(H)$, between 1.4 and 350 K (Fig. 1), and saturates to *ca.* 6 × 10^3 emu Oe mol^{-1} at 2 K and 19.5 kG. Assuming a Landé g value of 2, the expected maximum or saturation magnetization, M_s, for ferromagnetic coupling between S = 3/2 V^{II} and the two S = 1/2 [TCNE]$^{\cdot-}$ species (*ie.* S_{total} = 5/2) is 28 × 10^3 emu Oe mol^{-1}. In contrast, antiferromagnetic coupling, leading to ferrimagnetic behavior as observed for magnetite (Fe$_3$O$_4$), leads to an S_{total} of 1/2 with M_s expected to be 5.6 × 10^3 emu Oe mol^{-1}. The latter is in good agreement with the observed value. Hysteresis, characteristic of magnets' composition and shape, with a coercive field of 60 G is observed at room temperature (Fig. 2). The strong magnetic behavior is readily observed by its being attracted to a permanent magnet at room temperature (Fig. 3). Thus, **1a** is the first example of organic-based material with a critical temperature exceeding room temperature. The critical temperature exceeds 350 K, the thermal decomposition temperature of the sample, and a linear extrapolation to the

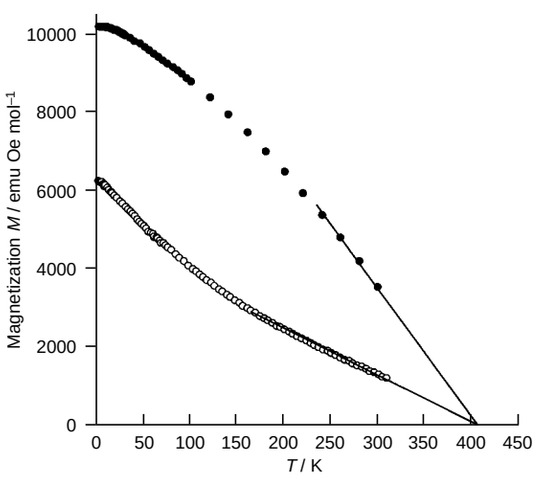

Fig. 1 Magnetization as a function of temperature [$M(T)$] at 1 kG for V(TCNE)$_x$·y(CH$_2$Cl$_2$) prepared from (○) V(C$_6$H$_6$)$_2$ **1a**[7] and (●) V(CO)$_6$ **1b**[8]

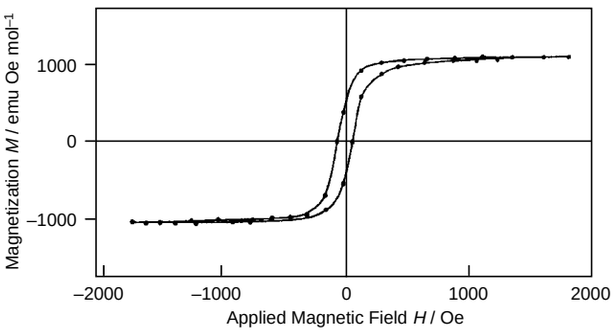

Fig. 2 Hysteresis $M(H)$, of $V(TCNE)_x{\cdot}y(CH_2Cl_2)$ **1a**, at room temperature

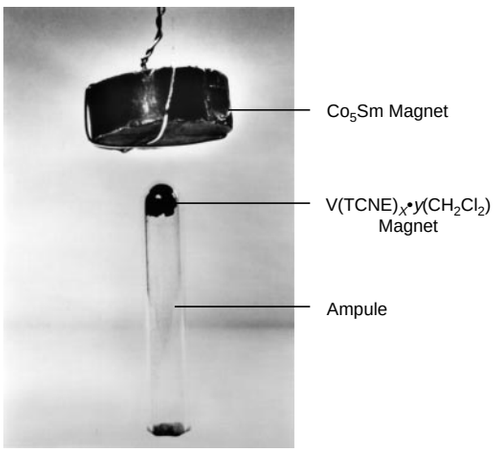

Fig. 3 Photograph of a powdered sample of **1a** being attracted to a Co_5Sm magnet at room temperature

temperature at which the magnetization should vanish leads to an estimate of $T_c \sim 400$ K (Fig. 1). Compound **1a** is also a semiconductor with a room temperature conductivity of $\sim 10^{-3}$ S cm^{-1} which decreases with decreasing temperature. At low temperatures the conductivity becomes frequency dependent, suggesting a hopping conduction mechanism.[7d]

Thermal treatment of **1a** reduces the magnetization. At room temperature **1a** has a *ca.* 50 day half-life. Sealed samples heated for 10 h at 100 °C are significantly less magnetic, while heating to 160 °C for 48 h destroys magnetic ordering; however, the number of spins remains essentially unchanged. Concomitantly, the infrared spectra in the ν_{CN} region are altered slightly with the absorption at 2195 cm^{-1} moving to higher energy at 2206 cm^{-1}. Air exposure further alters the infrared spectra, with the major absorption in the $\nu_{C\equiv N}$ region shifting to 2220 cm^{-1}. Likewise, **1a** rapidly decomposes in air and looses magnetic ordering. Infrared analysis of the decomposed product has much weaker absorptions at 2225 cm^{-1} which is in the region reported for TCNE[0 9] as well as TCNE π-bonds to metals atoms or ions.[10]

The reaction of $V(C_6H_6)_2$ and other strong acceptors such as TCNQ, perfluoro-TCNQ ($TCNQF_4$), $C_4(CN)_6$, 2,3,5,6-tetrachlorobenzoquinone (chloranil), 2,3-dichloro-5,6-dicyanobenzoquinone (DDQ) and 2,3,5,6-tetracyanobenzoquinone (cyanil)[11] led to insoluble precipitates of unknown composition. These materials do not exhibit field-dependent magnetic susceptibilities and their high temperature susceptibilities can be fitted to the Curie–Weiss expression with $\theta < 0$ characteristic of antiferromagnetic, not ferromagnetic, behavior. Hence, magnets of nominal $V(acceptor)_x{\cdot}y(solvent)$ composition based on strong acceptors other than TCNE have yet to be prepared.

Compound **1a** is a structurally disordered material; hence, improved preparative routes leading to less disorder as well as avoiding the difficult-to-obtain $V(C_6H_6)_2$ were sought. Unlike $V^0(C_6H_6)_2$, the reaction of isoelectronic $V^0(C_5H_5)(C_7H_7)$ with TCNE did not afford a room-temperature magnet.[8] This is due to the greater oxidation potential of $V^0(C_5H_5)(C_7H_7)$ (0.34 V *vs.* SCE) with respect to $V^0(C_6H_6)_2$ (−0.28 V). Similarly, the reactions of $[TCNE]^{\cdot-}$ and $[V^I(C_6H_6)_2]^+$ or TCNE and $V^{II}(C_5H_5)_2$ did not afford a room-temperature magnet. Since the reaction of $V^0(C_6H_6)_2$ and TCNE leads to a strongly magnetic material, but the reaction of $[V^I(C_6H_6)_2]^+$ and $[TCNE]^{\cdot-}$ does not, the mechanism of the reaction is crucial in the formation of the room-temperature magnet and it is presently being investigated. In contrast, the room-temperature reactions of $V^0(CO)_6$, $[V^I(C_6H_6)_2][V^{-I}(CO)_6]$, $[V^{II}(NCMe)_6][V^{-I}(CO)_6]_2$, $[V^{II}(NCMe)_6]^{2+}$ and $[V^{II}(THF)_6][V^{-I}(CO)_6]_2$ with TCNE led to room-temperature magnets; while the reactions of $[Et_4N][V^{-I}(CO)_6]$ and $Na[V^{-I}(CO)_6]{\cdot}2$diglyme did not.[8] The reaction of $V^0(CO)_6$ with TCNE was studied in detail.[8]

The elemental composition suggests that the magnets prepared from $V(C_6H_6)_2$ or $V(CO)_6$ have similar compositions. The similarity of the IR spectra for the magnets prepared from $V(C_6H_6)_2$ (*i.e.* **1a**) and $V(CO)_6$ (*i.e.* **1b**) and the absence of $\nu_{C\equiv O}$ stretches in the 1800 to 2000 cm^{-1} region for the latter magnet strongly suggest that all the carbonyls are expelled from the vanadium coordination sphere upon the reaction of $V(CO)_6$ with TCNE.[8] This was confirmed from the quantification of CO-loss *via* Toepler pump measurements for [eqn. (1)],

$$V(CO)_6 + y\ TCNE \rightarrow V(TCNE)_y(CO)_{6-x}\ (\mathbf{1b}) + x\ CO \quad (1)$$

with $x = 5.9 \pm 0.1$. Thus, all the six carbonyls are lost. Based on the lack of CO and the similarity between the IR spectra for the magnets prepared from $V(CO)_6$ (**1b**) and $V(C_6H_6)_2$ (**1a**), both are assigned the same structural building block **2**. Nonetheless, differences between the ν_{CN} absorptions for **1a** and **1b** indicate that the two magnets are structurally inequivalent and different magnetic behavior is observed, although both have a T_c 400 K (Fig. 1).

The M for **1b** (Fig. 1), is 10 300 emu Oe mol^{-1} at 4.2 K and 3600 emu Oe mol^{-1} at room temperature and an applied magnetic field of 1 kG; an increase of 67 and 133% at these temperatures, respectively, as compared to **1a**. Whereas M decreases monotonically with increasing T for **1a**, this is less evident at low temperatures for **1b**. The unusual linear decrease of M with increasing T is consistent with extensive disorder in the sample, and suggests that the **1b** is less disordered. Hysteresis with a coercive field of 15 Oe is observed at room temperature and at 4.2 K for the **1b**. This is significantly lower than the 60 Oe value observed for **1a** (Fig. 2).[7] The extrapolated T_c for **1b** is ~400 K, comparable to **1a** (Fig. 1).[7] The results of the magnetic behavior for **1** give hope that more molecular/organic/polymeric magnets with higher T_cs will be available in the future. Already a room temperature a Prussian blue-structured magnet, also based on vanadium, has been reported.[12]

In addition to forming **1** *via* the solution reaction of TCNE and $V(C_6H_6)_2$ or $V(CO)_6$, these reactions were also carried out without solvent. No reaction occurred upon the reaction of TCNE and $V(C_6H_6)_2$, while an immediate blue precipitate occurred with TCNE and $V(CO)_6$ at the surface of the TCNE crystals or on the walls of the reaction vessel if both TCNE to $V(CO)_6$ were co-sublimed. For the latter product, the IR spectrum and magnetic properties were very similar to materials prepared from solution. However, this material has reduced oxygen sensitivity. This difference is attributed to its much lower surface area when compared to the fine (~100 m^2 g^{-1}) powders that are formed from solution.[13]

Due to T_c exceeding room temperature, applications for this magnet can be envisioned.[14] One application is for magnetic shielding, the attenuation of magnetic fields found in many electronic applications, *e.g.* high voltage lines. The feasibility of using **1** for this applications has been demonstrated (Fig. 4).[15]

Synthesis of the $V(TCNE)_x{\cdot}y$(solvent) magnet using solvents other than CH_2Cl_2 results in similar materials with varying

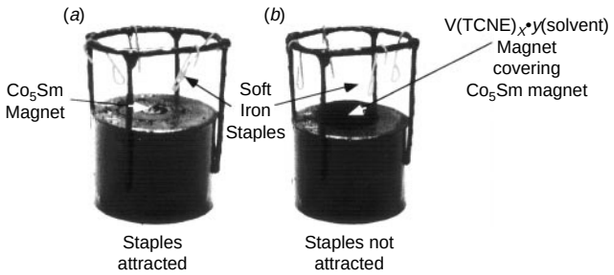

Fig. 4 Illustration of the $V(TCNE)_x{\cdot}y(CH_2Cl_2)$ magnet being an effective magnetic shield at room temperature; rods (paper clips) of soft-iron are attracted to a Co_5Sm permanent magnet (*a*); however, when a 1.7 mm pellet of $V(TCNE)_x{\cdot}y(CH_2Cl_2)$ is placed between the Co_5Sm magnet and the rods they hang freely (*b*) demonstrating magnetic shielding

degrees of structural order. For example, there is increasing disorder in the structure as the CH_2Cl_2 is replaced by THF[7b] (T_c ~ 210 K) and MeCN[7c] (T_c ~ 100 K). The exact magnetic ordering temperature varies with preparation conditions and resulting structural order. With increasing order these materials show features of correlated spin glass behavior. Additional examples of this class of magnets are needed to understand the chemistry and physics.[7,8] To date the reaction of $V(C_6H_6)_2$ or $V(CO)_6$ with other strong acceptors does not form magnetically ordered materials. Attempts to replace V with Cr, *i.e.* the reaction of TCNE with $Cr(C_6H_6)_2$ or $Cr(CO)_6$, lead to nonmagnetically ordered, but ferromagnetically coupled, $[Cr(C_6H_6)_2][TCNE]$[16] and a substitution reaction with $Cr(CO)_6$ forming $Cr(CO)_5(TCNE)$.[17] However, magnets of $M(TCNE)_2{\cdot}y$(solvent) stoichiometry have recently been reported.

$M(TCNE)_2{\cdot}y(CH_2Cl_2)$ (M = Mn, Fe, Co, Ni) have been prepared *via* the reaction of $MI_2{\cdot}x$MeCN in CH_2Cl_2.[18] The ν_{CN} absorption bands for $M(TCNE)_2{\cdot}xCH_2Cl_2$ are consistent with coordinated $[TCNE]^{\cdot-}$ and are similar, albeit sharper and occur at higher in energy, to that observed for $V(TCNE)_x{\cdot}y(CH_2Cl_2)$. In contrast to disordered $V(TCNE)_x{\cdot}y(CH_2Cl_2)$, $M(TCNE)_2{\cdot}xCH_2Cl_2$ (M = Mn, Fe) give X-ray powder patterns, which have yet to be indexed.

The spin and oxidation states of $Fe(TCNE)_2{\cdot}xCH_2Cl_2$ **3** were determined from ^{57}Fe Mössbauer spectroscopy.[18] Above 95 K, **3** has absorptions with large chemical shift [δ = 1.23 mm s^{-1}] and quadrupole coupling [ΔE_q = 3.26 mm s^{-1}] characteristic of hexacoordinate, high-spin Fe^{II} compounds[19] (Fig. 5). Below 95 K, the spectra become more complex due to magnetic

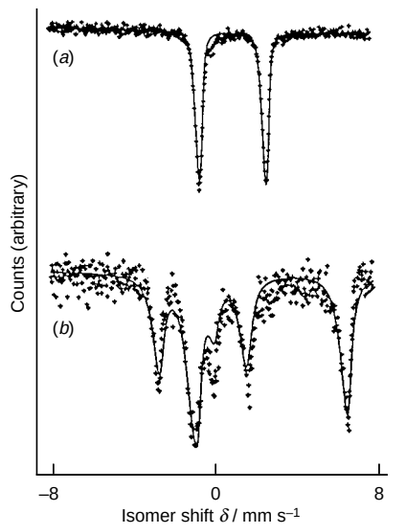

Fig. 5 ^{57}Fe Mössbauer spectra of $Fe(TCNE)_2{\cdot}xCH_2Cl_2$ at (*a*) 50 and (*b*) 100 K[18]

splitting [δ = 1.24 mm s^{-1}; ΔE_q = 3.31 mm s^{-1}, H_{int} = 229 KOe] (Fig. 5) in agreement with the critical temperature determined *via* magnetic studies (*vide infra*).

Complex **3** has a complex magnetic behavior which is essentially independent of preparation and amount of solvent.[18] The susceptibility cannot be fitted to the Curie–Weiss law, $\chi \propto (T - \theta)^{-1}$, as expected for high-spin d^6 Fe^{II} in an octahedral environment with spin-orbit coupling. A spontaneous magnetization occurs below a T_c of 121 K, taken here as the intercept with the temperature axis of the initial slope of the magnetization as a function of temperature (Fig. 6). At 2 K the

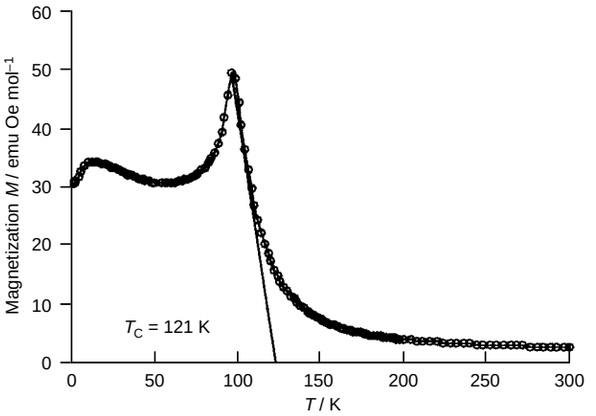

Fig. 6 Zero-field cooled magnetization as function of temperature for $Fe(TCNE)_2{\cdot}0.75CH_2Cl_2$

magnetization shows a complex, poorly understood response to the field, reminiscent of metamagnetic behavior. At 5 T and 2 K the observed magnetization is *ca.* 16 900 emu Oe mol^{-1}; however, higher fields are necessary to achieve saturation. This value of saturation magnetization corresponds to three S = 1/2 spins and exceeds the comparable value of 10 300 emu Oe mol^{-1} for $V(TCNE)_x{\cdot}y(CH_2Cl_2)$ prepared from $V(CO)_6$[8] by 63%, as well as exceeding the expectation of that from antiferromagnetically coupling between an S = 2 Fe^{II} site and two S = 1/2 $[TCNE]^{\cdot-}$, *i.e.* 11 200 emu Oe mol^{-1}, but is substantially less than the expectation from ferromagnetic coupling, *i.e.* 33,500 emu Oe mol^{-1}. Although the T_c shows little dependence on the synthetic route, hysteresis loops taken at 2 K show a strong variation in the coercive field ranging from 300 to 3000 G. Likewise, the detailed field and zero field cooled curves also have a strong dependency on reaction conditions and aging.

$Fe(TCNE)_2{\cdot}xCH_2Cl_2$ shows remarkable thermal stability. The IR spectrum and X-ray powder pattern, as well as magnetic data of a sample heated at 130 °C for 38 h, suggest that the chemical and structural features of the materials are preserved after the heat treatment, except for the apparent solvent loss. Some thermal degradation is observed from magnetic measurements on a sample treated at 180 °C, and massive decomposition is evident from IR studies when the material is heated to 200 °C. TGA data show that although desolvation starts at temperatures as low as 40 °C, it does not approach completion until the sample decomposes. Since CH_2Cl_2 is a poorly coordinating solvent, the high desolvation temperature may be attributed to CH_2Cl_2 being trapped into a three-dimensional network, and is only completely released when the structure collapses. $Fe(TCNE)_2{\cdot}xCH_2Cl_2$ is not pyrophoric as is $V(TCNE)_x{\cdot}y$(solvent), but it does decompose in air.

Reactions of TCNE and MeCN solvates of MI_2 (M = Mn, Co, Ni) led to $M(TCNE)_2{\cdot}xCH_2Cl_2$ species which magnetically order with T_c values of 44 (M = Ni, Co) and 107 K (M = Mn)[8] (Table 1). The nearest neighbor spin coupling energy, J, can be estimated from the mean-field expression of $T_c = JzS(S + 1)/3k_B$, where k_B = Boltzmann's constant, z = number of nearest neighbors, *i.e.* 6, and assuming $H = -2JS_a{\cdot}S_b$. The

Table 1 Summary of the infrared ν_{CN} absorption bands, saturation magnetization M_s, ordering temperature T_c and exchange energy J for $M(TCNE)_2{\cdot}xCH_2Cl_2$ (M = V, Mn, Fe, Co, Ni)[18]

Metal	Saturation magnetization[a] M_s/ emu Oe mol^{-1}	T_c/K	J/K[b]
V[c]	10 300	~400	53
Mn[d]	19 000	107	6.1
Fe[d]	16 900	121	10
Co[d]	8 000	44	5.9
Ni[d]	15 800	44	11

[a] 2 K and 5 T. [b] See text. [c] Ref. 7. [d] Ref. 18.

resulting estimates of J ranges as V ≫ Ni ~ Fe > Mn ~ Co (Table 1). $Mn(TCNE)_2{\cdot}xCH_2Cl_2$ is isostructural to $Fe(TCNE)_2{\cdot}xCH_2Cl_2$ based upon powder diffraction data; however, for M = Ni, Co the solids diffract poorly and do not appear to be isomorphous to $M(TCNE)_2{\cdot}xCH_2Cl_2$ (M = Fe, Mn). Hence, based upon the composition and the similarity of the ν_{CN} absorptions for M = Mn, Co and Ni, we assign all the metals as being divalent. Likewise, the elusive oxidation state of V in the room temperature $V(TCNE)_x{\cdot}yCH_2Cl_2$ magnet is again assigned the divalent oxidation state.[7,8]

Hysteresis is observed for all the magnets below T_c, however, as observed for $V(TCNE)_x{\cdot}y(CH_2Cl_2)$,[7,8] the coercive field varies from preparation to preparation. Nonetheless, the observed coercive fields range from 50 (M = Ni) to 6500 Oe (M = Co). The shape of the hysteresis curves is characteristic of metamagnetic behavior in some cases, *e.g.* for $Fe(TCNE)_2{\cdot}0.75CH_2Cl_2$ at 2 K (Fig. 7) and, along with more detailed magnetic studies, including ac measurements, is the focus of future research.

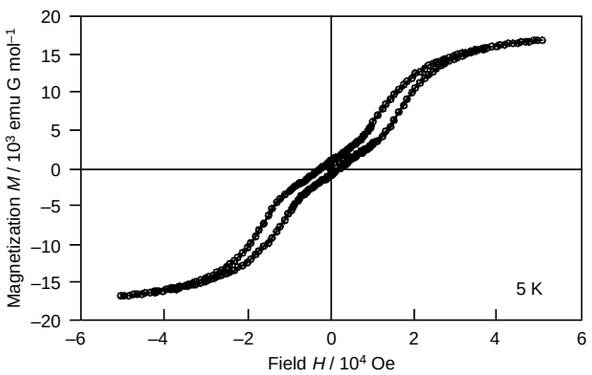

Fig. 7 An example of the observed hysteretic $M(H)$ for $Fe(TCNE)_2{\cdot}0.75CH_2Cl_2$ at 2 K. The observed coercive field for this sample is 2300 Oe and the sample saturates to 16 900 emu Oe mol^{-1}.

Hence, a new synthetic route enabling the preparation of several new examples of molecule-based magnets of $M^{II}(TCNE)_2{\cdot}xCH_2Cl_2$ composition has been identified. These new magnets have T_c values that exceed 100 K and coercive fields as great as 6500 Oe.

While preparing the $M^{II}(TCNE)_2{\cdot}xCH_2Cl_2$ magnets, crystals (light yellow for M = Mn; dark brown for M = Fe) which did not magnetically order were isolated. Single crystal X-ray diffraction studies revealed the unprecedented octacyanobutanediide dianion, $[C_4(CN)_8]^{2-}$ **4**, bound to four octahedral

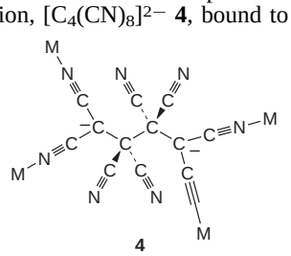

4

M^{II}s in a plane with the MeCN molecules filling the axial coordination sites, *i.e.* $Mn[C_4(CN)_8](NCMe)_2{\cdot}CH_2Cl_2$ **5** and $Fe[C_4(CN)_8](NCMe)_2{\cdot}MeCN$ **6**.[20] Compound **4** is disordered about the midpoint of the central C–C bond for M = Mn, but is ordered for M = Fe, and has long 1.59 (2) (M = Mn) and 1.627 (14) Å (M = Fe) central C–C bonds suggesting that it is a weak bond. This is the first example of a σ-dimer of $[TCNE]^{\cdot-}$, however, several examples of a structurally related σ-dimer of $[TCNQ]^{\cdot-}$ (TCNQ = 7,7,8,8-tetracyano-*p*-quinodimethane) have been reported.[21]

Compounds **5** and **6** are paramagnets obeying the Curie–Weiss law above 5 K. This is consistent with diamagnetic $[C_4(CN)_8]^{2-}$ weakly coupling the metal spin sites (S = 5/2 Mn^{II}). Upon desolvation of **5** and **6** at 100 °C the ν_{CN} IR absorptions disappear and new ν_{CN} bands characteristic of the $M(TCNE)_2{\cdot}xS$ magnets[20] (M = Mn, Fe) appear. Desolvated **5** magnetically orders at a T_c of 95 K,[20] in reasonable agreement with samples prepared from CH_2Cl_2.[18] Compound **6** behaves in a similar fashion upon desolvation. These observations suggest that upon desolvation the S = 0 μ_4-$[C_4(CN)_8]^{2-}$ reforms two S = 1/2 $[TCNE]^{\cdot-}$ units which can bind to additional metal centers, providing stronger spin coupling leading to the observed magnetic ordering. Evidence for this type of bond breaking has been reported for σ-dimers of $[TCNQ]^{\cdot-}$.[21a]

Hence, additional members of the $M(TCNE)_x$ class of magnets have been characterized, and in the case of Fe the metal is assigned to be divalent as previously proposed for $V(TCNE)_x{\cdot}y$solvent.[7] Furthermore, an intermediate in the formation of the $M(TCNE)_x$ class of magnets, namely $[C_4(CN)_8]^{2-}$ **6**, has been identified and structurally characterized.

[Mn(porphyrin)][TCNE]-based magnets

Another class of TCNE-based magnets is exemplified by $[Mn^{III}TPP]^{+}[TCNE]^{\cdot-}$ (TPP = *meso*-tetraphenylporphinato), which forms a coordination polymer (1-D) that was characterized to be a ferrimagnet with T_c 14 K.[22] With the goal of identifying the importance of 1-D with respect to 3-D interactions and developing a structure–function relationship for this class of magnetic materials, as well as preparing new molecule-based magnets with enhanced T_cs, we have pursued the study of this class of compounds.

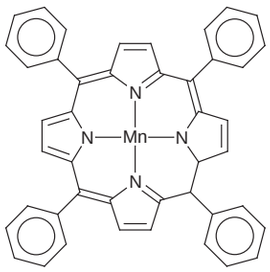

MnTPP

$[Mn^{III}TPP]^{+}[TCNE]^{\cdot-}$ forms uniform parallel 1-D chains in the solid state with each S = 2 Mn^{III} bonded to four porphyrin nitrogens (*ca.* 2.00 Å) and axially to two $[TCNE]^{\cdot-}$ nitrogens (*ca.* 2.30 Å), and each S = 1/2 $[TCNE]^{\cdot-}$ is *trans*-μ-bonded to two Mn^{III} species, [Fig. 8 (*a*)]. The magnetic susceptibility of $[MnTPP]^{+}[TCNE]^{\cdot-}{\cdot}2PhMe$ can be fitted to the Curie–Weiss expression above 280 K with θ ~ −15 K, and between 115 and 250 K with an effective θ, θ', of +61 K. A minimum in the value of χT, characteristic of 1-D ferrimagnetic behavior, is observed at ~310 K and field-dependent susceptibility is observed below 50 K. Magnetic ordering occurs below 13 K (as determined by scaling analysis[22c]) and hysteresis with a coercive field of 375 G was obtained at 5 K.[22] Thus, [MnTPP][TCNE] is a representative example of a new structure type of organic-based magnetic materials, and is an excellent model system for

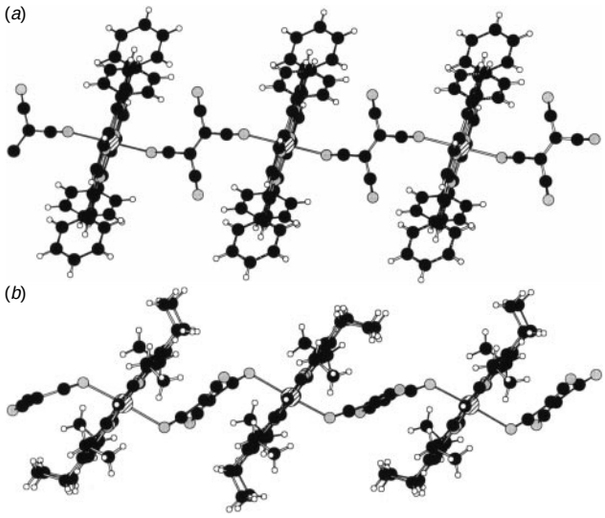

Fig. 8 (*a*) Segment of a uniform chain of the ferrimagnetic [Mn^{III}TPP]-[TCNE]·2PhMe coordination polymer (the solvent is omitted for clarity). (*b*) Alternating chain segment of the paramagnetic [Mn^{III}OEP][TCNE] coordination polymer.

studying a number of unusual magnetic phenomena, for example, the magnetic behavior of mixed quantum/classical spin systems.

In addition to modification of the porphyrin ring, the clathrate nature of this class of metalloporphryins[23] enables the introduction of different solvents into the structure to alter the inter- and intra-chain couplings and the magnetic properties. In this review we focus on modification of the [MnTPP][TCNE] structure type and discuss the consequent magnetic properties.

[MnTPP][TCNE]·2PhMe **6**[22*a*] has been crystallographically characterized. Likewise, the [TCNE]$^{\cdot-}$ salts of 4-methoxyphenyl (**7**),[24] 4-chlorophenyl (**8**)[25] and 2-fluorophenyl substituted [MnTPP]$^{+}$ (**9**)[24] and *meso*-tetrakis(3,5-di-*tert*-butyl-4-hydroxyphenyl)porphinatomanganese(III), MnTP′P[26] (**10**), have been studied by single crystal X-ray diffraction. Furthermore, to extend this system the analogous TCNE electron-transfer salt was prepared with the easier-to-oxidize MnOEP (OEP = octaethylporphyrinato).[27]

[MnOEP][TCNE] has weak ferromagnetic coupling as evidenced by the fitting of the susceptibility to the Curie–Weiss expression with a θ' of +7 K.[27] However, unlike [MnOEP][TCNE], magnetic ordering is not observed above 2 K. The differences in the magnetic properties are ascribed to structural differences. Although both [MnTPP][TCNE]·2PhMe and [MnOEP][TCNE] form parallel 1-D chains (Fig. 8), due to the differing orientations of [TCNE]$^{\cdot-}$ within a chain they are alternating chains for [MnOEP][TCNE] instead of being uniform chains as for [MnTPP][TCNE]·2PhMe. Thus, uniform chains appear to be important to achieve long range magnetic order.[27]

A correlation of the dihedral angle, ϕ, between the [Mn^{III}TPP]$^{+}$ MnN_4 and [TCNE]$^{\cdot-}$ mean planes and the magnitude of magnetic coupling has been observed for ditoluene solvates of five [TCNE]$^{\cdot-}$ salts, **6**–**10**.[28] The magnitude of magnetic coupling is determined from T_{min}, the temperature at which a minimum in $\chi T(T)$ or $\mu(T)$ plots occurs, as expected for antiferromagnetically coupling linear chain systems,[29] and the effective θ, θ', obtained from a fit of the data to the Curie–Weiss expression. A correlation to T_{min} is preferred as it is model independent; however, for strongly coupled systems T_{min} is not observed as it occurs at temperatures exceeding the measurement range. T_{min}, however, can be estimated from a fit of the data to the Seiden expression for isolated 1-D chains comprised of alternating quantum (S = 1/2) and classical (S > 1/2) spins.[30]

The smaller ϕ the stronger the magnetic coupling, *i.e.* the greater T_{min} and θ' (Fig. 9). Hence to attain strong intrachain coupling systems with more acute dihedral angles are sought and, based on **10**, 3,5-disubstituted [MnTPP]$^{+}$s are preferred over 2- or 4-substituted [MnTPP]$^{+}$s which from the data acquired to date have higher ϕ values. To test this postulate several 3,5-disubstituted systems are being studied. Likewise, pressure also may force such systems to have reduced angles and also lead to higher T_c values.

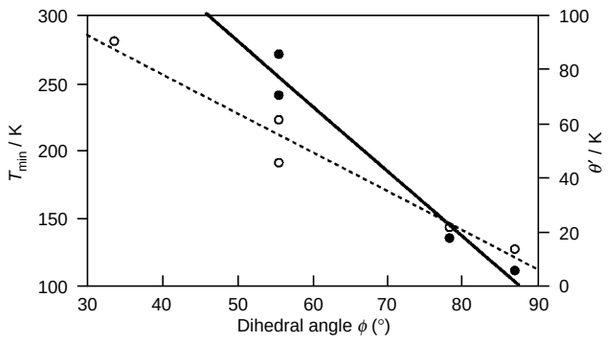

Fig. 9 Correlation of the dihedral angle ϕ between the MnN_4 and [TCNE]$^{\cdot-}$ mean planes with the temperature at which $\chi T(T)$ data has a minimum, (T_{min}, ● and solid line) and the effective θ value (θ'; ○ and dashed line)[28]

The aforementioned correlation between ϕ and T_{min} and θ' is attributed to the overlap between the [TCNE]$^{\cdot-}$ *N*-bound to Mn^{III} π* SOMO and the four Mn^{III} SOMO d orbitals. [The energy of the latter increase as $d_{xy}{}^1$ (b_1) < $d_{xz}{}^1$, $d_{yz}{}^1$ (e) < $d_{z^2}{}^1$ (a_1) < $d_{x^2-y^2}$ (b_1).[31]] From MO considerations (determined from semi-empirical INDO/SCF calculations) the expected d_π–p_z (d_π = d_{xz}, d_{yz}) overlap is not as important as the σ–d_{z^2}/p_z overlap between Mn^{III} and the [TCNE]$^{\cdot-}$ (Fig. 10).[28] Furthermore, the smaller ϕ increases the σ–d_{z^2}/p_z overlap between Mn^{III} and the [TCNE]$^{\cdot-}$ leading to an increased intrachain coupling, as reflected in T_{min} and θ' (Fig. 10).

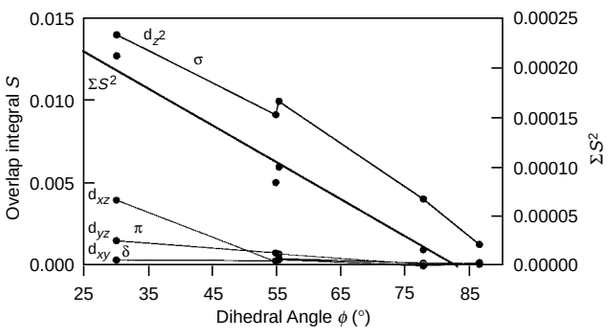

Fig. 10 Correlation of the dihedral angle ϕ between the MnN_4 and [TCNE]$^{\cdot-}$ mean planes with the semi-empirical INDO/SCF calculated d_{yz}-, d_{xz}-, d_{xy}- and d_{z^2}-like overlap integrals S with the [TCNE]$^{\cdot-}$ π* SOMO and the sum of the squares of these overlap integrals ΣS^2

While the σ overlap between the [TCNE]$^{\cdot-}$ p_z orbital and the Mn d_{z^2} orbital controls the intrachain magnetic exchange, the three-dimensional magnetic ordering temperature, T_c, depends upon this term *and* the interchain exchange. The later term is governed by the competition between antiferromagnetic exchange due to orbital overlap between porphyrin moieties of adjacent chains and an effective exchange due to dipolar interactions between chains. The dipolar term can be ferromagnetic or antiferromagnetic depending upon the structural order in the compound and the role of single ion anisotropy.[32]

Acknowledgments

The authors gratefully acknowledge support from the U.S. Department of Energy Division of Materials Science (Grant

Table 2 Summary of the structural and magnetic parameters for the several $[TCNE]^{\cdot-}$ magnets

Porphyrin	Mn–N_{TCNE} distance/Å	Dihedral angle (°)	Mn···Mn distance[a]/Å	Effective θ/K	T_{min}/K
[MNnTPP][TCNE]·2PhMe	2.306	55.4	10.116	61	270
[MnTClPP][TCNE]·2PhMe	2.267	86.8	10.189	13	110
[MnTOMePP][TCNE]·2PhMe	2.289	78.1	10.256	21	134
[MnTFPP][TCNE]·2PhMe	2.313	55.4	10.185	45	240
[MnTP′P[TCNE]·2PhMe	2.299	33.6	8.587	90	> 300[b]

[a] Intrachain. [b] Not plotted in Fig. 10.

Nos. DE-FG03-93ER45504 and DE-FG02-86ER45271.A000) and the U.S. National Science Foundation (Grant No. CHE-9320478).

Joel S. Miller was born in Detroit, MI and received his Bachelor of Science in Chemistry from Wayne State University (1967) and PhD from UCLA (1971). After a postdoctoral fellowship at Stanford University he joined the Xerox Webster Research Center in 1972 and later joined the now-defunct Occidental Research Corporation. He was Visiting Professor of Chemistry at the University of California, Irvine, CA. He joined the Central Research & Development Department at the Du Pont Company in 1983 where he was a Research Supervisor for solid state science. He has been a Visiting Scientist at the Weizmann Institute (1985) and a Visiting Professor of Chemistry at the University of Pennsylvania (1988). He joined the faculty of Department of Chemistry at the University of Utah in 1993. He is on the advisory board of *Advanced Materials* and *Journal of Materials Chemistry*, and a member of the Inorganic Synthesis Corporation. His research interests focus on the solid state magnetic, electrical and optical properties of molecular (organic, organometallic and inorganic coordination) compounds and electron transfer complexes as well as the surface modification of solids. Currently he is actively involved in synthesis and characterization of molecular/organic based ferromagnets. In addition to patents he has edited eleven monographs and published over 300 papers in these and other areas.

Arthur J. Epstein was born in Brooklyn, NY and received his BS in Physics from the Polytechnic Institute of Brooklyn in 1966 and his PhD in Physics from the University of Pennsylvania in 1971. After a year as Member of the Technical Staff of The MITRE Corporation and thirteen years at the Xerox Webster Research Center where he was Principal Scientist, he joined The Ohio State University in 1985 as Professor of Physics and Professor of Chemistry. In 1997 he was appointed as Distinguished University Professor. He has been the Director of The Ohio State University Center for Materials Research since 1989. He also has been adjunct Professor of Physics at the University of Florida and has been a visiting Professor at the Université Paris-Sud and the Technion—Israel Institute of Technology—and is presently Adjunct Professor of Chemistry at University of Utah. He is a Regional Editor for *Synthetic Metals*. His current research interests include experimental and theoretical study of magnetic, electronic/optical and transport phenomena of synthetic magnets (molecular, organic and polymeric magnets) and synthetic metals (conducting polymers, organic and molecular materials), including the study of excitations and their dynamics. He is also active in the exploration of potential applications of unconventional magnetic, electronic and optical materials for which he consults with several companies. In addition to having originated twenty patents and editing five conference proceedings, he has published over 500 papers in these and other areas.

Notes and References

† E-mail: jsmiller@chemistry.chem.utah.edu
‡ E-mail: epstein.2@osu.edu

1 P. W. Anderson, *Concepts in Solids*, W. A. Benjamin, Inc., 1963, p. 7; H. M. McConnell, *J. Chem. Phys.* 1963, **39**, 1910; H. M. McConnell, *Proc. Robert. A. Welch Found. Conf. Chem. Res.* 1967, **11**, 144.
2 J. S. Miller, A. J. Epstein and W. M. Reiff, *Mol. Cryst., Liq. Cryst.*, 1985, **120**, 27; J. S. Miller, J. C. Calabrese, A. J. Epstein, R. W. Bigelow, J. H. Zhang and W. M. Reiff, *J. Chem. Soc., Chem. Commun.* 1986, 1026; J. S. Miller, J. C. Calabrese, H. Rommelmann, S. Chittipeddi, A. J. Epstein, J. H. Zhang and W. M. Reiff, *J. Am. Chem. Soc.*, 1987, **109**, 769.
3 M. Kinoshita, *Jpn. J. Appl. Phys.* 1994, **33**, 5718; R. Chiarelli, A. Rassat, Y. Dromzee, Y. Jeannin, M. A. Novak and J. L. Tholence, *Phys. Scr.*, 1993, **T49**, 706.
4 J. S. Miller, and A. J. Epstein, *Angew. Chem.*, 1994, **106**, 399; *Angew. Chem. Int. Ed. Engl.*, 1994, **33**, 385; J. S. Miller and A. J. Epstein, *Chem. Eng. News*, 1995, **73**(#40), 30.
5 O. Kahn, *Molecular Magnetism*, VCH, Weinheim, 1993.
6 D. Gatteschi, *Adv; Mater.*, 1994, **6**, 635; A. Caneschi, D. Gatteschi, R. Sessoli and P. Rey, *Acc. Chem. Res.*, 1989, **22**, 392; A. Caneschi and D. Gatteschi, *Prog. Inorg. Chem.*, 1991, **37**, 331.
7 (*a*) J. M. Manriquez, G. T. Yee, R. S. McLean, A. J. Epstein and J. S. Miller, *Science*, 1991, **252**, 1415; J. S. Miller, G. T. Yee, J. M. Manriquez and A. J. Epstein, *Proceedings of Nobel Symposium #NS-81, Conjugated Polymers and Related Materials: The Interconnection of Chemical and Electronic Structure*, Oxford University Press, 1993, p. 461; *Chim. Ind.*, 1992, **74**, 845, A. J. Epstein and J. S. Miller, *Proceedings of Nobel Symposium #NS-81 Conjugated Polymers and Related Materials: The Interconnection of Chemical and Electronic Structure*, Oxford University Press, 1993, p. 475; *Chim. Ind.*, 1993, **75**, 185; (*b*) P. Zhou, B. Morin, A. J. Epstein and J. S. Miller, *Phys. Rev. B.*, 1993, **48**, 1325; (*c*) P. Zhou, S. M. Long, J. S. Miller and A. J. Epstein, *Phys. Lett. A*, 1993, **181**, 71; (*d*) G. Du, J. Joo, A. J. Epstein and J. S. Miller, *J. Appl. Phys.*, 1993, **73**, 6566.
8 J. Zhang, P. Zhou, W. B. Brinckerhoff, A. J. Epstein, C. Vazquez, R. S. McLean and J. S. Miller, *ACSSymp. Ser.*, 1996, **644**, 311.
9 D. A. Dixon and J. S. Miller, *J. Am. Chem. Soc.*, 1987, **109**, 3656.
10 *E.g.* W. Beck, R. Schlodder, and K. H. Lechler, *J. Organomet. Chem.*, 1973, **54**, 303; A. Maisonnat, J.-J. Bionnet and R. Poilblanc, *Inorg. Chem.*, 1980, **19**, 3168; M. I. Bruce, T. W. Hambley, M. R. Smow and A. G. Swincer, *J. Organomet. Chem.*, 1982, **235**, 105; W. H. Baddley, *J. Am. Chem. Soc.*, 1968, 90, 3705; W. H. Baddley and L. M. Venanzi, *Inorg. Chem.*, 1966, **5**, 33.
11 C. Vazquez, J. C. Calabrese, D. A. Dixon and J. S. Miller, *J. Org. Chem.*, 1993, **58**, 65.
12 T. Mallah, S. Thiébaut, M. Verdaguer and P. Veillet, *Science*, 1993, **262**, 1554.
13 D. G. Gordon and J. S. Miller, unpublished results.
14 J. S. Miller, *Adv. Mater.*, 1994, **6**, 322; C. P. Landee, D. Melville and J. S. Miller, in *NATO ARW Molecular Magnetic Materials*, ed. O. Kahn, D. Gatteschi, J. S. Miller and F. Palacio, 1991, **E198**, 395.
15 B. G. Morin, C. Hahm, A. J. Epstein and J. S. Miller, *J. Appl. Phys.*, 1994, **75**, 5782.
16 J. S. Miller, D. M. O'Hare, A. Chackraborty and A. J. Epstein, *J. Am. Chem. Soc.*, 1989, **111**, 7853.
17 B. Olbrich-Deussner, R. Gross and W. Kaim, *J. Organomet. Chem.*, 1989, **366**, 155; M. Heberhold, *Angew Chem., Int. Ed. Engl.*, 1968, **7**, 305; B. Olbrich-Deussner, W. Kaim and R. Gross-Lannert, *Inorg. Chem.*, 1989, **28**, 3113.
18 J. Zhang, J. Ensling, V. Ksenofontov, P. Gütlich, A. J. Epstein and J. S. Miller, *Angew. Chem. Int. Ed. Engl.*, 1998, **37**, 657.

19 P. Gütlich, R. Link and A. Trautwein, in *Inorganic Concepts 3: Mössbauer Spectroscopy and Transition Metal Chemistry*, Springer-Verlag, Berlin, Heidelberg, New York, 1988, pp. 19, 56–77.
20 J. Zhang, L. M. Liable-Sands, A. L. Rheingold, R. E. Del Sesto, D. C. Gordon, B. M. Burkhart and J. S. Miller, *Chem. Commun.*, 1998, 1385.
21 (*a*) R. H. Harms, H. J. Keller, D. Nöthe, M. Werner, D. Grundel, H. Sixl, Z. Soos and R. M. Metzger, *Mol. Cryst. Liq. Cryst.* 1981, **65**, 179; (*b*) S. K. Hoffman, P. J. Corvan, P. Singh, C. N. Sethuklekshmi, R. M. Metzger and W. E. Hatfield, *J. Am. Chem. Soc.*, 1983, **105**, 4608; (*c*) V. Dong, H. Endres, H. J. Keller, W. Moroni and D. Nöthe, *Acta Crystallogr.*, 1977, **B33**, 2428; H. Zhao, R. A. Heintz, K. R. Dunbar and R. D. Rogers, *J. Am. Chem. Soc.*, 1996, **118**, 12 844; B. Morosin, H. J. Plastas, L. B. Coleman and J. M. Stewart, *Acta Crystallogr.*, 1978, **B34**, 540.
22 (*a*) J. S. Miller, J. C. Calabrese, R. S. McLean and A. J. Epstein, *Adv. Mater.*, 1992, **4**, 498; (*b*) P. Zhou, B. G. Morin, A. J. Epstein, R. S. McLean and J. S. Miller, *J. Appl. Phys.*, 1993, **73**, 6569; (*c*) W. B. Brinckerhoff, B. G. Morin, E. J. Brandon, J. S. Miller and A. J. Epstein, *J. Appl. Phys.*, 1996, **79**, 6147.
23 I. Goldberg, H. Krupitsky, Z. Stein, Y. Hsiou and C. E. Strouse, *Supramol. Chem.*, 1995, **4,** 203; H. Krupitsky, Z. Stein and I. Goldberg, *Inclusion Phenom. Mol. Recognit.*, 1995, **20**, 211; I. Goldberg, *Mol. Cryst. Liq. Cryst.*, 1996, **278**, 767; M. P. Byrn, C. J. Curtis, Y. Hsiou, S. I. Kahn, P. A. Sawin, S. K. Tendick, A. Terzis and C. E. Strouse, *J. Am. Chem. Soc.*, 1993, **115**, 9480.
24 E. J. Brandon, A. M. Arif, B. M. Burkhart and J. S. Miller, unpublished work.
25 E. J. Brandon, D. K. Rittenberg, A. M. Arif and J. S. Miller, unpublished work.
26 A. Böhm, C. Vazquez, R. S. McLean, J. C. Calabrese, S. E. Kalm, J. L. Manson, A. J. Epstein and J. S. Miller, *Inorg. Chem.*, 1996, **35**, 3083.
27 J. S. Miller, C. Vazquez, N. L. Jones, R. S. McLean and A. J. Epstein, *J. Mater. Chem.*, 1995, **5**, 707.
28 E. J. Brandon, C. Kollmar and J. S. Miller, *J. Am. Chem. Soc.*, 1998, **120**, 1822; E. J. Brandon and J. S. Miller, *NATO ARW Supramolecular Engineering of Synthetic Metallic Materials: Conductors and Magnets*, ed. J. Veciana, C. Rovira and D. Amabilino, in the press.
29 E. Coronado, M. Drillon and R. Georges, in *Research Frontiers in Magnetochemistry*, ed. C. J. O'Connor, World Scientific, 1993, p. 26.
30 J. Seiden, *J. Phys. Lett.*, 1983, **44**, L947.
31 L. B. Dugad, D. V. Behere, V. R. Marathe and S. Mitra, *Chem. Phys. Lett.*, 1984, **104**, 353.
32 C. M. Wynn, M. Gîrtu, W. B. Brinckerhoff, K.-I. Sugiura, J. S. Miller and A. J. Epstein, *Chem. Mater.*, 1997, **9**, 2156.

8/00922H

Synthesis of fully sulfonated polyaniline: a novel approach using oxidative polymerisation under high pressure in the liquid phase

Hardy S. O. Chan,[a,b] Annette J. Neuendorf,[c] Siu-Choon Ng,*[a] Pauline M. L. Wong[a] and David J. Young*[c]†

[a] *Department of Chemistry, National University of Singapore, Singapore 119260*
[b] *Department of Materials Science, National University of Singapore, Singapore 119260*
[c] *School of Science, Griffith University, Queensland 4111, Australia*

The oxidative polymerisation of *o*- and *m*-aminobenzenesulfonic acid has been achieved for the first time at high pressures to yield fully sulfonated polyaniline (SPANI) which is self-doping, water soluble and electrically conducting.

Polyaniline (PANI) has received considerable attention over the past few decades on account of its high electrical conductivity, environmental stability and capacity for reversible doping to an electrically conductive state by external Brønsted acids.[1] More recently, the development of 'self-doped' PANI derivatives incorporating *N*-alkylsulfonic acid,[2] methylphosphonic acid[3] or sulfonic acid[4] moieties have been reported, of which the latter displayed the highest conductivity. This sulfonated polyaniline (SPANI) was synthesised by post-polymerisation treatment of PANI emeraldine base or pernigraniline base with fuming sulfuric acid[4a–d] to achieve 50% sulfonation, or by treatment of PANI leucoemeraldine base with fuming sulfuric acid[4e] to afford a 75% sulfonated polyaniline with electrical conductivity of *ca.* 0.1 and 1 S cm^{-1} respectively. The production of 100% sulfonated SPANI has hitherto not been reported but would be predicted to have even greater water solubility and possibly higher conductivity.[4e] The oxidative polymerisation of *o*-aminobenzenesulfonic acid **1** or *m*-aminobenzenesulfonic acid **2** would obviously provide fully sulfonated SPANI but attempts so far by both chemical or electrochemical methods[4b,5] have been unsuccessful, presumably due to steric hindrance and the strongly deactivating influence of the electron withdrawing sulfonic acid moiety. Incorporation of an electron donating methoxy group onto the monomer does, however, allow oxidative polymerisation and poly(3-amino-4-methoxybenzenesulfonic acid) has been prepared in this way[5,6] and has found applications for electron device fabrication[5] and in a novel polymer complex.[7] The room temperature conductivity of this methoxy-SPANI is, however, significantly less than that for 50 or 75% sulfonated SPANI[5,6] which has been attributed to the larger twist of the phenyl rings and increased interchain separation.[6] We now present the first report of a facile preparation of fully sulfonated SPANI by oxidative polymerisation of **1** and **2** under the influence of high pressures in the liquid phase (Scheme 1).

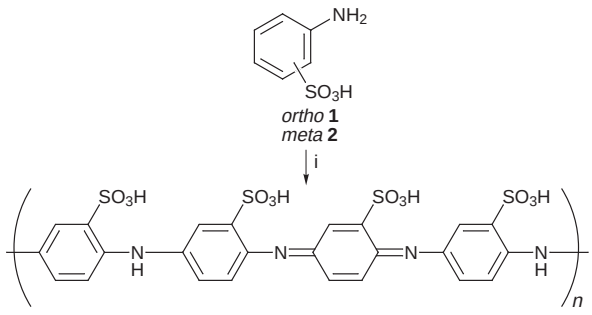

Scheme 1 *Reagents and conditions*: i, $Na_2S_2O_8$, high pressure, catalyst

Monomers **1** and **2** were polymerised at 19 kbar with $Na_2S_2O_8$ (1.25 equiv.) in aqueous LiCl (1.0 or 5.0 M) and with 5% $FeSO_4$ for 18 h at 20 °C. The usual requirement for added HCl to solubilise the monomer was not necessary and so the conductivity of the resulting polymers was exclusively due to self doping. After this period, the dark-green solution was freeze-dried, dissolved in a minimum amount of water and dialysed through cellulose acetate dialysis tubing with a molecular weight cut-off of 1000 g mol^{-1}. The yield of the polymers after dialysis and evaporation of the water was 10%. The addition of a small amount of aniline has been shown to facilitate the polymerisation of anilines bearing electron withdrawing nitro[8] or cyano[9] substituents. In combination with high pressure, the addition of 10% aniline had a dramatic effect on yield with essentially quantitative recovery of SPANI (Table 1) and no noticeable effect on the water solubility of the resulting polymer.

While the conductivity of polymers **3**–**8** was less than that reported for SPANI prepared by post-polymerisation sulfonation, these conductivity values are for 'as-synthesized' polymer (*i.e.* without addition of external dopant) and are comparable to externally doped *N*-alkylsulfonated polyaniline[2] and methoxy-SPANI.[5,6] The UV–VIS spectra of **3**–**8** gave three absorption bands. The band with λ_{max} at 306–324 nm is attributed to $\pi_B \rightarrow \pi^*$ and low lying $\pi_B \rightarrow \pi_Q$ transitions; the second with λ_{max} at 448–450 nm is consistent with low-lying π_B–π_S excitation to the polaron band whilst the third with λ_{max} at 565–624 nm is attributable to π_B–π_Q transition.[3b] Upon dedoping by addition of base, the absorption band at 448–450 nm was greatly diminished, showing the decreased contribution of the low-lying $\pi_B \rightarrow \pi_S$ transitions. The FTIR spectra gave the characteristic absorption bands for quinoidal and benzenoid stretchings at 1590 and 1500 cm^{-1} respectively, as well as absorption bands of the sulfonic acid group at 1200 and 1020–1072 cm^{-1}.

The bulk *S*/*N* ratios (Table 1) indicate 100% sulfonation for polymers **3**, **4**, **6** and **7** and a lower degree of sulfonation for polymers **5** and **8** for which 10 mol% aniline was used to assist initiation. We ascribe the higher than expected bulk hydrogen and surface oxygen content to the extremely hygroscopic nature of these zwitterionic polymers. The C1s XPS signals of the polymers can be deconvoluted into three components, each with a FWHM (full width at half maximum) of 1.6 eV; C–C or C–H at 285 eV, C–N or C=N at 286 eV and C–O at 287 eV. The N1s signals can be deconvoluted into four environments each with a FWHM of 1.6 eV; –NH– at 399.7 eV, –$^+$NH– at 401.2 eV, –$^+NH_2$– at 402.5 eV and an unidentified component at 400.7 eV. This last environment was also reported by Yue and Epstein.[4c]

In conclusion, we have demonstrated for the first time that high pressure in the liquid phase facilitates the direct oxidative polymerisation of **1** and **2** which is otherwise not possible at ambient pressure. The polymer yield is substantially increased by the addition of a small amount of aniline. The resulting SPANI is highly water soluble. Despite a higher degree of sulfonation than is possible by post-polymerisation sulfonation

Table 1 Summary of reaction conditions and polymer characterisation data

Monomer	SPANI	Reaction conditions	Yield (%)	Bulk atomic ratio (surface at. ratio)	σ^a/S cm^{-1}
1	**3**	1.0 M LiCl 0.05 equiv. $FeSO_4$	10	$C_{6.9}H_{8.9}N_{1.0}S_{1.0}$	10^{-4}
1	**4**	5.0 M LiCl 0.05 equiv. $FeSO_4$	10	$C_{7.1}H_{10.0}N_{1.0}S_{1.1}$ $(C_{18.1}N_{1.0}S_{0.8}O_{6.9})$	10^{-3}
1	**5**	5.0 M LiCl 0.05 equiv. $FeSO_4$ 0.1 equiv. aniline	98	$C_{6.3}H_{8.1}N_{1.0}S_{0.8}$ $(C_{8.1}N_{1.0}S_{1.0}O_{17.0})$	10^{-3}
2	**6**	1.0 M LiCl 0.05 equiv. $FeSO_4$	10	$C_{6.8}H_{9.6}N_{1.0}S_{1.0}$	10^{-5}
2	**7**	5.0 M LiCl 0.05 equiv. $FeSO_4$	10	$C_{6.2}H_{8.6}N_{1.0}S_{1.0}$ $(C_{16.0}N_{1.0}S_{0.9}O_{6.7})$	10^{-4}
2	**8**	5.0 M LiCl 0.05 equiv. $FeSO_4$ 0.1 equiv. aniline	100	$C_{6.4}H_{8.4}N_{1.0}S_{0.7}$	10^{-3}

[a] As determined using the four-point probe method.

of PANI,[4] the conductivity of the 'as-synthesised', high pressure SPANI is less than that of the latter and suggests the possibility of pressure induced defects. While these reactions were conducted at 19 kbar, we have observed that polymerisation of **1** will occur at pressures down to *ca.* 15 kbar, while **2** polymerises down to *ca.* 10 kbar. These reactions were catalysed with 5 mol% Co^{2+}. This difference in the reactivity of *ortho* and *meta* isomers has been reported for the oxidative polymerisation of cyanoanilines and ascribed to the relative effect of the electron withdrawing substituent on the spin densities at N and C4 in the oxidised monomers.[9] We are currently attempting to quantify the effect of pressure on reaction rate for the polymerisation of anilines. Preliminary rate measurements at different pressures for the ammonium persulfate oxidation of 2-methoxyaniline[10] conducted in a high pressure spectrophotometric cell[11] indicate a large, negative activation volume (ΔV^* of the order of -60 cm^3 mol^{-1}). Such a value would be consistent with charge development (and associated electrostriction of solvent) in the transition state[12] for the rate determining oxidation of aniline[13] and equates to a substantial rate enhancement (by a factor of *ca.* 12 at 1 kbar and a factor of *ca.* 10^{13} at 10 kbar, assuming a linear dependence of ln k on pressure[14]). This large effect suggests that the polymerisation of other unreactive aniline monomers may be viable at elevated pressures.

We gratefully acknowledge the National University of Singapore, Australian Research Council and the Australian Department of Industry, Science and Tourism for Financial Support.

Notes and References

† E-mail: d.young@sct.gu.edu.au

1 A. G. MacDiarmid, *Synth. Met.*, 1997, **84**, 27 and references cited therein.
2 S. A. Chen and G. W. Hwang, *J. Am. Chem. Soc.*, 1994, **116**, 7939.
3 (*a*) S. C. Ng, H. S. O. Chan, H. H. Huang and P. K. H. Ho, *J. Chem. Soc., Chem. Commun.*, 1995, 1327; (*b*) H. S. O. Chan, P. K. H. Ho, S. C. Ng, B. T. G. Tan and K. L. Tan, *J. Am. Chem. Soc.*, 1995, **117**, 8517.
4 (*a*) J. Yue and A. J. Epstein, *J. Am. Chem. Soc.*, 1990, **112**, 280; (*b*) J. Yue, Z. H. Wang, K. R. Cromack, A. J. Epstein and A. G. MacDiarmid, *J. Am. Chem. Soc.*, 1991, **113**, 2665; (*c*) J. Yue and A. J. Epstein, *Macromolecules*, 1991, **24**, 4441; (*d*) J. Yue, G. Gordon and A. J. Epstein, *Polymer*, 1992, **33**, 4410; (*e*) X.-L. Wei, Y. Z. Wang, S. M. Long, C. Bobeczko and A. J. Epstein, *J. Am. Chem. Soc.*, 1996, **118**, 2545.
5 S. Shimizu, T. Saitoh, M. Yuasa, K. Yano, T. Maruyama and K. Watanabe, *Synth. Met.*, 1997, **85**, 1337.
6 W. Lee, G. Du, S. M. Long, A. J. Epstein, S. Shimizu, T. Saitoh and M. Uzawa, *Synth. Met.*, 1997, **84**, 807.
7 D. E. Tallman and G. G. Wallace, *Synth. Met.*, 1997, **90**, 13.
8 B. C. Roy, M. D. Gupta and J. K. Ray, *Macromolecules*, 1995, **28**, 1727.
9 M. Ranger and M. Leclerc, *Synth. Met.*, 1997, **84**, 85.
10 W. A. Gazotti and M.-A. De Paoli, *Synth. Met.*, 1996, **80**, 263.
11 N. S. Isaacs and A. Laila, *J. Phys. Org. Chem.*, 1994, **7**, 178.
12 N. S. Isaacs and A. V. George, *Polymer Commun.*, 1984, **25**, 268.
13 Y. Wei, X. Tang and Y. Sun, *J. Polym. Sci. Part A: Polym. Chem.*, 1989, **27**, 2385; S. Mu, C. Chen and J. Wang, *Synth. Met.*, 1997, **88**, 249.
14 N. S. Isaacs, *Tetrahedron*, 1991, **47**, 8643.

Received in Cambridge, UK, 21st April 1998; 8/02970I

Calix[4]arenes with hard donor groups as efficient soft cation extractants. Remarkable extraction selectivity of calix[4]arene *N*-(X)sulfonylcarboxamides for Hg^{II}

Galina G. Talanova, Hong-Sik Hwang, Valdimir S. Talanov and Richard A. Bartsch*†

Department of Chemistry and Biochemistry, Texas Tech University, Lubbock, Texas 79409-1601, USA

Calix[4]arene *N*-(X)sulfonylcarboxamides efficiently extract Hg^{II} from acidic aqueous nitrate solutions with excellent selectivity over alkali, alkaline earth and many transition metal ions, including Pb^{II}, Ag^{I} and Pd^{II}.

Metal complexes of calixarene-based macrocyclic ligands are attracting ever-increasing attention,[1–3] especially for applications in metal ion separation processes. During the last decade, remarkable progress in the transition metal chemistry of calixarenes has been achieved.[3] Recently, several papers have appeared which report utilization of calixarene derivatives in separations of soft heavy metal ions, *e.g.* Ag^{I}, Au^{III}, Pd^{II}, Pt^{II} and Cd^{II}.[4,5] However, only very limited information on Hg^{II} extraction with calixarene-based ligands is available in the literature.[5]

Recently we synthesized new calix[4]arenes **1**–**4** with two

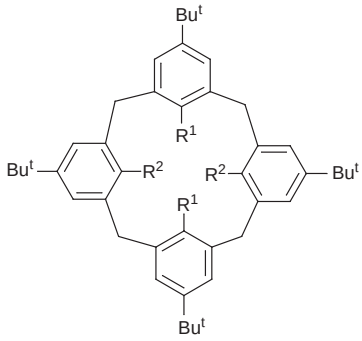

1 R^1 = OMe, R^2 = $OCH_2C(O)NHSO_2CF_3$
2 R^1 = OMe, R^2 = $OCH_2C(O)NHSO_2Me$
3 R^1 = OMe, R^2 = $OCH_2C(O)NHSO_2Ph$
4 R^1 = OMe, R^2 = $OCH_2C(O)NHSO_2C_6H_4NO_2$-4
5 R^1 = OBu, R^2 = $OCH_2C(O)NHSO_2Ph$
6 R^1 = OBu, R^2 = OCH_2CO_2H
7 R^1 = OBu, R^2 = OCH_2CO_2Et
8 R^1 = OMe, R^2 = OCH_2CO_2H
9 $R^1 = R^2$ = OMe
10 $R^1 = R^2$ = OH
11 R^1 = OBu, R^2 = OH

N-(X)sulfonylcarboxamide groups of 'tunable' acidity that exhibit good extraction selectivity for Pb^{II} over alkali and alkaline earth metal cations, as well as Cd^{II}, Co^{II}, Cu^{II}, Ni^{II} and Zn^{II}.[6] However, these ligands failed to extract Pb^{II} in the presence of Hg^{II}.[6] This unexpected favoring of a soft metal cation over a harder metal cation by ligands containing hard donor groups encouraged us to investigate the solvent extraction of Hg^{II}, Ag^{I} and Pd^{II} by **1**–**4** and related calix[4]arene derivatives **5**–**10** which have different pendant functional groups [*N*-(X)sulfonylcarboxamide, carboxylic acid, ester, ether, phenol]. To the best of our knowledge, this is the first report in which calixarene-type compounds without soft donor functions have been employed as Hg^{II} extractants.

The complexing abilities of calixarene-based ligands are known to vary significantly with alterations in their structures and conformations.[2] To study Hg^{II} extraction, we used the previously reported, conformationally mobile calix[4]arene *N*-(X)sulfonylcarboxamides **1**–**4**, as well as the related new compounds **5**–**7** which are restricted to the cone conformation. Calix[4]arene *N*-(X)sulfonylcarboxamide **5**‡ was prepared from the corresponding calixarene dicarboxylic acid **6**§ by the procedure described for the synthesis of **1**–**4**.[6] We also utilized proton-ionizable calixarenes **8**[8] and commercially available **10** which exist in cone conformations in $CHCl_3$ solution due to intramolecular hydrogen bonding, but may change into other conformations when converted into metal salts, and the conformationally flexible, non-ionizable derivative **9**[9] which is predominantly the partial cone conformer in $CHCl_3$.[10]

Although all of the calixarenes **1**–**10** were found to extract Hg^{II} from acidic (pH 2.5) aqueous nitrate solutions into $CHCl_3$¶ to some degree, the metal loadings of the ligands are noted to vary markedly with their structures and functional group types (Fig. 1). The calix[4]arene *N*-(X)sulfonylcarboxamides **1**–**4** extract Hg^{II} most efficiently. Even though the 'tunable' acidity of the calixarene *N*-(X)sulfonylcarboxamides alters their extraction properties for harder metal cations,[6] no significant difference in Hg^{II} loading was observed for **1**–**4** under the experimental conditions. For the conformationally flexible ligand **3**, the Hg^{II} loading was found to be considerably higher than that for analogue **5** which has a cone conformation. The calix[4]arene dicarboxylic acids **6** and **8** are weaker Hg^{II} extractants than the corresponding *N*-(X)sulfonylcarboxamides. The somewhat higher Hg^{II} loading for dicarboxylic acid **8** compared to **6** is ascribed to a greater conformational flexibility of the former. Conversion of calix[4]arene dicarboxylic acid **6** into the corresponding diester **7**, which also is restricted to the cone conformation, slightly reduces the level of Hg^{II} extraction. A conformational change from cone to partial cone is thought to be primarily responsible for the significant increase in Hg^{II} loading when the phenolic group in **10** was replaced with anisole units in **9**.

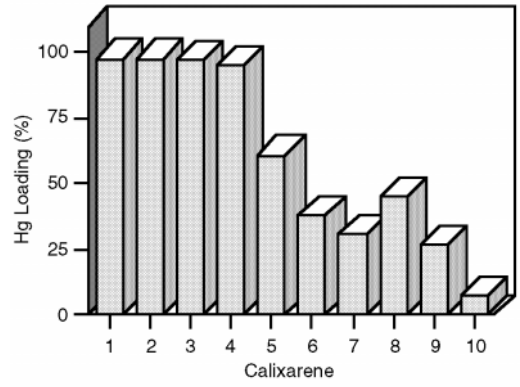

Fig. 1 Hg^{II} loading in extractions of 0.25 mM Hg^{II} from aqueous nitrate solutions at pH 2.5 into $CHCl_3$ with 0.25 mM calixarenes **1**–**10**

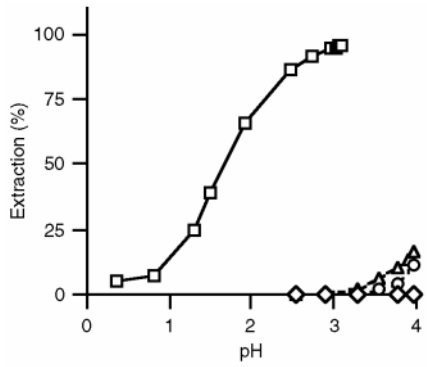

Fig. 2 pH profiles for Ag^{I} extraction from 1.00 mM aqueous $AgNO_3$ into $CHCl_3$ with 1.00 mM calix[4]arene *N*-(X)sulfonylcarboxamides **1**–**4**: (□) **1**, (◇) **2**, (○) **3** and (△) **4**

Coordination of Hg^{II} alters the UV spectra of calixarenes **1**–**10** in $CHCl_3$. The absorption bands at 270–279 nm (for the substituted benzene rings) undergo hypsochromic shifts that are greatest for **1**–**4** (17–23 nm). Analogous spectral changes were not observed when $CHCl_3$ solutions of the ligands were contacted with 1.0 M NaOH. With Cl^- as the counterion instead of NO_3^- under otherwise identical conditions, Hg^{II} extraction was found to decrease dramatically for all of the calixarenes **1**–**10**.

Further investigation of the conformationally flexible calixarene *N*-(X)sulfonylcarboxamides **1**–**4** reveals extraction complex stoichiometries of two metal ions per ligand molecule. The extraction constants determined for ligands **1**–**4** vary as X is changed in the order: CF_3 > Me > Ph > 4-$O_2NC_6H_4$. This ordering differs from that found for Pb^{II},[6] as well as alkali and alkaline earth metal cations, and indicates that the size rather than the electron-withdrawing ability of X is important in Hg^{II} extraction.

The results presented above suggest a significant contribution to the complex stability by π-interactions between Hg^{II} and the electron-rich aromatic rings in the calixarene framework. Previously, π-complexes of calixarenes with other soft heavy metal ions, Ag^{I} and platinides(II), have been reported.[2,3,11]

The calix[4]arene *N*-(X)sulfonylcarboxamides **1**–**4** are also efficient Ag^{I} extractants from acidic and neutral solutions.‖ Unlike Hg^{II} binding, the propensities of these ligands for Ag^{I} extraction are controlled by their acidities. Only ligand **1** extracts Ag^{I} at pH < 3, while a higher pH is required for weaker NH-acids **2**–**4** (Fig. 2). A similar trend is noted for extraction of Pd^{II} by **1**–**4**. Therefore, calixarene *N*-(X)sulfonylcarboxamides **2**–**4** are remarkably selective in Hg^{II} extraction from acidic (pH 2.0–2.5) nitrate solutions, since they efficiently extract Hg^{II} with negligible loadings of alkali, alkaline earth, and many transition metal cations, including Pb^{II}, Ag^{I} and Pd^{II}. Further investigation of soft metal ion separations with calix[4]arene *N*-(X)sulfonylcarboxamides is in progress.

This research was supported by the Division of Chemical Sciences of the Office of Basic Energy Sciences of the US Department of Energy (Grant DE-FGO3-94ER14416).

Notes and References

† E-mail: rabartsch@ttu.edu

‡ *Selected data* for **5**: yield 38%; mp 241–242 °C (Calc. for $C_{68}H_{86}N_2O_{10}S_2$: C, 70.68; H, 7.50; N, 2.42. Found: C, 70.74; H, 7.70; N, 2.28%); δ_H(200 MHz, $CDCl_3$) 0.85 (s, 18 H), 0.94 (t, *J* 7.1, 6 H), 1.25–1.44 (s + m, 22 H), 1.60–1.79 (m, 4 H), 3.21 (d, *J* 12.6, 4 H), 3.82–3.95 (m, 4 H), 4.33 (d, *J* 12.6, 4 H), 4.68 (s, 4 H), 6.54 (s, 4 H), 7.06 (s, 4 H), 7.42–7.72 (m, 6 H), 8.13–8.21 (m, 4 H), 10.41 (s, 2 H).

§ *Synthesis* of **6**: Calixarene **11**, prepared analogously to the dipropyl ether,[7] was stirred at 80 °C with ethyl bromoacetate and NaH in dry DMF for 48 h. After evaporation of the solvent *in vacuo*, the residue was acidified with 1 M HCl and CH_2Cl_2 was added. The CH_2Cl_2 layer was evaporated *in vacuo* and the crude product was chromatographed on alumina with EtOAc–hexanes as eluent. Recrystallization from CH_2Cl_2–MeOH gave the cone isomer of **7** as a white solid in 75% yield. Mp 195 °C (Calc. for $C_{60}H_{84}O_8$: C, 77.21; H, 9.01. Found: C, 77.51; H, 9.02%); δ_H(200 MHz, $CDCl_3$) 0.94–1.04 (s + t, 24 H), 1.17 (s, 18 H), 1.28 (t, *J* 7.1, 6 H), 1.36–1.55 (m, 4 H), 1.84–2.01 (m, 4 H), 3.17 (d, *J* 12.8, 4 H), 3.84 (t, *J* 7.4, 4 H), 4.20 (q, *J* 7.1, 4 H), 4.63 (d, *J* 12.8, 4 H), 4.83 (s, 4 H), 6.63 (s, 4 H), 6.90 (s, 4 H). Diester **7** was hydrolyzed to **6** by refluxing overnight with excess Me_4NOH in aq. THF. The THF was evaporated *in vacuo* and the residue was acidified with 6 M HCl. After extraction with CH_2Cl_2, the solvent was evaporated *in vacuo* to give **6** as a white solid in 97% yield. Mp 243 °C (Calc. for $C_{56}H_{76}O_8$·0.2CH_2Cl_2: C, 75.49; H, 8.61. Found: C, 75.33; H, 8.43%); δ_H(200 MHz, $CDCl_3$) 0.84 (s, 18 H), 0.94 (t, *J* 7.2, 6 H), 1.34 (s, 18 H), 1.23–1.42 (m, 4 H), 1.76–1.92 (m, 4 H), 3.29 (d, *J* 13.0, 4 H), 3.84–3.92 (m, 4 H), 4.24 (d, *J* 13.0, 4 H), 4.65 (s, 4 H), 6.56 (s, 4 H), 7.18 (s, 4 H), 11.34 (br s, 2 H). The presence of solvent in the analytical sample of **6** was evident in its ^1H NMR spectrum.

¶ Aqueous 0.25 mM Hg^{II} nitrate (pH 2.5, HNO_3) was extracted with a 0.25 mM calixarene solution in $CHCl_3$. The Hg^{II} concentration in the aqueous phase was determined spectrophotometrically after extraction into $CHCl_3$ containing 14.0 ppm dithizone (λ_{max} 495 nm).

‖ Aqueous 1.0 mM Ag^{I} nitrate (pH adjusted with HNO_3) was extracted with a 1.0 mM calixarene solution in $CHCl_3$. The Ag^{I} concentration in the aqueous phase was determined by atomic absorption spectrophotometry.

1 D. M. Roundhill, in *Progress in Inorganic Chemistry*, ed. K. D. Karlin, Wiley, New York, 1995, vol. 43, pp. 533–591; M. A. McKervey, M.-J. Schwing-Weill and F. Arnaud-Neu, in *Comprehensive Supramolecular Chemistry*, ed. G. W. Gokel, Elsevier, New York, 1996, vol. 1, pp. 537–603.
2 A. Ikeda and S. Shinkai, *Chem. Rev.*, 1997, **97**, 1713.
3 C. Wieser, C. B. Dieleman and D. Matt, *Coord. Chem. Rev.*, 1997, **165**, 93.
4 F. Arnaud-Neu, G. Barrett, D. Corry, S. Cremin, G. Ferguson, J. F. Gallagher, S. J. Harris, M. A. McKervey and M.-J. Schwing-Weill, *J. Chem. Soc., Perkin Trans. 2*, 1997, 575; M. R. Yaftian, M. Burgard, A. El Bachiri, D. Matt, C. Wieser and C. B. Dieleman, *J. Inclusion Phenom. Mol. Recog. Chem.*, 1997, **29**, 137; K. Ohto, H. Yamaga, E. Murakami and K. Inoue, *Talanta*, 1997, **44**, 1123; V. J. Mathew and S. M. Khopkar, *Talanta*, 1997, **44**, 1699; K. Ohto, E. Murakami, T. Shinohara, K. Shiratsuchi, K. Inoue and M. Iwasaki, *Anal. Chim. Acta*, 1997, **341**, 275; A. T. Yordanov, J. T. Mague and D. M. Roundhill, *Inorg. Chim. Acta*, 1995, **240**, 441; A. T. Yordanov and D. M. Roundhill, *Inorg. Chim. Acta*, 1997, **264**, 309.
5 A. T. Yordanov and D. M. Roundhill and J. T. Mague, *Inorg. Chim. Acta*, 1996, **250**, 295; A. T. Yordanov, O. M. Falana, H. F. Koch and D. M. Roundhill, *Inorg. Chem.*, 1997, **36**, 6468.
6 G. G. Talanova, H.-S. Hwang, V. S. Talanov and R. A. Bartsch, *Chem. Commun.*, 1998, 419.
7 K. Iwamoto, K. Araki and S. Shinkai, *J. Org. Chem.*, 1991, **56**, 4955.
8 R. Ostaszewski, T. W. Stevens, W. Verboom and D. N. Reinhoudt, *Recl. Trav. Chim. Pays-Bas*, 1991, **110**, 294.
9 C. D. Gutsche, B. Dhawan, J. A. Levine, K. H. No and L. J. Bauer, *Tetrahedron*, 1983, **39**, 409.
10 T. Harada, J. M. Rudzinski and S. M. Shinkai, *J. Chem. Soc., Perkin Trans. 2*, 1992, 2109.
11 T. Tsudera, A. Ikeda and S. Shinkai, *Tetrahedron*, 1997, **53**, 13 609; A. Ikeda, T. Tsudera and S. Shinkai, *J. Org. Chem.*, 1997, **62**, 3568; M. Kawaguchi, A. Ikeda and S. Shinkai, *J. Chem. Soc., Perkins Trans. 1*, 1998, 179; M. Staffilani, K. S. B. Hancock, J. W. Steed, K. T. Holman, J. L. Atwood, R. K. Juneja and R. S. Burkhalter, *J. Am. Chem. Soc.*, 1997, **119**, 6324.

Received in Corvallis, OR, USA, 11th March 1998; 8/01994K

Biphenyl-type electron acceptors exhibiting dynamic redox properties: a novel electrochromic system with 'write protect' option

Takanori Suzuki,*† Hyou Takahashi, Jun-ichi Nishida and Takashi Tsuji

Division of Chemistry, Graduate School of Science, Hokkaido University, Sapporo 060-0810, Japan

A novel redox pair undergoing reversible C–C bond making/breaking has been constructed based on a bis(dicyanovinyl)biphenyl derivative and a dianion with the dihydrophenanthrene skeleton; further cyclization of the latter to an enaminonitrile endows the 'write protect' option to its electrochromic response.

Recently much attention has been focused on molecules whose geometry and properties can be controlled by the external stimuli.[1] From this point of view redox systems undergoing reversible C–C bond making/breaking upon electron transfer (ET) are interesting[2] and might be applicable to the construction of electrochemical switches or molecular devices[3] based on their optical response and bistability. We have designed the novel redox pair shown in Scheme 1 which has the following interesting features: (*i*) 2,2′-bis(dicyanovinyl)biphenyls **1** are expected to undergo facile ring closure to dihydrophenanthrene-type dianions $\mathbf{2}^{2-}$ upon two-electron reduction; (*ii*) the resulting dianions are sterically congested molecules and will regenerate the starting material **1** by C–C bond cleavage upon oxidation; (*iii*) in the case of *p*-dimethylaminophenyl derivatives **1a** and $\mathbf{2a}^{2-}$, a sharp change in color is expected during ET because only the former shows strong absorption in the visible region due to the *p*-(dicyanovinyl)aniline skeleton; (*iv*) besides the reversible interconversion between **1** and $\mathbf{2}^{2-}$, further cyclization to **3** induced by protonation of $\mathbf{2}^{2-}$ endows the system with the 'write protect' option in its response (Scheme 2). Here, we report the preparation and unique redox properties of the title acceptors and their reduction products.

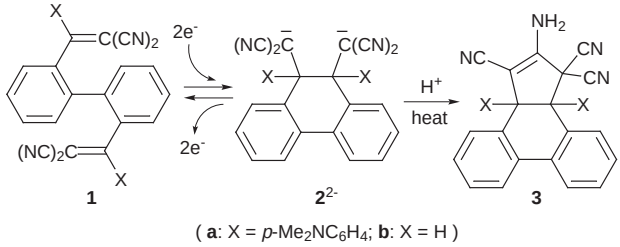

Scheme 1

Scheme 2

Condensation reaction of 2,2′-diformylbiphenyl with malononitrile in the presence of $TiCl_4$ and pyridine[4] gave **1b**‡ (mp 224–226 °C) as colorless crystals in 54% yield. Dye **1a**‡ (mp 333–334 °C) was prepared from 2,2′-diiodobiphenyl *via* its 2,2′-dilithio derivative[5] by successive reactions with *p*-dimethylaminobenzonitrile and malononitrile,[6] and obtained as orange plates [λ_{max} (MeCN): 455 nm (log ε 4.24), 279 (4.02)] in 7% yield.

Voltammetric analyses have revealed quite different behavior of **1a** compared with the *m,m*-isomer **4**.§ The redox behaviour of **4** is nearly identical to that of reference compound

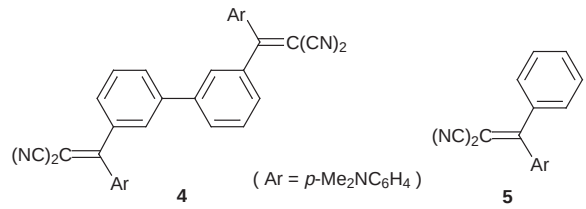

5,[6] which undergoes reversible one-electron reduction to $\mathbf{5}^{\cdot-}$ (E^{red} = −1.28 V) and oxidation to $\mathbf{5}^{\cdot+}$ (E^{ox} = +1.08 V). By contrast the reduction process of **1a** (E^{red} = −1.29 V) is irreversible in the sense that the corresponding anodic peak is absent in its cyclic voltammogram (Fig. 1). Instead, a new peak appeared in the anodic region (+0.04 V). This was assigned to the oxidation peak of $\mathbf{2a}^{2-}$ by independent measurement, and a new cathodic peak corresponding to the reduction of **1a** was observed after the oxidation of $\mathbf{2a}^{2-}$. Such hysteresis in redox waves is characteristic of 'dynamic' redox systems that undergo reversible and drastic structural change upon ET.[1b,2] Electrochromic behaviour was shown by spectrophotometric monitoring of the electrochemical reduction of **1a**, and the isosbestic point at 380 nm is indicative of the quantitative conversion to $\mathbf{2a}^{2-}$ (Fig. 2).

The stereospecific nature of the ring closure was evidenced by product analysis on the mixture obtained by the reaction of **1a** with SmI_2 then with acid.¶ Thus, *trans*-H_2**2a**‡ (mp 221–223 °C) was formed free from the *cis*-isomer and isolated in 64% yield as the sole product. Only by heating in EtOH, does this material isomerize quantitatively to *trans*-**3a**‡ (mp 198–200 °C) by Thorpe condensation[8] which no longer regenerates **1a** upon oxidation, suggesting that 'write protection' can be performed very easily.

Thorpe condensation occurred more rapidly in the absence of dimethylaminophenyl groups. Thus, the enaminonitrile *trans*-**3b**‡ (mp 276–278 °C; $^3J_{HH}$ 13.2 Hz) was obtained as the major

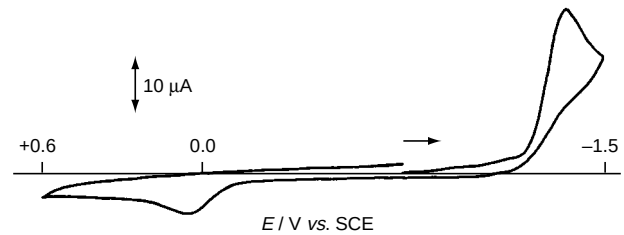

Fig. 1 Cyclic voltammogram of dye **1a** in MeCN (*E*/V *vs.* standard calomel electrode, 0.1 mol dm^{-3} NEt_4ClO_4, Pt electrode, scan rate 500 mV s^{-1}). The oxidation peak at +0.04 V is absent when the voltammogram was first scanned anodically. Another oxidation peak at +1.07 V was also observed but not shown, which corresponds to the oxidation of dimethylaniline moieties as in **4** and **5**.

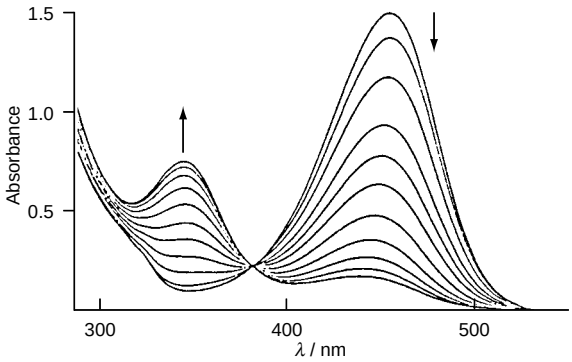

Fig. 2 Changes in UV–VIS spectrum of **1a** (3 ml soln., 7.34×10^{-5} mol dm^{-3} in MeCN containing 0.05 mol dm^{-3} NEt_4ClO_4) upon electrochemical reduction (480 μA) at 1 min intervals

product when **1b** [$E^{red} = -0.87$ V (irrev.)] was reduced with SmI_2. Although *trans*-H_2**2b**‡ (decomp. 250–270 °C) could be isolated as a primary product, the ratio of *trans*-H_2**2b** to *trans*-**3b** varied run-by-run depending on the work-up conditions, and in one case *trans*-**3b** free from *trans*-H_2**2b** was obtained in 83% yield. Careful examination of the mixture showed that *cis*-**3b**‡ (mp 281–282 °C; $^3J_{HH}$ 8.3 Hz) was also formed as a minor component [(*trans*-H_2**2b** + *trans*-**3b**): *cis*-**3b** = 10 : 1], which was separated and purified by reverse phase HPLC. These results indicate that the bulkiness of aryl groups in **1a** plays an important role in confining the stereochemical course of the reductive cyclization of **1**. At the same time, the aryl groups retard isomerization to **3**, thus preventing unintended 'write protection'.

This work was supported by the Ministry of Education, Science, and Culture, Japan (No. 08640664). NMR spectra were measured by Ms. Kazuyo Nakaoka at the Center for Instrumental Analysis (Hokkaido University).

Notes and References

† E-mail: tak@science.hokudai.ac.jp

‡ All new compounds gave satisfactory analytical values.

§ Compound **4**‡ (mp 202–204 °C) was also formed in 0.5% yield when the dilithiobiphenyl was generated from biphenyl and Bu^nLi–TMEDA[7] and used for the preparation of **1a**. This result suggests tht the direct lithiation of biphenyl affords a small amount of 3,3′-dilithio derivative.

¶ Similar reduction of *m*,*m*-isomer **4** with SmI_2 did not induce cyclization but instead hydrogenation of two vinyl groups thus giving the tetrahydro derivative H_4**4**‡ (mp 110–112 °C).

1 (*a*) P. R. Ashton, R. Ballardini, V. Balzani, A. Credi, M. T. Gandolfi, S. Menzer, L. Pérez-García, L. Prodi, J. F. Stoddart, M. Venturi, A. J. P. White and D. J. Williams, *J. Am. Chem. Soc.*, 1995, **117**, 11 171; (*b*) D. J. Cárdenas, A. Livoreil and J.-P. Sauvage, *J. Am. Chem. Soc.*, 1996, **118**, 11 980.

2 M. Horner and S. Hünig, *J. Am. Chem. Soc.*, 1977, **99**, 6122; W. Freund and S. Hünig, *J. Org. Chem.*, 1987, **52**, 2154; T. Suzuki, J. Nishida and T. Tsuji, *Angew. Chem., Int. Ed. Engl.*, 1997, **36**, 1329; T. Suzuki, M. Kondo, T. Nakamura, T. Fukushima and T. Miyashi, *Chem. Commun.*, 1997, 2325.

3 B. L. Feringa, W. F. Jager and B. de Lange, *Tetrahedron*, 1993, **49**, 8267.

4 W. Lehnert, *Tetrahedron Lett.*, 1970, 4723.

5 G. Wittig and W. Herwig, *Chem. Ber.*, 1954, **87**, 1511.

6 E. Campaigne, D. Mais and E. M. Yokley, *Synth. Commun.*, 1974, **4**, 379.

7 N. Neugebauer, A. J. Kos and P. von R. Schleyer, *J. Organomet. Chem.*, 1982, **228**, 107.

8 J. P. Schaefer and J. J. Bloomfield, *Org. React.* (*New York*), 1967, **15**, 1.

Received in Cambridge, UK, 20th February 1998; 8/01463I

Nanomolar determination of copper(II) and zinc(II) using supramolecular complexes of *meso*-tetrakis(4-*N*-methylpyridyl)porphine on polyglutamate

Emanuele Bellacchio,[a] Sergio Gurrieri,[b] Rosaria Lauceri,[a] Antonio Magrì,[a] Luigi Monsù Scolaro,[c] Roberto Purrello*[a]† and Andrea Romeo[c]

[a] *Dipartimento di Scienze Chimiche, Università di Catania, Viale A. Doria 6, 95125, Catania, Italy*
[b] *Istituto per lo Studio delle Sostanze Naturali di Interesse Alimentare e Chimico-Farmaceutico, CNR, Catania, Italy*
[c] *Dipartimento di Chimica Inorganica, Chimica Analitica e Chimica Fisica, Università di Messina, ICTPN CNR Sezione di Messina, Messina, Italy*

The remarkable acceleration of Cu^{II} and Zn^{II} insertion in cationic porphyrins monodispersed on a polyglutamate anionic surface allows determination of the two metal ions down to nanomolar concentrations.

In the last few years a large number of fluorescent sensors for pH or metal ions have been designed and synthesized by means of a supramolecular 'covalent' approach.[1] Most of them are two-component systems in which a 'receptor' unit is covalently linked to a 'sensing' one.

Owing to their high absorption coefficients and tunable fluorescence emission, porphyrins are excellent sensing units.[2] The introduction of polar groups at the periphery of the porphine ring makes them water-soluble and allows the formation of 'non-covalent' supramolecular species on oppositely charged templates.[3] Using this alternative supramolecular approach, it has been recently shown that the complexes of the tetraanionic *meso*-tetrakis(4-sulfonatophenyl)porphine on polylysine can be effective as pH-sensors.[3a] This 'non-covalent' strategy therefore allows one to achieve specific photochemical sensors‡ by mixing commercially available chemicals. On the other hand, the formation of these supramolecular complexes depends upon several factors (such as pH, ionic strength, *etc*.) and consequently they are less 'robust' than those obtained by the classical 'covalent' approach.

This report deals with supramolecular complexes formed by the tetracationic *meso*-tetrakis(4-*N*-methylpyridyl)porphine (H_2T4) and polyglutamate. As a result of a remarkable increase of the metallation reaction rate, this complex behaves as sensitive and specific fluorescent sensor for the determination of nanomolar concentrations of biologically relevant metal ions such as Zn^{II} and Cu^{II}.

Indeed, porphyrin metallation could be used, in principle, as a simple tool for analytical determination of trace amount of metal ions because, in most cases, the absorption and/or the emission properties of the metallo- and the free-porphyrins are quite different from each other, so that the two species can be clearly distinguished.§ Despite this, these reactions have been rarely used for analytical applications,[5] a major limitation being the slow rate of metal insertion.

Under the experimental conditions used in this work (succinate buffer 2 mM, pH = 5.6, [H_2T4] = 1 μM, [poly-L-glutamate] = 200 μM in residue) H_2T4 is mainly monodispersed on the anionic polypeptide.¶ In fact, only a small red shift ($\Delta\lambda$ = 4 nm) and hypochromicity (15%) of the Soret band was observed, while any characteristic feature of porphyrin assembly formation (such as resonance light scattering[6] or induced circular dichroism signals in the Soret region) was absent. Absorption experiments show that the addition of Zn^{II} to such H_2T4–polyglutamate supramolecular complexes leads to a shift of the Soret band at 440 nm (Fig. 1). Also, the main Q-band of H_2T4 (518 nm) is progressively replaced with that of ZnT4 (562 nm) (Fig. 1). These spectroscopic features are diagnostic

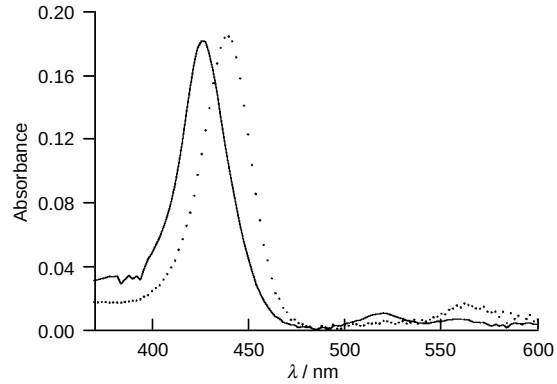

Fig. 1 Absorption spectra (pathlength = 1 cm) of H_2T4 (1 μM) in the presence of polyglutamate (200 μM) at pH 5.6 (succinate buffer 2 mM), before (—) and after (···) the addition of $ZnSO_4$ (0.05 μM)

of the formation of ZnT4. Note that the addition of successive aliquots, each containing a few pmol of Zn^{II}, leads to a linear increase of the fluorescence intensity at 622 nm‖ (ZnT4 emission maximum), as shown in Fig. 2.

The presence of polyglutamate turns out to be essential to observe a reasonable time response of the method. In the presence of the anionic polypeptide, Zn^{II} insertion was completed in about 10 min whereas in its absence, even after 24 h no evidence of metallation was observed *i.e.* the formation of the polyglutamate–H_2T4 supramolecular complex 'catalyzes' the insertion of Zn^{II}. Preliminary kinetic data show that the metallation rate under such conditions is about 1000 times higher compared to the 'uncatalyzed' reaction.**

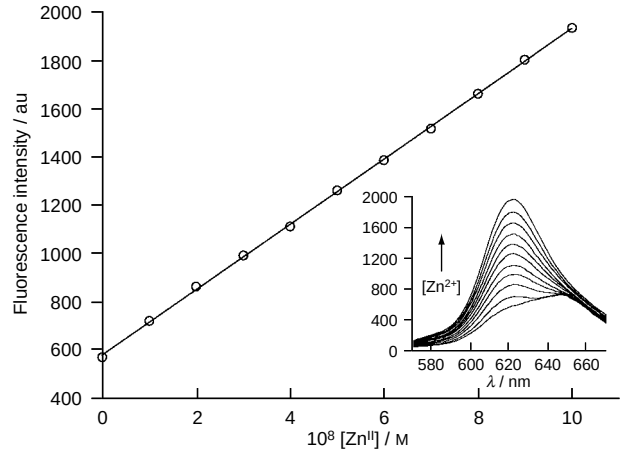

Fig. 2 Plot of fluorescence intensity at 622 nm (λ_{ex} = 445 nm) *vs.* Zn^{II} concentration, for a solution of H_2T4 (1 μM) in the presence of polyglutamate (200 μM) at pH 5.6 (succinate buffer 2 mM)

A similar behaviour was observed for the same system when Cu^{II} was employed in place of Zn^{II}. Here, the formation of the metalloporphyrin was confirmed by the gradual replacement of the H_2T4 Q-band (518 nm) with that of CuT4 (550 nm), as the Cu^{II} concentration was increased. However, since the CuT4 formed is non-fluorescent, we monitored the disappearance of H_2T4 monodispersed on polyglutamate. Here, as well, a plot of H_2T4 emission fluorescence intensity (λ_{ex} = 422 nm, λ_{em} = 655 nm) *vs*. Cu^{II} concentration (Fig. 3) shows a linear behavior.

Interestingly, the pH dependence of the metallation rate is also influenced by the presence of polyglutamate. For example, it has been reported that, in the presence of nitrate, the metallation rate is almost unaffected in the pH range 4.4–5.5 and accelerated at higher pH.[7] On the contrary, in the presence of polyglutamate the metallation rate increases with pH (*i.e.* with the number of negative charges on the polypeptide) in the range *ca*. 4.5–5.5 and then does not increase further at higher pHs. Also, at pHs lower than *ca*. 4.5 the insertion reaction is not catalyzed by polyglutamate. This observation suggests that, unlike other ligands,** the 'catalytic' role of the anionic template must be related to its electrostatic field by (i) increasing the 'local' concentration of metal ions,[8] and (ii) partially shielding the positive charges of the H_2T4 monodispersed on it (thus facilitating the approach of the cationic metal ions to the cationic porphyrins). As expected according to this hypothesis, no appreciable increase of metallation rate was observed when Zn^{II} or Cu^{II} were added to the solution containing the tetraanionic *meso*-tetrakis(4-sulfonatophenyl)-porphine monodispersed on the protonated polylysine. Most likely, the state of the porphyrins also plays a role in the reaction rate trend observed at pH lower than *ca*. 4.5. Decreasing the pH, H_2T4 tends to aggregate on polyglutamic acid.¶ In this case, the porphyrins face-to-face arrangement[9] should reduce the accessibility of the metal ions to the porphine 'core'. This hypothesis is in good agreement with previous experiments by Pasternack *et al.*[10] which show that aggregation and/or intercalation of porphyrins onto or into synthetic DNA have a negative influence on porphyrin metallation rate. Therefore, the nature of the matrix and of the supramolecular complex (*i.e.* of the molecular recognition processes) is crucial to allow the catalysis of the metal insertion by an anionic template.

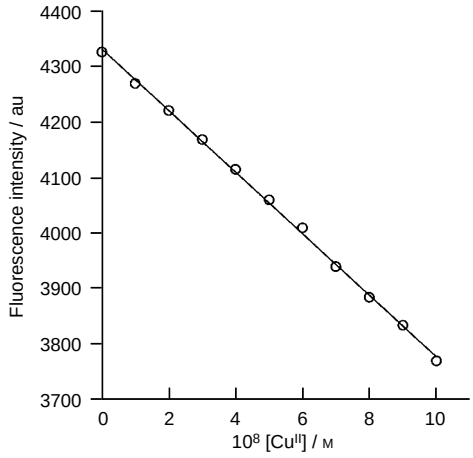

Fig. 3 Plot of fluorescence intensity at 655 nm (λ_{ex} = 422 nm) *vs.* Cu^{II} concentration, for a solution of H_2T4 (1 μM) in the presence of polyglutamate (200 μM) at pH 5.6 (succinate buffer 2 mM)

Finally, the addition of other metal ions, such as Co^{II}, Fe^{II}, Mg^{II}, Mn^{II} and Ni^{II} does not cause any of the spectroscopic variations described above in a time interval comparable to that observed for Zn^{II} and Cu^{II}. A reasonable explanation for this behavior is that the 'uncatalyzed' rate of insertion for Co^{II}, Fe^{II}, Mg^{II}, Mn^{II} and Ni^{II} in H_2T4 is much lower than that of Zn^{II} and Cu^{II}.

In conclusion, a selective and very sensitive supramolecular sensor for metal ions has been obtained by means of extremely simple routes. To date, the non-covalent nature of these species, and therefore their relatively low robustness, has hindered their application for the development of chemical devices. Further studies are currently in progress in our laboratory to investigate possible technological applications.

Notes and References

† E-mail: rpurrello@dipchi.unict.it

‡ The term sensor in the following context is not used to indicate a device, but rather a chemical system able to recognize a species and to report its recognition (*e.g.* by spectroscopic variations).

§ For example, absorption and emission maxima for ZnT4 and H_2T4 are λ_{ex} = 436 nm, λ_{em} = 622 nm, and λ_{ex} = 422 nm, λ_{em} = 655 nm, respectively. On the other hand, the insertion of Cu^{II} causes a complete quenching of the fluorescence of H_2T4 (a weak emission, centered at *ca.* 770 nm, has been found in water, but only when CuT4 is intercalated into natural or synthetic DNAs).[4]

¶ H_2T4 is aggregated on polyglutamate in the pH range 3.4–4.5, and is monodispersed on the polypeptide both at higher and lower pHs (E. Bellacchio, S. Gurrieri, L. Monsù Scolaro and R. Purrello, in progress).

‖ In order to minimize the contribution of H_2T4 fluorescence, the excitation wavelength used in these experiments is 445 nm.

** Acceleration of porphyrins metallation has been also observed in the presence of simple ligands such as acetate, pyridine, ammonia, nitrate and ascribed to labilization of the water molecules bound to the metal ion.[7]

1 R. A. Bissel, A. P. de Silva, H. Q. N. Gunaratne, P. M. L. Lynch, G. E. M. Maguire and K. R. A. S. Sandanayake, *Chem. Soc. Rev.*, 1992, 187; L. Fabbrizzi, M. Licchelli, P. Pallavicini, A. Perotti, A. Taglietti and D. Sacchi, *Chem. Eur. J.*, 1996, **2**, 75 and references therein.

2 R. Grigg and W. D. J. A. Norbert, *J. Chem. Soc., Chem. Commun.*, 1992, 1298.

3 (*a*) R. F. Pasternack and E. Gibbs, in *Metal Ion in Biological Systems*, ed. A. Sigel and H. Sigel, Marcel Dekker, Basel, 1996, p. 367 and references therein; (*b*) H.-J. Schneider and M. Wang, *J. Org. Chem.*, 1994, **59**, 7473; (*c*) R. Purrello, S. Gurrieri, E. Bellacchio, R. Lauceri and L. Monsù Scolaro, in *Spectroscopy of Biological Molecules: Modern Trends*, ed. P. Carmona, R. Navarro and A. Hernanz, Kluwer, Dordrecht, 1997, p. 91.

4 B. P. Hudson, J. Sou, D. J. Berg and D. R. McMillin, *J. Am. Chem. Soc.*, 1992, **114**, 8997.

5 C. V. Banks and R. E. Bisque, *Anal. Chem.*, 1957, **29**, 526; J.-I. Itoh, T. Yotsuyanagi and K. Aomura, *Anal. Chim. Acta*, 1975, **74**, 53; S. Funashi, Y. Ito, M. Inamo, Y. Hamada and M. Tanaka, *Mikrochim. Acta*, 1986, **1**, 33; M. Tabata, M. Kumamoto and J. Nishimoto, *Anal. Chem.*, 1996, **68**, 758.

6 R. F. Pasternack and P. J. Collings, *Science*, 1995, **269**, 935.

7 P. Hambright and P. B. Chock, *J. Am. Chem. Soc.*, 1974, **96**, 3123; M. Tabata and M. Tanaka, *Trends Anal. Chem.*, 1991, **10**, 128.

8 G. S. Manning, *J. Phys. Chem.*, 1981, **85**, 870.

9 C. A. Hunter and J. K. M. Sanders, *J. Am. Chem. Soc.*, 1990, **112**, 5525; J.-H. Fuhrhop, C. Demoulin, C. Boettcher, J. Köning and U. Siggel, *ibid.* 1992, **114**, 4159 and references therein.

10 R. F. Pasternack, E. J. Gibbs, R. Santucci, S. Schertel, P. Ellinas and S. C. Mah, *J. Chem. Soc., Chem. Commun.*, 1987, 1771.

Received in Basel, Switzerland, 5th March 1998; 8/01806E

Synthesis of highly branched block copolymers of enantiomerically pure amino acids

Andrew C. Birchall and Michael North*†

Department of Chemistry, University of Wales, Bangor, Gwynedd, UK LL57 2UW

The combination of multifunctional initiators and the use of lysine residues to introduce branch points into poly(amino acids) allow the synthesis of highly branched poly(amino acids).

In recent years, there has been considerable interest in the synthesis of synthetic polymers with non-linear molecular architectures.[1] Much work in this area has concentrated on the synthesis and investigation of dendrimers,[2] polymers which have precisely controlled molecular weights and geometry. However, for many applications, the variety of molecular weights found in conventional synthetic polymers leads to desirable physical properties. Thus there is a need for methodology which will allow the synthesis of polydisperse, highly branched polymers. We have an ongoing interest in the preparation of synthetic polymers derived from biomonomers,[3] and here the synthesis of highly branched, polydisperse poly(amino acid)s is reported.

The synthesis of the desired polymers is outlined in Scheme 1. An initiator **1a**–**d** containing one to four primary amino groups was used to polymerize the *N*-carboxy anhydride **2** of an amino acid.‡ This is a well known process for the preparation of poly(amino acid)s,[4] however it was anticipated that, provided termination reactions could be avoided, the addition of *N*,*N*′-di(benzyloxycarbonyl)lysine *p*-nitrophenyl ester **3** to the polymerization mixture would produce capped polymers **4**. Subsequent hydrogenation of polymers **4** would reveal two primary amino groups on each chain of the initial polymer which could be used to initiate the polymerization of a second *N*-carboxy anhydride of an amino acid. Capping of this polymerization by lysine derivative **3** would give the next generation of the polymer, and the process could be repeated indefinitely to give highly branched poly(amino acids).

In practice, unfunctionalized amino acid *N*-carboxy anhydrides **2** were employed in order to avoid the undesired termination reactions which are known to occur with functionalized amino acids such as γ-esters of glutamic acid.[5] It was also found to be advantageous to keep each polymer chain relatively short (5–10 amino acids) in order to avoid solubility problems, although even polymers prepared in this way were soluble only

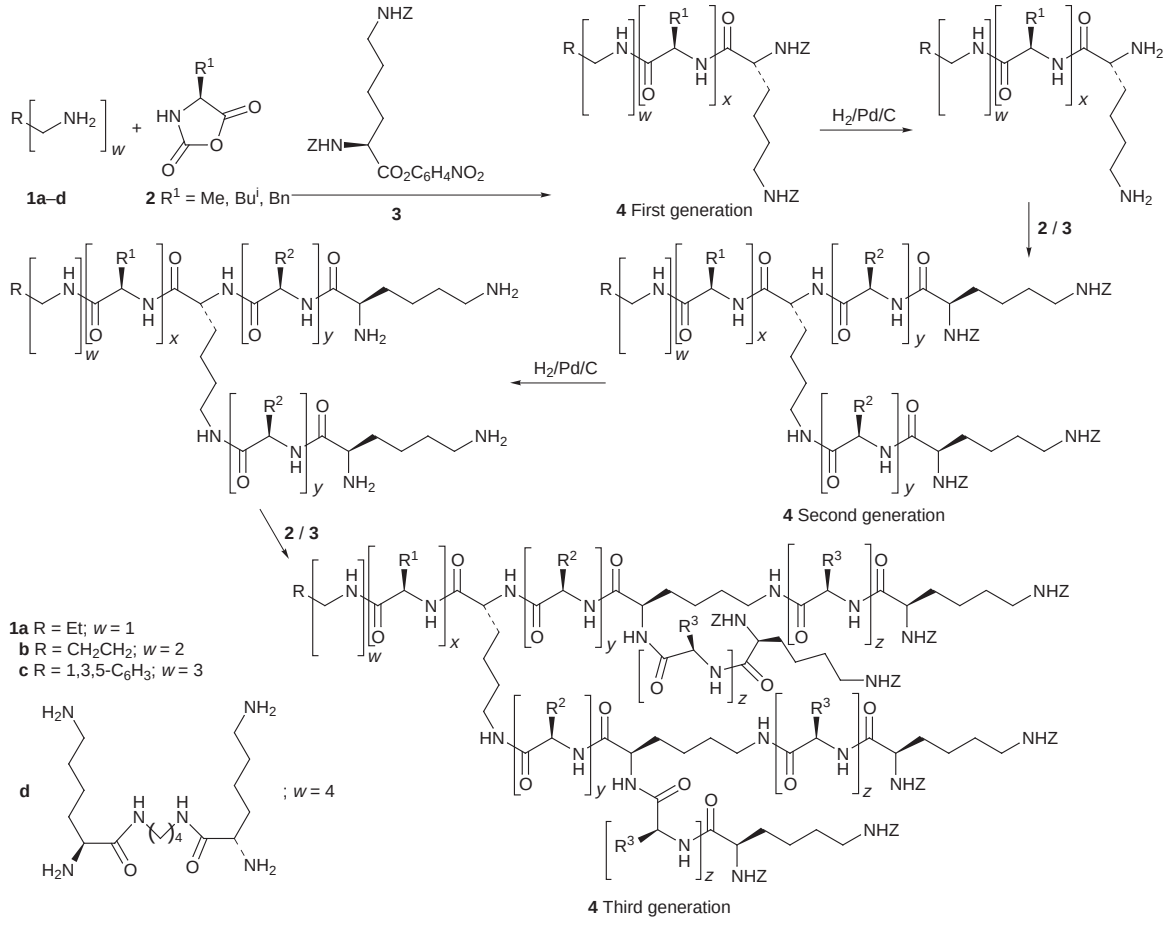

Scheme 1

Table 1 Structures and molecular weight data for polymers **4**

Entry	Initiator	AA1[a]	AA2[a]	AA3[a]	M_n[b]	M_w[b]	PDI	M_n[c] (calc.)	Yield (%)
1	**1a**	Leu (8)	—	—	1100	1230	1.1	1359	58
2	**1a**	Leu (8)	Ala (7)	—	3220	3720	1.2	2877	70
3	**1a**	Leu (8)	Ala (7)	Phe (4)	5240	7820	1.5	6277	56
4	**1a**	Phe (10)	—	—	1800	2000	1.1	1925	71
5	**1a**	Phe (10)	Leu (8)	—	1700	2000	1.2	4257	61
6	**1a**	Phe (10)	Leu (8)	Ala (4)	2200	2200	1.0	6441	94
7	**1b**	Ala (5)	—	—	2400	2900	1.2	1590	96
8	**1b**	Ala (5)	Leu (5)	—	2200	2700	1.2	4898	57
9	**1b**	Ala (5)	Leu (5)	Phe (4)	4300	7900	1.8	11798	66
10	**1b**	Leu (4)	—	—	2300	2640	1.1	1784	71
11	**1b**	Leu (4)	Phe (4)	—	3870	5300	1.4	5184	64
12	**1b**	Leu (4)	Phe (4)	Ala (4)	3570	5340	1.5	9552	57
13	**1b**	Phe (4)	—	—	2200	2680	1.2	2056	65
14	**1b**	Phe (4)	Leu (4)	—	3810	4890	1.3	4912	86
15	**1b**	Phe (4)	Leu (4)	Ala (4)	2430	4420	1.8	9280	74
16	**1c**	Phe (5)	—	—	2910	3740	1.3	3558	78
17	**1c**	Phe (5)	Leu (4)	—	2800	3600	1.3	7842	54
18	**1c**	Leu (5)	—	—	3500	4000	1.1	3048	63
19	**1c**	Leu (5)	Phe (4)	—	4500	5100	1.1	8148	81
20	**1d**	Phe (4)	—	—	4530	5440	1.2	4280	80
21	**1d**	Phe (4)	Leu (3)	—	4590	5920	1.3	9088	65
22	**1d**	Leu (4)	—	—	3070	4100	1.3	3736	60
23	**1d**	Leu (4)	Phe (3)	—	8270	33600	4.1	9360	77

[a] The numbers in brackets correspond to the average number of amino acids incorporated into each branch of the polymer as determined by ^{1}H NMR spectroscopy. [b] M_n and M_w values were obtained from GPC data calibrated with polystyrene standards. [c] Calculated from the integration trace of the ^{1}H NMR spectrum.

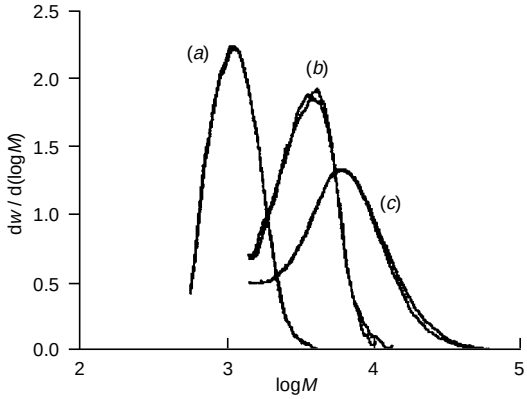

Fig. 1 The GPC chromatograms for the polymers corresponding to entries (*a*) 1, (*b*) 2 and (*c*) 3 in Table 1. Each chromatogram was run in duplicate.

in polar aprotic solvents, which restricted the methods which could be used for their characterization. Initial studies were carried out using propylamine **1a** as a monofunctional initiator, and the polymerizations were repeated to the third generation. The structures and molecular weights of the polymers are given in Table 1. In each case, the polymers were characterized by solution state ^{1}H NMR spectroscopy, solution or solid state ^{13}C NMR spectroscopy and GPC. Typical GPC chromatograms are shown in Fig. 1. It is apparent from Fig. 1 that the molecular weight of the polymer increases as each amino acid is added to the polymer, and that the peak corresponding to the precursor polymer disappears at each stage. In some cases (*e.g.* entries 4–6 in Table 1), however, the low molecular weights of alanine and leucine combined with the small number of residues being introduced meant that GPC was unable to detect the change in the size of the polymer.

Having shown that branched polymers could be prepared by this methodology, the use of initiators **1b**–**d**[6]§ bearing two to four primary amino groups was investigated. As Table 1 shows, in each case it was possible to obtain the desired branched poly(amino acid)s exactly as in the case of initiator **1a**. However, an increasing discrepancy between the calculated and experimental M_n values is apparent in these polymers (*e.g.* entries 7–9 in Table 1). This is probably due to the fact that GPC separation is based on molecular size rather than molecular weight, and for branched polymers, the relationshp between molecular size and molecular weight is non-linear.

In conclusion, we have shown that it is possible to prepare highly branched polymers derived from amino acids. The polymers are expected to have a number of applications including asymmetric catalysts, biomimetic polymers, biodegradable polymers and biocompatible polymers. Our work in this area is continuing.

The authors thank the EPSRC for a studentship (to A. C. B.), and the EPSRC GPC (RAPRA UK Ltd.), solid state NMR (Durham) and mass spectrometry (Swansea) services for their invaluable assistance with this work.

Notes and References

† E-mail: m.north@bangor.ac.uk

‡ All amino acids used in this work have the *S*-configuration.

§ Initiator **1d** was prepared by the reaction of lysine derivative **3** with 1,4-diaminobutane, followed by hydrogenolysis of the benzyloxycarbonyl protecting groups.

1 For recent examples see: A. Mueller, T. Kowalewski and K. L. Wooley, *Macromolecules*, 1998, **31**, 776; W. Radke, G. Litvinenko and A. H. E. Muller, *Macromolecules*, 1998, **31**, 239; L. J. Hobson, A. M. Kenwright and W. J. Feast, *Chem. Commun.*, 1997, 1877.

2 D. A. Tomalia, A. M. Naylor and W. A. Goddard III, *Angew. Chem., Int. Ed. Engl.*, 1990, **29**, 138; J. Issberner, R. Moors and F. Vogtle, *Angew. Chem., Int. Ed. Engl.*, 1994, **33**, 2413.

3 S. M. Bush and M. North, *Polymer*, 1998, **39**, 933; S. C. G. Biagini, M. P. Coles, V. C. Gibson, M. R. Giles, E. L. Marshall and M. North, *Polymer*, 1998, **39**, 1007 and references cited in these two papers.

4 H. R. Kricheldorf, *α-Amino Acid N-Carboxy Anhydrides and Related Materials*, Springer, New York, 1987.

5 D. Coleman, *J. Chem. Soc.*, 1951, 2294; W. E. Hanby, S. G. Waley and J. Watson, *J. Chem. Soc.*, 1950, 3239.

6 Y. Tor, J. Libman, A. Shanzer, C. E. Felder and S. Lifson, *J. Am. Chem. Soc.*, 1992, **114**, 6653.

Received in Liverpool, UK, 18th March 1998; 8/02158I

A stereoselective isomerization of allyl silyl ethers to (*E*)- or (*Z*)-silyl enol ethers using cationic iridium complexes

Toshimichi Ohmura, Yasuo Shirai, Yasunori Yamamoto and Norio Miyaura*†

Division of Molecular Chemistry, Graduate School of Engineering, Hokkaido University, Sapporo 060-8628, Japan

A cationic iridium complex, prepared *via* the hydrogenation of $[Ir(cod)_2]PF_6$–$2PPr_3$ is found to be an excellent catalyst for the stereoselective isomerization of primary allyl silyl ethers to (*E*)-enol ethers and secondary allyl ethers to (*Z*)-enol ethers.

The transition metal-catalyzed positional isomerization of double bonds is an excellent method which has been used in a variety of organic transformations,[1] such as the synthesis of ketones or aldehydes from allylic alcohols, the conversion of allylic ethers to enol ethers, and the transfer of double bonds to the carbon adjacent to carbonyl groups. Among them, the catalytic isomerization of allyl ethers to enol ethers has been studied quite extensively because the procedure is convenient and straightforward and uses readily available substrates, although their stereoselective transformation has not received much attention. The enol ethers thus obtained are either (*Z*)- or (*E*)-isomers, or a mixture of two in most cases. For example, a ruthenium complex gives an equilibrium mixture with the (*Z*)-enol ether predominating (*Z* > 55–68%),[2] while a cationic iridium(III) complex, in contrast, stereoselectively produces (*E*)-enol ethers (*E* > 97%).[3]

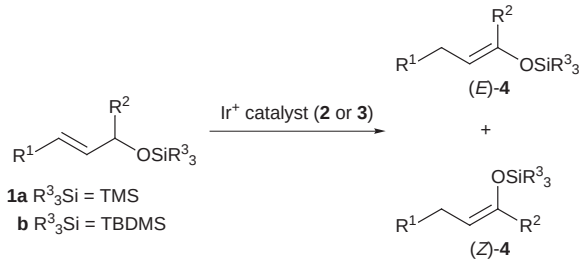

Scheme 1

We have recently demonstrated the efficiency of a cationic iridium catalyst for the stereoselective preparation of (*E*)-γ-alkoxyallylboronates from (3-alkoxy-1-alkenyl)boronates.[4] However, the difficulty in reproducing high stereoselectivities on various substrates prompted us to re-investigate the reactioin detail. One of the early, and still one of the most frequently used, routes to (*E*)- or (*Z*)-silyl enol ethers is the trapping of ketone or aldehyde enolates generated under conditions of either kinetic or equilibrium control conditions.[5] However, the catalytic isomerization may offer a reliable and economical route from readily available allylic alcohols (Scheme 1).

The cationic iridium(III) complex **2** generated *in situ* by hydrogenation of $[Ir(cod)(PMePh_2)_2]PF_6$ in THF, produced a very active catalyst, reported by Felkin, which isomerizes primary allyl ethers to (*E*)-enol ethers, but it was unfortunately

Table 1 Effect of catalysts on the isomerization of **1b** (R^1 = H, R^2 = Ph)[a]

Entry	Catalyst	Yield (%)	*E* : *Z*
1	$[Ir(cod)(PPh_2Me)_2]PF_6/H_2$	trace	
2	$[Ir(cod)(PPh_2Me)_2]PF_6$/catecholborane	12	36 : 64
3	$[Ir(cod)(PPh_3)_2]PF_6$/catecholborane	10	42 : 58
4	$[Ir(cod)_2]PF_6$–$2PMe_3/H_2$	0	
5	$[Ir(cod)_2]PF_6$–$2PEt_3/H_2$	76	8 : 92
6	$[Ir(cod)_2]PF_6$–$2PPr_3/H_2$	92	12 : 88
7	$[Ir(cod)_2]PF_6$–$2PBu_3/H_2$	96	10 : 90
8	$[Ir(cod)_2]PF_6$–$2PCy_3/H_2$	0	
9	$[Ir(cod)_2]PF_6$–dppe/H_2	0	

[a] To a solution of catalyst (3 mol%) in CH_2Cl_2 (3 ml)–acetone (0.5 mmol) was added **1b** (R^1 = H, R^2 = Ph) (0.5 mmol), and the resulting solution was then stirred for 30 min at room temperature. The catalysts were prepared *in situ* by bubbling hydrogen into a solution of $[Ir(cod)(PR_3)_2]PF_6$ or into a mixture of $[Ir(cod)_2]PF_6$ (0.015 mmol) and R_3P (0.03 mmol) (entries 1 and 4–9). To a solution of $[Ir(cod)(PR_3)_2]PF_6$ (3 mol%) and **1b** (0.5 mmol) was added catecholborane (3 mol%) at room temperature (entries 2 and 3).

Table 2 Synthesis of silyl enol ethers[a]

		Acetone		CH_2Cl_2–acetone	
Entry	Allyl silyl ether **1**	Yield (%)	*E* : *Z*	Yield (%)	*E* : *Z*
1	CH_2=CHCH$_2$OTBDMS	74	99 : 1	90	24 : 76
2	MeCH=CHCH$_2$OTBDMS	92	99 : 1[b]		
3	PrCH=CHCH$_2$OTBDMS	97	99 : 1[b]		
4	PrCH=CHCH$_2$OTBDMS	85	99 : 1[c]		
5	PhCH=CHCH$_2$OTBDMS	77	96 : 4		
6	CH_2=CHCHMeOTMS	—		71[d]	26 : 74
7	CH_2=CHCHMeOTBDMS	—		89[d]	28 : 72
8	CH_2=CHCHPr^{i}OTMS	—		89	*Z* > 99
9	CH_2=CHCHCyOTMS	—		96	*Z* > 99
10	CH_2=CHCHPhOTMS	—		96	18 : 82

[a] Hydrogen was bubbled into a mixture of $[Ir(cod)_2]PF_6$ (0.015 mmol) and PPr_3 (0.03 mmol) in acetone (3 ml) or CH_2Cl_2 (3 ml)–acetone (0.5 mmol) to give a pale yellow solution of the catalyst **3**. The excess hydrogen was then removed by bubbling argon into the solution. An allyl silyl ether (0.5 mmol) was added and the resulting mixture was then stirred for 30 min at room temperature. [b] The reaction was carried out for 10 min in the presence of 1 mol% of the catalyst because the conditions using 3 mol% catalyst for 30 min resulted in lower selectivity (*E* = 87–93%). [c] Catecholborane (0.015 mmol) was added to a mixture of $[Ir(cod)(PPh_2Me)_2]PF_6$ (0.015 mmol) and allyl silyl ether (0.5 mmol) in acetone. [d] The reaction accompanied by 5–6% of CH_2=CEtOSiR$^3{}_3$.

not effective for secondary allyl ethers such as **1b** (R^1 = H, R^2 = Ph) (entry 1 in Table 1). Similarly to the treatment with hydrogen, various metal hydrides were found to activate the Ir-cod complexes, presumably by removing the cod ligand *via* hydrometalation. The addition of catecholborane or DIBAL-H (1 equiv.) generated the more active catalyst solution than treatment with hydrogen, but the arylphosphine derivatives did not give good results due to their large steric hindrance (entries 2 and 3). Finally, Ir–trialkylphosphine complexes **3** obtained by hydrogenation of a mixture of $[Ir(cod)_2]PF_6$[6] and R_3P (R = Et, Pr, Bu) (2 equiv.) gave an excellent catalyst for the isomerization of secondary allyl ethers with (*Z*)-**4** predominating (*Z* = 88–92%) (entries 5–7). Trimethylphosphine, tricyclohexylphosphine (PCy_3) and bidentate phosphine ligands such as dppe are not effective (entries 4, 8 and 9).

The isomerization of the representative allyl silyl ethers with **3** (R = Pr) is summarized in Table 2. In an acetone solution, the isomerization of primary allyl ethers was completed within 30 min, provided (*E*)-**4** in high yields and with high selectivity, results which were comparable to those obtained for reactions catalyzed by **2** (entries 1–5). The reaction was further accelerated in a mixed solvent of acetone and CH_2Cl_2 giving (*Z*)-**4** predominantly (*E* : *Z* = 24 : 76) (entry 1), although all attempts for the stereoselective preparation of (*Z*)-**4** were unsuccessful. The *Z*-selectivity further improved for secondary allyl trimethylsilyl ethers (entries 6–10), especially when R^2 was a secondary alkyl unit (entries 8 and 9). Both catalysts reported by Felkin (**2**) and **3** worked well for primary allyl ethers (entry 4), but **3** demonstrated a higher catalytic efficiency for secondary allyl ethers.

The iridium-catalyzed isomerization of allyl ethers proceeds through the oxidative addition of an allylic C–H bond to the iridium(I) metal center giving a *syn*-π-allyliridium complex **6** which selectively led to (*E*)-**4** (Scheme 2).[1–3]

The ^1H NMR study reveled that the isomerization involves two process: the first and selective formation of (*E*)-**4** (kinetically controlled process) is followed by equilibration to a mixture of (*E*)- and (*Z*)-**4** through the *anti*-π-allyl intermediate (thermodynamically controlled process) which is slow in a solvent coordinating to the iridium metal center such as acetone.[7] Thus, the stereochemistry of **4** is highly dependent on the solvents and the substrates. When primary allyl ethers were

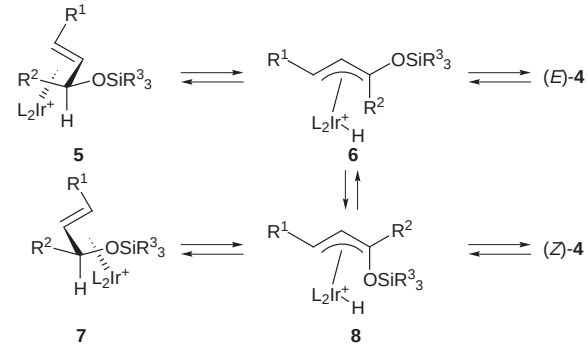

Scheme 2

reacted in acetone, the kinetic products [(*E*)-**4**] were obtained through the *syn*-π-allyl intermediate [**5** → **6** → (*E*)-**4**]. On the other hand, high *Z*-selectivity was achieved for secondary allyl ethers under conditions leading to equilibration, where the steric difference between the R^2 and R_3Si groups controls the stereochemistry of the products [**5** → **6** → **8** or **7** → **8** → (*Z*)-**4**].

Notes and References

† E-mail: miyaura@organ.hokudai.ac.jp

1 H. M. Colquhoun, J. Holton, D. J. Thompson and M. V. Twigg, *New Pathways for Organic Synthesis—Practical Applications of Transition Metals*, Plenum Press, London, 1984, pp. 173–193.
2 H. Suzuki, Y. Koyama, Y. Moro-oka and T. Ikawa, *Tetrahedron Lett.*, 1979, 1415.
3 D. Baudry, M. Ephritikhine and H. Felkin, *J. Chem. Soc., Chem. Commun.*, 1978, 694.
4 T. Moriya, A. Suzuki and N. Miyaura, *Tetrahedron Lett.*, 1995, **36**, 1887.
5 P. L. Hall, J. H. Gilchrist and D. B. Collum, *J. Am. Chem. Soc.*, 1991, **113**, 9571.
6 M. Green, T. A. Kuc and S. H. Taylor, *J. Chem. Soc. (A)*, 1971, 2334.
7 R. H. Crabtree, M. F. Mellea, J. M. Mihelcic and J. M. Quirk, *J. Am. Chem. Soc.*, 1982, **104**, 107.

Received in Cambridge, UK, 14th April 1998; 8/02760I

Mukaiyama aldol reactions of π-allyltricarbonyliron lactone and lactam complexes bearing trimethylsilyl enol ether side-chains. Not just formal, but genuine 1,7 induction of chirality

Steven V. Ley,*† Liam R. Cox, Ben Middleton and Julia M. Worrall

Department of Chemistry, University of Cambridge, Lensfield Road, Cambridge, UK CB2 1EW

A comparison of diastereoselectivities in the Mukaiyama aldol reactions of three types of trimethylsilyl enol ether substituted iron carbonyl complexes has provided evidence for the stereodirecting effect of remote substituents in π-allyltricarbonyliron lactone and lactam complexes.

The complexation of an organic ligand to a metal can influence the stereoselectivity of its reactions in a variety of ways. We have previously demonstrated the use of the π-allyltricarbonyliron lactone framework[1] as a chiral template to provide diastereocontrol in the manipulation of a ketone functionality appended to the allyl unit.[2,3] The reactions of such ketones with nucleophiles proceed with predictable stereochemistry, the ketone adopting an s-*cis* conformation and the nucleophile approaching *anti* to the bulky $Fe(CO)_3$ moiety. This parallels the reactivity pattern of the related η⁴ dienone tricarbonyliron complexes (Fig. 1).[4]

More recently, we have shown that trimethylsilyl enol ethers derived from *endo* substituted π-allyltricarbonyliron lactone complexes can undergo highly diastereoselective Mukaiyama aldol reactions with a variety of aldehydes under $BF_3{\cdot}OEt_2$ activation.[5] The selectivity in these reactions is more difficult to explain, as it is dependent only on the ability of the enol ether side-chain to distinguish between the prochiral faces of the Lewis acid–aldehyde complex. Interestingly, the trimethylsilyl enol ethers of η⁴ dienone tricarbonyliron complexes have been reported to show poor diastereoselectivity in their reactions with aldehydes under $BF_3{\cdot}OEt_2$ activation.[6] This apparent difference in the influence of the structurally similar enol ether substrates implies that the lactone portion of the π-allyl complexes might be involved in controlling the delivery of the aldehyde. More specifically, the *endo* substituent at the lactone tether, *seven* carbon atoms distant from the developing stereocentre, could interact directly with the incoming Lewis acid–aldehyde complex (Fig. 2).

This communication reports an investigation of diastereocontrol in the Mukaiyama aldol reactions of π-allyltricarbonyliron lactone and lactam complexes by variation of the substitution pattern at the tether and a direct comparison with a representative η⁴ diene tricarbonyliron complex.

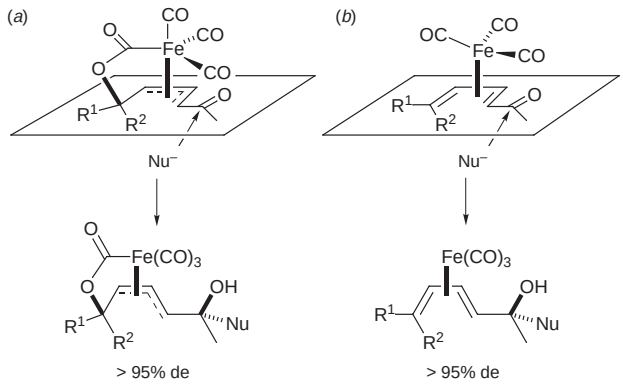

Fig. 1 Tricarbonyliron-mediated diastereocontrol: reaction of (*a*) ketone functionalised π-allyltricarbonyliron lactones and (*b*) η⁴-dienone complexes with nucleophiles

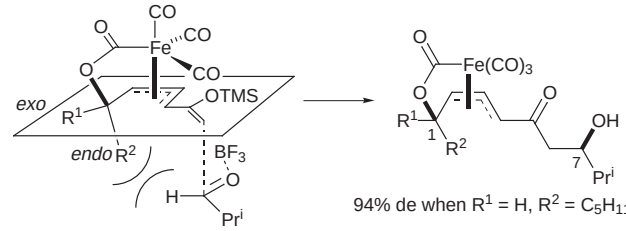

Fig. 2 Possible involvement of the *endo* substituent in directing Mukaiyama aldol reactions of π-allyltricarbonyliron lactone complexes

Trimethylsilyl enol ethers were prepared in excellent yields from the corresponding methyl ketone complexes by reaction with TMSOTf and Et_3N in CH_2Cl_2 at 0 °C. Treatment with premixed benzaldehyde and $BF_3{\cdot}OEt_2$ in Et_2O–CH_2Cl_2 at −78 °C afforded mixtures of TMS protected and unprotected aldol products which were desilylated using HF–pyridine during the work-up. A comparison of the yields and diastereoselectivities obtained using π-allyltricarbonyliron lactone and lactam complexes is shown in Table 1.

The *endo* substituted complexes **1**, **2**, **3** and **5** showed good to excellent levels of asymmetric induction in their reactions with benzaldehyde. The slightly lower diastereomeric excess obtained with the *endo* phenyl complex **3** may reflect the contribution of a favourable interaction between the aromatic rings of the complex and aldehyde. The diastereomeric excesses obtained when the complex was *exo* substituted (complexes **4** and **6**) were significantly reduced, showing that an important

Table 1 Mukaiyama aldol reaction of silyl enol ethers derived from π-allyltricarbonyliron lactone and lactam complexes with benzaldehyde

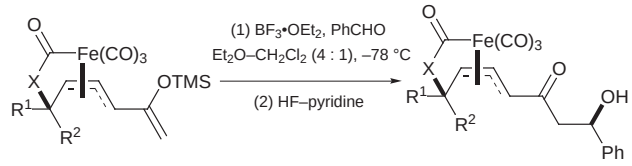

Complex	R^1	R^2	X	Yield (%)	De (%)[a]
1	H	C_5H_{11}	O	81	86
2	H	Me	O	81[b]	87
3	H	Ph	O	72	67
4	C_5H_{11}	H	O	53	55
5	H	Me	NBn	66[b]	90
6	Me	H	NBn	62[b]	57

[a] Diastereomeric excess determined by comparison of integrals in the ^1H NMR spectrum of the crude reaction mixture. [b] Reaction carried out in neat CH_2Cl_2 due to low Et_2O solubility of the substrate; this led to improved yields but did not affect the de.

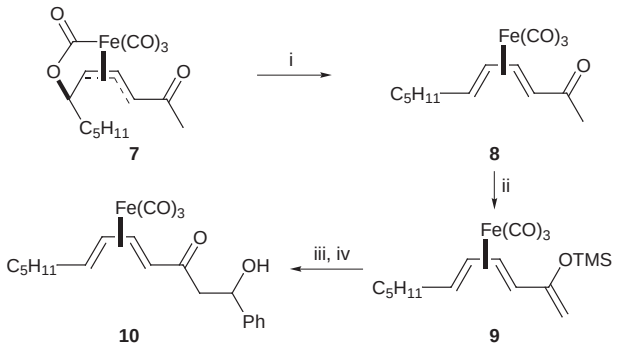

Scheme 1 *Reagents and conditions*: i, $Ba(OH)_2$ MeOH, room temp., 15 min, 92%; ii, Et_3N, TMSOTf, CH_2Cl_2, 0 °C, 90 min, 92%; iii, $BF_3{\cdot}OEt_2$, PhCHO, Et_2O–CH_2Cl_2 (4 : 1), − 78 °C, 1 h; iv, HF–Py, THF, 30 min, 64% yield over 2 steps, 25% de

element of the stereocontrol is indeed lost when the *endo* substituent R^2 is replaced by hydrogen. No significant difference in selectivity was observed between π-allyltricarbonyliron lactone and lactam complexes.

The (*E*,*E*) η^4-diene complex **8** was easily prepared from lactone complex **7** by treatment with barium hydroxide solution.[2b,7] Formation of the trimethylsilyl enol ether **9** in the usual way and reaction with benzaldehyde under standard conditions resulted in the formation of aldol product **10** with only 25% diastereomeric excess (Scheme 1). The selectivity is therefore significantly lower than even that achieved with *exo* substituted lactone and lactam complexes. The relative stereochemistry of the major diastereoisomer was determined for the reactions of complexes **1**, **6** and **9** by stereospecific reduction of the β-hydroxy ketone products to 1,3-diols followed by acetonide formation[5] and was found to be the same in each case as shown.

In summary, the Mukaiyama aldol reactions of a range of *endo* substituted π-allyltricarbonyliron lactone and lactam complexes proceed with high yields and diastereoselectivities. The lack of an *endo* substituent results in a significant decrease in the observed selectivity. A further decrease in selectivity occurs when the mode of attachment of the iron tricarbonyl unit is altered by conversion of the π-allyl complex into an η^4 diene complex. It therefore appears that the tricarbonyliron lactone or lactam unit provides control on a number of different levels during the reaction. The silyl enol ether functionality is maintained in a specific orientation and shielded from one face by the tricarbonyliron group, while on the opposite face a remote substituent is projected to create a chiral environment, restricting the possible orientations of the incoming boron trifluoride–aldehyde complex.

We gratefully acknowledge financial support from the EPSRC (to L. R. C., B. M. and J. M. W.), the Isaac Newton Trust (to L. R. C. and B. M.), Zeneca Pharmaceuticals (to L. R. C. and B. M.), the BP Endowment and the Novartis Research Fellowship (to S. V. L.).

Notes and References

† E-mail: svl1000@cam.ac.uk

1 For a general review on the synthetic utility of π-allyltricarbonyliron lactone complexes: S. V. Ley, L. R. Cox and G. Meek, *Chem. Rev*., 1996, **96**, 423.
2 (*a*) S. V. Ley, G. Meek, K-H. Metten and C. Piqué, *J. Chem. Soc., Chem. Commun*., 1994, 1931; (*b*) S. V. Ley, L. R. Cox, G. Meek, K-H. Metten, C. Piqué and J. M. Worrall, *J. Chem. Soc., Perkin Trans. 1*, 1997, 3299.
3 S. V. Ley and L. R. Cox, *Chem. Commun*., 1996, 657; *J. Chem. Soc., Perkin Trans. 1*, 1997, 3315.
4 M. Franck-Neumann, P. Chemla and D. Martina, *Synlett*, 1990, 641; N. A. Clinton and C. P. Lillya, *J. Am. Chem. Soc*., 1970, **92**, 3058.
5 S. V. Ley and L. R. Cox, *Chem. Commun*., 1998, 227.
6 M. Franck-Neumann, P. Bissinger and P. Geoffroy, *Tetrahedron Lett*., 1997, **38**, 4477.
7 R. Aumann, H. Ring, C. Krüger and R. Goddard, *Chem. Ber*., 1979, **112**, 3644.

Received in Cambridge, UK, 17th April 1998; 8/02878H

Synthesis and structure of the heterobimetallic oxo complex $[(thf)(Me_2NH)_2Cl_2Cr^{III}]_2\{ClSn^{II}(\mu\text{-}O)\}_2$

Michael A. Beswick,[a] Nick Choi,[b] Mary McPartlin,[b] Marta E. G. Mosquera,[a] Julie S. Palmer[a] and Dominic S. Wright*[a]†

[a] *Chemistry Department, University of Cambridge, Lensfield Road, Cambridge, UK CB2 1EW*
[b] *School of Chemistry, University of North London, Holloway Road, London, UK N7 8DB*

The reaction of $[Sn(NMe_2)_2]$ with a suspension of $CrCl_3$ and H_2O in thf gives the molecular $Cr^{III}Sn^{II}$ oxo complex $[(thf)(Me_2NH)_2Cl_2Cr]_2\{ClSn(\mu\text{-}O)\}_2$ 1, in which the O atoms of a central Sn_2O_2 ring coordinate two Cr^{III} cations.

Oxo complexes of Sn are an extensive and highly structurally varied class of compounds. Organotin(IV) oxo complexes are commonly prepared by hydrolysis of organotin(IV) halides or carboxylates or by the oxidation of organotin(II) complexes.[1] The functionality and steric bulk of the organic groups is crucial in dictating the geometries of the metal cores in these species and the nuclearity of the resulting cage arrangements. In contrast, structurally characterised tin(II) oxo complexes are rare and there are no general methods for their preparation.[2] The trapping of SnO fragments into molecular arrangements has been achieved by their incorporation into the frameworks of tin(II)/(IV) host complexes,[2a,c,e] by the formation of Lewis acid/base adducts with tin(II) complexes,[2b,d] or by coordination of transition metal carbonyls to the Sn lone pairs.[2f,g] In previous studies we showed that the low-temperature reactions of primary amines with dimethylamido p block metal reagents $\{[E(NMe_2)_x]$; E = Sn (x = 2), Sb (x = 3)$\}$ furnishes a simple route to imido and phosphinidene cage compounds [Scheme 1(*a*)].[3] We describe here the discovery that the analogous reactions of metal aqua complexes with dimethylamido p block reagents provide a new route to heterometallic oxo-complexes [Scheme 1(*b*)].

(*a*) $R{-}NH_2 + [E(NMe_2)_x] \longrightarrow [R{-}N\{E(NMe_2)_{x-2}\}] + 2Me_2N$

(*b*) $M{-}OH_2 + [E(NMe_2)_x] \longrightarrow [M{-}O\{E(NMe_2)_{x-2}\}] + 2Me_2N$

Scheme 1

The reaction of $[Sn(NMe_2)_2]$ with Bu^tNH_2–NH_3–1,4-dioxane in thf followed by addition of $CrCl_3$ was initially undertaken with a view to preparing a heterometallic Sn^{II}/Cr^{III} imido/nitrido complex. However, the product is a mixture of Sn^{II}/Cr^{III} oxo complexes $[(Me_2NH)_2(thf)CrCl_2]_2\{ClSn(\mu\text{-}O)\}_2\cdot L$ (L = 1,4-dioxane or Bu^tNH_2), the oxo ligand arising as a result of partial hydrolysis of the precursor $CrCl_3$. Further studies revealed that basic conditions catalyse this reaction and the stoichiometric reaction of a mixture of $CrCl_3$ and H_2O (1 : 1 equiv.) in thf–Bu^tNH_2 (1 equiv.) with $[Sn(NMe_2)_2]$ (1 equiv.) affords $[(Me_2NH)_2(thf)CrCl_2]_2\{ClSn(\mu\text{-}O)\}_2\cdot Bu^tNH_2$ (**1**·Bu^tNH_2) as the sole product (Scheme 2).‡

$$2CrCl_3 + 2H_2O \xrightarrow[\text{base}]{2[Sn(NMe_2)_2]} [\{(thf)(Me_2NH)_2CrCl_2\}_2\{ClSn(\mu\text{-}O)\}_2]$$
1

Scheme 2

An X-ray crystallographic study of **1**§ as the 1,4-dioxane solvate reveals that the complex is composed of bimetallic molecules $[(Me_2NH)_2(thf)CrCl_2]_2\{ClSn(\mu\text{-}O)\}_2$ (Fig. 1) which are loosely associated by lattice-bound 1,4-dioxane molecules into a hydrogen-bonded network *via* C–H···O hydrogen bonds to the terminal thf ligands. Although a few examples of mixed transition metal–p block metal oxo complexes have been structurally characterised, all of these have relied on alkoxide functionalities to support the association of the metals, *e.g.* in $[Pb_2Ti_2(\mu_4\text{-}O)(\mu_3\text{-}OPr^i)_2(\mu\text{-}OPr^i)_4(OPr^i)_4]$.[4] The molecular arrangement of **1**, effectively resulting from the trapping of a central $[ClSn(\mu\text{-}O)]_2$ fragment by the coordination of the O centres to two Cr^{III} cations, is unique among main group oxo compounds. The closest analogy is found in the tin(II) complex $[\{Me_3Si(NBu^t)_2Sn_2O\}SnCl_2]$ in which a $SnCl_2$ molecule is coordinated by the O atom of a $[Me_3Si(NBu^t)_2\{Sn_2(\mu\text{-}O)\}]$ ligand.[2b]

Despite the planarity of the O centres of **1** and the possibility of a degree of multiple bond character in the Cr–O bonds, the pattern of bond lengths and angles found in the $[Sn(\mu\text{-}O)]_2Cr_2$ portion of **1** is consistent with its formulation as a coordination complex between a $[ClSn(\mu\text{-}O)]_2^{2-}$ dianion and two Lewis base solvated $CrCl_2^+$ cations {rather than the alternative resonance extreme involving $[Cl_2Cr{=}O]^-$}. The central, planar $[Sn(\mu\text{-}O)]_2$ ring of **1** is rhombic shaped, with the internal angles at Sn and O [Sn–O–Sn 104.2(2), O–Sn–O 75.8(2)°] being similar to those present in the dimeric units of more elaborate tin(II) oxo compounds.[2e] In addition, the Sn–O bonds fall in the expected range (Sn–O av. 2.11 Å in **1**; *cf. ca.* 2.05–2.10 Å[2]). Significantly, the Cr–O bonds [1.893(4) Å] are only marginally below the value expected for single Cr–O bonds (*ca.* 1.93 Å)[5] and noticeably longer than those found for Sn–O–Cr linkages in organotin(IV) chromates.[6] In addition to their coordination by the O centres of the $[Sn(\mu\text{-}O)]_2$ ring, each of the Cr^{III} ions is also coordinated by two *trans*-Me_2NH ligands, by two *trans*-Cl^- ions and by one thf ligand, giving an octahedral geometry which is typical of Cr^{III}. The orientation of the Me_2NH groups, whose

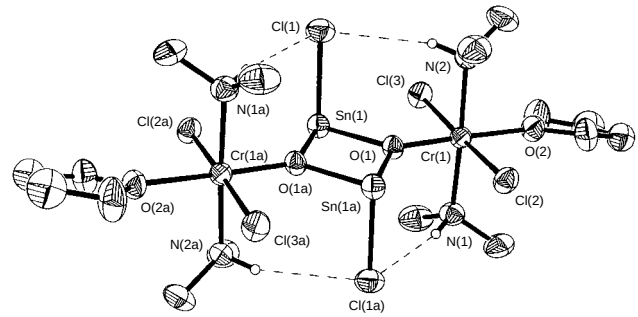

Fig. 1 ORTEP drawing of centrosymmetric molecular structure of **1**·1,4-dioxane. Thermal ellipsoids are at the 40% probability level. Selected bond lengths (Å) and angles (°); Sn(1)–Cl(1) 2.541(2), Sn(1)–O(1) 2.108(4), Sn(1)–O(1a) 2.103(4), Cr(1)–O(1) 1.893(4), Cr(1)–N(1) 2.140(5), Cr(1)–N(2) 2.135(5), Cr(1)–Cl(2) 2.327(2), Cr(1)–Cl(3) 2.334(2), Cr(1)–O(2) 2.108(4), H(2)···Cl(1) 2.59, H(1)···Cl(1a) 2.77, O(1)–Sn(1)–O(1a) 75.8(2), Sn(1)–O(1)–Sn(1a) 104.2(2), Cr(1)–O(1)–Sn(1, 1a) mean 127.9, O(1)–Cr–O(2) 178.4(2), N(1)–Cr(1)–N(2) 176.9(2), Cl(2)–Cr(1)–Cl(3) 177.94(8). Symmetry transformations used to generate equivalent atoms, a $-x + 1, -y - 1, -z + 1$.

H atoms are directed toward the Sn-bonded Cl^- ligands, and the presence of relatively short H···Cl contacts [H(2)···Cl(1) 2.59, H(1)···Cl(1a) 2.77 Å] indicates that the molecular arrangement of **1** is partially supported by hydrogen bonding. Further evidence for hydrogen bonding is the slight axial distortion of the Me_2NH groups towards the Cl atoms [N(2)–Cr(1)–N(3) 176.9(2)°]. These interactions give a reason for the *trans* coordination of the Cr^{III} cations by the Me_2NH and Cl^- ligands (as opposed to the alternative *cis* isomer).

Further studies are in hand to determine the generality of similar deprotonation reactions in the synthesis of hetero-metallic oxo and nitrido complexes containing a variety of mixed-metal compositions.

We gratefully acknowledge the EPSRC (M. A. B., J. S. P., M. McP.), the Royal Society (D. S. W.) and the Spanish Government (M. E. G. M.) for financial support.

Notes and References

† E-mail: dswl000@cus.cam.ac.uk

‡ *Synthesis of* **1**·Bu^tNH_2: to a suspension of anhydrous $CrCl_3$ [0.31 g, 2.5 mmol, (Aldrich 99.9%)] in thf (20 ml) was added degassed H_2O (0.05 ml, 2.5 mmol). The mixture was stirred for 24 h at 25 °C. Bu^tNH_2 (0.26 ml, 2.5 mmol) was added and after stirring at 25 °C (20 min) the temperature was lowered to −78 °C and $[Sn(NMe_2)_2]$ (0.52 g, 2.5 mmol) in thf (10 ml) was added slowly. The mixture was allowed to warm to room temperature and the green solution produced was filtered to remove a white precipitate. The filtrate was reduced to *ca*. 20 ml under vacuum and storage at 5 °C (48 h) gave light brown crystals of **1**·Bu^tNH_2. Yield 0.38 g, 31%. decomp. > 255 °C to black solid. IR (Nujol), ν_{max}/cm^{-1} 3352w, 3166w (N–H str), other bands at 1288w, 1256m, 1118s, 1080m, 1018s, 922m, 871m, 800m, 721w. ^1H NMR [$(CD_3)_2SO$, +25 °C, 250 MHz], 5.80 (br s, Me_2NH), 3.59 (s), 1.76 (s, thf), 2.32 (s, Me_2NH), 1.21 (s, Bu^tNH_2), overlapping of the resonances due to paramagnetic broadening made accurate integration impossible. Anal. calc. for **1**·Bu^tNH_2, C, 24.5; H, 5.2; N, 7.2; Cl, 21.8. Found; C, 23.8; H, 5.3; N, 7.2; Cl, 20.4%.

The reaction of $[Sn(NMe_2)_2]$ (0.53 g, 2.5 mmol) in thf (20 ml) with NH_3 (1.27 ml solution of 0.5 mol dm^{-3} in dioxane, 0.64 mmol) and Bu^tNH_2 (0.20 ml, 1.91 mmol) was aimed at the formation of the cubane $[Sn_4(NBu^t)_3NH]$. A red–brown solid formed after a few minutes. To this was added $CrCl_3$ (0.10 g, 0.81 mmol, 'anhydrous'). The mixture was stirred (1 h) giving a dark green solution. The insoluble material was filtered off and the filtrate concentrated to *ca.* 10 ml. Et_2O (3 ml) was added and storage at 5 °C (48 h) gave **1**·1,4-dioxane and **1**·Bu^tNH_2 as a mixture in low yield. The ^1H NMR spectrum is identical to that obtained separately for **1**·Bu^tNH_2 (δ 1.19, Bu^t) but with a dioxane resonance at δ 3.60. Only **1**·1,4-dioxane could be obtained as crystals from the mixture and repeated attempts to obtain single crystals of **1**·Bu^tNH_2 have so far failed.

§ *Crystal data* for **1**: $C_{10}H_{26}Cl_3CrN_2O_3Sn$, M = 998.74, monoclinic, space group $P2_1/n$, a = 8.002(1), b = 14.956(2), c = 15.855(2) Å, β = 99.81(1)°, U = 1869.9(5) $Å^3$, Z = 2, D_c = 1.77 Mg m^{-3}, λ = 0.710 73 Å, T = 223(2) K, μ(Mo-Kα) = 2.351 mm^{-1}, F(000) = 996. Data were collected on a Siemens P4 diffractometer using an oil-coated rapidly-cooled crystal of dimensions 0.30 × 0.30 × 0.30 mm by the ω–2θ method (1.88 ⩽ θ ⩽ 25.00°). Empirical absorption corrections were applied after initial refinement with isotropic displacement parameters.[7] Of a total of 4391 collected reflections, 3295 were independent (R_{int} = 0.027). The structure was solved by direct methods and refined by full-matrix least squares on F^2 to final values of $R1[F > 4\sigma(F)]$ = 0.040 and $wR2$ = 0.114 (all data) [$R1 = \Sigma(|F_o| - |F_c|)/\Sigma|F_o|$ and $wR2 = [\Sigma w(F_o^2 - F_c^2)^2/\Sigma w(F_o^2)^2]^{0.5}$, $w = 1/[\sigma^2(F_o^2) + (0.0535P)^2 + 2.9000P]$, $P = F_o^2 + (2F_c^2/3)$];[8] largest peak and hole in the final difference map 0.60 and −0.58 e $Å^{-3}$. Two of the C atoms of the Cr-bonded thf ligands are disordered. These were modelled with 1 : 1 occupancy. CCDC 182/869.

1 For a representative cross-section, see R. Graziani, G. Bombieri, E. Forsellini, R. Furlan, V. Peruzzo and G. Tayliarvini, *J. Organomet. Chem.*, 1977, **125**, 43; C. Glidewell and D. C. Liles, *Acta Crystallogr., Sect. B*, 1979, **35**, 1689; H. Puff, W. Schuh, R. Sievers and R. Zimmer, *Angew. Chem.*, 1981, **93**, 622; *Angew. Chem., Int. Ed. Engl.*, 1981, **20**, 591; M. Veith and M. Grosser, *J. Organomet. Chem.*, 1982, **229**, 247; H. Puff, J. Bung, E. Friedrichs and A. Jansen, *J. Organomet. Chem.*, 1983, **254**, 23; B. A. Narayanan and J. Kochi, *Inorg. Chim. Acta*, 1986, **122**, 85; S. Kerscul, B. Wrackmeyer, D. Manig, H. Nöth and R. Standigl, *Z. Naturforsch., Teil B*, 1987, **42**, 387; R. J. Batchelor, T. Birchall and J. P. Johnson, *Can. J. Chem.*, 1987, **65**, 2187; P. Brown, M. F. Mohon and K. C. Molloy, *J. Chem. Soc., Chem. Commun.*, 1989, 1621; R. R. Holmes, *Acc. Chem. Res.*, 1989, **22**, 190; M. A. Edelmann, P. P. Hitchcock and M. F. Lappert, *J. Chem. Soc., Chem. Commun.*, 1990, 1116; C. Vatsa, V. K. Jain, J. Kesavadas and E. T. R. Tiekink, *J. Organomet. Chem.*, 1991, **408**, 157; H. Reuter and M. Kremser, *Z. Anorg. Allg. Chem.*, 1992, **615**, 137; W. Bubenheim and U. Muller, *Z. Anorg. Allg. Chem.*, 1993, **619**, 779.

2 (*a*) P. F. R. Ewing, P. G. Harrison, T. J. King and A. Morris, *J. Chem. Soc., Chem. Commun.*, 1974, 53; (*b*) M. Veith, *Chem. Ber.*, 1978, **111**, 2536; (*c*) P. G. Harrison, P. J.Heylett and T. J. King, *J. Chem. Soc., Chem. Commun.*, 1978, 112; (*d*) M. Veith and O. Recktenwald, *Z. Anorg. Allg. Chem.*, 1979, **459**, 208; (*e*) T. Birchall and J. P. Johnson, *J. Chem. Soc., Dalton Trans.*, 1981, 69; (*f*) B. Schiemenz, F. Ettel, G. Huttner and L. Zsolnai, *J. Organomet. Chem.*, 1993, **458**, 159; (*g*) M. Veith and O. Recktenwald, *Z. Naturforsch., Teil B*, 1983, **38**, 1054; (*h*) B. Schiemenz, B. Antelmann, G. Huttner and L. Zsolnai, *Z. Anorg. Allg. Chem.*, 1994, **620**, 1760.

3 A. J. Edwards, N. E. Leadbeater, M. A. Paver, P. R. Raithby, C. A. Russell and D. S. Wright, *J. Chem. Soc., Dalton Trans.*, 1994, 1479; A. J. Edwards, M. A. Paver, M.-A. Rennie, C. A. Russell, P. R. Raithby and D. S. Wright, *J. Chem. Soc., Dalton Trans.*, 1994, 2963; M. A. Beswick, R. E. Allan, M. A. Paver, P. R. Raithby, M.-A. Rennie and D. S. Wright, *J. Chem. Soc., Dalton Trans.*, 1995, 1991; M. A. Beswick, R. E. Allan, M. A. Paver, P. R. Raithby, A. E. H. Wheatley and D. S. Wright, *Inorg. Chem.*, 1997, **36**, 2502.

4 S. Daniele, R. Rapiernik, L. G. Hubert-Pfalzgraf, S. Jagner and M. Hahansson, *Inorg. Chem.*, 1995, **34**, 628; P. J. Teff, J. C. Huffmann and K. G. Caulton, *J. Am. Chem. Soc.*, 1996, **118**, 4030.

5 F. A. Cotton and G. Wilkinson, *Advanced Inorganic Chemistry*, Wiley, New York, 5th edn., 1988; J. E. Huheey, *Inorganic Chemistry*, Harper and Row, London, 3rd edn. 1983; J. G. Stark and H. G. Wallace, *Chemistry Data Book*, John Murray, London, 1976.

6 For example, see A. M. Domingos and G. M. Sheldrick, *J. Chem. Soc., Dalton Trans.*, 1974, 477.

7 N. Walker and D. Stuart, *Acta Crystallogr., Sect. A*, 1983, **39**, 158.

8 SHELXTL PC version 5.03, Siemens Analytical Instruments, Madison, WI, 1994.

Received in Cambridge, UK, 20th March 1998; 8/02205D

Design, synthesis and cleaving activity of an abiotic nuclease based on a manganese(III) porphyrin complex bearing two acridine moieties

Cathy Drexler,[a] Mir Wais Hosseini,*[a]† Geneviève Pratviel[b] and Bernard Meunier[b]

[a] *Laboratoire de Chimie de Coordination Organique, Université Louis Pasteur, F-67000 Strasbourg, France*
[b] *Laboratoire de Chimie de Coordination du CNRS, 205 route de Narbonne, 31077 Toulouse cedex 4, France*

The synthesis of *meso*-5,15-bis(*m*-aminophenyl)porphyrin bearing two acridine derivatives and of its manganese(III) complex was achieved; in the presence of oxygen atom donors, the metalloporphyrin was shown to cleave double-stranded DNA.

Although the development of abiotic or biomimetic systems capable of probing[1] and/or cleaving[2] DNA has been a topic of active research over the last two decades, the design and synthesis of topo- and regio-selective artificial nucleases is still a current challenge.

The cleavage of DNA may either occur under hydrolytic or oxidative conditions. Dealing with the latter case, transition metal complexes,[3] in particular metalloporphyrins[4] have been shown to act, in the presence of oxygen donor reagents, by oxidation of the sugar units. The interactions between the tetracationic manganese porphyrins complexes such as *meso*-tetrakis(4-*N*-methylpyridiniumyl)porphyrinatomanganese(III) pentaacetate Mn–TMPyP[4] and DNA is believed to occur within the minor groove rich in A–T sequences by electrostatic charge/charge interactions with the negatively charged phosphodiester groups. Since the initial observation of interactions between acridine derivatives and double-stranded DNA (mainly by intercalation) by Lerman in 1961,[5] this mode of interaction between a large variety of intercalators such as acridine[6] and methidium[7] derivatives with nucleic acid oligomers has been well studied.

Our approach to the design of artificial nucleases was based on the positioning, by double intercalation using two acridine moieties, of oxidative cleaving centres such as metalloporphyrin complexes. In this vein, a class of abiotic DNA cleaving agent combining a metalloporphyrin core, two spacers and two 9-aminoacridine moieties was designed and prepared (Fig. 1). The spacer connecting the reactive centre to the intercalators may be amino acids of variable length such as aminobutyric, aminovaleric or aminocaproic acids allowing to control the distance between the porphyrin and the acridine centres. Dealing with geometrical features, *i.e.* the positioning of the acridines with respect to the porphyrin core, based on molecular models, the *meso*-5,15-diarylporphyrin bearing an amino function at the *meta* position of each phenyl group appeared to be the most appropriate choice. Analogues of bleomycin based on a porphyrin core functionalised at β-pyrrolic positions by two acridine derivatives have been reported.[8]

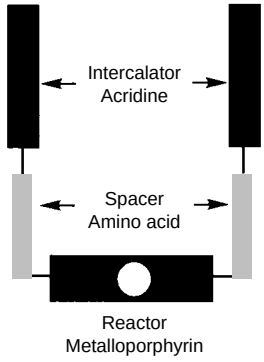

Fig. 1 Schematic representation of an abiotic nuclease based on a metalloporphyrin core functionalised by two acridine intercalators using amino acids as spacers

Here, we report the synthesis of compound **1** (Scheme 1) and the DNase activity of its manganese complex.

The synthetic strategy employed to prepare the compound **1** was based on the synthesis of bis(*m*-aminophenyl)porphyrin **2** followed by introduction of the spacer groups affording compound **3** and finally the introduction of acridine moieties. Whereas the synthesis of *meso*-arylporphyrins bearing amino groups at the *ortho* or *para* positions of the phenyl groups is well documented,[9] only few reports dealing with the preparation of the *meso*-*meta*-aminophenylporphyrins have been reported.[10,11] Compound **2** was prepared in two steps by modification of the described procedure for the bis(*o*-aminophenyl)porphyrin.[12] The condensation of 2,2-dipyrrylmethane,

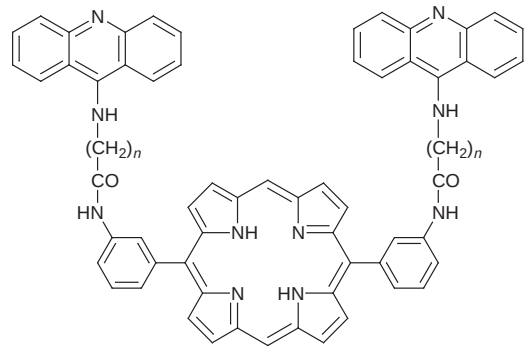

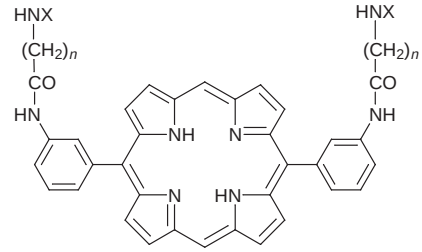

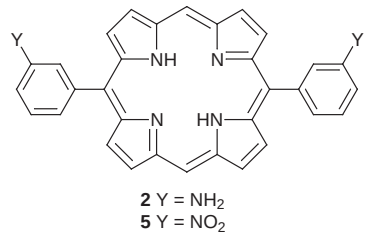

Scheme 1

prepared following reported procedures,[13] with 3-nitrobenzaldehyde (*ca.* 5 mM) in CH_2Cl_2 in the presence of catalytic amounts of CF_3CO_2H (TFA) afforded the nitroporphyrinogen which was oxidised by *p*-chloranil affording the nitroporphyrin **5**. The latter, owing to its rather poor solubility, was not isolated but directly reduced at 70 °C to the amino compound **2** by treatment with $SnCl_2$/HCl.[14] Since the overall yield was rather low (2%), in order to optimise it, both the nature of the acid and the ratio of reactants were varied. The use of a Lewis acid such as $BF_3{\cdot}OEt_2$ instead of the protonic acid TFA increased the yield to 7%. However the highest yield of 12% was reached by increasing the concentration of reactants to the 20 mM range. The rather poor yield may be related to the low reactivity of the aldehyde used.

On the other hand, starting with aminobutyric acid [$H_2N(CH_2)_3CO_2H$] the NH_2 group was protected using the Boc group [$HNBoc(CH_2)_3CO_2H$][15] and then the carboxylic acid moiety was activated by treatment with ethyl chloroformate [$BocHN(CH_2)_3CO_2COEt$].[16] The condensation of the latter in the presence of Et_3N with compound **2** in a mixture of THF and toluene afforded the protected compound **4** in 60% yield. The deprotection of the Boc group was achieved in quantitative yield by treatment with AcOH–HCl[16] affording **4**·2HCl. The condensation of the latter with 9-phenoxyacridine[17] in phenol at 120 °C gave, after recrystallisation from Et_2O–MeOH, the final compound **1** in 56% yield.

The **1**–Mn^{III} complex was prepared at 120 °C by reacting ligand **1** with $Mn(OAc)_2{\cdot}4H_2O$ in DMF in the presence of 2,4,6-trimethylpyridine for 2 h. The metallation was followed in DMF by UV-VIS spectroscopy which revealed a bathochromic shift of the Soret band from 408 to 458 nm and a reduction of the number of Q bands from four to two. After precipitation by adding diethyl ether and washing the solid with water, the complex was purified by column chromatography [basic alumina, CH_2Cl_2–MeOH (9/1)] and characterised by MS (FAB positive mode: $M^+ = 1070$).

The nuclease activity of the **1**–Mn complex was tested at room temperature on the supercoiled double-stranded ΦX174 DNA (form I) at various concentrations and pH values using phosphate buffer in the presence of either $KHSO_5$[18] or magnesium monoperphthalate (MMPP),[19] two oxidants able to generate high-valent manganese–oxo species.[20] The addition of the oxidant initiated the DNA cleavage reaction. The cleavage products were analysed on agarose gel by electrophoresis as previously reported.[18,19]

As expected, no degradation of DNA was observed under the same conditions in the absence of **1**–Mn or in the presence of free ligand **1**. The cleaving activity of **1**–Mn was observed at 1 μM and 500 nM concentrations in the presence of 1 or 10 mM $KHSO_5$, respectively. Although the cleavage of supercoiled DNA in the presence of 10 mM $KHSO_5$ appeared to be more spectacular since 90% of form I was transformed into forms II and III, the efficiency of the **1**–Mn complex was found to be below that observed with Mn–TMPyP for which DNA cleavage was detected at 5 nM in the presence of 10 μM $KHSO_5$.[18] However, in marked contrast with the tetracationic Mn–TMPyP complex for which a strong salt effect due to electrostatic interactions with DNA was observed,[18] the DNA cleavage activity of **1**–Mn was not affected by modification of the ionic strength of the reaction mixture by addition of NaCl. This absence of a salt effect is in agreement with the possible intercalation of the acridine moieties of the complex between DNA base pairs.

The nuclease activity of **1**–Mn with MMPP was one order of magnitude higher than with $KHSO_5$ (the same cleavage efficiency was observed at 0.1 mM with MMPP and at 1 mM with $KHSO_5$). A similar difference has been previously found with Mn–TMPyP as cleaver.[19]

Finally, the appearance of the linear DNA form III before the complete conversion of form I indicated that **1**–Mn is probably able to perform some direct double-strand breaks (see ref. 18 for a discussion of double-strand breaks resulting from the accumulation of single-strand breaks in opposition to direct double-strand breaks). This observation is in favour of a strong interaction, probably by intercalation of the acridine moieties, between the metalloporphyrin and DNA.

In conclusion, a new porphyrin bearing two acridine intercalators was designed and prepared. Its manganese complex was shown to cleave double-stranded DNA in the presence of different oxygen atom donors involving mainly single-strand breaks with a participation of direct double-strand breaks. Work is in progress to demonstrate the role of the spacer amino acid moieties and to investigate the physico-chemical aspects of the cleaving process and the possible bis-intercalation behaviour of this DNA cleaver.

Notes and References

† E-mail: hosseini@chimie.u-strasbg.fr

1 P. E. Nielsen, *J. Mol. Recognit.*, 1990, **3**, 1.
2 G. Pratviel, J. Bernadou and B. Meunier, *Angew. Chem., Int. Ed. Engl.*, 1995, **34**, 746.
3 D. S. Sigman, D. R. Graham, V. D'Aurora and A. M. Stern, *J. Mol. Biol.*, 1979, **254**, 12 269; R. E. Holmlin, P. J. Dandliker and J. K. Barton, *Angew. Chem., Int. Ed. Engl.*, 1997, **36**, 2715.
4 B. Ward, A. Skorobogaty and J. C. Dabrowiak, *Biochemistry*, 1986, **25**, 6875; E. Fouquet, G. Pratviel, J. Bernadou and B. Meunier, *J. Chem. Soc., Chem. Commun.*, 1987, 1169.
5 L. S. Lerman, *J. Mol. Biol.*, 1961, **3**, 18.
6 J. B. Le Pecq, M. Le Bret, J. Barbet and R. Roques, *Proc. Natl. Acad. Sci. USA*, 1975, **72**, 2915; H. D. King, W. D. Wilson and E. J. Gabbay, *Biochemistry*, 1982, **21**, 4982; G. J. Atwell, W. Leupin, S. J. Twigden and W. A. Denny, *J. Am. Chem. Soc.*, 1983, **105**, 2913.
7 P. B. Dervan and M. M. Becker, *J. Am. Chem. Soc.*, 1978, **100**, 1968; R. A. Ikeda and P. B. Dervan, *J. Am. Chem. Soc.*, 1982, **104**, 296.
8 J. W. Lown, S. M. Sondhi and C.-W. Ong, *Biochemistry*, 1986, **25**, 5111.
9 *The Porphyrins*, ed. D. Dolphin, Academic Press, New York, 1978; *Porphyrins and Metalloporphyrins*, ed. K. M. Smith, Elsevier, Amsterdam, 1978.
10 Y. Sun, A. E. Martell and M. Tsutsui, *J. Heterocycl. Chem.*, 1986, **23**, 561.
11 C. Drexler, M. W. Hosseini, A. De Cian and J. Fischer, *Tetrahedron Lett.*, 1997, **38**, 2993.
12 J. S. Manka and D. S. Lawrence, *Tetrahedron Lett.*, 1989, **30**, 6989.
13 P. S. Clezy and G. A. Smythe, *Aust. J. Chem.*, 1969, **22**, 239; R. Chong, P. S. Clezy, A. J. Liepa and A. W. Nichol, *Aust. J. Chem.*, 1969, **22**, 229.
14 M. J. Gunter and L. N. Mander, *J. Org. Chem.*, 1981, **46**, 4792.
15 O. Keller, W. E. Keller, G. van Look and G. Wersin, *Org. Synth.*, 1985, **63**, 160.
16 R. Young and C. K. Chang, *J. Am. Chem. Soc.*, 1985, **107**, 898.
17 D. J. Dupré and F. A. Robinson, *J. Am. Chem. Soc.*, 1945, 549.
18 J. Bernadou, G. Pratviel, F. Bennis, M. Girardet and B. Meunier, *Biochemistry*, 1989, **28**, 7268.
19 G. Pratviel, J. Bernadou, M. Ricci and B. Meunier, *Biochem. Biophys. Res. Commun.*, 1989, **160**, 1212.
20 M. Pitié, J. Bernadou and B. Meunier, *J. Am. Chem. Soc.*, 1994, **117**, 2935.

Received in Basel, Switzerland, 6th February 1998; 8/01095A

Sulfone-calixarenes: a new class of molecular building block

Gilles Mislin,[a] Ernest Graf,[a] Mir Wais Hosseini,*[a]† André De Cian[b] and Jean Fischer[b]

[a] *Laboratoire de Chimie de Coordination Organique, Université Louis Pasteur, (UMR 7513 CNRS), F-67000 Strasbourg, France*
[b] *Laboratoire de Cristallochimie et Chimie Structurale, Université Louis Pasteur, (UMR 7513 CNRS), F-67000 Strasbourg, France*

The synthesis of a new calix[4]arene derivative based on the linkage of the phenolic rings by four sulfone groups was achieved and its 1,3-alternate conformation in the crystalline phase, resulting from both inter- and intra-molecular H-bonding, was established by crystallography.

Over the past two decades, the calixarene framework has been the most used macrocyclic structure.[1,2] The increasing interest in these compounds seems to be due to their versatility. Indeed, a variety of calixarene based molecules displaying a wide range of properties ranging from molecular receptors and enzyme mimics as well as extractants to liquid crystals and conducting polymers have been reported. In our own hands, calix[4]arene derivatives have been used either for the design of hollow molecular modules[3,4] and their assembly into inclusion molecular networks in the crystalline phase,[5] or as backbones for the design of exo-ligands.[6–8]

In dealing with calix[4]arene **1**, its structural and functional tunings at various positions have been extensively studied. Whereas partial or complete substitution of the *p-tert*-butyl moieties by a variety of groups leads to the modification of the upper rim, the functionalisation of the hydroxyl moieties affords modified calixarenes at the lower rim. On the other hand, examples of partial[7] or complete[8,9] replacement of the OH by SH groups have been also reported. However, dealing with the linkage of the aromatic rings, only recently few examples of substitution of CH_2 groups by Me_2Si[10] or S[11,12] have been reported. An example of tetrathiacalix[4]arene based on four thiophene moieties has been also published.[13]

Here we report the first synthesis as well the solid state structural analysis of a new class of calix[4]arene analogues based on the linking of four phenolic rings by sulfone groups. These compounds may be of interest for the design of new receptors and backbones.

The synthetic strategy for the preparation of the tetrasulfone **6** was based on the complete oxidation of the thiacalix **3** (Scheme 1). The latter was obtained following the reported procedure.[11a] In a first attempt, all four OH moieties of **3** were protected as methoxy groups prior to the oxidation of the sulfide linkages to sulfones. The treatment of **3** under reflux with MeI in the presence of NaH in dry THF–DMF (1 : 9) for two days afforded, after recrystallisation from $CHCl_3$–MeOH, the desired compound **4** in 73% yield. The complete oxidation of **4** to the tetrasulfone **5** was first attempted by refluxing the compound **4** in a 30% H_2O_2–glacial AcOH mixture for eight days. Probably owing to the low solubility of **4**, the reaction isolated yield was only *ca.* 10%. The latter was increased to 88% when performing the oxidation with *m*-chloroperbenzoic acid in $CHCl_3$ at room temp. for 4 days. The pure compound **5** was isolated by recrystallisation from CH_2Cl_2–MeOH. Since the removal of the protecting groups by treatment with a large excess of BBr_3 in CH_2Cl_2 afforded the final compound **6** in only *ca.* 30% yield, the direct oxidation of the tetrasulfide **3** was carried out in 59% yield using 30% H_2O_2–glacial AcOH. The pure compound **6** was obtained after crystallisation from THF–hexane.

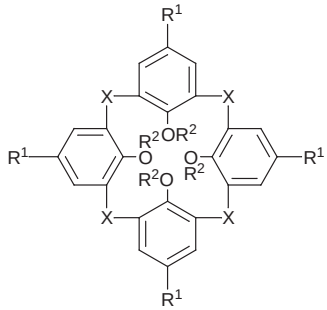

1 X = CH_2, R^1 = Bu^t, R^2 = H
2 X = S, R^1 = R^2 = H
3 X = S, R^1 = Bu^t, R^2 = H
4 X = S, R^1 = Bu^t, R^2 = Me
5 X = SO_2, R^1 = Bu^t, R^2 = Me
6 X = SO_2, R^1 = Bu^t, R^2 = H

Scheme 1

In solution, for all compounds **4**–**6**, both the ^1H and ^{13}C NMR spectra were extremely simple and in agreement with the proposed structure. In marked contrast with calix **1** derivatives for which both the ^1H and ^{13}C NMR signals corresponding to the methylene groups are usually used for conformational assignment in solution, due to the absence of such NMR probes for the thia- and sulfone-calix[4]arenes **2**–**6** their conformation could not be established unambiguously. For both compounds **4** and **5**, no changes in the proton spectra could be detected between −85 and 125 °C. However, bidimensional (^1H,^1H) ROESY experiments at room temp. showed correlations between the methoxy groups and both the CH_3 and CH aromatic proton indicating thus a rapid conformational interconversion. For the final compound **6** the dramatic changes observed upon cooling from 25 to −100 °C indicated temperature dependent conformational dynamics.

In the solid state, all compounds **4**–**6** were studied by X-ray diffraction methods on monocrystals. Suitable monocrystals‡ were obtained by slow diffusion of MeOH into a CH_2Cl_2 solution of either compound **4** or **5**, or by slow evaporation of a chlorobenzene solution of the compound **6**. In marked contrast with the tetramethoxy derivative of **1** which was shown to adopt a partial cone conformation,[14] and with the tetrathiacalix[4]-

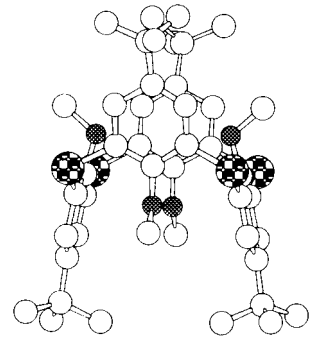

Fig. 1 X-Ray structure of the tetrasulfide **4** demonstrating the adopted 1,3-alternate conformation in the crystalline phase; for clarity H atoms are not presented

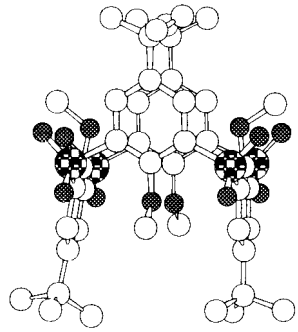

Fig. 2 X-Ray structure of the tetrasulfone **5** demonstrating the adopted 1,3-alternate conformation in the crystalline phase; for clarity H atoms are not presented

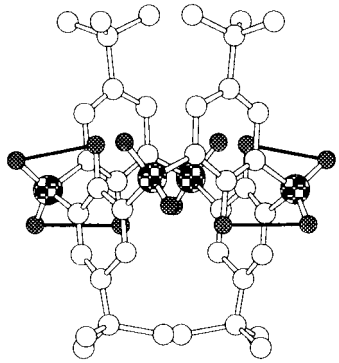

Fig. 3 X-Ray structure of the tetrasulfone **6** demonstrating the adopted 1,3-alternate conformation in the crystalline phase. The bold lines represent the intramolecular H-bonding pattern; for clarity H atoms are not presented.

arene **2** and the parent compound **3** which were present in cone conformation,[12] the thia analogue **4** was found to be in the 1,3-alternate conformation (Fig. 1).

For the two sulfone derivatives **5** (Fig. 2) and **6** (Fig. 3), again the conformation was found to be 1,3-alternate with oxygen atoms of the sulfones pointing outward. The average SO bond distance was *ca.* 1.43 and 1.44 Å for **5** and **6**, respectively. The average CS bond distance was *ca.* 1.77 Å for both cases. The average distance between two adjacent sulfur atoms was *ca.* 5.52 Å.

Based on the observed average O···O distance between two adjacent oxygen atoms of *ca.* 2.70, 2.85 and 2.64 Å for **1**, **2** and **3** respectively, as previously proposed in the case of **1**,[1] for both compounds **2**[12] and **3**[12] the cone conformation was, at least partially stabilised, by an array of intramolecular H-bonds. Interestingly, the 1,3-alternate conformation for compound **6** may be also rationalised in terms of H-bonding between the OH and SO_2 groups (Fig. 3). Indeed, O···OS distances varying from 2.81 to 3.02 Å were observed. Furthermore, compound **6** was found to form a 3-D network through intermolecular H-bonding between the OH and SO_2 groups belonging to adjacent units with an average O···OS distance of *ca.* 2.87 Å (Fig. 4).

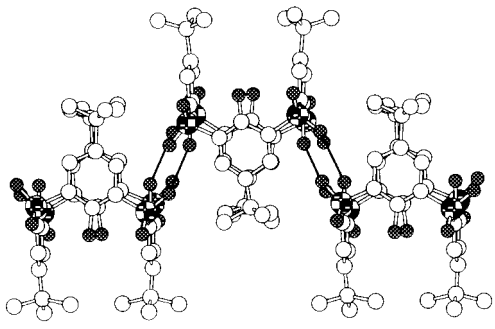

Fig. 4 A portion of the X-ray structure of the 3-D network formed between consecutive compounds **6**. The 3-D network is obtained by intermolecular H-bonding between OH and SO groups; for clarity H atoms are not presented.

In conclusion, the synthesis of new calix[4]arene derivatives based on sulfone linkages between the phenolic rings was achieved. All compounds were shown to adopt the 1,3-alternate conformation in the solid state. In the case of *p-tert*-butyltetrasulfonecalix[4]arene **6**, due to inter- and intra-molecular H-bonds, a 3-D network was observed in the solid state. The use of sulfonecalix derivatives for the design of receptors and building blocks is under current investigation.

We thank H. Akdas and L. Bringle for their help with the preparation of some of the reported compounds and the CNRS and the Institut Universitaire de France (IUF) for financial support.

Notes and References

† E-mail: hosseini@chimie.u-strasbg.fr

‡ *Crystallograpic data*: **4** (colorless, 173 K): $C_{44}H_{56}O_4S_4{\cdot}CH_2Cl_2$, M = 862.12, orthorhombic, a = 15.210(1), b = 12.747(1), c = 12.220(1) Å, U = 2369.2(5) Å^3, space group $P2_12_12_1$, Z = 2, D_c = 1.21 g cm^{-3}, Nonius CCD, Mo-Kα, μ/mm^{-1} = 0.343, 1523 data with $I > 3\sigma(I)$, R = 0.047, R_w = 0.054.

5 (colorless, 294 K): $C_{44}H_{56}O_{12}S_4$, M = 905.19, monoclinic, a = 10.9822(5), b = 18.567(2), c = 11.8055(6) Å, β = 101.941(4), U = 2355.1(5) Å^3, space group $P12_11$, Z = 2, D_c = 1.28 g cm^{-3}, MACH3 Nonius, Mo-Kα, μ/mm^{-1} = 0.248, 3435 data with $I > 3\sigma(I)$, R = 0.037, R_w = 0.047.

6 (colorless, 173 K): $C_{40}H_{48}O_{12}S_4$, M = 849.08, tetragonal, a = 15.992(1), b = 15.992(1), c = 17.712(1) Å, U = 4529.7(8) Å^3, space group $I4_1$, Z = 4, D_c = 1.24 g cm^{-3}, Nonius CCD, Mo-Kα, μ/mm^{-1} = 0.254, 1615 data with $I > 3\sigma(I)$, R = 0.055, R_w = 0.082. CCDC 182/856.

1 C. D. Gutsche, *Calixarenes*, ed. J. F. Stoddart, Monographs in Supramolecular Chemistry, RSC, London, 1989; *Calixarenes—A Versatile Class of Macrocyclic Compounds*, ed. J. Vicens and V. Böhmer, Kluwer, Dordrecht, 1991.
2 V. Böhmer, *Angew. Chem., Int. Ed. Engl.*, 1995, **34**, 713.
3 M. W. Hosseini and A. De Cian, *Chem. Commun.*, 1998, in press.
4 X. Delaigue, M. W. Hosseini, A. De Cian, J. Fischer, E. Leize, S. Kieffer and A. Van Dorsselaer, *Tetrahedron Lett.*, 1993, **34**, 3285; X. Delaigue, M. W. Hosseini, E. Leize, S. Kieffer and A. Van Dorsselaer, *Tetrahedron Lett.*, 1993, **34**, 7561; X. Delaigue, M. W. Hosseini, R. Graff, J.-P. Kintzinger and J. Raya, *Tetrahedron Lett.*, 1994, **35**, 1711; F. Hajek, E. Graf and M. W. Hosseini, *Tetrahedron Lett.*, 1996, **37**, 1409.
5 F. Hajek, E. Graf, M. W. Hosseini, X. Delaigue, A. De Cian and J. Fischer, *Tetrahedron Lett.*, 1996, **37**, 1401; F. Hajek, E. Graf, M. W. Hosseini, A. De Cian and J. Fischer, *Angew. Chem., Int. Ed. Engl.*, 1997, **36**, 1760; F. Hajek, E. Graf, M. W. Hosseini, A. De Cian and J. Fischer, *Mater. Res. Bull.*, 1998, in press.
6 G. Mislin, E. Graf and M. W. Hosseini, *Tetrahedron Lett.*, 1996, **37**, 4503.
7 Y. Ting, W. Verboom, L. G. Groenen, J.-D. van Loon and D. N. Reinhoudt, *J. Chem. Soc., Chem. Commun.*, 1990, 1432; X. Delaigue, M. W. Hosseini, A. De Cian, N. Kyritsakas and J. Fischer, *J. Chem. Soc., Chem. Commun.*, 1995, 609.
8 C. G. Gibbs and C. D. Gutsche, *J. Am. Chem. Soc.*, 1993, **115**, 5338; C. G. Gibbs, P. K. Sujeeth, J. S. Rogers, G. G. Stanley, M. Krawiec, W. H. Watson and C. D. Gutsche, *J. Org. Chem.*, 1995, **60**, 8394.
9 X. Delaigue, J. McB. Harrowfield, M. W. Hosseini, A. De Cian, J. Fischer and N. Kyritsakas, *J. Chem. Soc., Chem. Commun.*, 1994, 1579; X. Delaigue and M. W. Hosseini, *Tetrahedron Lett.*, 1993, **34**, 8112.
10 B. König, M. Rödel, P. Bubenitschek and P. G. Jones, *Angew. Chem., Int. Ed. Engl.*, 1995, **34**, 661.
11 (*a*) H. Kumagai, M. Hasegawa, S. Miyanari, Y. Sugawa, Y. Sato, T. Hori, S. Ueda, H. Kamiyama and S. Miyano, *Tetrahedron Lett.*, 1997, **38**, 3971; (*b*) T. Sone, Y. Ohba, K. Moriya, H. Kumada and K. Ito, *Tetrahedron*, 1997, **53**, 10 689.
12 H. Akdas, L. Bringel, E. Graf, M. W. Hosseini, G. Mislin, J. Pansanel, A. De Cian and J. Fischer, *Tetrahedron Lett.*, 1998, **39**, 2311.
13 B. König, M. Rödel, I. Dix and P. G. Jones, *J. Chem. Res.*, 1997, 0555.
14 P. D. J. Grootenhuis, P. A. Kollman, L. C. Groenen, D. N. Reinhoudt, G. J. van Hummel, F. Ugozzoli and G. D. Andreetti, *J. Am. Chem. Soc.*, 1990, **112**, 4165.

Received in Basel, Switzerland, 6th March 1998; 8/01860J

Comments on the elusive crystal structure of 4-iodo-4′-nitrobiphenyl

Norberto Masciocchi,*[a] Mirka Bergamo[b] and Angelo Sironi*[a]

[a] *Dipartimento di Chimica Strutturale e Stereochimica Inorganica, Università di Milano, via Venezian 21, 20133, Milano, Italy*
[b] *Dipartimento di Chimica Inorganica, Metallorganica ed Analitica, Università di Milano, via Venezian 21, 20133 Milano, Italy*

The recently proposed crystal structure of 4-iodo-4′-nitrobiphenyl is here confirmed on the basis of experimental diffraction data on single crystals and powders of high crystallinity; a reinterpretation of the nature of the (faulted) material studied in the original paper is also presented.

In a recent issue of Chemical Communications, Sarma *et al.* (hereafter, Sarma) reported[1] the design, based on the strength of Ar–NO_2···I–Ar interactions, of a new crystal phase, possessing second harmonic generation (SHG) properties. It was reported therein that single-crystal X-ray diffraction (XRD) on two crystals of 4-iodo-4′-nitrobiphenyl (INB) with different morphology (obtained by recrystallization from benzene or nitromethane) afforded, in both cases, an F-centered orthorhombic lattice, but no reliable structural model; accordingly, it was suggested that all samples chosen for single-crystal analysis were flawed, since the ordered structural model, obtained by the combination of XRD (cell/space group), semiempirical quantum chemistry calculations (molecular conformation), crystallochemical considerations (approximate location) and constrained lattice energy minimisation (final coordinates), did not match the observed intensity data.[1]

Sarma found that INB molecules form polar ribbons running along [001] through robust Ar–NO_2···I–Ar interactions (a well defined[2] supramolecular synthon[3]); however, in contrast with such robustness, the features observed in the XRPD pattern were modelled by a significant small-particle-size broadening effect along [001] (with an average coherent domain of 50 Å, accounting for three INB molecules only!). Suspecting a two-dimensional polytypic behaviour like that found in (C_5Me_5)ReO_3,[4] we decided to reconsider the INB problem by coupling XRPD, computer simulation of faulted crystals and conventional 'single-crystal' X-ray diffraction.

We have synthesized INB as described in refs. 1 and 5, and found that the reaction product is, according to GC–MS, a mixture of INB and of the symmetrically substituted dinitro- (DNB) and diiodo-biphenyls (DIB), in an approximate 90 : 9 : 1 ratio, while in the XRPD pattern only the two major phases (INB and DNB) could be recognized. Recrystallization from benzene, nitromethane or hexane eventually afforded only one crystal phase (INB, although, according to GC–MS, traces of DNB were still present), whose XRPD pattern revealed a well crystallized system with no anisotropic broadening (FWHM $< 0.2°$ 2θ). It was of note that our XRPD data (Fig. 1) can be indexed with the published INB cell parameters but show an intensity distribution different from that reported in Fig. 2 of ref. 1; in particular, two, previously unobserved, intense low angle peaks are now present.

Recrystallization from nitromethane spontaneously afforded light yellow INB crystals of very good quality, whose structure was easily solved and successfully refined in space group *Fdd*2 on data from two different crystals (which were found to differ only in the amount of racemic twinning present: none for crystal 1 and [73 : 27] for crystal 2).‡ The derived structural model is very similar to that proposed in ref. 1 and, allowing a rather good match (R_p = 0.10) between observed and calculated XRPD data (see Fig. 1), it correctly describes also the bulk. Accordingly, INB can afford highly crystalline samples.

In spite of our efforts, we were unable to prepare the poorly crystalline phase originally reported as INB. Nevertheless, we would like to tentatively propose, in the absence of direct experimental data, two possible explanations for Sarma's observations.

The substitution of one INB molecule by DNB generates an unstrained faulted ribbon, as schematically shown in Fig. 2, which, despite the inversion of the NO_2···I link, possesses fully ordered C and H atoms (note that DIB could act in the same manner while the copresence of DIB and DNB allows for any number of faults). The insertion of a single DNB molecule per

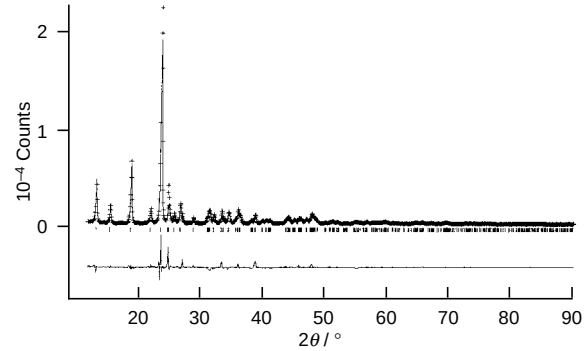

Fig. 1 Rietveld refinement plot of the INB phase with peak markers and difference plot at the bottom. Note that the first two log-angle peaks are consistent with the structural model and do not require any anisotropic broadening correction in order to spread their intensity into the background.

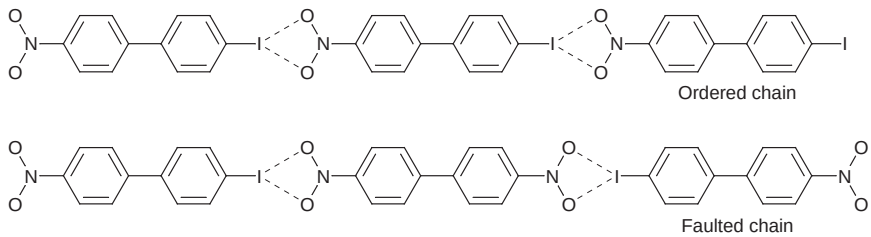

Fig. 2 Schematic drawing of the polarity inversion of one INB chain in the presence of a single DNB molecule per chain (conditioned disorder). Note that at most one DNB molecule can fit in an INB chain; DIB would act in the same manner, while the simultaneous presence of DIB and DNB allows for any number of faults (up to a random disorder).

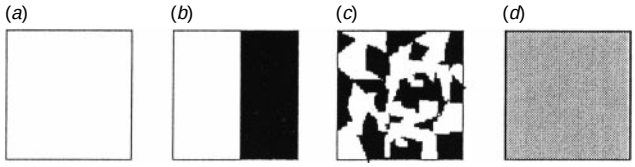

Fig. 3 Schematic drawing of the tiling of the *ab* plane of INB crystals with black and white dots (for up and down polar INB chains, respectively), showing a polar single crystal (*a*), a racemic (macro)twin (*b*), a faulted paracrystal with many twin boundaries (*c*) and a fully disordered *Fddd* (microtwinned) phase (*d*)

chain behaves similarly to a single error in the stacking sequence of pure INB which, however, would induce some strain. This kind of fault, as shown by Hulliger *et al*. for the 1,4-nitrophenylpiperazine–perhydrotriphenylene inclusion compound,[6] may evolve into a 180° [001] twinned macrostate with a fuzzy interface whose size depends on their intrinsic probability. However, since high error frequencies imply small interfaces, sharp XRPD peaks and possible SHG effects (while, low, non-zero probabilities lead to large 'interfaces', broad XRPD peaks§ and no SHG), the presence of DNB (or of less likely INB inversion faults) can be taken as responsible for all experimental evidences only if crystals of intermediate nature occur.

Alternatively, since inversion of the polarity of a whole (ordered) chain marginally affects the overall packing (more or less like an inversion fault, which inverts only 'half' a chain), Sarma's specimen may consist of a two-dimensional polytypic phase with (randomly distributed) microdomains of inverse polarity, large enough to guarantee SHG properties, but 'flawing' the original X-ray analysis, much like what is found for solid $(C_5Me_5)ReO_3$.[4] Indeed, juxtaposition of antiparallel domains in the *ab* plane can afford, on lowering the size of the homopolar regions, (*a*) untwinned *Fdd*2 single crystals (our crystal 1); (*b*) racemic (macro)twins (crystal 2); (*c*) two dimensional polytypes (Sarma's specimen); (*d*) disordered (*i.e.* microtwinned) *Fddd* 'single' crystals (Fig. 3). Since cases (*a*) and (*b*) would lead to sharp XRPD features and case (*d*) cannot be SHG active, only case (*c*) fits Sarma's experimental observations. That 2D polytypic crystals from different preparations may have different 'structures' should not surprise, particularly after it has been shown that crystals from the same batch and even different portions of the same good looking 'single' crystal may possess different peak intensities, reflecting the different ratio of ordered *vs*. disordered (*i.e.* boundary) regions.[4]

Summarizing, single-crystal and powder diffraction analyses of INB afforded an unambiguous crystal structure with long polar ribbons of INB molecules packed, in *Fdd*2, in a head-to-tail fashion, as originally inferred in ref. 1. This agrees well with the proposed robustness of the $NO_2\cdots I$ synthon, which has been extensively used in devising supramolecular assemblies of organic molecules.[7] Unfortunately, even if the outcome of the work reported by Sarma *et al*. happens to match the true INB crystal structure, the nature of their material (single crystals and bulk) remains obscure.

We acknowledge the Italian MURST and CNR (CSSMTBO) for funding. The courtesy of Dr G. A. Ardizzoia, who run the GC–MS measurements, is also acknowledged. We also thank Professor A. Gavezzotti for helpful discussions.

Notes and References

† E-mail: angelo@csmtbo.mi.cnr.it

‡ *Crystal data*: $C_{12}H_{10}INO_2$, M = 325.10; orthorhombic, space group *Fdd*2, a = 8.200(4), b = 18.887(4), c = 14.385(15) Å, U = 2228(3) Å^3, D_c = 1.938 g cm^{-3}; Single crystal results (crystal 1 and, in parentheses, crystal 2); CAD4, graphite monochromated Mo-Kα radiation, solution by Patterson and difference Fourier methods; refinement by full-matrix least squares, SHELX93[8]), $R1$ and $wR2$ = 0.014 (0.019) and 0.032 (0.044), respectively, for 567 (971, due to the presence of Friedel pairs) independent observed reflections [$I > 2\sigma(I)$] collected in the $3 < \theta < 26°$ (25°) range. Powder diffraction data (RIGAKU D-III/MAX, graphite monochromated Cu-Kα radiation, refinement by GSAS[9]), R_p, R_{wp} and R_F = 0.104, 0.144 and 0.085, respectively, for 3901 data collected in the $12 < 2\theta < 90°$ range (252 reflections). CCDC 182/877.

§ The explicit Fourier transform of such a model, computed with the aid of DISCUS on 20 × 20 × 20 cells (about 1 000 000 non-hydrogen atoms),[10] afforded some diffuse scattering and markedly asymmetric (111) or split (022) peaks; all these features are consistent with the broadening and lowering of peak intensity observed in Sarma's powder pattern.

1 J. A. R. P. Sarma, F. H. Allen, V. L. Hoy, J. A. K. Howard, R. Thaimattam, K. Biradha and G. R. Desiraju, *Chem. Commun.*, 1997, 101.
2 F. H. Allen, B. S. Goud, V. J. Hoy, J. A. K. Howard and G. R. Desiraju, *J. Chem. Soc., Chem. Commun.*, 1994, 2729; V. R. Thalladi, B. S. Goud, V. J. Hoy, F. H. Allen, J. A. K. Howard and G. R. Desiraju, *Chem. Commun.*, 1996, 401.
3 G. R. Desiraju, *Angew. Chem., Int. Ed. Engl.*, 1995, **34**, 2311.
4 N. Masciocchi, P. Cairati, F. Saiano and A. Sironi, *Inorg. Chem.*, 1996, **35**, 4060.
5 J. Harley-Mason and F. G. Mann, *J. Chem. Soc.*, 1940, 1379.
6 J. Hulliger, P. Rogin, A. Quintel, P. Rechsteiner, O. König and M. Wübbenhorst, *Adv. Mater.*, 1997, **9**, 677; O. König, H. B. Bürgi, T. Armbruster, J. Hulliger and T. Weber, *J. Am. Chem. Soc.*, 1997, **119**, 10 632.
7 F. H. Allen, J. P. M. Lommerse, V. J. Hoy, J. A. K. Howard and G. R. Desiraju, *Acta Crystallogr., Sect. B*, 1997, **53**, 1006 and references therein.
8 G. M. Sheldrick, SHELX93: Program for the refinement of crystal structures, University of Göttingen, 1993.
9 A. C. Larson and R. B. Von Dreele, GSAS, Generalized Structure Analysis System, LANSCE, Ms-H805, Los Alamos National Laboratory, New Mexico, 1994.
10 R. B. Neder and T. Proffen, *J. Appl. Crystallogr.*, 1996, **29**, 727.

Received in Cambridge, UK, 19th February 1998; revised manuscript received 8th May 1998; 8/03486I

5-Acceptor-substituted 4-amino-2-arylazothiazoles. A unique black monoazo chromophoric system

John Griffiths*† and Conrad J. Riepl

Department of Colour Chemistry, The University of Leeds, Leeds, UK LS2 9JT

Replacement of the chlorine substituent in blue dyes of the 5-acceptor-4-chloro-2-(4-*N*,*N*-dialkylaminophenylazo)thiazole type by a tertiary amino group produces a black monoazo chromophoric system with three π → π* bands spanning the whole of the visible spectrum.

Black dyes, *i.e.* those with two or more absorption bands extending across the whole of the visible spectrum, are rare, and known examples invariably have a large molecular size in order to provide the requisite conjugation and number of chromophoric sub-units for multiple π → π* transitions in the visible range. The most commonly encountered examples are bis-azo or higher poly-azo dyes; their large size can lead to problems associated with aggregation or low solubility and this can limit their technical application. The traditional alternative is to use mixtures of dyes, even though these may introduce dye compatibility and shade reproducibility problems. Given the currently increasing importance of soluble black colorants in areas such as ink-jet and other digital printing systems, liquid crystal displays and optical filters, there is a growing need for the development of new, relatively low molecular weight black chromophores which can overcome these difficulties. We now describe the synthesis of a unique 2-arylazothiazole chromophoric system, whereby simple replacement of a chlorine substituent by an amino group causes a dramatic change in the light absorption properties of the molecule, and the single visible π → π* absorption band is replaced by three intense π → π* bands more or less equally spaced across the visible spectrum.

The 5-acceptor-4-chloro-2-(4-*N*,*N*-dialkylaminophenylazo)-thiazole dyes, as exemplified by **1** and **2a**,[1] are highly polarised molecules that show a single intense π → π* absorption band in the range *ca.* 550–800 nm,[2] which can be considered to involve electron density migration from the amino group into the azo group, thiazole ring and the 5-acceptor substituents on the latter ring. Whilst normally violet to blue–green in colour, the use of multiple donor groups in the donor ring and powerful acceptor groups R in **1** (*e.g.* **3a**) can displace the band into the near IR region, leading to useful near-IR dyes.[2] The 4-chloro substituent in molecules such as **1**, **2a** and **3a** should be capable of nucleophilic replacement, particularly if the 5-substituent is strongly electron withdrawing, and this was investigated in the case of the indane-1,3-dione derivative **2a**.

A solution of the blue dye **2a** and piperidine (2 equiv.) in THF was heated under reflux, when the colour of the solution became black, and after 6 h the reaction was judged to be complete by TLC analysis. After filtration to remove piperidine hydrochloride, the solution was evaporated and the product recrystallised from a mixture of CH_2Cl_2 and EtOH to afford **2b** as black crystals in 65% yield. The structure was confirmed by microanalysis, mass spectrometry and NMR spectroscopy. The dye was readily soluble in solvents such as toluene and CH_2Cl_2, giving black solutions which showed three absorption bands in the visible region. The absorption spectra of **2a** and **2b** in cyclohexane are compared in Fig. 1(*a*) and (*b*). The second band of **2b** shows vibrational structure, which is most evident in non-polar solvents such as cyclohexane [Fig. 1(*b*)]. In CH_2Cl_2 the absorption maxima occurred at 437, 528 (shoulder at 500 nm) and 665 nm (ε_{max} 19 900, 26 500 and 29 400 l mol^{-1} cm^{-1}, respectively). Thus, introduction of the piperidino group into the thiazole ring generates three visible π → π* absorption

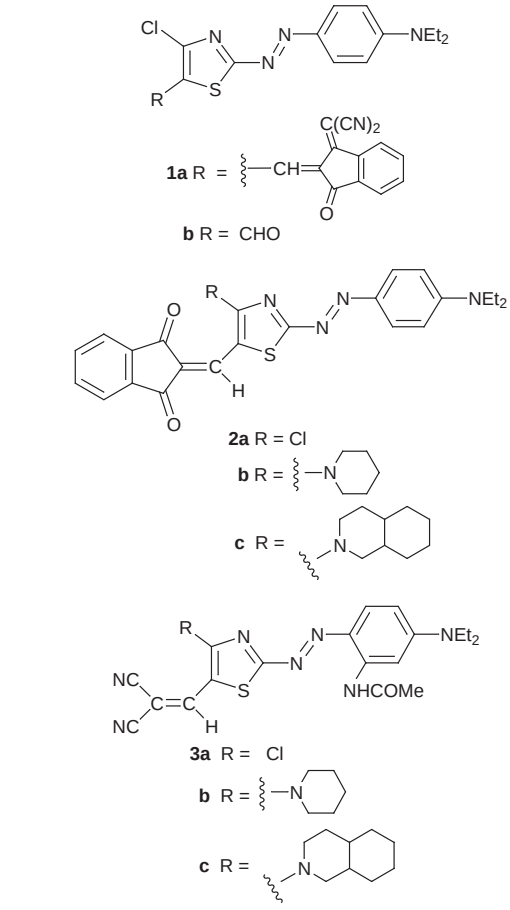

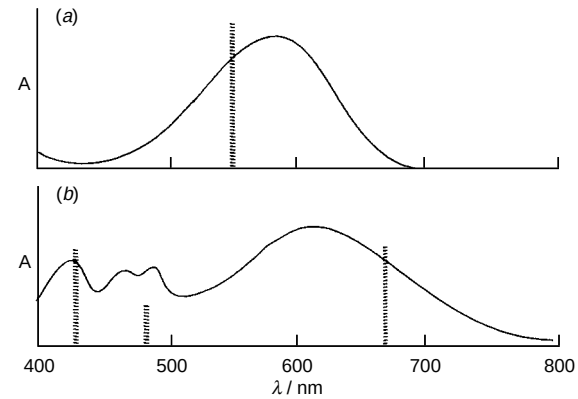

Fig. 1 Absorption spectra of (*a*) **2a**, and (*b*) **2b** in cyclohexane. Vertical broken lines represent the PPP-MO predicted absorption band λ_{max} values and relative intensities.

bands in place of the original single band. Such a dramatic change in the characteristics of a dye chromophore induced by a single substituent appears to be without precedent.

The electronic origin of the three bands was examined by application of PPP-MO theory to the π-chromophores of **2a** and **2b**.[3] Using standard parameters[3,4] the method predicted correctly that replacing the chlorine atom in **2a** by an amino group produces three visible absorption bands (Fig. 1).

The absorption bands, in order of increasing transition energy, approximate to the one electron excitation processes: HOMO → LUMO, HOMO → (LUMO + 1) and (HOMO-1) → (LUMO), although there is extensive configuration interaction between the three excited states. From the wavefunctions for these various orbitals one can deduce that the longest wavelength band involves the whole of the conjugated π system, the second band is associated predominantly with the 4-amino-5-acceptor-thiazole residue, and the shortest wavelength band is confined predominantly to the arylazo residue and the thiazole ring. All three bands show positive solvatochromism, shifting respectively from 608, 493 and 424 nm in cyclohexane to 677, 532 and 433 nm in DMF.

Replacement of the chlorine atom in the thiazole ring could also be effected with a variety of secondary amines, and with other 5-acceptor substituted analogues of **2a**. Thus the deeply coloured dyes **2c**, **3b**,**c** and **4**‡ were prepared in 50–95% yields by heating the appropriate chlorine-substituted dye and amine in solvents such as THF, EtOH and CH_2Cl_2. All showed the characteristic three visible absorption bands of this type of chromophore, their solutions ranging from dark blue, through greenish black to neutral black in colour. In general the rate of the replacement reaction and product yields were enhanced when the arylamine group had an acylamino substituent capable of hydrogen bonding to the azo group (*e.g.* **3**, **4b**,**c**,**e**).

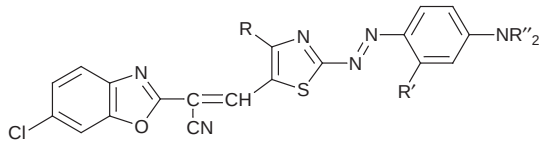

4a R = 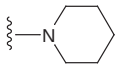 R′ = H, R″ = Et

b R = 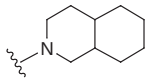 R′ = NHAc, R″ = Pr

c R = NMe_2, R′ = NHAc, R″ = Pr

d R = 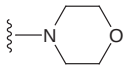 R′ = H, R″ = Et

e R = 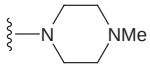 R′ = NHAc, R″ = Pr

The success of the chlorine replacement reaction is critically dependent on the nature of both the reacting amine and the thiazole 5-acceptor group. Weakly nucleophilic amines, *e.g.* primary and secondary arylamines, do not react, whereas primary alkylamines cause extensive decomposition of the chromophore, leading to (among other products) the parent aldehyde dye (*e.g.* formation of **1b** from **2a**). If the 5-acceptor group is particularly electron withdrawing then it undergoes preferential attack by the amine, leading to degradation of the chromophore and formation of red products. For example **1a** gave only decomposition products on reacting with a range of secondary amines. In the case of the aldehyde derivative **1b** reversible addition of the amine to the formyl group occurred, giving the unstable magenta aminohydroxy derivative.

The dyes **2b**,**c**, **3b**,**c** and **4** represent a new class of black chromophore that is capable of considerable structural diversity. Preliminary investigations have shown that hydrolytic, thermal and photochemical stability properties are typical for azo dyes of this general type and thus these systems offer considerable potential for the development of novel black colorants for many technical applications.

We thank the EPSRC National Mass Spectrometry Service Centre for provision of mass spectrometry services.

Notes and References

† E-mail: CCDJG@leeds.ac.uk

‡ Structures of new compounds were consistent with FAB-MS, 300 MHz NMR spectra and/or microanalytical data.

1 J. Fisher, M. Weaver and C. Coates, US Pat. 3 329 410, 1974.
2 K. A. Bello and J. Griffiths, *J. Chem. Soc., Chem. Commun.*, 1986, 1639.
3 J. Griffiths, *Dyes Pigments*, 1982, **3**, 211.
4 G. Hallas and R. Marsden, *Dyes Pigments*, 1985, **6**, 463.

Received in Liverpool, UK, 31st March 1998; 8/02495B

In aqua synthesis of a high molecular weight arylethynylene polymer with reversible hydrogel properties

Chao-Jun Li,*[a]† William T. Slaven IV,[a] Yi-Ping Chen,[b] Vijay T. John[c] and Suguna H. Rachakonda[c]

[a] *Department of Chemistry, Tulane University, New Orleans, LA 70118, USA*
[b] *Department of Cell and Molecular Biology, Tulane University, New Orleans, LA 70118, USA*
[c] *Department of Chemical Engineering, Tulane University, New Orleans, LA 70118, USA*

Palladium catalyzed copolymerization of 3,5-diiodobenzoic acid with acetylene gas in a basic aqueous medium provides a high molecular weight (~60 000), zig-zag phenylethynylene polymer; the polymer has been characterized by a variety of methods and has a high thermostability, is soluble in basic solutions and is reversibly switchable from soluble to hydrogel states in water by changing the pH of the solvent.

Poly(arylethynylene)[1] is an important class of conjugated polymer exhibiting properties such as photoluminescence,[2] electronic conductivity[3] and non-linear optical properties.[4] These polymers also exhibit exceptionally high quantum yields of fluorescence in comparison to other conjugated polymers.[5] Such properties render the polymer useful for applications in constructing polymer light emitting diodes (polymer LEDs),[6] organic magnetic materials,[7] molecular wires and antennas[8] and fluorescence sensors.[9] Recently, Nelson *et al.* have also shown that an arylethynylene-based oligomer mimics protein folding, which has exciting potential for biological applications.[10] However, the potential applications of these materials for electronic and optical purposes are often limited by their low solubility and low degree of the polymerization. The increased interest in the properties of polyarylethynylene-type materials has led to the attachment of various bulky substituents by various groups to increase their solubility in organic solvent.[1] Alternatively, Kondo *et al.* introduced irregularity in the polymer chain to increase their solubility and degree of polymerization.[11] However, the structural irregularity may also change its electronic and optical properties. During our studies of aqueous organic reactions,[12] and as part of our continuing interests in synthesizing arylethynylene-type polymers and oligomers,[13] we recently reported an efficient synthesis of arylethynylene polymer and oligomers through polymerization of aryl halides with acetylene gas in an aqueous medium.[14] However, the polymers that we generated had the same limitation of insolubility and low molecular weight. In an attempt to overcome these difficulties, we decided to explore the synthesis of water-soluble polyarylethynylenes. Here we report that the palladium catalyzed copolymerization of 3,5-diiodobenzoic acid with acetylene gas in a basic aqueous medium provides a high molecular weight, zig-zag arylethynylene polymer [eqn. (1)] which can be processed readily.

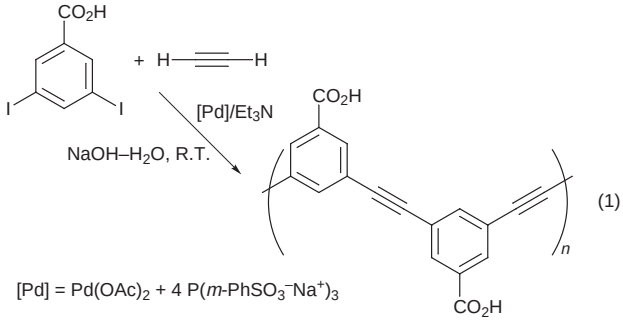

(1)

Previously, there has been a very limited study of the synthesis of water-soluble rigid-chain polyelectrolytes in the literature. The more noticeable advance in this area was the synthesis of a water-soluble poly(*p*-phenylene) reported by Wallow and Novak through the Suzuki reaction,[15] and a water-soluble poly(thiophene) sensor material reported by McCullough *et al.*[16] In the present investigation, the polymerization was carried out by reacting 3,5-diiodobenzoic acid with acetylene gas in the presence of a water-soluble palladium catalyst, cuprous iodide as a co-catalyst, 1 equiv. NaOH and 3 equiv. Et_3N in water. The water-soluble palladium catalyst was generated *in situ* from palladium acetate and tris(*m*-sulfophenyl)phosphine trisodium salt, as used by Casalnuovo and others.[17] The monomer used in the present study was prepared according to literature procedure.[18] After stirring the reaction mixture for three days at room temperature, the polymer was readily isolated by addition of dilute HCl, giving a dark brown solid in its free acid form. The polymer thus generated has no substantial solubility in all other solvents tested except in dilute aqueous NaOH solution. On the other hand, the polymer is readily soluble in dilute NaOH. Under neutral or slightly acidic conditions, the polymer becomes a hydrogel which holds water about eight times of its original weight after centrifuging. It can be reversibly transformed into the water-soluble and hydrogel states by changing the pH of the medium [eqn. (2)], which has

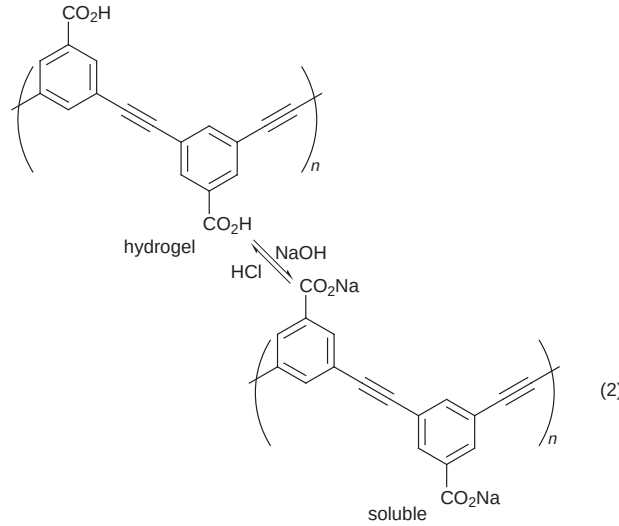

(2)

potential biomedical and environmental applications.[19] It should be noted that throughout the polymerization process, the polymer remained soluble in the reaction medium, which is essential for the formation of high molecular weight polymers.

The polymer thus generated has been characterized by a number of methods. The two potential types of aromatic hydrogens exhibited a broad resonance around 8.2–8.4 ppm in the ^1H NMR spectrum (D_2O–NaOD). The IR (KBr pellet)

spectrum displays typical absorption peaks corresponding to free carboxylic acid (3700–3100 and 1772 cm^{-1}) and aromatic functionality.[20] Absorption due to the acetylene stretch vibration (2100–2210 cm^{-1}) is insignificant. Raman spectroscopy of the aqueous solution of the corresponding sodium carboxylate salt showed several absorption peaks in the acetylene region, indicating the presence of polymers with different lengths.[21] The UV–VIS spectrum shows two major bands with absorption maxima at 210 and 288 nm respectively. The molecular weight (M_w = 66 000 g mol^{-1}) of the polymer was determined by agarose gel electrophoreses relative to double-stranded DNA markers.[22] Trace amounts of even higher molecular weight polymers were also observed. Thermogravimetric analysis (TGA) of the polymer showed the expected high thermal stability of common poly(arylethylene)s.[1] The polymer is stable up to 300 °C. It exhibited a one stage degradation with an onset decomposition at *ca.* 400 °C. Differential scanning calorimetry (DSC) measurements show an endotherm at 100 °C which may be due to removal of adsorbed water.

In conclusion, we have developed a simple process for obtaining high molecular mass poly(arylethylene)s. The polymer shows hydrogel properties in its carboxylic form and is reversibly switchable from water-soluble to hydrogel states. Presently, we are evaluating the potential applications of such water-soluble arylethynylene polymers.

Support of this research was provided in part by the Center of Bioenvironmental Research (DOD) and the Center for Photoinduced Processes (NSF-LEQSF). We thank the reviewers for their valuable comments. C. J. L. is an NSF CAREER Awardee (98-02).

Notes and References

† E-mail: cjli@mailhost.tcs.tulane.edu

1 For an excellent review on the synthesis and properties of poly(arylethynylene)s, see: R. Giesa, *J. Macromol. Sci., Rev. Macromol. Chem. Phys.*, 1996, C**36**, 631.
2 T. Yamamoto, M. Takagi, K. Kizu, T. Maruyama, K. Kubota, H. Kanbara, T. Kurihara and T. Kaino, *J. Chem. Soc., Chem. Commun.*, 1993, 797.
3 M. V. Lakshmikantham, J. Vartikar, K. Y. Jen, M. P. Cava, W. S. Huang and A. G. MacDiarmid, *Am. Chem. Soc., Polym. Prepr.*, 1983, **24**, 75; M. Tateishi, H. Nishihara and K. Aramaki, *Chem. Lett.*, 1987, 1727.
4 R. H. Baughman, J. L. Bredas, R. R. Chance, R. L. Elsenbaumer and L. W. Shacklett, *Chem. Rev.*, 1982, **82**, 209.
5 A. P. Davey, S. Elliott, O. O'Conner and W. Blau, *J. Chem. Soc., Chem. Commun.*, 1995, 1433.
6 D. D. C. Bradley, *Adv. Mater.*, 1992, **4**, 756; Q. X. Ni, L. S. Swanson, P. A. Lane, J. Shinar, Y. W. Ding, S. Ljadimaghsoodi and T. J. Barton, *Synth. Met.*, 1992, **49**–**50**, 447; L. S. Swanson, J. Shinar, Y. W. Ding and T. J. Barton, *ibid*, 1993, **55**–**57**, 1.
7 Y. Miura and Y. Ushitani, *Macromolcules*, 1993, **26**, 7079.
8 For a recent review, see: J. M. Tour, *Chem. Rev.*, 1996, **96**, 537. For representative examples, see: J. Zhang, J. S. Moore, Z. Xu and R. A. Arguirre, *J. Am. Chem. Soc.*, 1992, **114**, 2273; R. W. Wagener and J. S. Lindsey, *J. Am. Chem. Soc.*, 1994, **116**, 9759; J. S. Schumm, D. L. Pearson and J. M. Tour, *Angew. Chem., Int. Ed. Engl.*, 1994, **33**, 1360.
9 Q. Zhou and T. M. Swager, *J. Am. Chem. Soc.*, 1995, **117**, 7017; T. M. Swager, C. J. Gil and M. S. Wrighton, *J. Phys. Chem.*, 1995, **99**, 4886.
10 J. C. Nelson, J. G. Saven, J. S. Moore and P. G. Wolynes, *Science*, 1997, **277**, 1793.
11 K. Kondo, M. Okuda and T. Fujitani, *Macromolecules*, 1993, **26**, 7382.
12 C. J. Li, *Chem. Rev.*, 1993, **93**, 2023; C. J. Li, *Tetrahedron*, 1996, **52**, 5643; C. J. Li and T. H. Chan, *Organic Reactions in Aqueous Media*, Wiley, New York, 1997.
13 C. J. Li, D. Wang and W. T. Iv, Slaven, *Tetrahedron Lett.*, 1996, **37**, 4459; D. Wang, T. J. Liu, C. J. Li and W. T. Iv. Slaven, *Polym. Bull.*, 1997, **39**, 265; T. J. Liu, D. Wang, F. L. Bai, C. J. Li and W. T. Iv. Slaven, *Chin. J. Polym. Sci.*, in the press.
14 C. J. Li, W. T. Iv. Slaven, V. T. John and S. Banerjee, *Chem. Commun.*, 1997, 1569.
15 T. I. Wallow and B. M. Novak, *J. Am. Chem. Soc.*, 1991, **113**, 7411; see also references cited therein for other examples.
16 R. D. McCullough, P. C. Ewbank and R. S. Loewe, *J. Am. Chem. Soc.*, 1997, **119**, 633.
17 A. L. Casalnuovo and J. C. Calabrese, *J. Am. Chem. Soc.*, 1990, **112**, 4324. For other examples, see: M. Safi and D. Sinou, *Tetrahedron Lett.*, 1991, **32**, 2025; J. P. Genet, E. Blart and M. Savignac, *Synlett*, 1992, 715; N. A. Bumagin, V. V. Bykov and I. P. Beletskaya, *Russ. J. Org. Chem.*, 1995, **31**, 348; Z. Jiang and A. Sen, *Macromolecules*, 1994, **27**, 7215.
18 H. L. Wheeler and C. O. Johns, *Am. Chem. J.*, 1910, **43**, 398.
19 P. G. de Gennes, in *Physical Properties of Polymeric Gels*, ed. J. P. C. Addad, Wiley, Chichester, 1996; A. S. Hoffman, in *Polymer Gels, Fundamentals and Biomedical Applications*, ed. D. DeRossi, K. Kajiwara, Y. Osada and A. Yamauchi, Plenum Press, New York, 1991, p. 289–297.
20 R. M. Silverstein, G. C. Bassler and T. C. Morrill, *Spectrometric Identification of Organic Compounds*, Wiley, New York, 5th edn., 1991.
21 M. Moroni, J. L. Moigne and S. Luzzati, *Macromolecules*, 1994, **27**, 562.
22 J. Sambrook, E. F. Fritsch and T. Maniatis, *Molecular Cloning: A Laboratory Manual*, Cold Spring Harbor Laboratory Press, New York, 2nd edn., 1989.

Received in Columbia, MO, USA, 29th January 1998; 8/00843D

Total syntheses of (+)-castanospermine and (+)-6-epicastanospermine

Sung Ho Kang*† and Joon Seop Kim

Department of Chemistry, Korea Advanced Institute of Science and Technology, Taejon 305-701, Korea

A divergent synthetic route to (+)-castanospermine 1 and (+)-6-epicastanospermine 2 has been developed *via* phenylselenoamidation of trichloroacetimidate derived from allylic alcohol 7, and dihydroxylations of *trans*-olefins 14 and 18 to dispose the three contiguous asymmetric centers, one amino group and two hydroxy groups.

The naturally occurring hydroxylated indolizidine alkaloids such as (−)-swainsonine, (+)-castanospermine **1** and (+)-6-epicastanospermine **2** continue to enjoy considerable attention from synthetic and medicinal chemists due to their pronounced biological activities. Their inhibition of enzymatic glycosidic hydrolysis is closely related with the potential chemotherapeutic utility for the treatment of diabetes,[1] cancer,[2] viral diseases[3] and AIDS.[4] Their intriguing molecular structures and promising medicinal value led us to explore their efficient synthetic routes. Here we describe total syntheses[5] of (+)-castanospermine **1** and (+)-6-epicastanospermine **2**, which have been isolated from *Castanospermum australe*[6] and *Alexa leiopetala*.[7]

Based on our retrosynthetic analysis toward **1** and **2**, a crucial synthetic step was a stereoselective dihydroxylation of *trans*-olefin **3** (Scheme 1). While the effect of the allylic amino group in **3** on the stereochemical outcome was in question,[8] its allylic alkoxy group was properly disposed for the desired α-dihydroxylation according to Kishi's empirical rule.[9] Another key step was to produce a *syn*-amino alcohol as a prospective precursor to **3** *via* intramolecular phenylselenoamidation of trichloroacetimidate derived from *cis*-olefinic allylic alcohol **4**.[10]

(*S*)-Butane-1,2,4-triol reacted with *p*-anisaldehyde in the presence of PPTS in benzene using a Dean–Stark trap to give a 7.5–8 : 1 mixture of 6- and 5-membered benzylidenes (Scheme 2). After Swern oxidation[11] of the inseparable mixture, the resulting aldehydes were olefinated with phosphonium salt **5** prepared from (*S*)-butane-1,2,4-triol[12] to afford a 19 : 1 mixture of *cis*-olefin **6**, $[\alpha]_D^{28}$ +110.8 (*c* 1.5, $CHCl_3$), and the corresponding *trans*-olefin in 69% combined overall yield, along with 7% of the isomeric olefins generated from the 5-membered benzylidenes. Hydrolysis of **6** with PPTS in MeOH at 0 °C removed its *p*-methoxybenzylidene group chemoselectively to provide diol **4**, $[\alpha]_D^{27}$ +9.9 (*c* 1.3, $CHCl_3$), in 86% yield. The primary hydroxy group of **4** was regioselectively silylated with TBDPSCl in the presence of imidazole at −60 °C to furnish silyl ether **7**, $[\alpha]_D^{22}$ −2.6 (*c* 2.2, $CHCl_3$), in 92% yield. For the unprecedent phenylselenoamidation, **7** was treated with

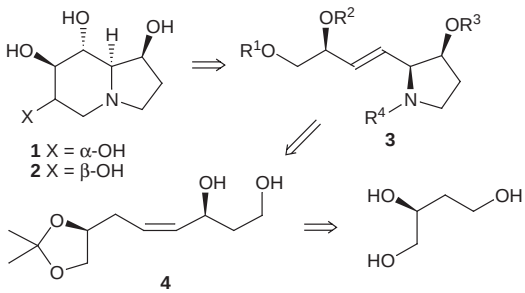

Scheme 1

Cl_3CCN in the presence of DBU in MeCN at 0 °C, and subsequently cyclized using phenylselenyl chloride in the presence of methyl 2,2,2-trichloroacetimidate and Et_3N in MeCN at −20 °C to produce an inseparable 15 : 1 mixture of *trans*-oxazoline **8** and the isomeric *cis*-oxazoline in 63% combined yield. In this cyclization, the addition of methyl 2,2,2-trichloroacetimidate was essential to suppress the formation of the corresponding trichloroacetate from trichloroacetimidate. Subjection of the mixture to PPTS in aqueous MeOH induced partial hydrolysis of the oxazoline groups to give hydroxy trichloroacetamides, of which the desired *syn*-stereoisomer, $[\alpha]_D^{22}$ −6.8 (*c* 2.0, $CHCl_3$), was readily separated in 87% yield from the *anti*-stereoisomer. Oxidative elimination of the *syn*-stereoisomer with H_2O_2 in THF afforded *trans*-olefin **9**, $[\alpha]_D^{24}$ +15.8 (*c* 3.7, $CHCl_3$), in 84% yield contaminated with less than 3% of *cis*-isomer.

The next event was a stereoselective dihydroxylation of the introduced *trans*-olefinic double bond. In order to attain better stereoselectivity, **9** was variously functionalized by changing the protecting groups and the molecular structural shapes. It was found that the most promising outcomes could be obtained with benzyloxycarbonyl (Z)-protected pyrrolidine derivatives. Accordingly, **9** was desilylated in 92% yield and then the resultant alcohol **10**, $[\alpha]_D^{21}$ +34.9 (*c* 0.7, $CHCl_3$), was cyclized under Mitsunobu conditions[13] using diisopropyl azodicarboxylate (DIAD) and PPh_3 in THF at 0 °C to provide pyrrolidine **11**, $[\alpha]_D^{24}$ +58.6 (*c* 1.0, $CHCl_3$), in 88% yield. Treatment of **11** with BnONa in THF resulted in the formation of Z-protected pyrrolidine **12**, $[\alpha]_D^{26}$ +54.9 (*c* 1.1, $CHCl_3$), in 90% yield. After removal of the acetonide group under acidic conditions, the obtained triol **13**, $[\alpha]_D^{25}$ +17.0 (*c* 3.0, MeOH), was regioselectively sulfonated with 2,4,6-triisopropylbenzenesulfonyl chloride (TIPBSCl) in pyridine to furnish monosulfonate **14**, $[\alpha]_D^{25}$ +18.9 (*c* 1.2, $CHCl_3$), in 83% overall yield based on 15% of the recovered **13**. Dihydroxylation of **14** with a catalytic amount of OsO_4 in the presence of NMO in aqueous acetone[14] at 0 °C produced the requisite tetraol **15**, $[\alpha]_D^{23}$ +9.2 (*c* 1.1, $CHCl_3$), in 88% yield along with less than 8% of **17**, which was undoubtedly formed by the spontaneous intramolecular etherification of the isomeric tetraol **16**. Subjection of **15** to hydrogenolysis followed by *in situ* cyclization in the presence of Et_3N gave (+)-6-epicastanospermine **2**, $[\alpha]_D^{23}$ +2.8 (*c* 0.6, MeOH), in 66% yield.[15]

For the synthesis of (+)-castanospermine, **12** was converted into silyl ether **18**, $[\alpha]_D^{25}$ −12.6 (*c* 1.7, $CHCl_3$), in 88% overall yield by protection of the secondary hydroxy group with $MeOCH_2Cl$ (MOMCl), hydrolysis of the acetonide group and monosilylation of the primary hydroxy group with TBDPSCl in sequence (Scheme 3). Osmylation of **18** gave triol **19**, $[\alpha]_D^{24}$ −4.9 (*c* 0.7, $CHCl_3$), in 91% yield along with 6% of the isomeric β-dihydroxylated triol. When **19** was exposed to acetone in the presence of TsOH, the desired dioxolane **20**, $[\alpha]_D^{23}$ −7.1 (*c* 1.5, $CHCl_3$), was prepared in 92% yield by ketalization of the two *syn*-hydroxy groups, accompanied by 2% of the regioisomeric dioxolane. In order to secure the correct stereochemistry at 6-position of (+)-castanospermine, the remaining hydroxy group of **20** was inverted by mesylation followed by desilylation to afford epoxide **21**, $[\alpha]_D^{21}$ −19.7 (*c* 1.2, $CHCl_3$), in 87% overall yield. Removal of the Z group in **21**

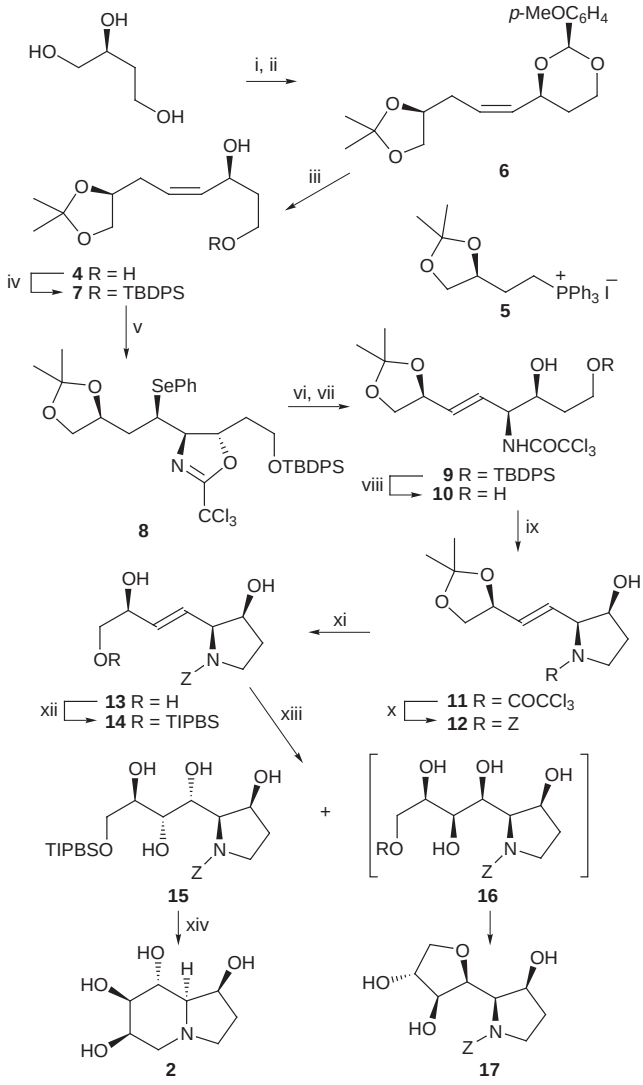

Scheme 2 *Reagents and conditions*: i, *p*-anisaldehyde, PPTS, PhH, Dean–Stark trap; ii, $(COCl)_2$, DMSO, Et_3N, then **5**, Bu^nLi, HMPA, THF, −78 to 0 °C; iii, PPTS, MeOH, 0 °C; iv, TBDPSCl, imidazole, DMF, CH_2Cl_2, −60 °C; v, Cl_3CCN, DBU, MeCN, 0 °C, then PhSeCl, $MeOC(=NH)CCl_3$, Et_3N, MeCN, −20 to −15 °C; vi, PPTS, H_2O, MeOH, 20 °C; vii, 30% H_2O_2, THF, 0 to 20 °C; viii, Bu_4NF, THF, −5 to 0 °C, then aq. NaH_2PO_4; ix, DIAD, Ph_3P, THF, 0 °C; x, NaOBn, THF, 20 °C; xi, TsOH, MeOH, 20 °C; xii, TIPBSCl, pyridine, 20 °C; xiii, OsO_4, NMO, acetone, 0 °C; xiv, H_2, 10% Pd/C, MeOH, 20 °C, then Et_3N, reflux

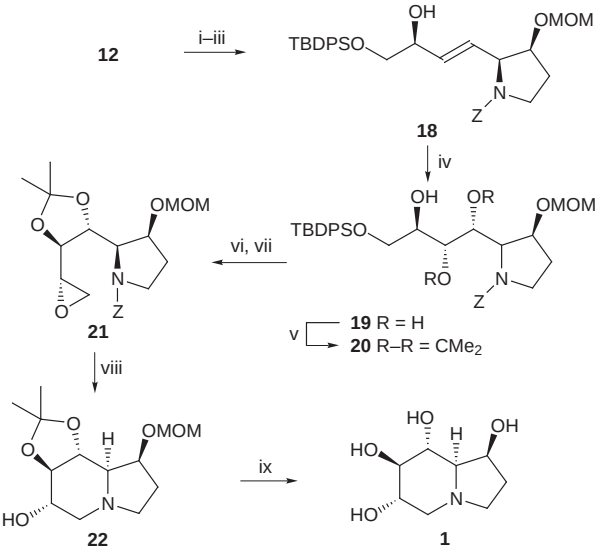

Scheme 3 *Reagents and conditions*: i, MOMCl, Et_3N, CH_2Cl_2, reflux; ii, TsOH, MeOH, 20 °C; iii, TBDPSCl, imidazole, DMF, CH_2Cl_2, −60 °C; iv, OsO_4, NMO, H_2O, acetone, 0 °C; v, TsOH, acetone, 20 °C; vi, MsCl, DMAP, Et_3N, CH_2Cl_2, 20 °C; vii, Bu_4NF, THF, 20 °C, then 5 M NaOH; viii, 5% Pd/C, cyclohexene, EtOH, reflux; ix, conc. HCl, MeOH, reflux, then Dowex 50WX8-100 ion-exchange resin

was anticipated to induce 6-*endo* cyclization rather than 5-*exo* cyclization due to the *anti* arrangement of the dioxolane ring. Indeed heating **21** under catalytic transfer hydrogenation conditions[16] provided only indolizidine **22**, $[\alpha]_D^{22}$ +39.5 (*c* 0.8, $CHCl_3$), in 76% yield. Finally methanolysis of **22** with methanolic HCl furnished (+)-castanospermine **1**, mp 205–207 °C (decomp.), $[\alpha]_D^{22}$ +79.7 (*c* 1.0, MeOH), in 96% yield.[15]

In summary, we have accomplished total syntheses of (+)-castanospermine **1** and (+)-6-epicastanospermine **2**, which culminated in the stereoselective phenylselenoamidation of trichloroacetimidate (from **7**) and the asymmetric dihydroxylation of **14** and **18** to establish the four contiguous chiral centers.

This work was supported by the Korea Advanced Institute of Science and Technology and the Organic Chemistry Research Center sponsored by the Korea Science and Engineering Foundation. Dedicated to Professor Yoshito Kishi on the occasion of his 60th birthday.

Notes and References

† E-mail: shkang@kaist.ac.kr

1 B. L. Rhinehart, K. M. Robinson, A. J. Payne, M. E. Wheatly, J. L. Fisher, P. S. Liu and W. Cheng, *Life Sci.*, 1987, **41**, 2325; K. M. Robinson, B. L. Rhinehart, J. B. Ducep and C. Danzin, *Drugs Future*, 1992, **17**, 705.
2 M. J. Humphries, K. Matsumoto, S. L. White and K. Olden, *Cancer Res.*, 1986, **46**, 5215; G. K. Ostrander, N. K. Scribner and L. R. Rohrschneider, *Cancer Res.*, 1988, **48**, 1091.
3 P. S. Sunkara, T. L. Bowlin, P. S. Liu and A. Sjoerdsma, *Biochem. Biophys. Res. Commun.*, 1987, **148**, 206; P. S. Sunkara, M. S. Kang, T. L. Bowlin, P. S. Liu, A. S. Tyms and A. Sjoerdsmar, *Ann. N.Y. Acad. Sci.*, 1990, **616**, 90.
4 R. A. Gruters, J. J. Neefjes, M. Tersmette, R. E. Y. de Goede, A. Tulp, H. G. Huisman, F. Miedema and H. L. Ploegh, *Nature*, 1987, **330**, 74; B. D. Walker, M. Kowalski, W. C. Goh, K. Kozarsky, M. Krieger, C. Rosen, L. Rohrschneider, W. A. Haseltine and J. Sodroski, *Proc. Natl. Acad. Sci. USA*, 1987, **84**, 8120; A. Karpas, G. W. J. Fleet, R. A. Dwek, S. Petursson, S. K. Namgoong, N. G. Ramsden, G. S. Jacob and T. W. Rademacher, *Proc. Natl. Acad. Sci. USA*, 1988, **85**, 9229.
5 K. Burgess and I. Henderson, *Tetrahedron*, 1991, **48**, 4045; H. Ina and C. Kibayashi, *J. Org. Chem.*, 1993, **58**, 52; N.-S. Kim, J.-R. Choi and J. K. Cha, *J. Org. Chem.*, 1993, **58**, 7096; H. S. Overkleeft and U. K. Pandit, *Tetrahedron Lett.*, 1996, **37**, 547.
6 L. D. Hohenschutz, E. A. Bell, P. J. Jewess, D. P. Leworthy, R. J. Pryce, E. Arnold and J. Clardy, *Phytochemistry*, 1981, **20**, 811.
7 R. J. Nash, L. E. Fellows, J. V. Dring, C. H. Stirton, D. Carter, M. P. Hegarty and E. A. Bell, *Phytochemistry*, 1988, **27**, 1403.
8 F. M. Hauser and R. P. Rhee, *J. Org. Chem.*, 1981, **46**, 227; H. Pettersson, A. Gogoll and J. E. Bäckvald, *J. Org. Chem.*, 1995, **60**, 1848.
9 J. K. Cha, W. J. Christ and Y. Kish, *Tetrahedron Lett.*, 1983, **24**, 3943 and 3947; G. Stork and M. Kahn, *Tetrahedron Lett.*, 1983, **24**, 3951.
10 S. H. Kang and G. T. Kim, *Tetrahedron Lett.*, 1995, **36**, 5049; S. H. Kang, G. T. Kim and Y. S. Yoo, *Tetrahedron Lett.*, 1997, **38**, 603.
11 A. J. Mancuso and D. Swern, *Synthesis*, 1981, 165.
12 S. H. Kang, T. S. Hwang, J. K. Lim and W. J. Kim, *Bull. Korean Chem. Soc.*, 1990, **11**, 455.
13 O. Mitsunobu, *Synthesis*, 1981, 1.
14 V. Vankheenen, R. C. Kelly and D. Y. Cha, *Tetrahedron Lett.*, 1976, 1973.
15 All new compounds showed satisfactory spectral data.
16 G. Brieger and T. J. Nestrick, *Chem. Rev.*, 1974, **74**, 567.

Received in Cambridge, UK, 14th April 1998; 8/02741B

The $^{18}O/^{16}O$ induced proton isotope shift in water

Natalia D. Sergeyeva,[a] J. P. Jacobsen*[b]† and N. M. Sergeyev[c]

[a] *Russian Peoples' Friendship University, 117198, Moscow, Russia*
[b] *Department of Chemistry, Odense University, 5230 Odense M, Denmark*
[c] *Department of Chemistry, Moscow State University, Moscow, 119899, Russia*

Measurements of proton NMR spectra at 750 MHz of dilute solutions of water in nitromethane reveals a small proton isotope shift due to $^{16}O/^{18}O$ substitution equal to about 1 ppb.

There has been much recent interest in the isotope shifts induced by the substitution of ^{18}O for ^{16}O. In the extensive review of Risley and van Etten[1] proton isotope shifts in water induced by $^{18}O/^{16}O$ substitution are reported as covering the very wide range from −70 to +300 ppb. In early work Pinchas and co-workers[2–4] used separate samples of the pure isotopomers in order to prevent proton exchange. The strong dependence of the water shielding upon concentration, temperature and certain uncontrolled impurities makes these results questionable.

Recently, we performed measurements of the $^{18}O/^{16}O$ induced proton isotope shift using dilute solutions of an $H_2{}^{16}O$ and $H_2{}^{18}O$ mixture in nitromethane.[5] At a proton NMR frequency of 300 MHz we found no splitting of the H_2O singlet. This suggested that the $H_2{}^{18}O/H_2{}^{16}O$ isotope shift is less than 0.5 Hz (about 2–3 ppb). The availability of NMR spectrometers with higher magnetic fields makes it possible to measure an isotope effect of this size. Here we describe a successful attempt to measure this isotope shift on a 750 MHz NMR spectrometer.

The crucial requirement in obtaining the NMR parameters of individual water molecules is to stop the proton (or proton–deuteron) exchange in order to prevent the collapse of spin multiplets and to exclude any effect on the NMR line shape. To obtain reliable results it is necessary to use dilute solutions of water in organic solvents.[6] The solvent has to be carefully dried to eliminate the residual water.

We used [$^2H_3$]nitromethane purchased from Merck with the deuteration levels of 99.44% (±0.01%) according to our estimates. The proton signal of the residual CHD_2NO_2 was used to determine the water content in the solvent. [$^2H_3$]Nitromethane was dried by several freezing–thaw–pumping cycles using P_2O_5 as a drying agent *in vacuo* and passed through a series of traps to eliminate traces of the drying agent. The final water content never exceeded 0.01 mol%. We used double distilled $H_2{}^{16}O$, 99.1% $H_2{}^{18}O$ and 30% $H_2{}^{17}O$ enriched water purchased from Isotech and 99.96% D_2O purchased from Merck. Small amounts of D_2O were added to the solutions of water to control the rate of exchange by monitoring of the HDO lines. A small amount of dried TMS was added to control the resolution and the water line shape. We used a Young sample tube for mixing the components to control *via* ^1H NMR spectra the water content at all stages of the sample preparation. The dosages of TMS and water mixtures were done by vaporization into the precalibrated volumes. The final solution was distilled in a 5 mm sample tube and sealed under vacuum. All bulbs and sample tubes used were treated according to the procedure described earlier[7] and kept under vacuum.

A 750 MHz Varian INOVA NMR spectrometer was used to obtain the ^1H NMR spectra. Typical proton NMR spectra of a 0.25 mol% solution of a 20 : 10 : 1 $H_2{}^{16}O$–$H_2{}^{18}O$–D_2O mixture in [$^2H_3$]nitromethane taken in the temperature range from 30 to 80 °C are shown in Fig. 1. Fig. 1(*a*) contains lines from $H_2{}^{16}O$–$H_2{}^{18}O$, while Fig. 1(*b*) contains lines from $H^{16}OD$–$H^{18}OD$. Values of the $^{18}O/^{16}O$ induced proton isotope shifts were measured to be the following: 30 °C: 0.79 ± 0.05; 45 °C: 0.93 ± 0.05; 60 °C: 1.04 ± 0.05; 80 °C: 1.08 ± 0.05 (all values are in ppb).

It is worth noting that the water linewidth is about 0.3 Hz, revealing a decrease with temperature. In all cases the $H_2{}^{18}O$ signal appears at higher field in accord with a very well known trend[8] that heavier isotopic substitution produces high fields displacements.

In Fig. 1(*b*) the multiplet for HDO is shifted to high field by about 23 Hz (*ca.* 30.6 ppb), in exact agreement with the previously found H/D induced proton isotope shift for water.[5,9] The HDO signal shows a superimposition of the triplet of $HD^{16}O$ and that of $HD^{18}O$, with the two low field components of the $HD^{18}O$ triplet almost overlapping the two high field components of the $HD^{16}O$ signal. It is of interest that the $^{18}O/^{16}O$ induced proton isotope shift for HDO estimated from spectra at 80 °C is equal to 1.1 Hz (1.4 ± 0.1 ppb). Comparing this value with the $^{16}O/^{18}O$ induced proton isotope shift for H_2O equal to 0.86 Hz (1.08 ± 0.05 ppb at 80 °C) we can suggest an anomalously strong (0.32 ± 0.15 ppb) nonadditivity effect.[10]

We also performed measurements of the proton NMR of water 30% enriched by ^{17}O. According to mass spectral analysis it contains ^{16}O, ^{17}O and ^{18}O in percentages of 25.5, 30.7 and 43.7%, respectively. The ^1H NMR spectrum of a 0.5% solution of this water in [$^2H_3$]nitromethane is shown in Fig. 2. Fig. 2(*b*)

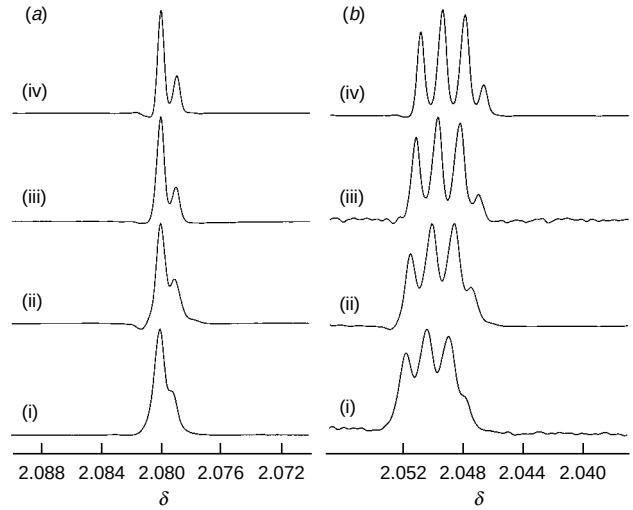

Fig. 1 Two different regions of the ^1H NMR spectrum of a 0.25 mol% solution of a $H_2{}^{16}O$–$H_2{}^{18}O$–D_2O mixture in [$^2H_3$]nitromethane at (i) 30, (ii) 45, (iii) 60 and (iv) 80 °C. The intensity of the signals in (*b*) has been multiplied by 25 compared to (*a*). In all four spectra the signal for $H_2{}^{16}O$ is referenced to δ 1.959 to reset the temperature effect on this signal. The spectrum was recorded at 750 MHz with a sweep width of 5000 Hz, an aquisition time of 8.0 s and 1 transient. The FID was processed using slight resolution enhancement and Fourier transformed in 128 K. (*a*) The signal from $H_2{}^{16}O$–$H_2{}^{18}O$ showing the increasing values of the isotope effect. (*b*) The signal from $HD^{16}O$–$HD^{18}O$ confirming the $^{16}O/^{18}O$ isotope effect.

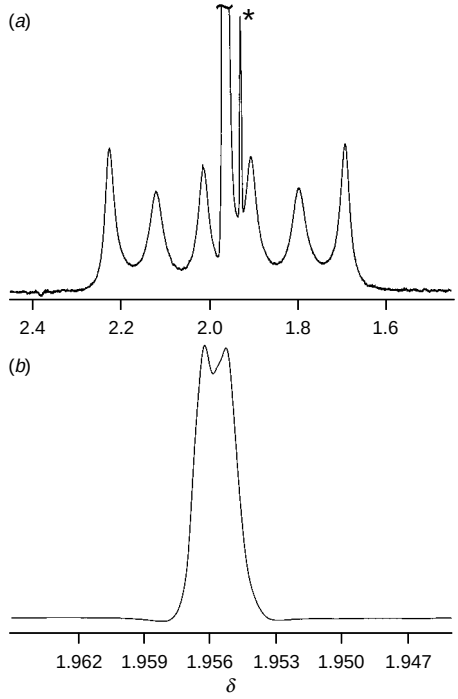

Fig. 2 The 750 MHz ^{1}H NMR spectrum of a 0.5 mol% solution of $H_2{}^{16}O$–$H_2{}^{17}O$–$H_2{}^{18}O$ in [$^2H_3$]nitromethane. The spectrum was recorded at 750 MHz with a sweep width of 5000 Hz, an aquisition time of 8.0 s and 1 transient. (*a*) The sextet of $H_2{}^{17}O$; the intensity of the signals has been multiplied by 100 compared to the upper trace. The signal due to HDO is marked by an asterisk (*). The FID was processed using exponential apodization and Fourier transformed in 128 K. (*b*) The signals corresponding to $H_2{}^{16}O$ and $H_2{}^{18}O$ are separated by an isotope shift equal to 1.1 ppb. The FID was processed using slight resolution enhancement and Fourier transformed in 128 K.

shows the central strong signal due to $H_2{}^{16}O$ and $H_2{}^{18}O$ with the $^{16}O/^{18}O$ induced proton isotope shift equal to (1.1 ± 0.1 ppb), in accord with the spectrum of pure ^{18}O water (Fig. 1).

The sextet of $H_2{}^{17}O$ caused by the coupling of protons in H_2O with ^{17}O (spin 5/2) is shown in Fig. 2(*a*). The small signal of HDO seen to the right of the $H_2{}^{16}O/H_2{}^{18}O$ signal is due to traces of heavy water in the solvent. All components of the sextet contain additional selective broadening due to the relatively slow ^{17}O relaxation.[11,12] The three low field components of the ^{17}O multiplet (less distorted by the central signal) have linewidths equal to *ca.* 20, 33 and 26 Hz, respectively, in full accord with theory.[11] It is interesting to note that, for a similar solution, we found in the ^{17}O NMR spectra at a similar temperature (*ca.* 60 °C) line widths of *ca.* 10 Hz.[5] This indicates that the measurement of ^{17}O–H coupling constants is best performed using ^{17}O rather than ^{1}H NMR spectroscopy. We intend to obtain accurate data on ^{17}O–^{1}H coupling constants and T_1 data for ^{17}O relaxation using iterative calculations with the QUADR program.[13] Also of interest is the possibility of checking the additivity of isotope shifts, as the $H_2{}^{16}O/H_2{}^{17}O$ isotope effect should be close to half of the $^{16}O/^{18}O$ induced proton isotope shift.

We can now state that disagreements with the old data are due to the inconsistent methods of measuring small isotope effects used in the early work.[2–4] The data now obtained are in good agreement with other data on proton isotope shifts due to heavier isotope substitution, *e.g.* of $^{12}C/^{13}C$ substitution.[8]

In parallel with this experimental study, the $^{18}O/^{17}O/^{16}O$ induced proton isotope shifts were studied theoretically[14] and the calculated values are in good agreement with the experimental ones.

The Danish Instrument Center for NMR Spectroscopy of Biological Macromolecules is acknowledged for the use of the 750 MHz NMR spectrometer. The authors thank the INTAS for a research grant (No. 94-448). The work was supported in part by the Danish Natural Science Research Foundation (Grant No. 9600856). The authors thank Professor J. Oddershede, Department of Chemistry, Odense University, for suggesting the experiments and Drs W. T. Raynes and R. Wigglesworth for fruitful discussions and for information about the results of the calculations.

Notes and References

† E-mail: jpj@oukemi.ou.dk

1 J. M. Risley and R. L. Van Etten, in *NMR: Basic Principles and Progress*, ed. P. Diehl, E. Fluck, H. Günther, R. Kosfeld and J. Seelig, Springer Verlag, Berlin, 1990, vol. 22, p. 81.
2 H. Pikman and S. Pinchas, *J. Inorg. Nucl. Chem.*, 1970, **32**, 2441.
3 S. Pinchas and E. Meshulam, *J. Chem. Soc., Chem. Commun.*, 1970, 1147.
4 B. Sredni and S. Pinchas, *J. Magn. Reson.*, 1972, **7**, 289.
5 N. M. Sergeyev, N. D. Sergeyeva, Yu. A. Strelenko and W. T. Raynes, *Chem. Phys. Lett.*, 1997, **227**, 142.
6 J. P. Kintzinger, in *NMR: Basic Principles and Progress*, ed. P. Diehl, E. Fluck, R. Kosfeld and J. Seelig, Springer Verlag, Berlin, 1981, vol. 17, p. 1.
7 D. Lankhors, J. Schriever and J. C. Leyte, *Ber. Bunsenges. Phys. Chem.*, 1982, **86**, 215.
8 P. E. Hansen, *Ann. Rep. NMR Spectrosc.*, 1983, **15**, 103.
9 J. R. Holmes, D. Kivelson and W. C. Drinkard, *J. Chem. Phys.*, 1962, **37**, 150.
10 N. M. Sergeyev, N. D. Sergeyeva and W. T. Raynes, *Chem. Phys. Lett.*, 1994, **221**, 385.
11 A. Abragam, *Principles of Nuclear Magnetism*, Clarendon Press, Oxford, 1961.
12 B. Halle and G. Karlstrøm, *J. Chem. Soc., Faraday Trans. 2*, 1983, **79**, 1031.
13 I. F. Leshcheva, V. N. Torocheshnikov, N. M. Sergeyev, V. A. Chertkov and V. N. Khlopkov, *J. Magn. Reson.*, 1991, **94**, 9.
14 J. Oddershedde, W. T. Raynes and R. D. Wigglesworth, personal communication.

Received in Cambridge, UK, 5th March 1998; 8/01819G

Synthesis and optical resolution of a fluorescent chiral calix[4]arene with two pyrene moieties forming an intramolecular excimer

Takashi Jin*[a]† and Kenji Monde[b]

[a] *Section of Intelligent Materials and Devices, Research Institute for Electronic Science, Hokkaido University, Sapporo, 060-0812, Japan*

[b] *Institute for Chemical Reaction Science, Tohoku University, 2-1-1 Katahira, Sendai, 980-8577, Japan*

An inherently fluorescent chiral calix[4]arene 2 with two pyrene moieties forming an intramolecular pyrene excimer has been synthesized and optically resolved by an HPLC method using a chiral-packed column.

Calixarenes are unique host molecules which have complexing abilities toward ions and/or organic molecules.[1] Recent interest in the synthesis of calixarenes has focused on chiral species, since such a chiral host has potential as an enantioselective artificial receptor of chiral or racemic ligands.[2] Chiral calix[4]arenes have been produced by the addition of chiral residues to calix[4]arene skeletons,[3] or by the introduction of asymmetric substituent patterns into the lower rim[4] or the phenolic rings.[5] Although more than twenty studies of the synthesis of chiral calix[4]arenes have been reported, there are only a few examples of fluorescent chiral calix[4]arenes.[4b,5g] Fluorescent-detectable chiral calixarenes have a great advantage in their high sensitivity as enantioselective sensors of biologically important organic molecules. Herein we describe a simple method for the synthesis of a tri-*O*-alkyated fluorescent chiral calix[4]arene (ABBH-type) that has two pyrene moieties *via* a two-step alkylation of the parent calix[4]arene.

The fluorescent calix[4]arene **2** was synthesised by the reaction of **1**‡ (92 mg) with 2 equiv. (100 mg) of pyren-1-ylmethyl iodoacetate (Molecular Prob. Inc.) in the presence of K_2CO_3 (103 mg) in anhydrous THF (Scheme 1). Racemic compound **2** was obtained as a white powder (55% yield) after a simple chromatographic purification. The structure of **2** was identified by ^{1}H NMR and FD mass spectroscopy.§

The ^{1}H NMR spectrum of **2** showed four singlets for the *tert*-butyl groups and four pairs of doublets from the bridging CH_2 groups, suggesting that the pyrene moieties were introduced to the proximal positions of the lower rim and that **2** adopted a cone conformation. Considering the intensity of the pyrene protons in the NMR spectrum and the results of the FD mass spectrum, calix[4]arene **2** should have an ABBH configuration with two pyrene moieties. To clarify the substituted pattern, a ^{1}H NMR spectrum of **2** in the presence of a chiral shift reagent was measured. The addition of Pirkle's reagent [(S)-(+)-1-(9-anthryl)-2,2,2-trifluoroethanol] to a $CDCl_3$-solution of **2** caused doubling of the methylene signals of the OCH_2CO groups (δ 4.56 and 4.69). This result confirmed that the substituted pattern of calix[4]arene **2** was of the ABBH type, not the ABHB type.

Optical resolution of **2** was performed *via* an HPLC method using a chiral-packed column (Chiracel OD, Daicel, 0.46 × 25 cm). Fig. 1(*a*) shows an HPLC chromatogram for the optical resolution of **2**. Up to 1 mg of **2** per injection could be separated completely in two fractions. To check the enantiomeric resolution, the first and second fractions were subjected to circular dichroism (CD) measurements. The CD spectra [Fig 1(*b*)] were mirror images of each other, indicating that the compounds from the first and second fractions were optical isomers.

The fluorescence spectrum of the first fraction was identical with that of the second fraction. Fig. 2(*a*) shows the fluorescence spectrum of the isomer from the first HPLC fraction. It shows a dual emission resulting from a pyrene monomer (*ca.* 390 nm) and excimer (480 nm),[6] while the fluorescence spectrum of pyrene at the same concentration as **2** afforded only monomer emissions [Fig. 2(*b*)]. The intensity ratio of the monomer/excimer emission **2** was less affected by the concentration in the range from 10^{-4} to 10^{-7} mol dm^{-3}. This indicates that the excimer emission results from an intramolecular excimer, not from an intermolecular excimer.

We examined the fluorescence properties of two enantiomers (the first and second fractions of **2**) toward three chiral guests in the $CHCl_3$–EtOH (30 : 1) at 25 °C. We found that the intensity of the excimer emission of **2** (3.9 μmol dm^{-3}) increased up to 2-fold by addition of L-phenylalanine methyl ester, L-alanine methyl ester or L-phenylglycinol in the presence of Na^+ (76 μmol dm^{-3}). However, differences in the fluorescence intensities between the two isomers of **2** in the presence of the

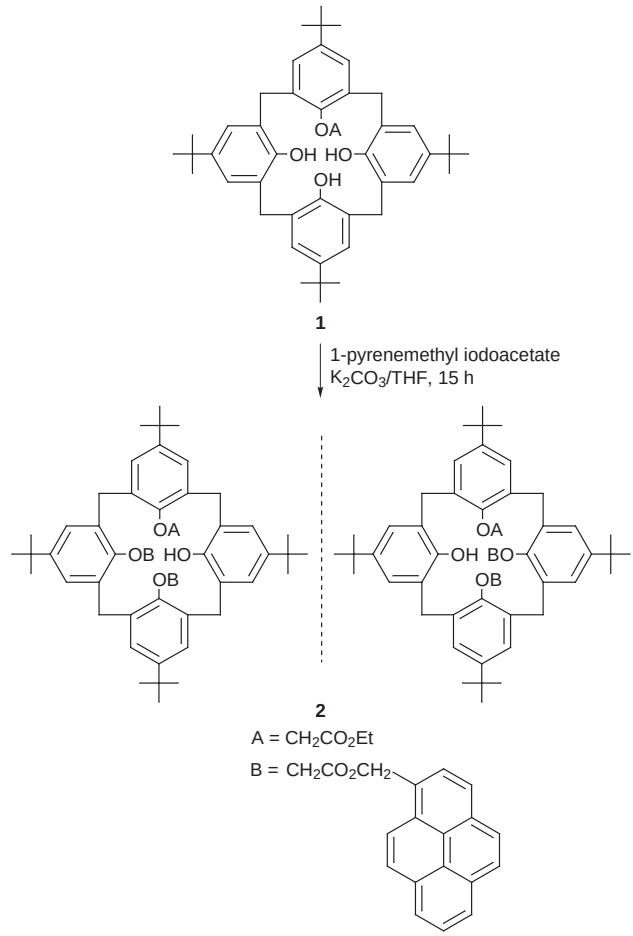

Scheme 1 *Reagents and conditions:* i, pyren-1-ylmethyl iodoacetate, K_2CO_3, THF, 15 h

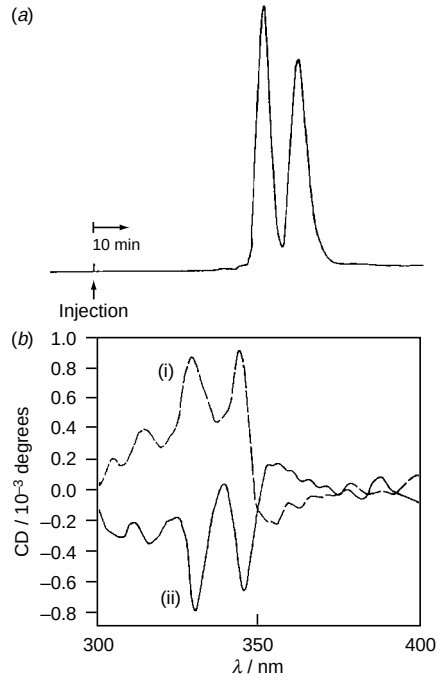

Fig. 1 (*a*) An HPLC chromatogram for optical resolution of racemic **2**. Column: Chiracel OD (0.46 × 25 cm); eluent: hexane–Pr^{i}OH (95 : 5); flow rate: 0.2 ml min^{-1}; T = 40 °C. (*b*) CD spectra of the enatiometric pair of **2** ($CHCl_3$, 25 °C): (i) first fraction, (ii) second fraction.

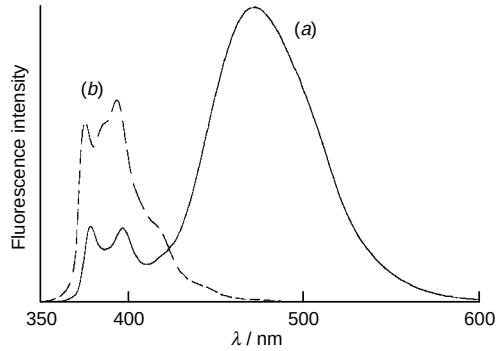

Fig. 2 Fluorescence spectra of the isomer (first fraction) of **2** and pyrene in $CHCl_3$ at 25 °C: (*a*) [**2**] = 3.9 μmol dm^{-3}, (*b*) [pyrene] = 3.9 μmol dm^{-3}

chiral guests were too small to evaluate the chiral discriminating ability of **2**.

To the best of our knowledge, compound **2** is the first example of a tri-*O*-alkylated fluorescent chiral calix[4]arene (ABBH type). So far, $Ba(OH)_2$ and BaO have been the only bases that stop the *O*-alkylation reaction at the tri-*O*-substituted stage.[7] Shinkai and co-workers have reported an inherently chiral calix[4]arene of the ABBH type *via* tri-*O*-alkylation of calix[4]arenes using $Ba(OH)_2$, where an excess amount of alkyl halide (*ca*. 10 equiv.) was used to accomplish alkylation.[4a,c] We found that a tri-*O*-alkylated chiral calix[4]arene **2** with a cone conformation could be easily prepared by a stoichiometric reaction with **1** and pyren-1-ylmethyl iodoacetate in the presence of K_2CO_3. Since chiral calix[4]arene **2** has a phenolic OH group, further modifications of **2** can be easily carried out. Applications for chiral calix[4]arene **2** are the subject of ongoing investigation in our laboratory.

This work was supported in part by a Grant-in-Aid from the Ministry of Education, Culture, and Science, Japan. We thank Professor M. Takasugi for his kind offer of the chiral-packed column.

Notes and References

† E-mail: jin@imdes.hokudai.ac.jp

‡ Compound **1** was synthesized by refluxing *p-tert*-butylcalix[4]arene (1 g, 1.5 mmol) and ethyl bromoacetate (171 μl, 1.5 mmol) in the presence of K_2CO_3 (0.213 g, 1.5 mmol) in anhydrous THF for 15 h.

§ *Selected data* for **2**: $\delta_H(CDCl_3)$ 0.820, 0.823, 1.27, 1.29 (s, 4 × 18 H, CMe_3), 1.10 (t, 3 H, OCH_2CH_3), 4.08 (m, 2 H, OCH_2CH_3), 4.08 (m, 2 H, OCH_2CH_3), 3.05, 3.17, 3.18, 3.19, 4.22, 4.31, 4.88, 4.89, (d, 2 H × 8, $ArCH_2Ar$), 4.43, 4.69 (dd, 2 H, OCH_2CO), 4.49, 4.56 (dd, 2 H, OCH_2CO), 5.19, 5.20 (s, 2 × 1 H, OCH_2CO), 5.68, 5.69 (s, 2 × 1 H, pyrene-CH_2), 5.75 (s, 2 H, pyrene-CH_2), 6.48–7.06 (m, 8 H, ArH), 6.64 (s, 1 H, ArOH), 7.83–8.13 (m, 18 H, pyrene); *m/z* (FD-MS) 1278 (M^+).

1 For reviews on calixarenes, see: C. D Gutshe, *Calixarenes*, The Royal Society of Chemistry, Cambridge, England, 1989; *Calixarenes: A Versatile Class of Macrocyclic Compounds*, ed. V. Böhmer and J. Vincens, Kluwer, Dordrecht, 1991.

2 K. Araki, K. Inada and S. Shinkai, *Angew. Chem., Int. Ed. Engl.*, 1996, **35**, 72; Y. Kubo, S. Maeda, S. Tokita and M. Kubo, *Nature*, 1996, **382**, 522.

3 S. Shinkai, T. Arimura, H. Saitoh and O. Manabe, *J. Chem. Soc., Chem. Commun*., 1987, 1495; T. Arimura, S. Edamitsu, S. Sinkai, O. Manabe, T. Muramatsu and M. Tashiro, *Chem. Lett.*, 1987, 2269; C. D. Gutshe and K. C. Nam, *J. Am. Chem. Soc.*, 1988, **110**, 6153; T. Arimura, H. Kuwabata, M. Matsuda, T. Muramatsu, H. Saitoh, K. Fujio, O. Manabe and S. Shinkai, *J. Org. Chem.*, 1991, **56**, 301; A. Marra, M.-C. Scherrmann, A. Dondoni, A Casnati, P. Minari and R. Ungaro, *Angew. Chem.*, 1994, **106**, 2533; *Angew. Chem., Int. Ed. Eng.*, 1994, **33**, 2479; P. Nari, A. Bottino, C. Geraci and M. Piattelli, *Tetrahedron: Asymmetry*, 1996, **7**, 17.

4 (*a*) K. Iwamoto, A. Yanagi, T. Arimura, T. Matsuda and S. Shinkai, *Chem. Lett.*, 1990, 1901; (*b*) S. Pappalardo, S. Caccamese and L. Giunta, *Tetrahedron. Lett.*, 1991, **32**, 7747; (*c*) K. Iwamoto, H. Shimizu, K. Araki and S. Shinkai, *J. Am. Chem. Soc.*, 1993, **115**, 3997; (*d*) G. Ferguson, J. F. Gallagher, L. Glunta, P. Neri and S. Pappalardo, *J. Org. Chem.*, 1994, **59**, 42; (*e*) S. Pappalardo, G. Ferguson, P. Neri and C. Rocco, *J. Org. Chem.*, 1995, **60**, 4576.

5 (*a*) H. Casabianca, J. Royer, A. Satrallah, A. Taty-C and J. Vicens, *Tetrahedron Lett.*, 1987, **28**, 6595; (*b*) S. Shinkai, T. Arimura, H. Kuwabata, H. Murakami, K. Araki, K. Iwamoto and T. Matsuda, *J. Chem. Soc., Chem. Commun.*, 1990, 1734; (*c*) S. Shinkai, T. Arimura, H. Kuwabata, H. Murakami and K. Iwamoto, *J. Chem. Soc., Perkin Trans. 1*, 1991, 2429; (*d*) P. A. Reddy and C. D. Gutshe, *J. Org. Chem.*, 1993, **58**, 3245; (*e*) G. D. Andreetti, V. Böhmer, J. G. Jordan, M. Tabatabai, F. Ugozzoli, W. Vogt and A. Wolff, *J. Org. Chem.*, 1993, **58**, 4023; (*f*) W. Verboom, P. J. Bodewes, G. van Essen, P. Timmerman, G. J. Van Hummel, S. Harkema and D. N. Reinhouldt, *Tetrahedron*, 1995, **51**, 499; (*g*) A. Ikeda, M. Yoshimura, P. Lhotak and S. Shinkai, *J. Chem. Soc., Perkin Trans. 1*, 1996, 1945.

6 W. R. Ware, *Time-Resolved Fluorescence Spectroscopy in Biochemistry*, ed. R. B. Cundall and R. E. Dale, Plenum, New York, 1983, p. 341; T. Jin, K. Ichikawa and T. Koyama, *J. Chem. Soc., Chem, Commun.*, 1992, 499.

7 C. D. Gutsche, B Dhawam, J. A. Levine, K. Hyun and L. J. Bauer, *Tetrahedron*, 1983, **39**, 409; K. Iwamoto, K. Araki and S. Shinkai, *Terahedron*, 1991, **47**, 4325.

Received in Cambridge, UK, 12th March 1998; 8/01995I

Reaction of triphenylbismuthonium 2-oxoalkylides with benzils. A novel one-pot conversion of symmetrical 1,2-diketones into *O*-aroyl enolates of unsymmetrical 1,3-diketones

M. Mizanur Rahman, Yoshihiro Matano and Hitomi Suzuki*†

Department of Chemistry, Graduate School of Science, Kyoto University, Sakyo-ku, Kyoto 606-8224, Japan

Triphenylbismuthonium 2-oxoalkylide 1, generated *in situ* from the corresponding onium salt 2 and base in THF at low temperatures, reacts with benzils 3 to give *O*-aroyl enolates of unsymmetrical 1,3-diketones 4 in moderate to good yields.

Ylide chemistry in carbon–carbon bond forming reactions has long been an active area of organic synthesis. However, in contrast to the extensive studies and general utility of phosphonium, arsonium and stibonium ylides,[1] little attention has been paid to the bismuthonium ylides.[2,3] Recently, we have found that triphenylbismuthonium 2-oxoalkylides **1** easily couple with aldehydes and *N*-sulfonylaldimines to give α,β-epoxy ketones and α,β-aziridino ketones, respectively.[4,5] This reaction mode is only observed for bismuth among all the group 15 elements; phosphonium, arsonium and stibonium 2-oxoalkylides are known to undergo Wittig-type reactions with these substrates.[1] Although ylides **1** do not react with simple ketones or esters, they readily couple with α-dicarbonyl compounds such as ethyl pyruvate and *ortho*-quinones, giving the epoxides or tropones depending on the structure of the substrates employed.[6] Here we report an unexpected result from the reaction of triphenylbismuthonium 2-oxoalkylides **1** with benzils **3**, where *O*-aroyl enolates of unsymmetrical 1,3-diketones **4** are formed *via* the carbon-to-oxygen migration of the aroyl moiety.

Treatment of benzil **3** with 1 equiv. of triphenylbismuthonium 2-oxoalkylide **1**, generated *in situ* from the corresponding onium salt **2** and a base in THF at low temperatures, readily gave an intimate *E*/*Z*-mixture of *O*-aroyl enolates **4** and triphenylbismuthane **5** (Scheme 1).‡ The reaction conditions were optimized using onium salt **2a** and 4,4′-dimethylbenzil **3a** (Table 1). Regardless of the order of adding the base and the substrate, enolates **4a** were obtained in similar yield (entries 1 and 2). Among several bases examined, KOBu^t gave the best results (entries 1–6). As for the solvent, a mixed solvent system THF–CH_2Cl_2 (1 : 1) gave better yields than THF alone, probably because of the improved solubility of **2a** in the former solvent (entries 1, 3, 8 *versus* 5, 6, 9). The stereoselectivity of the reaction was low, the *E*/*Z* isomeric ratio being around 4 : 6. Benzil **3b**, 4,4′-difluorobenzil **3c** and 4,4′-dichlorobenzil **3d** all underwent similar coupling reactions to yield the corresponding enolates **4b**–**d** and bismuthane **5**, respectively (entries 7–10). In contrast, 4,4′-dimethoxybenzil **3e** reacted with **2a** in the presence of KOBu^t to give enolate **4e** and triketone **6** in 12 and 10% yields, respectively (entry 11). The reaction between **3c** and ylide **1b**, generated *in situ* from **2b** and KOBu^t, afforded the corresponding enolate **4f** (entry 12).

O-Aroyl enolates **4** obtained were characterized by NMR, IR and mass spectroscopy as well as by elemental analysis.§ The ^{1}H NMR spectra of **4a**–**d** showed the olefinic protons of the *E*- and *Z*-isomers at around δ 6.7–6.9 (in $CDCl_3$) as two singlet peaks. In the IR spectra of **4a**–**d**, two strong carbonyl

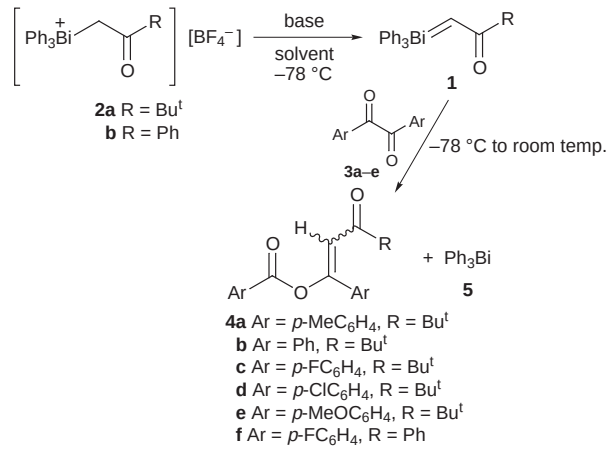

Scheme 1

Table 1 Reaction of bismuthonium salts **1** with benzils **3** in the presence of a base[a]

Entry	Salt	Benzil	Base	Solvent	Enolate	Yield (%)[b]	*E* : *Z* ratio
1	**2a**	**3a**	KOBu^t	THF	**4a**	53 (86)	42 : 58
2[c]	**2a**	**3a**	KOBu^t	THF	**4a**	55 (85)	42 : 58
3	**2a**	**3a**	$NaN(SiMe_3)_2$	THF	**4a**	43 (67)	41 : 59
4	**2a**	**3a**	$KN(SiMe_3)_2$	THF	**4a**	44 (69)	40 : 60
5	**2a**	**3a**	KOBu^t	THF–CH_2Cl_2	**4a**	65 (90)	42 : 58
6	**2a**	**3a**	$NaN(SiMe_3)_2$	THF–CH_2Cl_2	**4a**	47 (72)	41 : 59
7	**2a**	**3b**	KOBu^t	THF	**4b**	58 (88)	39 : 61
8	**2a**	**3c**	KOBu^t	THF	**4c**	55 (78)	50 : 50
9	**2a**	**3c**	KOBu^t	THF–CH_2Cl_2	**4c**	67 (91)	51 : 49
10	**2a**	**3d**	KOBu^t	THF	**4d**	63 (88)	45 : 55
11	**2a**	**3e**	KOBu^t	THF	**4e**	12 (42)[d]	40 : 60
12	**2b**	**3c**	KOBu^t	THF	**4f**	20 (80)	N.d.[e]

[a] All reactions were carried out using an equimolar amount of reagents. A 1 : 1 mixture of THF–CH_2Cl_2 was used in entries 5, 6 and 9. In every case, bismuthane **5** was recovered in good yield. [b] Isolated compounds. Numerals in parentheses refer to the conversion yields based on unrecovered benzil. [c] KOBu^t was added to a solution of **2a** and **3a** in THF at −78 °C. [d] Triketone **6** was obtained in 10% isolated yield. [e] Not determined.

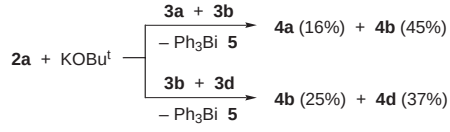

Scheme 2 *Reagents and conditions*: **2a** (1.0 mmol), **3a,b,d** (1.0 mmol), KOBu^t (1.0 mmol), THF (15 cm^3), −78 °C to room temp.

absorptions were observed at 1746–1760 and 1672–1684 cm^{-1}; the former was assigned to the ester carbonyl and the latter to the keto carbonyl stretching bands, respectively. These structural assignments were further confirmed by an X-ray diffraction analysis of the *Z* isomer of **4a**.¶

In order to shed light on the reaction pathway, competitive reactions were carried out for the pairs **3a**/**3b** and **3b**/**3d** (Scheme 2). As expected, the more electron-deficient benzil was more reactive toward ylide **1a**, suggesting that the nucleophilic attack of the ylide carbanion on the carbonyl function in **3** is the rate-determining stage of the present coupling reaction.

The 1,2-diketone structure seems to be indispensable for the present new type of 1,2-carbonyl transposition; ethyl benzoylformate **7**, which is an α-keto ester, reacted with ylide **1a** to give an epoxide **8** (Scheme 3). A plausible reaction mechanism is depicted in Scheme 4, where the negatively charged oxygen atom of the initial adduct **9** attacks the neighboring carbonyl carbon atom to form intermediate **10**, in which the carbon-to-oxygen migration of the aroyl group takes place under simultaneous elimination of the triphenylbismuthonio group as bismuthane **5**.‖ This interpretation is supported by the following findings. The Darzen reaction between α-bromopinacolone and benzil resulted in the formation of a mixture of *cis/trans*-2-aroyl-2-aryl-3-pivaloyl oxiranes **11**, which did not isomerize to enolate **4** under the present conditions. Moreover, on treatment with KOBu^t, triketone **6** derived from the reaction of **1a** and **3e** could not be converted to **4e**. Therefore, the reactivity inherent in **1** stands in marked contrast to that of its phosphorus counterpart, which is shown to undergo the Wittig reaction with benzil to afford α,β-unsaturated ketones.[7]

Homologation of 1,2-diketones to 1,3-diketones usually requires a multistep sequence. However, 1,2-diketones **3** can be directly transformed into unsymmetrical 1,3-diketones in the form of enolates **4** using triphenylbismuthonium 2-oxoalkylides **1** as the *in situ* reagent. This type of carbon–carbon bond construction based on 1,2-carbonyl migration is unprecedented in ylide chemistry[8] and is a potential new method in organic synthesis. Further investigation of this aspect of the chemistry of bismuthonium ylides is now in progress.

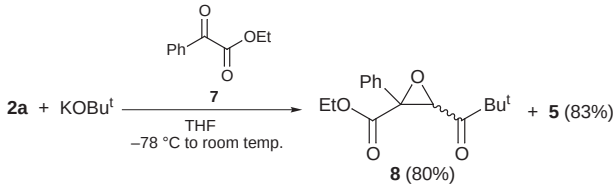

Scheme 3

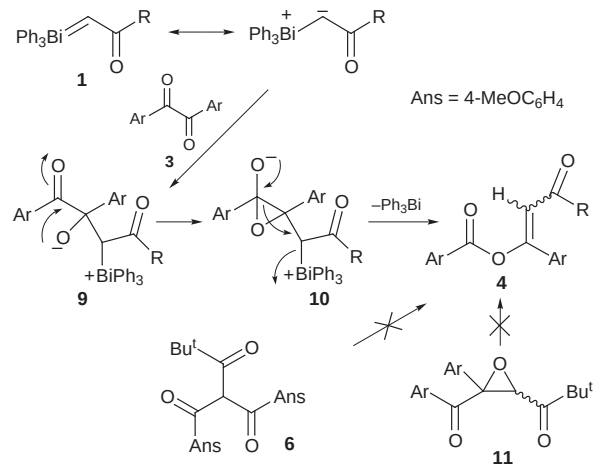

Scheme 4

Notes and References

† E-mail: suzuki@kuchem.kyoto-u.ac.jp

‡ *Typical procedure*: To a stirred suspension of onium salt **1a** (313 mg, 0.50 mmol) in THF (8 cm^3) was added KOBu^t (56 mg, 0.50 mmol) at −78 °C. After 10 min, 4,4′-dimethylbenzil **3a** (119 mg, 0.50 mmol) was added and the resulting mixture was allowed gradually to warm to room temperature. Evaporation of the solvent under reduced pressure gave an oily residue, which was chromatographed on silica gel (hexane–EtOAc) triphenylbismuthane **5** (185 mg, 84%), recovered **3a** (47 mg, 40%) and an intimate mixture of (*E*/*Z*)-enolates **4a** (90 mg, 53%; *E* : Z = 42 : 58) in this order. The *E*/*Z* isomer ratio was estimated by ^{1}H NMR integration of the olefinic protons. The equation proposed by Pascual *et al*.[10] was used for stereochemical assignment of compounds **4**, where the olefinic proton peak appearing at high field was always assigned to the *E*- isomer.

§ *Selected data* for **4a**: $\delta_H(CDCl_3)$ (*E*-isomer) 1.29 (9 H, s), 2.36 (3 H, s), 2.42 (3 H, s), 6.74 (1 H, s), 7.19 (d, 2 H, *J* 8), 7.29 (d, 2H, *J* 7), 7.78 (d, 2 H, *J* 8), 8.0 (d, 2 H, *J* 8); (*Z*-isomer) 1.20 (9 H, s), 2.36 (3 H, s), 2.42 (3 H, s), 6.90 (1 H, s), 7.19 (d, 2 H, *J* 8), 7.29 (d, 2 H, *J* 7), 7.55 (d, 2 H, *J* 8), 8.09 (d, 2 H, *J* 8); ν_{max} (KBr)/cm^{-1} 1746 (C=O), 1684 (C=O); *m*/*z* (EI) 279 (M$^+$ − 57). (Found: C, 78.43; H, 7.31. $C_{22}H_{24}O_3$ requires C, 78.54; H, 7.19%). For **6**: $\delta_H(CDCl_3)$ 1.24 (9 H, s), 3.85 (6 H, s), 6.60 (1 H, s), 6.91 (d, 4 H, *J* 9), 7.91 (d, 4 H, *J* 9); ν_{max}(KBr)/cm^{-1} 1707 (C=O), 1670 (C=O); *m*/*z* (EI) 368 (M$^+$) (Found: C, 72.37; H, 5.35. Requires C, 71.72; H, 6.57%).

¶ *Crystal data* for **4a**: $C_{22}H_{24}O_3$, *M* = 336.43, monoclinic, $P2_1/n$ (no. 14), *a* = 5.83(4), *b* = 17.42(3), *c* = 18.44(3) Å, β = 91.6(3)°, *V* = 1872(12) Å^3, *Z* = 4, D_c = 1.19 g cm^{-3}, μ(Cu-Kα) = 6.2 cm^{-1}, 3233 reflections measured, 2914 unique reflections, R_{int} = 0.013, *R* = 0.046, R_w = 0.076. CCDC 182/846.

‖ 2-Hydroxyacenaphthenone and acenaphthenequinone are known to undergo formally similar carbon-to-oxygen migration of the acyl group in the presence of a base (ref. 9).

1 For recent reviews of P, As and Sb ylides, see: A. W. Johnson, *Ylides and Imines of Phosphorus*, Wiley, Chichester, 1993; D. Lloyd, I. Gosney and R. A. Ormiston, *Chem. Soc. Rev*., 1987, **16**, 45; Y.-Z. Huang, *Acc. Chem. Res.*, 1992, **25**, 182; D, Lloyd and I. Gosney, *The Chemistry of Organic Arsenic, Antimony and Bismuth Compounds*, ed. S. Patai, Wiley, New York, l994, ch. 16, p. 657; W. I. Cross, S. M. Godfrey, C. A. McAuliffe, A. G. Mackie and R. G. Pritchard, *Chemistry of Arsenic, Antimony and Bismuth*, ed. N. C. Norman, Blackie Academic, London, 1998, ch. 5, p. 207.

2 For bismuthonium ylides, see: D. Loyd and M. I. C. Singer, *J. Chem. Soc., Chem. Commun.*, 1967, 1042; D. H. R. Barton, J.-C. Blazejewski, B. Charpiot, J.-P. Finet, W. B. Motherwell, M. T. B. Papoula and S. P. Stanforth, *J. Chem. Soc., Perkin Trans. 1*, 1985, 2667; N. V. Kirij, S. V. Pasenok, Y. L. Yagupolskii, D. Naumann and W. Tyrra, *J. Fluorine Chem.*, 1994, **66**, 75; H. Suzuki, T. Murafuji and T. Ogawa, *Chem. Lett.*, 1988, 847; Y. Matano and H. Suzuki, *Bull. Chem. Soc. Jpn.*, 1996, **69**, 2673 and references cited therein.

3 For C–C bond formation based on stabilized bismuthonium ylides, see: T. Ogawa, T. Murafuji and H. Suzuki, *Chem. Lett.*, 1989, 849; T. Ogawa, T. Murafuji and H. Suzuki, *J. Chem. Soc., Chem. Commun.*, 1989, 1749; T. Ogawa, T. Murafuji, K. Iwata and H. Suzuki, *Chem. Lett.*, 1989, 325.

4 Y. Matano, *J. Chem. Soc., Perkin Trans. 1*, 1994, 2703.

5 Y. Matano, M. Yoshimune and H. Suzuki, *J. Org. Chem.*, 1995, **60**, 4663.

6 Y. Matano and H. Suzuki, *Chem. Commun.*, 1996, 2697.

7 J. Parrick, *Can. J. Chem.*, 1964, **42**, 190.

8 For carbonyl transposition, see: V. V. Kane, V. Singh, A. Martin and D. L. Doyle, *Tetrahedron*, 1983, **39**, 345; D. G. Moris, *Chem. Soc. Rev.*, 1982, **11**, 397.

9 A. R. Miller, *J. Org. Chem.*, 1979, **44**, 1931; H. Bader and Y. H. Chiang, *Synthesis*, 1976, 249.

10 C. Pascual, J. Meier and W. Simon, *Helv. Chim. Acta*, 1966, **49**, 164.

Received in Cambridge, UK, 9th March 1998; 8/01879K

Highly active, stable, catalysts for the Heck reaction; further suggestions on the mechanism

Bernard L. Shaw,*† Sarath D. Perera and Elaine A. Staley

School of Chemistry, University of Leeds, Leeds, UK LS2 9JT

Tri(1-naphthyl)phosphine gives palladacycles which are very active catalysts for Heck reactions; mechanisms based on a Pd^{II}–Pd^{IV} cycle are proposed and a new, very efficient method of separating the product from the catalyst has been devised, which involves treatment with cyanide ion.

The Heck alkenation reaction [eqn. (1)] is very important in

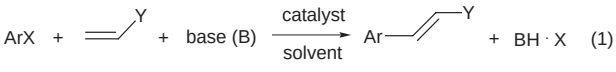

organic synthesis with many applications. Frequently, a Heck catalyst has been generated *in situ* from $Pd(OAc)_2$ and a tertiary phosphine, L = PPh_3 or $P(C_6H_4Me\text{-}o)_3$. This is assumed to give some PdL_2, which forms part of a catalytic cycle involving Pd^0–Pd^{II}. Recently, highly efficient catalysts using cyclopalladated $P(C_6H_4Me\text{-}o)_3$ have been reported.[1a,b] One of us has suggested a quite new mechanism for such catalyses with reversible nucleophilic attack on Pd^{II}-coordinated alkene being a key step in the promotion of oxidative addition of ArX, in a Pd^{II}–Pd^{IV} catalytic cycle.[2] Previously, as part of an extensive study on the effects of steric compression, we found that 1-naphthylphosphines could give particularly stable metallacycles,[3] with metallation in the 8- or *peri*-position. We have now found tri(1-naphthyl)phosphine (PNp_3) cyclopalladates to give very stable palladacycles, which are excellent catalysts for Heck reactions.

On heating PNp_3 with $Pd(OAc)_2$ in toluene the metallacycle **1a** was obtained. **1a** showed broad NMR spectra at 25 °C, probably due to exchange at the bridging acetates; the spectra sharpened at −60 °C. Broad NMR spectra were similarly found for the palladacycles prepared from $Pd(OAc)_2$ and $P(C_6H_4Me\text{-}o)_3$.[1a] We treated **1a** with acetylacetone and converted it into the mononuclear acetylacetonate **2a** which showed sharp NMR spectra at 25 °C. **2a** can be more conveniently made by treating $[Pd(acac)_2]$ with PNp_3 in hot benzene. **2b** was similarly prepared from PNp_3 and $[Pd(hfacac)_2]$. We have similarly cyclopalladated $P(C_6H_4Me\text{-}o)_3$ to give **3a** and **3b**. All these new palladacycles have been fully characterised.

The palladacycles **1a**, **2a** and **2b** are excellent catalysts for Heck reactions. Some of our catalytic results are summarised in Table 1. Thus treatment of iodobenzene with styrene at 120 °C for 5 days using 10^{-4} mol% catalyst **2b** gave stilbene in 65% isolated yield, *i.e.* a turn over number (TON) of 650 000. No palladium metal was formed and the final reaction solution was extremely pale yellow. Treatment of iodobenzene with methyl acrylate at 95 °C for 13 days using 5×10^{-5} mol% of catalyst **2b** gave methyl cinnamate with a TON of 1 120 000, the highest turnover number yet reported for a Heck reaction; with 10^{-3} mol% catalyst reacting at 95 °C for 5 d we isolated methyl cinnamate in 88% yield with a TON of 88 000. Herrmann and Beller's catalysts gave TONs of up to 100 000, or in the presence of much NBu_4Br as promoter, 1 000 000; NBu_4Br is expensive and we tried to achieve high TONs without it. 4-Bromoacetophenone reacted with styrene at 125 °C over 7 h to give 4-acetylstilbene in 94% isolated yield using catalyst **1a** (entry 5); similarly with 4-bromocyanobenzene (entry 6). Bromobenzene, a relatively inactive bromide, gave a 77% yield of stilbene after reacting with styrene at 115 °C for 30 h using catalyst **2b** (entry 7). In entry 8 we used sodium acetate as the base and the acetylacetonate catalyst **2a**. Examples of catalyses using **3a** and **3b** are also given. The entries given in Table 1 all refer to isolated yields of crystalline products. Apart from entry 3, where column chromatography was used, and entry 1, the products were separated from the palladium catalyst using an extraction process that we have devised. This depends on the enormous affinity of palladium for cyanide ion: the formation constant for $[Pd(CN)_4]^{2-}$ is *ca.* 10^{52}.[4] The extraction process works very well for the examples given in Table 1.‡

We suggest a mechanism for the Heck reactions catalysed by **1a**, **2a** or **2b** which is analogous to that proposed by one of us[2] for Heck reactions. The mechanism involves Pd^{II}–Pd^{IV}, with the alkene coordinating to the Pd^{II} being reversibly attacked by a nucleophile, such as OAc^-, $acac^-$, OH^-, Br^- or I^-, to give a negatively charged alkyl species **5** in which the Pd^{II} is electron rich and oxidatively adds ArX. Loss of nucleophile regenerates the coordinated alkene and migration of Ar from Pd^{IV} to coordinated alkene followed by β-hydrogen migration, gives the product ArCH=CHY and removal of HBr by the base regenerates the Pd^{II} catalyst of type **1**, (see Scheme 1).

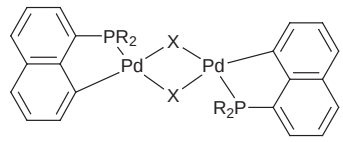

1a R = naphthyl, X = OAc
1b R = naphthyl, X = I
1c R = naphthyl, X = Br

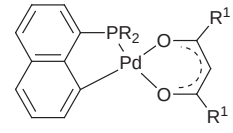

2a R = naphthyl, R^1 = Me
2b R = naphthyl, R^1 = CF_3

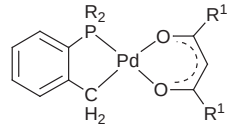

3a R = *o*-tolyl, R^1 = Me
3b R = *o*-tolyl, R^1 = CF_3

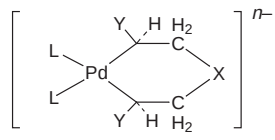

10a X = OC(=O)O
10b X = O

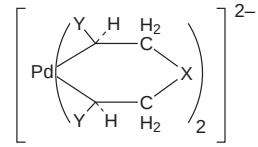

11a X = OC(=O)O
11b X = O

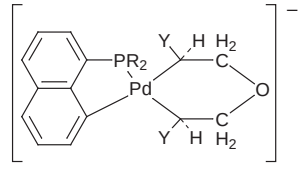

12

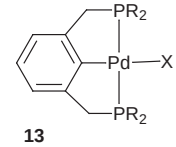

13

Table 1 Selected results of the Heck reactions catalysed by palladium chelates[a]

Entry	Aryl halide[b]	Alkene	ArX/alkene mmol/mmol	Catalyst/mmol	Time (T/°C)	Yield (%) (TON)
1	PhI	sty	10/12.5	**2b** (10^{-5})	5 d (120)	65 (650 000)
2	PhI	sty	10/12.5	**2b** (10^{-3})	17 h (95)	78 (7800)
3	PhI	mac	10/10	**2b** (5×10^{-6})	13 d (95)	56 (1 120 000)
4	PhI	mac	10/10	**2b** (10^{-4})	5 d (95)	88 (88 000)
5	bab	sty	2/2.6	**1a** (5.2×10^{-3})	7 h (125)	94 (180)
6	bcb	sty	2/3	**1a** (5.2×10^{-3})	7 h (125)	85 (165)
7	PhBr	sty	10/12.5	**2b** (10^{-2})	30 h (115)	77 (770)
8	PhI	sty	2/2.2	**2a** (10^{-2})	24 h (95)	56 (115)
9	PhI	sty	2/3	**3a** (7×10^{-3})	8 h (95)	83 (240)
10	PhI	sty	10/12.5	**3b** (10^{-2})	4 h (95)	90 (900)
11	PhI	mac	2/2.2	**2a** (1.9×10^{-3})	24 h (95)	72 (760)

[a] Except for entry 8, an equivalent amount of tri-(*n*-butyl)amine to the aryl halide was used as base; in entry 8, 4 mmol of sodium acetate was used. The catalyst was dissolved in dmf, *e.g.* 1 cm³ in entry 1. Experimental details available upon request from the authors. [b] bab = 4-bromoacetylbenzene, bcb = 4-bromocyanobenzene, sty = styrene, mac = methyl acrylate.

In the so-called exceptionally mild 'Jeffrey' conditions for effecting a Heck reaction, *viz* [$Pd(OAc)_2$], an aryl iodide and an alkene such as CH_2=CHY reacting in dmf at *ca.* 30 °C in the presence of sodium hydrogen carbonate or potassium carbonate, with much added NBu_4Cl as phase-transfer catalyst, very good yields are obtained. One of us suggested that the remarkable ability of aryl iodide to oxidatively add to Pd^{II} at such as low temperature arises because HCO_3^- or CO_3^{2-} attacks two coordinated alkenes to give chelated dialkyl species **10a** and **11a**, X = CO_3.[2] **11a** is an 'ate' complex with an extremely electron-rich palladium. We now suggest that under these conditions the bridging group X could be an oxygen atom, formed from water + base attacking two coordinated alkenes, *i.e.* **10b** and **11b**. Water is known to promote Heck reactions including under Jeffrey conditions.[5] We suggest that one function of the large cations such as NBu_4^+ is to help stabilise in solution large anions such as of type **10** or **11** and analogous species from palladacycles. Because of the beneficial effect of water we deliberately did not dry our reagents nor the dmf solvent (≥0.1% water). Electron rich 'ate' complexes of iron(II) or cobalt(II) *e.g.* $[FeMe_4]^{2-}$ or $[CoMe_4]^{2-}$, react with a series of vinyl bromides, such as β-bromostyrene, even at −78 °C, undergoing oxidative addition/reductive elimination:[6] 'ate' complexes of Pd^{II}, Ni^{II} and Pt^{IV} are known. We also suggest that attack on two-coordinated alkenes by H_2O + base could give **12**, as an electron rich Pd^{II} complex which oxidatively adds ArX and which could participate in a catalytic cycle similar to that shown in Scheme 1. Recently, the very stable and sterically hindered chelates of type **13** have been shown to be very stable catalysts for Heck reactions giving very high TON but requiring high reaction temperatures (140 °C) even with iodides.[7] We suggest a mechanism similar to that shown in Scheme 1 for catalyses by **13**.

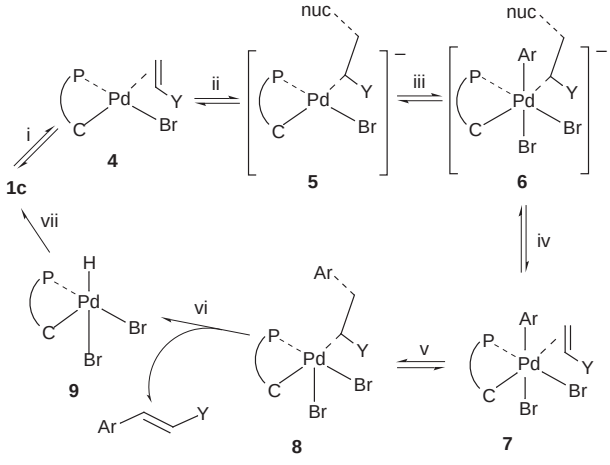

Scheme 1 Proposed mechanism for the Alkenation reaction using a palladacycle of type **1** or **2** and an aryl bromide. After several cycles the bromide **1c** will be formed and is used in the Scheme. i, CH_2=CHY; ii, reversible attack by nucleophile (OAc^-, Br^-, $acac^-$ or OH^-); attack is shown on the terminal carbon atom but it could be on the internal carbon; iii, oxidative addition of ArBr; iv, loss of nucleophile; v, migration of Ar to terminal carbon; vi, β-hydrogen elimination; vii, removal of HBr by base.

Notes and References

† E-mail: b.l.shaw@chem.leeds.ac.uk

‡ For entry 5 the reaction mixture was dissolved in CH_2Cl_2 (10 cm³) and the organic layer washed successively with water, with a solution of NaCN (2 mg) in water (5 cm³), with 2 M HCl, and finally with water; evaporation and crystallisation from MeOH gave the product;. similarly for the other entries. For syntheses involving methyl acrylate, diethyl ether was used in the work up. Preliminary work suggests that the treatment with NaCN gives a little PNp_3 but the main product seems to be a rapidly interconverting mixture of sodium salts of type $[Na^+]_n[Np_2PC_{10}H_6Pd(CN)_{n+1}]^{n-}$ which is not soluble in CH_2Cl_2 or Et_2O, is very soluble in MeOH and presumbably sufficiently soluble in dilute aqueous NaCN; very small quantities are involved, typically μg of Pd.

1 (*a*) W. A. Herrmann, C. Brossmer, C.-P. Reisinger, T. H. Riermeier, K. Öfele and M. Beller, *Chem. Eur. J.*, 1997, **3**, 1357; (*b*) M. Beller and T. H. Riermeier, *Eur. J. Inorg. Chem.*, 1998, **1**, 29.
2 B. L. Shaw, *New J. Chem.*, 1998, 77.
3 J. M. Duff and B. L. Shaw, *J. Chem. Soc., Dalton Trans.*, 1972, 2219.
4 M. T. Beck, *Pure Appl. Chem.*, 1987, **59**, 1703.
5 T. Jeffery, *Tetrahedron Lett.*, 1994, **35**, 3051 and references therein.
6 T. Kauffmann, B. Laarmann, D. Menges and G. Neiteler, *Chem. Ber.*, 1992, **125**, 163.
7 M. Ohff, A. Ohff, M. E. van der Boom and D. Milstein, *J. Am. Chem. Soc.*, 1997, **119**, 11 687.

Received in Cambridge, UK, 7th April 1998; 8/02642D

Synthesis and solid-state structure of $[K_3(thf)_2\{PH(Mes)\}_3]_\infty$ (Mes = 2,4,6-$Me_3C_6H_2$): the first potassium phosphanide with a polyhedral arrangement of K and P atoms

Christoph Frenzel, Peter Jörchel and Evamarie Hey-Hawkins*†

Institut für Anorganische Chemie der Universität Leipzig, Talstrasse 35, D-04103, Leipzig, Germany

KPH(Mes) (Mes = 2,4,6-$Me_3C_6H_2$), prepared from potassium and PH_2(Mes) in refluxing toluene, crystallises from thf–pentane as $[K_3(thf)_2\{PH(Mes)\}_3]_\infty$ 1, in which the basic structural feature is a chain of tetragonal pyramids of KP_5 units, which share common edges, and two additional K atoms located over two adjacent edges of one trigonal face of the pyramid.

While lithium phosphanides have been widely employed as phosphanide-transfer reagents,[1] their heavier congeners have remained largely unexplored. Furthermore, most structural studies have focused on the solid-state structures of lithium phosphanides,[2,3] and little is known about the structures of the heavier alkali metal analogues. A few examples of sodium,[3,4] potassium,[3a,5] and caesium phosphanides[4] have been reported, most of which, like the majority of lithium derivatives, exhibit dimeric M_2P_2 arrangements or polymeric one-dimensional ladders[5] consisting of alternating M–P and P–M steps. Lithium phosphanides also form one-dimensional polymeric zigzag or helical –M–P–M–P– chains.

In our studies on potential phosphinidene (PR) precursors, we are interested in the synthesis and solid-state structures of P–H functionalised alkali metal phosphanides, MPHR. We now report the synthesis and solid-state structure of $[K_3(thf)_2\{PH(Mes)\}_3]_\infty$ **1**.

When KPH(Mes)‡ is extracted with thf and the solution (10 ml) layered with pentane (10 ml), yellow crystals of $[K_3(thf)_2\{PH(Mes)\}_3]_\infty$ **1** are obtained on standing for two weeks at room temperature (yield of isolated product: 80%). **1** is insoluble in toluene or pentane and sparingly soluble in ether, but dissolves rapidly in thf. The proton-coupled ^{31}P NMR spectrum§ in thf exhibits a doublet at δ −141.6, which is shifted to low field relative to PH_2(Mes) (δ −153.9)[6] and Li(thf)$_2${PH(Mes)} (δ −163.4).[7]¶ The $^1J_{PH}$ coupling constant of 156 Hz is lower than those of PH_2(Mes) (207.3 Hz)[6] and Li(thf)$_2${PH(Mes)} (187 Hz).[7]

1 crystallises in the centrosymmetric monoclinic space group $P2_1/n$.‖ The asymmetric unit contains three types of potassium and phosphorus atoms. Potassium atom K(1) is surrounded in a tetragonal-pyramidal fashion by five P atoms, two of which [P(1A) and P(2A)] are generated by the 2_1 axis. Furthermore, the 2_1 axis generates a polymeric chain of edge-sharing tetragonal pyramids in which the apical P atoms alternately point upwards and downwards (Fig. 1). Potassium atom K(1) is almost coplanar with P(1), P(2), P(1A), P(2A) (deviation 0.08 Å), and the pyramidal structure is only slightly distorted, the P–K–P angles ranging from 88.28(4) to 92.32(4)°. The K–P distances range from 3.306(2) to 3.451(1) Å and are comparable to those in KPH(Mes*) [Mes* = 2,4,6-$Bu^t_3C_6H_2$, K–P 3.271(2), 3.181(2), 3.357(2) Å],[5] which, however, has an infinitely extended, centrosymmetric ladder structure, and the related compound [K(thf)$_2${P(Mes)(SiFBu$^t_2$)}]$_2$ [K–P 3.230(1) Å].[3a] Similar K–P distances are also found in [Cp*$_2$ZrP$_3$K(thf)$_{1.5}$] [Cp* = C_5Me_5, K–P 3.37(1)–3.61(1) Å],[8,9] [Cp$_2$ZrH{P(Mes*)}K(thf)$_2$]$_2$ [K–P 3.497(9), 3.67(1) Å],[9] a potassium phospholide [K–P 3.264(1), 3.256(1) Å],[10] and a phospholylsamarium complex [$(PC_4Me_4)_6Sm_2(KCl)_2$-$(C_6H_5Me)_3]_\infty$ [K–P 3.263(5), 3.383(5) Å].[11] In the solid-state compound KP, a polymeric helical chain of P atoms [$^1_\infty$ (P^-)] is surrounded by K atoms with short distances of 3.08–3.39 Å, and longer distances of 3.62–3.86 Å.[12]

The two remaining potassium atoms of **1**, K(2) and K(3), are located above the adjacent edges, P(3)–P(2A) and P(3)–P(1A), respectively, of a P_3 face of the tetragonal pyramid, with K–P distances in the expected range of 3.29–3.35 Å (Fig. 1). Both K atoms interact weakly with a third P atom [K(2)–P(1) 3.669(1), K(3)–P(2) 3.936(2) Å]. The coordination environment around the K(2) and K(3) atoms (Figs. 2 and 3) is completed by a disordered thf molecule and K–aryl interaction [η^3 and η^1

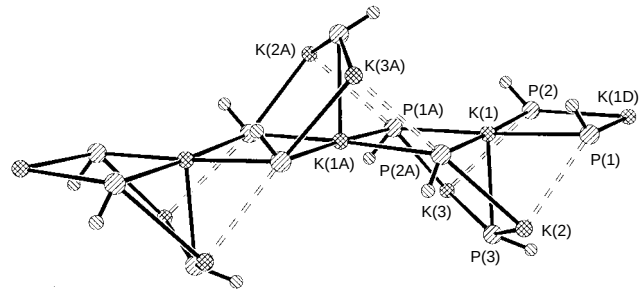

Fig. 1 Arrangement of the KP_5 fragment of **1** (SHELXTL PLUS; XP).[15] Only the K, P and H atoms (of P–H) are shown. Selected bond lengths (Å) and angles (°): K(1)–P(1) 3.368(1), K(1)–P(2) 3.397(1), K(1)–P(1A) 3.364(1), K(1)–P(2A) 3.451(1), K(1)–P(3) 3.306(2); P(1)–K(1)–P(2) 90.88(3), P(2)–K(1)–P(1A) 89.25(4), P(1A)–K(1)–P(2A) 91.46(3), P(2A)–K(1)–P(1) 88.28(4), P(1)–K(1)–P(1A) 177.25(3), P(2)–K(1)–P(2A) 177.23(3), P(1)–K(1)–P(3) 91.52(4), P(2)–K(1)–P(3) 90.34(4), P(1A)–K(1)–P(3) 91.23(4), P(2A)–K(1)–P(3) 92.32(4).

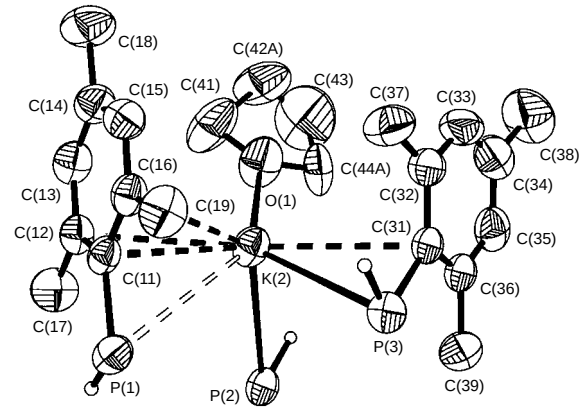

Fig. 2 Environment around K(2) (ORTEP, 50% probability, SHELXTL PLUS; XP).[15] Only one position of the disordered thf and the P–H hydrogen atoms are shown. Selected bond lengths (Å): K(2)–O(1) 2.654(3), K(2)–P(1) 3.669(1), K(2)–P(2A) 3.354(2), K(2)–P(3) 3.323(2), K(2)–C(31) 3.329(4), K(2)–C(12) 3.199(4), K(2)–C(11) 2.991(3), K(2)–C(16) 3.238(4).

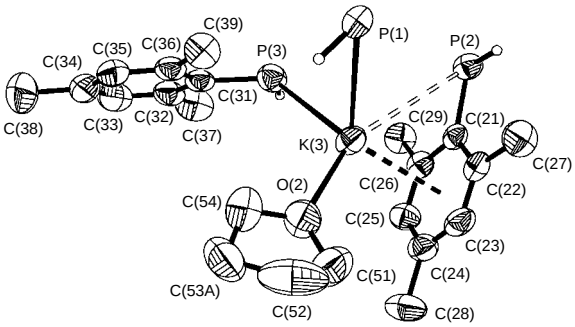

Fig. 3 Environment around K(3) (ORTEP, 50% probability, SHELXTL PLUS; XP).[15] Only one position of the disordered thf and the P–H hydrogen atoms are shown. Selected bond lengths (Å): K(3)–O(2) 2.666(3), K(3)–P(1A) 3.324(2), K(3)–P(2) 3.936(2), K(3)–P(3) 3.291(2), K(3)–C(21) 3.013(3), K(3)–C(22) 3.076(4), K(3)–C(23) 3.226(4), K(3)–C(24) 3.344(4), K(3)–C(25) 3.269(4), K(3)–C(26) 3.125(4).

coordination of the mesityl rings of P(1) and P(3) to K(2), and η^6 coordination of the mesityl ring of P(2) to K(3)] with K–C distances of 2.991(3)–3.344(4) Å. Similarly, K–aryl interaction was observed in KPH(Mes*) [η^3 coordination of Mes*, K–C 2.884(4)–3.197(4)], which is obtained solvent-free even on crystallisation from thf–toluene.[5]

In **1**, which was crystallised from thf–pentane, π interaction with the aryl rings is apparently preferred to coordination of additional thf molecules. Similarly, π coordination of arene ligands to potassium[11,13] and the heavier alkali metals[14] has often been reported in the literature. The caesium phosphanide $[Cs(thf)_{0.5}P(SiPr^i_3)\{Si(F)(Is)_2\}]_\infty$ (Is = 2,4,6-$Pr^i_3C_6H_2$) also exhibits η^3 and η^6 coordination of the aryl rings of the Is substituents to Cs.[4]

The alkali metal phosphanide presented here is the first example of a potassium phosphanide with a polyhedral arrangement of K and P atoms, in contrast to the corresponding lithium phosphanide, $[Li(thf)_2\{PH(Mes)\}]_\infty$,[7] which has a helical one-dimensional Li–P–Li–P arrangement. More information on the structural diversity of alkali metal phosphanides will be needed before the factors that determine the structural arrangement in the solid state are fully understood.

We gratefully acknowledge support from the Deutsche Forschungsgemeinschaft and the Fonds der Chemischen Industrie; the company Chemetall provided a generous donation of potassium metal.

Notes and References

† E-mail: hey@server1.rz.uni-leipzig.de

‡ The preparations were carried out under argon by Schlenk techniques. KPH(Mes) was prepared from K (1.00 g, 25.5 mmol) and excess $PH_2(Mes)$[6] (4.00 ml) in refluxing toluene (50 ml) (2 days), yield: quantitative.

§ In thf, one drop C_6D_6 for lock, 25 °C, Bruker DRX Avance 400, 161.9 MHz. ^{1}H NMR (400 MHz, [$^2H_8$]thf, 25 °C): δ 6.38 (s, 2 H, 2,4,6-$Me_3C_6H_2$), 2.11 (s, 6 H, *o*-Me in 2,4,6-$Me_3C_6H_2$), 2.01 (s, 3 H, *p*-Me in 2,4,6-$Me_3C_6H_2$), 1.88 (d, 1 H, P–H, $^1J_{PH}$ 156 Hz). ^{13}C NMR (100.6 MHz, [$^2H_8$]thf, 25 °C): δ 20.8 (*p*-CH_3 in 2,4,6-$Me_3C_6H_2$), 24.9 (*o*-CH_3 in 2,4,6-$Me_3C_6H_2$), 122.26 (*p*-C in 2,4,6-$Me_3C_6H_2$), 127.00 (*m*-C in 2,4,6-$Me_3C_6H_2$), 134.22 (*o*-C in 2,4,6-$Me_3C_6H_2$), 155.8 (br, *ipso*-C in 2,4,6-$Me_3C_6H_2$, no P–C coupling observed). IR for **1** (KBr) cm^{-1}: 2316, 2293m (P–H). Mp 189–207 °C.

‖ *Crystal data* for $[K_3(thf)_2\{PH(Mes)\}_3]_\infty$: $C_{35}H_{52}K_3P_3$, M = 714.98, yellow crystals, 0.45 × 0.20 × 0.15 mm, monoclinic, space group $P2_1/n$ (no. 14), T = 213(2) K, a = 16.511(3), b = 9.692(2), c = 25.337(5) Å, β = 97.72(3), U = 4017.9(14) Å^3, Z = 4, D_c = 1.182 Mg m^{-3}, F(000) = 1520, μ(Mo-Kα) = 0.486 mm^{-1}, 16 463 reflections collected with 1.4 < θ < 26.2°; of these 6909 were independent; 483 parameters, refinements converge to $R1$ = 0.0611, $wR2$ = 0.1175 [for reflections with $I > 2\sigma(I)$], $R1$ = 0.0818, $wR2$ = 0.1275 (all data). Data (Mo-Kα = 0.710 73 Å) were collected with a Siemens CCD (SMART). All observed reflections (2θ range: 2.8–52.4°) were used for determination of the unit cell parameters. The structure was solved by direct methods (SHELXTL PLUS[15]) and subsequent difference Fourier syntheses and refined by full-matrix least squares on F^2 (SHELXTL PLUS[15]); thf treated as disordered groups in two positions [C(42), C(44), A : B = 43 : 57; C(53), A : B = 73 : 27%]. K, P, O and C atoms anisotropic, H atoms of CH_3 groups and thf in idealized positions and refined isotropically, H atoms of P–H and C_6H_2 groups located and refined isotropically. Empirical absorption correction with SADABS.[16] CCDC 182/876.

¶ As the chemical shifts in the ^{31}P NMR spectra of alkali metal phosphanides are dependent on concentration, saturated solutions were always used for NMR spectroscopy. Apparently, the solid-state structure is not retained in solution, but discrete anions (and, by inference, cations) are formed.

1 *Organophosphorus Chemistry*, Royal Society of Chemistry, vol. 1–24; E. Hey-Hawkins, *Chem. Rev.*, 1994, **94**, 1661.
2 E. Hey-Hawkins and S. Kurz, *Phosphorus Sulfur Silicon*, 1994, **90**, 281; M. Drieß, H. Pritzkow, S. Martin, S. Rell, D. Fenske and G. Baum, *Angew. Chem.*, 1996, **108**, 1064; M. Drieß, S. Rell, H. Pritzkow and R. Janoschek, *Chem. Commun.*, 1996, 305; G. Becker, B. Eschbach, O. Mundt and N. Seidler, *Z. Anorg. Allg. Chem.*, 1994, **620**, 1381; Review: F. Pauer and P. P. Power, *Structures of Lithium Salts of Heteroatom Compounds*, in *Lithium Chemistry: A Theoretical and Experimental Overview*, ed. A.-M. Sapse and P. v. R. Schleyer, Wiley, New York, 1994, ch. 9, p. 361 and references therein.
3 (*a*) M. Andrianarison, D. Stalke and U. Klingebiel, *Chem. Ber.*, 1990, **123**, 71; (*b*) G. A. Koutsantonis, P. C. Andrews and C. L. Raston, *J. Chem. Soc., Chem. Commun.*, 1995, 47; (*c*) H. C. Aspinall and M. R. Tillotson, *Inorg. Chem.*, 1996, **35**, 5; (*d*) M. Drieß, G. Huttner, N. Knopf, H. Pritzkow and L. Zsolnai, *Angew. Chem.*, 1995, **107**, 354.
4 M. Drieß, H. Pritzkow, M. Skipinski and U. Winkler, *Organometallics*, 1997, **16**, 5108.
5 G. W. Rabe, G. P. A. Yap and A. L. Rheingold, *Inorg. Chem.*, 1997, **36**, 1990.
6 T. Oshikawa and M. Yamashita, *Chem. Ind.* (*London*), 1985, 126.
7 E. Hey and F. Weller, *J. Chem. Soc., Chem. Commun.*, 1988, 783.
8 M. C. Fermin, J. Ho and D. W. Stephan, *J. Am. Chem. Soc.*, 1994, **116**, 6033.
9 M. C. Fermin, J. Ho and D. W. Stephan, *Organometallics*, 1995, **14**, 4247.
10 F. Paul, D. Carmichael, L. Ricard and F. Mathey, *Angew. Chem.*, 1996, **108**, 1204.
11 H.-J. Gosink, F. Nief, L. Ricard and F. Mathey, *Inorg. Chem.*, 1995, **34**, 1306.
12 H. G. von Schnering and W. Hönle, *Z. Anorg. Allg. Chem.*, 1979, **456**, 194; *Chem. Rev.*, 1988, **88**, 243.
13 C. J. Schaverien and J. B. Van Mechelen, *Organometallics*, 1991, **10**, 1704.
14 B. Werner, T. Kräuter and B. Neumüller, *Organometallics*, 1996, **15**, 3746 and references therein.
15 SHELXTL PLUS, Siemens Analyt. X-ray Inst. Inc., 1990, XS: Program for Crystal Structure Solution, XL: Program for Crystal Determination, XP: Interactive Molecular Graphics.
16 R. H. Blessing, *Acta Crystallogr., Sect. A*, 1995, **51**, 33.

Received in Basel, Switzerland, 23rd February 1998; 8/01495G

Selective fluorescence detection of fluoride using boronic acids

Christopher R. Cooper, Neil Spencer and Tony D. James*†

School of Chemistry, The University of Birmingham, Edgbaston, Birmingham, UK B15 2TT

Fluorescent PET (photoinduced electron transfer) sensors 1,2 and 3 with boronic acid receptor units show F^- selective fluorescent quenching in aqueous solution at pH 5.5.

Neutral and ionic synthetic molecular receptors for anions are the focus of many research groups. Anion receptors can consist of protonated nitrogens, metal ions, hydrogen bonding sites and Lewis acid receptors.[1–6] The conversion of binding information between ions and synthetic molecular receptors into readable fluorescent outputs has attracted the attention of many research groups.[7–12] There is interest in following the uptake and metabolism of F^- in both plants and animals and in the analysis of drinking water. Fluoride concentrations are currently determined using electrodes prepared from LaF_3.[13] Electrodes for determining F^- concentrations are sensitive and selective, but, under certain circumstances a method for the direct visualisation of intracellular F^- would be of great advantage, especially to analytical biochemists.

The system presented here is based on the Lewis acid–base interaction between boron and anions. When boron binds with certain anions the hybridisation changes from sp^2 to sp^3.[14,15] Boron centred fluoride receptors were first studied by Katz, who trapped fluoride ions between two electron accepting boron atoms in 1,8-naphthalendiylbis(dimethylborane).[16,17] More recently Reetz combined a Lewis acid boron and crown ether to create a ditopic host for F^- and metal ions.[18] Paugam and Smith have used the tetrahedral fluoride adduct of phenyl boronic acid with fluoride to accelerate saccharide transport at neutral pH.[19] Shinkai and coworkers have recently developed a F^- receptor based on ferrocene boronic acids, the binding is measured electrochemically[20] or by the colour change of a redox coupled dye molecule.[21]

Work by the groups of Czarnik and Shinkai on saccharide sensors has shown that boronic acids exist as tetrahedral boronate anions at pH values above their pK_a, and that the tetrahedral boronate anion can quench the fluorescence of directly attached fluorophores by the mechanism of photoinduced electron transfer (PET).[22,23] With this work we decided to investigate whether F^- can also quench fluorescence on formation of a tetrahedral fluoride adduct.

When phenylboronic acid **1**‡ and 2-naphthylboronic acid **2**‡

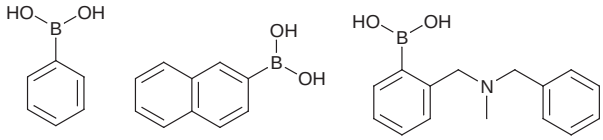

1 **2** **3**

are titrated with KF in a 50% (w/w) methanol–water buffer at pH 5.5[24] the fluorescence of the phenyl and naphthyl fluorophores decreases with added KF. (λ_{ex} = 265 nm, λ_{em} = 295 nm and λ_{ex} = 268 nm, λ_{em} = 344 nm, respectively) (Fig. 1). The experimental curves are fitted best using eqn. (1) assuming

$$I = \frac{I_0 + I_\infty K_n[F^-]^n}{1 + K_n[F^-]^n} \quad (1)$$

with:

$$K_n = \frac{[RB(OH)_{3-n}F_n]}{[RB(OH)_2][F^-]^n}$$

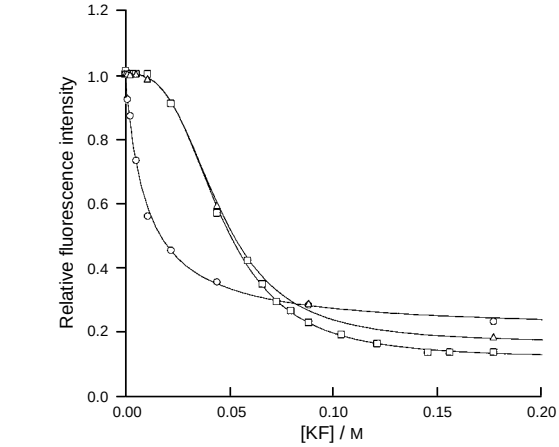

Fig. 1 Fluorescence intensity log [KF] profile of (□) **1**, (△) **2** and (○) **3** at 25 °C; 1.63×10^{-4} M **1** in 50% MeOH–H_2O, pH 5.5, λ_{ex} = 265 nm, λ_{em} = 295 nm; 1.16×10^{-4} M **2** in 50% MeOH–H_2O, pH 5.5, λ_{ex} = 268 nm, λ_{em} = 344 nm; 8.30×10^{-5} M **3** in 50% MeOH–H_2O, pH 5.5, λ_{ex} = 270 nm, λ_{em} = 309 nm

the formation of a trifluoro tetrahedral boronate (n = 3)[25] (Scheme 1). The stability constants K_3 determined from the best fit of these curves are 1.04×10^4 and 1.08×10^4 dm^9 mol^{-3} respectively. Compounds **1** and **2** can effectively detect concentrations of F^- in the range 50–70 mM. Compound **3** was prepared by alkylating 2-bromomethylphenylboronic acid with methyl aminomethylbenzene, an analytically pure sample was obtained by precipitation from $CHCl_3$ by hexane to give a 13% yield. Compound **3** was specifically designed to increase the strength of F^- binding relative to compound **1** by virtue of an additional hydrogen bonding site, which is available when the amine is protonated. The pK_a of the tertiary amine of compound **3** is 5.5, determined from a fluorescence pH titration. At a pH of 5.5 the amine is half protonated and can participate in hydrogen bonding with F^-.[8,10] Also at pH 5.5, **3** has a high fluorescence because PET from the nitrogen is reduced on protonation. When **3** is titrated with KF in a 50% (w/w) methanol–water buffer at pH 5.5[24] the fluorescence of the phenyl fluorophore decreases with added F^-. (λ_{ex} = 270 nm, λ_{em} = 309 nm) (Fig. 1). The experimental curve is fitted best using eqn. (1) and assuming the formation of monofluoro boronic acid derivative (n = 1)[25] (Scheme 1). The F^- stability constant K_1 determined from the best fit of this curve is 101 dm^3 mol^{-1}. Compound **3** can effectively detect concentrations of F^- in the range 5–30 mM. The single fluoride adduct of compound **1** is selectively stabilised by the additional hydrogen bonding from the protonated amine of compound **3** (Fig. 2). Titrations were also carried out using **1**, **2** and **3** with KCl and KBr but no change in fluorescence was observed until very high concentrations of

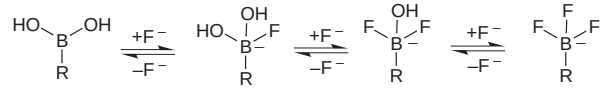

Scheme 1

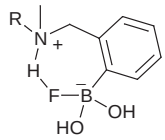

Fig. 2

these salts. A similar exclusive selectivity for F^- was observed by Shinkai and coworkers with ferrocene boronic acid.[20]

Both ^{11}B (128 MHz) and ^{19}F (376 MHz) NMR experiments were perfomed to confirm the presence of the F^- adducts depicted in Scheme 1. The ^{11}B NMR of compound **1** (0.205 M) in 33% (v/v) methanol-D_2O§ at 31 °C shows one boron signal at δ 13.2 relative to an external capillary of BMe_3 as reference. This signal shifted to δ 12.0 on addition of 1 equiv. of KF and to δ 7.4 on addition of 5 equiv. of KF. The ^{11}B NMR of **3** (0.137 M) in 70% (v/v) methanol–D_2O§ at 31 °C shows two boron signals at δ 14.5 and 2.5 corresponding to free boronic acid (sp^2) and nitrogen coordinated boronic acid (sp^3) respectively (At a pH of 5.5 the nitrogen atom of **3** is not fully protonated). On addition of 1 equiv. of KF the signal at high frequency moved to δ 13.5 while the other at low frequency remained at δ 2.5. On addition of 5 equiv. of KF only one signal at δ 2.5 was observed. The observed shifts from high to low frequency in the ^{11}B NMR are consistent with a shift from sp^2 to sp^3 boron on F^- binding.[26]

The ^{19}F NMR of compound **1** (0.205 M) in 33% (v/v) methanol–D_2O§ at 0 °C on the addition of 3 equiv. of KF shows signals at δ −126.9 [KF and $RB(OH)_2F^-$], −137.1 [$RB(OH)F_2^-$] and −147.5 [RBF_3^-] all relative to an external capillary of $CFCl_3$ as reference. The ^{19}F NMR of **3** (15.7 mM) in 50% (v/v) methanol–D_2O§ at 0 °C on addition of 3 equiv. of KF shows a signal at δ 131.6 [KF and $RB(OH)_2F$]. The species detected by ^{19}F NMR[27] are consistent with the F^- adducts depicted in Scheme 1 and the observed fluorescence behaviour. This work represents the first example where fluorescence has been used to detect F^- binding events. The use of these simple molecules has resulted in high F^- selectivity. We believe that with appropriate modifications of the Lewis acid and hydrogen bond donor, F^- selectivity can be fine tuned to any desired F^- concentration range. It is hoped that this work will lead to the development of fluorescent F^- sensors for a variety of industrial and medicinal applications.

T. D. J. wishes to acknowledge the Royal Society for support through the award of a University Fellowship. C. R. C. wishes to acknowledge the School of Chemistry for support through the award of a School Studentship.

Notes and References

† E-mail: tdjames@chemistry.bham.ac.uk

‡ Compounds **1** and **2** were purchased from Lancaster Synthesis Ltd., Eastgate, White Lund, Morecambe, Lancashire, UK LA3 3DY, and used without further purification.

§ The pH was adjusted to 5.5 by the addition of HCl.

1 M. M. G. Antonisse and D. N. Reinhoudt, *Chem. Commun.*, 1998, 443.
2 J. Scheerder, J. F. J. Engbersen and D. N. Reinhoudt, *Recl. Trav. Chim. Pays-Bas*, 1996, **115**, 307.
3 F. P. Schmidtchen and M. Berger, *Chem. Rev.*, 1997, **97**, 1609.
4 P. D. Beer, *Chem. Commun.*, 1996, 689.
5 J. L. Atwood, K. T. Holman and J. W. Steed, *Chem. Commun.*, 1996, 1401.
6 B. Dietrich, *Pure Appl. Chem.*, 1993, **65**, 1457.
7 A. W. Czarnik, *Acc. Chem. Res.*, 1994, **27**, 302.
8 A. P. deSilva, H. Q. N. Gunaratne, T. Gunnlaugsson, A. J. M. Huxley, C. P. McCoy, J. T. Rademacher and T. E. Rice, *Chem. Rev.*, 1997, **97**, 1515.
9 A. W. Czarnik, *Fluorescent Chemosensors for Ion and Molecule Recognition*, ed. A. W. Czarnik, ACS Books, Washington, DC, 1993.
10 T. D. James, K. Sandanayake, and S. Shinkai, *Angew. Chem., Int. Ed. Engl.*, 1996, **35**, 1911.
11 T. D. James, P. Linnane and S. Shinkai, *Chem. Commun.*, 1996, 281.
12 C. R. Cooper and T. D. James, *Chem. Commun.*, 1997, 1419.
13 M. S. Frant and J. W. Ross, *Science*, 1966, **154**, 1533.
14 K. Worm, F. P. Schmidtchen, A. Schier, A. Schafer and M. Hesse, *Angew. Chem., Int. Ed. Engl.*, 1994, **33**, 327.
15 S. Jacobson and R. Pizer, *J. Am. Chem. Soc.*, 1993, **115**, 11 216.
16 H. E. Katz, *J. Org. Chem.*, 1985, **50**, 5027.
17 H. E. Katz, *J. Am. Chem. Soc.*, 1986, **108**, 7640.
18 M. T. Reetz, C. M. Niemeyer and K. Harms, *Angew. Chem., Int. Ed. Engl.*, 1991, **30**, 1472.
19 M. F. Paugam and B. D. Smith, *Tetrahedron Lett.*, 1993, **34**, 3723.
20 C. Dusemund, K. Sandanayake and S. Shinkai, *J. Chem. Soc., Chem. Commun.*, 1995, 333.
21 H. Yamamoto, A. Ori, K. Ueda, C. Dusemund and S. Shinkai, *Chem. Commun.*, 1996, 407.
22 H. Suenaga, M. Mikami, K. Sandanayake and S. Shinkai, *Tetrahedron Lett.*, 1995, **36**, 4825.
23 J. Yoon and A. W. Czarnik, *J. Am. Chem. Soc.*, 1992, **114**, 5874.
24 D. D. Perrin and B. Dempsey, *Buffers for pH and Metal Ion Control*, Chapman and Hall, 1974.
25 B. Valeur, J. Pouget, J. Bourson, M. Kaschke and N. P. Ernsting, *J. Phys. Chem.*, 1992, **96**, 6545.
26 N. Farfan, P. Joseph-Nathan, L. M. Chiquete and R. Contreas, *J. Organomet. Chem*., 1988, **348**, 149.
27 R. E. Mesmer and A. C. Rutenberg, *Inorg. Chem*., 1972, **12**, 699.

Received in Cambridge, UK, 2nd March 1998; 8/01693C

Homogeneous ruthenium catalyzed hydrogenation of esters to alcohols‡

Herman T. Teunissen and Cornelis J. Elsevier*†

Institute of Molecular Chemistry, Universiteit van Amsterdam, Nieuwe Achtergracht 166, NL-1018 WV Amsterdam, The Netherlands

The homogeneous catalytic hydrogenation of aromatic and aliphatic esters to the corresponding alcohols, by a catalyst generated *in situ* from $[Ru(acac)_3]$ and $MeC(CH_2PPh_2)_3$ in an alcoholic solvent under H_2 pressure of 85 bar at 100–120 °C, is described.

The reduction of esters to the corresponding alcohols is an important reaction which is usually achieved by a stoichiometric reaction using lithium aluminium hydride,[1] whereas homogeneous catalytic routes have been scarcely explored.[2–4] For aromatic esters, the only example is concerned with the hydrogenation of dimethyl phthalate (DMP) to phthalide (PHT)

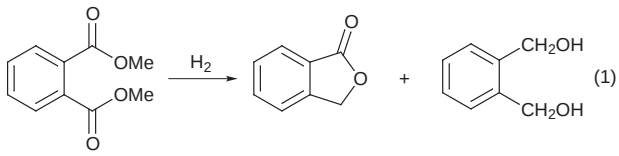

using a ruthenium hydride complex [eqn. (1)];[3a] PHT was obtained in a yield of 11.5% after 144 h at 180 °C under a hydrogen pressure of 130 bar.

Hydrogenation of PHT to 1,2-bis(hydroxymethyl)benzene (BHB) did not occur due to the absence of electron withdrawing substituents which enabled the conversion of DMP to PHT. Therefore, the hydrogenation of unactivated esters to the corresponding alcohols is one of the most intriguing challenges in contemporary hydrogenation catalysis. We have recently reported an important improvement using a catalyst based on $[Ru(acac)_3]$ and $MeC(CH_2PPh_2)_3$ in methanol,[4b] for the homogeneous hydrogenation of dimethyl oxalate. Now, we wish to report a catalytic system which is able to catalyse the hydrogenation of unactivated aromatic and aliphatic esters with very high turnover numbers.§

From Table 1 it is evident that the hydrogenation of DMP to give mainly PHT is feasible under relatively mild conditions (entry 1) employing a system consisting of $[Ru(acac)_3]$ and $MeC(CH_2PPh_2)_3$ in methanol. The catalytic activity (expressed as turnover number, TON) appeared to be strongly influenced by additives. Compared to entry 1, a negative effect is observed with Zn as an additive (entry 2) while positive effects are observed with NEt_3 (entry 3) and HBF_4 (entry 4). A further improvement is observed when the solvent MeOH is replaced by propan-2-ol (IPA). The combination IPA–HBF_4 shows the highest catalytic activity and gives rise to formation of BHB in high yield (entry 5) which was not observed in any previous experiment. Comparing our system with that of Matteoli *et al.*[3a] (entry 6) shows that we have achieved a considerable improvement with respect to turnover numbers and turnover frequencies under relatively mild conditions.

Next, we applied our system to the hydrogenation of benzyl benzoate (BZB, an unactivated ester) which is difficult to hydrogenate to benzyl alcohol (BZOH) (Table 2). In the presence of HBF_4 or NEt_3, we could achieve a TON of 33 (entry 1) and 105 (entry 2), respectively at 120 °C for this conversion. Furthermore, we investigated the influence of fluorinated alcohols on the hydrogenation of benzyl benzoate. These investigations were based on the results of Grey *et al.*,[2] who found that an ester is more easily hydrogenated when electron withdrawing substituents are present. Therefore, we postulated that an integration of transesterification (using *e.g.* 2,2,2-trifluoroethanol) and hydrogenation would lead to a substantial increase in catalytic activity due to substrate activation [eqn. (2)].

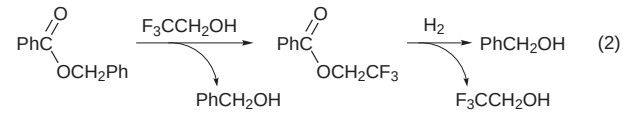

The hydrogenation of BZB to BZOH in 2,2,2-trifluoroethanol (TFE) at 120 °C turned out to be very successful (Table 2) and seems to confirm our hypothesis. Compared to the experiments in propan-2-ol (entry 2) the catalytic activity in TFE has drastically increased reaching a turnover number of nearly 900 in the presence of NEt_3 (entry 3). At 100 °C the catalytic activity was significantly lower, as expected (entry 4). Hydrogenation of BZB does not occur in the presence of HBF_4 (entry 5). Instead, three other products are formed: 2,2,2-trifluoroethyl benzoate, benzoic acid and a polymeric material. The formation of benzoic acid (82% isolated yield, TON 1412) was unexpected and is not readily explained. Hydrogenolysis of benzyl esters using heterogeneous palladium catalysts is common[5] but unprecedented for ruthenium complexes. Subsequently, the hydrogenation of BZB was carried out in 1,1,1,3,3,3-hexafluoropropan-2-ol (FIPA) which gave even

Table 1 Hydrogenation of DMP with the $[Ru(acac)_3]$–$MeC(CH_2PPh_2)_3$ system[a]

Entry	DMP/mmol	$[Ru(acac)_3]$/μmol	Additive/mmol	Conv. (%)	Yield PHT[b] (%)	Yield BHB[b] (%)	TON	TOF/h^{-1}
1	1.16	19.1	—	31	30	1	19	1.2
2	1.00	18.3	Zn (0.82)	25	18	0	10	0.6
3	1.05	15.3	NEt_3 (22.70)	87	82	0	56	3.5
4	1.14	17.1	HBF_4 (0.82)	91	79	0	53	3.4
5	1.17	18.1	IPA[c] + HBF_4 (0.27)	100	18	78	103	5.6
6	30.9		$[Ru_4H_4(CO)_8(PBu_3)_4]$[d]	21	12	0	51	0.4

[a] *Conditions*: 100 °C; 85 bar H_2; 16 h; 1.15–1.65 equiv. $MeC(CH_2PPh_2)_3$ in MeOH (12 ml). [b] Yield determined by GC or NMR (entry 5). [c] Propan-2-ol (12 ml, instead of MeOH). [d] From ref. 3(*a*); T = 180 °C; $p(H_2)$ = 130 bar, 144 h.

Table 2 Hydrogenation of esters in fluorinated alcohols[a]

Entry	Substrate/mmol	[Ru(acac)$_3$]/μmol	Additive/mmol	Solvent	Conv. (%)	Product[b]	Yield[c] (%)	TON
1	BZB (1.3)	21.3	HBF_4 (0.42)	IPA	63	BZOH	56	33
2	BZB (4.2)	18.3	NEt_3 (0.34)	IPA	87	BZOH	82	105
3	BZB (30.5)	18.1	NEt_3 (2.60)	TFE	65	BZOH	53	896
4[d]	BZB (17.3)	18.1	NEt_3 (2.46)	TFE	43	BZOH	23	219
5	BZB (29.5)	17.1	HBF_4 (0.47)	TFE	87	BZA	82[e]	1412
6	BZB (28.4)	13.1	NEt_3 (2.58)	FIPA	97	BZOH	95	2071
7[f]	BZB (25.9)	20.1	NEt_3 (2.55)	FIPA	7	BZOH	1	12
8	BZB (31.0)	10.8	NEt_3 (2.72)	FIPA–TFE	75	BZOH	67	1909
9	DMM (14.2)	14.1	NEt_3 (2.76)	FIPA	100	BDO	100	2019[g]
10	MP (8.3)	13.1	NEt_3 (2.66)	FIPA	94	HDO	94	596

[a] *Conditions*: 120 °C; 85 bar H_2; 16 h; [Ru(acac)$_3$]; 1.15–1.65 equiv. $MeC(CH_2PPh_2)_3$. [b] Apart from the alcohol, significant formation of transesterification product was observed: entry 3 (8%); entry 4 (16%); entry 5 not determined; entry 7 (1%); entry 8 (4%). [c] Yield determined by ^{1}H NMR. [d] T = 100 °C. [e] Isolated yield. [f] $p(H_2)$ = 0 bar. [g] The hydrogenation of the C=C bond is not included in the turnover number.

better results. Hydrogenation of BZB in FIPA occurs with a turnover number of > 2000 (entry 6), which is an enormous step forward in the homogeneous catalytic hydrogenation of unactivated esters. This result was completely unexpected and contradicts the hypothesis of transesterification prior to hydrogenation. In principle, a primary alcohol such as TFE should give rise to transesterification more easily than a secondary alcohol like FIPA.[6] In view of these facts we suggest that the high catalytic activity in FIPA is due to ionic hydrogenation (*vide infra*) rather than to an integration of transesterification and hydrogenation. Compared to the experiment in FIPA, a mixture of TFE and FIPA exhibited a slightly lower activity (entry 8), which also raises objection to our initial hypothesis. Finally, we investigated the possibility of transfer hydrogenation (entry 7). The low catalytic activity in this case emphasizes that a substantial hydrogen pressure is necessary for successful catalysis. Possibly, the ruthenium catalyzed oxidative transformation of BZOH to BZB[7] becomes feasible in the absence of hydrogen pressure thus obstructing a successful transfer hydrogenation.

Using the optimized catalytic system for the conversion of BZB (FIPA, entry 6), we explored the scope of this system using dimethyl maleate (DMM) [eqn. (3)] and methyl palmitate (MP) [eqn. (4)] as substrates. The results show that our system is able

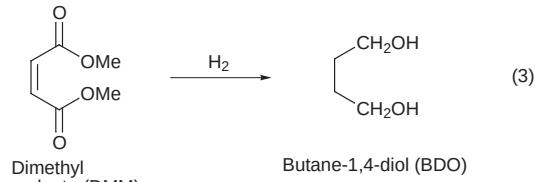

Dimethyl maleate (DMM) — Butane-1,4-diol (BDO) (3)

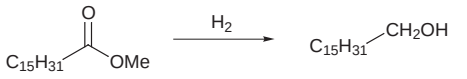

Methyl palmitate (MP) — Hexadecan-1-ol (HDO) (4)

to catalyze the hydrogenation of these substrates to the corresponding alcohols with, compared to BZB, a high activity for DMM (entry 9) and a slightly smaller activity for MP (entry 10). Altogether we can conclude that efficient hydrogenation of unactivated aromatic and aliphatic esters is possible using [Ru(acac)$_3$] and $MeC(CH_2PPh_2)_3$ in FIPA at 120 °C. Possibly, the remarkable activity in TFE and FIPA compared to IPA is related to the pK_a of the alcohols and not to transesterification. Berke and Burger showed that phenol[8a] and FIPA[8b] drastically influence the rate of insertion of aldehydes into the W–H bond in tungsten nitrosyl complexes. This influence was explained by ionic hydrogenation (*via* **A**).

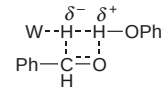

A

A comparable complex has been reported recently for a ruthenium hydride complex and FIPA.[8c] The unique features of our catalytic system are ascribed to ionic hydrogenation of the ester. Investigations pertaining to the mechanism of the hydrogenation of esters are currently in progress in our laboratory.

We gratefully acknowledge stimulating discussions with Dr J. G. de Vries (DSM, Geleen, NL) and Dr M. J. Doyle (SRTCA, Amsterdam, NL).

Notes and References

† E-mail: else4@anorg.chem.uva.nl

‡ NIOK publication UvA 98-03-03. This work was supported by the Innovation Oriented Research Programme (IOP-katalyse) under the auspices of the Netherlands' Ministry of Economic Affairs.

§ *General procedure*: first, a solution was prepared of [Ru(acac)$_3$], $MeC(CH_2PPh_2)_3$, the appropriate ester and additive (see Tables 1 and 2) in the appropriate solvent (15 ml) under N_2. Separately, a home-built stainless steel autoclave equipped with a magnetic stirring bar was flushed with dry nitrogen after which the dark red pre-catalyst solution was introduced *via* a needle. The autoclave was flushed with H_2 (at 50 bar), pressurized with hydrogen (85 bar at 20 °C) and heated for 16 h at the indicated temperature. The reaction products were characterized by GC–MS, the yields were determined with GC (internal standard) or ^{1}H NMR.

1 S. N. Ege, *Organic Chemistry*, D. C. Heath and Company, Lexington, 1989, p. 596.
2 R. A. Grey, G. P. Pez and A. Wallo, *J. Am. Chem. Soc.*, 1981, **103**, 7536.
3 (*a*) U. Matteoli, M. Bianchi, G. Menchi, P. Frediani and F. Piacenti, *J. Mol. Catal.*, 1984, **22**, 353; (*b*) U. Matteoli, G. Menchi, M. Bianchi and F. Piacenti, *J. Organomet. Chem.*, 1986, **299**, 233; (*c*) U. Matteoli, G. Menchi, M. Bianchi, F. Piacenti, S. Ianelli and M. Nardelli, *J. Organomet. Chem.*, 1995, **498**, 177 and refs. therein.
4 (*a*) Y. Hara, H. Inagaki, S. Nishimura and K. Wada, *Chem. Lett.*, 1992, 1983; (*b*) H. T. Teunissen and C. J. Elsevier, *Chem. Commun.*, 1997, 667.
5 J. S. Bajwa, *Tetrahedron Lett.*, 1992, **33**, 2299; W. H. Hartung and R. Simonoff, *Org. React.*, 1953, **7**, 263.
6 J. Otera, *Chem. Rev.*, 1993, **93**, 1449.
7 S. I. Murahashi, T. Naota, K. Ito, Y. Maeda and H. Taki, *J. Org. Chem.*, 1987, **52**, 4319; Y. Blum and Y. Shvo, *J. Organomet. Chem.*, 1985, **282**, C7.
8 (*a*) H. Berke and P. Burger, *Comments Inorg. Chem.*, 1994, **16**, 279; (*b*) H. Berke, *Book of abstracts, XIIth FECHEM Conference on Organometallic Chemistry*, Prague 1997, PL 9; (*c*) J. A. Ayllon, C. Gervaux, S. Sabo-Etienne and B. Chaudret, *Organometallics*, 1997, **16**, 2000.

Received in Basel, Switzerland, 5th March 1998; 8/01807C

Scanning tunnelling microscopy investigation of sintering in a model supported catalyst: nanoscale Pd on TiO_2(110)

Peter Stone, Stephen Poulston, Roger A. Bennett and Michael Bowker*†

Catalysis Research Centre, Department of Chemistry, University of Reading, Whiteknights Park, Reading, UK RG6 6AD

Vacuum annealing of metal vapour deposited Pd on TiO_2(110) results in particle formation and sintering with an increase in both the diameter and height of the particles measured using STM.

Metal vapour deposition on oxide single crystals provides a methodology for generating model catalysts which can be studied using conventional surface science techniques.[1,2] Of the wide range of techniques available scanning probe microscopy (SPM) is particularly valuable in that it allows the morphology and size distribution of metal particles on single crystal surfaces to be measured directly. The nucleation and growth of palladium on titania has previously been studied using STM by Goodman and coworkers[3] and Thornton and coworkers.[4] Here, we report the application of scanning tunnelling microscopy (STM) to the investigation of the sintering of Pd particles on TiO_2(110) upon heating in vacuum. STM is particularly advantageous compared to TEM as it measures the height of every particle in the scanned area. The magnitude of the reactivity relates to the area of supported particles which is available for reaction, and in this case particle–particle interactions in which size and shape distributions change will crucially affect the total reactivity. For example, sintering of small particles to form larger particles reduces the total surface area of the supported metal and results in a concomitant loss in catalytic activity. We present STM observations of the variation in particle size and height distributions and relate the observations to sintering. Annealing temperatures of 473 and 973 K correspond to the Hüttig and Tamman temperatures for Pd and roughly correspond to the expected onset of metal adatom and metal nanoparticle mobility respectively.[5] These observations represent the first analysis of the sintering process in this system by STM and the results are expected to be general for a wide variety of other systems.

Pd overlayers were prepared by Pd vapour deposition onto the TiO_2 surface at *ca.* 300 K. The Pd source consisted of a Pd wire wound tightly around a W filament. The TiO_2(110) surface was prepared by repeated sputter-anneal (>973 K) cycles to produce a slightly streaky (in the $<110>$ direction) (1×1) LEED pattern indicating the surface was slightly reduced. Pd deposition was monitored using Auger electron spectroscopy with the amount of Pd estimated from a calibration experiment of Pd deposition on Cu(110). The rate was estimated to be 2×10^{-3} ML s^{-1} where 1 ML is 1.1×10^{15} atoms cm^{-2}. The growth mode of Pd on TiO_2(110) at 300 K has been established to be of the classical nucleation type where Pd monomers are mobile while dimers form stable nuclei for subsequent growth in the Volmer–Weber mode (3D-islanding).[3]

Deposition of >1.5 ML Pd produced continuous, though rough Pd films which could be imaged in the STM. Annealing to 473 K produced particulate films, which is consistent with surface Pd mobility (Hüttig temperature) as small particles have been formed from a thin film. Deposition of <1.5 ML produces particles in the as-deposited overlayer. Fig. 1 shows STM images of 1.7 ML Pd on TiO_2 which has been vacuum annealed to (*a*) 473 K for 15 min and then (*b*) 973 K for a further 15 min. The Pd particles in Fig. 1(*a*) form a fairly homogeneous overlayer with some variation in particle size and height. This can be seen more quantitatively in Fig. 2 which shows (*a*) the particle size and (*b*) height distributions for this overlayer at this and two higher annealing temperatures (773 and 973 K). The same surface annealed to 973 K, Fig. 1(*b*), displays a significantly changed particulate array. The Pd particles show a reduction in particle number density from 7.5×10^{-2} to 6×10^{-3} nm^{-2} and display a much greater variety in size and height (Fig. 2). This change is characteristic of particle sintering as a result of mass transport of Pd particles on the surface (Tamman temperature). We believe that the mechanism of sintering in this system is by coalescence, that is, two or more particles join together to form the larger particles. Fig. 1(*b*) shows evidence of coalescence of the particles, in this image it is clear to see that some of the particles have merged together (see regions 1 and 2 on the image). In addition, if Ostwald ripening was the mechanism, we would expect to see smaller particles at some stage during the sintering process, which is not observed. The mean (s.d.) particle diameter varies between 42 (10 Å) after annealing at 473 K to 56 (11 Å) at 773 K and 87 (15 Å) at 973

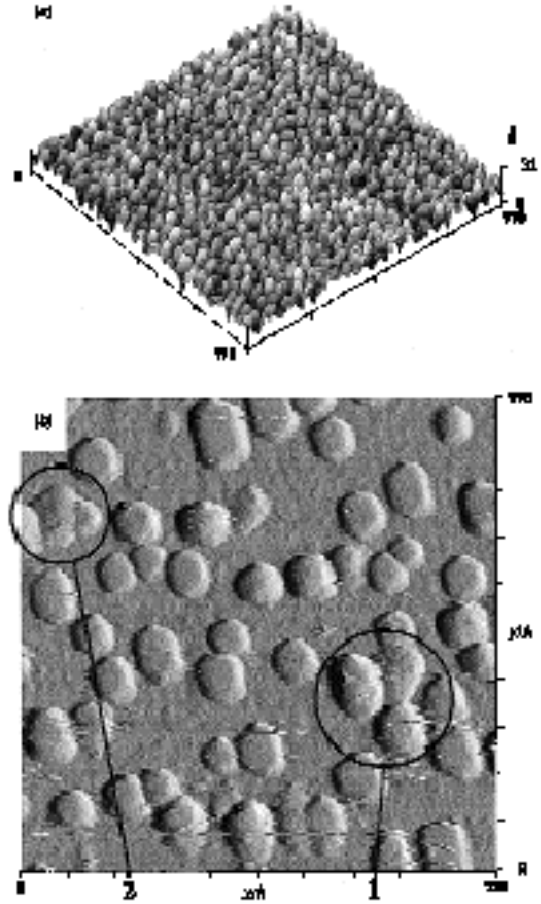

Fig. 1 STM images of 1.7 ML Pd on TiO_2(110) after annealing for 15 min at (*a*) 473 K (sample bias 0.5 V, tunnelling current 1 nA) and (*b*) 973 K (sample bias 2 V, tunnelling current 1 nA). The scan area of each image is 998×998 Å.

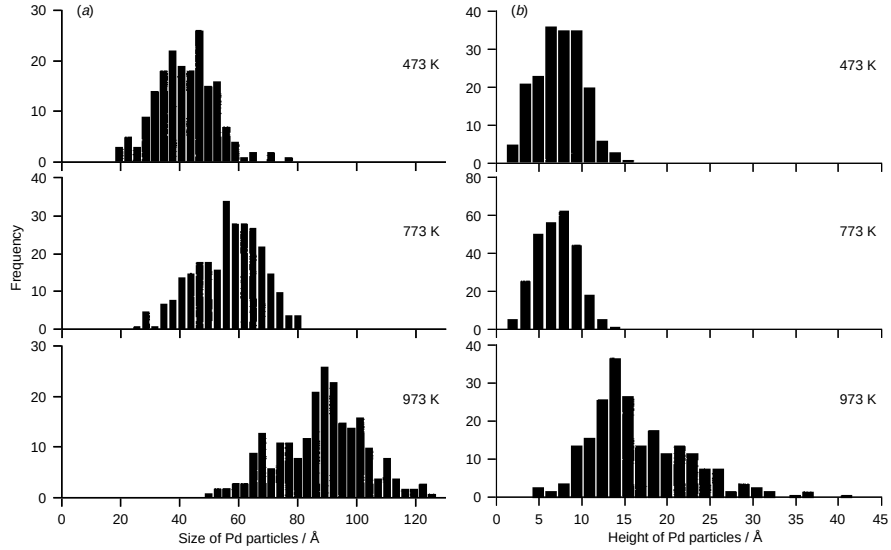

Fig. 2 Particle size distributions for 1.7 ML Pd on TiO_2(110) annealed to three different temperatures; 473, 773 and 973 K. (*a*) Size (diameter) and (*b*) height of particles.

K. The corresponding mean particle heights are 7.3 (2.7 Å), 6.8 (2.4 Å) and 16.6 (6.2 Å). The standard error for the mean particle diameter and height is (±1 Å) and (±0.5 Å) respectively.

At Pd coverages of 5 ML the same analysis of particle size with annealing temperature was not possible as well defined particulate arrays were not formed until the surface was annealed to 973 K. Other Pd coverages between 0.6 and 3 ML display the same trend on annealing as that shown above for the case of 1.7 ML though the measured particle densities after annealing to 973 K decrease with decreasing Pd coverage. After annealing at 973 K for lower Pd coverages it is possible to image the clean (1 × 1) surface between the particles.

In summary, we have investigated the sintering of particles in a model catalyst system, Pd on TiO_2. The as-deposited film displays little structure but annealing to 473 K produces distinct clusters, while further annealing at 973 K results in the sintering of these particles which we believe to be by the mechanism of coalescence.

Notes and References

† E-mail: m.bowker@reading.ac.uk

1 C. T. Campbell, *Surf. Sci. Rep.*, 1997, **27**, 1.
2 U. Diebold, J.-M. Pan and T. E. Madey, *Surf. Sci.*, 1995, **331**–**333**, 845.
3 C. Xu, X. Lai, G. W. Zajac and D. W. Goodman, *Phys. Rev. B*, 1997, **56**, 13464.
4 P. W. Murray, J. Shen, N. G. Condon, S. J. Pang and G. Thornton, *Surf. Sci.*, 1997, **380**, L455.
5 *Handbook of Heterogenous Catalysis*, ed. G. Ertl, H. Knözinger and J. Weitkamp, Wiley-VCH, New York, vol. 3.

Received in Cambridge, UK, 17th April 1998; 8/02881H

Cationic amphitropic gemini surfactants with hydrophilic oligo(oxyethylene) spacer chains

Michael Dreja,† Susanne Gramberg and Bernd Tieke*‡

Institut für Physikalische Chemie der Universität zu Köln, Luxemburger Straße 116, D-50939 Köln, Germany

New gemini diammonium surfactants have been synthesized in which the spacer chain consists of oligo(oxyethylene) units and which exhibit thermotropic liquid crystalline lamellar α and β as well as lyotropic mesophases.

Surfactant molecules usually consist of a hydrophilic headgroup attached to a hydrophobic alkyl chain. They self-assemble into micellar and lyotropic liquid crystalline mesophases when mixed with water. If the self-organization process occurs on heating, thermotropic liquid crystalline phases are often observed. Many amphiphilic compounds can form thermotropic as well as lyotropic mesophases, and therefore they are labelled as amphitropic.[1] Recently, bis(quaternary ammonium) surfactants ('gemini surfactants') have been prepared, in which two hydrophilic headgroups are linked *via* a hydrophobic alkylene or heteroatom-modified spacer chain.[2,3] Here we report on a new series of amphitropic gemini surfactants (12-EO$_x$-12) in which hydrophilic headgroups as well as hydrophilic spacer chains are simultaneously present for the first time. A study of the effect of the hydrophilic oligo(oxyethylene) spacer length on the amphitropic aggregation is presented.

Gemini surfactants 12-EO$_x$-12 with x = 2–5 were obtained in

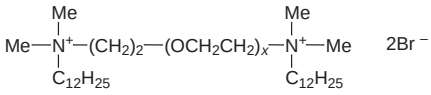

two steps *via* bromination of the corresponding oligo(oxyethylene)glycols HO–(CH$_2$)$_2$–(EO)$_x$–OH (0.1 mol) with PBr$_3$ (0.15 mol) in dry dioxane.[4] The resulting dibromides (0.06 mol) were quaternized with *N*,*N*-dimethyldodecylamine (0.13 mol) under reflux in anhydrous EtOH for two days. Evaporation yielded white solids which were recrystallized at least three times from ethyl acetate to give the desired products in good yields (50–70%). For comparison, 12-EO$_x$-12 with x = 0 or 1 were also prepared.[2,3a] The purity of all compounds was confirmed by elemental analysis and ^{1}H NMR spectroscopy.§

The thermotropic behaviour of the surfactants was characterized using polarized optical microscopy (POM), differential scanning calorimetry (DSC) and X-ray diffraction (XRD). The surfactants with $x \leqslant 4$ form one or two mesophases on heating, either an L$_\beta$ (viscous neat) or an L$_\alpha$ (smectic A) phase. The transition temperatures as well as the transition enthalpies are compiled in Table 1. The results were taken from the first DSC heating runs because the compounds are thermally unstable at high temperatures and partially decompose. Subsequent DSC scans are therefore significantly changed, as similarly observed by Fuller *et al.* for a series of conventional gemini surfactants.[5a] The first heating scans were always reproducible. For 12-EO$_0$-12, two mesophases were observed, while 12-EO$_1$-12 shows only one mesophase. For 12-EO$_2$-12, again two mesophases occur. 12-EO$_3$-12 and 12-EO$_4$-12 show a single mesophase each and clearing temperatures much lower than those of the compounds with shorter spacer chains. For 12-EO$_5$-12, no thermotropic mesophase was observed. This may be due to the higher flexibility of the spacer chains introduced by the additional oxygen atoms.

In Fig. 1, the first DSC heating run for 12-EO$_2$-12 is shown as a typical example. The four phase transitions are clearly recognizable. The occurrence of the mesophases was further identifed by the characteristic textures to be seen in the POM. In the case of 12-EO$_0$-12 and 12-EO$_1$-12, the optical textures are not easily discernable, since the materials exhibit a very high viscosity. Only after long thermal or mechanical treatment, birefringent cloudy textures occurred resembling that of a viscous neat phase. This effect was also reported for gemini surfactants with hydrophobic spacer chains.[5a] In contrast, the textures formed immediately for the compounds with x being 2–4. In Fig. 2(*a*) and (*b*), the fan-like textures of the viscous neat phase of 12-EO$_2$-12 at 120 °C and the mosaic texture of its smectic A phase at 180 °C are shown. Upon shearing, the mosaic texture at 180 °C is converted into oily streak textures.

The assignment of the mesophases was confirmed using XRD. The XRD spectrum of Fig. 3 indicates that the crystalline phase of 12-EO$_2$-12 has a layered structure with a period of 24.8

Table 1 Transition temperatures[a] (°C) of compounds 12-EO$_x$-12 and ΔH (kJ mol^{-1}) in parentheses determined by DSC at heating rate 10 °C min^{-1}

x	K$_1$		K$_2$		L$_\beta$		L$_\alpha$		I
0	•	88.7 (64.8)	•	97.4 (19.2)	•	151.5 (9.3)	•	204.0 (nd)	•
1	•			31.3 (70.9)	•			> 230 (nd)	•
2	•	33.1 (1.0)	•	82.7 (104.9)	•	150.5 (13.0)	•	196.7 (5.2)	•
3	•	31.3 (1.1)				55.4 (67.2)	•	79.4 (1.0)	•
4	•	34.2 (1.7)	•	83.0 (26.5)	•			120.8 (73.3)	•
5	•	32.9 (1.1)	•					81.9 (64.4)	•

[a] K = crystal; L$_\beta$, L$_\alpha$ = lamellar mesophases; I = isotropic liquid; nd = not determined.

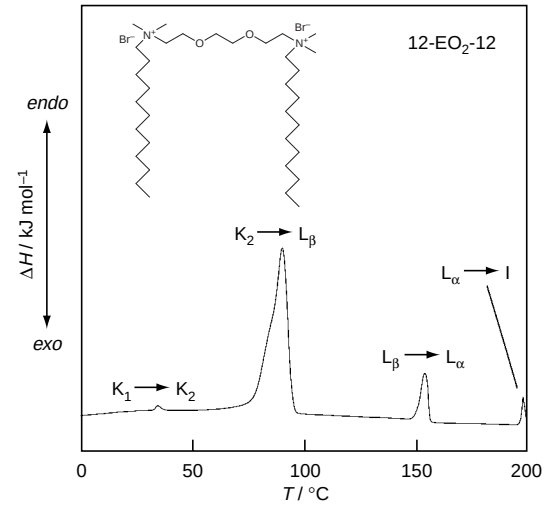

Fig. 1 First DSC heating scan of 12-EO$_2$-12 at 10 °C min^{-1}

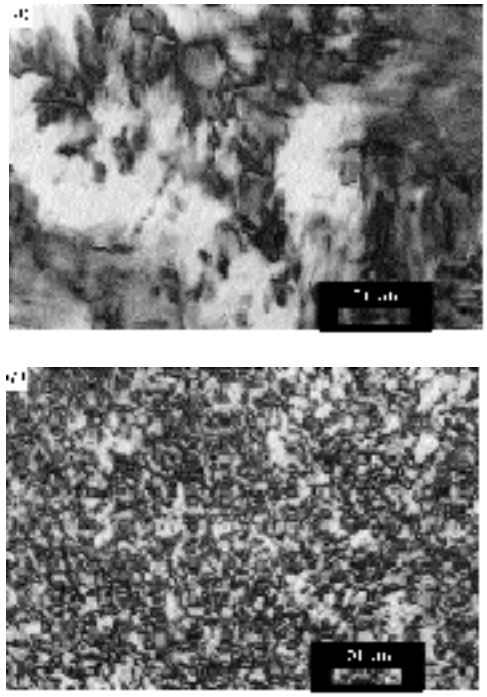

Fig. 2 Polarizing micrographs of the fan-like texture of 12-EO_2-12 at 120 °C (*a*) and of the mosaic textures at 180 °C (*b*)

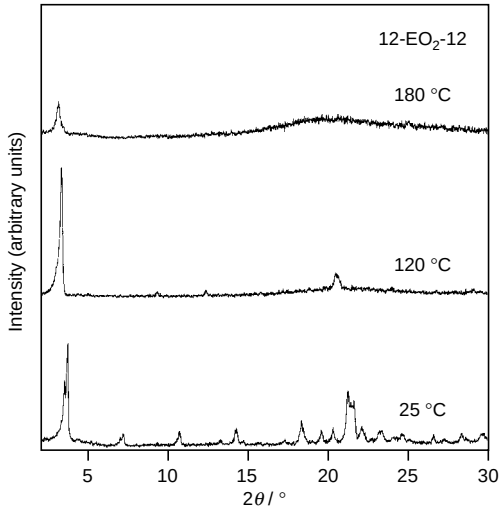

Fig. 3 XRD spectra of 12-EO_2-12 at 25, 120 and 180 °C

phase of 12-EO_2-12 has a layered structure with a period of 24.8 Å. The splitting of the low angle peak may indicate the presence of two coexisting crystalline modifications. At 120 °C, the typical diffraction pattern of an L_β phase is apparent,[6] indicating that the alkyl chains attain a hexagonal packing with fully extended chain conformation. The layer period is increased to 26.7 Å. At 180 °C, 12-EO_2-12 adopts a smectic A structure[6] indicating a disordered, liquid-like conformation of the alkyl chains and a layer period of 28.6 Å. Compared with a fully extended molecule (45.4 Å) or two extended C_{12} chains (33.4 Å), the repeat distance is much smaller. Therefore, we assume an interpenetrating bilayer structure, as similarly proposed for conventional gemini surfactants[5] and U-shaped benzimidazolium salts reported recently.[7] For the L_α-phase of 12-EO_3-12, a period of 29 Å was found, while 12-EO_4-12 has a layer spacing of 25.2 Å in the viscous neat phase. Both values are very similar to that of 12-EO_2-12 and indicate the same structural arrangements in the mesophases.

For all compounds, hexagonal (H_1), cubic (V_1) and lamellar (L_α) lyotropic mesophases were observed in water at certain concentration intervals in the temperature range from 25 to 100 °C using the contact preparation technique. Lyotropic phase behaviour sets in at concentrations above 36 ($x = 0$) to 66 wt% ($x = 5$). The hexagonal phase is stable in the whole temperature range for all surfactants except for $x = 0$, where it disappears above 50 °C. The bicontinuous cubic phase is formed for 12-EO_x-12 with $x = 2$–4 between 25 and 100 °C, for $x = 0$ only above 35 °C, and for $x = 1$, 4 above 50 °C. For $x = 0$, the lamellar phase occurs above 65 °C, for $x = 1$ above 50 °C and for $x = 2$ above 40 °C. For $x = 4$ it is stable during the whole temperature range and for $x = 3$, 5, only until the transition to the isotropic melt occurs (see Table 1).

In summary, the mesophase behaviour of the 12-EO_x-12 compounds is rather complex. Compared to geminis with short and hydrophobic spacer units, the 12-EO_x-12 compounds with $x \geqslant 2$ form thermotropic liquid crystalline phases quite readily, which can be easily identified. Therefore, such compounds may be useful as solvents for chemical reactions or as templating agents in the synthesis of inorganic materials. The lyotropic mesophase behaviour of the surfactants is also of considerable interest, since gemini surfactants with a hydrophobic spacer chain have been found to form ternary polymerizable microemulsions with styrene in water.[8] Gemini surfactants with hydrophilic oligo(oxyethylene) spacer are expected to exhibit similar or even improved properties due to a higher flexibility.

Financial support by the Deutsche Forschungsgemeinschaft (project Ti219/5-1) is gratefully acknowledged.

Notes and References

† Michael.Dreja@uni-koeln.de
‡ Tieke@uni-koeln.de

§ *Selected data* for 12-EO_2-12: $C_{34}H_{74}N_2O_2Br_2$ (702.28) (Calc. C, 58.11; H, 10.61; N, 3.99. Found C, 57.97; H, 10.75; N, 4.13); δ_H(300 MHz, $CDCl_3$) 0.85 (t, 6 H), 1.22, 1.32 (s, m 36 H), 1.7 (m, 4 H), 3.40 (s, 12 H), 3.54 (m, 4 H), 3.75 (s, 4 H), 3.90 (m, 4 H), 4.10 (m, 4 H); 12-EO_3-12: $C_{36}H_{78}N_2O_3Br_2$ (746.84) (Calc. C, 57.90; H, 10.53; N, 3.75. Found C, 57.48; H, 10.54; N, 3.76); δ_H(300 MHz, $CDCl_3$) 0.85 (t, 6 H), 1.22, 1.32 (s, m 36 H), 1.70 (m, 4 H), 3.41 (s, 12 H), 3.54 (m, 4 H), 3.61 (m, 4 H), 3.72 (m, 4 H), 3.90 (m, 4 H), 4.08 (m, 4 H). 12-EO_4-12: $C_{38}H_{82}N_2O_4Br_2$ (790.89) (Calc. 57.71; H, 10.45; N, 3.54. Found C, 57.81; H, 10.60; N, 3.67); δ_H(300 MHz, $CDCl_3$) 0.85 (t, 6 H), 1.22, 1.32 (s, m 36 H), 1.70 (m, 4 H), 3.42 (s, 12 H), 3.6 (m, 12 H), 3.72 (m, 4 H), 3.88 (m, 4 H), 4.08 (m, 4 H). 12-EO_5-12: $C_{40}H_{86}N_2O_5Br_2$ (834.94) (Calc. C, 57.54; H, 10.40; N, 3.36. Found C, 57.37; H, 10.59; N, 3.44) δ_H(300 MHz, $CDCl_3$) 0.85 (t, 6 H), 1.22, 1.32 (s, m 36 H), 1.70 (m, 4 H), 3.42 (s 12 H), 3.6 (m, 16 H), 3.72 (m, 4 H), 3.88 (m, 4 H), 4.08 (m, 4 H).

1 C. Tschierske, *Progr. Polym. Sci.*, 1996, **21**, 775.
2 C. A. Bunton, C. Robinson, J. Schaak and M. F. Stam, *J. Org. Chem.*, 1971, **34**, 780; F. Devinsky, I. Lacko and T. Imam, *J. Colloid Interface Sci.*, 1991, **143**, 336; R. Zana, M. Benrraou and R. Rueff, *Langmuir*, 1991, **7**, 1072.
3 (*a*) F. Devinsky, I. Lacko, F. Bitterova and L. Tomeckova, *J. Colloid Interface Sci.*, 1986, **114**, 314; (*b*) M. Diz, A. Mamresa, A. Pinazo, P. Erra and M. R. Infante, *J. Chem. Soc., Perkins Trans. 2*, 1994, 1871; (*c*) M. Pavlikova, I. Lucko, F. Devinsky and D. Mlgnarcik, *Collect. Czech. Chem. Commun.*, 1995, **60**, 1213; (*d*) L. D. Song and M. J. Rosen, *Langmuir*, 1996, **12**, 1149.
4 A. Lüttringhaus, F. Cramer, H. Prinzbach and F. M. Henglein, *Liebigs. Ann. Chem.*, 1958, **613**, 185.
5 (*a*) S. Fuller, N. N. Shinde, G. J. T. Tiddy, G. S. Attard and O. Howell, *Langmuir*, 1996, **12**, 1117; (*b*) E. Alami, H. Levy, R. Zana and A. Skoulios, *Langmuir*, 1993, **9**, 940.
6 D. Tsiourvas, C. M. Paleos and A. Skoulios, *Macromolecules*, 1997, **30**, 7191.
7 K. M. Lee, C. K. Lee and I. J. B. Lin, *Chem. Commun.*, 1997, 899.
8 M. Dreja and B. Tieke, *Langmuir*, 1998, **14**, 800.

Received in Bath, UK, 10th February 1998; 8/01448E

First uranium(IV) triflates

Jean Claude Berthet,[a] Monique Lance,[b] Martine Nierlich[b] and Michel Ephritikhine[a]

[a] *Laboratoire de Chimie de l'Uranium, Service de Chimie Moléculaire, CNRS URA 331, CEA Saclay, 91191 Gif sur Yvette, France*

[b] *Laboratoire de Cristallochimie, Service de Chimie Moléculaire, CNRS URA 331, CEA Saclay, 91191 Gif sur Yvette, France*

The uranium(IV) triflates $[U(Cp^*)_2(OTf)_2]$, $[U(Cp)_2(OTf)_2(py)]$, $[U(Cp)_3(OTf)]$, $[U(cot)(OTf)_2(py)]$ and $[U(OTf)_4(py)]$ have been synthesized by protonation of amide or alkyl precursors with pyridinium triflate; the crystal structures of $[U(Cp^*)_2(OTf)_2(OH_2)]$ and $[U(Cp)_3(OTf)(CNBu^t)]$ have been determined.

Transition metal triflates (trifluoromethanesulfonates) are much considered as Lewis acid catalysts in a variety of organic reactions, as well as precursors in inorganic and organometallic synthesis.[1] While the utility of lanthanide triflates has been clearly recognized in recent years,[2] scant attention has been paid to the actinide counterparts; a few thorium(IV) triflates have been reported[3,4] and the only uranium triflates are uranyl derivatives.[5] Here, we present the first uranium(IV) triflates, $[U(OTf)_4(py)]$, and a series of cyclopentadienyl and cyclooctatetraene derivatives; these were conveniently synthesized by using the pyridinium triflate as a novel reagent for the protonolysis of U–C and U–N bonds. We also describe the crystal structures of $[U(Cp^*)_2(OTf)_2(OH_2)]$ and $[U(Cp)_3(OTf)(CNBu^t)]$.

We first tried to prepare the cyclopentadienyl complexes $[U(Cp^*)_2(OTf)_2]$ **1** and $[U(Cp)_3(OTf)]$ **2** since $[U(Cp^*)_2X_2]$ and $[U(Cp)_3X]$ compounds are regarded, for most X groups, as models in organouranium chemistry. In an NMR test experiment, $[U(Cp^*)_2Me_2]$ was treated at 20 °C in toluene with 2 equiv. of HOTf; immediate evolution of gas was observed and the spectrum showed a new single signal at δ 20.1, corresponding to the Cp* groups. The solution was evaporated and crystallization of the red–brown powder from thf–pentane gave a few crystals of $[U(Cp^*)_2(OTf)_2(OH_2)]$; these were characterized by X-ray crystallography (*vide infra*). Difficulties were encountered when the above reaction was performed in a preparative scale; products resulting from protonation of Cp* ligands were also formed in variable yields. Other attempts to prepare **1** by treating the complexes $[U(Cp^*)_2X_2]$ (X = Me, NMe_2, Cl) with AgOTf in thf or benzene were unsuccessful; complicated mixtures were obtained and thf was quickly polymerized. We found that the best way to obtain complex **1** was the reaction of $[U(Cp^*)_2Me_2]$ with PyHOTf, which could be easily reproduced, and gave **1** in satisfactory yield. A solution of the pyridinium salt (219 mg) in thf (25 cm^3) was slowly added to the bis(alkyl) complex (215 mg) in thf (20 cm^3) at −70 °C; the mixture was stirred for 1 h at 20 °C and after evaporation to dryness, the red–brown powder was extracted in toluene and washed with pentane (78% yield). Similar treatment of $[U(Cp^*)_2(NMe_2)_2]$ also gave **1** in good yield. By following the same procedure, the organouranium compounds $[U(Cp)_3X]$ (X = NEt_2, Bu^n), $[U(Cp)_2(NEt_2)_2]$ and $[U(cot)\{N(SiMe_3)_2\}_2]$ were transformed into $[U(Cp)_3(OTf)]$ **2** (brown, 93%), $[U(Cp)_2(OTf)_2(py)]$ **3** (orange, 60%) and $[U(cot)(OTf)_2(py)]$ **4** (brown, 92%), respectively. It is noteworthy that **3** was stable towards ligand exchange reactions, whereas $[U(Cp)_2Cl_2]$ and its Lewis base adducts could not be isolated.[6] In the presence of an excess of Bu^tNC in thf–pentane, **2** was converted into $[U(Cp)_3(OTf)(CNBu^t)]$, the crystal structure of which was determined (*vide infra*); interestingly, the triflate group of **2** was not displaced by the isocyanide molecule.

The pyridinium triflate proved thus to be very efficient in the protonolysis reactions of U–C and U–N bonds. In contrast to triflic acid, this commercial powder is not hygroscopic, does not polymerize thf, can be stored for a long time and is easy to handle. This reagent was also useful to prepare a pyridine adduct of the homoleptic uranium(IV) triflate $[U(OTf)_4]$ while more classical routes, by reacting UCl_4 with HOTf or AgOTf, were not straightforward. The complex $[U(OTf)_4(py)]$ **5** was synthesized in 76% yield by treating the metallacycle $[U\{N(SiMe_3)(SiMe_2CH_2)\}\{N(SiMe_3)_2\}_2]$ (250 mg) with PyHOTf (319 mg) in pyridine (20 cm^3). The solution was heated at 110 °C for 20 h and after partial evaporation and addition of diethyl ether, deposited a green microcrystalline powder. Complex **5** would be a useful precursor for the synthesis of organometallic derivatives. For example, its reactions with K_2cot or $[U(cot)_2]$ in thf afforded **4** in almost quantitative yield (NMR experiments), providing a new access to monocyclooctatetraene uranium compounds; it is noteworthy that the chloride analogue $[U(cot)Cl_2(thf)_2]$ could not be obtained by similar treatment of UCl_4.[7]

Complexes **1**–**5** were characterized by elemental analyses (C, H, N or S) and ^1H NMR spectroscopy.‡ Besides a dimeric triflate bridged thorium compound,[3] $[U(Cp^*)_2(OTf)_2(OH_2)]$ and $[U(Cp)_3(OTf)(CNBu^t)]$ are the only actinide(IV) triflates to have been crystallographically characterized; the bis(triflate) derivative is also, from the data of the CCDC, the first structurally characterized organouranium compound with a coordinated H_2O molecule. The structures are shown in Fig. 1 and 2 together with selected data.§ The monomeric complexes adopt, respectively, a bent-sandwich configuration with an unsymmetrical arrangement of OTf and H_2O ligands in the

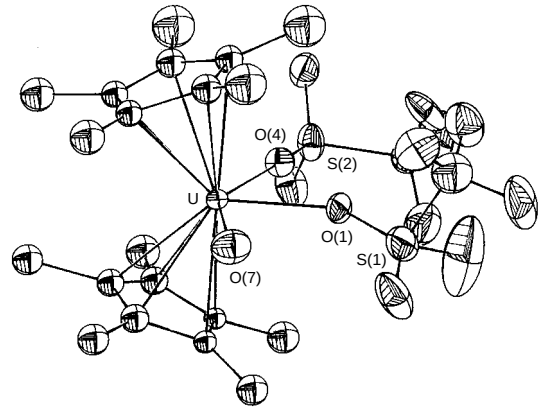

Fig. 1 X-Ray crystal structure of $[U(Cp^*)_2(OTf)_2(OH_2)]$. Displacement ellipsoids are shown at the 33% probability level. Selected bond distances (Å) and angles (°): U–O(1) 2.36(1), U–O(4) 2.40(1), U–O(7) 2.57(2), O(1)–S(1) 1.48(1), O(4)–S(2) 1.45(1); O(1)–U–O(4) 74.8(6), O(1)–U–O(7) 70.2(6), O(4)–U–O(7) 145.0(6), U–O(1)–S(1) 154.3(9), U–O(4)–S(2) 173.7(9).

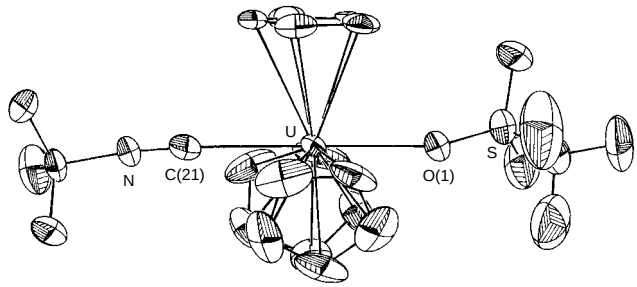

Fig. 2 X-Ray crystal structure of $[U(Cp)_3(OTf)(CNBu^t)]$. Displacement ellipsoids are shown at the 40% probability level. Selected bond distances (Å) and angles (°): U–O(1) 2.485(9), U–C(21) 2.59(2), O(1)–S 1.456(9), C(21)–N 1.13(2); O(1)–U–C(21) 179.3(4), U–O(1)–S 157.7(6), U–C(21)–N 175(1).

equatorial girdle,[8] and a nearly ideal trigonal bipyramidal structure with the Cp groups occupying the equatorial vertices.[9] Coordination of H_2O and Bu^tNC to the U^{IV} centre is unexceptional, with U–O(7) and U–C(21) bond distances of 2.57(2) and 2.59(2) Å. In both compounds, the triflate ligands are monodentate and, as expected for this weakly nucleophilic group, the U–O bond lengths which average 2.42(6) Å are longer than usual U–O σ bond distances (2.0–2.2 Å). In the bis(triflate) compound, the U–O–S angles are inequivalent and rather obtuse, with U–O(1)–S(1) and U–O(4)–S(2) equal to 154.3(9) and 173.7(9)°, respectively; similar structural features were previously noted in the yttrium complex $[Y\{C_6H_{12}N_3(CH_2CONH_2)_3\}(OTf)_2(H_2O)][OTf]$.[10]

In conclusion, the first uranium(IV) triflates were prepared by protonolysis of alkyl and amide precursors with pyridinium triflate; this convenient and efficient reaction should be of general interest for the synthesis of metal triflates. By comparison with their chloride analogues, uranium triflates should exhibit distinct structure and reactivity patterns, and open new perspectives in actinide chemistry.

Notes and References

† E-mail: ephri@nanga.saclay.cea.fr

‡ *Characterising data*: ^{1}H NMR (200 MHz, 30 °C, [$^2H_8$]thf). **1**, δ 20.1 (s, Cp*); **2**, δ −2.45 (s, Cp); **3**, δ 11.2 (10 H, Cp), 8.85, 8.8 and 6.9 (5 H, py); **4**, δ 7.6, 7.4 and 6.9 (5 H, py), −37.5 (8 H, s, cot); **5**, δ 8.8, 7.85 and 7.3 (py). Elemental analyses (%) (calculated values in parentheses). **1**: C, 32.8 (32.75); H, 3.75 (3.75); S, 7.85 (7.95). **2**: C, 32.85 (33.0); H, 2.7 (2.6). **3**: C, 26.65 (27.4); H, 2.0 (2.0); N, 2.05 (1.9), **4**: C, 25.0 (25.0); H, 1.9 (1.8); N, 2.1 (1.95). **5**: C, 12.05 (11.85), H, 0.7 (0.55); N, 1.6 (1.55).

§ *Crystal data* for $[U(Cp^*)_2(OTf)_2(OH_2)]$: $C_{22}H_{32}F_6O_7S_2U$, M = 824.64, crystal dimensions: 0.5 × 0.25 × 0.15 mm, monoclinic, space group *Cc*, a = 18.464(3), b = 10.847(3), c = 17.323(4) Å, β = 126.57(2)°, U = 2787(3) Å^3, Z = 4, D_c = 1.965 g cm^{-3}, 2 < 2θ < 44°, ω–2θ scan mode, μ = 57.44 cm^{-1}, F(000) = 1592, T = −30 °C. 1988 reflections collected, 1787 unique, 1680 reflections with $I > 3\sigma(I)$. Data were corrected for absorption (T_{min} = 0.571, T_{max} = 0.999),[11] Lorentz polarization effects and decay (10% in 30 h, linearly corrected). The structure was solved by the heavy-atom method and refined by full-matrix least squares (F) with anisotropic thermal parameters for all non-C atoms. H atoms were not introduced. The final R values were R = 0.030 and R_w = 0.047 {w = $1/(\sigma F)^2 = 4F^2/[\sigma I^2 + (pF^2)^2]^{1/2}$, p = 0.04}. The absolute structure was determined (R = 0.038 and R_w = 0.053). For $[U(Cp)_3(OTf)(CNBu^t)]$, $C_{21}H_{24}NF_3O_3SU$, M = 665.52, crystal dimensions: 0.4 × 0.35 × 0.15 mm, monoclinic, space group $P2_1/n$, a = 8.533(1), b = 19.545(4), c = 13.890(3) Å, β = 90.65(2)°, U = 2316(1) Å^3, Z = 4, D_c = 1.908 g cm^{-3}, 2 < 2θ < 44°, ω–2θ scan mode, μ = 67.75 cm^{-1}, F(000) = 1264, T = 22 °C. 3195 reflections collected, 2961 unique, 2018 reflections with $I > 3\sigma(I)$. Data were corrected for absorption (T_{min} = 0.452, T_{max} = 0.999),[11] Lorentz polarization effects and decay (19% in 39 h, linearly corrected). The structure was solved by the heavy-atom method and refined by full-matrix least squares (F) with anisotropic thermal parameters. H atoms were not introduced. The final R values were R = 0.031 and R_w = 0.042 {w = $1/(\sigma F)^2 = 4F^2/[\sigma I^2 + (pF^2)^2]^{1/2}$, p = 0.04}. For both compounds, diffraction data were recorded on an Enraf-Nonius CAD4 diffractometer using graphite-monochromatized Mo-Kα radiation (λ = 0.710 73 Å). All calculations were performed on a VAX 4000-200 computer with the Enraf-Nonius MolEN package.[12] CCDC 182/879.

1 G. A. Lawrance, *Chem. Rev.*, 1986, **86**, 17.
2 S. Kobayashi, *Synlett*, 1994, 689; F. T. Edelmann, *New. J. Chem.*, 1995, **19**, 535; H. Schumann, J. A. Meese-Marktscheffel, A. Dietrich and F. H. Görlitz, *J. Organomet. Chem.*, 1992, **430**, 299.
3 M. Schmeisser, B. Sartori and B. Lippsmeier, *Chem. Ber.*, 1970, **103**, 868; R. D. Gillespie, R. L. Burwell and T. J. Marks, *Langmuir*, 1990, **6**, 1465.
4 R. J. Butcher, D. L. Clark, S. K. Grumbine and J. G. Watkin, *Organometallics*, 1995, **14**, 2799.
5 P. Thuéry, M. Nierlich, N. Keller, M. Lance and J. D. Vigner, *Acta Crystallogr., Sect. C*, 1995, **51**, 1300.
6 R. D. Ernst, W. J. Kennelly, C. S. Day, V. W. Day and T. J. Marks, *J. Am. Chem. Soc.*, 1979, **101**, 2656.
7 T. R. Boussie, R. M. Moore, A. Streitwieser, A. Zalkin, J. G. Brennan and K. A. Smith, *Organometallics*, 1990, **9**, 2010.
8 R. S. Sternal, M. Sabat and T. J. Marks, *J. Am. Chem. Soc.*, 1987, **109**, 7920; Z. Lin, J. F. Le Maréchal, M. Sabat and T. J. Marks, *J. Am. Chem. Soc.*, 1987, **109**, 4127; C. W. Eigenbrot and K. N. Raymond, *Inorg. Chem.*, 1982, **21**, 2653.
9 H. Aslan, K. Yünlü, R. D. Fisher, G. Bombieri and F. Benetollo, *J. Organomet. Chem.*, 1988, **354**, 63; G. Bombieri, F. Benetollo, E. Klähne and R. D. Fisher, *J. Chem. Soc., Dalton Trans.*, 1983, 155.
10 S. Amin, C. Marks, L. M. Toomey, M. R. Churchill and J. R. Morrow, *Inorg. Chim. Acta*, 1996, **246**, 99.
11 A. C. T. North, D. C. Phillips and F. S. Mathews, *Acta Crystallogr., Sect. A*, 1968, **24**, 351.
12 MolEN, *An Interactive Structure Solution Procedure*, Enraf-Nonius, Delft, The Netherlands, 1990.

Received in Cambridge, UK, 10th March 1998; 8/01936C

A remarkable example of co-crystallisation: the crystal structure of the mononuclear and dinuclear diphenyl[2.2]paracyclophanylphosphine palladium(II) chloride complexes *trans*-$[Pd\{PPh_2(C_{16}H_{15})\}_2Cl_2]\cdot[Pd\{PPh_2(C_{16}H_{15})\}Cl_2]_2\cdot 0.6CH_2Cl_2$

Philip W. Dyer,[a] Paul J. Dyson,*[a]† Stuart L. James,[a] Priya Suman,[a] John E. Davies[b] and Caroline M. Martin[b]

[a] *Centre for Chemical Synthesis, Department of Chemistry, Imperial College of Science, Technology and Medicine, South Kensington, London, UK SW7 2AY*

[b] *Department of Chemistry, The University of Cambridge, Lensfield Road, Cambridge, UK CB2 1EW*

The reaction of $[Pd(cod)Cl_2]$ (cod = cycloocta-1,5-diene) with *rac*-diphenyl[2.2]paracyclophanylphosphine $PPh_2(C_{16}H_{15})$ affords *trans*-$[Pd\{PPh_2(C_{16}H_{15})\}_2Cl_2]$ and $[Pd\{PPh_2(C_{16}H_{15})\}Cl_2]_2$ in approximately equal yield which co-crystallise to form an unusual solid-state material.

Crystallisation of organic compounds is a common phenomenon and often of commercial value.[1] In inorganic/organometallic chemistry many anion–cation pairs[2] and to a lesser extent conformational isomers and polymorphs[3] have been recognised. However, co-crystals composed of two different neutral molecules are very rare and most can be classified as those which have two or more very similar molecules, often differing in a substituent on a ligand[4] or by the presence of slightly different ligand such as replacement of one halide for another.[5] Some co-crystals contain an inorganic/organometallic species in which a small or cylindrical 'solvent-like' molecule has been co-crystallised, for example, HgX_2 (X = I, Cl, F) and metallocenes.[6] We have also found one example of a co-crystal containing a neutral mononuclear and dinuclear complex[7] and one example involving clusters[8] in the literature.

We have been investigating the synthesis of [2.2]paracyclophanyl–phosphine ligands and studying their coordination chemistry.[9] This substituent was chosen as [2.2]paracyclophane has unusual nucleophilic behaviour with respect to its coordination chemistry.[10] Another group have also recently reported the synthesis of a chiral diphosphine with a [2.2]paracyclophane backbone which has some very impressive applications in catalysis.[11] We report here the synthesis of a new [2.2]paracyclophane containing phosphine and the discovery that it reacts with $[Pd(cod)Cl_2]$ to afford two $Pd^{II}Cl_2$ complexes which form a co-crystalline material in the solid-state.

The reaction of $C_{16}H_{15}Li$,[12] with PPh_2Cl, added dropwise in diethyl ether, affords diphenyl[2.2]paracyclophanylphosphine $PPh_2(C_{16}H_{15})$ in 62% yield after recrystallisation from ethanol. Reaction of this phosphine with $[Pd(cod)Cl_2]$ in dichloromethane at room temperature for 1 h affords an orange solution which exhibits two singlets of approximately equal intensity at δ 33.93 and 33.53 in its ^{31}P NMR spectrum. From later observations we assume these to be due to the two complexes *trans*-$[Pd\{PPh_2(C_{16}H_{15})\}_2Cl_2]$ **1** and $[Pd\{PPh_2(C_{16}H_{15})\}Cl_2]_2$ **2** and not from diastereomers of the same complex. The *cis*- and *trans*-platinum(II) chloride complexes of *rac*-$PPh_2(C_{16}H_{15})$ also show only one main resonance in their ^{31}P NMR spectra excluding the ^{195}Pt satellites.[13] Crystals were grown by removing the solvent and redissolving the solid in dichloromethane–diethyl ether. After allowing the solution to evaporate at room temperature for several days orange crystals formed which were suitable for single crystal X-ray diffraction analysis.‡ This reveals the remarkable co-crystalline structure described below.

The structures of **1** and **2** are shown in Figs. 1 and 2,

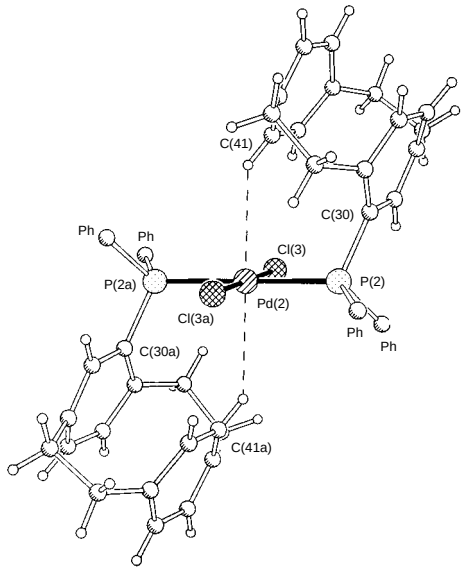

Fig. 1 Molecular geometry of **1**; selected bond lengths (Å) and angles (°): Pd(2)–P(2) 2.355(2), Pd(2)–Cl(3) 2.301(2), P(2)–C(30) 1.826(7), Pd(2)···H(41) 2.853, Cl(3)–Pd(2)–P(2) 88.07(7)

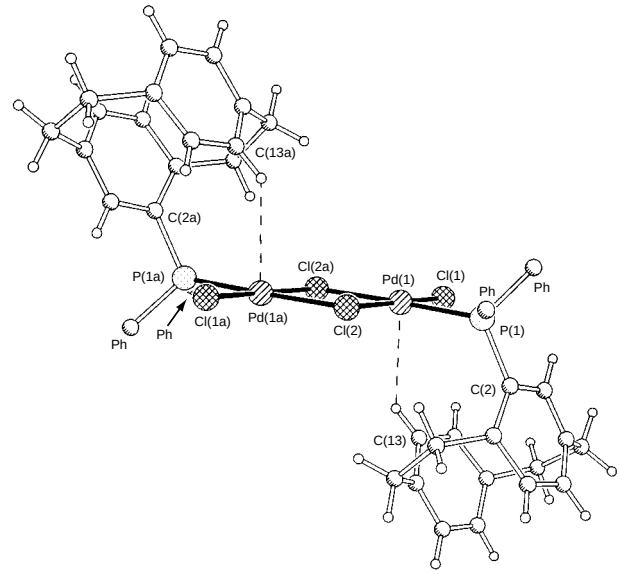

Fig. 2 Molecular geometry of **2**; selected bond lengths (Å) and angles (°): Pd(1)–P(1) 2.229(2), Pd(1)–Cl(1) 2.280(2), Pd(1)–Cl(2) 2.332(2), Pd(1)–Cl(2a) 2.429(2), P(1)–C(2) 1.816(7), Pd(1)···H(13) 2.933, P(1)–Pd(1)–Cl(2a) 177.29(8), Cl(1)–Pd(1)–Cl(2) 177.29(8)

respectively, together with principal bond parameters. In both **1** and **2** one of each enantiomer of $PPh_2(C_{16}H_{15})$ is present. The phosphines adopt a *trans*-conformation in **1** presumably due to the steric bulk of the [2.2]paracyclophanyl-substituent. The axial sites above and below the square plane are occupied by intramolecular interactions involving a proton on the [2.2]paracyclophane rings of each phosphine ligand (Pd···H 2.85 Å). The structure of **2** comprises a chloro-bridged dimer in which each palladium centre is approximately square planar. As in **1** and other similar square planar complexes[14] the axial sites form weak intra- or inter-molecular interactions in the solid state. In **2** the [2.2]paracyclophanyl group of each phosphine occupies one site on each of the palladium(II) centres (Pd···H 2.93 Å). The other site is occupied *via* an intermolecular interaction and it is this that possibly gives rise to the formation of the co-crystal (see below).

The crystal is composed of alternating layers of **1** and **2** intercalated with dichloromethane solvent molecules. There is one direct, albeit weak, hydrogen bond between **1** and **2** involving the Cl atoms on **1** with a phenyl ring proton on **2** (Cl···H 2.83 Å), shown in Fig. 3. Perhaps more importantly, compounds **1** and **2** are linked indirectly *via* one of the two CH_2Cl_2 solvent molecules as shown in Fig. 4. There is a bifurcated hydrogen bonding interaction between the H atom on the solvent with one terminal Cl (H···Cl 2.83 Å) and one bridging Cl (H···Cl 2.80 Å) of**2**. A Cl atom of this same solvent molecule also interacts with the H atom of a cyclophane attached to the phosphine in **1** (Cl···H 2.86 Å) thereby forming a **1**···Cl–C–H·**2** linkage (see Fig. 4). The second CH_2Cl_2 connects molecules of **1** *via* two interactions involving the H and Cl atoms of both the solvent and the complex. At this stage we can only speculate as to the precise role of the solvent but since it links **1** and **2** it may play a part in the co-crystallisation process. In this material partial desolvation has taken place but the co-crystal still retains its structure. We intend to examine the influence of solvents with various hydrogen bonding capabilities as well as the influence of the halide coordinated to the Pd^{II} centre.

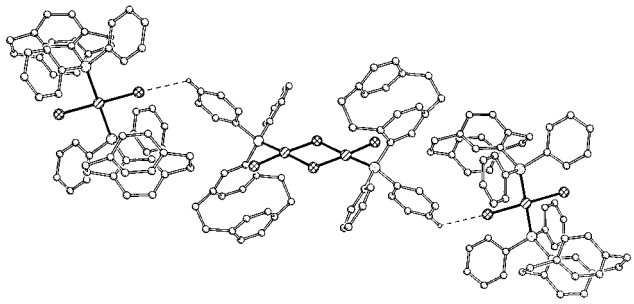

Fig. 3 The direct interaction, **1**··**2**

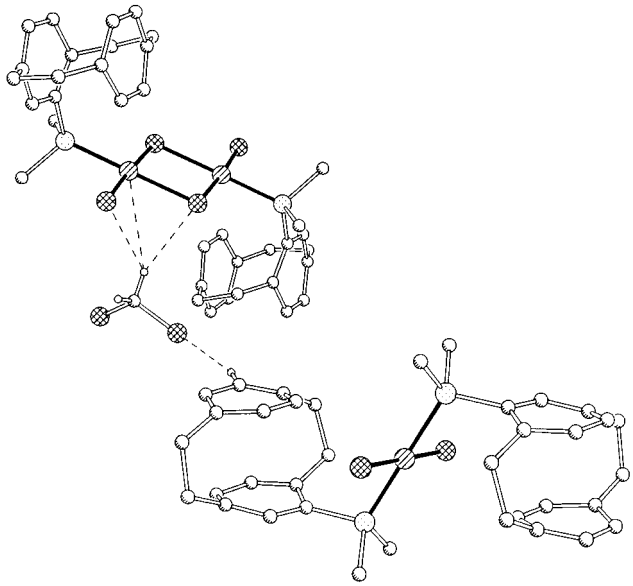

Fig. 4 The indirect solvent bridging interaction, **1**···Cl–C–H·**2**

We would like to thank the Royal Society for a University Research Fellowship (P. J. D.) and the EPSRC (P. S.) for financial support.

Notes and References

† E-mail: p.dyson@ic.ac.uk

‡ *Structural characterisation* of **1** and **2**: orange crystal, $C_{112.6}H_{101.2}Cl_{17.2}P_4Pd_3$, $[C_{56}H_{50}Cl_4P_2Pd_2\cdot C_{56}H_{50}Cl_2P_2Pd\cdot 0.6CH_2Cl_2]$, M = 2152.66, 0.20 × 0.20 × 0.20 mm, T = 180(2) K, triclinic, $P\bar{1}$, a = 12.033(3), b = 18.673(2), c = 11.871(2) Å, α = 95.20(1), β = 94.73(1), γ = 100.04(1)°, U = 2602.5(8) Å^3, Z = 1, F(000) = 1097, D_c = 1.374 Mg m^{-3}, λ = 0.71069 Å, $R1$ = 0.0555 [9152 intensity data with $I > 2\sigma(I)$] and $wR2$ = 0.1673 for 9156 independent reflections corrected for adsorption [μ(Mo-Kα) = 0.805 mm^{-1}] and 598 parameters (all non-H atoms anisotropic except solvent molecules). CCDC 182/882.

1 A. I. Kitaigorodsky, in *Mixed Crystals*, ed. M. Cardona, Solid State Sciences, vol. 33, Springer-Verlag, Berlin, 1984; G. R. Desiraju, *Crystal Engineering. The Design of Organic Solids*, Elsevier, Amsterdam, 1989.
2 See, for example: D. Braga, F. Grepioni, P. Milne and E. Parasini, *J. Am. Chem. Soc.*, 1993, **115**, 5115.
3 See, for example: D. Braga, F. Grepioni, P. J. Dyson, B. F. G. Johnson, P. Frediani, M. Bianchi and F. Piacenti, *J. Chem. Soc., Dalton Trans.*, 1992, 2565.
4 See, for example: C. A. Cotton, D. J. Darensbourg, A. Fang, B. W. S. Kolthammer, D. Reed and J. L. Thompson, *Inorg. Chem.*, 1981, **20**, 4090.
5 See, for example: P. A. Bianconi, R. N. Vrtis, C. P. Rao, I. D. Williams, M. P. Engeler and S. J. Lippard, *Organometallics*, 1987, **6**, 1968; C. J. Cardin, D. J. Cardin, D. A. Morton-Blake, H. E. Parge and A. Roy, *J. Chem. Soc., Dalton Trans.*, 1987, 1641.
6 G. K.-I. Magommedov, A. I. Gusev, A. S. Frenkel, V. G. Sirkin, L. I. Chaplina and S. N. Gourkova, *Koord. Khim.*, 1976, **2**, 257; J. Votinsky, L. Benes, J. Klikorka, J. Kalousova, J. Horak and P. Lostak, *J. Appl. Crystallogr.*, 1984, **17**, 363.
7 M. Maekawa, M. Munakata, T. Kuroda-Sowa and K. Hachiya, *Inorg. Chim. Acta*, 1995, **232**, 231.
8 D. Braga, F. Grepioni, C. M. Martin, E. Parisini, P. J. Dyson and B. F. G. Johnson, *Organometallics*, 1994, **13**, 2170.
9 P. W. Dyer, P. J. Dyson, S. L. James and P. Suman, in preparation.
10 P. J. Dyson, D. G. Humphrey, J. E. McGrady, D. M. P. Mingos and D. J. Wilson, *J. Chem. Soc., Dalton Trans.*, 1995, 4039.
11 P. J. Pye, K. Rossen, R. A. Reamer, N. N. Tsou, R. P. Volante and P. J. Reider, *J. Am. Chem. Soc.*, 1997, **119**, 6207; K. Rossen, P. J. Pye, A. Maliakal and R. P. Volante, *J. Org. Chem.*, 1997, **62**, 6462.
12 H. J. Reich and D. J. Cram, *J. Am. Chem. Soc.*, 1969, **91**, 3505.
13 P. J. Dyson and P. Suman, unpublished work.
14 E. C. Alyea, G. Ferguson and S. Kannan, *Chem. Commun.*, 1998, 345.

Received in Basel, Switzerland, 6th March 1998; 8/01863D

Enantioselective hydrogenation of a cyclic imidoketone over chirally modified Pt/Al_2O_3

Niklaus Künzle, Andras Szabo, Markus Schürch, Guozhi Wang, Tamas Mallat and Alfons Baiker*†

Laboratory of Technical Chemistry, Swiss Federal Institute of Technology, ETH-Zentrum, CH-8092 Zürich, Switzerland

1-Ethyl-4,4-dimethylpyrrolidine-2,3,5-trione 1 has been synthesized, and hydrogenated with 91% ee to (*R*)-1-ethyl-3-hydroxy-4,4-dimethylpyrrolidine-2,5-dione (2) using a 5 mass% Pt/Al_2O_3 catalyst modified by cinchonidine

In the past decade the enantioselective hydrogenation of carbonyl compounds has been one of the most intensively studied areas in asymmetric catalysis.[1] An efficient strategy for achieving reasonable enantioselectivity over solid catalysts is the modification of an active metal by adsorbed auxiliaries from the chiral pool.[2] Since the first application of cinchona-modified Pt,[3] considerable effort has been made to broaden the application range of this catalyst system. Good to high ee values were obtained in the hydrogenation of α-ketoesters[4] and acids,[5] and ketopantolactone.[6] The hydrogenation of other types of activated carbonyl compounds, such as α-diketones,[7] trifluoracetophenone[8] and pyruvamides,[9] was less successful affording only 60% ee or less. It seems that the Pt-cinchona system possesses unusually high substrate specificity.

In a systematic study, intended to reveal the nature of enantioselective hydrogenation of ketoimides over chirally modified Pt metals, a remarkable ee was obtained in the reduction of 1-ethyl-4,4-dimethylpyrrolidine-2,3,5-trione **1**. The starting material **1** was synthesized from racemic pantolactone [(*R*,*S*)-2-hydroxy-3,3-dimethyl-γ-butyrolactone] in two steps. The lactone ring was cleaved by ethylamine and oxidation of the resulting amide with pyridinium dichromate gave **1**.‡

The hydrogenation of the cyclic imidoketone **1** (Scheme 1) was carried out in a magnetically stirred (frequency: 1000 min^{-1}) 100 ml stainless steel Baskerville autoclave equipped with a glass liner and PTFE cover. 60 mg of a 5 mass% Pt/Al_2O_3 (Engelhard 4759) catalyst was pretreated for 90 min in a hydrogen stream at 400 °C, as described earlier.[6] Under standard conditions the reaction was carried out using 3.2 mmol **1** and 10 μmol cinchonidine in 5 ml toluene, at 15 °C and 70 bar hydrogen pressure. The reaction was stopped when hydrogen consumption ceased. No other product besides **2** could be detected by gas chromatography.

For the determination of the absolute configuration of the product, the pure (*R*)-enantiomer of **2** has been synthesized starting from (*R*)-pantolactone. The hydroxyl function of (*R*)-pantolactone was protected by a tetrahydropyranyl group. After treatment with ethylamine, the resulting hydroxyamide was oxidized by pyridinium dichromate in DMF. Deprotection in the presence of TsOH gave (*R*)-**2** in optically pure form. Gas chromatographic analysis using a chiral column (WCOT Cyclodextrin-β-2,3,6-M-19, Chrompack) proved that (*R*)-**2** was identical with the major enantiomer obtained in the hydrogenation.

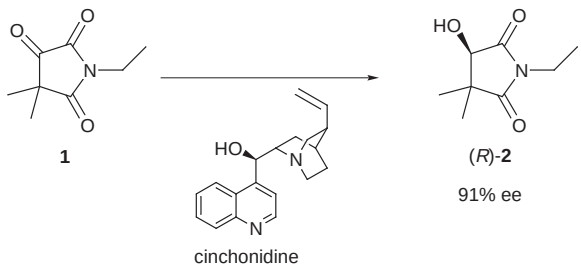

Scheme 1 Hydrogenation of **1**. *Conditions:* 5 mass% Pt/Al_2O_3, 9 μmol l^{-1} cinchonidine, 70 bar H_2, toluene, 15 °C.

Preliminary studies revealed that the enantiodifferentiation in the hydrogenation of **1** over the Pt–cinchonidine catalyst system was rather sensitive to the reaction medium. Good ee could be obtained only in weakly polar solvents, such as toluene. In polar and protic polar solvents (*e.g.* DMF, EtOH) the ee dropped to 20% or below. The only exception was acetic acid. The polarity of this solvent characterized by the empirical solvent parameter,[10] E^T_N, is about the same as that of EtOH, but the ee was remarkably higher (*ca.* 70 % instead of 20%, respectively, under standard conditions). Previously, the outstanding ee in acetic acid in the enantioselective hydrogenation of ethyl pyruvate was attributed to the protonation of the quinuclidine N atom of cinchonidine in acetic acid.[11] We assume that, similarly to the hydrogenation of ethyl pyruvate and ketopantolactone,[6] in the transition complex the quinuclidine N atom of cinchonidine interacts with the O atom of the activated carbonyl group *via* hydrogen bonding. Catalytic studies and molecular modeling are presently being carried out to confirm this assumption and uncover the role of acid in the enantiodifferentiation.

High hydrogen concentration on the Pt surface favoured the enantiodifferentiation, as illustrated in Fig. 1. This condition can be achieved by applying at least 30 bar hydrogen pressure and efficient stirring.

A reliable kinetic analysis based on the rate of hydrogen consumption could not be carried out owing to the small amount of substrate. In order to check the possible influence of mass transport limitation on the enantioselectivity, the stirring frequency was varied between 250 and 1000 min^{-1}. No significant change in ee was observed in this range of stirring frequency.

The influence of modifier concentration is illustrated in Fig. 2. A maximum of 91% ee was achieved at 9 μmol l^{-1} cinchonidine concentration in toluene; this value corresponds to a substrate : modifier molar ratio of 70 000. It should be

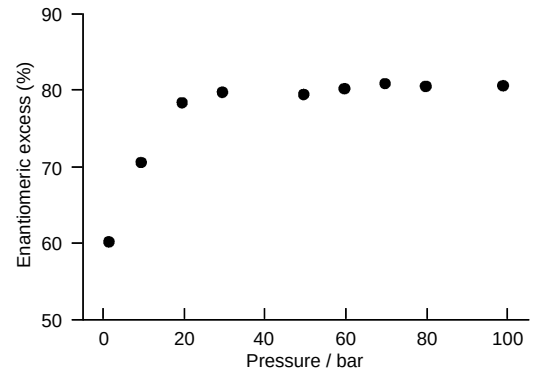

Fig. 1 Influence of hydrogen pressure on the enantiomeric excess (standard conditions except the pressure)

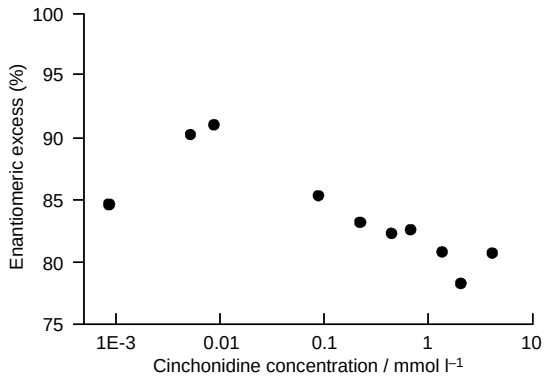

Fig. 2 Influence of modifier concentration on the enantiomeric excess (under otherwise standard conditions)

emphasized that no special pretreatment is required for establishing the 'chiral environment' on the Pt surface; the surface cinchonidine concentration is controlled by its bulk concentration and by the competitive adsorption of hydrogen, substrate and solvent.

The ee decreased with increasing temperature but the change (only 5% under standard conditions) was minor between +15 and −20 °C.

The influence of the above discussed reaction parameters is rather similar to those reported for the enantioselective hydrogenation of α-ketoesters[4] and ketopantolactone[6] over the same catalyst system, but distinctly different from that observed in the hydrogenation of trifluoracetophenone.[8]

Finally it should be mentioned that so far, there was no other substrate besides ethyl pyruvate[3] which could be hydrogenated with an ee exceeding 90% using the Pt–cinchona system. The chiral tertiary alcohol **2** can be used as an auxiliary in enantioselective Diels–Alder reactions. Promising results have already been reported for a similar application of (*R*)-pantolactone and an (*S*)-*N*-methyl-2-hydroxysuccinimide.[12]

Financial support by the Swiss National Science Foundation (Chiral 2) is kindly acknowledged.

Notes and References

† E-mail: baiker@tech.chem.ethz.ch

‡ A detailed description of the synthesis of **1** and (*R*)-**2** is available from the authors on request.

1 R. Noyori, *Chem. Soc. Rev*., 1989, 187; G. Zassinovich, G. Mestroni and S. Gladiali, *Chem. Rev.*, 1992, **92**, 1051; H. Takaya, T. Ohta and R. Noyori, in *Catalytic Asymmetric Synthesis*, ed. I. Ojima, VCH, New York, 1993, p.1.
2 Y. Izumi, *Adv. Catal.*, 1983, **32**, 215; H. U. Blaser, *Tetrahedron: Asymmetry*, 1991, **2**, 843; G. Webb and P. B. Wells, *Catal. Today*, 1992, **12**, 319; A. Baiker, *J. Mol. Catal. A: Chem.*, 1997, **115**, 473; T. Osawa, T. Harada and A. Tai, *Catal. Today*, 1997, **37**, 465.
3 Y. Orito, S. Imai, S. Niwa and G.-H. Nguyen, *J. Synth. Org. Chem. Jpn*., 1979, **37**, 173; Y. Orito, S. Imai and S. Niwa, *J. Chem. Soc. Jpn*., 1979, 1118.
4 H. U. Blaser, H. P. Jalett and J. Wiehl, *J. Mol. Catal.*, 1991, **68**, 215.
5 H. U. Blaser and H. P. Jalett, *Stud. Surf. Sci. Catal.*, 1993, **78**, 139.
6 M. Schürch, O. Schwalm, T. Mallat, J. Weber and A. Baiker, *J. Catal*., 1997, **169**, 275.
7 W. A. H. Vermeer, A. Fulford, P. Johnston and P. B. Wells, *J. Chem. Soc., Chem. Commun.*, 1993, 1053.
8 T. Mallat, M. Bodmer and A. Baiker, *Catal. Lett.*, 1997, **44**, 95.
9 G.-Z. Wang, T. Mallat and A. Baiker, *Tetrahedron Asymmetry*, 1997, **8**, 2133.
10 C. Reichardt, *Solvents and Solvent Effects in Organic Chemistry*, VCH, Weinheim, 2nd edn., 1988.
11 B. Minder, T. Mallat, P. Skrabal and A. Baiker, *Catal. Lett*., 1994, **29**, 115.
12 T. Poll, A. F. Abdel Hady, R. Karge, G. Linz and G. Helmchen, *Tetrahedron Lett*., 1989, **30**, 5595; G. Linz, J. Weetman, A. F. Abdel Hady and G. Helmchen, *Tetrahedron Lett*., 1989, **30**, 5599.

Received in Cambridge, UK, 3rd March 1998; 8/01760C

Enantioselective photoelectrocyclization within zeolites: tropolone methyl ether in chirally modified NaY

Abraham Joy,[a] John R. Scheffer,[b] David R. Corbin[c] and V. Ramamurthy*[a]†

[a] *Department of Chemistry, Tulane University, New Orleans, LA 70118, USA*
[b] *Department of Chemistry, University of British Columbia, Vancouver, Canada V6T 1Z1*
[c] *Central Research and Development, DuPont Company, Wilmington, DE 19880, USA*

Tropolone methyl ether, included within chirally modified Y zeolite, upon irradiation yields a product of 4e electrocyclization in *ca.* 40% ee.

During the past decade, many elegant and efficient chiral induction strategies have been developed for a variety of thermal reactions.[1] There are, however, considerably fewer examples of asymmetric induction in photochemical transformations.[2] A recent successful approach in this latter context has been to make use of confined media such as inclusion complexes and crystals.[3–5] Zeolites offer advantages over other confined media in that they can be used for catalysis,[6] and our long range objective is to prepare reusable zeolite-based materials for asymmetric catalysis of photochemical processes. First, however, we must establish the feasibility of employing zeolite matrices for non-catalytic asymmetric induction, and here we illustrate our strategy with the well known photocyclization of α-tropolone methyl ether **1** as an example.[7,8]

Upon exposure to UV light, α-tropolone methyl ether undergoes 4π-electron disrotatory electrocyclic ring closure to yield the bicyclic photoisomer **2** (Scheme 1).[7] Irradiation in solution results in a racemic mixture as the result of an equal probability of 'in' and 'out' rotation as illustrated in Scheme 1. An obvious approach to control the mode of cyclization is to adsorb compound **1** on a surface, since under these conditions, it is possible that the surface could interfere with one of the two modes of disrotation. Even then racemic products would be expected because compound **1** should not show any preference for adsorption from either enantiotopic face. On the other hand, when the surface is chiral, preferential adsorption from one of the two enantiotopic faces is likely, and under such conditions, one might anticipate enantioselectivity in the formation of photoproduct **2**. This is illustrated in Fig. 1. Enantioselectivity has indeed been achieved in this system by this strategy and the results are presented below. The medium we have used to achieve the desired goal is a zeolite. In the absence of readily available chiral zeolites, we have created an asymmetric environment within a zeolite by the adsorption of chiral organic molecules.[9]

A typical experimental procedure consisted of stirring tropolone methyl ether (0.01 M) and a chiral inductor (0.1 M) with activated NaY (300 mg) in dichloromethane–hexane (1 : 4) for 12 h at room temperature. The zeolite containing both the reactant and a chiral inductor was collected by filtration, washed with an excess of hexane and irradiated (450 W medium pressure mercury lamp, Pyrex filter) as a hexane slurry for 2 h. Sample handling was carried out under laboratory conditions (temperature = 20 °C, humidity 55%). The product was extracted with dichloromethane and analyzed by chiral GC (Supelco β-DEX column). The results are presented in Table 1.

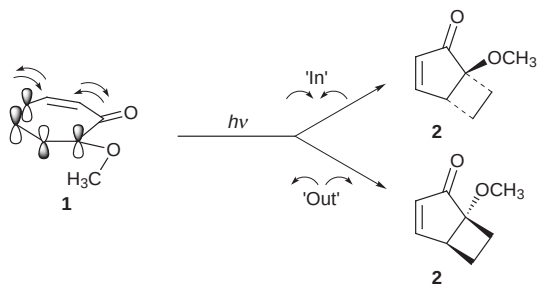

Scheme 1

Independent control experiments established that the numbers reported here are not skewed due to preferential adsorption of one enantiomer of the product within the chirally modified zeolite. The system is well behaved in the sense that, as expected, the optical antipode of the chiral inductor always gave the opposite enantiomer of the product (compare entries 2 and 7; 8 and 9; and 10 and 11 in Table 1). The need for a chiral inductor was clear, since irradiation of compound **1** in unmodified NaY gave racemic **2**. The zeolite is also essential as shown by the fact that none of the chiral inductors listed in Table 1 led to any enantioselectivity when photolyzed with compound **1** in solution (dichloromethane–hexane).

Examination of Table 1 reveals that not all chiral inductors are equally effective. Those that contain only one functional group (entries 15–18, Table 1) gave low or negligible chiral induction; more effective were those that contain both an amine and an alcohol functionality, and of these, norephedrine consistently gave good results. As a result, several additional experiments were carried out with norephedrine as the chiral inductor. In one set of experiments (entries 1, 2, 5–7, Table 1), the effect of changing the nature the alkali metal cation present within the zeolite was explored. While no clear trend was evident, this did indicate that NaY and RbY give the best results. In a second set of experiments (entries 2–4), the effect of temperature was briefly examined, which showed that −20 °C is optimum; above room temperature the enantiomeric excess (ee) also decreases and becomes zero at 60 °C.

At low conversions (< 10%, NaY, room temp.), the ee was relatively low (*ca.* 20%), which may be the result of reaction occurring faster at unencumbered sites with no chiral inductor

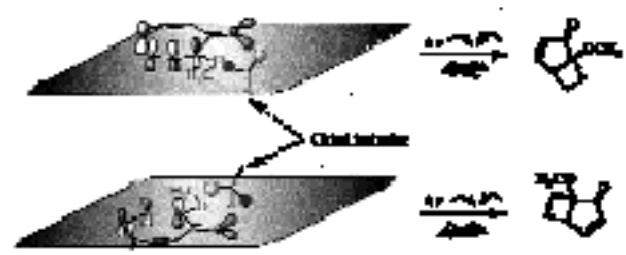

Fig. 1 Influence of a chiral agent on the mode of adsorption of tropolone methyl ether on a surface. On the top surface interactions are between methoxy and dark grey substituent, and carbonyl and light grey substituent. On the bottom surface they are reversed. Assuming one pair of interactions is preferred over the other, tropolone methyl ether will prefer to adsorb in this mode over the other.

Table 1 Dependence of enantiomeric excess on chiral inductor, zeolite and temperature[a–c]

Entry	Chiral auxiliary/zeolite/temp.[d]	ee (%)	Favored isomer[e]
1	(−)-Norephedrine/LiY	15	A
2	(−)-Norephedrine/NaY	35	A
3	(−)-Norephedrine/NaY/−20 °C	50	A
4	(−)-Norephedrine/NaY/−40 °C	31	A
5	(−)-Norephedrine/KY	31	A
6	(−)-Norephedrine/RbY	40	A
7	(−)-Norephedrine/CsY	20	A
8	(+)-Norephedrine/NaY	34	B
9	(−)-Ephedrine (anhydrous)/NaY	7	B
10	(+)-Ephedrine (hemihydrate)/NaY	5	A
11	(−)-Ephedrine hydrochloride/NaY	5	B
12	(+)-Ephedrine hydrochloride/NaY	5	A
13	(+)-Prolinol/NaY	6	B
14	L-Proline *tert*-butyl ester/NaY	7	B
15	(+)-Bornylamine/NaY	2	B
16	(−)-Camphorquinone-3-oxime/NaY	2	B
17	(−)-Menthol/NaY	< 1	—
18	(−)-Borneol/NaY	< 1	—

[a] All irradiations were done on samples that contained 1 mg of tropolone methyl ether and 25 mg of the chiral inductor in 200 mg of dry NaY. [b] Samples were irradiated for 2 h and conversions were within 50%. [c] Tropolone methyl ether and the chiral inductor were co-induced within NaY by three methods. In the first tropolone methyl ether and the chiral inductor were added simultaneously to a suspension of NaY and stirred, in the second the tropolone methyl ether was included into NaY and to the dried sample of tropolone methyl ether-NaY, the chiral inductor was added and stirred. In the third method the sequence in the second approach was reversed. [d] Unless indicated otherwise, the temperature of the reaction was 22 °C. [e] The peak with shorter retention time is arbitrarily assigned to be isomer A.

nearby. Beyond this point, the ee increased and reached a plateau of *ca.* 35% ee at 30% conversion; conversions beyond 50% were not attempted owing to secondary photoreactions of product **2**.[7] Values reported in Table 1 correspond to conversions in the range 35–50%.

From the results presented in Table 1, we tentatively conclude that a three point interaction between the reactant molecule, the chiral inductor and the zeolite interior is necessary to induce preferential adsorption of **1** from a single prochiral face. The fact that monofunctional chiral inductors fail to yield significant enantioselectivity supports this idea. The recognition points in the case of norephedrine are most likely the hydroxyl, amino and aryl groups of the inductor, the cations of the zeolite and the carbonyl and methoxy groups of tropolone methyl ether. The cations present in the zeolite help to anchor the chiral inductor to the interior surface. The overall arrangement as we visualize it is illustrated in Fig. 2,[10] which shows the hydrogen bonding between norephedrine and tropolone methyl ether as well as the electrostatic interaction between the cation on the zeolite and the phenyl group of norephedrine. This view reveals that one of the faces of tropolone methyl ether is fairly open while the other is encumbered by the zeolite surface. Such an arrangement is expected to favor one of the two modes of disrotatory cyclization. The fact that 100% enantioselectivity is not observed suggests that not all molecules are present in this idealized arrangement.

The results presented here provide encouragement for further exploration of chiral induction within modified zeolites.[11] For the first time, the phenomenon of asymmetric induction within a zeolite appears to be amenable to a simple model, a model that can be used to plan future experiments exploring the utility of zeolites as media for enantioselective photoreactions. Such research is under way in our laboratories.

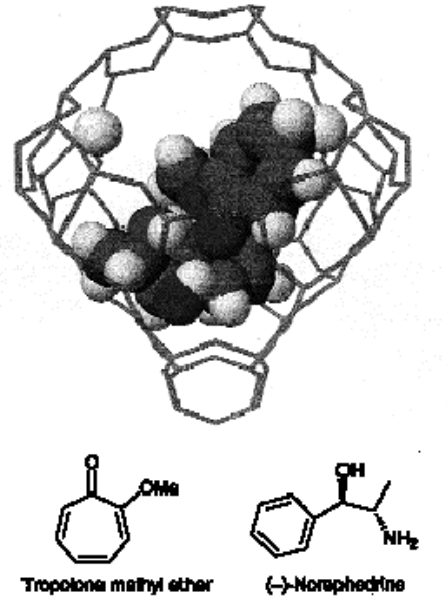

Fig. 2 Tropolone methyl ether and norephedrine included within a supercage of a NaY zeolite. The model shows hydrogen bonding interactions between the reactant and the chiral inductor and electrostatic interaction between the zeolitic cation and the chiral inductor. The cations help to anchor the chiral inductor and the chiral inductor helps to adsorb tropolone methyl ether preferentially from one enantiotopic face.

The authors thank the donors of the Petroleum Research Fund, administered by the American Chemical Society, for partial support of this research (V. R. and J. R. S.). Financial support by the Natural Sciences and Engineering Research Council of Canada (J. R. S.) is also gratefully acknowledged.

Notes and References

† E-mail: murthy@mailhost.tos.tulane.edu

1 *Asymmetric Synthesis*, ed. J. D. Morrison, Academic Press, Inc., New York, 1985, vol. 1–5; R. Noyori, *Asymmetric Catalysis in Organic Synthesis*, Wiley-Interscience, New York, 1994; O. Cervinka, *Enantioselective Reactions in Organic Chemistry*, Ellis Horwood, London, 1995.
2 Y. Inoue, *Chem. Rev.*, 1992, **92**, 741; H. Rau, *Chem. Rev.*, 1983, **83**, 535; J. P. Pete, *Adv. Photochem.*, 1996, **21**, 135.
3 M. Vaida, R. Popovitz-Biro, L. Leserowitz and M. Lahav, in *Photochemistry in Organized and Constrained Media*, ed. V. Ramamurthy, VCH, New York 1991, p. 247.
4 M. Leibovitch, G. Olovsson, J. R. Scheffer and J. Trotter, *Pure Appl. Chem.*, 1997, **69**, 815.
5 F. Toda, *Acc. Chem. Res.*, 1995, **28**, 480.
6 D. W. Breck, *Zeolite Molecular Sieves: Structure, Chemistry and Use*, Wiley, New York, 1974.
7 W. G. Dauben, K. Koch, S. L. Smith and O. L. Chapman, *J. Am. Chem. Soc.*, 1963, **85**, 2616.
8 H. Takashita, M. Kumamoto and I. Koino, *Bull. Chem. Soc. Jpn.*, 1980, **53**, 1006; F. Toda and K. Tanaka, *J. Chem. Soc., Chem. Commun.*, 1986, 1429.
9 M. Leibovitch, G. Olovsson, G. Sundarababu, V. Ramamurthy, J. R. Scheffer and J. Trotter, *J. Am. Chem. Soc.*, 1996, **118**, 1219; G. Sundarababu, M. Leibovitch, D. R. Corbin, J. R. Scheffer and V. Ramamurthy, *Chem. Commun.*, 1996, 2159; A. Joy, R. Robbins, K. Pitcumani and V. Ramamurthy, *Tetrahedron Lett.*, 1997, **38**, 8825.
10 Calculations were performed on a CAChe STEREO Worksystem using the standard software programs, including molecular mechanics employing MM2 parameters.
11 Very recently we found that ee could be improved to 65% when the samples are very dry. Experiments are underway to examine the effect of water on the extent of ee.

Received in Columbia, MO, USA, 10th December 1997; 7/08912K

Structure and dynamics of all of the stereoisomers of europium complexes of tetra(carboxyethyl) derivatives of dota: ring inversion is decoupled from cooperative arm rotation in the *RRRR* and *RRRS* isomers

Judith A. K. Howard,[a] Alan M. Kenwright,[a] Janet M. Moloney,[a] David Parker,*[a]† Marc Port,[b] Michel Navet,[b] Olivier Rousseau[b] and Mark Woods[a]

[a] *Department of Chemistry, University of Durham, South Road, Durham, UK DH1 3LE*
[b] *Guerbet s.a., Aulnay-sous-Bois, 95943 Roissy-Charles de Gaulle, France*

The absolute configuration of the four stereoisomeric α-substituted derivatives of dota has been defined; in their Eu complexes, 2D-NMR methods have revealed that in solution ring inversion is independent of pendant arm rotation and the (*RRRR*)-[EuL^{1a}] complex which in the solid state crystallises as a square antiprismatic structure.

The octadentate ligands derived from 1,4,7,10-tetraazacyclododecane (cyclen) by tetra-*N*-substitution define an important subgroup of modern lanthanide complexation chemistry.[1] Eight-coordinate tetraacetate ('dota'), phosphinate and carboxamide derivatives form kinetically robust complexes in aqueous solution, permitting their use in targeted radiotherapy,[2] as contrast agents in magnetic resonance imaging (MRI)[3] and as single-component luminescent probes in biochemical analyses.[4] In the lanthanide complexes of dota, or its achiral carboxamide derivatives, there are two independent elements of chirality, associated with the ring N–C–C–N and side-arm N–C–C–O torsion angles (*i.e.* each five-ring chelate is δ or λ). Accordingly there are four stereoisomers, related as two pairs of enantiomers, which may interconvert in solution *via* ring inversion (δδδδ → λλλλ) or concerted arm rotation (Δ → Λ). Either motion, in isolation, will exchange the coordination geometry between a square-antiprismatic arrangement, [Δ(λλλλ)/Λ(δδδδ)], with an N_4/O_4 twist angle of *ca.* 40°, and a more open twisted square antiprism [Δ(δδδδ)/Λ(λλλλ)] with a twist angle of *ca.* 29°. Introduction of a stereogenic centre β or γ to the ring nitrogen has been shown to impart considerable rigidity into the complex, inhibiting arm rotation in particular, as shown with the tetraphosphinoxymethyl complexes, and leading to preferential formation of one major stereoisomer in solution.[1,5,6] The effect of introducing a substituent α to each ring nitrogen on the structure and solution dynamics of the derived europium complexes is now described.[5b] Such a substitution gives rise to 6 ligand stereoisomers L^1 defined by the absolute configuration at carbon: *RRRR* (*SSSS*), *RSSS* (*SRRR*), *RSRS* and *RRSS*. In the corresponding lanthanide complexes, for a given ligand configuration, there are theoretically four stereoisomeric complexes (Fig. 1), which in principle may exchange by sequential arm rotation and/or ring inversion.

Alkylation of cyclen with racemic dimethyl-2-bromoglutarate (K_2CO_3–MeCN) led to formation of a mixture‡ of the expected diastereoisomeric esters. Base hydrolysis (6 M NaOH, 80 °C) afforded a mixture of ligands L^{1a}–L^{1d} which was separated by factional crystallisation and analysed by reverse-phase HPLC. The absolute configuration of each ligand was established by an X-ray structural analysis. Europium complexes of each ligand were formed by heating with $Eu(NO_3)_3$ at pH 5.5 (18 h, 90 °C). The complexes were purified by crystallisation from water. Proton NMR spectra for each complex were recorded (Fig. 2), highlighting the symmetry of the complex in solution. Thus in the high frequency region of the shifted spectrum, the C_4-symmetric complex [EuL^{1a}] gave rise to only two signals (δ_H 24.2 and 44.0) in ratio 4 : 1. ^{1}H–^{1}H COSY NMR showed that these resonances correspond to an axial ring proton in each of the isomeric species, consistent with earlier NMR analyses of such systems.[7,8] With the 'C_2-symmetric' complex [EuL^{1c}], two pairs of axial ring protons were observed also in a ratio of 4 : 1; with both [EuL^{1b}] and [EuL^{1d}] which lack any rotational symmetry, each of the four 'axial' ring hydrogens gave rise to a separate resonance and the observed ratio of stereoisomers was *ca.* 2 : 1 and ⩾ 12 : 1 respectively.

A concerted arm rotation will interconvert the axial protons of the major isomer with the axial protons of the minor isomer. However, a ring inversion interconverts the axial protons of the major isomer with equatorial protons of the minor (Fig. 1). Such processes have been observed with [Eu(dota)]$^-$ at room temperature.[8,9] Two-dimensional exchange spectroscopy (^{1}H

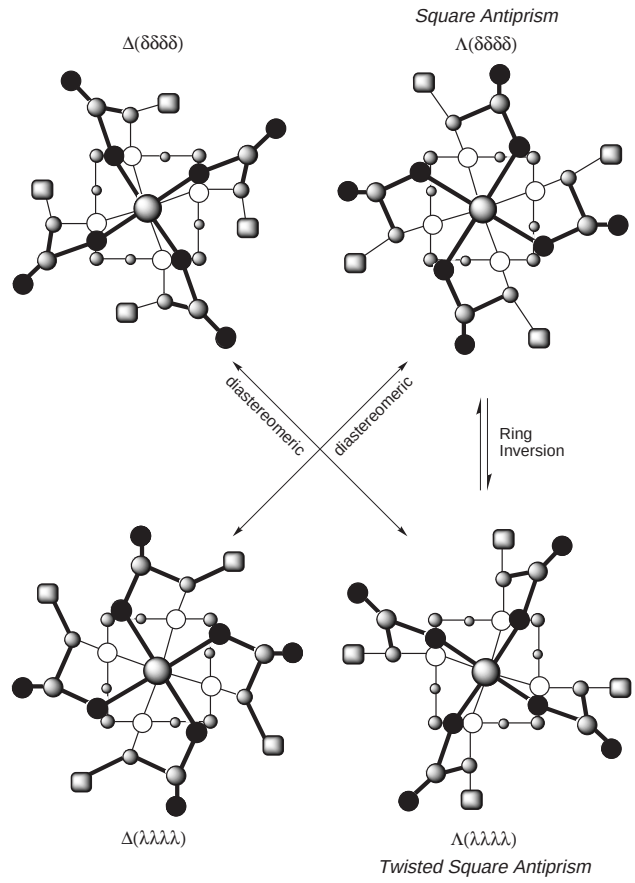

Fig. 1 Stereoisomerism in chiral eight- or nine-coordinate lanthanide complexes of α-alkylated derivatives of dota: ring inversion interconverts (δδδδ) and (λλλλ) isomers, and concerted arm rotation allows Δ and Λ isomers to exchange. The shaded square represents an alkyl group.

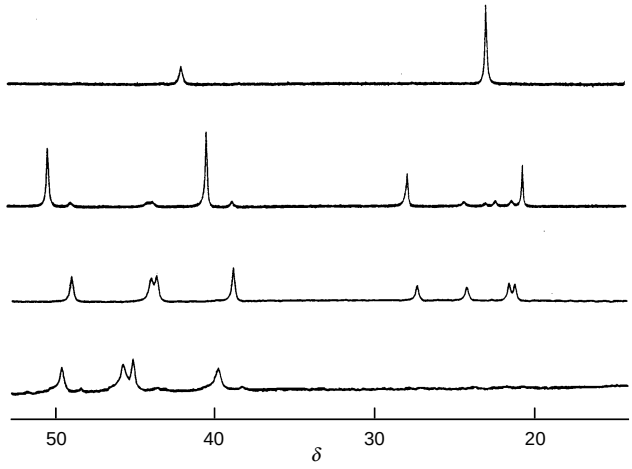

Fig. 2 ^{1}H NMR spectra (pD 6, D_2O, 293 K) of the europium complexes of (from top to bottom), (*a*) L^{1a}, (*b*) L^{1c}, (*c*) L^{1b}, (*d*) L^{1d} showing the shifted axial ring proton resonances which define the nature and relative proportion of complex stereoisomers

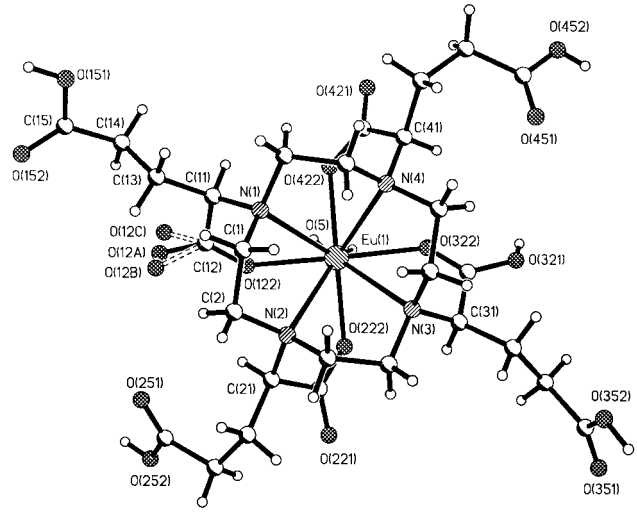

Fig. 3 Structure of (*RRRR*)-[Eu(H_5L^{1a})(H_2O)] in the crystal showing the mono-capped square antiprismatic geometry about the Eu ion, and the left-handed lay-out of the pendant arms

EXSY) was used to probe these processes in the complexes [EuL^{1a}], [EuL^{1b}] and [EuL^{1c}] (293 K, pD 6). The 2-D EXSY spectra of [EuL^{1a}] and [EuL^{1b}] showed cross-correlations between related axial and equatorial protons, indicating that ring inversion is occurring at room temperature. No cross-peaks were observed arising from the interconversion of axial protons in the major and minor isomers. This is consistent with fast ring inversion but slow arm rotation, on the NMR timescale. Thus, major/minor isomer interconversion occurs primarily through ring inversion, rendering two of the four possible diastereoisomeric structures less accessible. This accounts for the observation of just two species in solution in the ^{1}H NMR spectrum (Fig. 2). On warming the sample, the two high frequency axial protons began to broaden and the minor resonance moved towards the major, with coalescence not observed but likely to be not much above 60 °C. The rate of exchange between the two isomers through ring inversion (λλλλ to δδδδ), was measured by selective pulse inversion methods, examining the axial proton (H_{ax}, δ 44) to equatorial (H_{eq}, δ −8) exchange process. The measured rate was 45 ± 15 s^{-1}, very similar to that found for [Eu(dota)]$^-$,[8] indicating clearly that the process of ring inversion is independent of arm rotation. The situation with [EuL^{1c}] was quite different: at room temperature, cross-peaks associated with both arm rotation and ring inversion were observed indicating that both processes were occurring at comparable rates. Indeed the EXSY spectra were very similar to those defined for [Eu(dota)]$^-$.[8]

The structure of the neutral complex [Eu(H_5L^{1a})] was determined by X-ray crystallography§ and both the (*RRRR*) and (*SSSS*) complexes crystallised together (in $P\bar{1}$) (Fig. 3). The Eu ion is nine-coordinate with Eu–O and Eu–N distances averaging 2.38 and 2.68 Å and the Eu–water oxygen bond distance was 2.445(7) Å. For the (*RRRR*)-enantiomer, the ring adopted a square [3333] conformation with each five-ring (N–C–C–N) chelate in a δ configuration (N–C–C–N torsion angle averaging +59.4°) and the N–C–C–O torsion angles were all negative (averaging −34.1°) consistent with a Λ configuration. For the (*SSSS*)-enantiomer, both sets of torsion angles were of opposite sign. Thus the configuration of the stereogenic centre at carbon in the ligand determines both the overall helicity of the complex and its 'macrocyclic' ring configuration, in the solid-state structures. In solution (Fig. 2), comparison of the ^{1}H NMR spectrum of [EuL^{1a}] with those of its three diastereoisomers and [Eu(dota)]$^-$,[9] suggests that the minor isomer also possesses the Λ(δδδδ) configuration (specifying *R* configuration). The major isomer in solution must then adopt the Λ(λλλλ) configuration. In the complexes of [EuL^{1b}], [EuL^{1c}] and [EuL^{1d}], it follows that the major isomer must adopt a square antiprismatic geometry. Thus it is the minor isomer of [EuL^{1a}] that has crystallised preferentially.

We thank EPSRC for support.

Notes and References

† E-mail: david.parker@durham.ac.uk

‡ Statistically, this reaction leads to 50% of the *RRRS*/*SSSR* L^{1b}, 25% of the *RRSS* L^{1d} and 12.5% of each of L^{1a} and L^{1c}.

§ *Crystal data* for $C_{28}H_{49}EuN_4O_{20.25}$, M = 917.67, triclinic, space group $P\bar{1}$, a = 9.637(2), b = 12.690(4), c = 16.186(5), α = 102.47(2), β = 101.28(3), γ = 110.42(3)°, U = 1729.8(1) Å^3, D_c = 1.762 g cm^{-3}, λ(Mo-Kα) 0.710 73 Å, Z = 2, μ = 1.906 mm^{-1}. Data were collected on a SMART at 150(2) K. Refinement of 627 parameters by full matrix least squares on F^2 (SHELX 93) converged at R = 0.031, wR_2 = 0.067 for 7242 reflections with $I > 2\sigma(I)$. CCDC 182/875.

1 D. Parker and J. A. G. Williams, *J. Chem. Soc., Dalton Trans.*, 1996, 3613.
2 D. Parker, in *Comprehensive Supramolecular Chemistry*, ed. D. N. Reinhoudt, J. E. Atwood, F. Vogtle, D. D. MacNicol and J.-M. Lehn, Pergamon, Oxford, 1996, vol. 10. ch. 17.
3 S. Aime, M. Botta, M. Fasano and E. Terreno, *Chem. Soc. Rev.*, 1998, **27**, 19; K. Kumar and M. F. Tweedle, *Pure Appl. Chem.*, 1993, **65**, 515; J. A. Peters, J. Huskens and D. J. Raber, *Prog. NMR Spectrosc.*, 1996, **28**, 283.
4 D. Parker, K. Senanayake and J. A. G. Williams, *Chem. Commun.*, 1997, 1777; D. Parker and J. A. G. Williams, *Chem. Commun.*, 1998, 245; D. Parker and T. Gunnlaugsson, *Chem. Commun.*, 1998, 511; D. Parker and J. A. G. Williams, *J. Chem. Soc., Perkin Trans. 2*, 1998, in press.
5 (*a*) S. Amin, J. R. Morrow, C. H. Lake and M. R. Churchill, *Angew. Chem., Int. Ed. Engl.*, 1994, **33**, 773; (*b*) M. Spirlet, J. Rebizant, J. F. Desreux and M.-F. Loncin, *Inorg. Chem.*, 1984, **23**, 359.
6 R. S. Dickins, J. A. K. Howard, C. W. Lehmann, J. M. Moloney, D. Parker and R. D. Peacock, *Angew. Chem., Int. Ed. Engl.*, 1997, **36**, 521.
7 S. Aime, M. Botta, M. Fasano, M. P. M. Harques, C. F. G. C. Geraldes, D. Pubanz and A. E. Merbach, *Inorg. Chem.*, 1997, **36**, 2059 and references therein.
8 S. Hoeft and K. Roth, *Chem. Ber.*, 1993, **126**, 869; V. Jacques and J. F. Desreux, *Inorg. Chem.*, 1994, **33**, 4048.
9 S. Aime, M. Botta and G. Ermondi, *Inorg. Chem.*, 1992, **31**, 4291.

Received in Cambridge, UK, 16th April 1998; 8/02847H

$[(DippNH)_2Al(\mu\text{-}NHDipp)_2Li\cdot thf]$ and $[thf\cdot Li(\mu\text{-}NHCy)_3Sn(\mu\text{-}NHCy)_3Li\cdot thf]\cdot C_6H_5Me$, potential building blocks for heterometallic imido compounds (Dipp = 2,6-$Pr^i_2C_6H_3$)

Michael A. Beswick,[a] Nick Choi,[b] Christopher N. Harmer,[a] Mary McPartlin,[b] Marta E. G. Mosquera,[a] Paul R. Raithby,[a] Mustafa Tombul[a] and Dominic S. Wright*[a]

[a] *Chemistry Department, University of Cambridge, Lensfield Road, Cambridge, UK CB2 1EW*
[b] *Department of Applied Chemistry, University of North London, London, UK N7 8DB*

$[(DippNH)_2Al(\mu\text{-}NHDipp)_2Li\cdot thf]$ 1 and $[thf\cdot Li(\mu\text{-}NHCy)_3Sn(\mu\text{-}NHCy)_3Li\cdot thf]\cdot C_6H_5Me$ 2 are produced from the reactions of $AlCl_3$ and $SnCl_4$ or $MeAlCl_2$ and $MeSn(NMe_2)_3$ with the apporopriate primary amido lithium precursors [RNHLi; R = 2,6-$Pr^i_2C_6H_3$ (Dipp), C_6H_{11} (Cy)]; both complexes have ion-paired structures in the solid state with the retention of potentially reactive N–H functionality providing precursors for heterometallic species containing $[M(NR)_x(NHR)_{n-x}]^{(1+x)-}$ anions (M = Al, n = 4; M = Sn, n = 6).

One area of current interest to us is the investigation of the metallation reactions of primary amido and phosphido p block and transition metal complexes [of the type $M(NHR)_n^{x-}$] with a series of main group metal reagents (such as dimethylamido complexes).[1] Some indication of the scope of this approach to the synthesis of heterometallic arrangements is provided by the reaction of the $[Sb(NHCy)_4]^-$ (Cy = C_6H_{11}) with $Sb(NMe_2)_3$ which gives the *spiro* anion $[(Me_2N)Sb(\mu\text{-}NCy)_2Sb]^-$.[2] However, further in-roads in this area have been hampered by the surprising lack of well defined homoleptic primary amido and phosphido metal complexes which we sought as precursors for metallation. In some cases this situation reflects the ease of formation of imido complexes in the reactions of REHLi with metal halides.[3] We report here the syntheses and X-ray crystal structures of $[(DippNH)_2Al(\mu\text{-}NHDipp)_2Li\cdot thf]$ **1** (Dipp = 2,6-$Pr^i_2C_6H_3$) and $[thf\cdot Li(\mu\text{-}NHCy)_3Sn(\mu\text{-}NHCy)_3Li\cdot thf]\cdot C_6H_5Me$ **2**.

Compounds **1** and **2** can be prepared directly by the reactions of $AlCl_3$ with DippNHLi (1 : 4 equiv., respectively) and $SnCl_4$ with CyNHLi (1 : 6 equiv., respectively) (Scheme 1). The same complexes are also formed in the reactions of $MeAlCl_2$ with DippNHLi (1 : 3 equiv., respectively) and $MeSn(NMe_2)_3$ with CyNHLi (1 : 3 equiv., respectively). These reactions presumably involve intra- or inter-molecular deprotonation of RNH– groups by the Me groups of $MeAlCl_2$ and $MeSn(NMe_2)_3$.‡

The X-ray study of **1**§ reveals that it exists as an ion-paired complex in the solid state in which an $[Al(NHDipp)_4]^-$ anion is attached through two μ-NDipp groups of a thf solvated Li^+ cation (Fig. 1). The effect of the bridging of two of the DippNH groups to the Li^+ cation is to elongate the associated Al–N bonds (av. 1.95 Å) compared to those made with the terminal DippNH ligands (av. 1.85 Å). The coordination to the Li^+ cation also has a large affect on the geometry of the $[Al(NHDipp)_4]^-$ anion, with the N–Al–N angle within the $Al(\mu\text{-}N)_2Li$ rings being compressed (av. 93.6°) and the N–Al–N angle between the terminal ligands being expanded (av. 117.7°) as a result. Similar structural variations are found in the related amido complexes $[(pyrN)_2Al(\mu\text{-}Npyr)_2Li\cdot L_2]$ (pyr = pyrrolidinido; L = pyrNH, thf),[4] although the mono- rather than bis-solvation of the Li^+ cation in **1** leads to slightly longer Al–(μ-N) bonds and slightly shorter Li–N bonds. In addition, the resulting planar, three-coordinate geometry of the Li^+ cation of **1** gives rise to further α-C–H···Li interactions (range Li···H av. 2.30 Å) with a Pr^i group of each of the bridging DippNH ligands. These

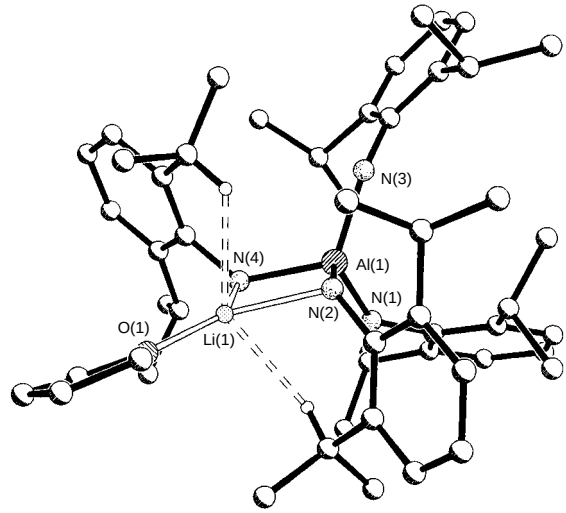

Fig. 1 Crystal structure of $[(DippNH)_2Al(\mu\text{-}NHDipp)_2Li\cdot thf]$ **1**. Only one of the independent molecules is shown. H atoms, except those attached to N, have been omitted for clarity. Key bond lengths (Å) and angles (°); molecule A: Al(1)–N(1) 1.846(9), Al(1)–N(2) 1.898(9), Al(1)–N(3) 1.844(9), Al(1)–N(4) 1.91(1), Li(1)–N(2) 2.03(2), Li(1)–N(4) 2.04(2), Li(1)–O(1) 1.81(2), Li(1)···H av. 2.39; N(1)–Al(1)–N(2) 119.5(5), N(1)–Al(1)–N(3) 121.3(5), N(1)–Al(1)–N(4) 98.9(5), N(2)–Al(1)–N(3) 100.6(5), N(2)–Al(1)–N(4) 95.5(5), N(3)–Al(1)–N(4) 119.2(5), Al(1)–N(2)–Li(1) 88.4(6), Al(1)–N(4)–Li(1) 88.4(6), N(2)–Li(1)–N(4) 87.7(8); molecule B: Al(2)–N(5) 1.907(9) Al(2)–N(6) 1.82(1), Al(2)–N(7) 1.830(9), Al(2)–N(8) 1.938(9), Li(2)–N(5) 2.03(2), Li(2)–N(8) 2.04(2), Li(2)–O(2) 1.83(2), Li(2)···H av. 2.36; N(5)–Al(2)–N(6) 99.4(4), N(5)–Al(2)–N(7) 121.4(4), N(5)–Al(2)–N(8) 95.8(4), N(6)–Al(2)–N(7) 121.7(5), N(6)–Al(2)–N(8) 119.0(5), N(7)–Al(1)–N(8) 97.9(4) Al(2)–N(5)–Li(2) 88.1(6), Al(1)–N(8)–Li(2) 87.0(6), N(5)–Li(2)–N(8), 89.1(8).

$$AlCl_3 + 4\ [DippNHLi] \xrightarrow{thf} [(DippNH)_2Al(\mu\text{-}NHDipp)_2Li\bullet thf] + 3LiCl$$
1

$$SnCl_4 + 6\ [CyNHLi] \xrightarrow[thf]{toluene} [thf\bullet Li(\mu\text{-}NHCy)_3Sn(\mu\text{-}NHCy)_3Li\bullet thf]\bullet C_6H_5Me + 4LiCl$$
2

Scheme 1

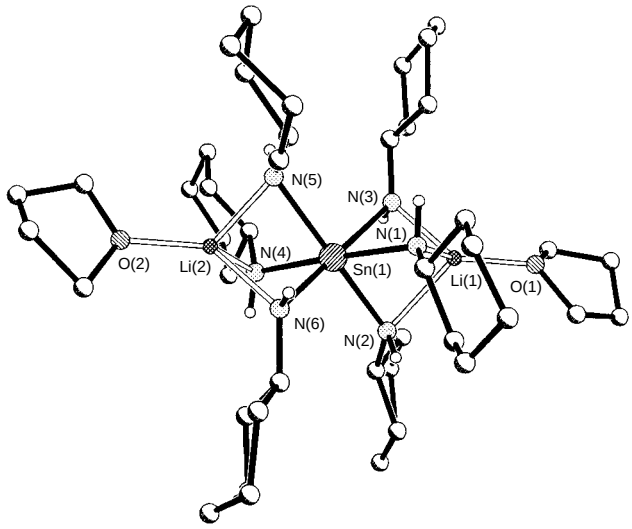

Fig. 2 Crystal structure of [thf·Li(μ-NHCy)$_3$Sn(μ-NHCy)$_3$Li·thf]·C$_6$H$_5$Me **2**. H atoms and the lattice-bond toluene molecule have been omitted for clarity. Key bond lengths (Å) and angles (°); range Sn–N 2.06(2)–2.27(2), range Li–N 1.98(4)–2.17(4), range N–Sn–N [Sn(μ-N)$_3$Li] 81.0(7)–83.6(7), Sn(1)···Li(1) 2.71(4), Sn(1)···Li(2) 2.67(4); N(1)–Sn(1)–N(4) 177(1), N(2)–Sn(1)–N(5) 178.1(9), N(3)–Sn(1)–N(6) 176.4(9), range N–Li–N 81(2)–92(2).

interactions appear to be relatively weak and have no apparent effect on the geometry of the Al(μ-N)$_2$Li rings. Similar interactions are now commonplace in organolithium chemistry[5] and are also found in other lithium aluminate complexes in which the alkali metal cation has a low coordination number.[6]

Although an extensive range of primary amido Al complexes have been reported previously, the vast majority of these have been neutral oligomers of the type [R′$_2$Al(μ-NHR′)]$_n$ prepared by metallation of RNH$_2$ with AlR′$_3$.[7] Complexes containing primary amido Al anions are far rarer and, to our knowledge, the only compounds of this type to be structurally elucidated are the heteroleptic organo-primary amido complexes [(Ph$_3$CNH)$_2$AlBu$^t_2$]Li,[8] [(Mes)$_2$Al(NHBu^t)$_2$Li·*n*(thf)] (Mes = 2,4,6-Me$_3$C$_6$H$_2$; *n* = 1, 2),[9] [Li(thf)$_4$] [(DippNH)AlBu$^i_2$Bu^t],[9] and [(DippNH)AlBu^{t}Me$_2$]Li·3thf.[9,10] Although several tetrakis(amido) complexes adopt similar structures to **1**,[4,11] this complex is the first example containing a primary amido anion of the type [Al(NHR)$_4$]$^-$. The formation of this unit in the reaction of MeAlCl$_2$ with DippNHLi is of particular interest bearing in mind the apparently low basicity of the Me groups in [(DippNH)AlBu^{t}Me$_2$]Li·3thf,[9,10] which even when subjected to prolonged reflux fails to eliminate methane.

The X-ray structure of **2**§ shows that the complex is the ion-paired species [thf·Li(μ-NHCy)$_3$Sn(μ-NHCy)$_3$Li·thf]·C$_6$H$_5$Me, composed of a central [Sn(NHCy)$_6$]$^{2-}$ dianion which uses all six of its NHCy groups to bond to two thf solvated Li$^+$ cations (Fig. 2). There is one lattice-bound molecule of toluene per formula unit. The coordination of the two Li$^+$ cations gives rise to a contraction in the skeletal N–Sn–N angles of the resulting Sn(μ-N)$_3$Li units (av. 82.3°) and introduces considerable distortion in the geometry of the Sn^{IV} centre away from pure octahedral. Despite the apparent similarity of the geometries of two Li$^+$ cations of **2**, they are crystallographically different. The large variation in the Sn–N bond lengths within the [Sn(NHCy)$_6$]$^{2-}$ dianion [range 2.06(2)–2.27(2) Å] roughly mirrors the different degrees of interaction of the bridging NHCy groups with each Li$^+$ cation, the longest Sn–N bonds being associated with the shortest Li–N interactions and the shortest Sn–N bonds with longer Li–N contacts. The distortions within the framework of **2** suggest that this arrangement is highly strained. Although the structure of **2** is comparatively simple, few related Sn–N bonded compounds appear to have been structurally characterised. The closest relatives to **2** are ion-separated species containing inorganic EX$_6^{2-}$ anions (E = Si–Pb; X = N$_3^-$, SCN$^-$, SeCN$^-$, CN$^-$).[12] Complex **2** contains the first example of a hexa(amido) group 14 dianion to be characterised in the solid state.

Our studies of the reactions of homoleptic complexes of groups 13 and 14 with a range of metallating reagents [such as E(NMe$_2$)$_x$ (E = Sb, *x* = 3; E = Sn, *x* = 2)] are still at an early stage. However, there are good reasons for thinking that complexes like **1** and **2** (containing reactive N–H functionalities) will be of value as precursors in the synthesis of heterometallic species containing [M(NR)$_x$(NHR)$_{n-x}$]$^{(1+x)-}$ anions (M = Al, *n* = 4; M = Sn, *n* = 6). Recent work by Rutherford and Atwood has shown that deprotonation of species of the type [R$_2$AlNHR′] can be easily accomplished with organolithium reagents[9,10] and our own studies have revealed that various p block metal bases readily deprotonate primary amido metal complexes.[1,2] Further studies will be aimed at the synthesis of such 'multianion' species and the applications of these as new ligands to a range of main group and transition metals.

We gratefully acknowledge the EPSRC (C. N. H., M. McP.), The Leverhulme Trust (M. A. B.), The Turkish Government (M. T.) and The Spanish Government (M. E. G. M.) for financial support.

Note added at proof. During the proof stage another example of a primary amido Al^{III} complex was reported (J. S. Silverman, C. J. Carmalt, D. A. Neumayer, A. H. Cowley, B. G. Burnett and A. Decken, *Polyhedron*, 1998, **17**, 977).

Notes and References

† E-mail: dsw1000@cus.cam.ac.uk

‡ Synthetic details will be reported in a full paper.

§ *Crystal data*: C$_{52}$H$_{76}$AlLiN$_4$O **1**, *M* = 807.09, monoclinic, space group *P*2$_1$/*c*, *a* = 23.913(4), *b* = 20.756(3), *c* = 22.833(3) Å, *β* = 116.25(1)°, *U* = 10 164(3) Å^3, *Z* = 8, *D*$_c$ = 1.055 Mg m^{-3}, *λ* = 0.71 073 Å, *T* = 293(2) K, *μ*(Mo-K*α*) = 0.078 mm^{-1}, *F*(000) = 3520. 11 986 collected reflections, 10 190 independent (*R*$_{int}$ = 0.098). *R*1 [*F* > 4*σ*(*F*) = 0.099 and *wR*2 = 0.425 (all data).[13] C$_{51}$H$_{93}$Li$_2$N$_6$O$_2$Sn **2**, *M* = 954.88, monoclinic, space group *Cc*, *a* = 14.81(2), *b* = 16.574(1), *c* = 23.24(2) Å, *β* = 106.48(8)°, *U* = 5473(9) Å^3, *Z* = 4, *D*$_c$ = 1.159 Mg m^{-3}, *λ* = 0.710 73 Å, *T* = 203(2) K, *μ*(Mo-K*α*) = 0.507 mm^{-1}, *F*(000) = 2052. 6227 collected reflections, 6051 independent (*R*$_{int}$ = 0.048). *R*1[*F* > 4*σ*(*F*)] = 0.094 and *wR*2 = 0.438 (all data).[13] CCDC 182/880.

1 M. A. Beswick and D. S. Wright, *Coord. Chem. Rev.*, in press.
2 A. J. Edwards, D. A. Paver, M.-A. Rennie, C. A. Russell, P. R. Raithby and D. S. Wright, *Angew. Chem.*, 1994, **106**, 1334; *Angew. Chem., Int. Ed. Engl.*, 1994, **33**, 1277.
3 For examples from group 15 see, S. C. James, N. C. Norman, A. G. Orpen and M. J. Quayle, *J. Chem. Soc., Dalton Trans.*, 1996, 1455; M. Noltemeyer, H. W. Roesky, H. Schmidt and U. Wirringa, *Inorg. Chem.*, 1994, **33**, 4607.
4 M. M. Andrianarison, M. C. Ellerby, I. B. Gorrell, P. B. Hitchcock, J. D. Smith and D. R. Stanley, *J. Chem. Soc., Dalton Trans.*, 1996, 211.
5 K. Gregory, P. v. R. Schleyer and R. Snaith, *Adv. Inorg. Chem.*, 1991, **37**, 47; R. E. Mulvey, *Chem. Rev.*, 1991, **20**, 167.
6 See, for example: N. Niemeyer and P. P. Power, *Organometallics*, 1995, **14**, 5488.
7 For some typical examples of dimeric and trimeric complexes, see A.-A. I. Al-Wassil, P. B. Hitchcock, S. Sarisaban, J. D. Smith and C. L. Wilson, *J. Chem. Soc., Dalton Trans.*, 1985, 1929; W. Clegg, M. Haase, U. Klingebiel, J. Neeman and G. M. Sheldrick, *J. Organomet. Chem.*, 1983, **252**, 281; G. M. McLaughlin, G. A. Sin and J. D. Smith, *J. Chem. Soc., Dalton Trans.*, 1972, 2197.
8 M. Petrie, K. Ruhlandt-Senge and P. P. Power, *Inorg. Chem.*, 1993, **32**, 1135.
9 D. Rutherford and D. A. Atwood, *J. Am. Chem. Soc.*, 1996, **118**, 11 535.
10 D. A. Atwood and D. Rutherford, *Chem. Commun.*, 1996, 1251.
11 St. Böck, H. Nöth and P. Rahm, *Z. Naturforsch., Teil B*, 1988, **43**, 53.
12 For example see M. Fitz, D. Rieger, E. Bar, G. Beck, J. Fuchs, G. Holzmann and W. P. Fehlhammer, *Inorg. Chem.*, 1992, **198**, 513.
13 SHELXTL PC version 5.03, Siemens Analytical Instruments, Madison, WI, 1994.

Received in Cambridge, UK, 6th April 1998; 8/02590H

Isolation and structural determination of octacyanobutanediide, $[C_4(CN)_8]^{2-}$; precursors to $M(TCNE)_x$ magnets‡

Jie Zhang,[a] Louise M. Liable-Sands,[b] Arnold L. Rheingold,*[b] Rico E. Del Sesto,[a] Douglas C. Gordon,[a] Brian M. Burkhart[c] and Joel S. Miller*[a]†

[a] *Department of Chemistry, University of Utah, Salt Lake City, UT 84112-0850, USA*
[b] *Department of Chemistry, University of Delaware, Newark, DE 19716, USA*
[c] *Hauptman-Woodward Medical Research Institute, Buffalo, NY 14203, USA*

The reaction of $MI_2{\cdot}x$Me$_3$CN (M = Mn, Fe) and TCNE (tetracyanoethylene) leads to unprecedented $[C_4(CN)_8]^{2-}$ μ_4-metal complexes which have been crystallographically characterized and are precursors to $M(TCNE)_x{\cdot}y$S magnets.

The study of cyanocarbons has led to the discovery of both molecule-based conductors[1] and magnets[2] as well as several new classes of compounds based upon reduction of the nitrile triple bond.[3,4] While generalizing the room-temperature molecule-based magnet $V(TCNE)_x{\cdot}yCH_2Cl_2$[5] to magnetic systems based upon other metals, we discovered several new magnets in this class: $M(TCNE)_2{\cdot}x$S (M = Mn, Fe, Co, Ni; S = MeCN, CH_2Cl_2).[6] In contrast to the V magnet, the Fe and Mn magnets exhibit X-ray powder diffraction. Therefore, we attempted to grow single crystals of these magnets *via* slow diffusion of $MI_2{\cdot}x$MeCN (M = Mn, Fe) and TCNE in a H-tube using either MeCN–CH_2Cl_2 (M = Mn) or pure MeCN (M = Fe). Crystals of new compounds (light yellow for M = Mn; dark brown for M = Fe) were isolated with ν_{CN} IR absorptions at 2304m, 2275m, 2212s, 2205s, 2153s, and 2096m (sh) cm^{-1} for M = Mn and 2307m, 2280m, 2213s, 2154s, and 2108w cm^{-1} for M = Fe. These ν_{CN} absorptions are similar to, but distinguishable from, those observed for the $M(TCNE)_2{\cdot}xCH_2Cl_2$.[6] magnets. The absorptions above 2230 cm^{-1} are assigned to coordinated MeCN, while the latter are assigned to reduced nitriles and were initially thought to be associated with a metal-bound reduced form of TCNE.

Single crystal X-ray diffraction studies‡ of $Mn[C_4(CN)_8](NCMe)_2{\cdot}CH_2Cl_2$ **1** and $Fe[C_4(CN)_8](NCMe)_2{\cdot}$MeCN **2** each revealed the unprecedented octacyanobutanediide dianion, $[C_4(CN)_8]^{2-}$ **3**. This dianion is bound to four

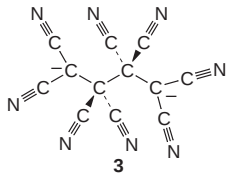

3

octahedral M^{II} centres (M = Mn, Fe) in a plane with the MeCN molecules filling the axial coordination sites, and the non-coordinated CH_2Cl_2 (**1**) and MeCN (**2**) lying in diamond-shaped holes in the structure, Figs. 1 and 2. Adjacent planes are eclipsed. The interlayer M···M separaions are 7.626(2) and 9.356(4) Å, respectively, for **1**, and **2**, while the intralayer M···M separations are 7.581(2) and 9.344(2) Å for **1**, 7.562(4) and 9.368(4) for **2**.

Compound **3** is disordered about the midpoint of the C(5)–C(5′) bond for M = Mn and ordered for M = Fe. The chemically equivalent M–N, C≡N, NC–C and $(MNC)_2$C–C distances average 2.218(4), 1.151(6), 1.389(7) and 1.615(10) Å, respectively, for Me = Mn, and average 2.221(7), 1.151(10), 1.398(11) and 1.508(9) Å, respectively, for M = Fe. The central C–C bond is 1.59(2) (M = Mn) and 1.627(14) Å (M = Fe). The terminal C_4-backbone carbon atoms are sp^2 hybridized as indicated by the average angle of 119.0° (M = Mn) and 119.8° (M = Fe) while the central carbon atoms are sp^3 hybridized [average angles are 109.5° (M = Mn) and 109.4° (M = Fe)].

This is the first example of a σ-dimer of $[TCNE]^{\cdot-}$, however, several examples of a structurally related σ-dimer of $[TCNQ]^{\cdot-}$ (TCNQ = 7,7,8,8-tetracyano-*p*-quinodimethane) have been reported.[7] The backbone C–C bonds are significantly longer[8] than the conventionally accepted value of 1.54 Å for an sp^3–sp^3 C–C bond length and are comparable to the central C–C bond for the σ-dimers of $[TCNQ]^{\cdot-}$ (1.630–1.659 Å).

For **1** thermogravimetric analysis–mass spectrometry (TGA–MS) reveals a one-step mass loss between 100 and 120 °C, during which both MeCN and CH_2Cl_2 are simultaneously observed in the effluent gas. The 34.3% mass loss is in good agreement with the formula $Mn[C_4(CN)_8](NCME)_2{\cdot}CH_2Cl_2$ (34.9%). At *ca*. 250 °C a second mass loss occurs which is accompanied by the generation of C_2N_2 and HCN. An exothermic event is also observed in the DSC data at this temperature. This mass loss is only 4%, corresponding to *ca.* 0.7 CN per Mn. The observation of C_2N_2 and HCN is consistent with the formation of CN˙ radicals which either combine or

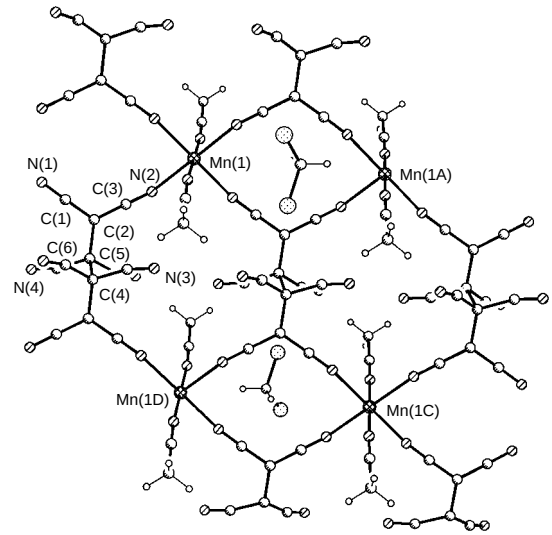

Fig. 1 Structure and labeling diagram of $Mn[C_4(CN)_8](NCMe)_2{\cdot}CH_2Cl_2$. Selected bond lengths (Å) and angles (°): Mn(1)–N(2) 2.206(3) Å, N(2)–C(3) 1.154(5), C(3)–C(2) 1.389(7), C(2)–C(1) 1.389(7), C(1)–N(1) 1.148(6), N(1)–Mn(1^a) 2.230(4), C(2)–C(5) 1.615(10), C(5)–C(5^b) 1.59(2); N(2)–Mn(1)–(N1^a) 86.08(13), Mn(1)–N(1^a)–C(1^a) 154.4(4), N(1)–C(1)–C(2) 179.0(5), C(1)–C(2)–C(3) 118.7(4), C(2)–C(3)–N(2) 178.0(5), C(3)–N(2)–Mn(1) 165.7(3), N(1^b)–Mn(1)–N(2) 93.92(13), C(3)–C(2)–C(5) 116.6(4), C(2)–C(5)–C(5^b) 105.2(7), C(5^b):C(2^b)–C(1^b) 121.8(4). ^{a} $-x, -y, -z$; ^{b} $x-1, y, z$.

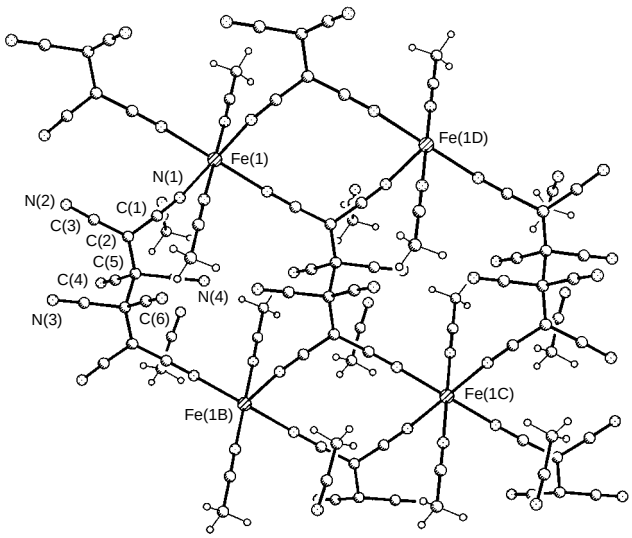

Fig. 2 Structure and labeling diagram of $Fe[C_4(CN)_8](NCMe)_2 \cdot MeCN$. Selected bond lengths (Å) and angles (°): Fe(1)–N(1) 2.218(7), N(1)–C(1) 1.147(10), C(1)–C(2) 1.395(12), C(2)–C(3) 1.401(11), C(3)–N(2) 1.144(9), N(2)–Fe(1^c) 2.224(6), C(2)–C(5) 1.508(9), C(2^b)–C(5^b) 1.508(9), C(5^b)–C(5^b)–C(5^a) 1.627(14); N(1)–Fe(1)–N(2^d) 86.4(2), C(1^d)–N(1^d)–Fe(1^c) 163.0(6), Fe(1^c)–N(2)–C(3) 165.3(6), N(2)–C(3)–C(2) 177.4(7), C(3)–C(2)–C(1) 118.2(6), N(2^a)–Fe(1)–N(1) 93.6(2), Fe(1)–N(1)–C(1) 163.0(6), N(1)–C(1)–C(2) 177.9(7), C(1)–C(2)–C(5) 120.3(6), C(2^b)–(C5^b)–C(5^a) 113.2(7), C(5^a)–C(2^a)–C(3^a) 120.9(6). ^{a} $x-1, y, z$; ^{b} $-x+1, -y+1, -z+1$; ^{c} $x+1, y, z$; ^{d} $-x+1, -y+1, -z+2$.

abstract hydrogen. Despite the lower volatility of MeCN as compared to CH_2Cl_2, **2** loses solvent very rapidly when removed from the mother-liquor and cannot be isolated with all three MeCN molecules present. A sample with 1.7 MeCN per Fe was obtained after drying *in vacuo* at room temperature. TGA–MS on this material shows that it loses the remaining solvent at 100 °C and formation of C_2N_2 begins at *ca.* 150 °C and peaks at 320 °C. We have observed similar thermal decomposition processes in other compounds containing $[TCNE]^{\cdot-}$ such as $[NBu_4][TCNE]$ and K[TCNE]. Thus, we believed that desolvation leads to cleavage of the long central C–C bond of $[C_4(CN)_8]^{2-}$ to reform $[TCNE]^{\cdot-}$ which subsequently decomposes to form the observed byproducts, HCN and C_2N_2.

Compound **1** is a paramagnet with a room temperature effective moment of 6.7 μ_B and obeys the Curie–Weiss law above 5 K. This is consistent with a diamagnetic $[C_4(CN)_8]^{2-}$ which weakly couples the metal spin sites ($S = 5/2$ Mn^{II}), albeit with a larger than expected room temperature moment. The magnetic properties of **2** are as yet undetermined since it cannot be isolated without loss of solvent.

Upon desolvation of **1** at 100 °C the ν_{CN} absorptions disappear and new ν_{CN} bands characteristic of the $Mn(TCNE)_2 \cdot xCH_2Cl_2$ magnet (2225, 2182, and 2170 cm^{-1})[6] appear. In addition the room temperature moment increases. The desolvated sample magnetically orders at a T_c of 95 K, in reasonable agreement with the value previously reported (107 K) for $Mn(TCNE)_2 \cdot xCH_2Cl_2$ prepared directly in CH_2Cl_2.[6] **2** behaves in a similar fashion upon desolvation. The desolvated material has ν_{CN} IR absorptions characteristic of the $Fe(TCNE)_2 \cdot x$MeCN ($x = 1.7$) magnet (2280, 2220, 2164 and 2117 cm^{-1}) and orders magnetically at *ca.* 6 K $[Fe(TCNE)_2 \cdot x$MeCN orders at *ca.* 8 K].[6] These observations are consistent with the TGA–MS data and indicate that desolvation leads to formation of $S = 1/2$ $[TCNE]^{\cdot-}$ which can bind to additional metal centers and provide strong spin coupling leading to the observed magnetic ordering. Evidence for this bond breaking has been reported for σ-dimers of $[TCNQ]^{\cdot-}$.[7a]

The authors gratefully acknowledge discussions with D. K. Rittenberg and the support of the Department of Energy (Grant Nos. DE-FG03-93ER45504 and DEFG-0296ER12198).

Notes and References

† E-mail: jsmiller@chemistry.utah.edu

‡ Dedicated to Professor Roald Hoffmann on the occasion of his 60th birthday.

§ *Crystal data*: $Mn[C_4(CN)_8](NCMe)_2 \cdot CH_2Cl_2$, **1**: $C_{17}H_8C_{12}MnN_{10}$, triclinic, space group $P\bar{1}$, $a = 7.5805(6)$, $b = 7.6259(6)$, $c = 9.3443(7)$ Å, $\alpha = 89.1436(12)$, $\beta = 88.8320(20)$, $\gamma = 87.2979(14)°$, $V = 538.85(7)$ Å^3, $Z = 1$, $T = 223(2)$ K, $D_c = 1.472$ g cm^{-1}, $R(F) = 0.0501$, $R(wF^2) = 0.1512$ for 1103 independent observed reflections ($3 \leqslant 2\theta \leqslant 58°$).

$Fe[C_4(CN)_8](NCMe)_2 \cdot MeCN$, **2**: $C_{20}H_{12}FeN_{12}$, monoclinic, space group $P2_1/c$, $a = 7.5623(5)$, $b = 16.1971(11)$, $c = 9.3682(6)$ Å, $\beta = 90.8167(9)°$, $V = 1147.37(13)$ Å^3, $Z = 2$, $T = 233(2)$ K, $D_c = 1.379$ g cm^{-1}, $R(F) = 0.0796$, $R(wF^2) = 0.2149$ for 1324 independent observed reflections ($3 \leqslant 2\theta \leqslant 58°$). Further details of either crystal structure investigation may be obtained from the Fachinformationszentrum Karlsruhe, D-76344 Eggenstein-Leopoldshafen (Germany), on quoting depository number CSD-407730 and 407731, respectively. CCDC 182/887.

1 Recent reviews: P. Cassoux and J. S. Miller, *Chemistry of Advanced Materials: A New Discipline*, ed. L. V. Interrante and M. Hampton-Smith, VCH Publishers, New York, 1998, 19; M. R. Bryce, *Chem. Soc. Rev.*, 1991, **20**, 355.

2 Recent reviews: J. S. Miller and A. J. Epstein, *Angew. Chem., Int. Ed. Engl.*, 1994, **33**, 385, *Angew. Chem.*, 1994, **106**, 399; *Adv. Chem. Ser.*, 1995, **245**, 161. D. Gatteschi, *Adv. Mater.*, 1994, **6**, 635; O. Kahn, *Molecular Magnetism*, VCH Publishers, Inc., New York, 1993.

3 O. W. Webster, *Kirk-Othmer Encyclo. Chem. Tech.*, 1993, **7**, 809; R. P. Suprayan and P. G. Rasmussen, *Trend. Polym. Sci.*, 1995, **3**, 165.

4 W. E. Buschmann, A. M. Arif and J. S. Miller, *J. Chem. Soc., Chem. Commun.*, 1995, 2343.

5 J. M. Manriquez, G. T. Yee, R. S. McLean, A. J. Epstein and J. S. Miller, *Science*, 1991, **252**, 1415; J. S. Miller, G. T. Yee, J. M., Manriquez and A. J. Epstein, in *Proceedings of Nobel Symposium #NS-81, Conjugated Polymers and Related Materials: The Interconnection of Chemical and Electronic Structure*, Oxford University Press, 1993, 461; *La Chim.*, 1992, **74**, 845; A. J. Epstein and J. S. Miller, in *Proceedings of Nobel Symposium #NS-81, Conjugated Polymers and Related Materials: The Interconnection of Chemical and Electronic Structure*, Oxford University Press, 1992, 475; *La Chim.*, 1993, **75**, 185.

6 J. Zhang, J. Ensling, V. Ksenofontov, P. Gütlich, A. J. Epstein and J. S. Miller, *Angew. Chem., Int. Ed. Engl.*, 1998, **37**, 656.

7 (*a*) R. H. Harms, H. J. Keller, D. Nöthe, M. Werner, D. Grundel, H. Sixl, Z. G. Soos and R. M. Metzger, *Mol. Cryst., Liq. Cryst.*, 1981, **65**, 179; S. K. Hoffman, P. J. Corvan, P. Singh, C. N. Sethuklekshmi, R. M. Metzer and W. E. Hatfield, *J. Am. Chem. Soc.*, 1983, **105**, 4608; (*b*) V. Dong, H. Endres, H. J. Keller, W. Moroni and D. Nöthe, *Acta Crystallogr., Sect. B*, 1977, **33**, 2428; H. Zhao, R. A. Heintz, K. R. Dunbar and R. D. Rogers, *J. Am. Chem. Soc.*, 1996, **118**, 12844; B. Morosin, H. J. Plastas, L. B. Coleman and J. M. Stewart, *Acta Crystallogr., Sect. B*, 1978, **34**, 540.

8 G. Kaupp and J. Boy, *Angew. Chem., Int. Ed. Engl.*, 1997, **36**, 48.

Received in Bloomington, IN, USA, 23rd March 1998; 8/02273I

Silica condensation reaction: an *ab initio* study

J. C. G. Pereira,[a,b] C. R. A. Catlow*[a]† and G. D. Price[b]

[a] *Davy Faraday Research Laboratory, The Royal Institution of Great Britain, 21 Albermarle Street, London, UK W1X 4BS*
[b] *University College London, Department of Geological Sciences, Gower Street, London, UK WC1E 6BT*

***Ab initio* techniques are used to investigate the mechanisms and energetics of condensation of two $Si(OH)_4$ monomers in a simulated hydrated environment; the calculated activation energies accord well with those measured for silica condensation in sol–gel systems.**

The kinetics of the silica-based condensation reaction have been widely investigated, using a variety of spectroscopies and scattering techniques.[1] Silicate clusters in solution have also been identified[2,3] using NMR and gas chromatographic techniques. However, because of the multitude of simultaneous reactions in solution, it is difficult to extract information about individual events using only experimental data.

The chemistry of silica has also been studied extensively using theoretical techniques.[4] A simple mechanism for the silica hydrolysis reaction was suggested,[5] with an activation energy of 21.9 kcal mol^{-1}, close to the experimental energy barrier for silicate and quartz dissolution. All these calculations were carried out in the gas phase, ignoring hydration effects. Moreover, no systematic *ab initio* studies of the silica condensation reaction have been reported to date, even for gas phase systems.

We have therefore studied the simplest condensation reaction, $2Si(OH)_4 \rightarrow Si_2O(OH)_6 + H_2O$, using DF theory coupled with a continuum dielectric model, COSMO,[6,7] to describe the electrostatic conditions found in real silica solutions. This conductor-like screening model is a continuum dielectric model, where a solute molecule is embedded in a dielectric continuum of permittivity ε. The interface between the cavity formed by the solute and the dielectric, the solvent accessible surface, has thus a surface charge distribution, arising from the polarisation of the dielectric medium in response to the charge distribution of the solute. The COSMO model calculates the screening charges in a conductor ($\varepsilon = \infty$), for arbitrarily shaped cavities, using a non-iterative procedure, and then the dielectric screening energy and its gradient are scaled by $(\varepsilon - 1)/(\varepsilon + \frac{1}{2})$, to take into account the effect of the dielectric.

All calculations used the DMOL code[8] with the local BLYP functional[9,10] and a DNP double numerical basis set.[11] All atomic arrangements were first optimised *in vacuo* and subsequently recalculated including hydration effects, as a single energy point, without reoptimisation. We considered mechanisms effected by acid catalysis (corresponding to pH < 3) as in most experimental work.[12,13] A methanol environment was chosen for the COSMO calculations, to fit better the electrostatic conditions found in real sol–gel solutions, where the alcohol is usually the main component. Typical compositions are water/alkoxide = 2–4 and alcohol/alkoxide = 4–10.

Acid catalysed condensation reactions are effected by the attack of a neutral monomer on a protonated monomer resulting in a protonated dimer and a water molecule; $Si(OH)_4H^+$ and $Si_2OH(OH)_6^+$ are therefore key species in the condensation reaction. The protonation energy for both clusters, presented in Table 1, shows that this process is exothermic in the gas phase and endothermic in the methanol environment. In addition, we find that it is more energetically favourable to protonate the cluster rather than the monomer. In gas phase calculations, the key factor is always the additional charge, which may generally be delocalised more effectively in larger systems; consequently, the side of the equilibrium where the charge is hosted by a larger species tends to have a lower energy. In the solvated medium, simulated by the COSMO methodology, this charge stabilisation effect is drastically reduced: it now requires more energy to protonate the $Si_2O(OH)_2$ dimer than the $Si(OH)_4$ monomer. As the electron-withdrawing effect of OSi groups is greater than that of OH groups,[1] the bridging O in $Si_2O(OH)_6$ is less basic than the four terminal O in $Si(OH)_4$. The general implication of this effect is that in acid conditions, larger neutral species attack the smaller, protonated monomers, as observed.[12]

Protonated species formation

$Si(OH)_4 + H_3O^+ + \Delta E \rightarrow Si(OH)_3(H_2O)^+ + H_2O$	
without hydration	$\Delta E = -18.8$
with hydration	$\Delta E = +7.4$
$Si_2O(OH)_6 + H_3O^+ + \Delta E \rightarrow Si_2OH(OH)_6^+ + H_2O$	
without hydration	$\Delta E = -22.3$
with hydration	$\Delta E = +12.9$

Table 1 Formation energies, *in vacuo* and methanol environments

The energy for the condensation reaction, from the protonated reactants to the protonated products, is presented in Table 2. The results for the reaction in the gas phase are again dominated by the effects of charge distribution. The energy of the condensation reaction is negative, because the dimer is larger than the monomer. In the solvated environment, where these charge effects are relatively unimportant, the reaction is endothermic, essentially because the products have groups that are more electron withdrawing than those of the reactants. The results for the calculations with a solvated environment agree with the trends predicted experimentally for these clusters in solution.[12]

Protonated species reactions

$Si(OH)_4 + Si(OH)_3(H_2O)^+ + \Delta E \rightarrow Si_2OH(OH)_6^+ + H_2O$	
without hydration	$\Delta E = -6.3$
with hydration	$\Delta E = +5.1$

Table 2 Condensation energy, *in vacuo* and methanol environments

We now study two detailed mechanisms of condensation: the S_N2 attack (illustrated in Fig. 1) in which the attack occurs from the opposite side to the leaving group and the lateral attack (Fig. 2) in which the attack occurs sideways. To ensure that the energy surface for the reaction was adequately searched we performed, in each case, two sets of calculations. In the first, we started from the reactants, with the protonated monomer having its equilibrium $Si–O^+$ distance of 1.88 Å. During the course of the reaction, the distance, *d*, between the oxygen of the attacking monomer and the Si of the protonated monomer was reduced in a succession of steps from *ca.* 8 Å to the equilibrium value (for the protonated dimer) of 1.83 Å; at each step along the path, *d* was held fixed and all other parameters were optimised. In the second set of calculations, we started from the products, with the protonated dimer having its equilibrium O^+–Si distance of 1.83 Å. We successively decreased the distance, *d′*, between the oxygen of the leaving water molecule and the Si of the

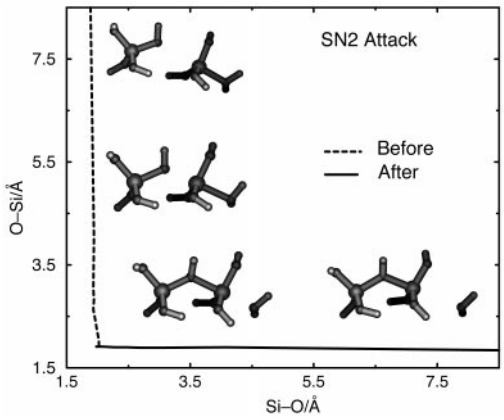

Fig. 1 S_N2 mechanism for the condensation reaction $Si(OH)_4 + Si(OH)_4H^+ \rightarrow Si_2OH(OH)_6^+ + H_2O$. The *y* axis represents the oxygen–silicon distance, (O–Si), between the attacking monomer and the protonated monomer; the *x* axis represents the silicon–oxygen distance, (Si–O), between the protonated dimer and the departing water molecule.

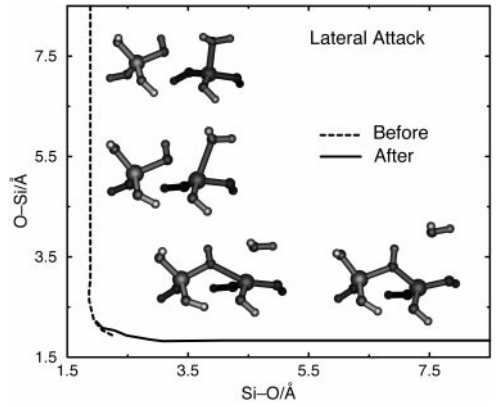

Fig. 2 Lateral attack mechanism for the condensation reaction $Si(OH)_4 + Si(OH)_4H^+ \rightarrow Si_2O(OH)_6H^+ + H_2O$. The *x* and *y* axes are as in Fig. 1.

protonated dimer, from a value of *ca.* 8 Å to the equilibrium value (for the protonated monomer) of 1.88 Å. Again *d′* was fixed in the individual calculations, with all other parameters being optimised. The two sets of calculations, denoted 'before' and 'after', result in similar energy profiles in the intermediate region where they overlap. We note that this step-by-step analysis gives valuable information about the evolution of the charge distribution, which is fundamental in understanding the full transformation from the reactants to the products.

The S_N2 and lateral attack reaction paths, optimised in the gas phase, are very different. While the S_N2 path is composed of two almost straight lines, suggesting a negligible activation energy, the lateral attack path exhibits a small energy barrier.

In the solvated environment, simulated by the COSMO methodology, the energy evolution along the S_N2 reaction path shows first a small energy barrier of 2.5 kcal mol^{-1} before decreasing to a five-silicon intermediate, which is 3.4 kcal mol^{-1} more stable than the reactants, with O–Si 1.91 Å and Si–O 1.98 Å. A second energy barrier of 11.3 kcal mol^{-1}, the largest in the whole reaction process, occurs later, when the Si–O distance is already 4.08 Å.

In the lateral attack mechanism in the solvated environment, after the first 2.5 kcal mol^{-1} energy barrier, a five-coordinate silicon intermediate occurs at O–Si 2.83 Å and Si–O 1.86 (1.9 kcal mol^{-1} less stable than the other reactants). As in the gas phase, a pronounced peak occurs at Si–O 2.48 Å, forming the largest energy barrier in the overall mechanism: 17.3 kcal mol^{-1} (6 kcal mol^{-1} larger than in the S_N2 mechanism). The S_N2 mechanism seems therefore to be an easier route for the conversion of the reactants into the products. However, as the study for the lateral attack shows, several other mechanisms that

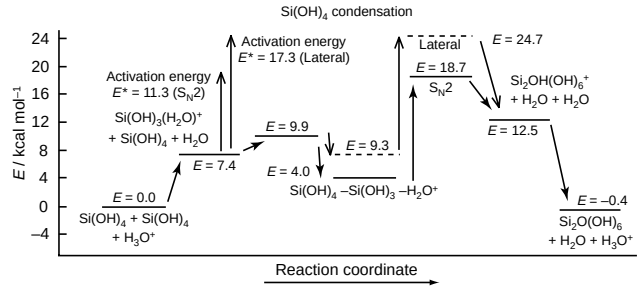

Fig. 3 Energy evolution (kcal mol^{-1}) during the $Si(OH)_4$ condensation reaction, for both S_N2 and lateral attack mechanisms

are energetically and statistically less favourable, should still be possible and may occur simultaneously in the solution.

The global energy evolution from the neutral reactants to the neutral products is depicted in Fig. 3. The difference in energy between reactants and products is small: only −0.4 kcal mol^{-1}. On fully optimising both reactants and products in the COSMO environment, this difference increases to −3.2 kcal mol^{-1}, which is still relatively small. Most significant, however, is the fact that our calculated activation energies are within the range of those measured experimentally for silica condensation reactions in sol–gel systems, in the range 12–15 kcal mol^{-1}.[14,15] We may be confident therefore that we have identified the main mechanisms for this crucially important process. Further calculations will explore stabilities and condensation mechanisms for larger clusters.

We are very grateful to EPSRC for providing both local and national computer resources. One of us (J. C. G. P.) is greatly indebted to Instituto Superior Técnico, Dept. Eng. Materials, Lisboa, and JNICT, Programa Ciência and Programa Praxis XXI, Lisboa, for financial support.

Notes and References

† E-mail: richard@ri.ac.uk

1 J.-C. Pouxviel and J. P. Boilot, in *Better Ceramics Through Chemistry III*, ed. C. J. Brinker, D. E. Clark and D. R. Ulrich, Materials Research Society, Elsevier, 1986, vol. 121, p. 37; I. Artaki, M. Bradley, T. W. Zerda, J. Jonas, G. Orcel and L. L. Hench, in *Science of Ceramic Chemical Processing*, ed. L. L. Hench and D. R. Ulrich, Wiley, 1986, p. 73; C. W. Turner and C. J. Franklin, in *Science of Ceramic Processing*, ed. L. L. Hench and D. R. Ulrich, Wiley, 1986, p. 81; K. D. Keefer, in *Better Ceramics Through Chemistry*, ed. C. J. Brinker, D. E. Clark and D. R. Ulrich, Elsevier, 1984, vol. 32, p. 15.
2 L. W. Kelts and N. J. Armstrong, *J. Mater. Res.*, 1989, **4**, 423.
3 W. G. Klemperer and S. D. Ramamurthi, in *Fifth International Workshop on Glasses and Glass Ceramics from Gels*, ed. M. A. Aegerter; *J. Non-Cryst. Solids*, 1990, **121**, 16.
4 L. P. David, L. W. Burgraff and M. S. Gordon, *J. Am. Chem. Soc.*, 1988, **110**, 3056; J. Hill and J. Sauer, *J. Phys. C: Solid State Phys.*, 1994, **98**, 1238; I. Pápai, A. Goursot and F. Fajula, *J. Phys. C: Solid State Phys.*, 1994, **98**, 4654; J. A. Pople, *Ab Initio Molecular Orbital Theory*, Wiley, New York, 1986; R. G. Parr and W. Wang, *Density Functional Theory of Atoms and Molecules*, OUP, Oxford, 1989.
5 A. C. Lasaga and G. Gibbs, *Am. J. Sci.*, 1990, **290**, 263.
6 A. Klamt and G. Schüürmann, *J. Chem. Soc., Perkins Trans. 2*, 1993, 799.
7 J. Andzelm and C. Kölmel, *J. Chem. Phys.*, 1995, **103**, 9312.
8 DMOL Manual, Molecular Simulations Inc., 9685 Scranton Road, San Diego, CA, 1966.
9 A. D. Becke, *Phys. Rev. A*, 1988, **3**, 3098.
10 C. Lee, W. Yang and R. G. Parr, *Phys. Rev. B*, 1988, **37**, 785.
11 B. Delley, *J. Chem. Phys.*, 1990, **92**, 508.
12 C. J. Brinker and G. W. Scherer, *Sol–Gel Science: The Physics and Chemistry of Sol–Gel Processing*, Academic Press, London, 1989.
13 R. K. Iler, *The Chemistry of Silica*, Wiley, 1979.
14 L. W. Burggraf, L. P. Davies and M. S. Gordon, in *Ultrastructure Processing of Advanced Materials*, ed. D. R. Uhlmann and D. R. Ulrich, Wiley, 1992, p. 47.
15 S. H. Garofalini and G. Martin, *J. Phys. C: Solid State Phys.*, 1994, **98**, 1311.

Received in Cambridge, UK, 5th March 1988; 8/01816B

Assembly based on μ_4-bridging thiolate: a new type of polymeric silver(I) complex having a one dimensional chain structure

Weipin Su, Rong Cao, Maochun Hong,*† Jiutong Chen and Jiaxi Lu

State Key Laboratory of Structural Chemistry, Fujian Institute of Research on the Structure of Matter, Fuzhou, Fujian 350002, PR China

The polymeric silver(I)–thiolate complex $[\{Ag_8(\mu_4\text{-}SC_2H_4NH_3)_6Cl_6\}Cl_2]_n$ has been prepared from the assembling reaction of silver chloride and 2-mercaptoethylamine hydrochloride in DMF; X-ray diffraction analysis shows the complex has a one dimensional chain structure and all the sulfur atoms of the thiolates exhibit μ_4 bonding bridging four silver(I) centers.

Thiolates are a subject of great interest in the chemistry of transition-metal complexes.[1–4] Dithiolates acting as μ_2 or μ_3 bridging ligands have been used to link metal ions such as Cu^I or Ag^I giving rise to complexes with infinite-chain structures.[5–8] Simple monothiolate ligands acting as μ_2 or μ_3 bridges are very common in transition metal chemistry,[8,9] however, those acting as μ_4 bridges and linking metal atoms to form polymeric complexes in one infinite chain or in network structures are unknown.[10] Recently, we have explored ways to design syntheses of polymeric complexes with chain structures by using coinage metal ions and dithiolate ligands.[11] By changing from dithiolate to monothiolate bridging ligands, we obtained a new type of polymeric silver(I) complex having a one dimensional chain structure and metal–metal interactions in which the thiolates show μ_4 bridging linking four Ag^I centers.

We have found that it is possible to use this simple monothiolate ligand to generate an unusual one dimensional molecular component of ligand bridged Ag^I ions.

By very slowly mixing a DMF solution of AgCl and NEt_4Cl and a DMF solution of 2-mercaptoethylamine hydrogen chloride in an H-tube at room temperature, a large quantity of colorless prismatic crystals deposited.‡ Clearly, the synthesis of the polymeric silver(I) 2-mercaptoethylamine complex can be approached from the controlled assembling reaction of $[AgCl_2]^-$ and $HSC_2H_4NH_2{\cdot}HCl$ in DMF [eqn. (1)]. In this

$$8n[NEt_4][AgCl_2] + 8nHSC_2H_4NH_2{\bullet}HCl \rightarrow \underset{\mathbf{1}}{[\{Ag_8(\mu_4\text{–}SC_2H_4NH_3)_6Cl_6\}Cl_2]_n} + 8n[NEt_4]Cl + 2nHSC_2H_4NH_2{\bullet}HCl \quad (1)$$

reaction, one mole of HCl is liberated for each Ag^+ added and shows the zwitterion $^-SC_2H_4NH_3^+$ acts as a ligand to form the complex. A crystallographic analysis reveals that the complex is a polymer and the octanuclear cation $[Ag_8(SC_2H_4NH_3)_6Cl_6]^{2+}$ constitutes the building-block unit. The octanuclear units, possessing a crystallographic mirror plane through Ag(1), Ag(3) and S(2) (Fig. 1), are bound by Ag–S and Ag–Ag interactions to form a one dimensional chain structure along the *b* axis and the chains are linked by hydrogen bonds in the crystal (Fig. 2). Two types of coordination environments for Ag^I ions are present: six Ag^I ions have a distorted tetrahedral S_3Cl coordination environment, generated by the sulfur atoms of the zwitterions and terminal chloride; the other two are trigonal planar with an S_3 coordination environment from the sulfur atoms of the zwitterion. All six zwitterions $^-SC_2H_4NH_3^+$ exhibit μ_4 bridge linking four metal centers. The occurrence of μ_4 bridging coordination of thiolate ligands in transition metal chemistry is very limited.[10] This is the first example of an $Ag_4(\mu_4\text{-}S)$ bridge coordination mode for thiolate found in silver(I) chemistry and the third example of a $M_4(\mu_4\text{-}S)$ bridge coordination mode of the zwitterion found in transition metal thiolate chemistry (the other examples being $[Cu_{13}Cl_{13}(SC_2H_4NH_3)_6]$[10a] and $[\{Cu_8Cl_6(SC_2H_4NH_3)_6\}Cl_2]_n$[10b]). The coordination geometry of all the sulfur atoms is a highly distorted square pyramidal $CSAg_4$ unit with one carbon atom at the apex and four silver atoms in the equatorial plane. The four Ag–S bonds in the μ_4-S(1)Ag_4 unit are all similar in length [2.577(5), 2.583(5), 2.611(5), 2.690(5) Å], while those in the μ_4-S(2)Ag_4 unit are non-equivalent, one shorter at 2.440(7) Å, two at 2.626(4) Å and one longer at 2.917(7) Å. The average Ag–S bond distance [2.634(7) Å] is much longer than that [2.248 Å] in $[Cu_{13}Cl_{13}(SC_2H_4NH_3)_6]$[10a] and slightly longer than those for Ag^I–SR involving three- or four-coordinate silver (2.40–2.55 Å).[3,4] The Ag–Ag separations range from 2.976(2) to 3.046(3) Å with an average value of 3.003 Å. All are best considered as non-bonding,[3] although the values are very similar to those present in metallic silver (2.88 Å).[12] The average Ag–Cl bond distance [2.489(5) Å] is slightly longer than that (2.448 Å) in $[Cu_{13}Cl_{13}(SC_2H_4NH_3)_6]$[10a] and lies in the normal range for Ag^I–Cl bonds.[4] Two Cl^- are not coordinated to silver atoms, but are bonded to NH_3^+ *via* a strong hydrogen bond N–H···Cl (N···Cl= 3.20 Å) in the crystal.

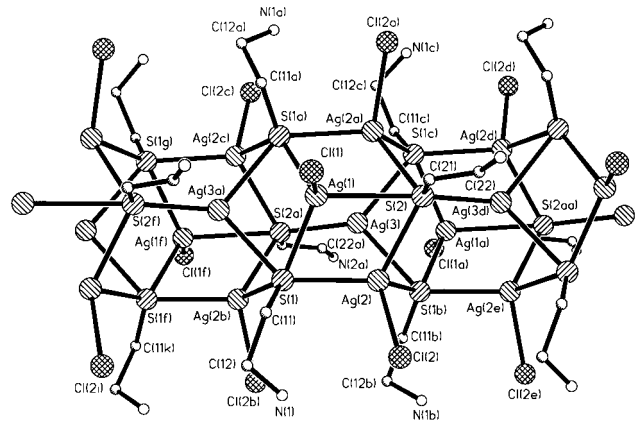

Fig. 1 Perspective view of an octanuclear unit in the polymeric chain in $[\{Ag_8(\mu_4\text{-}SC_2H_4NH_3)_6Cl_6\}Cl_2]_n$. Selected bond lengths (Å) and angles (°): Ag(1)–Ag(2) 2.976(3), Ag(1)–Ag(3a) 2.994(3), Ag(1)–Ag(2a) 2.976(3), Ag(2)–Ag(3) 3.046(3), Ag(3)–Ag(1a) 2.994(3), Ag(3)–Ag(2a) 3.046(3), Ag(1)–S(1) 2.577(5), Ag(1)–S(2) 2.917(7), Ag(1)–Cl(1) 2.464(7), Ag(1)–S(1a) 2.577(5), Ag(2)–S(1) 2.611(5), Ag(2)–S(2) 2.626(4), Ag(2)–Cl(2) 2.514(5), Ag(2)–S(1b) 2.583(5), Ag(3)–S(1b) 2.690(5), Ag(3)–S(1c) 2.690(5), Ag(3)–S(2a) 2.440(7); C(11)–S(1)–Ag(1) 104.1(6), C(11)–S(1)–Ag(2) 103.8(7), C(11)–S(1)–Ag(2b) 119.5(6), C(11)–S(1)–Ag(3a) 110.3(6), Ag(1)–S(1)–Ag(2) 70.0(1), Ag(1)–S(1)–Ag(3a) 69.2(1), Ag(2)–S(1)–Ag(2b) 119.7(1), Ag(2b)–S(1)–Ag(3a) 70.5(1), C(21)–S(2)–Ag(1) 94.1(13), C(21)–S(2)–Ag(2) 114.6(6); C(21)–S(2)–Ag(2a) 114.6(6), C(21)–S(2)–Ag(3d) 101.3(13), Ag(1)–S(2)–Ag(2) 64.7(1), Ag(1)–S(2)–Ag(2a) 64.7(1), Ag(2)–S(2)–Ag(3d) 108.1(2), Ag(2a)–S(2)–Ag(3d) 108.1(2).

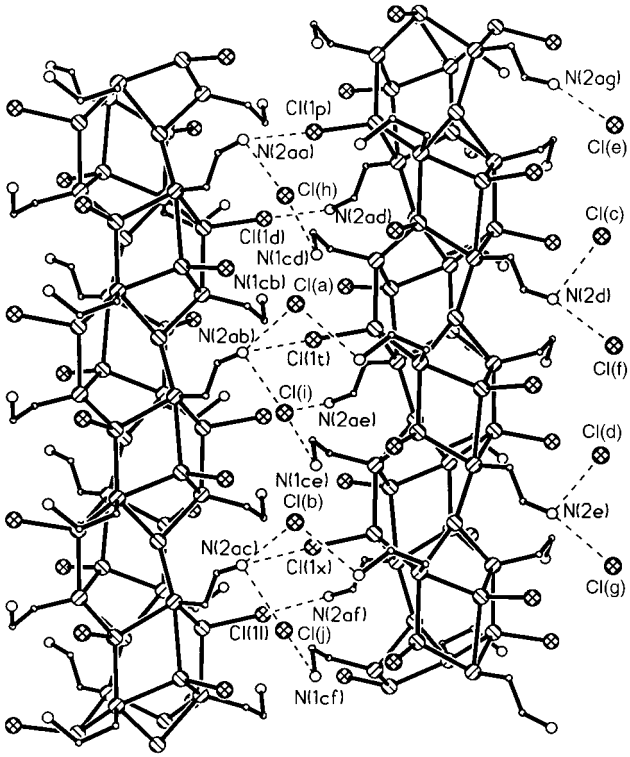

Fig. 2 View of the one dimensional chains and hydrogen bonds between the chains running along the *b* axis in $[\{Ag_8(\mu_4\text{-}SC_2H_4NH_3)_6Cl_6\}Cl_2]_n$

The IR spectrum of the complex exhibit a shift of the C–S stretching band from 659 cm^{-1} for the free mercaptoethylamine to 644 cm^{-1} upon coordination. The C–H and N–H stretching bands are complicated and occur between 2798 and 3162 cm^{-1} for the complex.

The authors acknowledge NNSF of China for financial support.

Notes and References

† E-mail: hmc@ms.fjirsm.ac.cn

‡ *Crystal data*: crystal dimensions 0.12 × 0.15 × 0.30 mm, $C_{12}H_{42}N_6Ag_8S_6Cl_8$, M = 1609.4, orthorhombic, space group *Pnma*, a = 7.831(1), b = 15.180(1), c = 16.410(1) Å, U = 1951.1(4) Å^3, Z = 2. D_c = 2.743 g cm^{-3}. 5955 intensity data were collected on a Siemens SMART CCD diffractometer with graphite-monochromated Mo-Kα radiation at room temperature, of which 1471 (R_{int} = 0.0492) are independent. $R(R_w)$ = 0.082 (0.090) for 1178 reflections with $I \geqslant 2.0\sigma(F_o)$ and 103 refined parameters. $\Delta\rho_{max}$ = 1.44 e Å^{-3} near the silver atoms. CCDC 182/871.

1 B. Krebs and G. Henkel, *Angew. Chem., Int. Ed. Engl.*, 1991, **30**, 769; G. Henkel, P. Petz and B. Krebs, *Angew. Chem., Int. Ed. Engl.*, 1987, **26**, 145; G. Henkel, B. Krebs and P. Petz, *Angew. Chem., Int. Ed. Engl.*, 1988, **27**, 1326.
2 I. G. Dance, *Inorg. Chem.*, 1981, **20**, 1487; I. G. Dance, L. J. Fitzpatrick, A. D. Rae and M. A. Scudder, *Inorg. Chem.*, 1983, **22**, 3785; I. G. Dance, *Polyhedron*, 1986, **5**, 1037.
3 P. J. Blower and J. R. Dilworth, *Coord. Chem. Rev.*, 1987, **76**, 121.
4 T. E. Wolf, J. M. Berg, P. P. Power, K. O. Hodgson and R. H. Holm, *Inorg. Chem.*, 1980, **19**, 430; P. A. Pírez-Lourido, J. A. García-Vazquez, J. Romero, M. S. Louro, A. Sousa, Q. Chen, Y. Chang and J. Zubieta, *J. Chem. Soc., Dalton Trans.*, 1996, 2047; Z. Y. Huang, X. J. Lei, M. C. Hong and H. Q. Liu, *Inorg. Chem.*, 1992, **31**, 2991; W. P. Su, M. C. Hong, F. L. Jiang, H. Q. Liu, Z. Y. Zhou, D. D. Wu and C. T. W. Mak, *Polyhedron*, 1996, **15**, 4047.
5 L. Carlucci, G. Ciani, D. M. Proserpio and A. Sironi, *J. Chem. Soc., Chem. Commun.*, 1994, 2755.
6 S. B. Copp, S. Subramanian and M. J. Zaworotko, *J. Chem. Soc., Chem. Commun.*, 1993, 1078; S. B. Copp, S. Subramanian and M. J. Zaworoko, *J. Am. Chem. Soc.*, 1992, **114**, 8719; S. B. Copp, K. T. Holman, J. O. S. Sangster and S. Subramanian, *J. Chem. Soc., Dalton Trans.*, 1995, 2233.
7 S. Kawata, S. Kitagawa, M. Kondo, I. Furuchi and M. Munakata, *Angew. Chem., Int. Ed. Engl.*, 1994, **33**, 1759; T. Kuroda-Sowa, M. Munakata, H. Matsuda, S. Akiyama and M. Maekawa, *J. Chem. Soc., Dalton Trans.*, 1995, 2201.
8 K. L. Tang, M. Aslam, E. Block, T. Nicholson and J. Zubieta, *Inorg. Chem.*, 1987, **26**, 1488; M. L. Tang, X. L. Jin, Q. N. Xiao and Y. Q. Tang, *Jiegou Huaxue* (*J. Struct. Chem.*), 1988, **7**, 159.
9 H. Anacker-Eickhoff, R. Hesse, P. Jennische and A. Wahlberg, *Acta Chem. Scand., Part A*, 1982, **36**, 251; A. M. M. Lanfredi, F. Ugozzoli, A. Camus and N. Marsich, *J. Chem. Crystallogr.*, 1995, **25**, 37.
10 (*a*) R. V. Parish, Z. Salehi and R. Z. Pritchard, *Angew. Chem., Int. Ed. Engl.*, 1997, **36**, 251; (*b*) Z. Salehi, R. V. Parish and R. Z. Pritchard, *J. Chem. Soc., Dalton Trans.*, 1997, 4241; G. W. Adamson, N. A. Bell and H. M. M. Shearer, *Acta Crystallogr., Sect. B*, 1982, **38**, 462.
11 M. C. Hong, X. J. Lei, Z. Y. Huang, B. S. Kang, F. L. Jiang and H. Q. Liu, *Chinese Sci. Bull.*, 1993, **38**, 912.
12 N. N. Greenwood and A. Earnshow, *Chemistry of the Elements*, Pergamon, Oxford, 1989, p. 1368.

Received in Cambridge, UK, 24th March 1998; 8/02286K

Photopromoted oxidative cyclization of an *o*-phenylene-bridged Schiff base *via* a manganese(III) complex, leading to a fluorescent compound, 2-(2-hydroxyphenyl)benzimidazole

Takashi Fukuda,[a] Fuminori Sakamoto,[a] Minoru Sato,[b] Yoshiharu Nakano,[a] Xiang Shi Tan[a] and Yuki Fujii*[a]†

[a] *Department of Chemistry, Faculty of Science, Ibaraki University, Mito, 310-8512, Japan*
[b] *Department of Chemistry and Engineering, Ibaraki National College of Technology, Hitachinaka 344-1200, Japan*

Visible light photolysis of [*N*,*N*′-*o*-phenylenebis(salicylideneaminato)]diaquamanganese(III) resulted in the fluorescent compound 2-(2-hydroxyphenyl)benzimidazole by a one electron redox reaction between Mn^{III} and the Schiff base ligand, followed by the base-hydrolysis of the oxidized Schiff base, and then the cyclization of the base-hydrolyzed product.

The photoactivation of manganese complexes is an attractive theme both in the modeling of PSII and in the development of a new photoreaction.[1–4] It has been known that, upon visible light irradiation, in the presence of *p*-quinone, manganese(III) complexes with tetradentate Schiff base ligands having the salen-type skeleton generate molecular oxygen;[5–7] in the absence of *p*-quinone, rearrangement of the coordinated Schiff base ligand occurs.[8] Recently, we examined the photolysis of [*N*,*N*′-*o*-phenylenebis(salicylideneaminato]diaquamanganese-(III) **1** and observed a photopromoted oxidative cyclization of the coordinated Schiff base ligand, and the effective formation of the fluorescent compound 2-(2-hydroxyphenyl)benzimidazole **2**, which is useful as a laser dye, high-energy radiation detector, molecular energy storage system, and fluorescent probe.[9–11] **2** is usually prepared from salicylic acid and *o*-phenylenediamine in polyphospholic acid at 190 °C in 14% yield.[12] This photoreaction thus provides a new and effective synthetic method for the fluorescent compound **2** and its derivatives.‡

Cation **1** was prepared by a literature method,[13] and isolated as its perchlorate salt.§ Absence of Mn^{II} was confirmed by EPR spectroscopy. Slow evaporation of methanol solution of the complex produced crystals suitable for single crystal X-ray structure analysis.¶ An ORTEP drawing of **1** is shown in Fig. 1. The structure of the complex cation comprises a planar tetradentate Schiff base ligand tightly bound to the Mn^{III} center *via* two Mn–N bonds [1.981(2), 1.978(2) Å] and two Mn–O bonds [1.859(1), 1.875(1) Å], and by axial methanol and water molecules which complete an octahedron around the Mn^{III} ion. Longer Mn–O distances to the apical ligands [2.272(2) Å for Mn–H_2O and 2.291(2) Å for MeOH] may be partly attributed to the Jahn–Tellar effect for the d^4 ion, although it is common for solvated Mn–O distances to be longer than chelated ones.[14] No hydrogen bond between the phenolic oxygen atoms of the Schiff base ligand and apical water or methanol was observed.[6]

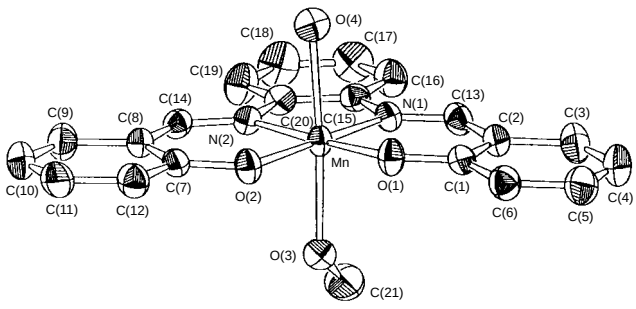

Fig. 1 An ORTEP drawing of cation **1** with thermal ellipsoids at 50% probability. Hydrogen atoms are omitted for clarify.

Fig. 2 shows the time courses of UV–VIS (320 nm), fluorescence (432 nm), and EPR spectra of **1** in water at initial pH = 6.4 under irradiation with visible light (150 W tungsten halogen lamp with UV cut filter L-39). The UV–VIS spectral change exhibited an isosbestic point at 223 nm, and the half life ($t_{1/2}$) of **1** was 11–15 h at pH 6.4.‖ A similar spectral change also occurred in the dark but was very slow ($t_{1/2}$ ≈55 h). Our preliminary experiments revealed that the photopromotion occurs by the irradiation into the CT band (400 ± 20 nm), but hardly for the π → π* (335 ± 20 nm) and d → d (540 ± 20 nm) bands. Further, the reaction becomes faster with increase of solution pH ($t_{1/2}$ ≈ 9 h at pH 7.5, ≈ 5 h at pH 8.6).

On the other hand, the fluorescence and EPR intensities of the photoreaction solution increased with the decay of **1**, indicating that the fluorescent compound, assigned as 2-(2-hydroxyphenyl)benzimidazole **2**, was formed at early stages of the reaction. The EPR spectra show typical six-line Mn^{II} signals (g = 2.013), which proves that the Mn^{III} was reduced to Mn^{II} during this reaction. Since neither molecular oxygen nor hydrogen peroxide were detected in the photoreaction solution, it is strongly suggested that intramolecular one electron redox occurred between Mn^{III} and the coordinated Schiff base ligand. A similar photoreaction also occurred under vacuum, however, no EPR signal corresponding to an organic radical was observed.

From the photoreaction solution, **2** and salicylaldehyde **3** could be separated both in about 40% yield by extraction with ethyl acetate, followed by silica-gel column separation using ethyl acetate–*n*-hexane (1 : 2) as eluent (R_f = 0.6 for **2**, R_f = 0.8 for **3**).** In addition to **2** and **3**, under argon, *N*,*N*′-

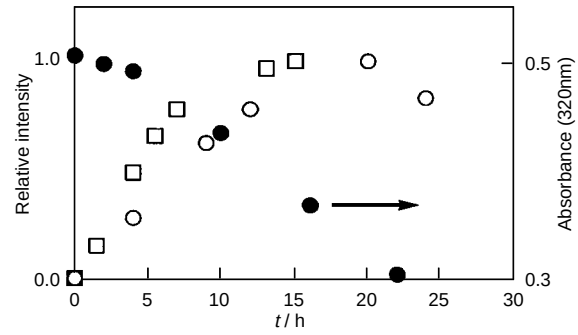

Fig. 2 Time courses of UV–VIS, fluorescence and X-band EPR spectra of the photolysis solution of **1** at pH = 6.4 and 25 °C. The complex concentration is 2.0 × 10^{-5} mol dm^{-3} for UV–VIS (●) and fluorescence (○) and 1.0 × 10^{-3} mol dm^{-3} for EPR (□). Fluorescence: λ_{ex} = 325 nm, λ_{em} = 432 nm, EPR: microwave power = 5 mW, microwave frequency = 9.238 GHz, 0.5 mT modulation amplitude, 25 °C.

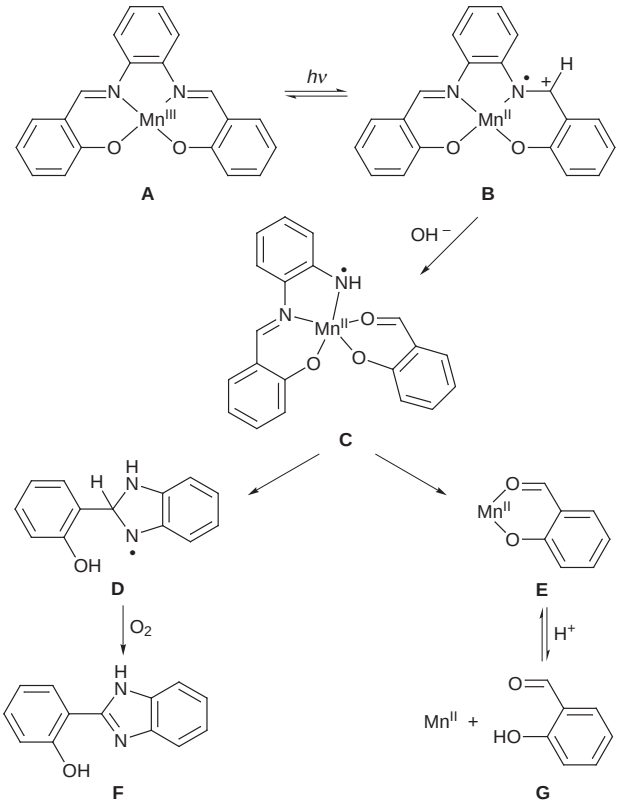

Scheme 1

o-phenylenebis(salicylideneamine) **4** was isolated in *ca*. 10% yield as a photoreaction product of **1**.

On the basis of these facts, the reaction mechanism (Scheme 1) is suggested as follows: (*i*) Mn^{III}–Schiff base complex **A** is reduced to Mn^{II} complex **B** with partially oxidized Schiff base ligand, for which visible light promotes the reaction (the reaction has been shown to be enhanced by excitation at the CT band of **1**, probably by LMCT). **B** is thought to be a transient radical and a similar radical has been proposed by Floriani and coworkers.[15] (*ii*) **B** is base-hydrolyzed to form radical **C**, followed by cyclization of the partially oxidized Schiff base ligand to produce radical **D** and Mn^{II} complex **E**, **D** is oxidized by O_2 to produce **F**. These processes are very fast, since final products **F** and Mn^{II} appear from the start of the reaction with no organic radical being detected in the timescale of EPR measurement. No detection of radical **D** under vacuum may be due to a redox reaction between **A** and **D**, which results in the formation of the corresponding Mn^{II}–Schiff base complex and **F**. This is partly supported by the fact that the Schiff base ligand **4** is detected under argon but not under air. Evidence for base-hydrolysis of **B** is the formation of salicylaldehyde **G** and rate enhancement with increase of solution pH. A study of the detailed reaction mechanism is under way.

This work was partly supported by a Grant-in-Aid for Science Research (No. 09440224 and No. 97370) from the Ministry of Education, Science and Culture of Japan.

Notes and References

† E-mail: yuki@mito.ipc.ibaraki.ac.jp

‡ This method is also applicable for the preparation of the cationic fluorescent compound 2-(2-hydroxy-5-trimethylammoniomethylphenyl)-benzimidazole chloride.

§ This complex contains methanol as apical ligand in the crystal state, however the methanol is thought to be substituted by water in aqueous solution.

¶ *Crystal data*: $C_{21}H_{20}N_2O_8MNCl$, M = 518.79, monoclinic, space group $P2_1/c$, Z = 4, a = 11.804(2), b = 13.435(2), c = 14.358(2) Å, β = 109.108(9)°, U = 2151.5(5) Å^3, D_c = 1.601 g cm^{-3}, Mo-Kα radiation (λ = 0.710 73 Å), R = 0.033 and R_w = 0.032 for 3585 observed reflections with $I > 3\sigma(I)$. CCDC 182/878.

‖ Since the reaction occurs with irregular induction time, $t_{1/2}$ is variable.

** **2**: ^{1}H NMR [$(CD_3)_2SO$, TMS standard], δ 13.18 (br, 1 H), 8.057 (d, 1 H), 7.664 (d, 2 H), 7.400 (t, 1 H), 7.303 (br, 2 H), 7.074–7.019 (m, 2 H). ^{13}C NMR [$(CD_3)_2SO$], δ 158.07, 151.68, 140.93, 133.14, 126.19, 123.27, 122.38, 119.11, 117.93, 112.58, 111.51. EI-MS: *m/z* 210 (M^+)

1 A. Harriman, *Coord. Chem. Rev.*, 1979, **28**, 147.
2 V. L. Pecoraro, *Photochem. Photobiol.*, 1988, **48**, 247.
3 K. Wieghardt, *Angew. Chem., Int. Ed. Engl.*, 1989, **28**, 1153.
4 V. L. Pecoraro, M. J. Baldwin and A. Gelasco, *Chem. Rev.*, 1994, **94**, 807.
5 F. M. Ashmawy, C. A. McAuliffe, R. V. Parish and J. Tames, *J. Chem. Soc., Dalton Trans.*, 1985, 1391.
6 N. Aurangzeb, C. E. Hulme, C. A. McAuliffe, R. G. Pritchard, M. Watkinson, M. R. Bermejo, A. Garcia-Deibe, M. Rey, J. Sanmartin and A. Sousa, *J. Chem. Soc., Chem. Commun.*, 1994, 1153.
7 M. Watkinson, A. Whiting and C. A. McAuliffe, *J. Chem. Soc., Chem. Commun.*, 1994, 2141.
8 A. Garcia-Deibe, A. Sousa, M. R. Bermejo, P. P. MacRory, C. A. McAuliffe, R. G. Pritchard and M. Helliwell, *J. Chem. Soc., Chem. Commun.*, 1991, 728.
9 D. L. Williams and A. Heller, *J. Phys. Chem.*, 1970, **74**, 4473.
10 A. U. Acuna, F. Amat, J. Catalan, A. Costela, J. M. Figuera and J. M. Munoz, *Chem. Phys. Lett.*, 1986, **132**, 567.
11 E. L. Roberts, J. Dey and I. M. Warner, *J.Phys. Chem., A*, 1997, **101**, 5296.
12 C. M. Oelando Jr., J. G. Wirth and D. R. Heath, *J. Org. Chem.*, 1970, **35**, 3147.
13 L. J. Boucher and C. G. Coe, *Inorg. Chem.*, 1975, **14**, 1289.
14 C. A. McAuliffe, A. Nabhan, R. G. Pritchard, M. Watkinson, M. Bermejo and A. Sousa, *Acta Crystallogr., Sect. C*, 1994, **50**, 1676.
15 E. Gallo, E. Solari, N. Re, C. Floriani, A. Chiesi-Villa and C. Rizzoli, *Angew. Chem., Int. Ed. Engl.*, 1996, **35**, 1981.

Received in Cambridge, UK, 30th March 1998; 8/02405G

Three-dimensional redox-active layered composites of Au–Au, Ag–Ag and Au–Ag colloids

Ron Blonder, Laila Sheeney and Itamar Willner*†

Institute of Chemistry and The Farkas Center for Light-Induced Processes, The Hebrew University of Jerusalem, Jerusalem 91904, Israel

Ordered layered three-dimensional networks of Au, Ag and Au/Ag colloids are assembled in a stepwise synthesis using *N*,*N*′-bis(2-aminoethyl)-4,4′-bipyridinium as a redox-active crosslinker.

The ordered assembly of metal particles on solid supports, *i.e*. glass or conductive ITO-glass attracts substantial research effort due to the unique electronic and optical properties of nanoscale metal colloid particles.[1,2] Surface-enhanced Raman spectroscopy (SERS) of adsorbate monolayers on Au-colloids,[3,4] electrochemistry of redox-active monolayers associated with rough Au-colloid monolayers,[5] conductivity of three-dimensional Au-colloid assemblies,[6] and second-harmonic generation at layered Au-colloids,[7] were examined. Nanometer-size organization of the metal colloids is of importance to tailor microelectronic nano-devices. Indeed, it was shown that two Au_{55} clusters could act as a tunnel resonance resistor.[8] The assembly of metal colloid monolayers was accomplished by the functionalization of glass or conductive glass supports with surface thiolate or surface amino groups, acting as a ligation monolayer for the association of the colloids.[3,4] Alternatively, functionalized capped-metal colloids were reacted with modified surfaces to yield the respective monolayers. Colloid arrays were deposited on solid supports using dithiolate crosslinkers[10] or thiol-tagged oligonucleotides.[11] The bridging units separating the dithiol or the double-stranded oligonucleotide units control the inter-particle distances and the resulting conductivity features of the colloid arrays. The optical and electronic properties of metal colloids can be tuned by the preparation of bimetallic particles. Specifically, gold/silver composites or alloys have received interest with respect to their optical and electronic features.[4–6] Layered and ordered colloidal Au/Ag composites have been studied to date only to the extent that Ag-clad Au layers are generated by the electrochemical deposition of Ag on Au nanoparticles.[12]

In the present study, we describe the novel assembly of ordered three-dimensional metal colloids composed of Au colloids, Ag colloids and composite Au and Ag colloids. The colloids are crosslinked by a redox-active molecular bridging unit. We find that the molecular redox-active unit is electroactive in the three-dimensional colloid array, implying that electron transport through the colloid particles is feasible. To our knowledge, we present for the first time a synthetic method to assemble mixed composites of Au and Ag in an ordered way.

Au colloids were prepared by citrate reduction of an $HAuCl_4$ solution to yield Au particles of 12 ± 2 nm size.[13] Ag colloids were similarly prepared by citrate reduction of $AgNO_3$ solution [in the presence of iron(II) sulfate] to generate particles exhibiting a diameter corresponding to 31 ± 2 nm.[14] Glass slides or indium tin oxide (ITO) conductive glass were functionalized with triethoxy aminopropylsilane to yield an amino-functionalized surface. Interaction of the functionalized surface with the Au or the Ag colloid for 1.5 h yields the primary metal colloid monolayer, Scheme 1. These monolayers were subsequently reacted with *N*,*N*′-bis(2-aminoethyl)-4,4′-bipyridinium **1**, as the crosslinking reagent of the colloid monolayers. Further interaction of the surfaces with the Au colloid or the Ag colloid yield the respective two-layer Au/Au, Ag/Ag or Au/Ag assemblies, Scheme 1. By the additional interaction of the layered colloid assemblies with the crosslinking unit **1** and the respective metal colloid, a controlled number of metal particles with the respective ordering of the metal colloid layers, could be deposited onto the glass supports. Fig. 1(A) shows the absorption spectra changes upon assembly of a four-layer assembly of Au colloids. The absorption band, λ_{max} = 522 nm, increases almost linearly upon increasing the number of colloid layers associated with the surface. At high surface coverages, an additional absorbance at *ca*. 640 nm is observed. This band was attributed to a collective interparticle clustered plasmon.[3] Similarly, Fig. 1(B) shows the absorbance changes upon the assembly of a four-layer structure of Ag colloids. The absorbance of the Ag colloid, λ_{max} = 430 nm, increases as the number of layers is increased. Fig. 1(C) shows the absorbance spectra of a composite monolayer composed of one Au and one Ag layer. The composite assembly consists of two absorbance

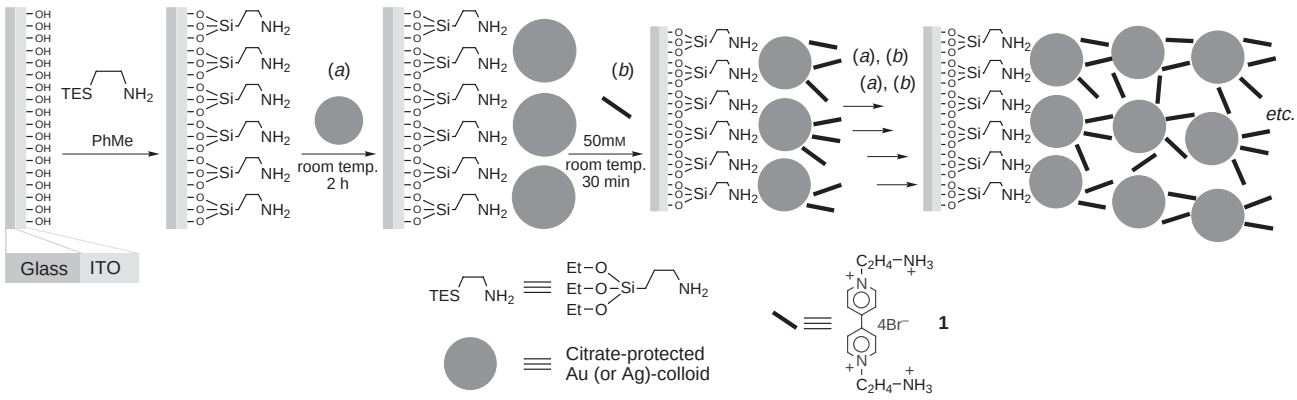

Scheme 1 Stepwise assembly of metal particle multilayer arrays

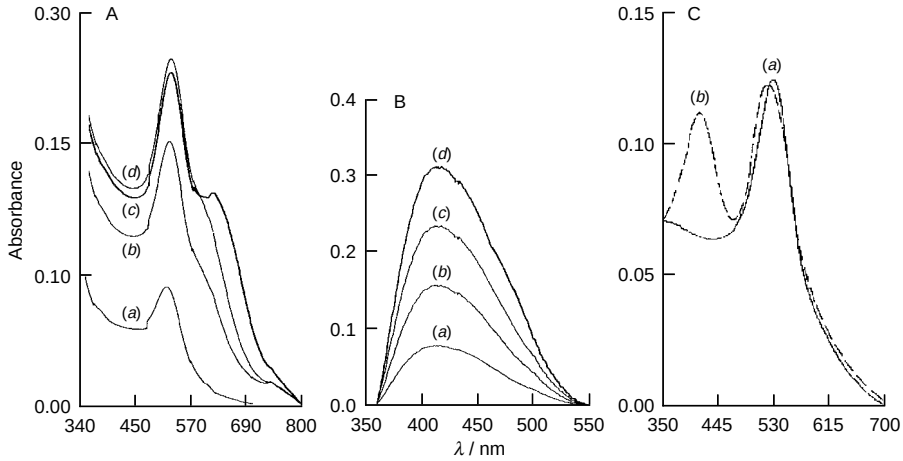

Fig. 1 (A) Absorbance spectra of an ITO glass upon the stepwise assembly of Au colloid (12 ± 2 nm, diameter layers); (*a*) 1, (*b*) 2, (*c*) 3, (*d*) 4 layers. (B) Absorbance spectra of an ITO glass upon the stepwise assembly of Ag colloid (31 ± 2 nm, diameter); (*a*) 1, (*b*) 2, (*c*) 3, (*d*) 4 layers. (C) Absorbance spectra of a composite Au/Ag metal colloid array; (*a*) one Au colloid layer assembled on an aminopropyl siloxane functionalized monolayer, (*b*) Ag colloid deposited onto the Au monolayer using **1** as crosslinker. All multilayers were assembled by functionalization of the respective colloid layer with the crosslinker **1** by the interaction of the colloid with a 50 mM solution of **1** for 0.5 h.

maxima at 520 and 430 nm, characteristic of the Au and Ag colloids, respectively.

Fig. 2 shows the cyclic voltammograms of the *N*,*N*′-bis(2-aminoethyl)-4,4′-bipyridinium redox-active crosslinking units upon the assembly of the four-layered Au colloid. The electrochemical response of the bipyridinium units is enhanced as the number of layers is increased. Coulometric analysis of the bipyridinium relay units associated with the first Au colloid layer, reveals a surface coverage of 7.3×10^{-11} mol cm^{-2} (geometrical area). As the surface coverage of Au colloids on glass was estimated by electromicroscopy measurements[4,5] to be *ca*. 1×10^{11} particles cm^{-2}, it suggests that *ca*. 450 bipyridinium bridging units are associated with each Au particle. Coulometric analysis indicates that the surface coverage of the bipyridinium units associated with the four-layer Au colloid assembly increases almost linearly upon the formation of the three-dimensional network (Fig. 2, inset).

In conclusion, we have demonstrated a novel method to assemble three-dimensional metal colloid networks consisting of Au, Ag or composite Au/Ag colloids and an amino-bifunctional redox-active briding unit as crosslinker. Electrostatic attraction between the crosslinker and the citrate-protected metal particles presumably leads to the assembly of the systems. The results demonstrate the formation of ordered composite layered assemblies of Au and Ag particles and reveal a means for the pre-planned structuring of composite multilayer assemblies. The electrochemical characterization of the bridged colloid assembly reveals that the redox-active molecular components are electrically contacted in the colloid lattice. This supports the suggestion that the Au particles act as nanoparticle conductive layers for electron transport through the network.

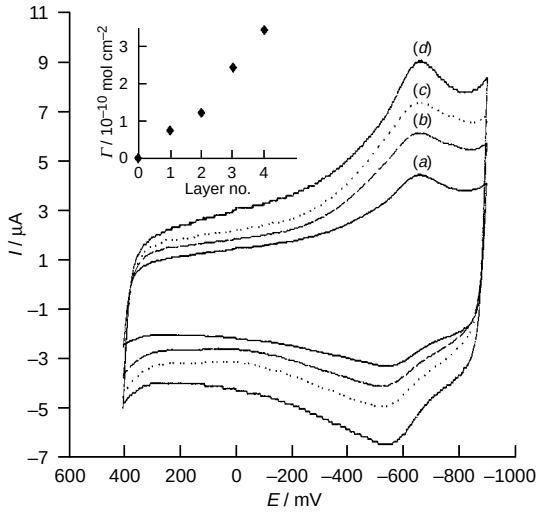

Fig. 2 Cyclic voltammograms of the Au-colloid layers functionalized by *N*,*N*′-bis(2-aminoethyl)-4,4′-bipyridinium **1**; (*a*) 1, (*b*) 2, (*c*) 3, (*d*) 4 layers. All measurements were recorded in phosphate buffer, pH = 7.0, scan rate 100 mV s^{-1}. Inset: Surface coverage of **1** *vs*. number of Au colloid layers.

This study is supported by the Israel Ministry of Science as an Infrastructure Project on Material Science.

Notes and References

† E-mail: willnea@vms.huji.ac.il

1 *Clusters and Colloids*, ed. G. Schmid, VCH, Weinheim 1994.
2 M. Antonietti and C. Göltner, *Angew Chem., Int. Ed. Engl*., 1997, **36**, 910.
3 R. G. Freeman, M. B. Hommer, K. C. Graber, M. A. Jackson and M. J. Natan, *J. Phys. Chem*., 1996, **100**, 718; P. G. Freeman, K. C. Garber, K. J. Allison, R. M. Bright, J. A. Davis, A. P. Guthrie, M. B. Hommer, M. A. Jackson, P. C. Smith, D. G. Walter and M. J. Natan, *Science*, 1995, **267**, 1629.
4 K. C. Garber, K. J. Allison, B. E. Baker, R. M. Bright, K. R. Brown, R. G. Freeman, A. P. Fox, C. D. Keating, M. D. Musick and M. J. Natan, *Langmuir*, 1996, **12**, 2353.
5 A. Doron, E. Katz, and I. Willner, *Langmuir*, 1995, **11**, 1313; A. Doron, E. Yoselevich, A. Schlittner and I. Willner, *Thin Solid Films*, in press.
6 M. D. Musick, C. D. Keating, M. H. Keefe and M. J. Natan, *Chem. Mater*., 1997, **9**, 1499; D. Bethell, M. Brust, D. J. Schiffrin and C. Kiely, *J. Electroanal. Chem.*, 1996, **409**, 137.
7 K. Kadono, T. Sakaguchi, M. Miya, J. Matsuoka, T. Fukumi and H. Tanaka, *J. Mater. Sci.: Mater. Electron.*, 1993, **4**, 59; A. Liebsch, *Surf. Sci.*, 1994, **307**, 1007.
8 U. Simon, G. Schön and G. Schmid, *Angew. Chem., Int. Ed. Engl.*, 1993, **32**, 250.
9 S. Peschel and G. Schmid, *Angew. Chem., Int. Ed. Engl*., 1995, **34**, 1442.
10 M. Brust, D. Bethell, D. J. Schiffrin and C. J. Kiely, *Adv. Mater*., 1995, **7**, 795.
11 (a) C. A. Mirkin, R. L. Lestinger, R. C. Mucic and J. J. Storhoff, *Nature*, 1996, **382**, 607; (b) S. P. Alivisatos, K. P. Johnsson, X. Peng, T. E. Wilson, C. J. Loweth, M. P. Bruchez Jr. and P. G. Schultz, *Nature*, 1996, **382**, 609.
12 R. M. Bright, D. G. Walter, M. D. Musick, M. A. Jackson, K. J. Allison and M. J. Natan, *Langmuir*, 1996, **12**, 810.
13 J. Turakevich, J. Stevenson and P. C. Hillier, *Discuss, Faraday Soc*., 1951, **11**, 55.
14 O. Siiman, L. A. Bumm, R. Callaghan, C. G. Blatchford and M. Kerker, *J. Phys. Chem*. 1983, **87**, 1014; U. Nickel, P. Halbig, H. Gliemann and S. Schneider, *Ber. Bunsenges. Phys. Chem*., 1977, **41**, 101.

Received in Cambridge, UK, 14th April 1998; 8/02727G

Palladium-catalysed carbon–carbon bond formation in supercritical carbon dioxide

Michael A. Carroll and Andrew B. Holmes*†

Melville Laboratory for Polymer Synthesis, Department of Chemistry, University of Cambridge, Pembroke Street, Cambridge, CB2 3RA UK

Novel fluorinated phosphine palladium complexes are prepared and employed in the first examples of palladium-catalysed carbon–carbon bond formation in supercritical carbon dioxide.

Supercritical carbon dioxide ($scCO_2$) has recently emerged as an environmentally benign substitute for volatile organic solvents.[1] Above the critical temperature (31.1 °C) and pressure (73.8 bar) carbon dioxide possesses hybrid properties of both a liquid and a gas. Control of the solvent density by variation of the temperature and pressure enables the solvent properties to be 'tuned' to substrates and reactants. These aspects have been used to advantage in polymer synthesis[2–4] and more recently in the preparation of 'small molecules'.[4,5] The particular attraction of $scCO_2$ must reside in the 'added value' as has been recognised in its application to heterogeneous catalytic processes and in asymmetric catalytic hydrogenation/hydroformylation.[6,7] In this respect synthetic transformations on small molecules could be coupled with the advantages of processing (separation/purification) technologies[8] to provide significant benefits over the use of conventional solvents.

We have chosen to study metal-catalysed bond forming reactions, but the majority of the commercially available metal-based catalysts, typically those bearing phosphine or amine ligands, are unsuitable for use in CO_2 owing to their low solubility.[9] Here we describe the synthesis of a range of fluorinated phosphines which enable various palladium-mediated reactions to be conducted in $scCO_2$.

Highly fluorinated compounds have been shown to have unusually high solubility in $scCO_2$, and their incorporation into phosphine-based ligands was expected to improve the solubility of the corresponding metal complexes. Such compounds can be prepared by adding the Grignard reagent $C_6F_{13}CH_2CH_2MgI$ to chlorophosphines to give a range of potential ligands for the solubilisation of palladium complexes in carbon dioxide (Scheme 1). Similar work has recently been reported regarding the preparation of these and other, similar ligands for applications in the 'fluorous' phase.[10] A simple but indirect means of purification of the required phosphines was achieved by temporary conversion to the corresponding oxide. Regeneration of the phosphine was achieved in excellent yield by treatment with Cl_3SiH and Et_3N.

The effect of the fluorinated phosphines **1** and **2** on the solubility of palladium complexes in $scCO_2$ was then examined, and the results are summarised in Table 1. It is evident that the solubility of the palladium complexes was dramatically improved. However, the degree of 'fluorination' required to confer solubility is dependent on the particular complex, those species having a higher degree of ionic character requiring an increased level of fluorination (Table 1, entries 4 and 7).‡

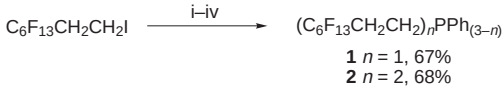

Scheme 1 *Reagents and conditions*: i, Mg, Et_2O, room temp., 12 h; ii, $Cl_nPPh_{(3-n)}$, Et_2O, room temp., 3 h; iii, $NaIO_4$, acetone, room temp., 12 h; iv, Et_3N, Cl_3SiH, toluene, 100 °C, 12 h

The soluble palladium complexes§ (Table 1, entries 5 and 8) were then used to catalyse three important carbon–carbon bond forming reactions, namely the Heck, Suzuki and Sonogashira couplings. The Heck reaction has emerged as one of the most versatile members of this group.[11] Table 2 (entry 1) illustrates that the reaction in $scCO_2$ with electron deficient alkenes occurs in a superior yield to that reported for conventional solvents; intramolecular processes are also possible (entry 2). The palladium-catalysed coupling of boronic acids with aryl or vinyl halides, the Suzuki reaction, has certain advantages for the coupling of two sp^2 centres.[12] This too can be conducted in $scCO_2$ (entries 3 and 4) in yields that are comparable to those achieved in conventional solvents. Finally, the Sonogashira coupling reaction[13] affords functionalised acetylenic compounds also in satisfactory yield.¶ The use of a more basic (secondary rather than tertiary) amine in palladium-mediated transformations typically leads to an improvement in yield. However, in $scCO_2$ very little difference is observed between the two. It is not yet clear whether this is due to carbamic acid formation.[14] Electron deficient amines, such as perfluorotrihexylamine, despite having improved solubility, exhibit a detrimental effect.

It is of note that the work-up procedures are significantly easier than those associated with standard reaction conditions. Typically the use of a polar solvent such as DMF and a water soluble base (carbonate or alkoxide) requires extraction of the product with an organic solvent according to conventional isolation techniques. By contrast, a simple pressure change in the $scCO_2$ reactor allows the gaseous/liquid reaction medium to be vented (possibly through a conventional solvent) thus eliminating liquid/liquid partition.

In summary, new fluorinated phosphine palladium complexes have been prepared and used as homogeneous catalysts in supercritical carbon dioxide. Important palladium-mediated carbon–carbon bond forming processes are now accessible and are expected to lead to considerable advances in synthetic methodology in due course.[15]

Table 1 Solubility of phosphine palladium complexes in $scCO_2$

Entry	Complex	L	Solubility
1	PdL_2Cl_2	PPh_3	Insoluble
2	PdL_2Cl_2	PCy_3	Insoluble
3	PdL_2Cl_2	dppf[a]	Insoluble
4	PdL_2Cl_2	**1**[b]	Partial[c]
5	PdL_2Cl_2	**2**[b]	Soluble
6	$PdL_2(OAc)_2$	PPh_3	Insoluble
7	$PdL_2(OAc)_2$	**1**[d]	Soluble[e]
8	$PdL_2(OAc)_2$	**2**[d]	Soluble

[a] 1,1′-Bis(diphenylphosphino)ferrocene. [b] Prepared in CH_2Cl_2 by the reaction (25 °C) of the phosphine (2 equiv.) and $(MeCN)_2PdCl_2$ (1 equiv.). [c] Incomplete disappearance of solid coupled with an increase in colour intensity on warming. [d] Prepared *in situ* from the phosphine (2 equiv.) and $Pd(OAc)_2$ (1 equiv.). [e] Decomposes at $T > 45$ °C.

Table 2 Palladium-catalysed carbon–carbon bond formation in $scCO_2$

Entry	Substrate 1	Substrate 2	Product	Catalyst[a]	*T*/°C	Yield (%)[b]
1	PhI	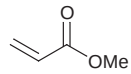	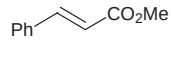	$PdL_2(OAc)_2$[c]	100	91
2		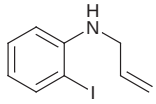	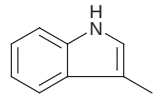	$PdL_2(OAc)_2$[c]	100	37
3	PhI	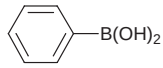	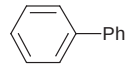	PdL_2Cl_2	100	52
4	PhI	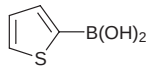	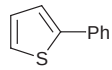	PdL_2Cl_2	100	49
5	PhI	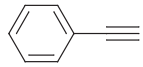	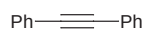	PdL_2Cl_2[d]	60	62
6	PhI	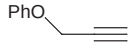	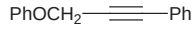	PdL_2Cl_2[d]	60	18

[a] L = **2** (5 mol%) for 64 h with Et_3N (1.1 equiv.) added. [b] Isolated yield, not optimised. [c] Prepared *in situ* from the phosphine **2** (2 equiv.) and $Pd(OAc)_2$ (1 equiv.). [d] 5 mol% CuI added.

We thank the EPSRC for financial support and provision of the Swansea Mass Spectrometry Service, and ICI Acrylics for financial support. We thank Dr A. I. Cooper and Mr S. A. Mang for their interest in this work. Dedicated to the memory of Professor Ralph Raphael.

Notes and References

† E-mail: abh1@cus.cam.ac.uk

‡ *Typical procedure* for determining solubility in supercritical carbon dioxide: $Pd(PPh_3)_2Cl_2$ (7 mg, 0.01 mmol) was placed in a 10 ml stainless steel cell. The cell was sealed and completely filled with liquid carbon dioxide (*ca.* 1000 psi). The cell was then heated to 70 °C and the state of the solid was monitored by viewing through a sapphire observation window. After 10 min at the final temperature the cell was allowed to cool. When the pressure had dropped below 2000 psi the cell was vented into CH_2Cl_2 (100 ml), the cell was opened once atmospheric pressure was reached and was washed out with a further quantity of CH_2Cl_2 (20 ml).

§The determination of the crystal structure of PdL_2Cl_2 (L = **2**) is currently under investigation.

¶ *Typical procedure* for the Sonogashira reaction using the catalyst PdL_2Cl_2 (L = **2**) in $scCO_2$: Bis[bis(1*H*, 1*H*, 2*H*, 2*H*-perfluorooctyl)-phenylphosphino]palladium dichloride‖ (89 mg, 0.05 mmol), copper(I) iodide (9 mg, 0.05 mmol), iodobenzene (0.11 ml, 1 mmol), phenylacetylene (0.11 ml, 1 mmol) and triethylamine (0.15 ml, 1.1 mmol) were placed in a 10 ml stainless steel cell. The cell was sealed and pressurised to approximately 1000 psi (full of carbon dioxide). The suspended reagents were magnetically stirred and afforded a dark red-coloured medium as the cell was heated to 60 °C. The reagents were stirred at this temperature for 64 h when a crystalline deposit formed on the sapphire window. The cell was then cooled, and when the pressure had dropped below 2000 psi the cell was vented into Et_2O (100 ml). The cell was opened once atmospheric pressure was reached and washed out with a quantity of CH_2Cl_2 (10 ml). The organic fractions were combined and concentrated *in vacuo* to give the crude product. The product was purified by flash column chromatography on silica gel, eluting with hexane to give diphenylacetylene as a white crystalline solid (110 mg, 0.62 mmol, 62%), mp 58–60 °C; δ_H(250 MHz; $CDCl_3$) 7.56–7.61 (4 H, m, *o*-Ph), 7.33–7.43 (6 H, m, *m/p*-Ph); δ_C 131.7 (*o*-C), 128.5 (*m*-Ph), 128.4 (*p*-Ph), 123.4 (quaternary Ph), 89.5 (alkyne). A similar procedure (excluding CuI) was used for the Suzuki reaction. The Heck procedure employed the *in situ* generated palladium acetate complex. All reactions showed similar colour and physical behaviour.

‖ All new compounds gave spectroscopic (NMR, IR, HRMS) data in accordance with their proposed structure.

1 D. A. Morgenstern, R. M. LeLacheur, D. K. Morita, S. L. Borokowsky, S. Feng, G. H. Brown, L. Luan, M. F. Gross, M. J. Burk and W. Tumas, *ACS Symp. Ser*., 1996, **626**, 132.
2 A. I. Cooper and J. M. DeSimone, *Curr. Opin. Solid State Mater. Sci*., 1996, **1**, 761.
3 T. M. Yong, W. P. Hems, J. L. M. van Nunen, A. B. Holmes, J. H. G. Steinke, P. L. Taylor, J. A. Segal and D. A. Griffin, *Chem. Commun*., 1997, 1811.
4 A. Fürstner, D. Koch, K. Langemann, W. Leitner and C. Six, *Angew. Chem., Int. Ed. Engl*., 1997, **36**, 2466.
5 A. R. Renslo, R. D. Weinstein, J. W. Tester and R. L. Danheiser, *J. Org. Chem*., 1997, **62**, 4530; M. G. Hitzler, F. R. Smail, S. K. Ross and M. Poliakoff, *Chem. Commun*., 1998, 359.
6 M. G. Hitzler and M. Poliakoff, *Chem. Commun*., 1997, 1667; P. G. Jessop, Y. Hsaio, T. Ikariya and R. Noyori, *J. Am. Chem. Soc*., 1996, **118**, 344; M. J. Burk, S. Feng, M. F. Gross and W. Tumas, *J. Am. Chem. Soc*., 1995, **117**, 8277.
7 S. Kainz, D. Koch, W. Baumann and W. Leitner, *Angew. Chem., Int. Ed. Engl*., 1997, **36**, 1628.
8 M. A. McHugh and V. J. Krukonis, *Supercritical Fluid Extraction*, 2nd edn., Butterworth-Heinman, Stoneham, MA, 1994.
9 D. R. Palo and C. Erkey, *J. Chem. Eng. Data*, 1998, **43**, 47.
10 P. Bhattacharyya, D. Gudmunsen, E. G. Hope, R. D. W. Kemmitt, D. R. Paige and A. M. Stuart, *J. Chem. Soc., Perkin Trans. 1*, 1997, 3609.
11 R. F. Heck, *Palladium Reagents in Organic Synthesis*. Academic Press, Orlando, 1985.
12 N. Migaura, T. Yanagi and A. Suzuki, *Synth. Commun*., 1981, **11**, 513.
13 K. Sonogashira, Y. Tohda and N. Hagihara, *Tetrahedron. Lett*., 1975, 4467.
14 V. P. Savin, V. P. Talzi and N. O. Bek, *Zh. Org. Khim.*, 1984, **20**, 1842 (*J. Org. Chem. USSR*, 1984, **20**, 1680).
15 D. K. Morita, D. R. Pesiri, S. A. David, W. H. Glaze and W. Tumas, *Chem. Commun*., 1998, 1397.

Received in Cambridge, UK, 23rd March 1998; 8/02235F

Palladium-catalyzed cross-coupling reactions in supercritical carbon dioxide

David K. Morita,[a] David R. Pesiri,[b] Scott A. David,[a] William H. Glaze[c] and William Tumas*[a]†

[a] *Los Alamos Catalysis Initiative, Chemical Science and Technology Division, Los Alamos National Laboratory, Los Alamos, NM 87545, USA*
[b] *Department of Environmental Sciences and Engineering, University of North Carolina, Chapel Hill, NC 27599, USA*
[c] *Carolina Environmental Program, University of North Carolina, Chapel Hill, NC 27599, USA*

Palladium-catalyzed carbon–carbon bond coupling reactions, the Heck and Stille reactions, proceed in supercritical carbon dioxide with a number of phosphine ligands including tris[3,5-bis(trifluoromethyl)phenyl]phosphine, which affords high conversions and selectivities.

Elevated pressures[1] have been reported to offer benefits for homogeneous catalyst lifetime[2] and selectivity.[3] Such pressure-related advantages, in combination with the properties of supercritical carbon dioxide ($scCO_2$), led us to explore homogeneous catalytic reactions in this medium. A number of recent reports describe examples of homogeneous catalytic reactions in $scCO_2$ including hydrogenations,[4] hydroformylations,[5] epoxidations[6] and polymerizations.[7] We report the first demonstration that palladium-catalyzed carbon–carbon coupling reactions can be carried out in supercritical CO_2. We have examined catalyst activity, selectivity and ligand effects in $scCO_2$ in a first step toward capitalizing on the benefits of high pressures for homogeneous palladium-catalyzed reactions. The reactivity and selectivity of Heck[8] and Stille[9] reactions using several different phosphine ligands in $scCO_2$[10] were compared to those in organic solvents (THF and toluene).

All reactions in $scCO_2$ were carried out batchwise in magnetically stirred, custom built 316 stainless steel reactors with sapphire windows to allow viewing of the contents at high pressure.[11] Stille cross-coupling reactions of PhI and vinyl(tributyl)tin in CO_2 (345 bar) were run at 90 °C for 5 h using a number of different ligands (Table 1). The highest conversion in $scCO_2$ was achieved with the tris[3,5-bis(trifluoromethyl)phenyl]phosphine ligand **4** (> 99%) which was comparable to the results using tri-2-furylphosphine **3** (86%), a ligand noted for high palladium-coupling activity.[9c] PPh_3 **2** and tri-*o*-tolylphosphine **1** were characterized by significantly lower turnover numbers, with PPh_3 **2** resulting in conversions only slightly higher than the reaction in the absence of added ligand. We also ran the Stille coupling reaction of PhI with vinyl(tributyl)tin with the same ligands in CO_2 and THF at 50 °C and found that the conversions were considerably higher in THF. For example, in THF at 50 °C the tri-2-furylphosphine and tris[3,5-bis(trifluoromethyl)phenyl]phosphine ligands both resulted in conversions above 95% while slightly lower conversions (81%) were measured with PPh_3. The conversion in $scCO_2$ at 50 °C for the Stille reaction was only 28% after 5 h using the tri-2-furylphosphine ligand.

The much higher conversions in $scCO_2$ for tris[3,5-bis(trifluoromethyl)phenyl] phosphine appear to arise from the enhanced solubilization of the catalytically active palladium–phosphine complexes. A number of reports have demonstrated the ability of fluorine substitution on organic polymers and ligands to enhance solubility in $scCO_2$.[7a,7b,12,13] In particular, Leitner has recently reported catalytic activity in $scCO_2$ for rhodium catalysts containing perfluoroalkyl-substituted arylphosphines.[12] Although we have not carried out any quantitative solubility studies, we observed no visible precipitation for the Stille coupling reactions in CO_2 using the tris[3,5-bis(trifluoromethyl)phenyl]phosphine ligand. We did, however, observe significant precipitation in CO_2 (presumably palladium–phosphine complexes) under identical conditions with PPh_3. The perfluorinated ligand, tris(pentafluorophenyl)-phosphine, also conferred solubility indicated by no observed precipitation, although lower conversions (≤ 75%) were obtained.

In order to further probe these ligand effects, and to benchmark the chemical reactivity in CO_2 with organic solvents, we carried out preliminary kinetic studies of the Stille coupling of PhI and vinyl(tributyl)tin at 75 °C in $scCO_2$ and toluene. Reaction rates were determined as initial rates[14] using a high pressure reactor with a six-port sampling valve for CO_2, which has been described previously,[11] and standard Schlenk-ware for toluene. As shown in Table 2, the initial rate of reaction using tris[3,5-bis(trifluoromethyl)phenyl]phosphine **4** was twice that of PPh_3 **2** in both CO_2 and toluene. Moreover, the

Table 1 Stille cross-coupling of PhI with vinyl(tributyl)tin using $Pd_2(dba)_3$ in supercritical CO_2[a]

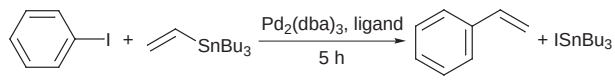

Ligand	Conversion (%)	Selectivity[c] (%)	TON[d]/h^{-1}
Tri-*o*-tolylphosphine **1**	9	99	0.5
No ligand	38	96	1.9
PPh_3 **2**	49	96	2.5
Tri-2-furylphosphine **3**	86	97	4.3
$P[3,5\text{-}(CF_3)_2C_6H_3]_3$ **4**	> 99	99	> 5

[a] 90 °C, 5 h, 345 bar CO_2, 2 equiv. of phosphine ligand for each equiv. of palladium(0) in all coupling reactions, [2.7 mmol (0.790 ml) vinyl(tributyl)tin, 2.7 mmol (0.3 ml) PhI, 0.054 mmol (0.048 g) $Pd_2(dba)_3$, 0.216 mmol phosphine ligand], reactions were quenched in acetone and analyzed by GC using known standards and confirmed by GC–MS and/or ^{1}H NMR spectroscopy. [b] Conversion = iodobenzene reacted (%). [c] Selectivity = styrene (%) with respect to all products formed. [d] TON/h^{-1} = [(moles of iodobenzene) × (% conversion)]/[(moles of catalyst added) × (hours of reaction)].

Table 2 Rates of Stille coupling reactions in supercritical CO_2 and toluene[a]

	k/min^{-1}	
Ligand	CO_2	Toluene
PPh_3 **2**	0.016	0.034
$P[3,5\text{-}(CF_3)_2C_6H_3]_3$ **4**	0.036	0.057

[a] 75 °C, 0.024 mmol (0.022 g) $Pd_2(dba)_3$, 2.4 mmol vinyl(tributyl)tin, 2.4 mmol PhI, 33 ml toluene or 33 ml CO_2 at 310 bar used. Initial rates measured by GC with internal standard (octafluoronaphthalene). Initial rates (30 min) were obtained from a ln [c/c_o] *vs.* time plot and are accurate to within 10%.

Table 3 Heck cross-coupling reaction in supercritical CO_2[a]

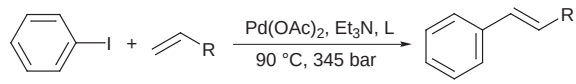

	R = CO_2Me			R = Ph		
L	Conversion (%)	Selectivity (%)	TON/h^{-1}	Conversion (%)	Selectivity (%)	TON/h^{-1}
Tri-*o*-tolylphosphine **1**	35	80	1	—	—	—
No ligand	17	82	0.5	37	99	1
PPh_3 **2**	—	—	—	20	99	0.6
Tri-2-furylphosphine **3**	96	78	2.7	—	—	—
$P[3,5\text{-}(CF_3)_2C_6H_3]_3$ **4**	94	91	2.6	99	99	2.8
$P(C_6F_5)_3$ **5**	—	—	—	99	99	2.8

[a] 90 °C, 24 h (R = CO_2Me), 12 h, 0.3 mmol ligand, 0.15 mmol (0.034 g) $Pd(OAc)_2$, 15 mmol (2.25 ml) Et_3N, 5 mmol (0.560 ml) PhI, 25 mmol (2.25 ml) methyl acrylate, octafluoronaphthalene internal standard. Reactions were analyzed as in Table 1.

observed rates in $scCO_2$ were within a factor of two of those observed in toluene for both phosphine ligands (Table 2). The initial rates of the PPh_3 **2** and tris[3,5-bis(trifluoromethyl)phenyl]phosphine **4** ligands are similar but the conversions are so different, suggesting that the enhanced solubility of the trifluoromethyl substituted system is probably more important than any increased activity through electronic effects. We found that the much less basic fluorinated ligand, tris(pentafluorophenyl)phosphine **5**, also enhanced solubility relative to PPh_3 **2** but the initial rate was two orders of magnitude less than the other ligands, presumably due to electronic effects.

We have also examined the palladium-catalyzed Heck coupling of PhI with simple olefins using several phosphines in $scCO_2$ at 90 °C. As Table 3 illustrates, we observe that the fluorinated phosphines result in high conversions for both styrene and methyl acrylate (> 94%), similar to the proven tri-2-furylphosphine ligand. The non-fluorinated triarylphosphines led to lower conversions (20–35%), which were comparable to reactions run in the absence of added ligand. Unlike the Stille couplings, the reaction solution for all the Heck couplings was dark and opaque and prevented even qualitative observation of precipitation; however, we believe the higher turnovers for the fluorinated phosphines probably arise from enhanced solubilization of the palladium complexes.

In summary, we have observed that both Heck and Stille couplings can proceed in supercritical CO_2 with rates and selectivites comparable to those in toluene. Of particular note, we find that fluorinated phosphines, particularly tris[3,5-bis(trifluoromethyl)phenyl]phosphine, result in high conversions due to the ability of these ligands to enhance the solubility of the metal complexes in $scCO_2$. 'CO_2-philic' ligands such as fluorinated phosphines should expand the utility of $scCO_2$ for homogeneous catalysis. Another logical extension of our work would be to explore supercritical fluids at pressures reported[2] to be high enough (> 1 kbar) to enhance some catalytic reactions.

This work was supported as part of the Los Alamos Catalysis Initiative by The Department of Energy through Laboratory Directed Research and Development (LDRD) funding, and a grant from the US EPA, Office of Pollution Prevention and Toxics (Grant Number 1877-97-1). We would like to acknowledge many helpful discussions with Dr Tom Baker and Dr Steve Buelow.

Notes and References

† E-mail: tumas@lanl.gov

1 *Organic Synthesis at High Pressures*, ed. K. Matsumoto and R. M. Acheson, Wiley, New York, 1990; J. H. Espenson, *Chemical Kinetics and Reaction Mechanisms*, McGraw-Hill, New York, 1981.
2 S. Hillers, S. Sartori and O. Reiser, *J. Am. Chem. Soc*., 1996, **118**, 2087.
3 Y. Sun, R. N. Landau, J. Wang, C. LeBland and D. G. Blackmond, *J. Am. Chem. Soc.*, 1996, **118**, 1348.
4 P. G. Jessop, T. Ikariya and R. Noyori, *Science*, 1995, **269**, 1065; P. G. Jessop, T. Ikariya and R. Noyori, *Chem. Rev*., 1995, **95**, 259; M. J. Burk, S. Feng, M. F. Gross and W. Tumas, *J. Am. Chem. Soc*., 1995, **117**, 8277.
5 J. W. Rathke, R. J. Klingler and T. B. Krause, *Organometallics*, 1991, **10**, 1350.
6 D. R. Pesiri, D. K. Morita, W. H. Glaze and W. Tumas, *Chem. Commum*., 1998, 1015.
7 (*a*) J. B. McClain, D. E. Betts, D. A. Canelas, E. T. Samulski, J. M. DeSimone, J. D. London, H. D. Cochran, G. D. Wignall, D. Chillura-Martino and R. Triolo, *Science*, 1996, **274**, 2049; (*b*) C. A. Mertdogan, T. P. DiNoia and M. A. McHugh, *Macromolecules*, 1997, **30**, 7511.
8 R. F. Heck, *Palladium Reagents in Organic Synthesis*, Academic Press, London, 1985; R. F. Heck and J. P. Nolley Jr., *J. Org. Chem.*, 1972, **37**, 2320.
9 (*a*) J. K. Stille, *Angew. Chem., Int. Ed. Engl.*, 1986, **25**, 508; (*b*) I. P. Beletskaya, *J. Organomet. Chem*., 1983, **250**, 551; (*c*) V. Farina and G. P. Roth, in *Advances in Metal-Organic Chemistry*, ed. L. S. Liebeskind, JAI Press, Greenwich, CT, 1996, vol. 5, p. 1.
10 For similar reactions and conditions please see: M. A. Carroll and A. B. Holmes, *Chem. Commun.*, 1998, 1395.
11 S. Buelow, P. Dell'Orco, D. K. Morita, D. R. Pesiri, E. Birnbaum, S. Borkowsky, G. Brown, S. Feng, L. Luan, D. A. Morgenstern and W. Tumas, *Recent Advances in Chemical Processing in Dense Phase Carbon Dioxide at Los Alamos*, in *Frontiers in Benign Chemical Synthesis and Processing*, ed. P. T. Anastas and T. C. Williamson, Oxford University Press, in the press.
12 S. Kainz, D. Koch, W. Baumann and W. Leitner, *Angew. Chem., Int. Ed. Engl*., 1997, **36**, 1628.
13 B. Betzemeier and P. Knochel, *Angew. Chem., Int. Ed. Engl*., 1997, **36**, 2623; I. T. Horvarth and J. Rábai, *Science*, 1994, **266**, 72; K. Laintz, C. Wai, C. Yonker and R. Smith, *J. Supercritical Fluids*, 1991, **4**, 194; A. Yazdi, C. Lepilleur, E. Singley, W. Liu, F. Adamsky, R. Encik and E. Beckman, *Fluid Phase Equilib*., 1996, **117**, 297.
14 V. Farina and B. Krishnan, *J. Am. Chem. Soc.*, 1991, **113**, 9585.

Received in Cambridge, UK, 6th April 1998; 8/02621A

ortho-Vinylation reaction of anilines

Masahiko Yamaguchi,*[a]† Mieko Arisawa[a] and Masahiro Hirama[b]

[a] *Faculty of Pharmaceutical Sciences, Tohoku University, Aoba, Sendai 980-8578, Japan*
[b] *Department of Chemistry, Graduate School of Science, Tohoku University, Aoba, Sendai 980-8578, Japan*

_N_-Alkylanilines and anilines are vinylated at the *ortho*-position with ethyne in the presence of $SnCl_4$–Bu_3N.

Vinylanilines are versatile intermediates for the synthesis of heterocyclic compounds and functionalized polymers, and the elimination reaction of (aminophenyl)ethanol derivatives is the most common method used to prepare these compounds.[1] The Wittig reaction has also been used for the formation of aryl olefins.[2] The vinyl group can be introduced to haloanilines employing either the Heck reaction or the Stille coupling reaction.[3] Cleavage of heterocyclic compounds has also been examined.[4] In some cases, such sequences of reactions were conducted *via* vinylated nitroarenes.[5] All these methods, however, required stepwise transformations, and direct introduction of the vinyl group to the aniline nucleus was desired. In this context, the vinylation of cyclopalladated acetanilide reported by Horino is interesting, although the use of a stoichiometric amount of the palladium compound is inconvenient from a synthetic point of view.[6] Previously, we reported the direct *ortho*-vinylation of phenols with ethyne,[7] and the methodology is extended here to the direct *ortho*-vinylation of anilines (Scheme 1).

Scheme 1

Ethyne was bubbled into a chlorobenzene solution of *N*-methylaniline and $SnCl_4$–Bu_3N (4 equiv.) at −50 °C for 30 min. Then, the mixture was heated at 80 °C for 40 min, during which time ethyne was continuously introduced. The reaction was quenched by treating with 2 M KOH and THF at reflux for 1 h. After aqueous workup, the crude products were trifluoroacetylated with TFAA and Et_3N giving *N*-methyl-2′-vinyl trifluoroacetanilide in 77% yield. In contrast to the vinylation of phenol, the aniline reaction required the continuous introduction of ethyne during heating to obtain satisfactory results.

Several *para*- and *meta*-substituted *N*-methylanilines were treated with ethyne under the above conditions, and the results are summarized in Scheme 2. The vinylation was applicable to various substituted *N*-alkylanilines including halogen and methoxy derivatives. *N*-Benzyl- and *N*-butyl-aniline could also be vinylated. In the case of *meta*-substituted derivatives, the reaction took place at the less hindered site predominantly. It may be interesting to note that 3-fluoroaniline showed higher selectivity than the chloro derivative, and electronic effect also appeared to affect the selectivity. *ortho*-Substituted anilines such as 2-methyl-*N*-methylaniline did not give the expected product. This may be due to steric reasons, since *ortho*-substituted anilines lacking the nitrogen substituent gave the vinylated products (*vide infra*). Absence of the divinylated product in the reaction of *N*-methylanilines could be ascribed to the same reason.[8] The trifluoroacetyl group could readily be removed by treatment with KOH and MeOH at reflux for 10 min. The present methodology was also used to alkenylate *N*-methylanilines with aromatic and aliphatic alk-1-ynes.

The vinylation of anilines lacking the nitrogen substituent required modification of the workup procedures. *para*-Methylaniline was treated with ethyne at 80 °C for 2 h, and worked up in 2 M KOH and THF in the presence of excess ethylenediamine at reflux for 5–8 h to give a mixture of 2-vinylaniline,

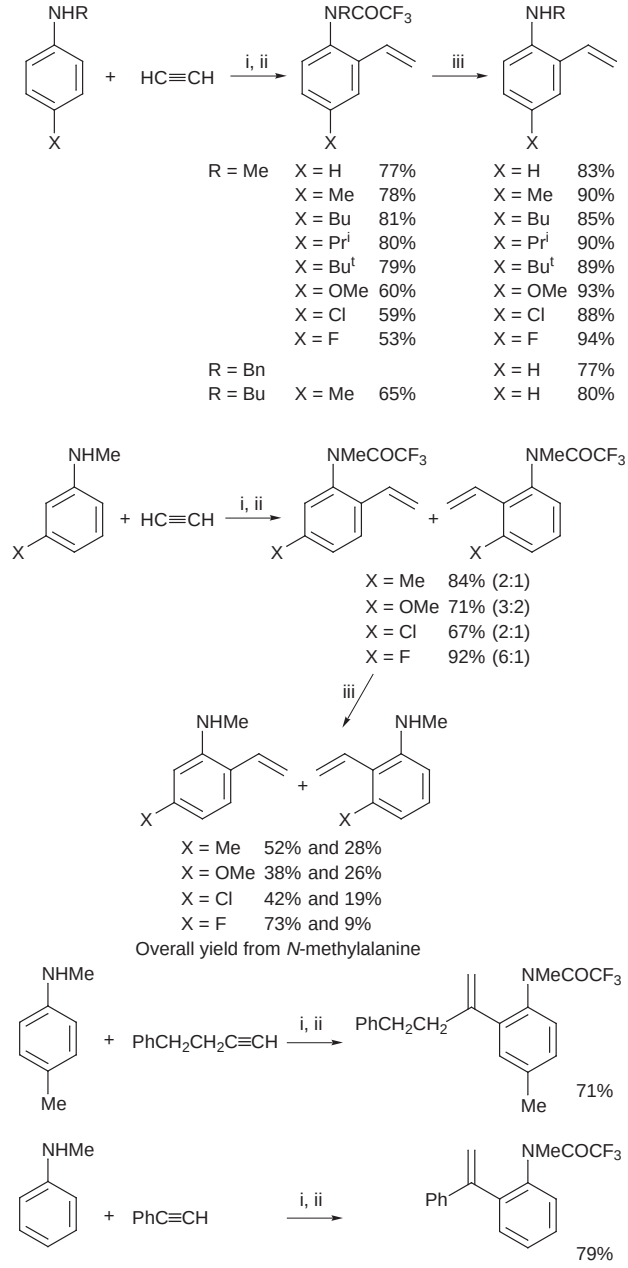

Scheme 2 *Reagents and conditions*: i, $SnCl_4$–Bu_3N; ii, TFAA, Et_3N; iii, KOH, MeOH

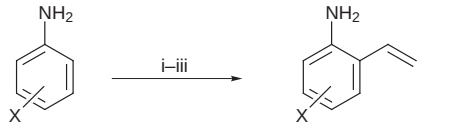

X = H 39%
X = 2-Me 58% (78%)
X = 2-Et 43% (60%)
X = 2-F 42%
X = 2-Cl 45%
X = 3-Cl 32%
X = 4-Me 41% (61%)
X = 4-MeO 30% (53%)

Scheme 3 *Reagents and conditions*: i, $SnCl_4$–Bu_3N, HC≡CH; ii, TFAA, Et_3N; iii, KOH, MeOH, H_2O. Yields shown in parentheses are based on consumed aniline.

2,6-divinylaniline and the starting material in yields of 46, 5 and 23%, respectively. The chelating reagent was required in the workup for the effective protonation of vinylstannane, which is an intermediate of the present vinylation reaction.[7,8] The protonation of the organotin compound appeared to be slower for vinylanilines than for *N*-methylvinylanilines and vinylphenols. The considerable amount of starting material recovered is not due to nitrogen protonation, since aniline hydrochloride could be converted to the vinylaniline. *N*-Vinylation was also excluded since reactions of alk-1-ynes with *para*-methylaniline gave no trace of the corresponding methyl ketones. When 4-methylaniline was treated with the $SnCl_4$–Bu_3N in C_6D_5Cl, at least two species were detected by ^1H NMR spectroscopy. Probably only a part of the stannylated aniline could participate in the vinylation. The secondary trifluoroacetamide moiety of these products hydrolyzed more slowly than the *N*-methyl derivatives, and harsh conditions were required: heating with KOH in MeOH–H_2O (96 : 4) for 35–48 h. Based on these experiments a method to convert anilines to *ortho*-vinylanilines was established which involved vinylation, trifluoroacetylation and deprotection (Scheme 3). The synthesis gave the vinylated products in moderate overall yields.

Vinylaniline derivatives are one of the most attractive precursors for the synthesis of indoles. While sulfonylated anilines are known to cyclize effectively,[9] the reaction of unprotected aniline is rare. Although Hegedus reported the palladium-catalyzed reaction of *ortho*-vinylaniline,[9] their applicability remained unexplored. When 2-vinyl-*N*-methylanilines prepared in the present study were treated with $PdCl_2(MeCN)_2$ at THF reflux for 18 h in the presence of quinone and LiCl, *N*-methylindoles were obtained in high yields (Scheme 4). A shorter reaction time of 10 h was employed for 2-vinylanilines to avoid decomposition. Thus, the applicability of the Hegedus method turned out to be broad.

Typical procedures are as follows. Ethyne was bubbled into a solution of Bu_3N (24.0 mmol, 5.76 ml), $SnCl_4$ (24.0 mmol, 2.76 ml) and *N*-methylaniline (6.0 mmol, 642.6 mg) in chlorobenzene (60 ml) at −50 °C for 1 h. The reaction mixture was heated at 80 °C for 1.5 h, during which bubbling was continued. 2 M KOH (240 ml) and THF (40 ml) were added, and the mixture was heated at reflux for another 1 h. On cooling the organic materials were extracted with Et_2O, washed with brine, dried over $MgSO_4$ and filtered. After removal of Et_2O under reduced pressure, Et_3N (8.4 ml) and TFAA (8.5 ml) were added to the resultant chlorobenzene solution, and the mixture was stirred at −10 °C for 12 h. An aqueous workup followed by flash chromatography (hexane–EtOAc, 30 : 1) over silica gel gave *N*-methyl-2′-vinyl trifluoroacetanilide (72%, 990 mg).

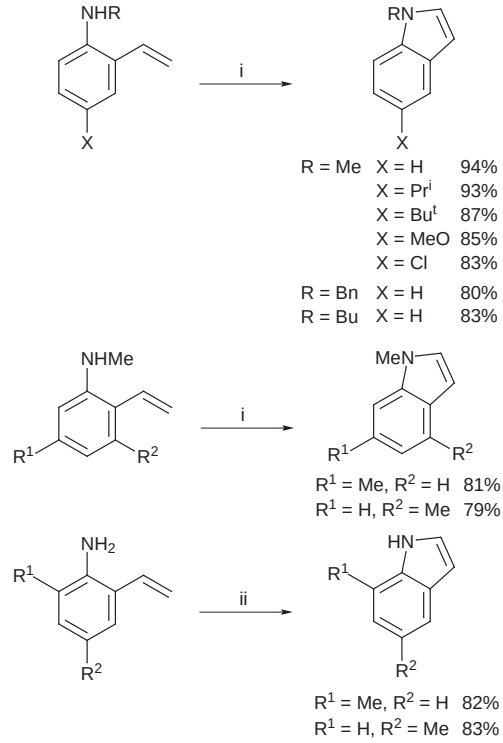

R = Me X = H 94%
X = Pr^i 93%
X = Bu^t 87%
X = MeO 85%
X = Cl 83%
R = Bn X = H 80%
R = Bu X = H 83%

R^1 = Me, R^2 = H 81%
R^1 = H, R^2 = Me 79%

R^1 = Me, R^2 = H 82%
R^1 = H, R^2 = Me 83%

Scheme 4 *Reagents and conditions*: i, $PdCl_2(MeCN)_2$, THF, reflux, 18 h; ii, $PdCl_2(MeCN)_2$, THF, reflux, 10 h

This work was supported by grants from the Japan Society of Promotion of Science (RFTF 97P00302) and the Ministry of Education, Science and Culture, Japan (No. 08404050).

Notes and References

† E-mail: yama@mail.pharm.tohoku.ac.jp

1 For example; S. Sabetay and T. Mintsou, *Bull. Soc. Chim. Fr.*, 1929, **45**, 842; S. Sabetay, J. Bléger and Y. de Lestrange, *Bull. Soc. Chim. Fr.*, 1931, **49**, 3; T. Sato, S. Ishida, H. Ishibashi and M. Ikeda, *J. Chem. Soc., Perkin Trans 1*, 1991, 353.
2 S. Hibino and E. Sugino, *Heterocycles*, 1987, **26**, 1883.
3 J. E. Plevyak and R. F. Heck, *J. Org. Chem.*, 1978, **43**, 2454; H. Jung and W. Heitz, *Makromol. Chem., Rapid Commun.*, 1988, **9**, 373; M. E. Krolski, A. F. Renaldo, D. E. Rudisill and J. K. Stille, *J. Org. Chem.*, 1988, **53**, 1170.
4 M. Harmata and M. Kahraman, *Synthesis*, 1995, **713**; M. Lancaster and D. J. H. Smith, *J. Chem. Soc., Chem. Commun.*, 1980, 471.
5 For example, J. H. Boyer and H. Alul, *J. Am. Chem. Soc.*, 1959, **81**, 2136; M. K. Cooper and D. W. Yaniuk, *J. Organomet. Chem.*, 1981, **221**, 231; C. Subramanyam, M. Noguchi and S. M. Weinreb, *J. Org. Chem.*, 1989, **54**, 5580.
6 H. Horino and N. Inoue, *J. Org. Chem.*, 1981, **46**, 4416.
7 M. Yamaguchi, A. Hayashi and M. Hirama, *J. Am. Chem. Soc.*, 1995, **117**, 1151.
8 *Cf.* M. Yamaguchi, M. Arisawa, Y. Kido and M. Hirama, *Chem. Commun.*, 1997, 1663.
9 L. S. Hegedus, G. F. Allen, J. J. Bozell and E. L. Waterman, *J. Am. Chem. Soc.*, 1978, **100**, 5800; P. J. Harrington and L. S. Hegedus, *J. Org. Chem.*, 1984, **49**, 2657; P. J. Harrington, L. S. Hegedus and K. F. McDaniel, *J. Am. Chem. Soc.*, 1987, **109**, 4335.

Received in Cambridge, UK, 17th April 1998; 8/02879F

Pyrrole-embedded [60]fullerenes

Uwe Reuther and Andreas Hirsch†

Institut für Organische Chemie, Henkestraße 42, D-91054 Erlangen, Germany

The treatment of the monoarylated azafullerenes $ArC_{59}N$ with iodine monochloride in carbon disulfide leads to the exclusive formation of the tetrachlorinated heterofullerenes $Cl_4ArC_{59}N$ which contain a pyrrole moiety in the fullerene cage.

Recently, we reported on the synthesis of arylated heterofullerenes $ArC_{59}N$.[1] These systems are suitable compounds for the investigation of the chemistry of azafullerenes, because they are stable and more soluble than the parent dimer $(C_{59}N)_2$.

Here, we report on the facile chlorination of azafullerenes $ArC_{59}N$ with ICl. The reaction of C_{60} with ICl was previously described by Birkett *et al.*[2] and leads to the quantitative formation of $C_{60}Cl_6$. This C_s symmetrical compound exhibits an addition pattern with five Cl atoms attached in 1,4 positions at the outer and one at the inner perimeter of a corannulene substructure, leaving a cyclopentadiene moiety within the fullerene framework. Consequently, the reaction with azafullerene derivatives $ArC_{59}N$ should yield the related tetrachlorinated species $Cl_4ArC_{59}N$ containing an integral pyrrole moiety decoupled from the conjugated π-system of the fullerene cage.

For the synthesis of the pyrrole-embedded fullerenes **4**–**6** a freshly prepared solution of 25 equiv. of ICl in CS_2 was added to a solution of 1 equiv. of the azafullerene derivatives **1**–**3** in CS_2 at room temperature (Scheme 1). This mixture was stirred for 10 min and then allowed to stand in the dark for three days for the decomposition of the excess ICl. Subsequently, the solvent and most of the iodine were removed *in vacuo*. After chromatography on silical gel (toluene) the chlorinated compounds **4**–**6** were isolated in 50–60% yield as orange powders (**6** had to be further purified by HPLC on a semipreparative Cosmosil column). The reaction can easily be monitored by HPLC using a Cosmosil column and toluene as eluent, since compounds **4**–**6** show a significantly longer retention time than the corresponding educts. Compounds **4** and **5** are only sparingly soluble in CS_2. This turned out to be a serious problem, as no ^{13}C NMR spectra of sufficient intensity could be obtained. Compound **6** however is soluble enough (about 3 mg ml^{-1} in CS_2) to obtain a well-resolved ^{13}C NMR spectrum corroborating the depicted structure.‡ The spectrum shows 26 resolved of the 28 expected signals for the sp^2 C-atoms of the fullerene cage between δ 160 and 128. The eight different carbon atoms of the isopentoxyphenyl moiety resonate at δ 22.54, 25.15, 37.93, 66.25, 115.19, 126.35, 128.78 and 159.95. Because of the long relaxation times of the sp^3 C-atoms of the fullerene cage their signals do not show up using a delay time of 6 s. To detect these signals longer pulse delay times, *e.g.* 16 s, are required.[3] In order to avoid very long measurements, we decided to use undeuterated 1,2-dichlorobenzene as solvent making use of the solvent heteronuclear NOE.[4] The two expected sp^3 signals appear at δ 57.31 and 58.42‡ In $C_{60}Cl_6$, the corresponding C-atoms resonate at δ 54.93 and 55.42.[2] The signal for Cl (Fig. 1) appears at δ 70.19. The ^1H NMR spectra of **4**–**6** resemble those of the educts **1**–**3**.‡ All signals show an upfield shift which is stronger for those hydrogens closer to the fullerene cage. The resonances are centred at δ 2.52, 7.42 and 8.06 for **4**, 3.91, 7.16 and 8.11 for **5** and 1.01, 1.73, 1.87, 4.05, 7.05 and 8.06 for **6**. The UV–VIS spectrum of **6** is very similar to that of $C_{60}Cl_6$,[2] with the λ_{max} values‡ located at 237, 283, 345, 394, 434, 475 and 518 nm. The FTIR spectrum of **6** displays intense bands‡ for the C–Cl vibrations at 846 and 817 cm^{-1}. The FTIR and UV–VIS spectra of **4** and **5** are basically identical to those of **6**.‡ In the mass spectra (FAB, MALDI-TOF, EI) of **4**–**6** no M^+ peak could be detected due to facile loss of the Cl addends.[5]

An AM1 calculation (SPARTAN 4.0) on **4** (Fig. 1) reveals a geometry of the integral pyrrole moiety which is very similar to

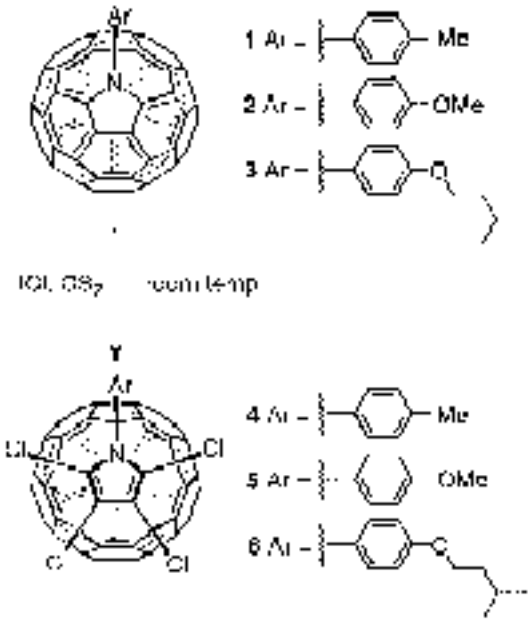

Scheme 1

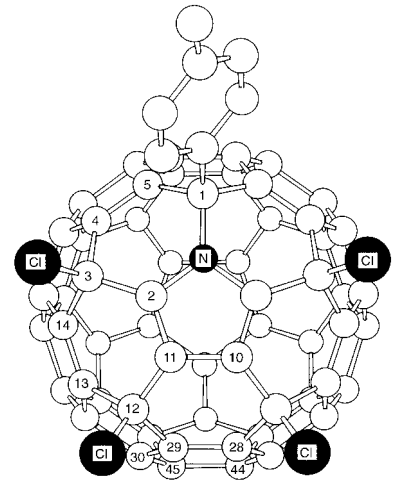

Fig. 1 AMl calculated structure of **4**. Selected bond lengths (pm): N–C2 140.8, C2–C11 140.7, C10–C11 143.4, C1–N 148.0, C2–C3 149.8, C11–C12 148.4, C1–C5 155.1, C4–C5 136.7, C3–C4 152.9, C3–C14 153.9, C13–C14 136.9, C12–C13 153.5, C12–C29 153.7, C28–C29 137.0, C29–C30 145.0, C30–C45 138.8, C44–C45 145.4.

the parent pyrrole. For example, the bond distances between C2–N, C2–C11 and C10–C11 are 140.8, 140.7 and 143.4 pm. Those of the parent compound are 139.2, 140.2 and 142.5 pm (AM1) or 137.0, 138.2 and 141.7 pm (exp.).[6] The pyrrole moiety is not completely planar; the dihedral angle between N–C2–C11–C10 is about 4°. The cage-centred HOMO of **4** has its coefficients exclusively on the [6,6]-bonds forming the equatorial belt of **4**, *e.g.* between C30 and C45. The shortest remaining double bonds are those located at the outer perimeter of the corannulene subunit. For example, the bond length between C4 and C5 is 136.7 pm. The highest Mulliken charges are also found at these C-atoms, whereas the charges at the C-atoms of the southern hemisphere are zero. These factors could be relevant for the regioselectivity of further addition reactions to systems like **4**–**6**.

The chlorine addends can be easily removed from the cage by treatment of **4**–**6** in 1,2-dichlorobenzene with an excess of PPh_3 at room temperature. The parent compounds **1**–**3** were obtained in good yield.[5,7]

Investigations on the chemistry of fulleropyrroles like **4**–**6**, and especially on their use as potential precursors for $C_{58}N_2$ derivatives formed by an azide addition/dechlorination sequence, are currently underway.

We thank the Deutsche Forschungsgemeinschaft (DFG) for financial support.

Notes and References

† E-mail: hirsch@organik.uni-erlangen.de

‡ *Selected data* for **3**: ν(KBr)/cm^{-1} 2953, 2924, 2867, 1734, 1606, 1580, 1509, 1462, 1418, 1384, 1366, 1308, 1251, 1222, 1178, 1114, 1058, 1012, 838, 555 and 525; λ_{max}(cyclohexane)/nm 256, 315, 355 and 441; δ_H(400 MHz, CS_2–20% $CDCl_3$) 8.67 (ddd, J_{AB} 8.6, 2 H), 7.30 (ddd, J_{AB} 8.6, 2 H), 4.18 (t, *J* 6.35, 2 H), 1.95 (m, 1 H), 1.81 (m, 2 H) and 1.07 (d, *J* 6.8, 6 H); δ_C(100.5 MHz, CS_2–20% $CDCl_3$) 159.97 (C-OR, 1 C), 154.16 (2 C), 148.72 (2 C), 147.62 (1 C), 147.49 (2 C), 147.42 (2 C), 147.09 (2 C), 146.98 (2 C), 146.43 (2 C), 146.23 (2 C), 146.05 (2 C), 145.70 (2 C), 145.67 (1 C), 145.50 (2 C), 144.88 (4 C), 144.41 (2 C), 144.13 (2 C), 143.84 (2 C), 142.96 (2 C), 142.58 (2 C), 141.92 (2 C), 141.63 (2 C), 141.39 (2 C), 141.26 (2C), 140.82 (2 C), 140.72 (2 C), 139.64 (2 C), 137.35 (2 C), 132.75 (4 C), 128.47 (phenyl, 2 C), 123.94 (q, 1 C), 115.52 (phenyl, 2 C), 82.39 (q, 1 C), 66.35 (C-CH_2CHMe$_2$, 1 C), 38.03 (C-CHMe$_2$, 1 C), 25.22 (C-Me$_2$, 1 C) and 22.60 (Me, 2 C); *m*/*z* (EI) 885 (M^+) and 722 ($C_{59}N^+$).

For **4**: ν(KBr)/cm^{-1} 3027, 2919, 2854, 1735, 1626, 1511, 1462, 1443, 1420, 1377, 1341, 1316, 1265, 1239, 1189, 1104, 1073, 1054, 1021, 966, 945, 904, 845, 824, 779, 761, 709, 670, 625, 576, 563, 547, 513, 496, 452 and 434; λ_{max}(cyclohexane)/nm 239, 284, 337, 393, 433 and 470; δ_H(400 MHz, CS_2–20% $CDCl_3$) 8.06 (ddd, J_{AB} 8.3, 2 H), 7.42 (ddd, J_{AB} 8.3, 2 H) and 2.52 (s, 3 H).

For **5**: ν(KBr)/cm^{-1} 3000, 2953, 2927, 2901, 2833, 1640, 1606, 1511, 1461, 1439, 1420, 1340, 1302, 1257, 1181, 1103, 1073, 1033, 967, 945, 905, 846, 820, 779, 760, 709, 671, 649, 625, 577, 563, 546, 512, 454 and 433; λ_{max}(cyclohexane)/nm 239, 283, 337, 393, 435 and 477; δ_H(400 MHz, CS_2–20% $CDCl_3$) 8.11 (ddd, J_{AB} 8.8, 2 H), *ca.* 7.25 (ddd, covered by $CHCl_3$) and 3.91 (s, 3 H).

For **6**: ν(KBr)/cm^{-1} 2951, 2921, 2868, 2850, 1608, 1578, 1511, 1463, 1421, 1384, 1301, 1254, 1219, 1181, 1103, 1073, 1054, 1021, 967, 945, 905, 846, 817, 760, 709, 671, 624, 578, 563, 547, 512 and 434; λ_{max}(cyclohexane)/nm 237, 283, 345, 394, 434 and 475; δ_H(400 MHz, CS_2–20% $CDCl_3$) 8.06 (ddd, J_{AB} 8.8, 2 H), 7.05 (ddd, J_{AB} 8.8, 2 H), 4.05 (t, *J* 6.59, 2 H), 1.86 (m, 1 H), 1.72 (m, 2 H) and 1.01 (d, *J* 6.26, 6 H); δ_C(100.5 MHz, CS_2–20% $CDCl_3$) 160.06 (C-OR, 1 C), 150.10, 149.64, 149.27, 148.90, 148.78, 147.29, 147.24, 147.20, 147.05, 147.00, 146.85, 146.13, 146.00, 145.62, 145.01, 144.37, 144.29, 143.75, 143.67, 143.44, 143.18, 143.13, 140.68, 136.18, 129.04, 128.84 (phenyl, 2 C), 128.07, 126.41 (q, 1 C), 115.25 (phenyl, 2 C), 66.24 (C-CH_2-CHMe$_2$, 1 C), 37.88 (C-CHMe$_2$, 1 C), 25.10 (C-Me$_2$, 1 C) and 22.48 (Me, 2 C); δ_C(125.65 MHz, 1,2-dichlorobenzene–20% $CDCl_3$) 70.19 (q), 58.42 (C-Cl) and 57.31 (C-Cl).

1 B. Nuber and A. Hirsch, *Chem. Commun.*, 1998, 405.
2 P. R. Birkett, A. G. Avent, A. D. Darwish, H. W. Kroto, R. Taylor and D. R. M. Walton, *J. Chem. Soc., Chem. Commun.*, 1993, 1230.
3 C. Bellavia-Lund, M. Keshavarz-K., T. Collins and F. Wudl, *J. Am. Chem. Soc.*, 1997, **119**, 8101.
4 W. Bauer, personal communication.
5 F. N. Tebbe, J. Y. Becker, D. B. Chase, L. E. Firment, E. R. Holler, B. S. Malone, P. J. Krusic and E. Wasserman, *J. Am. Chem. Soc.*, 1991, **113**, 9900.
6 T. L. Gilchrist, *Heterocyclic Chemistry*, Pittman Publishing Ltd., London 1985, p. 13.
7 S. D. Darling and R. L. Kidwell, *J. Org. Chem.*, 1968, **33**, 3974.

Received in Cambridge, UK, 27th April 1998; 8/03112F

Synthesis of cholesterol-polyamine carbamates: pK_a studies and condensation of calf thymus DNA

Andrew J. Geall,[a] Richard J. Taylor,[b] Mark E. Earll,[b] Michael A. W. Eaton[b] and Ian S. Blagbrough[a]*†

[a] *Department of Pharmacy and Pharmacology, University of Bath, Claverton Down, Bath, UK BA2 7AY*
[b] *Celltech Therapeutics Ltd., Bath Road, Slough, UK SL1 4EN*

Novel cholesterol-polyamine carbamates have been prepared and their pK_as determined potentiometrically for conjugates substituted with up to five amino functional groups and the binding affinity for calf thymus DNA has also been determined; these polyamine carbamates are models for lipoplex formation with respect to gene delivery (lipofection), a key first step in gene therapy.

Polyamines such as tetra-amine spermine **1** are widely distributed in nature and display a variety of important biological activities.[1,2] Polyamines affect DNA replication and translation, protein synthesis, membrane stabilization and the activity of certain kinases and topoisomerases. Stabilization of specific DNA conformations and charge neutralisation of intracellular polyanions (*e.g.* DNA and RNA) may be among the most important physiological roles of polyamines. Their binding has a profound effect on DNA structure, causing transitions from B to both A and Z forms, and at higher concentrations conformational changes, *e.g.* aggregation and condensation.[2,3] Condensation is caused by alleviation of charge repulsion between neighbouring phosphates on the DNA helix allowing collapse into a more compact structure.[3] Polyamine mediated condensation is a rapidly expanding area of research for non-viral vectors in gene therapy (lipoplexes in lipofection).[4]

The application of synthetic lipo-polyamines constitutes a safer and more efficient gene transfer strategy which, unlike the use of viral vectors, does not elicit immune responses.[5] Within the prerequisites for delivery of DNA across an intact cytoplasmic membrane are condensation and masking the negative charge of the phosphate backbone; polyammonium ions are therefore suitable for use as gene delivery systems.[6,7] Covalent attachment of a lipid moiety,[8] such as an aliphatic chain[2,7,9] or a steroid,[6,10,11] further enhances polyamine-mediated DNA condensation.[12] The mechanism by which these compounds cause lipofection is poorly understood. Knowledge about the pK_as, especially accurate prediction along a polyamine (polyammonium) chain, will allow protonation states at physiological pH to be determined and therefore DNA binding affinities can be predicted with greater confidence. Such physicochemical properties are important in the design of lipoplexes for efficient lipofection.

Herein we report the design and synthesis of polyamine carbamates of cholesterol (at position 3), using our orthogonal protection stragegy for efficient syntheses of unsymmetrical polyamine amides.[13] Six compounds have been made using polyamines: 1,12-diamino-4,9-diazadodecane **1** (spermine, 3.4.3), 1,11-diamino-4,8-diazaundecane (thermine, norspermine, 3.3.3), 1,10-diamino-4,7-diazadecane (3.2.3), 1,9-diamino-3,7-diazanonane (2.3.2), tetraethylenepentamine **2** (2.2.2.2) and pentaethylenehexamine (2.2.2.2.2) affording **6**–**11** respectively. Our protocol for the synthesis of carbamate **10** is outlined.‡ The pK_a values of these compounds were then measured using a Sirius PCA101 automated pK_a titrator, in 0.15 M KCl ionic strength adjusted water; values obtained for spermine (3.4.3) **1** are comparable with literature values determined both potentiometrically and spectroscopically.[14–16]

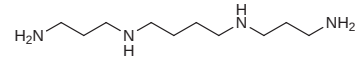

Spermine (3.4.3) **1**

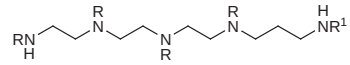

2 R = H, R^1 = H
3 R = H, R^1 = $COCF_3$
4 R = Boc, R^1 = $COCF_3$
5 R = Boc, R^1 = H

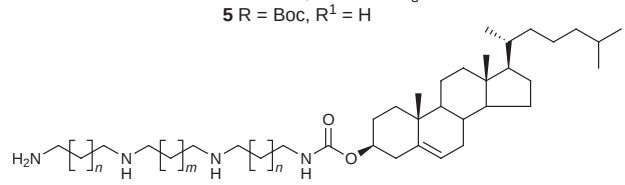

6 *m* = 2, *n* = 1
7 *m* = 1, *n* = 1
8 *m* = 0, *n* = 1
9 *m* = 1, *n* = 0

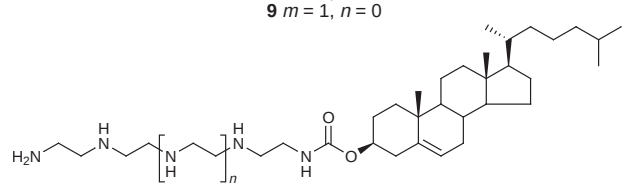

10 *n* = 1
11 *n* = 2

The DNA binding affinities for this series of polyamine conjugates **6**–**11** were determined using calf thymus DNA (6 μg, [DNA base-pair] = 3.0 μM),§ and a fluorescence quenching assay based upon exclusion of ethidium bromide which is effectively present in excess (1.3 μM).[11,12] The binding affinities are critically compared as both the charge ratio[4] and concentration at which 50% of the ethidium bromide fluorescence was quenched (in 20 mM NaCl, see Table 1). These data give support to our hypothesis that binding is a function of charge and that the regiochemical distribution of such charges is also significant for DNA affinity; conjugates 3.4.3 **6**, 3.3.3 **7**, 3.2.3 **8** and 2.3.2 **9** show this trend. Likewise, polyethylene imine conjugates **10** and **11** were (respectively) weaker with only 2.0 charges at pH 7.4 and stronger wtih 2.3 charges distributed along the polyamine. Carbamates **7** and **11** have comparable pK_as across the first three protonation sites, but their structural differences are reflected in their DNA binding affinities (Table 1). These subtle differences in DNA condensation as a function of charge distribution are clearly important for lipoplex formation when compared with the higher charge on unconjugated spermine (3.8 at pH 7.4).

In a recent, comprehensive paper on the role of charge in polyamine analogue recognition, Bergeron *et al.* demonstrated that small structural alterations resulted in substantial differences in biological activities.[15] pK_as are a function of the interamine distance as well as their substituents. It is important to recognise that any charge is shared across several of the basic

Table 1 Polyamine pK_as and ethidium bromide exclusion data

Polyamine	Measured pK_as	Net charge[a]	Charge ratio[b]	Conc./μM[c]
1	10.9 ± 0.01	3.8	> 4.0	> 17.0
	10.1 ± 0.01			
	8.9 ± 0.01			
	8.1 ± 0.01			
6	10.1 ± 0.06	2.4	0.62	1.3
	8.6 ± 0.06			
	7.3 ± 0.05			
7	10.7 ± 0.04	2.3	0.76	1.6
	8.8 ± 0.02			
	7.2 ± 0.02			
8	10.0 ± 0.02	1.8	0.80	1.7
	8.0 ± 0.02			
	5.5 ± 0.02			
9	9.3 ± 0.01	1.6	0.88	2.4
	7.6 ± 0.01			
	5.7 ± 0.01			
10	9.9 ± 0.20	2.0	0.92	2.7
	8.4 ± 0.20			
	6.3 ± 0.21			
	3.9 ± 0.21			
11	10.2 ± 0.10	2.3	0.66	1.3
	8.6 ± 0.08			
	7.2 ± 0.09			
	4.4 ± 0.09			
	2.5 ± 0.28			

[a] Net positive charge calculated from the Henderson–Hasselbach equation at pH 7.4. [b] Charge ratio[4] at which 50% exclusion of ethidium bromide is effected using calf thymus DNA at pH 7.4. [c] Concentration of polyamine conjugate at which 50% exclusion of ethidium bromide (1.3 μM) is effected using calf thymus DNA (3.0 μM) at pH 7.4.

centres and that it cannot be attributed to a single point. Even when the first charge is introduced principally on the primary amine, it is also distributed on to the secondary amines. This has been shown using unsymmetrical triamine, spermidine.[17]

The four methylene central spacer found in spermine **1** has also been shown to be important for binding affinity, confirming that both the number of positive charges and their distribution has a profound effect on the polyamine's ability to induce DNA conformational changes.[18] The measured pK_as for polyamines containing aminopropyl[16] and aminoethyl[10] units and Transfectam (DOGS)[7,19] add further weight to this hypothesis. These results will be of use in gene therapy studies and should find ready application in the design of lipoplexes with particular reference to spermidine and spermine class alkaloids. This evaluation of pK_a data, the number and regiochemical distribution of charges along the polyamine backbone, may lead to a clearer understanding of lipoplex modes of action.

We thank the EPSRC and Celltech Therapeutics Ltd, for a CASE studentship (to A. J. G.). We acknowledge some preliminary experimental work of Ms Dima Al-Hadithi (University of Bath) and useful discussions with Dr Ian S. Haworth (University of Southern California). I. S. B. and I. S. H. are recipients of a NATO grant (CRG 970290).

Notes and References

† E-mail: prsisb@bath.ac.uk

‡ An important first step is the ready purification of technical grade (~80%) 2.2.2.2-pentamine **2** by selective protection of one primary amino functional group by reaction with ethyl trifluoroacetate (1.0 equiv., MeOH, −78 °C for 1 h then to 0 °C over 1 h) to form trifluoroacetamide **3**. Immediately, in this solution, the remaining four amino functional groups were Boc protected with di-*tert*-butyl dicarbonate (5 equiv., 0–25 °C over 1 h then 14 h) to afford fully protected polyamine **4**. The trifluoroacetyl protecting group was then cleaved by increasing the pH to 11 with conc. aq. ammonia, stirring (25 °C, 15 h) to afford, after flash chromatography over silica gel (CH_2Cl_2–MeOH–conc. aq. NH_4OH 200 : 10 : 1 to 150 : 10 : 1 v/v/v), tetra-Boc protected polyamine **5** (19%). Reaction of the free primary amine of **5** with 3-cholesteryl chloroformate (1.2 equiv., 3.0 equiv. TEA, CH_2Cl_2, 0 °C for 10 min then to 25 °C for 12 h) afforded, after purification over silica gel (EtOAc–hexane 8 : 2 to 6 : 4 v/v) fully protected carbamate **10** (81%). Deprotection (CH_2Cl_2–TFA 10 : 90 v/v, 0 °C, 2 h) and purification by RP-HPLC over ABZ + Plus (5 μm, Supelcosil) (MeCN–0.1% aq. TFA 1 : 1 v/v, λ = 220 nm) afforded the polytrifluoroacetate salt of polyamine carbamate **10** (50%) HR-FABMS (+ve ion in *m*-NBA) [Found 602.5380 (M + 1). $C_{36}H_{68}N_5O_2$ requires 602.5380].

§ Using the literature average weight per nucleotide of 330 Da.[4]

1 For selected reviews on polyamines, see B. Ganem, *Acc. Chem. Res.*, 1982, **15**, 290; R. J. Bergeron, *Acc. Chem. Res.*, 1986, **19**, 105; I. S. Blagbrough, S. Carrington and A. J. Geall, *Pharm. Sci.*, 1997, **3**, 223 and refs. cited therein.
2 J.-P. Behr, *Tetrahedron Lett.*, 1986, **27**, 5861; J.-P. Behr, *Acc. Chem. Res.*, 1993, **26**, 274; N. Schmid and J.-P. Behr, *Tetrahedron Lett.*, 1995, **36**, 1447 and refs. cited therein.
3 S. C. Tam and R. J. P. Williams, *Struct. Bonding*, 1985, **63**, 103; E. Rowatt and R. J. P. Williams, *J. Inorg. Biochem.*, 1992, **46**, 87; K. D. Stewart and T. A. Gray, *J. Phys. Org. Chem.*, 1992, **5**, 461; V. A. Bloomfield, *Curr. Opin. Struct. Biol.*, 1996, **6**, 334.
4 P. L. Felgner, Y. Barenholz, J. P. Behr, S. H. Cheng, P. Cullis, L. Huang, J. A. Jessee, L. Seymour, F. Szoka, A. R. Thierry, E. Wagner and G. Wu, *Hum. Gene Ther.*, 1997, **8**, 511.
5 R. G. Crystal, *Science*, 1995, **270**, 404; P. L. Felgner, *Sci. Am.*, 1997, **276**, 86; C. O'Driscoll, *Chem. Brit.*, 1997, **33**, 66; R. I. Mahato, A. Rolland and E. Tomlinson, *Pharm. Res.*, 1997, **14**, 853; I. M. Verma and N. Somia, *Nature*, 1997, **389**, 239.
6 E. R. Lee, J. Marshall, C. S. Siegel, C. Jiang, N. S. Yew, M. R. Nichols, J. B. Nietupski, R. J. Ziegler, M. B. Lane, K. X. Wang, N. C. Wan, R. K. Scheule, D. J. Harris, A. E. Smith and S. H. Cheng, *Hum. Gene Ther.*, 1996, **7**, 1701; R. G. Cooper, C. J. Etheridge, L. Stewart, J. Marshall, S. Rudginsky, S. H. Cheng and A. D. Miller, *Chem. Eur. J.*, 1988, **4**, 137.
7 J.-P. Behr, B. Demeneix, J.-P. Loeffler and J. Perez-Mutul, *Proc. Natl. Acad. Sci. USA*, 1989, **86**, 6982.
8 I. S. Blagbrough, S. Taylor, M. L. Carpenter, V. Novoselskiy, T. Shamma and I. S. Haworth, *Chem. Commun.*, 1998, 929.
9 G. Byk, C. Dubertret, V. Escriou, M. Frederic, G. Jaslin, R. Rangara, B. Pitard, J. Crouzet, P. Wils, B. Schwartz and D. Scherman, *J. Med. Chem.*, 1998, **41**, 224.
10 J. K. Guy–Caffey, V. Bodepudi, J. S. Bishop, K. Jayaraman and N. Chaudhary, *J. Biol. Chem.*, 1995, **270**, 31 391; D. Moradpour, J. I. Schauer, V. R. Zurawski, Jr., J. R. Wands and R. H. Boutin, *Biochem. Biophys. Res. Commun.*, 1996, **221**, 82; S. Walker, M. J. Sofia, R. Kakarla, N. A. Kogan, L. Wierichs, C. B. Longley, K. Bruker, H. R. Axelrod, S. Midha, S. Babu and D. Kahne, *Proc. Natl. Acad. Sci. USA*, 1996, **93**, 1585.
11 H.-P. Hsieh, J. G. Muller and C. J. Burrows, *J. Am. Chem. Soc.*, 1994, **116**, 12 077.
12 A. J. Geall and I. S. Blagbrough, *Tetrahedron Lett.*, 1998, **39**, 443.
13 I. S. Blagbrough and A. J. Geall, *Tetrahedron Lett.*, 1998, **39**, 439.
14 G. Anderegg and P. Bläuenstein, *Helv. Chim. Acta*, 1982, **65**, 162.
15 R. J. Bergeron, J. S. McManis, W. R. Weimar, K. M. Schreier, F. Gao, Q. Wu, J. Ortiz-Ocasio, G. R. Luchetta, C. Porter and J. R. T. Vinson, *J. Med. Chem.*, 1995, **38**, 2278.
16 Y. Takeda, K. Samejima, K. Nagano, M. Watanabe, H. Sugeta and Y. Kyogoku, *Eur. J. Biochem.*, 1983, **130**, 383; D. Aikens, S. Bunce, F. Onasch, R. Parker, III, C. Hurwitz and S. Clemans, *Biophys. Chem.*, 1993, **17**, 67.
17 M. M. Kimberly and J. H. Goldstein, *Anal. Chem.*, 1981, **53**, 789; D. A. Aikens, S. C. Bunce, O. F. Onasch, H. M. Schwartz and C. Hurwitz, *J. Chem. Soc., Chem. Commun.*, 1983, 42.
18 H. S. Basu, H. C. A. Schwietert, B. G. Feuerstein and L. J. Marton, *Biochem. J.*, 1990, **269**, 329.
19 J.-S. Remy, C. Sirlin, P. Vierling and J.-P. Behr, *Bioconjugate Chem.*, 1994, **5**, 647.

Received in Glasgow, UK, 30th April 1998; 8/03284J

Chelation-assisted alkylation of benzylamine derivatives by Ru^0 catalyst

Chul-Ho Jun,*† Duck-Chul Hwang and Sang-Jin Na

Department of Chemistry, Yonsei University, Seoul 120-749, Korea

***N*-Benzyl-*N*-(3-methyl-2-pyridyl)amine 1 reacts with various alkenes *via* sp³ C–H bond cleavage by catalytic $Ru_3(CO)_{12}$ to give the corresponding alkylated products.**

C–H bond activation is currently of interest in organometallic chemistry.[1] In particular, its application to organic synthesis has been under intensive development in recent years.[2] One useful method by which to achieve C–H bond activation by transition metal complexes is cyclometallation utilizing nearby heteroatoms.[3] Stoichiometric cleavage of a C–H bond of a methyl group through cyclopalladation has been applied to functionalization of organic molecules.[4] Vinyl,[5] imine,[6] aldehyde[7] and aromatic groups[8] were catalytically alkylated through chelation-assisted C–H bond cleavage by a transition metal catalyst and subsequent cross coupling with an alkene. Many chelation-assisted alkylations are centered on the sp² C–H bond, and not on the sp³ C–H bond, probably due to the better thermodynamic stability of the metal–sp² carbon bond compared to that of the metal–sp³ carbon bond.[9] Here we report the catalytic addition of a benzylic sp³ C–H bond to an alkene to give alkylated products.

N-Benzyl-*N*-(3-methyl-2-pyridyl)amine **1** reacted with 500 mol% of hex-1-ene **2a** in toluene at 130 °C for 6 h under 10 mol% of $Ru_3(CO)_{12}$ **3** based on **1**. After the reaction, the corresponding alkylated product **4a** was isolated in 95% yield by column chromatography (Scheme 1). The reaction mechanism is shown in Scheme 2. The first step is likely to be the oxidative addition of a Ru^0 catalyst to the benzylic C–H bond in **1** to generate **5**, a stable 5-membered ring metallacycle complex. The coordination of **2a** to **5**, hydride-insertion into **2a** and the subsequent reductive elimination of the resulting metal–hexyl complex **7** produces **4a** with the regeneration of catalyst **3**. Alkylations of various amine substrates with **2a** were carried out. In this reaction, it was found that the geometrical structure of **1**, in which the methyl group is placed in the 3-position of the pyridyl group, is prerequisite. When **8–10**, in which the methyl

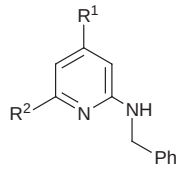

8 R^1 = Me, R^2 = H
9 R^1 = H, R^2 = Me
10 R^1 = R^2 = H

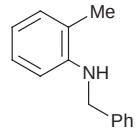

11

group is either placed in the 4- or 6-position or is replaced by hydrogen, trace amounts of alkylated products were obtained under identical reaction conditions (1–2% GC yield). These

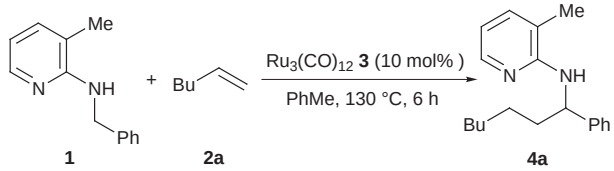

1 **2a** **4a**

Scheme 1

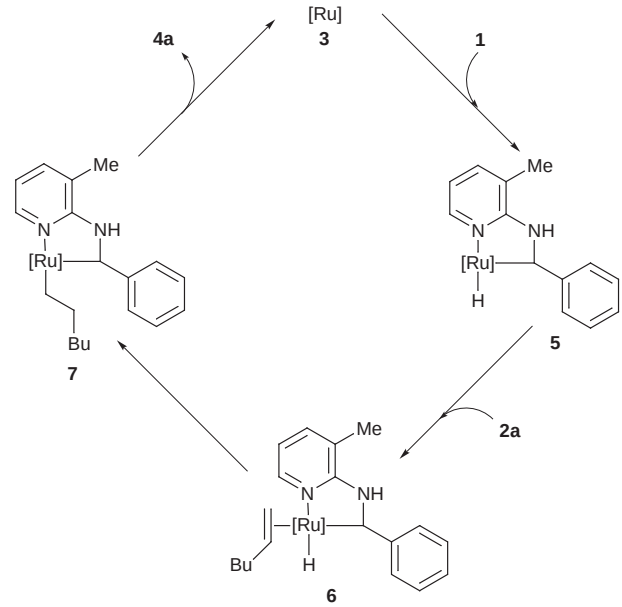

Scheme 2

results demonstrate that the 3-methyl group in **1** may retard the free rotation of the benzyl group around the amine group, and help the benzylic C–H bond to approach the Ru catalyst after the coordination of the nitrogen atom in the pyridyl group to the Ru catalyst. Also, precoordination of the metal complex is a very important requirement for cleaving the C–H bond since **11** bearing no coordination site gave no alkylated product and was fully recovered. The reactions between **1** and various alkenes were examined, and the results are shown in Table 1. For terminal olefins (entries 1–6), linear alkylated products were obtained. Sterically hindered alkenes such as **2c** and **2d** reacted with **1** to give the alkylated products **4c** and **4d** in a lower yield (72 and 75%) than unhindered alkenes such as **2a** and **2b**. Styrene **2e** was also formed in a low yield (70%) due to a side reaction, polymerization (entry 5). When internal olefins such as **2i** and **2j** were used, the linear alkylated product **4a** was isolated in 85 and 81% yield respectively (Scheme 3). No branched alkylated product was detected. The reason must be that the 2- or 3-hexyl–metal complex initially generated from hydride insertion into **2i** or **2j**, may isomerize to the 1-hexyl–metal complex due to the steric congestion of the secondary alkyl group. This type of isomerization has already been studied.[10] However, for cyclic alkenes such as **2g** and **2h**, the corresponding cycloalkyl compounds, **4g** and **4h,** were isolated in 70 and 60% yield, respectively. To examine the effect of phenyl substituents, competitive alkylation between benzyl-

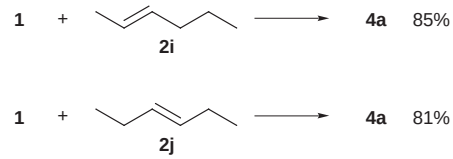

Scheme 3

Table 1 Alkylation of **1** with various alkenes **2**[a] in the presence of **3**

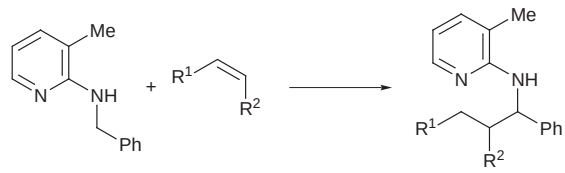

1 **2** **4**

Entry	Alkene	R^1	R^2	Product	Isolated yield (%)
1	**2a**	Bu	H	**4a**	95
2	**2b**	C_8H_{17}	H	**4b**	93
3	**2c**	Bu^t	H	**4c**	72
4	**2d**	Cyclohexyl	H	**4d**	75
5	**2e**	Ph	H	**4e**	70
6	**2f**	Bn	H	**4f**	85
7	**2g**	$-(CH_2)_3-$		**4g**	70
8	**2h**	$-(CH_2)_4$		**4h**	60

[a] 500 mol% based on **1**.

amines bearing electron-donating and electron-withdrawing groups was carried out. When a mixture of **12** and **13** was

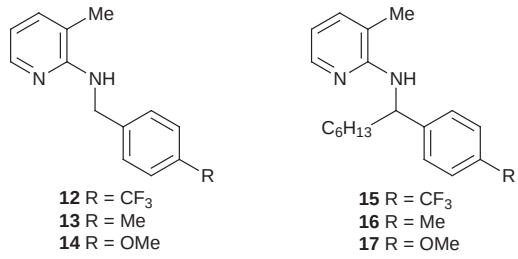

12 R = CF_3
13 R = Me
14 R = OMe

15 R = CF_3
16 R = Me
17 R = OMe

allowed to react with **2a** under 20 mol% of catalyst **3** at 130 °C for 1.2 h, 39 and 70% yield of **15** and **16** (**15**:**16** = 1:1.8) were determined by GC, indicating that the electron-donating group activates benzylic C–H bond cleavage better than the electron-withdrawing group. For the competitive reaction of **12** and **14** with **2a**, a mixture of **15** and **17** was obtained in 26 and 60% yield (**15**:**17** = 1:2.3). The higher ratio of 1:2.3 for **15**:**17** compared with that of 1:1.8 for **15**:**16** can be rationalised by a more electron-donating substituent such as the methoxy group in **14** showing higher activity for C–H bond activation than the moderately electron-donating methyl group in **13**.

In conclusion, the sp^3 C–H bond of benzylamine bearing the 3-methyl-2-pyridyl group was readily alkylated with various alkenes *via* cyclometallation by a $Ru_3(CO)_{12}$ catalyst.

This research was supported by the Korean Science and Engineering Foundation (Grant No. 97-05-01-05-01-3). We also thank Mr Dae-Yon Lee for technical assistance.

Notes and References

† E-mail: junch@alchemy.yonsei.ac.kr

1 R. H. Crabtree, *Chem. Rev*., 1985, **85**, 245.
2 S. Cenini, F. Ragaini, S. Tollari and D. Paone, *J. Am. Chem. Soc*., 1996, **118**, 11 964; N. Chatani, T. Fukuyama, F. Kakiuchi and S. Murai, *J. Am. Chem. Soc*., 1996, **118**, 493; B. S. Jaynes and C. L. Hill, *J. Am. Chem. Soc*., 1995, **117**, 4704; F. Kakiuchi, Y. Tanaka, T. Sato, N. Chatani and S. Murai, *Chem. Lett*., 1995, 679; 1995, 682; E. J. Moore, W. R. Pretzer, T. J. O'Connell, J. Harris, L. LaBounty, L. Chou and S. S. Grimmer, *J. Am. Chem. Soc*., 1992, **114**, 5888; R. F. Jordan and D. F. Taylor, *J. Am. Chem. Soc*., 1989, **111**, 778; T. Sakakura and M. Tanaka, *J. Chem. Soc., Chem. Commun*., 1987, 758; Y. Ishii, N. Chatani, F. Kakiuchi and S. Murai, *Organometallics*, 1997, **16**, 3615.
3 M. I. Bruce, *Angew. Chem., Int. Ed. Engl*., 1977, **16**, 73.
4 K. Carr, H. M. Saxton and J. K. Sutherland, *J. Chem. Soc., Perkin Trans. 1*, 1988, 1599; J. E. Baldwin, C. Najera and M. Yus, *J. Chem. Soc., Chem. Commun*., 1985, 126; J. E. Baldwin, R. H. Jones, C. Najera and M. Yus, *Tetrahedron*, 1985, **41**, 699; K. Carr and J. K. Sutherland, *J. Chem. Soc., Chem. Commun*., 1984, 1227.
5 N. Fujii, F. Kakiuchi, N. Chatani and S. Murai, *Chem. Lett*., 1996, 939; Y.-G. Lim, J.-B. Kang and Y. H. Kim, *Chem. Commun*., 1996, 585; B. M. Trost, K. Imi and I. W. Davies, *J. Am. Chem. Soc*., 1995, **117**, 5371.
6 C.-H. Jun, J.-B. Kang and J.-Y. Kim, *J. Organomet. Chem*., 1993, **458**, 193; J. W. Suggs, *J. Am. Chem. Soc*., 1979, **101**, 489.
7 C.-H. Jun, H. Lee and J.-B. Hong, *J. Org. Chem*. 1997, **62**, 1200; J. W. Suggs, *J. Am. Chem. Soc*., 1978, **100**, 640.
8 T. Fukuyama, N. Chatani, F. Kakiuchi and S. Murai, *J. Org. Chem*., 1997, **62**, 5647; N. Chatani, Y. Ie, F. Kakiuchi and S. Murai, *J. Org. Chem*., 1997, **62**, 2604; M. Sonoda, F. Kakiuchi, A. Kamatani, N. Chatani and S. Murai, *Chem. Lett*., 1996, 109; 1996, 111; F. Kakiuchi, S. Sekine, Y. Tanaka, A. Kamatani, M. Sonoda, N. Chatani and S. Murai, *Bull. Chem. Soc. Jpn*., 1995, **68**, 62; M. Sonoda, F. Kakiuchi, N. Chatani and S. Murai, *J. Organomet. Chem*., 1995, **504**, 151; Y.-G. Lim, Y. H. Kim and J.-B. Kang, *J. Chem. Soc., Chem. Commun*., 1994, 2267; S. Murai, F. Kakiuchi, S. Sekine, Y. Tanaka, A. Kamatani, M. Sonoda and N. Chatani, *Nature*, 1993, **336**, 529.
9 P. O. Stoutland, R. G. Bergman, S. P. Nolan and C. D. Hoff, *Polyhedron*, 1988, **7**, 1429.
10 D. L. Reger, D. G. Garza and J. C. Baxter, *Organometallics*, 1990, **9**, 873.

Received in Cambridge, UK, 16th February 1998; 8/01298I

Supercritical fluid extraction of surfactant template from MCM-41

Sibudjing Kawi*† and Man Wai Lai

Department of Chemical Engineering, National University of Singapore, Kent Ridge Crescent, Republic of Singapore 119260

Supercritical fluid extraction was used to extract and recover >90% of the surfactant template from the pores of as-synthesized pure siliceous MCM-41 and the MCM-41 after supercritical fluid extraction shows more uniform pore size distribution than the calcined MCM-41.

Since the discovery of the M41S family of mesoporous materials by Mobil scientists in 1992,[1,2] intensive research has been undertaken by various researchers on the synthesis mechanism and applications of these new materials. Current synthesis involves the use of liquid surfactant as the liquid-crystal templates and these templates are normally removed by calcination to yield the porous materials.

Removal of the template by calcination destroys the template which constitutes *ca.* 50 mass% of the as-synthesized material.[3] Recently, the use of liquid extraction to remove the templates has been reported.[4–6]

The present work describes a new and alternative method of recovering the surfactant templates from as-synthesized materials using supercritical fluid extraction (SFE). This should result in significant savings as the recovered templates can be reused in future synthesis. The MCM-41 materials and the extracted templates were shown to have retained their structures and properties after SFE. In addition, SFE may be used to remove surfactant templates at much lower temperatures from new mesoporous materials, which mesopores could easily collapse under high temperature calcination.

The pure siliceous MCM-41 material were synthesized using cetyltrimethylammonium hydroxide (CTMAOH) and fumed silica. A gel with a molar composition of 1 CTMAOH : 1.04 SiO_2 : 62.50 H_2O was prepared and loaded into polypropylene bottles. The gel was heated at 96 °C for 48 h after which the as-synthesized materials were washed by centrifugation and recovered by filtration. A small part of the as-synthesized sample was calcined in air at 550 °C for 15 h in order to serve as a comparison to samples that underwent SFE. SFE was performed on the remaining samples under different extraction conditions. Supercritical CO_2 modified with MeOH (which was used to increase the solvating power of the supercritical fluid) was used for extraction. The range of pressures and temperatures investigated in this study span from 150 to 350 bar and from 35 to 125 °C, respectively.

The SFE experiments were carried out using a Jasco SFE system consisting of a HPLC pump for carbon dioxide, a syringe pump for the modifier, a chiller for cooling the pump head, an oven for controlling the extraction temperature, an extraction vessel for holding the sample during extraction and a back pressure regulator for controlling the extraction pressure. Powder X-ray diffraction (XRD), which was performed using a Shimadzu XRD-6000 Spectrometer, and N_2 absorption and desorption, which was performed using Quantachrome Autosorb-1 at 77 K, were used to characterize the MCM-41 materials after calcination and after SFE. FTIR (Shimadzu DR-8001) and GC–MS (Hewlett Packard Model 6890) were used to identify the chemical structures and composition of the extracted surfactants. Using TGA (Shimadzu DTG-50), extraction efficiencies of the SFE process were determined by comparing the mass loss between the as-synthesized sample and the samples after SFE.

Table 1 shows the extraction efficiencies under different conditions. The results show that no surfactant template was extracted when pure CO_2 was used as the supercritical fluid since it does not have sufficient solvating strength at the typical working pressures to quantitatively extract surfactants that are quite polar.[7] However, by adding a small amount of methanol into the supercritical CO_2, substantial extraction of the template was achieved. In fact, the highest extraction efficiency (*i.e.* 93.2%) was achieved using a methanol flow rate of 0.2 ml min^{-1}. The addition of methanol as a modifier dramatically increases the bulk solubility of the analytes (extracted surfactants). The enhanced bulk solubility properties of the supercritical fluid cause a shift in the matrix/fluid distribution of the analyte, resulting in favorable partitioning to the supercritical fluid.[8] Using the methanol-modified supercritical CO_2 an increase in the extraction pressure increases the extraction efficiency due to the increase in the solvating power of the supercritical fluid.[9,10]

The results in Table 1 also indicate that there exists an optimum temperature for maximum extraction efficiency since the extraction efficiency achieved at 85 °C is much higher than that at 45 or 125 °C. It has also been shown that, by increasing the extraction temperatures, the energy barrier of desorption can be overcome, resulting in higher extraction efficiencies.[11,12] Hence, the extraction of the surfactant template from MCM-41 is facilitated by the higher temperature at 85 °C. However, at 125 °C, the increase in temperature results in a lower density of the supercritical fluid, thereby lowering the solvating power of the fluid and hence the extraction efficiency.

Fig. 1 shows the powder X-ray diffraction patterns of the calcined MCM-41 and the MCM-41 after SFE (with extraction efficiency of 93.2%). The results show that both the XRD patterns correspond well with those reported for pure siliceous MCM-41. The 2θ position for the MCM-41 after SFE is lower than that of the calcined MCM-41, indicating a larger unit cell size for the MCM-41 after SFE. In fact, the 2θ position for the MCM-41 after SFE is similar to the as-synthesized sample, indicating that pore contraction did not occur during the removal of the surfactant template by SFE. The narrower XRD pattern for the sample after SFE may also indicate that the sample after SFE possesses better crystallinity than the calcined

Table 1 Extraction efficiencies under various conditions for a CO_2 flow rate of 1 ml min^{-1} for 3 h[a]

Extraction temperature/°C	Extraction pressure/bar	Methanol flow rate/ ml min^{-1}	Extraction efficiency (%)
85	350	0.0	0.0
45	350	0.1	55.6
85	350	0.1	81.0
125	350	0.1	61.7
85	250	0.1	57.3
85	150	0.1	41.5
85	350	0.2	93.2

[a] Flow rate of CO_2 measured at the pump head cooled to −5 °C. Using Peng Robinson equation of state, the variation in the density of CO_2 at −5 °C between 150 and 350 bar is only 3%.

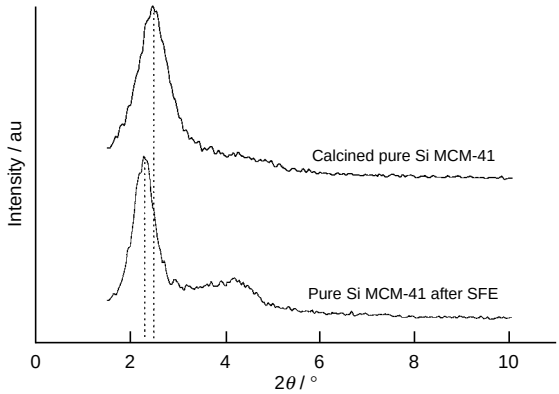

Fig. 1 X-Ray diffraction patterns of the calcined MCM-41 and MCM-41 after SFE

Table 2 Properties of as-synthesized, calcined and SFE samples

Sample	a_o/Å	Pore diameter, d_p/Å	A_{BET}/ $m^2\ g^{-1}$	Pore volume/ $cm^3\ g^{-1}$
As-synthesized	44.7	—	—	—
Calcined	41.5	26.4	1031	0.95
SFE	44.7	29.4	1007	1.08

sample. Assuming hexagonal symmetry, the unit cell sizes of the materials are calculated and tabulated in Table 2.

The N_2 isotherms (not shown) also show no hysteresis in both the calcined and SFE samples. The surface areas were calculated using BET analysis while the pore diameters were calculated from the desorption branch of the isotherms using BJH analysis. The results of these calculations are also collected in Table 2. The surface areas of both the calcined and SFE samples are comparable. In agreement with the XRD results, the pore size of the calcined sample is lower than the SFE sample, indicating again that SFE is able to remove the surfactant template without affecting the pore size and the pore structure of MCM-41. Also, the pore size distribution of the SFE sample is sharper than the calcined sample, indicating that the samples after SFE have slightly more uniform pores than the calcined samples.

GC–MS was performed to identify the constituents of the extracted surfactant and the MS results of the extracted surfactant were compared with the MS results of CTMAOH dissolved in methanol (used as a standard). Fig. 2 shows the MS results obtained and both Fig. 2(*a*) and (*b*) have peaks at the same *m*/*z* values, indicating that the extracted material is CTMAOH.

FTIR (results not shown) was also used to identify the extracted surfactant. The absorbance spectrum of the extracted organic template is similar to that of pure CTMAOH, indicating again that no changes to the structure of the CTMAOH were detected after SFE. The GC–MS and FTIR results show that as the chemical structure and composition of the extracted surfactant remain the same as those of the fresh surfactant, the

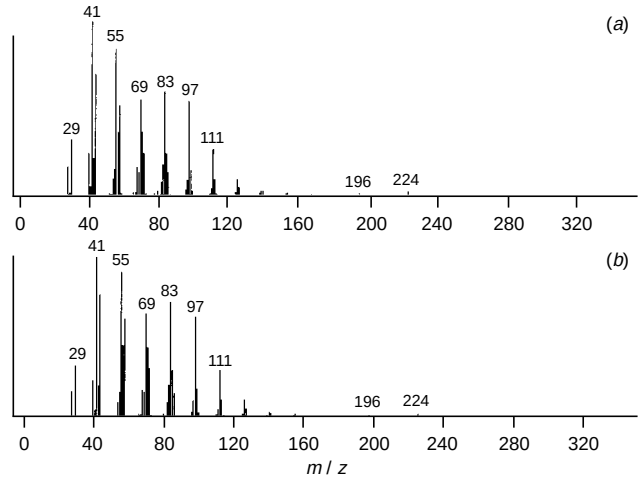

Fig. 2 The mass spectra of (*a*) a standard solution of methanol and CTMAOH and (*b*) extracted surfactant in methanol

extracted surfactant could be recycled and reused as a template in the synthesis of MCM-41 materials.

In conclusion, supercritical fluid extraction is effective in extracting the organic template from the pores of as-synthesized MCM-41. The MCM-41 materials after SFE retained their uniform pore size distribution and high surface areas and in fact have a larger pore size than the calcined MCM-41. The structure of the surfactant extracted by SFE was also unmodified and may be reused in the future synthesis of MCM-41.

Notes and References

† E-mail: chekawis@nus.sg

1 C. T. Kresge, M. E. Leonowicz, W. J. Roth, J. C. Vartuli and J. S. Beck, *Nature*, 1992, **359**, 710.
2 J. S. Beck, J. C. Vartuli, W. J. Roth, M. E. Leonowicz, C. T. Kresge, K. D. Schmidt, C. T.-W. Chu, D. H. Olson, E. W. Sheppard, S. B. McCullen, J. B. Higgens and J. L. Schlenker, *J. Am. Chem. Soc.*, 1992, **114**, 10 384.
3 C. Y. Chen, M. E. Davis and H. X. Li, *Microporous Mater.*, 1993, **2**, 17.
4 D. D. Whitehurst, *US Pat.*, 5 143 879, 1992.
5 R. Schmidt, D. Akporiaye, M. Stocker and O. H. Ellestad, *Zeolites and Related Microporous Materials: State of the Art 1994*, Elsevier Science B. V., Amsterdam, 1994, p. 61.
6 S. Hitz and R. Prins, *J. Catal.*, 1997, **168**, 194.
7 S. B. Hawthorne, *Anal. Chem. A*, 1990, **62**, 633.
8 J. J. Langenfeld, S. B. Hawthorne, D. J. Miller and J. Pawliszyn, *Anal. Chem.*, 1994, **66**, 909.
9 J. W. King, *J. Chromatogr. Sci.*, 1989, **27**, 355.
10 M. Ashraf-Khorassani, S. Gidanian and Y. Yamini, *J. Chromatogr. Sci.*, 1995, **33**, 658.
11 N. Alexandrou, M. J. Lawrence and J. Pawliszyn, *Anal. Chem.*, 1992, **64**, 301.
12 J. J. Langenfeld, S. B. Hawthorne, D. J. Miller and J. Pawliszyn, *Anal. Chem.*, 1993, **65**, 338.

Received in Cambridge, UK, 20th April 1998; 8/02907E

C–H··π hydrogen bonding *vs.* anion complexation in rhodium(I) complexes of cyclotriveratrylene

Kirsty S. B. Hancock and Jonathan W. Steed*†

Department of Chemistry, King's College London, Strand, London, UK WC2R 2LS

The bimetallic rhodium(I) complex [{Rh(nbd)}$_2$(CTV)][BF$_4$]$_2$ exists as an infinite self-included chain in the solid state with intracavity CH···π interactions linking the inclusion polymer together; the analogous monometallic complex co-crystallises with the dinuclear species as an inclusion compound with acetone as the guest.

In the past decade the topic of supramolecular anion complexation has received ever increasing attention as a consequence of the relatively challenging and hitherto unexplored nature of the field.[1–5] This culminated last year in the publication of the first book dealing solely with the area.[6] The key to the production of useful anion hosts for applications in areas such as environmental and biochemical sensors, and in bulk waste remediation is the selectivity of the host for a given anionic guest (*e.g. in vivo* sensing of Cl^- [3] or monitoring the environmental levels of nutrients such as phosphates and nitrate[2,6]). Our initial approach to this problem has been based upon a simple consideration of electrostatic attraction of the anion to the site of greatest positive charge density on a host mediated by the steric requirements of this cationic binding pocket. The host is thus selective for anions possessing the most complementary size and symmetry match to the host binding pocket since it is these anions which are able to make the closest approach to the host positive charge. This simple concept has been demonstrated by the synthesis of organometallic hosts **1**[7,8] and **2**[9,10] in which the calix[4]arene[11]

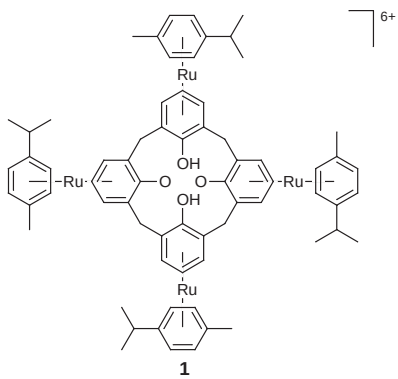

1

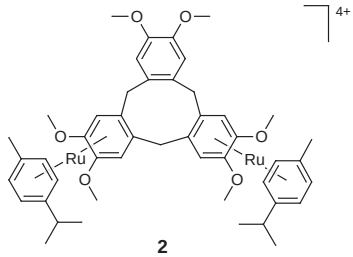

2

or cyclotriveratrylene (CTV)[12] cavities have been shown by X-ray crystallography to be occupied by tightly fitting anionic guests. In the case of host **1** the crystallographically demonstrated poor fit of I^- is borne out by ^{1}H NMR titration results in solution which give binding constants in aqueous solution decreasing in the order Cl^- > Br^- > I^-.[7] The selectivity of hosts such as **1** and **2** is reduced however, as a consequence of their multiply charged nature in as much as the host cavity is not the only site available for anion binding. Host **1** in particular binds up to five additional anions outside the host cavity. We now report preliminary results in a programme of research designed to reduce the overall host charge, in the anticipation of thus increasing host selectivity.

The synthesis of monocationic complexes of type '(arene)-Rh(diene)' [arene = benzene, xylenes, hexamethyl benzene *etc.*, diene = norbornadiene (nbd) or cyclooctadiene] was reported by Green and Kue in 1972[13] starting from the [Rh(diene)$_2$]$^+$ **3** cations. Complexes of type **3** are relatively tedious to prepare, however, and we accordingly adopted the simpler procedure of direct reaction of [{Rh(nbd)Cl}$_2$] **4**[14] with CTV in CH_2Cl_2–acetone in the presence of 2 equiv. of Ag[BF$_4$]. After removal of precipitated AgCl this resulted in a clear yellow solution from which the complexes [Rh(η^4-nbd)(η^6-CTV)][BF$_4$] **5** and [{Rh(η^4-nbd)}$_2$(η^6:η^6-CTV)][BF$_4$]$_2$ **6** were obtained upon evaporation of the bulk of the solvent. Compounds were characterised by FABMS and ^{1}H NMR spectroscopy.

Crystals suitable for X-ray crystallography were prepared by slow diffusion of diethyl ether into an acetone solution of complex **6** over a period of *ca.* three weeks. Surprisingly, during the course of the crystal growth, partial solvolysis of **6** to give **5** occurred such that a co-crystallised product of formula [Rh(η^4-nbd)(η^6-CTV)][BF$_4$]·[{Rh(η^4-nbd)}$_2$-(η^6:η^6-CTV)][BF$_4$]$_2$·0.5 Me$_2$CO was eventually isolated. This fortuitous circumstance resulted in structure determinations (at −150 °C) for both **5** and **6** in the same experiment, Fig. 1.‡ Strikingly, the structure reveals that for **6**, in contrast to a wide range of bimetallic complexes related to the tetracation **2**,[10] the CTV cavity in **6** is not occupied by one of the BF_4^- anions. Instead **6** forms an inclusion polymer in which the norbornadiene ligand of one dicationic molecule engages in two short chelating, C–H··π hydrogen bonding interactions with the CTV carbon atoms C(3A) and C(4A) of the ring attached to Rh(1A); distances C(13A)···C(3A) 3.431(14), C(10A)···C(4A) 3.451(14), H(13A)···C(3A), 2.99, H(10A)···C(4A) 3.00 Å (C–H bond lengths normalised to 0.95 Å), Fig. 2. This may be compared to H···C distances in the range 2.73–3.05 Å recently reported for the organic system 2,3,7,8-tetraphenyl-1,9,10-anthyridine·toluene[15] in which there is much less steric hindrance at the arene (enabling a short C–H··π-centroid interaction), and falls well within the range associated with carbon acid hydrogen bonding interactions.[16,17] The observation of short intermolecular contacts alone does not however, necessarily mean an attractive intermolecular interaction. However, in this case the hydrogen bond acid–base complementarity between the donor and acceptor is clearly evident. Increased acidity of alkenes upon coordination to a metal centre arises from delocalisation of the metal positive charge, while it is the carbon atoms adjacent to the electron donating methoxy substituents which are the most electron rich on the CTV framework.

This result may be compared to the inclusion of iron(II) cations of type [Fe(arene)(Cp)]$^{-1}$ by free CTV recently

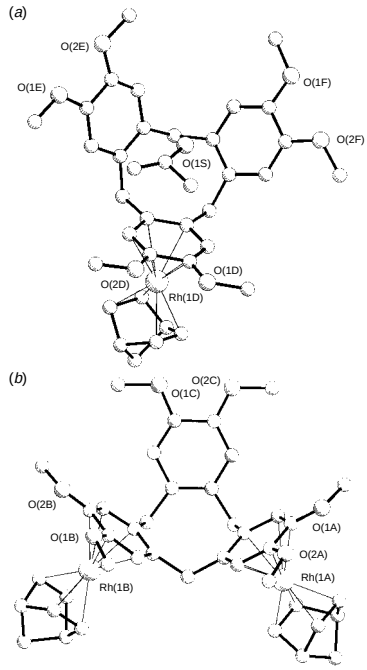

Fig. 1 (*a*) The monometallic and (*b*) bimetallic CTV based host complexes found in the structure of $[Rh(\eta^4\text{-nbd})(\eta^6\text{-CTV})][BF_4]\cdot[\{Rh(\eta^4\text{-nbd})\}_2(\eta^6:\eta^6\text{-CTV})][BF_4]_2\cdot 0.5Me_2CO$

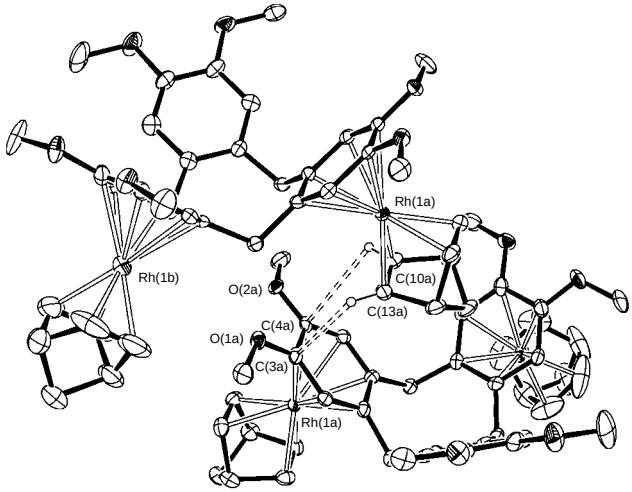

Fig. 2 C–H···π hydrogen bonding in the bimetallic complex **6**

reported by us,[18] in which shortest cyclopentadiene to CTV C···C contacts range from 3.44 to 3.59 Å depending on the identity of the arene. Curiously, however, in **6** it is the metallated ring attached to Rh(1A) which interacts with the C-acid guest. In contrast to compounds such as **2**, back bonding from the Rh^I centre will render the metalated CTV rings relatively electron rich, and it is presumably for this reason that intracavity anion binding is not observed in this case, in contrast to all other such systems with more than one metal centre.[2,7–10,19] However, the metallated ring should not be as electron rich as the free ring C(1C)–C(6C) and it seems that stacking of the anions external to the cavity around the two stacked Rh centres is maximised by the observed inclusion arrangement. This results in a short C(2A)–H···F(1A) contact; C(2A)···F(1A) 3.148(12) Å. Hence, it is clear that the electrostatic forces between cations and anions and the chelating C–H···π hydrogen bonding interactions act synergically.

The structure of the co-crystallised molecule of **5** is of the solvent-inclusion type, with the CTV cavity being occupied by a partial molecule of acetone, the crystals apparently having undergone some desolvation even at the very low temperature of the experiment. The acetone is approximately parallel with the metallated ring C(1D)–C(6D) with guest–host contacts in the range 3.4–4.0 Å.

The fact that no intracavity anion inclusion by even the bimetallic host **6** is observed in the solid state correlates with its anion binding ability in solution. Addition of 10 mol equiv. of $[NBu^n_4]I$ to a sample of **6** in $(CD_3)_2CO$ resulted in no change whatsoever in its ^1H NMR spectrum. This contrasts to the tetracationic ruthenium species **2** in which a similar experiment results in chemical shift changes of 0.89 ppm for the protons of the CTV rings.[20] In an attempt to estimate the strength of the double C–H···π interaction in solution, the ^1H NMR spectrum of **6** was monitored at a variety of concentrations from 0.02 to 0.002 M. This did result in slight downfield shifts (*ca.* 0.1 ppm) for the resonances assigned to the protons of the CTV rings, suggesting some degree of self-association. However, similar changes were also noted upon addition of excess $[NBu^n_4][BF_4]$ and hence this is probably not representative of significant C–H···π interactions in solution.

We thank Johnson Matthey plc for generous loans of rhodium trichloride, the Nuffield Foundation for the provision of computing equipment. We thank King's College London and the EPSRC for provision of the diffractometer system and the EPSRC for a studentship (to K. S. B. H.).

Notes and References

† E-mail: jon.steed@kcl.ac.uk

‡ *Crystal data*: $C_{76,50}H_{87}B_3F_{12}O_{12,50}Rh_3$, M = 1775.62, monoclinic, space group $C2/c$, a = 30.4514(9), b = 13.3577(4), c = 38.6258(7) Å, β = 92.790(1)°, U = 15692.8(7) Å^3, Z = 8, 10 167 data, 977 parameters, R_1 [$F_2 > 2\sigma(F^2)$] = 0.0838, wR_2 (all data) = 0.2375. CCDC 182/853.

1 K. T. Holman, J. L. Atwood and J. W. Steed, in *Advances in Supramolecular Chemistry, vol. 4*, ed. G. W. Gokel, JAI Press, London, 1997, pp. 287–331.
2 J. L. Atwood, K. T. Holman and J. W. Steed, *Chem. Commun.*, 1996, 1401.
3 P. D. Beer, *Chem. Commun.*, 1996, 689.
4 B. Dietrich, *Pure Appl. Chem.*, 1993, **65**, 1457.
5 M. M. G. Antonisse and D. N. Reinhoudt, *Chem. Commun.*, 1998, 443.
6 *Supramolecular Chemistry of Anions*, ed. A. Bianchi, K. Bowman-James and E. Garcia-Espana, Wiley–VCH, New York, 1997.
7 M. Staffilani, K. S. B. Hancock, J. W. Steed, K. T. Holman, J. L. Atwood, R. K. Juneja and R. S. Burkhalter, *J. Am. Chem. Soc.*, 1997, **119**, 6324.
8 J. W. Steed, R. K. Juneja and J. L. Atwood, *Angew. Chem., Int. Ed. Engl.*, 1994, **33**, 2456.
9 K. T. Holman, M. M. Halihan, J. W. Steed, S. S. Jurisson and J. L. Atwood, *J. Am. Chem. Soc.*, 1995, **117**, 7848.
10 A. B. Mitchell, J. W. Steed, K. T. Holman, M. M. Halihan, J. Montgomery, S. S. Jurisson, J. L. Atwood and R. S. Burkhalter, *J. Am. Chem. Soc.*, 1996, **118**, 9567.
11 C. D. Gutsche, *Calixarenes*, ed. J. F. Stoddart, Royal Society of Chemistry, Cambridge, 1989.
12 A. Collet, *Tetrahedron*, 1987, **43**, 5725.
13 M. Green and T. A. Kuc, *J. Chem. Soc., Dalton Trans.*, 1972, 832.
14 J. Chatt and L. M. Venanzi, *J. Chem. Soc.*, 1957, 4735.
15 N. N. L. Madhavi, A. K. Katz, H. L. Carrell, A. Nangia and G. R. Desiraju, *Chem. Commun.*, 1997, 1953.
16 G. R. Desiraju, *Acc. Chem. Res.*, 1996, **29**, 441.
17 M. J. Zaworotko, *Chem. Soc. Rev.*, 1994, **23**, 283.
18 K. T. Holman, J. L. Atwood and J. W. Steed, *Angew. Chem., Int. Ed. Engl.*, 1997, **36**, 1736.
19 J. W. Steed, P. C. Junk, J. L. Atwood, M. J. Barnes, C. L. Raston and R. L. Burkhalter, *J. Am. Chem. Soc.*, 1994, **116**, 10 346.
20 M. Staffilani, G. Bonvicini, J. W. Steed, K. T. Holman, J. L. Atwood and M. R. J. Elsegood, *Organometallics*, 1998, **17**, 1732.

Received in Columbia, MO, USA, 2nd March 1998; 8/01745J

High yield selective synthesis of C_{60} dimers

Y. Iwasa,*[a]† K. Tanoue,[a] T. Mitani,[a] A. Izuoka,[b] T. Sugawara[b] and T. Yagi[c]

[a] *Japan Advanced Institute of Science and Technology, Tatsunokuchi, Ishikawa, 923-12, Japan*
[b] *Department of Pure and Applied Sciences, University of Tokyo, Meguro-ku, Tokyo, 153, Japan*
[c] *Institute for Solid State Physics, University of Tokyo, Minato-ku, Tokyo, 106, Japan*

Squeezing the organic molecular crystal $(ET)_2C_{60}$ at 5 GPa and 200 °C followed by removing unreacted ET molecules produces C_{60} dimers, with a yield of *ca.* 80%.

Polymeric fullerenes have attracted considerable interest because of their various structures and properties.[1] Both neutral and doped polymers have been synthesized by various techniques. While doped polymers are found to be formed spontaneously by slow cooling to room temperature,[2] polymerization in the neutral state requires activation of C_{60} *via* light irradiation[3] or application of external pressure at high temperature.[4,5] An advantage of high pressure synthesis is that by tuning the temperature and pressure, one can selectively synthesize one- and two-dimensional polymers in bulk. Recently, a new technique, called the mechanochemical method, produced a bulk amount of C_{60} dimers in 25–30% yield.[6] X-Ray crystallographic analysis of the dimer revealed that the dimer is formed *via* a 2 + 2 cycloaddition [Fig. 1 (*b*)].

To control the dimensionality and the degree of polymerization, here we report a novel method of squeezing the crystals of a molecular compound of C_{60} and ET [ET = bis(ethylenedithio)tetrathiafulvalene].[7] In the $(ET)_2C_{60}$ crystal, a novel arrangement of C_{60} is achieved by covering a part of the C_{60} molecules with ET molecules. Fig. 1(*a*) shows the arrangement of C_{60} in a crystal of $(ET)_2C_{60}$, where C_{60} molecules form a one-dimensional closest packing arrangement with a regular triangle lattice framework along the *c*-axis.[7] Interfullerene distances parallel and diagonal to the *c*-axis are 9.923(2) and 9.919(3) Å, respectively. Since they are very close to that of the face-centred cubic lattice of neat C_{60} (10.02 Å), pressure-induced cross-linking of C_{60} molecules in the $(ET)_2C_{60}$ crystals is highly promising. Incidentally, the charge transfer interaction between ET and C_{60} in this crystal is estimated to be small, as judged by the difference between redox potentials of each element.

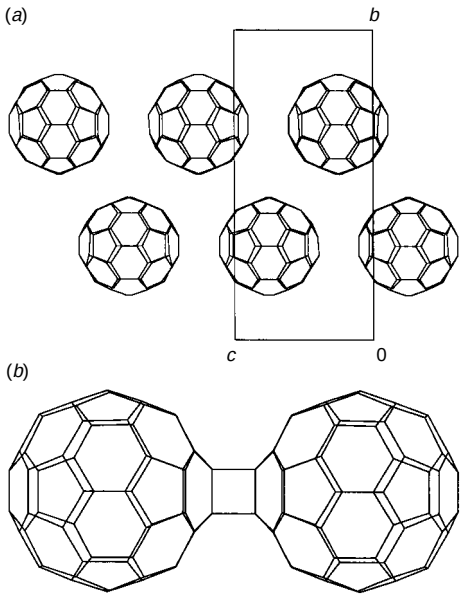

Fig. 1 (*a*) Arrangement of C_{60} in $(ET)_2C_{60}$ crystal; (*b*) C_{60} dimer

The starting $(ET)_2C_{60}$ crystals were obtained by slow evaporation of a CS_2 solution of a stoichiometric amount of C_{60} and ET. High pressure treatment was performed following previously described procedures.[4] Polycrystalline $(ET)_2C_{60}$ (50–100 mg) loaded in a gold capsule was reacted at 5 GPa and 200 °C using a wedge-type cubic anvil high pressure apparatus. After squeezing, the sample was recovered from the reaction capsule, and subjected to characterization under at ambient conditions.

Raman spectra of the pentagonal pinch mode $A_g(2)$ for the I_h of C_{60}, which is a sensitive probe for the occurrence of interfullerene bonds, were obtained.[3] Reflecting the almost neutral nature of the $(ET)_2C_{60}$ complex, the $A_g(2)$ mode was observed at 1469.3 cm^{-1}, which is identical to the position for pure C_{60}. In the as-pressurized $(ET)_2C_{60}$, the corresponding mode appeared at 1462.9 cm^{-1}, displaying a 6.4 cm^{-1} red-shift. This result indicates that interfullerene bonds are formed in the pressurized sample.

Earlier work has proved that infrared spectroscopy is a useful tool to identify the C_{60} polymer phases.[8,9] Fig. 2 shows the infrared absorption spectra of several samples dispersed in KBr pellets. The spectrum of starting $(ET)_2C_{60}$ is shown in Fig. 2(*c*). This spectrum is approximately explained as the sum of those for the constituent molecules, C_{60} [Fig. 2(*a*)] and ET [Fig. 2(*b*)], this being consistent with the absence of charge transfer suggested by the structural analysis. The spectrum of the as-

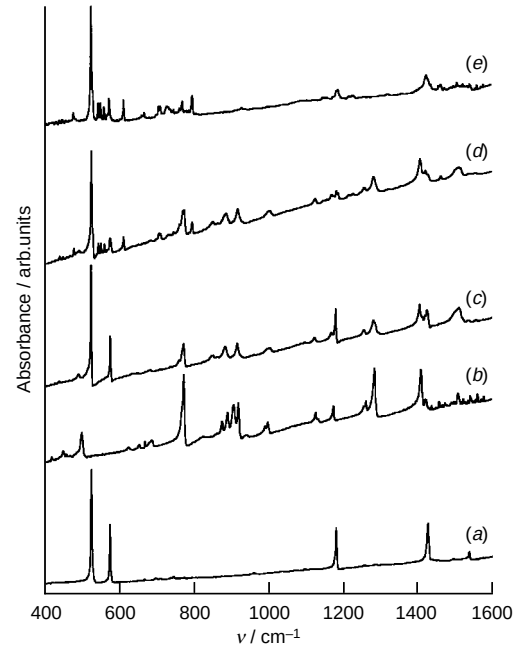

Fig. 2 Infrared absorption spectra for (*a*) C_{60}, (*b*) ET, (*c*) pristine $(ET)_2C_{60}$, (*d*) as-pressurized $(ET)_2C_{60}$, and (*e*) $(ET)_2C_{60}$ washed by CH_2Cl_2. ET molecules were removed in the final product.

pressurized sample is displayed in Fig. 2(*d*), which is remarkably different from the spectrum of the starting $(ET)_2C_{60}$. By a careful comparison between the two spectra, we found that the peaks attributable to ET were not changed by pressurization, while those from C_{60} exhibited notable changes. In order to confirm the change more precisely, the unreacted ET molecules were removed by sonication in CH_2Cl_2. The infrared spectrum [Fig. 2(*e*)] of the washed sample shows no trance of ET and can be ascribed to reacted C_{60}. Since this substance was soluble to *o*-dichlorobenzene, the degree of polymerization is expected to be substantially smaller than those for the one- and two-dimensional polymers, which are insoluble to *o*-dichlorobenzene.

The infrared spectrum [Fig. 2 (*e*)] of the obtained sample differs significantly from those for the polymers reported in previous papers, but is very similar to that for photodimerized C_{60}.[10] Furthermore, the spectrum of the mechanochemically synthesized dimer[6] turned out to be almost identical to Fig. 2(*e*), including the peak positions and intensity distributions. These spectral results strongly indicate that the dominant product of high pressure treatment of $(ET)_2C_{60}$ is the C_{60} dimer [Fig. 1(*b*)].

High performance liquid chromatographic analysis of the obtained sample was performed on a Cosmosil Buckyprep column with toluene as the eluent. The retention volume (14.5 ml) of the main peak was exactly the same as that for the mechanochemically obtained dimer.[6] Although several weak peaks are observed in the chromatogram, no signal derived from unreacted monomer C_{60} was found. The purity of C_{60} dimer was estimated to be about 79% based on the peak area of the chromatogram, detected by monitoring UV light at 326 nm. Since the weight-loss during the pressure treatment and purification is negligible, we can conclude that roughly 80% of the C_{60} monomer is converted to the dimer. This yield is considerably higher than that of the mechanochemical method.

Although most of the product of the above method is soluble in *o*-dichlorobenzene, there remains a small amount of insoluble material. Thus a substantial amount of one-dimensional oligomers or ladder polymers might be synthesized according to the current method by optimizing the reaction conditions. The reaction mechanism in the restricted spaces in such types of molecular compounds could be an interesting issue to be explored in the future.

Authors are grateful to Professor K. Komatsu and Dr Y. Murata, Kyoto University, for their help in sample characterization, and to Mr. T. Uchida, University of Tokyo, for his help in high pressure synthesis. This work was supported by a Grant from the Japan Society for Promotion of Science (JSPS-RFTF96P00l04 and NPCR-36396-0326), from the Ministry of Education, Science, Sports, and Culture, and from Yamada Science Foundation.

Notes and References

† E-mail: iwasa@jaist.ac.jp

1 For example, *Appl. Phys. A*, 1997, **64** (Special issue, *Polymeric Fullerenes)*, *Fullerene Polymers and Fullerene-Polymer Composites*, ed. P. C. Eklund and A. M. Rao, Springer, 1997.
2 O. Chauvet, G. Oszlanyi, L. Forro, P. W. Stephens, M. Tegze, G. Faigel and A. Janossy, *Phys. Rev. Lett.*, 1994, **72**, 2721.
3 A. M. Rao, P. Zhou, K.-A. Wang, G. T. Hager, J. M. Holden, Y. Wang, W.-T. Lee, X.-X. Bi, P. C. klund, D. S. Cornett, M. A. Duncan and I. J. Amster, *Science*, 1993, **259**, 955.
4 Y. Iwasa, T. Arima, R. M. Fleming, T. Siegrist, O. Zhou, R. C. Haddon, L. J. Rothberg, K. B. Lyons, H. L. Carter Jr., A. F. Hebard, R. Tycko, G. Dabbagh, J. J. Krajewski, G. A. Thomas and T. Yagi, *Science*, 1994, **264**, 1570.
5 M. Nunez-Regueiro, L. Marques, J.-L. Hodeau, O. Bethoux and M. Perroux, *Phys. Rev. Lett.*, 1995, **74**, 278.
6 G.-W. Wang, K. Komatsu, Y. Murata and M. Shiro, *Nature*, 1997, **387**, 583.
7 A. Izuoka, T. Tachikawa, T. Sugawara, Y. Suzuki, M. Konno, Y. Saito and H. Shinohara, *J. Chem. Soc., Chem. Commun.*, 1992, 1472.
8 A. M. Rao, P. C. Eklund, J.-L. Hodeau, L. Marques and M. Nunez-Regueiro, *Phys. Rev. B*, 1997, **55**, 4766.
9 K. Kamaras, Y. Iwasa and L. Forro, *Phys. Rev. B*, 1997, **55**, 10 999.
10 J. Onoe and K. Takeuchi, *Phys. Rev. B*, 1996, **54**, 6167.

Received in Cambridge, UK, 27th March 1998; 8/02382D

Radical-chain reductive carboxyalkylation of electron-rich alkenes: carbon–carbon bond formation mediated by silanes in the presence of thiols as polarity-reversal catalysts

Hai-Shan Dang, Kyoung-Mahn Kim and Brian P. Roberts*†

Christopher Ingold Laboratories, Department of Chemistry, University College London, 20 Gordon Street, London, UK WC1H 0AJ

The reductive carboxyalkylation of electron-rich alkenes by α-halogenoesters in the presence of triphenylsilane under free-radical conditions is catalysed by thiols: prochiral alkenes give optically-active adducts when the thiol catalyst is homochiral.

The reductive alkylation of electron-poor alkenes, using alkyl halides or psuedohalides in the presence of tributyltin hydride, is a radical-chain reaction of considerable importance for intermolecular C–C bond formation.[1] The propagation stage of this process, which is sometimes referred to as the 'tin method' or the 'Giese reaction', is illustrated in Scheme 1.

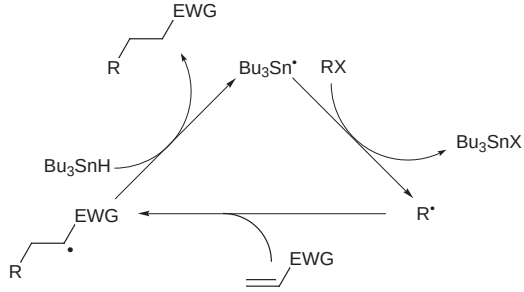

Scheme 1

This reaction suffers from certain limitations, notably the use of toxic organotin compounds and the need to keep the tin hydride concentration low in order to avoid trapping the radical R• to form RH before it has time to add to the alkene. The latter problem is more severe when the alkene is electron-rich, because simple alkyl radicals are nucleophilic, and the reaction is not then a practical method for C–C bond formation. Trialkylgermanes[2] and tris(trimethylsilyl)silane[3] have been employed in place of the tin hydride as they are less toxic and also less efficient hydrogen-atom donors. There are also a few examples of the successful use of α-halogenoesters, which yield relatively electrophilic α-alkoxycarbonylalkyl radicals, in conjunction with tributyltin hydride to bring about reductive alkylation of electron-rich alkenes.[4]

We have reported that the principle of polarity-reversal catalysis,[5] in this instance by thiols, may be applied to promote the overall abstraction of electron-rich hydrogen by nucleophilic alkyl radicals from silicon in simple triorganosilanes, through the catalytic cycle of reactions (1) and (2), and we have described how this silane–thiol couple can serve as an effective replacement for trialkyltin hydrides in many radical-chain processes.[6]

$$R^{\bullet} + XSH \rightarrow RH + XS^{\bullet} \quad (1)$$

$$XS^{\bullet} + R_3SiH \rightarrow XSH + R_3Si^{\bullet} \quad (2)$$

$$Bu^tON{=}NOBu^t \rightarrow 2Bu^tO^{\bullet} + N_2 \quad (3)$$

The SH group of a thiol provides electron-deficient hydrogen, which favours hydrogen-atom transfer to the nucleophilic alkyl radicals that are formed by addition to electron-rich alkenes, while polar effects will discriminate against the abstraction of hydrogen from thiols by electrophilic radicals.[7] With these considerations in mind, we reasoned that reductive alkylation of electron-rich alkenes, mediated by the silane–thiol couple, could be a viable method for C–C bond formation when the alkyl halide provides an electrophilic alkyl radical. In this communication we report the translation of these ideas into practice, along with the results of preliminary attempts to develop asymmetric syntheses based on this new methodology.

Table 1 Reductive carboxyalkylation of alkenes using organic halides in the presence of triphenylsilane, catalysed by thiol and initiated by TBHN in dioxane at 60 °C

Entry	Alkene	R³Hal	Thiol	Adduct	Adduct yield (%)[a]
1	**1a**	**2a**	MTG	**3aa**	78
2	**1a**	**2a**	TPST	**3aa**	88[b]
3	**1a**	**2b**	MTG	**3ab**	75
4	**1a**	**2b**	TPST	**3ab**	72
5	**1a**	**2c**	TPST	**3ac**	78
6	**1b**	**2a**	TPST	**3ba**	86
7	**1b**	**2b**	TPST	**3bb**	75
8	**1c**	**2a**	TPST	**3ca**	85
9	**1d**	**2a**	TPST	**3da**	78
10	**1e**	**2a**	TPST	**3ea**	60
11	**1f**	**2a**	TPST	**3fa**	63
12	**5**	**2a**	TPST	**6**	76
13	**7**	**2a**	TPST	**8**	63[b]
14	**7**	**2a**	**10**	**8**	63 (24% ee)[c]
15	**7**	**2a**	**11**	**8**	64 (27% ee)[c]
16	**7**	**2b**	**10**	**9**	72 (19% ee)[d,e]

[a] Isolated yields based on alkene; satisfactory spectroscopic and analytical data were obtained for all new compounds. [b] The yield was similar in benzene solvent. Only a trace of adduct was formed in the absence of thiol. [c] The ee was determined by chiral-stationary-phase HPLC analysis (Chiralcel-OD column, eluent: hexane–isopropyl alcohol 99 : 1); the enantiomer in excess was eluted second. [d] The ee was determined by ^{1}H NMR analysis using a homochiral shift reagent [Eu(hfc)$_3$]. [e] The ee was the same when **11** was used as catalyst.

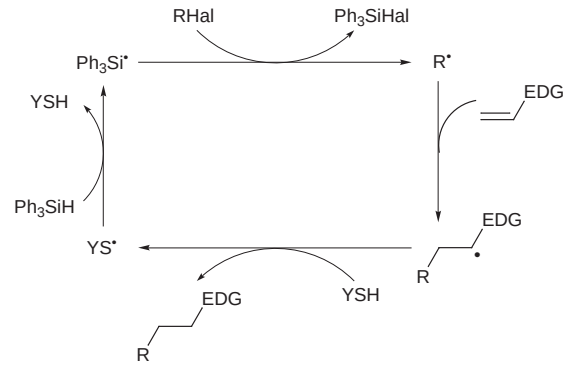

Scheme 2

All reactions were carried out at 60 °C and were initiated by thermal decomposition of di-*tert*-butyl hyponitrite (TBHN, $t_{\frac{1}{2}}$ = *ca.* 55 min),[8] which produces *tert*-butoxyl radicals [eqn. (3)] that go on to abstract hydrogen from the silane and/or the thiol to afford chain-carrying silyl or thiyl radicals. When a dioxane solution containing isopropenyl acetate **1a** (2.50 mmol), triphenylsilane (3.25 mmol), dimethyl chloromalonate **2a** (3.75 mmol) and TBHN (0.125 mmol) was heated under argon for 2 h, examination of the reaction mixture by ^{1}H NMR spectroscopy showed that < 1% of the adduct **3aa**‡ had been formed. However, when the experiment was repeated in the presence of methyl thioglycolate (MeO_2CCH_2SH, MTG, 0.125 mmol, 5 mol% based on alkene) under otherwise identical conditions, the adduct **3aa** was isolated in 78% yield. A somewhat higher yield was obtained in the presence of triphenylsilanethiol (TPST, 5 mol%) as catalyst (Table 1, entries 1 and 2). The reductive carboxyalkylation of **1a** [eqn. (4)] evidently proceeds

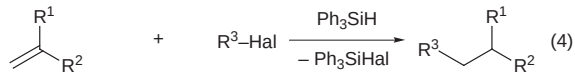

(4)

1a R^1 = OAc, R^2 = Me
b R^1 = OAc, R^2 = Bu^t
c R^1 = $OSiMe_2Bu^t$, R^2 = Me
d R^1 = OBu, R^2 = H
e R^1 = Pentyl, R^2 = Me
f R^1 = CH_2OAc, R^2 = Me

2a $(MeO_2C)_2CH$–Cl
b MeO_2CCH_2–Br
c $(EtO_2C)_2CMe$–Br

3

by a radical-chain mechanism, the propagation stage of which is shown in Scheme 2. A similarly high yield of the adduct **3ab** was obtained when dimethyl chloromalonate was replaced with methyl bromoacetate **2b** in the presence of either MTG or TPST (entries 3 and 4), but with methyl chloroacetate under the same conditions the yield of **3ab** was reduced to 40% and a large amount (50%) of the adduct **4** was also isolated. Evidently, the

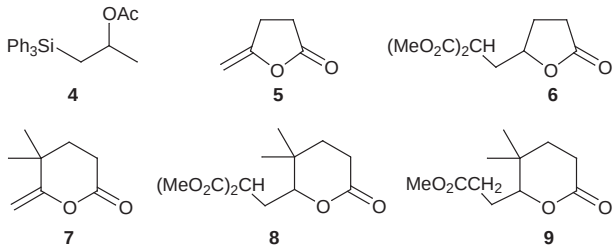

4 **5** **6** **7** **8** **9**

triphenylsilyl radical adds to the C=C bond[6d,e] in **1a** at about the same rate as it abstracts halogen from the chloroacetate, while with the more reactive bromoacetate halogen-atom abstraction is much faster than addition to the alkene. A good yield of the adduct **3ac** was obtained from the reductive carboxyalkylation of isopropenyl acetate with diethyl 2-bromo-2-methylmalonate (entry 5).§

Similar addition reactions were carried out with the alkenes **1b**–**f** and the results are summarised in Table 1:¶ essentially no adduct formation occurred in the absence of thiol catalyst. The methylenelactones **5** and **7** also functioned well as acceptors (entries 12 and 13).‖

The stereogenic centres in the adducts **8** and **9** are formed when the prochiral chain-carrying radicals, produced by addition to these alkenes, abstract hydrogen from the thiol catalyst (Scheme 2). If the thiol is homochiral then the hydrogen-atom transfer will be enantioselective and optically-active adducts should result. Reductive carboxyalkylation of the methylenelactone **7** using the carbohydrate-derived thiols **10** and **11** as catalysts gave the adducts **8** and **9** with an enantiomeric excess (ee) up to 27% (entries 14–16).** Although the optical purities obtained so far are low, the results

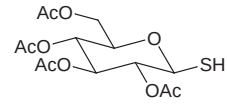

10

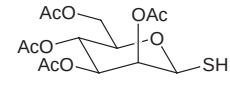

11

are encouraging because the transfer of chirality is catalytic and the reactions are carried out at relatively high temperatures. Efforts to design more effective homochiral thiol catalysts are underway.

Financial support for this work was provided by the EPSRC.

Notes and References

† E-mail: b.p.roberts@ucl.ac.uk

‡ The adduct **3aa** arises from **1a** and **2a**, the adduct **3ab** arises from **1a** and **2b** and so on.

§ Triphenylbromosilane is formed in reactions involving bromides. This bromosilane is a Lewis acid and is also very sensitive to hydrolysis, so that care must be taken if the reactants or adduct are sensitive to acid.

¶ No adducts could be obtained from the enol acetate $PhC(OAc)=CH_2$. It is likely that the oxygen-conjugated benzylic radicals formed by addition to this alkene do not abstract hydrogen from the thiol catalyst at a sufficient rate to maintain a chain reaction.

‖ *Typical procedure*. A solution in dry dioxane (4 cm^3) containing isopropenyl acetate **1a** (0.250 g, 2.50 mmol), triphenylsilane (0.846 g, 3.25 mmol), dimethyl chloromalonate (0.625 g, 3.75 mmol), TBHN (22 mg) and triphenylsilanethiol (37 mg) was stirred and heated at 60 °C under an atmosphere of dry argon for 2 h. The solvent was removed by evaporation under reduced pressure, the residue was dissolved in Et_2O (10 cm^3) and the solution was washed with 5% aqueous $NaHCO_3$, then with saturated brine and then dried ($MgSO_4$). After evaporation of the ether, light petroleum (bp 40–60 °C) (5 cm^3) was added and the slurry was filtered to remove most of the triphenylsilanol, which was washed on the sinter with a little petroleum. After evaporation of the solvent from the filtrate, the residue was purified by flash-chromatography (eluent: petroleum–Et_2O 95 : 5 to 5 : 1) to give the adduct **3aa** as a clear oil (0.511 g, 88%). δ_H 1.24 (3 H, d, *J* 6.2, Me), 2.00 (3 H, s, Ac), 2.35 (2 H, m, C*H*$_2$CH), 3.46 [1 H, dd, *J* 8.6 and 6.1 $(MeO_2C)_2$C*H*], 3.72(7) (3 H, s, OMe^A), 3.73(2) (3 H, s, OMe^B), 4.89 (1 H, m, C*H*OAc); δ_C 20.1, 21.1, 34.7, 48.4, 52.7 (2C), 68.7, 169.3, 169.5, 170.4.

** Enantioselective reductive carboxylkylation of **7** could also be mediated by tributyltin hydride. When triphenylsilane was replaced by tin hydride (1.3 equiv.), added slowly during 2 h as a dioxane solution also containing TBHN, but otherwise essentially under the conditions of entry 14, the adduct **8** was isolated in 80% yield and showed an ee of 25%. This result also demonstrates that thiols can act as polarity-reversal catalysts for the abstraction of hydrogen from tin hydrides by alkyl radicals.

1 B. Giese, *Radicals in Organic Synthesis: Formation of Carbon-Carbon Bonds*, Pergamon Press, Oxford, 1986; W. B. Motherwell and D. Crich, *Free Radical Chain Reactions in Organic Synthesis*, Academic Press, London, 1992.
2 P. Pike, S. Hershberger and J. Hershberger, *Tetrahedron Lett.*, 1985, **26**, 6289.
3 B. Giese, B. Kopping and C. Chatgilialoglu, *Tetrahedron Lett.*, 1989, **30**, 681.
4 B. Giese, H. Horler and M. Leising, *Chem. Ber.*, 1986, **119**, 444; T. F. Herpin, W. B. Motherwell and M. J. Tozer, *Tetrahedron: Asymmetry*, 1994, **5**, 2269.
5 V. Paul and B. P. Roberts, *J. Chem. Soc., Chem. Commun.*, 1987, 1322; V. Paul and B. P. Roberts, *J. Chem. Soc., Perkin Trans. 2*, 1988, 1183; H.-S. Dang and B. P. Roberts, *J. Chem. Soc., Perkin Trans. 1*, 1993, 891.
6 (*a*) R. P. Allen, B. P. Roberts and C. R. Willis, *J. Chem. Soc., Chem. Commun.*, 1989, 1387; (*b*) J. N. Kirwan, B. P. Roberts and C. R. Willis, *Tetrahedron Lett.*, 1990, **31**, 5093; (*c*) S. J. Cole, J. N. Kirwan, B. P. Roberts and C. R. Willis, *J. Chem. Soc., Perkin Trans. 1*, 1991, 103; (*d*) H.-S. Dang and B. P. Roberts, *Tetrahedron Lett.*, 1995, **36**, 2875; (*e*) M. B. Haque and B. P. Roberts, *Tetrahedron Lett.*, 1996, **37**, 9123; (*f*) H.-S. Dang and B. P. Roberts, *J. Chem. Soc., Perkin Trans. 1*, 1998, 67.
7 B. P. Roberts and A. J. Steel, *J. Chem. Soc., Perkin Trans. 2*, 1994, 2155; B. P. Roberts, *J. Chem. Soc., Perkin Trans. 2*, 1996, 2719.
8 H. Kiefer and T. G. Traylor, *Tetrahedron Lett.*, 1966, 6163; G. D. Mendenhall, *Tetrahedron Lett.*, 1983, **24**, 451.

Received in Liverpool, UK, 15th April 1998; 8/02826E

Amphiphilic core–shell nanospheres obtained by intramicellar shell crosslinking of polymer micelles with poly(ethylene oxide) linkers

Haiyong Huang,[a] Edward E. Remsen[b] and Karen L. Wooley*[a]†

[a] *Department of Chemistry, Washington University, One Brookings Drive, St Louis, MO, 63130, USA*
[b] *Monsanto Company, 800 N. Lindbergh Blvd., St. Louis, MO 63167, USA*

Intramicellar crosslinking of the polymer chains within the shells of polystyrene-*b*-poly(acrylic acid) micelles by reaction with difunctional poly(ethylene oxide) afforded unimolecular amphiphilic core–shell nanospheres (50 nm hydrodynamic radius); the resulting surface hydrogel layer gives an approximate fivefold increase of particle volume from the dry state to aqueous solution.

The concept of shell crosslinked knedel-like structures (SCKs)[1] has been applied to synthesize nanoparticles with core–shell structures, composed of poly(ethylene oxide) (PEO) chains as covalent crosslinks binding together the peripheral layer of polymer micelles. The unique combination of size, structure, stability and composition of these nanospheres renders them great potential for drug delivery systems. Extensive efforts have been undertaken by other researchers to understand the structurally related drug delivery properties of the submicrometer-sized polymeric particles.[2–6] For example, the sub-100 nm diameter of PEO-adsorbed polystyrene nanoparticles allowed for evasion of sequestration by the phagocytosis process,[2] and the hydrophilicity of PEO facilitated the transportation of these particles through the interstitum by aqueous channels.[7] Moreover, the surface PEO blocks of polymer micelles sterically stabilized the nanospheres and prolonged the circulation lifetime in the blood.[3]

The shell-crosslinked nanospheres in this study offer some advantageous features, such as the ability to maintain structural integrity upon infinite dilution and mechanical stresses, the stability of covalently bound PEO within the surface domain, and the potential to attach receptor-recognizing ligands to the residual carboxylate side groups on the PAA block. SCKs have previously been prepared with coupling *via* short difunctional oligomeric crosslinkers,[8] in which the chemical composition of the crosslinkers resulted in differences in the nature of the shell. This report demonstrates that PEO can be incorporated into the SCK shell as a polymeric crosslinker to greatly increase the shell thickness and to modify the surface properties[9] of the SCKs (*e.g.* permeability and flexibility), without the evidence of intermicellar reactions occurring.

SCKs are essentially unimolecular polymer micelles, which are prepared by stabilization of the basic structure of the spherical micellar assembly through linking together of the hydrophilic portions of the chains within the micelle shell. Therefore, the synthesis of the SCKs involves only three steps: (*i*) preparation of an amphiphilic block copolymer; (*ii*) self-assembly of the amphiphilic block copolymer into polymer micelles; (*iii*) crosslinking through side groups along the blocks occupying the shell of the polymer micelles.

The preparation of the SCKs began from the diblock copolymer, polystyrene-*b*-poly(acrylic acid) (PS-*b*-PAA), which was conveniently synthesized by living free radical polymerization.[10] The living free radical polymerization was accomplished by a stepwise atom transfer radical polymerization technique, similar to the procedures reported by Matyjaszewski and coworkers.[11] Micelles composed of PS-*b*-PAA were formed by addition of water to a solution of the polymer in THF,[12] and an aqueous solution of micelles was obtained by dialyzing against distilled water. The crosslinking was accomplished by condensation reactions of diamino linkers with PAA, facilitated by a carbodiimide coupling agent (Scheme 1).

The carboxylic acid groups on the PAA block were first activated by reaction with the water soluble carbodiimide, 1-(3-dimethylaminopropyl)-3-ethylcarbodiimide methiodide (1 equiv. based upon the acrylic acid groups). The crosslinker, poly(ethylene glycol) diamine (M_w = 3400 Da, 0.5 equiv. based upon the acrylic acid groups), was then added to crosslink the PAA domain by formation of amide bonds[13] and yield SCK **1**. For evaluation of the effects of the crosslinker length, SCK **2** was crosslinked *via* a short tri(ethylene oxide) linker in a similar fashion using 2,2′-(ethylenedioxy)bis(ethylamine).[8] In both cases, the urea by-product was removed by dialysis against distilled water.

^{1}H NMR resonance signals could not be detected in D_2O solutions, due to the colloidal nature of **1** and **2**. Therefore, solid samples of the SCKs were obtained by lyophilization, and the compositions of **1** and **2** were characterized by IR spectroscopy. Upon formation of **1**, absorption bands corresponding to free carboxylic acid groups (3600–2500 and 1710 cm^{-1}) of the polymer micelles attenuated to 10–30% of their original intensity, as amide I and II bands appeared at 1650 and 1540 cm^{-1}. Solid-state NMR experiments are in progress to determine the extent of amidation and the effects on the shell permeability. In contrast, upon formation of **2**, the carbonyl stretch of the carboxylic acid band disappeared in the IR spectrum, and only the amide carbonyl bands were observed. Strong absorption from C–O stretching of the ethylene oxide linkers was observed at 1108 cm^{-1} for both **1** and **2**. The compositions of the SCKs were quantitatively confirmed by elemental analysis.

Transmission electron microscopy (TEM) provided further evidence for structural differences between **1** and **2** (Fig. 1). The cores of **1** and **2** appear to be approximately the same diameter, however, the shell thicknesses are very different. SCK **1** has a distinct corona owing to the poly(ethylene oxide) linker [Fig. 1(*a*), the PEO coronas are the gray areas surrounding the brighter center cores], whereas SCK **2** has a sharp edge [Fig. 1(*b*)]. The average diameters of the nanospheres were determined in aqueous solution by dynamic light scattering (DLS)[8]

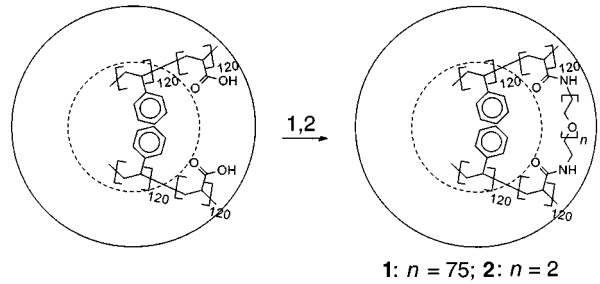

1: n = 75; **2**: n = 2

Scheme 1 Amidation chemistry used for crosslinking of poly(acrylic acid) groups located in the shell of Ps-*b*-PAA polymer micelles to form the SCK nanospheres. 1, $CH_3CH_2N{=}C{=}N(CH_2)_3N(CH_3)_3I$; 2, $H_2N(CH_2CH_2O)_n$-$CH_2CH_2NH_2$.

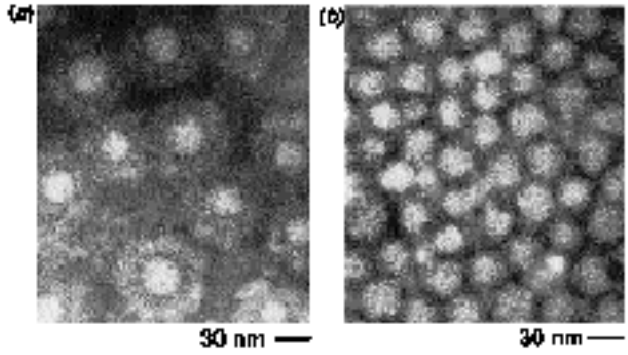

Fig. 1 Negatively stained transmission electron microscopy (TEM) images at 300 K magnification of the SCKs crosslinked by (*a*) PEO linkers to yield a thick hydrogel-like crosslinked shell surrounding and covalently bound to the PS core, and (*b*) tri(ethylene oxide) linkers to yield SCKs possessing a relatively thin shell of oligo(ethylene oxide)-crosslinked polyacrylamide. The TEM samples were prepared by dropping 1 : 1 mixtures of aqueous solutions of the SCK sample and uranyl acetate (2.5% solution), upon a carbon-coated copper grid and allowing to dry.

to be 100 ± 3 nm for **1** and 37 ± 2 nm for **2**. Based on the size of the precursor polymer micelles in the dry state (average diameter is 26 nm, core diameter is 22 nm and shell thickness is 2 nm, determined by TEM and AFM)[8] and the increment of volume added from the linkers, the theoretical[14] diameters of SCKs **1** and **2** in the compact dry state were calculated to be 56 and 29 nm, respectively. Because both **1** and **2** result from the same polymer micelle, with an average core diameter of 22 nm, the shell thicknesses in the compact dry state are calculated as 17 and 3.5 nm, respectively. The extent of swelling of the crosslinked hydrogel peripheral layer when placed within water was determined to be about twofold in thickness, corresponding to an approximate eightfold increase in shell volume. Considering the differences in shell thickness **1** experiences a fivefold increase in overall SCK volume, whereas only a twofold total volume increase occurs for **2**.

Differential scanning calorimetry (DSC) experiments were performed to deduce structural information for the dried samples of **1** and **2**. SCK **1** exhibits a melting transition (T_m) at 45 °C, which corresponds to the T_m of PEO,[15] however no T_g is observable for the PS core. This indicates that PEO in the shell exists as a phase separated crystalline domain, and that the PS content may be too low for detection by our DSC instrumentation. In contrast, a glass transition (T_g) for the PS core at 105 °C is evident for SCK **2**, but no detectable T_m or T_g corresponding to PEO is observed. These results support the compositional and structural differences between **1** and **2**.

The ethylene oxide surface layer covalently attached throughout the SCK shell provides a stable, steric barrier between the hydrophobic core and aqueous media. Poly(ethylene glycol)diamine incorporates a higher degree of ethylene oxide units than 2,2′-(ethylenedioxy)bis(ethylamine), which allows phase separation of the PEO, demonstration of behavior characteristic of pure PEO, formation of a thicker hydrogel-like exterior layer, and greater extents of overall nanoparticle swelling in water. The SCKs thus prepared have many enhanced features that should serve well when applied as artificial drug carriers. Investigations into protein binding for early *in vitro* screening of potential biocompatibility are in progress.

This work was funded by a National Science Foundation National Young Investigator Award (DMR 9458025) and Monsanto Company. The authors are grateful to Mr Michael Veith for TEM experiments.

Notes and References

† E-mail: klwooley@artsci.wustl.edu

1 K. B. Thurmond II, T. Kowalewski and K. L. Wooley, *J. Am. Chem. Soc.*, 1997, **119**, 6656; 1996, **118**, 7239; K. L. Wooley, *Chem. Eur. J.*, 1997, **3**, 1397.
2 S. E. Dunn, A. G. A. Coombes, M. C. Garnett, S. S. Davis, M. C. Davies and L. Illum, *J. Controlled Release*, 1997, **44**, 65.
3 M. T. Peracchia, R. Gref, Y. Minamitake, A. Domb, N. Lotan and R. Langer, *J. Controlled Release*, 1997, **46**, 223.
4 A. Rolland, J. O'Mullane, P. Goddard, L. Brookman and K. Petrak, *J. Appl. Polym. Sci.*, 1992, **44**, 1195.
5 K. Kataoka, in *Controlled Drug Delivery: the Next Generation*, ed. K. Park, American Chemical Society, Washington, DC, 1997, ch. 4.
6 E. Mathiowitz, J. S. Jacob, Y. S. Jong, G. P. Carino, D. E. Chickering, P. Chaturvedi, C. A. Santos, K. Vijayaraghavan, S. Montgomery, M. Bassett and C. Morrell, *Nature*, 1997, **386**, 410.
7 S. M.Moghim, A. E. Hawley, N. M. Christy, T. Gray, L. Illum and S. S. Davis, *FEBS Lett.*, 1994, **344**, 25.
8 (*a*) H. Huang, K. L. Wooley, R. Gertzmann and T. Kowalewski, *ACS Polym. Prepr.*, 1997, **38**, 119; (*b*) H. Huang, T. Kowalewski, E. E. Remsen, R. Gertzmann and K. L. Wooley, *J. Am. Chem. Soc.*, 1997, **119**, 11 653.
9 S. I. Jeon, J. H. Lee, J. D. Andrade and P. G. de Gennes, *J. Colloid Interface Sci.*, 1991, **142**, 149.
10 C. J. Hawker, *J. Am. Chem. Soc.*, 1994, **116**, 11 185; J.-S. Wang and K. Matyjaszewski, *J. Am. Chem. Soc.*, 1995, **117**, 5614.
11 The PS-*b*-PAA was prepared by living atom transfer radical polymerization of styrene and then methyl acrylate, followed by HCl catalyzed hydrolysis of the methyl ester functionalities. The polystyrene block was prepared by polymerization of styrene, using a mixture of copper(I) bromide (0.8 mol%), 4,4′-di(5-nonyl)-2,2-bipyridine (1.5 mol%) and 1-bromoethylbenzene (0.8 mol%). This bromo-terminated polystyrene (0.8 mol%) was isolated by precipitation into methanol. The dried bromo-terminated polystyrene was then used to initiate the polymerization of methyl acrylate, in the presence of copper(I) bromide (0.8 mol%) and 4,4′-di(5-nonyl)-2,2′-bipyridine (1.7 mol%). The diblock copolymer was made amphiphilic by hydrolysis of the methyl ester functionalities along the poly(methyl acrylate) block in HCl–dioxane. The PS block was of M_n = 12 500, determined from GPC calibrated with polystyrene standards. Based on the ratio of integration values for resonances of respective protons in the ^{1}H NMR spectrum, the average numbers of styrene units and acrylic acid units in the PS-*b*-PAA copolymer were determined to both be approximately 120. J. S. Wang, D. Greszta and K. Matyjaszewski, *ACS Polym. Mater. Sci. Eng.*, 1995, **73**, 416.
12 The SCK syntheses were performed on up to 200 mg scales, with the formation of the polymer micelles following similar procedure to that found in ref 8(*b*) as well as L. Zhang and A. Eisenburg, *Science*, 1995, **268**, 1728; Y. Yu and A. Eisenburg, *J. Am. Chem. Soc.*, 1997, **119**, 8383.
13 The single alkyl bromide located at the chain end of each polymer chain resulting from the ATRP chemistry may also undergo reaction with the diamino crosslinkers.
14 The sizes of SCK particles of **1** shown by TEM cannot be taken as the compact dry-state diameters, owing to distortion of the PEO-containing corona of the nanospheres upon drying on the carbon-coated copper grid substrate. Therefore, the SCK size was predicted by adding the volume of the precursor micelle to the additional volume from the linkers (calculated from the product of moles of linker, linker molecular mass and linker density), followed by conversion to the diameter for a spherical SCK. The 29 nm calculated diameter of **2** agrees with the particle sizes observed in the TEM image.
15 T_m of PEO–$(NH_2)_2$ (M_w = 3400) is 45 °C.

Received in Columbia, MO, USA; 1st December 1997; 7/08686E

Typeset and printed by Black Bear Press Limited, Cambridge, England

ChemComm
FEATURE ARTICLE

The domino cycloaddition/*N*-acyliminium ion cyclization cascade

Albert Padwa

Department of Chemistry, Emory University, Atlanta, GA 30322, USA

Various applications of the domino cycloaddition/ *N*-acyliminium ion cyclization cascade are reported. The key step in the process involves the generation of a reactive *N*-acyliminium ion by fragmentation of an amino substituted [4 + 2]-cycloadduct. The successful synthesis of a number of alkaloids by this sequence of reactions reveals the usefulness and importance of this unique domino cascade.

Introduction

Domino processes belong to a growing family of reactions which allow for the regio- and stereo-controlled formation of several carbon–carbon bonds and/or ring systems in a single operation.[1] Cationic reactions that proceed in a domino fashion are featured in the biosynthesis of important natural products, and synthetic applications of both biomimetic and non-biomimetic cationic cyclizations have been widely developed.[2] Important contributions to this area have also been realized utilizing a combination of anionic, radical, carbenoid and transition metal-catalyzed processes.[3] The combination of a sequence of individually powerful methods often has a value significantly greater than the sum of the individual reactions and has become of great interest to the synthetic community. Corey has termed such a sequence as a tactical combination.[4]

In recent years, consecutive pericyclic reactions involving at least one cycloaddition have also been utilized for the synthesis of complex polycyclic ring systems.[5] In the realm of synthesis, in which a premium is put on the rapid construction of polyfunctional, highly bridged carbon and heteroatom networks, the [4 + 2]-cycloaddition has emerged as one of the foremost synthetic methods.[6] Well known and extensively studied for many decades, the Diels–Alder reaction is frequently employed for the construction of six-membered ring systems. The high regio- and stereo-selectivity typically displayed by this pericyclic process and the ease of execution have contributed toward its popularity. Carbon–carbon bond-forming reactions involving *N*-acyliminium ions play an extremely important role in the synthesis of nitrogen heterocycles. Speckamp[7] and Hart,[8] in particular, were the pioneers in this area, showing that *N*-acyliminium ions are valuable intermediates in the synthesis of a broad range of alkaloids. A combination of these two powerful synthetic methods would allow for the rapid, stereocontrolled synthesis of a variety of azapolycyclic products. This feature article describes some of our recent work in this area.

Cycloaddition of 1,3-oxazolium 4-oxides

In 1994 we started work in our laboratory to synthesize ring-fused polyheterocycles based on a *sequential cycloaddition/* N-*acyliminium ion cyclization process.*[9] These two types of reaction provide an opportunity for linking two disparate ring-forming reactions in a novel sequential manner. We believed that such a protocol would provide one-pot access to target molecules possessing a high degree of complexity which would otherwise require technically demanding multi-step syntheses. Our early studies showed that 1,3-oxazolium 4-oxides (isomünchnones) **2** can be generated by the rhodium(II)-catalyzed cyclization of a suitable diazo imide **1** (Scheme 1).[10] This type

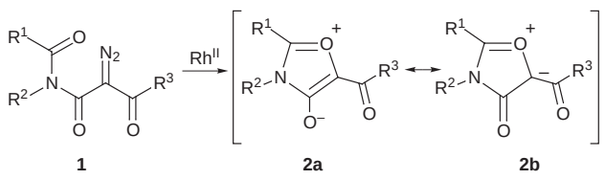

1 **2a** **2b**

Scheme 1

of mesoionic ylide corresponds to the cyclic equivalent of a carbonyl ylide and was found to readily undergo [4 + 2]-cycloaddition with suitable dipolarophiles.[10] Construction of the prerequisite diazo imides necessary for betaine generation was accomplished by the transformation of the corresponding carboxylic acids to their respective amides. Conversion to the diazo imides was straightforward using established malonylacylation and diazotization procedures.[11] Formation of the isomünchnone ring proceeds by initial generation of a rhodium carbenoid species, followed by an intramolecular cyclization onto the neighboring carbonyl oxygen to form the mesoionic ylide **2**.[10] The resultant isomünchnone may be trapped with electron-rich or electron-deficient dipolarophiles to give the cycloadducts in high yield. These uniquely functionalized cycloadducts (*i.e.* **5**) contain a 'masked' *N*-acyliminium ion which is generated by its treatment with a Lewis acid.[12] By incorporating an internal nucleophile on the tether, annulation of the original cycloadduct **5** allows for the construction of a more complex nitrogen heterocyclic system, particularly B-ring homologues of the erythrinane family of alkaloids. Starting from simple acyclic diazo imides **3**, we established a *domino carbenoid cyclization/[4 + 2]-cycloaddition/cationic* π-cyclization protocol as a method for the construction of complex nitrogen polyheterocycles of type **6** (Scheme 2). This

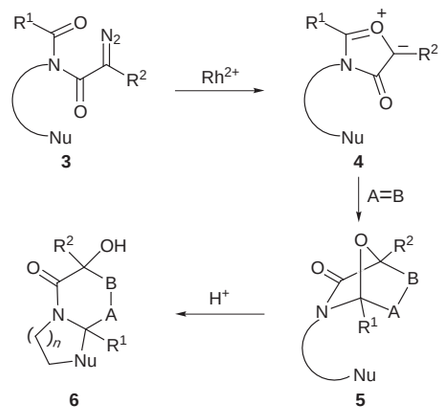

3 **4** **6** **5**

Scheme 2

sequence represents the first example where a [4 + 2]-cycloaddition and *N*-acyliminium ion cyclization are coupled in a one-pot sequence. The novelty of the process lies in the method of *N*-acyliminium ion generation, which to the best of our knowledge is unprecedented. *N*-Acyliminium ions are traditionally generated from the *N*-acylation of imines,[13]

N-protonation[14] and oxidation of amides,[15] electrophilic additions to enamides,[16] and the heterolysis of amides bearing a leaving group adjacent to nitrogen.[7] These reactive intermediates readily react with a wide assortment of nucleophiles to effect an overall α-amido alkylation.

An early application of the domino cascade process toward the construction of alkaloids involved the synthesis of (±)-lycopodine **11** (Scheme 3).[17] The isomünchnone cycloadduct **8** was

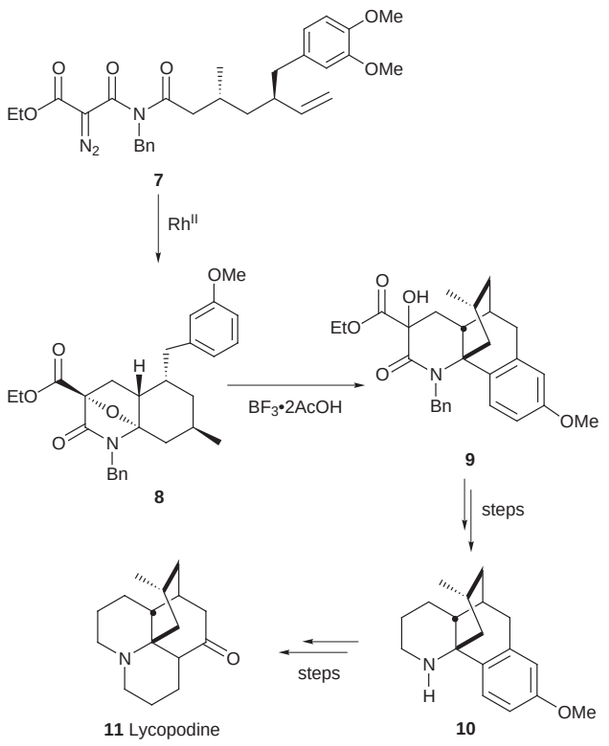

Scheme 3

formed from the Rh^{II}-catalyzed reaction of diazo imide **7** and was found to be the precursor of the key Stork intermediate **10** (*via* 9).[18] Our plan involved formation of **9** by a Pictet–Spengler cyclization of the *N*-acyliminium ion derived from **8**. Central to this strategy was the expectation that the bicyclic iminium ion originating from **8** would exist in a chair-like conformation.[18,19] Indeed, cyclization of the aromatic ring onto the *N*-acyliminium ion center readily occurred from the axial position.[20] The rearranged product **9** was then converted into the key intermediate previously used by Stork for the synthesis of (±)-lycopodine **11**.[18]

Application of the domino cyclization/cycloaddition sequence to the pentacyclic skeleton of the aspidosperma ring system

Prompted by our work dealing with the internal [4 + 2]-cycloaddition reaction of mesoionic oxazolium ylides,[10] we became interested in the rhodium(II)-catalyzed reactions of diazo ketoamides such as **12**. Attack of the amido oxygen at the rhodium carbenoid produced a carbonyl ylide dipole (*i.e.* **13**) that is isomeric with the isomünchnone class of mesoionic betaines **4**. We found that the rhodium(II)-catalyzed formation of carbonyl ylide intermediates derived from cyclic diazo amides furnished tetracycles such as **14b** in good yield, provided that the tether engaged in ring formation carried a carbonyl group (*i.e.* **12b**, X = O) (Scheme 4).[21]

Without the C=O functionality (*i.e.* **12a**, X = H), only decomposition products were observed. By performing *ab initio* transition state geometry optimizations, we learned that a severe

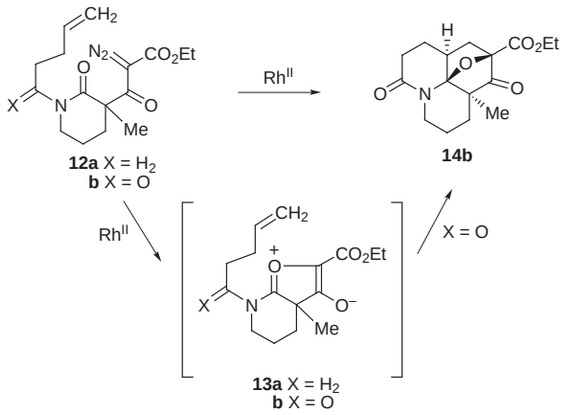

Scheme 4

cross-ring 1,3-diaxial interaction caused by the bridgehead methyl group promoted a boat or twist-boat conformation in the piperidine ring fused to the newly forming one.[21] The presence of a carbonyl group on the tether apparently helps to relieve the steric congestion by favoring a second boat conformation in the latter ring. When the side chain is devoid of a carbonyl group, the calculated reaction barrier is much larger, thereby permitting competing processes to intervene. Thus, the reactivity discrepancy between diazo amido esters **12a** and **12b** can be attributed to steric effects in the transition states.[21]

As an extension of these studies, we have developed a fundamentally new approach to the construction of the pentacyclic skeleton of the aspidosperma ring system which involves a related domino cascade sequence.[22] This strategy was successfully applied to the synthesis of desacetoxy-4-oxo-6,7-dihydrovindorosine **15**. The approach used is outlined in Scheme 5 and is centered on the construction of the key oxabicyclic intermediate **16**. We reasoned that **15** should be accessible by reduction of the *N*-acyliminium ion derived from **16**, which, by analogy with our previous work, should be available by the *tandem rhodium*(II)-*catalyzed cyclization/cycloaddition* of α-diazoimide **17**. Cycloaddition of the initially formed dipole across the pendant indole π-system[23] would be expected to result in the simultaneous generation of the CD-rings of the aspidosperma skeleton.[24] The stereospecific nature of the internal cycloaddition reaction should also lead to the correct relative stereochemistry of the four chiral centers about the C-ring. In a recent publication, we described our results which verified the underlying viability of this approach to the aspidosperma skeleton (Scheme 5).[22]

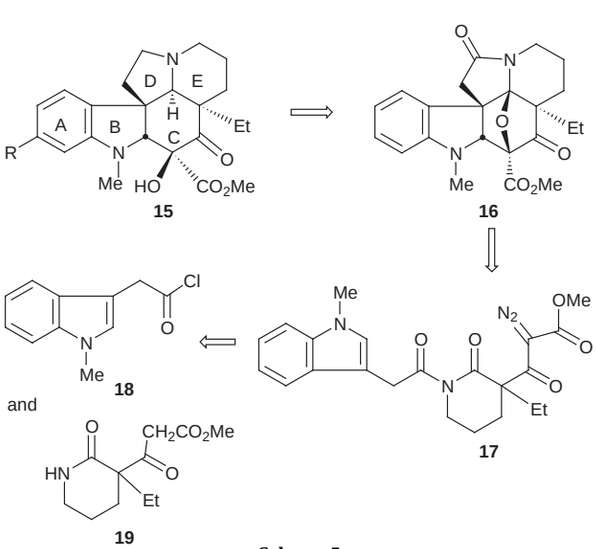

Scheme 5

The 2-aminofuran Diels–Alder strategy

In the next phase of our work, we decided to reconsider some aspects of our domino cascade strategy. It occurred to us that we could also utilize a series of 2-amino-substituted furans for the critical [4 + 2]-cycloaddition step rather than the highly reactive 1,3-dipole, which on occasion was prone to undergo hydrolytic decomposition.[10] Our long-range goal involved using 2-amino-substituted furans such as **20** that contain both a suitable leaving group (LG) and an olefinic tether to allow for an intramolecular Diels–Alder reaction (Scheme 6). The resultant cycloadduct

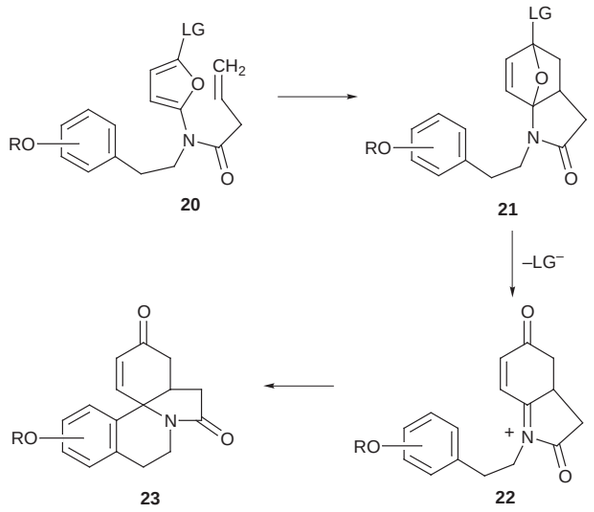

Scheme 6

was expected to undergo ring opening to generate a vinylogous *C*-acyliminium ion of type **22**. Our intention was to use this sequence of reactions for a rapid entry into the erythrinane family of alkaloids. With this goal in mind, some model studies were undertaken to determine the facility with which 2-amino-furans would undergo Diels–Alder cycloadditions.[25]

Heterocycles such as furan, thiophene and pyrrole undergo Diels–Alder reactions despite their stabilized 6π-aromatic electronic configuration.[26] By far the most extensively studied heteroaromatic system for Diels–Alder cycloaddition is furan and its substituted derivatives.[26] The resultant 7-oxabicyclo[2.2.1]heptanes are valuable synthetic intermediates that have been further elaborated to substituted arenes, carbohydrate derivatives and various natural products.[26] A crucial synthetic transformation employing these intermediates involves the cleavage of the oxygen bridge to produce functionalized cyclohexene derivatives.[27] In many cases, however, this strategy is not feasible because of the low reactivity of furan toward monoactivated dienophiles. Lewis acid catalysis, interaction with metals, or use of high pressure helps to overcome the sluggishness of furan toward Diels–Alder cycloaddition.[26] MO calculations show that the presence of an electron-donating substituent such as an amino group in the 2-position of the furan nucleus increases its HOMO energy relative to that of furan.[28] A significant increase in the HOMO coefficient at the C-5 position compared to that at the C-2 position also occurs, consistent with an increase in electron density at that position due to resonance interaction with the amino substituent. In this regard, we have recently demonstrated that simple 2-aminofurans such as **24** react with various dienophiles in an intermolecular fashion with high regioselectivity.[28] The initial cycloadducts were not isolated, as they readily undergo ring opening to cyclohexadienols **26**, assisted by the lone pair of electrons on the adjacent nitrogen atom (Scheme 7). The influence of the amino group is evident by the extremely facile cleavage of the oxybridge intermediates under the thermal conditions used in the reaction. This behavior stands in contrast to the related oxabicyclic system **28**, which was reported to undergo ring

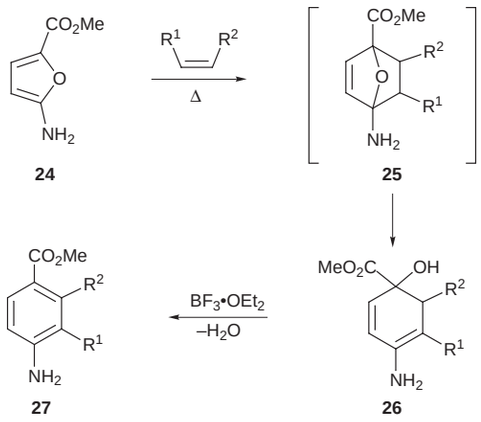

Scheme 7

cleavage only when treated with acetic acid at elevated temperatures (125 °C) (Scheme 8).[29]

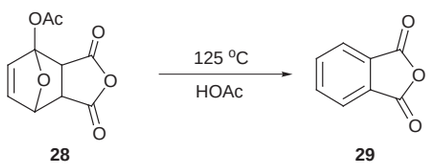

Scheme 8

IMDAF Cycloaddition as a method for the preparation of pyrrolophenanthridine alkaloids

The intramolecular Diels–Alder reaction of furans, often designated as IMDAF, helps to overcome the sluggishness of this heteroaromatic ring system toward [4 + 2]-cycloaddition.[26] Not only do IMDAF reactions allow for the preparation of complex oxygenated polycyclic compounds, they often proceed at lower temperatures than their intermolecular counterparts.[30] Even more significantly, unactivated π-bonds are often suitable dienophiles for the internal cycloaddition. While the carbocyclic IMDAF reaction has been the subject of many reports in the literature, much less is known regarding the cycloaddition behavior of furan Diels–Alder systems that contain heteroatoms. Even more rare are examples in which the heteroatom is directly attached to the furan ring.[25] In an effort to investigate the scope of these reactions, a number of new furan substrates were prepared in our laboratory and tested for the *cycloaddition/cyclization* cascade. Tethered amidofurans **30** and **31** were easily synthesized starting from aminofuran **24** and pent-4-enoyl chloride. The thermal reaction of **30** at 200 °C for 24 h afforded tetrahydroquinolinone **32** in 66% yield. Likewise, heating a sample of the *N*-methylated analog **31** at 160 °C furnished a 6 : 1-mixture of cyclohexadienol **33** (77%) and tetrahydroquinoline **34** (13%), the former being easily converted to **34** by treatment with $BF_3 \cdot OEt_2$. In both cases, the initial cycloadducts were not isolated, as they readily underwent ring opening, assisted by the lone pair of electrons on the adjacent nitrogen (Scheme 9).

During the course of our studies we have found that the IMDAF cycloadditions of furanamides such as **35** can also be performed by using 4 M ethereal $LiClO_4$ as solvent.[31] Under these conditions, furanamide **35** underwent cycloaddition at a much lower temperature and in higher yield than under strictly thermal conditions. The major product formed corresponded to cyclohexenone **38**. This reaction presumably involves an initial [4 + 2]-cycloaddition to give **36** followed by a rapid ring opening to afford iminium ion **37** which is subsequently converted to **38** upon reaction with water (Scheme 10). The Grieco conditions[31] were also successfully employed using the unactivated four-carbon tethered furanamide **39** which gave dihydroindole **40** in 73% isolated yield.

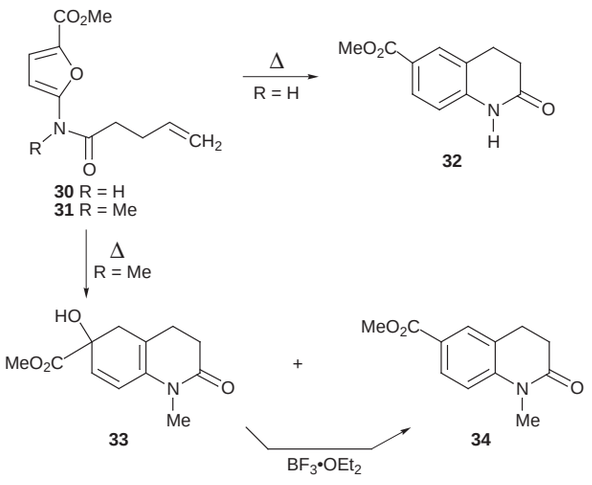

Scheme 9

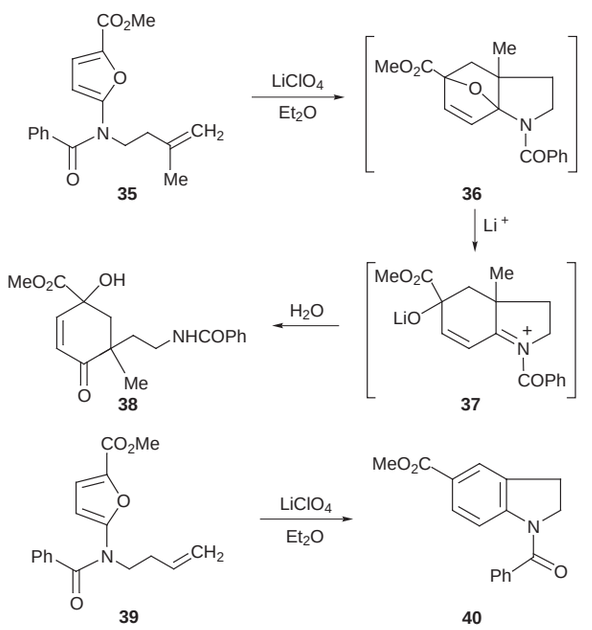

Scheme 10

Having established the suitability of 2-amidofurans to generate dihydroindoles, we turned our attention to the application of the method toward the synthesis of oxoassoanine[32] **42** and anhydrolycorin-7-one **43**.[33] These compounds are

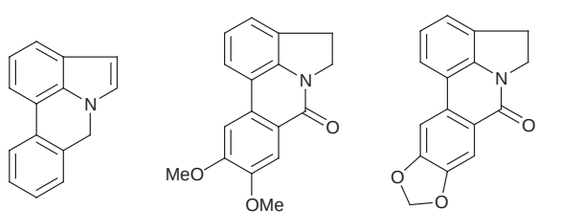

members of the pyrrolophenanthridine class of alkaloids which have been isolated from various species of amaryllidaceae.[34] The 1*H*-pyrrolo[3,2,1-*de*]phenanthridine ring system **41** constitutes the core structural framework of the pyrrolophenanthridine alkaloids. Although a number of synthetic routes are available for this ring system, many of these suffer from low yields and lack generality.[35] A short synthesis of **42** and **43** was carried out as depicted in Scheme 11. This approach is centered

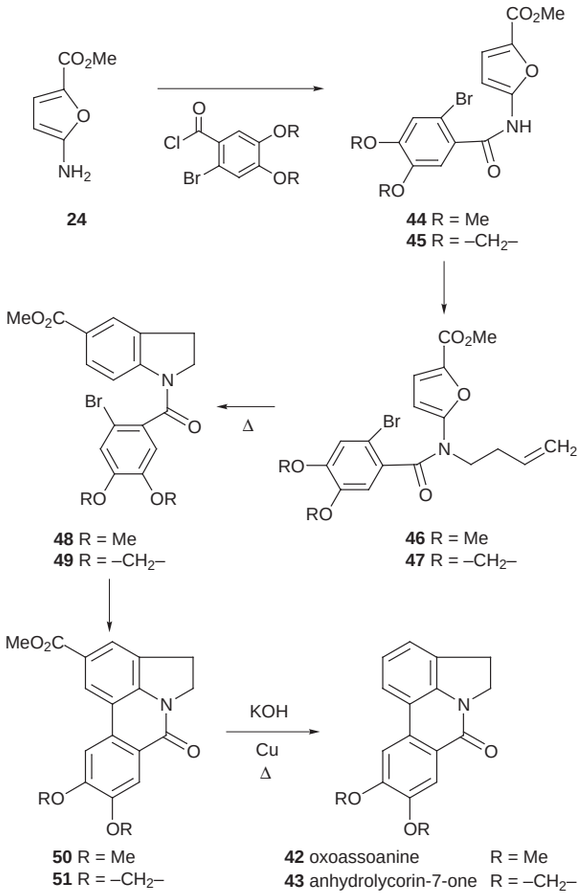

Scheme 11

on the construction of the key dihydroindoles **48** and **49** which are formed by a IMDAF cycloaddition followed by subsequent nitrogen atom lone pair assisted ring opening of the initially formed oxa-bridged cycloadducts. After some experimentation, it was found that using bis(tributyltin) under photochemical conditions afforded the aryl-coupled products **50** and **51** in high yield from the corresponding dihydroindoles **48** and **49**. Both compounds were converted to the natural products by a saponification-decarboxylation protocol.

The domino Pummerer Diels–Alder sequence

Much of the chemistry utilized in the two preceding sections relied on our ability to synthesize the requisite 2-aminofurans. One limitation of the method is that sometimes the 2-aminofuran system is not easily accessible. In the context of our studies dealing with *domino cycloaddition/Mannich cyclizations*, we discovered that the Pummerer reaction can be effectively utilized to prepare the required furans.[36] α-Acyl thionium ions generated from α-acyl sulfoxides under Pummerer conditions are powerful electrophiles, reacting efficiently with nucleophilic carbon species.[37] Bimolecular addition of the cation to various carbon–carbon double bonds is well known.[38] In the realm of natural product synthesis, most success has been achieved using intramolecular Friedel–Crafts cyclization of the Pummerer thionium ion intermediate.[39] Far fewer examples exist for heteroatom interception of the Pummerer intermediate.[40] De Groot and co-workers recently developed an efficient procedure for butenolide formation in which the key step involves a Pummerer induced cyclization of aldehydic sulfoxides of type **52** into butenolides **54** (Scheme 12).[41] It was assumed that the neighboring carbonyl group attacks the initially formed thionium ion to give an oxy-stabilized cation **53** which loses a proton to generate a 2-thio-substituted furan

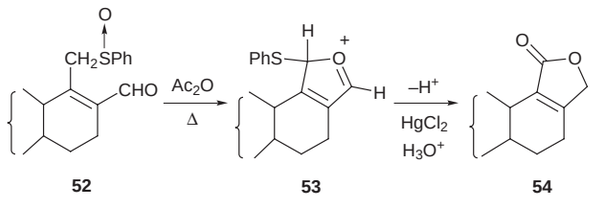

Scheme 12

which is subsequently converted to the butenolide upon hydrolysis. On the basis of this transformation we decided to explore the internal trapping of the Pummerer cation with adjacent carbonyl groups as a method to prepare a variety of substituted furans. The strategy was first tested on keto sulfoxide **55** (Scheme 13). The α-thiocarbocation derived from

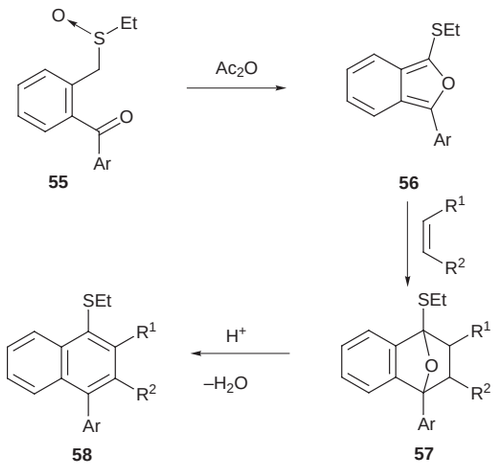

Scheme 13

the Pummerer reaction of **55** was readily intercepted by the adjacent keto group to produce isobenzofuran **56** as a transient intermediate which underwent a subsequent Diels–Alder cycloaddition with an added dienophile. The resulting cycloadduct **57** was readily converted to representatives of several types of arylnaphthalene lignans.[42]

As heteroaromatic isobenzofuran analogs have not been extensively studied in the literature, we focused our attention on the Pummerer reaction of several *o*-heteroaroyl substituted sulfoxides as a method to generate reactive heteroaromatic *o*-xylylenes. Most notable among the heteroaromatic isobenzofurans **60** reported in recent years are the furo[3,4-*b*]furans,

thieno[2,3-*c*]furans, furo[3,4-*d*]isoxazoles and furo[3,4-*b*]indoles.[43] These 10π-systems are isoelectronic with the pentalene dianion and have been of some theoretical interest.[43] MO calculations on these heteroisobenzofurans indicate that they possess little or no aromatic character, and this is reflected in their high chemical reactivity.[43] Using the *domino Pummerer/Diels–Alder sequence* we were able to synthesize several thieno[2,3-*c*]furans and furo[3,4-*b*]indoles.[44] In the presence of a suitable dienophile, the reactive *o*-xylylene underwent [4 + 2]-cycloaddition followed by an acid-catalyzed ring-opening and aromatization to give heteroaromatic naphthalene derivatives (Scheme 14). The *domino Pummerer cyclization/cycloaddition sequence* also occurred intramolecularly using unactivated alkenyl tethers of variable length. The results clearly indicate that the domino cascade process is a powerful method for the construction of complex heteroaromatic *o*-quinodimethanes.

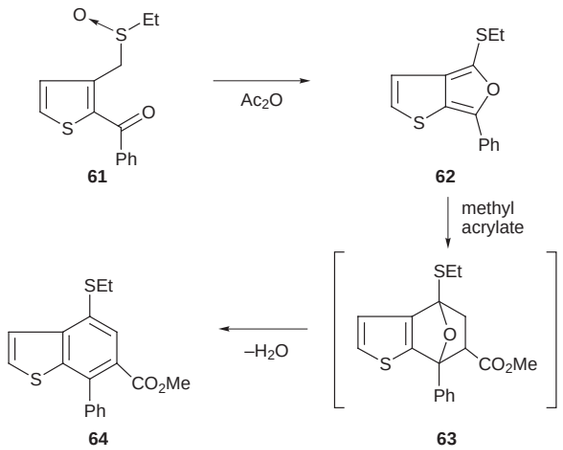

Scheme 14

Cycloaddition/ring opening/elimination sequence of 2-amino substituted isobenzofurans

Prompted by the above results, we became interested in extending the Pummerer-promoted cyclization reaction to *o*-amido-substituted sulfoxides since this would allow for the rapid stereocontrolled synthesis of a variety of azapolycyclic products. Indeed, the *domino Pummerer/Diels–Alder* sequence readily afforded 2-amino-substituted isobenzofurans as transient species which were too labile to isolate but underwent rapid [4 + 2]-cycloaddition with added dienophiles.[45] When dimethyl acetylenedicarboxylate (DMAD) was used as the trapping agent, the initially formed iminium ion **68** could not undergo proton loss (Scheme 15). Instead, **68** rearranged by means of a 1,2-ethylthio shift to afford the tetralone derivative **69**. Compound **69** was converted to naphthol **70** in high yield upon further heating. This process presumably proceeds by elimination of thioacetaldehyde in a hetero-retro-ene fashion, for which there is ample precedence in the literature.[46]

In order to access synthetically more valuable targets, we focused our attention on an intramolecular variation of the *domino amido-Pummerer/Diels–Alder reaction sequence.* The one-pot intramolecular cascade process occurred smoothly when the olefin tether was activated by an ester or when a carbonyl group was located adjacent to the nitrogen atom of the 2-amino-substituted isobenzofuran (Scheme 16).[45] The intramolecular cycloaddition behavior of the incipient isobenzofurans in response to the presence of a C=O group is striking. Five- and six-membered ring precursors **71a** and **71b** delivered cyclized products bearing a carbonyl within the newly formed rings in good to excellent yields. Externalization of the C=O as in **73** likewise led to a facile internal cyclization. Removal of the C=O functionality, however, suppressed intramolecular cycloaddition in favor of the traditional Pummerer reaction. The amine-amide effect is not limited to isobenzofurans. In our previous study of the intramolecular cycloaddition of carbonyl ylide dipoles and tethered alkenyl π-bonds, a similar phenomenon was observed (*i.e.* **12** → **14**).[21] Intermediates with carbonyl groups in the tether provided cycloaddition products; those lacking the C=O group failed to cyclize. The reactivity discrepancy in both cases can be traced to steric effects in the transition states. The incorporation of an amido group is clearly of synthetic advantage as it offers the opportunity to accelerate intramolecular cycloaddition by steric adjustment of ground state and transition state energies either separately or simultaneously. Both examples underscore the unexpected complexity of intramolecular cycloaddition processes that create several fused rings in a domino cascade and simultaneously induce steric effects remote from the reacting centers. Amide tethers have

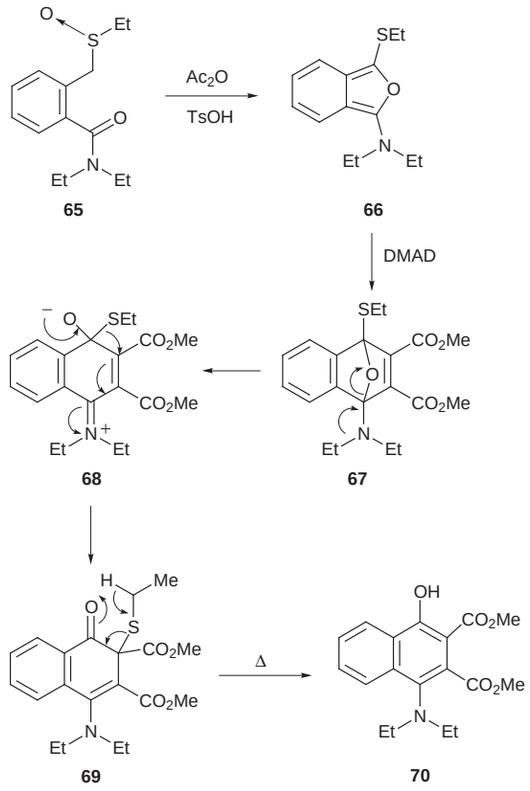

65 **66** **67** **68** **69** **70**

Scheme 15

emerged as remote-site promoters of intramolecular cycloaddition for tandem processes yielding products containing multiple fused rings.

Triple cascade sequence for construction of the erythrinane alkaloid skeleton

Having established the facility with which *N*-acyliminium ions can be formed from the Pummerer reaction of *o*-amido-substituted sulfoxides, we next focused our attention on the final cyclization step of the proposed cascade process (*i.e.* **22** → **23** in Scheme 6).[47] In order to avoid the deprotonation (aromatization) step, we prepared sulfoxides **75** and **76**, each possessing a

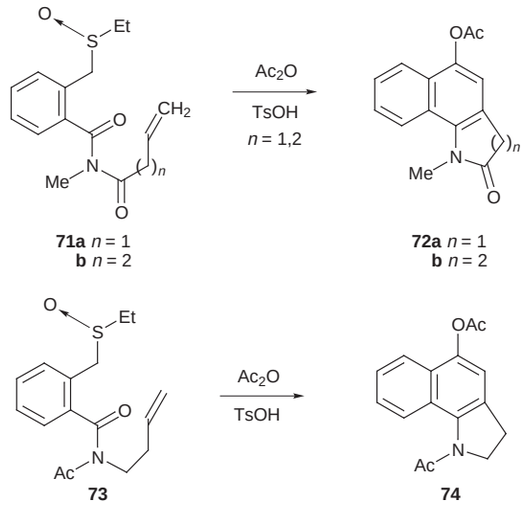

71a *n* = 1
b *n* = 2

72a *n* = 1
b *n* = 2

73 **74**

Scheme 16

methoxycarbonyl group attached to the olefin tether. This substituent was selected not only to prevent deprotonation, but also because the presence of an electron-withdrawing group on the double bond enhances [4 + 2]-cycloaddition based on FMO considerations. *N*-Acyliminium ion **78** derived from the internal cycloadduct **77** underwent stereoselective spirocyclization to furnish the *cis*-3,4-benzoerythrinane **79** or homoerythrinane derivative **80** in good yield (Scheme 17). The overall triple cascade sequence represents an efficient one-pot approach towards the erythrinane alkaloid skeleton[34] in which the spirocyclic ABC skeleton is assembled in a single operation.

At this point, we decided to undertake a synthesis of (±)-erysotramidine **90** in order to further test the viability of the triple cascade process as an entry into the erythrinane skeleton.[34] The requisite starting imido sulfoxide **81**, possessing both a dienophilic and diactivated aromatic π-tether, was efficiently synthesized from known starting materials. Subjection of **81** to the Pummerer conditions gave compound **87** as a single diastereomer in 83% yield. The *cis* A/B ring fusion present in **87** was unequivocally established by an X-ray crystallographic analysis and is identical to the stereochemical relationship found in the naturally occurring erythrina alkaloids. The conversion of **81** into **87** is believed to follow the pathway

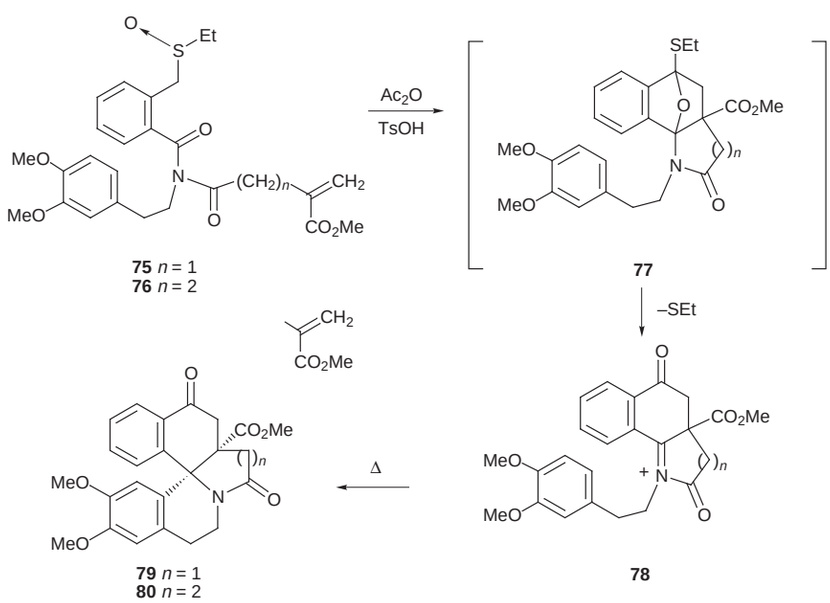

75 *n* = 1
76 *n* = 2

77

78

79 *n* = 1
80 *n* = 2

Scheme 17

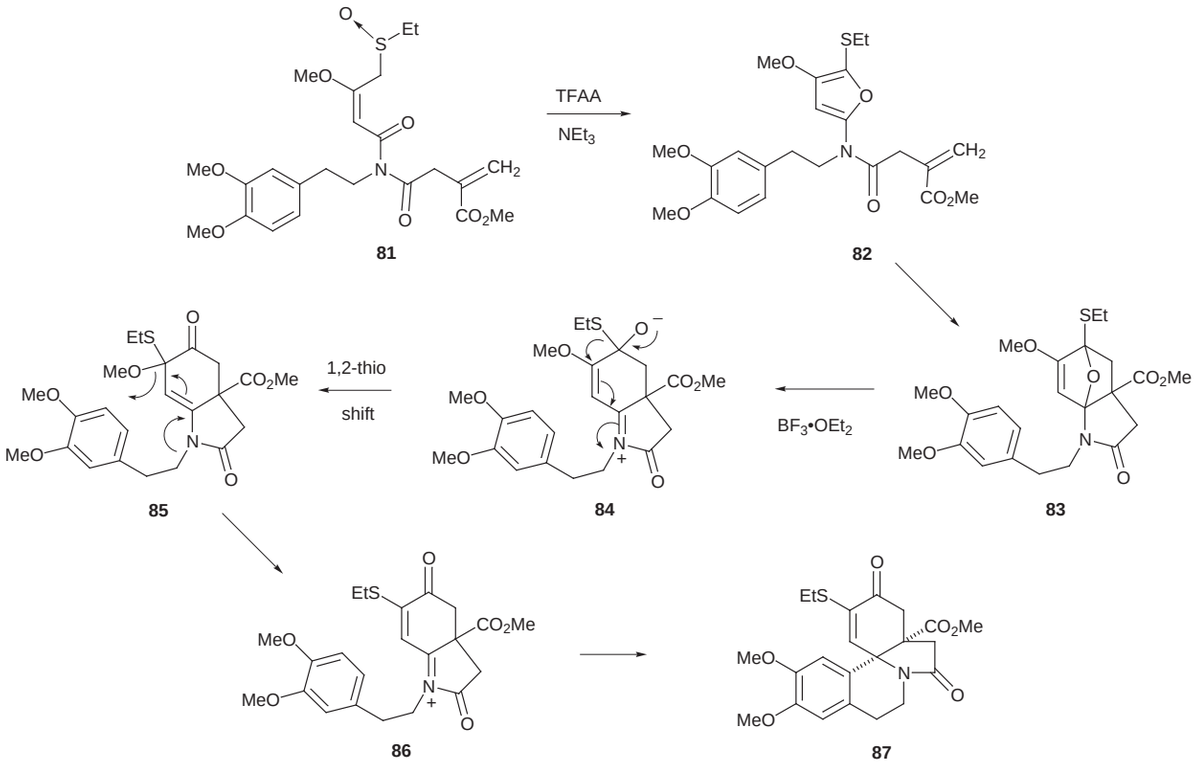

Scheme 18

outlined below (Scheme 18). The initially formed α-thiocarbocation intermediate generated from the Pummerer reaction of **81** is intercepted by the adjacent imido carbonyl to produce the α-amido substituted furan **82**. This transient intermediate undergoes a subsequent intramolecular Diels–Alder cycloaddition across the tethered π-bond to furnish cycloadduct **83**. Nitrogen-assisted ring opening of the oxabicyclic bridge results in the formation of zwitterionic intermediate **84** which undergoes a 1,2-thioethyl shift followed by methoxide ion ejection. Cyclization of the diactivated aromatic tether onto *N*-acyliminium ion **86** ultimately provides the tetracyclic amide **87**.

With a supply of **87** in hand, this enone was converted into the corresponding vinyl triflate which, in turn, was subjected to a palladium-catalyzed formate reduction to give **88**. The resulting thio-substituted diene was subsequently transformed into ketone **89** *via* a titanium mediated hydrolysis.[48] The present sequence constitutes a formal synthesis of (±)-erysotramidine **90** based on the successful conversion of **89** into **90** by Tsuda.[49]

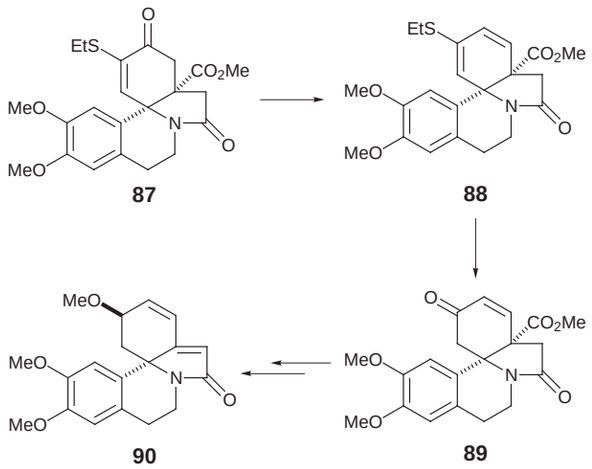

Scheme 19

Concluding remarks

Over the past four years we have shown that many structurally diverse heterocyclic compounds can be readily accessed *via* the *domino cycloaddition*/N-*acyliminium ion cyclization cascade*. The key step in this process involves the generation of a reactive *N*-acyliminium ion by fragmentation of an amino substituted [4 + 2]-cycloadduct. This triple cascade is applicable toward the preparation of a broad range of alkaloids. It is a reasonable expectation that future years will see a continued evolution of this unique domino cascade toward other synthetic targets.

Acknowledgments

I thank my enthusiastic and gifted co-workers, whose names appear in the appropriate references, and the National Institute of Health for financial support.

Albert Padwa is the William Patterson Timmie Professor of Chemistry at Emory University. Before that he was on the faculty at Ohio State University (1963–1966) and the State University of New York at Buffalo (1966–1979). He has held visiting positions at University Claude Bernard, France (1978), University of California at Berkeley (1982), the University of Wurzburg, Germany (1985) and Imperial College, UK (1990). Professor Padwa has been the recipient of an Alfred P. Sloan Fellowship (1968–1970), John S. Guggenheim Fellowship (1981–1982), Alexander von Humboldt Senior Scientist Award (1983–1985) and a Fulbright Hays Scholarship (1990). He was elected as the Chairman of the Organic Division of the ACS (1985–1986) and more recently served as president of the International Society of Heterocyclic Chemistry (1994–1996). He has also served as a member of the editorial board of the Journal of the American Chemical Society, Journal of Organic Chemistry, Heterocyclic Communications, Internet Journal of

Chemistry and has been the volume editor of Comprehensive Heterocyclic Chemistry. He is the coauthor of more than 520 publications. His research interests include heterocyclic chemistry, reactive intermediates, dipolar cycloadditions, alkaloid synthesis and transition metal chemistry. Aside from Chemistry, his other passion is mountain climbing in South America.

Notes and References

E-mail: chemap@emory.edu

1 T.-L. Ho, *Tandem Organic Reactions*, Wiley-Interscience, New York, 1992; *Frontiers in Organic Synthesis*, *Chem. Rev.*, 1996, **96**, pp. 1–600; L. F. Tietze and U. Beifuss, *Angew. Chem., Int. Ed. Engl.*, 1993, **32**, 131.

2 J. K. Sutherland, in *Comprehensive Organic Synthesis*, ed. B. M. Trost and I. Fleming, Pergamon, Oxford, 1991, vol. 3, p. 341.

3 P. Canonne, R. Boulanger and M. Bernatchez, *Tetrahedron Lett.*, 1987, **28**, 4997; D. P. Curran, in *Comprehensive Organic Synthesis*, ed. B. M. Trost and I. Flemming, Pergamon, Oxford, 1991, vol. 4, ch. 4.2; H. M. L. Davies, T. J. Clark and H. D. Smith, *J. Org. Chem.*, 1991, **56**, 3817; R. Grigg, P. Kennewell and A. J. Teasdale,. *Tetrahedron Lett.*, 1992, **33**, 7789.

4 E. J. Corey and X. M. Cheng, *The Logic of Chemical Synthesis*, Wiley-Interscience: New York, 1989, p. 31.

5 S. E. Denmark and A. Thorarensen, *Chem. Rev.*, 1996, **96**, 137.

6 J. D. Winkler, *Chem. Rev.*, 1996, **96**, 167; W. R. Roush, in *Comprehensive Organic Synthesis*, ed. B. M. Trost, Pergamon, New York, 1991, vol. 5, p. 513; *1,3-Dipolar Cycloaddition Chemistry*, ed. A. Padwa, Wiley-Interscience, New York, 1984, vols. I and II.

7 H. Hiemstra and W. N. Speckamp, in *Comprehensive Organic Synthesis*, ed. B. M. Trost and I. Fleming, Pergamon, Oxford, 1991, vol. 2, pp. 1047–1082; W. N. Speckamp and H. Hiemstra, *Tetrahedron*, 1985, **41**, 4367.

8 D. J. Hart, *J. Org. Chem.*, 1981, **46**, 367; D. J. Hart, *J. Org. Chem.*, 1981, **46**, 3576; D. J. Hart and K. Kanai, *J. Org. Chem.*, 1982, **47**, 1555; D. J. Hart and and T. K. Yang, *Tetrahedron Lett.*, 1982, **23**, 2671; D. J. Hart and K. Kanai, *J. Am. Chem. Soc.*, 1983, **105**, 1255.

9 J. P. Marino, Jr., M. H. Osterhout, A. T. Price, M. A. Semones and A. Padwa, *J. Org. Chem.*, 1994, **59**, 5518.

10 A. Padwa and M. D. Weingarten, *Chem. Rev.*, 1996, **96**, 223; A. Padwa, J. P. Marino, Jr. and M. H. Osterhout, *J. Org. Chem.*, 1995, **60**, 2704; A. Padwa, D. L. Hertzog, W. R. Nadler, M. H. Osterhout and A. T. Price, *J. Org. Chem.*, 1994, **59**, 1418; D. L. Hertzog, D. J. Austin, W. R. Nadler and A. Padwa, *Tetrahedron Lett.*, 1992, **33**, 4731; M. H. Osterhout, W. R. Nadler and A. Padwa, *Synthesis*, 1994, 123.

11 M. Sato, N. Kanuma and T. Kato, *Chem. Pharm. Bull.*, 1982, **30**, 1315; M. Regitz, J. Hocker and A. Leidhergener, *Org. Synth.*, 1973, **Coll. Vol. V**, 179.

12 A. Padwa, M. A. Brodney, J. P. Marino, Jr., M. H. Osterhout and A. T. Price, *J. Org. Chem.*, 1997, **62**, 67.

13 H. Böhme and K. Hartkke, *Chem. Ber.*, 1963, **96**, 600; H. Hiemstra, H. P. Fortgens, S. Stegenga and N. W. Speckamp, *Tetrahedron Lett.*, 1985, **26**, 3151.

14 S. M. Weinreb and J. I. Levin, *Heterocycles*, 1979, **12**, 949; S. Jendrzejewski and W. Steglich, *Chem. Ber.* 1981, **114**, 1337.

15 T. Shono, H. Hamaguchi and Y. Matsumura, *J. Am. Chem. Soc.*, 1975, **97**, 4264.

16 V. M. Csizmadia, K. M. Koshy, K. C. M. Lau, R. A. McClelland, V. J. Nowlan and T. T. Tidwell, *J. Am. Chem. Soc.*, 1979, **101**, 974; A. Brossi, L. A. Dolan, and S. Teital, *Org. Synth.*, 1977, **56**, 3.

17 A. Padwa, M. A. Brodney, J. P. Marino, Jr. and S. M. Sheehan, *J. Org. Chem.*, 1997, **62**, 78.

18 G. Stork, R. A. Kretchmer, and R. H. Schlessinger, *J. Am. Chem. Soc.*, 1968, **90**, 1647; G. Stork, *Pure Appl. Chem.*, 1968, **17**, 383.

19 C. H. Heathcock, E. Kleinman and E. S. Binkley, *J. Am. Chem. Soc.*, 1978, **100**, 8036.

20 A. Mondon, K. F. Hansen, K. Boehme, H. P. Faro, J. H. Nestler, H. G. Vilhuber and K. Böttcher, *Chem. Ber.*, 1970, **103**, 615; A. Mondon and P. R. Seidel, *Chem. Ber.*, 1971, **104**, 2937; A. Mondon, and H. J. Nestler, *Chem. Ber.*, 1979, **112**, 1329.

21 M. D. Weingarten, M. Prein, A. T. Price, J. P. Snyder and A. Padwa, *J. Org. Chem.*, 1997, **62**, 2001.

22 A. Padwa, and A. T. Price, *J. Org. Chem.*, 1995, **60**, 6258; A. Padwa and A. T. Price, *J. Org. Chem.*, 1998, **63**, 556.

23 A. Padwa, D. L. Hertzog and W. R. Nadler, *J. Org. Chem.*, 1994, **59**, 7072.

24 G. A. Cordell, in *The Alkaloids*, ed. R. H. F. Manske and R. G. A. Rodrigo, Academic Press, New York, 1979, vol. 17, pp. 199–384; J. E. Saxton, *Nat. Prod. Rep.*, 1993, **10**, 349; 1994, **11**, 493.

25 For some examples of amino-substituted furan Diels–Alder reactions, see J. E. Cochran, T. Wu and A. Padwa, *Tetrahedron Lett.*, 1996, **37**, 2903; R. H. Schlessinger and C. P. Bergstrom, *Tetrahedron Lett.*, 1996, **37**, 2133; R. H. Schlessinger, X. H. Wu, and T. R. R. Pettus, *Synlett*, 1995, 536; R. H. Schlessinger, T. R. R. Pettus, J. P. Springer and K. Hoogsteen, *J. Org. Chem.*, 1994, **59**, 3246; R. H. Schlessinger and C. P. Bergstrom, *J. Org. Chem.*, 1995, **60**, 16.

26 C. O. Kappe, S. S. Murphree and A. Padwa, *Tetrahedron*, 1997, **53**, 14179; S. Woo, and B. Keay, *Synthesis*, 1996, 669; F. M. Dean, *Adv. Heterocycl. Chem.*, 1981, **30**, 168.

27 P. Chiu and M. Lautens, *Top. Curr. Chem.*, 1997, **190**, 1.

28 A. Padwa, M. Dimitroff, A. G. Waterson and T. Wu, *J. Org. Chem.*, 1997, **62**, 4088.

29 M. P. Cava, C. L. Wilson and C. J. Williams, *J. Am. Chem. Soc.*, 1956, **78**, 2303.

30 D. D. Sternbach, D. M. Rossana and K. D. Onan, *J. Org. Chem.*, 1984, **49**, 3427; M. E. Jung and J. Gervey, *J. Am. Chem. Soc.*, 1989, **111**, 5469; L. L. Klein, *J. Org. Chem.*, 1985, **50**, 1770.

31 P. A. Grieco, *Aldrichim. Acta*, 1991, **24**, 61; P. A. Grieco, J. J.; Nunes, and M. D. Gaul, *J. Am. Chem. Soc.*, 1990, **112**, 4595; H. Waldman, *Angew. Chem., Int. Ed. Engl.*, 1991, **30**, 1306.

32 J. M. Llabres, F. Viladomat, J. Bastida, C. Codina and M. Rubiralta, *Phytochemistry*, 1986, **25**, 2637.

33 S. Ghosal, P. H. Rao, D. K. Jaiswal, Y. Kumar and A. W. Frahm, *Phytochemistry* 1985, **24**, 1825; D. Perez, G. Bures, E. Guitian, and L. Castedo, *J. Org. Chem.*, 1996, **61**, 1650.

34 R. K. Hill, in *The Alkaloids*, ed. R. H. F. Manske, Academic Press, New York, 1967, vol. 9, p. 483.

35 R. H. Hutchings and A. I. Meyers, *J. Org. Chem.*, 1996, **61**, 1004 and references cited therein.

36 O. DeLucchi, U. Miotti and G. Modena, *Organic Reactions*, ed. L. A. Paquette, Wiley, 1991, ch. 3, pp. 157–184.

37 D. S. Grierson and H. P. Husson, in *Comprehensive Organic Synthesis*, ed. B. M. Trost, Pergamon, Oxford, 1991, vol. 6, pp. 909–947.

38 M. Kennedy and M. A. McKervey in *Comprehensive Organic Synthesis*, ed. B. M. Trost, Pergamon, Oxford, 1991, vol. 7, pp. 193–216.

39 P. D. Magnus, T. Gallagher, P. Brown and J. C. Huffman, *J. Am. Chem. Soc.*, 1984, **106**, 2105; P. Magnus, M. Giles, R. Bonnert, G. Johnson, C. McQuire, M. Deluca, A. Merrit, C. S. Kim and N. Vicker, *J. Am. Chem. Soc.*, 1993, **115**, 8116.

40 A. Padwa, D. E. Gunn and M. H. Osterhout, *Synthesis*, 1997, 1353.

41 A. De Groot and B. J. M. Jansen, *J. Org. Chem.*, 1984, **49**, 2034; B. J. M. Jansen, C. T. Bouwman and A. De Groot, *Tetrahedron Lett.*, 1994, **35**, 2977.

42 J. E. Cochran and A. Padwa, *Tetrahedron Lett.*, 1995, **36**, 3495; J. E. Cochran and A. Padwa, *J. Org. Chen.*, 1995, **60**, 3938; A. Padwa, J. E. Cochran, C. O. Kappe, *J. Org. Chem.*, 1996, **61**, 3706.

43 W. Eberbach, H. Fritz and N. Laber, *Angew. Chem., Int. Ed. Engl.*, 1988, **27**, 568; A. Schönig, T. Debaerdemaeker, M. Zander and W. Friedrichsen, *Chem. Ber.*, 1989, **122**, 1119; L. Aßmann, L. Palm, M. Zander and W. Friedrichsen, *Chem. Ber.*, 1991, **124**, 2481; G. W. Gribble, D. J. Keavy, D. A. Davis, M. G. Saulnier, B. Pelcman, T. C. Barden, M. P. Sibi, E. R. Olson and J. BelBruno, *J. Org. Chem.*, 1992, **57**, 5878.

44 C. O. Kappe and A. Padwa, *J. Org. Chem.*, 1996, **61**, 6166.

45 A. Padwa, C. O. Kappe, J. E. Cochran and J. P. Snyder, *J. Org. Chem.*, 1997, **62**, 2786.

46 J. L. Ripoll and Y. Vallee, *Synthesis*, 1993, 659.

47 A. Padwa, C. O. Kappe and T. S. Reger, *J. Org. Chem.*, 1996, **61**, 4888; A. Padwa, R. Hennig, C. O. Kappe and T. S. Reger, *J. Org. Chem.*, 1988, **63**, in the press.

48 T. Mukaiyama, K. Kamio, S. Kobayashi and H. Takei, *Bull. Chem. Soc. Jpn.*, 1972, **45**, 3723.

49 Y. Tsuda, S. Hosoi, A. Nakai, Y. Sakai, T. Abe, Y. Ishi, F. Kiuchi and T. Sano, *Chem. Pharm. Bull.*, 1991, **39**, 1365.

8/01467A

Nanosized rhodium oxide particles in the MCM-41 mesoporous molecular sieve

Ravichandra S. Mulukutla,[a] Kiyotaka Asakura,[b] Seitaro Namba[c] and Yasuhiro Iwasawa*[a]†

[a] *Department of Chemistry, Graduate School of Science, The University of Tokyo, Hongo, Bunkyo-Ku, Tokyo 113-0033, Japan*
[b] *Research Center for Spectrochemistry, Graduate School of Science, The University of Tokyo, Hongo, Bunkyo-Ku, Tokyo 113-0033, Japan*
[c] *Department of Materials, Teikyo University of Science and Technology, Uenohara-machi, Kitatsuru-gun, Yamanashi 409-0193, Japan*

Nanosized rhodium oxide-containing MCM-41 (Rh-MCM-41) mesoporous molecular sieves are synthesized and characterized by XRD, TEM, N_2 adsorption, NMR, XPS and EXAFS.

The discovery[1,2] of the novel mesoporous silicate based MCM-41 molecular sieve has generated much interest to design hybrid atom-containing MCM-41 by isomorphous substitution of transition metals into the framework or by functionalisation of the silanols in the pore channels for their applications to catalysis and advanced materials.[3–5] Noble metals such as Pt,[6,7] Pd,[8,9] and Ru[10] were supported on MCM-41, and Ag/Ru bimetallic nanoparticles[11] were supported inside the MCM-41 channels and found to be active compared with the corresponding conventional supported catalysts. However there is no study related to the synthesis of noble metal-containing MCM-41 by addition of noble metals to mixed silicate surfactant gels prior to the hydrothermal synthesis. We have systematically studied the formation of hexagonal structure of MCM-41 and the formation of rhodium oxide nanoparticles, while changing the temperature, aging time and Si/Rh ratio during the hydrothermal synthesis. We report here the first synthesis and characterization of Rh-MCM-41.

The synthesis‡ of Rh-MCM-41 was achieved by modifying the recently reported procedure.[12] The Si/Rh ratio in the synthesis was varied in the range 200–70, and the hydrothermal synthesis was carried out *via* two different pathways [route A: 373 K for 10 days (Rh-MCM-41-A) and route B: 423 K for 48 h (Rh-MCM-41-B)] to study the formation of rhodium oxide particles and also the MCM-41 framework. Supporting Rh on MCM-41 (Rh-su-MCM-41) by an impregnated method was also conducted§ for comparison with Rh-MCM-41. The powder XRD patterns of the calcined forms of Rh-MCM-41 are shown and indexed in Fig. 1. The d_{100} spacings and the unit cell parameters (a_0) are listed in Table 1. A highly ordered hexagonal structure was identified for the Rh-MCM-41-A, which resembled pure Si-MCM-41 reported in the literature.[1,12] A shift of the d_{100} peak was noticed for the Rh-MCM-41-B, indicating that the a_0 (5.47–5.71 nm) became larger. The increase in the a_0 implies the promotion of polymerization of the silica precursor by the presence of Rh ions in the gel, and eventually thicker pore walls were produced as compared to the pure Si-MCM-41 (a_0 = 5.00 nm, pore wall thickness: 1.69 nm) prepared under the similar conditions. The increase of a_0 may be due to a catalytic role of rhodium during the construction of the mesoporous framework at 423 K.

The (114) XRD peak of Rh_2O_3 at 2θ = 34.3° was not detected for the Rh-MCM-41-B, indicating that rhodium oxides are highly dispersed and/or amorphous. Rh K-edge EXAFS spectra for Rh-MCM-41-A and Rh-MCM-41-B were measured at 20 K using synchrotron radiation at Photon factory (proposal No. 97G002). The curve fitting analysis using the empirical parameters derived from Rh_2O_3 (Rh–O 0.211 nm, coordination number six), revealed the Rh–O bond distance at 0.205 nm with the coordination number of 4.3–4.5. Preliminary analysis for the second shell also indicated the presence of Rh–Rh bonds at 0.299 nm for Rh-MCM-41-A and at 0.307 nm for Rh-MCM-41-B, the distance being > 0.292 nm for Rh_2O_3. Hence the rhodium oxide particles in the Rh-MCM-41 seem to have different structures from Rh_2O_3.

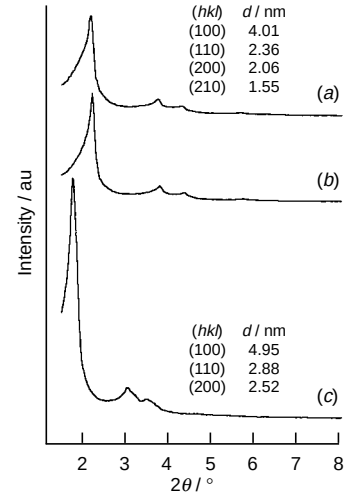

Fig. 1 Powder X-ray diffraction patterns of the calcined forms of Rh-MCM-41; (*a*) Rh-MCM-41-A, (Si/Rh = 200); (*b*) Rh-MCM-41-A(104); (*c*) Rh-MCM-41-B (200)

Table 1 Properties of the Rh-MCM-41 molecular sieves

Sample	Si/Rh ratio[a]	d_{100}[b]/nm	a_0[c]/nm	Pore diameter[d]/nm	S_{BET}/m^2 g^{-1}	Pore volume/ cm^3 g^{-1}	PWT[e]/nm	XPS Si/Rh ratio
Rh-MCM-41-A	200	4.01	4.63	3.02	1016	0.96	1.61	907
Rh-MCM-41-A	70	4.01	4.63	3.02	1028	1.06	1.61	554
Rh-MCM-41-B	200	4.95	5.71	3.40	623	0.80	2.31	415
Rh-MCM-41-B	104	4.74	5.47	3.26	464	0.55	2.21	355
Rh-su-MCM-41	104	4.57	5.27	3.40	1175	0.88	1.87	91

[a] At the synthesis stage. [b] Spacing after calcination. [c] Calculated $a_0 = 2d_{100}\sqrt{3}$. [d] Dollimore–Heal method. [e] PWT (pore wall thickness) = a_0 − pore diameter.

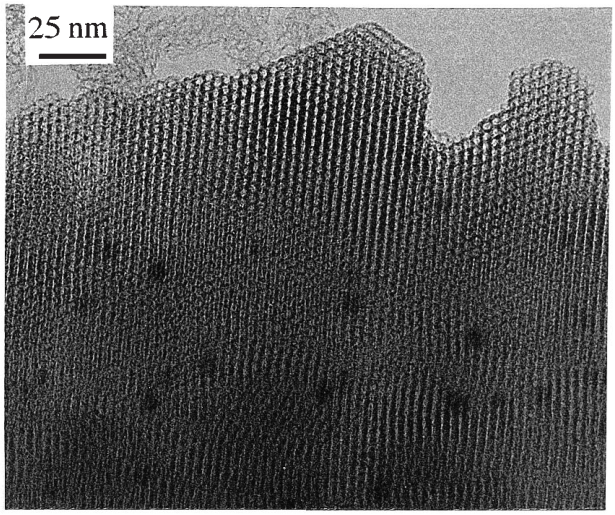

Fig. 2 TEM micrograph (200 kV; ×80 000) of the calcined form of Rh-MCM-41-A with Si/Rh ratio of 200

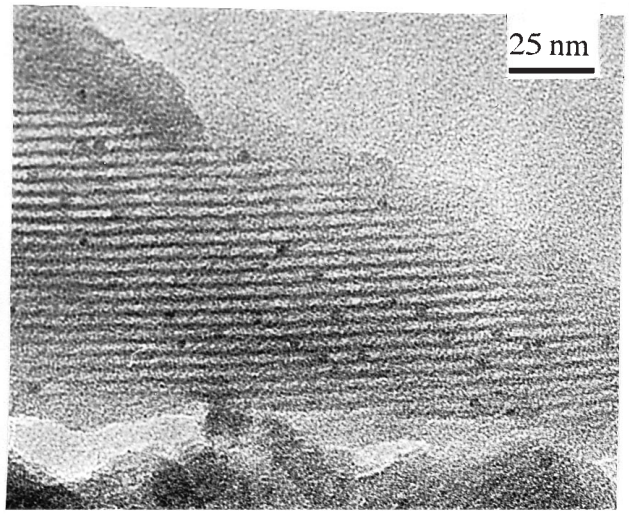

Fig. 3 TEM micrograph viewed perpendicular to the pore axis (200 kV; ×100 000) of the calcined form of Rh-MCM-41-B with Si/Rh ratio of 200

The TEM image of calcined Rh-MCM-41-A is shown in Fig. 2, where the hexagonally packed MCM-41 with dispersed rhodium oxide particles with an average particle size of 6 nm is observed. Fig. 3 is the TEM image viewed perpendicular to the pore axis of the calcined Rh-MCM-41-B, which depicts the uniformly packed channels containing dispersed rhodium oxide nanoparticles (< 3 nm), and the d_{100} value calculated from the TEM image is in agreement with the value from XRD. The thickness of pore walls in TEM is also in agreement with that calculated from XRD in Table 1.

The adsorption–desorption isotherms of N_2 at 77 K were of type IV for Rh-MCM-41 samples which is typical of mesoporous solids and has a narrow pore size distribution. The surface area, pore diameter and pore wall thickness are listed in Table 1. Further characterization of the calcined Rh-MCM-41 samples was performed by ^{29}Si solid state MAS NMR using cross polarization (CP) technique to examine the formation of thicker pore walls in case of Rh-MCM-41-B. The intensity ratio of the two NMR peaks $Q^3 : Q^4$ for Rh-MCM-41-B was 66 : 34, while that for pure Si-MCM-41 was 76 : 24, and this $Q^3 : Q^4$ ratio obtained by CP technique for the Si-MCM-41 is in agreement with that reported by Zhao *et al.*[13] The large increase in the intensity of the Q^4 silicon peak at δ −122 for Rh-MCM-41-B indicates the enhancement of cross-linking by rhodium. The $Q^3 : Q^4$ ratio for Rh-MCM-41-A was identical with that for Si-MCM-41.

The location of rhodium oxide particles in Rh-MCM-41 may be deduced by the Si/Rh ratio in XPS spectra. The Si/Rh XPS ratio for Rh-su-MCM-41 with the Si/Rh bulk ratio of 104 was 91, whereas that for Rh-MCM-41-B with the Si/Rh bulk ratio of 104 was 355. All the Rh-MCM-41 samples in Table 1 showed much larger Si/Rh XPS ratios than the values expected from the bulk composition. These results demonstrate that most of rhodium oxide particles in the Rh-MCM-41-A and Rh-MCM-41-B samples are located in the bulk or the mesopore channel, as imaged in Fig. 2 and 3, respectively, whereas rhodium oxides in Rh-su-MCM-41 are thought to be supported at the external surfaces and near the surfaces.

The comprehensive characterization data demonstrate that the growth of nanosized rhodium oxide particles < 3 nm in the mesopore channel of MCM-41 can be controlled with the appropriate selection of synthesis conditions, and that rhodium plays a catalytic role in the polymeric formation of silica walls of the MCM-41 framework. The application of Rh-MCM-41 to catalysis is in progress.

This work has been supported by CREST (Core Research for Evolutionary Science and Technology) of the Japan Science and Technology Corporation (JST). We thank Dr T. Kogure for assistance with some of the TEM observations which were completed in the Electron Microbeam Analysis Facility of the Mineralogical Institute, The University of Tokyo.

Notes and References

† E-mail: iwasawa@chem.s.u-tokyo.ac.jp

‡ Tetramethylammonium hydroxide pentahydrate (TMAOH) was added to distilled water followed by addition of cetyltrimethylammonium bromide (CTABr) at 303 K. $RhCl_3 \cdot 3H_2O$ (Wako Chemicals) was added to the solution and stirred for 10 min until the solution became clear, then fumed silica obtained from Sigma was slowly added to the solution. The gel composition was 1.0 SiO_2 : 0.19 TMAOH : 0.27 CTABr : 40 H_2O : 0.0049–0.14 $RhCl_3 \cdot 3H_2O$. The gel was aged for 24 h at room temperature and aged at 373 K for 10 days or at 423 K for 48 h. It was filtered, washed with distilled water and dried at 373 K for 12 h, followed by calcination in air at 823 K for 8 h.

§ A methanol solution of $RhCl_3 \cdot 3H_2O$ was added to the calcined pure Si-MCM-41 and the methanol was evaporated with rotary pump and the resultant solid was dried at 373 K for 12 h, followed by calcination at 823 K for 8 h.

1 C. T. Kresge, M. E. Leonowicz, W. J. Roth, J. C. Vartuli and J. C. Beck, *Nature*, 1992, **359**, 710.
2 J. S. Beck, J. C. Vartuli, W. J. Roth, M. E. Leonowicz, C. T. Kresge, K. D. Schmitt, C. T-W. Chu, D. H. Olson, E. W. Sheppard, S. B. McCullen, J. B. Higgins and J. L. Schlenker, *J. Am. Chem. Soc.*, 1992, **114**, 10834.
3 X. S. Zhao, G. Q. Lu and G. J. Millar, *Ind. Eng. Chem. Res.*, 1996, **35**, 2075.
4 A. Sayari, *Chem. Mater*., 1996, **8**, 1840.
5 A. Corma, *Chem. Rev*., 1997, **97**, 2373.
6 U. Junges, W. Jacobs, I. Voigt-Martin, B. Krutzsch and F. Schüth, *J. Chem. Soc., Chem. Commun.*, 1995, 2283.
7 A. Corma, A. Martínez and V. Martínez-Soria, *J. Catal*., 1997, **169**, 480.
8 J. N. Armor, *Appl. Catal. A*, 1994, **112**, N21.
9 C. A. Koh, R. Nooney and S. Tahir, *Catal. Lett*., 1997, **47**, 199.
10 C. T. Fishel, R. J. Davis and J. M. Garces, *J. Catal*., 1996, **163**, 148.
11 D. S. Shephard, T. Maschmeyer, B. F. G. Johnson, J. M. Thomas, G. Sankar, D. Ozkaya, W. Zhou, R. D. Oldroyd and R. G. Bell, *Angew. Chem., Int. Ed. Engl*., 1997, **36**, 2242.
12 C. F. Cheng, D. H. Park and J. Klinowski, *J. Chem. Soc., Faraday Trans*., 1997, **93**, 193.
13 X. S. Zhao, G. Q. Lu, A. K. Whittaker, G. J. Millar and H. Y. Zhu, *J. Phys. Chem. B*, 1997, **101**, 6525.

Received in Cambridge, UK, 23rd March 1998; 8/02259C

Novel unsymmetrical triphenylene discotic liquid crystals: first synthesis of 1,2,3,6,7,10,11-heptaalkoxytriphenylenes

Sandeep Kumar*† and M. Manickam

Centre for Liquid Crystal Research, PO Box 1329, Jalahalli, Bangalore-560 013, India

Oxidation of 2-hydroxy-3,6,7,10,11-pentaalkoxytriphenylene yields the pentaalkoxytriphenylene-1,2-quinone; reductive acetylation of this *o*-quinone furnishes the diacetate that can be directly alkylated to 1,2,3,6,7,10,11-heptaalkoxytriphenylene derivatives showing columnar D_h phases.

Mesophases formed by discotic liquid crystals (LCs) are now well-recognised to be suitable for many device applications.[1,2] Most of the discogens reported to date consist of a flat, or nearly flat, rigid core surrounded by a number of aliphatic side chains having binary, trigonal, tetragonal or hexagonal symmetries. Symmetrically substituted hexethers of triphenylene are the most widely synthesised and studied discotic mesogens. The potential uses of these materials as one-dimensional conductors,[2,3] photoconductors[4] and light emitting diodes[5] are attracting considerable attention. Several research groups are currently working on the synthesis of symmetrical, unsymmetrical and functionalized triphenylene discotic liquid crystals.[6–14]

Triphenylene derivatives show mesomorphism only when the six peripheral positions are substituted with aliphatic chains. Whereas the synthesis of symmetrical hexalkoxytriphenylenes by oxidative trimerisation of 1,2-dialkoxybenzenes is quite easy, the synthesis of well-defined unsymmetrically substituted derivatives is more complicated. Breaking of symmetry in a hexaalkoxytriphenylene can be achieved by different ways, *e.g.* by changing the chain length of some of the side chains, by changing the nature of one or more side chain or by using lower or higher degrees of substitution. Tinh *et al.* reported the synthesis of several dissymmetrical hexasubstituted triphenylenes by incorporating different alkyl chains into the periphery using a statistical approach and found that introduction of dissymmetric side-chains does not affect the nature of the D_h phase but does result in the reduction of the mesophase stability.[15] An easy route to unsymmetrically-substituted triphenylenes was recently reported using the so-called biphenyl route.[6e,7e] A well-defined synthesis of unsymmetrical and low degree substituted triphenylenes has also been reported recently using organometallic chemistry.[10] When one out of the six ether side chains in hexaalkoxytriphenylenes was replaced by an ester group, the stability of the mesophase was enhanced significantly.[16] A plastic columnar discotic phase is reported in this type of unsymmetric triphenylene derivatives.[17] In an another approach to the preparation of unsymmetrical triphenylenes and to the induction of molecular dipole, colour, *etc.*, nitration and halogenation of hexaalkoxytriphenylenes has been investigated.[6a–d,9] While the nitro or halogen group in these triphenylene derivatives could not be replaced by an alkylthio group by nucleophilic aromatic substitution,[9] reduction of the nitro group followed by acylation with various acid chlorides yielded 'seven tail' triphenylene discotics.[6a] However, because of the presence of the amide group, the clearing temperature of these derivatives are rather high.

We have very recently reported a highly improved synthesis of symmetrical, unsymmetrical and mono-functionalized triphenylene derivatives using $MoCl_5$.[8c] We have also reported the synthesis of various functionalized triphenylene,[7f,8d] mixed tail triphenylene,[7b] low symmetry fluorescent triphenylene[7a] and core functionalized triphenylene discotic LCs.[8b,c]

All the triphenylene derivatives hitherto known have six or less alkoxy chains. While triphenylene derivatives with six alkoxy chains are mesomorphic, triphenylenes having less than six alkoxy chains are nonmesomorphic but can be made mesomorphic by putting other substituents onto the periphery.[7a,b] To the best of our knowledge, there are no examples of triphenylene discotic species having more than six alkoxy chains. Here we report on a novel approach to the synthesis of triphenylene-based discotic liquid crystals containing seven alkoxy chains in the periphery. The synthesis of these novel heptaalkoxytriphenylenes is outlined in Scheme 1.

During the nitration 2-hydroxy-3,6,7,10,11-pentabutoxytriphenylene, we always found a black product in addition to the nitrated and some unreacted starting material.[8e] If the reaction is not monitored carefully, this black material becomes the major product. We suspected that the formation of this black material was due to ring oxidation to an *o*-quinone. Oxidation of 2-hydroxy-3,6,7,10,11-pentabutoxytriphenylene **1a** with other known oxidising agents such as chromium trioxide and cerium(IV) ammonium nitrate yielded the same product. The structure of this compound was assigned as 3,6,7,10,11-petabutyloxytriphenylene-1,2-dione **2a** on the bases of its ^{1}H NMR and mass spectral data. Reductive acetylation of this *o*-quinone resulted in the formation of diacetate **3a**. The diacetate was directly alkylated[8a] with alkyl halide to heptabutoxytriphenylene **4a** in very high yield. Heptapentoxytriphenylene was prepared in the same manner. The ^{1}H NMR data of the products were found to be in perfect agreement with the structure.‡

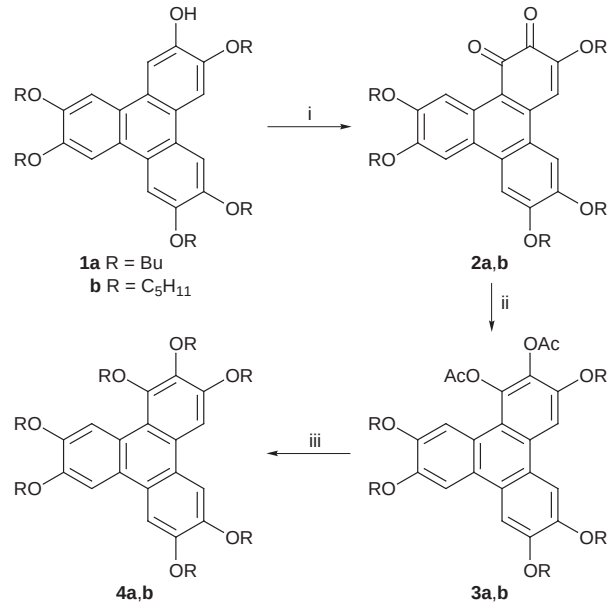

Scheme 1 *Reagents and conditions*: i, CAN, MeCN, room temp., 2 min, 94%; ii, Ac_2O, Zn, NEt_3, reflux, 0.5 h, 92%; iii, DMSO, KOH, RBr, 60 °C, 1 h, 95%

Both heptaalkoxytriphenylenes **4a** and **4b** are mesogenic. While compound **4a** melted at 65.7 °C and clears at 70.1 °C, compound **4b** exhibited a very broad mesophase from room temperature to 65 °C. The mesophase–isotropic transition temperatures of both heptaalkoxytriphenylenes are very low compared to their hexasubstituted analogues (*ca.* 145 °C for hexabutoxy- and 122 °C for hexapentoxytriphenylene). This could be due to the presence of the extra alkoxy chain and the steric hindrance caused by this chain.

This methodology provides an easy, high-yielding process for the preparation of various unsymmetrical, low clearing temperature, broad mesophase triphenylene discotics. It can also be extended to other discotic cores. The potential of this new method is currently under investigation for the synthesis of various hepta-, octa-, nona- and per-alkoxytriphenylene derivatives.

We are very grateful to Professor S. Chandrasekhar for many helpful discussions. The authors also gratefully acknowledge the technical assistance of Mr Sanjay K. Varshney.

Notes and References

† E-mail: uclcr@giasbg01.vsnl.net.in

‡ *Selected data* for **2a**: *m*/*z* (FAB) 620.2 ($M^+ + 2$ H); $\delta_H(CDCl_3)$ 8.91 (s, 1 H), 7.64 (s, 1 H), 7.61 (s, 1 H), 7.35 (s, 1 H), 6.98 (s, 1 H), 4.20 (m, 10 H), 1.89 (m, 10 H), 1.55 (m, 10 H) and 1.05 (m, 15 H). For **2b**: $\delta_H(CDCl_3)$ 8.98 (s, 1 H), 7.72 (s, 1 H), 7.68 (s, 1 H), 7.45 (s, 1 H), 7.08 (s, 1 H), 4.20 (m, 10 H), 1.95 (m, 10 H), 1.48 (m, 20 H) and 0.98 (m, 15 H). **3a**: $\delta_H(CDCl_3)$ 8.48 (s, 1 H), 7.84 (s, 1 H), 7.83 (s, 1 H), 7.81 (s, 1 H), 7.78 (s, 1 H), 4.19 (m, 10 H), 2.44 (s, 3 H), 2.38 (s, 3 H), 1.92 (m, 10 H), 1.60 (m, 10 H) and 1.03 (m, 15 H). For **3b**: $\delta_H(CDCl_3)$ 8.48 (s, 1 H), 7.84 (s, 1 H), 7.83 (s, 1 H), 7.81 (s, 1 H), 7.78 (s, 1 H), 4.18 (m, 10 H), 2.44 (s, 3 H), 2.38 (s, 3 H), 1.88 (m, 10 H), 1.47 (m, 20 H) and 0.97 (m, 15 H). For **4a**: $\delta_H(CDCl_3)$ 9.22 (s, 1 H), 7.83 (s, 2 H), 7.81 (s, 1 H), 7.66 (s, 1 H), 4.20 (m, 12 H), 4.01 (t, *J* 7.1, 2 H), 1.88 (m, 14 H), 1.56 (m, 14 H) and 0.99 (m, 21 H). For **4b**: $\delta_H(CDCl_3)$ 9.21 (s, 1 H), 7.83 (s, 2 H), 7.81 (s, 1 H), 7.66 (s, 1 H), 4.20 (m, 12 H), 4.01 (t, *J* 7.1, 2 H), 1.83 (m, 14 H), 1.49 (m, 28 H) and 1.02 (m, 21 H).

1 S. Chandrasekhar and S. Kumar, *Science Spectra,* 1997, **8**, 66.
2 N. Boden, R. Bissell, J. Clements and B. Movaghar, *Liq. Crystal. Today,* 1996, **6**, 1.
3 N. Boden, R. J. Bushby, J. Clements, M. V. Jesudason, P. F. Knowles and G. Williams, *Chem. Phys. Lett.,* 1988, **152**, 94; N. Boden, R. J. Bushby and J. Clements, *J. Chem. Phys.,* 1993, **98**, 5920; N. Boden, R. J. Bushby, A. N. Cammidge, J. Clements and R. Luo, *Mol. Cryst. Liq. Cryst.,* 1995, **261**, 251; E. O. Arikainen, N. Boden, R. J. Bushby, J. Clements, B. Movaghar and A. Wood, *J. Mater. Chem.,* 1995, **5**, 2161.
4 D. Adams, F. Closs, T. Frey, D. Funhoff, D. Haarer, H. Ringsdorf, P. Schuhmacher and K. Siemensmeyer, *Phys. Rev. Lett.,* 1993, **70**, 457; D. Adam, F. Closs, T. Frey, D. Funhoff, D. Haarer, H. Ringsdorf, P. Schuhmacher and K. Siemensmeyer, *Ber. Bunsenges. Phys. Chem.,* 1993, **97**, 1366; D. Adam, P. Schuhmacher, J. Simmerer, L. Häussling, W. Paulus, K. Siemensmeyer, K. H. Etzbach, H. Ringsdorf and D. Haarer, *Adv. Mater.,* 1995, **7**, 276; J. Simmerer, B. Glusen, W. Paulus, A. Kettner, P. Schuhmacher, D. Adam, K. H. Etzbach, K. Siemensmeyer, J. H. Wendorff, H. Ringsdorf and D. Haarer, *Adv. Mater.,* 1996, **8**, 815.
5 I. H. Stapff, V. Stumpflen, J. H. Wendorff, D. B. Spohn and D. Mobius, *Liq. Cryst.,* 1997, **23**, 613.
6 (*a*) N. Boden, R. J. Bushby, A. N. Cammidge, S. Duckworth and G. Headdoc, *J. Mater. Chem.,* 1997, **7**, 601; (*b*) N. Boden, R. J. Bushby and A. N. Cammidge, *Mol. Cryst. Liq. Cryst.,* 1995, **260**, 307; (*c*) N. Boden, R. J. Bushby and A. N. Cammidge, *Liq. Cryst.,* 1995, **18**, 673; (*d*) N. Boden, R. J. Bushby, A. N. Cammidge and G. Headdock, *J. Mater. Chem.,* 1995, **5**, 2275; (*e*) N. Boden, R. J. Bushby, A. N. Cammidge and G. Headdock, *Synthesis,* 1995, 31; (*f*) N. Boden, R. J. Bushby and A. N. Cammidge, *J. Chem. Soc., Chem. Commun.,* 1994, 465; (*g*) N. Boden, R. C. Borner, R. J. Bushby, A. N. Cammidge and M. V. Jesudason, *Liq. Cryst.,* 1993, **15**, 851.
7 (*a*) J. A. Rego, S. Kumar and H. Ringsdorf, *Chem. Mater.,* 1996, **8**, 1402; (*b*) J. A. Rego, S. Kumar, I. J. Dmochowski and H. Ringsdorf, *Chem. Commun.,* 1996, 1031; (*c*) P. Henderson, S. Kumar, J. A. Rego, H. Ringsdorf and P. Schuhmacher, *J. Chem. Soc., Chem. Commun.,* 1995, 1059; (*d*) F. Closs, L. Häussling, P. Henderson, H. Ringsdorf and P. Schuhmacher, *J. Chem. Soc., Perkin Trans. 1,* 1995, 829; (*e*) P. Henderson, H. Ringsdorf and P. Schuhmacher, *Liq. Cryst.,* 1995, **18**, 191; (*f*) S. Kumar, P. Schuhmacher, P. Henderson, J. Rego and H. Ringsdorf, *Mol. Cryst. Liq. Cryst.,* 1996, **288**, 211.
8 (*a*) S. Kumar, *Mol. Cryst. Liq. Cryst.,* 1996, **289**, 247; (*b*) S. Kumar and M. Manickam, *Mol. Cryst. Liq. Cryst.,* 1998, **309**, 291; (*c*) S. Kumar and M. Manickam, *Chem. Commun.,* 1997, 1615; (*d*) S. Kumar and M. Manickam, *Synthesis,* 1998, in the press; (*e*) S. Kumar, M. Manickam, V. S. K. Balagurusamy and H. Schonherr, unpublished work.
9 K. Praefcke, A. Eckert and D. Blunk, *Liq. Cryst.,* 1997, **22**, 113.
10 R. C. Borner and R. F. W. Jackson, *J. Chem. Soc., Chem. Commun.,* 1994, 845.
11 J. W. Goodby, M. Hird, K. J. Toyne and T. Watson, *J. Chem. Soc., Chem. Commun.,* 1994, 1701.
12 H. Naarmann, M. Hanack and R. Mattmer, *Synthesis,* 1994, 477.
13 F. C. Krebs, N. C. Schiodt, W. Batsberg and K. Bechgaard, *Synthesis,* 1997, 1285; K. Bechgaard and V. D. Parker, *J. Am. Chem. Soc.,* 1972, **94**, 4749.
14 V. Le Berre, L. Angely, N. Simonet-Gueguen and J. Simonet, *J. Chem. Soc., Chem. Commun.,* 1987, 984; V. Le Berre, J. Simonet and P. Batail, *J. Electroanal. Chem.,* 1984, **169**, 325; J. Chapuzet and J. Simonet, *Tetrahedron,* 1991, **47**, 791.
15 N. H. Tinh, M. C. Bernaud, G. Sigaud and C. Destrade, *Mol. Cryst. Liq. Cryst.,* 1981, **65**, 307.
16 M. Werth, S. U. Valklerien and H. W. Spiess, *Liq. Cryst.,* 1991, **10**, 759.
17 B. Glausen, A. Kettner and J. H. Wendorff, *Mol. Cryst. Liq. Cryst.,* 1997, **303**, 115.

Received in Cambridge, UK, 9th April 1998; 8/02698I

A highly coupled Ru^{III}–Ru^{II} system incorporating sulfur donor ligands

Sue Roche,[a] Lesley J. Yellowlees[b] and Jim A. Thomas*[a]†

[a] *Department of Chemistry, University of Sheffield, Sheffield, UK S3 7HF*
[b] *Department of Chemistry, University of Edinburgh, Edinburgh, UK EH9 3JJ*

Bimetallic complex 1, which is based on a Ru^{II} metal centre incorporating sulfur donor ligands, shows strong intermetallic coupling in its mixed valence state comparable to those observed in complexes incorporating conventional nitrogen donors.

Mixed valence coordination chemistry has been dominated for some time by ruthenium(III/II) complexes,[1] most of them being modelled on the Creutz–Taube ion.[2] Theoretical models[3] have been used to understand their spectral properties, especially of the characteristic metal-to-metal charge transfer or intervalence transitions.

Previous research has revealed that the electron transfer properties of such systems are highly dependent on the nature of the metal centres and ligand bridge. Such systems have also played an important part in the development of devices for molecular electronics,[4] where they have formed the basic components of molecular wires and molecular switches. The goal of such research is to develop systems displaying electronic communication between metal centres and thus long range electron transfer and photoinduced charge separation.[5] So far, research has involved changing the bridging ligands[6] and the metal ion.[7] However, all of the metal centres in these complexes contain nitrogen based ligands, such as NH_3 and 2,2′-bipyridine (bpy), coordinated to the metal ion. Our attempt has been to broaden the experimental basis of mixed valence chemistry, by introducing new metal organic fragments incorporating sulfur donor ligands such as the crown ether 1,4,7-trithiacyclononane.

An ideal starting material for these complexes is the previously reported $[Ru(Me_2SO)Cl_2([9]aneS_3)]$.[8] When refluxed overnight with the ligand 3,6-bis(2-pyridyl)-1,2,4,5-tetrazine[9] (bptz) in ethanol–water (1 : 1), a crude product is isolated on the addition of ammonium hexafluorophosphate. After alumina column chromatography, the bimetallic complex cation $\mathbf{1}^{2+}$ was isolated as its PF_6 salt as a blue powder in 48% yield. This compound is air and moisture stable and has been characterised by ^{1}H NMR, UV–VIS and FAB mass spectroscopy.‡

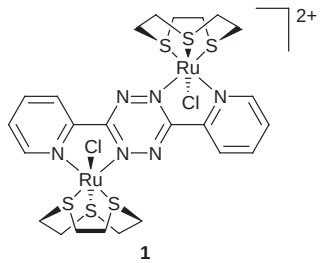

1

The UV–VIS spectrum of $\mathbf{1}^{2+}$ shows two bands (Table 1). The first at 302 nm has a large absorption coefficient (ε = 3497 $dm^3\ mol^{-1}\ cm^{-1}$) and has been assigned to a π–π* transition. The second intense band has ε = 2281 $dm^3\ mol^{-1}\ cm^{-1}$ and occurs at 751 nm. A comparison with structurally similar complexes allows this band to be to assigned metal-to-ligand charge transfer (MLCT).[1b]

Table 1 UV–VIS spectra data for complex **1** in acetonitrile

Complex	λ_{max}/nm	ε/ $dm^3\ mol^{-1}\ cm^{-1}$	Assignment
$\mathbf{1}^{2+}$	302	3497	π–π*
	751	2281	MLCT
$\mathbf{1}^{3+}$	310	3158	π–π*
	678	2312	MLCT
	1852	519	IVCT

In an attempt to quantify the ligand bridge mediated intermetallic interaction, cyclic voltammetry was used. This was carried out in acetonitrile (Table 2). Complex $\mathbf{1}^{2+}$ displays a first oxidation at $E_{1/2}$ 1.36 V. The first oxidations for the related complexes $[\{Ru(NH_3)_4\}_2(bptz)]^{4+}$ ($\mathbf{2}^{4+}$) and $[\{Ru(bpy)_2\}_2(bptz)]^{4+}$ ($\mathbf{3}^{4+}$) occur at 0.72 and 1.52 V respectively. The difference in these values can be explained by considering the nature of the coordination bonding in these complexes. While NH_3 is a purely σ-donor ligand, bpy ligands are also π-acceptors and as such stabilise the Ru^{II} oxidation state producing the observed anodic potential shifts. The electrochemical behaviour of $\mathbf{1}^{2+}$ indicates that the $[RuCl([9]aneS_3)]^+$ metal centre is also appreciably stabilised by π back-donation interactions. Such an observation is consistent with, and confirms, recent findings on the coordination chemistry of thioether ligands.[10]

Complex $\mathbf{1}^{3+}$ displays a strong intermetallic interaction with $\Delta E_{1/2}$ = 0.48 V resulting in a comproportionation constant (K_c) of 1.48×10^8, suggesting that it is a Robin and Day class III system.[12] This value is greater than the previously reported value of $\Delta E_{1/2}$ = 0.39 V for the Creutz–Taube ion,[13] and is similar to complex $\mathbf{3}^{5+}$ ($\Delta E_{1/2}$ = 0.5 V) but less than the value for complex $\mathbf{2}^{5+}$ ($\Delta E_{1/2}$ = 0.84 V). On this evidence, it would appear that $\mathbf{1}^{2+}$ is a less strongly interacting system than $\mathbf{2}^{4+}$. However, a comparison of the optical properties of the mixed valence complexes is more informative.

The intermetallic interaction in $\mathbf{1}^{3+}$ was further investigated using spectroelectrochemistry. The formation of several isosbetic points after the oxidation of $\mathbf{1}^{2+}$ shows a clean conversion taking place, with the MLCT band showing a hypsochromic shift (Table 1). A significant observation is the formation of an new band at 1852 nm (5375 cm^{-1}). This band, which has been assigned to an intervalence charge transfer (IVCT), has an absorption coefficient of ε = 519 $dm^3\ mol^{-1}\ cm^{-1}$. By

Table 2 Electrochemical data[a] for some ruthenium complexes

Complex	$E_{1/2}(1)$/V	$E_{1/2}(2)$/V	$\Delta E_{1/2}$/V	K_c[b]	Ref.
$\mathbf{1}^{2+}$	1.36	1.84	0.48	1.4×10^8	This work
$\mathbf{2}^{4+}$	0.72	1.56	0.84	1×10^{15}	1(*a*)
$\mathbf{3}^{4+}$	1.52	2.02	0.5	3×10^8	11

[a] Cyclic voltammogram of complex cation $\mathbf{1}^{2+}$ was carried out at a scan rate of 200 mV s^{-1} in acetonitrile containing tetrabutylammonium hexafluorophosphate as supporting electrolyte (0.1 M). Potentials were measured *vs.* SCE. All couples were reversible with I_{pc} and I_{pa} equal and ΔE_p < 100 mV. [b] K_c values calculated using $\log K_c = \Delta E_{1/2}/0.059$.

comparison, the IVCT band found for $\mathbf{2}^{5+}$ is observed at 1453 nm with ε = 500 dm^3 mol^{-1} cm^{-1}.[1a]

Application of Hush theory[3b,c] to the IVCT spectral data of $\mathbf{1}^{3+}$ yields a bandwidth at half-height, $\Delta\nu_{1/2}$, which is much higher than the experimental value: $\Delta\nu_{1/2} = (2310\nu)^{1/2}$ cm^{-1}, $\Delta\nu_{1/2}$ ($\mathbf{1}^{3+}$, calc.) = 3524 cm^{-1}, $\Delta\nu_{1/2}$ ($\mathbf{1}^{3+}$, exptl.) ≈ 1375 cm^{-1}.

This discrepancy indicates that, like $\mathbf{2}^{5+}$, $\mathbf{1}^{3+}$ is a delocalised (class III) system, to which the above treatment is not applicable. Accordingly, the degree of electronic coupling, H_{AB}, can be estimated to approximately $1/2\nu$ = 2687.5 cm^{-1}.[3c]

Concluding, not only is this a new structural motif for such studies, it also seems effective in facilitating bridge mediated intermetallic interactions. With an aim to designing functional molecular devices, future studies will concentrate on variations in the metal ion, co-ordination sphere of the metal centre, and the bridging ligand.

We gratefully acknowledge the support of The Royal Society (J. A. T.) and the EPSRC.

Notes and References

† E-mail: james.thomas@sheffield.ac.uk

‡ *Elemental analysis*. Found C, 23.49; H, 3.06; N, 6.74. Calc. for $Ru_2C_{24}H_{40}S_6N_6Cl_2P_2F_{12}$: C, 23.39; H, 3.25; N, 6.82%. ^{1}H NMR (200 MHz, CD_3COCD_3): δ 8.00 (dt, 2 H), 8.40 (dt, 2 H), 8.89 (dd, 2 H), 9.31 (dd, 2 H). FABMS: peaks at *m*/*z* 1016 [(**1** + PF_6)$^+$, 15%], 871 [(**1**)$^{2+}$, 30%].

1 See, for example: (*a*) J. Poppe, M. Moscherosch and W. Kaim, *Inorg. Chem.*, 1993, **32**, 1640; (*b*) J. E. B. Johnson, C. DeGroff and R. R. Ruminski, *Inorg. Chim. Acta*, 1991, **187**, 73; (*c*) D. E. Richardson and H. Taube, *Coord. Chem. Rev.*, 1984, **60**, 107.
2 C. Creutz and H. Taube, *J. Am. Chem. Soc.*, 1969, **91**, 3988; 1973, **95**, 1086.
3 (*a*) J. R. Miller, *Electron transfer in Inorganic, Organic, and Biological systems*, ch. 17, ed. J. R. Bolton, N. Mataga and G. McLendon, Advances in Chemistry Series, 228, American Chemical Society, Washington, DC, 1991; (*b*) N. S. Hush, *Prog. Inorg. Chem.*, 1967, **8**, 391; (*c*) C. Creutz, *Prog. Inorg. Chem.*, 1983, **30**, 1; (*d*) R. J. Crutchley, *Adv. Inorg. Chem.*, 1994, **41**, 273.
4 M. D. Ward, *Chem. Ind. (London)*, 1996, 568; 1997, 640.
5 V. Balzani and F. Scandola, *Pure Appl. Chem.*, 1990, **8**, 1457.
6 W. Kaim, V. Kasack, H. Binder, E. Roth and J. Jordanov, *Angew. Chem., Int. Ed. Engl.*, 1988, **27**, 1174; M. Haga, T. Ano, K. Kano and S. Yamabe, *Inorg. Chem.*, 1991, **30**, 3843; J.-P. Collin, R. Laine, J.-P. Launay, J.-P. Sauvage and A. Sour, *J. Chem. Soc., Chem. Commun.*, 1994, 434; M. A. S. Aquino, F. L. Lee, E. J. Gabe, C. Bensimon, J. E. Greedau and R. J. Crutchley, *J. Am. Chem. Soc.*, 1992, **114**, 5130.
7 E. M. Kober, K. A. Goldsby, D. N. S. Narayana and T. J. Meyer, *J. Am. Chem. Soc.*, 1983, **105**, 4303; S. Ernst, V. Kasack and W. Kaim, *Inorg. Chem.*, 1988, **27**, 1146; S. Ernst and W. Kaim, *Inorg. Chem.*, 1989, **28**, 1520; W. Kaim and S. Kohlmann, *Inorg. Chem.*, 1990, **29**, 2909.
8 C. Landgrafe and W. S. Sheldrick, *J. Chem. Soc., Dalton Trans.*, 1994, 1885.
9 E. S. Lewis and M. D. Johnson, *J. Am. Chem. Soc.*, 1959, **81**, 2070.
10 G. E. D. Mullen, M. J. Went, S. Wocadlo, A. K. Powell and P. J. Blower, *Angew. Chem., Int. Ed. Engl.*, 1997, **36**, 1205.
11 S. Kohlmann, S. Ernst and W. Kaim, *Angew. Chem., Int. Ed. Engl.*, 1985, **24**, 8684.
12 M. B. Robin and P. Day, *Adv. Inorg. Chem. Radiochem.*, 1967, **10**, 247.
13 H. S. Lim, J. Barclay and F. C. Anson, *Inorg. Chem.*, 1972, **11**, 1460.

Received in Basel, Switzerland, 28th April 1998; 8/03212B

Diastereoselective hydrogenation of *o*-toluic acid derivatives over supported rhodium and ruthenium heterogeneous catalysts

Michèle Besson,*† Pierre Gallezot, Samuel Neto and Catherine Pinel

Institut de Recherches sur la Catalyse-CNRS, 2 avenue Albert Einstein, 69626 Villeurbanne Cedex, France

Asymmetric hydrogenation of an *o*-toluic acid derivative to 2-methylcyclohexanoic acid with high optical selectivity (up to 95%) was performed by using (*S*)-pyroglutamic acid methyl ester as a chiral auxiliary and Rh–Al_2O_3 as the catalyst.

Diastereoselective catalytic hydrogenation with heterogeneous metal catalysts has been applied for the reduction of C=C, C=O or C=N bonds.[1,2] Modest to high diastereoselectivities were obtained, depending on the chiral auxiliary used and the nature of the heterogeneous catalyst. Recently, this method was proposed to hydrogenate aromatic rings.[3,4] Thus, (*S*)-*N*-(2-methylbenzoyl)proline methyl ester was hydrogenated quantitatively on pretreated Rh–Al_2O_3 in the presence of a bulky amine (ethyldicyclohexylamine = EDCA); the *cis* isomer was obtained preferentially (yield > 97%) with diastereoisomeric excess (de) values reaching 67%.[5] We now report on the use of a pyroglutamic acid derivative as a chiral auxiliary which permits the diastereoselective reduction of aromatic moities with higher than 90% de.

Substrate **1** was synthesized with a 82% yield, after purification, by coupling under mild conditions *o*-toluoyl chloride with pyroglutamic acid methyl ester (Scheme 1).[6]‡ The hydrogenation was carried out in a stirred autoclave at a hydrogen pressure of 5 MPa at room temperature. The substrate was dissolved in EtOH and supported rhodium or ruthenium catalysts (2–5 mol%) were added. EDCA (2–3 equiv. with respect to metal) was optionally added. The typical product distribution as a function of time (entry 5) is given in Fig. 1 for a hydrogenation performed over Ru–C catalyst. The aromatic substrate was hydrogenated to **3a** and **b** with a constant de; some

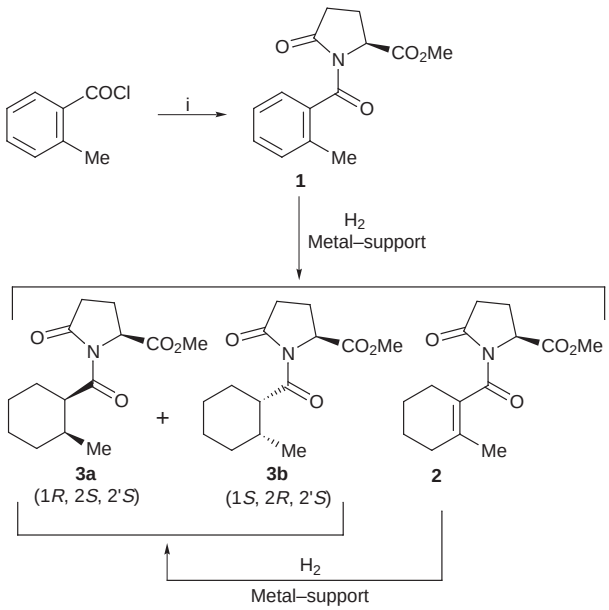

Scheme 1 *Reagents and conditions*: i, (*S*)-pyroglutamic acid methyl ester, toluene, 80 °C, N_2

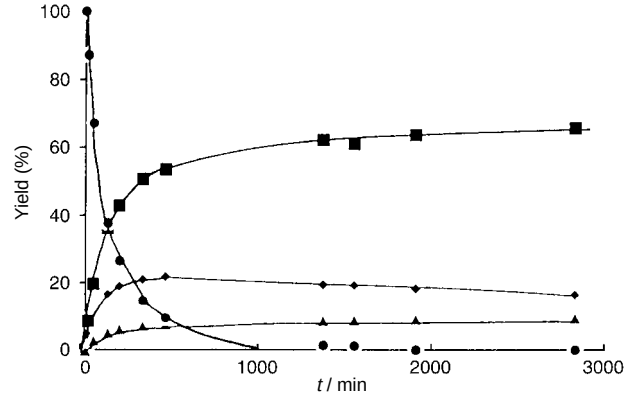

Fig. 1 Distribution of products *versus* time for hydrogenation of **1** over Ru–C (entry 5, Table 1). Reaction conditions: 2.26 mmol **1**, 0.063 mmol Ru, 130 ml EtOH, room temp., 5 MPa H_2. Less than 3% of the *trans* compound was detected. (●) **1**, (◆) **2**, (■) **3a** and (▲) **3b**.

cyclohexenic compound **2** was formed transiently and consecutively hydrogenated to **3**. An overview of the most significant catalytic results is summarized in Table 1.

In all reactions, only small amounts of *trans*-cyclohexane derivative were found (< 3%) and the absolute configuration of the major *cis* product was *(1S,2R,2′S)*. Hydrogenation of (*S*)-*N*-(2-methylbenzoyl) pyroglutamic acid methyl ester **1** in the presence of Rh–C catalyst resulted in 35% de, whereas on Rh–Al_2O_3 the conversion was slightly lower, although the diastereoselectivity was 90%. Addition of a bulky amine (EDCA) to the reaction medium lowered the reaction rate in both cases, but excellent diastereoisomeric excesses were observed, both on carbon (90% de) and on alumina (95% de). Compound **2** was detected in significant amounts only in the case of Rh–C; its hydrogenation gave preferentially **3b** and lowered the de.

In the case of the ruthenium catalyst, high diastereoselectivities were achieved without amine, irrrespective of the support (74 and 85% de on carbon and alumina, respectively). However, it was found that the reaction was slower on the alumina-supported catalyst. The semi-hydrogenated compound **2** was

Table 1 Results for hydrogenation of *o*-toluic acid derivatives **1**

Entry	Metal–support	EDCA : metal[a]	Conversion (%)[b] after 24 h	Yield **2** (%)[b]	De (%)[b,c]
1	Rh–C (Aldrich, 3.6%)	—	100[d]	13	35
2	Rh–Al_2O_3 (Degussa, 3.7%)	—	89	5	90
3	Rh–C (Aldrich, 3.6%)	2	49	3.5	90
4	Rh–Al_2O_3 (Degussa, 3.7%)	3	49	2	95
5	Ru–C (Aldrich, 5%)[e]	—	99	19	74
6	Ru–Al_2O_3 (Degussa, 3.7%)[e]	—	61	11	85
7	Ru–C (Aldrich, 5%)[e]	3	61	10	83

[a] Molar ratio. [b] Determined by GC analysis (DB 1701). [c] The determination of the major configuration (1*S*,2*R*,2′*S*) was carried out by measuring the optical purity of the hydrolyzed product. [d] The conversion was complete after 100 min reaction. [e] Pretreated under H_2 at 300 °C for 2 h.

present in up to 19%, and due to steric constraints, it was hydrogenated with reduced de. The diastereoselectivity was increased from 74 to 83% when EDCA was added to the Ru–C catalyst.

These results clearly show that (*S*)-pyroglutamic acid methyl ester exerts much stronger chiral induction than (*S*)-proline derivatives since the de increased to 95% from 67%. This is probably due to the presence of the ketone group in the auxiliary, which plays a crucial role by interacting with the catalyst surface and blocking one of the faces of the aromatic ring.

Notes and References

† E-mail : mbesson@catalyse.univ-lyon1.fr

‡ *Selected data* for **1** : white crystals; mp 108 °C; $[\alpha]_D^{25}$ −28.9 (*c* 1, $CHCl_3$); δ_H ($CDCl_3$) 7.25 (m, 4 H), 4.96 (dd, 1 H, *J* 3.4, 5.8), 3.83 (s, 3 H), 2.74–2.07 (m, 4 H), 2.36 (s, 3 H); δ_C ($CDCl_3$) 173.0 (C), 171.5 (C), 170.4 (C), 135.5 (C), 135.0 (C), 130.4 (CH), 130.2 (CH), 126.9 (CH), 125.3 (CH), 57.9 (CH), 52.8 (CH_3), 31.7 (CH_2), 21.6 (CH_2), 19.2 (CH_3); *ν* (KBr) cm^{-1} 2928, 1751, 1679, 1304, 1218 [C, 64.62 (64.34); H, 5.77 (5.74); N, 5.32 (5.36); O, 24.07% (24.50)].

1 A. Tungler and K. Fodor, *Catal. Today*, 1997, **37**, 191.
2 M. Besson and C. Pinel, *Top. Catal.*, 1998, **5**, 25 and references cited therein.
3 M. Besson, B. Blanc, M. Champelet, P. Gallezot, K. Nasar and C. Pinel, *J. Catal.*, 1997, **170**, 254.
4 C. Exl, E. Ferstl, H. Hönig and R. Rogi-Kohlenprath, *Chirality*, 1995, **7**, 211.
5 M. Besson, P. Gallezot, C. Pinel and S. Neto, *Studies in Surface Science, Heterogeneous Catalysis and Fine Chemicals*, ed. H.-U. Blaser, Elsevier Science B. V., Amsterdam, 1997, vol. **108**, p. 215.
6 J. B. Behr, A. Defoin, J. Pires, J. Streith, L. Macko and M. Zehnder, *Tetrahedron*, 1996, **52**, 3283.

Received in Liverpool, UK, 15th April 1998; 8/02822B

Single stranded DNA-poly(*N*-isopropylacrylamide) conjugate for affinity precipitation separation of oligonucleotides

Daisuke Umeno, Takeshi Mori and Mizuo Maeda*†

Department of Materials Physics and Chemistry, Graduate School of Engineering, Kyushu University, 6-10-1, Hakozaki, Higashi-ku, Fukuoka 812-8581, Japan

The conjugate between single-stranded DNA and the temperature-responsive polymer poly(*N*-isopropylacrylamide) was synthesized, and was demonstrated to distinguish its target sequence from mismatch DNAs and separate it from aqueous solution when heated.

Single stranded (ss) DNA has been widely used as an affinity ligand for detection[1] and separation[2] of DNA and RNA having specific sequences because of its high precision in molecular recognition. For affinity separation of a specific sequence, ss DNA-carrying materials such as silica gel,[3] cellulose,[4] and latex particles[5] have been widely applied in the field of molecular and cellular biology. Especially, affinity columns immobilized with poly(dT) or poly(U) are invariably used for the purification of mRNAs from the crude cell extracts.[6] However, the affinity interaction between target sequences and ligand DNA immobilized on the solid materials has been indicated to be weaker and slower than that in homogeneous conditions.[7] Here we describe an alternative system using a conjugate between oligonucleotides and poly(*N*-isopropylacrylamide) (polyNIPAAm) which is known to undergo temperature-directed phase-transition between soluble (< 31 °C) and insoluble (> 31 °C) forms.[8] This conjugate hybridizes with the target sequence in homogeneous solution, and precipitates with the target by the slight change in solution temperature (Fig. 1). The concept of 'thermally-induced affinity precipitation separation' was first proposed by Chen and Hoffman for the separation of IgG using a polyNIPAAm–protein A conjugate.[9]

The vinyl derivative of $(dT)_8$ (**1**) was synthesized by the coupling of 5′-amino-terminated $(dT)_8$ with methacryloyloxy succinimide according to the previous report.[10] **1** (75 μM) and NIPAAm (150 mM) were copolymerized in buffer solution (10 mM Tris–HCl, pH 7.4) at 20 °C using ammonium persulfate (1.3 mM) and *N*,*N*,*N*′,*N*′-tetramethylethylenediamine (86 mM) as a redox initiator couple in nitrogen atmosphere to give a polyNIPAAm-$(dT)_8$ conjugate with the structure illustrated in Scheme 1. By monitoring the peak area of the monomers on a reversed phase-HPLC, conversions of **1** and NIPAAm were determined to be 71 and 75%, respectively, indicating that the amount of $(dT)_8$ incorporated in the resulting copolymer is almost the same as the feed ratio of **1** to NIPAAm (0.05 mol%) at the polymerization step. The reaction mixture was dialyzed against 10 l of deionized water for a day, followed by lyophilization. The white powder obtained was dissolved in water to 1.0 m/v %. The aqueous solution was then centrifuged at 40 °C. After removal of the supernatant, the precipitated fraction was re-dissolved in water to give a stock solution which was stored at 4 °C. Removal of the unpolymerized constituents (**1** and NIPAAm) was confirmed by disappearance of their peaks on HPLC.

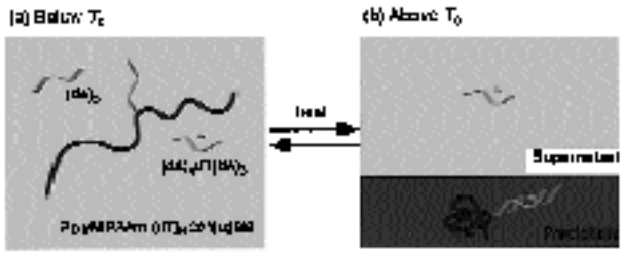

Fig. 1 Schematic illustration of the temperature-directed precipitation of oligonucleotides using polyNIPAAm–$(dT)_8$ conjugate. (*a*) At the temperature below the phase transition point (T_c) of polyNIPAAm, the conjugate is soluble in water and captures its complementary sequence in homogeneous condition. (*b*) At temperatures above T_c, the target sequence is separated to the precipitate with the conjugate. This process is fully reversible.

The resultant conjugate between polyNIPAAm and $(dT)_8$ was applied to the one-pot separation of its complementary sequence $(dA)_8$. The conjugate [0.45 m/v %; 20 μM of $(dT)_8$ in strand] was mixed with the target DNA [$(dA)_8$; 10 μM in strand]. Then 1.0 m/v % of polyNIPAAm was added to the mixture because we found that a certain concentration (> 1 m/v %) of homopolymer was required for the reproducible precipitation of polyNIPAAm-$(dT)_8$ conjugate. The concentration of NaCl and $MgCl_2$ was adjusted to be 1.5 and 0.1 M, respectively. The melting curve of the duplex between $(dT)_8$ and $(dA)_8$ and transmittance curve of polyNIPAAm conjugated with $(dT)_8$ under these solution conditions is shown in Fig. 2. From the curves, melting temperature of the duplex between $(dT)_8$ and $(dA)_8$ was determined to be 16.2 °C, while the transition temperature of the conjugate was *ca.* 14 °C.‡ The mixture (150 μl) was incubated at 0 °C for 6 h for hybridization and then heated to 15 °C for desolubilization of the conjugate. The resulting turbid mixture was centrifuged at the temperature, and the supernatant was collected. The amount of $(dA)_8$ in the supernatant was evaluated by the peak area on HPLC. The precipitate fractions were dissolved in 150 μl of water and analyzed similarly.

As is shown in Table 1, 84% of $(dA)_8$ in the system was concentrated into the precipitate fraction in the presence of conjugate. On the other hand, only a small amount of $(dA)_8$ (*ca.* 6%) was distributed to the precipitate when the separation experiment was performed in the absence of the conjugate. The precipitation % of $(dT)_8$ did not depend on the presence of the conjugate, being a small value of *ca.* 5% which should be ascribed to the incompleteness in the collection of the aqueous phase.

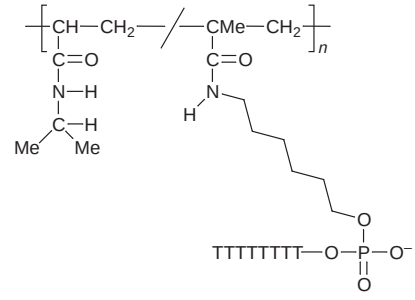

Scheme 1 Chemical structure of the polyNIPAAm–$(dT)_8$ conjugate

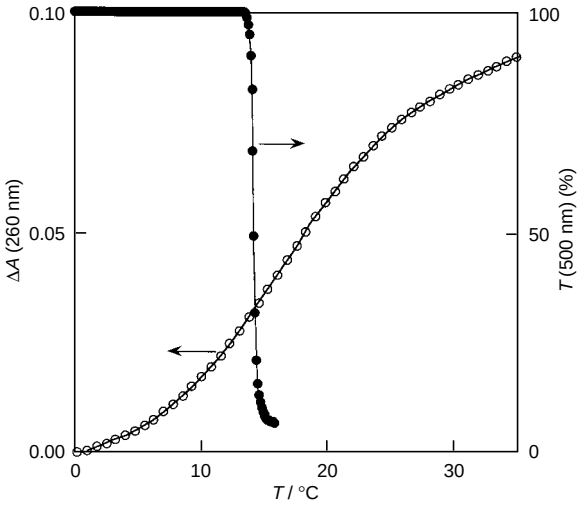

Fig. 2 Melting curve of the $(dA)_8 \cdot (dT)_8$ duplex and transmittance (at 500 nm) curve of the polyNIPAAm–$(dT)_8$ conjugate under the following solution conditions: 1.5 M NaCl, 0.1 M $MgCl_2$ and 10 mM Tris–HCl (pH 7.4). The $(dA)_8 \cdot (dT)_8$ concentration was 3 μM in the strand in the melting temperature measurement, and the concentration of polyNIPAAm–$(dT)_8$ conjugate was 0.068 m/v % [$(dT)_8$ unit, 3 μM in strand] at the transition temperature measurement. Heating rate at both measurements was 0.25 °C min^{-1}.

Table 1 Precipitation efficiency (%) of the oligonucleotides by heating and centrifugation in the presence of the polyNIPAAm–$(dT)_8$ conjugate

	Precipitation %	
Target DNA	+ Conjugate	− Conjugate
$(dA)_8$	83.6 ± 0.8	5.5 ± 0.3
$(dT)_8$	5.3	4.6

An aqueous solution of polyNIPAAm (1 m/v %) and target DNA (10 μM in strand) was heated and centrifuged at 40 °C in the presence (+) or absence (−) of polyNIPAAm–$(dT)_8$ conjugate. Precipitation % was calculated as follows; % = 100 × [DNA found in precipitate fraction]/{[DNA in supernatant] + [DNA in precipitate fraction]}. The precipitation % of $(dA)_8$ is given as mean ± standard error (n = 3).

The applicability of this separation system was further examined for a mixture of $(dA)_8$ and $(dA)_3dT(dA)_4$ (10 μM each). A typical example is shown in Fig. 3: 84.0 ± 1.4 (n = 3) % of $(dA)_8$ was concentrated into the precipitate by the procedure, while 91.7 ± 0.8 (n = 3) % of $(dA)_3dT(dA)_4$ remained in the supernatant. This result clearly indicates that the polyNIPAAm–$(dT)_8$ conjugate distinguished $(dA)_8$ from $(dA)_3dT(dA)_4$, and isolated the complementary DNA selectively from the aqueous solution. In fact, 99% of the precipitated $(dA)_8$ was recovered when the precipitate was resuspended in deionized water and centrifuged at 40 °C.‡

Here we have proposed a simple method for the one-pot separation of ss DNAs with a unique sequence. We have described the separation of $(dA)_8$ using polyNIPAAm–$(dT)_8$ conjugate, because the conjugate having poly(dT) will be useful for the separation of polyadenylated mRNAs which are of great importance in cDNA cloning.

Wolf *et al*. reported that ss DNA attached to latex particles hybridized, in certain conditions, with its complementary oligonucleotide at a comparable rate with free DNA, while it

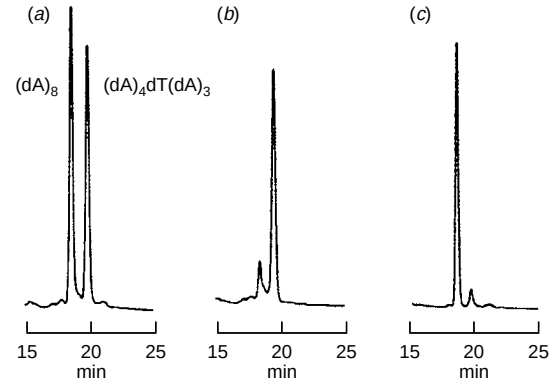

Fig. 3 HPLC chromatograms of $(dA)_8$ and $(dA)_3dT(dA)_4$ before and after the precipitation separation using polyNIPAAm–$(dT)_8$ conjugate. The equimolar mixture of $(dA)_8$ and $(dA)_3dT(dA)_4$ was heated in the presence of polyNIPAAm–$(dT)_8$ conjugate and centrifuged. (*a*) HPLC chromatogram before the process. (*b*) HPLC chromatogram of the supernatant fraction after the process. (*c*) HPLC chromatogram of the precipitated fraction after the process.

hybridized much slower with the larger DNAs,[11] probably because of the steric repulsion due to the latex surface. In this sense, the soluble conjugate described here would be advantageous especially for the larger target molecules such as mRNAs. In addition, this property would be also advantageous even in the post-separation stages. For instance, we hypothesize that cDNA synthesis of the separated mRNA on the polyNIPAAm–poly(dT) conjugate would be much more efficient than that on solid materials such as poly(dT)–silica.[12] These conjectures are under further investigation.

This work was partly supported by a Grant-in-Aid for Scientific Research from Ministry of Education, Science, Sports and Culture of Japan. Financial support by the General Sekiyu Research and Development Encouragement and Assistance Foundation is also acknowledged.

Notes and References

† E-mail: maedatcm@mbox.nc.kyushu-u.ac.jp

‡ PolyNIPAAm undergoes dehydration (and precipitation) at *ca.* 31 °C in deionized water, as was also the case for the polyNIPAAm–$(dT)_8$ conjugate. However, the addition of salt lowers the transition temperature of polyNIPAAm,[8] which was found to be 14 °C in the present solution conditions for the one-pot separation.

1 S. R. Mikkelsen, *Electroanalysis*, 1996, **8**, 15.
2 H. G. Jarrett, *J. Chromatogr*., 1993, **618**, 315.
3 J. T. Kadonaga and R. Tjian, *Proc. Natl. Acad. Sci.*, 1986, **83**, 5889.
4 B. Alberts and G. Herrik, *Methods Enzymol.*, 1971, **21**, 198.
5 T. Imai, Y. Sumi, M. Hatakeyama, K. Fujimoto, H. Kawaguchi, N. Hayashida, K. Shiozaki, K. Terada, H. Yajima and H. Handa, *J. Colloid Interface Sci.*, 1996, **177**, 245.
6 N. Tanner, *Methods Enzymol.*, 1989, **180**, 25.
7 H. Bunneman, *Nucleic Acids Res.*, 1982, **10**, 7181.
8 H. G. Schild, *Prog. Polym. Sci.*, 1992, **17**, 163.
9 J. P. Chen and A. S. Hoffman, *Biomaterials*, 1990, **11**, 631.
10 Y. Ozaki, T. Ihara, Y. Katayama and M. Maeda, *Nucleic Acids Res. Symp. Ser*., 1997, **37**, 235.
11 S. F. Wolf, L. Haines, J. Fisch, J. N. Kremski, J. P. Doughertly and K. Jacob, *Nucleic Acids Res.*, 1987, **15**, 2911.
12 L. R. Solomon, L. R. Masson and H. W. Jarrett, *Anal. Biochem.*, 1992, **203**, 58.

Received in Cambridge, UK, 30th March 1998; 8/02431F

Crystal engineering with tetraarylporphyrins, an exceptionally versatile building block for the design of multidimensional supramolecular structures

R. Krishna Kumar, S. Balasubramanian and Israel Goldberg*†

School of Chemistry, Sackler Faculty of Exact Sciences, Tel-Aviv University, 69978 Ramat-Aviv, Tel-Aviv, Israel

Zinc *meso*-tetra(4-amidophenyl)porphyrin assembles into open two-dimensional arrays parallel to the porphyrin plane by self-complementary hydrogen bonding between the –$CONH_2$ recognition sites of adjacent molecules; manganese *meso*-tetraphenylporphyrin perchlorate and the bidentate 4,4′-bipyridyl ligand afford one-dimensional coordination polymers, which propagate in a direction perpendicular to the porphyrin plane; simultaneous application of these two modules of supramolecular design may lead to porous porphyrin-based materials with enhanced structural integrity.

The design of multiporphyrin architectures has drawn considerable attention in recent years, as such materials have diverse potential for scientific and technological applications as biomimetic models of photosynthetic systems or as functional molecular devices.[1,2] Tetraarylporphyrin molecules have a number of features that make them attractive building blocks for crystal engineering. These molecules are quite rigid, highly symmetric, and easily synthesized, and they exhibit a high degree of thermal and oxidative stability. The porphyrins can be easily 'programmed' by addition of various substituents and recognition sites to either the pyrrole or aryl groups, as well as by varying the nature of the metal atom inserted into the porphyrin core. Several successful attempts to assemble supramolecular porphyrin aggregates, in solution as well as in the solid state, have been reported recently.[3] In this context we have previously described formation of one-, two- and three-dimensional coordination polymers of zinc tetra(4-pyridyl)porphyrin and of zinc tetra(4-cyanophenyl)porphyrin.[4] We have also demonstrated, along with others, the utilization of hydrogen-bonding as an effective means of structural control in the design of homogeneous multiporphyrin architectures.[5,6] As part of this ongoing investigation we now report the structures of new materials based on controlled multiporphyrin aggregation which demonstrate two of the most plausible modes of supramolecular design, utilizing effective synthons for hydrogen-bonding and coordination polymerization.

Zinc *meso*-tetra(4-amidophenyl)porphyrin **1a** is representative of building blocks containing self-complementary recognition sites at the peripheral 4-position of the phenyl rings. The square-shaped tetraamide functionality and its hydrogen bonding capacity can dictate the formation of planar and rigid hollow networks sustained by hydrogen bonds.[7] On the other hand, the use of manganese *meso*-tetraphenylporphyrin **1b** should facilitate the construction of coordination polymers with suitable multidentate ligands, as Mn^{III} reveals high affinity for a six-coordinate environment. In view of the paramagnetic properties of the latter, these materials may also have significant potential as molecular magnets.[8a] Literature survey shows, however, that only a very small number of coordination polymers with metalloporphyrin frameworks have been successfully prepared thus far,[8] while the occurrence of monomeric Mn^{III} complexes is considerably more common. Compounds **1a** and **1b** were prepared by standard procedures of porphyrin synthesis. Single crystals of zinc tetra(4-amidophenyl)porphyrin·$4Me_2SO·H_2O$ **2** suitable for X-ray diffraction analysis were grown by very slow cooling of the solution of **1a** in Me_2SO. Similarly, single crystals of the 1 : 1 complex of MnTPP·ClO_4 with neutral 4,4′-bipyridyl (**3**; crystallizing as a nitrobenzene solvate) were grown from a slowly cooled stoichiometric mixture of these two components in nitrobenzene. The structure and composition of these crystals were determined unequivocally by X-ray diffraction analysis.‡

Fig. 1 illustrates the interporphyrin arrangement in the crystal structure of **2**. As anticipated, the self-assembly process utilizes cooperatively the hydrogen-bonding potential of the amide functions,[7] affording open two-dimensional networks with no inter-penetration between them. Each porphyrin unit is involved in eight hydrogen-bonding interactions at NH···OC distances within 2.984–3.068 Å. The interporphyrin cavities in each layer are *ca.* 5.9–6.8 Å wide and *ca.* 10 Å long (estimated distances between the van der Waals surfaces of the surrounding environment). They are accommodated by two guest molecules of Me_2SO at each of the two crystallographically independent sites. One of the four species axially ligates to the metal center of a porphyrin unit in an adjacent layer at a Zn···O=S coordination distance of 2.151(7) Å. The five-coordinate Zn ion deviates by 0.28 Å from its porphyrin plane towards the axial ligand. The two-dimensional networks relate to each other by crystallographic inversion. They stack in the crystal in an offset manner with a characteristic average spacing of 4.6 Å[4a] to optimize van der Waals stabilization and the fit of the axial ligands from one layer into the interporphyrin cavities of the next layer. As shown earlier, the cavity size characteristics in such layered multiporphyrin motifs depend directly on the functional substituents attached to the porphyrin framework, which allows one to control to a considerable extent the porosity

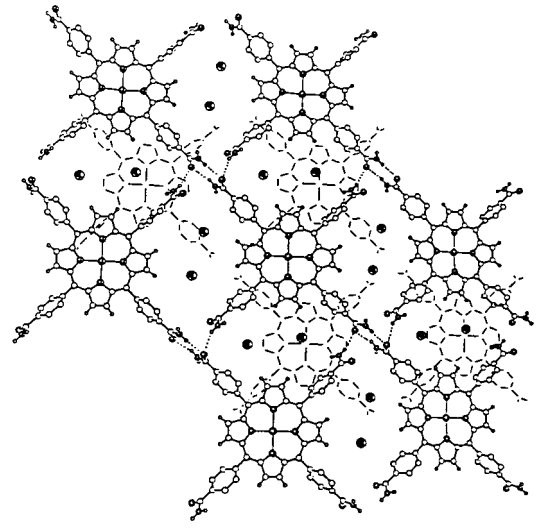

Fig. 1 Assembly of zinc tetra(4-amidophenyl)porphyrin building blocks in the form of two-dimensional open networks sustained by N–H···O=C hydrogen bonds. Each of the oval shaped interporphyrin cavities is occupied by two molecules of Me_2SO. For clarity, the positions of the latter are indicated by large darkened circles. The stick-only frameworks illustrate porphyrin molecules in a neighboring network and indicate the layered nature of the crystal structure.

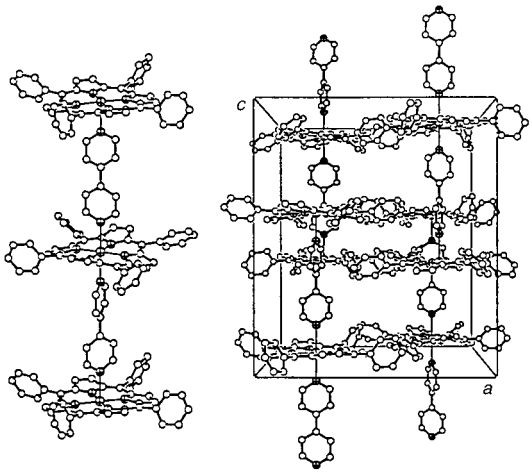

Fig. 2 (Left) Molecular structure of the coordination polymer composed of Mn^{III}–TPP and 4,4′-bipyridyl components. (Right) Perspective view of the crystal structure of this compound down the *b*-axis, showing the 'hollow' lattice of the crystal-packed polymers. The cavities are occupied by the perchlorate counter ions and by disordered solvent (not shown for clarity).

of the porphyrin layers thus formed. In relation to the present observation, the interporphyrin cavity dimensions found in homogeneous layered networks composed of tetra(4-hydroxyphenyl)porphyrin and of tetra(4-carboxyphenyl)porphyrin are 3.5 × 9.5 and 16 × 21 Å, respectively.[5]

The molecular structure of the coordination polymer units which compose **3** is displayed in Fig. 2(left). The linear polymeric strands consist of alternating metalloporphyrin and bipyridyl building blocks linked to each other from both ends by metal–ligand coordination, at Mn···N_{py} distances ranging from 2.321(7) Å to 2.409(7) Å. Along the chains the Mn···Mn separation is 11.79 Å, while between the chains the shortest Mn···Mn distance is 11.05 Å. The polymers are located on axes of twofold rotation at ($\frac{1}{4}$, 0, *z*), and extend along the *c*-axis [Fig. 2(right)]. Their side packing in the *ab* plane is stabilized by dispersive interactions between the TPP frameworks (deformed from planarity to adopt a saddle conformation) as well as by coulombic forces through the anions located in between. The parallel alignment of the polymeric chains in the crystal leads to a nanoporous architecture of the three-dimensional assembly, with tubular shaped voids between the thinner bipyridyl sections of the polymers along the *a* and *b* crystal axes (directions parallel to the porphyrin planes), that are occupied by molecules of the nitrobenzene solvent (near 0.2, $\frac{1}{4}$, $\frac{1}{4}$ and 0.8, $\frac{1}{4}$, $\frac{1}{4}$) and the perchlorate counter ions (centered at 0.50, 0.08, 0.24). The smallest cross-section distance between the van der Waals surfaces of the channel walls is *ca.* 5 Å.

The structural integrity of the multiporphyrin architectures in **2** and **3** can be in principle increased by combination of the coordination polymerization and the lateral hydrogen-bonding features in the same material. Thus, cooperative hydrogen bonding between neighboring polymeric entities in **3** (which in that structure are displaced along the *a* and *b* crystal axes) can be introduced by substituting the TPP building block with suitable recognition groups on the porphyrin periphery (*e.g.* as observed in **2**). The structure of such a designed lattice can be fine-tuned by changing the size and shape of the bridging ligand as well as of the hydrogen-bonding sites on the porphyrin periphery. We are currently exploiting this promising methodology in an effort to construct a new series of structurally robust porous organic crystals and evaluate the potential applications of such molecular-sieve materials in molecular separation, transport and controlled release.

This research was supported in part by the United States-Israel Binational Science Foundation (BSF-grant No. 94-00344), Jerusalem, Israel. The assistance of Dr Leo Straver and Nonius B.V. with diffraction measurements on the KappaCCD diffractometer is gratefully acknowledged.

Notes and References

† E-mail: goldberg@post.tau.ac.il

‡ *Crystal data*: **2**: $C_{48}H_{32}N_8O_4Zn·4C_2H_6SO·H_2O$, M_r = 1180.7, triclinic, space group $P\bar{1}$, a = 11.653(1), b = 13.901(1), c = 17.708(1) Å, α = 78.38(1), β = 88.83(1), γ = 83.47(1)°, U = 2791.5 Å^3, Z = 2, D_c = 1.405 g cm^{-3}, $F(000)$ = 1232, μ(Mo-Kα) = 6.53 cm^{-1}, crystal size ≈0.20 × 0.10 × 0.10 mm, $2\theta_{max}$ = 46.6°, 6188 unique reflections, final $R1$ = 0.086 for 3461 reflections with $F > 4\sigma(F)$, $R1$ = 0.145, $wR2$ = 0.279 and GOF = 1.026 for all 6188 data. Two out of the four Me_2SO molecules in the asymmetric unit were found disordered; for one of them a twofold orientational disorder could be recognized and modeled accordingly.

3: $C_{44}H_{28}ClMnN_4O_4·C_{10}H_8N_2·C_6H_5NO_2$, M_r = 1046.4, orthorhombic, space group *Pnna*, a = 20.489(1), b = 20.611(1), c = 23.653(1) Å, U = 9988.6 Å^3, Z = 8, D_c = 1.392 g cm^{-3}, $F(000)$ = 4320, μ(Mo-Kα) = 3.80 cm^{-1}, crystal size ≈0.30 × 0.25 × 0.10 mm, $2\theta_{max}$ = 52.7°, 9896 unique reflections, final $R1$ = 0.099 for 4823 reflections with $F > 4\sigma(F)$, $R1$ = 0.175, $wR2$ = 0.40 and GOF = 0.961 for all 9896 data. The nitrobenzene solvent molecule was found translationally as well as orientationally disordered, and could not be modeled precisely. When its contribution to the structure factors was substracted by the 'Bypass' procedure,[9] $R1$ = 0.084 for 4754 reflections with $F > 4\sigma(F)$, $R1$ = 0.144 and $wR2$ = 0.315 for all 9896 data. The large atomic displacement parameters of the perchlorate oxygens are also indicative of wide-amplitude rotational motion of this ion. The diffraction data of the poorly diffracting crystals were collected at 293(2) K on a KappaCCD diffractometer system, using Mo-Kα (λ = 0.7107 Å) radiation and 0.6° ϕ scans. CCDC 182/886.

1 V. S.-Y. Lin, S. G. DiMagno and M. J. Therien, *Science*, 1994, **264**, 1105; S. Prathapan, T. E. Johnson and J. S. Lindsey, *J. Am. Chem. Soc.*, 1993, **115**, 7519; C. A. Hunter and R. K. Hyde, *Angew. Chem., Int. Ed. Engl.*, 1996, **35**, 1936; S. Anderson, H. L. Anderson, A. Bashall, M. McPartlin and J. K. M. Sanders, *ibid.*, 1955, **34**, 1096.

2 T. J. Marks, *Angew. Chem., Int. Ed. Engl.*, 1990, **29**, 857; S. Miller and A. J. Epstein, *C&EN*, 1995, October 2nd issue, 30–41.

3 C. M. Drain and J.-M. Lehn, *Chem. Commun.*, 1994, 2313; B. F. Abrahams, B. F. Hoskins, D. M. Michail and R. Robson, *Nature*, 1994, **369**, 727; R. T. Stilbrany, J. Vasudevan, S. Knapp, J. A. Potenza, T. Emge and H. J. Schugar, *J. Am. Chem. Soc.*, 1996, **118**, 3980; E. B. Fleischer and A. M. Shachter, *Inorg. Chem.*, 1991, **30**, 3763.

4 (*a*) R. Krishna Kumar, S. Balasubramanian and I. Goldberg, *Inorg. Chem.*, 1998, **37**, 541; (*b*) H. Krupitsky, Z. Stein, I. Goldberg and C. E. Strouse, *J. Incl. Phenom.*, 1994, **18**, 177.

5 P. Dastidar, Z. Stein, I. Goldberg and C. E. Strouse, *Supramol. Chem.*, 1996, **7**, 257; I. Goldberg, H. Krupitsky, Z. Stein, Y. Hsiou and C. E. Strouse, *ibid.*, 1995, **4**, 203.

6 P. Bhyrappa, S. R. Wilson and K. S. Suslick, *J. Am. Chem. Soc.*, 1997, **119**, 8492. It has been demonstrated also that the collective effect of hydrogen bonding may lead to the formation of quite robust molecular networks of porous nature: P. Brunet, M. Simard and J. D. Wuest, *J. Am. Chem. Soc.*, 1997, **119**, 2737.

7 Y.-L. Chang, M.-A. West, F. W. Fowler and J. W. Lauher, *J. Am. Chem. Soc.*, 1993, **115**, 5991.

8 (*a*) A. Böhm, C. Vazquez, R. S. McLean, J. C. Calabrese, S. E. Kalm, J. L. Manson, A. J. Epstein and J. S. Miller, *Inorg. Chem.*, 1996, **35**, 3083 and references therein; (*b*) P. Turner, M. J. Gunter, T. W. Hambley, A. H. White and B. W. Skelton, *Inorg. Chem.*, 1992, **31**, 2297; (*c*) J. T. Lantrum, K. Hatano, W. R. Scheidt and C. A. Reed, *J. Am. Chem. Soc.*, 1980, **102**, 6729.

9 P. Van der Sluis and A. L. Spek, *Acta Crystallogr., Sect. A*, 1990, **46**, 194.

Received in Basel, Switzerland, 3rd April 1998; 8/02549E

Molecular riveting: high yield preparation of a [3]-rotaxane

Alexander G. Kolchinski,[a] Nathaniel W. Alcock,[b] Rebecca A. Roesner[a] and Daryle H. Busch*[a]†

[a] *Department of Chemistry, University of Kansas, Lawrence, Kansas 66045, USA*
[b] *Department of Chemistry, University of Warwick, Coventry, UK CV4 7AL*

An aminothiol axle molecule is so efficient at threading through the macrocycle 24-crown-8 that iodine oxidation produces a [3]-rotaxane in record yield (84%) by literally riveting two rings together.

Molecular motifs incorporating mechanically interlocked molecules, such as rotaxanes, catenanes and knots, are harbingers to a virtual molecular macrame of orderly molecular entanglements that will constitute new materials for the 21st century.[1] But the preparation of mechanically interlocked molecules presents a significant challenge,[2] and the probability of success decreases as the number of interlocked molecules increases. For example, only a few [3]- and higher rotaxanes[3] have been prepared and their yields are often low, with the highest reported yield for a [3]-rotaxane being 55%.[3] Reaping the potential of the field will depend on the detailed understanding of template reactions, including such elementary processes as molecular threading, which underlies the work reported here. In on-going studies of the relationships that favor the threading of linear molecules through cyclic molecules, we have found a methodology that produces a [3]-rotaxane in record yield (84%) by literally riveting two rings together. Such high yields open the way to molecularly interlocked polymers based on rotaxane formation.

Having learned from the threading of rings onto polymers[4] that closely positioned coordination sites strongly favor rotaxane formation, we first applied a new methodology to [2]-rotaxane formation.[5] Interaction between a functional group at the terminus of the linear component and its cyclic partner positions the tip of the linear molecule for penetration into the ring and prepays the entropic price of threading. Relaying of the binding site for the cyclic molecule from the terminal to the internal functional group completes the threading process. Closely related syntheses, based on the coordination of secondary ammonium groups to crown ethers were described shortly thereafter.[3b,e,6]

The success of our relay threading and the ease with which secondary amines form pseudo rotaxanes led to the hypothesis that, for maximum threading, the internal function of the axle molecule should bind the cyclic component substantially more strongly than does the terminal function. Further guidance, specifically applicable to [3]-rotaxanes, is provided by the recent work of Stoddart and co-workers,[3e] which relies solely on the crown ether–secondary ammonium ion interaction. For closely related structures, the yields of two [2]-rotaxanes were found to be 24 and 31%, while that for the [3]-rotaxane was only 10%. It may be significant that the fractional yield of the [3]-rotaxane is approximately the square of that for a [2]-rotaxane [$0.1 \approx (0.31)^2$]. These admittedly very limited data correspond to a simple model in which the yield of the blocking reaction may be largely controlled by the preequilibrium concentration of pseudo rotaxane. In such a case, the yield of the [3]-rotaxane is likely to be limited by the product of the yields (preequilibrium concentrations) of the two required threading processes. Therefore we suggest that the preparation of a [3]-rotaxane constitutes a powerful test for the efficiency of a given methodology for molecular threading.

A secondary ammonium group provides the primary binding site in our new axle molecule and the thiol group was selected as the terminal function because (a) it should not compete significantly with the secondary ammonium group for coordination to the crown ether, (b) it should, however, exert a relatively weak, reversible attraction for the crown ether and (c) it is well suited for a number of blocking reactions. To the best of our knowledge, the formation of strong crown ether–thiol complexes has not been reported, while, on the other hand, thiols do form easily detectable hydrogen bonds with a variety of nitrogen and oxygen containing functional groups.[7] The thioammonium salt, **I**Br, was synthesized by Schiff base condensation of 9-anthraldehyde with 2-aminoethanethiol, followed by borohydride reduction.

The oxidative coupling of the thiol groups of two pseudo rotaxane molecules provided a very convenient route for [3]-rotaxane formation (Scheme 1). Complexation of **I** with excess crown ether **II** and subsequent oxidation of the resulting complex with a small excess of iodine gave the [3]-rotaxane triiodide, **III**$(I_3)_2$, in remarkably high yield (84%) (Scheme 1). The high yield synthesis proceeds as follows: 9-anthrylmethyl(2-mercaptoethyl)ammonium bromide (**I**) (0.347 g, 1 mmol) and dibenzo-24-crown-8 (**II**) (1.344 g, 3 mmol) were dissolved at room temperature in the presence of air in a mixture of MeOH (7 ml) and $CHCl_3$ (10 ml). I_2 (0.381 g, 1.5 mmol) in $CHCl_3$ (10 ml) was slowly added over 10 min. Crystallization began after standing for 30 min. After 12 h the reaction mixture was refrigerated for 1 h and then filtered. The resulting brown crystalline product was washed with MeOH and dried in air. Larger iodine concentrations resulted in the formation of a highly crystalline adduct, **III**$(I_3)_2 \cdot 1\frac{1}{2}I_2 \cdot 2$MeOH. The mechanics of this molecular riveting reaction are closely analogous to the familar macroscopic riveting process, *i.e.* the rivet is inserted in

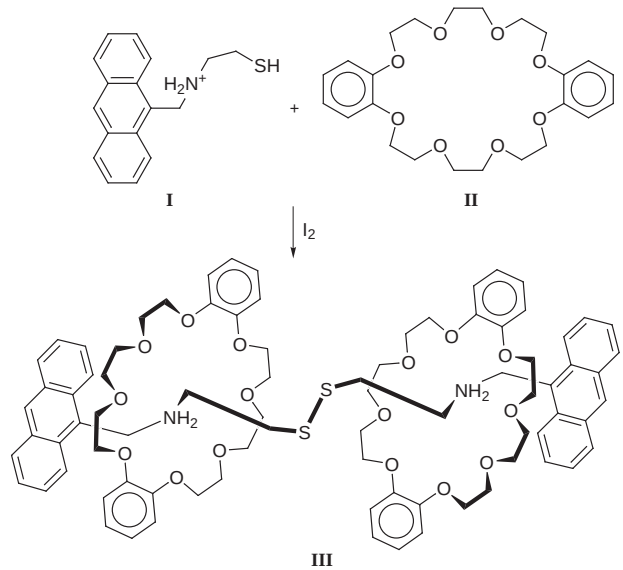

Scheme 1

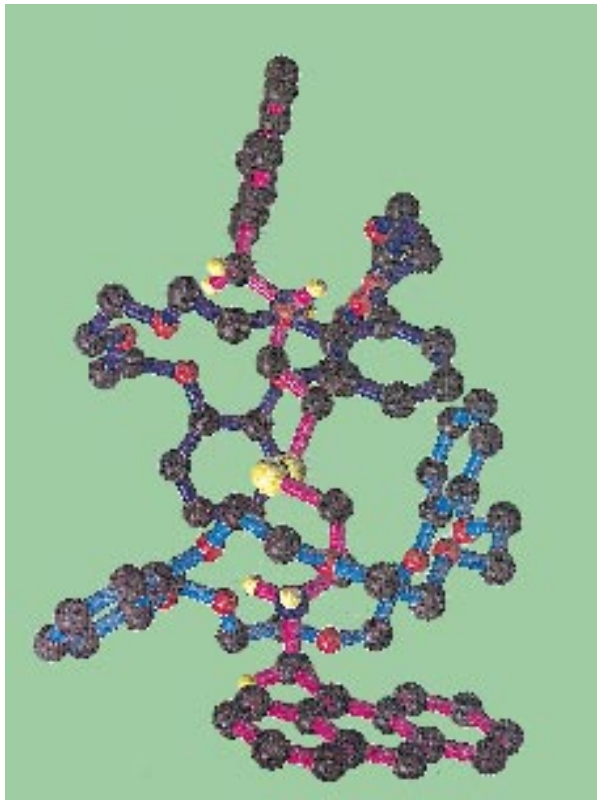

Fig. 1 Structure of the cationic [3]-rotaxane

holes in two parts that are subsequently joined together when the rivet is made complete with massive heads at each end. Referring back to the model described above, if the yield of this reaction were determined by the pseudo rotaxane preequilibrium, the pseudo rotaxane must be present in an equilibrium concentration exceeding 90%.

The crystal structure‡ of the [3]-rotaxane (Fig. 1) confirms the threading of the crown ether and clearly shows the axle–torus interactions. These include H-bonds between the amine nitrogen and the oxygen atoms of the crown, as well as [N^+–C–H···O] interactions between the methylene group adjacent to the anthryl unit and the crown ether oxygens.

The substantially higher yield obtained for **III** compared to all other rotaxanes based on secondary ammonium salt–crown ether partners, as well as the data obtained for polymeric rotaxanes,[4] strongly supports the relay threading hypothesis. Clearly, the close proximity of two binding sites on the axle molecule and the relative coordinating abilities of those two sites play important roles in facilitating these threading reactions. Further, this process of linking two molecules together by a highly efficient reaction gives promise of much new chemistry. For example, we suggest that molecular riveting will ultimately be used to produce new families of polymers and films.

This research was supported in part by the US National Science Foundation under grant number 9550487 and matching support from the state of Kansas. We thank the EPSRC and Siemens Analytical Instruments for grants in support of the diffractometer. We also thank Professor J. Fraser Stoddart for providing preprints of his publications.

Notes and References

† E-mail: DBusch@$CaCO_3$.Chem.ukans.edu

‡ *Crystal data* for **3**: 2[$C_{82}H_{98}N_2O_{16}S_2$]4[I_3]3[I_2]4MeOH, M = 5204.0, triclinic, space group $P\bar{1}$, a = 15.805(1), b = 16.0197(5), c = 19.7166(5) Å, α = 95.999(5), β = 102.880(5), γ = 94.478(5)°, U = 4813.23(7) Å^3. T = 180(2) K, Mo-Kα radiation, λ = 0.71073 Å, Z = 1, D(cal) = 1.679 mg m^{-3} μ(Mo-Kα) = 3.283 mm^{-1}. Siemens SMART three-circle system with CCD area detector. 21 986 reflections measured, 14 644 unique [R(int) = 0.0414]. Absorption correction by psi-scan. The crystals are weakly diffracting; one anthracene unit is disordered between two positions; three of the iodine positions in the polyiodide anion are incompletely occupied; and, of the two MeOH molecules in the asymmetric unit, one has a disordered oxygen position. Refinement on F^2 was accomplished using SHELXL 96 (Sheldrick, 1996) with 1049 parameters. $R1$ [for 8361 reflections with $I > 2\sigma(I)$] = 0.0980, $wR2$ (all reflections) = 0.3091. Goodness-of-fit on F^2 = 0.943. CCDC 182/873.

1 D. H. Busch, in *Transition Metal Ions in Supramolecular Chemistry*, ed. L. Fabbrizzi, Kluwer, Dordrecht, Boston, London, 1994, pp. 55–79.

2 J.-C. Chambron, C. Dietrich-Buchecker and J.-P. Sauvage, *Compr. Supramol. Chem.*, 1996, **2**, 43; D. Philp and J. F. Stoddart, *Angew. Chem., Int. Ed. Engl.*, 1996, **35**, 1154; D. B. Amabilino, F. M. Raymo and J. F. Stoddart, *Compr. Supramol. Chem.*, 1996, **2**, 85; M. Bělohradsky, F. M. Raymo and J. F. Stoddart, *Collect. Czech. Chem. Commun.*, 1996, **61**, 1; D. B. Amabilino and J. F. Stoddart, *Chem. Rev.*, 1995, **95**, 2725; H. W. Gibson, M. C. Bheda and P. T. Engen, *Prog. Polym. Sci.*, 1994, **19**, 843.

3 (*a*) S. Anderson and H. L Anderson, *Angew. Chem., Int. Ed. Engl.*, 1996, **35**, 1956; (*b*) P. R. Ashton, P. T. Glink, J. F. Stoddart, S. Menzer, P. A. Tasker, A. J. P. White and D. J. Williams, *Tetrahedron Lett.*, 1996, **37**, 6217; (*c*) M. Asakawa, P. R. Ashton, R. Ballardini, V. Balzani, M. Bělohradsky, M. T. Gandolfi, O. Kocian, L. Prodi, F. M. Raymo, J. F. Stoddart and M. Venturi, *J. Am. Chem. Soc*., 1997, **119**, 302; (*d*) D. B. Amabilino, P. R. Ashton, V. Balzani, C. L. Brown, A. Credi, J. M. J. Fréchet, J. W. Leon, F. M. Raymo, N. Spencer, J. F. Stoddart and M. Venturi, *J. Am. Chem. Soc.*, 1996, **118**, 12 012; (*e*) P. R. Ashton, P. T. Glink, J. F. Stoddart, P. A. Tasker, A. J. P. White and D. J. Williams, *Chem. Eur. J.*, 1996, **2**, 729; (*f*) N. Solladié, J.-C. Chambron, C. O. Dietrich-Buchecker and J.-P. Sauvage, *Angew. Chem., Int. Ed. Engl.*, 1996, **35**, 906; (*g*) P. R Ashton, R Ballardini, V. Balzani, M. Bělohradsky, M. T. Gandolfi, D. Philp, L. Prodi, F. M. Raymo, M. V. Reddington, N. Spencer, J. F. Stoddart, M. Venturi and D. J. Williams, *J. Am. Chem. Soc*., 1996, **118**, 4931; (*h*) F. Voegtle, T. Duennwald, M. Haendel, R. Jaeger, S. Meier and G. Harder, *Chem. Eur. J*., 1996, **2**, 640; (*i*) M. Bělohradsky, D. Philp, F. M. Raymo and J. F. Stoddart, *Organic Reactivity: Physical and Biological Aspects*, ed. B. T. Golding, R. J. Griffin and H. Maskill, Special Publication 148, Royal Society of Chemistry, Cambridge, 1955, p. 387.

4 G. Wenz and B. Keller, *Angew. Chem., Int. Ed. Engl.*, 1992, **31**, 197; D. Whang, Y.-M. Jeon, J. Heo and K. Kim, *J. Am. Chem. Soc*., 1996, **118**, 11 333.

5 A. G. Kolchinski, D. H. Busch and N. W. Alcock, *J. Chem. Soc., Chem. Commun.*, 1995, 1289.

6 P. R. Ashton, P. J. Campbell, E. J. T. Chrystal, P. T. Glink, S. Menzer, D. Philp, N. Spencer, J. F. Stoddart, P. A. Tasker and D. J. Williams, *Angew. Chem., Int. Ed. Engl.*, 1995, **34**, 1865; P. R. Ashton, E. J. T. Chrystal, P. T. Glink, S. Menzer, C. Schiavo, N. Spencer, J. F. Stoddart, P. A. Tasker, A. J. P. White and D. J. Williams, *Chem. Eur. J.*, 1996, **2**, 709; P. R. Ashton, E. J. T. Chrystal, P. T. Glink, S. Menzer, C. Schiavo, J. F. Stoddart, P. A. Tasker and D. J. Williams, *Angew. Chem., Int. Ed. Engl.*, 1995, **34**, 1869.

7 H. Mollendal, *J. Mol. Struct.*, 1983, **97**, 303; H. Wolff, in *Hydrogen Bond*, ed. P. Schuster, G. Zundel and C. Sandorfy, North-Holland, Amsterdam, 1976, vol. 3, pp. 1225–60; M. R. Crampton, in *Chem. Thiol Group, Part 1*, ed. S. Patai, Wiley, Chichester, 1974, pp. 379–415.

Received in Bloomington, IN, USA, 23rd January 1998; 8/00639C

Immobilization of semiconductor nanoparticles formed in reverse micelles into polyurea *via in situ* polymerization of diisocyanates

Susumu Shiojiri,[a] Takayuki Hirai*[a]† and Isao Komasawa[a,b]

[a] *Department of Chemical Science and Engineering, Graduate School of Engineering Science, Osaka University, Toyonaka, Osaka 560-8531, Japan*

[b] *Research Center for Photoenergetics of Organic Materials, Osaka University, Toyonaka, Osaka 560-8531, Japan*

Nanoparticles of CdS, ZnS, TiO_2 or AgI, formed in reverse micelles, have been immobilized into polyurea *via in situ* polymerization of hexamethylene diisocyanate; the CdS– or ZnS–polyurea composites obtained were utilized as photocatalysts.

There has been much recent interest in the preparation and processing methods for nanoparticles formed from various materials, including metals,[1,2] metal selenides,[3] sulfides[1,3–8] and oxides,[9] using reverse micellar systems. One of the most powerful methods for recovering the metal sulfide particles is that of particle surface modification using thiols.[3,6–8] The binding of the thiols, however, passivates the surface sulfur vacancies of the sulfide particles, and may substantially change the particle surface characteristics. Moreover, thiol modification cannot be applied to metal oxides; some of which are no less important than sulfides as catalysts and photocatalysts. The present study describes a novel immobilization method for nanoparticles formed in reverse micelles into polymer particles synthesized *in situ*. Addition of a diisocyanate, which reacts with water to form polyurea,[10] to the reverse micellar solution leads to the formation of polyurea fine particles. This polymerization in the presence of nanoparticles formed *in situ* brings about the encapsulation of the nanoparticles into the formed polyurea particles.

A reverse micellar system consisting of sodium bis(2-ethylhexyl) sulfosuccinate (AOT, 0.1 mol l^{-1}), water and isooctane (2,2,4-trimethylpentane) was used for the nanoparticle preparation. CdS or ZnS nanoparticles were prepared by the rapid addition of an AOT–isooctane micellar solution {100 ml, W_0 (= $[H_2O]/[AOT]$) = 6} containing $Cd(NO_3)_2$ or $Zn(NO_3)_2$ to another micellar solution (100 ml, W_0 = 6) containing Na_2S and stirring vigorously with a magnetic stirrer at 298 K. A glass vessel covered with aluminium film and a final composition of $[S^{2-}] = [Cd^{2+}]$ or $[Zn^{2+}] = 6.0 \times 10^{-4}$ mol l^{-1} was used. Hexamethylene diisocyanate [HDI, 0.385 ml (0.0024 mol)] was added rapidly to the nanoparticle-containing reverse micellar solution 2 min after nanoparticle formation.

The broken lines in Fig. 1 represent the absorption spectra for (*a*) CdS and (*b*) ZnS nanoparticles, 1 min after their formation in the reverse micellar systems. The absorption spectra after the HDI addition gradually increased owing to the turbidity of the polyurea (PUA) formation in the solutions. After stirring for 18 h for CdS (19.5 h for ZnS) the nanoparticles were collected together with the formed polymer powder by centrifugation. The precipitate was washed with *n*-hexane and diethyl ether and dried *in vacuo* overnight. The CdS or ZnS nanoparticle–polyurea composites are denoted CdS–PUA or ZnS–PUA, and were yellow and white, respectively, reflecting the colour of the corresponding metal sulfide particles.

Polymerization in a water–acetone homogeneous system produced irregularly shaped PUA particles of *ca.* 1 μm in diameter. Fig. 2(a) shows an FE-SEM image for metal sulfide-free PUA particles formed in the reverse micellar system and in which the PUA has led to a rather ordered morphology consisting of twisted rods. Polymerization in the presence of CdS nanoparticles, however, produced fused rod-like aggregates [Fig. 2(b)]. The presence of nanoparticles or NO_3^- may also influence polymer morphology. The PUA particles showed IR absorption peaks (1260, 1570, 1650 and 3300 cm^{-1}) attributable to urea bonds. Elemental analysis for the CdS-free PUA gave: C, 58.5; H, 10.5; N, 17.5 (calc. C, 59.1; H, 9.92; N 19.7%). The polyurea and PUA composites were slightly soluble in *m*-cresol but insoluble in most organic solvents.

The solid lines in Fig. 1 represent the absorption spectra for CdS (*c*) and ZnS (*d*) nanoparticles in PUA composites (measurement was by diffuse reflectance, owing to the turbid disperison of PUA composites in the photoreaction solution, as described below). The red shifts of the absorption onset compared with spectra (*a*) and (*b*) of Fig. 1 are due to particle growth following HDI addition. The values of the band gap for immobilized CdS and ZnS, as calculated in a previous report[5] were 2.75 and 3.92 eV, respectively, which are larger than the bulk values for CdS (2.5 eV[11]) and ZnS (3.7 eV[11]) owing to the quantum size effect.[12] The diameter of the immobilized CdS and ZnS nanoparticles was estimated using the above obtained values and the Brus' equation,[12] as also in the previous report,[5] to be 4.70 and 4.37 nm, respectively.

The metal content of the PUA composites (total analysis) was determined[8] by decomposing a given quantity of a PUA composite in concentrated H_2SO_4 and measuring the eluted metal ions, using an inductively coupled argon plasma atomic emission spectrophotometer. Since the PUA was not decomposed in HCl (6 mol l^{-1}), only the exposed sulfide particles from the PUA composite were dissolved in the acid and this was also measured. The ratio of the partial dissolved quantity, obtained *via* contact with 6 mol l^{-1} HCl, to that of the total quantity obtained *via* H_2SO_4 decomposition is denoted as particle exposed fraction *F*.[8] Table 1 lists the total metal content and the particle exposed fraction for CdS–PUA and ZnS–PUA.

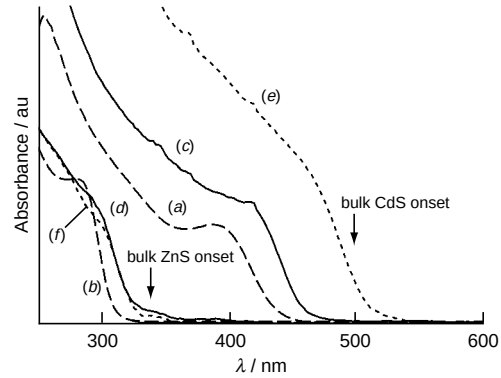

Fig. 1 Broken lines: absorption spectra of metal sulfide nanoparticles in reverse micellar systems 1 min after formation [(*a*) CdS; (*b*) ZnS]. (*c*)–(*f*): absorption spectra of metal sulfide nanoparticles immobilized in PUA composites [(*c*) and (*e*) CdS; (*d*) and (*f*) ZnS] before [solid lines, (*c*) and (*d*)] and after [dotted lines, (*e*) and (*f*)] photoirradiation for 18 h (diffuse reflectance spectra, scattering was subtracted).

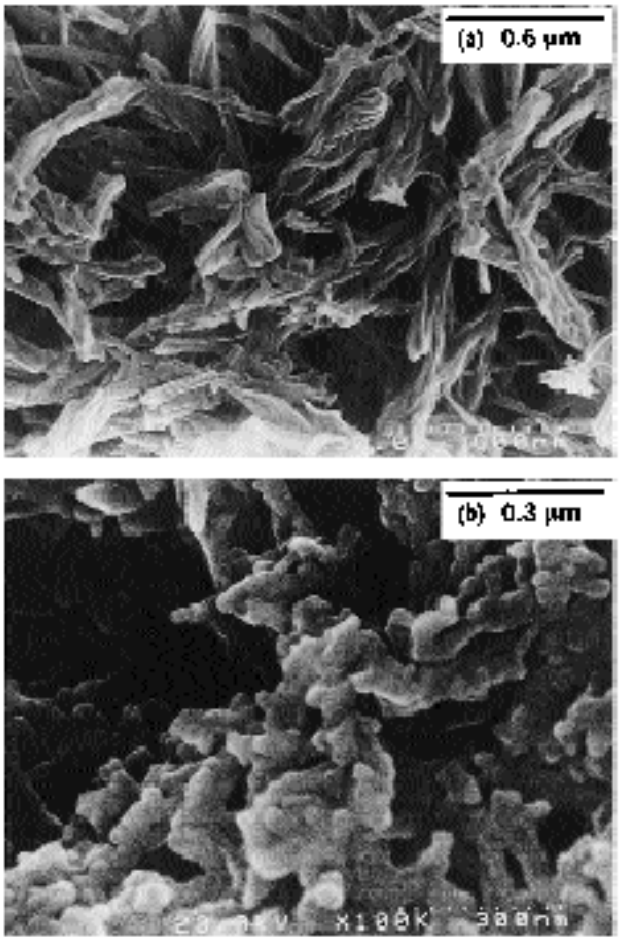

Fig. 2 SEM images for (a) metal sulfide-free PUA particles and (b) CdS–PUA prepared in a reverse micellar system

Table 1 Metal content and particle exposed fraction *F* of CdS–PUA and ZnS–PUA composites and results of photocatalytic H_2 generation

PUA composite	Total Cd or Zn content/ μmol (mg PUA composite)$^{-1}$	*F*	H_2 formed (18 h irradiation)	
			μmol (mg PUA composite)$^{-1}$	μmol (μmol exposed Cd or Zn)$^{-1}$
CdS–PUA	1.71	0.969	2.63	1.59
ZnS–PUA	1.56	0.866	8.56	6.34
CdS–PUA	1.71	0.969	0.0077	0.0047[a]
CdS-free PUA	—	—	0	—

[a] No propan-2-ol present.

The values of *F* obtained for both approach unity, thus indicating almost all sulfide nanoparticles are more or less exposed to the external solution.

Photocatalytic generation of hydrogen on the CdS–PUA or ZnS–PUA composites in a 10 vol% propan-2-ol aqueous solution was demonstrated. Such experiments, *ca.* 4 mg of PUA composite was dispersed in 25 ml of a 10 vol% propan-2-ol aqueous solution by ultrasonication with sodium hexametaphosphate (0.0125 g). 20 ml of this mixture was purged with argon for 1 h, sealed with a septum and photo-irradiated with a 2 kW xenon lamp. Irradiation light with wavelength < 300 nm and light in the IR range was cut off by the Pyrex glass of the tube and by the water filter, respectively. The quantity of H_2 formed in the gas phase in the tube was measured by gas chromatography.

The quantities of H_2 formed during the photo-irradiation of CdS–PUA or ZnS–PUA are also listed in Table 1. The H_2 generation with the PUA composites, probably *via* the reduction of water with propan-2-ol as the sacrificial agent, is very prominent as compared with the results of control experiments. ZnS–PUA is superior to CdS–PUA under the present experimental conditions, owing to the greater reducing ability of the conduction band electrons in ZnS than in CdS.

The dotted lines in Fig. 1 show the absorption spectra (diffuse reflectance spectra) for CdS–PUA (*e*) and ZnS–PUA (*f*) after photo-irradiation. The absorption onset for CdS–PUA shifts towards a longer wavelength and appears to reach that of bulk CdS, thus indicating photo-induced CdS growth *via* the fusion of CdS particles adjacent to each other in the PUA composites. The band gap for the CdS particles, after photo-irradiation, was calculated to be 2.5 eV, the same as that for bulk CdS. On the other hand, a relatively small red shift is seen for ZnS–PUA, with the band gap for the ZnS particles in ZnS–PUA after the photo-irradiation being calculated as 3.86 eV, which is larger than the bulk value of 3.7 eV.

The HDI polymerization method was also applied to nanoparticles of TiO_2 and AgI. These nanoparticles were prepared in AOT–isoocatane systems as described previously.[9,13] The nanoparticles of TiO_2 or AgI were also easily recovered from the micellar system *via in situ* polymerization of HDI and centrifugation, although the method for measuring the particle exposed fraction could not be employed in these cases.

The present study thus describes a novel immobilization method for semiconductor nanoparticles formed in reverse micelles into polyurea *via in situ* polymerization of hexamethylene diisocyanate. This may prove to be a universal method applicable to nanoparticles of any material formed in reverse micellar systems, since the surface properties of the target nanoparticles can be chosen freely. The effect of micellar conditions on PUA morphology and the photocatalytic properties of metal sulfide–PUA materials is worthy of further study.

The authors are grateful to the Division of Chemical Engineering, Department of Chemical Science and Engineering, Osaka University for the scientific support by 'Gas-Hydrate Analyzing System (GHAS)' constructed by a supplementary budget for 1995 and the financial support by a Grant-in-Aid for Scientific Research (No. 08455357) from the Ministry of Education, Science, Sports and Culture, Japan. S. S. is grateful for financial support from the Research Fellowships of the Japan Society for the Promotion of Science for Young Scientists.

Notes and References

† E-mail: hirai@cheng.es.osaka-u.ac.jp

1 M. P. Pileni, *J. Phys. Chem.*, 1993, **97**, 6961.
2 M. Kishida, T. Fujita, K. Umakoshi, J. Ishiyama, H. Nagata and K. Wakabayashi, *J. Chem. Soc., Chem. Commun.*, 1995, 763.
3 A. R. Kortan, R. Hull, R. L. Opila, M. G. Bawendi, M. L. Steigerwald, P. J. Carroll and L. E. Brus, *J. Am. Chem. Soc.*, 1990, **112**, 1327.
4 M. Meyer, C. Wallberg, K. Kurihara and J. H. Fendler, *J. Chem. Soc., Chem. Commun.*, 1984, 90.
5 T. Hirai, S. Shiojiri and I. Komasawa, *J. Chem. Eng. Jpn.*, 1994, **27**, 590.
6 J. Cizeron and M. P. Pileni, *J. Phys. Chem.*, 1995, **99**, 17 410.
7 S. Shiojiri, T. Hirai and I. Komasawa, *J. Chem. Eng. Jpn.*, 1997, **30**, 86.
8 S. Shiojiri, M. Miyamoto, T. Hirai and I. Komasawa, *J. Chem. Eng. Jpn.*, 1998, **31**, in press.
9 T. Hirai, H. Sato and I. Komasawa, *Ind. Eng. Chem. Res.*, 1993, **32**, 3014.
10 Y. Iwakura, K. Uno and K. Hamatani, *Nippon Kagaku Zasshi*, 1957, **78**, 1416.
11 P. E. Lippens and M. Lannoo, *Phys. Rev. B*, 1989, **39**, 10 935.
12 L. E. Brus, *J. Chem. Phys.*, 1984, **80**, 4403.
13 H. Sato, T. Hirai and I. Komasawa, *J. Chem. Eng. Jpn.*, 1996, **29**, 501.

Received in Cambridge, UK, 6th April 1998; 8/02588F

Reactions of ruthenium cyclopropenyl complexes with trimethylsilyl azide

Ku-Hsien Chang and Ying-Chih Lin*

Department of Chemistry, National Taiwan University Taipei, Taiwan 106, Republic of China

Treatment of three cyclopropenyl complexes [Ru]–C=C(Ph)CHR {[Ru] = (η^5-C_5H_5)(PPh_3)$_2$Ru; R = Ph 1a, CN 1b, CH=CH_2 1c} with Me_3SiN_3 afforded the nitrile complex 3a, the zwitterionic tetrazolate complex 6, and 7, respectively; for 1c, the triazole 8 was also obtained.

Organic cyclopropene is highly strained and its estimated strain energy is > 50 kcal mol^{-1} (1 cal = 4.184 J).[1] This molecule has played a crucial role in the development of important concepts such as aromaticity and chemical reactivities.[2] A few recent papers focused on applications of various cyclopropenes in organic synthesis.[3] In organometallic systems, deprotonation of a number of vinylidene complexes {[Ru]=C=C(Ph)CH_2R}I {[Ru] = (η^5-C_5H_5)(PPh_3)$_2$Ru; R = CN, Ph, CH=CH_2} readily afforded ruthenium cyclopropenyl complexes.[4] Protonation opens the three-membered rings of these Ru complexes to give back the vinylidene moiety. Nevertheless, in the ruthenium system, the cyclopropenyl and the vinylidene complexes display distinctive reactivities. We carried out reactions of cyclopropenyl complexes with various organic substrates. Herein we report the reaction of Me_3SiN_3 ($TMSN_3$) with a number of ruthenium cyclopropenyl complexes containing different substituents at the cyclopropenyl ring to yield various products.

Upon addition of a fivefold excess of $TMSN_3$ to **1a** in THF at room temperature, the solution displayed color changes during the course of the reaction. The light yellow solution of **1a** turned to deep red at the initial stage then became light orange in *ca.* 3 h and, after 5 h, turned yellow again. We thus carried out the reaction at −10 °C and, while the solution was deep red, isolated **2a**‡ as the major product and the N-coordinated nitrile complex **3a**‡ as the minor product, Scheme 1. From the light orange solution of the same reaction at room temperature, **3a** could be isolated in high yield. Finally with a 5 h reaction time the reaction gave **4**[5] and **5**.[6]‡ As a precursor of **3a**, **2a** is unstable at room temperature.

Complex **3a** is also unstable and decomposes to give **4** and **5**. Exchange of the N_3^- counter anion with PF_6^- made **2a** and **3a** more stable. In the ^{1}H NMR spectrum of **2a**, a singlet resonance at δ 3.50 is assigned to the CH_2 group. The ^{31}P NMR spectrum displays a singlet resonance at δ 42.5. However, in the ^{31}P NMR spectrum of **3a** two doublet resonances at δ 41.7 and 41.2 with J_{PP} 35.3 Hz indicate the presence of a diastereotopic center in the N-coordinated nitrile ligand and, in the ^{1}H NMR spectrum, two resonances at 3.15 (J_{HH} 16.6, 6.5 Hz) and 3.00 (J_{HH} 16.6, 10.0 Hz) are assigned to the CH_2 group. The parent peak of the mass spectrum of **3a** clearly indicates addition of one nitrogen atom to **2a**.

Treatment of **1b** with $TMSN_3$ at room temperature caused addition of four nitrogen atoms to **1b** and afforded the yellow tetrazolate complex **6**‡ in high yield and **7**‡ in *ca.* 5% yield, Scheme 1. Complex **6** is stable at room temperature, and in the course of the reaction only a deep red color attributed to a vinylidene intermediate **2b** was observed. The intermediate **2b** could be isolated at 0 °C. In the ^{1}H NMR spectrum of **6**, a dd resonance at δ 4.32 (J_{HH} 7.4, 7.7 Hz) is assigned to the methyne proton and two multiplet resonances displaying doublets of an AB pattern at δ 2.66 (J_{HH} 16.6, 7.4 Hz) and 2.44 (J_{HH} 16.6, 7.7 Hz) are assigned to two methylene protons. In the ^{31}P NMR spectrum of **6**, two doublet resonances at δ 43.8 and 41.7 with J_{PP} 38.0 Hz are assigned to the two PPh_3 ligands owing to the presence of a diastereotopic center. The proton source of the reactions of **1a** and **1b** is believed to come from water in $TMSN_3$ (no attempt was made to dry $TMSN_3$ due to potential hazards) and protons are incorporated into the product through hydrolysis of the TMS substituents. TMSOH was distilled off with THF solvent from the reaction mixture and identified by mass spectrometry. In both reactions, addition of D_2O to THF led to incorporation of two deuterium atoms at two vicinal carbon atoms of both **5** and **6**. No reaction was observed between {[Ru]=C=C(Ph)CH_2CH}PF_6 and $TMSN_3$ possibly owing to the covalent character of the Si–N bond in $TMSN_3$ and weak nucleophilicity of the cationic vinylidene complex to cleave the Si–N bond.

The reaction of **1a** with $TMSN_3$ may proceed by an electrophilic addition of a TMS group followed by hydrolysis to afford **2a**. Further nucleophilic addition of N_3^- at C_α and electrophilic addition of a second TMS group at C_β followed by loss of N_2 gives the N-coordinated nitrile complex **3a**,[5] Scheme 1. In the reaction of **1b** with $TMSN_3$, formation of **6** is

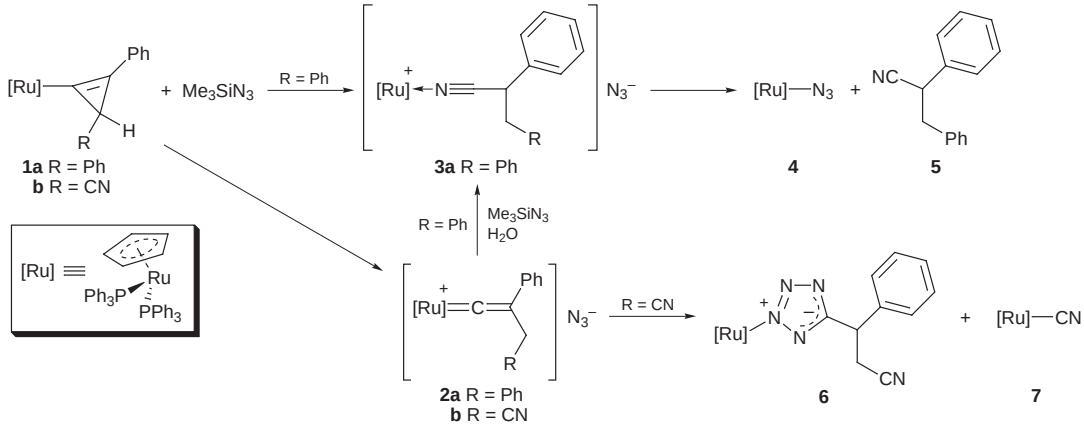

Scheme 1

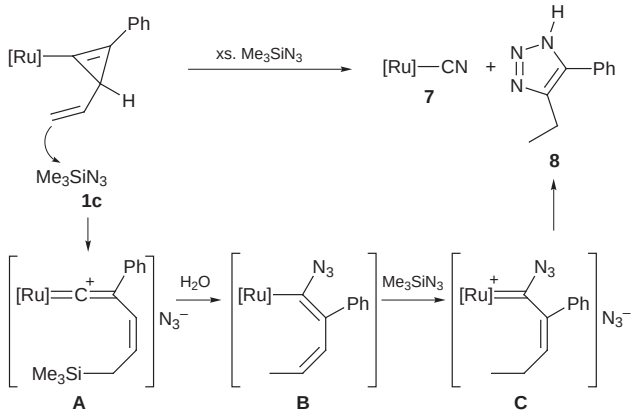

Scheme 2

rationalized by a [3 + 2] cycloaddition of the CN bond with a second N_3^-.[7] As early as 1958, formation of tetrazolate ring structure has been observed in the [3 + 2] cycloaddition reaction of a nitrile group with azide.[8] Metal-coordinated azide ligands undergo 1,3-dipolar cycloaddition reactions with carbon–carbon and carbon–heteroatom multiple bonds. Among others, this chemistry has been investigated by the group of Beck. The metals involved are most often palladium(II),[9] platinum(II)[10] and cobalt(III)[11] although a whole range of other transition metals[12] has been used. These metal azido complexes react with nitrile to give various tetrazolate complexes.[13] Formation of the tetrazolate ring in **6** is derived from the reaction of nitrile with [Ru]–N_3 since under our mild reaction condition, no such reaction was observed. The reaction of the acetylide complex [Ru]–C≡CPh with an excess of $TMSN_3$ afforded **4** and $PhCH_2CN$, identified by elemental analysis and high resolution mass spectroscopy. Conversion of a vinylidene precursor to N-coordinated nitrile by hydrazine, an organometallic Beckmann rearrangement, has been reported in an iron system.[14]

Interestingly, treatment of **1c** with an excess of $TMSN_3$ afforded **7** and **8**,‡ Scheme 2. The organic product is identified by elemental analysis and high resolution mass spectrometry. Formation of **7** and **8** by cleavage of the C=C double bond of the cyclopropenyl ring and transformation of the vinyl to an ethyl group could be explained as followed. Addition of a TMS group to the terminal carbon atom of the vinyl group accompanied by opening of the three-membered ring resulted in formation of **A**, Scheme 2. We previously reported that the reaction of TCNQ with **1c** gave similar addition at the terminal carbon of the vinyl group.[4] Subsequent nucleophilic addition of N_3^- at C_α followed by hydrolysis gave **B**. Further addition of $TMSN_3$ at C_δ followed by hydrolysis led to the formation of **C**. The single bond character of the C_α–C_β in **C** facilitates its cleavage, which is accompanied by a [3 + 2] cycloaddition of the C_β–C_γ double bond with N_3^- to give the triazole compound **8** and **7**. The fact that **7** is isolated in this reaction as the only organometallic product suggests that it is not likely to have an intermediate with a terminal N-coordinated nitrile ligand. Formation of **7** as a minor product in the reaction of **1b** with $TMSN_3$ could proceed through the same pathway. A detailed mechanism for these processes is currently under investigation.

We are grateful for support of this work by the National Science Council, Taiwan, the Republic of China.

Notes and References

† E-mail: yclin@mail.ch.ntu.edu.tw

‡ *Selected spectroscopic data*: ^{1}H and ^{13}C-{^{1}H} NMR were recorded in $CDCl_3$ relative to $SiMe_4$ and ^{31}P NMR data with H_3PO_4 as external standard in $CDCl_3$. **2a**: ^{1}H NMR, δ 7.41–6.80 (m, 45 H, Ph), 5.21 (s, 5 H, Cp), 3.56 (s, 2 H, CH_2); ^{31}P NMR, δ 42.5 (s). FAB MS: *m*/*z* 883 (M^+), 691 ($M^+ - CCPhCH_2Ph$). **2b**: ^{1}H NMR, δ 7.50–6.96 (m, 35 H, Ph), 5.21 (s, 5 H, Cp), 3.22 (s, 2 H, CH_2). **3a**: ^{1}H NMR (253 K), δ 7.43–6.85 (m, 45 H, Ph), 4.50 (t, J_{HH} 10.0, 6.5 Hz, 1 H, CH), 4.33 (s, 5 H, Cp), 3.15, (J_{HH} 16.6, 6.5 Hz, 1 H, CH_2), 3.00 (J_{HH} 16.6, 10.0 Hz, 1 H, CH_2). ^{13}C NMR (253 K), δ 136.4–127.2 (Ph), 83.6 (Cp), 41.3 (CH), 40.0 (CH_2). ^{31}P NMR, δ 41.7, 41.2 (two d, J_{PP} 35.3 Hz). FAB MS: *m*/*z* 898 (M^+), 691 ($M^+ - NCCHPhCH_2Ph$). **4**: ^{1}H NMR, δ 7.68–7.07 (m, 30 H, Ph), 4.18 (s, 5 H, Cp); ^{13}C NMR, δ 138.4–127.4 (Ph), 81.3 (Cp); ^{31}P NMR, δ 41.8 (s). FAB MS: *m*/*z* 733.1 (M^+); 705.0 ($M^+ - N_2$). Anal. Calc. for $C_{41}H_{35}N_3P_2Ru$: C, 67.20; H, 4.81; N, 5.73. Found: C, 67.92; H, 4.95; N, 4.91%. **5**: ^{1}H NMR, δ 7.43–7.09 (m, 10 H, Ph), 3.98 (dd, J_{HH} 8.4, 6.7 Hz, 1 H, CH), 3.17, (dd, J_{HH} 13.7, 6.7 Hz, 1 H, CH_2) 3.11 (dd, J_{HH} 13.7, 8.4 Hz, 1 H, CH_2). HRMS: *m*/*z* 207.1050 (M^+). Anal. Calc. for $C_{15}H_{13}N$: C, 86.92; H, 6.32; N, 6.76. Found: C. 87.01; H, 6.30; N, 6.65%. **6**: ^{1}H NMR (C_6D_6), δ 7.59–6.81 (m, 35 H, Ph), 4.45 (dd, J_{HH} 7.4, 7.7 Hz, 1 H, CH), 4.30 (s, 5 H, Cp), 2.66, (J_{HH} 16.6, 7.4 Hz, 1 H, CH), 2.44 (J_{HH} 16.6, 7.7 Hz, 1 H, CH_2); ^{13}C NMR, δ 164.1 (CNN, C_α), 140.2 (C_{ipso}), 138.3–127.1 (Ph), 118.6 (CN), 83.1 (Cp), 39.9 (CH), 23.5 (CH_2). ^{31}P NMR, δ 43.8, 41.7 (two d, J_{PP} 38.0 Hz). FABMS: *m*/*z* 889.2 (M^+ + 1, Ru = 104), 691 ($M^+ - N_4C_2HPhCH_2CN$), 429 ($M^+ - PPh_3$, $N_4C_2HPhCH_2CN$). Anal. Calc. for $C_{51}H_{43}N_5P_2Ru$: C, 68.91; H, 4.88; N, 7.88. Found: C, 69.20; H, 4.96; N, 7.96%. **7**: ^{1}H NMR, δ 7.69–6.95 (m, 30 H, Ph, 4.36 (s, 5 H, Cp); ^{13}C NMR, δ 138.2–127.3 (Ph), 85.0 (Cp); ^{31}P NMR, δ 50.3 (s). FABMS: *m*/*z* 717.0 (M^+); 691.0 ($M^+ - CN$). Anal. Calc. for $C_{42}H_{35}NP_2Ru$: C, 70.38; H, 4.92; N, 1.95. Found: C, 69.94; H, 4.85; N, 2.06%. **8**: ^{1}H NMR, δ 7.31–7.19 (m, 5 H, Ph), 2.89 (q, J_{HH} 7.6 Hz, 2 H, CH_2), 1.30 (t, J_{HH} 7.6 Hz, 3 H, CH_3). HRMS: *m*/*z* 173.0952 (M^+). Anal. Calc. for $C_{10}H_{11}N_3$: C, 69.34; H, 6.40; N, 24.26. Found: C, 69.53; H, 6.21; N, 23.98%.

1 J. F. Liebman and A. Greenberg, *Strained Organic Molecules*, Wiley, New York, 1978, p. 91; special issue on srained organic compounds, *Chem. Rev.*, 1989, 89.
2 B. Halton and M. G. Banwell, in *The Chemistry of the Cyclopropyl Group. Part 2*, ed. S. Patai and Z. Rappoport, Wiley, Chichester, 1987, ch. 21, p. 1223.
3 Y-T. Jeong, J-H. Jung and S-K. Choi, *J. Chem. Soc., Perkin Trans. 1*, 1997, 823; A. Chiang, A. S. Grant, A. J. Kresge and S. W. Paine, *J. Am. Chem. Soc.*, 1996, **118**, 4366.
4 P. C. Ting, Y. C. Lin, M. C. Cheng and Y. Wang, *Organometallics*, 1994, **13**, 2150; P. C. Ting, Y. C. Lin, G. H. Lee, M. C. Cheng and Y. Wang, *J. Am. Chem. Soc.*, 1996, **112**, 6433.
5 H. L. Ji, J. H. Nelson, A. DeCian, J. Fischer, L. Solujic and E. B. Milosavljevic, *Organometallics*, 1992, **11**, 401.
6 F. D. Lewis, B. E. Zebrowski and P. E. Correa, *J. Am. Chem. Soc.*, 1984, **106**, 187.
7 W. R. Ellis, Jr. and W. L. Purcell, *Inorg. Chem.*, 1982, **21**, 834; W. G. Jackson and S. Cortez, *Inorg. Chem.*, 1994, **33**, 1921.
8 W. G. Finnegan, R. A. Henry and R. J. Lofquist, *J. Am. Chem. Soc.*, 1958, **80**, 3908.
9 W. P. Fehlhammer and W. Beck, *Z. Naturforsch., Teil B*, 1983, **38**, 546; J. Geisenberger, J. Erbe, J. Heidrich, U. Nagel and W. Beck, *Z. Naturforsch., Teil B*, 1987, **42**, 55.
10 W. Beck and K. Schorpp, *Chem. Ber.*, 1975, **108**, 3317.
11 B. T. Hsieh, J. H. Nelson, E. B. Milosavljevic, W. Beck and T. Kemmerich, *Inorg. Chim. Acta*, 1987, 267; T. Kemmerich, J. H. Nelson, N. E. Takach, H. Bohme, B. Jablonski and W. Beck, *Inorg. Chem.*, 1982, **21**, 1226.
12 S. Kozima, T. Itano, N. Mihara, N. Sisido and T. Isida, *J. Organomet. Chem.*, 1972, **44**, 117.
13 J. C. Weis and W. Beck, *Chem. Ber.*, 1972, **105**, 3203.
14 A. G. M. Barrett, N. E. Carpenter and M. Sabat, *J. Organomet. Chem.*, 1988, **352**, C8.

Received in Cambridge, UK, 20th March 1998; 8/02199F

Phosphines exchange in quadruply bonded metal dimers: theoretical proposal for an alternative to the internal flip mechanism

Yves Jean*[a]† and Agusti Lledos*[b]‡

[a] *Laboratoire de Chimie Théorique, URA 506, Bât. 490, Université de Paris-Sud, 91405 Orsay Cedex, France*
[b] *Departament de Quimica, Universitat Autonoma de Barcelona, 08193 Bellaterra, Catalonia, Spain*

The non-concerted jumping of two phosphine ligands from one metal center to the other in $[Mo_2Cl_4(PH_3)_4]$ is found to be < 30 kcal mol^{-1} (1 cal = 4.184 J) energy costing process (DFT calculations).

Quadruply bonded complexes of $[Mo_2X_4(dpe)_2]$ type (X = halide, dpe = diphosphinoethane) may exist in two isomeric forms:[1] the α isomer with two chelating diphosphines and the β isomer with two bridging diphosphines (Fig. 1). In the former, the $Mo_2X_2P_2$ units are essentially eclipsed while internal rotational angles between 25 and 65° have been found in the latter.[2]

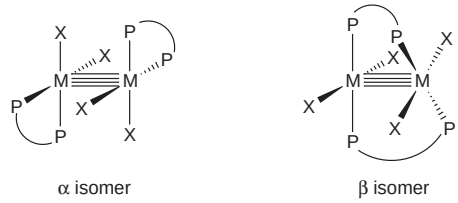

Fig. 1 Schematic structure of α and β isomers in $[Mo_2X_4(P–P)_2]$ complexes

The α → β isomerization has been observed both in solution[3–6] and in the solid state.[5,7] From the experimental data on $[Mo_2Cl_4(dppe)_2]$,[5] two mechanisms are believed to be competitive in solution: (*i*) a dissociative process in which one or both dppe ligands would break one of their M–P bonds; (*ii*) a unimolecular non-dissociative process. In the solid state, only the latter would be at work.[5] A fascinating mechanism has been proposed[4–6] for the non-dissociative process, the so-called internal flip mechanism. It involves as the rate-determining step the internal rotation of the Mo_2 unit inside the cavity formed by the eight ligand atoms (Scheme 1), followed by some internal rotation around the Mo–Mo bond. At the mid-point structure, four ligands (2P, 2X) would bridge the two metal centers. An activation energy of *ca.* 24 kcal mol^{-1} has been estimated for the non-dissociative mechanism in $[Mo_2Br_4(dppe)_2]$ (solution).[4] In the related $[Mo_2Cl_4(dppe)_2]$ complex, a similar activation energy has been measured in solution (28.9 ± 1 kcal mol^{-1}).[3] However, a much higher value (80 ± 7 kcal mol^{-1}) has been found for the solid-state reaction,[7] although the flip mechanism was believed to be at work in both phases. Since 1985 until very recently, this mechanism has been invoked for ligands exchange processes in various bimetallic complexes,[8]

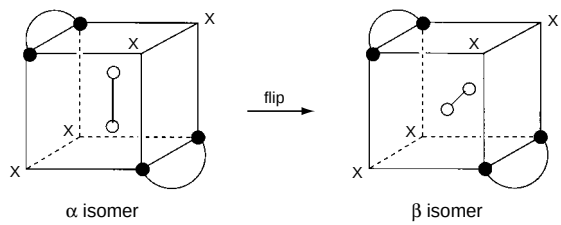

Scheme 1 Schematic picturing of the internal flip mechanism in $[M_2X_4(P–P)_2]$ complexes

the activation energies in solution lying between 20 and 29 kcal mol^{-1}.[8c,e,f]

Cayton and Chisholm have addressed the feasibility of such an intriguing process *via* an orbital symmetry analysis.[9] Fenske–Hall calculations on the $[Mo_2Cl_8]^{4-}$ complex have shown the rigid rotation of the Mo_2 unit to be a symmetry allowed process, but the Walsh diagram revealed that one π bonding MO was destabilized by about 2.5 eV and that the Mo–Mo bond should be elongated in the intermediate structure. These calculations did not however allow the authors to estimate the energy barrier associated to this mechanism.

Here we report the results of DFT calculations on the $[Mo_2Cl_4(PH_3)_4]$ complex used as a model for the real $Mo_2X_4(P–P)_2$ systems. Calculations were performed with the B3LYP functional[10] within both the restricted (RB3LYP) and the unrestricted broken-symmetry (UB3LYP-bs) formalisms.§[11,12] Structures **1** and **2**, with *cis* and *trans* phosphines on each metal center, respectively, were used as models for the α and β isomers. Full geometry optimizations led to structures of C_{2h} and D_{2d} symmetry, respectively.[13] The β isomer (**2**) was found to be the most stable, the energy difference being almost independent of the method of calculation (12.3 and 13.2 kcal mol^{-1} for RB3LYP and UB3LYP-bs methods, respectively).

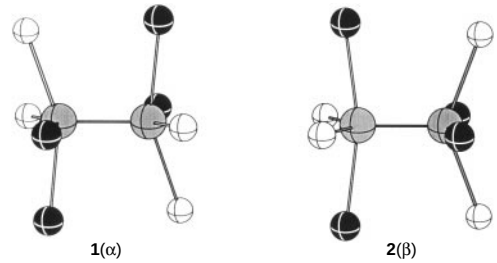

The mid-point structure associated with the flip mechanism was optimized within C_i constraint and keeping the four bridging ligands in a plane perpendicular to the Mo–Mo bond. The RB3LYP structure was found to be located 86.4 kcal mol^{-1} above the α isomer (**1**) with an Mo–Mo distance elongated to 2.525 Å. Single-point energy-only calculation of this structure using the UB3LYP-bs method led to a very similar result (89.2 kcal mol^{-1}). It is noteworthy that these values are close to the experimental activation energy reported for the α → β conversion of $[Mo_2Cl_4(dppe)_2]$ in the solid state (80 ± 7 kcal mol^{-1}).[7] Although we failed in locating a stationary point in this region of the potential energy surface, the possibility for the flip mechanism to be operative in the solid state is, at least, left open by our calculations. However, it is unlikely on energetic grounds for the reaction in solution (E_a < 30 kcal mol^{-1}). Therefore, we searched for another mechanism for the α → β isomerization reaction.

Exploration of the potential energy surface for phosphine(s) migration processes led to the localization of a stationary point which was further characterized as a transition state (a single imaginary frequency of 124i cm^{-1}). Moving along the reaction coordinate on both sides of the transition state confirmed it

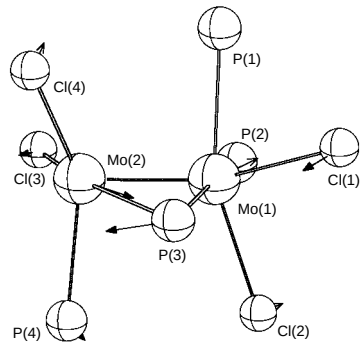

Fig. 2 Optimized geometry of the transition state for the α (**1**) → β (**2**) conversion. Hydrogen atoms of the phosphine ligands are omitted for clarity. The transition vector is also pictured.

connects the α (**1**) and β (**2**) isomers through a one-step mechanism. The main feature of the transition state structure (Fig. 2) is the presence of a single bridging phosphine (P3, initially bound to Mo2 in the α isomer), with Mo1–P3 2.820 Å and Mo2–P3 3.150 Å (UB3LYP-bs). Although P3 is closer to Mo1 than to Mo2, no Mo–P bond is fully broken at the transition state. Another interesting feature is that the Mo–Mo distance (2.181 and 2.240 Å at the RB3LYP and UB3LYP-bs levels, respectively) is *ca.* 0.3 Å shorter than in the mid-point associated with the flip mechanism and close to that found at the same level of calculations in the quadruply bonded structures **1** and **2**.[13] Last but not least, the computed activation energy (28.4 and 28.8 kcal mol^{-1} at the RB3LYP and UB3LYP-bs levels, respectively) is in good agreement with the experimental estimates for the α → β conversion of quadruply bonded metal dimers in solution.

The whole reaction mechanism is pictured in Scheme 2 (for the atom numbering, see Fig. 2). It involves first the migration of one phosphine (P3) from Mo2 toward Mo1, leading to the bridged transition state. Next P3 binds definitely Mo1, thus creating a vacancy at the Mo2 center and a distorted octahedral arrangement around Mo1. Finally P1, which is more suitably oriented than P2 with respect to the vacant site, migrates from Mo1 to Mo2 to form the β isomer. This mechanism can thus be described as the successive jumping of two phosphine ligands from one metal center to the other.

Although satisfactory in several aspects with respect to the experimental data in solution, there is however one result this mechanism does not account for: in the $[Mo_2Cl_4(dpdbp)_2]$ complex, it has been shown that the α-*syn* and α-*anti* isomers convert to the β-*syn* and β-*anti* isomers, respectively.[6] Such a stereoselectivity would require the migration of P2 instead of that of P1 in the last stage of the reaction path (Scheme 2). Such change might be due to the constraints exerted by the bridging diphosphines in real β-$[Mo_2X_4(P–P)_2]$ systems,[2] the P–Mo–Mo–P dihedral angles being smaller than in our model complex **2** (90°). These constraints should be at work not only at the very end of the reaction (β isomer) but just after the transition state has been reached, when P3 binds Mo1 (one 'bridging diphosphine' involving P4 and P3 atoms). Therefore, the reaction path for $[Mo_2Cl_4(dpe)_2]$ systems should be modified in its last stage by an internal rotation around the Mo–Mo bond which might in turn make P2 more suitably oriented than P1 for migration from Mo1 to Mo2.

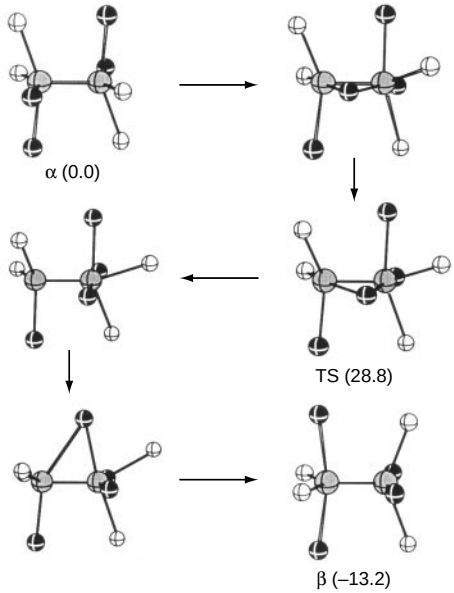

Scheme 2 Mechanism for the α (**1**) → β (**2**) conversion going through the transition state given in Fig. 2. Hydrogen atoms of the phosphine ligands are omitted for clarity.

A. L. acknowledges financial support from the DGES of Spain (Project No. PB95-0639-CO2-01). The use of computational facilities of the Institut du Développement et des Ressources en Informatique Scientifique (IDRIS) is gratefully appreciated by Y. J. Support is also acknowledged by the authors from the Action Intégrée Franco-Espagnole (96034/0236).

Notes and References

† E-mail: jean@cth.u-psud.fr
‡ E-mail: agusti@klingon.uab.es

§ Calculations were performed with the GAUSSIAN 94 series of programs[11] with a basis set of valence double-ζ quality on the metal atom[11,12a] and valence double-ζ[11,12b] + d polarization functions[12c] for the P and Cl atoms. Effective core potentials (ECP) were used to represent the 28 innermost electrons of the Mo atom[12a] as well as the electron core of the P and Cl atoms.[12b] 6-31G basis set was used for the H atoms.[12d]

1 F. A. Cotton and R. A. Walton, *Multiple Bonds between Metal Atoms*, Wiley, New York, 1982.
2 F. A. Cotton, J. L. Eglin, B. Hong and C. A. James, *Inorg. Chem.*, 1993, **32**, 2104.
3 I. F. Fraser, A. McVitie and R. D. Peacock, *J. Chem. Res. (S)*, 1984, 420.
4 P. A. Agaskar, F. A. Cotton, D. R. Derringer, G. L. Powell, D. R. Root and T. J. Smith, *Inorg. Chem.*, 1985, **24**, 2786.
5 P. A. Agaskar and F. A. Cotton, *Inorg. Chem.*, 1986, **25**, 15.
6 F. A. Cotton and S. Kitagawa, *Polyhedron*, 1988, **7**, 463.
7 A. McVitie and R. D. Peacock, *Polyhedron*, 1992, **11**, 2531.
8 (*a*) F. A. Cotton and R. L. Luck, *Inorg. Chem.*, 1989, **28**, 4522; (*b*) R. G. Abbott, F. A. Cotton and L. R. Falvello, *Polyhedron*, 1990, **9**, 1821; (*c*) H. Chen, F. A. Cotton and Z. Yao, *Inorg. Chem.*, 1994, **33**, 4255; (*d*) F. A. Cotton, E. V. Dikarev and W.-Y. Wong, *Inorg. Chem.*, 1997, **36**, 2670; (*e*) F. A. Cotton, E. V. Dikarev and W.-Y. Wong, *Inorg. Chem.*, 1997, **36**, 3268; (*f*) M. H. Chisholm, J.-H. Huang, J. C. Huffman and I. P. Parkin, *Inorg. Chem.*, 1997, **36**, 1642; (*g*) M. H. Chisholm, K. Folting, W. E. Streib and D.-D. Wu, *Inorg. Chem.*, 1998, **37**, 50.
9 R. H. Cayton and M. H. Chisholm, *Inorg. Chem.*, 1991, **30**, 1422.
10 C. Lee, W. Yang and R. G. Parr, *Phys. Rev. B*, 1988, **37**, 785; A. D. Becke, *J. Chem. Phys.*, 1993, **98**, 5648; P. J. Stephens, F. J. Delvin, C. F. Chabalowski and M. J. Frisch, *J. Phys. Chem.*, 1994, **98**, 11 623.
11 M. J. Frisch, G. W. Trucks, H. B. Schlegel, P. M. W. Gill, B. G. Johnson, M. A. Robb, J. R. Cheeseman, T. A. Keith, G. A. Petersson, J. A. Montgomery, K. Raghavachari, M. A. Al-Laham, V. G. Zakrzewski, J. V. Ortiz, J. B. Foresman, J. Cioslowski, B. B. Stefanov, A. Nanayakkara, M. Challacombe, C. Y. Peng, P. Y. Ayala, W. Chen, M. W. Wong, J. L. Andres, E. S. Replogle, R. Bomperts, R. L. Martin, D. J. Fox, J. S. Binkley, D. J. Defrees, J. Baker, J. J. P. Stewart, M. Head-Gordon, C. Gonzalez, J. A. Pople, *Gaussian 94*, Gaussian, Inc., Pittsburgh PA, 1995.
12 (*a*) P. J. Hay and W. R. Wadt, *J. Chem. Phys.*, 1985, **82**, 299; (*b*) W. R. Wadt and P. J. Hay, *J. Chem. Phys.*, 1985, **82**, 284; (*c*) A. Höllwarth, M. Böhme, S. Dapprich, A. W. Ehlers, A. Gobbi, V. Jonas, K. F. Köhler, R. Stegman, A. Veldkamp and G. Frenking, *Chem. Phys. Lett.*, 1993, **208**, 237; (*d*) W. J. Hehre, R. Ditchifeld and J. A. Pople, *J. Chem. Phys.*, 1972, **56**, 2257.
13 A. Lledos and Y. Jean, *Chem. Phys. Lett.*, 1998, **287**, 243.

Received in Basel, Switzerland, 9th April 1998; 8/02706D

The first example of a poly(ethylene oxide)–poly(methylphenylsilane) amphiphilic block copolymer: vesicle formation in water

Simon J. Holder,*[a] Roger C. Hiorns,[b] Nico A. J. M. Sommerdijk,[a] Stuart J. Williams,[a] Richard G. Jones[b] and Roeland J. M. Nolte[a]

[a] *Department of Organic Chemistry, NSR Centre, University of Nijmegen, Toernooiveld, Nijmegen 6525 ED, The Netherlands*
[b] *Centre for Materials Research, School of Physical Sciences, University of Kent, Canterbury, Kent, UK CT2 7NH*

A new amphiphilic multiblock copolymer of polymethylphenylsilane and poly(ethylene oxide) has been synthesised and demonstrated to form well-defined aggregates in water.

Polysilanes have been the subject of extensive research over the past decade due to their remarkable electronic properties that allow for a number of potential applications as conductive, electroluminescent, non-linear optical and lithograpic materials.[1] Many of these properties can be expected to be more fully exploited through the incorporation of polysilanes into copolymer systems[2] which would allow for greater processability but also allow for the manipulation of the macroscopic order of the materials by supramolecular assembly (*e.g.* by microphase separation or aggregation in aqueous dispersions). The majority of amphiphilic block copolymers, none of which are derived from polysilanes, form spherical micellar structures in aqueous dispersions.[3] Recently, further morphologies have been observed in aqueous dispersons such as rodlike, lamellar and vesicular aggregates.[4] However the formation of vesicles by block copolymers remains rare and is confined to copolymers where the component blocks are monodisperse. We report here the formation of vesicles from the multiblock poly(methylphenylsilane)-co-poly(ethylene oxide) (PMPS-PEO), in which the PMPS blocks have a normal size distribution. We believe that this is the first example of vesicle formation by a multiblock copolymer and the first defined aqueous aggregate formed by a polysilane.

The PMPS-PEO copolymer was synthesised according to Scheme 1 utilising Schlenk techniques under a dry argon atmosphere. A solution of 4.78 g of poly(ethylene oxide) (M_n = 7000, 6.8×10^{-4} mol, M_n/M_w = 1.03) in toluene was added to a solution of α,ω-dihalopoly(methylphenylsilane)[5] (M_n = 4400, 6.8×10^{-4} mol, M_n/M_w = 2.00) in THF and toluene. Subsequently pyridine (3 ml, 3.7×10^{-2} mol) was added and the reaction solution was stirred for 30 min. This solution was then added dropwise to MeOH (300 ml) and pentane (400 ml) was slowly added to the resultant mixture. PMPS-PEO was obtained as a yellowish white powder (60% yield, M_n = 27 000, M_w/M_n = 1.6) after filtration and vacuum drying for 72 h. The molecular weights quoted are based upon size-exclusion chromatography (SEC) measurements of THF solutions relative to polystyrene standards using a refractive index (RI) detector. The block structure of the copolymer was confirmed by ^{1}H, ^{13}C and ^{29}Si NMR spectroscopy and also by analysis of the molecular weight determinations of the copolymer and its precursors using both UV and RI detectors in the SEC experiment.[6]

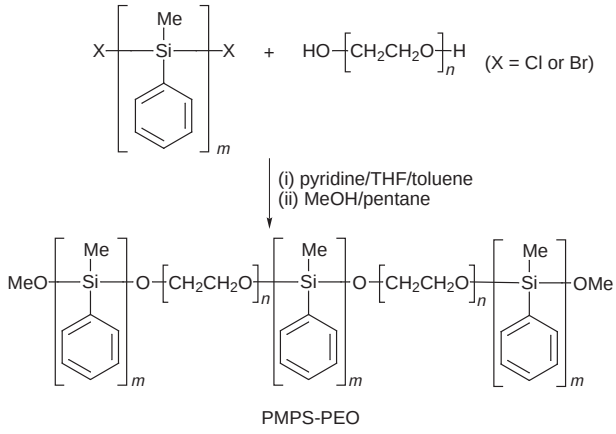

Scheme 1

Although the molecular weights have been determined relative to polystyrene standards it can be assumed that the hydrodynamic properties of the parent homopolymers and the segments in the copolymer structure are very similar. Thus the M_n value of 27 000 for the copolymer corresponds closely to the structure shown in Scheme 1, $[PMPS\text{-}PEO]_2$-PMPS, with a degree of polymerisation (DP) of 2.5.‡ This is merely the most abundant structure and comprises up to 30% of the overall distribution which ranges from PMPS-PEO to $(PMPS\text{-}PEO)_{16}$.

Direct addition of the copolymer to water (1 mg PMPS-PEO/1 ml H_2O) gave poor quality dispersions with most of the PMPS-PEO remaining as bulk solid. However transmission electron microscopic (TEM) analysis of samples of the aqueous portion of the mixture revealed vesicles [Fig. 1(*a*)].

Homogenous dispersions of the copolymer in water could be prepared in two ways. The copolymer was dissolved in THF (100 mg/10 ml THF) and water (3.5 ml) was added dropwise to the stirred solution (the solution became turbid after the addition of *ca.* 1.5 ml water). Subsequently the mixture was subjected to ultrafiltration with continuous concentration and water dilution (3 × 10 ml water). A homogenous white opaque dispersion resulted (concentration = 1.2 g l^{-1}). TEM analysis of freeze fractured samples of this dispersion showed that the copolymer existed as vesicles with remarkably little micellar material [Fig. 1(*b*)]. Both convex and concave hemispheres are clearly visible. The diameters of the vesicles ranged from *ca.* 100 nm to *ca.* 180 nm.

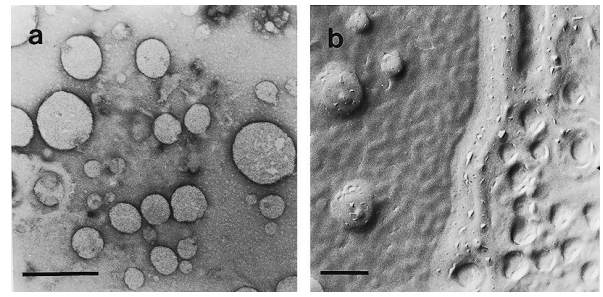

Fig. 1 Transmission electron micrographs of vesicles observed for copolymer dispersions obtained by (*a*) direct addition to water (negative staining), (*b*) ultrafiltration/dilution method (freeze-fracture). Bars represent 300 nm.

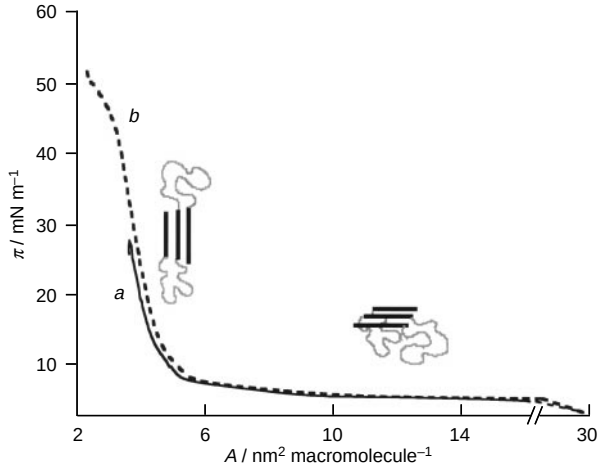

Fig. 2 π–*A* isotherms of PMPS-PEO at (*a*) pure water interface and (*b*) 100 mM $NaCl_{(aq)}$ interface

Vesicle dispersions could also be prepared by the dialysis procedure reported by Zhang and Eisenberg.[7] The copolymer dispersion in water–THF was prepared in a similar manner to the aforementioned procedure (3 ml THF, 1 ml water) and placed in a dialysis bag (exclusion limit = 20 000 Da) and dialysed against pure water (500 ml) for 72 h. EM analysis of negatively stained and platinum shadowed samples of the dispersion after this time again showed vesicles to be the predominant aggregate structure.

To confirm that the observed structures were vesicles an encapsulation experiment was performed utilising the water soluble fluorescent dye 5-carboxyfluorescein in the dialysis procedure.[8] After 72 h the dispersion was eluted (in water) through a Sephadex column (G150, mesh size 40–120 μ). The elution volume of the encapsulated dye (30–110 ml, emission at 519.5 nm) coincided with that of the copolymer (emission 355 nm) indicating that closed vesicles are formed. The elution volume of the free dye was substantially larger (160–190 ml).

To investigate the orientation of the copolymer chains in the vesicle walls surface pressure–area isotherms were recorded for a monolayer of PMS-PEO at the air/water interface.§ The isotherm revealed a very large lift-off area of *ca.* 30 nm^2 $molecule^{-1}$ which would correspond to the approximate area for three PMPS chains orientated parallel to the water surface. The observed plateau from 30 to 5 nm^2 $molecule^{-1}$ (Fig. 2) and the transition to a state characterised by a macromolecular area of 4.7 nm^2 $molecule^{-1}$ indicates a pseudo-first-order transition to a phase in which the PMPS chains become orientated perpendicular to the air/water interface. The collapse point is reached at a pressure of *ca.* 27 mN m^{-1} where the area per polymer chain is 3.7 nm^2, which is in remarkably good agreement with the estimated cross-sectional area for three PMPS rods (*ca.* 3.6 nm^2 based upon models). When PMPS-PEO was spread upon a subphase containing 0.1 M NaCl the monolayer behaviour was essentially the same, the only substantial exception being the higher collapse pressure. This tends to confirm the above model where the limiting area is defined by the PMPS segments.

UV spectroscopic analysis of the dispersion prepared by ultrafiltration revealed a very weak absorption, due to the σ–σ* transition, with a maximum at 342 nm (λ_{max} in THF = 339 nm) superimposed upon the scattering background. This is tentatively attributed to chain straightening and an extension of the effective conjugation length.

The freeze fracture electron micrographs, monolayer studies, structural considerations and UV data support a tentative model

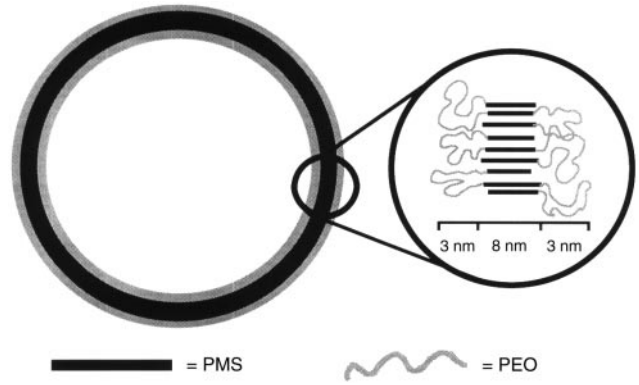

Fig. 3 Proposed model for copolymer organisation in the vesicle walls

of the packing in the vesicle walls as shown in Fig. 3.¶ It is apparent from our results that well-defined and very low polydispersity systems need not necessarily be requirements for the self-assembly of well-defined aggregates. Further work is in progress to study the structures adopted by this remarkable copolymer system.

Notes and References

† E-mail: sjh4@sci.kun.nl

‡ A polydispersity of 1.6 (recorded by SEC) corresponds to an extent of reaction, *p*, of 0.6 in terms of the kinetics of the linear step-reaction polymerisation involved in the block copolymer formation. This in turn specifies a number average degree of polymerisation (DP) of 2.5 in excellent agreement with the expected Flory distribution.[9]

§ Monolayer experiments were carried out at 20.0 ± 0.1 °C using a double barrier R&K trough of dimensions 6 × 25 cm with a compression speed of 8.8 cm^2 min^{-1}. The copolymer was spread from a solution of $CHCl_3$.

¶ The lengths of the PMPS segments were calculated from literature data;[10] light-scattering experiments have shown a strong correlation between the molecular weights obtained for polystyrene and PMPS in THF solutions by SEC.[11] The lengths of the PEO chains were based upon the molecular weight characteristics supplied by Aldrich; the width of the PEO coronae were calculated assuming repeated folding of the chain parallel to the orientation of the PMPS chains and the value given is therefore the minimum width expected.

1 R. D. Miller and J. Michl, *Chem. Rev.*, 1989, **89**, 1359; *Inorganic Polymers*, ed. J. E. Mark, H. R. Allcock and R. West, Prentice-Hall, New Jersey, 1992, ch. 5, p. 186.
2 K. Sakamoto, K. Obata, H. Hirata, M. Nakajima and H. Sakurai, *J. Am. Chem. Soc.*, 1989, **111**, 7641; S. Demoustier-Champagne, A.-F. de Mahieu, J. Devaux, R. Fayt and P. J. Teyssie, *J. Polm. Sci., Polym. Chem.*, 1993, **31**, 2009; E. Fossum, K. Matyjaszewski, S. S. Sheiko and M. Möller, *Macromolecules*, 1997, **30**, 1765.
3 C. Price, in *Developments in block copolymers*, ed. I. Goodman, Applied Science Publishers, London, 1982, vol. 1, p. 39; J. Selb and Y. Gallot, in *Developments in block copolymers*, ed. I. Goodman, Applied Science Publishers, London, 1985, vol. 2, p. 327; Z. Tuzar and P. Kratochvil, in *Surface and Colloid Science*, ed. E. Matijevic, Plenum Press, New York, 1993, vol. 15, p. 1.
4 L. Zhang and A. Eisenberg, *Science*, 1995, **268**, 1728.
5 R. C. Hiorns, R. G. Jones and F. Schue, unpublished results.
6 R. G. Jones and S. J. Holder, *Macromol. Chem. Phys.*, 1997, **198**, 3571.
7 L. Zhang and A. Eisenberg, *J. Am. Chem. Soc.*, 1996, **118**, 3168.
8 J. M. Fendler, *Membrane Mimetic Chemistry*, Wiley, New York, 1982.
9 P. J. Flory, *Principles of Polymer Chemistry*, Cornell University Press, Ithaca, New York, 1953, ch. 8.
10 W. J. Welsh, J. R. Damewood, Jr. and R. C. West, 1989, **22**, 2947.
11 C. Strazielle, A.-F. de Mahieu, D. Daoust and J. Devaux, *Polymer*, 1992, **33**, 4171.

Received in Cambridge, UK, 29th April 1998; 8/03250E

A two-step low pressure chemical vapour deposition process for the production of tungsten metal thin films

David V. Baxter, Kenneth G. Caulton, Malcolm H. Chisholm,*† Shiow-Huey Chuang and Coey D. Minear

Departments of Chemistry and Physics, Indiana University, Bloomington, IN 47405 USA

A two-step process for the production of $W_{(m)}$ thin films on Si(100) and SiO_2/Si(100) is described involving the initial low pressure chemical vapour deposition of tungsten carbide from $(Bu^tCH_2)_3W{\equiv}CBu^t$ at 350 °C followed by a post-treatment with H_2 (500–700 °C) or H_2 plasma at 350–700 °C.

Metal films find several industrial applications because of their refractory characteristics. Also applications from wear and corrosion protection to conducting layers and diffusion barriers in electronic devices are of importance. For the latter, the metals of primary interest are W, Al, Cu, Pd, Pt, Au and Ti.[1] The CVD of both $Al_{(m)}$ and $Cu_{(m)}$ have received much attention and a considerable knowledge of the chemistry involved in depositing these metals is now available. Among other things this has allowed the use of surface modification in order to obtain selectivity in deposition.[2] Of the metals noted above tungsten offers certain distinct advantages with respect to its inertness in contact with all major III–V semiconductors even at high temperatures and prolonged contact times.[3] Traditional routes to tungsten films involve reactions between WF_6 and H_2 or SiH_4.[4] These methods are not environmentally friendly because they lead to the formation of the noxious gases, HF and SiF_4. In addition, silane and WF_6 are themselves extremely reactive and require elaborate safety procedures. We describe here the first report of the production of tungsten films by a two-step low pressure chemical vapour deposition (LPCVD) process involving the use a metalloorganic precursor, $(Bu^tCH_2)_3W{\equiv}CBu^t$.

$(Bu^tCH_2)_3W{\equiv}CBu^t$ was prepared by the reacton between $(Bu^tO)_3W{\equiv}CBu^t$ and excess Bu^tCH_2MgCl in diethyl ether.[5] Low-pressure chemical vapour depositions were carried out with a simple hot-walled reactor. The substrates chosen for this study are p-type Si(100) and SiO_2/p-type Si(100) wafers. They were washed with isopropyl alcohol and light petroleum (bp 60 °C) and rinsed with distilled water (in the case of the Si wafers, HF was used) and were stored in isopropyl alcohol. The substrates were placed at the center of the hot zone (350 °C). In the first step, the precursor was transported at 55 ± 2 °C under vacuum to the deposition chamber.[5,6] Highly reflective and smooth tungsten carbide films formed on the substrates and on the wall of the hot chamber. In the second step, the amorphous tungsten carbide films were treated with H_2 (500–700 °C) or H_2 plasma in the temperature range 350–700 °C, for 2 h [eqn. (1)].

$$(Bu^tCH_2)_3W{\equiv}CBu^t \xrightarrow[\text{LPCVD}]{350\ ^\circ C} \text{Tungsten carbide} \xrightarrow[H_2 \text{ or } H_2 \text{ plasma}]{500\text{–}700\ ^\circ C} W_{(m)} \quad (1)$$

The H_2 plasma was inductively coupled at 13.5 MHz with a power density on the order of 5 W cm^{-2}.

The thin films produced after this post-deposition annealing were studied by XRD, XPS, Auger, SEM and four-point sheet resistance probes. Annealing at temperatures below 500 °C leaves amorphous films [broad XRD band centered near 39° (Cu-Kα radiation)]. Annealing at temperatures above 500 °C in an H_2 plasma produced crystalline α-W X-ray patterns but SEM revealed a rough and pitted surface morphology for these films. Films annealed in an H_2 atmosphere retained the high density and surface morphology of the original tungsten carbide films but did not produce pure α-W X-ray patterns at temperatures below 600 °C within 2 h. The XRD of a $W_{(m)}$ film on Si(100) prepared at 700 °C is shown in Fig. 1.

The chemical purity of the films was estimated by Auger spectroscopy (with depth profiling) and XPS. Figs. 2 and 3

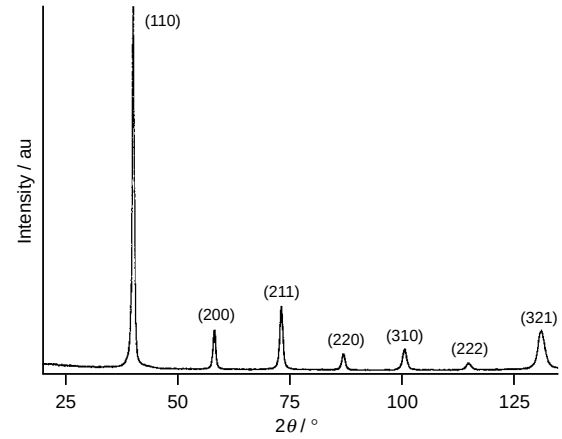

Fig. 1 X-Ray diffraction (Cu-Kα radiation) spectra of W metal film on SiO_2/Si(100) after post processing under H_2, flowing at 10 sccm, at 973 K for 2 h

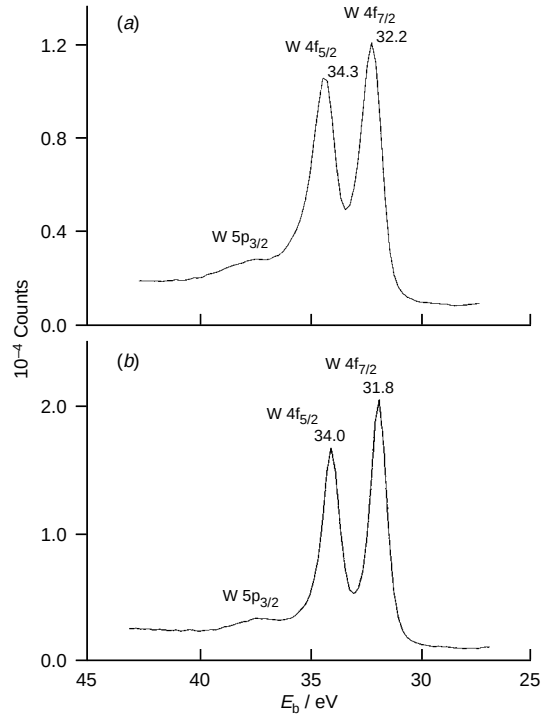

Fig. 2 (*a*) XPS spectra on W 4f region of the tungsten carbide film deposited on Si(100) under vacuum at 623 K for 2 h by $(Bu^tCH_2)_3W{\equiv}CBu^t$. (*b*) XPS spectra on the W 4f region of the tungsten metal film on Si(100) produced after post-treatment with H_2, flowing at 10 sccm, at 973 K for 2 h.

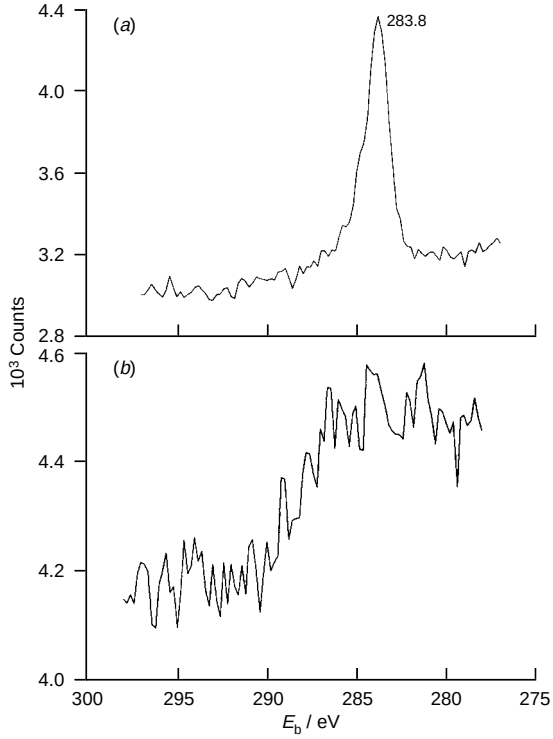

Fig. 3 (*a*) XPS spectra on the C 1s region of tungsten carbide film deposited on Si(100) under vacuum at 623 K for 2 h by $(Bu^tCH_2)_3W{\equiv}CBu^t$. (*b*) XPS spectra on the C 1s region of the tungsten metal film on Si(100) produced after post-treatment with H_2, flowing at 10 sccm, at 973 K for 2 h.

show the XPS data collected near the W 4f and C 1s energies for WC films as originally deposited and after 700 °C, H_2 annealing. These figures demonstrate a carbon content below the detection limit (*ca.* 2%) for this method.

The resistivities for all the films were $> 50\ \mu\Omega$ m, a value too large to be of direct interest for integrated circuit metallization. At least for the plasma annealed films this large resistivity could reflect the poor morphology noted above. It may be that a more gentle remote plasma treatment could produce more conductive films while still removing the carbon impurities. However, the resisitivity of our films of $W_{(m)}$ compare favorably with others produced by CVD.[7]

It should be noted that this two-step process for the production of $W_{(m)}$ films avoids the problems of high carbon content contamination that a one-step process entails when using an organometallic such as $W(CO)_6$, $W(\eta\text{-}C_6H_6)_2$, Cp_2WH_2 or $W(allyl)_4$ in the presence of an H_2 carrier gas.[1d] Indeed, in our studies we find that attempts to prepare $W_{(m)}$ from $(Bu^tCH_2)_3W{\equiv}CBu^t$ by LPCVD in the presence of H_2 results in carbonaceous films.

To conclude, we have discovered a new route for the formation of $W_{(m)}$ films by a two-step LPCVD process. The two step process may be compared with the industrially significant process employing $Ti(NMe_2)_4$ in the synthesis of TiN,[8] wherein Ti(C,N) is first formed by CVD and then in a post treatment with NH_3, converted to pure TiN. The potential advantage of the use of a volatile organometallic tungsten precursor clearly lies in the avoidance of noxious substances such as SiH_4, HF and WF_6. Other organotungsten compounds can be used to prepare tungsten carbide films[9] so one is not limited to the volatile liquid precursor $(Bu^tCH_2)_3W{\equiv}CBu^t$, though this precursor does offer the advantage of minimizing graphite content in the films. Also the present procedure does not require the use of ultrahigh vacuum procedures as has been claimed in the synthesis of $W_{(m)}$ from $W(CO)_6$ at 540 °C.[10] Further investigations of this approach seem justified.

We thank the National Science Foundation for support of this work and Professor H.-T. Chiu at the National Chiao Tung University, Taiwan, for assistance in the XPS characterization.

Notes and References

† E-mail: chisholm@indiana.edu

1 (*a*) W. Kern, *Chemical Methods of Film Deposition in Thin Film Processes*, ed. J. L. Vossen and W. Kern, Academic Press, New York, 1978; (*b*) W. Lin, B. C. Wiegand, R. G. Nuzzo and G. S. Girolami, *J. Am. Chem. Soc.*, 1996, **118**, 5977; (*c*) W. Lin, R. G. Nuzzo and G. S. Girolami, *J. Am. Chem. Soc.*, 1996, **118**, 5988; (*d*) T. Kodas and M. J. Hampden-Smith, *The Chemistry of Metal CVD*, VCH, New York, Mannheim, 1994.

2 W. L. Gladfelter, D. C. Boyd and K. F. Jensen, *Chem. Mater.*, 1989, **1**, 339; M. J. Hampden-Smith and T. T. Kodax, *Chem. Vap. Deposition*, 1995, **1**, 8; M. J. Hampden-Smith and T. T. Kodas, *Chem. Vap. Deposition*, 1995, **1**, 39; M. J. Hampden-Smith and T. T. Kodas, *Polyhedron*, 1995, **14**, 699; H.-K. Shin, K.-M. Chi, M. J. Hampden-Smith, T. T. Kodas, J. D. Farr and M. Paffet, *Mater. Res. Soc. Symp. Proc.*, 1990, **204**, 415; A. C. Jones, D. J. Houlton, S. A. Rushworth, J. A. Flanagan, J. R. Brown and G. W. Critchlow, *Chem. Vap. Deposition*, 1995, **1**, 24.

3 R. S. Williams, J. R. Lince, T. C. Tsai and J. H. Pugh, *Mater. Res. Soc. Symp. Proc.*, 1986, **54**, 335.

4 E. K. Broadbent and C. L. Ramiller, *J. Electrochem. Soc.*, 1984, **131**, 1427; H. Körner, *Thin Solid Films*, 1989, **175**, 55; C. A. van der Jeugd, G. C. A. M. Janssen and S. Radelaar, *Appl. Phys. Lett.*, 1990, **57**, 354; M. L. Yu and B. N. Eldridge, *J. Vac. Sci. Technol. A*, 1989, **7**, 1441.

5 Z. Xue, K. G. Caulton and M. H. Chisholm, *Chem. Mater.*, 1991, **3**, 384.

6 Z. Xue, S.-H. Chuang, K. G. Caulton and M. H. Chisholm, *Chem. Mater.*, in press.

7 X. Lu, J. Zhang and M. Qui, *Thin Solid Films*, 1991, **196**, 95; A. A. Zinn, B. Niemer and H. D. Kaesz, *Adv.Mater.*, 1992, **4**, 375; C. I. M. A. Spee, F. Verbeek, J. G. Kraaijkamp, J. L. Linden, T. Rutten, H. Delhaye, E. A. van der Zouwen and H. A. McInema, *Mater. Sci. Eng. B*, 1993, **17**, 108.

8 L. H. Dubois, *Polyhedron*, 1994, **13**, 1329.

9 K. K. Lai and H. H. Lamb, *Chem. Mater.*, 1995, **7**, 2284.

10 K. K. Lai, Ph.D. Thesis, North Carolina State University, Raleigh, NC, 1994; ref. 13 in ref. 9 above.

Received in Cambridge, UK, 20th March 1998; 8/02202J

First efficient synthesis of α-MAPI

Robert J. Broadbridge, Ram P. Sharma*† and Muhammad Akhtar

Division of Biochemistry and Molecular Biology, School of Biological Sciences, University of Southampton, Bassett Crescent East, Southampton, UK SO16 7PX

α-MAPI 1 and its analogues have been synthesised using tri-*tert*- butoxysilyl protected amino acids in conjunction with a solid-phase N→C assembly; the terminal aldehyde group of the peptide is generated from a C-modified amino acid containing a *gem*-diol.

MAPI (*microbial alkaline proteinase inhibitor*) is a mixture of three compounds, α-, β- and γ-MAPI possessing similar activity which are produced by *streptomyces nigrescens* WT-27.[1–3] The unique features of these peptides are that they contain terminal carboxy and aldehyde groups and a ureido (–NH–CO–NH–) function. Furthermore, α-MAPI **1** has been shown to inhibit HIV-I protease.[4] Recently, a closely related family of tetrapeptides **3**, **5** and **6** which inhibit HIV-protease has been reported.[5–7] It is hoped that these compounds may ultimately lead to the development of effective anti-proteolytic drugs for the treatment of AIDS. There is no report on the synthesis of **1** and **2**. Therefore, the synthesis of these compounds and their analogues is of paramount importance.

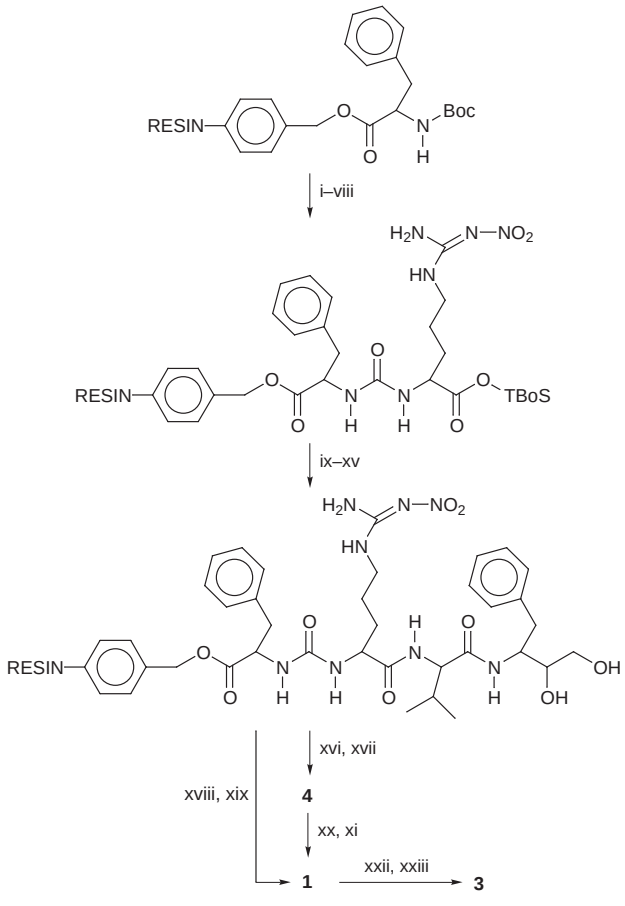

Scheme 1 *Reagents and conditions*: i, CH_2Cl_2 (2 × 1 min); ii, 50% TFA–CH_2Cl_2 (5 and 25 min); iii, CH_2Cl_2 (4 × 1 min); iv, CDI (78 mg, 0.48 mmol), CH_2Cl_2, 30 min; v, repeat iii; vi, remove 2–3 mg resin for ninhydrin assay; vii, Arg–TBos (223 mg, 0.48 mmol), CH_2Cl_2, 120 min; viii, repeat iii; ix, 25% TFA–CH_2Cl_2 (2 × 5 min); x, repeat iii; xi, Val-TBos (172 mg, 0.48 mmol); BOP–HOBt–DIPEA (1 1 : 1 : 3 equiv.), CH_2Cl_2, 120 min; xii, repeat iii, xiii, repeat ix, x; xiv, Phe-diol (87 mg)–BOP–HOBt–DIPEA (1 : 1 : 1 : 3 equiv.), DMF, 120 min; xv, DMF (2 × 1 min), CH_2Cl_2 (2 × 1 min); xvi, HF; xvii, RP-HPLC; xviii, $NaIO_4$, MeOH, 90 min; xix, repeat xv–xvii; xx, $NaIO_4$, MeOH–H_2O (80%, 2 ml), 45 min; xxi, repeat xvii; xxii, $NaBH_4$, MeOH, 30 min, AcOH; xxiii, repeat xvii. The solvent used was 10 ml throughout for 200 mg of resin.

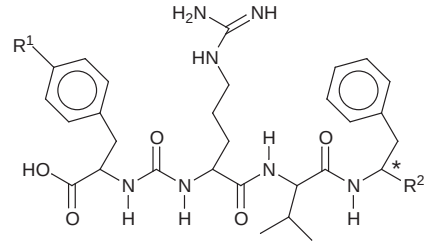

Table 1 Configuration data for **1**–**6**

Compound	R^1	R^2	Config. at *
1 α-MAPI	H	CHO	*S*
2 β-MAPI	H	CHO	*R*
3 Mer-N5075A	H	CH_2OH	*S*
4 α-MAPI-diol	H	$CHOHCH_2OH$	*S*
5 GE20372A	OH	CHO	*S*
6 GE20372B	OH	CHO	*R*

Our recently reported[8] new approach for the assembly of peptides on solid-phase from N→C direction was extended for the synthesis of α-MAPI **1** and its analogues **3** and **4** as illustrated in Scheme 1.

Boc-Phe-Merrifield resin was treated with TFA to remove the Boc group. The resin was thoroughly washed (CH_2Cl_2) and incubated with *N*,*N*′-carbonyldiimidazole (CDI). The reaction was monitored by ninhydrin assay.[9] Arginine-(N^G-NO_2)-tri-*tert*-butoxysilyl ester[8] (TBos)† was added and the mixture was shaken for 2 h. The removal of tri-*tert*-butoxysilyl group was accomplished in quantitative yield with 25% TFA. The peptide chain was further elongated by coupling valine-tri-*tert*-butoxysilyl ester followed by the deprotection of the ester group as before. Finally, the resulting peptidyl-resin was coupled to phenylalanine diol[10] in DMF to give the required peptidyl-resin. The peptide was then cleaved from the resin using liquid HF[11] and after preparative RP-HPLC followed by lyophilisation gave α-MAPI-diol **4** in 75% yield.§ Analytical and spectral data are in agreement with the assigned structure.¶

The diol **4** was smoothly oxidized with $NaIO_4$ to give α-MAPI **1**. The extent of reaction completeness was monitored by RP-HPLC and mass spectrometry. The oxidation was complete in 45 min. RP-HPLC purification afforded α-MAPI **1** in 84% yield§ and gave the expected spectral data.¶ The oxidation of the diol was also carried out on the solid-phase to give the aldehyde **1** in good yield.

α-MAPI **1** was treated with $NaBH_4$ and gave after purification the expected alcohol **3** in 64% yield.¶ Further work in this area is continuing.

Notes and References

† E-mail: RPS2@soton.ac.uk

‡ All amino acids described in this work are of L-configuration. TBos refers to the tri-*tert*-butoxysilyl group.

§ Analytical and preparative reversed-phase HPLC (RP-HLPC) experiments were performed on a Gilson 715 instrument equipped with a multi-wave length detector (Applied Biosystems 759A) and two slave 306 pumps. Retention times are given for gradient elution using the following conditions: Column, Vydac C_{18} (10 μm, 0.46 and 2.2 × 25 cm); eluent A, 0.1% (v/v) TFA in H_2O; eluent B, 0.1% (v/v) TFA in acetonitrile, gradient, 0% B over 2 min, 0–80% B over 32 min; flow rate 1 ml min^{-1} (analytical) and 10 ml min^{-1} (preparative); absorbance, 216 nm. Molecular weight determinations were carried out by electrospray (ES) Micromass Quattro II mass spectrometer.

¶ All compounds reported herein are white solids and exhibited satisfactory analytical and spectral data. *Selected data* for α-MAPI-diol **4**: single peak, retention time, 16.5 min HPLC; ESMS, *m/z* 628 $[M + H]^+$. *Selected data* for α-MAPI **1**: single peak, retention time, 16.8 min HPLC; mp 211–213 °C (decomp.) (lit.,[2] 204–205 °C); $[\alpha]_D^{24}$ 22.2 (*c* 0.9, AcOH) (lit.,[2] −18); ESMS, *m/z* 596 $[M + H]^+$ and 614 $[M + H_2O]^+$, hemi-acetal; δ_H (360 MHz, $[^2H_7]$DMF) 0.79 (d, 3H, *J* 6.7 CH–C*H*$_3$, Val), 0.81 (d, 3H, *J* 6.9, CH-C*H*$_3$, Val), 1.5–1.75 (m, 4H, CH–C*H*$_2$–C*H*$_2$, Arg), 2.08 (h, 1H, *J* 6.55, C*H*$[CH_3]_2$, Val), 3.0–3.35 (m, 4*H*, 2 × C*H*$_2$, Phe), 3.6 (2H, obscured by solvent, –CH_2–NH, Arg), 4.3–4.6 (m, 4H, 4 × methines), 6.5 (d, 1H, *J* 8), 6.7 (d, 1H, *J* 7.8), 7.2 (m, 10H, 2 × C_6H_5, Phe), 7.55 (br), 7.85 (d, 1H, *J* 8.6), 8.5 (d, 1H, *J* 7.1), 9.58 (s, 1H, C*H*O). *Selected data* for alcohol **3**: single peak, retention time, 16.8 min HPLC; mp 155 °C, softens and 180–182 °C, (decomp. lit.,[5] 182 °C); $[\alpha]_D^{24}$ −24.0 (*c* 0.5, AcOH) (lit.,[5] –24.4); ESMS, *m/z* 598 $[M + H]^+$; ^1H NMR (360 MHz) and ^{13}C NMR (90 MHz) gave expected chemical shift values.

1 S. Murao and T. Watanabe, *Agric. Biol. Chem.*, 1977, **41**, 1313.
2 T. Watanabe, K. Fukuhara and S. Murao, *Tetrahedron Lett.*, 1979, 625.
3 T. Shin-Watanabe, K. Fukuhara and S. Murao, *Tetrahedron*, 1982, **38**, 1775.
4 R. Kaneto, H. Chiba, K. Dobashi, I. Kojima, K. Sasaki, N. Shibamoto, H. Nishida, R. Okamoto, H. Akagawa and S. J. Mizuno, *J. Antibiot.*, 1993, **46**, 1622.
5 Y. Konda, Y. Takahashi, H. Mita, K. Takeda and Y. Harigaya, *Chem. Lett.*, 1997, 345.
6 E. Sarubbi, P. F. Seneci, M. R. Angelastro, N. P. Peet, M. Denaro and K. Islam, *FEBS Lett.*, 1993, **319**, 253.
7 S. Stefanelli, E. Cavaletti, E. Sarubbi, L. Ragg, L. Colombo and E. Selva, *J. Antibiot.*, 1995, 48, 332.
8 R. P. Sharma, D. A. Jones, R. J. Broadbridge, D. L. Corina and M. Akhtar, in *Innovation and Perspectives in Solid Phase Synthesis, Peptides, Proteins and Nucleic Acids, Biological and Biomedical Applications*, ed. R. Epton, Mayflower Worldwide Ltd., Birmingham, UK, 1994, p. 353; R. P. Sharma, D. A. Jones, R. J. Broadbridge, D. L. Corina and M. Akhtar, in *Peptides: Chemistry, Structure and Biology*, ed. R. S. Hodges and J. A. Smith, Leiden, ESCOM, 1994, 127; R. P. Sharma, R. J. Broadbridge, D. A. Jones, D. L. Corina and M. Akhtar, in *Peptides: Biology and Chemistry*, ed. G. Lu and J. P. Tam, Leiden, ESCOM, 1995, p. 31.
9 V. K. Sarin, S. B. H. Kent, J. P. Tam and R. B. Merrifield, *Anal. Biochem.*, 1981, **117**, 147.
10 R. P. Sharma, M. G. Gore and M. Akhtar, *J. Chem. Soc., Chem. Commun.*, 1979, 875.
11 J. P. Tam, W. F. Heath and R. B. Merrifield, *J. Am. Chem. Soc.*, 1983, **105**, 6442.

Received in Cambridge, UK, 27th March 1998; 8/02380H

Solvent and substituent effects on the sense of the enantioselective hydrogenation of pyruvate esters catalysed by Pd and Pt in colloidal and supported forms

Paul J. Collier,[a] Tracey J. Hall,[b] Jonathan A. Iggo,*[a]† Peter Johnston,[b]‡ J. Anton Slipszenko,[b] Peter B. Wells*[b] and Robin Whyman*[a]

[a] *Department of Chemistry, University of Liverpool, PO Box 147, Liverpool, UK L69 7ZD*
[b] *Department of Chemistry, University of Hull, Hull, UK HU6 7RX*

The outcome of the enantioselective hydrogenation of pyruvate esters using cinchona alkaloid-modified palladium catalysts is dependent on the choice of solvent/substituent; the sense of the enantioselectivity can be switched from *S* to *R* whilst maintaining the magnitude of the enantiomeric excess.

The enantioselective hydrogenation of methyl pyruvate (MP) and ethyl pyruvate (EP) catalysed by Pt modified by the cinchona alkaloids cinchonidine (CD) and cinchonine (CN) has received much attention over the last decade as one of only a few effective heterogeneous enantioselective systems (Scheme 1).[1–4] It is generally accepted that the adsorption of such modifiers onto a Pt surface *via* the quinoline moiety[5] provides an adjacent site at which *selective enantioface adsorption* of pyruvate occurs and at which subsequent hydrogenation provides lactate product with one enantiomer formed in excess, cinchonidine favouring the *R*- and cinchonine the *S*-enantiomer (Table 1, entries 1 and 2). Concomitant with enantioselectivity is an increase in rate, the enantioselective reaction typically being 20 to 50 times faster than the reaction in the absence of alkaloid. The corresponding Pd-catalysed reactions have been less well studied.[6–9] Two distinctive features of the Pd-catalysed reaction are that (i) the sense of the enantioselectivity is reversed with respect to that of the Pt system (*i.e.* CD directs the reaction to the *S* product and CN to the *R* product), and (ii) there is no rate enhancement.[6–8] Deuterium tracer studies have shown that, over platinum, there is direct addition of two deuterium atoms across the carbon–oxygen double bond but over palladium the main product-forming route is *via* the enolate tautomer and carbon–carbon double bond hydrogenation.[8,10]

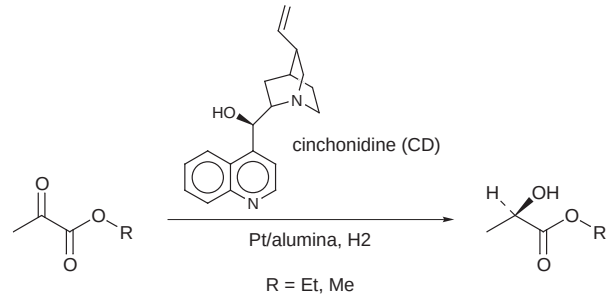

Scheme 1

Table 1 The catalytic enantioselective hydrogenation of pyruvate esters

Run	Catalyst	Reactant	Solvent/ substituent	Modifier	Pressure/bar	Initial rate[a]/ mmol s^{-1} mol_{metal}^{-1}	Ee[b] (%)
1	6.3% Pt/silica	MP	EtOH	CD	10	1550	70 (*R*)
2	6.3% Pt/silica	MP	EtOH	CN	10	1375	65 (*S*)
3	colloidal Pt/KD1	EP	MEK	CD	70	635	12 (*R*)
4	colloidal Pt/KD1	EP	MEK	CN	70	795	12 (*S*)
5	colloidal Pt/KD1	EP	MEK	none	70	35	0
6	colloidal Pt	EP	MEK	CD	70	1025	25 (*R*)
7	colloidal Pt	EP	MEK	CN	70	830	15 (*S*)
8	colloidal Pd/KD1	EP	MEK	CD	70	45	29 (*R*)
9	colloidal Pd/KD1	EP	MEK	none	70	< 5	0
10	colloidal Pd/KD1	EP	MEK	CN	70	5	12 (*S*)
11	5% Pd/alumina[c]	MP	THF	CD	10	15	10 (*S*)
12	5% Pd/alumina[c]	MP	THF	CN	10	25	12 (*R*)
13	5% Pd/alumina[c]	MP	EtOH	none	10	80	0
14	5% Pd/alumina[c]	MP	EtOH	CD	10	20	5 (*S*)
15	5% Pd/alumina[c]	MP	EtOH	CN	10	30	11 (*R*)
16	Pd/carbon[d]	MP	MeOH	CD	70	n/r	4 (*S*)
17	5% Pd/alumina[c]	MP	MEK	CD	70	30	7 (*S*)
18	5% Pd/alumina[e]	EP	MEK	CD	70	30	32 (*R*)
19	5% Pd/alumina[e]	EP	MEK	CN	70	15	7 (*S*)
20	5% Pd/alumina[c]	EP	MEK	CD	70	10	14 (*R*)
21	5% Pd/alumina[c]	EP	MEK	CN	70	5	1 (*R*)
22	5% Pd/alumina[c]	EP	EtOH	CD	70	10	8 (*R*)
23	5% Pd/alumina[c]	EP	THF	CD	10	20	15 (*R*)
24	Pd/carbon[f]	EP	EtOH	CD	70	n/r	14 (*S*)

[a] n/r = not reported. [b] Uncertainty ± 2%. [c] Johnson Matthey type 24C. Experiment performed in Hull. [d] Ref. 6. [e] Englehardt ESCAT14. Experiment performed in Liverpool. [f] Ref. 7.

We now report that the catalysis over palladium surfaces shows a more diverse chemistry than was hitherto suspected and that, depending on the choice of solvent/substituent, *each* alkaloid may give *either* enantiomer in excess.

Pt and Pd colloids stabilized with KD1, a proprietary protecting agent, were prepared by a metal vapour synthesis route[11]§ and used as catalysts in the enantioselective hydrogenation of EP.[12,13]¶ The Pt colloids gave the expected direction of enantioselectivity and rate enhancement on the basis of the known chemistry of supported platinum catalysts, *i.e.* CD and CN modification gave (*R*)- and (*S*)-lactate, respectively (Table 1, entries 3–5). The KD1 stabilizing agent was found to have only a marginal effect on the performance of the catalysts (Table 1, compare entries 3 and 4 with 6 and 7).

Surprisingly however, when modified by addition of a butan-2-one (MEK) solution of CD, the palladium colloids also gave (*R*)-lactate with ees of up to 30% in the hydrogenation of EP (entry 8), *i.e.* in the opposite sense to that previously reported for CD-modified Pd catalysts (*e.g.* entry 24).[6–8] In contrast to reactions using oxide-supported Pd catalysts these reactions also appear to show rate enhancement, the rate of the unmodified reaction being very slow (compare entries 8 and 9). The enantioselectivity induced by CN was more muted, in agreement with previous reports that CN is a less effective modifier than CD, and was in favour of (*S*)-lactate (entry 10). This is the *first* report of palladium emulating platinum in the sense of the enantioselectivity induced in pyruvate ester hydrogenation.

Previous studies of oxide-supported palladium catalysed reactions have used EtOH rather than MEK as the solvent[6,8] or have used the methyl rather than the ethyl ester as reactant.[7] In order to investigate the possibility of unprecedented solvent and/or substituent effects in Orito-type reactions, several oxide-supported palladium catalysts were modified either *in situ* or by the Orito procedure[14]‖ in EtOH, THF and MEK and used as catalysts in the hydrogenation of ethyl and methyl pyruvates. All these catalysts gave the expected[6–8] enantioselectivity, *i.e.* in the opposite sense to that observed for platinum catalysts, CD giving (*S*)- and CN (*R*)- product, and showed a reduced rate in MP hydrogenation, (entries 11–17). However, when used in ethyl pyruvate hydrogenation, CD modified catalysts gave (*R*)-lactate in substantial ee and CN modified catalysts (*S*)-lactate, (entries 18–23), *i.e. in the opposite sense to that previously reported*.[6–8] These results originate in independent studies in Liverpool (entries 18 and 19) and Hull (entries 20–23). Thus, this work is not only the *first* report of Pd following Pt in the sense of the observed enantioselectivity, but is also the *only* report, for *either* platinum or palladium, *of the direction of the enantioselectivity being solvent and/or substituent dependent.*

The mechanistic pathway of the palladium-catalysed reaction is not well-understood. Deuterium labelling experiments have shown that, in contrast to the case with Pt, over Pd the main product forming route is *via* the enol and carbon–carbon double bond hydrogenation.[8] Deuterium tracer experiments are in progress to test whether the palladium catalysed reaction in MEK also follows this mechanistic pathway.

These observations reveal that the palladium catalysed enantioselective hydrogenation of pyruvate esters is a much more complicated system than the analogous platinum-catalysed reaction and that coadsorption of solvent/substituent molecules on the Pd surface both during the modification procedure and thereafter during enantioselective hydrogenation is crucial in determining the stereochemical outcome of the reaction.

The authors thank the Catalysis Initiative of the EPSRC (J. A. I. and R. W.) and Johnson Matthey (P. B. W.) for financial support and the provision of studentships (P. J. C., T. J. H and J. A. S.).

Notes and References

† E-mail: iggo@liverpool.ac.uk
‡ Current address: Johnson Matthey PLC, Orchard Road, Royston, Herts, UK SG8 5HE

§ Colloidal metal solutions were prepared by metal vapour deposition in a Torrovap reactor. Typically 2.5 g of KD1, a proprietary protecting agent (ICI), was melted and dispersed onto the walls of the 5 l spherical chamber, after which the chamber was evacuated to 10^{-7} Torr and cooled in liquid nitrogen. 11.3 mmol of Pd was then evaporated over 2 h and co-condensed with 145 cm^3 of butan-2-one (MEK) which was simultaneously added to the vessel as vapour. After deposition the chamber was warmed to room temperature during which period a further 2.5 g KD1 in 60 cm^3 of MEK was added. Pt colloids were prepared by an analogous procedure. High resolution transmission electron microscopy showed the Pd colloids typically to have a particle size distribution ranging from 1.75 to 4.75 nm, with a maximum at 2.5 nm. After use in catalysis the particle size had increased to 2 to 9 nm with a maximum at 4 nm.

¶ A solution of the colloid containing 1 mg of Pd, modifier (6 mg, 2.0×10^{-5} mol), freshly distilled ethyl pyruvate (2.7 mg, 0.024 mol) (Aldrich)[15] and solvent/substituent (total reaction volume: 20 ml) was added to a Parr 4592 autoclave. The autoclave was sealed, purged three times with H_2 to 50 bar and then pressurized to 70 bar with H_2 and maintained at 25 ± 1 °C for 1 h.

‖ The reduced catalyst was first immersed in a solution of the alkaloid in the appropriate solvent and the slurry was then stirred in air for about 1 h before the catalyst was loaded into the high pressure reactor.

1 P. B. Wells and A. G. Wilkinson, *Top. Catal.*, in the press.
2 A. Baiker, *J. Mol. Catal. A,*, 1997, **115**, 473.
3 H-U. Blaser, H. P. Jalett, M. Muller and M. Studer, *Catal. Today*, 1997, **37**, 441.
4 R. L. Augustine and S. K. Tanielyan, *J. Mol. Catal. A*, 1997, **118**, 79.
5 G. Bond and P. B. Wells, *J. Catal.*, 1994, **150**, 329.
6 H-U. Blaser, H. P. Jallett, D. M. Monti, J. F. Reber and J. T. Wehrli, *Stud. Surf. Sci. Catal.*, 1988, **41**, 153.
7 H-U. Blaser, H. P. Jallett, M. Muller and M. Studer, *Catal. Today*, 1997, **37**, 441.
8 T. J. Hall, P. Johnston, W. A. H. Vermeer, S. R. Watson and P. B. Wells, *Stud. Surf. Sci. Catal.*, 1996, **101**, 221.
9 T. Mallat, S. Szabo, M. Schurch, U. W. Gobel and A. Baiker, *Catal. Lett.*, 1997, **47**, 221.
10 I. M. Sutherland, A. Ibbotson, R. B. Moyes and P. B. Wells, *J. Catal.*, 1990, **125**, 77.
11 R. W. Devenish, T. Goulding, B. T. Heaton and R. Whyman, *J. Chem. Soc., Dalton Trans.*, 1996, 673.
12 J. U. Kohler and J. S. Bradley, *Catal. Lett.*, 1997, **45**, 203.
13 H. Bonnemann and G. A. Braun, *Angew. Chem., Int. Ed. Engl.*, 1996, **35**, 1992; H. Bonnemann and G. A. Braun, *Chem. Eur. J.*, 1997, **3**, 1200.
14 Y. Orito, S. Imai and S. Niwa, *Nippon Kagaku Kaishi*, 1979, 1118.
15 Impurities in the pyruvate reactant can have an effect on both the rate and ee in these reactions. Ethyl pyruvate was therefore distilled daily. The same batch of ethyl pyruvate was used in the comparative study. Ethyl pyruvate supplied by Aldrich has been reported as suffering fewest problems in this regard. H-U. Blaser, H. P. Jalett and F. Spindler, *J. Mol. Catal. A*, 1996, **107**, 85; T. Mallat, Z. Bodmer, B. Minder, K. Borszelay and A. Baiker, *J. Catal.*, 1997, **168**, 183.

Received in Cambridge, UK, 9th February 1998; revised manuscript received, 18th May 1998; 8/03901A

Measurement of chiral amino acid discrimination by cyclic oligosaccharides: a direct FAB mass spectrometric approach

Masami Sawada,*[a]† Motohiro Shizuma,[b] Yoshio Takai,[a] Hiroshi Adachi,[c] Tokuji Takeda[b] and Takao Uchiyama[d]

[a] *Institute of the Scientific and Industrial Research, Osaka University, Ibaraki, Osaka 567, Japan*
[b] *Technochemistry Department, Osaka Municipal Technical Research Institute, Joto-ku, Osaka 536, Japan*
[c] *Faculty of Science, Osaka University, Toyonaka, Osaka 560, Japan*
[d] *Department of Biology, Osaka Kyoiku University, Kashihara, Osaka 582, Japan*

The novel cyclic oligosaccharides, permethylated cyclofructans MECF, 1b and 2b, discriminate enantiomers of chiral amino acid ester hydrochlorides.

Chiral discrimination of amino acids by cyclodextrins (CD) has been widely investigated in the field of liquid chromatographic and electrophoretic enantioseparations,[1–4] but that by cyclofructans (CF)[5,6] has not as yet been examined. With the application of the FAB mass spectrometry (MS)–enantiomer labelled (EL) guest method,[7–9] one of the rare methods for estimation of the chiral recognition ability of new hosts,[10] we found for the first time that permethylated cyclofructans (MECF) exhibit various degrees of chiral discrimination towards amino acid esters. This is the first successful detection of the chiral amino acid-discriminating ability of cyclic oligosaccharides on a unified scale covering the two series, where various types of complexation mechanism, such as charge-dipole electrostatic, hydrophobic and hydrogen bonding interactions are operative. An oligosaccharide host (H) is complexed with a 1:1 amino acid guest mixture of an unlabelled (*R*)-enantiomer (G_R^+) and a deuterium labelled (*S*)-enantiomer ($G_{S\text{-}Dn}^+$). The enantioselectivity of a given oligosaccharide (host) toward a given racemic amino acid (guest) is quantitatively estimated from the relative peak intensity value $\{I[(H + G_R)^+]/I[(H + G_{S\text{-}Dn})^+] = I_R/I_{S\text{-}Dn}\}$ of the two host–guest diastereomeric complex ion peaks in the FAB mass spectrum.

The cyclic oligosaccharide hosts **1b**–**5b** were permethylated so that their complex ions were sensitively detected by FAB MS. Amino acid 2-propyl ester hydrochlorides[11] were used as guests so that natural abundance correction[7] was unnecessary. All (*S*)-enantiomers were labelled with deuterium (2-propyl ester: n = 6 or 7). A 1:1 racemic mixture solution of enantiomer guests was prepared by mixing an equal amount of a 0.67 M MeOH solution of each enantiomer. A 10 μl aliquot of the guest solution and a 5 μl aliquot of a 0.20 M host $CHCl_3$ solution were added to 15 μl of the 3-nitrobenzyl alcohol (NBA) matrix. A 1 μl sample of the final mixture was used for obtaining FAB mass spectra. A typical FAB mass spectrum is shown in Fig. 1, and the $I_R/I_{S\text{-}Dn}$ values obtained are summarized in Table 1. MECF6 **1b** and MECF7 **2b** showed higher (*R*)-enantioselectivity for $[Trp\text{-}O\text{-}Pr^i]^+$ ($I_R/I_{S\text{-}Dn}$ = 1.38–1.29; $-\Delta\Delta G_{enan}$ = 150–190 cal mol^{-1}) [$-\Delta\Delta G_{enan} = RT\ln(I_R/I_{S\text{-}Dn})$ was employed for interconversion].[7–9] MECF6 **1b** for $[Tle\text{-}O\text{-}Pr^i]^+$ and MECF7 **2b** for $[Ser\text{-}O\text{-}Pr^i]^+$ or $[Pro\text{-}O\text{-}Pr^i]^+$ provided the next best (*R*)-enantioselectivities. On the other hand, MECF7 **2b** for $[Pgly\text{-}O\text{-}Pr^i]^+$ showed an inverse (*S*)-enantioselectivity ($I_R/I_{S\text{-}Dn}$ = 0.76). β-MECD **4b** and γ-MECD **5b** indicated (*R*)-enantioselectivity for $[Ser\text{-}O\text{-}Pr^i]^+$ and $[Pro\text{-}O\text{-}Pr^i]^+$ ($I_R/I_{S\text{-}Dn}$ = *ca.* 1.15; $-\Delta\Delta G_{enan}$ = *ca.* 80 cal mol^{-1}).

Among many thermodynamic chiral discrimination studies, the chiral discrimination of simple amino acids by CDs on the basis of the host–guest (1:1) intermolecular interactions has rarely been reported until now. In one of the reports, Lincoln determined the relative binding constant (K_R/K_S = 0.92 in water at 295.5 K) of α-MECD **3b** with 4-fluorophenylglycine hydrochloride using the ^{19}F NMR titration method.[12,13] The enantioselectivity of α-MECD **3b** for the corresponding $[Pgly\text{-}O\text{-}Pr^i]^+$ under our FAB MS conditions ($I_R/I_{S\text{-}Dn}$ = 0.94) was in a good agreement with the above K_R/K_S value. It is worthwhile to note that this is further experimental evidence for the parallels between the $I_R/I_{S\text{-}Dn}$ and K_R/K_S values which have been described previously.[7–9] The NOE behavior of α-CD **3a** with Trp using ^1H NMR analysis suggested (*R*)-enantioselectivity,[14]

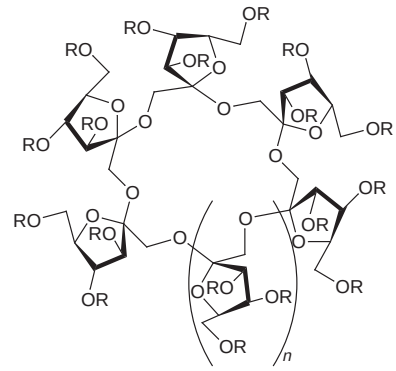

1a CF6, n = 1, R = H
b MECF6, n = 1, R = Me
2a CF7, n = 2, R = H
b MECF7, n = 2, R = Me

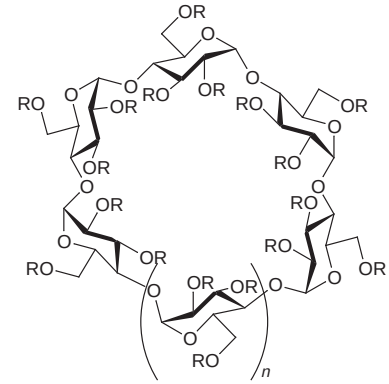

3a α-CD, n = 1, R = H
b α-MECD, n = 1, R = Me
4a β-CD, n = 2, R = H
b β-MECD, n = 2, R = Me
5a γ-CD, n = 3, R = H
b γ-MECD, n 3, R = Me

Table 1 $I_R/I_{S\text{-}Dn}$ values of permethylated cyclic oligosaccharide hosts with amino acid ester hydrochloride guests[a]

Guest (counter anion: Cl^-)	Host: MECF6 **1b**	MECF7 **2b**	α-MECD **3b**	β-MECD **4b**	γ-MECD **5b**	18-C-6
$[Trp\text{-}O\text{-}Pr^i]^+$	1.38	1.29	1.29	1.23	1.17	0.98
$[Pgly\text{-}O\text{-}Pr^i]^+$	0.99	0.76	0.94	0.91	0.89	0.99
$[Phe\text{-}O\text{-}Pr^i]^+$	1.00	1.01	1.02	1.01	1.00	1.02
$[Tle\text{-}O\text{-}Pr^i]^+$	1.18	1.00	0.95	0.94	0.93	0.97
$[Met\text{-}O\text{-}Pr^i]^+$	1.04	0.95	0.91	0.91	0.92	0.96
$[Ser\text{-}O\text{-}Pr^i]^+$	1.01	1.18	0.95	1.15	0.99	0.96
$[Pro\text{-}O\text{-}Pr^i]^+$	1.08	1.16	1.07	1.07	1.14	0.96
$[Gly\text{-}O\text{-}Pr^i]^+$	1.01	0.99	0.97	0.98		0.99

[a] 18-crown-6 (18-C-6) is the typical achiral host employed. Glycine 2-propyl ester $(Gly\text{-}O\text{-}Pr^i)^+$ is the typical achiral guest employed. Averaged value (n = 4) of 10th, 20th, 30th and 40th scan data. Errors of the $I_R/I_{S\text{-}Dn}$ values are estimated within ±0.04. Tle = *tert*-leucine, Pgly = phenylglycine.

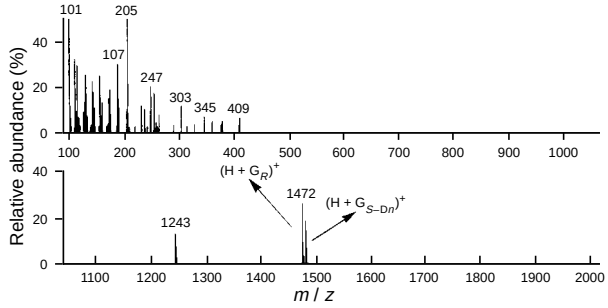

Fig. 1 An example of a FAB mass spectrum from the FABMS/EL guest method. Host: MECF6 **1b**; guest: $[Trp\text{-}O\text{-}Pr^i]^+$. The left peak ($m/z$ 1472) is a complex ion $(H + G_R)^+$ and the right (m/z 1478) is $(H + G_{S\text{-}Dn})^+$.

which was also in line with our results obtained by FAB MS (α-MECD **3b** with $[Trp\text{-}O\text{-}Pr^i]^+$; $I_R/I_{S\text{-}Dn}$ = 1.29).

The crystalline structure of a complex of MECF6 **1b** with Ba^{2+} (counter anion: SCN^-) that was reported previously showed that the cation was coordinated at ten points to the host, four 3-OMe oxygens of the furanose rings and six oxygens in the 18-crown-6 skeleton (Fig. 2).[6] In the case of a complex of MECF6 with amino acid ester hydrochlorides, it is expected that the 3-OMe groups become chiral barriers for the indole or *tert*-butyl groups of the corresponding chiral guest. The difference in the stereochemical complementarity would be origin of the chiral discrimination of MECF6 **1b**.

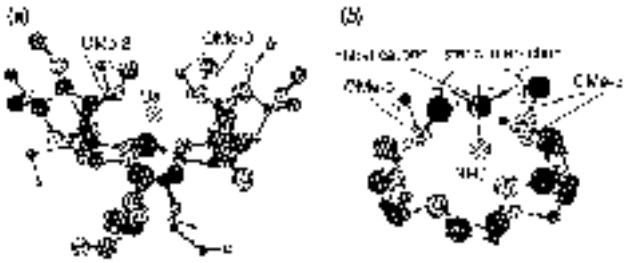

Fig. 2 (*a*) Crystalline complex of **1b** with barium cation (counter anion: SCN^-). Hydrogen atoms are not shown. (*b*) Imaged illustration of a complex of **1b** with an alkylammonium ion. The nitrogen cation of the alkylammonium replaced the barium from (*a*). The α-carbon of the alkylammonium ion was localized at a position of 1.49 Å from the nitrogen, an average C–N distance in amino acids.

We are studying in detail the mechanism of chiral discrimination of the cyclofructans. We hope that cyclofructans and their derivative hosts will be amenable to the further development of new chiral stationary phases and chiral selectors.

We are very grateful to Mitsubishi Chemical Co. for the kind gift of cyclofructans (**1a**, **2a** and the other oligomers).

Notes and References

† E-mail: m-sawada@sanken.osaka-u.ac.jp

1 D. W. Armstrong, A. M. Stalcup, M. H. Hilton, J. D. Duncan, J. R. Faulkner and S. C. Chang, *Anal. Chem.*, 1990, **62**, 1610.
2 A. Berthod, S. C. Chang and D. W. Armstrong, *Anal. Chem.*, 1992, **64**, 395.
3 S. Fanali, *J. Chromatogr.*, 1989, **474**, 441.
4 V. Schurig and H.-P. Nowotny, *Angew. Chem., Int. Ed. Engl.*, 1990, **29**, 939.
5 M. Kawamura, T. Uchiyama, T. Kuramoto, Y. Tamura and K. Mizutani, *Carbohydr. Res.*, 1989, **192**, 83.
6 Y. Takai, Y. Okumura, T. Takana, M. Sawada, S. Takahashi, M. Shiro, M. Kawamura and T. Uchiyama, *J. Org. Chem.*, 1994, **59**, 2967.
7 X. X. Zhang, J. S. Bradshaw and R. M. Izatt, *Chem. Rev.*, 1997, **97**, 3133.
8 M. Sawada, Y. Takai, H. Yamada, S. Hirayama, T. Kaneda, T. Tanaka, K. Kamada, T. Mizooku, S. Takeuchi, K. Ueno, K. Hirose, Y. Tobe and K. Naemura, *J. Am. Chem. Soc.*, 1995, **117**, 7726.
9 M. Sawada, *Mass Spectrom. Rev.*, 1997, **16**, 73.
10 M. Sawada, Y. Takai, H. Yamada, J. Nishida, T. Kaneda, R. Arakawa, M. Okamoto, K. Hirose, T. Tanaka and K. Naemura, *J. Chem. Soc., Perkin Trans. 2*, 1998, 701.
11 E. P. Kyba, J. M. Timko, L. J. Kaplan, F. de Jong, G. W. Gokel and D. J. Cram, *J. Am. Chem. Soc.*, 1978, **100**, 4555.
12 C. J. Easton and S. F. Lincoln, *Chem. Soc. Rev.*, 1996, 163.
13 S. E. Brown, C. J. Easton and S. F. Lincoln, *J. Chem. Res.* (*S*), 1995, 2.
14 K. B. Lipkowitz, S. Raghothama and J. Yang, *J. Am. Chem. Soc.*, 1992, **114**, 1554.

Received in Cambridge, UK, 23rd April 1998; 8/03023E

Importance of intramolecular hydrogen bonding for preorganization and binding of molecular guests by water-soluble calix[6]arene hosts

Julio Alvarez, Yun Wang, Marielle Gómez-Kaifer and Angel E. Kaifer*†

Chemistry Department, University of Miami, Coral Gables, FL 33124-0431, USA

The binding affinity of calix[6]arene hexasulfonate hosts for ferrocene or cobaltocenium guests is highly dependent on the extent of intramolecular hydrogen bonding in the lower rim of the calixarene.

The calixarenes[1] are an interesting and extensively studied class of host molecules characterized by their aromatic character and conformational flexibility. Water-soluble calixarenes are commonly prepared by sulfonation of the aromatic rings, yielding a family of negatively charged hosts.[2] We have previously reported on the binding ability in aqueous solution of sulfonated calixarene hosts with different molecular guests.[3,4] Here, we concentrate our attention on calix[6]arenes **1** and **2** (Fig. 1) and report our findings on the striking differences in the binding affinity exhibited by these two calixarene hosts towards the same guests (ferrocene and cobaltocenium derivatives, Fig. 1). The differences observed can be rationalized on grounds of host preorganization due to intramolecular hydrogen bonding in the calixarene's lower rim.

Calixarene **1** exists in neutral aqueous solution as an octaanion due to the deprotonation of two of its phenolic OH groups. Atwood *et al.* reported the X-ray crystal structure of the sodium salt of $\mathbf{1}^{8-}$.[5] They found that this host exhibits a partial cone conformation with three adjacent sulfonate groups pointing to one side of the cavity and the remaining three sulfonates pointing to the opposite end. The structure is rigidified by hydrogen bonding of each negatively charged phenolate to the two neighboring phenolic OH groups, as shown in Fig. 1. This crystal structure was postulated to be very close to the average solution structure due to the high level of hydration of the crystal.[5]

The accessible electroactivity of the selected guests‡ allowed us to readily examine the binding interactions between each calixarene–guest pair using voltammetric techniques. Relevant electrochemical data are given in Tables 1 and 2. Host **1** forms stable complexes in pH 7.0 aqueous media with all the guests surveyed. This is shown by the decreased current levels observed upon addition of $\mathbf{1}^{8-}$ on the voltammetric waves for the oxidation of the ferrocene guests as well as on those for the reduction of the cobaltocenium guests. This current decrease reveals the association of $\mathbf{1}^{8-}$ with all the guests prior to any electrochemical conversions. In addition to this, the half-wave potential ($E_{1/2}$) for the oxidation of the ferrocene guests shifts to less positive values in the presence of $\mathbf{1}^{8-}$ and the $E_{1/2}$ values for reduction of the cobaltocenium guests shift to more negative values. This is consistent with the octaanionic host binding more strongly to the oxidation states of the guests bearing a higher positive charge.

Similar experiments with $\mathbf{2}^{6-}$, the O-methylated analog of calixarene host $\mathbf{1}^{8-}$, yield very different results. First, addition of this calixarene does not affect the current levels of the voltammetric waves. Secondly the $E_{1/2}$ values also remain

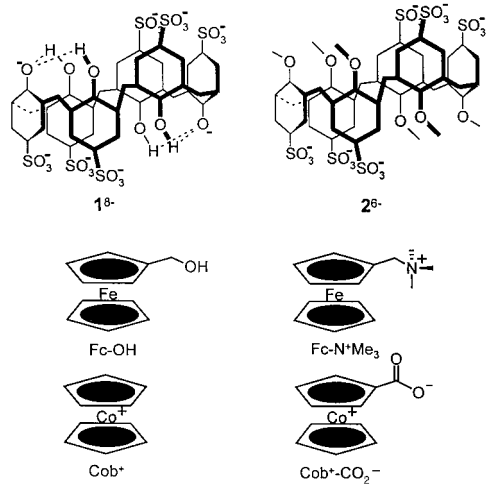

Fig. 1 Structures of calixarene hosts and molecular guests studied in this work

Table 1 Voltammetric data at 25 °C for different guests (1.0 mM) in the absence and in the presence of two calixarene hosts. Medium: 0.1 M phosphate buffer (pH 7)

		Host $\mathbf{1}^{8-}$		Host $\mathbf{2}^{6-}$	
Guest	[Host]/[Guest]	$E_{1/2}{}^a$/V	$i_p{}^b$/μA cm^{-2}	$E_{1/2}{}^a$/V	$i_p{}^b$/μA cm^{-2}
Fe–OH	0 : 1	0.234	336.5	0.229	350.1
	1 : 1	0.175	260.1	0.230	350.0
	4 : 1	0.114	274.2	0.224	350.1
Fc–N$^+$Me$_3$	0 : 1	0.446	216.4	0.445	223.0
	1 : 1	0.342	143.9	0.437	216.2
	5 : 1	0.331	139.9	0.421	209.6
Cob$^+$	0 : 1	−1.112[c]	334.2[c]	−1.112[c]	336.4[c]
	1 : 1	−1.228[c]	149.5[c]	−1.124[c]	334.6[c]
	4 : 1	−1.272[c]	136.8[c]	−1.128[c]	320.6[c]
Cob$^+$–CO$_2^-$	0 : 1	−0.992	210.9	−0.992	203.8
	1 : 1	−1.016	153.1	−0.996	204.2
	4 : 1	−1.044	142.6	−0.997	201.2

[a] V *vs.* Ag/AgCl reference electrode. [b] Peak current densities, cathodic for cobaltocenium and anodic for ferrocene derivatives. [c] These values are strongly affected by the precipitation of the reduced form (Cob); to minimize these effects, we determined the half-wave potentials using normal pulse voltammetry.

Table 2 Voltammetric data at 25 °C for ferrocene-based guests (1.0 mM) in the absence and in the presence of calixarene host $\mathbf{1}^{6-}$. Medium: 0.1 M chloroacetate buffer (pH 2.6)

Guest	[Host]/[Guest]	$E_{1/2}{}^a$/V	$i_p{}^b$/μA cm^{-2}
Fc–OH	0 : 1	0.227	183.5
	1 : 1	0.215	185.3
	4 : 1	0.191	165.2
Fc–N$^+$Me$_3$	0 : 1	0.441	175.4
	1 : 1	0.411	170.2
	5 : 1	0.393	142.0

[a] V *vs.* Ag/AgCl reference electrode. [b] Anodic peak current densities.

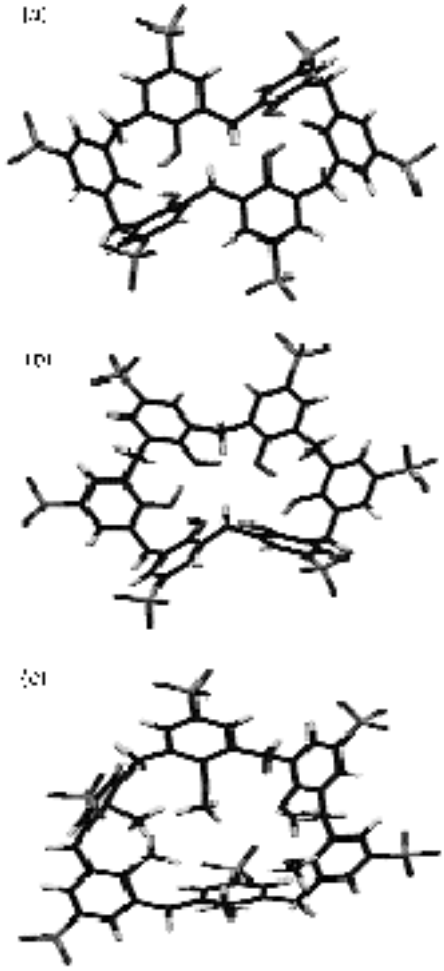

Fig. 2 Minimum energy conformations obtained with computational methods for (*a*) $\mathbf{1}^{8-}$, (*b*) $\mathbf{1}^{6-}$ and (*c*) $\mathbf{2}^{6-}$§

essentially unchanged in the presence of $\mathbf{2}^{6-}$. These data reveal that this hexaanionic calixarene host is ineffective at binding all these guests in any of their two accessible oxidation states. In an attempt to understand the striking binding ability differences between $\mathbf{1}^{8-}$ and $\mathbf{2}^{6-}$, we also performed experiments with $\mathbf{1}^{6-}$, prepared by dissolving the unmethylated calixarene **1** in a solution buffered at pH = 2.6 to insure the full protonation of its phenolic lower rim.[6] The corresponding voltammetric results (Table 2) clearly indicate that this host loses a fraction of its binding ability under these conditions compared to the same host in neutral (pH = 7) media.

It seems dubious that these effects could be rationalized with electrostatic arguments. While calixarene **1** at neutral pH bears eight negative charges, both calixarene **2** at the two pH values surveyed here and calixarene **1** at pH = 2.6 are hexaanions. These less charged hosts still have six negative charges, certainly enough to attract positively charged guests if electrostatic forces were to control the host–guest interactions. To further clarify the observed binding properties we have run a series of molecular modeling calculations§ aimed at finding relevant conformational differences between these hosts. The computational results show that, at neutral pH, the most stable conformation of the octaanionic host $\mathbf{1}^{8-}$ is very similar to the crystal structure reported by Atwood and coworkers [Fig. 2(*a*)]. After full protonation of its lower phenolic rim, the same host (now $\mathbf{1}^{6-}$) adopts a very different, flattened and puckered conformation [Fig. 2(*b*)], which lacks well defined binding pockets in spite of its relative rigid character. This conformational change may be responsible for the diminished binding ability exhibited by this host in acidic media. Finally, the methylated host $\mathbf{2}^{6-}$ exhibits a lot more flexibility since intramolecular hydrogen bonding in the lower rim is no longer possible. In this case, we could not locate a clearly defined energy minimum. The lowest energy conformation found is shown in Fig. 2(*c*), but many other equally disorganized conformations are readily accessible. The flexibility and absence of molecular preorganization are the key factors that determine the poor binding ability demonstrated by this host. Conversely, the octaanionic form of **1** (present at neutral pH) is an excellent host¶ for the guests surveyed here because of its preorganized and rigid character which is determined by the network of hydrogen bonds in its lower rim.

The authors are grateful to the US National Science Foundation for the support of this research work (to A. E. K., CHE-9633434).

Notes and References

† E-mail: akaifer@umiami.ir.miami.edu

‡ The two ferrocene derivatives, Fc–OH and Fc–N^+Me_3, undergo reversible one-electron oxidation to the corresponding ferrocenium forms, Fc^+–OH and Fc^+–N^+Me_3, respectively. We have previously reported on the binding of these two guests by calixarene **1** in unbuffered aqueous media, see ref. 3(*a*). The two cobaltocenium derivatives, Cob^+ and Cob^+–CO_2^-, undergo reversible one-electron reduction to the corresponding cobaltocene forms, Cob and Cob–CO_2^-, respectively, at a potential which is accessible at neutral pH but inaccessible at pH = 2.6. The pK_a of Cob^+–CO_2H is *ca.* 1.3 so that complete ionization is expected in the pH range used in this work.

§ All calculations were run with the Macromodel software package (version 6.0) running on a O2 Silicon Graphics workstation. The energy of each calixarene was minimized, after setting the solvent option to water, using the OPLS force field. Conformtional searches were done using Monte Carlo simulations with an energy range of 100 kJ mol^{-1} (1 cal = 4.184 J). On average, 400–500 unique conformations were identified for each host *en route* to a global minimum. At least two full conformational searches were performed with each host.

¶ ^{1}H NMR spectroscopic experiments indicate that the complexes formed between the guests Fc–N^+Me_3 and Cob^+ with host $\mathbf{1}^{8-}$ have 2 : 1 (guest : host) stoichiometry under these experimental conditions (see the following communication in this issue).

1 C. D. Gutsche, *Calixarenes*, in *Monographs in Supramolecular Chemistry*, ed. J. F. Stoddart, Royal Society of Chemistry, London, 1989; *Calixarenes: A Versatile Class of Macrocyclic Compounds*, ed. V. Böhmer and J. Vicens, Kluwer Academic, Dordrecht, Germany, 1991; C. D. Gutsche, *Aldrichim. Acta*, 1995, **28**, 3; V. Böhmer, *Angew. Chem., Int. Ed. Engl.*, 1995, **34**, 713.

2 S. Shinkai, S. Mori, H, Koreishi, T. Tsubaki and O. Manabe, *J. Am. Chem. Soc.*, 1986, **108**, 2409.

3 (*a*) L. Zhang, A. Macias, T. Lu, J. I. Gordon, G. W. Gokel and A. E. Kaifer, *J. Chem. Soc., Chem. Commun.*, 1993, 1017; 235; (*b*) A. R. Bernardo, T. Lu, E. Córdova, L. Zhang, G. W. Gokel and A. E. Kaifer, *J. Chem. Soc., Chem. Commun.*, 1994, 529; (*c*) L. Zhang, L. A. Godinez, T. Lu, G. W. Gokel and A. E. Kaifer, *Angew. Chem., Int. Ed. Engl.*, 1995, **34**, 235.

4 R. Castro, L. A. Godínez, C. M. Criss, S. G. Bott and A. E. Kaifer, *Chem. Commun.*, 1997, 935; R. Castro, L. A. Godínez, C. M. Criss and A. E. Kaifer, *J. Org. Chem.*, 1997, **62**, 4928.

5 J. L. Atwood, D. L. Clark, R. K. Juneja, G. W. Orr, K. D. Robinson and R. L. Vincent, *J. Am. Chem. Soc.*, 1992, 7558.

6 G. Arena, A. Cantino, G. G. Lombardo and D. Sciotto, *Thermochim. Acta*, 1995, **264**, 1; Y. Zhang, R. A. Agbaria, N. E. Mukundan and I. M. Warner, *J. Incl. Phenom.*, 1996, **24**, 353.

Received in Columbia, MO, USA, 30th January 1998; 8/00846I

Redox control of host–guest recognition: a case of host selection determined by the oxidation state of the guest

Yun Wang, Julio Alvarez and Angel E. Kaifer*†

Chemistry Department, University of Miami, Coral Gables, FL 33124-0431, USA

In the presence of β-CD, reduction of the strong complex between two cobaltocenium guests and the octaanionic form of calix[6]arene hexasulfonate leads to the formation of 1 : 1 complexes between cobaltocene and β-CD.

Redox conversions have been effectively used to control the strength of host–guest interactions. Typically, changes in the oxidation state of one of the interacting partners (either the host or the guest) lead to substantial modifications in the stability of the host–guest complex. Redox switchable hosts,[1] for instance, contain a redox subunit which can be acted upon (electrochemically or chemically) to alter their binding affinity for certain guests. Here, we extend these ideas to the concept of host selection. We describe a system composed of two redox inactive hosts and one redox active guest in which the oxidation state of the guest determines which of the two hosts is selected for complex formation.[2]

Fig. 1 shows the structures of the host and guest compounds used in this work. The solubilities of hosts and guests permit the investigation of this system in aqueous solution. The two hosts selected are the sulfonated calix[6]arene $\mathbf{1}^{8-}$ and β-cyclodextrin (β-CD). The anionic character and conformational rigidity‡ of host $\mathbf{1}^{8-}$ make it an excellent host for positively charged guests, while β-CD is well known to exhibit a strong binding affinity for suitably sized non-polar guests.[3] The two guests selected are cobaltocenium and carboxycobaltocenium. The cobaltocenium subunit undergoes a fast and reversible one-electron reduction to neutral cobaltocene. Very recently we have reported that, while β-CD does not interact appreciably with the positively charged cobaltocenium (Cob^+), it does form a stable 1 : 1 inclusion complex with the reduced form, cobaltocene (Cob).[4]

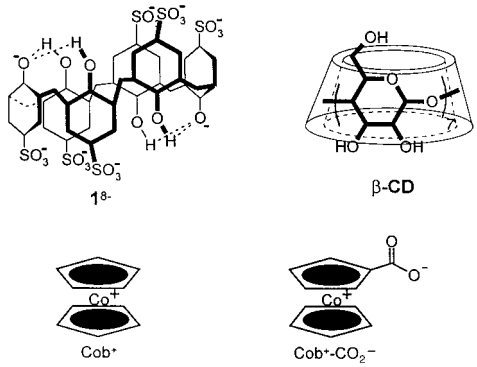

Fig. 1 Structures of calixarene hosts and molecular guests studied in this work

The voltammetric reduction of cobaltocenium yields the hydrophobic Cob form, which precipitates on the electrode surface. These precipitation effects distort the cyclic voltammogram [see Fig. 2(*a*)] from the otherwise anticipated nernstian, reversible shape. Addition of host $\mathbf{1}^{8-}$ shifts the Cob^+–Cob voltammetric wave to more negative potentials but the distortions associated with deposition of the reduced form persist [Fig. 2(*a*)]. These findings are consistent with (*i*) complexation

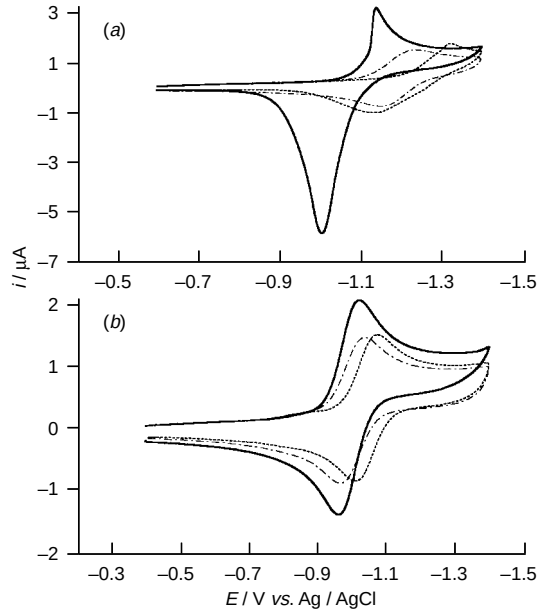

Fig. 2 (*a*) Voltammetric response on a glassy carbon electrode (0.008 cm^2) of a 1.0 mM solution of Cob^+ also containing 0.1 M phosphate buffer (pH = 7) in the absence of any host compound (——), in the presence of 4.0 mM $\mathbf{1}^{8-}$ (------), and in the presence of 4.0 mM $\mathbf{1}^{8-}$ and 4.0 mM β-CD (-·-·-·). Scan rate = 0.1 V s^{-1}. (*b*) Same for 1.0 mM Cob^+–CO_2^- solution.

of Cob^+ by the anionic calixarene host and (*ii*) lack of substantial interaction between $\mathbf{1}^{8-}$ and Cob. NMR titrations (^1H, 400 MHz) of buffered (pD = 7) D_2O solutions of $\mathbf{1}^{8-}$ with increasing concentrations of Cob^+ produce strong evidence for the formation of a stable complex containing two Cob^+ guests bound to the anionic host.[5] The Cob^+-induced splitting patterns of both the aromatic proton and the methylene proton resonances of the calixarene (Fig. 3) constitute strong evidence for the formation of the 2 : 1 complex shown in Scheme 1. In 1992, Atwood *et al.* solved the crystal structure of the hydrated sodium salt of $\mathbf{1}^{8-}$ (crystallized from neutral aqueous solution) and found that the calixarene adopts a double partial cone conformation exhibiting two clearly defined binding pockets.[6] To the best of our knowledge, our NMR data constitute the first unequivocal spectroscopic evidence for the adoption by host $\mathbf{1}^{8-}$ of the same conformation in neutral aqueous solution. In the absence of Cob^+, the aromatic units of the calixarene undergo fast interconversions and, thus, only two proton resonances are observed (one for the methylene protons and another for the aromatic protons). In the presence of more than 2 equiv. of Cob^+, each one of these resonances splits into the patterns shown in Fig. 3. These resonances are consistent with a double partial cone conformation for the calixarene (see assignments in Fig. 3) and can only be rationalized by the formation of a complex in which one Cob^+ guest binds to each of the two cavity openings of the calixarene.§ Complexation of $\mathbf{1}^{8-}$ to two Cob^+ guests slows down the otherwise fast averaging of the

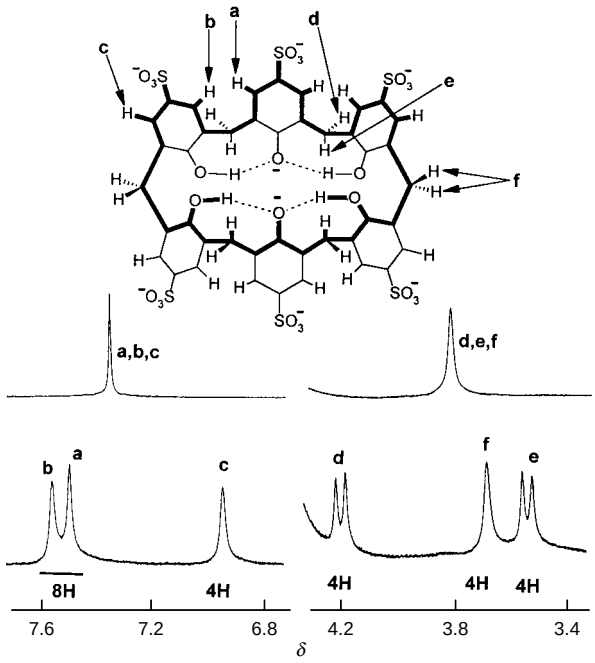

Fig. 3 ^{1}H NMR (400 MHz) of a 2.0 mM solution of $\mathbf{1}^{8-}$ in D_2O also containing 0.1 M phosphate buffer (pD = 7) in the absence (top) and in the presence (bottom) of 6.0 mM Cob^+

host's proton resonances, giving rise to the distinctive splitting patterns shown in Fig. 3.

The $\mathbf{1}^{8-}$–Cob^+ host–guest system is further affected by the addition of β-CD to the medium [Fig. 2(*a*)]. In the presence of this neutral host, the precipitation effects associated with the generation of the hydrophobic Cob form (which is not effectively complexed by $\mathbf{1}^{8-}$) completely disappear, revealing that Cob forms a stable 1 : 1 inclusion complex with the β-CD host, as anticipated from our previous work.[4] Therefore, we must conclude that, while Cob^+ forms a stable 2 : 1 complex with the anionic calixarene host $\mathbf{1}^{8-}$, its reduced form, Cob, is preferentially bound by β-CD. Since the binding interactions between the Cob^+–β-CD and Cob–$\mathbf{1}^{8-}$ pairs are indeed quite weak, the electrochemical reduction of Cob^+ has a profound effect not only on the selection of host by this redox active guest but also on the stoichiometry of the resulting complex as represented in Scheme 1. The voltammetric results obtained with the more water soluble Cob^+–COO^- guest are shown in Fig. 2(*b*). No precipitation of the reduced Cob–CO_2^- form is observed, but the shifts recorded in the $E_{1/2}$ values upon addition of $\mathbf{1}^{8-}$ and β-CD indicate that similar host selection phenomena also take place with this guest.

We have shown here that the redox chemistry of cobaltocenium guests can be used to select the appropriate host between calixarene $\mathbf{1}^{8-}$ and β-CD. These results add to the arsenal of mechanisms and schemes by which redox conversions can be used to control molecular recognition interactions.

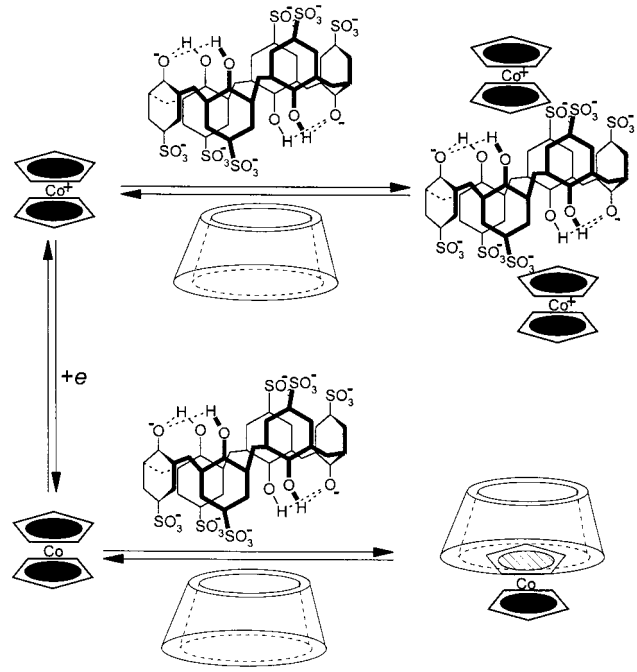

Scheme 1

The authors are grateful to the US National Science Foundation for the support of this work (to A. E. K. CHE-9633434) and Cerestar for continued and generous gifts of cyclodextrins.

Notes and References

† E-mail: akaifer@umiani.ir.miami.edu

‡ For more details on the solution conformation of this calixarene host, see the preceding communication in this same issue.

§ From our NMR data we estimate that the association constant for the overall equilibrium 2 Cob^+ + $\mathbf{1}^{8-}$ = $\mathbf{1}\cdot(Cob)_2^{6-}$ is at least 2×10^6 $dm^6\ mol^{-2}$.

1 A. E. Kaifer and S. Mendoza, in *Comprehensive Supramolecular Chemistry*, ed. J. L. Atwood, J. E. D. Davies, D. D. MacNicol and F. Vogtle, vol. 1, *Molecular Recognition: Receptors for Cationic Guests*, ed. G. W. Gokel, Elsevier, New York, 1996, p. 701.
2 Another example of redox-induced host switching has been reported very recently: R. Deans, A. Niemz, E. C. Breinlinger and V. M. Rotello, *J. Am. Chem. Soc.*, 1997, **119**, 10 863.
3 K. A. Connors, *Chem. Rev.*, 1997, **97**, 1325.
4 Y. Wang, S. Mendoza and A. E. Kaifer, *Inorg. Chem.*, 1998, **37**, 317.
5 Shinkai *et al.* have demonstrated the formation of a 2 : 1 complex between a cationic guest and a water-soluble calix[8]arene: S. Shinkai, K. Araki and O. Manabe, *J. Am. Chem. Soc.*, 1988, **110**, 7214.
6 J. L. Atwood, D. L. Clark, R. K. Kuneja, G. W. Orr, K. D. Robinson and R. L. Vincent, *J. Am. Chem. Soc.*, 1992, **114**, 7558.

Received in Columbia, MO, USA; 30th January 1998; 8/00845K

Spiro[4.4] and spiro[4.5] lactones from phthaloyl chloride and 1,4- and 1,5-bis-nucleophiles

Mary J. O'Mahony,[a] Charles W. Rees,*[b] Elizabeth A. Saville-Stones,[a] Andrew J. P. White[b] and David J. Williams[b]

[a] *AgrEvo UK Limited, Chesterford Park, Saffron Walden, Essex, UK CB10 1XL*
[b] *Department of Chemistry, Imperial College of Science, Technology and Medicine, London, UK SW7 2AY*

Phthaloyl chloride reacts with the 1,4-bis-nucleophiles 3 to give spiro[4.4] lactones 7 and 9 and with the 1,5-bis-nucleophiles 10 to give spiro[4.5] lactones 12, as proved by X-ray crystallography, and not the 8- and 9-membered heterocyclic systems previously claimed.

4,5-Dichloro-1,2,3-dithiazolium chloride ('Appel Salt') **1** is a remarkably versatile reagent in organic synthesis.[1–4] When treated with primary aromatic amines followed by secondary aliphatic amines it gives the dithiazoles **2** which can be hydrolysed to the amidino thioamides **3**.[2] As reactive 1,4-bis-nucleophiles compounds **3** are useful in heterocyclic synthesis, particularly when treated with 1,1-bis-electrophiles to give five-membered rings **4** (X = CS, CNPh, SO and SO_2) (Scheme 1),[3] and with 1,2-bis-electrophiles to give six-membered rings.[4] A more unusual application was the reported reaction of compound **3** with the 1,4-bis-electrophile, phthaloyl chloride, in CH_2Cl_2 containing pyridine at room temperature to give the 8-membered ring compounds, 2,5-benzothiazocine-1,6-diones **5** (Scheme 2). Nine examples, selected from R = Pr, Bu and Ar = 4-XC_6H_4 (X = Cl, Br, Me, MeO, NO_2) and 3-$O_2NC_6H_4$, were reported in 45–83% yield.[3]

These unusual 2,5-benzothiazocines were unknown, and if valid, this route would render them readily available. However displacement of the second chlorine in phthaloyl chloride to form a highly unsaturated 8-membered ring seems questionable on mechanistic grounds; furthermore it overlooks the possibility of a lower energy process involving interaction between the two acid chloride groups, typified by the long-known isomerisation of phthaloyl chloride into 3,3-dichlorophthalide.[5] It occurred to us that attack of the second carbonyl group could be through the first, as shown in **6** for example, to give the strain-free spiro[4,4] lactones **7** (or **9**) rather than the 8-membered ring (Scheme 3). This we have now shown to be the case.

We repeated the preparation of the amidino thioamides **3** (R = Pr, Ar = 4-$O_2NC_6H_4$, 4-$MeOC_6H_4$), and treated them with phthaloyl chloride and pyridine, exactly as reported,[3] to obtain 1 : 1 adducts (44 and 47% yield, respectively). By spectroscopic comparison these were clearly the same products as described in the literature.[3] Careful chromatography and slow crystallisation from Pr^i_2O–hexane gave the 4-nitrophenyl product as yellow crystals, mp 229–231 °C, suitable for X-ray crystallography† which revealed the structure to be the racemic spiro lactone **9** (R = Pr, Ar = 4-$O_2NC_6H_4$). It is clear from their IR, ^1H and ^{13}C NMR and mass spectra that all the claimed benzothiazocines **5** are structurally very similar and thus we deduce that they are all spiro compounds **9**; indeed this structure is in better agreement with the spectroscopic data than the benzothiazocine **5**, which remains unknown.

The X-ray structure of **9** (R = Pr, Ar = 4-$O_2NC_6H_4$) is illustrated in Fig. 1. There are only minor differences in the geometries of the four independent molecules: small changes in the conformations of the NPr_2 groups and in the twist angle between the planes of the imidazole and nitrophenyl ring systems. The only other structural features of note are a pronounced double bond character for N(3)–C(4) and delocalisation within the thioamide [N(1)–C(5)–S(5)].

In the reaction of the amidino thioamides **3** with phthaloyl chloride there are various possibilities for the order of nucleophilic attack. Because of the high nucleophilicity of sulfur we consider **6** to be the more likely first intermediate and this would result in the formation of **7** rather than **9**. It is possible that **7** is the kinetic product which then undergoes a Dimroth type rearrangement to the more stable thioamide structure **9**, through the stabilised ring-opened intermediate **8**. This view was strongly supported by studying the reactions of phthaloyl

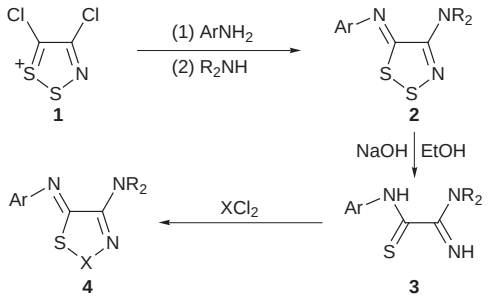

Scheme 1

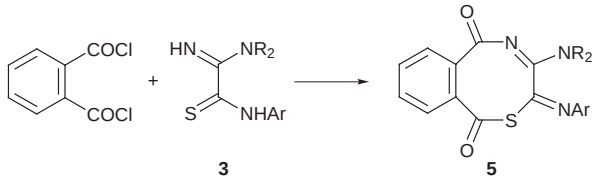

Scheme 2

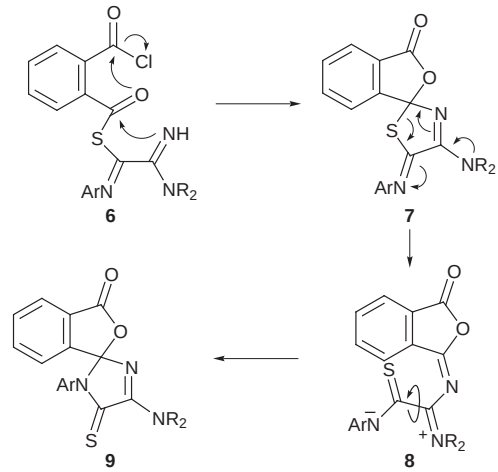

Scheme 3

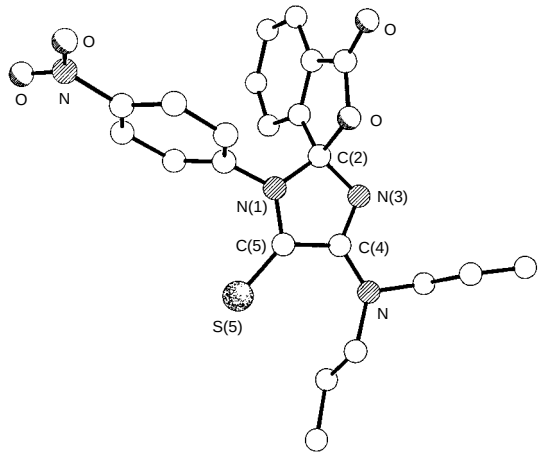

Fig. 1 The structure of one of the four crystallographically independent molecules of **9** (R = Pr, Ar = 4-$O_2NC_6H_4$). Selected bond lengths (Å) [averaged over the four molecules]; N(3)–C(4) 1.29(2), N(1)–C(5) 1.35(2), C(5)–S(5) 1.622(13).

chloride with the amidino thioamides **3** (R = Pr, Ar = 2,6-$Me_2C_6H_3$ and R = Pr, Ar = 2,4,6-$Me_3C_6H_2$) where the bulkier *N*-aryl groups should favour the less congested structure **7** over **9**. From each of these reactions two isomeric products were isolated and shown spectroscopically to be **7** (62%) and **9** (32%) for the dimethyl and **7** (65%) and **9** (28%) for the trimethyl compounds. The products **7** in the dimethyl and trimethyl series are labile and isomerise slowly to **9** on standing in CH_2Cl_2 at room temperature; this rearrangement is markedly catalysed by acid (HCl in $CDCl_3$). In view of the possible formation of structural isomers in the cyclisation of compound **3**, the five-membered ring structures **4**, proposed above,[3] should also be treated with caution and isomeric thioamide structures be considered.

In similar vein the condensation of phthaloyl chloride with the 1,5-bis-nucleophiles **10** has been reported to give the equally striking 9-membered ring system, 2,6-benzothiazonine-1,5,7-trione **11**.[6] Eleven such products (R = Me, Et, allyl, cyclohexyl, Bn, substituted benzyl) were obtained as colourless solids, mostly in very high yields, and all exhibit very similar spectroscopic properties.[6] If correct this would provide an attractive route to this new ring system, but again it seemed likely that the 1,5-bis-nucleophiles **10** could be reacting by the same general mechanism as the 1,4-bis-nucleophiles **3**, to give the analogous spiro[4,5] lactones **12**.

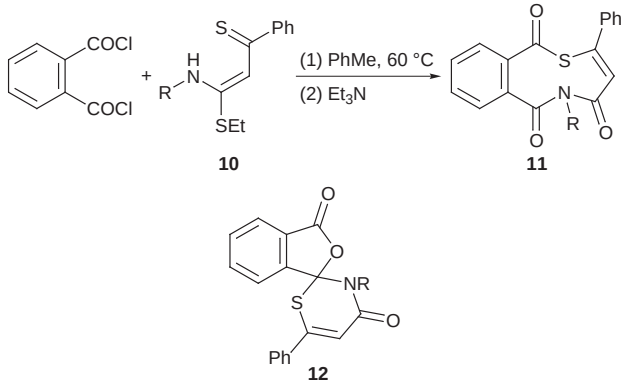

We therefore prepared the thione **10** (R = Et) and treated this with phthaloyl chloride as reported,[6] to give a colourless crystalline product, mp 132–133 °C (61%). X-Ray crystallography reveals a spiro junction between the phthalide and thiazinone ring systems, thus confirming the alternative structure **12** (Fig. 2). The thiazinone ring has a half-chair conformation with the spiro centre C(2) lying 0.64 Å out of the plane of the remaining atoms–which are co-planar to within 0.04 Å.

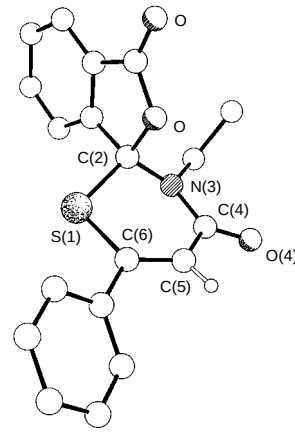

Fig. 2 The molecular structure of **12**, (R = Et). Selected bond lengths (Å); S(1)–C(6) 1.738(3), C(6)–(5) 1.343(4), N(3)–C(4) 1.373(4), C(4)–O(4) 1.226(4), C(4)–C(5) 1.466(4).

The spectroscopic data for **12** (R = Et) agreed well with the spiro structure and with the data reported for the other products, indicating that these too are all spiro compounds, and that the nine-membered ring of **11** is still unknown. A similar spirolactone structure has been assigned to the product from phthaloyl chloride and 2-(dihydroimidazol-2-yl)thiophenol, on the basis of its ^{13}C NMR spectrum which agreed well with that of our product.[7]

It follows from these results that spiro lactone (phthalide) structures should always be considered for the products of condensation of phthaloyl chloride, and related 1,2-bis-carboxylic acid halides, with 1,4 and higher bis-nucleophiles.

We gratefully acknowledge support from AgrEvo UK Limited and Dr P. J. Dudfield and we thank the Wolfson Foundation for establishing the Wolfson Centre for Organic Chemistry in Medical Science at Imperial College.

Notes and References

† *Crystal data* for **9** (R = Pr, Ar = 4-$O_2NC_6H_4$): $C_{22}H_{22}N_4O_4S$, M = 438.5, monoclinic, Pc (no. 7), a = 12.699(3), b = 20.079(3), c = 18.900(3) Å, β = 109.03(1)°, V = 4555(1) Å^3, Z = 8 (there are four crystallographically independent molecules in the asymmetric unit), D_c = 1.279 g cm^{-3}, μ(Mo-Kα) = 1.78 cm^{-1}, F(000) = 1840. A yellow block of dimensions 0.77 × 0.50 × 0.20 mm was used. For **12** (R = Et): $C_{19}H_{15}NO_3S$, M = 337.4, monoclinic, $P2_1/n$ (no. 14), a = 10.159(1), b = 8.330(1), c = 19.638(1) Å, β = 101.33(1)°, V = 1629.4(2) Å^3, Z = 4, D_c = 1.375 g cm^{-3}, μ(Cu-Kα) = 19.1 cm^{-1}, F(000) = 704. A thin clear plate of dimensions 0.40 × 0.27 × 0.02 mm was used. 8304 (1940) Independent reflections were measured on Siemens P4/PC diffractometers with Mo-Kα (Cu-Kα) radiation using ω-scans for **9** (**12**) respectively. The structures were solved by direct methods and all of the major occupancy non-hydrogen atoms were refined anisotropically using full-matrix least-squares based on F^2 to give R_1 = 0.073 (0.036), wR_2 = 0.183 (0.089) for 4269 (1616) independent observed (and absorption corrected for **12**) reflections [$|F_o| > 4\sigma(|F_o|)$, $2\theta \leqslant 50°$ (125°)] and 1117 (218) parameters for **9**, (**12**) respectively. The polarity of **9** could not be reliably determined, probably due to the presence of a non-crystallographic inversion centre at 0.878, 0.393, 0.580. CCDC 182/884.

1 R. Appel, H. Janssen, M. Siray and F. Knoch, *Chem. Ber*., 1985, **118**, 1632; J. J. Folmer and S. M. Weinreb, *Tetrahedron Lett*., 1993, **34**, 2737; T. Besson and C. W. Rees, *J. Chem. Soc*., *Perkin Trans. 1*, 1996, 2857; R. F. English, O. A. Rakitin, C. W. Rees and O. G. Vlasova, *J. Chem. Soc*., *Perkin Trans. 1*, 1997, 201 and references cited therein.
2 H. Lee, K. Kim, D. Whang and K. Kim, *J. Org. Chem*., 1994, **59**, 6179.
3 S.-H. Choi and K. Kim, *Tetrahedron*, 1996, **52**, 8413.
4 M.-K. Jeon and K. Kim, *Tetrahedron*, 1998, **54**, 2459.
5 D. V. Banthorpe and B. V. Smith, in *The Chemistry of Acyl Halides*, ed. S. Patai, Interscience, London, 1972, ch. 8; P. R. Jones, *Chem. Rev*., 1963, **63**, 461.
6 S. H. Kim and K. Kim, *Heteroatom Chem*., 1995, **6**, 387.
7 W. Reid and A. von der Eltz, *Liebigs Ann. Chem*., 1988, 599.

Received in Liverpool, UK, 7th April 1998; 8/02630K

A supramolecular assembly controlled by anions: threading and unthreading of a pseudorotaxane

Marco Montalti and Luca Prodi*†

Dipartimento di Chimica 'G. Ciamician', Università di Bologna, via Selmi 2, Bologna, 40126, Italy

The pseudorotaxane formed in CH_2Cl_2 solution by (9-anthrylmethyl)methylammonium hexafluorophosphate salt and dibenzo-24-crown-8 can be unthreaded by addition of NBu_4Cl through the formation of a strong ammonium chloride ion pair, while pseudorotaxane rethreading can be performed by addition of $NHBu_3PF_6$; all these processes can be followed by pronounced changes in the luminescence spectra, which could allow the use of this system as a fluorescent sensor for chloride ions.

The association between crown ethers and ammonium salts has been widely studied and employed to synthesise self-assembling supramolecular systems.[1–5] In particular, the remarkable capability of the ammonium–crown interaction to be switched on/off through acid–base equilibria has also been exploited to induce mechanical movements in systems such as rotaxanes and pseudorotaxanes.[6–8] In this context, we previously examined the photophysical properties of adducts between fluorescent ammonium ions and aromatic crown ethers, pointing out that the nature of the counteranion of the ammonium cation could influence its association with crown ethers in low polarity solvents where strong ion pairs are formed. Starting from this point, we have conceived a new way, based on anion exchange, of controlling the threading and unthreading of a previously examined pseudorotaxane.[6,8]

All experiments were carried out in CH_2Cl_2 solution at room temperature. The experimental equipment and procedures have been previously described.[6] PF_6^- and Cl^- salts were prepared from commercial (9-anthrylmethyl)methylamine. The other compounds were commercial products. All fluorescence spectra were appropriately corrected.[9]

We have already reported the absorption and fluorescence spectra of (9-anthrylmethyl)methylammonium (**1**H$^+$) hexafluorophosphate and dibenzo-24-crown-8 (**2**), together with the properties of the adduct they origin.[6] Absorption and fluorescence spectra of **1**·HCl present some differences from those of **1**·HPF_6; in particular, the fluorescence intensity is about 35% weaker and the maximum is shifted from 421 to 419 nm. A decrease in the fluorescence lifetime from 8.5 to 5.5 ns is also observed. These findings give clear evidence for the formation of a highly associated ion pair with Cl^-, since the fluorescence of the anthracene moiety is very sensitive to the electronic density on the nearby nitrogen atom, which can be responsible for electron transfer quenching processes.[10] If 1 equiv. NBu_4Cl is added to a 2×10^{-4} M solution of **1**·HPF_6, a decrease in the fluorescence intensity and lifetime is observed as expected for the formation of the **1**H$^+$Cl$^-$ ion pair. On addition of an excess of the $NHBu_3PF_6$ salt, the fluorescence of **1**H$^+$ increases although it does not reach the initial intensity, because of the competition between **1**H$^+$ and $NHBu_3^+$ to form ion pairs with Cl^- [eqn. (1)].

$$\mathbf{1}H^+Cl^- + NHBu_3^+ \overset{K_{exc}}{\rightleftharpoons} NHBu_3^+Cl^- + \mathbf{1}H^+ \qquad (1)$$

An even larger effect of the chloride ion on the fluorescence spectra is observed when **2** is present. If equimolar amounts (2×10^{-4} M) of **1**·HPF_6 and **2** are mixed in a CH_2Cl_2 solution, the adduct **1H2**$^{2+}$ $2PF_6^-$ is formed, where the fluorescence of **2** is completely quenched by an energy transfer process to the anthracene moiety. On the contrary, in a solution of **1**·HCl (2×10^{-4} M) and **2** (2×10^{-4} M) no association is observed, and, as a consequence, no sensitization of the fluorescence of **1**H$^+$ on excitation of **2** is detected. This behaviour in solution can be described on the basis of equilibria (2) and (3)

$$\mathbf{1}H^+ + A^- \overset{K_{ip}}{\rightleftharpoons} \mathbf{1}\cdot HA \qquad (2)$$

$$\mathbf{1}H^+ + \mathbf{2} \overset{K_{as}}{\rightleftharpoons} \mathbf{1}H\mathbf{2}^+ \qquad (3)$$

where A^- is the counteranion. If K_{ip} is very large, as it is for Cl^-, equilibrium (3) cannot compete with equilibrium (2), and the adduct with **2** cannot be formed, while if it is small (as for PF_6^-) the adduct formation is observed. This set of equilibria, together with the different affinity of the chloride ions for the different ammonium ions ($NH_2R_2^+ > NHR_3^+ >> NR_4^+$) can be used for controlling the threading and unthreading of this pseudorotaxane. In a solution of **1**·HPF_6 (2×10^{-4} M) and **2** (2×10^{-4} M) the fluorescence of **2** is, as already observed, completely quenched while sensitised fluorescence of **1**H$^+$ is observed (Fig. 1). On addition of 1 equiv. NBu_4Cl the fluorescence of **2** is completely recovered and the sensitised fluorescence of anthracene disappears (Fig. 1). Simultaneously

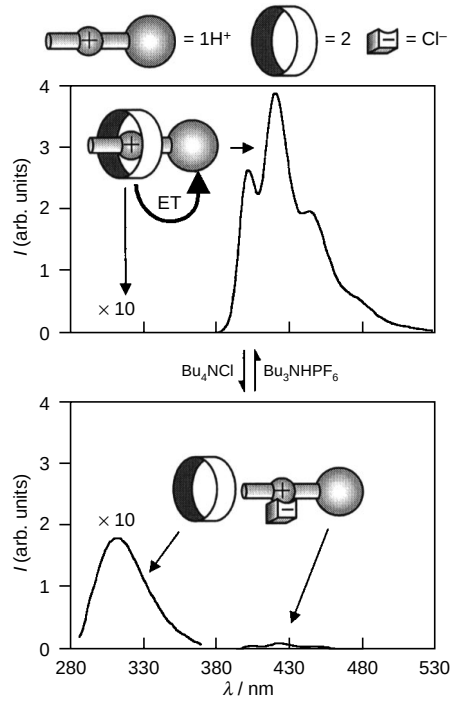

Fig. 1 Changes in the fluorescence spectrum of a CH_2Cl_2 solution of **1**H$^+$ (2×10^{-4} M) and **2** (2×10^{-4} M) upon unthreading and threading of the pseudorotaxane structure caused by addition of NBu_4Cl and $NHBu_3PF_6$, respectively

the anthracene fluorescence (on excitation at λ = 381 nm, where only the anthracene moiety absorbs) decreases to the intensity expected for the **1**H^+Cl^- ion pair formation and the fluorescence lifetime decreases to 5.5 ns. These results indicate that addition of NBu_4Cl leads to the formation of the **1**H^+Cl^- ion pair, preventing the ammonium cation from binding to the crown ether (Fig. 1). Further addition of 1 equiv. $NHBu_3PF_6$ leads again to complete quenching of the fluorescence of **2**, while the **1**H^+ fluorescence intensity and lifetime increase to the initial values, indicating that the pseudorotaxane structure is regenerated. In this case, addition of the $NHBu_3^+$ cation, more strongly bound to Cl^- than to the NBu_4^+ ion, gives rise to equilibrium (1), that, although spontaneously shifted to the left side, can be driven in the presence of **2** to the right side by the occurrence of equilibrium 3, allowing the almost complete formation of the **1**H·**2**$^+$ pseudorotaxane. As can be seen from Fig. 1, dramatic changes in the fluorescence intensities of **1**H^+ and **2** can be observed on every step of the working cycle. This cycle could be repeated several times on the same system, without losing its efficiency, also because tertiary and quaternary ammonium salts cannot compete with **1**H^+ on the association with **2** [equilibrium (3)]. Ion pairing results in a new way of controlling the association of hydrogen bonded supramolecular systems. As a consequence, the pseudorotaxane **1**H**2**$^+$ can be unthreaded and threaded again in three different ways: (i) by adding an acid and then a base, (ii) by adding a base and then an acid or (iii) by adding NBu_4Cl and then $NHBu_3PF_6$. New supramolecular systems could be conceived which, through the combination of these three different modes, would carry out various and complicated logical operations.[11]

Moreover the sensitivity of the ammonium–crown supramolecular systems to the chloride concentration could be usefully employed for the development of new fluorescent chemosensors for chloride ions.[12] Studies in this direction are actually in progress.

We thank Professor V. Balzani and Dr A. Credi for stimulating discussions. This research is being supported by the University of Bologna (Funds for Selected Topics).

Notes and References

† lprodi@ciam.unibo.it

1 J.-M. Lehn, *Angew. Chem., Int. Ed. Engl.*, 1988, **27**, 89.
2 D. J. Cram, *Angew. Chem., Int. Ed. Engl.*, 1988, **27**, 1009.
3 C. J. Pedersen, *Angew. Chem., Int. Ed. Engl.*, 1988, **27**, 1021.
4 P. R. Ashton, A. N. Collins, M. C. T. Fyfe, P. T. Glink, S. Menzer, J. F. Stoddart and D. J. Williams, *Angew. Chem., Int. Ed. Engl.*, 1997, **36**, 59.
5 P. R. Ashton, P. T. Glink, J. F. Stoddart, P. A. Tasker, A. J. P. White and D. J. Williams, *Chem. Eur. J.*, 1996, **2**, 731.
6 P. R. Ashton, R. Ballardini, V. Balzani, M. Gómez-López, S. E. Lawrence, M. V.Martínez-Díaz, M. Montalti, A. Piersanti, L. Prodi, J. F. Stoddart and D. J. Williams, *J. Am. Chem. Soc*., 1997, **119**, 10 641.
7 M. V. Martínez-Díaz, N. Spencer and J. F. Stoddart, *Angew. Chem., Int. Ed. Engl.*, 1997, **36**, 1904.
8 M. Montalti, R. Ballardini, L. Prodi and V. Balzani, *Chem. Commun.*, 1996, 2011.
9 A. Credi and L. Prodi, *Spectrochim. Acta, Part A*, 1998, **54**, 159.
10 L. Fabbrizzi and A. Poggi, *Chem. Soc. Rev.*, 1995, 197.
11 A. Credi, V. Balzani, S. J. Langford and J. F. Stoddart, *J. Am. Chem. Soc*., 1997, **119**, 2679.
12 For a recent and complete review on fluorescent chemosensors, see A. P. de Silva, H. Q. N. Gunaratne, T. Gunnlaugsson, A. J. M. Huxley, C. P. McCoy, J. T. Rademacher and T. E. Rice, *Chem. Rev.*, 1997, **97**, 1515.

Received in Liverpool, UK, 18th March 1998; 8/02157K

Hydroformylation of hex-1-ene in supercritical carbon dioxide catalysed by rhodium trialkylphosphine complexes

Ingrid Bach and David J. Cole-Hamilton*†

School of Chemistry, University of St. Andrews, St. Andrews, Fife, Scotland, UK KY16 9ST

Triethylphosphine complexes of rhodium catalyse the hydroformylation of hex-1-ene in supercritical carbon dioxide at rates similar to those obtained in toluene, but with a slightly improved n : i ratio; using trioctylphosphine, much lower rates are observed.

Supercritical carbon dioxide is potentially an excellent solvent for carrying out homogeneous catalytic reactions because it is easily separated from the catalyst and the products and is environmentally benign.[1,2] In addition, the high solubility of gases (totally miscible with $scCO_2$) means that problems associated with transport of gases across interfaces are removed and the gas-like nature of the medium means that diffusion is much faster than in solution reactions.

Extensive studies have been made of hydroformylation of alkenes using $[Co_2(CO)_8]$[3,4] but there have been problems with studying the more active and selective rhodium based species because the triarylphosphine complexes that are usually employed in liquid phase reactions have very low solubility in $scCO_2$.[5] A brief report has appeared in which this problem has been overcome by derivatising the aryl groups with fluorinated chains.[6]

We now report that simple trialkylphosphines such as PEt_3, which are readily available, do not involve the use of costly fluorinated derivatives and have low molecular masses so the relatively small amounts can be employed, can provide highly active catalysts for the hydroformylation of hex-1-ene in $scCO_2$. Trimethylphosphine complexes of ruthenium have been used for the hydrogenation of CO_2[5] and for the formation of DMF from CO_2, hydrogen and dimethylamine in $scCO_2$.[7,8]

Using a catalyst prepared *in situ* from $[Rh_2(OAc)_4]$ and PEt_3, complete conversion to C_7 aldehydes, with a trace of C_7 alcohols [total straight to branched (n : i) ratio = 2.4] is obtained within 2 h at 100 °C.‡ [SAFETY WARNING: All reactions involving $scCO_2$ are carried out at very high pressures (up to 250 bar). They should only be attempted in autoclaves that have been specially designed to withstand such pressures.] Comparison of the pressures within the autoclave during the heating period (10 min), with those obtained during heating an identical solution in the absence of catalyst shows that the onset of reaction occurs at 80 °C, and visual inspection through a sapphire window shows that the mixture becomes homogeneous (monophasic pale yellow solution) at *ca.* 70 °C. Table 1 lists the results of a series of different experiments and shows that the rate is very similar to that obtained with the same catalyst under identical conditions using toluene as the solvent, but the n : i ratio is slightly higher in $scCO_2$. The reaction is retarded by addition of excess of PEt_3, but enhanced by increased p_{CO} or p_{H_2}.

In the solution phase system, we have previously shown[9] that C_7 alcohols can be products of the hydroformylation of hex-1-ene, either formed in a sequential reaction (thf as solvent) or as primary products (alcoholic solvents). In the hydroformylation of hex-1-ene carried out in $scCO_2$, C_7-alcohols are products (*ca.* 8%) after 2 h reaction and become significant (31%) products after longer reaction times. Adding ethanol to the mixture does not increase the amount of alcohol produced, but somewhat reduces the overall rate. We have shown[9] that, in liquid phase reactions, protonation of an acyl intermediate by ethanol is the key step that leads to C_7 alcohol production. It is presumably the inability of $scCO_2$ to solvate the ionic species formed by the protonation, that prevents the direct formation of C_7 alcohols when the reaction is carried out in $scCO_2$ in the presence of ethanol. Interestingly, addition of the fluorinated alcohol, $C_6F_{13}CH_2CH_2OH$, does lead to an increase in the amount of alcohol produced and to a higher reaction rate.

We have also studied other trialkylphosphine ligands. Replacing one ethyl group in PEt_3 with a fluorinated chain ($-CH_2CH_2C_6F_{13}$) increases the reaction rate, presumably because of electron density changes on the rhodium rather than

Table 1 Conditions and yields of products from the hydroformylation of hex-1-ene catalysed by rhodium complexes‡

Solvent	Phosphine	[Rh]/mmol dm^{-3}	p_{CO}/bar	p_{H_2}/bar	t/h	Aldehydes[a] (%)	Heptanol (%)	n : i	TOF/ Rh^{-1} h^{-1}
Toluene	PEt_3	6.58	20	20	1	74	4.8	2.1	53
$scCO_2$	PEt_3	6.54	10	20	1	56	1	2.4	38
$scCO_2$	PEt_3[b]	6.48	10	20	1	23	—	2.2	16
$scCO_2$	PEt_3	6.43	10	10	1	38	—	2.5	27
$scCO_2$	PEt_3	6.57	5	20	1	35	—	2.6	24
$scCO_2$	PEt_3	6.48	20	20	1	82	2.3	2.4	57
$scCO_2$	PEt_3	6.52	20	20	2	89	8.1	2.5	
$scCO_2$	PEt_3	6.58	20	30	22	54	28[c]	2.5	
$scCO_2$/EtOH[d]	PEt_3	6.48	20	20	1	60	3	2.4	44
$scCO_2$/R_fOH[d,e]	PEt_3	6.42	20	20	1	82	11	2.5	62
$scCO_2$	PEt_2R_f[e,f]	6.45	20	20	1	81	—	2.4	58
$scCO_2$	$P(C_8H_{17})_3$	6.57	5	10	2	8.2	—	3.3	2.7
$scCO_2$	$P(C_8H_{17})_3$	6.56	5	20	2	12	—	3.9	4.2
$scCO_2$	$P(C_8H_{17})_3$	6.69	10	10	2	17	1.5	2.8	6.3
$scCO_2$	$P(C_8H_{17})_3$	6.61	15	10	2	20	2.3	2.8	7.5

[a] Traces of isomerised alkenes are also observed. [b] 0.2 cm^3. [c] 2-Methylhexanol (3%) and hexane are also observed. [d] 2 cm^3. [e] R_f = $C_6F_{13}CH_2CH_2$. [f] 90 °C.

changes in solubility (both reactions are fully homogeneous). Using tri-*n*-octylphosphine, the rate is very much reduced, two phases are apparent in the system and higher n : i ratios (up to 3.9) are obtained with low p_{CO}, although the conversion is low. We have shown that higher n : i ratios can be obtained at low conversion in the solution phase system.[9]

We conclude that hydroformylation of hex-1-ene can be successfully carried out in $scCO_2$ using rhodium based catalysts containing cheap, readily available trialkylphosphine ligands, and that different chemoselectivities can be observed from those observed under some conditions in organic solvents.

We thank the EPSRC and the EC TMR programme for a Fellowship (I. B) and Professor M. Poliakoff for helpful discussion.

Notes and References

† E-mail: djc@st-and.ac.uk

‡ Reactions were carried out in a 36 cm^3 Hastelloy autoclave fitted with a mechanical stirrer and a sapphire base for visual observation of the contents. All manipulations were carried out under nitrogen. $[Rh_2(OAc)_4]$ (0.052 g, 0.1176 mmol) was dissolved in PEt_3 (0.1 cm^3, 0.67 mmol) to give a red solution. Degassed hex-1-ene (2 cm^3, 16 mmol) was added and the mixture transferred into the autoclave, pressurised with CO and H_2 and stirred at room temperature for 1 h. Liquid CO_2 was then transferred into the autoclave using a cooled head hplc pump to give a total pressure 65 bar above that of the CO–H_2. The autoclave was then heated for the desired reaction time, with the pressure and temperature being monitored throughout. After the reaction, the autoclave was allowed to cool in dry ice to −50 °C. The CO_2 was vented and the liquid product, typically 1.8 cm^3, was collected and analysed by GLC (quantitative analysis) and GC–MS (identification of products). ^{31}P NMR studies of the final liquid indicated that the major species in solution is $[RhH(CO)_2(PEt_3)_2]$.[9]

For reactions in toluene, the reaction was carried out in the same autoclave using half the amounts of all the reagents, 17 cm^3 of toluene and the same gas pressure. This ensures that all the concentrations are the same as in the $scCO_2$ experiments and that the pressure drop for the same percentage conversion of substrate is also the same.

1 R. Noyori, *Science*, 1995, **269**, 1065.
2 P. G. Jessop, T. Ikariya and R. Noyori, *Chem. Rev*., 1995, **95**, 259.
3 J. W. Rathke, R. J. Klinger and T. R. Krause, *Organometallics*, 1991, **10**, 1350.
4 R. J. Klinger and J. W. Rathke, *J. Am. Chem. Soc*., 1994, **116**, 4772.
5 P. G. Jessop, Y. Hsiao, T. Ikariya and R. Noyori, *J. Am. Chem. Soc*., 1996, **118**, 344.
6 S. Kainz, D. Koch, W. Baumann and W. Leitner, *Angew. Chem., Int. Ed. Engl*., 1997, **36**, 1628.
7 P. G. Jessop, T. Ikariya and R. Noyori, *J. Am. Chem. Soc*., 1994, **116**, 8851.
8 P. G. Jessop, Y. Hsiao, T. Ikariya and R. Noyori, *J. Am. Chem. Soc*., 1996, **118**, 344.
9 J. K. MacDougall, M. C. Simpson, M. J. Green and D. J. Cole-Hamilton, *J. Chem. Soc., Dalton Trans*., 1996, 1161.

Received in Cambridge, UK, 21st May 1998; 8/03855D

Remarkable synergy between microwave heating and the addition of seed crystals in zeolite synthesis—a suggestion verified

Colin S. Cundy,*† Richard J. Plaisted and Jing Ping Zhao

Centre for Microporous Materials, Department of Chemistry, UMIST, PO Box 88, Manchester, UK M60 1QD

A recent suggestion that there can be a nucleation-related bottleneck in microwave zeolite synthesis has been verified: ZSM-5 has been synthesised very rapidly in seeded systems with and without an organic template.

Microwave dielectric heating is becoming an increasingly important accessory in chemical synthesis.[1–3] Remarkable reductions in synthesis time (by up to a factor of 10^3)[4] are observed and selectivity to particular product isomers has been achieved in naphthalene sulfonation.[5] Following an early study,[6] the microwave-mediated synthesis of micro- and mesoporous materials has been the subject of a number of recent reports, with zeolites,[7,8] $AlPO_4$-type materials[9,10] and MCM-41[11] being successfully prepared. In the microwave synthesis of zeolite Y, crystallisation of undesired phases is suppressed[7] and phase selectivity can be maintained at an unusually high synthesis temperature (150 °C).[12]

The crystallisation of zeotype materials is frequently constrained by limitations at the nucleation stage so that it is common practice to age reaction mixtures or add nucleants to them.[13] There are two potential effects of these procedures on the synthesis reaction: (*a*) reduction of the induction period preceding the detection of crystalline product and (*b*) promotion of a dominant crystalline phase (usually that of the seeding material). Thus, overall synthesis time can be shortened and product purity improved. Different aspects of these two effects have been demonstrated in recent studies on the synthesis of zeolite A with conventional[14] and microwave[8] heating. In one report,[8] microwave heating of zeolite A reaction mixtures which had been aged for various periods led to reaction times as short as 1 min and it was suggested that the rearrangement of the synthesis mixture to yield nuclei was the bottleneck in a microwave synthesis. We demonstrate below using a different zeolite system as a model that this is indeed the case and furthermore that the effects achievable by microwave heating and seeding techniques are strongly synergistic.

The synthesis of zeolite ZSM-5 has been studied using two optimised reaction systems.‡ In the first case, Na, TPA-ZSM-5 was synthesised using the composition:[12] 5.0 Na_2O : 0.2 Al_2O_3 : 60 SiO_2 : 4.0 TPABr : 900 H_2O where the silica source was a silica sol, the alumina source was sodium aluminate and TPA is the templating cation tetrapropylammonium. The second system used similar reagents but contained no organic template:[15] 10.0 Na_2O : 1.0 Al_2O_3 : 60 SiO_2 : 3000 H_2O.

In each case, reactions were carried out in the presence and absence of seed material and using both microwave and traditional heating methods. The seed employed (5% by mass of total silica) was a fully characterised TPA-silicalite (Al-free ZSM-5) sol[16,17] consisting of near-monodisperse nanometre-sized crystalline zeolite particles in water. Reaction temperature was 175 °C throughout and times were recorded from the start of the heating period.

The results are illustrated in Fig. 1. In the unseeded TPA-templated thermal preparation [curve (*e*)], crystalline MFI product was detected (XRD) after 2 h and the synthesis was complete at 5.5 h. Carrying out the reaction at the same indicated temperature using microwave heating reduced the synthesis time to 3 h following the appearance of crystallinity at t = 1 h [curve (*d*)]. The crystallisation of the oven-heated mixture was considerably accelerated by the presence of the nanosized seed material with 15% crystallinity apparent after only 1 h and completion in 2 h [curve (*c*)]. However, the combined effect of nanocrystal seeding and microwave heating produced the remarkable result seen in curve (*a*) where crystallisation was almost complete by the time that the reaction mixture had reached working temperature (3 min).

With no organic template and in the absence of seed crystals, no crystalline product was found after 3 h of microwave heating, whilst only a trace of product was detectable by X-ray diffraction after 7 h of oven heating. The inclusion of colloidal seed material brought reaction rates within the time frame of Fig. 1, although the thermal reaction was the slowest recorded overall [curve (*f*)]. However, the corresponding microwave-mediated synthesis [curve (*b*)] was only a little slower than its templated counterpart [curve (*a*)].

These results may be rationalised by consideration of three factors contributing to the overall reaction time, namely (1) thermal lag, (2) the induction period and (3) crystal growth. The first of these probably accounts for about 0.5 h in the experiments with the oven-heated autoclaves (as determined by separate tests). This is essentially eliminated in the microwave experiments, where the rise to operating temperature of the reactor contents is extremely rapid (≤3 min). It is clear from Fig. 1 that, although the induction period is reduced by the presence of the nanocrystal seed, a notable synergism occurs when microwave heating is additionally employed. Possible reasons for this are discussed in more detail below. The third factor allows for a reaction time adjustment which depends on the pattern of nucleation and crystal growth. The unseeded TPABr-containing compositions produce products of broader particle size range (up to *ca.* 5 μm thermal, 12 μm microwave) than the seeded preparations (≤1 μm), necessitating a longer period of crystal growth for the largest crystals to reach their final size. There are also differences in linear growth rate (templated synthesis > inorganic and microwave > thermal). A more detailed study of crystal growth rates[18] will be reported elsewhere.

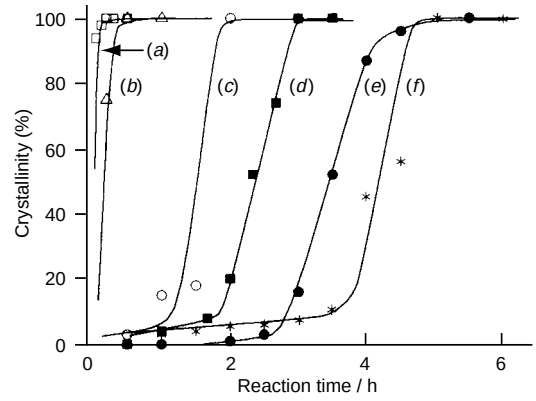

Fig. 1 Growth curves for ZSM-5: (*a*) seeded, TPA, microwave; (*b*) seeded, inorganic, microwave; (*c*) seeded, TPA, thermal; (*d*) unseeded, TPA, microwave; (*e*) unseeded, TPA, thermal; (*f*) seeded, inorganic, thermal

The results above confirm the suggested[8] nucleation-related bottleneck. However, it is useful to make a distinction between the equilibration of the reaction mixture (as evidenced by, for example, changes in pH and silicate anion distribution) and the generation of nuclei, since it can be shown that these are separate, although interlinked, processes.[19] In both the zeolite A and the ZSM-5 cases (but perhaps not universally), the microwave heating rate far outstrips the crystal nucleation rate so that no zeolite product is formed at short heating times in the absence of added seed crystals or sources of nuclei. However, in the earlier work,[8] it was also proposed that the almost instantaneous heat-up allowed the reaction to take place in a synthesis mixture that had hardly changed during the heating process. The very rapid onset of crystal growth which occurs under microwave heating conditions in the presence of added nanocrystalline seed [*e.g.* curve (*a*) *vs.* curve (*d*)] confirms that it is the time to form nuclei rather than the preceding equilibration of the reaction mixture which is the slowest step. However, such rapid and complete crystallisation could not occur unless any slow reagent digestion steps were complete. Hence, the reaction mixture has to be regarded as essentially fully equilibrated rather than hardly changed.

Finally, we consider the differences apparent from Fig. 1 between comparable microwave and thermal reactions. Since both thermal and microwave syntheses are carried out under conditions of controlled and measured temperature, a significant overall temperature difference due to microwave superheating[3] is unlikely. A more probable cause lies in differential microwave heating effects due to the heterogeneity of the dielectric (*i.e.* the reaction mixture) which at all times contains colloidal or particulate material. Local superheating could result from a number of energy-loss mechanisms:[3] (*i*) dipolar polarisation losses varying with local composition, (*ii*) interfacial (Maxwell–Wagner) polarisation losses and (*iii*) conduction losses associated with clusters or arrays of ions. Thus, one component of the enhanced rates observed in the microwave syntheses may derive from an acceleration of reagent digestion and aluminosilicate equilibration processes to produce a medium which is more homogeneous on a molecular scale. However, perhaps an even more significant effect may be occurring at crystal surfaces where microwave energisation of the hydroxylated surface or of associated water molecules in the boundary layer may be linked to specific energy dissipation through modes (*ii*) and (*iii*) above. This could account for the rapid activation of seed crystals under microwave conditions seen in curves (*a*) and (*b*) of Fig. 1.

The authors would like to thank John Dwyer for his interest in this work and the EPSRC for partial support under Grant No. GR/K 06877. The support for the Centre for Microporous Materials provided by BNFL, BOC, Engelhard and ICI is also gratefully acknowledged.

Notes and References

† E-mail: colin.cundy@umist.ac.uk

‡ *Experimental details* for the zeolite syntheses: TPA-templated composition: sodium aluminate (0.49 g, BDH, 21.3 mass% Na, 20.8 mass% Al) dissolved in a solution of sodium hydroxide (1.80 g, Prolabo AR) in water (35 g) was added with stirring to a solution of tetrapropylammonium bromide (5.03 g, ABM Chemicals) in 42.5 g of Ludox AS 40 silica sol (40 mass% SiO_2, Dupont). To one half of this mixture was added water (7.5 g) and, to the other, an aqueous colloidal sol of TPA-silicalite (7.5 g, 5.8 mass% solids, mean particle size *ca.* 70 nm). Reaction mixture aliquots were heated in PTFE-lined autoclaves at 175 °C either in a conventional oven or in a CEM MDS-2100 microwave reactor (2.45 GHz).

Inorganic composition: aluminium nitrate nonahydrate (12.75 g, Merck AR) dissolved in water (100 g) was added to a vigorously stirred solution of sodium hydroxide (17.65 g, Prolabo AR) in water (150 g). The resulting clear solution was added to a mixture of Syton X 30 silica sol (203.8 g, 30 mass% SiO_2, Monsanto) and water (456 g). Further water or silicalite sol was added as above to give a seed concentration of 5% by mass (based on total silica) and the comparative syntheses carried out as before.

1 S. Caddick, *Tetrahedron*, 1995, **51**, 10 403.
2 C. R. Strauss and R. W. Trainor, *Aust. J. Chem.*, 1995, **48**, 1665.
3 D. M. P. Mingos and D. R. Baghurst, *Chem. Soc. Rev.*, 1991, **20**, 1.
4 R. N. Gedye, F. E. Smith and K. C. Westaway, *Can. J. Chem.*, 1988, **66**, 17.
5 D. Stuerga, K. Gonon and M. Lallemant, *Tetrahedron*, 1993, **49**, 6229.
6 P. Chu, F. G. Dwyer and J. C. Vartuli, *US Pat*. 4 778 666, 1988.
7 A. Arafat, J. C. Jansen, A. R. Ebaid and H. van Bekkum, *Zeolites*, 1993, **13**, 162.
8 P. M. Slangen, J. C. Jansen and H. van Bekkum, *Microporous Mater.*, 1997, **9**, 259.
9 I. Girnus, K. Jancke, R. Vetter, J. Richter-Mendau and J. Caro, *Zeolites*, 1995, **15**, 33; I. Girnus, K. Hoffmann, F. Marlow, J. Caro and G. Doering, *Microporous Mater.*, 1994, **2**, 537.
10 S. L. Cresswell. J. R. Parsonage, P. G. Riby and M. J. K. Thomas, *J. Chem. Soc., Dalton Trans.*, 1995, 2315.
11 C. G. Wu and T. Bein, *Chem. Commun.*, 1996, 925.
12 J. P. Zhao, C. S. Cundy and J. Dwyer in *Progress in Zeolites and Microporous Materials*, ed. H. Chon, S.-K. Ihm and Y. S. Uh, *Studies in Surface Science and Catalysis*, Elsevier, Amsterdam, 1997, vol. 105, part A, p. 181.
13 R. M. Barrer, *Hydrothermal Chemistry of Zeolites*, Academic Press, New York, 1982, ch. 4.
14 L. Gora and R. W. Thompson, *Zeolites*, 1997, **18**, 132.
15 A. Araya and B. M. Lowe, *Zeolites*, 1986, **6**, 111.
16 A. E. Persson, B. J. Schoeman, J. Sterte and J.-E. Otterstedt, *Zeolites*, 1994, **14**, 557.
17 J. P. Verduijn, *World Pat.*, 9308124, 1993.
18 For earlier work, see C. S. Cundy, B. M. Lowe and D. M. Sinclair, *Faraday Discuss. Chem. Soc.*, 1993, **95**, 235 and references therein.
19 C. S. Cundy, M. S. Henty and R. J. Plaisted, paper in preparation.

Received in Cambridge, UK, 5th May 1998; 8/03324B

Molecular design and testing of organophosphonates for inhibition of crystallisation of ettringite and cement hydration

Peter V. Coveney,*[a]† Roger J. Davey,[b] Jonathan L. W. Griffin[c] and Andrew Whiting[c]

[a] *Schlumberger Cambridge Research, High Cross, Madingley Road, Cambridge, UK CB3 0EL*
[b] *Department of Chemical Engineering, UMIST, PO Box 88, Manchester, UK M60 1QD*
[c] *Department of Chemistry, Faraday Building, UMIST, PO Box 88, Manchester, UK M60 1QD*

We report the synthesis and testing of novel macrocyclic organophosphonate retarders which have been proposed using rational molecular design methods based on the selective inhibition of the crystallisation of ettringite, a product of the early stages of cement hydration.

Cementitious materials are among the most widely used by mankind while being among the least well understood. The detailed physicochemical processes involved in the hydration and setting of cement slurries are very complex, and a clearly defined quantitative account is still lacking; indeed, even the precise composition of the cement powder is unknown. Although numerous additives are known and used to retard the cement setting process, little is understood of the mechanism by which they act. Here, we show how it is possible to design and synthesize novel macrocyclic organophosphonate retarders by rational molecular design methods[1] based on the selective inhibition of the crystallisation of ettringite, a product of the early stages of cement hydration. This delays the setting process without altering the setting properties (development of compressive strength, *etc*.) once this process begins.

It is known that phosphonate-based organic compounds, such as **1**, **2** and **3** in Fig. 1, are able to retard the onset of setting in cement slurries under ambient conditions;[1,2] however, the mechanism by which such retarders work has hitherto not been established. Furthermore, some phosphonates (such as **1**) are such powerful cement setting retarders that they also cause the time taken for setting (that is, the compressive strength development, once setting commences) to increase substantially.[1] From the point of view of engineering applications of cement in the oil and construction industries,[3–5] it is usually desirable for cement slurries to set rapidly once the setting process is initiated, thus ensuring the development of the required mechanical properties of the resulting concrete matrix as rapidly as possible. There is, therefore, a need to devise cement setting retarders which not only accurately control the time taken for setting to take place, but also maintain the setting characteristics of neat (untreated) cement once set is initiated. To enable the development of such retarders, however, it is necessary to have an accurate understanding of the processes which control the setting of cement.

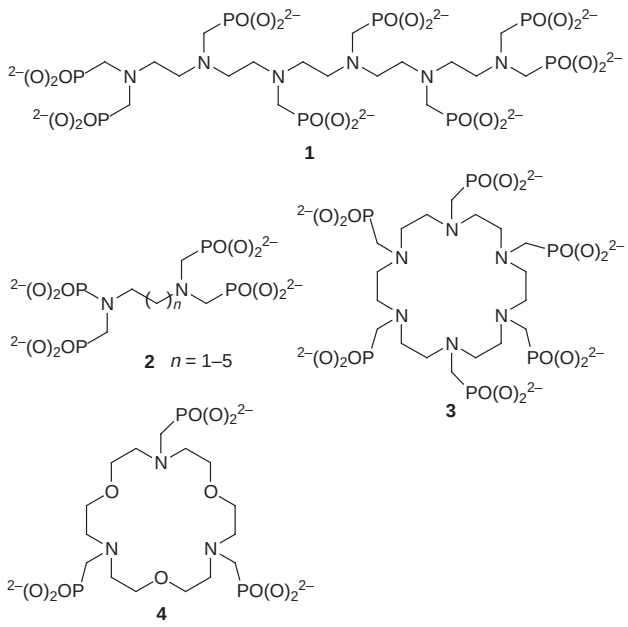

Fig. 1 Some phosphonate cement-setting retarders: **1** and **2**, linear phosphonates; hexaaza-18-crown-6 **3** and trioxotriaza-18-crown-6 **4** macrocyclic phosphonates designed by computer modelling techniques[1]

The work reported here makes use of a recently proposed theoretical model for the setting of cement involving the initial nucleation and growth of crystalline ettringite, $[Ca_3Al(OH)_6]_2[SO_4]_3{\cdot}26H_2O$, from a gelatinous precursor.[1,6,7] An important consequence of this model is that, if retarders can be designed which interfere solely with the process of ettringite nucleation and growth, then cement slurries should set normally once the silicate hydration process is initiated, thus ensuring mechanical integrity of the resulting cured product; a separate mechanism for the retardation of silicate hydration has also recently been proposed.[8] The structural basis for the design of such ettringite-specific retarding agents has been discussed previously[1] and is based on the strategy exemplified earlier by Davey *et al*.[9–12] in which the geometry and functionality of additive molecules are chosen such that they are capable of recognising and binding to the growing surface of nuclei or crystals, thereby accomplishing inhibition of nucleation and/or crystal growth.[1] In turn, if such specific retarding agents designed for an ettringite substrate also exhibit an ability to inhibit the setting of cement, without changing its essential setting properties, then this would be consistent with the nonlinear chemical clock-type hypothesis of Billingham and Coveney[6] in which the autocatalytic formation of crystalline ettringite is the rate determining step.

Although molecular modelling studies have proved useful for the rational design of crystal growth inhibitors for simple inorganic systems,[9–12] the design of crystal growth inhibitors for ettringite is a much more challenging prospect due to the complexity of the inorganic matrix. It was however possible to propose that compounds such as **3** and **4** should be effective agents for inhibiting the crystal growth of ettringite, since they possess the ideal structural motifs for molecular recognition with the most rapidly growing [001] face of the ettringite matrix.[1] In particular, the geometry of the phosphonate functions of **3** and **4** in Fig. 1 are such that they fit into the sulfate binding sites of ettringite ensuring enhanced molecular recognition compared to acyclic phosphonates **1** and **2**.[13] Compound **4** exhibits a greater level of conformational flexibility and is expected to be the more active of the two.[1]

Hexaphosphonate **3** was prepared as reported previously[1,14] and triphosphonate **4** was prepared using analogous methods.[14–17] These two compounds were then used as additives during the formation of ettringite and also in cement samples.

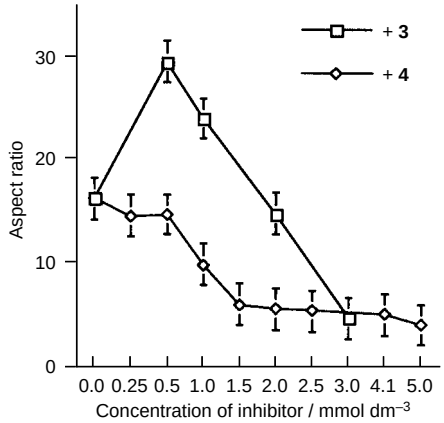

Fig. 2 The influence of additives **3** and **4** on the aspect ratio of ettringite crystals; the data were obtained from SEM images. Note that the trioxygen containing macrocycle **4** is more efficient at limiting ettringite crystal growth at lower concentrations than the macrocycle **3**.

Ettringite crystals,[18] prepared by reacting aqueous $Al_2(SO_4)_3$ with a calcium hydroxide suspension for 30 min at 70 °C, exhibit a prismatic morphology, being elongated about the *c*-axis. Additives **3** and **4** had a profound effect on ettringite crystal morphology, producing a remarkable reduction in the length of the ettringite crystals even at low concentrations: for example at concentrations of **3** and **4** of 1.00 mmol dm^{-3}, there were respectively 45 and 75% reductions in crystal lengths compared to untreated ettringite. Fig. 2 shows the data as the change in measured aspect ratios and indicates clearly the transition from needle to prism. These results are in agreement with the prediction that both compounds **3** and **4** are pre-organised to recognise and bind to the growing {001} faces of ettringite, and that **4** should be a superior inhibitor to **3**.[1]

These results are supported by X-ray powder diffractograms of the solid products of ettringite crystallisations carried out in the absence of additive and in the presence of 4.0 mmol dm^{-3} of additives **3** and **4**. The diffractogram for a pure ettringite sample exhibits the preferred orientation expected for *c*-axis needles, with all {*hkl*} reflections having significantly reduced intensities. This X-ray pattern is entirely consistent with pure, well crystalline ettringite; the relative intensities of diffraction from the (100) and (114) lattice planes at 9 and 22.8° would be 2 : 1 in a powder comprising isometric crystals. The observed enhancement to 4 : 1 is consistent with a product comprising *c*-axis needle shaped crystals. In the presence of additive **3**, this relative intensity is 1 : 1, implying significantly more equant crystal habits; at the same time the pattern indicates the presence of two other crystalline phases, calcium hydroxide and gypsum, not normally seen as a product in these reactions (the relatively intense diffraction peaks at 29.3 and 47.3° are consistent with the existence of gypsum [(111) reflection] and calcium hydroxide [(102) reflection] respectively). In the presence of additive **4** the result is even more extreme, indicating significantly lower levels of ettringite, some gypsum, and calcium hydroxide, together with significant amounts of amorphous material. These data confirm the observed morphological change in the ettringite crystals and also suggest that ettringite nucleation is indeed inhibited by these additives, leading to the production of amorphous material and crystalline gypsum together with a reduction in the overall reaction rate, resulting in unreacted calcium hydroxide. Again molecule **4** is found to be the more active as originally predicted.

The effect of these same additives on the setting of cement slurries was then examined. Rates and extent of setting of samples taken from one batch of class G oilfield cement were measured at additive concentrations of 1.0 mmol dm^{-3} by heat flow calorimetry[1] in which the magnitude and time evolution of the heat of reaction were recorded. It was found that hexaphosphonate **3** doubles the induction time for the onset of setting of cement while triphosphonate **4** extends this period threefold. In addition, however, it is evident that in both cases the setting characteristics, as judged by the profile of the heat flow curves, remain unchanged compared with the case of neat cement, suggesting that these compounds act to inhibit nucleation of ettringite and do not interfere with compressive strength development once that nucleation process has occurred. This is in marked contrast with the general behaviour of acyclic phosphonate cement setting retarders which both delay the onset of setting and inhibit the setting process once it has begun.[1] It is important to note that aged cements, which have been exposed to atmospheric humidity for extended periods, show no delay in the onset of setting and display calorimetric profiles identical to neat cement when treated with these additives. This result is consistent both with the specificity of these additives towards ettringite, which has presumably already formed in these aged materials, and their inability to influence other hydration products such as calcium silicate or hydroxide.

Our results show that additives designed as selective inhibitors for the crystallisation of ettringite can be used to delay the onset of setting of cement slurries without interfering with the eventual setting process itself. This behaviour was discovered on the basis of two central concepts: firstly, that the formation of crystalline ettringite from an amorphous precursor plays a rate determining role in cement setting, and secondly, that it is possible to rationally design compounds which are preorganised for molecular recognition at the surfaces of complex inorganic matrices, such as ettringite, and thus act as powerful crystallisation inhibitors. In the case of cement slurries, the use of such phase-selective retarders should result in the production of cured concrete with very similar mechanical properties to that from the untreated cement.

Jon Griffin is grateful to the EPSRC (GR94007291) and Schlumberger Cambridge Research for the award of a Total Technology grant.

Notes and References

† E-mail: coveney@cambridge.scr.slb.com

1 P. V. Coveney and W. Humphries, *J. Chem. Soc., Faraday Trans.*, 1996, **92**, 831.
2 H. Taylor, *Cement Chemistry*, Academic Press, London, 1989.
3 *Schlumberger Oilfield Rev.*, 1991, **3**: Special Issue on Cementing.
4 P. V. Coveney, T. L. Hughes and P. Fletcher, *Proceedings of the 1996 Annual Conference of the American Association for Artificial Intelligence*, Portland, Oregon, USA, vol. 2, p. 1471.
5 P. V. Coveney, T. L. Hughes and P. Fletcher, *AI Mag.*, 1996, **17**, 41; *Well Cementing*, ed. E. Nelson, Schlumberger Educational Services, Houston, 1990.
6 J. Billingham and P. V. Coveney, *J. Chem. Soc., Faraday Trans.*, 1993, **89**, 3021.
7 J. A. D. Wattis and P. V. Coveney, *J. Chem. Phys.*, 1997, **106**, 9122.
8 I. S. Bell and P. V. Coveney, *Mol. Sim.*, 1998, **20**, 331.
9 R. J. Davey, S. N. Black, L. A. Bromley, D. Cottier, B. Dobbs and J. E. Rout, *Nature*, 1991, **353**, 549.
10 S. N. Black, L. A. Bromley, D. Cottier, R. J. Davey, B. Dobbs and J. E. Rout, *J. Chem. Soc., Faraday Trans.*, 1991, **87**, 3409.
11 L. A. Bromley, D. Cottier, R. J. Davey, B. Dobbs, S. Smith and B. R. Heywood, *Langmuir*, 1993, **9**, 3594.
12 A. L. Rohl, D. H. Gay, R. J. Davey and C. R. A. Catlow, *J. Am. Chem. Soc.*, 1996, **118**, 6042.
13 V. S. Ramachandran, M. S. Lowery, T. Wise and G. M. Polomark, *Mater. Struct.*, 1993, **26**, 425.
14 G. W. Morris, N. D. Feasey, P. A. Ferguson, D. Van Hemelrijk and M. Charlot, *UK Pat.*, GB 88-17185 880719, 1988.
15 E. Graf and J. M. Lehn, *Helv. Chim. Acta*, 1981, **64**, 1040.
16 D. Chen, P. J. Squattrito, A. E. Martell and A. Clearfield, *Inorg. Chem.*, 1990, **29**, 4368.
17 K. Moedritzer and R. Irani, *J. Org. Chem.*, 1966, **31**, 1603.
18 M. Atkins, F. P. Glasser and A. Kindness, *Cement Concr. Res.*, 1992, **22**, 241.

Received in Cambridge, UK, 12th May 1998; 8/02371I

Octafunctionalized polyhedral oligosilsesquioxanes as scaffolds: synthesis of peptidyl silsesquioxanes‡

Frank J. Feher,*[a]† Kevin D. Wyndham,[a] Mark A. Scialdone*[b] and Yoshitomo Hamuro

[a] *Department of Chemistry, University of California, Irvine, California 92697-2025, USA*
[b] *E. I. du Pont de Nemours & Co., Inc., Central Research and Development, Experimental Station, Wilmington, Delaware 19880-0328, USA*

The first use of polyhedral silsesquioxanes to organize ensembles of biologically relevant motifs is described. N-Protected amino acids and peptides can be attached to $[H_2N(CH_2)_3]_8Si_8O_{12}$ 1 and $[p\text{-}HOCH_2C_6H_4]_8Si_8O_{12}$ 2 in either a convergent fashion or a divergent fashion to produce peptidyl silsesquioxanes in excellent yield and purity.

Symmetric core scaffolds possessing multiple reactive functional groups have recently attracted much interest as templates for the presentation of molecular domains of biological relevance. For example, symmetrical tetrafunctional xanthene and cubane have been used as scaffolds to create combinatorial libraries of trypsin inhibitors with moderate activities,[1–3] while porphyrins,[4,5] polyfunctional cyclic peptides[6] and cyclotriphosphazenes[7] have been used as scaffolds for helical bundles of peptides in models for ion channels. Similarly, calixarenes have been used as templates to assist the spatial arrangement of cyclic peptides[8] and sugars.[9] In principle, any polyfunctional molecule may serve as a scaffold to present multiple copies of a biologically relevant pendant group, but the most attractive cores are those which have particular geometrical parameters (*e.g.* size, shape, symmetry) to allow unique ligand presentation. Here, we describe the first use of polyhedral oligosilsesquioxanes as scaffolds for peptides. These robust, readily available Si/O frameworks offer interesting possibilities as cores for ensembles of biologically relevant pendant groups.

A wide range of polyhedral oligosilsesquioxanes can be prepared *via* hydrolytic condensation reactions of trifunctional organosilicon monomers.[10] Two known frameworks that possess terminal protic nucleophilic functionality are octaamine **1** and octaalcohol **2**. Octaamine **1** is readily available as a hydrochloride salt in one step (35% yield) from $H_2N(CH_2)_3Si(OEt)_3$.[11,12] Octaalcohol **2** is prepared in approximately 5% overall yield in three steps from $p\text{-}ClCH_2C_6H_4SiCl_3$.[13]

Octaamine **1** undergoes octafunctionalization with N-protected amino acids and N-protected di- and tri-peptides under standard coupling conditions.[14–16] As outlined in Scheme 1 and Table 1, high yields of coupled products can be obtained by reacting **1** with an excess of an N-protected amino acid (*e.g.* Z-Pro-OH) and *O*-(7-benzotriazol-l-yl)-1,1,3,3-tetramethyluronium (TBTU) in DMF–*N*,*N*′-diisopropylethylamine (DIPEA), and then precipitating the product with aqueous acid.§ The course of these reactions can be conveniently monitored by ^{1}H NMR spectroscopy because the chemical shift for the CH_2N of **1** shifts from δ 2.8 to 3.0 [$(CD_3)_2SO$] upon condensation with the amino acid. The only Si-containing species detectable by ^{1}H, ^{13}C and ^{29}Si NMR spectroscopy in the crude materials are the desired octafunctional derivatives and they are spectroscopically pure. In most cases, the ^{1}H and ^{13}C NMR spectra of peptidyl silsesquioxane are well defined and fully assignable on the basis of COSY, HMQC and DEPT experiments.

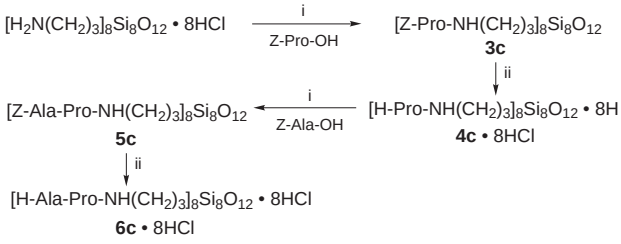

Scheme 1 *Reagents and conditions*: i, protected amino acid (1.2–4 equiv. per NH_2), TBTU (2–4 equiv. per NH_2), HOBt + H_2O (4 equiv. per NH_2) and DIPEA (9 equiv. per NH_2) in DMF, 10–24 h, 25 °C; ii, H_2 (100 psi), 10% Pd/C, 1 M HCl–MeOH, 8 h, 25 °C

The syntheses of **3d** and **3e** *via* coupling reactions of **1** with N-protected peptides represent convergent syntheses of peptidyl silsesquioxanes, which are attractive when the desired peptide sequence can be prepared in advance. It is also possible to synthesize peptidyl silsesquioxanes in a divergent fashion by iteratively coupling and deprotecting Z-protected amino acids. For example, removal of the Z-group from **3c** *via* hydrogenolysis over 10% Pd/C in aqueous acidic methanol (100 psi, 25 °C, 8 h)¶ gives **4c**·8HCl in high yield, which can be subsequently coupled with Z-Ala-OH and deprotected to give dipeptidyl silsesquioxane **6c**·8HCl (Scheme 1).

Octaalcohol **2** is also a useful scaffold for peptidyl silsesquioxanes, which may exhibit different properties because of its rigid *para*-phenylene spacer. The synthesis of peptidyl silsesquioxanes derived from **2** is analogous to the preparation of peptidyl silsesquioxanes derived from **1** (Fig. 1 and Table 2). However, the poorer nucleophilicity of the benzylic hydroxyl group requires a much longer reaction time and a generous excess of N-protected amino acid and TBTU for complete coupling to occur. For example, the reaction of **2** with 2 equiv. of Fmoc-Ala-OH and TBTU per OH for 17 h in DMF–DIPEA produces **7c** in only 26% yield. The major product (40%) is the incompletely-substituted product derived from coupling of **2** with seven Fmoc-Ala-OH; small amounts (6%) of incom-

Table 1 Preparation of peptidyl silsesquioxanes derived from **1**

$[R^1NH(CH_2)_3]_8Si_8O_{12} \rightarrow [R^2NH(CH_2)_3]_8Si_8O_{12}$

Starting material	R^1	Product	R^2	Isolated yield (%)
1·8HCl	H	**3a**	Z-Gly	91
1·8HCl	H	**3b**	Z-Ala	98
1·8HCl	H	**3c**	Z-Pro	44
1·8HCl	H	**3d**	Z-Phe-Leu	94
1·8HCl	H	**3e**	Z-Phe-Leu-Ala	73
3c	Z-Pro	**4c**·8HCl	H-Pro	89
3d	Z-Phe-Leu	**4d**·8HCl	H-Phe-Leu	87
4c·8HCl	H-Pro	**5c**	Z-Ala-Pro	100
4d·8HCl	H-Phe-Leu	**5d**	Z-Ala-Phe-Leu	92
5c	Z-Ala-Pro	**6c**·8HCl	H-Ala-Pro	89

See Scheme 1 for reaction conditions. R^1 and R^2 refer to neutral organic substituents on N. Where indicated, starting materials and products were used or isolated as salts containing 8HCl.

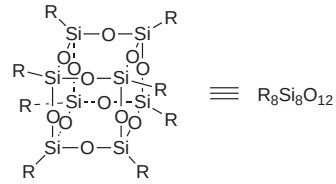

1 R = $CH_2CH_2CH_2NH_2$
2 *p*-$C_6H_4CH_2OH$

Fig. 1

Table 2 Preparation of peptidyl silsesquioxanes derived from **2**

[*p*-$R^1OCH_2C_6H_4]_8Si_8O_{12}$ → [*p*-$R^2OCH_2C_6H_4]_8Si_8O_{12}$

Starting material	R^1	Product	R^2	Isolated yield (%)
2	H	**7a**	Fmoc-Ala	26
2	H	**7b**	Fmoc-Phe	28
2	H	**7c**	Boc-Ala	72
7c	Boc-Ala	**8c**·8TFA	H-Ala	100
8c·8TFA	H-Ala	**9c**	Boc-Phe-Ala	46

See Scheme 1 for reaction conditions. R^1 and R^2 refer to neutral organic substituents on O. Where indicated, starting materials and products were used or isolated as salts containing 8TFA (*i.e.* CF_3CO_2H).

pletely-substituted products containing six Fmoc-Ala groups are also isolated. These compounds can be readily separated by flash chromatography on SiO_2 (20 : 1 CH_2Cl_2–MeOH) and fully characterized by multinuclear NMR spectroscopy and MALDI-TOF mass spectrometry. Complete functionalization of **2** by Boc-Ala-OH was accomplished by using 4 equiv. of the protected amino acid (per CH_2OH), 4 equiv. of TBTU and a reaction time of 7 days. Removal of Boc protecting groups can be efficiently accomplished with TFA in CH_2Cl_2, but the cleavage of Fmoc protecting groups with piperidine (20% in THF, 25 °C) does not occur cleanly, presumably because of base-induced decomposition of the Si_8O_{12} framework.[11]

In summary, we have demonstrated the first use of polyhedral silsesquioxanes to organize ensembles of biologically relevant motifs. Peptides can be attached to octaamine **1** and octaalcohol **2** in either a convergent fashion or a divergent fashion to produce peptidyl silsesquioxanes in excellent yields and purity. In the case of octaalcohol **2**, coupling reactions are more difficult to complete due to the poor nucleophilicity of hydroxy groups, but the octasubstituted compound can be easily separated from less extensively substituted derivatives by column chromatography. These large frameworks can be synthetically manipulated by standard solution methods and characterized by NMR spectroscopy and mass spectroscopy (MALDI-TOF). We have only begun to explore the use of silsesquioxanes as scaffolds for biologically relevant pendant groups, but the ready availability of discrete polyhedral frameworks containing 6–16 silicon atoms offers many interesting possibilities in areas of molecular recognition, biomimetics and drug design. Our work in these and other areas will be reported separately.[17,18]

This work was supported by the National Science Foundation. We thank Dr Keith J. Weller (Witco/OSi Specialties) for a generous gift of silanes and Professor William F. DeGrado (University of Pennsylvania) for helpful discussions.

Notes and References

† E-mail: fjfeher@uci.edu
‡ Contribution No. 7751.
§ Peptidyl silsesquioxane **3c** was prepared by adding DIPEA (0.8 ml, 46 mmol) to a solution of **1**·8HCl (0.074 g, 0.063 mmol), CBZ-Pro-OH (0.501 g, 2.02 mmol), TBTU (642 mg, 2.00 mmol), and 1-hydroxybenzotriazole hydrate (306 mg, 2.00 mmol) in DMF (3 ml). After stirring for 1 day, the crude product was precipitated by dropwise addition of the reaction mixture to ice-cold 0.2 M aqueous citric acid (200 ml). Filtration, extraction with methanol, precipitation with a 0.5 M $NaHCO_3$, washing and drying *in vacuo* (25 °C, 0.01 Torr) afforded **3c** in 44% yield (76 mg). For **3c**, which possesses proline pendants with two rotameric forms (a : b 1.3 : 1): ^{1}H NMR [500.0 MHz, $(CD_3)_2SO$, 25 °C] δ 7.98 (t, NHCO, rotamer a), 7.90 (t, NHCO, rotamer b), 7.35–7.22 (m, C_6H_5), 5.10–4.98 (m, $CH_2C_6H_5$), 4.13 (m, COCH), 3.41 [s, $CH_2(N)CH_2$], 3.35 [s, $CH_2(N)CH_2$], 2.98 (br, $SiCH_2CH_2CH_2$), 2.05 [d, $COCH(N)CH_2$], 1.73 (br, $COCHCH_2CH_2$), 1.42 (br, $SiCH_2CH_2$), 0.53 (br, $SiCH_2$); ^{13}C{^{1}H} [125.7 MHz, $(CD_3)_2SO$, 25 °C] δ 172.06, 153.78, 65.70, 59.63, 47.10, 31.29, 23.07 (rotamer a), 171.75, 154.05, 65.87, 60.12, 46.49, 30.23, 23.95 (rotamer b), 136.95, 128.36, 128.15, 127.75, 127.50, 127.46, 127.00, 41.01, 22.43, 8.75; ^{29}Si NMR [99.3 MHz, $(CD_3)_2SO$, 25 °C) δ −66.2 (s); Elemental analysis for $C_{128}H_{168}O_{36}Si_8N_{16}$. Found (calc.); C, 56.22 (56.28), H, 6.14 (6.20), N, 8.08 (8.20).

¶ Hydrogenolysis of **3c** (250 mg, 0.090 mmol) was performed by using 10% Pd/C (50 mg) in a mixture of methanol (25 ml) and 1 M HCl (10 ml) for 24 h at 25 °C and 100 psig H_2. Filtration and evaporation of the solvent *in vacuo* (25 °C, 0.01 Torr) gave **4c**·8HCl in quantitative yield. For **4c**·8HCl: ^{1}H NMR (500.2 MHz, CD_3OD, 25 °C) δ 9.46, 8.53 (s, NH), 4.26 [s, $CH(N)CH_2$], 3.37 [m, $CH_2N(CH)$], 3.30 [m, $CH_2N(CH)$], 3.18 (br, $SiCH_2CH_2CH_2$), 2.43 (br, $COCHCH_2CH_2$), 2.00 (br, $COCHCH_2CH_2$); ^{13}C{^{1}H} (125.8 MHz, CD_3OD, 25 °C) δ169.32 (CO), 61.04 (COCH), 47.48 ($CHCH_2CH_2CH_2N$), 42.90 ($SiCH_2CH_2$), 31.26, 25.14 (CH_2), 23.64 ($SiCH_2CH_2$), 97.6 ($SiCH_2$). ^{29}Si NMR (99.4 MHz, CD_3OD, 25 °C) δ −66.5 (s); MS (MALDI). Calc. for $C_{64}H_{121}N_{16}O_{20}Si_8$ ($M + H^+$) *m/z* 1658.7, found 1658.7.

1 T. Carell, E. A. Wintner and J. Rebek, *Angew. Chem., Int. Ed. Engl.*, 1994, **33**, 2061.
2 T. Carell, E. A. Wintner, A. Bashir-Hashemi and J. Rebek, *Angew. Chem., Int. Ed. Engl.*, 1994, **33**, 2059.
3 R. Beerli and J. Rebek, *Tetrahedron Lett.*, 1995, **36**, 1813.
4 T. Sasaki and E. T. Kaiser, *J. Am. Chem. Soc.*, 1989, **111**, 380.
5 K. S. Akerfeldt, R. M. Kim, D. Camac, J. T. Groves, J. D. Lear and W. F. DeGrado, *J. Am. Chem. Soc.*, 1992, **114**, 9656.
6 M. Mutter, G. G. Tuchscherer, C. Miller, K. H. Altmann, R. I. Carey, D. F. Wyss, A. M. Labhardt and J. E. Rivier, *J. Am. Chem. Soc.*, 1992, **114**, 1463.
7 K. Inoue, A. Miyahara and T. Itaya, *J. Am. Chem. Soc.*, 1997, **119**, 6191.
8 Y. Hamuro, M. C. Calama, H. S. Park and A. D. Hamilton, *Angew. Chem., Int. Ed. Engl.*, 1997, **36**, 2680.
9 A. Marra, A. Dondoni and F. Sansone, *J. Org. Chem.*, 1996, **61**, 5155.
10 M. G. Voronkov and V. I. Lavrent'yev, *Top. Curr. Chem.*, 1982, **102**, 199.
11 F. J. Feher and K. D. Wyndham, *Chem. Commun.*, 1998, 323.
12 R. Wiedner, N. Zeller, B. Deubzer and V. Frey, *US Pat.* 5 047 492, 1991 (Wacker-Chemie).
13 F. J. Feher and T. A. Budzichowski, *J. Organomet. Chem.*, 1989, **379**, 33.
14 L. A. Carpino, *J. Am. Chem. Soc.*, 1993, **115**, 4397.
15 L. A. Carpino, A. El-Faham and F. Albericio, *Tetrahedron Lett.*, 1994, **35**, 2279.
16 A. Ehrlich, H.-U. Heyne, R. Winter, M. Beyermann, H. Haber, L. A. Carpino and M. Bienert, *J. Org. Chem.*, 1996, **61**, 8831.
17 F. J. Feher and K. D. Wyndham, *Chem. Commun.*, submitted.
18 F. J. Feher, K. D. Wyndham, M. A. Scialdone and Y. Hamuro, *J. Org. Chem.*, in preparation.

Received in Bloomington, IN, USA, 8th April 1998; 8/02671H

Supramolecular assembly of mesostructured tin oxide

Kathryn G. Severin, Tarek M. Abdel-Fattah and Thomas J. Pinnavaia

Department of Chemistry and Center for Fundamental Materials Research, Michigan State University, East Lansing, MI 48824, USA

The first example of a mesostructured tin oxide that is stable to surfactant removal has been prepared by hydrolysis of tin isopropoxide in the presence of a neutral amine surfactant (tetradecylamine).

Since the discovery of mesoporous silica molecular sieves in 1992[1,2] several supramolecular assembly pathways have been reported and extended to the synthesis of a variety of mesoporous metal oxide compositions including alumina, titania, niobia and zirconia.[3] Other surfactant metal oxide mesostructures also have been reported, but they have not been stable with respect to surfactant removal. Among them is a tin oxide assembled by the hydrolysis of $SnCl_4$ in the presence of an anionic surfactant.[4] Tin oxide is particularly interesting because it has semiconductive properties and its performance in semiconductor gas sensor applications is highly dependent upon its structure and morphology.[5,6] The structure directing capabilities of a supramolecular assembly pathway may allow for the controlled optimization of a mesostructured form of SnO_2 for chemical sensing.

In this study we use a neutral S^0I^0 assembly pathway‡ to produce the first stable mesostructured tin oxide. The mesostructure is synthesized using a neutral primary amine surfactant as the structure director (S^0) and tin isopropoxide as the inorganic precursor (I^0). We have chosen this pathway because it tends to provide mesostructured materials with thick pore walls.[7] Materials with thick walls may be less susceptible to collapse upon surfactant removal.[8] We have successfully prepared stable mesostructured tin oxide using a range of primary amines including octylamine, dodecylamine, tetradecylamine and hexadecylamine.[9] We report here on mesostructured SnO_2 assembled from tetradecylamine and compare it to the oxide prepared in an analogous manner in the absence of surfactant.

The XRD patterns of the as-synthesized products prepared in the presence and absence of tetradecylamine and that of a commercial SnO_2 sample are presented in Fig. 1. The pattern of tin oxide assembled with tetradecylamine contains the low angle peak (*d*-spacing: ≈ 46 Å) characteristic of mesostructured materials,[1–4,7,8] whereas the tin oxide prepared in the absence of surfactant and the commercial oxide do not exhibit a low angle reflection. However, all three materials exhibit reflections of comparable integral intensity in the region 2θ 20–80° that are characteristic of cassiterite, signifying that the as synthesized materials are largely crystalline in nature. On the basis of the < 110 > line widths, the products obtained by hydrolysis in the presence or absence of surfactant have the same average domain size (15 Å). The hydrolysis and condensation processes are apparently similar in both reaction systems, except that SnO_2 crystallites are assembled into a mesostructure in the presence of tetradecylamine. The presence of a single low angle XRD reflection is consistent with a sponge-like or wormhole channel motif.[7]

XRD patterns of the mesostructured SnO_2 after calcination at different temperatures are shown in Fig. 2. It can be seen that the average *d*-spacing for the mesostructure is largely unchanged by calcination at 300 °C, which indicates that the surfactant has been removed without structural collapse. Also, the average crystallite domain size has increased from 15 to 18 Å. Although low temperature sintering is commonly observed for tin oxide materials,[10] the mesostructured SnO_2 shows a lower tendency toward sintering than the tin oxide prepared in the absence of a surfactant. The domain size of the latter oxide after calcination at 300 °C is 27 Å. Thus, the surfactant acts not only as a structure director, but it also inhibits crystallite growth during calcination.

The mesostructured SnO_2 produced after calcination 300 °C has a BET surface area of 314 $m^2\ g^{-1}$ (Table 1), approximately twice that of the SnO_2 prepared in the absence of surfactant calcined at the same temperature (158 $m^2\ g^{-1}$). In contrast the surface areas reported for SnO_2 gels obtained from aqueous $SnCl_4$ solutions and calcined at 300 °C are only 110–120

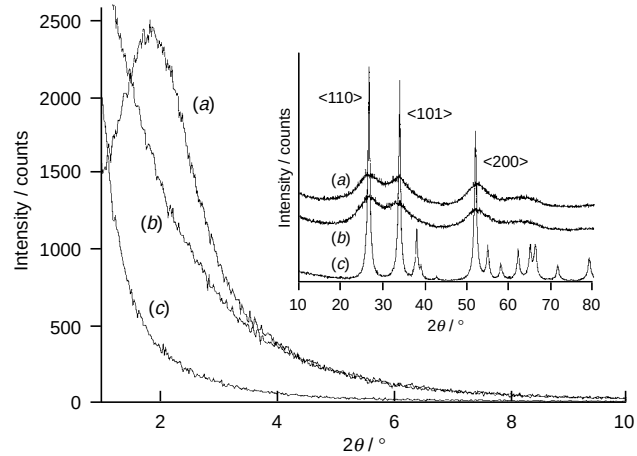

Fig. 1 XRD patterns of tin oxides: (*a*) as-synthesized product obtained by S^0I^0 assembly at ambient temperature, (*b*) as-synthesized product obtained by hydrolysis of tin isopropoxide in the absence of a surfactant, and (*c*) commercial sample of polycrystalline tin(IV) oxide

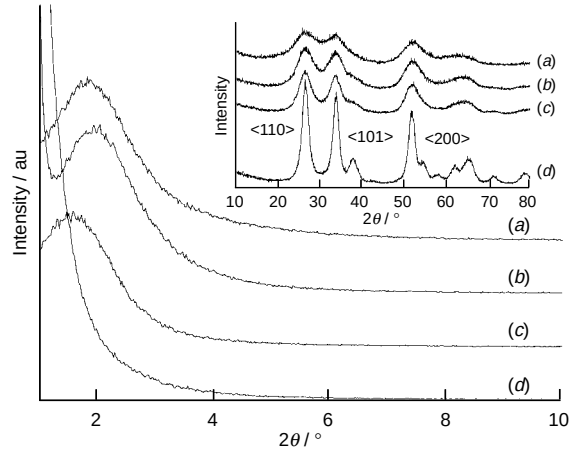

Fig. 2 XRD patterns of tin oxide assembled in the presence of tetradecylamine: (*a*) as-synthesized and after calcination at (*b*) 300, (*c*) 350 and (*d*) 400 °C

Table 1 Characterization of tin oxide prepared from tin isopropoxide in the presence of tetradecylamine surfactant

Calcination temp./°C	*d*-Spacing[a]/Å	Crystallite domain size[b]/Å	BET surface area/m^2 g^{-1}	Average pore diameter[c]/Å
As made	46	15	—	—
300	46	18	314	14
350	56	24	300	18
400	None	44	99	43

[a] As determined from 2θ of the low angle XRD peak. [b] As determined using Scherrer equation from the width of the < 110 > peak at 26.5° (2θ) in the XRD pattern. [c] BJH adsorption average pore diameter.

m^2 g^{-1}.[11,12] Because the density of crystalline tin oxide is more than three times that of amorphous SiO_2, our mesostructured tin oxide has a surface to framework volume ratio comparable to that of mesoporous silicas.[7] No hysteresis is observed in the N_2 isotherms (Fig. 3). Therefore, the pores are relatively free of constrictions and of uniform diameter. The average pore diameter is 14 Å and the pore size distribution is relatively narrow in comparison to the pore distribution observed for the SnO_2 prepared in the absence of surfactant (Fig. 3 inset).

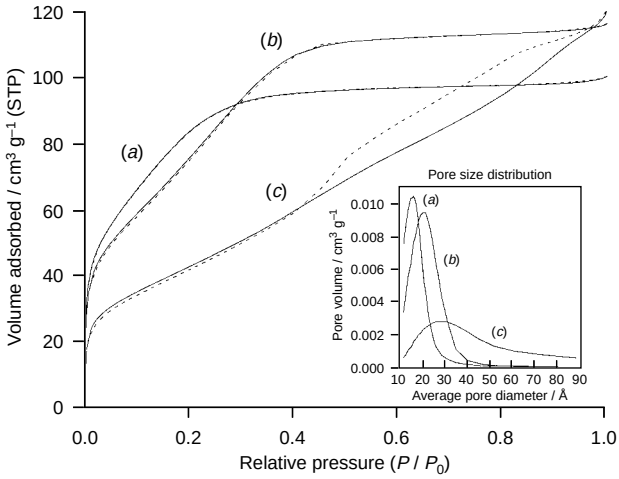

Fig. 3 N_2 adsorption–desorption isotherms of mesostructured SnO_2 synthesized in the presence of tetradecylamine and calcined at (*a*) 300 and (*b*) 350 °C, and (*c*) tin oxide prepared without surfactant and calcined at 300 °C. Inset shows pore size distributions for these materials as determined using the BJH model and the adsorption branch isotherm.

The low angle diffraction peak for the calcined product provides an estimate of the average distance between framework pores (46 Å). Since the average pore size is 14 Å, the pore walls are *ca.* 32 Å thick, almost twice the average crystallite domain size (Table 1). These values are in reasonable agreement with those inferred from TEM micrographs of the as-synthesized mesostructure. We may conclude, therefore, that the walls are comprised largely of aggregates of small crystallites, but we can not preclude the possibility of the crystallites being encapsulated in a matrix of amorphous SnO_2. Small crystalline domains surrounded by amorphous grain boundaries could account for the increase in crystallite domain size without a change in the *d*-spacing of the mesostructure upon calcination.

In contrast to the mesostructured SnO_2 calcined at 300 °C, SnO_2 prepared in the absence of surfactant has an average pore diameter of 28 Å, a value similar to its average crystallite size. The pore size distribution is very broad [Fig. 3(*c*) inset] and consistent with a pore structure resulting from the irregular packing of small crystalline particles. Thus, the role of the surfactant in forming mesostructured SnO_2 is to organize the small oxide crystallites into a structure sufficiently ordered to generate regular pores and a low angle Bragg reflection.

Calcination of the mesostructured tin oxide at 350 °C lowers the BET surface area only slightly to 300 m^2 g^{-1}, but the average crystallite size (24 Å), pore diameter (18 Å), pore volume (0.15 cm^3 g^{-1}) and *d*-spacing (56 Å) are all significantly larger than those measured for the sample calcined at 300 °C (Table 1). As inferred from these measurements, the average pore wall thickness has also increased, to a value of 38 Å. Although more restructuring occurs at 350 °C than at the lower calcination temperature, the lack of hysteresis in the N_2 isotherms (Fig. 3) again indicates that the pore channels remain quite uniform, despite their increased diameters. This thermal dependence of pore size and wall thickness is not typical of a mesostructure formed by micellar assembly and further suggests a mechanism based on the packing of surfactant-decorated crystallites of uniform size.

Upon calcination at 400 °C the mesostructured framework collapses and the surface area is lowered to 99 m^2 g^{-1}. The low 2θ peak is no longer present (Fig. 2) in the XRD pattern and the average crystallite domain size increases to 44 Å (Table 1). In addition, the average pore size has increased to 43 Å, the pore size distribution has broadened and necking has developed in the channels (average diameter *ca.* 37 Å). These results are consistent with a material comprised entirely of cassiterite crystallites. TGA analysis[9] indicates that at this calcination temperature the surface hydroxyl groups condense, and this process may lead to extensive sintering.

Support of this research by NSF CRG grant CHE-9633798 is gratefully acknowledged.

Notes and References

† E-mail: pinnavai@cem.msu.edu

‡ *Experimental methods*: mesostructured SnO_2 was prepared quiescently from a 1 $Sn(OPr^i)_4$: 0.2 tetradecylamine : 60 Pr^iOH mixture under water-saturated air at RT. After 2 days the product was filtered and washed with water and ethanol. The surfactant was removed by a 2 h reflux in ethanol (*ca.* 80% remained) After filtration, the product was calcined (4 h) at the reported temperature (heating rate 1 °C min^{-1}).

1 C. T. Kresge, M. E. Leonowicz, W. J. Roth, J. C. Vartuli and J. S. Beck, *Nature*, 1992, **359**, 710.
2 J. S. Beck, J. C. Vartuli, W. J. Roth, M. E. Leonowicz, C. T. Kresge, K. D. Schmitt, C. T. W. Chu, D. H. Olson, E. W. Sheppard, S. B. McCullen, J. B. Higgins and J. L. Schlenker, *J. Am. Chem. Soc.*, 1992, **114**, 10 834.
3 P. Behrens, *Angew. Chem., Int. Ed. Engl.*, 1996, **35**, 515.
4 N. Ulagappan and C. N. R. Rao, *Chem. Commun.*, 1996, 1685; L. Qi, J. Ma, H. Cheng and Z. Zhao, *Langmuir*, 1998, **14**, 2579.
5 M. Ando, S. Suto, T. Suzuki, T. Tsuchida, C. Nakayama, N. Miura and N. Yamazoe, *J. Ceram. Soc. Jpn.*, 1996, **104**, 409.
6 J. Takahashi, M. Takatsu, T. Ota and I. N. Yamai, *J. Ceram. Soc. Jpn.*, 1989, **97**, 1274.
7 P. T. Tanev and T. J. Pinnavaia, *Science*, 1995, **267**, 865; S. A. Bagshaw and T. J. Pinnavaia, *Angew. Chem., Int. Ed. Engl.*, 1996, **35**, 1102.
8 S. B. McCullen and J. C. Vartuli, *US Pat.* 5, 156 829, 1992; N. Coustel, F. Di Renzo and F. J. Fajula, *Chem. Soc., Chem. Commun.*, 1994, 967.
9 K. G. Severin, T. Abdel-Fattah and T. J. Pinnavaia, in preparation.
10 J. F. Goodman and S. J. Gregg, *J. Chem. Soc.*, 1960, 1162.
11 M. J. Fuller, M. E. Warwick and A. Walton, *J. Appl. Chem. Biotechnol.*, 1978, **28**, 396.
12 P. G. Harrison and A. Guest, *J. Chem. Soc., Faraday Trans. 1*, 1987, **83**, 3383.

Received in Columbia, MO, USA, 17th December 1997; 7/09067F

Photoactive ruthenium(II) cyclodextrins responsive to guest binding

Steffen Weidner and Zoe Pikramenou*

Department of Chemistry, The University of Edinburgh, King's Buildings, West Mains Road, Edinburgh, UK EH9 3JJ

A terpyridine functionalised cyclodextrin has been synthesised and ruthenium photoactive centres appended to give luminescent metallo-cyclodextrins which respond to guest binding.

Biology provides many examples of light-sensitive macro- or supra-molecular intelligent systems that are capable of inducing directional motion of electrons and excitation energy. The design of supramolecular systems[1] that perform similar functions is of great interest particularly for their application towards the development of photomolecular devices.[2] Photoactive transition metal systems are very attractive candidates as units for the construction of molecular devices due to their photosensitisation and electrochemical properties.

Research in this area has mainly concentrated on building covalently linked metal complexes.[2] Photophysical studies have shown that the spatial organisation of the photoactive units is important for both energy and electron transfer processes and consequently this has led to the development of rigid polymetallic arrays using appropriate spacer units to covalently link metal centres.[3] High molecular complexity is inevitable in this approach since several features are accumulated in a single molecular component and synthetic challenges limit the choice of photoactive units. In this paper we introduce an alternative approach based on non-covalent links between components. It involves the design of photoactive metal-appended receptors that can act as sensor units upon introduction of a guest molecule in their cavity. When the guest is a metal complex the communication between the appended metal centre and the metallo-guest, brought together in space *via* non-covalent interactions, may then be established. Few examples of the previously reported metallo-receptors[4] have demonstrated their sensor properties.[5] Our design involves a terpyridine functionalised cyclodextrin which can form complexes with photoactive metals. The hydrophobic microenvironment of the cyclodextrin cavity allows the binding of appropriate guest molecules that trigger a change in the luminescence of the appended metal centre. We have synthesised a β-cyclodextrin functionalised with a tolyl-terpyridine unit (β-CD–ttp, **II**) and studied the formation of its luminescent complexes with ruthenium (Scheme 1). When an electron-accepting guest is added to the ruthenium functionalised CD, quenching of the ruthenium emission is observed.

An important precursor for the synthesis is the mono-6-hydroxy permethylated β-CD **I** which allows selective monofunctionalisation of the primary cyclodextrin side and solubility in organic solvents. A recently developed synthetic route for this derivative[6] proposed a convenient method to easily access compound **I** in good yield. Coupling of the cyclodextrin to the terpyridyl fragment was achieved through the reaction of **I** with 4′-[*p*-(bromomethyl)phenyl]-2,2′:6′,2″-terpyridine, ttpCH_2Br, under Williamson ether conditions using an excess of NaH in THF. The reaction was followed by TLC (Al_2O_3; ethyl acetate–methanol 30:1; R_f: β-CD–ttp = 0.7 and β-CDOH = 0.22) and after three days the terpyridine functionalised CD **II** was isolated in 50% yield after extraction by CH_2Cl_2 and size exclusion chromatography.

The 600 MHz ^{1}H NMR spectrum of **II** in $CDCl_3$ shows the fourteen aromatic protons in the range 7.2–8.8 ppm, the seven anomeric protons of the cyclodextrin at 5.0–5.2 and the rest of the cyclodextrin protons in the range 3.0–4.1 ppm. The methylene protons of the tolyl-terpyridine unit are diastereotopic due to the chirality of the CD and appear as two doublets at 4.62 and 4.68 ppm. The connectivities were elucidated by ^{1}H–^{1}H TOCSY spectroscopy. The formula of the compound was also confirmed by FAB-MS and elemental analysis.

Reaction of equimolar quantities of **II** with Ru(tpy)Cl_3 or Ru(ttp)Cl_3 in methanol with addition of *N*-ethyl morpholine afforded [(β-CD–ttp)Ru(tpy)][PF_6]$_2$ **III** and [(β-CD–ttp)Ru(ttp)][PF_6]$_2$ **IV** respectively after precipitation with ammonium hexafluorophosphate and size-exclusion chromatography (BioBeads SX2, DMF–THF 1:1) (tpy = 2,2′:6′,2″-terpyridine, ttp = 4′-(*p*-tolyl)-2,2′:6′,2″-terpyridine). The FAB mass spectra of **III** and **IV** show peaks at *m*/*z* = 2216 and 2306 corresponding to {M − [PF_6]}$^+$ and at *m*/*z* = 2071 and 2161 corresponding to {M − 2[PF_6]}$^{2+}$, respectively. The 600 MHz ^{1}H NMR spectra of **III** and **IV** show the characteristic aromatic proton patterns of terpyridine and tolyl-terpyridine in the region 7.0–9.2 ppm similar to the ones observed for [Ru(ttp)(tpy)]$^{2+}$ and [Ru(ttp)$_2$]$^{2+}$.[7] Complex **III** exhibits an MLCT absorption at 484 nm but it does not emit at room temperature upon excitation at the MLCT band. It is known that [Ru(tpy)$_2$]$^{2+}$ emits only at low temperature at λ_{max} = 598 nm and that [Ru(ttp)$_2$]$^{2+}$ emits at 640 nm at room temperature.[8] Interestingly, [(β-CD–ttp)Ru(tpy)][PF_6]$_2$ **III** emits at 77 K with an emission maximum at 622 nm (Fig. 1) which lies in between the values of the [Ru(tpy)$_2$]$^{2+}$ and [Ru(ttp)$_2$]$^{2+}$ emissions, as expected due to the electronic effects of the ligands. We have independently synthesised [Ru(tpy)(ttp)]$^{2+}$ and it shows the same emission behaviour as **III**.[9] The MLCT absorption of [(β-CD–ttp)Ru(ttp)][PF_6]$_2$ **IV** is centred at 490 nm and leads to room temperature emission with λ_{max} at 635 nm consistent with the expected MLCT emission. The UV-transparent cyclodextrin cavity does not perturb the luminescence properties of the complexes.

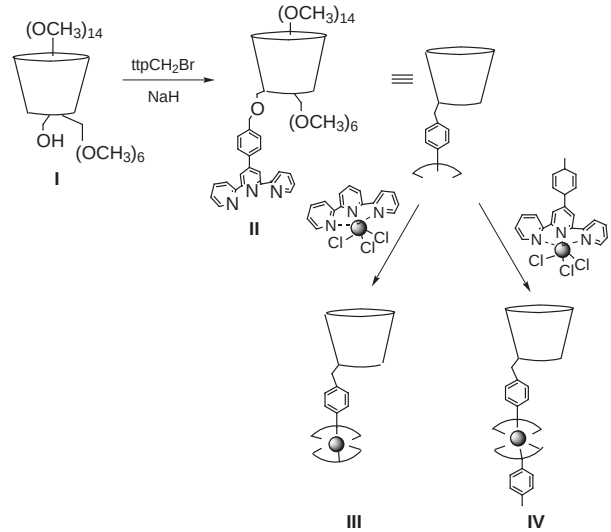

Scheme 1

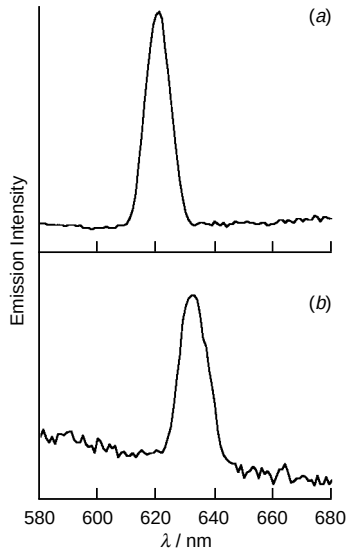

Fig. 1 Emission spectra of (*a*) [(β-CD–ttp)Ru(tpy)][PF_6]$_2$ in acetonitrile at 77 K, λ_{exc} = 480 nm, and (*b*) [(β-CD–ttp)Ru(ttp)][PF_6]$_2$ in acetonitrile at room temperature, λ_{exc} = 490 nm

In order to study the potential of metallo-CDs to participate in energy and electron transfer processes between the appended metal and a guest we initially selected an organic redox active guest, anthraquinone-2-carboxylic acid. The effect on the MLCT emission of the ruthenium centre of complex **IV** upon introduction of an equimolar amount of the guest was examined. Addition of microliter quantities of a 9.8×10^{-4} M solution of the guest in acetonitrile induced partial quenching, up to 20%, of the MLCT emission of complex **IV** (Fig. 2). We attribute this quenching effect to electron transfer between the appended metal and the guest, consistent with previous cases when quinones covalently attached to ligands of ruthenium complexes quench the MLCT emission.[10] In the absence of the cyclodextrin receptor the quenching of the MLCT emission is not observed upon addition of anthraquinone-2-carboxylic acid to a solution of $[Ru(ttp)_2]^{2+}$ under similar conditions. Further photophysical studies of the electron transfer process, and examination of the relation of the guest with the binding constant and the distance of the ruthenium centre, are in progress.

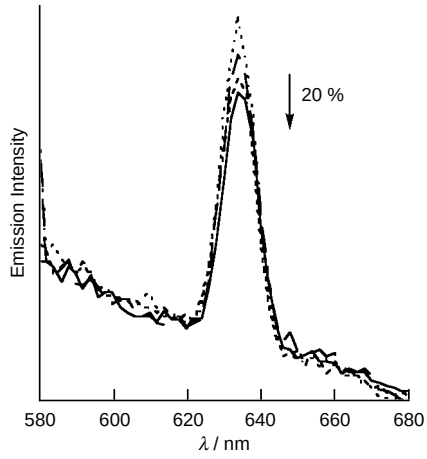

Fig. 2 Emission spectra of 1.9×10^{-5} M [(β-CD–ttp)Ru(ttp)][PF_6]$_2$ in 10% acetonitrile in water upon addition of 0.25, 0.5, 1 molar equivalents of anthraquinone-2-carboxylic acid, λ_{exc} = 490 nm

We have established the formation of photoactive metallocyclodextrins based on a new terpyridine functionalised cyclodextrin and confirmed the communication between guest molecules in the cavity and a ruthenium centre appended to the cyclodextrin cavity. We are currently extending our approach to the inclusion of metallo-guests in the ruthenium cyclodextrins and studying their involvement in energy and electron transfer processes between the appended metal and the metallo-guest.

We are grateful to the Nuffield Foundation for an Award to Newly Appointed Science Lecturers (Z. P.), the ERASMUS exchange scheme for support (S.W.) and the Swansea National Mass Spectrometry Centre for recording the mass spectra. We also thank Dr. Hewage for obtaining the NMR data in the EPSRC/BBSRC supported National Ultra-high Field NMR Centre in Edinburgh.

Notes and References

† E mail: z.pikramenou@ed.ac.uk

1 J.-M. Lehn, *Supramolecular Chemistry*, VCH, Weinheim, 1995.
2 V. Balzani and F. Scandola, *Supramolecular Photochemistry*, Ellis Horwood, Chichester, 1991.
3 A. Harriman and R. Ziessel, *Chem. Commun.*, 1996, 1707; F. Barigelletti, L. Flamigni, J. P. Collin and J. P. Sauvage, *Chem. Commun.*, 1997, 333; F. Barigelletti, L. Flamigni, V. Balzani, J.-P. Collin, J.-P. Sauvage, A. Sour, E. C. Constable and A. M. W. Cargill Thompson, *J. Am. Chem. Soc.*, 1994, **116**, 7692; F. Vögtle, M. Frank, M. Nieger, P. Belser, A. von Zelewsky, V. Balzani, F. Barigelletti, L. De Cola and L. Flamigni, *Angew. Chem., Int. Ed. Engl.*, 1993, **32**, 1643.
4 B. Zhang and R. Breslow, *J. Am. Chem. Soc.*, 1997, **119**, 1676; R. Deschenaux, T. Ruch, P-F. Deschenaux, A. Juris and R. Ziessel, *Helv. Chim. Acta*, 1995, **78**, 619; R. Deschenaux, A. Greppi, T. Ruch, H-P. Kriemler, F. Raschdorf and R. Ziessel, *Tetrahedron Lett.*, 1994, **35**, 2165; R. Deschenaux, M. M. Harding and T. Ruch, *J. Chem. Soc., Perkin Trans. 2*, 1993, 1251.
5 M. A. Mortellaro and D. G. Nocera, *J. Am. Chem. Soc.*, 1996, **118**, 7414; Z. Pikramenou, J-a. Yu, A. Ponce and D. G. Nocera, *Coord. Chem. Rev.*, 1994, **132**, 181; F. Szemes, D. Hesek, Z. Chen, S. W. Dent, M. G. B. Drew, A. J. Goulden, A. R. Graydon, A. Grieve, R. J. Mortimer, T. Wear, J. S. Weightman and P. D. Beer, *Inorg. Chem.*, 1996, **35**, 5868; A. Nakamura, S. Okutsu, Y. Oda, A. Ueno and F. Toda, *Tetrahedron Lett.*, 1994, **35**, 7241.
6 Z. Chen, J. S. Bradshaw and M. L. Lee, *Tetrahedron Lett.*, 1996, **37**, 6831.
7 E. C. Constable and A. M. W. Cargill Thompson, *New J. Chem.*, 1992, **16**, 855.
8 J.-P. Sauvage, J.-P. Collin, J.-C. Chambron, S. Guillerez, V. Balzani, F. Barigelletti, L. De Cola and L. Flamigni, *Chem. Rev.*, 1994, **94**, 993.
9 R. A. J. Cameron and Z. Pikramenou, unpublished results.
10 K. A. Opperman, S. L. Mecklenburg and T. J. Meyer, *Inorg. Chem.*, 1994, **33**, 5295; V. Goulle, A. Harriman and J.-M. Lehn, *J. Chem. Soc., Chem. Commun.*, 1993, 1034.

Received in Cambridge, UK, 24th March 1998; 8/02301H

Self-assembly of a helical dicopper(I) metallophane

Thomas Bark,[a] Thomas Weyhermüller[b] and Fenton Heirtzler*[a]†

[a] *Departement Chemie der Universität, Spitalstrasse 51, CH-4056, Basel Switzerland*
[b] *Max-Planck-Institut für Strahlenchemie, Stiftstrasse 34-36, D-45470 Mülheim, Germany*

X-Ray crystallographic and ^{1}H NMR spectroscopic studies show that, in the presence of copper(I), an oligopyridyl pyrazine derivative spontaneously forms a single chiral, cyclophane-like dimeric complex and that this is the sole species present in solution and the solid state.

The self-assembly[1,2] of appropriate ligands and labile metal centers to result in double-stranded helicates[1a,c–e] and cyclophane-like structures[2] is well documented. Either linear[1c–e] or knotted [1a] shapes are typical for the former, and a distinguishing characteristic of the latter is frequently the coplanar orientation of aromatic spacer units. In some of these 'metallophanes', this results in a cavity, whilst in others, the non-bonding distances between the spacers are within those values considered to be crucial for π-stacking interactions[3] (*cf.* [2.2]paracyclophane[4]). In several of the latter cases, the spacer directly participates in metal binding.[2a,b]

While helicates are, by definition chiral,[5] this is not so for metallophanes. The majority of such complexes are achiral (*meso*)[2a–d,f] although studies describing a chiral, dizinc(II) metallophane which is stable in dilute solution have also recently appeared.[2e] Chiral metallophanes,whose formation is templated by the inclusion of an aromatic guest molecule, have also been recently described,[2d,e] as have equilibrating mixtures of similar chiral and *meso* complexes.[2d,g,6]

We are interested in the preparation[7] and supramolecular complexation chemistry[2a] of 2,3-bis(2,2′-oligopyridyl)pyrazines. We anticipate that the influences of internitrogen pyrazine base strength within the plane of that ring[8a] and stacking effects perpendicular to it[8b] should together determine the behaviour of this ligand class. Simpler pyrazine-containing ligand systems are known to form cyclic trimeric or tetrameric supramolecular complexes.[8a,9]

Along these lines, we have already shown that the symmetrical 2,3-bis(2,2′-bipyridyl)pyrazine **1** and Co^{II} self-assemble to

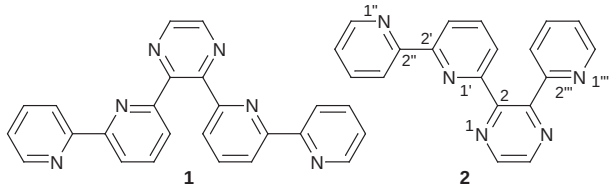

give a dimetallic *meso*-metallophane in which two roughly orthogonal binding domains having different dendicity are generated to geometrically satisfy the metal coordination requirements.[2a] We wished to further test these premises on a 2,3-bis(2,2′-oligopyridyl)pyrazine derivative possessing oligopyridyl groups of explicitly unlike dendicity. The simplest such ligand is the previously unknown 2-(2,2′-bipyridyl)-3-(2-pyridyl)pyrazine **2**. Either tridentate/monodentate or bidentate/bidentate binding modes are conceivable for **2**, and thus we anticipated that it should bind cooperatively with tetrahedral Cu^I.

A crude, but reasonable synthesis of **2** is described in Scheme 1. Thus, condensation of 2,2′-bipyridine-6-carbaldehyde **3**[7] with an excess of pyridine-2-carbaldehyde in the presence of potassium cyanide afforded a mixture of the enediol **4** and 1,2-bis(2′-pyridyl)-1,2-dihydroxyethene. This mixture was directly oxidized with iodine to the corresponding α-diketones, from which the desired product **5** was purified in 14% overall yield. Condensation of **5** with 1,2-diaminoethane, then chloranil-oxidation, afforded **2** in 64% yield.‡

Treatment of **2** with 1 equiv. of [Cu(MeCN)$_4$][BF$_4$] in methanol under reflux and addition of an excess of [NH$_4$][BF$_4$] resulted in the precipitation of a dark red complex which could be recrystallized from nitromethane–diethyl ether. This substance analysed as {[Cu**2**][BF$_4$]}$_n$‡ and in its FABMS spectrum (noba matrix) prominent signals centered at m/z = 750 and 837 were observed, corresponding to [Cu**2**]$_2^+$ and [Cu**2**]$_2$[BF$_4$]$^+$, respectively, and thus we assume a dimeric structure [Cu**2**]$_2$[BF$_4$]$_2$. In its electronic spectrum in acetonitrile, metal–ligand charge-transfer bands centered around 460 (1400) and 570 nm (700 dm^3 mol^{-1} cm^{-1}) were visible, and suggest an N$_4$-environment for Cu^I.[10] The cyclovoltammogram in MeCN indicated a single, reversible Cu^I–Cu^{II} redox process at −0.16 V *vs.* Fc–Fc$^+$. In analogy to literature precedent,[2b,10] we ascribe this to a dimetallic complex containing two identical non-interactive Cu^I centers.

We were, however uncertain of its exact structure, as both *meso*-Λ,Δ and Λ, Λ/Δ,Δ-configured diasteromeric pairs were reasonable structures. The ^{1}H NMR spectrum of [Cu**2**]$_2$[BF$_4$]$_2$ (400 MHz, CD$_3$CN), recorded at 21 °C, displayed a single set of broad resonances, integrating to 13 protons [Fig. 1(*a*)]. This suggested either the ready interconversion of the three diasteromers, like in other dimeric oligopyridine complexes[2d,f,g,6,11] or some type of exchange process with the coordinating solvent, as has been observed for other dicopper(I) bis-N$_4$ systems[2g,10] were occurring. Upon cooling to −40 °C [Fig. 1(*b*)], these absorption sharpened to result in the profile of a single compound, while at 40 °C, a broadening of the same shifts is apparent. As well, the ^{13}C NMR spectrum of the complex, recorded at −40 °C, exhibited 13 C–H correlated resonances displaying NOE enhancement. At no temperature could a decoalescence of signals in the ^{1}H NMR spectra be observed, and the chemical shifts were essentially temperature independent. Since others have already demonstrated that low-temperature

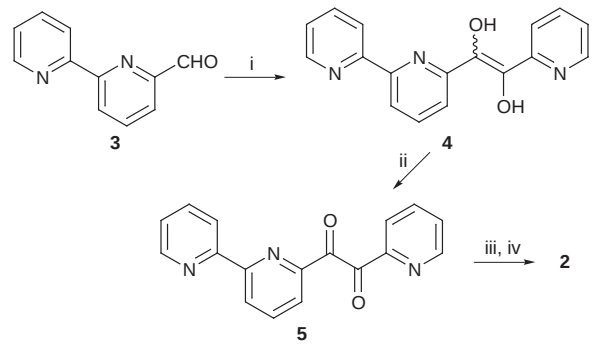

Scheme 1 Preparation of ligand **2**. *Reagents and conditions:* i, 15 equiv. pyridine-2-carbaldehyde, KCN, EtOH–H$_2$O, reflux, 2 h; ii, 1 equiv. I$_2$, CH$_2$Cl$_2$, 25 °C, 15 h; iii, 1 equiv. 1,2-diaminoethane, EtOH, reflux, 2 h; iv, 1 equiv. chloranil, xylenes, reflux, 16 h.

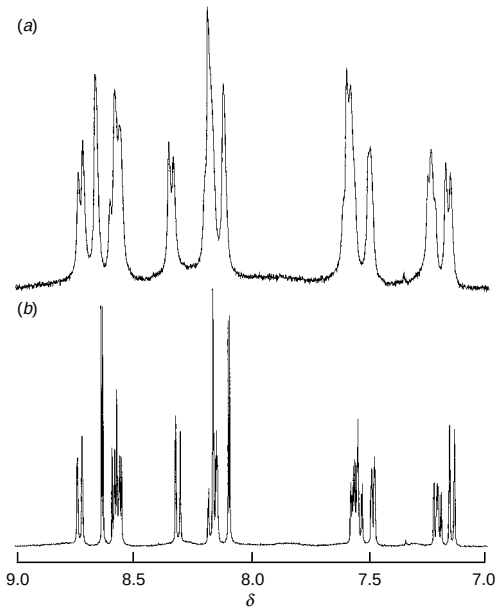

Fig. 1 ^{1}H NMR spectra of $[Cu\mathbf{2}]_2[BF_4]_2$ at (*a*) 21 and (*b*) −40 °C

^{1}H NMR spectroscopy can distinguish equilibrating mixtures of diastereomeric metallophanes[2g] it is evident that $[Cu\mathbf{2}]_2[BF_4]_2$ undergoes no such phenomenon.

In order to determine the stereochemistry of the dinuclear complex, its crystal structure was determined.§ Complex $[Cu\mathbf{2}]_2[BF_4]_2$ crystallizes in a centrosymmetric space group. Consequently, the dication occurs as a racemic mixture of Λ,Λ- and Δ,Δ-configured enantiomers, whereby the equivalent Cu**2** fragments are inter-related by the C_2 axis which runs parallel to the pyridyl pyrazine surfaces and between the bipyridyl flanks.¶ The *P*-helical enantiomer is displayed in Fig. 2. The pyridyl pyrazine copper(I) 'decks' of the metallophane are arranged in a head-to-head fashion. Interdeck non-bonding distances between closest pairs of atoms are 3.47–3.57 Å for the pyrazine rings and 3.42–3.62 Å for the monosubstituted pyridine rings; the pairs of pyrazine and pyridine rings are parallel to within 2.10 and 2.03°, respectively. The bipyridyl and pyridylpyrazine binding domains are twisted by 72.3° with respect to one another, giving the observed rectangular molecular geometry. The intermetallic distance is 5.08 Å. All metal–ligand bonding parameters are within expected values.

Ligand **2** diastereoselectively self-assembles to form a chiral metallophane, which is also stable in solution. That this phenomenon is influenced by stacking of metal-binding pyridyl pyrazine fragments is suggested by molecular models of the Λ,Λ/Δ,Δ-and *meso*-Λ,Δ-disastereomers, which indicate more efficient overlap for the former compound.

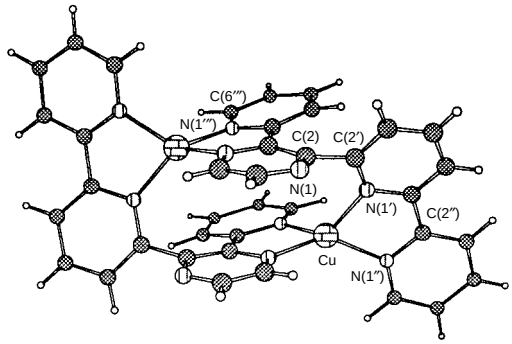

Fig. 2 Crystal structure of the $[Cu\mathbf{2}]_2$-dication. Selected bond angles (°) and lengths (Å): N(4)–Cu–N(1″) 138.46(7), N(1″)–Cu–N(1′) 82.17(7), N(1″)–Cu–N(1‴) 114.39, N(4)–Cu–N(1′) 120.80(7), N(4)–Cu–N(1‴) 80.91(7), N(1′)–Cu–N(1‴) 126.72(7); Cu–N(4) 1.991(2), Cu–N(1′) 2.033(2), Cu–N(1″) 2.005(2), Cu–N(1‴) 2.038(2).

We are currently investigating the extent which stacking interactions control self-assembly in related substances.

We thank the companies Novartis Ag, Biosynth AG and Shell Oil for chemical donations, the Treubel Fond for a stipend (F. H.) and Professors E. C. Constable and K. Wieghardt for encouraging this work.

Notes and References

† E-mail: heirtzler@ubaclu.unibas.ch

‡ Correct spectral and analytical data (C, H, N) were obtained for **2** and **5**. Spectral data for $[Cu\mathbf{2}]_2[BF_4]_2$: ^{1}H NMR (400 MHz, CD_3CN, −40 °C), δ 8.72 (dd, *J* 1.0, 8.2 Hz, 1 H, H-3′/5′), 8.63 (d, *J* 2.7 Hz, 1 H, H-5/6), 8.57 (t, *J* 7.8 Hz, 1 H, H-4′), 8.56 (d, *J* 8.2 Hz, 1 H, H-3″), 8.31 (dd, *J* 0.7, 7.6 Hz, 1 H,H-5′/3′), 8.14–8.19 (m, 2 H, H-4″, H-5″/6″), 8.09 (d, *J* 2.4 Hz, 1 H, H-6/5), 7.53–7.58 (m, 3 H, H-6″/5″, H-4‴,), 7.48 (dt, *J* 1.2, 4.8 Hz, 1 H, H-6‴), 7.21 (ddd, *J* 1.0, 5.3, 8.2 Hz, 1 H, H-5‴), 7.15 (d, *J* 8.2 Hz, 1 H, H-3‴); ^{13}C NMR (100 MHz, CD_3CN −40 °C), δ 149.35 (2C), 146.46, 141.96 (2C), 139.63, 137.79, 129.29, 127.68 (2C), 125.74, 124.18, 123.42. Anal. Calc. for $C_{38}H_{26}B_2Cu_2F_8N_{10}$: C, 48.8; H, 2.97; N, 15.3. Found: C, 49.4; H, 2.84; N, 15.2%.

§ *Crystallographic data* for $[Cu\mathbf{2}]_2[BF_4]_2$, $C_{38}H_{26}B_2Cu_2F_8N_{10}$, M_r = 923.39, dark red blocks, 0,43 × 0.28 × 0.25 mm, monoclinic, space group *C*2/*c*, *a* = 13.271(2), *b* = 11.368(2), *c* = 24.200(4) Å, β = 95.72(2)°, *U* = 3632.7(10) Å^3, *Z* = 4, D_c = 1.688 Mg m^{-3}, μ = 1.259 mm^{-1}, *F*(000) = 1856, graphite monochromated radiation with λ(Mo-Kα) = 0.710 73 Å, *T* = 100(2) K, 17 678 reflections measured (1.69 < θ < 30.00°) of which 5262 were independent (R_{int} = 0.0241), collected on a Siemens SMART diffractometer with CCD detector taking frames at 0.3° in ω. Data corrected for Lorentz and polarization effects, absorption correction using SADABS[11] (min., max. transmission factors: 0,572, 0.832) and structure solution and refinement on F^2 using Siemens ShelXTL-V5. All non-hydrogen atoms refined anisotropically, hydrogen atoms placed at calculated positions and refined isotropically. R_1 = 0.0426, wR_2 = 0.1041, goodness-of-fit: 1.049 for 4353 reflections with $I > 2\sigma(I)$ and 271 parameters. Residual positive, negative electron density: +1.34, −0.49 Å^{-3}. CCDC 182/883.

¶ The hypothetical *meso*-dicopper(I) metallophane is characterized by a 'head-to-tail' orientation of the pyridylpyrazine decks and an inversion axis (S_2) in roughly the same location as for the chiral form.

1 (*a*) J.-C. Chambron, C. Dietrich-Buchecker and J.-P. Sauvage, *Top. Curr. Chem.*, 1993, **165**, 131; (*b*) P. J. Stang and B. Olenyuk, *Acc. Chem. Res.*, 1997, **30**, 502; (*c*) C. Piguet, G. Bernardinelli and G. Hopfgartner, *Chem. Rev.*, 1997, **97**, 2005; (*d*) J. M. Lehn, *Supramolecular Chemistry, Concepts and Perspectives*, VCH, New York, 1995; (*e*) E. C. Constable, *Tetrahedron*, 1992, **48**, 10 013.

2 (*a*) F. Heirtzler and T. Weyhermüller, *J. Chem. Soc., Dalton Trans.*, 1997, 3653; (*b*) M. J. Hannon, C. L. Painting and W. Errington, *Chem. Commun.*, 1997, 307; (*c*) A. K. Burrell, D. L. Officer, D. C. W. Reid and K. Y. Wild, *Angew. Chem., Int. Ed. Engl.*, 1998, **37**, 114; (*d*) A. Bilyk, M. M. Harding, P. Turner and T. W. Hambley, *J. Chem. Soc., Dalton Trans.*, 1995, 2549; (*e*) M. H. Houghton, A. Bilyk, M. M. Harding, P. Turner and T. W. Hambley, *J. Chem. Soc., Dalton Trans.*, 1997, 2725; 1998, 723; (*f*) A. Bilyk, M. Harding, P. Turner and T. W. Hambley, *J. Chem. Soc., Dalton Trans.*, 1994, 2783. (*g*) A. Bilyk and M. M. Harding, *J. Chem. Soc., Dalton Trans.*, 1994, 77.

3 C. A. Hunter, *Chem. Soc. Rev.*, 1994, **23**, 101.

4 H. Hope, *Acta Crystallogr., Sect. B*, 1972, **28**, 1733.

5 See, however, M. Albrecht and C. Riether, *Chem. Ber.*, 1996, **129**, 829 and references therein.

6 C. O. Dietrich-Buchecker, J.-F. Nierengarten, J.-P. Sauvage, N. Armaroli, V. Balzani and L. De Cola, *J. Am. Chem. Soc.*, 1993, **115**, 11 237.

7 F. R. Heirtzler, M. Neuburger, M. Zehnder and E. C. Constable, *Liebigs Ann./Recueil*, 1997, 297.

8 (*a*) R.-D. Schnebeck, L. Randaccio, E. Zangrando and B. Lippert, *Angew. Chem., Int. Ed. Engl.*, 1998, **37**, 119; (*b*) L. Carlucci, G. Ciani, D. M. Proserpio and A. Sironi, *J. Am. Chem. Soc.*, 1995, **117**, 4562.

9 (*a*) T. Otieno, S. J. Rettig, R. C. Thompson and J. Trotter, *Inorg. Chem.*, 1993, **32**, 1607; (*b*) R. V. Stone, J. P. Hupp, C. L. Stern and T. E. Albrecht-Schmitt, *Inorg. Chem.*, 1996, **35**, 4096.

10 E. C. Constable, M. J. Hannon, A. J. Edwards and P. R. Raithby, *J. Chem. Soc., Dalton Trans.*, 1994, 2669.

11 G. Sheldrick, University of Göttingen, 1994.

Received in Basel, Switzerland, 9th April 1998; 8/02709I

Organic gels are useful as a template for the preparation of hollow fiber silica

Yoshiyuki Ono,[a] Kazuaki Nakashima,[a] Masahito Sano,[a] Yasumasa Kanekiyo,[a] Kazuhiko Inoue,[a] Junichi Hojo[b] and Seiji Shinkai*[a]†

[a] *Chemotransfiguration Project, Japan Science and Technology Corporation (JST), 2432 Aikawa, Kurume, Fukuoka 839-0861, Japan*
[b] *Department of Chemistry and Biochemistry, Graduate School of Engineering, Kyushu University, Hakozaki, Higashi-ku, Fukuoka 812-8581, Japan*

A novel mesoporous silica with a tubular structure has been prepared using organic gel fibers as a template.

Increasing attention has been paid to low molecular-mass compounds that can gelatinize various organic solvents efficiently.[1–11] These phenomena are interesting in that the fibrous aggregates formed by non-covalent interactions are responsible for the gelation. In particular, cholesterol-based gelators, which can form stable gels using only non-hydrogen-bonding interactions, show an excellent gelation ability towards a wide variety of organic solvents at sufficiently low concentrations.[5–9,11] In addition, the resulting gels have chirally oriented structures which are imparted from the characteristic cholesterol skeleton. Through this study we found that even liquid silanol derivatives can be gelatinized by some cholesterol-based gelators.[7,12] It thus occurred to us that if the sol–gel polymerization of the silanol derivatives proceeds in the organic gel state, the gelator fibrils should act as a template which eventually creates a void in the resultant silica. After trial-and-error, we have found that under certain reaction conditions the gelator fibrils survive in the sol–gel process and construct a tubular structure in the fibrous silica.

It is known that compound **1** can gelatinize tetraethoxysilane

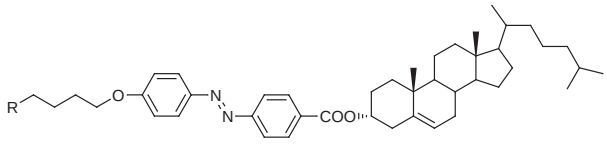

R = H **1**, R = $NMe_3^+Br^-$ **2**

(TEOS).[12] First, this gel was polymerized under acidic or basic reaction conditions. SEM observation showed, however, that the structure which might be constructed using this gelator fibrils as a template was not found in the resultant silica. Hence, we newly synthesized compound **2** which contains a quaternary ammonium cation like conventional cationic surfactants generally used as templates for sol–gel polymerization.[13,14] Compound **2** was synthesized according to Scheme 1 and identified by IR and ^{1}H NMR spectral evidence and elemental analysis. Since PPh_3 and azodicarboxylic acid diethyl ester were used for the condensation with cholesterol, the C-3 atom has the unnatural inverted (*R*)-configuration.[7]

The gelation ability was tested using several organic solvents (Table 1). It is seen from Table 1 that **2** is not very soluble in organic solvents but can gelatinize some solvents such as MeOH, EtOH and $MeCO_2H$. As a gelator, therefore, **2** is not so versatile as **1**. Fig. 1 shows a SEM image of a dried gel prepared from $MeCO_2H$ (3.0 mass%). Well grown fibrils with diameters of 50–200 nm are observed in this photograph.

Sol–gel polymerization was carried out as follows: **2** (5.0 mg) was dissolved in CH_2Cl_2 (0.3 g). To this solution were added $MeCO_2H$ (0.32 g), TEOS (0.045 g) and water (0.016 g) in this order. The resultant solution was evaporated *in vacuo* until the CH_2Cl_2 was removed (monitored by the mass decrease) to give a turbid acetic acid gel. This gel was sealed in a glass tube and left at 20 °C for 10 days. We also prepared a reference sample which was treated according to the same procedure in the absence of **2**. After 10 days, both mixtures were totally solidified, indicating that sol–gel polymerization of TEOS proceeded sufficiently. In order to preserve the original organic gel structure and the formed silica structure they must be dried under mild conditions. Thus, the products were dried at room temp. for 2 days to remove $MeCO_2H$ and water. Subsequently,

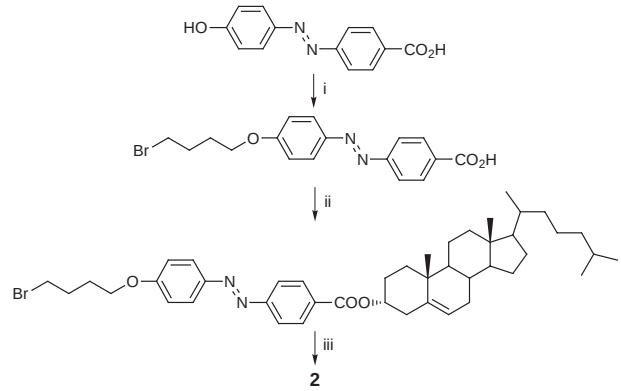

Scheme 1 *Reagents and conditions*: i, 1,4-dibromobutane, KOH, EtOH, reflux, 15%; ii, cholesterol, PPh_3, azodicarboxylic acid diethyl ester, THF, 20 °C, 18%; iii, NMe_3, THF, 20 °C, 69%

Table 1 Gelation ability of **1** and **2**[a]

Solvent	**1**[b]	**2**
n-Hexane	G	I
Toluene	S	I
Dichloromethane	S	S
Chloroform	S	S
Diethyl ether	G[c]	I
Tetrahydrofuran	S	I
Acetone	G	I
Methyl ethyl ketone	G	I
Acetonitrile	SG[d]	I
Methanol	SG	G
Ethanol	SG	G
Acetic acid	SG	G
n-Propylamine	S	I
Diethylamine	Gf[e]	I
Benzylamine	—	G[c]
TEOS	G	I
Water	I	I

[a] The solution (5 mass%) was warmed and then cooled to 4 °C to grow the gel: G = stable gel formed at room temperature, S = solution, I = insoluble. [b] Cited from refs. 7 and 12. [c] The gel was formed at 4 °C but turned into a solution at room temp. [d] Super-gelator in which the gel was formed at a concentration of < 1 mass%. [e] Gel formed when cooled in a refrigerator (at −6 °C) and was stable at room temp.

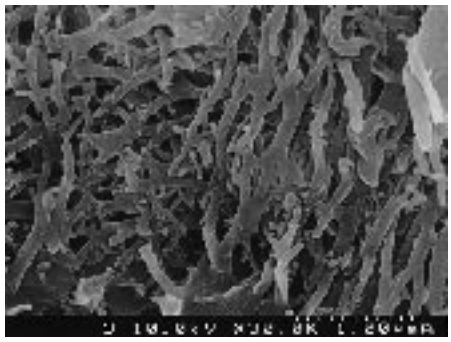

Fig. 1 SEM image for the gel of **2**–$MeCO_2H$: the gel was frozen in liquid N_2 and dried under reduced pressure for 2 h

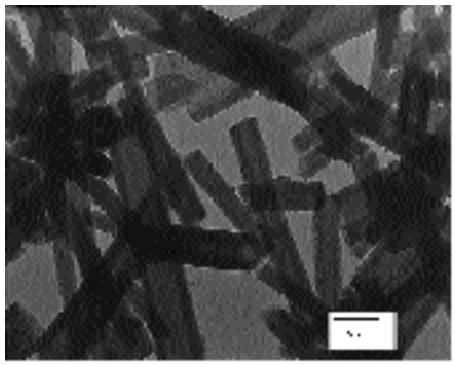

Fig. 2 TEM image for the silica (sample B) with a tubular structure (125 kV Hitachi H7100 TEM)

they were heated at 60 °C for 5 h *in vacuo* in order to entirely remove residual liquid and to accelerate the TEOS polymerization. At this stage a portion of the samples was subjected to SEM observation (sample A). They were further heated at 200 °C for 6 h under an N_2 stream for the polymerization and the removal of the residual stress evolved by shrinkage of the silica network. Finally, they were heated at 500 °C for 2 h under an N_2 stream and for 4 h in air (sample B) for the pyrolytic decomposition of **2**.

The SEM image of sample B is shown in the Graphical Abstract. It is clearly seen that sol–gel polymerization results in well grown fibrous silica and very interestingly, the tube edges contain cavities. In order to view the inside of the strand we obtained a TEM image (Fig. 2). It is clearly seen that these fibers have a tubular structure with inner diameters of 10–200 nm. Although the silica may shrink to some extent during calcination, the size is nearly comparable with that of the organic gelator fibrils (50–200 nm: Fig. 1). On the other hand, sample A obtained after treatment at 60 °C also gave fibrous silica but the tubular structure was not observed in the SEM picture. These results indicate that the organic gelator fibrils of **2** act as a template in the sol–gel process, create the tubular structure and finally are removed by pyrolysis at 500 °C.

Here, we consider why **2** can act as the template while **1** cannot although both gelators aggregate into fibers in the organic solvents. When the sol–gel polymerization is carried out in $MeCO_2H$, the propagation species is considered to be anionic.[15,16] Hence, the oligomeric silica species are adsorbed onto the cationic gelator fibrils and the polymerization further proceeds along these fibrils. This propagation mode can eventually yield fibrous silica with tubular structure. This proposal is further supported by the effect of added alcohol: when the sol–gel polymerization was initiated in **2**–$MeCO_2H$–TEOS–H_2O–EtOH (1 : 63 : 10 : 4 : 22, m/m), the resultant silica had a well developed fibrous network structure but tubular structure was not observed (SEM). Since EtOH facilitates the polymerization, the resultant silica becomes the network structure but cannot construct the isolated silica fibers.[16]‡ In contrast, the organic gelator fibrils of **1** without the cationic charge cannot adsorb the oligomeric silica species even in the absence of EtOH, so that the resultant silica showed only the granular structure (SEM). Similar granular structure was also observed for the silica obtained in the absence of the gelator.

In conclusion, the present paper has demonstrated a novel application of organic gels as a template to prepare a novel porous silica with tubular structure.

We thank Dr P. C. Ewbank for helpful discussions.

Notes and References

† E-mail: seijitcm@mbox.nc.kyushu-u.ac.jp

‡ It is not yet clear if this network silica also has the tubular structure. The sample is too thick to view the inside with TEM.

1 E. J. de Vries and R. M. Kellogg, *J. Chem. Soc., Chem. Commun.*, 1993, 238; M. de Loos, J. van Esch, I. Stokroos, R. M. Kellogg and B. L. Feringa, *J. Am. Chem. Soc.*, 1997, **119**, 12 675.
2 M. Aoki, K. Nakashima, H. Kawabata, S. Tsutsui and S. Shinkai, *J. Chem. Soc., Perkin Trans. 2*, 1993, 347.
3 K. Hanabusa, K. Okui, K. Karaki, T. Koyama and H. Shirai, *J. Chem. Soc., Chem. Commun.*, 1992, 1371; K. Hanabusa, A. Kawakami, M. Kimura and H. Shirai, *Chem. Lett.*, 1997, 191 and references therein.
4 J.-E. S. Sohna and F. Fages, *Chem. Commun.*, 1997, 327.
5 E. Otsuni, P. Kamaras and R. G. Weiss, *Angew. Chem., Int. Ed. Engl.*, 1996, **35**, 1324 and references therein.
6 P. Terech, I. Furman and R. G. Weiss, *J. Phys. Chem.*, 1995, **99**, 9558 and references therein.
7 K. Murata, M. Aoki, T. Suzuki, T. Harada, H. Kawabata, T. Komori, F. Ohseto, K. Ueda and S. Shinkai, *J. Am. Chem. Soc.*, 1994, **116**, 6664 and references therein.
8 T. D. James, K. Murata, T. Harada, K. Ueda and S. Shinkai, *Chem. Lett.*, 1994, 273.
9 S. W. Jeong, K. Murata and S. Shinkai, *Supramol. Sci.*, 1996, **3**, 83.
10 T. Brotin, R. Utermöhlen, F. Fages, H. Bouas-Laurent and J.-P. Desvergne, *J. Chem. Soc., Chem. Commun.*, 1991, 416.
11 For recent comprehensive reviews, see: P. Terech and R. G. Weiss, *Chem. Rev.*, 1997, **97**, 3133; S. Shinkai and K. Murata, *J. Mater. Chem.* (*Feature Article*), 1998, **8**, 485.
12 K. Murata, Ph.D. Thesis, Graduate School of Engineering, Kyushu University, 1997.
13 C. T. Kresge, M. E. Leonowicz, W. J. Roth, J. C. Vartuli and J. S. Beck, *Nature*, 1992, **359**, 710.
14 J. S. Beck, J. C. Vartuli, W. J. Roth, M. E. Leonowicz, C. T. Kresge, K. D. Schmitt, C. T-W. Chu, D. H. Olson, E. W. Sheppard, S. B. McCullen, J. B. Higgins and J. L. Schlenker, *J. Am. Chem. Soc.*, 1992, **114**, 10 834.
15 Q. Huo, D. I. Margolese, U. Ciesla, P. Feng, T. E. Gier, P. Sieger, R. Leon, P. M. Petroff, F. Schüth and G. D. Stucky, *Nature*, 1994, **368**, 317.
16 C. J. Brinker and G. W. Scherer, *Sol–Gel Science*, Academic Press, San Diego, 1990, p. 97.

Received in Cambridge, UK, 15th April 1998; 8/02829J

Oxonium-ion crown ether complexes from *aqua regia*

Karin Johnson and Jonathan W. Steed*†

Department of Chemistry, King's College London, Stand, London, UK WC2R 2LS

Reaction of an *aqua regia* solution of gold metal with 15-crown-5 and its derivatives results in the formation of the hydrogen bonded aggregates $[H_7O_3][AuCl_4]\cdot$15-crown-5 1 and $[H_5O_2][AuCl_4]\cdot$(benzo-15-crown-5)$_2$ 2; complex 1 exhibits a complex, cross-linked structure in which the $H_7O_3^+$ unit hydrogen bonds to two adjacent crown ethers and a chloride ligand of the anion; the Au^{III} centre also engages in long-range interactions wtih the crown oxygen atoms.

Recent work in acidic liquid clathrate[1,2] media has indicated that the selective crystallisation of various forms of the hydrated proton (H_3O^+, $H_5O_2^+$, *etc.*) may sometimes be achieved by isolation in the presence of a crown ether of the complementary dimensions to the desired oxonium species. A good fit is observed for 18-crown-6 with H_3O^+,[3,4] whereas larger crown ethers such as 21-crown-7 select $H_5O_2^+$.[5,6] Dibenzo-30-crown-10 is able to encapsulate two H_3O^+ ions.[5] In the case of the smaller crown ethers the nature of the oxonium species is variable, and depends considerably on the counter anion.[7] Indeed, $[H_{13}O_6][PtCl_5(H_2O)]\cdot H_2O\cdot$(18-crown-6)$_2$ shows that the oxonium ion species isolated by larger crown ethers may be strikingly influenced by the nature of the anion.[8] For protonated derivatives of 2,6-pyrido-21-crown-7 a water molecule is included within the cavity, while the analogous 2,6-pyrido-24-crown-8 complex encapsulates two water molecules with hydrogen bonding interactions to the protonated nitrogen.[9] We have recently begun a programme of research into host–guest species which exhibit a symmetry or steric mismatch.[10] As an extension of this work we now report the results of our investigations into oxonium ion complexes of tetrachloroaurate(III) containing small and intermediate-sized crown ethers.

Aqua regia [HCl–HNO_3 (3 : 1)] has been known since the thirteenth century as the only reagent capable of dissolving metallic gold.[11] A stock solution containing gold in *aqua regia* was prepared, resulting in oxidation of the gold to $H[AuCl_4]$. To aliquots of this solution were added equimolar amounts (relative to Au) of 15-crown-5 and benzo-15-crown-5 in aqueous ethanol. This resulted in the very rapid formation of bright orange–yellow crystalline products from each solution over periods of 1–4 h in good yields. The products were subjected to analysis by X-ray crystallography at −150 °C,‡ which gave the formulations $[H_7O_3][AuCl_4]\cdot$15-crown-5 **1** and $[H_5O_2][AuCl_4]\cdot$(benzo-15-crown-5)$_2$ **2**. The $H_7O_3^+$ ion in particular is relatively uncommon, though it has been observed in hydrogen bromide tetrahydrate.[12]

Complex **1** consists of an unusual, infinite hydrogen bonded chain containing alternating oxonium ion···crown pairs separated by $AuCl_4^-$ anions. The structure of the repeating unit of the infinite $H_7O_3^+\cdot$15-crown-5 chain is shown in Fig. 1, while the overall crystal packing arrangement is illustrated in Fig. 2.

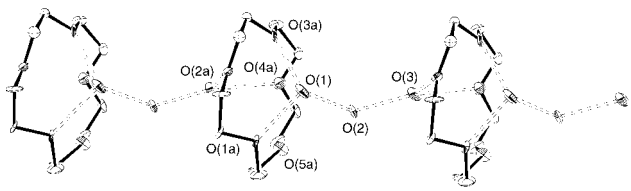

Fig. 1 Structure of the infinite $H_7O_3^+\cdot$15-crown-5 chain repeating unit in **1**

The $H_7O_3^+$ ion exhibits an unsymmetrical conformation with a short O(1)···O(2) distance comparable to that found in $H_5O_2^+$ systems[6,13,14] and a longer O(2)···O(3) interaction, 2.43(2) *vs.* 2.536(18) Å, O(1)–O(2)–O(3) angle 121(2)°. In contrast, a somewhat more symmetrical example is found in $[H_7O_3][H_9O_4]Br_2\cdot H_2O$ in which the inter oxygen separations are 2.465 and 2.498 Å,[12] whereas the hydrogen bonded $H_5O_2^+\cdots H_2O$ pair exhibits very different distances of 2.424 and 2.721 Å.[15] In complex **1** the oxonium ion hydrogen bonds to the crown oxygen atoms O(1a) and O(3a); O···O 2.64(2) and 2.63(3) Å respectively. The opposite end of the $H_7O_3^+$ unit interacts with an adjacent crown *via* longer hydrogen bonds; O(3)···O(2a) 2.75(2), O(3)···O(4a) 2.820(18) Å. This presumably results from the conflicting steric requirements of the $AuCl_4^-$ anion and the oxonium cation, although it may also be influenced by an additional, albeit long hydrogen bond from the central atom of the oxonium ion to one of the chloride ligands of the tetrachloroaurate(III) anion, O(2)···Cl(1) 3.30(2) Å. The gold(III) ion exhibits a square-planar coordination geometry, with Au–Cl distances falling into two groups; Au–Cl(1), –Cl(4) 2.296(7) Å and Au–Cl(2), –Cl(3) 2.267(7) Å (average). Interestingly, the Au^{III} ions also exhibit very long axial interactions with crown oxygen atom O(5a) (which does not take part in a hydrogen bond) and O(3a); Au–O(3a) 3.342(16), Au–O(5a) 3.381(19) Å, resulting in a cross-linked polymeric structure.

Given the polymeric nature of **1**, the structure of the benzo-15-crown-5 derivative **2** is somewhat surprising. Complex **2** contains discrete $H_5O_2^+\cdot$(benzo-15-crown-5)$_2$ units in which a pair of crowns sandwich the oxonium ion (Fig. 3). The syntheses of both **1** and **2** were carried out under identical conditions, in a 1 : 1 ratio of Au : crown. Examination of Fig. 2, however, suggests that the long range Au–O_{crown} interactions seen for **1** as well as the hydrogen bond to O(2), would not be sterically feasible for an analogous benzo-15-crown-5 complex. Indeed, the closest axial approach to the $AuCl_4^-$ anions in **2** is

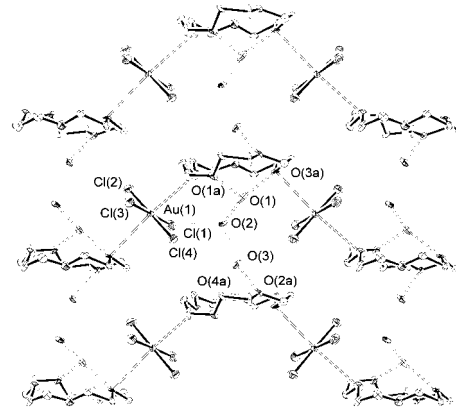

Fig. 2 Crystal packing arrangement in $[H_7O_3^+][AuCl_4]\cdot$15-crown-5 **1** showing long-range axial interactions from the crown ether to the $AuCl_4^-$ anions. Au–Cl(1–4) 2.297(7), 2.268(8), 2.266(7), 2.295(7) Å; Au–O(3a) 3.342(16), Au–O(5a) 3.381(19) Å. Hydrogen bonds: O(1)–O(1a) 2.64(2), O(1)–O(3a) 2.63(3), O(3)–O(2a) 2.75(2), O(3)–O(4a) 2.820(18) Å. Oxonium ion: O(1)–O(2) 2.43(2), O(2)–O(3) 2.536(18) Å.

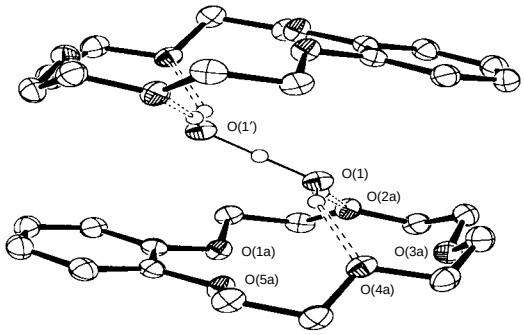

Fig. 3 The discrete H_2O_2'·(benzo-15-crown-5)$_2$ unit in **2**. Hydrogen bonds: O(1)–O(2a) 2.715(4), O(1)–O(4a) 2.642(4) Å. Oxonium ion: O(1)–O(1′) 2.420(6) Å.

by the hydrogen atoms of a crown ethylene moiety, and hence it seems likely that in the absence of these stabilisations a simple ion paired structure results.

Interaction of H[$AuCl_4$] with other crown ethers also results in the formation of oxonium ion–crown ether salts of tetrachloroaurate(III). In particular, reactions with larger crown ethers, namely 18-crown-6 and dibenzo-24-crown-8, give respectively the H_3O^+ and $H_5O_2^+$ containing species [H_5O][$AuCl_4$]·18-crown-6 and [H_5O_2][$AuCl_4$]·dibenzo-24-crown-8. Full details of this work will be reported separately.

We thank the EPSRC and King's College London for funding of the diffractometer system and the Nuffield Foundation for the provision of computing equipment.

Notes and References

† E-mail: jon.steed@kcl.ac.uk

‡ *Crystal data* **1**: $C_{10}H_{27}AuCl_4O_8$, M = 614.08, monoclinic, space group $P2_1$, a = 7.9485(3), b = 18.7082(7), c = 13.9930(6) Å, β = 104.34(1)°, U = 2015.95(14) Å^3, Z = 4, 7868 unique data ($2\theta \leqslant 52°$), 406 parameters, R_1 [$F^2 > 2\sigma(F^2)$] = 0.058, wR_2 (all data) = 0.174. **2**: $C_{28}H_{45}AuCl_4O_{12}$, M = 912.41, triclinic, space group $P\bar{1}$, a = 9.2950(6), b = 10.2293(11), c = 11.6412(11) Å, α = 64.77(1), β = 88.63(1), γ = 66.99(1)°, U = 907.99(14) Å^3, Z = 1, 3321 unique data ($2\theta \leqslant 52°$), 214 parameters, R_t [$F^2 > 2\sigma(F^2)$] = 0.028, wR_2 (all data) = 0.064. Crystals were mounted using a fast setting epoxy resin on the end of a glass fibre and cooled on the diffractometer. All crystallographic measurements were carried out with a Nonius KappaCCD diffractometer equipped with graphite monochromated Mo-Kα radiation using ϕ rotations with 2° frames and a detector to crystal distance of 25 mm. Integration was carried out by the program DENZO-SMN.[16] Data sets were corrected for Lorentz and polarization effects and for the effects of absorption using the program Scalepack.[16] Structures were solved using the direct methods option of SHELXS-97[17] and developed using conventional alternating cycles of least squares refinement and difference Fourier synthesis (SHELXL-97).[17] In general, all non-hydrogen atoms were refined anisotropically, whilst hydrogen atoms were fixed in idealized positions and allowed to ride on the atom to which they were attached. Hydrogen atom thermal parameters were tied to those of the atom to which they were attached. In the case of **2** oxonium ion protons were located experimentally and refined freely. Oxonium ion protons could not be located for **1**. All calculations were carried out either on a Silicon Graphics Indy workstation or an IBM-PC compatible personal computer. CCDC 182/889.

1 J. L. Atwood, in *Chemical Separations*, ed. C. J. King and J. D. Navratil, Litarvan, Denver, 1986.
2 J. L. Atwood, in *Separation Technology*, ed. N. N. Li and H. Strathmann, United Engineering Trustees, New York, 1988.
3 J. L. Atwood, S. G. Bott, A. W. Coleman, K. D. Robinson, S. B. Whetstone and C. M. Means, *J. Am. Chem. Soc.*, 1987, **109**, 8100.
4 J. L. Atwood, S. G. Bott, K. D. Robinson, E. J. Bishop and M. T. May, *J. Cryst. Spectrosc. Res.*, 1991, **21**, 459.
5 P. C. Junk and J. L. Atwood, *J. Chem. Soc., Dalton Trans.*, 1997, 4393.
6 P. C. Junk and J. L. Atwood, *J. Chem. Soc., Chem. Commun.*, 1995, 1551.
7 J. L. Atwood and P. C. Junk, *Chem. Commun.*, submitted.
8 D. Steinborn, O. Gravenhorst, H. Hartung and U. Baumeister, *Inorg. Chem.*, 1997, **36**, 2195.
9 P. D. J. Grootenhuis, J. W. H. M. Uiterwijk, D. N. Reinhoudt, C. J. van-Stavren, E. J. R. Sudhölter, M. Bos, J. van-Eerden, W. T. Klooster, L. Kruise and S. Harkema, *J. Am. Chem. Soc.*, 1986, **108**, 780.
10 J. W. Steed, H. Hassaballa and P. C. Junk, *Chem. Commun.*, 1998, 577.
11 N. N. Greenwood and A. Earnshaw, *Chemistry of the Elements*, Pergamon, Oxford, 1984.
12 J.-O. Lundgren and I. Olovsson, *J. Chem. Phys.*, 1968, **49**, 1068.
13 C. I. Ratcliffe and D. E. Irish, in *The Nature of the Hydrated Proton*, ed. F. Franks, Cambridge, 1986.
14 A. Bino and F. A. Cotton, *J. Am. Chem. Soc.*, 1979, **101**, 4150.
15 R. Attig and J. M. Williams, *Inorg. Chem.*, 1976, **15**, 3057.
16 Z. Otwinowski and W. Minor, in *Methods in Enzymology*, ed. C. W. Carter and R. M. Sweet, Academic Press, New York, 1996.
17 G. M. Sheldrick, in 'SHELX-97', University of Göttingen, 1997.

Received in Columbia, MO, USA, 30th March 1998; 8/02537A

A double sandwich silver(I) polymer with 1,1′-bis(diethyldithiocarbamate)-ferrocene

Olga Crespo,[a] M. Concepción Gimeno,[a] Peter G. Jones,[b] Antonio Laguna*[a]† and Cristina Sarroca[a]

[a] *Departamento de Química Inorgánica, Instituto de Ciencia de Materiales de Aragón, Universidad de Zaragoza-CSIC, 50009 Zaragoza, Spain*

[b] *Institut für Anorganische und Analytische Chemie der Technischen Universität, Postfach 3329, D-38023 Braunschweig, Germany*

The polymeric complex $[Ag\{Fc(S_2CNEt_2)_2\}]_n[ClO_4]_n$, in which the silver centres are bonded to two sulfur atoms of different ferrocene moieties and also to the cyclopentadienyl rings in an η^2 fashion, is reported.

In the last few years the chemistry of ferrocene and the design of new compounds containing the ferrocene unit has received much attention, associated with utility in many fields such as organic synthesis, catalysis and material chemistry.[1,2] Numerous derivatives in which the metallocene is bonded to a chelate ligand have been described. Interesting effects such as redox-switched bonding of metal ions within ferrocene crown ethers or investigations into the potential use of such compounds as amperometric sensors for metal ions or protons have been among the highlights of this development.[3–8] It seems that the performance of such molecular devices depends on the efficient electronic communication between the ferrocene and the metal ion coordinated within the chelating ligand.

The compound 1,1′-bis(diethyldithiocarbamate)ferrocene, $Fc(S_2CNEt_2)_2$ [Fc = $Fe(C_5H_4)_2$], although synthesized more than ten years ago,[9] has not been studied as a ligand. Here we report on the reaction of $Fc(S_2CNEt_2)_2$ with $AgClO_4$ to give a polymeric chain with stoichiometry $[Ag\{Fc(S_2CNEt_2)_2\}]_n[ClO_4]_n$, in which the silver centres are bonded to two sulfur atoms of different ferrocene moieties and are also bonded to the cyclopentadienyl rings in an η^2 fashion. Thus the silver atoms can be regarded as being four-coordinate and the molecule as a double sandwich of iron and silver. This is the first example where an η^5-Cp ring of the ferrocene unit is bonded to another metal centre through the π system. Recently Grossel *et al.* suggested the presence of a stabilising interaction between the metallocene π system of ferrocenyl substituted aza crown ethers and the cation bound to the crown moiety.[10] The complex $[Ag\{Fc(S_2CNEt_2)_2\}]_n[ClO_4]_n$ will be interesting in order to study the physical properties, mainly due to the possible existence of the delocalized aromatic conduction electrons.

The reaction of $Fc(S_2CNEt_2)_2$ with $AgClO_4$ (1 : 1 molar ratio) in diethyl ether gives a yellow precipitate from which the complex $[Ag\{Fc(S_2CNEt_2)_2\}]_n[ClO_4]_n$ **1** (Scheme 1) can be isolated.‡ It is stable to air and moisture and behaves as a 1 : 1 electrolyte in acetone. The ^{1}H NMR spectrum is in agreement with the presence of one type of 1,1′-bis(diethyldithiocarbamate)ferrocene ligand. The positive liquid secondary-ion mass spectrum shows the peak $[Ag\{Fc(S_2CNEt_2)_2\}]^+$ at m/z = 589 as the most intense.

The structure of complex **1** has been confirmed by an X-ray diffraction study (Fig. 1).§ The molecule consists of 1,1′-bis(diethyldithiocarbamate)ferrocene units bridged by silver atoms. Each silver centre is coordinated to sulfur atoms of different ferrocene moieties. The silver atom lies on an inversion centre and the iron atom on a twofold axis; consequently only half of the monomeric formula unit represents the asymmetric unit. Of necessity the grouping S–Ag–S^i (i = $-x + 1, -y + 1, -z + 1$) is perfectly linear; additionally, the silver centre is weakly bonded to two carbon atoms of each of two cyclopentadienyl rings. The Ag–C distances, 2.972(8) and 3.027(8) Å, are only slightly longer than the longest found in complexes of silver(I) with aromatic systems (2.47–2.92 Å).[11–20]

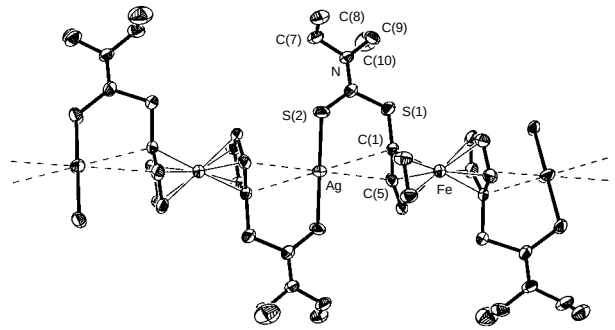

Fig. 1 Part of the polymeric chain of the cation of complex **1** in the crystal showing the atom numbering scheme. Ellipsoids represent 50% probability surfaces. H atoms are omitted for clarity.

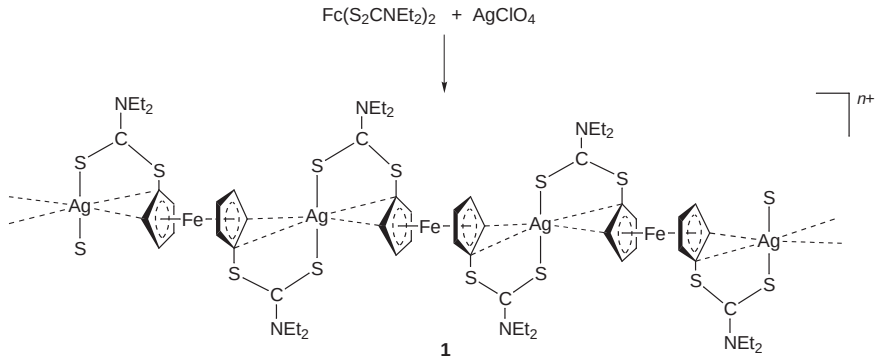

1

Scheme 1

It is also noteworthy that aromatic silver(I) complexes usually show an asymmetry in their Ag–C interactions (as do copper complexes).[21,22] According to Mulliken's model[23] the most favourable position for a silver ion is at the point of highest π-electron density, directly above one of the carbon atoms of the ring. Dewar[24] maintained that silver(I) could act not only as an electron acceptor, but also as a donor of electrons from a filled d orbital to an empty molecular orbital of the aromatic. If this 'back donation' interaction is of importance in the stabilization of the complex, the best overlap is achieved when the silver is located in the π cloud equidistant between the two carbon atoms. This situation has only been observed for naphthalene-tetrakis(silver perchlorate) tetrahydrate (2.59, 2.61 Å).[19] In complex **1** the interaction is weaker, as discussed above.

The interaction of the silver atom with the C(1)–C(5) bond produces only a small effect on the ring geometry, as was previously observed in other silver–aromatic species. However the C(1)–C(5) bond is marginally longer at 1.448(11) Å, although the difference may not be significant, while the C_5 ring remains planar (σ = 0.003 Å).

The Ag–S(2) distance is 2.386(3) Å and compares well with those observed for linear Ag–S bonds in complexes such as $[Ag_2(CH_2PPh_2S)_2]$ [2.382(3) Å].[25]

This work is supported by the Dirección General de Investigación Cientifica y Técnica (No. PB94-0079), the Caja de Ahorros de la Inmaculada (No. CB8/97) and the Fonds der Chemischen Industrie.

Notes and References

† E-mail: alaguna@posta.unizar.es

‡ *Preparation*: to a solution of $AgClO_4$ (0.1 mmol, 0.021 g) in diethyl ether $Fc(S_2NEt_2)_2$ (0.1 mmol, 0.048 g) was added. The mixture was stirred for 1 h and the resulting yellow solid filtered off and dried *in vacuo*. Yield 60%. Elemental analysis (%): Calc. for $C_{20}H_{28}AgClFeN_2O_4S_4$: C, 34.9; H, 4.1; N, 4.05; S, 18.65. Found: C, 34.95; H, 4.35; N, 4.25; S, 18.70%. ^{1}H NMR (300 MHz, $CDCl_3$), δ 4.46 (m, br, 4 H, C_5H_4), 4.38 (m, br, 4 H, C_5H_4), 3.94 (m, br, 4 H, C*H*$_2$CH$_3$), 3.77 (m, br, 4 H, C*H*$_2$CH$_3$), 1.33 (m, br, 6 H, CH$_2$C*H*$_3$), 1.18 (m, br, 6 H, CH$_2$C*H*$_3$).

§ *Crystal data*: $[Ag\{Fc(S_2CNEt_2)_2\}]_n[ClO_4]_n$, **1**·2$CH_2Cl_2$, $C_{22}H_{32}AgCl_5FeN_2O_4S_4$, M = 857.71, monoclinic, space group $C2/c$, a = 20.066(5), b = 9.859(3), c = 18.463(5) Å, β = 113.02(2)°, U = 3362(2) Å^3, Z = 4, μ(Mo-Kα) = 1.69 mm^{-1}. A yellow plate 0.35 × 0.25 × 0.04 mm was used to collect 2935 reflections with intensities to $2\theta_{max}$ 50°, of which 2924 (R_{int} = 0.018) were unique. The structure was solved by direct methods and subjected to full-matrix least-squares refinement on F^2 (SHELXL-93). Refinement proceeded to $wR(F^2)$ = 0.17 for 2924 reflections, 183 parameters and 26 restraints, conventional $R(F)$ [$I > 2\sigma(I)$] 0.064. CCDC 182/891.

1 *Ferrocenes*, ed. A. Togni and T. Hayashi, VCH, Weinheim, Germany 1995.
2 N. J. Long, *Angew. Chem., Int. Ed. Engl.*, 1995, **34**, 21.
3 F. C. J. M. van Veggel, W. Verboom and D. N. Reinhoudt, *Chem. Rev.*, 1994, **94**, 279.
4 P. D. Beer, *Adv. Inorg. Chem.*, 1992, **39**, 79.
5 H. Plenio and R. Diodone, *J. Organomet. Chem.*, 1995, **492**, 73.
6 H. J. L. Tendero, A. Benito, R. Martinez-Manez, J. Soto, J. Paya, A. J. Edwards and P. R. Raithby, *J. Chem. Soc., Dalton Trans.*, 1996, 343.
7 H. Plenio, J. Yang, R. Diodone and J. Heinze, *Chem. Ber.*, 1993, **126**, 2403.
8 H. Plenio and D. Burth, *Organometallics*, 1996, **15**, 4054.
9 B. McCulloch and C. H. Brubaker Jr., *Organometallics*, 1984, **3**, 1707.
10 M. C. Grossel, D. G. Hamilton, J. I. Fuller and E. Millan-Barios, *J. Chem. Soc., Dalton Trans.*, 1997, 3471.
11 R. W. Turner and E. L. Amma, *J. Am. Chem. Soc.*, 1996, **88**, 3243.
12 E. A. H. Griffith and E. L. Amma, *J. Am. Chem. Soc.*, 1971, **93**, 3167.
13 S. H. Strauss, M. D. Noirot and O. P. Anderson, *Inorg. Chem.*, 1985, **24**, 4307.
14 J. C. Barners and C. S. Blyth, *Inorg. Chim. Acta*, 1985, **98**, 181.
15 H. Schmidbaur, W. Bublak, B. Huber, G. Reber and G. Müller, *Angew. Chem., Int. Ed. Engl.*, 1986, **25**, 1089.
16 H. C. Kang, A. W. Hanson, B. Eaton and V. Boekelheide, *J. Am. Chem. Soc.*, 1985, **107**, 1979.
17 P. F. Rodesiler, E. A. H. Griffith and B. L. Amma, *J. Am. Chem. Soc.*, 1972, **94**, 761.
18 P. F. Rodesiler and E. L. Amma, *Inorg. Chem.*, 1972, **11**, 388.
19 E. A. H. Griffith and E. L. Amma, *J. Am. Chem. Soc.*, 1974, **96**, 743, 5407.
20 M. Munakata, L. P. Wu, T. Kuroda-Sowa, M. Maekawa, Y. Suenaga and K. Sugimoto, *Inorg. Chem.*, 1997, **36**, 4903.
21 R. W. Turner and E. L. Amma, *J. Am. Chem. Soc.*, 1963, **85**, 4046.
22 R. W. Turner and E. L. Amma, *J. Am. Chem. Soc.*, 1966, **88**, 1877.
23 M. S. Mulliken, *J. Am. Chem. Soc.*, 1952, **74**, 811.
24 M. J. S. Dewar, *Bull. Soc. Chim. Fr.*, 1951, 71.
25 S. Wang, J. P. Fackler, Jr. and T. F. Carlson, *Organometallics*, 1990, **9**, 1973.

Received in Basel, Switzerland, 24th April 1998; 8/03087A

Multilayer formation in an azacrown [18]N_6 Langmuir film

P. A. Heiney,*[a]† D. Gidalevitz,[a]‡ N. C. Maliszewskyj,[b] S. Satija,[b] D. Vaknin,[c] Y. Pan[d] and W. T. Ford[d]

[a] *Department of Physics and Astronomy, University of Pennsylvania, Philadelphia PA 19104, USA*
[b] *NIST Center for Neutron Research, National Institute of Standards and Technology, Gaithersburg MD 20899, USA*
[c] *Ames Laboratory, Iowa State University, Ames IA 50011, USA*
[d] *Department of Chemistry, Oklahoma State University, Stillwater OK 74078, USA*

A neutron reflectivity study of a deuterated azacrown [18]N_6 at the air–water interface shows that it forms multilayers upon compression, with monolayers and trilayers being more stable than bilayers.

Typical Langmuir films are composed of a monolayer of amphiphilic molecules at the air–water interface. Upon compression, they are stable up to an irreversible 'collapse point', beyond which three-dimensional droplets are formed and/or the molecules dissolve in the water subphase. Recently, a number of compounds have been shown to form equilibrium multilayers, and in some cases trilayers are more stable than bilayers.[1,2] In other cases,[3] anomalous features in pressure–area isotherms have been associated with structural rearrangements of the molecules themselves.

We have now used neutron reflectivity to study deuterated Langmuir films of 1,4,7,10,13,16-hexakis(4-dodecyloxybenzoyl)-1,4,7,10,13,16-hexazacyclooctadecane **1**.

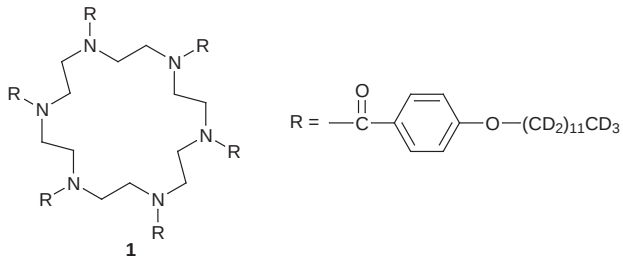

1

The bulk liquid crystal properties of **1** have excited considerable interest,[4–7] due in part to the potential existence of a hollow channel structure and also to the difficulty in distinguishing between columnar and smectic structures. Langmuir films of **1** are also unusual. Published pressure–area isotherms[5,6,8] measured on compression all show a rise beginning around 200 Å^2 molecule^{-1}, with an inflection point near 160 Å^2 molecule^{-1}, followed by a nonequilibrium 'bump' at slightly higher concentrations. This feature was variously ascribed to intramolecular reorientations, two-dimensional rearrangement of the film or multilayer formation.

To enhance neutron contrast, the alkyl chains were deuterated. Monolayers were spread at 20 °C from 10^{-3} to 10^{-4} M solutions on Millipore purified H_2O (resistivity 18.2 MΩ cm^{-1}). Neutron reflectivity measurements were made on beamline NG-7 of the Center for Neutron Research at the National Institute of Standards and Technology. After each compression, the film was allowed to equilibrate for 30 min before a measurement was made; each measurement took *ca.* 90 min to perform. Typical reflectivity profiles are shown in Fig. 1. The most dramatic feature is the evolution of a minimum at Q = 0.11 Å^{-1}, corresponding to a 60 Å film. This is approximately the thickness expected for a trilayer film. No minimum was ever observed in the vicinity of 0.16 Å^{-1}, as would be expected for a bilayer film.

The reflectivity data were analyzed[9] by modeling the film as a stack of uniform slabs, or boxes, each with a different scattering length density ρ, thickness L and roughness σ. We used in each case the minimum number of adjustable parameters required to obtain an acceptable fit to the data, with at most two slabs being employed. The profiles resulting from these fits are shown in Fig. 2. The general trends are as follows: at low concentrations, the reflectivity profiles are well described by a single flat slab of thickness 21.4 Å and roughness 3 Å. The thickness and scattering length density are close to those expected for a monolayer film with the central cores in contact with the subphase and the alkyl tails projecting away from the interface. As the concentration is increased beyond 1 molecule per 200 Å^2, a second well-defined 22 Å layer is formed. However, this layer does not grow to completion. Well before a concentration of 2 molecules per 200 Å^2 is achieved, the second layer roughens, so that the actual structure consists of a well-defined first layer plus patches of two-layer and three-layer film. At a nominal concentration of 3 molecules per 200 Å^2, the best fit structure is a rough trilayer film, consisting predominantly of a single sharp monolayer with regions of 1, 2 and 3 layers above that, as shown in Fig. 2.

The 'slab' model implicitly assumes that mono- and multilayer regions coexist on short length scales. It is also possible that domains larger than the neutron transverse coherence length are formed, in which case it would be more appropriate to sum reflectivity intensities for the different regions. Our central conclusion, that monolayers and trilayers are more stable than bilayers, still holds in this case, however, since we

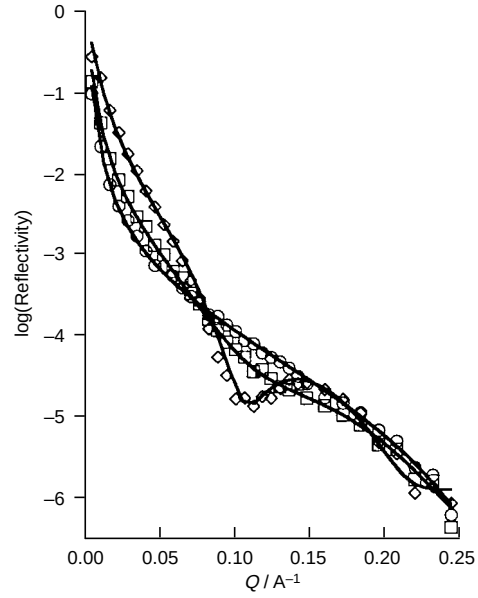

Fig. 1 Log of absolute neutron reflectivity *vs.* momentum transfer perpendicular to surface for three typical film concentrations of **1**: (○) 1.0, (□) 1.5 and (◇) 3.0 molecules per 200 Å^2

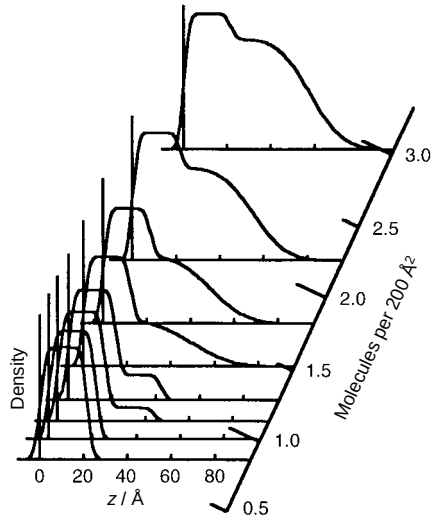

Fig. 2 Density profiles corresponding to 1- and 2-slab fits to the reflectivity data. Scattering length density (arbitrary units) is plotted *vs.* distance from the air–water interface, at a variety of surface concentrations (scaled to a nominal monolayer coverage of 1 molecule per 200 Å^2).

never observe the dip at 0.16 Å^{-1} expected for a bilayer film. We also note that there are systematic uncertainties in the calculated layer thickness, on the order of 15–20%, arising from the assumption of uniform density slabs; models incorporating the possibility of intraslab density variations may yield somewhat different thicknesses.

The relative instability of a bilayer film to trilayer formation most likely arises from the differing character of the hydrophilic amide cores and the hydrophobic hydrocarbon tails. We expect that the molecular orientation should alternate from layer to layer, with the hydrocarbon tails in the first and third tails directed away from the water and those in the second layer directed towards the first layer. The lower interfacial tension between hydrocarbon and air than between hydrated amide groups and air, which is known from X-ray photoelectron spectroscopy of amphiphilic polymers,[10] should then stabilize the third layer relative to the second.

In summary, we have shown that the nonequilibrium maximum observed in pressure–area isotherms of **1** is the result of multilayer formation upon compression. Furthermore, we have found that a bilayer structure is less stable than either a monolayer or a trilayer structure.

We thank L. Sung for her technical assistance. D. G. and P. A. H. were supported by National Science Foundation grants DMR MRL 92-20668 and DMR 93-15341. Y. P. and W. T. F. were supported by the US Army Research Office. Ames Laboratory is operated by Iowa State University for the US Department of Energy under Contract No. W-7405-Eng-82. The work at Ames was supported by the Director for Energy Research, Office of Basic Energy Sciences.

Notes and References

† E-mail: heiney@dept.physics.upenn.edu
‡ Present address: James Franck Institute, University of Chicago, Chicago IL 60637, USA.

1 J. Xue, C. S. Tag and M. W. Kim, *Phys. Rev. Lett.*, 1992, **69**, 474.
2 S. P. Weinbach, K. Kjaer, W. G. Bouwman, G. Grübel, J.-F. Legrand, J. Als-Nielsen, M. Lehav and L. Leiserowitz, *Science*, 1994, **264**, 1566.
3 A. El Abed, L. Tamisier, G. Dumas, B. Mangeot, K. Tanazefti, P. Peretti and J. Billard, *Mol. Cryst. Liq. Cryst.*, 1995, **265**, 151.
4 J.-M. Lehn, J. Malthête and A.-M. Levelut, *J. Chem. Soc., Chem. Commun.*, 1985, 1794.
5 J. J. Malthête, D. Poupinet, R. Vilanove and J.-M. Lehn, *J. Chem. Soc., Chem. Commun.*, 1989, 1016.
6 C. Mertesdorf and H. Ringsdorf, *Liq. Cryst.*, 1989, **5**, 1757.
7 M. Zhao, W. T. Ford, S. H. J. Idziak, N. C. Maliszewskyj and P. A. Heiney, *Liq. Cryst.*, 1994, **16**, 583 and references cited therein.
8 N. C. Maliszewskyj, P. A. Heiney, J. K. Blasie, J. P. McCauley, Jr. and A. B. Smith, III, *J. Phys. II*, 1992, **2**, 75.
9 K. Kjaer, J. Als-Nielsen, C. A. Helm, P. Tippman-Krayer and H. Möhlwald, *J. Phys. Chem.*, 1989, **93**, 3200.
10 W. R. Salaneck, H. W. Gibson, F. C. Bailey, J. M. Pochan and H. R. Thomas, *J. Polym. Sci., Polym. Lett. Ed.*, 1978, **16**, 447.

Received in Corvallis, OR, USA, 13th January 1998; 8/00388B

Biosynthesis of kelsoene in cultured cells of liverworts *Ptychanthus striatus*

Kensuke Nabeta,[a] Kanae Yamamoto,[a] Makoto Hashimoto,[a] Hiroyuki Koshino,[b] Kenzo Funatsuki[c] and Kenji Katoh[c]

[a] *Department of Bioresource Science, Obihiro University of Agriculture and Veterinary Medicine, Obihiro 080-8555, Japan*
[b] *The Institute of Physical and Chemical Research, Wako, 351-0198 Japan*
[c] *Shionogi Abrahi Laboratory, Kohga-cho, Shiga- ken 520-3423, Japan*

The most uncommon tricyclic sesquiterpenes, kelsoene 1 and prespatane 2, were isolated from cultured cells of liverwort *Ptychanthus striatus*, and the labelling pattern of kelsoene biosynthesized from exogenous [2-^{13}C]-mevalonate suggested that kelsoene is biosynthesized from germacradienyl cation *via* alloaromadendranyl cation.

Sesquiterpenes kelsoene **1** and prespatane **2** were isolated for the first time from the tropical marine sponge *Cymbastella hooperi*.[1] Although the formation of an uncommon tricyclo[5.3.0.0^{2,5}]-decane ring system in kelsoene can be explained by the cyclization between C-1 and C-4 in alloaromadendranyl cation **6** with breaking of the C-4/C-11 bond and elimination of one proton from the *gem*-dimethyl groups, there was no experimental evidence provided regarding the biosynthesis of this compound.[1] Here we described the isolation of kelsoene **1** and prespatane **2** from suspension cultured cells of liverwort *Ptychanthus striatus* (Lejeuneaceae), which seems to have almost no phylogenetic relationship with tropical marine sponge, and the biosynthesis of kelsoene. Intact plants of *P. striatus* produce striatane-type sesquiterpenes[2] striatene, striatol and β-monocyclonerolidol.

A callus was induced from the leafy gametophytes of *P. striatus*, transfered on MSK-4 medium with 4% glucose but without 2,4-dichlorophenoxyacetic acid,[3] successively subcultured every four weeks for more than four years, and then used for suspension culture. The suspension culture was propagated routinely in 100 cm^3 of MSK-4 medium under continuous light of 3000 Lux at 25 °C for more than three years. Cells (1200 g fresh weight) were harvested and extracted with EtOAc (6.23 g). Kelsoene **1** (6.6 mg) and prespatane **2** (2.3 mg were isolated from the extract by a judicious combination of liquid chromatography (silica gel and silica gel–$AgNO_3$). Full assignment of the natural abundance ^{1}H and ^{13}C NMR spectra of (+)-kelsoene {[α]$_D$ +77.1 (lit.,[1] +78.1)} was identified by extensive 1D (^{1}H, ^{13}C and differential NOE) and 2D NMR experiments (PFG-DQF-COSY,[4] PFG-HMQC,[5] PFG-HMBC[6]). Prespetane **2** was identified by comparison of ^{1}H and ^{13}C NMR and mass spectral data with those reported previously.[1]

Table 1 ^{13}C enrichment of kelsoene incorporating [2-^{13}C]-mevalonate[a]

Carbon	δ_C	^{13}C Enrichment[b] (atom% excess)	J_{C-H}/Hz[c]
1	45.7	–	–
2	33.0	3.62	136
3	14.6	–	136
4	47.4	–	144
5	48.1	–	131
6	49.9	–	131
7	36.3	–	–
8	33.2	4.52	131
9	26.0	–	131
10	57.8	–	131
11	145.6	–	–
12	109.8	0.98	156
13	24.2	0.90	127
14	23.5	–	124
15	17.7	–	126
Average		3.34	

[a] All assignments are based on extensive 1D and 2D NMR measurements and previously reported data. [b] ^{13}C Enrichment was calculated on the basis of relative peak intensity of ^{13}C enriched peak to non-labelled carbon in biosynthetically labelled compound. [c] C–H coupling constants were determined by gated ^{1}H decoupling ^{13}C NMR analysis.

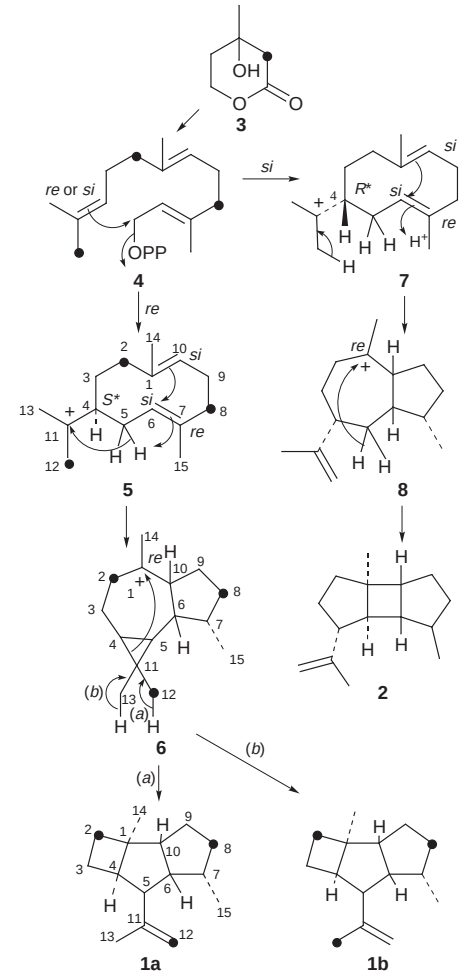

Scheme 1 Biosynthetic pathway to kelsoene **1** from [2-^{13}C]-mevalonate in cultured cells of *P. striatus*

Potassium [2-^{13}C]-mevalonate (MVA, 0.5 mmol) was then fed to the culture (100 cm^3). Cells were harvested after 21 days and extracted with EtOAc. The enriched kelsoene was purified by repeated liquid chromatography as described above.

The ^{13}C{^{1}H} NMR spectrum of kelsoene derived from [2-^{13}C]-mevalonate (average ^{13}C enrichment: 3.34 atom%

excess, Table 1) showed enrichment at the C-2, C-8, C-12 and C-13 positions (4.52, 3.62, 0.98 and 0.90 atom% excess, respectively). Randomization of label between C-12 and C-13 was observed. The level of ^{13}C enrichment in each carbon was determined by comparing the relative intensities of ^{13}C enriched carbons in each carbon with those of the corresponding carbons in the non-labelled compound.

These results may be rationalized by the sequence illustrated in Scheme 1. Cyclization of farnesyl diphosphate **4** to germacradienyl cation **5** *via* the (4*S**)-isopropyl cation would be followed by concomitant intramolecular cyclization between C-6 and C-10 and between C-5 and C-11 of **5** with loss of a proton at C-5 to form a *cis* fused cyclopentane ring and a cyclopropane ring in the resultant alloaromadendranyl cation **6**. Cleavage of the cyclopropane ring and ring closure between C-1 and C-4 with loss of one proton from the *gem*-dimethyl groups generates kelsoene **1**. Observed randomization of label between C-12 and C-13 in kelsoene suggested that the protons of the *gem*-dimethyl groups on the cyclopropane ring in the cation **6** were almost equally eliminated during the conversion of **6** to **1**. Alternatively, the cation at C-11 of **5** might be attacked at both the *re* and *si* faces to form **6a** and **6b**. A proton is then eliminated specifically from a methyl group in either of the two planes of the cyclopropane ring. The co-metabolite, prespatane **2**, might be biosynthesized from a guaianyl cation **8** *via* cation **7** with a (4*R**) isopropyl cation.

Although kelsoene and prospatane were isolated from the marine sponge, they may represent a simple accumulation of constituents from a dietary source such as marine algae, since

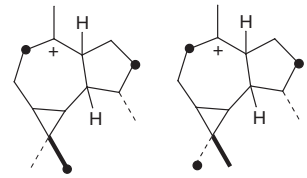

6a **6b**

there is a hypothesis that bryophytes originate in green algae.[7]

Notes and References

† E-mail: knabeta@obihiro.ac.jp

1 G. M. Konig and A. D. Wright, *J. Org. Chem*., 1997, **62**, 3837.
2 R. Takeda, H. Naoki, T. Iwashita, K. Mizukami, Y. Horose, T. Ishida and M. Inoue, *Bull. Chem. Soc. Jpn.*, 1983, **56**, 1125.
3 R. Takeda and K. Katoh, *Planta*, 1981, **151**, 525.
4 R. E. Hurd, *J. Magn. Reson*., 1990, **87**, 422.
5 R. E. Hurd and B. K. John, *J. Magn. Reson.*, 1991, **91**, 648.
6 W. Willker, D. Leibfrinz, R. Kerssebaum and W. Bermel, *Magn. Reson. Chem*., 1993, **31**, 287.
7 Y. Asakawa, in *Progress in the Organic Natural Products*, ed. W. Herz, G. W. Kirby, R. E. Moore, W. Steglich and C. Tamm, Springer-Verlag, vol. 65, pp. 1–618.

Received in Cambridge, UK, 20th April 1998; 8/02908C

Simple azetidine *N*-oxides: synthesis, structure and reactivity

Ian A. O'Neil*† and Andrew J. Potter‡

Robert Robinson Laboratories, Department of Chemistry, University of Liverpool, Crown St, Liverpool, UK L69 7ZD

The preparation of two stable azetidine *N*-oxides is described; one structure was confirmed by X-ray crystallography and the second was found to undergo a quantitative ring expansion to yield a new 6-hydroxy tetrahydro-1,2-oxazine, a potentially useful reagent for further synthetic transformations.

Azetidine *N*-oxides are usually unstable at room temperature, undergoing a [1,2] rearrangement.[1] Only one example of an azetidine *N*-oxide stable at room temperature has been reported.[2] In this case the azetidine ring was fused to a six membered ring. Related compounds include azetidine aminoxyls and nitrones.[3]

Recent work has shown that tertiary amine oxides derived from proline and pipecolic acid derivatives are stabilised by intramolecular hydrogen bonding if a suitable hydrogen bonding donor group is present in the carboxylic acid side chain. The amine oxides are formed as single diastereoisomers where the amine oxide is *syn* to the carboxylic acid side chain (Scheme 1).[4]

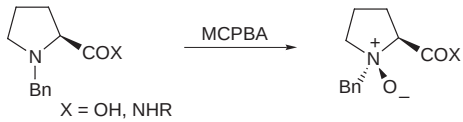

Scheme 1

We were intrigued by the possibility of synthesising the corresponding *N*-benzyl-2-carbonylazetidine *N*-oxides in order to establish if they would be stablised by intramolecular hydrogen bonding. In addition, such compounds should possess novel and useful synthetic potential as a consequence of ring strain.

Racemic ethyl *N*-benzylazetidine-2-carboxylate **1** was prepared according to route of Wasserman.[5] Saponification of the ester with $Ba(OH)_2$ followed by acidification gave the free acid **2**. Oxidation with MCPBA furnished the desired azetidine *N*-oxide **3** in 30% yield as a stable compound (Scheme 2). In contrast, all attempts to form the *N*-oxide of ester **1** led to complex mixtures of products and none of the desired material was ever isolated.

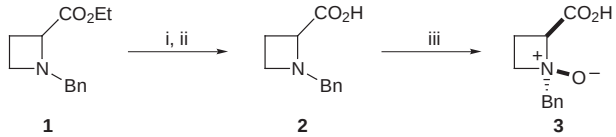

Scheme 2 *Reagents and conditions*: i, $Ba(OH)_2$; ii, H_3O^+; iii, MCPBA, 30% over 3 steps

From spectroscopic data the *N*-oxide **3** had clearly been formed as a single diastereoisomer. Crystals of suitable quality for X-ray analysis were grown and the X-ray structure clearly showed that the amine oxide had been formed *syn* to the carboxylic acid and that there was an intramolecular hydrogen bond between the amine oxide oxygen and the carboxylic acid (Fig. 1). To the best of our knowledge this is the first example of a simple, stable azetidine *N*-oxide characterised by X-ray crystallography.[6]

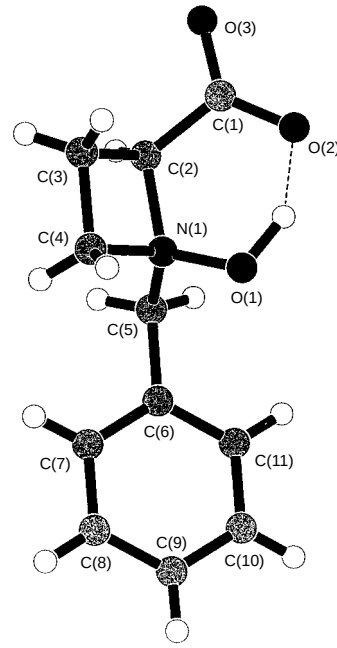

Fig. 1 Crystal structure of **3**

In order to establish if other hydrogen bond donor groups could stabilise azetidine *N*-oxides, the ester **1** was reduced to the primary alcohol **4** with $LiAlH_4$. Oxidation with MCPBA yielded the amine oxide **5** as a single diastereoisomer, in a much higher yield of 63% (Scheme 3). Again this compound was stable at room temperature and full spectroscopic data were obtained.

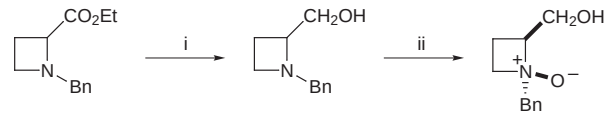

Scheme 3 *Reagents and conditions*: i, $LiAlH_4$, THF, −78 °C to room temp., 90%; ii, MCPBA, 63%

Upon attempted recrystallisation from hot CH_2Cl_2, the amine oxide underwent a quanitative conversion to a new less polar material (Scheme 4).

The presence of a signal at δ 5.2 in the ^{1}H NMR spectrum suggested that oxazine **6** had been formed. We can rationalise this conversion either as a Cope-type elimination followed by tautomerism of the enol to an aldehyde and lactol formation, or as a [1,2] rearrangement. Such rearrangements have precedent,

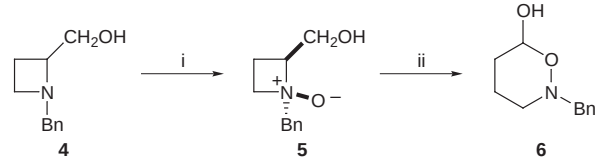

Scheme 4 *Reagents and conditions*: i, MCPBA, 63%; ii, CH_2Cl_2, reflux, quant.

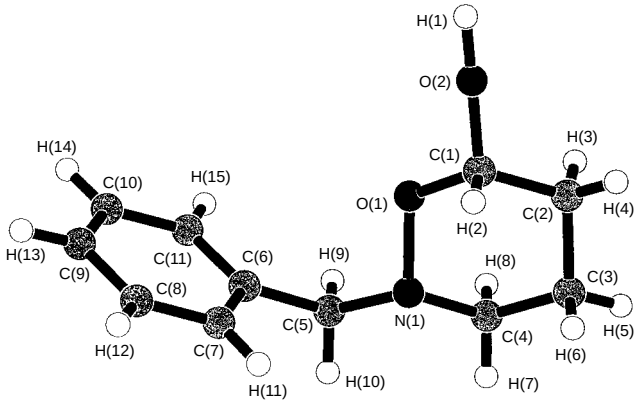

Fig. 2 Crystal structure of **6**

exemplified by the conversion of physostigimine *N*-oxide to geneserine.[7] The structure of tetrahydrooxazine **6** was confirmed by single crystal X-ray analysis of the product (Fig. 2).[6]

This 6-hydroxytetrahydrooxazine in which the nitrogen bears a benzyl group has not been previously prepared. Interestingly, the crystal structure shows that the anomeric hydroxy group is in an equatorial position. We have carried out some preliminary studies on the chemistry of this ring system and have established that it undergoes reactions typical of a lactol. For example, treatment of tetrahydrooxazine **6** with the stabilised ylide shown gave the ester **7** *via* initial alkene formation followed by an intramolecular Michael addition.[8] Conversion of the tetrahydrooxazine **6** to its acetate followed by reaction with allyltrimethylsilane in the presence of BF_3–OEt_2 yielded the allyl adduct **8** (Scheme 5).

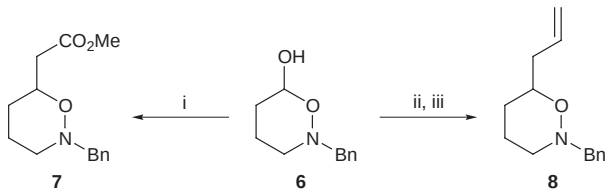

7 **6** **8**

Scheme 5 *Reagents and conditions*: i, Ph_3P = $CHCO_2Me$, THF, 68%; ii, AcCl, NEt_3, CH_2Cl_2; iii, $AllylSiMe_3$, $BF_3{\cdot}OEt_2$, 30% over 2 steps

In summary, we have prepared and characterised the first stable simple azetidine *N*-oxide **3** and shown that it is stabilised by intramolecular hydrogen bonding to the carboxylic acid. The corresponding *N*-benzyl-2-hydroxymethylazetidine *N*-oxide **5** undergoes rearrangement in warm CH_2Cl_2 to give a novel tetrahydrooxazine **6**, which shows coupling reactions typical of a lactol.

We thank the EPSRC for their support of this work (grant GR/K50719). I.A.O.N. thanks the James Black Foundation for their continued financial support and Zeneca for a generous unrestricted research grant.

Notes and References

† E-mail: ion@liv.ac.uk

‡ *Present address*: Ribotargets Ltd, Kett House, 1 Station Road, Cambridge, UK CB1 2JP.

1 R. Yoneda, Y. Sakamoto, Y. Oketo, S. Harusawa and T. Kurihara, *Tetrahedron*, 1996, **52**, 14 563; T. Kurihara, Y. Sakamoto, M. Takai, K. Ohuchi, S. Harusawa and R. Yoneda, *Chem. Pharm. Bull*., 1993, **41**, 1221.

2 T. Kurihara, K. Ohuchi, M. Kawamoto, S. Harusawa and R. Yoneda, *Chem. Lett.*, 1991, 1781.

3 J. C. Espie, R. Ramasseul and A. Rassat, *Tetrahedron Lett.*, 1978, 795; J. B. Aragao and M. H. Loucheux, *Bull. Soc. Chim. Fr*., 1971, 4387; A. D. de Wit, M. L. M. Pennings, W. P. Trompenaars, D. N. Reinhoudt, S. Harkema and O. Nevestveit, *J. Chem. Soc., Chem. Commun.*, 1979, 993.

4 I. A. O'Neil, N. D. Miller, J. Peake, J. V. Barkley, C. M. R. Low and S. B. Kalindjian, *Synlett*., 1993, 515; I. A. O'Neil, N. D. Miller, J. V. Barkley, C. M. R. Low and S. B. Kalindjian, *Synlett*, 1995, 617; I. A. O'Neil, N. D. Miller, J. V. Barkley, C. M. R. Low and S. B. Kalindjian, *Synlett*, 1995, 619; I. A. O'Neil, C. D. Turner and S. B. Kalindjian, *Synlett*, 1997, 777; I. A. O'Neil and A. J. Potter, *Tetrahedron Lett.*, 1997, **38**, 5731.

5 H. H. Wasserman, B. H. Lipshutz, A. W. Tremper and J. S. Wu, *J. Org. Chem.*, 1981, **46**, 2991.

6 *Crystal data* for **3** (from CH_2Cl_2): $C_{11}H_{13}NO_3$, M = 207.23, orthorhombic, space group *Pbca*, Z = 8, a = 10.998(3), b = 16.750(4), c = 10.837 Å, U = 1996.3(10) Å^3, D_c = 1.379 g cm^{-3}; T = 153 K; max 2θ = 49.9°, graphite-monochromated Mo-Kα radiation (λ = 0.71069Å), 2020 reflections were measured; of these, 1277 with $F > 0.30\sigma(F)$ were used in the refinement; R = 0.077, R_w = 0.081, residual electron density 0.44/−0.48 e Å^{-3}. For **6** (from CH_2Cl_2): $C_{11}H_{15}NO_2$, M = 193.24, monoclinic, space group $P2_1/c$ (no 14), Z = 4, a = 9.036(6), b = 13.551(6), c = 8.478(4) Å, β = 99.70(4), U = 1023.4(9) Å^3, D_c = 1.254 g cm^{-3}; T = 153 K; max 2θ = 50.0°, graphite-monochromated Mo-Kα radiation (λ = 0.71069Å), 2008 reflections were measured; of these, 1877 were unique with 1325 $F > 1.00\sigma(F)$ used in the refinement; R = 0.052, R_w = 0.040, residual electron density 0.81/−0.96 e Å^{-3}. CCDC 182/893.

7 S. Takano and K. Ogasawara, *Alkaloids of the Calabar Bean*, in *The Alkaloids, Chemistry and Pharmacology*, Academic Press, San Diego, 1989, vol. 36, pp. 225–251; C. Hootelé, *Tetrahedron Lett*., 1969, 2713.

8 B. Maurer, A. Grieder and W. Thommen, *Helv. Chim. Acta*., 1979, **62**, 44.

Received in Cambridge, UK, 2nd April 1998; 8/02503G

Inhomogeneity in the interaction between methanol molecules and Brønsted acid sites of H-ZSM-5 directly detected by 2D CPMAS ^{13}C NMR spectroscopy

Kei Inumaru,*†‡ Ni Jin, Sayaka Uchida and Makoto Misono

Department of Applied Chemistry, Graduate School of Engineering, The University of Tokyo, 7-3-1, Hongo, Bunkyo-Ku, Tokyo 113-8656, Japan

1D and 2D exchange ^{13}C NMR investigation of the states of methanol adsorbed on H-ZSM-5 at ambient temperature demonstrates the coexistence of methanol strongly interacting with Brønsted acid sites and methanol physisorbed or hydrogen-bonded, and provides the first spectroscopic evidence of a wide distribution in the strength of its interaction with Brønsted acid sites.

In the micropores of zeolites, the electric field induced by the pore walls has often been assumed to assist the activation of molecules, although no direct evidence has been provided. A recent theoretical calculation[1] predicted that the ionic effect of the zeolite framework alters the state of MeOH adsorbed at a Brønsted acid site: a methoxonium ion is preferred in the narrow channel of chabazite, while a hydrogen-bonded neutral complex is stable in the larger cage of sodalite. H-ZSM-5, an important catalyst for chemical processes such as the MTG (methanol to gasoline) reaction,[2] would exhibit interesting characterisitics with respect to the ionic effect on the acid sites because its pore size is intermediate.[1] There are sites in the two kinds of channel and at their intersections in H-ZSM-5, and the local electric field must be reflected in the states of the molecules adsorbed.[3] There have been extensive experimental studies on the state of MeOH using *in situ* IR analysis,[4–7] temperature programmed desorption,[8,9] and solid-state NMR analysis,[5,10–15] as well as theoretical calculations.[1,16–18] High-resolution solid-state ^{1}H NMR spectroscopy has recently shown that MeOH molecules form 'clusters' on the Brønsted acid sites of H-ZSM-5 at high coverages at ambient temperature.[5,12–14] The hydroxy protons of MeOH and the acidic protons rapidly exchanged in these clusters. IR investigations indicated the formation of hydrogen-bonded species on the acid sites.[6,7] Two research groups recently reached different conclusions based on careful NMR studies of the state of adsorbed MeOH, favouring either a resonant structure including adsorbed methoxonium ion[13] or a hydrogen-bonded neutral complex.[14] One of the major differences between the two studies appears in the observed ^{13}C NMR spectra, with peaks of 53.6 *vs.* 50.5 ppm reported. So, the state of MeOH stoichiometrically adsorbed on the acid sites is still controversial. To the best of our knowledge, all NMR studies on this subject were carried out with MeOH/acidic sites ≥ 1.

In this study, by focusing on low coverages of MeOH, we provide spectroscopic (2D exchange ^{13}C NMR) evidence for the co-existence of the two different species and a wide distribution in strength of interaction between the MeOH molecules and the acid sites. These species adsorbed so firmly that they did not exchange their positions at 298 K even on an NMR timescale of 0.5 s. The present results explain the previous results, which are apparently contradictory.

H-ZSM-5 was prepared from Na-ZSM-5 (Si/Al = 11.9, 7.4 Al atoms per unit cell) which was kindly supplied by Toso Co. Ltd. After ion exchange with ammonium nitrate, the zeolite was heated in a dry He stream at a rate of 0.3 K min^{-1} and was finally calcined at 673 K for 10 h. In the ^{27}Al NMR spectrum of the fully hydrated H-ZSM-5, the intensity of the octahedral Al (extraframework Al) resonance at around 0 ppm was less than one twelfth of that of tetrahedral Al in the framework (*ca.* 50 ppm). The samples for ^{13}C NMR analysis were prepared using a glass high vacuum system (*ca.* 100 cm^3). After H-ZSM-5 had been dehydrated at 673 K (heating rate: usually 1 K min^{-1}, *in vacuo*), a calculated amount of $^{13}CH_3OH$ (99 atom% ^{13}C) was introduced at 298 K. The amount of MeOH was varied from 0.5 to 12 molecules per unit cell (MeOH/Al = 0.07–1.6). Then the zeolite was transferred into a small glass cell (*ca.* 0.1 cm^3) and the cell was sealed while the sample was cooled with liquid N_2. The cell was set in a zirconia rotor, and 1D ^{13}C and ^{27}Al NMR spectra were recorded using a JNM-EX270 spectrometer with a cross-polarisation magic angle spinning (CPMAS) probe. 2D ^{13}C NMR exchange experiments (CP excitation)[19] were carried out with a Chemagnetics CMX-300 Infinity spectrometer. 48 1D spectra with 840 scans for each were recorded. All NMR spectra were recorded at 298 K.

Fig. 1 shows the CPMAS ^{13}C NMR spectra for samples having 0.5–12 molecules per unit cell (molecule uc^{-1}) of MeOH adsorbed on H-ZSM-5. The spectra in Fig. 1(*a*) were recorded by single pulse excitation with proton decoupling and the ordinate for each spectrum was normalized by the sample weight. Therefore, the peak intensities are proportional to the number of nuclear spins. The spectra in Fig. 1(*b*) were recorded by CP to improve the signal-to-noise ratio. Similar spectra were obtained using the two methods. This indicates that the CP efficiencies for the signals were similar in these measurements and the relative intensities in each spectrum in Fig. 1(*b*) can be regarded as nearly quantitative. In the case of 12 molecule uc^{-1} (MeOH/Al = 1.6), a broad peak was observed at 51.5 ppm. When the amount of MeOH was decreased to 8 molecule uc^{-1} (MeOH/Al = 1.1), the peak shifted downfield to 52.7 ppm, suggesting an increased interaction of MeOH with the acid sites. A further decrease in the amount of MeOH to 4 molecule uc^{-1} (MeOH/Al = 0.54) caused a splitting of the signal into a narrow peak at 51.5 ppm and a broad shoulder at *ca.* 54 ppm. These two signals were observed more clearly at 2 molecule uc^{-1}. As the

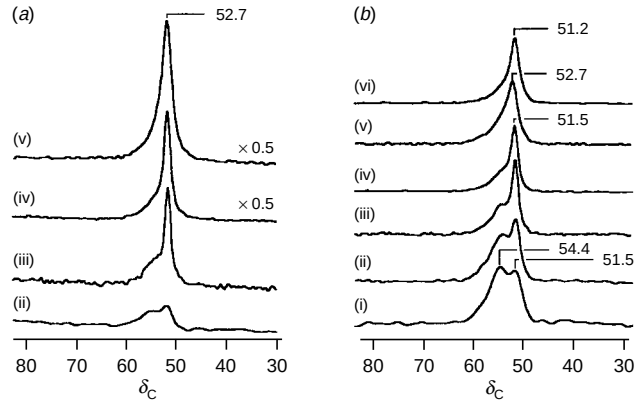

Fig. 1 CPMAS ^{13}C NMR spectra of $^{13}CH_3OH$ adsorbed on H-ZSM-5 at various coverages of MeOH at 298 K; (*a*) single pulse excitation with proton decoupling and (*b*) cross polarization. (i) 0.5 (0.07), (ii) 1 (0.13), (iii) 2 (0.27), (iv) 4 (0.54), (v) 8 (1.1) and (vi) 12 molecule uc^{-1} (MeOH/Al = 1.6). MAS rate = 6 kHz.

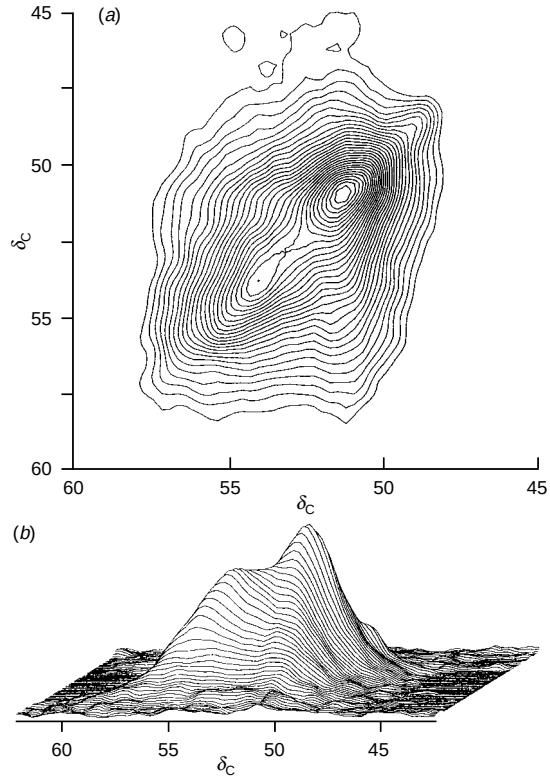

Fig. 2 2D exchange ^{13}C NMR spectrum of $^{13}CH_3OH$ adsorbed on H-ZSM-5 at 298 K; (*a*) contour plot and (*b*) stack plot. Adsorption = 1 molecule uc^{-1}. Mixing time = 0.5 s. MAS rate = 3.5 kHz.

amount of MeOH decreased to 1 molecule uc^{-1} (MeOH/Al = 0.13) and 0.5 molecule uc^{-1} (MeOH/Al = 0.07), the peak at 51.5 ppm decreased and the broad signal at *ca.* 54 ppm became dominant.

The origins of these signals were investigated by the following experiments. First, the ^{13}C NMR spectrum of adsorbed MeOH was measured for H-ZSM-5 with a higher Si/Al ratio (26) at 1 molecule uc^{-1}. The intensity of the broad peak at 54 ppm decreased as compared with H-ZSM-5 with Si/Al = 11.9, while its linewidth was almost unchanged. Next, the degree of dealumination of H-ZSM-5 was increased by accelerating the rate of temperature rise in the pretreatment *in vacuo* from 1 to 3, and then to 10 K min^{-1}. Accordingly, the peak intensity at *ca.* 0 ppm (extraframework Al) relative to that at *ca.* 50 ppm (Al in framework) in the ^{27}Al NMR spectrum (measured after full rehydration) increased from 0.13 to 0.15, and then to 0.17. ^{13}C NMR measurements for these zeolite samples at 1 MeOH molecule uc^{-1} showed that the broad signal at 54 ppm decreased with an increase in the dealumination. On the basis of these two experiments, it may be concluded that the broad signal is not connected with extraframework aluminium sites, but it corresponds to a species strongly interacting with the Brønsted acid sites. In the case of silicalite, the ^{13}C NMR spectrum at 1 MeOH molecule uc^{-1} gave a single sharp peak at 51.0 ppm. This shows that the narrow peak at *ca.* 51 ppm is due to MeOH weakly interacting with the zeolite.

Two research groups recently performed careful studies using temperature-variable ^{1}H, ^{13}C and ^{2}D NMR spectroscopy, and reached different conclusions. Thursfield and Anderson observed a signal at 53.6 ppm and proposed a resonance structure between an adsorbed methoxonium ion and a hydrogen-bonded MeOH molecule.[13] On the other hand, Hunger and Horvath found a peak at 50.5 ppm and assigned it to a hydrogen-bonded neutral complex in which the hydroxy proton of MeOH and the acidic proton of H-ZSM-5 rapidly exchange their positions.[14] These two different results become consistent if the variation of the major species with coverage shown in Fig. 1 is taken into account: the major species at MeOH/Al = 1 gives a peak at 51 ppm, while at low coverage the species strongly interacting with the Brønsted acid sites and hydrogen-bonded MeOH coexist. The two species do not exchange with each other on the NMR timescale.

The broadness of the ^{13}C NMR peak of the strongly bonded species (54 ppm) is notable. In order to elucidate the mechanism of broadening and the exchangeability of the species, a 2D exchange ^{13}C NMR spectrum was measured at 1 molecule uc^{-1} with a mixing time of 0.5 s. As shown in Fig. 2, no cross-peak was observed, so the species observed do not exchange at 298 K at low coverage even on the long timescale of 0.5 s. Fig. 2 provides additional important information. The broad peak for the strongly adsorbed species appears as a long narrow ridge along the diagonal, demonstrating the presence of inhomogeneous broadening. That is, the width of the peak is not due to a short T_2 induced, for example, by strong dipole interactions with other nuclei such as ^{27}Al and neighbouring ^{13}C. The linewidth, which is insensitive to change in the MAS rate, shows that it is not due to residual anisotropy of the chemical shifts or a misadjusted magic angle. Therefore, it was concluded that the broad peak came from several species which have different chemical shifts, reflecting the different strengths of interaction between MeOH and the Brønsted acid sites. This is the first NMR detection of inhomogeneous adsorption states presumably due to the different environments of adsorption in the zeolites. Since the linewidth of the peak is almost unchanged when the Si/Al ratio is varied, this inhomogeneity of adsorbed MeOH is thought to be intrinsic to the H-ZSM-5 structure.

Some of the experimental results in this communication were presented at the Spring Meeting of the Chemical Society of Japan, 1996 (No. 3D538).

Notes and References

† E-mail: inumaru@ipc.hiroshima-u.ac.jp
‡ Present Address: Department of Applied Chemistry, Faculty of Engineering, Hiroshima University, 1-4-1 Kagamiyama, Higashi-Hiroshima 739-8527, Japan.

1 R. Shah, M. C. Payne and M.-H. Lee, J. D. Gale, *Science*, 1996, **271**, 1395.
2 S. L. Meisel, J. P. McCullough, C. H. Lechthaler and P. B. Weisz, *CHEMTECH*, 1976, **6**, 86.
3 J. S. Haw, T. Xu, J. B. Nicholas and P. W. Goguen, *Nature*, 1997, **389**, 832.
4 T. R. Forester and R. F. Howe, *J. Am. Chem. Soc.*, 1987, **109**, 5076.
5 G. Mirth, J. A. Lercher, M. W. Anderson and J. Klinowski, *J. Chem. Soc., Faraday Trans.*, 1990, **86**, 3039.
6 A. Kogelbauer, C. Gründling and J. A. Lercher, *J. Phys. Chem.*, 1996, **100**, 1852.
7 F. Wakabayashi, M. Kashitani, T. Fujino, J. N. Kondo, K. Domen and C. Hirose, *Stud. Surf. Sci. Catal.*, 1996, **105**, 1739.
8 M. Jayamurthy and S. Vasudevan, *Ber. Bunsenges. Phys. Chem.*, 1995, **99**, 1521.
9 B. Hunger, S. Matysik, M. Heuchel and W.-D. Einicke, *Langmuir*, 1997, **13**, 6249.
10 E. J. Munson, A. A. Kheir, N. D. Lazo and J. F. Haw, *J. Phys. Chem.*, 1992, **96**, 7740.
11 C. Tsiao, D. R. Corbin and C. Dybowski, *J. Am. Chem. Soc.*, 1990, **112**, 7140.
12 M. W. Anderson, P. J. Barrie and J. Klinowski, *J. Phys. Chem.*, 1991, **95**, 235.
13 A. Thursfield and M. W. Anderson, *J. Phys. Chem.*, 1996, **100**, 6698.
14 M. Hunger and T. Horvath, *J. Am. Chem. Soc.*, 1996, **118**, 12302.
15 L. Heeribout, C. Dorémie-Morin, L. Kubelkova, R. Vincent and J. Fraissard, *Catal. Lett.*, 1997, **43**, 143.
16 F. Haase and J. Sauer, *J. Am. Chem. Soc.*, 1995, **117**, 3780.
17 P. E. Sinclair and C. R. A. Catlow, *J. Chem. Soc., Faraday Trans.*, 1997, **93**, 333.
18 E. Nusterer, P. E. Blöchl and K. Schwarz, *Angew. Chem., Int. Ed. Engl.*, 1996, **35**, 175.
19 N. M. Szeverenyi, M. J. Sullivan and G. E. Maciel, *J. Magn. Reson.*, 1982, **47**, 462.

Received in Cambridge, UK, 23rd March 1998; 8/02268B

Synthesis and characterization of $[NBu_4]_4[Ag_2\{Mo_5O_{13}(OMe)_4(NO)\}_2]$, a novel polyoxomolybdate complex with a short $Ag^I\cdots Ag^I$ distance

Richard Villanneau, Anna Proust, Francis Robert‡ and Pierre Gouzerh*†

Laboratoire de Chimie des Métaux de Transition, U.R.A. C.N.R.S. No 419, Université Pierre et Marie Curie, 4 Place Jussieu, 75252 Paris Cedex 05, France

In methanol, the defect nitrosylpolyoxomolybdate $[Mo_5O_{13}(OMe)_4(NO)]^{3-}$ reacts with Ag^+ to give the complex $[Ag_2\{Mo_5O_{13}(OMe)_4(NO)\}_2]^{4-}$ which displays attractive interactions between the two square-planar closed-shell Ag^I cations.

The molecular building block approach, *i.e.* the linking of preorganized units, has proved efficient in the synthesis of polyoxometalates with increasing complexity.[1–6] Whereas the structures of large polyoxomolybdates are mainly based on $\{Mo_7\}$, $\{Mo_8\}$ and $\{Mo_{17}\}$ units, those of polyoxotungstates are mainly based on defect $\{XW_{11}\}$ and $\{XW_9\}$ Keggin subunits but also may include defect $\{W_5\}$ Lindqvist subunits.[1] While the defect anion $\{W_5O_{18}\}^{6-}$ has been characterized in lanthanide[7,8] and actinide[9] complexes and in a palladium complex,[10] complexes of the related $\{Mo_5O_{18}\}^{6-}$ have not yet been reported. However, a derivatized Lindqvist-type $\{Mo_5\}$ unit, $[Mo_5O_{13}(OMe)_4(NO)]^{3-}$, has been characterized,[11] and its coordination chemistry has been investigated. We report herein the synthesis and characterization of $[NBu_4]_4[Ag_2\{Mo_5O_{13}(OMe)_4(NO)\}_2]$, the anion of which displays several unusual features.

To the best of our knowledge, silver complexes of polyoxometalates have not been previously reported, with the exception of the cyclic $[As_4W_{40}O_{140}]^{28-}$ anion where each of the four lacunary sites S_2 may be occupied by Ag^I.[12] The compound $[NBu_4]_4[Ag_2\{Mo_5O_{13}(OMe)_4(NO)\}_2]$ **2** was obtained by reacting $[NBu_4]_2[Mo_5O_{13}(OMe)_4(NO)\{Na(MeOH)\}]\cdot 3MeOH$ **1**[11] with $AgNO_3$ in methanol.§ Compound **2** was characterized by elemental analysis, spectroscopic methods (IR and UV–VIS)¶ and single-crystal X-ray structure analysis.‖ The structure of **2** consists of discrete centrosymmetrical $[Ag_2\{Mo_5O_{13}(OMe)_4(NO)\}_2]^{4-}$ anions (Fig. 1) and of tetrabutylammonium cations. The silver complex $[Ag_2\{Mo_5O_{13}(OMe)_4(NO)\}_2]^{4-}$ appears to be roughly similar to the palladium complex $[Pd_2\{W_5O_{18}\}_2]^{8-}$.[10] In both cases, each defect polyoxoanion bridges between two cations in slightly distorted square-planar environments. The Ag–O distances range from 2.342 to 2.477 Å (av. 2.381 Å) and the O–Ag–O angles range from 76.1(2) to 102.0(2)°, the larger angles occurring between two oxygen atoms of the same Mo_5 unit. The silver atom is displaced inside by 0.23 Å from the mean plane of its surrounding oxygen atoms. Square-planar coordination is precedented for Ag^I cations, *e.g.* in $[\{(NH_3)_4Pt_2(C_5H_5N_2O_2)_2\}_2Ag]^{5+}$ where Ag^+ is coordinated to four oxygen atoms of 1-methyluracil ligands.[13] The average Ag–O distance of 2.381 Å in $[Ag_2\{Mo_5O_{13}(OMe)_4(NO)\}_2]^{4-}$ is close to the average Ag–O distance of 2.39 Å in the Pt_4Ag complex. In contrast to $[Pd_2\{W_5O_{18}\}_2]^{8-}$ in which the symmetry of the overall anion approaches D_{2h},[10] the Ag···Ag vector deviates by 40.5° from the normal to the mean coordination planes of the silver cations. Another unexpected feature of the molecular structure of $[Ag_2\{Mo_5O_{13}(OMe)_4(NO)\}_2]^{4-}$ is the short distance between the two Ag^I cations. Indeed the Ag···Ag distance of 2.873(2) Å in $[Ag\{Mo_5O_{13}(OMe)_4(NO)\}_2]^{4-}$ is less than the Ag···Ag distance in the metal, which suggests significant Ag···Ag bonding interaction. Closed-shell interactions in inorganic chemistry are well documented, especially for Au^I which has a strong tendency for metallophilic attraction.[14,15] Although the shortest $Ag^I\cdots Ag^I$ contacts have been observed for ligand-supported metal pairs, *e.g.* in $[Ag_2(PhNNNPh)_2]$,[16a] $[Ag_2(ArNCHNAr)_2]$ (Ar = *p*-tolyl,[16b] *o*-methoxyphenyl[16c]), $[Ag_2(1,8\text{-naphthyridine})_2][ClO_4]_2$,[16d] and in $[Ag_3(1,8\text{-diisocyano-}p\text{-menthane})_2I_3]$,[16e] attractive Ag···Ag interactions do exist in the absence of any bridging ligand.[17] The bridging polyoxoanions most probably play a role in the Ag···Ag separation; however, it is noteworthy that the Ag···Ag distance is significantly shorter than the ligand bite distance of *ca.* 3.15 Å. In contrast, the $Pd^{II}\cdots Pd^{I}$ distance in $[Pd_2\{W_5O_{18}\}_2]^{8-}$ is longer (3.034 Å)[10] than it would be expected in case of a significant direct interaction.[18] Altogether, these features support the view that attractive $Ag^I\cdots Ag^I$ interactions exist in $[Ag_2\{Mo_5O_{13}(OMe)_4(NO)\}_2]^{4-}$.

The reason for the difference between $[Ag_2\{Mo_5O_{13}(OMe)_4(NO)\}_2]^{4-}$ and $[Pd_2\{W_5O_{18}\}_2]^{8-}$ with respect to metal–metal interaction is not straightforward. It should be pointed out that there are some systematic differences between $[Mo_5O_{13}(OMe)_4(NO)]^{3-}$ and $[W_5O_{18}]^{6-}$, according to the molecular structures of their respective complexes.[7b,8,10,11,19] In particular, the Mo–O distances involving the coordinated axial oxygen atoms (O_a, av. 1.717 Å in **2**) are comparable with those to equatorial oxygen atoms [O_e, av. 1.698(7) Å in **2**), while the W–O_a distances {av. 1.805(5) Å in $[Pd_2\{W_5O_{18}\}_2]^{8-}$}[10] are significantly lengthened by comparison with W–O_e {av. 1.718(6) Å in $[Pd_2\{W_5O_{18}\}_2]^{3-}$}.[10] In addition, the central oxygen atom is much more displaced from the plane of the four basal M atoms toward the apical M atom in the complexes of $[Mo_5O_{13}(OMe)_4(NO)]^{3-}$ (*e.g.* 0.41 Å in **2**) than in those of $[W_5O_{18}]^{6-}$ {*e.g.* 0.14 Å in $[Pd_2\{W_5O_{18}\}_2]^{8-}$}. Therefore the

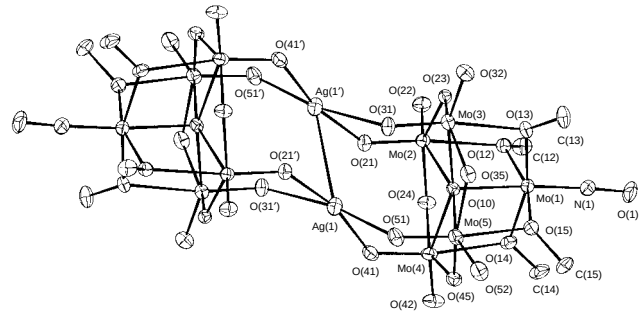

Fig. 1 Molecular drawing of $[Ag_2\{Mo_5O_{13}(OMe)_4(NO)\}_2]^{4-}$ in **2**.[21] Selected bond lengths (Å) and angles (°): Mo(1)–N(1) 1.746(9), N(1)–O(1) 1.22(1), Mo(2)–O(21) 1.720(7), Mo(2)–O(22) 1.698(6), Mo(3)–O(31) 1.716(6), Mo(3)–O(32) 1.704(7), Mo(4)–O(41) 1.717(7), Mo(4)–O(42) 1.700(7), Mo(5)–O(51) 1.717(7), Mo(5)–O(52) 1.692(7), Ag(1)–O(41) 2.342(8), Ag(1)–O(51) 2.346(7), Ag(1′)–O(21) 2.361(7), Ag(1′)–O(31) 2.477(7), Ag(1)–Ag(1′) 2.873(2); O(41)–Ag(1)–O(51) 82.3(3), O(41)–Ag(1)–O(21′) 167.4(2), O(51)–Ag(1)–O(31′) 169.1(2), O(21)–Ag(1′)–O(31) 76.1(2), O(41)–Ag(1)–Ag(1′) 121.4(2), O(51)–Ag(1)–Ag(1′) 126.5(2), O(21′)–Ag(1)–Ag(1′) 65.6(2), O(31′)–Ag(1)–Ag(1′) 62.8(2). The coordinates of the halves of the anion are related *via* the transformation $[x', y', z'] = [-x, -y, -z]$.

comparison of $[Ag_2\{Mo_5O_{13}(OMe)_4(NO)\}_2]^{4-}$ with $[Pd_2\{Mo_5O_{13}(OMe)_4(NO)\}_2]^{2-}$ should have been more appropriate. Unfortunately, our efforts to obtain the palladium analogue of **2**, *i.e.* $[NBu_4]_2[Pd_2\{Mo_5O_{13}(OMe)_4(NO)\}_2]$ by reaction of **1** with either $PdCl_2$ or $Na_2[PdCl_4]$ have failed up to now. Only nitrosyl reduced decamolybdates[20] were obtained in these reactions. The behaviour of $[Mo_5O_{13}(OMe)_4(NO)]^{3-}$ towards other main-group cations has been investigated. Both Ba^{2+} and Bi^{3+} form eight-coordinate complexes of the type $[M\{Mo_5O_{13}(OMe)_4(NO)\}_2]^{n-}$ (M = Ba, n = 4; M = Bi, n = 3). However, these complexes differ in the geometry of the coordination polyhedron which is best described as an elongated cube for Ba and a tetragonal antiprism for Bi.[19]

Notes and References

† E-mail: pg@ccr.jussieu.fr
‡ Deceased, February 5, 1998.

§ An equimolar mixture of $[NBu_4]_2[Mo_5O_{13}(OMe)_4(NO)\{Na(MeOH)\}]\cdot 3MeOH$ **1** (0.34 g, 0.25 mmol) and $AgNO_3$ (0.042 g, 0.25 mmol) in MeOH (10 ml) was stirred for 4 h at room temperature. After separation of the yellow precipitate of $[NBu_4]_2[Mo_6O_{19}]$, purple crystals of $[NBu_4]_4[Ag_2\{Mo_5O_{13}(OMe)_4(NO)\}_2]$ **2** were obtained in 56% yield by keeping the filtrate overnight at −30 °C.

¶ IR (KBr pellet, ν/cm^{-1}): 1605 (NO), 924, 906, 885, 865, 698. UV–VIS [MeOH, λ/nm (ε/dm^3 mol^{-1} cm^{-1})]: 540 (148) {Mo^{IV}(NO)}.

‖ *Crystal data*: **2**: orthorhombic, space group *Pbca*, a = 18.439(2), b = 24.354(3), c = 24.739(3) Å, U = 11 109(3) Å^3, Z = 4, D_c = 1.715 g cm^{-3}; structure solution and refinement based on 5522 reflections with $I > 3\sigma(I)$ [λ(Mo-Kα) = 0.710 69 Å] converged at R = 0.043 and R_w = 0.047 (w = 1.0). CCDC 182/898.

1 A. Müller, F. Peters, M. T. Pope and D. Gatteschi, *Chem. Rev.*, 1988, **98**, 239.
2 *From Simplicity to Complexity in Chemistry—and Beyond*, Part I, ed. A. Müller, A. Dress and F. Vögtle, Vieweg, 1996: A. Müller and K. Mainzer, p. 1; M. T. Pope, p. 137.
3 A. Müller, *J. Mol. Struct.*, 1994, **325**, 13; A. Müller, H. Reuter and S. Dillinger, *Angew. Chem., Int. Ed. Engl.*, 1995, **34**, 2328.
4 A. Müller, E. Krickemeyer, S. Dillinger, J. Meyer, H. Bögge and A. Stammler, *Angew. Chem., Int. Ed. Engl.*, 1996, **35**, 171; A. Müller, E. Krickemeyer, H. Bögge, M. Schmidtmann, F. Peters, C. Menke and J. Meyer, *Angew. Chem., Int. Ed. Engl.*, 1997, **36**, 484.
5 M. Bösing, I. Loose, H. Pohlmann and B. Krebs, *Chem. Eur. J.*, 1997, **3**, 1232.
6 K. Wassermann, M. H. Dickman and M. T. Pope, *Angew. Chem., Int. Ed. Engl.*, 1997, **36**, 1445.
7 (*a*) R. D. Peacock and T. J. R. Weakley, *J. Chem. Soc. A*, 1971, 1836; (*b*) J. Iball, J. N. Low and T. J. R. Weakley, *J. Chem. Soc., Dalton Trans.*, 1974, 2021.
8 T. Yamase, H. Naruke and Y. J. Sasaki, *J. Chem. Soc., Dalton Trans.*, 1990, 1687; M. Sugeta and T. Yamase, *Bull. Chem. Soc. Jpn.*, 1993, **66**, 444; T. Yamase, T. Ozeki and M. Tosaka, *Acta Crystallogr., Sect. C*, 1994, **50**, 1849 and references therein.
9 A. M. Goulbev, L. P. Kazanskii, E. A. Torchenkova, V. I. Simonov and V. I. Spitzyn, *Dokl. Chem.*, Proceedings of the Academy of Sciences of the USSR (English translation), 1975, **221**, 198.
10 S. J. Angus-Dunne, R. C. Burns, D. C. Craig and G. A. Lawrence, *J. Chem. Soc., Chem. Commun.*, 1994, 523.
11 P. Gouzerh, Y. Jeannin, A. Proust and F. Robert, *Angew. Chem., Int. Ed. Engl.*, 1989, **28**, 1363; A. Proust, P. Gouzerh and F. Robert, *Inorg. Chem.*, 1993, **32**, 5291.
12 M. Leyrie and G. Hervé, *Nouv. J. Chim.*, 1978, **2**, 233.
13 B. Lippert and D. Neugebauer, *Inorg. Chem.*, 1982, **21**, 451.
14 P. Pyykkö, *Chem. Rev.*, 1988, **88**, 563, 1977, **97**, 597.
15 M. Jansen, *Angew. Chem., Int. Ed. Engl.*, 1987, **26**, 1098.
16 (*a*) J. Beck and J. Strahle, *Z. Naturforsch., Teil B*, 1986, **41**, 4; (*b*) F. A. Cotton, X. Feng, M. Matusz and R. Poli, *J. Am. Chem. Soc.*, 1988, **110**, 7077; (*c*) T. Ren, C. Lin, P. Amalberti, D. Macikenas, J. D. Protasiewicz, J. C. Baum, T. L. Gibson, *Inorg. Chem. Commun.*, 1998, **1**, 23; (*d*) T. Tsuda, S. Ohba, M. Takahashi and M. Ito, *Acta Crystallogr., Sect. C*, 1989, **45**, 887; (*e*) P. D. Harvey, M. Drouin, A. Michel and D. Perreault, *J. Chem. Soc., Dalton Trans.*, 1993, 1365.
17 K. Singh, J. R. Long and P. Stavropoulos, *J. Am. Chem. Soc.*, 1997, **119**, 2942; M. A. Omary, T. R. Webb, Z. Assefa, G. E. Shankle and H. H. Patterson, *Inorg. Chem.*, 1998, **37**, 1380.
18 H. Engelking, S. Karentzopoulos, G. Reusmann and B. Krebs, *Chem. Ber.*, 1994, **127**, 2355.
19 R. Villanneau, A. Proust, F. Robert and P. Gouzerh, manuscript in preparation.
20 A. Proust, F. Robert, P. Gouzerh, Q. Chen and J. Zubieta, *J. Am. Chem. Soc.*, 1997, **119**, 3523.
21 J. J. Pearce and D. J. Watkin, CAMERON, Chemical Crystallography Laboratory, University of Oxford.

Received in Basel, Switzerland, 3rd April 1998; 8/02548G

Efficient photo-assisted Fenton catalysis mediated by Fe ions on Nafion membranes active in the abatement of non-biodegradable azo-dye

Javier Fernandez,[a] Jayasundera Bandara,[a] Antonio Lopez,[b] Peter Albers[c] and John Kiwi*[a]†

[a] *Institute of Physical Chemistry II, Swiss Federal Institute of Technology, 1015, Lausanne, Switzerland*
[b] *IRSA, Water Research Institute, Department of Chemistry and Technology, Via de Blasio 5, 70123 Bari, Italy*
[c] *Degussa AG, Postfach 1345, ZFE-OT, Wolfgang, 63457 Hanau, Germany*

Highly dispersed Fe ions on Nafion membranes are shown to decompose H_2O_2 with similar kinetics as found for homogeneous solutions containing Fe^{3+} ions during the photo-assisted Fenton degradation of Orange II, avoiding the drawbacks of the homogeneous treatment.

Membrane related research has attracted much attention in recent years as a structured medium for a variety of chemical reactions. Nafion perfluorinated membranes have been used during the last decade in a variety of catalytic/electrocatalytical integrated chemical reactions.[1] Polymer membranes have also been used for charge transfer in inorganic and biological systems.[2] Few studies of chemical transformations with CdS or TiO_2 loaded membranes using photochemical activation have been reported until now.[3–6] This study is concerned with the degradation of non-biodegradable azo-dye Orange II by Fenton photo-assisted reactions in Fe-free solutions. This dye does not undergo bacterial degradation in a waste-water treatment plant due to the aromatic and sulfo-aromatic group found the ring structure. Azo dyes, which account for more than 22% of industrial dye production, are commonly found in effluents of the textile industry.[7]

Experiments were conducted with Nafion perfluorinated cation transfer membrane (Dupont 117, 0.007 in, Aldrich #7.467-4) containing hydrophilic sulfonate groups immobilized on the fluorocarbon matrix. Exchange with $FeCl_3 \cdot 6H_2O$ (Fluka) at room temperature was carried out for a few minutes after the Nafion was immersed in HCl. After the ion exchange, the membrane was washed with water followed by immersion in 1 M NaOH to convert Fe^{3+} to its hydrated form. The Fe-ion content of the Nafion was found to be 1.78 mass% after digestion in concentrated HNO_3 (Teflon coated autoclave) under high pressure and temperature. The solution obtained in this way was subsequently diluted and the Fe content measured by AAS (flame detector, Philips 20 M). Photolysis experiments were carried out by means of a Hanau Suntest Lamp with tunable light intensity equipped with an IR filter to remove IR radiation. The short UV radiation ($\lambda \leqslant 305$ nm) was removed by the Pyrex wall of the reaction vessels. Light irradiation reached the Nafion/Fe membrane which was positioned immediately behind the wall of the reaction vessel (60 ml volume containing 40 ml solution) as the only light absorber in this two phase system. The detection of Orange II in solution was carried out *via* an HPLC (Varian 9065 Diode Array) provided with a Phenomenex C-18 inverse phase column. The azo-dye peak was detected at $\lambda = 486$ nm with a retention time of 11.1 min. The solution gradient during the analysis was regulated with a buffer consisting of ammonium acetate and acetonitrile.

The disappearance of Orange II (pH 2.8) under light irradiation on a Fe-loaded Nafion membrane by a Suntest lamp was recorded as a function of time for different concentrations of H_2O_2 in the solution. With increasing concentration of H_2O_2 the Orange II degradation kinetics was accelerated. At H_2O_2 concentrations > 0.8 mM, no further acceleration was observed. This effect is due to the known scavenging effect when using higher H_2O_2 concentration on the further generation of hydroxyl radicals in solution.[8] The concomitant total organic carbon (TOC) decrease was observed to be modest changing from 16 to 11 ppm C after 120 min. Within this time of the azo dye was observed to completely disappear from the solution. Concomitant CO_2 evolution was checked by gas chromatography (GC) confirming that mineralization of the dye proceeds with a much slower kinetics than the Orange II disappearance. This reveals the formation of longer lived intermediates in solution. The decoloration shown in Fig. 1 reflects azo-bond breakage in Orange II.[9,10] During dye abatement where H_2O_2 (0.8 mM) is added, the solution pH was seen to increase from 2.8 to ≈ 3.2. This corresponds to about a fourfould increase in the OH^- concentration in the solution and suggests reaction (1) as the main pathway for

$$\text{Nafion/Fe}^{II} + H_2O_2 \rightarrow \text{Nafion/Fe}^{III} + {}^{\bullet}OH + OH^- \quad (1)$$

Orange II degradation rather than reaction (2).

$$\text{Nafion/Fe}^{III} + H_2O_2 \rightarrow \text{Nafion/Fe}^{II} + HO_2^{\bullet} + H^+ \quad (2)$$

Three experimental observations substantiate further the mechanism suggested in eqn. (1): (*a*) methanol (0.26 M) precluded the abatement of the azo dye due to its $^{\bullet}OH$ radical scavenging properties, (*b*) spectrophotometric results showed that the initial Nafion/Fe^{III} membrane decolored substantially during the photolysis due to the build-up of Nafion/Fe^{II} absorbing at much lower wavelengths. Since the iron has been exchanged at room temperature in aqueous solution the exchanged-hydrated Nafion/Fe^{III} would involve the presence in the Nafion of the Fe-species $Fe(OH)^{2+}$ ($\varepsilon_{366nm} = 275$ dm^3 mol^{-1} cm^{-1}) and $Fe_2(OH)_2^{4+}$ ($\varepsilon_{366nm} = 1000$ dm^3 mol^{-1} cm^{-1}).[18] During the

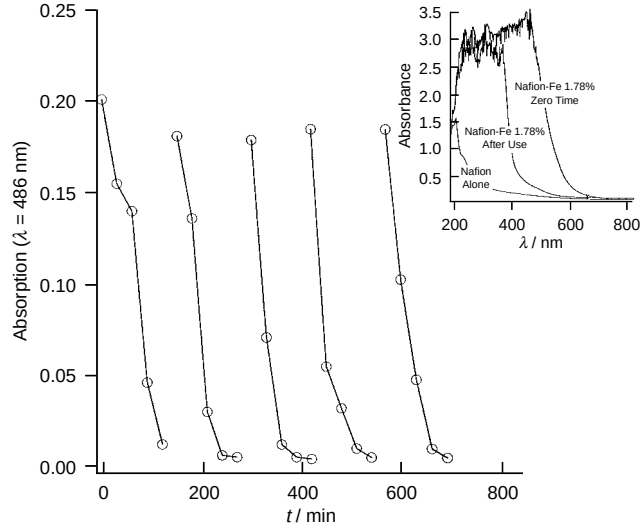

Fig. 1 Nafion/Fe loaded induced degradation of Orange II as a function of time followed by visible spectral observations at the Orange II peak of 486 nm up to the fifth cycle. The inset shows the Fe content in the solution after 26.6 days (1600 min). [Orange II] = 0.05 mM, pH = 2.8, H_2O_2 = 4.85 mM, irradiation intensity = 50 mW cm^{-2}.

dye decoloration (Fig. 1) the orange–brown color of Nafion/Fe^{III} gradually disappears due to the much lower absorption from the charge transfer band of $Fe(H_2O)_6^{2+}$ observed below λ = 265 nm with ε_{254nm} = 20 dm^3 mol^{-1} cm^{-1}.[19] Finally, (*c*) the superoxide radical $HO_2^{\cdot}$ (pK_a = 4.8) photoproduced according to eqn. (2) has a considerably lower one electron standard reduction potential of $E°$ = 0.75 V *vs.* NHE ($HO_2^{\cdot}/O_2^{\cdot -}$) than the $^{\cdot}OH$ radical with $E°$ = 1.90 V *vs.* NHE[20] ($^{\cdot}OH/OH^-$) in eqn. (1). The fast oxidation of the Orange II cannot possibly be explained in terms of this kinetically slower and less energetic $HO_2^{\cdot}$ radical [eqn. (2)].

Fig. 1 shows the repetitive nature of the Orange II photodegradation in the presence of Nafion/Fe-loaded membrane and H_2O_2. After *ca.* 25 cycles, the membrane was regenerated by immersion in 1 M NaOH. The timing of this regeneration was determined by two factors: (*a*) during use, the initial orange–brown coloration with absorption up to λ = 600 nm slowly changed to gray–yellowish with absorption reaching only an upper limit of *ca.* 410 nm. This indicated that during the photolysis the Fe^{III} content in the Nafion membrane decreased leading to the formation of colorless Fe^{II} since the total iron content of the membrane was seen to remain constant (see below). The Nafion without any Fe-loading absorbed only below 300 nm; and (*b*) during the degradation cycles the membrane become more active with time. A faster Orange II degradation of *ca.* 40% was observed compared to the first degradation run. Highly stable Nafion/Fe^{II} species are probably responsible for the observed acceleration as the reaction progresses.

The assessment of the oxidation state of Fe during the reaction was carried out by XPS in a Leybold–Heraeus instrument. Quantitative evaluation of the Fe^{III} and Fe^{II} species revealed 78% Fe^{III} (E_b = 710.0 eV) and 22% Fe^{III}/Fe^{II} (E_b = 713.8 eV) at time zero. The former species appeared mainly as Fe_2O_3 while the latter species consisted mainly of the composite Fe_3O_4 oxide showing the peaks for the constituent oxides. After reaction, the Nafion membrane showed 16% Fe^{III} and 84% Fe^{III}/Fe^{II} oxidation states. The correction for electrostatic charging of the particles during the measurements was carried out by a polynomial fit of the data with a Shirley-type background subtraction. The XPS experimental result further confirms the spectral change in the Fe-Nafion membrane observed during the photocatalysis. The size of the Fe-clusters on the Nafion was determined by TEM to be 37 ± 4 Å (Philips 20 M instrument). The particles were seen to be uniformly deposited on the Nafion and the size distribution was narrowly centered around the median value.

Membranes were regenerated after 500 h irradiation to attain the same Orange II degradation kinetics as observed during the initial cycle. The highly dispersed Fe^{III} ions could be regenerated in the Nafion. In solution the degradation of Orange II proceeded according to eqn. (3).[3,4]

$$^{\cdot}OH + \text{Orange II} \rightarrow [\text{Orange II–OH}^{\cdot}] \rightarrow \text{hydroxylated azo-bond scission intermediates} \quad (3)$$

The inset in Fig. 1 shows the change in absorption of the Nafion membranes with time. After 500 h irradiation a substantial change in absorption of the Nafion/Fe^{III} was seen. A decrease in the absorption of Nafion/Fe^{III} is observed along with concomitant growth of the lower absorbing Nafion/Fe^{II}. This change in absorption is consistent with the molar absorption coefficients and the XPS evidence presented above. The optical absorption of Nafion membranes is shown in the left hand side of the inset. The formation of Q-sized Fe^{III}/Fe^{II} clusters in the Nafion upon irradiation has been confirmed by X-ray diffraction. The exchange procedure used to incorporate Fe ions in the membrane is therefore also a method to produce discrete small sized particles of iron oxides embedded in the polymer structure.

Based on the experimental results a simplified scheme of the reaction is presented (Scheme 1). Scheme 1 shows the photocatalytic degradation of Orange II in acidic solutions due to the photoproduction of oxidative radicals in solution and the build up of Nafion/$Fe^{III}Fe^{II}$ species during the degradation process.

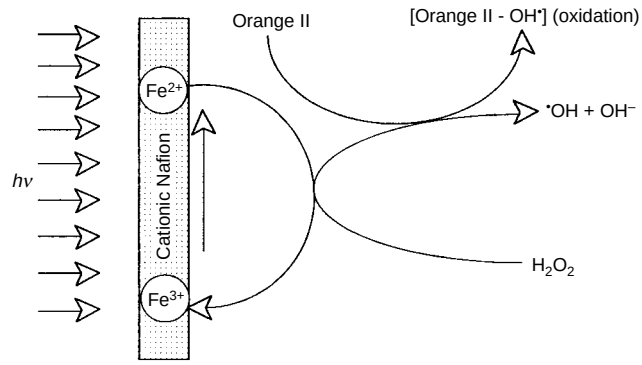

Scheme 1

The redox processes involving H_2O_2 decomposition induce Orange II hydroxylation. Less than 60 min pretreatment were necessary to reach a BOD_5 value of *ca.* 100 mg O_2 1^{-1}. This is indicative for the presence of biodegradable intermediates in solution since no biodegradation was observed for Orange II in the absence of pretreatment. Azo bonds have been reported not to be susceptible to biological degradation.[13]

In conclusion, we have presented the first evidence for a Fenton-like reaction in a Fe-free solution using Orange II as a model compound. Fig. 1 shows a kinetically significant rate of azo dye disappearance in solution. A similar rate is observed in homogeneous Fe ion–H_2O_2 solutions containing ≈100 times higher concentration of Fe^{3+}. This work demonstrates the possibility of degradation of otherwise recalcitrant azo compounds removing the need to dispose of Fe ions after reaction to meet EU directives.[12]

This work was supported by the European Community Environmental program ENV-CT95-0064, OFES No. 96.350, Bern) and the INTAS cooperation program with Russia (94-0642).

Notes and References

† E-mail: john.kiwi@dcmq.epfl.ch

1 J. Bard, *Integrated Chemical Systems*, Wiley, New York, 1994.
2 R. Lawson, D. B. Kiang and R. Martin, *Chem. Mater.*, 1933, **5**, 400.
3 G. Meissner, R. Memming and B. Kastening, *Chem. Phys. Lett.*, 1993, **96**, 34.
4 I. Bellobono, A. Carrara, B. Barni and A. Gazzotti, *J. Photochem. Photobiol., A*, 1994, **84**, 83.
5 R. Pozzo, M. Baltanas and A. Cassano, *Catal. Today*, 1997, **39**, 219.
6 H. Miyoshi, S. Nippa, H. Uchida and H. Yoneyama, *Bull. Chem. Soc. Jpn.*, 1994, **63**, 3880.
7 H. Zollinger, in *Color Chemistry–Syntheses and Applications of Organic Dyes and Pigments*, VCH, New York, 1987.
8 J. Edwards and R. Curci, *Catalytic Oxidation with* H_2O_2 *as Oxidant*, ed. G. Strukul, Kluwer Academic Press, Dordrecht, 1982.
9 J. Bandara, C. Morrison, P. Pulgarin and J. Kiwi, *J. Photochem. Photobiol. A*, 1996, **99**, 5764.
10 V. Nadtochenko and J. Kiwi, *J. Chem. Soc., Faraday Trans.*, 1996, **93**, 2373.
11 C. Pulgarin, P. Peringer, P. Albers and J. Kiwi, *J. Mol. Catal. A*, 1995, **95**, 61.
12 European Economic Community, EEC, *List of Council Directives 76/4647*, Brussels, Belgium 1982.
13 P. Peter and P. Chudoba, *Biodegradability of Organic Substances in the Aquatic Environment*, CRC Press, Boca Raton, FL, 1994.

Received in Bath, UK, 27th March 1998; 8/02539H

Typeset and printed by Black Bear Press Limited, Cambridge, England

ChemComm
FEATURE ARTICLE

Dynamic anion recognition by macrocyclic polyamines in neutral pH aqueous solution: development from static anion complexes to an enolate complex

Eiichi Kimura*† and Tohru Koike

Department of Medicinal Chemistry, School of Medicine, Hiroshima University, Kasumi, Minami-ku, Hiroshima, 734-8551, Japan

Multiprotonated macrocyclic polyamines are useful host molecules for anion guests at neutral pH in aqueous solution. An intramolecular uracil anion complex with a diprotonated macrocyclic tetraamine recently provided a unique example of electrostatic stabilization of the uracil N^1 anion at neutral pH, which may be relevant to the facile glycosylation and deglycosylation of uracil at N^1 in DNA. Macrocyclic polyamine complexes with Zn^{2+} possess strong anion affinities and hence can deprotonate weak acids at neutral pH to bind with the resulting conjugate bases: *e.g.* $H_2O \rightarrow HO^-$, $ROH \rightarrow RO^-$, $ArSO_2NH_2 \rightarrow ArSO_2NH^-$, $RCONHR' \rightarrow RCON^-R'$, $RCONHCOR' \rightarrow RCON^-COR'$. The Zn^{2+}–conjugate base complexes act as catalytic nucleophiles (*i.e.* HO^-–Zn^{2+}, RO^-–Zn^{2+}), fluorescence sensors ($ArSO_2NH^-$–Zn^{2+}), and thymine or barbital recognition hosts, which are often found in zinc–enzyme functions. Enolate anion complex formation has recently been observed in intramolecular interaction of carbonyl oxygen with Zn^{2+}.

1 Anion complexes with multiprotonated macrocyclic polyamines

Macrocyclic polyamines have long been demonstrated to be good host molecules for polyanions (*e.g.* di- and tri-carboxylates, phosphates, carbonates) and form stable 1 : 1 complexes at neutral pH in aqueous solution, where macrocyclic polyamines are multiprotonated and highly charged.[1–10] For instance, the hexaazamacrocyclic polyamine [18]aneN$_6$ **1** which has pK_a values of 10.2, 9.2, 8.7, 4.1, < 2, and < 2, is mostly present in the [18]aneN$_6$·3H$^+$ form **2** at pH *ca.* 7, which binds with citrate^{3-} (log K = 2.4), AMP^{2-} (log K = 3.3), or ATP^{4-} (log K = 6.4) in 1 : 1 anion complexes **3** (Scheme 1).[2,5] Electrostatic and hydrogen bonding interactions account for the fairly strong complexation.

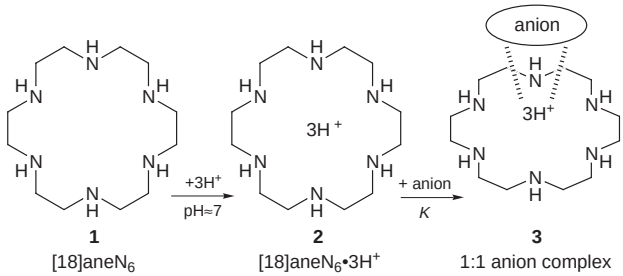

Scheme 1

Enolization of carbonyl compounds is crucial in a wide variety of key reactions in biochemical transformations; enzymes include aldolase, racemase and isomerase. Of special interest is how weak bases of enzymes (*e.g.* imidazole, aspartate or glutamate), with pK_a values < 7, can effectively abstract a proton from carbonyl substrates having much higher pK_a values and there must be some mechanism which lowers pK_a values of the methylene protons adjacent to a carbonyl group.[11] Uracil–DNA glycosylase (UDGase), which disrupts the N(1)–C(1′) bond (see **4**) at neutral pH, is an example of one

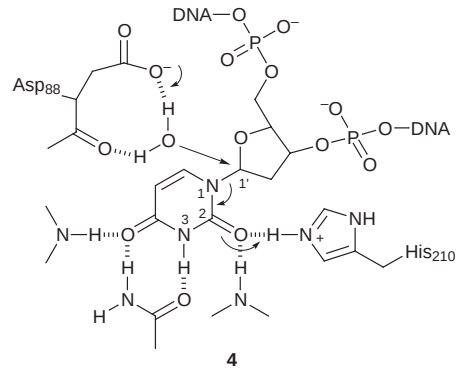

of these enzymes.[12,13] The amide carbonyl group C^2=O must be activated (probably by hydrogen bonding with protonated His$_{210}$), so as to lower the electron density of the uracil group to allow a concerted nucleophilic attack by a water molecule (activated by Asp$_{88}$) on the C$^{1'}$ atom. Concerning this mechanism, chemical questions arise: how much is the product uracil anion stabilized by the protonated imidazole or how is uracil N^{1}H selectively deprotonated for activation in the reverse reaction to form the glycosyl bond at neutral pH. These questions are translated into whether the uracil N^{1}H (pK_a *ca.* 9.5) can be rendered more acidic.

In order to address such basic chemical questions, we synthesized a diprotonated cyclen-attached uracil **5**.[14] It is remarkable to find that the uracil N^{1}H group of **5** (Scheme 2) is

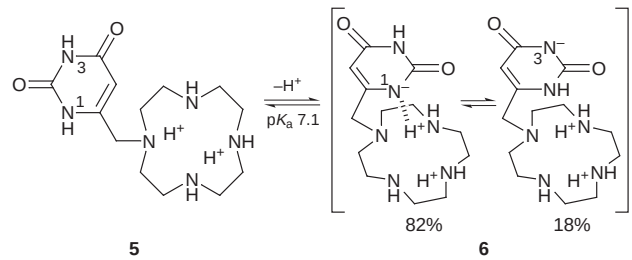

Scheme 2

readily deprotonated to the anionic species **6** in aqueous solution [pK_a = 7.14 at 25 °C (I = 0.1)]. The lowered pK_a by more than two units is due to an electrostatic stabilization of the conjugate base (N^1)$^-$ anion by the diprotonated cycle at physiological pH. Furthermore, the negative charge is highly localized at N^1 (82% according to UV and NMR studies), under the strong influence of cyclen NH$^+$. At higher pH where the two protons are removed from the cyclen, the negative charge at N^1 becomes delocalized and the (N^3)$^-$ anionic tautomer becomes more predominant (18% at pH → 63% at pH 12.5).

This simple model may illustrate how easily the uracil N^1H can be deprotonated so as to be a good leaving group in deglycosylation and also to be a good nucleophile for glycosylation at neutral pH. The uracil N^1 site should be especially subject to the electrostatic effect by protonic acids. Thus, uracil may be appropriately chosen for the DNA repair mechanism.

2 Dynamic anion complexes by interaction of macrocyclic polyamine–zinc(II) complexes with water and alcohols

When a strong Lewis acid such as a divalent metal ion replaces protons in macrocyclic polyamine cavities, more acidic macrocyclic molecules are obtained. This is particularly true for Zn^{2+}, which along with Cu^{2+} is one of the strongest Lewis acids, and is characteristically non-directional (no ligand field effect) owing to its d^{10} electronic state (*cf.* the directional d^9 Cu^{2+} ion[15–19]) and Zn^{2+} can be regarded as a condensed multiproton site. The Zn^{2+} ion complexes in four-, five- or six-coordinate structures. Taking full advantage of the properties of Zn^{2+} and rigid macrocyclic configurations, one can design appropriate zinc(II) complexes as host molecules for anions. In this connection, it should be noted that halogen ions X^- or inorganic hydrogen phosphate $HOPO_3^{2-}$ bind to Zn^{2+} at active centers of zinc enzymes to inhibit the enzymatic activities and that zinc enzymes are active towards anionic substrates (*e.g.* $HOCO_2^-$ for carbonic anhydrase, $ROPO_3^{2-}$ for alkaline phosphatase) or neutral molecules (with weak acidity) that are developed into anionic reaction intermediates or transition states [*e.g.* amides for carboxypeptidase, CO_2 (or H_2CO_3) for carbonic anhydrase].[20] Thus, zinc(II) macrocyclic polyamine complexes can be static as well as dynamic receptor molecules for anions, showing more versatile behavior than mere protonated macrocyclic polyamines or other conventional organic anion receptors.[21–23]

The most revealing example is ready deprotonation of water bound to Zn^{2+} in macrocyclic polyamines (**7a** ⇄ **7b** + H^+ and **8a** ⇄ **8b** + H^+), as reflected in the pK_a values (7.3 and 7.9,

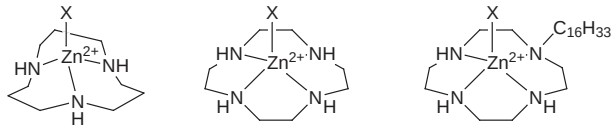

7a X = OH_2 **b** X = OH^- Zn^{2+}-[12]aneN_3

8a X = OH_2 **b** X = OH^- Zn^{2+}-cyclen

9a X = OH_2 **b** X = OH^-

respectively).[24,25] Alternatively, one can view the HO^- anion binding to Zn^{2+}, which is measured in terms of the anion affinity constant K ($10^{6.7}$ and $10^{6.1}$ dm^3 mol^{-1}, respectively). Although HO^-–Zn^{2+} bonds are fairly strong they are characteristically labile. In line with their pK_a values, HO^-–Zn^{2+} complexes are appreciably and rapidly generated at physiological pH, which then act as nucleophiles toward carboxyesters, β-lactam and phosphoesters for catalytic hydrolyses.[24–27] When appended with a hexadecyl group (see **9**), the HO^- anion complex is generated as readily (pK_a = 7.6 for **9a** ⇄ **9b** + H^+) and the resulting anion can migrate into Triton X-100 micelles, whereby the Zn^{2+}-bound OH^- becomes more desolvated and its nucleophilicity towards lipophilic esters such as tris(4-nitrophenyl) phosphate is 290 times stronger than HO^-–Zn^{2+} of **8b**.[28]

It is of interest to point out that the anion affinity of Zn^{2+} is of central importance in the active center of zinc enzymes such as carbonic anhydrase (CA).[17] In the forward (CO_2 hydration) and reverse ($HOCO_2^-$ dehydration) reactions, two anionic reactants OH^- (a good nucleophile toward CO_2) and $HOCO_2^-$ (a substrate) always compete for Zn^{2+}. The successful binding to Zn^{2+} depends on the pH of the medium (*i.e.* concentration of OH^-) and $HOCO_2^-$. This equilibrium then determines the direction of the enzyme reaction: at higher pH hydration of CO_2 and at lower pH dehydration of $HOCO_2^-$ predominate. The 12-membered macrocyclic triamine ([12]aneN_3) zinc(II) complex **7a** (pK_a = 7.3 at 25 °C) has for the first time mimicked such pH-dependent CA behavior of CO_2 hydration and $HOCO_2^-$ dehydration at physiological pH.[29]

The Zn^{2+}-bound OH^- anion can also behave as a catalytic base. When propan-2-ol was heated with catalytic amounts of **7b** in dimethylformamide in the presence of 4-nitrobenzaldehyde or *N*-methyl nicotinamide, hydride transfer occurred from propan-2-ol to 4-nitrobenzaldehyde (yielding 4-nitrobenzyl alcohol) or *N*-methyl nicotinamide (yielding 1,4-dihydronicotinamide).[30] The reaction mechanism (Scheme 3) was

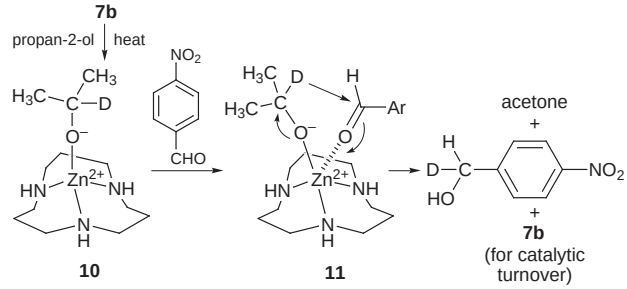

Scheme 3

established by using $(CH_3)_2CDOH$. An essential step is generation of an alkoxide at the acidic Zn^{2+} center (**10**), which still leaves the fifth coordination site open for the other reactants coordinating through carbonyl oxygen to permit hydride transfer in the aldehyde-bound complex **11**. This system is a good model for Zn^{2+}-containing alcohol dehydrogenase.

With an alcohol-pendant zinc(II)–cyclen complex **12**, deprotonation occurs with a pK_a value of 7.7 in aqueous solution (Scheme 4).[31] Available evidence supports the HO^-–Zn^{2+}

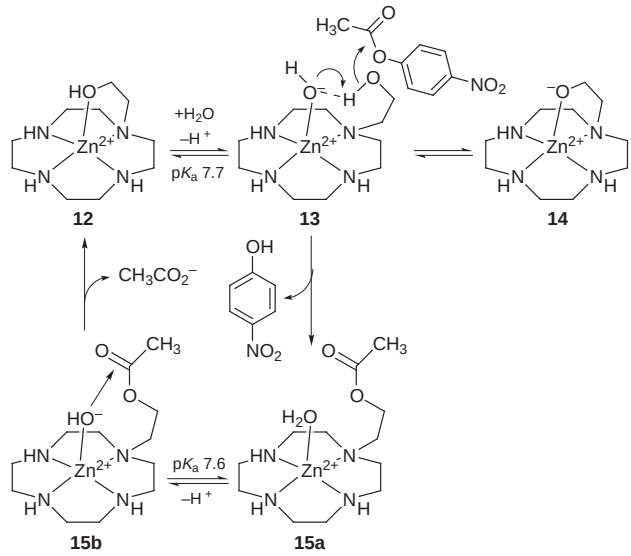

Scheme 4

structure **13** rather than Zn^{2+}–alkoxide complex **14**. In terms of reactivity, the pendant alcohol in **13** is more nucleophilic than a reference Zn^{2+}-bound OH^- complex **8b**. The product from the reaction of **13** (at pH > 8) with 4-nitrophenyl acetate was exclusively an acetyl-transferred complex **15a**. The pendant acetate in **15a** immediately undergoes hydrolysis by the proximate Zn^{2+}-bound HO^- in **15b** which is immediately generated (pK_a = 7.6). Another alcohol–pendant Zn^{2+} complex **16** is at equilibrium with its monodeprotonated complex **17** in neutral aqueous solution with a pK_a value of 7.5 (Scheme 5).[32] In this case, the alkoxide-bound complex **17** rather than an

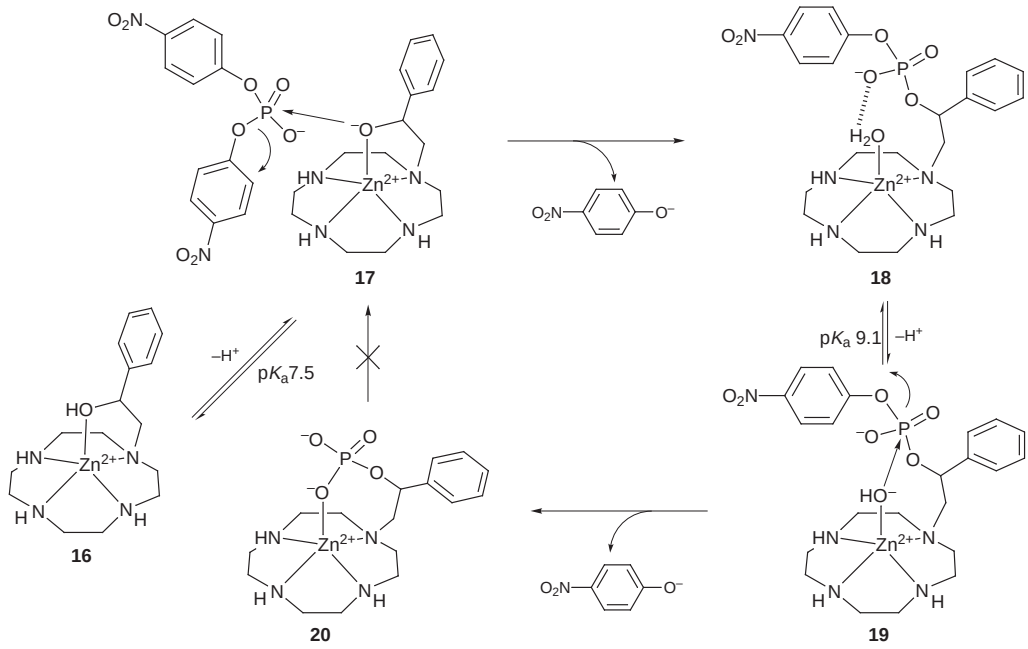

Scheme 5

equivalent **13**-type complex is predominant in alkaline solution. The alkoxide anion complex was isolated and its X-ray crystal structure was determined. The Zn^{2+}-bound alkoxide ion in **17** is again a better nucleophile than HO^-–[zinc(II)–cyclen] **8b**. The alkoxide complex **17** reacted with a phosphodiester to yield an isolable 'phosphate-transfer' product **18**, which is then subject to intramolecular attack by an immediately generated Zn^{2+}-bound OH^- in **19**. The reactions led eventually to a very stable Zn^{2+}-bound phosphomonoester anion complex **20**. Here, we see the appearance of various anions each having different dynamic behaviour in neutral aqueous solution during the reaction processes.

A dinuclear zinc(II) cryptate **21** is a potential receptor of phosphomonoester dianions such as 4-nitrophenyl phosphate (NP^{2-}), although the two Zn^{2+} ions (separated at a distance of 3.42 Å) in the cryptate appear coordinatively saturated in a rigid five-coordinate configuration.[33] However NP^{2-} can transiently bind to **21** at pH *ca.* 6 in aqueous solution to give **22** and cleavage of the P–O ester bond by nucleophilic attack of one of the apically coordinated NH groups yields the phosphoramide product **23** (Scheme 6). The driving force for the recognition by the two Zn^{2+} centres in **22** arises from formation of the stable zinc(II)–phosphate O^- bonds in **23**.

3 Application of anion complexes for recognition of Zn^{2+} and weakly acidic neutral molecules

Just like H_2O and alcohols, other weak acids, *e.g.* aromatic sulfonamides (pK_a *ca.* 10) are deprotonated at physiological pH by macrocyclic polyamine zinc(II) complexes. The recognition

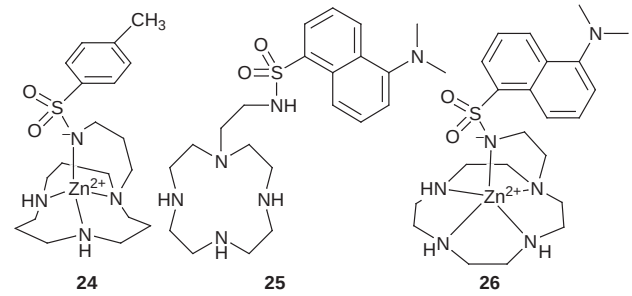

of the deprotonated sulfonamide anion by Zn^{2+} in **24** is a good chemical model designed to explain the inhibition of carbonic anhydrase by aromatic sulfonamides.[34] Attachment of a dansylamide pendant to cyclen **25** has led to a very sensitive and selective fluorescent probe for Zn^{2+} at neutral pH in aqueous solution (owing to formation of **26**).[35] The Zn^{2+}-dependent fluorescence with 5 μM **25** (at pH 7.3) is quantitatively responsive to 0.01–5 μM concentrations of Zn^{2+}, and is unaffected by the presence of mM concentrations of biologically important metal ions such as Na^+, K^+, Ca^{2+} and Mg^{2+}. The zinc fluorophore **25** forms a far more stable 1 : 1 Zn^{2+} complex (K_d = 6×10^{-13} mol dm^{-3} at pH 7.8) than any previously prepared zinc fluorophore[36] and can be regarded as a new prototype of zinc fluorophore.

The zinc(II)–cyclen complex **8a** can act as a good anion receptor for imide-containing weakly acidic molecules at neutral pH in aqueous solution. Typical guests are thymidine (or

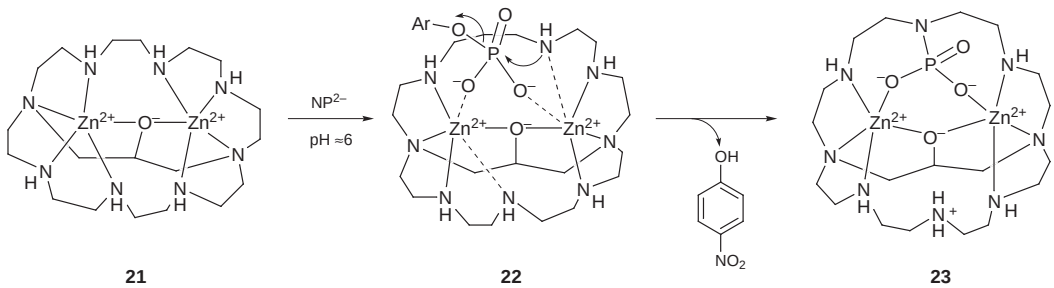

Scheme 6

uridine) and barbiturates, which are deprotonated and form 1 : 1 complexes **27a**[37] and **28**[38] upon interaction with **8a**. Complexes **27a** and **28** result from Zn^{2+} deprotonating the imide protons

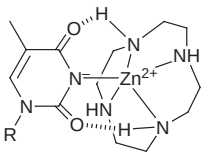

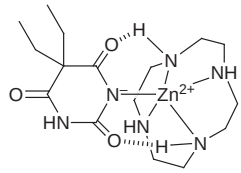

27a R = 2'-deoxy-1'-ribosyl
b R = 3'-azido-2',3'-dideoxy-1'-ribosyl

28

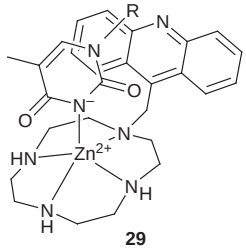

29

and the resulting Zn^{2+}–N^- (imide) bond is reinforced by the two complementary hydrogen bonds between the two imide oxygen atoms and two NH groups of cyclen; K_d values (at 25 °C) are 8×10^{-4} mol dm^{-3} for **27a** at pH 7.4 and 6×10^{-5} mol dm^{-3} for **28** at pH 8. The X-ray crystal structure of the AZT$^-$–[zinc(II)–cyclen] complex **27b** reinforces the stability of these complexes. The major stabilization comes from the Zn^{2+}–N^-(imide) bonding with the two hydrogen bonds providing a supplementary contribution. The zinc(II)–acridinylmethylcyclen complex binds 50 times more strongly with thymine, owing to an additional π–π stacking interaction (see **29**).[39] It is remarkable that zinc(II)–cyclen complexes preferentially recognize neutral thymine or uracil bases over biological anions such as phosphate monoanions in DNA or RNA.

In the light of the fact that zinc(II)–cyclen yielded only the 1 : 1 complex **28** with barbital, although barbital potentially has two imide donor sites, a bis[zinc(II)–cyclen] connected with a *p*-xylene bridge **30** was synthesized to match the dianionic barbital anion.[40] A number of host molecules (*e.g.* **31**[41]) have been synthesized for barbiturates; however, such barbiturate–host complexes are stable only in non-aqueous environments (*e.g.* $K_d = 10^{-2}$–10^{-6} in $CDCl_3$ for **31**): and they dissociate immediately in aqueous solution. Potentiometric pH titration of **30** and barbital (both at 1 mM) led to extremely facile deprotonation of the two imide groups at pH < 7, leading to the formation of the 1 : 1 complex barbital^{2-}–bis[zinc(II)–cyclen] **32**.[40] From an aqueous solution of an equimolar mixture of **30** and barbital at pH 8, a cyclic 2 : 2 complex **33** was isolated and characterized by X-ray crystal analysis. An NMR study of isolated **33** in 10% (v/v) D_2O–H_2O revealed the dissociation of **33** into the original target 1 : 1 complex **32**, establishing a dimerization constant K of $10^{3.4}$ dm^3 mol^{-1} for **32** + **32** ⇄ **33**. Thus, **30** was established to be an excellent host for barbital at neutral pH in aqueous solution.

The acridine-pendant complex, zinc(II)–acridinylmethylcyclen (*cf.* thymidine complex **29**) also acts as a selective host molecule for terephthalic acid by supramolecular self-assembly.[42] In neutral pH aqueous solution, zinc(II)–acridinylmethylcyclen yields a 1 : 1 complex with terephthalate with dissociation constant $K_d = 10^{-2.3}$ mol dm^{-3} at 25 °C. Despite its relatively weak affinity, crystalline **34** [a ternary complex of one terephthalate and two zinc(II)–acridinylmethylcyclen molecules] precipitated almost quantitatively when zinc(II)–acridinylmethylcyclen (10 mM) was mixed with terephthalic acid (5 mM) in an aqueous solution containing excess ClO_4 at pH 8.4. It was found that zinc(II)–acridinylmethylcyclen selectively separates terephthalate as insoluble

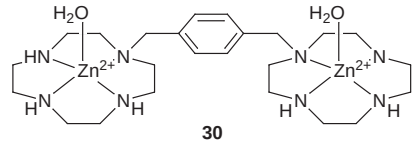

30

Bis(Zn^{2+}-cyclen)

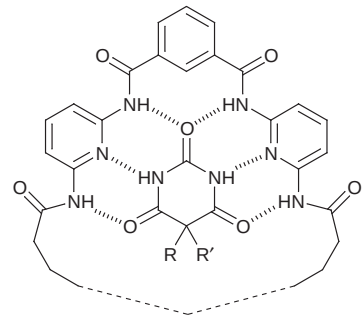

31

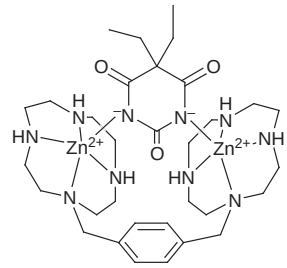

32

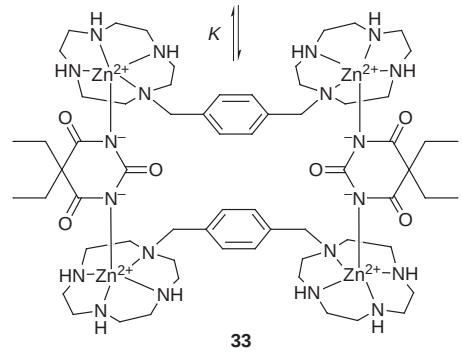

33

crystals of the 2 : 1 complex **34** from a mixture with its isomers (*o*- and *m*-phthalate). This is a consequence of the fact that **34** in the solid state is additionally stabilized by self-assembly in a highly ordered aggregate with π–π stacking (schematic representation **35**), as revealed by X-ray crystal analysis. Metal complexes with aromatic pendants like zinc(II)–acridinylmethylcyclen would be useful for the molecular recognition of other anionic molecules in aqueous media.

The recognition of thymine (or uracil) by zinc(II)–cyclens has been extended to a single-stranded polynucleotide poly(U) and double-stranded poly(U)–poly(A).[43–46] The affinity constant of zinc(II)–cyclen **8a** for each N^3-deprotonated uracil base in poly(U) is $K = 10^{5.1}$ dm^3 mol^{-1} at 25 °C, which is almost the same ($10^{5.2}$ dm^3 mol^{-1}) for the interaction of zinc(II)–cyclen and N^3-deprotonated uridine. This fact imples that zinc(II)–cyclen shows a negligible interaction with the monoanionic phosphodiester backbone of poly(U). Moreover, zinc(II)–cyclen disrupts U–A hydrogen bonds to unzip the duplex of poly(U)–poly(A) (see **36**), as demonstrated by the decreasing melting temperatures (T_m) of poly(U)–poly(A) in aqueous solution at pH 7.6 (5 mM Tris-HCl, 10 mM NaCl) with an increase in the concentration of zinc(II)–cyclen. A bidentate host molecule, bis[zinc(II)–cyclen] **30**, is a more potent zipper of the poly(U)–poly(A) double strand. Very recently, we have determined an

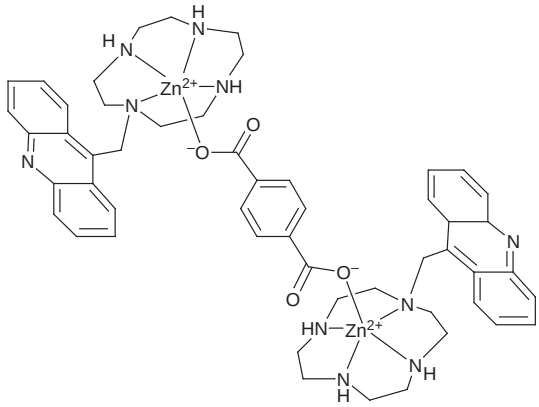

34

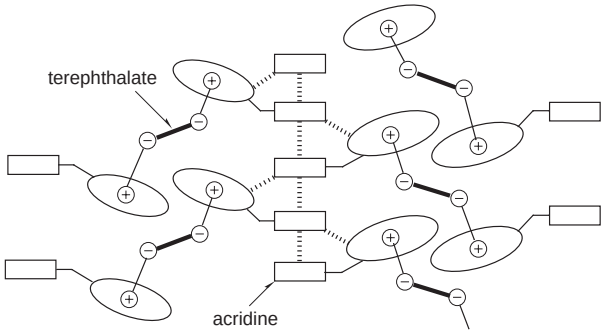

35

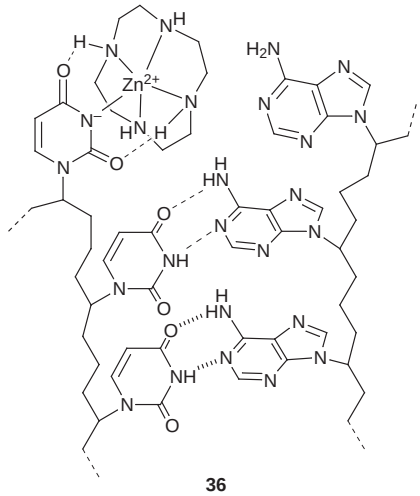

36

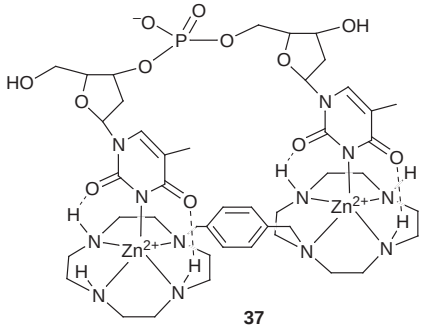

37

extremely strong interaction of bis[zinc(II)–cyclen] with thymidinylthymidine (TpT) in aqueous solution at pH 7.4 to yield a much more stable complex **37** *cf.* T$^-$–[zinc(II)–cyclen] **27a**.[47] The dissociation constant K_d of 10^{-6} mol dm^{-3} for **37** is almost 10^3 times smaller than that for **27a** ($K_d = 8 \times 10^{-4}$ mol dm^{-3}). This fact, along with the widened T–T plane distance (*ca.* 10 Å) determined by molecular mechanics calculation (MM2) well accounts for the more effective disruption of the poly(U)–poly(A) double strand by **30**. Thus, **30** can act as a useful TpT sequence-selective ligand in biochemical applications.

In section 1, it was stated that uracil N^{1}H is two orders of magnitude more acidic when proximate to a diprotonated macrocyclic tetraamine (see **5** and **6**). When Zn^{2+} is used in place of the two protons in **5**, the acidic Zn^{2+} in the cyclen exerts an even stronger effect on the deprotonation of the uracil N^{1}H to below pH 5.[14] The resulting zinc(II) complex **38** contains a very stable Zn^{2+}–(N^1)$^-$ coordination bond.

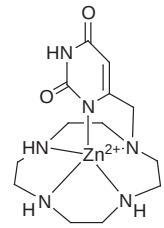

38

Finally, the acidic Zn^{2+} centre in the substituted cyclen ligand 1-(4-bromophenacyl)-1,4,7,10-tetraazacyclododecane **39** has recently been found to deprotonate a methylene hydrogen adjacent to the carbonyl group to yield an enolate complex **40** in aqueous solution (Scheme 7), which is in equilibrium with an

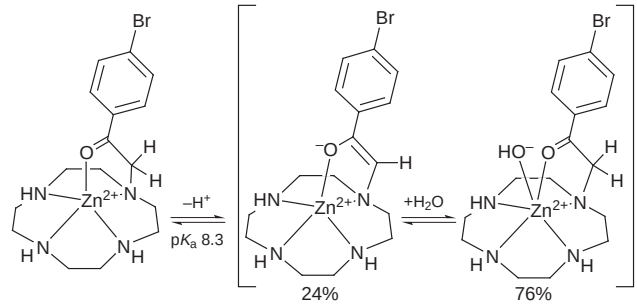

39 **40** **41**

Scheme 7

equivalent OH$^-$-bound complex **41** (ratio of **40**:**41** = 24:76).[48] Surprisingly, its pK_a value is as low as 8.3 at 25 °C (I = 0.1, $NaNO_3$), which is probably the first successful identification of enolate formation in aqueous solution. It is of interest to note that type II aldolase is a zinc enzyme, which also forms an enolate-bound zinc(II) complex (see **42**).[20]

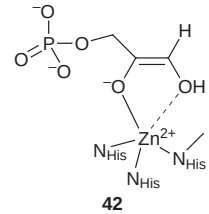

42

4 Conclusions

This article illustrates that macrocyclic polyamines either in multiprotonated forms or in zinc(II) complexes act as static anion receptors in aqueous solution. The macrocyclic 12-membered N_3– or N_4–Zn^{2+} complexes can, moreover, recognize netural molecules having weak acid protons to yield stable

anion complexes. These anion complexes possess dynamic functions as exemplified by HO^{-}–Zn^{2+} and RO^{-}–Zn^{2+} acting as strong nucleophiles for catalytic hydrolysis of esters or as bases for thymine recognition. This basic principle has been further developed to hydride transfer reactions from Zn^{2+}-bound alkoxides, a Zn^{2+} sensor, DNA base recognition, or stabilization of unusual anions such as enolate in aqueous solution.

Acknowledgments

E. K. is grateful to the Grant-in-Aid for Priority Project 'Biometallics' (No. 08249103) from the Ministry of Education, Science and Culture in Japan.

Professor Eiichi Kimura was born in Shizuoka in 1938. He obtained BSc and MSc degrees from the University of Tokyo and his PhD from the University of North Carolina under Professor James P. Collman in 1967. After postdoctoral years at Syntex and Chicago University, he became an Associate Professor at Hiroshima University in 1970 where he is presently a Professor. His research interest include supramolecular chemistry with macrocyclic polyamines such as in molecular recognition and zinc–enzyme models. He was given the 2nd Izatt–Christensen award for macrocyclic chemistry in 1992.

Dr Tohru Koike was born in Hiroshima in 1959. After receiving his PhD in 1986 from Hiroshima University under the direction of Professor Eiichi Kimura, he became a research assistant at Hiroshima University where he is presently an Associate Professor. His research interest is bioinorganic chemistry. He has been innovating original macrocyclic polyamines to disclose the intrinsic properties of Zn^{2+} in metalloproteins.

Notes and References

† E-mail: ekimura@ipc.hiroshima-u.ac.jp

1 E. Kimura, *Top. Curr. Chem.*, 1985, **128**, 113.
2 E. Kimura, A. Sakonaka, T. Yatsunami and M. Kodama, *J. Am. Chem. Soc.*, 1981, **103**, 3041.
3 T. Yatsunami, A. Sakonaka and E. Kimura, *Anal. Chem.*, 1981, **53**, 477.
4 B. Dietrich, M. W. Hosseini and J. M. Lehn, *J. Am. Chem. Soc.*, 1981, **103**, 1283.
5 E. Kimura, M. Kodama and T. Yatsunami, *J. Am. Chem. Soc.*, 1982, **104**, 3182.
6 E. Kimura and A. Sakonaka, *J. Am. Chem. Soc.*, 1982, **104**, 4984.
7 M. W. Hosseini and J. M. Lehn, *J. Am. Chem. Soc.*, 1982, **104**, 3525.
8 Y. Umezawa, M. Kataoka, W. Takami, E. Kimura, T. Koike and H. Nada, *Anal. Chem.*, 1988, **60**, 2392.
9 M. Kataoka, R. Naganawa, K. Odashima, Y. Umezawa, E. Kimura and T. Koike, *Anal. Lett.*, 1989, **22**, 1089.
10 E. Kimura, Y. Kuramoto, T. Koike, H. Fujioka and M. Kodama, *J. Org. Chem.*, 1990, **55**, 42.
11 W. W. Cleland and M. M. Kreevoy, *Science*, 1994, **264**, 1887.
12 R. Savva, K. McAuley-Hecht, T. Brown and L. Pearl, *Nature*, 1995, **373**, 487.
13 G. Slupphaug, C. D. Mol, B. Kavli, A. S. Arvai, H. E. Krokan and J. A. Tainer, *Nature*, 1996, **384**, 87.
14 E. Kimura, H. Kitamura, T. Koike and M. Shiro, *J. Am. Chem. Soc.*, 1997, **119**, 10 909.
15 E. Kimura, *Prog. Inorg. Chem.*, 1993, **41**, 443.
16 E. Kimura and T. Koike, *Comments Inorg. Chem.*, 1991, **11**, 285.
17 E. Kimura and T. Koike, in *Comprehensive Supramolecular Chemistry*, ed. D. N. Reinhoudt, Elsevier Science, Oxford, 1966, vol. 10, p. 429.
18 E. Kimura and T. Koike, *Adv. Inorg. Chem.*, 1997, **44**, 229.
19 E. Kimura and T. Koike, *Struct. Bonding* (*Berlin*), 1997, **89**, 1.
20 W. N. Lipscomb and N. Sträter, *Chem. Rev.*, 1996, **96**, 2375.
21 F. P. Schmidtchen and M. Berger, *Chem. Rev.*, 1997, **97**, 1609.
22 M. M. G. Antonisse and D. N. Reinhoudt, *Chem. Commun.*, 1998, 443.
23 V. Král, P. A. Gale, P. Anzenbacher Jr., K. Jursíková, V. Lynch and J. L. Sessler, *Chem. Commun.*, 1998, 9.
24 E. Kimura, T. Shiota, T. Koike, M. Shiro and M. Kodama, *J. Am. Chem. Soc.*, 1990, **112**, 5805.
25 T. Koike, M. Takamura and E. Kimura, *J. Am. Chem. Soc.*, 1994, **116**, 8443.
26 T. Koike and E. Kimura, *J. Am. Chem. Soc.*, 1991, **113**, 8935.
27 E. Kimura, I. Nakamura, T. Koike, M. Shionoya, Y. Kodama, T. Ikeda and M. Shiro, *J. Am. Chem. Soc.*, 1994, **116**, 4764.
28 E. Kimura, H. Hashimoto and T. Koike, *J. Am. Chem. Soc.*, 1996, **118**, 10 963.
29 X. Zhang, R. van Eldik, T. Koike and E. Kimura, *Inorg. Chem.*, 1993, **32**, 5749.
30 E. Kimura, M. Shionoya, A. Hoshino, T. Ikeda and Y. Yamada, *J. Am. Chem. Soc.*, 1992, **114**, 10 134.
31 T. Koike, S. Sakonaka, I. Nakamura, E. Kimura and M. Shiro, *J. Am. Chem. Soc.*, 1995, **117**, 1210.
32 E. Kimura, Y. Kodama, T. Koike and M. Shiro, *J. Am. Chem. Soc.*, 1995, **117**, 8304.
33 T. Koike, M. Inoue, E. Kimura and M. Shiro, *J. Am. Chem. Soc.*, 1996, **118**, 3091.
34 T. Koike, E. Kimura, I. Nakamura, Y. Hashimoto and M. Shiro, *J. Am. Chem. Soc.*, 1992, **114**, 7338.
35 T. Koike, T. Watanabe, S. Aoki, E. Kimura and M. Shiro, *J. Am. Chem. Soc.*, 1996, **118**, 12 696.
36 E. Kimura and T. Koike, *Chem. Soc. Rev.*, 1998, **27**, in press.
37 M. Shionoya, E. Kimura and M. Shiro, *J. Am. Chem. Soc.*, 1993, **115**, 6730.
38 H. Fujioka, T. Koike, N. Yamada and E. Kimura, *Heterocycles*, 1996, **42**, 775.
39 M. Shionoya, T. Ikeda, E. Kimura and M. Shiro, *J. Am. Chem. Soc.*, 1994, **116**, 3848.
40 T. Koike, M. Takashige, E. Kimura, H. Fujioka and M. Shiro, *Chem. Eur. J.*, 1996, **2**, 617.
41 D. H. Hamilton, in *Bioorganic Chemistry Frontiers*, ed. H. Dugas, Springer, Berlin, 1991, p. 115.
42 E. Kimura, T. Ikeda, M. Shionoya and M. Shiro, *Angew. Chem., Int. Ed. Engl.*, 1995, **34**, 663.
43 M. Shionoya, M. Sugiyama and E. Kimura, *J. Chem. Soc., Chem. Commun.*, 1994, 1747.
44 E. Kimura, T. Ikeda and M. Shionoya, *Pure Appl. Chem.*, 1997, **69**, 2187.
45 E. Kimura and M. Shionoya, in *Metal Ions in Biological Systems*, ed. A. Siegel and H. Sigel, Marcel Dekker, New York, 1966, p. 29.
46 E. Kimura, T. Ikeda, S. Aoki and M. Shionoya, *J. Biol. Inorg. Chem.*, 1998, **3**, in press.
47 E. Kimura, M. Kikuchi and T. Koike, submitted.
48 E. Kimura, T. Goto and T. Koike, unpublished work.

8/02285B

Exchanged ligands on the surface of a giant cluster: $[(MoO_3)_{176}(H_2O)_{63}(CH_3OH)_{17}H_n]^{(32-n)-}$

Achim Müller,*† Michael Koop, Hartmut Bögge, Marc Schmidtmann and Christian Beugholt

Fakultät für Chemie der Universität, D-33501 Bielefeld, Germany

The synthesis of 1a·(32 − *n*)Na^+·*ca.* 600 H_2O·*ca.* 30 CH_3OH 1 containing the ring-shaped, mixed-valence (Mo^V/Mo^{VI}) cluster $[(MoO_3)_{176}(H_2O)_{63}(CH_3OH)_{17}H_n]^{(32-n)-}$ 1a as a discrete unit in the crystal lattice is reported, which for the first time yields a compound of this type *via* a facile synthetic method and without amorphous reaction products; remarkably, H_2O ligands can be replaced by CH_3OH on the surface of a giant metal-oxide based cluster which has a nanometer sized cavity and, in contrast to zeolites, reducing properties.

Early reports on the giant reduced ring-shaped, metal-oxide cluster $[Mo_{154}(NO)_{14}O_{420}(\mu_3\text{-}O)_{28}(H_m)_{14}(H_2O)_{70}]^{(42-n)-}$ **2**[1,2] and more recently on the even larger analogue $[(MoO_3)_{176}(H_2O)_{80}H_n]^{(32-n)-}$ **3**[3] (a reduced, protonated giant molecular molybdenum oxide with H_2O ligands), have shown the difficulties associated with the synthesis, isolation, identification and characterization of such systems, especially of the *m* and *n* values which correspond to the different protonations; see below.[1–4] Here we report a facile synthetic method for the pure crystalline blue mixed-valence compound (type III according to the Robin–Day classification)[5] **1a**·(32 − *n*)Na^+·*ca.* 600 H_2O·*ca.* 30 CH_3OH **1** containing the discrete cluster $[(MoO_3)_{176}(H_2O)_{63}(CH_3OH)_{17}H_n]^{(32-n)-}$ **1a** with CH_3OH ligands.‡ In contrast, all previously reported compounds of this type were obtained only under less lucid reaction conditions and not completely in crystalline form.

1 was simply prepared by addition of a methanolic solution of $MoCl_5$ to an acidified solution of molybdate§ and characterized by elemental analysis, single crystal X-ray structure analysis¶ [including bond valence sum (BVS) calculations for determination of the positions of the H atoms and the (formal) number of Mo^V centres], vibrational as well as VIS–NIR spectra, and redox titrations for the (additional) determination of the (formal) number of Mo^V centres.

The single crystal X-ray structure analysis¶ of compound **1** shows eight ring-shaped clusters in the unit cell, the (large) volume of which is comparable to that of protein structures (Fig. 1). The rings are packed only approximately parallel to the *a*,*b* plane, whereby they are tilted slightly relative to one another along the *a* and *b* axes. The cluster **1a** (Fig. 2) consists of sixteen sets of the three characteristic building blocks[2,6] $\{Mo_2\}$, $\{Mo_8\}$ and $\{Mo_1\}$ corresponding to the formula of the hexadecameric cluster $[\{Mo_2\}\{Mo_8\}\{Mo_1\}]_{16}$ ($\equiv[\{Mo^{VI}{}_2O_5(H_2O)_2\}\text{-}\{Mo^{VI/V}{}_8O_{26}(\mu_3\text{-}O)_2(H_m)L_3Mo^{VI/V}\}]_{16}$ with L = H_2O, CH_3OH and *m* = 0, 1 or 2 corresponding to the overall charge related to *n* = 0, 16 or 32).‡ The positions of the CH_3OH ligands in **1a** can be best described by referring to the sixteen characteristic Mo_6O_6 rings which are formed by two adjacent $\{Mo_8\}$-type units and one $\{Mo_2\}$ group. In every such Mo_6O_6 ring but three, a CH_3OH ligand is found coordinated to one or two Mo centres, respectively (for details see Fig. 2; referring to the packing in the crystal structure, the CH_3OH ligands are located at regions in the direct neighbourhood of adjacent rings).

Whereas **1a** is a mixed-valence cluster with an *S* = 0 spin ground state but no metal–metal bonds, the (rather) large diamagnetic mixed-valence $\{Mo_{43}\}$-type cluster[7] $[H_{13}Mo_{43}O_{112}\{(OCH_2)_3CCH_3\}_7]^{9-}$ contains 'dumb-bells' or pairs of covalently bonded Mo^V centres. On the other hand, in the largest reported polyoxotungstate $[Ln_{16}As_{12}W_{148}O_{524}(H_2O)_{36}]^{76-}$ all the W centres exist in completely oxidized W^{VI} form.[8]

The fast formation of cluster **1a** as well as the subsequent crystallization of compound **1**, free from amorphous precipitates, is facilitated not only by the use of aqueous methanol as solvent (with lower solubility than in water, as was used in previous preparation methods) but also by the addition of a solution containing Mo^V centres which become direct constituents of the reaction product **1**. In this context it should be mentioned that generations of chemists have tried to isolate crystals from molybdenum-blue solutions without success.[9,10] Another important result of the present study is that it is in principle possible to substitute ligands on the reducing surface of a giant metal-oxide based cluster with the possible consequence of influencing the activation of the ligands.

We thank F. Peters for his assistance. The financial support of the Deutsche Forschungsgemeinschaft and the Fonds der Chemischen Industrie is gratefully acknowledged.

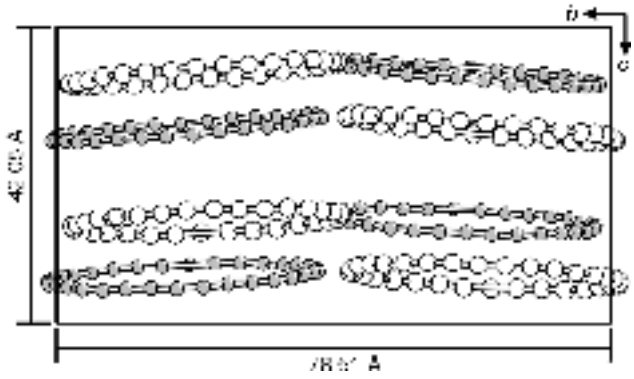

Fig. 1 Unit cell of **1** viewed along the *a* axis showing the packing of the rings. For the sake of clarity only the equatorial $\{Mo_1\}$-type atoms are shown (rings at the rear of the unit cell: grey).

Notes and References

† E-mail: amueller@cheops.chemie.uni-bielefeld.de

‡ The cluster charge 32 − *n* corresponds to the difference between the (formal) number of Mo^V centres (32 according to redox titrations and Mo-BVS values) and the number of protonations at the 32 μ_3-O atoms having BVS values of 1.20 ± 0.05. As these are practically constant in *ca.* 20 related structures in the corresponding $(\mu_3\text{-}O)_2O_2$ tetrahedra (see Fig. 2) we have an identical situation in all compounds which have either two, one or no protons in each such tetrahedron corresponding to *n* = 32, 16 or 0; but *n* = 28, 14 or 0 in tetradecameric species like **2**. The determination of the exact formula and the charge of the large investigated protonated mixed-valence cluster by single-crystal X-ray structure analysis therefore presents an almost invincible problem, in particular as charged lattice components like Na^+ located in cavities and channels and large amounts of crystal water molecules or solvent molecules cannot be clearly localized due to disorder phenomena. The analytical data, however, also have only limited accuracy because the concentration of the mentioned charged lattice components is very small (but not the number of ions in the formula unit!) and because the

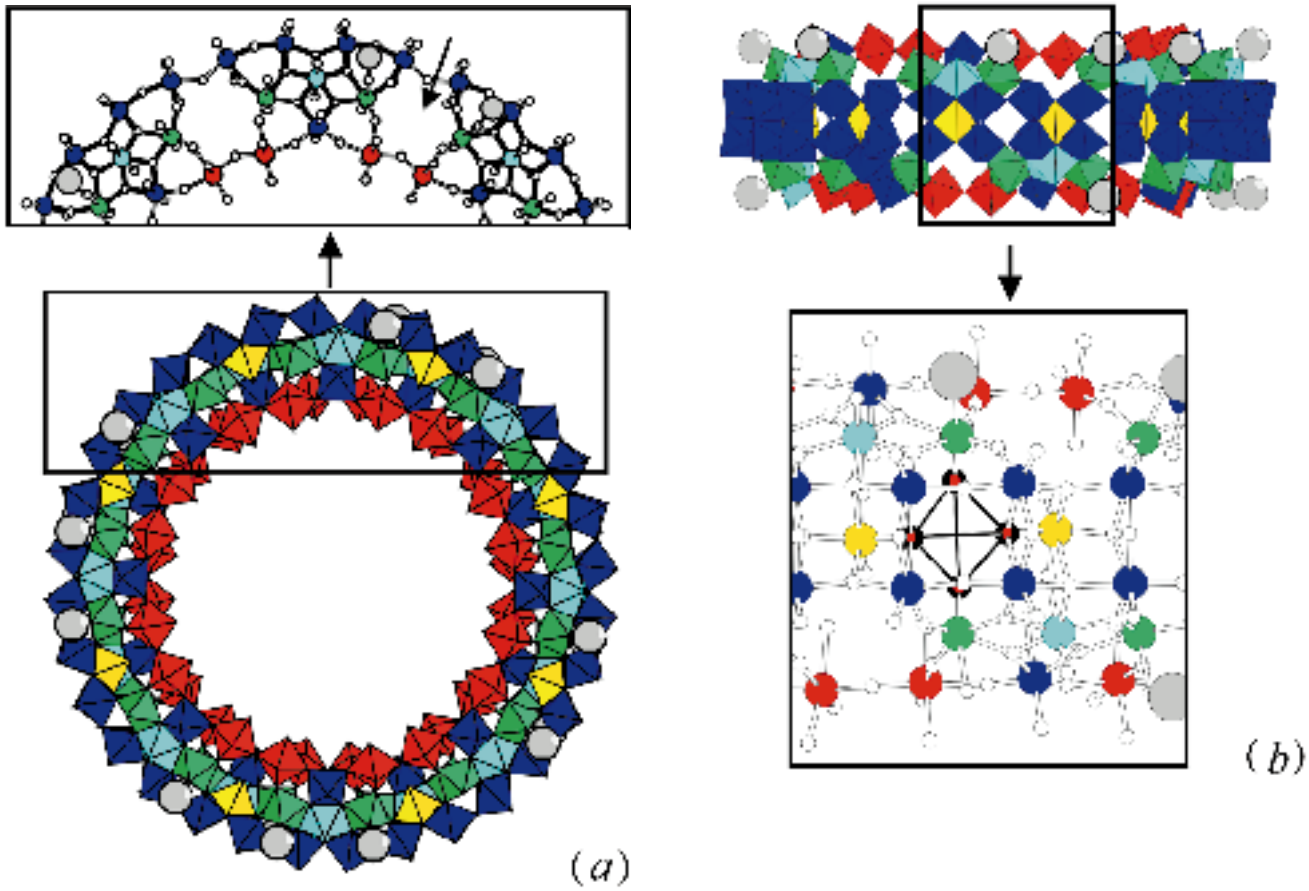

Fig. 2 Polyhedral representations of the structure of **1a** in two perspectives. (*a*) Top view, including an additional enlarged segment in ball-and-stick representation depicting the {Mo_8}-type units and {Mo_2} groups forming the Mo_6O_6 rings (see arrow) on the upper half of the cluster structure, showing the typical positions of the CH_3OH ligands with respect to the {Mo_8} units, as well as the twelve–membered rings. (*b*) Side view including an enlarged segment in ball-and-stick representation showing one of the sixteen $(\mu_3\text{-}O)_2O_2$ tetrahedra (highlighted by black lines) between two incomplete double-cubane-type fragments formed by five Mo and the related six O atoms of the {Mo_8} and {Mo_1} units, whereby the two μ_3-O atoms, highly accessible for protonation, are coordinated to (partly reduced) Mo centres. ({Mo_8} units: blue with the central pentagonal bipyramids (light blue) and the MoO_6 octahedra (green) at the right and left sides of these as (possible) coordination sites for the CH_3OH ligands; {Mo_2} units: red; {Mo_1} units: yellow; C atoms of CH_3OH ligands: grey; O atoms forming the $(\mu_3\text{-}O)_2O_2$ tetrahedron in the enlarged segment of (*b*): red connected by black lines).

large content of solvent molecules in the structure varies due to pronounced weathering. In any event, we consider an *n* value of 16 for the hexadecameric clusters **1a** and **3** (*n* = 14 for tetradecameric species) to be most suitable according to the sodium analysis together with the (only) possible *n* values.

§ A solution of $MoCl_5$ (0.5g; 1.83 mmol in 13.2 ml dry CH_3OH) was added dropwise to a stirred aqueous solution of $Na_2MoO_4{\cdot}2H_2O$ (2.01 g; 8.3 mmol in 18.5 ml H_2O) acidified with 1.0 ml 25% hydrochloric acid. The resulting blue solution was subsequently adjusted with 10% hydrochloric acid to pH 1.4 and stored under exclusion of air. Blue tetragonal-prismatic crystals which precipitated from the filtrate within 4 days were filtered and dried quickly in an argon stream. Yield: 0.64 g, 31.6% based on $MoCl_5$ used. Found: Na, 1.00; C, 1.51; H, 3.85 (Cl, 0.2). Calc.: Na, 0.94 (for 16 Na); C, 1.44; H, 3.94%. Subtraction of the estimated volume of the structurally localized atoms (using increments) from the total volume of the unit cell shows that a maximum of *ca.* 600 crystal water molecules can in principle be present per formula unit. **1**, however, loses a large amount of solvent molecules (about 60%) due to extremely strong and rapid weathering even at room temperature within 2 h. The analytical data which could therefore only be obtained for the partly weathered compound are corrected for this effect (based on time-dependent TG measurements), so that they can be compared to the calculated values which refer to the compound with the maximum crystal water content. IR ν/cm^{-1} (KBr pellet prepared under argon, 1700–400 cm^{-1}): 970m, 910wm [ν(Mo=O)], 820sh, 747s, 669sh, 634s, 559s. Resonance-Raman ν/cm^{-1} (KBr matrix, λ_e = 1064 nm): 804s, 536m, 465m, 325m, 217m. UV–VIS λ_{max}/nm (methanol): 743 (IVCT), 1072 (IVCT).

¶ *Crystal data* for **1**: $C_{47}H_{1530}Mo_{176}Na_{16}O_{1238}$, M = 39 166.5 g mol^{-1}, tetragonal, space group $P42_1c$, a = 78.508(5), c = 42.050(3) Å, U = 259 180(30) Å^3, Z = 8, D_c = 2.008 g cm^{-3}, μ = 1.76 mm^{-1}, F(000) = 154 270, crystal size = 0.35 × 0.35 × 0.35 mm^3. Crystals of **1** were removed from the mother liquor and immediately cooled to 198(2) K on a Bruker AXS SMART diffractometer (Mo-Kα, graphite monochromator). A total of 861 055 reflections (1.70 < θ < 22.49°) were collected of which 168 666 unique reflections (R_{int} = 0.1277) were used. The structure was solved using the program SHELXS-97 and refined using the program SHELXL-97 to R = 0.0951 for 111 621 reflections with $I > 2\sigma(I)$. CCDC 182/911.

1 A. Müller, E. Krickemeyer, J. Meyer, H. Bögge, F. Peters, W. Plass, E. Diemann, S. Dillinger, F. Nonnenbruch, M. Randerath and C. Menke, *Angew. Chem., Int. Ed. Engl.*, 1995, **34**, 2122.
2 A. Müller, F. Peters, M.T. Pope and D. Gatteschi, *Chem. Rev.*, 1998, **98**, 239.
3 A. Müller, E. Krickemeyer, H. Bögge, M. Schmidtmann, C. Beugholt, P. Kögerler and C. Lu, *Angew. Chem., Int. Ed. Engl.*, 1998, **37**, 1220.
4 A. Müller, J. Meyer, E. Krickemeyer and E. Diemann, *Angew. Chem., Int. Ed. Engl.*, 1996, **35**, 1206.
5 M. B. Robin and P. Day, *Adv. Inorg. Chem. Radiochem.*, 1967, **10**, 247.
6 A. Müller, E. Krickemeyer, H. Bögge, M. Schmidtmann, F. Peters, C. Menke and J. Meyer, *Angew. Chem., Int. Ed. Engl.*, 1997, **36**, 484.
7 M. I. Khan and J. Zubieta, *J. Am. Chem. Soc.*, 1992, **114**, 10 058; H. K. Chea, W. G. Klemperer and T. A. Marquart, *Coord. Chem. Rev.*, 1993, **128**, 209.
8 K. Wassermann, M. H. Dickman and M. T. Pope, *Angew. Chem., Int. Ed. Engl.*, 1997, **36**, 1445.
9 *Gmelins Handbuch der Anorganischen Chemie*, Verlag Chemie, Berlin, 1935: Mo, pp.134–137.
10 *Gmelin Handbook of Inorganic Chemistry*, Springer, Berlin, 1989: Mo Suppl. B3, pp. 61–68.

Received in Basel, Switzerland, 5th March 1998; 8/01804I

Chemically amplified photolithography of a conjugated polymer

Jianfei Yu, Michael Abley, Cheng Yang and Steven Holdcroft*†

Department of Chemistry, Simon Fraser University, Burnaby, BC, Canada V5A 1S6

The solid state photocatalytic reaction between trifluoromethanesulfonic acid and poly{3-[2-(tetrahydropyran-2-yloxy)ethyl]thiophene} is employed to fabricate polymeric patterns of conjugated polymer.

Microelectronic technologies routinely image polymer films using photolithography. Similar techniques have been employed to deposit conjugated polymers because of their attractive microelectronic and optoelectronic properties.[1] Here we describe a strategy which enhances the photoreactivity of conjugated polymers and facilitates their photolithography. The concept uses chemical amplification which was first demonstrated in photolithography with polystyrene based polymers.[2] The first example of chemical amplification in the photolithography of a conjugated polymer is demonstrated below (Scheme 1) for a polythiophene derivative possessing pendant THP functionality in the presence of a photoacid generator (PAG).

Poly{3-[2-(tetrahydropyran-2-yloxy)ethyl]thiophene} (PTHPET) was synthesized by the following procedure. 2-(3-Thienyl)ethanol was brominated selectively with 1 equiv. of NBS in DMF, and was protected by reacting with 5 equiv. of dihydropyran to afford 2-bromo-3-[2-(tetrahydropyran-2-yloxy)ethyl]thiophene.[3] The regioregular polymer PTHPET was prepared by cross-coupling of the corresponding 5-Grignard reagent.[4] The polymer was precipitated and purified from MeOH. The structure of the polymer was confirmed by NMR spectroscopy: resonance peaks in the ^{1}H NMR spectra centered at 7.12, 4.56 and 3.09 ppm were assigned to the thienyl ring, the methine of the THP moiety, and the α-methylene, respectively.[3a] Eleven resonance peaks were observed in the ^{13}C NMR spectra. Four peaks at 129.5, 132.0, 133.7 and 136.5 ppm were assigned to thienyl ring carbons.[4] The observed peaks at 98.8, 19.5, 25.6, 30.7 and 62.1 ppm are characteristic of the THP group.[5] Peaks at 30.0 and 67.1 ppm were assigned to α- and β-methylene carbons, respectively. The regioregularity of the polymer is evidenced by the fact that only four aromatic carbon signals and only one α-methylene carbon signal were observed. Molecular weight and molecular weight distribution were measured by GPC in THF solution and calibrated against poly(3-hexylthiophene) standards:[6] M_w = 1.15 × 10^4, M_w/M_n = 1.73. The photoacid generator, *N*-(trifluoromethylsulfonyloxy)-1,8-naphthalimide, was a gift from the IBM Research Division, San Jose, CA.

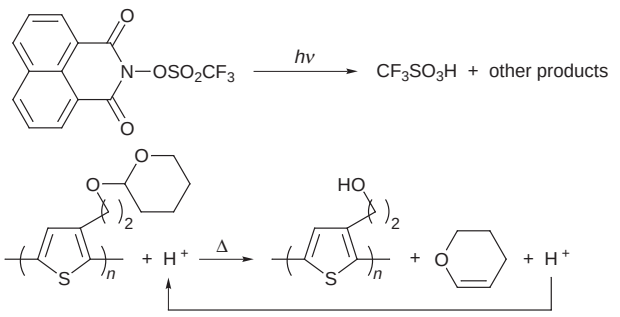

Scheme 1 Reaction scheme for chemically amplified photolithography of PTHPET

PTHPET is thermally stable up to ~220 °C whereupon a 30% weight loss was observed between 220 and 275 °C by TGA. The weight loss is consistent with the deprotection scheme shown in Scheme 1 in the absence of a catalytic proton. When mixed with trifluoromethanesulfonic (triflic) acid (5 mol% based on the thienyl unit), films of PTHPET are chemically stable at room temperature. However, upon heating, the deprotection temperature for the polymer was lowered to 120 °C. Furthermore, deprotection is complete indicating that the reaction is catalyzed by the presence of acid.

Upon thermolysis of PTHPET in the presence of triflic acid, FTIR showed the emergence of a broad signal at ~3400 cm^{-1} due to –OH. This occurred concomittently with the deprotection temperatures determined by TGA. There was also a significant decrease in the signals due to the THP group. Cleavage of THP from PTHPET gave rise to dramatic changes in the absorption spectra. PTHPET alone yielded classical reversible thermochromism between 20 and 210 °C (Fig. 1) but in the presence of 5 mol% triflic acid, λ_{max} dramatically increased at 130 °C upon heating. The red-shift is explained by the sudden release of steric hindrance caused upon elimination of the bulky THP group. The absorption spectra and λ_{max} became independent of temperature upon further heating or subsequent cooling cycles which is consistent with the increase in compactness associated with the shorter side-chain polymer and/or the existence of strong hydrogen bonding between ethanolic side-chains.

PTHPET is completely soluble in common organic solvents, whereas the resultant polymer following cleavage is not. This is the result of a significant change in the length and polarity of the side-chain. This observation, in conjunction with the acid-catalyzed nature of the deprotection process, gave the impetus to examine chemically amplified photolithography of PTHPET in the presence of a photoacid generator (Scheme 1). Films of PTHPET containing 20 mol% of the PAG were cast from THF solution. The PAG exhibited a broad absorption spectrum, λ_{max} 336 nm, and generates triflic acid when irradiated. Films were irradiated with UV–VIS light from a 1000 W Xe lamp through a 361 nm broadband filter with an irradiation intensity of 0.18 mW cm^{-2}. The temperature dependant absorption spectra of

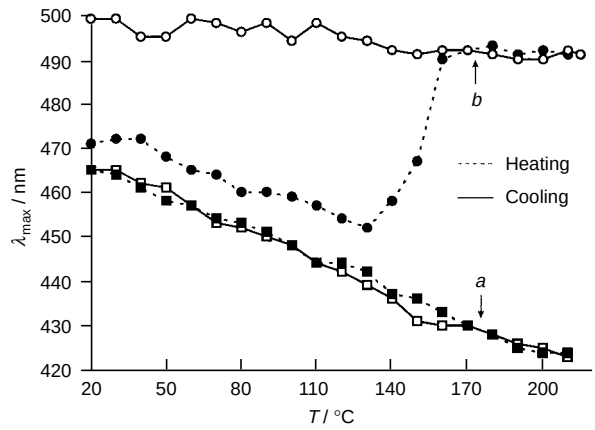

Fig. 1 Temperature dependence of λ_{max} for films of PTHPET (*a*) in the absence, and (*b*) presence of 5 mol% triflic acid

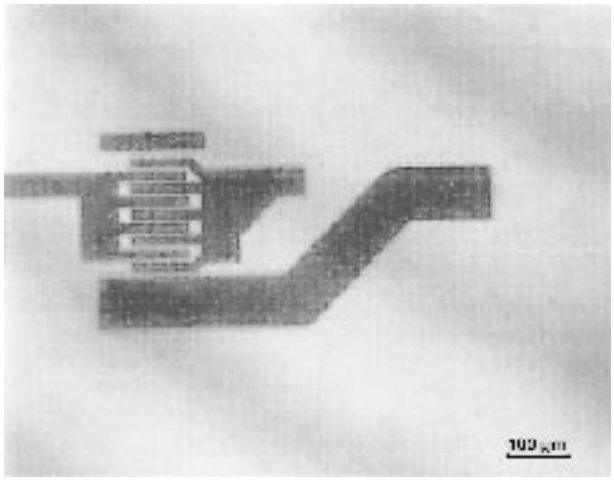

Fig. 2 Micrograph of conjugated polymer obtained by chemically amplified photolithography

photolyzed composite films was recorded following irradiation and showed a dramatic red-shift λ_{max} at 120 °C, *i.e.* similar to that observed for films containing triflic acid (Fig. 1). This is strong evidence for the catalytic cleavage of THP initiated through photogeneration of triflic acid. FTIR confirmed the reaction and the resultant photolyzed films were insoluble in common organic solvents.

Chemically amplified photolithography was demonstrated by irradiating similar composite films (~ 300 nm thick) through a photomask. The films were subsequently heated to 125 °C for 2.5 min and developed with THF, whereupon only the unexposed polymer dissolved. A patterned image of the conjugated polymer is presented in Fig. 2. The resolution of the smallest features is 15 μm and is limited by the optical apparatus. Due to the catalytic nature of this reaction relatively low irradiation doses were required for imaging (65 mJ cm^{-2}). Thus, the degree of photobleaching of the polymer was negligible. Conductivity measurements on the photochemically deprotected polymer doped with a variety of oxidants yielded conductivities very similar (1–4 S cm^{-1}) to the triflic acid deprotected polymer, confirming that π-conjugation was retained.

Spectroscopic, thermogravimetric, solubility and microscopic analyses confirm the reaction presented in Scheme 1. The reaction does not proceed in the solid state at room temperature at an appreciable rate. Upon heating, the reaction rate is increased either through an increase in free volume of the polymer and/or an increase in the rate constant. This is a favourable observation since it infers that the spatial extent of the imaging chemistry can be controlled following irradiation. Studies are underway to determine the electronic, optical and photonic properties of micron-sized polymeric patterns fabricated using this and similar chemical schemes.

We thank the Natural Sciences and Engineering Research Council of Canada for financial support and Dr R. D. Miller, IBM Research Division, San Jose, CA for generously providing photoacid generators.

Notes and References

† E-mail: holdcrof@sfu.ca

1 M. S. A. Abdou, Z. Xie, A. Leung and S. Holdcroft, *Synth. Met.*, 1992, **52**, 159; P. C. Allen, D. C. Bott, C. S. Brown, L. M. Connors, S. Gray, N. S. Walker, P. I. Clemonson and W. J. Feast, *Electronic Properties of Conjugated Polymers III*, ed. H. Kuzmany, M. Mehring and S. Roth, Springer-Verlag, Berlin, 1989; A. Torres-Filho and R. W. Lenz, *J. Polym. Sci., Part B: Polym. Phys.*, 1993, **31**, 959; M. Angelopoulos, J. M. Shaw, K.-L. Lee, W.-S. Huang, M.-A. Lecorre and M. Tissier, *Mol. Cryst. Liq. Cryst.*, 1990, **189**, 221; G. Venugopal, X. Quan, G. E. Johnson, F. M. Houlihan, E. Chin and O. Nalamasu, *Chem. Mater.*, 1995, **7**, 271.

2 H. Ito, C. G. Willson, J. M. J. Frechet, M. J. Farrall and E. Eichler, *Macromolecules*, 1983, **16**, 1510.

3 (*a*) K. A. Murray, S. C. Moratti, D. R. Baigent, N. C. Greenham, K. Pichler, A. B. Holmes and R. H. Friend, *Synth. Met.*, 1995, **69**, 395; (*b*) A. Bolognesi, R. Mendichi, A. Schieroni and D. Villa, *Macromol. Chem. Phys.*, 1997, **198**, 3277.

4 R. D. McCullough, R. D. Lowe, M. Jayaraman and D. L. Anderson, *J. Org. Chem.*, 1993, **58**, 904.

5 T. Sakamizu, H. Shiraish, H. Yamaguchi, T. Ueno and N. Hayashi, *Jpn. J. Appl. Phys.*, 1992, **31**, 4288.

6 S. Holdcroft, *J. Polym. Sci., Polym. Phys. Ed.*, 1991, **29**, 1585.

Received in Colombia, MO, USA, 20th December 1997; revised manuscript received 18th May 1998; 8/04117B

Radical cyclisation of carbohydrate alkynes: synthesis of highly functionalised cyclohexanes and carbasugars

Elise Maudru,[a] Gurdial Singh*[a]† and Richard H. Wightman*[b]

[a] *Department of Chemistry, University of Sunderland, Sunderland, UK SR1 3SD*
[b] *Department of Chemistry, Heriot-Watt University, Edinburgh, UK EH14 4AS*

Carbohydrate alkynes undergo 6-*exo* radical cyclisation to afford cyclohexanes resulting in the synthesis of carbasugars.

The use of carbohydrates as synthetic precursors of many functionalised carbocyclic compounds is widespread.[1] The first conversion of a sugar to a cyclohexane ring involved the preparation of nitroinositols from 6-deoxy-6-nitrohexose.[2] In the intervening years there have been numerous examples of the use of radical chemistry for the synthesis of cyclopentane derivatives,[3] with notable work in the carbohydrate area coming from the Fraser-Reid group.[4] It is thus surprising that there are few examples of the preparation of six-membered aliphatic rings employing radical cyclisation onto an alkyne.[5] Some reasons for this can be inferred from work on cyclisations of ω-alkenyl radicals. The formation of six-membered rings by radical chain reactions involving 6-*exo* cyclisation is some 40 times slower than that of the hex-5-enyl cyclisation.[6] The consequence of this is that chain transfer by attack of the acyclic radical on the stannane usually present is a much more effective process than with the hex-5-enyl radical. The second problem is that 1,5-hydrogen abstraction leading to a resonance stabilised allyl radical is favourable and in fact this can become synthetically useful.[3b]

We have been interested in the development of 6-*exo* cyclisations of alk-6-ynyl radicals as these would allow the preparation of heavily substituted hydroxycyclohexanes and of carbasugars. In this regard we chose to prepare alkynes derived from D-ribose[7] and to investigate their chemistry. Treatment of the protected silyl-D-ribose derivative **1** with lithium phenylacetylide afforded an inseparable diastereomeric mixture of the diols **2a** in 90% yield (Scheme 1). The protection of both the hydroxy groups as methoxymethyl (MOM) ethers[8] proceeded in a yield of 89% and allowed chromatographic separation of the diastereomers **3a** and **3b** with an *anti*:*syn* ratio of 3 : 2. Alternatively the *syn* isomer **3b** could be prepared almost exclusively using D-ribonolactone as the starting material.[9] Desilylation of **3a** was effected with TBAF in THF in 92% yield and afforded the primary alcohol **6a** which was converted to the corresponding iodide **7a** in 76% yield with triphenylphosphine, imidazole and iodine.[10] Similar chemistry with the isomer **3b** gave the alcohol **6b** and subsequently the iodide **7b** in comparable yields. With both the iodides **7a** and **7b** in hand we investigated their radical cyclisation reactions. Treatment of the iodide **7a** with tri-*n*-butyltin hydride in refluxing benzene in the presence of AIBN effected the 6-*exo* cyclisation affording only the substituted cyclohexanes **10** in 93% yield (Scheme 2) as an inseparable mixture of *E* and *Z* geometric isomers in a ratio of 1 : 1 as determined by ^{1}H NMR analysis. Analogous reaction of the diastereomer **7b** afforded the corresponding cyclohexanes **11** and **12** in 70% yield. In this case we were able to separate the *E* and *Z* stereoisomers by chromatography, in a ratio of 2 : 3. The major isomer **11** was assigned the *Z* geometry about the double bond on the basis of NOE experiments.

Having been successful in our initial goal we turned our attention to the syntheses of compounds with an unsubstituted *exo*-methylene group. Thus the protected ribose **1** was treated with lithium trimethylsilylacetylide in THF and afforded the diols **2b**, in a combined yield of 45% along with the alkynes **2c**, in 28% yield. The diastereomeric mixture **2b** was converted to

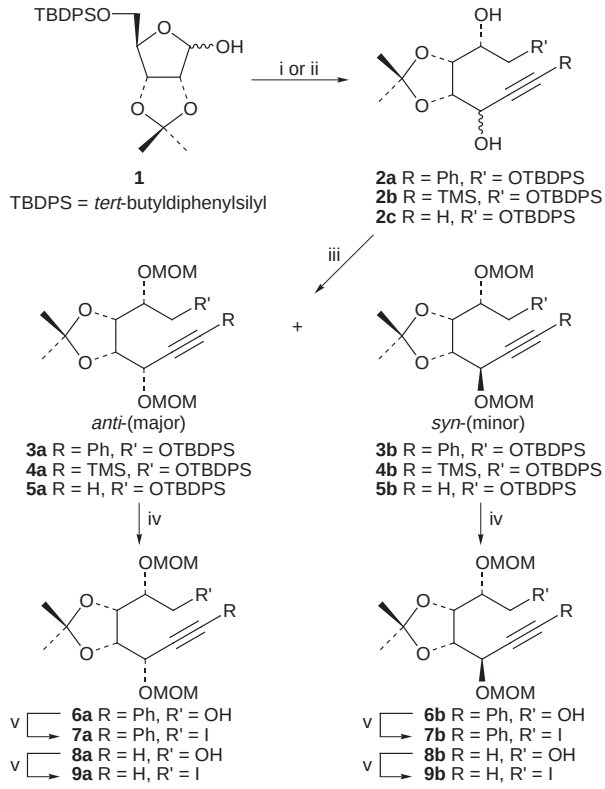

Scheme 1 *Reagents and conditions:* i, LiC≡CPh, THF, −78 °C; ii, LiC≡CTMS, THF, −78 °C; iii, MOMCl, NEt_2Pr^i, CH_2Cl_2, RT; iv, Bu_4NF, THF, RT; v, I_2, PPh_3, Im, PhMe, Δ

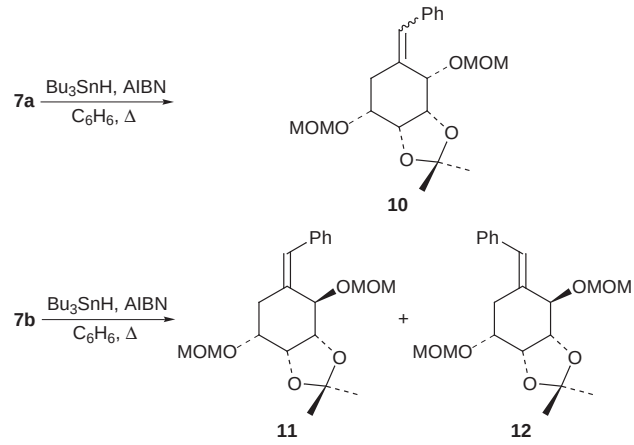

Scheme 2

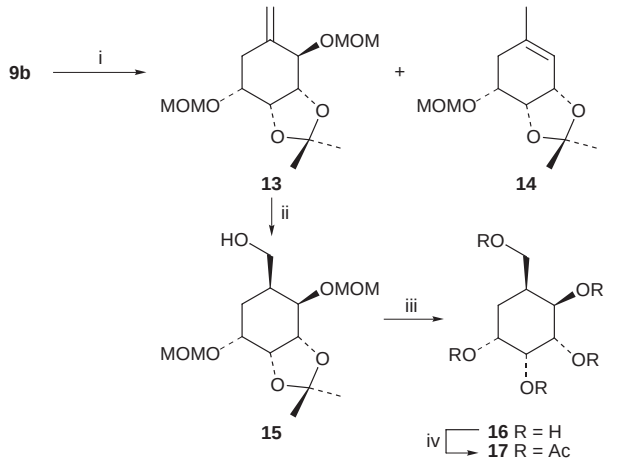

Scheme 3 *Reagents and conditions:* i, Bu_3SnH, AIBN, PhH, Δ; ii, BH_3–Me_2S, THF; 0 °C, H_2O_2, NaOH; iii, 6 M HCl, MeOH; iv, Ac_2O, Py, RT

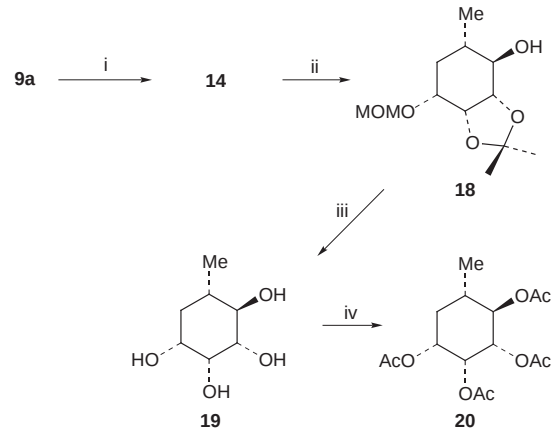

Scheme 4 *Reagents and conditions:* i, Bu_3SnH, PhH, AIBN, Δ; ii, BH_3–Me_2S, THF; 0 °C, H_2O_2, NaOH; iii, 6 M HCl, MeOH; iv, Ac_2O, Py, RT

the MOM ethers **4a** and **4b** that could be separated in a combined yield of 71% with an *anti*:*syn* ratio of 3.5 : 1. Both of these diastereomers were processed separately. Desilylation of **4a** and **4b** gave the corresponding primary alcohols **8a** and **8b** in 91 and 96% yields respectively. These compounds were identical to those obtained from **2c** after the diastereoisomers had been subjected to protection by MOM chloride to afford **5a**, **5b** and desilylation, the *anti*:*syn* ratio being 3 : 1. The *syn*-product was correlated with material prepared from the pure *syn*-isomer **2c**, which we have described in our earlier report.[9] The alcohols **8a** and **8b** were converted smoothly to the corresponding iodides **9a** and **9b** in 71 and 78% yields respectively. At this juncture we were in a position to study the 6-*exo* radical cyclisation of these iodides. Thus (Scheme 3) the *syn* isomer **9b** was treated with tri-*n*-butyltin hydride and AIBN in refluxing benzene and afforded the expected *exo*-methylene-cyclohexane **13** in 49% yield along with the cyclohexene **14** in 39% yield where the MOM group had been lost. The structure of **14** was clearly evident from the ^{1}H NMR spectrum which had resonances due to only one MOM group and in addition there was a resonance at δ 5.33 due to the vinylic proton and a resonance at δ 1.75 due to a methyl group. We next subjected the iodide **9a** to these conditions (Scheme 4) and we observed that in this case the cyclisation reaction was appreciably slower, taking 24 h to reach completion, but much cleaner in that only **14** was obtained in 99% yield. The formation of **14** can be rationalised by cyclisation of a primary radical in a 6-*exo* mode onto the alkyne, resulting in the formation of a vinyl radical which then abstracts a hydrogen from the methylene carbon of the MOM group followed by β-scission[11] resulting in an allylic radical which subsequently affords the observed product. The formation of **14** is a reflection of the geometry of the vinyl radical in that these are bent with a bond angle of *ca*. 135° whilst the α-phenyl substituted vinyl radical is linear.[12]

The *exo*-methylenecyclohexane **13** (Scheme 3) was hydroborated and gave after oxidation the primary alcohol **15** in 94% yield. Removal of the protecting groups of **15** with 6 M HCl gave carba-α-L-gulopyranose **16** whose spectral properties were in accord with those reported in the literature.[13] Additional structural proof was obtained by acetylation of **16** with excess acetic anhydride and pyridine which afforded the pentaacetate **17** in 100% yield. The cyclohexene **14** underwent hydroboration/oxidation (Scheme 4) with BH_3–Me_2S and afforded the protected carba-β-D-rhamnose derivative **18** in 77% yield. The stereochemistry of the newly formed chiral centres was *anti* with the C-4 hydroxy group β as a result of hydroboration occurring from the opposite face from the *O*-isopropylidene group, and this was confirmed by NOE experiments. Removal of the MOM and isopropylidene protection proceeded uneventfully with 6 M HCl and afforded the fully deprotected carba-β-D-rhamnose **19** in 99% yield. Further structural integrity of **19** was established by acetylation with excess acetic anhydride and pyridine which resulted in formation of the tetraacetate **20** in 99% yield.

We thank the EPSRC for access to central facilities for high resolution mass spectrometric data at the University of Wales, Swansea (Director, Dr J. A. Ballantine) and Professor W. T. Borden (University of Washington) for enlightening discussions regarding vinyl radicals. We thank Dr K. M. Morgan (Heriot-Watt University) for Monte Carlo Calculations.

Notes and References

† E-mail: gurdial.singh@sunderland.ac.uk

1 R. J. Ferrier and S. Middleton, *Chem. Rev*., 1993, **93**, 2779.
2 H. O. L. Fischer and J. M. Grosheintz, *J. Am. Chem. Soc*., 1948, **70**, 1476; H. O. L. Fischer and B. Iselin, *J. Am. Chem. Soc*., 1948, **70**, 3946.
3 For excellent reviews on radical cyclisation reactions see: (*a*) B. Giese, B. Kopping, T. Gobel, J. Dickhaut, G. Thoma, K. J. Kulicke and F. Trach, *Org. React.*, 1996, **48**, ch. 2; (*b*) W. B. Motherwell and D. Crich, *Free Radical Chain Reactions in Organic Synthesis*, Academic Press, New York, 1992.
4 B. Fraser-Reid and R. Tsang, *Strategies and Tactics in Organic Synthesis*, Academic Press, New York, 1989, vol. 2.
5 G. Büchi and H. Wüest, *J. Org. Chem*., 1979, **44**, 546; M. D. Bachi and C. Hoornaert, *Tetrahedron Lett*., 1982, **23**, 2502; D. L. J. Clive, P. L. Beaulieu and L. Set, *J. Org. Chem*., 1984, **49**, 1313; J. K. Crandell and W. I. Michaley, *J. Org. Chem*., 1984, **49**, 4244; G. Just and G. Sacripante, *Can. J. Chem*., 1987, **65**, 104, A. V. Rama Rao, J. S. Yadav, C. S. Rao and S. Chandrasekhar, *J. Chem. Soc., Perkin Trans. 1*, 1990, 1211; C. K. Sha, T. S. Jean and D. C. Wang, *Tetrahedron Lett*., 1990, **31**, 3745; D. L. Boger and R. J. Mathvink, *J. Am. Chem. Soc*., 1990, **112**, 4003; T. Honda, M. Satoh and Y. Kobayashi, *J. Chem. Soc., Perkin Trans. 1*, 1992, 1557; J. Marco-Contelles, *Synth Commun*., 1994, **24**, 1293; J. Marco-Contelles, M. Bernabe, D. Ayala and B. Sanchez, *J. Org. Chem*., 1994, **59**, 1234; this details a 6-*endo-dig* cyclisation; R. E. McDevitt and B. Fraser-Reid, *J. Org. Chem*., 1994, **59**, 3250.
6 A. L. J. Beckwith, *Tetrahedron*, 1981, **37**, 3073; A. L. J. Beckwith and C. J. Easton, *J. Am. Chem. Soc*., 1981, **103**, 615; V. Malatesta and K. U. Ingold, *J. Am. Chem. Soc*., 1981, **103**, 609, A. L. J. Beckwith and C. H. Schiesser, *Tetrahedron*, 1985, **41**, 3925; P. R. Jenkins, M. C. R. Symons, S. E. Booth and C. J. Swain, *Tetrahedron Lett*., 1992, **33**, 3545.
7 B. Mekki, G. Singh and R. H. Wightman, *Tetrahedron Lett*., 1991, **32**, 5143 and references cited therein.
8 G. Stork and T. Takahashi, *J. Am. Chem. Soc*., 1977, **99**, 1275.
9 S. Jiang, G. Singh and R. H. Wightman, *Chem. Lett*., 1996, 67.
10 P. J. Garegg and B. Samuelsson, *J. Chem. Soc., Perkin Trans. 1*, 1980, 2866.
11 J.-C. Malanda and A. Doutheau, *J. Carbohydr. Chem*., 1993, **12**, 999.
12 W. T. Borden and A. Nicolaides, *J. Am. Chem. Soc*., 1991, **113**, 6750 and refs. therein.
13 L. Pingli and M. Vandewalle, *Tetrahedron*, 1994, **50**, 7061; L. Pingli and M. Vandewalle, *Synlett*., 1994, 228.

Received in Liverpool, UK, 20th March 1998; 8/02228C

Preparation and catalytic properties of single phase Ni–Sn intermetallic compound particles by CVD of $Sn(CH_3)_4$ onto Ni/silica

Ayumu Onda, Takayuki Komatsu*† and Tatsuaki Yashima

Department of Chemistry, Tokyo Institute of Technology, Meguro-ku, Tokyo 152-8551, Japan

Particles of each of the single phase Ni–Sn intermetallic compounds Ni_3Sn, Ni_3Sn_2 and Ni_3Sn_4 have been formed on silica by chemical vapor deposition (CVD) of $Sn(CH_3)_4$ onto Ni/SiO_2 and used as catalysts for cyclohexane dehydrogenation.

We have previously reported unique catalytic selectivities of Co or Pt containing intermetallic compounds (IMCs) for the partial hydrogenation of acetylene[1] or buta-1,3-diene;[2] however, their catalytic activities suffered from low specific surface areas. It was reported that Sn–M (M = Rh, Pt, Pd or Ni) bimetallic catalysts were prepared by CVD of organotin complexes on M/SiO_2.[3–5] Tin species are deposited by the CVD method preferentially onto the particles of these noble metals. In this study, we applied the CVD method to prepare fine particles of single phase Ni–Sn IMCs on SiO_2, which were found to have unique catalytic selectivities in the dehydrogenation of cyclohexane.

Ni (5 wt%)/SiO_2 was first prepared by an incipient wetness method using $Ni(NO_3)_2$ and silica gel (Fuji-Silysia, Caliact 6), followed by reduction at 723 K in H_2. The average diameter of the Ni particles measured by TEM, XRD and chemisorption of H_2 was about 7 nm. CVD of $Sn(CH_3)_4$ (Soekawa Chemicals) onto Ni/SiO_2 was carried out at 373–523 K with flowing H_2 containing 33 Torr of $Sn(CH_3)_4$, followed by hydrogen treatment at 873–1173 K. The samples were dissolved in hydrochloric acid and the amounts of Ni and Sn were determined by ICP. Unsupported Ni–Sn IMCs were prepared by melting a mixture of Ni and Sn powders in an electric furnace at 1730 K under flowing argon, and the resulting ingot was crushed into 25–38 μm particles. A glass circulation system was used for the pretreatment of catalysts with H_2 and subsequent catalytic reactions.

CVD of $Sn(CH_3)_4$ was carried out at various temperatures for 1 h to prepare each Ni–Sn IMC (Ni_3Sn, Ni_3Sn_2 and Ni_3Sn_4). Fig. 1 shows the amount of deposited Sn as a function of CVD temperature on Ni/SiO_2 (*a*) or SiO_2 (*b*). The amounts of deposited Sn increased with CVD temperature on both supports.

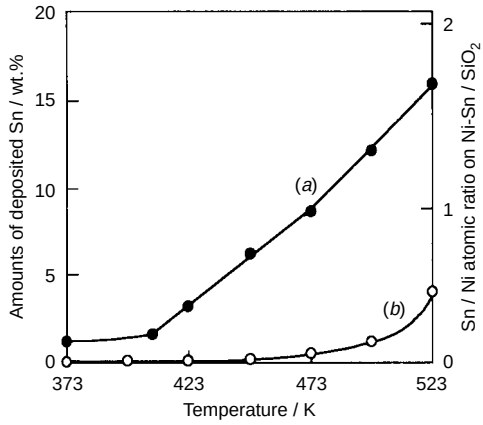

Fig. 1 Effect of CVD temperature on the amount of Sn supported by $Sn(CH_3)_4$ on Ni/SiO_2 (*a*) or on SiO_2 (*b*)

However, the amounts of deposited Sn on Ni/SiO_2 were much larger than those on SiO_2. In particular, no appreciable deposition of Sn was observed on SiO_2 below 423 K. $Sn(CH_3)_4$ was selectively decomposed on Ni particles owing to the high activity of Ni for the hydrogenolysis of $Sn(CH_3)_4$. When CVD of $Sn(CH_3)_4$ was carried out onto Ni/SiO_2 at 423, 448 and 498 K, the Ni/Sn atomic ratios of the samples became very close to 3/1, 3/2 and 3/4, respectively. If Sn atoms are deposited on the surface of Ni particles to form a few Sn layers, the Ni/Sn ratio must be much higher than unity. Therefore, during the CVD treatment, some of the deposited Sn atoms will enter into the bulk of the Ni particles after the hydrogenation of $Sn(CH_3)_4$ with the evolution of methane. In fact, the X-ray diffraction pattern of Ni–Sn/SiO_2 samples just after CVD included weak peaks of Ni–Sn IMCs in addition to those of Ni metal. Hydrogen treatment after CVD was then performed in order to form single phase Ni_3Sn, Ni_3Sn_2 and Ni_3Sn_4 particles.

Fig. 2 shows the X-ray diffraction patterns of the silica-supported Ni–Sn IMC (Ni/Sn = 3/1) after hydrogen treatment at 1173 K for 1 h (*a*) and of the unsupported Ni_3Sn powder (*b*). The supported sample did not show the same diffraction peaks as those of pure Ni supported on SiO_2 (*c*) and pure Sn supported on SiO_2 (*d*), but showed almost exclusively peaks at the same positions as those of unsupported Ni_3Sn. This result confirmed that single phase Ni_3Sn particles were formed on SiO_2 by the CVD and subsequent hydrogen treatment. Generally, Ni_3Sn is formed above 1730 K, because the melting points of Ni and Sn are 1730 K and 505 K, respectively. In this study, we succeeded in the formation of single phase Ni_3Sn particles by hydrogen treatment at much lower temperature after the CVD process.

The XRD measurements showed that single phase Ni_3Sn_2 and Ni_3Sn_4 particles were also formed on SiO_2 by hydrogen treatment at 873 and 723 K after CVD at 448 and 498 K, respectively. It is revealed that the lower the Ni/Sn ratio, the

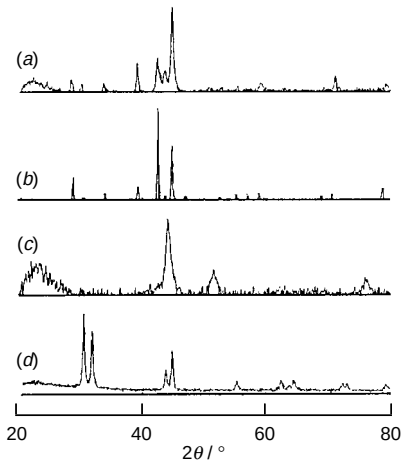

Fig. 2 XRD patterns of supported Ni–Sn IMCs (Ni/Sn = 3/1) on SiO_2 prepared by CVD after hydrogen treatment at 1173 K for 1 h (*a*), unsupported Ni_3Sn (*b*), Ni/SiO_2 prepared by the incipient wetness method after reduction (*c*) and Sn/SiO_2 prepared by CVD of $Sn(CH_3)_4$ on SiO_2 (*d*)

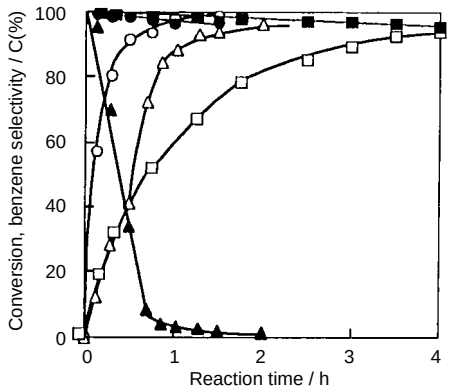

Fig. 3 Conversion of cyclohexane (open symbols) and selectivity to benzene (closed symbols) at 823 K on 0.05 g of Ni_3Sn/SiO_2 (○,●), 0.5 g of unsupported Ni_3Sn (■,□) and 0.5 g of unsupported Ni (△,▲)

lower the temperature of hydrogen treatment necessary for the formation of single phase Ni–Sn IMCs. The broad diffraction peaks of supported Ni_3Sn [Fig. 2(*a*)] suggest that the Ni_3Sn particles have much smaller diameters than those of unsupported Ni_3Sn. The particle sizes of Ni_3Sn, Ni_3Sn_2 and Ni_3Sn_4 determined by XRD were about 18, 12 and 12 nm, respectively. These values correspond roughly with the diameters estimated by TEM. Ni_3Sn particles had the largest diameter as these were formed at the highest temperature in the hydrogen treatment. The use of Ni/SiO_2 with smaller Ni particles would lead to Ni–Sn IMCs with smaller particles. It is concluded that all kinds of single phase Ni–Sn intermetallic compounds are obtained on silica by the CVD of $Sn(CH_3)_4$ and subsequent hydrogen treatment at temperatures much lower than the melting point of Ni.

The reaction profiles of cyclohexane in hydrogen at 823 K on silica-supported and unsupported Ni_3Sn IMCs and pure Ni catalysts are shown in Fig. 3. The initial molar ratio of hydrogen to cyclohexane was 6. On the unsupported Ni, benzene was formed as an initial product and was then converted completely into methane in 2 h. On the other hand, the unsupported Ni_3Sn catalyst scarcely converted the initially produced benzene into methane even at higher cyclohexane conversions, though the activity was lower than Ni. The high selectivity to benzene was revealed to be the characteristic catalysis of Ni_3Sn IMC, which would be due to the weaker adsorption of benzene on Ni_3Sn than on Ni. Silica-supported Ni_3Sn showed almost the same selectivity as the unsupported Ni_3Sn. This implies that no pure Ni particles that are too small to be detected by XRD exist on the silica-supported catalyst. Ni_3Sn has the composition richest in Ni among the Ni–Sn IMCs studied. Therefore, it is also indicated that there would be few Ni_3Sn_2, Ni_3Sn_4 or Sn small particles on the silica gel because the Ni/Sn atomic ratio of this sample (3.1/1) was very close to the stoichiometry of Ni_3Sn. Comparing the activity per weight of Ni_3Sn, the supported Ni_3Sn was 500 times more active than the unsupported Ni_3Sn, though the activities of both catalysts per surface area of Ni_3Sn were almost the same. It is clear that the CVD method has resulted in the preparation of silica-supported Ni–Sn IMC catalysts with higher activities than the unsupported ones, owing to the much higher specific surface areas, with retention of the high selectivity to benzene.

Notes and References

† E-mail: komatsu@chem.titech.ac.jp

1 T. Komatsu, M. Fukui and T. Yashima, *Stud. Surf. Sci. Catal.*, 1996, **101**, 1095.
2 T. Komatsu, S. Hyodo and T. Yashima, *J. Phys. Chem. B*, 1997, **101**, 5565.
3 J. P. Candy, A. E. Mansour, O. A. Ferretti, G. Mablion, J. P. Bournonville J. M. Basset and G. Martino, *J. Catal.*, 1988, **112**, 201.
4 P. Lesage, O. Clause, P. Moral, B. Didillon, J. P. Candy and J. M. Basset, *J. Catal.*, 1995 **155**, 238.
5 K. Tomishige, K. Asakura and Y. Iwasawa, *J. Catal.*, 1994, **149**, 70.

Received in Cambridge, UK, 24th April 1998; 8/03071E

Palladium-catalyzed amination of aromatic halides in water-containing solvent systems: a two-phase protocol

Guido Wüllner, Helge Jänsch, Sven Kannenberg, Frank Schubert and Gernot Boche*†

Fachbereich Chemie, Philipps-Universität, Marburg, D-35032, Germany

The use of the six-fold sulfonated ligand BINAS-6 1 permits the Pd⁰-catalyzed amination of aromatic halides in water containing single- or two-phase systems.

Following the initial investigations of Kosugi *et al.*,[1] both Buchwald[2] and Hartwig[3] and their co-workers have developed in recent years a new methodology for the amination of aromatic halides and triflates (ArX: X = Cl, Br, I, OSO_2CF_3) with amines RR^1NH to yield aromatic amines of the type $ArNRR^1$.[4] ArX and RR^1NH were reacted with (di)phosphine-complexed palladium [Pd^0L, 1–5 mol%] and sodium *tert*-butoxide (1.4 equiv.) in PhMe at 80–100°C under homogeneous reaction conditions [eqn. (1)].

$$ArX + HNRR^1 \xrightarrow[\text{toluene, 80–100 °C}]{Pd^0L,\ NaOBu^t} ArNRR^1 \qquad (1)$$

X = Cl, Br, I, OSO_2CF_3 R = H, alkyl, aryl R^1 = aryl

Under such conditions reapplication of the Pd^0 catalyst would be difficult as is reuse of the relatively expensive (di)phosphine ligand L. In contrast, by using a two-phase protocol, the separation of products (and unreacted starting material) from the catalyst and subsequent reapplication of the catalyst in further reactions is made facile.[5] For this reason there is increasing interest in two-phase catalysis both in the laboratory[6,7] and for industrial applications.[8] Here we report on a two-phase protocol of the aforementioned Pd^0-catalyzed amination reaction.

The ligand used here is the six-fold sulfonated 2,2′-bis(diphenylphosphinomethyl)-1,1′-binaphthyl **1** (BINAS-6) dissolved in water.[9]

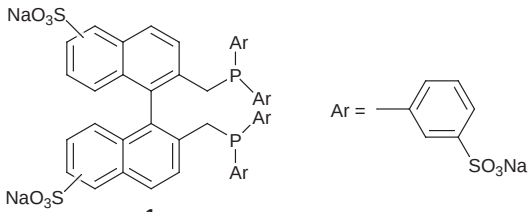

1

The reaction of 4-bromoacetophenone **2** with *N*-methylaniline **3a** in water–MeOH (1:3; solvent A) using NaOH as the base and the aforementioned catalyst Pd^0–**1** afforded 1-[4-(*N*-methylanilino)phenyl]ethan-1-one **4a** in 88% yield [eqn. (2); Table 1, entry 1].

Reacting **2** with **3b** in the presence of Pd^0–**1** and NaOH as the base in water–MeOH (1 : 6; solvent B) resulted in the formation of 1-(4-anilinophenyl)ethan-1-one **4b** in 91% yield [eqn. (2); Table 1, entry 2]. The Pd^0–**1** catalyst, which is dissolved in the aqueous phase, can be reused after separation of the products. The reaction was repeated under similar conditions. The following yields were achieved: second reaction 85% **4b**, (5 h); third reaction 53% **4b**, (7 h); fourth reaction 36% **4b**, (7 h).

The use of a two-phase H_2O–MeOH–PhMe system (1 : 2 : 2; solvent C) in the reaction of **2** with **3a** afforded only low yields

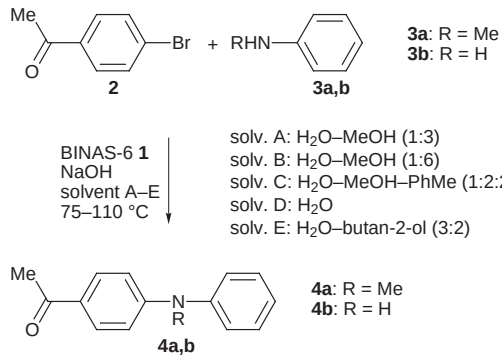

(2)

(36%) of **4a** [eqn. (2); Table 1, entry 3]. The use of emulsifying agents like tetradecyltrimethylammoniumbromide did not increase the yield of **4a**, but resulted in considerable problems during product recovery. With only water as the solvent (solvent D) **4a** was obtained in 36% yield [eqn. (2); Table 1, entry 4].

Butan-2-ol and water form a biphasic system with good miscibility of the two solvents. Thus in the reaction of **2** with **3b** in the presence of Pd^0–**1** and water–butan-2-ol (3 : 2, solvent E) the product **4b** was obtained in 89% yield [eqn. (2); Table 1, entry 5]. NaOH was found to give the best results as compared to other group I hydroxides. The catalyst Pd^0–**1** remains in the aqueous phase while the products can be collected conveniently by separation of the organic layer. Only small amounts of

Table 1 Pd^0–**1** catalysed aminations of ArX in water-containing solvent systems. All reactions were carried out under argon with degassed solvents and starting materials. **1** was applied in an aqueous solution (140 mmol l^{-1}). Physical and spectroscopic data of the products were consistent with those reported previously in the literature.

Entry[a]	Halide	Amine	Solvent	Reaction time/h	Product	Yield (%)
1	**2**	**3a**	A	2	**4a**	88
2	**2**	**3b**	B	3	**4b**	91
3	**2**	**3a**	C	32	**4a**	36
4	**2**	**3a**	D	25	**4a**	36
5	**2**	**3b**	E	6	**4b**	89
6	**5**	**3b**	E	6	**6a**	81
7	**5**	**3c**	E	8	**6b**	71

[a] Details of entries 1–7. 1: 160 μmol **1**, 20 μmol $Pd(OAc)_2$, 3 ml MeOH, 1 mmol ArX, 1.3 mmol amine, 1.3 mmol NaOH, 75 °C; products were extracted with Et_2O. 2: 70 μmol **1**, 9 μmol $Pd(OAc)_2$, 6 ml MeOH, 1 mmol ArX, 1.3 mmol amine, 1.4 mmol NaOH, 75 °C; products were extracted with Et_2O. 3: 840 μmol **1**, 100 μmol $Pd(OAc)_2$, 12 ml MeOH, 12 ml PhMe, 6 ml water, 2 mmol ArX, 2.4 mmol amine, 2.8 mmol NaOH, 70 °C; products were collected by separation of the organic layer. 4: 840 μmol **1**, 100 μmol $Pd(OAc)_2$, 12 ml water, 2 mmol ArX, 2.4 mmol amine, 2.8 mmol NaOH, 90 °C; products were extracted with Et_2O. 5–7: 80 μmol **1**, 11 μmol $Pd(OAc)_2$, 3 ml water, 2 ml butan-2-ol, 1 mmol ArX, 1.3 mmol amine, 1.3 mmol NaOH, 110 °C; products were collected by separation of the organic layer.

product (< 5%) remain in the aqueous phase. In this solvent system the catalyst can be reused as well.

Reacting 1-chloroanthraquinone **5** with aniline **3b** in the presence of Pd^0–**1** and NaOH in water–butan-2-ol (3 : 2) allowed amination of **5**, affording 1-anilinoanthraquinone **6a** in 81% yield [eqn. (3); Table 1, entry 6]. The use of *o*-toluidine **3c** under similar conditions gave 1-(*o*-toluidino)anthraquinone **6b** in 71% yield [eqn. (3); Table 1, entry 7].

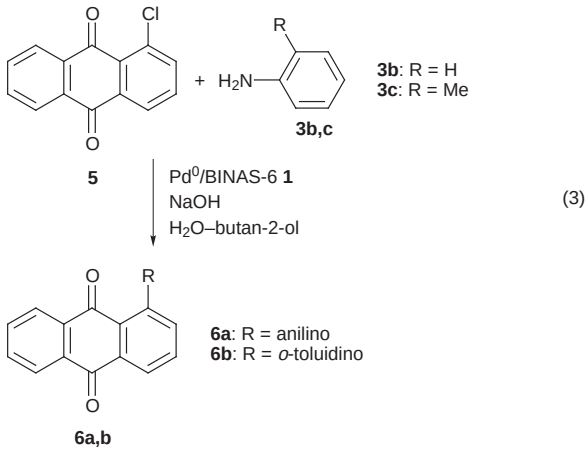

In conclusion, it has been demonstrated that the Pd^0-catalyzed amination of aromatic halides with amines can be performed by means of a two-phase protocol with NaOH instead of the expensive $NaOBu^t$ as the base. Further advantages are the facile catalyst/product separation and the reusability of the water-soluble Pd^0/BINAS-6 catalyst. The catalyst system is also suitable for the preparation of substituted anthraquinones, which are important in dye stuff production.[10] Further work is being conducted to optimise the reaction conditions and to perform selective single amination reactions of dichloro-substituted anthraquinones.

We are grateful to the Deutsche Forschungsgemeinschaft (Sonderforschungsbereich 260 and Graduiertenkolleg Metallorganische Chemie) and the Fonds der Chemischen Industrie for financial support, and Dr H. Bahrmann, Celanese GmbH, Werk Ruhrchemie, for BINAS-6 **1** as well as helpful discussions. The Degussa AG provided us with $Pd(OAc)_2$.

Notes and References

† E-mail: boche@ps1515.chemie.uni-marburg.de

1 M. Kosugi, M. Kameyama and T. Migita, *Chem. Lett.*, 1983, 927; M. Kosugi, M. Kameyama and T. Migita, *Nippon Kagaku Kaishi*, 1985, **3** 547.
2 A. S. Guram, R. A. Rennels and S. L. Buchwald, *Angew. Chem.*, 1995, **107**, 1456; *Angew. Chem., Int. Ed. Engl.*, 1995, **34**, 1348; J. P. Wolfe, R. A. Rennels and S. L. Buchwald, *Tetrahedron*, 1996, **52**, 7525; J. P. Wolfe, S. Wagaw and S. L. Buchwald, *J. Am. Chem. Soc.*, 1996, **118**, 7215; S. Wagaw and S. L. Buchwald, *J. Org. Chem.*, 1996, **61**, 7240; palladium-catalyzed aminations of triflate-arenes J. P. Wolfe and S. L. Buchwald, *J. Org. Chem.*, 1996, **61**, 1133; J. P. Wolfe and S. L. Buchwald, *J. Org. Chem.*, 1997, **62**, 1264.
3 J. Louie and J. F. Hartwig, *Tetrahedron Lett.*, 1995, **36**, 3609; M. S. Driver and J. F. Hartwig, *J. Am. Chem. Soc.*, 1996, **118**, 7217; J. Louie, M. S. Driver and B. C. Hamann and J. F. Hartwig, *J. Org. Chem.*, 1997, **62**, 1268.
4 See also M. Beller, T. M. Riermeier, C.-P. Reisinger and W. A. Herrmann, *Tetrahedron Lett.*, 1997, **38**, 2073; N. P. Reddy and M. Tanaka, *Tetrahedron Lett.*, 1997, **38**, 4807.
5 B. Cornils, *Angew. Chem.*, 1995, **107**, 1709; *Angew. Chem., Int. Ed. Engl.*, 1995, **34**, 1575.
6 W. A. Herrmann and C. W. Kohlpaintner, *Angew. Chem.*, 1993, **105**, 1588; *Angew. Chem., Int. Ed. Engl.*, 1993, **32**, 1524; P. Kalck and F. Monteil, *Adv. Org. Chem.*, 1992, **34**, 219.
7 T. Prinz, W. Keim and B. Drießen-Hölscher, *Angew. Chem.*, 1996, **108**, 1835; *Angew. Chem., Int. Ed. Engl.*, 1996, **35**, 1708.
8 W. Keim, *Chem Ing. Tech*., 1984, **56**, 850; G. Mercier and P. Chabardes, *Pure Appl. Chem.*, 1994, **66**, 1509; Y. Tokitoh, N. Yoshimura, T. Higashi, K. Mino and M. Murasawa, EP 436226, 1991; *Chem. Abstr.*, 1991, **115**, 158508z; A. Behr and W. Keim, *Arab. J. Sci. Eng.*, 1985, **10**, 377.
9 H. Bahrmann, K. Bergrath, H.-J. Kleiner, P. Lappe, C. Naumann, D. Peters and D. Regnat, *J. Organomet. Chem.*, 1996, **520**, 97.
10 H. S. Bien, J. Stawitz and K. Wunderlich, *Ullmann's Encyclopedia of Industrial Chemistry*, VCH, Weinheim, 1985, vol. A2, p. 355.

Received in Liverpool, UK, 20th May 1998; 8/03819H

Formation of thermotropic and lyotropic smectic and columnar liquid crystalline phases by a novel type of rigid rod-like amphiphilic molecule

Marius Kölbel,[a] Carsten Tschierske*[a]† and Siegmar Diele[b]

[a] *Institut für Organische Chemie der Martin-Luther-Universität Halle-Wittenberg, D-06120 Halle, Kurt-Mothes-Str. 2, Germany*
[b] *Institut für Physikalische Chemie der Martin-Luther-Universität Halle-Wittenberg, D-06108 Halle, Mühlpforte 1, Germany*

4-Benzyloxy-4′-(2,3-dihydroxypropyloxy)biphenyls with lateral methyl substituents are a novel class of amphiphilic mesogens displaying thermotropic and lyotropic smectic and columnar mesophases due to microsegregation of hydrophilic regions from all-aromatic segments in the absence of a flexible alkyl chain.

The liquid crystalline state which combines order and mobility on a molecular level is of great interest for material science as well as for life science and is found in different classes of compounds. Most are anisometric (rod-shaped or disc-like) molecules and amphiphilic molecules. These molecules consist of an anisometric or a polar basic unit to which one or more flexible chains are grafted. Usually these are alkyl chains and provide the mobility whereas the order is provided by the packing of the anisometric groups or by the attractive forces between the polar groups. Liquid crystalline materials without flexible chains are rare. Examples are *p*-oligophenylenes[1] and high molecular mass condensed polyaromatic compounds (carbonaceous materials).[2] More recently columnar liquid crystalline properties have been found for some polyhalogenated small aromatic compounds such as indene derivatives and pseudoazulenes[3] and for salts of 3-phenyloxyphenyl-2-propionic acid, important non-steroidal antiinflammatory drugs (fenoprofens).[4] Also molecules consisting of aromatic systems with polar groups around their peripheries such as, for example, some drugs, dyes, nucleic acids and antibiotics, can form lyotropic mesophases with protic solvents. In these chromonic liquid crystals[5] the solvent provides the mobility.

Here, we report on a novel type of amphiphiles without flexible alkyl chains, consisting only of a hydrophilic *rac*-2,3-dihydroxypropyl group and a linear array of three *p*-substituted benzene rings providing a rather rigid lipophilic unit.[6] Both the attractive interactions between the rigid aromatic units and the hydrogen bonding provided by the 1,2-diol[7] unit give rise to the very high melting point of **1**. In order to diminish the attractive interactions between the aromatic units a single methyl group was grafted at different positions laterally to the biphenyl unit of **1**. Indeed, a dramatic decrease in the melting temperature was possible and liquid crystalline properties can be observed for all methyl-substituted compounds **2**–**5**.‡ The influence of the position of the lateral substituent on the thermotropic properties is shown in Table 1.

Compounds **2** and **4** show a monotropic phase easily identified as a smectic layer structure (S_A phase) by its typical fan like texture and regions with homeotropic orientation and oily streaks, observed by microscopy between crossed polarisers. For compound **3** one observes a monotropic tilted smectic phase (S_C phase), identified by its typical *schlieren* texture, which on further cooling turns into a highly viscous and optically isotropic (probably cubic) phase. Owing to the monotropic nature of these mesophases, a more detailed investigation by X-ray scattering was however not possible.

An enantiotropic mesophase was found for **5** between 128 and 151 °C. It is characterised by regions with spherulitic as well as broken fan shaped texture (Fig. 1). No homeotropic orientation can be obtained by shearing the sample. Therefore an S_A phase can be ruled out. X-Ray studies provide a diffuse scattering in the wide angle region and three non-equidistant reflections in the small angle region (d_1 = 3.55, d_2 = 1.93, d_3 = 1.27 nm), excluding a smectic layer structure. As there are no references to a hexagonal or a rectangular 2D lattice, we evaluated the pattern under the assumption of a two-dimensional oblique cell, assigning the observed reflections to (10), (01) and (11) with increasing ϕ-values and obtained lattice parameters a = 9.95, c = 5.41 nm and β = 159.1°. In the light of the fact that the aromatic unit should provide a rod-like molecular shape and that the mesophases of **2**–**4** represent layer structures, it seems likely that the columnar phase results from the collapse of smectic layers into band-like segments (ribbons). The collapse can be caused either by an incompatibility of two incommensurate length scales or by a different space filling of microsegregated regions. The first case is found at the transition between smectic bilayer and monolayer structures ($S_{\tilde{C}}$, $S_{\tilde{A}}$ phases).[8] The second type is known from the thermotropic mesophases of pure soaps[9] and has been proposed for columnar mesophases of polycatenar compounds,[10] and several types of calamitic amphiphiles containing oligo(oxyethylene) units.[11,12]

In the crystalline state of **5** in the small angle region three equidistant reflections are observed with a period of d = 3.55

Table 1 Phase transition temperatures of **1**–**5** as determined by polarising microscopy. Abbreviations: K = crystalline solid, S_A = smectic A phase, Col = columnar phase, Cub? = optically isotropic, probably cubic mesophase, Iso = isotropic liquid

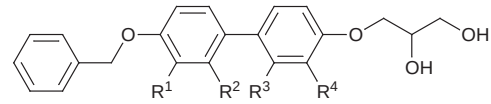

	R1	R2	R3	R4	*T*/°C (pure compounds)	*T*/°C (glycerol saturated samples)
1	H	H	H	H	K 230 Iso	—
2	H	H	H	Me	K 147 (S_A 130) Iso	S_A 140 Iso
3	H	H	Me	H	K 103 (Cub? 70 S_C 73) Iso	Col 96 Iso
4	H	Me	H	H	K 95 (S_A 62) Iso	S_A 70 Col 79 Iso
5	Me	H	H	H	K 128 Col_{ob} 151 Iso	Col 125 S_A 143 Iso

Fig. 1 Polarised optical micrograph of the columnar phase of **5** at 150 °C

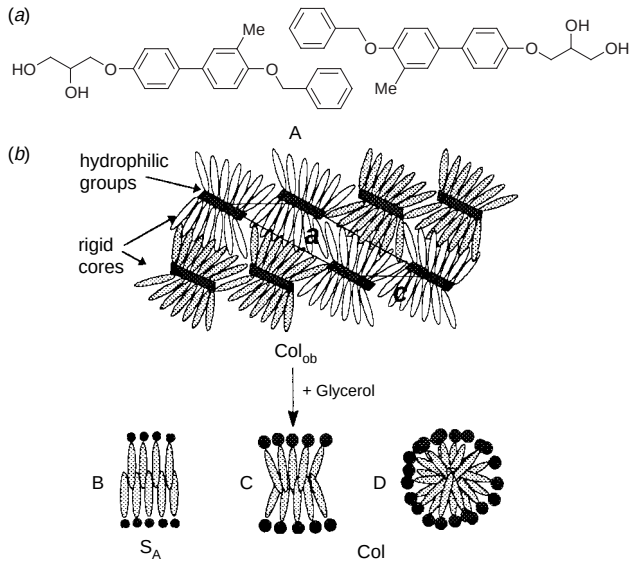

Fig. 2 Schematic presentation of the proposed arrangement of the molecules of **5** in its mesophases. (*a*) Intercalation of two molecules, (*b*) cross-section through a possible thermotropic Col_{ob} phase (A) and through aggregates of possible lyotropic mesophases, formed on addition of glycerol: layer of an S_A-phase (B), ribbon (C) and cylindrical aggregate (D).

nm. The corresponding scattering vector remains on heating the sample whereas the higher orders are significantly shifted at the transition to the liquid crystalline state. Therefore, we assume that the thickness of the ribbons is *ca.* 3.5 nm. The molecular length *L* obtained from CPK models is 2.3 nm. Thus we can conclude on a bilayer arrangement with strongly tilted molecules and/or with a high degree of intercalation. Intercalation of the terminal benzyl groups seems to be likely because the methyl groups provide a partial tapering of the molecules which should facilitate their intercalation [Fig. 2(*a*)]. The shape of the molecules and the intercalation increase the diameter of the aromatic regions with respect to the polar regions of the head groups. Thus, the frustration of the bilayer structure can be explained by the different space filling of the segregated regions of the polar and the aromatic molecular parts.

A possible model which is in accord with the obtained lattice parameter is shown in Fig. 2(*b*), arrangement A. According to this model the oblique lattice results from the organisation of pairs of ribbons (grey and white) consisting of partly intercalated and tilted molecules. Each pair differs from the neighbouring pairs by the average tilt direction of the molecules. The individual ribbons should have a lateral diameter of *ca.* 5 nm and *ca.* ten molecules are arranged side by side an average.

Being amphiphilic, the liquid crystalline properties of **2**–**5** should be influenced by solvents. Their behaviour in the solvent saturated state and in the contact region with the protic solvent glycerol§ was investigated by polarising microscopy. In the contact region between **5** and glycerol the columnar mesophase is destabilised and the formation of an S_A phase with a maximum clearing temperature of 143 °C is observed. In a medium concentration range no columnar mesophase can be found. However, on further increasing the glycerol content a second columnar mesophase appears. This observation confirms the proposed model of the organisation of **5** in the columnar mesophase. The solvent molecules are built in between the polar head groups and increase the diameter of these regions. At a certain solvent content an equivalent space filling of the aromatic and the polar regions is reached, the ribbons fuse and a stable layer structure is found (S_A phase). On further increased solvent content the size of the polar regions could exceed that of the aromatic regions and again the layers break up with formation of a columnar phase. Thus, with respect to the space filling of the different regions the two columnar phases should be inverted to each other. The second columnar phase could again represent a ribbon phase [Fig. 2(*b*), arrangement C], but a columnar phase consisting of cylindrical aggregates [Fig. 2(*b*), arrangement D], cannot be excluded. Columnar phases can also be induced on addition of glycerol to **3** and **4** (Table 1). These induced columnar phases have the same optical texture as that induced in the system **5**–glycerol and should be related to it.

In summary, it was found that rigid all-aromatic amphiphiles represent novel amphotropic liquid crystals.[13] They show the same diversity of different mesophases as thermotropic and lyotropic systems of classical flexible amphiphiles. However, the hydrophobic interactions between flexible alkyl chains are replaced by interactions of rigid aromatic units and therefore ribbon structures are formed. Moreover, a tilted S_C phase was detected which has never been found in the mesophase sequence of conventional flexible amphiphiles and also its appearance is related to the rigid molecular structure.

This work was supported by the Deutsche Forschungsgemeinshaft and the Fonds der Chemischen Industrie.

Notes and References

† E-mail: coqfx@mlucom6.urz.uni-halle.de

‡ All analytical data of the investigated compounds are in accord with the proposed structures, *e.g.* **5**: $C_{23}H_{24}O_4$ requires (found): C, 75.80 (75.54); H, 6.64 (6.38%). ^{1}H NMR [$(CD_3)_2SO$, 200 MHz], δ 7.56–7.31 (9 H, m, Ar-H), 7.09–6.97 (3 H, m, Ar-H), 5.18 (2 H, s, $ArCH_2O$), 4.95 (1 H, d, *J* 4.9 Hz, sec. OH), 4.67 (1 H, t, *J* 5.7 Hz, prim. OH), 4.08–3.81 (3 H, m, $ArOCH_2CHOH$), 3.48 (2 H, dd, *J* 5.6 Hz, CH_2OH), 2.28 (3 H, s, CH_3).

§ Glycerol was chosen because of its high boiling point and because it represents the basic unit of the hydrophilic groups of compounds **1**–**5**.

1 G. W. Smith, *Mol. Cryst. Liq. Cryst.*, 1979, **49**, 207; I. C. Lewis and J. B. Barr, *Mol. Cryst. Liq. Cryst.*, 1981, **72**, 65.
2 H. Honda, *Carbon*, 1988, **26**, 139.
3 J. Barbera, O. A. Rakitin, M. B. Ros and T. Torroba, *Angew. Chem.*, 1998, **110**, 308.
4 T. Rades and C. C. Müller-Goymann, *Eur. J. Pharm. Biopharm.*, 1994, **40**, 277.
5 T. K. Attwood and J. E. Lydon, *Mol. Cryst. Liq. Cryst.*, 1984, **108**, 349.
6 Spiro-tensides and -phospholipids have recently been investigated as non-aromatic rigid amphiphiles: F. M. Menger and J. Ding, *Angew. Chem.*, 1996, **108**, 2266.
7 A. S. C. Lawrence, *Mol. Cryst. Liq. Cryst.*, 1969, **7**, 1; C. Tschierske, G. Brezesinski, F. Kuschel and H. Zaschke, *Mol. Cryst. Liq. Cryst., Lett.*, 1989, **6**, 139.
8 F. Hardouin, A. M. Levelut, M. F. Achard and G. Sigaud, *J. Chim. Phys.*, 1983, **80**, 53.
9 A. Skoulios and V. Luzzati, *Nature*, 1959, **183**, 1310.
10 H. T. Nguyen, C. Destrade and J. Malthete, *Adv. Mater.*, 1997, **9**, 375.
11 J. A. Schröter, C. Tschierske, M. Wittenberg and J. H. Wendorff, *Angew. Chem.*, 1997, **109**, 1160; *Angew. Chem., Int. Ed. Engl.*, 1997, **36**, 1119; F. Hildebrandt, J. A. Schröter, C. Tschierske, R. Festag, M. Wittenberg and J. H. Wendorff, *Adv. Mater.*, 1997, **9**, 564; B. Neumann, C. Sauer, S. Diele and C. Tschierske, *J. Mater. Chem.*, 1996, **6**, 1087.
12 M. Lee, N.-K. Oh and W.-C. Zin, *Chem. Commun.*, 1996, 1787; M. Lee, N.-K. Oh, H. K. Lee and W.-C. Zin, *Macromolecules*, 1996, **29**, 5567.
13 C. Tschierske, *Prog. Polym. Sci.*, 1996, **21**, 775.

Received in Bath, UK, 27th March 1998; 8/02540A

Rare M_7O_2 double tetrahedral core in molecular species: preparation, structure and properties of $[Zn_7O_2(O_2CMe)_{10}(1\text{-Meim})_2]$ (1-Meim = 1-methylimidazole)

Nikolia Lalioti,[a] Catherine P. Raptopoulou,[b] Aris Terzis,[b] Abil E. Aliev,[c] Spyros P. Perlepes,*[a] Ioannis P. Gerothanassis*[d] and Evy Manessi-Zoupa*[a]†

[a] *Department of Chemistry, University of Patras, 265 00 Patras, Greece*
[b] *Institute of Materials Science, NCSR "Demokritos", 153 10 Aghia Paraskevi Attikis, Greece*
[c] *Chemistry Department, University College London, 20 Gordon Street, London, UK WC1H OAJ*
[d] *Department of Chemistry, University of Ioannina, 451 10 Ioannina, Greece*

The 2 : 1 reaction between $Zn(O_2CMe)_2\cdot 2H_2O$ and 1-Meim in refluxing MeCN gives $[Zn_7O_2(O_2CMe)_{10}(1\text{-Meim})_2]$ 1 which comprises two vertex-sharing tetranuclear $Zn_4(\mu_4\text{-O})(\eta^1:\eta^1:\mu_2\text{-}O_2CMe)_5(1\text{-Meim})$ units; solid-state ^{13}C and ^{15}N NMR spectra reveal structural details of the complex.

We have recently become interested in the synthesis of mono- and di-/tri-nuclear zinc complexes containing carboxylate and imidazole ligands which would be satisfactory models for the carboxylate–histidine–metal triad catalytic centres in hydrolytic zinc enzymes.[1–4] This area of Zn chemistry has been poorly explored. Two groups have reported[5,6] the preparation and X-ray structures of the mononuclear, four-coordinate complexes $[Zn(O_2CR)_2L_2]$, where R = Me, Et and L = imidazole, 2-ethylimidazole.

For the better investigation of the Zn^{II}–RCO_2^-–L systems (L = various monodentate imidazoles), we have systematically varied the nature of R, L and solvent, and both the Zn^{II} : L and Zn^{II} : RCO_2^- ratios. We have found all these parameters to have an important effect on the chemical and structural identity of obtained products. We herein report that the 2 : 1 and 3.5 : 1 reactions of $Zn(O_2CMe)_2\cdot 2H_2O$ with 1-methylimidazole (1-Meim) in MeCN lead to the assembly of the remarkable high-nuclearity product $[Zn_7O_2(O_2CMe)_{10}(1\text{-Meim})_2]$ **1**.

$Zn(O_2CMe)_2\cdot 2H_2O$ (4.0 mmol) and 1-Meim (2.0 mmol) were refluxed for 30 min in MeCN (30 ml) to form a colourless solution. Layering this solution with an equal volume of Et_2O afforded colourless crystals of $[Zn_7O_2(O_2CMe)_{10}(1\text{-Meim})_2]\cdot$ 2MeCN, **1**·2MeCN in typical yields of *ca.* 45%; the dried solid analysed as **1**.‡ Employing a Zn^{II} : 1-Meim ratio of 3.5 : 1 in either MeCN or MeOH complex **1** again results. The same procedure in EtOH can be employed for the 1,2-dimethylimidazole (1,2-diMeim) analogue of **1** ($[Zn_7O_2(O_2CMe)_{10}(1,2\text{-diMeim})_2]$ **2**).§

The structrure of **1**¶ (Fig. 1) is extremely unusual and consists of a $[Zn_7(\mu_4\text{-O})_2]^{10+}$ core. The central Zn site [Zn(1)] lies on a crystallographic inversion centre and is the shared vertex of two $Zn_4(\mu_4\text{-O})$ units; this unit is well established in Zn chemistry.[7] The peripheral ligation is provided by ten $\eta^1:\eta^1:\mu_2$-acetate groups and two 1-Meim ligands bonded to Zn(4) atoms; each of the five crystallographically independent acetates spans one edge of the Zn_4 tetrahedron. The Zn_4O tetrahedron is slightly irregular, the Zn···Zn distances being between 3.081(1) and 3.199(1) Å and the Zn–O–Zn angles varying from 103.5 to 112.5(1)°. The shortest Zn···Zn distance between the tetrahedral subunits is the Zn(2)···Zn(4) one [5.333(1) Å]. The geometry at the central Zn is distorted octahedral, while that at the peripheral metal ions can be described as distorted tetrahedral with the distortion at Zn(4) being more severe. Bond distances to Zn(1) are distinctly longer [1.979(2)–2.203(2) Å] as expected for a higher coordination number. There appear to be stacking interactions between the centrosymmetrically parallel 1-Meim ligands that belong to neighbouring heptanuclear molecules [closest interatomic separation, N(1)···C(3) = C(3)···N(1), between opposite ligands is 3.340(5) Å]; these interactions create a form of 'chains' along the *b* axis and aid in stabilizing the crystal structure.

Complex **1** joins a small family of discrete heptanuclear zinc(II) clusters,[8–11] the first reported example being $[Zn_7Me_6(OMe)_8]$.[8] Complex **1** becomes the second member of a homometallic molecular complex containing the $[M_7(\mu_4\text{-O})_2]$ double tetrahedral unit, the only other known example[10] being also a zinc(II) cluster.

The compound is practically insoluble in all organic solvents; its high-resolution solid-state ^{13}C NMR spectrum (recorded[12] at 75.5 MHz) indicates a 2 : 1 : 1 : 1 splitting of the carboxylate carbons[13,14] (δ 181.4–179.4) and 1 : 2 : 1 : 1 splitting of the methyl carbons (δ 24.2–22.2). Evidently, polynuclear zinc(II) complexes are excellent candidates for a comparative study of X-ray structure with solid-state NMR properties because of the

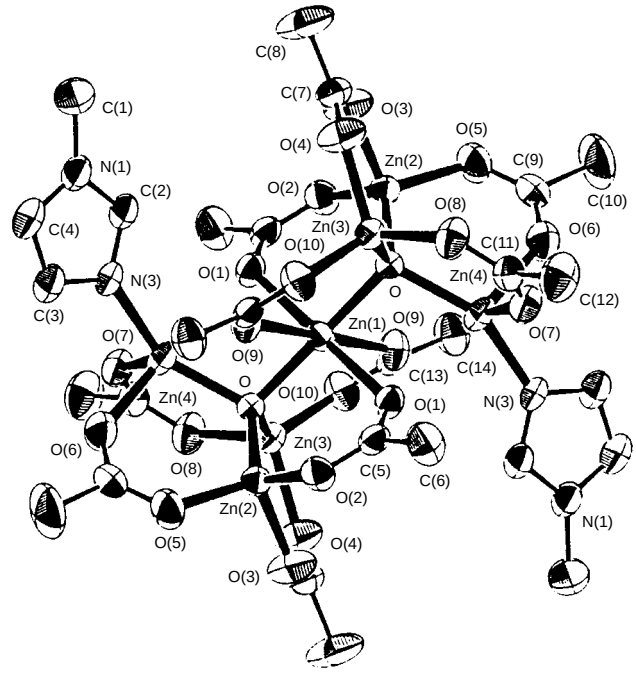

Fig. 1 ORTEP representation of $[Zn_7O_2(O_2CMe)_{10}(1\text{-Meim})_2]$ **1**. Some symmetry equivalent atoms are not labelled. Selected interatomic distance ranges (Å): Zn–O(oxo) 1.914(2)–1.979(2), Zn–O(acetate) 1.944(3)–2.203(2), Zn(4)–N(3) 2.004(3), Zn···Zn 3.081–6.375(1). Selected bond angle ranges (°): *trans* at Zn(1), 180.0; *cis* at Zn(1), 81.3(1)–98.7(1); around Zn(2), 102.4(1)–120.6(1); around Zn(3), 101.5(1)–120.4(1); around Zn(4), 93.0(1)–146.2(1); Zn–O(oxo)–Zn 103.5(1)–112.5(1).

very high quality ^{13}C CP MAS spectra produced and the fact that shieldings of both CO_2^- and acetate CH_3 groups are very sensitive to the precise crystallographic environment. In the present complex, two of the five crystallographically inequivalent acetate ligands present in the unit cell have degenerate ^{13}C chemical shifts for both methyl and carboxylate groups. The solid-state ^{15}N CP MAS NMR spectrum of complex **1** indicates the presence of two resonances at δ −163.6 [N(3)] and δ −212.7 [N(1)] for the bound 1-Meim. Both resonances are significantly shifted to those of the free ligand (δ −120.3 [N(3)] and δ −219.9 [N(1)], neat liquid at 300 K, relative to CH_3NO_2 as reference).

From a synthetic inorganic viewpoint, the preparation of **1** and **2** shows that it is possible to generate polynuclear zinc carboxylate complexes with unusual structures and nuclearities significantly greater than those known to date by relatively minor perturbations to the Zn^{II}–RCO_2^-–L system, in this case, the use of a high Zn^{II} to L ratio. We are currently investigating the reactivity chemistry of **1** and **2** and seeking access to additional structural types.

We thank University of London Intercollegiate Research Service for the provision of solid-state NMR facilities.

Notes and References

† E-mail: emane@upatras.gr

‡ The vacuum-dried complex analysed satisfactorily (C, H, N) as **1**.

§ Complex **2** has been characterised by single-crystal X-ray crystallography and microanalyses.

¶ *Crystal data* for **1**·2MeCN: $C_{32}H_{48}Zn_7O_{22}N_6$, M_r = 1326.36, triclinic, space group $P\bar{1}$, a = 11.771(1), b = 12.616(2), c = 10.384(1) Å, α = 107.36(1), β = 93.39(1), γ = 117.03(1)°, U = 1276.2(3) Å^3, Z = 1, T = 298 K, μ(Cu-Kα) = 4.283 mm^{-1}, D_c = 1.726 g cm^{-3}, $2\theta_{max}$ = 143°, $wR2$ (on F^2) = 0.1044, $R1$ (on F) = 0.0372 for 4289 unique reflections with $I > 2\sigma(I)$. The number of refined parameters is 360. The structure was solved by direct methods using SHELXS- 86[15] and refined by full-matrix least-squares techniques using SHELXL-93.[16] All hydrogen atoms were located by difference maps and refined isotropically. All non-hydrogen atoms were refined anisotropically. CCDC 182/890.

1 H. Bertini and C. Luchinat, in *Bioinorganic Chemistry*, ed. I. Bertini, H. B. Gray, S. J. Lippard and J. Valentine, University Science Books, Mill Valley, CA, 1994.
2 N. Sträter, W. N. Lipscomb, T. Klabunde and B. Krebs, *Angew. Chem., Int. Ed. Engl.*, 1996, **35**, 2024.
3 D. E. Fenton and H. Okawa, *J. Chem. Soc., Dalton Trans.*, 1993, 1349.
4 A. Abufarag and H. Vahrenkamp, *Inorg. Chem.*, 1995, **34**, 2207.
5 W. D. Horrocks, Jr., J. N. Ishley and R. R. Whittle, *Inorg. Chem.*, 1982, **21**, 3265, 3270.
6 X.-M. Chen, B.-H. Ye, X.-C. Huang and Z.-T. Xu, *J. Chem. Soc., Dalton Trans.*, 1996, 3465.
7 F. A. Cotton, L. M. Daniels, L. R. Falvello, J. H. Matonic, C. A. Murillo, X. Wang and H. Zhou, *Inorg. Chim. Acta*, 1997, **266**, 91 and references therein.
8 M. L. Ziegler and J. Weiss, *Angew. Chem., Int. Ed. Engl.*, 1970, **9**, 905.
9 M. Ishimori, T. Hagiwara, T. Tsuruta, Y. Kai, N. Yasuoka and N. Kasai, *Bull. Chem. Soc. Jpn.*, 1976, **49**, 1165.
10 D. Attanasio, G. Dessy and V. Fares, *J. Chem. Soc., Dalton Trans.*, 1979, 28.
11 M. Tesmer, B. Muller and H. Vahrenkamp, *Chem. Commun.*, 1997, 721.
12 Experimental details will be given in the full paper.
13 S.-J. Lin, T.-N. Hong, J.-Y. Tung and J.-H. Chen, *Inorg. Chem.*, 1997, **36**, 3886.
14 P. A. Hunt, B. P. Straughan, A. A. M. Ali, R. K. Harris and B. J. Say, *J. Chem. Soc., Dalton Trans.*, 1990, 2131.
15 G. M. Sheldrick, SHELXS-86, Structure Solving Program, University of Göttingen, Germany, 1986.
16 G. M. Sheldrick, SHELXL-93, Program for Refinement of Crystal Structure, University of Göttingen, Germany, 1993.

Received in Basel, Switzerland, 15th April 1998; 8/02844C

Energy gap dependence of electron transfer rates in porphyrin–imide supramolecular assemblies

Joe Otsuki,*[a]† Kenkichi Harada,[a] Koji Toyama,[b] Yoshio Hirose,[b] Koji Araki,[a] Manabu Seno,[b] Kikuo Takatera[a] and Tadashi Watanabe[a]

[a] *Institute of Industrial Science, University of Tokyo, 7-22-1 Roppongi, Minato-ku,Tokyo 106-8558, Japan*
[b] *College of Science and Technology, Nihon University, 1-8-14 Kanda Surugadai, Chiyoda-ku, Tokyo 101-8308, Japan*

The energy gap dependence of the rate of electron transfer has been revealed for donor–acceptor supramolecular assemblies composed of zinc–tetraphenylporphyrin and a series of spacer–acceptor conjugate molecules which are structurally similar but with varying redox potentials.

Artificial photosynthetic devices rely on spatially organised units with suitable photochemical and electrochemical properties.[1] An increasing number of reports use non-covalent interactions, such as metal–ligand coordinate bonds, hydrogen bonding and so on, to construct a donor–acceptor supramolecular architecture.[2] We noticed, however, that there have been very few cases dealing with systematic variations in supramolecular donor–acceptor assemblies. As such little is known about the energy gap dependence of electron transfer rates through non-covalent interactions in well defined synthetic systems, while several systematic studies have been conducted for covalent donor–acceptor conjugates.[3–7]

Hunter and coworkers reported on a very simple way to assemble donor–[spacer–acceptor] supermolecules, *i.e.* to use axial ligation of pyridine ligands to zinc–porphyrin (*e.g.* Fig. 1 with **1**).[8] We reasoned that systematic variations on the redox potential of the imide unit would be made possible by this strategy and synthesised a series of pyridine–imide conjugates, **2–7**, which were structurally similar but with varying redox potentials (Table 1). Two ethoxy groups were introduced in the pyridine spacer to impart enough solubility to be used in excess, in order to ensure nearly complete complexation of Zn–tetraphenylporphyrin (ZnTPP). The key intermediate, 3,5-diethoxy-4-aminomethylpyridine, was prepared according to a literature method.[9] Once this material was obtained in a fair amount, a variety of commercially available phthalic anhydride derivatives were reacted with it to prepare **2–7**.‡

Upon addition of pyridine–imide conjugates to a solution of ZnTPP in CH_2Cl_2, the Q bands exhibit a red-shift of *ca.* 15 nm, which is characteristic of the axial coordination to the metal centre of ZnTPP. From the change in the electronic spectra, binding constants were determined, as shown in Table 1, which are virtually constant (log K 4.0 ± 0.2, 25 °C, CH_2Cl_2) for the whole series of pyridine–imide conjugates employed.§ Owing to the intense ring-current effect of the porphyrin macrocycle, ^{1}H NMR spectroscopy is a powerful tool to probe the complexation.[11,12] For example, in the limit of complete complexation, protons at pyridine-H2, pyridine-H3, and methylene of **1** experience upfield shifts of 6.29, 1.91 and 1.25 ppm, respectively, which are in accord with the axial coordination of the pyridine ligand. The minimum energy conformation of pyridine–imide conjugates was systematically searched with a molecular mechanics calculation by incrementally rotating C(pyridine)–CH_2 and CH_2–N bonds. The result suggests that, in the most stable conformation, the imide ring lies more or less in a face-to-face orientation with the porphyrin plane, assuming that the pyridine moiety coordinates perpendicular to the porphyrin plane.[13] All this evidence indicates that a supermolecule as depicted schematically in Fig. 1 is formed exclusively.

Fluorescence from the singlet excited state of ZnTPP is quenched upon addition of pyridine–imide conjugates due to electron transfer to the imide[14,15] as shown in Fig. 2. The degree of quenching is in proportion to the amount of complex formed and in quantitative accordance with the curve obtained from the binding constant determined as above. A slight increase in fluorescence intensity (5%) is noted upon complexation with 4-picoline which is used to serve as a model compound to differentiate the effect of axial coordination from that of electron transfer. Quenching by dihexylpyromellitic diimide, which is a model compound for **1** and **7** and lacks coordination capability, is also noted. However, this collisional quenching rate is more than two orders of magnitude smaller than that of **1** or **7** in the concentration range studied and can be safely neglected. Thus the collisional quenching is assumed negligible also for the other acceptors.

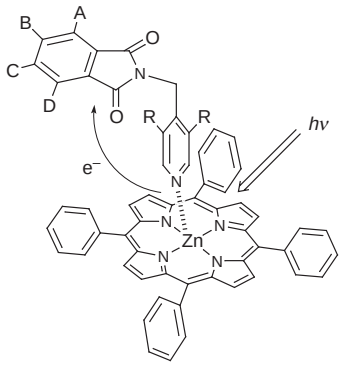

Fig. 1 A supramolecular assembly from ZnTPP and [spacer–acceptor] conjugates with various redox potentials

Table 1 Structures and properties of imides and porphyrin–imide assemblies

	R	A	B	C	D	$E°^a$/V *vs.* Fc/Fc$^+$	log K^b/ M^{-1}	$\phi_{eT}{}^c$	log $k_{eT}{}^d$/ s^{-1}
1	H	H	$(CO)_2NC_6H_{13}$		H	−1.34	3.8	0.91	9.7
2	OEt	H	H	H	H	−2.06	4.1	0.11	7.8
3	OEt	F	H	H	F	−1.81	4.1	0.13	7.9
4	OEt	F	F	F	F	−1.68	4.2	0.24	8.2
5	OEt	NO_2	H	H	H	−1.44	4.1	0.55	8.8
6	OEt	H	NO_2	H	H	−1.26	4.1	0.83	9.4
7	OEt	H	$(CO)_2NC_6H_{13}$		H	−1.37	4.0	0.85	9.5

[a] One-electron reduction potentials. The cyclic voltammetry was conducted with glassy C, Pt and Ag/Ag$^+$ as working, counter and reference electrodes, respectively, under a N_2 atmosphere. Millimolar amount of samples were used in CH_2Cl_2 containing 0.1 M Bu_4NClO_4. [b] Binding constants in CH_2Cl_2 at 25 °C. [c] The quantum yields of intrasupramolecular electron transfer. Repeated runs agreed within ±2% with respect to the initial fluorescent intensity. [d] See footnote ¶. The propagated errors are indicated in Fig. 3.

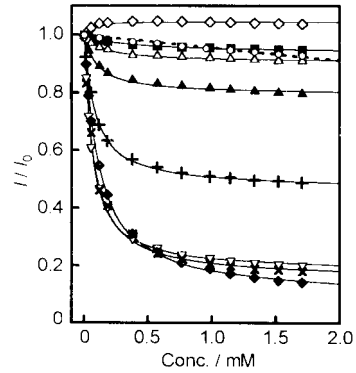

Fig. 2 Quenching of ZnTPP fluorescence upon addition of coordinating acceptors and model compounds (ZnTPP 10 μM in CH_2Cl_2 at 25 °C in air). 4-Picoline (◇), **2** (■), **3** (△), **4** (▲), **5** (+), **6** (▽), **7** (×), **1** (◆) and dihexylpyromellitic diimide (dotted line).

In the limit of complexation, the quantum yields of the intrasupramolecular electron transfer, ϕ_{eT}, are obtained and listed in Table 1. For the studied acceptors with redox potentials varying in the range of 0.8 V, the electron transfer yield varies from 0.11 for **2** to as high as 0.91 for **1**. The rates of electron transfer obtained from these data¶ are plotted against the free energy gap ($\Delta G°$)‖ between the singlet excited state of ZnTPP and acceptors. Increasing energy gap results in increasing electron transfer rate, which is apparently 'normal' behaviour.

In the classical Marcus theory for nonadiabatic electron transfer for the case of weak coupling, the rate of electron transfer, k_{eT}, is given by

$$k_{eT} = (\pi/\hbar^2\lambda k_B T)^{1/2}|V|^2\exp[-(\Delta G° + \lambda)^2/4\lambda k_B T]$$

where $\hbar$ is Planck's constant divided by 2π, λ is the reorganisation energy, k_B is the Boltzmann constant, T is the temperature (298 K), and V is the coupling matrix element.[3,16] Here the two parameters, λ and V, are to be determined by experiment. Assuming that these parameters are constant throughout the series of acceptors, which may be justified on account of their chemical and structural similarity, possible curves from some combinations of these parameters are shown in Fig. 3. It is impossible to single out parameter values to fit all the observed data, especially when the data point for **2** is included. This system awaits further detailed photophysical scrutiny, including transient absorption measurements, to reveal the nature of electron transfer through space or intermolecular bonds.

We have shown that the supramolecular approach is powerful in constructing donor–acceptor architecture with relative ease that can be systematically addressed. In addition, the data presented herein may provide a guide to acceptors to be used in more elaborate donor–acceptor assemblies to obtain desired

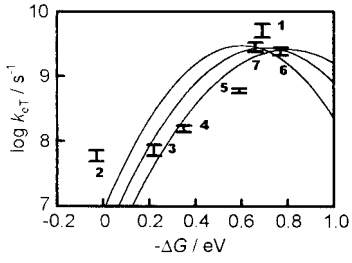

Fig. 3 The dependence of intrasupramolecular electron transfer rate on the energy gap. Curves are also shown according to the Marcus equation with V = 3 cm^{-1} and λ = 0.6, 0.7, 0.8 eV from left to right.

electron transfer rates. This work was supported by Nissan Science Foundation and Foundation Advanced Technology Institute.

Notes and References

† E-mail: otsuki@iis.u-tokyo.ac.jp

‡ Typically, separate solutions of 3,5-diethoxy-4-aminomethylpyridine and substituted phthalic anhydride in MeOH were mixed and heated on a hot plate, letting MeOH evaporate. The reaction mixture was purified by PLC. All compounds obtained had the expected ^{1}H NMR, IR spectra, and HRMS or elemental analyses and purity checked by TLC.

§ The Q bands obey Beer's Law around the concentration (10 μM) used in the absorption and fluorescence measurements and no broadening or splitting of the Soret band[10] is observed, indicating that ZnTPP exists as monomers before complexation. Clear isosbectic points upon addition of the pyridine-containing compounds indicate that only the 1 : 1 complex forms.

¶ The electron transfer rates were determined from $k_{eT} = k_P\Phi_{eT}/(1 - \Phi_{eT})$, where k_P is the decay rate constant of ZnTPP in the absence of quenching ligand, which is 4.9×10^8 s^{-1}. Some of the values (due to our instrumental limit) were independently confirmed by measurement of fluorescence decays, which were single exponential.

‖ The redox potential of the lowest excited state of ZnTPP ($E_P°$) was estimated to be −1.84 V *vs.* Fc/Fc^+ from the ground state redox potential (0.22 V) and the energy of the Q(0,0) band (2.06 eV) of pyridine-complexed ZnTPP. The energy gap, $\Delta G°$, was obtained according to the equation

$$\Delta G° = E° - E_P° + e^2/\varepsilon r$$

where the last term is the Coulomb correction in which ε is the relative permittivity of CH_2Cl_2 and r is the donor–acceptor distance. This term was set to be 0.20 eV based upon the estimated value of r (9.5 Å) from the molecular mechanics calculation described in the text and the known geometry of a pyridine–porphyrin complex.[13]

1 J. Otsuki, in *Recent Research Developments in Pure & Applied Chemistry*, Transworld Research Network, Trivandrum, in press; J. Otsuki, N. Okuda, T. Amamiya, K. Araki and M. Seno, *Chem. Commun.*, 1997, 311; J. Otsuki, H. Ogawa, N. Okuda, K. Araki and M. Seno, *Bull. Chem. Soc. Jpn.*, 1997, **70**, 2077.
2 M. D. Ward, *Chem. Soc. Rev.*, 1997, **26**, 365 and references therein.
3 G. L. Closs and J. R. Miller, *Science*, 1988, **240**, 440; G. L. Closs, L. T. Calcaterra, N. J. Green, K. W. Penfield and J. R. Miller, *J. Phys. Chem.*, 1986, **90**, 3673.
4 G. L. Gaines, III, M. P. O'Neil, W. A. Svec, M. P. Niemczyk and M. R. Wasielewski, *J. Am. Chem. Soc.*, 1991, **113**, 719.
5 H. Heitele, F. Pöllinger, K. Kremer, M. E. M.-Beyerle, M. Futscher, G. Voit, J. Weiser and H. A. Staab, *Chem. Phys. Lett.*, 1992, **188**, 270.
6 T. Asahi, M. Ohkohchi, R. Matsusaka, N. Mataga, R. P. Zhang, A. Osuka and K. Maruyama, *J. Am. Chem. Soc.*, 1993, **115**, 5665.
7 C. C. Moser, J. M. Keske, K. Warncke, R. S. Farid and P. L. Dutton, *Nature*, 1992, **355**, 796.
8 C. A. Hunter, J. K. M. Sanders, G. S. Beddard and S. Evans, *J. Chem. Soc., Chem. Commun.*, 1989, 1765.
9 V. Bertini, F. Lucchesini, M. Pocci and A. D. Munno, *Heterocycles*, 1995, **41**, 675.
10 R. T. Stibrany, J. Vasudevan, S. Knapp, J. A. Potenza, T. Emge and H. J. Schugar, *J. Am. Chem. Soc.*, 1996, **118**, 3980.
11 R. J. Abraham, G. R. Bedford, D. McNeillie and B. Wright, *Org. Magn. Reson.*, 1980, **14**, 418; R. J. Abraham, S. C. M. Fell and K. M. Smith, *Org. Magn. Reson.*, 1977, **9**, 367.
12 C. Chachaty, D. Gust, T. A. Moore, G. A. Nemeth, P. A. Liddell and A. L. Moore, *Org. Magn. Reson.*, 1984, **22**, 39.
13 D. M. Collins and J. L. Hoard, *J. Am. Chem. Soc.*, 1970, **92**, 3761.
14 A. Osuka, I. Yamazaki, Y. Nishimura, T. Ohno and K. Nozaki, *J. Am. Chem. Soc.*, 1996, **118**, 155; A. Osuka, S. Nakajima, K. Maruyama, N. Mataga and T. Asahi, *Chem. Lett.*, 1991, 1003.
15 M. P. Debreczeny, W. A. Svec and M. R. Wasielewsky, *Science*, 1996, **274**, 584; G. P. Wiederrecht, M. P. Niemczyk, W. A. Svec and M. R. Wasielewski, *J. Am. Chem. Soc.*, 1996, **118**, 81.
16 H. Kurreck and M. Huber, *Angew. Chem., Int. Ed. Engl.*, 1995, **34**, 849.

Received in Cambridge, UK, 20th February 1998; 8/01453A

Highly enantioselective construction of the key azetidin-2-ones for the synthesis of carbapenem antibiotics *via* intramolecular C–H insertion reactions of α-methoxycarbonyl-α-diazoacetamides catalysed by chiral dirhodium(II) carboxylates

Masahiro Anada, Nobuhide Watanabe and Shun-ichi Hashimoto*†

Graduate School of Pharmaceutical Sciences, Hokkaido University, Sapporo 060-0812, Japan

A highly enantioselective construction of 3-oxa-1-azabicyclo[4.2.0]octanes (up to 96% ee) has been achieved by intramolecular C–H insertion of α-methoxycarbonyl-α-diazoacetamides catalysed by dirhodium(II) complexes incorporating *N*-phthaloyl-(*S*)-amino acids as chiral bridging ligands, which provides a new, catalytic asymmetric route to key intermediates for carbapenem antibiotics.

Among a variety of transition metal complexes used to catalyse a broad spectrum of transformations of α-diazo carbonyl

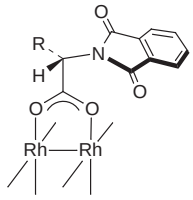

Rh_2(*S*-PTPA)$_4$ R = Bn
Rh_2(*S*-PTA)$_4$ R = Me
Rh_2(*S*-PTV)$_4$ R = Pr^i
Rh_2(*S*-PTPG)$_4$ R = Ph
Rh_2(*S*-PTTL)$_4$ R = Bu^t

compounds, dirhodium(II) complexes have distinguished themselves by their superiority in C–H insertion reactions.[1] Consequently, a great deal of effort is being devoted to the design, synthesis and evaluation of chiral dirhodium(II) catalysts which make it possible to construct both carbocyclic and hetereocyclic systems with high enantioselectivities.[1,2] Our efforts in this area have led to the development of dirhodium(II) carboxylates incorporating *N*-phthaloyl-(*S*)-amino acids as the bridging ligands, which catalyse intramolecular C–H insertion reactions of α-diazo carbonyl compounds to give optically active cyclopentanone and indan-2-one derivatives in high yields and with up to 80 and 98% ee, respectively.[3,4] Herein we report the highly enantioselective construction of 3-oxa-1-azabicyclo-[4.2.0]octanes, which lead to the key azetidin-2-ones for the synthesis of 1-unsubstituted and 1β-methyl carbapenem antibiotics.[5]

We previously demonstrated that cyclisation of *N*-alkyl-*N*-*tert*-butyl-α-methoxycarbonyl-α-diazoacetamides catalysed by dirhodium(II) tetrakis[*N*-phthaloyl-(*S*)-phenylalaninate], Rh_2(*S*-PTPA)$_4$, led to the exclusive formation of azetidin-2-one derivatives of up to 74% ee,[6] wherein installation of a *tert*-butyl group as an *N*-substituent proved to be crucial to enantiocontrol as well as regiocontrol; however, the inability to remove the *tert*-butyl group precluded its application to the synthesis of carbapenem antibiotics. In this respect, of particular interest is the pioneering work of Ponsford and Southgate dating back to 1979.[7] They developed a racemic route to the thienamycin key intermediate *via* the $Rh_2(OAc)_4$-catalysed C–H insertion reaction of α-diazoacetoacetamides **1a** and **1b** tethered to a tetrahydro-1,3-oxazine system. Following the suggestion that the *N*,*O*-acetal moiety could function as a substitute for the *tert*-butyl group, we then examined cyclisation of **1a** and **1b** with the aid of 10 mol% of Rh_2(*S*-PTPA)$_4$. Cyclisation proceeded smoothly to give the 3,4-*trans*-azetidin-2-one derivatives **2a** and **2b**, but we were disappointed to find that there was no asymmetric induction in either case [eqn. (1)].

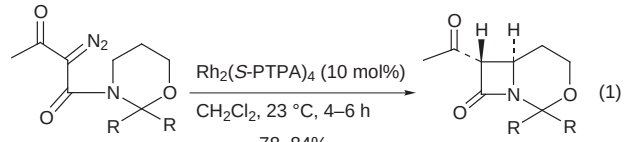

(1)

Although the steric and electronic differences between the acetyl and methoxycarbonyl groups as the α-substituent of the diazo carbon was thought to be small, we next explored the feasibility of asymmetric induction with α-methoxycarbonyl-α-diazoacetamide **3a**. To our surprise, cyclisation of **3a** under the influence of 5 mol% of Rh_2(*S*-PTPA)$_4$ afforded the 3,4-*trans*-azetidin-2-one derivative **4a** as the sole product in 89% yield and with 90% ee (Table 1, entry 1). While the mechanistic profile is not clear at present, the beneficial effect of the ester group in this system should be underscored.‡ To further enhance the enantioselectivity, we then screened other chiral dirhodium(II) carboxylates, Rh_2(*S*-PTA)$_4$, Rh_2(*S*-PTV)$_4$, Rh_2(*S*-PTPG)$_4$ and Rh_2(*S*-PTTL)$_4$, derived from *N*-phthaloyl-(*S*)-alanine, -valine, -phenylglycine and -*tert*-leucine, respectively. While the catalysis of **3a** provided **4a** with a consistent sense of enantioselection at the insertion site and in more than

Table 1 Enantioselective C–H insertion reaction of **3** catalysed by chiral Rh^{II} complexes[a]

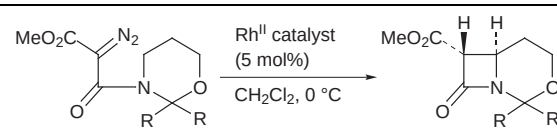

3a–c **4a–c**

	Substrate				Lactam		
Entry	**3**	R,R	Catalyst	*t*/h	**4**	Yield[b] (%)	Ee[c] (%)
1	**3a**	–(CH$_2$)$_5$–	Rh_2(*S*-PTPA)$_4$	3	**4a**	89	90
2	**3a**	–(CH$_2$)$_5$–	Rh_2(*S*-PTV)$_4$	3	**4a**	86	92
3	**3a**	–(CH$_2$)$_5$–	Rh_2(*S*-PTPG)$_4$	3	**4a**	85	92
4	**3a**	–(CH$_2$)$_5$–	Rh_2(*S*-PTTL)$_4$	4	**4a**	85	93
5	**3a**	–(CH$_2$)$_5$–	Rh_2(*S*-PTA)$_4$	2	**4a**	94	96
6	**3b**	Me,Me	Rh_2(*S*-PTA)$_4$	6	**4b**	89	93
7	**3c**	Et,Et	Rh_2(*S*-PTA)$_4$	8	**4c**	89	83

[a] Reactions were carried out as follows: 5 mol% of the catalyst was added to a stirred solution of the α-diazo amide **3** (1 mmol) in anhydrous CH_2Cl_2 (2 ml) at 0 °C under argon. [b] Isolated yield. [c] Determined by a chiral stationary phase column (Daicel Chiralcel OJ) after reduction with $LiBH_4$ and subsequent benzoylation.

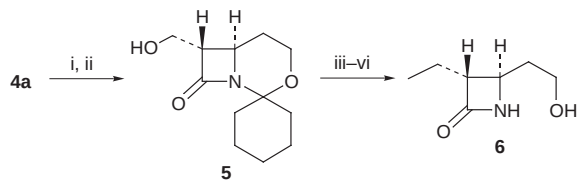

Scheme 1 *Reagents and conditions*: i, $LiBH_4$, THF, 0 °C, 2 h, 94%; ii, recrystallisation from Pr^i_2O–hexane, 90%; iii, Dess–Martin periodinane, CH_2Cl_2, 0 °C, 3 h, 94%; iv, CH_2I_2, Zn, Me_3Al, THF, 0 °C, 2 h, 89%; v, H_2, Pd–C, EtOH, 23 °C, 2 h, 96%; vi, aq. AcOH, 70 °C, 2 h, 97%

92% ee in all cases (entries 2–5), Rh_2(*S*-PTA)$_4$ proved to be the catalyst of choice for displaying the highest degree of enantioselectivity (96% ee, entry 5). With regard to the *N*,*O*-acetal protection, the isopropylidene acetal **3b** exhibited almost the same enantioselectivity as **3a** (entry 6), whereas a dramatic drop in enantioselectivity was observed with the pentylidene acetal **3c** (entry 7). It should be emphasised here that **3a** has distinct advantages over **3b** from the standpoint of its preparative yield.

The azetidin-2-one **4a** {96% ee, $[\alpha]_D^{25}$ +57.7 (*c* 1.02, $CHCl_3$)} thus obtained was then transformed to the key synthetic intermediate **6** for PS-5, which also determined the preferred absolute configuration at the insertion site (Scheme 1). Reduction of **4a** with $LiBH_4$ gave the alcohol **5**, which, upon one recrystallisation from Pr^i_2O–hexane, produced an optically pure sample {mp 89–90 °C, $[\alpha]_D^{25}$ +17.7 (*c* 1.03, $CHCl_3$)}. Oxidation of **5** with the Dess–Martin periodinane followed by sequential methylenation,[8] hydrogenation and hydrolysis afforded the PS-5 intermediate **6** {$[\alpha]_D^{25}$ +25.0 (*c* 1.16, CH_2Cl_2); lit.,[9] +24.3 (*c* 1.33, CH_2Cl_2)}.

Finally, we extended the present protocol to the synthesis of the pivotal intermediate for 1β-methylcarbapenems (Scheme 2).

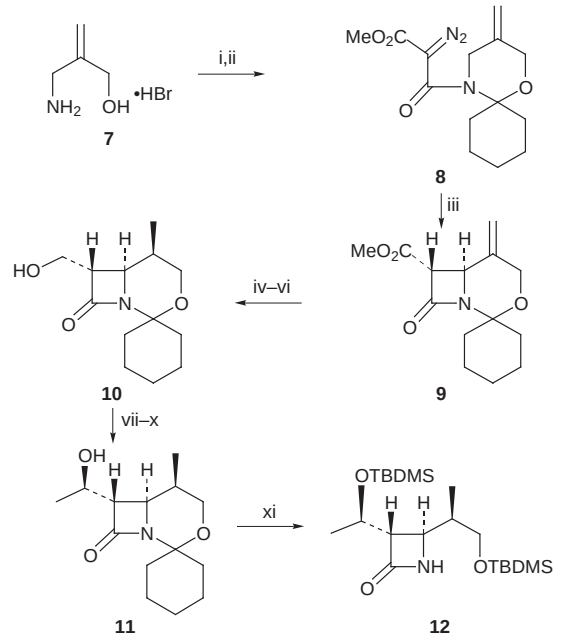

Scheme 2 *Reagents and conditions*: i, cyclohexanone, $NaHCO_3$, benzene, reflux, azeotropic distillation, 6 h, then methyl malonyl chloride, $PhNMe_2$, CH_2Cl_2, 0 °C, 1 h, 68%; ii, *p*-$AcNHC_6H_4SO_2N_3$, DBU, MeCN, 0 °C, 2 h, 91%; iii, Rh_2(*S*-PTA)$_4$, CH_2Cl_2, 23 °C, 13 h, 83%, 88% ee; iv, $LiBH_4$, THF, 0 °C, 2 h, 91; v, H_2, Raney-Ni (W2), EtOH–EtOAc, 0 °C, 6 h, 96%; vi, recrystallisation from AcOEt–hexane, 82%; vii, Dess–Martin periodinane, CH_2Cl_2, 0 °C, 3 h, 94%; viii, Me_3Al, CH_2Cl_2, 0 °C, 2.5 h, 87%; ix, DMSO, $(COCl)_2$, Et_3N, CH_2Cl_2, −60 °C, 1 h, 95%; x, K-Selectride®, Et_2O, −20 °C, 2 h, 90%; xi, aq. AcOH, 70 °C, 2 h, then TBDMSCl, imidazole, CH_2Cl_2, 0 °C, 4 h, 94%

Toward this end, α-methoxycarbonyl-α-diazoacetamide **8** bearing an exocyclic olefin was prepared from **7**§ by condensation with cyclohexanone followed by *N*-acylation with methyl malonyl chloride and subsequent diazo transfer. Cyclisation of **8** with the aid of 5 mol% of Rh_2(*S*-PTA)$_4$ proceeded uneventfully to afford the desired azetidin-2-one **9** {$[\alpha]_D^{25}$ +0.90 (*c* 1.05, $CHCl_3$)} in 83% yield and with 88% ee.¶ Reduction of **9** with $LiBH_4$ followed by stereocontrolled hydrogenation[11] furnished the alcohol **10**, which, upon one recrystallisation from AcOEt–hexane, produced an optically pure sample {mp 159–160 °C, $[\alpha]_D^{25}$ +16.9 (*c* 1.06, $CHCl_3$)}. Treatment of **10** with the Dess–Martin periodinane followed by alkylation with Me_3Al,[12] oxidation under standard Swern conditions and stereocontrolled reduction with K-Selectride®[13] produced the alcohol **11**. Hydrolysis and subsequent silylation provided the known intermediate **12** {mp 96–98 °C, $[\alpha]_D^{25}$ −7.93 (*c* 0.98, $CHCl_3$); lit.,[14] −7.88 (*c* 1.03, $CHCl_3$)}. The above transformation also established that the preferred absolute configuration at the insertion site in this cyclisation was the same as that with **4a**, suggesting a common stereochemical reaction course in both series.

The present protocol provides a new, efficient and general method for the catalytic asymmetric synthesis of carbapenems.[15] Further extension of the present method to trinem antibiotics as well as mechanistic and stereochemical studies are currently in progress.

Notes and References

† E-mail: hsmt@pharm.hokudai.ac.jp

‡ Reaction of the corresponding α-diazoacetamides in the presence of Rh_2(*S*-PTPA)$_4$ gave a complex mixture of products.

§ Compound **7** was prepared from ethyl α-(bromomethyl)acrylate (ref. 10) in 65% yield by the following sequence: DIBAL-H, CH_2Cl_2, −78 °C, 1 h, then NH_3, MeOH, 23 °C, 6 h.

¶ The enantiomeric purity of **9** was determined by a chiral stationary phase column (Daicel Chiralpak AD) after reduction with $LiBH_4$ and subsequent benzoylation.

1 M. P. Doyle, M. A. McKerney and T. Ye, *Modern Catalytic Methods for Organic Synthesis with Diazo Compounds*, Wiley, New York, 1998.
2 M. P. Doyle and D. C. Forbes, *Chem. Rev.*, 1998, **98**, 911.
3 S. Hashimoto, N. Watanabe, T. Sato, M. Shiro and S. Ikegami, *Tetrahedron Lett.*, 1993, **34**, 5109; S. Hashimoto, N. Watanabe and S. Ikegami, *Synlett*, 1994, 353.
4 N. Watanabe, Y. Ohtake, S. Hashimoto, M. Shiro and S. Ikegami, *Tetrahedron Lett.*, 1995, **36**, 1491; N. Watanabe, T. Ogawa, Y. Ohtake, S. Ikegami and S. Hashimoto, *Synlett*, 1996, 85.
5 C. Palomo, in *Recent Progress in the Chemical Synthesis of Antibiotics*, ed. G. Lukacs and M. Ohno, Springer-Verlag, Berlin, 1990, p. 565; A. H. Berks, *Tetrahedron*, 1996, **52**, 331.
6 N. Watanabe, M. Anada, S. Hashimoto and S. Ikegami, *Synlett*, 1994, 1031.
7 R. J. Ponsford and R. Southgate, *J. Chem. Soc., Chem. Commun.*, 1979, 846.
8 K. Takai, Y. Hotta, K. Oshima and H. Nozaki, *Bull. Chem. Soc. Jpn.*, 1980, **53**, 1698.
9 D. Tanner and P. Somfai, *Tetrahedron*, 1988, **44**, 619.
10 K. Ramarajan, K. Ramalingam, D. J. O'Donnell and K. D. Berlin, *Org. Synth.*, 1982, **61**, 56.
11 L. M. Fuentes, I. Shinkai, A. King, R. Purick, R. A. Reamer, S. M. Schmitt, L. Cama and B. G. Christensen, *J. Org. Chem.*, 1987, **52**, 2563.
12 M. Taniguchi, H. Fujii, K. Oshima and K. Utimoto, *Bull. Chem. Soc. Jpn.*, 1994, **67**, 2514.
13 F. A. Bouffard and B. G. Christensen, *J. Org. Chem.*, 1981, **46**, 2208.
14 N. Tsukada, T. Shimada, Y. S. Gyoung, N. Asao and Y. Yamamoto, *J. Org. Chem.*, 1995, **60**, 143.
15 R. Noyori, T. Ikeda, T. Ohkuma, M. Widhalm, M. Kitamura, H. Takaya, S. Akutagawa, N. Sayo, T. Saito, T. Taketomi and H. Kumobayashi, *J. Am. Chem. Soc.*, 1989, **111**, 9134; S.-I. Murahashi, T. Naota, T. Kuwabara, T. Saito, H. Kumobayashi and S. Akutagawa, *J. Am. Chem. Soc.*, 1990, **112**, 7820.

Received in Cambridge, UK, 28th April 1998; 8/03176B

Zinc-promoted direct amination of nitropyridines with methoxyamine *via* vicarious nucleophilic substitution

Shinzo Seko*† and Kunihito Miyake

Organic Synthesis Research Laboratory, Sumitomo Chemical Co., Ltd, Tsukahara, Takatsuki, Osaka 569-1093, Japan

Direct amination of nitropyridines with methoxyamine in the presence of a stoichiometric amount of zinc(II) chloride under basic conditions proceeds to give aminonitropyridines.

Direct amination of nitropyridine is a simple synthetic approach to aminonitropyridines, which are of great importance as intermediates of various biologically active compounds containing imidazopyridine, triazolopyridine *etc*.[1] The well-known Chichibabin amination,[2] in which the α-position of the pyridine ring is aminated by an alkali metal amide, fails to aminate nitropyridines.[3] Although oxidative direct amination of 3-nitropyridines using liquid ammonia/potassium permanganate has been reported,[4] 2- and 4-nitropyridines do not react in this system. On the other hand, alkylation of nitropyridines[5] and amination of nitrobenzenes[6] *via* vicarious nucleophilic substitution (VNS),[7] which has been extensively studied by Makosza, has been reported. However, little attention has been given to the VNS amination of nitropyridines.[8] Recently, we have found that alkoxyamines, in particular methoxyamine,[9] efficiently aminate nitrobenzenes in the presence of a copper catalyst *via* VNS.[10] As part of our investigations to develop new amination, we report here the direct amination of nitropyridines with methoxyamine in the presence of a stoichiometric amount of a zinc salt.

Treatment of 6-methoxy-3-nitropyridine with methoxyamine in the presence of a stoichiometric amount of zinc(II) chloride under strongly basic conditions in DMSO at room temperature gave 2-amino-6-methoxy-3-nitropyridine in 87% yield (Table 1, entry 1). The yield of the amination was strongly influenced by the combination of substrates and solvents used. In diethoxymethane (DEM), THF, DME, toluene and DMF, yields of 2-amino-6-methoxy-3-nitropyridine were 62, 59, 43, 19 and 0%, respectively (entries 2, 3, 4, 5 and 6). In DMF, the reaction with 2-chloro-3-nitropyridine also did not give the aminated products (entry 12). However, with 4-nitropyridine or 2-amino-3-nitropyridine, DMF was a good solvent (entries 7, 8 and 15). In general, DMSO was relatively favored in this reaction. DMSO may play a significant role in the activation of a Meisenheimer intermediate,[11] which result from nucleophilic attack of methoxyamine *ortho* or *para* to the nitro group.

4-Nitropyridine and 4-nitropyridine *N*-oxide were aminated with methoxyamine to afford 3-amino-4-nitropyridine and 3-amino-4-nitropyridine *N*-oxide, respectively (entries 7 and 8). The *N*-oxide provided the better result. The product is a precursor of 3,4-diaminopyridine, an important intermediate of many pharmaceuticals, which is presently synthesized from pyridin-4-ol *via* a tedious reaction sequence.[1c] Our methodology provides a new efficient route to 3,4-diaminopyridine from 4-nitropyridine *N*-oxide, which is cheaper than pyridin-4-ol. The use of other metallic halides as a promoter of the reaction with 4-nitropyridine *N*-oxide was examined. In the presence of titanium(IV) chloride, manganese(II) chloride, cobalt(II) chloride, nickel(II) chloride, copper(I) chloride or aluminum(III) chloride instead of zinc(II) chloride, the reaction gave 3-amino-4-nitropyridine *N*-oxide in 2, 8, 17, 0, 35 and 0% yields, respectively. The result with copper(I) chloride lacked reproducibility although it was similar to that with zinc(II) chloride. Thus zinc(II) chloride was found to be the best promoter of this amination. In the absence of zinc catalyst, the reaction did not proceed and starting material was recovered. The zinc(II) salt may act as an acceptor of an unshared electron pair from the nitrogen in pyridine ring or the oxygen of the *N*-oxide, and thus activates the substrate. A catalytic amount of zinc salt is insufficient to promote the amination since zinc also forms a coordination complex with the product as well as the substrate. This differs from the previously reported copper-catalyzed amination of nitrobenzenes with methoxyamine, in which interaction between the copper catalyst and methoxyamine was observed.[10]

An *ortho* selectivity with respect to the nitro group was observed in the case of 2-chloro-3-nitropyridine (entries 10 and 11). This selectivity is in good agreement with those observed in the amination of nitrobenzenes with methoxyamine.[10] We presume that in both cases (Scheme 1, X = C,N), *ortho* selectivity was observed because the neighboring nitro group in the σ-adduct **3**, derived from the *ortho* attack of methoxyamine on the nitroarene, assists in the elimination of the methoxy anion *via* a five-membered intermediate **4**.[6b] In contrast, Wozniak has reported that the same substrate was aminated by liquid ammonia/potassium permanganate with *para* selectivity to give mainly 6-amino-2-chloro-3-nitropyridine in 40% yield.

Table 1 Direct amination of nitropyridines **1** with methoxyamine[a]

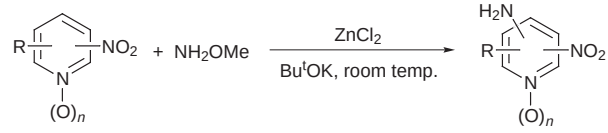

1 **2**

Entry	R	*n*	Position of NO_2	Solvent	Position of amination	Yields[b] (%) of **2**
1	6-MeO	0	3	DMSO	2	87
2	6-MeO	0	3	DEM	2	62 (70)[c]
3	6-MeO	0	3	THF	2	59 (63)[c]
4	6-MeO	0	3	DME	2	43 (50)[c]
5	6-MeO	0	3	Toluene	2	19 (24)[c]
6	6-MeO	0	3	DMF	—	0
7	H	0	4	DMF	3	25
8	H	1	4	DMF	3	38
9	3-EtO	0	2	DMSO	5	7 (10)[c]
10	2-Cl	0	3	DME	4	34
11	2-Cl	0	3	DMSO	4/6	28/8
12	2-Cl	0	3	DMF	—	0
13	6-Cl	0	3	DEM	2/4	9/13
14[d]	2-NH_2	0	3	DMSO	6	58 (85)[c]
15[d]	2-NH_2	0	3	DMF	6	53
16[d]	2-NH_2	0	5	DEM	6	17 (26)[c]
17[d]	2-OH	0	5	DEM	6	9 (17)[c]

[a] Unless otherwise noted, the amination of **1** was carried out with methoxyamine (1.5 equiv.), zinc(II) chloride (1 equiv.) and potassium *tert*-butoxide (3 equiv.) in solvent at room temperature for 1–10 h. [b] Isolated yields. [c] Yields in parentheses are based on the conversion of **1**. [d] 4 equiv. of potassium *tert*-butoxide was used.

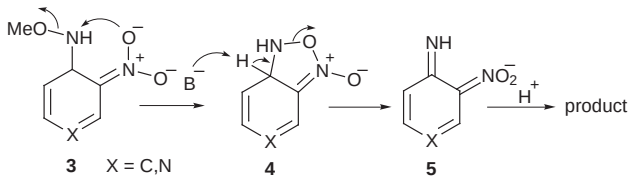

Scheme 1

He explained that the orientation of this reaction was controlled by the charge distribution.[4] However, neither charge control nor orbital control obtained by molecular calculations could explain our results.

It is noteworthy that the amination of 2-amino-3-nitropyridine, 2-amino-5-nitropyridine and 5-nitropyridin-2-ol in the presence of excess base (4 equiv.) proceeded (entries 14, 15, 16 and 17), despite no previous reports of VNS reactions of *o*- or *p*-nitroaniline and *o*- or *p*-nitrophenol. Under strongly basic conditions, *o*- or *p*-nitroaniline, *o*- or *p*-nitrophenol, 2-amino-3-nitropyridine, 2-amino-5-nitropyridine, 3-nitropyridin-2-ol and 5-nitropyridin-2-ol are easily deprotonated to form **6** or **7**. A

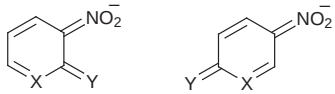

a X = C, Y = NH, O
b X = N, Y = NH, O

nucleophile cannot attack **6a** and **7a** because of the lack of an electrophilic carbon center. However nitropyridine derivatives **6b** and **7b** are susceptible to addition of a nucleophile at the α-position of the pyridine ring as well as to the Chichibabin reaction. Therefore, the amination of 2-amino-3-nitropyridine did not proceed with *ortho* selectivity but proceeded with *para* selectivity to give 2,6-diamino-3-nitropyridine (entries 14 and 15).

Similarly 4-nitroquinoline *N*-oxide was aminated, although in low yield (Scheme 2). This is important because, in spite of many reports of direct amination of bicyclic nitroarenes[12] with hydroxylamine or liquid ammonia/potassium permanganate, direct amination of 4-nitroquinoline derivatives has not been previously reported.

A typical experimental procedure is as follows. To a suspension of $ZnCl_2$ (1 mmol) and Bu^{t}OK (3 mmol) in DMSO

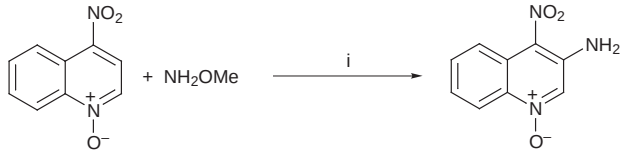

Scheme 2 *Reagents and conditions:* i, $ZnCl_2$, Bu^{t}OK, DMF, room temp., 21%.

(3 ml) was added dropwise a solution of the nitropyridine (1 mmol) and NH_2OMe (1.5 mmol) in DMSO (2 ml), and the mixture was stirred at room temperature. After 1–10 h, the reaction was quenched in saturated aq. NH_4Cl and the products were extracted with EtOAc. The combined organic layers were washed with water, dried, filtered and concentrated. The crude products were purified by silica gel thin layer chromatography to afford the pure aminonitropyridine.

In conclusion, we have developed a new direct amination of nitropyridines with methoxyamine in the presence of a stoichiometric amount of zinc salt. An *ortho* selectivity to the nitro group was observed, which is useful for the synthesis of many pharmaceuticals containing imidazopyridine, triazolopyridine and so on. The general, industrially practical method for direct amination of aromatic compounds has yet to be achieved, especially from the viewpoint of environmental protection. Further studies in this field are in progress in our laboratory.

We thank Professor Z. Yoshida and Professor M. Tokuda for helpful discussions.

Notes and References

† E-mail: seko@sc.sumitomo-chem.co.jp

1 (*a*) J. A. May, Jr. and L. B. Townsend, *J. Org. Chem*., 1976, **41**, 1449; (*b*) K. B. de Roos and C. A. Salemink, *Recueil*, 1969, **88**, 1263; (*c*) J. B. Campbell, J. M. Greene, E. R. Lavagnino, D. N. Gardner, A. J. Pike and J. Snoddy, *J. Heterocycl. Chem*., 1986, **23**, 669 and references cited therein.
2 R. A. Abramovitch and J. G. Saha, *Adv. Heterocycl. Chem*., 1966, **6**, 229.
3 D. A. de Bie, B. Geurtsen and H. C. van der Plas, *J. Org. Chem*., 1985, **50**, 484.
4 M. Wozniak, A. Baranski and B. Szpakiewicz, *Liebigs Ann. Chem.*, 1991, 875.
5 M. Makosza and K. Wojciechowski, *Liebigs Ann./Recueil*, 1997, 1805.
6 (*a*) A. R. Katritzky and K. S. Laurenzo, *J. Org. Chem*., 1986, **51**, 5039; (*b*) A. R. Katritzky and K. S. Laurenzo, *J. Org. Chem*., 1988, **53**, 3978; (*c*) M. Makosza and M. Bialecki, *J. Org. Chem*., 1992, **57**, 4784; (*d*) P. F. Pagoria, A. R. Mitchell and R. D. Schmidt, *J. Org. Chem*., 1996, **61**, 2934.
7 M. Makosza and J. Winiarski, *Acc. Chem. Res*., 1987, **20**, 282.
8 J. H. Boyer and W. Schoen, *J. Am. Chem. Soc*., 1956, **78**, 423.
9 T. C. Bissot, R. W. Parry and D. H. Campbell, *J. Am. Chem. Soc*., 1957, **79**, 796.
10 S. Seko and N. Kawamura, *J. Org, Chem*., 1996, **61**, 442.
11 N. R. Ayyangar, S. N. Naik and K. V. Srinivasan, *Tetrahedron Lett*., 1990, **31**, 3217
12 J. Meisenheimer and E. Patzig, *Chem. Ber*., 1906, **39**, 2533; H. E. Baumgarten, *J. Am. Chem. Soc*., 1955, **77**, 5109; O. N. Chupakhin, V. N. Charushin and H. C. van der Plas, *Tetrahedron*, 1988, **44**, 1; H. C. van der Plas, M. Wozniak and H. J. W. van der Haak, *Adv. Heterocycl. Chem*., 1983, **33**, 95; R. Nasielski-Hinkens, J. Kotel, T. Lecloux and J. Nasielski, *Synth. Commun*., 1989, **19**, 511.

Received in Cambridge, UK, 11th May 1998; 8/03497D

An efficient method for total syntheses of avenaciolide and isoavenaciolide *via* tungsten-π-allyl complexes

Kesavaram Narkunan and Rai-Shung Liu*†

Department of Chemistry, National Tsing-Hua University, Hsinchu, 30043, Taiwan, ROC

Total syntheses of avenaciolide and isoavenaciolide were achieved in six and three steps respectively based on starting chloropropargyl derivatives; the key step in such syntheses involves intramolecular alkoxycarbonylation of tungsten-η¹-propargyl complexes.

There has been increasing interest in the utilization of molybdenum- or tungsten-π-allyl compounds for organic syntheses.[1,2] Faller *et al.* reported[3] that CpMo(NO)Cl(η³-allyl)[3] condensed with aldehydes *via* a chairlike transition state, yielding homoallylic alcohols with excellent diastereoselectivities (Scheme 1). We applied this method to the syntheses of acyclic 1,3-diols, 1,3,5-triols and other oxygen heterocycles.[4] Despite numerous studies on these π-allyl species, there is no precedent for the synthesis of natural products based on these organometallics. Avenaciolide **1** and isoavenaciolide **2** are secondary metabolites isolated from *Aspergillus* and *Penicillium*; total syntheses of these two compounds have attracted considerable attention[4,5] because of their diverse and potent biological activities. In this paper, we report total syntheses of these two bislactones based on tungsten-π-allyl complexes; this synthetic protocol is highly efficient because only a few steps are required from the starting chloropropargyl derivatives **3** and **9**.

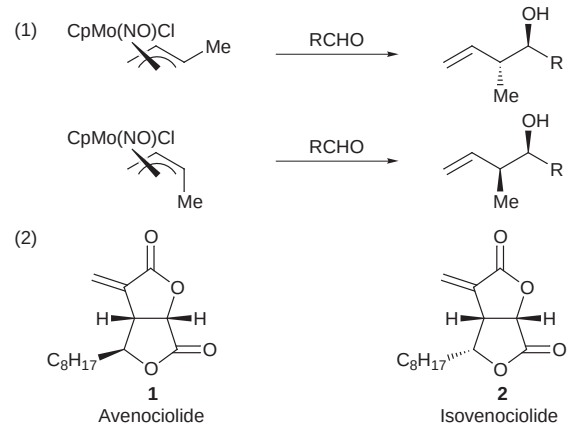

Scheme 1

The starting compound **3** is readily available from propargyl chloride and *n*-butylglyoxalate.[6] As shown in Scheme 2, treatment of **3** with $CpW(CO)_3Na$ (1.3 equiv.) yielded tungsten-η¹-propargyl complex **A** which was not isolated due to its high reactivity. Elution of this tungsten species through a silica

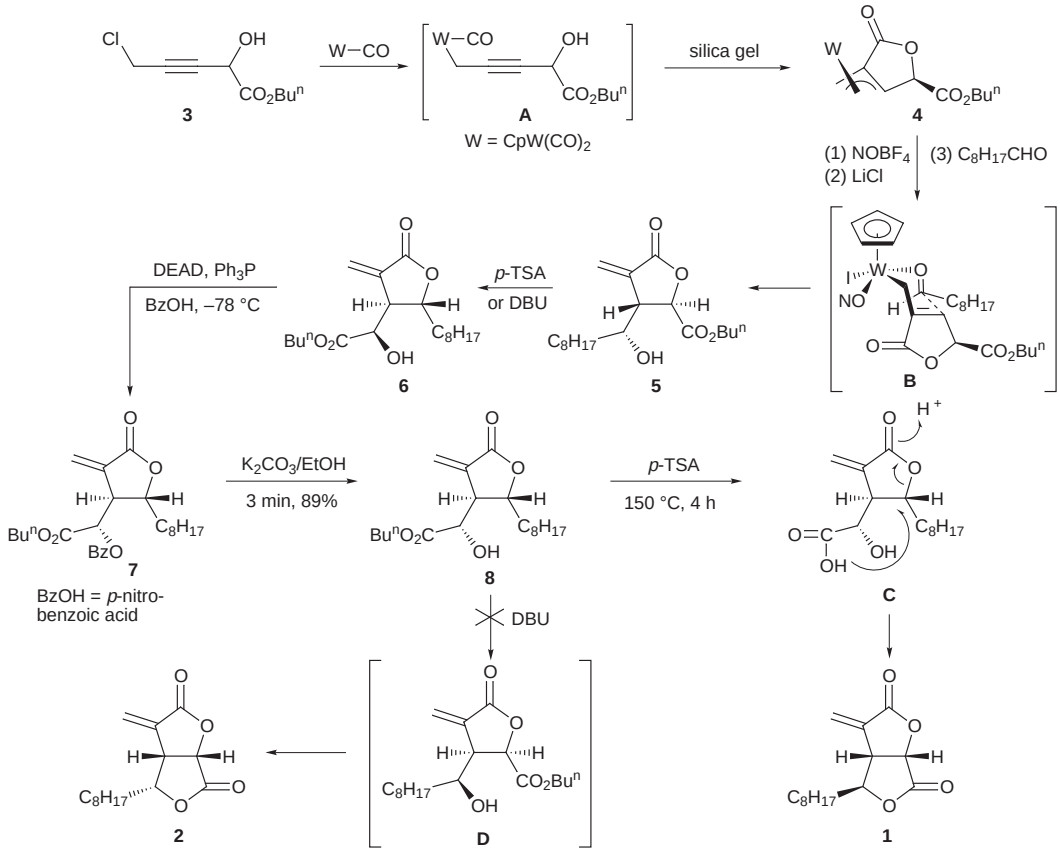

Scheme 2

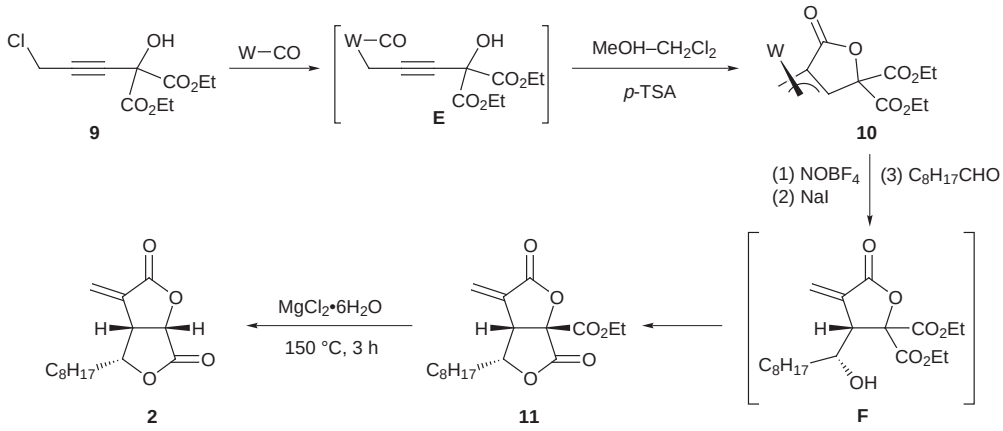

Scheme 3

column induced intramolecular alkoxycarbonylation[4a,b] to yield tungsten-*syn*-π-allyl complex **4** in 70% yield. The *syn*-configuration of **4** is indicated by the coupling constant J_{34} = 3.1 Hz.[4a,b] Sequential treatment of **4** with $NOBF_4$ (1.0 equiv.) and LiCl (2.0 equiv.) in CH_3CN generated an allyl anion equivalent[3] that reacted with $C_8H_{17}CHO$ to yield α-methylene butyrolactone **5** in 62% isolated yield. The *trans*-configuration of **5** was confirmed by a proton NOE experiment. Determination of the remaining $CH(OH)C_8H_{18}$ configuration relies on its transacylation product **6**. The stereochemistry of **5** can be rationalized based on a chairlike transition structure **B** in which the new carbon–carbon bond is formed opposite the CO_2Bu^n substituent. Although compound **5** has a structural skeleton like those for avenaciolide **1** and isoavenaciolide **2**, inversions of configuration of the C(5) and C(1′) carbons and at the C(5) carbon of **5** are required to produce bislactones **1** and **2** respectively. Notably, epimerization at the C(5) carbon of **5** is expected to give isoavenaciolide **2**. Toward this direction, compound **5** was heated in toluene for 7 hours with the DBU catalyst (0.30 equiv.), however transacylation occurred to yield a new α-methylene butyrolactone **6** in 86% yield that also has a *trans*-configuration. Under the same conditions, the *p*-TSA (*p*-toluenesulfonic acid) catalyst (0.20 equiv.) also gave compound **6** in 91% yield. Hence, we sought to invert the configuration at the CH(OH) carbon of **6**; this was achieved by the Mitsunobu reaction,[7] sequentially giving **7** and **8** in 90% and 89% yields respectively. Heating **8** with excess *p*-TSA·H_2O (2.0 equiv.) in toluene in a sealed tube (150 °C, 4 h) produced the desired avenaciolide **1** in 62% yield together with isoavenaciolide **2** in 5% yield. The generation of **1** can be envisaged to proceed from intramolecular attack of the acid group of **8** at its C(5) carbon to invert its stereoconfiguration,[5c,d] ultimately yielding avenaciolide **1**. Attempts to synthesise isoavenaciolide **2** *via* base-catalyzed transacylation of compound **8** were unsuccessful. Heating a mixture of DBU (0.2–2.0 equiv.) and **8** in toluene at reflux for 72 h did not show any sign of chemical reaction, and the starting material **8** was recovered exclusively.

We sought to develop an alternative approach to the synthesis of isoavenaciolide **2** *via* tungsten-π-allyl complexes; the whole synthesis requires only a few steps from chloropropargyl species **9**.[8] As shown in Scheme 3, treatment of **9** with $CpW(CO)_3Na$ (2.0 equiv.) in THF at 23 °C gave the expected tungsten-η^1-propargyl species **E** which was subsequently treated with *p*-TSA·H_2O (1.0 equiv.) in a MeOH–CH_2Cl_2 mixture (volume ratio = 1 : 10) to induce alkoxycarbonylation to yield tungsten-π-allyl complex **10** in 65% yield. Further conversion of **10** produced a π-allyl anion equivalent *via* sequential treatment with $NOBF_4$ (1.0 equiv.) and NaI (2.0 equiv.), which then reacted with $C_8H_{17}CHO$ to yield a 62% yield of bislactone species **11** which was presumably produced *via* lactonization of the primary species **F**. Decarboxylation of **11** proceeded smoothly through heating its dimethylacetamide solution (150 °C, 3 h) containing $MgCl_2·6H_2O$ (5.0 equiv.)[9] to afford the desired isoavenaciolide **2** in 59% yield.

In summary, we report here the first example of the use of tungsten-π-allyl complexes for the efficient syntheses of naturally occurring compounds such as avenaciolide and isoavenaciolide. The overall synthetic scheme‡ is considered to be the most efficient of the known methods. This demonstration highlights the use of tungsten-allyl complexes in the syntheses of natural products.

Notes and References

† E-mail: rsliu@faculty.nthu.edu.tw

‡ All the new compounds gave satisfactory microanalytical data.

1 A. J. Pearson, *Synlett*, 1990, 10.

2 A. J. Pearson, in *Comprehensive Organometallic Chemistry*, ed. G. Wilkinson, F. G. A. Stone and E. W. Abel, Pergamon Press, Oxford, 1995, vol. 12, p. 637.

3 (*a*) J. W. Faller and D. L. Linebarrier, *J. Am. Chem. Soc.*, 1989, **111,** 1939; (*b*) J. W. Faller, J. A. John and M. R. Mazzier, *Tetrahedron Lett.*, 1989, **31**, 1769.

4 (*a*) W.-J. Vong, S.-M. Peng, S.-H. Peng, S.-H. Lin, W.-J. Lin and R.-S. Liu, *J. Am. Chem. Soc*., 1991, **113**, 573; (*b*) C.-H. Chen, J.-S. Fan, G.-H. Lee, S.-M. Peng, S.-L. Wang and R.-S. Liu, *J. Am. Chem. Soc*., 1995, **117**, 2933; (*c*) C.-H. Chen, J.-S. Fan, G.-H. Lee, S.-J. Shieh, S.-L. Wang, S.-M. Peng, S.-L. Wang and R.-S. Liu, *J. Am. Chem. Soc*., 1996, **118,** 9279.

5 (*a*) S. Tsuboi, J.-I. Sakamoto, H. Yamashita, T. Sakai and M. Utaka, *J. Org. Chem*., 1998, **63**, 1102; (*b*) W. L. Parker and F. Johnson, *J. Org. Chem*., 1973, **38**, 2489; (*c*) C. M. Rodriguez, T. Martin and V. S. Martin, *J. Org. Chem*., 1996, **61**, 8448; (*d*) S. D. Burke, G. J. Pacofsky and A. D. Piscopio, *J. Org. Chem.*, 1992, **57**, 2228; (*e*) J. H. Udding, K. J. M. Tuijp, M. N. A. Van Zanden, H. Hiemstra and W. N. Speckamp, *J. Org. Chem.*, 1994, **59**, 1993.

6 L. Brandsma, in *Preparative Acetylenic Chemistry*, Elsevier, Amsterdam, 1988.

7 (*a*) L. E. Overman, K. L. Bell and F. Ito, *J. Am. Chem. Soc*., 1984, **106**, 4192; (*b*) M. Okabe, R. C. Sun and G. B. Zenchoff, *J. Org. Chem*., 1991, **56,** 4392.

8 Y. Nagao, K. Kim, S. Sano, H. Kakegawa, W. S. Lee, H. Shimizu, M. Shiro and N. Katunuma, *Tetrahedron Lett.*, 1996, **37,** 861.

9 J. A. J. M. Vekemans, C. W. M. Dapperens, R. C. Laessen, A. M. J. Koten and E. J. F. Chittenden, *J. Org. Chem*., 1990, **55**, 5336.

Received in Cambridge, UK, 11th May 1998; 8/03491E

Hydroxylation of alkanes by molecular oxygen with dinuclear Fe^{II} macrocyclic complexes as catalysts

Zheng Wang, Arthur E. Martell*† and R. J. Motekaitis

Department of Chemistry, Texas A&M University, College Station, Texas TX77843-3255, USA

The iron(II) complexes of two new macrocyclic ligands: [24]RBPyBC (L24), a 24-membered macrocycle containing phenol, pyridine and amino donor groups, and [30]RBBPyBC (L30), a 30-membered macrocycle containing phenol, bipyridine, and amino donor groups, were found to be effective for the hydroxylation of alkanes, including cyclohexane and adamantane, with H_2S as a two-electron reductant.

The synthesis, characterization, and metal-binding properties of two new macrocyclic ligands [24]RBPyBC (L24) and [30]RBBPyBC (L30) have been reported,[1–3] and the stabilities of their mixed-valence dinuclear iron(II,III) chelates were described. It has now been discovered that the dinuclear iron(II) complexes of these ligands catalyze the hydroxylation of the hydrocarbons cyclohexane and adamantane in the presence of a two-electron reductant (H_2S) and thus may serve as functional models of methane monooxygenase.

Methane monooxygenase is known to contain a binuclear iron active center[4] and has been mimicked by a number of dinuclear model complexes,[5] but in most cases an oxidant such as H_2O_2 or ROOH was used. Descriptions of model systems containing porphyrin ligands in which the oxidant was molecular oxygen have been published.[6] Of the model systems that have molecular oxygen as an oxidant and do not contain porphyrin ligands are the GIF systems of Barton *et al.*,[7] an O_2/Zn/HOAc system of Christou *et al.*[5] and of Kitajima *et al.*,[8] and the present work.

The new dinuclear iron(II) complexes of the macrocyclic ligands designated above, L24 and L30, are indicated below by **1** and **2**, respectively. These dinuclear Fe^{II} complexes are believed to react with oxygen to form a diiron–peroxide intermediate. The active species may decay to a dinuclear Fe^{III} complex with an oxo bridge, releasing an oxygen atom for insertion (hydroxylation) of a hydrocarbon. In the presence of a two-electron reductant the dinuclear Fe^{III} species may revert back to the dinuclear Fe^{II} complex to complete the catalytic cycle.

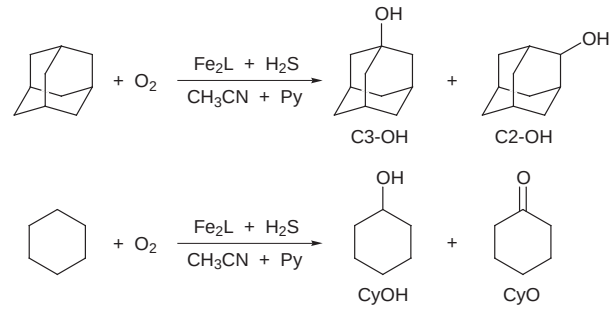

Scheme 1 Oxidation of adamantane and cyclohexane by molecular dioxygen with diiron complexes as catalysts

The overall oxidation reactions are shown in Scheme 1, which shows the organic substrates and reaction products. The results obtained for the hydroxylation of adamantane and cyclohexane are summarized in Tables 1 and 2. Typical oxidation reaction procedures were as follows: at room temperature and atmospheric pressure, 0.10 mmol of free macrocyclic ligand L24 or L30 was dissolved in 40 ml of CH_3CN. $FeCl_2{\cdot}4H_2O$ (0.20 mmol) was added to initiate iron complex formation. After the mixture was stirred for 10 min, the solution turned dark violet signifying the formation of the dinuclear iron complexes Fe_2L24, **1**, or Fe_2L30, **2**. While stirring was continued, 20 mmol cyclohexane or adamantane was added, then 1.0 ml pyridine was added. Hydrogen sulfide (2 ml min^{-1}) and dioxygen (20 ml min^{-1}) were simultaneously passed through the solution. After successive 2 h periods, the reaction mixture was filtered from the deposited sulfur and the solution was analyzed.

An aliquot (1.0 ml) was taken from the reaction solution and added to an aqueous NaOH solution (5%, 2 ml) at 0 °C. The products were extracted with diethyl ether (3 × 5 ml) and dried over $MgSO_4$. A naphthalene solution (1.0 ml, 0.080 M in diethyl ether) was added as an internal standard. The organic products were quantitatively analyzed by gas chromatography.

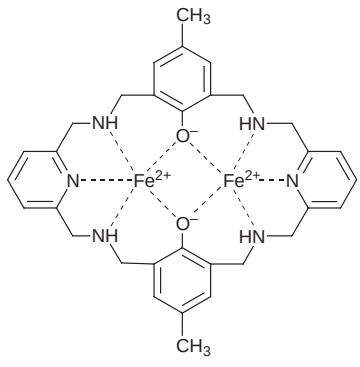

1

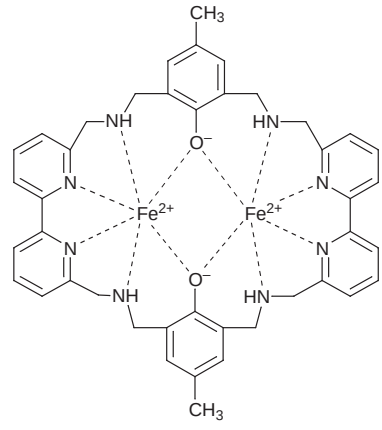

2

Table 1 Oxidation of adamantane by molecular oxygen with diiron complexes as catalysts and hydrogen sulfide as reductant[a]

Catalyst	Time/h	C3-OH/ mmol	C2-OH/ mmol	C3-OH/ C2-OH	Turnover
Fe_2L24	2	0.099	0.29	0.37	3.7
	4	0.867	0.749	1.16	16.2
	6	1.13	0.882	1.28	20.1
	8	1.27	1.05	1.21	23.2
	10	1.51	1.22	1.24	27.3
	20	2.38	2.13	1.12	45.1
Fe_2L30	2	0.360	0.355	1.01	7.2
	4	0.502	0.400	1.26	9.0
	6	0.621	0.492	1.26	11.1
	8	0.782	0.574	1.36	13.6
	10	0.79	0.642	1.24	14.4
	12	0.850	0.719	1.18	15.7

[a] Reaction conditions: $FeCl_2$ (0.20 mmol), ligand (0.10 mmol), adamantane (20 mmol), pyridine (1.0 ml), and CH_3CN (40 ml) at 25 °C. Oxygen and hydrogen sulfide were purged through the solution. Turnover is based on mmols of the products per mmol of the catalyst used.

Table 2 Oxidation of cyclohexane by molecular oxygen with diiron complexes as catalysts and hydrogen sulfide as reductant[a]

Catalyst	Time/h	CyOH/ mmol	CyO/ mmol	CyOH/ CyO	Turnover
Fe_2L24	2	0.96	0.50	1.92	14.6
	4	1.38	0.70	1.97	20.8
	6	1.61	0.73	1.94	24.4
	8	1.85	0.99	1.87	28.4
	10	2.06	1.04	1.98	31.0
	12	2.33	1.26	1.85	35.9
Fe_2L30	2	0.64	0.60	1.07	12.4
	4	0.89	0.83	1.07	17.2
	6	1.10	1.04	1.06	21.4

[a] Reaction conditions: $FeCl_2$ (0.20 mmol), ligand (0.10 mmol), cyclohexane (20 mmol), pyridine (1.0 ml), and CH_3CN (40 ml) at 25 °C. Oxygen and hydrogen sulfide were purged through the solution. Turnover is based on mmols of the products per mmol of the catalyst used.

The mmols of products = $P_{product}/P_{naphthalene} \times 40$ ml $\times$ 0.080 M. The turnovers = the sum of mmols of products/mmol of catalyst. The turnover numbers show that these macrocyclic iron complexes are several times more effective as hydroxylating catalysts for cyclohexane than are the μ-oxo dinuclear iron complexes containing a tris(pyrazol-1-yl)borate ligand described by Kitajima *et al.*[8b] The effectiveness in the catalytic oxidation of adamantane is approximately at the same level as Kitajima's catalyst.[8b] Thus the dinuclear macrocyclic iron(II) complexes described in this paper are among the most effective functional models of methane monooxygenase reported thus far.

The oxidation of cyclohexane gives cyclohexanol and cyclohexanone. The turnovers are 24.4 after 6 h for the 24-membered macrocyclic diiron complex as a catalyst, or 21.4 after 6 h with the 30-membered macrocyclic complex. The ratios of cyclohexanol to cyclohexanone are 1.9 and 1.1 for **1** and **2**, respectively, during the whole period of time of the oxidation reactions. This result shows that the mechanisms of oxidation are similar but slightly different for the two catalysts.

The recent stability studies of dinuclear and mononuclear Fe^{II} and Fe^{III} complexes of the ligand indicate the dinuclearity of the complexes under reaction conditions. Accordingly, the electronic spectra of the reaction mixture before and after the reactions show the same characteristic absorption bands that are attributed to hydroxo dinuclear iron complexes. Thus, we suggest that the active center is a diiron species and the reaction mechanism probably resembles that of MMO.

H_2S serves as both an electron and a proton donor, the equivalent of NADH in MMO systems. The diiron(II) complex can be regenerated from the oxidized diiron(III) complex with H_2S as a two electron reductant to produce a sulfur precipitate which was analyzed quantitatively after the experiment.

In the control experiments for the oxidation of cyclohexane, the turnover is 1.1 in 8 h with Fe^{II} as a catalyst and is 1.7 in 8 h with pyridine as a ligand. Significantly, the turnover is 28.4 in 8 h with the use of the macrocyclic ligand. Autoxidation is clearly ruled out by comparison with these turnover numbers.

It is interesting that the oxidation of adamantane produces only hydroxylation products. The ratio of tertiary adamantanol to secondary adamantanol is around 1.2 for both catalysts. No ketonization product is observed even when the turnover is 45.1 after 20 h. A similar result was obtained by Kitajima *et al.*,[8b] who reported only a trace of ketonization product. This result seems to imply a difference in the mechanisms of oxidation of cyclohexane and adamantane.

The turnover numbers show that the iron complex of the 24-membered macrocycle is a better catalyst for these oxidation reactions than that of the 30-membered macrocycle.

This research was supported by The Robert A. Welch Foundation under Grant No. A-0259. The authors thank Dr Li Tingsheng for assistance with gas chromatography.

Notes and References

† E-mail: martell@chemvx.tamu.edu

1 Z. Wang, J. H. Reibenspies and A. E. Martell, *Inorg. Chem.*, 1997, **36**, 629.
2 Z. Wang, Ph.D. Dissertation, Texas A&M University, 1997.
3 Z. Wang and A. E. Martell, *Inorg. Chem.*, submitted.
4 M. P. Woodland, D. S. Patil, R. Cammack and H. Dalton, *Biochem. Biophys. Acta*,1986, **873**, 237; A. Ericson, B. Hedman, K. O. Hodgson, J. Green, H. Dalton, J. G. Bentsen, R. H. Beer and S. J. Lippard, *J. Am. Chem. Soc.*, 1988, **110**, 2330; B. G. Fox, W. A. Froland, J. Dege and J. D. Lipscomb, *J. Biol. Chem.*, 1989, **263**, 10023.
5 D. Mansuy, J. F. Bartoli and M. Mometeau, *Tetrahedron Lett.*, 1982, **23**, 2781; B. de Poorter, M. Ricci and B. Mounier, *Tetrahedron Lett.*, 1985, **26**, 4459; P. Battioni, J. P. Renaud, J. F. Bartoli and D. Mansuy, *J. Chem. Soc., Chem. Commun.*, 1986, 341; J. B. Vincent, J. C. Huffman, G. Christou, Q. Li, M. A. Nanny, D. N. Hendrickson, R. H. Fong and R. H. Fish, *J. Am. Chem. Soc.*, 1988, **110**, 6898; R. H. Fish, R. H. Fong, J. B. Vincent and G. Christou, *J. Chem. Soc., Chem. Commun.*, 1988, 1504.
6 E. I. Karasevich, A. M. Khenkin and A. E. Shilov, *J. Chem. Soc., Chem. Commun.*, 1987, 731; P. Battioni, J. F. Bartoli, P. Leduc, M. Fontecave and D. Mansuy, *J. Chem. Soc., Chem. Commun.*, 1987, 791; P. E. Ellis, Jr. and J. E. Lyons, *J. Chem. Soc., Chem. Commun.*, 1989, 1189; P. E. Ellis, Jr. and J. E. Lyons, *J. Chem. Soc., Chem. Commun.*, 1989, 1315.
7 D. H. R. Barton, R. S. Hay-Motherwell and W. B. Motherwell, *J. Chem. Soc., Perkin Trans. 1*, 1983, 445; D. H. R. Barton, J. Boivin, M. Bastiger, J. Morzyck, R. S. Hay-Motherwell, W. B. Motherwell, N. Ozbalik and K. Schwartzentruber, *J. Chem. Soc., Perkin Trans. 1*, 1986, 947; C. Balavoine, D. H. R. Barton, J. Boivin, A. Gref, P. L. Coupanec, N. Ozbalik, J. A. X. Pestana and H. Riviere, *Tetrahedron*, 1988, **44**, 1091; D. H. R. Barton, F. Halley, N. Ozbalik, E Young, G. Balavoin, A. Gref and J. Boivin, *New J. Chem.*, 1989, **13**, 177.
8 (*a*) N. Kitajima, H. Fukui and Y. Moro-oka, *J. Chem. Soc., Chem. Commun.*, 1988, 485; (*b*) N. Kitajima, M. Ito, H. Fukui and Y. Moro-oka, *J. Chem. Soc., Chem. Commun.*, 1991, 102.

Received in Cambridge, UK, 6th February 1998; revised manuscript received 29th May 1998; 8/04258F

Large aligned-nanotube bundles from ferrocene pyrolysis

C. N. R. Rao,*† Rahul Sen, B. C. Satishkumar and A. Govindaraj

CSIR Centre of Excellence in Chemistry, Solid State and Structural Chemistry Unit and Materials Research Centre, Indian Institute of Science, Bangalore, 560012, India

Aligned-nanotube bundles have been obtained in copious quantities by the pyrolysis of ferrocene or ferrocene–acetylene mixtures.

Aligned carbon nanotubes have aroused much interest because of their mechanical properties[1,2] as well as their interesting anisotropic optical and other properties.[2] Aligned carbon nanotube films have also been considered to be good candidates as electron field emitters.[3] One of the procedures employed to prepare nanotube films is to pass a dispersion of arc-produced carbon nanotubes in ethanol through an alumina micropore filter and then press the nanotube-covered filter onto a polymer sheet.[4] Under pressure, the nanotubes are printed onto the sheet in an aligned manner. Aligned nanotubes have also been obtained by the chemical vapor deposition of acetylene catalyzed by iron nanoparticles embedded in mesoporous silica,[5] the pores of the silica controlling the growth direction of the nanotubes. Recently, aligned-nanotube bundles have been prepared by the pyrolysis of 2-amino-4,6-dichloro-*s*-triazine over thin films of a cobalt catalyst, patterned on a silica substrate by laser etching.[6] We have been interested in finding a simple means of producing aligned nanotubes in large quantities and were encouraged in this direction by the discovery that the pyrolysis of hydrocarbons in the presence of organometallic precursor molecules gives good yields of carbon nanotubes.[7] Realizing that a precursor such as ferrocene not only gives rise to small catalytic metal particles but also acts as a carbon source, we carried out systematic experiments on the pyrolysis of ferrocene. Initial experiments showed that aligned nanotubes are produced under certain conditions. We have varied the conditions of the pyrolysis of ferrocene and also carried out the pyrolysis in the presence of acetylene which acts as an additional carbon source, and have found these methods to yield large quantities of aligned-nanotube bundles. In this communication, we report this rather impressive result obtained by a very simple technique.

The procedure employed for the pyrolysis of ferrocene was as follows. A known quantity (100 mg) of ferrocene (presublimed, *ca*. 99.99% purity) was placed in a quartz boat located at one end of a narrow quartz tube (10 mm i.d.), which in turn was placed in a dual furnace system. The part of the quartz tube containing the ferrocene was in the first furnace and the ferrocene was sublimed by raising the temperature of this furnace to 620 K at a controlled heating rate. Argon gas was passed through the quartz tube at a desired rate. The ferrocene vapour was carried by the Ar gas into the second furnace, maintained at 1370 K, where pyrolysis occurred. The main variables in the experiments were the heating rate of ferrocene, the flow rate of the argon gas and the pyrolysis temperature. Large quantities of deposits accumulated at the inlet of the second furnace. These carbon deposits, mainly containing carbon nanotubes, were examined by a LEICA S440i scanning electron microscope (SEM) and a JEOL 3010 transmission electron microscope (TEM).

In Fig. 1(*a*) and (*b*), we show the SEM images of the nanotubes obtained by carrying out the pyrolysis of ferrocene at 1370 K with a fast heating rate of ferrocene (100 °C min^{-1}) and a high flow rate of Ar (1000 sccm; sccm = standard cubic cm per min). The images in Fig. 1(*a*) and (*b*), which are recorded in two different directions with respect to the axis of the nanotubes, clearly reveal the extraordinary alignment. TEM images of these nanotubes revealed that they were multi-walled, some of them partially filled with metallic iron. Pyrolysis of ferrocene at 1170 K under vacuum (10^{-5} Torr) also yielded good quantities of aligned-nanotube bundles. In Fig. 1(*c*) we

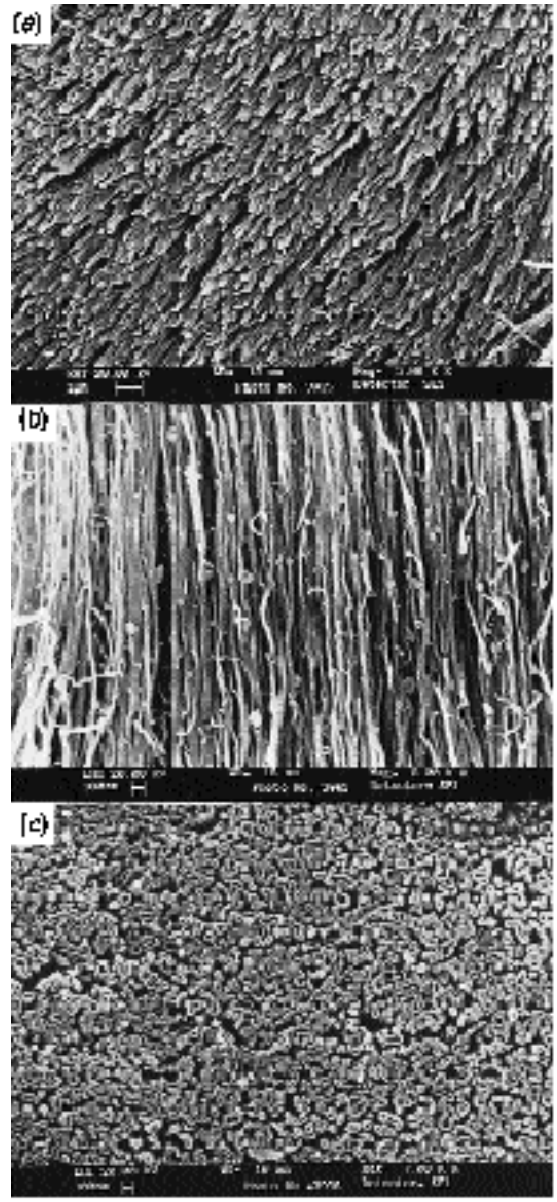

Fig. 1 SEM images of aligned carbon nanotubes obtained by the pyrolysis of ferrocene: (*a*) and (*b*) show views of the aligned nanotubes along and perpendicular to the axis of the nanotubes, (*c*) shows a top view of aligned nanotubes obtained by the pyrolysis of ferrocene under vacuum (10^{-5} Torr) at a slow heating rate (1 °C min^{-1})

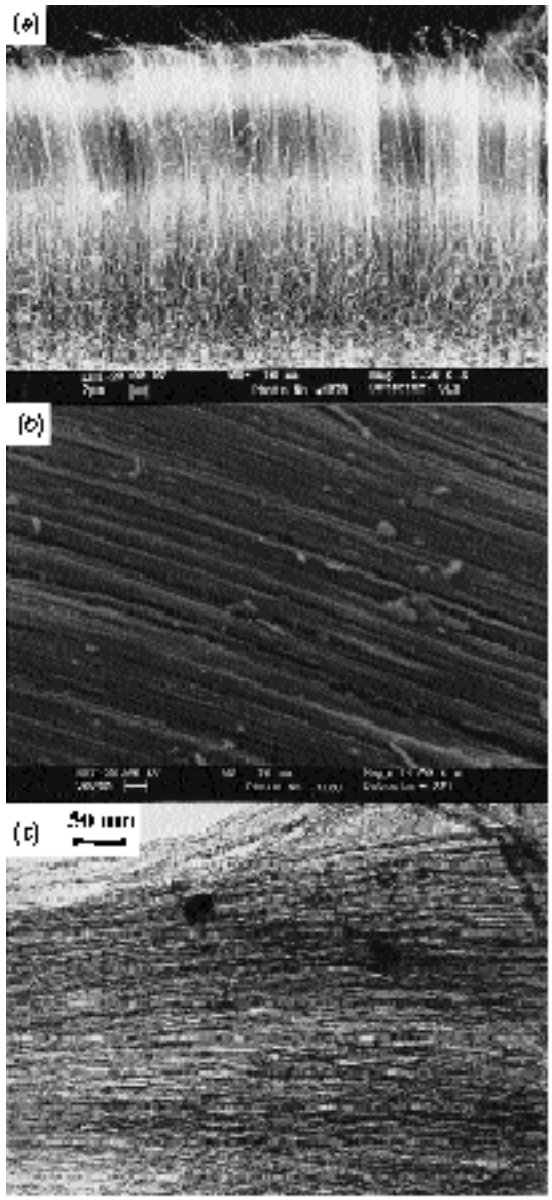

Fig. 2 (*a*) An SEM image of aligned nanotubes obtained by the pyrolysis of ferrocene at 1370 K under a flow of C_2H_2 (5 sccm) and Ar (1000 sccm). In (*b*) and (*c*), we show SEM and TEM images of densely packed aligned nanotubes obtained by the pyrolysis of ferrocene at 1370 K in the presence of a higher proportion of C_2H_2 [flow of C_2H_2 (85 sccm) and Ar (1000 sccm)].

show a top view of such nanotubes. When the rate of heating of ferrocene (1 °C min^{-1}) and the flow rate of argon (10 sccm) were low, fewer aligned nanotubes were obtained at a pyrolysis temperature of 1370 K.

We carried out the pyrolysis of ferrocene with acetylene, by passing a mixture of argon and acetylene through the quartz tube. In Fig. 2(*a*), we show an SEM image of the aligned nanotubes obtained by the pyrolysis of a mixture of ferrocene and acetylene (5 sccm) at 1370 K in flowing Ar (1000 sccm). The alignment could be further improved by increasing the flow rate of C_2H_2. The SEM image in Fig. 2(*b*) obtained in this manner shows densely packed aligned nanotubes. The TEM image in Fig. 2(*c*) reveals how well aligned these nanotubes are. The nanotubes in the bundles were generally closed and were 5–10 μm in length.

Pyrolysis of ferrocene was carried out at a heating rate of 50 °C min^{-1} under a vacuum (10^{-5} Torr). Here, the ferrocene sublimed under vacuum and the vapour was drawn into the pyrolysis zone. In these experiments we mainly obtained

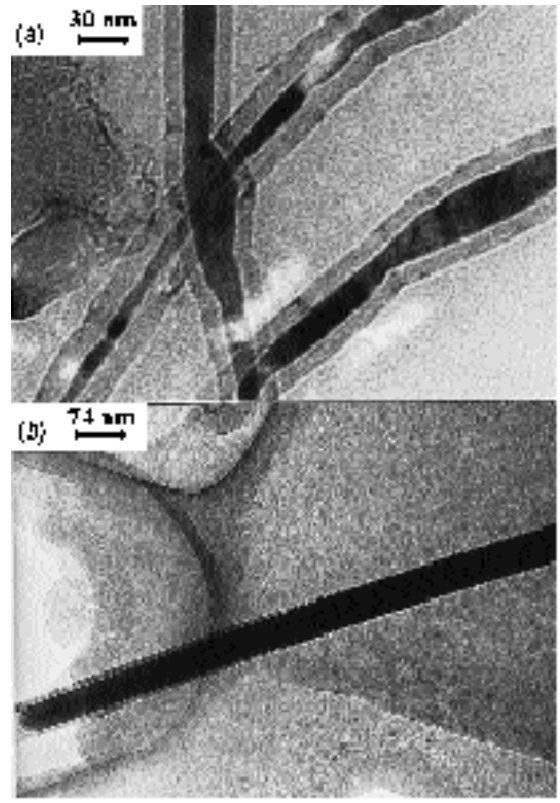

Fig. 3 TEM images of carbon-coated iron nanorods obtained by the pyrolysis of ferrocene (*a*) at 1170 K under vacuum (10^{-5} Torr) and (*b*) at 1370 K under a flow of Ar (10 sccm)

carbon-coated iron nanorods (yield ≥60%). In Fig. 3(*a*), we show a TEM image of metal nanorods with a thick carbon coating, obtained by the pyrolysis of ferrocene at 1170 K under vacuum. We also obtained a fair proportion of nanorods when the flow rate of Ar was low (10 sccm). In Fig. 3(*b*) we show a TEM image of a nanorod obtained by the pyrolysis of ferrocene at 1370 K under an Ar flow of 10 sccm. Note that such nanorods have been reported in the literature, produced by the reaction of carbon nanotubes with volatile oxide or halide species.[8] The present method of producing nanorods is much simpler. The formation of metallic iron in the form of particles or rods in the pyrolysis of ferrocene suggests that the mechanism of alignment of the nanotubes may be related to the magnetic nature of the nanorods or particles of iron.

Notes and References

† E-mail: cnrrao@sscu.iisc.ernet.in

1 P. M. Ajayan, O. Stephan, C. Colliex and D. Trauth, *Science*, 1994, **265**, 1212.
2 P. M. Ajayan, *Adv. Mater*., 1995, **7**, 489.
3 W. A. de Heer, A. Chatelain and D. Ugarte, *Science*, 1995, **270**, 1179.
4 W. A. de Heer, W. S. Basca, A. Chatelain, T. Gerfin, R. Humphrey-Baker, L. Forro and D. Ugarte, *Science*, 1995, **268**, 845.
5 W. Z. Li, S. S. Xie, L. X. Qian, B. H. Chang, B. S. Zou, W. Y. Zhou, R. A. Zhao and G. Wang, *Science*, 1996, **274**, 1701.
6 M. Terrones, N. Grobert, J. Olivares, J. P. Zhang, H. Terrones, K. Kordatos, W. K. Hsu, J. P. Hare, P. D. Townsend, K. Prassides, A. K. Cheetham, H. W. Kroto and D. R. M. Walton, *Nature*, 1997, **388**, 52.
7 R. Sen, A. Govindaraj and C. N. R. Rao, *Chem. Phys. Lett.*, 1997, **267**, 276.
8 H. Dai, E. W. Wong, Y. Z. Lu, S. Fan and C. M. Lieber, *Nature*, 1995, **375**, 769.

Received in Cambridge, UK, 23rd March 1998; 8/02258E

Synthesis and structure of $[\{Bu^tP)_2H\}K\cdot pmdeta]_2$, containing an organo diphosphido ligand [pmdeta = $(Me_2NCH_2CH_2)_2NMe$]

Michael A. Beswick,[a] Alexander D. Hopkins,[a] Lesley C. Kerr,[a] Marta E. G. Mosquera,[a] Julie S. Palmer,[a] Paul R. Raithby,[a] Alexander Rothenberger,[a] D. Stalke,[b] Alexander Steiner,[c] Andrew E. H. Wheatley[a] and Dominic S. Wright*[a]

[a] *Chemistry Department, University of Cambridge, Lensfield Road, Cambridge, UK CB2 1EW*
[b] *Institut für Anorganische Chemie, Universität Würzburg, Am Hubland, 97074 Würzburg, Germany*
[c] *Department of Chemistry, Liverpool University, Crown Street, Liverpool, UK L69 7ZD*

Reduction of $[Bu^tP]_4$ with K metal (1 : 5 equiv.) followed by the addition of pmdeta and stoichiometric hydrolysis gives $[\{(Bu^tP)_2H\}K\cdot pmdeta]_2$, a unique complex containing a $[Bu^tP(H)PBu^t]^-$ anion ligand homologous with a phosphido anion (R_2P^-).

Early investigations showed that the reduction of $[RP]_4$ by alkali metals leads to fragmentation of the cyclic P_4 rings, giving species containing various anions {such as $[RP]_4^{2-}$, $[RP]_3^{2-}$, $[RP]_2^{2-}$ and $[(RP)_2(H)]^-$} depending on the reaction stoichiometries.[1] However, the solids isolated were mainly characterised by elemental analysis and NMR spectroscopic studies on these and related systems indicated later that mixtures of anions are produced in solution.[2] Owing to the lack of X-ray structural data on the alkali metal complexes and the difficulty in isolating the pure components there have been few systematic investigations of the coordination chemistry of the organopolyphosphido anions and their reactivity with other metal centres is poorly understood.[3] Our emerging interest in the potential use of these anions as ligands to main group elements has lead us to reinvestigate the reduction of $[Bu^tP]_4$ with alkali metals, with the aim of developing well defined reagents for transmetallation.

We report here that the reaction of $[Bu^tP]_4$ with potassium metal (1 : 5 equiv.) in thf followed by the addition of pmdeta and stoichiometric hydrolysis gives the crystalline complex $[\{(Bu^tP)_2H\}K\cdot pmdeta]_2$ **1** (Scheme 1).‡ This complex is the first representative of this type of alkali metal complex to be fully characterised in pure form. Evidence for the presence of the H atom in the anion of **1** is obtained from the IR spectrum (ν_{P-H} 2005 cm^{-1}). In addition, the room-temperature ^{31}P NMR spectrum is similar to that previously reported for $[\{(Bu^tP)_2H\}K]$ in thf (produced in trace amounts in the reaction of K metal with $[Bu^tP]_4$),[2a] although with a markedly larger $^1J_{PH}$ coupling constant in **1** (*ca.* 201 Hz;[5] *cf. ca.* 137 Hz[2a]). The ^{31}P NMR spectrum illustrates that the anion has a rigid structure in solution in which the proton is bonded solely to one P centre (with no intra- or inter-molecular exchange occurring).

The low-temperature X-ray structure of **1**§ shows that it exists as dimeric molecules in the solid state in which two $[(Bu^tP)_2H]^-$ anions are associated into a ring structure by two pmdeta-solvated K^+ cations [Fig. 1(*a*)]. Although a number of lithium organophosphides (containing R_2P^-) have been structurally characterised in recent years,[6] very few complexes of the heavier alkali metals have been reported.[7] Complex **1** is the first containing an organodiphosphide anion, the second homologue of a potential series of organo polyphosphide chain anions of the type $[R_{2x+1}P_x]^-$. The closest analogues of **1** are phosphoramides[8] such as the dimer $[\{Ph_2PN(Ph)\}Li\cdot Et_2O]_2$, containing a $[\{Ph_2PN(Ph)\}]^-$ anion.[8a] The only other alkali metal organo polyphosphide to be reported is $[\{(Bu^t_2P)_2P\}Li\cdot 2thf]$, containing a 'branched' $[(Bu^tP)_2P]^-$ anion.[9]

The anionic P centres of the $[(Bu^tP)_2H]^-$ ligands form the central K_2P_2 ring of the dimeric structure of **1** [K(1)–P(1) 3.340(3), K(1)–P(1a) 3.251(2) Å]. Secondary coordinative interactions occur with the neutral P centres of each $[(Bu^tP)_2H]^-$ anion [P(2)–K(1) 3.658(3) Å]. The bidentate

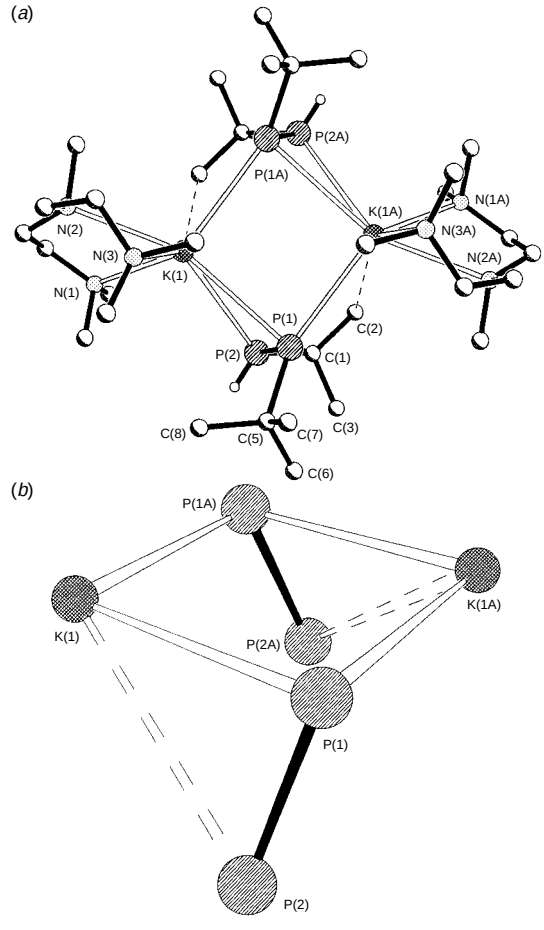

Fig. 1 Dimer structure of **1**. H atoms (except that bonded to P) have been omitted for clarity. Key bond lengths (Å) and angles (°); K(1)–P(1a) 3.251(2), K(1)–P(1) 3.340(3), K(1)–P(2) 3.658(3), P(1)–P(2) 2.135(3), K(1)–N(1) 2.936(6), K(1)–N(2) 2.865(6), K(1)–N(3) 2.894(7), K(1a)···C(2) 3.685(3) [K(1)···H(2a) 3.01]; P(1)–K(1)–P(1a) 94.98(6), K(1)–P(1)–K(1a) 84.93(6), P(1)–K(1)–P(2) 35.15(5), P(2)–P(1)–K(1) 84.93(6), P(2)–P(1)–K(1a) 110.11(9).

$$[Bu^tP]_4 \xrightarrow[\text{ii pmdeta, } H_2O]{\text{i K}} [\{(Bu^tP)_2H\}K\bullet pmdeta]_2$$

1

Scheme 1

coordination mode of the $[(Bu^tP)_2H]^-$ ligands in **1** is similar to that found in dimeric alkali metal phosphoramides[8] and hydrazides,[10] in which P,N and N,N chelation of the alkali metals by the $[R_2PNR]^-$ and $[R_2NNR]^-$ anions occurs. However, one significant difference with the latter is the unusual *cis* orientation of the $[(Bu^tP)_2H]^-$ ligands with respect to the K_2P_2 dimer ring of **1** [giving a 'boat-like' rather than 'chair-like' core, Fig. 1(*b*)]. This orientation seems most likely to be steric in origin. A noteworthy feature in **1** is the presence of a relatively short P–P bond [2.135(3) Å] which is well below distances normally anticipated for single bonds (*ca*. 2.20 Å) and similar to those found in transition metal complexes containing η^2-RP=PR ligands (*ca*. 2.1 Å).[3] In dimeric complexes containing isoelectronic $[R_2NNR]^-$ anions the N–N bonds are generally longer than in neutral hydrazines, as a result of enhanced lone pair repulsion.[10] The shortening of the P–N bonds in complexes containing $[R_2PNR]^-$ ligands may partly be a result of $p_\pi(N)$–$d_\pi(P)$ bonding. However, although the possibility of such bonding cannot be discounted in the $[(Bu^tP)_2H]^-$ anion the principal reason for the short P–P bond length probably stems from compression arising from the chelation of the K^+ cations.

The isolation and full characterisation of **1** provides a well defined and readily accessible source of the $[(Bu^tP)_2H]^-$ anion for application as a ligand to a range of metals. In addition, the presence of a reactive proton also furnishes the potential for further metallation. In this regard preliminary ^{31}P studies indicate that the major product formed by the reaction of **1** with Bu^nLi is not the expected $[Bu^tP]_2^{2-}$ dianion but the $[Bu^tP]_3^{2-}$ dianion.‡

We gratefully acknowledge the EPSRC (A. D. H., L. C. K., J. S. P., A. E. H. W.), The Spanish Government (M. E. G. M.), the Leverhulme Trust (M. A. B.), Electron Tubes, Ltd. (UK) (A. D. H.), the Gottlieb Daimler- und Karl Benz-Stiftung (A. R.) and the Royal Society (D. S. W., P. R. R.) for financial support.

Notes and References

† E-mail: dsw1000@cus.cam.ac.uk

‡ *Synthesis* of **1**; to a solution of $[Bu^tP]_4$ (1.0 g, 2.84 mmol)[1a] in thf (40 ml) was added K metal (0.56 g, 14.2 mmol) and the mixture brought to reflux for 24 h. After this period all the K had reacted (if 8 equiv. are used then only 5 equiv. is consumed even after reflux for 48 h). The mixture was filtered while hot (Celite) and pmdeta (2.1 ml, 10 mmol, distilled over Na) was added. The orange–yellow solution was cooled (−78 °C) and a standard solution of H_2O in thf was added dropwise (10.2 ml, 0.56 mol dm^{-3}, 5.68 mmol). The mixture was allowed to warm to room temperature and stirred (12 h), resulting in a yellow solution and the precipitation of KOH. Filtration (Celite) followed by concentration to *ca*. 8 ml gave a light yellow precipitate which was heated into solution. Storage at 25 °C (12 h) gave large light yellow crystalline needles of **1**; yield 0.33 g (15%) (the low yield reflects the high solubility of the complex in thf); decomp. > 115 °C to orange oil; IR (Nujol), 2205m (P–H str.), other major bands at 1345m, 1309m, 1162s, 1023s, 945m, 900m, 809m, 784m; ^1H NMR (250 MHz, +25 °C, $[^2H_8]$thf), δ 2.75 (1 H, br d, P–H, $J_{^1H^{31}P}$ *ca.* 200 Hz), 2.34 (8 H, m, CH_2CH_2 of pmdeta), 2.21 (3 H, s., NMe of pmdeta), 2.13 (12 H, s., NMe_2 of pmdeta), 1.15 (9 H, br s, Bu^t), 0.99 (9 H, br s, Bu^t); ^{31}P NMR (101.256 MHz, +25 °C, $[^2H_8]$thf, rel. to 85% H_3PO_4), δ −8.90 (dd, Bu^tPH, $J_{^1H^{31}P}$ 201.4 ± 1.1, $J_{^{31}P^{31}P}$ 321.5 Hz), −57.37 (d Bu^tP, $J_{^{31}P^{31}P}$ 321.5 Hz), the ^1H decoupled spectrum gave $J_{^{31}P^{31}P}$ 321.6 ± 0.6 Hz; Anal., Calc. for $[C_{17}H_{42}\}P_2N_3K]_n$: C, 52.4; H, 10.8; N, 10.8; P, 15.9. Found: C, 50.2; H, 10.5; N, 10.5; P 15.3%. The reaction of **1** with Bu^nLi (*ca*. 1 equiv.) in thf was monitored by ^{31}P NMR spectroscopy (+25 °C). This preliminary study reveals that the major product contains the $[Bu^tP]_3^{2-}$ dianion, with a triplet (δ 4.74) and a doublet (δ −44.96) being observed (ratio 1 : 2 respectively, $J_{^{31}P^{31}P}$ *ca* 170 Hz).

§ *Crystal data* for **1**; $C_{34}H_{84}K_2N_6P_4$, M = 779.15, orthorhombic, space group *Pnn*2, a = 14.457(7), b = 16.255(8), c = 10.502(5) Å, U = 2468(2) Å^3, Z = 2, D_c = 1.048 g cm^{-3}. Data were collected on a Siemens-Stoe AED diffractometer (2θ–ω scans) using an oil-coated[11] rapidly cooled crystal of dimensions 0.30 × 0.30 × 0.25 mm (3.64 < θ < 22.48°). Of a total of 3410 reflections collected, 3052 were independent (R_{int} = 0.036). An absorption correction based on ψ-scans was applied (max.,min. transmission = 0.978,0.618). The structure was solved by direct methods and refined by full-matrix least squares on F^2 using all data to final values of $R1$ [$F > 4\sigma(F)$] = 0.058 and $wR2$ = 0.140;[12] largest peak, hole in the final difference map = 0.30, −0.32 e Å^{-3}. All non-hydrogen atoms were refined anisotropically and H-positions were set geometrically. C-atoms of the pmdeta ligand were disordered and were split into two positions using restraints. CCD8 182/900.

1 (*a*) K. Issleib and M. Hoffmann, *Chem. Ber.*, 1966, **100**, 1320; (*b*) K. Issleib and K. Krech, *Chem. Ber.*, 1966, **100**, 1311.
2 (*a*) M. Baudler, C. Grunerm, G. Fürstenberg, B. Kloth, F. Saykowski and U. Özer, *Z. Anorg. Allg. Chem.*, 1978, **446**, 169; (*b*) P. R. Hoffmann and K. G. Caulton, *J. Am. Chem. Soc.*, 1975, **97**, 6370.
3 For example, the reaction of $[(Bu^tP)_2Li_2]$ with $[(Ph_3P)_2NiCl_2]$ gives [(*cyclo*-Bu^tP_4)Ni(η^2-Bu^tP=PBu^t)], P. A. Jones, M. H. Seeberger and B. R. Whittlesey, *J. Am. Chem. Soc.*, 1985, **107**, 6424.
5 $^1J_{PH}$ in **1** is similar to that found in $(RPH)_2$ [R = Bu^t (*ca*. 191 Hz), Ph (*ca.* 206 Hz)], M. Baudler, C. Gruner, H. Tschäbunin and J. Hahn, *Chem. Ber.*, 1982, **115**, 1739; M. Baudler, B. Carlsohn, D. Koch and P. K. Medda, *Chem. Ber.*, 1978, **111**, 1210.
6 M. A. Beswick and D. S. Wright, *Comprehensive Organometallic Chemistry II*, ed. E. W. Abel, F. G. A. Stone and G. Wilkinson, vol. ed. C. E. Housecroft, Pergamon, Oxford, 1995, vol. 1, p. 1.
7 There appear to be no simple K phosphides; G. A. Koutsantonsi, P. C. Andrews and C. L. Raston, *J. Chem. Soc., Chem. Commun.*, 1995, 47; H. C. Aspinall and M. R. Tillotson, *Inorg. Chem.*, 1990, **35**, 5.
8 (*a*) M. T. Ashby and Z. Li, *Inorg. Chem.*, 1992, **31**, 1321; (*b*) A. Müller, B. Neumüller, K. Dehniche, J. Magull and D. Fenske, *Z. Anorg. Allg. Chem.*, 1997, **623**, 1306.
9 I. Kovacs, H. Krautscheid, E. Matern, E. Satler, G. Fritz, W. Houle, H. Borrmann and H. v. Schnering, *Z. Anorg. Allg. Chem.*, 1996, **622**, 1564.
10 M. Metzler, H. Nöth and H. Sachdev, *Angew. Chem., Int. Ed. Engl.*, 1994, **33**, 1746; (*b*) C. Dost, C. Jager, U. Klingebiel, C. Freire-Erdbrugger, R. Herbst-Irmer and M. Schafer, *Z. Naturforsch. Teil B*, 1995, **50**, 76; B. Gemund, H. Nöth, H. Sachdev and M. Schmidt, *Chem. Ber.*, 1996, **129**, 1335.
11 T. Kottke and D. Stalke, *J. Appl. Crystallogr.*, 1993, **26**, 615.
12 G. M. Sheldrick, SHELX-97, Universität Göttingen, 1997.

Received in Cambridge, UK, 21st May 1998; 8/03834A

Transylidation of a transiently formed nitrilium phosphane ylide complex

Hendrik Wilkens, Frank Ruthe, Peter G. Jones and Rainer Streubel*†

Institut für Anorganische und Analytische Chemie der Technischen Universität Braunschweig, D-38106 Postfach 3329, Braunschweig, State, Germany

Thermal decomposition of the 3-phenyl-substituted 2*H*-azaphosphirene complex 1 in the presence of dimethyl cyanamide and dimethyl acetylenedicarboxylate (DMAD) yielded dimethylamino-substituted products, the 2*H*-1,2-azaphosphole complex 4b and the diastereoisomeric Δ³-1,3,2-oxazaphospholene complexes 5a,b; this represents the first example of 1,3-dipolar cycloaddition reactions of a nitrilium phosphane ylide complex that is generated *in situ* by transylidation.

Recently, we reported the first evidence for transiently formed nitrilium phosphane ylide complexes by two different trapping experiments. Thermal ring opening of the 2*H*-azaphosphirene complex **1** in toluene in the presence of dimethyl acetylenedicarboxylate (DMAD) yielded a product mixture consisting of the 1*H*-phosphirene complex **3** and the 2*H*-1,2-azaphosphole complex **4a**.[1,2] With dimethyl cyanamide in benzonitrile the trapping resulted in the formation of a 2*H*-1,3,2-diazaphosphole complex;[3] based on the observed selectivity and non-formation of a 4,5-diphenyl-substituted 2*H*-1,3,2-diazaphosphole complex, we assumed a transylidation during the reaction course. To the best of our knowledge transylidation processes among nitrilium betaines have been reported so far only for nitrile sulfides[4] (Scheme 1); neither is their mechanism known nor has this methodology been synthetically exploited. With respect to the enormous potential of 1,3-dipoles such as nitrilium betaines in [3 + 2] cycloaddition reactions and, therefore, in heterocyclic chemistry,[5] we decided to examine this aspect more thoroughly for the case of nitrilium phosphane ylide complexes and performed a trapping experiment with two suitable, but different trapping reagents, DMAD and dimethyl cyanamide.

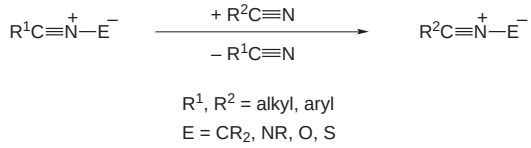

Scheme 1

Thermal decomposition of the 2*H*-azaphosphirene tungsten complex **1** in the presence of 2 equiv. of DMAD and 2 equiv. of dimethyl cyanamide yielded the 2*H*-1,2-azaphosphole complex **4b** and the two diastereoisomeric Δ³-1,3,2-oxazaphospholene complexes **5a,b** (*meso* and racemate) in an estimated ratio of 1 : 1 : 1 (³¹P NMR integration). The formation of both five-membered heterocycles is rationalized by 1,3-dipolar cycloaddition reactions of the *in situ* generated nitrilium phosphane ylide complex **2b** to the C≡C triple bond and the C=O double bond of dimethyl acetylenedicarboxylate [Scheme 2, path (*b*)].

This result has several noteworthy aspects. It is a rare example of a dual reactivity of DMAD towards a 1,3-dipole and it is remarkable that neither the 1*H*-phosphirene complex **3** nor the phenyl-substituted five-membered heterocycle complex **4a** was detected [path *a*)]. Furthermore, during the reaction course a transylidation must have taken place, such that the benzonitrile unit in **2a** was substituted, at least formally, by dimethyl cyanamide, thus forming the nitrilium phosphane ylide complex **2b**. We performed additionally control experiments to check this interpretation. Firstly, we heated a solution of 1*H*-phosphirene complex **3** and dimethylcyanamide to exclude a subsequent ring enlargement reaction, but up to 85 °C no reaction was observed. Secondly, we examined the possible reaction sequence: DMAD gives initially an azete derivative with dimethyl cyanamide, which then could yield 2*H*-1,2-azaphosphole complex **4b** by insertion of transiently formed terminal phosphanediyl complex [$(OC)_5$WPCH-$(SiMe_3)_2$] (*cf.* ref. 2) into a C–N bond of the azete ring; but azete formation could not be detected upon heating a solution of DMAD and dimethyl cyanamide for 2 h at 85 °C.

The composition of the 2*H*-1,2-azaphosphole complex **4b** and the Δ³-1,3,2-oxazaphospholene complexes **5a,b** are confirmed by elemental analysis and mass spectrometry;‡ the structural formulation is based on their characteristic NMR spectral data‡ in solution and that of **5a** was confirmed by X-ray structure analysis.§ The phosphorus nucleus of **4b** displays a resonance at δ 85.6, which is significantly high-field shifted compared to other 2*H*-1,2-azaphosphole complexes (δ 102–105[2]) with a markedly increased phosphorus–tungsten coupling constant of 249.7 Hz (*vs.* 236–238 Hz[2]). The ³¹P NMR parameters of the diastereoisomeric Δ³-1,3,2-oxazaphospholene complexes are δ 191.6 [$^1J_{PW}$ 303.1 Hz (**5a**)] and δ 198.6 [$^1J_{PW}$ 305.9 Hz (**5b**)]. In view of the strong influence of the phosphorus-bonded oxygen atom on the

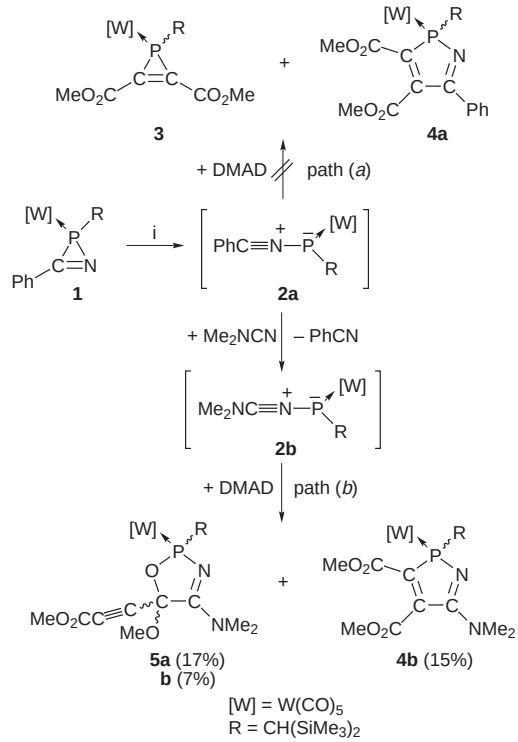

Scheme 2 *Reagents and conditions*: i, DMAD (2 equiv.), Me_2NCN (2 equiv.), toluene (3 ml), 75 °C, 1.5 h.

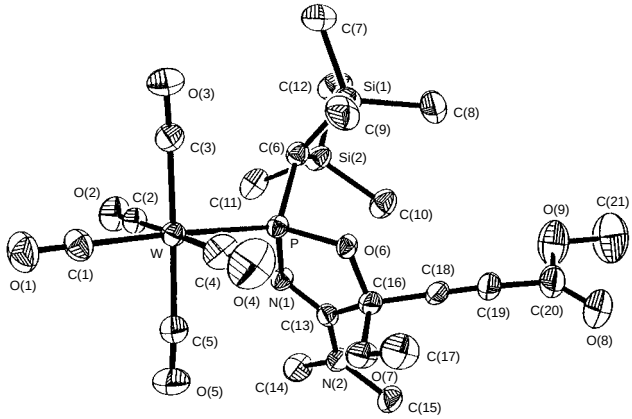

Fig. 1 Molecular structure of complex **5a** in the crystal. Radii are arbitrary. Selected bond lengths (Å) and angles (°): P–W 2.4748(9), P–N(1) 1.677(3), N(2)–C(13) 1.337(4), O(6)-C(16) 1.413(4), C(13)–C(16) 1.552(4), C(18)–C(19) 1.180(5), P–O(6) 1.683(2), N(1)–C(13) 1.301(4); N(1)–C(13)–N(2) 1.242(3), N(1)–P–O(6) 95.23(12), C(13)–N(1)–P 111.5(2), C(16)–O–P 111.9(2), N(1)–C(13)–C(16) 114.8(3), O(6)–C(16)–C(13) 105.3(2).

phosphorus resonances, the almost constant imino carbon resonances of **4b** and **5a,b** (δ 158.0–158.4) are surprising. All these carbon resonances display small carbon–phosphorus coupling constants (1.1-5.3 Hz), which seems to be characteristic for such heterocyclic ring systems; these magnitudes most probably derive from ^2J and ^3J scalar couplings.

The five-membered ring system of the Δ^3-1,3,2-oxazaphospholene complex **5a**, which is the first to be reported, is almost planar; the best plane is given by P–N(1)–C(13)–C(16) (deviation: 0.005 Å) and the oxygen atom lies 0.17 Å out of this plane. The N(1)–C(13) distance [1.301(4) Å] is in the typical range of nitrogen–carbon double bonds, while the coordination sphere of the phosphorus atom is distorted tetrahedral with a phosphorus–tungsten bond length of 2.4748(9) Å.

We are currently investigating the synthetic potential of nitrilium phosphane ylide complexes that are generated *in situ* by transylidations.

This work was supported by the Fonds der Chemischen Industrie and by the Deutsche Forschungsgemeinschaft.

Notes and References

† E-mail: r.streubel@tu-bs.de

‡ Satisfactory elemental analyses were obtained for complexes **4b** and **5a,b**. NMR data [$CDCl_3$], 30.3 MHz (^{13}C), 81.0 MHz (^{31}P), TMS and 85% H_3PO_4 were used as standard references. *Selected data* for **4b**: mp 123 °C; δ_C 139.2 (d, J_{PC} 21.1, P–*C*=C), 158.4 (d, $^{(2+3)}J_{PC}$ 5.3, P–N=*C*), 161.8 (d, $^{(2+3)}J_{PC}$ 7.3, P–C=*C*); δ_P 85.6 (d, $^1H_{PW}$ 249.7); *m/z* (EI) 726 (M^+). For **5a**: mp 158 °C; δ_C 99.1 (d, $^{(2+3)}J_{PC}$ 6.9, P–O–C), 158.1 (d, $^{(2+3)}J_{PC}$ 1.1, P–N=C); δ_P 191.6 (d, $^1J_{PW}$ 305.9); *m/z* (EI) 726 (M^+). For **5b**: mp 164 °C; δ_C 99.2 (d, $^{(2+3)}J_{PC}$ 4.0, P–O–C), 158.0 (d, $^{(2+3)}J_{PC}$ 1.3, P–N=C); δ_P 198.6 (d, $^1J_{PW}$ 303.1); *m/z* (EI) 726 (M^+).

§ *Crystal data* for **5a**: $C_{21}H_{31}N_2O_9PSi_2W$; M = 726.48, triclinic, space group $P\bar{1}$, a = 10.0074(10), b = 10.073(2), c = 15.8415 Å, α = 97.711(8), β = 92.631(8), γ = 106.817(8)°, U = 1508.8(3) Å^3, Z = 2, D_c = 1.599 mg m^{-3}, μ = 4.006 mm^{-1}, F(000) = 720, 5290 independent reflections to $2\theta_{max}$. = 50°, T = 173 K, S = 0.962, R [F, $>4\sigma(F)$] = 0.0217, $R_w(F^2)$ = 0.0505, 164 restraints and 336 parameters, highest peak = 0.994, deepest hole = −0.527 e Å^{-3}. The X-ray data set was collected with monochromated Mo-Kα radiation (λ = 0.71073 Å) on a Siemens P4 four-circle diffractometer. Absorption correction was based on ψ-scans. The structure was solved by the heavy-atom method and refined anisotropically by full-matrix least-squares on F^2. H atoms were included using a riding model for all non-methyl group protons. Methyls were refined as rigid groups. CCDC 182/894.

1 A. Ostrowski, J. Jeske, P. G. Jones and R. Streubel, *J. Chem. Soc., Chem. Commun., 1995, 2507.*
2 R. Streubel, H. Wilkens, A. Ostrowski, C. Neumann, F. Ruthe and P. G. Jones, *Angew. Chem., Int. Ed. Engl.*, 1997, **36**, 1492.
3 H. Wilkens, J. Jeske, P. G. Jones and R. Streubel, *Chem. Commun.*, 1997, 2317.
4 R. K. Howe and J. E. Franz, *J. Org. Chem.*, 1974, **39**, 962.
5 A. Padwa, *1,3-Dipolar Cycloaddition Chemistry*, Wiley, New York, 1984.

Received in Cambridge, UK, 3rd April 1998; 8/02569J

Nickel-catalyzed generation of 2-methylhex-5-enyl ethers from allyl ethers with trimethylaluminium

Takahiko Taniguchi and Kunio Ogasawara*†

Pharmaceutical Institute, Tohoku University, Aobayama, Sendai 980-8578, Japan

Allyl ethers have been converted into the corresponding 2-methylhex-5-enyl ethers in one step on treatment with trimethylaluminium in the presence of a catalytic amount of (dppp)$NiCl_2$.

We recently found that allyl ethers **1** are cleaved facilely and selectively to give the alcohols **2** with expulsion of propene on treatment with DIBAL-H in the presence of a catalytic amount of dichloro[bis(diphenylphosphino)propane] nickel [(dppp)$NiCl_2$] in an aprotic solvent[1] (Scheme 1). The reaction may be applied to allyl acetals, such as **1a**,**b**, using triethylaluminium in place of DIBAL-H to give the same hemiacetal mixture **2a**/**b**, in good yield, without causing reduction of the hemiacetal functionality, although the fate of the allyl functionality was uncertain[1] (Scheme 2). We report here an unprecedented type of C–C bond formation reaction which was observed during the examination of the reaction of the allyl acetals **1a**,**b** with trimethylaluminium in place of triethylaluminium in the presence of the same nickel catalyst.

Thus, when the α-H allyl acetal **1a** was treated with trimethylaluminium (1.3 equiv.) in the presence of (dppp)$NiCl_2$ (2 mol%) in toluene at 0 °C to room temperature for 0.5 h, an inseparable mixture of **3a**‡ consisting of two diastereomers was generated in a substantial yield as well as the expected hemiacetal mixture **2a**/**b**. On the same treatment, the β-H epimer **1b** gave the diastereoisomeric mixture **3b** consisting of two diastereomers and the same hemiacetal mixture **2a**/**b** above. The sugar moiety, including the hemiacetal stereochemistry, of the products was recognized to be unchanged during the reaction by examination of ^1H NMR and mass spectra which indicated that the change occurred in the allyl moiety of **1** with an increment of 56 mass numbers attributed to one Me on a tertiary stereogenic center and one allyl unit. It was also concluded that the reaction that occurred was essentially a dimerization and, therefore, the yields of **3a**,**b** were calculated as 61 and 60%, respectively. The same reaction occurred with another sugar derivative **4** having a bis-allyl ether moiety in the molecule to give the bis(2-methylhex-5-enyl) ether **5** and the mono-2-methylhex-5-enyl ether **6** both as diastereomeric mixtures in yields of 10 and 40% as well as 34% of the double deallylated diol in the presence of 2.6 equiv. of trimethylaluminium (Scheme 3).

The other simple allyl ethers **1c**–**l**, those that gave the corresponding alcohols **2c**–**l** with DIBAL-H and (dppp)$NiCl_2$, were, therefore, subjected to the same reaction with trimethylaluminium in the presence of (dppp)$NiCl_2$ and it was found that all but the aryl ether gave the corresponding products having the same ether moiety in addition to the corresponding deallylated products. The aryl ether gave the phenol quantitatively as the sole product. Most importantly, neither the coupling reaction nor the cleavage reaction occurred at all in the absence of

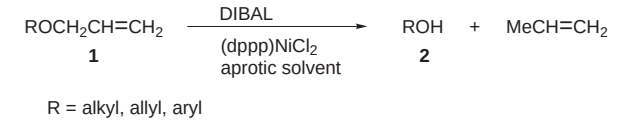

Scheme 1

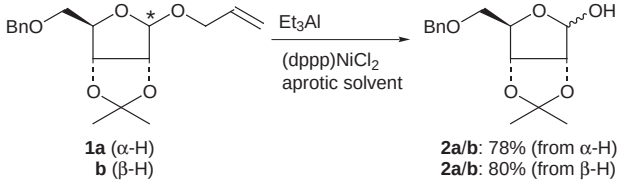

Scheme 2

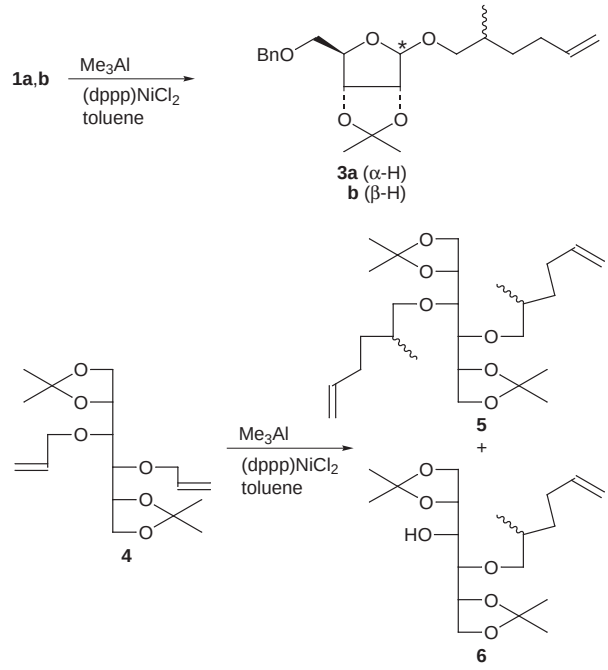

Scheme 3

Table 1 Reaction of allyl ethers **1** with Me_3Al and (dppp)$NiCl_2$

Entry	Substrate **1**	Product **3**	R	Yield[a]
1	**a**	**a**[b]	Scheme 3	61[c]
2	**b**	**b**[b]	Scheme 3	60[c]
3	**c**	**c**	$HO(CH_2)_2O$	27
4	**d**	**d**	$HO(CH_2)_3O$	27
5	**e**	**e**	4-MeOPh	0
6	**f**	**f**	$PhCH_2$	45[c]
7	**g**	**g**	$PhCH_2CH_2$	42[c]
8	**h**	**h**	$AcO(CH_2)_4$	44[c]
9	**i**	**i**	Ph_2CH	30[c]
10	**j**	**j**	$Me_2C{=}CHCH_2O(CH_2)_4$	39[c]
11	**k**	**k**	(*S*)-PhCHMe	42[c]
12	**l**	**l**	THP	48[c]

[a] Isolated yield after SiO_2 column chromatography. [b] Obtained as a diastereomeric mixture. [c] Yield was calculated based on consumption of 2 equiv. of the substrate per product.

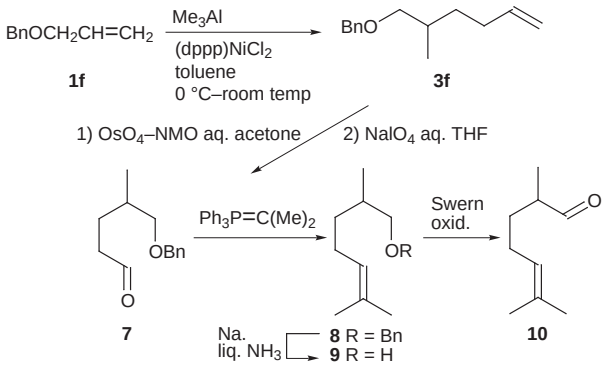

Scheme 4

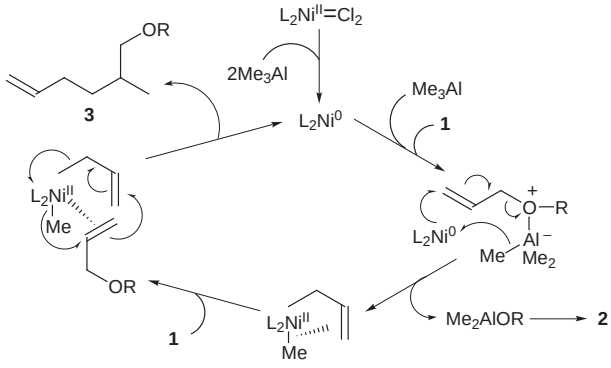

Scheme 5

(dppp)$NiCl_2$ and only the cleavage reaction occurred when triethylaluminium in place of trimethylaluminium was used under the same catalytic conditions (Table 1).

To confirm the structure of the products **3a–l**, the benzyl ether **3f** generated from allyl benzyl ether **1f** was transformed into the known compound (±)-norcitronellal[2] **10** in 69% overall yield *via* sequential olefin cleavage, Wittig condensation, reductive debenzylation and oxidation through the aldehyde **7**, the ether **8** and the alcohol **9**. This confirmed unambiguously the structure of the common ether half as a 2-methylhex-5-enyl functionality (Scheme 4).

Formation of the 2-methylhex-5-enyl functionality indicated that a concurrent regioselective addition of a methyl moiety from trimethylaluminium and of the allyl moiety from the substrate allyl ether to the allyl double bond of another molecule of the substrate occurred under the conditions used. It is plausible that the reaction was initiated by generation of a Ni^0 complex[3] which led to formation of an allyl–methyl–Ni^{II} complex by reaction with trimethylaluminium and an allyl ether to induce the ether cleavage at the first stage. The complex then interacted with another molecule of allyl ether to allow the regioselective addition[4] of the methyl and allyl functionalities from Ni^{II} to the allyl ether double bond *via* a reductive elimination pathway that reformed the Ni^0 complex (Scheme 5).

Notes and References

† E-mail: konol@mail.cc.tohoku.ac.jp

‡ All new compounds had spectroscopic [IR, ^{1}H NMR, mass] and analytical (HRMS) data consistent with the assigned structure.

1 T. Taniguchi and K. Ogasawara, *Angew. Chem., Int. Ed. Engl.*, 1998, **37**, 1136.
2 S. Takano, S. Satoh and K. Ogasawara, *Heterocycles*, 1985, **23**, 41.
3 K. Fischer, K. Jonas, P. Misbach, R. Stabba and G. Wilke, *Angew. Chem., Int. Ed. Engl.*, 1973, **12**, 943; G. Wilke, *Angew. Chem., Int. Ed. Engl.*, 1988, **27**, 186.
4 H. Felkin and G. Swievczewski, *Tetrahedron*, 1975, **31**, 2735.

Received in Cambridge, UK, 30th March 1998; 8/02430H

Reaction field for efficient porphyrin metallation catalysis produced by self-assembly of a short DNA oligonucleotide

Naoki Sugimoto,*† Takeshi Toda and Tatsuo Ohmichi

Department of Chemistry, Faculty of Science, Konan University, 8-9-1 Okamoto, Higashinada-ku, Kobe 658-8501, Japan

The G-wire structure, which is formed by dGTGGGTTGGGTGGGTTGG in the presence of 50 mM K^+, becomes a catalytic reaction field for porphyrin metallation, inserting Zn^{2+} into porphyrin efficiently.

Many protein enzymes provide a reaction field for their substrates. RNA or DNA can catalyze the cleavage or ligation reaction of nucleic acids, and then has the potential to provide a reaction field for its substrate.[1–4] The catalytic RNA– or DNA–substrate complexes consist of many unpaired regions such as internal loops, hairpin loops and bulges, and the catalysis reactions occur in these unpaired regions.[1–4] Thus, catalytic RNA or DNA produces the reaction fields. If these reaction fields can be made by designing specific sequences of catalytic RNA or DNA, it would be an important development for ribozyme engineering. Recently, a DNA enzyme that can catalyze insertion of Zn^{2+} into mesoporphyrin IX (MPIX) was isolated from a DNA library using *in vitro* selection.[5,6] This minimum DNA enzyme is a 24-mer oligonucleotide and consists of a G-rich sequence that is able to form a G-quartet structure.[6] Although this reaction mechanism was investigated,[7] little is known about the detailed active structure of this DNA enzyme except for the G-quartet that produces the reaction field to catalyze the metallation reaction. Here, in order to develop the chemical engineering of nucleic acids, we have investigated the active structure of the DNA enzyme with catalytic activity for the porphyrin metallation by using an 18-mer DNA sequence, dGTGGGTTGGGTGGGTTGG. This oligonucleotide was designed to contain the G-rich sequence that forms the G-quartet structure and to be shorter than the previous minimum DNA enzyme isolated by Li and Sen.[5,6]

The ability of this 18-mer DNA to catalyze the insertion of Zn^{2+} into MPIX was investigated by HPLC. The reaction yields of the porphyrin metallation were calculated by the ratio of the peak areas at 400 nm between the reactant and the product (ZnMPIX). The metallation reactions were performed in the presence of 50 mM K^+ or Na^+, because the formation of the G-quartet structure is easier in the presence of K^+ than Na^+.[8–12] At the single turnover condition,‡ the reaction yield in the presence of 50 mM K^+ was 91% after 8 h. On the other hand, the reaction yield in the presence of 50 mM Na^+ was 46%. The reaction yields in the absence of K^+ or Na^+ were 20 or 17%, respectively. Further, the k_{cat} values of the 18-mer DNA in the presence of 50 mM Na^+ and K^+ were 8.0×10^{-3} and 1.0 min^{-1}, respectively.§ This value in the presence of K^+ is of the same order as that for ferrochlatase.[13] Thus, the 18-mer DNA was able to catalyze efficiently the porphyrin metallation and played a role as an enzyme in the presence of K^+. The result also suggests that the active structure of this novel DNA enzyme consists of the G-quartets. In order to investigate the effect of DNA sequences other than the G-rich sequence, the activity of 16-mer DNA, dGTGGGTGGGTGGGTGG (which lacks the sixth and fifteenth T residues of the 18-mer DNA oligonucleotide), was also measured in the presence of K^+. Under the single turnover condition, the reaction yield was 55% after 8 h, which is much smaller than that for the 18-mer DNA. The k_{cat} value was 5.6×10^{-3} min^{-1}. Thus, the sequence that joins the G-rich sequence is also important for the formation of the active structure.

The CD spectra of the DNA oligonucleotides were measured to determine the active structure, since CD spectra of nucleic acids are very sensitive to their overall structure.[14] Fig. 1 shows the CD spectrum of the 18-mer DNA oligonucleotide in 50 mM Tris-OAc (pH 7.4) solution containing 50 mM K^+ and 1 mM spermidine at 25 °C. The spectrum has a positive peak around 265 nm and a relatively weak and negative peak around 240 nm. On the other hand, the spectra of the 18-mer DNA in the presence of Na^+ and the 16-mer DNA in the presence of K^+ have two positive peaks around 265 and 295 nm and a relatively weak and negative peak around 230 nm. The intensity at 265 nm of the 18-mer DNA in the presence of K^+ was about 15-fold higher than those of the 18-mer DNA in the presence of Na^+ and the 16-mer DNA in the presence of K^+. The difference in metallation activities between the DNA species corresponds to the difference in the intensity values at 265 nm. Thus, the structural component that produces the positive peak around 265 nm in the CD spectrum must be the active structure for the metallation catalysis. The G-rich DNA species form a parallel or antiparallel G-quartet structure.[8–12,15,16] Previous studies indicated that the CD spectrum of the antiparallel G-quartet structure had 295 nm positive and 265 nm negative bands, while a parallel G-quartet structure with four or more strands exhibits a strong positive band at 260 nm and negative band at 240 nm.[15,16] Since the CD spectrum of the active structure of the DNA enzyme showed a strong positive band at 260 nm, the structure with the catalytic activity for the metallation should have mainly a parallel G-quartet structure with four or more strands. The structures of these DNA species were also investigated by nondenaturing gel electrophoresis. The mobility of the 18-mer DNA in the presence of 50 mM K^+ at 25 °C was demonstrated by the smearing of the band. This suggests that

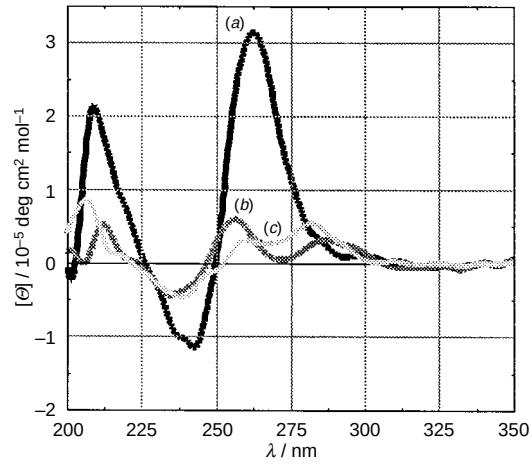

Fig. 1 CD spectra of dGTGGGTTGGGTGGGTTGG in the presence of (*a*) 50 mM K^+ and (*b*) 50 mM Na^+, and (*c*) dGTGGGTGGGTGGGTGG in the presence of 50 mM K^+ at 25 °C. Buffer contains 50 mM Tris-OAc (pH 7.4) and 1 mM spermidine. Concentration of each oligonucleotide was 20 μM.

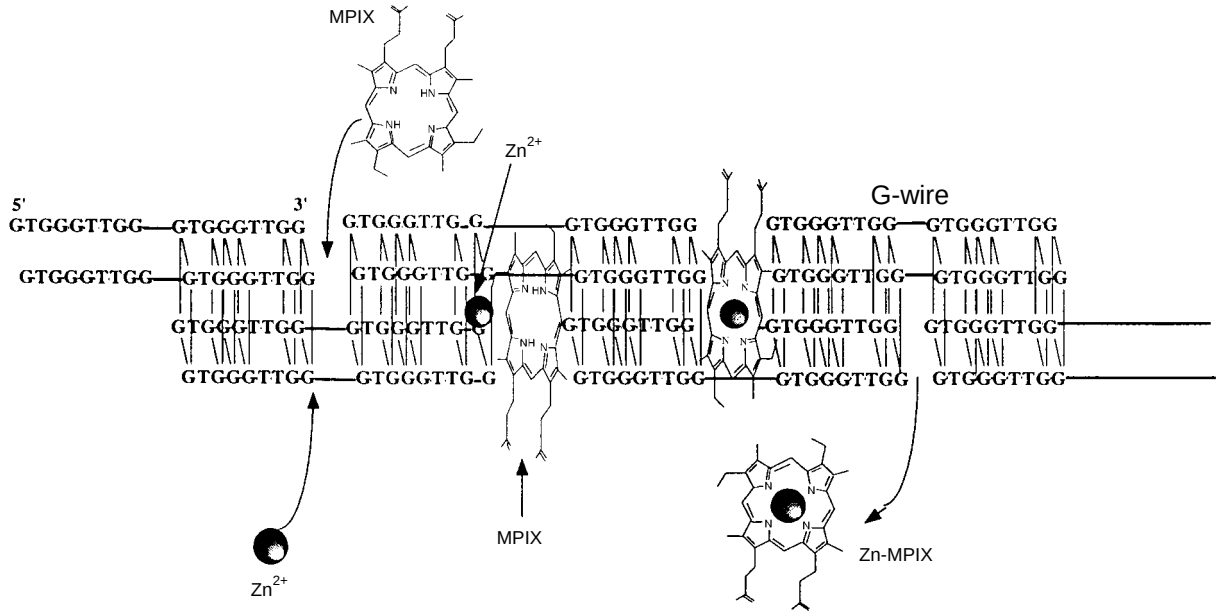

Fig. 2 Schematic illustration of the reaction mechanism between Zn^{2+} and MPIX in the G-wire of the 18-mer DNA species

the structure of the G-wire consists of a slipped tetraplex structure.[17,18] Thus, the results of the CD spectra and gel bands indicate that the active structure of the DNA enzyme is a G-wire structure stabilized by K^+.[17–19]

Fig. 2 shows our proposed reaction field for the porphyrin metallation. In the G-wire field, the porphyrin intercalates into the pocket formed by the junction between the G-quartet domains. Zn^{2+} also inserts into the cavity between two G-quartet planes near the pocket formed by the junction between the G-quartet domains. Following these intercalations, the porphyrin is close to Zn^{2+} so that the metallation occurs easily. The K_m value of the 18-mer DNA in the presence of K^+ was about two orders larger than the others. This value would suggest the possibility that G-wire DNA enzymes are easily able to release the complex between the porphyrin and Zn^{2+} as a product. Furthermore, the G-wire structure has many pockets into which the porphyrins may enter. Thus, this structure produces a good reaction field for the catalytic reaction. In this G-wire structure, the two T residues removed from the 18-mer DNA enzyme locate in the junction site between continuing G-quartet domains. If this region is shortened, the G-wire structure is destabilized by repulsion between the G-quartet domains. Thus, the difference in G-wire formation between the 18-mer and 16-mer DNA species is due to this repulsion between the junctions.

In summary, it was found that a novel 18-mer DNA enzyme, which was shorter than a previously reported DNA enzyme, catalyzed porphyrin metallation. This DNA enzyme formed a G-wire structure as the reaction field to catalyze the insertion of Zn^{2+} into mesoporphyrin IX. This G-wire structure shows promise as a reaction field for other catalytic reactions. Thus, our results in the present study indicate the possibility of DNA usage as materials and reaction fields in chemical nanotechnology.

This work was supported in part by Grants-in-Aid from the Ministry of Education, Science, Sports and Culture, Japan and Grants from the 'Research for the Future' Program of the Japan Society for the Promotion of Science and the Hirao Taro Foundation of the Konan University Association for Academic Research.

Notes and References

† E-mail: sugimoto@konan-u.ac.jp

‡ The metallation reaction was carried out in 50 mM Tris-OAc (pH 7.4) solution containing 5 μM DNA, 1 mM Zn^{2+}, 33 μM MPIX, 50 mM KOAc, 1 mM spermidine, 5% DMSO and 0.5% Triton X-100 at 25 °C for 8 h. Before the reaction was initiated, the DNA was reannealed by heating to 90 °C for 2 min, cooled to 25 °C, and incubated for 24 h in the reaction buffer without MPIX and Zn^{2+}. Then, the DNA was preincubated with MPIX for 10 min, and combined with appropriate volumes of the same solution containing $Zn(OAc)_2$. The reactions were stopped by the addition of a solution containing 200 mM Tris (pH 9.0) and 15 mM EDTA. The reactions were monitored by HPLC. The column used was a C18 column, and the mobile phase was 85% methanol and 15% 1 M ammonium acetate, pH 5.2.

§ The rates of metallation in the presence of the 18-mer or 16-mer DNA species were assayed for the concentration range of MPIX from 30 to 500 μM at a fixed concentration of 1 mM Zn^{2+} and 5 μM DNA. For initial rate measurements, good linear relationships between product formation and time were found in each case. The K_m and k_{cat} values were calculated form Lineweaver–Burk plots of $1/(V_{obs}-V_{background})$ *vs.* 1/[MPIX]. Each data point represents the average of at least two sets of independent measurement.

References

1 T. R. Cech, in *The RNA World*, ed G. Atkins, Cold Spring Harbor Laboratory Press, New York, 1993, p. 239.
2 T. Pan, D. M. Long and O. C. Uhlenbeck, in *The RNA World*, ed. G. Atkins, Cold Spring Harbor Laboratory Press, New York, 1993, p. 271.
3 N. Sugimoto and T. Ohmichi, *FEBS Lett.*, 1996, **393**, 97.
4 T. Ohmichi and N. Sugimoto, *Biochemistry*, 1997, **36**, 3514.
5 Y. Li and D. Sen, *Nat. Struct. Biol.*, 1996, **3**, 743.
6 Y. Li and D. Sen, *Biochemistry*, 1997, **36**, 5589.
7 Y. Li and D. Sen, *Chem. Biol.*, 1998, **5**, 1.
8 J. R. Wiliamson, M. K. Raghuraman and T. R. Cech, *Cell*, 1989, **59**, 871.
9 E. H. Blackburn, *Nature*, 1991, **350**, 569.
10 C. C. Hardin, E. Henderson, T. Watson, and J. K. Prosser, *Biochemistry*, 1991, **30**, 4460.
11 D. Sen and W. Gilbert, *Biochemistry*, 1992, **31**, 65.
12 N. Sugimoto, T. Ohmichi and M. Sasaki, *Nucleosides Nucleotides*, 1996, **15**, 559.
13 M. Okuda, H. Kohno, T. Furukawa, R. Tokunaga and S. Taketani, *Biochim. Biophys. Acta*, 1994, **1200**, 123.
14 W. Saenger, *Principles of Nucleic Acid Structure*, Springer-Verlag, Berlin, Heidelberg, NY, 1984.
15 P. Balagurumoorthy, S. K. Brathmachari, D. Mohanty, M. Bansal and V. Sasisekharan, *Nucleic Acid Res.*, 1992, **20**, 4061.
16 M. Lu, Q. Guo and N. R. Kallenback, *Biochemistry*, 1993, **32**, 598.
17 T. C. Marsh and E. Henderson, *Biochemistry*, 1994, **33**, 10718.
18 S. P. Marotta, P. A. Tamburri and R. D. Sheardy, *Biochemistry*, 1996, **35**, 10484.
19 F. M. Chen, *Biophys. J.*, 1997, **73**, 348.

Received in Cambridge, UK, 12th March 1998; 8/01998C

Experimental charge density study of the Mn–Mn bond in $Mn_2(CO)_{10}$ at 120 K

R. Bianchi,[a] G. Gervasio[b]† and D. Marabello[b]

[a] *Centro CNR per lo Studio delle Relazioni tra Struttura e Reattività Chimica, Milano, Italy*
[b] *Dipartimento di Chimica I.F.M. dell'Università, Torino, Italy*

This paper presents an analysis of the charge density, $\rho(r)$, for the Mn–Mn bond in $Mn_2(CO)_{10}$, determined by a multipole model from accurate X-ray data measured at 120 K.

The experimental deformation charge densities of some binuclear metal carbonyls, $[CpFe(CO)_2]_2$, $(\mu\text{-}CH_2)[CpMn(CO)_2]_2$ and $Mn_2(CO)_{10}$, were determined by X-ray diffraction some years ago.[1–3] The theoretical deformation densities for other similar complexes, $Fe_2(CO)_9$ and $Co_2(CO)_8$, and for $Mn_2(CO)_{10}$ were also reported in refs. 4 and 5.

In all the three complexes examined by X-ray diffraction, the deformation maps showed no evidence of significant density accumulation in the metal–metal bonding region. This result was justified by the presence of bridging groups (CH_2 or CO), which join the two metallic fragments to form the entire molecule. This explanation was also supported by the theoretical calculations made for $Fe_2(CO)_9$ and $Co_2(CO)_8$. However, in the case of $Mn_2(CO)_{10}$, which has only terminal carbonyl groups, two Mn–Mn bonding hypotheses were considered: the first is a direct metal–metal bond and the second is an interaction between the d_{xz} or d_{yz} orbitals of one manganese and the π^* orbital of the equatorial carbonyls of the other manganese.[3,6,7] The last hypothesis could be also supported by the bending of equatorial carbonyls towards the opposite Mn atom. Note that the above two hypotheses are not supported by experimental evidence, but a theoretical study, based on Bader's quantum theory of atoms in molecules (QTAM),[8] proved the existence of the Mn–Mn bond in $Mn_2(CO)_{10}$.[9]

Here we report the experimental charge density of the title compound, determined by accurate X-ray data, measured at 120 K and interpreted by the aspherical-atom formalism developed by Stewart.[10] Further, the results of the Bader analysis on the experimental charge density are reported, in order to confirm the existence of the Mn–Mn bond. This is the first topological analysis of the experimental charge density in binuclear metal complexes.

A crystal of $Mn_2(CO)_{10}$ recrystallized from a light petroleum solution was made spherical to a diameter of 0.51 mm and put in a Lindemann glass capillary. The intensity data were collected on a Siemens P4 diffractometer equipped with a low temperature device using liquid nitrogen. 20507 reflections were collected at 120 K, up to $2\theta = 110°$, with Mo-Kα radiation (λ = 0.71073 Å) and with the θ–2θ scan method. Other experimental data are summarized in Table 1. Further information on data collection will be given in the full paper. However, our data collection is not better than that of ref. 3, because they measured the low-order reflections ($\sin\theta/\lambda < 0.76$ Å^{-1}) with the same crystal but two different X-ray wavelengths, Ag-Kα and Mo-Kα.

The quantity minimized in the multipole refinement was $\Sigma w(|F_o|^2 - k^2|F_c|^2)^2$ based on 6217 independent reflections with $I > 2\sigma(I)$ and weights $w = 1/\sigma^2(|F_o|^2)$. The data were corrected for absorption effects, extinction corrections were not introduced and the anomalous dispersion was considered only for the Mn atom. The final aspherical fit to X-ray data was obtained with the following multipole model (POP). Each pseudoatom is assigned a small finite multipole expansion of the atomic form factor. The multipole expansion included two monopoles for C and O atoms and three monopoles for Mn atom and the higher terms were up to the octupole level, except for Mn (up to hexadecapole level). The monopoles consist of shells constructed from the canonical SCF s-, p- and d-orbitals.[11] For the higher multipoles, Slater-type radial functions with fixed standard molecular exponents were used for all carbons and oxygens[12] and the radial exponents of Mn atom were determined in the refinement procedure. All calculations were performed using a modified version of the VALRAY program.[13] The final agreement factors and some other refinement information are listed in Table 1.

Table 1 Crystal data and multipole POP refinement information

Lattice type; space group	monoclinic; *C*2/*c*
a/Å	17.314(4)
b/Å	6.898(1)
c/Å	14.110(3)
β/°	126.94(3)
Z	4
N_o (number of reflections)	6217
N_p (number of parameters)	290
R(int) = $\Sigma\|\|F_o\|^2 - \|F_o\|^2$(mean)$\|/\Sigma\|F_o\|^2$	0.033
R(sigma) = $\Sigma[\sigma(\|F_o\|^2)]/\Sigma[\|F_o\|^2]$	0.039
$R(F) = \Sigma\|\|F_o\| - k\|F_c\|\|/\Sigma\|F_o\|$	0.0326
$wR(F) = [\Sigma w(\|F_o\| - \|F_c\|)^2/\Sigma w\|F_o\|^2]^{1/2}$	0.0216
$R(F^2) = \Sigma\|\|F_o\|^2 - k^2\|F_c\|^2\|/\Sigma\|F_o\|^2$	0.0424
$wR(F^2) = [\Sigma w(\|F_o\|^2 - k^2\|F_c\|^2)^2/\Sigma w\|F_o\|^4]^{1/2}$	0.0403
$S = [\Sigma w(\|F_o\|^2 - k^2\|F_c\|^2)^2/(N_o - N_p)]^{1/2}$	1.209
k (scale factor)	0.2477(5)
$(\text{shift/e.s.d.})_{max}$	< 0.02

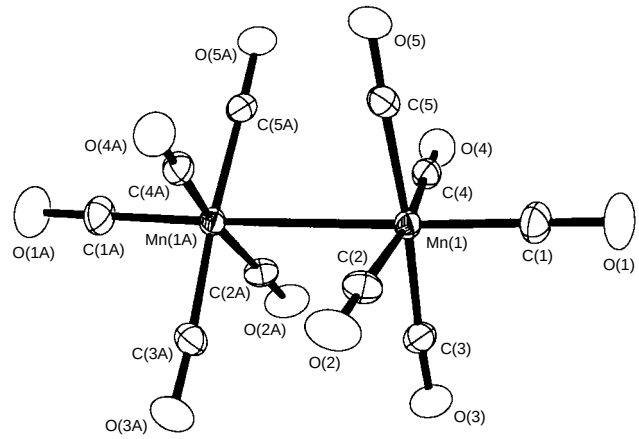

Fig. 1 An ORTEP plot (30% probability) of the entire molecule of $Mn_2(CO)_{10}$.[16] The molecule has crystallographic C_2 symmetry with the two-fold axis passing through the middle of the Mn–Mn bond. Each Mn atom links four equatorial and one axial CO groups in a pseudo-octahedral environment. The equatorial CO groups of the two Mn atoms are staggered [51° between the CO(1)–Mn(1)–CO(2) and CO(1A)–Mn(1A)–CO(2A) planes]. The Mn–Mn bond distance is 2.9042(8) Å; this value is in keeping with the observed dependence on the temperature [2.923(3) Å r.t., 2.9042(8) Å 120 K, 2.8950(6) Å 74 K].[3]

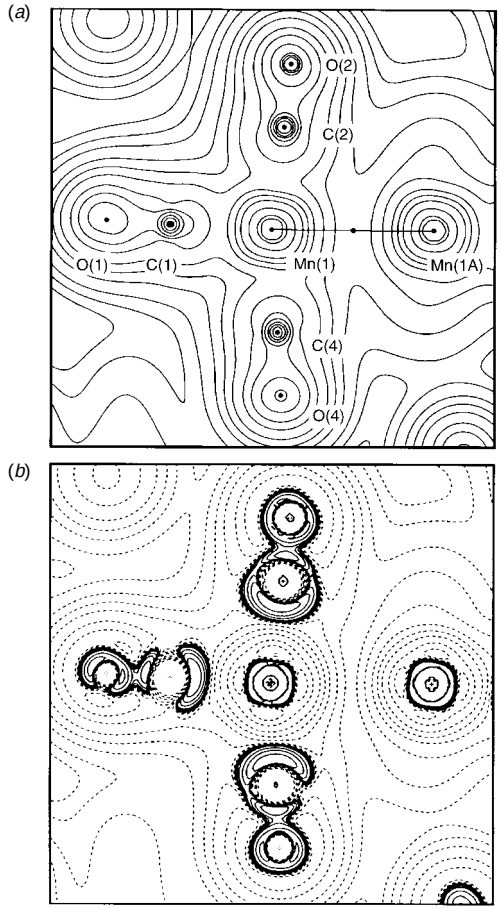

Fig. 2 Experimental charge density, $\nabla\rho(\boldsymbol{r})$ (*a*), and its Laplacian, $\nabla^2\rho(\boldsymbol{r})$ (*b*), on the plane defined by Mn(1), Mn(1A) and C(2). The absolute values of the contours (atomic units) increase from the outermost one inwards in steps of 2×10^n, 4×10^n and 8×10^n with n beginning at -3 and increasing in steps of 1. It has been shown that a necessary and sufficient condition for two atoms to be involved in a bonding interaction is the existence in $\nabla\rho(\boldsymbol{r})$ of a line linking the nuclei along which the charge density is at a maximum with respect to any lateral displacement. Such a line is called a bond path, and the interatomic critical point $\boldsymbol{r}_c$ [where $\nabla\rho(\boldsymbol{r}_c) = 0$] occurring on it is a bond critical point (bcp). At the bcp, there are two negative curvatures (λ_1 and λ_2) that determine the contraction of ρ towards $\boldsymbol{r}_c$ in the directions perpendicular to the bond path, and one positive curvature, λ_3, parallel to the interaction line. The values of $\rho(\boldsymbol{r}_c)$ and of $\nabla^2\rho(\boldsymbol{r}_c) = \lambda_1 + \lambda_2 + \lambda_3$ characterize the atomic interaction. In (*a*) the bond paths of $\nabla\rho(\boldsymbol{r})$ which originate at bcp are superimposed on the same map and the bcp position is denoted by a black dot. In (*b*) positive values are denoted by dashed contours, negative values are denoted by solid contours.

The total electron density, $\rho(\boldsymbol{r})$, based on the multipole model, the gradient and Hessian of $\rho(\boldsymbol{r})$ were calculated with a direct space lattice sum. The topological analysis of $\rho(\boldsymbol{r})$ (search of critical points and bond paths[14]) was carried out using the TOPOND program,[15] interfaced to VALRAY. The topology of $\rho(\boldsymbol{r})$ has been fully described by Bader in the QTAM.

The molecular structure, with the atomic labeling, is shown in Fig. 1. The largest peak in the residual density (based on $F_{obs} - F_{multipole}$) is 0.33 e Å^{-3} and it is close to the Mn position. We observe a slightly positive and not significant deformation density of 0.1(1) e Å^{-3} (total density minus free spherical atoms) at the midpoint of the Mn–Mn bond. On the other hand a very small deformation density has also been observed between the two metal atoms in previous works.[1,3]

Fig. 2 shows the total electron density map and its Laplacian, derived from the multipole POP model, in the plane containing the axial [C(1)–O(1)], the two equatorial carbonyl groups [C(2)–O(2) and C(4)–O(4)] and the two Mn atoms. The number of bcps we found in the experimental electron density corresponds to the expected number of bonds for $Mn_2(CO)_{10}$, including the interaction between the two Mn atoms as illustrated in Fig. 2(*a*). The density at the bcp between the two heavy atoms is 0.190(4) e Å^{-3}. No bcps were found for any cross interaction between one metal and the equatorial COs linked to the other metal atom. The positive value of $\nabla^2\rho(\boldsymbol{r})$ at the Mn—Mn bcp [0.815(8) e Å^{-5}; Fig. 2(*b*)] indicates an unshared interaction[14] between the two Mn atoms: the density is contracted towards each Mn nucleus. Indeed, one finds that $\lambda_3 = 1.209(3)$ e Å^{-5} is here dominant with respect to $\lambda_1 = \lambda_2 = -0.199(3)$ e Å^{-5}. This behaviour is similar to that found in the ionic and van der Waals interactions and clearly indicates a totally different nature with respect to a typical covalent interaction.

In conclusion, an accurate description of the total electron density has been obtained from a multipole analysis of the X-ray data. The low temperature (120 K) at which the diffraction experiment was performed allowed us to obtain a significant total electron density in the metal–metal region and the Bader analysis of this density was a useful tool to characterize the nature of their interaction.

Notes and References

† E-mail: gervasio@ch.unito.it

1 A. Mitschler, B. Rees and M. S. Lehmann, *J. Am. Chem. Soc*., 1978, **100**, 3390.
2 D. A. Clemente, M. Cingi Biagini, B. Rees and W. A. Hermann, *Inorg. Chem*., 1982, **21**, 3741.
3 M. Martin, B. Rees and A. Mitschler, *Acta Crystallogr*., *Sect. B*, 1982, **38**, 6.
4 W. Heiser, E. J. Baerends and P. Ros, *Discuss. Faraday Soc.*, 1980, **14**, 211.
5 A. Veillard and M.-M. Rhomer, *Int. J. Quantum Chem.*, 1992, **42**, 965.
6 R. Bau, S. W. Kirtley, T. N. Sorrel and S. Winark, *J. Am. Chem. Soc*., 1974, **96**, 988.
7 D. A. Brown, W. J. Chambers, N. J. Fitzpatrick and R. M. Rawlinson, *J. Chem. Soc. A*, 1971, 720.
8 R. F. W. Bader, *Atoms in molecules—a Quantum Theory*, Oxford University Press, Oxford, 1990.
9 P. J. McDougall, Ph.D. Thesis, McMaster University, 1989; P. J. McDougall and M. B. Hall, *Trans. Am. Crystallogr. Assoc*., 1990, **26**, 101.
10 R. F. Stewart, *Acta Crystallogr*., *Sect. A*, 1976, **32**, 565.
11 E. Clementi and C. Roetti, *At. Data Nucl. Data Tables*, 1974, **14**, 177.
12 W. J. Hehre, R. Ditchfield, R. F. Stewart and J. A. Pople, *J. Chem. Phys*., 1970, **51**, 2769.
13 R. F. Stewart and M. A. Spackman, VALRAY User's Manual, Department of Chemistry, Carnegie-Mellon University, Pittsburgh, PA, 1983.
14 R. F. W. Bader and H. Essen, *J. Chem. Phys.*, 1984, **80**, 1943.
15 C. Gatti, V. R. Saunders and C. Roetti, *J. Chem. Phys.*, 1993, **101**, 10 686.
16 C. K. Johnson, ORTEP, Report ORNL-5138, Oak Ridge National Laboratory, Oak Ridge, TN, 1976.

Received in Cambridge, UK, 27th March 1998; 8/02386G

Synthesis and coordination chemistry of 1,3,5-triphosphabicyclo[2.1.0]-pent-2-ene

Vinicius Caliman, Peter B. Hitchcock and John F. Nixon*†

School of Chemistry, Physics and Environmental Science, University of Sussex, Brighton, UK, BN1 9QJ

Room temperature electrocyclisation of the 1,2,4-triphosphole $P_3C_2Bu^t_2CH(SiMe_3)_2$ affords the new 1,3,5-triphosphabicyclo[2.1.0]pent-2-ene which undergoes a very rapid [1,3]-phosphorus migration which can be stopped by coordination of $[W(CO)_5]$; the two isomeric phosphorus compounds react differently with $[PtCl_2(PEt_3)]_2$, the latter *via* an insertion of the metal into the P–P bond and a chlorine migration reaction to afford *trans*-$[PtCl(PEt_3)P_2C_2Bu^t_2PClCH(SiMe_3)_2]$, the molecular structure of which has been determined by a single crystal X-ray diffraction study.

We recently showed[1] that the activation barrier for the [1,3]-phosphorus migration in the hypothetical 1,3,5-triphosphabicyclo[2.1.0]pent-2-ene $P_3C_2H_3$ **1** is estimated (MP4SDTQ/6-31G*//MP2/6-31G*+ZPE) to be only 11.62 kcal mol^{-1}, which is considerably smaller than the barrier (31.13 kcal mol^{-1}) for the corresponding [1,3]-carbon migration in the structurally related hydrocarbon C_5H_6 **2**. We attributed the much more facile migration within the phosphorus system to favourable cleavage of the weak P–P bond in **1** compared to the strong C–C bond in **2** and to the suprafacial pathway in both systems, which requires the migrating atom to become planar, and is therefore much more favourable for phosphorus than carbon (see Scheme 1). We now present the first experimental support for these proposals with the synthesis of 1-bis-(trimethylsilylmethyl)-1,3,5-triphosphabicyclo[2.1.0]-pent-2-ene **3** and a study of its dynamic behaviour and ligating properties.

The recently described[2] 1,2,4-triphosphole $P_3C_2Bu^t_2CH(SiMe_3)_2$ **4** readily undergoes a slow electrocyclisation reaction on long standing in sunlight at room temperature, to afford the new isomeric 1,3,5-triphosphabicyclo[2.1.0]pent-2-ene **3** (Fig. 1). The reaction, which is accelerated by irradiation with a tungsten lamp (100 W), is about 60% complete after one week.

When the electrocyclisation reaction is monitored by $^{31}P\{^1H\}$ NMR spectroscopy , the original three doublet-of-doublets resonances (δ_P 244.4 $P_{(A)}$, 180.0 $P_{(B)}$ and 112.0 $P_{(X)}$) of **4** steadily disappear and are replaced by two new resonances attributed to **3** (a doublet δ_P 166.6 and a triplet δ_P 24.1). The simplicity of the $^{31}P\{^1H\}$ NMR spectrum of **3** shows that two phosphorus atoms $P_{(A)}$ and $P_{(B)}$ become magnetically equivalent because of the fast [1,3]-sigmatropic rearrangement of **3**. On cooling the sample the doublet resonance broadens but the dynamic proces is still evident even at −110 °C.

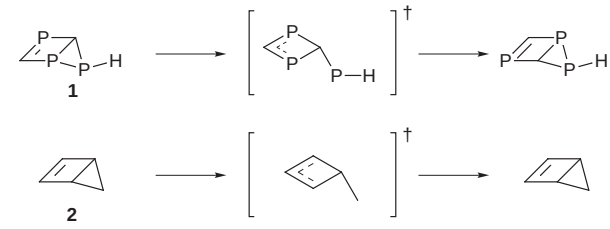

Scheme 1

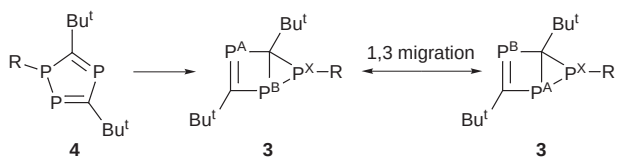

Fig. 1 R = $CH(SiMe_3)_2$

The migration process of $P_{(X)}$ from $P_{(A)}$ to $P_{(B)}$ can however be stopped completely by ligation of a $[W(CO)_5]$ fragment to **3**. Thus $[W(CO)_5(THF)]$ readily reacts with **3** in THF at room temperature to afford the red η^1-complex $[W(CO)_5P_3C_2Bu^t_2CH(SiMe_3)_2]$ **5** in 70% yield. The mode of attachment of the $[W(CO)_5]$ fragment was established as being *via* the unique sp^2-hybridised phosphorus $P_{(A)}$, by its $^1P\{^1H\}$ NMR spectrum which shows three resonances (δ_P 270.7 $P_{(A)}$, 33.8 $P_{(M)}$ and −78.8 $P_{(X)}$), each occurring as a doublet of doublets. The high field shifts of $P_{(M)}$ and $P_{(X)}$ are typical for sp^3-hybridised phosphorus atoms and each exhibits the expected large direct one-bond coupling ($^1J_{P(M)P(X)}$ = 151.3 Hz). The low field $P_{(A)}$ resonance, which is typical of an sp^2-hybridised phosphorus, also shows two additional two-bond couplings ($^2J_{P(A)P(M)}$ = 83.8 Hz and $^2J_{P(A)P(X)}$ = 21.7 Hz) and the characteristic ^{183}W satellites ($^1J_{PW}$ = 229.3 Hz). Isomers **3** and **4** thus behave quite differently towards zerovalent tungsten, the latter giving only the η^5-complex $[W(CO)_3P_3C_2Bu^t_2CH(SiMe_3)_2]$ **8** under a variety of reaction conditions.[3]

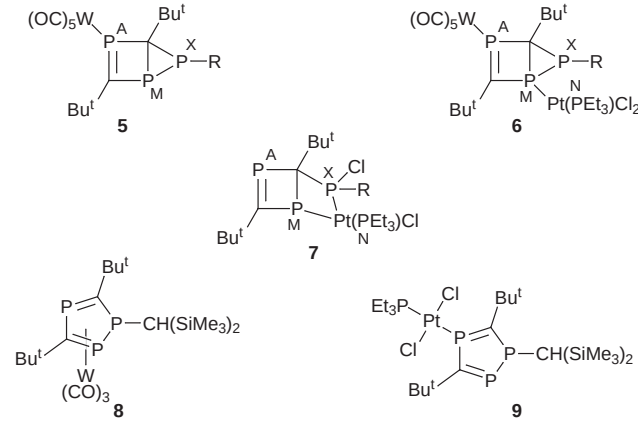

$[PtCl_2(PEt_3)]_2$ reacts with **5** in THF at room temperature to afford the yellow bimetallic complex *trans*-$[PtCl_2(PEt_3)W(CO)_5P_3C_2Bu^t_2CH(SiMe_3)_2]$ **6** (79% yield) with a similar structure to **5**, in which the additional $[PtCl_2(PEt_3)]$ fragment becomes attached to the sp^3-hybridised phosphorus at the junction of the 3- and 4-membered rings, as was established spectroscopically.‡

The identity of the 1,3,5-triphosphabicyclo[2.1.0]pent-2-ene, **3**, was confirmed by its unusual reaction with $[PtCl_2(PEt_3)]_2$ at room temperature, to give the yellow air-stable complex *trans*-$[PtCl(PEt_3)P_2C_2Bu^t_2PClCH(SiMe_3)_2]$ **7** (77% yield), the molecular structure of which was confirmed spectroscopically‡ and by a single crystal X-ray diffraction study. The reaction

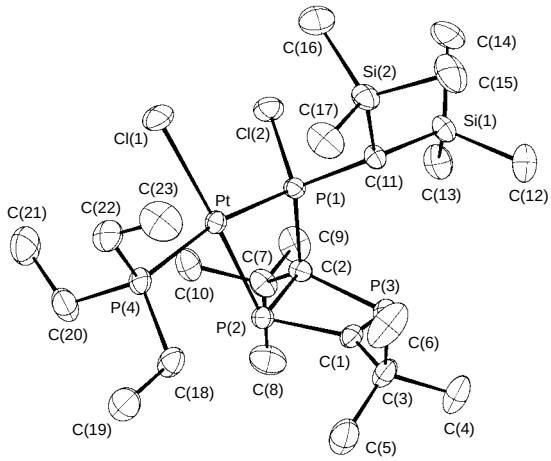

Fig. 2 Molecular structure of *trans*-[PtCl(PEt_3)$P_2C_2Bu^t_2PClCH(SiMe_3)_2$] **7** together with the atomic numbering scheme and some selected bond lengths (Å) and angles (°): Pt–P(1) 2.263(1), Pt–P(2) 2.299(1), Pt–P(4) 2.322(2), Pt–Cl(1) 2.381(2), P(1)–C(11) 1.826(5), P(1)–C(2) 1.877(5), P(1)–Cl(2) 2.062(2), P(2)–C(1) 1.820(5), P(2)–C(2) 1.907(5), P(3)–C(1) 1.698(5), P(3)–C(2) 1.876(5), P(1)–Pt–P(2) 71.90(5), P(1)–Pt–P(4) 167.25(5), P(2)–Pt–P(4) 95.42(5), P(1)–Pt–Cl(1) 100.38(6), P(2)–Pt–Cl(1) 164.50(6), P(4)–Pt–Cl(1) 91.63(6)

involves both an insertion of the metal–ligand fragment into the weak P–P bond of the three-membered ring of **3** and a chlorine migration from platinum to phosphorus. Clearly the dynamic behaviour of **3**, involving rapid breaking and remaking of the P–P bond, facilitates the insertion step.

We previously reported[4] a similar ring opening and chlorine transfer from Pt^{II} to phosphorus in the reaction of [$PtCl_2(CNR)_2$] (R = Bu^t, *p*-$MeOC_6H_4$) with the three-membered phosphirene ring PPhCPh=CPh to form the dimeric chlorophosphane complex [PtCl(PClPhCPh=CPh)($CNBu^t$)]$_2$.

The mass spectrum of compound **7** exhibits a molecular ion peak at *m*/*z* 774 and the expected fragmentation pattern and the $^{31}P\{^1H\}$ NMR spectrum exhibits the anticipated pattern of lines arising from an [AMNX] spin system.§ The molecular structure of **7**, shown in Fig. 2, was established by a single crystal X-ray diffraction study¶ and is in full accord with the NMR spectroscopic data. The symmetry around the Pt^{II} atom is close to idealised square planar geometry, and the Pt–P distances and the P=C double bond length [P(3)–C(1) 1.698(5) Å] are typical.[5,6] Isomers **3** and **4** thus also behave quite differently towards divalent platinum, the latter giving the η^1-complex *trans*-[$PtCl_2(PEt_3)P_3C_2Bu^t_2CH(SiMe_3)_2$] **9** in which the platinum is attached to the unsaturated phosphorus lying between the two ring carbon atoms.[7]

We thank the Brazilian Government (CNPq) for a scholarship (to V. C.).

Notes and References

† E-mail: j.nixon@sussex.ac.uk

‡ *Synthesis. trans*-[($PtCl_2(PEt_3)${$W(CO)_5$}$P_3C_2Bu^t_2CH(SiMe_3)_2$] **6**: to a solution of [{$W(CO)_5$}$P_3C_2Bu^t_2CH(SiMe_3)_2$] **5** (120 mg, 0.195 mmol) in chloroform (5 ml), at room temperature, was slowly added a solution of [$PtCl_2(PEt_3)]_2$ (75.0 mg, 0.097 mmol) dissolved in chloroform (10 ml). The resulting mixture was stirred for 8 h and the solvent removed *in vacuo*. The yellow solid was washed with light petroleum (bp 60–80 °C; 5 ml) to give **6** (155 mg, 79%).$^{31}P\{^1H\}$ NMR data (101.3 MHz, $CDCl_3$, 25 °C): δ_P 304.6 (dd, $P_{(A)}$, $^1J_{P(A)W}$ = 251.2, $^2J_{P(A)P(M)}$ = 65.1, $^2J_{P(A)P(X)}$ = 26.8 Hz); 82.9 (ddd, $P_{(M)}$, $^1J_{P(M)Pt}$ = 2422, $^2J_{P(M)P(N)}$ = 529.1, $^1J_{P(M)P(X)}$ = 200.3, $^2J_{P(M)P(A)}$ = 65.1 Hz); 11.1 (dd, $P_{(N)}$, $^1J_{P(N)Pt}$ = 2767, $^2J_{P(N)P(M)}$ = 529.1 Hz); −99.4 (dd, $P_{(X)}$, $^1J_{P(X)P(M)}$ = 200.3, $^2J_{P(X)P(A)}$ = 26.8 Hz).

§ *Synthesis*. *trans*-[PtCl(PEt_3)$P_2C_2Bu^t_2PClCH(SiMe_3)_2$] **7**: [$PtCl_2(PEt_3)]_2$ (145 mg, 0.19 mmol) was added, as a solid, to a solution of $P_3C_2Bu^t_2CH(SiMe_3)_2$ **3** (160 mg, 0.41 mmol) in chloroform (10 ml), and stirred for 8 h. The yellow solid was filtered and washed with light petroleum (bp 60–80 °C; 5 ml) to give **7** (230 mg, 77% yield). Recrystallisation from THF–light petroleum (bp 30–40 °C) gave yellow crystals (mp 186 °C) suitable for the X-ray diffraction study (Found: C, 35.70; H, 6.71; $C_{23}H_{52}Cl_2Si_2P_4Pt$ requires C, 35.66; H, 6.77%). $^{195}Pt\{^1H\}$ NMR data (53.8 MHz, $CDCl_3$, 25 °C): δ −3974 (dddd, Pt, $^1J_{PtP(X)}$ = 2884, $^1J_{PtP(N)}$ = 2778, $^1J_{PtP(M)}$ = 564.5, $^3J_{PtP(A)}$ = 216.2 Hz). $^{31}P\{^1H\}$ NMR data (101.3 MHz, $CDCl_3$, 25 °C): δ_P 371.0 (dd, $P_{(A)}$, $^3J_{P(A)Pt}$ = 216.2, $^2J_{P(A)P(M)}$ = 59.0, $^2J_{P(A)P(X)}$ = 11.2 Hz); 117.6 (dd, $P_{(X)}$, $^1J_{P(X)Pt}$ = 2884, $^2J_{P(X)P(N)}$ = 540.1, $^2J_{P(X)P(A)}$ = 11.2 Hz); 10.2 (d, $P_{(N)}$, $^1J_{P(N)Pt}$ = 2778, $^2J_{P(N)P(X)}$ = 540.1 Hz); −13.9 (d, $P_{(M)}$, $^1J_{P(M)Pt}$ = 564.5, $^2J_{P(M)P(A)}$ = 59.0 Hz). ^1H NMR data (250.2 MHz, $CDCl_3$, 25 °C): δ 1.94 (d, 1 H, CH, $^2J_{HP}$ = 6.3 Hz); 1.90 [m, 6 H, 3(CH_2)]; 1.47 [s, 9 H, C(CH_3)$_3$]; 1.27 [s, 9 H, C(CH_3)$_3$]; 1.13 [dt, 9 H, 3(CH_3), $^3J_{HP}$ = 16.0, $^3J_{HH}$ = 7.5 Hz); 0.58 [s, 9 H, Si(CH_3)$_3$]; 0.35 [s, 9 H, Si(CH_3)$_3$]. Mass spectrum (EI): *m*/*z* 774 [$PtCl(PEt_3)P_2C_2Bu^t_2PClCH(SiMe_3)_2]^+$ (30 %), 674 [$PtCl(PEt_3)PCBu^tPClCH(SiMe_3)_2]^+$, 390 [$P_2C_2Bu^t_2PCH(SiMe_3)_2]^+$, 73 [$SiMe_3]^+$.

¶ *Crystal data* for **7,** $C_{23}H_{52}Cl_2Si_2P_4Pt$, *M* = 774.7, monoclinic, space group $P2_1/c$ (no. 14), *a* = 18.545(2), *b* = 10.943(5), *c* = 16.745(3) Å, β = 95.14(1)°, *U* = 3385(2) Å^3, *Z* = 4, D_c = 1.52 g cm^{-3}. Crystal size 0.3× 0.3 × 0.2 mm. Data were collected at 293 K on an Enraf-Nonius CAD4 diffractometer using Mo-Kα radiation, λ = 0.71073 Å, μ = 45.8 cm^{-1}. A total of 9818 unique reflections were measured, of which 6979 had $I > 2\sigma(I)$. Non-H atoms were located by direct methods (SHELXS-86) and the structure was refined by full-matrix least-squares (SHELXL-93), non-H atoms anisotropic. R_1 = 0.042, wR_2 = 0.117 (all data). CCDC 182/897.

1 S. M. Bachrach, V. Caliman and J. F. Nixon, *J. Chem. Soc., Chem. Commun.*, 1995, 2395.
2 V. Caliman, P. B. Hitchcock and J. F. Nixon, *J. Chem. Soc., Chem. Commun.*, 1995, 1661.
3 V. Caliman, P. B. Hitchcock, J. F. Nixon, L. Nyulaszi and N. Sakarya, *Chem. Commun.*, 1997, 1305.
4 F. A. Ajulu, P. B. Hitchcock, J. F. Nixon, R. A. Michelin and A. J. L. Pombeiro, *J. Chem. Soc., Chem. Commun*., 1993, 142.
5 R. Appel, C. Casser, M. Immenkeppel and F. Knoch, *Angew. Chem., Int. Ed. Engl.*, 1984, **23**, 895.
6 D. Gudat, E. Niecke, A. M. Arif, A. H. Cowley and S. Quashie, *Organometallics*, 1986, **5**, 593.
7 V. Caliman, P. B. Hitchcock and J. F. Nixon, *Heteroatom. Chem.*, 1998, **9**, 1.

Received in Cambridge, UK, 6th May 1998; 8/03402H

Coordination control of intramolecular electron transfer in boronate ester-bridged donor–acceptor molecules

Hideo Shiratori,[a] Takeshi Ohno,[b] Koichi Nozaki,[b] Iwao Yamazaki,[c] Yoshinobu Nishimura[c] and Atsuhiro Osuka*[a]†

[a] *Department of Chemistry, Graduate School of Science, Kyoto University, Kyoto, 606-8502, Japan*
[b] *Department of Chemistry, Graduate School of Science, Osaka University, Toyonaka, 560-8531, Japan*
[c] *Department of Chemical Process Engineering, Graduate School of Engineering, Hokkaido University, Sapporo, 060-8628, Japan*

Acid–base reaction at the bridge in a donor–acceptor molecule can influence intramolecular electron-transfer reactions; this has been demonstrated in boronate ester bridged zinc porphyrin–diimide dyads in which intramolecular electron transfer reaction has been completely suppressed by coordination of F^- on the bridge boron.

Intramolecular electron transfer (ET) is the subject of many studies that are aimed at elucidating the role of the various parameters which govern the ET rate.[1] Among these, the chemical identity and nature of the bridge that connects donor and acceptor are important, since ET reactions can be facilitated by appropriate molecular orbitals provided by the bridge.[2] When a donor–acceptor molecule undergoes ET with a rate tunable by external physical and/or chemical input, it may constitute a switching ET molecular system. We report here intramolecular photoinduced electron transfer in boronate ester bridged zinc porphyrin–pyromellitimide (ZP–PI, **1b**) and zinc porphyrin–1,8:4,5-naphthalenetetracarboxylic diimide (ZP–NI, **1c**) (Scheme 1) in which the Lewis acidic boronate ester may enable alteration of the ET rate upon base coordination. This has indeed been demonstrated by addition of fluoride anion (F^-) which suppresses the ET.

Porphyrin **1a** was prepared according to the method reported by Toi *et al.*[3] Attempted hydrolysis of **1a** was unsuccessful in our hands under both basic[3] and acidic conditions.[4] Thus, boronic acid **3** was prepared by the cross-condensation of 4-formylphenylboronic acid **4** and 3,5-di-*tert*-butylbenzaldehyde **5** with dipyrrylmethane **6** followed by oxidation with *p*-chloranil under mild conditions (0 °C, 30 min) in 35% yield. Boron-bridged dyads **1b** and **1c** were prepared by refluxing a toluene solution of **3** in the presence of diol **7** or **8** with 84% and 90% isolated yields, respectively.

In benzene, the fluorescence of ^{1}ZP* in **2b** and **2c** is quenched by the attached PI or NI; the relative fluorescence intensities of **2b** and **2c** to **2a** are 0.89 and 0.36, respectively, and the fluorescence decays of **2b** and **2c** measured by the time-correlated single photon counting technique have been found to obey a single exponential function with lifetimes of 1.21 ns and 0.49 ns, respectively, which are shorter than the lifetime (1.39 ns) of **2a**. The observed fluorescence quenching suggests charge separation (CS) between ^{1}ZP* and PI or NI. The ET quenching has been confirmed by picosecond time resolved transient absorption spectroscopy. The transient absorption spectra taken for excitation with a 17 ps laser pulse at 532 nm revealed the appearance of a 715 nm absorption band due to PI^- for **2b** (not shown) and of 480 nm and 610 nm bands due to NI^- for **2c** [Fig. 1(*b*)],[5] respectively, clearly indicating ion-pair formation. Charge recombination kinetics of the ion pair to the ground state in **2b** measured by monitoring the 715 nm absorbance change follows a single exponential decay with $\tau = 84 \pm 6$ ns, while the similar kinetic trace at 480 nm in **2c** follows a biphasic decay with $\tau_1 = 77 \pm 16$ ns (66%) and $\tau_2 = 380 \pm 100$ ns (34%).[6] The boronate ester-bridged models, **1b** and **1c**, undergo essentially the same ET reactions as those of **2b** and **2c**; the relative fluorescence intensities of **1b** and **1c** to **1a** are 0.70 and 0.36, and the fluorescence lifetimes of **1b** and **1c** are 1.18 ns and 0.57 ns, respectively, which are both shorter than the lifetime (1.40 ns) of **1a**. Transient absorption spectroscopy also revealed the formation of the ion-pair state, and the lifetimes of the ion-pair state are 40 ± 5 ns for **1b** (not shown) and 13 ± 1 ns (60%) and 290 ± 10 ns (40%) for **1c** [Fig. 1(*a*), solid line].

The ET dynamics were also examined in the presence of tetra-*n*-butylammonium fluoride (TBAF). In the ^{11}B NMR spectra taken in benzene, a broad boron signal of **1a** appearing at around 10 ppm with respect to a trimethylborate internal standard was shifted to −14 ppm upon an addition of 1 equiv. of TBAF, indicating the complete coordination of F^- on the

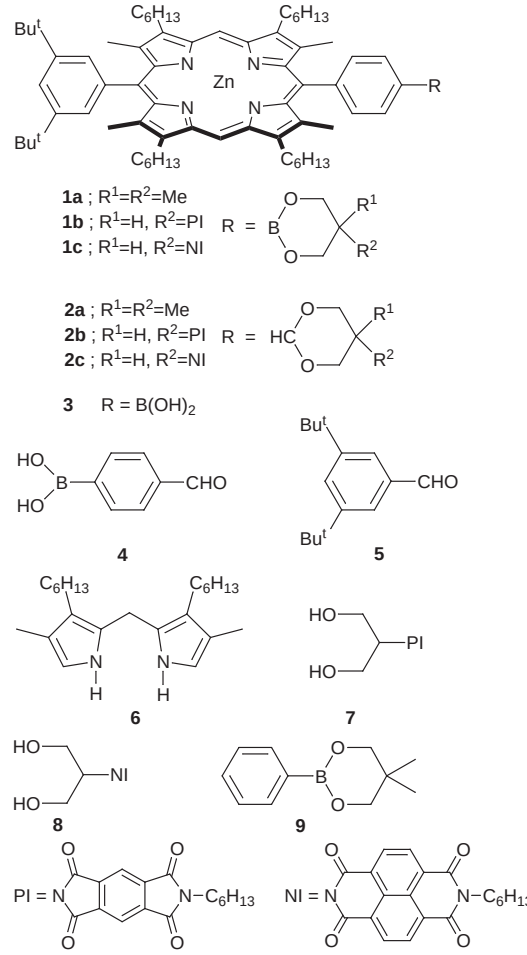

Scheme 1 Structures of models studied

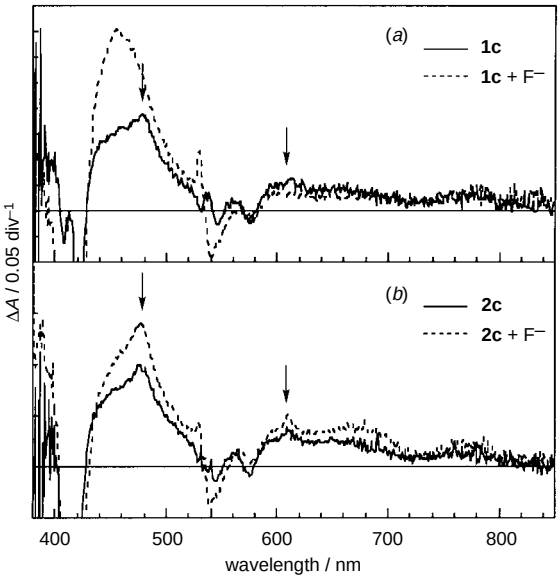

Fig. 1 Transient absorption spectra of **1c** (*a*) and **2c** (*b*) in benzene, at a delay time of 6 ns. Solid lines: in the absence of F^-; dotted lines: in the presence of 1.2 equiv. F^-.

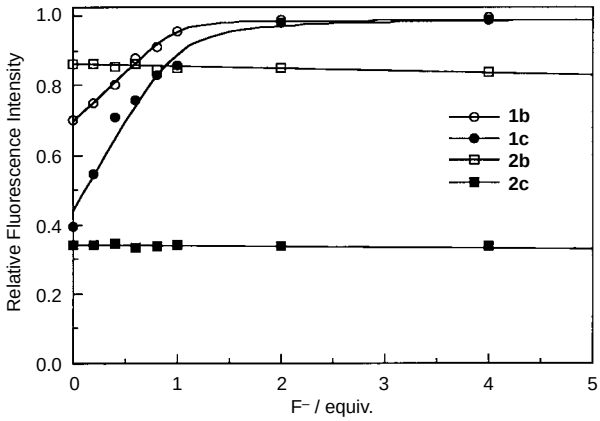

Fig. 2 Change of fluorescence intensities of diimide-linked models upon addition of F^-. Data for **1b**,**c** and **2b**,**c** were recorded relative to **1a** and **2a**, respectively. Concentrations of models were 1 μM.

boron atom. Similar shifts were observed for **1b** and **1c**. Fig. 2 shows the effects of TBAF addition on the fluorescence intensities of **1b**,**c** and **2b**,**c**. It is evident that the fluorescence intensity of **1c** increased with increasing amount of TBAF and returned to the original unquenched level with *ca*. 1 equiv. of TBAF, while the fluorescence intensity of **2c** remained quenched to a constant level up to 5 equiv. of TBAF added. Essentially the same trend was observed for **1b** and **2b**. Upon addition of 5 equiv. TBAF, the short fluorescence lifetimes of free **1b** and **1c** were restored to the unquenched levels (1.56 and 1.57 ns, respectively), which are almost the same as that (1.58 ns) of the acceptor-free reference compound **1a** under the same conditions. In contrast to the ET reactions of **2b** and **2c**, which are rather independent of TBAF [Fig. 1(*b*)], the transient absorption spectra of **1b** and **1c** in the presence of 1.2 equiv. TBAF are practically the same as those of the acceptor-free **1c** with no indication of ion-pair formation [Fig. 1(*a*), dotted line].[7] Therefore it is concluded that the CS reactions in **1b** and **1c** are completely blocked by F^- coordination. Since restoring the initial ET activities of **1b** and **1c** after the addition of F^- is important for constructing a real ON/OFF system, the addition of a large amount of **9** to solutions of F^--complexed **1b** and **1c** was examined but did not lead to the recovery of the ET activities. Finally, note that the CS reactions in **1b** and **1c** are also completely blocked in solvents with high donor numbers such as DMF and triethylamine but such solvent effects are not observed for **2b** and **2c**.

At the present stage, it seems difficult to identify the main reason for this CS inhibition by F^- coordination. The energy levels of the ion-pair states, geometrical parameters, and electronic coupling should be changed upon F^- coordination. Since the addition of TBAF had almost no effect on the redox potentials of these models,[8] the energy levels of the ion-pair states do not change significantly, at least in polar DMF solution, but are more difficult to estimate in nonpolar benzene solution. Since the center-to-center distance between ZP and the boron is estimated to be longer than that between the boron and the diimide,[9] the negative charge at the boron may raise the energy level of the ion-pair state, thereby decreasing the k_{CS} value. A change from a neutral trigonal boron to a tetrahedral 'ate' anion induces a slight shortening of the donor–acceptor distance by 0.4 Å as well as changes in the molecular orbitals of the bridge that will alter the electronic coupling between ZP and the diimide acceptor, relevant for CS. The former structural change seems to be unimportant since comparable k_{CS} rates were observed for the structural analogues, **2b** and **2c**. The latter effect, which may be evaluated by considering the molecular orbitals of the phenylboronate **9**, causes a considerable increase in the LUMO energy of the bridge upon F^- coordination,[10] suggesting the decreased electronic coupling due to the high LUMO energy to be critical in the observed CS inhibition.

Coordination on a neutral bridging boron may provide a convenient method of controlling the intramolecular ET. The generality of this method will be tested in other ET systems and also in triplet–triplet energy transfer systems. Studies in this direction are ongoing and will be reported soon elsewhere.

This work was partly supported by a Grant-in-Aid for Scientific Research (No. 09440217) from the Ministry of Education, Science, Sports and Culture of Japan and by CREST (Core Research for Evolutional Science and Technology) of Japan Science and Technology Corporation (JST).

Notes and References

† E-mail: osuka@kuchem.kyoto-u.ac.jp

1 M. R. Wasielewski, *Chem. Rev.*, 1992, **92**, 435, and references therein.
2 H. M. McConnell, *J. Chem. Phys.*, 1961, **35**, 508; S. Lasson, *J. Am. Chem. Soc.*, 1981, **103**, 4034; M. N. Paddon-Row, *Acc. Chem. Res.*, 1994, **27**, 18, and references therein.
3 H. Toi, Y. Nagai, Y. Aoyama, H. Kawabe, K. Aizawa and H. Ogoshi, *Chem. Lett.*, 1993, 1043.
4 M. Takeuchi, Y. Chin, T. Imada and S. Shinkai, *Chem. Commun.*, 1996, 1867.
5 A. Osuka, S. Nakajima, K. Maruyama, N. Mataga, T. Asahi, I. Yamazaki, Y. Nishimura, T. Ohno and K. Nozaki, *J. Am. Chem. Soc.*, 1993, **115**, 4577; A. Osuka, R.-P. Zhang, K. Maruyama, N. Mataga, Y. Tanaka and T. Okada, *Chem. Phys. Lett.*, 1993, **215**, 179.
6 This biphasic decay behavior may be accounted for by considering the singlet–triplet intersystem crossing within the ion-pair since the rate of charge recombination is comparable to the rate of the singlet–triplet intersystem crossing of the ion-pair state. W. Udo, Y. Sakaguchi, H. Hayashi, G. Nohya, R. Yoneshima, S. Nakajima and A. Osuka, *J. Phys. Chem.*, 1995, **99**, 13 930.
7 The transient absorption spectra indicate that the S_1 state of the ZP does not undergo any ET and is converted to the T_1 state absorbing at 455 nm.
8 The one-electron redox potentials of the donor and the acceptor moieties have been measured in DMF by cyclic voltammetry: E_{ox}(ZP) = 0.22, E_{red}(PI) = −1.24 and E_{ox}(NI) = −0.98 V for **1a–c**, and E_{ox}(ZP) = 0.22, E_{red}(PI) = −1.18 and E_{red}(NI) = −0.94 V for **2a–c** *vs*. ferrocene–ferrocenium ion.
9 Estimated distance between the ZP and the boron is 9.4 Å and those between the boron and the diimide are 7.6 and 7.8 Å in **1b** and **1c**, respectively.
10 MO calculations were performed using MacSpartan Plus (*ab initio*, 3-21G basis set). Calculated LUMO energies are 3.4, 8.2, and 4.1 eV for neutral **9**, F^--coordinated **9**, and an acetal reference bridge, respectively.

Received in Cambridge, UK, 1st April 1998; 8/02473A

Mechanistic studies on the photogeneration of *o*- and *p*-xylylenes from α,α′-dichloroxylenes

Miguel A. Miranda,*[a]† Julia Pérez-Prieto,*[b] Enrique Font-Sanchis,[a] and J. C. Scaiano*[c]

[a] *Instituto de Tecnología Química/Departamento de Química, Universidad Politécnica de Valencia, Camino de Vera s/n, 46071 Valencia, Spain*

[b] *Departamento de Química Orgánica, Facultad de Farmacia, Universidad de Valencia, Vicént Andrés Estellés s/n, Burjasot, 46100 Valencia, Spain*

[c] *Department of Chemistry, University of Ottawa, Ottawa, Canada K1N 6N5*

Two-colour two-laser techniques have unambiguously proved that photolysis of the *o*-/*p*-(chloromethyl)benzyl radical leads to the sequential two-photon generation of *o*-/*p*-xylylene from α,α′-dichloro-*o*-/*p*-xylene.

Xylylenes are molecules of considerable theoretical and synthetic interest, which have been detected and characterized by different spectroscopic methods.[1] Although benzylic dichlorides have been used as very simple and readily accessible precursors, the involved mechanisms are not completely understood.[2] It has been recently reported[3] that 266 nm laser irradiation of α,α′-dichloro-*o*-xylene (**1a**) produces the dissociation of both C–X bonds *via* a two-photon process; however, the nature of the intermediate species which absorbs the second photon is uncertain. Three possibilities have been considered: the S_1 and T_1 states of **1a** and the *o*-(chloromethyl)benzyl radical (**2a**). Based on the short lifetime of the singlet state of the dichloride and the apparent relative yields of the observed transients, the undetected T_1 state of the dichloride has been suggested as the photochemical precursor of *o*-xylylene.

Our aim was to explore the photochemistry of the benzyl radical **2a** produced after dissociation of one C–X bond of α,α′-dichloro-*o*-xylene, using two-laser two-colour techniques, in order to obtain new data to support or reject the intermediacy of **2a** in the formation of *o*-xylylene. We report here our findings and compare them with those obtained in the photolysis of α,α′-dichloro-*p*-xylene. Based on the obtained results, a mechanism for the formation of *o*- and *p*-xylylenes from their corresponding dichloro precursors is presented.

Laser flash photolysis of deaerated 1.5 mM solutions of **1a** in cyclohexane at 266 nm (Nd: YAG laser, fourth harmonic, < 10 ns, ⩽20 mJ pulse^{-1}) yielded the transient absorption spectra shown in Fig. 1. Two transients with different lifetimes were obtained. According to the literature,[3] they were assigned to **2a** (with a maximum at 330 nm) and *o*-xylylene (**3a**) (maximum at 360 nm, $\varepsilon_{max} = 3 \times 10^3$ dm^3 mol^{-1} cm^{-1}),[4] generated through one- and two-photon processes, respectively.

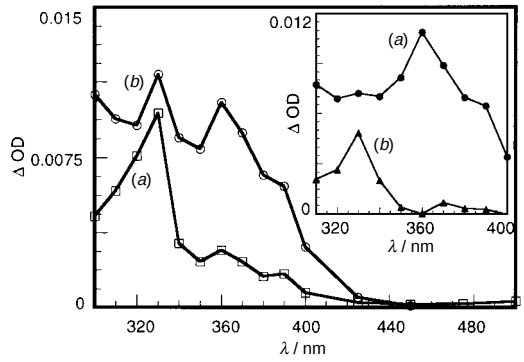

Fig. 1 Transient absorption spectra recorded following laser excitation (266 nm) of **1a** under nitrogen 2 μs after laser pulse (*a*) with diffuser and (*b*) without diffuser. Insert: (*a*) spectrum of *o*-xylylene obtained 2.32 μs after irradiation in the presence of oxygen without diffuser; (*b*) spectrum of **2a** obtained by normalizing and subtracting the spectrum of *o*-xylylene from the spectrum obtained in the absence of oxygen.

When irradiating with a 266 nm laser it is useful to place a beam diffuser (which eliminates 'hot' spots in the laser beam) close to the sample in order to get a better observation of monophotonic transients.[5] Actually, a new spectrum obtained under these conditions showed a higher ratio of radical **2a** to the two photon intermediate, **3a** (Fig. 1).

To confirm the radical nature of the transient at 330 nm, oxygenated samples were examined, showing that, while the band at 330 nm was quenched at close to the diffusion controlled limit (see insert Fig. 1), the lifetime of the transient at 360 nm appeared insensitive to the presence or absence of oxygen (data not shown).

Furthermore, to study the photobehaviour of **2a**, two-colour two-laser flash photolysis experiments[6] were carried out using 266 nm laser pulses (20 mJ pulse^{-1}) to photolyze **1a** and a 308 nm excimer laser (90 mJ pulse^{-1}) to irradiate **2a**. The two pulses were typically separated by *ca.* 2.5 μs, a time sufficiently long that the irradiation of excited states of **1a** by the 308 nm laser is impossible. We note that **1a** is transparent at 308 nm. That the benzyl radical **2a** can be the precursor of *o*-xylylene is clearly demonstrated by comparing the spectra obtained upon irradiation with the first and the second laser (Fig. 2). The permanent and irreversible bleaching of the transient with a maximum at 330 nm was concurrent with the jump of the band with a maximum at 360 nm.

Thus, it seems clear that **2a** photolyzes to *o*-xylylene, and a mechanism for the photogeneration of *o*-xylylene from α,α′-dichloro-*o*-xylene is shown in Scheme 1; while triplet **1a** may or may not produce *o*-xylylene, it is clear that there is no need to invoke this undetected process.

On the other hand, laser flash photolysis of deaerated 1.5 mM solutions of α,α′-dichloro-*p*-xylene (**1b**) in cyclohexane at 266 nm (with a beam diffuser) yielded the transient absorption spectrum shown in Fig. 3. Irradiation of oxygenated samples showed that the band at 320 nm was quenched at close to the diffusion controlled limit, but the lifetime of the transient at 290 nm appeared to be insensitive to the presence of oxygen. Thus, the band at 320 nm can be assigned to the *p*-(chloromethyl)benzyl radical (**2b**) by comparison with the band of the *p*-methylbenzyl radical in solution.[7] On the other hand, the band at 290 nm is assigned to *p*-xylylene in accordance with literature data.[8] At first glimpse, the formation of *p*-xylylene from **1b** appeared to be more efficient than the generation of *o*-xylylene from **1a**, even if both dihalides were photolyzed under the same conditions [compare curve (*b*) in Fig. 1 and the transient in Fig. 3]. However, this could also reflect a different molar extinction coefficient of both xylylenes. Although ε_{max} of **3b** has not been reported, electronic spectra calculated for xylylenes[9] indicate that a much higher intensity should be expected for the absorption of the *para* than for the *ortho* derivative.

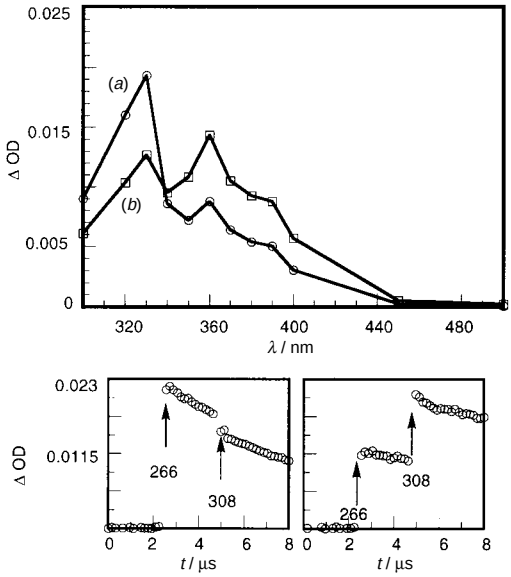

Fig. 2 Top: (*a*) Transient absorption spectrum recorded following laser excitation (266 nm) of **1a** under nitrogen 1.12 μs after laser pulse. (*b*) Transient absorption spectrum obtained upon two laser-two colour excitation of **1a**. The intermediate generated by means of a 266 nm laser pulse is photolyzed after 2 μs by a second laser at 308 nm. Bottom: Kinetic trace at 330 (left) and 360 nm (right); the bleaching at 330 nm corresponds to the disappearance of **2a** and the jump at 360 nm corresponds to the formation of **3b**.

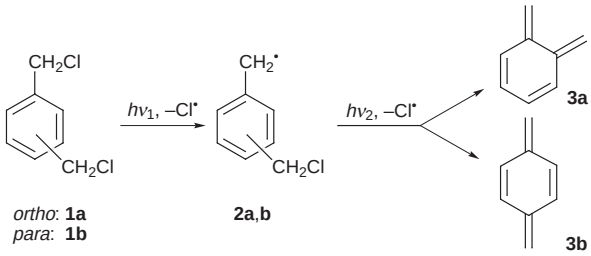

Scheme 1

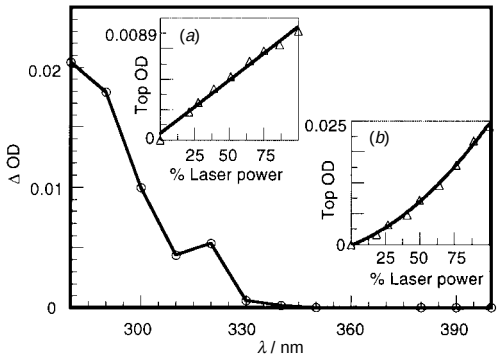

Fig. 3 Transient absorption spectrum recorded following laser excitation (266 nm) of **1b** under nitrogen 0.8 μs after laser pulse. Inserts (*a*) and (*b*) show the effect of the laser power on signal intensities monitored at 320 and 290 nm, respectively.

To establish the nature of the process leading to radical **2b** and *p*-xylylene, an investigation of the effects of light intensity on the relative intensity of their signals was carried out by attenuating the laser beam with a set of calibrated neutral density filters. Inserts (*a*) and (*b*) in Fig. 3 show that there is a linear relationship between the formation of **2b** and the laser power, while a parabola is obtained in the case of **3b**; thus, the evidence supports a one-photon process for the benzylic radical and a two-photon process for *p*-xylylene.

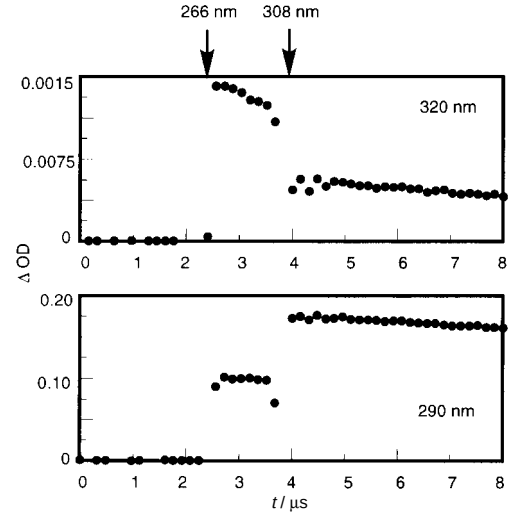

Fig. 4 Two laser-two colour photolysis of **1b**. Top: kinetic trace at 320 nm; the bleaching corresponds to the disappearance of **2b**. Bottom: kinetic trace at 290 nm; the jump corresponds to the formatio of **3b**.

The photobehaviour of radical **2b** was studied by using two-colour two-laser experiments; the 266 nm laser was used to generate this radical, which was further irradiated with pulses from the 308 nm laser. That **2b** can be the precursor of **3b** is clearly demonstrated by comparing traces obtained for both transients (Fig. 4). Thus, the bleaching at 320 nm was coincident with the jump at 290 nm. Based on this evidence the mechanism for the photogeneration of *p*-xylylene from α,α′-dichloro-*p*-xylene is also that of Scheme 1.

In summary, this work has demonstrated that benzyl radicals are the key light absorbing transients in the two-photon generation of *o*- and *p*-xylylenes from the corresponding dichloroxylenes.

J. C. S. thanks the National Sciences and Engineering Research Council of Canada for support. Spanish DGICYT (MAM, Project no. PB94-0539) and Spanish Ministry of Education (EFS, Grant) are gratefully acknowledged.

Notes and References

† E-mail: mmiranda@qim.upv.es

1 L. A. Errede, *J. Am. Chem. Soc.*, 1961, **83**, 949; E. Migirdicyan and J. Baudet, *J. Am. Chem. Soc.*, 1975, **97**, 7400; J. J. McCullough, *Acc. Chem. Res.*, 1980, **13**, 270; Y. Ito, M. Nakatsuka and T. Saegusa, *J. Am. Chem. Soc.*, 1982, **104**, 7609; V. Wintgens, J. C. Netto-Ferreira, H. L. Casal and J. C. Scaiano, *J. Am. Chem. Soc.*, 1990, **112**, 2363.
2 K. L. Tseng and J. Michl, *J. Am. Chem. Soc.*, 1977, **99**, 4840; K. Haider, M. S. Platz, A. Despres, V. Lejeune, E. Migirdicyan, T. Bally and E. Haselbach, *J. Am. Chem. Soc.*, 1988, **110**, 2318.
3 M. Fujiwara, K. Mishima, K. Tamai, Y. Tanimoto, K. Mizuno and Y. Ishii, *J. Phys. Chem.*, 1997, **101**, 4912.
4 W. S. Trahanovsky and J. R. Macias, *J. Am. Chem. Soc.*, 1986, **108**, 6820.
5 M. A. Miranda, J. Pérez-Prieto, E. Font-Sanchis, K. Kónya and J. C. Scaiano, *J. Org. Chem.*, 1997, **62**, 5713.
6 J. C. Scaiano, L. J. Johnston, W. G. McGimpsey and D. Weir, *Acc. Chem. Res.*, 1988, **21**, 22.
7 R. F. C. Claridge and H. Fisher, *J. Phys. Chem.*, 1983, **87**, 1960.
8 G. Kaupp, *Angew. Chem., Int. Ed. Engl.*, 1976, **15**, 442; J. M. Pearson, M. A. Six, D. J. Williams and M. Levy, *J. Am. Chem. Soc.*, 1971, **93**, 5034; R. Marquardt, W. Sander, T. Laue and H. Hopf, *Leibigs Ann.*, 1995, 1643.
9 C. R. Flynn and J. Michl, *J. Am. Chem. Soc.*, 1974, **96**, 3280.

Received in Liverpool, UK, 12th March 1998; 8/02016G

Photoinduced reduction of thymine and uracil derivatives by hypophosphite: unusual high quantum yield of chromophore loss

Kongjiang Wang,*† and Zhifang Chai

Institute of High Energy Physics, The Chinese Academy of Sciences, PO Box 2732, Beijing 100080, PR China

The quantum yield of chromophore loss of thymine, uracil and their corresponding nucleosides and nucleoside-5′-monophosphates undergoing irradiation with 254 nm UV light was found to be sharply enhanced by hypophosphite; thymine and uracil were reduced by hypophosphite to give 5,6-dihydrothymine and 5,6-dihydrouracil respectively.

In the photochemistry of nucleic acids, there has been much interest in oxidative damage to DNA and its biological consequences in living cells.[1,2] Here we report the photoinduced reduction (hydrogenation) of thymine (**1a**), uracil (**1b**) and their derivatives by hypophosphite, which was initially found in our tentative simulation of the photochemistry of the primitive sea, by irradiation with a medium pressure mercury lamp.[3] Contrary to the wavelength dependence of the enhancement of the photolysis of nucleic acid monomers by orthophosphates and pyrophosphate on UV light for photoionization of phosphates (< 210 nm),[3,4] no obvious wavelength dependence has been observed in photoinduced reduction by hypophosphite. We present the results obtained by the irradiation with 254 nm UV light.

For actinometry of the low pressure mercury lamp, we repeatedly used the chromophore loss of uridine in areated aqueous solution at pH 6.[5] A 20% $MeCO_2H$ solution of 1 cm pathlength was employed to filter off the photochemically significant quantities of 184.9, 194.2 and 222.4 nm UV light. The quantum yield of chromophore loss (ϕ^{cl}) was determined from the decrease of absorbance at λ_{max} of the substrates. Fig. 1 shows the concentration dependence of ϕ^{cl} of thymine, uracil and their corresponding nucleosides and nucleoside-5′-monophosphates. It is clear from this figure that ϕ^{cl} of thymine, uracil and their derivatives increases when the concentration of sodium hypophosphite is about 3×10^{-3} M or higher. ϕ^{cl} for uracil and thymidine is higher than for the other derivatives. Note that ϕ^{cl} for thymine, thymidine and thymidine-5′-monophosphate increases so sharply that at 1 M sodium hypophosphite ϕ^{cl} for thymine, thymidine and thymidine-5′-monophosphate is 0.016, 0.046 and 0.029, ϕ^{cl} being 0.064, 0.16 and 0.11 for uracil and its derivatives under the same conditions. However, no significant ϕ^{cl} change for uracil and thymine has been observed in the presence of 0.1 M concentrations of other anions (SO_4^{2-}, Cl^-, CO_3^{2-}, citrate, acetate, arsenate, cacodylate, orthophosphates, pyrophosphate), 0.1 M urea and 0.004 M metaphosphate under irradiation with 254 nm UV light. In contrast to the enhancement of the photolysis of nucleic acid monomers by orthophosphates and pyrophosphate,[4] no obvious ϕ^{cl} increase has been observed for cytosine, cytidine and cytidine-5′-monophosphate in the range 10^{-5}–1 M hypophosphite. For adenine, guanine and their derivatives, ϕ^{cl} was observed to increase when the concentration rises to more than 0.01 M, but the relative ϕ^{cl} value is < 5.

Hydrate formation of uracil, uridine and uridine-5-monophosphate was quantified using both HPLC[6] and the method introduced by Moore and Thomson[7] because the latter method has been demonstrated to bring about total dehydration.[6] HPLC elution demonstrates that hydrate formation of uracil and uridine in the concentration range corresponding to photoinduced reduction by hypophosphite ($> 3 \times 10^{-3}$ M) decreases sharply. The low reversibility or irreversibility of the irradiated samples of uracil, uridine and uridine-5-monophosphate in the concentration range corresponding to photoinduced reduction by hypophosphite also indicates that hydrates are not the main products. In dilute solution, dimers of pyrimidine bases and their derivatives arise through the triplet state.[1] ϕ for thymine dimer formation is small (< 0.1), while the reversal quantum yield is about 1.[8] This, combined with the reported limiting concentrations for uracil dimerization (> 0.1 mM)[9] and the aerated aqueous media (O_2 as triplet quencher) in the current system eliminates the possibility of forming the dimers in large quantity.

Fig. 2 indicates that major photoproducts have been formed in aqueous solutions of uracil and thymine containing sodium hypophosphite, which have been purified‡ and characterized.§ Using the authentic samples (Sigma) as internal standard, the retention time of the purified products was found to be the same to 5,6-dihydrothymine (**2a**) and 5,6-dihydrouracil (**2b**). The corresponding peaks were found to disappear by HPLC analysis after incubating the photoproducts in 0.2 M KOH for 1 h at room temperature. This is in agreement with the alkaline lability of dihydrouracil and dihydrothymine.[10] However, after heating the aqueous solution of the photoproducts with or without 0.1 M HCl in a boiling water bath for 10 min, no obvious change was observed *via* HPLC. Both IR and NMR spectra of the purified samples were found to be the same as those of the authentic samples. Overall these data indicate that the major product of

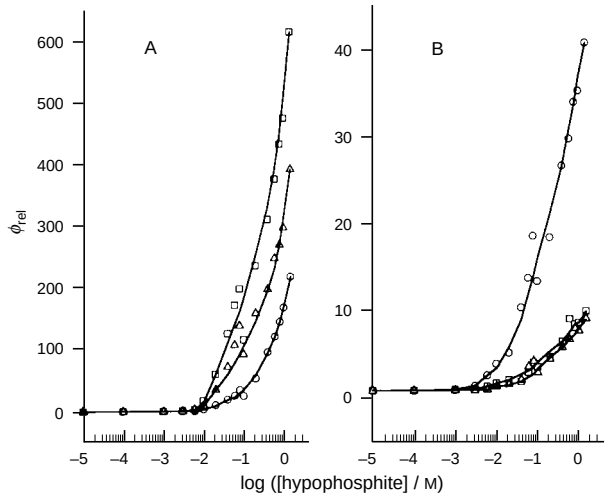

Fig. 1 ϕ^{cl} for thymine (A), uracil (B) and their derivatives as a function of the molar concentration of sodium hypophosphite undergoing the irradiation with 254 nm UV light (6.05×10^{-4} Einstein min^{-1}): (○) the base, (□) the corresponding nucleoside and (△) nucleoside-5′-monophosphate. Generally, 1×10^{-4} M aerated pyrimidines or their mixed solutions with sodium hypophosphite (pH 7 ± 0.3) were irradiated so as to facilitate UV absorbance and spectrum assay. ϕ^{cl} for thymine, thymidine and thymidine-5'-monophosphate in the absence of hypophosphite is 9.7×10^{-5}, ϕ^{cl} for uracil, uridine and uridine-5′-monophosphate in the absence of hypophosphite is 1.8×10^{-3}, 0.018 and 0.014. ϕ^{cl} in the presence of hypophosphite has been normalized to ϕ^{cl} in the absence of hypophosphite.

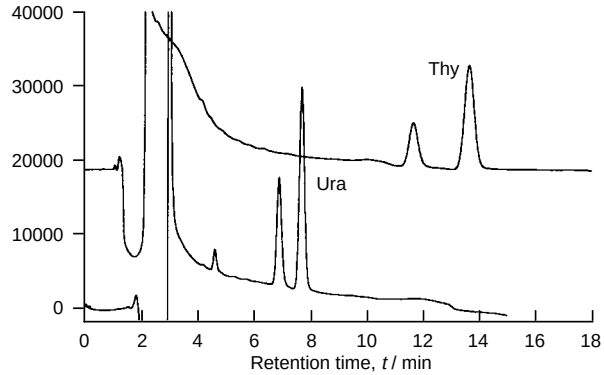

Fig. 2. HPLC elution profiles of products from irradiated 1×10^{-4} M thymine (Thy) and uracil (Ura) containing 0.2 M hypophosphite. The products were eluted from the μBondapak C_{18} column (Waters, 3.9×300 mm) at a flow rate of 1.4 ml min^{-1} (Thy) and 1 ml min^{-1} (Ura). The chromatograms were monitored at 210 nm.

thymine and uracil containing hypophosphite is 5,6-dihydrothymine (**2a**) and 5,6-dihydrouracil (**2b**). UV absorbance at 254 nm of 1 M sodium hypophosphite is 0.009, eliminating complications in the reaction mechanism owing to the competitive UV absorbance of hypophosphite. This, combined with detection of the quantitative oxidated hypophosphite (600 MHz, ^{13}P NMR spectrum), indicates that the enhancement of the chromophore loss by hypophosphite is indeed the photoinduced reduction by hypophosphite [eqn. (1)].

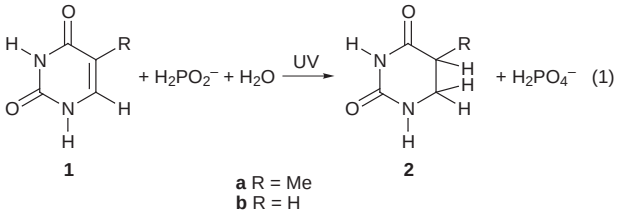

The fact that no obvious difference in the quantum yield has been found between the aerated and nitrogen-saturated samples favors the singlet pathway as the reaction mechanism.

This work was supported by the Presidential Foundation and is a major project of the Chinese Academy of Sciences.

Notes and References

† E-mail: wangkj@lnat.ihepa.ac.cn

‡ The major photoproducts were prepared by 254 nm irradiation of 1×10^{-3} M aerated thymine or uracil aqueous solution containing 1 M sodium hypophosphite (pH 7 ± 0.3). The photoproducts were extracted using ethyl acetate (for photoproducts of thymine) and a mixed solution of butanone and ethyl acetate (80 : 20, v/v) (for photoproducts of uracil). The collected samples were concentrated on a rotary evaporator. The residue was taken up in water, the products were purified by reversed-phase HPLC (Waters 600, Waters μBondapak C_{18} 19 × 300) with aqueous solution (uracil) or 2% MeOH aqueous solution (thymine). The collected samples were lyophilized to dryness.

§ *Selected spectroscopic data*: **1**, UV spectrum of **2a** and **2b** shows the disappearance of the characteristic absorption (> 230 nm) of uracil and thymine. **1**, **2a** ($C_5H_8N_2O_2$), Anal. Calc. for $C_5H_8N_2O_2$: C, 46.88; H, 6.25; N, 21.88; O, 25. Found: C, 47.1; H, 7.1; N, 22.1; O, 23.8%. FTIR (ν/cm^{-1}) 3236m, 3088m, 2892w, 1736vs, 1715vs, 1496m, 1392w, 1240s; 819w, 696w, 448w; δ_H(DSS, 600 MHz) 1.079 and 1.096 (d, Me), 2.647–2.723 (m, 5 H), 3.043–3.099 (m, 6 H), 3.036–3.045 (m, 6 H). *m/z* (atmosphere pressure chemical ionization), 129 $(M + 1)^+$. **2, 2b** ($C_4H_6N_2O_2$), Anal. Calc. for $C_4H_6N_2O_2$: C, 42.1; H, 5.26; N, 24.56; O, 28.07. Found: C, 42; H, 5.1, N, 24.6, O, 28.54%. FTIR (ν/cm^{-1}) 3236m, 3087m, 2892w, 1736vs, 1715vs, 1678m, 1496m, 1391w, 1239s, 820w, 756w, 453w; δ_H(DSS, 600 MHz) 2.554–2.589 (t, 5 H), 3.324–3.405 (t, 6 H); *m/z* 115 $(M + 1)^+$.

1 J. Cadet and P. Vigny, *Bioorganic Photochemistry, Photochemistry and Nucleic Acids*, ed. M. Morrision, Wiley-Interscience, New York, 1989, vol. 1, pp 53–184; G. J. Fisher and H. E. Johns, *Photochemistry and Photobiology of Nucleic Acids*, ed. S. Y. Wang, Academic Press, New York, 1976, vol. 1, pp. 226–295; S. T. Reid, *Advances in Heterocyclic Chemistry*, ed. A. R. Katritzky and A. J. Boulton, Academic Press, New York, 1982, vol. 30, pp. 278–291.
2 C. Sheu and C. S. Foote, *J. Am. Chem. Soc*., 1995**, 117**, 474 and refs. cited therein.
3 K. J. Wang, Ph.D. Thesis, 1995, Peking University, pp. 70–73.
4 K. J. Wang, X. M. Pan, J. L. Wu and W. Q. Wang, *Photochem. Photobiol.*, 1997**, 65**, 656; K. J. Wang, Z. F. Chai and X. M. Pan, *Origin Life Evol. Biosphere*, 1998**,** in the press.
5 G. J. Fisher and H. E. Johns, *Photochemistry and Photobiology of Nucleic Acids*, ed. S. Y. Wang, Academic Press, New York, 1976, vol. 1, pp. 169–224; G. G. Gurzadyan and H. Gorner, *Photochem. Photobiol.*, 1993, **58**, 477; H. Gorner, *J. Photochem. Photobiol. B: Biol*., 1991, **10**, 91; V. A. Ivanchenko, A. I. Titschenko, E. I. Budowsky, N. A. Simokova and N. S. Wulfson, *Nucleic Acids Res*., 1975, **2**, 1365; G. G. Gurzadyan and H. Gorner, *Photochem. Photobiol.*, 1994, **60**, 323; G. G. Gurzadyan and H. Gorner, *Photochem. Photobiol.*, 1996, **63**, 143.
6 K. J. Wang and Z. F. Chai, *J. Photochem. Photobiol. A: Chem.*, 1997, **107**, 143.
7 A. M. Moore and C. H. Thomson, *Can. J. Chem*., 1957, **35**, 163; A. M. Moore and C. H. Thomson, *Science*, 1955**, 122**, 594.
8 M. A. Herbert, L. C. LeBlanc and D. Weiblum, *Photochem. Photobiol.*, 1969, **9**, 33; R. B. Setlow, *Biochim. Biophys. Acta*, 1961**, 49**, 237.
9 I. H. Brown and H. E. Johns, *Photochem. Photobiol*., 1968**, 8**, 273.
10 R. D. Batt, K. Martin, J. M. Ploesser and J. Murphy, *J. Chem. Soc*., 1954**,** 3663; R. E. Cline and R. M. Fink, *Anal. Chem*., 1956**, 28**, 52; A. J. Varghese, *Biochemistry*, 1971, **10**, 4283.

Received in Cambridge, UK, 15th April 1998; 8/02836B

Dynamic *cis*/*trans* isomerisation in a porphyrin–fullerene conjugate

Jean-François Nierengarten,*† Laurence Oswald and Jean-François Nicoud

Groupe des Matériaux Organiques, Institut de Physique et Chimie des Matériaux de Strasbourg, Université Louis Pasteur and CNRS, 23 rue du Loess, F-67037 Strasbourg, France

A porphyrin with two fullerene substituents is prepared by condensation of a C_{60} aldehyde derivative and dipyrrol-2-yl methane and by reaction of a preconstructed porphyrin with C_{60} itself; it is obtained as a mixture of two conformers in slow equilibrium, as shown by a variable temperature NMR study.

Since the first reported preparation of a C_{60}-linked porphyrin by Gust,[1] several other fullerene–porphyrin hybrids have been described.[2] Intramolecular processes such as electron and energy transfer have been observed in some of these compounds and C_{60} appears as a particularly interesting electron acceptor in photochemical molecular devices because of its symmetrical shape, large size and the properties of its π-electron system.[3] Concerning their synthesis, all the previously reported porphyrin–C_{60} hybrids have been prepared by reaction of a preconstructed porphyrin with C_{60} itself or a C_{60} acid derivative.[2] We have recently shown that a porphyrin could be constructed starting from a C_{60} aldehyde derivative and pyrrole.[4] As a part of this research, we now report the synthesis of the novel porphyrin **1** with two C_{60} groups directly attached to the core using our methodology. Furthermore, the corresponding Zn^{II}–porphyrin **2** has been prepared by metalation of **1**, but also by reaction of a preconstructed Zn^{II}–porphyrin with C_{60} itself. Interestingly, both **1** and **2** have been obtained as a mixture of two conformers and an NMR study reveals a previously unreported type of dynamic *cis*/*trans* isomerisation.

The synthesis of porphyrin **1** and its Zn^{II} complex **2** is depicted in Scheme 1. Aldehyde **3**,[4] compound **4**[4] and dipyrrol-2-yl methane **5**[5] were prepared according to previously reported methods. The condensation of **3** and **5** was performed in $CHCl_3$ at room temperature in the presence of $BF_3{\cdot}Et_2O$. After 12 h, *p*-chloranil was added to irreversibly convert the porphyrinogen to the porphyrin. The desired porphyrin **1** was isolated in 38% yield and subsequent metalation with $Zn(OAc)_2$ gave **2** in 97% yield. Compound **2** could also be prepared starting from **4**: deprotection (TFA, CH_2Cl_2, H_2O), subsequent condensation of the resulting aldehyde **6** with **5** in $CHCl_3$ with $BF_3{\cdot}Et_2O$ as catalyst and *p*-chloranil oxidation yielded porphyrin **7**, which was metalated with $Zn(OAc)_2$ to give **8**. Fullerene incorporation was based on the regioselective macrocyclisation reaction of the carbon sphere with bismalonate derivatives developed by Diederich and co-workers.[6] Treatment of C_{60} with **8**, I_2 and DBU in toluene at room temperature afforded a mixture of compounds from which the desired Zn^{II}–porphyrin **2** could be subsequently isolated in 2% yield by tedious chromatographic separations. This poor yield could be easily explained by a low selectivity of the intramolecular addition to C_{60} due to competition between the different available reactive malonic units on the porphyrin core after its first intermolecular reaction with C_{60}.

All of the spectroscopic studies and elemental analysis results were consistent with the proposed molecular structures.‡ The ^1H NMR spectrum of **1** at room temperature showed the presence of two conformers in a 1 : 1 ratio (Fig. 1). Molecular modelling studies on compound **1** revealed that each fullerene group is located to one side of the plane of its bridging phenyl ring. Therefore due to the high barrier to rotation of the phenyl substituents on the porphyrin, two conformers are possible for **1**. The two carbon spheres in **1** can be in either a *cis* or *trans* relative orientation (Fig. 1). Whereas the two porphyrin *meso*-

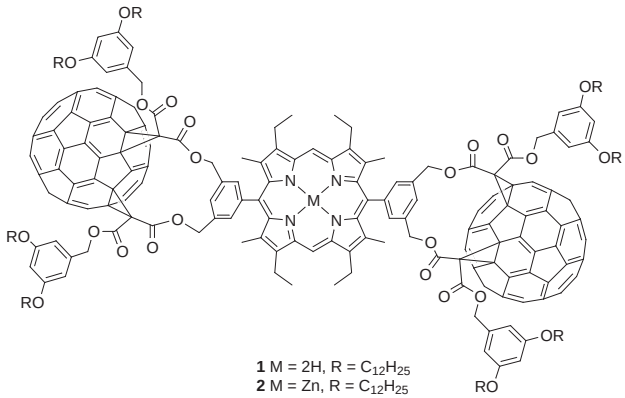

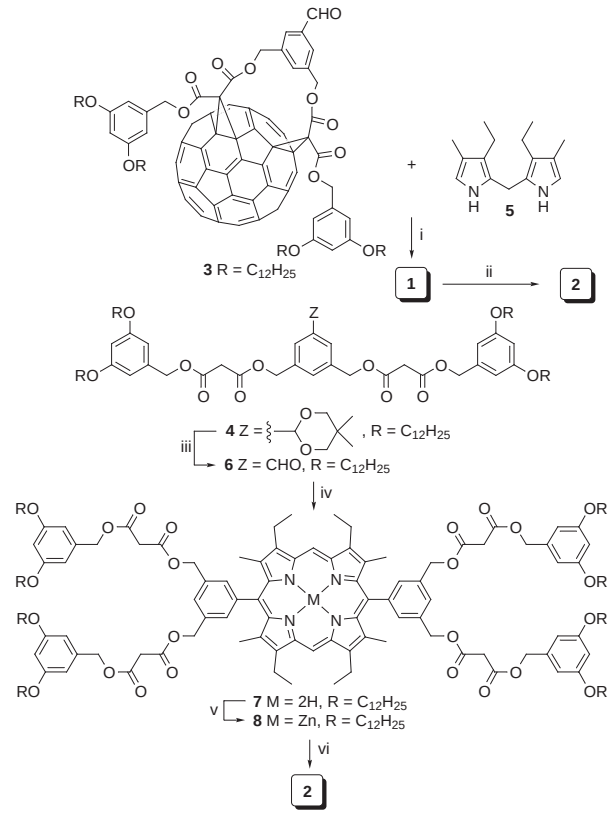

Scheme 1 *Reagents and conditions*: i, $CHCl_3$, $BF_3{\cdot}Et_2O$, room temp., 12 h, then *p*-chloranil, reflux, 2 h, 38%; ii, $Zn(OAc)_2$, $CHCl_3$, MeOH, reflux, 2 h, 97%; iii, TFA, CH_2Cl_2, H_2O, room temp., 5 h, 80%; iv, **5**, $CHCl_3$, $BF_3{\cdot}Et_2O$, room temp., 12 h, then *p*-chloranil, reflux, 2 h, 47%; v, $Zn(OAc)_2$, $CHCl_3$, MeOH, reflux, 3 h, 92%; vi, C_{60}, DBU, I_2, toluene, room temp., 12 h, 2%

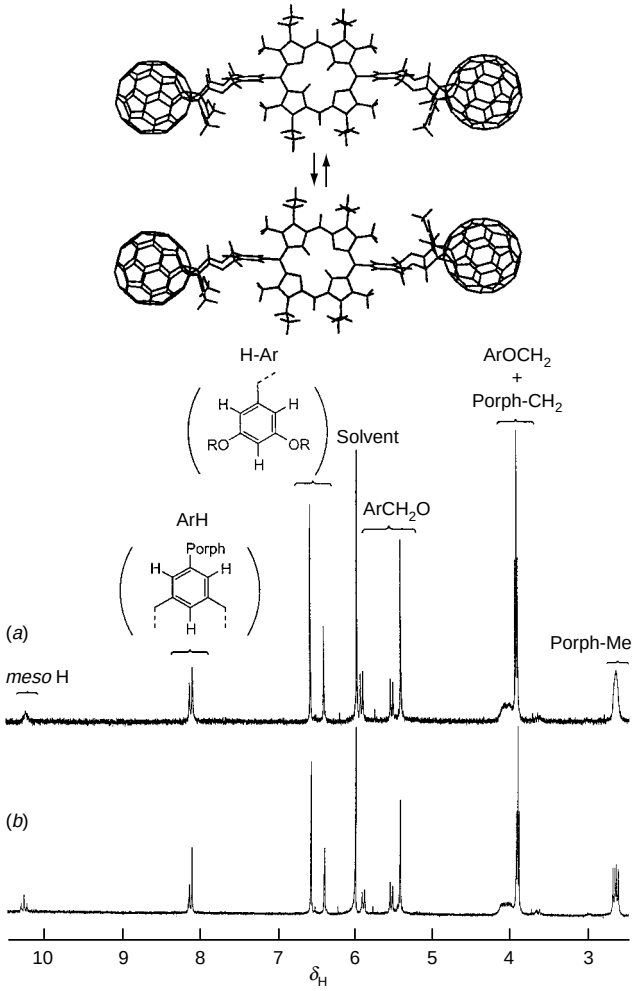

Fig. 1 ^{1}H NMR spectra of **1** ($CDCl_2CDCl_2$, 400 MHz) at (a) 125 and (*b*) 25 °C, and molecular models of the two conformers of compound **1** (the four didodecyloxyphenyl groups have been omitted for clarity)

Hs are equivalent in the *trans* conformer, they are non-equivalent in the *cis* one. As expected, three singlets in a 1 : 2 : 1 ratio are observed at δ 10.20, 10.23 and 10.27, respectively, for the *meso*-Hs in the 1 : 1 mixture of conformers. Furthermore, the four methyl groups on the porphyrin form equivalent pairs in both conformers and the expected four singlets are clearly observed (δ 2.60, 2.63, 2.64 and 2.67) in the ^{1}H NMR spectrum. A variable-temperature NMR study showed a clear coalescence at 125 °C (Fig. 1). By monitoring the coalescence of the porphyrin *meso*-Hs, the free energy barrier for the conformational equilibrium was calculated as $\Delta G^{\ddagger}$ = 85 kJ mol^{-1}.[7] A sharp symmetric spectrum could not be obtained below the limit of heating, however the observed reversible narrowing of all the peaks unambiguously shows that a dynamic effect does occur. This *cis*/*trans* isomerism has also been seen for compound **2** and can be related to the diastereoisomerism observed for some terphenyl systems.[8] Whereas atropisomerism in bis(*o*-substituted phenyl) porphyrins is well known, the conformational isomerism observed for **1** and **2** is, to the best of our knowledge, the first example of a bis(*m*-substituted phenyl) porphyrin for which the barrier to free rotation is high enough at room temperature to be able to distinguish the *cis* and *trans* conformers.

Preliminary luminescence measurements show a strong quenching of the porphyrin emission in **1** and **2** and their photophysical properties are currently under investigation.

We thank the CNRS for financial support, C. Bourgogne for his help with the molecular modelling, Hoechst AG for samples of C_{60} and Professor F. Diederich (Zürich, Swiss) for his interest in our work and his support.

Notes and References

† E-mail: niereng@michelangelo.u-strasbg.fr

‡ *Selected data* for **1**: $\lambda_{max}(CH_2Cl_2)$/nm (ε/dm^3 mol^{-1} cm^{-1}) 259 (275 580), 317 (96 370), 382 (sh, 133 130), 408 (284 740), 506 (27 000), 539 (10 580), 573 (11 050), 624 (2680); $\nu_{max}(CHCl_3)$/cm^{-1} 1748 (C=O); *m*/*z* (ESI) 4360 (M^+) (Calc. for $C_{304}H_{270}N_4O_{24}$: C, 83.68; H, 6.24; N, 1.28. Found: C, 83.79; H, 6.29; N, 1.27%).

1 P. A. Liddell, J. P. Sumida, A. N. Macpherson, L. Noss, G. R. Seely, K. N. Clark, A. L. Moore, T. A. Moore and D. Gust, *Photochem. Photobiol.*, 1994, **60**, 537.
2 H. Imahori, K. Hagiwara, T. Akiyama, S. Taniguchi, T. Okada and Y. Sakata, *Chem. Lett.*, 1995, 265; T. Drovetskaya, C. A. Reed and P. Boyd, *Tetrahedron Lett.*, 1995, **36**, 7971; H. Imahori and Y. Sakata, *Chem. Lett.*, 1996, 199; H. Imahori, K. Hagiwara, M. Aoki, T. Akiyama, S. Taniguchi, T. Okada, M. Shirakawa and Y. Sakata, *J. Am. Chem. Soc.*, 1996, **118**, 11 771; M. G. Ranasinghe, A. M. Olivier, D. F. Rothenfluh, A. Salek and M. N. Paddon-Row, *Tetrahedron Lett.*, 1996, **37**, 4797; H. Imahori, K. Yamada, M. Hasegawa, S. Taniguchi, T. Okada and Y. Sakata, *Angew. Chem., Int. Ed. Engl.*, 1997, **36**, 2626; I. G. Safanov, P. S. Baran and D. I. Schuster, *Tetrahedron Lett.*, 1997, **38**, 8133.
3 H. Imahori and Y. Sakata, *Adv. Mater*., 1997, **9**, 537.
4 J.-F. Nierengarten, C. Schall and J.-F. Nicoud, *Angew. Chem.*, in the press.
5 R. Young and C. K. Chang, *J. Am. Chem. Soc.*, 1985, **107**, 898.
6 J.-F. Nierengarten, V. Gramlich, F. Cardullo and F. Diederich, *Angew. Chem., Int. Ed. Engl.*, 1996, **35**, 2101; J.-F. Nierengarten, A. Herrmann, R. R. Tykwinski, M. Rüttimann, F. Diederich, C. Boudon, J.-P. Gisselbrecht and M. Gross, *Helv. Chim. Acta*, 1997, **80**, 293; J.-F. Nierengarten, T. Habicher, R. Kessinger, F. Cardullo, F. Diederich, V. Gramlich, J.-P. Gisselbrecht, C. Boudon and M. Gross, *Helv. Chim. Acta*, 1997, **80**, 2238.
7 H. Günther, *NMR-Spektroskopie*, 2nd edn., Thieme, Stuttgart, 1983.
8 E. L. Eliel, S. H. Wilen and L. N. Mander, *Stereochemistry of Organic Compounds*, Wiley, New York, 1994.

Received in Cambridge, UK, 7th May 1998; 8/03434F

Non-covalent control of site-selective incorporation of the pyridoxal phosphate cofactor into a folded polypeptide motif—mimicking a key step in enzymatic transamination

Malin Allert, Martin Kjellstrand, Klas Broo, Åke Nilsson and Lars Baltzer*†

Department of Chemistry, Göteborg University, S-412 96, Göteborg, Sweden

The site-selective incorporation of the pyridoxal phosphate cofactor into a designed polypeptide motif has been achieved and shown to be controlled by the non-covalent interactions between the phosphate group of the cofactor and a single arginine residue on the surface of the folded polypeptide.

The *de novo* design of functionalized proteins is an attractive alternative in the construction of new catalysts because of the inherent capacity of polypeptides for folding into complex three-dimensional structures determined by non-covalent bonds. Folded polypeptide catalysts, with reactive sites formed by naturally occurring amino acids, are now emerging that catalyse multistep reactions with rate enhancements that rival those of typical catalytic antibodies.[1–3] Coenzyme-based catalysts have, perhaps, an even greater potential because of their intrinsic reactivities, provided that efficient strategies can be found to embed the cofactors into reactive sites in template peptides. The site-selective incorporation of residues for which no codons exist has so far been accomplished by the cumbersome synthesis of artificial amino acids[4,5] or by the site-selective functionalization of lysine, ornithine, diaminobutyric acid[6–8] and cysteine residues.[9,10] Here we report that for the first time non-covalent interactions have been used to control the incorporation of a complex cofactor into a folded polypeptide. Understanding the principles that govern the recognition of functional groups by folded polypeptides opens up efficient routes for the engineering of new proteins with tailor-made specificities.

PP-42, a polypeptide with 42 residues, was designed to fold into a helix-loop-helix motif and dimerise in aqueous solution to form a four-helix bundle protein (Fig. 1). Its design was based on the sequence and solution structure of SA-42[11,12] with the objective of engineering a template polypeptide into which a pyridoxal cofactor could be introduced. PP-42 was synthesised by solid-phase peptide synthesis using Fmoc chemistry, purified by reversed-phase HPLC and identified from the electrospray mass spectrum (calc. 4532.1; found 4531.5).‡ The mean residue ellipticity of PP-42 at a concentration of 0.60 mM is -24500 ± 1000 deg cm^2 dmol^{-1} in aqueous solution at pH 7.0 and ambient temperature, which is comparable to those of other designed helix-loop-helix dimers.[13] The helical content of amphiphilic helix-loop-helix dimers is known to decrease substantially upon dissociation, therefore the measured mean residue ellipticity of PP-42 provides strong evidence that it folds into the designed four-helix bundle motif.

The mechanism of transamination in native enzymes includes the formation of an aldimine from the pyridoxal phosphate cofactor **I** and the side chain of a lysine residue in the active site. Upon introduction of the amino acid substrate into the active site, the lysine side chain is replaced by the amino group of the amino acid, which is transformed to an α-keto acid in a multistep reaction.[14] In order to incorporate the cofactor into the folded helix-loop-helix motif, to mimic the initial step of the enzymatic reaction, a lysine residue was targeted for aldimine formation by placing an arginine side chain in a position to interact with the phosphate group of the cofactor. In the computer modelled structure the guanidino group of Arg-19 is ideally positioned to bind the phosphate group upon aldimine formation at the side chain of Lys-30. Two more lysine residues were introduced into PP-42 to probe whether the phosphate-arginine interaction would be strong enough to make the incorporation site-selective. The sequence of PP-42 contains three lysine and four arginine residues, Lys-11, Lys-15, Lys-30, Arg-10, Arg-19, Arg-33 and Arg-40 (Fig. 1).

The reaction between **I** and PP-42 to form the aldimine was followed by the increase in absorbance at 390 nm, using an extinction coefficient for the aldimine of 4000 M^{-1} cm^{-1} (Fig. 2).§ The degree of aldimine formation was determined from the 400 MHz ^{1}H NMR spectrum recorded in D_2O at pH 4.4 by measuring the reduction of the intensity of the aldehyde proton of **I** at δ 10.43 upon addition of PP-42 under these conditions. More than 95% of the monofunctionalised peptide was obtained using approximately 0.6 mM PP-42 and a five-fold excess of **I**. At pH 4.4 the reaction is rapid and equilibrium is established within a few minutes. The UV spectrum of a solution of 0.6 mM PP-42 and 3.1 mM of **I** at 25 °C and pH 4.4 is shown in Fig. 2 and shows that more than 95% of the PP-42 is bound. In contrast, under identical reaction conditions, the equilibrium

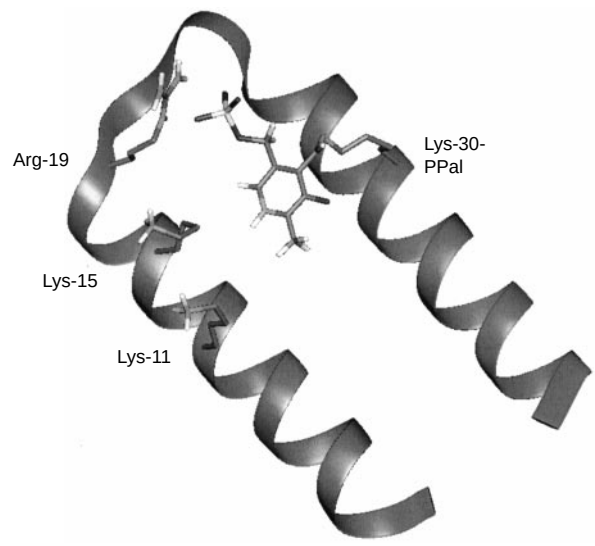

Fig. 1 The amino acid sequence and the modelled structure of PP-42 showing the positions of arginine and lysine side chains on the surface of the folded motif. The amino acid residues are given in the one-letter code where Nle is the artificial amino acid norleucine. Only the monomer is shown for simplicity.

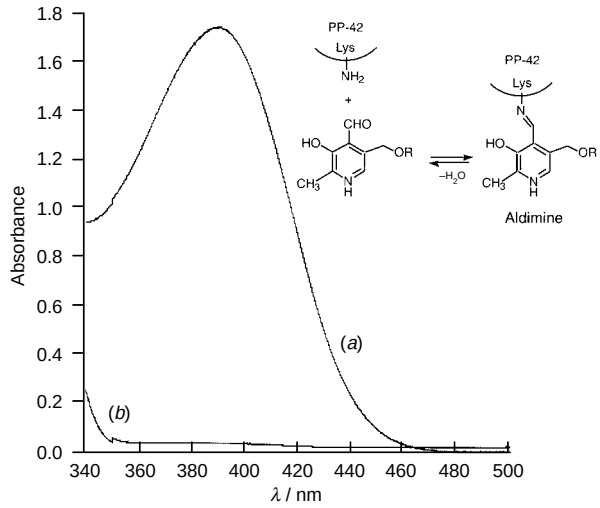

Fig. 2 The UV spectrum recorded in aqueous solution, at 25 °C and pH 4.4, of 0.6 mM PP-42 in the presence of (*a*) 3.1 mM pyridoxal phosphate **I** (R = PO_3^{2-}) and (*b*) 3.1 mM pyridoxal II (R = H). The aldimine formation was followed at 390 nm.

concentration of aldimine upon reaction between PP-42 and pyridoxal **II**, that has no phosphate residue, is insignificant. It can be estimated from the ratio of the absorbances of the two aldimines that the equilibrium constants differ by more than two orders of magnitude, although the absorbance of the pyridoxal-containing mixture is too weak to permit an accurate determination. A strong interaction between the negatively charged phosphate residue and the peptide is thus demonstrated.

The site of incorporation of pyridoxal phosphate into PP-42 was determined by $NaBH_4$ reduction of the aldimine in aqueous solution to form the corresponding secondary amine, followed by trypsin cleavage of the functionalised peptide. The site of functionalization was determined by LC-ESMS of the polypeptide digest. Trypsin cleaves polypeptides on the C-terminal side of basic residues. No cleavage was expected at the lysine side chain that had been functionalized.

A fragment from the reduced form of the functionalized peptide (dication 835.91 and trication 557.61), which corresponded to the molecular mass of the sequence from Gly-20 to Arg-33 (1438.64) plus the mass of pyridoxal phosphate (247.2) and 2H (2.02), less the weight of water (18.02) amounting to approximately 85% of the total amount of reduced functionalized peptide, were found in the LC-ESMS spectrum. The dominant site of aldimine formation was therefore the side chain of Lys-30. A minor amount of aldimine formation at the side chain of Lys-11 was also observed, whereas no aldimine formation involving the side chain of Lys-15 could be detected.

Arg-19 is apparently in a good position relative to Lys-30 to control the functionalization of its side chain, but the proximity of Arg-10 to Lys-11 in a helical conformation appears to give rise to small amounts of aldimine, too, under conditions of excess **I** over peptide. The absence of detectable amounts of aldimine at the side chain of Lys-15 shows that a lysine side chain that is not flanked by an arginine in PP-42 does not form an aldimine with **I** to a measurable extent.

Arg-19 and Lys-30 thus form a two-residue site that competes favourably with other lysine residues in PP-42, and the aldimine formation with **I** is controlled by the binding of phosphate by arginine. The engineering of a Lys-Arg two-residue site is therefore sufficient to ensure the incorporation of the cofactor provided that the arginine side chain has a similar orientation towards the lysine side chain as that of Arg-19 towards Lys-30. The incorporation of **I** can thus be made site-selective in the presence of other lysine residues. To enhance the selectivity further Arg-(*i*)-Lys-(*i*+1) configurations in helical segments should be avoided. In the second step of the catalytic cycle the amino group of an amino acid will replace the lysine side chain in an exchange reaction. Further design of the polypeptide motif is now under way so that the second intermediate, too, will be bound to the peptide catalyst. It can for example be envisioned that the trianion formed in the reaction between **I** and Asp will be bound by arginine residues.

The demonstration of non-covalent control of the incorporation of **I** shows that the interaction between the phosphate group and an arginine side chain in aqueous solution at pH 4.4 is strong enough to ensure the site-selectivite funtionalization of the folded polypeptide. A well-defined two-residue site on the surface of the folded polypeptide can therefore be used to create a molecule of high complexity in a one-step reaction in aqueous solution. The use of the arginine–phosphate bond should be of general interest in a wide range of applications involving phosphates and phospho esters. The results suggest that understanding the interplay between functional amino acid side chains, organised in three-dimensional space by polypeptide templates, is a key element in the rational design of functionalised polypeptides with tailor-made specificities.

Financial support from the Swedish Natural Science Research Council and from Carl Tryggers Stiftelse is gratefully acknowledged. We are indebted to Dr Gunnar Stenhagen for mass spectrometric determinations.

Notes and References

† E-mail: baltzer@oc.chalmers.se

‡ The solid-phase peptide synthesis, cleavage and purification strategies have been described in detail for the four-helix bundle proteins SA-42[11,12] and KO-42[1] that have similar sequences.

§ The extinction coefficient at pH 4.4 and 25 °C was estimated from the absorbance of an aqueous solution containing 0.3 mM PP-42 and 0.3 mM **I**.

1 K. S. Broo, L. Brive, P. Ahlberg and L. Baltzer, *J. Am. Chem. Soc.*, 1997, **119,** 11362.
2 K. Johnsson, R. K. Allemann, H. Widmer and S. A. Benner, *Nature*, 1993, **365**, 530.
3 K. Severin, D. H. Lee, A. J. Kennan and R. M. Ghadiri, *Nature*, 1997, **389**, 706.
4 B. Imperiali and R. Sinha Roy, *J. Org. Chem.*, 1995, **60**, 1891.
5 R. Sinha Roy and B. Imperiali, *Tetrahedron Lett.*, 1996, **37**, 2129.
6 L. Baltzer, A.-C. Lundh, K. Broo, S. Olofsson and P. Ahlberg. *J. Chem. Soc., Perkin Trans. 2*, 1996, 1671.
7 K. Broo, L. Brive, A.-C. Lundh, P. Ahlberg and L. Baltzer, *J. Am. Chem. Soc.*, 1996, **118**, 8172.
8 K. Broo, M. Allert, L. Andersson, P. Erlandsson, G. Stenhagen, J. Wigström, P. Ahlberg and L. Baltzer, *J. Chem. Soc., Perkin Trans. 2*, 1997, 397.
9 H. Mihara, Y. Tanaka, Y. Fujimoto and N. Nishino, *J. Chem. Soc., Perkin Trans. 2*, 1995, 1915.
10 H. Mihara, K. Tomizaki, N. Nishino and T. Fujimoto, *Chem. Lett.*, 1993, 1533.
11 S. Olofsson, G. Johansson and L. Baltzer, *J. Chem. Soc., Perkin Trans. 2*, 1995, 2047.
12 S. Olofsson and L. Baltzer, *Folding Des.*, 1996, **1**, 347.
13 S. Ho and W. DeGrado, *J. Am. Chem. Soc.*, 1987, **109**, 6751.
14 H. Dugas, *Bioorganic Chemistry*, Springer-Verlag, New York, 3rd edn., 1996, p. 523.

Received in Glasgow, UK, 2nd March 1998; 8/01741G

Novel application of chiral micellar media to the Diels–Alder reaction

Michael J. Diego-Castro and Helen C. Hailes*†

Department of Chemistry, University College London, London, UK WC1H 0AJ

A novel chiral surfactant has been used in the first reported aqueous chiral micellar catalysis of a Diels–Alder reaction and enantioselectivities have been observed.

The chemical industry is undergoing an important transition period in which they are reacting to ever increasing governmental and public pressure to reduce the use of volatile organic solvents. In the context of Diels–Alder reactions, there is also an urgent need to seek alternatives to Lewis acids, since they are typically dumped when spent.

There is good reason to believe that chiral micellar media offer a viable clean alternative to more traditional methods of accomplishing many organic reactions. In particular, aqueous micellar media have the potential to confer special properties on reactions due to their ability to, for example, solubilise substrates and concentrate and preorientate reactants within the micellar core.[1] Furthermore, they are recyclable; there is the potential for enantioselection; they can be prepared at low cost, particularly when using synthons from the chiral pool; they can be applied to a range of different reactions; they are more versatile than other chiral aqueous systems such as cyclodextrins due to the potential number of structural variations; and they are more robust than enzymes. Whilst this field exhibits considerable promise, it is at an early stage in its development. Consequently, there are relatively few currently reported applications of chiral micellar media[2] and, until now, none at all for their application to Diels–Alder reactions.

Here we outline our initial investigations into a methodology, which enabled us to perform a Diels–Alder reaction using chiral micellar media, with enantioselectivities comparable with the best obtained for cyclodextrin based aqueous Diels–Alder reactions.[3] The reaction in question was performed using a novel (*S*)-leucine-derived surfactant **1**[4] to catalyse the reaction between cyclopentadiene and nonyl acrylate, under a variety of conditions.

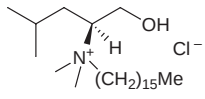

1

In a previous paper,[5] we demonstrated that a variety of factors influence the overall efficiency of the cycloaddition and the diastereoselective *endo* : *exo* (*N*/*X*) ratio. Amongst these are the chain length of the acrylate, the selection of the surfactant concentration and the pH of the solution. In view of the first of these factors, we chose to use nonyl acrylate as the test substrate to explore the feasability of the methodology, both because its long alkyl chain increases the pre-orientation effects within the micellar structure, and because the cycloadduct is stable to chiral HPLC analysis.

In order to ascertain the concentration at which micelles or micellar-like aggregates will be present and some enantioselective induction could be expected, we initially utilised a dye method which gave a value of *ca.* 0.011 g l^{-1} (0.027 mM).[6] Whilst it is well known that the critical micellar concentration (cmc) for a particular surfactant can vary depending on the method that is used,[7] and indeed, surface tension experiments indicated a higher value,[4,6] we felt that in our synthetic applications a dye method gave an appropriate starting point. This is because, in the micellar reaction system with nonyl acrylate present mixed micellar aggregates will be generated, as is also likely when the indicator dye is present.

Analysis of our initial experiments in the presence of the chiral surfactant **1** indicated some chiral induction in the *endo* adduct but negligible induction in the *exo* isomer. It was therefore necessary to assess whether the *R* or the *S endo* adduct was formed preferentially. To this end, we correlated our products using Oppolzer's sultam auxiliary methodology.[8] As outlined in Scheme 1, (*S*)-camphorsulfonyl chloride was treated with aq. NH_3, heated in the presence of Amberlyst-15, then reduced to a cyclic amine which was coupled with acryloyl chloride. The subsequent Diels–Alder cycloaddition reaction with cylopentadiene and the Lewis acid $TiCl_4$, followed by reduction and reaction with benzoyl chloride generated the *endo-S* isomer **2**. An analogous route using (*R*)-camphorsulfonyl chloride was used to synthesise the *R endo* ester **3**. The Diels–Alder *endo* cycloadducts generated in the reaction between nonyl acrylate and cyclopentadiene with **1** present were then isolated from the *endo–exo* mixture using chromatographic techniques. These were converted into a mixture of **2** and **3** *via* reduction and ester formation. Finally, HPLC analysis revealed that the *R* isomer was formed preferentially.‡

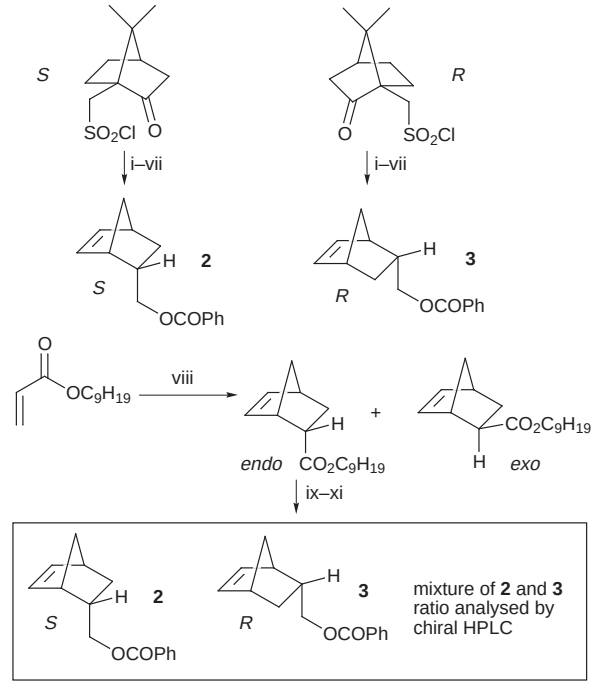

Scheme 1 *Reagents and conditions*: i, NH_4OH, THF, 83%; ii, Amberlyst-15, toluene, 110 °C, 18 h, 99%; iii, $LiAlH_4$, THF, 69%; iv, NaH, acryloyl chloride, 65%; v, $TiCl_4$, Et_2O, cyclopentadiene, −78 °C, 20 h, 55%; vi, $LiAlH_4$, Et_2O, 99%, vii, BzCl, CH_2Cl_2, 54%, viii, cyclopentadiene, 20 h, surfactant **1**, 55%; ix, only *endo* isomer was carried through subsequent steps (SiO_2, 4% Et_2O in hexane); x, $LiAlH_4$, Et_2O, 99%; xi, BzCl, CH_2Cl_2, 55%

Table 1 Addition of cyclopentadiene to nonyl acrylate in water containing surfactant **1**

Entry	[Surfactant]/g l^{-1}	Yield[a] (%)	*N*/*X*	Ee[b] (%) (*R*)
1	0.011	55	2.1	10
2	0.022	72	2.1	12
3	0.006	43	2.0	7
4	0.011[c]	29	2.1	13
5	0.011[d]	75	2.2	15

[a] Isolated yields. [b] Determined by chiral HPLC. [c] pH 3. [d] pH 3 with LiCl.

In view of the initial uncertainty in the optimum surfactant concentration for use in such applications, the concentration of **1** was varied and the effects on enantioselectivities and yield were noted,§ see summarised results in Table 1. For comparison purposes, the reaction in water alone under identical conditions, gave a yield of 70% and an *N*/*X* selectivity of 1.7.

At the starting point, an ee of 10% was observed (entry 1), rising slightly (entry 2) as surfactant concentration was increased then falling as the concentration was decreased (entry 3) together with a lowering of the yield, which could be due to the presence of non-micellar aggregates. Previously, we had seen the greatest yields and *N*/*X* selectivities in acrylate systems in the absence of surfactant when operating at pH 3.[5] In this instance, we found that when the solution was at pH 3 the enantioselectivity increased, although the yield of cycloadduct that was isolated was poor (entry 4). In determining how to increase the yield in this system, we reasoned that a salting-out agent would tend to remove the reactants from the aqueous pseudo-phase, increasing the complexation of the substrates to the micelles. Further, it is known that an increased concentration of chloride counterions can cause a shrinkage in the Stern layer, leading to a concentration of reactants[1] which, in our system, could translate to greater pre-orientation and enhanced yield and ees. In view of these factors, we added lithium chloride (4.86 M) to the reaction at pH 3, thence obtaining both the highest yield (75%) and the greatest ee (15%). This result compares well with the results quoted for Diels–Alder reactions in cyclodextrins in which maximum enantioselectivities of 21% are reported.[3]

A number of conformations of the surfactant **1** could be considered (since surfactants are dynamic in nature) and a representative one, consistent with NOE difference experiments is shown below in Scheme 2, in an attempt to provide a tentative simplistic model which nevertheless helps to visualise the observed preferences. All possible conformations have the common feature of a more hindered top face of the molecule as drawn due to the chirality present. Alignment of nonyl acrylate with the underside of **1** results in the cyclopentadiene having to approach from below the acrylate. As shown in Scheme 2 (for the reaction under neutral conditions), the carbonyl moiety can complex to the nitrogen and hydrogen bond to the O–H group with the alkene beneath the isopropyl group in **A**, with subsequent approach of cyclopentadiene beneath the complex leading to the formation of the *R*-isomer. However, in **B**, reaction with the diene would generate the *S*-isomer. Since **A** is complexed more favourably (with possible hydrogen bonding and carbonyl complexation) as well as having the polar carbonyl moiety directed towards the Stern layer, the *R*-isomer would be expected to be more prevalent. Future work will shed more light on this model.

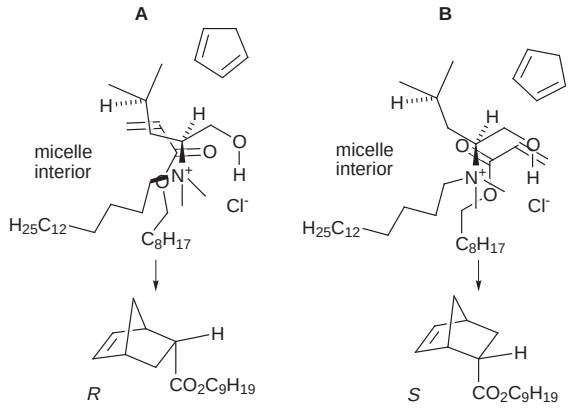

Scheme 2 Positioning of the acrylate with respect to the surfactant head group

In summary, we have performed the first Diels–Alder reaction in aqueous chiral micellar media, obtaining selectivities comparable with the best reported for other non-enzymic aqueous Diels–Alder reactions. We established that the *R* enantiomer in the *endo* isomer was formed preferentially in this system and have rationalised these results.

Subsidiary results include a further confirmation of the fact that the selection of the surfactant concentration is an important but elusive parameter in organic synthesis and that the pH is significant in chiral micellar catalysis. Finally, we have seen that lithium chloride may prove to be useful in such systems.

This work is part of a series of ongoing projects. We are aiming at further enhancing selectivity in Diels–Alder reactions by investigating a range of substrates with the aim of reducing the effects of the competing reaction in the water phase. We are also investigating the use of chiral surfactants in other classes of reaction as well as exploring the effect of more conformationally constrained surfactants.

We are grateful to University College London (Access Funds for M. J. D.-C.), Bush Boake Allen, Central Research Fund University of London, The Royal Society, and The Nuffield Foundation for funding. We thank Dr P. Sandor for running NOE experiments.

Notes and References

† E-mail: h.c.hailes@ucl.ac.uk

‡ Chiralcel OD column, 0.5% propan-2-ol–hexane, 1 ml min^{-1}. Retention times: **2** 7.0 min; **3** 4.8 min. Optical rotations were: **3** *via* $TiCl_4$ catalysis, $[\alpha]_D$ +8.1 (*c* 1.00, in CH_2Cl_2, 20 °C), **2** and **3** *via* micellar catalysis $[\alpha]_D$ +5.0 (*c* 1.03, in CH_2Cl_2, 20 °C).

§ Reactions were repeated a minimum of three times, giving enantioselectivities consistent to ± 0.5%. Cyclopentadiene (3.8 mmol) was reacted with nonyl acrylate (1.9 mmol) in water (25 ml) containing surfactant **1** for 20 h. Acidity adjusted with HCl. Chiralcel OD column, 0.1% propan-2-ol–hexane, 0.75 ml min^{-1}. Retention times: *exo*, 6.7 and 6.9 min; *endo*, 7.9 and 9.0 min.

1 T. Tascioglu, *Tetrahedron*, 1996, **52**, 11 113.
2 Y. M. Zhang, W. Fan, P. Lu and W. Wang, *Synth. Commun.*, 1988, **18**, 1495; Y. M. Zhang and W. Li, *Synth. Commun.*, 1988, **18**, 1685; Y. M. Zhang, S. Qu and W. Bao, *Synth. Commun.*, 1994, **24**, 2437; Y. M. Zhang and W. D. Wu, *Tetrahedron: Asymmetry*, 1997, **8**, 3573; Y. M. Zhang and W. D. Wu, *Tetrahedron: Asymmetry*, 1997, **8**, 2723.
3 H.-J. Schneider and N. K. Sangwan, *Angew. Chem., Int. Ed. Engl.*, 1987, **26**, 896.
4 M. J. Diego-Castro, H. C. Hailes and M. J. Lawrence, unpublished results.
5 M. J. Diego-Castro and H. C. Hailes, *Tetrahedron Lett.*, 1988, **39**, 2211.
6 M. J. Diego-Castro, H. C. Hailes, M. J. Lawrence and D. J. Barlow, unpublished results.
7 B. Lindman and H. Wennerstrom, *Top. Curr. Chem.*, 1981, **87**, 1.
8 M. Vanderwalle, J. Van der Eyeken, W. Oppolzer and C. Vullioud, *Tetrahedron*, 1986, **42**, 4035.

Received in Liverpool, UK, 15th April 1998; 8/02825G

Construction of two- and three-dimensional supramolecular networks with an encapsulated lanthanide(III) complex as building block and hydrogen-bonded 4,4′-bipyridyl as spacer

Cheng-Yong Su,[a,b] Bei-Sheng Kang,[b] Han-Qin Liu,[b] Qi-Guang Wang[a] and Thomas C. W. Mak[a]*†

[a] *Department of Chemistry, The Chinese University of Hong Kong, Shatin, New Territories, Hong Kong*
[b] *Institute of Physical Chemistry, School of Chemistry and Chemical Engineering, Zhongshang University, Guangzhou 510275, PR China*

Reaction of the tripodal ligand tris(2-benzimidazolylmethyl)amine (ntb) with hydrated lanthanide(III) perchlorates in methanol affords the complexes $[Ln(ntb)_2]^{3+}$ (Ln = Pr, Eu and Tb) in which the central Ln^{3+} ion is well encapsulated in a cubic coordination environment; *in situ* co-crystallization of the complexes in the presence of 4,4′-bipyridyl produces either a double salt containing the bipyridinium(1+) cation or adducts with two to three bipyridyl molecules, the latter adducts forming doubly interpenetrating two- or three-dimensional cationic networks.

The control of molecular assembly using supramolecular interactions represents a new area of considerable general and topical interest.[1] In particular, strong, selective and directional hydrogen bonding has been exploited for molecular recognition associated with biological activity, and for crystal engineering of molecular solids.[2] Much progress has been made in the construction of organic building blocks into one-, two- or three-dimensional hydrogen-bonded architectures;[2,3] however, the use of metal complexes for assembly or self-assembly by hydrogen bonding has attracted little attention until recently,[4] although the resulting products are often expected to exhibit certain desirable electronic, magnetic, or inclusion behavior.[1b]

The specific spectroscopic and magnetic properties of lanthanide(III) ions have made them essential components in the preparation of new materials and ideal probes in studies of biological systems.[5] The incorporation of trivalent lanthanide ions into supramolecular complexes that act as molecular photonic devices is currently of great interest in supramolecular chemistry.[6] Probes based on Eu^{III} and Tb^{III} are of special relevance because of their long-lived $^5D_0$ and $^5D_4$ excited states and their large Stokes' shift. However, the design of a good lanthanide luminescent probe has to overcome difficulties arising from the low oscillator strengths of the f–f transitions and from the easy de-excitation of the Ln^{III} excited state.[6a,c]

Current research has mainly focused on the encapsulation of the Ln^{III} ions using pre-organized ligands such as coronands, cryptands, podands, calixarenes or Schiff bases.[5c,6d] We now report the syntheses and crystal structures of new lanthanide complexes with the tripodal ligand tris(2-benzimidazolylmethyl)amine (ntb), in which the central Ln^{III} ion displays a rarely found cubic coordination environment and is well encapsulated from interaction with its surroundings by the rigid heterocyclic rings of ntb. Employing the linear difunctional H-bond acceptor 4,4′-bipyridyl as a spacer, the bipyridinium(1+) double salt $[Eu(ntb)_2](ClO_4)_3\cdot(bipyH)ClO_4\cdot 3H_2O$ **1** and two types of bipyridyl adducts bearing different lanthanide/bipy molar ratios, namely $[Pr(ntb)_2](ClO_4)_3\cdot 2bipy\cdot 1.5H_2O$ **2** and $[Ln(ntb)_2](ClO_4)_3\cdot 3bipy\cdot nH_2O$ (**3,** Ln = Eu, n = 2; **4**, Ln = Tb, n = 1) were obtained. Doubly interpenetrating two- or three-dimensional extended networks are formed in complexes **2–4**.

In the presence of 4,4′-bipyridyl, reaction of ntb with hydrated lanthanide(III) perchlorates afforded complexes **1–4.**‡ The nature of the products isolated is evidently sensitive to the presence of a trace amount of acid[8] and different equivalents of 4,4′-bipyridyl. Single crystals suitable for X-ray analyses were obtained by slow diffusion of diethyl ether into a dilute reaction mixture.§

The main structural feature common to all four complexes is the presence of the $[Ln(ntb)_2]^{3+}$ motif, in which the Ln^{III} ion is coordinated by eight nitrogen atoms from the two ntb ligands to give a slightly distorted cubic environment (Fig. 1). Both ntb ligands display a tripod-type tetradentate coordination mode in wrapping around the central lanthanide ion. This kind of coordination geometry is seldom found for eight-coordinated Ln^{III} ions, although Wood *et al*.[9] suggested long ago that the cube should not be energetically unfavorable relative to either the square antiprism (D_{4d}) or the triangular dodecahedron (D_{2d}). The ability of two ntb tripods to shield completely a Ln^{III} ion with N-donor sites without additional bound solvent molecules, especially water or alcohol, is important for the design of lanthanide(III) supramolecular photonic devices since such coordinated solvent molecules are frequently efficient quenchers of Ln^{III} luminescence.[6d]

Since each ntb ligand possesses three NH groups that are potential hydrogen-bond donors (see Fig. 1), the possibility of controlling the assembly of $[Ln(ntb)_2]^{3+}$ moieties by employing the linear difunctional hydrogen-bond acceptor 4,4'-bipyridyl as a spacer component was explored. X-Ray crystal structure analysis showed that in complex **1**, one nitrogen atom of ($bipyH^+$) forms an acceptor hydrogen bond to $[Eu(ntb)_2]^{3+}$ (N···N, 2.900 Å) while the protonated nitrogen atom is connected to one oxygen atom of a perchlorate anion (N···O,

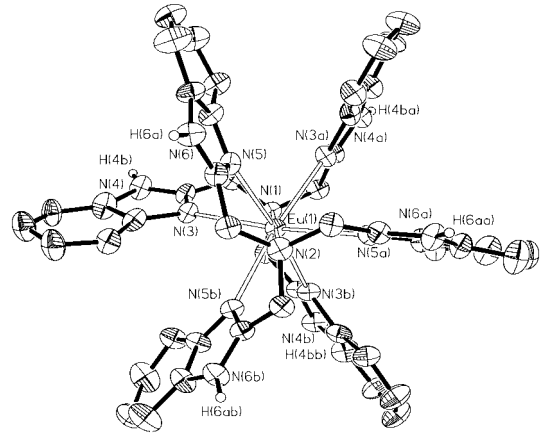

Fig. 1 Perspective view of the $[Eu(ntb)_2]^{3+}$ cation in **3** showing atoms as thermal ellipsoids at the 30% probability level. All H atoms have been omitted, except those of the NH groups that are shown as small spheres.

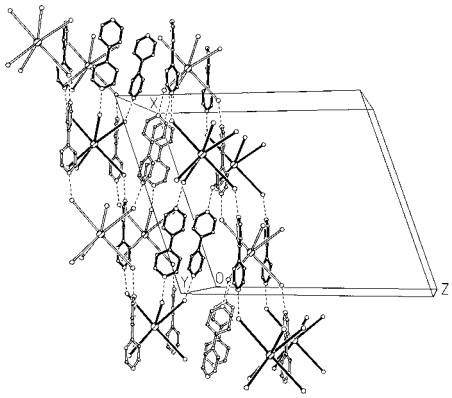

Fig. 2 Interlocking two-dimensional cationic frameworks constituting a layer matching the (001) plane in the crystal structure of **2**. For clarity, each 2-benzimidazolylmethyl arm of the ntb ligand is represented by a long rod joining each NH group to the lanthanide atom, so that each $[Pr(ntb)_2]^{3+}$ cation takes the appearance of an octahedron. All hydrogen atoms, water molecules and perchlorate ions have been omitted. The independent interlocking frameworks are differentiated by solid and open shading.

2.942 Å), thus precluding the formation of the linear chain $\cdots[Eu(ntb)_2]^{3+}\cdots bipy\cdots[Eu(ntb)_2]^{3+}\cdots bipy\cdots$. In complex **2**, each bipy forms a pair of acceptor hydrogen bonds with two different $[Pr(ntb)_2]^{3+}$ cations (N⋯N distances lie in the range 2.783–2.852 Å), thereby generating an open, two-dimensional cationic framework with each $[Pr(ntb)_2]^{3+}$ cation alternately connected to one and three bipy molecules in the *a* direction. Moreover, two independent frameworks of this type interpenetrate each other to form an extended layer corresponding to the (001) plane (Fig. 2), with the perchlorate ions and water molecules located in the inter-layer region. In complex **4** the NH groups of both independent ntb ligands in the $[Tb(ntb)_2]^{3+}$ ion and the bipy molecule are involved in the supramolecular hydrogen-bonding scheme (N⋯N range 2.818–2.871 Å). Linkage between each $[Tb(ntb)_2]^{3+}$ cation and six neighbouring bipy units leads to an open, three-dimensional cationic network, leaving large voids to be filled by another identical, interlocking network (Fig. 3), and the perchlorate ions and water molecules are located in the residual interstices. Compound **3**, in which the $[Eu(ntb)_2]^{3+}$ ion lies on a three-fold symmetry axis (Fig. 1), exhibits the same type of supramolecular structure as **4**, although the two adducts crystallize in different space groups.

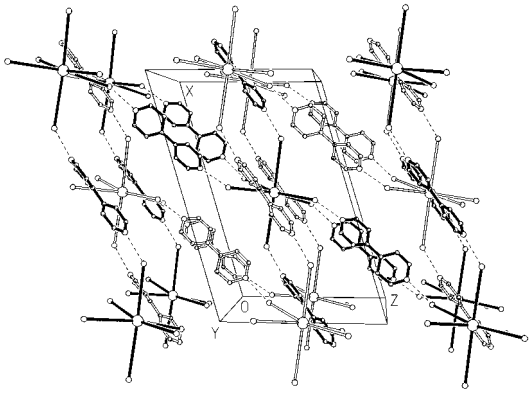

Fig. 3 Three-dimensional doubly interpenetrating networks in the crystal structure of **4**. Representation of the supramolecular structure is simplified in the same manner as in Fig. 2.

In summary, the present study has demonstrated that the intrinsic steric constraints of the tripodal ligand ntb facilitate complete encapsulation of a lanthanide(III) ion in a rare cubic coordination geometry. Assembly of $[Ln(ntb)_2]^{3+}$ building blocks with bipy spacers using supramolecular NH⋯bipy⋯HN hydrogen bonds results in two- or three-dimensional two-fold interpenetrating networks, which may be profoundly influenced by the presence of acid and different equivalents of the spacer component.

This work is supported by Hong Kong Research Grants Council Earmarked Grant Ref. No. CUHK 303/96P and the National Natural Science Foundation of China.

Notes and References

† E-mail: tcwmak@cuhk.edu.hk

‡ All complexes were prepared using a similar procedure: 0.2 mmol of tris(2-benzimidazolylmethyl)amine[7] (ntb) and 0.1 mmol of $Ln(ClO_4)_3{\cdot}nH_2O$ (prepared by dissolving the corresponding lanthanide oxides (99.99%) in 50% perchloric acid) were dissolved in 5 ml methanol. To this solution was added 5 ml of a methanolic solution of 4,4'-bipyridyl (0.1 mmol for **1**, 0.2 mmol for **2** and 0.3 mmol for **3** or **4**, respectively). The resulting mixture was left standing for several hours to give microcrystals. Complex **1**: Found: C, 44.07; H, 3.61; N, 13.93. Calc. for $C_{58}H_{57}N_{16}O_{19}Cl_4Eu$: C, 44.20; H, 3.65; N, 14.22%; **2**: Found: C, 50.23; H, 3.71; N, 15.55. Calc. for $C_{68}H_{61}N_{18}O_{13.5}Cl_3Pr$: C, 51.25; H, 3.86; N, 15.82%; **3**: Found: C, 52.62; H, 3.71; N, 15.55. Calc. for $C_{78}H_{70}N_{20}O_{14}Cl_3Eu$: C, 52.93; H, 3.99; N, 15.84%; **4**: Found: C, 52.46; H, 3.67; N, 15.53. Calc. for $C_{78}H_{68}N_{20}O_{13}Cl_3Tb$: C, 53.27; H, 3.90; N, 15.93%. For **1**–**4**: IR (KBr, cm^{-1}), 4200 [broad, ν(O–H)], 1623–1625, 1596 [ν(C=N)], 1085–1091, 626 [ν(Cl–O)]; UV–VIS (CH_3CN), λ/nm: 280, 273 and 198–201. Emission spectra (excited at 280 nm, 77 K) for complexes **1** and **3** are nearly identical, λ/nm: 598 ($^5D_0$–$^7F_1$) and 615 ($^5D_0$–$^7F_2$).

§ *Crystal data*: **1**: M = 1593.6, orthorhombic, space group $Pca2_1$, a = 26.109(3), b = 12.7780(10), c = 20.755(3) Å, Z = 4, yellowish crystal 0.6 × 0.7 × 0.8 mm, 7772 reflections measured, final $R1$ = 0.071 and $wR2$ = 0.149 for 4656 observed [$I > 2\sigma(I)$] reflections. **2**: M = 1593.6, monoclinic, $C2$, a = 20.562(2), b = 16.303(1), c = 24.079(2) Å, β = 109.04(1)°, Z = 4, colorless crystal 0.2 × 0.2× 0.15 mm, 9088 reflections measured, final $R1$ = 0.078 and $wR2$ = 0.208 for 7779 observed reflections. **3**: M = 1769.9, trigonal, $R3$, a = 16.449(2), c = 27.354(4) Å, Z = 3, yellowish crystal 0.4× 0.55 × 0.6 mm, 4906 reflections measured, final $R1$ = 0.078 and $wR2$ = 0.199 for 3305 observed reflections. **4**: M = 1758.8, monoclinic, $C2$, a = 20.503(2), b = 16.323(1), c = 13.083(1) Å, β = 106.61(1)°, Z = 2, colorless crystal 0.3 × 0.2 × 0.2 mm, 4982 reflections measured, final $R1$ = 0.068 and $wR2$ = 0.179 for 4780 observed reflections. CCDC 182/896.

1 (*a*) A. D. Burrows, C.-W. Chan, M. M. Chowdhry, J. E. McGrady and D. M. P. Mingos, *Chem. Soc. Rev.*, 1995, **24**, 329; (*b*) O. M. Yaghi, H. Li and T. L. Groy, *J. Am. Chem. Soc.*, 1996, **118**, 9096; (*c*) W. A. Herrmann, N. W. Huber and O. Runte, *Angew. Chem., Int. Ed. Engl.*, 1995, **34**, 2187.

2 G. R. Desiraju, *Chem. Commun.*, 1997, 1475; G. M. Whitesides, E. E. Simanek, J. P. Mathias, C. T. Seto, D. N. Chin, M. Mammen and D. M. Gordan, *Acc. Chem. Res.*, 1995, **28**, 37.

3 J.-M. Lehn, *Supramolecular Chemistry—Concepts and Perspectives*, VCH, Weinheim, 1995; K. Endo, T. Sawaki, M. Kobayashi, H. Masuda and Y. Aoyama, *J. Am. Chem. Soc.*, 1995, **117**, 8341; G. R. Desiraju, *Angew. Chem., Int. Ed. Engl.*, 1995, **34**, 2311.

4 V. Y. Kukushkin, T. Nishioka, D. Tudela and I. Kinoshita, *Inorg. Chem.*, 1997, **36**, 6157; M. Munakata, L. P. Wu, M. Yamamoto, T. Kuroda-Sowa and M. Mackawa, *J. Am. Chem. Soc.*, 1996, **118**, 3117; S. B. Copp, K. T. Holman, J. O. S. Sangster, S. Subramanian and M. J. Zaworotko, *J. Chem. Soc., Dalton Trans.*, 1995, 2233.

5 (*a*) J.-C. G. Bünzli, in *Lanthanide Probes in life, Chemical and Earth Sciences*, ed. J.-C. G. Bünzli and G. R. Choppin, Elsevier, Amsterdam, 1989, ch. 7; (*b*) P. G. Sammes and G. Yahioglu, *Nat. Prod. Rep.*, 1996, **13**, 1; (*c*) P. Guerriero, S. Tamburini and P. A. Vigato, *Coord. Chem. Rev.*, 1995, **139**, 17.

6 (*a*) S. Petoud, J.-C. G. Bünzli, F. Renaud, C. Piguet, K. J. Schenk and G. Hopfgartner, *Inorg. Chem.*, 1997, **36**, 5750; (*b*) C. Piguet, J.-C. G. Bünzli, G. Bernardinelli, G. Hopfgartner, S. Petoud and O. Schaad, *J. Am. Chem. Soc.*, 1996, **118**, 6681; (*c*) J.-C. G. Bünzli, P. Froidevaux and C. Piguet, *New J. Chem.*, 1995, **19**, 661; (*d*) N. Sabbatini, M. Guardigli and J.-M. Lehn, *Coord. Chem. Rev.*, 1993, **123**, 201.

7 A. R. Oki, P. K. Bommarreddy, H. M. Zhang and N. Hosmane, *Inorg. Chim. Acta*, 1995, **231**, 109.

8 K. Al-Rasoul and T. J. R. Weakley, *Inorg. Chim. Acta*, 1982, **60**, 191.

9 A. R. Al-Karaghouli and J. S. Wood, *Inorg. Chem.*, 1979, **18**, 1177; A. R. Al-Karaghouli, R. O. Day and J. S. Wood, *Inorg. Chem.*, 1978, **17**, 3702.

Received in Cambridge, UK, 20th April 1998; 8/02918K

Bipyridine functionalized molecular clips. Self-assembly of their ruthenium complexes in water

Johannes A. A. W. Elemans,[a] René de Gelder,[b] Alan E. Rowan[a] and Roeland J. M. Nolte*[a]†

[a] *Department of Organic Chemistry, NSR Center, University of Nijmegen, Toernooiveld, 6525 ED, The Netherlands*
[b] *Crystallography Laboratory, NSR Center, University of Nijmegen, Toernooiveld, 6525 ED, The Netherlands*

Ruthenium-bipyridine complexes of molecular clips self-assemble in water to form scroll- and cigar-like nanostructures.

The development of artificial self-assembled structures with specific shape and size is a topic of fundamental importance.[1,2] Incorporation of metal centers into these structures is of great interest as it may eventually lead to functional nanosized devices, for which many applications can be foreseen.

In our work to construct well defined nanosized assemblies by means of molecular recognition, we recently reported the formation of 'razorblade-like' aggregates in water, which were built up from diphenylglycoluril (DPG) derived molecular clips with water-soluble groups on their convex side.[3] Dimerization of these clips, in which the cavity of one clip is filled by the sidewall of its neighbour and *vice versa*, was found to play a major role in the assembly process. In order to be able to incorporate metal centers in these assemblies, a new type of molecular clip was developed having a bipyridine ligand on its convex side. Here the synthesis and properties of two of these clips are presented, as well as the self-assembling behaviour of their ruthenium-bipyridine complexes in water.

Bipyridine-glycoluril **1** was prepared in 81% yield by acid catalyzed condensation of 1,10-phenanthroline-5,6-quinone[4] and urea in toluene. Clip molecules **2** and **3** were synthesized in 32% and 16% yields, respectively, from **1** and 1,2-bis-(bromomethyl)benzene and from **1** and 2,3-bis(bromomethyl)naphthalene according to a standard procedure.[3]‡

Single crystals of **2** were grown by slow diffusion of methanol into a chloroform solution of this compound.§ The crystal structure [Fig. 1(*a*)] reveals that a large steric interaction exists between the γ-bipyridine and methylene protons of **2** resulting in a more squeezed cavity compared to cavities of other DPG-derived clips. This is reflected in the smaller distance between the aromatic side-walls of **2** (6.18 Å, as compared to 6.67 Å in the crystal structure of **4b**[5]). To investigate the consequences of this narrower cavity on the binding properties of **2** and **3** in $CDCl_3$, ^1H NMR binding studies with various 5-substituted 1,3-dihydroxybenzenes were carried out. It can clearly be seen in Table 1 that binding of guests in **2** is significantly weaker than in the reference compound **4a**, which is in agreement with the observed squeezed cavity of **2**. The host–guest binding properties of **3** in $CDCl_3$ are even weaker than those of **2**, as was observed before in DPG-derived clips containing 2,3-connected naphthalene walls.[6]

Clips **2** and **3** were then complexed with $[Ru(bipy)_2]Cl_2{\cdot}2H_2O$[7] to give water-soluble metalloclips **5** and **6** in 56% and 42% yields, respectively.‡ ^1H NMR experiments indicated that when a solution of **5** in D_2O was diluted, the resonances of the wall protons H_a and H_b and the bipyridine protons H_4 and H_5 shifted downfield, whereas the resonances of all the other protons of **5** did not undergo significant shifts. From an NMR dilution titration (500 MHz) in D_2O, the self-association constant of two molecules of **5** was determined to be $K_{dimer} = 50 \pm 10$ dm^3 mol^{-1}; the same value was calculated for each shifting proton. A 2D NOESY experiment of **5** in D_2O revealed several NOE contacts between the sidewall protons of one molecule of **5** and the bipyridine protons of its neighbour. Combining these results, we propose that **5** forms head-to-tail associates in water, clipping the sterically least hindered side of one of the bipyridine ligands of its neighbour between its cavity walls. From the calculated complexation induced shift values for the shifting protons (H_a: −0.85 ppm; H_b: −0.45 ppm; H_4: −1.41 ppm; H_5: −0.58 ppm), the geometry of the self-associated complex can be predicted, see Fig. 1(*b*). Because of steric hindrance it is not possible for **5** to bind simultaneously two neighbours at both bipyridines.¶

A ^1H NMR dilution titration of complex **6** in D_2O (0.1–2 mM) showed downfield shifts of the resonances of H_4, H_5, H_c and H_d. At concentrations above 2 mM the solutions of **6** became turbid and severe line broadening occurred, which was attributed to the

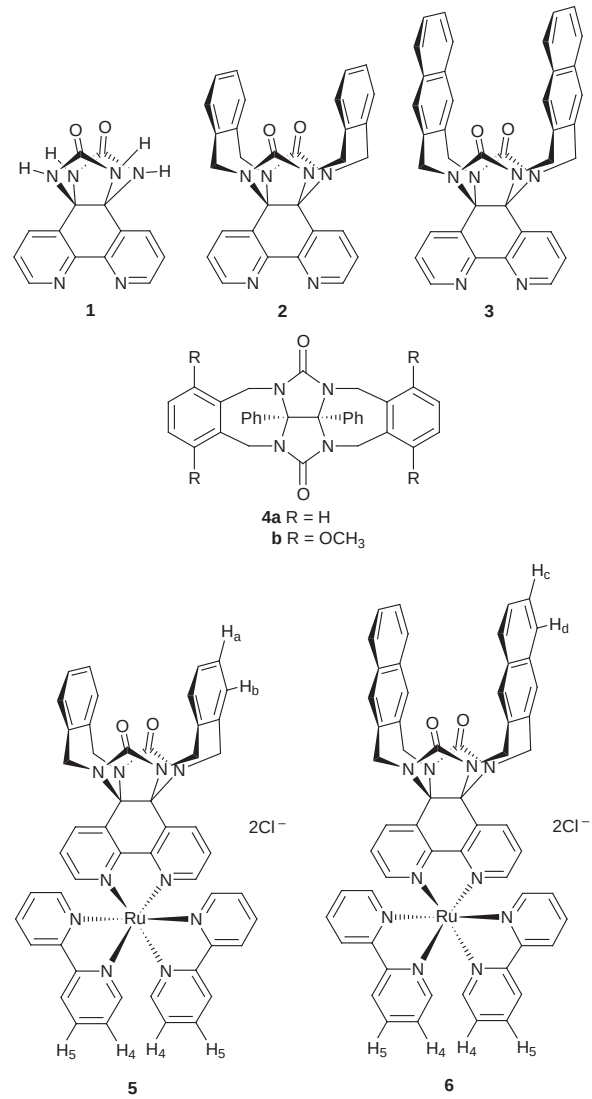

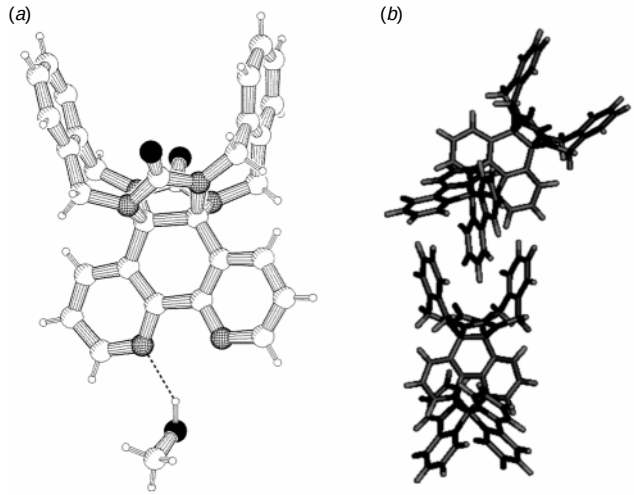

Fig. 1 (*a*) X-Ray structure of **2**·CH_3OH; (*b*) ^1H NMR based and computer generated (Quanta Charmm) structure of two molecules of **5** in D_2O

Table 1 Association constants ($dm^3\ mol^{-1}$) of complexes between various host and guest molecules in $CDCl_3$ (T = 298 K)

	Host		
Guest	**2**[a]	**4a**[b]	**3**[a]
5-Pentylresorcinol	20	74	< 5
Resorcinol	50	175	—[c]
5-Methoxyresorcinol	60	195	—[c]
5-Chlororesorcinol	100	475	—[c]
Methyl 3,5-dihydroxybenzoate	100	850	20
5-Cyanoresorcinol	240	3500	—[c]

[a] Estimated errors 20%. [b] Values taken from ref. 6. [c] Not determined.

formation of larger aggregates (*vide infra*). The calculated K_{dimer} using H_c or H_d as a probe (21000 ± 5000 $dm^3\ mol^{-1}$) was much larger than the calculated K_{dimer} using H_4 or H_5 as a probe (2500 ± 500 $dm^3\ mol^{-1}$). These values indicate that **6**, in contrast to **5**, can self-associate in two competing geometries, *viz*. head-to-head and head-to-tail, in which the interaction between the large hydrophobic cavities of **6** in the former geometry is stronger than the clipping of a bipyridine ligand between the cavity side-walls in the latter. The existence of both head-to-head and head-to-tail geometries has been observed before in the case of naphthalene-walled pyridinium-functionalized clips.[3] The self-association of **6** in D_2O is much stronger than the self-association of **5**, which is in contrast with the binding of guests in $CDCl_3$ solution, where **2** is a better host than **3**. In aqueous solution, however, the self-association geometry is dominated by hydrophobic interactions, and since **6** has a much larger hydrophobic cavity than **5** it is expected that **6** forms stronger self-associated complexes.

To further study the aggregates formed, samples of **5** and **6** in D_2O were investigated by electron microscopy (TEM). For **5**, rather undefined scroll-like structures were observed with lengths up to 10 μm [Fig. 2(*a*)]. In contrast, for **6**, well defined 'cigar-like' aggregates were found [Fig. 2(*b*),(*c*)] which displayed a very high monodispersity in size [aspect ratio (length/width) = 11 ± 2]. X-Ray powder diffraction on samples of **5** and **6** revealed no clear reflections, implying that the aggregates are built up from molecular units that interact in a very diverse way or assemble in a variety of geometries. Since the complexes are racemic mixtures of Λ and Δ enantiomers, and in the head-to-tail self-association geometry one molecule of **5** or **6** has the possibility to choose between different bipyridine ligands of a neighbouring clip molecule for binding in its cleft and, additionally, has the option to use each of its own bipyridines to hold another clip molecule, such diversity in binding can be easily envisaged.

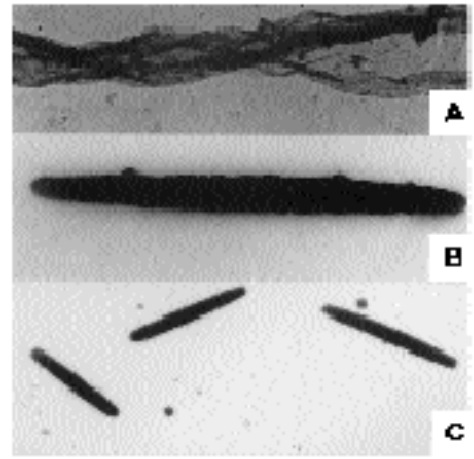

Fig. 2 Electron microscopic pictures of aggregates formed by **5** and **6** in water: (*a*) TEM picture of a scroll formed by **5**, 1 cm = 100 nm; (*b*),(*c*) TEM pictures of 'cigar-like' aggregates formed by **6**, 1 cm = 500 nm (*b*), 1 cm = 1750 nm (*c*). No shadowing or staining techniques were applied.

The observation that **6** assembles into a better defined supramolecular structure than **5** is attributed to the stronger self-association behaviour of **6**. We propose that the molecules of **6** self-assemble in a similar fashion to that reported before for the 'razorblade-like' nanostructures formed by molecular clips with pyridinium functions.[3] With their large hydrophobic cavities, molecules of **6** initially form head-to-head dimers, to which monomers of **6** can be further attached in a head-to-tail fashion. In this way, assemblies are formed that always have a hydrophilic outer surface. What is unique about these assemblies is that they grow until they reach a finite size. Apparently, at a certain point further growth is no longer energetically favoured.

Preliminary fluorescence experiments on solutions of both **5** and **6** in water indicate that upon excitation of the CT band the emission is quenched at higher concentrations due to aggregate formation. Further studies aimed at understanding the mechanism of assembly and the photophysical and electrochemical properties of the 'cigar-like' aggregates are in progress and will be reported in a forthcoming full paper.

Notes and References

† E-mail: tijdink@sci.kun.nl

‡ All new compounds were fully characterized. Full experimental details will be reported in a forthcoming full paper.

§ *Crystal data* for **2**·CH_3OH: $C_{31}H_{26}N_6O_3$, M_r = 530.58, space group $P2_1/n$, monoclinic, a = 10.5690(3), b = 18.2221(5), c = 12.9211(2) Å, β = 92.241(2)°; V = 2486.57(10) $Å^3$, Z = 4, ρ_{calc} = 1.364 g cm^{-3}; $2\theta_{max}$ = 139.92°, Cu-Kα radiation (graphite monochromator) λ = 1.54184 Å, μ = 0.765 mm^{-1}, T = 293(2) K, scan type: θ–2θ; 4974 reflections collected, 4710 independent of which 4016 observed. Final $wR2$ = 0.1078, final $R1$ = 0.0410 [for $I > 2\sigma(I)$]. CCDC 182/906.

¶ A 1 : 1 self-association is also supported by the data of the dilution titration, which could only be fitted by assuming a 1 : 1 complex.

1 G. M. Whitesides, J. P. Mathias and C. T. Seto, *Science*, 1991, **254**, 1312; R. F. Service, *ibid*., 1994, **265**, 316.
2 B. Hasenknopf, J.-M. Lehn, N. Boumediene, A. Dupont-Gervais, A. Van Dorsselaer, B. Kneisel and D. Fenske, *J. Am. Chem. Soc*., 1997, **119**, 10 956; M. Fujita, D. Oguro, M. Miyazawa, H.Oka, K. Yamaguchi and K. Ogura, *Nature*, 1995, **378**, 469; P. J. Stang and B. Olenyuk, *Acc. Chem. Res.*, 1997, **30**, 502 and references therein.
3 J. N. H. Reek, A. Kros and R. J. M. Nolte, *Chem. Commun*., 1996, 245.
4 M. Yamada, Y. Tanaka, Y. Yoshimoto, S. Kuroda and I. Shimao, *Bull. Chem. Soc. Jpn*., 1992, **65**, 1006.
5 R. P. Sijbesma, A. P. M. Kentgens, E. T. G. Lutz, J. H. van der Maas and R. J. M. Nolte, *J. Am. Chem. Soc*., 1993, **115**, 8999.
6 J. N. H. Reek, A. H. Priem, H. Engelkamp, A. E. Rowan, J. A. A. W. Elemans and R. J. M. Nolte, *J. Am. Chem. Soc.*, 1997, **119**, 9956.
7 B. P. Sullivan, D. J. Salmon and T. J. Meyer, *Inorg. Chem*., 1978, **17**, 3334.

Received in Cambridge, UK, 5th May 1998; 8/03327G

A bridging coordination mode of urea and carbamate at a dinuclear nickel(II) centre

Franc Meyer*† and Hans Pritzkow

Anorganisch-Chemisches Institut der Universität Heidelberg, Im Neuenheimer Feld 270, D-69120 Heidelberg, Germany

Starting from an active O_2H_3-bridged bimetallic complex, a bridging coordination mode of both urea and carbamate—the substrate and its first hydrolytic product in urease activity—at a dinickel(II) centre relevant to the active site of the metalloenzyme has been characterised structurally.

The nickel containing enzyme urease—which is present in a variety of plants, fungi and bacterial species—catalyses the hydrolysis of urea to form ammonia and carbamate, with the latter decomposing further to yield carbonic acid and another molecule of ammonia.[1] The X-ray crystal structure[2] of the microbial urease from *Klebsiella aerogenes* revealed two nickel ions 3.5 Å apart within the dinuclear active site and corroborated previously suggested models for its hydrolytic activity.[3] It is assumed that urea is activated by coordination to one nickel(II) ion in conjunction with extensive hydrogen bonding within the active site pocket of the protein and is subsequently attacked by a nucleophilic hydroxide bound to the opposite nickel centre.[3,4] However, the exact binding mode of the substrate as well as details of the operative mechanism are not yet unambiguously resolved, however. Considerable effort has therefore been devoted to the search of model complexes featuring a dinickel(II) core with accessible co-ordination sites at the metal centres[5–8] in order to elucidate the possible binding modes of urea at such urease-like systems and finally mimic the enzymatic reactivity. Nevertheless, only in a few cases has co-ordination of urea[7] (generally O-coordination) or even its hydrolytic cleavage[7b] hitherto been observed.

We recently described a class of pyrazolate-based dinuclear complexes, where appropriate chelating side arms attached to the heterocycle enforce metal–metal separations large enough to prevent small monoatomic units like HO^- from spanning both metal centres, thus favouring the formation of intramolecular O_2H_3 secondary bridges like in **1**.[9,10] For a related FHO(H)-bridged dicobalt(II) complex experimental evidence suggested that H_2O can reversibly be extruded from these moieties.[9b] Such a process in the case of **1** would generate an open coordination site for potential substrate binding adjacent to a hydroxide bound to the proximate second nickel ion, thus explaining the hydrolytic activity of **1** towards, for example, nitriles.[11] The similarity of this assumption with the proposed mechanism of urease activity prompted us to investigate the reaction of **1** with urea, especially because urea has been found to exhibit a greater affinity than water for binding to certain metal ions.[12]

Treatment of an acetone solution of **1** with urea or *N*,*N*-bis(trimethylsilyl)urea (Scheme 1) caused a slight change in its UV–VIS spectrum, and the resulting green complex **2**$(ClO_4)_2$‡ could be isolated from the reaction mixture. Single crystals were obtained by layering an acetone solution of the product with light petroleum. A crystallographic study (Fig. 1; two independent molecular entities with similar molecular dimensions were found in the unit cell)§ revealed that a tetraatomic trigonal planar moiety is situated within the coordination pocket created by the basic bimetallic framework, this being identified as a N,O-bridging deprotonated urea on the basis of the combined analytical data.‡ In particular, FAB mass spectrometry showed signals for $LNi_2[NH(O)CNH_2](ClO_4)^+$ and $LNi_2[NH(O)CNH_2]^+$ with the expected isotopic distribution pattern as the most intense peaks. The protons attached to the terminal nitrogen atoms N(9) were located as hydrogen bridges to oxygen atoms of the perchlorate counter anions [*d*(N···O) in the range 3.08–3.21 Å], while the Ni-bound O and N atoms of the bridging urea could not be distinguished crystallographically and are presumably disordered over both positions.

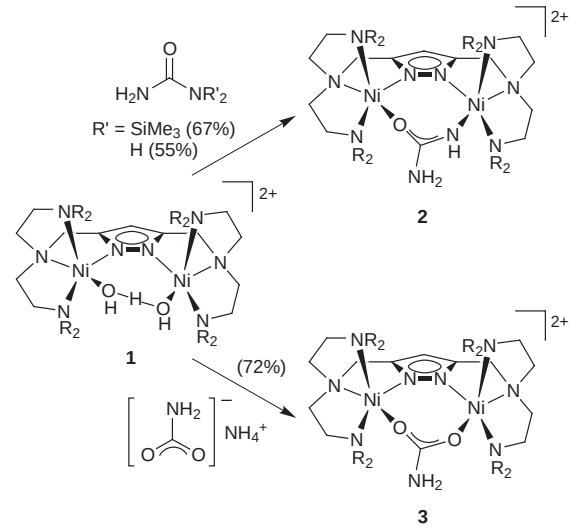

Scheme 1 Syntheses of the complexes. Yields are based on **1** and refer to isolated crystalline product.

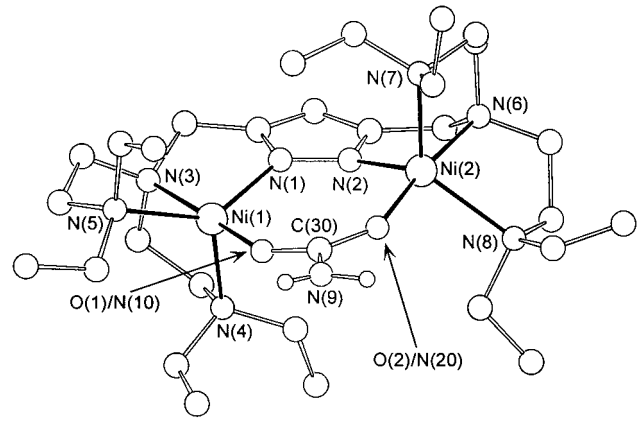

Fig. 1 Molecular structure of **2**. Selected atom distances (Å) and bond angles (°); values for the second independent molecule in square brackets: Ni(1)–O(1)/N(10) 1.971(7) [1.988(6)], Ni(1)–N(1) 2.014(8) [2.019(8)], Ni(1)–N(3) 2.159(8) [2.141(7)], Ni(1)–N(4) 2.099(8) [2.133(7)], Ni(1)–N(5) 2.214(8) [2.204(8)], Ni(2)–O(2)/N(20) 1.964(7) [1.987(6)], Ni(2)–N(2) 1.990(8) [2.007(7)], Ni(2)–N(6) 2.128(7) [2.157(8)], Ni(2)–N(7) 2.126(7) [2.168(8)], Ni(2)–N(8) 2.248(9) [2.234(8)], Ni(1)···Ni(2) 4.257(2) [4.253(2)]; O(1)/N(10)–Ni(1)–N(3) 174.1(3) [176.3(3)], O(2)/N(20)–Ni(2)–N(6) 173.5(3) [172.4(3)], O(1)/N(10)–C(30)–O(2)/N(20) 127.2(9) [125.6(9)].

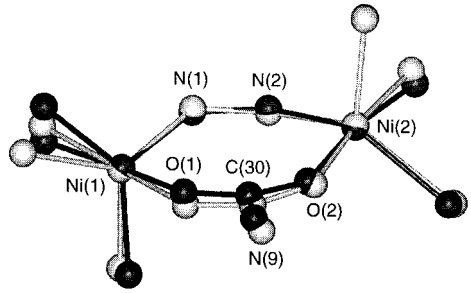

Fig. 2 Overlay of the crystallographically determined dinuclear sites of **2** (light) and **3** (dark). Selected atom distances (Å) and bond angles (°) for **3**: Ni(1)–O(1) 1.971(3), Ni(1)–N(1) 1.979(4), Ni(2)–O(2) 1.982(4), Ni(2)–N(2) 1.987(4), Ni(1)···Ni(2) 4.229(1), O(1)–C(30)–O(2) 127.3(5).

Formation of **2** from urea and *N*,*N*-bis(trimethylsilyl)urea implies the cleavage of the N–$SiMe_3$ bonds in the latter case, which is in accord with the known facility of N–Si bond hydrolysis in N-silylated amides.[13] The resulting trimethylsilanol was identified by GC–MS and ^{29}Si NMR spectroscopy among the volatile products of the present reaction. The observed deprotonation of parent urea by nickel-bound hydroxide to form **2** is understandable in the light of the drastic increase in substrate acidity upon its co-ordination to metal ions.[14] Thereby ureas are several orders of magnitude more acidic when N-bonded (pK_A < 6) then when O-bonded (pK_A > 11), and in the former case may even be more acidic than co-ordinated water.[14] It has thus been noted that isomerisation of the urea substrate from initial O-bonding to N-bonding can be thermally driven at intermediate pH, with the resulting deprotonated urea being kinetically inert and providing a thermodynamic sink for the linkage isomerisation.[14] A decisive driving force for the present reaction to form **2** certainly stems from the exceedingly strong tendency of these pyrazolate-based bimetallic complexes to incorporate secondary bridging ligands at the inner co-ordination site.[9,15]

In order to definitely exclude the presence of an O,O-bridging carbamate in **2**, complex **3** was synthesised independently for comparison (Scheme 1). At the same time this provides further insight into the possible coordination mode of this latter moiety—assumed to be the primary hydrolytic product of urease activity—at a dinickel(II) centre.[6] The IR absorptions of **3** assigned to the coordinating carbamate unit‡ clearly differ from those of the urea bridge in **2**, and mass spectrometry afforded a dominant signal with the expected isotopic distribution pattern for the molecular ion $LNi_2(O_2CNH_2)^+$. This is one mass unit higher than those observed for **2** and thus allows an unambiguous distinction between the two complexes and further corroborates the presence of a bridging urea in **2**.

As shown by an X-ray single crystal analysis of **3**$(BPh_4)_2$ the overall molecular geometry of the bimetallic cation is quite similar to that of **2** (Fig. 2), however the Ni···Ni separation is slightly shortened [**2**: 4.255(2) Å; **3**: 4.229(1) Å], as are the C(30)–O/NH bond lengths {**2**: *d*[C(30)–O/NH] = 1.28(1)–1.31(1) Å *vs.* **3**: *d*[C(30)–O] = 1.249(6)/1.242(6) Å] in accordance with the difference in covalent radii of either a bridging O–C–O (**3**) or disordered O–C–NH (**2**) moiety spanning the metal centres. Two acetonitrile solvent molecules included in the crystal lattice of **3**$(BPh_4)_2$ are positioned suitably for weak hydrogen bonding with the protons attached to N(9) {*d*[N(9)···N(10)] = 3.190 Å; *d*[N(9)···N(11)] = 3.423 Å}, although the latter could not be located in the crystallographic analysis.

2 and **3** thus represent first structurally characterised examples of a bridging coordination mode of both deprotonated urea and carbamate at a dinickel(II) core. These molecular arrangements obviously have considerable thermal stability as both DSC and TGA measurements of **2**$(ClO_4)_2$ and **3**$(BPh_4)_2$ indicate no degradation or loss of weight until above 200 °C, and consequently the corresponding coordination modes should be taken into consideration when studying the interaction and reactivity of urea with urease-mimetic dinickel model systems. The findings furthermore underline that a bridging carbamate ligand, which is present in the form of a carbamylated lysine residue in the urease active site itself, is a reasonable alternative to the ubiquitous carboxylate bridges in dinuclear metal arrangements.

Acknowledgement is made to Professor Dr G. Huttner for his generous and continuous support of our work as well as to the Deutsche Forschungsgemeinschaft (Habilitandenstipendium for F. M.) and the Fonds der Chemischen Industrie. We thank Dr F. Rominger and Professor Dr P. Hofmann for collecting the X-ray data of complex **3**$(BPh_4)_2$.

Notes and References

† E-mail: Franc@sun0.urz.uni-heidelberg.de

‡ Satisfactory elemental analyses could be obtained for all new complexes. Selected IR bands for **2**$(ClO_4)_2$: ν_{max}/cm^{-1} (KBr) 3479s, 3376s, 1614s, 1572vs, 1486s, 1455s. For **3**$(BPh_4)_2$: ν_{max}/cm^{-1} (KBr) 3499m, 3385s, 1590s, 1571sh, 1558vs, 1473s, 1422vs.

§ *Crystal data* for **2**$(ClO_4)_2$: $C_{30}H_{64}Cl_2N_{10}Ni_2O_9$, M = 897.2, orthorhombic, space group $P2_12_12_1$, a = 14.646(7), b = 22.77(1), c = 24.26(1) Å, V = 8090(7) Å^3, Z = 8, ρ_{calc} = 1.475 g cm^{-3}, μ(Mo-Kα) = 1.12 mm^{-1}, 9596 unique reflections measured, 6479 observed [$I > 2\sigma(I)$], 992 parameters, largest diff. peak 0.70 e Å^{-3}, final $R1[I > 2\sigma(I)]$ = 0.060, $wR2$ = 0.172, goodness of fit on F^2 = 1.038. For **3**$(BPh_4)_2$·2MeCN: $C_{78}H_{103}B_2N_9Ni_2O_2$·2MeCN, M = 1419.8, monoclinic, space group $C2/c$, a = 58.3029(6), b = 11.0423(3), c = 28.4945(3) Å, β = 118.549(1)°, V = 16114.1(4) Å^3, Z = 8, ρ_{calc} = 1.171 g cm^{-3}, μ(Mo-Kα) = 0.51 mm^{-1}, 13951 unique reflections measured, 7794 observed [$I > 2\sigma(I)$], 909 parameters, largest diff. peak 0.93 e Å^{-3}, final $R1[I > 2\sigma(I)]$ = 0.063, $wR2$ = 0.207, goodness of fit on F^2 = 1.10. All structures were solved by direct methods with SHELXS-97 and refined with SHELXL-97.[16] CCDC 182/901.

1 R. K. Andrews, R. L. Blakeley and B. Zerner, in *The Bioinorganic Chemistry of Nickel*, ed. J. R. Lancaster, Jr., VCH, New York 1988.
2 E. Jabri, M. B. Carr, R. P. Hausinger and P. A. Karplus, *Science*, 1995, **268**, 998.
3 (*a*) N. E. Dixon, P. W. Riddles, C. Gazzola, R. L. Blakeley and B. Zerner, *Can. J. Biochem.*, 1980, **58**, 1335; (*b*) S. J. Lippard, *Science*, 1995, **268**, 996.
4 P. A. Karplus, M. A. Paerson and R. P. Hausinger, *Acc. Chem. Res.*, 1997, **30**, 330.
5 D. Volkmer, A. Hörstmann, K. Griesar, W. Haase and B. Krebs, *Inorg. Chem.*, 1996, **35**, 1132; D. Volkmer, B. Hommerich, K. Griesar, W. Haase and B. Krebs, *Inorg. Chem.*, 1996, **35**, 3792.
6 R. M. Buchanan, M. S. Mashuta, K. J. Oberhausen and J. F. Richardson, *J. Am. Chem. Soc.*, 1989, **111**, 4497.
7 (*a*) H. E. Wages, K. L. Taft and S. J. Lippard, *Inorg. Chem.*, 1993, **32**, 4985; (*b*) K. Yamaguchi, S. Koshino, F. Akagi, M. Suzuki, A. Uehara and S. Suzuki, *J. Am. Chem. Soc.*, 1997, **119**, 5752; (*c*) T. Koga, H. Furutachi, T. Nakamura, N. Fukita, M. Ohba, K. Takahashi and H. Okawa, *Inorg. Chem.*, 1998, **37**, 989.
8 F. Meyer, A. Jacobi, B. Nuber, P. Rutsch and L. Zsolnai, *Inorg. Chem.*, 1998, **37**, 1213.
9 (*a*) F. Meyer, S. Beyreuther, K. Heinze and L. Zsolnai, *Chem. Ber./Recueil*, 1997, **130**, 605; (*b*) F. Meyer, K. Heinze, B. Nuber and L. Zsolnai, *J. Chem. Soc., Dalton Trans.*, 1998, 207.
10 F. Meyer and P. Rutsch, *Chem. Commun.*, 1998, 1037.
11 F. Meyer, E. Kaifer, H. Pritzkow, F. Rominger, K. Heinze and L. Zsolnai, manuscript in preparation.
12 N. V. Kaminskaia and N. M. Kostic, *Inorg. Chem.*, 1997, **36**, 5917.
13 L. Birkofer, A. Ritter and H. Dickopp, *Chem. Ber.*, 1963, **96**, 1473.
14 T. C. Woon, W. A. Wickramasinghe and D. P. Fairlie, *Inorg. Chem.*, 1993, **32**, 2190.
15 T. G. Schenck, J. M. Downes, C. R. C. Milne, P. B. Mackenzie, H. Boucher, J. Whelan and B. Bosnich, *Inorg. Chem.*, 1985, **24**, 2334.
16 G. M. Sheldrick, SHELXL-97, Program for Crystal Structure Refinement, Universität Göttingen, 1997; SHELXS-97, Program for Crystal Structure Solution, Universität Göttingen, 1997.

Received in Cambridge, UK, 3rd April 1998; 8/02554A

Catalytic asymmetric imidation of selenides into selenimides

Hiroya Takada, Masamitsu Oda, Yoshihiro Miyake, Kouichi Ohe and Sakae Uemura*†

Department of Energy and Hydrocarbon Chemistry, Graduate School of Engineering, Kyoto University, Sakyo-ku, Kyoto 606-8501, Japan

The direct catalytic imidation of various prochiral selenides with TsN=IPh in the presence of CuOTf using chiral 4,4′-disubstituted 2,2′-bis(oxazoline) ligand afforded the corresponding chiral selenimides (~ 36% ee).

The synthesis and the synthetic application of optically active organosulfur compounds have been widely studied.[1] Recently, we succeeded in developing direct catalytic sulfimidation of prochiral sulfides to chiral sulfimides with *N*-(*p*-tolylsulfonyl)-imino(phenyl)-λ³-iodane (TsN=IPh)[2] in the presence of CuOTf and the chiral ligands, 4,4′-disubstituted bis(oxazoline).[3] In contrast, the asymmetric synthesis of analogous organoselenium compounds, selenimides, has been much less studied.[4–6] In 1981, Krasnov *et al.* reported the first synthesis of the optically active selenimides by starting from dialkyl- and diaryl-selenium dichlorides,[4] but the scope of this reaction has not been fully developed probably because of low yields of the products as well as their quite low optical activity. Recently, Kamigata and co-workers have shown an example of conversion of a chiral selenoxide obtained by optical resolution of a diastereomeric mixture[7] into the corresponding enantiomerically pure selenimide, ascertaining the detailed stereochemistry of the compound.[6] We have already demonstrated the diastereoselective imidation of chiral allylic selenides using TsN=IPh or chloramine-T (TsNClNa) as an imidation reagent.[8] We report here a first example of the direct catalytic enantioselective imidation of simple selenides into the corresponding selenimides (Scheme 1).

As described above, a direct catalytic imidation of prochiral sulfides to chiral sulfimides proceeded with TsN=IPh in the presence of CuOTf and bis(oxazoline) in various solvents. We first looked for the solvent in which imidation of prochiral

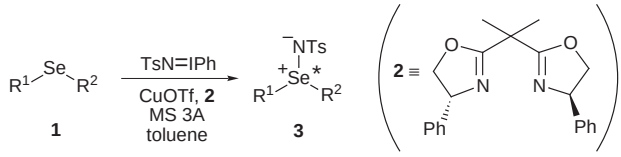

Scheme 1

Table 1 Catalytic asymmetric imidation of selenides **1**[a]

Entry	Selenide	*T*/°C	Product	Yield (%)	Ee (%)[b]
1[c]	PhSeBn	25	**3a**	40	0
2	PhSeBn	25	**3a**	53	32
3	PhSeBn	0	**3a**	18	33
4	4-$MeOC_6H_4SeBn$	25	**3b**	37	20
5	1-NaphthylSeBn	25	**3c**	23	29
6[d]	2-NaphthylSeBn	25	**3d**[e]	64	36
7	2,4,6-$Bu^t_3C_6H_2SeBn$	25	**3e**	nr	—

[a] All the reactions were performed in toluene (0.02 M) in the presence of 12 mol% chiral ligand **2** and 10 mol% CuOTf for 24 h unless otherwise noted. [b] Enantiometric excesses were determined by HPLC using suitable chiral columns. [c] The reaction was performed without MS 3A. [d] MS 4A, for 48 h. [e] See footnote §.

Scheme 2

selenide **1** with TsN=IPh did not proceed in the absence of CuOTf. Treatment of benzyl phenyl selenide with TsN=IPh in MeCN and CH_2Cl_2 at 25 °C for 24 h afforded benzyl phenyl selenimide in 46% and in a trace amount, respectively, but in toluene no reaction occurred. Therefore, we chose toluene as solvent[9] and carried out imidation of benzyl phenyl selenide with TsN=IPh in the presence of CuOTf (10 mol%) and the optically active bis(oxazoline) **2** (12 mol%) at 25 °C for 24 h under N_2 (Scheme 1).[10] Benzyl phenyl selenimide was formed in 40% yield, but no asymmetric induction occurred. Fortunately, further studies revealed that the reaction proceeded enantioselectively when molecular sieves were added (compare entry 1 in Table 1). This is probably due to the interference of the rapid selenimide–selenoxide equilibrium[11] (Scheme 2) by removal of water present in the reaction mixture. A rapid racemization of the selenoxide is well known.[12] At a lower temperature the reaction was slower (entry 3). The reaction also proceeded with several other aryl benzyl selenides, but the selenide having bulky substitutents on an aryl ring such as benzyl 2,4,6-tri-*tert*-butylphenyl selenide (**1e**) did not react at all. Typical results are shown in Table 1. The desired product was isolated in moderate yield without racemization by removal of the precipitate through Celite and purification of the residue by column chromatography (SiO_2). When this reaction was applied to various aryl cinnamyl selenides **4**, the expected chiral allylic amides (~ 30% ee) were obtained selectively in moderate to good yield *via* [2,3] sigmatropic rearrangement of the

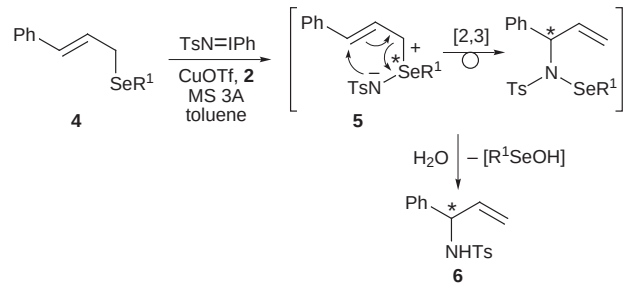

Scheme 3

Table 2 Catalytic asymmetric imidation of cinnamyl selenides **4**[a]

Entry	R^1	Product	Yield (%)	Ee (%)[b]
1	Ph	**6a**	63	20
2	1-Naphthyl	**6b**	71	28
3	2-Naphthyl	**6c**	52	30
4	Ferrocenyl	**6d**	35	17
5	2-$NO_2C_6H_4$	**6e**	Trace	—

[a] All the reactions were performed in toluene (0.02 M) in the presence of 12 mol% chiral ligand **2** and 10 mol% CuOTf for 24 h. [b] Enantiomeric excesses were determined by HPLC using suitable chiral columns.

intermediate chiral allylic selenimide (Scheme 3, Table 2), clearly showing that the chirality transfer occurred at the rearrangement step.

Although the enantioselectivity obtained here is not yet satisfactory (~ 36% ee) and lower than the corresponding sulfur case,[3] the finding presented here is the first example of the direct catalytic enantioselective imidation of organic selenides into the corresponding selenimides.

Notes and References

† E-mail: uemura@scl.kyoto-u.ac.jp

‡ Representative procedure for the imidation of selenide: to a solution of MS 3A (*ca.* 300 mg), CuOTf (0.010 mmol, 0.10 equiv.) and chiral 2,2′-bis(oxazoline) **2** (0.012 mmol, 0.12 equiv., Aldrich) in 5.0 ml of toluene were added first TsN=IPh (0.10 mmol, 1.0 equiv.) and then the selenide (0.20 mmol, 2.0 equiv.)[10] and the resulting mixture was stirred under nitrogen at 25 °C for 24 h. Removal of the precipitate through Celite and evaporation of the solvent gave a crude product. Purification by silica gel column chromatography gave a pure chiral selenimide.

§ *Selected data* for **3d**: white solid; 64% yield; 36% ee by Daicel chiralcel OD column with 25% Pr^{i}OH–hexane; eluent AcOEt; mp 156.0–157.0 °C; ν_{max}(KBr)/cm^{-1} 1264, 1161, 1132, 1084, 946, 937, 814, 697; δ_H($CDCl_3$, 270 MHz) 2.27 (s, 3 H), 4.26 (d, *J* 11.3, 1 H), 4.58 (d, *J* 11.3, 1 H), 6.94–7.92 (m, 16 H); δ_C($CDCl_3$, 67.8 MHz) 21.2, 57.2, 122.7, 125.9, 127.5, 128.0, 128.3, 128.4, 128.5, 128.8, 129.1, 129.21, 129.22, 129.9, 130.4, 132.8, 134.6, 141.0, 142.7; *m/z* (FAB LRMS) 468; FAB HRMS: calc. for $C_{24}H_{22}O_2NSSe$ $(M + H)^+$: 468.0537. Found: 468.0535.

1 See for example: *Sulfur Reagents in Organic Synthesis*, ed. P. Metzner and A. Thuillier, Academic Press, London, 1994.

2 Y. Yamada, T. Yamamoto and M. Okawara, *Chem. Lett.*, 1975, 361.

3 H. Takada, Y. Nishibayashi, K. Ohe and S. Uemura, *Chem. Commun.*, 1996, 931; H. Takada, Y. Nishibayashi, K. Ohe, S. Uemura, C. P. Baird, T. J. Sparey and P. C. Taylor, *J. Org. Chem.*, 1997, **62**, 6512; H. Takada, Y. Nishibayashi, K. Ohe and S. Uemura, *Phosphorus Sulfur Silicon Relat. Elem.*, 1997, **120**–**121**, 363.

4 V. P. Krasnov, V. I. Naddaka and V. I. Minkin, *Zh. Org. Khim.*, 1981, **17**, 445; *Chem. Abstr.*, 1981, **95**, 42551x.

5 F. A. Davis, J. M. Billmers and O. D. Stringer, *Tetrahedron Lett.*, 1983, **24**, 3191.

6 T. Shimizu, N. Seki, H. Taka and N. Kamigata, *J. Org. Chem.*, 1996, **61**, 6013; T. Shimizu and N. Kamigata, *Org. Prep. Proced. Int.*, 1997, **29**, 603.

7 T. Shimizu, K. Kikuchi, Y. Ishikawa, I. Ikemoto, M. Kobayashi and N. Kamigata, *J. Chem. Soc., Perkin Trans. 1*, 1989, 597.

8 Y. Nishibayashi, T. Chiba, K. Ohe and S. Uemura, *J. Chem. Soc., Chem. Commun.*, 1995, 1243.

9 Toluene was also revealed to be the solvent of choice for asymmetric sulfimidation of organic sulfides.[3]

10 Excess selenide was employed (2.0 equiv.) and TsN=IPh served as the limiting reagent.

11 S. Tamagaki, S. Oae and K. Sakaki, *Tetrahedron Lett.*, 1975, 649.

12 F. A. Davis and R. T. Reddy, *Tetrahedron*, 1985, **41**, 4747; K. B. Sharpless, M. W. Young and R. F. Lauer, *Tetrahedron Lett.*, 1973, 1979; M. Oki and H. Iwamura, *Tetrahedron Lett.*, 1966, 2917; W. J. Burlant and E. S. Gould, *J. Am. Chem. Soc.*, 1954, **76**, 5775; T. W. Campbell, H. G. Walker and G. M. Coppinger, *Chem. Rev.*, 1952, **50**, 297; R. W. Gaithwaite, J. Kenyon and H. Phillips, *J. Chem. Soc.*, 1928, 2080.

Received in Cambridge, UK, 11th May 1998; 8/03494J

The 'valence tautomers' of *o*-iodosobenzoic acid: the case of 4-pentyl-2-iodosobenzoic acid

Robert A. Moss,*† Saketh Vijayaraghavan and T. J. Emge

Department of Chemistry, Rutgers, The State University of New Jersey, New Brunswick, New Jersey 08903, USA

Contrary to a previous report, only the closed (iodoxolone) form of 4-pentyl-2-iodosobenzoic acid (3a) can be isolated; the previously assigned open (iodoso) form (3b) is actually 4-pentanoyl-2-iodobenzoic acid.

o-Iodosobenzoic acid (IBA, **1**) has long been known[1] to exist in the cyclic 1-hydroxy-1,2-benziodoxol-3(1*H*)-one form (**2**).[2,3] X-Ray crystal structure[4] and theoretical studies[5] agree that the cyclic form is the better representation, although the internal I–O bond is longer than a 'normal' single I–O bond, indicating significant 'open' character.[4b,c,5]

A valence tautomeric representation of IBA (**1** ⇌ **2**) suggests that both **1** and **2** can exist as separate entities. Such

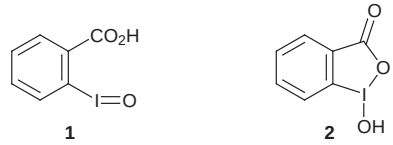

1 **2**

representations have often appeared,[6] even if they were not intended to imply the simultaneous presence of interconverting open ('iodoso') and closed (iodoxolone) forms. Thus, in 1990, Panetta *et al*. reported the *separate isolation* of the iodoxolone and iodoso valence tautomers of 4-propyl- as well as 4-pentyl-2-iodosobenzoic acids.[7] These extraordinary results have been reiterated in a recent authoritative review,[3b] so that it becomes imperative to verify them, particularly because of the importance of IBA and its analogues as decontamination agents for toxic phosphonates and phosphates.[4b,c,5–8]

We have now reinvestigated the case of the 4-pentyl 'tautomers' (**3a** and **3b**), and report here that the previously described[7] compounds were misassigned; in fact, only a single 4-pentyl-2-iodosobenzoic acid can be isolated, and it is best represented as the 'closed' iodoxolone compound, **3a**.

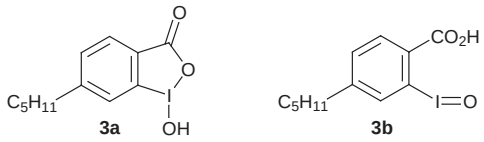

3a **3b**

The origin of the misassignments in ref. 7 lies in the synthetic sequence, which we summarize in Scheme 1. 4-Pentylbenzyl alcohol (**4**) was first regiospecifically iodinated to **5**.[7,9]

In the following and key step, iodo alcohol **5** was oxidized to 4-pentyl-2-iodobenzoic acid (**6**) using phase transfer catalysis in a $KMnO_4$–water–benzene system.[7,10] This reaction led not only to the desired **6**, in 63% yield, but also to a second, chromatographically-separated product, **X** (25%, mp 115–116 °C), assigned[7] as 4-pentyl-2-iodosobenzoic acid in its cyclic (iodoxolone) form, **3a**. A separate H_2O_2/Ac_2O oxidation[7,11] of **6** afforded 4-pentyl-2-iodosobenzoic acid **Y** (mp 188.5–189.5 °C) assigned[7] as the open (iodoso) valence tautomer, **3b**.

The assignments[7] of **X** and **Y** rest on acceptable elemental analyses for $C_{12}H_{15}IO_3$, suggestive of isomerism, as well as IR

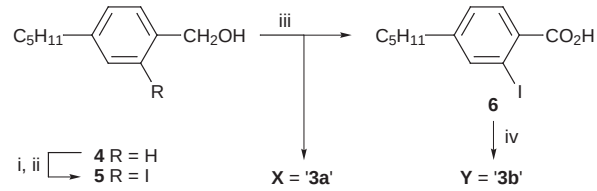

Scheme 1 *Reagents and conditions*: i, BuLi, $Me_2NCH_2CH_2NMe_2$; ii, I_2; iii, $KMnO_4$–H_2O, C_6H_6, cat. $Bu_4P^+Cl^-$; iv, 30% H_2O_2, Ac_2O, 40 °C, 20 h

carbonyl bands for **X** at 1710 cm^{-1} and **Y** at 1650 cm^{-1}. The higher frequency C=O band of **X** was considered indicative of a 'lactone' structure as in **3a**.[7] However, it is known[2] that the carbonyl band of IBA, in its iodoxolone form, is at 1633 cm^{-1} (Nujol), so that the reported IR band of **X** at 1710 cm^{-1} is inconsistent with structure **3a**; it is **Y** (1650 cm^{-1}) that is more likely to merit this assignment.

We repeated the synthetic sequence of Scheme 1.[7] In particular, the permanganate oxidation of **5**, after chromatography of the product on silica gel (hexanes–EtOAc–HOAc, 79 : 20 : 1 to 28 : 70 : 2) afforded **6** (48%, mp 67.5–68.5 °C, lit.[7] 68.0–69.0 °C) and **X** (10%, mp 115–116 °C, lit.[7] 115–116 °C).

Our sample of **X** displayed the same mp, an experimentally comparable elemental analysis, and a similar IR C=O band (1707 cm^{-1}) relative to those reported[7] for '**3a**'. Nevertheless, several observations indicated that **X** was not **3a**. (1) The NMR spectrum of **X**‡ revealed only four sets of alkyl protons rather than the anticipated five. (2) The pentyl benzylic resonance of **5** (a triplet at δ 2.55) was missing in **X**, while a more deshielded triplet appeared at δ 3.1. (3) The IR spectrum (KBr) of **X** revealed two intense C=O absorptions at 1707 and 1686 cm^{-1}. The Supplementary Material for ref. 7 reports this band at 1685 cm^{-1}; it can be assigned to an aromatic CO_2H. The former band was assigned[7] to the carbonyl of **3a**, but the 'lactone' carbonyl group of (*e.g.*) **2** is known to absorb at 1633 cm^{-1} (Nujol).[2] (4) Compound **X** was kinetically inactive toward *p*-nitrophenyl diphenyl phosphate (PNPDPP) in aqueous micellar cetyltrimethylammonium chloride (CTACl) at pH 8 (see Table 1), whereas authentic benziodoxolones (*e.g.* **2**) rapidly cleave PNPDPP under these conditions.[8a,b] (5) Additionally, **X** did not oxidize iodide to iodine, a common property of iodosobenzoates.[8b]

Accordingly, an X-ray crystal structure determination was carried out for **X**,§ revealing it to be not an iodoso compound at all, but 4-pentanoyl-2-iodobenzoic acid (**7**) (Fig. 1). Clearly, the $KMnO_4$ oxidation of **5** to **6** must have been accompanied by overoxidation[12] at the benzylic position of the pentyl chain, affording (both) ketone **7** (and iodoterphthalic acid). Structure **7** immediately accounts for the spectral characteristics of **X** itemized above in points (1)–(3),¶ and, of course, **7** should also be inactive in the hydrolysis of PNPDPP or the oxidation of iodide [points (4) and (5)].

Compound **Y**, which we obtained from the peroxide oxidation of **6** (Scheme 1) had a mp identical to the compound previously obtained,[7] and is actually 4-pentyl-2-iodosobenzoic

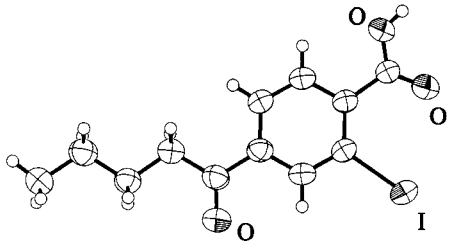

Fig. 1 ORTEP diagram of **X** (4-pentanoyl-2-iodobenzoic acid, **7**)

acid, best represented as **3a** (not **3b**[7]). Thus, **Y** (**3a**) gave both an appropriate elemental analysis [C, 43.l; H, 4.53; I, 38.0%) and NMR spectrum.‖ The IR (KBr) spectrum of **3a** displayed its C=O band at 1602 cm^{-1}, considerably lower than the reported[7] 1650 cm^{-1}. However, benziodoxolone carbonyl bands are very sensitive to conditions of their determination; the C=O absorption of **2** has been variously reported at 1633,[2] 1612,[6b] and 1605[6b] cm^{-1}. Additionally, **3a** showed the expected[2] (I)OH absorptions at 2928 and 2444 cm^{-1}. A standard iodometric titration[13] of **3a** gave 93% of I=O oxidative activity.

Most importantly, **3a** was very reactive toward PNPDPP. Its kinetic properties were assessed from a rate constant–[surfactant] profile for the cleavage of PNPDPP in micellar CTACl;[8b] conditions and results appear in Table 1. Not only is **Y** (**3a**) highly reactive toward PNPDPP, where **X** (**7**) is inactive (entry 2), but **3a** affords an acceleration of 1460 relative to micellar CTACl alone (entry 1), 4.6 times greater than the acceleration provided by the parent IBA (**2**) (entry 3). This reactivity advantage is an expected consequence of the hydrophobic pentyl group of **3a**, which affords better binding of **3a** to the micellar phase in which the phosphorolytic reaction occurs.[8b,c]

Table 1 Rate constants for the cleavage of PNPDPP[a]

Entry	Catalyst	$k_\psi/10^{-4}$ s^{-1}	k_{rel}
1	None[b]	2.05[c]	1.00
2	**X** (**7**)	2.00	0.98
3	**2**	640[d]	312
4	**Y** (**3a**)[e]	3000[f]	1460
5[g]	**2**	18.3	8.9
6[g]	**Y** (**3a**)	63.3	30.9

[a] For background, see ref. 8(*b*). Conditions for entries 1–4: [CTACl] = 1.0×10^{-3} M, [PNPDPP] = 1.0×10^{-5} M, [catalyst] = 1.0×10^{-4} M, pH 8, 0.02 M phosphate buffer, μ = 0.08 (NaCl), 25 °C. Rate constants were determined by monitoring the time dependent absorbance of the released *p*-nitrophenylate ion at 400 nm. [b] CTACl alone. [c] Given as 1.8×10^{-4} s^{-1} in ref. 6(*a*). [d] Ref. 8(*b*). [e] [PNPDPP] = 3.0×10^{-5} M, [Y] = 3.0×10^{-4} M. [f] Stopped-flow determination. [g] Microemulsion conditions:[7] 8% (w/w) CTABr, 8% *N*-methylpyrrolidinone, 4% toluene, 80% 0.03 M aqueous $Na_2B_4O_7 \cdot 10H_2O$ buffer, pH 9.4, 25 °C; [PNPDPP] = 3×10^{-5} M, [catalyst] = 3×10^{-4} M.

Although we could not obtain crystals of **3a** suitable for X-ray analysis, its closed, 'lactone' structure follows from the IR spectrum,[2] and from its kinetic properties toward PNPDPP (which link **3a** to other phosphorolytically reactive iodosobenzoates for which the closed structure has been established).[4–6,8] True 'iodoso' compounds, such as *m*-iodosobenzoic acid, show little esterolytic reactivity.[8a] Additionally, we determined the pK_a of **3a** as 6.8 from a pH–rate constant profile[4c,5,8b] for the cleavage of PNPDPP by **3a** in 0.02 M micellar CTACl and 0.02 M phosphate buffer over the pH range 5.35–7.68. A pK_a ~7 is appropriate for an *o*-iodosobenzoate in the iodoxolone form.[2,8]

Finally, **3a** was reported to be 477 times *less* reactive than IBA itself toward PNPDPP in a CTABr–*N*-methylpyrollidinone–toluene–aqueous borate microemulsion, a phenomenon attributed to incorporation of the more hydrophobic catalyst into the oily interior of the microemulsion.[7] However, we find **3a** to be quite reactive toward PNPDPP under these conditions (Table 1, entry 6); indeed, it is actually ~3.5 times more reactive than IBA (entry 5), paralleling the results in micellar CTACl (see above, and entries 3 and 4). Note (Table 1) that both IBA and **3a** are less reactive toward PNPDPP in the microemulsion than in micellar CTACl, an expected consequence of lessened mutual catalyst/substrate concentration in the microemulsion.[14]

In conclusion, only one 4-pentyl-2-iodosobenzoic acid can be isolated, and it is best represented as iodoxolone **3a**. A similar situation is likely to hold for 4-propyl-2-iodosobenzoic acid[7] as well.

We are grateful to the US Army Research Office for financial support.

Notes and References

† E-mail: moss@rutchem.rutgers.edu

‡ δ_H[$(CD_3)_2CO$, 200 MHz] 0.92 (t, *J* 8, 3H), 1.4 (sext., *J* 8, 2H), 1.7 (pent., *J* 8, 2H), 3.1 (t, *J* 8, 2H), 7.9 (d, *J* 8, 1H), 8.1 (AB dd, *J* 8, 1.6, 1H), 8.5 (d, *J* 1.6, 1H).

§ *Crystal data* for **7**: $C_{12}H_{13}O_3I$, M = 332.12, colorless rods, 0.06 × 0.54 × 0.60 mm, monoclinic, space group $P2_1/n$, a = 4.2397(11), b = 29.477(5), c = 10.222(2) Å, β = 101.92(2)° U = 1249.9(5) $Å^3$, Z = 4, D_c = 1.765 g cm^{-3}, μ(Mo-Kα) = 25.52 cm^{-1}, F(000) = 648. The 2340 total data were collected at 20 °C using graphite monochromatized Mo-Kα radiation (λ = 0.71073 Å), and converged at R_1 = 0.0507, wR_2 = 0.0889 for all 2157 unique data. CCDC 182/910.

¶ Note too that the calculated elemental analysis of **7**, $C_{12}H_{13}IO_3$ [C, 43.4; H, 3.94; I, 38.2%] is nearly within accepted limits of the calculated analysis for **3**, $C_{12}H_{15}IO_3$ [C, 43.1; H, 4.52; I, 38.0%].

‖ δ[$[^2H_6]$DMSO, 200 MHz) 0.83 (t, *J* 8, 3H), 1.3 (m, $2CH_2$, 4H), 1.62 (pent., *J* 8, 2H), 2.75 (t, *J* 8, 2H), 7.5 (d, *J* 8, 1H), 7.6 (s, 1H), 7.9 (d, *J* 8, 2H), 7.95 (s, 1H, OH exchangeable with D_2O).

1 V. Meyer and W. Wachter, *Chem. Ber.*, 1892, **25**, 2632; C. Wilgerodt, *Die Organische Verbindungen mit Mehrwertigen Jod*, Enke, Stuttgart, 1914, p. 134; D.E. Banks, *Chem. Rev.*, 1966, **66**, 243 (see p. 255).

2 G. P. Baker, F. G. Mann, N. Sheppard and A. J. Tetlow, *J. Chem. Soc.*, 1965, 3721.

3 (*a*) G. F. Koser, in *The Chemistry of Functional Groups, Suppl. D*, ed. S. Patai and Z. Rappoport, Wiley, New York, 1983, pp. 721f; (*b*) P. J. Stang and V. V. Zhdankin, *Chem. Rev.*, 1996, **96**, 1123; (*c*) A. Varvoglis, *The Organic Chemistry of Polycoordinated Iodine*, VCH, New York, 1992, p. 168f.

4 (*a*) E. Shefter and W. Wolf, *J. Pharm. Sci.*, 1965, **54**, 104; (*b*) A. R. Katritzky, G. P. Savage, G. J. Palenik, K. Qian, Z. Zhang and H. D. Durst, *J. Chem. Soc., Perkin Trans. 2*, 1990, 1657; (*c*) R. A. Moss, K. Bracken and T. J. Emge, *J. Org. Chem.*, 1995, **60**, 7739.

5 R. A. Moss, B. Wilk, K. Krogh-Jespersen, J. T. Blair and J. D. Westbrook, *J. Am. Chem. Soc.*, 1989, **111**, 250; R. A. Moss, B. Wilk, K. Krogh-Jespersen and J. D. Westbrook, *J. Am. Chem. Soc.*, 1989, **111**, 6729.

6 (*a*) R. A. Moss, S. Chatterjee and B. Wilk, *J. Org. Chem.*, 1986, **51**, 4303; (*b*) A. R. Katritzky, G. P. Savage, J. K. Gallos, and H. D. Durst, *J. Chem. Soc., Perkin Trans. 2*, 1990, 1515.

7 C. A. Panetta, S. M. Garlick, H. D. Durst, F. R. Longo and J. R. Ward, *J. Org. Chem.*, 1990, **55**, 5202.

8 (*a*) R. A. Moss, K. Alwis and G. O. Bizzigotti, *J. Am. Chem. Soc.*, 1983, **105**, 681; (*b*) R. A. Moss, K. W. Alwis and J.-S. Shin, *J. Am. Chem. Soc.*, 1984, **106**, 2651; (*c*) R. A. Moss, K. Y. Kim and S. Swarup, *J. Am. Chem. Soc.*, 1986, **108**, 788; (*d*) P. S. Hammond, J. S. Forster, C. N. Lieske and H. D. Durst, *J. Am. Chem. Soc.*, 1989, **111**, 7860.

9 N. Meyer and D. Seebach, *Angew. Chem., Int. Ed. Engl.*, 1978, **17**, 521.

10 A. W. Herriott and D. Picker, *Tetrahedron Lett.*, 1974, **16**, 1511.

11 A. R. Katritzky, B. L. Duell, H. D. Durst and B. L. Knier, *J. Org. Chem.*, 1988, **53**, 3972.

12 H-J. Schmidt and H.J. Schäfer, *Angew. Chem., Int. Ed. Engl.*, 1979, **18**, 68.

13 H. J. Lucas and E. R. Kennedy, *Org. Synth.*, 1955, **Coll. Vol. 3**, 482.

14 (*a*) R. A. Moss, R. Fujiyama, H. Zhang, Y.-C. Chung and K. McSorley, *Langmuir*, 1993, **9**, 2902; (*b*) R. Mackay, F. R. Longo, B. L. Knier and H. D. Durst, *J. Phys. Chem.*, 1987, **91**, 861.

Received in Corvallis, OR, USA, 17th April 1998; 8/02902D

A three-dimensional open-framework tin(II) phosphate exhibiting reversible dehydration and ion-exchange properties

Srinivasan Natarajan,[a] M. Eswaramoorthy,[a] Anthony K. Cheetham[b] and C. N. R. Rao[a]†

[a] *Chemistry and Physics of Materials Unit, Jawaharlal Nehru Centre for Advanced Scientific Research Jakkur P.O., Bangalore 560 064, India*

[b] *Materials Research Laboratory, University of California, Santa Barbara, CA 93106, USA*

A three-dimensional open-framework tin(II) phosphate, prepared hydrothermally with 1,3-diaminopentane as the template, is shown to exhibit reversible dehydration and ion-exchange properties.

The synthesis of microporous solids with different connectivities and pore chemistry from those obtained in zeolitic materials is of considerable interest because of the potential applications of these materials as catalysts, molecular sieves and ion exchangers.[1,2] Investigations in this direction have led to the discovery of many materials with interesting structures. Recently, open-framework tin(II) phosphates with novel building motifs, such as vertex-sharing trigonal pyramidal SnO_3 units and truncated square-pyramidal SnO_4 units, have been synthesized.[3–5] It would be most desirable to design a more open, three-dimensional network with channels running along the crystallographic axes and to facilitate the formation of such a structure, we have employed a branched diamine as a structure-directing agent, in place of the linear diamines. With 1,3-diaminopentane, we have been able to obtain a tin phosphate with three different channel systems. The structure possesses two molecules of water which can be reversibly intercalated and, more significantly, exhibits remarkable ion-exchange properties reminiscent of aluminosilicate zeolites. Here we describe the synthesis, structure and characterization of this unique open-framework material.

The structure of the new Sn^{II} phosphate‡ involves networking of strictly alternating SnO_3 and PO_4 units in which all the vertices are shared. The SnO_3 and PO_4 units form a framework with the formula $[Sn_4P_3O_{12}]^-$. Charge neutrality is achieved by the incorporation of the diprotonated organic cation $[NH_3CH_2CH_2CH(NH_3)CH_2CH_3]^{2+}$. There is half a unit of the organic cation per formula unit and the structure contains two molecules of water. Thus, the composition of the material is $[Sn_4P_3O_{12}]^-\{[NH_3CH_2CH_2CH(NH_3)CH_2CH_3]^{2+}\}_{0.5}\cdot 2H_2O$. The asymmetric unit (Fig. 1) contains 27 independent non-hydrogen atoms.

The entire framework structure can be considered to be made from a networking of four-, six-, eight- and twelve-membered rings formed by T atoms (T = Sn, P). The four-, six- and twelve-membered rings are connected to each other in such a way that they form a uniform 8-ring channels bound by 8 T atoms (T = Sn and P) along the *a* and *b* axes [Fig. 2(*a*) and (*b*)]. The widths of these channels are 7.0 × 6.1 Å along the *a* axis and 8.3 × 8.8 Å along the *b* axis (longest and shortest atom–atom contact distances, not including van der Waals radii). The widths of the channels suggest that the eight-membered channels along the *b* axis are more regular [Fig. 2(*b*)]; the amine molecules sit in the middle of these channels. When viewed along the *a* axis, the two water molecules occupy the distorted six- and twelve-membered channels [Fig. 2(*a*)]. The lone pair of electrons of the Sn^{II} protrude into the twelve-membered channel rendering it ineffective for sorption of a guest molecule. Along the *c* axis, the 4-, 6- and 8-rings are connected to form a twelve-membered ring channel which has the appearance of a six-membered channel due to distortion. The amine and the water molecules are both present in this channel. Most of the distortions in the channels arise due to the three coordination of the tin(II) with the oxygens in this structure. The Sn atoms coordinated to three oxygens occupy the vertex of a trigonal pyramid; the lone pair presumably occupies the fourth vertex of the tetrahedron. The M–O bond lengths and O–M–O bond angles (M = Sn, P) are similar to those observed for other tin phosphate materials.

Since the synthesis involved the use of two different optical isomers of the branched organic diamine, we expected the isomers to be resolved and form different channels. We find, however, that the two amine isomers are located at the crystallographic center of inversion in the structure creating a new type of disorder (Fig. 1). A low-temperature single crystal X-ray diffraction study ($T \approx 100$ K) showed no change in the disorder, indicating it to be static rather than dynamic.

Thermogravimetric analysis (TGA) in an oxygen atmosphere showed a mass loss of *ca.* 3.9% at 125 °C due to the removal of two molecules of water present in the channels (calc. 4.1%). Careful experiments showed that the material (heated to 125 °C) reabsorbs the water on cooling and storage for a few hours under atmospheric conditions (typically 4 h). This feature is indeed noteworthy as this is the first time such a complete reversible dehydration–hydration process has been observed in an open-framework tin phosphate material. TGA studies also reveal that the protonated 1,3-diaminopentane is removed at 350 °C. The crystal structure collapsed after the removal of the amine.

In our effort to remove the template molecule from the open-framework structure by other methods, we employed soft chemical routes, including ion-exchange. Since the structure is open and the framework is anionic, we used an NaCl (1.0 M) solution for the ion-exchange with the expectation that the Na^+ cations might exchange for the protonated diamine. After 4 days of continuous stirring at room temperature (the solution was

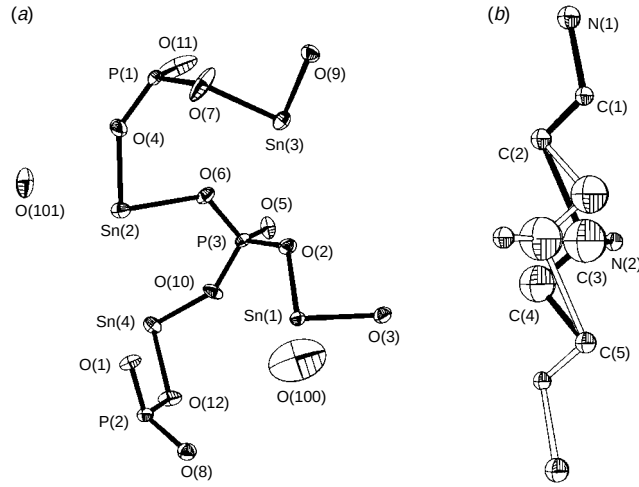

Fig. 1 ORTEP plots of (*a*) the framework along with the water molecule and (*b*) the organic template molecule showing the disorder

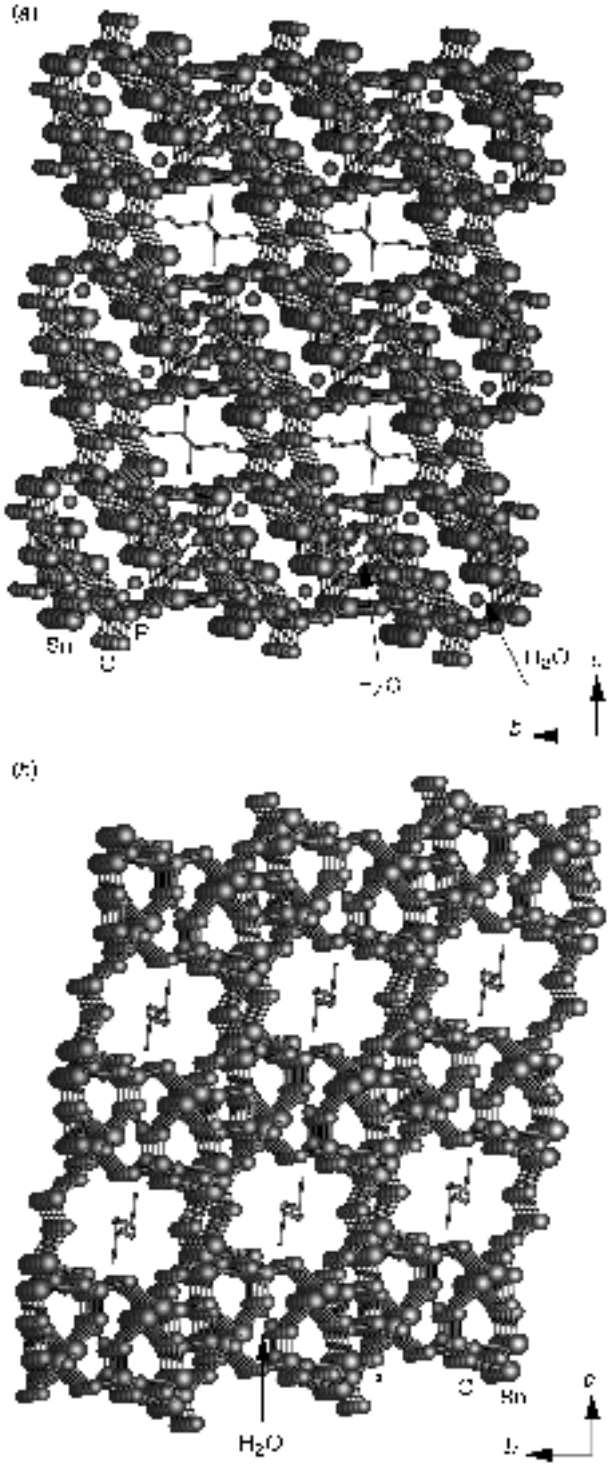

Fig. 2 Structures of $[Sn_4P_3O_{12}]^-\{[NH_3CH_2CH_2CH(NH_3)CH_2CH_3]^{2+}\}_{0.5}\cdot 2H_2O$ viewed down the *a* axis (*a*) and *b* axis (*b*). Note that the amine and the water molecule occupy different channels in both cases.

replenished every 24 h), *ca*. 50% of the amine was exchanged, as indicated by FTIR and TGA studies. The powder XRD pattern of the ion-exchanged sample was consistent with that of the parent material. Gravimetric adsorption studies were carried out on the parent material and the Na^+-exchanged sample after dehydration at 175 °C, by employing N_2 and MeOH as adsorbants. Methanol exhibits a Langmuir type I isotherm corresponding to about 1 molecule per unit cell (at higher pressures, $p/p_o \geqslant 0.8$, the results indicate some type II component as well) and N_2 shows a type IV isotherm for the dehydrated Na^+-exchanged sample (Fig. 3). The parent material, however, showed no significant adsorption of these molecules. This study suggests that there is considerably greater free volume in the dehydrated Na^+-exchanged sample. Further experiments on the ion-exchange properties of this novel three dimensional tin(II) phosphate material and its catalytic properties are currently in progress and the results will be reported elsewhere.

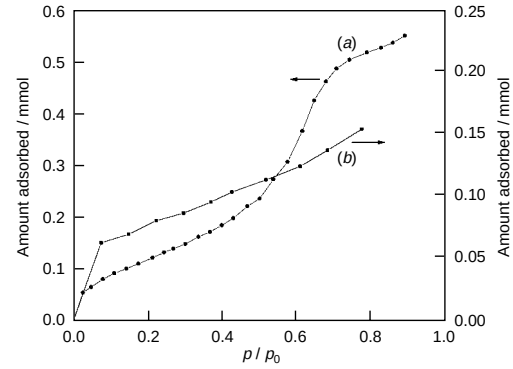

Fig. 3 Sorption isotherms (at 77 K) for (*a*) nitrogen and at room temp. for (*b*) methanol (p/p_o ratio of partial pressure of sorbate to its saturated vapour pressure)

A. K. C. thanks the MRSEC program of the US National Science Foundation under the award no. DMR-9632716.

Notes and References

† E-mail: cnrrao@sscu.iisc.ernet.in

‡ The title compound was synthesized from a starting tin phosphate gel containing a mixture of the two optical isomers of 1,3-diaminopentane as the structure directing agent. Tin(II) oxalate (Aldrich), phosphoric acid (85 wt%, Merck), 1,3-diaminopentane (DYTEK, Aldrich) and water in the ratio SnC_2O_4 : 0.5 P_2O_5 : 1.0 1,3-diaminopentane : 55 H_2O were mixed, sealed and heated at 170 °C for 3 days under autogeneous pressure. The resulting product, containing a mixture of white powder and a few colorless single crystals, was filtered and washed thoroughly with deionised water. The single crystals were separated easily under a polarizing microscope. The powder X-ray diffraction patterns taken independently on both the white powder and the single crystals were found to be identical indicating that the product was a new material. A suitable, needle-like single crystal (0.06 × 0.05 × 0.04 mm) was selected and mounted at the tip of a glass fiber using cyanoacrylate adhesive. Crystal structure determination by X-ray diffraction was performed on a Siemens Smart-CCD diffractometer (Mo-Kα radiation, λ = 0.71073 Å). A hemisphere of intensity data was collected at room temperature in 1321 frames with ω scans (width of 0.30° and exposure time of 30 s per frame).

Crystal data for the title compound: triclinic, space group $P\bar{1}$ (no. 2), a = 9.417(1), b = 9.754(1), c = 11.002(1) Å; α = 80.51(1), β = 71.64(2), γ = 61.68(1)°, U = 844.2(2) Å^3, Z = 2, M = 861.85(1) and ρ_{calc} = 3.39(1) g cm^{-3}. A total of 3352 reflections were collected in the range $-8 \leqslant h \leqslant 10$, $-8 \leqslant k \leqslant 10$, $-12 \leqslant l \leqslant 11$. These were merged to give 2383 unique data (R_{merg} = 2.3). The absorption correction was based on symmetry equivalent reflections using the SADABS[6] program. Because of the heavy disorder on the carbon and nitrogen atoms of the amine molecule, hydrogen atoms though found on the Fourier map were not used for refinement purposes. The last cycles of refinement included atomic positions, anisotropic thermal parameters for all the atoms. Final R = 0.0397, R_w = 0.0937 and S = 1.04 were obtained for 215 parameters. The final Fourier map minimum and maximum: −1.26 and 1.68 e Å^{-3}. The structure was solved and refined using the SHELXSTL-PLUS[7,8] package of programs. CCDC 182/895.

1 G. Ozin, *Adv. Mater.*, 1992, **4**, 612.
2 J. M. Thomas, *Angew. Chem., Int. Ed. Engl.*, 1994, **33**, 913.
3 S. Natarajan, M. P. Attfield and A. K. Cheetham, *Angew. Chem., Int. Ed. Engl.*, 1997, **36**, 978.
4 S. Natarajan and A. K. Cheetham, *Chem. Commun.*, 1997, 1089.
5 S. Natarajan and A. K. Cheetham, *J. Solid State Chem.*, 1997, **134**, 207.
6 G. M. Sheldrick, SADABS Users guide, University of Göttingen, Germany, 1995.
7 G. M. Sheldrick, SHELXL-86: A program for the solution of crystal structures, University of Göttingen, Germany, 1993.
8 G. M. Sheldrick, SHELXL-93: A program for crystal structure determination, University of Göttingen, Germany, 1993.

Received in Cambridge, UK, 1st April 1998; 8/02478B

Self-assembled thin films from lamellar metal disulfides and organic polymers

Patricia J. Ollivier,[a] Nina I. Kovtyukhova,[b] Steven W. Keller[c] and Thomas E. Mallouk*[a]†

[a] *Department of Chemistry, The Pennsylvania State University, University Park, PA 16802, USA*
[b] *Institute of Surface Chemistry, National Academy of Science of Ukraine, Kiev, Ukraine 252022*
[c] *Department of Chemsitry, The University of Missouri-Columbia, Columbia, MO 65211, USA*

The intercalation/exfoliation reactions of MoS_2 and SnS_2 yield lamellar colloids, which may be grown layer-by-layer on cationic surfaces by alternate adsorption of cationic clusters or polymers.

Over the past several years, self-assembly has become increasingly useful as a simple and inexpensive method for making functional thin films.[1] While much of this work has focused on organic monolayers, inorganic surface heterostructures are also interesting because of the structural,[2] magnetic,[3] electrochemical[4] and other properties associated with inorganic compounds. Unfortunately, to date, the building blocks of these thin films have been electronic insulators: clays, metal phosphates and lamellar oxides.[5] Here, we report the successful extension of this technique to lamellar chalcogenides, which in bulk form are semiconductors, semimetals, and metals. These materials have been used previously to prepare interesting bulk nanocomposites.[6]

Lamellar metal disulfides (MoS_2, SnS_2) were reductively intercalated by reaction with excess Bu^nLi in hexane, then added to water to make exfoliated suspensions that were approximatley 5 mass% MS_2.[7] As prepared, these suspensions were basic, but upon dilution to 1 mass%, the pH decreased to 8–9. Attempts to lower the pH further resulted in flocculation. These 1% suspensions were stable for periods of days (orange–brown SnS_2) to weeks (brown–black MoS_2), and transmission electron microscopy (Fig. 1) revealed intact single- and multiple-sheet aggregates ranging in lateral dimensions from *ca.* 20–500 nm.

Growth of the metal disulfide films was initiated by first priming polished silicon wafers with a cationic monolayer. This was accomplished by hydroxylating the surface, by 30 min sonication in 'piranha' solution (4 : 1 conc. H_2SO_4–30% H_2O_2), and then adsorbing a monolayer of aluminium Keggin ions [$Al_{13}O_4(OH)_{24}(H_2O)_{12}^{7+}$], (5 min adsorption from an 80 °C solution of the chloride salt[8]), or poly(allylamine hydrochloride), PAH (15 min adsorption from a 0.01 M aqueous solution at pH 8 and ambient temperature). Both surface priming procedures create a high charge density surface, which binds the anionic MS_2 sheets. The first monolayer of MS_2 sheets was adsorbed by immersing the primed silicon into the appropriate colloidal suspension for 15 min, and rinsing with water. These MS_2 monolayers tile the surface incompletely, as shown in tapping-mode atomic force microscopy (AFM) images, Fig. 2. The adsorption process appears to select relatively small sheets from the broad distribution of sizes present in the colloid (Fig. 1). Surface coverage was estimated at about 75% for MoS_2 on the Al-Keggin-primed surface, and about 50% on the PAH-primed surface. While it was not possible to resolve the lattice structure of the MS_2 sheets, AFM line scans over the terraces of sheets showed mean roughness of the order of 1–2 Å, consistent with exposure of the basal planes. The step height from the primed substrate to the top of the sheets was typically 13–15 Å, which corresponds roughly to the thickness of a single layer of MoS_2 sheets (6 Å) plus a layer of hydrated Li^+ cations.

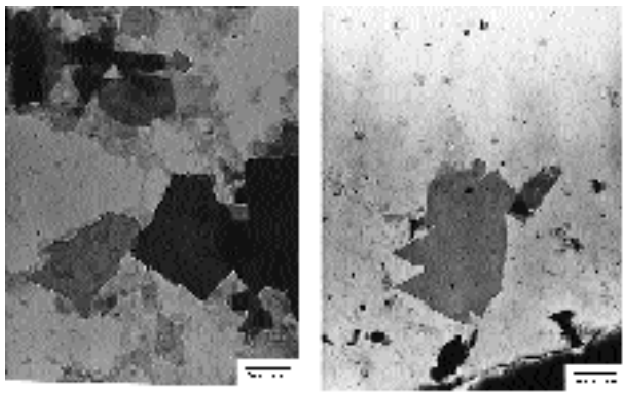

Fig. 1 Transmission electron micrographs of (left) colloidal MoS_2 and (right) SnS_2 particles

Multilayer films were grown by sequentially adsorbing the MS_2 colloids and polymeric PAH cations in 15 min cycles, with intermediate washing steps. The layer growth was monitored by ellipsometry, transmission UV–VIS spectroscopy (using quartz substrates), and AFM. The observed change in average layer thickness per adsorption cycle, Fig. 3, was consistently 14.8(3) Å per layer pair for MoS_2/PAH and 23.8(3) Å for SnS_2/PAH. UV–VIS spectra confirmed the regular stepwise growth of film thickness. In the case of MoS_2, the layer pair thickness is approximately that expected for a monolayer of PAH plus a single sheet of MoS_2, whereas for SnS_2 it is apparent that more than one monolayer is deposited in each adsorption cycle. Consistent with this observation, TEM studies of the SnS_2 colloid show that it is not completely exfoliated. For both MoS_2 and SnS_2, the layer pair thickness was quite insensitive to the adsorption time, up to several hours. This observation is consistent with the model of electrostatic self-assembly as a self-limiting process in which film growth ceases once the layer charge is inverted by adsorption of poly-anions or -cations.[9]

In contrast to the more regularly tiled surfaces observed with zirconium phosphate/polymer multilayers,[10] AFM images of the MoS_2 multilayer films reveal a 'spongy' morphology, in which sheets and polymer appear randomly oriented. The rms roughness of a four layer pair film of MoS_2/PAH was 16 Å on the PAH-anchored substrate, and 8 Å on the Al-Keggin derivatized surface. This is consistent with the model proposed by Kleinfeld and Ferguson for multilayer growth on islands, which eventually coalesce into smoother films.[11] The more densely tiled first monolayer that grows on the Keggin-primed surface yields a smoother film after a few layers are grown. XPS analysis of Si–SiO_x–Al Keggin–$(MoS_2\text{-PAH})_n$–MoS_2 (n = 0, 3; Table 1) films confirms that the sheets are intact and cover the surface relatively well after deposition of four layers. In the monolayer spectra, the surface coverage is low and the XPS spectrum is dominated by adventitious carbon and signals from the Si/SiO_x substrate. Both Mo and S are present in the film, but their ratio cannot be determined accurately because of counting errors. With multilayer films, the Si, Al and O signals from the buried substrate and primer layer are attenuated relative to Mo and S, which are present in the expected 1 : 2 ratio.

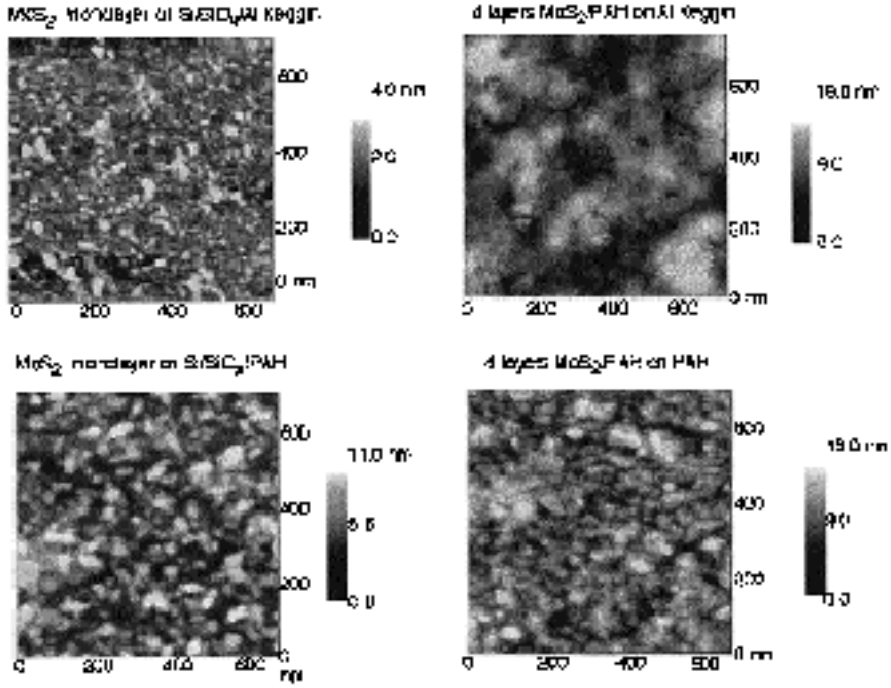

Fig. 2 Tapping-mode AFM images of monolayer MoS_2 and $(MoS_2/PAH)_3MoS_2$ films on Si/SiO_x/PAH and Si/SiO_x/Al Keggin substrates

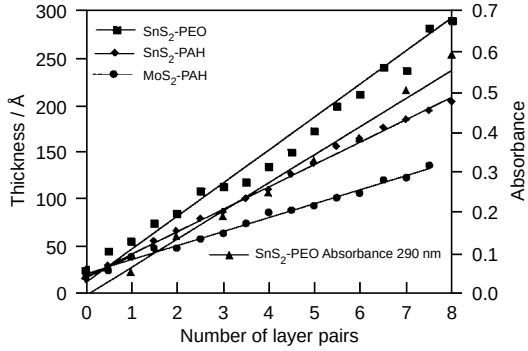

Fig. 3 Ellipsometric and UV absorbance data showing the thickness and change in absorbance of MS_2/polymer films *vs.* number of layer pairs. The thickness of 'zero' layers corresponds to the SiO_x and primer (PAH or Al-Keggin). Half-integer abscissa values refer to films terminated by an MS_2 layer, and integer values by a PAH or PEO layer.

Table 1 Relative integrated peak areas, corrected for atomic sensitivity, for $Si–SiO_x$–Al Keggin–$(MoS_2\text{-}PAH)_n$–MoS_2 (n = 0, 3) films

	n = 0	n = 3
Si	21.3	4.4
Al	3.4	0.2
Mo	0.7	1.9
S	0.7	3.7
C	44.0	72.9
O	29.9	16.9

The basal plane surface of MS_2 colloids is relatively non-polar, relative to previously studied clay, metal oxide and metal phosphate lamellar colloids. MoS_2 and SnS_2 exfoliated colloids can be re-stacked by neutral polymers, such as poly(ethylene oxide), PEO.[12] Accordingly, the cationic PAH polymer was replaced by a solution of neutral PEO, and multilayer films were grown by the same method. The film growth, monitored by ellipsometry and UV–VIS spectroscopy, is regular and the trend is similar to that found with PAH, 15 Å per layer pair with MoS_2 and 35 Å per layer pair with SnS_2. Apparently, PEO complexes the Li^+ ions that charge-compensate the colloid sheets, much as it does in the bulk intercalation compounds.[12b] This interaction is sufficiently strong to persistently bind sequentially adsorbed layers.

This work was supported by a grants from the National Science Foundation (CHE-9529202) and Civilian Research and Development Foundation. Instrumentation for AFM experiments was provided by National Science Foundation grant CHE-9626326.

Notes and References

† E-mail: pjo@chem.psu.edu

1 A. Ulman, *An Introduction to Ultrathin Organic Films: From Langmuir–Blodgett to Self-Assembly*, Harcourt Brace Jovanovich, Boston, 1991; G. A. Ozin, *Adv. Mater.*, 1992, **4**, 612; S. Mann, *J. Mater. Chem.*, 1995 **5**, 935.
2 H. E. Katz, *Chem. Mater.*, 1994, **6**, 2227; J. A. Gavin and T. E. Mallouk, *Acc. Chem. Res.*, 1998, **31**, 209.
3 C. T. Seip, G. E. Granroth, M. W. Meisel and D. R. Talham, *J. Am. Chem. Soc.*, 1997, **119**, 7084.
4 M. E. Thompson, *Chem. Mater.*, 1994, **6**, 1168; J. L. Snover, H. Bryd, E. P. Suponeva, E. Vincenzi and M. E. Thompson, *Chem. Mater.*, 1996, **8**, 1490.
5 E. R. Kleinfeld and G. S. Ferguson *Science* 1994, **265**, 370; S. W. Keller, H. N. Kim and T. E. Mallouk, *J. Am. Chem. Soc.*, 1994, **116**, 8817; N. A. Kotov, I. Dekany and J. H. Fendler, *Adv. Mater.*, 1996, **8**, 1414.
6 H.-L. Tsai, J. Heising, J. L. Schindler, C. R. Kannewurf and M. G. Kanatzidis, *Chem. Mater.*, 1997, **9**, 879; H.-L. Tai, J. L. Schindler, C. R. Kannewurf and M. G. Kanatzidis, *Chem. Mater.*, 1997, **9**, 875.
7 P. Joensen, F. Frindt and S. R. Morrison, *Mater. Res. Bull.*, 1996, **21**, 457; W. M. R. Divigalpitiya, S. R. Morrison and R. F. Frindt, *Thin Solid Films*, 1990, **186**, 177; B. K. Miremadi and S. R. Morrison, *J. Appl. Phys.*, 1988, **63**, 4970. The butyllithium/dry hexane/MS_2 suspension was stirred for 3–4 days under Ar, filtered in an Ar dry-box, and then rinsed with dry hexane. The intercalated solid was then added to deionized water and sonicated for 20 min to promote exfoliation.
8 S. Schönherr, G. Görz, D. Müller and W. Gessner, *Z. Anorg. Allg. Chem.*, 1981, **476**, 188.
9 G. Decher, *Science*, 1997, **277**, 1232.
10 M. Fang, D. M. Kaschak, A. C. Sutorik and T. E. Mallouk, *J. Am. Chem. Soc.*, 1997, **119**, 12 184.
11 E. R. Kleinfeld and G. R. Ferguson, *Chem. Mater.*, 1996, **8**, 1575.
12 (*a*) C. D. England, G. E. Collins, T. J. Schuerlein and N. R. Armstrong, *Langmuir*, 1994, **10**, 2748; (*b*) R. Bissessur, M. G. Kanatzidis, J. L. Schindler and C. R. Kannewurf, *J. Chem. Soc., Chem. Commun.*, 1993, 1582.

Received in Columbia, MO, USA, 19th February 1998; 8/01454J

A convenient synthesis of the cruciferous phytoalexins brassicanal A and brassilexin by mimicry of a fungal detoxification pathway

M. Soledade C. Pedras*† and Francis I. Okanga

Department of Chemistry, University of Saskatchewan, 110 Science Place, Saskatoon, SK, Canada S7N 5C9

The cruciferous phytoalexin brassilexin 3 has been synthesized in four steps from indoline-2-thione *via* 3-(aminomethylene)indole-2-thione 2, a metabolic intermediate of the detoxification pathway of the phytoalexin cyclobrassinin 1; in addition, the phytoalexin brassicanal A 8 has been synthesized in two steps from 2-indolinethione.

It is now well-recognized that the blackleg fungus [*Phoma lingam* (Tode ex Fr.) Desm., perfect stage *Leptosphaeria maculans* (Desm.) Ces. et de Not.], one of the most destructive fungal pathogens of rapeseed (*Brassica napus, B. rapa*), can overcome the plant's induced chemical defenses, *i.e.* phytoalexins, by enzymatic detoxification.[1–6] Recently, we reported[6] an unprecedented detoxification of the cruciferous phytoalexin cyclobrassinin **1**[7] *via* the phytoalexins brassilexin **3**[8] and dioxibrassinin **4**[9,10] by isolates of *P. lingam*‡ (Scheme 1). A detailed analysis of the metabolites involved in that fungal biotransformation of cyclobrassinin **1** indicated that 3-(aminomethylene)indole-2-thione **2**, or its thiol tautomer(s), was a precursor of brassilexin **3** (Scheme 1).[6] In continuation of that work we have now accomplished the synthesis of brassilexin **3** by mimicry of that detoxification pathway, utilizing the key intermediate **2** (Scheme 2). This route provides a very convenient process for preparation of both compounds **2** and **3**,

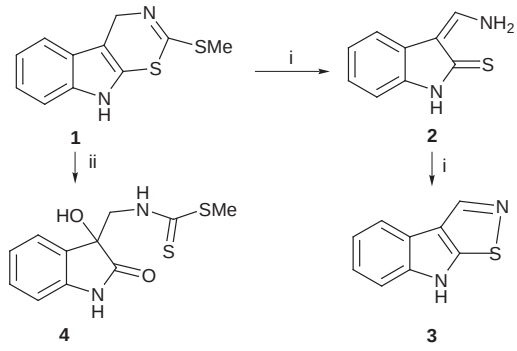

Scheme 1 Transformation of cyclobrassinin by the phytopathogenic fungus *Phoma lingam*: i, 'avirulent' isolate Unity; ii, 'virulent' isolate BJ −125

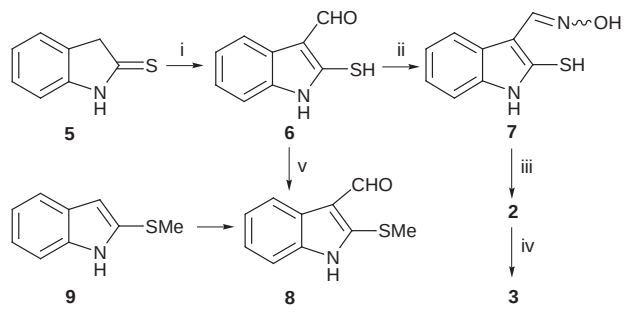

Scheme 2 *Reagents and conditions*: i, NaH, HCO_2Et, 25 °C, 92%; ii, $NH_2OH·HCl$, AcONa, EtOH, reflux, quant.; iii, $TiCl_3$, $NaBH_3CN$, MeOH, 25 °C, 85%; iv, activated charcoal, 25 °C, 82%; v, CH_2N_2, Et_2O, 25 °C, quant.

offering also the possibility of introducing carbon and/or nitrogen isotopes into the indol-3-yl substituents in good yield. Previous syntheses of brassilexin **3** from indole-3-carbaldehyde *via* cyclobrassinin **1** (11% overall yield),[11–13] or directly from indole-3-carbaldehyde (11–30% overall yield),[14] have been reported. However, our route affords the best overall yield to date while following the simplest process in terms of purification and reaction conditions. Utilizing the route shown on Scheme 2, brassilexin **3** was obtained from indolinethione **5**[15] in four steps (typically 50 mg scale reactions) in *ca.* 64% overall yield. In addition, this route provided aldehyde **6**, which on reaction with CH_2N_2 quantitatively yielded brassicanal A **8**, another cruciferous phytoalexin,[16] in *ca.* 92% yield. This synthesis of brassicanal A **8** also presents a great improvement to the previously reported procedure, which employed methylation of indolinethione **5** followed by Vilsmeier formylation of the corresponding 2-thiomethyl ether **9** (Scheme 2, 39% overall yield from **5**).[4]

During previous biotransformation studies,[6] we observed that brassilexin **3** could be obtained from metabolite **2** after standing in solution or on silica gel TLC plates. Interestingly, this transformation was catalyzed by activated charcoal to afford brassilexin almost quantitatively, demonstrating that metabolite **2** would be a synthetically useful brassilexin precursor if available in reasonable yields. One apparent method for the preparation of **2** was the reduction of amino derivatives of 3-(hydroxymethylene)indole-2-thione (or equivalent tautomer, *e.g.* **6**) similar to the preparation of 3-hydroxymethylene-2-oxoindole derivatives.[17] Thus, formylation of thione **5**[15] with EtO_2CH afforded aldehyde **6**, whose ^1H and ^{13}C NMR spectroscopic data§ indicated that only the thiol tautomeric form was present. Oximination of **6** under standard conditions[18] yielded quantitatively oxime **7**, which was readily reduced to the desired intermediate **2** with $NaBH_3CN$ in the presence of $TiCl_3$.[19] Finally, treatment of **2** with activated charcoal afforded brassilexin in excellent yield.¶

It is worth noting that thione **2** was hypothesized to be a biogenetic precursor of brassilexin **3** *in planta*.[6] In addition, although thiol **6** does not appear to have been prepared previously, it was proposed as a precursor of brassicanal A *in planta*.[20] Our facile synthesis of intermediates **2** and **6** offers the possibility of isotopic labelling and should facilitate future biosynthetic studies on brassilexin **3** and brassicanal A **8**. Particularly because brassilexin **3** appears to be involved in the blackleg disease resistance of several agriculturally important cruciferous oilseeds (*e.g. B. juncea*, *B. carinata*),[21] its biosynthesis has tremendous potential application and is presently under investigation in our laboratory.

We gratefully acknowledge the financial support of the Natural Sciences and Engineering Research Council of Canada and the University of Saskatchewan.

Notes and References

† E-mail: pedras@sask.usask.ca

‡ The fungal species *Phoma lingam* is subdivided in various groups (*cf.* M. S. C. Pedras, J. L. Taylor and V. M. Morales, *Phytochemistry*, 1995, **38**, 1215; J. L. Taylor, M. S. C. Pedras and V. M. Morales, *Trends Microbiol.*,

1995, **3**, 202); the so-called 'avirulent' group, *e.g.* isolate Unity, is now considered a species different from that of the 'virulent' group, *e.g.* BJ-125, although no formal reclassification has been carried out.

§ *Selected data* for **6**: δ_H(500 MHz, CD_3OD) 9.49 (s, CHO), 8.15 (d, *J* 8.0, 1 H), 7.48 (d, *J* 8.0, 1 H), 7.37 (dd, *J* 8.0, 7.5, 1 H), 7.27 (dd, *J* 8.0, 7.5, 1 H); δ_H(500 MHz, [$^2H_6$]DMSO) 12.77 (br s, NH), 9.49 (s, CHO), 8.06 (d, *J* 8.0, 1 H), 7.50 (d, *J* 8.0, 1 H), 7.35 (dd, *J* 8.0, 7.0, 1 H), 7.26 (dd, *J* 8.0, 7.0, 1 H); δ_C(125.5 MHz, [$^2H_6$]DMSO) 184.3, 138.5, 137.1, 125.2, 124.6, 122.9, 120.8, 119.8, 112.3; HRMS: found 177.0249 (calc. for C_9H_7NOS: 177.0248); *m/z* (EI) 177 (M^+, 100%), 149 (18), 148 (24), 121 (15); *m/z* (CI) 178 ($M^+ + 1$, 19%), 164 (32), 150 (24), 146 (100), 132 (50). For **7**: δ_H(300 MHz, CD_3CN): δ 9.88 (br s, NH), 8.52 (br s, OH), 8.03 (d, *J* 8.0, 1 H), 7.95 (s, H-1'), 7.42 (d, *J* 8.0, 1 H), 7.31 (dd, *J* 8.0, 7.0, 1 H), 7.21 (dd, *J* 8.0, 7.0, 1 H); δ_C(75.5 MHz, CD_3CN) 145.2, 138.9, 131.1, 126.0, 125.7, 123.5, 122.4, 117.2, 112.6; HRMS: found 174.0251 (calc. for $C_9H_8N_2OS - H_2O$: 174.0252); *m/z* (EI) 174 ($M^+ - H_2O$, 100%), 149 (51), 142 (24); *m/z* (CI) 175 ($M^+ + 1 - H_2O$, 100%).

¶ All compounds gave satisfactory spectroscopic data.

1 M. S. C. Pedras and J. L. Taylor, *J. Org. Chem.*, 1991, **56**, 2619.
2 M. S. C. Pedras, I. Borgmann and J. L. Taylor, *Phytochem. (Life Sci. Adv.)*, 1992, **11**, 1.
3 M. S. C. Pedras and J. L. Taylor, *J. Nat. Prod*., 1993, **56**, 731.
4 M. S. C. Pedras and A. Q. Khan, *J. Agric. Food Chem.*, 1996, **44**, 3403.
5 M. S. C. Pedras, A. Q. Khan and J. L. Taylor, in *Phytochemicals for Pest Control*, ed. P. A. Hedin, R. M. Hollingworth, E. P. Masler, J. Miyamoto and D. G. Thompson, *ACS Symp. Ser*., 1997, **658**, 155.
6 M. S. C. Pedras and F. I. Okanga, *Chem. Commun*., 1998, 67.
7 First isolation and synthesis: M. Takasugi, N. Katsui and A. Shirata, *J. Chem. Soc., Chem. Commun*. 1986, 1077.
8 First isolation: M. Devys, M. Barbier, I. Loiselet, T. Rouxel, A. Sarniguet, A. Kollmann and J. Bousquet, *Tetrahedron Lett*., 1988, **29**, 6447.
9 First isolation: K. Monde, K. Sasaki, A. Shirata and M. Takasugi, *Phytochemistry*, 1991, **30**, 2915.
10 Synthesis: K. Monde, M. Takasugi and T. Ohnishi, *J. Am. Chem. Soc*., 1994, **116**, 6650.
11 M. Devys and M. Barbier, *Synthesis*, 1990, 214.
12 M. Devys and M. Barbier, *J. Chem. Soc., Perkin Trans. 1*, 1990, 2856.
13 M. Devys and M. Barbier, *Z. Naturforsch*., 1992, **47C**, 318
14 M. Devys and M. Barbier, *Org. Prep. Proced. Int.*, 1993, **25**, 344.
15 T. Hino, K. Tsuneoka, M. Nakagawa and S. Akaboshi, *Chem. Pharm. Bull*., 1969, **17**, 550.
16 K. Monde, N. Katsui, A. Shirata and M. Takasugi, *Chem. Lett.*, 1990, 209.
17 E. Wenkert, N. K. Bhattacharyya, T. L. Reid and T. E. Stevens, *J. Am. Chem. Soc*., 1956, **78**, 797.
18 E. Wenkert, B. S. Bernstein and J. H. Udelhofen, *J. Am. Chem. Soc*., 1958, **80**, 4899.
19 J. P. Leeds and H. A. Kirst, *Synth. Commun.*, 1988, **18**, 777.
20 K. Monde, A. Tanaka and M. Takasugi, *J. Org. Chem.*, 1996, **61**, 9053.
21 T. Rouxel, A. Kollmann, L. Boulidard and R. Mithen, *Planta*, 1991, **184** 271.

Received in Corvallis, OR, USA, 8th May, 1998; 8/03485K

Electron transfer in a hydrogen-bonded assembly consisting of porphyrin–diimide

Atsuhiro Osuka,*[a] Ryusho Yoneshima,[a] Hideo Shiratori,[a] Tadashi Okada,*[b] Seiji Taniguchi[b] and Noboru Mataga[c]

[a] *Department of Chemistry, Graduate School of Science, Kyoto University, Kyoto 606-8502, Japan*
[b] *Department of Chemistry, Graduate School of Engineering Science and Research Center for Materials Science at Extreme Conditions, Osaka University, Toyonaka 560-8531, Japan*
[c] *Institute for Laser Technology, Utsubo Honmachi, Nishi-ku, Osaka 550-0004, Japan*

Electron-transfer reactions in an H-bonded assembly composed of a diacylaminopyridine bearing zinc porphyrin and 1,8 : 4,5-naphthalenetetracarboxylic diimide (K_a = 2.8 × 10² dm³ mol⁻¹) in benzene occur with k_{CS} = 4.1 × 10¹⁰ s⁻¹ and k_{CR} = 3.7 × 10⁹ s⁻¹, while the corresponding covalently linked model with a comparable distance and energy gap undergoes electron transfer with k_{CS} = 9.9 × 10¹⁰ s⁻¹ and k_{CR} = 6.7 × 10⁸ s⁻¹.

In recent years there has been a considerable upsurge in the development of hydrogen (H)-bonded assemblies that can undergo efficient electron-transfer (ET) reactions,[1–6] since most biological electron transfers take place in non-covalently assembled arrays of several chromophores where the overall electronic coupling between the donor and acceptor seems to depend on the electronic interaction at a non-covalent H-bonded motif. Although several synthetic models have been presented to display ET within H-bonded assemblies, key aspects of ET dynamics still remain unclarified. In particular, ion-pair states have been only scarcely identified by transient absorption spectroscopy, leaving behavior of photogenerated ion pairs across H-bonds unknown except for a limited number of examples.[3,6,7]

Here, we study an H-bonded assembly of a photoexcitable electron-donor zinc porphyrin **9** and electron-acceptor 1,8 : 4,5-naphthalenetetracarboxylic diimide **10** and ET dynamics within the assembly. Porphyrin **9** bears a *meso*-substituted 2,6-diacylaminopyridyl group that is expected to form a strong H bond to the diimide **10**.[8] The radical anion of **10** possesses sharp and characteristic absorption bands that have proven to be particularly useful for analysis of electron-transfer kinetics.[9] Aldehyde **5** was prepared in six steps from citrazinic acid (Scheme 1). The cross-condensation of 3,5-di-*tert*-butylbenzaldehyde, aldehyde **5** and 4,4′-diethyl-3,3′-dimethyldipyrrylmethane gave porphyrin **6** in 62% yield (on the basis of **5**), which was converted to a 2,6-diaminopyridyl-substituted porphyrin **7** in 67% yield by hydrolysis under acidic conditions (HBr–phenol–acetic acid). Porphyrin **9** was prepared by the reaction of **7** with hexanoyl chloride and subsequent insertion of Zn.‡ Diimides **10** and **11** were prepared by the cross-condensation of 1,8 : 4,5-naphthalenetetracarboxylic dianhydride with urea and 2-aminopropane-1,3-diol followed by silylation with *tert*-butyldimethylsilyl chloride in *ca.* 30 and 13% yields, respectively. The siloxyl substituents were introduced in order to increase the solubilities of these diimides in non-polar organic solvents.

To confirm the complexation *via* H-bonding, the ^{1}H NMR spectra of **9** in the absence and presence of increasing amounts of **10** were examined in C_6D_6, $CDCl_3$ and CD_2Cl_2. Typical chemical shift changes upon complexation of **9** and **10** in $CDCl_3$ are summarized in Scheme 2. Most prominently the imide H_a proton and the amide H_b protons were downfield shifted, while the other protons were essentially unperturbed. The fact that no particular upfield shift was observed for the aromatic protons of **10** precludes the coordination of **10** to the zinc centre in **9**. Similar shifts were observed in C_6D_6 and CD_2Cl_2, while no such shifts were detected in [$^2H_8$]THF or [$^2H_6$]DMF. The observed chemical shift changes are consistent with a complexation by three-points H-bonding as depicted in Scheme 2. From the ^{1}H NMR titration, the binding constants were determined using a standard non-linear least-square curve fitting method: 2.8 × 10² dm³ mol⁻¹ in benzene, 1.0 × 10² dm³ mol⁻¹ in $CDCl_3$ and 79 dm³ mol⁻¹ in CD_2Cl_2. Further, the continuous variation method (Job's plot) was used to determine the complexation stoichiometry as 1 : 1.

Steady-state fluorescence studies carried with a benzene solution of **9** (1.0 × 10⁻⁵ M)) in the presence of **10** (5.0 × 10⁻³

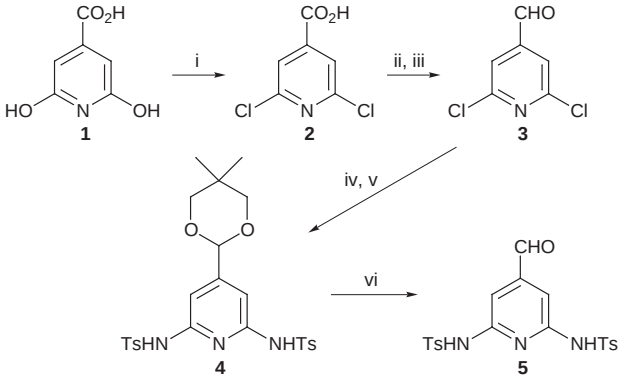

Scheme 1 *Reagents and conditions*: i, $POCl_3$, 160 °C, 78%; ii, $BF_3{\cdot}OEt_2$, $NaBH_4$, 74%; iii, activated MnO_2, 66%; iv, neopentyl glycol, *p*-TsOH, 99%; v, toluene-*p*-sulfamide, Cu powder, 190 °C, 63%; vi, 10% H_2SO_4, TFA, 76%

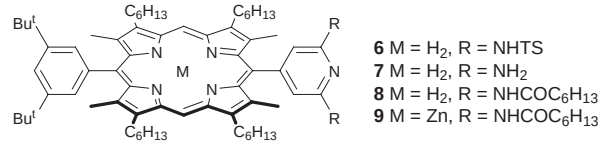

6 M = H_2, R = NHTS
7 M = H_2, R = NH_2
8 M = H_2, R = $NHCOC_6H_{13}$
9 M = Zn, R = $NHCOC_6H_{13}$

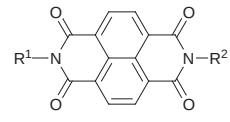

10 R^1 = H, R^2 = $CH(CH_2OTBDMS)_2$
11 R^1 = R^2 = $CH(CH_2OTBDMS)_2$
12 R^1 = D, R^2 = $CH(CH_2OTBDMS)_2$

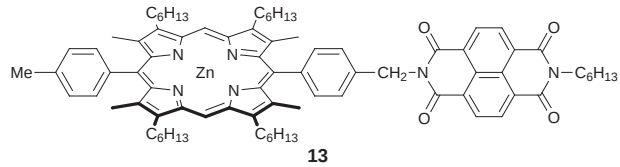

13

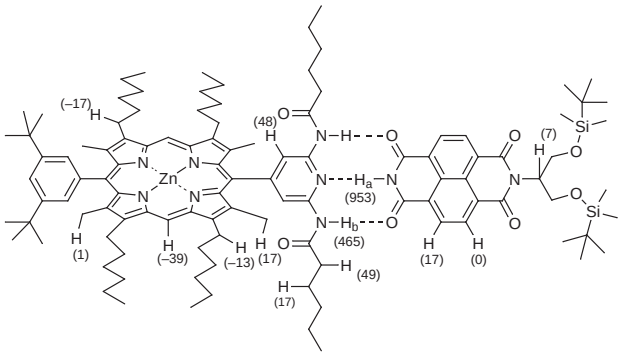

Scheme 2 Complexation-induced (20%) changes in ^{1}H NMR chemical shifts (ppb) for **9**–**10** in $CDCl_3$

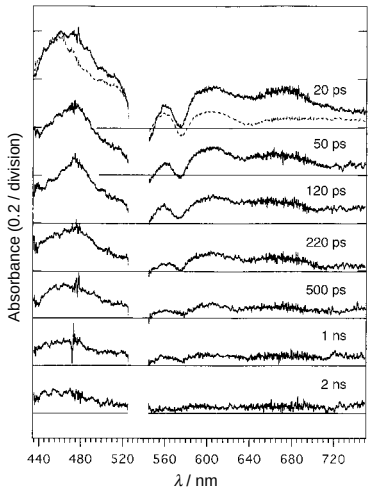

Fig. 1 Transient absorption spectra of a benzene solution of **9** (2.0×10^{-4} M) and **10** (1×10^{-2} M) at λ_{ex} = 532 nm. The dotted line shows the spectrum at a 20 ps delay time for **9** alone.

M) revealed substantial fluorescence quenching (70%) compared with the fluorescence of **9** alone. Such fluorescence quenching was not observed in THF and DMF nor for a solution of **9** and **11**, indicating that a complexation *via* H-bonding was crucial for fluorescence quenching, rather than diffusional encounters.

To provide further support for ET *via* H-bonding, time-resolved transient absorption studies were carried out. Fig. 1 shows the picosecond transient absorption spectra of **9** alone and in the presence of **10** at λ_{ex} = 532 nm in benzene. Under the conditions used, > 95% of **9** was complexed with **10** and the fluorescence of **9** was completely quenched. The transient spectrum of **9** alone (shown by dotted line at a delay time of 20 ps) is a typical transient absorption spectrum of a 5,15-diaryl-octaalkyl zinc porphyrin, in which the absorption band at 458 nm is due to $S_n \leftarrow S_1$ absorption and the bleaching at 640 nm is due to stimulated emission of the S_1 state and these two bands decay with τ = 1.6 ns. The transient absorption spectra of the complex **9**–**10** provided clear evidence for the formation of a diimide anion radical (474 nm) and a zinc porphyrin cation radical (655 nm), both of which were observed early at 20 ps delay time and decayed with τ = 270 ps. Thus, the rate of charge recombination within the complex **9**–**10** is 3.7×10^9 s^{-1}. By analyzing the time profile at 458 nm where the main absorbing species is the S_1 state of the zinc porphyrin, the rate of charge separation has been determined to be 4.1×10^{10} s^{-1}. These ET rates across an H-bond were compared with those in a related covalently linked model **13**, which has a similar energy diagram and a slightly shorter center-to-center distance, to characterize ET across an H-bond bridge.§¶ The transient absorption studies revealed that the rates of charge separation and recombination in **13** are 9.9×10^{10} and 6.7×10^8 s^{-1}, respectively. Thus it may be concluded that (1) electronic coupling across an H-bond interface necessary for charge separation is comparable to that across two C–C single bonds, in line with recent results reported by Therien and coworkers,[5] and (2) an ion-pair across H-bonds is considerably shorter-lived in comparison to a covalently linked ion-pair. The latter aspect that can account for difficulty in detecting an ion-pair across H-bonds may be understood in terms of stabilization of the ion pair, thus the decrease in $-\Delta G$ in the inverted region, by H-bond reorganization which is accompanied by the charge separation.[7] The assembly **9**–**12** has been also studied by transient absorption spectroscopy and found to undergo ET-reaction with $k_{CS} = 2.9 \times 10^{10}$ s^{-1} and $k_{CR} = 2.4 \times 10^9$ s^{-1}, revealing that the isotope effect k_H/k_D is 1.4 and 1.5 for charge separation and recombination, respectively, roughly in line with results reported by Nocera and coworkers.[3a] Our next target will be the development of a H-bonded asembly of donor–acceptor triads and tetrads which can realize long-lived charge separation in spite of inherently shorter-lived ion-pairs across H-bonds. Our attempts in this direction will be reported elsewhere.

This work was supported by Grant-in-Aids for Scientific Research (No. 09440217 and 08874074) from the Ministry of Education, Science, Sports and Culture of Japan and by CREST (Core Research for Evolutional Science and Technology) of Japan Science and Technology Corporation (JST).

Notes and References

† E-mail: osuka@kuchem.kyoto-u.ac.jp

‡ All new compounds were fully characterized by 500 MHz ^{1}H NMR and FAB mass spectra.

§ The one-electron redox potentials of the donor and the acceptor moieties have been measured in $CHCl_3$ by cyclic voltammetry *vs.* ferrocene–ferrocenium ion. The oxidation potential of **9** was 0.16 V and the reduction potential of **10** was −1.05 V in the free form and −0.97 V in an H-bonded assembly with 2,6-dihexanoylaminopyridine, while the oxidation and reduction potentials of **13** were 0.11 and −1.06 V.

¶ Estimated center-to-center distances are 14.7 and 12.8 Å for **9**–**10** and **13**, respectively.

1 Y. Aoyama, M. Asakawa, Y. Matsui and H. Ogoshi, *J. Am. Chem. Soc.*, 1991, **113**, 6233; T. Hayashi, T. Miyahara, N. Hashizume and H. Ogoshi, *J. Am. Chem. Soc.*, 1993, **115**, 2049.

2 A. Harriman, Y. Kubo and J. L. Sessler, *J. Am. Chem. Soc.*, 1992, **114**, 388; T. Arimura, C. T. Brown, S. L. Springs and J. L. Sessler, *Chem. Commun.*, 1996, 2293.

3 (*a*) C. Turro, C. K. Chang, G. E. Leroi, R. I. Cukier and D. G. Nocera, *J. Am. Chem. Soc.*, 1992, **114**, 4013; (*b*) T. Hayashi, T. Miyahara, S. Kumazaki, H. Ogoshi and K. Yoshihara, *Angew. Chem., Int. Ed. Engl.*, 1996, **35**, 1964.

4 J. P. Kirby, N. A. van Dantzig, C. K. Chang and D. G. Nocera, *Tetrahedron Lett.*, 1995, **36**, 3477; J. A. Roberts, J. P. Kirby and D. G. Nocera, *J. Am. Chem. Soc.*, 1995, **117**, 8051; J. P. Kirby, J. A. Roberts and D. G. Nocera, *J. Am. Chem. Soc.*, 1997, **119**, 9230; Y. Deng, J. A. Roberts, S.-M., Peng, C. K. Chang and D. Nocera, *Angew. Chem., Int. Ed. Engl.*, 1997, **36**, 2124.

5 P. J. F. de Rege, S. A. Williams and M. J. Therien, *Science*, 1995, **269**, 1409.

6 A. Osuka, H. Shiratori, R. Yoneshima, T. Okada, S. Taniguchi and N. Mataga, *Chem. Lett.*, 1995, 913.

7 H. Miyasaka, A. Tabane, K. Kamada and N. Mataga, *J. Am. Chem. Soc.*, 1993, **115**, 7335 and references therein.

8 A. D. Hamilton, N. Pant and A. Muehldorf, *Pure Appl. Chem.*, 1988, **60**, 535; M. Kotera, J.-M. Lehn and J. P. Vigneron, *Tetrahedron*, 1995, **51**, 1953.

9 A. Osuka, S. Nakajima, K. Maruyama, N. Mataga, T. Asahi, I. Yamazaki, Y. Nishimura, T. Ohno and K. Nozaki, *J. Am. Chem. Soc.*, 1993, **115**, 4577; G. P. Wiederrecht, M. P. Niemczyk, W. A. Svec and M. R. Wasielewski, *J. Am. Chem. Soc.*, 1996, **118**, 81.

Received in Cambridge, UK, 12th May 1998; 8/03541E

Determination of enantiomeric excess for amino acid ester salts using FAB mass spectrometry

Masami Sawada,*[a]† Hiroshi Yamaoka,*[b] Yoshio Takai,[a] Yorito Kawai,[c] Hitoshi Yamada,[a] Tomoko Azuma,[b] Tamaki Fujioka[b] and Toshikazu Tanaka[c]

[a] *Materials Analysis Center, the Institute of Scientific and Industrial Research, Osaka University, Ibaraki, Osaka, 567, Japan*
[b] *Department of Natural Science, Osaka Women's University, Sakai, Osaka, 590, Japan*
[c] *Faculty of Engineering, Osaka Institute of Technology, Asahi-ku, Osaka, 535, Japan*

The enantiomeric excess of α-amino acid ester hydrochlorides is determined for the first time using FAB mass spectrometry coupled with enantiomer-labelled host method.

The simple determination of enantiomeric excess using FAB mass spectrometry, without chromatographic separation of the enantiomers,[1,2] has been demonstrated for the first time using *R*/*S* mixtures of α-amino acid esters or, more generally, organic primary amine hydrochlorides. The principle of this method is based on the FAB mass spectrometric detection (nitrobenzyl alcohol matrix)[3–6] of enantiomeric recognition of primary amines by chiral macrocyclic host compounds.[7,8] This method uses a 1:1 mixture [for example, (*R*)-nonlabelled/(*S*)-deuterium-labelled] of chiral crown ethers [for example, (*RRRR*)-**1** and [$^2H_6$]-(*SSSS*)-**1**], and is known as the enantiomer-labelled (EL) host method. In other words, the hosts are utilized as a pair of specific reagents for determining the ee of organic primary amines.

The relative peak intensity of the diastereomeric host–guest complex ions, which are produced from the complexation between a 1:1 mixture of the enantiomeric hosts (H_{RRRR}):[^2H_n]-(H_{SSSS}) and the primary amine salt guest (G^+), is taken as a quantitative measure; *n* is the number of deuterium labels [eqn. (1)].

$$I[(H_{RRRR} + G)^+]/I[[^2H_n]\text{-}(H_{SSSS} + G)^+] = I_R/I_S = IRIS \text{ (abbreviation)} \quad (1)$$

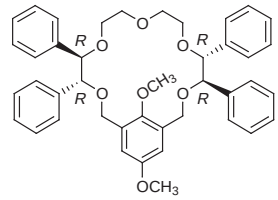

(*RRRR*)-**1**

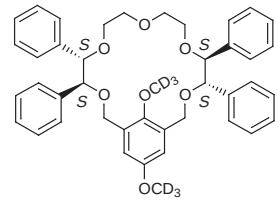

[$^2H_6$]-(*SSSS*)-**1**

The fundamental concept of this methodology is schematically shown in Fig. 1, where the diastereomeric host–guest complex ion peaks are given. For the conceptual data shown in Fig. 1, the (*R*)-guest complexes the (*RRRR*)-host by an arbitrary factor of 2.0 better than the (*SSSS*)-host (run 1, *IRIS* = 2.0). Accordingly, the (*S*)-guest should complex the (*SSSS*)-host by a factor of 2.0 better than the (*RRRR*)-host (run 2, *IRIS* = 0.50) because of the mirror image relationship between the host–guest complex ions produced. Furthermore, the racemic (*RS*)-guest should provide a pair of equal peak intensities (run 3, *IRIS* = 1.0) because of the net compensation of a racemic host–racemic guest combination. Therefore, in the case of a given guest with unknown ee, one can expect to determine the percent enantiomeric excess from the relationship between the *IRIS* and the ee values.

The (*RRRR*)-**1** host was prepared by a route previously reported by Kaneda, Hirose and Misumi.[9,10] The corresponding

Run	Host	Guest	Pattern of H–G diastereomeric complex ion peaks	I_R/I_S
A:	**FABMS/EL host method**			
1	*RRRR* / [^2H_n]-*SSSS*	*R* (*R*)100% ee		2.0
2	*RRRR* / [^2H_n]-*SSSS*	*S* (*S*)100% ee		0.5
3	*RRRR* / [^2H_n]-*SSSS*	*R* / *S* 1:1 racemic	^2H_n	1.0
4	*RRRR* / [^2H_n]-*SSSS*	*R/S* unknown	Various	Various
B:	**FABMS/EL guest method**			
5	*RRRR*	*R* / [^2H_n]-*S* 1:1 racemic		2.0
6	*SSSS*	*R* / [^2H_n]-*S* 1:1 racemic	^2H_n	0.5

Fig. 1 FAB mass spectrometry with the enantiomer-labelled host and guest methods

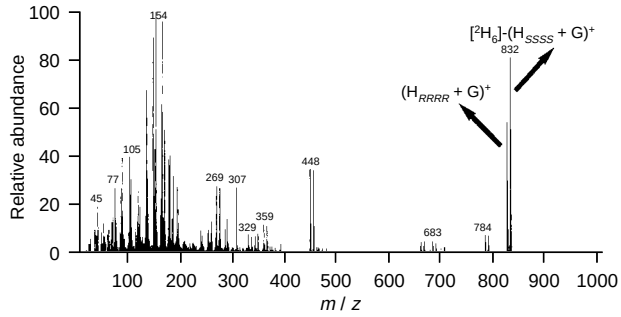

Fig. 2 A typical FAB mass spectrum (nitrobenzyl alcohol matrix) using the enantiomer-labelled host method [host: (*RRRR*)-**1** and [$^2H_6$]-(*SSSS*)-**1**; guest: (*S*)-PglyOMe•HCl (80% ee)]

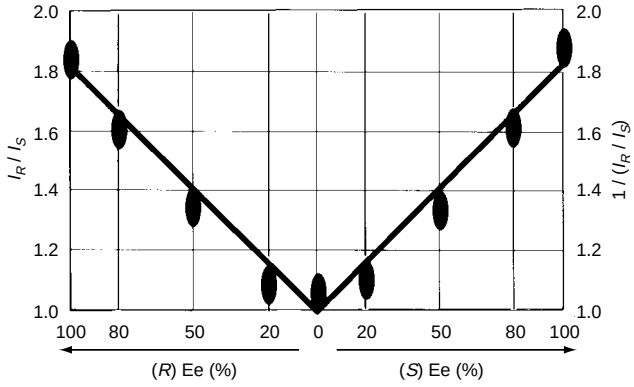

Fig. 3 A plot of $I[(H_{RRRR} + G)^+]/I[[^2H_6]\text{-}(H_{SSSS} + G)^+]$ *vs.* ee

enantiomer-labelled [$^2H_6$]-(*SSSS*)-**1** was similarly prepared *via* 2,6-bis(bromomethyl)hydroquinone [$^2H_6$]dimethyl ether.

A FABMS solution was prepared by mixing the following three solutions: (i) 5 μl of a 1:1 mixture of a 0.16 mmol dm^{-3} $CHCl_3$ solution (25 μl) of (*RRRR*)-**1** and a 0.16 mmol dm^{-3} $CHCl_3$ solution (25 μl) of [$^2H_6$]-(*SSSS*)-**1**, (ii) 5 μl of a 0.08 mmol dm^{-3} MeOH solution of a given guest, and (iii) 30 μl of NBA matrix. After evaporation of MeOH and $CHCl_3$ in the ion source, the concentrations in NBA were calculated to $[H_{RRRR}] = [H_{SSSS}] = [G] = 0.0133$ mmol dm^{-3}. Several guest solutions with different ees were prepared by appropriate mixing of solutions of both the (*R*)- and (*S*)-phenylglycine methyl ester (PglyOMe) hydrochloride salts, and the *IRIS* values were determined by FAB mass spectrometry (Table 1). A typical FAB mass spectrum is shown in Fig. 2. In order to see the characteristic relationship, the *IRIS* value is plotted on the ordinate when the (*R*)-guest is in excess, and the reciprocal of the *IRIS* value is plotted when the (*S*)-guest is in excess (Fig. 3). The *IRIS* value varies in a linear fashion with the ee quantity and produces a symmetric V-shaped plot. Therefore, it is clear that the ee value of a given guest with unknown ee can be determined from the *IRIS* values obtained for both the guests with unknown and known (100%) ee. As mentioned previously,[5] there exist, in general, weak concentration effects of the host and guest solutions upon the *IRIS* values, so it is necessary to measure the FAB mass spectra under fixed sample concentration conditions.

The *IRIS* value of run 1 (or run 2) (the EL host method) should be equivalent to the *IRIS* value of run 5 (or run 6) (the EL guest method)[5] for the mirror image relationship between the complex ions. Therefore, using the EL host method with a series of enantiomerically pure guests (run 1 or run 2), we can determine the chiral recognition abilities of this host toward a series of guests using the same *IRIS* scale derived from the EL guest method (run 5 or run 6). Table 1 shows several *IRIS* values

Table 1 The $I[(H_{RRRR} + G)^+]/I[[^2H_6]\text{-}(H_{SSSS} + G)^+]$ values toward various primary amine hydrochlorides

Amine	*IRIS* values[a]
GlyOMe	1.00
(*R*)-PglyOMe	1.84
(*S*)-PglyOMe	0.53
(*R*)-PglyOEt	1.98
(*R*)-PglyOPr^i	2.00
(*S*)-AspOMe[b]	0.37
(*S*)-AsnOMe	0.51
(*S*)-PheOMe	0.51
(*S*)-ValOEt	0.35
(*R*)-1-Phenylethylamine	0.95
(*R*)-1-Phenyl-2-hydroxyethylamine	0.62
(*R*)-1-(*p*-Nitrophenyl)ethylamine	1.03

[a] Averaged values of 10th, 20th, 30th and 40th scans ($n = 4$). The standard deviations were within ±5%. [b] (*S*)-Aspartic acid dimethyl ester hydrochloride.

obtained experimentally using the EL host method with a series of hydrochloride salts of enantiomerically pure amino acid esters and organic primary amines. These data have shown which type of guest is suitable to the ee determination. Since the *IRIS* values of the PglyOR$^+$, AspOR$^+$, AsnOR$^+$ and ValOR$^+$ guests show relatively high degrees of chiral recognition character [*IRIS* $\geqslant$ *ca.* 2.0 for (*RRRR*)-host preference or *IRIS* $\leqslant$ 0.5 for (*SSSS*)-host preference], these guests are applicable to determine the ee quantities. On the other hand, the *IRIS* values of the 1-phenylethylamine hydrochloride guests are close to unity, so these are not appropriate for such a purpose. These differences strongly suggest the importance of the COOR function in the guest part for higher chiral recognition ability in the present system.

We have described a conceptually novel method for ee determination of amino acid ester salts using FAB mass spectrometry (positive mode). The methodology is potentially applicable to other host–guest systems with relatively high degrees of chiral recognition.

The authors thank Professor T. Kaneda and Dr K. Hirose for their kind instruction of the synthesis of the chiral crown hosts.

Notes and References

† E-mail: m-sawada@sanken.osaka-u.ac.jp

1 M. A. Baldwin, S. A. Howell, K. J. Welham and F. J. Winkler, *Biomed. Environ. Mass Spectrom.*, 1988, **16**, 357.
2 D. W. Armstrong, *Anal. Chem.*, 1987, **59**, 84A; L. R. Sousa, G. D. Sogah, D. H. Hoffman and D. J. Cram, *J. Am. Chem. Soc.*, 1978, **100**, 4569.
3 M. Sawada, *Mass Spectrom. Rev.*, 1997, **16**, 73.
4 M. Sawada, *J. Mass Spectrom. Soc. Jpn.*, 1997, **45**, 439.
5 M. Sawada, Y. Takai, H. Yamada, S. Hirayama, T. Kaneda, T. Tanaka, K. Kamada, T. Mizooku, S. Takeuchi, K. Ueno, K. Hirose, Y. Tobe and K. Naemura, *J. Am. Chem. Soc.*, 1995, **117**, 7726.
6 M. Sawada, Y. Takai, H. Yamada, J. Nishida, T. Kaneda, R. Arakawa, M. Okamoto, K. Hirose, T. Tanaka and K. Naemura, *J. Chem. Soc., Perkin Trans. 2*, 1998, 701.
7 X. X. Zhang, J. S. Bradshaw and R. M. Izatt, *Chem. Rev.*, 1997, **97**, 3313.
8 F. Vögtle and E. Weber, *The Chemistry of Ethers, Crown Ethers, Hydroxyl Groups and their Sulphur Analogues*, ed. S. Patai, John Wiley, New York, 1980, Part 1, ch. 2.
9 T. Kaneda, K. Hirose and S. Misumi, *J. Am. Chem. Soc.*, 1989, **111**, 742.
10 M. Sawada, Y. Okumura, M. Shizuma, Y. Takai, Y. Hidaka, H. Yamada, T. Tanaka, T. Kaneda, K. Hirose, S. Misumi and S. Takahashi, *J. Am. Chem. Soc.*, 1993, **115**, 7381.

Received in Cambridge, UK, 13th March 1998; 8/02029I

An efficient synthesis of analogues of unsymmetrical archaeal tetraether glycolipids

Grégory Lecollinet,[a] Rachel Auzély-Velty,[a] Thierry Benvegnu,*[a]† Grahame Mackenzie,[b] John W. Goodby[b] and Daniel Plusquellec[a]

[a] *Ecole Nationale Supérieure de Chimie de Rennes, Laboratoire de Synthèses et Activations de Biomolécules, associé au CNRS, Avenue du Général Leclerc, PO Box, 35700 Rennes, France*
[b] *The Department of Chemistry, Faculty of Science and the Environment, The University of Hull, Hull, UK HU6 7RX*

Unsymmetrical tetraether analogues of glycolipids found in archaebacteria, possessing either two different carbohydrate units or a saccharidic moiety and a phosphate group as polar heads and a quasi-macrocyclic lipid core, are efficiently synthesized from versatile chiral building blocks.

The Archaea domain, composed of a variety of extremophilic microorganisms, belongs to a third kingdom of life which is clearly distinct from the well-known Bacteria and Eucarya domains.[1–3] Preservation of the membrane function under extreme conditions such as high temperatures and strong acidity lies with the unique structure of archaebacterial lipids, which fundamentally differ from those of their bacterial and eucaryotic counterparts.[4] Of particular interest is the unusual molecular architecture of the macrocyclic tetraether lipids found in methanogenic and thermoacidophilic species.[5] These lipids are characterized by a bipolar structure with two head groups linked together by two C40 polyisoprenoid chains. Recently, Gräther and Arigoni demonstrated that several natural lipids were in fact nearly statistical mixtures of regioisomers differing in the relative orientation of their glycerol units.[6] The dimensions of the tetraether lipids are therefore sufficient to form monolayered membranes[5] and the presence of two head groups with different sizes at opposite sides of the monolayer is expected to induce membrane curvature.[4b] The presence of galactofuranose units in some glycolipids is puzzling since hexoses appear only in the pyranose form in mammalian glycoconjugates. The unique chemical design of these archaeal lipids represents an interesting opportunity to build exceptionally thermal stable vesicles which might be suitable for nano-scale technologies and for drug-delivery applications.[7]

We report here the first synthesis of the chiral unsymmetrical quasi-macrocyclic tetraethers **3** and **4** as models of the natural

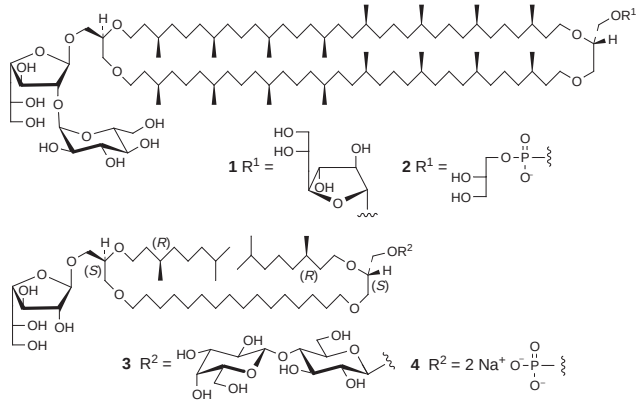

lipids **1** and **2** isolated from *Methanospirillum hungatei*, which is a methanogenic species.[5] The most characteristic structural features of the target molecules lies with (i) a lipid core consisting in a linear hexadecanemethylene spacer and two (*R*)-dihydrocitronellyl chains having a combined length equal to that of the bridging unit, attached to glycerol respectively at *sn*-3 and *sn*-2 positions, (ii) either a D-galactofuranose and a phosphate group or the former and a lactosyl unit as polar head groups at opposite ends of the lipid core, and (iii) an *S* stereogenic center at each glycerol backbone similar to that of the corresponding natural glycolipids **1** and **2**.[5] These synthetic bolaamphiphiles might show similar behaviour to cyclic lipids when aggregated or inserted into membranes.[8]

The general synthetic pathway for **3** and **4** (Scheme 1) involved the preparation of the key diol intermediate **9**, subsequent monoprotection of one of the hydroxy groups and sequential introduction of the polar heads. The crucial glycosylation or phosphorylation step of the monoglycosylated compound **12** should be performed under extremely mild conditions in order to preserve the highly hydrolysable β-D-galactofuranosidic linkage. Hemimacrocyclic diol **9** was obtained from (*S*)-(+)-2,2-dimethyl-1,3-dioxolan-4-ylmethanol [(*S*)-(+)-solketal],‡ hexadecane-1,16-diyl ditriflate **5**, and (*R*)-(−)-citronellyl bromide as the starting materials. After experimentation, we found that reaction of hexadecane-1,16-diol with Tf_2O in the presence of the hindered base 2,6-lutidine resulted in the efficient formation of the expected ditriflate **5**. Separation of the ditriflate from the base was easily accomplished by flash chromatography, thus affording compound **5** in 80% yield. Alkylation of two (*S*)-solketal units by **5** proceeded efficiently (83%) in refluxing CH_2Cl_2 for 24 h using 1,8-bis(dimethylamino)naphthalene (proton sponge: PS) as a base. Removal of the isopropylidene groups in the presence of a Dowex acidic resin in refluxing MeOH gave the tetraol (73%) which was selectively protected by *p*-methoxytritylation of the primary hydroxy groups. Williamson coupling of the remaining secondary hydroxy groups using commercially available (*R*)-(−)-citronellyl bromide provided the unsaturated tetraether **8** (80% yield). Palladium-catalyzed hydrogenation of **8** led to the formation of byproducts due to the unexpected cleavage of the ether linkages at the *sn*-2 glycerol sites. Addition of 1 equiv. of triethylamine in the hydrogenation media avoided this side reaction and furnished quasi-quantitatively the corresponding saturated lipid. Finally, the key diol **9** was readily prepared by removal of the trityl groups under acidic conditions.[9]

At this stage, the next challenging problem involved the selective protection of **9** so as to introduce two different polar head groups at opposite ends. After experimentation, we found that the protocol reported by Bouzide and Sauvé[10] was the most efficient methodology for the monoprotection of the diol. Treatment of **9** with Ag_2O and BnBr in CH_2Cl_2 led to the formation of the monobenzylated product **10** (50% yield) in addition to the dibenzylated derivative (10% yield) and the unreacted recyclable diol (36%). The introduction of the β-D-galactofuranoside unit was performed stereospecifically by way of *n*-pentenyl glycoside (NPG) glycosylation[11] from the key galactofuranosyl donor **11**.[12] After hydrogenolysis of the benzyloxy group, we envisaged either the glycosylation or the

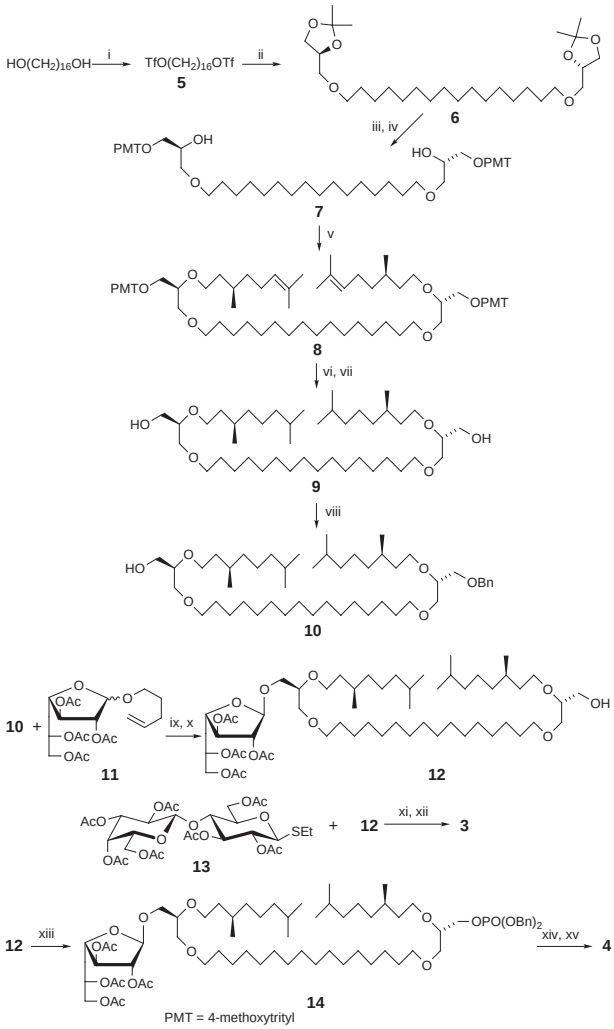

Scheme 1 *Reagents and conditions*: i, Tf_2O, 2,6-lutidine, CH_2Cl_2, 0 °C, then room temp., 80%; ii, (*S*)-solketal, PS, CH_2Cl_2, reflux, 83%; iii, Dowex H^+ resin, MeOH, reflux; iv, 4-methoxytrityl chloride, pyridine, DMAP, THF, reflux, 60% over two steps; v, (*R*)-citronellyl bromide, NaH, 130 °C, 80%; vi, H_2, Pd/C, Et_3N, AcOEt; vii, HCO_2H, Et_2O, 70% over two steps; viii, Ag_2O, BnBr, CH_2Cl_2, 50%; ix, NIS, Et_3SiOTf, CH_2Cl_2; x, H_2, Pd/C, EtOH, 73% over two steps; xi, NIS, TESOTf, 4 Å molecular sieves, CH_2Cl_2; xii, MeONa, MeOH, 65% over two steps; xiii, 1*H*-tetrazole, $(BnO)_2PNPr^i_2$, CH_2Cl_2, then MCPBA, CH_2Cl_2, −40 to 0 °C, 80%; xiv, MeONa, MeOH; xv, H_2, Pd/C, MeOH, acetate buffer (pH 5) (3:1 v/v), then Amberlite® IR-120 (Na^+), MeOH, then gel-filtration on Sephadex LH-20 (1:2 CH_2Cl_2–MeOH), 85% over two steps

phosphorylation of the free alcohol under mild conditions in order to prevent any hydrolysis of the former β-D-galactofuranosidic bond. The glycosylation of **12** using lactosyl thioglycoside **13** as a donor[13] was carried out under NIS–Et_3SiOTf conditions and provided the desired β-D-glycoside in 70% yield. Deacetylation of the glycosyl hydroxy groups under standard conditions gave the totally deprotected bipolar lipid **3** in 93% yield.§

Having successfully prepared the bis-glycoside **3**, we turned our attention towards the introduction of a phosphate group onto intermediate **12**. Alkyl dibenzyl phosphate **14** was prepared by reacting alcohol **12** with dibenzyl *N*,*N*-diisopropylphosphoramidite and 1*H*-tetrazole followed by *in situ* mild oxidation of the resultant alkyl dibenzyl phosphite with MCPBA (80% yield).[14] The transformation of **14** into the phosphate salt **4** was performed by sequential deacetylation of the galactosyl unit, catalytic hydrogenolysis (Pd/C) in a buffered solvent mixture (MeOH–AcOH–NaOAc, pH 5) avoiding the glycoside hydrolysis and treatment with Amberlite® IR-120 (Na^+ form, water).

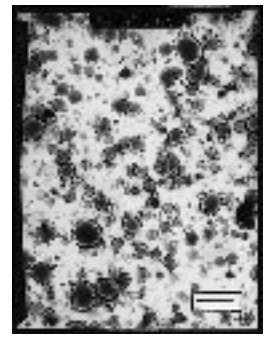

Fig. 1 Transmission electron micrograph of compound **4** vesicles negatively stained with uranyl acetate. The bar is 1500 nm.

Purification by gel filtration chromatography with Sephadex LH-20 furnished the targeted unsymmetrical glycolipid analogue **4** in 85% yield.

Aqueous dispersions of glycolipids **3** and **4** were sonicated at 60 °C for 20 min. Transmission electron microscopy revealed that phosphate **4** furnished spherical vesicles of 100–1000 nm diameter stable for several weeks at ambient temperature as shown in a representative micrograph (Fig. 1). Compound **3** provided myelin-type aggregates (not shown).

Further physicochemical measurements are under investigation.

We are grateful to the CNRS and the Région Bretagne for grants to R. A.-V. and G. L., respectively, to M. Lefeuvre for assistance with NMR experiments, and to P. Guenot for mass spectrometry measurements.

Notes and References

† E-mail: thierry.benvegnu@ensc-rennes.fr

‡ (*S*)-(+)-Solketal and its (*R*)-(−)-isomer are currently available on a kilogram scale. (*S*)-(+)-Solketal was obtained from Chemi S.p.A., 20092 Cinisello Balsamo, Italy.

§ All yields reported herein refer to isolated pure materials which have ^1H and ^{13}C NMR spectra, elemental analyses and high resolution mass spectral characteristics in accordance with the proposed structures. *Selected data* for **3**: $[\alpha]_D^{20}$ −26.7 (*c* 0.78 in MeOH); FABMS (*m*-nitrobenzyl alcohol matrix): Calc. for $[M + Na]^+$: 1195.7907. Found: 1195.7880. For **4**: $[\alpha]_D^{20}$ −26.4 (*c* 0.72 in MeOH); FABMS (*m*-nitrobenzyl alcohol matrix): Calc. for $[M + H]^+$: 973.6333. Found: 973.6331; Calc. for $[M - Na + 2H]^+$: 951.6514. Found: 951.6524.

1 C. R. Woese and G. E. Fox, *Proc. Natl. Acad. Sci. USA*, 1977, **74**, 5088.
2 J. A. Fuhrman, K. McCallum and A. A. Davis, *Nature*, 1992, **356**, 148.
3 E. F. Delong, K. Y. Wu, B. B. Prézelin and R. V. M. Jovine, *Nature*, 1994, **371**, 695.
4 (*a*) M. De Rosa and A. Morana, in *Neural Networks and Biomolecular Engineering to Bioelectronics*, ed. C. Nicolini, Plenum Press, New York, 1995, p. 217; (*b*) K. Yamauchi and M. Kinoshita, *Prog. Polym. Sci*., 1993, **18**, 763.
5 G. D. Sprott, *J. Bioenerg. Biomembr.*, 1992, **24**, 555.
6 O. Gräther and D. Arigoni, *Chem. Commun.*, 1995, 405.
7 A. Gambarcorta, A. Gliozzi and M. De Rosa, *World J. Microbiol. Biotechnol.*, 1995, **11**, 115.
8 R. A. Moss, T. Fujita and Y. Okumura, *Langmuir*, 1991, **7**, 2415.
9 M. Bessodes, D. Komiotis and K. Antonakis, *Tetrahedron Lett.*, 1986, **27**, 579.
10 A. Bouzide and G. Sauvé, *Tetrahedron Lett.*, 1997, **38**, 5945.
11 B. Fraser-Reid, U. E. Ododong, Z. Wu, H. Ottoson, J. R. Merritt, C. S. Rao, C. Roberts and R. Madsen, *Synlett*, 1992, 927.
12 R. Velty, T. Benvegnu, M. Gelin, E. Privat and D. Plusquellec, *Carbohydr. Res.*, 1997, **299**, 7.
13 M. O. Contour, J. Defaye, M. Little and E. Wong, *Carbohydr. Res.*, 1989, **193**, 283.
14 J. W. Perich and R. B. Johns, *Tetrahedron Lett.*, 1987, **28**, 101.

Received in Glasgow, UK, 24th March 1998; 8/02338G

Chiral aminoborane as a chiral proton source for asymmetric protonation of lithium enolates derived from 2-arylcycloalkanones

Akira Yanagisawa, Hiroshi Inanami and Hisashi Yamamoto*†

Graduate School of Engineering, Nagoya University, CREST, Japan Science and Technology Corporation (JST), Chikusa, Nagoya, 464-8603, Japan

Reaction of lithium enolates of 2-arylcycloalkanones 2 with (*R*,*R*)-aminoborane 1, prepared from (1*R*,2*R*)-1,2-diaminocyclohexane 4 and $PhBCl_2$, gives the corresponding optically active ketones 3 with up to 93% ee; this is the first example of enantioselective protonation using a metal-containing chiral proton source.

Asymmetric protonation of prochiral metal enolates has proved to be an efficient method for the synthesis of chiral carbonyl compounds.[1] The success of this process depends on the structure and acidity of the chiral proton source. Several chiral acids have been developed so far, and have been applied to enantioselective protonations.[2–4] However, as far as we know, there are no reports on a proton source containing metal atoms. We describe here a new enantioselective protonation of lithium enolates **2** with chiral aminoborane **1** [eqn. (1)].

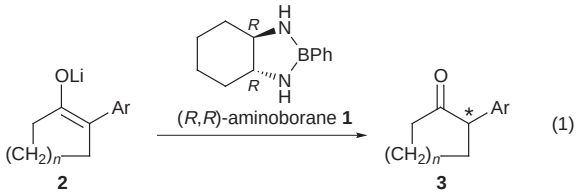

Heteroatom-substituted chiral boron compounds such as oxazaborolidines and acyloxyboranes are well-known as chiral Lewis acid catalysts for various asymmetric reactions.[5] High levels of asymmetric induction are obtained in Diels–Alder reactions or Mukaiyama aldol reactions, and the formation of a stable complex of a boron catalyst with a carbonyl compound is regarded as the key to success. We considered that if a chiral aminoborane could form a rigid cyclic transition state structure with a lithium enolate, and if the amide proton is acidic enough, a highly enantioselective protonation might occur.

Chiral aminoborane **1** was synthesized from (1*R*,2*R*)-1,2-diaminocyclohexane **4** (2 equiv.) and $PhBCl_2$ (1 equiv.) in toluene [eqn. (2)].[6] The resulting ammonium salt was filtered

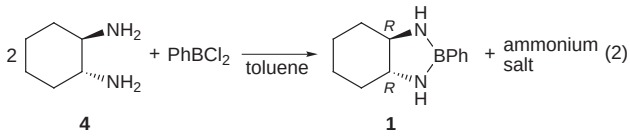

off. Treatment of lithium enolate **6**, generated from silyl enol ether **5** and Bu^nLi/hexane (1.1 equiv.) in THF at 0 °C,[7] with a solution of (*R*,*R*)-aminoborane **1** (1.5 equiv.) in toluene–THF (1:1) at −78 °C for 2 h followed by quenching with Me_3SiCl (to remove unreacted **6**) at −78 °C gave (*S*)-enriched 2-phenylcyclohexanone **7** in 94% yield and 84% ee (Table 1, entry 1).‡ Using various chiral aminoboranes, we studied the enantioselectivity of this protonation; yields and enantiomeric excesses of the product **7** obtained by reactions with other chiral aminoboranes **8**–**15** in THF at −78 °C are shown in Table 1. Substitution of the phenyl group of **1** by a chlorine atom resulted in a lower

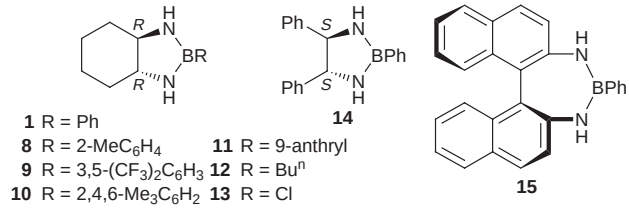

enantioselectivity, while the chemical yield increased (entry 7). As a consequence, (*R*,*R*)-aminoborane **1** was the most effective chiral proton source for the protonation of **6**.

This asymmetric protonation was applied to a variety of lithium enolates of ketones **17**, and the results with (*R*,*R*)-aminoborane **1** are summarized in Table 2. These reactions have the following characteristics: (i) all of the reactions proceeded to give a satisfactory yield at −78 °C for 2 h, except for the lithium enolate of 2-methylindanone **22**, which gave a low yield due to concomitant side reactions (entry 5); (ii) moderate to high asymmetric induction occurred in the protonation of lithium enolates **6**, **19**–**21** and **29**, which possess an aryl group at the C-2 position (entries 1–4 and 12). The highest enantioselectivity (93% ee) was obtained with the enolate of 2-(2-naphthyl)cyclohexanone **21** (entry 4). The enolates **22**, **23**, **27** and **28** derived from 2-methylindanone, 2-methyltetralone and their derivatives also gave good optical purities (entries 5, 6, 10, and 11). However, the use of simple substrates bearing no aromatic

Table 1 Protonation of the lithium enolate **6** with chiral aminoboranes **1** and **8**–**15**[a]

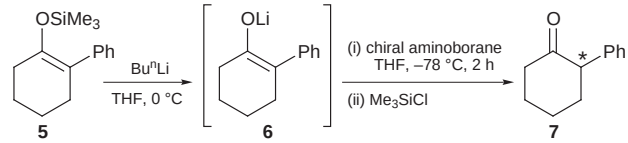

Entry	Chiral aminoborane	Yield (%)[b]	Ee (%)[c]	Configuration[d]
1	**1**	94	84	*S*
2	**8**	83	60	*S*
3	**9**	65	47	*S*
4	**10**	17	5	*S*
5	**11**	14	3	*R*
6	**12**	74	20	*S*
7	**13**	> 99	44	*S*
8	**14**	20	32	*R*
9	**15**	19	6	*S*

[a] The lithium enolate **6** was generated from the corresponding silyl enol ether **5** (1 equiv.) and a solution of Bu^nLi/hexane (1.1 equiv.) in THF at 0 °C for 2 h. The following protonation was carried out using a chiral aminoborane (1.5 equiv.) in THF at −78 °C for 2 h. The reaction was quenched by TMSCl at −78 °C to exclude the unreacted enolate **6**. [b] Isolated yield. [c] Determined by HPLC analysis (Chiralcel OD-H, Daicel Chemical Industries, Ltd.). [d] The absolute configuration was determined by comparison of the $[\alpha]_D$ value with reported data [ref. 3(*c*)].

Table 2 Enantioselective protonation of various enolates with (*R*,*R*)-aminoborane **1**[a]

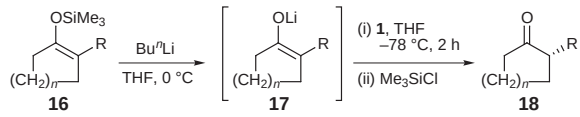

Entry	Lithium enolate[b]	Yield (%)[c]	Ee (%)[d]	Configuration[e]
1	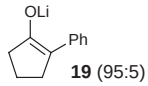 **19** (95:5)	70	34[f] (36)[f,g]	—
2	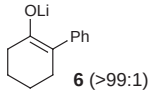 **6** (>99:1)	94	84	*S*[h]
3	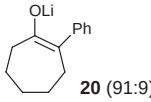 **20** (91:9)	69	70[f] (77)[f,g]	—
4	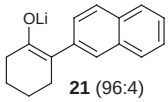 **21** (96:4)	84	89 (93)[g]	—
5	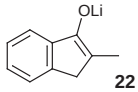 **22**	26	60	—
6	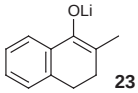 **23**	80	70	*S*[i]
7	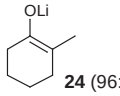 **24** (96:4)	69	1[j]	*S*[i]
8	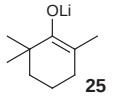 **25**	>99	16[k]	*S*[l]
9	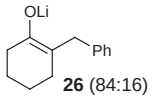 **26** (84:16)	93	8[m] (10)[g,m]	*R*[i]
10	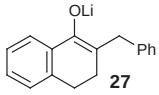 **27**	64	47	—
11	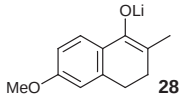 **28**	88	78	—
12	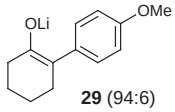 **29** (94:6)	92	81 (86)[g]	—

[a] All conditions are the same as in Table 1. [b] Parentheses indicate the regioisomeric ratio of the starting silyl enol ethers **16**. [c] Isolated yield. [d] Determined by HPLC analysis (Chiralcel OD-H, Daicel Chemical Industries, Ltd.). [e] The absolute configuration was determined by comparison of the $[\alpha]_D$ value with reported data. [f] Determined by HPLC analysis (Chiralpak AS, Daicel Chemical Industries, Ltd.). [g] Corrected value based on the regioisomeric ratio of the starting silyl enol ether **16**. [h] Ref. 3(*c*). [i] Ref. 8. [j] Determined by GC analysis with chiral column (ChiraldexTM B-TA, astec). [k] Determined by GC analysis with chiral column (ChiraldexTM G-TA, astec). [l] Ref. 4(*b*). [m] Determined by HPLC analysis (Chiralcel OJ, Daicel Chemical Industries, Ltd.).

groups gave unsatisfactory results (entries 7 and 8); (iii) a lithium enolate of 2-phenylcyclohexanone is superior to that of 2-phenylcyclopentanone or 2-phenylcycloheptanone with respect to enantioselectivity (compare entries 1–3); and (iv) introduction of an electron-donating group to the aromatic ring improved the enantiomeric ratios to some extent (entries 11 and 12).

Notes and References

† E-mail: j45988a@nucc.cc.nagoya-u.ac.jp

‡ Procedure for protonation of lithium enolate **6** with (*R*,*R*)-aminoborane **1**: To a solution of (1*R*,2*R*)-1,2-diaminocyclohexane (172 mg, 1.5 mmol) in dry toluene (4 ml) was added $PhBCl_2$ (97 µl, 0.75 mmol) at −78 °C. The mixture was warmed to room temperature and again stirred for 2.5 h at this temperature. The resulting ammonium salt was filtered off under an argon atmosphere and washed with dry THF (2 ml). To the filtrate was added at −78 °C a solution of lithium enolate **6**, prepared from trimethylsilyl enol ether **5** (123 mg, 0.5 mmol) and BunLi (1.67 M hexane solution, 0.33 ml, 0.55 mmol) in dry THF (2.3 ml) at 0 °C, through a stainless steel cannula under an argon stream. After being stirred for 2 h at −78 °C, TMSCl (65 µl, 0.5 mmol) was added, and stirring continued for another 30 min at this temperature. The reaction mixture was treated with saturated aqueous NH_4Cl, extracted with Et_2O , dried (Na_2SO_4), and finally purified by column chromatography on silica gel to give (*S*)-enriched 2-phenylcyclohexanone [(*S*)-**7**, 94% yield] with 84% ee. The enantiomeric ratio was determined by HPLC analysis using a chiral column (Chiralcel OD-H, Daicel Chemical Industries, Ltd.). The absolute configuration was determined by comparison of its optical rotation with published data; (*S*)-isomer (87% ee): $[\alpha]_D^{29}$ −88.9 (*c* 1.0, $CHCl_3$) [ref. 3(*c*)]. Observed value of (*S*)-isomer (84% ee): $[\alpha]_D^{28}$ −94.1 (*c* 1.1, $CHCl_3$).

1 Reviews: L. Duhamel, P. Duhamel, J.-C. Launay and J.-C. Plaquevent, *Bull. Soc. Chim. Fr.*, 1984, II-421; C. Fehr, *Chimia*, 1991, **45**, 253; H. Waldmann, *Nachr. Chem., Tech. Lab.*, 1991, **39**, 413; S. Hünig, in *Houben-Weyl: Methods of Organic Chemistry*; ed. G. Helmchen, R. W. Hoffmann, J. Mulzer and E. Schaumann, Georg Thieme Verlag, Stuttgart, 1995, vol. E 21, p. 3851; C. Fehr, *Angew. Chem., Int. Ed. Engl.*, 1996, **35**, 2566.

2 Recent reports: Y. Nakamura, S. Takeuchi, A. Ohira and Y. Ohgo, *Tetrahedron Lett.*, 1996, **37**, 2805; J. Muzart, F. Hénin and S. J. Aboulhoda, *Tetrahedron: Asymmetry*, 1997, **8**, 381; Y. Nakamura, S. Takeuchi, Y. Ohgo, M. Yamaoka, A. Yoshida and K. Mikami, *Tetrahedron Lett.*, 1997, **38**, 2709; H. Kosugi, M. Abe, R. Hatsuda, H. Uda and M. Kato, *Chem. Commun.*, 1997, 1857; J. Martin, M.-C. Lasne, J.-C. Plaquevent and L. Duhamel, *Tetrahedron Lett.*, 1997, **38**, 7181.

3 Enantioselective protonation of silyl enol ethers and ketene silyl acetals: (*a*) F. Cavelier, S. Gomez, R. Jacquire and J. Verducci, *Tetrahedron: Asymmetry*, 1993, **4**, 2501; (*b*) F. Cavelier, S. Gomez, R. Jacquire and J. Verducci, *Tetrahedron Lett.*, 1994, **35**, 2891; (*c*) K. Ishihara, M. Kaneeda and H. Yamamoto, *J. Am. Chem. Soc.*, 1994, **116**, 11 179; (*d*) K. Ishihara, S. Nakamura and H. Yamamoto, *Croat. Chem. Acta*, 1996, **69**, 513; (*e*) K. Ishihara, S. Nakamura, M. Kaneeda and H. Yamamoto, *J. Am. Chem. Soc.*, 1996, **118**, 12854; (*f*) T. Taniguchi and K. Ogasawara, *Tetrahedron Lett.*, 1997, **38**, 6429; (*g*) M. Takahashi and K. Ogasawara, *Tetrahedron: Asymmetry*, 1997, **8**, 3125; (*h*) M. Sugiura and T. Nakai, *Angew. Chem., Int. Ed. Engl.*, 1997, **36**, 2366.

4 For examples of simple enolates: (*a*) H. Hogeveen and L. Zwart, *Tetrahedron Lett.*, 1982, **23**, 105; (*b*) M. B. Eleveld and H. Hogeveen, *Tetrahedron Lett.*, 1986, **27**, 631; (*c*) K. Matsumoto and H. Ohta, *Tetrahedron Lett.*, 1991, **32**, 4729; (*d*) K. Fuji, K. Tanaka and H. Miyamoto, *Tetrahedron: Asymmetry*, 1993, **4**, 247; (*e*) K. Fuji, T. Kawabata and A. Kuroda, *J. Org. Chem.*, 1995, **60**, 1914; (*f*) T. Takahashi, N. Nakao and T. Koizumi, *Chem. Lett.*, 1996, 207; (*g*) H. Kosugi, K. Hoshino and H. Uda, *Tetrahedron Lett.*, 1997, **38**, 6861; (*h*) T. Tsunoda, H. Kaku, M. Nagaku and E. Okuyama, *Tetrahedron Lett.*, 1997, **38**, 7759; (*i*) P. Riviere and K. Koga, *Tetrahedron Lett.*, 1997, **38**, 7589; (*j*) T. Takahashi, N. Nakao and T. Koizumi, *Tetrahedron: Asymmetry*, 1997, **8**, 3293.

5 M. Vaultier and B. Carboni, in *Comprehensive Organometallic Chemistry II*, ed. E. W. Abel, F. G. A. Stone and G. Wilkinson, Pergamon, Oxford, 1995, vol. 11, p. 247.

6 A review of the preparation of aminoboranes: M. F. Lappert, P. P. Power, A. R. Sanger and R. C. Srivastava, *Metal and Metalloid Amides*, Ellis Horwood, Chichester, 1980, p. 76.

7 BunLi can be used for cleavage of the Si–O bond of silyl enol ether **5** instead of MeLi. Generation of lithium enolates: E. W. Colvin, *Silicon in Organic Synthesis*; Butterworth: London, 1981, p. 217.

8 A. I. Meyers, D. R. Williams, G. W. Erickson, S. White and M. Druelinger, *J. Am. Chem. Soc.*, 1981, **103**, 3081.

Received in Cambridge, UK, 19th May 1998; 8/03756F

Electrochemical reduction of halogenosugars on silver: a new approach to *C*-disaccharide-like mimics

Marco Guerrini,[a] Patrizia Mussini,[b] Sandra Rondinini,[b] Giangiacomo Torri[a] and Elena Vismara*[c]†

[a] *Istituto di Chimica e Biochimica 'Giuliana Ronzoni', via G. Colombo 81, 20133 Milano Italy*
[b] *Dipartimento di Chimica Fisica ed Elettrochimica, Università degli Studi di Milano, via Golgi 19, 20133 Milano, Italy*
[c] *Dipartimento di Chimica del Politecnico di Milano, via Mancinelli 7, 20131 Milano, Italy*

Electrochemical reduction on silver of tri-*O*-acetyl-α-D-fucopyranosyl bromide 3 affords (1 → 1′)-linked *C*-disaccharide-like mimics 6–8; reduction of 1,2 : 3,4-di-*O*-isopropylidene-6-deoxy-6-iodo-α-D-galactopyranose 5 provides 1,2:3,4-di-*O*-isopropylidene-6-deoxy-6-(1′,2′ : 3′,4′-di-O-isopropylidene-6′-deoxy-α-D-galactopyranos-6′-yl)-α-D-galactopyranose 9; simultaneous reduction of 5 and tetra-*O*-acetyl-α-D-glucopyranosyl bromide 1 or tri-*O*-acetyl-α-L-fucopyranosyl bromide 4 gives 9 and methylene-bridged *C*-disaccharide-like mimics 11, 12 or 13, 14, respectively.

C-Glycosides are of interest as molecules of potential biological activity and are also useful for enzymatic and metabolic studies.[1] Some *C*-disaccharides have also been investigated.[2]

Here we describe an electrochemical approach to *C*-disaccharide-like mimics, the reduction of halogenosugars in MeCN at a silver electrode, a method already extensively applied to glycosides syntheses.[3,4] This approach was confirmed by the electroreduction using the above conditions of tetra-*O*-acetyl-α-D-glucopyranosyl bromide **1** which mainly provides 1,3,4,5,8,9,10,12-octa-*O*-acetyl-D-gluco-L-altro-L-erythro-2,6 : 7,11-dianhydrododecitol,[8] 1,3,4,5,8,9,10,12-octa-*O*-acetyl-D-gluco-D-galacto-L-erythro-2,6 : 7,11-dianhydrododecitol and 1,3,4,5,8,9,10,12-octa-*O*-acetyl-D-gluco-L-ido-L-erythro-2,6 : 7,11-dianhydrododecitol[8] with an overall yield of 50%, the ratio being *ca.* 2 : 1 : 1.[5] We can account for the formation of these biglucosyl derivatives *via* a radical pathway, *i.e.* the dimerisation of tetra-*O*-acetyl-D-glucopyranosyl radical **2**.[3,4]

The *O*-glucosides themselves formed in the electrolyses of **1** on silver in the presence of phenols can be accounted for by coupling of an anomeric radical and a phenoxyl radical.[3,5] These electrolyses were carried out in MeCN *via* cyclic voltammetry of **1** at a silver electrode which displays one irreversible peak at E_p = −1.3 V (*vs.* aq. SCE). Electrochemical reduction of **1** at a mercury electrode in DMF or MeCN was proposed by Vianello and co-workers as a new approach to 3,4,6-tri-*O*-acetyl-D-glucal, the cyclic voltammetry of **1** displaying one irreversible peak at E_p = −1.9 V (*vs.* SCE).[6] No dimers were observed. Different mechanisms are no doubt involved in electrolyses of **1** using mercury or silver electrodes. On mercury, the overall electrode process of **1** was interpreted as a two electron C–Br bond cleavage coupled to a very fast elimination of the acetate anion, which leads to 3,4,6-tri-*O*-acetyl-D-glucal. 1,2,3,4,6-Penta-*O*-acetyl-β-D-glucopyranose was also isolated, *via* nucleophilic substitution.[6] The electrode process on the silver cathode appears more complex. Compound **1** undergoes a single electron-transfer reduction; the following elimination of the bromide anion leads to the intermediate radical **2**, which affords dimers (50%); 3,4,6-tri-*O*-acetyl-D-glucal (20%) and 1,2,3,4,6-penta-*O*-acetyl-β-D-glucopyranose (15%) are also isolated, thus indicating that a further reduction of **2** occurs.

On the basis of these results, we have investigated whether silver cathodic reduction of halogenosugars could be suitable to generate carbohydrate radicals, with the aim of developing new synthetic methods. The voltammetric behaviour of **1**, tri-*O*-acetyl-α-D-fucopyranosyl bromide **3**,[7] tri-*O*-acetyl-α-L-fucopyranosyl bromide **4**[7] and 1,2 : 3,4-di-*O*-isopropylidene-6-deoxy-6-iodo-α-D-galactopyranose **5**[8] were studied both at silver and mercury electrodes in MeCN (Table 1).

Table 1 Reduction peak potentials

Halogenosugar	E_p (Ag)/V (*vs.* SCE)	E_p (Hg)/V (*vs.* SCE)
1	−1.30	−1.95
3[a]	−1.20	−1.95
5	−1.23	−1.81

[a] Compound **4** is reduced at the same E_p as **3**.

Data in Table 1 confirm the remarkable electrocatalytic activity of silver with respect to mercury. Compounds **1**,**3**–**5** were submitted to preparative electrolyses on a silver cathode in MeCN. Tri-*O*-acetyl-α-D-fucopyranosyl bromide **3** was electrolysed at −1.5 V. 3,4,5,8,9,10-Hexa-*O*-acetyl-D-galacto-L-ido-D-threo-1,12-deoxy-2,6 : 7,11-dianhydrododecitol **6**‡ (15%), 3,4,5,8,9,10-hexa-*O*-acetyl-D-galacto-L-altro-D-threo-1,12-deoxy-2,6 : 7,11-dianhydrododecitol **7**‡ (15%) and 3,4,5,8,9,10-hexa-*O*-acetyl-D-galacto-D-galacto-D-threo-1,12-deoxy-2,6 : 7,1-dianhydrododecitol **8**‡ (4%) (Scheme 1) were recovered, together with 3,4-di-*O*-acetyl-D-fucal (11%) and fucose tetraacetate (10%).

The product distribution of **3** appears similar to that of **1**, except for the dimer ratio. 1,2 : 3,4-Di-*O*-isopropylidene-6-deoxy-6-iodo-α-D-galactopyranose **5** is suitable for generating a non-anomeric radical and for derivatisation to occur at the other end of the sugar skeleton. The reduction of **5** at −1.7 V provides 1,2 : 3,4-di-*O*-isopropylidene-6-deoxy-6-(1′,2′ : 3′,4′-di-*O*-isopropylidene-6′-deoxy-α-D-galactopyranos-6′-yl)-α-D-galactopyranose **9**[4,9] as the only product (Scheme 2). Once again its formation can be explained by the presence of an intermediate radical like 1,2 : 3,4-di-*O*-isopropylidene-6-deoxy-α-D-galactopyranos-6-yl radical **10**.

On the basis of these results and of the similar redox potentials of the investigated substrates (Table 1), we asked

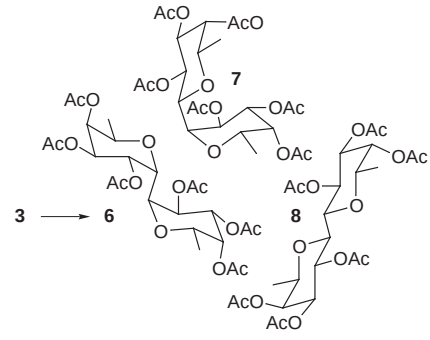

Scheme 1

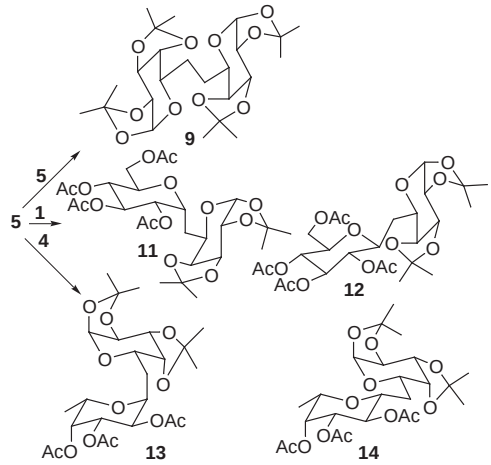

Scheme 2

ourselves if it was possible to couple two different radicals generated at the same stage. Our goal was the synthesis of non-symmetrical *C*-disaccharides-like mimics. Radical **2** is a secondary radical, to some extent stabilised by an O atom in the α-position, while **10** is an unstabilized primary radical. So could the so-called anomeric radical **2** behave as a persistent radical[10] and act as a scavenger of the more reactive **10**? Compounds **1** and **5** were simultaneously reduced at −1.5 V in the ratio 1.5 : 1. 1,2 : 3,4-Di-*O*-isopropylidene-6-deoxy-6-(2′,3′,4′,6′-tetra-*O*-acetyl-α-D-glucopyranosyl)-α-D-galactopyranose **11**§ (9%) and 1,2 : 3,4-di-*O*-isopropylidene-6-deoxy-6-(2′,3′,4′,6′-tetra-*O*-acetyl-β-D-glucopyranosyl)-α-D-galacto-pyranose **12**§ (9%) were isolated (Scheme 2) together with **9** (17%), with only a very small amount of glucosyl dimers (> 3%).

Compounds **4**[7] and **5** in the ratio 2 : 1 were also simultaneously reduced at −1.5 V. 1,2 : 3,4-Di-*O*-isopropylidene-6-deoxy-6-(2′,3′,4′-tri-*O*-acetyl-α-L-fucopyranosyl)-α-D-galactopyranose **13**¶ (11%) and 1,2:3,4-di-*O*-isopropylidene-6-deoxy-6-(2′,3′,4′-tri-*O*-acetyl-β-L-fucopyranosyl)-α-D-galactopyranose **14**¶ (11%) were isolated together with **9** (34%) (Scheme 2).

In both cases glycals and penta- or tetra-acetyl derivatives were also isolated. The product distributions show that dimerisation of **10** competes well with its trapping by glycosyl radicals, but also that there is no dimerisation of glycosyl radicals in the presence of **10** or that it is significantly reduced.

The mechanism of these reductions is very intriguing as we could argue that not only are carbohydrate radicals involved as intermediates, but also that dimerisation is the only termination reaction, which would be very unusual. The glucopyranosyl radical **2**, for instance, has been extensively studied especially by Giese. In the absence of a radical scavenger, it mainly undergoes migration of the acetate group from position 2 to 1.[11] In the electroreduction we did not actually observe any migration at all! We extensively studied the chemical behaviour of **10**.[8] Although it acts as a good hydrogen abstractor even from MeCN, in the electroreduction we did not observe any hydrogen abstraction at all! Some coupling of **10** was observed, but only in the presence of Fe^{II}[12] and, in that particular case, the effect of Fe^{II} was interpreted using Kochi's hypothesis as being due to 'metal ion–free radical complexes of relatively longer life than a simple alkyl radical'.[13]

In conclusion, we have provided evidence for the ability of a silver cathode to generate carbohydrate radicals and perhaps to induce their dimerisation, but, for the moment, we are not able to give any satisfactory interpretation of the mechanism. Indeed, even if yields are lowered by the presence of glycals and acetate derivatives, this peculiar electroreduction affords different kinds of *C*-disaccharide-like mimics, and in this sense it could be proposed as a mild, clean, one-pot method with which to form stable interglycosidic bonds.

We gratefully acknowledge MURST and CNR for the financial support, the student Daniela Beccati for the experimental work.

Notes and References

† E-mail: vismara@dept.chem.polimi.it

‡ *Selected data* for **6**: δ_H(500 MHz, C_6D_6) 1.12 (d, 3 H, H-6, $J_{5\text{-}6}$ 6.6), 4.33 (dq, 1 H, H-5, $J_{4\text{-}5}$ 3.6), 4.40 (d, 1 H, H-1, $J_{1\text{-}2}$ 3.9), 5.48 (t, 1 H, H-4, $J_{3\text{-}4}$ 3.5), 5.57 (dd, 1 H, H-2, $J_{2\text{-}3}$ 7.8), 5.78 (dd, 1 H, H-3). For **7**: δ_H(500 MHz, C_6D_6) 0.95 (d, 3 H, H-6′, $J_{5'\text{-}6'}$ 6.5), 1.19 (d, 3 H, H-6, $J_{5\text{-}6}$ 6.7), 2.85 (dq, 1 H, H-5′, $J_{4'\text{-}5'}$ 0.9), 3.60 (dd, 1 H, H-1′, $J_{1\text{-}1'}$ 4.9, $J_{1'\text{-}2'}$ 9.9), 4.12 (dq, 1 H, H-5, $J_{4\text{-}5}$ 3.8), 4.33 (dd, 1 H, H-1, $J_{1\text{-}2}$ 4.3), 5.11 (dd, 1 H, H-3′, $J_{2'\text{-}3'}$ 10.0, $J_{3'\text{-}4'}$ 3.4), 5.24 (dd, 1 H, H-4′), 5.51 (t, 1 H, H-4, $J_{3\text{-}4}$ 3.5), 5.67 (t, 1 H, H-2′), 5.80 (dd, 1 H, H-2, $J_{2\text{-}3}$ 7.1), 5.89 (dd, 1 H, H-3). For **8**: δ_H(500 MHz, C_6D_6) 1.0 (d, 3 H, H-6, $J_{5\text{-}6}$ 6.4), 2.97 (q, 1 H, H-5, $J_{4\text{-}5}$ 0), 3.37 (d, 1 H, H-1, $J_{1\text{-}2}$ 9.0), 5.22 (dd, 1 H, H-3, $J_{2\text{-}3}$ 9.0, $J_{3\text{-}4}$ 3.7), 5.22 (d, 1 H, H-4), 5.90 (t, 1 H, H-2).

§ *Selected data* for **11**: δ_H(500 MHz, C_6D_6) 1.99 (ddd, 1 H, H-6a, $J_{1'\text{-}6a}$ 11.7, $J_{5\text{-}6a}$ 2.9, $J_{6a\text{-}6b}$ 14.9), 2.12 (ddd, 1 H, H-6b, $J_{1'\text{-}6b}$ 2.5, $J_{5\text{-}6b}$ 10.0), 3.86 (dd, 1 H, H-4, $J_{3\text{-}4}$ 8.0, $J_{4\text{-}5}$ 1.9), 3.93 (ddd, 1 H, H-5′, $J_{4'\text{-}5'}$ 8.0, $J_{5'\text{-}6'a}$ 4.5, $J_{5'\text{-}6'b}$ 4.3), 4.14 (ddd, 1 H, H-5), 4.15 (dd, H-2, $J_{1\text{-}2}$ 5.0, $J_{2\text{-}3}$ 2.4), 4.33 (ddd, 1 H, H-6′a, $J_{6'a\text{-}6'b}$ 11.9), 4.38 (ddd, 1 H, H- 6′b), 4.49 (dd, 1 H, H-3), 4.60 (ddd, 1 H, H-1′, $J_{1'\text{-}2'}$ 5.1), 5.24 (dd, 1 H, H-2′, $J_{2'\text{-}3'}$ 8.0), 5.26 (t, 1 H, H-4′, $J_{3'\text{-}4'}$ ≈ 7.9), 5.43 (d, 1 H, H-1), 5.53 (t, 1 H, H-3′). For **12**: δ_H(500 MHz, C_6D_6) 2.07–2.08 (dd, 2 H, H-6a, H-6b, $J_{1'\text{-}6}$ 4.6–4.8, $J_{5\text{-}6}$ 2.0), 3.22 (ddd, 1 H, H-5′, $J_{4'\text{-}5'}$ 10.0, $J_{5'\text{-}6'a}$ 2.0, $J_{5'\text{-}6'b}$ 4.9), 3.52 (dt, 1 H, H-1′, $J_{1'\text{-}2'}$ 9.2), 3.94 (dd, 1 H, H-4, $J_{3\text{-}4}$ 7.8, $J_{4\text{-}5}$ 1.6), 4.03 (dd, 1 H, H-6′a, $J_{6'a\text{-}6'b}$ 12.1), 4.16 (dd, 1 H, H-2, $J_{1\text{-}2}$ 5.2, $J_{2\text{-}3}$ 2.4), 4.26 (dd, 1 H, H-6′b), 4.26 (dt, 1 H, H-5), 4.51 (dd, 1 H, H-3), 5.23 (dd, 1 H, H-4′, $J_{3'\text{-}4'}$ 9.3), 5.30 (dd, 1 H, H-2′), 5.30 (dd, 1 H, H-3′), 5.48 (d, 1 H, H-1).

¶ *Selected data* for **13**: δ_H(500 MHz, $CDCl_3$) 1.12 (d, 3 H, H-6′, $J_{5'\text{-}6'}$ 6.4), 1.84 (ddd, 1 H, H-6a, $J_{1'\text{-}6a}$ 4.2, $J_{5\text{-}6a}$ 8.2, $J_{6a\text{-}6b}$ 14.5), 2.00–2.05 (m, 1 H, H-6b), 3.85 (ddd, 1 H, H-5, $J_{4\text{-}5}$ 1.9, $J_{5\text{-}6b}$ 5.7), 4.05 (dq, 1 H, H-5′, $J_{4'\text{-}5'}$ 1.9), 4.17 (dd, 1 H, H-4, $J_{3\text{-}4}$ 7.9), 4.27 (dd, 1 H, H-2, $J_{1\text{-}2}$ 5.2, $J_{2\text{-}3}$ 2.4), 4.35 (ddd, 1 H, H-1′, $J_{1'\text{-}2'}$ 5.6, $J_{1'\text{-}6b}$ 11.6), 4.57 (dd, 1 H, H-3, $J_{2\text{-}3}$ 2.4), 5.20 (dd, 1 H, H-3′, $J_{2'\text{-}3'}$ 10.0, $J_{3'\text{-}4'}$ 3.0), 5.25 (dd, 1 H, H-4′), 5.28 (dd, 1 H, H-2′), 5.47 (d, 1 H, H-1). For **14**: δ_H(500 MHz, $CDCl_3$) 1.12 (d, 3 H, H-6′, $J_{5'\text{-}6'}$ 6.4), 1.55 (ddd, 1 H, H-6a, $J_{1'\text{-}6a}$ 11.0, $J_{5\text{-}6a}$ 2.0, $J_{6a\text{-}6b}$ 14.7), 1.86 (ddd, 1 H, H-6b, $J_{1'\text{-}6b}$ 1.9, $J_{5\text{-}6b}$ 10.6), 3.63 (dt, 1 H, H- 1′, $J_{1'\text{-}2'}$ 9.6), 3.79 (q, 1 H, H-5′), 4.02 (dd, 1 H, H-4, $J_{3\text{-}4}$ 7.9, $J_{4\text{-}5}$ 1.9), 4.07 (dd, 1 H, H-5), 4.25 (dd, 1 H, H-2, $J_{1\text{-}2}$ 4.9, $J_{2\text{-}3}$ 2.4), 4.54 (dd, 1 H, H-3), 4.98 (dd, 1 H, H-3′, J3′-4′ 3.4, $J_{2'\text{-}3'}$ 10.1), 5.05 (t, 1 H, H-2′), 5.25 (d, 1 H, H-4′), 5.47 (d, 1 H, H-1).

1 For a comprehensive description of *C*-glycosides, see D. E. Levy and C. Tang, *The Chemistry of* C-*glycosides*, Tetrahedron Organic Chemistry Series, Pergamon Press, 1995, vol. 13.
2 P. Sinaÿ, *Pure Appl. Chem.*, 1997, **69**, 459; Y. Wang, P. G. Goekjian, D. M. Ryckman, W. H. Miller, S. A. Babirad and Y. Kishi, *J. Org. Chem.*, 1992, **57**, 482; J.-F. Espinoza, F. J. Cañada, J. L. Asensio, M. Martin-Lomas, R. R. Schmidt and J. Jiménes-Barbero, *J. Am. Chem. Soc.*, 1996, **118**, 10 862; G. Rubinstenn, P. Sinaÿ and P. Berthault, *J. Phys. Chem., A*, 1997, **101**, 2536.
3 M. Benedetto, G. Miglierini, P. Mussini, F. Pelizzoni, S. Rondinini and G. Sello, *Carbohydr. Lett.*, 1995, **1**, 321.
4 S. Rondinini, P. Mussini, G. Sello and E. Vismara, *J. Electrochem. Soc.*, 1998, **145**, 1108.
5 A. Alberti, M. Della Bona, D. Macciantelli, F. Pelizzoni, G. Sello, G. Torri and E. Vismara, *Tetrahedron*, 1996, **52**, 10 241.
6 F. Maran, E. Vianello, G. Catellani and F. D'Angeli, *Electrochim. Acta*, 1989, **34**, 587.
7 H. Shah and O. P. Bahl, *Carbohydr. Res.*, 1974, **32**, 15.
8 E. Vismara, A. Donna, F. Minisci, A. Naggi, N. Pastori and G. Torri, *J. Org. Chem.*, 1993, **58**, 959.
9 E. I. Stout , W. M. Doane and V. C. Trinkus, *Carbohydr. Res.*, 1976, **50**, 282.
10 A. Bravo, H.-R. Bjørsvig, F. Fontana, L. Liguori and F. Minisci, *J. Org. Chem.*, 1997, **62**, 3849 and references cited therein.
11 B. Giese, B. Rückert, K. S. Gröningen, R. Muhn and H. J. Lindner, *Liebigs Ann. Chem.*, 1988, 997.
12 E. Vismara, N. Pastori, M. Guerrini, L. Liguori, A. Naggi and G. Torri, Abstracts XVIIth International Carbohydrate Symposium, Ottawa, Canada, 1994, 338.
13 J. Kochi and F. F. Rust, *J. Am. Chem. Soc.*, 1961, **83**, 2017.

Received in Liverpool, UK, 27th March 1998; 8/02392A

The activation of carbon disulfide by a cluster. The reaction of the μ_3-CS complex $[\{Co(\eta\text{-}C_5H_5)\}_2\{Fe(CO)_2PPh_3\}(\mu_3\text{-}S)(\mu_3\text{-}CS)]$ with CS_2

Anthony R. Manning,[a]† Anthony J. Palmer,[a] John McAdam,[b] Brian H. Robinson[b] and Jim Simpson[b]†

[a] *Department of Chemistry, University College, Belfield, Dublin 4 Ireland,*
[b] *Department of Chemistry, University of Otago, Dunedin, New Zealand*

When $[\{Co(\eta\text{-}C_5H_5)\}_2\{Fe(CO)_2PPh_3\}(\mu_3\text{-}S)(\mu_3\text{-}CS)]$ is refluxed in CS_2 solution, it is converted to $[\{Co(\eta\text{-}C_5H_5)\}_2\{Fe(CO)PPh_3\}(\mu_3\text{-}S)\{\mu_3\text{-}CSC(S)S\}]$ which contains an unusual C_2S_3 bridging ligand.

$[\{Co(\eta\text{-}C_5H_5)\}_2\{Fe(CO)_2PPh_3\}(\mu_3\text{-}S)(\mu_3\text{-}CS)]$ **I** is formed when the η^2-CS_2 ligand in $[Fe(PPh_3)_2(CO)_2(\eta^2\text{-}CS_2)]$ is cleaved by $[Co(\eta\text{-}C_5H_5)(PPh_3)_2]$.[1,2] When a solution of this compound in carbon disulfide is heated to reflux for 12 hours, a further molecule of CS_2 is taken up and CO is lost. The product, **II**, is obtained in 75% yield. It is a brown crystalline solid which, when crystallized from carbon disulfide solution, analyses as $Co_2(\eta\text{-}C_5H_5)_2Fe(CO)(PPh_3)(S)(CS)\cdot 2CS_2$. This is consistent with NMR and IR spectroscopic data,‡ but does not define the actual structure of **II** which was determined by X-ray crystallography on a crystal grown from benzene solution which analyzed as $[\{Co(\eta\text{-}C_5H_5)\}_2\{Fe(CO)PPh_3\}(\mu_3\text{-}S)\{\mu_3\text{-}CSC(S)S\}]\cdot 2C_6H_6$.§ It is illustrated in Fig. 1.

The molecular structure of **II** is closely related to that of **I**[1,2] and is based on an $FeCo_2$ triangle capped on one face by a μ_3-S ligand and on the other by a μ_3-C atom. The coordination about each of the two Co atoms is completed by a η^5-C_5H_5 group whilst that about Fe is completed by a CO and a Ph_3P ligand and the S* atom of a S*C(S)S moiety which is also bonded to the μ_3-C atom. The coordination about Fe is severely distorted from that found in **I** where the $Fe(L)_3$ fragment is more or less symmetrical with respect to an axis from Fe to the midpoint of the Co–Co bond. Furthermore the $FeCo_2$ triangle is no longer an isosceles triangle as it is in **I** [Fe–Co = 2.5099(6), 2.5061(6) Å] as Fe(1)–Co(1) at 2.642(3) Å is very much longer than Fe(1)–Co(2) at 2.502(4) Å.

The C_2S_3 ligand has no precedent. The various C–S bond lengths lie between those for a C=S (*ca.* 1.62 Å in thioketones)[3] and a C–S (*ca.* 1.82 Å in thioethers)[3] which is indicative of delocalised bonding. In particular the μ_3-C–S distance in **II** [1.774(11) Å] is very long compared with that in **I** [1.638(3) Å] or its S-methylated derivative, $[\{Co(\eta\text{-}C_5H_5)\}_2\{Fe(CO)_2PPh_3\}(\mu_3\text{-}S)(\mu_3\text{-}CSMe)]I$, [**III**]I,[2] [1.728(7) Å]. The C–S distances are all longer than the comparable ones in $[Co(\eta\text{-}C_5H_5)(CNBu^t)(S_2C{=}S)]$.[4] The overall reaction which gives rise to **II** is shown in Scheme 1. It is reminiscent of that of a thiolate anion, RS^-, which with CS_2 forms a thioxanthate anion $[RSCS_2]^-$[5] and is a reflection of the nucleophilicity of the μ_3-CS ligand which has been illustrated by the ease with which **I** is alkylated to **III**$^+$ salts. The related complex $[\{Co(\eta\text{-}C_5H_5)\}_3(\mu_3\text{-}S)(\mu_3\text{-}CS)]$ is also readily alkylated at S to give $[\{Co(\eta\text{-}C_5H_5)\}_3(\mu_3\text{-}S)(\mu_3\text{-}CSMe)]I$, but it does not react with CS_2. This implies that the conversion of **I** to **II** takes place because the first-formed $[\{Co(\eta\text{-}C_5H_5)\}_2\{Fe(CO)_2PPh_3\}(\mu_3\text{-}S)(\mu_3\text{-}CS{\rightarrow}CS_2]$ intermediate can undergo CO loss with the formation of an Fe–S bond which stabilizes the C_2S_3 ligand.

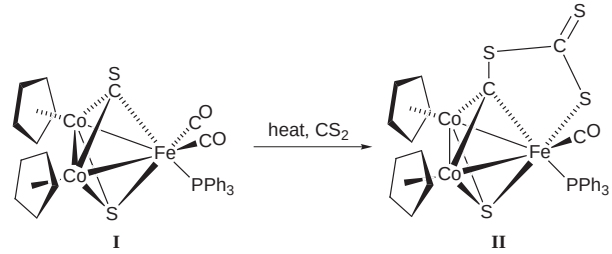

Scheme 1

Analogues of **II** are obtained when Ph_3P in **I** is replaced by $(PhO)_3P$ or $Bu^n{}_3P$, but not when it is replaced by $(MeO)_3P$. The extent of this reaction is being investigated at present.

The exocyclic S atom in **II** is nucleophilic and with electrophiles E such as $Me^+(I^-)$ or $HgCl_2$ gives $[\{Co(\eta\text{-}C_5H_5)\}_2\{Fe(CO)PPh_3\}(\mu_3\text{-}S)\{\mu_3\text{-}CSC(S{\rightarrow}E)S\}]$ adducts. These have been characterized by elemental analysis and spectroscopy.

Attempts to use **I** to activate other cumulenes such as CO_2, COS and MeNCS have not, as yet, been successful. The only isolable product has been $[\{Co(\eta\text{-}C_5H_5)\}_3(\mu_3\text{-}S)(\mu_3\text{-}CS)]$,[6] which is a thermal decomposition product of **I**.

We thank Professor W.T. Robinson, University of Christchurch, Christchurch, New Zealand for collecting the X-ray data, and Labkem Ltd. (Dublin) for financial assistance to A. J. P.

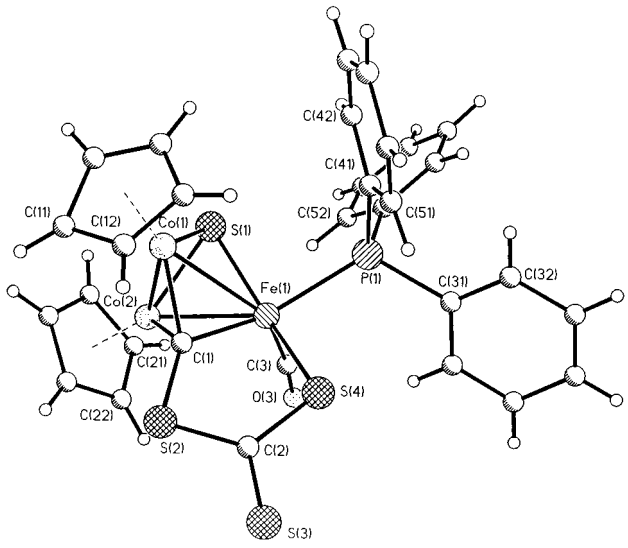

Fig. 1 Structure of $\{Co(\eta\text{-}C_5H_5)\}_2\{Fe(CO)(CS_2)PPh_3\}(\mu_3\text{-}S)(\mu_3\text{-}CS)]$

Notes and References

† E-mail: armannin@ollamh.ucd.ie; jsimpson@alkali.otago.ac.nz

‡ *Spectroscopic data* for **II**: υ(CO) 1922 cm^{-1} (KBr disc); ^1H NMR ($CDCl_3$ solution) δ 4.11(s) and 4.90(s) (C_5H_5); 7.40 (m) (PPh_3); ^{13}C NMR ($CDCl_3$ solution) δ 84.93 and 86.08 (C_5H_5); 128.3(d), 130.2(s), 133.5(d), 135.0(d) (PPh_3); 218.7 (d, J = 22.2 Hz; CO); 243.4 (d, J = 18.7 Hz; SCS); 346.1 (d, J = 15.3 Hz; μ_3-C) [all downfield from $(CH_3)_4Si$; d = doublet].

§ *Crystal data* for **II**: $C_{43}H_{37}Co_2FeOPS_4$, M = 902.65, monoclinic, space group $P2_1/n$, a = 9.853(13), b = 19.97(2), c = 20.61(2) Å, α = 90, β =

91.79(4), $\gamma = 90°$, $U = 4055(8)$ Å^3; $Z = 4$; $D_c = 1.478$ Mg m^{-3}; absorption coefficient 1.440 mm^{-1}; $F(000)$ 1848; data collection $2.04 < \theta < 25.01°$, $-11 < h < 0$, $0 < k < 23$, $-24 < l < 24$, reflections collected 6687, independent reflections collected 6380. Solved by direct methods.[8] Refined by full-matrix least-squares[9] to $R_1 = 0.0692$ and $wR_2 = 0.1575$ [$I = 2\sigma(I)$], and $R_1 = 0.1488$ and $wR_2 = 0.1823$; max. and min. residual electron densities = 1.482 and −0.620 e Å^{-3}, respectively. CCDC 182/907.

1 A. R. Manning, L. O′Dwyer, P. A. McArdle and D. Cunningham, *J. Chem. Soc., Chem. Commun*., 1992, 897.
2 A. R. Manning, L. O′Dwyer, P. A. McArdle and D. Cunningham, *J. Organomet. Chem*., in press, and references therein.
3 F. H. Allen, O. Kennard, D. G. Watson, L. Brammer, A. G. Orpen and R. Taylor, *J. Chem. Soc., Perkin Trans. 2,* 1987, S1.
4 J. Doherty, J. Fortune, A. R. Manning and F. S. Stephens, *J. Chem. Soc., Dalton Trans.*, 1984, 1111.
5 D. Coucouvanis, *Prog. Inorg. Chem.*, 1970, **11**, 233.
6 H. Werner and K. Leonhard, *Angew. Chem., Int. Ed. Engl.*, 1979, **18**, 627. H. Werner, K. Leonhard, O. Kolb, E. Röttinger and H. Vahrenkamp, *Chem. Ber*., 1980, **113,** 1654.
7 J. Fortune and A. R. Manning, *Organometallics*, 1983, **2**, 1719.
8 G. M. Sheldrick, SHELXS-86, A program for the solution of crystal structures from diffraction data, University of Göttingen, Germany, 1986; G. M. Sheldrick, *Acta Crystallogr., Sect. A*, 1990, **46,** 467.
9 G. M. Sheldrick, SHELXL-96, A program for the solution of crystal structures from diffraction data, University of Göttingen, Germany, 1996.

Received in Cambridge, UK, 20th April 1998; 8/02906G

The MTO-catalyzed oxidative conversion of *N*,*N*-dimethylhydrazones to nitriles

Saša Stanković and James H. Espenson*†

Ames Laboratory and Department of Chemistry, Iowa State University, Ames, Iowa, 50011, USA,

Methyltrioxorhenium catalyzes the fast and efficient oxidation of aldehyde *N*,*N*-dimethylhydrazones to the corresponding nitriles in high yield.

N,*N*-Dimethylhydrazones derived from aldehydes (**1**) can be oxidatively transformed into nitriles (**2**) using hydrogen peroxide as the oxidizing agent and methyltrioxorhenium (CH_3ReO_3, abbreviated as MTO) as the catalyst, usually at the 1% level, as shown in eqn. (1). Ten specific examples are

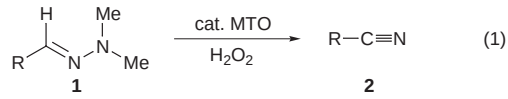

presented in Table 1.

MTO is a well established catalyst for oxidations utilizing hydrogen peroxide,[1,2] including oxidations of various nitrogen-containing compounds.[3–7] The reactions were best carried out in acetonitrile–acetic acid–pyridine solvent, 94.5 : 5 : 0.5. The use of acetic acid was mandatory since the hydrazones are sufficiently basic to deactivate MTO to the inactive perrhenate.[8] Without pyridine, however, the reaction was accompanied by 5–10% hydrolysis to the parent aldehyde. Hydrolysis can effectively be suppressed by a small amount of pyridine, to reduce the Lewis acidity of MTO and its peroxo adducts. This procedure prevents the hydrolysis of epoxides formed by the oxidation of alkenes by MTO–hydrogen peroxide.[9] Pyridine also accelerates the formation of the catalytically active peroxorhenium complexes as in eqn. (2).

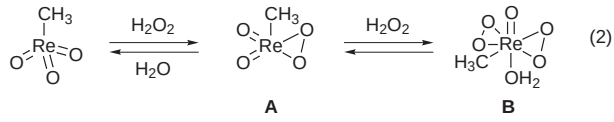

Under the described conditions the hydrazones **1** were completely transformed into the corresponding nitriles after several minutes as indicated by GC–MS analysis. The reaction is quite general: *N*,*N*-dimethylhydrazones of aliphatic, unsaturated, aromatic and heterocyclic aldehydes were successfully oxidized to the corresponding nitriles. Other present oxidizable functionalities did not interfere (see Table 1, entry 8 where the hydrazone was oxidized without the pyridine *N*-oxide being formed). In this particular example pyridine was not used, since the starting hydrazone itself functions in this regard. Also in entry 10, as expected, the double bond was not epoxidized during the reaction, indicating far greater reactivity of the hydrazone moiety compared to the double bond.

The oxidation of **1** presumably goes through the oxide **2**, which undergoes a Cope-type elimination[10] to yield the nitrile **3** and dimethylhydroxylamine **4**, eqn. (3). *N*,*N*-Dialkylhydroxylamines are known to undergo oxidation to nitrones with H_2O_2–MTO.[7] No attempts were made to detect either dimethylhydroxylamine or its oxidation product.

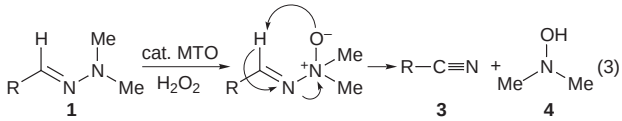

N,*N*-Dialkylhydrazones are versatile and useful intermediates in organic synthesis, especially in carbon–carbon bond forming[11] reactions, which has led to considerable interest in the development of mild methods for their transformation into nitriles. Non-oxidative procedures *via N*,*N*,*N*-trimethylhydrazonium salts or directly, in hyperbasic media,[12,13] have been used, but they require high temperatures and strong bases. Several mild oxidative procedures for the use of hydrogen peroxide, using 3-chloroperbenzoic acid and magnesium monoperoxyphthalate, have been reported.[10,14,15] These reactions, however, are rather slow; for example, the 3-chloroperbenzoic acid reactions require several hours.

Hydrogen peroxide is a desirable reagent on several counts. Selenium dioxide and 2-nitrobenzeneselenic acid catalyze its reactions, giving good yields of nitriles from aromatic and

Table 1 Preparation of nitriles from aldehyde *N*,*N*-dimethylhydrazones[a]

Entry	Hydrazone	Product	Yield[b] (%)
1	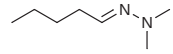		88
2	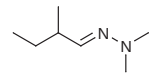		90
3	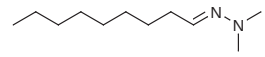	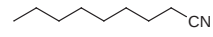	92
4	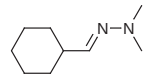		95
5	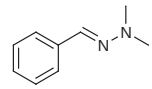		93
6	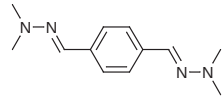	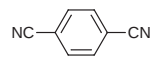	94
7	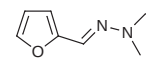		93
8	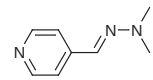		92[c]
9	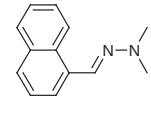	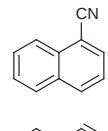	94
10	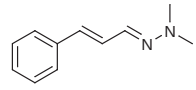	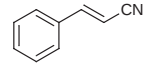	91

[a] With 10 mM substrate, 300 mM H_2O_2, 25 mM pyridine and 1 mM MTO in acetonitrile, acetic acid, pyridine (94.5:5:0.5) for 15 min. [b] Isolated yield. [c] Without pyridine.

unsaturated *N*,*N*-dimethylhydrazones, but hours, even days, are required. Moreover, these catalysts give poor results with aliphatic *N*,*N*-dimethylhydrazones which are largely hydrolyzed. Phosphomolybdic acid, $H_3PO_4 \cdot 12MoO_3 \cdot 12H_2O$, performs better with aliphatic hydrazones but it gives by-products such as the corresponding acids. Compared to these catalysts, MTO is clearly superior. MTO also catalyzes the oxidative cleavage of ketone hydrazones to the parent carbonyl compounds; these reactions are now being investigated.

A typical experimental procedure is as follows: **1** (100 mmol) was added to a rapidly stirred solution of MTO (1 mM), hydrogen peroxide (0.3 M, added as 30% solution in water), pyridine (25 mM) in 100 ml of acetonitrile containing 5 vol% HOAc. After 15 min, most of the acetonitrile was removed by rotary evaporation, and the residue poured into 300 ml of diethyl ether, washed successively with 0.1 M HCl and saturated sodium hydrogen carbonate. (In the case of 4-cyanopyridine, entry 8, the ether solution was washed only once with saturated sodium hydrogen carbonate.) The ethereal solution was then dried over anhydrous sodium sulfate, and the product obtained after evaporation. The crude nitriles were purified by column chromatography (*n*-hexane–acetone).

This research was supported by the US Department of Energy, Office of Basic Energy Sciences, Division of Chemical Sciences under contract W-7405-Eng-82.

Notes and References

† E-mail: espenson@ameslab.gov

1 W. A. Herrmann and F. E. Kühn, *Acc. Chem. Res.*, 1997, **30**, 169.
2 J. H. Espenson and M. M. Abu-Omar, *Adv. Chem. Ser.*, 1997, **253**, 99.
3 S. Yamazaki, *Bull. Chem. Soc. Jpn.*, 1997, **70**, 877.
4 R. W. Murray, K. Iyanar, J. Chen and J. T. Wearing, *Tetrahedron Lett.*, 1996, **37**, 805.
5 R. W. Murray, K. Iyanar, J. Chen and J. T. Wearing, *J. Org. Chem.*, 1996, **61**, 8009.
6 A. Goti and L. Nanneli, *Tetrahedron Lett.*, 1996, **37**, 6025.
7 T. H. Zauche and J. H. Espenson, *Inorg. Chem.*, 1997**, 36**, 5257.
8 M. M. Abu-Omar, P. J. Hansen and J. H. Espenson, *J. Am. Chem. Soc.*, 1996, **118**, 4966.
9 J. Rudolph, K. L. Reddy, J. P. Chiang and K. B. Sharpless, *J. Am. Chem. Soc.*, 1997, **119**, 6189.
10 R. Fernandez, C. Gasch, J. Lassaletta, J. Llera and J. Vazquez, *Tetrahedron Lett.*, 1993, **34**, 141.
11 E. J. Corey and D. Enders, *Chem. Ber.*, 1978, **111**, 1337, 1362.
12 R. F. Smith and R. E. J. Walker, *Org. Chem.*, 1962, **27**, 4372.
13 T. Cuvigny, J. F. Le Borgne, M. Larcheveque and H. Normant, *Synthesis*, 1977, 237.
14 S. B. Said, J. Skarzewski and J. Mlochowski, *Synthesis*, 1989, 223.
15 J. Mlochowski, K. Kloc and E. Kubicz, *J. Prakt. Chem.*, 1994, **336**, 467.

Received in Bloomington, IN, USA, 14th April 1998; 8/02723D

Dithioamide metal ion receptors on fluorescent lipid bilayers for the selective optical detection of mercuric ion

Darryl Y. Sasaki*† and Benjamin E. Padilla

Sandia National Laboratories, Albuquerque, NM 87185, USA

Functionalized lipid bilayers with dithioamide receptors at the surface and pyrene labels in the hydrophobic interior showed a selective fluorescence response to mercuric ion with sensitivity limits at the ppb level.

The release of mercury into the environment originates from a variety of man-made and natural sources, including fossil fuel combustion and the electronics industry.[1] As many mercurial compounds are highly toxic, the monitoring of mercurials in the environment and in industrial waste streams is highly desirable. The development of optically responsive sensor materials for the detection of heavy metal ions has received much attention in recent years offering an inexpensive and robust sensor platform with remote detection capability. Often the sensor material employs the use of ion recognition sites to selectively bind specific analytes from solution. In particular, sensors that can detect mercuric ion have been prepared using porphyrins,[2] bioreceptors,[3] borates[4] and polyamines[5] as the ion recognition ligands. Typically the recognition group operates in conjunction with a neighboring chromophore that produces a change in spectral properties upon binding. We describe here a novel sensor material that uses a molecular assembly as a platform for ion recognition as well as a reversible and sensitive optical transducer to the binding event.

Previously[6] we showed that a distearylphosphatidylcholine (DSPC) bilayer doped with a synthetic lipid having an iminodiacetic acid headgroup and a pyrene label in the tail could detect sub-ppb levels of Cu^{2+} selectively. The selectivity was determined to be a function of the ion binding headgroup, however, the mechanism of the fluorescence response and generality of the detection approach was uncertain. Herein, we describe a new sensor tailored for the binding and detection of 'soft' metal ions previously not recognized by the iminodiacetic acid group. As the recognition ligand we chose the thioamide functional group for selective detection of mercuric ion.[7,8] Lipid **1**,‡ which contains the dithioamide headgroup, was prepared by a series of steps starting from compound **2**.[9] The alcohol headgroup of **2** was converted to the primary amine by mesylation of the alcohol, followed by azide substitution with sodium azide in DMF, and then LAH reduction. The reaction of this amine with 8-(4-nitrophenyl)-3,6-dioxaoctanoate-1-dibutylamide, prepared through two steps from 3,6-dioxaoctanedioic acid, yielded the diamide product **3** in 83% yield. The dithioamide **1** was obtained as a light yellow–green viscous liquid in 75% yield through the reaction of **3** with P_2S_5 in pyridine at elevated temperature for 24 h followed by flash column chromatography.

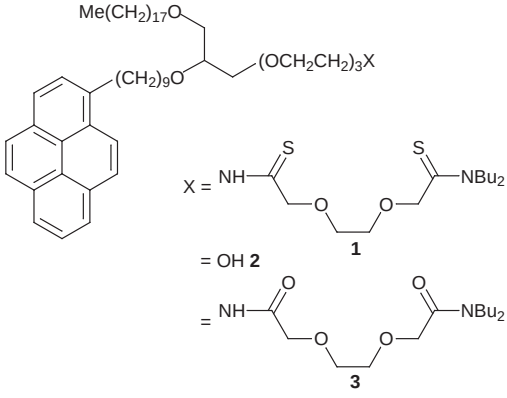

Lipid bilayer preparation is briefly described below; a more detailed description can be found elsewhere.[10] Films of 5% **1** in DSPC were prepared by evaporation of a chloroform solution of the lipids on the inside of a conical tube. The films were then hydrated in a MOPS buffer solution (pH 7.4, 0.02 M morpholinopropanesulfonic acid–0.10 M NaCl) at 65 °C with vortex mixing. The solution temperature was maintained near room temperature while being probe sonicated for 12 min using a 2 mm tip at a power of 25 W under a nitrogen atmosphere. Following sonication the solution was centrifuged and the supernatant passed through a 0.2 μm filter. Total lipid incorporated into the bilayers was 50% as determined by phosphate analysis.[11] The **1**/DSPC aggregates imaged with transmission electron microscopy (not shown here), using a 1% ammonium molybdate stain, formed disc-like structures with no apparent inner volume unlike the typical spherical structures found with DSPC liposomes. Although the structural geometry and headgroup polarity of the lipid components determine the packing geometry of the bilayer,[11] it is interesting to find that incorporation of small amounts of **1** can significantly alter the DSPC bilayer geometry. Details of these and related results will be described elsewhere.

The fluorescence spectrum of the 5% **1**/DSPC lipid bilayers in buffered solution shows emission maxima from both the pyrene monomer at 376 nm and the excimer at near 470 nm [Fig. 1(*a*)]. With a total lipid concentration of 0.05 mM the observed excimer to monomer intensity ratio (*E*/*M*) is 2.2. Addition of certain metal ions (chloride salts) into solution causes a decrease in the fluorescence intensity of the pyrene excimer with a concomitant increase in the monomer emission. A highly selective response was found for mercuric ion with a limit of detection at 100 nM (20 μg l^{-1}). Fig. 1(*b*) shows an example of the fluorescence response from the 5% **1**/DSPC bilayers to the presence of 1.0 mM Hg^{2+}. The *E*/*M* response for Hg^{2+} was linear from a concentration of 10^{-7} to 10^{-4} M on a semilogarithmic plot shown in Fig. 2. Against the heavy metal

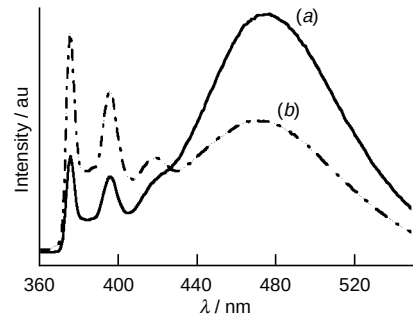

Fig. 1 Fluorescence spectra of 5% **1**/DSPC lipid bilayers in MOPS buffer solution (pH 7.4) in the absence (*a*) and presence of 1.0 mM $HgCl_2$ (*b*)

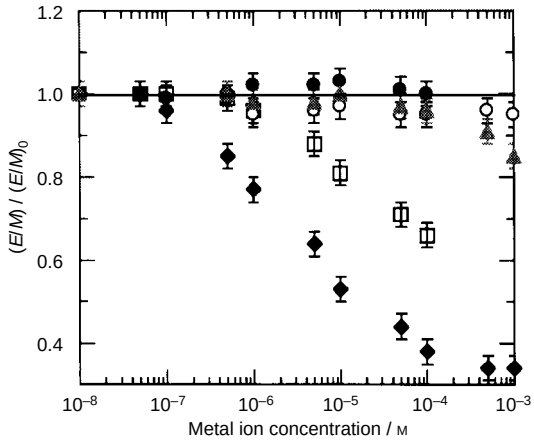

Fig. 2 Plot of the normalized ratio of fluorescence intensities from pyrene excimer to monomer (*E/M*) *vs.* metal ion concentration, showing metal ion selectivity of the 5% **1**/DSPC bilayers. Selectivity was in the order Hg^{2+} (◆) > Cu^{2+} (□) ≫ Cd^{2+} (▲) > Pb^{2+} (●) and Mn^{2+} (○). Equilibration of response took only moments following addition of metal ion and slight stirring.

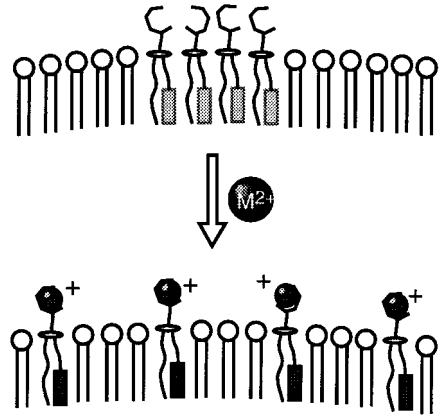

Fig. 3 Illustration of lipid molecule aggregational changes upon metal ion binding to receptor sites. Initially the receptor **1** is phase separated from the DSPC matrix. Metal ion complexation with the receptor and formation of charged headgroups causes static repulsion of the pyrene labeled molecules and loss of local aggregation.

ions Mn^{2+}, Ni^{2+}, Ca^{2+}, Cr^{3+}, Co^{2+} and Pb^{2+}, the bilayers were unresponsive up to mM concentrations. Of the metals evaluated only Cu^{2+} and Cd^{2+} gave responses with 10- and 1000-fold lower sensitivity, respectively, compared to Hg^{2+}. The material was also insensitive to high concentrations (100 mM) of monovalent alkali metals (*i.e.* Na^+, Li^+, K^+). Response times were rapid, limited only by the rate of mixing of the solution. To regenerate the material an excess of EDTA was added to solution to remove metal ions bound to the recognition sites. Complete fluorescence recovery was realized in a few minutes and the material could be reused. As a control, compound **3**, which has a poor metal chelating headgroup, when prepared as a bilayer with DSPC and tested for metal sensitivity showed no response to any of the above mentioned metal ions.

The observed fluorescence response to selected metal ions is due to a change in aggregational properties of the pyrene labeled lipid in the DSPC matrix. In the absence of metal ion, molecules of lipid **1** tend to aggregate into pools within the bilayer due to differences between the physical state of the two membrane components. At room temperature, DSPC (T_c = 55 °C) forms crystalline domains causing a partitioning from the liquid phase of lipid **1** (T_c < room temperature). This creates high local concentrations of pyrene which increases the collision rate of the fluorophores subsequently producing a large population of pyrene excimers compared to monomers.[12] Metal ion binding to the dithioamide headgroup induces a reorganization of molecules in the molecular assembly. Aggregates of **1** are dispersed into the DSPC matrix reducing the local concentration of pyrene resulting in a population shift in the excited state species and the observed loss in intensity of excimer emission and gain in monomer emission. Of the changes that could result from metal ion complexation, formation of a charged headgroup on **1** producing static repulsion between **1**–M^{2+} chelates would lead to the observed changes in molecular organization in the bilayer. Fig. 3 illustrates the molecular aggregate state before and after metal complexation. Initially, when **1** is neutrally charged, lipid organization is controlled by differences in the crystalline and liquid behavior of the components. Following metal ion binding and formation of charged headgroups on **1** electrostatic repulsion overcomes the separation of physical phases resulting in a dispersal of **1** in the matrix.

Although dithioamides have been used as ionophores for 'soft' metals, such as Hg^{2+}, Pb^{2+} and Cd^{2+}, the present sensor shows almost exclusive selectivity for Hg^{2+}. Some slight structural differences that exist between those in literature[7,8] and that on **1**, and the use of a lipid bilayer as the site of recognition, may account for the differences in selectivity. We are continuing to pursue new metal chelating headgroups to increase the range of metal ion selectivities for eventual configuration into a sensor array system for evaluation of mixed wastes.

Sandia is a multiprogram laboratory operated by Sandia Corporation, a Lockheed Martin Company, for the United States Department of Energy under Contract DE-AC04-94AL85000.

Notes and References

† E-mail: dysasak@sandia.com

‡ *Selected data* for **1**: ^{1}H NMR (400 MHz, $CDCl_3$) δ 8.86 (br s, 1 H, NH), 8.28 (d, 1 H, *J* 9.3 Hz, Py-H), 8.10 (m, 7 H, Py-H), 7.87 (d, 1 H, *J* 7.8 Hz, Py-H), 4.54 [s, 2 H, $OCH_2C(S)NBu_2$], 4.39 [s, 2 H, $OCH_2C(S)NH$], 3.92 [dt, *J* 5.4, 5.4 Hz, 2 H, $CH_2NHC(S)$], 3.85 (t, *J* 7.5 Hz, 2 H, CH_2O), 3.76–3.40 (m, 25 H, CH_2O, CH_2N), 3.33 (t, *J* 7.7 Hz, 2 H, $PyCH_2$), 1.85 (tt, *J* 7.7, 7.7 Hz, 2 H, $PyCH_2CH_2$), 1.72–1.24 (m, 57 H, aliphatic CH_2), 0.95 [t, *J* 7.4 Hz, 6 H, $N(CH_2)_3CH_3$], 0.87 [t, *J* 6.9 Hz, 3 H, $(CH_2)_{17}CH_3$]. Anal. Calc. for $C_{66}H_{108}N_2O_7S_2$: C, 71.69; H, 9.84; N, 2.53; S, 5.80. Found: C, 71.51; H, 9.96; N, 2.50; S, 6.11%.

1 *Metals in the Environment*, ed. H. A. Waldron, Academic Press, London, 1980.
2 R. Czolk, J. Reichert and H. J. Ache, *Sens. Actuators B*, 1992, **7**, 540.
3 M. Virta, J. Lampinen and M. Karp, *Anal. Chem.*, 1995, **67**, 667.
4 I. Murkovic and O. S. Wolfbeis, *Sens. Actuators B*, 1997, **38**–**39**, 246.
5 J. Yoon, N. E. Ohler, D. H. Vance, W. D. Aumiller and A. W. Czarnik, *Chemosensors of Ion and Molecule Recognition*, ed. J. P. Desvergne and A. W. Czarnik, 1997, vol. 492, p. 189.
6 D. Y. Sasaki, D. R. Shnek, D. W. Pack and F. H. Arnold, *Angew. Chem., Int. Ed. Engl.*, 1995, **34**, 905.
7 M. Lerchi, E. Bakker, B. Rusterholz and W. Simon, *Anal. Chem.*, 1992, **64**, 1534.
8 A. Borraccino, L. Campanella, M. P. Sammartino, M. Tomassetti and M. Battilotti, *Sens. Actuators B*, 1992, **7**, 535.
9 Synthetic preparation can be found in: K. Ng, D. W. Pack, D. Y. Sasaki and F. H. Arnold, *Langmuir*, 1995, **11**, 4048.
10 S. A. Yamanaka, D. H. Charych, D. A. Loy and D. Y. Sasaki, *Langmuir*, 1997, **13**, 5049.
11 R. R. C. New, *Liposomes*, ed. D. Rickwood and B. D. Hames, Oxford University Press, New York, 1990, ch. 3.
12 H.-J. Galla and W. Hartman, *Chem. Phys. Lipids*, 1980, **27**, 199.

Received in Columbia, MO, USA; 24th March 1998; 8/02534G

Aerobic enantioselective alkene epoxidation by a chiral *trans*-dioxo(D_4-porphyrinato)ruthenium(VI) complex

Tat-Shing Lai,[a] Rui Zhang,[a] Kung-Kai Cheung,[a] Hoi-Lun Kwong[b] and Chi-Ming Che*[a]†

[a] *Department of Chemistry, The University of Hong Kong, Pokfulam Road, Hong Kong, PR China*
[b] *Department of Biology and Chemistry, City University of Hong Kong, Tat Chee Avenue, Kowloon Tong, Hong Kong, PR China*

A dioxoruthenium(VI) complex with a D_4-chiral porphyrin ligand has been prepared and characterized by spectroscopic methods and X-ray crystal analysis; the complex exhibits catalytic activity towards aerobic enantioselective epoxidation of prochiral alkenes with enantioselectivity up to 73% ee at an oxygen pressure of 8 atm.

Among various terminal oxidants used in metalloporphyrin-catalysed organic oxidations,[1] dioxygen is the most appealing since it is both economical and environmental friendly,[2,3] but reports on the use of dioxygen in enantioselective alkene epoxidations are sparse. Chiral Mn(β-ketoiminato) complexes were reported to catalyse asymmetric aerobic alkene epoxidations but aldehyde is required as a sacrificial reducing agent.[4] We herein report the first example of aerobic enantioselective epoxidation of alkenes that does not rely on the use of a co-reductant. The D_4-porphyrin was synthesized according to the literature procedure.[5] The catalyst precursor is [Ru^{II}(por*)(CO)(EtOH)] **1**[6,7] which has been characterized by X-ray crystallography.[7] Oxidation of complex **1** with

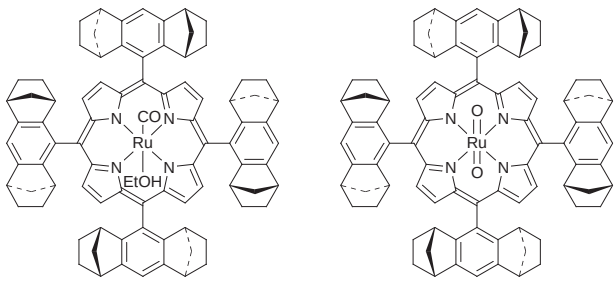

1 **2**

m-chloroperoxybenzoic acid in CH_2Cl_2 afforded [Ru^{VI}(por*)O_2] **2** in 60–70% yield after purification by column chromatography.‡ Complex **2** is diamagnetic. Its FAB spectrum shows peaks attributed to M^+, [$M^+ - O$] and [$M^+ - 2O$]. The $\nu_{as}(RuO_2)$ stretch and the oxidation marker band are positioned at 822 and 1019 cm^{-1} respectively. These spectroscopic data agree with the *trans*-dioxoruthenium(VI) formulation.[8,9] The structure with a high R_w value was established by an X-ray diffraction study (Fig. 1).§ The Ru=O distances average 1.74 Å, as expected for a Ru=O bond.[10] Unlike other reported [Ru^{VI}(por)O_2] (por = porphyrinato dianion) complexes,[2,8,9] complex **2** is stable in solid state for months and in purified MeCN or CH_2Cl_2 for more than 24 h. However in the presence of pyrazole, it reacts with alkenes to give the corresponding epoxides with moderate to good enantioselectivities and a paramagnetic ruthenium product that was formulated to be [Ru^{IV}(por*)$(pz)_2$] [pz = pyrazolate, μ_{eff} = 2.94 μ_B (solid sample) at room temp., FABMS *m/z* = 1375] (Scheme 1). The results are summarized in Table 1. For the five alkenes studied, the ee ranged from 20 to 72%. The 65% ee of styrene oxide (entry 1) is among the highest obtained with chiral porphyrin catalysts.[11,12] However, the ee obtained for *cis*-disubstituted alkenes are not as high as those obtained with chiral Mn–Schiff base catalytic system.[13] The absolute configurations of the major enantiomers of styrene oxide and *cis*-β-methylstyrene oxide were determined to be (*R*) and (1*R*, 2*S*) respectively. The epoxidation of *cis*-β-methylstyrene (entry 2) proceeded with high retention of configuration. Epoxidation of *trans*-β-methylstyrene gave only 20% ee and complete retention of configuration (entry 3).

Interestingly, the dioxoruthenium complex catalysed enantioselective aerobic oxidation of alkenes with moderate to good ee (Scheme 2). The results are listed in Table 1. Catalytic oxygenation of styrene using air at 1 atm pressure in CH_2Cl_2 gave very low turnover. However, under 8 atm pressure of oxygen, styrene oxide was obtained with 10 turnovers and 70% ee (entry 1). With *cis*-β-methylstyrene as the substrate, *cis*-β-methylstyrene oxide was observed with 20 turnovers and 69% ee and the ee increased to 73% if toluene was used as the solvent. The *cis*/*trans* ratio was 10 (entry 2), a value similar to that obtained in the stoichiometric reaction. Prolonged reaction time from one to two days did not increase the total turnovers. At the end of the reaction, UV–VIS spectrophotometric analysis of the reaction mixture revealed that the ruthenium–porphyrinato moiety remained intact (Soret band was at 411 nm). A brown diamagnetic complex, which showed no ν(C=O) IR band, was isolated after silica gel-column chromatography using ethyl acetate as the eluent. Its FABMS spectrum revealed

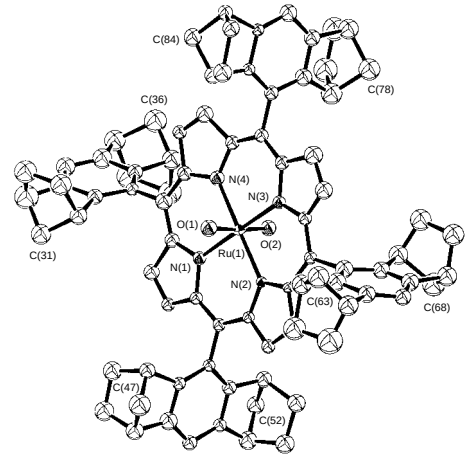

Fig. 1 Perspective drawing of **2**. Selected bond lengths (Å) and angles (°): Ru–O(1) 1.73(1), Ru–O(2) 1.75(1), Ru–N(1) 2.08(1), Ru–N(2) 2.069(10), Ru–N(3) 2.05(1), Ru–N(4) 2.05(1); O(1)–Ru–O(2) 175.4(5), O(1)–Ru–N(1) 91.1(5), N(1)–Ru–N(2) 90.3(4), N(1)–Ru–N(3) 178.3(5).

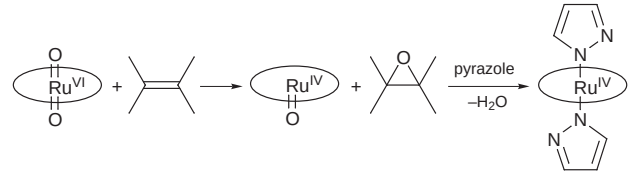

Scheme 1

Table 1 Enantioselective epoxidation of alkenes by $[Ru^{VI}(por^*)O_2]$

Entry	Substrate	Product	Stoichiometric[a]		Catalytic aerobic[b]	
			% yield[c]	% ee[d]	turnover no.[e]	% ee[d]
1	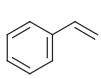	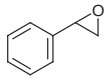	61[f]	65 (*R*)[f,g]	10	70 (*R*)
		benzaldehyde	22		5	
		2-phenylacetaldehyde	13		1	
2	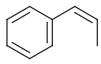	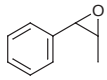	64	72 (1*R*, 2*S*)[h]	20	69 (1*R*, 2*S*)
					21[i]	73 (1*R*, 2*S*)[i]
		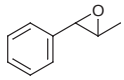	5	n.d.	2	n.d.
					3[i]	n.d.
3	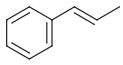	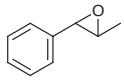	66[f]	20[f]	—	—
4	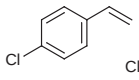	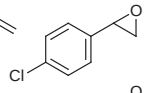	71	45 (*R*)[j]	11	52 (*R*)
5	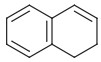	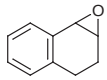	61	71	14	56

[a] Stoichiometric reactions were conducted at room temperature for 12 h; oxidant 4 mg, substrate 200 mg, pyrazole 50 mg in 5 ml CH_2Cl_2 unless otherwise stated. [b] Reactions were performed at room temp. at *ca.* 8 atm for 22–24 h; catalyst 4 mg and substrate 40 mg in 4 ml CH_2Cl_2 unless otherwise stated. [c] Yield were calculated based on the amount of ruthenium complex. [d] Enantiomeric excesses were determined by chiral GC (J&W Scientific Cyclodex B; length 30 m for entries 1, 2, 4 and 5, chiraldex G-TA, 30 m for entry 3). [e] The product yields for the calculation of turnover no. were determined by GC with *p*-dichlorobenzene or *p*-bromochlorobenzene as internal standards. [f] In benzene. [g] Absolute configuration was determined by comparison with an authentic sample. [h] Absolute configuration was determined by matching the order of elution of the two enantiomers on a Cyclodex-B column. [i] In toluene. [j] Absolute configuration was determined by comparing its ^{1}H NMR spectrum in the presence of $Eu(hfc)_3$ with that of a sample of known enantiomeric composition, J. T. Groves and R. S. Myres, *J. Am. Chem. Soc.*, 1983, **105**, 5791.

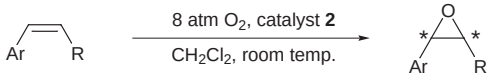

Scheme 2

a $[Ru(por^*)(C_9H_{10}O)]$ ion peak [*m/z* = 1377 (20%)]. The dioxoruthenium(VI) complex is likely to be the active intermediate of the reaction, since with the exception of 1,2-dihydronaphthalene, both the catalytic and stoichiometric reactions produced similar ee for the same substrate, and thus the mechanism of this reaction could be similar to that of the $[Ru(tmp)O_2]$ (H_2tmp = tetramesitylporphyrin) system reported by Groves and Quinn.[2] As the Ru–D_4-porphyrin moiety has survived the oxidation, we envisage that high catalytic turnovers can be achieved through optimizing the reaction conditions. Thus this work has provided a starting point for designing future catalysts for efficient aerobic enantioselective epoxidation without the need of a sacrificial reducing agent.

Supports from the Hong Kong Research Grants Council, The University of Hong Kong and City University of Hong Kong are gratefully acknowledged.

Notes and References

†E-mail: cmche@hkucc.hku.hk

‡ ^{1}H NMR (300 MHz, $CDCl_3$), δ 0.8–2.4 (m), 2.58 (s, 8 H), 3.80 (s, 8 H), 7.44 (m, 4 H, ArH), 8.73 (s, 8 H, pyrrolic H). ^{13}C NMR (300 MHz, $CDCl_3$), δ 27.183, 27.565, 42.417, 44.403, 49.339, 113.988, 118.923, 127.908, 130.780, 141.533, 144.272, 148.062. FABMS+: *m/z* 1274 (M^+, 35%), 1258 ($M^+ - O$, 23%), 1242 ($M^+ - 2O$, 98%).

§ *Crystallographic data* for **2**: $[Ru(por^*)O_2]\cdot 3MeCN$: $C_{90}H_{85}N_7O_2Ru$, M = 1397.78, monoclinic, space group $P2_1$ (no. 4), a = 14.734(2), b = 18.447(3), c = 15.627(3) Å, β = 110.61(2)°, U = 3975(1) Å^3, Z = 2, D_c = 1.170 g cm^{-3}, $F(000)$ = 1468, μ = 2.48 cm^{-1}, crystal dimensions 0.10 × 0.05 × 0.30 mm. Diffraction data were collected at 28 °C on a MAR diffractometer with a 300 mm image plate detector using graphite monochromated Mo-Kα radiation (λ = 0.710 73 Å). The images were interpreted and intensities integrated using program DENZO. 3692 Unique and independent reflections were obtained, 3048 with $I > 3\sigma(I)$ were used in the structural analysis. These reflections were in the range h 0–13, k 0–17, l −15 to 15 with $2\theta_{max}$ = 51.2°. The structure was solved by Patterson methods and expanded by Fourier methods (PATTY) and refinement by full-matrix least squares using the software package TeXsan on a Silicon Graphics Indy computer. In the least-squares refinement, in view of the large thermal parameters of the four chiral radical $C_{16}H_{17}$, only the Ru atom was refined anisotropically and all the other 99 non-H atoms were refined isotropically and 88 H atoms at calculated positions with thermal parameters equal to 1.3 times that of the attached C atoms were not refined. Convergence for 405 variable parameters by least-squares refinement on F with $w = 4F_o^2/\sigma^2(F_o^2)$, where $\sigma^2(F_o^2) = [\sigma^2(I) + (0.063F_o^2)^2]$ for 3048 reflections with $I > 3\sigma(I)$ was reached at R = 0.084 and wR = 0.117 with a goodness-of-fit of 3.00, $(\Delta/\sigma)_{max}$ = 0.04 for atoms of the porphyrin skeleton. The final difference Fourier map had maximum positive and negative peaks of 1.15 and 0.51 e Å^{-3} respectively. CCDC 182/892.

1 *Metalloporphyrins in Catalytic Oxidations*, ed. R. S. Sheldon, M. Dekker, New York, 1994; B. Meunier, *Chem. Rev.*, 1992, **92**, 1411.
2 J. T. Groves and R. Quinn, *J. Am. Chem. Soc.*, 1985, **107**, 5790.
3 W. H. Leung, C. M. Che, C. H. Yeung and C. K. Poon, *Polyhedron*, 1993, **12**, 2331.
4 T. Mukaiyama, T. Yamada, T. Nagata and K. Imagawa, *Chem. Lett.*, 1993, 327.
5 R. L. Halterman and S. T. Jan, *J. Org. Chem.*, 1991, **56**, 5253.
6 A. Berkessel and M. Frauenkron, *J. Chem. Soc., Perkin Trans. 1*, 1997, 2265.
7 W. C. Lo, C.-M. Che, K. F. Cheng and T. C. W. Mak, *Chem. Commun.*, 1997, 1205.
8 J. T. Groves and R. Quinn, *Inorg. Chem.*, 1984, **23**, 3844.
9 W. H. Leung and C.M. Che, *J. Am. Chem. Soc.*, 1989, **111**, 8812.
10 W. C. Cheng, W. Y. Yu, K. K. Cheung and C. M. Che, *J. Chem. Soc., Dalton Trans.*, 1994, 57.
11 J. P. Collman, X. Zhang, V. J. Lee, E. S. Uffelman and J. I. Brauman, *Science*, 1993, **261**, 1404.
12 R. L. Halterman, S. T. Jan, H. L. Nimmons, D. J. Standlee and M. A. Khan, *Tetrahedron*, 1997, **53**, 11257.
13 E. N. Jacobsen, W. Zhang, A. R. Muci, J. R. Ecker and L. Deng, *J. Am. Chem. Soc.*, 1991, **113**, 7063.

Received in Cambridge, UK, 12th March 1998; 8/02009D

‘Phospha-Wittig’ reactions using isolable phosphoranylidenephosphines ArP=PR$_3$ (Ar = 2,6-Mes$_2$C$_6$H$_3$ or 2,4,6-But$_3$C$_6$H$_2$)

Shashin Shah and John D. Protasiewicz*†

Department of Chemistry, Case Western Reserve University, Cleveland, OH 44106-7708, USA

Phosphoranylidenephosphines DmpP=PMe$_3$ (1a, Dmp = 2,6-Mes$_2$C$_6$H$_3$) and Mes*P=PMe$_3$ (1b, Mes* = 2,4,6-But$_3$C$_6$H$_2$) act as ‘Phospha-Wittig’ reagents with aldehydes providing phosphaalkenes [ArP=C(H)R] in high yields.

The successful synthesis of a ‘true phosphobenzene’, Mes*P=PMes* (Mes* = 2,4,6-But$_3$C$_6$H$_2$),[1] signaled a new era in the study of phosphorus–phosphorus double bonds.[2] We have recently uncovered reactions of [Cp$_2$Zr=PDmp(PR$_3$)] (Dmp = 2,6-Mes$_2$C$_6$H$_3$) which produce phosphoranylidenephosphines DmpP=PR$_3$ (R = Me or Bu).[3] Phosphoranylidenephosphines are formally the products of phosphinidene transfer to phosphines.[4] These novel materials contain PP multiple bonding of a very differing nature, as exemplified by the following resonance forms:

$$\mathrm{ArP{=}PR_3 \leftrightarrow Ar\bar{P}{-}\overset{+}{P}R_3}$$

Similar resonance forms are commonly drawn for Wittig reagents R$_2$C=PR$_3$, and the nature of the bonding between the P and C atoms in these species has been reviewed.[5] Bearing such a close kinship to Wittig reagents, it was anticipated that phosphoranylidenephosphines could act as potential ‘phospha-Wittig’ reagents by reacting with aldehydes to generate phosphaalkenes RP=C(H)R [eqn. (1)]. Several transition metal containing systems have been reported that accomplish similar transformations.[6–8] Herein we present the reactivity of the phosphoranylidenephosphines DmpP=PMe$_3$ **1a** and Mes*P=PMe$_3$ **1b** with aldehydes to generate phosphaalkenes.

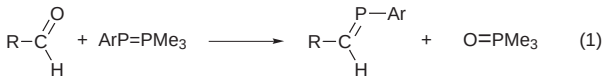

(1)

Compounds **1a** and **1b** are conveniently prepared by reduction of either DmpPCl$_2$ or Mes*PCl$_2$ with Zn dust in the presence of excess PMe$_3$ in 88–95% yields [**1a**: ^{31}P NMR (C$_6$D$_6$), δ −2.8, −114.7 (J_{PP} 582 Hz); **1b**: ^{31}P NMR (C$_6$D$_6$), δ 4.7, −134.0 (J_{PP} 581 Hz)].[3]‡ In the absence of air and water, compounds **1a**, **b** are stable yellow crystalline solids. Both **1a** and **1b** slowly decompose in solution to lose PMe$_3$ and form DmpP=PDmp and Mes*P=PMes*, respectively (days to weeks).[9]

Reactions of **1a** and **1b** with C=O containing molecules were thus examined. A series of *para*-substituted benzaldehydes reacted with **1a**, **b** in THF to produce the desired phosphaalkenes in excellent isolated yields (Table 1). Work-up involves removal of THF and extraction of the phosphaalkene into hexanes to remove the relatively insoluble O=PMe$_3$. Reaction times, as well as product yields, varied with the nature of the substituent; the most electron releasing substituents required the longest reactions times (2–24 h) and provided the lowest yields. Each reaction produced a single isomer of the phosphaalkene, and the $^2J_{PH}$ coupling constants (24–25 Hz) are consistent with an assignment of *E*-isomers for the products.[10]§

Our new protocol can be contrasted to multistep procedures utilizing sterically hindered primary phosphines such as Mes*PH$_2$. For example, compound **2b** has been prepared in 80% yield after purification by chromatography [eqn. (2)].[10] The primary phosphine Mes*PH$_2$ is obtained by LiAlH$_4$ reduction of Mes*PCl$_2$ and isolated in 80% yield after recrystallization.[11] Our procedure thus represents not only a saving in time but also of material due to phosphaalkene access from the more readily available dichlorophosphine precursors. A more dramatic advance in the utility of the current reaction was realized by the discovery that compounds **1a** and **1b** can be generated and used *in situ*. For example, reaction of DmpPCl$_2$, benzaldehyde, zinc dust and excess PMe$_3$ gives an isolated yield of 95% of DmpP=C(H)Ph. Likewise, Mes*P=C(H)Ph is obtained in 87% yield from Mes*PCl$_2$ under the same conditions.

(2)

The scope of the phosphaalkene forming reactions using **1a** was also investigated. Pentafluorobenzaldehyde, ferrocenecarboxaldehyde and pivaldehyde provided phosphaalkenes **7a**–**9a** in good yields, demonstrating the remarkable tolerance of the phosphoranylidenephosphines to varying functional groups. Reactions of **1a** with ketones proved more problematic,

Table 1 Reactions of aldehydes to give phosphaalkenes

Aldehyde R(H)C=O		Phosphaalkene R(H)C=PAr	Yield (%)	^{31}P{^{1}H} (C$_6$D$_6$)§ δ
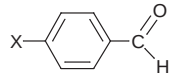	X = H	**2a**	94	240.9
		2b	93	258.5[10]
	Cl	**3a**	90	243.8
		3b	90	261.4
	NO_2	**4a**	92	265.6
		4b	92	284.6
	OMe	**5a**	97	225.4
		5b	87	245.1[15]
	NMe_2	**6a**	78	210.4
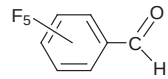		**7a**	96	286.8 (t, J_{PF} 98Hz)
		7b	97	304.3 (t, J_{PF} 93Hz)
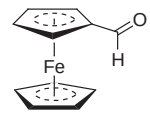		**8a**	61	222.1
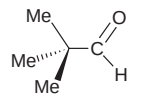		**9a**	91	221.2

however. Acetophenone, benzophenone and cyclohexanone showed no evidence of phosphaalkene formation and yielded extensive amounts of DmpP=PDmp over time.

Effords to extend the reactivity of phosphoranylidenephosphines to systems having less steric hindrance than Dmp or Mes* have been partially successful. Attempts to isolate TripP=PMe_3 (Trip = 2,4,6-$Pr^i_3C_6H_2$) by reduction of $TripPCl_2$ with Zn dust in the presence of PMe_3 resulted in rapid formation of $(TripP)_3$.[12] Addition of benzaldehyde, however, to such reactions results in mixtures of $(TripP)_3$ and TripP=C(H)Ph {$^{31}P\{^1H\}$ (C_6D_6), δ 254.7; ^1H NMR, δ 8.99 [TripP=C(*H*)Ph, d, J_{HP} 25.6 Hz]}, suggesting the presence of a transient TripP=PMe_3 capable of effecting phosphaalkene formation.

Reactions of phosphoranylidenephosphines with aldehydes would be of greater synthetic value if the more readily handled (and cheaper) PPh_3 could replace PMe_3 in these reactions. Unfortunately, efforts to prepare DmpP=PPh_3 by reduction of $DmpPCl_2$ with Zn in the presence of PPh_3 resulted in isolation of DmpP=PDmp. Attempts to generate DmpP=PPh_3 *in situ* for reaction with benzaldehyde also failed. Exchange of the PMe_3 unit in **1a** with added PPh_3 also proved futile. The PMe_3 groups in **1a** and **1b** do undergo exchange with certain non-hindered trialkylphosphines in solution. For example, **1a** and **1b** react quickly with PBu_3 to produce mixtures of **1a**, PMe_3 and DmpP=PBu_3 [**1c**, ^{31}P NMR(C_6D_6), δ 24.1, −151.3 (J_{PP} 589 Hz)] and mixtures of **1b**, PMe_3 and Mes*P=PBu_3 [**1d**, ^{31}P NMR(C_6D_6), δ 19.9, −153.7 (J_{PP} 612 Hz)], respectively.[13,14] Compound **1c** can also be generated *in situ* (as above) from PBu_3 and $DmpPCl_2$, which in the presence of benzaldehyde yields the phosphaalkene DmpP=C(H)Ph and O=PBu_3 in good yields. Work-up, however, requires more effort than the PMe_3 system due to the decreased volatility of PBu_3.

In conclusion, we have demonstrated that readily prepared and isolable phosphoranylidenephosphines are apt phosphinidene carriers in phospha-Wittig reactions. Our procedure represents a significant advance for the synthesis of phosphaalkenes as it utilizes dichlorophosphines directly, rather than derived primary phosphines. High yields and functional group tolerance are further highlights of this phospha-Wittig approach. Further studies of the phosphinidene and atom transfer reactions of these conveniently prepared phosphinidene-carriers are underway.

We thank the National Science Foundation (CHE-9733412) and the Department of Chemistry (CWRU) for support of this research.

Notes and References

† E-mail: jdp5@po.cwru.edu

‡ Compound **1a**: ^1H NMR(C_6D_6), δ 7.08 (t, 1 H, J_{HH} 8 Hz), 6.96 (d, 2 H, J_{HH} 8 Hz), 6.90 (s, 4 H), 2.37 (s, 12 H), 2.22 (s, 6 H), 0.58 (dd, 9 H, $^2J_{HP}$ 12 Hz, $^3J_{HPP}$ 3 Hz). HRMS (EI) *m/z* calc. for $C_{27}H_{34}P_2$ 420.2138; found 420.2127. Compound **1a** has also been structurally characterized.[3] Compound **1b**: ^1H NMR(C_6D_6), δ 7.42 (s, 2 H), 1.90 (s, 18 H), 1.36 (s, 9 H), 0.69 (d, 9 H, $^2J_{HP}$ 11.5 Hz). HRMS (EI) *m/z* calc. for $C_{21}H_{38}P_2$ 352.2451; found 352.2446.

§ Other data for phosphaalkenes: **2a**: mp 162–164 °C; ^1H NMR(C_6D_6), δ 9.00 (d, $^2J_{HP}$ 25.0 Hz, 1 H), 7.21 (t, J_{HH} 8.0 Hz, 1 H), 7.16 (m, 2 H), 7.00 (d, J_{HH} 7.6 Hz, 2 H), 6.78 (s, 4 H), 6.73 (m, 1 H), 2.20 (s, 12 H), 2.07 (s, 6 H); HRMS (EI) *m/z* calc. for $C_{31}H_{31}P$ 434.2165; found 434.2141. **2b**: mp 149–152 °C (lit. 152–153 °C[10]); ^1H NMR (C_6D_6), δ 8.19 (d, $^2J_{HP}$ 25.4 Hz, 1 H), 7.64 (d, $^4J_{HP}$ 1.2 Hz, 2 H), 7.46 (m, 2 H), 7.00 (m, 3 H), 1.60 (s, 18 H), 1.35 (s, 9 H). **3a**: mp 113–115 °C; ^1H NMR(C_6D_6), δ 8.80 (d, $^2J_{HP}$ 24.9 Hz, 1 H), 7.20 (t, J_{HH} 7.6 Hz, 1 H), 6.98 (d, J_{HH} 7.4 Hz, 2 H), 6.83 (m, 2 H), 6.80 (s, 4 H), 6.66 (d, J_{HH} 8.5 Hz, 2 H), 2.18 (s, 12 H), 2.08 (s, 6 H); HRMS (EI) *m/z* calc. for $C_{31}H_{30}PCl$ 468.1776; found 468.1788. **3b**: mp 124–126 °C; ^1H NMR(C_6D_6), δ 7.97 (d, $^2J_{HP}$ 25.1 Hz, 1 H), 7.63 (s, 2 H), 7.13 (m, 2 H), 6.96 (d, J_{HH} 8.6 Hz, 2 H), 1.57 (s, 18 H), 1.35 (s, 9 H); HRMS (EI) *m/z* calc. for $C_{25}H_{34}PCl$ 400.2089; found 400.2086. **4a**: mp 131–132 °C; ^1H NMR(C_6D_6), δ 8.67 (d, $^2J_{HP}$ 24.9 Hz, 1 H), 7.40 (d, J_{HH} 8.6 Hz, 2 H), 7.20 (t, J_{HH} 7.7 Hz, 1 H), 6.96 (d, J_{HH} 7.7 Hz, 2 H), 6.80 (s, 4 H), 6.70 (m, 2 H), 2.14 (s, 12 H), 2.08 (s, 6 H); HRMS (EI) *m/z* calc. for $C_{31}H_{30}PNO_2$ 479.2016; found 479.2028. **4b**: mp 129–131 °C; ^1H NMR(C_6D_6), δ 7.83 (d, $^2J_{HP}$ 24.8 Hz, 1 H), 7.73 (d, J_{HH} 8.8 Hz, 2 H), 7.62 (s, 2 H), 7.01 (m, 2 H), 1.52 (s, 18 H), 1.35 (s, 9 H); HRMS (EI) *m/z* calc. for $C_{25}H_{34}PNO_2$ 411.2329; found 411.2329. **5a**: mp 121–122 °C; ^1H NMR(C_6D_6), δ 9.00 (d, $^2J_{HP}$ 24.9 Hz, 1 H), 7.22 (t, J_{HH} 7.6 Hz, 1 H), 7.11 (m, 2 H), 7.02 (d, J_{HH} 7.6 Hz, 2 H), 6.81 (s, 4 H), 6.34 (d, J_{HH} 8.6 Hz, 2 H), 3.04 (s, 3 H), 2.23 (s, 12 H), 2.09 (s, 6 H); HRMS (EI) *m/z* calc. for $C_{32}H_{33}PO$ 464.2271; found 464.2260. **5b**: mp 164–166 °C; ^1H (C_6D_6): δ 8.20 (d, $^2J_{HP}$ 25.1 Hz, 1 H), 7.66 (d, $^4J_{HP}$ 1 Hz, 2 H), 7.41 (m, 2 H), 6.44 (d, J_{HH} 8.4 Hz, 2 H), 3.20 (s, 3 H), 1.64 (s, 18 H), 1.37 (s, 9 H); HRMS (EI) *m/z* calc. for $C_{26}H_{37}PO$ 396.2584; found 396.2584. **6a**: mp 181–183 °C; ^1H NMR (C_6D_6): δ 9.06 (d, $^2J_{HP}$ 24.4 Hz, 1 H), 7.22 (m, 3 H), 7.04 (d, J_{HH} 7.6 Hz, 2 H), 6.82 (s, 4 H), 6.09 (d, J_{HH} 8.8 Hz, 2 H), 2.27 (s, 12 H), 2.22 (s, 6 H), 2.10 (s, 6 H); HRMS (EI) *m/z* calc. for $C_{33}H_{36}PN$ 477.2588; found 477.2596. **7a**: mp 159–161 °C; ^1H NMR (C_6D_6), δ 8.73 (d, $^2J_{HP}$ 24.9 Hz, 1 H), 7.21 (t, J_{HH} 7.7 Hz, 1 H), 6.97 (d, J_{HH} 7.4 Hz, 2 H), 6.82 (s, 4 H), 2.19 (s, 12 H), 2.06 (s, 6 H); HRMS (EI) *m/z* calc. for $C_{31}H_{26}PF_5$ 524.1694; found 524.1704. **7b**: mp 130–133 °C; ^1H NMR (C_6D_6), δ 7.94 (d, $^2J_{HP}$ 24.8 Hz, 1 H), 7.63 (d, J_{HP} 1.0 Hz, 2 H), 1.58 (s, 18 H), 1.32 (s, 9 H); HRMS (EI) *m/z* calc. for $C_{25}H_{30}PF_5$ 456.2007; found 456.2010. **8a**: mp 104–106 °C; ^1H (C_6D_6), δ 8.77 (d, $^2J_{HP}$ 24.2 Hz, 1 H), 7.20 (t, J_{HH} 7.7 Hz, 1 H), 6.96 (d, J_{HH} 8.1 Hz, 2 H), 6.84 (s, 4 H), 4.15 (m, 2 H), 3.89 (m, 2 H), 3.73 (d, *J* 0.5 Hz, 5 H), 2.21 (s, 12 H), 2.14 (s, 6 H); HRMS (EI) *m/z* calc. for $C_{35}H_{35}PFe$ 542.1817; found 542.1837. **9a**: mp 127–129 °C; ^1H NMR (C_6D_6), δ 8.37 (d, $^2J_{HP}$ 25.1 Hz, 1 H), 7.18 (t, J_{HH} 7.6 Hz, 1 H), 6.97 (d, J_{HH} 8.1 Hz, 2 H), 6.83 (s, 4 H), 2.16 (s, 12 H), 2.15 (s, 6 H), 0.79 (d, $^4J_{HH}$ 1.9 Hz, 9 H); HRMS (EI) *m/z* calc. for $C_{29}H_{35}P$ 414.2479; found 414.2474.

1 M. Yoshifuji, I. Shima, N. Inamoto, K. Hirotsu and T. Higuchi, *J. Am. Chem. Soc.*, 1981, **103**, 4587.
2 L. Weber, *Chem. Rev.*, 1992, **92**, 1839.
3 E. Urnezius, S. Shah, G. P. Yap and J. D. Protasiewicz, manuscript in preparation.
4 In, *Multiple Bonds and Low Coordination in Phosphorus Chemistry*, ed. M. Regitz and O. J. Schere, Thieme Verlag, Stuttgart, 1990.
5 D. G. Gilheany, *Chem. Rev.*, 1994, **94**, 1339; P. V. Sudhakar and K. Lammertsma, *J. Am. Chem. Soc.*, 1991, **113**, 1899.
6 T. L. Breen and D. W. Stephan, *J. Am. Chem. Soc.*, 1995, **117**, 11 914; *Organometallics*, 1996, **15**, 4223; 1997, **16**, 365.
7 C. C. Cummins, R. R. Schrock and W. M. Davis, *Angew. Chem., Int. Ed. Engl.*, 1993, **32**, 756.
8 P. Le Floch, A. Marinetti, L. Ricard and F. Mathey, *J. Am. Chem. Soc.*, 1990, **112**, 2407; P. Le Floch and F. Mathey, *Synlett.*, 1990, 171; P. Floch and F. Mathey, *Synlett.*, 1991, 743.
9 E. Urnezius and J. D. Protasiewicz, *Main Group Chem.*, 1996, **1**, 369.
10 M. Yoshifuji, K. Toyota and N. Inamoto, *Tetrahedron Lett.*, 1985, **26**, 1727.
11 A. H. Cowley, N. C. Norman and M. Pakulski, *Inorg. Synth.*, 1990, **27**, 235.
12 C. N. Smit, T. A. van der Knaap and F. Bickelhaupt, *Tetrahedron Lett.*, 1983, **24**, 2031.
13 A. B. Burg, and W. Mahler, *J. Am. Chem. Soc.*, 1961, **83**, 2388.
14 A. H. Cowley and M. C. Cushner, *Inorg. Chem.*, 1980, **19**, 515.
15 K. Issleib, H. Schmidt and E. Leibring, *Z. Chem.*, 1986, **26**, 406.

Received in Bloomington, IN, USA; 14th April 1998; 8/02722F

Unique cationic, neutral and anionic copper(II) nitrite species in a single compound

Alexander J. Blake, Stuart J. Hill and Peter Hubberstey*†

Department of Chemistry, University of Nottingham, University Park, Nottingham, UK NG7 2RD

Crystallisation from an aqueous/acetonitrile solution of copper(II) nitrite containing bdmppy {bdmppy = 2,6-bis[(3,5-dimethyl)pyrazol-1-yl]pyridine} affords a compound with a unique arrangement of cationic [{Cu(bdmppy)(NO_2)}$_2$(μ-NO_2-κ*O*:κ*N*)]$^+$, neutral [Cu(bdmppy)(NO_2)$_2$] and anionic [Cu(NO_2)$_4$]$^{2-}$ copper(II) nitrite species, which feature diverse copper–nitrite coordination modes.

Copper nitrite complexes with ancillary *N*-donor ligands are of current interest[1–4] following the elucidation of the structures of several copper-containing nitrite reductase enzymes, such as *Achromobacter Cycloclastes*[5] or *Alicaligenes Xylosoxidans.*[6] The nitrite anion is a versatile ligand to copper(II)[7,8] exhibiting nitro (*via* the nitrogen),[9] nitrito (*via* an oxygen),[10] chelating (*via* both oxygens),[8] or bridging (*via* the nitrogen and an oxygen)[11] coordination modes. This versatility is displayed in the complex [Cu(L)(NO_2)][PF_6] {L = tris[(2-pyridyl)methyl]-amine}, where two structural isomers have been determined, differing only in nitro or nitrito co-ordination.[2b] In nitrite reductases the site of nitrite binding has been shown to involve three histidine donors;[5,6] the mode of nitrite coordination, although still to be confirmed, is thought to be asymmetric bidentate (*cis*-monodentate).[6]

Using the tridentate *N*-donor ligands 2,6-bis(pyrazol-1-yl)-pyridine (bppy) and its tetramethyl analogue 2,6-bis[(3,5-dimethyl)pyrazol-1-yl]pyridine (bdmppy) to mimic the three histidine donors of the enzymes, we have investigated the chemistry of Cu(bppy) and Cu(bdmppy) moieties with the nitrite anion. As part of this work we have synthesised and structurally characterisated the unique complex [{Cu-(bdmppy)(NO_2)}$_2$(μ-NO_2-κ*O*:κ*N*)]$_2$[Cu(bdmppy)(NO_2)$_2$]$_2$[Cu-(NO_2)$_4$]·MeCN **1**, which we describe herein.

The stoichiometric addition of an aqueous solution of 'copper nitrite' [prepared by the addition of an aqueous solution of $CuSO_4$·5H_2O to a stoichiometric amount of Ba(NO_2)$_2$] to a solution of bdmppy resulted in a green solution, slow evaporation of which in air gave a green crystalline product **1**. Single crystal IR spectroscopy confirmed the presence of ligand and nitrite **1**.‡

The structure of complex **1** (Fig. 1) was determined by single crystal X-ray diffraction.§ Its unit cell consists of seven copper centres; two dimeric cationic [{Cu(bdmppy)(NO_2)}$_2$(μ-NO_2-κ*O*:κ*N*)]$^+$ units, two neutral [Cu(bdmppy)(NO_2)$_2$] units, a [Cu(NO_2)$_4$]$^{2-}$ anion and an acetonitrile solvent molecule. Three distinct copper–nitrite coordination modes occur (Scheme 1). Following precedence[7] these are defined as (i) *cis*-monodentate, (ii) *trans*-monodentate and (iii) bridging. For all *cis*-monodentate nitrites, the second oxygen atom is remotely located (> 2.50 Å) in an axial coordination position. This contact is ignored, however, in describing the nitrite coordination mode and the copper(II) coordination geometry owing to the fact that it is a consequence of constraints imposed by the anion geometry.[7]

The [{Cu(bdmppy)(NO_2)}$_2$(μ-NO_2-κ*O*:κ*N*)]$^+$ units [Fig. 1(*a*)] are dimeric [Cu··Cu 5.304(1) Å] and represent the first fully structurally characterised example of the κ*O*:κ*N* bridging motif in copper(II) chemistry. Previously, a disordered example has been described in [{Cu(dien)}$_2$(μ-bimpydz)][NO_2]-[BF_4]$_3$·MeCN [dien = diethylenetriamine; bimpydz = 3,6-bis-(imidazol-1-yl)pyridazine].[11] Each of the two independent copper atoms has all three nitrogen atoms from the bdmppy ligand and an oxygen atom from a *cis*-monodentate nitrite in the basal positions of a square pyramidal geometry [Cu(2)–N 1.964(3), 1.997(3), 2.010(3); Cu(2)–O(31) 1.962(3); Cu(3)–N 1.968(3), 2.006(4), 2.011(4); Cu(3)–O(51) 1.957(3) Å]. The bridging nitrite occupies the apical position of both copper co-ordination spheres [Cu(2)–N(4) 2.307(4), Cu(3)–O(41) 2.267(3) Å]. The second oxygen atoms of each of the *cis*-

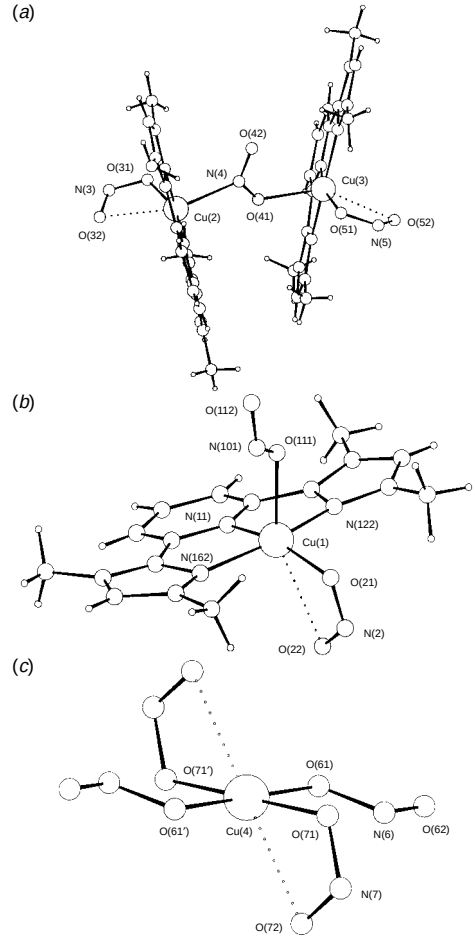

Fig. 1 The molecular structures of the three unique copper nitrite species in **1**: (*a*) the dinuclear [{Cu(bdmppy)(NO_2)}$_2$(μ-NO_2-κ*O*:κ*N*)]$^+$ cation, (*b*) the neutral [Cu(bdmppy)(NO_2)$_2$] species and (*c*) the [Cu(NO_2)$_4$]$^{2-}$ anion

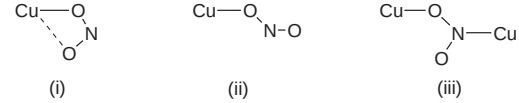

Scheme 1 Copper–nitrite coordination modes: (i) *cis*-monodentate (asymmetric bidentate); (ii) *trans*-monodentate; (iii) bridging

monodentate nitrites are weakly bound in axial positions [Cu(2)–O(32) 2.577(3), Cu(3)–O(52) 2.576(3) Å].

In the neutral [Cu(bdmppy)$(NO_2)_2$] species [Fig. 1(*b*)], the copper atom has a coordination geometry based on a square pyramid, with the three nitrogen atoms of the bdmppy ligand occupying three of the basal positions [Cu(1)–N(11) 1.978(4), Cu(1)–N(122) 1.990(5), Cu(1)–N(162) 1.984(4) Å]. The remaining basal site is occupied by a *cis*-monodentate nitrite [Cu(1)–O(21) 1.958(4) Å]. The apical position is occupied by a weakly bound disordered nitrite which adopts either a *trans*-monodentate [67%; Cu(1)–O(111) 2.168(8) Å] or *cis*-monodentate [33%; Cu(1)–O(121) 2.15(3), Cu(1)–O(122) 2.90(3) Å] co-ordination mode. Overall the copper atom adopts an N_3O_2 donor set. Again the second oxygen atom of the basally located *cis*-monodentate nitrite is weakly bound in the remaining axial position [Cu(1)–O(22) 2.655(4) Å].

The $[Cu(NO_2)_4]^{2-}$ anion [Fig. 1(*c*)] is situated on a centre of inversion, and comprises two symmetry related *cis*-monodentate [Cu(4)–O(71) 2.039(5) Å] and two symmetry related *trans*-monodentate nitrites [Cu(4)–O(61) 1.955(4) Å], resulting in a square planar CuO_4 coordination sphere. The second oxygen atoms of the *cis*-monodentate nitrites are weakly bound in the two remaining axial positions [Cu(4)–O(72) 2.518(5) Å]. Although the anions $[Cu(NO_2)_5]^{3-}$ and $[Cu(NO_2)_6]^{4-}$ are well documented in the literature as salts of the form $M^I_3[Cu(NO_2)_5]$ (M^I = K, Cs),[12] and $M^I_2M^{II}[Cu(NO_2)_6]$ (M^I = Tl, K, Rb, Cs; M^{II} = Ca, Sr, Ba, Pb)[13] or $M^I_5M^{III}[Cu(NO_2)_6]_2$ (M^I = Tl, K, Rb, Cs; M^{III} = Ce)[14] there is only one previous report of the $[Cu(NO_2)_4]^{2-}$ anion, as the structurally uncharacterised 1,2-xylylenebis(triphenylphosphonium) salt.[15] Hence this is the first reported structure containing the tetranitritocuprate(II) anion.

The only other copper(II) nitrite in the literature containing a *mer*-directed tridentate N-donor ligand is [Cu(terpy)(NO_2)-$(H_2O)][NO_2]\cdot H_2O$, **2** (terpy = 2,2′:6′,2″-terpyridyl). Despite the similarity of the tridentate ligands, the two complexes show very different formulations. Complex **2** has a square based pyramidal geometry and is ligated by the three N-donors of the terpy ligand, a monodentate nitrite anion and an axially located water molecule.[9]

We thank the EPSRC for a maintenance grant (to S. J. H.) and for the provision of a four-circle diffractometer.

Notes and References

† E-mail: peter.hubberstey@nottingham.ac.uk

‡ Single crystal IR spectroscopy for **1**: ν/cm^{-1} (unassigned bands are presumed to be associated with the various modes of coordinated nitrite): 3125m (bdmppy), 1616s (bdmppy), 1596s (bdmppy), 1569s (bdmppy), 1488s (bdmppy), 1476s, 1455s (bdmppy), 1432s, 1396br, 1365s (bdmppy), 1318br, 1301br, 1182m, 1144m, 1057m (bdmppy), 1040m (bdmppy), 1014m (bdmppy), 999m (bdmppy), 827m, 809m, 798m (bdmppy).

§ *Crystal data*: $C_{90}H_{102}Cu_7N_{44}O_{28}\cdot 2CH_3CN$, M = 2775.02, triclinic, space group $P\bar{1}$ (no. 2), a = 10.785(3), b = 15.192(3), c = 18.917(4) Å, α = 101.83(2), β = 96.63(3), γ = 107.81(2)°, U = 2834.97 Å^3, Z = 1, μ = 1.38 mm^{-1}, 9375 unique data. T = 150.0(2) K. Refinement converged to give conventional R = 0.0762, R' = 0.0847 for all data and 0.0668, 0.0789 for 8212 data with $I \geqslant 2\sigma(I)$. CCDC 182/912.

1 L. Casella, O. Carugo, M. Gullotti, S. Doldi and M. Frassoni, *Inorg. Chem.*, 1996, **35**, 1101.
2 (*a*) N. Komeda, H. Nagao, Y. Kushi, G. Adachi, M. Suzuki and A. Uehara, *Bull. Chem. Soc. Jpn.*, 1995, **68**, 581; (*b*) H. Nagao, N. Komeda, M. Mukaida, M. Suzuki and K. Tanaka, *Inorg. Chem.*, 1996, **35**, 6809.
3 F. Jiang, R. R. Conroy, L. Bubacco, Z. Tyeklar, R. R. Jacobson, K. D. Karlin and J. Peisach, *J. Am. Chem. Soc.*, 1993, **115**, 2093.
4 W. B. Tolman, *Inorg. Chem.*, 1991, **30**, 4877.
5 J. W. Godden, S. Turley, P. L. Teller, E. T. Adman, M. Y. Liu, W. J. Payne and J. Legall, *Science*, 1991, **253**, 458.
6 F. E. Dodd, S. S. Hasnain, Z. H. L. Abraham, R. R. Eady and B. E. Smith, *Acta Crystallogr., Sect. D*, 1997, **53**, 406; R. R. Eady, B. E. Smith, Z. H. L. Abraham, F. E. Dodd, J. G. Grossmann, L. M. Murphy, W. Strange and S. S. Hasnain, *J. Phys. (IV) France*, 1997, **7**, 2-611.
7 M. A. Hitchman and G. L. Rowbottom, *Coord. Chem. Rev.*, 1982, **42**, 55; B. J. Hathaway, *Comprehensive Coordination Chemistry*, Pergamon, Oxford, 1987, vol. 2, p. 413; vol. 5, p. 533.
8 S. J. Hill, P. Hubberstey and W.-S. Li, *Polyhedron*, 1997, **16**, 2447.
9 A. Pajunen and I. Belinski, *Suom. Kemistil. B*, 1970, **43**, 70.
10 R. Allman, S. Kremer and D. Kucharzyck, *Inorg. Chim. Acta*, 1984, **85**, L19.
11 A. S. Batsanov, M. J. Begley, P. Hubberstey and J. Stroud, *J. Chem. Soc., Dalton Trans.*, 1996, 4295.
12 K. A. Klanderman, W. C. Hamilton and I. Bernal, *Inorg. Chim. Acta*, 1977, **23**, 117; A. Ozarowski, R. Allmann, A. Pour-Ibrahim and D. Reinen, *Z. Anorg. Allg. Chem.*, 1991, **592**, 187.
13 For example, S. Tagaki, P. G. Lenhert and M. D. Joesten, *J. Am. Chem. Soc.*, 1974, **96**, 6606; D. L. Cullen and E. C. Lingafelter, *Inorg. Chem.*, 1971, **81**, 1264; M. D. Joesten, S. Tagaki and P. G. Lenhert, *Inorg. Chem.*, 1977, **16**, 2680; S. Klein and D. Reinen, *J. Solid State Chem.*, 1978, **25**, 295.
14 A. Ferrari, L. Cavalca and M. Nardelli, *Gazz. Chim. Ital.*, 1951, **81**, 964.
15 D. M. L. Goodgame and M. A. Hitchman, *J. Chem. Soc. (A)*, 1967, 612.

Received in Cambridge, UK, 19th May 1998; 8/03762K

An intramolecular rhodium carbenoid C–H insertion approach to chiral isotwistanes. Synthesis of (−)-neopupukean-4,10-dione and (−)-neopupukean-10-one

A. Srikrishna*† and Santosh J. Gharpure

Department of Organic Chemistry, Indian Institute of Science, Bangalore 560012, India

The first synthesis of a chiral neopupukeanane starting, from (*R*)-carvone and employing a double Michael reaction and a regioselective intramolecular rhodium carbenoid C–H insertion reaction as key steps, is described.

Recently, Scheuer and co-workers, during their biosynthetic experiments directed towards discovering the origin of the isocyano group in marine sponges, isolated[1] a new rearranged tricyclic sesquiterpene, 9-isocyanoneopupukeanane **1**, from the sponge *Ciocalypta* sp. whose relative stereostructure was established with the help of extensive 2D NMR spectroscopy. Subsequently, the research groups of Scheuer and Higa reported[2] the isolation of two thiocyanato derivatives of this new class of sesquiterpenes, 2-thiocyanatoneopupukeanane **2** from the sponge *Phycopsis terpnis* from Okinawa and 4-thiocyanatoneopupukeanane **3** from an unidentified species from Pohnpei. A characteristic of the structures of these neopupukeananes is the presence of a unique 9-isopropyl-3,6-dimethyltricyclo[4.3.1.0^{3,7}]decane carbon framework incorporating two quaternary carbon atoms besides the presence of the isocyano and thiocyanato functionalities, making them challenging synthetic targets. In continuation of our interest in the synthesis of chiral pupukeanones from (*R*)-carvone,[3] we herein report the first total synthesis of a chiral neopupukeanane[4] employing a regioselective intramolecular rhodium carbenoid C–H insertion reaction[5] as the key step for the generation of the isotwistane **4** carbon framework.

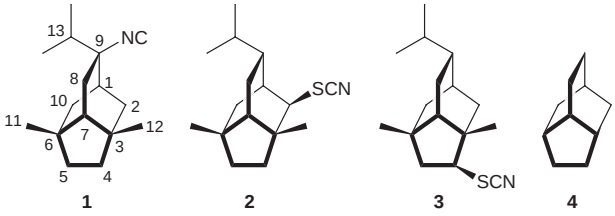

1 **2** **3** **4**

It was envisaged that the rhodium catalysed decomposition of the bicyclic diazo ketone **5** will generate the isotwistane **6** (Scheme 1) in a regioselective manner *via* the preferential formation of a five-membered ring by the insertion of the intermediate rhodium carbenoid into the only available C–H bond. A double Michael reaction on carvone[6] was chosen for the generation of an appropriate bicyclic precursor of an analogue of the diazo ketone **5**, which could be suitable for

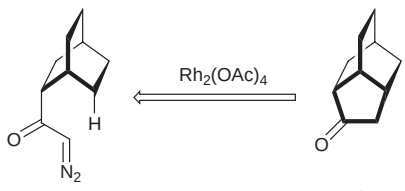

5 **6**

Scheme 1

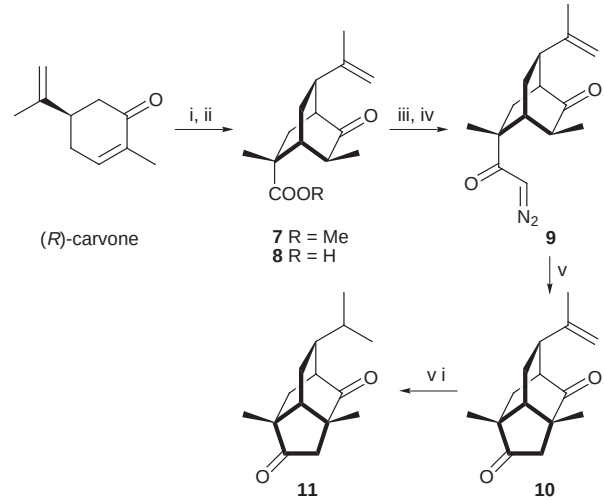

(*R*)-carvone **7** R = Me **8** R = H **9** **11** **10**

Scheme 2 *Reagents and conditions*: i, LiHMDS, $H_2C{=}CMeCO_2Me$, hexane–Et_2O (9 : 1), −78 °C → room temp., 50%; ii, 10% aq. NaOH, MeOH, reflux, 8 h, 92%; iii, $(COCl)_2$, C_6H_6, 2 h; iv, CH_2N_2, Et_2O, 0 °C → room temp., 2 h 90% (2 steps); v, $Rh_2(OAc)_4$ (cat.), CH_2Cl_2, reflux, 2 h, 90%; vi, H_2 (1 atm), 10% Pt/C, EtOH, 4 h, 96%

further elaboration into chiral neopupukeananes. Thus, double Michael reaction of (*R*)-carvone with LiHMDS and methyl methacrylate furnished the bicyclic keto ester **7** in a regio- and stereo-selective manner (Scheme 2) which, on base-catalysed hydrolysis, furnished the keto acid **8**. It is worth mentioning that in the keto acid **8**, the stereochemistry of the secondary methyl group at the carbon α to the keto group is *anti* with respect to the acid group, which was perfectly suited for the projected C–H insertion reaction for the generation of the tricyclic system. Reaction of the acid **8** with oxalyl chloride followed by treatment of the resulting acid chloride with an excess of ethereal CH_2N_2 furnished the diazo ketone **9**. Treatment of the diazo ketone **9** with a catalytic amount of rhodium acetate in refluxing CH_2Cl_2 led to the formation of the isotwistane dione **10** containing the complete carbon framework of neopupukeananes, *via* the regioselective C–H insertion of the intermediate keto carbenoid. The structure of neopupukean-13-en-4,10-dione **10** was established from its spectral data.‡ Catalytic hydrogenation in EtOH using 10% Pt/C transformed the dione **10** into neopupukean-4,10-dione **11**.‡ To test the generality of the C–H insertion, the reaction was carried out with three other bicyclic diazo ketones **12**–**14** to generate the isotwistanes **11**,**15** and **16** (Scheme 3). It is interesting to note that the reaction was not so facile when there is no tertiary methyl group at the α′-position of the diazo ketone, *cf.* **13**; perhaps the steric crowding due to the tertiary methyl group forces the rhodium carbenoid to occupy the *syn* orientation.

The difference in the steric crowding of the two ketones in dione **11** was exploited for the conversion of neopupukean-4,10-dione into neopupukean-10-one **17** (or 9-epineopupukean-2-one). Thus, treatment of dione **11** with $HS(CH_2)_2SH$

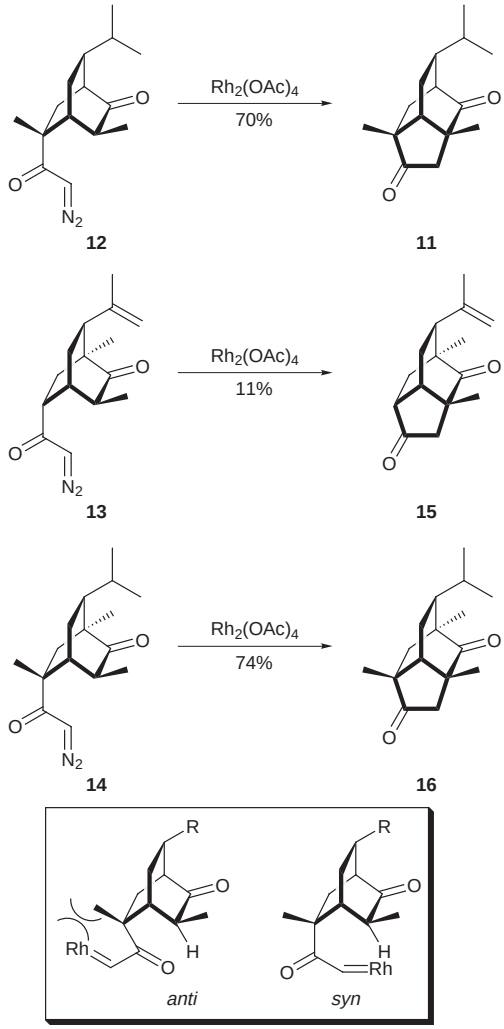

Scheme 3

(1 equiv.) in the presence of $BF_3{\cdot}OEt_2$ in benzene at room temperature generated the thioketal **18** (Scheme 4), which on desulfurisation with Raney nickel furnished neopupukean-10-one **17**.‡

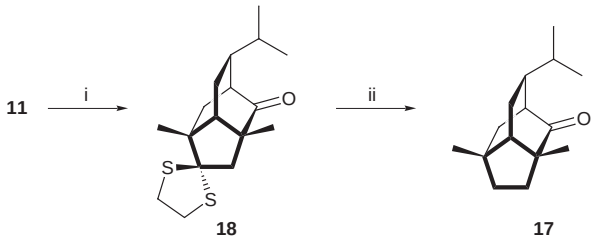

Scheme 4 *Reagents and conditions*: i, $HS(CH_2)_2SH$, $BF_3{\cdot}OEt_2$, C_6H_6, room temp., 8 h, 82%; ii, Raney Ni, EtOH, reflux, 9 h, 85%

In conclusion, we have developed a rapid methodology for the generation of chiral isotwistanes, containing the neopupukeanane carbon framework, employing a regioselective intramolecular rhodium carbenoid C–H insertion reaction. In addition to being the first synthesis of neopupukeanones, the generation of the chiral compounds, brevity and simplicity are the highlights of the present strategy. Currently, we are investigating the extension of this methodology for the synthesis of other neopupukeananes to establish the absolute stereochemistry of the natural products.

We thank the Department of Science and Technology, New Delhi, for financial support and the Council of Scientific and Industrial Research for the award of a research fellowship to S. J. G.

Notes and References

† E-mail: ask@orgchem.iisc.ernet.in

‡ All the compounds exhibited spectral data consistent with their structures. *Selected data* for **10**: mp 111–113 °C; $[\alpha]_D^{26}$ −45.5 (*c* 1.32, $CHCl_3$); ν_{max}/cm^{-1} 1740, 1710, 1640, 900, 890; δ_H(300 MHz, $CDCl_3$) 4.82 (1 H, s) and 4.79 (1 H, s) (C=CH_2), 2.55–2.50 (2 H, m, H-1 and 9), 2.52 (1 H, d, *J* 18.9, H-5a), 2.21 (1 H, ddd, *J* 14.5, 10.5 and 3.3, H-8a), 2.10 (1 H, d, *J* 18.9, H-5b), 1.94 (1 H, ddd, *J* 14.5, 6.3 and 2.7, H-8b), 1.90 (1 H, br s, H-7), 1.80 (1 H, dd, *J* 14.7 and 4.2, H-2a), 1.76 (3 H, s, olefinic CH_3), 1.59 (1 H, d, *J* 14.7, H-2b), 1.25 (3 H, s) and 1.24 (3 H, s) (2 × *tert*-CH_3); δ_C(75 MHz, $CDCl_3$, DEPT) 218.6 (C=O), 217.6 (C=O), 146.8 (*C*=CH_2), 110.4 (C=*C*H_2), 50.9 (quat. C), 49.0 (CH, C-1), 48.5 (quat. C), 48.1 (CH_2), 46.3 (CH), 45.1 (CH), 35.2 (CH_2), 22.0 (CH_3), 20.7 (CH_2), 19.5 (CH_3), 18.1 (CH_3); *m*/*z* 232 (M^+) (Calc. C, 77.5; H, 8.8. $C_{15}H_{20}O_2$ requires C, 77.55; H 8.7%). For **11**: mp 131–133 °C; $[\alpha]_D^{26}$ −48.9 (*c* 1.48, $CHCl_3$); ν_{max}/cm^{-1} 1740, 1720; δ_H(300 MHz, $CDCl_3$) 2.47 (1 H, d, *J* 19.2, H-5a), 2.48 (1 H, br s), 2.07 (1 H, d, *J* 18.9, H-5b), 2.05–2.20 (1 H, m), 1.86 (1 H, t, *J* 3.3), 1.78 (1 H, dd, *J* 14.7 and 4.5, H-2a), 1.60–1.75 (2 H, m), 1.47 (1 H, d, *J* 15, H-2b), 1.45–1.55 (1 H, m), 1.26 (3 H, s) and 1.20 (3 H, s) (2 × *tert*-CH_3), 0.94 (3 H, d, *J* 6.3) and 0.91 (3 H, d, *J* 6.6) (2 × *sec*-CH_3); δ_C(22.5 MHz, $CDCl_3$) 218.3 (s, C=O), 217.6 (s, C=O), 50.6 (s, quat. C), 49.1, 48.1 (s, quat. C), 47.6, 46.7, 45.0 (d, CH), 34.4 (t, CH_2), 33.9 (t, CH_2), 21.3, 20.5, 19.7, 19.2, 17.8; *m*/*z* 234 (M^+) (Calc. C, 76.98; H, 9.64. $C_{15}H_{22}O_2$ requires C, 76.88; H, 9.46%). For **17**: $[\alpha]_D^{27}$ −84.1 (*c* 1.70, $CHCl_3$); ν_{max}/cm^{-1} 1715; δ_H(300 MHz, $CDCl_3$) 2.32 (1 H, br s), 1.20–2.10 (11 H, m), 1.16 (3 H, s) and 1.11 (3 H, s) (2 × *tert*-CH_3), 0.893 (3 H, d, *J* 6.3) and 0.886 (3 H, d, *J* 6.3) (2 × *sec*-CH_3]; δ_C(75 MHz, $CDCl_3$) 222.4 (C=O), 55.5 (quat. C), 51.8, 46.6, 45.6, 40.2, 39.7, 35.5 (quat. C), 35.2, 34.0, 26.5, 21.9, 20.8, 20.3, 18.6; *m*/*z* 220 (M^+).

1 P. Karuso, A. Poiner and P. J. Scheuer, *J. Org. Chem.*, 1989, **54**, 2095.
2 A. T. Pham, T. Ichiba, W. Y. Yoshida, P. J. Scheuer, T. Uchida, J.-i. Tanaka and T. Higa, *Tetrahedron Lett.*, 1991, **32**, 4843.
3 A. Srikrishna, P. Hemamalini and G. V. R. Sharma, *J. Org. Chem.*, 1993, **58**, 2509; A. Srikrishna and T. J. Reddy, *J. Chem. Soc., Perkin Trans. 1*, 1997, 3293.
4 To the best of our knowledge, there are no reports in the literature of the synthesis of either racemic or chiral neopupukeanane carbon frameworks.
5 T. Ye and M. A. McKervey, *Chem. Rev.*, 1994, **94**, 1091; M. P. Doyle, in *Comprehensive Organometallic Chemistry II*, ed. L. S. Hegedus, Pergamon Press, New York, 1995, vol. 12, ch. 5.2; M. P. Doyle, *Aldrichim. Acta*, 1996, **29**, 3.
6 R.-B. Zhao, Y.-F. Zhao, G. Q. Song and Y.-L. Wu, *Tetrahedron Lett.*, 1990, **31**, 3559.

Received in Cambridge, UK, 28th May 1998; 8/04001J

Further evidence that the polycyclization reaction by oxidosqualene-lanosterol cyclase proceeds *via* a ring expansion of the 5-membered C-ring formed by Markovnikov closure. On the enzymic products of the oxidosqualene analogue having an ethyl residue at the 15-position

Tsutomu Hoshino*[a,b]† and Yoshiyuki Sakai[b]

[a] *Department of Applied Biological Chemistry, Faculty of Agriculture, Niigata University, Ikarashi, Niigata, 950-2181, Japan*
[b] *Graduate School of Science and Technology, Niigata University, Ikarashi, Niigata, 950-2181, Japan*

The incubation of the substrate analogue, (3*S*)-(6*E*,10*E*,14*E*,18*E*)-15-ethyl-2,6,19,23-tetramethyl-2,3-epoxytetracosa-6,10,14,18,22-pentaene (-)-1 with 2,3-oxidosqualene-lanosterol cyclase from pig liver gave products 2 (a lanosterol homologue) and 3 (a tricyclic product), definitively demonstrating that the cyclization of oxidosqualene proceeds *via* the expansion reaction from a 5- to a 6-membered ring for the C-ring formation of lanosterol.

In a preceding paper,[1] we reported the unprecedented cyclization products given by 2,3-oxidosqualene cyclase: substitution of the ethyl groups with methyl groups at both C-10 and C-15 of oxidosqualene halts the enzymic reaction at the monocyclic ring stage. This demonstrated that the cyclizing reaction to the protosterol cation proceeds *via* discrete carbocation intermediates, although usually this reaction has been assumed to be concerted, and gives the first example of the cyclase reaction being stopped at the stage of the initial A-ring formation. To gain more insight into the fine control of the polyolefin cyclization, we have now examined the enzymic reaction of the analogue **1**, in which only the methyl group at C-15 in the squalene backbone has been replaced by an ethyl group. Here, we report the tricyclic and tetracyclic formed products by the cyclase and give further evidence for the involvement of a C-ring expansion process in the formation of lanosterol.

The synthesis of (±)-**1** was essentially the same as previous papers.[1,2] The coupling reaction of (2*E*,6*E*)-1,10-dibromo-3,7,11-trimethyldodeca-2,6-diene-11-ol with (2*E*,6*E*)-1-bromo-

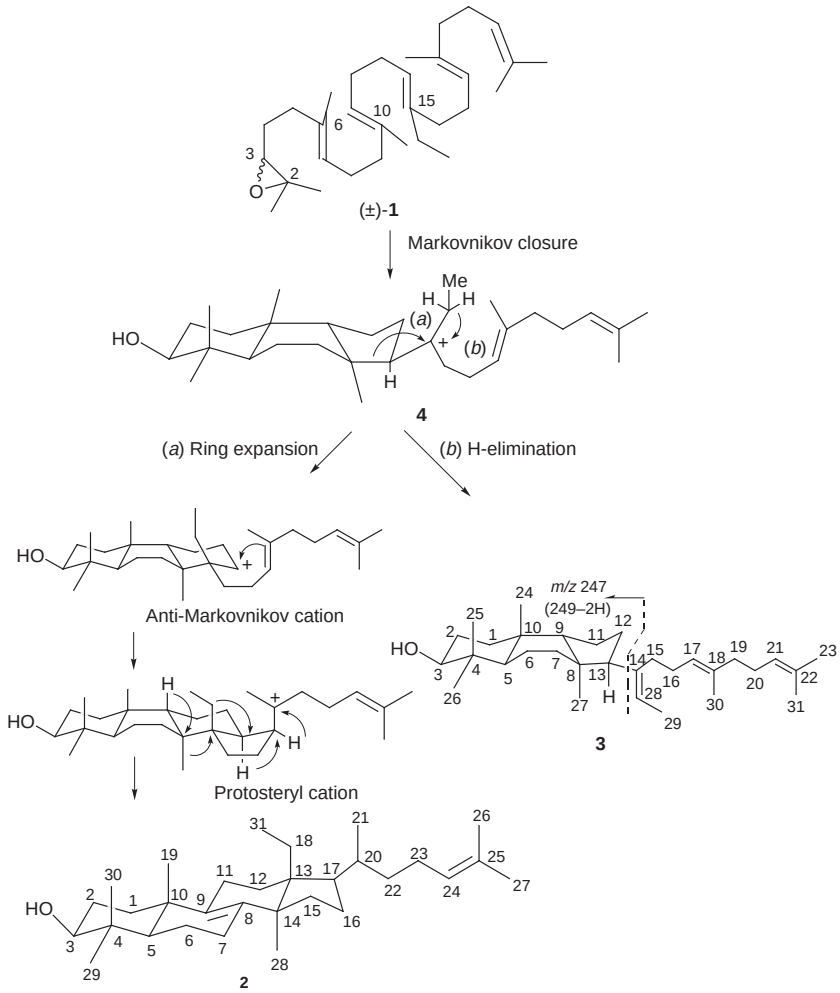

Scheme 1

3,7,11-trimethyldodeca-2,6,10-triene, by treatment of cuprous iodide with lithium pyrrolidide,[3] afforded the desired **1**, the squalene derivative having ethyl groups at C-10 and C-15, and 2,3:22,23-dioxidosqualene in the yields of 36, 29 and 6%, respectively, which could be easily separated by SiO_2 column chromatography due to remarkable differences of the products' polarity. Enzyme preparation from the microsomal fractions of pig liver was carried out according to the literature.[1,4] A sample of (±) **1** (38 mg) was anaerobically incubated for 24 h at 37 °C and lyophilized. Extraction of the reaction residues with hexane gave two new peaks (**2** and **3**) *via* GLC. The behavior of **2** and **3** on SiO_2 TLC was the same, irrespective of solvent system. By using an argentation SiO_2 column (10%), the metabolites **2** (solid) and **3** (oil) were isolated in yields of 5.8 and 2.2 mg, respectively. The total conversion was 42% based on one enantiomer of (±)-**1**. The specific rotations of **2**, **3** and the recovered **1** were +21.58 (*c* 0.417, $CHCl_3$), +13.25 (*c* 0.083, $CHCl_3$) and +1.93 (*c* 0.497, EtOH), respectively, indicating that the 3*S* form, (-)-**1**, was selectively transformed. The molecular composition of **2** was determined to be $C_{31}H_{52}O$ from EI-HRMS (*m/z* 440.4043; requires 440.4018) and the following characteristic mass fragments were observed: *m/z* 440 (M^+, 56%), 425 (M^+-Me, 100%), 407 (M^+-Me-H_2O, 21%); the fission patterns and peak intensities were the same as authentic lanosterol (*m/z* 426, 411, 393). The molecular composition of **3** was also determined to be $C_{31}H_{52}O$ from EI-HRMS (*m/z* 440.4035); *m/z* 440 (M^+), 247 (249-2H; tricyclic moiety). The hydroxy groups of **2** and **3** were confirmed to be equatorial from the coupling constants of H-3 (dd, *J* 4.5, 12 Hz). Detailed analyses of NMR spectra including ^1H–^1H COSY 45, HOHAHA, NOESY, DEPT, HMQC and HMBC experiments unambiguously verified the structures of **2** and **3** to be a lanosterol homologue and a tricyclic compound, respectively. In the HMBC spectrum of **2**, the crosspeak of 19-Me with the sp^2 quaternary C-9 and that of 28-Me with C-8 confirmed the position of the double bond, and the correlations of 28-Me and 31-Me to C-13 also proved the ethyl position. The clear NOEs of 31-Me with 21-Me and of 19-Me with 31-Me indicated that all the stereo-orientations of **2** were identical to those of lanosterol. The stereochemistry at C-20 has yet to be established, but it should have the same *R* configuration as natural lanosterol; the chemical shift (δ_C 35.1) of C-20 was homogenous. On the other hand, **3** had a partially cyclized 6/6/5 fused-ring system possessing a chair/boat geometry. The boat geometry of the B-ring was confirmed by the apparent correlation of H-5 with 27-Me and that of H-9 with 24-Me in the NOESY spectrum. The NOE correlation of 27-Me with H-13 indicated the α-orientation of H-13. The ethylidene moiety was also inferred from the HMBC data.

Formation of the two products **2** and **3** suggests that a common precursor **4**, the tricyclic cation having a 6/6/5-fused system, should be produced before the subsequent reactions occur (Scheme 1). The carbocation intermediate **4**, a thermodynamically favored product by Markovnikov closure, undergoes ring expansion toward the anti-Markovnikov cation of the 6-membered C-ring to form the protosterol cation, which is then subjected to four sequential antiparallel 1,2-shifts of two hydrogens, the ethyl group and the methyl group, followed by deprotonation leading to double bond formation [path (*a*)], just as does the natural substrate. It is noticeable that the *ethyl* group also underwent the migration reaction. If a proton is eliminated from the ethyl group, the tricyclic **3** is formed [path (*b*)]. The ring expansion competes with the deprotonation process from the ethyl group. The tricyclic fused-A/B/C ring system has also been isolated from the enzyme products of the $\Delta^{18,19}$ double bond *Z*-isomer,[5] the truncated substrate[6] and the 20-oxa analogue.[6] Recently, Corey proposed the idea, on the basis of the enzyme reactions of the truncated C_{20} and 20-oxa analogues, that the 6-membered C-ring of lanosterol is formed *via* ring expansion of the 5-membered cation, previously produced by Markovnikov closure. However, the enzyme reactions were halted at the intermediate stage without completion of the cyclase reaction, thus, the ring expansion process remained unclear. In contrast, analogue **1** afforded the complete lanosterol skeleton **2** along with capture of the intermediate **3**; therefore, this finding provides strong evidence for the involvement of a ring expansion process. The intermediate **4** would have been formed in a Markovnikov fashion and as a result of the longer lifetime of **4** due to the enhanced steric repulsion between the methyl at C-10 and the ethyl at C-15, compared to that between the two methyl groups of natural squalene, the detailed mechanism of which has been discussed.[6b] Kyler and co-workers have assumed that substitution on the β-side of the folded conformation interferes with the normal cyclization.[7] A good conversion of **1** to **2**, despite the ethyl moiety being situated on the β-face, was a contrast to this hypothesis inferred from Bakers' yeast. This inconsistency may originate from the difference in the biological source used. Indeed, no reaction was detectable for **1** or the diethylated oxidosqualene with the yeast cyclase.[1] The binding site and/or cavity size for the methyl group at C-15 may be different for the yeast and mammal enzymes. In the case of the diethylated analogue, only the initially cyclized A-ring was formed,[1] while the monoethylated **1** gave the subsequent tricyclic and tetracyclic reaction products. These results also imply that the 10-methyl group plays a critical role in the normal polycyclizaton reaction by the mammalian cyclase, which is consistent with a previous report.[8]

This work was partly supported by a Grant-in-Aid to T. H. (No. 0966011) from the Ministry of Education, Science and Culture, Japan.

Notes and References

† E-mail: hoshitsu@agr.niigata-u.ac.jp

1 T. Hoshino, E. Ishibashi and K. Kaneko, *J. Chem. Soc., Chem. Commun.*, 1995, 2401.
2 T. Hoshino, H. J. Williams, K. Shishido and A. I. Scott, *J. Labelled Compd. Radiopharm.*, 1990, **28**, 1285.
3 Y. Kitagawa, K. Oshima, H. Yamamoto and H. Nozaki, *Tetrahedron Lett.*, 1975, 1859.
4 I. Abe, M. Bai, X.-y. Xiao and G. D. Prestwich, *Biochem. Biophys. Res. Commun.*, 1992, **187**, 32; T. Hoshino, N. Kobayashi, E. Ishibashi and S. Hashimoto, *Biosci. Biotechnol. Biochem.*, 1995, **59**, 602.
5 A. Krief, J. R. Scauder, E. Guittet, C. Herve du Penhoat and J. Y. Lallemand, *J. Am. Chem. Soc.*, 1987, **109**, 7910; A. Krief, P. Pasau and L. Quéré, *Bioorg. Med. Chem. Lett.*, 1991, **1**, 365; A. Krief, P. Pasau, E. Guittet, Y. Y. Shan and M. Herin, *Bioorg. Med. Chem. Lett.*, 1993, **3**, 365.
6 (*a*) E. J. Corey and H. Cheng, *Tetrahedron Lett.*, 1996, **37**, 2709; (*b*) E. J. Corey, S. C. Virgil, H. Cheng, C. H. Baker, S. P. T. Matsuda, V. Singh and S. Sarshar, *J. Am. Chem. Soc.*, 1995, **117**, 11 819; (*c*) E. J. Corey, H. Cheng, C. H. Baker, S. P. T. Matsuda, D. Li and X. Song, *J. Am. Chem. Soc.*, 1997, **119**, 1289.
7 J. C. Medina and K. S. Kyler, *J. Am. Chem. Soc.*, 1988, **110**, 4818; J. C. Medina, R. Guajardo and K. Kyler, *J. Am. Chem. Soc.*, 1989, **111**, 2310.
8 E. J. Corey, S. C. Virgil, D. R. Liu and S. Sarshar, *J. Am. Chem. Soc.*, 1992, **114**, 11 524.

Received in Cambridge, UK, 1st June 1998; 8/04074E

Weak intermolecular interactions in sulfonamide salts: structure of 1-ethyl-2-methyl-3-benzyl imidazolium bis[(trifluoromethyl)sulfonyl]amide

Jacob J. Golding,*[a] Douglas R. MacFarlane,[a] Leone Spiccia,[a] Maria Forsyth,[b] Brian W. Skelton[c] and Alan H. White[c]

[a] *Department of Chemistry, Monash University, Clayton, Victoria, 3168, Australia*
[b] *Department of Materials Engineering, Monash University, Clayton, Victoria, 3168, Australia*
[c] *Department of Chemistry, University of Western Australia, Nedlands, Western Australia, 6907, Australia*

The crystal structure of a 1,2,3-trisubstituted imidazolium salt of the bis[(trifluoromethyl)sulfonyl)]amide ion is presented; this salt is a prototype for similar, room temperature liquid, imidazolium salts; the structure shows that the anion and cation interact weakly, with little if any hydrogen bonding present.

The use of molten organic salts as electrolytes in a variety of electrochemical devices, such as photo-electrochemical cells,[1] is becoming more widespread. As these applications become more varied,[2] the need for a variety of new, low melting point, fluid, ionic liquids is apparent. In the investigation of novel ionic liquids, interactions between the anion and cation are of great interest, as are the conformational states of each component of the salt, since the key transport properties (conductivity and diffusivity) are determined to a significant extent by these interactions. The relationship between structure and physical characteristics of many ionic liquids is yet to be fully quantified. The direct insight into the spatial relationship between cation and anion afforded by the elucidation of crystal structures provides a basis from which features of the ionic liquid itself can be understood, since the short range order and interactions of related, non-crystalline compounds may be similar to those of the crystalline form.

It is becoming clear[1–3] that anions (and cations) with diffuse charges and negligible hydrogen bonding yield the lowest melting points and hence have the greatest potential to produce ionic compounds that are liquid at room temperature. For example, the bis[(trifluoromethyl)sulfonyl]amide ion, $(CF_3SO_2)_2N^-$, has been found to produce low melting point (sub-room temperature in some cases, and completely non-crystalline in others) salts which are also characterized by their high fluidity and high ionic conductivity relative to other molten salts.[3] Owing to a lack of structural information on these types of complexes, the origins of these two important effects (low mp and high fluidity) are not well understood. In this work we present crystal structure data for a low melting (mp ≈ 50 °C) organic salt, 1-ethyl-2-methyl-3-benzyl imidazolium bis[(trifluoromethyl]sulfonyl)amide **1**.‡§

In the only previously reported crystal structure[4] determination of a salt of this anion {magnesium hexaaquobis[(trifluoromethyl)sulfonyl]amide dihydrate}, the anion was subject to molecular distortions[4] due to hydrogen bonding to the water molecules coordinated to the $[Mg(H_2O)_6]^{2+}$ cation. The structure presented here allows a clearer picture of the geometric features of this anion to be observed, in the absence of the hydrogen-bonding interactions which are present in the previous structure.

Fig. 1 shows the crystal structure of **1**. The imidazolium ring lies above the amide nitrogen, with the $-SO_2CF_3$ groups positioned away from the benzyl group. The distances between oxygen, nitrogen or fluorine and the closest hydrogen atoms approximate to van der Waals separations (*ca*. 2.6, 2.7 and 2.55 Å, respectively) indicating no evidence of the presence of strong hydrogen bonding in the crystal lattice.[5] The large degree of thermal motion evident in both ions is also consistent with the absence of any strong interaction between the anion and cation. This implies that ionic, rather than covalent, interactions hold the salt in a low melting point crystalline form.

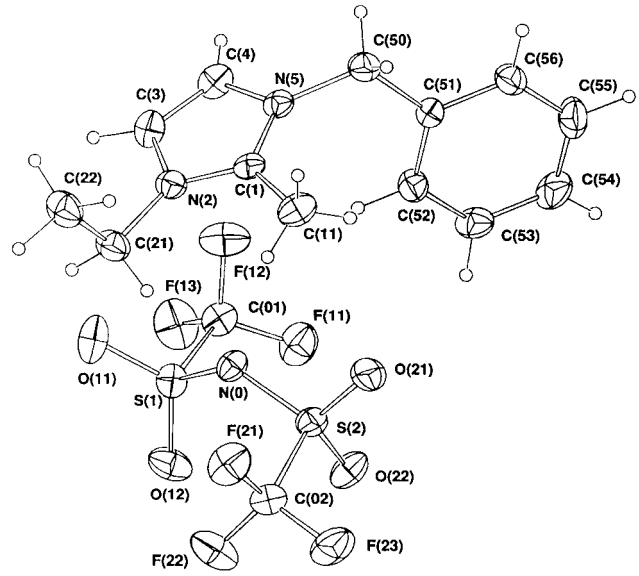

Fig. 1 Projection of the salt **1**. 20% Thermal ellipsoids are shown for the non-hydrogen atoms, hydrogen atoms having arbitrary radii of 0.1 Å.

Bond length and angle data for the 1-ethyl-2-methyl-3-benzyl imidazolium cation in this salt (Fig. 2), agree with previously reported imidazolium cations[5–7] (the majority of which are unsubstituted in the 2-position). The imidazole ring remains planar and the bond lengths in the imidazolium ring show strong residual double bond character at C(3)–C(4) with only partial delocalization of the positive charge, as previously reported.[5–7] It is perhaps not surprising that this and related trisubstituted imidazolium salts (*i.e.* 1-alkyl-2-methyl-3-benzyl imidazolium salts) do not easily form salts which are liquid at

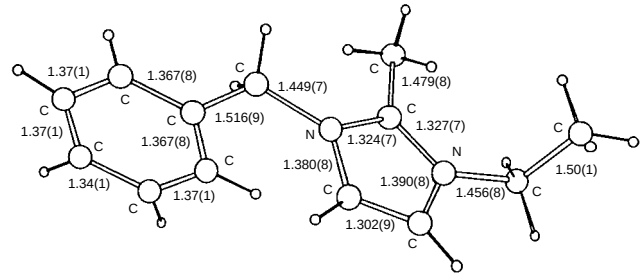

Fig. 2 Ball and stick representation of imidazolium cation including bond lengths (Å)

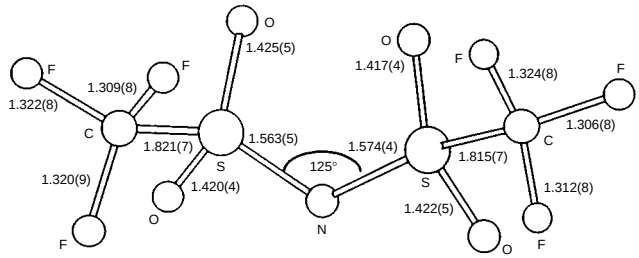

Fig. 3 Ball and stick representation of the bis[(trifluoromethyl)sulfonyl]amide anion including bond lengths (Å)

room temperature, when the influence of the size and orientation of the benzyl group, perpendicular to the plane of the imidazole ring [dihedral angle 86.7(3)°], are taken into account.

Fig. 3 shows the bond lengths and spatial arrangement of the anion. The anion as a whole has near C_2 symmetry, and the sulfonyl moieties have distorted tetrahedral symmetry with bond angles ranging from 102 to 115°.

Previous investigations of sulfonyl amide anions[4,8] have supported Cruickshank's[9] description, which proposed d_π–p_π interaction between neighbouring sulfur and nitrogen atoms. This interaction effectively delocalizes the negative charge across the S–N–S moiety but not necessarily onto the sulfonyl oxygens, as might have been expected on the basis of simpler models. The structure determined in this work supports this model, the S–O bond lengths all being quite characteristic of the S–O double bond in SO_2 (1.43 Å) and showing no evidence of lengthening due to charge delocalization onto the sulfonyl oxygens. The lengthening of the S–O bonds (0.07 Å) observed by Haas *et al.*[4] when the sulfonyl amine was converted to the amide can be partially explained by the increased charge density across the S–N–S moiety. Given the strong hydrogen bonding present in their compound, no conclusive evidence of charge delocalization onto the sulfonyl oxygens can be deduced from that structure. On the other hand, the S–N bond lengths shown in Fig. 3 (1.56–1.57 Å) are significantly shorter than typical S–N single bonds ($\approx$1.75 Å) as a result of the S–N–S charge delocalization, hence charge delocalization onto the sulfurs is clearly indicated.

The key features of this anion in promoting a low melting point in its compounds, concomitant with high fluidity, would therefore appear to be this charge delocalization coupled with the lack of hydrogen bonding. The slightly larger than trigonal S–N–S angle (125°) will also, combined with the bulk of the $–SO_2CF_3$ groups, provide steric impediments to close interactions with neighbouring cations.

The crystal structure presented here provides a contrasting view of the interaction of organic cations, *vs.* solvated inorganic cations, *e.g.* aquo ions, with this anion. In the case of $[Mg(H_2O)_6][N(SO_2CF_3)_2]_2$, the intermolecular hydrogen bonding distorted the geometric features of the anion. In the structure presented here, however, the relatively unperturbed intramolecular features of the anion have been elucidated. This has been possible because only weak electrostatic interactions are evident between the sulfonamide anion and the imidazolium cation.

The support of the Australian Research Council is gratefully acknowledged.

Notes and References

† E-mail: j.golding@sci.monash.edu.au.

‡ *Crystal data*: $C_{15}H_{17}F_6N_3O_4S_2$, M = 481.4. Monoclinic, space group $P2_1/n$, a = 8.862(2), b = 11.051(3), c = 21.271(7) Å, β = 98.42(2)°, U = 2061 Å^3, D_c (Z = 4) = 1.552 g cm^{-3}. F(000) = 984. μ_{Mo} = 3.4 cm^{-1}; specimen: 0.50 × 0.26 × 0.17 mm; $A^*_{min,max}$ (gaussian correction) 1.05, 1.10. 1795 'observed' [$I > 3(I)$] out of 3612 independent four-circle diffractometer reflections (monochromatic Mo-Kα radiation, λ = 0.7107$_3$ Å; $2\theta_{max}$ = 50°; T = 295 K) refining to conventional R on $|F|$ 0.050, R_W (statistical weights) = 0.059. (x, y, z, U_{iso})$_H$ refined; anisotropic thermal parameter forms refined for non-hydrogen atoms (full-matrix). CCDC 182/881.

§ After reacting ethyl iodide with 1-benzyl-2-methylimidazole, the resultant iodide salt was converted to a nitrate (using $AgNO_{3(aq)}$), and subsequently $LiN(SO_2CF_3)_2$ was added in a minimum of EtOH. The hydrophobic salt **1** was isolated and dissolved in CH_2Cl_2 [to remove residual $LiN(SO_2CF_3)_2$] and dried over $MgSO_4$. Crystals were grown from a CH_2Cl_2–$C_2H_3Cl_3$–MeCN mixture.

1 P. Bonhote, A. Dias, N. Papageorgiou, K. Kalyanasundaram and M. Gratzel, *Inorg. Chem.*, 1996, **35**, 1168.
2 K. R. Seddon, *J. Chem. Technol. Biotechnol.*, 1997, **68**, 351.
3 J. Sun, D. Macfarlane and M. Forsyth, *Proceedings of 5th International Symposium on Molten salt Chemistry and Technology*, Dresden, in press. V. R. Koch, C. Nanjundah, G. Battista Appetecchi and B. Scrosati, *J. Electrochem. Soc.*, 1995, **142**, L116.
4 A. Haas, Ch. Klare, P. Betz, C. Kruger, Y-H. Tsay and F. Aubke, *Inorg. Chem.*, 1996, **35**, 1918.
5 A. K. Abdul-Sada, A. M. Geenway, P. B. Hitchcock, T. J. Mohammed, K. R. Seddon and J. A. Zora, *J. Chem. Soc., Chem. Commun.*, 1986, 1753.
6 J. S. Wilkes and M. J. Zaworotko, *J. Chem. Soc., Chem Commun.*, 1986, 965.
7 J. Fuller, R. T. Carlin, H. C. De Long and D. Haworth, *J. Chem. Soc., Chem. Commun.*, 1994, 299.
8 F. A. Cotton and P. F. Stokely, *J. Am. Chem. Soc.*, 1970, **92**, 294.
9 D. W. J. Cruickshank, *J. Chem. Soc.*, 1961, 5486.

Received in Cambridge, UK, 14th April 1998; 8/02745E

First example of a sixteen membered Jäger macrocycle having a 'Z' conformation

James H. Cameron,*† Duncan P. Nicol and Georgina M. Rosair

Chemistry Department, Heriot-Watt University, Riccarton, Edinburgh, UK EH14 4AS

The crystal structure of the first sixteen membered Jäger type macrocycle having a Z conformation rather than the expected saddle shaped geometry has been determined.

The family of tetraaza macrocycles first reported by Jäger[1] displays a fascinating interplay of structure–reactivity relationships and this has been exploited to interesting effect, in particular by Busch and Cairns, in the production of the so-called 'cyclidene' macrocyclic complexes[2] where examples have been used in reversible oxygen binding,[3] as models for cytochrome P-450,[4] and in supramolecular chemistry.[5]

The solid state structure of the Jäger macrocycles varies widely with ring size.[6] The fourteen membered rings are planar, the fifteen membered rings adopt one of two possible geometries (either 'saddle shaped' or a Z conformation) while the sixteen membered ring, until now, has been found exclusively in the saddle shaped geometry (**I**). The saddle shape of the

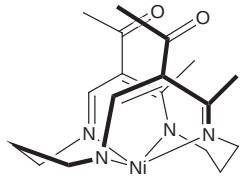

I

sixteen membered species arises due to the conformations adopted by the two saturated six membered metallochelate rings present in the structure.[6]

As part of a study into the steric control of reactions of superstructured macrocycles[7] we prepared a new example of a sixteen membered Jäger type complex, **1**, with neopentyl

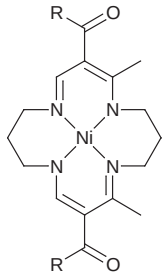

1a R = Bu^t
2a R = Me

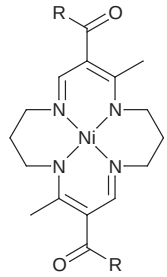

1b R = Bu^t
2b R = Me

substitutents,‡ and found that it exists as a 1 : 1 ratio of two isomers: the conventional species, with *cis* related ring methyl groups (**1a**) and an unusual *trans* isomer (**1b**). The complex was prepared by the general scheme described in the literature, except using neopentanoyl chloride as the acylation reagent.[8] The isomers were separated using preparative TLC on neutral alumina, with $CHCl_3$–MeCN (10 : 1) as eluent and the isomeric nature of the two fractions was confirmed by mass spectrometry and by microanalysis. The slower moving isomer had a ^{1}H NMR spectrum consistent with those of saddle shaped (*cis*) Jäger complexes, while both the ^{1}H and ^{13}C NMR spectra of the other isomer indicated that it possessed higher symmetry.

Single crystals of each isomer were grown from $CHCl_3$–MeCN and the structures of **1a** (Fig. 1) and **1b** (Fig. 2) were determined.§ Complex **1a** has the expected saddle shape and the most interesting feature of the structure is the disorder in the position of C(10), arising from the presence of both boat (22%) and chair (78%) conformations for the metallochelate ring containing this carbon atom. In **1b**, the ring methyl groups appear in a *trans* relationship, rather than the usual *cis*, and this causes the keto oxygen atoms also to adopt a *trans* relationship, to minimise steric repulsion between ring and acyl methyl groups. Further, also to avoid steric interaction with the ring methyls, both saturated metallochelate rings adopt a skewed conformation, forcing the molecule to adopt a structure that has one unsaturated chelate ring above and one below the Ni–N_4 plane, producing the unprecedented (for a sixteen membered ring) Z isomer. Notably this structure possesses a centre of inversion at the nickel centre and the NiN_4 unit is exactly planar. In both molecules there are intermolecular contacts between the keto oxygens and hydrogen atoms on the saturated portion of the macrocycle [in **1b**: O(1)···H(4) 2.534(3), in **1a**: O(1)···H(10B) 2.581(5), O(2)···H(3B) 2.589(4) and O(2)···H(5A) 2.359(4) Å].

Identification of the existence of **1b** opens the way for the production of new sixteen membered Jäger macrocyclic ligands with a radically different supramolecular structural motif from that of the *cis* isomer. For example the extended Z structure could be used as the basis for new polymeric systems, by bridging across the keto functions. Our work in this interesting area is continuing.

Initially we believed that the new type of structural isomer was being formed during the addition of the neopentyl group,

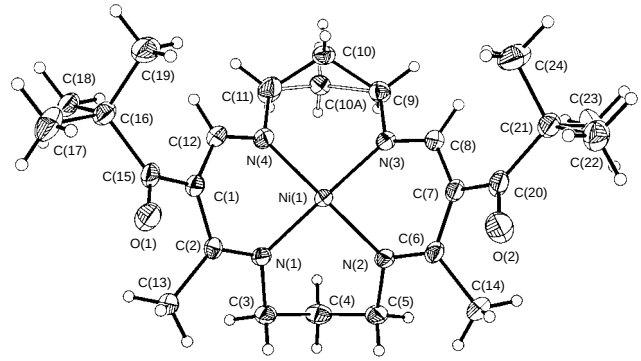

Fig. 1 Perspective view of compound **1a**; probability displacement ellipsoids are drawn at the 40% level. Selected bond lengths (Å) and angles (°) for **1a**: Ni(1)–N(4) 1.876(3), Ni(1)–N(3) 1.883(2), Ni(1)–N(2) 1.894(2), Ni(1)–N(1) 1.895(2), N(1)–C(2) 1.312(4), N(1)–C(3) 1.480(4), N(2)–C(6) 1.312(4), N(2)–C(5) 1.478(4), N(3)–C(8) 1.305(4), N(3)–C(9) 1.474(4), N(4)–C(12) 1.301(4), N(4)–C(11) 1.474(4); N(4)–Ni(1)–N(3) 92.22(11), N(4)–Ni(1)–N(2) 175.67(12), N(3)–Ni(1)–N(2) 88.09(10), N(4)–Ni(1)–N(1) 88.45(11), N(3)–Ni(1)–N(1) 174.90(11), N(2)–Ni(1)–N(1) 90.87(10), C(2)–N(1)–C(3) 118.2(3), C(6)–N(2)–C(5) 119.0(3), C(8)–N(3)–C(9) 117.2(3), C(12)–N(4)–C(11) 118.0(3).

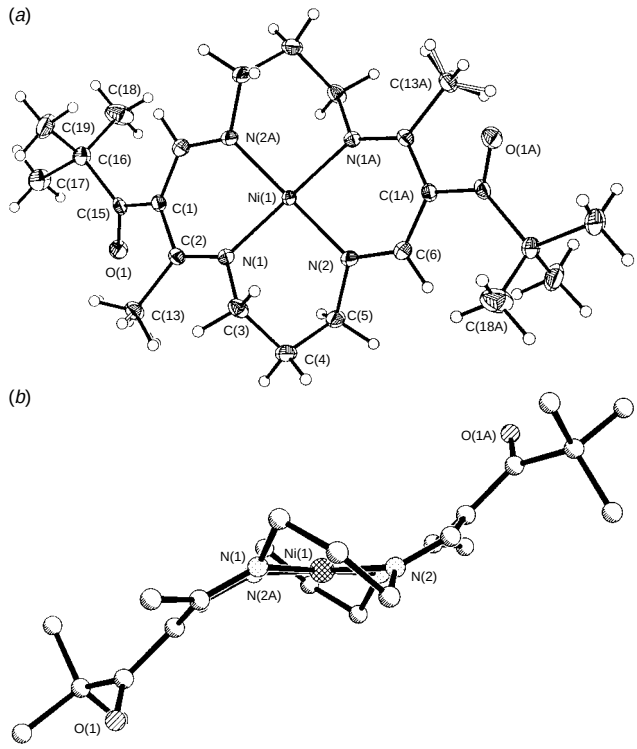

Fig. 2 (*a*) Perspective view of compound **1b**; probability displacement ellipsoids are drawn at the 40% level. Selected bond lengths (Å) and angles (°) for **1b**: Ni(1)–N(2) 1.874(2), Ni(1)–N(2A) 1.874(2), Ni(1)–N(1) 1.895(2), Ni(1)–N(1A) 1.895(2), N(1)–C(2) 1.308(3), N(1)–C(3) 1.479(3), N(2)–C(6) 1.296(4), N(2)–C(5) 1.469(3); N(2)–Ni(1)–N(2A) 180.0, N(2)–Ni(1)–N(1) 91.08(10), N(2A)–Ni(1)–N(1) 88.92(10), N(2)–Ni(1)–N(1A) 88.92(10), N(2A)–Ni(1)–N(1A) 91.08(10), N(1)–Ni(1)–N(1A) 180.0, C(2)–N(1)–C(3) 121.2(2), C(2)–N(1)–Ni(1) 126.6(2), C(3)–N(1)–Ni(1) 112.2(2), C(6)–N(2)–C(5) 118.1(2), C(6)–N(2)–Ni(1) 122.9(2), C(5)–N(2)–Ni(1) 118.7(2). Symmetry transformations used to generate equivalent atoms: A $-x, -y, -z + 1$. (*b*) Side view of **1b**, emphasising the *Z* conformation.

but this required a major rearrangement of the parent macrocycle which mechanistically seemed unlikely. Careful scrutiny of the reactions revealed that in fact both *cis* (**2a**) and *trans* (**2b**) forms of the parent sixteen membered complex were produced in the Schiff's base condensation reaction used to form this Jäger macrocycle from its acyclic precursor, and both **2a** and **2b** have now been structurally characterised.[9] Prior to this work, the *trans* form had not been recognised as a product of the cyclisation reaction, and we believe that this is because it is usually the minor isomer and also it is rather more soluble than the *cis* isomer, hence previously only the *cis* form had been isolated and characterised. We have now carried out a detailed study of the conditions of the ring closure reaction and have found that it is possible to favour the formation of the *trans* isomer relative to the *cis*, and the details of this work, and the X-ray structures of **2a** and **2b**, will be reported in a separate publication.[9]

We thank Professor D. H. Busch and Dr N. W. Alcock for helpful discussion, and EPSRC for the award of a Postgraduate Studentship (to D. P. N.).

Notes and References

† E-mail: J.H.Cameron@hw.ac.uk

‡ *Spectroscopic data*: for **1a**: ^{1}H NMR ($CDCl_3$, 200 MHz), δ 7.42 (s, 2 H), 3.10 (t, 4 H), 2.90 (s, 6 H), 2.10 (s, 6 H), 1.92 (m, 2 H) and 1.25 (s, 18 H); ^{13}C NMR ($CDCl_3$, 50 MHz), δ 201.8, 167.6, 157.1, 113.8, 54.9, 50.0, 42.8, 30.7, 29.8, 29.5 and 20.2. For **1b**: ^{1}H NMR ($CDCl_3$, 400 MHz), δ 7.40 (s, 2 H), 3.00 (t, 4 H), 2.91 (t, 4 H), 2.30 (m, 4 H), 2.05 (s, 6 H) and 1.22 (s, 18 H); ^{13}C NMR ($CDCl_3$, 100.6 MHz), δ 202.2, 166.7, 156.2, 114.2, 52.0, 48.7, 42.3, 29.1, 28.7 and 19.6.

§ For **1a** and **1b** intensity data were measured on a Siemens P4 diffractometer with Mo-Kα radiation, λ = 0.710 73 Å, ω mode, θ range 2.0–25.00° at 160 K. Data collection and reduction were performed using the program XSCANS.[10] Direct methods solution and refinements (full-matrix least squares on F^2) were performed using SHELXTL/PC[11] Version 5.03.

Crystal data: for **1a**: red crystal (0.80 × 0.52 × 0.64 mm) from $CHCl_3$–MeCN coated with Nujol mounted on a glass fibre, $C_{24}H_{38}N_4NiO_2{\cdot}C_2H_3N$, M = 514.34, monoclinic, space group $P2_1/n$, a = 10.1000(10), b = 10.5670(10), c = 25.414(3) Å, β = 90.950(10)°, U = 2712.0(5) Å^3, Z = 4, D_c = 1.252 g cm^{-3}, μ = 0.746 mm^{-1}. The structure was refined to $R1$ = 0.0501, $wR2$ = 0.1367 and goodness of fit 1.011 for 3988 unique observed [$I > 2\sigma(I)$] data and 317 parameters.

For **1b**: red crystal (0.6 × 0.4 × 0.25 mm) from $CHCl_3$–MeCN coated with Nujol mounted on a glass fibre, $C_{24}H_{38}N_4NiO_2{\cdot}2CHCl_3$, M = 712.03, orthorhombic, space group *Pbca*, a = 15.721(2) b = 10.493(2), c = 19.668(3) Å, U = 3244.4(9) Å^3, Z = 4, D_c = 1.458 g cm^{-3}, μ = 1.123 mm^{-1}. The structure was refined to $R1$ = 0.0361, $wR2$ = 0.0801 and goodness of fit 1.021 for 2158 unique observed [$I > 2\sigma(I)$] data and 178 parameters. CCDC 182/913.

1 E. G. Jäger, *Z. Chem.*, 1968, **8**, 392.
2 D. H. Busch and C. J. Cairns, in *Progress in Macrocyclic Chemistry*, ed. R. M. Izatt and J. J. Christensen, Wiley, New York, 1987.
3 N. Herron, L. L. Zimmer, J. J. Grzybowski, D. J. Olszanski, S. C. Jackels, R. W. Callahan, J. H. Cameron, G. G. Christoph and D. H. Busch, *J. Am. Chem. Soc.*, 1983, **105**, 6585.
4 T. J. Meade, K. J. Takeuchi and D. H. Busch, *J. Am. Chem. Soc.*, 1987, **109**, 725.
5 D. H. Busch and N. A. Stephenson, *J. Inclusion Phenom. Mol. Recognit. Chem.*, 1989, **7**, 137.
6 N. W. Alcock, W.-K. Lin, A. Jircitano, J. D. Mokren, P. W. R. Corfield, G. Johnson, G. Novotnak, C. Cairns and D. H. Busch, *Inorg. Chem.*, 1987, **26**, 440.
7 J. H. Cameron, C. A. Clarke, G. M. Rosair and E. L. Scott, *Coord. Chem. Rev.*, 1998, in press.
8 J. H. Cameron, M. Kojima, B. K. Daskiewicz, B. K. Coltrain, T. J. Meade, N. W. Alcock and D. H. Busch, *Inorg. Chem.*, 1987, **26**, 427.
9 J. H. Cameron, C. R. Ginoux, K. J. McCullough, D. P. Nicol and G. M. Rosair, manuscript in preparation.
10 Siemens Analytical Instruments, Inc., Madison, WI, 1994.
11 G. M. Sheldrick, SHELXTL/PC. Siemens Analytical X-ray Instruments Inc., Madison, WI, 1994.

Received in Basel, Switzerland, 3rd April 1998; 8/02550I

Total synthesis of (−)-epothilone B

Scott A. May and Paul A. Grieco*†

Department of Chemistry and Biochemistry, Montana State Univeristy, Bozeman, Montana 59717, USA

The sixteen-membered ring macrolide (−)-epothilone B 1 has been synthesized by a route which features stereospecific methylation of an (*E*)-γ,δ-epoxy acrylate, the use of a double asymmetric reaction employing (*R*,*R*)-diisopropyltartrate and (*E*)-crotylboronate, and ring closure by means of an olefin metathesis reaction.

(–)-Epothilone B **1**, isolated by Höfle and co-workers[1] from the myxobacteria *Sorangium cellulosum* strain 90, has been the object of intense synthetic activity.[2,3] The excitement surrounding the epothilones stems, in part, from research conducted at the Merck Research Laboratories by Bollag[4] and co-workers who demonstrated that the epothilones function *via* a paclitaxel-like mode of action by binding to and stabilizing cell microtubule assemblies. Particularly significant has been the finding[4] that (−)-epothilone B appears to be effective against a number of drug-resistant tumor cell lines. We detail below an intramolecular olefin metathesis strategy for the construction of (−)-epothilone B which features preparation of the C(3)-C(12) fragment **2** and its elaboration into **3**, and subsequent conversion of **3** into **1**.

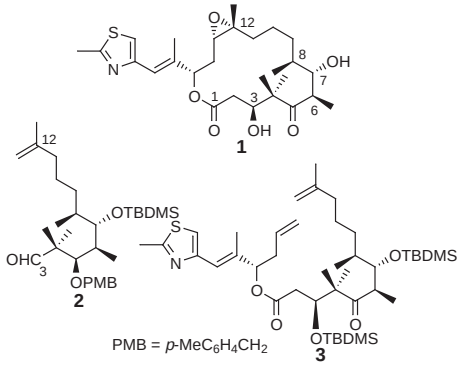

Synthesis of the chiral C(3)-C(12) fragment **2** commenced with the optically active epoxide **5**, $[\alpha]_D^{25}$ −10.1 (*c* 2.5, $CHCl_3$), which was prepared from allylic alcohol **4**[5] *via* a Sharpless epoxidation[6] [diethyl L-tartrate (0.26 equiv.), $Ti(O\text{-}Pr^i)_4$ (0.2 equiv.), Bu^tOOH (3.0 equiv.), CH_2Cl_2, 4 Å mol sieves, −40 °C (8 h) → −10 °C (8 h)]. With the ready availability of **5**, efforts were focused on introduction of the C(6) methyl group. Toward this end, **5** was transformed, in 87% overall yield, into the (*E*)-γ,δ-epoxy acrylate **6** *via* a Swern oxidation [DMSO, $(COCl)_2$, CH_2Cl_2, −78 °C, 1 h, then Et_3N, 0 °C, 1 h] and an (*E*)-selective Horner–Wadsworth–Emmons reaction [NaH, THF, $(EtO)_2POCH_2CO_2Et$, 0 °C, 1 h, then RCHO, THF, 0 °C, 30 min]. Treatment of a 0.07 M solution of **6** in 1,2-dichloroethane in the presence of 6.0 equiv. of water cooled to −30 °C with 10.0 equiv. of Me_3Al (2.0 M in hexane) gave rise to **7** (R = H), $[\alpha]_D^{25}$ +11.7 (*c* 2.5, $CHCl_3$), as the sole product in 87% yield.[7] The methylation of **6** is stereospecific, proceeding with net inversion of configuration about C(6). Note that, in the absence of water, the transformation of **6** into **7** (R = H) does not proceed to any appreciable extent.

Elaboration of the remaining two stereocenters at C(7) and C(8) necessitated conversion of substrate **7** into aldehyde **8** which was realized (95% overall yield) *via* a three step protocol

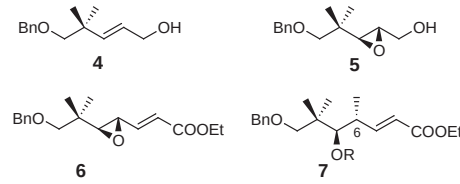

[TESOTf, 2,6-lutidine, CH_2Cl_2, 45 min, then OsO_4 (catalytic), NMO, acetone–water–Bu^tOH (2:5:1), 7 h, followed by $NaHSO_3$, 14 h, then $Pb(OAc)_4$, C_6H_6, 15 min]. Exposure of **8** to (*R*,*R*)-diisopropyltartrate and (*E*)-crotylboronate[8] in toluene [−78 °C (3 h) → room temp. (12 h)] in the presence of 4 Å molecular sieves gave rise to **9**, $[\alpha]_D^{25}$ −8.6 (*c* 2.1, $CHCl_3$), as the sole product in 93% yield, thus establishing the required *syn*,*anti* arrangement about C(6)–C(7) and C(7)–C(8). Prior to functionalization of the $\Delta^{9,10}$ terminal olefin, the triethylsilyl ether was cleaved (TBAF, THF, 30 min) and the resulting 1,3-*anti* diol was converted, upon exposure (15 min) to 2,2-dimethoxypropane and catalytic TsOH, into the 1,3-*anti* acetonide **10**, $[\alpha]_D^{25}$ +11.6 (*c* 1.7, $CHCl_3$), in 93% overall yield. The stereochemical assignment for the *anti* acetonide follows from the ^{13}C NMR spectrum of **10**. The observed chemical shifts for the acetonide carbons (δ 23.4, 25.7 and 100.1) in **10** are in excellent agreement with previous data from independent studies on 1,3-*anti* acetonides by Rychnovsky[9] and Evans.[10]

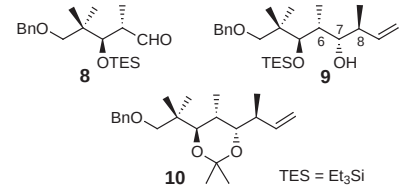

Completion of the synthesis of the C(3)-C(12) fragment **2** was realized as follows. Hydroboration [catecholborane, $(PPh_3)_3RhCl$ (catalytic), THF, 45 min; NaOH, H_2O_2][11] of **10** followed by oxidation (Swern conditions) and subsequent Horner–Wadsworth–Emmons condensation (THF, 4 h) of the resulting aldehyde with the sodium anion derived from diethyl (2-oxopropyl)phosphonate gave rise, in 55% overall yield, to **11**, $[\alpha]_D^{25}$ +26.0 (*c* 1.05, $CHCl_3$). Enone **11** was transformed (77% overall) into triol **12** *via* a three step sequence [H_2, 10% Pd/C, EtOH–EtOAc (1:1), 5 h, then $Ph_3P{=}CH_2$, THF, 3 h, then 1.0 M HCl–THF (1:1), 50 °C, 3 h] which set the stage for selective protection of the C(5) and C(7) hydroxy groups, which proved critical for completion of the total synthesis of epothilone B since the 1,3-diol acetonide present in **11** was not compatible with the olefin metathesis reaction in the late stages of the synthesis.

Exposure (30 min) of **12** to *p*-anisaldehyde dimethylacetal in benzene containing catalytic TsOH gave rise (90%) to **13** (R = H) which, upon silylation [TBDMSOTf, 2,6-lutidine, CH_2Cl_2, −78 °C, 4 h], provided (94%) **13** (R = TBDMS), $[\alpha]_D^{25}$ +19.7 (*c* 3.9, $CHCl_3$). Protection of the C(5) hydroxy group as its 4-methoxybenzyl (PMB) ether was realized *via* regioselective

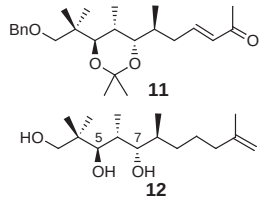

reductive ring cleavage[12] of the 1,3-dioxane ring of the 4-methoxybenzylidene acetal **13** (R = TBDMS). Thus, a 0.04 M solution of **13** (R = TBDMS) in CH_2Cl_2 , cooled to −78 °C, was treated with 10.0 equiv. of a 1.0 M solution of DIBAL-H in CH_2Cl_2. After warming to −15 °C (1.5 h), a 75% yield of primary alcohol **14** was isolated. Oxidation (Swern conditions) of **14** provided the intact C(3)-C(12) fragment **2**, $[\alpha]_D^{25}$ −7.6 (*c* 4.6, $CHCl_3$), in 98% yield.

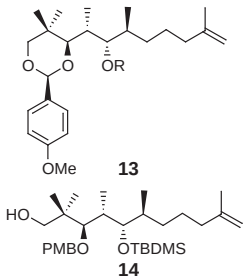

In order to complete the total synthesis of **1**, the ester enolate derived (LDA, THF, −78 °C) from the known acetate **15**[2] was condensed with **2** giving rise (83%) to a readily separable mixture (1.7 : 1) of diastereomers favoring **16**, $[\alpha]_D^{25}$ −28.6 (*c* 1.4, $CHCl_3$), possessing the correct configuration at C(3). Protection [TBDMSOTf, 2,6-lutidine, CH_2Cl_2, −50 °C, 4 h] of the C(3) hydroxy group, followed by cleavage [DDQ, CH_2Cl_2–H_2O (18 : 1), 0 °C, 3 h] of the C(5) 4-methoxybenzyl ether and subsequent Dess–Martin oxidation gave rise to **17**, $[\alpha]_D^{25}$ −44.0 (*c* 2.4, $CHCl_3$), in 65% overall yield.

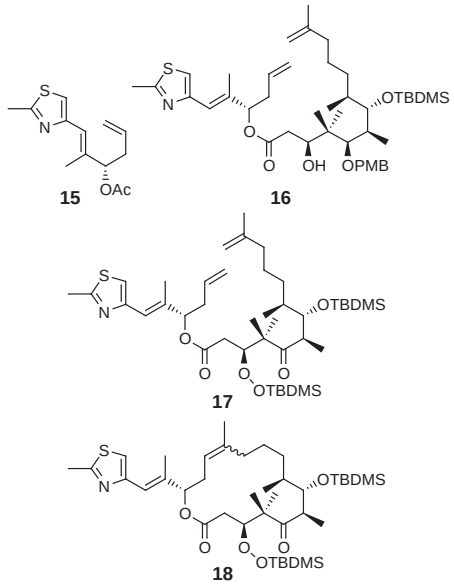

Ring closure to complete the formation of the sixteen-membered ring of **1** was realized by an intramolecular olefin metathesis reaction.[13,14] Exposure (4 h) of a 0.001 M solution of **17** in benzene (heated to 55 °C) to 20 mol% of the molybdenum-based catalyst [$Mo(CHMe_2Ph)\{N(2,6\text{-}Pr^i_2C_6H_3)\}\{OCMe(CF_3)_2\}_2$] of Schrock[13] afforded in 55% yield a 1 : 1 mixture of *Z* and *E* isomers (*cf.* **18**) which could be separated by preparative TLC. Upon treatment of the enantiomerically pure *Z*-isomer with HF·pyridine (THF, 3 h), a 60% yield of pre-epothilone B **19** was obtained. Epoxidation (dimethyldioxirane,[15] CH_2Cl_2, −50 °C, 4 h) of **19** provided crystalline **1**, mp 93–94 °C (lit.,[2] 93.6–94.7 °C), $[\alpha]_D^{25}$ −32.2 (*c* 0.09, $CHCl_3$) [lit.,[2] −31.0 (*c* 0.045, $CHCl_3$)] in 86% yield. The ^{1}H NMR spectrum of synthetic **1** was identical in all respects with a spectrum of natural (-)-epothilone B.

We thank Professor S. Danishefsky for helpful discussions and the ^{1}H NMR spectra of natural (−)-**1** and synthetic (−)-**17**. This research was supported by a grant from the U.S. NIH (CA 28865).

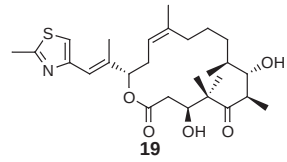

Notes and References

† E-mail: grieco@chemistry.montana.edu

1 G. Höfle, N. Bedorf, H. Steinmetz, D. Schomburg, K. Gerth and H. Reichenbach, *Angew. Chem., Int. Ed. Engl.*, 1996, **35**, 1567.
2 D. Meng, P. Bertinato, A. Balog, D.-S. Su, T. Kamenecka, E. J. Sorensen and S. J. Danishefsky, *J. Am. Chem. Soc.*, 1997, **119**, 10073 and references cited therein.
3 K. C. Nicolaou, S. Ninkovic, F. Sarabia, D. Vourloumis, Y. He, H. Vallberg, M. R. V. Finlay and Z. Yang, *J. Am. Chem. Soc.*, 1997, **119**, 7974.
4 D. M. Bollag, P. A. McQueney, J. Zhu, O. Hensens, L. Koupal, J. Liesch, M. Goetz, E. Lazarides and C. M. Woods, *Cancer Res.*, 1995, **55**, 2325.
5 M. A. Blanchette, M. S. Malamas, M. H. Nantz, J. C. Roberts, P. Somfai, D. C. Whritenour, S. Masamune, M. Kageyama and T. Tamura, *J. Org. Chem.*, 1989, **54**, 2817.
6 T. Katsuki and K. B. Sharpless, *J. Am. Chem. Soc.*, 1980, **102**, 5974.
7 M. Miyashita, M. Hoshino and A. Yoshikoshi, *J. Org. Chem.*, 1991, **56**, 6483; M. Miyashita, K. Yoshihara, K. Kawamine, M. Hoshino and H. Irie, *Tetrahedron Lett.*, 1993, **39**, 6285; M. Miyashita, T. Shiratani, K. Kawamine, S. Hatakeyama and H. Irie, *Chem. Commun.* 1996, 1027; P. A. Grieco, J. D. Speake, S. K. Yeo and M. Miyashita, *Tetrahedron Lett.*, 1998, **39**, 1125.
8 W. R. Roush, K. Ando, D. B. Powers, A. D. Palkowitz and R. L. Halterman, *J. Am. Chem. Soc.*, 1990, **112**, 6339; W. R. Roush, A. D. Palkowitz and K. Ando, *J. Am. Chem. Soc.*, 1990, **112**, 6348.
9 S. D. Rychnovsky and D. J. Skalitzky, *Tetrahedron Lett.*, 1990, **31**, 945.
10 D. A. Evans, D. L. Rieger and J. R. Gage, *Tetrahedron Lett.*, 1990, **31**, 7099.
11 D. Männig and H. Nöth, *Angew. Chem., Int. Ed. Engl.*, 1985, **24**, 878; D. A. Evans, G. C. Fu and A. H. Hoveyda, *J. Am. Chem. Soc.*, 1992, **114**, 6671.
12 S. Takano, M. Akiyama, S. Sato and K. Ogasawara, *Chem. Lett.*, 1983, 1593.
13 R. R. Schrock, J. S. Murdzek, G. C. Bazan, J. Robbins, M. DiMare and M. O'Regan, *J. Am. Chem. Soc.*, 1990, **112**, 3875.
14 P. Schwab, M. B. France, J. W. Ziller and R. H. Grubbs, *Angew. Chem., Int. Ed. Engl.*, 1995, **34**, 2039. Also See: A. Houri, Z. Xu, D. A. Cogan and A. H. Hoveyda, *J. Am. Chem. Soc*., 1995, **117**, 2943.
15 R. W. Murray and R. Jeyaraman, *J. Org. Chem*., 1985, **50**, 2847.

Received in Corvallis, OR, USA, 20th April 1998; 8/02947D

Crystal structure of a chiral nitrido-manganese salen complex. The nitrogen analogue to the intermediate in the Jacobsen epoxidation reaction

Aase Sejr Jepsen, Mark Roberson, Rita G. Hazell and Karl Anker Jørgensen*†

Center for Metal Catalyzed Reactions, Department of Chemistry, Aarhus University, Aarhus C, DK-8000, Denmark

A chiral nitrido-manganese salen complex has been synthesised and characterised by X-ray diffraction; the geometrical and electronic structure of the complex are discussed in relation to the intermediate in asymmetric reactions.

The transfer of an oxygen atom(s) from high-valent oxo-metal complexes to alkenes in an enantioselective manner has been developed to be highly successful using asymmetric catalysis.[1] For the epoxidation of alkenes the use of chiral manganese salen complexes as the catalyst is among the most useful and widely applicable as it has proven effective for a variety of different alkenes.[1a,2]

The intermediate in reactions using chiral manganese(III) salen complexes as the catalyst has been postulated to be an oxo-manganese(V) salen complex.[1a,3] There are a number of indirect proofs for the oxo-manganese(V) salen intermediate, and recently direct proof by application of electrospray tandem MS appeared.[4] A further aspect of reactions catalyzed by chiral manganese salen complexes, which also relates to the intermediate in the reaction, is the mechanism for the oxygen transfer process. The majority of the experimental results for the epoxidation reaction point to a mechanism starting with addition of the alkene to the oxygen atom in the oxo-manganese salen intermediate and the epoxide is formed by collapse involving a rotation of the carbon–carbon bond.[1a,5] An alternative mechanism is based on the concept of metallaoxetanes as intermediates in oxygen-transfer reactions[6] and assumes that the alkene adds to the oxo–manganese bond in a [2 + 2] fashion followed by collapse giving the epoxide.[7]

Although much attention has been devoted to the intermediate in reactions catalyzed by chiral manganese(III) salen complexes no direct structural evidence for the intermediate is available. One way to obtain structural information about the intermediate could be to turn attention to the corresponding nitrogen analogue of the chiral oxo-manganese(V) salen complex as the structural difference between an O=Mn^V and a N≡Mn^V bond is small (*vide infra*). Here we present the preparation, characterisation and electronic structure analysis of the nitrogen analogue to the intermediate in the Jacobsen epoxidation reaction.

The dark brown chiral manganese(III) salen complex **1** reacts with NH_3 in CH_2Cl_2 at −50 °C using NBS as the oxidant to yield a deep green complex **2** isolated in 89% yield [reaction (1)].[8]‡

^{1}H NMR spectroscopic investigations of **2** give the following resonances in $CDCl_3$: δ_H 1.47 (s, 9H), 1.50 (s, 9H), 2.14 (s, 3H), 2.15 (s, 3H), 4.70 (d, *J* 11 Hz, 1H), 5.14 (d, *J* 11 Hz, 1H), 6.57 (s, 2H), 7.09–7.37 (m, 14 H), 7.55 (s, 1H), 7.62 (s, 1H). The ^{1}H NMR data show that the Bu^t, Me, CH=N and CH(Ph)CH(Ph) hydrogen atoms are non-equivalent. The ^{13}C NMR spectrum for **2** shows the following resonances: δ_C 20.4, 29.7, 35.6, 81.2, 81.4, 119.4, 120.5, 124.0, 128.8, 129.1, 129.4, 129.5, 131.3, 131.7, 134.7, 134.9, 135.6, 137.9, 141.1, 166.0, 166.2, 167.3, 167.5. These data for **2** show also the non-equivalence of several signals, most notably the signal for the chiral carbon and imine carbon atoms. The IR spectrum for **2** shows a N≡Mn stretch at 1049 cm^{-1}. Recrystallisation of the green complex gave crystals from MeOH (mp 206–208 °C) which were useable for X-ray analysis.

The structure of **2** is depicted in Fig. 1§ and shows the presence of the N≡Mn bond. The N≡Mn bond length is found to be 1.537 Å and similar to other N≡Mn bonds characterized.[8,9] Other selected bond distances and angles are in the legend to Fig. 1. If one compares the N≡Mn^V bond length in **2** with, according to our knowledge, the only two other characterised O=Mn^V bonds (1.548 and 1.558 Å) in related types of complexes,[10] the structural similarity between the N≡Mn^V and O=Mn^V fragments is obvious. It is also notable for the structure of **2** that the oxidation of the manganese atom causes a displacement of this atom by 0.49 Å out of the plane consisting of the four atoms coordinating to manganese. The displacement of the manganese atom when forming the N≡Mn^V complex probably causes the change in electronic environment at the chiral ligand which accounts for the non-equivalent resonances observed in the NMR spectra of **2**. The reactivity of **2** has also been briefly investigated under various reaction conditions, but compared with the corresponding chiral oxo-manganese(V) salen complex it is much less reactive.[11]

In an attempt to obtain further insight into the structure and the chemical properties of the chiral nitrido-manganese(V) salen complex **2** the electronic structure has been investigated. A

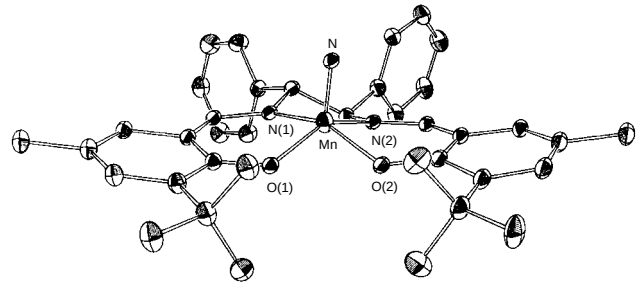

Fig. 1 Molecular structure of **2**. C–H hydrogen atoms are not shown (the other molecule is similar except that 12% have Mn and N on the other side of the salen plane). Selected distances (Å) and angles (°) for **2**: Mn–N 1.537(6), Mn–N(1) 1.949(6), Mn–N(2) 1.968(6), Mn–O(1) 1.903(6), Mn–O(2) 1.915(6), O(1)–Mn–N 109.8(3), O(2)–Mn–N 103.2(3), N(1)–Mn–N 101.6(3), N(2)–Mn–N 104.0(3).

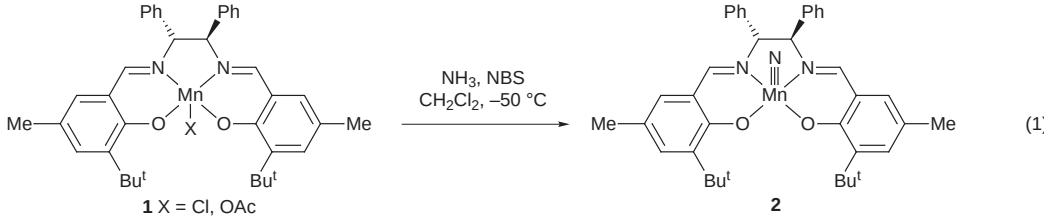

(1)

model compound (**3**) for **2** was optimised using *ab initio* DFT calculations applying a B3LYP/6-31G* basis set and a TZV basis set for manganese.[12] For the singlet state of **3** the optimised structure is shown below with the calculated bond lengths at the manganese atom and it is notable that the N≡Mn, Mn–N and Mn–O bond lengths for **3** are similar to the same bonds in **2**. Furthermore, the displacement of the manganese atom (0.45 Å) out of the plane consisting of the four heteroatoms coordinating to manganese in **3** is also similar to the displacement in **2**. The simple model **3** seems thus to be a reliable model for **2**.

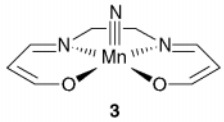

3

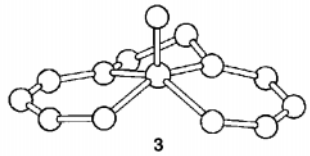

3

Mn≡N: 1.497 Å
Mn–N: 1.970 Å
Mn–O: 1.965 Å

The calculations give a N≡Mn bond order of 2.8 indicating a bond with triple bond character. The charges on the nitrogen and manganese atoms are −0.15 and 0.87, respectively. The frontier orbitals calculated for the N≡Mn bond in **3** give the HOMO at −5.71 eV and with only a minor contribution of the bonding combination of N p_x–Mn $d_{x^2-y^2}$, but this orbital is mainly located on the ligand. The second HOMO is at −6.00 eV and is mainly on the manganese atom as $d_{x^2-y^2}$; while the fourth HOMO at −7.62 eV is the bonding combination of N p_y–Mn d_{yz}. The LUMO and the third LUMO, at −1.60 eV and −0.95 eV, respectively, are the antibonding combination of N p_y–Mn d_{yz} and N p_x–Mn d_{xz} orbitals, respectively. The antibonding combination of N p_z–Mn d_{z^2}, the σ^*_{N-Mn} orbital, is at −0.20 eV.

It is interesting to compare the structure of the nitrido-manganese(v) salen complex **3** with the closely related oxo-manganese(v) salen complex. The structure of the latter is unknown, but the similarity in $N{\equiv}Mn^{V}$ and $O{=}Mn^{V}$ bond lengths (*vide supra*) is striking; however, the structural similarity does not account for the difference in reactivity. A comparison of the electronic structure for both the $O{=}Mn^{V+}$ and $O{=}Mn^{V}$–Cl (optimised structures) obtained by *ab initio* DFT calculations[12] gives important information. The results for the two oxo-manganese complexes are alike, so only the former will be discussed here. The O=Mn bond length is optimised to be 1.546 Å which is similar to the two characterised $O{=}Mn^{V}$ bonds (1.548 and 1.558 Å) in related types of complexes.[10] The charges at oxygen and manganese are −0.20 and 1.18, respectively. The bond length and charge considerations of the $N{\equiv}Mn^{V}$ and $O{=}Mn^{V}$ complexes are thus not that different. However, the O=Mn bond order is calculated to be 2.3, showing a much weaker bond than the N≡Mn bond, and, furthermore, the $O{=}Mn^{V}$ complex also shows a different frontier orbital picture compared with the $N{\equiv}Mn^{V}$ complex, as the related frontier orbitals of the former are found at lower energies, the HOMO at −10.65 eV, while the LUMO is at −7.92 eV. The lowering of the LUMO in $O{=}Mn^{V}$ by 6.3 eV points to a significant difference in reactivity, when reacting with electron-rich alkenes. The more reactive chiral oxo-manganese(v) salen complex compared with the closely related chiral nitrido-manganese(v) salen complex is thus probably due to a much weaker O=Mn bond and lower lying unoccupied MOs in the former complex.

With the structural knowledge of the chiral nitrido-manganese(v) salen complex the remarkable enantioselectivity of the related oxo-manganese(v) salen complex might begin to be understood in detail as the present results allow one to analyse the approach of *e.g.* alkenes to the intermediate.

The work presented here was made possible by a grant from The Danish National Science Foundation.

Notes and References

† E-mail: kaj@kemi.aau.dk

‡ Reaction conditions for the preparation of **2**. A solution of [(*R*,*R*)-diphenyl-*tert*-butylmethylsalen]Mn(Cl) (360 mg, 0.56 mmol) in 30 ml CH_2Cl_2 was cooled to −50 °C. NBS was added (470 mg, 2.8 mmol). Gaseous NH_3 was fed through the reaction mixture for 5–10 min and a colour change to green was observed. The reaction mixture was warmed and the contents transferred to a separator funnel with 25 ml H_2O added. The dark green organic phase was isolated and the aqueous layer extracted with 25 ml CH_2Cl_2. The combined organic phases were washed with 4 × 25 ml H_2O and the solvent removed. The solid material was re-dissolved in CH_2Cl_2 and purified by chromatography (Al_2O_3, 4 × 18 cm) with CH_2Cl_2 as the eluent. A dark green band was collected and recrystallized in MeOH.

§ *Crystallographic data* for **2**: $C_{38}H_{42}N_3O_2Mn$; M_w: 627.72; triclinic, space group *P*1, a = 10.2919(8), b = 12.0062(9), c = 14.139(1) Å, α = 88.543(1), β = 76.608(1), γ = 77.637(1)°, V = 1659.7(2) Å^3, Z = 2. 6542 independent reflections measured at 120 K on a Siemens SMART CCD diffractometer. Mo-Kα radiation. 4697 reflections with $I > 3\sigma(I)$ and 329 variables yield R = 0.052, R_w = 0.057. The two molecules are related by an approximate center of symmetry except for the chiral centers. This necessitated the use of severe constraints on the refinement.[13] CCDC 182/904.

1 For example, (*a*) asymmetric epoxidations: E. N. Jacobsen, in *Catalytic Asymmetric Synthesis*, ed. I. Ojima, VCH, New York, 1993, ch. 4.2; (*b*) asymmetric dihydroxylation: H. C. Kolb, M. S. VanNieuwenhze and K. B. Sharpless, *Chem. Rev.*, 1994, **94**, 2483.

2 See *e.g.*: E. N. Jacobsen, in *Comprehensive Organometallic Chemistry II*, ed. G. Wilkinson, F. G. A. Stone, E. W. Abel and L. S. Hegedus, Pergamon, New York, 1995, vol. 12, ch. 11.1; T. Katsuki, *Coord. Chem. Rev.*, 1995, **140**, 189.

3 See *e.g.*: E. N. Jacobsen, W. Zhang, A. R. Muci and M. L. Güler, *J. Am. Chem. Soc.*, 1991, **113**, 7063; P. J. Pospisil, D. H. Carstens and E. N. Jacobsen, *Chem. Eur. J.*, 1996, **2**, 974.

4 D. Ferringer and D. A. Plattner, *Angew. Chem., Int. Ed. Engl.*, 1997, **36**, 1718.

5 See *e.g.*: M. Palucki, N. S. Finney, P. J. Pospisil, M. L. Güler, T. Ishida and E. N. Jacobsen, *J. Am. Chem. Soc.*, 1998, **120**, 948; N. S. Finney, P. J. Pospisil, S. Chang, M. Palucki, R. G. Konsler, K. B. Hansen and E. N. Jacobsen, *Angew. Chem., Int. Ed. Engl.*, 1997, **36**, 1720.

6 K. A. Jørgensen and B. Schiøtt, *Chem. Rev.*, 1990, **90**, 1483.

7 P.-O. Norrby, C. Linde and B. Åkermark, *J. Am. Chem. Soc.*, 1995, **117**, 11035; T. Hamada, T. Fukuda, H. Imanishi and T. Katsuki, *Tetrahedron*, 1996, **52**, 515; C. Linde, M. Arnold, P.-O. Norrby and B. Åkermark, *Angew. Chem., Int. Ed. Engl.*, 1997, **36**, 1723.

8 J. du Bois, J. Hong, E. M. Carreira and M. W. Day, *J. Am. Chem. Soc.*, 1996, **118,** 915; J. du Bois, C. S. Tomooka, J. Hong, E. M. Carreira and M. W. Day, *Angew. Chem., Int. Ed. Engl.*, 1997, **36**, 1645; J. du Bois, C. S. Tomooka, J. Hong and E. M. Carreira, *Acc. Chem. Res.*, 1997, **30**, 364.

9 J. W. Bucjler, C. Dreher, K.-L. Lay, Y. J. A. Lee and W. R. Scheidt, *Inorg. Chem.*, 1983, **22**, 888.

10 T. J. Collins and S. W. Gordon-Wylie, *J. Am. Chem. Soc.*, 1989, **111**, 4511; F. M. MacDonnell, N. L. P. Fackler, C. Stern and T. V. O′Halloran, *J. Am. Chem. Soc.*, 1994, **116**, 7431.

11 A. S. Jepsen, A. Bøgevig and K. A. Jørgensen, unpublished results.

12 Gaussian 94, Revision E. 2, M. J. Frisch, G. W. Trucks, H. B. Schlegel, P. M. W. Gill, B. G. Jonhson, M. A. Robb, J. R. Cheeseman, T. Keith, G. A. Petersson, J. A. Montgomery, K. Raghavachari, M. A. Al-Laham, V. G. Zakrezewski, J. V. Ortiz, J. B. Foresman, J. Cioslowski, B. B. Stefanov, A. Nanayakkara, M. Challacombe, C. Y. Peng, P. Y. Ayala, W. Chen, M. W. Wong, J. L. Andres, E. S. Replogle, R. Gomperts, R. L. Martin, D. J. Fox, J. S. Binkley, D. J. Defrees, J. Baker, J. P. Stewart, M. Head-Gordon, C. Gonzales and J. A. Pople, Gaussian, Inc., Pittsburgh, PA, 1995.

13 X-Ray programs: SIR97, G. Cascarano, A. Altomare, C. Giacovazzo, A. Guagliardi, A. G. G. Moliterni, D. Siliqi, M. C. Burla, G. Polidori and M. Camalli, *Acta Crystallogr., Sect. A*, 1996, **52**, C50; G. S: Pawley, *Adv. Struct. Res. Diffract. Methods*, 1972, **4**, 1; ORTEP III, M. N. Burnett and C. K. Johnson, Report ORNL-6895, Oak Ridge National Laboratory, Tennessee, 1996.

Received in Cambridge, UK, 6th April 1998; 8/02592D

Catalytic heterogeneous aziridination of alkenes using microporous materials

Christopher Langham,[a] Paola Piaggio,[a] Donald Bethell,[b] Darren F. Lee,[b] Paul McMorn,[a] Philip C. Bulman Page,[c] David J. Willock,[a], Chris Sly,[d] Frederick E. Hancock,[e] Frank King[e] and Graham J. Hutchings[a,b]†

[a] *Department of Chemistry, University of Wales Cardiff, PO Box 912, Cardiff, UK CF1 3TB*
[b] *Leverhulme Centre for Innovative Catalysis, Department of Chemistry, University of Liverpool, Liverpool, UK L69 3BX*
[c] *Department of Chemistry, Loughborough University, Loughborough, Leicestershire, UK LE11 3TU*
[d] *Robinson Brothers Ltd., Phoenix Street, PO Box, West Bromwich, West Midlands, UK B70 OAH*
[e] *ICI Katalco, R & T Division, Street, PO Box 1, Billingham, Teeside, UK TS23 1LB*

Copper-exchanged zeolite Y is a highly active catalyst for the aziridination of alkenes; modification using bis(oxazolines) leads to preparation of the first heterogeneous enantioselective aziridination catalyst.

The design of asymmetric catalysts is of intense current interest,[1] and procedures making use of chiral transition metal complexes have been described for epoxidation, cyclopropanation, aziridination and hydrogenation of alkenes in homogeneous solution.[2–6] There is increasing recognition that heterogeneous catalysts have practical advantages over homogeneous ones.[6–8] We describe here a generic approach to the design of heterogeneous transition-metal catalysts by making use of the well-known ability of zeolites to undergo metal cation exchange,[9] together with their acid–base properties.[10] By constructing transition-metal complexes within the spatially restricted environment of the zeolite pores, enantioselective organic transformations can be catalysed with comparable or even greater efficiency than in the corresponding homogeneous process. We exemplify this approach with the first heterogeneous catalyst for asymmetric aziridination of alkenes.

We have found that CuHY zeolite is successful in catalysing the aziridination of a range of alkenes employing [*N*-(tolyl-*p*-sulfonyl)imino]phenyliodinane (PhI = NTs) as the nitrogen source. The results are shown in Table 1. The Cu-exchanged zeolite (CuHY) was prepared by conventional ion-exchange methods with aqueous $Cu(OAc)_2$ solution, the concentration of which was chosen so as to obtain the required exchange level (*ca*. 50–60% of available H^+). The cation-exchanged zeolite was then washed with distilled water and dried at 110 °C in air. CuHY was initially screened in the aziridination of styrene (Table 1, entries 1–3), since this alkene affords good yields of aziridine when copper triflate is used as a homogeneous catalyst.[4] Using a five-fold molar excess of styrene, the desired *N*-tosylaziridine was obtained in 90% yield (entry 1). These initial results confirmed our contention that cations within zeolites could be used as heterogeneous counterparts of known homogeneous catalysts, and, to the best of our knowledge, this is the first example of an aziridination reaction catalysed heterogeneously.

Table 1 CuHY-catalysed aziridination of representative alkenes

Entry	Alkene[a]	Cu (mol%)	Yield (%)[b]
1	Styrene	25	90 (92)
2	Styrene[c]	25	87 (35)
3	Styrene	5	62
4	α-Methylstyrene	25	33
5	*p*-Chlorostyrene	25	76
6	*p*-Methylstyrene	25	66
7	Cyclohexene	25	50 (60)
8	Methyl cinnamate	25	84 (73)
9	*trans*-Stilbene	25	0 (52)
10	*trans*-Hex-2-ene	25	44

[a] Unless otherwise specified reaction conditions were: MeCN, 25 °C, styrene : PhI=NTs = 5 : 1. [b] Isolated yield of aziridine based on PhI=NTs. Values in parentheses indicate yields obtained from homogeneous reactions. [c] styrene : PhI=NTs = 1 : 1 molar ratio.

In order to confirm the absence of homogeneously catalysed reaction, following reaction the zeolite catalyst was recovered by filtration and another aliquot of reactants (styrene: PhI=NTs = 5 : 1 molar ratio) was added to the recovered filtrate; no further product was observed. Further, the removed catalyst was reused with fresh reagents and solvent, and the zeolite demonstrated similar activity to when it was used initially.

It was noted in earlier studies that, in the homogeneously catalysed reaction,[4] the yield of aziridine decreased to 37% when the molar ratio of styrene : PhI=NTs = 1 : 1 was employed, due to the competing breakdown of the PhI=NTs reagent. This decrease was found to be less significant using our heterogeneous catalyst, where 87% yield was obtained when a styrene : PhI=NTs = 1 : 1 molar ratio was used (Table 1, entry 2) as compared to a yield of 90% when a styrene : PhI=NTs = 1 : 1 molar ratio was used (Table 1, entry 1).

CuHY was found to be successful in catalysing the aziridination of a range of alkenes (Table 1) in addition to styrene. It is observed that the catalyst gives best results with phenyl-substituted alkenes and lower yields are observed with cyclohexene and *trans*-hex-2-ene. Interestingly, for the aziridination of *trans*-stilbene no product could be observed. This was considered to be the due to the relatively bulky aziridine product being too large to be accommodated within the supercages of CuHY. However, the aziridination of *trans*-methyl cinnamate inside CuHY proceeded in 84% yield, despite being similar in structure type to the *trans*-stilbene product. We used molecular modeling to investigate the ease with which these two aziridines could be placed into the pore structure of zeolite Y. These calculations suggest that the *N*-tosylaziridine formed from *trans*-methyl cinnamate can adopt a conformation which can easily be accommodated in the pores of zeolite Y. The aziridine derived from *trans*-stilbene can be constructed within the supercages but is indeed too bulky to diffuse through the connecting channels of the zeolite. We consider this to be a crucial piece of evidence since it shows that the aziridination reaction with the CuHY catalyst occurs within the intracrystalline space. Furthermore, this exciting result illustrates the potential for a heterogeneous catalyst to possess size-specificity to a precise degree. Such a property could be exploited by constructing zeolites with a range of pore sizes, and could also be developed to achieve regioselectivity in a reagent containing two or more double bonds.

Evans *et al.*[4] have shown that modification of the copper homogeneous catalysts using chiral bis(oxazoline) ligands induces enantioselectivity. We have examined modification of the CuHY catalyst with a range of oxazolines and have observed *N*-tosylaziridine products with up to 61% ee. The optimum conditions for racemic heterogeneous aziridination of alkene, in

the absence of bis(oxazoline), was observed to be at 25 °C using MeCN as solvent. As expected, for the enantioselective reaction, the use of lower reaction temperatures was found to give the highest enantioselectivities. We have found that a temperature of −10 °C provides the highest enantioselectivity of 42% ee without compromising yield when using MeCN solvent and 2,2-bis{2-[(4*R*)-1-phenyl-1,3-oxazolinyl]}propane **1** as the chiral modifier. It would be reasonable to assume that one chiral modifier would be required per zeolite supercage to obtain maximum enantioselectivity. We have, however, found that very low levels of the expensive modifier can be used without resulting in decreases in yield or enantioselectivity. An excess of **1** significantly reduces the yield of aziridine, due to pore-blocking, but both yield and enantioselectivity were maximized with a molar ratio of only PhI=NTs : **1** = 1 : 0.05. This corresponds to a molar ratio of Cu^{2+} : **1** of 2 : 1, indicating that not all the Cu^{2+} cations are modified in our experiments. In a subsequent experiment, an excess of **1** was stirred with CuHY (Cu^{2+} : **1** = 1 : 60) in MeCN. The zeolite was filtered and washed with acetonitrile, then used as the catalyst in fresh solvent and reactants. Both yield and enantioselectivity observed were identical to that obtained when **1** was added directly to the reaction mixture (molar ratio of PhI=NTs : **1** = 1 : 1.05). It is clear that very low levels of the modifier are required to obtain the enantioselectivities reported.

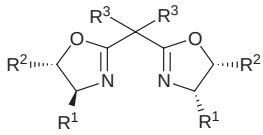

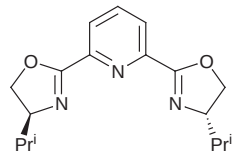

1 R^1 = Ph, R^2 = H, R^3 = Me
2 R^1 = Bu^t, R^2 = H, R^3 = Me
3 R^1 = Ph, R^2 = R^3 = H
4 R^1 = R^2 = Ph, R^3 = H

5

With the optimum conditions established for the enantioselective aziridination of styrene, other bis(oxazolines) and alkenes were screened with CuHY as the catalyst (Table 2). *trans*-β-Methylstyrene was found to show similar degrees of enantioselectivity to styrene. However, *trans*-methyl cinnamate gave a much higher result of 61% ee, albeit in poorer yield. The *tert*-butyl substituted bis(oxazoline) **2**, when used in MeCN, gave racemic aziridine. We suggest this is because MeCN, a ligand for Cu^{2+}, binds more strongly to the active sites than does this bis(oxazoline). Support for this interpretation comes from our observation that, by carrying out the reaction using styrene as the solvent, enantioselectivity was restored, although both yield and ee were then lower than for the homogenous reaction. To provide further evidence that the reaction is proceeding within the supercages of the zeolite, reactions were carried out using a simple phenyl-substituted bis(oxazoline) **3**, which is known to fit inside the zeolite, and using a diphenyl substituted analogue **4**, which was considered as the result of molecular simulations to be too bulky to fit inside the zeolite pores. At 25 °C the smaller bis(oxazoline) **3** gave 10% ee for both the heterogeneous and homogeneous reactions. However, for the heterogeneously catalysed reaction, using CuHY as catalyst, the bulky diphenyl bis(oxazoline) **4** gave racemic product, despite inducing 15% ee for the equivalent homogeneously catalysed reaction. This is again evidence that the reaction is truly heterogeneous and is occurring within the pores of the zeolite. Further modification of the bis(oxazaline) has shown that the pyridine-bridged bis(oxazoline) **5** gives the highest enantioselectivity of 61% ee for the aziridination of styrene (Table 2). We consider that these initial results are encouraging and that careful optimization of the chiral ligand will result in further improvements in ee and yield.

The major advantage of the use of CuHY as a catalyst for this reaction is the ease with which it can be recovered from the reaction mixture by simple filtration if used in a batch reactor (alternatively it can be used in a continuous flow fixed bed reactor). We have carried out the heterogeneous asymmetric aziridination of styrene until completion, filtered and washed the zeolite then added fresh styrene, PhI=NTs and solvent, without further addition of bis(oxazoline) **1**, for several consecutive experiments and have found that both yield and enantioselectivity are retained. After each consecutive experiment a portion of CuHY was retained to determine the concentration of copper still present in the zeolite. For each experiment we found that only traces of the copper were removed from the catalyst (< 0.5% of the total Cu^{2+} is lost from the catalyst). Filtrate containing trace Cu^{2+} has been used in a reaction and was not found to catalyse aziridination. We have noted that adsorbed water can build up within the pores of the zeolite on continued use and this can lead to some loss of activity. However, full enantioselectivity and yield can be recovered if the catalyst is simply dried in air prior to reuse. We are therefore confident that this catalyst system can form the basis of a commercial heterogeneous catalyst for the aziridination of alkenes.

Table 2 Representative bis(oxazolines) for the enantioselective aziridination of alkenes

Oxazoline	Alkene[a]	*T*/°C	Yield (%)[b]	Ee (%)[b,c]
1	*trans*-Methyl cinnamate	−10	8 (21)	61 (70)
1	*trans*-β-Methylstyrene	−10	74	36
1	Styrene	−10	82	44
1	Styrene	25	87	29
2	Styrene	−20	64	0
2	Styrene[d]	−20	15 (89)	18 (63)
3	Styrene	25	78 (75)	10 (10)
4	Styrene	25	73 (74)	0 (15)
5	Styrene	−10	4	61

[a] Unless otherwise specified, reaction conditions were: MeCN, alkene: PhI=NTs = 5 : 1. [b] Values in parentheses indicate yields obtained from homogeneous reactions. [c] Enantioselectivity determined by chiral HPLC. Absolute configurations of major products, determined by optical rotation, are (*S*) for *trans*-β-methylstyrene and *trans*-β-methyl cinnamate, (*R*) for styrene. [d] Styrene was used as solvent.

Notes and References

† E-mail: hutch@cf.ac.uk

1 R. Noyari, *Asymmetric Catalysis in Organic Synthesis*, Wiley, New York, 1994.
2 T. Katsuki and K. B. Sharpless, *J. Am. Chem. Soc*., 1980, **102**, 5974.
3 D. A. Evans, K. A. Woerpel, M. M. Hinman and M. M Faul, *J. Am. Chem. Soc*., 1991, **113**, 726.
4 D. A. Evans, M. M. Faul and M. T. Bilodeau, *J. Am. Chem. Soc*., 1994, **116**, 2742.
5 K. Srinivasan, P. Michaud and J. K. Kochi, *J. Am. Chem. Soc*., 1986, **108**, 2309; W. Zhang, J. L. Loebach, S. R. W. Wilson and E. N. Jacobsen, *J. Am. Chem. Soc*., 1990, **112**, 2801.
6 K. T. Wan and M. E. Davis, *Nature* 1994, **370**, 449.
7 H. U. Blasser, *Tetrahedron: Asymmetry*, 1997, **8**, 1693.
8 P. P. Knops-Gerrits, D. De Vos, F. Thibault-Starzyk and P. A. Jacobs, *Nature*, 1994, **369**, 543.
9 K. Klier, *Langmuir*, 1998, **4**, 13.
10 C. B. Dartt and M. E. Davis, *Catal. Today*, 1994, **19**, 151.

Received in Cambridge, UK, 12th March 1998; 8/01997E

$Tl_2Au_4S_3$: $x = 4/3$ member of the series $A_{2-x}Au_xQ$. Preparation and an analysis of its gold–gold bonding

Sandra Löken, Claudia Felser and Wolfgang Tremel*†

Institut für Anorganische Chemie und Analytische Chemie, Universität Mainz, Becher Weg 24, Mainz D-55099, Germany

$Tl_2Au_4S_3$ was synthesized by reacting gold with reactive fluxes of Tl_2S and S; its crystal structure is characterised by sheets of buckled 16-membered rings of Au and S with short Au–Au contacts between the sheets; the Au–Au bonding has been analysed through high-level band structure calculations.

The chemistry of ternary gold chalcogenides continues to attract interest because of the richness of structures displayed by them. Thus even in the simple formulation AAuQ, the anionic species found include linear, molecular AuQ_2 units in KAuQ (Q = S, Se),[1] AuQ chains in AAuQ (A = Rb, Cs and Q = S, Se, Te),[2] planar hexagonal Au–Te networks in AAuTe (A = Na, K),[2] *etc.* The unique feature of many of these compounds is the presence of short Au–Au distances arising from mixing of gold 5d, 6s and 6p levels; these are usually described in terms of d^{10}–d^{10} interactions. Computational difficulties abound in handling an element such as gold whose electronic structure is influenced by relativistic effects, and there seem to be few high-level band structure calculations detailing the nature of bonding between gold atoms in extended solids. Much of the previous theoretical work on d^{10}–d^{10} interactions has focussed on molecular systems with the exception of some alkali-metal aurides.[3]

We have noted short Au–Au distances in many quaternary gold chalcogenides from the A–Au–X–Q systems where X (= Ge, Sn, P, As) is a main group element that forms chalcogeno anions.[4] Gold chalcogenides and related systems have been studied extensively during the past few years.[4–9] In the course of these investigations we have found the first ternary gold chalcogenide with thallium (replacing the alkali metal).‡ The compound $Tl_2Au_4S_3$ turns out to be the $x = 4/3$ member of the series $A_{2-x}Au_xQ$. With A = alkali metal and Q = chalcogen, the members with $x = 1/2$,[6] 5/6,[7] 1,[2] 6/5,[8] and 3/2[9] have been previously characterised. To understand the nature of the short Au–Au contacts in the title compound, we have used scalar-relativistic TB-LMTO band-structure calculations in conjunction with an analysis of the crystal orbital hamiltonian population (COHP) which we present here. Apart from the bonding situation, these compounds are of interest because they display direct band gaps suggesting uses such as in infrared detection.

The crystal structure of $Tl_2Au_4S_3$ is shown in Fig. 1.§ It is characterised by buckled sheets comprising 16-membered rings of Au and S arranged in an alternating manner. The confirmation of the rings are boat-like. The S–Au–S units in the ring are linear or nearly so. Acute Au(1)–S(1)–Au(2) angles [91.8(3)°] at the corners of the rings lead to an Au–Au distance of 3.350(1) Å within the rings. However, the stacking of the sheets along *c* results in an intersheet Au–Au distance of 3.010(1) Å. These distances are emphasised in the [100] projection by light grey lines. The Tl atoms are in a distorted trigonal prismatic S coordination and sit in the boats defined by the buckling of the Au–S sheets. They are moved off the prism centers; as a result, there are short Tl–Tl contacts of 3.307(3) Å (*cf.* Tl metal where it is about 3.36 Å[10]). The presence of 16-membered rings in the structure is to be contrasted to previous $A_{2-x}Au_xQ$ structures which have (so far) been reported as having 6 ($x = 1$),[2a] 8 ($x = 1$),[2b] 12 ($x = 3/2$),[9] and 24 ($x = 6/5$)[8b]-membered rings.

Fig. 2(*a*) and (*b*) display the decomposed LMTO densities of state (DOS) of the $Tl_2Au_4S_3$ near the Fermi energy. It is clear from Fig. 2(*a*) that there is strong mixing of the s, p and d states of gold. Interestingly, despite short Au–Au contacts, the states closest to E_F are actually derived from a mixing of Tl 6s and S 3p [Fig. 2(*b*)]. Thus Tl acts not only as an inert countercation, in contrast to the other ternaries described earlier, where K^+, Rb^+, *etc.* serve only to balance charge. This is also seen from the COHP plots displayed in Fig. 2(*c*). Strong Au–Au interaction leads to bonding and antibonding states below E_F, with the bonding states being much greater in number. Above E_F, the COHP is flat but slightly bonding. This is because the Au 6s and 6p states are mixed in with the 5d states. This behaviour has been previously remarked in some silver oxides.[11] The principle Au–Au bonding interaction around 5 eV below E_F arise due to Au d states as seen from the DOS. The Au–S interactions lead to well separated bonding and antibonding states below and above the E_F. However, the occupied states closest to E_F are associated with the (shorter) Tl–S distance of 2.978(1) Å. The gap between filled and empty states in the LMTO DOS is in agreement with the measured optical band gap of 1.5 eV obtained from the diffuse-reflectance spectra [Fig. 2(*d*)]. From the preceding discussion, the transition that causes this direct band gap is from filled Tl 6s–6p to the empty, hybridised Tl 6p–S 3p states.

This research has been suppported by the Fonds der Chemischen Industrie. The donation of quartz tubes from

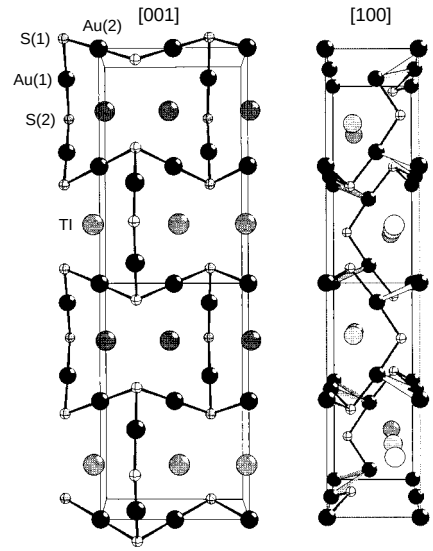

Fig. 1 [100] and [001] projection of the $Tl_2Au_4S_3$ structure (Tl, grey spheres; Au, black spheres; S, crossed spheres). Important bond distances and angles are given in the footnotes. Au(1)–S(2) 2.315(7), Au(1)–S(1) 2.320(9), Au(2)–S(1) 2.343(5) ×2, mean Au-S 2.330, Au(1)–Au(2) 3.0098(1) ×2, Au(1)–Au(2) 3.3502(1) ×2, Au(1)–Tl 3.152(2) ×2, Au(2)–Tl 3.2405(8) ×2, Tl—Tl 3.307(3), Tl–S(1) 3.563(8) ×2, Tl–S(1) 3.645(8) ×2, Tl–S(2) 2.978(1), Tl–S(2) 3.324(1), mean Tl–S 3.453; S(2)–Au(1)–S(1) 175.0(3), S(1)–Au(2)–S(1) 180.0, Au(1)–S(1)–Au(2) 91.8(3), Au(1)–S(2)–Au(1) 114.3(6), S(1)–Tl–S(2) 81.5(2), S(1)–Tl–S(1) 73.5(3), S(1)–Tl–S(1) 81.1(2), S(1)–Tl–S(2) 143.0(1), S(1)–Tl–S(1) 125.4(1).

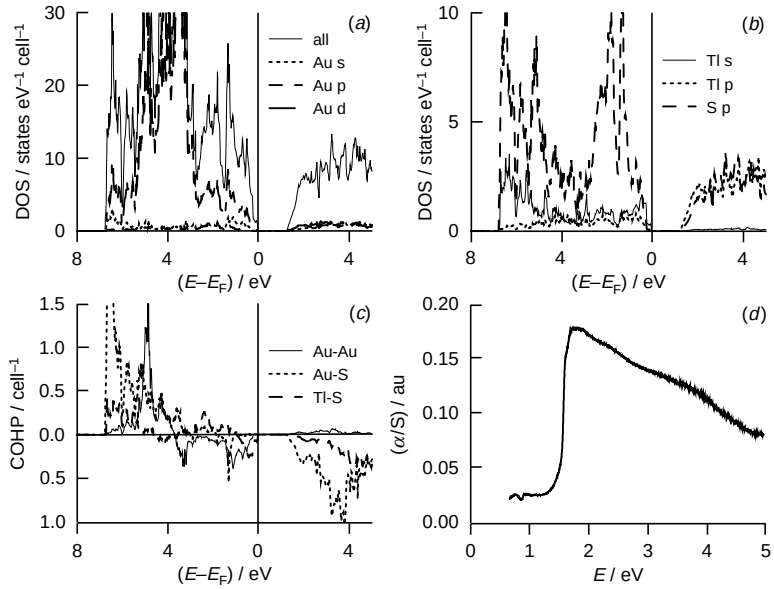

Fig. 2 Densities of states of $Tl_2Au_4S_3$ showing the Au (*a*) and Tl (*b*) contributions. (*c*) Crystal orbital hamiltonian populations for Au–Au, Au–S and Tl–S interactions (positive values are bonding, negative values antibonding). (*d*) Diffuse reflectance UV–VIS spectrum of $Tl_2Au_4S_3$ after transformation by the Kubelka–Munk function.

Heraues Quarzschmelze, Hanau (Dr Hofer) and gold from Degussa AG is gratefully acknowledged.

Notes and References

† E-mail: tremel@indigotrem1.chemie.uni-mainz.de

‡ $Tl_2Au_4S_3$ was prepared by combining 0.315 g (1.6 mmol) of Au powder, 0.176 g (0.4 mmol) Tl_2S and 0.026 g (0.8 mmol) S in a vacuum-sealed quartz tube. It was heated to 650 °C and kept at this temperature for 4 days and then cooled to room temperature at 4 °C h^{-1}. X-Ray powder patterns of the sample are single phase. IR data (KBr pellet): 1358w, 1059s, 668m, 590s, 467w, 296s cm^{-1}. Differential thermal analysis shows a congruent melting point endotherm at 436 °C and a crystallization point exotherm at 548 °C. UV–VIS–NIR spectra were acquired on a spectrometer equipped with a diffuse reflectance integrating sphere, with the sample diluted in $BaSO_4$.

§ *Crystal data* for $Tl_2Au_4S_3$ at 25 °C: orthorhombic, space group *Pmmm* (no. 59), a = 7.507(2), b = 11.919(2)(2), c = 4.688(1) Å, U = 419.5(2) Å^3, Z = 2, λ = 0.710 73 Å, M_R = 1292.79, D_c = 10.236 g cm^{-3}, μ = 108.61 mm^{-1}, platelike crystal, dark red, dimensions 0.4 × 0.16 × 0.14 mm, $2\theta_{max}$ = 54°, data collected at 25 °C on a Nicolet P2$_1$ four circle diffractometer, θ–2θ scan, absorption correction (ψ-scan), transmission factors 0.719–0.461, 975 reflections collected, 512 independent reflections, 436 reflections with $I > 2\sigma(I)$, 30 parameters. The structure was solved by direct methods (SHELXL-86). Full-matrix least-squares refinement of this model against F_o^2 (SHELXL-93) converged to final residual indices $R(R_w)$ = 0.055(0.112). CCDC 182/888.

¶ *Band structure calculations:* tight-binding linearised muffin-tin orbital (TB-LMTO)[12] calculations were carried out using version 47c of the program kindly provided by Professor O. K. Anderson. 315 irreducible *k*-points were used in the calculations.

1 K. O. Klepp and W. Bronger, *J. Less-Common Met.*, 1987, **127**, 65.
2 (*a*) W. Bronger and H. U. Kathage, *J. Alloys Compd.*, 1992, **184**, 87; (*b*) K. O. Klepp, *J. Alloys Compd.*, 1996, **234**, 199.
3 K. M. Merz, Jr. and R. Hoffmann, *Inorg. Chem.*, 1988, **27**, 2120; P. Pyykkö, *Chem. Rev.*, 1997, **97**, 597; for DFT calculations on alkali-metal aurides, see: G. H. Grosch and K.-J. Range, *J. Alloys Compd.*, 1996, **233**, 30, 39; M. Jansen, *Angew. Chem.*, 1987, **99**, 1136; for anionic gold compounds, see: C. Feldmann and M. Jansen, *Angew. Chem.*, 1993, **105**, 1107; J. Jäger, D. Stahl, P. C. Schmidt and R. Kniep, *Angew. Chem.*, 1993, **105**, 738; *Unkonventionelle Wechselwirkungen in der Chemie metallischer Elemente*, ed. B. Krebs, VCH, Weinheim, 1992; K. P. Hall and D. M. P. Mingos, *Prog. Inorg. Chem.*, 1983, **32**, 239.
4 S. Löken and W. Tremel, *Eur. J. Inorg. Chem.*, 1998, **2**, 283; *Z. Anorg. Allg. Chem.*, in press.
5 J.-H. Liao and M. G. Kanatzidis, *Chem. Mater.*, 1993, **5**, 1561; K. Chondroudis, J. A. Hanko and M. G. Kanatzidis, *Inorg. Chem.*, 1997, **36**, 2623.
6 Na_3AuS_2: K. O. Klepp and W. Bronger, *J. Less-Common Met.*, 1987, **132**, 173; K_3AuSe_2: K. O. Klepp and C. Weithaler, *Z. Kristallogr.*, 1995, **210**, 221.
7 K. O. Klepp and G. Brunnbauer, *J. Alloys Compd.*, 1992, **183**, 252.
8 (*a*) $K_4Au_6S_5$: K. O. Klepp and W. Bronger, *J. Alloys Compd.*, 1988, **137**, 13; (*b*) $Cs_4Au_6S_5$, $Rb_4Au_6S_5$: K. O. Klepp and C. Weithaler, *J. Alloys Compd.*, 1996, **243**, 12.
9 K. O. Klepp and C. Weithaler, *J. Alloys Compd.*, 1996, **243**, 1.
10 J. Donohue, *The Structures of the Elements*, Wiley, New York, 1974.
11 T. D. Brennan and J. K. Burdett, *Inorg. Chem.*, 1994, **33**, 4794; M. Jansen, M. Bortz and K. Heidebrecht, *J. Less-Common Met.*, 1990, **161**, 17; R. Seshadri, C. Felser and W. Tremel, *Chem. Mater.*, in press.
12 O. K. Andersen, *Phys. Rev. B*, 1975, **12**, 3060; G. Krier, O. Jepsen, A. Burkhardt and O. K. Andersen, Program TB-LMTO-ASA 47c, Stuttgart, 1996.

Received in Cambridge, UK, 3rd April 1998; 8/02571A

New symmetry-breaking deprotonation reactions of cyclic imides using a chiral lithium amide base

David J. Adams, Nigel S. Simpkins*† and Torben J. N. Smith

Department of Chemistry, The University of Nottingham, University Park, Nottingham, UK NG7 2RD

Treatment of various *N*-substituted succinimides, possessing additional three-, four- or five-membered ring-fusion, with a mixture of chiral lithium amide base and Me_3SiCl, enables enantioselective silylation to give products in up to 95% ee.

During the past few years there have been great developments in the application of chiral lithium amide base reactions to asymmetric synthesis.[1] Most of the enantioselective deprotonation reactions of these chiral bases described to date involve discrimination between enantiotopic hydrogens activated by a single common functional group. The best developed chemistry of this type is the asymmetric enolisation of cyclic ketones, although somewhat analogous situations involving metallation of sulfoxides and prochiral organometallics have also been described.[2]

We considered that a considerable broadening in the scope for applications of chiral lithium amides would be possible if *multifunctional* substrates could be employed. In a general sense this could involve desymmetrisation of a prochiral molecule having a number of functional groups deployed on a suitable conformationally constrained template (most likely a carbocyclic or saturated heterocyclic or polycyclic system). In this type of chiral base reaction the key step would involve kinetically controlled discrimination between hydrogens which are activated by *separate* functional groups. For a situation in which just two functional groups are involved (as the activating groups for two enantiotopic methine hydrogens), the transformation can be illustrated as the conversion of **1** into **2** (Scheme 1).[3]

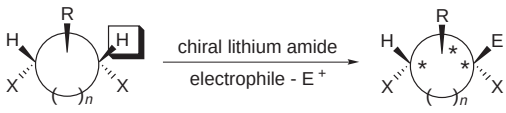

1 **2**

Scheme 1

The two activating groups X could be typical carbonyl types, including ketone, ester or amide, or other types such as sulfone. These two functions could be close together or somewhat remote (variation in *n*) and the overall framework could bear substituents R as long as the overall symmetry is retained in substrate **1**. As can be seen, the chiral base transformation, involving selective substitution at one activated position would be expected to generate chiral products having a number of asymmetric centres (marked *).

Herein we describe our initial results in this new area of chiral lithium amide base chemistry in which we have examined the desymmetrisation of a number of ring–fused imides, *i.e.* $n = 0$ and X = amide (X groups linked to form a five-membered ring imide).

Initial work showed that treatment of cyclopropane derivative **3** with chiral base **4** at low temperature in the presence of Me_3SiCl resulted in the formation of the desired product **5** in 80% yield and 95% ee (Scheme 2).[4]‡

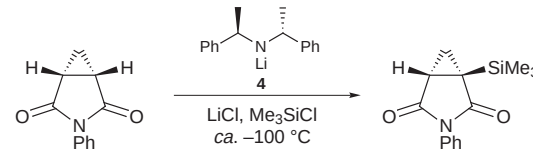

3 **5** 80% (95% ee)

Scheme 2

Imide **5** proved to be crystalline, which enabled us to determine the absolute configuration shown by single crystal X-ray structure determination.§ Our delight at this excellent result was tempered by the observation that only the use of Me_3SiCl as an *in situ* electrophile appears to enable clean substitution, with the attempted reaction with alkylating agents such as MeI resulting only in the destruction of starting material. Although this is a drawback, we were able to circumvent this apparent limitation by substitution of the remaining acidic hydrogen by conventional means (Table 1).

Table 1 Substitution of **5** using LDA

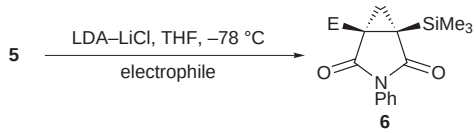

6

Compound	Electrophile	Yield of **6** (%)
6a	MeI	93
6b	AllylBr	73
6c	BnBr	67
6d	PhSSPh	71
6e	PhCHO[a]	61
6f	PhCOCl	57

[a] Formed as a *ca.* 1 : 1 ratio of diastereoisomers.

Thus, introduction of a range of different substituents was possible in good to excellent yield by use of LDA–LiCl as the base.[5] In the case of **6a** we have confirmed that removal of the silicon group is possible, to give the expected methylated imide. As an alternative approach to the problem we have found that fluoride-mediated substitution of the Me_3Si group of **5** is possible by a narrow range of electrophiles (PhCHO, PhSSPh and PhCOF), to give directly the imide products **7** (Scheme 3).[6] We expect that no loss of ee takes place in this process, although this has not been confirmed to date.

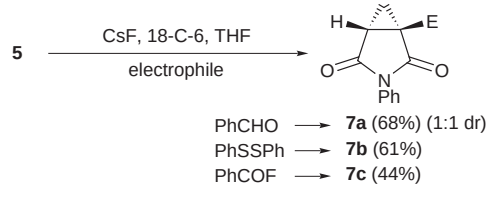

Scheme 3

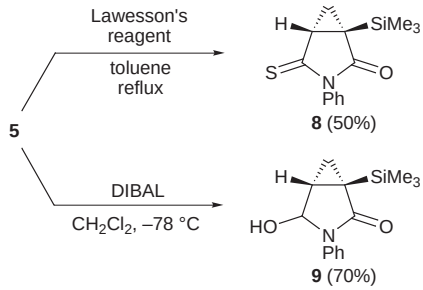

Scheme 4

Since one of the main objectives of this new chiral base chemistry is to enable the synthesis of varied enantiomerically enriched products, it was important to establish if the initial enantioselective substitution to give **5** enabled subsequent regiocontrolled reactions of the imide. In line with our expectations, imide **5** undergoes highly regioselective thionation and reduction reactions, to give **8** and **9** respectively (Scheme 4).[7,8]

Taken in combination with the highly enantioselective access to compounds of type **6** and **7**, this chemistry begins to indicate some of the potential of our new approach for the synthesis of lactams, lactones, pyrrolidines, *etc*.

Finally, we were able to extend this new asymmetric process to several other imide systems, the silylated products **10**–**12**

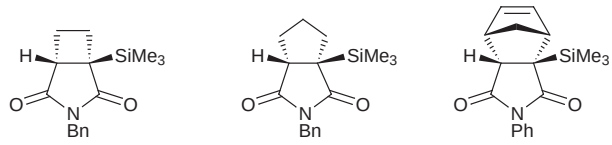

being isolated in excellent levels of ee from reaction of the appropriate symmetrical imide starting material with a mixture of **4** and Me_3SiCl at low temperature.[9]¶

These results show that the concept outlined in Scheme 1 can be realised, and the products clearly have some potential for target synthesis. However, these asymmetric transformations of ring-fused imides form but a small sub-group of the chemistry implicit in Scheme 1, and efforts to realise further examples of this diverse group of reactions are underway.

We are grateful to the EPSRC and Chiroscience Limited (Cambridge Science Park, Milton Road, Cambridge, UK CB4 4WE) for support of T. J. N. S under the CASE scheme. We are also very grateful to Professor H. Hiemstra of the University of Amsterdam for samples of certain ring-fused imides.

Notes and References

† E-mail: nigel.simpkins@nottingham.ac.uk

‡ In a typical asymmetric silylation, a solution of the chiral lithium amide base **4** mixed with LiCl was added dropwise to a mixture of starting imide and Me_3SiCl (excess) in THF at *ca.* −100 °C (internal temperature). The mixture was then allowed to warm slowly (4 h) to ambient temperature before standard aqueous work-up and chromatography on silica gel. All products have been fully characterised by spectroscopic methods and give satisfactory elemental analysis and/or HRMS results. Enantiomeric excess values were established by HPLC (UV detection) using Pr^iOH–hexane as eluent, using a Chiralcel OD column for **5**, **11** and **12**, and a Chiralcel OJ column for **10**.

§ The absolute configuration of **5** was established by the collection of low temperature data, including Friedel equivalents, and by refinement of a Flack parameter, value 0.05(19), see H. D. Flack, *Acta Crystallogr., Sect. A*, 1983, **39**, 876. The absolute stereochemistry of product **12** was likewise established; Flack parameter −0.12(14). We thank Dr A. J. Blake of this Department for these determinations; full details will be published elsewhere.

¶ These reactions have not been optimised; the absolute configurations shown for **10** and **11** are based on analogy with **5** and **12**.

1 For reviews, see P. O'Brien, *J. Chem. Soc., Perkin Trans. 1*, 1998, 1439; P. J. Cox and N. S. Simpkins, *Tetrahedron: Asymmetry*, 1991, **2**, 1; N. S. Simpkins, *Advances in Asymmetric Synthesis*, ed. G. R. Stephenson, Blackie Academic, 1996; K. Koga, *Pure Appl. Chem*., 1994, **66**, 1487.

2 For leading references in these two areas, see A. J. Blake, S. M. Westaway and N. S. Simpkins, *Synlett*, 1997, 919 (sulfoxides); R. A. Ewin, D. A. Price, N. S. Simpkins, A. M. MacLeod and A. P. Watt, *J. Chem. Soc., Perkin Trans. 1*, 1997, 401 (organometallics).

3 We have recently described an enantioselective elimination reaction akin to the process outlined in Scheme 1, see C. D. Jones, N. S. Simpkins and G. M. P. Giblin, *Tetrahedron Lett*., 1998, **39**, 1023.

4 The starting imide **5** was prepared *via* reaction of the corresponding anhydride (J. J. Tufariello, A. S. Milowsky, M. Al-Nuri and S. Goldstein, *Tetrahedron Lett*., 1987, **28**, 267) with aniline, see A. L. J. Beckwith and D. R. Boate, *J. Org. Chem.*, 1988, **53**, 4339. See also A. Mustafa, S. M. A. D. Zayed and S. Khattab, *J. Am. Chem. Soc*., 1956, **78**, 145 for an alternative synthesis, and ref. 9.

5 In the past we have observed increased rates of metallation by addition of LiCl to lithium amides, see for example D. A. Price, N. S. Simpkins, A. M. MacLeod and A. P. Watt, *Tetrahedron Lett*., 1994, **35**, 6159; B. J. Bunn, N. S. Simpkins, Z. Spavold and M. J. Crimmin, *J. Chem. Soc., Perkin Trans. 1*, 1993, 3113. Recently, little effect of LiCl on the rate of deprotonation of a simple ketone by LDA was observed, see M. Majewski and P. Nowak, *Tetrahedron Lett*., 1998, **39**, 1661.

6 These reactions were modelled on analogous substitutions of episulfones that we examined previously, see A. P. Dishington, R. E. Douthwaite, A. Mortlock, A. B. Muccioli and N. S. Simpkins, *J. Chem. Soc., Perkin Trans. 1*, 1997, 323.

7 M. J. Milewska, M. Gdaniec and T. M. Polonski, *J. Org. Chem*., 1997, **62**, 1860.

8 T. Mukaiyama, H. Yamashita and M. Asami, *Chem. Lett*., 1983, 385.

9 For details of the preparation and enantioselective reduction of these types of *meso*-imide, see M. Ostendorf, R. Romagnoli, I. C. Pereiro, E. C. Roos, M. J. Moolenaar and W. N. Speckamp and H. Hiemstra, *Tetrahedron: Asymmetry*, 1997, **8**, 1773.

Received in Liverpool, UK, 12th May 1998; 8/03574A

ChemComm
FEATURE ARTICLE

The mechanism of catalysis and the inhibition of β-lactamases

Michael I. Page*† and Andrew P. Laws

Department of Chemical and Biological Sciences, The University of Huddersfield, Queensgate, Huddersfield, UK HD1 3DH

Formation of a tetrahedral intermediate by nucleophilic attack on the β-lactam carbonyl carbon of penicillins generates a lone pair on the β-lactam nitrogen which is *syn* to the incoming nucleophile, in contrast to the normal *anti* arrangement found in peptides. Ring opening of the β-lactam requires protonation of the β-lactam nitrogen by a general acid catalyst. The general acid/base catalyst in β-lactamases is probably a glutamate and a tyrosine residue in class A and C enzymes, respectively. Phosphonamidates inactivate class C β-lactamases by phosphonylation of the active site serine, the rate of which is enhanced by a factor of at least 10^6. The enzyme's catalytic machinery used for hydrolysis is also used for phosphonylation. The rate enhancement may be greater than 10^9 if the mechanism occurs by an inhibitor assisted reaction involving intramolecular general acid catalysis. Class B metallo-β-lactamases are inhibited by thiol derivatives with K_i as low as 10 μM. The mechanism of hydrolysis of the metallo-β-lactamase involves a dianionic tetrahedral intermediate stabilised by zinc(II).

β-Lactam antibiotics account for 50% of the world's total antibiotic market. They have high anti-bacterial activity and low toxicity.[1] In addition to the traditional families of penicillins and

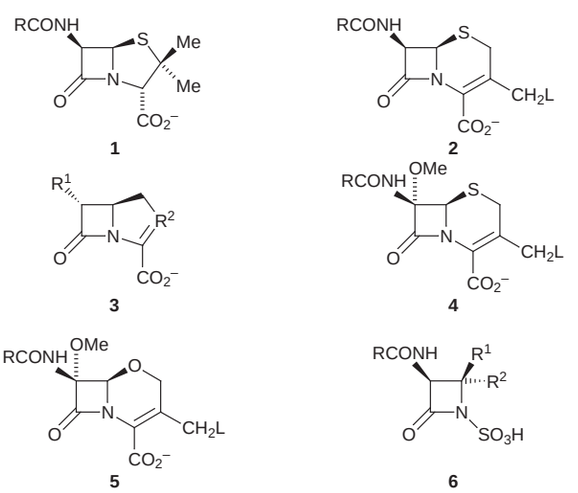

cephalosporins—the penams **1** and cephems **2**, respectively—there are the carbapenems **3**, the cephamycins **4**, the oxacephamycins **5** and the monobactams **6**.[2] This battalion of structures differ in their spectrum of antibacterial activity—from narrow anti-*Staphylococcal* agents to broad spectrum β-lactams capable of killing a wide variety of Gram positive and negative bacteria—and in their ability not to be susceptible to the β-lactamase hydrolytic enzymes which are the most common, and growing, form of bacterial resistance to their normally lethal action. β-Lactamases catalyse the hydrolysis of the β-lactam to give the ring opened and bacterially inert β-amino acid (Scheme 1).[3]

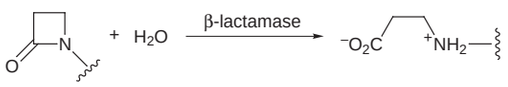

Scheme 1

Two main therapeutic strategies have been adopted to counteract bacterial resistance to β-lactam antibiotics. One involves the design of antibiotics which are not susceptible to β-lactamase catalysed hydrolysis. The other is to use an inhibitor or inactivator of β-lactamase together with a normal β-lactam antibiotic. Unfortunately, bacteria seem to be able to produce new β-lactamases which catalyse the hydrolysis of previously poor substrates and which are no longer susceptible to previous inhibitors. For example, when the carbapenems **3**, such as imipenem, were first introduced in the 1970s they were seen as versatile broad-spectrum antibacterials resistant to hydrolysis by most β-lactamases. However, now 'carbapenamases' are increasingly produced by a variety of bacteria.[4] There are two distinct types of β-lactamase production in bacteria and so far about 200 different enzymes have been identified.[5] Inducible enzymes may be chromosomal or plasmid encoded but the more common constitutive β-lactamase production is predominantly plasmid mediated. Constitutive mutants of Gram-negative strains produce enormous amounts of enzyme so that periplasmic β-lactamase concentrations[6] may be up to 1 mM—about 10^4-fold greater than that used in most laboratory kinetic experiments. Such high concentrations of catalyst combined with their high efficiency means that there is little chance of β-lactam antibiotics reaching their targets without being hydrolysed.

Chemical reactivity of β-lactams

Four membered β-lactams occur relatively rarely in nature, therefore it is not surprising that the biological activity of these compounds should be attributed to the chemical reactivity of the β-lactam ring. Shortly after the introduction of penicillin to the medical world it was suggested that the antibiotic's activity was due to the inherent strain of the four-membered ring or to reduced amide resonance.[7] The non-planar butterfly shape of the penicillin molecule **7** could reduce amide resonance and thus increase the susceptibility of the carbonyl group to nucleophilic attack, compared with planar amides. However, there is little evidence to suggest that the kinetic reactivity of β-lactams in penicillins and cephalosporins is due to an unusually strained or an amide-resonance inhibited β-lactam.[2] Interestingly, although the rate of alkaline hydrolysis of the simple β-lactam **8** is only three-fold greater than that of **9**,[2] the corresponding 4-membered β-sultams[8] and β-phospholactams[9] are 10^7–10^9 fold more reactive than the corresponding acyclic sulfonamides and phosphonamidates, respectively.

Nucleophilic substitution at the carbonyl of β-lactams is an acyl transfer process involving covalent bond formation between the carbonyl carbon and the nucleophile and C–N bond fission of the β-lactam (Scheme 2). In these types of reactions the mechanism involves, at least, a two-step process.[2,7] Covalent bond formation to the incoming nucleophile occurs before C–N bond fission, resulting in the reversible formation of

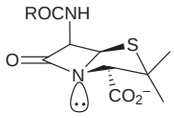

7

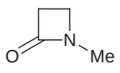

8

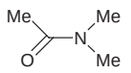

9

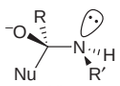

10

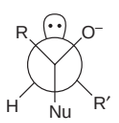

11

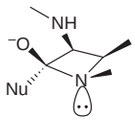

12

a tetrahedral intermediate. Contrary to expectations, opening the four-membered ring is not a facile process.[10] In many of these nucleophilic substitution reactions the rate-limiting step is often not the first addition step but a subsequent one which may sometimes even be ring-opening itself.[2]

Those reactions which involve the attack of a neutral nucleophile which has an ionisable hydrogen (Scheme 2) invariably require general base catalysis to remove the proton.[2,7] The requirement for proton removal is paramount—and in extreme cases only the reaction of the anionic nucleophile is observed (Scheme 2). For example, there is no pH-independent

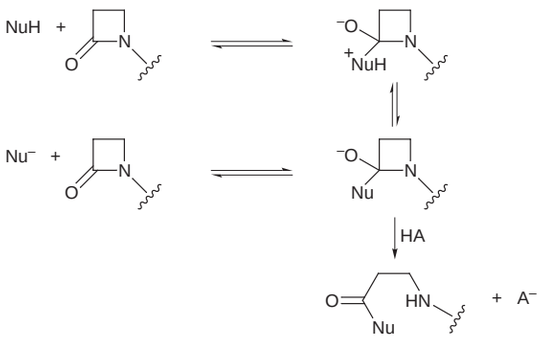

Scheme 2

reaction of water with penicillin, and alcohols react only through their anions.[11] The importance of general base catalysis is a reflection of the fact that contrary to expectations penicillins are not powerful acylating agents.[11] Similarly, C–N bond fission requires protonation of the amine nitrogen.[2,7]

It has been suggested that ring opening does not occur by stretching of the C–N bond but rather by a rotational motion.[10,12] This minimises strain effects and maximises favourable orbital interactions. The unusual mode of C–N bond fission could have interesting consequences in the enzyme-catalysed hydrolysis of β-lactams for the geometrical relationship of the proton donor in the protein and the amine leaving group.

Another interesting difference between nucleophilic substitution in penicillins and peptides/amides is the preferred direction of attack and the geometry of the initially formed tetrahedral intermediate. It is usually assumed that nucleophilic attack on the carbonyl carbon of a planar peptide will generate a tetrahedral intermediate with the lone pair on nitrogen *anti* to the incoming nucleophile, (**10**, **11**). Conversely, nucleophilic attack on β-lactams occurs from the least hindered α-face (*exo*) so that the β-lactam nitrogen lone pair is *syn* to the incoming nucleophile in the tetrahedral intermediate (**12**).[13, 14] This has obvious consequences for the placement of catalytic groups—particularly the general acid donating a proton to the departing amine of the β-lactam.[12]

β-Lactamases

The main mechanistic division of β-lactamases is into serine enzymes and zinc enzymes.[3] The former have an active site serine residue and the catalytic mechanism involves the formation of an acyl–enzyme intermediate. The metallo-enzymes appear to involve only non-covalently bound intermediates. On the basis of their amino acid sequences, the serine β-lactamases are sub-divided into three classes—A, C and D—whereas the class B β-lactamases consist of the zinc enzymes.[3]

Serine β-lactamases

Structure

The class A and class C enzymes are monomeric medium-sized proteins with M_r values of about 29 000 and 39 000, respectively.[3] The structures of four class A[15–17] and two class C[18,19] β-lactamases have been reported. There are two major structural domains—all-α and α/β—with the active site situated in a groove between the two domains. The class C β-lactamases have additional loops and secondary structure on the all-α domain. The active site serine is situated at the N-terminus of the long, relatively hydrophobic, first α-helix of the all α-domain. There are several highly-conserved residues surrounding the active site which may be involved in substrate recognition and the catalytic process of bond making and breaking. Firstly, a lysine residue is always present as the third amino acid and one helix-turn further down the chain from the serine and pointing into the active site. Two other residues forming one side of the catalytic cavity are Ser-Xaa-Asn (class A) or Tyr-Xaa-Asn (classes C and D) with the side chains of the first and third residues pointing into the active site. The Ser130-Asp131-Asn132 (the SDN loop) motif is also almost invariant in class A. The other side of the cavity is formed from the β-sheet of the α/β domain and is generally Lys-Thr-Gly. In class A enzymes there is also a conserved glutamate which, in the static crystal structure, is hydrogen-bonded to a conserved water molecule which in turn is hydrogen-bonded to the active site serine.

Mechanism of hydrolysis

There is very strong evidence for the formation of an acyl enzyme intermediate (Scheme 3)—including electrospray mass

Scheme 3

spectrometry,[20] infra-red measurements,[21] trapping experiments,[22] the determination of the rate constants for their formation and breakdown[23] and even an X-ray crystal structure.[24]

The two experimental kinetic parameters associated with simple systems exhibiting Michaelis–Menten behaviour are the second-order rate constant k_{cat}/K_m determined below saturation and the first order rate constant k_{cat} determined above saturation.[25] The *interpretation* of these experimental macroscopic rate constants as they vary with parameters such as pH, substituents in the substrate[26,27] and amino acid replacement in the enzyme[28] depends upon the model assumed for the reaction pathway. The overall reaction pathway for the serine β-lactamases is given in eqn. (1).

$$E + S \underset{k_{-1}}{\overset{k_1}{\rightleftharpoons}} ES \underset{k_{-2}}{\overset{k_2}{\rightleftharpoons}} EA \xrightarrow{k_3} E + P \qquad (1)$$

It is usually assumed that formation of the usually relatively unstable acyl enzyme (EA) is irreversible, *i.e.* $k_{-2} = 0$ and the second-order rate constant k_{cat}/K_m, determined below saturation

conditions, is then given by eqn. (2) and hence always reflects the rate of acylation *irrespective* of the value of k_2 and k_3.

$$\frac{\text{Rate}}{(\mathbf{E})(\mathbf{S})} = \frac{k_{cat}}{K_m} = \frac{k_1 k_2}{k_{-1} + k_2} \quad (2)$$

Under saturation conditions the observed rate constant, k_{cat}, is independent of substrate concentration and is given by eqn. (3) and so simplifies to the rate of acylation k_2, if $k_3 >> k_2$ and the enzyme is essentially present as the enzyme–substrate complex. Conversely, k_{cat} reflects the rate of deacylation, k_3, when $k_2 >> k_3$ and the enzyme is present mainly as the acyl enzyme.

$$k_{cat} = \frac{k_2 k_3}{k_2 + k_3} \quad (3)$$

However, if formation of the acyl enzyme is *reversible* then k_{cat}/K_m and k_{cat} are given by eqns. (4) and (5), respectively. For

$$\frac{k_{cat}}{K_m} = \frac{k_1 k_2 k_3}{k_3(k_{-1} + k_2) + k_{-1}k_{-2}} \quad (4)$$

$$k_{cat} = \frac{k_2 k_3}{k_2 + k_{-2} + k_3} \quad (5)$$

serine proteases, k_{-2} represents the 'intermolecular' aminolysis of the acylenzyme to regenerate the peptide substrate. For the hydrolysis of β-lactams catalysed by β-lactamases the k_{-2} step corresponds to 'intramolecular' aminolysis to regenerate the β-lactam substrate (Scheme 3). Although the formation of a strained four-membered β-lactam is likely to have a significant activation energy it is not totally inconceivable that this intramolecular step has an entropic advantage[29] and is competitive with intermolecular hydrolysis of the acylenzyme. For example, we have demonstrated, using esterase enzymes, that lactams can be formed from amino esters in water in preference to the hydrolysis product.[30] The interpretation of the macroscopic rate constant k_{cat}/K_m may then become ambiguous because it reflects all microscopic rate constants up to and including the first effectively irreversible step.

Formation of the acyl enzyme intermediate requires at least two proton transfers—proton removal from the attacking serine and proton donation to the departing β-lactam amine (Scheme 4). Despite the availability of a number of X-ray crystal

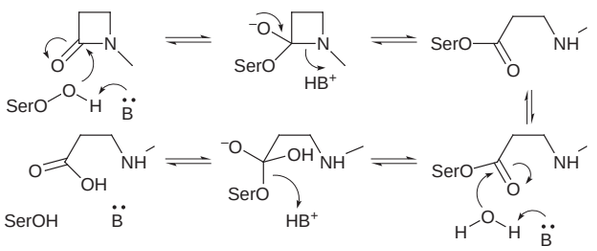

Scheme 4

structures of several class A and class C β-lactamases[15–19] and many site-directed mutagenesis studies,[28] the indentity of the catalytic groups involved in these proton transfer steps remain elusive.

In principle, the general base which accepts a proton from the nucleophilic serine is not necessarily the same residue which then acts as a general acid to donate a proton to the departing β-lactam nitrogen. Conceptually this is neater and our prejudices are reinforced by the juxtaposition of the nitrogen lone pair, the serine and the general base/acid being on the same (*exo*) α-face of the substrate in the tetrahedral intermediate **12**. Similarly, the hydrolysis of the acyl enzyme requires two proton transfer steps—from water and to the departing serine—and only our preference for simplicity requires these to be one and the same residue *and* the same as that involved in the acylation step (Scheme 4). This hydrolytic water probably also approaches from the α-face and can be displaced by a 6α- or 7α-substituent in the penicillin or cephalosporin nucleus, respectively, which explains the poor activity of class A β-lactamases against imipenem[31] and cephamycins.[32] Protein stability measurements of covalently-bound phosphonates to a class A β-lactamase also support this hypothesis.[33]

There are therefore at least four transition states corresponding to formation and breakdown of the tetrahedral intermediate to give initially the acyl enzyme followed by its hydrolysis (Scheme 4). The concept of a unique 'transition state analogue' as an inhibitor for an enzyme catalysing a reaction through many steps becomes ambiguous—there could be many analogues corresponding to different transition states.[34] The evolutionarily-perfect enzyme reduces the transition state energies for all steps in the conversion of reactants to products without 'over-stabilising' any intermediates.[35] The maximum second-order rate constant for an enzyme-catalysed reaction is that corresponding to diffusion control (*ca.* 10^8 M^{-1} s^{-1}) and some β-lactamases appear to be near this limit and are 'perfect catalysts'.[36]

In class A β-lactamases there are two serious contenders for the general base/acid—Glu166 and Lys73. The pH-dependence of k_{cat}/K_m indicates two ionising residues are important for catalysis—one of pK_a *ca.* 5 and formally required in its basic form and one of pK_a *ca.* 9 and formally required in its acidic form. If the low pK_a group corresponds to the general base then this is acceptable for the carboxylic acid of Glu166 but is rather low for an ammonium ion of Lys73. Although it has been suggested that Lys73[24,37] may have a reduced pK_a it is difficult to envisage the required reduction of 5.6 pK_a units given the close proximity to Glu166 (2.8 to 3.4 Å).[15–17] A normal pK_a of Lys73 is supported by ^{13}C NMR studies[38] and theoretical calculations.[39] In class A β-lactamases[15–17] the Glu166 carboxylate oxygen distance to Ser70 oxygen is 3.5–4.0 Å whereas the Lys73 nitrogen distance to the Ser70 oxygen is 2.5–2.9 Å. It is possible that the intervening water molecule, seen in the crystal structure, can act as a bridge for proton transfer from Ser70 to Glu166, acting as a general base catalyst. Alternatively, the flexibility of the Ω-loop on which Glu166 resides may allow the distance between the two residues to shorten during the acylation process. The internal structures of proteins are in a state of constant motion at ambient temperature and a degree of flexibility in β-lactamases has been proposed for many years.[40] The ability of β-lactamases to accommodate substrates of diverse structure is indicative of their flexibility.

Site-directed mutagenesis of Glu166 shows that the rates of both acylation and deacylation are affected, although the latter is more so.[28] However, in general base-catalysed reactions the dependence of reactivity upon the basicity of the catalyst and the geometrical relationship between the acid-base pair is not usually strong.[25] It is quite conceivable for mutants to act as reasonable catalysts even when the amino acid residue acting as the general base/acid in the wild type is replaced because another residue, or even the peptide link itself,[14] can take over the role of proton acceptor/donor without significant loss of activity.

On balance it appears that the evidence supports Glu166 (Scheme 4, B = $GluCO_2^-$) acting as the unique proton transfer agent—as a general base and acid in the formation and breakdown of the tetrahedral intermediate, respectively, and in the same role for the hydrolysis of the acyl enzyme intermediate.

Class C β-lactamases

Historically, class C β-lactamases were often referred to as 'cephalosporinases' because of the characteristic higher turnover numbers, k_{cat}, observed for cephalosporins compared with penicillins. However, the k_{cat}/K_m values for the two classes of enzymes are generally similar and high for both penicillins and

cephalosporins (10^5 to 10^8 M^{-1} s^{-1}).[41] A major difference between the two classes is that for class C β-lactamases deacylation is often rate-limiting, so that the acyl enzyme intermediate may accumulate, giving rise to low values of K_m.[41] Furthermore, class C enzymes are weak catalysts for the hydrolysis of non β-lactam substrates such as esters and thioesters.[42] In class C β-lactamase there is no equivalent glutamate residue but Tyr150 may take its role with Lys67 equivalent to Lys73 in the class A enzyme.[18,19] In addition, it has been suggested that the hydrolytic water involved in deacylation of the acylenzyme approaches from the β-face[43] and that this hydrolysis may be substrate-assisted by the expelled amine, which was the β-lactam nitrogen, acting as a general base catalyst.[44] In class C β-lactamase it has been suggested that the phenol of Tyr150 has a severely reduced pK_a and acts as a general base catalyst for proton removal from Ser64[18,42] although this is not supported by site-directed mutagenesis of Tyr150.[45]

The *E.cloacae* P99 class C β-lactamase catalysed hydrolysis of benzylpenicillin has been shown to yield, in addition to the normal hydrolysis product, the penicilloyl α-methyl ester in the presence of methanol.[22] This is presumably due to the partitioning of the acyl enzyme intermediate between its reaction with water to give the hydrolysis product and its reaction with methanol to produce the penicilloyl ester. At pH 8, with 1 M methanol, up to 30% of the product is the methyl ester. Under saturation conditions the pH-dependence for the second-order rate constant for methanolysis gives two apparent pK_as for the methanolysis reaction which are similar to those observed for hydrolysis, implying that the same catalytically important groups are being used for both reactions.[22]

The absolute values of the pK_a and their shift in D_2O indicate differences between the acidic and basic limbs of the pH–rate profiles. The shift in pK_a^2 in D_2O obtained from k_{cat}/K_m and k_{cat} for hydrolysis is about 0.4 and is that expected from fractionation factors for common acidic groups.[46] However, ΔpK_a^1 is 0.85 from k_{cat}/K_m and k_{cat} for both methanolysis and hydrolysis. This shift and the observed inverse kinetic solvent isotope effect on k_{cat}/K_m is unusual and is indicative of a system with an abnormally low fractionation factor for the basic species formed and/or a high fractionation factor for the protonic state undergoing dissociation.[47] The most likely basic group responsible for the acid limb of the pH–rate profile for both acylation and deacylation is Tyr150, which is hydrogen-bonded to Lys315 and Lys67[22] (Scheme 5).

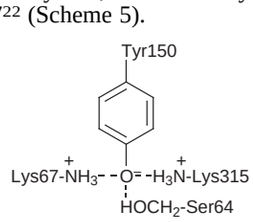

Scheme 5

Because of its relatively positive environment and the strong hydrogen bonding of the phenoxide ion by lysine residues, Tyr150 has a severely reduced pK_a. It appears that the Tyr150 residue is a very strong candidate for the role of a general base catalyst in class C β-lactamases (Scheme 4, B = TyrO$^-$).[22]

Catalytic efficiency of β-lactamase-catalysed acyl and phosphyl transfer

Nucleophilic substitution at acyl centres generally proceeds *via* the formation of an unstable tetrahedral intermediate (TI).[25] The reaction pathway involves a change in geometry as the carbonyl carbon is converted from three- to four-coordination. Furthermore, it is usually assumed that there is some preferential direction of nucleophilic attack such that the incoming nucleophile approaches at approximately the tetrahedral angle to the carbonyl group.[48] By contrast, the associative mechanism for phosphyl group transfer involves a pentacoordinate intermediate with trigonal bipyramidal geometry.[25,49] An initially four-coordinate and tetrahedral phosphorus centre is converted to a five-coordinate one and, in general, it is assumed that the preferential pathway involves the nucleophile taking up the apical position and the leaving group departing from an apical position of the trigonal bipyramidal intermediate (TBPI).[49] Nucleophilic attack at both carbonyl and phosphyl centres is often facilitated by general base catalysis when the nucleophile generates an acidic centre upon covalent bond formation in the intermediate. Similarly if the leaving group is very basic, bond fission and expulsion of the leaving group may be assisted by general acid catalysis. Given the preferential geometrical requirements for incoming nucleophiles and departing leaving groups, there must be a favoured relative positioning of the general base and general acid catalysts (Scheme 6).

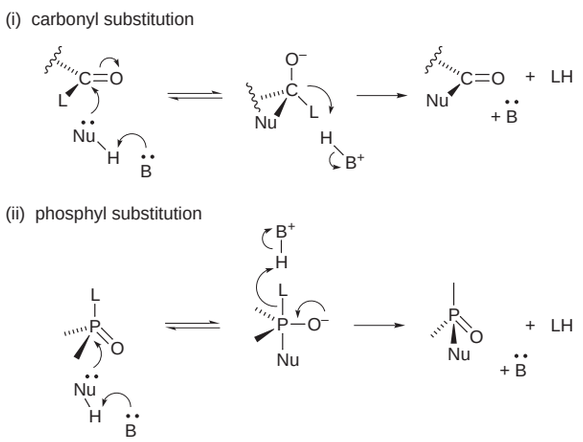

Scheme 6

It is often assumed, but with little actual supporting evidence, that enzymes catalyse reactions by an exquisite positioning of the catalytic groups.[50] This is obviously not the case for β-lactamases, which efficiently catalyse the hydrolysis of both penicillins and cephalosporins where there are significant geometrical differences, *e.g.* between the β-lactam carbonyl and nitrogen and the C-3 carboxylic acid in penicillins and that at C4 in cephalosporins. Also if rigid positioning of catalytic groups was so important then it is doubtful if an enzyme with a primary function as a catalyst for acyl transfer could be an effective catalyst for phosphyl transfer because of the geometrical differences in the displacement mechanisms (Scheme 6), although the possibility of pseudorotation in the intermediate may make matters even more complicated.

The class C β-lactamase is, in fact, extremely efficient in enhancing the rate of phosphyl transfer[51] and the pH dependence of the kinetic parameters indicate that similar catalytic machinery is used for both acyl and phosphyl transfer. The class C β-lactamase from *Enterobacter cloacae* P99 is inactivated by the phosphonamidate **13** (R = BnO)[51] by a phosphonylation process analogous to the enzyme-catalysed acylation by the penicillins (Scheme 7).

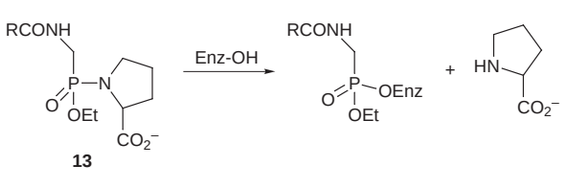

13

Scheme 7

It is necessary to demonstrate that the enzyme actually *enhances* the rate of the phosphonylation reaction. It is well-known that enzymes can catalyse the same reaction of a variety

of substrates and even different reactions with alternative substrates.[52] However, demonstrating the efficiency of the catalysis when the substrate is modified is not straightforward. Modification of the substrate structure can affect the absolute free energies of both the initial reactant state and the transition state, whereas the observed differences in rate constants for the enzyme catalysed reaction only reflect the *difference* in energies between these two states.[53] Different chemical structures can affect the ease of bond-making and -breaking *via* classical electronic factors such as inductive, resonance and steric effects. However, the free energy of activation of an enzyme-catalysed reaction is also affected by the favourable binding energies between the protein and substrate substituents not directly involved with the reaction site. It is therefore necessary to separate these two effects before conclusions about the efficiency of enzyme catalysis can be made. We have suggested[26] that an 'enzyme rate-enhancement factor' (EREF) can be evaluated by dividing the second-order rate constant for the enzyme catalysed reaction, k_{cat}/K_m, by that for hydrolysis of the same substrate catalysed by hydroxide ion, k_{OH}. These factors 'normalise' substrate reactivity and indicate the true efficiency of catalysis.

Both diastereoisomers of the phosphonamidate **13** (R = BnO) completely and irreversibly inactivate the P99 class C β-lactamase in a time-dependent manner to give apparent first order rate constants, k_{obs}, for inactivation. These in turn show a first-order dependence on the concentration of the phosphonamidate to give the second-order rate constants, k_i, for inactivation. The two diastereoisomers show different rate constants for inactivation (5.10 and 0.14 $dm^3\ mol^{-1}\ s^{-1}$). There is no discernible difference in the chemical reactivity of the two diastereoisomers towards alkaline hydrolysis. The 36-fold difference in reactivity is therefore good evidence of selectivity in the reaction of the enzyme with the two phosphonamidates and indicative of specific interactions between the inactivators and the protein. Further evidence of selectivity is seen from the fact that the phosphonamidate **13** (R = BnO) is not a significant inhibitor of either the class A β-lactamase or the class B zinc-dependent β-lactamase from *B. cereus*. The time-dependent inactivation is indicative of covalent bond formation between the enzyme and the phosphonamidate, which is confirmed by electrospray mass spectrometry (ESMS).[51] For the most reactive diastereoisomer, inactivation of the enzyme occurs by formation of a 1 : 1 covalently bound enzyme–inactivator complex in which a proline residue has been displaced by a nucleophilic group on the enzyme—presumably the active site serine. Conversely, the less reactive diastereoisomer reacts with β-lactamase by displacing ethanol, which can be detected by gas chromatography. The observation that the enzyme reacts with one diastereoisomer by displacing proline and with another by displacing ethanol is again indicative of a stereoselective reaction occurring at the active site.

Phosphonamidates are relatively chemically stable and the fast reaction with the β-lactamase indicates that the catalytic machinery of the enzyme used for hydrolysis is also used for phosphonylation and inactivation. This is confirmed by the enzyme rate enhancement factors. The P99 β-lactamase catalyses the hydrolysis of benzylpenicillin with an EREF of 2.6×10^8. Phosphonylation of β-lactamase by the most reactive diastereoisomer of the phosphonamidate **13** occurs by P–N fission and displacement of proline, but the hydroxide ion-catalysed hydrolysis of the phosphonamidate **13** occurs with P–O fission, so the EREF value for phosphonylation is therefore $> 2 \times 10^6$. Clearly, the enzyme is facilitating P–N fission almost as effectively as it does C–N fission in β-lactams. Despite the differences in geometrical requirements for substitution at acyl and phosphyl centres and the enormous differences in intrinsic chemical reactivities between the β-lactam in penicillin and the phosphonamidate, the β-lactamase enzyme is able to significantly lower the activation energy for reactions of both compounds.

The generation of a formal negative charge on oxygen in the tetrahedral intermediate is accompanied by a large change in the basicity of the oxygen—a change in pK_a of the corresponding conjugate acids of at least 12 pK_a units (Scheme 6). The kinetically important species of the tetrahedral intermediate is its anion even though the thermodynamically more stable form is the neutral conjugate acid at neutral pH. Nonetheless, the anion must be strongly solvated by hydrogen-bonding and many enzymes which catalyse acyl transfer reactions have an 'oxyanion hole' which stabilises the tetrahedral intermediate by hydrogen-bonding from adjacent peptide links. The *difference* in this interaction between the initial state carbonyl oxygen and the tetrahedral intermediate as a result of the change in oxygen basicity makes a major contribution to the lowering of the activation energy compared with the non-enzyme-catalysed reaction.[54] Such an 'oxyanion hole' exists for the serine β-lactamases[55] and, in common with serine proteases, one of the peptide N–H hydrogen-bond donors is that belonging to the serine residue—Ser70 in the class A enzymes and Ser64 in the class C enzymes. The 'intramolecular' hydrogen-bond with the active site serine peptide NH presents a fairly well-defined geometry. In the equivalent pentavalent phosphyl enzyme the negative charge on the oxygen presumably takes up an equatorial position so that it is *ca*. 90° to the newly formed serine O–P bond compared with the approximately tetrahedral angle formed with the β-lactam substrate (Scheme 6). Despite these differences, the enzyme is capable of catalysing the phosphonylation with extreme efficiency.

It is often assumed that the phosphylation of serine enzymes can only occur with organophosphorus compounds with good leaving groups because these do not require proton transfer from general acid catalysts to aid departure.[56] However, the class C β-lactamase is obviously capable of displacing the proline residue from the phosphonamidate **13** despite the poor leaving group and the presumed need for protonation of the amine nitrogen.

There are two ionisations in class C β-lactamase which control hydrolytic catalytic activity (Fig. 1)—corresponding to

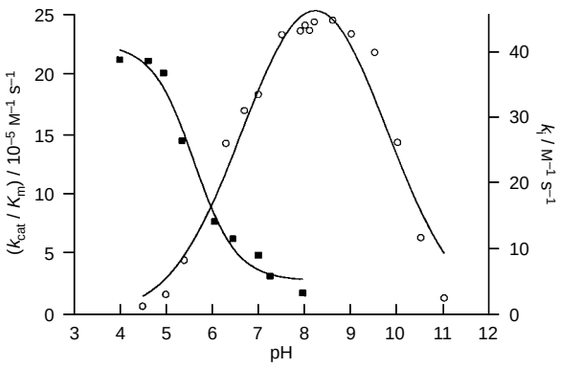

Fig. 1 (○) A plot of k_{cat}/K_m (left hand axis) for the class C *E.cloacae* β-lactamase-catalysed hydrolysis of benzylpenicillin against pH and (■) k_i (right hand axis) against pH for the inactivation of the enzyme by the phosphonamidate **13 (R = BnO)**

groups of pK_a *ca.* 6.1 and 10.1.[22] The pH-dependence of k_i (Fig. 1) shows that inactivation also depends on a catalytic group of pK_a 6.2, which suggests that the catalytic machinery used for hydrolysis is also used for the phosphonylation of **13**. However, the pH–rate profile for inactivation indicates an additional proton is required, *i.e.* whereas hydrolysis apparently requires the group of pK_a 6 to be in its deprotonated, basic form, phosphonylation apparently requires this group to be in its protonated, acidic form, which is probably the result of kinetic ambiguity. The rate of hydrolysis of the substrate **S** is proportional to [**EH**][**S**] where [**EH**] is the protonic form of the enzyme with the groups of pK_a 6 and 10 in their basic and acidic forms, respectively (Scheme 8). The observed kinetics (Fig. 1)

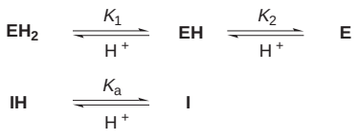

Scheme 8

for inactivation by the inhibitor **I** indicate a rate proportional to [$\mathbf{EH_2}$][**I**], which, for a process of phosphonylation of the active site serine (Scheme 7) is difficult to interpret mechanistically. Of course, the rate law can have various kinetic equivalents [eqn. (6)].

$$\text{Rate} = k_i[\mathbf{EH}_2][\mathbf{I}] = \frac{k_i}{K_1}[\mathbf{EH}][\mathbf{I}][\mathbf{H}^+] = \frac{k_i K_a}{K_1}[\mathbf{EH}][\mathbf{IH}] \quad (6)$$

Phosphonylation could occur through **EH** with the group of pK_a 6 acting as a general base for serine attack as in the hydrolytic reaction (Scheme 9). Breakdown of the trigonal bipyramidal

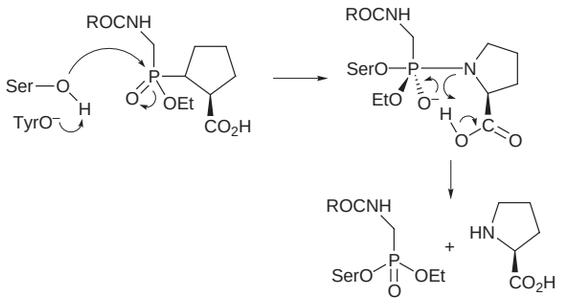

Scheme 9

intermediate, however, could occur by proton donation to the proline nitrogen from the solvent hydronium ion and not the protein [eqn. (6)]. Only the L-proline phosphonamidate **13** (R = BnO) is an effective inhibitor; the corresponding ester is ineffective and the D-proline isomers are much weaker. This could reflect the normal requirement of a carboxylate anion for molecular recognition. It could, however, indicate that the reaction occurs through **EH** and **IH** [eqn. (6)] where the latter is the conjugate acid of the phosphonamidate **13**, *i.e.* with the carboxylic acid group undissociated. The pK_a of this carboxylic acid is 3.86, so, over the pH range studied for inactivation, the major species present is the carboxylate anion of the phosphonamidate **13**. The pH-dependence for inactivation (Fig. 1) would then be given by eqn. (7). The true second-order rate constant for phosphonylation would then be k_iK_1/K_a =

$$k_{obs}^{inact} = k_i \cdot \frac{K_1}{K_a} \cdot \frac{H^+}{K_1 + H^+} \quad (7)$$

6.43×10^3 dm^3 mol^{-1} s^{-1}, giving an EREF of $> 3\times 10^9$. The class C β-lactamase is indeed very effective at enhancing the rate of phosphonylation. If the mechanism does involve the undissociated carboxylic acid of the phosphonamidate as 'substrate' then this is probably the result of 'substrate'-assisted catalysis, with the carboxylic acid acting as an intramolecular general acid catalyst facilitating P–N fission from the trigonal bipyramidal intermediate (Scheme 9).

Class B metallo-β-lactamases

Class B β-lactamases are metalloproteins which require zinc(II) ions for their activity. The first of these enzymes discovered was called β-lactamase II[57] and is produced by *Bacillus cereus*, which also produces two distinct class A enzymes. In 1985 there were just two species identified as producing metallo-β-lactamases. Now there are at least 20 bacterial sources of the metallo-enzyme including those found in *Pseudomonas maltophilia* (L-1), *Aeromonas hydrophila* (A2) and *Bacteroides fragilis*.[58]

Although these metallo-enzymes were initially thought to be clinically unimportant, some pernicious strains have been shown to owe their antibiotic resistance to their ability to produce zinc-β-lactamases.[59] The mechanism-based inactivators which have been used against the serine enzymes are generally ineffective against the Zn^{II}-dependent enzymes, and, at present, there are no clinically-useful inhibitors known. One of the main characteristics of the zinc-enzyme is its ability to catalyse the hydrolysis of nearly all β-lactams including carbapenems **3**. These β-lactamases are extremely efficient at catalysing the hydrolysis of imipenem with values of k_{cat}/K_m of *ca*. 10^6 M^{-1} s^{-1}, which is at least a 1000-fold greater than that shown by 'classical' class A β-lactamases such as TEM-1. A review of the catalytic properties of the well-characterised class B β-lactamases shows that the *A. hydrophila* enzyme exhibits the most specific substrate profile, while the other enzymes are rather broad-spectrum.[60]

The sequences of the metallo-β-lactamases have been established and they all contain a single peptide chain, composed of 220–230 residues.[61] A sequence comparison indicates that the *P. maltophilia* enzyme is only remotely related to the others, which do appear to constitute a more homogenous group and exhibit 37 strictly conserved residues. Surprisingly, His86, one of the histidine residues which seems to be involved as Zn^{II}-binding ligands in the *Bacillus cereus* enzyme, is replaced by an Asn residue in the *A. hydrophila* β-lactamase.

Of particular ambiguity is the number of zinc ions per molecule of β-lactamase. A low resolution crystal structure of the *B. cereus* (569/H/9) β-lactamase showed 1 mol of Zn^{II} in the active site bound by three histidines and one cysteine.[62] A second metal-binding site was identified, but this only weakly bound Zn^{II}. However, more recently, a second crystal structure of the same enzyme showed only a single metal-binding site, with other significant differences. The zinc ion, in the *B. cereus* (569/H/9) β-lactamase is coordinated by three histidine residues (86, 88 and 149) and, probably, a water molecule in a distorted tetrahedral arrangement.[63] Equilibrium dialysis[64] and ^{1}H NMR analysis[65] indicate that the *B. cereus* II enzyme is capable of binding two zinc ions but computer-assisted molecular modelling indicates there is just one major metal ion binding site.[62] As with many metallo-β-lactamases, the zinc ion of the *B. cereus* II enzyme can be replaced by different metal ions and still retain some β-lactamase activity.[64] Most mechanistic and structural information is derived from the *B. cereus* enzyme. However, there has very recently been a structure reported for the binuclear zinc β-lactamase from *B. fragilis*[66] which tightly binds both Zn^{II} ions, although the loss of a single Zn^{II} is not catastrophic for β-lactamase activity.[67].

The mechanism of action of *B. cereus* II metallo-β-lactamase is generally thought to be similar to that of carboxypeptidase A and to involve a water molecule, bound to the zinc ion of the active site, attacking the carbonyl group of the β-lactam ring. It was originally proposed that glutamate-37 acts as a general base and deprotonates the water molecule with the proton subsequently being donated to the nitrogen atom of the β-lactam ring to cause cleavage.[68] However, glutamate-37 is too far from the zinc ion to perform this function and site-directed mutagenesis studies have shown this glutamate is not essential for the catalytic function of the enzyme.[69] It has been demonstrated that aspartate-90 is essential for enzyme activity and consequently suggested that this residue acts as the general base to assist in the hydrolysis of the amide bond of β-lactam substrates.[63,70] In summary, it is not known whether the hydrolysis of β-lactams catalysed by class B β-lactamases occurs by general base catalysis or whether zinc acts simply as an electrophile or as a provider of zinc-bound hydroxide ion. Furthermore, if there is a second binding site for zinc its exact role is not known.

Inhibition of metallo-β-lactamases

Whatever the detailed mechanism of action of β-lactamase, it is likely that zinc(II) stabilises the tetrahedral intermediate **12** presumed to be formed during the catalytic process. Thiols are well-known inhibitors of metallo-proteases because of their ability to coordinate to the active site zinc.[34] We have synthesised several thiol derivatives with structures containing suitable sites for molecular recognition (**14**) as potential

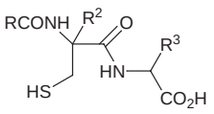

14

inhibitors of the class B metallo-β-lactamases.[71,72] The thiols are indeed competitive inhibitors of the *B.cereus* class B β-lactamase and values of K_i were determined by the effect of varying concentrations of the thiol on the value of the second-order rate constant k_{cat}/K_m for the hydrolysis of benzylpenicillin and cephaloridine. The inhibition constants vary from 10 to 400 μM and are dependent on the nature of the substituents and the stereochemistry at R^2 and R^3.[71] The antihypertensive drug and ACE thiol inhibitor captopril is also an effective inhibitor with a K_i of 27 μM. Replacing the CH_2SH moiety in **14** by CO_2H gives far less effective inhibitors. As described later, these thiol inhibitors were useful in determining the pK_a of the zinc bound water.[72]

Despite the increasing clinical importance of the metallo-β-lactamases there have been few reports of effective inhibitors.[73]

Mechanism of hydrolysis

The number of binding sites for zinc(II) per molecule of class B β-lactamases appears to be one[63] or two.[66] The crystal structure of the enzyme from *B.cereus* 569/H used in our studies has one tightly bound zinc.[63] The effect of additional zinc(II) in solution on the catalytic activity of the enzyme is minimal. Between pH 5.5 and 7.0 a ten thousand-fold excess of zinc(II) increases k_{cat}/K_m by less than 36%, indicating that for this enzyme, at least, there is no catalytically important second site for zinc(II).[72]

The pH-dependence of the rate of hydrolysis of β-lactams catalysed by the class B metallo-β-lactamase from *B. cereus* is very unusual. The pH-dependence of the logarithm of the rate constants, k_{cat}/K_m and k_{cat}, for the hydrolysis of benzylpenicillin and cephaloridine show characteristic bell-shaped behaviour, but, amazingly, *the slope on the acidic limb is 2.0* and not the usual 1.0. The variations in kinetic constants are the result of reversible ionisation and are not due to acid-catalysed inactivation/degradation of the protein.[72] There is no evidence for rapid and reversible denaturation of the enzyme at pH 4.5 from changes in the CD spectrum.

It therefore appears that the rate is suppressed at lower pH because of *two* protonation processes. Because similar behaviour is observed for the two substrates, a penicillin and a cephalosporin, this unusual behaviour is attributable to protonation of the enzyme. The pK_as corresponding to these two equilibrium processes, *i.e.* pK_{a1} and pK_{a2} in Scheme 10, must be

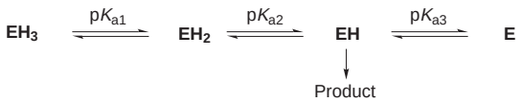

Scheme 10

similar, with pK_{a1} = pK_{a2} = 5.60 ± 0.20. Altogether, there are *three* kinetically important ionising groups including one with a pK_a of 9.5 (Scheme 10). The mechanism may not necessarily involve the two groups of pK_a 5.6 and that of pK_a 9.5 in their deprotonated and acidic forms, respectively. The kinetics simply indicate that there are three basic residues and a proton controlling activity. Two of the most likely candidates for these ionisations are the zinc-bound water molecule and Asp90. The zinc of *B. cereus* β-lactamase is co-ordinated to three protein ligands—His86, His88 and His149—and a water molecule.[63] Formally, either the pK_a of 5.6 or 9.5 could conceivably correspond to the ionisation of zinc-bound water. The pK_a of hydrated Zn^{2+} is 9.5 but the enzyme environment and the nitrogen ligands could modify this. For example, the pK_a of zinc-bound water in carbonic anhydrase is 6.8[74] and in carboxypeptidase A it is 6.2.[75] The most likely amino acid candidate for the pK_a of 5.6 is aspartate-90, which is highly conserved.

It has been possible to deduce the pK_a of the zinc-bound water in β-lactamase by determining the dependence of the inhibition constant pK_i of the thiols **14** against pH. Binding is *pH-independent* between pH 6 and 9 but decreases in both acidic and basic solution—the inflections are very similar to those observed for enzyme-catalysed hydrolysis which indicates that the ionisation states of the enzyme required for catalysis are also those required for binding the inhibitor. However, the slope on the acidic limb is 1.0, in contrast to that observed for hydrolysis, which implies that only one acidic group in the enzyme has an effect on binding the inhibitor. The pH-independent binding of the thiol inhibitor between pH 6 and 9 indicates that the pK_a of the zinc-bound water is the low value of 5.6 because the only scheme which gives pH-independent binding between pH 6 and 9 would be if the neutral undissociated thiol, pK_a 9.5, binds to the species of enzyme in which the water bound to the zinc is fully deprotonated [eqn. (8)].[73]

$$EZn{\cdot}OH + RSH \rightleftharpoons EZn{\cdot}SR + H \qquad (8)$$

A major problem with the widely accepted mechanism of general base-catalysed removal of a proton from zinc(II)-bound water in a process which is concerted with nucleophilic attack on the β-lactam carbonyl group is the relative acidity of this proton. Even if the pK_a of the zinc(II)-bound water is about 9 then 10% of the species already exists in the fully deprotonated form at pH 8 and 1% at pH 7. Presumably, the deprotonated form is a much better nucleophile than the species which is only partially deprotonated. There is little or no catalytic advantage in having a general base remove a proton when the more active species is already present. Although C–N bond fission is the most energetically difficult process in amides hydrolysis, little attention is normally given to the mechanism of the breakdown of the tetrahedral intermediate.

The mechanism which is compatible with the observation that two catalytically important groups of pK_a *ca.* 5.6 are both required in their *deprotonated* forms is shown in Scheme 11.

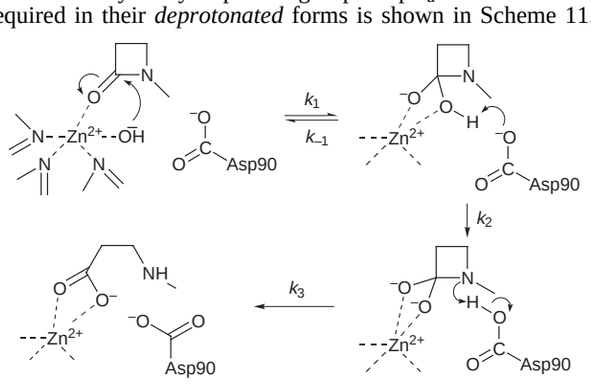

Scheme 11

Zinc(II)-bound water is present at neutral pH in its deprotonated form and acts directly as the nucleophile to attack the β-lactam carbonyl. Zinc(II) also acts as an electrophile to stabilise the negative charge generated on the carbonyl oxygen on forming the tetrahedral intermediate. Ring opening of the β-lactam ring is not a facile process and this first step is likely to be reversible,

i.e. collapse of the tetrahedral intermediate to regenerate the β-lactam occurs at a faster rate than C–N bond fission ($k_{-1} >> k_2$, Scheme 11). This is not surprising; carbon–oxygen bond fission expels a reasonable leaving group—the zinc bound hydroxide ion, the conjugate acid of which has a pK_a of 5.6. Carbon–nitrogen bond fission to expel the amine leaving group will not occur without protonation of nitrogen. In amide hydrolysis carbon–nitrogen bond fission is sometimes facilitated by deprotonation of the tetrahedral intermediate to generate a dianionic tetrahedral intermediate. In the metallo-β-lactamase mechanism this process could occur by the carboxylate anion of Asp90 (Scheme 11) to give a dianionic system with two negatively charged oxygens bound to zinc. The formation of the dianion of the tetrahedral intermediate nicely explains the requirement for two negative charges in the transition state. Deprotonation of the attacking zinc-bound hydroxide also avoids formation of an unstable system of a neutral undissociated carboxylic acid bound to zinc(II). The final step would then involve general acid-catalysed breakdown of the zinc-bound dianionic tetrahedral intermediate with the now undissociated Asp90 donating a proton to the departing amine nitrogen (Scheme 11). Either k_2 or k_3 could be rate-limiting, and kinetic solvent isotope effects do not distinguish between these. The proposed mechanism also suggests structures which may be suitable for inhibiting the metallo-β-lactamases.

Summary

The battle between humans and bacteria appears relentless and the ability of bacteria to develop and pass on resistance to antibiotics seems never-ending. Understanding the mechanisms of the broad classes of β-lactamases makes one contribution to overcoming this conflict.

Although there is superficial similarity between the serine β-lactamases and the more familiar serine proteases the details of the mechanisms of the necessary proton transfer steps remains unknown. We need to know more about the mechanics of C–N bond fission in the β-lactam leading to ring opening. Given the relative conformational inflexibility of the normal β-lactam substrates it is intriguing to note the apparent flexibility of the enzyme in efficiently catalysing the reactions of a wide variety of substrates and inactivators. There does *not* appear to be an exquisite positioning of the catalytic groups and, indeed, the detailed mechanism may vary with substrate structure. This may be an advantage with respect to the design of potential enzyme inactivators and inhibitors. In addition to acyl and phosphyl transfer the serine β-lactamases may catalyse other reactions.

The metallo-β-lactamases are becoming clinically more important as a form of bacterial resistance. The mechanism of their action again appears to be different from the formally similar metallo-proteases. Now that it appears that a dianionic tetrahedral intermediate is involved, the design of suitable transition state analogues may lead to effective inhibitors of the zinc-dependent β-lactamases. The importance of a second metal ion in the metallo-β-lactamases remains unknown.

Mike Page is Dean of the School of Applied Sciences at the University of Huddersfield. He obtained his Ph.D. under the supervision of Brian Capon at the University of Glasgow in 1970 and subsequently worked with Bill Jencks at Brandeis on the energetics of intramolecular reactions and enzyme catalysis. Following a post-doctoral position with Ronnie Bell at Stirling on proton-transfer he moved to Huddersfield in 1973. His research interests are organic and bioorganic reaction mechanisms, enzyme catalysis and inhibition and the use of enzymes in synthesis. In 1991 he was a recipient of the 150th anniversary *Perkin Transactions* prize.

Andy Laws graduated from Lancaster University before moving to undertake a Ph.D. in Physical Organic Chemistry at Sussex University with Dr R. Taylor. In 1987 he took up a post-doctoral fellowship at Huddersfield University with M. I. Page. Presently he holds the post of Senior Lecturer in Organic Chemistry and still works very closely with Mike Page.

Notes and References

† E-mail: m.i.page@hud.ac.uk

1 H. C. Neu, in *The Chemistry of β-Lactam*s, ed. M. I. Page, Blackie, Glasgow, 1992, pp. 101–128.
2 M. I. Page, *Adv. Phys. Org. Chem.*, 1987, **23**, 165.
3 S. G. Waley, in *The Chemistry of β-Lactams*, ed. M. I. Page, Blackie, Glasgow, 1992, pp. 198–226.
4 D. J. Payne, *J. Med. Microbiol.*, 1993, **39**, 93; P. Nordmann, S. Mariotte, T. Naas, R. Labia and M. H. Nicolas, *Antimicrob. Agents Chemother.*, 1993, **37**, 939; T. Naas, L. Vandel, W. Sougakoff, D. M. Livermore and P. Nordmann, *Antimicrob. Agents Chemother.*, 1994, **38**, 1262.
5 K. Bush, G. A. Jacoby and A. A. Modeiros, *Antimicrob. Agents Chemother.*, 1995, **39**, 1211.
6 V. Hechler, M. Van den Weghe, H. H. Martin and J.-M. Frère, *J. Gen. Microbiol.*, 1989, **135**, 1275.
7 M. I. Page, *The Chemistry of β-Lactams*, ed. M. I. Page, Blackie, Glasgow, 1992, pp. 79–100.
8 N. J. Baxter, A. P. Laws, L. Rigoreau and M. I. Page, *J. Chem. Soc., Perkin Trans. 2*, 1996, 2245.
9 A. P. Laws, J. R. Stone and M. I. Page, *J. Chem. Soc., Chem. Commun.*, 1994, 1223.
10 P. Webster, L. Ghosez and M. I. Page, *J. Chem. Soc., Perkin Trans. 2*, 1990, 805.
11 A. M. Davis, P. Proctor and M. I. Page, *J. Chem. Soc., Perkin Trans. 2*, 1991, 1213.
12 M. I. Page, *Phil. Trans. R. Soc. Lond. Ser. B*, 1991, **332**, 149.
13 A. F. Martin, J. J. Morris and M. I. Page, *J. Chem. Soc., Chem. Commun.*, 1979, 298; N. P. Gensmantel and M. I. Page, *J. Chem. Soc., Perkin Trans. 2*, 1979, **137**; J. J. Morris and M. I. Page, *J. Chem. Soc., Perkin Trans. 2*, 1980, 212.
14 A. Llinas-Marti, B. Vilanova, J. Frau, F. Munoz, J. Donoso and M. I. Page, submitted for publication in *J. Org. Chem*.
15 J. A. Kelly, O. Dideberg, P. Charlier, J. Wery, M. Libert, P. Moews, J. Knox, C. Duez, C. Fraipont, B. Joris, J. Dusart, J.-M. Frère and J. M. Ghuysen, *Science*, 1986, **231**, 1429.
16 B. Samraoui, B. Sutton, R. Todd, P. Artmiuk, S. G. Waley and D. Phillips, *Nature*, 1986, **320**, 378.
17 J. R. Knox and P. C. Moews, *J. Mol. Biol.*, 1991, **220**, 435; P. C. Moews, J. R. Knox, O. Dideberg, P. Charlier and J.-M. Frère, *Proteins Struct. Funct. Genet.*, 1990, **7**, 156; O. Herzberg and J.-M. Moult, *Science*, 1987, **236**, 694; O. Herzberg, *J. Mol. Biol.*, 1991, **217**, 701; O. Dideberg, O. Charlier, J.-P. Wéry, P. Dehottay, J. Dusart, T. Erpicum, J.-M. Frère and J.-M. Ghuysen, *Biochem. J.*, 1987, **245**, 911; J. Lamotte-Brasseur, G. Dive, O. Dideberg, P. Charlier, J.-M. Frère and J.-M. Ghuysen, *Biochem. J.*, 1991, **279**, 213; C. Jelsch, L. Mourey, J.-M. Masson and J.-P. Samama, *Proteins Struct. Funct. Genet.*, 1993, **16**, 364.
18 C. Oefner, A. Darcy, J. J. Daly, K. Gubernator, R. L. Charnes, I. Heinze, C. Hubschwerlen and F. K. Winkler, *Nature*, 1990, **343**, 284.
19 E. Lobkovsky, P. C. Moews, L. Hansong, Z. Haiching, J.-M. Frère and J. R. Knox, *Proc. Natl. Acad. Sci. U.S.A.*, 1993, **90**, 11 257.
20 Y.-C. Leung, C. V. Robinson, R. T. Aplin and S. G. Waley, *Biochem. J.*, 1994, **299**, 671; R. P. A. Brown, R. T. Aplin and C. J. Schofield, *Biochemistry*, 1996, **35**, 12421.
21 J. Fisher, J. G. Belasco, S. Khosla and J. R. Knowles, *Biochemistry*, 1980, **19**, 2895.
22 M. I. Page, B. Vilanova and N. J. Layland, *J. Am. Chem. Soc.*, 1995, **117**, 12 092.
23 H. Christensen, M. T. Martin and S. G. Waley, *Biochem. J.*, 1990, **266**, 853.
24 N. C. J. Strynadka, H. Adachi, S. E. Jensen, K. Johns, A. Sielecki, C. Betzel, K. Sutoh and M. N. G. James, *Nature*, 1992, **359**, 700.
25 M. I. Page and A. Williams, in *Organic and Bioorganic Mechanisms*, Longman, 1997.
26 A. P. Laws and M. I. Page, *J. Chem. Soc., Perkin Trans. 2*, 1989, 1577.
27 S. C. Buckwell, M. I. Page and J. L. Longridge, *J. Chem. Soc., Perkin Trans. 2*, 1988, 1809; S. C. Buckwell, M. I. Page, S. G. Waley and J. L. Longridge, *J. Chem. Soc., Perkin Trans. 2*, 1988, 1815; S. C. Buckwell, M. I. Page, J. L. Longridge and S. G. Waley, *J. Chem. Soc., Perkin Trans. 2*, 1988, 1823; A. P. Laws, N. J. Layland, D. G. Proctor and M.

I. Page, *J. Chem. Soc., Perkin Trans. 2*, 1993, 17; N. J. Layland, A. P. Laws, B. Vilanova and M. I. Page, *J. Chem. Soc., Perkin Trans. 2*, 1995, 869.
28 A. Matagne and J.-M. Frère, *Biochem. Biophys. Acta*, 1995, **1246**, 109.
29 M. I. Page, *Chem. Soc. Rev*., 1973, **2**, 295; M. I. Page and W. P. Jencks, *Gazz. Chim. Ital*., 1987, **117**, 455.
30 C. V. Barker and M. I. Page, unpublished results.
31 K. Miyashita, I. Massova, P. Taibi and S. Mobashery, *J. Am. Chem. Soc*., 1995, **117**, 11 055; I. Massova and S. Mobashery, *Acc. Chem. Res.*, 1997, **30**, 162.
32 A. Matagne, J. Lamotte-Brasseur, G. Dive, J. R. Knox and J.-M. Frère, *Biochem. J*., 1993, **293**, 607.
33 J. Rahil and R. F. Pratt, *Biochemistry*, 1994, **33**, 116.
34 M. I. Page, in *Comprehensive Medicinal Chemistry*, ed. P. G. Sammes, Pergamon, Oxford, 1990, vol. 2, pp. 61–87.
35 W. J. Albery and J. R. Knowles, *Biochemistry*, 1976, **15**, 5631; M. I. Page, in *The Chemistry of Enzyme Action*, ed. M. I. Page, Elsevier, Oxford, 1984 pp. 1–54; M. I. Page, in *Comprehensive Medicinal Chemistry*, ed. P. G. Sammes, Pergamon, Oxford, 1990, vol. 2, pp. 45–60.
36 H. Christensen, M. T. Martin and S. G. Waley, *Biochem. J.*, 1990, **266**, 853.
37 O. Herzberg and J. Moult, *Curr. Opin. Struct. Biol.*, 1991, **1**, 946; N. C. J. Strynadka, R. Martin, S. E. Jensen, M. Gold and J. B. Jones, *Nature Struct. Biol.*, 1996, **3**, 688.
38 C. Damblon, X. Raquet, L. Lu-Yun, J. Lamotte-Brasseur, E. Fonzé, P. Charlier, G. C. K. Roberts and J.-M. Frère, *Proc. Natl. Acad. Sci. U.S.A.*, 1996, **93**, 1747.
39 X. Raquet, V. Lounnas, J. Lamotte-Brassuer, J.-M. Frère and R. C. Wade, *Biophys. J.*, 1997, **73**, 2416.
40 M. G. P. Page, *Biochem J.*, 1993, **295**, 295; A. Samuni and N. Citri, *Biochem. Biophys. Res. Commun.*, 1975, **62**, 7; P. Taibi-Tronche, I. Massova, S. B. Vakulenko, S. A. Lerner and S. Mobashery, *J. Am. Chem. Soc.*, 1996, **118**, 7441.
41 M. Galleni, G. Amicosante and J.-M. Frère, *Biochem. J*., 1988, **255**, 123.
42 C. Damblon, G. H. Zao, M. Jamin, P. Ledent, A. Dubus, M. Vanhove, X. Raquet, L. Christiaens and J.-M. Frère, *Biochem. J.*, 1995, **309**, 431; Y. Xu, G. Soto, K. R. Hirsch and R. F. Pratt, *Biochemistry*, 1996, **35**, 3595; B. P. Murphy and R. F. Pratt, *Biochemistry*, 1991, **30**, 3640.
43 E. Lobovsky, E. M. Billings, P. C. Moews, J. Rahil, R. Pratt and J. R. Knox, *Biochemistry*, 1994, **33**, 6762.
44 A. Bulychev, I. Massova, K. Miyashita and S. Mobashery, *J. Am. Chem. Soc*, 1997, **33**, 7620.
45 A. Dubus, S. Normark, M. Kania and M. G. P. Page, *Biochemistry*, 1994, **33**, 8577.
46 K. B. Schowen and R. L. Schowen, *Methods Enzymol.*, 1982, **87**, 551; D. M. Quinn and L. D. Sutton, *Enzyme Mechanisms from Isotope Effects*, ed. P. F. Cooke, CRC Press, 1991, pp. 73–126; A. J. Kresge, R. A. More O'Ferrall and M. F. Powell, *Isotopes in Organic Chemistry*, ed. E. Buncel and C. C. Lee, Elsevier, Amsterdam, 1987, pp. 177–273.
47 Y. Chiang, A. J. Kresge and R. A. More O'Ferrall, *J. Chem. Soc., Perkin Trans. 2*, 1980, 1832; F. Hibbert and H. J. Robbins, *J. Chem. Soc., Chem. Commun.*, 1980, 141.
48 H. B. Burgi and J. D. Dunitz, *Acc. Chem. Res.*, 1983, **16**, 153.
49 G. R. J. Thatcher and R. Kluger, *Adv. Phys. Org. Chem.*, 1989, **25**, 99.
50 F. M. Menger, *Acc. Chem. Res.*, 1985, **18**, 128; F. M. Menger, *Acc. Chem. Res.*, 1993, **26**, 206; A. Daffron and D. E. Koshland, *Proc. Natl. Acad. Sci. U.S.A.*, 1971, **68**, 2463; A. D. Mesecar, B. L. Stoddard and D. E. Koshland, Jr., *Science*, 1997, **277**, 202; A. J. Kirby, *Acc. Chem. Res.*, 1997, **30**, 290; A. J. Kirby, *Angew. Chem., Int. Ed. Engl.*, 1996, **35**, 707.
51 M. I. Page, A. P. Laws, M. J. Slater and J. R. Stone, *Pure Appl. Chem.*, 1995, **67**, 711; A. P. Laws, M. I. Page and M. J. Slater, *Bioorg. Med. Chem. Lett.*, 1993, **3**, 2317.
52 M. Jones and M. I. Page, *Chem. Commun.*, 1991, 316.
53 M. I. Page, *J. Mol. Catal.*, 1988, **47**, 241.
54 See however: W. L. Mock and D. C. Y. Chua, *J. Chem. Soc., Perkin Trans 2*., 1995, 2069.
55 B. P. Murphy and R. F. Pratt, *Biochem. J*., 1988, **256**, 669.
56 I. M. Kovach, *J. Enzyme Inhibition*, 1988, **2**, 199; I. M. Kovach and E. J. Enyedy, *J. Am. Chem. Soc.*, 1998, **120**, 258.
57 S. Kubawara and E. P. Abraham, *Biochem. J*., 1967, **103**, 23C.
58 Y. Saino, F. Kobayashi, M. Inoue and S. Mitsuhashi, *Antimocrob. Agents Chemother*., 1982, **34**, 1590; R. Bicknell, E. L. Emmanuel, J. Gagnon and S. G. Waley, *Biochem. J*., 1985, **229**, 791; J. P. Iaconis and C. C. Sanders, *Antimicrob. Agents Chemother*., 1990, **34**, 44; G. J. Cuchural, Jr., M. H. Malamy and F. P. Tally, *Antimicrob. Agents Chemother*., 1986, **30**, 645.
59 D. J. Payne, *J. Med. Microbiol.*, 1993, **39**, 93.
60 A. Felici, G. Amicosante, A. Oratore, R. Strom, P. Ledent, B. Joris, L. Fanuel and J.-M. Frère, *Biochem. J*., 1993, **291**, 151.
61 H. M. Lim, J. J. Pène and R. Shaw, *J. Bacteriol*., 1988, **170**, 2873; J.-M. Frère. *Mol. Microbiol.*, 1995, **16**, 385; O. Massidda, G. M. Rossolini and G. Salta, *J. Bacteriol.*, 1991, **173**, 4611; B. A. Rasmussen, Y. Gluzman and F. P. Tally, *Antimicrob. Agents Chemother*., 1990, **34**, 1590; J. S. Thompson and M. H. Malamy, *J. Bacteriol.*, 1990, **172**, 2584; M. Hussain, A. Carlino, M. J. Madonnam and J. O. Lampen, *J. Bacteriol.*, 1985, **164**, 223; R. P. Ambler, M. Daniel, J. Fleming, J.-M. Hermoso, C. Pang and S. G. Waley, *FEBS Lett.*, 1986, **189**, 207.
62 B. J. Sutton, P. J. Artymiuk, A. E. Cordero-Borboa, C. Little, D. C. Phillips and S. G. Waley, *Biochem. J.*, 1987, **248**, 181.
63 A. Carfi, S. Pares, U. Duée, M. Galleni, C. Duez, J.-M. Frère and O. Dideberg, *EMBO J*., 1995, **14**, 4914.
64 R. B. Davies and E. P. Abraham, *Biochem. J*., 1974, **143**, 129.
65 G. S. Baldwin, A. Galdes, H. A. O. Hill, B. E. Smith, S. G. Waley and E. P. Abraham, *Biochem. J*., 1978, **175**, 441.
66 N. O. Concha, B. A. Rasmussen, K. Bush and O. Herzberg, *Structure*, 1996, **4**, 823; *Protein Sci.*, 1997, **6**, 2671; A. Carfi, R. Paul-Soto, L. Martin, Y. Petillot, J.-M. Frère and O. Dideberg, *Acta. Crystallogr., Sect. D*, 1997, **53**, 485.
67 M. W. Crowder; Z. Wang, S. C. Franklin, E. P. Zovinka and S. J. Benkovic, *Biochemistry*, 1996, **35**, 12126.
68 C. Little, E. L. Emanuel, J. Gagnon and S. G. Waley, *Biochem. J*., 1986, **233**, 465.
69 H. M. Lim and J. J. Pène, *J. Biol. Chem.*, 1989, **264**, 11 682.
70 H. M. Lim, R. K. Iyer and J. J. Pène, *Biochem. J*, 1991, **276**, 401.
71 S. Bounaga and M. I. Page, unpublished results.
72 S. Bounaga, A. P. Laws, M. Galleni and M. I. Page, *Biochem. J*., 1998, **331.**
73 M. W. Walker, A. Felici, M. Galleni, R. P. Soto, R. M. Adlington, J. E. Baldwin, J.-M. Frère, M. Gololobov and C. J. Schofield, *Bioorg. Med. Chem Lett.*, 1996, **6**, 2455; D. J. Payne, J. H. Bateson, B. C. Gasson, D. Proctor, T. Khushi, T. H. Farmer, D. A. Tolson, D. Bell, P. W. Skett, A. C. Marshall, R. Reid, L. Ghosez, Y. Combret and J. Marchand-Brynaert, *Antimicrob. Agents Chemother*., 1997, **41**, 135; J. T. Toney, P. M. D. Fitzgerald, N. Grover-Sharma, S. H. Olsen, W. J. May, J. G. Sundelot, D. E. Vanderwall, K. A. Cleary, S. K. Grant, J. K. Wu, J. W. Kozarich, D. L. Pompliano and G. H. Hammond, *Chem. Biol.*, 1998, **5**, 185.
74 Y. Pocker and D. W. Bjorkquist, *Biochemistry*, 1977, **16**, 5698; E. Kimura, T. Shiota, T. Koike, M. Shiro and M. Kodama, *J. Am. Chem. Soc.*, 1990, **112**, 5805.
75 W. L. Mock and J.-T. Tsay, *Biochemistry*, 1986, **25**, 2920; W. L. Mock and J.-T. Tsay, *J. Biol. Chem.*, 1988, **263**, 8635.

8/03578D

Experimental evidence for a [2 + 2] mechanism in the Lewis acid-promoted formation of α,β-unsaturated esters from ethoxyacetylene and aldehydes. Synthesis and characterisation of 4-ethoxyoxetes.

Magali Oblin,[a] Jean-Luc Parrain,[b] Michel Rajzmann[b] and Jean-Marc Pons*[a]†

[a] *Laboratoire Réactivité en Synthèse Organique (RéSo), UMR 6516, Faculté de St-Jérôme, boîte D12,13397 Marseille Cedex 20, France*

[b] *Laboratoire de Synthèse Organique, ESA 6009, Faculté de St-Jérôme, boîte D12, F-13397 Marseille Cedex 20, France*

4-Ethoxy-2*H*-oxetes 3a–c were prepared from ethoxyacetylene and alkoxy aldehydes 1a–c through $MgBr_2$–Et_2O promoted [2 + 2] cycloaddition reaction and were characterized at room temperature; their synthesis, which could occur *via* the formation of a chelate, establishes cycloaddition as the initial step in the formation of α,β-unsaturated esters 4a–c.

The formation of α,β-unsaturated esters from aldehydes or ketones and alkoxyacetylenes, under Lewis acid catalysis was first reported by Vieregge *et al*. in 1959.[1] The reaction immediately met with success as demonstrated in a review article published seven years later by the same authors.[2] In the same paper, the authors proposed that the mechanism involves the formation of an intermediate alkoxyoxete and its conrotatory ring-opening to give the corresponding α,β-unsaturated ester (Scheme 1).

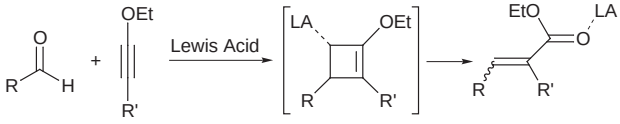

Scheme 1

The strongest evidence supporting such a mechanism at that time was the isolation by Middleton of an alkoxyoxete resulting from the non-catalyzed reaction between hexafluoroacetone and ethoxyacetylene.[3] Furthermore this oxete underwent a rearrangement to yield the corresponding unsaturated ester. Since then this reaction has attracted many experimental studies[4] and has even found application in synthesis where it can sometimes be used instead of the Wittig reaction.[5] However, to the best of our knowledge, no experimental evidence of the occurrence of a non-metallated oxete[6] in a Lewis acid catalyzed process has yet been reported. This is probably due to the instability of oxetes which have been seldom isolated or characterized.[7] Examples of alkoxyoxetes are also very scarce: in addition to the examples reported by Middleton[3] and Zaitseva *et al*.,[6] two others can be found in the literature.[8,9]

As part of an ongoing interest in Lewis acid-promoted [2 + 2] cycloadditions involving aldehydes,[10] we report the observation and characterization, at room temperature, of 2-ethoxy-2*H*-oxetes **3a**–**c**.

3-Benzyloxytetradecanal **1a** reacts with ethoxyacetylene **2** under $MgBr_2$–Et_2O catalysis in CH_2Cl_2 to yield after 30 min 2-(2-benzyloxytridecyl)-4-ethoxy-2*H*-oxete **3a** as a 4 : 1 mixture of diastereomers (Scheme 2, Table 1, entry 1).‡ 4-Ethoxy-2*H*-oxetes **3b,c**§ were also obtained (both as 9 : 1 mixtures of diastereomers) from aldehydes **1b,c** and were observed under the same conditions (Scheme 2, Table 1, entries 3 and 4).

The obtention of oxetes **3a**–**c** could result from the formation of chelate **A**[11] which then would lead to the 'bicyclic' cycloadduct-chelate **B**. The rigidity of the chelate structure of **B**, *i.e.* its 'bicyclic' structure, under the reaction conditions, could then prevent the ring opening rearrangement. We have undertaken *ab initio* calculations on a model chelate **C** to establish that such an intermediate is indeed a minimum on a potential energy surface. Calculations were run at the HF/6-31G* level of theory. The total energy of **C** was found to be −1693.424205 au.

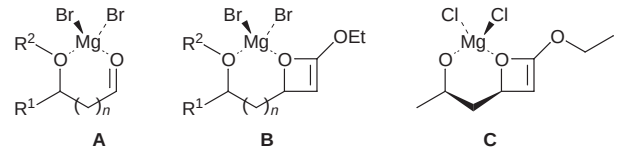

A **B** **C**

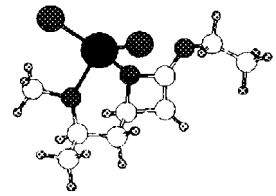

Further support for this explanation was found in the following experimental results (Table 1). When **2** and **1a** react under BF_3–Et_2O catalysis, the only product we were able to observe is α,β-unsaturated ester **4a** (Table 1, entry 2). Only traces of **3a** were identified during the monitoring of the reaction by TLC. The reaction between **2** and 3-(*tert*-butyldimethylsiloxy)tetradecanal **1d** (R^1 = $C_{11}H_{23}$; R^2 = TBDMS; n = 1) or hexanal **1e** under BF_3–Et_2O or $MgBr_2$–Et_2O catalysis leads, in all four cases (Table 1, entries 5–8), to the expected corresponding (*E*)-unsaturated esters **4d,e**. Indeed, in all these cases, the formation of chelates analogous to chelates **A** and

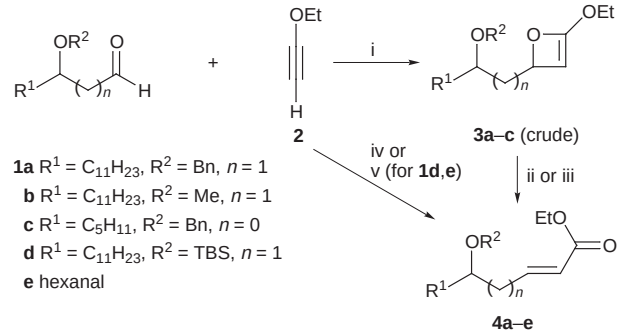

1a R^1 = $C_{11}H_{23}$, R^2 = Bn, n = 1
b R^1 = $C_{11}H_{23}$, R^2 = Me, n = 1
c R^1 = C_5H_{11}, R^2 = Bn, n = 0
d R^1 = $C_{11}H_{23}$, R^2 = TBS, n = 1
e hexanal

2 **3a–c** (crude) **4a–e**

Scheme 2 *Reagents and conditions*: i, $MgBr_2$–OEt_2 (3 equiv.), CH_2Cl_2, 15 min, −60 °C; ii, BF_3–OEt_2 (cal.), CH_2Cl_2, 1 min, −30 °C; iii, CH_2Cl_2 or $CDCl_3$, 2–3 h, room temp.; iv, BF_3–OEt_2 (1 equiv.), CH_2Cl_2, 30 min, −60 °C; v, $MgBr_2$–OEt_2 (3 equiv.), CH_2Cl_2, 15 min, −60 °C

Table 1 Preparation of oxetes **3a–c** and esters **4a–e** (yields are unoptimized) from aldehydes **1a–e**

Entry	Aldehyde	Lewis acid	Oxete (d.r.)	(*E*)-Ester (yield)
1	**1a**	$MgBr_2$–OEt_2	**3a** (4 : 1)	**4a** (88%)
2	**1a**	BF_3–OEt_2	—	**4a** (70%)
3	**1b**	$MgBr_2$–OEt_2	**3b** (9 : 1)	**4b** (67%)
4	**1c**	$MgBr_2$–OEt_2	**3c** (9 : 1)	**4c** (75%)
5	**1d**	BF_3–OEt_2	—	**4d** (60%)
6	**1d**	$MgBr_2$–OEt_2	—	**4d** (71%)
7	**1e**	BF_3–OEt_2	—	**4e** (56%)
8	**1e**	$MgBr_2$–OEt_2	—	**4e** (73%)

therefore **B** is not possible[12] and hence the conrotatory ring opening takes place.

Finally, although **3a–c** are stable in $CDCl_3$ solution at −20 °C,¶ their life-time at room temperature does not exceed 1 or 2 h and is a few seconds in solution at −30 °C in the presence of BF_3–Et_2O (in all three cases, ring opening leads to esters **4a–c**). This last observation gives further support for the structure of **3a–c** and to our hypothesis of the rigidity of chelate **B**.

In conclusion, we have provided the first evidence of a [2 + 2] mechanism for the studied reaction. We think that the isolation of oxetes **3a–c** at room temperature rests upon the formation of stable chelates **B** which prevents the conrotatory ring opening step of the reaction. Since the formation of **3a–c** occurs with good diasteroselectivity, studies are currently underway to use these as intermediates in synthesis.

We are grateful to Dr François Volatron (CNRS-Orsay) for useful discussions, and to Mrs Roselyne Rosas and Dr Robert Faure (Université d'Aix-Marseille) for NMR experiments.

Notes and References

† E-mail: jean-marc.pons@reso.u-3mrs.fr

‡ The structure of **3a** lies upon extensive 2D homo- and hetero-nuclear ^{1}H NMR experiments at 400 MHz. Experimental procedure: a solution of **1a** (0.35 mmol; 111 mg) in CH_2Cl_2 (1 cm^3) was added to a suspension of $MgBr_2$–OEt_2 (1.05 mmol; 270 mg) in CH_2Cl_2 (3 cm^3) at −60 °C under argon. After 15 min, a solution of **2** (0.70 mmol; 49 mg) in CH_2Cl_2 (2 cm^3) at room temp. was added dropwise to the suspension at −60 °C. TLC monitoring showed the reaction to be completed (no starting material left) after 15 min. The reaction mixture was diluted in light petroleum (10 cm^3) and hydrolyzed with ice–water (2 cm^3). Filtration and concentration *in vacuo* gave 126 mg of crude product; ^{1}H NMR (400 MHz) was used to establish the presence of **3a** as a 4 : 1 mixture of the two diastereomers. An increase in the temperature of the reaction mixture, up to −30 °C, prior to the hydrolysis led to unsaturated ester **4a** (88%). R_f (light petroleum–Et_2O = 7 : 3) **1a** : 0.5; **3a** : 0.25; **4a** : 0.75.

3a: major isomer: δ_H (400 MHz, $CDCl_3$) 7.35–7.25 (5 H, m, PhH), 5.12 (1 H, d, *J* 7.9, =CH), 4.60 (1 H, m, CH–O–), 4.59 (1 H, part A of AB system, J_{AB} 11.9, –O–C*H*$_a$H–Ph), 4.52 (1 H, part B of AB system, J_{AB} 11.9, –O–CH*H*$_b$–Ph), 3.89 (1 H, part A of ABX_3 system, J_{AB} 9.6, J_{AX} 7.1, O–C*H*$_a$H–Me), 3.86 (1 H, part B of ABX_3 system, J_{AB} 9.6, J_{AX} 7.0, O–CH*H*$_b$–Me), 3.66 (1 H, m, CH–OBn), 1.82 (1 H, part A of ABXY system, J_{AB} 14.5, J_{AX} 8.7, J_{AY} 3.7, O–CH–C*H*$_a$H–CH–O), 1.72 (1 H, part B of ABXY system, J_{AB} 14.5, J_{AX} 7.1, J_{AY} 3.3, O–CH–CH*H*$_b$–CH–O), 1.88–1.46 (6 H, m), 1.37–1.18 (14 H, m), 0.87 (3 H, t, *J* 7.0, –Me), 0.85 (3 H, br t, O–CH_2–*Me*); δ_C (50.3 MHz, $CDCl_3$) 138.3 (s), 138.0 (s), 128.5 (d, 2C), 128.0 (d, 2C), 127.9 (d), 111.8 (d), 77.0 (d), 77.1 (t), 68.7 (t), 68.6 (d), 39.8 (t), 33.4 (t), 32.0 (t), 29.8 (t), 29.7 (t, 2C), 29.6 (t, 2C), 29.4 (t), 25.4 (t), 22.8 (t), 14.2 (q, 2C).

§ ^{1}H and ^{13}C NMR data of **3b,c** are similar to those described for **3a**.

¶ Oxete **3c** was, for example, kept over 2 months in a NMR tube (^{1}H concentration). We first imagine that the relative stability of Lewis acid-free **3a** could result from an intramolecular π-stacking (between the double bond and the aromatic ring), but both the formation of **3b** and semiempirical (AM1) calculations were in disagreement with such an explanation.

1 H. Vieregge, H. J. T. Bos and J. F. Arens, *Recl. Trav. Chim. Pays-Bas*, 1959, **78**, 664; see also H. Vieregge and J. F. Arens, *Recl. Trav. Chim. Pays-Bays*, 1959, **78**, 921.
2 H. Vieregge, H. M. Schmidt, J. Renema, H. J. T. Bos and J. F. Arens, *Recl. Trav. Chim Pays-Bas*, 1966, **85**, 929.
3 W. J. Middleton, *J. Org. Chem.*, 1965, **30**, 1307.
4 J. Pornet, A. Rayadh and L. Miginiac, *Tetrahedron Lett.*, 1986, **27**, 5479; J. Pornet, A. Rayadh and L. Miginiac, *Tetrahedron Lett.*, 1988, **29**, 3065; D. Zakarya, A. Rayadh, M. Samih and T. Lakhlifi, *Tetrahedron Lett.*, 1994, **35**, 405; D. Zakarya, A. Rayadh, M. Samih and T. Lakhlifi, *Tetrahedron Lett.*, 1994, **35**, 2345; C. J. Kowalski and S. Sakdarat, *J. Org. Chem.*, 1990, **55**, 1977.
5 D. Crich and J. Z. Crich, *Tetrahedron Lett.*, 1994, **35**, 2469.
6 A trimethylgermyloxete resulting from the Lewis acid catalyzed cyclization of the *O*-(trimethylgermyl) derivative of 4-ethoxy-1,1,1-trifluoro-2-(trifluoromethyl)but-3-yn-2-ol has been described: G. S. Zaitseva, L. I. Livantsova, N. A. Orlova, Yu. L. Baukov and I. F. Lutsenko, *Zh. Obshch. Khim.*, 1982, **52**, 2076.
7 L. E. Friedrich and G. B. Schuster, *J. Am. Chem. Soc.*, 1969, **91**, 7204; L. E. Friedrich and G. B. Schuster, *J. Am. Chem. Soc.*, 1971, **93**, 4603; L. E. Friedrich and J. D. Bower, *J. Am. Chem. Soc.*, 1973, **95**, 6869; Y. Kobayashi, Y.Hanzawa, W. Miyashita, J. Kashiwagi, T. Nakano and I. Kumadaki, *J. Am. Chem. Soc.*, 1979, **101**, 6445.
8 Y. I. Baukov, G. S. Zaisteva, L. I. Livanstova, R. A. Bekker and L. A. Savost'yanova, *Zh. Obshch. Khim.*, 1981, **51**, 1304.
9 D. C. England and C. G. Krespan, *J. Org. Chem.*, 1970, **35**, 3312.
10 A. Pommier, J.-M. Pons, P. J. Kocienski and L. Wong, *Synthesis*, 1994, 1294; A. Pommier, J.-M. Pons and P. J. Kocienski, *J. Org. Chem.*, 1995, **60**, 7334; J.-M. Pons, M. Oblin, A. Pommier, M. Rajzmann and D. Liotard, *J. Am. Chem. Soc.*, 1997, **119**, 3333; B. W. Dymock, P. J. Kocienski and J.-M. Pons, *Chem. Commun.*, 1996, 1053.
11 For X-ray structure and NMR evidence of chelates similar to **A**, see G. E. Keck and S. Castellino, *J. Am. Chem. Soc.*, 1986, **108**, 3847 (NMR); M. T. Reetz, K. Harmsand and W. Reif, *Tetrahedron Lett.*, 1988, **29**, 5881 (X-ray).
12 It is well known that TBDMS ethers do not give chelates but rather 2 : 1 complexes with bidentate Lewis acids. G. E. Keck and S. Castellino, *Tetrahedron Lett.*, 1987, **28**, 281. For other examples, see M. Santelli and J.-M. Pons, in *Lewis Acids and Selectivity in Organic Synthesis*, CRC Press, Boca Raton, 1996, ch. 1.

Received in Liverpool, UK, 5th May 1998; 8/03395A

Hydrophobic proteins: synthesis and characterisation of organic-soluble alkylated ferritins

Kim K. W. Wong,[a] Nicola T. Whilton,[a] Helmut Cölfen,[b] Trevor Douglas[a] and Stephen Mann[a]†

[a] *Department of Chemistry, University of Bath, Bath, UK BA2 7AY*
[b] *Max Planck Institute of Colloids and Interfaces, Kanstr. 55, D-14513, Teltow, Germany*

Alkylated derivatives of the iron storage protein, ferritin, have been prepared by carbodiimide-activated coupling of long chain primary amines to surface carboxylic acid residues; the proteins are soluble in dichloromethane as intact, non-aggregated biomolecules.

Ferritin is an unusual metalloprotein in that the inorganic centre consists of a large number of ions (up to 4500 Fe atoms) present as a biomineral (ferrihydrite, $Fe_2O_3{\cdot}nH_2O$) encapsulated within a 24-subunit polypeptide shell.[1] The organic shell is remarkably stable to thermal and chemical degradation due to strong subunit–subunit interactions, a property which offers much scope in using the protein micelle as a nanoreactor for the synthesis of biocompatible nanocolloids. Recently, we have developed synthetic routes to biomimetic ferritins reconstituted with non-native inorganic nanoparticles such as Fe_3O_4,[2,3] MnOOH,[4] FeS[5] or CdS.[6] These routes are generally dependent on a balance between the redox chemistry, oxidation kinetics and hydrolytic behaviour of metal ions, and are limited to aqueous-based media. Further developments should be possible if ferritin could be solubilized in organic media because this would allow a wide range of organometallic precursors to be used. In particular, sol–gel reactions based on alkoxide hydrolysis could be achieved within the polypeptide cage by preparing organic-soluble ferritin molecules which have a water-filled hydrophilic inner cavity and a hydrophobically modified outer surface. Such derivatives would be analogous to the reverse micellar (water-in-oil) phase of many surfactants but would have enhanced stability owing to the absence of dynamic exchange between ferritin subunits.

Here, we describe the first step towards this goal in which ferritins soluble in dichloromethane (DCM) have been prepared by alkylation reactions using long chain primary amines (C_n, n = 6, 9, 12, 14, 18). The method involves the carbodiimide activation of surface carboxylic acid groups[7] of the native protein or a demetallated derivative (apoferritin) followed by nucleophilic substitution in the presence of a large excess of the amine.‡ Coupling of hexyl, nonyl or lauryl chains produced clear red–orange (ferritin) or colourless (apoferritin) THF–H_2O solutions which were stable for at least 12 months. Similar reactions with tetradecylamine or stearylamine gave turbid mixtures which precipitated after a few days due to the reduced solubility of the longer chain amines. Each of the alkylated proteins, except for the hexyl-derivatized ferritin, were readily extracted into DCM by addition of small amounts of NaCl to give clear red–orange (ferritin) or colourless (apoferritin) organic solutions. In contrast, control experiments involving native (apo)ferritin, or reaction mixtures of (apo)ferritin in the absence of either the amine or EDC coupling reagent, showed no evidence of phase transfer into DCM. For the alkylated proteins, UV–VIS spectra of the DCM layer showed a shouldered peak at approximately 280 nm indicative of the aromatic amino acid side chains of the transferred ferritin. The ease of transfer of the alkylated ferritins into DCM was in the order tetradecyl- > lauryl- > nonyl-amine. In general, the alkylated proteins were stable for as long as six months in the DCM layer.

TEM images of unstained samples of the alkylated ferritins transferred into DCM showed discrete, electron dense iron oxide cores with an average size of 5 nm (Fig. 1). The non-aggregated and monodisperse nature of the protein when dried onto the TEM grid indicates that the derivatized polypeptide shell is structurally intact. Unlike native ferritin, the alkylated proteins could not be stained with uranyl acetate, indicating significant changes in the surface chemistry. Staining of the samples did however show evidence of a surfactant lamellar phase, presumably formed by self-assembly of excess amine molecules during air-drying of the DCM solutions.

Polyacrylamide gel electrophoresis (PAGE) showed that the native and nonyl-derivatized proteins migrated towards the positive and negative electrodes, respectively, under non-denaturing conditions (data not shown). Migration of the alkylated ferritin terminated, however, at the interface between the stacking and resolving gels, indicating only a small net positive charge on the derivatized protein.

Analytical ultracentrifuge (AUC) analysis§ of nonyl-derivatized ferritin showed evidence of a floating (excess nonylamine) and a sedimenting component (derivatized protein) in the DCM solutions. The sedimentation coefficient distributions [$g(s^*)$] showed the presence of two well defined species corresponding to nonyl-derivatized ferritin [s^* = 12.1 Sv (77.5%)] and a larger species [s^* = 21.4 Sv (21.4%), Fig. 2]. The sedimentation coefficients were consistent with those expected for a monomer–dimer system of spherical molecules, according to $s_n = s_1 n^{2/3}$ with n = 2. Significantly, the relative proportions of monomeric and dimeric species were similar to those previously measured for native ferritin (69.4% monomer, 19.5% dimer and 11.1% trimer) using flow-field–flow-fractionation.[8] This strongly suggests that the hydrophobic ferritin is structurally intact and that negligible degradation occurs during

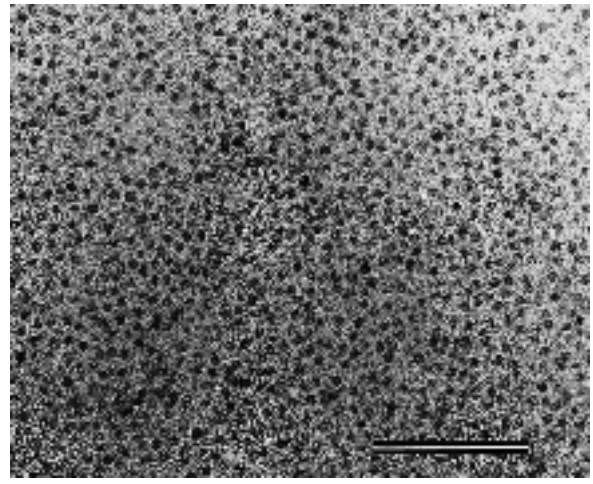

Fig. 1 TEM image of a DCM solution of nonyl-derivatized ferritin showing discrete electron dense iron oxide cores, each of which is encapsulated within an alkylated protein shell; scale bar = 100 nm

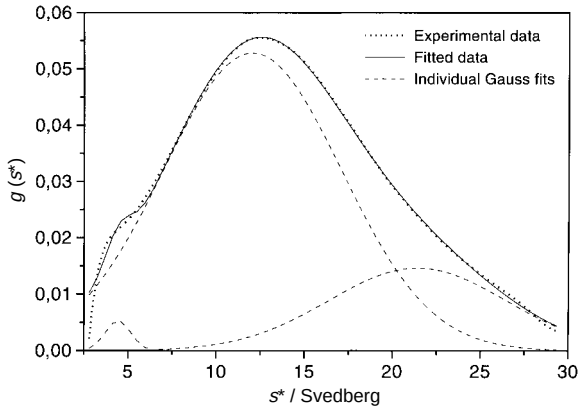

Fig. 2 Sedimentation coefficient distribution [$g(s^*)$] for a DCM solution of nonyl-derivatized ferritin showing the presence of alkylated ferritin monomers and dimers. A minor contaminant with s^* = 4.5 Sv (1.1%) is also present.

chemical functionalization in the THF–water reaction mixture.

The molar mass of nonylamine-derivatized ferritin in DCM was determined as M_w = 675 kDa from sedimentation equilibrium results. This was an approximate value because the density could only be estimated from the sample composition. However, the value was consistent with results obtained from sedimentation equilibrium data for native ferritin (M_w = 622.8 ± 4.3 kDa), assuming a similar monomer : dimer ratio and iron loading in the samples, and an additional mass due to the covalently attached nonylamine chains. The M_w for apoferritin was determined as 497.0 ± 5.0 kDa by sedimentation equilibrium, giving molar masses, M_w of 20.7 kDa and 125.8 kDa for the native subunit and FeOOH core, respectively. Assuming, M_w = 675 kDa for the derivatized ferritin, gives a value of approximately 550 kDa for the molar mass of the derivatized apoferritin (22.9 kDa per subunit) which corresponds to approximately 400 covalently coupled nonylamine groups per protein molecule. This is approximately 75% of the theoretical number of amino acid carboxyl groups (*ca.* 520) in the protein molecule.[1]

Dynamic light scattering for nonyl-derivatized ferritin in DCM gave an average hydrodynamic diameter of 35 nm, compared with 12 mm for aqueous solutions of native ferritin. Although further work is required, the results suggest that the derivatized protein is associated to some extent with the excess amine molecules present in the DCM solution. Reversed-phase HPLC data for native ferritin showed a sharp peak for the monomer at 15 min with a shoulder at 11.5 min corresponding to the dimer, whereas nonyl-derivatized ferritin showed a broad protein peak with a retention time centred at 24 min. Because the derivatized sample was run directly from the reaction mixture without dialysis, excess amine and coupling agent, as well as small molecule byproducts, were observed as relatively sharp peaks between 2 and 5 min. The reconstructed data from the electrospray mass spectra of the proteins showed a narrow (m/z 19.9–20.5 k) and wide distribution of molecular masses (m/z 20–30 k) for the native and nonyl-derivatized ferritin subunits, respectively. These values were consistent with the derivatized subunit molar mass of 22.9 kDa determined by AUC analysis.

The results indicate that alkylated ferritins with long term solubility in DCM can be readily prepared. TEM, PAGE and AUC were consistent with the preparation of intact protein molecules with significantly modified surface charge. However, HPLC and electrospray mass spectroscopy suggest that the degree of derivatization varies significantly between ferritin molecules and that a heterogeneous product is obtained. Furthermore, significant amounts of non-covalently bound amine may be strongly associated with the chemically modified protein. In this regard, it seems feasible that surfactant micellization could enhance the transfer of the alkylated ferritins into DCM, although native ferrintin could not be transferred into DCM in the presence of uncoupled amine molecules alone, indicating that alkylation is the dominant factor determining the solubility in the organic medium. Further work is in progress to expand these studies and to exploit the alkylated proteins in sol–gel reactions involving metal alkoxides.

We thank Armelle Buzy (University of Warwick) for electrospray MS, Franziska Gröhn (Teltow) for light scattering measurements, and BBSRC for financial support.

Notes and References

† E-mail: s.mann@bath.ac.uk

‡ Nonylamine (1.11 g, 7.77 mmol, 1.5 ml) was added to THF–H_2O (1 : 1 v/v, 8.5 ml) and the pH adjusted to *ca.* 5.5. THF was found to be a suitable solvent for amine solubilization without protein degradation. Ferritin or apoferritin (10 mg, 2.22 × 10^{-5} mmol) was slowly added, and the pH readjusted to 5.5 if required. The mole ratio of nonylamine to carboxylic acid residues was *ca.* 700 : 1, assuming a total of 520 aspartic and glutamic acid residues in the 24-meric protein.[1] 1-(3-Dimethylaminopropyl)-3-ethyl carbodiimide hydrochloride (EDC, 150 mg, 0.78 mmol) dissolved in THF–H_2O (1 : 1 v/v, 1 ml), was slowly added dropwise whilst maintaining the pH at 5.5 for 2–3 h, and the reaction mixture stirred overnight at room temperature. Samples (*ca.* 1 mg) of the alkylated protein were transferred from the reaction mixture into DCM by addition of small quantitites (5–10 mg) of dry NaCl followed by shaking. Reactions were also performed at lower concentrations of nonylamine, equivalent to 0.5, 7, 70, 170 or 340 molecules per protein carboxylic acid group. In general, ratios < 1 : 170 did not result in efficient phase transfer into DCM. Other primary amines, such as hexyl, lauryl (C_{12}), tetradecyl (C_{14}) and stearyl (C_{18}) amine were reacted with ferritin at concentrations equivalent to 125 or 500 molecules per carboxylate group, using the above procedure.

§ The sedimentation coefficient distributions [$g(s^*)$] were evaluated from sedimentation velocity data using the time-derivative method[9] and fitted with Gaussian curves. The weight average molar mass M_w was obtained from sedimentation equilibrium distributions for a concentration series by extrapolation of $M_{w,app}$ to infinite dilution. $M_{w,app}$ values were derived from direct fitting to an ideal one-component model system,[10] and also independently from the cumulative M^* approach.[11]

1 P. M. Harrison, S. C. Andrews, P. J. Artymiuk, G. C. Ford, J. R. Guest, J. Hirzmann, D. M. Lawson, J. C. Livingstone, J. M. A. Smith, A. Treffry and S. J. Yewdall, *Adv. Inorg. Chem.*, 1991, **36**, 449.
2 F. C. Meldrum, B. R. Heywood and S. Mann, *Science*, 1992, **257**, 522.
3 K. K. W. Wong, T. Douglas, S. Gider, D. D. Awschalom and S. Mann, *Chem. Mater.*, 1988, **10**, 279.
4 F. C. Meldrum, V. J. Wade, D. L. Nimmo, B. R. Heywood and S. Mann, *Nature*, 1991, **349**, 684.
5 T. Douglas, D. P. E. Dickson, S. Betteridge, J. Charnock, C. D. Garner and S. Mann, *Science*, 1995, **269**, 54.
6 K. K. W. Wong and S. Mann, *Adv. Mater.*, 1996, **8**, 928.
7 D. Danon, L. Goldstein, Y. Marikovsky and E. Skutelsky, *J. Ultrastruct. Res.*, 1972, **38**, 500.
8 T. Pauck and H. Cölfen, *Anal. Chem.*, in press.
9 W. F. Stafford, in *Analytical Ultracentrifugation in Biochemistry and Polymer Science*, ed. S. E. Harding, A. J. Rowe and J. C. Horton, Royal Society of Chemistry, Cambridge, 1992, pp. 359–393.
10 D. K. McRorie and P. J. Voelker, *Self-associating Systems in the Analytical Ultracentrifuge*, Beckman Instruments, Fullerton, CA, 1993.
11 H. Cölfen and S. E. Harding, *Eur. Biophys. J.*, 1997, **25**, 333.

Received in Cambridge, UK, 6th April 1998; 8/02627K

Luminescence response of the solid state polynuclear copper(I) iodide materials $[CuI(4\text{-picoline})]_x$ to volatile organic compounds

Elena Cariati, James Bourassa and Peter C. Ford*†

Department of Chemistry, University of California, Santa Barbara, CA 93106, USA

Exposure of the polymeric solid $[CuI(4\text{-pic})]_\infty$ to either liquid or vapor toluene leads to disappearance of this material's characteristic room temperature blue emission (λ_{max} 437 nm) and the appearance of the yellow emission (λ_{max} 580 nm) indicative of the $[CuI(4\text{-pic})]_4$ tetramer; the process is reversed when the latter is exposed to liquid or vapor *n*-pentane.

Polynuclear d^{10} metal complexes exhibit remarkably rich photoluminescent properties coupled in part to their diverse structural motifs.[1–3] The copper(I) halide adducts CuXL (X = halide, L = a nitrogen donor ligand) are particularly fascinating for the variety of structural formats which can be altered by varying the reagent stoichiometry, crystallization conditions and the reaction medium.[4–7] Many are brightly luminescent, even at ambient temperature, and the emission behavior varies markedly with structure and with environment. For example, the solid state luminescence spectrum of $[CuIpy]_\infty$ (py = pyridine), a 'stair step' polymer [Fig. 1(a)], displays a broad blue emission band at room temperature (λ_{max} = 437 nm), which does not shift upon cooling, and is probably due to an excited state with iodide to pyridine charge transfer (XLCT) character.[7,8] In contrast, the 'cubane' isomer $[CuIpy]_4$ [Fig. 1(b)] shows 'luminescence thermochromism'.[9] Room temperature, solid $[CuIpy]_4$ displays a broad yellow emission (λ_{max} = 580 nm), but, at 77 K, two bands are seen (λ_{max} = 438, 618 nm);[6,7] the higher energy one is largely XLCT in character, while that at lower energy has been assigned to a mixed halide to metal charge transfer (XMCT), d→(s,p) 'cluster centered' excited state.[8] Here we report that, for the related material $[CuI(4\text{-pic})]_x$ (x = 4 or ∞, 4-pic = 4-picoline), exposure of the solid to the liquid or the vapor phase of certain volatile organic compounds (VOCs) reversibly induces structural changes readily seen in the luminescent behavior.

Addition of neat 4-picoline to an aqueous CuI–KI solution at room temperature results in the formation of $[CuI(4\text{-pic})]_\infty$ (**A**) as revealed by a single crystal X-ray structure study.[10] Under UV illumination, the emission from this material is distinctly blue, and the room temperature luminescence spectrum displays a single broad band centered at 426 nm, which is shifted to slightly lower energy (λ_{max} 450 nm) at 77 K. Notably, similar addition of excess neat 3-picoline to aqueous CuI–KI solution gives the 'cubane' solid $[CuI(3\text{-pic})]_4$ as confirmed by a single crystal X-ray structure determination.[10] The luminescence spectrum of this solid displays a single, broad band centered at λ_{max} 614 nm at room temperature, but two bands at 77 K, one at 590 nm and one centered at 456 nm, as previously described.[6] These results may explain the observation by Hardt and Pierre that, for solids of stoichiometry CuIL, the derivative with 3-picoline emits yellow while that with 4-picoline emits blue.[11] In this context, it is notable that dissolving 3-picoline in methanol before addition to the CuI–KI aqueous solution directs the reaction pathway toward formation of the blue emitting stair-step polymer $[CuI(3\text{-pic})]_\infty$ (λ_{max} 452 nm at room temperature) whose structure was confirmed by a single crystal X-ray study.

The polymeric $[CuI(4\text{-pic})]_\infty$ solid is only very slightly soluble in most organic solvents. Despite this, we found that the addition of a small amount of toluene (far less than that needed for substantial dissolution) to a vial containing solid **A** leads to disappearance of the characteristic room temperature blue luminescence and subsequent appearance of yellow luminescence from the solid with an emission band centered at 578 nm (Fig. 2). This band corresponds to that of the tetranuclear 4-picoline complex $[CuI(4\text{-pic})]_4$ (**B**) which was independently prepared as described below and confirmed by a single crystal X-ray diffraction study. Notably, there appears to be an intermediate non-emitting species formed rapidly upon exposure of **A** to liquid toluene which more gradually undergoes

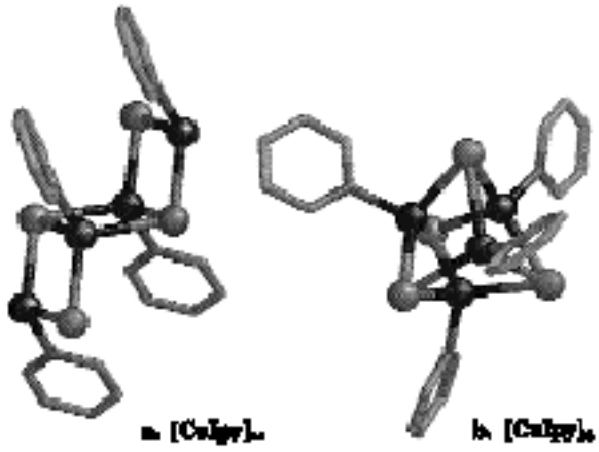

Fig. 1 Representations of the structures of the 'stair step' (a) and 'cubane' (b) forms of the compounds $[CuIpy]_x$ adapted from crystallographic data (refs. 5 and 6). Only a four copper fragment of the stair step chain of $[CuIpy]_\infty$ is shown.

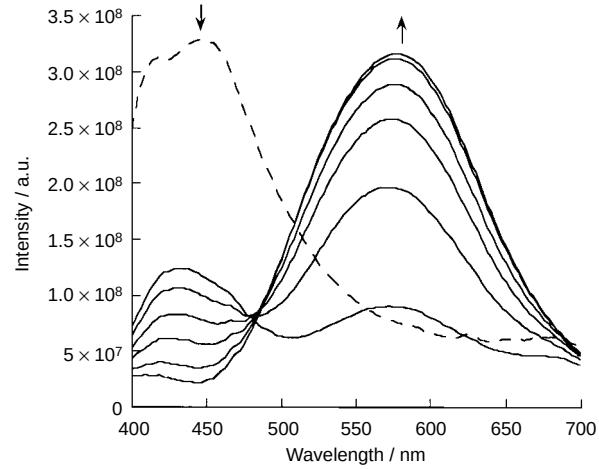

Fig. 2 Temporal emission spectra of solid $[CuI(4\text{-pic})]_\infty$ at ambient temperature before (- - -) and after (—) exposure to liquid toluene. Spectra were collected every 5 min (arrows indicate sequence of data collection).

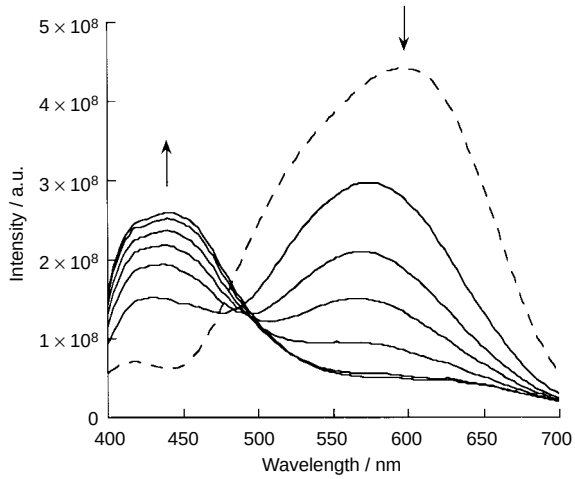

Fig. 3 Temporal emission spectra of solid $[CuI(4\text{-pic})]_4$ at ambient temperature before (- - -) and after (—) exposure to liquid pentane. Spectra were collected every 15 min (arrows indicate sequence of data collection).

transformation into **B** in a few minutes. We are attempting to characterize the non-emitting intermediate.

The toluene supernatant solution isolated from the above experiment shows a room temperature emission band at 684 nm, considerably different from the solid state emission behavior, as previously observed in the case of $[CuIpy]_4$.[7] Addition of pentane to this solution led to the isolation of trace amounts of **B**. However, exposure of the room temperature cubane solid to a small amount of liquid pentane caused it to revert to the blue emitting polymer over the course of 2 h (Fig. 3).

These surprising observations prompted us to examine the solid state behavior of the two $[CuI(4\text{-pic})]_x$ derivatives **A** and **B** in the presence of toluene and pentane vapors to test whether the same transformations could be effected by exposure to the vapors as well as to the liquids of these two solvents. This indeed turned out to be the case. When the blue emitting solid $[CuI(4\text{-pic})]_\infty$ was left in a sealed vial in contact with toluene vapors at the room temperature partial pressure, the transformation to the yellow emitting cubane solid was complete within two days. The reverse process, transformation back to **A,** was effected by exposing this sample to pentane vapors for 3 hours. Remarkably, while transformation **B** to **A** can be carried out in a few minutes by heating the sample to 343 K and appears to occur thermally over several days when simply left standing in air, the process is at least an order of magnitude faster at ambient temperature under pentane vapor. The analogous transformations between the cubane and polymeric forms do not occur when the 3-picoline analogs $[CuI(3\text{-pic})]_x$ are similarly treated with liquid or vapor toluene or pentane.

In conclusion, an unusual chromic photoluminescent behavior linked to a solid state structural change induced by exposure to the liquid or vapor phase of two VOCs has been demonstrated. This behavior is strongly ligand dependent, as revealed by our analogous studies with 3-picoline. X-Ray crystal structure determinations currently in progress[10] indicate that the cubane form of $[CuI(4\text{-pic})]_x$ displaying the yellow emission band at 578 nm has incorporated toluene into the crystal packing, and it is likely that this plays an important role in effecting the solid state isomerization from the blue emitting stair-step polymer. We have not detected analogous pentane incorporation into the structure of **B**, and are uncertain as to what role pentane plays in reformation of the more stable polymer. A recent study by Eisenberg and coworkers has described a similar 'luminescent switch for the detection of volatile organic compounds' using gold(I) dimers[12] following pioneering work by Mann and coworkers on absorption and emission spectra vapochromic Pt^{II} and Pd^{II} compounds.[13] The present work demonstrates the greater generality of such behavior, as well as the extension of this to much less expensive copper compounds, expense being a possible consideration in the design of practical sensors. An advantage of the present system is the very distinctive differences in the emission colors of the polymeric and cubane forms of $[CuI(4\text{-pic})]_4$, although the relatively slow response times would not be acceptable in the design of a practical sensor. Ongoing studies are concerned with defining the mechanisms of these structural transformations induced by exposure to VOCs as well as the photophysical mechanisms responsible for the differing luminescence responses.

This work was supported by the National Science Foundation (CHE 9400919 and CHE 9726889). Dr Cariati thanks Università di Milano for a postdoctoral fellowship and the Fulbright Commission for support of her postdoctoral stay at UC Santa Barbara.

Notes and References

† E-mail: ford@chem.ucsb.edu

1 V. W-W. Yam and K. K-W. Lo, *Comments Inorg. Chem.*, 1997, 62 and refs. therein.
2 P. C. Ford and A. Vogler, *Acc. Chem. Res.*, 1993, **26,** 220 and refs. therein.
3 P. C. Ford, *Coord. Chem. Rev.*, 1994, **132**, 129.
4 P. C. Healy, C. Pakawatchai and A. H. White, *J. Chem. Soc., Dalton Trans.*, 1983, 1917; J. A. Campbell, C. L. Raston and A. H. White, *Aust. J. Chem.*, 1977, **30**, 1937.
5 C. L. Raston and A. H. White, *J. Chem. Soc., Dalton Trans.*, 1976, 2153.
6 E. Eitel, D. Oelkrug, W. Hiller and J. Strahle, *Z. Naturforsch., B: Anorg. Chem., Org. Chem.*, 1980, **35**, 1247.
7 K. R. Kyle, C. K. Ryu, J. A. DiBenedetto and P. C. Ford, *J. Am. Chem. Soc.*, 1991, **113**, 2954.
8 M. Vitale, W. E. Palke and P. C. Ford, *J. Phys. Chem.*, 1992, **96**, 8329.
9 H. D. Hardt and A. Pierre, *Inorg. Chim. Acta*, 1977, **25**, L59 and refs. therein.
10 E. Cariati, J. Bourassa, X. Bu and P. C. Ford, to be published.
11 H. D. Hardt and A. Pierre, *Z. Anorg. Allg. Chem.*, 1972, **387**, 61.
12 M. A. Mansour, W. B. Connick, R. J. Lachicotte, H. J. Gysling and R. Eisenberg, *J. Am. Chem. Soc.*, 1998, **120**, 1329.
13 C. Exstrom, J. R. Sowa, Jr., C. A. Daws, D. Janzen and K. R. Mann, *Chem. Mater.*, 1995, **7**, 15.

Received in Bloomington, IN, USA, 14th April 1998; 8/02805B

Exo-ligands based on two *p*-aminopyridine interconnection by tuneable alkyl chains: design, synthesis and structural analysis of silver and palladium metallamacrocycles

Raoul Schneider,[a] Mir Wais Hosseini,*[a]† Jean-Marc Planeix,[a] André De Cian[b] and Jean Fischer[b]

[a] *Laboratoire de Chimie de Coordination Organique, Université Louis Pasteur, F-67000 Strasbourg, France, UMR CNRS 7513*
[b] *Laboratoire de Cristallochimie et Chimie Structurale, Université Louis Pasteur, F-67000 Strasbourg, France, UMR CNRS 7513*

Exo-ligands based on functionalisation of diazacyclic cores of variable size by two pyridines has been achieved; under self-assembly conditions, their ability to form metallamacrocycles in the presence of Pd^{II} or Ag^{II} was demonstrated by X-ray crystallography.

Since the pioneering investigations by Fujita *et al.*[1] and by Saalfranck *et al.*[2] on metallamacrocycles considerable efforts have been focused on the design and synthesis of macrocyclic and macrobicyclic structures composed of metal centres connected by organic fragments.[3] The majority of metallmacrocycles reported so far are based on bis-monodentate ligands such as 4,4′-bipyridine, pyrimidine, bipyrazine, 4,7-phenanthroline or bis-pyridines interconnected by rigid or flexible spacers.[4] The same type of ligands has been also used for the formation of coordination networks.[5] *p*-Dimethylaminopyridine (dmap) shows strong alkaline character. We thought that one could take advantage of its peculiar electronic distribution for the design of ligands capable of forming metallamacrocycles. In order to interconnect two or more metals into a cyclic framework, the ligand needs to be of the *exo* type, *i.e.* it should possess at least two coordination sites oriented in divergent fashion. We have previously reported *exo*-ligands based on 2,2′-bipyridine derivatives,[6] catechol units[7] or of mercaptocalixarene type.[8] We now report the design, synthesis and structural analysis of *exo*-bis-monodentate ligands based on two dmap derivatives and of their binuclear silver and palladium metallamacrocycles.

The design of *exo*-ligands **4**–**6** (Scheme 1) was based on the interconnection of two *p*-aminopyridine substructures at the 4 position by two tuneable alkyl bridges. Ligands **4**–**6** may also be regarded as diazacycloalkanes[9] **1**–**3** bearing two pyridines. We have previously used cyclic diamines for the design of cyclospermidines and cyclospermines[10] and as backbones connecting donor and acceptor groups.[11] The design of **4**–**6** is rather versatile since, by controlling the size and thus the conformation of the medium size cyclic core and by choosing metals with specific coordination demands, one may investigate structural aspects in the formation of metallamacrocycles under self-assembly conditions.

The synthesis of **4**–**6** was achieved by treating under reflux a mixture of 4-chloropyridine, PhLi and compounds **1**–**3** in a 1 : 2.2 : 2.5 ratio in diethylether.[12] The yields reported are based on 4-chloropyridine. In all cases studied, in addition to **4**–**6**, the mono-substituted compounds **7**–**9** were also isolated. Thus,

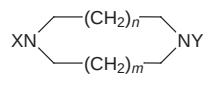

1 X = Y = H, *n* = *m* = 0
2 X = Y = H, *n* = 0, *m* = 1
3 X = Y = H, *n* = 1, *m* = 2
4 X = Y = Py, *n* = *m* = 0
5 X = Y = Py, *n* = 0, *m* = 1
6 X = Y = Py, *n* = 1, *m* = 2
7 X = H, Y = Py, *n* = *m* = 0
8 X = H, Y = Py, *n* = 0, *m* = 1
9 X = H, Y = Py, *n* = 1, *m* = 2

Scheme 1

treatment of **1**, **2** or **3**[13] with 4-chloropyridine gave compounds **4** (20%) and **7** (22%), **5** (39%) and **8** (28%) or **6** (13%) and **9** (38%) respectively.

The formation of metallamacrocycles using Pd^{II} was achieved by mixing at room temp. an EtOH solution of ligands **4**–**6** with an aqueous solution of $[Pd(NO_3)_2(en)]$ (en = ethylenediamine). Upon addition of EtOH and Et_2O complexes were collected after several days as colourless crystalline materials. In addition to solution NMR spectroscopy, crystals were analysed by FAB^+ spectrometry which revealed the formation of a trinuclear complex $\{[\mathbf{4}_3\{Pd(en)\}_3(NO_3)_6]\}$ for the ligand **4** and binuclear complexes $\{[L_2\{Pd(en)\}_2(NO_3)_4]$, L = **5** or **6**$\}$ for ligands **5** and **6**. For the $[\mathbf{6}_2\{Pd(en)\}_2(NO_3)_4]$ complex the structure could be determined by X-ray crystallography which indeed revealed the formation of a Pd^{II} binuclear metallamacrocycle.‡ Although in the crystal H_2O and EtOH molecules were present none of them nor NO_3^- anions were clathrated in the cavity of the macrocycle. In principle, owing to the non-symmetric nature of **6**, two different isomeric complexes, one with C_{2v} and the other with D_{2h} ideal symmetry may be envisaged (Fig. 1). The difference between these two isomers originates from the mutual orientation of the cyclic cores. However in the solid state, only the complex with C_{2v} symmetry was observed (Fig. 2). The crystal structure showed the following features: (*i*) two ligands **6** bridge two Pd centres by adopting a bent conformation; (*ii*) as expected, both nitrogen atoms of the diaza core show a marked sp^2 character with an average C–N–C angle of *ca.* 120.3° and N–C distance of 1.37 Å demonstrating the delocalization of the nitrogen lone pairs on the pyridine rings; (*iii*) the coordination geometry around Pd atoms is almost square planar with the N–Pd–N angle varying from 83.7 to 93.5°; (*iv*) the average N–Pd distance is *ca.* 2.03 Å; (*v*) with Pd···Pd distance is 11.35 Å.

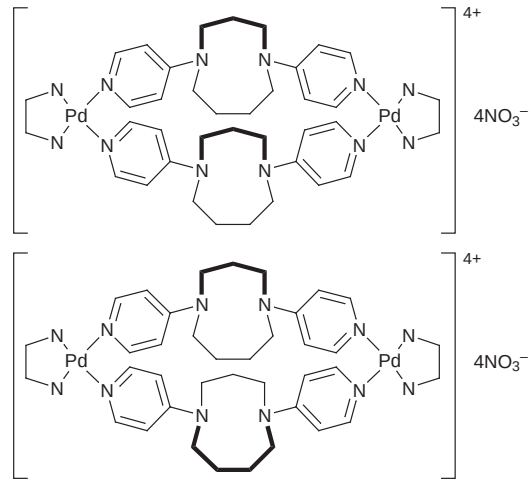

Fig. 1 Two possible isomeric structures D_{2h} (top) and C_{2v} (bottom) for the $[\mathbf{6}_2\{Pd(en)\}_2]$ metallamacrocycle

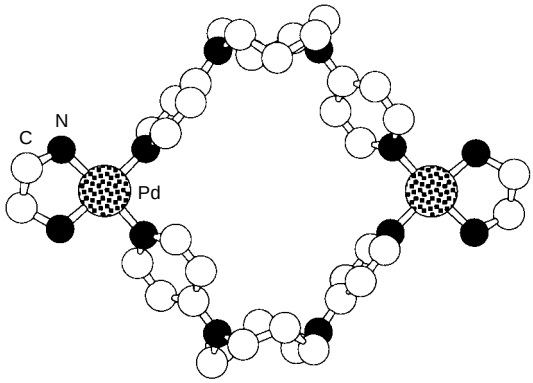

Fig. 2 Crystal structure of the [$\mathbf{6}_2${Pd(en)}$_2$ $(NO_3)_4$] metallamacrocycle (see text for bond angles and distances). Solvent molecules, anions and H atoms are not presented for sake of calrity.

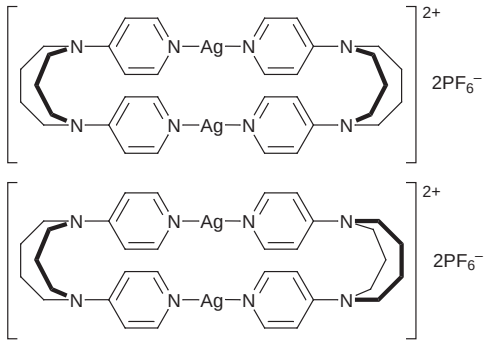

Fig. 3 Two possible isomeric structures D_{2h} (top) and C_{2v} (bottom) for the [$\mathbf{6}_2Ag_2$] metallamacrocycle

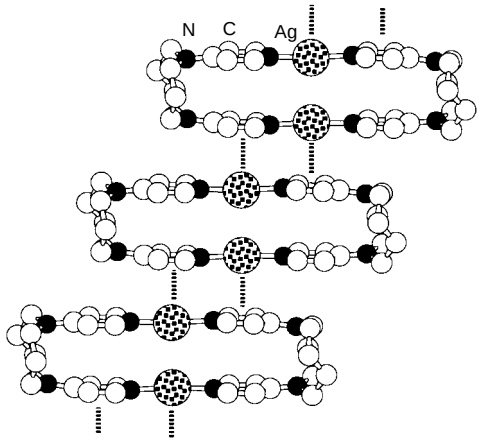

Fig. 4 A portion of the crystal structure of the [$\mathbf{6}_2Ag_2(PF_6)_2$] metallamacrocycle (see text for bond angles and distances) showing the formation of an infinite network formed by double Ag–aromatic interactions between consecutive units. Anions and H atoms are not presented for sake of clarity.

The formation of metallamacrocycles using Ag^I was investigated by diffusion at room temp. of a EtOH solution of ligand **6** with an aqueous solution of $AgPF_6$. After several days colourless crystals of the complex were filtered and further washed with Et_2O. The complex was characterised by NMR and by FAB spectrometry. Furthermore, in the solid state the structure of [$\mathbf{6}_2Ag_2(PF_6)_2$] complex was elucidated by X-ray crystallography.‡ Again, as in the above mentioned Pd case, two different isomeric complexes may be envisagted (Fig. 3). Once again the complex with C_{2v} symmetry was observed (Fig. 4). The crystal analysis showed the following features: (*i*) the binuclear metallamacrocycle is formed through the bridging of two Ag^I atoms by two pyridine units belonging to two ligands **6** which adopt a bent conformation; (*ii*) as in the previous case, both nitrogen atoms of the diaza core show a marked sp^2 character with an average C–N–C angle of *ca.* 121.1° and N–C distance of 1.36 Å; (*iii*) the coordination geometry around Ag atoms is almost linear with an average N–Ag–N angle of *ca.* 175.8°; (*iv*) the average N–Ag distance is *ca.* 2.10 Å; (*v*) the Ag···Ag distance is 3.36 Å; (*vi*) quite interestingly, in the crystal the metallamacrocycles form a one dimensional network through four strong silver–aromatic (pyridine) interactions per unit with an average Ag–centroid distance of 3.43 Å (Fig. 4).

In conclusion, it has been demonstrated that a class of exo ligands based on the interconnection of two *p*-aminopyridines forms by self-assembly metallamacrocycles in the presence of Pd^{II} or Ag^I metals. A systematic investigation on the role of the conformation of the cyclic core is under current investigation.

Notes and References

† E-mail: hosseini@chimie.u-strasbg.fr

‡ *Crystallographic data*: [$\mathbf{6}_2${Pd(en)}$_2(NO_3)_4$] (colorless, 173 K): $C_{19}H_{30}N_6Pd{\cdot}4NO_3{\cdot}2C_2H_5OH{\cdot}5H_2O$, M = 1328.02, monoclininc, space group $P2_1/c$, a = 13.005(2) b = 16.532(2), c = 13.622(1) Å, U = 2927(1) Å^3, β = 91.603(9)°, Z = 2, D_c = 1.34 g cm^{-3}, MACH3 Nonius, Mo-Kα, μ/mm^{-1} = 0.657, 4549 data with $I > 3\sigma(I)$, R = 0.057, R_w = 0.075.

[$\mathbf{6}_2Ag_2(PF_6)_2$] (colorless, 173 K): $C_{34}H_{44}N_8Ag_2{\cdot}2PF_6$, M = 1070.45, monoclinic, space group $P2_1/c$, a = 7.6250(2), b = 23.5140(9), c = 10.9360(4) Å, β = 93.105(7)°, U = 1957.9(2) Å^3, Z = 2, D_c = 1.82 g cm^{-3}, Nonius Kappa CCD, Mo-Kα, μ/mm^{-1} = 1.164, 2958 data with $I > 3\sigma(I)$, R = 0.053, R_w = 0.073. CCDC 182/885.

1 M. Fujita, J. Yakaki and K. Ogura, *J. Am. Chem. Soc.*, 1990, **112**, 5645; M. Fujita, *J. Synth. Org. Chem. Jpn.*, 1996, **54**, 953.
2 R. W. Saalfrank, A. Stark, K. Peters and H.-G. von Schnering, *Angew. Chem., Int. Ed. Engl.*, 1988, **27**, 851.
3 J. K. M. Sanders, *Comprehensive Supramolecular Chemistry*, ed. J. L. Atwood, J. E. D. Davies, D. D. MacNicol and F. Vögtle, vol. 9 (ed. J. P. Sauvage and M. W. Hosseini), Elsevier, Amsterdam, 1996, pp. 131–164; P. J. Stang and B. Olenyuk, *Acc. Chem. Res.*, 1997, **30**, 502; C. M. Drain and J.-M. Lehn, *J. Chem. Soc., Chem. Commun.*, 1994, 2313; T. Beissel, R. E. Powers and K. N. Raymond, *Angew. Chem., Int. Ed. Engl.*, 1996, **35**, 1084.
4 C. V. Krishnamohan Sharma, S. T. Griffin and R. D. Rogers, *Chem. Commun.*, 1998, 215; R.-D. Schnebeck, L. Randaccio, E. Zangrando and B. Lippert, *Angew. Chem., Int. Ed. Engl.*, 1998, **37**, 119; J. R. Hall, S. J. Loeb, G. K. H. Shimizu and G. P. A. Yap, *Angew. Chem., Int. Ed. Engl.*, 1998, **37**, 121.
5 R. Robson, in *Comprehensive Supramolecular Chemistry*, ed. D. D. Macnicol, F. Toda and R. Bishop, Pergamon, New York, 1996, vol. 6, p. 733; L. Carluci, G. Ciani, D. M. Proserpio and A. Sironi, *J. Am. Chem. Soc.*, 1995, **117**, 4562; T. L. Hennigar, D. C. MacQuarrie, P. Losier, R. D. Rogers and M. J. Zaworotko, *Angew. Chem., Int. Ed. Engl.*, 1997, **36**, 972; M. A. Withersby, A. J. Blake, N. R. Champness, P. Hubberstey, W.-S. Li and M. Schröder, *Angew. Chem., Int. Ed. Engl.*, 1997, **36**, 2327; D. Whang and K. Kim, *J. Am. Chem. Soc.*, 1997, **119**, 451; O. M. Yaghi, H. Li and T. L. Groy, *Inorg. Chem.*, 1997, **36**, 4292.
6 C. Kaes, M. W. Hosseini, R. Ruppert, A. De Cian and J. Fischer, *Tetrahedron Lett.*, 1994, **35**, 7233; *J. Chem. Soc., Chem. Commun.*, 1995, 1445; C. Kaes, M. W. Hosseini, A. De Cian and J. Fischer, *Tetrahedron Lett.*, 1997, **38**, 3901; 4389; *Chem. Commun.*, 1997, 229.
7 E. Graf, M. W. Hosseini and R. Ruppert, *Tetrahedron Lett.*, 1994, **35**, 7779; C. Drexler, M. W. Hosseini, A. De Cian and J. Fischer, *Tetrahedron Lett.*, 1997, **38**, 2993; C. M. Drexler, M. W. Hosseini, G. Stupka, J.-M. Planeix, A. De Cian and J. Fischer, *Chem. Commun.*, 1998, 689; G. Mislin, E. Graf and M. W. Hosseini, *Tetrahedron Lett.*, 1996, **37**, 4503.
8 X. Delaigue, J. McB. Harrowfield, M. W. Hosseini, A. De Cian, J. Fischer and N. Kyritsakas, *J. Chem. Soc., Chem. Commun.*, 1994, 1579; X. Delaigue, M. W. Hosseini, A. De Cian, N. Kyritsakas and J. Fischer, *J. Chem. Soc., Chem. Commun.*, 1995, 609.
9 R. W. Alder, *Acc. Chem. Res.*, 1983, **16**, 321.
10 G. Brand, M. W. Hosseini and R. Ruppert, *Tetrahedron Lett.*, 1994, **35**, 8609.
11 R. Schneider, M. W. Hosseini and J.-M. Planeix, *Tetrahedron Lett.*, 1996, **35**, 4721.
12 T. Kauffmann and F.-P. Boettcher, *Chem. Ber.*, 1962, **88**, 1528.
13 H. Yamamoto and K. Maruoka, *J. Am. Chem. Soc.*, 1981, **103**, 4186.

Received in Basel, Switzerland, 27th April 1998, 8/03166E

‘CMPO-substituted’ calix[4]arenes, extractants with selectivity among trivalent lanthanides and between trivalent actinides and lanthanides

Lætitia H. Delmau,‡ Nicole Simon,*[a]† Marie-José Schwing-Weill,*[b]† Françoise Arnaud-Neu,[b] Jean-François Dozol,[a] Serge Eymard,[a] Bernard Tournois,[a] Volker Böhmer,[c] Cordula Grüttner,[c] Christian Musigmann[c] and Abdi Tunayar[c]

[a] *CEA Cadarache, DESD/SEP/LPTE, 13108 St Paul lez Durance Cedex, France*
[b] *ECPM, 1 rue Blaise Pascal, 67008 Strasbourg Cedex, France*
[c] *Institut für Organische Chemie, Johannes Gutenberg Universität, Becher Weg 34, Mainz, D-55099, Germany*

Calix[4]arenes substituted by acetamidophosphine oxide groups at their wider (upper) rim not only exhibit excellent extraction efficiency towards trivalent cations but also show pronounced selectivity for the light lanthanides and actinides in their extraction from highly saline or acidic media.

Calixarenes[1] are readily available molecular platforms, on which various functional groups may be assembled in a well defined mutual arrangement. Numerous cation extractants derived from calixarenes have been developed in the past decade, in which the preorganization of ligating functions adds favorably to their specificity.[2] Crown ethers derived from calix[4]arenes fixed in the 1,3-alternate conformation may be cited as one of the most typical examples, showing the highest potassium over sodium (crown-5)[3] and caesium over sodium (crown-6)[4] selectivities ever reported.

Carbamoylphosphine oxides **1** (CMPOs) are known to extract trivalent cations from highly acidic and highly saline media,[5] and **1a** is industrially used in the TRUEX process.[6] The extracted complex requires three molecules of **1a** per cation,[7] thus attachment of CMPO-like functions to the calixarene scaffold in the cone conformation should achieve cooperativity. Indeed, calix[4]arenes such as **2a** bearing four diphenyl acetamidophosphine oxide functions on the wider rim[8] are powerful extractants for europium and tri- and tetravalent

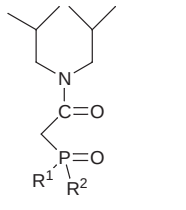

1a $R^1 = C_6H_5$, $R^2 = C_8H_{17}$
1b $R^1 = R^2 = C_6H_5$
1c $R^1 = R^2 = C_4H_9$

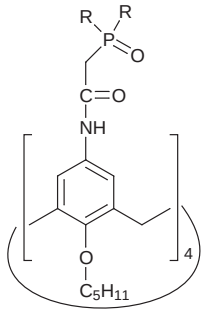

2a $R = C_6H_5$
2b $R = C_6H_{13}$

actinides with an efficiency highly superior to that of **1a**. Here we compare the two ligands **1a** and **2a**[8] with respect to their extraction efficiencies towards nine lanthanides (La, Pm, Sm, Eu, Gd, Tb, Ho, Er, Yb) and two actinides (Am, Cm).

Extractions were followed by radiotracers and were quantified by the distribution coefficient of the metallic cation M ($D_M = \Sigma[M]_{org,eq}/\Sigma[M]_{aq,eq}$). The concentrations of **1a** and **2a** were chosen to obtain comparable distribution coefficients. Preliminary experiments showed that the extraction kinetics are rapid; all reported distribution coefficients are at equilibrium.

The behavior of CMPO **1a** is in agreement with literature data,[5] while we observe for **2a** a marked decrease of the distribution coefficients along the lanthanide series, from 140 for lanthanum to 0.19 for ytterbium (Fig. 1). This corresponds to a separation factor (ratio of the distribution coefficients) of nearly three orders of magnitude. It is important to point out that distribution coefficients are independent of the equilibrium aqueous metal ion concentration. This eliminates any influence of cation concentrations on the selectivity.

In order to determine one of the possible origins of the selectivity, we modified the functional groups present on the phosphorus. The observed size selectivity nearly disappears for **2b**,[9] in which the phenyl groups of **2a** have been replaced by *n*-hexyl groups (Fig. 2). This observation is in agreement with the results obtained for the two CMPO type molecules **1b** and **1c**.[10] While the diarylphosphine oxide **1b** shows a small selectivity (separation factor $D_{La}/D_{Lu} \approx 10$), no selectivity is found for the dialkylphosphine oxide **1c**. We can conclude, therefore, that the attachment of four CMPO functions with diphenylphosphine oxide groups to the calixarene skeleton leads to a significant increase of their discriminating properties towards lanthanides and actinides.

The selectivity discussed so far is related to the extraction of trivalent cations from a highly saline but moderately acidic medium. A topic of current interest is actinide–lanthanide group mixtures separation at high acidity, which, at low acid

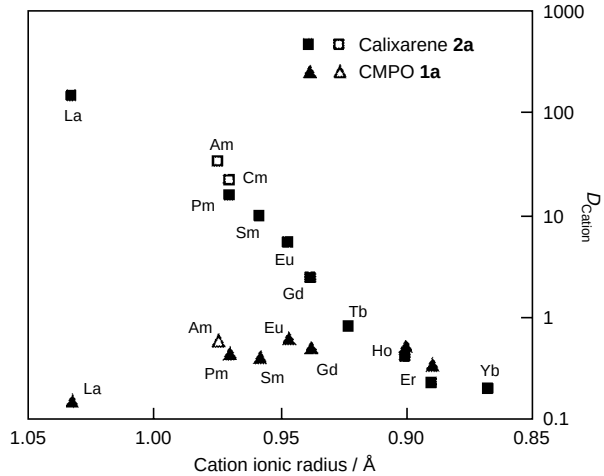

Fig. 1 Comparison of the extraction efficiencies of CMPO **1a** and calixarene **2a**. Organic phase: chloroform containing either $[\mathbf{1a}]_{init} = 0.2$ M or $[\mathbf{2a}]_{init} = 10^{-3}$ M. Aqueous phase: $[NaNO_3] = 4$ M, $[HNO_3] = 10^{-2}$ M, $[Ln^{3+}] = 10^{-6}$ M. Promethium and actinides were used at trace levels. Phase ratio 1:1. $T = 25$ °C. Filled symbols: lanthanides; open symbols: actinides.

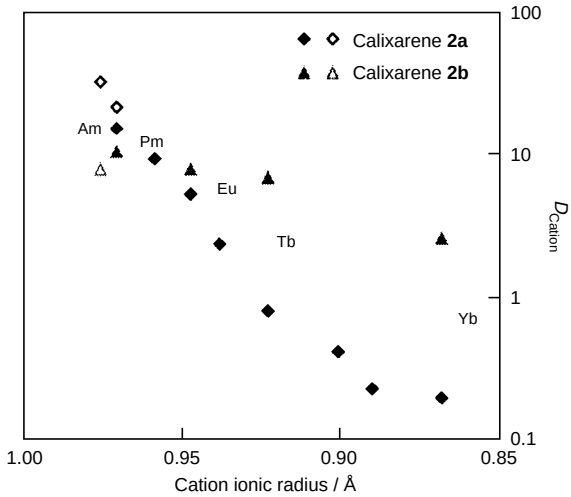

Fig. 2 Comparison of extraction efficiencies of calixarenes **2a** and **2b.** Organic phase: chloroform containing either $[\mathbf{2a}]_{init} = 10^{-3}$ M or $[\mathbf{2b}]_{init} = 10^{-3}$ M. Aqueous phase: $[NaNO_3] = 4$ M, $[HNO_3] = 10^{-2}$ M, $[Ln^{3+}]_{init} = 10^{-6}$ M. Promethium and actinides were used at trace levels. Phase ratio 1:1. $T = 25$ °C. Filled symbols: lanthanides; open symbols: actinides.

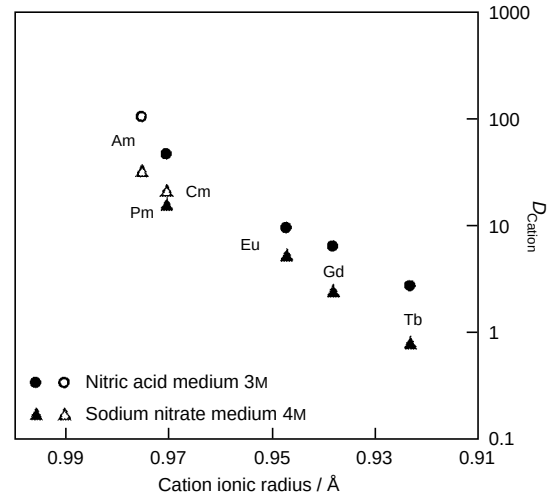

Fig. 3 Extraction of trivalent lanthanides and actinides by calixarene **2a** from two different media, $[NaNO_3] = 4$ M/$[HNO_3] = 0.01$ M or $[HNO_3] = 3$ M. Organic phase: chloroform containing $[\mathbf{2a}]_{init} = 10^{-3}$ M. Aqueous phase: $[Ln^{3+}]_{init} = 10^{-6}$ M. Promethium and actinides were used at trace levels. Phase ratio 1:1. $T = 25$ °C. Filled symbols: lanthanides; open symbols: actinides.

concentrations (pH > 1) can usually be achieved by extractants containing soft donors (sulfur or nitrogen).[11] Although a recent publication shows that calix[6]arene derivatives bearing acid and amide functions can be used for this group separation, the same pH limitations (pH > 2.5) apply.[12]

We have repeated some of our experiments with **2a** extracting the trivalent cations from 3 M nitric acid (Fig. 3). We observe essentially the same trend for both media (4 M sodium nitrate or 3 M nitric acid), which suggests the selectivity is not caused by a constituent of the aqueous phase. In particular, the potential interaction between nitric acid and the ligand has no effect on the selectivity. The separation factor D_{Am}/D_{Eu} for 3 M nitric acid (10.2) is slightly better than that for 4 M sodium nitrate (7.5), and is probably one of the best ever obtained at this acidity and this ionic strength.

In conclusion, calixarene **2a**, and more general calix[4]arenes bearing four CMPO moieties on their upper rim where the phosphorus atoms are substituted with phenyl groups, are not only excellent extractants for trivalent lanthanides and actinides, they also exhibit remarkable selectivity based mainly on the size of the cations. This selectivity can reach nearly three orders of magnitude and remains even under strongly acidic conditions. It does not yet allow complete actinide–lanthanide group mixtures separation but the separation factors could be useful for the selective extraction of actinides (or light lanthanides) from heavy lanthanides.

This work has been partly sponsored by the European Community (contract no. F12-W-CT-0062). L. H. D. would like to thank personally C. Beuchot for helpful discussions.

Notes and References

† E-mail: simon@desdcad.cea.fr, schwing@chimie.u-strasbg.fr
‡ Present address: ORNL, CASD/Chemical Separations Group, Oak Ridge, TN 37831-6119, USA.

1 V. Böhmer, *Angew. Chem*., 1995, **107**, 785.
2 M. A. McKervey, M. J. Schwing-Weill and F. Arnaud-Neu, in *Comprehensive Supramolecular Chemistry*, ed. G. W. Gokel, Pergamon, Oxford, 1996, vol. 1, p. 537.
3 A. Casnati, A. Pochini, R. Ungaro, C. Bocchi, F. Ugozzoli, R. J. M. Egberink, H. Struijk, R. Lugtenberg, F. de Jong and D. N. Reinhoudt, *Chem. Eur. J.*, 1996, **2**, 436.
4 A. Casnati, A. Pochini, R. Ungaro, F. Ugozzoli, F. Arnaud-Neu, S. Fanni, M. J. Schwing-Weill, R. J. M. Egberink, F. de Jong and D. N. Reinhoudt, *J. Am. Chem. Soc.*, 1995, **117**, 2767.
5 E. P. Horwitz and D. G. Kalina, *Solv. Extr. Ion Exch*., 1984, **2**, 179.
6 E. P. Horwitz, D. G. Kalina, G. F. Vandegrift and W. W. Schulz, *Solv. Extr. Ion Exch*., 1985, **3**, 75.
7 E. P. Horwitz, K. A. Martin, H. Diamond and L. Kaplan, *Solv. Extr. Ion Exch*., 1986, **4**, 449.
8 F. Arnaud-Neu, V. Böhmer, J. F. Dozol, C. Grüttner, R. A. Jakobi, D. Kraft, O. Mauprivez, H. Rouquette, M. J. Schwing-Weill, N. Simon and W. Vogt, *J. Chem. Soc., Perkin Trans. 2*, 1996, 1175.
9 The synthesis of **2b** was carried out in analogy to **2a** and will be published separately.
10 M. N. Litvina, M. K. Chmutova, B. F. Myasoedov and M. I. Kabachnik, *Radiochemistry*, 1996, **38**, 494.
11 C. Musikas, Rapport CEA-CONF-7706.
12 R. Ludwig, K. Kunogi, N. Dung and S. Tachimori, *Chem. Commun*., 1997, 1985.

Received in Cambridge, UK, 3rd April 1998; 8/02555J

Novel hyperbranched polymer based on urea linkages

Anil Kumar and E. W. Meijer*†

Laboratory of Macromolecular and Organic Chemistry, Eindhoven University of Technology, PO Box 513, 5600MB Eindhoven, The Netherlands

The thermal decomposition of 3,5-diaminobenzoyl azide, to generate *in situ* the corresponding 3,5-diaminophenyl isocyanate, was found to give hyperbranched polyureas, whose structure was established using IR and NMR spectroscopy.

In the last decade synthesis of three-dimensional dendritic polymers by constructing branches upon branches, either in a stepwise fashion to get dendrimers or in a one-step process to get hyperbranched polymers, has received much attention. These highly branched, untangled and globular structures have been explored because of their unusual properties.[1–5] Although dendrimers have been studied extensively for their size, shape and surface functional group related properties, their large scale synthesis has been limited to only a few structures because of the inherent difficulties in the stepwise growth process. However, whilst the one step approach for the synthesis of hyperbranched polymers has potential for large scale preparation, it lacks well defined and monodisperse dendrimers.

Hyperbranched polymers have been synthesized by self-condensation polymerization using an AB_x type monomer in which A and B are functional groups that react with each other and not with themselves. These hyperbranched polymers can be divided into two major categories depending upon the growth process. One is the classical polycondensation involving an AB_x type monomer where the growth of the polymer starts only at the already existing reaction sites A and B; in other words there is no generation of a new growing site during the polymerization. Some examples of this class are polyphenylenes,[6,7] polyesters,[8–12] polyethers,[13,14] polyurethanes,[15–17] polyamines,[18] polyamides[19] and polysiloxanes.[20] The second category is where new growing sites are generated during the polymerization reaction and examples of this class include polystyrene [21–23] and polyacrylates.[24] The consequence of these new reaction sites during polymerization is an increased number of subunits in the polymer. This leads to difficulties in estimating the degree of branching as quantification of each of the subunit structures is not possible.

Dendritic and hyperbranched structures based on amide linkage[25–31] have received considerable attention due to the fact that polyamides are commercially important and these linkages are the backbone of all the naturally occurring proteins and enzymes. Linear polyureas have been studied extensively in order to produce alternative fiber-forming polymers analogous to the polyamides.[32] There is now a much wider range of commercial polymers containing urea groups.[33] Surprisingly there are no reports on the synthesis of hyperbranched or dendritic polymers based on urea linkages. This could be due to the inherent difficulties in the synthesis and purification of monomers containing both amine and isocyanate groups, to obtain the urea linkage, as they are not compatible. Here we report synthesis and characterization of the first example of a hyperbranched polymer based on urea linkages. We developed a novel one-pot route to wholly aromatic hyperbranched polyureas, *via* the *in situ* generation of a diaminophenyl isocyanate monomer **5** by the thermal decomposition of the corresponding carbonyl azide **4** (Scheme 1).

3,5-Diaminobenzoyl azide was prepared starting from 3,5-diaminobenzoic acid as described in Scheme 1. The amine groups were protected with a Boc group[34] and the carboxylic acid was converted to carbonyl azide using the procedure described by Ghatge and Jadhav.[35] Removal of the Boc group with TFA in CH_2Cl_2 followed by treatment with saturated $NaHCO_3$ solution gave pure **4** in an overall yield of 59%. The FTIR spectrum of **4** exhibits a strong absorption at 2136 cm^{-1} indicating the presence of azide groups. Thermal decomposition of the aromatic carbonyl azides has been reported[15,16] to occur at *ca.* 107 °C and, hence, the polymerization was carried out at 110 °C by heating a solution of **4** in NMP. Rapid evolution of N_2 was observed during the initial stages of the reaction, after which the solution was maintained at 110 °C for 7 h. The polymers were precipitated into water, centrifuged, washed with acetone and vacuum dried at 90 °C to give around 90% yields of the wholly aromatic polyureas which are soluble in solvents like DMSO, NMP and DMF. The FTIR spectrum of the polymer indicates the absence of any residual azide (no absorption at 2136 cm^{-1}) or isocyanate (no absorption at 2200 cm^{-1}) and shows strong absorption at 1656 and 3352 cm^{-1} indicating the formation of

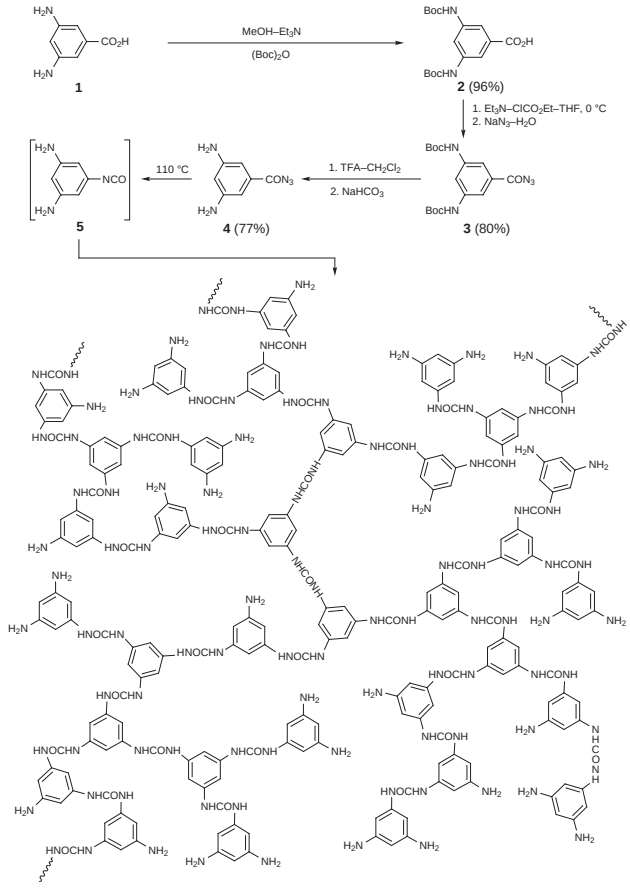

Scheme 1

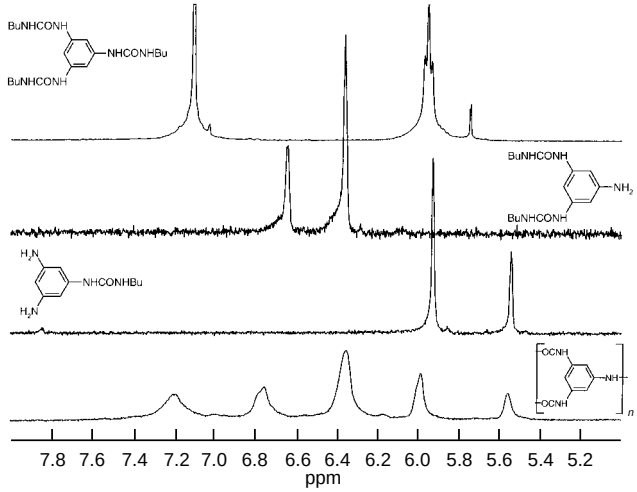

Fig. 1 300 MHz ^{1}H NMR spectra of the polymer and the model compounds in $(CD_3)_2SO$–D_2O

urea linkages. The ^{1}H NMR spectrum of the hyperbranched polyurea (Fig. 1) was analyzed based upon the various possible subunits (**A**–**C**) that may be present. Various peaks in the NMR spectrum of the polymer (Fig. 1) were assigned upon the NMR spectrum of three model compounds that resemble subunits **A**–**C**. The degree of branching calculated based on the ^{1}H NMR

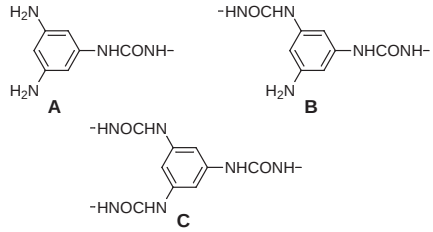

spectrum was found to be 0.55. This suggests that the growth process is statistical in nature in agreement with other systems.[36] The molecular mass of the samples was determined by GPC using NMP as solvent and polystyrene as standard. M_w was found to be 19 500 with a polydispersity of 1.56.

The wholly aromatic linear polyureas are generally difficult to process because of their limited solubility and high melt temperatures.[32,37] One approach to increase solubility in organic solvents is the introduction of *N*-alkyl or *N*-aryl substituents along the polymer backbone. Here we have shown that the wholly aromatic hyperbranched polyureas are completely soluble. A closer look at the Boc-protected carbonyl azide **3** reveals that its a novel AB_2 type building block where both A and B groups are protected and can be generated when needed. These types of structures are ideal candidates for the stepwise synthesis of the dendrimers. Currently, work is in progress to generate the corresponding perfect polyurea dendrimers.

This work was supported by the Netherlands Foundation for Chemical Research (SON).

Notes and References

† E-mail: tgtobm@chem.tue.nl

1 J. M. J. Frechet, *Science*, 1994, **263**, 1710.
2 K. L. Wooley, J. M. J. Frëchet and C. J. Hawker, *Polymer*, 1994, **35**, 4489.
3 C. J. Hawker, P. Farrington, M. Mackay, J. M. J. Frëchet and K. L. Wooley, *J. Am. Chem. Soc.*, 1995, **117**, 6123.
4 J. F. G. A. Jansen, E. M. de Brabander van den Berg and E. W. Meijer, *Science*, **266**, 1226.
5 J. F. G. A. Jansen, E. W. Meijer and E. M. de Brabander van den Berg, *J. Am. Chem. Soc.*, 1995, **117**, 4417.
6 Y. H. Kim and O. W. Webster, *J. Am. Chem. Soc.*, 1990, **112**, 4592.
7 Y. H. Kim and O. W. Webster, *Macromolecules*, 1992, **25**, 5561.
8 C. J. Hawker, R. Lee and J. M. J. Frëchet, *J. Am. Chem. Soc.*, 1991, **113**, 4583.
9 S. R. Turner, B. I. Voit and T. M. Mourey, *Macromolecules*, 1993, **26**, 4617.
10 W. J. Feast and N. M. J. Stainton, *J. Mater. Chem.*, 1995, **5**, 405.
11 A. Kumar and S. Ramakrishnan, *Macromolecules*, 1996, **29**, 2524.
12 E. Malmstorm, M. Johansson and A. Hult, *Macromolecules*, 1996, **29**, 1222.
13 V. Percec, P. Chu, G. Unger and J. Zhou, *J. Am. Chem. Soc.*, 1995, **117**, 1441.
14 T. M. Miller, T. X. Neenan, E. W. Kwock and S. M. Stein, *J. Am. Chem. Soc.*, 1993, **115**, 356.
15 A. Kumar and S. Ramakrishnan, *J. Chem. Soc., Chem. Commun.*, 1993, 1453.
16 A. Kumar and S. Ramakrishnan, *J. Polym. Sci., Polym. Chem. Ed.*, 1996, **34**, 839.
17 R. Spindler and J. M. J. Frechet, *Macromolecules*, 1993, **26**, 4809.
18 M. Suzuki, A. Li and T. Saegusa, *Macromolecules*, 1992, **25**, 7071.
19 Y. H. Kim, *J. Am. Chem. Soc.*, 1992, **114**, 4947.
20 L. J. Mathias and T. W. Carothers, *J. Am. Chem. Soc.*, 1991, **1134**, 4043.
21 J. M. J. Frechet, M. Henmi, I. Gitsov, S. Aoshima, M. R. Leduc and R. B. Grubbs, *Science*, 1995, **269**, 1080.
22 S. G. Gaynor, S. Edelman and K. Matyjaszewski, *Macromolecules*, 1996, **29**, 1079.
23 C. J. Hawker, J. M. J. Frëchet, R. B. Grubbs and J. Dao, *J. Am. Chem. Soc.*, 1995, **117**, 10763.
24 K. Matyjaszewski, S. G. Gaynor, A. Kulfan and M. Podwika, *Macromolecules*, 1997, **30**, 5192.
25 G. R. Newkome, X. Lin and C. D. Weis, *Tetrahedron: Asymmetry*, 1991, **2**, 957.
26 K. E. Uhrich and J. M. J. Frechet, *J. Chem. Soc., Perkin Trans. 1*, 1992, 1623.
27 R. G. Dekewalter, J. F. Kolc and W. J. Lukasavage, *US Pat.* 4410688/1983.
28 C. Rao and J. P. Tam, *J. Am. Chem. Soc.*, 1994, **116**, 6975.
29 J. Shao and J. P. Tam, *J. Am. Chem. Soc.*, 1995, **117**, 3893.
30 P. J. Dandliker, F. Diederich, M. Gross, C. B. Knobler, A. Louati and E. M. Sanford, *Angew. Chem., Int. Ed. Engl.*, 1994, **33**, 1739.
31 P. J. Dandliker, F. Diederich, J.-P. Gisselbrecht, A. Louati and M. Gross, *Angew. Chem., Int. Ed. Engl.*, 1995, **34**, 2725.
32 M. Katz, *US Pat.* 2888438/1959; *Chem. Abstr.*, 1959, **53**, 17582b.
33 A. J. Ryan and J. L. Standord, in *Comprehensive Polymer Science*, ed. G. C. Eastmond, A. Ledwith, S. Russo and P. Sigwalt, Pergamon, Oxford, 1989, vol. 5, p. 427.
34 E. Ponnusamy, V. Fotadar, A. Spisni and D. Fiat, *Synthesis*, 1986, 48.
35 N. D. Ghatge and J. Y.Jadhav, *J. Polym. Sci., Polym. Chem. Ed.*, 1983, **21**, 1941.
36 For a critical review see: D. Hölter, A. Burgath and H. Frey, *Acta Polym.*, 1997, **48**, 30.
37 Y. Oishi, M.-A. Kakimoto and Y. Imai, *J. Polym. Sci., Polym. Chem. Ed.*, 1987, **25**, 2185.

Received in Liverpool, UK, 13th May 1998; 8/03676D

Irreversible conductivity change of $Li_{1-x}CoO_2$ on electrochemical lithium insertion/extraction, desirable for battery applications

Matsuhiko Nishizawa, Satoru Yamamura, Takashi Itoh and Isamu Uchida*†

Department of Applied Chemistry, Graduate School of Engineering, Tohoku University, Aramaki-aoba, Aoba-ku, Sendai, 980-8579, Japan

Electrical conductivity of a sputter-deposited $LiCoO_2$ thin film was studied *in situ* during electrochemical lithium extraction/insertion, revealing that the metallic behavior of $Li_{1-x}CoO_2$ induced by the initial lithium extraction did not revert to its original insulating state in the following successive reduction/oxidation cycles.

$LiCoO_2$ is one of the most promising cathode active materials for lithium secondary batteries, and the battery system based on the $LiCoO_2$/carbon couple has been used commercially in many types of electronic equipment.[1–8] Since the electrical conductivity of active materials is an important characteristic for the design of high performance batteries, there have been a number of reports measuring the conductivity upon taking the electrode out of the electrochemical cell; *i.e. ex situ* characterization.[9–11] In contrast, work in our laboratory has shown that the interdigitated microarray (IDA) electrode is a powerful tool for studying the dynamic changes in the DC conductivity of electroactive films *in situ*.[12–17] We recently reported that the conductivity of $Li_{1-x}CoO_2$ increased by several orders of magnitude when a very small amount of lithium was extracted ($x < 0.1$),[16] as was predicted theoretically.[1,9] Such a drastic conductivity change requires that care must be taken when using $LiCoO_2$ as a battery active material. Since our previous work was on a composite film consisting of $LiCoO_2$ powders mixed with poly(vinylidene fluoride) and acetylene black, we could not treat the measured conductivity as that of $LiCoO_2$ itself.[16] Therefore, in this study we prepared a fine $LiCoO_2$ film by sputtering onto IDA electrodes to obtain more precise and reproducible results. It was found that the metallic behavior of $Li_{1-x}CoO_2$ induced by the initial lithium extraction (charge) did not revert to its original insulating state in the following reduction/oxidation cycles, indicating that this electrode material maintains its high conductivity during the successive use of secondary batteries.

The IDA electrode was fabricated by photolithography with a sputter-deposited Pt film on a thermally oxidized silicon wafer,[12–16] to have two sets of comb-type Pt arrays; each array has 50 band-electrode elements of 10 μm wide, 2.4 mm long and 0.1 μm thick, separated by 10 μm from its adjacent elements. A $LiCoO_2$ film of 0.2 μm thickness was deposited onto the IDA electrode by RF-sputtering and annealed in air at 700 °C for 15 min. Each peak in the X-ray diffraction spectrum of the annealed film was assigned to $LiCoO_2$. During the sputtering of the $LiCoO_2$ films, the IDA substrate was masked to limit the exposed area to a 0.2 cm × 0.3 cm rectangle. Each electrochemical measurement was conducted in a glove box filled with dried Ar, by using propylene carbonate (PC) containing 1 M $LiClO_4$ as the electrolyte solution. Lithium foils were used as the reference and counter electrodes. The *in situ* conductivity measurements were carried out, as previously,[15,16] using a bipotentiostat to maintain a 5 mV potential difference between the two working electrodes. The specific conductivity of the film was calculated from the ohmic current flowing through the film under the 5 mV bias voltage.[14,15] Note, however, that our measurement is a two-point probe method and that the film is thicker than the Pt film electrodes, therefore it is still dangerous to discuss the obtained conductivity as an absolute value. Rather, this method is suited to the study of dynamic, relative changes in the conductivity taking place with redox reactions.[12–14]

Fig. 1 shows cyclic voltammograms (CVs, solid lines) and *in situ* potential–conductivity profiles (dashed lines), which were measured simultaneously. The results for the first and the sixth cycles are presented. During the initial extraction of lithium, the conductivity of the film increased by more than four orders of magnitude and saturated around the main CV peak at 3.9 V, as observed for the $Li_{1-x}CoO_2$ composite film.[16] The saturated conductivity was not varied even upon expansion of the potential range up to 4.2 V ($x \approx 0.5$ in $Li_{1-x}CoO_2$). The drastic conductivity change which appeared before the CV peak is known to be the metal–insulator transition (MIT) resulting from the possible direct overlap of cobalt t_{2g} orbitals across a shared octahedral edge.[1,9] It was found here that the increased conductivity did not revert to the initial low value in the following reduction process, and that the conductivity value remained within the same order of magnitude during the successive charging/discharging cycles. This conductivity profile hysteresis was not removed even upon reduction of the potential scan rate to 10 μV s^{-1}. Fig. 2 shows the conductivity measured under open-circuit conditions to examine the above potentiodynamic results. A known amount of charge was induced using a galvanostat (typically, 150 μC with 0.1 μA), and then the rest potential and conductivity of the $Li_{1-x}CoO_2$ film were measured after more than 2 h. The correlation between the rest potential and the conductivity, shown in Fig. 2(*a*), was essentially the same as the result obtained by potentiodynamic measurements; the initial insulating state was not reproduced. Fig. 2(*b*) represents the conductivity changes as a function of *x*, calculated using the apparent volume of the film and the density of a single crystal of $LiCoO_2$. Although the

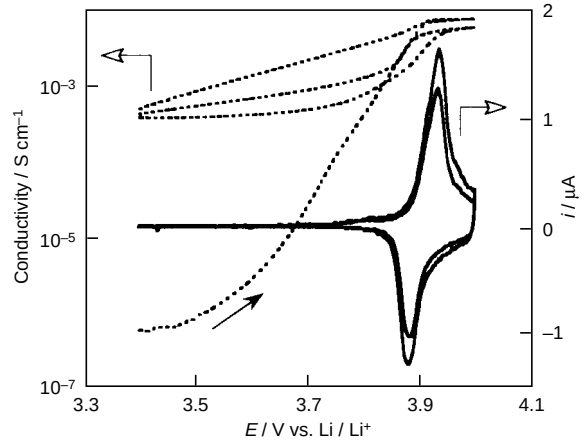

Fig. 1 Cyclic voltammograms (solid lines) and potential–conductivity profiles (dashed lines) of a $LiCoO_2$ film (0.2 μm thickness) sputter-deposited onto a Pt IDA electrode, taken in 1 M $LiClO_4$/PC at a scan rate of 0.1 mV s^{-1}. The bias voltage set between arrays was 5 mV. The first and the sixth cycles are presented.

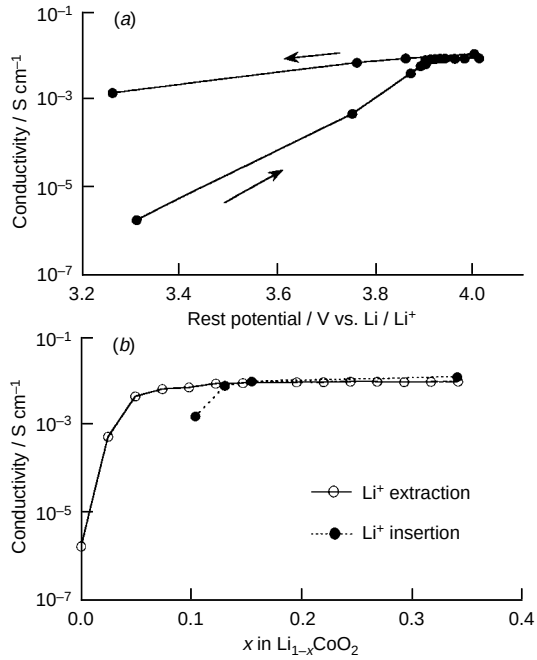

Fig. 2 The variations of the conductivity of a $LiCoO_2$ film during the first extraction/insertion of lithium as functions of (*a*) the rest potential and (*b*) x in $Li_{1-x}CoO_2$, taken in 1 M $LiClO_4$/PC with a bias voltage of 5 mV

calculated x values are not strictly accurate because of the polycrystallinity of the film and some side reactions, it was roughly confirmed that the MIT was induced by extraction of a very small amount of lithium (less than 10%) and the conductivity of the film could not revert to the initial insulating state due to the difficulty in reinserting this small amount of lithium. There are many reports showing similar irreversible capacities for the first charge/discharge cycle.[2,6–8] Crystallographic irreversibility may be the reason for this hysteresis because of the fact that a structural transformation occurs around $x = 0.1$ in $Li_{1-x}CoO_2$; within the composition range $0 < x < 0.1$, a single hexagonal phase exists, whereas within the range $0.1 < x < 0.22$, two hexagonal phases coexist.[1,6,7] Furthermore, electrochemical processes accompanied by growth of insulating phases are kinetically unfavorable in general, as seen for conducting polymers such as polyaniline.[18] Anyway, the insulating nature of $LiCoO_2$, which may be serious for battery applications, was found not to be regained within the time scale of battery applications.

The present work was supported by Grant-in-Aids for Scientific Research on Priority Area (No. 10148205 and No. 10131211 for 'Electrochemistry of Ordered Interfaces') and for Encouragement of Young Scientists (No. 09750906) from the Ministry of Education, Science, Sports and Culture, Japan, and partly by The Osaka Science & Technology Center.

Notes and References

† E-mail: uchida@est.che.tohoku.ac.jp

1 P. G. Bruce, *Chem Commun*., 1997, 1818.
2 B. Scrosati, *Electrochemistry of Novel Materials*, ed. J. Lipkowski and P. N. Ross, VCH Publishers, New York, 1994, p. 111.
3 K. Ozawa, *Solid State Ionics*, 1994, **69**, 212.
4 K. Mizushima, P. C. Jones, P. J. Wiseman and J. B. Goodenough, *Mater. Res. Bull*., 1980, **15**, 783.
5 M. G. S. R. Thomas, P. G. Bruce and J. B. Goodenough, *J. Electrochem. Soc*., 1985, **132**, 1521.
6 J. N. Reimers and J. R. Dahn, *J. Electrochem. Soc.*, 1992, **139**, 2091.
7 G. G. Amatucci, J. M. Tarascon and L. C. Klein, *J. Electrochem. Soc*., 1996, **143**, 1114.
8 T. Ohzuku and A. Ueda, *J. Electrochem. Soc*., 1994, **141**, 2972.
9 J. Molenda, A. Stoklosa and T. Bak, *Solid State Ionics*, 1989, **36**, 53.
10 N. K. Appandairjan, B. Viswanathan and J. Gopalakrishnan, *J. Solid State Chem*., 1981, **40**, 117.
11 G. Wei, T. E. Haas and R. B. Goldner, *Solid State Ionics*, 1992, **58**, 115.
12 M. Nishizawa, M. Shibuya, T. Sawaguchi, T. Matsue and I. Uchida, *J. Phys. Chem*., 1991, **95**, 9042.
13 M. Nishizawa, T. Matsue and I. Uchida, *Anal. Chem*., 1992, **64**, 2642.
14 M. Nishizawa, K. Tomura, T. Matsue and I. Uchida, *J. Electroanal. Chem*., 1994, **379**, 233.
15 M. Shibuya, S. Yamamura, T. Matsue and I. Uchida, *Chem. Lett*., 1995, 749.
16 M. Shibuya, T. Nishina, T. Matsue and I. Uchida, *J. Electrochem. Soc*., 1996, **143**, 3157.
17 M. J. Natan and M. S. Wrighton, *Prog. Inorg. Chem.*, 1987, **37**, 391.
18 K. Aoki, T. Edo and J. Cao, *Electrochim. Acta*, 1997, **43**, 285.

Received in Cambridge, UK, 21st April 1998; 8/02962H

Strong coordination of cycloheptynes by gold(I) chloride: synthesis and structure of two complexes of the type [(alkyne)AuCl]

Petra Schulte and Ulrich Behrens*†

Institut für Anorganische und Angewandte Chemie der Universität Hamburg, Martin-Luther-King-Platz 6, D-20146 Hamburg, Germany

Gold(I) chloride (stabilized by tetrahydrothiophene) reacts with the cycloheptynes 3,3,6,6-tetramethyl-1-thiacyclohept-4-yne-1,1-dioxide (SO_2-alkyne) and 3,3,6,6-tetramethyl-1-thiacyclohept-4-yne (S-alkyne) to afford the complexes [(η^2-alkyne)AuCl]$_n$ [n = 2 (SO_2-alkyne), n = ∞ (S-alkyne)]; the X-ray structures of both compounds show trigonal-planar gold(I) centres and very short Au–C(alkyne) bonds.

Although gold(I) complexes (*e.g.* R_3PAuNO_3) are excellent catalysts for the addition reaction of nucleophiles to alkynes,[1] little is known about the interaction of gold(I) with the C≡C triple bond. Some efforts to prepare simple gold(I) alkyne complexes were made in 1972 by Hüttel and Wittig, but most of the obtained gold compounds were thermally unstable and all were poorly characterized.[2] In 1996–97 Lang *et al*. synthesized five stable organogold(I) 3-titanapenta-1,4-diyne complexes [$Cp_2Ti(C{\equiv}CR)_2AuR$] with a trigonal-planar coordination of the gold(I) centre. These complexes were properly characterized, three of them by X-ray structure analysis.[3] The compounds can be considered as alkyne complexes although in reality heterometallic acetylide coordination compounds are present. Furthermore, in 1995 Mingos *et al*. reported on the compound [Au(C≡CBu^t)] within the structure of which η^2(C≡C)-coordinated acetylide moieties also exist.[4]

In this study, we report on the first examples of structurally well characterized [(η^2-alkyne)AuCl]$_n$ complexes (n = 2, ∞) with the gold(I) ion in a trigonal-planar environment. Complexes **1** and **2** were prepared by the reaction of [AuCl(tht)] (tht = tetrahydrothiophene) with equal amounts of the cycloheptynes 3,3,6,6-tetramethyl-1-thiacyclohept-4-yne-1,1-dioxide (SO_2-alkyne) and 3,3,6,6-tetramethyl-1-thiacyclohept-4-yne (S-alkyne), respectively (yield 90–97%).‡ Both complexes **1** and **2** form colourless crystalline powders which are thermally stable up to 150 °C. The solid compounds can be handled in air for short periods. In solution they decompose slowly when exposed to air or light. Compound **1** is soluble in tetrahydrofuran and dichloromethane, while complex **2**, due to its polymeric character in the solid state, only dissolves in strongly coordinating solvents such as mixtures of dimethyl sulfide–dichloromethane or dimethyl sulfide–tetrahydrofuran. In acetonitrile a molecular mass of 447 was found osmometrically for **1** which shows that the chloro bridges in solid **1** have been cleaved by the coordinating solvent (calc. M = 432.7 for the monomer). In chloroform a somewhat higher value (M = 580) was observed (monomer–dimer mixture in solution).

X-Ray diffraction studies were carried out on both **1** and **2** (Fig. 1 and 2).§ Compound **1** forms dimeric molecules with the gold(I) ions bridged by two chloro ligands (Fig. 1), whereas complex **2** contains a polymeric chain built up by AuCl units which are connected by S-alkyne ligands (coordination *via* the C≡C bond and the S atom; Fig. 2). The gold(I) centres exist in a trigonal-planar environment. The alkyne carbon atoms as well as the η^1-bonded Cl and S atoms are arranged in-plane, which is a typical feature for copper(I) and silver(I) η^2-alkyne complexes.[5] A very strong alkyne–gold bond is found, with the Au–C bond distances ranging from 2.050(7) to 2.100(8) Å.[6] This is close to the range for a normal Au–C-σ bond [*e.g.* Au–R-σ bond

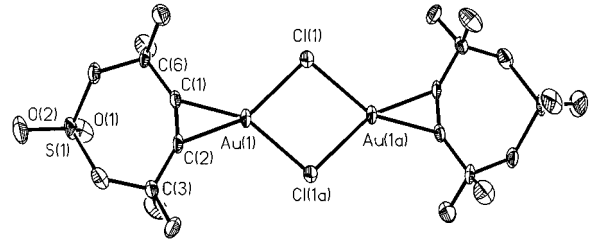

Fig. 1 View of the molecular structure of [AuCl(SO_2-alkyne)]$_2$ **1** with atomic numbering scheme (60% thermal ellipsoids). Selected bond lengths (Å) and angles (°): Au(1)···Au(1a) 3.666(1), Au(1)–Cl(1) 2.456(2), Au(1)–Cl(1a) 2.473(3), Au(1)–C(1) 2.075(9), Au(1)–C(2) 2.055(9), C(1)–C(2) 1.259(12); Cl(1)–Au(1)–Cl(1a) 83.9(1), Cl(1)–Au(1)–C(1) 121.4(2) Cl(1a)–Au(1)–C(2) 119.2(3), C(1)–Au(1)–C(2) 35.5(3), Au(1)–Cl(1)–Au(1a) 96.1(1), C(2)–C(1)–C(6) 147.3(8), C(1)–C(2)–C(3) 146.4(9).

lengths of 2.00(1), 2.018(6) and 2.079(7) Å were observed for three trigonally coordinated Au^I complexes $Cp_2Ti(C{\equiv}CR)_2AuR$].[3] The C≡C bonds are lengthened from 1.194 Å (C≡C bond distance for the free SO_2-alkyne)[7] and 1.209 Å (C≡C bond distance for the free S-alkyne)[7] to 1.259(11) Å (**1**) and 1.244(11) Å (**2**), which also proves the existence of a strong Au–η^2(C≡C) interaction. For a gold(I) complex with trigonal-planar coordination, an extremely short Au–Cl bond length of 2.409(2) Å is observed in **2**. For instance, in the complex $(Ph_3P)_2AuCl$, an Au–Cl distance above 2.50 Å is observed.[8] A value of about 2.40 Å, as in **2**, is normally found for Au–Cl bonds in square-planar neutral organyl Au^{II} complexes.[9] We therefore think that strong back-bonding from Au^I to the cycloalkyne ligand occurs in **2** (and also in **1**), which is equivalent to partial oxidation of the Au^I ion to Au^{III}. Also complex **1** is the first example of a gold(I) complex where two chloro ligands bridge two Au^I ions.[10] In gold(III) chemistry such bridging chloro ligands are only known for the structure of gold(III) chloride.[11] No aurophilic attractions (weak inter- or intramolecular Au^I···Au^I interactions resulting in Au–Au distances shorter than 3.40 Å) between the Au^I ions are found in **1** or **2**.[12] The intramolecular

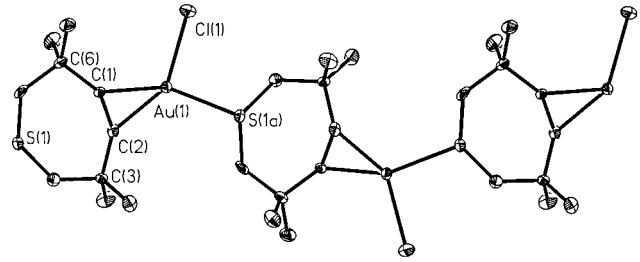

Fig. 2 Part of the polymeric chain of solid [AuCl(S-alkyne)] **2** with atomic numbering scheme (60% thermal ellipsoids). Selected bond lengths (Å) and angles (°): Au(1)–Cl(1) 2.409(2), Au(1)–S(1a) 2.415(2), Au(1)–C(1) 2.050(7), Au(1)–C(2) 2.100(8), C(1)–C(2) 1.244(11); Cl(1)–Au(1)–S(1a) 96.1(1), Cl(1)–Au(1)–C(1) 110.5(2), S(1a)–Au(1)–C(2) 118.7(2), C(1)–Au(1)–C(2) 34.9(3), C(2)–C(1)–C(6) 146.3(7), C(1)–C(2)–C(3) 146.6(7).

Au···Au distance in **1** is 3.666(1) Å; the Au–Cl–Au angle is 96.1(1)°.

The strong η^2-coordination of the alkyne triple bond is also confirmed by IR spectroscopy. The C≡C stretching vibration is shifted from 2177 cm^{-1} to 1949, 1928 cm^{-1} (**1**) and from 2188, 2161 cm^{-1} to 1930, 1910 cm^{-1} (**2**). These shifts of about 250 cm^{-1} are much larger than those found in cycloheptyne copper(I) chloride complexes (180 cm^{-1}).[13]

This study shows that angle-strained alkynes are able to interact strongly with the gold(I) ion, thus forming thermally stable complexes. An investigation of the coordination behaviour of other alkynes with gold(I) is in progress.

This work was supported by the Deutsche Forschungsgemeinschaft and the Fonds der Chemischen Industrie.

Notes and References

† behrens@xray.chemie.uni-hamburg.de

‡ *Experimental data* for **1**: [AuCl(tht)][14] (1.00 g, 3.1 mmol) was suspended at 0 °C in tetrahydrofuran (30 ml). 3,3,6,6-Tetramethyl-1-thiacycloheptyne-1,1-dioxide[15] (0.75 g, 3.7 mmol) was added and the solution stirred at 0 °C for 1 h. The clear solution was evaporated to dryness to remove the released tetrahydrothiophene. Cyclopentane (25 ml, 0 °C) was added to extract excess alkyne ligand. Filtration of the precipitate (washed twice with 3 ml cyclopentane) gave a yield of 1.2 g (2.8 mmol, 90%) of complex **1** in the form of a colourless crystalline powder (mp 176 °C, decomp.). The compound is insoluble in cyclopentane and benzene, but soluble in acetonitrile, dichloromethane, chloroform and tetrahydrofuran. IR (KBr) ν/cm^{-1} 1949, 1928; ^{1}H NMR (200 MHz, $CDCl_3$) δ 1.39 (s, 12H, CH_3), 3.32 (s, 4H, CH_2); ^{13}C NMR (50.3 MHz, $CDCl_3$) δ 27.89 (CH_3), 30.35 (CCH_3), 66.76 (CH_2), 97.15 (C≡C); elemental analysis: found C 28.07, H 3.97%; calc. C 27.76, H 3.73%. For **2**: [AuCl(tht)][14] (1.00 g, 3.1 mmol) was suspended at 0 °C in tetrahydrofuran (25 ml). 3,3,6,6-tetramethyl-1-thiacycloheptyne[16] (0.9 g, 5.3 mmol) was added and the slurry stirred at 20 °C (3 days, exclusion of light). The mixture was evaporated to dryness to remove the released tetrahydrothiophene. Tetrahydofuran (20 ml) was added to extract excess alkyne ligand. Filtration of the precipitate (washed twice with 3 ml tetrahydrofuran) gave a yield of 1.2 g (3.0 mmol, 97%) of complex **2** in the form of a colourless crystalline powder (mp 245 °C, decomp.). The compound is insoluble in acetonitrile, benzene, dichloromethane, chloroform and tetrahydrofuran, but soluble in tetrahydrothiophene, dimethyl sulfide, and in mixtures of dimethyl sulfide with dichloromethane and tetrahydrofuran. IR (KBr) ν/cm^{-1} 1930, 1910; elemental analysis: found C 30.07, H 3.99%; calc. C 29.97, H 4.03%.

§ Single crystals of **1** were grown from a solution in tetrahydrofuran to which cyclopentane was slowly added *via* the gas phase. Single-crystals of **2** were grown from a solution in dichloromethane–dimethyl sulfide (15 : 1) to which cyclopentane was slowly added *via* the gas phase.

Crystal data for **1**: $C_{10}H_{16}AuClO_2S$, M = 432.70, triclinic, space group $P\bar{1}$, a = 6.897(9), b = 8.563(2), c = 11.957(3) Å, α = 75.68(1), β = 78.41(4), γ = 69.54(4)°, U = 635.9(9) Å^3, Z = 2, D_c = 2.260 g cm^{-3}, μ(Mo-Kα) = 11.92 mm^{-1} (absorption correction by the ψ scan method). P4 Siemens diffractometer, using θ–2θ scan technique [2θ limits 5.0–55.0°] and Mo-Kα radiation (λ = 0.71073 Å). Crystal dimensions: 0.6 × 0.6 × 0.25 mm, 2397 observed data [$I \geqslant 2\sigma(I)$] of 2575 independent data measured (T = 173 K). Refinement (on F^2) to R_1 = 0.048 and wR_2 = 0.127. No. of refined parameters: 143. For **2**: $C_{10}H_{16}AuClS$, M = 400.72, monoclinic, space group $P2_1/n$, a = 8.880(2), b = 13.547(2), c = 10.513(2) Å, β = 109.93(2)°, U = 1188.9(4) Å^3, Z = 4, D_c = 2.239 g cm^{-3}, μ(Mo-Kα) = 12.73 mm^{-1} (absorption correction carried out with DIFABS program).[17] P4 Siemens diffractometer, using θ–2θ scan technique [2θ limits 5.0–55.0°] and Mo-Kα radiation (λ = 0.71073 Å). Crystal dimensions: 0.6 × 0.4 × 0.1 mm, 2307 observed data [$I \geqslant 2\sigma(I)$] of 2735 independent data measured (T = 173 K). Refinement (on F^2) to R_1 = 0.046 and wR_2 = 0.116. No. of refined parameters: 125. In both structures all atoms (excluding hydrogens) were refined using anisotropic displacement parameters (riding model for hydrogens). The structures were solved by direct methods (SHELXS-86 and SHELXL-93).[18] CCDC 182/915.

1 J. H. Teles, S. Brode and M. Chabanas, *Angew. Chem.*, 1998, **110**, 1475; *Angew. Chem., Int. Ed. Engl.*, 1998, **37**, 1415. For the catalytic effect of the $[AuCl_4]^-$ anion, see Y. Fukuda and K. Utimoto, *J. Org. Chem.*, 1991, **56**, 3729; *Bull. Chem. Soc. Jpn.*, 1991, **64**, 2013.

2 R. Hüttel and H. Forkl, *Chem. Ber.*, 1972, **105**, 1664; G. Wittig and S. Fischer, *Chem. Ber.*, 1972, **105**, 3542. For the general literature on alkyne complexes of gold and on alkynylgold(I) compounds, see H. Schmidbaur, in *Organogold Compounds*, *Gmelin Handbook of Inorganic Chemistry*, Springer Verlag, Berlin, 1980, pp. 209–211 and 191–194; A. Grohmann and H. Schmidbaur, in *Comprehensive Organometallic Chemistry II*, ed. E. W. Abel, F. G. A. Stone and G. Wilkinson, Elsevier Science, Oxford, 1995, vol. 3, pp. 44 and 6–9; R. J. Puddephatt, in *Comprehensive Organometallic Chemistry*, ed. G. Wilkinson, F. G. A. Stone and E. W. Abel, Pergamon, Oxford, 1982, vol. 2, pp. 812–814 and 766–774.

3 H. Lang, K. Köhler and L. Zsolnai, *Chem. Commun.*, 1996, 2043; K. Köhler, S. J. Silverio, I. Hyla-Kryspin, R. Gleiter, L. Zsolnai, A. Driess, G. Huttner and H. Lang, *Organometallics*, 1997, **16**, 4970.

4 D. M. P. Mingos, J. Yau, S. Menzer and D. J. Williams, *Angew. Chem.*, 1995, **107**, 2045; *Angew. Chem., Int. Ed. Engl.*, 1995, **34**, 1894.

5 H. Lang, K. Köhler and S. Blau, *Coord. Chem. Rev.*, 1995, **143**, 113; P. Schulte and U. Behrens, *J. Organomet. Chem.*, 1998, in press, and references therein.

6 Considerably longer Au–η^2(C≡C) bond lengths were found for the complexes $Cp_2Ti(C{\equiv}CR)_2AuR$ [2.22(1)–2.27(1) Å].[3]

7 P. J. Stang and F. Diederich, *Modern Acetylene Chemistry*, VCH Verlagsgesellschaft, Weinheim, 1995, p. 296.

8 N. C. Baenziger, K. M. Dittemore and J. R. Doyle, *Inorg. Chem.*, 1974, **13**, 805; G. A. Bowmaker, J. C. Dyson, P. C. Healy, L. M. Engelhardt, C. Pakawatchai and A. H. White, *J. Chem. Soc., Dalton Trans.*, 1987, 1089.

9 H. Schmidbaur, J. R. Mandl, A. Frank and G. Huttner, *Chem. Ber.*, 1976, **109**, 466; H. H. Murray III, J. P. Fackler, Jr., L. C. Porter and A. M. Mazany, *J. Chem. Soc., Chem. Commun.*, 1986, 321.

10 In copper(I) chloride alkyne complexes this type of structure is quite common: H. Lang, K. Köhler and S. Blau, *Coord. Chem. Rev.*, 1995, **143**, 113; P. Schulte, G. Schmidt, C.-P. Kramer, A. Krebs and U. Behrens, *J. Organomet. Chem.*, 1997, **530**, 95, and references therein. On the other hand, gold(I) chloride alkene complexes show linear coordination geometry at the metal: D. B. Dell'Amico, F. Calderazzo, R. Dantona, J. Strähle and H. Weiss, *Organometallics*, 1987, **6**, 1207.

11 E. S. Clark, D. H. Templeton and C. H. MacGillavry, *Acta Crystallogr.*, 1958, **11**, 284.

12 H. Schmidbaur, *Chem. Soc. Rev.*, 1995, 391; P. Pyykkö, N. Runeberg and F. Mendizabal, *Chem. Eur. J.*, 1997, **3**, 1451; P. Pyykkö and F. Mendizabal, *Chem. Eur. J.*, 1997, **3**, 1458.

13 P. Schulte, G. Schmidt, C.-P. Kramer, A. Krebs and U. Behrens, *J. Organomet. Chem.*, 1997, **530**, 95.

14 R. Usón and A. Laguna, *Organomet. Synth.*, 1986, **3**, 322.

15 U. Höpfner, diploma, University of Heidelberg, 1976.

16 A. Krebs and H. Kimling, *Tetrahedron Lett.*, 1970, 761; *Liebigs Ann. Chem.*, 1974, 2074.

17 A. L. Spek, DIFABS, Part of program PLATON95, *Acta Crystallogr., Sect. A*, 1990, **46**, C34; N. Walker and D. Stuart, *Acta Crystallogr., Sect. A*, 1983, **39**, 158.

18 G. M. Sheldrick, Program for Crystal Structure Solution (SHELXS) and Program for Crystal Structure Refinement (SHELXL), University of Göttingen, 1986 and 1993.

Received in Cambridge, UK, 20th May 1998; 8/03791D

Isolation and characterization of an oxidative degradation product of a polypyridine ligand

Michael Renz, Catherine Hemmert, Bruno Donnadieu and Bernard Meunier*†

Laboratoire de Chimie de Coordination du CNRS, 205 route de Narbonne, 31077 Toulouse cedex 4, France

The origin of the fragility of a polypyridine ligand under oxidizing conditions is discussed.

The catalytic activity of non-heme complexes has been recently investigated in relation to non-heme containing enzymes having one or two iron centers.[1] Mononuclear iron complexes with polypyridine ligands have been studied as potential oxidation catalysts.[2] In order to compare the activity of a mononuclear polypyridine–iron complex with porphyrin or phthalocyanine iron catalysts in the oxidative degradation of chlorophenols,[3] we synthesized a new symmetric tetrapyridine ligand, bis[bis(2-pyridyl)methyl]amine (BDPMA, Scheme 1).[4] The iron(III) complex of this ligand, $Fe(BDPMA)(NO_3)_3$, is able to catalyze the oxidative degradation of aromatic pollutants such as chlorinated phenols in the presence of $KHSO_5$.[5] Unfortunately, the oxidation stopped at the quinone level (without formation of ring cleavage products which are observed with an iron–phthalocyanine catalyst)[3] and the catalyst seemed to be short-lived. In attempts to crystallize the iron(III) complex of this tetrapyridyl ligand, we found the reason for the low catalytic activity that we observed in chlorophenol oxidations. Instead of a metal complex, the cationic compound 1,3,3-tris(2-pyridyl)-3*H*-imidazo[1,5-*a*]pyridin-4-ium (TPIP) was surprisingly obtained.‡ This degradation product of the BDPMA ligand was completely characterized by ^1H NMR, FAB-MS spectrometry and X-ray analysis (Fig. 1).§ The key feature of this structure is the presence of a pyridinium entity with the three other pyridine substituents still intact. Formally, this modified ligand TPIP can be obtained from BDPMA by abstraction of four electrons and three protons. In the crystal structure, the bond lengths of the pyridinium moiety are as expected for such rings and the shortest bond length [N(1)–C(7)] of the imidazole moiety is in agreement with a double bond. The N(2)–C(1) bond of the five-membered ring is around 4 pm longer than the N(1)–C(1) bond, as expected for a $C–N^+$ bond of a pyridinium entity (Fig. 1). The angle between the two planes formed by the imidazopyridinium and the pyridine connected to the C(7) carbon atom (Fig. 1) is only 5°, strongly suggesting that the conjugation is extended to this pyridine.

The formation of TPIP can be explained by the oxidation of BDPMA in the presence of Fe^{III} species (in the absence of metal traces BDPMA is stable and has been completely characterized). The first step consists of a two-electron oxidation of BDPMA by 2 equiv. of iron(III). The resulting imine can be activated by protonation and then attacked by a pyridine nitrogen acting as internal nucleophile to generate a five-membered ring (Scheme 1). This reaction is already known for pyridyl substituted imines, which after cyclization, are further oxidized to imidazo[1,5-*a*]pyridines.[6] This is not possible in the present case because a quaternary carbon is created during the cyclization (C^3, Scheme 1). Consequently, only one C–N double bond can be obtained by dehydrogenation of the five-membered ring (step 3, Scheme 1), and the pyridinium nitrogen remains positively charged. The cationic TPIP was obtained with nitrate as counterion (Scheme 1).

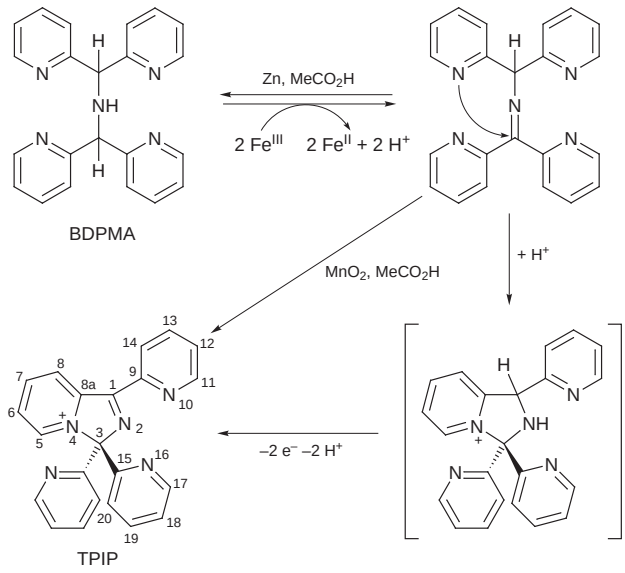

Scheme 1 Mechanism of the oxidative cyclization of BDPMA

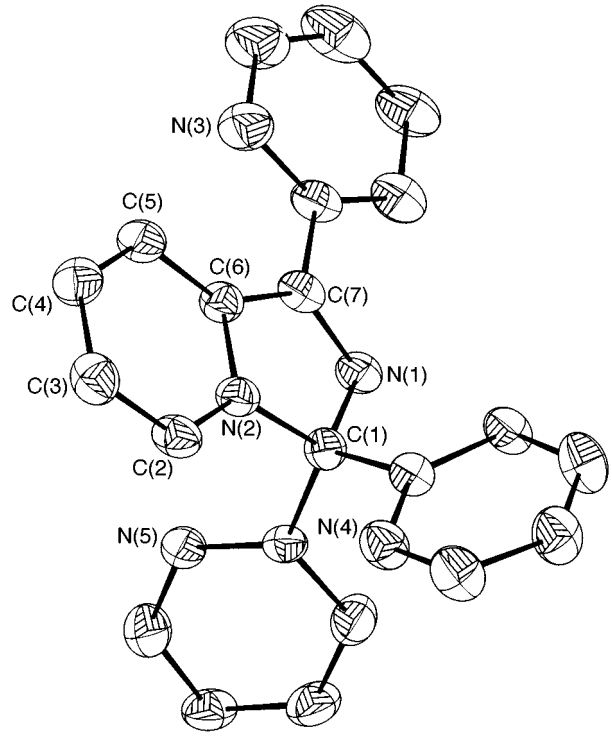

Fig. 1 Crystal structure of TPIP (atom numbering is differing from that presented in Scheme 1).§ Selected bond lengths (Å): N(1)–C(1) 1.457(4), N(1)–C(7) 1.293(5), N(2)–C(1) 1.498(4), N(2)–C(2) 1.336(4), N(2)–C(6) 1.364(4), C(2)–C(3) 1.374(5), C(3)–C(4) 1.383(6), C(4)–C(5) 1.388(5), C(5)–C(6) 1.377(5), C(6)–C(7) 1.471(5).

To prove this mechanism, we synthesized TPIP on a large scale *via* the imine. The latter is already known as precursor of BDPMA and has been reduced by Zn to obtain BDPMA.[4] For the oxidation, MnO_2 has been employed and TPIP was isolated in 73% yield.‡ A slow oxidation leading to the C–N double bond was observed in the presence of molecular oxygen, but we found that MnO_2 was the suitable oxidant to efficiently prepare TPIP.

The isolation and characterization of this degradation product is a significant illustration of the denaturation of a polypyridine ligand in oxidative conditions. The mechanism of the degradation was confirmed by the synthesis of the obtained product from the intermediary imine. The present work shows that ligands having easily oxidizable C–H bonds, *i.e.* activated in benzylic position or in α-position of a hetero atom, have to be avoided for stability reasons in the design of effective and long-lived oxidation catalysts.

We are grateful to the CNRS for financial support, especially M. R. for a postdoctoral fellowship.

Notes and References

† E-mail: bmeunier@lcc-toulouse.fr

‡ *Preparations*: TPIP [oxidation of BDPMA with $Fe(NO_3)_3$]: BDPMA (100 mg, 0.283 mmol) in methanol (2 ml) was added to a solution of $Fe(NO_3)_3{\cdot}9H_2O$ (105 mg, 0.260 mmol) in methanol (2 ml) and the mixture allowed to stand for 1 h. The solvent was evaporated and the residue dried under oil-pump vacuum for 3 h at 60 °C and *ca.* 10 mg of the obtained powder were dissolved in acetone. The solution was allowed to stand in an atmosphere of diethyl ether for two weeks. The solution became colorless, brown drops condensed and a large branched crystal was obtained, on which an X-ray analysis could be carried out. A yellow crystal was also obtained from an ethanolic solution in a methyl *tert*-butyl ether (MTBE) atmosphere. A part of this was cut and used for the presented X-ray structure. The remaining crystal was dissolved in dry $(CD_3)_2SO$ for ^{1}H NMR analysis and mass spectrometry. ^{1}H NMR [250 MHz, $(CD_3)_2SO$, 25 °C] δ 7.69 [dd, ^3J(HH) 7.7, ^3J(HH) 4.8 Hz, 2 H, 18-H], 7.91 [d, ^3J(HH) 7.9 Hz, 2 H, 20-H], 7.93 [ddd, ^3J(HH) 7.8, ^3J(HH) 4.8, ^4J(HH) 1.0 Hz, 1 H, 12-H], 8.14 [td, ^3J(HH) 7.7, ^4J(HH) 1.7 Hz, 2-H, 19-H], 8.32 [td, ^3J(HH) = 7.8 Hz, ^4J(HH) 1.7 Hz, 1 H, 13-H], 8.51 [ddd, ^3J(HH) 7.7, ^3J(HH) 6.2, ^4J(HH) 1.1 Hz, 1 H, 6-H], 8.75 [d, ^3J(HH) 4.8 Hz, 2 H, 17-H), 8.76 [d, ^3J(HH) 7.8 Hz, 1 H, 14-H], 9.08 [d, ^3J(HH) = 4.8 Hz, 1 H, 11-H], 9.13 [td, ^3J(HH) 7.7, ^4J(HH) 1.0 Hz, 1 H, 7-H], 9.60 [d, ^3J(HH) 8.0 Hz, 1 H, 8-H], 10.18 [d, ^3J(HH) 6.2 Hz, 1 H, 5-H]; FAB-MS (*meta*-nitrobenzyl alcohol): *m*/*z* (%): 350 (100).

TPIP (preparative synthesis): 300 mg (1.63 mmol) of bis(2-pyridyl)-ketone and 300 mg (1.63 mmol) of bis(2-pyridyl)methylamine[4] were dissolved in 10 ml of absolute isopropanol and dried over molecular sieves 3 Å for 1 h at room temperature. 350 μl (5.5 mmol) of glacial acetic acid was added under N_2 atmosphere and the reaction mixture refluxed for 5 h. 1.42 g (16.3 mmol) of MnO_2 was added (the oil bath was removed for the addition). After 1 h heating was switched off and the reaction mixture allowed to cool slowly. After 16 h, solids were removed by filtration. The solvent was evaporated (50 °C, 30 Torr) and the residue dissolved in 10 ml CH_2Cl_2 and washed with brine (2 × 5 ml). The crude reaction mixture was dissolved in MeOH and exposed to a MTBE atmosphere. 498 mg (1.19 mmol, 73%) of yellow crystals were obtained.

§ *Crystal data* for $C_{22}H_{16}N_6O_3$ (TPIP): M = 412.41, yellow pale crystal (0.20 × 0.20 × 0.10 mm), monoclinic, space group $I2/a$, a = 22.665(3), b = 8.4832(8), c = 23.415(3) Å, β = 117.83(2)°, U = 3982 Å^3, Z = 8, D_c = 1.37 g cm^{-3}, λ = 0.71073 Å, T = 160(2) K, μ(Mo-Kα) = 0.89 cm^{-1}, 25822 reflections (3166 independent) were collected on a STOE-IPDS diffractometer, 281 parameters were refined using the least-squares method on F[7], R = 0.051 and R_w = 0.055. CCDC: 182/925.

1 B. J. Wallar and J. D. Lipscomb, *Chem. Rev.*, 1996, **96**, 2625; L. Que Jr. and R. Y. N. Ho, *Chem. Rev.*, 1996, **96**, 2607.
2 P. A. MacFaul, I. W. C. E. Arends, K. U. Ingold and D. D. M. Wayner, *J. Chem. Soc., Perkin Trans. 2*, 1997, 135; M. Lubben, A. Meetsma, E. C. Wilkinson, B. Feringa and L. Que Jr., *Angew. Chem., Int. Ed. Engl.*, 1995, **34**, 1512.
3 A. Hadasch, A. Sorokin, A. Rabion and B. Meunier, *New J. Chem.*, 1998, **22**, 45; B. Meunier and A. Sorokin, *Acc. Chem. Res.*, 1997, **30**, 470; A. Sorokin, J. L. Séris and B. Meunier, *Science*, 1995, **268**, 1163.
4 M. Renz, C. Hemmert and B. Meunier, *Eur. J. Org. Chem.*, 1998, in press.
5 C. Hemmert, M. Renz and B. Meunier, *J. Mol. Catal. A*, 1998, in press.
6 A. P. Krapcho and J. R. Powell, *Tetrahedron Lett.*, 1986, **27**, 3713.
7 D. J. Watkin, C. K. Prout and L. J. Pearce, CAMERON, Chemical Crystallography Laboratory, University of Oxford, 1996.

Received in Basel, Switzerland, 30th April 1998; 8/03255F

Polymer pendant crown thioethers: synthesis and Hg^{II} extraction studies of a novel thiacrown polymer

Theodore F. Baumann,*† John G. Reynolds and Glenn A. Fox

Lawrence Livermore National Laboratory, University of California, PO Box 808, Livermore, CA 94551, USA

A novel C-substituted crown thioether has been synthesized and used to prepare a cross-linked polystyrene polymer containing pendant crown thioethers and that product has been shown to be effective in extracting Hg^{II} from acidic aqueous solutions.

Owing to increasing environmental concerns about waste water remediation, major efforts are under way to design new materials that can effectively remove and recover toxic metal ions from aqueous solutions. One approach to this problem has been to utilize organic ligands anchored to solid supports.[1] Specific binding properties of the ligands can be exploited to selectively remove a desired metal ion from a complex solution of cations. The utility of polymer pendant ligands for the extraction of a variety of metal ions from aqueous media has been previously demonstrated.[2]

We are interested in designing polymeric materials for Hg^{II} remediation in mixed waste streams. Typically, these waste streams are not only very acidic, but also contain a wide variety of other metal ions. As a result, removal of Hg^{II} requires a robust and selective sequestering agent. To address this difficult and expensive problem, we have developed the synthesis of polymer pendant crown thioethers for the selective removal of Hg^{II} from acidic aqueous media.[3] Crown thioethers[4] are well suited for this task owing to the high affinity that sulfur crowns have for the Hg^{II} ion[5] as well as their resistance to degradation under acidic conditions.[6] As pendant ligands on solid supports, crown thioethers have been shown to remove soft metal ions, such as Ag^{I}, Hg^{II} and Pb^{II}, directly from aqueous solutions.[7] Here we present the novel synthesis of a thiacrown polymer and initial results in the extraction of the Hg^{II} ion from acidic aqueous solutions.

Preparation of thiacrown polymers first required the synthesis of a sulfur crown containing a pendant arm incorporated into the carbon framework. Functionalization of this pendant arm would allow for either the attachment of the crown to a polymer support or direct polymerization of the thiacrown monomer. While there are reported syntheses for C-substituted sulfur crowns,[7d,8] those methods were not practical for our purposes, requiring a new method for the synthesis of pendant-arm crown thioethers.

The new crown thioether, 2-hydroxymethyl-1,4,8,11,14-pentathiacycloheptadecane[9] ([17]aneS_5-OH), **1**, was synthesized in a 25% yield through reaction of 2,3-dimercaptopropan-1-ol[10] with 4,7,10-trithiatridecane-1,13-di(toluene-*p*-sulfonate) (Scheme 1), using caesium carbonate mediated cyclization.[11] Advantages of this technique are: (1) it is general for synthesizing sulfur crowns of various sizes,[12] and (2) the hydroxymethyl moiety does not need to be protected prior to the condensation reaction. [17]aneS_5-OH was then treated with thionyl chloride to form 2-chloromethyl-1,4,8,11,14-pentathiacycloheptadecane ([17]aneS_5-Cl), **2** (89%), followed by conversion to 2-(*N*-methyl)aminomethyl-1,4,8,11,14-pentathiacycloheptadecane ([17]aneS_5-NHMe), **3** (65%), through reaction with methylamine. The synthesis of the 4-vinylbenzyl-substituted thiacrown **4** (60%) was readily accomplished by treating **3** with 4-vinylbenzyl chloride. Copolymerization of the 4-vinylbenzyl-substituted thiacrown **4** with DVB (80% divinylbenzene) using AIBN as the radical initiator generated the highly cross-linked crown thioether polymer **5**.[13] Elemental analysis of the resulting polymeric material showed that each gram of the polymer contained 1.53 mmol of [17]aneS_5 crown (based on % by weight of sulfur).

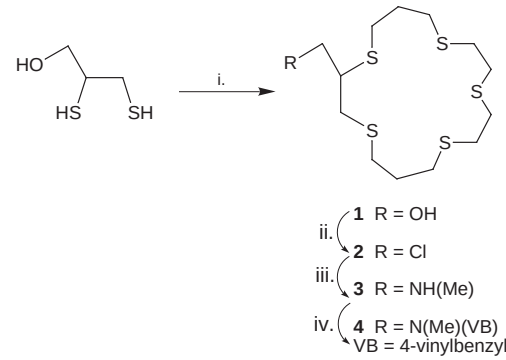

Scheme 1 *Reagents and conditions*: i. $S(CH_2CH_2SCH_2CH_2CH_2OTs)_2$, Cs_2CO_3, DMF, 90 °C; ii. $SOCl_2$, CH_2Cl_2, RT; iii. $MeNH_2$, Na_2CO_3, MeCN, 0 °C; iv. 4-vinylbenzyl chloride, Na_2CO_3, MeCN, 81 °C

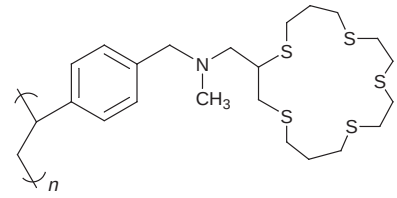

5

Solid–liquid extraction capabilities of the polymer pendant crown thioethers were tested in aqueous solutions. Twenty milligrams of the polymer were stirred in 5 ml of a buffered solution (ammonium acetate) containing 2.0×10^{-5} g of Hg^{II} [as $Hg(NO_3)_2$] at pH 3.60. Mixing times ranged from 30 minutes to 18 hours. At the end of the mixing, the polymer powder was separated from each solution by filtering through a cotton plug. The concentration of Hg^{II} remaining in the buffer solution was quantified spectrophotometrically using a diphenylthiocarbazone extraction method adapted from the methods of Charlot.[14] Using this method, the accuracy in determining the Hg^{II} concentration was ±1 ppm. In all cases, Hg^{II} removal was determined to be 99+%, indicating the high reactivity and extraction efficiency of the thiacrown polymer. The mercury extraction performance of the polymer under different conditions (pH and Hg concentrations), in addition to metal ion competition studies, will be reported in a full paper.

Work was performed under the auspices of the U.S. Department of Energy by the Lawrence Livermore National Laboratory under contract number W-7405-ENG-48.

Notes and References

† E-mail: baumann2@llnl.gov

1 For a recent review, see: C. Kantipuly, S. Katragadda, A. Chow and H. D. Gesser, *Talanta*, 1990, **37**, 491 and references therein.

2 For some recent examples, see: (*a*) H. Chen, M. M. Olmstead, R. L. Albright, J. Devenyi and R. H. Fish, *Angew. Chem., Int. Ed. Engl.*, 1997, **36**, 642; (*b*) S. Huang, K. J. Franz, E. H. Arnold, J. Devenyi and R. H. Fish, *Polyhedron*, 1996, **15**, 4241; (*c*) W. Li, M. Couglin, R. L. Albright and R. H. Fish, *React. Funct. Polym.*, 1995, **28**, 89; (*d*) S. Huang, W. Li, K. J. Franz, R. L. Albright and R. H. Fish, *Inorg. Chem.*, 1995, **34**, 2813; (*e*) M. Andrei, J. M. G. Cowie and P. Prosperi, *Electrochim. Acta*, 1992, **37**, 1545; (*f*) R. Shah and S. Devi, *React. Funct. Polym.*, 1996, **31**, 1.

3 T. F. Baumann, J. G. Reynolds and G. A. Fox, *Synthesis of Novel Pendant Arm Crown Thioethers for Mercury Removal from Mixed Waste Streams, Abstracts of Papers*, 214th National Meeting of the American Chemical Society, Las Vegas, NV, Sept. 7–11, 1997; ENVR 117.

4 S. R. Cooper, *Acc. Chem. Res.*, 1988, **21**, 141.

5 (*a*) D. Sevdic and H. Meider, *J. Inorg. Nucl. Chem.*, 1977, **39**, 1409; (*b*) D. Sevdic, L. Fekete and H. Meider, *J. Inorg. Nucl. Chem.*, 1980, **42**, 885; (*c*) D. Sevdic and H. Meider, *J. Inorg. Nucl. Chem.*, 1981, **43**, 153.

6 B. A. Moyer, G. N. Case, S. D. Alexandratos and A. A. Kriger, *Anal. Chem.*, 1993, **65**, 3389.

7 (*a*) M. Tomoi, O. Abe, N. Takasu and H. Kakiuchi, *Makromol. Chem.*, 1983, **184**, 2431; (*b*) K. Yamashita, K. Kurita, K. Ohara, K. Tamura, M. Nango and K. Tsuda, *React. Funct. Polym.*, 1996, **31**, 47; (*c*) M. Oue, K. Kimura and T. Shono, *Analyst*, 1988, **113**, 551; (*d*) E. I. Troyansky, M. S. Pogosyan, N. M. Samoshina, G. I. Nikishin, V. V. Samoshin, L. K. Shpigun, N. E. Kopytova and P. M. Kamilova, *Mendeleev Commun.*, 1996, 9.

8 (*a*) R. J. Smith, G. D. Admans, A. P. Richardson, H. Küppers and P. J. Blowers, *J. Chem. Soc., Chem. Commun.*, 1991, 475; (*b*) V. B. Pett, G. H. Leggett, T. H. Cooper, P. R. Reed, D. Situmeang, L. A. Ochrymowycz and D. B. Rorabacher, *Inorg. Chem.*, 1988, **27**, 2164.

9 Characterization for [17]aneS_5-OH (**1**)**:** mp 30–32 °C. Anal. Found (calc. for $C_{13}H_{26}OS_5$): C, 43.32 (43.57); H, 7.27 (7.32); S, 44.51 (44.65). ^{1}H NMR ($CDCl_3$) δ 1.8–2.0 (4 H, m, $CH_2CH_2CH_2$), 2.3 (1 H, br s, OH), 2.6–2.85 (14 H, m, CH_2SCH_2), 2.95 (1 H, qnt, CH_2CHS), 3.65 (1 H, dd, $HOCH_2CH$), 3.80 (1 H, dd, $HOCH_2CH$). ES-MS *m*/*z* ($C_{13}H_{26}OS_5$, 358): 357 ($M - H^+$), 417 ($M + OAc^-$) (Courtesy of Hugh Gregg, LLNL).

10 This compound has been used to synthesize 2-hydroxymethyldithia-18-crown-6: J. S. Bradshaw, K. E. Krakowiak, R. M. Izatt, R. L. Bruening and B. J. Tarbet, *J. Heterocycl. Chem.*, 1990, **27**, 347.

11 J. Buter and R. M. Kellogg, *Org. Synth.*, 1987, **65**, 150.

12 We have also used this method to synthesize the [14]aneS_4-OH crown and its synthesis and characterization will be presented as part of a full paper.

13 Characterization for thiacrown polymer **5**: Anal. Found: C, 62.30; H, 7.46; N, 2.42; S, 24.51. IR (KBr, ν/cm^{-1}): 3017w, 2920s, 2848w, 1699w, 1603w, 1509w, 1437m, 1421s, 1384m, 1300m, 1259m, 1203w, 1122w, 1034m, 1018m, 922w, 825m, 799m, 711m, 567w.

14 A. G. Charlot, *Colorimetric Determination of Elements*; Elsevier, Amsterdam, 1964, pp. 295–297.

Received in Bloomington, IN, USA, 5th May 1998; 8/03383H

A new protocol for the syntheses of (*E*)-3-benzylidenechroman-4-ones: a simple synthesis of the methyl ether of bonducellin

Deevi Basavaiah,*† Manickam Bakthadoss and Subramanian Pandiaraju

School of Chemistry, University of Hyderabad, Hyderabad-500 046, India

Development of a simple new methodology for the synthesis of (*E*)-3-benzylidenechroman-4-ones using methyl 3-aryl-3-hydroxy-2-methylenepropanoates, the Baylis–Hillman adducts derived from methyl acrylate, and the application of this methodology for the synthesis of the methyl ether of bonducellin, an important natural product, and 3-(4-methoxybenzylidene)-6-methoxychroman-4-one, an antifungal agent, are described.

The (*E*)-3-benzylidenechroman-4-one moiety occupies a special place in the field of heterocycles as this skeleton is an integral part of many natural products and biologically active

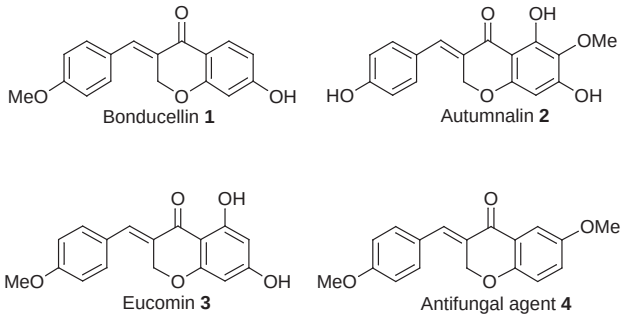

molecules. For example, bonducellin **1** is an important natural product occurring in *Caesalpinia bonducella*[1] and *Caesalpinia pulcherrima*.[2] Autumnalin **2**[3] and Eucomin **3**[4] are interesting naturally occurring molecules present respectively in *Eucomis autumnalis* GRAEB (Liliaceae) and *Eucomis bicolor* BAK (Liliaceae). (*E*)-3-(4-Methoxybenzylidene)-6-methoxychroman-4-one **4** is an antifungal agent.[5] Therefore the development of simple, general and new protocols for the synthesis of the (*E*)-3-benzylidenechroman-4-one skeleton is of considerable importance today in synthetic organic chemistry.

The classical and most of the literature methods for the synthesis of (*E*)-3-benzylidenechroman-4-ones involve the initial synthesis of the chroman-4-one skeleton, followed by the construction of the benzylidene moiety *via* acid or base catalyzed aldol condensation with aryl aldehydes.[6–8] However, to the best of our knowledge, there is no report in the literature of the synthesis of (*E*)-3-benzylidenechroman-4-one involving the initial preparation of the benzylidene moiety and then the construction of the chroman-4-one ring system. We herein disclose the first such methodology, thus developing a new protocol for the synthesis of (*E*)-3-benzylidenechroman-4-ones using methyl 3-aryl-3-hydroxy-2-methylenepropanoates, the Baylis–Hillman adducts derived from methyl acrylate.

The Baylis–Hillman reaction[9–13] has attracted the attention of organic chemists in recent years as this reaction provides synthetically useful multifunctional molecules which have been successfully employed in various stereoselective processes. In continuation of our interest in the Baylis–Hillman reaction[14–17] we have examined the possible application of methyl (2*Z*)-2-bromomethylalk-2-enoates‡ **5** derived from methyl 3-hydroxy-2-methylenealkanoates for the synthesis of (*E*)-3-benzylidenechroman-4-ones **8** according to Scheme 1.

We first selected (2*E*)-2-phenoxymethyl-3-phenylprop-2-enoic acid **7a**, which was obtained *via* the reaction of allyl

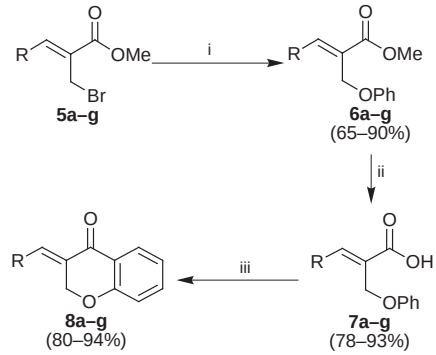

Scheme 1 *Reagents and conditions*: i, PhOH, K_2CO_3, acetone, reflux, 3 h; ii, KOH, H_2O, acetone, room temp., 14 h; iii, TFAA, CH_2Cl_2, reflux, 1 h

Table 1 Synthesis of (*E*)-3-benzylidene- or (*E*)-3-alkylidene-chroman-4-ones (**5**→**6**→**7**→**8**)

Allyl bromide[a]	R	Product[a,b]	Yield[c] (%)	Product[a,d]	Yield[e] (%)	Product[f,g,h]	Yield[i] (%)
5a	Ph	**6a**	73	**7a**	87	**8a**[j]	91
5b	*p*-MeC_6H_4	**6b**	75	**7b**	83	**8b**	94
5c	*o*-MeC_6H_4	**6c**	87	**7c**	93	**8c**	90
5d	*p*-EtC_6H_4	**6d**	90	**7d**	92	**8d**	93
5e	*p*-$Pr^iC_6H_4$	**6e**	71	**7e**	84	**8e**	91
5f	*p*-$MeOC_6H_4$	**6f**	77	**7f**	90	**8f**	92
5g	Pr	**6g**	65	**7g**	78	**8g**	80

[a] See footnote ‖. [b] All reactions were carried out in 10 mmol scale of bromide with 10 mmol of phenol in the presence of K_2CO_3 in acetone at reflux temperature for 3 h. [c] Yields of pure esters obtained after silica gel column chromatography (3% EtOAc–hexane). [d] Hydrolysis of these esters was carried out on a 5 mmol scale with aq. KOH–acetone at room temperature. [e] Isolated yields of the pure acids after crystallization. [f] See footnote **. [g] All the reactions were carried out on a 1 mmol scale for the acid with TFAA (1 mmol) in refluxing CH_2Cl_2 for 1 h. [h] All the products gave satisfactory IR, ^1H NMR (200 MHz), ^{13}C NMR (50 MHz) and mass spectral data and elemental analyses. [i] Yields of the pure chromanones obtained after crystallization (**8a–f**) from EtOAc–hexane (2:98) or after silica gel column chromatography (**8g**) (3% EtOAc–hexane). [j] See footnote §.

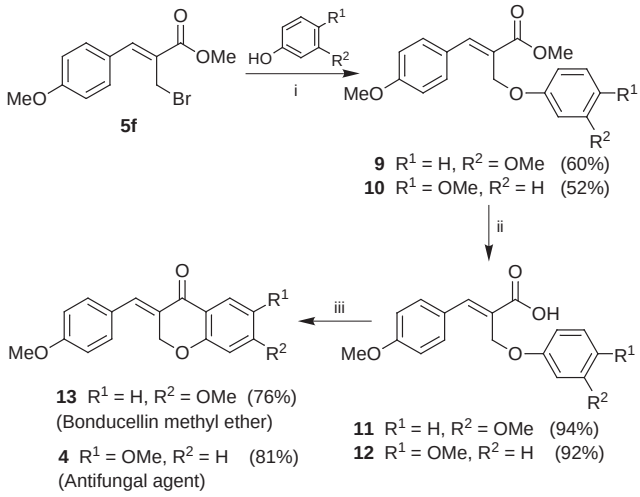

Scheme 2 *Reagents and conditions*: i, K_2CO_3, acetone, reflux, 3 h; ii, KOH, H_2O, acetone, room temp., 14 h; iii, TFAA, CH_2Cl_2, reflux, 1 h

bromide **5a**‡ with phenol followed by hydrolysis, as a substrate having a benzylidene moiety. Treatment of **7a** with TFAA in CH_2Cl_2 provided the desired (*E*)-3-benzylidenechroman-4-one **8a**§ in 91% yield. Encouraged by this success we prepared a representative class of (*E*)-3-benzylidenechroman-4-ones **8b**–**f** using (2*E*)-3-aryl-2-phenoxymethylprop-2-enoic acids **7b**–**f** obtained from methyl 3-aryl-3-hydroxy-2-methylenepropanoates (Scheme 1, Table 1). With a view to the generalization of this methodology we also synthesized (*E*)-3-butylidenechroman-4-one **8g** (R = Pr) (Table 1) starting from methyl (2*Z*)-2-bromomethylhex-2-enoate **5g**.¶

The efficiency of this methodology has been demonstrated *via* the synthesis of the methyl ether of bonducellin **13** and (*E*)-3-(4-methoxybenzylidene)-6-methoxychroman-4-one **4**, an antifungal agent, according to Scheme 2.

In conclusion, we have developed a new protocol for the synthesis of (*E*)-3-benzylidenechroman-4-ones involving the initial synthesis of the benzylidene moiety, followed by construction of the chroman-4-one system. Further application of this methodology for the synthesis of biologically active molecules is in progress in our laboratory.

We thank DST (New Delhi) for funding this research project. We thank UGC (New Delhi) for COSIST and the Special Assistance Program at the School of Chemistry, University of Hyderabad, Hyderabad. M. B. thanks UGC (New Delhi) and S. P. thanks CSIR (New Delhi) for their research fellowships.

Footnotes and References

† E-mail: dbsc@uohyd.ernet.in

‡ The (*Z*)-allyl bromides **5** were prepared from the corresponding 3-hydroxy-2-methylenealkanoates following the literature method (ref. 18).

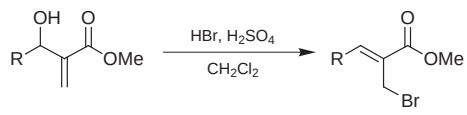

§ *Selected data* for **8a**: mp 110–111 °C (lit. 110–112 °C) (ref. 19); ν_{max}(KBr)/cm^{-1} 1668, 1601; δ_H(200 MHz, $CDCl_3$) 5.35 (d, 2 H, *J* 1.6) 6.95–7.60 (m, 8 H), 7.88 (s, 1 H), 8.03 (d, 1 H, *J* 7.8); δ_C(50 MHz, $CDCl_3$) 67.63, 117.93, 121.91, 122.06, 127.96, 128.74, 129.46, 129.99, 130.97, 134.43, 135.85, 137.44, 161.17, 182.17; *m/z* 236 (M^+); Calc. for $C_{16}H_{12}O_2$: C, 81.34; H, 5.12. Found: C, 81.45; H, 5.12%.

¶ The reaction of methyl (2*Z*)-2-bromomethylhex-2-enoate **5g** with phenol in the presence of K_2CO_3 also provided *ca.* 15% of a side product, presumably methyl 2-methylene-3-phenoxyhexanoate (S_N2' product). However, the major compound methyl (2*E*)-2-phenoxymethylhex-2-enoate **6g** was obtained in pure form after silica gel column chromatography (3% EtOAc–hexane).

‖ The (*Z*)-stereochemistry of the molecules **5** and the (*E*)-stereochemistry of the molecules **6** and **7** were confirmed by ^{1}H NMR spectral analysis. It is well documented in the literature that in the ^{1}H NMR spectrum the chemical shifts of the vinylic β-proton *cis* to the ketone, ester and acid carbonyl groups and of the corresponding vinylic *trans* β-proton are well-differentiated and vinylic *cis* β-protons appear downfield in comparison with *trans* protons (ref. 20). The (*Z*)-stereochemistry of the allyl bromides **5** was assigned on the basis of the chemical shift values of the β-vinylic protons, *i.e.* δ 7.78–7.91 (when R = Ar) and 6.97 (when R = Pr) (refs. 18, 21). The (*E*)-stereochemistry of the molecules **6, 7** and **9**–**12** was assigned on the basis of the chemical shift values of the β-vinylic protons, *i.e.* δ 8.02–8.25 (when R = Ar) and 6.93–7.11 (when R = Pr) (refs. 18, 22).

** It is well established that in the ^{1}H NMR spectra of 3-benzylidenechroman-4-ones the vinylic β- proton *cis* to the carbonyl group appears at δ *ca.* 7.7 (refs. 4, 23) while the corresponding *trans* β-proton appears at δ *ca.* 6.7 (ref. 4). In the case of compounds **4**, **8a**–**f** and **13** the vinylic β-protons appear at δ 7.81–7.96. Hence (*E*)-stereochemistry was assigned to the compounds **4, 8a**–**f** and **13**. In the case of butylidenechroman-4-one **8g** (R = Pr) the vinylic β-proton appears at δ 7.04. Therefore (*E*)-stereochemistry was assigned to **8g**.

1 K. K. Purushothaman, K. Kalyani, K. Subramaniam and S. P. Shanmughanathan, *Indian J. Chem., Sect. B*, 1982, **21**, 383.
2 D. D. McPherson, G. A. Cordell, D. D. Soejarto, J. M. Pezzuto and H. H. S. Fong, *Phytochemistry*, 1983, **22**, 2835.
3 W. T. L. Sidwell and C. Tamm, *Tetrahedron Lett*., 1970, 475.
4 P. Bohler and C. Tamm, *Tetrahedron Lett*., 1967, 3479.
5 T. Al Nakib, V. Bezjak, M. J. Meegan and R. Chandy, *Eur. J. Med. Chem.*, 1990**, 25**, 455; *Chem. Abstr*., 1990, **113**, 231160v.
6 W. Heller and C. Tamm, *Progress in the chemistry of organic natural products*, ed. W. Herz, H. Grisebach and G. W. Kirby, Springer-Verlag, New York, 1981, vol. 40, pp. 105–252.
7 S. Malhotra, V. K. Sharma and V. S. Parmar, *J. Chem. Res. (S)*, 1988, 179.
8 L. Farkas, A. Gottsegen and M. Nogradi, *Tetrahedron*, 1970, **26**, 2787.
9 D. Basavaiah, P. D. Rao and R. S. Hyma, *Tetrahedron*, 1996, **52**, 8001.
10 E. Ciganek, *Org. React.*, 1997, **51**, 201.
11 S. E. Drewes and G. H. P. Roos, *Tetrahedron*, 1988, **44**, 4653.
12 A. Chamakh and H. Amri, *Tetrahedron. Lett*., 1998, **39**, 375.
13 H. M. R. Hoffmann and J. Rabe, *J. Org. Chem*., 1985, **50**, 3849.
14 D. Basavaiah and P. K. S. Sarma, *J. Chem. Soc., Chem. Commun*., 1992, 955.
15 D. Basavaiah, P. K. S. Sarma and A. K. D. Bhavani, *J. Chem. Soc., Chem. Commun*., 1994, 1091.
16 D. Basavaiah, S. Pandiaraju and P. K. S. Sarma, *Tetrahedron. Lett*., 1994, **35**, 4227.
17 D. Basavaiah, V. V. L. Gowriswari, P. K. S. Sarma and P. D. Rao, *Tetrahedron Lett*., 1990, **31**, 1621.
18 R. Buchholz and H. M. R. Hoffmann, *Helv. Chim. Acta*., 1991, **74**, 1213.
19 O. Dann and H. Hofmann, *Chem. Ber*., 1962, **95**, 1446.
20 L. M. Jackman and S. Sternhell, *Applications of nuclear magnetic resonance spectroscopy in organic chemistry*, 2nd edn., Pergamon, Oxford, 1969, vol. 5; S. W. Tobey, *J. Org. Chem*., 1969, **34**, 1281.
21 A. Gruiec and A. Foucaud, *New. J. Chem*., 1991, **15**, 943.
22 E. Ciganek, *J. Org. Chem*., 1995, **60**, 4635; S. Wang, K. Yamamoto, H. Yamada and T. Takahashi, *Tetrahedron*, 1992, **48**, 2333.
23 M. Namikoshi, H. Nakata and T. Saitoh, *Phytochemistry*, 1987, **26**, 1831.

Received in Cambridge, UK, 5th May 1998; revised manuscript received 22nd June 1998; 8/04796K

Synthesis of cadmium sulfide nanoparticles *in situ* using γ-radiation

Yadong Yin, Xiangling Xu,*† Xuewu Ge, Chuanjun Xia and Zhicheng Zhang

Department of Applied Chemistry, University of Science and Technology of China, Hefei 230026, People's Republic of China

Cadmium sulfide nanoparticles have been produced *in situ* in aqueous solution at room temperature by precipitating Cd^{2+} ions with homogeneously released S^{2-} ions, which were generated from the decomposition of $Na_2S_2O_3$ by γ-irradiation.

Semiconductor particles in the nanometric range with dimensions comparable to the Bohr radius exhibit strongly size dependent optical and electrical properties. Such particles may lead to quantum dot lasers, single electron transistors and a host of other applications.[1] It is important to synthesize such particles at the desired size with a narrow size distribution and in an easy-to-handle condition. Many of the studies have focused on group II–VI semiconductor nanoparticles, in particular cadmium sulfide, because of their technological importance. Nanosized CdS particles are often prepared by precipitating Cd^{2+} ions with gaseous H_2S[2,3] as the source of S^{2-} ions. Because Cd^{2+} ions and H_2S are in separate phases and mix unevenly, the formation and aggregation of CdS particles is inevitably uneven. Other reports are of efforts in preparing CdS nanometer particles by mixing Cd^{2+} ions with Na_2S in aqueous solutions, water/oil microemulsions or other media.[4–6] As the precipitation of Cd^{2+} with S^{2-} is quicker than their homogeneous mixing, the inhomogenity at early stages results in a broadening of the size distribution. Also, deoxygenation and fresh Na_2S aqueous stock solutions are necessary in these methods to avoid the formation of colloidal sulfur and other species because of the instability of Na_2S. On the other hand, some reports have utilized other S^{2-} reservoirs, such as P_2S_5 or thioacetamide (TAA), to provide a homogeneous and rapid release of S^{2-} ions.[7,8] However, it is difficult to control the decomposition rate of P_2S_5 and TAA because non-aqueous or other complex manipulations are required.

Here we report a novel method for synthesis of the CdS nanoparticles at room temperature by utilizing homogeneous release of S^{2-} from the decomposition of sodium thiosulfate ($Na_2S_2O_3$) upon γ-irradiation.[9,10] In the presence of metal cations such as Cd^{2+} in solution, sulfide particles are formed by precipitation. To prevent the small CdS particles from coming into close contact and undergoing further aggregation, a surfactant, sodium dodecyl sulfate (SDS), is also needed in the system. Isopropyl alcohol, which is a scavenger of oxidative radicals such as ·OH, is thus added to improve the yield of nanoparticles.

Analytically pure $Na_2S_2O_3$, $3CdSO_4 \cdot 8H_2O$, isopropyl alcohol and SDS were mixed in appropriate proportions in distilled water. The solutions were irradiated by a ^{60}Co γ-ray source. After irradiation, the pale yellow product was collected and washed with distilled water. Finally, the product was dried in vacuum at 50 °C for 3 h.

X-Ray powder diffraction (XRD) was carried out on a Rigaku Dmax γ_A X-ray diffractometer with Cu-Kα radiation (λ = 0.154 178 nm). The absorption spectrum was recorded on a UV-2100 Schimadzu UV–VIS spectrophotometer using quartz cells. Transition electron microscopy (TEM) micrographs were taken with a Hitachi Model H-800 transmission electron microscope, using an accelerating voltage of 200 kV.

Fig. 1 shows the XRD pattern of a sample of CdS produced by γ-irradiation and is compared with the data of the JCPDS file.[11] The CdS particles were identified as β-CdS which belongs to the cubic crystal system. The broad peaks indicate that the dimensions of the CdS nanoparticles are very small. Employing Scherrer's equation,[12] the mean size of the CdS nanoparticles was estimated to be 2.3 nm.

The TEM image of the CdS sample of Fig. 1 is shown in Fig. 2, which reveals that small particles aggregate into secondary particles because of their extremely small dimensions and high surface energy. Therefore the size and the size distribution of the nanoparticles is difficult to determine precisely by simply viewing the TEM image.

The influence of the absorbed dose on the CdS nanoparticle size was studied by recording the absorption spectra of solutions irradiated with different absorbed doses, using aqueous solutions containing the same concentration of SDS as reference. Fig. 3 shows that the absorption spectra are structured and their absorption onset is in the violet wavelength range. It has been established that for relatively small semiconductor particles, the absorption spectrum provides a direct measure of the size of the crystallites.[2,13–15] By comparing the position of shoulders with the results of ref. 2, the particles are estimated to be *ca.* 1.5 nm in diameter. Fig. 3 also shows the progressive shift of the

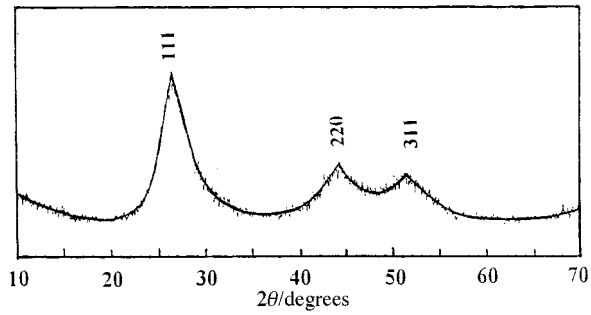

Fig. 1 XRD pattern of a CdS sample produced by γ-irradiation

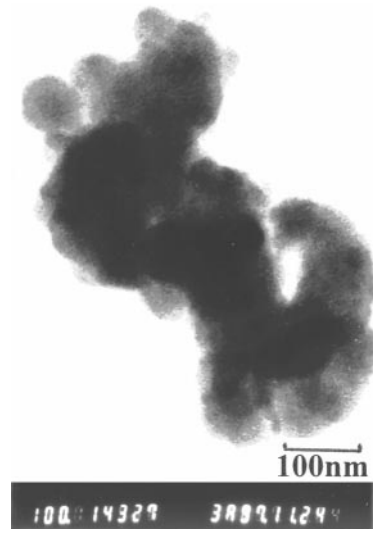

Fig. 2 TEM image of the CdS sample shown in Fig. 1

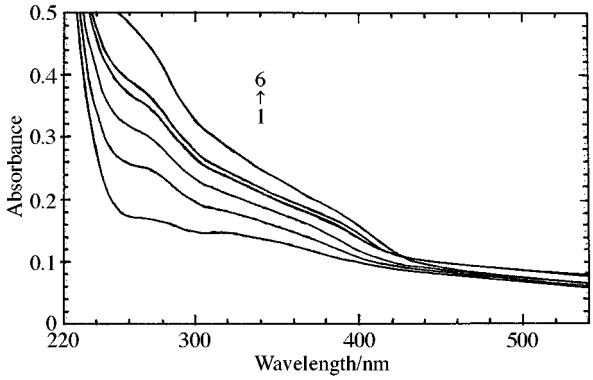

Fig. 3 Absorption spectra of irradiated CdS solutions with various absorbed doses: (1) 1000 Gy, (2) 1500 Gy, (3) 2000 Gy, (4) 2500 Gy, (5) 3000 Gy, (6) 4000 Gy. Solution: 2×10^{-4} M $CdSO_4 \cdot 8/3H_2O$, 2×10^{-4} M $Na_2S_2O_3$, 0.3 M Pr^iOH, 0.05 M SDS. Reference: aqueous solution containing the same concentration of SDS.

absorption onset with increasing irradiation dose, indicating that CdS particles gradually grow larger. The difference (in nm) between the position of the onset and the mean position of the shoulders characterizes the size polydispersity.[16] Fig. 3 reveals that the size polydispersity of the particles increases as the absorbed dose increases but does not change distinctly. It seems that the observed homogeneity is a direct consequence of the homogeneous mixing of $S_2O_3^{2-}$ and Cd^{2+}, and the even production of S^{2-} upon γ-irradiation.

Upon standing for ten days, the irradiated solutions show almost no change in absorption spectra. The system in the absence of SDS displays a weaker absorption, which shifts to longer wavelength and decays quickly upon aging. The surfactant layer around the small particles provides a microenvironment without water and other ions and inhibits the reverse (corrosion) reaction as well as coalescence; this favors the stabilization of small colloidal semiconductor particles.

In summary, γ-irradiation of the mixture provides promptly released and evenly dispersed S^{2-} ions, which then rapidly precipitate with Cd^{2+} ions and aggregate *in situ*. The surfactant prevents the small particles from coming into close contact and growing larger. A detailed study of the mechanism of the γ-irradiation route is underway and will be reported elsewhere.

Notes and References

† E-mail: xlxu@mail.ach.ustc.edu.cn

1 R. F. Service, *Science*, 1996, **271**, 920.
2 A. Henglein, *Chem. Rev.*, 1989, **89**, 1861.
3 M. L. Steigerwald and L. E. Brus, *Acc. Chem. Res.*, 1990, **23**, 183.
4 N. Herron, Y. Wang and H. Eckert, *J. Am. Chem. Soc.*, 1990, **112**, 1322.
5 P. Lianos and J. K. Thomas, *Chem. Phys. Lett.*, 1986, **125**, 299.
6 W. Chen, Z. Lin, Z. Wang and L. Lin, *Solid State Commun.*, 1996, **100**, 101.
7 M. K. Oda, K. Eguchi and H. Ari, *Chem. Commun.*, 1996, 1209.
8 T. Sugimoto, G. E. Dirige and A. Muramatsu, *J. Colloid Interface Sci.*, 1996, **182**, 444.
9 A. J. Elliot, D. R. McCracken, G. V. Buxton and N. D. Wood, *J. Chem. Soc., Faraday Trans.*, 1990, **86**, 1539.
10 G. V. Buxton and D. C. Walker, *Radiat. Phys. Chem.*, 1984, **23**, 207.
11 Joint Committee on Powder Diffraction Standards, *Diffraction Data File*, No. 10-454, JCPDS International Center for Diffraction Data, Pennsylvania, 1991.
12 H. P. Klug and E. A. Leroy, *X Ray Diffraction Procedures*, Wiley, New York, 1974, p. 656.
13 T. Vossmeyer, L. Katsikas, M. Giersig, I. G. Popovic and H. Weller, *J. Phys. Chem.*, 1994, **98**, 7665.
14 R. Rossetti, J. L. Ellison, J. M. Gibson and L. E. Brus, *J. Chem. Phys.*, 1984, **80**, 4464.
15 A. P. Alivisatos, *Science*, 1996, **271**, 933.
16 S. Modes and P. Lianos, *J. Phys. Chem.*, 1989, **93**, 5854.

Received in Cambridge, UK, 20th April 1998; 8/02910E

Reversible anion binding in aqueous solution at a cationic heptacoordinate lanthanide centre: selective bicarbonate sensing by time-delayed luminescence

Rachel S. Dickins,[a] Thorfinnur Gunnlaugsson,[a] David Parker*[a]† and Robert D. Peacock[b]

[a] *Department of Chemistry, University of Durham, South Road, Durham, UK DH1 3LE*
[b] *Department of Chemistry, University of Glasgow, Glasgow, UK G12 8QQ*

Reversible displacement of up to two metal bound water molecules at a coordinately unsaturated, cationic lanthanide centre is signalled by increases in the luminescence intensity or lifetime of the emissive lanthanide: selective chelation of hydrogencarbonate is consistent with emission spectroscopic, ESMS and CPL measurements.

Intrigued by the prospect of using a charged luminescent lanthanide receptor for the time-gated signalling of anion binding (hinted at by a brief communication[1]), we set out to prepare well-defined coordinately unsaturated Tb and Eu complexes wherein stepwise displacement of quenching metal-bound water molecules by a given anion would be signalled by increases in the lifetime or emission intensity of the lanthanide luminescence. Accordingly the enantiopure complexes $[EuL^1]^{3+}$ and $[TbL^1]^{3+}$ were devised, wherein the remote chiral centre at carbon determines the chirality of the complex in a similar fashion to that established with the Ln complexes of L^2.[2] In aqueous solution, the complexes complete their coordination number by binding two displaceable water molecules.

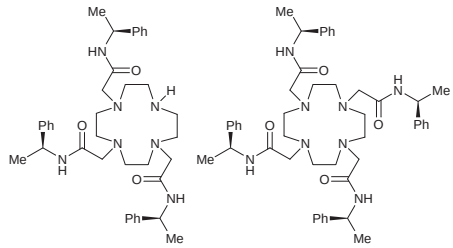

L^1 L^2

Reaction of 3 equiv. of (*R*)-*N*-(2-chloroethanoyl)-2-phenylethylamine with 1-(4-methoxyphenylsulfonyl)-1,4,7,10-tetraazacyclododecane (Cs_2CO_3, DMF, 70 °C) followed by reductive deprotection (Na, aq. NH_3, EtOH–THF) allowed isolation of the heptadentate, tri-*N*-substituted ligand L^1 (mp 64 °C), following chromatography on neutral alumina (CH_2Cl_2 to 1% MeOH–CH_2Cl_2). Complexation with $Eu(CF_3SO_3)_3$ or $Tb(CF_3SO_3)_3$ in anhydrous MeCN gave tripositive complexes. Analysis of $[EuL^1]^{3+}$ by ^1H NMR spectroscopy in D_2O and CD_3OD revealed only one set of four distinct broadened resonances for the most shifted axial ring proton (293 K, D_2O: +27.0, +16.1, +13.5, +8.8 ppm). A low temperature EXSY spectrum at −20 °C, clearly indicated that there were four stereoisomeric complexes (in a ratio of *ca.* 3.5 : 1 : 0.5 : 0.25) undergoing exchange by arm rotation but not ring inversion at this temperature.

The luminescence lifetimes for each complex were measured in H_2O and D_2O, initially in the absence and presence of a 10-fold excess of a selection of halides and oxyanions (Table 1). Such measurements allow the estimation of the number of coordinated water molecules ($q' = 2$ for each in the absence of added anions). A correction has been made in each case to account for the quenching effect of closely diffusing OH and amide NH oscillators.[3] In the presence of base (I = 0.14 NaCl), the lifetime of $[TbL^1]^{3+}\cdot(OH_2)_2$ increased by almost 50% and the q' value fell from 1.9 to 0.4, consistent with deprotonation and concomitant displacement of the second water molecule by Cl^-—leaving one quenching OH oscillator. The labilisation of metal bound water molecules following deprotonation is well-known with di- and poly-aqua metal ion species.[4]

Lifetimes for $[TbL^1]^{3+}$ in the presence of $I^-/Br^-/Cl^-$ and NO_3^- (pH 5.5–6.5) were virtually unchanged, whereas F^-, acetate and sulfate competed with H_2O for binding and led to the displacement of up to one of the quenching water molecules. Most striking was the behaviour of hydrogencarbonate (pH 6.5) and carbonate (pH 11) in which *both* water molecules were displaced leading to a large change in the measured lifetime (Table 1). This pattern of behaviour was echoed in lifetime measurements with $[EuL^1]^{3+}$, suggesting formation of a chelated adduct with HCO_3^-/CO_3^{2-} (Scheme 1).[5]

Further support for the distinctive nature of the anion adduct was provided by examination of the Eu emission spectra wherein the hypersensitive $\Delta J = 2$ transition at 618 nm is particularly sensitive to coordination environment.[2] The intensity ratio of the $\Delta J = 2 : \Delta J = 1$ emission bands was 4 : 1 (10-fold excess of anion in D_2O) for HCO_3^-, and the other values measured were all lower (*e.g.* F^-, 4 : 3; $H_2PO_4^-$, 2 : 1). A titration of the change in the intensity of one component of the 620 nm band as a function of added bicarbonate ($[Eu\cdot L^1]^{3+}$ = 2 × 10^{-3} M, 0–40 mM $NaHCO_3$, 293 K, 0.1 M MES buffer,

Table 1 Effect of added anions (10 mM complex) on the rate constants (±10%) for depopulation of the excited states of $[Eu\cdot L^1]^{3+}$ and $[Tb\cdot L^1]^{3+}$, and corrected inner-sphere hydration numbers, q'

Complex/anion	k_{H_2O}/ms^{-1}	k_{D_2O}/ms^{-1}	$\Delta k_{corr.}$/ms^{-1}	q'_{is} (±0.15)
$[Tb\cdot L^1]^a$ ($CF_3SO_3^-$)	0.84	0.39	0.39	1.91
OH^- (pH 11)	0.59	0.45	0.08	0.39
F^-	0.61	0.36	0.19	0.93
I^-, Br^- or Cl^-	0.87	0.39	0.42	2.06
NO_3^-	0.84	0.42	0.36	1.76
$CH_3CO_2^-$	0.74	0.42	0.26	1.27
SO_4^{2-}	0.66	0.37	0.23	1.13
$H_2PO_4^-$	0.57	0.37	0.14	0.69
Citrate	0.55	0.41	0.08	0.39
HCO_3^-	0.54	0.45	0.03	0.15
CO_3^{2-c}	0.53	0.46	0.01	0.05
$[Eu\cdot L^1]^d$ ($CF_3SO_3^-$)	3.85	1.54	1.81	2.14
CO_3^{2-}	2.33	1.64	0.19	0.24
HCO_3^{-b}	2.44	1.67	0.27	0.34
$H_2PO_4^-$	2.63	1.54	0.59	0.74
SO_4^{2-}	2.94	1.67	0.77	0.96
$CH_3CO_2^-$	3.45	1.69	1.26	1.58
F^-	2.70	1.39	0.81	1.01

[a] Corrections for Tb complexes were to allow for the effect of closely diffusing OH oscillators (−0.06 $^{-1}$ in Δk) and used $q'_{is} = A'\Delta k_{corr.}$ where $A' = 4.9$. [b] Unchanged in 0.14 M NaCl; reduces to $q' = 0.25$ in 50 mM HCO_3^-. [c] At pH 11. [d] For Eu complexes, the correction for closely diffusing OH oscillators was −0.25 and −0.08 ms^{-1} for each amide NH, with $A' = 1.25$.

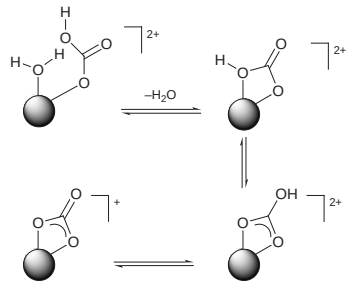

Scheme 1

Figs. 1 and 2), revealed an increase in the intensity of the band, with a switching factor of six, consistent with reversible formation of a 1:1 adduct. A similar titration with added dihydrogenphosphate showed much less change, with an enhancement factor of two in the range 0–5 mM. It is well known that hydrogenphosphate prefers to bind in a monodentate manner,[6] while carboxylates and carbonates often chelate, particularly to metal centres in higher coordination numbers.[7] Support for the existence of such a species came from ESMS, where in addition to the observation of an $[TbL^1OH]^+$ species at 831, peaks at 875.2 and 876.2 were apparent, together with 437.6/438.2 (⅔), whose relative abundance was in agreement with the isotope pattern calculated for $[TbL^1 + HCO_3]^+$ [calc.: 875.34 (100%) and 876.34 (51%)]. The structure of the excited state of lanthanide complexes is probed sensitively by circularly polarised luminescence (CPL).[8] CPL spectra for $[EuL^1]^{3+}$ in the presence of $CF_3SO_3^-$, $H_2PO_4^-$ and HCO_3^- (at pH 6.5 in an

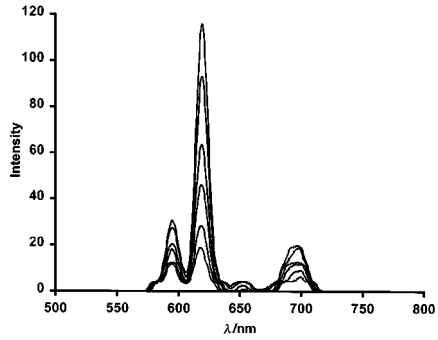

Fig. 1 Variation of luminescence intensity at 620 nm for $[EuL^1](CF_3SO_3)_3$ (pH 6.4 to 7.3 in 0.1 M MES buffer, 293 K, 1 mM) as a function of added $NaHCO_3$ in the range 1–30 mM. Emission intensities and lifetimes were unchanged (±7%) in the presence of 140 mM NaCl and in control experiments varying pH only (Perkin Elmer LS50B fluorimeter).

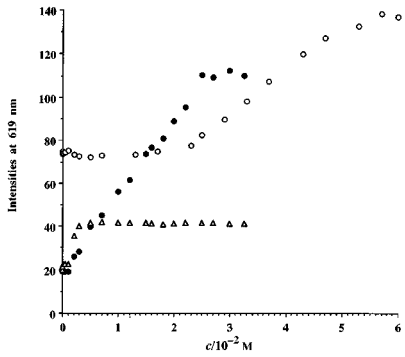

Fig. 2 Increase in the Eu emission intensity as a function of added $NaHCO_3$ (●; 293 K, pH 6.5–7.3 in an 0.1 M MES buffer, $\lambda_{exc.}$ 257 nm), NaH_2PO_4 (△) and $NaHCO_3$ (○) in a simulated clinical background of anions ($H_2PO_4^-$ 0.9 mM, 2.3 mM lactate, 145 mM Cl^-, 0.13 mM citrate)

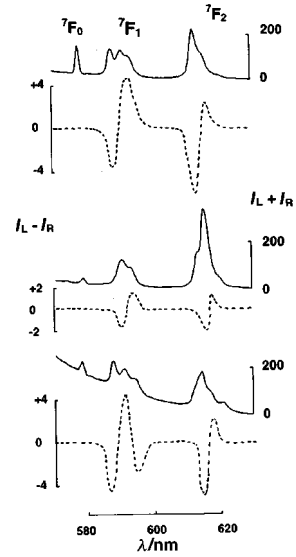

Fig. 3 Circularly polarised luminescence spectra for $[EuL^1](CF_3SO_3)_3$ (pD 6.9, 293 K, 1.0 mmol dm^{-3} in 0.1 M MES) (upper), and in the presence of 10 mM $H_2PO_4^-$ (bottom) and 40 mM HCO_3^- (centre). With $H_2PO_4^-$, the three $\Delta J = 1$ components have alternating signs while with HCO_3^- the highest energy component is absent and the signs are reversed.

0.1 M MES buffer) (Fig. 3) were measured. Distinctively different CPL spectra were found in the presence of both HCO_3^- and HPO_4^{2-} consistent with a pronounced change in the helicity of the 'anion-bound' europium excited-state structure.

In summary, measurements of the luminescence lifetime or intensity of emissive, coordinatively unsaturated enantiopure lanthanide complexes in aqueous media afford a new way of signalling the presence of selected oxyanions. Such systems may also act as simple models for studying anion binding in water that is relevant to the mode of action of alkaline phosphatase and carbonic anhydrase.

We thank the EPSRC, the BBSRC, the Royal Society and the University of Durham for support.

Notes and References

† E-mail: david.parker@durham.ac.uk

1 N. Sabbatini, M. Guardigli, J.-M. Lehn and G. Mathis, *J. Alloys Compds.*, 1992, **180**, 363.
2 R. S. Dickins, J. A. K. Howard, C. W. Lehmann, J. M. Moloney, D. Parker and R. D. Peacock, *Angew. Chem., Int. Ed. Engl.*, 1997, **36**, 521; R. S. Dickins, J. A. K. Howard, J. M. Moloney, D. Parker, R. D. Peacock and G. Siligardi, *Chem. Commun.*, 1997, 1747.
3 D. Parker and J. A. G. Williams, *J. Chem. Soc., Dalton Trans.*, 1996, 3613; M. P. O. Wolbers, F. C. J. M. van Veggel, J. W. Hofstraat, F. A. J. Geurts and D. N. Reinhoudt, *J. Chem. Soc., Perkin. Trans. 2*, 1997, 2275.
4 D. T. Richens, *The Chemistry of Aqua Ions*, Wiley, Chichester, 1997.
5 In Scheme 1, chelation in principle may involve attack by bound bicarbonate at the metal centre or nucleophilic attack by the bound OH group at the trigonal carbonyl centre: such mechanisms may be distinguishable by appropriately controlled isotope incorporation experiments in $^{18}OH_2$.
6 B. Schneider and M. Kabelac, *J. Am. Chem. Soc.*, 1998, **120**, 161.
7 C. J. Carrell, H. L. Carrell, J. Erlebacher and J. P. Glusker, *J. Am. Chem. Soc.*, 1988, **110**, 8651.
8 J. P. Riehl and F. S. Richardson, *Chem. Rev.*, 1986, **86**, 1; E. Huskowska, C. L. Maupin, D. Parker, J. A. G. Williams and J. P. Riehl, *Enantiomer*, 1997, **2**, 381.

Received in Cambridge, UK, 5th June 1998; 8/04255A

Zirconocene-coupling routes to conjugated polymers: soluble poly(arylenedienylene)s

Brett L. Lucht and T. Don Tilley*†

Department of Chemistry, University of California, Berkeley, Berkeley, California, 94720-1460, USA

Zirconocene-coupling of (–C≡CCH$_2$C(CH$_2$OC$_6$H$_{13}$)$_2$CH$_2$C≡C–arylene–)$_n$ polymers, followed by hydrolysis, provides a convenient, versatile route to soluble, diene-arylene polymers.

During the past decade, there have been extensive investigations on the synthesis and properties of conjugated polymers.[1] Since conjugated polymers tend to have poor solubility properties, they are frequently synthesized from more soluble precursor polymers,[2] or their solubilities are increased *via* incorporation of alkyl or alkoxy substituents as solubilizing groups.[3] Soluble conjugated polymers are desired as processible materials for numerous optoelectronic applications.[1] Particular attention has focused on poly(*p*-phenylenevinylene) derivatives, but it is clear that rather small changes in chemical structure can result in substantial changes in electronic properties for the polymer.[4]

We have recently developed a metal-coupling route to soluble poly(*p*-phenylenedienylene)s,[5] which involves palladium-catalyzed cross-coupling of diiodobenzenes with terminal dialkynylalkanes,[6] intramolecular zirconocene coupling of the alkyne units, and hydrolysis of the resulting zirconacyclopentadiene polymers[7] (Scheme 1). Variations of substituents on the phenyl ring (alkyl *versus* alkoxy) and the size of the exocyclic ring allow tuning of optical absorbances from 316–524 nm and emissions from 437–619 nm.[5] We now report a new method for the preparation of soluble conjugated polymers, based on zirconocene coupling (Scheme 2). This procedure is more versatile in that it allows for incorporation of a wide variety of aromatic units into the backbone of soluble poly(arylenedienylene)s.

Polycondensations of **1** with dibromoarenes were catalyzed by Pd(PPh$_3$)$_4$/CuI in a mixture of THF and diisopropylamine for 12–16 h at 50 °C.‡ Polymers **2a–g** were isolated as brown tars in 76–86% yield after purification by standard aqueous workup and removal of solvent. The crude polymers, which are highly soluble in THF, toluene and CHCl$_3$, contained trace quantities of the catalyst (by NMR spectroscopy). However, their structures were confirmed by ^{1}H NMR and IR spectroscopy. The IR spectra of **2a–g** contain ν(C≡C) stretches in the range 2212–2230 cm^{-1}, and their molecular weights (as determined by gel permeation chromatography, GPC; polystyrene standards) varied from 6100–20 000 (M_w; PDI ≈ 2).

Polymers **2a–g** were converted to deeply colored arylene-zirconacyclopentadiene polymers *via* additions to a solution of zirconocene, generated by the addition of Bu^{n}Li to zirconocene dichloride at −78 °C.[7b] These metal-containing polymers were converted directly to the corresponding poly(arylenedienylene)s **3a–g** by addition of aqueous HCl.§ Polymers **3a–g** were isolated as waxy solids in 82–91% yield after purification by standard aqueous workups. They are quite soluble in toluene, CHCl$_3$ and THF, and their molecular weights (Table 1) are similar to those for the precursor polymers **2a–g**, indicating that no chain degradation had occurred. The chemical structures of the polymers were determined by ^{1}H NMR and IR spectroscopies and combustion analyses.¶ The spectral data for polymers **3a–e** are consistent with the structures given in Scheme 2. Thus, the ^{1}H NMR spectra for these polymers contain vinylic and allylic resonances in the expected integrated ratios. Also, the IR spectra reveal no evidence for ν(C≡C) absorbances, indicating nearly quantitative conversion of alkyne to alkene units.

Our previous study indicated that the preparation of poly(*p*-phenylenedienylene)s *via* a multi-step process involving the conversion of one polymer to another is potentially susceptible to incomplete conversions and incorporation of defects into the backbone.[5] The vinylic and allylic regions of the ^{1}H NMR spectra of poly(arylenedienylene)s **3f** and **3g** suggest incomplete conversion. The vinylic and allylic ^{1}H NMR resonances for **3f** consist of one primary set of resonances (> 80% by integration) along with additional resonances with lower intensities. This suggests that the polymer contains minor defects (< 20%). The vinylic and allylic ^{1}H NMR resonances for **3g** are extremely broad and ill-defined, suggesting that the conversion of **2g** to **3g** results in a complex mixture of products with few diene units. The lack of observed ν(C≡C) absorbances in IR spectra of polymers **3f** and **3g** is consistent with partial conversion, since the alkynyl absorbances of **2f** and **2g** are very weak. Given the steric bulk of the arene spacers in **2f** and **2g**, we attribute the incomplete conversions for these polymers to unfavorable interactions between the arene group and the

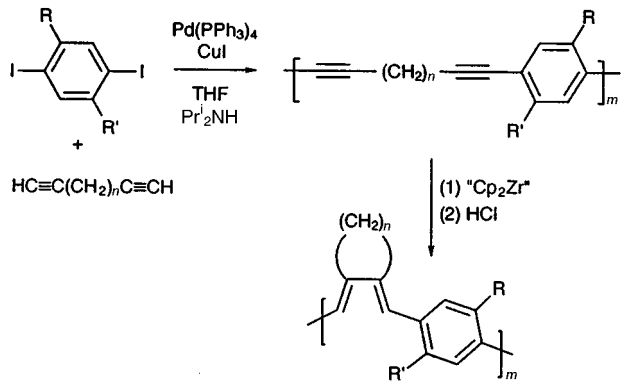

Scheme 1

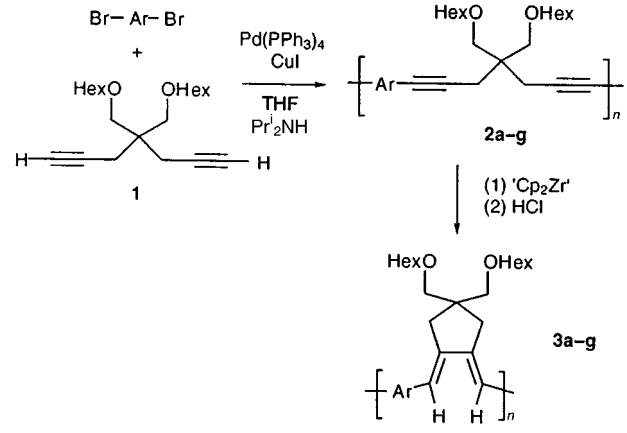

Scheme 2

Table 1 Optical and molecular weight data for polymers **3a–g**

	Ar	M_n/M_w[a]	λ_{max} (Abs)/nm	λ_{max} (Em)/nm	Color
a		3700/7400	422	482	Orange
b	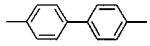	3500/7000	396	470	Blue–green
c		4700/12000	446	548	Orange
d		3600/7200	538	569	Violet
e		13000/27000	360	463	Yellow
f		5000/11000	410	490	Orange
g	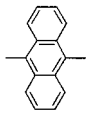	4800/13000	[b]	[b]	Orange

[a] Molecular weights were determined by GPC *vs*. polystyrene standards. [b] The optical properties were not investigated due to incomplete conversion.

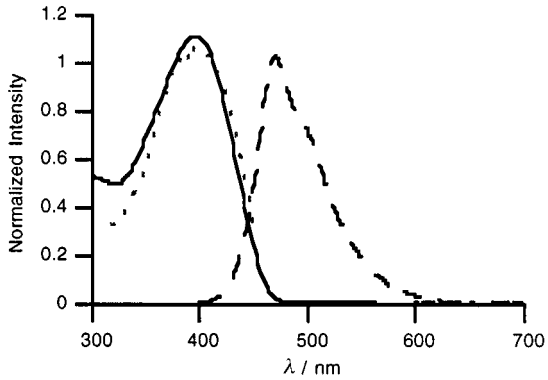

Fig. 1 Absorption (——), emission (-----) and excitation (·····) spectra of **3b**

zirconocene fragment. This is supported by observations on model zirconocene couplings with alkynes,[8] and semi-empirical PM3 calculations.

The optical properties of polymers **3a–g** were investigated by absorption, emission and excitation spectroscopy. The spectral data for polymers **3a–g** are summarized in Table 1, and Fig. 1 presents absorption, emission and excitation spectra for polymer **3b**. The observed optical properties vary considerably, according to the structure of the aromatic rings. The absorption spectrum of the pyridine-containing polymer **3c** is red-shifted (λ_{max} = 548 nm) upon treatment with 3.0 M HCl to form the pyridinium cation **3c**·HCl, as has been observed in related polymers.[9] Note that incorporation of a thiophene group leads to a red-shift (with respect to polymer **3a**), while incorporation of tetrafluorophenylene results in a blue shift. For polymer **3b**, the excitation spectrum reproduces the absorption spectrum, and the photoluminescence quantum yield is 0.043.[5,10] The photoluminescence quantum yields for **3a** and **3c–f**, on the other hand, are low ($\Phi < 0.01$). The excitation spectra for **3a** and **3c–f** exhibit maxima at shorter wavelength (by 40–120 nm) than the respective absorption λ_{max} values. Based on our previous study, we suggest that this may be attributed to efficient emission from defect sites resulting from incomplete conversion to the diene-polymer.[5]

We are currently investigating the photoluminescent and electroluminescent properties of thin films of polymer **3b**. In addition, further evaluation of the use of zirconocene couplings for the preparation of conjugated polymers is in progress.

Notes and References

† E-mail: tdtilley@socrates.berkeley.edu

‡ Polymer **2a**. A 100 ml Schlenk flask was charged with 1,4-dibromobenzene (0.59 g, 2.5 mmol), $Pd(PPh_3)_4$ (0.13 g, 0.12 mmol), CuI (0.04 g, 0.21 mmol), Pr^i_2NH (7.0 ml) and THF (15.0 ml). To this solution was added **1** (0.80 g, 2.5 mmol), and the reaction mixture was allowed to stir for 16 h at 50 °C. The reaction mixture was diluted with $CHCl_3$ (100 ml) and washed with diluted NH_4OH (2 × 75 ml, 1.0 M) and H_2O (75 ml). The organic layer was dried with Na_2SO_4 and the solvent was removed by rotary evaporation. This yields **2a** (79%, 0.78 g) as a light yellow–brown gummy solid. δ_H(300 MHz, $CDCl_3$) 0.86 (t, *J* 7.2, 6 H, CH_3), 1.27 (m, 8 H, CH_2), 1.33 (m, 4 H, CH_2), 1.55 (m, 4 H, CH_2), 2.61 (s, 4 H, CH_2), 3.43 (t, *J* 6.8, 4 H, CH_2O), 3.47 (s, 4 H, CH_2O), 7.29 (s, C_6H_4, 4 H); ν(film, KBr)/cm^{-1} 2954, 2930, 2859, 2223 (C≡C), 1507, 1465, 1376, 1261, 1113, 1020, 836, 800; M_n/M_w = 3600/6100 by GPC.

§ Polymer **3a**. A 100 ml Schlenk flask was charged with Cp_2ZrCl_2 (1.0 g, 3.4 mmol) and 30 ml of dry THF. The solution was cooled to −78 °C and Bu^nLi (4.0 ml, 1.6 M, 6.5 mmol) was added dropwise over 5 min. The reaction mixture was allowed to stir for 15 min at −78 °C, and then crude **2a** (0.78 g, 2.0 mmol of diyne) in 10 ml of dry THF was slowly added *via* cannula over 5 min. The reaction was allowed to stir under N_2 while warming to room temperature over 3–4 h, and was then stirred for an additional 1 h at room temperature. The phenylene zirconocyclopentadiene polymer was not isolated, but was converted directly to **3a** by addition of HCl (15 ml, 6 M). The reaction mixture was diluted with $CDCl_3$ (100 ml) and washed with HCl (75 ml, 0.5 M), H_2O (75 ml), $NaHCO_3$ (75 ml, 1.0 M), and H_2O (75 ml). The organic layer was dried over Na_2SO_4, and then the solvent was removed by rotory evaporation. This yields **3a** (85%, 0.66 g) as an orange wax. δ_H(300 MHz, $CDCl_3$) 0.87 (br, 6 H, CH_3), 1.26 (br, 12 H, CH_2), 1.53 (br, 4 H, CH_2), 2.75 (br, 4 H, CH_2), 3.23 (br, 4 H, CH_2), 3.39 (br, 4 H, CH_2), 6.99 (br, 2 H, CH), 7.43 (br, 4 H, C_6H_4); ν(film, KBr)/cm^{-1} 3021, 2954, 2930, 2857, 2793, 1598, 1464, 1376, 1261, 1112, 877; M_n/M_w 3700/7400 by GPC; (Calc. for $C_{27}H_{40}O_2$: C, 81.8; H, 10.18. Found: C, 77.5; H, 9.62%).

¶ As expected for conjugated polymers, the combustion analyses typically gave values for the carbon content that were low by a few percent.

1 W. J. Feast and R. H. Friend, *J. Mater. Sci*., 1990, **25**, 3796; A. G. MacDiarmid and A. J. Epstein, *Faraday Discuss. Chem. Soc*., 1989, 317; A. O. Patil, A. J. Heeger and F. Wudl, *Chem. Rev*., 1988, **88**, 183; H. W. Gibson, *Polymer*, 1984, **25**, 3; J. M. Tour, *Chem. Rev*., 1996, **96**, 537; D. D. C. Bradley, *Synth. Met*., 1993, **54**, 410; J. Roncali, *Chem. Rev*., 1997, **97**, 173; A. Kraft, A. C. Grimsdale and A. B. Holmes, *Angew. Chem., Int. Ed. Engl*., 1988, **37**, 402.

2 P. M. Lahti, D. A. Modarelli, F. R. Denton, R. W. Lenz and F. E. Karasz, *J. Am. Chem. Soc*., 1988, **110**, 7258; D. L. Gin, V. P. Conticello and R. H. Grubbs, *J. Am. Chem. Soc*., 1992, **114**, 3167; J. H. Burroughs, D. D. C. Bradley, A. R. Brown, R. N. Marks, K. Mackay, R. H. Friend, P. L. Burns and A. B. Holmes, *Nature*, 1990, **347**, 539; D. R. Gagnon, J. D. Capistran, F. E. Karasz and R. W. Lenz, *Polym. Bull*., 1984, **12**, 293.

3 R. Duran, M. Balluff, M. Wenzel and G. Wegner, *Macromolecules*, 1988, **21**, 2897; C. L. Gettinger, A. J. Heeger, J. M. Drake and D. J. Pine, *J. Chem. Phys*., 1994, **101**, 1673.

4 J. J. M. Halls, C. A. Walsh, N. C. Greenham, E. A. Marseeglia, R. H. Friend, S. C. Moratti and A. B. Holmes, *Science*, 1995, **376**, 498; M. Pan, Z. Bao and L. Yu, *Macromolecules*, 1995, **28**, 5151.

5 B. L. Lucht, S. S. H. Mao and T. D. Tilley, *J. Am. Chem. Soc*., 1998, **120**, 4354.

6 K. Sonogashira, Y. Tohda and N. Hagihara, *Tetrahedron Lett*., 1975, 4467; K. Sonogashira and S. Takahashi, *J. Synth. Org. Chem. Jpn*., 1993, **51**, 1053; D. L. Trumdo and C. S. Marvel, *J. Polym. Sci., Part A: Polym. Chem*., 1987, **25**, 839.

7 (*a*) W. A. Nugent, D. L. Thorn and R. L. Harlow, *J. Am. Chem. Soc*., 1987, **109**, 2788; (*b*) E. Negishi, F. E. Cederbaum and T. Takahashi, *Tetrahedron Lett*., 1986, **27**, 2829; (*c*) E. Negishi and T. Takahashi, *Acc. Chem. Res*., 1994, **27**, 124; (*d*) R. D. Broene and S. L. Buchwald, *Science*, 1993, **261**, 1696.

8 G. Harder, J. Nitschke, B. L. Lucht and T. D. Tilley, unpublished results.

9 M. J. Marsella, D. K. Fu and T. M. Swager, *Adv. Mater*., 1995, **7**, 145; J. Tian, C.-C. Wu, M. E. Thompson, J. C. Sturn and R. A. Register, *Chem. Mater*., 1995, **7**, 2190; J. Tian, C.-C. Wu, M. E. Thompson, J. C. Sturm, R. A. Register, M. J. Marsella and T. M. Swager, *Adv. Mater*., 1995, **7**, 395.

10 *Handbook of Organic Photochemistry*, ed. J. C. Scaiano, CRC Press, Boca Raton, FL, 1989; vol. 1, ch. 8, p 231.

Received in Columbia, MO, USA, 19th March 1998; 8/02538J

Influence of oxygen and nitrogen on ^{7}Li MAS NMR spectra of zeolite LiX-1.0

M. Feuerstein and R. F. Lobo*†

Center for Catalytic Science and Technology, Department of Chemical Engineering, University of Delaware, Newark, DE 19716, USA

Nitrogen and oxygen were adsorbed in dehydrated samples of zeolite LiX-1.0 [$(SiAlO_4)_{96}Li_{96}$]; the ^{7}Li MAS NMR spectra of these samples were compared with the spectrum of a sample studied in vacuum; it has been shown that the line assigned to Li cations at position SIII ($\delta_{iso} = -0.7$) is influenced by the different gases, whereas lines belonging to Li cations in front of six-rings do not change (SI′ line $\delta_{iso} = 0.4$, SII line $\delta_{iso} = -0.3$).

Characterization of the acid and adsorption sites of porous materials is a key issue for understanding the adsorption process and its technical applications. LiX zeolites are commercially useful adsorbents for the production of nitrogen from air in the PSA (pressure swing adsorption) process.[1] Adsorption experiments have shown that the capacity of nitrogen adsorption correlates with the amount of the Li extraframework cations in these zeolites.[2] Recently, Plevert and coworkers[3] investigated zeolite LiX-1.0 by neutron diffraction and located Li cations in four crystallographic sites (SI′, SII, SIII and SIII′). Li cations in zeolite LiX were also studied using a combination of ^{6}Li and ^{7}Li MAS NMR spectroscopy and neutron diffraction by Feuerstein and Lobo.[4] ^{6}Li and ^{7}Li MAS NMR spectra of dehydrated LiX-1.0 show three lines belonging to Li cations in sites SI′ (δ_{iso} = 0.4), SII ($\delta_{iso} = -0.3$), and SIII ($\delta_{iso} = -0.7$). Variable temperature ^{7}Li MAS NMR spectra have shown that the cations at SIII have to be considered mobile. In this earlier study zeolite samples were dehydrated in MAS NMR glass inserts and the inserts sealed while under vacuum. Here we discuss the changes in the ^{7}Li MAS NMR spectra caused by the presence of nitrogen and oxygen on LiX-1.0.

NaKX-1.0 zeolite was prepared following a method similar to the one published by Kuehl[5] and the as-synthesized form was exchanged to the Li form by several ion exchanges (see ref. 4). The LiX-1.0 zeolites were dehydrated at 673 K and 10^{-1} Pa. The integrity of the faujasite structure was confirmed by X-ray powder diffraction. ^{29}Si MAS NMR spectra show an Si/Al ratio of 1.0 and ^{27}Al MAS NMR spectra show only the existence of tetrahedral coordinated aluminium. ^{7}Li MAS NMR spectra were recorded at a resonance frequency of 116.6 MHz using a Bruker MSL-300 spectrometer and a 4 mm double bearing Bruker probe. The sample studied in vacuum was prepared in MAS glass inserts. For the oxygen adsorption a sample was dehydrated in a MAS glass insert and sealed after filling the tube with dry oxygen (79.1 kPa). Studies of adsorption of nitrogen were performed by packing the MAS NMR rotor in a nitrogen atmosphere using a glove box.

Fig. 1 shows the ^{7}Li MAS NMR spectra of zeolite LiX under three different sets of conditions: at vacuum, and after the adsorption of nitrogen and oxygen. The lines belonging to the Li cations in front of the six-ring windows [SI′ (δ_{iso} = 0.4), and SII ($\delta_{iso} = -0.3$)] do not change after the adsorption of the different gases. Cations at SI′ do not interact with the gas molecules because the van der Waals radii of N_2 and O_2 are too large to enter the β-cages and interact with this site. On the other hand, it is known from the refinements of the neutron diffraction data of LiX-1.0 that Li cations at SII are located inside the six-ring.[3,4] Therefore, the SII cations are effectively shielded by the framework atoms and do not interact with molecules in the supercages.

The line observed at $\delta_{iso} = -0.7$ in the ^{7}Li MAS NMR spectrum of the sample studied in vacuum and attributed to the SIII cations shifts slightly to a lower frequency after the adsorption of nitrogen. This observation is explained by the preferred interaction of the nitrogen molecules with the Li cations at SIII. Interestingly, ^{23}Na and ^{7}Li MAS NMR experiments of LiNaX zeolites having different Li exchange levels had shown that the site population of Li cations at SIII correlate directly with its nitrogen adsorption capacity.[6] The presence of oxygen causes a down-field shift of the SIII line. The shift to higher frequency is explained by the paramagnetism of the oxygen molecules. Several authors have observed shorter spin–lattice relaxation times (T_1) caused by the adsorption of oxygen.[7] Recently, Norby *et al.*[8] also observed a down-field shift of lines in ^{133}Cs MAS NMR spectra (recorded at variable temperature) of a CsNaY zeolite. The down-field shift was explained by the paramagnetic interaction between the unpaired electrons of the oxygen molecules and the Cs nucleus. Variable temperature ^{7}Li MAS NMR spectra of zeolite LiX-1.0 loaded with oxygen are depicted in Fig. 2. It can be observed that as a function of temperature, (i) the lines belonging to the six-ring cations show a small high-field shift, (ii) the line at high field belonging to the cations at SIII shows a down-field shift with decreasing temperature, (iii) the line width of the SIII line is increasing with decreasing temperature.

The high-field shift of the SI′ and SII components was also observed in ^{7}Li MAS NMR spectra of LiX-1.0 recorded at variable temperature with samples studied under vacuum in a MAS glass insert. Neutron diffraction experiments have shown that in LiX-1.0 a phase transition occurs at T = 220–230 K.[4] The symmetry changes from the cubic space group *Fd*3 to the orthorhombic space group *Fddd*. This phase transition might cause a slightly different environment of the Li cations and accounts for the change in the chemical shifts of the SI′ and SII lines. This point, however, is not completely understood and needs additional study. The down-field shift of the SIII line at lower temperatures is due to the temperature dependence of the

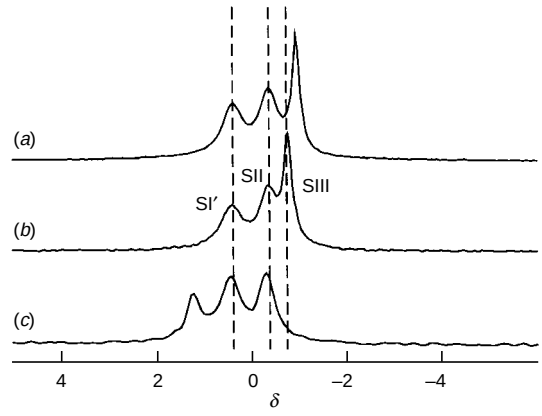

Fig. 1 ^{7}Li MAS NMR spectra of LiX-1.0, (*a*) after adsorption of nitrogen, (*b*) in vacuum, and (*c*) after adsorption of oxygen

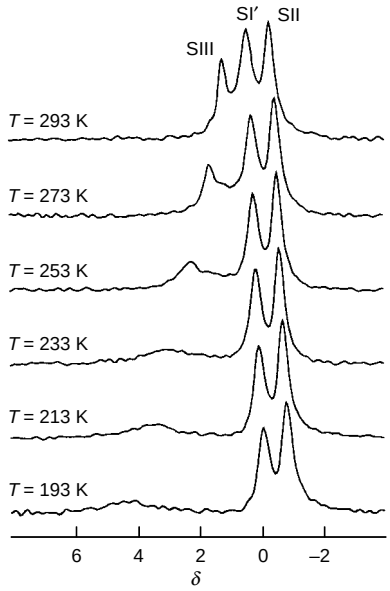

Fig. 2 Variable temperature ^{7}Li MAS NMR spectra of zeolite LiX after adsorption of oxygen

paramagnetic shift $\Delta\nu \approx 1/T$. The increase of the line broadening at lower temperatures is caused by two effects: a line broadening of the SIII line was previously observed in a study of ^{7}Li MAS NMR spectra of LiX in vacuum in the temperature range 233–253 K.[4] This effect is related to motion of the SIII cations and the line narrowing by the MAS NMR experiment. However, at temperatures below 233 K a narrow SIII line was again observed in the sample studied in vacuum. The ^{7}Li MAS NMR spectra shown in Fig. 2 differ in this point and the SIII line broadens further at temperatures below 233 K. The source of the other broadening is the paramagnetic shift due to the anisotropic interaction of the nuclear spin with the electron spin.[9]

The adsorption of oxygen can be easily used to test for accessibility of a cation site in microporous materials in general. The present work shows clearly the advantage of using ^{7}Li MAS NMR spectroscopy to study the adsorption sites in zeolite LiX, namely the Li cations at site SIII. We will discuss this topic in more detail in the future and compare the ^{7}Li MAS NMR spectra of different zeolites recorded under vacuum and after adsorption of nitrogen and oxygen.

Note added at proof: Plevert *et al.*[10] very recently reported a study of the paramagnetic shift of ^{6}Li in zeolite Li-X. Their results are fully consistent with the results presented here for ^{7}Li in zeolite Li-X.

Notes and References

† E-mail: lobo@che.udel.edu

1 C. C. Chao, *U.S. Pat.* 4 859 217, 1989.
2 J. F. Kirner, *U.S. Pat.* 5 268 023, 1993.
3 J. Plevert, F. Di Renzo, F. Fajula and G. Chiari, *J. Phys. Chem. B*, 1997, **101**, 10 340.
4 M. Feuerstein and R. F. Lobo, *Chem. Mater.*, in press.
5 G. H. Kuehl, *Zeolites*, 1987, **7**, 451.
6 M. Feuerstein, G. Engelhardt, P. L. McDaniel, J. E. MacDougall and T. D. Gaffney, submitted.
7 (*a*) R. H. Meinhold and D. M. Bibby, *Zeolites*, 1990, **10**, 74; (*b*) D. J. Cookson and B. E. Smith, *J. Magn. Reson.*, 1985, **63**, 217; (*c*) J. Klinowski, T. A. Carpenter and J. M. Thomas, *J. Chem. Soc., Chem. Commun.*, 1986, 956.
8 P Norby, F. I. Poshni, A. F. Gualtiere, J. C. Hanson and C. P. Grey, *J. Phys. Chem. B*, 1998, **102**, 839.
9 A. Nayeem and J. P. Yesinowski, *J. Chem. Phys.*, 1988, **89**, 4600.
10 J. Plevert, L. C. de Menorval, F. Di Renzo and F. Fajula, *J. Phys. Chem. B*, 1998, **102**, 3412.

Received in Bloomington, IN, USA, 21st April 1998; 8/02961J

Directed reactivity at a vanadium(II) thiolate center: synthesis and structure of a novel vanadium thiolate complex and its reaction product with azobenzene

John A. Davis, Christopher P. Davie, David B. Sable and William H. Armstrong*†

Department of Chemistry, Eugene F. Merkert Chemistry Center, Boston College, Chestnut Hill, Massachusetts, 02167-3860, USA

The vanadium(II) thiolate complex [V(tmeda)(DCTP)$_2$] [DCTP = 2,6-dichlorothiophenolate; tmeda = *N,N,N′,N′*-tetramethylethylenediamine] is obtained by the reaction of 2 equiv. of LiDCTP with [VCl$_2$(tmeda)$_2$] and reacts with azobenzene to yield the imido-containing complex [V(tmeda)(DCTP)$_2$(≡NPh)].

Low-valent vanadium thiolate complexes are of interest due in part to their potential relevance to the functioning of the alternative nitrogenase cofactor,[1] and to their presumed reactivity toward small reducible molecules in general. Recently, Coucouvanis and coworkers have shown that vanadium in a sulfur- and nitrogen-containing environment can catalyze the reduction of hydrazine to ammonia.[2] We have had considerable interest in lower-valent vanadium chalcogenide complexes, particularly with respect to their reactivity toward small molecules.[3] Herein we report the synthesis and structural characterization of a novel and rare mononuclear vanadium(II) thiolate complex containing labile coordination sites. We also provide an initial report on its reactivity with a substrate of relevance to dinitrogen reduction.

Complex **1**, [V(tmeda)(DCTP)$_2$] (DCTP = 2,6-dichlorothiophenolate; tmeda = *N,N,N′,N′*-tetramethylethylenediamine), is formed from the reaction of 2 equiv. of the lithium salt of 2,6-dichlorothiophenol (LiDCTP)‡ with 1 equiv. of [VCl$_2$(tmeda)$_2$].§[4] The crystal structure of **1** is shown in Fig. 1.¶ Bond distances and angles for **1** are consistent with those observed for other complexes of this sort, though crystallographically characterized vanadium(II) thiolates are still quite uncommon.[5] The structure of **1** reveals as well the presence of two dative, aryl–halide bonds. The observed V–Cl distances [2.515(2) Å, 2.510(2) Å] are well within the sum of radii of the atoms (3.131 Å),[6] and there is a slight lengthening of the Cl–C bond [1.758(9) Å] relative to the bond for the non-coordinated chlorine [1.727(9) Å]. While the ability of DCTP$^-$ to act as a bidentate ligand through sulfur and chlorine is unknown in the literature, such dative bonds with other halides are not unprecedented,[7] including one at a vanadium center.[8] The occurrence of such potentially labile bonds at a vanadium(II) center, and particularly at an electron-rich vanadium(II) thiolate center, gives hope that these might be sites for reactivity.

These hopes were realized in the reaction that yields complex **2**, [V(tmeda)(DCTP)$_2$(≡NPh)]. Complex **2**, whose ORTEP is shown in Fig. 2,¶ is obtained from the reaction of **1** with 0.5 equiv. of azobenzene.‖ The azobenzene is cleaved to give one phenylimido group per vanadium, with concomitant dissociation of one of the chlorine dative bonds of **1**. The other dative chlorine bond is now located *trans* to the imido group, and the V–Cl bond distance is, as expected from the strongly electron donating nature of the imido functionality, significantly lengthened relative to that seen in **1** [2.671(3) *vs*. 2.510(2) Å]. Structurally, **2** is quite similar to other vanadium(IV) and vanadium(V) arylimido complexes,[9] with the short V–N distance [1.670(7) Å] and nearly linear V–N–C angle [171.2(7)°] indicating a V≡NAr bonding moiety.[9] Other distances are as expected, though again it should be noted that

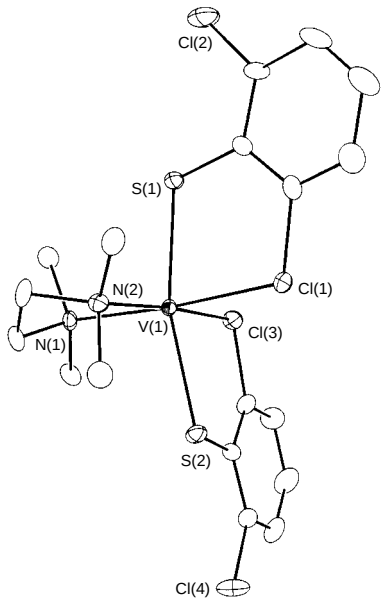

Fig. 1 ORTEP of [V(tmeda)(DCTP)$_2$], **1**, showing the 30% probability thermal ellipsoids and atom labelling scheme. Hydrogen atoms are omitted for clarity. Selected bond distances (Å) and angles (°) are as follows: V(1)–S(1) 2.468(2), V(1)–S(2) 2.464(2), V(1)–Cl(1) 2.515(2), V(1)–Cl(3) 2.510(2), V(1)–N(1) 2.206(6), V(1)–N(2) 2.220(7), S(1)–V(1)–S(2) 165.19(7), Cl(1)–V(1)–Cl(3) 92.84(6).

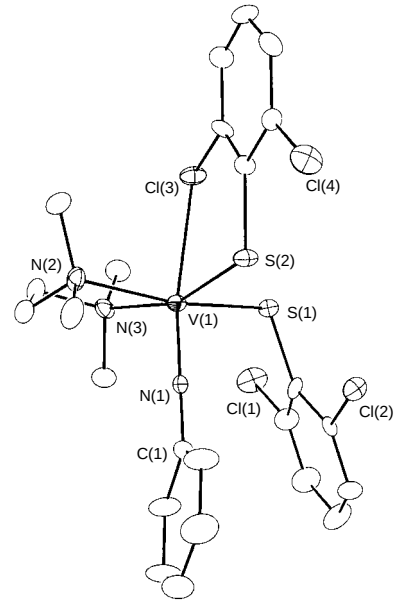

Fig. 2 ORTEP of [V(tmeda)(DCTP)$_2$(≡NPh)], **2**, showing the 30% probability thermal ellipsoids and atom labelling scheme. Hydrogen atoms are omitted for clarity. Selected bond distances (Å) and angles (°) are as follows: V(1)–N(1) 1.670(7), V(1)–S(1) 2.465(3), V(1)–S(2) 2.434(3), V(1)–Cl(3) 2.671(3), V(1)–N(2) 2.245(8), V(1)–N(3) 2.243(7), V(1)–N(1)–C(1) 171.2(7).

very few vanadium(IV) imido complexes have been structurally characterized.[10] Perhaps more interestingly, of those that have, none have been prepared from reduction of a diazo moiety. In fact, of all reported vanadium imido complexes, only one other is formed as the result of the reductive cleavage of a dinitrogen analogue.[11]

Compound **1** has also shown reactivity with many other small molecules such as *tert*-butyl isocyanide, 1,2-diphenylhydrazine and organic aldehydes. Elucidation of other reaction products and details of the reactivity of related compounds will be reported elsewhere. Further development of chemistry at other low-valent vanadium thiolate centers is under way.

For funding this work we thank the National Science Foundation (Grant CHE-8857455). We also thank the National Institutes of Health (Grant 1 S10 RR09008) and Boston College for providing funds for the purchase of a Siemens SMART single crystal X-ray diffractometer.

Notes and References

† E-mail: william.armstrong@bc.edu

‡ In a typical preparation, 5.372 g (30.00 mmol) of 2,6-dichlorothiophenol (Lancaster) were added to 20 ml of toluene. 18.75 ml (30.00 mmol) of 1.6 M *n*-butyllithium (Aldrich, in hexanes) were added over 0.5 h to the thiol solution with vigorous stirring. The resulting white precipitate was washed with hexane and dried, affording an approximately quantitative yield.

§ In a typical preparation, 1.00 g (2.82 mmol) of $[VCl_2(tmeda)_2]$[4] was dissolved in 20 ml of THF. Then 1.04 g (5.65 mmol) of LiDCTP were added at once with stirring. The light blue solution turned homogeneous and emerald green. Over 0.2 h a light green precipitate of $[V(tmeda)(DCTP)_2]$ appeared. The precipitate was filtered off, washed with diethyl ether and dried *in vacuo* to give analytically pure product in 68% yield. The yield could be improved by treating the remaining filtrate with pentane. The green precipitate was filtered off and rinsed with 5 ml of diethyl ether and then 5 ml of THF. The combined solids then afforded an 82% yield. Elemental analysis was satisfactory. EPR (X-band, CH_2Cl_2, 77 K): g = 5.33, multiline.

¶ *Crystal data* for **1**: a single crystal was mounted under the cold stream (−90 °C) of a Siemens SMART system. An initial collection of 60 frames of data yielded the crystal system (hexagonal) and unit cell [a = 7.6735(1), c = 65.3685(2) Å]. 20749 reflections were collected, of which 5003 were unique. The space group ($P6_1$, Z = 6) was chosen by systematic absences and successful refinement of the structure. No absorption correction was used. The structure was solved using SHELX 5.0 using anisotropic thermal parameters for all non-hydrogen atoms to values of R_1 = 7.35%, wR_2 = 15.7% for $I > 2\sigma(I)$. For **2**·thf: a single crystal was mounted under the cold stream (−90 °C) of a Siemens SMART system. An initial collection of 60 frames of data yielded the crystal system (orthorhombic) and unit cell [a = 13.621(4), b = 15.254(4), c = 30.410(7) Å]. 17675 reflections were collected, of which 10152 were unique. The space group ($P2_12_12_1$, Z = 2) was chosen by systematic absences and successful refinement of the structure. No absorption correction was used. The structure was solved using SHELX 5.0 using anisotropic thermal parameters for all non-hydrogen atoms to values of R_1 = 8.40%, wR_2 = 13.72% for $I > 2\sigma(I)$. CCDC 182/902.

‖ In a typical preparation, 0.25 g (0.478 mmol) of **1** was suspended with stirring in 20 ml of THF. Addition of 0.044 g (0.239 mmol) of azobenzene (Aldrich) yielded a yellow–green heterogeneous mixture which was then refluxed and became dark brown and homogeneous over 2 h. The solution was filtered, concentrated and cooled, affording brown crystals in 65% yield. Analysis was satisfactory. EPR (X-band, THF, 77 K): g = 2.0, 8 lines.

1 R. R. Eady, in *Advances in Inorganic Chemistry*, ed. A. G. Sykes, Academic, San Diego, 1991, vol. 36, pp. 77–101 and references therein.
2 S. M. Malinak, K. D. Demadis and D. Coucouvanis, *J. Am. Chem. Soc*., 1995, **117**, 3126.
3 W. C. A. Wilisch, M. J. Scott and W. H. Armstrong, *Inorg. Chem*., 1988, **27**, 4333; C. R. Randall and W. H. Armstrong, *J. Chem. Soc., Chem. Commun*., 1988, 986; L. Gelmini and W. H. Armstrong, *J. Chem. Soc., Chem. Commun*., 1989, 1904; M. J. Scott, W. C. A. Wilisch and W. H. Armstrong, *J. Am. Chem. Soc*., 1990, **112**, 2429; D. B. Sable and W. H. Armstrong, *Inorg. Chem*., 1992, **31**, 161; H. H. Murray, S. G. Novick, W. H. Armstrong and C. S. Day, *J. Cluster Sci*., 1993, **4**, 439; P. J. Bonitatebus, Jr., S. K. Mandal and W. H. Armstrong, *Chem. Commun.*, 1998, 939.
4 J. J. H. Edema, S. Gambarotta, A. Meetsma, A. L. Spek and N. Veldman, *Inorg. Chem*., 1991, **30**, 2062.
5 D. W. Stephan and T. T. Nadasdi, *Coord. Chem. Rev*., 1996, **147**, 147; $[V(pyt)_3]^-$: G. Henkel, B. Krebs and W. Schmidt, *Angew. Chem., Int. Ed. Engl*., 1992, **31**, 1366; $[V(tmeda)(pyt)_2]$: J. G. Reynolds, S. C. Sendlinger, A. M. Murray, J. C. Huffman and G. Christou, *Angew. Chem., Int. Ed. Engl*., 1992, **31**, 1253; J. G. Reynolds, S. C. Sendlinger, A. M. Murray, J. C. Huffman and G. Christou, *Inorg. Chem*., 1995, **34**, 5745; [V(tmeda)('S_4')]: W. Tsagkalidis, D. Rodewald and D. Rehder, *J. Chem. Soc., Chem. Commun*., 1995, 165.
6 Values for Cl (van der Waals) and V (atomic) taken from J. Emsley, *The Elements*, Oxford University Press, Oxford, 1991, pp. 50, 210.
7 R. M. Catala, D. Cruz-Garritz, P. Sosa, P. Terreros, H. Torrens, A. Hills, D. L. Hughes and R. L. Richards, *J. Organomet. Chem*., 1989, **359**, 219; R. M. Catala, D. Cruz-Garritz, A. Hills, D. L. Hughes, R. L. Richards, P. Sosa and H. Torrens, *J. Chem. Soc., Chem. Commun*., 1987, 261; Y. A. Simonov, A. A. Dvorkin, G. S. Matuzenko, M. A. Yampol'skaya, T. S. Gifeisman, N. V. Berbeleu and T. I. Malinovskii, *Koord. Khim*., 1984, **10**, 1247; Y. A. Simonov, G. S. Matuzenko, M. M. Botoshanskii, M. A. Yampol'skaya, N. V. Gerbeleu and T. I Malinovskii, *Zh. Neorg. Khim*., 1982, **27**, 407; M. J. Burk, R. H. Crabtree and E. M. Holt, *J. Organomet. Chem*., 1988, **341**, 495; J. M. Casas, L. R. Falvello, J. Forniés and A. Martín, *Inorg. Chem*., 1996, **35**, 56.
8 V. C. Gibson, C. Redshaw, L. J. Sequeira, K. B. Dillon, W. Clegg and M. R. J. Elsegood, *Chem. Commun*., 1996, 2151.
9 D. E. Wigley, *Prog. Inorg. Chem*., 1995, **42**, 239, and references therein; W. A. Nugent and J. M. Mayer, *Metal Ligand Multiple Bonds*, John Wiley and Sons, New York, 1988.
10 N. Wiberg, H.-W. Häring and U. Schubert, *Inorg. Chem*., 1978, **17**, 1880; F. Preuss, H. Becker, J. Kaub and W. A. Sheldrick, *Z. Naturforsch., B: Anorg. Chem. Org. Chem*., 1988, **43**, 1195; S. Gambarotta, A. Chiesi-Villa and C. Guastini, *J. Organomet. Chem*., 1984, **270**, C49; J. H. Osborne, A. L. Rheingold and W. C. Trogler, *J. Am. Chem. Soc*., 1985, **107**, 7945.
11 For compound $[V(\equiv NPh)Cl(\mu\text{-}Cl)]_2$, M. Mazzanti, M. Khadkhodayan and W. H. Armstrong, *Abstracts of the 203rd National Meeting, ACS*, INOR No. 461, San Francisco, CA, 1992.

Received in Bloomington, IN, USA, 5th January 1998; revised manuscript received 27th May 1998; 8/04231D

Chromium(III) complexes bearing N,N-chelate ligands as ethene polymerization catalysts

Vernon C. Gibson,*[a]† Peter J. Maddox,[b] Claire Newton,[a] Carl Redshaw,[a] Gregory A. Solan,[a] Andrew J. P. White[a] and David J. Williams[a]

[a] *Department of Chemistry, Imperial College, Exhibition Road, London, UK SW7 2AY*
[b] *BP Chemicals, Sunbury Research Centre, Chertsey Road, Sunbury on Thames, Middlesex, UK TW16 7LN*

Novel chromium(III) ethene polymerization catalysts bearing bulky monoanionic N,N-chelate ligands are described.

Chromium supported on silica plays a central role in the world-wide production of polyethylene.[1] As heterogeneous catalysts they have not proved amenable to intimate study, and even to this day there remains an on-going debate about the oxidation state of the active chromium centres.[2] The development of homogeneous molecular chromium catalysts is therefore an important objective, since these offer the potential for understanding the *modus operandi* of supported chromium catalysts and may provide new opportunities for tuning activity and selectivity. A number of reports of molecular chromium catalysts have appeared in the recent literature,[3–6] the majority on half-sandwich chromium species as models for the active sites of chromocene-derived systems.[3,4]

Here we describe a series of coordinatively unsaturated chromium(III) ethene polymerization procatalysts bearing either β-diketimate or pyrrolide-imine ligands. A general feature of these ligands is the presence of bulky aryl substituents which offer protection to the active centre, a strategy that has proved successful for the stabilisation of new N,N-chelate catalysts based on early[7] and late transition metal systems.[8] A similar strategy has also recently been applied to a new catalyst system based on iron and cobalt.[9]

The chromium chloride complexes, **1** and **3**, were prepared in high yield by the treatment of $[CrCl_3(thf)_3]$ with the lithium salts of the β-diketimate ligand or the pyrrolide-imine ligand, respectively (Scheme 1).‡ The structures of **1** and **3** were confirmed by X-ray structure determinations.[10] Interestingly, only one β-diketimate ligand can be coordinated to chromium in **1**, while in **3** the less sterically demanding pyrrolide-imine ligand allows bis-chelation. It is also of note that the vacant sixth coordination site in **3** is unexpectedly occupied by a molecule of lithium chloride (as a thf solvate).

Complex **2**, the dimethyl derivative of **1**, has been prepared in good yield by treatment of **1** with trimethylaluminium (TMA). Crystals of **2** suitable for an X-ray structure determination§ were grown from a concentrated pentane solution. The structure is dimeric, the two crystallographically independent molecules both having C_{2h} symmetry and comprising in each case two slightly distorted square pyramidal Cr^{III} centres linked by chloride bridges, the remaining basal sites being occupied by bidentate β-diketimate ligands (Fig. 1). The apical position on each chromium centre is filled by a terminal methyl group with Cr–C distances of 2.037(7) and 2.042(8) Å for the two independent molecules. The 2,6-diisopropylphenyl rings are oriented almost orthogonally (*ca.* 87°) with respect to the basal plane.

In a similar way, complex **4** was obtained by treatment of **3** with TMA (Scheme 1). Crystals of **4** suitable for X-ray analysis were grown from a concentrated light petroleum (bp 40–60 °C) solution. The structure again reveals a five-coordinate square pyramidal Cr^{III} centre, this time coordinated basally to two chelating pyrrolide-imine ligands and apically to a terminal methyl group at 2.037(9) Å (Fig. 2). The complex has crystallographic C_2 symmetry about an axis passing through the Cr–Me bond, and the two independent Cr–N distances differ significantly, with that to the pyrrolide [2.026(5) Å] markedly shorter than that to the imine [2.073(4) Å] reflecting the formal anionic nature of N(1). The double bond character of the imine has been retained [1.318(7) Å] though there is some evidence for delocalisation between the imine and pyrrolide systems, C(5)–C(6) being short at 1.410(8) Å. As in **2**, the 2,6-diisopropylphenyl rings are steeply inclined (*ca.* 65°) to the basal plane. It is noteworthy that both of these structures provide rare examples of five-coordinate chromium(III) alkyls, only two other examples having been found on the CCDC database [to March 1998, 175 093 entries].[11]

A summary of the ethene polymerization tests for **1**–**4** is shown in Table 1. Solid polyethylene is obtained in all cases with samples displaying high molecular weights¶ and virtually no branching (by NMR). A comparison of the polymerisation runs 1–12 shows that similar activities are found for procatalysts bearing either β-diketimate (**1** and **2**) or pyrrolide-imine ligands (**3** and **4**), the highest activity being 75 g $mmol^{-1}$ h^{-1} bar^{-1} using **1** and diethylaluminium chloride (Et_2AlCl) activator (see run 2).

The nature of the activator is seen to have an important influence on activity; for example, alkylaluminium chloride activators are found to be more compatible with these

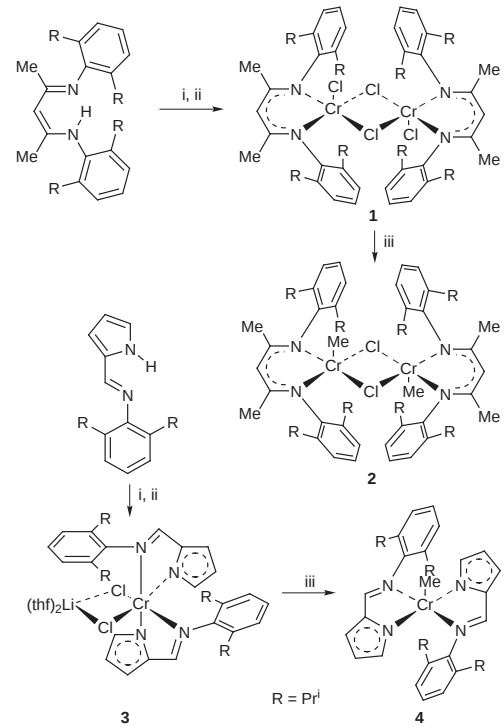

Scheme 1 Preparation of chromium complexes **1**–**4**. *Reagents and conditions*: i, Bu^nLi, −78 °C, thf; ii, $[CrCl_3(thf)_3]$, −78 °C, thf; iii, $AlMe_3$, thf.

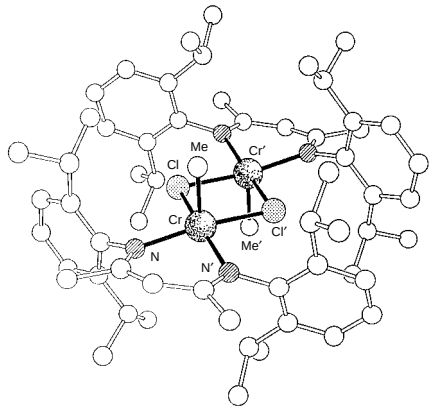

Fig. 1 The molecular structure of **2**. Selected bond lengths (Å) and angles (°) (values for the second independent molecule are in square brackets); Cr–Me 2.037(7) [2.042(8)], Cr–N 2.028(4) [2.031(4)], Cr–Cl 2.395(1) [2.393(1)]; Me–Cr–N 95.4(2) [96.8(2)], Me–Cr–Cl 97.8(2) [96.8(2)], N–Cr–N′ 91.3(2) [90.8(2)], Cl–Cr–Cl′ 80.3(1) [80.6(1)], N–Cr–Cl 92.7(1) [92.7(1)], N–Cr–Cl′ 165.7(1) [165.4(1)], Cr–Cl–Cr′ 99.7(1) [99.4(1)]. The transannular Cr···Cr distance is 3.66 Å [3.65 Å] and the chromium atom lies 0.25 Å [0.26 Å] out of its basal plane.

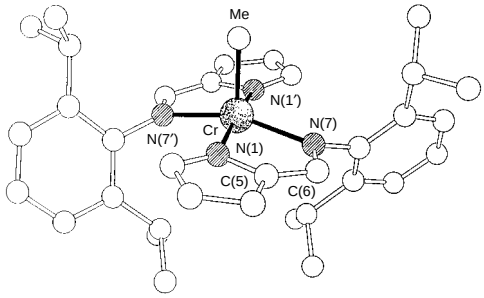

Fig. 2 The molecular structure of **4**. Selected bond lengths (Å) and angles (°); Cr–Me 2.037(9), Cr–N(1) 2.026(5), Cr–N(7) 2.073(4), C(5)–C(6) 1.410(8), C(6)–N(7) 1.318(7); Me–Cr–N(1) 93.4(2), Me–Cr–N(7) 100.4(1), N(1)–Cr–N(7) 80.9(2), N(1)–Cr–N(7′) 97.9(2), N(1)–Cr–N(1′) 173.2(4), N(7)–Cr–N(7′) 159.2(3).

Table 1 Results of ethene polymerisation runs using procatalysts **1**–**4**[a]

Run	Proctalyst (0.015 mmol)	Activator[b] (mmol/equiv.)	Yield PE[c]/g	Activity[d]/ g mmol^{-1} h^{-1} bar^{-1}
1	1	MAO (6.0/400)	0.12	4
2	1	Et_2AlCl (0.45/30)	2.25	75
3	1	$Et_2AlCl{\cdot}EtAlCl_2$ (0.3/20)	0.69	23
4	2	MAO (6.0/400)	0.15	10
5	2	Et_2AlCl (0.45/30)	0.80	54
6	2	$Et_2AlCl{\cdot}EtAlCl_2$ (0.3/20)	0.48	32
7	3	MAO (6.0/400)	0.08	5
8	3	Et_2AlCl (0.45/30)	1.04	69
9	3	$Et_2AlCl{\cdot}EtAlCl_2$ (0.45/30)	0.40	27
10	4	MAO (6.0/400)	0.04	3
11	4	Et_2AlCl (0.45/30)	1.05	70
12	4	$Et_2AlCl{\cdot}EtAlCl_2$ (0.45/30)	0.23	15

[a] *General conditions*: 1 bar ethene Schlenk test carried out in toluene (40 cm^3) at 25 °C, over 60 min, reaction quenched with dil. HCl and the solid PE washed with methanol (50 cm^3) and dried in a vacuum oven at 40 °C. [b] MAO = methylaluminoxane. [c] Solid polyethylene. [d] Activity reported per chromium centre.

procatalysts than methylaluminoxane (MAO). Moreover, diethylaluminium chloride (Et_2AlCl) is superior to aluminium sesquichloride ($Et_2AlCl{\cdot}EtAlCl_2$). Notably, the alkyl procatalysts **2** and **4** are inactive in the absence of activator.

The new catalyst types described herein represent a notable addition to the limited list of non-cyclopentadienyl chromium ethene polymerization catalysts[5,6] and highlight the importance of the choice of co-catalyst for optimal catalyst performance.

BP Chemicals Ltd is thanked for financial support. Dr W. Reed and Dr J. Boyle are thanked for GPC and NMR measurements, respectively.

Notes and References

† E-mail: V.Gibson@ic.ac.uk

‡ Satisfactory elemental analyses have been obtained.

¶ As a representative example, GPC analysis of the polyethylene obtained from run 8 afforded M_w = 293,000, M_n = 113,000; M_w/M_n 2.2. Care should be taken in the interpretation of these values, however, since in general the polymers derived from these polymerisations are not fully soluble in the 1,2,4-trichlorobenzene GPC solvent, even upon heating at 160 °C for several hours.

§ *Crystal data*: for **2**: $C_{60}H_{88}Cl_2Cr_2N_4{\cdot}0.5C_5H_{12}$, M = 1076.3, monoclinic, space group $C2/m$ (no. 12), a = 19.434(3), b = 21.764(2), c = 15.098(2) Å, β = 90.58(1)°, U = 6386(1) Å^3, Z = 4 (there are two crystallographically independent C_{2h} symmetric molecules in the asymmetric unit), D_c = 1.120 g cm^{-3}, μ(Cu-Kα) = 38.5 cm^{-1}, F(000) = 2316. A crimson prismatic needle of dimensions 0.33 × 0.17 × 0.13 mm was used. For **4**: $C_{35}H_{45}CrN_4$, M = 573.8, orthorhombic, space group $Fdd2$ (no. 43), a = 20.280(2), b = 34.103(4), c = 9.420(1) Å, U = 6515(2) Å^3, Z = 8 (the molecule has crystallographic C_2 symmetry), D_c = 1.170 g cm^{-3}, μ(Mo-Kα) = 3.79 cm^{-1}, F(000) = 2456. A green block of dimensions 0.37 × 0.37 × 0.10 mm was used. 4866 (1530) independent reflections were measured at 203 K on Siemens P4(PC) diffractometers with Cu-Kα—rotating anode source—(Mo-Kα) radiation using ω-scans for **2** (**4**), respectively. The structures were solved by direct methods and all of the major occupancy non-hydrogen atoms were refined anisotropically using full matrix least squares based on F^2 to give R_1 = 0.065 (0.049), wR_2 = 0.164 (0.094) for 3370 (1193) independent observed reflections [$|F_o| > 4\sigma(|F_o|)$, $2\theta \leqslant 120(50°)$] and 340 (182) parameters for **2** (**4**), respectively. The polarity of **4** was determined by a combination of R-factor tests [R_1^+ = 0.048, R_1^- = 0.050] and by use of the Flack parameter [x^+ = 0.10(1), x^- = 0.90(1)]. CCDC 182/903.

1 F. J. Karol, G. L. Garapinka, C. Wu, A. W. Dow, R. N. Johnson and W. I. Carrick, *J. Polym. Sci., Part A*, 1972, **10**, 2621; J. P. Hogan, *J. Polym. Sci., Part A*, 1972, **8**, 2637.
2 M. P. McDaniel, *Adv. Catal.*, 1985, **33**, 47; J. A. N. Ajjou, S. L. Scott and V. Paquet, *J. Am. Chem. Soc.*, 1998, **120**, 415.
3 For recent reviews, see: K. H. Theopold, *Chem. Eur. J.*, 1998, **3**, 15; K. H. Theopold, *CHEMTECH*, 1997, **27**, 26.
4 R. Emrich, O. Heinemann, P. W. Jolly, C. Krüger and G. P. J. Verhovnik, *Organometallics*, 1997, **16**, 1511.
5 F. J. Feher and R. L. Blanski, *J. Chem. Soc., Chem. Commun.*, 1990, 1614.
6 M. P. Coles, C. I. Dalby, V. C. Gibson, W. Clegg and M. R. J. Elsegood, *J. Chem. Soc., Chem. Commun.*, 1995, 1709.
7 J. D. Scollard and D. H. McConville, *J. Am. Chem. Soc.*, 1996, **118**, 10 008; V. C. Gibson, B. S. Kimberley, A. J. P. White, D. J. Williams and P. Howard, *Chem. Commun.*, 1998, 313.
8 L. K. Johnson, C. M. Killian and M. Brookhart, *J. Am. Chem. Soc.*, 1995, **117**, 6414; L. K. Johnson, S. Meeking and M. Brookhart, *J. Am. Chem. Soc.*, 1996, **118**, 267; C. M. Killian, D. J. Tempel, L. K. Johnson and M. Brookhart, *J. Am. Chem. Soc.*, 1996, **118**, 11 664; L. K. Johnson, C. M. Killian, S. D. Arthur, J. Feldman, E. F. McCord, S. J. McLain, K. A. Kreutzer, M. A. Bennett, E. B. Coughlin, S. D. Ittel, A. Parthasarathy, D. J. Tempel and M. S. Brookhart, *Pat. Appl.*, WO 96/23010, 1996, DuPont.
9 G. J. P. Britovsek, V. C. Gibson, B. S. Kimberley, P. J. Maddox, S. J. McTavish, G. A. Solan, A. J. P. White and D. J. Williams, *Chem. Commun.*, 1998, 849; B. L. Small, M. Brookhart and M. A. Bennett, *J. Am. Chem. Soc.*, 1998, **120**, 4049.
10 X-Ray data for **1** and **3** will be published elsehwere.
11 M. D. Fryzuk, D. B. Leznoff and S. J. Rettig, *Organometallics*, 1997, **16**, 5116; Y. Liang, G. P. A. Rheingold and K. H. Theopold, *Organometallics*, 1996, **15**, 5284.

Received in Exeter, UK, 14th April 1998; 8/02797H

Intramolecular macrocyclization of bis(5-methylthio-1,2-dithiole-3-thione)s with triethyl phosphite. A stereoselective route to macrocyclic (*Z*)-thioxodesaurines

Sandra Rudershausen,[a] Hans-Jürgen Holdt,*[a]† Helmut Reinke,[a] Hans-Joachim Drexler,[a] Manfred Michalik[b] and Joachim Teller[a]

[a] *Universität Rostock, Fachbereich Chemie, Buchbinderstraße 9, D-18051 Rostock, Germany*
[b] *Institut für Organische Katalyseforschung an der Universität Rostock e.V., D-18055 Rostock, Germany*

Intramolecular macrocyclizations of [oligo(oxyethylene)-ethylenedithio]bridged bis(5-methylthio-1,2-dithiole-3-thione)s 5a and b with $P(OEt)_3$ in *p*-xylene furnished the macrocyclic thioxodesaurin (*Z*)-6, thioxodesaurin (*E*)-7 and 1,3-dithiafulvene (*E*)-8, respectively.

2,4-Bis(2-oxoethylidene)-1,3-dithietanes are well-known as desaurines.[1,2] In these compounds, the electron-withdrawing groups at the 2,4-dimethylene-1,3-dithietane unit can be (*E*)- or (*Z*)-configured. (*E*)-Configuration was determined for the desaurines **1a**–**d** by X-ray analysis.[3] The well-known desaurin

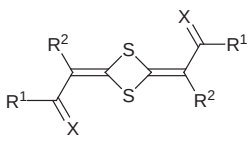

	X	R^1	R^2	ref.
1a	O	Ph	H	3(*a*)
1b	O	Me	Me	3(*b*)
1c	O	MeO	NC	3(*c*)
1d	O	Et	Ph	3(*d*)
(*E*)-**2**	S	MeS	MeS	5,7(*a*)

syntheses lead predominately to the thermodynamically stabilized (*E*)-isomer, or an (*E*)-/(*Z*)-mixture.[4] To the best of our knowledge the stereoselective synthesis of a (*Z*)-desaurin has not yet been reported.

Thioxoanalogous desaurines can be synthesized by reductive dimerization of 1,2-dithiole-3-thione derivatives containing an alkylthio substituent in the 5-position with $P(OEt)_3$.[5] Reaction of 4,5-bis(methylthio)-1,2-dithiole-3-thione[6] with $P(OMe)_3$, in refluxing benzene, yielded the (*E*)-thioxodesaurin (*E*)-**2** (35%) and its (*Z*)-isomer (*Z*)-**2** (15%).[5] We confirmed the stereochemistry of (*E*)-**2** by X-ray analysis.[7a] In (*E*)-**2** the eight sulfur and the six central carbon atoms lie almost in-plane. (*E*)-Isomers were formed exclusively by the dimerization of dodecylthio-substituted 1,2-dithiole-3-thiones and crowned 4,5-dithio-1,2-dithiole-3-thiones.[7b]

Here, we describe a novel macrocyclization reaction using bridged bis(5-methylthio-1,2-dithiole-3-thione)s **5** as precursors. Intramolecular cyclization of **5a** and **b** with $P(OEt)_3$ yielded the macrocyclic thioxodesaurin (*Z*)-**6**, thioxodesaurin (*E*)-**7** and 1,3-dithiafulvene (*E*)-**8**, respectively (Scheme 1). The length of the [oligo(oxyethylene)ethylene]dithio bridge in **5** determines the stereochemistry of the thioxodesaurin formed. With **5a** the crowned (*Z*)-thioxodesaurin (*Z*)-**6** was stereoselectively synthesized.

The precursors **5a**,**b** are obtainable in yields of up to 75% by alkylation of 4-mercapto-5-methylthio-1,2-dithiole-3-thione **3**‡ (2 equiv.) with 1,8-dibromo-3,6-dioxaoctane **4a** and 1,11-dibromo-3,6,9-trioxaundecane **4b**, respectively, in the presence of Cs_2CO_3 in DMF. Correct spectral data were obtained for both compounds. Compounds **5a**,**b** were intramolecularly cyclized under high dilution conditions with $P(OEt)_3$ in *p*-xylene. Compound **5a** provides one macrocyclic reaction product (*Z*)-**6** (20–25 %) as well as unidentified polymeric material. The ^{13}C NMR spectrum of (*Z*)-**6** revealed that this macrocycle contains the expected thioxodesaurin unit.§ The configuration of the thioxodesaurin unit in (*Z*)-**6** was determined by X-ray crystallographic analysis.¶ The crystal structure of (*Z*)-**6** shows a (*Z*)-configured planar thioxodesaurin moiety which is incorporated in a macrocyclic framework by a [bis(oxyethylene)ethylene]dithio chain [Fig. 1(*a*)]. Attempts to build CPK models of the (*E*)-isomer of (*Z*)-**6** revealed that the [bis(oxyethylene)ethylene]dithio chain is too short to bridge a planar (*E*)-thioxodesaurine unit. This is possibly the reason why the intramolecular cyclization of **5a** furnishes the (*Z*)-isomer stereoselectively. In the (*Z*)-thioxodesaurin moiety of (*Z*)-**6** the

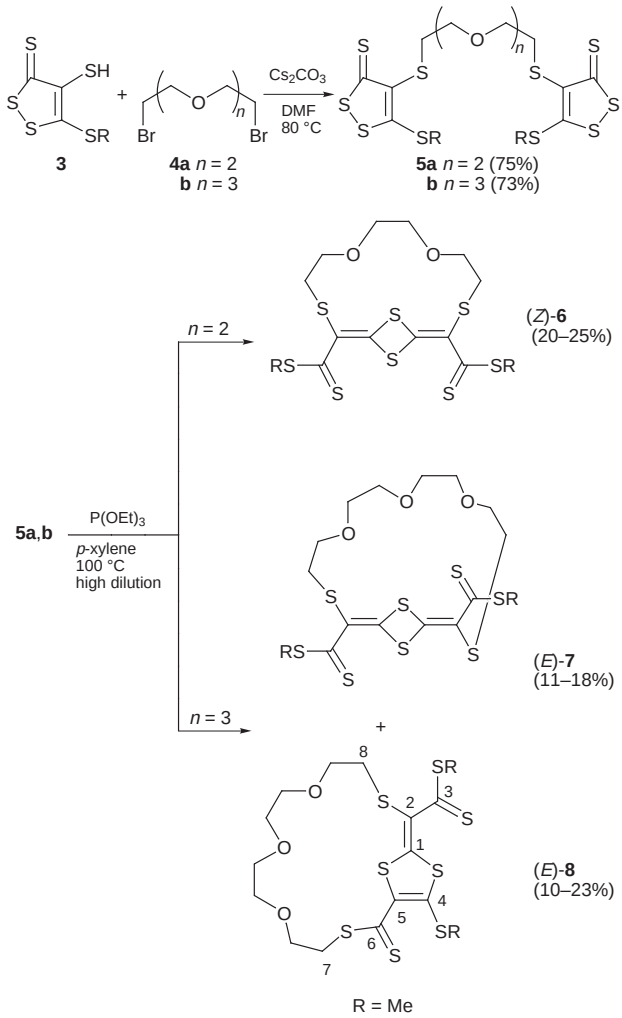

Scheme 1

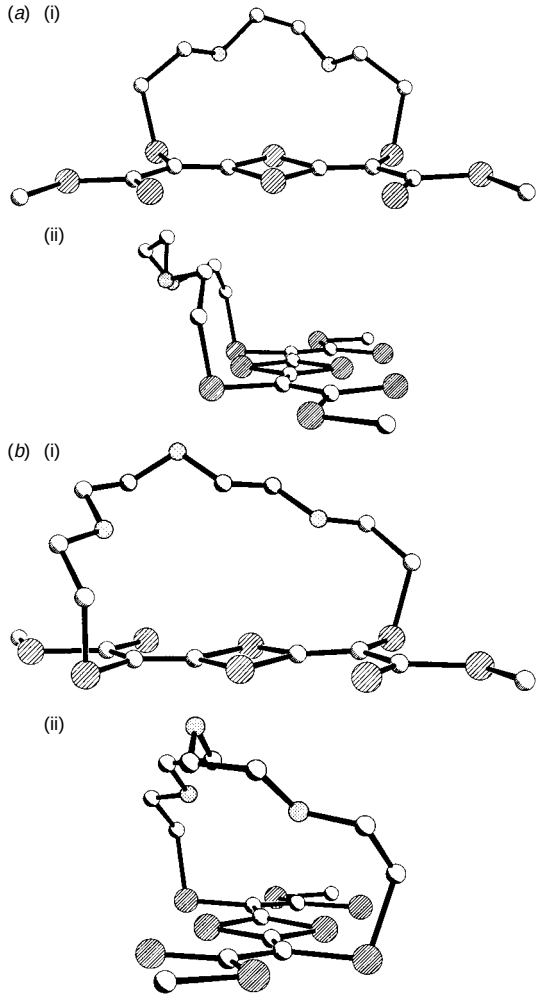

Fig. 1 Structures of the macrocyclic thioxodesaurines (*a*) (*Z*)-**6** and (*b*) (*E*)-**7** in the crystal: view of the molecules (i) orthogonal and (ii) parallel to the central 2,4-dimethylene-1,3-dithietane moiety

two carbon–carbon double bonds do not lie in line, as it is observed for the bonds in the (*E*)-thioxodesaurin units of (*E*)-**2**[7a] and (*E*)-**7** [Fig. 1(*b*)]. This deviation from 180° amounts to 9°.

In comparision to **5a**, bis(1,2-dithiole-3-thione) **5b** has a bridging chain with one more oxyethylene moiety. This chain is long enough to enable the intramolecular cyclization to form the (*E*)-thioxodesaurine (*E*)-**7** (11–18%). X-Ray analysis of crowned (*E*)-**7**¶ shows an *ansa*-compound-like molecular structure. The [tris(oxyethylene)ethylene]dithio chain, bridges the planar (*E*)-configurated thioxodesaurin unit like a handle. Since rotation of the (*E*)-thioxodesaurin moiety around the axis along the H_2C–S bonds is not possible, (*E*)-**7** has planar chirality. No (*Z*)-isomer was detected at the intramolecular cyclization of **5b**. On the contrary, we obtained the crowned 1,3-dithiafulvene (*E*)-**8** (10–23%). The molecular structure of (*E*)-**8** was determined *via* an X-ray structural investigation.[7b]

Mollier[5] and Pedersen[8] postulated thioacyl thioketenes as intermediates for the reaction of 5-alkylthio-1,2-dithiole-3-thiones with trialkyl phosphite, which dimerize in [2+2] cycloadditions to the thioxodesaurines. In a similar way bis(thioketene) intermediates of **5a**,**b** should form intramolecular macrocyclic thioxodesaurines (*Z*)-**6** und (*E*)-**7**. Compound (*E*)-**8**, which in its turn furnishes the thioxodesaurin (*E*)-**7,** cannot be formed by an intramolecular [2+3] cycloaddition of the bis(thioketene) intermediate. Therefore other thioketene intermediates must exist, at least in the reaction solution of **5b** with $P(OEt)_3$. The formation of a thioxodesaurin and a 1,3-dithiafulvene from α-thioxothioketene intermediates was recently proposed by Hartke *et al*.[9] A desaurin and a 1,3-dithiafulvene were obtained from α-oxothioketenes earlier by Voronkov.[10]

The intramolecular macrocyclization of bridged bis(5-methylthio-1,2-dithiole-3-thione)s with $P(OEt)_3$ is a simple synthetic route to macrocyclic (*Z*)- and (*E*)-thioxodesaurines and 1,3-dithiafulvenes.

We are synthesizing macrocyclic (*Z*)- and (*E*)-thioxodesaurines and 1,3-dithiafulvenes since we are interested in their redox properties and coordination chemistry. We would like to use these new macrocyclic and sulfur-rich ligands containing both endocyclic and exocyclic donor sites for the preparation of dinuclear metal complexes comprising simultaneously hard and soft metal centers, and as new components for supramolecular compounds. Full results will be reported in a full paper.

S. R. thanks the Bundesland Mecklenburg Vorpommern for a graduate stipendium.

Notes and References

† E-mail: hans-juergen.holdt@chemie.uni-rostock.de

‡ Synthesized from 4-benzoylthio-5-methylthio-1,2-dithiole-3-thione (ref. 6) by saponification with NaOMe in MeOH and reaction of the corresponding sodium thiolate with dilute HCl [ref. 7(*c*)].

§ *Selected data* for (*Z*)-**6**: δ_C(75.48 MHz, $CDCl_3$) 20.70 (SCH_3), 35.82 (SCH_2), 67.22 (SCH_2CH_2O), 70.42 (OCH_2CH_2O), 124.58 (*C*=CS_2), 163.79 (CS_2), 219.22 (C=S); For (*E*)-**7**: δ_C 20.70 (SCH_3), 35.78 (SCH_2), 69.96–71.11 (m, $SCH_2CH_2OCH_2CH_2O$), 72.27 ($OCH_2CH_2OCH_2CH_2O$), 124.79 (*C*=CS_2), 162.27 (CS_2), 218.90 (C=S); For (*E*)-**8**: δ_C 18.18 (C=CS*C*H_3), 21.05 (SCS*C*H_3), 36.64 (C-8), 38.11 (C-7), 67.08–71.66 (m; OCH_2), 117.48 (C-2), 129.92 (C-5), 149.60 (C-4), 166.75 (C-1), 204.96 (C-6), 211.53 (C-3).

¶ *Crystal data* for (*Z*)-**6**·$(CHCl_3)_{0.3}$: $C_{14.3}H_{18.3}Cl_{0.9}O_2S_8$, M = 514.56 g·mol^{-1}, trigonal, space group $R\bar{3}$, $a = b = c$ = 1689.0(1) pm, $\alpha = \beta = \gamma$ = 112.044(4)°, V = 3.3092(3) nm^3, D_c. = 1.532 Mg m^{-3}, Z = 6, F(000) = 1574.7, μ = 0.92 mm^{-1}, 3150 reflections collected in the scan range of $4.36 \leqslant 2\theta \leqslant 43.00°$, 2480 independent reflections, 2079 observed reflections, R1 [$2\sigma(I)$] = 0.0453, $R1$ (all data) = 0.0558, $wR2$ (all data) = 0.0773, GoF = 1.079 for 242 parameters and 3 restraints. On the three-fold axis 0.3 disordered molecules of $CHCl_3$ per molecule (*Z*)-**6** are found.

For (*E*)-**7**: $C_{16}H_{22}O_3S_8$, M = 518.82 g·mol^{-1}, triclinic, space group $P\bar{1}$, a = 960.0(3), b = 1066.1(4), c = 1221.2(5) pm, α = 70.16(2), β = 82.33(2), γ = 72.82(3)°, V = 1.1224(7) nm^3, D_c. = 1.535 Mg m^{-3}, Z = 2, F(000) = 540, μ = 0.81 mm^{-1}, 3324 reflections collected in the scan range of $3.54 \leqslant 2\theta \leqslant 44.00°$, 2724 independent reflections, 1573 observed reflections, $R1$ [$2\sigma(I)$] = 0.0566, $R1$ (all data) = 0.1155, $wR2$ (all data) = 0.1120, GoF = 1.329 for 244 parameters.

Siemens P4 diffractometer, Mo-Kα radiation (λ = 71.073 pm), room temperature. CCDC 182/908.

1 H. Bergreen, *Ber. Dtsch. Chem. Ges.*, 1888, **21**, 337.
2 P. Yates, D. R. Moore and T. R. Lynch, *Can. J. Chem.*, 1971, **49**, 1456.
3 (*a*) T. R. Lynch, I. P. Mellor, S. C. Nyburg and P. Yates, *Tetrahedron Lett.*, 1967, 373; (*b*) J. A. Kapecki, J. E. Baldwin and I. C. Paul, *J. Am. Chem. Soc.*, 1968, **90**, 5800; (*c*) G. Lábbe, P. Vangheluwe, S. Toppet, G. S. D. King and L. Van Meervelt, *Bull. Soc. Chim. Belg*., 1984, **93**, 405; (*d*) E. Schaumann, S. Scheiblich, U. Wriede and G. Adiwidjaja, *Chem. Ber.*, 1988, **121**, 1165.
4 H. Meier and N. Hanold, *Methoden Org. Chem., Houben-Weyl*, 4th edn., 1985, vol. E11/2, pp. 1584–1597.
5 J. Amzil, J.-M. Catel, G. LeCoustumer, Y. Mollier and J.-P. Sauve, *Bull. Soc. Chim. Fr.*, 1988, 101.
6 G. Steimecke, H.-J. Sieler, R. Kirmse, W. Dietzsch and E. Hoyer, *Phosphorus Sulfur*, 1982, **12**, 237.
7 (*a*) S. Rudershausen, H.-J. Drexler, H. Reinke, A. Knöchel and H.-J. Holdt, *Sulfur Lett*., 1995, **18**, 233; (*b*) S. Rudershausen, H.-J. Holdt and H.-J. Drexler, unpublished work.
8 C. O. Kappe, C. T. Pedersen, J.-M. Catel and Y. Mollier, *J. Chem. Soc., Perkin Trans. 2*, 1994, 351
9 K. Hartke, N. Rettberg, D. Dutta and H.-D. Gerber, *Liebigs Ann. Chem.*, 1993, 1081.
10 A. N. Mirskova, G. G. Levkovskaya, I. D. Kalikham, T. I. Vakulśkaya, V. A. Pestunovich and M. G. Voronkov, *Izv. Akad. Nauk. SSSR, Ser. Khim*., 1976, 2040 (*Chem. Abstr.*, 1977, **86**, 106439r). See also a review on thioketenes: E. Schaumann, *Tetrahedron*, 1988, **44**, 1827.

Received in Liverpool, UK, 7th April 1998; 8/02658K

Gas phase protonation of diazirines: a route to N-protonated diazomethanes

Takatsugu Matsumoto,[a] Shinjiro Kobayashi,[a] Masaaki Mishima,[a] Gennady V. Shustov[b] and Michael T. H. Liu*[c]†

[a] *IFOC, Kyushu University, Hakozaki, Higashi-ku, Fukuoka 812-81, Japan*
[b] *Department of Chemistry, University of Calgary, Calgary, AB, Canada T2N 1N4*
[c] *Department of Chemistry, University of Prince Edward Island, Charlottetown, PE, Canada C1A 4P3*

N-Protonated diazomethanes have been generated successfully *via* gas phase protonation of the corresponding diazirines.

The electronic distribution in diazoalkanes is usually represented by the resonance forms **I**–**IV**. The reactivities of diazo-

I **II** **III** **IV**

alkanes with acids and electrophiles are dominated by forms **II** and **III**; forms **I** and **IV** play no role at all. An early study by Wiberg[1] postulated N-protonation, which was subsequently revised in the light of more extensive data.[2–4] Conventionally, protonation occurs at the C atom of the diazoalkanes. Since their discovery in 1966, the diazirines, cyclic diazo compounds with three-membered rings, have been added to the ranks of the well-known aliphatic diazo compounds.[5] Herein we report the successful generation of the N-protonated diazoalkanes **4a**–**d** *via* the protonation of the corresponding diazirines **1a**–**d** (Scheme 1).

The gas phase protonation of diazirines **1a**–**d** and the equilibrium constant experiments were performed on an Extrel FTMS 2001 Fourier transform mass spectrometer equipped with a 3.0 T superconducting magnet with an inlet system described in previous studies.[6] The experiment was initiated by a pulsed electron beam (electron energy of 20 eV). The detectable intermediates in the cell are evidently either the protonated diazirines **3a**–**d** or the N-protonated diazoalkanes **4a**–**d**. Since the spectra gave only the masses of the protonated species, it is not possible to distinguish whether the protonated species appear in the closed (**3**) or open form (**4**).

In order to clarify this process, we determined the gas phase basicity (GB) of diazirines **1a**–**d** and proceeded with high-level *ab initio* computations of proton affinities of diazirines **1c**,**d** and their open forms **2c**,**d** (Scheme 1). In the case of the large molecules **1a**,**b** and **2a**,**b**, proton affinities for model com-

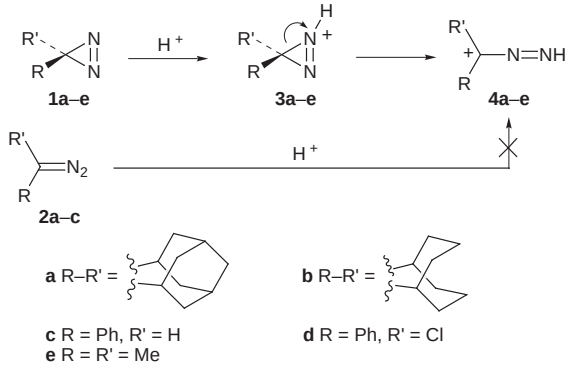

Scheme 1

pounds, 3,3-dimethyldiazirine **1e** and 2-diazopropane **2e** were calculated.

The GB of diazirine (D) was determined by measuring the equilibrium constants of the proton-transfer reactions between D and a reference base (B_0) of known basicity [eqn. (1)].[7]

$$D + B_0H^+ \rightleftharpoons DH^+ + B_0 \quad (1)$$

The equilibrium constants are given by the ratio of pressures for a reference base to a diazirine, $[B_0]/[D]$, and the ratio of intensities of spectra for the corresponding conjugate acid, $[DH^+]/[B_0H^+]$ [eqn. (2)]. In most cases, equilibrium was

$$K = \frac{[DH^+][B_0]}{[D][B_0H^+]} \quad (2)$$

attained after a reaction period of several hundred milliseconds to 1 s. The observed free energy changes [eqn. (3)] for

$$\Delta G° = -RT \ln K \quad (3)$$

respective proton transfer equilibria and the selected GB values are summarized in Table 1. For the case of **1d**, we adopted the threshold technique[8] instead of the equilibrium method because the amount of the conjugate acid ion formed in the cell was too small to be measured quantitatively. When bases having lower basicity than butyronitrile (GB = 184.4 kcal mol^{-1}) were used as reference bases, the proton transfer reaction from the protonated reference base to the neutral **1d** occurred to give the protonated **1d**. On the other hand, when reference bases with higher basicity than acetone (GB = 187.9 kcal mol^{-1}) were used, the proton transfer reaction from the protonated reference base to the neutral **1d** was not observed. The results suggest that the basicity of **1d** would be intermediate between those of acetone and butyronitrile, *i.e.* GB = 186.4 ± 1 kcal mol^{-1}. The ΔGB values are provided for comparison. The basicities of

Table 1 Gas phase basicities[a] and proton affinities[b] of ammonia, diazirines **1a**–**e** and diazoalkanes **2c**–**e**

Species	GB/ kcal mol^{-1}	ΔGB/ kcal mol^{-1}	PA/ kcal mol^{-1}	ΔPA/ kcal mol^{-1}
NH_3	195.6	0.0	202.4	0.0
			(202.5)	(0.0)
1a	194.2	1.4		
1b	193.7	1.9		
1c	187.6	8.0	176.7	25.7
			(178.7)	(23.8)
1d	186.3	9.3	171.0	31.4
1e			177.1	25.3
			(179.6)	(22.9)
2c			192.8	9.6
			(193.7)	(8.8)
2d			194.1	8.3
2e			197.2	5.2
			(199.0)	(3.5)

[a] Experimental data. [b] Derived with B3LYP/6-31 + G* and B3LYP/6-311 + G** (in parenthesis).

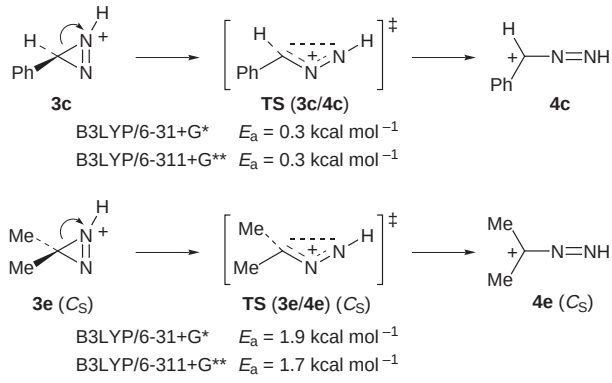

Scheme 2

diazirines **1a** and **1b** are stronger than **1c** and **1d** by approximately 6 kcal mol^{-1}.

The geometry optimizations and frequency calculations were carried out at the B3LYP hybrid density functional theoretical level with the internal 6-31 + G* and 6-311 + G** basis sets, using procedures implemented in the GAUSSIAN 94 system of programs.[9] Zero-point vibrational energy (ZPVE) corrections were scaled by a 0.98 factor. The proton affinities of diazirines **1c**–**e** and diazoalkanes **2c**–**e** obtained as the differences in the total energies of the neutral and the protonated forms, including the ZPVE corrections, are given in Table 1. The differences (ΔPA) in the calculated proton affinities (PA) between species **1c**–**e**, **2c**–**e** and a reference compound (NH_3) are also provided. Because the measured ΔGB values of the 3,3-dialkyldiazirines **1a** and **1b**, of 1.4 and 1.9 kcal mol^{-1}, and of the 3-aryldiazirines **1c** and **1d**, of 8.0 and 9.3 kcal mol^{-1}, are in much closer agreement with the ΔPA values calculated (B3LYP/6-31 + G*) for model diazoalkane **2e** (5.2 kcal mol^{-1}), and the aryldiazoalkanes **2c** (9.6 kcal mol^{-1}) and **2d** (8.3 kcal mol^{-1}) than for diazirines, we deduce that the detected species in the cell are the N-protonated diazoalkanes. As expected, the calculated PA for C-protonation of 2-diazopropane is higher (217.2 kcal mol^{-1}, B3LYP/6-311 + G**) than the PA for its N-protonation (199.0 kcal mol^{-1}). Moreover, the low calculated activation barriers for the conversion of N-protonated diazirines **3c**,**e** into the corresponding N-protonated diazoalkanes **4c**,**e** (Scheme 2) confirm the ease of the ring opening in the N-protonated diazirines under the experimental conditions.

The chemistry of the N-protonated diazoalkane in the cell is interesting due to the following observations. In particular, protonation of **3a** leads to an ion with the mass of the protonated azine **5a**, and this could occur by ring opening of the protonated diazirine **3a** into N-protonated 2-diazoadamantane **4a**, which reacts with neutral diazirine **1a** to yield the expected the protonated azine **5a**. The N-protonated 2-diazoadamantane **4a**, *m*/*z* 163, decays with the concomitant growth of the protonated azine **5a**, *m*/*z* 297, in the time frame of the experiment (1 s). A plausible mechanism of this reaction is the nucleophilic displacement by the neutral diazirine **1a** of the activated N-protonated 2-diazoadamantane **4a**. This is followed by proton transfer in concert with nitrogen extrusion to yield the protonated azine, as depicted in Scheme 3.

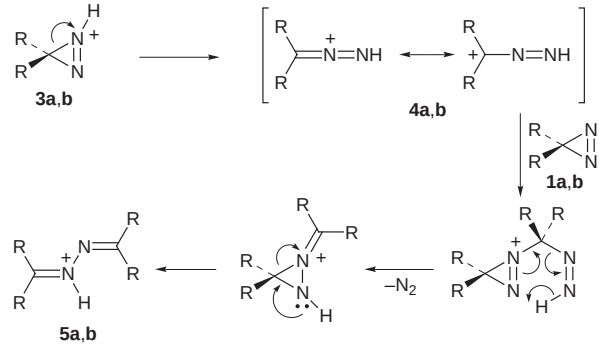

Scheme 3

The diazoalkane **2b** (*m*/*z* 151) has a gas phase basicity similar to that of **2a** but the formation of the protonated azine **5b** (*m*/*z* 273) occurs at a slower rate, possibly resulting from the steric effects of the flexibility on the bicyclo ring in **4b**. In contrast, the N-protonated diazoalkanes **4c**,**d** remain unreactive with their respective neutral diazirine parents even after 3 s. This may be so because the phenyl substituent in these species decreases the electrophilicity of the targeted carbon owing to the π-donor ability of the phenyl ring.

In conclusion, we have shown that N-protonated diazomethanes can be generated *via* protonation of the corresponding diazirines. Our experiments also indicate that some of the N-protonated species are reactive and can undergo further reaction with neighbouring molecules.

M. T. H. Liu thanks the NSERC of Canada for financial support.

Notes and References

† E-mail: liu@upei.ca

1 K. B. Wiberg and J. M. Lavanish, *J. Am. Chem. Soc.*, 1966, **88**, 365.
2 K. B. Wiberg and J. M. Lavanish, *J. Am. Chem. Soc.*, 1966, **88**, 5272.
3 F. Cook, H. Shechter, J. Bayless, L. Friedman, R. L. Foltz and R. Randall, *J. Am. Chem. Soc.*, 1966, **88**, 3870.
4 H. Zollinger, *Diazo Chemistry 1 and 2*, VCH, New York, 1994.
5 *Chemistry of Diazirines*, ed. M. T. H. Liu, CRC Press, Boca Raton, Florida, 1987.
6 M. Mishima, S. Usui, H. Inoue, M. Fujio and Y. Tsuno, *Nippon Kagaku Kaishi*, 1989, 1262; M. Mishima, T. Ariga, T. Matsumoto, S. Kobayashi, H. Taniguchi, M. Fujio, Y. Tsuno and Z. Rappoport, *Bull. Chem. Soc. Jpn.*, 1996, **69**, 445.
7 R. W. Taft, *Prog. Phys. Org. Chem.*, 1983, **14**, 247.
8 J.-L. M. Abboud, R. Notario, E. Ballesteros, M. Herreros, O. Mó, M. Yáñez, J. Elguero, G. Boyer and R. Claramunt, *J. Am. Chem. Soc.*, 1994, **116**, 2486.
9 M. J. Frisch, G. W. Trucks, H. B. Schlegel, P. M. W. Gill, B. G. Johnson, M. A. Robb, J. R. Cheeseman, T. A. Keith, G. A. Petersson, J. A. Montgomery, K. Raghavachari, M. A. Al-Laham, V. G. Zakrewski, J. V. Oritz, J. B. Foresman, J. Cioslowski, B. B. Stefanov, A. Nanayakkara, M. Challacombe, C. Y. Peng, P. Y. Ayala, W. Chen, M. W. Wong, J. L. Andres, E. S. Replogle, R. Gomperts, R. L. Martin, D. J. Fox, J. S. Binkley, D. J. Defrees, J. Baker, J. P. Stewart, M. Head-Gordon, C. Gonzalez and J. A. Pople, GAUSSIAN 94 (Revision D.2), Gaussian, Inc., Pittsburgh, PA, 1995.

Received in Corvallis, OR, USA, 6th April 1998; 8/02640H

Synthesis and properties of novel tetrathiafulvalene vinylogues

Yoshiro Yamashita,*† Masaaki Tomura, M. Badruz Zaman and Kenichi Imaeda

Institute for Molecular Science, Myodaiji, Okazaki 444-8585, Japan

The cation radical states of novel TTF vinylogues with *o*-substituted phenyl groups at the vinyl positions are thermodynamically stable, and X-ray analyses of the cation radical salts have revealed the planar structures of the TTF vinylogue parts and unique crystal structures.

Tetrathiafulvalene (TTF) vinylogues **1** with extended π-conjugation are promising electron donors for organic

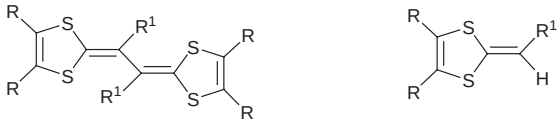

1

2

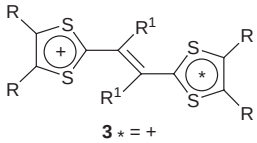

3 * = +
4 * = •

conductors due to their highly electron-donating properties and reduced on-site Coulombic repulsion.[1] The parent compound[2] and the ethylenedithio derivative[3] were synthesized several years ago. Recently the derivatives of **1** containing substituents such as aryl groups at the vinyl positions have been prepared by several groups.[4] They have been considered to be non-planar molecules due to the steric interactions between the substituents and the 1,3-dithiole parts, and X-ray analyses revealed the severely deformed structures.[4c,d,e] Therefore, those TTF molecules have not been used as components for organic conductors. However, the TTF vinylogue skeletons can be planar when the aryl substituents are twisted away from the π-conjugated framework. These compounds are expected to afford conductors with unusual structures since good molecular overlapping is disturbed by the bulky substituents. We have now prepared various derivatives **1** by a convenient method and have found that the cation radicals of **1** containing *o*-substituted phenyl groups are thermodynamically stable and can be isolated as single crystals.

The derivatives of **1** were previously prepared by electrochemical oxidative coupling of the corresponding 1,4-dithiafulvenes **2**.[4b,c,e,5] We have recently reported oxidative intramolecular cyclization to give bis(1,3-dithiole) electron donors by using tris(4-bromophenyl)aminium hexachloroantimonate as the oxidation reagent.[6] We have now used this chemical oxidation for the synthesis of **1**. First, 1,4-dithiafulvene derivatives **2** were prepared by either Wittig reaction of a phosphonium salt (for the dibenzo derivatives) or Wittig–Horner reaction of a phosphonium ester (for the ethylenedithio derivatives) with the corresponding aldehydes. Reaction of **2** with the aminium salt in CH_2Cl_2 afforded dication salts **3** which are formed by oxidative dimerization followed by oxidation. The salts **3** were reduced with zinc in MeCN to give **1**. The yields of **1** from **2** were 20–85%. It is noteworthy that the naphthyl and pyrenyl derivatives as well as phenyl derivatives were prepared.

The oxidation potentials of the donors **1** (Table 1) were measured by cyclic voltammetry (CV). The methyl derivatives **1a**,**m** and the phenyl ones **1b**,**n** show reversible one-stage two-electron redox waves. The *p*-substituted derivatives **1g**,**h**,**q** and the *m*-substituted one **1i** also undergo the similar two-electron oxidation. This fact suggests that the cation radical states of these compounds are thermodynamically unstable due to non-planar structures, similar to the reported examples. On the other hand, the *o*-substituted derivatives **1c–f**,**j**,**o**,**p**,**r** showed two reversible one-electron oxidation waves similar to the non-substituted one **1t**. This result suggests that the cation radicals of the *o*-substituted phenyl derivatives are thermodynamically stable. This can be explained by considering that the TTF vinylogue skeletons are planar when there are *o*-substituents, which increase the steric interactions and make the phenyl parts twist away from the π-conjugated framework. In the case of 1-naphthyl derivatives **1k**,**s** and 1-pyrenyl one **1l**, the cation radicals are also stable since they are also *o*-substituted phenyl derivatives. The values of the oxidation potentials are dependent on the substituents. BEDT-TTF analogues **1o**,**s** show lower first oxidation potentials than the non-substituted one **1t** and even TTF, indicating that they are stronger electron donors. The differences between the first and second oxidation potentials are smaller than those of TTF and BEDT-TTF, indicating the reduced on-site Coulombic repulsion in **1** due to the extended π-conjugation.

Electrochemical oxidation of **1j** and **1p** gave the cation radical salts **1j**·PF_6 and **1p**·$Au(CN)_2$ as stable single crystals with stoichiometries of 1:1. These are the first examples of cation radical salts of TTF vinylogues containing substituents at the vinyl positions. In order to investigate the geometries of the donors, X-ray structure analyses of the neutral compounds **1a**,**j**

Table 1 Oxidation potentials of donors **1**[a]

Compound	R,R	R^1	*E*/V
1a	$(CH{=}CH)_2$	Me	0.71 (2e)
1b	$(CH{=}CH)_2$	Ph	0.61 (2e)
1c	$(CH{=}CH)_2$	*o*-MeC_6H_4	0.44, 0.62
1d	$(CH{=}CH)_2$	*o*-ClC_6H_4	0.53, 0.75
1e	$(CH{=}CH)_2$	*o*-$OMeC_6H_4$	0.42, 0.63
1f	$(CH{=}CH)_2$	*o*-$NO_2C_6H_4$	0.59, 0.76
1g	$(CH{=}CH)_2$	*p*-ClC_6H_4	0.67 (2e)
1h	$(CH{=}CH)_2$	*p*-$OMeC_6H_4$	0.58 (2e)
1i	$(CH{=}CH)_2$	*m*-$NO_2C_6H_4$	0.73 (2e)
1j	$(CH{=}CH)_2$	2,6-$F_2C_6H_3$	0.66, 0.85
1k	$(CH{=}CH)_2$	1-naphthyl	0.47, 0.71
1l	$(CH{=}CH)_2$	1-pyrenyl	0.50, 0.70
1m	SCH_2CH_2S	Me	0.51 (2e)
1n	SCH_2CH_2S	Ph	0.49 (2e)
1o	SCH_2CH_2S	*o*-MeC_6H_4	0.30, 0.54
1p	SCH_2CH_2S	*o*-ClC_6H_4	0.38, 0.60
1q	SCH_2CH_2S	*p*-ClC_6H_4	0.52 (2e)
1r	SCH_2CH_2S	2,6-$F_2C_6H_3$	0.51, 0.70
1s	SCH_2CH_2S	1-naphthyl	0.33, 0.58
1t	SCH_2CH_2S	H	0.37, 0.56
1u	H	2,6-$F_2C_6H_3$	0.42, 0.65
TTF			0.35, 0.79
BEDT-TTF			0.50, 0.85

[a] 0.1 mol dm^{-3} Bu_4NPF_6 in PhCN, Pt electrode, scan rate 100 mV s^{-1}, *E*/V *vs.* SCE.

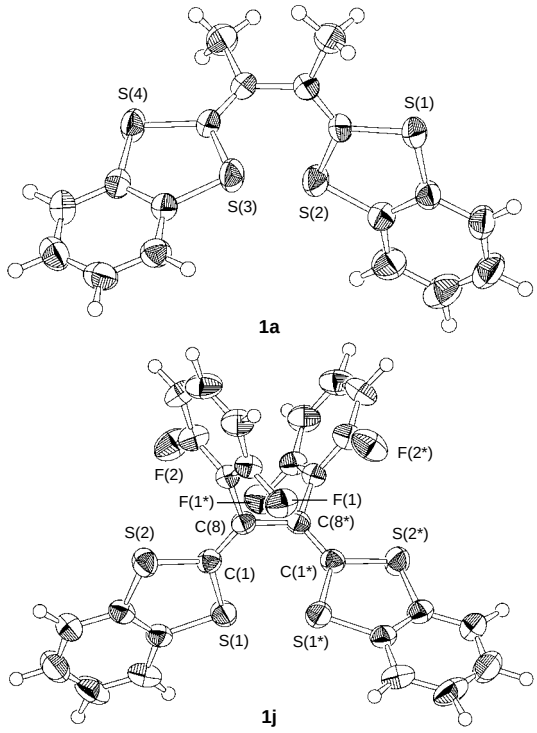

Fig. 1 Molecular structures of **1a** and **1j**

and the cation radical salts **1j**·PF_6 and **1p**·$Au(CN)_2$ were carried out.‡ As expected from the CV data, the methyl derivative **1a** has a non-planar structure (Fig. 1) as found in the substituted TTF vinylogues.[4c,d,e] The *o*-substituted phenyl derivative **1j** which undergoes step-wise oxidation was expected to have a planar TTF vinylogue framework. However, the structure was revealed to be similarly non-planar, as shown in Fig 1. In contrast, the molecular structure is drastically changed upon oxidation. The cation radical salt **1j**·PF_6 has a planar TTF vinylogue skeleton, as shown in Fig. 2. The aryl groups are twisted and almost orthogonal to the TTF vinylogue framework. The dihedral angle between the aryl group and the 1,3-dithiole ring is 83.9°. The C(1)–C(8) bond length [1.400(8) Å] in the cation radical salt is longer than that of the neutral **1j** [1.354(6) Å], while the C(8)–C(8*) bond length [1.41(1) Å] is shorter than the corresponding one in the neutral species [1.481(8) Å]. This fact suggests the contribution of a delocalized structure **4**. The donor molecules form an interesting two-dimensional columnar structure, as shown in Fig. 2. The bulky aryl groups disturb good overlapping between molecules. Instead, one molecule bridges two others; the 1,3-benzodithiole moieties form a stacking with an equal intermolecular distance of 3.6 Å. The side view of the crystal structure (Fig. 2, bottom) clearly shows a stair-like network where two-dimensional interactions can be expected. The donor molecule in **1p**·$Au(CN)_2$ also has a planar geometry of its TTF vinylogue framework. The unique crystal structure will be reported elsewhere. Unfortunately, these cation radical salts have a 1:1 stoichiometry and so they showed semiconducting behavior (**1j**·PF_6: $\sigma = 3 \times 10^{-6}$ S cm^{-1}, $E_a = 0.18$ eV; **1p**·$Au(CN)_2$: $\sigma = 10^{-2}$ S cm^{-1}, $E_a = 0.11$ eV). Studies on the preparation of other cation radical salts of **1** are now in progress.

This work was supported by a Grant-in-Aid for Scientific Research from the Ministry of Education, Science, Sports and Culture, Japan.

Notes and References

† E-mail: yoshiro@ims.ac.jp

‡ *Crystal data* for **1a**: $C_{18}H_{14}S_4$, $M = 358.55$, monoclinic, $P2_1/c$, $a = 12.1233(4)$, $b = 7.4016(3)$, $c = 18.5788(6)$ Å, $\beta = 98.196(3)°$, $V = 1650.08(9)$ Å^3, $Z = 4$, $T = 296$ K, μ(Cu-Kα) = 52.11 cm^{-1}, independent reflections 3640, $R = 0.055$ for 2812 data with $I > 3\sigma(I)$. For **1j**: $C_{28}H_{14}F_4S_4$, $M = 554.65$, orthorhombic, *Pbcn*, $a = 20.124(9)$, $b = 8.724(7)$, $c = 14.258(5)$ Å, $V = 2503(3)$ Å^3, $Z = 4$, $T = 296$ K, μ(Mo-Kα) = 4.26 cm^{-1}, independent reflections 3283, $R = 0.037$ for 1166 data with $I > 3\sigma(I)$. For **1j**·PF_6: $C_{28}H_{14}F_{10}PS_4$, $M = 699.62$, monoclinic, $C2/c$, $a = 19.814(2)$, $b = 7.1181(6)$, $c = 20.069(1)$ Å, $\beta = 104.588(6)°$, $V = 2739.3(4)$ Å^3, $Z = 4$, $T = 296$ K, μ(Cu-Kα) = 45.65 cm^{-1}, independent reflections 3036, $R = 0.058$ for 1303 data with $I > 3\sigma(I)$. For **1p**·$Au(CN)_2$: $C_{28}H_{16}AuCl_2N_2S_8$, $M = 880.78$, monoclinic, $P2_1/c$, $a = 10.527(1)$, $b = 11.025(1)$, $c = 13.001(3)$ Å, $\beta = 100.26(2)°$, $V = 1484.8(4)$ Å^3, $Z = 2$, $T = 296$ K, μ(Cu-Kα) = 164.1 cm^{-1}, independent reflections 3021, $R = 0.056$ for 2173 data with $I > 2\sigma(I)$. CCDC 182/905

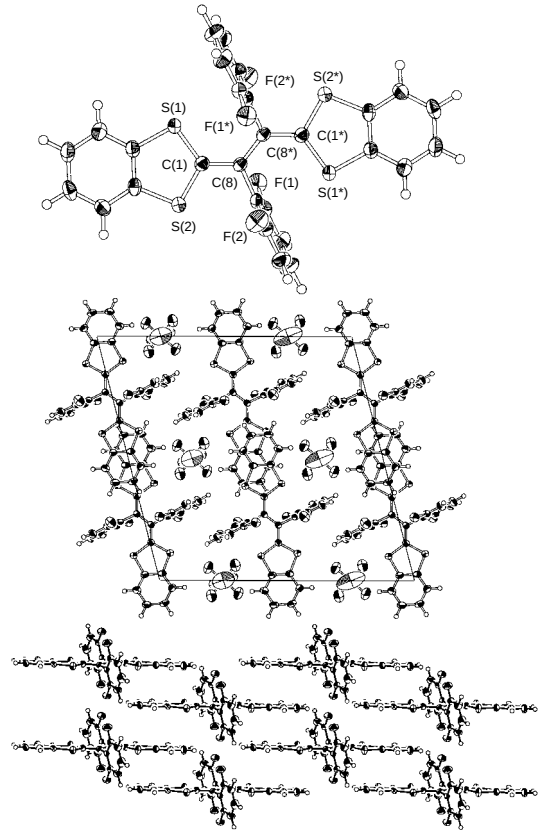

Fig. 2 Crystal structure of **1j**•PF_6. Top: structure of the donor molecule. Middle: projection along the *b*-axis. Bottom: view perpendicular to the stacking axis *b*.

1 J. Roncali, *J. Mater. Chem*., 1997, **7**, 2307.
2 Z. Yoshida, T. Kawase, H. Awaji, I. Sugimoto, T. Sugimoto and S. Yoneda, *Tetrahedron Lett*., 1983, **24**, 3469; T. Sugimoto, H. Awaji, I. Sugimoto, Y. Misaki, T. Kawase, S. Yoneda and Z. Yoshida, *Chem. Mater*., 1989, **1**, 535.
3 A. J. Moore, M. R. Bryce, D. J. Ando and M. B. Hursthouse, *J. Chem. Soc., Chem. Commun*., 1991, 320; T. K. Hansen, M. V. Lakshmikantham, M. P. Cava, R. M. Metzger and J. Becher, *J. Org. Chem*., 1991, **56**, 2720.
4 (*a*) U. Schöberl, J. Salbeck and J. Daub, *Adv. Mater*., 1992, **4**, 41; (*b*) A. Benahmed-Gasmi, P. Frère, J. Roncali, E. Elandaloussi, J. Orduna, J. Garín, M. Jubault and A. Gorgues, *Tetrahedron Lett*., 1995, **36**, 2983; (*c*) D. Lorcy, R. Carlier, A. Robert, A. Tallec, P. Le Maguerès and L. Ouahab, *J. Org. Chem*., 1995, **60**, 2443; (*d*) A. J. Moore, M. R. Bryce, P. J. Skabara, A. S. Batsanov, L. M. Goldenberg and J. A. K. Howard, *J. Chem. Soc., Perkin Trans. 1*, 1997, 3443; (*e*) P. Hascoat, D. Lorcy, A. Robert, R. Carlier, A. Tallec, K. Boubekeur and P. Batail, *J. Org. Chem*., 1997, **62**, 6086.
5 P. Hapiot, D. Lorcy, A. Tallec, R. Carlier and A. Robert, *J. Phys. Chem*., 1996, **100**, 14823.
6 A. Ohta and Y. Yamashita, *J. Chem. Soc., Chem. Commun*., 1995, 1761.

Received in Cambridge, UK, 12th May 1998; 8/03531H

A novel intramolecular photocyclization of methyl 2-(2,3-dimethylbut-2-enyloxymethyl)naphthalene-1-carboxylate *via* 1,9-hydrogen abstraction

Kazuhiko Mizuno,*† Shin-ichi Konishi, Yasuharu Yoshimi and Akira Sugimoto

Department of Applied Chemistry, College of Engineering, Osaka Prefecture University, 1-1 Gakuen-cho, Sakai, Osaka 599-8531, Japan

Irradiation of a benzene solution containing methyl 2-(2,3-dimethylbut-2-enyloxymethyl)naphthalene-1-carboxylate 1 gave an eight-membered keto ether 2 as the main product *via* a novel 1,9-hydrogen abstraction of the ester carbonyl group.

Photochemical hydrogen abstraction reactions have been extensively investigated from synthetic and mechanistic viewpoints.[1] Intramolecular long-range hydrogen abstraction such as 'remote oxidation' is one of the most attractive subjects in the photochemistry of carbonyl groups.[2] However, little is known about the hydrogen abstraction of an excited state of an ester carbonyl group except for an intramolecular 1,5-hydrogen abstraction *via* a 6-membered transition state.[3] Intermolecular hydrogen abstraction has also been reported as a rare case although the efficiency was quite low.[4] We now report a novel intramolecular 1,9-hydrogen abstraction of an ester carbonyl group to give an eight-membered keto ether *via* an exciplex.

Irradiation of a benzene solution containing methyl 2-(2,3-dimethylbut-2-enyloxymethyl)naphthalene-1-carboxylate **1** through a Pyrex filter (> 280 nm light) under an argon atmosphere gave **2** as the main product accompanied by (2π + 2π) photocycloadducts **3** and **4** and C–O bond cleavage product **5** (Scheme 1). Similar irradiation of **1** in MeCN also gave **2**, but **5** was mainly obtained (Table 1). Irradiation of **6** in benzene did not afford the corresponding eight-membered ring compound,

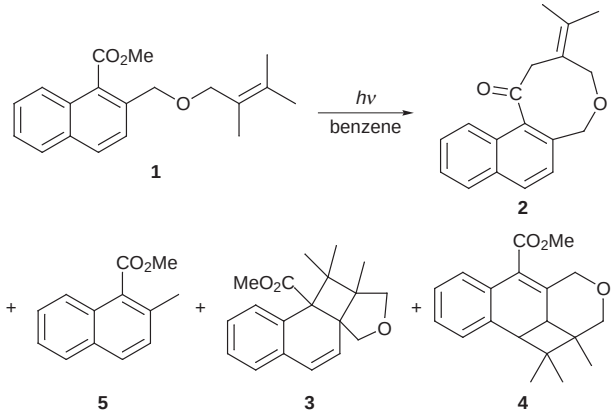

1 **2** **5** **3** **4**

Scheme 1

Table 1 Yields for photoreaction of **1** in benzene and MeCN

	Yield (%)[a]			
Solvent	**2**	**3**	**4**	**5**
Benzene	48	6	33	13
MeCN	10	< 5	< 5	80

[a] Yields based on unrecovered **1** were determined by GLC analysis after irradiation with a 500 W high-pressure mercury lamp for 100 h.

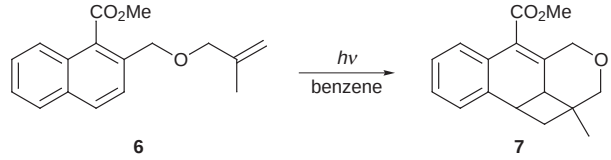

6 **7**

Scheme 2

but instead gave (2π + 2π) photocycloadduct **7** in low yield (Scheme 2).

The products were isolated by column chromatography on silica gel. The structure of **2** was determined from its spectral data.‡ The FT-IR spectrum of **2** showed the disappearance of the ester carbonyl group of **1** at 1743 cm^{-1} and the appearance of an aromatic carbonyl group at 1682 cm^{-1}. The ^1H NMR spectrum showed the existence of three kinds of methylene group, two nonequivalent methyl groups and six aromatic protons. These data indicate the elimination of MeOH from the starting material **1**. Finally, the structure of **2** was confirmed by X-ray crystallography (Fig. 1). The structures of (2π + 2π) photocycloadducts **3** and **4** were determined from their spectral properties and comparison with the intramolecular photocycloadducts obtained from 2-(2,3-dimethylbut-2-enyloxymethyl)naphthalene-1-nitrile, previously reported by McCullough *et al.*[5] and by us.[6]

The formation of the eight-membered keto ether **2** and the photocycloadducts **3** and **4** was not sensitized by the addition of 0.1 mol dm^{-3} of Michler's ketone (E_T = 275 kJ mol^{-1}),[7] and was not quenched by 0.5 mol dm^{-3} of 2-methylbuta-1,3-diene (E_T = 251 kJ mol^{-1})[7] and molecular dioxygen. The relative intensity of the fluorescence of **1** in cyclohexane was smaller than that of methyl naphthalene-1-carboxylate. This is due to the intramolecular quenching of the fluorescence of the methyl naphthalene-1-carboxylate chromophore by the alkene moiety, although an intramolecular exciplex emission between the methyl naphthalene-1-carboxylate chromophore and the 2,3-dimethylbut-2-ene chromophore was not observed. When the

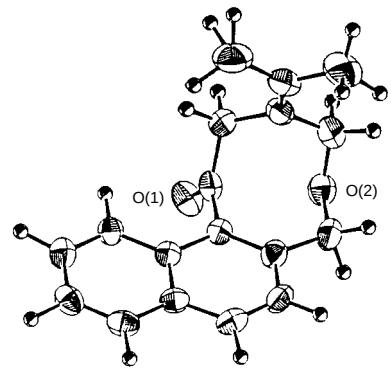

Fig. 1 X-Ray crystal structure of **2**

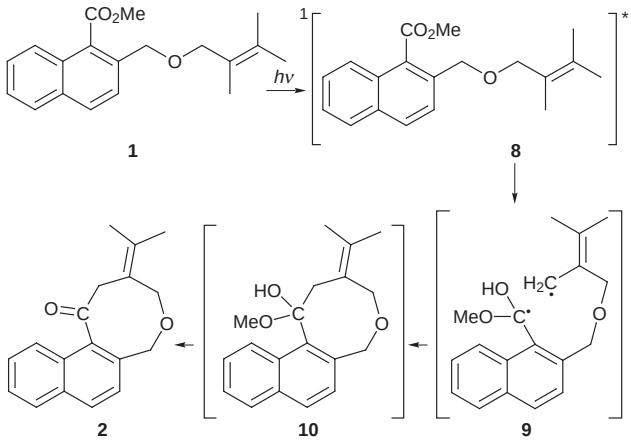

Scheme 3

fluorescence lifetime of **1** was measured by single photon counting in cyclohexane, the major component (short-lived, < 0.3 ns) was assigned to the methyl naphthalene-1-carboxylate moiety and the minor component (long-lived, 5.8 ns) to the singlet exciplex, because the fluorescence lifetime of methyl naphthalene-1-carboxylate has a value of 1.3 ns.

From these results, we propose the mechanism for the formation of the eight-membered keto ether shown in Scheme 3. The first step is the formation of an intramolecular exciplex **8** *via* the excited singlet state of the methyl naphthalene-1-carboxylate chromophore. The second step is the abstraction of an allylic hydrogen by the ester carbonyl group followed by radical coupling of **9** to give the hemiacetal **10**, which then eliminates MeOH to afford the eight-membered keto ether **2**. Although intramolecular 1,5-hydrogen abstraction by an ester carbonyl group *via* a six-memebered transition state is known, long-range intramolecular hydrogen abstraction has never been reported. The exciplex **8** also gives (2π + 2π) photocycloadducts **3** and **4**. The cleavage product **5** is probably produced *via* **9**. In the photoreaction of **1**, the charge transfer nature of the intramolecular exciplex plays an important role in the novel intramolecular 1,9-hydrogen abstraction. It is because the ester carbonyl group of **6** has a less electron donating alkene that it did not abstract the allylic hydrogen. In MeCN, the formation of the eight-membered keto ether **2** is observed in trace amounts, but the C–O bond cleavage product **5** was mainly obtained. This is reasonably explained by a photoinduced electron transfer process.[8]

We are indebted to Professor T. Takata and Emeritus Professor H. Inoue (Osaka Prefecture University) for helpful discussions. This work is partially supported by a Grant-in-Aid for Scientific Research from the Ministry of Education, Science, Sports, and Culture of Japan, and the Nagase Science and Technology Foundation.

Notes and References

† E-mail: mizuno@chem.osakafu-u.ac.jp

‡ *Selected data* for **2**: mp 172–173 °C; δ_H(270 MHz, $CDCl_3$) 7.82–7.69 (m, 3 H), 7.50–7.45 (m, 2 H), 7.07 (d, *J* 8.54, 1 H), 4.89 (br s, 2 H), 4.41 (s, 2 H), 3.51 (s, 2 H); δ_C(68 MHz, $CDCl_3$) 135.5, 133.8, 132.5, 132.2, 129.2, 128.8, 128.2, 127.2, 125.9, 125.8, 123.7, 121.9, 73.5, 73.4, 48.4, 20.8, 20.2; ν_{max}(KBr)/cm^{-1} 1682; *m*/*z* 266 (M^+).

Crystal data for **2**: $C_{18}H_{18}O_2$, *M* = 266.34, monoclinic, space group $P2_1/n$ (#14), *a* = 8.6862(6), *b* = 12.468(2), *c* = 13.468(1) Å, β = 105.418(7)°, *V* = 1406.0(3) Å^3, *Z* = 4, D_c = 1.258 g cm^{-3}, *T* = 296 K, μ = 0.80 cm^{-1}, *F*(000) = 568, crystal size = 0.650 × 0.600 × 0.330 mm, Rigaku AFC5R diffractometer. Final *R* value was 0.038 for 2105 reflections (R_w = 0.043). CCDC 182/914.

1 For a review, see: P. J. Wagner, *Acc. Chem. Res.*, 1971, **4**, 168; 1983, **16**, 461; 1989, **22**, 83.
2 For a review, see: R. Breslow, *Acc. Chem. Res.*, 1980, **13**, 170.
3 R. M. Duhaime, D. A. Lombardo, I. A. Skinner and A. C. Weedon, *J. Org. Chem.*, 1985, **50**, 873; T. Gomibuchi, K. Fujiwara, T. Nehira and M. Hirama, *Tetrahedron Lett.*, 1993, **34**, 5753.
4 K. Fukui and Y. Odaira, *Tetrahedron Lett.*, 1969, **10**, 2887.
5 J. J. McCullough, W. K. MacInnis, C. J. L. Lock and R. Faggiani, *J. Am. Chem. Soc.*, 1982, **104**, 4644.
6 K. Mizuno, S. Konishi, T. Takata and H. Inoue, *Tetrahedron Lett.*, 1996, **37**, 7775.
7 Methyl naphthalene-1-carboxylate (E_T = 256 kJ mol^{-1}); S. L. Murov, I. Carmichael and G. L. Hug, *Handbook of Photochemistry*, Marcel Dekker, New York, 1993, p. 17, 76 and 77.
8 Photocleavage reaction *via* photoinduced electron transfer: F. D. Saeva, in *Photoinduced Electron Transfer I*, ed. J. Mattay, Springer-Verlag, Berlin, 1990, pp. 59–92.

Received in Cambridge, UK, 18th May 1998; 8/03711F

A new synthesis of benzoporphyrins using 4,7-dihydro-4,7-ethano-*2H*-isoindole as a synthon of isoindole

Satoshi Ito,[a] Takashi Murashima,[a] Hidemitsu Uno[b] and Noboru Ono*[a]†

[a] *Department of Chemistry, Faculty of Science, Ehime University, Bunkyo-cho 2-5, Matsuyama 790-8577, Japan*
[b] *Advanced Instrumentation Center for Chemical Analysis, Ehime University, Bunkyo-cho 2-5, Matsuyama 790-8577, Japan*

Heating 4,7-dihydro-4,7-ethano-2*H*-isoindole at 200 °C induces the retro-Diels–Alder reaction to give isoindole in essentially quantitative yield, which can be applied to a new synthesis of tetrabenzoporphyrins and monobenzoporphyrins.

Pyrroles fused with aromatic rings, namely isoindoles, may be useful as precursors of polypyrroles with low band gap[1] and benzoporphyrins.[2] However, unsubstituted isoindole is too unstable to be used directly for the preparation of such compounds.[3] Recently we have developed a new synthesis of isoindoles *via* the Barton–Zard pyrrole synthesis using aromatic nitro compounds and ethyl isocyanoacetate, from which polypyrroles and porphyrins fused with various aromatic rings have been prepared.[1,2] However, this method is not applicable to the synthesis of unsubstituted isoindole, for nitrobenzene does not react with ethyl isocyanoacetate. Here we report a very simple method for the synthesis of isoindole. Ethyl 4,7-dihydro-4,7-ethano-*2H*-isoindole-1-carboxylate **1** was prepared by the reaction of the Diels–Alder reaction of 1,3-cyclohexadiene with β-sulfonylnitroethylene followed by the treatment with ethyl isocyanoacetate.[4] De-ethoxycarbonylation by heating **1** with KOH in ethylene glycol at 170 °C gave **2**,‡ which acted as a masked isoindole (Scheme 1). Namely, heating **2** at 200–230 °C causes a retro-Diels–Alder reaction, the product of which can be trapped in about 70% yield with reactive dienophiles such as *N*-phenylmalenimide[5] Although there are many possibilities for the use of **1** or **2** as an isoindole synthon, here we focus on the synthesis of benzoporphyrins. Porphyrin **3**,[4] which was prepared from **1** *via* reduction of the ester function with $LiAlH_4$ followed by tetramerization and oxidation, was converted into tetrabenzoporphyrin **4** in 100% yield by heating at 200 °C for 10 min. In general, it is rather difficult to handle tetrabenzoporphyrin and its metal complexes due to their low solubility in most organic solvents. This difficulty is now resolved by the use of porphyrin **3** and its metal complexes, as they are soluble in CH_2Cl_2 and can be converted into **4** in quantitative yield by simply heating at 200 °C. Various kinds of metal complexes (Zn, Cu, Ni, Fe, *etc.*) of **3** were readily prepared by the conventional method[6] and purified by column chromatography and recrystallization from CH_2Cl_2–MeOH. They were soluble in $CHCl_3$ and CH_2Cl_2. The metal complexes of porpyrin **3** were converted into the corresponding metal complexes of **4** in essentially quantitative yield by heating at 200 °C. By using this method, various materials coated with metal complexes of **4** which may be important for electronic applications are readily prepared. For example, a glass slide coated with Zn-**3** (λ_{max} 405, 525, 560 nm) was prepared using a solution of Zn-**3** in CH_2Cl_2; this was changed into a glass slide coated with Zn-**4** (λ_{max} 454, 617, 696 nm) by heating at 200 °C for 10 min.

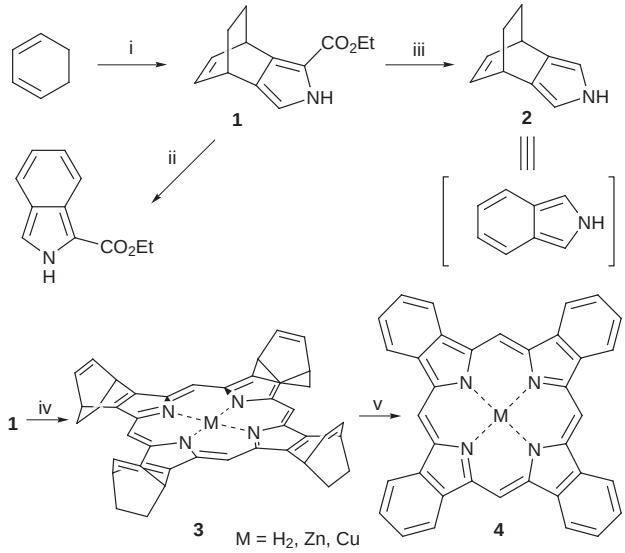

Scheme 1 *Reagents and conditions*: i, ref. 4, 60% for two steps; ii, 200 °C, 10 min; iii, KOH, $HOCH_2CH_2OH$, 170 °C, 2 h, 81%; iv, ref. 4, 30%; v, 200 °C, 10 min, quant.

Other syntheses of benzoporphyrins using **2** as an isoindole synthon are shown in Schemes 2 and 3. The reaction of **2** with aromatic aldehydes in the presence of $BF_3{\cdot}OEt_2$ followed by oxidation gave *meso*-tetraarylated porphyrins **5** in 25–35% yield, which were converted into the corresponding benzoporphyrins **6** in quantitative yield by heating at 200 °C for 10 min. Thus, pyrrole **2** can be used as a masked isoindole in benzoporphyrin synthesis. As pointed out by Bonnet, the chemistry of benzoporphyrins has been relatively neglected due to their synthesis being difficult, although they have potential uses as electro-optical, molecular electronic and photodynamic therapeutic materials.[7] Now various types of benzoporphyrins can be prepared *via* the use of **2** as an isoindole synthon. As a typical example, monobenzoporphyrin **9** was prepared in quantitative yield by heating porphyrin **8** at 200 °C for 10 min, as shown in Scheme 3. Porphyrin **8** was prepared by the well-established method *via* a 3 + 1 approach consisting of the reaction of tripyrrane **7** with pyrrole-2,5-dicarbaldehyde followed by oxidation.[8] The requisite **7** was readily prepared by the reaction of **2** with 2-acetoxymethylpyrroles. The UV–VIS

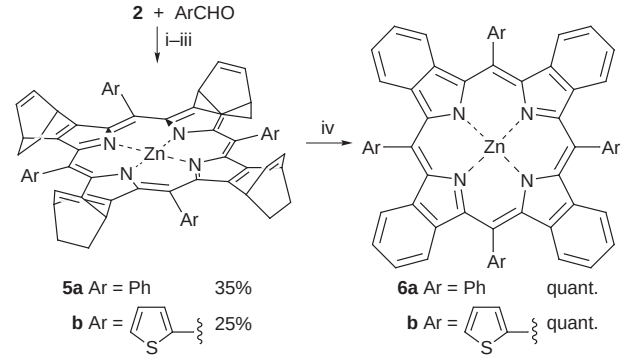

Scheme 2 *Reagents and conditions*: i, $BF_3{\cdot}OEt_2$; ii, $Zn(OAc)_2$; iii, *p*-chloranil; iv, 200 °C, 10 min

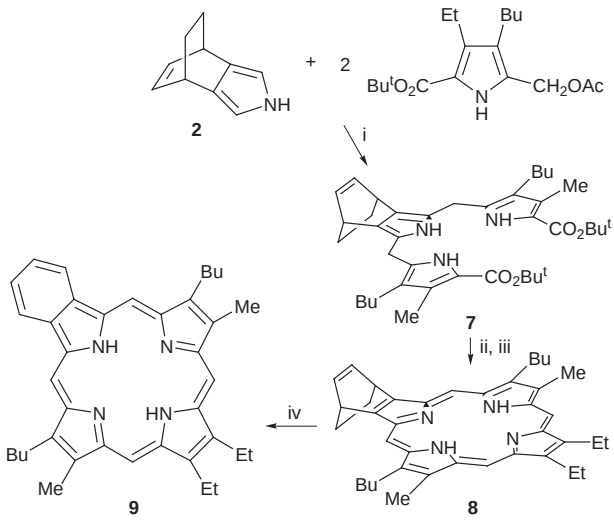

Scheme 3 *Reagents and conditions*: i, AcOH–EtOH, reflux, 16 h; ii, 3,4-diethylpyrrole-2,5-dicarbaldehyde, TFA, room temp., 2 h; iii, DDQ, $CHCl_3$, room temp., 1 h, 11% for three steps; iv, 200 °C, 10 min, quant.

spectrum of **8** (λ_{max} 398, 497, 529, 566, 619 nm; band strength IV > III > II > I) indicated that **8** was readily converted to **9** (λ_{max} 404, 504, 541, 574, 629 nm; band strength III > I > IV > II); these were in good agreement with those reported in the literature.[7,9]

In conclusion, we have described a new synthesis of benzoporphyrins using **1** or **2** as insoindole synthons which is superior to the existing methods in its simplicity and generality. It should be emphasized that formation of benzoporphyrns **4**, **6** and **9** can be achieved by simple heating. This process is a very clean reaction and purification of products is not usually necessary if precursors **3**, **5** and **8** are pure. This method could be extended to the preparation of other π-extended molecules including polypyrroles fused with aromatic rings, which is now in progress in our laboratory.

The work was partly supported by Grants-in aid for Scientific Research from the Ministry of Education, Science, Sports and Culture of Japan.

Notes and References

† E-mail: ononbr@dpc.ehime-u.ac.jp

‡ All new compounds gave satisfactory elementary analyses. *Selected data* for **2**: mp 130–131 °C, $\delta_H(CDCl_3)$ 1.54 (4 H, m), 3.85 (2 H, m), 6.45 (2 H, d, *J* 2.1), 6.50 (1 H, d, *J* 4.27), 6.52 (1 H, d, *J* 4.27), 7.53 (1 H, NH); *m/z* (EI) 145 (M^+, 7), 117 (100). For Zn-**3:** λ_{max}(solid on glass)/ nm 405, 525, 560; $\lambda_{max}(CHCl_3)$/nm 400, 534, 561. For Cu-**3**: λ_{max}(solid)/nm 402, 520, 560. For **4**: λ_{max}(solid)/nm 454, 617, 696; $\lambda_{max}[(CHCl_3+CF_3CO_2H)]$/nm 431, 605, 660 nm. For Zn-**4:** λ_{max}(solid on glass)/nm 450, 690; λ_{max}(THF–pyridine)/nm 425, 622; For Cu-**4**: λ_{max}(solid)/nm 420, 663; λ_{max}(THF–pyridine)/nm 416, 61. For Zn-**5a**: $\delta_H(CDCl_3)$ 1.44 (16 H, m), 3.39 (8 H, m), 6.45 (8 H, m), 7.78–7.8 (12 H, m), 8.24 (8 H, m); $\lambda_{max}(CHCl_3)$/nm (log ε) 425 (6.45), 550 (5.15); *m/z* (FAB) 988 (M^++1). For Zn-**6a**: $\delta_H(CDCl_3)$ 7.17 (8 H, dd, *J* 6.35, 3.42), 7.28 (8 H, dd, *J* 6.35, 2.92), 7.87 (8 H, t, *J* 7.33), 7.95 (4 H, t, *J* 7.81), 8.30 (8 H, d, *J* 6.84); $\lambda_{max}(CHCl_3)$/nm (log ε) 463 (6.44), 609 (5.09), 652 (5.68); *m/z* (FAB) 876 (M^+ +1). For **8**: $\delta_H(CDCl_3)$ −3.99 (2 H, s), 1.18 (6 H, t, *J* 7.3), 1.48 (6 H, s), 1.79 (6 H, t, *J* 7.3), 2.1–2.3 (8 H, m), 4.07 (4 H, t, *J* 7.3), 4.13 (4 H, q, *J* 7.3), 5.72 (2 H, s), 7.20 (2 H, m), 10.12 (2 H, s), 10.17 (2 H, s); $\lambda_{max}(CHCl_3)$/nm 398 (6.21), 497 (5.15), 529 (4.89), 566 (4.73), 620 (4.54); *m/z* (FAB) 585 (M^++1). For **9**: $\delta_H(CDCl_3)$ −3.64 (2 H, m), 1.14 (6 H, t, *J* 7.3), 1.52 (6 H, s), 1.80 (4 H, m), 1.89 (6 H, t, *J* 7.3), 2.30 (4 H, m), 4.02 (4 H, q, *J* 7.3), 4.16 (4 H, t, *J* 7.3), 8.08 (2 H, dd, *J* 1.1), 9.34 (2 H, dd, *J* 1.1). 10.08 (2 H, s), 10.39 (2 H, s); $\lambda_{max}(CHCl_3)$/ nm (log ε) 404 (6.48), 504 (5.12), 541 (5.40), 574 (4.91), 629 (5.17); *m/z* (FAB) 557 (M^++1).

1 N. Ono, H. Hironaga, K. Simidzu, K. Ono and T. Ogawa, *J. Chem. Soc., Chem. Commun*., 1994, 1019; N. Ono, C. Tsukamura, Y. Nomura, H. Hironaga, T. Murashima and T. Ogawa, *Adv. Mater*., **9**, 1997, 149. Polypyrroles fused with aromatic rings have been little studied, while the corresponding polythiophenes have been well-studied, see F. Wudl, M. Kobayashi and A. J. Heager, *J. Org. Chem*., 1984, **49**, 3382; M. Hanack, U. Schmid, S. Echingerr, F. Teichert and J. Heiber, *Syntheis*, 1993, 634.

2 N. Ono, H. Hironaga, K. Ono, S. Kaneko, T. Murashima, T. Ueda, C. Tsukamura and T. Ogawa, *J. Chem. Soc., Perkin Trans. 1*, 1996, 417; T. D. Lash and B. H. Novak, *Angew. Chem., Int. Ed. Engl*., 1995, **34**, 683; P. Chandrasekar and T. D. Lash, *Tetrahedron Lett.*, 1996, **28**, 4873 and references cited therein.

3 R. Bonnett and R. C. Brown, *J. Chem. Soc., Chem. Commun*., 1972, 393; R. Bonnett and S. A. North, in *Advances in heterocyclic chemistry*, ed. A. R. Katritzky and A. J. Boulton, Academic Press, New York, 1981, vol. 29, pp. 341–399; R. Kreher, N. Kohl and G. Use, *Angew. Chem., Int. Ed. Engl*, 1982, **21**, 621; M. Lee, H. Morimoto and K. Kanematsu, *J. Chem. Soc., Chem. Commun*., 1994, 1535.

4 S. Ito, T. Murashima and N. Ono, *J. Chem. Soc., Perkin Trans. 1*, 1997, 3161.

5 The retro-Diels–Alder reaction of **1** or **2** takes place at 200–230 °C, the bridged moiety of **1** and **2** being stable during de-ethoxycarbonylation of **1** at 170 °C. The formation of isoindoles from **1** or **2** by heating was monitored *via* NMR spectroscopy.

6 K. M. Smith, *Porphyrins and Metalloporphyrins*, Elsevier, Amsterdam, 1975.

7 Existing methods for benzoporphyrin synthesis are summarized in R. Bonnett and K. A. McManus, *J. Chem. Soc., Perkin Trans. 1*, 1996, 2461; for a recent synthesis of benzoporphyrins, see M. G. H. Vicente, A. C. Tome, A. Walter and J. A. S. Cavaleiro, *Tetrahedron Lett*., 1997, **38**, 3639 and references cited therein.

8 T. D. Lash, *Chem. Eur. J*., 1996, **2**, 1197; A. Boudif and M. Momenteau, *J. Chem. Soc., Perkin Trans. 1*, 1996, 1235; L. T. Nguyen, M. O. Senge and K. M. Smith, *J. Org. Chem*., 1996, **61,** 998 and references cited therein.

9 P. S. Clezy and A. H. Mirza, *Aust. J. Chem*., 1982, **35**, 197; T. D. Lash, *Energy Fuels*, 1993, **7**, 166.

Received in Cambridge, UK, 15th May 1998; 8/03656J

Synthesis of novel imidazolidinones from hexose–peptide adducts: model studies of the Maillard reaction with possible significance in protein glycation

Štefica Horvat,*† Lidija Varga-Defterdarović, Maja Roščić and Jaroslav Horvat

Department of Organic Chemistry and Biochemistry, Ruđer Bošković Institute, POB 1016, 10001 Zagreb, Croatia

Novel hexose-related imidazolidin-4-ones are prepared by intramolecular rearrangements of monosaccharide esters in which D-mannose, D-glucose, or D-galactose are linked through their C-6 hydroxy groups to the endogenous opioid pentapeptide, leucine-enkephalin.

Non-enzymatic glycation of proteins has been increasingly identified as an important factor in the age-dependent chemical modification and cross-linking of tissue proteins,[1] as well as in the pathogenesis of the long term complications of diabetes.[2] The sequence of non-enzymatic glycation involves the reaction of an aldose (or ketose) sugar with free amino groups of proteins (Maillard reaction) leading initially to the formation of labile Schiff bases. With the subsequent Amadori rearrangement, the aminoketoses formed undergo a variety of reactions[3] such as dehydrations, fragmentations, and the formation of highly reactive carbonyl compounds, which continue to react with free amino groups, thus leading to cross-linking of proteins *via* advanced glycation end products (AGEs) which are mainly responsible for the diabetic complications.[2] A few such adducts have been structurally identified by *in vitro* glycation of proteins or by monitoring the breakdown of isolated Amadori compounds.[4]

This study demonstrates for the first time, by *in vitro* experiments, that, in addition to Amadori rearrangement, an alternative pathway for carbohydrate-induced modification of peptides is possible, yielding imidazolidin-4-ones from the initially formed hexose–peptide adducts.

We recently reported[5] on the products of intramolecular Amadori rearrangements formed in pyridine–AcOH as the solvent from monosaccharide esters **1a**–**c**[6] in which D-mannose (**1a**), D-glucose (**1b**), or D-galactose (**1c**) are linked through their C-6 hydroxy groups to the C-terminal carboxy group of the endogenous opioid pentapeptide leucine-enkephalin (H-Tyr-Gly-Gly-Phe-Leu-OH).[7] Herein we provide evidence that synthons **1a**–**c** are also transformed to carbohydrate-related imidazolidinones **3a**–**c** (Scheme 1). Thus, incubation of monosaccharide esters **1a**–**c** in MeOH at 50–60 °C afforded, after purification by semipreparative reverse-phase high-performance liquid chromatography (RP HPLC), the corresponding imidazolidin-4-ones **2a**–**c** in acceptable yields (Table 1). We assume that, in a similar fashion to Amadori product formation from esters **1a**–**c**,[5] the first step of this reaction requires the open-chain form of the carbohydrate moieties in compounds **1a**–**c**, which is attacked by the free amino terminus of the peptide moiety. In the subsequent step, the Schiff base formed, instead of Amadori rearrangement to the corresponding keto-sugar, undergoes nucleophilic attack by the Gly[2] nitrogen to yield imidazolidin-4-ones **2a**–**c** in which C-1 of the sugar moiety forms a bridge between the α-amino group of the *N*-terminal tyrosine residue and the amide nitrogen of the Tyr[1]-Gly[2] peptide bond. As presented in Table 1, the transformation **1a**→**2a** took place completely stereospecifically, while the conversion of esters **1b** and **1c** to the corresponding imidazolidinones exhibited a low degree of stereocontrol. Rearrangements of **1a**–**c** in MeOH yield only 5% of the corresponding Amadori products.

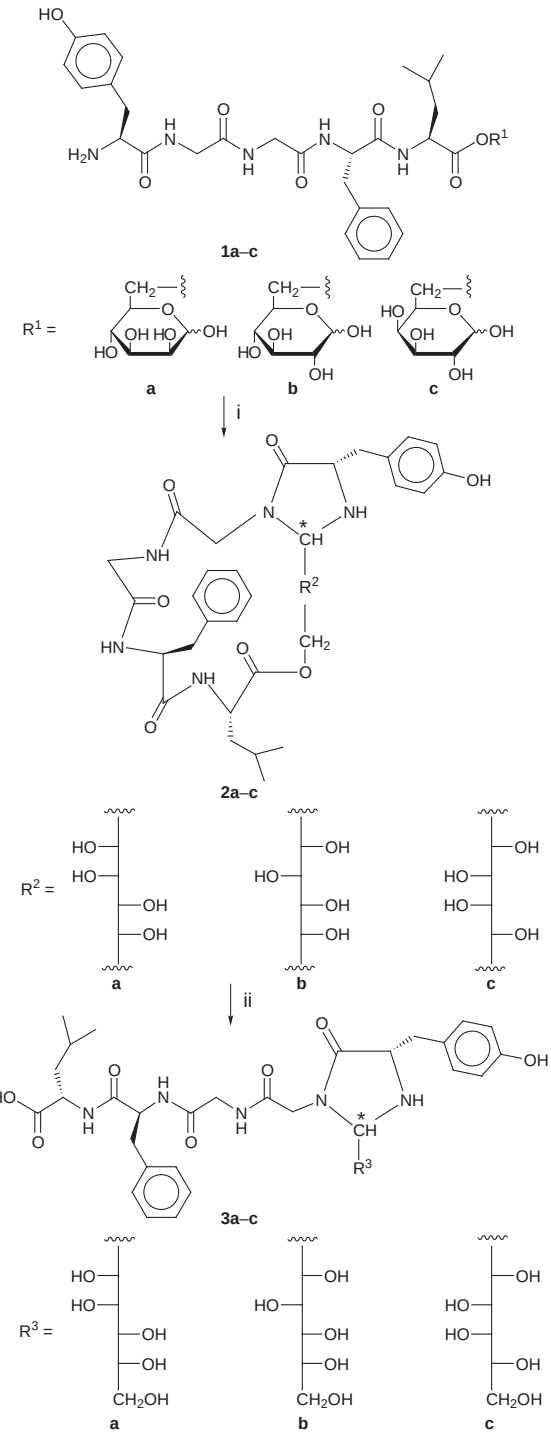

Scheme 1 *Reagents and conditions*: i, MeOH, 50–60 °C; ii, 0.1 M NaOH, 25 °C. Asterisk indicates either (*S*)- or (*R*)-configuration at the new *N*,*N*'-acetal centre.

Table 1 Intramolecular rearrangement of esters **1a**–**c** in MeOH

Starting compound	*t*/h	*T*/°C	Product[a]	Yield (%)[b] Major	Minor
1a	24	50	**2a**	49	—
1b	72	60	**2b**	34	9
1c	48	60	**2c**	12	10

[a] Mixture of diastereomers for **2b** and **2c**. [b] Isolated yields after RP HPLC purification.

Cleavage of the ester bond in both the major and minor isomers of compounds **2a**–**c** was carried out in 0.1 M NaOH at room temperature and led to the corresponding chiral imidazolidin-4-ones of D-mannose (**3a**), D-glucose (**3b**) or D-galactose (**3c**) in 77–95% yield after RP HPLC chromatography.‡

The experimental fact that the monosaccharide esters **1a**–**c**, the behaviour of which closely resembles the reactivity of hexose 6-phosphates, yield either the corresponding Amadori products[5] or imidazolidinones **2a**–**c** points, in our understanding, to the possibility that, depending on the physiological environment, similar imidazolidinon-4-one adducts may be also generated *in vivo*.

In conclusion, the method outlined above, which is based on the intramolecular rearrangement of 6-*O*-peptidyl esters **1a**–**c,** represents an innovative route for the synthesis of hexose-related imidazolidin-4-ones, compounds useful in understanding the details of the mechanism of non-enzymatic glycation *in vivo*.

This work was funded by the Ministry of Science and Technology of Croatia (Grant No. 00980704).

Notes and References

† E-mail: shorvat@rudjer.irb.hr

‡ All new compounds have been fully characterized and have spectroscopic properties compatible with the structures assigned.

1 R. G. Paul and A. J. Bailey, *Int. J. Biochem. Cell Biol.*, 1996, **28**, 1297; R. Sullivan, *Arch. Physiol. Biochem.*, 1996, **104**, 797; D. R. Sell, *Mech. Ageing Dev.*, 1997, **95**, 81.

2 M. Brownlee, *Diabetes*, 1994, **43**, 836; E. Schleicher and A. Nerlich, *Horm. Metab. Res.*, 1996, **28**, 367; H. Vlassara, *Diabetes*, 1997, **46** (Suppl. 2), S19.

3 V.A. Yaylayan and A. Huyghues-Despointes, *Crit. Rev. Food Sci. Nutr.*, 1994, **34**, 321; F. Ledl and E. Schleicher, *Angew. Chem., Int. Ed. Engl.*, 1990, **29**, 565.

4 V. M. Monnier, D. R. Sell, R. H. Nagaraj, S. Miyata, S. Grandhee, P. Odetti and S. A. Ibrahim, *Diabetes*, 1992, **41** (Suppl. 2), 36; P. R. Smith and P. J. Thornalley, *Eur. J. Biochem.*, 1992, **210**, 729; A. Cerami, in *Maillard Reactions in Chemistry, Food and Health*, ed. T. P. Labuza, G. A. Reineccius, V. M. Monnier, J. O'Brien and J. W. Baines, The Royal Society of Chemistry, Cambridge, England, 1994, pp. 1–10.

5 Š. Horvat, M. Roščić, L. Varga-Defterdarović and J. Horvat, *J. Chem. Soc., Perkin Trans. 1*, 1998, 909.

6 Š. Horvat, J. Horvat, D. Kantoci and L. Varga, *Tetrahedron*, 1989, **45**, 4579; Š. Horvat, L. Varga-Defterdarović, J. Horvat, S. Modrić-Žganjar, N. N. Chung and P. W. Schiller, *Lett. Pept. Sci.*, 1995, **2**, 363.

7 G. A. Olson, R. D. Olson and A. J. Kastin, *Peptides*, 1996, **17**, 1421.

Receieved in Glasgow, UK, 24th April 1998; 8/03099E

Evidence for actinide metal to ligand π backbonding. Density functional investigations of the electronic structure of [{$(NH_2)_3(NH_3)U$}$_2(\mu^2$-η^2:η^2-$N_2)$]

Nikolas Kaltsoyannis*[a]† and Peter Scott[b]‡

[a] *Centre for Theoretical and Computational Chemistry, University College London, 20 Gordon Street, London, UK WC1H 0AJ*
[b] *Department of Chemistry, University of Warwick, Coventry, UK CV4 7AL*

The electronic structure of [{$(NH_2)_3(NH_3)U$}$_2(\mu^2$-η^2:η^2-$N_2)$], a model for the first dinitrogen compound of an actinide, is investigated computationally using quasi-relativistic non-local density functional theory; the only significant U–N_2–U interaction is found to be U→N_2 π backbonding.

The instability of f element complexes with π acid ligands is presumed to arise from the inability of these metals to take part in metal→ligand backbonding. Indeed the bonding in f element compounds is widely regarded as being essentially electrostatic. Nevertheless the physicochemical properties of certain actinide systems cannot be satisfactorily explained without invoking appreciable metal–ligand covalency.[1–4]

We have recently reported our discovery of the first dinitrogen complex of an actinide element, [{$(NN'_3)U$}$_2(\mu^2$-η^2:η^2-N_2)] [NN'_3 = $N(CH_2CH_2NSiBu^tMe_2)_3$] **1** (Fig. 1).[5] This compound, synthesised by the exposure of the 'base-free' triamidoamine [$(NN'_3)U$] to rigorously pure dinitrogen, features an N_2 unit bridging the two uranium centres in a side-on manner. This coordination geometry raises the intriguing and fundamental question of how the N_2 ligand interacts with the metal atoms. The N–N distance [1.109(7) Å] is similar to that found in dinitrogen gas (1.0975 Å), and the magnetic susceptibility and UV–VIS spectrum are very close to those of the parent [$(NN'_3)U$]. These data led us to suggest that **1** contains essentially N_2→U σ bonds, with [$(NN'_3)U$] acting as an extremely potent Lewis acid. We noted, however, that since the unobserved 1 : 1 intermediate [$(NN'_3)U$–(N_2)] is clearly more basic than free dinitrogen, some degree of U→N_2 backbonding may be present.

In order to gain insight into the electronic structure of **1** and hence to evaluate the above suggestions, we have carried out density functional calculations§ on the model complex [{$(NH_2)_3(NH_3)U$}$_2(\mu^2$-η^2:η^2-N_2)] **2**. Bond lengths and angles were taken from the crystallographic data obtained on **1**, and the molecular structure was idealised to C_{2h} symmetry. The replacement of the triamidoamine ligand by $(NH_2)_3(NH_3)$ is necessary for calculational feasibility and, while such a simplification is not insignificant, we anticipate that the fundamental features of the U–N_2–U interaction will not be greatly affected. Indeed, we have previously used this ligand replacement in other studies.[6]

1 is paramagnetic, with a susceptibility of 3.22 μ_B per uranium atom.[5] It is therefore appropriate to address the electronic structure of **2** using the spin unrestricted approach, in which α and β spin electrons occupying a molecular orbital (MO) of a given number and symmetry are not constrained to have the same spatial wavefunction. The excess α over β spin density is a user-defined parameter within ADF, raising the question of how many unpaired electrons **1** and **2** possess. The spin-only formula is inappropriate for actinide complexes, and thus the magnetic susceptibility of **1** cannot be straightforwardly related to the number of unpaired electrons. Consideration of all the available experimental data suggests that **1** has six unpaired electrons per molecule, *i.e.* that each uranium atom is best regarded as a U^{III} f^3 centre. We have carried out a range of spin unrestricted calculations of **2**, and have found that the most stable electronic arrangement has four unpaired electrons. Imposition of six unpaired electrons produces a non-Aufbau orbital occupation and a markedly less stable structure.¶ We stress, however, that the general features of the electronic structure are very similar in all cases, and it is to these that we now turn.‖

A MO energy level diagram for **2** with four unpaired electrons is given in Fig. 2. The orbitals are labelled according to the C_{2h} irreducible representations that they span, together with an α or β designation to indicate the spin of the electron in that orbital. The use of the spin unrestricted approach doubles the number of MOs, and there are 42 such energy levels in the eigenvalue range −8.3 to −2.3 eV. Fortunately the MOs are concentrated in a few groups of similar energy and composition (represented by rectangles on Fig. 2), simplifying the analysis of the valence electronic structure. MOs around the highest occupied orbital are shown on an expanded scale.

The three groups of MOs with energies centred around −8.2, −7.5 and −5.5 eV are largely localised on the NH_2 and NH_3 ligands, with some levels also containing small contributions from the uranium atoms. These orbitals are primarily responsible for binding the NH_2 and NH_3 groups to the metal atoms, as

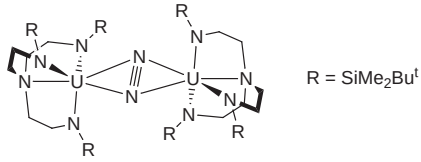

Fig. 1 The geometric structure of [{$(NN'_3)U$}$_2(\mu^2$-η^2:η^2-N_2)] [NN'_3 = $N(CH_2CH_2NSiBu^tMe_2)_3$] **1**

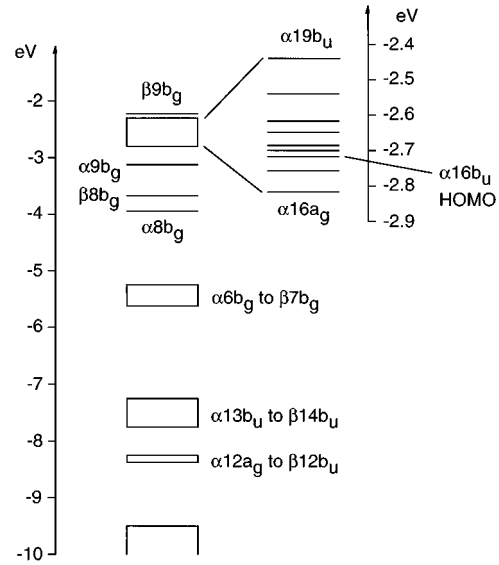

Fig. 2 Molecular orbital energy level diagram of C_{2h} symmetric [{$(NH_2)_3(NH_3)U$}$_2(\mu^2$-η^2:η^2-N_2)] **2**

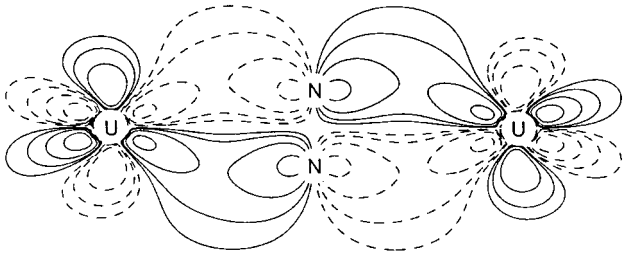

Fig. 3 Contour plot of the $\alpha 8b_g$ molecular orbital of $[\{(NH_2)_3(NH_3)U\}_2(\mu^2\text{-}\eta^2\text{:}\eta^2\text{-}N_2)]$ **2**, viewed in the plane defined by the two uranium atoms and the N_2 unit. Contour levels are ±0.2, ±0.1, ±0.05 and ±0.025.

well as for some N–H bonding. Given that we are concerned mainly with the U–N_2–U interaction, these orbitals will not be discussed further.

The six least stable electrons occupy the $\alpha 8b_g$ to $\alpha 16b_u$ orbitals. Five of these levels have α spin and one has β spin, and the spatial symmetry of the unpaired electrons is such that the overall molecular electronic state is ^5A_u. The four orbitals of α spin that have no filled β spin counterpart ($\alpha 9b_g$ to $\alpha 16b_u$) are predominantly uranium f based (⩾75% in all cases). The α and β $8b_g$ orbitals, however, are rather different from this group, in terms of both energy (> 0.6 eV more stable) and composition. These two levels are mixtures of uranium f and the N–N antibonding π_g orbital of the N_2 ligand,** and are U→N_2 π backbonding. A contour plot of the $\alpha 8b_g$ orbital is shown in Fig. 3. Analysis of all of the filled MOs of **2** shows that this is the only significant U–N_2–U interaction. MOs with contributions from the π_u N–N bonding orbital lie at much more negative eigenvalues (*ca.* −11 to −12 eV) and have negligible uranium character. The Mulliken overlap population between the uranium atoms and the N_2 fragment is +0.25 electrons, reinforcing the conclusion of appreciable U–N_2–U covalency, and the calculated charge on the nitrogen atoms of the N_2 unit (−0.49) indicates a net transfer of electron density from metal to ligand.

Population of the N_2 π_g antibonding MO would be expected to produce a lengthening of the N–N bond. That no significant increase is observed experimentally merits further investigation. The strong directionality of f orbitals (arising from their high nodality) suggests one possible explanation. Lengthening the N–N bond would reduce the overlap between the metal f and N_2 π_g levels, weakening the U–N_2–U bonding interaction. Work is in progress to evaluate this and other hypotheses.††

N. K. thanks the Royal Society for equipment grants, and the UK Computational Chemistry Working Party for a grant of computer time on the EPSRC's 'Columbus/Magellan' facility. P. S. thanks BNFL for their support.

Notes and References

† E-mail: n.kaltsoyannis@ucl.ac.uk; http://calcium.chem.ucl.ac.uk/webstuff/people/nkalt/index.html

‡ E-mail: peter.scott@csv.warwick.ac.uk; http://www.warwick.ac.uk/fac/sci/Chemistry/astaff/psc.html

§ Calculations were performed with the Amsterdam Density Functional program suite.[7,8] Quasi-relativistic[9] frozen cores were used for N (1s) and U (5d). Relativistic core potentials were computed using the ADF auxiliary program 'Dirac'. An uncontracted triple-zeta Slater-type orbital valence basis set was employed for all atoms, supplemented with p and d polarisation functions for H (ADF Type V), and d and f polarisation functions for N (ADF Type V). No polarisation functions were included for U (ADF Type IV). The density functional of Vosko *et al.*[10] was employed in conjunction with Becke's gradient correction[11] to the exchange part of the potential and the correlation correction due to Perdew.[12] Mulliken population analyses were performed.[13] The calculations were performed on IBM RS/6000 and DEC 433au workstations and the EPSRC's 'Columbus/Magellan' computer.

¶ The non-Aufbau, six unpaired electron arrangement is 102 kJ mol^{-1} less stable than that with four unpaired electrons, which has an Aufbau orbital occupancy and which is 68 kJ mol^{-1} more stable than the Aufbau restricted (*i.e.* no unpaired electrons) arrangement.

‖ It should be noted that a full description of the electronic structure of **2** must include the effects of spin–orbit coupling.[14] Under these circumstances the number of unpaired electrons is a meaningless quantity, as the electronic spin and orbital angular momenta cannot be separated. We will address this issue in further studies of triamidoamine–uranium systems.

** *E.g.* the principal contributions to the $\alpha 8b_g$ orbital are 24.34% U $f_{z(x^2 - y^2)}$, 14.97% U f_{z^3}, 6.13% U d_{yz} and 40.23% N_2 π_g.

†† Two areas that we will concentrate on are (a) geometry optimisations of **2** (in order to establish if the lack of N–N lengthening is indeed a result of f-orbital/π_g overlap requirements) and (b) replacement of one of the NH_2 H atoms by a SiH_3 unit in order to model the $N(CH_2CH_2NSiBu^tMe_2)_3$ ligand more closely.

1 J. B. Brennan, J. C. Green and C. M. Redfern, *J. Am. Chem. Soc.*, 1989, **111**, 2373.
2 D. L. Clark, S. K. Grumbine, B. L. Scott and J. G. Watkin, *Organometallics*, 1996, **15**, 949.
3 R. J. Butcher, D. L. Clark, S. K. Grumbine, B. L. Scott and J. G. Watkin, *Organometallics*, 1996, **15**, 1488.
4 N. Kaltsoyannis and B. E. Bursten, *J. Organomet. Chem.*, 1997, **528**, 19.
5 P. Roussel and P. Scott, *J. Am. Chem. Soc.*, 1998, **120**, 1070.
6 N. Kaltsoyannis, *J. Chem. Soc., Dalton Trans.*, 1996, 1583.
7 G. te Velde and E. J. Baerends, *J. Comput. Phys.*, 1992, **99**, 84.
8 ADF < 2.3 > , Department of Theoretical Chemistry, Vrije Universiteit, Amsterdam, 1997.
9 T. Ziegler, V. Tschinke, E. J. Baerends, J. G. Snijders and W. Ravenek, *J. Phys. Chem.*, 1989, **93**, 3050.
10 S. H. Vosko, L. Wilk and M. Nusair, *Can. J. Phys.*, 1980, **58**, 1200.
11 A. Becke, *Phys. Rev. A*, 1988, **38**, 3098.
12 J. P. Perdew, *Phys. Rev. B*, 1986, **33**, 8822.
13 R. S. Mulliken, *J. Chem. Phys.*, 1955, **23**, 1833.
14 N. Kaltsoyannis, *J. Chem. Soc., Dalton Trans.*, 1997, 1 (Perspective article).

Received in Cambridge, UK, 21st May 1998; 8/03833C

The coordination chemistry of amine triphenolate tripod ligands with iron(III). Old organic compounds but new tripod ligands

JungWon Hwang, Kumar Govindaswamy and Stephen A. Koch*†

Department of Chemistry, State University of New York at Stony Brook, Stony Brook, NY 11794-3400, USA

The coordination chemistry of new C_3 symmetric triphenolate amine tripod ligands has been demonstrated with Fe^{III}.

A key feature of the coordination chemistry of tripod ligands is their ability to divide the metal–ligand coordination sphere into non-labile sites and reactive sites. Saconni and the Florence school first demonstrated the rich coordination chemistry of tripod ligands in the 1960s and 1970s.[1,2] In the 1990s the chemistry of tripod ligands has undergone a renaissance.[3–5] We report the coordination chemistry of new polyphenolate amine tripod ligands: tris(2-hydroxybenzyl)amine (**1**) and tris(2-hydroxy-3,5-dimethylbenzyl)amine (**2**). Phenolate containing ligands are valuable in modeling the active sites of metal–tyrosine centers in metalloproteins[6] and homogeneous and heterogeneous catalysts.[7] Historically, the hydrochloride salt of **1** was the subject of its first and only report in 1922,[8] while the synthesis of **2** appeared in the literature in 1949.[9] The coordination chemistry of compounds **1** and **2** has never been previously reported.

Our route to **1,** which differs from the original synthesis, is outlined in Scheme 1. The reaction of 2 equiv. of 2-methoxybenzyl bromide[10] (**3**) with commercially available 2-methoxybenzylamine (**4**) in refluxing CH_3CN with added K_2CO_3 gives tris(2-methoxybenzyl)amine (**5**) in 80–85% yield. The methyl protecting groups are removed by refluxing **5** in toluene with 5 equiv. of $AlCl_3$ to give **1** in 70% yield. We were able to reproduce the synthesis of **2** by the one step Mannich reaction of 2,4-dimethylphenol with hexamethylenetetramine.[9] Since both **1** and **2**‡ were reported before the advent of modern spectroscopic techniques, the congruence of our compounds with the literature compounds was established by melting point comparisons.

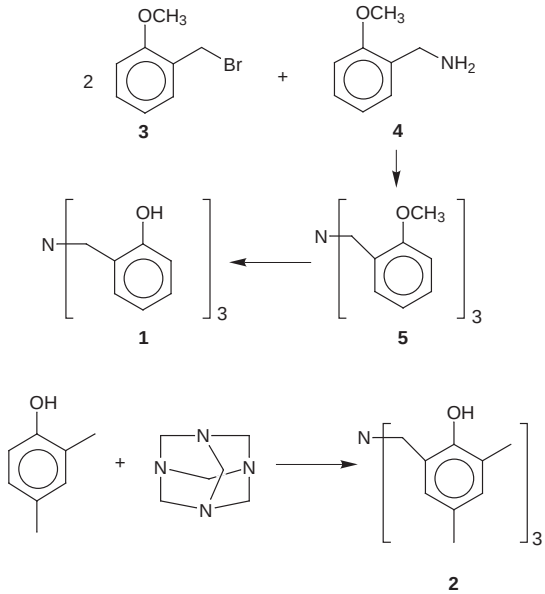

Scheme 1

The reaction of the trilithium salt of **1** with $FeCl_3$ in the presence of 3 equiv. of 1-methylimidazole (1-Meim) in MeOH gave dark red crystals of [Fe{N(CH_2-*o*-C_6H_4O)$_3$}(1-Meim)] (**6**) in 65% yield. The structure of **6**, which was determined by X-ray crystallographic analysis§ (Fig. 1), consists of a trigonal bipyramidal structure with an N1–Fe–N2 angle of 173.4(1)°. The Fe atom is 0.045 Å out of the plane of the three oxygen donors toward the imidazole nitrogen. The FeO_3 plane shows small deviations from trigonal symmetry with O–Fe–O angles of 117.4(1) to 126.3(1)°. The average Fe–O bond distance [1.876(15) Å] is intermediate between the Fe–O in tetrahedral [Fe^{III}(OC_6HMe_4-2,3,5,6)$_4$]$^-$ [1.847(13) Å] and in octahedral Fe tris-catecholate complexes (2.02 Å).[11,12] The analogous compound, [Fe{N[CH_2-*o*-C_6H_2(OMe)$_2$-3,5]$_3$}(1-Meim)] (**7**), has also been characterized with ligand **2**.

The tripod ligand coordinates to the metal to generate a chiral C_3 conformation[13] with both enantiomeric structures present in the centric crystal lattice. These tripod ligands **1** and **2** differ from the well studied N(CH_2CH_2OH)$_3$ and N(CH_2CO_2H)$_3$ ligands in the phenolate *versus* alkoxide and carboxylate donors and by having six- *versus* five-membered metal ligand chelate rings. The aminetriphenolate ligand N(*o*-C_6H_4O)$_3$ and its coordination chemistry with Al have been reported.[14]

The thiol analog of **1** and its [Fe^{III}{N(CH_2-*o*-C_6H_4S)$_3$}(1-Meim)] complex has recently been reported.[15] The 0.43 Å change in Fe–O *versus* Fe–S bond distance reflects the difference in the ionic radii of S and O. The larger average Fe–O–C angle [134(1)°] in **6** *versus* the Fe–S–C [110(1)°] angle is

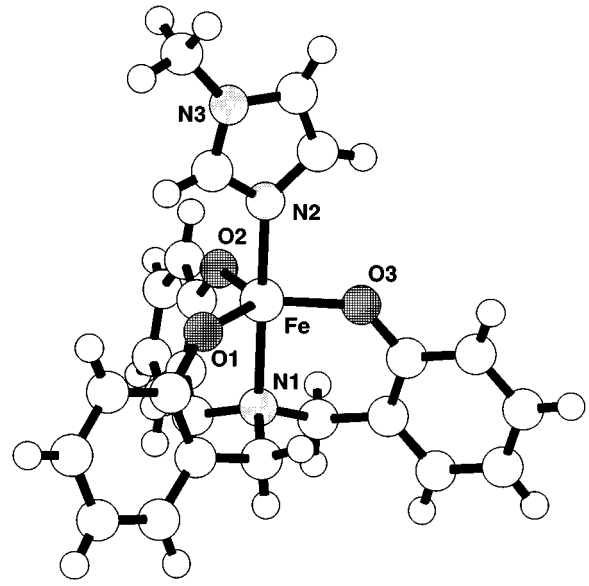

Fig. 1 Structural diagram for [Fe{N(CH_2-*o*-C_6H_4O)$_3$}(1-Meim)] (**6**). Selected distances (Å) and angles (°) Fe1–O1 1.881(3); Fe1–O2 1.888(3); Fe1–O3 1.859(3); Fe1–N1 2.191(3); Fe1–N2 2.090(4); O1–Fe1–O2–126.3(1); O1–Fe1–O3–117.4(1); O2–Fe1–O3 116.2(1); O1–Fe1–N1 87.1(1); O1–Fe1–N2 87.6(1); O2–Fe1–N1 88.9(1); O2–Fe1–N2 91.1(1); O3–Fe1–N1 89.9(1); O3–Fe1–N2 96.0(1); N1–Fe1–N2 173.4(1); Fe1–O–C_{avg} 134(1).

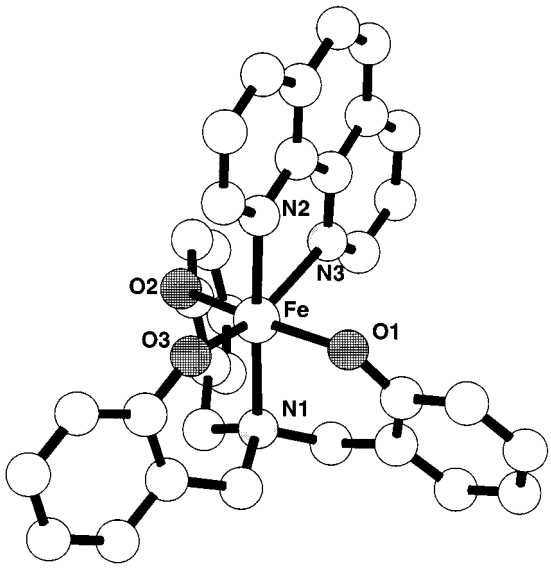

Fig. 2 Structural diagram for [Fe{N(CH_2-*o*-C_6H_4O)$_3$}(phen)] (**9**). Selected distances (Å) and angles (°): Fe1–O1 1.897(6); Fe1–O2 1.926(6); Fe1–O3 1.893(7); Fe1–N1 2.225(8); Fe1–N2 2.158(7); Fe1–N3 2.340(7); N1–Fe–O3 91.5(3); O3–Fe–N2 87.7(3); N2–Fe–N3 73.9(3); N3–Fe–N1 107.0(3); O1–Fe–O2 164.1(3); N–Fe–$O2_{avg}$ 88.4(3); N–Fe–$O1_{avg}$ 87.5(3); Fe–O–C_{avg} 128.5(7).

consistent with the known Fe^{III} coordination chemistry of thiolate and phenolate ligands.[11,16,17] In an attempt to prepare a four coordinate complex, the reaction of $Li_3N(CH_2$-*o*-$C_6H_4O)_3$] with $FeCl_3$ was repeated in the absence of 1-Meim. However the X-ray structure§ of the product, [Fe{N(CH_2-*o*-$C_6H_4O)_3$}(DMF)] (**8**), revealed that a molecule of solvent was coordinated to the iron. The crystal of **8** is isomorphous and is essentially isostructural with **6**. The atomic positions of the non-hydrogen atoms of the DMF molecule are structurally equivalent to five of the atoms of the 1-Meim in **6**. The reaction of **8** with 1,10-phenanthroline in DMF followed by the addition of MeOH gave dark red crystals of [Fe{N(CH_2-*o*-$C_6H_4O)_3$}(phen)] (**9**) in 50% yield. The structure of **9**§ (Fig. 2) demonstrates that the tripod ligands can support an octahedral coordination center. The phen ligand has a distinctly asymmetric coordination with Fe–N2 2.158(7) Å and Fe–N3 2.340(7) Å distances. The distortion results from a short contact between a benzyl proton and the hydrogen atom *ortho* to N3.

Compounds **6**–**9** have magnetic moments indicative of high spin Fe^{3+} and have an intense phenolate to Fe charge transfer transition at 399 nm (ε = 7960 dm^3 mol^{-1} cm^{-1}), 422 (8320), 405 (9700), and 399 (7751) respectively.[18] A quasireversible Fe^{III}–Fe^{II} redox couple was observed in the cyclic voltammogram of **7** occurring at $E_{1/2}$ = −0.78 V (ΔE = 107 mV) *versus* Ag/AgCl in DMF solution. Only irreversible oxidation processes were observed for all the compounds.[19]

The chemistry of these tripod ligands with other metal ions is under investigation. We thank the National Institutes of Health for support.

Notes and References

† E-mail: stephen.koch@sunysb.edu

‡ Compound **1**: ^{1}H NMR ([$^2H_6$]DMSO): δ 4.25 (s; 6 H; CH_2), 6.82 (t; 3 H; 3-H), 6.93 (d; 3 H; 1-H), 7.24 (m; 6 H; 3,4-H), 8.40 [s(br); 1 H; NH^+], 10.5 (s; 3 H; OH). FAB-MS**:** 335 [M^+]. Compound **2**: ^{1}H NMR ($CDCl_3$): δ 2.23 (s; 18 H; CH_3), 3.61 (s; 6 H; CH_2), 6.52 [s(br); 3 H; OH], 6.72 (s; 3 H; 6-H), 6.84 (s; 3 H; 4-H). FAB-MS**:** 419 [M^+].

§ *Crystal data* for **6** (crystallized from DMF–isopropanol): $FeC_{25}H_{24}N_3O_3$, M = 469.85, monoclinic, space group $P2_1/c$, a = 14.837(3), b = 9.410(8), c = 17.162(3) Å, β = 110.836(9)°, U = 2239(1) Å^3, Z = 4, Mo-Kα radiation (λ = 0.71073 Å), μ = 7.016 cm^{-1}. The structure was solved and refined using standard crystallographic techniques with $R(R_w)$ = 0.040(0.039) for 1993 observed reflections $I > 3\sigma(I)$. For **7**: $FeC_{31}H_{36}O_3N_3$, M = 554.49, monoclinic, space group $P2_1/n$, a = 16.409(4), b = 10.841(1), c = 17.082(4) Å, β = 110.37(1)°, U = 2849(1) Å^3, Z = 4, μ(Mo-Kα) = 7.127 cm^{-1}; $R(R_w)$ = 0.053(0.025) for 1733 reflections $I > 3\sigma(I)$. For **8**: $FeC_{24}H_{25}N_2O_4$, M = 449.3, monoclinic, space group $P2_1/c$, a = 14.670(3), b = 9.413(9), c = 16.807(3) Å, β = 108.054(8)°, U = 2206(1) Å^3, Z = 4, μ(Mo-Kα) = 5.65 cm^{-1}, $R(R_w)$ = 0.039(0.047) for 2888 observed reflections $I > 3\sigma(I)$. For **9** (crystallized from DMF–MeOH): $FeC_{33}H_{26}N_3O_3$, M = 568.44, monoclinic, space group $P2_1/c$, a = 12.042(3), b = 18.356(3), c = 12.713(4) Å, β = 110.02(1)°, U = 2640(2) Å^3, Z = 4, μ(Mo-Kα) = 6.087 cm^{-1}, $R(R_w)$ = 0.050(0.044) for 2888 observed reflections $I > 3\sigma(I)$. CCDC 182/921.

1 L. Sacconi and F. Mani, *Transition Met. Chem.*, 1982, **8**, 179.
2 F. Mani and L. Sacconi, *Comments Inorg. Chem.*, 1983, **2**, 157.
3 C. Bianchini, A. Meli, M. Peruzzini, F. Vizza and F. Zanobini, *Coord. Chem. Rev.*, 1992, **120**, 193.
4 J. G. Verkade, *Acc. Chem. Res.*, 1993, **26**, 483.
5 R. R. Schrock, *Acc. Chem. Res.*, 1997, **30**, 9.
6 D. H. Ohlendorf, A. M. Orville and J. D. Lipscomb, *J. Mol. Biol.*, 1994, **244**, 586; T. Klabunde, N. Sträter, R. Fröhlich, H. Witzel and B. Krebs, *J. Mol. Biol.*, 1996, **259**, 737; B. F. Anderson, H. M. Baker, G. E. Norris, D. W. Rice and E. N. Baker, *J. Mol. Biol.*, 1989, **209**, 711; N. Ito, S. E. V. Phillips, C. Stevens, Z. B. Ogel, M. J. McPherson, J. N. Keen, K. D. S. Yadav and P. F. Knowles, *Nature*, 1991, **350**, 87.
7 M. H. Chisholm, J.-H. Huang, J. C. Huffman, W. E. Strieb and D. Tiedtke, *Polyhedron*, 1997, **17**, 2941; K. J. Weller, P. A. Fox, S. D. Gray and D. E. Wigley, *Polyhedron*, 1997, **17**, 3139 and references therein.
8 G. Zemplén and A. Kunz, *Chem. Ber.*, 1922, **55**, 979.
9 K. Hultzsch, *Chem. Ber.*, 1949, **82**, 16.
10 J. L. Kelley, J. A. Linn and J. W. T. Selway, *J. Med. Chem.*, 1989, **32**; 1757.
11 S. A. Koch and M. Millar, *J. Am. Chem. Soc.*, 1982, **104**, 5255.
12 K. N. Raymond, S. S. Isied, L. D. Brown, F. R. Fronczek and J. H. Nibert, *J. Am. Chem. Soc.*, 1976, **98**, 1767.
13 C. Moberg, *Angew. Chem., Int. Ed. Engl.*, 1998, **37**, 249
14 E. Müller and H.-B. Bürgi, *Helv. Chim. Acta*, 1987, **70**, 520.
15 N. Govindaswamy, D. A. Quarless Jr. and S. A. Koch, *J. Am. Chem. Soc.*, 1995, **117**, 8468.
16 L. E. Maelia, M. Millar and S. A. Koch, *Inorg. Chem.*, 1992, **31**, 4594.
17 M. Millar, J. F. Lee, T. O'Sullivan, S. A. Koch and R. Fikar, *Inorg. Chim. Acta*, 1996, **243**, 333.
18 J. W. Pyrz, A. L. Roe, L. J. Stern and L. Que Jr., *J. Am. Chem. Soc.*, 1985, **107**, 614.
19 A. Sokolowski, J. Müller, T. Weyhermüller, R. Schnepf, P. Hildebrandt, K. Hildenbrand, E. Bothe and K. Wieghardt, *J. Am. Chem. Soc.*, 1997, **119**, 8889.

Received in Bloomington, IN, USA, 14th April 1998; 8/02725K

Transition metal imide/organic imine metathesis reactions: *unexpected observations*

Jacqueline M. McInnes and Philip Mountford*†‡

Department of Chemistry, University of Nottingham, Nottingham, UK NG7 2RD

Mixtures of [Ti(NBu^t)Cl$_2$(py)$_3$] 1 and PhC(NAr)H (Ar = C$_6$H$_3$Me$_2$-2,6 or C$_6$H$_4$Me-4) gave quantitative conversion to [Ti(NAr)Cl$_2$(py)$_3$] and PhC(NBu^t)H, the products of Ti=N-Bu^t/C=NAr transition metal imide/organic imine metathesis; examination of the kinetics for Ar = C$_6$H$_4$Me-4 showed that the rate limiting step for this process is zero order in [1], demonstrating that these reactions do not involve metal imide participation in the rate limiting step.

One attraction of transition metal imido compounds is their potential use in metal-mediated imido group (NR) transfer reactions. The addition of unsaturated substrates to M=NR linkages is now well documented, but examples of reactions resulting in complete removal (functional group transfer) of NR from metal to substrate are still somewhat more restricted, especially by comparison with the rich functional group transfer chemistry of metal oxo complexes.[1] Very recently there have been reports of transition metal imide/organic imine (L$_n$M=NR/R$_2$C=NR′) functional group metathesis reactions,[2] and these have been proposed in some instances to arise *via* metal imide-mediated processes, possibly involving cycloaddition of C=NR′ to M=NR. Such processes appear to be the aza-analogues of the widely used metal alkylidene (L$_n$M=CR$_2$)/alkene (R′$_2$C=CR′$_2$) metathesis reaction[3] and are therefore potentially hugely important transformations in stoichiometric and catalytic synthesis. Identification of the possible role(s) of the metal centre in such processes is clearly essential. As part of an ongoing study of early transition metal imido chemistry, we found that a number of titanium imido complexes undergo well characterised cycloaddition and other coupling reactions of the Ti=NR group (R = Bu^t or aryl) with organic substrates.[4] In parallel studies we have observed reactions of [Ti(NBu^t)Cl$_2$-(py)$_3$][4b] with certain mono- and α-di-imines that yield the expected products of imide/imine functional group metathesis. The results herein show that examples of apparently metal-mediated imide/imine metathesis reactions must be subjected to mechanistic investigations before they can be properly authenticated.

Reaction of [Ti(NBu^t)Cl$_2$(py)$_3$] **1** with one equivalent of the *N*-2,6-dimethylphenylbenzaldehyde imine **2** at 60 °C for 96 hours in CDCl$_3$ gave (by NMR) quantitative and stoichiometric conversion to PhC(NBu^t)H **4** and the arylimido compound [Ti(NC$_6$H$_3$Me$_2$-2,6)Cl$_2$(py)$_3$] **3** [eqn. (1)].§ Repeating the

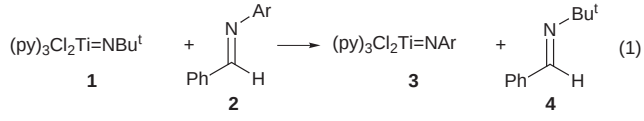

(1)

Ar = C$_6$H$_3$Me$_2$-2,6

reaction on a preparative scale confirmed the exchange of *tert*-butylimide for the 2,6-dimethylphenylimide ligand. Similarly, reaction of **1** with one equivalent of the less bulky *N*-arylimine PhC(NTol)H **5** (Tol = C$_6$H$_4$Me-4) gave a quantitative yield of **4** after only 4 hours at 60 °C in CDCl$_3$, along with the tolylimido product **6** [eqn. (2)]. Products **3**, **4** and **6** were identified by comparison with authentic samples[4b] and the reactions were

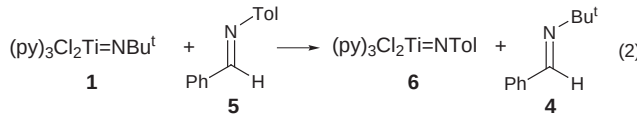

(2)

fully reproducible in both CDCl$_3$ and C$_6$D$_6$. At first sight, eqns. (1) and (2) are apparently straightforward examples of metal-mediated imide/imine metathesis reactions. Furthermore, reaction of **1** with certain *N*-aryl-α-diimines also leads to the expected arylimido titanium products and the corresponding *N*-*tert*-butyl-α-diimines.

In a separate experiment [eqn. (3)] an equimolar mixture of

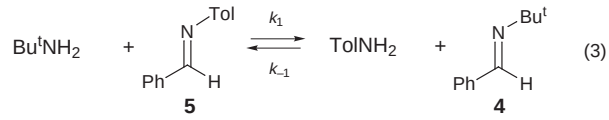

(3)

Bu^{t}NH$_2$ with **5** in CDCl$_3$ (no titanium imido compound added) gave an equilibrium mixture (K_{eq} *ca.* 1, *i.e.* $k_1 \approx k_{-1}$) containing the two starting compounds along with the products TolNH$_2$ and imine **4** after 8 hours at 30 °C. Similarly, starting with an equimolar mixture of pure TolNH$_2$ and **4** also gave an equilibrium mixture of TolNH$_2$, **4**, Bu^{t}NH$_2$ and **5**. Since there is no thermodynamic driving force in eqn. (3) to account for the net quantitative reactions in eqns. (1) and (2), we infer that it is formation of the arylimide products **3** and **6** that causes these two reactions to go to completion. This hypothesis is supported by eqn. (4) which shows that addition of a stoichiometric

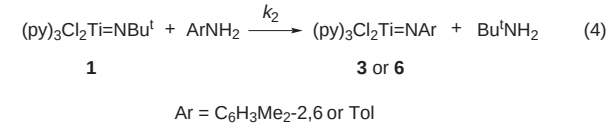

(4)

Ar = C$_6$H$_3$Me$_2$-2,6 or Tol

amount of arylamine to [Ti(NBu^t)Cl$_2$(py)$_3$] **1** gives quantitative formation of Bu^{t}NH$_2$ and the corresponding arylimide **3** or **6**.[4b] This process is (qualitatively) very much faster than any of the other three [*i.e.* eqns. (1)–(3)]. Further evidence for the role of **1** as an effective trap for ArNH$_2$ came from NMR experiments in which **1** was added to a pre-equilibrated mixture of Bu^{t}NH$_2$, **5**, TolNH$_2$ and **4** [eqn. (3)]: **1** and TolNH$_2$ were consumed and there was quantitative conversion of **5** to **4**.

Examination of the kinetics of eqn. (3) under pseudo-first order conditions established that this reaction [from left to right as shown in eqn. (3)] is first order in both Bu^{t}NH$_2$ and imine **5** and also allowed the direct deduction of k_1. However, reaction of [Ti(NBu^t)Cl$_2$(py)$_3$] **1** with PhC(NTol)H **5** (10, 16.5 and 20 equivs.) under otherwise identical pseudo-first order conditions showed (Fig.1) that the rate for eqn. (2) is zero order with respect to **1** and has no simple dependence on [**5**]. These observations are clearly not consistent with the expected titanium imide-mediated metathesis mechanism of the type illustrated in Scheme 1, in which a diazametallacycle **7** is formed in the rate limiting step. For such a process a rate dependency on [**1**] is required.¶ Indeed, to our knowledge, all

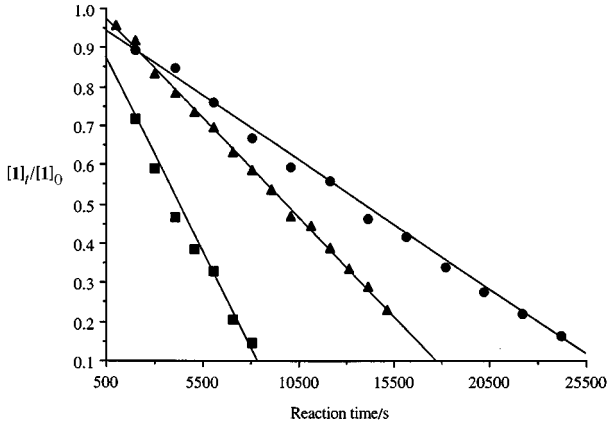

Fig. 1 Linear plots of $[\mathbf{1}]_t/[\mathbf{1}]_0$ *versus* time for the reactions with an excess of PhC(NTol)H **5** in $CDCl_3$ showing clearly the zero order dependence of rate on [**1**]. Legend: ● 10 equivalents of **5**; ▲, 16.5 equivalents of **5**; ■, 20 equivalents of **5**.

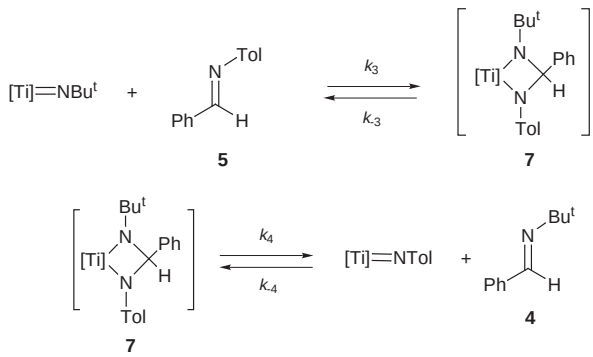

Scheme 1

kinetically characterised examples of alkene metathesis by homogeneous metal alkylidene (carbene) complexes (which proceed *via* metallacyclobutane intermediates) show a first order dependence on metal concentration.[5] Furthermore, studies by Lee and Bergman of cycloaddition reactions of the imido zirconium complex $[Cp_2Zr(NR)(L)]$ (R = But or $C_6H_3Me_2$-2,6, L = THF, $OPPh_3$ or 4-*tert*-butylpyridine) have shown them to be first order in imido complex.[6] Previously reported zirconium-mediated imine metathesis reactions also follow a first order relationship between reaction rate and metal complex, although in this instance the resting state of the complex is a diazametallacycle.[2a]

The absence of a rate dependence on [**1**] implies that one or more alternative mechanisms (to that shown in Scheme 1) must be operating in eqns. (1) and (2). At first sight, one possibility appears to be a tandem combination of eqns. (3) and (4) where traces of Bu^tNH_2 (in principle impossible to exclude for these very moisture sensitive systems, although we have no NMR evidence for its presence in mixtures of **1** and **5**) give rise to formation of imine **4**, the liberated $TolNH_2$ being scavenged by **1** forming the imido product **6**. However, the kinetic results do not support this mechanism since the rate law in this case‖ requires a first-order dependence on [**5**]. Furthermore there is no evidence for significant enough concentrations of Bu^tNH_2 in these NMR mixtures to account for the observed rate of formation of **4** and **6** in these reactions.**

In summary we have demonstrated that apparently straightforward transition metal imide/organic imine metathesis reactions do not necessarily involve metal imide participation in the rate determining step. This is in sharp contrast to the well known metal alkylidene/alkene metathesis reactions. Cases of metal imide/imine metathesis must clearly be subjected to mechanistic scrutiny before conclusions concerning either the role of the metal centre or any structure–activity relationships can be reached. Further investigations of these and other related reactions are currently under way.

We thank the EPSRC and Leverhulme Trust for support, Professors M. Bochmann, R. H. Grubbs and J. J. Turner for helpful comments and Dr P. Scott for a gift of $[Sc(OTf)_3]$.

Notes and References

† Email: Philip.Mountford@Nottingham.ac.uk,
www: http://www.nottingham.ac.uk/~pczwww/Inorganic/PMount.html
‡ Philip Mountford is the Royal Society of Chemistry Sir Edward Frankland Fellow.

§ For all the rate determinations the disappearance of $[Ti(NBu^t)Cl_2(py)_3]$ **1** or Bu^tNH_2 was monitored over at least three half-lives under pseudo-first-order conditions with *p*-dimethoxybenzene as the internal standard. Both before and after each experiment the temperature in the NMR probe was calibrated using ethylene glycol (80%) in DMSO. The temperature did not vary by more than 1 °C. The samples were prepared in a dry-box using Teflon valve (Young's) 5 mm tubes, which had been rigorously dried. $CDCl_3$ and C_6D_6 were dried over calcium hydride and potassium respectively, at rt, then distilled under reduced pressure. ^{1}H NMR spectra were recorded on a Bruker DPX 300 spectrometer at 30 °C.

¶ For the process shown in Scheme 1, rate = k_{obs}[metal imide][organic imine], where $k_{obs} = k_3k_4/(k_{-3} + k_4)$, assuming the k_{-4} step is not significant at low concentrations of product imine and a steady state approximation for [**7**]. In the reactions in eqns. (1) and (2), pyridine dissociation may be required before formation of hypothetical **7**. In this instance the rate should still be dependent on [metal imide], but k_{obs} would show a dependence on [pyridine]. However, we have found that the five-coordinate bis(pyridine) complex $[Ti(NBu^t)Cl_2(py)_2]$ also reacts with organic imines at a rate not significantly different from that of **1** under the same conditions and so the presence of the third pyridine molecule is not important.

‖ Combining eqns. (3) and (4) and assuming a steady state approximation of $[TolNH_2]$ leads to the expression: rate = $k_1[Bu^tNH_2][\mathbf{5}]$ since, under the pseudo-first order conditions used here, [**5**] ≫ [**4**] and hence the k_{-1} back-reaction is negligible, especially since **1** is an effective trap for $TolNH_2$.

** From kinetic analysis of eqn. (3) we know independently the value of k_1 (1.35×10^{-3} M^{-1}s^{-1}) under analogous reaction conditions. Therefore, if indeed rate = $k_1[Bu^tNH_2][\mathbf{5}]$ then $[Bu^tNH_2]$ has to be approximately 0.10 to 0.43 M for the experiments shown in Fig. 1. From the NMR spectra the maximum possible value of $[Bu^tNH_2]$ in these experiments is < 0.005 M. However, it is possible that under the reaction conditions of eqns. (1) or (2), eqn. (3) is accelerated by Lewis and/or Brønsted acids. Indeed, tests of this hypothesis for eqn. (3) with added $[Sc(OTf)_3]$ demonstrated a rate acceleration suggesting that Lewis acids (*e.g.* **1** and/or its trace decomposition products) may make a tandem combination of eqns. (3) and (4) a possibility. Toluene-*p*-sulfonic acid had no measurable effect on the rate of eqn. (3). We cannot directly determine the influence of additional Bu^tNH_2 on the rate of reaction of **1** with **5** [eqn. (2)]: any Bu^tNH_2 added would be rapidly scavenged by **5** [eqn. (3)] since $t_{1/2}$ for the consumption of **5** in eqn. (3) is *ca.* 25 times shorter than for **5** in eqn. (2) under otherwise identical conditions.

1 D. E. Wigley, *Prog. Inorg. Chem.*, 1994, **42**, 239; W. A. Nugent and J. M. Mayer, *Metal-Ligand Multiple Bonds*, Wiley-Interscience, New York, 1988; R. H. Holm, *Chem. Rev.*, 1987, **87**, 1401; E. W. Harlan and R. H. Holm, *J. Am. Chem. Soc.*, 1990, **112**, 186; L. K. Woo, *Chem. Rev.*, 1993, **93**, 1125.

2 (*a*) K. E. Meyer, P. J. Walsh and R. G. Bergman, *J. Am. Chem. Soc.*, 1995, **117**, 974; (*b*) G. K. Cantrell and T. Y. Meyer, *Organometallics*, 1997, **16**, 5381; (*c*) G. K. Cantrell and T. Y. Meyer, *Chem. Commun.*, 1997, 1551; (*d*) G. K. Cantrell, T. Pontz and T. Y. Meyer, *Abstracts of Papers of the American Chemical Society*, 1997, **214**, 312-INOR.

3 For reviews see: V. C. Gibson, *Adv. Mater.*, 1994, **6**, 37; R. H. Grubbs and S. Chang, *Tetrahedron*, 1998, **54**, 4413, and references therein.

4 (*a*) P. Mountford, *Chem. Commun.*, 1997, 2127 (Feature Article); (*b*) A. J. Blake, P. E. Collier, S. C. Dunn, W.-S. Li, P. Mountford and O. V. Shishkin., *J. Chem. Soc., Dalton Trans.*, 1997, 1549; (*c*) A. J. Blake, P. E. Collier, L. H. Gade, P. Mountford, M. Schubart and I. J. Scowen, *Chem. Commun.*, 1997, 1555.

5 E. L. Dias, S. T. Nguyen and R. H. Grubbs, *J. Am. Chem. Soc.*, 1997, **119**, 3887 and references therein.

6 S. Y. Lee and R. G. Bergman, *Tetrahedron*, 1995, **51**, 4255 and references therein.

Received in Cambridge, UK, 18th May 1998; 8/03719A

Phosphoramidate-mediated conversion of metal carbonyls into metal isonitriles

Susan E. Gibson (née Thomas),*† Thomas W. Hinkamp, Mark A. Peplow and Mark F. Ward

Department of Chemistry, Imperial College of Science, Technology and Medicine, South Kensington, London, UK SW7 2AY

The reaction of metal carbonyls with readily-available phosphoramidate anions provides a new route to metal isonitriles; in particular, enantiomerically pure isonitrile complexes are easily accessed by this method.

Our recent interest in tricarbonyl(vinylketene)iron(0) complexes and their nitrogen analogues, tricarbonyl(vinylketenimine)iron(0) complexes, led us to devise a method for the conversion of the former into the latter, central to which were the anions of diethyl *N*-alkylphosphoramidates.[1] We subsequently questioned whether or not this approach could be used to convert metal carbonyls into metal isonitriles, a transformation worthy of investigation in view of the ubiquity of carbonyl and isonitrile ligands in organometallic chemistry.

We report herein our preliminary results in this area which reveal that the phosphoramidate-mediated conversion of metal carbonyls to metal isonitriles is indeed a viable process. The reaction's potential may be summarised by the following points: (i) unlike the 'classical' carbonyl–isonitrile exchange approach to isonitrile ligands[2] the process avoids the use of 'free' isonitriles, compounds which are frequently volatile, smelly and toxic; (ii) the method introduces isonitrile ligands in a controlled manner, again in contrast to the 'classical' carbonyl–isonitrile exchange reaction which frequently delivers mixtures of products;[3] (iii) phosphoramidates are easy to synthesise[4] and handle;‡ and (iv) the method provides rapid access to non-racemic chiral isonitrile ligands, a class of ligand which has received remarkably little attention to date.§

An initial experiment was carried out using phosphoramidate **1** and the tricarbonyliron cation **2**. Phosphoramidate **1** was synthesised by stirring together 2.2 equiv. of *tert*-butylamine and 1.0 equiv. of diethyl phosphite in CCl_4–light petroleum according to literature precedent;[4a,c] work-up gave **1** as a colourless stable liquid in 89% yield (Scheme 1). The iron cation **2** was synthesised from $[(C_5H_5)(CO)_2Fe]_2$ by reduction with sodium amalgam, and sequential addition of ethyl chloroformate, hydrogen chloride and ammonim hexafluorophosphate.[8] This produced cation **2** in 81% overall yield as an orange–yellow crystalline solid.

Phosphoramidate **1** was dissolved in THF, cooled to −78 °C and treated with 1 equiv. of butyllithium.¶ To this solution was added to a stirred suspension of 1 equiv. of cation **2** in THF. The resulting mixture was held at −78 °C for 6 h during which time the suspension gradually gave way to a yellow solution. Work-up of the product mixture by column chromatography and crystallisation produced a light yellow solid which was identified as the dicarbonyl isonitrile complex **3** by comparison of its ^{1}H NMR and IR spectra with literature values.[9] Cation **3** was generated in an acceptable 58% yield on a 1.0 mmol scale, thus indicating that the phosphoramidate-mediated conversion of carbonyl ligands to isonitrile ligands is indeed feasible.

Experiments to probe the scope and limitations of this process with respect to the phosphoramidate were performed next. Thus cation **2** was reacted with 2 equiv. of the ethylamine-derived phosphoramidate **4** and methyllithium. This experiment gave the diisonitrile product **5**[10] in 77% yield. Moreover reaction of cation **3** with 1 equiv. of phosphoramidate **4** and methyllithium gave the novel‖ cation **6** in 63% yield. These experiments demonstrate not only that the degree of carbonyl–isonitrile conversion can be controlled by the amount of phosphoramidate used and that the method is useful for the controlled formation of mixed isonitrile complexes, but also that complexes of volatile isonitriles are readily and conveniently formed by this approach.

In view of the rarity of non-racemic chiral isonitrile complexes, phosphoramidate (*S*)-**7** was synthesised from (*S*)-α-methylbenzylamine. Reaction of the anion of **7** with cation **2** smoothly generated the novel cation **8** in 55% yield. Thus the

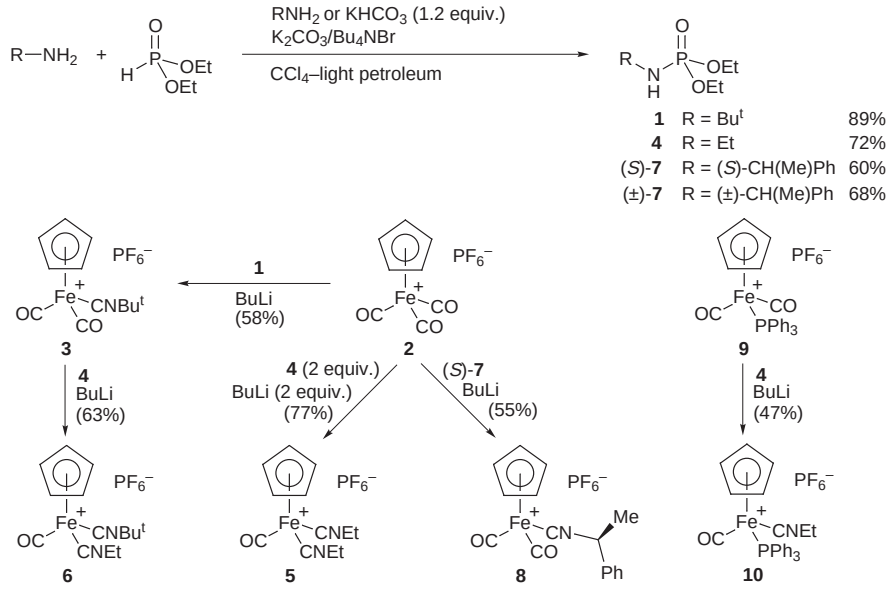

Scheme 1

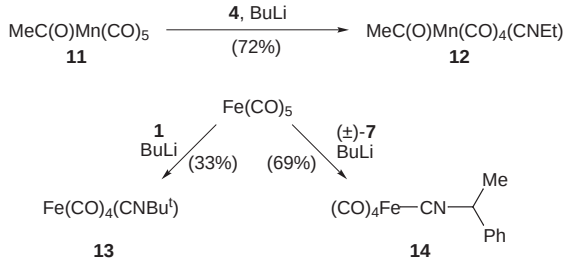

Scheme 2

method provides a straightforward and new way of incorporating chirality into transition metal complexes. Moreover, a wide variety of amines, which provide the chirality, is readily available.

Initial experiments on the scope and limitations of the conversion with respect to transition metal substrates have also been performed. Thus the triphenylphosphine-substituted iron cation **9** was synthesised according to a literature procedure[11] and reacted with the anion of phosphoramidate **4** to give the isonitrile **10**[12] in 47% yield. Likewise the manganese acetyl complex **11** was synthesised[13] and reacted with the anion derived from phosphoramidate **4** thus producing the novel manganese isonitrile complex **12** in 72% yield (Scheme 2), and iron pentacarbonyl was reacted with the anions of **1** and (±)-**7** to give isonitrile complex **13**[14] and the novel complex **14** respectively.

Finally, to check the stereochemical consequences of the metal isonitrile synthesis, iron pentacarbonyl was reacted with the anion of (*S*)-**7**. Chiral HPLC analysis of the products** from the reactions of iron pentacarbonyl with the anions of (±)-**7** and (*S*)-**7** revealed that the product derived from (*S*)-**7** was formed in 99 ± 1% ee, indicating that racemisation of the amine does not occur during its incorporation into the isonitrile ligand.

Notes and References

† E-mail: s.gibson@ic.ac.uk

‡ Phosphinimines, $Ph_3P{=}NR$, are known to convert metal carbonyl ligands into metal isonitrile ligands (ref. 5). In contrast to phosphoramidates, however, phosphinimines are frequently moisture and/or air-sensitivity (refs. 5, 6).

§ For example, a recent report on the enantioselective bis-silylation of alkenes using a palladium(0) chiral isonitrile catalyst (ref. 7), represents, to the best of our knowledge, the only use of chiral isonitriles in asymmetric catalysis to date.

¶ The method used for the conversion of cation **2** to cation **3** is in fact typical of the protocols used for all the other carbonyl–isonitrile conversions discussed herein. Thus, Bu^nLi (1.6 mol dm^{-3}; 0.63 cm^3, 1.0 mmol) was added dropwise to a solution of *N*-(*tert*-butyl)phosphoramidate **1** (0.209 g, 1.00 mmol) in THF (10 cm^3) held at −78 °C under nitrogen. The solution was allowed to warm to room temperature and then recooled to −78 °C for the addition, *via* a cannula and under nitrogen, of a suspension of cation **2** (0.350 g, 1.00 mmol) in THF (30 cm^3). The reaction mixture was stirred at −78 °C for 6 h. Solvent removal gave a brown solid which was subjected to column chromatography [SiO_2; light petroleum (bp 40–60 °C)–acetone, 1 : 1]. The resulting yellow solid was crystallised from acetone–CH_2Cl_2 to give cation **3** (0.235 g, 58%) as yellow crystals.

‖ The novel complexes **6**, **8**, **12** and **14** all gave satisfactory spectroscopic (IR, ^1H NMR, ^{13}C NMR and low resolution MS) and microanalytical or high resolution MS data.

** Chiralcel OD-H; Pr^iOH–hexane (1 : 40), 900 μl min^{-1}; retention times of enantiomers: 6.37 and 6.83 min.

1 S. A. Benyunes, S. E. Gibson (née Thomas) and J. A. Stern, *J. Chem. Soc., Perkin Trans. 1*, 1995, 1333.
2 E. Singleton and H. E. Oosthuizen, *Adv. Organomet. Chem.*, 1983, **22**, 209.
3 For example, see M. J. Mays and P. D. Gavens, *J. Chem. Soc., Dalton Trans.*, 1980, 911.
4 (*a*) F. R. Atherton, H. T. Openshaw and A. R. Todd, *J. Chem. Soc.*, 1945, 660; (*b*) A. Zwierzak and K. Osowska, *Synthesis*, 1984, 223; (*c*) W. S. Wadsworth and W. D. Emmons, *J. Org. Chem.*, 1964, **29**, 2816; (*d*) A. Koziara, B. Olejniczak, K. Osowska and A. Zwierzak, *Synthesis*, 1982, 918; (*e*) E. K. Ryu and L. A. Cates, *J. Med. Chem.*, 1971, **14**, 1022.
5 C.-Y. Liu, D.-Y. Chen, M.-C. Cheng, S.-M. Peng and S.-T. Liu, *Organometallics*, 1995, **14**, 1983 and references cited therein.
6 H. Zimmer and G. Singh, *J. Org. Chem.*, 1963, **28**, 483.
7 M. Suginome, H. Nakamura and Y. Ito, *Tetrahedron Lett.*, 1997, **38**, 555.
8 L. Busetto and R. J. Angelici, *Inorg. Chim. Acta*, 1968, **2**, 391.
9 P. Johnston, G. J. Hutchings, L. Demer, J. C. A. Boeyens and N. J. Colville, *Organometallics*, 1987, **6**, 1293.
10 J. A. Dineen and P. L. Pauson, *J. Organomet. Chem.*, 1974, **71**, 77.
11 P. M. Treichel, R. L. Shubkin, K. W. Barnett and D. Reichard, *Inorg. Chem.*, 1966, **5**, 1177.
12 D. L. Reger, *Inorg. Chem.*, 1975, **14**, 660.
13 C. M. Lukehart, G. P. Torrence and J. V. Zeile, *Inorg. Synth.*, 1990, **28**, 199.
14 F. A. Cotton and R. V. Parish, *J. Chem. Soc.*, 1960, 1440; M. O. Albers and N. J. Colville, *J. Chem. Soc., Dalton Trans.*, 1982, 1069.

Received in Cambridge, UK, 8th June 1998; 8/04302G

Polystyrene supports for vanadium ethylene polymerisation catalysts

Michael C. W. Chan,[a] Kong Chin Chew,[a] Christopher I. Dalby,[a] Vernon C. Gibson,*[a]† A. Kohlmann,[a] Ian R. Little[b] and Warren Reed[b]

[a] *Department of Chemistry, Imperial College, South Kensington, London, UK SW7 2AY*
[b] *BP Chemicals, Sunbury Research Centre, Chertsey Road, Sunbury on Thames, Middlesex, UK TW16 7LN*

Amino-functionalised polystyrene resins have been synthesised and used as well-defined supports for imidovanadium ethylene polymerisation catalysts; a dramatic enhancement in the lifetime and productivity of the supported catalysts compared to their unsupported (homogeneous) analogues is found.

During the past decade there has been tremendous industrial and academic interest in the development of new generation, highly tunable catalysts for α-olefin polymerisation.[1] Advances in catalyst design, especially the development of well-defined 'single-site' systems,[2] and the technologically significant discovery of high performance cocatalysts such as methylaluminoxane (MAO),[3] have played a key role in driving this interest. A third and equally important component of industrially relevant catalyst systems, especially for those that operate in the gas phase, is the solid support to which the procatalyst and cocatalyst are often attached and through which the resultant polymer morphology may be controlled. A significant proportion of the world's supply of polyolefins is manufactured using catalysts supported on inorganic materials such as $MgCl_2$ (especially Ziegler-type catalysts)[4] or silica (especially chromium catalysts).[5] Silica especially is highly reactive due to the presence of surface hydroxy groups, even after prolonged calcination, and therefore is not particularly well-suited as a support for the latest generation well-defined catalyst systems which may undergo drastic chemical modification upon attachment to the SiO_2 surface. By contrast, inert organic supports can be synthesised with precision and control[6] and are readily functionalised in such a way as to allow a specific well-defined covalent linkage to be formed between the procatalyst, and possibly also the cocatalyst, and the support. Moreover, through free-radical suspension polymerisation methods, spherical polymer beads can be obtained of controlled size and porosity.[7] Carefully tailored organic supports thus offer a potentially significant development in the heterogenisation of well-defined homogeneous olefin polymerisation catalysts. Polystyrene resins impregnated with catalysts have been the focus of recent attention in industrial research laboratories[8] and covalently attached metallocenes have previously been investigated as hydrogenation catalysts.[9]

We describe herein the dramatic influence of an appropriately functionalised polystyrene on the kinetic profile of a model vanadium system. In previous work we have shown that complexes of the type $CpV(NR)Cl_2$ are active procatalysts for ethylene polymerisation.[10] However, it was found that they deactivate within minutes due to a reductive bimolecular decomposition process.[11] Recognising that isolating the active sites within an inert matrix should increase the longevity of this catalyst system, we targeted an appropriately functionalised polystyrene resin that would allow the organometallic procatalyst to be supported without loss of its integrity. In previous work, we have established that *tert*-butylimido ligands can be readily exchanged for arylimido groups upon treatment with an appropriate aniline.[11,12] This methodology offered an opportunity to (covalently) attach imidovanadium procatalysts to an inert organic support.

The amino-functionalised resins shown in Scheme 1 were targeted. The first samples were prepared *via* the living anionic polymerisation method reported by Nakahama and co-workers[13] [Scheme 1(*a*)] which involves silyl protection of the amino functionality followed by copolymerisation with styrene using sodium naphthalenide as an initiator. The resultant linear copolymers‡ were characterised by ^1H NMR spectroscopy and by GPC. The proportion of amino styrene in the polymer was determined by integration of the trimethylsilyl resonance (δ 0.05) *versus* the polystyryl backbone hydrogens. For this study we did not seek to obtain information concerning the uniformity of blockiness of the distribution of the aminostyryl units. After deprotection with HCl, the amino-functionalised polystyrene was treated with a toluene solution of $CpV(NBu^t)Cl_2$ for several days at 80 °C during which time the polymer took on the dark red coloration of the half-sandwich imido complex (Scheme 2). This supported procatalyst was then tested for ethylene polymerisation in a 1 l reactor; the results are collected in Table 1.

For comparison purposes, entry 1 shows the result of a polymerisation experiment using unsupported $CpV(NBu^t)Cl_2$ which, in combination with diethylaluminium chloride (DEAC) cocatalyst, is short-lived (< 10 min) and affords a catalyst productivity of 6.8 g mmol^{-1} h^{-1}. By contrast, treatment of the polystyrene-supported procatalyst with DEAC at 50 °C in the presence of ethylene (10 atm) affords a catalyst productivity of 77.2 g mmol^{-1} h^{-1}. Significantly, however, a steady rate of ethylene uptake ensues over the 60 min duration of the run and the polymer was obtained as a flocculent product rather than the stringy material obtained from homogeneous polymerisations.[10] The polyethylene product is unimodal, of relatively

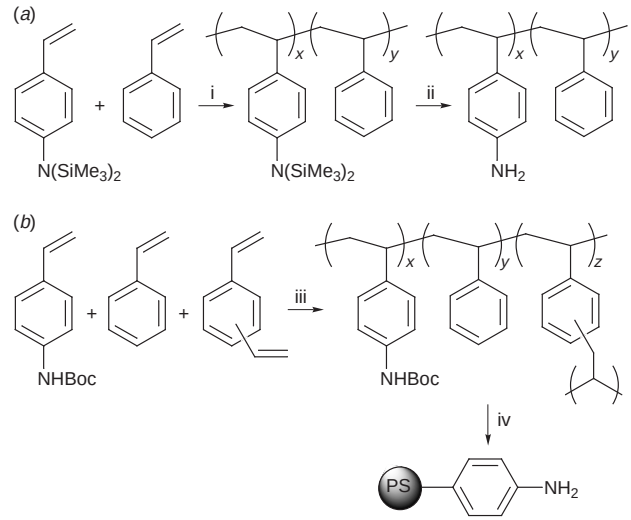

Scheme 1 *Reagents and conditions*: i, ii, ref. 13; iii, styrene, divinylbenzene, Boc-protected vinylaniline dissolved in chlorobenzene. The initiator AlBN (2 mol%) and monomer solution added to water (100 cm^3) containing calcium orthophosphate, calcium sulfate and poly(vinylpyrrolidone) as droplet stabilisers, stirring speed 200 rpm, 15 h; iv, HCl (aq) (12.6 M), THF, ultrasonic bath, 1 h

Table 1 Results of ethylene polymerisation

Run	Procatalyst[a]	Aminostyrene (mol%)	Activator (equiv.)	Ethylene pressure/atm	*T*/°C	*t*/min	Yield/g	Productivity§/ g mmol^{-1} h^{-1}
1	CpV(NBu^t)Cl$_2$ (unsupported)	—	DEAC (40)	10	50	60	1.00	6.8
2	PS–N=VCpCl$_2$	6.3	DEAC (34)	10	50	60	10.8	77.2
3	PS–N=VCpCl$_2$	6.3	DEAC (34)	10	75	60	1.9	13.7
4	PS–N=VCpCl$_2$	6.3	MAO (1000)	10	50	60	11.4	81.4
5	PS′–N=VCpCl$_2$	4.5	DEAC (20)	1	25	60	2.1	10.7

[a] PS = linear styrene–*p*-aminostyrene copolymer: PS′ = polystyrene–*p*-aminostyrene beads.

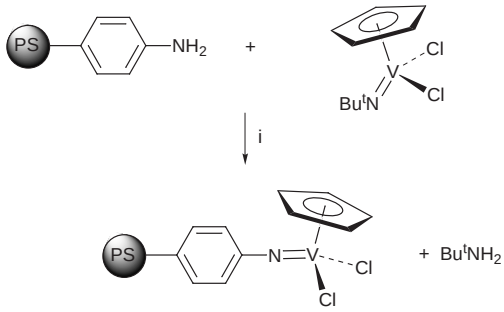

Scheme 2 *Reagents and conditions*: i, toluene, 80 °C, 9 d

high molecular weight (M_w 1.9 × 10^6, M_n 3.9 × 10^5) with little branching (< 1 per 5000 carbons) and with a molecular weight distribution (M_w/M_n) of 4.9. Raising the reactor temperature to 75 °C (entry 3) led to a reduction in productivity indicating that catalyst deactivation starts to become significant at elevated temperature. The use of a large excess of methylaluminoxane (MAO), in place of DEAC cocatalyst, whilst also giving a long-lived catalyst, did not lead to a significant increase in productivity.

The study was then extended to amino-functionalised cross-linked polystyrene beads [Scheme 1(*b*)] as a first step towards controlling the morphology of the resultant polyethylene particles. A mixture of Boc-protected *p*-aminostyrene, styrene and divinylbenzene was polymerised in an equal volume of chlorobenzene in a conventional suspension polymerisation reactor to give solvent expanded highly cross-linked (~ 12% mol%) spherical beads of fairly uniform diameter (typically 100–150 μm). After deprotection and treatment with CpV(NBu^t)Cl$_2$ under analogous conditions to those described previously, polymerisation at room temperature, this time at 1 atm ethylene pressure, gave a productivity of 10.7 g mmol^{-1} h^{-1}, a figure of merit comparable to the other supported catalysts. Once again steady uptake of ethylene was observed over the 60 min duration of the run.

In summary, the results described here on a model vanadium catalyst system highlight a strategy for covalently attaching transition metal procatalysts to an inert polystyrene support, and importantly demonstrate that dramatically improved kinetic profiles for the polymerisation of ethylene relative to their unsupported analogues can be obtained. There is considerable potential for extending this approach to differently functionalised polystyrenes that will be suited to other classes of transition metal procatalyst, offering the possibility for developing well-defined supports tailored to specific well-defined organometallic procatalysts. The fragmentation of the support will be an important future consideration for controlling the shape and morphology of the growing polyethylene particles.

The EPSRC and BP Chemicals Ltd are thanked for financial support.

Notes and References

† E-mail: V.Gibson@ic.ac.uk

‡ δ_H 0.05 (SiMe$_3$). 1.38 (–C*H*$_2$–CHAr–), 1.46 (–C*H*$_2$–CHPh–), 1.68 (–C*H*Ph–), 1.80 (–C*H*Ar–), 6.5–7.1 (aryl H); M_w 76 700, M_n 51 400, M_w/M_n 1.49. 6.3% bis(trimethylsilyl)aminostyrene copolymer.

§ This figure is a conservative value calculated on the assumption that all of the vanadium in solution is transferred onto the solid support and that all of the supported procatalyst is successfully injected into the reactor.

1 See, for example, K. B. Sinclair and R. B. Wilson, *Chem. Ind.*, 1994, 857; A. M. Thayer, *Chem. Eng. News*, Sept. 11, 1995, 15; R. G. Harvan, *Chem. Ind.*, 1997, 212.

2 R. F. Jordan, W. E. Dasher and S. F. Echols, *J. Am. Chem. Soc.*, 1986, **108**, 1718; R. F. Jordan, C. S. Bajgur, R. Willett and B. Scott, *J. Am. Chem. Soc.*, 1986, **108**, 7410; R. F. Jordan, R. E. LaPointe, C. S. Bajgur, S. F. Echols and R. Willett, *J. Am. Chem. Soc.*, 1987, **109**, 4111; G. G. Hlatky, H. W. Turner and R. R. Eckman, *J. Am. Chem. Soc.*, 1989, **111**, 2728; S. L. Borkowsky, R. F. Jordan and G. D. Hinch, *Organometallics*, 1991, **10**, 1268; M. Bochmann, A. J. Jaggar and J. C. Nicholls, *Angew. Chem., Int. Ed. Engl.*, 1990, **29**, 780; M. Bochmann and A. J. Jaggar, *J. Organomet. Chem.*, 1992, **424**, C5; M. Bochmann and S. J. Lancaster, *Organometallics*, 1993, **12**, 633; X. Yang, C. L. Stern and T. J. Marks, *J. Am. Chem. Soc.*, 1991, **113**, 3623.

3 H. Sinn, W. Kaminsky, H.-J. Vollmer and R. Woldt, *Angew. Chem., Int. Ed. Engl.*, 1980, **19**, 390; W. Kaminsky, M. Miri, H. Sinn and R. Woldt, *Makromol. Chem. Rapid Commun.*, 1983, **4**, 417; W. Kaminsky and H. Luker, *Makromol. Chem. Rapid Commun.*, 1984, **5**, 225.

4 B. C. Gates, J. R. Katzer and G. C. A. Schuit, *Chemistry of Catalytic Processes*, McGraw-Hill, New York, 1979.

5 M. P. McDaniel, *Adv. Catal.*, 1985, **33**, 47; A. Clark, *Catal. Rev.*, 1969, **3**, 145; F. J. Karol, G. L. Brown and J. M. Davidson, *J. Polym. Sci., Polym. Chem. Ed.*, 1973, **11**, 413; F. J. Karol, G. L. Karapinka, C. Wu, A. W. Dow, R. N. Johnson and W. L. Carrick, *J. Polym. Sci., Part A-1*, 1972, **10**, 2621.

6 See, for example, J. Lieto, D. Milstein, R. L. Albright, J. V. Minkiewicz and B. C. Gates, *Chemtech.*, 1983, 46.

7 *Polymer-supported reactions in organic synthesis*, ed. P. Hodge and D. C. Sherrington, Wiley, New York, 1980.

8 A. B. Furtek, N. J. Warren and R. S. Shinomoto (Mobil Oil Corp.), *US Pat.* 5 362 824, 1995.

9 R. H. Grubbs, *Chemtech.*, 1977, 512.

10 M. P. Coles and V. C. Gibson, *Polym. Bull.*, 1994, **33**, 529.

11 M. C. W. Chan, J. M. Cole, V. C. Gibson and J. A. K. Howard, *Chem. Commun.*, 1997, 2345.

12 P. W. Dyer, V. C. Gibson, E. L. Marshall, W. Clegg, M. J. Elsegood and A. Bell, *J. Chem. Soc., Chem. Commun.*, 1994, 2247; P. W. Dyer, V. C. Gibson, E. L. Marshall, W. Clegg, M. J. Elsegood and A. Bell, *J. Chem. Soc., Chem. Commun.*, 1994, 2547; M. P. Coles, C. I. Dalby, V. C. Gibson, W. Clegg and M. R. J. Elsegood, *Polyhedron*, 1995, **14**, 2455.

13 K. Suzuki, K. Yamaguchi, A. Hirao and S. Nakahama, *Macromolecules*, 1998, **22**, 2607.

Received in Liverpool, UK, 7th April 1998; 8/02656D

Ultra rigid cross-bridged tetraazamacrocycles as ligands—the challenge and the solution

Timothy J. Hubin,[a] James M. McCormick,[a] Simon R. Collinson,[a] Nathaniel W. Alcock[b] and Daryle H. Busch*[a]†

[a] *Chemistry Department, University of Kansas, Lawrence, KS 66045, USA*
[b] *Chemistry Department, University of Warwick, Coventry, UK CV4 7AL*

The challenge to metal ion binding that is represented by the proton-sponge nature of two-carbon cross-bridged tetraazamacrocycles has been overcome and a general method developed for the synthesis of their transiton, and other, metal complexes; these ultra-rigid ligands form complexes having remarkable kinetic stabilities.

According to modern coordination chemistry principles,[1] ligands of great rigidity impart enormous kinetic stability to their complexes, and such a property facilitates the exploitation of transition metal ions in biomimicry, catalysis, and numerous other areas. In this context, we have reexamined the cross-bridged tetraazamacrocycles[2,3] of Weisman and Ciampolini and focus on the *ultra-rigid* two-carbon cross-bridged ligands[2] **1**–**7**.

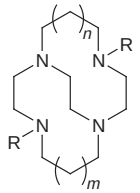

1 *n* = *m* = 0, R = H
2 *n* = *m* = 0, R = Me
3 *n* = *m* = 0, R = Bn
4 *n* = *m* = 1, R = H
5 *n* = *m* = 1, R = Me
6 *n* = *m* = 1, R = Bn
7 *n* = 1, *m* = 0, R = Me

These ligands are proton sponges (for **5**, $pK_{a1} > 24$ and $pK_{a2} = 10.8$).[2] Consequently, in protonic solvents only the proton-like Li^+ ion[2] and the most strongly binding divalent transition metal ions, Cu^{2+} and Ni^{2+}, form complexes with such ligands.[4]

We have overcome this obstacle; reaction of anhydrous metal salts with strictly deprotonated ligands (distillation from KOH after extraction from pH ⩾ 14 water) in rigorously dry aprotic solvents under a dry, inert atmosphere has yielded the first complexes of a broad array of transition metal ions. With routinely high yields, complexes of Cr^{II}, Mn^{II}, Mn^{III}, Fe^{II}, Fe^{III}, Co^{II}, Ni^{II}, Cu^{I}, Cu^{II} and Zn^{II} have been obtained.‡ In many cases, elimination of any source of protons is crucial for complexation. X-Ray crystal structures have been obtained of the Mn^{II}, Mn^{III}, Fe^{II}, Fe^{III} , Co^{II}, Ni^{II}, Cu^{I}, Cu^{II} and Zn^{II} complexes with ligands having 12- and 14-membered rings and a variety of R groups. In all cases, the ligand is folded, and in most cases it occupies two axial and two *cis* equatorial sites of a distorted octahedra. Exceptions occur with pentacoordinate copper(II) and tetracoordinate copper(I). For complexes of **5**, there is a clear correlation between the ionic radius of the metal ion and the N_{ax}–M–N_{ax} bond angle, which increases smoothly from Mn^{II} through Cu^{II} as the smaller metal ions can more easily be engulfed by the macrobicycle. Mn^{II}(**5**)Cl_2 (Fig. 1) exemplifies these structures,§ and in this example the N(3)–Mn(1)–N(4) angle is 158.0°.

Because of their great importance in catalysis[5] and bio-inorganic chemistry,[6] this report focuses on the manganese, iron and copper derivatives. Magnetic susceptibility data for [Mn(**5**)Cl_2] indicates that it is high spin d^5. Accordingly, there are no intense electronic transitions and the X-band EPR spectrum in EtOH at 77 K contains a six-line signal centered at $g = 2.026$. The cyclic voltammogram of [Mn(**5**)Cl_2] in MeCN exhibits reversible oxidation-reduction processes at +0.585 (Mn^{2+}/Mn^{3+}) and +1.343 V (Mn^{3+}/Mn^{4+}) *versus* SHE that are sensitive to solvent, macrocycle ring size and N-substitution. Since the proton-sponge behavior of the ligands that complicates complexation also interferes with the potentiometric determination of stability constants, other methods have been used to demonstrate the exceptional stabilities of these complexes. [Fe(**2**)Cl_2] and [Fe(**5**)Cl_2] show no degradation in either acidic (pH 1) or basic (pH 13) aqueous media in air for periods up to one month. After standing for several weeks in aqueous 2 M NaOH in air at room temperature, [Mn(**5**)Cl_2] produced a pure Mn^{III} complex and only traces of MnO_2 (probably from unreacted Mn^{2+} impurities).

Copper(II), known for forming the most stable, yet most labile, divalent transition metal complexes, provides a fascinating insight into the stabilities of these ultra-rigid complexes. The UV–VIS spectrum of a 0.1 mM solution of Cu(**5**)$^{2+}$ in 1 M $HClO_4$ remains unchanged over several weeks at 40 °C; from estimated errors, the lower limit of the half-life for ligand dissociation is > 6 years. This is to be compared with the rate of dissociation of Cu(tmc)$^{2+}$ (tmc = *N*,*N*′,*N*″,*N*‴-tetramethylcyclam) whose ligand is the nearest unbridged structural analogue of **5**. The ligand tmc differs from **5**, hypothetically, by breaking the C–C bridge bond and converting the residual methylenes into methyl groups. The half-life of Cu(tmc)$^{2+}$ at 25 °C in 1 M HNO_3 is only 2.0 s (calculated from the rate law[7]), at least eight orders of magnitude smaller than that of Cu(**5**)$^{2+}$. ($> 2 \times 10^8$ s

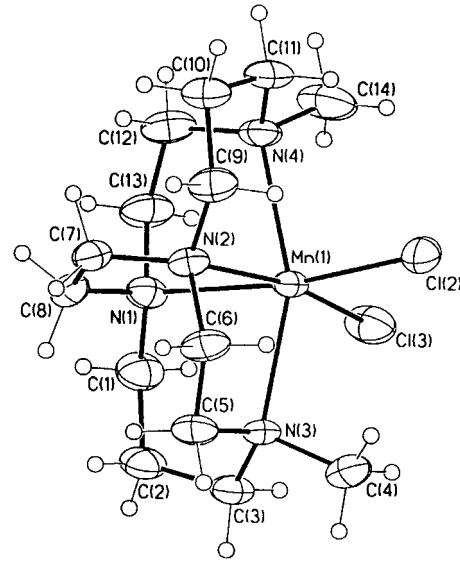

Fig. 1 Molecular structure of [Mn(**5**)Cl_2]. Selected bond lengths (Å) and angles (°): Mn(1)–N(1) 2.347(4); Mn(1)–N(2) 2.332(4); Mn(1)–N(3) 2.325(4); Mn(1)–N(4) 2.333(4); Mn(1)–Cl(2) 2.456(2); Mn(1)–Cl(3) 2.455(2); N(3)–Mn(1)–N(4) 158.0(2); N(1)–Mn(1)–N(2) 75.6(2); Cl(2)–Mn(1)–Cl(3) 98.85(6).

in 1 M $HClO_4$). The classic example of a kinetically stable Cu^{2+} complex,[8] $Cu(tet\text{-}A)^{2+}$ (tet-A = 5,5,7,12,12,14-hexamethyl-1,4,8,11-tetraazacyclotetradecane), provides significant comparisons. Its blue isomer is believed to contain tet-A in the folded form, the same conformation that the bridged cyclam ligand is forced to adopt. This complex, *cis*-$Cu(tet\text{-}A)^{2+}$, loses its macrocyclic ligand in 6.1 M HCl with a half-life of about 3 min; replacement of the six *C*-methyls in tet-A by two *N*-methyl groups and the short two-carbon cross-bridge in **5** increases the kinetic stability of the corresponding complex by at least six orders of magnitude. Even the square planar red isomer of $Cu(tetA)^{2+}$ is at least 100 times more labile than the folded bridged cyclam complex $Cu(\mathbf{5})^{2+}$. Hence ultra-rigid, cross-bridged tetraazamacrocyclic complexes are indeed ultra-stable, at least in the kinetic sense.

T. J. H. thanks the Madison and Lila Self Graduate Fellowship of the University of Kansas for financial support. This Warwick/Kansas collaboration is made possible by a travel grant from NATO. We also thank the EPSRC and Siemens Analytical Instruments for their support.

Notes and References

† E-mail: dbusch@eureka.chem.ukans.edu

‡ *Typical Complexation Reaction* for $[Mn(\mathbf{5})Cl_2]$: All steps were performed in an inert atmosphere glovebox with solvents distilled over CaH_2 and degassed by three freeze/pump/thaw cycles before introduction to the glovebox. To 1.00 g (0.004 mol) of **5** [obtained by literature procedures (ref. 2)] suspended in 40 ml MeCN was added 1.14 g (0.004 mol) $Mn(py)_2Cl_2$ [obtained by literature procedures (ref.9)] with stirring. The ligand and initially slightly soluble metal source were completely dissolved after 2 h stirring at room temperature. The reaction mixture was allowed to stir an additional 12 h, then filtered. The product was obtained upon evaporation of the solvent. The yield was 1.16 g (77%). The FAB^+ mass spectrum in MeCN (NBA matrix) exhibitted peaks at *m/z* 344 $[Mn(\mathbf{5})Cl]$ and 379 $[Mn(\mathbf{5})Cl_2]$. Calc. for $Mn(\mathbf{5})Cl_2$: C, 44.22; H, 7.95; N, 14.73. Found: C, 44.48; H, 7.86; N, 14.98%. Crystals suitable for X-ray diffraction were grown by the slow evaporation of an MeCN solution under an inert atmosphere.

§ *Crystal data* for $[Mn(\mathbf{5})Cl_2]$: $C_{14}H_{30}N_4Cl_2Mn$, M = 380.26, green–yellow badly-formed blocks, crystal dimensions 0.38× 0.20× 0.18 mm, monoclinic, space group $P2(1)/c$, a = 8.2967(2), b = 13.9194(4), c = 15.9010(5) Å, β = 100.6210(10)°, V = 1804.87(9) Å^3 (by least squares refinement on 4500 reflection positions), Z = 4, T = 293(2) K, D_c = 1.399 g cm^{-3}, Mo-Kα radiation (0.71073 Å), μ(Mo-Kα) = 1.027 mm^{-1}, $F(000)$ = 804, Siemens SMART three-circle system with CCD area detector. Maximum θ was 28.35°, *hkl* ranges were −11/10, −18/18, −10/20. Absorption correction by ψ-scan; crystal decay compensated for in data processing. The structure was solved by direct methods using SHELXS (TREF) with additional light atoms found by Fourier methods. Heavy atoms were located by the Patterson interpretation section of SHELXS and the light atoms then found by E-map expansion and successive Fourier syntheses. Refinement used SHELXL 96. Hydrogen atoms were added at calculated positions and refined using a riding model. Anisotropic displacement parameters were used for all non-H atoms; H-atoms were given isotropic displacement parameters equal to 1.2 (or 1.5 for methyl hydrogen atoms) times the equivalent isotropic displacement parameter of the atom to which the H-atom is attached. Goodness-of-fit on F^2 was 1.133, $R1$ = 0.0819 for 2710 reflections with $I > 2\sigma(I)$, $wR2$ = 0.2228, 10463 measured reflections, 4145 unique reflections [R(int) = 0.1040], number of refined parameters 192, largest difference peak and hole 1.153 and −1.259 e Å^{-3}.

1 D. H. Busch, *Chem. Rev.*, 1993, **93**, 847.
2 G. R. Weisman, M. E. Rogers, E. H. Wong, J. P. Jasinski and E. S. Paight, *J. Am. Chem. Soc.*, 1990, **112**, 8604.
3 M. Ciampolini, N. Nardi, B. Voltaconi and M. Micheloni, *Coord. Chem. Rev.*, 1992, **120**, 223.
4 This limitation, originally reported in G. R. Weisman, E. H. Wong, D. C. Hill, M. E. Rogers, D. P. Reed and J. C. Calabrese, *Chem. Commun.*, 1996, 947, has been confirmed in our work.
5 E. N. Jacobsen, in *Catalytic Asymmetric Synthesis*, ed. by I. Ojima, VCH, New York, 1993; D. Mansuy, *Coord. Chem. Rev.*, 1993, **125**, 129.
6 B. Meunier, in *Metalloporphyrin Catalyzed Oxidations;* Kluwer, Netherlands, 1994, pp. 1–47; V. L. Pecoraro, M. J. Baldwin and A. Gelasco, *Chem. Rev.*, 1994, **94**, 807; J. P. Caradonna and A. Stassinopoulow, *Adv. Inorg. Biochem.*, 1994, **9**, 245.
7 L. Hertli and T. A. Kaden, *Helv. Chim. Acta*, 1974, **57**, 1328.
8 D. K. Cabbiness and D. W. Margerum, *J. Am. Chem. Soc.*, 1970, **92**, 2151.
9 H. T. Witteveen, B. Nieuwenhuijse and J. Reedijk, *J. Inorg. Nucl. Chem.*, 1974, **36**, 1535.

Received in Bloomington, IN, USA, 16th March 1998; 8/02060D

C–H Bond activation by alumina: facile hydroxylation of chlorins at their saturated β-carbon by molecular oxygen and alumina

Dennis H. Burns,*† Yue Hu Li, Dong Chuan Shi and Michael O. Delaney‡

Department of Chemistry, Wichita State University, Wichita, Kansas, 67260, USA

The mono-hydroxylation of a β-methylene carbon in the pyrroline ring of a chlorin requires only alumina and molecular oxygen as reagents, with good yields (70–80%) of the hydroxy chlorin obtained at room temperature in 2 h; this is the first example of a hydroxylated chlorin that has been prepared in a regiospecific manner starting from a chlorin, and the first demonstration of the mild activation of a C–H bond by alumina for its oxidation into a hydroxy group.

Chlorins serve as prosthetic groups for proteins that perform a diverse set of biological functions. Magnesium chlorins (chlorophylls) are found in the photosynthetic proteins of green plants.[1] Iron chlorins are the prosthetic groups for a number of redox proteins, such as the heme in sulfmyoglobin,[2] in the green catalases from *Neurospora crassa* and *Escherichia coli*,[3] as well as the heme (heme *d*) in cytochrome *d* of *E. coli*.[4] Additionally, several dihydroporphyrins have been isolated from marine organisms, such as the sex-differentiating pigment, bonellin, as well as (possible antioxidants) tunichlorin, cyclopheophorbide and chlorophyllone *a*.[5] Like porphyrins, the hydroporphyrins are ubiquitous in nature.

A major thrust of our efforts has been the development of facile methods to prepare the chlorin macrocycle in a regioselective manner directly from linear tetrapyrroles, and also to develop useful pathways for their further elaboration. In this latter vein, we now report the facile mono-hydroxylation of chlorins **1** and **2** (Scheme 1) on their β-methylene carbons in the pyrroline ring. Hydroxylated chlorins are of interest because the iron chlorin prosthetic group of the bacterial oxidases, heme *d*, is thought to contain a bis-hydroxylated pyrroline ring.[4] The hydroxy functional group modifies the heme *d*'s π-system, enabling it to more strongly bind molecular oxygen than heme *b* (protoheme),[6] and presumably making it less prone to oxidation. Additionally, hydroxylated chlorins have elicited interest because they exhibit potential as PDT agents.[4b] The new and simple oxidation reported here represents the first example of a hydroxylated chlorin that has been prepared in a regiospecific manner starting from a chlorin.§ Even more interesting, these results are the first demonstration of the mild activation of a C–H bond by alumina for its oxidation into a hydroxy group.¶

Preparation of chlorins **1** and **2** *via* rearrangement of their metallated porphodimethenes,[9] occurred in a regioselective manner (*i.e.* only one pyrroline ring isomer produced), as shown in Scheme 1. Monohydroxylation of chlorin **1** furnished chlorins **3a**,**b**, while mono-hydroxylation of the more symmetrically substituted chlorin **2** furnished only the one chlorin **4**. In each case, oxidation was confined to the pyrroline ring. The oxidation′s experimental procedure was simple and straightforward. A column was prepared with a slurry of Grade 3 alumina gel,‖ and a solution of the chlorin was allowed to penetrate the alumina gel column to maximize the surface area of adsorption. The mixture was allowed to stand for 2 h, whereupon the hydroxylated chlorin was eluted off the column. This remarkable oxidation of the β-carbon resulted in 70–80 % yields of the mono-hydroxylated chlorin, with little oxidation of the macrocycle to porphyrin. While chlorin isomers **3a** and **3b** were not separated efficiently by chromatography, isomer **3a** crystallized out of hexane–EtOAc in preference to **3b** (as determined by a difference NOE experiment).

The hydroxylated chlorin **3a** was characterized by IR, UV–VIS and NMR spectroscopy and high resolution mass spectrometry and elemental analysis, as well as by chemical transformation (*vide infra*).** The 400 MHz ^{1}H NMR spectrum of chlorin **1** in $CDCl_3$ exhibited a singlet proton resonance at δ 4.60, indicative of the four hydrogens on the pyrroline ring.[9] The substitution of a pyrroline ring hydrogen with a hydroxy group produced a spectrum that exhibited three new resonances for the three remaining protons on the pyrroline ring, which resonated as doublets of doublets at δ 6.60, 4.78 and 4.38, while the hydroxy proton resonated as a broad singlet at δ 2.61. The COSY spectra of chlorin **3a** (Fig. 1) clearly shows that the three proton resonances at δ 6.60, 4.78 and 4.38 are coupled to each other, as would be expected from the three protons on the pyrroline ring. Further corroboration of the structure of chlorin **3a** came from a comparison of the DEPT spectra of chlorin **1** and **3a** (Fig. 2). The spectra exhibit similar methoxy ester and ring methyl and methylene substituent ^{13}C resonances at δ 52.0 and < 22, respectively. The difference in the resonances of the pyrroline ring β-carbons was striking, however. Chlorin **1** exhibited three methylene resonances between δ 36–38, indicative of the two pyrroline ring β-carbon methylenes and

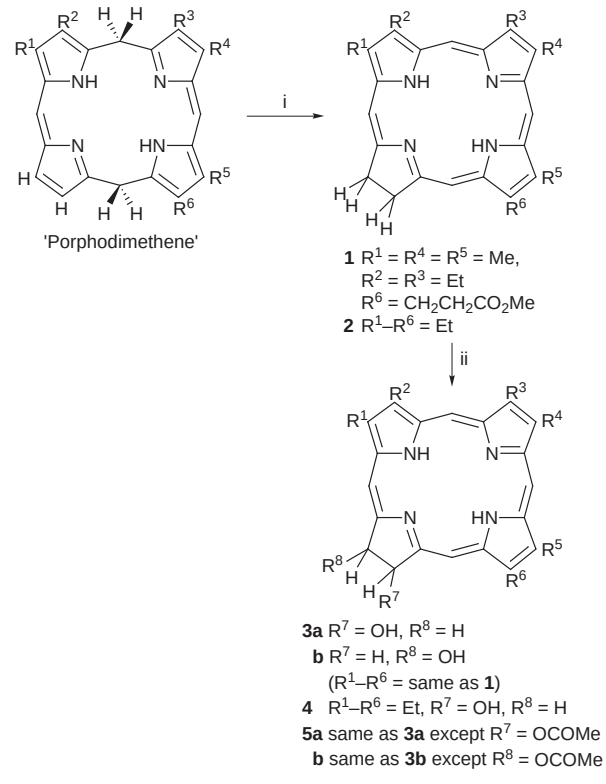

Scheme 1 *Reagents and conditions*: i, $Zn(OAc)_2$, 65 °C; ii, Al_2O_3, O_2, 25 °C

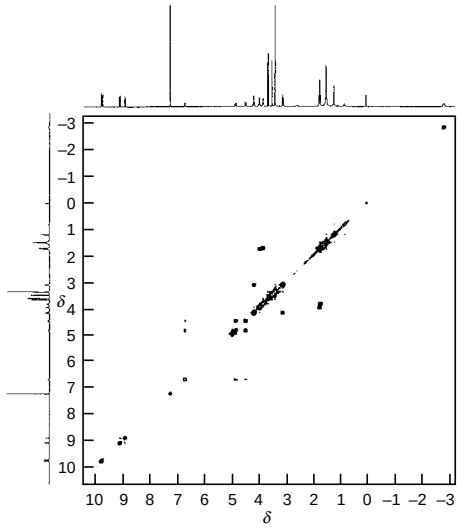

Fig. 1 400 MHz COSY spectrum of chlorin **3a** ($CDCl_3$)

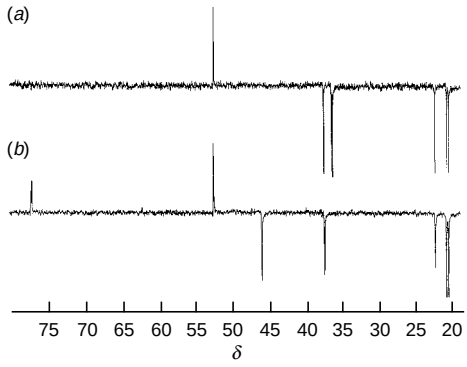

Fig. 2 100.5 MHz DEPT spectra ($3\pi/4$ pulse angle) of chlorins (*a*) **1** and (*b*) **3a** ($CDCl_3$). Peaks directed up are due to methyl and methine carbons, peaks directed down are due to methylene carbons.

the propanoate methylene adjacent to the carbonyl. While chlorin **3a** exhibited a similar propanoate methylene resonance at δ 37, the pyrroline ring β-carbon ^{13}C resonances were markedly shifted downfield. The one remaining methylene β-carbon exhibited a resonance at δ 45, and the carbon that contained the hydroxy functional group exhibited a new methine resonance at δ 77.

The mechanism of the oxidation is not well understood. The mono-hydroxylation of chlorins **1** or **2** required the presence of both alumina and molecular oxygen; no reaction occurred when the solvent was degassed with argon and the column packed and run in a glove box. Zn-chlorins were hydroxylated in the same manner as free-base chlorins, and the reaction took place in the dark. Bis-hydroxylation was not observed, even when the chlorins were left on the alumina for extended periods of time (at room temperature). One might speculate that in the tight confines of the basic alumina surface, adsorbed chlorin could be deprotonated at the pyrroline ring.†† Reaction of the newly formed chlorin anion with correctly positioned adsorbed triplet oxygen to form the chlorin radical, followed by recombination with a hydroxyl radical, is a scenario similar to the much slower, basic solution oxidation (allomerization) observed with chlorophyll *a*. The latter mechanism requires formation of an (exocyclic ring) enolate that reacts with triplet oxygen to form the chlorophyll radical, which then recombines with a hydroxyl radical to form the 13^2-hydroxy chlorophyll derivative.[11] Recombination of the chlorin radical with triplet oxygen to form the peroxyl radical, followed by decomposition to form the hydroxy group, cannot be ruled out. However, in the allomerization of chlorophyll *a*, this leads to the formation of a carbonyl and not a hydroxy functional group. While there are literature examples of hydroxy groups that undergo addition to alkenes and epoxides in the presence of alumina,[7] there is no precedence for the hydroxylation of an unfunctionalized carbon.

The hydroxylated chlorins were stable to air oxidation (unlike chlorin **1**, which slowly formed porphyrin), and stable to high temperatures under vacuum. Under strongly acidic conditions (H_2SO_4, MeOH), chlorin **3a** was slowly transformed into porphyrin (half-life of 24 h), presumably *via* loss of water. The Zn-metallochlorin was easily formed, and demetallation with TFA produced no porphyrin. Due to the apparent stability of chlorins **3** and **4**, it was anticipated that the hydroxy function could be utilized to allow for the further elaboration of the chlorin macrocycle. As an initial attempt, acetylation of a mixture of **3a** and **3b** (Ac_2O, pyridine, 10 mol% DMAP) furnished chlorins **5a** and **5b** (Scheme 1) in 95% yield. The production of **5**, which exhibited a pyrroline ring methine ester proton resonance at δ 7.65, and an acetate methyl proton resonance at δ 2.20, was additional proof for the structure of the hydroxy chlorin. Further study of the chemistry of hydroxy chlorins and their derivatives, and their use in the preparation of more complex molecules, is an ongoing project in our group.

We thank J. Homan for his assistance in the preparation of chlorin **3a**. D.H.B. gratefully acknowledges the support of this work by the National Science Foundation (CHE - 9508653), and for the support of NSF in the purchase of a departmental 400 MHz NMR spectrometer (CHE-9700421).

Notes and References

† E-mail: burns@wsuhub.uc.twsu.edu
‡ Undergraduate researcher

§ Vicinal bis-hydroxy chlorins have been prepared from porphyrins with OsO_4. The formation of the bis-hydroxy chlorins in this manner produces four regioisomers when starting from asymmetrically substituted porphyrins (ref. 4).

¶ The utilization of alumina for the oxidation of hydroxy compounds (ref.7) or the dehydrogenation of arenes (ref. 8) required an oxidant other than oxygen, or a transition metal catalyst plus oxygen.

‖ The oxidation reaction has been accomplished with several different batches of neutral alumina (60–325 mesh), received from Fisher Scientific.

** The IR spectrum of chlorin **1** exhibited only one absorption above 3000 cm^{-1} at 3345 cm^{-1}, indicative of the N–H stretch, while the hydroxy chlorin **3a** exhibited two absorptions above 3000 cm^{-1}, one at 3342 (with a shoulder at 3430) cm^{-1} and a second, weaker absorption at 3586 cm^{-1}, indicative of the N–H and O–H stretches, respectively. The UV–VIS spectrum of chlorin **3a** shows a small (10 nm) hypsochromatic shift of the Q band relative to chlorin **1**. Both HRFABMS and elemental analysis were consistent with the hydroxy chlorin.

†† Deprotonation of the pyrroline hydrogens on tetraphenylchlorin occurs with *tert*-butoxide (ref. 10).

1 H. Scheer, in *Chlorophylls*, ed. H. Scheer, CRC Press, Boca Raton, 1991, pp. 3–30.
2 M. A. Scharberg and G. N. La Mar, *J. Am. Chem. Soc.*, 1993, **115**, 6513; L. A. Andersson, T. M. Loehr, A. R. Lim and A. G. Mauk, *J. Biol. Chem.*, 1984, **259**, 15 340.
3 S. Ozawa, Y. Watanabe, S. Nakashima, T. Kitagawa and I. Morishima, *J. Am. Chem. Soc.*, 1994, **116**, 634.
4 C. Sotiriou and C. K. Chang, *J. Am. Chem. Soc.*, 1988, **110**, 2264; K. M. Barkigia, C. K. Chang and J. Fajer, *J. Am. Chem. Soc.*, 1991, **113**, 7445.
5 F. P. Montforts, B. Gerlach and F. Höper, *Chem. Rev.*, 1994, **94**, 327.
6 L. A. Andersson, C. Sotiriou, C. K. Chang and T. M. Loehr, *J. Am. Chem. Soc.*, 1987, **109**, 258.
7 G. H. Posner, *Angew. Chem., Int. Ed. Engl.*, 1978, **17**, 487.
8 T. Sakamoto, H. Yonehara and C. Pac, *J. Org. Chem.*, 1997,**62**, 3194.
9 D. H. Burns, T. M. Caldwell and M. W. Burden, *Tetrahedron Lett.*, 1993, **34**, 2883.
10 J. W. Whitlock and M. Y. Oester, *J. Am. Chem. Soc.*, 1973, **95**, 5738.
11 P. H. Hynninen, in *Chlorophylls*, ed. H. Scheer, CRC Press, Boca Raton, 1991, pp. 176–180.

Received in Corvallis, OR, USA, 16th March 1998; 8/02165A

Solution- and solid-phase synthesis of novel hydantoin and isoxazoline-containing heterocycles

Kyung-Ho Park,[a] Eric Abbate,[a] Samir Najdi,[b]† Marilyn M. Olmstead[a] and Mark J. Kurth*[a]‡

[a] *Department of Chemistry, University of California, One Shields Avenue, Davis, CA 95616, USA*
[b] *Department of Chemistry, Al-Quds University, East Jerusalem, Israel*

Exploiting 1,3-dipolar cycloaddition and carbanilide cyclization transformations, novel isoxazolylmethylimidazolidinedione heterocycles have been prepared using both solution- and solid-phase methods.

The hydantoin moiety has important medicinal[1] as well as agrochemical[2,3] activities and a large number of hydantoins have been synthesized for various biological applications.[4] Moreover, the isoxazoline heterocycle has been used extensively to modulate various other biologically active motifs.[5] As part of our efforts toward the preparation and biological evaluation of novel hydantoin-containing heterocycles, we disclose here a useful route for the synthesis of isoxazoline-containing hydantoins[6] as well as present a synthetic strategy applicable to solid-phase combinatorial approaches.

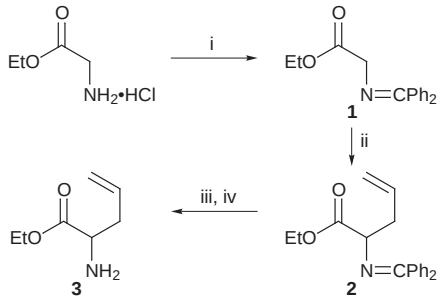

Scheme 1 *Reagents and conditions*: i, $HN{=}CPh_2$, CH_2Cl_2, room temp., ii, allyl bromide, NaH, DMF, room temp.; iii, HCl (1 M); iv, NaOH (1 M)

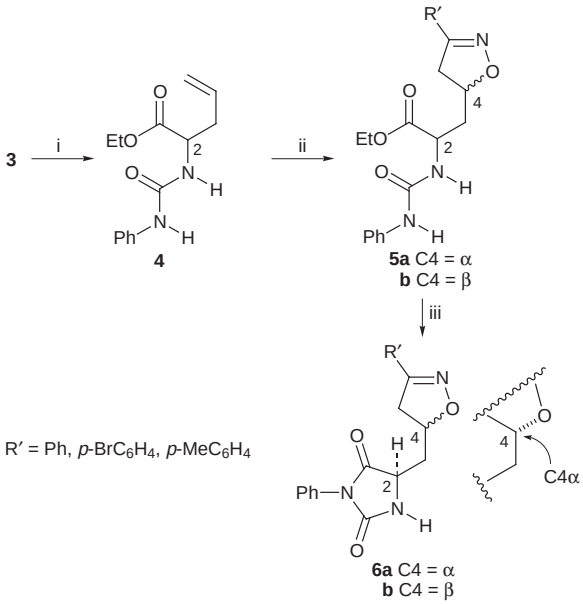

Scheme 2 *Reagents and conditions*: i, PhN=C=O, CH_2Cl_2, room temp.; ii, RCH_2NO_2, PhN=C=O, Et_3N, THF, 60 °C; iii, NaOEt, EtOH, room temp.

The condensation of glycine ethyl ester HCl salt with benzophenone imine gave benzophenone Schiff base **1**[7] (5 mmol scale, 95% yield) which was alkylated with allyl bromide to give protected amino ester **2** (5 mmol scale, 90% yield) (Scheme 1). Hydrolysis of the imine moiety in **2** with aq. HCl and subsequent neutralization of the resulting ammonium salt with aq. NaOH delivered **3** (5 mmol scale, 86%).

The free amine of **3** was reacted with phenyl isocyanate in CH_2Cl_2 at ambient temperature for 2 h to give urea **4** in 90% yield (5 mmol scale) (Scheme 2). 1,3 Dipolar cycloaddition to the alkene in **4** with a Mukaiyama-generated nitrile oxide[8] gave isoxazoline heterocycle **5**[9] as a C4α and C4β mixture of

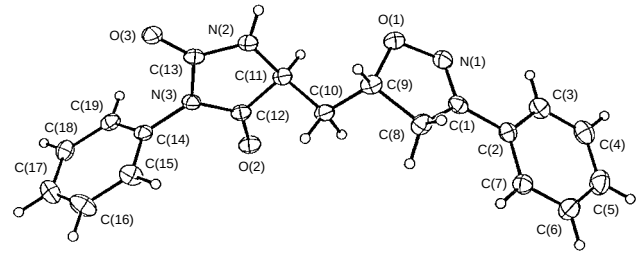

Fig. 1 Crystallographic projection of 6a (R = Ph)

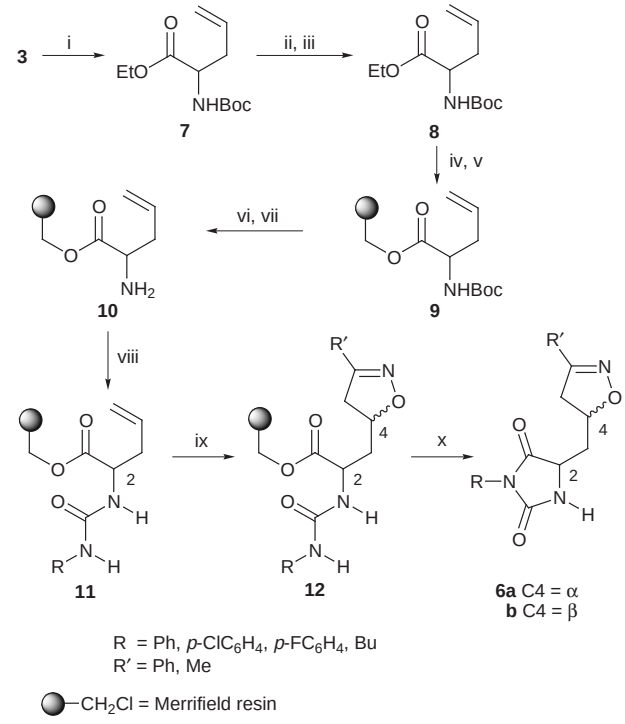

Scheme 3 *Reagents and conditions*: i, Boc_2O, CH_2Cl_2, reflux; ii, NaOH (1 M); iii, HCl (1 M); iv, KOH; v, 18-crown-6, Merrifield resin, DMF, 70 °C; vi, TFA, CH_2Cl_2; vii, Et_3N, CH_2Cl_2; viii, RN=C=O, CH_2Cl_2, room temp.; ix, $R'CH_2NO_2$, PhN=C=O, Et_3N, THF, 60 °C; x, Et_3N, THF, 60 °C

diastereomers (4 mmol scale, **5a** : **5b** : 1 : 1 ratio, yield 60–70%). While separable by flash-column chromatography, each diastereomer of **5** gave the same mixture of two diastereomeric isoxazoloimidazolidinediones **6** upon treatment with NaOEt (1.0 equiv.) in EtOH. Due to this propensity for C2 epimerization during the carbanilide cyclization (**5a**→**6a** + **6b** or **5b**→**6a** + **6b**; 4 mmol scale; **6a** : **6b** : 1 : 1; 80% yield), it was in fact most expedient to effect this transformation on the **5a**/**5b** mixture. X-Ray crystallographic analysis§ of **6a** (R = Ph) (Fig. 1) verified the relative stereochemistries of **5a**/**5b** and **6a**/**6b**.

Our solid-phase approach[10] to isoxazolylmethylimidazolidinedione **6** began with amino ester **3**, which was Boc-protected to give **7** (4 mmol scale, 95% yield) (Scheme 3). Saponification delivered **8** (4 mmol scale, 90% yield) which was coupled with Merrifield resin to give resin **9.**[11]¶ TFA-mediated removal of the Boc protecting group followed by a resin wash with Et_3N–CH_2Cl_2 delivered **10**, the solid-phase analog of **3**. Paralleling the solution results, isocyanate treatment of **10** gave urea **11** and subsequent 1,3-dipolar cycloaddition with a Mukaiyama-generated nitrile oxide gave **12**. A *ca.* 1 : 1 mixture of isoxazolylmethylimidazolidinedione diastereomers (**6a**/**6b**) was obtained on cyclative release.

We thank the National Science Foundation and Novartis Crop Protection AG for financial support of this research.

Notes and References

† Fulbright Fellow, 1996–1997, University of California, Davis, USA.
‡ E-mail: mjkurth@ucdavis.edu

§ *Crystal data:* for **6a** (R = Ph): $C_{19}H_{17}N_3O_3$, colorless crystals, M = 335.36, orthorhombic, space group *Pbca*, a = 9.0062(11), b = 11.1037(10), c = 32.472(3) Å, U = 3247.3(6) Å^3, Z = 8, D_c = 1.372 Mg m^{-3}, μ = 0.776 mm^{-1}, R = 0.0392, wR = 0.0955, GOF = 1.092, T = 130(2) K, F(000) = 1408, 2189 independent reflections were collected on a Syntex $P2_1$ diffractometer using graphite-monochromated Cu-Kα radiation. CCDC 182/917.

¶ Typical procedure for solid-phase isoxazolylmethylimidazolidinedione synthesis: Boc-protected glycine acid **8** (130 mg, 0.6 mmol) was neutralized (room temp., 1 h) with KOH (1.0 equiv., 0.6 mmol) in EtOH–H_2O (2:1) and, after removing the solvent and drying *in vacuo*, the potassium salt was dissolved in DMF (20 ml) and reacted with Merrifield resin (300 mg, 0.3 mmol; loading *ca.* 1 mmol Cl g^{-1}) and 18-crown-6 (158 mg, 0.6 mmol). The resulting mixture was stirred at 70 °C for 40 h and then washed with DMF (20 ml), THF (20 ml), THF–H_2O (20 ml× 2), and THF (20 ml). Dried resin **9** (ν_{max}/cm^{-1} 1723) was treated with 50% TFA–CH_2Cl_2 (20 ml) at ambient temperature for 1 h, after which time the resin was washed with CH_2Cl_2 (20 ml), dioxane (20 ml) and CH_2Cl_2 (20 ml× 2). An Et_3N wash (10% in CH_2Cl_2, 20 ml) followed by CH_2Cl_2 washes (20 ml× 2) gave resin **10** (ν_{max}/cm^{-1} 3383, 1735). Phenyl isocyanate (107 mg, 0.9 mmol) in CH_2Cl_2 (20 ml) was added and, after 10 h at ambient temperature, the resin was washed with DMF (20 ml), THF (20 ml) and CH_2Cl_2 (20 ml) and dried to give resin **11** (R = Ph; ν_{max}/cm^{-1} 1740, 1700, 1662). α-Nitrotoluene (123 mg, 0.9 mmol), phenyl isocyanate (214 mg, 1.8 mmol) and Et_3N (10 µl) were added to this resin in THF (20 ml). After incubating at 60 °C for 20 h, washing the resin with DMF (20 ml), THF (20 ml) and CH_2Cl_2 (20 ml) gave resin **12** (R = R′ = Ph; ν_{max}/cm^{-1} 1738, 1699) which was finally treated with Et_3N (1 ml) in THF (20 ml) at 60 °C for 20 h. Resin was removed from the liberated product to give **6a**/**6b** (R = R′ = Ph) in 35% overall yield from Merrifield resin. These two isomers were easily separated by flash chromatography (EtOAc–hexane 1:2) to give **6a** (R = R′ = Ph; 16 mg, 16% overall yield) and **6b** (R = R′ = Ph; 19 mg, 19% overall yield). The optimized solid-phase overall yield of **6a** + **6b** is 35%, which translates to *ca.* 84% yield per step from **8**. With catalytic Et_3N, we saw no evidence for formation of **6** in **11**→**12**.

1 E. Ware, *Chem. Rev.*, 1950, **46**, 403; A. Spinks and W.S. Waring, *Prog. Med. Chem.*, 1963, **3**, 313; J. Karolakwojciechowska, W. Kwiatkowski and K. Kieckonono, *Pharmazie*, 1995, **50**, 114; W. J. Brouillette, V. P. Jestkov, M. L. Brown and M. S. Akhtar, *J. Med. Chem.*, 1994, **37**, 3289; W. J. Brouillette, G. B. Brown, T. M. Deloreg and G. Liang, *J. Pharm. Sci.*, 1990, **79**, 871.
2 C.J. Mappes, E.H. Pommer, C. Rentzea and B. Zeeh, *U.S. Pat.*, 1980, 4,198,423.
3 H. Ohta, T. Jikihara, K. Wakabayashi and T. Fujita, *Pestic. Biochem. Physiol.*, 1980, **14**, 153.
4 C. Avendano Lopez and G. Gonzalez Trigo, *Adv. Heterocycl. Chem.*, 1985, **38**, 177.
5 M. A. Khalil, M. F. Maponya, D.-H. Ko, Z. You, E. T. Oriaku and H. J. Lee, *Med. Chem. Res.*, 1996, **6**, 52; W. C. Groutas, R. Venkataraman, L. S. Chong, J. E. Yooder, J. B. Epp, M. A. Stanga and E.-H. Kim, *Bioorg. Med. Chem.*, 1995, **3**, 125; J. I. Levin, P. S. Chan, J. Coupet, T. K. Bailey, G. Vice, L. Thibault, F. Lai, A. M. Venkatesan and A. Cobuzzi, *Bioorg. Med. Chem. Lett.*, 1994, **4**, 1703.
6 K.-H. Park, M. M. Olmstead and M. J. Kurth, *J. Org. Chem*., 1998, **63**, 113; J. Wityak, T. M. Sielecki, D. J. Pinto, G. Emmett, J. Y. Sze, J. Liu, A. E. Tobin, S. Wang, B. Jiang, P. Ma, S. A. Mousa, R. R. Wexler and R. E. Olson, *J. Med. Chem*., 1997, **40**, 50.
7 M. J. O′Donnell and R. L. Polt, *J. Org. Chem*., 1982, **47**, 2663.
8 T. Mukaiyama and T. Hoshin, *J. Am. Chem. Soc*., 1960, **62**, 5339.
9 D. P. Curran, *Adv. Cycloaddition*, 1988, **1**, 129; K. B. G. Torssel, *Nitrile Oxides, Nitrones and Nitronates in Organic Synthesis*, VCH, Weinheim, 1988.
10 S. H. DeWitt, J. S. Kiely, C. J. Stankovic, M. C. Schroeder, D. R. Cody and M. R. Pavia, *Proc. Natl. Acad. Sci. U.S.A.*, 1993**, 90**, 6909; B. A. Dressman, L. A. Spangle and S. W. Kaldor, *Tetrahedron Lett.*, 1996, **37**, 937.
11 R. W. Roeske and P. D. Gesellchen, *Tetrahedron Lett.*, 1976, **38**, 3369.

Received in Corvallis, OR, USA, 5th May 1998; 8/03400A

Self-assembly of a supramolecular cube

Sue Roche, Claire Haslam, Harry Adams, Sarah L. Heath and Jim A. Thomas*†

Department of Chemistry, University of Sheffield, Sheffield, UK S3 7HF

In one step, 8 octahedral metal 'corners' and 12 ligand 'edges' come together to form a supramolecular cube.

Self-assembly[1] templated by metal ions has been used as a strategy to construct compounds with large cavities.[2] Previously, using pyridyl ligands with two coordination sites and square planar metal complexes as corner templates, two-dimensional squares[3] have been synthesised. Three-dimensional architectures result when ligands with a higher number of coordination sites,[4] or metal ions with tetrahedral[5] or octahedral[6] coordination geometries, are used in the self-assembly process. It has been suggested that an appropriate octahedral metal centre could template the self-assembly of a supramolecular cube.[2] Here, we report the one-step self-assembly of 20 components into such a structure.

Reaction of [([9]aneS_3)Ru(DMSO)Cl_2][7] with a large excess of 4,4-bipyridine, bpy, yielded cationic complex **1** which would appear ideally suited to act as a corner for a supramolecular cube. X-Ray crystallography confirms that the three bpy ligands are oriented at mutual right angles‡ (Fig. 1). As a solid, and in non-coordinating solvents such as dichloromethane and nitromethane, **1** is air and moisture stable. However, solutions of **1** in coordinating solvents are unstable toward solvolysis. Using ^{1}H NMR spectroscopy, the solvolysis of **1** by acetonitrile was monitored. At room temperature, during a process which takes 2 weeks to reach completion, **1** is converted to [([9]aneS_3)Ru(bpy)$(MeCN)_2$]$^{2+}$ which has been isolated as its hexafluorophosphate salt and fully characterised by NMR and mass spectrometry, as well as elemental analysis.

Entropic and enthalpic arguments indicate that discrete supramolecular architectures are favoured over polymeric products.[8] Therefore, it was reasoned that the relative lability of **1** could be used to construct supramolecular architectures. If the correct ratio of metal ions and bpy ligands are mixed together in a non-coordinating environment, these components will undergo substitution processes, searching through possible product states to obtain the thermodynamically most stable product. Using nitromethane as the non-coordinating solvent, [([9]aneS_3)Ru(DMSO)Cl_2] was treated with bpy in an 8 : 12 stoichiometry and the reaction was monitored by ^{1}H NMR spectroscopy.

Changes in the spectral region due to bpy resonances are highly diagnostic of any self-assembly processes.[3a,4] In contrast to the synthesis of **1**, where the final product is obtained within 3 hours (Fig. 2a), a complex mixture of products is initially formed (Fig. 2b). However, further measurements taken over a period of four weeks (Fig. 2c–e) show a gradual simplification towards a single product, **2.** The slight shift observed in the bpy signals of **2** is due to the hygroscopic nature of the complex, causing the reaction solvent to absorb atmospheric water during the course of the experiment. Addition of diethyl ether to the reaction mixture isolates **2** as a hygroscopic, air and moisture stable, brown–black solid. A variety of data confirm that the structure of **2** is a cube (Fig. 3).

When compared to the ^{1}H NMR spectrum of **1,** it is clear that **2** possesses high symmetry as all the 4-pyridyl rings are now equivalent. Furthermore, the integration confirms that the ratio of bpy 'edge' to [9]aneS_3 'corner' protons is 1 : 1. This ratio, and the elemental analysis of **2**, is only consistent with closed, highly symmetrical structures such as a cube, or tetrahedron.

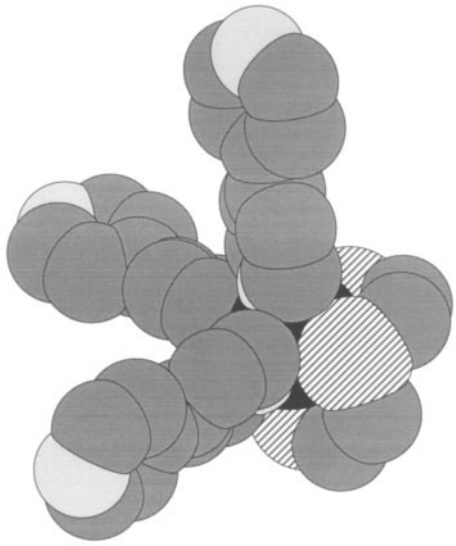

Fig. 1 Space filling model of the crystal structure of cationic complex **1**

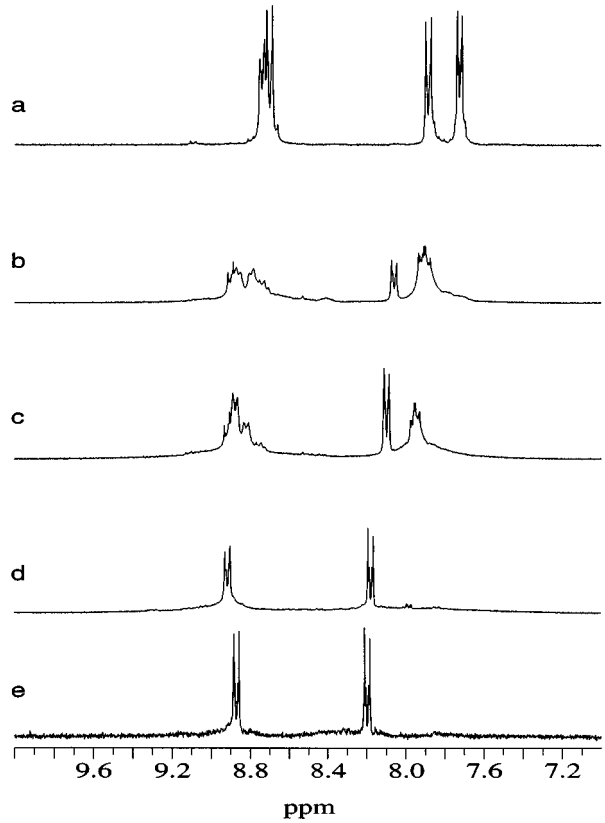

Fig. 2 ^{1}H NMR data for **1** and **2**. a, bpy region (300 Hz in nitromethane) for **1**; b, bpy region (300 Hz in nitromethane) for **2** after 3 days; c, after 1 week; d, after 4 weeks; e, isolated product in MeCN

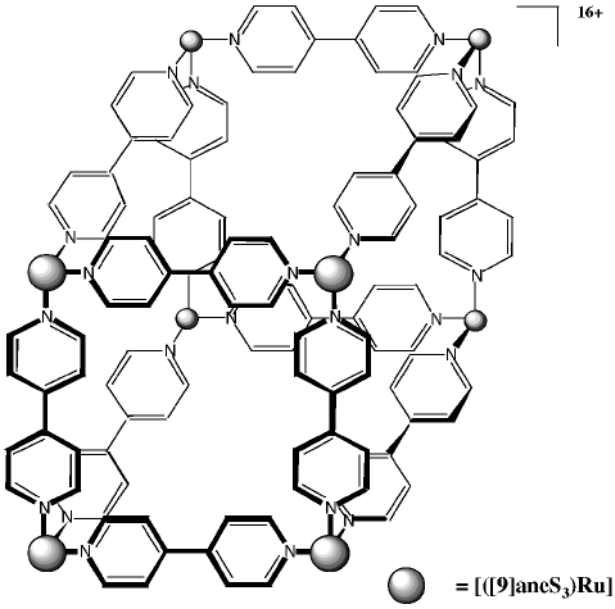

Fig. 3 Structure of **2**

However, structures other than a cube are inconsistent with the crystallographic data for **1** and highly unlikely due to steric reasons**.** For example, a tetrahedral structure would produce strained corners, with three ligands held at mutual 60° angles as they coordinate to each metal ion.

ES-MS studies on **2** show peaks centred on *m*/*z* 285 ($[\mathbf{2}\cdot(CF_3SO_3^-)]^{15+}$ requires 285), 351.8 ($[\mathbf{2}\cdot(CF_3SO_3^-)_3]^{13+}$ requires 351.78) 393.5 ($[\mathbf{2}\cdot(CF_3SO_3^-)_4]^{12+}$ requires 393.5), and 502 ($[\mathbf{2}\cdot(CF_3SO_3^-)_6]^{10+}$ requires 502.1). These peaks are not observed by conventional techniques such as FAB-MS and their shapes are consistent with theoretical isotopic patterns.

Unlike **1**, solutions of **2** in coordinating solvents such as acetonitrile are perfectly stable, showing no changes in their ^{1}H NMR spectra over a period of weeks. Again, this anomalous kinetic stability is only consistent with an unstrained cubic structure for **2**, where cooperative interactions within the assembly will 'lock' the ligands into position.

Complexes incorporating Ru^{II} metal centres bridged by oligopyridyl ligands show electrochemical interactions.[9] If the metal centres of **3** are interacting in this manner they will not all oxidise at the same potential. From simple electronic and electrostatic arguments, it is expected that the oxidation of the metal centres in **2** should occur in four steps. During each step a pair of metal ions in diagonally opposed corners of **2** will be oxidised and, for each oxidation, the required anodic potential should be progressively greater.

The electrochemistry of **2** was investigated using cyclic voltammetry. Since all the oxidation processes for **1** and **2** showed varying degrees of irreversibility E_p was obtained using convolution/deconvolution techniques.[10] In contrast to **1**, which displays only one oxidation process, **2** displays three oxidations. The first oxidation wave is at 1.18 V (*vs.* SCE) while the second and third are at 1.38 V and 1.63 V respectively. The first oxidation wave is notably broader than the second and third, consistent with it incorporating two closely overlapping oxidation couples.

The incorporation of electroactive metal centres into the assembly is significant, it opens up the possibility of constructing a variety of novel molecular devices, such as tuneable sensors or multiple state switches. In this context, the host–guest chemistry of **2**, and physical studies on electron/energy transfer within its molecular architecture, are being investigated. The self-assembly of similar structures incorporating other ligands and metal ions will be described elsewhere.

We gratefully acknowledge the support of The Royal Society (J. A. T., S. A. H.), the EPSRC (S. R.) and Professor Bill Clegg, University of Newcastle-upon-Tyne, for use of the diffractometer.

Notes and References

† E-mail: james.thomas@shef.ac.ukur

‡ *Crystal data* for $C_{40}H_{42}F_{12}N_8P_2RuS_3$: M = 1122.01; crystallises from acetonitrile–ethanol as yellow blocks; crystal dimensions 0.43 × 0.21 × 0.13 mm. Triclinic, a = 10.9913(2), b = 13.2679(2), c = 16.5469(2) Å, α = 88.5080(10), β = 80.7680(10), γ = 88.1760(10)°, U = 2380.06(6) Å^3 (based on 10110 reflections, θ range 1.25 to 22.5°), Z = 2, D_c = 1.566 Mg m^{-3}, space group $P\bar{1}$ (C_i^1, no. 2), Mo-Kα radiation (λ = 0.71073 Å), μ(Mo-Kα) = 0.615 mm^{-1}, F(000) = 1136, T = 160 K, 5779 independent reflections [$|F|/\sigma(|F|) > 4.0$]. Refinement converged at a final R = 0.0697 ($wR2$ = 0.1787, for all 6156 unique data, 719 parameters) with allowance for the thermal anisotropy of all non-hydrogen atoms. Minimum and maximum final electron density −0.860 and 1.251 e Å^{-3}. A weighting scheme $w = 1/[\sigma^2(F_o^2) + (0.0703P)^2 + 16.38P]$ where $P = (F_o^2 + 2F_c^2)/3$ was used in the latter stages of refinement. Data collected were measured on a Siemens Smart CCD area detector with a Siemens LT2 temperature system. Reflections were measured from a hemisphere of data collected of frames each covering 0.3° in ω. Hydrogen atoms were placed geometrically and refined with a riding model (including torsional freedom for methyl groups) and with U_{iso} constrained to be 1.2 (1.5 for methyl groups) × U_{eq} of the carrier atom. Complex scattering factors were taken from the program SHELXTL.[11] CCDC 182/927.

1 (*a*) J.-M. Lehn, *Angew. Chem., Int. Ed. Engl.*, 1990, **29**, 1304; (*b*) J. S. Lindsey, *New J. Chem*., 1991, **15**, 153.
2 C. A. Hunter, *Angew. Chem., Int. Ed. Engl*., 1995, **34**, 1079.
3 (*a*) M. Fujita, J. Yazaki and K. Ogura, *J. Am. Chem. Soc.*, 1990, **112**, 5645; (*b*) P. J. Stang and D. H. Cao, *J. Am. Chem. Soc.*, 1994, **116**, 4981; (*c*) M. Fujita, J. Yazaki and K. Ogura, *Tetrahedron Lett*., 1991, **32**, 5589.
4 (*a*) M. Fujita, D. Oguro, M. Miyazawa, H. Oka, K. Yamaguchi and K. Ogura, *Nature*, 1995, **378**, 469; (*b*) M. Fujita, S. Nagao and K. Ogura, *J. Am. Chem. Soc.*, 1995, **117**, 1648.
5 (*a*) P. N. W. Baxter, J.-M. Lehn, J. Fischer and M.-T. Youinou, *Angew. Chem., Int. Ed. Engl.*, 1993, **32**, 69; (*b*) A. Marquis-Rigault, A. Dupont-Gervais, P. N. W. Baxter, A. Vandorsselaer and J.-M. Lehn, *Inorg. Chem*., 1996, **35**, 2307.
6 (*a*) R. W. Saalfrank, B. Hörner, D. Stalke and J. Salbeck, *Angew. Chem., Int. Ed. Engl.*, 1993, **32**, 1179; (*b*) R. W. Salfrank, R. Burak, S. Reihs, N. Löw, F. Hampel, H.-D. Stachel, J. Lentmaier, K. Peters, E. M. Peters and H. G. von Schneering, *Angew. Chem., Int. Ed. Engl.*, 1995, **34**, 993.
7 C. Landgrafe and W. S. Sheldrick, *J. Chem. Soc., Dalton Trans.*, 1994, 1885.
8 (*a*) P. J. Stang, N. E. Persky and J. Manna, *J. Am. Chem. Soc*., 1997, **119**, 4777; (*b*) X. Chi, A. J. Guerin, R. A. Haycock, C. A. Hunter and L. D. Sarson, *J. Chem. Soc., Chem. Commun*., 1995, 2563.
9 (*a*) C. Creutz, *Prog. Inorg. Chem*., 1983, **30**, 1; (*b*) R. J. Crutchley, *Adv. Inorg. Chem.*, 1994, **41**, 273.
10 A. J. Bard and L. R. Faulkner, *Electrochemical Methods. Fundamentals and Applications*, John Wiley and Sons, New York, 1980, pp. 236–241.
11 G. M. Sheldrick, SHELXTL manual, revision 5, Siemens Analytical X-ray Instruments, Madison, WI, 1995.

Received in Basel, Switzerland, 5th May 1998; 8/03318H

The azuliporphyrin-carbaporphyrin connection†

Timothy D. Lash*‡

Department of Chemistry, Illinois State University, Normal, Illinois 61790-4160, USA

Under base catalyzed conditions, reaction of azuliporphyrin 3 with *tert*-butyl hydroperoxide affords the benzocarbaporphyrins 2a and 2b; a mechanism for the formation of 2b is proposed.

Recently, diverse monocyclic dialdehydes have been shown to condense with tripyrranes [2,5-bis(pyrrol-2-ylmethyl)pyrroles] under the so-called '3 + 1' conditions[1] to give structural analogs of the porphyrins including oxybenziporphyrin **1**[2] and carbaporphyrins **2**.[3–6] Lash and Chaney reported[4] that azulene-1,3-dicarbaldehyde condensed with a tripyrrane in the presence of 5% TFA in CH_2Cl_2 to give the unique borderline aromatic macrocycle 'azuliporphyrin' **3** (Scheme 1) in good yield. In complete contrast, Breitmaier[5] found that under somewhat different conditions these reactants afforded low yields of benzocarbaporphyrins **2a–c** where the seven-membered ring of the azulene precursor has undergone a ring contraction to give the fused benzo moiety of **2**. No explanation for the origins of these materials was offered, but it should be noted that **2a** can be more directly obtained in excellent yields and isomerically pure form from 1,3-diformylindene.[3] Azuliporphyrin **3** is a cross-conjugated system for which dipolar resonance contributors (*e.g.* **4**) can be written that impart a degree of porphyrinoid aromaticity onto the macrocycle and this view is supported by the observation of a weak diatropic ring current in the proton NMR spectrum of **3**.[4] This feature is greatly enhanced in the presence of acid due to the increased ability of the aromatic species to allow charge delocalization.[4]

1

2a X = Y = H
b X = CHO, Y = H
c X = H, Y = CHO

Scheme 1

During the course of our studies, we noted that addition of small amounts of pyrrolidine to an NMR solution of the sparingly soluble azuliporphyrin caused the green solution to turn brown. The resulting NMR spectrum (Fig. 1) displayed a carbaporphyrin-like ring current[3] where the internal CH was shifted upfield from δ 1.5 in **3** to δ −7 and the external *meso*-protons were similarly deshielded to resonate near δ 10. The seven-membered ring protons nearest to the macrocycle produced a broadened 2H doublet at δ 7.85 and a 2H dd was noted near δ 6. These data implied that **3** had undergone a nucleophilic substitution on the seven-membered ring to give the pyrrolidine–carbaporphyrin adduct **5** (Scheme 1). The process must be regioselective as a single symmetrical isomer dominates the NMR spectrum, but the reaction is reversible and removal of pyrrolidine simply afforded starting material. Further evidence for the formation of a carbaporphyrin structure comes from UV–VIS spectroscopy; addition of pyrrolidine causes a Soret-like band to emerge near 400 nm (Fig. 2).

The observed reactivity of the seven-membered ring suggested that the azuliporphyrin system could be functionalized

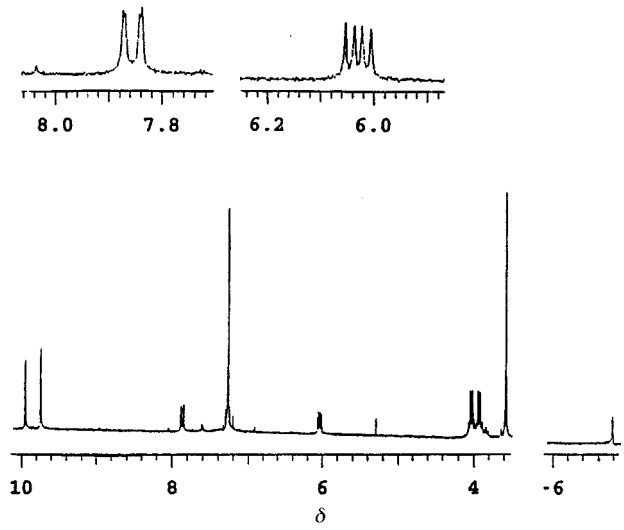

Fig. 1 Partial 300 MHz ^{1}H NMR spectrum of azuliporphyrin **3** in the presence of trace pyrrolidine in $CDCl_3$. The region between δ 1 and 4 is obscured by the pyrrolidine absorptions.

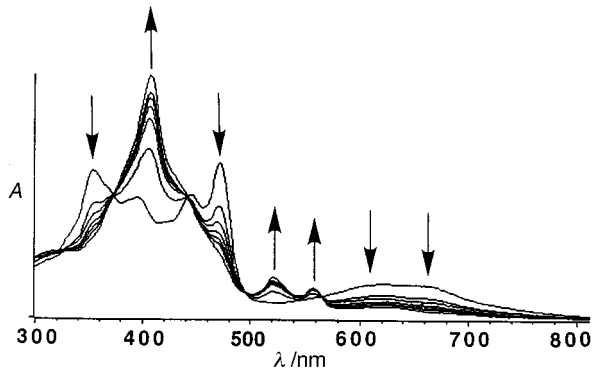

Fig. 2 Electronic absorption spectra of azuliporphyrin **3** in $CHCl_3$ with 0, 1000, 2000, 3000, 4000, 5000 or 9000 equiv. of pyrrolidine. The development of a Soret band near 400 nm is clearly evident.

under suitable reaction conditions. We were particularly interested in the possibility of generating the fused tropone structure **6**, which might be formed by an addition-elimination process. However, attempts to form **6** by reacting **3** with NaOCl were unsuccessful. Alkaline solutions of H_2O_2 reacted with **3** to give complex mixtures of products that appeared to be carbaporphyrins, and this prompted us to investigate the reaction of **3** with *tert*-butyl hydroperoxide. Interestingly, when the reaction was carried out with Bu^{t}OOH (5 equiv.) in KOH–MeOH and CH_2Cl_2 at room temperature, benzoporphyrin **2a** was the main isolatable product (30%) together with a small amount of **2b**. On the other hand, the formyl derivative **2b** was the predominant product (40%) when the reaction was carried out with Bu^{t}OOH and Bu^{t}OK in CH_2Cl_2, although some **2a** (15%) was also isolated in this case. Carbaporphyrin **2a** was identical to our previously synthesized material[3] and structure **2b** was fully characterized by NMR and mass analysis.§

The formation of **2b** can be rationalized by the mechanism shown in Scheme 2. Following nucleophilic attack by the *tert*-butyl peroxide anion, the adduct **7** may undergo a Cope rearrangement to give the cyclopropane **8** and subsequent elimination of *tert*-butyl alcohol would give the aldehyde **2b**. A third carbaporphyrin appears to be present by TLC (very minor) and may correspond to **2c**; this would result from the initial nucleophilic attack occurring at a different position on the azulene ring. The formation of **2a** may also arise from intermediate **8**, in this case by elimination of *tert*-butyl alcohol and carbon monoxide. Aldehyde **2b** cannot be an intermediate in the formation of **2a** as it does not decarbonylate or oxidize under these reaction conditions, although it is possible that **2a** arises from the elusive tropone **6** instead. It is noteworthy that tropylium salts also ring contract, in this case to form benzene, upon oxidation with hydrogen peroxide or MCPBA and a similar mechanism has been proposed for this chemistry.[7] Clearly our observations help to explain the results obtained by the Bonn group, although the complex mixtures of reagents used in their studies makes mechanistic investigations impractical. The new results also demonstrate that isomerically pure functionalized carbaporphyrins are easily obtainable from azuliporphyrin and this will allow further aspects of the chemistry of this remarkable new carbaporphyrin family to be explored.

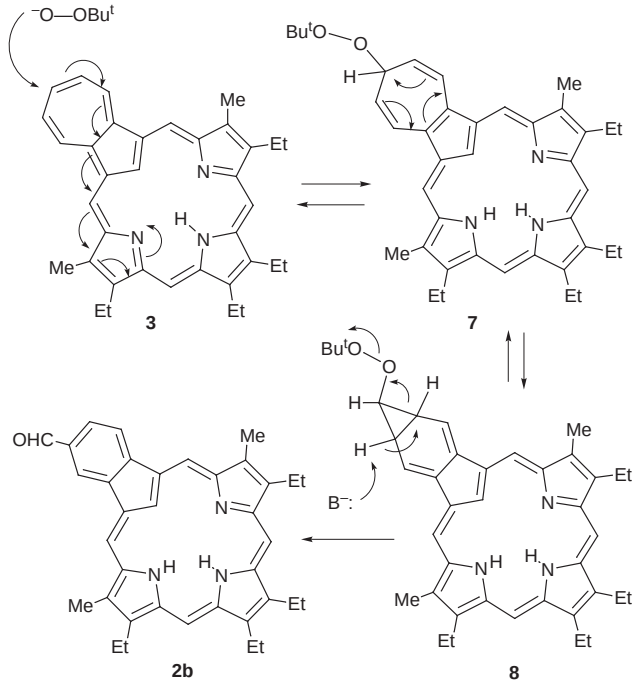

Scheme 2

This work was supported by the National Science Foundation under Grant No. CHE-9500630 and the Donors of the Petroleum Research Fund, administered by the American Chemical Society. The assistance of Ms S. T. Chaney with the early phases of this project is also acknowledged.

Notes and References

† Part 11 of the series 'Conjugated Macrocycles Relalted to the Porphyrins'. Part 10: M. J. Hayes and T. D. Lash, *Chem. Eur. J.*, 1998, **4**, 508.

‡ E-mail: tdlash@rs6000.cmp.ilstu.edu

§ *Selected data* for **2b**: δ_H(300 MHz, $CDCl_3$) −7.12 (1H, s), −4.45 (2H, br s), 1.79–1.89 (12H, 4 overlapping triplets), 3.51 (3H, s), 3.52 (3H, s), 3.90–4.05 (8H, 4 overlapping quartets), 8.10 (1H, d, *J* 7.5), 8.67 (1H, d, *J* 7.5), 9.06 (1H, s), 9.70 (1H, s), 9.71 (1H, s), 9.78 (1H, s), 9.80 (1H, s), 10.36 (1H, s); HRMS: Calc. for $C_{36}H_{37}N_3O$: 527.2937. Found: 527.2933. The proton NMR spectrum shows no indication of tautomeric species at room temperature, adding further support to our previous suggestion (ref. 3) that the German group had isolated isomeric mixtures of carbaporphyrins in their studies (ref. 5).

1 T. D. Lash, *Chem. Eur. J.* 1996, **2**, 1197; T. D. Lash, *J. Porphyrins Phthalocyanines*, 1997, **1**, 29.
2 T. D. Lash, *Angew. Chem., Int. Ed. Engl.*, 1995, **34**, 2533.
3 T. D. Lash and M. J. Hayes, *Angew. Chem., Int. Ed. Engl.*, 1997, **36**, 840.
4 T. D. Lash and S. T. Chaney, *Angew. Chem., Int. Ed. Engl.*, 1997, **36**, 839.
5 K. Berlin, C. Steinbeck and E. Breitmaier, *Synthesis*, 1996, 336.
6 See also: T. D. Lash and S. T. Chaney, *Chem. Eur. J.*, 1996, **2**, 944; T. D. Lash and S. T. Chaney, *Tetrahedron Lett.*, 1996, **37**, 8825.
7 K. Nakasuji, T. Nakamura and I. Murata, *Tetrahedron Lett.*, 1978, 1539.

Received in Corvallis, OR, USA, 12th May 1998; 8/03575J

Two novel reactions of ruthenated aniline. Structure and bonding in bis-chelated ruthenium complexes of quinone related ligands

Kedar Nath Mitra,[a] Shie-Ming Peng[b] and Sreebrata Goswami*[a]†

[a] *Department of Inorganic Chemistry, Indian Association for the Cultivation of Science, Calcutta, 700032, India*
[b] *Department of Chemistry, National Taiwan University, Taipei, Taiwan, Republic of China*

Two novel examples of oxidative *ortho* coupling of ruthenated aniline are described; the products are fully characterised by X-ray and other physicochemical data.

In a recent communication[1] we reported the formation of $RuCl_2(PhNH_2)_2(L^1)$, **1** (L^1 = *N*-phenyl-1,2-phenylenediimine), from the reaction of hydrated $RuCl_3$ and $PhNH_2$ [eqn. (1)].

$$RuCl_3{\bullet}3H_2O \xrightarrow{\text{aniline}} \underset{\mathbf{1}}{RuCl_2(PhNH_2)_2(L^1)} \qquad (1)$$

Although ruthenium(II) aniline complexes are known,[2] complex **1** represents the first example of a structurally characterised aniline complex of ruthenium. One of the principal interests in **1** was the possibility to study the chemical reactions of the coordinated aniline. In this report we present two such novel examples.

The reaction of $RuCl_2(PhNH_2)_2(L^1)$ and 3,5-di-*tert*-butylcatechol occurs smoothly in methanol at room temperature to produce a blue compound of composition $RuCl_2(L^1)(L^2)$, **2** [eqn. (2)], in 55% yield. This compound is highly soluble in

$$\underset{\mathbf{1}}{RuCl_2(PhNH_2)_2(L^1)} + \text{3,5-di-}\textit{tert}\text{-butylcatechol} \xrightarrow{CH_3OH} \underset{\mathbf{2}}{RuCl_2(L^1)(L^2)} \qquad (2)$$

common organic solvents and the solution shows an intense transition in the visible region at 627 nm. Verification of the composition and geometry of **2** was ascertained by the

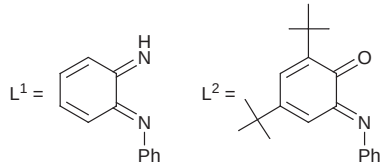

determination of its single crystal X-ray structure.‡ A view of the molecule is shown in Fig. 1 and selected bond distances are collected in Table 1. The results reveal the oxidative coupling of coordinated aniline and catechol to result in an *N*-phenyliminoquinone ligand, L^2, with the formation of a C–N bond. This transformation was not known previously. The formulation of the diimine oxidation state of L^1 (N,N) is evident[1] from the structural data of **2**. The imine C–N bond lengths, average 1.315(6) Å, are considerably shorter than the C7–N2 single bond, 1.444(6) Å, present in the same ligand. Considering the diimine oxidation state of the ligand L^1, two charge distributions for the RuL^2 moiety are possible in the above complex, either Ru^{II}–L^2 BQ (**2a**) or Ru^{III}–L^2 SQ (**2b**). Compound **2** is diamagnetic and shows two sharp *tert*-butyl proton resonances at δ 0.993 and 1.267. The C14–O bond length of the coordinated L^2 is 1.280(5) Å and the C13–N3 bond length is 1.339(6) Å. This C–O bond length is longer than the C=O bond length [1.239(7) Å] observed[3] in free 2,4,6,8-tetra-*tert*-butylphenoxazin-1-one (Phenox BQ) but it falls below the range observed[4] (1.29 Å and above) for a coordinated semiquinone ligand. For comparison, the C–O bond length[3a] in $Ru(PPh_3)_2Cl_2$-(phenox SQ) (phenox SQ = 1-hydroxy-2,4,6,8-tetra-*tert*-butylphenoxyzinyl radical) is 1.300(4) Å and the average C–O bond length[5] in $Ru(bpy)_2(DBSQ)^+$ (bpy = 2,2′-bipyridine, DBSQ = 3,5-di-*tert*-butyl-1,2-semiquinone) is 1.308 Å. The C–N bond length of coordinated L^2 is within the range of values expected[6] for imine ligands. Moreover, the C15–C16 and C17–C18 bonds have almost localised double bond character which is also consistent[4b] with the iminobenzoquinone formulation (**2a**). Their average distance of 1.355(6) Å is significantly shorter than the other four bonds of the ring (Table 1). To the

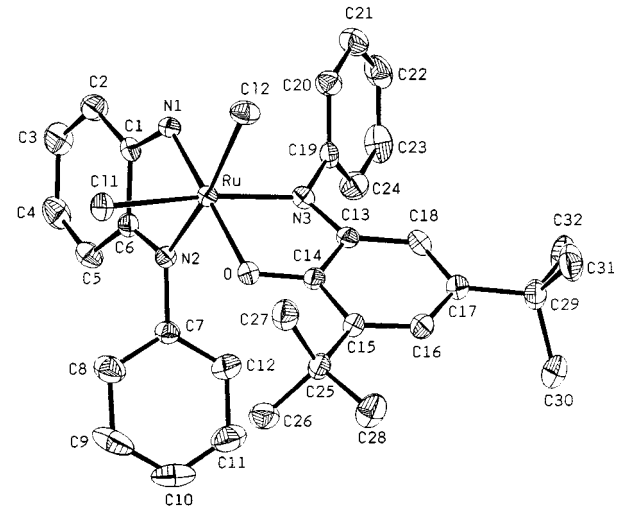

Fig. 1 Molecular structure of $RuCl_2(L^1)(L^2)$ showing the atom numbering scheme

Table 1 Selected bond distances (Å) for $RuCl_2(L^1)(L^2)\cdot CH_2Cl_2$

Ru–O	2.022(3)	N3–C13	1.339(6)	C5–C6	1.434(6)
Ru–N1	1.950(4)	O–C14	1.280(5)	C6–C1	1.447(6)
Ru–N2	2.001(4)	N2–C7	1.444(6)	C13–C14	1.439(6)
Ru–N3	1.974(4)	N3–C19	1.446(6)	C14–C15	1.439(6)
Ru–Cl1	2.364(13)	C1–C2	1.421(7)	C15–C16	1.355(6)
Ru–Cl2	2.385(13)	C2–C3	1.341(7)	C16–C17	1.441(7)
N1–C1	1.317(6)	C3–C4	1.417(8)	C17–C18	1.355(7)
N2–C6	1.313(6)	C4–C5	1.338(8)	C18–C13	1.420(6)

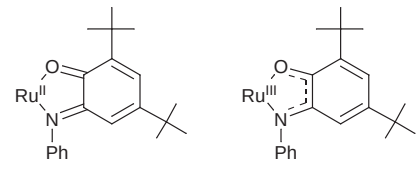

2a **2b**

best of our knowledge compound **2** represents the first example[7] of a mixed ligand compound containing both 1,2-diimine (N,N) and 1,2-iminoquinone (N,O) which gives an opportunity for the direct comparison of bonding between an (N,N) and an (N,O) donor. Furthermore, we wish to note here that structurally characterised Ru 1,2-diimines (N,N) are scarce[6] and there is only one example[3] of a ruthenium complex of 1,2-iminosemiquinone, the structure of which has been reported. Synthetic difficulties[7] have inhibited the study of iminoquinone complexes.

It was observed that prolonged exposure of a brown solution of **1** to air led to formation of a blue solution. A similar transformation occurs instantaneously and smoothly when a solution of **1** in CH_2Cl_2 is treated with H_2O_2. Chromatographic work up followed by crystallisation of the crude product yielded crystalline $RuCl_2(L^1)_2$, **3**, in 45% yield [eqn. (3)]. The three-

$$\underset{\mathbf{1}}{RuCl_2(PhNH_2)_2(L^1)} \xrightarrow[CH_2Cl_2]{H_2O_2} \underset{\mathbf{3}}{RuCl_2(L^1)_2} \qquad (3)$$

dimensional X-ray structure of **3** authenticates the formation of the compound from reaction (3). The isomer geometry of the ruthenium complex is identical[8] to that of the analogous dibromo osmium complex, $OsBr_2(L^1)_2$. The bond distances of the coordinated diimine ligand in the above two ruthenium and osmium compounds are similar. (Details of the X-ray structure of **3** will be reported elsewhere.) The compound shows an intense transition at 590 nm in the visible region.

The above coupling reactions [(2) and (3)] do not occur with uncoordinated aniline. These reactions therefore may be classified as reactions of the activated coordinated aniline. In reaction (2) one of the coordinated anilines coupled with externally added 3,5-di-*tert*-butyl catechol to form an *N*-phenyl substituted derivative of *o*-iminobenzoquinone.[7] It is possible that oxidation of catechol followed by condensation with the coordinated aniline have occurred during the above transformation. Reaction (3) formally involves many operations which are believed to occur simultaneously: isomerization of the starting compound to bring the two interacting aniline molecules into close proximity, oxidative coupling of two aniline molecules to *o*-semidine and further oxidation of *o*-semidine to diimine. For comparison, the reaction[8] of aniline with $[OsBr_6]^{2-}$ resulted in formation of a bis-chelated complex, $OsBr_2(L^1)_2$, directly. In contrast, a similar reaction[1] using hydrated $RuCl_3$ as the starting material yielded only a monochelated diimine complex, $RuCl_2(PhNH_2)_2(L^1)$, where two out of the four coordinated aniline molecules underwent oxidative dimerisation. Our present results have been able to demonstrate clearly that further oxidative coupling of the coordinated anilines in $RuCl_2(PhNH_2)_2(L^1)$ is possible by the use of a suitable oxidant. Our preliminary results in the area of oxidative coupling reactions of coordinated aromatic amines[2] in $[Ru(ArNH_2)_6]^{2+}$ and related substrates are highly encouraging and the scope of these reactions is very high.

We are grateful to the referees for their suggestions. Financial support received from the Council of Scientific and Industrial Research, New Delhi is gratefully acknowledged.

Notes and References

† E-mail: icsg@iacs.ernet.in

‡ *Crystal data*: $[RuCl_2(L^1)(L^2)]\cdot CH_2Cl_2$ **2**: $C_{33}H_{37}N_3OCl_4Ru$, M = 734.55, monoclinic, space group $P2_1/n$, a = 12.1035(20), b = 14.7953(11), c = 19.718(3) Å, β = 104.715(11)°, U = 3415.2(8) Å^3, Z = 4, D_c = 1.429 g cm^{-3}, crystal dimensions 0.25 × 0.25 × 0.20 mm, T = 298 K, μ = 6.259 cm^{-1}. Intensity data were collected on an Enraf-Nonius CAD4 diffractometer with graphite-monochromated Mo-Kα radiation (λ = 0.7107 Å). 6007 unique reflections were measured and 3728 with $I \geqslant 2\sigma(I)$ were used in the refinement. Refinement[9] of positional and anisotropic thermal parameters for all non-hydrogen atoms converged to R = 0.037. The final Fourier difference map showed residual extrema at 0.410, −0.430 e Å^{-3}. CCDC 182/919.

1 K. N. Mitra, P. Majumdar, S.-M. Peng, A. Castiñeiras and S. Goswami, *Chem.Commun*., 1997, 1267.
2 D. L. Key, L. F. Larkworthy and J. E. Salmon, *J. Chem. Soc. (A)*, 1971, 2583.
3 (*a*) S. Bhattacharya and C. G. Pierpont, *Inorg. Chem.*, 1992, **31**, 2020; (*b*) S. Bhattacharya, S. R. Boone and C. G. Pierpont, *J. Am. Chem. Soc.*, 1990, **112**, 4561.
4 (*a*) S. Bhattacharya and C. G. Pierpont, *Inorg. Chem.*, 1991, **30**, 1511; (*b*) C. G. Pierpont and R. M. Buchanan, *Coord. Chem. Rev.*, 1981, **38**, 45.
5 S. R. Boone and C. G. Pierpont, *Inorg. Chem.*, 1987, **26**, 1769.
6 T. Jüstel, J. Bendix, N. M. Nolte, T. Weyhermuller, B. Nuber and K. Wieghardt, *Inorg. Chem*., 1998, **37**, 35; P. Belser, A. von. Zelewsky and M. Zehnder, *Inorg. Chem.*, 1981, **20**, 3098; C. J. da. Cunha, S. S. Fielder, D. V. Stynes, H. Masui, P. R. Auburn and A. B. P. Lever, *Inorg. Chim. Acta*, 1996, **242**, 293.
7 H. Masui, A. B. P. Lever and P. R. Auburn, *Inorg. Chem.*, 1991, **30**, 2402.
8 K. N. Mitra and S. Goswami, *Chem. Commun.*, 1997, 49.
9 G. M. Sheldrick, SHELXS 86, Program for the solution of crystal structures, University of Göttingen. 1986.

Received in Cambridge, UK, 3rd April 1998; revised manuscript received 8th June 1998; 8/04794D

Novel products from bromination reactions of 5,10,15,20-tetraisopropylporphyrins

Nora Y. Nelson, Craig J. Medforth, Richard G. Khoury, Daniel J. Nurco and Kevin M. Smith*†

Department of Chemistry, University of California, Davis, CA 95616, USA

Bromination reactions of nickel(II) or copper(II) complexes of 5,10,15,20-tetraisopropylporphyrin afford the unusual porphodimethenes 2–5; crystallographic data for some of these compounds are presented and possible mechanisms for their formation are discussed.

2,3,7,8,12,13,17,18-Octahalo-5,10,15,20-tetraarylporphyrins have recently received considerable attention due to their usefulness as catalysts for the oxidation of organic substrates.[1] Although the syntheses and properties of these porphyrins have been extensively investigated, comparatively little is known about the bromination reactions of other porphyrins such as those with alkyl substituents. Bonnett *et al.*[2] have reported that halogenation of deuteroporphyrins preferentially yields peripherally as opposed to *meso* halogenated products, and that attempts to brominate 2,3,7,8,12,13,17,18-octaethylporphyrin (H_2OEP) resulted in bromodealkylation and benzylic-type subsitution reactions. Vicente and Smith[3] have also shown that treatment of H_2OEP with NBS in the presence of AIBN affords *trans*-(2-bromovinyl)heptaethylporphyrin, as well as (1-alkoxyethyl)heptaethylporphyrins when alcohols are present. We have recently described the novel chemical and spectroscopic properties of some 5,10,15,20-tetraalkylporphyrins with isopropyl or *tert*-butyl substituents.[4,5] We now show that one of these porphyrins also yields unexpected and unusual products upon bromination with NBS or Br_2.

When the nickel(II) complex of 5,10,15,20-tetraisopropylporphyrin **1a** was treated with 8 equiv. of NBS, or excess Br_2 in $CHCl_3$ in the dark at room temperature, a dark green solid **2** was isolated as the major product in 7.2 and 46% yield, respectively. The structure of **2**, as determined by X-ray crystallography,‡ is shown in Fig. 1. The structure reveals a cyclic tetrapyrrole in which all of the pyrrole 3,4-positions have been brominated. Remarkably, the macrocycle is no longer a porphyrin but has a porphodimethene-like structure with two exocyclic double bonds on opposite *meso* positions. The molecule also adopts an extremely nonplanar ruffled conformation, with a maximum deviation of the 24 core atoms from the mean plane of 1.44 Å (for a *meso* carbon atom) and an average deviation from the mean plane of 0.57 Å. As is expected for such a nonplanar macrocycle, the average Ni–N distance is very short (1.88 Å). The absorption spectrum, which shows two broad bands at 482 nm (ε 48 100) and 594 (30 700), resembles that of 5,15-dimethyl-2,3,7,8,12,13,17,18-octaethyl-5H,15H-porphinato)nickel(II).[6] The ^{1}H NMR spectrum, which features two sets of methyl protons [δ 1.74 (d, 12H), 2.11 (s, 12H)] and one set of isopropyl methine protons [δ 4.42 (septet, 2H)], is consistent with the observed symmetrical structure.

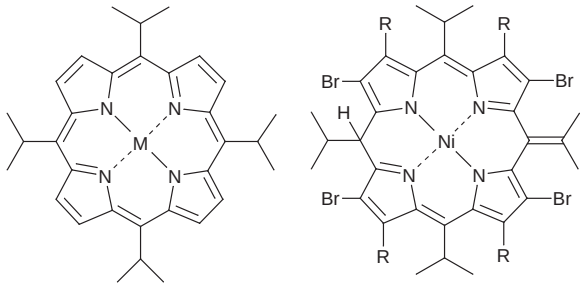

1a M = Ni
b M = Cu

3 R = Br
4 R = H

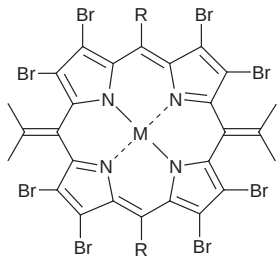

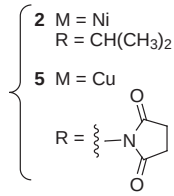

2 M = Ni
R = $CH(CH_3)_2$

5 M = Cu

Only a few porphyrins bearing exocyclic double bonds have been described in the literature; these include a cyclic tetrapyrrole bearing four *meso* exocyclic carbonyl groups (octaethylxanthoporphyrinogen),[7] the exocyclic alkene analogue octaethyl-*meso*-tetrakis(methylene)porphyrinogen,[8] and certain oxidation products of *meso*-tetrakis(3,5-di-*tert*-butyl-4-hydroxyphenyl)porphyirn described by Milgrom.[9] The formation of compounds with exocyclic double bonds from the bromination of **1a** suggests that the reaction may involve the addition of HBr or Br_2 across the opposite *meso* carbons of a partially brominated species, followed by elimination of one or two molecules of HBr, respectively, to yield compounds **3** and **4** or compound **2**. Addition of molecules to the porphyrin periphery in this fashion has previously been observed in

When compound **1a** was treated with 8 equiv. or less of Br_2, two other compounds were also isolated. These materials did not yield crystals suitable for X-ray structure determination but the structures **3** (10% yield) and **4** (75%) were established from NMR experiments and mass spectral data. Both compounds share a common porphodimethene-type structure with one exocyclic double bond and one sp^3 *meso* carbon atom. Interestingly, in compound **4** the β-pyrrolic carbons have been brominated in a regiospecific fashion.

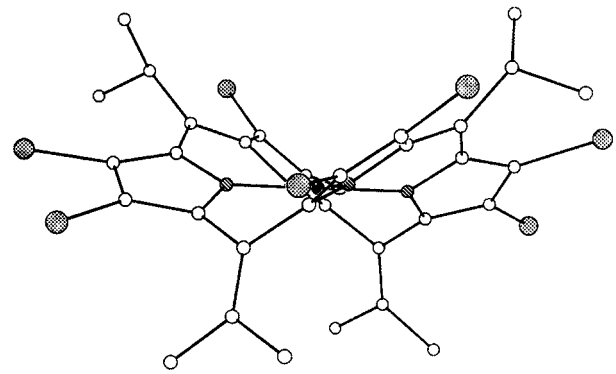

Fig. 1 Molecular structure of **2**. Hydrogen atoms are omitted for clarity.

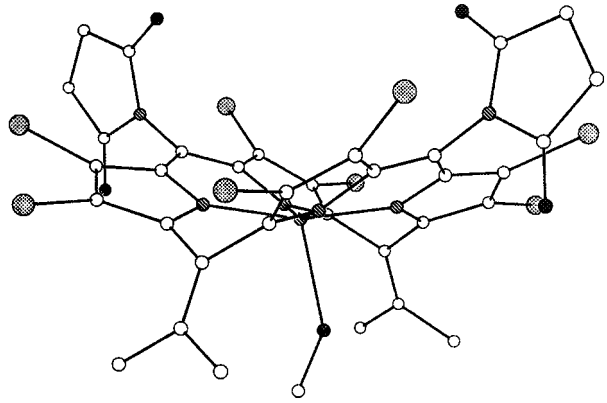

Fig. 2 Molecular structure of **5**. Hydrogen atoms are omitted for clarity.

5,10,15,20-tetra-*tert*-butylporphyrin and some of its metal complexes.[4] We believe that similar addition reactions may occur for compound **1a** because they result in a release of steric congestion between the *meso* isopropyl and the adjacent pyrrole bromo groups. In theory, bromination could also occur at the isopropyl benzylic positions *via* a radical mechanism when NBS is used as the brominating agent. If followed by elimination of the benzylic bromine atom and loss of a methine proton from the opposite isopropyl group, this would also furnish the two opposite exocyclic double bonds seen in compound **2**.

In order to investigate the effects of different metals on the bromination reaction, the copper(II) complex (**1b**) of 5,10,15,20-tetraisopropylporphyrin was treated with 8 equiv. of NBS in $CHCl_3$ in the dark at room temperature. One of three major products (**5**) isolated from this reaction gave high quality crystals enabling its definitive characterization by X-ray crystallography§ (Fig. 2). Compound **5** is similar to compound **2** in that all of the pyrrole positions have been brominated, and the macrocycle has a very ruffled porphodimethene-like structure; the maximum and average deviations of the 24 core atoms from the macrocycle mean plane in **5** of 1.27 and 0.51 Å, respectively, are slightly smaller than those seen for **2**. An unusual feature of the structure is that it no longer has any isopropyl groups attached to the porphyrin periphery! Instead, it bears two exocyclic alkene groups and two succinimido moieties. In addition, the copper atom is penta-coordinated, with a MeOH molecule serving as the fifth ligand (Cu–O 2.29 Å, Cu–$N_{average}$ 1.98 Å**).** This unusual axial ligation is presumably a consequence of the very electron-deficient nature of the macrocycle. It has previously been shown that 5-succinimido-OEP can be obtained when zinc(II)-OEP is treated with NBS in the presence of AIBN.[3] When *N*-chlorosuccinimide was used in place of NBS under the same conditions, however, only the mono- and di-*meso*-chloroporphyrins were obtained. This, and our current data, suggest that bromodeprotonation and bromodealkylation of the *meso* proton and isopropyl groups, respectively, could be intermediate steps in the formation of these unusual *meso*-succinimido products.

This work was supported by grants from the National Institutes of Health (HL 22252) and the National Science Foundation (CHE-96-23117). C. J. M. gratefully acknowledges financial support from Professor J. A. Shelnutt (Sandia National Laboratories) through U. S. Department of Energy Contract DE-AC04-94AL85000.

Notes and References

† E-mail: kmsmith@ucdavis.edu

‡ *Crystal data* for **2** ($C_{32}H_{26}N_4Br_8Ni{\cdot}CH_2Cl_2$): crystals were grown by the slow diffusion of MeOH into a solution of **2** in CH_2Cl_2. The selected crystal was cut to dimensions of 0.22 × 0.14 × 0.06 mm for cell determination and data collection. The unit cell was triclinic, space group $P\bar{1}$ with cell dimensions a = 11.6952(13), b = 13.214(3), c = 14.909(3) Å, α = 98.04(2), β = 106.547(14), γ = 115.526(14)°, V = 1899.0(6) Å^3, and Z = 2 (FW = 1249.5). Diffraction data were collected on a Siemens P4 diffractometer with a rotating anode [λ(Cu-Kα) = 1.54178 Å] at 130(2) K in $\theta/2\theta$ scan mode to $2\theta_{max}$ = 112.8°. Of 5310 reflections measured (+h, ±k, ±l), 5007 were independent (R_{int} = 0.081), and 4315 had $I > 2\sigma$ (T_{min} = 0.25, T_{max} = 0.55 °C, ρ_{calc} = 2.182 g cm^{-3}, μ = 12.14 mm^{-1}). The structure was solved by direct methods and refined (based on F^2 using all independent data) by full-matrix least-squares methods with 253 parameters (Siemens SHELXTL ver. 5.03). All bromines and the central nickel ion were refined with anisotropic thermal parameters; all other atoms were refined with isotropic thermal parameters. Hydrogen atom positions were generated by their idealized geometry and refined using a riding model. An empirical absorption correction was applied (XABS2) (ref. 10). The final difference map had a largest peak of 1.37 e Å^{-3} and a largest hole of −1.19 e Å^{-3}. Final R factors were $R1$ = 0.054 (observed data) and w$R2$ = 0.147 (all data).

§ *Crystal data* for **5** ($C_{35}H_{23}N_6O_5Br_8Cu$): crystals were grown by the slow diffusion of MeOH into a solution of **5** in CH_2Cl_2. The single crystal was selected with dimensions of 0.46 × 0.22 × 0.10 mm. The unit cell was monoclinic, space group $C2/c$ with cell dimensions a = 26.977(4), b = 6.7493(14), c = 25.623(4) Å, β = 121.561(9)°, V = 3975.2(11) Å^3, and Z = 2 (FW = 1310.41). Diffraction data were collected on a Siemens P4 diffractometer with a rotating anode [λ(Cu-Kα) = 1.54178 Å] at 130(2) K in $\theta/2\theta$ scan mode to $2\theta_{max}$ = 113°. Of 3655 reflections measured (+h, +k, ±l), 2573 were independent (R_{int} = 0.077), and 2309 had $I > 2\sigma$ (T_{min} = 0.13, T_{max} = 0.41 °C, ρ_{calc} = 2.19 g cm^{-3}, μ = 10.65 mm^{-1}). The final difference map had a largest peak of 1.834 e Å^{-3} and a largest hole of −1.287 e Å^{-3}. Final R factors were $R1$ = 0.0729 (observed data) and w$R2$ = 0.218 (all data). The structure was solved by direct methods and refined (based on F^2 using all independent data) by full-matrix least-squares methods with 136 parameters (Siemens SHELXTL V. 5.03). The bromines and the central nickel ion were refined with anisotropic thermal parameters. Hydrogen atom positions were generated by their idealized geometry and refined using a riding model. An empirical absorption correction was applied (XABS2) (ref. 10). CCDC 182/920.

1 R. A. Sheldon, *Metalloporphyrins in Catalytic Oxidations*, Marcel Dekker, New York, 1994 and references cited therein.
2 R. Bonnett, I. H. Campion-Smith, A. N. Kozyrev and A. F. Mironov, *J. Chem. Res. (S).*, 1990, 138.
3 M. G. H. Vicente and K. M. Smith, *Tetrahedron*, 1991, **47**, 6887.
4 T. Ema, M. O. Senge, J. A. Roberts, N. Y. Nelson, H. Ogoshi and K. M. Smith, *Angew. Chem., Int. Ed. Engl.*, 1994, **33**, 1879.
5 C. M. Drain, S. Gentemann, J. A. Roberts, N. Y. Nelson, C. J. Medforth, S. Jia, M. C. Simpson, K. M. Smith, J. Fajer, J. A. Shelnutt and D. Holten, *J. Am. Chem. Soc*., 1998, **120**, 3781 and references cited therein.
6 M. W. Renner and J. W. Buchler, *J. Phys. Chem.*, 1995, **99**, 8045.
7 H. Fisher and H. Orth, *Die Chemie des Pyrrols*, Akademische Verlag, Leipzig, 1940, vol. 2, part 2, pp. 423–429; W.S. Sheldrick, *J. Chem. Soc., Perkin Trans. 2*, 1976, 453 and references cited therein.
8 C. Otto and E. Breitmaier, *Liebigs Ann. Chem*., 1991, 1347.
9 L. R. Milgrom, J. P. Hill and G. Yahioglu, *J. Heterocycl. Chem.*, 1995, **32**, 97 and references cited therein.
10 S. R. Parkin, B. Moezzi and H. Hope, *J. Appl. Crystalogr*., 1995, **28**, 53.

Received in Corvallis, OR, USA, 17th April 1998; 8/02901F

Synthesis and characterization of the monomeric molybdenum trithiolate Mo(η⁷-dmpt)(η¹-dmpt)$_2$ (dmpt = 2,6-dimesitylphenylthiolate)

Birsen S. Buyuktas, Marilyn M. Olmstead and Philip P. Power*†

Department of Chemistry, University of California, Davis, California 95616, USA

Treatment of $MoCl_3(THF)_3$ with 3 equiv. of $LiSC_6H_3Mes_2$-2,6 (Mes = $C_6H_2Me_3$-2,4,6) (Lidmpt) affords the monomeric molybdenum trithiolate Mo(η⁷-dmpt)(η¹-dmpt)$_2$, 1, which is spectroscopically and structurally characterized; the MoS_3 array has distorted trigonal pyramidal geometry which is caused by strong π-interactions between molybdenum and an *ortho*-mesityl group from one of the thiolate substituents.

Stable, well characterized examples of monomeric, three-coordinate Mo^{III} complexes are rare. In general, such compounds are dimerized to form triply bonded species of formula $L_3Mo{\equiv}MoL_3$ (L = uninegative ligand) which have been extensively studied.[1] Although it is probable that the incompletely characterized, sterically encumbered derivatives $Mo\{N(Pr^i)_2\}_3$ and $Mo\{N(SiMe_3)_2\}_3$ are monomers,[2] the first well established three-coordinate Mo^{III} compound was $Mo[N\{C(CD_3)_2CH_3\}C_6H_3Me_2\text{-}3,5]_3$[3] which, like the related molybdenum triamidoamine derivative [Mo(OTf)({C_6F_5N-$(CH_2)_2$}$_3$N)],[4] activates dinitrogen at room temperature to form a variety of complexes, including imines and nitrides. The stabilization of these unusual and interesting complexes by bulky aryl amido substituents suggested that it should be possible to isolate further examples of monomeric, low coordinate trivalent complexes with other ligands. Here it is shown that the use of the thiolate ligand $SC_6H_3Mes_2$-2,6 (dmpt)[5] enables the isolation of the first monomeric homoleptic molybdenum trithiolate complex Mo(η⁷-dmpt)(η¹-dmpt)$_2$, **1**.

Complex **1** was synthesized in moderate yield‡ by the reaction of 3 equiv. of $LiSC_6H_3Mes_2$-2,6 with $MoCl_3(THF)_3$.[6] The dark red, almost black, crystalline product, **1**, has good solubility in hydrocarbon solvents. The electronic absorption spectrum is almost featureless with a rapid rise in absorption at < 400 nm and a very weak shoulder at 490 nm (ε = 4600) is apparent. Magnetic studies confirm the paramagnetic character with μ_B = 3.6 (T = 293 K). The monomeric structure of **1** was established by a single crystal X-ray crystal study of its pentane solvate, **1**·0.25pentane.§ The Mo atom is bound to three thiolate sulfurs and two of the Mo–S distances have almost equal values of 2.393(2) and 2.394(2) Å, whereas the other is slightly shortened to 2.314(2) Å. The MoS_3 array is grossly distorted from planarity as indicated in the three S–Mo–S angles, which have the values 88.68(6), 105.59(7), and 91.67(7)°. The Mo–S–C angles also are different with an angle of 102.3(2)° being observed at S(1) (which bears the mesityl ring that interacts with Mo, *vide infra*) which is 14–16° narrower than the corresponding angles at S(2) and S(3). The coordination sphere of Mo is completed by a strong interaction with the C(11) *ortho*-mesityl ring. This ring is bent along the C(7)···C(10) axis (fold angle = 159.4°) such that these two atoms are closest to Mo [Mo–C distances = 2.220(6) and 2.248(7) Å] while the Mo–C distances to the remaining ring carbons are in the range 2.295(6)–2.502(6) Å.

Previous examples of related Mo^{III} thiolates [*e.g.* $Mo_2(SMes)_6$[7] or the heteroleptic species $Mo_2\{S(Bu^t)\}_2(NMe_2)_4$[8]] have been shown to be dimeric with Mo–Mo triple bonds. The monomeric structure observed for **1** (Fig. 1) is a consequence of the large size of the $SC_6H_3Mes_2$-2,6 ligand and the π-interaction between one of the mesityl groups on the ligand and the metal. The metal–ligand π-interaction may arise in part from the unique reactivity of the trigonal Mo^{III} fragment[4] which in the case of the $Mo[N\{C(CD_3)_2CH_3\}C_6H_3Me_2\text{-}3,5]_3$ complex is capable of activating N_2[3b,9] to afford, *inter alia*, the nitride $N{\equiv}Mo[N\{C(CD_3)_2CH_3\}C_6H_3Me_2\text{-}3,5]_3$. In the case of **1**, the strong interaction between the metal and a π-ring system apparently prevents the dinitrogen activation observed for the amide complexes. Note that the synthesis and manipulation of **1** were conducted under an N_2 atmosphere. Furthermore, hexane solutions of purified **1** show no sign of reaction with N_2 upon standing for 3 days at room temperature. Although the structure of **1** is unique it may be compared to that described for the Mo^{II} species [Mo(η⁷-dpt)(η¹-dpt)(CO)], **2** (dpt = $SC_6H_3Ph_2$-2,6)[10a] which also possesses a Mo–η⁶-Ph ring interaction involving a thiolate ligand.[10b] However, the η⁶-coordination of the *ortho*-phenyl ring may be displaced by the addition of CO or bidentate neutral ligands such as 2,2′-bipyridyl. The Mo–S distances in **2** [2.239(4) and 2.358(3) Å] are quite similar to those in **1**. However, the distortions in the geometry of the η⁶-interacting Mes ring in **1** are not observed in the η⁶-Ph ring of **2** although in the latter the *ipso*-carbon is displaced slightly (by *ca*. 0.14 Å) from the averaged plane of the other five ring carbon atoms.

The structural distortion observed in the mesityl ring which interacts with Mo has similarities to those observed in a variety of transition metal complexes.[11] In many instances this results in a 1,4-diene type of localization of multiple bond character within the aromatic ring. In **1**, however, the localization does not show a regular pattern. Thus, although the C(8)–C(9) distance, 1.360(9) Å, is short, the C(11)–C(12) distance, 1.420(10) Å, is

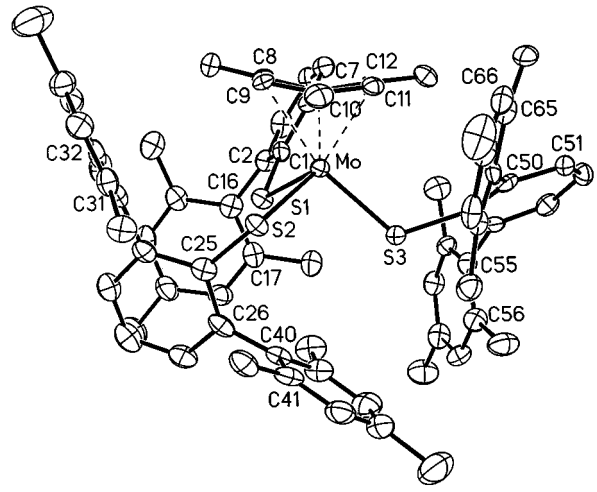

Fig. 1 Thermal ellipsoid plot of **1**. Important bond distances (Å) and angles (°) are as follows: Mo–S(1) 2.393(2), Mo–S(2) 2.394(2), Mo–S(3) 2.314(2), Mo–C(7) 2.220(6), Mo–C(8) 2.502(6), Mo–C(9) 2.433(6), Mo–C(10) 2.248(7), Mo–C(11) 2.295(6), Mo–C(12) 2.389(8), S(1)–Mo–S(2) 88.68(6), S(1)–Mo–S(3) 105.59(7), S(2)–Mo–S(3) 91.67(7), Mo–S(1)–C(1) 102.3(2), Mo–S(2)–C(25) 116.1(2), Mo–S(3)–C(49) 118.6(2)°.

near normal for an aromatic ring, whereas the C(7)–C(8) bond is lengthened to 1.494(9) Å. Perhaps the most structurally related Mo environment to that seen in **1** is in $[\{(\eta^6\text{-PhMe})Mo(\mu\text{-}SMe)_2\}_2][PF_6]_2$.[12] In this case, the oxidation state of Mo is also 3+; however, the Mo–S distances [2.451(1)–2.462(1) Å] are, of course, considerably longer owing to their bridging nature. Nonetheless, the range of Mo–C distances [2.287(3)–2.416(3) Å] is similar to the 2.220(6)–2.502(6) Å range observed in **1**. In essence, the Mo–ring π-interaction in **1** is as strong as that seen for other Mo species with neutral 6π-electron ring donors. Furthermore, the Mo–S distances are similar to those observed in $Mo_2(SMes)_6$[7] but longer than the 2.262(1) Å in the Mo^{4+} species $Mo(SC_6H_2\text{-}Pr^i_3\text{-}2,4,6)_4$.[13]

In summary, the $SC_6H_3Mes_2$-2,6 ligand permits the isolation of the first monomeric complex of formula $Mo(SR)_3$ (R = alkyl or aryl group). However, intramolecular interactions between the Mo atom and a ligand Mes ring prevent the molecule from displaying significant reactivity toward N_2 under ambient conditions.

We thank the National Science Foundation and the Donors of the Petroleum Research Fund administered by the American Chemical Society for financial support and TUBITAK (Turkish Scientific and Technical Research Institution) for fellowship support for B. B.

Notes and References

† E-mail: pppower@uc.davis.edu

‡ All manipulations were carried out under anaerobic and anhydrous conditions. The thiol $HSC_6H_3Mes_2$-2,6 was synthesized as described in the literature.[5] **1**·0.25pentane: $HSC_6H_3Mes_2$-2,6[5] (1.91 g, 5.5 mmol) was dissolved in diethyl ether (25 ml) and treated slowly with Bu^nLi (3.6 ml of a 1.6 M solution in hexane; 5.5 mmol) with cooling in an ice bath. The mixture was stirred for 30 min at 0 °C and allowed to warm to room temperature with continuous stirring for a further 1 h. The solution was then added slowly to a suspension of $MoCl_3(THF)_3$[6] (0.767 g, 1.83 mmol) in diethyl ether (25 ml) at *ca.* 0 °C. The mixture became deep red and stirring was continued for 18 h at room temperature. The precipitate was allowed to settle and the supernatant, deep red solution was decanted to another Schlenk tube *via* a cannula. The ether was evaporated under reduced pressure and hexane (40 ml) was added to the dark red residue. Filtration through Celite gave a clear, dark red solution. Reduction of the volume under reduced pressure to *ca.* 15 ml and storage of the solution in a −20 °C freezer gave black crystals of **1**·0.25pentane, which were suitable for X-ray structure determination. Total yield: 1.08 g, 51%, mp 112–115 °C. Anal. Calc. for **1**, $C_{72}H_{75}S_3Mo$: C, 76.36; H, 6.68. Found C, 75.94; H, 6.81%. UV–VIS (λ_{max}, ε): 490 nm (sh), 4600 $dm^3\ mol^{-1}\ cm^{-1}$. IR (Nujol, ν/cm^{-1}): 3040sh, 2950s, 2920s, 2850s, 2720w, 1720w, 1610m, 1560w, 1460s, 1450s, 1370s, 1255m, 1090w, 1020w, 845, 800m, 740w, 730w, 710w. Magnetic moment μ_B = 3.6 (T = 293 K).

§ *Crystal data* for **1** at T = 130 K with Mo-Kα (λ = 0.71073 Å) radiation: M = 1150.48, a = 27.927(6), b = 19.974(4), c = 23.346(5) Å, β = 103.82(3)°, V = 12646(4) $Å^3$, μ = 0.347 mm^{-1}, monoclinic, space group $C2/c$, Z = 8, R_1 = 0.062 for 6177 [$I > 2\sigma(I)$] data. CCDC 182/922.

1 F. A. Cotton and R. A. Walton, *Multiple Bonds between Metal Atoms*, Clarendon, Oxford, 2nd edn., 1993.
2 M. H. Chisholm, *Acc. Chem. Res*., 1990, **23**, 419; M. H. Chisholm and W. Reichert, *Adv. Chem. Ser*., 1976, **150**, 273; D. C. Bradley and M. H. Chisholm, *Acc. Chem. Res*., 1976, **9**, 273.
3 (*a*) C. E. Laplaza, A. L. Odom, W. M. Davis, C. C. Cummins and J. D. Protasiewicz, *J. Am. Chem. Soc*., 1995, **117**, 4999; (*b*) C. E. Laplaza, M. J. A. Johnson, J. Peters, A. L. Odom, E. Kim, C. C. Cummins, G. N. George and I. J. Pickering, *J. Am. Chem. Soc*., 1996, **118**, 8623; (*c*) C. C. Cummins, *Prog. Inorg. Chem*., 1998, **47**, 685.
4 R. R. Schrock, *Acc. Chem. Res*., 1997, **30**, 9 and references therein.
5 J. J. Ellison, K. Ruhlandt-Senge and P. P. Power, *Angew. Chem., Int. Ed. Engl*., 1994, **33**, 1178.
6 J. R. Dilworth and J. Zubieta, *Inorg. Synth*., 1986, **24**, 193.
7 M. H. Chisholm, J. F. Corning and J. C. Huffman, *J. Am. Chem. Soc*., 1983, **105**, 5924.
8 M. H. Chisholm, J. F. Corning and J. C. Huffman, *Inorg. Chem*., 1983, **22**, 38; M. H. Chisholm, J. F. Corning, K. Folting and J. C. Huffman, *Polyhedron*, 1985, **4**, 383.
9 C. E. Laplaza and C. C. Cummins, *Science*, 1995, **268**, 861.
10 (*a*) P. T. Bishop, J. R. Dilworth, T. Nicholson and J. Zubieta, *J. Chem. Soc., Dalton Trans*., 1991, 385; (*b*) for *ortho*-aryl phenoxide–group 6 metal interactions see: M. A. Lockwood, P. E. Farwick, O. Eisenstein and I. P. Rothwell, *J. Am. Chem. Soc*., 1996, **118**, 2762.
11 D. J. Arney, P. A. Wexler and D. E. Wigley, *Organometallics*, 1990, **9**, 1282.
12 W. E. Silverthorn, C. Couldwell and K. Prout, *J. Chem. Soc., Chem. Commun*., 1978, 1009.
13 E. Roland, E. C. Walborsky, J. C. Dewan and R. R. Schrock, *J. Am. Chem. Soc*., 1985, **107**, 5795.

Received in Bloomington, IN, USA, 24th April 1998; 8/03064B

Tertiary cyclopropanol systems as synthetic intermediates: novel ring-cleavage of tertiary cyclopropanol systems using vanadyl acetylacetonate

Masayuki Kirihara,*† Motohiro Ichinose, Shinobu Takizawa and Takefumi Momose

Faculty of Pharmaceutical Sciences, Toyama Medical and Pharmaceutical University, Sugitani 2630, Toyama 930-0194, Japan

Tertiary cyclopropanol systems react with a catalytic amount of vanadyl acetylacetonate under an oxygen atmosphere to afford β-hydroxyketones and β-diketones.

Tertiary cyclopropyl silyl ethers (**1**), readily available from the cyclopropanation of enol silyl ethers, are important synthetic

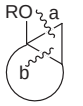

a: $Hg(OAc)_2$, ZnI_2, base, halogen, $AgBF_4$, $Cu(BF_4)_2$, $SnCl_4$, PhPdOTf, $[Pt(C_2H_4)Cl_2]_2$
b: $FeCl_3$, $Mn(pic)_3$, electrolysis
a & b: $PhI(OAc)_2$, $Pb(OAc)_4$

1 (R = TMS, H)

intermediates due to their high reactivity,[1] and simple fragmentation at their cyclopropanol system is familiar as the procedure for the α-homologation of ketones. Several methods have been developed to achieve specific cleavage at bond 'a'[2] or 'b'.[3] The methods of bond cleavage at both 'a' and 'b' have been reported by Rubottom and co-workers[4] and ourselves.[5]

Here we describe a novel reaction involving the treatment of tertiary cyclopropyl silyl ethers or tertiary cyclopropanols (**1**) with a catalytic amount of vanadyl actylacetonate‡ under an O_2 atmosphere in EtOH to cause a ring fragmentation resulting in the formation of β-hydroxy ketones and β-diketones§ (Scheme 1). These results are summarised in Table 1. In the case of 1-(trimethylsiloxy)bicyclo[*n*.1.0]alkanes or bicyclo[*n*.1.0]alkanols (entries 1–6), the 'b' bond was specifically cleaved to afford ring-enlarged β-hydroxy ketones and β-diketones. As noted in entry 6, the cyclopropane ring without oxygen-functionality did not react under these reaction conditions.

β-Diketones were not obtained by the reaction of β-hydroxy ketones with $VO(acac)_2$. These results mean that β-diketones were directly produced from the cyclopropanol systems. Molecular oxygen acts as the co-oxidant and reoxidises the low valent vanadium compound formed, thus a stoichiometric amount of $VO(acac)_2$ reacted with 1-(trimethylsiloxy)-bicyclo[4.1.0]heptane in the absence of oxygen (Scheme 2).

Although $VO(acac)_2$ did not react with **1** in an aprotic solvent (*e.g.* CH_2Cl_2), it reacted with **1** in trifluoroethanol to afford β-diketones (**3**) predominantly (Scheme 3).

Interestingly, 5-but-3-enylbicyclo[4.1.0]heptan-1-ol (**4**) did not cause tandem ring expansion–cyclisation but caused simple ring expansion to afford **5** and **6**. This result is in sharp contrast to iron(III) chloride[3c,d] or manganese(III) picolinate[3g] that causes the tandem reaction (Scheme 4). We also found that a radical inhibitor [2,6-di(*tert*-butyl)-*p*-cresol] did not interfere with the reaction of $VO(acac)_2$ with **1**.

Although the reaction mechanism is unknown, these results suggest that this reaction is different from the other specific 'b'

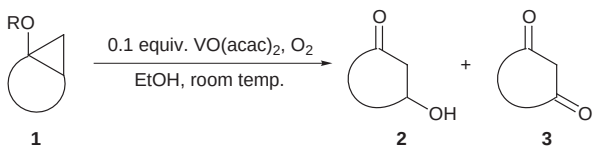

Scheme 1

Table 1 Results of ring-cleavage reactions[a]

Entry	Starting Material	Products	
1	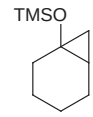	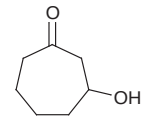 41%	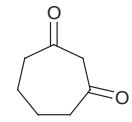 24%
2	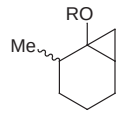	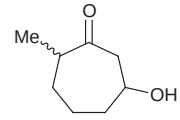 R = TMS (40%) R = H (36%)	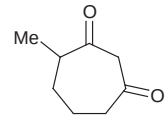 R = TMS (25%) R = H (39%)
3	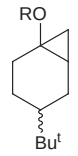	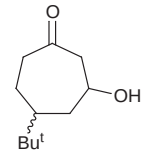 R = TMS (25%) R = H (21%)	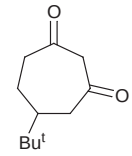 R = TMS (30%) R = H (35%)
4	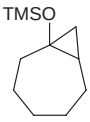	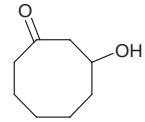 31%	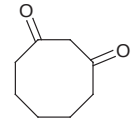 33%
5		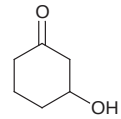 75%	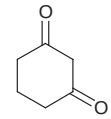 10%
6	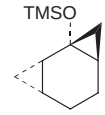	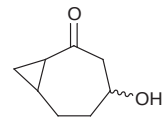 29%	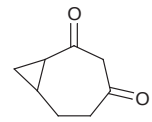 31%
7	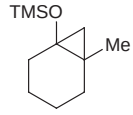	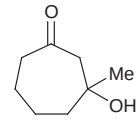 53%	
8	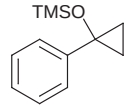	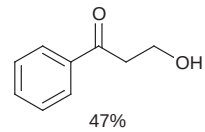 47%	
9	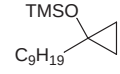	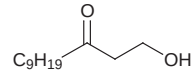 46%	

[a] All known products were identifed by comparison with authentic samples, and new compounds were characterized on the basis of mass, IR, and NMR spectral data.

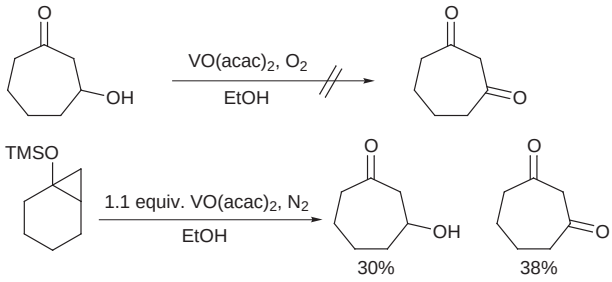

Scheme 2

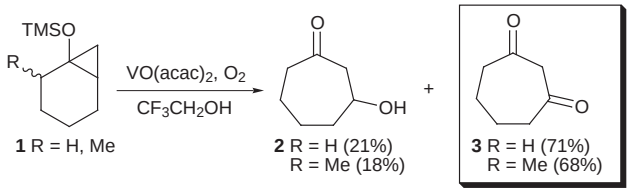

Scheme 3

bond cleavage reactions[3] which proceed through a simple radical oxidation. Further details of the mechanism are currently under investigation.

This work was supported in part by The Tamura Foundation for Promotion of Science and Technology and a Grant-in-Aid (No. 09672139) for Scientific Research from the Ministry of Education, Science, Sports and Culture, Japan.

Notes and References

† E-mail: kirihara@ms.toyama-mpu.ac.jp

‡ The reaction with pentavalent vanadium compounds [*e.g.* dichloro(ethoxy)(oxy)vanadium] did not afford β-hydroxy ketones or β-diketones, giving instead complex mixtures.

§ A typical experimental procedure is as follows: a mixture containing tertiary cyclopropyl silyl ethers (or tertiary cyclopropanols) (0.5 mmol), $VO(acac)_2$ (0.05 mmol) and EtOH (5 ml) was stirred at room temperature under an oxygen atmosphere for 1.5–35 h. Water (3 ml) was added to the reaction mixture, and the resulting mixture was extracted with ethyl acetate (20 ml × 3). The combined organic extracts were washed with brine, dried over magnesium sulfate, and evaporated to afford the crude mixture of β-hydroxy ketones and β-diketones. Separation and purification by chromatography (silica gel, hexane–ethyl acetate) gave pure samples.

1 Reviews: I. Kuwajima and E. Nakamura, *Top. Curr. Chem.*, 1990, **155**, 1.

2 S. Murai, T. Aya, T. Renge and N. Sonoda, *J. Org. Chem.*, 1974, **39**, 858; G. M. Rubottom and M. I. Lopez, *J. Org. Chem.*, 1973, **38**, 2097; J. M. Conia and C. Girard, *Tetrahedron Lett.*, 1973, 2767; S. Murai, Y. Seki and N. Sonoda, *J. Chem. Soc., Chem. Commun.*, 1974, 1032; I. Ryu, K. Matsumoto, M. Ando, S. Murai and N. Sonoda, *Tetrahedron Lett.*, 1980, **21**, 4283; I. Ryu, M. Ando, A. Ozawa, S. Murai and N. Sonoda, *J. Am. Chem. Soc.*, 1983, **105**, 7192; I. Ryu, K. Matsumoto, Y. Kameyama, M. Ando, N. Kusumoto, A. Ogawa, N. Kambe, S. Murai and N. Sonoda, *J. Am. Chem. Soc.*, 1993, **115**, 12 330; I. Ryu, S. Murai and N. Sonoda, *J. Org. Chem.*, 1986, **51**, 2389; S. Aoki, T. Fujimura, E. Nakamura and I. Kuwajima, *J. Am. Chem. Soc.*, 1988, **110**, 3296; K. Ikura, I. Ryu, N. Kambe and N. Sonoda, *J. Am. Chem. Soc.*, 1992, **114**, 1520.

3 (*a*) Y. Ito, S. Fujii and T. Saegusa, *J. Org. Chem.*, 1976, **41**, 2073; (*b*) S. Lewicka-Pickut and W. H. Okamura, *Synth. Commun.*, 1980, **10**, 415; (*c*) K. I. Booker-Milburn, *Synlett*, 1992, 809; (*d*) K. I. Booker-Milburn and D. F. Thompson, *Synlett*, 1993, 592; (*e*) L. Blanco and A. Massauri, *Tetrahedron Lett.*, 1988, **29**, 7239; (*f*) S. Torii, T. Okamoto and N. Ueno, *J. Chem. Soc., Chem. Commun.*, 1978, 293; (*g*) N. Iwasawa, M. Funahashi, S. Hayakawa and K. Narasaka, *Chem. Lett.*, 1993, 545.

4 G. M. Rubottom, R. Marrero, D. S. Krueger and J. L. Schreiner, *Tetrahedron Lett.*, 1977, 4013; G. M. Rubottom, E. C. Beedle, C.-W. Kim and R. C. Mott, *J. Am. Chem. Soc.*, 1985, **107**, 4230.

5 M. Kirihara, S. Yokoyama, H. Kakuda and T. Momose, *Tetrahedron Lett.*, 1995, **36**, 6907; M. Kirihara, S. Yokoyama and T. Momose, *Synth. Commun.*, 1998, **28**, 1947.

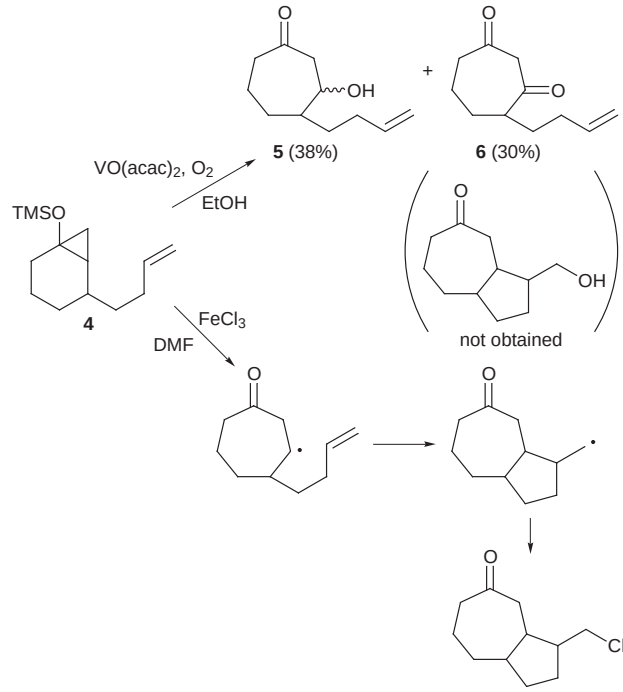

Scheme 4

Received in Cambridge, UK, 28th April 1998; 8/03178I

Electrochemical reduction of CCl_2F_2 on Nafion solid polymer electrolyte composite electrodes

E. Delli, S. Kouloumtzoglou, G. Kyriacou*† and C. Lambrou

Department of Chemical Engineering, Aristotle University of Thessaloniki, Thessaloniki 54006, Greece

The electrochemical reduction of CCl_2F_2 (CFC-12) was carried out at Pd, Au, Cu and Ag cathodes, which were chemically deposited on Nafion 117 (H^+ form) membrane; the main electrolysis product at −1.0 V *vs.* Ag/AgCl at Au, Pd and Cu was CH_4, with current efficiencies (CE) of 14, 15 and 47% respectively, while at Ag cathode, in addition to CH_4, a considerable quantity of CH_2F_2 (CE 60%) was also detected, which might be used as a new technology refrigerant.

The production of chlorofluorocarbons (CFCs) has been stopped since 1996, in line with the Montreal Protocol, because of their ability to react in ways that destroy tropospheric ozone.[1] At present, almost 2×10^6 tonnes of these compounds are stored in various freezing devices, the bigger percentage of which is CFC-12.[2] These large quantities must be destroyed or preferentially converted to other useful products. Recently Cabot and co-workers[3,4] achieved the electrosynthesis of trifluoroethene and difluoroethene from 1,1,2-trichloro-1,2,2-trifluoroethane (CFC-113) in organic solvents.

This work deals with the possible conversion of CFC-12 to non-polluting substances *via* electrochemical reduction at metallic electrodes which are deposited on Nafion 117 (H^+ form) membrane. These electrodes enable us to perform electrochemical reactions with reactants that are insoluble in water, without employing organic solvents.

For the metal deposition, aqueous 0.1 M solutions of $AgNO_3$, $HAuCl_4$, $Pd(OAc)_2$ and $CuSO_4$ were used, combined with 10% aqueous $NaBH_4$ solution, using the method previously described for copper.[5] The charged side of the metal surface of the membrane, having an apparent effective area of 2.35 cm^2 was in contact with CFC-12, while the other side was in contact with 2 M aqueous NaOH solution (10 cm^3), as shown in Fig. 1. As a reference, an Ag/AgCl electrode was used. The analysis of the products was performed by gas chromatography using a flame ionization detector and a Porapak QS 1/8 in, 4 m column at 120 °C.

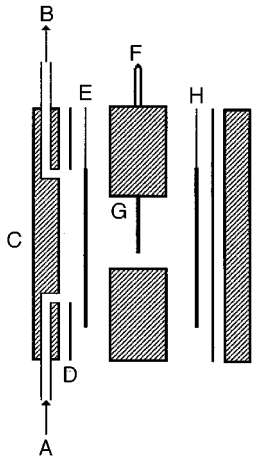

Fig. 1 Exploded view of the electrolysis cell: (A) gas inlet, (B) gas outlet, (C) PTFE gasket, (D) silicone screen spacer, (E) Nafion SPE electrode, (F) reference electrode, (G) electrolyte chamber and (H) Pt anode

The voltammogram at the Ag electrode, between −0.7 and −1.6 V *vs.* Ag/AgCl (Fig. 2), showed that the reduction of CCl_2F_2 was taking place at potentials more negative than −0. 8 V, while hydrogen was produced at cathodic potentials more negative than −1.3 V. This value is in accordance with hydrogen evolution at Ag wire at the same pH value.[6]

Based on the voltammetry results, constant potential electrolysis was performed in the region −0.8 to −1.6 V *vs.* Ag/AgCl. The main products of the electrolysis were CH_2F_2 and CH_4 at all potentials examined. CH_2F_2 is a compound of great practical importance, due to its application as a new technology refrigerant which does not cause ozone depletion.[7] Small amounts of $CHClF_2$, CH_3F and HCF_2CF_2H were also detected in the reaction products.

Fig. 3 illustrates the rate of CF_2H_2 production *vs.* cathodic potential where a sharp maximum was observed at about −1.4 V. The rate of CH_4 production was slightly increased at potentials more negative than −1.4 V. The CEs of CF_2H_2 and CH_4 formation at −1.4 V were 60 and 30%, respectively. Repeated experiments showed that the distribution of products was as shown by the curves of Fig. 3, with a reproducibility of about 15%. The form of these curves can be explained by a consecutive reaction mechanism corresponding to $CCl_2F_2 \rightarrow CH_2F_2 \rightarrow CH_4$.

Theoretical analysis of consecutive electrochemical reactions showed that the effect of potential on the selectivity and yield of the intermediate compound could be considered analogous to that of temperature in the conventional chemical reactions. In this case the selectivity of the intermediate product *vs.* potential

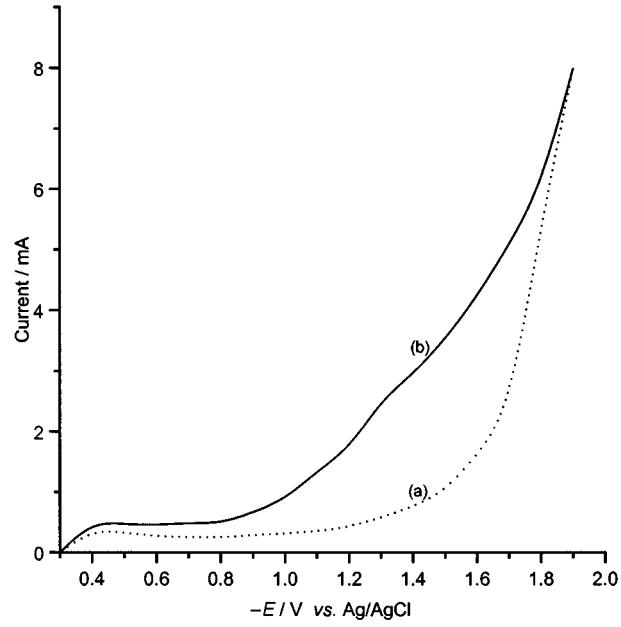

Fig. 2 Polarization curves at silver cathode, in 2 M KOH electrolyte at 10 mV s^{-1} (a) with N_2 and (b) with CFC-12

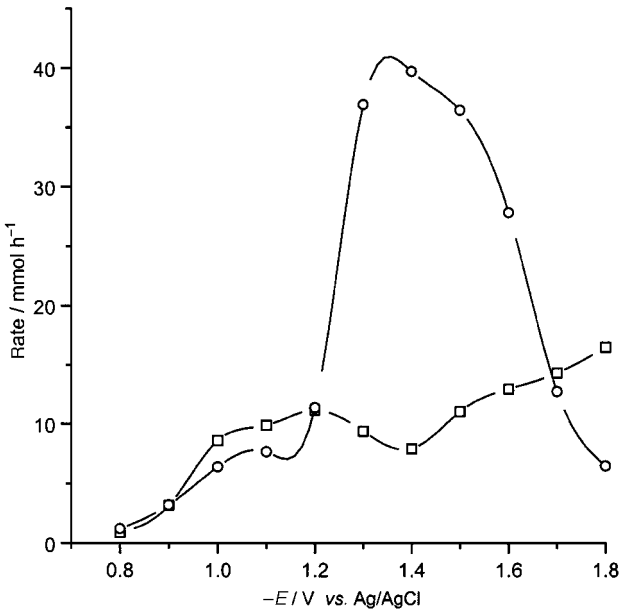

Fig. 3 Rate of (○) CH_2F_2 and (□) CH_4 production *vs*. cathodic potential at a silver electrode in 2 M KOH electrolyte

could show one or more maxima.[8] A similar consecutive reaction mechanism scheme was proposed for the hydrogenolysis of CCl_2F_2 in the gas phase.[9]

The electroreduction of CCl_2F_2 was also studied at −1.0 V *vs*. Ag/AgCl using Pd, Au and Cu electrodes. In all cases, the main product of the reduction was CH_4, with mean CEs of 14, 15 and 47%, respectively. The current density and time function shows that the current density stabilises after 30 min and remains stable for a long period of time. This implies that the electrode is not deactivated and the membrane is not destroyed. The current density at Ag, Cu and Pd was about 5 mA cm^{-2}, whereas at Au it is four times smaller.

Note and References

† E-mail: kyriakou@vergina.eng.auth.gr

1 M. J. Molina and F. S. Rowland, *Nature*, 1974, **249,** 810.
2 I. Kirk and D. Othmer, *Encyclopedia of Chemical Technology*, 4th edn, Wiley and Sons, New York, 1991, vol. 11, p. 508.
3 P. Cabot, M. Centelles, L. Segarra and J. Casado, *J. Electrochem. Soc*., 1997, **144,** 3749.
4 P. Cabot, M. Centelles, L. Segarra and J. Casado, *J. Electroanal. Chem*., 1997, **435,** 255.
5 S. Komatsu, M. Tanaka, A. Okumura and A. Kungi, *Electrochim. Acta*, 1995, **40,** 745.
6 D. Kyriacou, *Basics of Electroorganic Synthesis*, Wiley, New York, 1981, p. 114
7 W. Wojdon and M. George, *Hydrocarbon Process., Int. Ed.,* 1994, **73**, 107.
8 G. Sakellaropoulos, *AlChE J*., 1979, **25,** 781.
9 B. Coq, J. Cognion, F. Figueras and D. Tournigant, *J. Catal*., 1993, **141**, 21.

Received in Cambridge, UK, 4th June 1998; 8/04210A

A test for the reverse anomeric effect

Peter G. Jones, Anthony J. Kirby,*† Igor V. Komarov‡ and Peter D. Wothers

University Chemical Laboratory, Cambridge, UK CB2 1EW

Conformational preferences and the geometry at the anomeric centre of a 1,3-dioxane with a trialkylammonium group in the 2-position (stable because part of a 1-azaadamantane) are consistent with a small, normal anomeric effect.

The anomeric effect—the preference for an electronegative substituent X in the 2-position of a tetrahydropyran for the axial conformation (**1a**)—is a well-characterised exception to the usual rules of conformational analysis.[1,2] The reverse anomeric effect (RAE)[3]—an apparent increased preference of a positively charged electronegative substituent for the *equatorial* conformation (**1e**)—is thus an exception to the exception, and presents something of a conceptual problem. The simplest solution to the problem would be that the effect does not exist.[3–6] We report the conformational preferences of a novel sterically balanced system (general structure **2**) consistent with this conclusion.

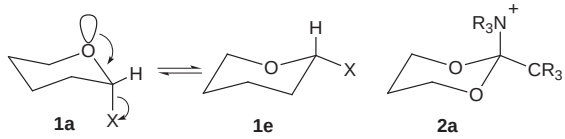

The normal anomeric effect can be understood in terms of a stereoelectronic effect involving the lone pair electrons of the ring oxygen: the stabilising n_O–$\sigma^*_{C–X}$ interaction (arrows in **1a**, possible only for the axial geometry) outweighing the steric preference for the equatorial position.[1,2] Through-bond interactions of this sort play an important role in controlling reactivity as well as conformation[7,8] and thus in the way we think about both. They should not depend on the charge on the electronegative substituent X—hence the conceptual problem.

Experimental support for the RAE is neither extensive, nor generally clear-cut. The best experimental evidence,[9] recently reconfirmed,[10] is that N-protonation of *N*-triacetyl-α-D-xylopyranosylimidazole **3a** leads to an increase in the (already

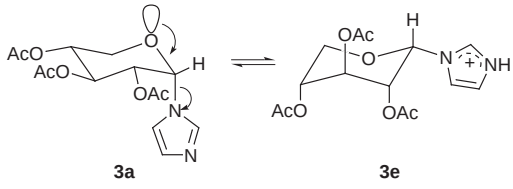

considerable) population of the $^1C_4$-conformation **3e**: corresponding to a RAE of 0.8–1.4 kcal mol^{-1}. On the other hand Perrin[5] concluded that the corresponding shift in the position of this equilibrium for a series of glucopyranosylamines could be accounted for on the basis of steric effects and a small, normal anomeric effect. (These results are not necessarily contradictory: the positions of such anomeric equilibria are known to depend on the structure of the sugar, with acetoxy groups in particular showing unusually small 1,3-diaxial interactions;[11] it has been suggested that the steric effect of an imidazole group may be increased on protonation.[5]) The most convincing evidence consistent with the operation of a small, normal anomeric effect comes from the NMR titration experiments of Fabian *et al.*,[6] which show that the axial imidazole is the more basic in an anomeric mixture of glucosylimidazoles.

We sought a direct experimental test for the existence of the RAE in a simple sterically balanced system, uncomplicated as far as possible by solvation effects. In order to maximise stereoelectronic effects we chose to work with the dioxane ring, and to set trialkylammonium, with a full positive charge on N, against an isosteric tertiary alkyl group. The problems involved are illustrated by the following sequence of results. Simple systems with X = R_3N^+ already have a strong steric preference for the equatorial conformation:[12] thus 2-trialkylammonium systems **4e**, although stable, are exclusively equatorial. But the sterically balanced system **5e** is not isolable: addition of Me_3N to the dioxocarbenium ion **6** probably gives **5a** as a kinetic product, but what we isolate is the pivalate ester **7**, formed by the alternative (S_N2) reaction shown (Scheme 1).

To encourage the three heteroatoms to stay together on the quaternary center of interest we embedded it in the azaadamantane structure **8**. The critical test for RAE *vs.* normal anomeric effect now becomes simply the conformational preference of the dioxane ring. The conformational equilibrium **8a**⇌**8e** is as far as possible sterically neutral: because the CH_3–N^+ bond is shorter than CH_3–C it will have a slight preference for the conformation (**8e**) favored by RAE. In solution we find a clear preference for a conformation closer to **8a**, and in the crystal the pattern of bond lengths at the 'anomeric' centre expected if a normal anomeric effect is operating. However, the evidence from two crystal structures shows that the conformational picture is not as simple as depicted by **8a**⇌**8e**.

In the ^{1}H NMR spectrum protons H^a and H^b of **8** show nuclear Overhauser effects[13] of 12.3% to the $^+NCH_3$ and 2.0% to the CCH_3 groups, respectively, and vicinal couplings (*J* 11.4, 5.6 Hz for H^a, *J* 2.4, 2.4 Hz for H^b) not far from the expected magnitudes for conformation **8a**. However, X-ray structure determinations[14] of two different salts show pronounced flattening of the dioxane ring at the two oxygen centres. This is the not unexpected result of steric interactions—almost equally severe in either chair conformation—between the two O–CH_2 bonds and the $^+$N–CH_3 and C–CH_3 groups (in **8a** and **8e**, respectively: indicated by the open arrows in Fig. 1). What *is* unexpected is that the conformations of the iodide and hydrogenfluoride salts in the crystalline state differ sig-

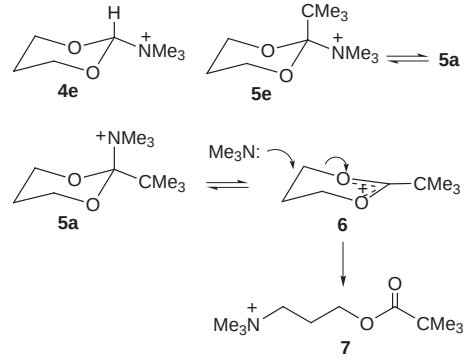

Scheme 1

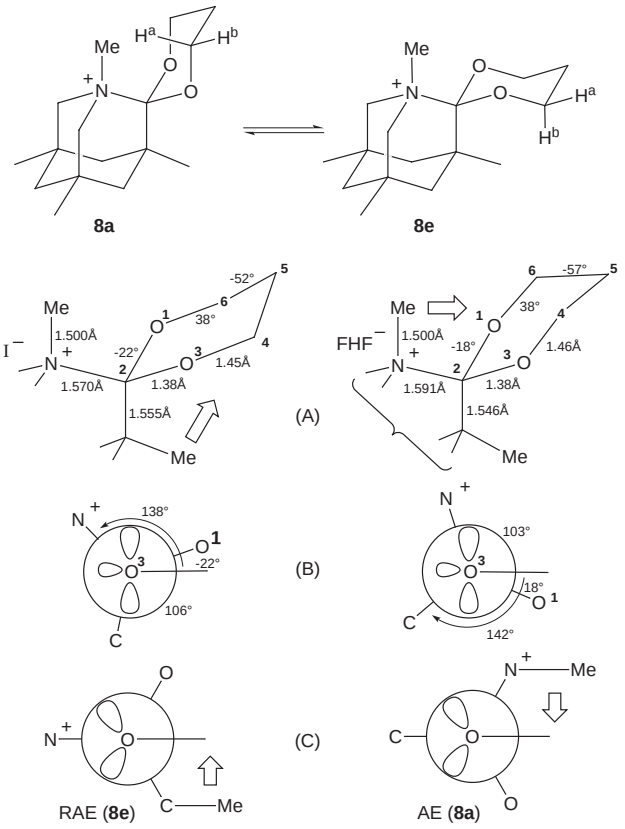

Fig. 1 Selected structural features at the anomeric centre of the iodide (left) and hydrogenfluoride (right) salts of **8**. The cation is formally (although not crystallographically) symmetrical about the mirror plane through C(2) and C(5) of the dioxane ring: mean values of bond lengths and angles are given. Individual bond lengths and angles have esd values of ±0.003 Å and 0.2°, respectively. (A) Observed conformations of the dioxane ring (in-ring torsion angles are given) and bond lengths at the anomeric centre. (B) Torsion angles at the anomeric centre, compared with (C) the geometry expected for a (hypothetical) system with normal bond angles showing the reverse (RAE) or normal (AE) anomeric effect. The open arrows represent major steric interactions responsible for flattening the dioxane chair of **8** (see the text).

nificantly, being closer in the former case to **8e** and in the latter to **8a**.

The differences are limited to the $(CH_2)_3$ chain of the dioxane ring: the structures are otherwise identical—and remarkable. The COC bond angles (120 ± 1.4°) show that the two dioxane oxygens are effectively sp²-hybridised. This, together with the large OCO bond angle (118.0 ± 0.5°) and very long C(2)–N^+ and short O–C(2) bonds at the anomeric centre [Fig. 1(A)] is consistent with a well-developed n_O–$\sigma^*_{C–N}$ interaction, and thus a normal anomeric effect, with C–N^+ bond breaking being well advanced in the ground state. (The extent of the effect shows very clearly why simpler systems like **5** are not viable synthetic targets.) The C(2)–N^+ bonds are in both cases close to parallel to p-type non-bonding electron pairs on oxygen, which allows relatively efficient p_O–$\sigma^*_{C–N}$ overlap: closer in the case of the hydrogenfluoride [Fig. 1(B)], which—presumably consequently—has the longer C(2)–N^+ bond. This lengthening of the bond to N^+ can be interpreted as the stereoelectronically most efficient means of relieving strain at the crowded anomeric centre: there is very little lengthening of the equally crowded C(2)–C bond.

The observed conformations of the dioxane ring of the cation **8** represent two different compromises between stereoelectronic effects and powerful steric forces. It is reasonable to expect a unique minimum energy conformation, so the difference in the crystalline state may be presumed to derive from anion-related packing forces.§ (Iodide and hydrogenfluoride differ markedly in size, shape and charge-density.) Since the conformation in solution is clearly closer to **8a** we conclude that there is no conclusive evidence for a reverse anomeric effect in this test system. As found by Perrin,[5] in a very different system, the observed conformations can be explained on the basis of steric effects and a small, normal anomeric effect.[15]

Notes and References

† E-mail: ajk1@cam.ac.uk
‡ Permanent address: Chemistry Department, Organic Chemistry Chair, Taras Shevchenko University, Kiev 252033 Ukraine.
§ The inference is clear that this difference in conformation is driven by a packing-induced ring-flip at C(5), the most flexible part of the system. The conformation of the rest of the dioxane ring must adjust to accommodate this change: ending up much the way it started, except that N^+ and C have changed places [Fig. 1(B)].

1 A. J. Kirby, *The Anomeric Effect and Related Stereoelectronic Effects at Oxygen*, Springer-Verlag, Berlin, 1983.
2 *The Anomeric Effect and Associated Stereoelectronic Effects*, *ACS Symp. Ser.*, ed. G. R. J. Thatcher, 1993, **539**.
3 C. L. Perrin, *Tetrahedron*, 1995, **51**, 11 901.
4 A. J. Kirby and N. H. Williams, in *Anomeric and Gauche Effects: Some Basic Stereoelectronics*, ref. 2, pp. 55–69.
5 C. L. Perrin and K. B. Armstrong, *J. Am. Chem. Soc*., 1993, **115**, 6825.
6 M. A. Fabian, C. L. Perrin and M. L. Sinnott, *J. Am. Chem. Soc*., 1994, **116**, 8398.
7 P. Deslongchamps, *Stereoelectronic Effects in Organic Chemistry*, Pergamon, Oxford, 1983.
8 A. J. Kirby, *Stereoelectronic Effects*, Oxford University Press, Oxford, 1996.
9 H. Paulsen, Z. Gyorgydeak and M. Friedmann, *Chem. Ber.*, 1974, **107**, 1590.
10 A. R. Vaino, S. S. C. Chan, W. A. Szarek and G. R. J. Thatcher, *J. Org. Chem.*, 1996, **61**, 4514.
11 Ref. 1, p. 13.
12 P. D. Wothers, PhD Thesis, University of Cambridge, 1996.
13 NMR spectra were measured in $CDCl_3$ on a Bruker 500 MHscz instrument. NOEs were obtained from NOE build-up curves according to K. Stott, J.H. Keeler, Q. N. Van and A. J. Shaka, *J. Magn. Reson*., 1997, **125**, 302.
14 *Crystal data* for **8** (iodide salt): $C_{16}H_{28}INO_2$, colourless tablet, 0.4 × 0.3 × 0.15 mm, monoclinic, *Cc*, a = 7.8145(6), b = 14.9324(12), c = 14.5044(14) Å, β = 96.171(8)° (at −100 °C), μ = 1.906 mm^{-1}, Z = 4. Final $wR2$ = 0.040, $R1$ = 0.018, S = 1.00 for 3349 reflections and 186 parameters. For **8** (hydrogenfluoride salt): $C_{16}H_{29}F_2NO_2$, colourless tablet, 0.6 × 0.6 × 0.3 mm, monoclinic, $P2_1/c$, a = 10.206(2), b = 11.797(3), c = 26.344(7) Å, β = 92.09(3)° (at −130 °C), μ = 0.098 mm^{-1}, Z = 8 (two independent molecules). Final $wR2$ = 0.129, $R1$ = 0.049, S = 1.02 for 5584 reflections and 395 parameters. The nitrogen atoms were clearly distinguished from their carbon counterparts at C2 (Fig. 1) by comparison with the R values and displacement parameters for a refinement with C and N transposed. For the iodide salt, which represents an extreme case (heavy-atom structure, non-centrosymmetric), refinement of a C/N disorder model gave the occupation factor 0.89(2) for the structure as reported, *i.e*. there is no significant component with C and N exchanged. CCDC 182/929.
15 We find further support for this conclusion in the crystal structures of two *gem*-diols, hydrates corresponding to the acetal **8** (N. Feeder, A. J. Kirby and I. V. Komarov, *J. Am. Chem. Soc*., in the press, and unpublished work). For both NH^+ and NMe^+ compounds the two O–H bonds adopt conformations corresponding to **8a**. Steric effects are reduced in these systems, and C–O–H angles are closer to tetrahedral values.

Received in Liverpool, UK, 9th June 1998; 8/04354J

A macrobicyclic Ag^{I}_3 cage encapsulating two cobalt(III) ions: synthesis, structure and reactivity

Takumi Konno,*[a]† Keiji Tokuda[a] and Ken-ichi Okamoto[b]

[a] *Department of Chemistry, Faculty of Engineering, Gunma University, Kiryu, Gunma, 376, Japan*
[b] *Department of Chemistry, University of Tsukuba, Tsukuba, Ibaraki 305, Japan*

Reaction of the S-bridged $Co^{III}_2Ag^{I}_3$ pentanuclear complex, $[Ag^{I}_3\{Co^{III}(aet)_3\}_2]^{3+}$ (1; aet = $NH_2CH_2CH_2S^-$), with paraformaldehyde in basic acetonitrile, followed by adding aqueous ammonia, produces the aza-capped complex, $[Ag^{I}_3\{Co^{III}(L)\}_2]^{3+}$ [2; L = $N(CH_2NHCH_2CH_2S^-)_3$] , in which two Co^{III} atoms are encapsulated in a macrobicyclic cage consisting of two aza-capped ligands L and three Ag^{I} atoms; 2 is converted to the aza-capped $Co^{III}_4Zn^{II}_4$ octanuclear complex, $[Zn^{II}_4O\{Co^{III}(L)\}_4]^{6+}$, by the reaction with I^- in the presence of ZnO and Zn^{2+} in water, retaining the chiral configuration of the aza-capped $[Co^{III}(L)]$ units.

Since the discovery of the formation of the aza-capped cage complex, $[Co(sepulchrate)]^{3+}$, by the facile condensation of formaldehyde and ammonia with $[Co(en)_3]^{3+}$ (en = $NH_2CH_2CH_2NH_2$),[1] similar preparative techniques have been applied to obtain analogous metal complexes with a macrobicyclic cage, which exhibit unique stereochemical and redox properties.[2–10] The cage complexes of this type have been derived from mononuclear metal complexes and thus contain only one metal ion. In order to expand the co-ordination chemistry of metal ions encapsulated in a macrobicyclic cage, it is desirable to introduce two or more metal ions in one cage. We report here the synthesis and structure of a new class of macrobicyclic cage complex encapsulating two cobalt(III) ions, $[Ag_3\{Co(L)\}_2]^{3+}$ [L = $N(CH_2NHCH_2CH_2S^-)_3$], together with its conversion to the $Co^{III}_4Zn^{II}_4$ octanuclear complex, $[Zn_4O\{Co(L)\}_4]^{6+}$.

Treatment of a dark purple acetonitrile solution of the S-bridged $Co^{III}_2Ag^{I}_3$ pentanuclear complex, $[Ag_3\{Co(aet)_3\}_2](BF_4)_3\cdot H_2O$ [**1**$(BF_4)_3\cdot H_2O$; aet = $NH_2CH_2CH_2S^-$],[11] with paraformaldehyde and triethylamine at room temperature gave a dark red solution, which turned dark purple upon the addition of aqueous ammonia. A dark purple powder [**2**$(NO_3)_3\cdot 4H_2O$] was isolated from the dark purple reaction solution by adding an aqueous solution of $NaNO_3$ (80% yield).‡ The absorption spectrum of **2** is quite similar to that of **1** over the whole region. In the ^{13}C NMR spectrum **2** gives three sharp signals at δ 34.64, 61.62, and 69.76, which is distinct from the two ^{13}C NMR signals at δ 36.64 and 51.41 observed for **1**.[11] From these facts and elemental analysis, it is assumed that **2** has an aza-capped $Co^{III}_2Ag^{I}_3$ pentanuclear structure in $[Ag_3\{Co(L)\}_2]^{3+}$ [L = $N(CH_2NHCH_2CH_2S^-)_3$]. **2** was optically resolved into its enantiomers, $(+)^{CD}_{580}$ and $(-)^{CD}_{580}$, by SP-Sephadex C-25 column chromatography using $[Sb_2(R,R\text{-tartrato})_2]^{2-}$ as eluent. The CD spectrum of $(-)^{CD}_{580}$-**2** corresponds well with that of the $\Delta\Delta$ isomer of **1**, which implies that the two [Co(L)] units in $(-)^{CD}_{580}$-**2** have the Δ configuration.

The structure of **2** was established by a single crystal X-ray analysis of the PF_6^- salt [**2**$(PF_6)_3\cdot H_2O$], which was prepared by adding an aqueous solution of $NaPF_6$ to the aqueous solution of **2**$(NO_3)_3\cdot 4H_2O$.§ The total occupancy factor of the PF_6^- anions implies that the entire complex cation **2** is trivalent. As shown in Fig. 1, the entire complex cation **2** contains two Co^{III} and three Ag^{I} atoms. Each Co^{III} atom is surrounded by an aza-capped hexadentate N_3S_3 ligand L to form an approximately octahedral $[Co^{III}(L)]$ unit. The two $[Co^{III}(L)]$ units are spanned by three Ag^{I} atoms, such that the three S–Ag–S linkages form a triple helical structure. As a result, the two Co^{III} atoms are encapsulated in a macrobicyclic metallo-cage, $[Ag^{I}_3(L)_2]^{3-}$, in which each of three Ag^{I} atoms is linearly coordinated by two S atoms from two aza-capped ligands L. Except for the presence of the two terminal aza caps, the overall structure of **2** is similar to that of the parent complex **1**.[11] In particular, the bond distances and angles around the Co^{III} atoms in **2** [average Co–S = 2.243(8) Å, Co–N = 2.02(3) Å, S–Co–S = 91.3(3)°, N–Co–N = 89(1)°] are in good agreement with those in **1** [average Co–S = 2.248(8) Å, Co–N = 2.03(3) Å, S–Co–S = 92.1(3)°, N–Co–N = 90(1)°]. However, the averaged Ag–S distance in **2** [2.417(8) Å] is *ca*. 0.04 Å longer than that found in **1** [2.378(8) Å]. Moreover, the S–Ag–S angles [average 177.9(4)°] in **2** are closer to 180° than those in **1** [average 174.6(3)°], which permits the slightly shorter Ag···Ag separations in **2** [average 2.956(4) Å], compared with the separations in **1** [average 3.029(3) Å].

The two [Co(L)] units in **2** have the same chiral configuration to form the $\Delta\Delta$ and $\Lambda\Lambda$ isomers; the former isomer is illustrated in Fig. 1. This is compatible with the fact that **2** was optically resolved into its enantiomers. In the crystal lattice the $\Delta\Delta$ and $\Lambda\Lambda$ isomers co-exist in a disordered manner with a site occupancy of 0.5, which indicates that crystal **2** is not a racemic compound but a solid solution.[12] All the six bridging S atoms are fixed to the *S* configuration for the $\Delta\Delta$ isomer and *R* for the $\Lambda\Lambda$ isomer. The helical structure due to three S–Ag–S linkages is left-handed for the $\Delta\Delta$ isomer and right-handed for the $\Lambda\Lambda$ isomer. These stereochemical properties are the same as those in **1**.[11] However, it should be noted that in **2** all the five-membered N,S-chelate rings adopt the *lel* conformation, which is in contrast to the fact that the *ob* conformation as well as the *lel* one has been found in **1**. All the six asymmetric N atoms in **2** have the *R* configuration for the $\Delta\Delta$ isomer and *S* for the $\Lambda\Lambda$ isomer.

Attempts to fit the S-bridged $Co^{III}_4Zn^{II}_4$ octanuclear complex, $[Zn_4O\{Co(aet)_3\}_4]^{6+}$,[13] with aza caps by a similar condensation reaction were unsuccessful, because of the decomposition of $[Zn_4O\{Co(aet)_3\}_4]^{6+}$ in basic conditions. Instead, the corresponding aza-capped complex, $[Zn^{II}_4O\{Co^{III}(L)\}_4]^{6+}$ (**3**), was successfully derived from **2** (Scheme 1). That is, treatment of **2** with a stoichiometric amount of NaI in the presence of excess ZnO and $Zn(NO_3)_2\cdot 6H_2O$ in water at

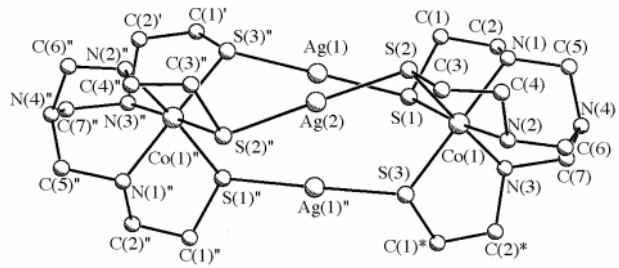

Fig. 1 A perspective view of the complex cation **2** (the $\Delta\Delta$ isomer) with the atomic labeling scheme. The overlapped $\Lambda\Lambda$ isomer is omitted for clarity

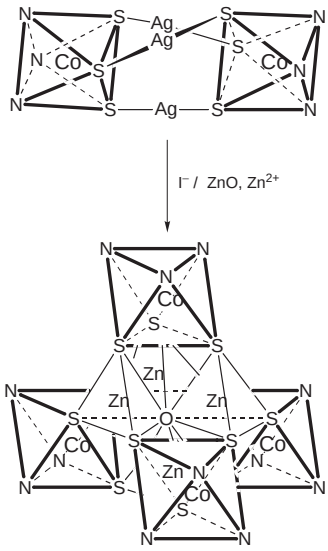

2

3

Scheme 1 Conversion of the $Co^{III}_2Ag^{I}_3$ pentanuclear structure in **2** to the $Co^{III}_4Zn^{II}_4$ octanuclear structure in **3**

room temperature gave a dark blue–purple solution, from which a black powder [**3**$(ClO_4)_6$·$7H_2O$] was isolated by adding an aqueous solution of $NaClO_4$ (50% yield).¶Compound **3** was characterized by (i) elemental and plasma emission spectral analyses, (ii) electronic absorption spectroscopy, the spectral features of which coincide well with that of $[Zn_4O\{Co(aet)_3\}_4]^{6+}$, and (iii) ^{13}C NMR spectroscopy which gives three sharp signals at δ 32.63, 61.15, and 69.51. The cyclic voltammogram of **3** at a glassy-carbon electrode in a 0.2 mol dm^{-3} aqueous $NaNO_3$ solution yields four consecutive redox couples (E = −0.43, −0.55, −0.62, and −0.75 V *vs*. Ag/AgCl, 100 mV s^{-1}). Similar redox behavior is characteristically observed for $[M_4O\{Co(aet)_3\}_4]^{6+}$ (M = Zn, Hg) having a *T*-symmetrical $Co^{III}_4M^{II}_4$ octanuclear structure.[13,14] Thus, it is confirmed that **3** has the S-bridged $Co^{III}_4Zn^{II}_4$ octanuclear structure in $[Zn^{II}_4O\{Co^{III}(L)\}_4]^{6+}$. Compound **3** was optically resolved into its enantiomers, $(+)^{CD}_{580}$ and $(-)^{CD}_{580}$, by SP-Sephadex C-25 column chromatography. Since the CD spectrum of $(-)^{CD}_{580}$-**3** is very similar to that of the ΔΔΔΔ isomer of $[Zn_4\{Co(aet)_3\}_4]^{6+}$, it is assumed that the four [Co(L)] units in $(-)^{CD}_{580}$-**3** have the Δ configuration. When ΔΔ-**2** was used as the starting complex, instead of the racemate of **2**, only the ΔΔΔΔ isomer of **3** was formed. This result indicates that the $Co^{III}_2Ag^{I}_3$ pentanuclear structure in **2** is converted to the $Co^{III}_4Zn^{II}_4$ octanuclear structure in **3** with retention of the chiral configuration of the [Co(L)] unit. Similar conversion reactions of **2** to other S-bridged polynuclear structures are currently under way.

Notes and References

† E-mail: konno@chem.gunma-u.ac.jp

‡ Anal. Calc. for **2**$(NO_3)_3$·$4H_2O$ = $C_{18}H_{50}Ag_3Co_2N_{11}O_{13}S_6$: C, 17.12, H; 3.99; N, 12.20; Co, 9.34; Ag, 25.63. Found: C, 17.05; H, 3.78; N, 12.25; Co, 9.28; Ag, 25.63%. VIS–UV spectrum in H_2O [ν/10^3 cm^{-1} (log ε/mol^{-1} dm^3 cm^{-1})]: 17.54 (2.97), 23.5 sh (2.90), 36.36 (4.62), 37.9 sh (4.6). The sh label denotes a shoulder. CD spectrum in H_2O [ν/10^3 cm^{-1} ($\Delta\varepsilon$/mol^{-1} dm^3 cm^{-1})]: 17.73 (−16.36), 22.62 (+21.72), 25.71 (−13.25), 30.12 (+14.77), 36.76 (−129.22), 42.92 (+83.04). ^{13}C NMR (500 MHz, D_2O, ppm from DSS): δ 34.64 (CH_2S), 61.62 ($NHCH_2$), 69.76 (NCH_2NH) (DSS = 4,4′-dimethyl-4-silapentane-1-sulfonate).

§ Anal. Calc. for **2**$(PF_6)_3$·H_2O = $C_{18}H_{44}Ag_3Co_2F_{18}N_8OP_3S_6$: C, 14.83, H; 3.04; N, 7.69. Found: C, 15.13; H, 3.03; N, 7.73%. *Crystal data* for **2**$(PF_6)_3$·H_2O: $C_{18}H_{44}Ag_3Co_2F_{18}N_8OP_3S_6$, M = 1457.3, tetragonal, space group $I\bar{4}2m$ (no. 121), a = 13.012(1), c = 24.707(2) Å, U = 4182.8(8) $Å^3$, Z = 4, μ(Mo-Kα) = 26.81 cm^{-1}, 1413 unique reflections at 296 K, R = 0.055 for 1025 reflections with $I > 1.5\sigma(I)$. For the atoms of the complex cation, Co(1), Ag(1), N(4), C(3) and C(4) were constrained to the special positions of symmetry *m* with a site occupancy factor of 0.5, while Ag(2) was constrained to the position of symmetry 2*mm* with a site occupancy factor of 0.25. The site occupancy factor of other atoms of the complex cation, except C(1) and C(2), was fixed to 0.5. The symmetry-expansion operation showed that a pair of enantiomers co-exist in each of four sites in the unit cell, sharing the C atoms of the N,S-chelate rings, besides the Ag, Co and aza-capped N atoms. CCDC 182/923.

¶ Anal. Calc. for **3**$(ClO_4)_6$·$7H_2O$ = $C_{36}H_{98}Cl_6Co_4N_{16}O_{32}S_{12}Zn_4$: C, 18.31, H;4.18; N,9.49; Co, 9.98; Zn, 11.07. Found: C, 18.16; H, 4.24; N, 9.76; Co, 10.25; Zn, 11.45%. VIS–UV spectrum in H_2O [ν/10^3 cm^{-1} (log ε/mol^{-1} dm^3 cm^{-1})]: 17.54 (3.31), 23.41 (3.41), 29.87 (4.32), 37.31 (4.94). CD spectrum in H_2O [ν/10^3 cm^{-1} ($\Delta\varepsilon$/mol^{-1} dm^3 cm^{-1})]: 17.18 (−19.44), 21.82 (+8.83), 26.68 (+12.40), 34.60 (−111.75), 39.52 (+120.15), 43.67 (+143.24). ^{13}C NMR (500 MHz, D_2O, ppm from DSS): δ 32.63 (CH_2S), 61.15 ($NHCH_2$), 69.51 (NCH_2NH).

1 I. I. Creaser, J. M. Harrowfield, A. J. Herlt, A. M. Sargeson, J. Springborg, R. J. Geue and M. R. Snow, *J. Am. Chem. Soc.*, 1977, **99**, 3181; I. I. Creaser, R. J. Geue, J. M. Harrowfield, A. J. Herlt, A. M. Sargeson, M. R. Snow and J. Springborg, *J. Am. Chem. Soc*., 1982, **104**, 6016.
2 L. R. Gahan, T. W. Hambley, A. M. Sargeson and M. R. Snow, *Inorg. Chem*., 1982, **21**, 2699.
3 H. A. Boucher, G. A. Lawrance, P. A. Lay, A. M. Sargeson, A. M. Bond, D. F. Sangster and J. C. Sullivan, *J. Am. Chem. Soc*., 1983, **105**, 4652.
4 J. M. Harrowfield, A. J. Herlt, P. A. Lay and A. M. Sargeson, *J. Am. Chem. Soc*., 1983, **105**, 5503.
5 L. R. Gahan, T. W. Hambley, J. M. Harrowfield, A. M. Sargeson and M. R. Snow, *J. Am. Chem. Soc*., 1984, **106**, 5478.
6 A. Hohn, R. J. Geue, A. M. Sargeson and A. C. Willis, *J. Chem. Soc., Chem. Commun.*, 1989, 1644.
7 L. R. Gahan, T. M. Donlevy and T. W. Hambley, *Inorg. Chem*., 1990, **29**, 1451.
8 T. M. Donlevy, L. R. Gahan, T. W. Hambley and R. Stranger, *Inorg. Chem*., 1992, **31**, 4376.
9 J. I. Bruce, L. R. Gahan, T. W. Hambley and R. Stranger, *Inorg. Chem.*, 1993, **32**, 5997.
10 R. Bhula, A. P. Arnold, G. J. Gainsford and W. G. Jackson, *Chem. Commun.*, 1996, 143.
11 T. Konno, K. Tokuda, T. Suzuki and K. Okamoto, *Bull. Chem. Soc. Jpn.*, 1998, **71**, 1049.
12 J. Jacques, A. Collet and S. H. Wilen, *Enantiomers, Racemates and Resolutions*, John Wiley & Sons Ltd., New York, 1981.
13 T. Konno, T. Nagashio, K. Okamoto and J. Hidaka, *Inorg. Chem.*, 1992, **31**, 1160.
14 Y. Kageyama, T. Konno, K. Okamoto and J. Hidaka, *Inorg. Chim. Acta*, 1995, **239**, 19.

Received in Cambridge, UK, 30th April 1998; 8/03257B

DNA alkylation sites of nitrogen mustards conjugated to polyamines and their implications for polyamine–DNA interactions

Paul M. Cullis,*† Louise Merson-Davies, Michael J. Sutcliffe and Richard Weaver

Department of Chemistry and the Centre for Mechanisms of Human Toxicity, Leicester University, Leicester, UK LE1 7RH

Polyamines conjugated to the nitrogen mustard chlorambucil increase the efficiency of DNA alkylation at N^7 of guanine by factors in the range 10^3 to 10^4; the sequence selectivity of this alkylation (the alkylation 'finger-print') is largely unchanged, which is consistent with flexible, electrostatic binding and incompatible with tight, sequence-specific binding of the polyamine moiety.

Polyamines are low molecular weight cations, essential for growth and differentiation,[1,2] that are present in high concentration in all cells. Polyamine–DNA interaction is associated with the physiological role of polyamines,[3–9] and there has been conflicting speculation concerning the nature and site of such interactions including reports of binding in the major[3] and minor groove,[4] spanning the minor groove[5,8] and theoretical studies that suggest interaction with the phosphate backbone or some sequence-specific interaction.[6] The crystal structure of a spermine–B-DNA complex[9] exhibits aspects of both charge–charge interactions with the phosphate backbone, and direct or water-mediated hydrogen bonds with bases and van der Waals interactions with hydrophobic regions. We previously determined the preferred cross-linking site on DNA for chlorambucil and both a spermidine– and spermine–chlorambucil conjugate.[10] The interstrand cross-link for each of these was at a 5'-GNC sequence within defined oligonucleotides, and this did not appear to be perturbed by the polyammonium moiety, despite a major enhancement of the efficiency of cross-linking. We interpreted this observation in terms of non-specific electrostatic interaction between the polyammonium cation and DNA. However, there may be a rather tight structural requirement for successful cross-linking which could be expressed in the second, interstrand alkylation step and which might potentially overwhelm the polyammonium ion binding preferences. Here we report the sequence specificities for mono-alkylation of DNA at N^7 of guanine shown by chlorambucil–polyamine conjugates and compare this to the known selectivity shown by chlorambucil itself.

The major alkylation site of DNA by chlorambucil is the N^7 of guanine bases.[11] The sequence selectivity in terms of guanine N^7 alkylation is demonstrated by converting these sites into strand breaks on treatment with hot piperidine and analysing the resulting fragments by denaturing polyacrylamide gel electrophoresis (PAGE). It has been shown that chlorambucil shows a significant sequence dependence in terms of the mono-alkylation sites,[11] with guanosine residues within runs of Gs being the most reactive.[12] In energetic terms, the enhanced reactivity in such regions as compared with isolated Gs represents a comparatively small difference, and a degree of alkylation at each G site can be detected on denaturing PAGE analysis of the cleavage products. In the case of the polyamine–chlorambucil conjugates it would be reasonable to expect that such small rate differences between the various alkylation reactions might be readily perturbed by the non-covalent binding interactions with the polyammonium moieties that are clearly promoting in some manner the eventual covalent step. We therefore anticipated that the alkylation selectivity could provide a potentially sensitive probe of the nature of the interaction between DNA and polyammonium cations. For example, it has been shown that the alkylation specificity of some aromatic nitrogen mustards is perturbed on conjugation to intercalators such as acridine, in a manner that reflects the acridine binding specificity.[13]

A DNA sequence of 276 base pairs was 5′-end-labelled and cleaved from linearised pBR322. Treatment of this double-stranded DNA with chlorambucil, or one of the polyamine–chlorambucil conjugates **1**–**4**,[14] followed by exposure of the

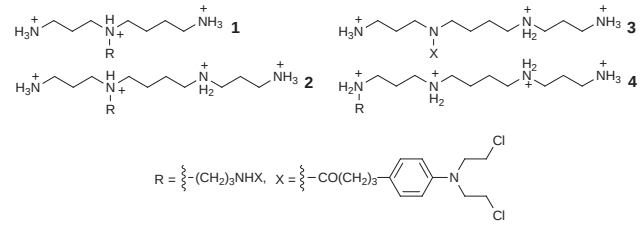

alkylated DNA to hot aqueous piperidine led to a family of DNA fragments that arise because of the lability of the DNA

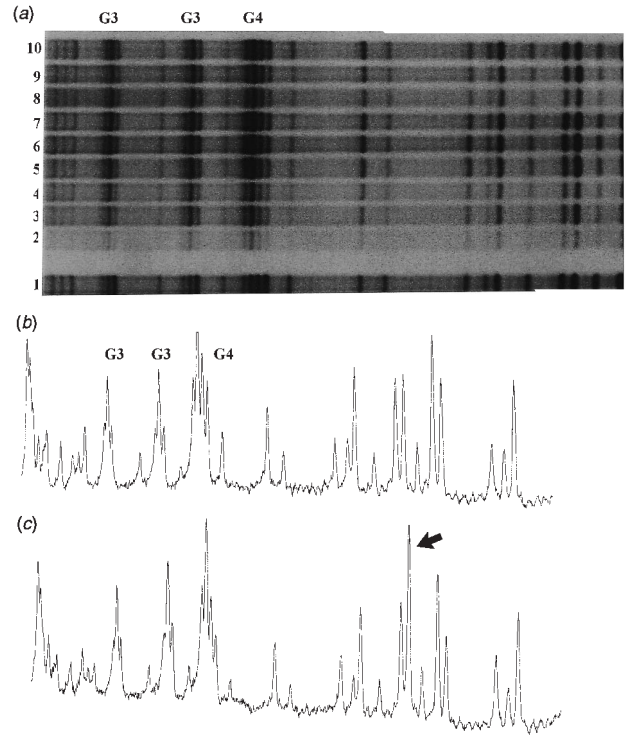

Fig. 1 (*a*) Autoradiograph of a denaturing PAGE gel showing sequence selective alkylation of guanine N^7 by chlorambucil–polyamne conjugates; lane 1: Maxam–Gilbert G track; lane 2: conjugate **1**; lane 3: conjugate **2**; lane 4: N^4–chlorambucil–spermidine conjugate (no linker); lane 5: conjugate **3**; lane 6: N^4–chlorambucil–norspermidine linked conjugate; lane 7: N^4–chlorambucil–homospermidine linked conjugate; lane 8: N^1–chlorambucil–spermidine linked conjugate; lane 9: conjugate **4** [0.1 μM; phosphorimager gel scan shown in (*c*)]; lane 10: DNA treated with chlorambucil [200 μM Phosphorimager gel scan shown in (*b*)]. DNA sequence: 5′-CGCGAGTACTCGGGCTTCACCGCTCGGGCTAG-AAGGGGTAGCCACTACAGCCGCTATATCCGCGGTCGTTGGCGT-GGACACCGC).

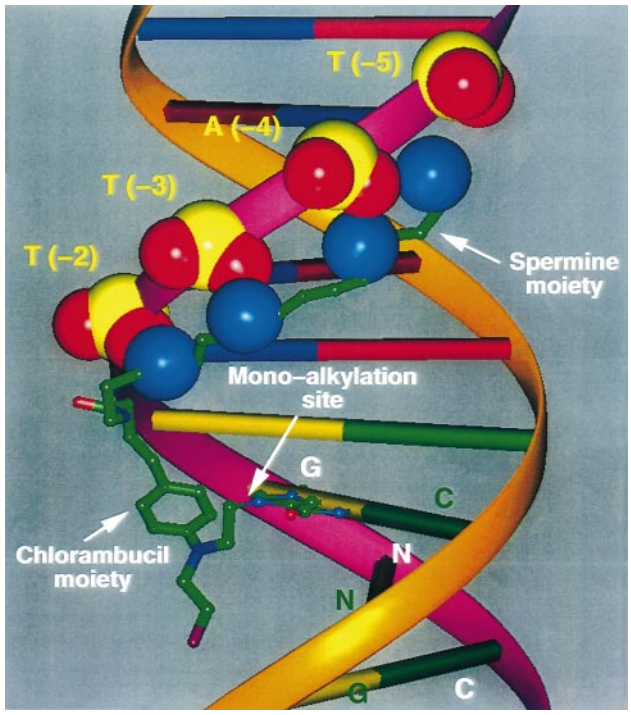

Fig. 2 Schematic representation of one of the molecular models for the B-DNA duplex d(CTATATTG**G**GCGGGATTAA)/d(TTAATCCCGCC-CAATATAG) monoalkylated by conjugate **4**, showing a low energy conformation in which the polyamine interacts with the phosphates 5′ to the alkylation site

alkylated at N^7 of the guanine bases. These cleavage products could be distinguished by denaturing PAGE (Fig. 1).[15] For chlorambucil the intensities of individual bands vary depending on the neighbouring sequence, confirming that guanine alkylation shows significant sequence selectivity, as reported previously[11] for a number of aromatic nitrogen mustards. More interestingly, all of the polyamine–chlorambucil conjugates show identical alkylation 'finger-prints', over a range of concentrations and molar ratios, but comparable levels of alkylation being observed with chlorambucil at 0.2 mM and conjugate **4** at 0.1 μM. Thus the presence of the polyamine moiety significantly enhances the alkylation by factors in the range 10^3 to 10^4 but does not alter the selectivity.

We have reported that chlorambucil and conjugate **1** hydrolyse and react with simple nucleophiles at the same rate and by the same mechanism.[16] The enhanced reactivity of the conjugates with DNA compared to chlorambucil is therefore a result of the polyamine–DNA interaction and in free energy terms this corresponds to about 23 kJ mol^{-1} (calculated for a 10^4-fold increased reactivity). The degree of enhanced reactivity, as with the observations on cross-linking efficacy, depends on the number of positive charges. The selectivity between different individual guanine bases is typically a factor of 2–3, which corresponds to an energy difference of 2–3 kJ mol^{-1}. The close similarity between the gel scans shown in Fig. 1, despite significant changes to the structure of the polyamine conjugate, must mean that the presence of the polyammonium moiety in the conjugate is able to enhance the reactivity at *all* of the guanine sites *and to the same extent.* A corollary to this is that although the polyammonium moiety has a high affinity for the DNA, it is not interacting at discrete sites and that there must therefore be significant mobility in the complex. This is consistent with a non-sequence selective, largely electrostatic interaction, and incompatible with sequence-specific H-bonded interactions. The similarities between the alkylation profiles is striking; however, close inspection of Fig. 1 does reveal a greater extent of alkylation by the polyammonium conjugate at a single site in the sequence GTCGTTG**G***CGTGGA [arrow in Fig. 1(*c*)]. This enhanced alkylation is reproducible but its structural basis is not evident.

Preliminary molecular modelling studies were performed to probe the nature of the interactions between DNA and these conjugates.[17] We have explored the covalent and non-covalent interactions of the spermine–chlorambucil conjugate by using B-DNA as the target and forming the first covalent link to N^7 of the more reactive guanine residue. Using this constrained adduct we have sought to probe three aspects: (i) whether the polyammonium moiety can make reasonable electrostatic interactions in such an adduct; (ii) whether the interactions are sensitive to the conjugate structure; and (iii) whether the cross-linking step involves much distortion of the conjugate or DNA structure. It is clear from the structure shown in Fig. 2 that in the adduct the polyammonium moiety can adopt a conformation that places the positive charges in good juxtaposition to the phosphate anions of the backbone. It is also clear that several alternative orientations of the polyammonium moiety are possible and of very similar energy. Similar interactions are possible for all of the conjugates **1**–**4** despite the structural differences, *e.g.* branched *vs.* non-branched. There is a trend in the strength of the interaction which increases with the number of positive charges. However, the differences in these values are close to the errors in the calculations and therefore should not be over-interpreted. It is very clear from the modelling that the formation of the cross-link requires appreciable distortion of the conjugate–DNA structure, and that this can be achieved whilst maintaining the interaction between the polyammonium moiety and the DNA. Thus the computational modelling is fully consistent with the conclusions drawn from the experiments.

Notes and References

E-mail: pmc@leicester.ac.uk

1 O. Heby, *Differentiation*, 1981, **19**, 1.
2 C.W. Tabor and H. Tabor, *Annu. Rev. Biochem.* 1984, **53**, 749.
3 H. R. Drew and R. E. Dickerson, *J. Mol. Biol.*, 1981, **151**, 535.
4 D. Bancroft, L. D. Williams, A. Rich and M. Egli, *Biochemistry*, 1994, **33**, 1073.
5 A.M. Liquori, L. Constantino, V. Crescenzi, V. Elia, E. Giglio, R. Puliti, S. M. DeSantis and V. Vitigliano, *J. Mol. Biol.*, 1967, **24,** 113.
6 I. S. Haworth, A. Rodger and W.G. Richards, *J. Biomol. Struct. Dyn.*, 1992, **10**, 195.
7 H-J. Schneider and T. Blatter, *Angew. Chem., Int. Ed. Engl.*, 1992, **31**, 1207.
8 K. Zakrzewski and B. Pullman, *Biopolymers*, 1986, **25**, 375.
9 L. W. Tari and A. S. Secco, *Nucleic Acids Res.*, 1995, **23**, 2065.
10 P. M. Cullis, L. Merson-Davies and R. Weaver, *J. Am. Chem. Soc.*, 1995,**117**, 8033.
11 K. W. Kohn, J. A. Hartley and W. B. Mattes, *Nucleic Acids Res.*, 1987, **15**, 10 531; A. Sunters, C. J. Springer, K. D. Bagshawe, R. L. Souhami and J. A. Hartley, *Biochem. Pharmacol.*, 1992, **44**, 59.
12 A. Pullman and B. Pullman, *Quart. Rev. Biophys.*, 1981, **14**, 289.
13 A. S. Prakash, W. A. Denny, T. A. Gourdie, K. K. Valu, P. D. Woodgate and L. P. Wakelin, *Biochemistry*, 1990, **29**, 9799.
14 Conjugate **1** was synthesised by our published method (G. M. Cohen, P. M. Cullis, J. A. Hartley, A. Mather, M. C. R. Symons and R. T. Wheelhouse, *J. Chem. Soc., Chem. Commun.*, 1992, 298) and the remaining conjugates by analogous methods (R Weaver, PhD Thesis, University of Leicester) to be published elsewhere. The identity and purity of all compounds were confirmed to be > 95% by NMR, HPLC and HRMS analysis. All are stable as HCl salts at −40 °C but hydrolyse at very similar rates ($t_{1/2}$ of *ca.* 20 min) in aqueous solutions at pH 7, 37 °C.
15 W.B. Mattes, J.A. Hartley and K.W. Kohn, *Nucleic Acids Res.*, 1986, **14**, 2971.
16 P. M. Cullis, R. E. Green and M. E. Malone, *J. Chem. Soc., Perkin Trans. 2*, 1995, 1503.
17 Molecular modeling and molecular dynamics refinements were performed on a duplex 19-mer canonical B-DNA, sequence d(CTA-TATTG**G**GCGGGATTAA)/d(TTAATCCCGCCCAATATAG) [where **G** is the first alkylation site], alkylated by **4** using InsightII and Discover (AMBER forcefield; MSI, San Diego, USA).

Received in Glasgow, UK, 5th May 1998; 8/03399D

Valence delocalisation in a strongly coupled (K_c = 10^{14}) molecule-bridged cyanodiiron(III,II) species

Michael Ketterle,[a] Jan Fiedler[b] and Wolfgang Kaim*[a]†

[a] *Institut für Anorganische Chemie, Universität Stuttgart, Pfaffenwaldring 55, D-70550 Stuttgart, Germany*
[b] *J. Heyrovsky Institute of Physical Chemistry, Academy of Sciences of the Czech Republic, Dolejškova 3, 18223 Prague, Czech Republic*

A hybrid between the Prussian Blue and Creutz–Taube mixed valent species is presented in the form of the bmtz-bridged bis[tetracyanoiron(+2.5)] complex 1^{3-} [bmtz = 3,6-bis(2-pyrimidyl)-1,2,4,5-tetrazine] which exhibits a very large comproportionation constant of 10^{14} and a delocalised structure, according to UV–VIS–NIR–IR spectroelectrochemistry in acetonitrile solution.

Mixed-valent compounds with electron transfer sites of similar or identical composition have become the focus of research for a number of reasons.[1–3] These include their function in biochemical systems,[1a] their model character for inner-sphere electron transfer,[1b,c] their special spectroscopic or other physical properties,[1d] their potential in 'molecular electronics'[1e] and their role as test systems for theory.[1d,f] Among the best known such mixed-valent coordination compounds are the cyanoferrate(III,II) species[2] Prussian Blue $Fe^{III}_4[Fe^{II}(CN)_6]_3$ and the molecule-bridged dinuclear Creutz–Taube ion $[(H_3N)_5Ru(\mu\text{-}pz)Ru(NH_3)_5]^{5+}$ (pz = pyrazine) with delocalised valencies of +2.5 for the equivalent metal centres.[1b,c,3] Although molecule-bridged diiron(III,II) species have been reported with various comproportionation constants K_c,[4] cyanoiron compounds like $[(NC)_5Fe(\mu\text{-}pz)Fe(CN)_5]^{5-}$ or $[(NC)_4Fe(\mu,\eta^4\text{-}bpym)Fe(CN)_4]^{3-}$, bpym = 2,2′-bipyrimidine, showed only small values $K_c < 10^3$ in aqueous media and thus weak metal–metal interaction.[5]

$$K_c = 10^{\Delta E/59\ mV} = [M^{(n-1)}]^2/[M^n][M^{(n-2)}] \qquad (1)$$
$$M^n + M^{(n-2)} \rightleftharpoons 2\ M^{(n-1)}$$

In the course of exploring the potentially tetrafunctional ligand bmtz [3,6-bis(2-pyrimidyl)-1,2,4,5-tetrazine][6] we discovered that the ligand can serve as an efficient bridge for promoting metal–metal interactions. The diruthenium compound $[(bpy)_2Ru(\mu,\eta^4\text{-}bmtz)Ru(bpy)_2]^{5+}$ [6] and the related $[(H_3N)_4Ru(\mu,\eta^4\text{-}bptz)Ru(NH_3)_4]^{5+}$ [7] showed unusually large K_c values of $> 10^{10}$ and $10^{15.0}$, respectively. Reacting bmtz with $FeCl_2$ and $[NEt_4]CN$‡,§ we have now found that the resulting redox system $[(NC)_4Fe(\mu,\eta^4\text{-}bmtz)Fe(CN)_4]^{n-}$ $\mathbf{1}^{n-}$ exhibits a diiron(III,II) state (n = 3) with an enormous stability constant K_c and delocalised vacancies.

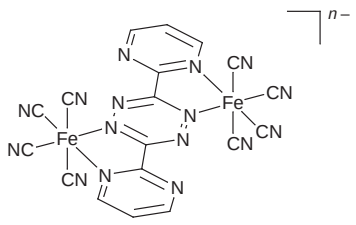

In MeCN–0.1 M $[NBu_4]PF_6$ the redox system $\mathbf{1}^{n-}$ exhibits four reversible one-electron waves between the n = 6 and n = 2 oxidation states at −1.92, −1.41, −0.32 and +0.52 V *vs.* $Fc–Fc^+$. The paramagnetic intermediate states with n = 3 (K_c = $10^{14.1}$) and n = 5 (K_c = $10^{8.7}$) could be characterised by EPR after *in situ* electrolytic generation from the diiron(II) precursor (n = 4).[8] Whereas the reduced form clearly shows a ligand-centered radical species at g = 1.998,[6–9] the oxidation produces an EPR signal with g components at 2.57, 2.44 and 1.78 in frozen acetonitrile solution. This result points to a metal-based oxidation process, implying the formation of a mixed-valent species.[1a,4] The corresponding data for the Creutz–Taube ion showed a similar splitting of g components at 2.799, 2.489 and 1.346,[10] the larger g anisotropy resulting from higher spin–orbit coupling effects from the heavier element (Ru *vs.* Fe).

Electronic absorption spectra of the n = 3, 4, 5 forms were obtained by spectroelectrochemistry in MeCN–0.1 M $[NBu_4]PF_6$, the isolated n = 4‡ and 3§ forms could also be studied separately. The intense (ε = 19 840 $dm^3\ mol^{-1}\ cm^{-1}$) metal-to-ligand charge transfer (MLCT) band at 831 nm of the diiron(II) form is shifted to higher energy, both on reduction and oxidation (Fig. 1). Oxidation to the mixed-valent state produces an asymmetrical intervalence charge transfer (IVCT) transition at 2245 nm. While the corresponding energy of 4450 cm^{-1} suggests weaker metal–metal interaction than in the Creutz–Taube ion,[3] the low intensity at ε = 750 $dm^3\ mol^{-1}\ cm^{-1}$ reflects the bis-chelate nature of the system with a chelate-enforced orientation unfavourable for orbital overlap. It was shown previously[7,11] that the IVCT features in dinuclear complexes with related bis(bidentate) bridging ligands exhibit very low-intensity IVCT bands in spite of large comproportionation constants K_c.

The question of localisation or delocalisation in mixed-valent complexes in solution may be most elegantly answered by vibrational spectroscopy.[12,13] On the corresponding time scale of about 10^{-12} s the appearance of averaged bands in relation to the neighbouring oxidation states suggests delocalisation whereas the appearance of separate or broadened features indicates localisation. The redox system $\mathbf{1}^{n-}$ was thus studied in the cyanide stretching region for n = 3, 4 and 5 (Fig. 2). The direction of shifts of the typically single band (very close A_1, B_1 and B_2 features) corresponds to charge alteration,[11–13] however, the oxidation to a metal-based mixed-valent species and the

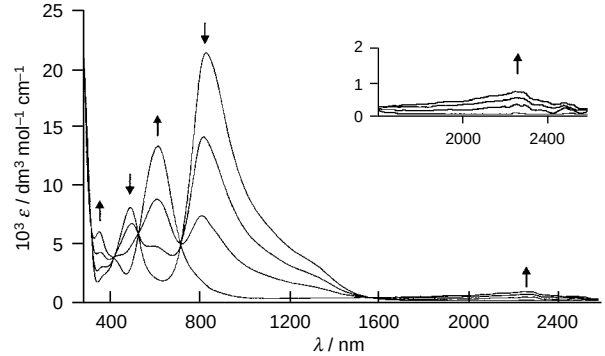

Fig. 1 UV–VIS–NIR spectroelectrochemical response of the $\mathbf{1}^{4-}$ ion (831 and 489 nm) on one-electron oxidation (2245, 613 and 354 nm) in MeCN–0.1 M $[NBu_4]PF_6$

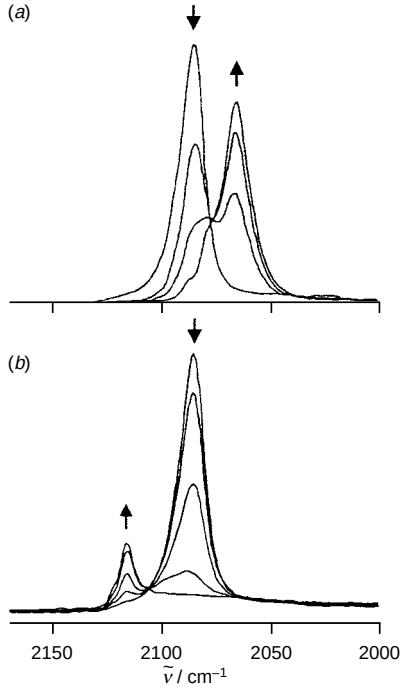

Fig. 2 IR-spectroelectrochemical response of the $\mathbf{1}^{4-}$ ion (ν_{CN} = 2085 cm^{-1}) on one-electron reduction (*a*) (2064 cm^{-1}) and oxidation (*b*) (2116 cm^{-1}) in MeCN–0.1 M [NBu_4]PF_6

reduction to a ligand-centered radical complex produce rather similar amounts of high- and low-energy shifts, respectively. As noted previously,[11] such band energy differences are thus not suitable to unambiguously clarify the site of electron addition or removal. However, the appearance of only one albeit intensity-diminished CN stretching band at an intermediate value after one-electron oxidation clearly confirms the delocalised nature of the mixed-valent Fe_2[2,5] species $\mathbf{1}^{3-}$ in agreement with the very large K_c value and the relatively narrow IVCT band ($\Delta\nu_{\frac{1}{2}}$ = 1200 cm^{-1}). Further studies of this and related systems will also focus on the solid state properties of such materials.

We thank Deutsche Forschungsgemeinschaft and Volkswagen Foundation for support.

Notes and References

† E-mail: kaim@iac.uni-stuttgart.de

‡ A solution of 940 mg (6.0 mmol) [NEt_4]CN in 50 ml MeOH was slowly added to a mixture containing 60 mg (0.25 mmol) bmtz[6] and 190 mg (1.5 mmol) $FeCl_2$ in 50 ml MeOH. After completion of the reaction the green solution was concentrated and the product precipitated by adding acetone and diethyl ether. Recrystallization from EtOH–Et_2O–acetone (1 : 6 : 3) yielded 35% of [NEt_4^+]$_4$ [$\mathbf{1}^{4-}$] as black microcrystals. Correct C, H, N analysis; ^{1}H NMR (CD_3OD): δ 9.67 (dd, H^4), 7.56 (dd, H^5), 8.93 (dd, H^6). UV–VIS (MeCN): λ_{max} = 831 nm (ε = 19 840 dm^3 mol^{-1} cm^{-1}).

§ 50 mg (0.05 mmol) of [NEt_4^+]$_4$[$\mathbf{1}^{4-}$] were oxidized electrolytically at a platinum electrode in MeCN–0.1 M [NBu_4]PF_6. The reaction was monitored by UV–VIS spectroscopy. Precipitation with diethyl ether and washing twice with THF yielded 10 mg (12%) of deep blue [NBu_4^+]$_3$[$\mathbf{1}^{3-}$], identified *via* EPR, IR and UV–VIS–NIR spectroscopy.

1 (*a*) W. Kaim, W. Bruns, J. Poppe and V. Kasack, *J. Mol. Struct.*, 1993, **292**, 221; (*b*) H. Taube, *Ann. N.Y. Acad. Sci.*, 1978, **313**, 481; (*c*) D. Astruc, *Electron Transfer and Radical Processes in Transition Metal Chemistry*, VCH, New York, 1995; (*d*) *Mixed Valency Systems—Applications in Chemistry, Physics and Biology*, ed. K. Prassides, Kluwer Academic Publishers, Dordrecht, 1991; (*e*) M. D. Ward, *Chem. Soc. Rev.*, 1995, **34**, 121; (*f*) N. S. Hush, *Coord. Chem. Rev.*, 1985, **64**, 135.
2 H. Vahrenkamp, A. Geiss and G. N. Richardson, *J. Chem. Soc., Dalton Trans.*, 1997, 3643.
3 C. Creutz, *Prog. Inorg. Chem.*, 1983, **30**, 1.
4 D. Astruc, *Acc. Chem. Res.*, 1997, **30**, 383; B. A. Etzenhouser, M. D. Cavanaugh, H. N. Sprugeon and M. B. Sponsler, *J. Am. Chem. Soc.*, 1994, **116**, 2221; H. S. Mountford, L. O. Spreer, J. W. Otvos, M. Calvin, K. J. Brewer, M. Richter and B. Scott, *Inorg. Chem.*, 1992, **31**, 717.
5 F. Felix, U. Hauser, H. Siegenthaler, F. Wenk and A. Ludi, *Inorg. Chim. Acta*, 1975, **15**, L7; F. Felix and A. Ludi, *Inorg. Chem.*, 1978, **17**, 1782; K. J. Brewer, W. R. Murphy, Jr. and J. D. Petersen, *Inorg. Chem.*, 1987, **26**, 3376.
6 W. Kaim and J. Fees, *Z. Naturforsch., Teil B*, 1995, **50**, 123.
7 J. Poppe, M. Moscherosch and W. Kaim, *Inorg. Chem.*, 1993, **32**, 2640.
8 E. Waldhör, J. Poppe, W. Kaim, E. Cutin, M. Garcia Posse and N. E. Katz, *Inorg. Chem.*, 1995, **34**, 3093; E. Waldhör, W. Kaim, J. A. Olabe, L. D. Slep and J. Fiedler, *Inorg. Chem.*, 1997, **36**, 2969.
9 W. Kaim, *Coord. Chem. Rev.*, 1987, **76**, 187.
10 A. Stebler, J. H. Ammeter, U. Fürholz and A. Ludi, *Inorg. Chem.*, 1984, **23**, 2764.
11 W. Kaim, W. Bruns, S. Kohlmann and M. Krejcik, *Inorg. Chim. Acta*, 1995, **229**, 143.
12 T. T. Chin, S. R. Lovelace, W. E. Geiger, C. M. Davis and R. N. Grimes, *J. Am. Chem. Soc.*, 1994, **116**, 9359.
13 W. Bruns, W. Kaim, E. Waldhör and M. Krejcik, *J. Chem. Soc., Chem. Commun.*, 1993, 1868; W. Bruns, W. Kaim, E. Waldhör and M. Krejcik, *Inorg. Chem.*, 1995, **34**, 663.

Received in Basel, Switzerland, 5th June 1998; 8/04279I

Effects of metal ion complexation on the spiropyran–merocyanine interconversion: development of a thermally stable photo-switch

James T.C. Wojtyk,[a] Peter M. Kazmaier[b] and Erwin Buncel*[a]†

[a] *Department of Chemistry, Queen's University, Kingston, Canada K7L 3N6*
[b] *Xerox Research Center of Canada, Mississauga, Canada L5K 2A1*

Spectrophotometric absorption and fluorescence measurements of spiropyrans 2 and 3 modified with chelating functionalities, in the presence of Ca^{2+} and Zn^{2+}, provide evidence of a thermally stable spiropyran–merocyanine photoswitch that is modulated by the metal cations.

The potential application of spiropyran–merocyanine equilibria (SP⇌MC), *e.g.* **1a⇌1b**, in molecular devices (sensors, switches, signal transducers) has led to burgeoning activity aimed at exploitation of these systems.[1] A conceptually attractive possibility is the modification of the spiropyran moiety to enable chelation by metal ions and preferentially, stabilize the open MC form.[2] Other approaches to a molecular switch exploit the photoactive anthracene moiety bound to an aza crown ether which upon irradiation undergoes photocyclisation to form a cryptand, with the forward and the thermal reverse reactions strongly affected by metal cations.[3] One can thus envisage a photosensitive molecular switch with selectivity for particular metal cations. However, none of the studies reported to date have provided the necessary requirements[4] of a molecular switch: two thermodynamically stable states, or bistability, with facile interconversion between the two states.

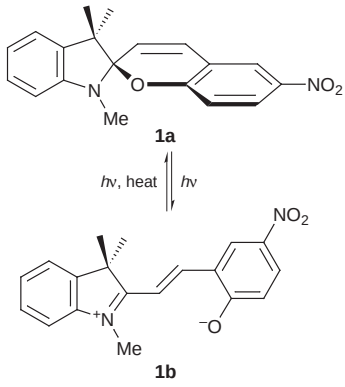

Following our previous studies of SP⇌MC systems and structural/solvent changes thereupon,[5] here we report our results on intramolecular electrostatic bridging in molecules **2** and **3**, *via* addition of a divalent metal ion to stabilize the MC form from thermal decay. Furthermore, the open MC forms of these molecules undergo the ring closure back-reaction through photo-activation at wavelengths appreciably different from the SP→MC light irradiation. Evidence for a dual wavelength photoactivation molecular switch is presented.

Spiropyrans **2** and **3** were synthesized by reaction of 2,3,3-trimethylindolenine with β-iodopropionic acid[6] and γ-sultone, respectively, followed by condensation with 5-nitrosalicaldehyde in the presence of Et_3N and were fully characterized. Studies on the effects of $CaCl_2$ and $ZnCl_2$ on the SP⇌MC process for **2**, **3** and **1a** as a control were conducted in acetone. Following the injection of 1, 2, 5 and 10 equiv. of the dry metal halide salt in acetone into the cuvette containing an acetone solution of the SP (1×10^{-5} M), the cuvette was

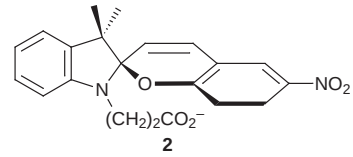

2

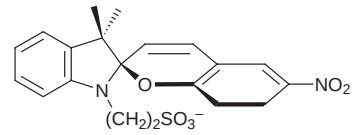

3

irradiated with a 15 W UV lamp (λ = 254 nm) for 1 min; the MC→SP reaction was monitored spectrophotometrically, scanning at 1 min intervals over a period of 30 min at 25 °C.

A control experiment on the decay of the MC form (λ_{max} = 572 nm) of **1** showed a first-order process, $k_{obs} = 7.30\times 10^{-3}$ s^{-1} [Fig. 1(*a*)], and addition of $CaCl_2$ had no effect on the rate or on the nature of the spectra. However, addition of $ZnCl_2$ resulted in the appearance of two distinct photo-reversible species: one corresponding to the free MC (λ_{max} = 566nm) and the other to a MC–Zn^{2+} complex (λ_{max} = 502 nm). Spectra [Fig. 1(*b*)] generated in the presence of 10:1 ratio of $ZnCl_2$:**1** showed that the amount of the MC–Zn^{2+} complex depended on the $ZnCl_2$:SP ratio. Furthermore, there was a significant decrease in the rate constant for MC decay, from $k_{obs} = 7.3\times 10^{-3}$ s^{-1} when $[Zn^{2+}] = 0$ to $k_{obs} = 3.3\times 10^{-3}$ s^{-1} when $ZnCl_2$:**1** = 10:1. A similar hypsochromic shift was observed upon addition of $ZnCl_2$ or $CaCl_2$ to sodium *p*-nitrophenoxide in acetone, with λ_{max} shifting from 428 nm when $[M^{2+}] = 0$, to 310 nm upon addition of 1 equiv. of MCl_2. Addition of either

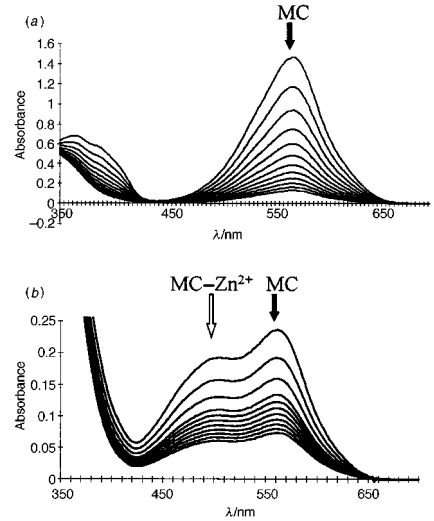

Fig. 1(*a*) Spectra illustrating the first order thermal reversion of the MC form **1b** at 25 °C in acetone (scanning at 1 min intervals). (*b*) Thermal reversion of the free and complexed forms of **1b** (MC and MC–Zn^{2+}) in the presence of $ZnCl_2$:**1** = 10:1.

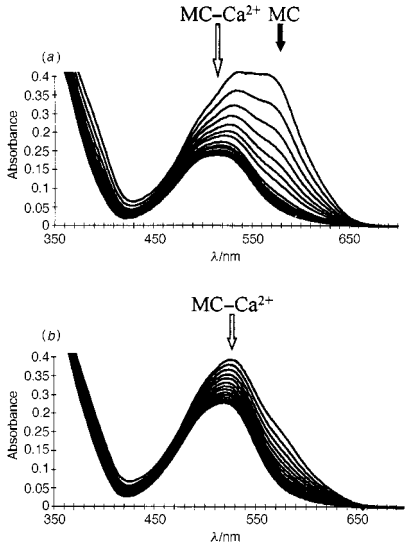

Fig. 2 Illustration of the thermal reversion of the MC and MC–Ca^{2+} forms of **2** in the presence of (*a*) 1 and (*b*) 10 equiv. $CaCl_2$

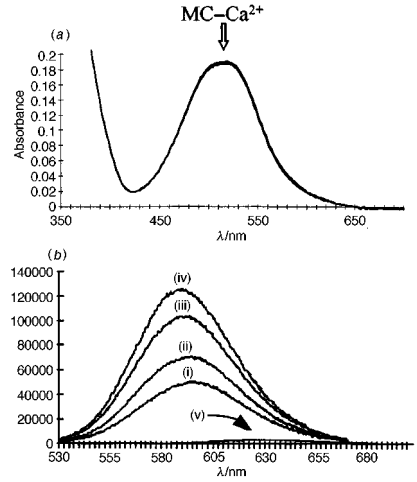

Fig. 3 (*a*) Overlay spectra illustrating the stabilization of the MC–Ca^{2+} form of **3** to thermal reversion in the presence of $CaCl_2$:**3** = 1:1. (*b*) Emission spectra (λ_{ex} = 520 nm) of the MC–Ca^{2+} form of **2** with increasing Ca^{2+}:SP ratios of (i) 1:1, (ii) 2:1, (iii) 5:1 and (iv) 10:1 compared to (v) MC.

metal salt to *p*-nitrophenol had no effect on the absorption spectra, which points to complexation of M^{2+} to the phenoxide moiety in the case of **1b** as the cause of the spectral changes.

For **2** in the absence of metal ion, the first-order decay of the MC form (λ_{max} = 572 nm) occurred with $k_{obs} = 20.0 \times 10^{-3}$ s^{-1} . Addition of Zn^{2+} generated a new photo-reversible peak (λ_{max} = 502 nm) with peak intensity and k_{obs} both being dependent on added [$ZnCl_2$]: $k_{obs} = 9.70 \times 10^{-3}$ s^{-1} for a 5:1 ratio of $ZnCl_2$:**2.** Addition of Ca^{2+} similarly generated a new photo-reversible peak at λ_{max} = 520 nm, the intensity and k_{obs} being dependent on added Ca^{2+} [Fig. 2(*a*),(*b*)]: $k_{obs} = 9.03 \times 10^{-3}$ s^{-1} for $CaCl_2$:**2** = 5:1, *i.e.* half the initial value.

The above results show that introduction of a chelating moiety onto the SP indoline ring results in an electrostatic bridge being formed that inhibits the thermal reversion of the MC form to the SP. In contrast to the lack of effect of Ca^{2+} on ring closure with control SP **1,** Ca^{2+} had a significant effect on the ring-closure of **2**. In addition, the contrasting k_{obs} values and λ_{max} for MC–Ca^{2+} and MC–Zn^{2+} complexes of **2** and the free MC forms demonstrate that stabilization of the MC form to thermal reversion through complexation is metal-dependent.

Similar experiments with **3** showed totally different behaviour. With a 1:1 ratio of Ca^{2+} and Zn^{2+}, complete stabilization of the MC form towards thermal decay was observed [Fig. 3(*a*)], no free MC being detected. The photo-stable form was found to persist for at least three days in the dark but exposure to visible light resulted in rapid decay of the spectrum of the complex.

Fluorescence measurements provided further information on the roles of Ca^{2+} and Zn^{2+} complexation with the MC form of **2** and **3**. As shown in Fig. 3(*b*), the fluorescence intensity increased on increasing the metal halide concentration. Moreover, Fig. 3(*b*) illustrates the overlapped emission spectra using excitation wavelengths of 520 nm for the MC–Ca^{2+} complex (for the MC–Zn^{2+} complex, λ_{oxc} = 502 nm). These observations reveal two main features which inherently facilitate application of these MC–M^{2+} complexes to optical data storage. The first is that fluorescence of the complexed forms is more intense compared to the free MC form, which fluoresces only weakly at these wavelengths. Secondly, the fact that fluorescence occurs at 587 nm for both Ca^{2+} and Zn^{2+} complexed forms, and that the absorption and fluorescence envelopes do not overlap, eliminates the possibility of 'cross-talk' and points to the suitability of fluorescence as the method of choice for 'reading' data that has been 'written' into these systems.

In order to investigate the light-induced reversion of the metal-complexed MC form to SP, a solution of **3**–Ca^{2+} was irradiated continuously with a 520 nm light source. The measured fluorescence intensity decreased gradually over a 30 min period, signifying reversion to the closed SP form. Since the above UV–VIS measurements have shown that the MC form of **3** does not decay over a three day period, this reversion of the complexed MC to the SP form must be a photo-induced process. Clearly, the reversion would be more efficient upon irradiation at shorter wavelengths. Hence switching between the colorless SP and the colored MC–M^{2+} forms can be modulated *via* irradiation at two wavelengths: SP→MC–M^{2+}, 254 nm; MC–M^{2+}→SP, 520 nm (or lower λ).

The results of this work have shown that the MC form of **3** has been stabilized towards thermal reversion, a key requirement of optical data storage systems.[4] Importantly, this system exhibits bistability at room temperature and is photo-switchable with two different light energies.

In conclusion, this report documents the first thermally stable SP–MC photo-switch *via* intramolecular bidentate metal ion chelation. Further investigations are ongoing into the effects of alkyl chain length and metal ion complexation ability in stabilizing the MC form. Optimization, *via* molecular modeling, enforcing ligand conformation and varying the heteroatom substitution and the nature of the metal, may lead to a prototypical device based on these systems.

The authors thank the Natural Sciences and Engineering Research Council of Canada for support of this research.

Notes and References

† E-mail: buncele@chem.queensu.ca

1 *Photochromism: Molecules and Systems*, ed. H. Durr and H. Bouas-Laurent, Elsevier, London, 1992; B. L. Feringa, W. F. Jager and B. de Lange, *Tetrahedron*, 1993, **49**, 37 and 8267; A. S. Dvornikov, J. Malkin and P. M. Rentzepis, *J. Phys. Chem*., 1994, **98**, 6746.

2 T. Tamaki and K. Ichimura, *J. Chem. Soc., Chem. Commun*., 1989, 1477; M. Priegh, F.-Y. Lin, K. Z. Ismail and S. G. Weber, *J. Chem. Soc., Chem. Commun*., 1995, 2091; M. Inouye, K. Akamatsu and H. Nakazumi, *J. Am. Chem. Soc*., 1997, **119**, 9160.

3 J. H. R. Tucker, H. Bouas-Laurent, P. Marsau, S.W. Riley and J.-P. Desvergne, *Chem. Commun*., 1997, 1165.

4 D. Rouvary, *Chem. Br*., 1998, **34**, 26; S. Janicki and G. B. Schuster, *J. Am. Chem. Soc*., 1995, **117**, 8524; F. Pina, M. J. Melo, M. Maestri, R. Ballardini and V. Balzani, *J. Am. Chem. Soc*., 1997, **119**, 5556.

5 S.-R. Keum, M.-S. Hur, P. M. Kazmaier and E. Buncel, *Can. J. Chem*., 1991, **69**, 1940; S.-R. Keum, K.-B. Lee, P. M. Kazmaier and E. Buncel, *Tetrahedron Lett*., 1994, **35,** 1015.

Received in Cambridge, UK, 28th April 1998; revised manuscript received, 22nd June 1998; 8/04908D

Reaction in supercritical CO_2; an intercalation of 4-phenylazoaniline between layers of montmorillonite pillared with tetramethylammonium ions

Ryo Ishii,*† Hideo Wada and Kenta Ooi

Shikoku National Industrial Research Institute, 2217-14 Hayashi-cho, Takamatsu-shi, Kagawa, 761-0395, Japan

The intercalation reaction of 4-phenylazoaniline into montmorillonite pillared with tetramethylammonium ions has been performed successfully in supercritical CO_2 (SCC) at T = 313 K (P = 15 MPa), demonstrating that SCC is a better medium than organic solutions for intercalating large amounts of guest molecules into a host compound without the contamination of solvent.

The host–guest chemistry of intercalation systems have attracted attention for synthesis strategies for nanostructured functional materials.[1] These syntheses are usually achieved by promoting the intercalation reaction in the liquid phase. However, the solvent molecules inevitably participate in diffusion and adsorption of solutes in the reaction. A supercritical fluid (SCF) has several advantages for such an adsorption reaction with porous materials. First, solute transfer through the solid–SCF interface is smooth because of the low surface tension of SCF as well as its low viscosity. Second, the adsorption amount can be varied by controlling the dissolving power for the solute *via* the temperature and the pressure of the SCF. Third, the competitive adsorption of the solvent on the porous material is rare because of the weaker interactions between the solid surface and solvent molecules in a supercritical state than in the interaction in the liquid state. For material processing, these advantages lead us to anticipate the development of composite materials containing a large amount of functional adsorbate in the pores, but little contaminant by solvent molecules. Here we present a new intercalation technique using supercritical CO_2 (SCC) as the reaction medium. 4-Phenylazoaniline (PAA) was used as the intercalating molecule and montmorillonite (Mnt) pillared with tetramethyl ammonium (TMA) ions as the layered host (TMA-Mnt). This composite material is of interest as a candidate for photo-functional molecular devices.[2]

Gray colored TMA-Mnt was synthesized *via* the ion exchange method reported by J.-F. Lee *et. al.*[3] using tetramethylammonium chloride (Tokyo Kasei Co., purity : > 98%) and montmorillonite (Kunimine Industries Co., cation exchange capacity: 119 mequiv per 100 g). Chemical analysis of the nitrogen and carbon in TMA-Mnt indicated that 80 ± 3% of Na^+ ions were replaced by TMA ions. XRD analysis showed a layered structure for TMA-Mnt with basal spacing of 1.387 nm. The N_2 adsorption at 77.4 K indicated the presence of slit-shaped pores with a BET surface area of 180 $m^2\ g^{-1}$ and a pore volume of 0.068 $cm^3\ g^{-1}$.

The intercalation of PAA into TMA-Mnt was performed using a critical point dryer (HCP-2, Hitachi Koki Co.). After batches of TMA-Mnt (400 mg) and PAA (100 mg) were placed separately in the high pressure cell of the apparatus, CO_2 gas was supplied and then liquefied in the cell at 263 K. The liquid CO_2 was gradually heated to 313 K (pressure: 15.0 ± 0.5 MPa), at which point the CO_2 (T_c = 304.21 K, P_c = 7.13 MPa) was in a supercritical state. Separate batches were maintained in this state for 1, 6, 12, 24, 48 and 72 h, respectively. The cell temperature was then cooled to 293 K and the CO_2 liquid vented. The samples after SCC treatment were washed once with 50 cm^3 n-hexane to remove the residual PAA from the surface. Total nitrogen (TN) and total carbon (TC) contents of the SCC treated samples were determined by GC with a SUMIGRAPH GCT-12N (Sumika Bunseki Center Co.). The PAA uptake by TMA-Mnt in each sample was evaluated from the TN value by subtracting that due to TMA ions. The solubility of PAA in the SCC phase was roughly determined from the weight loss of PAA solid by SCC treatment in the absence of TMA-Mnt. The solubility was estimated as 0.3 mg cm^{-3}, considered reasonable since Hildebrand's solubility parameter of SCC at T = 313 K and P = 15 MPa is similar to that of n-hexane, which shows saturated solubility of 1.8 mg cm^{-3}.[4]

Yellowish samples were obtained by the SCF treatment. The PAA contents estimated from the TN values are listed in Table 1. The CO_2 residue was found to be negligible since the ratios of TN uptake to TC uptake were between 0.20 and 0.25; these are close to the TN to TC ratio (0.25) of PAA molecules. The PAA content increases rapidly during the first 24 h of treatment and is then almost constant from 24 to 72 h. The adsorption rate is relatively slow compared to the conventional dissolution rate of solute in SCF media.[5] The relatively slow rate may be caused by the slow diffusion of PAA molecules through the internal pores of TMA-Mnt. Since the pore size is near the lower limit for PAA diffusion, the intraparticle diffusion of PAA molecules may be the rate determining step in the present case, rather than the PAA transfer through the SCC–solid interface. The N_2 adsorption isotherms are analyzed with V_l *vs.* t plots, using the t values of Lecloux and Pirard[6] and C constants determined by BET plots, as shown in Fig.1. The V_l *vs.* t plot for the untreated TMA-Mnt shows a downward deviation from the straight line at t > 0.4 nm, indicating the presence of micropores around 0.4 nm in width. The downward deviation is not observed for the samples treated with SCC for 6 h or more. This demonstrates that the micropores disappear with the increase in the PAA uptake. The BET surface area, micropore volume, and the basal spacing determined by XRD analysis are given for the SCC-treated samples in Table 1. The specific surface area and the micropore volume decrease significantly with the PAA content.

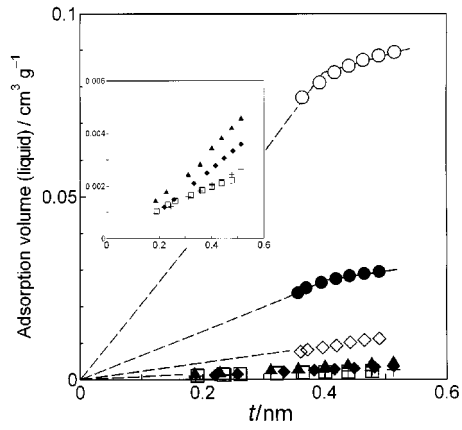

Fig. 1 V_l *vs.* t plots of TMA-Mnt and PAA-TMA-Mnt composites: (○) untreated TMA-Mnt, and SCC treatment for (●) 1, (◇) 6, (□) 12, (▲) 24, (◆) 48 and (+) 72 h

Table 1 PAA content, basal spacing, BET surface area and micropore volume of PAA-TMA-Mnt composites produced with SCC as a medium

Reaction time/h	PAA content/ mg g^{-1}	Basal spacing/ nm	BET surface area/m^2 g^{-1}	Pore volume/ cm^3 g^{-1}
0	0	1.38(7)	180	0.068
1	8.6	1.39(6)	60	0.018
6	29	1.40(7)	22	n.d.[a]
12	38	1.41(3)	5	n.d.
24	70	1.43(6)	7	n.d.
48	75	1.43(9)	6	n.d.
72	80	1.43(9)	4	n.d.

[a] n.d. = Values not determined.

In addition, the basal spacing, which corresponds to the interlayer distance of the PAA-TMA-Mnt composite, increases slightly with an increase in the adsorbed amount. These results clearly indicate that most of the PAA molecules are intercalated in the interlayer of TMA-Mnt. The equilibrium PAA uptake is evaluated as 75 mg g^{-1} (0.38 mmol g^{-1}) from the time courses of PAA adsorption in Table 1. The intercalation capacity is calculated as 124 mg g^{-1} from the micropore volume of TMA-Mnt and the geometric volume of a PAA molecule ($1.2 \times 0.5 \times 0.3$ nm). The PAA uptake reached 60% of the intercalation capacity, indicating that SCC is an efficient intercalation medium as compared with PAA uptakes in the solution stated below.

Liquid-phase intercalation reactions at 313 K for 48 h with acetone and n-hexane were investigated for comparison with the reaction in SCC phase. We confirmed that the liquid-phase reactions attain equilibrium after treatment for 48 h. The adsorption isotherms of PAA in the organic solutions are given in Fig. 2 together with the PAA uptake in the SCC system. The PAA adsorptivity is much higher in the SCC phase than those in the organic systems at the same PAA concentration. The PAA uptake (31 mg g^{-1}) in n-hexane solution is less than half that (80 mg g^{-1}) in the SCC phase at a PAA concentration of 0.3 mg cm^{-3}. The PAA uptake is estimated to be negligible in acetone solution at the same PAA concentration. The difference in PAA adsorptivity can be explained by considering two factors; the dissolving power of the solvent for the solute and the influence of competitive adsorption of solvent on the intercalation site. The lower dissolving power of SCC makes the PAA molecules unstable in the fluid phase, driving the migration of solutes from the fluid to the TMA-Mnt phase. Also, competitive adsorption may not occur in the SCC system, since the kinetic energy of CO_2 molecules is higher than the interaction energy between CO_2 and the pore wall.[7] On the other hand, TMA-Mnt shows high adsorptivity (more than 50 mg g^{-1}) for hydrocarbon and organic solvents at 323 K.[8] The competitive adsorption of solvent molecules causes a decrease of PAA uptake, depending on PAA concentration. These two factors are likely to be responsible for the higher PAA adsorptivity in the SCC system.

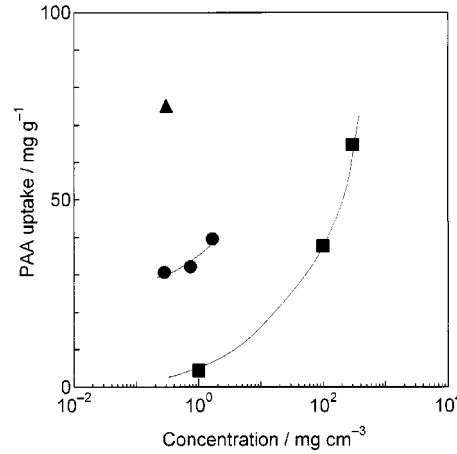

Fig. 2 PAA uptakes into TMA-Mnt in (●) n-hexane, (■) acetone and (▲) SCC

In conclusion, we have successfully intercalated PAA into TMA-Mnt using SCC as a medium. The resultant PAA-TMA-Mnt composite has relatively large amounts of PAA without CO_2 contamination. This demonstrates that SCC is a highly suitable medium for the intercalation reaction. The SCF technique can be expected to find application as a unique method for the synthesis of the nanostructural functional materials.

The authors are grateful for invaluable discussions and suggestions from Dr E. Kanezaki at the University of Tokushima. We also thank Kunimine Co. Ltd., for supplying Mnt samples.

Notes and References

† E-mail: ishii@sniri.go.jp

1 R. Schöllhorn, *Chem. Mater.*, 1996, **8**, 1747.
2 M. Ogawa, M. Takahashi and K. Kuroda, *Chem. Mater.*, 1994, **6**, 715; M. Ogawa, T. Handa, K. Kuroda, C. Kato and T. Tani, *J. Phys. Chem.*, 1992, **96**, 8116.
3 J.-F. Lee, M. M. Mortland, S. A. Boyd and C. T. Chiou, *J. Chem. Soc., Faraday Trans. 1*, 1989, **85**, 2953.
4 J. C. Giddings, M. N. Myers, L. McLaren and R. A. Keller, *Science*, 1968, **162**, 67.
5 G. Madras, C. Erkey and A. Akgerman, *Ind. Eng. Chem. Res.*, 1993, **32**, 1163.
6 A. Lecloux and J. P. Pirard, *J. Colloid Interfac. Sci.*, 1972, **38**, 109.
7 T. Shigeta and T. Nitta, *J. Chem. Eng. Jpn.*, 1996, **29**, 516.
8 R. M. Barrer and D. M. Macleod, *Trans. Faraday Soc.*, 1955, **51**, 1290.

Received in Cambridge, UK, 12th May 1998; 8/03540G

Solid state coordination chemistry of the copper cyanide–organoamine system: hydrothermal syntheses and structural characterization of $[\{Cu_2(bpy)_2(CN)\}Cu_5(CN)_6]$ and $[Cu_4(CN)_4(biquin)]$

Douglas J. Chesnut and Jon Zubieta*†

Department of Chemistry, Syracuse University, Syracuse, NY 13244, USA

The hydrothermal reactions of CuCN and $Cu(NO_3)_2{\cdot}2.5H_2O$ with the appropriate organonitrogen ligand in water yielded a one-dimensional chain, $[Cu_4(CN)_4(biquin)]$ 1, and a material with a two-dimensional anionic honeycomb network and interpenetrating binuclear cations, $[\{Cu_2(bpy)_2(CN)\}Cu_5(CN)_6]$ 2.

The contemporary interest in solid state inorganic materials reflects their properties, which endow these materials with applications ranging from heavy construction to microcircuitry.[1] A powerful synthetic approach for the manipulation of the microstructures of solid state inorganic materials exploits the incorporation of organic components, which contribute to the increased complexity as one constituent in a hierarchical structure exhibiting a synergistic interaction between the organic and inorganic substructures.[2,3] Organic materials have been demonstrated to play an important role in five subclasses of the oxide family of materials: zeolites,[4] mesoporous oxides of the MCM-41 type,[5] biomineralized materials,[6] microporous octahedral–tetrahedral framework transition metal phosphates[7] and organically templated molybdenum oxides.[8] We have recently extended this concept of templating anionic inorganic networks with organic constituents to the copper halide system, as represented by $[\{Cu(en)_2\}_2Cu_7Cl_{11}]$.[9] The rich supramolecular chemistry of the metal derivatives of the pseudohalide cyanide[10] encouraged us to expand our investigations to the copper–cyanide–organoamine family of materials, exploiting the bridging cyano ligand as a rigid tether in the propagation of Cu^I geometry in solid state materials. These studies have resulted in a variety of one- and two-dimensional materials of which $[Cu_4(CN)_4(biquin)]$ **1** and $[\{Cu_2(bpy)_2(CN)\}Cu_5(CN)_6]$ **2** are representative (biquin = 2,2′-biquinoline; bpy = 2,2′-bipyridine).

Compound **1** was prepared as yellow–orange crystals in *ca.* 15–25% yield from the reaction of CuCN, $Cu(NO_3)_2{\cdot}2.5H_2O$, 2,2′-biquinoline and H_2O in the mole ratio 4.2 : 0.99 : 1.0 : 280 at 170 °C for 86.5 h. Compound **2** was prepared as light orange crystals in *ca.* 35% yield in a similar fashion from the reaction of CuCN, $Cu(NO_3)_2{\cdot}2.5H_2O$, 2,2′-bipyridine and water in the mole ratio 6.3 : 1.0 : 1.0 : 290. Compound **1** cocrystallized with a red phase, identified as $[Cu_2(CN)_2(biquin)]$, while compound **2** cocrystallized with bright red crystals of [Cu(CN)(bpy)].[11] Curiously, the preparation of **1** and **2** in crystalline form and reasonable yields requires the presence of a Cu^{II} precursor. We have noted previously[12] that organoamines function as reducing agents in hydrothermal reactions, perhaps serving to generate a repository of reduced metal species for further aggregation. Optimization of yields may be accomplished by employing an excess of organonitrogen ligand to Cu^{II} precursor.

As shown in Fig. 1, the structure of **1**‡ exhibits a backbone constructed from a zigzag chain of two-coordinate $\{Cu(CN)_2\}$ sites and three-coordinate $\{Cu(CN)_3\}$ sites, with $\{Cu_2(CN)(biquin)\}$ groups projecting from the chain. The Cu–CN backbone and its attendant side chains are nearly planar with the best plane parallel to the 101 crystallographic plane.

While Cu–CN chain structures have been reported,[13] the greater structural complexity of **1** derives from the presence of the biquinoline ligand, which may serve to passivate the copper chain with respect to extension in two or three dimensions.

The structure of **2**† consists of sheets of fused 36-membered puckered honeycomb rings interpenetrated by $[(bipyCu)_2CN]^+$ cations, shown in Fig. 2. The rings are composed of two nearly linear $\{Cu(CN)_2\}$ sites, four 'bent' $\{Cu(CN)_2\}$ moieties and six $\{Cu(CN)_3\}$ distorted trigonal planar sites which serve as junctions between adjacent rings. As illustrated by the view of Fig. 3, each ring is interpenetrated by two space-filling and charge compensating $[Cu_2(bpy)_2(CN)]^+$ cations at an oblique angle to the {Cu(CN)Cu} axis of the cation with respect to the face of the ring. The honeycomb layers are offset along the stacking axis *b*, so as to generate channels of approximate dimensions 5.4 × 9.0 Å occupied by the cations (Fig. 4). Each cation interpenetrates rings from two adjacent layers, which are separated by 3.5 Å. While two-dimensional Cu–CN networks have been observed for $[Cu_3(en)_2(CN)_4]{\cdot}6H_2O$[14] and $K[Cu_2(CN)_3]{\cdot}H_2O$,[15] the layers are constructed from significantly smaller 15 and 18 membered rings.

The structures of **1** and **2** demonstrate the power of hydrothermal synthesis in the preparation of organic–inorganic composite materials. Not only are differential solubility problems avoided, reducing the tendency to phase segregate, but structurally more complex metastable phases are favored.[16] The structural complexity, in general, reflects the versatility of the organonitrogen component which may function as counterion,

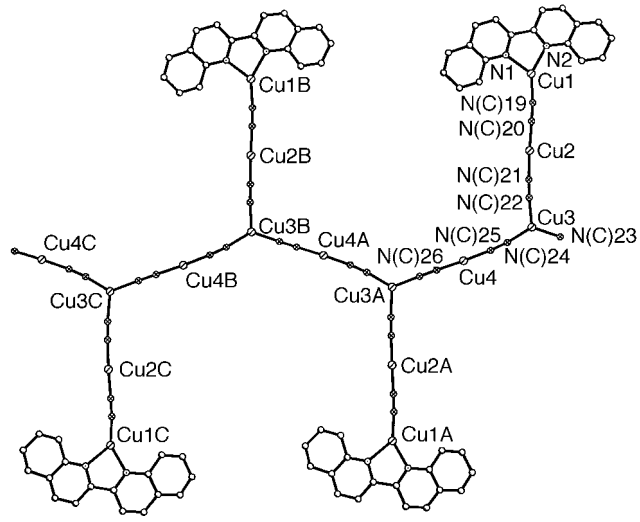

Fig. 1 A view of the structure of **1**. Selected bond lengths (Å) and angles (°): Cu1–N1 2.03(1), Cu1–N2 2.01(1), Cu1–N(C)19 1.84(2), Cu2–N(C)20 1.84(1), Cu2–N(C)21 1.85(2), Cu3–N(C)22 1.93(1), Cu3–N(C)23 1.91(2), Cu3–N(C)24 1.86(2), Cu4–N(C)25 1.84(2), Cu4–N(C)26 1.84(2), N1–Cu1–N2 81.3(5), N1–Cu1–N(C)19 130.6(7), N(2)–Cu1–N(C)19 147.5(7), N(C)20–Cu2–N(C)21 174.0(6), N(C)22–Cu3–N(C)24 118.4(6), N(C)22–Cu3–N(C)23 113.7(6), N(C)23–Cu3–N(C)24 128.0(6), N(C)25–Cu4–N(C)26 175.1(6).

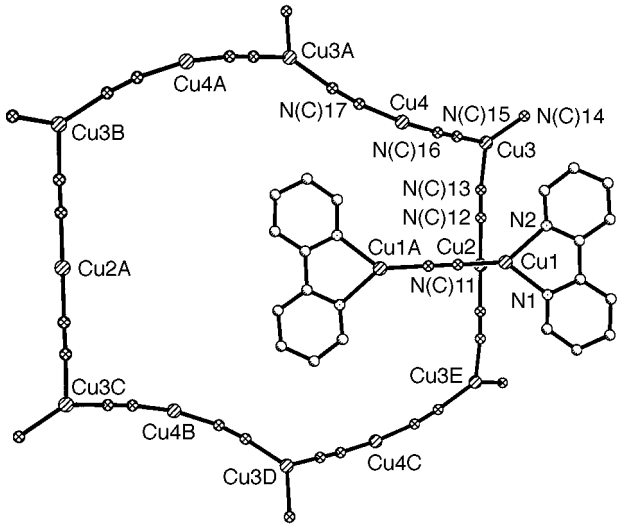

Fig. 2 A view of the honeycomb anionic network of **2** and of the location of the $[Cu_2(bipy)_2CN]^+$ cations. Selected bond lengths (Å) and angles (°): Cu1–N1 2.026(6), Cu1–N2 2.054(7), Cu1–N(C)11 1.846(7), Cu2–N(C)12 1.865(9), Cu3–N(C)13 1.994(8), Cu3–N(C)14 1.907(9), Cu(3)–N(C)15 1.924(8), Cu4–N(C)16 1.863(9), Cu4–N(C)17 1.843(7), N1–Cu1–N2 81.1(3), N1–Cu1–N(C)11 139.8(3), N2–Cu1–N(C)11 136.5(3), N(C)12–Cu2–N(C)12A 180.000(2), N(C)13–Cu3–N(C)14 116.6(3), N(C)13–Cu3–N(C)15 111.4(3), N(C)14–Cu3–N(C)15 130.1(4), N(C)16–Cu4–N(C)17 161.6(4).

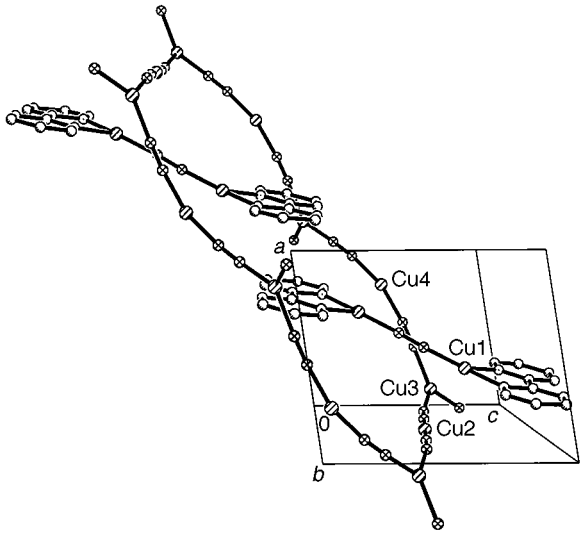

Fig. 3 A view of the interpenetration of a $\{Cu_{12}(CN)_{12}\}$ ring by two $[Cu_2(bipy)_2(CN)]^{1+}$ cations

ligand to the copper cyanide backbone or ligand in a coordination complex anion. In its role as ligand, the biquinoline in **1** serves to passivate the copper so as to prevent extension of the structure in more than one dimension. The increased hydrophobicity of biquinoline relative to bipyridine may result in the larger nonpolar domains localized in the interstrand regions. The role of the organic ligand as a component of a coordination complex cation, a recurring theme in metal oxide–organoamine chemistry,[17] appears to extend to the metal–halide and metal–psuedohalide phases. The large ring sizes of the copper cyanide networks of **2** are required to accommodate the large binuclear cations, suggesting that cation size in such structures may be a determinant not of interlamellar spacing but of ring topology and channel dimensions. We are investigating the roles of coordination complex cations of various sizes and shapes in defining the structures of metal halide and metal pseudohalide phases.

This work was supported by NSF Grant CHE9617232.

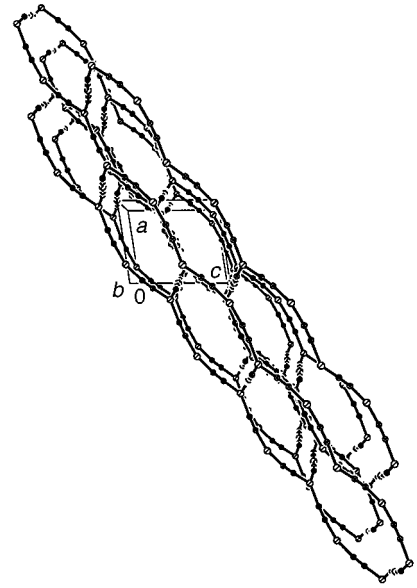

Fig. 4 A view down the crystallographic *b*-axis of the channels formed by offsetting of honeycomb layers in **2**

Notes and References

† E-mail: jazubiet@syr.edu

‡ *Crystal data*: for **1**: $C_{22}H_{12}Cu_4N_6$, monoclinic, space group $P2_1/c$, a = 7.3947(7), b = 18.041(2), c = 16.002(1) Å, β = 98.550(2)°, V = 2111.1(3) Å^3, Z = 4, M_w = 614.54, D_c = 1.934 mg m^{-3}, T = 293(2) K, μ = 39.98 cm^{-1} (Mo-Kα, λ = 0.71073 Å), R_1 = 0.0866; wR_2 = 0.1770 (3626 reflections, all collected).

For **2**: $C_{27}H_{16}Cu_7N_{11}$, monoclinic, space group $P2_1/c$, a = 7.2422(2), b = 24.2930(2), c = 8.6645(2) Å, β = 98.742(1)°, V = 1506.68(6) Å^3, Z = 4, M_w = 939.28, D_c = 2.070 mg m^{-3}, T = 293(2) K, μ = 48.84 cm^{-1} (Mo-Kα, λ = 0.71073 Å), R_1 = 0.0590; wR_2 = 0.1223 (2653 reflections). CCDC 182/934.

1 A. K. Cheetham, *Science*, 1994, **264**, 794.
2 S. Mann, *J. Chem. Soc., Dalton Trans.*, 1997, 3953.
3 S. Mann and G. A. Ozin, *Nature*, 1996, **382**, 313.
4 J. V. Smith, *Chem. Rev.*, 1988, **88**, 149; M. L. Occelli and H. C. Robson, *Zeolite Syntheses*, American Chemical Society, Washington, DC, 1989.
5 C. T. Kresge, M. E. Leonowicz, W. J. Roth, J. C. Vartuli and J. S. Beck, *Nature*, 1992, **359**, 710.
6 S. Mann, *Nature*, 1993, **365**, 499.
7 R. C. Haushalter and L. A. Mundi, *Chem. Mater.*, 1992, **4**, 31; M. I. Khan, L. M. Meyer, R. C. Haushalter, C. L. Schweitzer, J. Zubieta and J. L. Dye, *Chem. Mater.*, 1996, **8**, 43.
8 D. Hagrman, C. Zubieta, D. J. Rose, J. Zubieta and R. C. Haushalter, *Angew. Chem., Int. Ed. Engl.*, 1997, **36**, 873.
9 J. R. D. Debord, Y. Lu, C. J. Warren, R. C. Haushalter and J. Zubieta, *Chem. Commun.*, 1997, 1365; R. D. Willet, *Coord. Chem. Rev.*, 1991, **109**, 181.
10 T. Iwamoto, in *Comprehensive Supramolecular Chemistry*, ed. J. L. Atwood, J. E. D. Davies and D. D. MacNicol, Pergamon, New York, 1996, vol. 6, 643.
11 D. J. Chesnut and J. Zubieta, unpublished work.
12 M. I. Khan, R. C. Haushalter, C. J. O'Connor, C. Tao and J. Zubieta, *Chem. Mater.*, 1995, **7**, 593.
13 D. T. Cromer, *J. Phys. Chem.*, 1957, 1388; D. T. Cromer, A. C. Larson and R. B. Roof Jr., *Acta Crystallogr.*, 1965, **19**, 192; R. J. Williams, D. T. Cromer and A. C. Larson, *Acta Crystallogr. Sect. B*, 1971, **27**, 1701.
14 R. J. Williams, A. C. Larson and D. T. Cromer, *Acta Crystallogr. Sect. B*, 1972, **28**, 858.
15 D. T. Cromer and A. C. Larson, *Acta Crystallogr.*, 1962, **15**, 397.
16 J. Gopalakrishnan, *Chem. Mater.*, 1995, **7**, 1265.
17 Y. Zhang, J. R. D. DeBord, C. J. O'Connor, R. C. Haushalter, A. Clearfield and J. Zubieta, *Angew. Chem., Int. Ed. Engl.*, 1996, **35**, 989.

Received in Columbia, MO, USA, 7th April 1998; 8/02641F

Hydrothermal synthesis and structure of a three-dimensional open-framework cobalt molybdenum(VI) phosphate containing ethylenediammonium ions: $(C_2H_9N_2)_6[Co_3Mo_4P_4O_{28}]$

Jian J. Lu, Yan Xu,*† Ngoh K. Goh and Lian S. Chia

Division of Chemistry, School of Science, Nanyang Technological University Singapore 259756, Republic of Singapore

The first microporous cobalt molybdenum(VI) phosphate, crystallised under hydrothermal conditions, is constructed from unique $CoMo_2P$ tetrahedral units connected by CoO_4 tetrahedra and by sharing corners; the framework contains interlocking cavity units and unusual 7-ring intersecting channels that are filled with charge-compensating ethylenediammonium ions.

While the synthesis and characterisation of three-dimensional framework aluminosilicate zeolites[1] and aluminophosphate materials[2] has been an actively pursued area of materials chemistry, only in recent years have other open-framework inorganic materials started to emerge. The driving force behind the effort is to engineer open-framework materials with desired chemical and catalytic reactivities. One of the strategies adopted is to incorporate d-block elements into these materials as stoichiometric framework constituents through the combined effects of hydrothermal synthesis and amine templates. Practicing this strategy results in the successful synthesis of open-framework reduced molybdenum phosphates,[3] mixed valent molybdenotungsten phosphates,[4] vanadium phosphates,[5] cobalt phosphates,[6] vanadium oxides,[7] non-oxide solids[8] and a number of layered molybdenum(VI) solids.[9] However, three-dimensional open-framework molybdenum(VI) solids remain largely unexplored except for a hexagonal molybdenum trioxide phase.[10]

In the course of our investigation on the synthesis of molybdenum(VI) polyoxoanion based solid materials, we have hydrothermally synthesised a series of novel one- and two-dimensional organically templated solids.[11] Extending this idea, we explored the incorporation of 'heteroatoms' as tetrahedral tethers and applied the 'magic' F^- mineraliser[12] to assemble molybdenum(VI) polyoxoanions forming three-dimensional open frameworks. Here, we report the synthesis and structural characterisation of the first open-framework cobalt molybdenum phosphate with entrenched charge-compensating ethylenediammonium ions, $(C_2H_9N_2)_6[Co_3Mo_4P_4O_{28}]$ **1**.

Compound **1** was prepared from the hydrothermal reaction of $CoCl_2{\cdot}6H_2O$, $MoO_3{\cdot}H_2O$, H_3PO_4 (85 mass%), NaF, ethylenediamine and H_2O in a mole ratio of 1 : 2.2 : 3.3 : 3.1 : 1.2 : 407. Ethylenediamine was introduced at the last stage into the clear solution of $CoCl_2{\cdot}6H_2O$, $MoO_3{\cdot}H_2O$, H_3PO_4, NaF and H_2O resulting in a pinkish slurry. Crystallisation was carried out in a sealed Teflon-lined stainless-steel autoclave reactor at 160 °C and autogenous pressure for 3 days. The presence of NaF was found to be critical for the successful synthesis of **1**. The use of $Co(NO_3)_2{\cdot}6H_2O$ instead of $CoCl_2{\cdot}6H_2O$ resulted in the crystallisation of the same product **1**. The chemical analysis in combination with the single crystal X-ray structure determination‡ and thermogravimetric analysis confirmed the chemical formula of $C_3H_{13.5}N_3Co_{0.75}MoPO_7$ and the absence of F^- ions from the crystal structure of **1**. Simultaneous TG/DT analysis and *in-situ* powder XRD studies§ indicated that ethylenediamine can be removed at 360 °C and the structure of **1** remained intact until *ca.* 700 °C. By replacing the heteroatom Co^{2+} with Al^{3+} and Zn^{2+}, a few new organic/MoPO hybrid phases crystallised as identified by both the single and powder X-ray diffraction methods. One of the organic/MoPO hybrid phases, $(C_2N_2H_{10})_2[Mo_5P_2O_{22}]{\cdot}H_2O$, crystallised in monoclinic symmetry.¶

As shown in Fig. 1, the three-dimensional framework of **1** is constructed from the unique $CoMo_2P$ pseudo-tetrahedral building units (Fig. 1 inset) which consist of crystallographically independent one MoO_6 octahedron, one PO_4 tetrahedron and a half CoO_6 octahedron. The $CoMo_2P$ units are linked into a covalently bonded three-dimensional framework through (i) direct and (ii) indirect connection modes as shown in Fig. 2(*a*). The direct connection mode refers to the connection between two adjacent $CoMo_2P$ units by corner-sharing Mo and Co atoms. The indirect connection mode refers to the connection of four 4_1-screw-axis-related $CoMo_2P$ units, each linking to a common CoO_4 tetrahedron *via* a corner-shared oxygen atom from PO_4 of the respective $CoMo_2P$ unit. This gives rise to two cavity units, A and B, of **1** as shown in Fig. 2(*b*). The cavity A is circumscribed by four MoO_6, four CoO_6, four PO_4 and two CoO_4 units and contains four identical 3- and 7-ring windows. In the cavity B, five MoO_6, five PO_4, two CoO_6 and two CoO_4 units are linked up *via* corner-shared oxygen atoms forming one 8-ring window, three distinct 3-ring windows and three 7-ring windows of two distinct types (I: $Mo_2Co_3P_2$ and II: $Mo_3Co_2P_2$). The cavities **A** and **B** are interlocked by a single 7-ring window encircled by one CoO_4, two PO_4, two MoO_6 and two CoO_6 units (highlighted). The three-dimensional framework of **1** can also

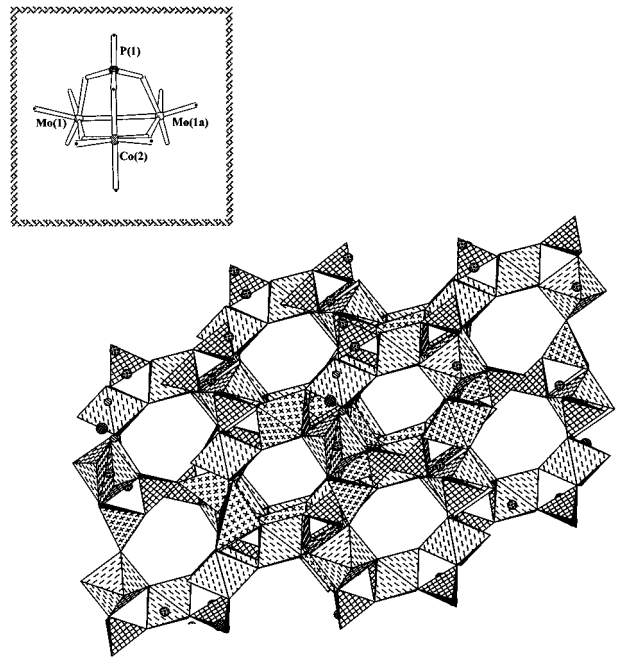

Fig. 1 A polyhedral view of $(C_2H_9N_2)_6[Co_3Mo_4P_4O_{28}]$ **1** showing the intersecting 7-ring channels. Inset shows the $CoMo_2P$ tetrahedral unit.

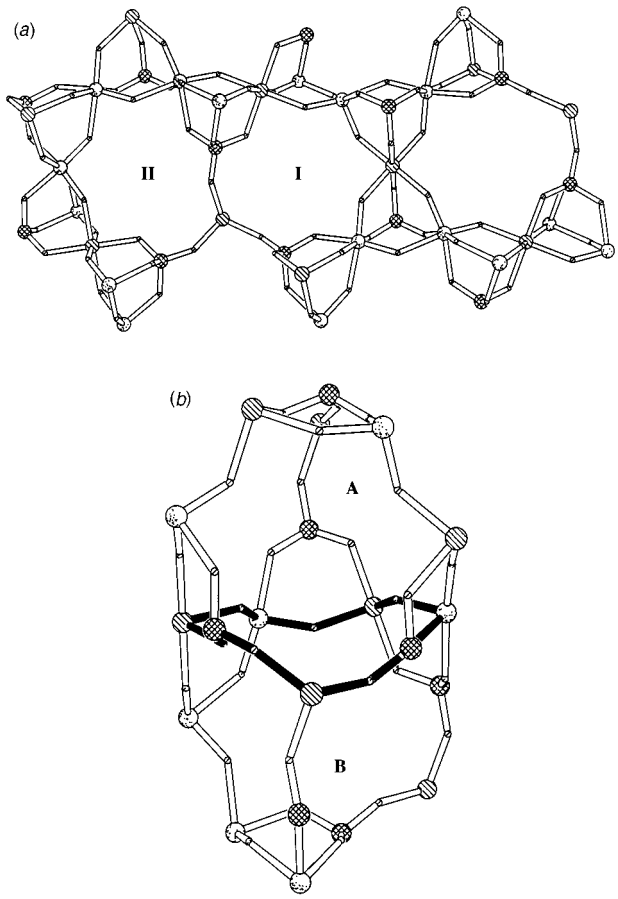

Fig. 2 (*a*) A general view of $(C_2H_9N_2)_6[Co_3Mo_4P_4O_{28}]$ **1** showing the two types of connection modes of the $CoMo_2P$ units and two types of 7-ring windows. (*b*) A view of interlocked cavities **A** and **B** by a single 7-ring window (with highlighted bonds) showing the 3-, 7- and 8-ring windows. The atoms shown are: dotted circles for Mo, cross-hatched circles for P, shaded circles for Co and small circles for O.

be envisioned as being built up in space group $I4_1/a$ from the aforementioned interlocking cavity units [**A** + **B**] by sharing the $CoMo_2P$ units. Two types of intersecting 7-ring channels are formed in the so-packed cobalt molybdenum phosphate framework as shown in Fig. 1 and 2(*a*).

The 7-ring channels of **1** are filled with partially protonated ethylenediamine molecules. The ethylenediammonium ions interact with the framework through contacts between the N atoms of the ethylenediammonium ions and the O atoms of the framework with N(H)···O 2.82–2.94 Å. One of the two nitrogen atoms of the ethylenediammonium ion is found to be involved in the N(H)···O interactions, supporting the assignment of partial protonation of ethylenediamine molecules. However, uncertainty is encountered in locating H atoms attached to the N atoms due to the severe disordering of the ethylenediammonium ions in the crystal packing of **1**.

The asymmetric unit of **1** consists of one MoO_6 octahedron, one PO_4 tetrahedron, a half CoO_6 octahedron, a quarter CoO_4 tetrahedron, and one and a half ethylenediammonium ions. The coordination geometry of the three framework atoms, Mo, P and Co, is exclusively defined by unsymmetrically corner-shared oxo groups. The geometric parameters of the cobalt molybdenum phosphate framework which are reasonably well determined (data:parameters ratio *ca.* 10:1) show that the Mo–O contacts are in the range 1.767(3)–2.198(3) Å, the P–O contacts in the range 1.517(4)–1.556(3) Å, the Co(1)–O contact 1.928(4) Å (tetrahedral Co, T_{Co}) and the Co(2)–O contacts in the range 2.066(3)–2.102(3) Å (octahedral Co, O_{Co}). The P–O and Co–O (at both T_{Co} and O_{Co} sites) contacts are within the expected range.[6a,13] The molybdenum site exhibits short-to-medium bond length pattern regardless of the absence of terminal oxo groups which is not uncommon to molybdenum(VI) oxides containing unsymmetrical bridging oxo groups.[14] This may also be attributed to the existence of moderate hydrogen bonds involving some of the O atoms of the MoO_6 units.

The cobalt molybdenum phosphate **1** reported here represents the first successful synthesis and characterisation of covalently bonded three-dimensional open-framework structure in the metal molybdenum(VI) phosphate compositional domain. The enhanced solvating effect of water and mineralising effect of F^- under the hydrothermal autogenous conditions evidently provide the environment required for the assembly of an open-framework from molecular precursors. It opens up the possibility of applying this method for assembling other three-dimensional metal molybdenum phosphates with potentially interesting or useful properties.

We thank Nanyang Technological University, Singapore, for financial support (Research grant: RP 23/96XY).

Notes and References

† E-mail: urxuy@nievax.nie.ac.sgur

‡ *Crystal data* for $(C_2H_9N_2)_6[Co_3Mo_4P_4O_{28}]$ **1**: $C_3H_{13.5}N_3Co_{0.75}MoPO_7$, M_w = 374.78, tetragonal, space group $I4_1/a$, a = 17.163(2), c = 10.764(2) Å, V = 3170.7(9) Å^3, Z = 16, D_c = 3.140 g cm^{-3}, μ = 3.40 mm^{-1}, T = 296 K, dark blue prism, crystal size *ca.* 0.15 × 0.10 × 0.08 mm, and max., min. peak on final Fourier difference map 0.647, −0.994 e Å^{-3} respectively. Intensity data were collected by $\theta/2\theta$ scans on a Siemens P4 X-ray diffractometer with graphite-monochromated Mo-Kα radiation. Empirical absorption corrections were made from ψ-scan data using an applied program at the data reduction stage along with the correction of Lorentz and polarization factors. The structure was solved by direct methods and refined using full-matrix least squares on F^2 using the SHELXTL-PLUS package. The final refinement was based on 1384 reflections with $I > 2.0\sigma(I)$ for 135 parameters and converged to R_1/wR_2 = 0.0303/0.0742 (R_1/wR_2 = 0.0388/0.0896 for all data). CCDC 182/933.

§ *Powder XRD data*: *in situ* XRD patterns were collected on a Siemens D5005 diffractometer with graphite-monochromated Cu-Kα radiation (λ = 1.5406 Å). Heating was conducted in the temperature range room temp.–1000 °C under vacuum.

¶ *Crystal data* for the monoclinic $(C_2N_2H_{10})_2[Mo_5P_2O_{22}]\cdot H_2O$ phase: M_w = 1035.9, space group $C2/c$ with unit cell dimensions a = 17.642(4), b = 10.039(2), c = 13.777(3) Å, β = 96.92(3)°, V = 2422.4(8) Å^3.

1 D. Breck, *Zeolite Molecular Sieves*: *Structure, Chemistry and Use*, Wiley, New York, 1974; R. Barrer, *Hydrothermal Chemistry of Zeolites*, Academic Press, New York, 1982.
2 S. Wilson, T. Cannan, E. Flanigen, B. Lok and C. Messina, *ACS Symp. Ser.*, 1983, **218**, 79.
3 R. Haushalter and L. Mundi, *Chem. Mater.*, 1992, **4**, 31 and references therein.
4 A. Leclaire, M. Borel, J. Chardon and B. Raveau, *J. Solid State Chem.*, 1997, **128**, 215.
5 Y. Lu, R. Haushalter and J. Zubieta, *Inorg. Chim. Acta*, 1998, **268**, 257; V. Soghomonian, Q. Chen, R. Haushalter and J. Zubieta, *Chem. Mater.*, 1993, **5**, 1595.
6 (*a*) J. Chen, R. Jones, S. Natarajan, M. Hursthouse and J. Thomas, *Angew. Chem., Int. Ed. Engl.*, 1994, **33**, 639; (*b*) P. Feng, X. Bu, S. Tolbert and G. Stucky, *J. Am. Chem. Soc.*, 1997, **119**, 2497.
7 Y. Zhang, R. Haushalter and A. Clearfield, *Inorg. Chem.*, 1996, **35**, 4950.
8 C. Bowes and G. Ozin, *Adv. Mater.*, 1996, **8**, 13 and references therein.
9 W. Harrison, L. Dussack and A. Jacobson, *Inorg. Chem.*, 1994, **33**, 6043.
10 J. Guo, P. Zavalij and M. Whittingham, *J. Solid State Chem.*, 1995, **117**, 323.
11 Y. Xu, L. An and L. Koh, *Chem. Mater.*, 1996, **8**, 814; Y. Xu, L. Koh, L. An, D. Roshan and L. Gan, *Stud. Surf. Sci. Catal.*, 1997, **105**, 2123; Y. Xu, B. Zhang, N. Goh and L. Chia, *Inorg. Chim. Acta*, 1998, in press; Y. Xu, J. Lu, N. Goh and L. Chia, to be published.
12 G. Ferey, *J. Fluorine Chem.*, 1995, **72**, 187 and references therein.
13 P. Lightfoot, A. Cheetham and A. Sleight, *J. Solid State Chem.*, 1990, **85**, 275.
14 W. Harrison, L. Dussack and A. Jacobson, *J. Solid State Chem.*, 1995, **116**, 95.

Received in Cambridge, UK, 22nd June 1998; 8/04693J

Reaction of *S*-nitrosothiols with ascorbate: clear evidence of two reactions

Anthony J. Holmes and D. Lyn H. Williams*†

Chemistry Department, University of Durham, South Road, Durham, UK DH1 3LE

Ascorbate reacts with *S*-nitrosothiols at pH 7.4 *via* two pathways, in which ascorbate (at low concentration) acts as a reducing agent generating Cu^{I}, and (at high concentration) acts as a nucleophile, attacking the nitroso group.

We have shown[1] that *S*-nitrosothiols (RSNO) decompose in aqueous buffer at pH 7.4 to give nitric oxide and the corresponding disulfides, in a reaction brought about by Cu^{I} [eqn. (2)], which is generated from Cu^{II} by reduction with thiolate anion [eqn. (1)]. Often there is enough Cu^{II} present in the water/buffer system to effect reaction, and usually there is enough thiolate present in equilibrium[2] with RSNO [eqn. (3)] to bring about the reduction. In addition it has been shown[3] that Cu^{II} bound in proteins, peptides and amino acids can also be reduced by thiolate and effect RSNO decomposition, so that it is not necessary for the Cu^{II} to be present as free solvated Cu^{2+}. It follows that other reducing agents should be capable of the copper reduction, and it has been shown[1] that added ascorbate does indeed behave in a similar fashion to added *N*-acetylpenicillamine in the decomposition of *S*-nitroso-*N*-acetylpenicillamine, but hitherto no detailed mechanistic study has been carried out.

$$2Cu^{2+} + 2RS^{-} = 2Cu^{+} + RSSR \quad (1)$$

$$Cu^{+} + RSNO = Cu^{2+} + RS^{-} + NO \quad (2)$$

$$RSH + HNO_2 = RSNO + H_2O \quad (3)$$

Recently, however, it has been reported, (i) that ascorbate will promote NO release from *S*-nitroso albumin and *S*-nitroso glutathione (GSNO) in blood plasma even in the presence of metal chelating agents,[4] and (ii) in a separate study[5] using plasma and fractions of liver and kidney extracts, it is also claimed that ascorbate promotes the decomposition of GSNO, again in the absence of copper ions. A further paper in the biological literature[6] found glutathione and nitrite as the products of the reaction of GSNO with ascorbate. These findings prompted us to examine further the effect of ascorbate on RSNO decomposition.

We have examined the decomposition at pH 7.4 of GSNO, generated in solution from glutathione and nitrous acid, in the presence of a low concentration of ascorbic acid and with added Cu^{2+} (1×10^{-4} mol dm^{-3}). Fig. 1 shows the resulting absorbance–time plots measured at 545 nm.‡ Trace (*a*) shows the small extent of decomposition (< 10% in 3 h) which occurs when no ascorbic acid is present. This probably represents the spontaneous thermal decomposition. This is in marked contrast to trace (*b*) which results from the same experiment with added ascorbic acid (2×10^{-4} mol dm^{-3}). Here, reaction goes to completion by a first order process with a half life of *ca.* 18 min.

This reaction is dramatically stopped, virtually completely (over the time scale examined), by the addition, at the start, of EDTA (1×10^{-3} mol dm^{-3}), as shown in trace (*c*). Further, when the experiment of trace (*b*) is repeated, and EDTA (1×10^{-3} mol dm^{-3}) is added after about one half life, then the reaction is stopped suddenly at this time point, as shown in trace (*d*). These experiments show clearly that the GSNO decomposition under these conditions *is* a metal ion promoted reaction, almost certainly a Cu^{+} catalysed reaction, in which the ascorbate ion is acting as a reducing agent for Cu^{2+}, in the same way as thiolate does in the earlier experiments,[1] and leading to disulfide formation. A similar reaction using *S*-nitrosocysteine (which is much faster than the reaction of GSNO), with added Cu^{2+} (5×10^{-6} mol dm^{-3}) and ascorbic acid (5×10^{-6} mol dm^{-3}), generated 86% NO as detected by a commercial NO electrode.

However at higher ascorbate concentrations the situation is somewhat different. For example, when the GSNO experiments are repeated with ascorbate at a ten-fold higher concentration (2×10^{-3} mol dm^{-3}), there is a slow first order decomposition, which is completely unaffected by the addition of EDTA (1×10^{-3} mol dm^{-3}) after roughly one half life. Furthermore the reaction seems to be quite general, since the decomposition of the more reactive *S*-nitrosopenicillamine occurs readily in the presence of EDTA, and the rate is clearly dependent on the [ascorbate], as shown in Fig. 2. When reactions are carried out under conditions of [ascorbate] >> [RSNO], then we find a good first order dependence on both reactants, for a number of RSNO structures. The products of this reaction at higher [ascorbate] are NO and the thiol. For example, in the reaction of *S*-nitrosocysteine with 0.1 mol dm^{-3} ascorbate, the thiol was detected by the Ellman procedure[8] in > 80% yield. This contrasts markedly with the copper-promoted reaction carried out at 1×10^{-5} mol dm^{-3} ascorbate, where the thiol

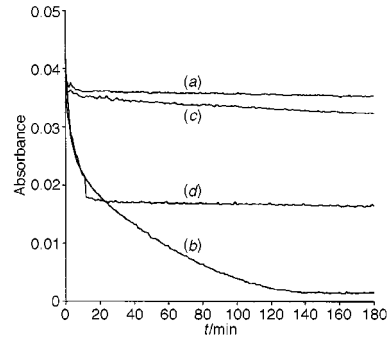

Fig. 1 Absorbance–time plots (measured at 545 nm) for the decomposition of GSNO (2×10^{-3} mol dm^{-3}) with added Cu^{2+} (1×10^{-4} mol dm^{-3}) at pH 7.4: (*a*) with no added ascorbic acid, but with added EDTA (1×10^{-3} mol dm^{-3}); (*b*) with added ascorbic acid (2×10^{-4} mol dm^{-3}); (*c*) as (*b*) but with added EDTA (1×10^{-3} mol dm^{-3}); (*d*) as (*b*) but with EDTA (1×10^{-3} mol dm^{-3}) added after 14 min

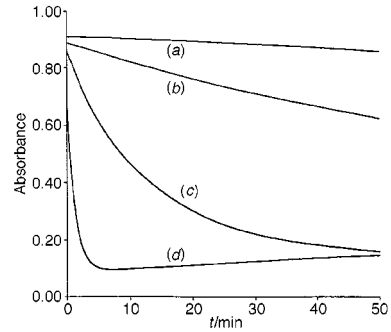

Fig. 2 Absorbance–time plots (measured at 340 nm) for the decomposition of *S*-nitrosopenicillamine (1×10^{-3} mol dm^{-3}) in the presence of EDTA (1×10^{-3} mol dm^{-3}) and (*a*) 0, (*b*) 1×10^{-4}, (*c*) 1×10^{-3} and (*d*) 1×10^{-2} mol dm^{-3} ascorbate

concentration in the product is < 5%. Similarly we were able to detect NO in high yield (78%) from the same reaction at high [ascorbate] (0.01 mol dm^{-3}) in the presence of EDTA (1×10^{-3} mol dm^{-3}) using the NO electrode. Similar results were obtained for the *S*-nitrosothiols derived from captopril, *N*-acetylpenicillamine, homocysteine and thioglycerol.

This reaction bears a close similarity to that recently reported for the reaction of ascorbate with an alkyl nitrite.[9] That reaction, also yielding NO, was studied at high pH (10–12), and was thought to involve initial attack at the nitroso nitrogen atom by the dianion of ascorbic acid. In our case, it is likely at pH 7.4 that the reactant is the monoanion of ascorbic acid, given that the two pK_a values of ascorbic acid are 4.3 and 11.8.

Nucleophilic attack at the nitroso nitrogen atom of *S*-nitrosothiols (and alkyl nitrites) is well-known for the thiolate ion [eqn. (4)], as the transnitrosation reaction, and has been

$$\text{RSNO (or RONO)} + \text{R}'\text{S}^- = \text{RS}^- \text{ (or RO}^-\text{)} + \text{R}'\text{SNO} \quad (4)$$

studied mechanistically.[10,11] More recently we have found[12] that other nucleophiles, such as amines, hydrazine, azide ion, and sulfite ion, will also act in this way; in each case the *S*-nitrosothiol acts as an electrophilic nitrosating species. *N*-Nitroso species, particularly *N*-nitrososulfonamides, have also been shown to be able to act as electrophilic nitrosating species towards a large range of nucleophiles.[13]

It is therefore not surprising that the ascorbate ion can also be nitrosated in a direct reaction with *S*-nitrosothiols. Nitrosation of ascorbic acid by nitrous acid is a well-known reaction which has been studied mechanistically.[14,15] Reaction is thought to involve *O*-nitrosation, followed by homolytic cleavage of the O–NO bond to give NO and a radical or radical ion species, which yields dehydroascorbic acid as the final product, by reaction with more nitrous acid. Alternatively, initial attack could (by analogy with nitrosation of some phenols[16]) occur at carbon, as an electrophilic addition to a very reactive alkene, followed by homolytic fission to give NO.

Whatever the detailed mechanism of NO release in these reactions with ascorbate, it is clear that there is a reaction pathway for NO formation from *S*-nitrosothiols which is independent of the presence of metal ions, particularly Cu^{2+}. This reaction is dominant at high [ascorbate], whereas at low [ascorbate], where the direct ascorbate reaction is too slow to be significant, the Cu^+-promoted reaction takes over. Presumably the copper reaction is suppressed anyway at high [ascorbate], by complexation and hence removal of Cu^{2+}, just as is the case for many of the Cu^+-promoted reactions where thiolate ion is the reducing agent.

These results show clearly that there are two reactions between ascorbate and *S*-nitrosothiols, and explain the observations[4,5] that GSNO can still undergo decomposition in the presence of ascorbate, even when Cu^{2+} ions are removed, so long as the [ascorbate] is high enough to ensure a reasonable rate of reaction.

We thank the EPSRC for a research studentship to A. J. H.

Notes and References

† E-mail: d.l.h.williams@durham.ac.uk

‡ For the slower reactions we worked at 545 nm, rather than at the more usual wavelength of 340 nm (where there is a higher extinction coefficient), to avoid the increasing absorbance towards the end of the reactions in the 340 nm region, which occurs because of the decomposition reaction of the product dehydroascorbic acid (ref. 7).

1 A. P. Dicks, H. R. Swift, D. L. H. Williams, A. R. Butler, H. H. Al-Sadoni and B. G. Cox, *J. Chem. Soc., Perkin Trans. 2*, 1996, 481.
2 P. H. Beloso and D. L. H. Williams, *Chem. Commun.*, 1997, 89.
3 A. P. Dicks and D. L. H. Williams, *Chem. Biol.*, 1996, **3**, 655.
4 G. Scorza, D. Pietraforte and M. Minetti, *Free Radical Biol. Med.*, 1997, **22**, 633.
5 M. Kashiba-Iwatsuki, K. Kitoh, E. Kasahara, H. Yu, M. Nisikawa, M. Matsuo and M. Inoue, *J. Biochem.*, 1997, **122**, 1208.
6 M. Kashiba-Iwatsuki, M. Yamaguchi and M. Inoue, *FEBS Lett.*, 1996, **389**, 149.
7 E. L. Hirst, E. G. V. Percival, R. W. Herbert, R. J. W. Reynolds and F. Smith, *J. Chem. Soc.*, 1933, 1270.
8 P. W. Riddles, R. L. Blakeley and B. Zerner, *Anal. Biochem.*, 1979, **94**, 75.
9 J. R. Leis and A. Rios, *J. Chem. Soc., Chem. Commun.*, 1995, 169.
10 D. J. Barnett, A. M. Rios and D. L. H. Williams, *J. Chem. Soc., Perkin Trans. 2*, 1995, 1279.
11 H. M. S. Patel and D. L. H. Williams, *J. Chem. Soc., Perkin Trans. 2*, 1990, 37.
12 A. P. Munro and D. L. H. Williams, unpublished work.
13 J. R. Leis, M. E. Pena and A. Rios, *J. Chem. Soc., Perkin Trans. 2*, 1996, 863 and references cited therein.
14 C. A. Bunton, H. Dahn and L. Loewe, *Helv. Chim. Acta*, 1960, **43**, 303, 317 and 320 and earlier papers.
15 B. D. Beake, R. B. Moodie and D. Smith, *J. Chem. Soc., Perkin Trans. 2*, 1995, 1251.
16 B. D. Beake, R. B. Moodie and J. P. B. Sandall, *J. Chem. Soc., Perkin Trans. 2*, 1994, 957.

Received in Liverpool, UK, 27th May, 1998; 8/03983F

Unprecedented electron deficient bridging between zinc atoms by boron atoms of *nido*-carborane anions: preparation, crystal and molecular structure of the dimer $[(nido\text{-}C_2B_9H_{11})ZnNMe_3]_2$

Andrés E. Goeta, Judith. A. K. Howard,* Andrew K. Hughes,*† Andrew L. Johnson and Ken Wade*

Department of Chemistry, University of Durham, South Road, Durham, UK DH1 3LE

The alkane elimination reaction between $ZnMe_2$ and $[(NMe_3H)^+(nido\text{-}C_2B_9H_{12})^-]$ gives the macropolyhedral dimer $[(nido\text{-}C_2B_9H_{11})ZnNMe_3]_2$, containing an unprecedented planar diamond-shaped Zn_2B_2 ring at its core.

The capacity of the *nido*-carborane anion $[C_2B_9H_{11}]^{2-}$ to bond cationic metallic units at sites on its open pentagonal face that reflect the frontier orbital characteristics of the metallic cations has long been recognised.[1] The σ^2,π^4 arrangement of the frontier orbitals of $[C_2B_9H_{11}]^{2-}$ is similar to those of the cyclopentadienyl, $(C_5H_5)^-$, and imido, RN^{2-}, ligands.[2] Both $[C_2B_9H_{11}]^{2-}$ and RN^{2-} act as 4 electron LX_2 ligands.[3] Metallic residues that are isolobal with BH^{2+} can bond η^5 to the face, and so effectively complete the c*loso*-metallacarborane. It has been recognised that metal fragments with full, or almost full, d shells tend to occupy 'slipped' positions over the open face, even though the metal fragment formally has the three vacant orbitals of a BH^{2+} unit (one radially, two tangentially oriented).[4] Coordination in an η^1 mode is also observed when the metal fragment has fewer than 3 vacant orbitals, as in $[(\eta^1\text{-}C_2B_9H_{11})SnPh_3]^-$.[5] Alternative cluster geometries may also be observed even when the metal fragment has three vacant orbitals but is not isolobal with HB^{2+}.[6]

Noting that the only structurally characterised zinc borane species are a number of tetrahydridoborate complexes,[7] ionic compounds containing the $[Zn(B_{10}H_{12})_2]^{2-}$ anion,[8] and small zinc boranes,[9] and that complexes of boranes or carboranes[10] with group 2[11] or group 12 metals are rare (except for linear complexes of Hg^{2+}), we explored the reaction‡ between $[(Me_3NH)^+(nido\text{-}C_2B_9H_{12})^-]$ and $ZnMe_2$, which by loss of two moles of methane was expected to afford a monomeric icosahedral metallacarborane $Me_3N\text{-}ZnC_2B_9H_{11}$, Scheme 1. The units $Me_3N\text{-}Zn^{2+}$ and HB^{2+} are formally isolobal, and so in principle HB^{2+} units of borane clusters might be expected to be replaced by $Me_3N\text{-}Zn^{2+}$ units. The analogous beryllium complex, $[Me_3N\text{-}BeC_2B_9H_{11}]$, is believed to be isostructural and isoelectronic with *closo*-$C_2B_{10}H_{12}$.[12] The stoichiometry of our product was indeed as expected; however, an X-ray crystallographic study§ has shown it to have an alternative remarkable macropolyhedral dimeric structure, $[(nido\text{-}C_2B_9H_{11})ZnNMe_3]_2$ **1**, shown in Fig. 1. Although the molecule has approximate C_{2v} molecular symmetry it has no crystallographically imposed symmetry. Two *nido*-$C_2B_9H_{11}$ fragments are connected through the unique boron atoms of the *nido* carborane residues and a $Me_3NZnZnNMe_3$ unit, in which the two zinc atoms are at a separation of 2.800(1) Å (*cf.* 2.665 Å for the shortest Zn–Zn distance in metallic Zn). The bonding of these boron atoms (coordination number 7) and of the zinc atoms (coordination number 8) are we believe unprecedented, and involve a planar diamond-shaped Zn_2B_2 ring system [angles at Zn 108.1(1)° and 105.5(1)°; two equal angles at B 73.2(1)°]. This is reminiscent of the 3-centre 2-electron (3c2e) bonds in the M_2C_2 ring systems of electropositive metal alkyls, as in Al_2Me_6,[13] or $(BeMe_2)_n$,[14] with characteristically acute angles at the alkyl carbon and obtuse angles at the electropositive metals. By contrast, zinc alkyls, ZnR_2 (R = Me, Et, Pr^n) are monomeric by gas-phase electron diffraction,[15] although in the solid state, diphenyl zinc is dimeric, $[(C_6H_5Zn)_2(\mu\text{-}C_6H_5)_2]$ [Zn–Zn = 2.685 Å], with unsymmetrical bridges, assigned to σ-covalent and π-dative bonds.[16] The Zn–Zn separations observed in amide-bridged $[(MeZn)(\mu\text{-}NPh_2)]_2$ (2.913 Å),[17] chloride-bridged $[Zn_2Cl_6]^{2-}$ (typically 3.06 to 3.3 Å)[18] and other electron-precise species, are longer than that in **1**.

In addition to the Zn_2B_2 ring the coordination about each zinc atom is completed by one NMe_3 ligand and interaction of a pair of B–H bonds with each zinc atom. Since Me_3N-Zn is isolobal with BH, compound **1** would be isolobal with the (unknown) species $C_4B_{20}H_{24}$ and $[B_{24}H_{24}]^{4-}$. The closest known carborane is $C_4B_{18}H_{22}$, which contains two $C_2B_9H_{11}$ residues directly fused.[19] Other clusters distantly related to **1** include *syn*-$B_{14}H_{20}$[20] and *anti*-$\{[Pt(PMe_2Ph)]_2(nido\text{-}B_6H_9)_2\}$ containing

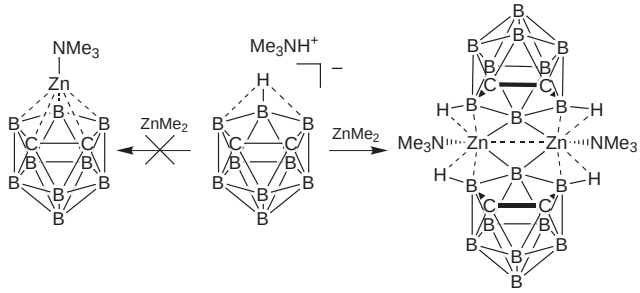

Scheme 1 Expected and isolated products from the reaction of $ZnMe_2$ and $[(NMe_3H)^+(nido\text{-}C_2B_9H_{12})^-]$. Terminal hydrogens on each boron and carbon atom are omitted.

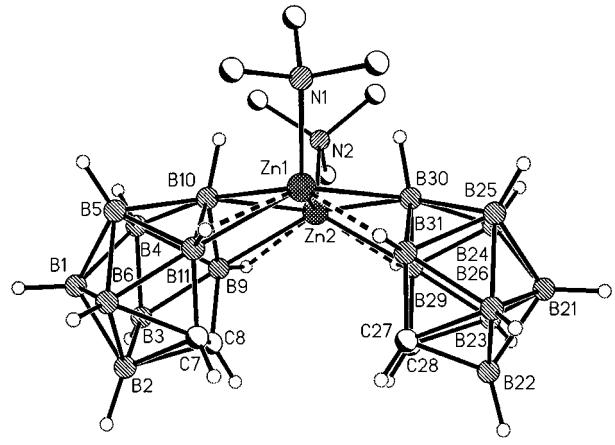

Fig. 1 A view of the 'head-set' or 'ear-muff' molecular structure of $[(nido\text{-}C_2B_9H_{11})ZnNMe_3]_2$, showing the adopted atom numbering scheme. Hydrogen atoms on the NMe_3 ligands are omitted for clarity. Selected bond lengths (Å) and angles (°): Zn(1)–B(10) 2.315(3), Zn(1)–B(11) 2.177(3), Zn(1)–B(30) 2.340(3), Zn(1)–B(31) 2.165(3), Zn(2)–B(9) 2.160(3), Zn(2)–B(10) 2.380(3), Zn(2)–B(29) 2.163(3), Zn(2)–B(30) 2.352, Zn(1)–N(1) 2.065(2), Zn(2)–N(2) 2.062(2), Zn(1)–Zn(2)–N(2) 127.30(8), Zn(2)–Zn(1)–N(1) 126.87(6); other values are given in the text.

square planar 16 electron platinum.[21] There is some structural resemblance to the μ-allyl ligand bridging two metal atoms in $[W_2(\mu;\eta^3\text{-}C_3H_5)_2(NMe_2)_4]$,[22] though in this allyl complex the central W_2C_2 ring is far from planar.

The geometry of the Zn_2B_2 ring at the centre of the structure of **1** prompts us to interpret the metal–ligand bonding primarily in terms of two 3c2e Zn–B–Zn bonds. However, it should be noted that there is a roughly tetrahedral coordination about each metal atom if one counts the other metal atom, and trimethylamine ligand, and two BH units (connected to the bridging B atom) as defining the ligand sphere and ignores the bridging boron atoms. It is clear that a rationalisation of this structure in terms of a localised bonding model has its limitations. We are undertaking more detailed investigations of the bonding in $[(nido\text{-}C_2B_9H_{11})ZnNMe_3]_2$ using molecular orbital methods, and these will be reported in a subsequent publication.

We acknowledge the award by the University of Durham of a Sir Derman Christopherson Fellowship to J. A. K. H. and the support of the EPSRC and Kværner Process Technology (CASE award to A. L. J.).

Notes and References

† E-mail: a.k.hughes@durham.ac.uk

‡ *Selected data* for **1**. A stirred suspension of $[nido\text{-}C_2B_9H_{12}][NMe_3H]$ (0.288 g, 1.5 mmol) in toluene (20 ml) was treated dropwise with Me_2Zn (0.75 ml of 2 M solution in toluene, 1.5 mmol). After stirring for 18 h the solution was briefly refluxed and filtered whilst hot. Slow cooling to room temperature gave three crops of colourless crystals of $[(nido\text{-}C_2B_9H_{11})ZnNMe_3]_2$. Total yield 1.00 g, 96%. δ_H (300 MHz, $[^2H_5]$pyridine, $^1H\{^{11}B\}$) 2.57 (2H, BH), 2.44 (1H, BH), 2.37 (2H, BH), 2.27 (2H, BH), 2.07 (9H, NMe_3), 1.88 (1H, BH), 1.37 (1H, BH), 1.24 (2H, CH). δ_B (96.2 MHz, $[^2H_5]$pyridine) −16.3 (5B), −21.5 (2B), −32.3 (1B), −38.5 (1B). (Found: C, 36.3; H, 7.9; N, 4.9. $C_{10}H_{40}N_2B_{18}Zn_2(C_7H_8)_{1.35}$ requires C, 36.6; H, 8.0; N, 4.4%.)

§ *Crystal data* for $[(nido\text{-}C_2B_9H_{11})ZnNMe_3]_2\cdot 1.5(C_7H_8)$: $C_{20.5}H_{52}B_{18}N_2Zn_2$, M = 651.96, triclinic, space group $P\bar{1}$, a = 10.528(3), b = 10.915(3), c = 16.612(4) Å, α = 102.677(4), β = 96.566(4), γ = 107.892(4)°, U = 1738.0(7) Å^3, Z = 2, D_c = 1.246 Mg m^{-3}, μ = 1.398 mm^{-1}, 7914 unique data, 444 refined parameters, 1.28 < θ < 27.48°, R_1 = 0.0414, wR_2 = 0.1055 [all data]. X-Ray diffraction data were collected on a Siemens SMART CCD diffractometer at 150 K. Data Collection Software, SMART, Ver. 4.050, 1996, Siemens Analytical X-ray Instruments Inc., Madison, Wisconsin, USA. Data Reduction Software, SAINT, Version 4.050, 1996, Siemens Analytical X-ray Instruments Inc., Madison, Wisconsin, USA. Interactive Molecular Graphics, SHELXTL 5.04/VMS, 1995, Siemens Analytical X-ray Instruments Inc., Madison, Wisconsin, USA. One of the toluene solvates and the NMe_3 ligand containing atom N(2) each display disorder of their constituent carbon atoms. For the amine ligand only the major component is shown in Fig. 1. CCDC 182/937.

1 R. N. Grimes, in *Comprehensive Organometallic Chemistry II*, ed. E. W. Abel, F. G. A. Stone and G. Wilkinson, Pergamon Press, Oxford, 1995, vol. 1, ch. 9; A. K. Saxena and N. S. Hosmane, *Chem. Rev.*, 1993, **93**, 1081; A. K. Saxena, J. A. Maguire and N. S. Hosmane, *Chem. Rev.*, 1997, **97**, 2421.
2 V. C. Gibson, *J. Chem. Soc., Dalton Trans.*, 1994, 1607; T. P. Hanusa, *Polyhedron*, 1982, **1**, 663; D. M. P. Mingos, M. I. Forsyth and A. J. Welch, *J. Chem. Soc., Dalton Trans.*, 1978, 1363.
3 M. L. H. Green, *J. Organomet. Chem.*, 1995, **500**, 127.
4 M. F. Hawthorne, *J. Organomet. Chem.*, 1975, **100**, 97; H. M. Colquhoun, T. J. Greenhough and M. G. H. Wallbridge, *J. Chem. Soc., Dalton Trans.*, 1979, 619; D. M. P. Mingos, M. I. Forsyth and A. J. Welch, *J. Chem. Soc., Dalton Trans.*, 1978, 1363; M. J. Calhorda, D. M. P. Mingos and A. J. Welch, *J. Organomet. Chem.*, 1982, **228**, 309; E. J. M. Hamilton and A. J. Welch, *Polyhedron*, 1990, **9**, 2407.
5 J. Kim, S. Kim and Y. Do, *J. Chem. Soc., Chem. Commun.*, 1992, 938.
6 M. A. Beckett, J. E. Crook, N. N. Greenwood and J. D. Kennedy, *J. Chem. Soc., Dalton Trans.*, 1986, 1879.
7 S. Aldridge, A. J. Blake, A. J. Downs, S. Parsons and C. R. Pulham, *J. Chem. Soc., Dalton Trans.*, 1996, 853; R. L. Bansamer, J. C. Huffman and K. G. Caulton, *J. Am. Chem. Soc.*, 1983, **105**, 6163; A. P. Borisov, N. N. Mal'tseva and N. S. Kedrova, *Koord. Khim.*, 1991, **17**, 405; M. A. Porai Koshits, A. S. Antsyshkina, A. A. Pasynskii, G. G. Sadikov, Yu. V. Skripkin and V. N. Ostrikova, *Koord. Khim.*, 1979, **5**, 1103; G. A. Koutsantonis, F. C. Lee and C. L. Raston, *J. Chem. Soc., Chem. Commun.*, 1994, 1975.
8 N. N. Greenwood, J. A. McGinnety and J. D. Owen, *J. Chem. Soc. A*, 1971, 809; R. Allmann, V. Batzel, R. Pfeil and G. Schmid, *Z. Naturforsch., Teil B*, 1976, **31**, 1329.
9 S. Aldridge, A. J. Blake, A. J. Downs and S. Parsons, *J. Chem. Soc., Chem. Commun.*, 1995, 1363; S. A. Snow, M. Shimoi, C. D. Ostler, B. K. Thompson, G. Kodama and R. W. Parry, *Inorg. Chem.*, 1984, **23**, 511.
10 D. A. Owen and M. F. Hawthorne, *J. Am. Chem. Soc.*, 1971, **93**, 873.
11 N. S. Hosmane, D. Zhu, J. E. McDonald, H. Zhang, J. A. Maguire, T. G. Gray and S. C. Helfert, *Organometallics*, 1998, **17**, 1426.
12 G. Popp and M. F. Hawthorne, *Inorg. Chem.*, 1971, **10**, 391.
13 J. C. Huffman and W. E. Streib, *J. Chem. Soc. D*, 1971, 911.
14 A. I. Snow and R. E. Rundle, *Acta Crystallogr.*, 1951, **4**, 348
15 A. Almenningen, T. U. Helgaker, A. Haaland and S. Samdal, *Acta Chem. Scand., Ser. A*, 1982, **36**, 159.
16 P. R. Markies, G. Schat, O. S. Akkerman, F. Bickelhaupt, W. J. J. Smeets and A. L. Spek, *Organometallics*, 1990, **9**, 2243.
17 N. A. Bell, H. M. M. Shearer and C. B. Spencer, *Acta Crystallogr., Sect. C.*, 1983, **39**, 1182.
18 Search of Cambridge Structural Database; F. H. Allen and O. Kennard, *Chem. Des. Automat. News*, 1993, **8**, 1; 31.
19 Z. Janoušek, B. Štíbr, X. L. R. Fontaine, J. D. Kennedy and M. Thornton-Pett, *J. Chem. Soc., Dalton Trans.*, 1996, 3813.
20 J. C. Huffman, D. C. Moody and R. Schaeffer, *Inorg. Chem.*, 1981, **20**, 741.
21 N. N. Greenwood, M. J. Hails, J. D. Kennedy and W. S. McDonald, *J. Chem. Soc., Dalton Trans.*, 1985, 953.
22 R. H. Cayton, M. H. Chisholm, M. J. Hampden-Smith, J. C. Huffman and K. G. Moodley, *Polyhedron*, 1992, **11**, 3197.

Received in Cambridge, UK, 8th June 1998; 8/04305A

A novel layered indium sulfide material consisting of corner and edge shared InS_4 tetrahedra: synthesis and structural characterization of DPA-InS-SB3

Christopher L. Cahill,*[a] Biagio Gugliotta[a] and John B. Parise[a,b]

[a] *Department of Chemistry, State University of New York at Stony Brook, Stony Brook, NY 11794, USA. E-mail: Christopher.Cahill@sunysb.edu; John.Parise@sunysb.edu*

[b] *Department of Geosciences, State University of New York at Stony Brook, Stony Brook NY 11794-2100, USA*

A novel layered indium sulfide inorganic/organic composite material has been synthesized under solvothermal conditions and characterized *via* single crystal X-ray diffraction.

Metal sulfide based microporous solids were first reported by Bedard *et al.* in 1989.[1] The ability of main group metals to coordinate tetrahedrally with sulfur, as Al and Si do with oxygen in the molecular sieve oxides[2] suggested that a new family of materials with structures resembling those of the zeolites (for example) could exist. These compounds however, did not contain the MS_4 tetrahedra that might be expected in materials structurally related to the oxides. Rather, complex building units such as the $Sb_3S_6^{3-}$ semi-cube,[3] the Sn_3S_4 semi-cube,[1,4] the $[Ge_4S_{10}]^{4-}$ adamantine unit,[5] and the $[In_{10}S_{20}]^{10-}$ and $[Sn_{10}S_{20}O_4]^{8-}$ supertetrahedra[6,7] condense to form structures analogous to zeolites,[5c] neso-,[5d] iono-[5e] and tecto-silicate materials.[5a,b] We report here the synthesis and structure of a novel layered sulfide material consisting of linked InS_4 tetrahedra: DPA-InS-SB3 [DPA = dipropylamine, $(C_3H_7)_2NH$].

The synthesis of DPA-InS-SB3 (**1**) was achieved by reacting elemental In and elemental S with the organic structure directing agent dipropylamine in the approximate molar ratio 1 : 2.3 : 3.5. Reactant slurries were sealed in Pyrex tubes and held static at 180 °C under autogenous pressures for 5 days. The resultant product, a white powder, was washed with ethanol and water and allowed to air dry. Large single crystals up to 0.2 mm on edge were obtained and isolated for X-ray diffraction. Qualitative electron probe microanalysis (EPMA) on the crystals revealed the presence of In, S, and N.

The structure of **1** was determined from single crystal X-ray diffraction† data and is shown in Fig. 1. The primary structural building units of this material are InS_4 tetrahedra which corner and edge link to form layers that stack along (100). Alternatively, the structure can be viewed in terms of In_6S_{11} subunits that form infinite chains running along (010) [Fig. 1(*b*)]. Within the chains, all tetrahedra are linked to one another *via* corner sharing of vertex sulfur atoms. Between chains however, InS_4 tetrahedra edge share [In6–S11–In6; Fig. 1(*b*)] to stitch the chains together approximately along (011) and (0$\bar{1}$1). This connectivity gives rise to pores within the layers that measure 6.9 × 12.8 Å and an interlayer spacing of 8.8 Å as determined from the shortest S–S distances. The layers are similar to those found in Sn–S compounds,[4] but stack such that the pores are aligned throughout the entire structure in a direction perpendicular to the In–S sheets. Although the structure of **1** is not a three-dimensional framework, its unidimensional pore topology (Fig. 1) resembles zeolites such as theta-1[8] and ZSM-23[9] and certain aluminophosphates.[10]

The In–S bond lengths range from 2.420 to 2.534 Å, with an average of 2.432 Å. These values are consistent with those reported in other In–S materials containing tetrahedrally coordinated In.[11] Bond valence sums[12] gave no indication of any mixed valency in indium, which has been observed previously in In–S compounds.[13] Sulfur coordination with In ranges from one to three. The singly coordinated sulfur [S7, Fig. 1(*b*)], is also bound to a hydrogen atom to form a terminal –SH group. The edge sharing of two InS_4 tetrahedra gives one short In–In (In6–In6) contact of 3.299 Å, as opposed to an average of about 3.9 Å for other In–In distances within **1**, and 3.24 Å in indium metal.[14]

The strain associated with this geometry is reflected in the S–In6–S [S11, 10, 6; Fig. 1(*b*)] bond angles which range from

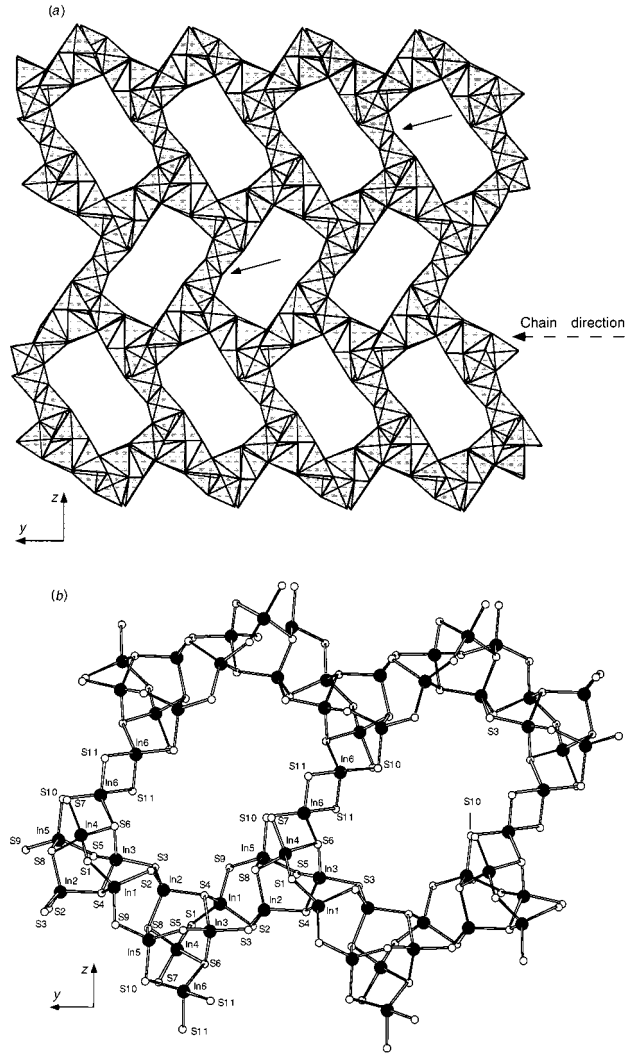

Fig. 1 (*a*) A view down (100) of a single layer of DPA-InS-SB3: $[(C_3H_7)_2NH_2]_3In_6S_{11}H$. This polyhedral representation shows the corner linking of tetrahedra within the In–S chains along (010) (dashed arrow) and the edge sharing of tetrahedra (bold arrows) to link chains together. For clarity, the ordered DPA cations have been omitted and only two edge sharing locations are labeled. (*b*) A labeled portion of two pores from a single layer of **1** in the same orientation as in (*a*). The pore size (6.9 × 12.8 Å) was determined from S3–S3 and S10–S10 distances.

96.23(6) to 120.01(8)° as opposed to an ideal tetrahedral value of 109.5°.

The organic component of **1** is located within the extra-framework voids of the structure. A hydrogen bonded host/guest relationship is proposed as protons on the nitrogen atoms are within 2.3–2.6 Å of sulfur atoms on the In–S framework. IR spectroscopy suggests that the DPA molecules are protonated although a second hydrogen on one of the three N atoms was not located in the X-ray analysis. A medium absorption band at 1579 cm^{-1} corresponding to a N–H bend of a secondary amine salt and strong N–H stretching bands (3000–2700 cm^{-1}) were observed.[15] A weak band at 2515 cm^{-1} was assigned to the S–H stretching vibration[15] of S7–H (see above). With respect to these designations, all nitrogen atoms were assumed to be protonated to balance the 3− charge on the $In_6S_{11}H$ framework, thus giving an overall stoichiometry of $[(C_3H_7)_2NH_2]_3In_6S_{11}H$.

Other experiments involving treatment of elemental In and S in the presence of amines have resulted in formation of the $[In_{10}S_{20}]^{10-}$ supertetrahedral building unit.[6] It is possible that the amount of water or the size of the amine in a preparation dictates which building unit will form. An investigation of the mother liquors from which these In–S materials crystallize is in progress.

This study was supported by the National Science Foundation (DMR 94-13003). The authors wish to thank Dr Victor G. Young Jr. of the X-ray crystallography Laboratory, University of Minnesota (Minneapolis), for data collection and structure solution.

Notes and References

† *Crystal structure data* for DPA-InS-SB3 $[(C_3H_7)_2NH_2]_3In_6S_{11}H$: M = 1346.15, monoclinic, space group $P2_1/c$, a = 12.2366(3), b = 12.2834(3), c = 28.5484(6) Å, β = 101.960(1), Z = 4, μ(Mo-Kα) = 3.804 mm^{-1}; Data collection at 298(2) K; Siemens SMART Platform CCD: 20 419 reflections collected, 7334 unique; R indices [$I > 2\sigma(I)$ = 5965]: R_1 = 0.0370, wR_2 = 0.0721; R indices (all data): R_1 = 0.0531, wR_2 = 0.0722. CCDC 182/935.

1 R. L. Bedard, S. T. Wilson, L. D. Vail, J. M. Bennett and E. M. Flanigen, *The next generation: Synthesis, characterization and structure of metal–sulfide-based microporous solids, Proceedings of the Zeolites: Facts, Figures, Future. Proceedings of the 8th International Zeolite Conference*, Amsterdam, 1989.
2 D. W. Breck, *Zeolite Molecular Sieves*, Krieger, Malabar, FL, 1984.
3 J. B. Parise, *Science*, 1991, **251**, 292; J. B. Parise and Y. Ko, *Chem. Mater.*, 1992, **4**, 1446.
4 Y. Ko, K. Tan, D. M. Nellis, S. Koch and J. B. Parise, *J. Solid State Chem.*, 1995, **114**, 506; T. Jiang, A. J. Lough, G. A. Ozin and D. Young, *Chem. Mater.*, 1995, **7**, 245; T. Jiang, G. A. Ozin and R. L. Bedard, *Adv. Mater.*, 1995, **7**, 166; T. Jiang, G. A. Ozin and R. L. Bedard, *Adv. Mater.*, 1994, **6**, 860; Y. Ko, C. Cahill and J. B. Parise, *J. Chem. Soc., Chem. Commun.*, 1994, 69.
5 (*a*) C. L. Bowes, W. U. Huynh, S. J. Kirkby, A. Malek, G. A. Ozin, S. Petrov, M. Twardowski and D. Young, *Chem. Mater.*, 1996, **8**, 2147; (*b*) O. M. Yaghi, Z. Sun, D. A. Richardson and T. L. Groy, *J. Am. Chem. Soc.*, 1994, **116**, 807; (*c*) C. L. Cahill and J. B. Parise, *Chem. Mater.*, 1997, **9**, 807; (*d*) J. Y. Pivan, O. Achak, M. Louer and D. Louer, *Chem. Mater.*, 1994, **6**, 827; (*e*) D. M. Nellis, Y. Ko, K. Tan, S. Koch and J. B. Parise, *J. Chem. Soc., Chem. Commun.*, 1995, 541; (*f*) C. L. Cahill, Y. Ko, J. C. Hanson, K. Tan and J. B. Parise, *Chem. Mater.*, 1998, **10**, 1453.
6 C. L. Cahill, Y. Ko and J. B. Parise, *Chem. Mater.*, 1998, **10**, 19.
7 J. B. Parise, Y. Ko, K. Tan, D. M. Nellis and S. Koch, *J. Solid State Chem.*, 1995, **117**, 219; J. B. Parise and Y. Ko, *Chem. Mater.*, 1994, **6**, 718.
8 S. A. I. Barri, G. W. Smith, D. White and D. Young, *Nature*, 1985, **312**, 533.
9 P. A. Wright, J. M. Thomas, G. R. Millward, S. Ramadas and S. A. I. Barri, *J. Chem. Soc., Chem. Commun.*, 1985, 1117.
10 J. M. Bennet, J. P. Cohen, E. M. Flanigen J. Pluth and J. V. Smith, *ACS Symp. Ser.*, 1983, **218**, 79; J. M. Thomas, R. H. Jones, R. Xu, J. Chen, A. M. Chippendale, S. Natarajan and A. K. Cheetham, *J. Chem. Soc., Chem. Commun.*, 1992, 929.
11 B. Krebs, D. Voelker and K.-O. Stiller, *Inorg. Chim. Acta*, 1982, **65**, L101; B. Eisenmann and A. Hoffma, *Z. Kristallogr.*, 1991, **195**, 318.
12 N. E. Brese and M. O'Keefe, *Acta Crystallogr. Sect. B*, 1991, **47**, 192.
13 H. J. Deiseroth, H. Pfeifer and A. Stupperich, *Z. Kristallogr.*, 1993, **207**, 45.
14 A. F. Wells, *Structural Inorganic Chemistry*, Clarendon Press, Oxford, 1984.
15 R. M. Silverstein, G. C. Bassler and T. C. Morril, *Spectrometric Identification of Organic Compounds*, Wiley, New York, 1991.

Received in Columbia, MO, 6th April 1998; 8/02628I

Reversible occlusion of CO in Cs-impregnated X and Y zeolites

E. Garrone,*[a] N. Russo,[a,b] P. Marturano,[a] B. Onida,[b] F. Di Renzo[c] and M. Laspéras[c]

[a] *Dipartimento di Chimica Inorganica, Fisica e dei Materiali,Università di Torino, Via P. Giuria 7, 10125, Torino, Italy. E-mail: garrone@ch,unito.it*

[b] *Dipartimento di Scienza dei Materiali e Ingegneria Chimica, Politecnico di Torino, C.so Duca degli Abruzzi 24, 10129, Torino, Italy*

[c] *Laboratoire de Matériaux Catalytiques et Catalyse en Chimie Organique, ENSCM, 8 rue Ecole Normale, 34296 Montpellier France*

Cs_2O in the supercages of Cs-impregnated X and Y zeolites attacks the siliceous portions of the lattice (siloxane bridges), with formation of $(Si–O^-Cs^+)_2$ groups which allow the occlusion (reversible at high temperature) of CO in the sodalite units, as indicated by the formation of an IR band at 2150 cm^{-1}.

Basic zeolites (bearing alkali metal counterions) arouse much interest these days, because they may possibly replace in catalysis harsh chemicals like sodium hydroxide. Besides cationic exchange of the original Na^+ for Cs^+, to increase basicity, samples are further impregnated[1] with Cs acetate, which, on thermal treatment, converts to Cs_2O. The nature of such an oxide in the zeolite matrix depends on the activation conditions and is currently under discussion.[2]

In the course of a systematic study of basic centres in Cs-exchanged and Cs-impregnated X and Y zeolites,[3] we made the intriguing observation that a weak band at 2150 cm^{-1} is formed in the IR background spectrum, recorded at room temperature, of impregnated (but not simply exchanged) samples in the activation step (lower curve in Fig. 1). This activation step consists of thermal treatment (during which decomposition of the acetate takes place) and subsequent oxidation under oxygen at 823 K as described by Laspéras *et al*.[3]

Two Cs impregnated samples, with different Cs contents (8 and 24 atoms per unit cell) were considered, with both Y and X zeolites. IR spectra were recorded on a Perkin-Elmer 1760-X spectrophotometer equipped with a MCT cryodetector, at a resolution of 2 cm^{-1}.

The intensity of the IR band at 2150 cm^{-1} was larger for Y than for X zeolites, and it varied with the Cs_2O content. Outgassing at about 820 K depletes the band. Its peak position is strongly indicative of CO interacting with Na^+ cations, which

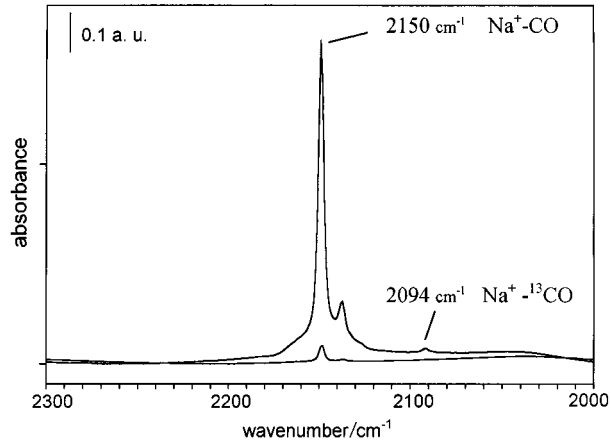

Fig. 1 Infrared spectra of Cs impregnated X zeolite (24 Cs per unit cell). Lower curve: after activation at 823 K; upper curve: after heating in CO atmosphere at 770 K for 1 hour and cooling in the same atmosphere.

are left behind in the exchange process. Thermal decomposition of the acetate is likely to yield CO: such an assignment cannot, however, be made lightly, because CO adsorption on alkali-exchanged zeolites only takes place at temperatures around 77 K[4,5] under substantial CO pressure.

Heating of the impregnated samples in a CO atmosphere at temperatures around 770 K followed by cooling in the same atmosphere leads to an enormous increase in the intensity of the 2150 cm^{-1} band (upper curve in Fig. 1), so that even the ^{13}C satellite band can be observed, though the natural abundance of ^{13}C is only 1%. This confirms beyond doubt that the band is due to CO held in the solid. The nature of the species giving rise to the peak appearing at 2137 cm^{-1} is not discussed here. If heating in CO is followed by evacuation at the same temperature before cooling, a decrease of the original band is observed: CO contact at room temperature has no effect. Prolonged heating of the samples holding CO at 823 K in vacuum depletes the band.

A plausible assignment of the band under discussion is the stretching mode of CO molecules interacting with Na^+ cations: these latter, however, are not those normally exposed at the supercages, but are instead the Na^+ cations inside the sodalite cages, usually not accessible to molecules, though the mineral sodalite is known to occlude large rare-gas atoms like Kr.[6]

We favour Na^+ over Cs^+ as the centre of interaction for the following reasons: (i) the ν(CO) frequency is closer to the values reported in the literature for the former cation; (ii) if reference is made to the standard geometry of the sodalite cage. There is not enough room for Cs^+ cations and CO molecules to coexist in the cage.

We have checked, by means of computer graphics, that a CO molecule may be occluded in the sodalite cages of an X zeolite, of composition close to the one studied by us, for which structural data are available.[7] One CO molecule may be hosted in the cavity: little room is left, however, so that the molecule is actually trapped in the sodalite cage. Indeed, the ratio between the frequencies of ^{12}CO and ^{13}CO (see Fig. 1) indicates that the motion is particularly anharmonic. The peculiarity of such an interaction occurring at room temperature also accounts for the lower frequency observed for related CO in comparison with that observed for CO interacting at 77 K with Na^+ cations in supercages (2154 cm^{-1}).

Thermal treatments in CO, even at high temperatures, of the simply exchanged samples do not cause the appearance of the 2150 cm^{-1} band. This is therefore strictly related to the presence of Cs_2O. On the other hand, the intensity of the 2150 cm^{-1} band is much higher with Y than with X zeolite, *i.e.* the occlusion of CO is greater, the larger the Si content of the sample. Chemical attack of the lattice by Cs_2O is indicated by the loss of crystallinity we observed in the XRD patterns for thermal treatment above 670 K. A plausible mechanism is then the reaction of siloxane bridges with caesium oxide: $Si–O–Si + Cs_2O \rightarrow (Si–O^-Cs^+)_2$, to yield a microcluster of Cs silicate, according to rather elementary chemistry. The cleavage of the

siloxane bridge widens the window giving access to the sodalite cage, which is partially obstructed by the Si–O^{-}Cs^{+} groups. At high temperatures, thermal movement of these groups may give CO molecules access to sodalite cavities, which is then prevented at low temperatures.

Whereas occlusion phenomena are known in some fields of chemistry (clathrates, matrix isolation), to our knowledge, the phenomenon reported here is the first case of reversible occlusion in the solid state: it may probably be extended to other suitably sized molecules like nitrogen and oxygen, and to other zeolitic systems.

Notes and References

1 C. Lacroix, A. Deluzarche, A. Kiennemann and A. Boyer, *J. Chim. Phys*., 1984, **81**, 473; P. E. Hathaway and M. E. Davis, *J. Catal*., 1989, **116**, 263.

2 F. Yagi, N. Kanuka, H. Tsuji, S. Nakata, H. Kita and H. Hattori, *Microporous Mater*., 1997, **9**, 229.

3 M. Laspéras, H. Cambon, D. Brunel, I. Rodriguez and P. Geneste, *Microporous Mater*., 1996, **7**, 61.

4 A. Zecchina, S. Bordiga, C. Lamberti, G. Spoto, L. Carnelli and C. Otero Aréan, *J. Phys. Chem*., 1994, **98**, 9577.

5 S. Bordiga, E. Garrone, C. Lamberti, A. Zecchina, C. Otero Aréan, V. B. Kazansky and L. M. Kustov, *J. Chem. Soc., Faraday Trans*., 1994, **90**, 3367.

6 R. M. Barrer, *Zeolites and Clay Minerals as Adsorbents and Molecular Sieves*, Academic Press, London, 1978, pp. 148–335.

7 Y. F. Shepelov, I. K. Butikova and Y. I. Smolin, *Zeolites*, 1991, **11**, 287.

Received in Cambridge, UK, 21st May 1998; 8/03829E

Halogen exchange during atom transfer polymerisation of methyl methacrylate mediated by copper(I) *N*-alkyl-2-pyridylmethanimine complexes

David M. Haddleton,*† Alex M. Heming, Dax Kukulj and Stuart G. Jackson

Department of Chemistry, University of Warwick, Coventry, UK CV4 7AL

Highly efficient exchange between the halogen arising from the copper(I) halide and the alkyl halide originating from the initiator occurs during atom transfer polymerisation of methyl methacrylate mediated by copper(I) *N*-alkyl-2-pyridylmethanimine complexes.

Living/controlled polymerisations of vinyl monomers lead to the synthesis of polymers with well controlled architecture and predetermined molecular weight. Living/controlled *radical* polymerisation is of increasing importance due to the resilience of free-radical polymerisations to impurities and protic species invariably present in the monomer, solvent, *etc*. Transition metal mediated atom transfer polymerisation has been pioneered by Matyjaszewski, using $Cu^{I}X$ (X = Cl, Br) in conjunction with 2,2-bipyridine[1] and substituted bipyridines,[2–5] and Sawamoto, using $[Ru(PPh_3)_3Cl_2]$.[6–8] Since then a number of different systems using transition metal complexes to polymerise styrenes, methacrylates and acrylates have been reported including $[Ni(PPh_3)_3X_2]$,[9] $[Ni\{o,o\text{-}(Me_2NCH_2)_2C_6H_3\}Br]$,[10] $[Pd(OAc)_2(PPh_3)_4]$,[11] $[Rh(PPh_3)_3Cl]$,[12] and [Cu(*N*-alkyl-2-pyridylmethanimine)$_2$X].[13] More recently Teyssie has reported $FeCl_3$ mediated polymerisation in the presence of PPh_3 for the living/controlled polymerisation of methyl methacrylate (MMA) initiated with a conventional free-radical initiator, AIBN.[14]

It has been previously demonstrated that atom transfer polymerisation is an excellent one step method for the preparation of α-functional polymers.[15–17] The alkyl halide initiator can possess a wide variety of functionalities without causing loss of performance or control over the reaction. Although the existence of several different functionalities at the α-terminal end group has been demonstrated, no detailed study has been made on the nature of the ω-terminal end group. The assumption has been that the ω-terminal end group contains the halogen atom originating from the initiator molecule.

The aim of the work reported here was to investigate the possibility, and extent, of halogen exchange between polymer and catalyst in the polymerisation of methyl methacrylate mediated by [Cu(*N*-alkyl-2-pyridylmethanimine)$_2$X] complexes. During the course of this work two papers appeared referring to the possibility of halogen exchange in atom transfer polymerisation. Sawamoto reported observing the presence of both bromide and chloride ω-end groups in the ^{1}H NMR spectrum of PMMA from bromomalonate initiation catalysed with $Ru(PPh_3)_3Cl_2$.[18] Matyjaszewski *et al.* stated that exchange can occur between the halogen from the initiator and the halogen on the catalyst for BnBr and 2-bromopropionate with $Cu^{I}X$/4,4-di(nonan-5-yl)-2,2-bipyridine catalyst; however, no experimental details were provided.[19] In addition, Matyjaszewski reported similar exchange occurring during the polymerisation of MMA based on matrix-assisted laser desorption ionisation time of flight (MALDI-TOF) and electro-spray ionisation (ESI) mass spectrometry;[19] again, no spectra or experimental details were provided. We have found that this approach is fraught with difficulties due to the ease of fragmentation of these type of polymers within the mass spectrometer.[20]

Table 1 Reaction conditions and results for poly(methyl methacrylate) produced using atom transfer polymerisation with sulfonyl halide initiators and copper halide catalysts

Reaction[a]	Initiator[b]	Mediator	*t*/h	M_n[c]	PDI[d]	Halogen on ω-end group
A	TsBr	CuBr	3	4130	1.10	Br
B	TsCl	CuCl	48	2170	1.06	Cl
C	TsCl	CuBr	22	1900	1.08	Cl
D	TsBr	CuCl	11	4170	1.09	Cl

[a] See footnote ‡. [b] Synthesis of TsBr modified from the preparation of TsI by Truce *et al*. (ref. 22). [c] Number average molecular weight measured by SEC, using THF as eluent at 1 ml min^{-1} calibrated with narrow molecular weight distribution PMMA standards. [d] Polydispersity index from SEC.

In order to study the effects of halogen exchange, PMMA was synthesised using four different combinations of initiator and copper(I) halide (Table 1, reactions A–D). In each case the ligand used to complex copper(I) was *N*-pentyl-2-pyridylmethanimine and the polymerisation was carried out in xylene solution (35% w/w). The polymerisations were allowed to proceed until the number average molecular weight, M_n, reached approximately 2000–4000 g mol^{-1} (20–40% conversion), as monitored by size exclusion chromatography (SEC). Polymerisations were stopped, by cooling to room temperature, at low conversion in order to minimise termination by conventional radical-radical interactions. Low molecular weights were targeted to enable end group analysis by ^{13}C NMR spectroscopy. Fig. 1 shows the ^{13}C NMR spectra of the products from reactions A–D between δ 68 and 58, the –*C*–X region, to focus on the nature of the ω-end group. For reaction A the ω-terminal [–*C*(CH$_3$)(CO$_2$Me)Br] can be seen as three peaks between δ 58.9 and 58.3, Fig. 1(*a*), which correspond to *racemic*

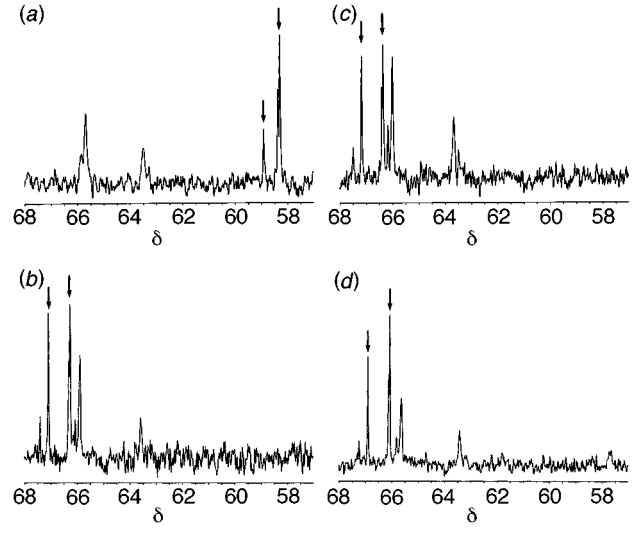

Fig. 1 ^{13}C NMR spectra of PMMA made by ATP, initiated with (*a*) TsBr and CuBr, (*b*) TsCl and CuCl, (*c*) TsCl and CuBr, and (*d*) TsBr and CuCl. Marked peaks are from halogenated ω-end groups.

(syndiotactic) and *meso* (isotactic) terminal units respectively. The position of the halogenated carbon atom was verified by comparison with a spectrum of a model compound, methyl-2-bromoisobutyrate, $[(CH_3)_2C(CO_2Me)Br]$, δ 55.4. The product from reaction B shows a similar set of peaks due to $[-C(CH_3)(CO_2Me)Cl]$ shifted downfield, between δ 67.1 and 66.3 [Fig. 1(*b*)], as expected for a chlorinated carbon relative to a brominated one. On examining the spectrum from the product of reaction C [Fig. 1(*c*)] it can be seen that the polymer has exclusively chlorinated ω-end groups with peaks between δ 67.2 and 66.4, *i.e.* the product is the same as that from reaction B. There are no peaks observed in the region δ 58.0 to 60.0 corresponding to a bromine ω-end group functionality. Thus, no observable halogen exchange occurs between the bromide originating from copper(I) bromide and the propagating polymer end capping group, a chlorine atom originating from the initiator. This result is what might be expected for the generally accepted mechanism for atom transfer polymerisation (Scheme 1), *viz.* the halogen atom that originated on the initiator is

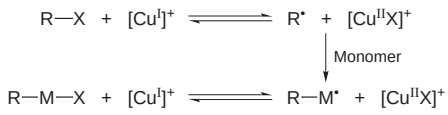

Scheme 1

transferred between transition metal complex and polymer chain end throughout the reaction and is present as the ω-end group of product. For reaction D, three peaks between δ 66.9 and 66.1 are observed corresponding to $[-C(CH_3)(CO_2Me)Cl]$ with no peaks upfield due to brominated ω-end groups [Fig. 1(*d*)]. This result is surprising because the polymer exclusively has chlorinated ω-end groups even though a sulfonyl bromide initiator was employed, so complete halogen exchange has occurred.

Our results show that polymerisation of MMA by atom transfer polymerisation mediated by a Cu(*N*-alkyl-2-pyridylmethanimine)$_2$X complex in xylene at 90 °C in the presence of both bromine and chlorine atoms results in solely chloro ω-functional polymer. This can be attributed to the greater strength of the C–Cl bond compared with the C–Br one, *i.e.* the formation of a C–Cl bond is energetically favourable and its homolysis is less facile. This result differs from that of Sawamoto, who found a mixture of Cl and Br in the ω-end group when polymerising MMA initiated with a bromomalonate compound and $Ru(PPh_3)_3Cl_2/Al(OPr^i)_3$ in toluene at 80 °C,[18] and Matyjaszewski, who claimed to have observed a mixture of Cl and Br ω-end groups.[19] Therefore, the tendency for exchange to occur must be effected by the transition metal complex and/or reaction conditions.

The observation of halogen exchange shows that the mechanism of atom transfer polymerisation is more complicated than first thought.[13,19] It is likely that, in reactions where both Cl and Br species are present, the Cu^{II} species contains both in similar states regardless of their origin (initiator or catalyst) and exchange could then occur as the propagating polymer centre abstracts one or other halogen in the deactivation step. Alternatively, exchange may occur by nucleophilic attack of the halide counter-anion from the catalyst at the alkyl halide group of initiator or deactivated polymer. The reaction may also involve bimetallic species with bridging halide or oxygen containing ligands.[3,21] It is not yet known whether exchange occurs at the first reaction step or whether several halogen transfer cycles are involved.

The occurrence of halogen exchange results in competitive rates of polymerisation which complicates the polymerisation kinetics. This may result in a broadening of the molecular weight distribution of the product and also effect the evolution of number average molecular mass with conversion when the reaction is carried out to high conversion. To avoid these effects, therefore, it is advisable to match the halides between the copper(I) salt and the initiator. This is currently under further investigation in our laboratory. It is also noted that this is the first instance of sulfonyl bromides being used as effective initiators for atom transfer polymerisation.

We thank the EPSRC for funding of this work (A. M. H. studentship and D. K. GR/L10314).

Notes and References

† E-mail: msrgs@snow.csv.warwick.ac.uk

‡ In a typical polymerisation, CuX (0.93 mmol) and TsX (0.93 mmol) ([Cu]:[initiator] = 1:1) were placed in a predried Schlenk flask which was evacuated and then flushed with dry nitrogen three times. Methyl methacrylate (10 ml, 93 mmol) was added and the suspension stirred while adding *N*-pentyl-2-pyridylmethanimine (1.87 mmol, [ligand]:[Cu] = 2:1) which instantaneously formed a deep brown solution. Xylene (20 ml) was added and the flask was heated in a thermostatted oil bath at 90 °C. The polymer was isolated by passing the cooled reaction solution down a column of activated basic aluminium oxide to remove catalyst and precipitating into hexane. ^{13}C NMR spectra were recorded on a Bruker 400 MHz spectrometer with a minimum of 4000 scans.

1 J.-S. Wang and K. Matyjaszewski, *Macromolecules*, 1995, **28**, 7901.
2 J.-S. Wang and K. Matyjaszewski, *J. Am. Chem. Soc.*, 1995, **117**, 5614.
3 J.-L. Wang, T. Grimaud and K. Matyjaszewski, *Macromolecules*, 1997, **30**, 6507.
4 J. Xia and K. Matyjaszewski, *Macromolecules*, 1997, **30**, 7697.
5 T. E. Patten, J. H. Xia, T. Abernathy and K. Matyjaszewski, *Science*, 1996, **272**, 866.
6 M. Kato, M. Kamigaito, M. Sawamoto and T. Higashimura, *Macromolecules*, 1995, **28**, 1721.
7 T. Ando, M. Kato, M. Kamigaito and M. Sawamoto, *Macromolecules*, 1996, **29**, 1070.
8 M. Sawamoto and M. Kamigaito, *Trends Polym. Sci.*, 1996, **4**, 371.
9 H. Uegaki, Y. Kotani, M. Kamigaito and M. Sawamoto, *Macromolecules*, 1997, **30**, 2249.
10 C. Granel, P. Teyssie, P. DuBois and R. Jerome, *Macromolecules*, 1996, **29**, 8576.
11 P. Lecomte, I. Drapier, P. DuBois, P. Teyssie and R. Jerome, *Macromolecules*, 1997, **30**, 7631.
12 G. Moineau, C. Granel, P. DuBois, R. Jerome and P. Teyssie, *Macromolecules*, 1998, **31**, 542.
13 D. M. Haddleton, C. B. Jasieczek, M. J. Hannon and A. J. Shooter, *Macromolecules*, 1997, **30**, 2190.
14 G. Moineau, P. Dubois, R. Jerome, T. Senninger and P. Teyssie, *Macromolecules*, 1998, **31**, 545.
15 D. M. Haddleton, C. Waterson, P. J. Derrick, C. Jasieczek and A. J. Shooter, *Chem. Commun.*, 1997, 683.
16 M. Sawamoto and M. Kamigaito, *Abstr. Pap. Am. Chem. Soc.*, 1997, **213**, 87.
17 K. Matyjaszewski, S. Coca, Y. Nakagawa and J. H. Xia, *Abstr. Pap. Am. Chem. Soc.*, 1997, **213**, 83.
18 T. Ando, M. Kamigaito and M. Sawamoto, *Tetrahedron*, 1997, **53**, 15 445.
19 K. Matyjaszewski, J.-L. Wang, T. Grimaud and D. A. Shipp, *Macromolecules*, 1998, **31**, 1527.
20 D. M. Haddleton, C. Waterson and P. J. Derrick, unpublished results.
21 D. M. Haddleton, A. J. Clark, D. J. Duncalf, A. M. Heming, D. Kukulj and A. J. Shooter, *J. Chem. Soc., Dalton Trans.*, 1998, 381.
22 W. Truce, D. Heuring and G. Wolf, *J. Org. Chem.*, 1974, ***39***, 241.

Received in Cambridge, UK, 29th May 1998; 8/04046J

Synthesis and first structural characterisation of a homoleptic tetraorganochromate(III) salt

Pablo J. Alonso, Larry R. Falvello, Juan Forniés,* M. Angeles García-Monforte, Antonio Martín, Babil Menjón and Gerardo Rodríguez

Instituto de Ciencia de Materiales de Aragón, Facultad de Ciencias, Universidad de Zaragoza-C.S.I.C., Pza. S. Francisco s/n, E-50009 Zaragoza, Spain. E-mail: forniesj@posta.unizar.es

The homoleptic, pseudo-octahedral, d³ species $[Li(thf)_4][Cr^{III}(C_6Cl_5)_4]$ 1 has been obtained and characterised by analytical, spectroscopic and X-ray diffraction methods.

The synthesis of aryl derivatives of chromium(III) and the study of their properties have drawn the attention of numerous research groups since the very beginning of this century, shortly after the synthesis of the first organomagnesium reagents. Early reports, however, were discouraging[1] or puzzling[2] and it was not until the late fifties that σ-aryl complexes of chromium(III) were isolated and recognised as species of limited stability, which are prone to rearrange, eventually yielding π-arene compounds of low-valent chromium.[3] This tendency to decompose is more pronounced in compounds with some degree of coordinative unsaturation,† which may be a principal reason for the lack of homoleptic (*i.e.*, not bearing additional stabilising ligands) organometallic compounds of formula $[Cr^{III}R_4]^-$. As far as we know, the only organometallic precedents for this stoichiometry are probably the salts $Li[Cr(C_6H_4OMe\text{-}2)_4]\cdot Et_2O$[5] and $Li[Cr(C_6H_2Me_3\text{-}2,4,6)_4]\cdot 4thf$;[6] however, no structural information is available for them.‡ Interestingly, some related tetraalkylchromate(III) salts had also been detected as solution species but could not even be isolated because they readily suffered oxidation giving the more stable neutral tetraalkychromium(IV) derivatives.[8]

We have prepared the tetraorganochromate(III) salt $[Li(thf)_4][Cr^{III}(C_6Cl_5)_4]$ **1** by arylation of $[CrCl_3(thf)_3]$[9] with LiC_6Cl_5[10] in 1 : 5 molar ratio.§ Complex **1** is a violet solid of limited thermal stability; since it is also air- and moisture-sensitive, it must be synthesised, stored and handled under an inert atmosphere and at low temperatue (below 0 °C).

The solid-state structure of **1** has been established by single-crystal X-ray diffraction analysis.¶ The lattice contains the separate ions $[Li(thf)_4]^+$ and $[Cr(C_6Cl_5)_4]^-$ together with interstitial solvent molecules. The cation has a tetrahedral geometry (local at the Li^+ ion) as usually found in other salts.[13] The core of the anion contains four σ Cr–C bonds and two additional Cr–Cl interactions, thus resulting in a pseudo-octahedral environment for the Cr atom (Fig. 1). Two of the C_6Cl_5 groups act as monodentate σ-bonded ligands, while the other two act as chelating ligands through their *ipso*-C and one of the *o*-Cl atoms. The small bite-angle of the chelating C_6Cl_5 group yields two strained four-membered metallacycles with C–Cr–Cl angles of *ca*. 60°. These acute angles are responsible for the severe deviations of the metal coordination environment from the ideal octahedral geometry. The two Cr–C distances involving C-*trans*-to-Cl atoms are virtually identical and in good agreement with those described in other σ-aryl derivatives of Cr^{III} (mean value 207 pm).[14] The two Cr–C distances involving C-*trans*-to-C atoms are slightly longer, probably due to the higher *trans* influence exerted by the anionic C atom of the aryl group. The Cr–Cl distances are clearly dissimilar and much longer than found in standard terminal chloro-complexes of chromium (mean value 232 pm).[14] The long Cr–Cl distances can be ascribed to both the poor donating ability of halocarbons and the strain of the metallacycle formed. The overall geometry of the $[Cr(C_6Cl_5)_4]^-$ anion is similar to that found in the related heavy-metal complexes $[Pt(C_6Cl_5)_4]$[15] and $[Rh(C_6Cl_5)_4]^-$.[16]

The EPR spectrum of **1** was registered (Fig. 2)‖ and analysed as a particular case** of an (S = 3/2) spin system that behaves as an (S = 1/2) system with the following spin Hamiltonian:

$$H = \mu_B B(g_x' l_x S_x + g_y' l_y S_y + g_z' l_z S_z) \qquad (1)$$

In the preceding equation l_i ($i = x, y, z$) are the direction cosines of the magnetic field of magnitude B referred to the principal axes of the $\tilde{\boldsymbol{g}}$-tensor. Using this spin-Hamiltonian and assuming Lorentzian line shapes, we have obtained an excellent agreement between the experimental [Fig. 2(*a*)] and calculated [Fig. 2(*b*)] spectra for the following set of effective principal g-values and band halfwidths: $g_x' = 4.02$, $g_y' = 3.55$, $g_z' = 1.946$; W_x = 15.0 mT, W_y = 22.5 mT, W_z = 10.0 mT. The relationship between the effective and true principal g-factors is a function of the *a priori* unknown η-parameter which accounts for the departure from axial symmetry.** Since the observed EPR spectrum is practically axial it is reasonable to assume an axial true $\tilde{\boldsymbol{g}}$-tensor as well. Under this assumption the following true g-values have been derived: $g_\parallel = 1.98$ and $g_\perp = 1.90$ with η = 0.08(1). It is interesting that, while the $g_\parallel$-value is typical for a Cr^{3+} ion, the $g_\perp$-value departs from that of the free electron by more than what is usually observed for this paramagnetic entity. This could be attributed to an extra orbital contribution due to the ligand as a consequence of the covalent bonding.

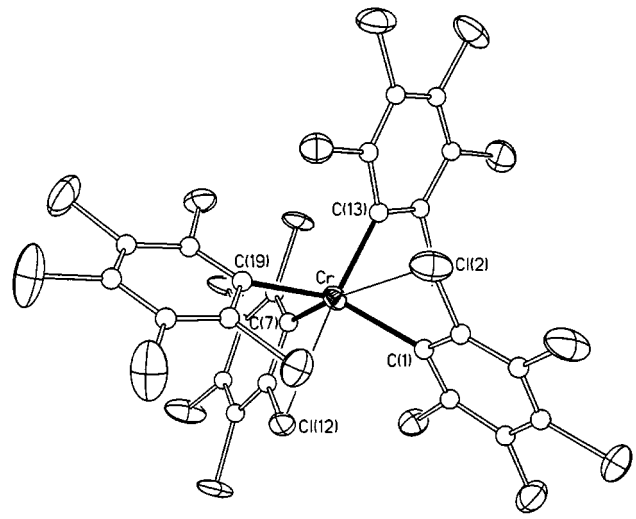

Fig. 1 Thermal ellipsoid diagram of the anion of **1**. Selected distances (pm) and angles (°): Cr–C(1) 213.7(11), Cr–C(7) 207.3(10), Cr–C(13) 208.1(10), Cr–C(19) 217.3(11), Cr–Cl(2) 300.1(4), Cr–Cl(12) 281.8(4); C(1)–Cr–C(7) 111.7(4), C(1)–Cr–C(13) 94.2(4), C(1)–Cr–C(19) 141.5(4), C(1)–Cr–Cl(2) 59.5(3), C(1)–Cr–Cl(12) 83.1(3), C(7)–Cr–C(13) 103.2(4), C(7)–Cr–C(19) 90.8(4), C(7)–Cr–Cl(2) 170.1(3), C(7)–Cr–Cl(12) 63.2(3), C(13)–Cr–C(19) 111.1(4), C(13)–Cr–Cl(2) 74.2(3), C(13)–Cr–Cl(12) 163.4(3), C(19)–Cr–Cl(2) 99.0(3), C(19)–Cr–Cl(12) 79.8(4), Cl(2)–Cr–Cl(12) 117.4(1).

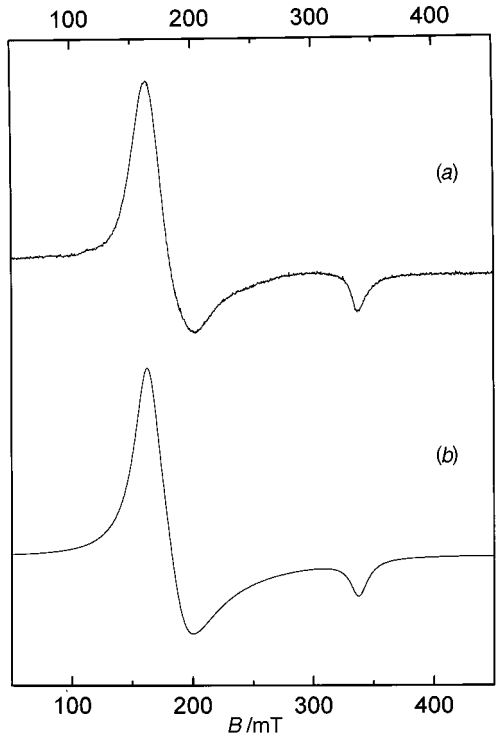

Fig. 2 EPR spectrum of a frozen CH_2Cl_2 solution of **1** at liquid nitrogen temperature (microwave frequency: 9.49 GHz): experimental (*a*) and calculated (*b*)

The homoleptic tetraorganochromate(III) salt **1** is stable enough to allow its isolation and characterisation. This reasonable stability can be ascribed to the versatility of the C_6Cl_5-group which is able to act as a standard monodentate σ-aryl ligand as well as a poor didentate one depending on the electronic and steric demands of the metal centre. Further studies aimed at exploring the chemical reactivity and redox behaviour of the new compound **1** are in progress.

We thank the Dirección General de Enseñanza Superior (Projects PB95-0003-C02-01 and PB95-0792) for financial support.

Notes and References

† The use of the very bulky bis(trimethylsilyl)methyl group has enabled Lappert and coworkers to isolate and characterise a highly unusual, coordinatively unsaturated neutral complex of formula $[CrR_3]$ (ref. 4).

‡ Hein and Schmiedeknecht reported on the synthesis of sodium and lithium tetraphenylchromate(III) salts, but the authors concluded that they were, in fact, solvent-stabilised species of formula $M[CrPh_4\cdot 2dme]\cdot 2dme$ (M = Na or Li; dme = 1,2-dimethoxyethane). The analogous thf-stabilised salts $MCrPh_4\cdot x$thf were too unstable to be isolated (ref. 7).

§ *Experimental procedure:* to a solution of LiC_6Cl_5 (*ca*. 34 mmol) in Et_2O (130 cm^3) at −78 °C was added $[CrCl_3(thf)_3]$ (2.57 g, 6.85 mmol). The suspension was allowed to warm to −10 °C and after about 4 h of stirring, the by then violet solid was filtered and extracted in CH_2Cl_2 (60 cm^3). The solvent in the extract was replaced by thf (20 cm^3) and the slow diffusion of an *n*-hexane layer (60 cm^3) into it at −30 °C yielded **1** as a violet solid in 57% yield. Anal. Found: C 36.21, H 2.02; $C_{40}H_{32}Cl_{20}CrLiO_4$ requires: C 35.73, H 2.40%. IR (KBr; cm^{-1}): 1321s, 1311s, 1281vs, 1219m, 1125m, 1059s [$\nu(COC)_{asym}$], 1043vs [$\nu(COC)_{asym}$], 915m, 887s [$\nu(COC)_{sym}$], 822vs (C_6Cl_5: X-sensitive vibr.),[11] 667vs, 600w, 415m and 349m. MS (FAB−): *m/z* 1040 $[Cr(C_6Cl_5)_4]^-$ and 828 $[Cr(C_6Cl_5)_3Cl]^-$.

¶ *Crystal data* for $\mathbf{1}\cdot 0.5OEt_2\cdot 0.5C_6H_{14}$: $C_{45}H_{44}Cl_{20}CrLiO_{4.5}$, M = 1424.74, monoclinic, a = 4151.3(6), b = 1288.25(10), c = 2387.8(3) pm, β = 117.324(12)°, U = 11.345(3) nm^3, T = 150(1) K, space group *C*2/*c* (no. 15), graphite-monochromated Mo-Kα radiation, λ = 71.073 pm, Z = 8, D_c = 1.668 g cm^{-3}, $F(000)$ = 5736, violet, approx. crystal dimensions: 0.40 × 0.25 × 0.10 mm, μ(Mo-Kα) = 1.187 mm^{-1}, measured absorption correction based on ψ scans, transmission factors: 0.899–0.793; Enraf-Nonius CAD4 diffractometer, ω–θ scans, data collection range $4.0 < 2\theta < 50.0°$, $+h$, $+k$, $\pm l$, three standard reflections showed no significant variation in intensity; 10 103 intensity data collected, 9956 unique (R_{int} = 0.0887) which were used in all calculations. The structure was solved by Patterson and Fourier methods and refined anisotropically (except for the solvent atoms) by full-matrix least squares on F^2 (program SHELXL 93; ref. 12) to final values of R_1 = 0.0870 [for 4366 data with $I > 2\sigma(I)$] and wR_2 = 0.2324 (all data) for 635 parameters; GOF = 1.037, maximum Δ/σ = 0.001, maximum $\Delta\rho$ = 1063 e nm^{-3} (−1053 e nm^{-3}) located very near the chromium atom. Hydrogen atoms were set geometrically. The weighting scheme was $w = [\sigma^2(F_o^2) + (0.0590P)^2 + 115.07P]^{-1}$, where $P = (1/3)[\max\{F_o^2,0\} + 2F_c^2]$. CCDC 182/936.

‖ EPR data were taken on a Varian E-112 spectrometer working in the X-band. The magnetic field was measured with a Bruker ER035M gaussmeter. The diphenylpicrylhydrazyl resonance signal [g = 2.0037(2)] was used to determine the microwave frequencies. The program WIN-EPR SimFonia (supplied by Bruker) was used to perform the simulation. In the calculations, the following interpolating halfwidth formula was used: $W^2(l_x,l_y,l_z) = W_x^2l_x^2 + W_y^2l_y^2 + W_z^2l_z^2$.

** The relevant spin Hamiltonian for the paramagnetic centre in **1** [Cr^{III}, d^3, S = 3/2] should read:

$$H = \mu_B\mathbf{B}\cdot\tilde{\mathbf{g}}\cdot\mathbf{S} + \mathbf{S}\cdot\tilde{\mathbf{D}}\cdot\mathbf{S}$$

where μ_B is the Bohr magneton. The first term accounts for the electronic Zeeman interaction and the second one for the zero field splitting. In the principal axes of the $\tilde{\boldsymbol{D}}$-tensor, the latter term is given by

$$\mathbf{S}\cdot\tilde{\mathbf{D}}\cdot\mathbf{S} = D[\{S_z^2 - \tfrac{1}{3}S(S+1)\} + \eta(S_x^2 - S_y^2)]$$

where η can always be set to a value of $< 1/3$ by an appropriate choice of principal axes. In the absence of any applied magnetic field, the quartet corresponding to the (S = 3/2)-system splits into two doublets separated by $\Delta_o = 2D(1 + 3\eta^2)^{\frac{1}{2}}$, which can be treated independently if Δ_o is greater than the Zeeman energy. Moreover, for low values of the rhombic parameter, the only transition actually observed is the one among the states of the $S = \pm 1/2$ doublet. Under these conditions, the initlal S = 3/2 problem reduces to a quasi-axial S = 1/2 spin system, with the spin Hamiltonian given in eqn. (1). If the principal axes of the $\tilde{\boldsymbol{g}}$- and $\tilde{\boldsymbol{D}}$-tensors coincide the relationship between the effective (g_i') and the principal (g_i) true g-factors is given by

$$g_x' = g_x(1 + \cos 2\beta + \sqrt{3}\sin 2\beta)$$
$$g_y' = g_y(1 + \cos 2\beta - \sqrt{3}\sin 2\beta)$$
$$g_z' = g_z(2\cos 2\beta - 1),$$

where $\tan 2\beta = (\sqrt{3})\eta$.

1 J. Sand and F. Singer, *Liebigs Ann. Chem*., 1903, **329**, 190; G. M. Bennett and E. E. Turner, *J. Chem. Soc*., 1914, 1057.
2 F. Hein, *Ber. Deutsch. Chem. Ges*., 1919, **52**, 195. This is the first of a series of papers dealing with so-called polyphenylchromium derivatives. For an almost contemporary survey of this subject see: H. J. Emeléus and J. S. Anderson, *Modern Aspects of Inorganic Chemistry*, D. van Nostrand, New York, 1938, pp. 419–426.
3 W. Herwig and H. H. Zeiss, *J. Am. Chem. Soc*., 1957, **79**, 6561; 1959, **81**, 4798.
4 G. K. Barker, M. F. Lappert and J. A. K. Howard, *J. Chem. Soc., Dalton Trans*., 1978, 734.
5 F. Hein and D. Tille, *Z. Anorg. Allg. Chem*., 1964, **329**, 72.
6 W. Seidel and G. Kreisel, *Z. Anorg. Allg. Chem*., 1976, **426**, 150.
7 F. Hein and K. Schmiedeknecht, *J. Organomet. Chem*., 1967, **8**, 503.
8 W. Mowat, A. J. Shortland, N. J. Hill and G. Wilkinson, *J. Chem. Soc., Dalton Trans*., 1973, 770; W. Mowat, A. Shortland, G. Yagupsky, N. J. Hill, M. Yagupsky and G. Wilkinson, *J. Chem. Soc., Dalton Trans*., 1972, 533.
9 P. Boudjouk and J.-H. So, *Inorg. Synth*., 1992, **29**, 108.
10 M. D. Rausch, F. E. Tibbets and H. B. Gordon, *J. Organomet. Chem*., 1966, **5**, 493.
11 R. Usón and J. Forniés, *Adv. Organomet. Chem*., 1988, **28**, 219; E. Maslowsky, Jr., *Vibrational Spectra of Organometallic Compounds*, Wiley, New York, 1977, pp. 437–442.
12 G. M. Sheldrick, SHELXL 93, Program for the Refinement of Crystal Structures from Diffraction Data, University of Göttingen, Germany, 1993.
13 W. N. Setzer and P. von Ragué Schleyer, *Adv. Organomet. Chem*., 1985, **24**, 353.
14 A. G. Orpen, L. Brammer, F. H. Allen, O. Kennard, D. G. Watson and R. Taylor, *J. Chem. Soc., Dalton Trans*., 1989, S1.
15 J. Forniés, B. Menjón, R. M.ª Sanz-Carrillo, M. Tomás, N. G. Connelly, J. G. Crossley and A. G. Orpen, *J. Am. Chem. Soc*., 1995, **117**, 4295.
16 M. P. García, M. V. Jiménez, A. Cuesta, C. Siurana, L. A. Oro, F. J. Lahoz, J. A. López, M. P. Catalán, A. Tiripicchio and M. Lanfranchi, *Organometallics*, 1997, **16**, 1026.

Received in Basel, Switzerland, 15th June 1998; 8/04473B

Regioselective directed lithiation of *N*-Boc 3-hydroxypyrrolidine. Synthesis of 2-substituted 4-hydroxypyrrolidines

Mihiro Sunose,[a] Torren M. Peakman,[a] Jonathan P. H. Charmant,[a] Timothy Gallagher*[a]† and Simon J. F. Macdonald[b]

[a] *School of Chemistry, University of Bristol, Bristol, UK BS8 1TS*
[b] *GlaxoWellcome Research and Development, Medicines Research Centre, Gunnels Wood Road., Stevenage, UK SG1 2NY*

***N*-Boc 3-hydroxypyrrolidine 1 undergoes directed *C*-lithiation at C5 and not, as previously reported, at C2; the resulting dilithiated intermediate 6 has been trapped by a range of electrophiles to give 2-substituted 4-hydroxypyrrolidines 7.**

Directed metallation provides a versatile method for achieving substitution adjacent (α) to an amino moiety and this is a process which has found widespread application within heterocyclic chemistry.[1] The presence of additional and appropriately positioned heteroatom residues can, by providing additional activation, also enable regiochemical control to be exercised in the metallation (usually lithiation) step.[2–4] For example, *N*-Boc pyrrolidines[3] and piperidines[4] carrying a methoxy residue at C3 have been shown to undergo lithiation at C2 which is then followed by loss of MeOLi to give the corresponding cyclic enamine. Choosing a C3 substituent that is a poorer leaving group should, by suppressing β-elimination, allow this residue to be retained in the resulting product and this concept has been successfully applied to *O*-based heterocycles.[5]

More recently, this approach has also been utilised for *N*-heterocycles and Pandey and Chakrabarti[6] have reported that *N*-Boc 3-hydroxypyrrolidine **1** undergoes lithiation (at −78 °C using Bu^{s}Li, THF–TMEDA) followed by silylation to give exclusively the *C,O*-disilylated adduct **3** (in 86% yield), an intermediate that was then later employed in an alkaloid synthesis (Scheme 1).‡ These authors suggest that the sense of regiocontrol 'was expected due to the directing effects of the hydroxy group for the initial metallation reaction' and the implication of this claim is that the *C,O*-dilithiated species **2** is involved.

As part of a broader programme, we have had cause to examine the lithiation of **1** and two key issues are apparent. Firstly, in our hands, *C*-lithiation of **1** does not occur at −78 °C and, secondly, at higher temperatures when *C*-lithiation does take place, the only products observed are those resulting from lithiation distal to the C3 hydroxy, rather than proximal as claimed by Pandey. We have achieved lithiation of *N*-Boc 3-hydroxypyrrolidine **1** using Bu^{s}Li (2.2 equiv.) in THF–TMEDA at −78 °C and then allowing the solution to warm to −46 °C. After 2 h, the mixture is then recooled (to −78 °C) and Me_3SiCl (2.2 equiv.) was added giving, after work up, the *cis*-2,4-disubstituted adduct **4** as the only observed disilylated product (Scheme 1).

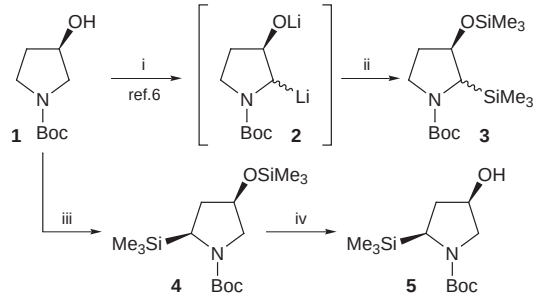

Scheme 1 *Reagents and conditions*: i, (ref. 6) Bu^{s}Li, THF–TMEDA, −78 °C; ii, Me_3SiCl (2.2 equiv.); iii, (this work) Bu^{s}Li (2.2 equiv.), THF–TMEDA, −78 °C to −46 °C, 2 h, cool to −78 °C, then Me_3SiCl (75%); iv, Bu_4NCl, KF, MeCN (100%)

Adduct **4** was then desilylated (at oxygen) to give **5** which proved to be a more suitable intermediate for assignment of both regio- and stereo-chemistry. This was carried out by ^{1}H NMR (COSY and NOE difference) analysis and, in addition, the relative stereochemistry of **5** has been established by X-ray crystallographic analysis (Fig. 1).§

The results of our study point towards the intermediacy of the *C,O*-dilithiated species **6** (and not **2**) as the only detectable intermediate (based on trapping) produced by lithiation of *N*-Boc-3-hydroxypyrrolidine **1**, however, the relative configuration of **6** has not been investigated.

The broader synthetic scope of this regiospecific lithiation chemistry has been further developed and intermediate **6** has been trapped with a range of electrophiles, including primary alkyl halides and enolizable aldehydes, to give the corresponding *N*-Boc 2-substituted 4-hydroxypyrrolidines **7** (Scheme 2, Table 1).¶ Yields for adducts **7**‖ have not been optimised because in most cases only modest *cis*/*trans* selectivity was observed. This likely reflects a combination of a highly reactive intermediate, *i.e.* **6**, with a lack of a significant conformational bias associated with the five membered ring, but we have established that *cis*/*trans* is kinetically controlled: attempts to lithiate *cis*-**7e** (using the standard reaction conditions), and thereby provide evidence for an equilibration pathway, failed.

In summary, *C*-lithiation of *N*-Boc 3-hydroxypyrrolidine (**1**) takes place distal to the hydroxy (lithioalkoxy) function but nevertheless offers a versatile and synthetically useful entry into 2-substituted 4-hydroxypyrrolidines. Our observations con-

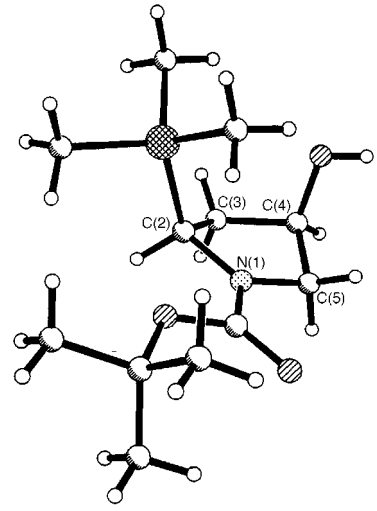

Fig. 1 Molecular structure of **5**

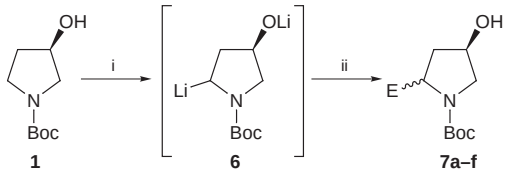

Scheme 2 *Reagents and conditions*: Bu^{s}Li (2.2 equiv.), THF–TMEDA, −78 °C to −46 °C, 2 h; ii, cool to −78 °C, then E^+ (2.2 equiv.) (see Table 1)

Table 1 Trapping of **6** with different electrophiles

Electrophile	2-Substituted 4-hydroxypyrrolidine (**7**) % yield and *trans*/*cis* ratio
Bu_3SnCl	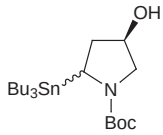 **7a** 50% 1 : 1
Br–Me	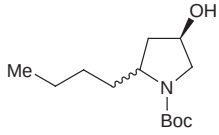 **7b** 37% 1 : 1
Br–Me	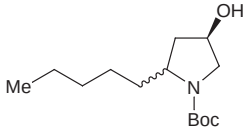 **7c** 39% 1 : 1
Br	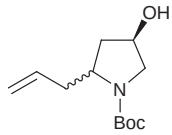 **7d** 59% 1 : 1
Me_2SO_4	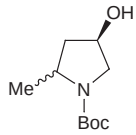 **7e** 65% 5 : 1 (see text)
Octanal	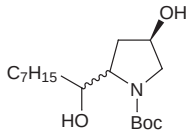 **7f** 39% 1 : 1 (see text)

cerning *C*-lithiation clearly conflict with those described earlier[6] by Pandey and Chakrabarti. This is a concern but until this group publishes either detailed experimental protocols or compound data, it is not possible to identify those factors that might account for this apparent contradiction.

We thank The Overseas Research Students Awards Scheme and GlaxoWellcome Research and Development for financial support (to M. S.), and acknowledge use of the EPSRC's Chemical Database Service at Daresbury.[7]

Notes and References

† E-mail: t.gallagher@bristol.ac.uk

‡ Metallation of **1** is described[6] as having taken place at −78 °C. No spectroscopic data was reported for the *C*,*O*-disilylated adduct **3** which was also indicated as an unspecified mixture of diastereomers.

§ When we carried out lithiation and quenching of **1** at −78 °C (and the solution was not allowed to warm above this temperature) then only the *O*-silyl ether of **1** was observed. This monosilylated product was also observed as a minor component (in 15% yield) in the generation of **4**. The exclusive formation of *cis*-**4** has not yet been investigated but intramolecular delivery involving participation by oxygen cannot be ruled out. Data for **4**: $[\alpha]_D^{24}$ + 43.3 (*c* 1, CH_2Cl_2); δ_H(400 MHz, C_6D_6) 4.03 (1 H, m, H4), 3.69 (1 H, m, H5), 3.30–3.23 (2 H, m, H2 and H5), 1.91 (1 H, m H3), 1.78 (1 H, m, H3), 1.56 (9 H, s); δ_C(100 MHz, $CDCl_3$) (doubling due to rotamer populations) 154.9/154.5, 79.6/78.6, 71.0/70.2, 54.5/54.3, 46.3/46.0, 37.3/36.8, 28.5, −0.2, −1.8. Data for **5**: mp 107–110 °C (pentane–EtOAc); $[\alpha]_D^{24}$ + 57.4 (*c* 1, CH_2Cl_2); δ_H(300 MHz, $CDCl_3$) 4.39 (1 H, pentet, *J* 5.9, H 4α), 3.78 (1 H, d d, *J* 11.7, 5.9, H5α), 3.30 (1 H, dd, *J* 9.2, 7.2, H2α), 3.05 (1H, dd, *J* 11.7, 5.9, H5β), 2.26 (1 H, dddd, *J* 12.8, 9.2, 5.9, 0.7, H3α), 1.78 (1 H, m, H3β), 1.69 (1 H, br s, OH), 1.46 (9 H, s, Bu^t) and 0.10 (9 H, s, Me_3Si). Stereochemical assignments are based on NOE difference studies. The crystal structure of **5** was determined from data collected on a Siemens SMART diffractometer (λ = 0.71073 Å) at 173(2) K. The structure was solved by direct and Fourier methods and refined by least squares against all F^2 data corrected for absorption. *Crystal data*: $C_{12}H_{25}NO_3Si$, *M* = 259.4, orthorhombic, space group $P2_12_12_1$, *a* = 6.159(1), *b* = 24.957(4), *c* = 9.709(2) Å, *U* = 1492.5(5) Å^3, *Z* = 4, D_c = 1.15 g cm^{-3}, μ = 0.156 mm^{-1}, 3382 unique data, θ < 27.4°, R_1 = 0.043. CCDC 182/194.

¶ All lithiation reactions shown in Table 1 were carried out as described in the following example: to a solution of *N*-Boc (3*R*)-hydroxypyrrolidine **1** (189 mg, 1 mmol) in THF (5 cm^3) at −78 °C was added TMEDA (0.34 cm^3, 2.21 mmol) followed by Bu^{s}Li (1.7 cm^3, 1.3 M in cyclohexane, 2.21 mmol). The resulting bright yellow reaction mixture was warmed to −46 °C, stirred for 2 h, then recooled to −78 °C, and dimethyl sulfate (0.21 cm^3, 2.21 mmol, dried over 4 Å MS) was added dropwise. The reaction mixture was then allowed to warm slowly to room temperature (over 5 h) and, after this time, water (5 cm^3) and CH_2Cl_2 (7 cm^3) were added and the organic layer was separated. The aqueous layer was extracted with CH_2Cl_2 (2 × 5 cm^3), the organic extracts were combined, and dried (K_2CO_3). Concentration *in vacuo* and purification of the residue by flash chromatography (light petroleum–EtOAc) gave *N*-Boc 2-methyl-4-hydroxypyrrolidine **7e** (131 mg, 65%) as a 5 : 1 mixture of diastereomers. Recrystallisation gave the major (*cis*) diastereomer as colourless crystals. Data for *cis*-**7e**: mp 88–89 °C (light petroleum–EtOAc); $[\alpha]_D^{24}$ + 21.1 (*c* 1, CH_2Cl_2). The *cis* stereochemistry of this major adduct has also been conformed by X-ray crystallographic analysis, details of which will be described elsewhere.)

‖ Enantiomerically pure (*R*)-**1** was used in these initial studies. Carbamate resonance complicated interpretation of the NMR data associated with adducts **7** but where this was an issue it was overcome by *N*-deprotection (using TFA, CH_2Cl_2, room temp.) to give the corresponding free amine. The formation of stereoisomers at C2, rather than a mixture of C2/C5 regioisomers, was confirmed by Swern oxidation of the *cis*/*trans* mixture to give a single 2-substituted pyrrolidin-4-one; this process was carried out for adducts **7b**–**e**. Octanal gave **7f** as an inseparable 1 : 1 mixture of two of the four possible products, but the stereochemistry of these products has not been assigned. In addition, all new compounds have been characterised by spectroscopic methods and either elemental analysis or HRMS.

1 P. Beak, A. Basu, D. J. Gallagher, Y. S. Park and S. Thayumanavan, *Acc. Chem. Res.*, 1996, **29**, 552; M. Gray, M. Tinkl and V. Snieckus, in *Comprehensive Organometallic Chemistry*, ed. E. W. Abel and F. G. A. Stone, Elsevier, New York, vol. 11, ch. 1; P. Beak, W. J. Zajdel and D. B. Reitz, *Chem. Rev.*, 1984, **84**, 471.

2 D. L. Comins and M. A. Weglarz, *J. Org. Chem.*, 1988, **53**, 4437; for a recent example involving a desymmetrisation process, see M. Lautens, E. Fillion and M. Sampat, *J. Org. Chem.*, 1997, **62**, 7080. Steric factors also play a role in determining regiochemical control in spite of the presence of a (sulfur-based) directing group, see D. J. Hart, J. Li, W.-L. Wu and A. P. Kozikowski, *J. Org. Chem.*, 1997, **62**, 5023.

3 M. Giles, M. S. Hadley and T. Gallagher, *J. Chem. Soc., Chem. Commun.*, 1990, 831.

4 P. Beak and W. K. Lee, *J. Org. Chem.*, 1993, **58**, 1109.

5 V. Wittmann and H. Kessler, *Angew. Chem., Int. Ed. Engl.*, 1993, **32**, 1091; P. Lesimple and J.-M. Beau, *Bioorg. Med. Chem.*, 1994, **2**, 1319; O. Frey, M. Hoffmann, V. Wittmann, H. Kessler, P. Uhlmann and A. Vasella, *Helv. Chim. Acta*, 1994, **77**, 2060; D. Mazeas, T. Skrydstrup and J.-M. Beau, *Angew. Chem., Int. Ed. Engl.*, 1994, **33**, 1383; M. Hoffmann and H. Kessler, *Tetrahedron Lett.*, 1994, **35**, 6067; D. Urban, T. Skrydstrup, C. Riche, A. Chiaroni and J.-M. Beau, *Chem. Commun.*, 1996, 1883. For a review of carbohydrate-based C1 nucleophiles, see J.-M. Beau and T. Gallagher, *Top. Curr. Chem.*, 1997, **87**, 1.

6 G. Pandey and D. Chakrabarti, *Tetrahedron Lett.*, 1996, **37**, 2285.

7 D. A. Fletcher, R. F. McMeeking and D. J. Parkin, *J. Chem. Inf. Comput. Sci.*, 1996, **36**, 746.

Received in Cambridge, UK, 4th June 1998; 8/04211J

The synthesis of the new zeolite, ERS-7, and the determination of its structure by simulated annealing and synchrotron X-ray powder diffraction

Branton J. Campbell,[a] Giuseppe Bellussi,[b] Luciano Carluccio,[b] Giovanni Perego,[b] Anthony K. Cheetham,*[a]† David E. Cox[c] and Roberto Millini*[b]

[a] *Materials Research Laboratory, University of California, Santa Barbara, CA 93106, USA*
[b] *EniTecnologie S.p.A., Via F. Maritano 26, I-20097 San Donato Milanese, Milan, Italy*
[c] *Physics Department, Brookhaven National Laboratory, Upton, NY 11973, USA*

The new zeolite ERS-7 (EniRicerche-molecular-Sieve-7), which was synthesized within a narrow temperature and compositional range using *N*,*N*-dimethylpiperidinium as a structure directing agent, has a structure consisting of 17-sided ($4^6 5^4 6^5 8^2$) picnic-basket-shaped cages connected by 8-membered ring windows.

The discovery of new zeolites is closely linked to the use of increasingly complex and novel structure directing agents (SDAs). The syntheses of extra-large pore UTD-1[1] and CIT-5[2] zeolites, for example, were recently accomplished by using Cp_2Co^+ and N(16)-methylsparteinium, respectively. Because of the lack of selectivity typical of many SDAs, good results may also be achieved by carefully controlling other synthesis parameters. This is the case with the 'simple' *N*,*N*-dimethylpiperidinium cation, which was reported to favor the crystallization of ZSM-51 (NON).[3] By systematic investigation of different synthesis parameters (*i.e*. temperature, crystallization time, and the SiO_2/Al_2O_3, SDA/SiO_2, OH^-/SiO_2 and H_2O/SiO_2 molar ratios), we have obtained several known microporous framework compounds (MOR, MTW, LEV, NON),‡ together with the hitherto unknown ERS-7 phase.[4]

To synthesize ERS-7, a reaction mixture with the composition $0.2SDA : 0.3Na_2O : 0.04Al_2O_3 : 1SiO_2 : 40H_2O$ was prepared by using sodium silicate (Carlo Erba, 27 wt.% SiO_2, 8 wt.% Na_2O) and $Al_2(SO_4)_3 \cdot 16H_2O$ as sources of silica and aluminium, respectively. Aqueous *N*,*N*-dimethylpiperidinium hydroxide (30 wt.%) was synthesized by refluxing an ethanol solution of 1,5-dibromopentane and dimethylamine; the bromide salt obtained was filtered, washed with ethanol, dried under N_2, dissolved in demineralized water and finally exchanged to the OH^- form by electrodialysis. The reaction mixture was then charged in a Teflon-lined stainless steel autoclave and heated under autogeneous pressure at 170 °C for 7 days.

The pure and well crystallized ERS-7 product was only obtained in a narrow range of SiO_2/Al_2O_3 molar ratios near 25. Increasing the aluminium content in the reaction mixture resulted in the formation of LEV (SiO_2/Al_2O_3 = 15) or a small amount of an unidentified crystalline phase (SiO_2/Al_2O_3 = 20). Pure MTW was obtained when the SiO_2/Al_2O_3 ratio was increased to 80, while NON crystallized from reaction mixtures containing little (SiO_2/Al_2O_3 = 214) or no aluminium. If instead, the SDA/SiO_2 molar ratio was decreased, MOR was formed as a product. At 155 °C, ANA crystallized first, while ERS-7 started to appear only after 7 days, the pure phase being obtained after 14 days with the consumption of ANA. Similar kinetics were observed at 170 °C, with MOR forming first, and ERS-7 completely crystallizing after 5 days.

The framework structure of ERS-7 was determined by simulated annealing.[5] As implemented by MSI for zeolite-like structures,[6] the simulated annealing algorithm required the unit cell dimensions, the space group symmetry, the total number of T-sites (or more precisely, the number of cationic framework atoms) in the unit cell, and the number of crystallographically independent T-sites. High resolution synchrotron X-ray powder diffraction data were collected at room temperature on dehydrated template-free H^+ ERS-7§ at beamline X7A of the Brookhaven National Synchrotron Light Source. The first 30 large reflections were indexed with the TREOR90 software package[7] to obtain a primitive orthorhombic unit cell (M_{30} = 50, F_{30} = 242). The space group *Pnma* was selected as a starting-point based on the unambiguous determination of extinction class and the absence of significant second-harmonic-generation emission. The framework density was determined by measuring the density of an ERS-7 precursor (2.04 g cm^{-3} using a Micromeritics AccuPyc 1330 helium displacement pycnometer) and then correcting for the thermogravimetric loss of H_2O and SDA trapped inside the pores (15.5 wt.% using a Mettler TG50 thermobalance) as well as the Na^+ content (1.2 wt.% from elemental analysis); the final value was 1.70 g cm^{-3} which corresponds to 48.1 T-sites per unit cell.

Assuming 48 total T-sites and *Pnma* symmetry, simulated annealing runs with different initial random seeds were performed for each possible number of symmetry-independent T-sites, from 6 to 12. From the 1000 runs that assumed 6 symmetry-independent T-sites, 373 unique framework topologies were generated. The correct structure was identified among these by geometry optimizing[8] the simulated structures, sim-

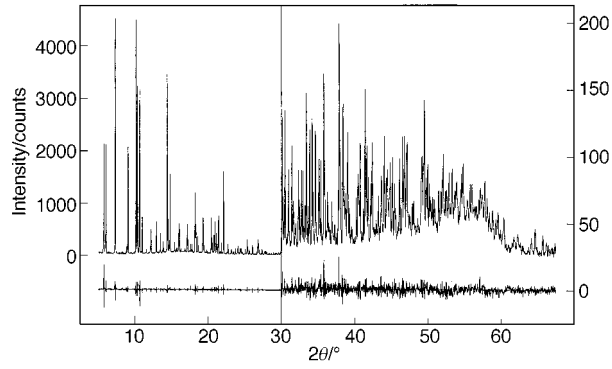

Fig. 1 Experimental and difference XRD patterns from the Rietveld refinement of the ERS-7 structure. The scale of the high angle data is expanded to better illustrate its detail. R_{wp} = 6.11%, R_p = 5.60%, χ^2 = 1.566, R_B = 3.28%, 1407 reflections, 12491 data points. A total of 195 parameters were refined: scale (1), profile shape (6), positional parameters (56), anisotropic thermal parameters (112), and 20 evenly spaced background points with linear interpolation between points. Lattice parameters were refined during the LeBail fit to the profile, but fixed during the model refinement due to slight oscillation. The pseudo-Voigt profile shape of Thompson *et al.*[10] was used including the asymmetry correction of Finger *et al.*[11] Refined profile parameters were U = 0.597, V = −0.057, and W = 0.008 (degrees squared), Lorentzian strain broadening = 0.005°, anisotropic (011) strain broadening = 0.131, and S/L = 0.013 (H/L was fixed at the measured value of 0.011). The thermal ellipsoid of O9 has one slightly negative root.

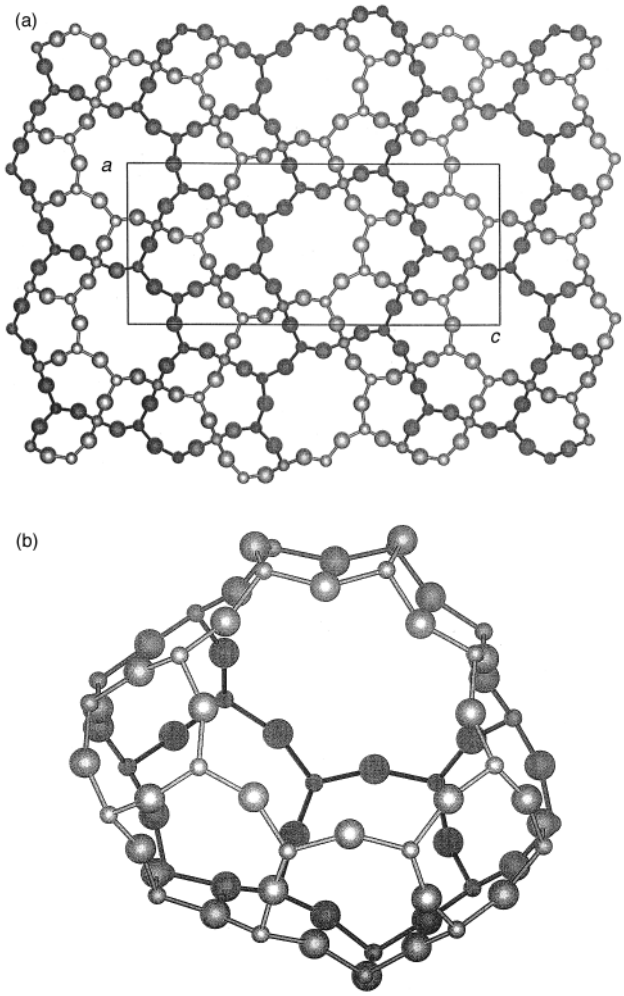

Fig. 2 (a) The [010] projection of ERS-7 showing the 8-membered ring channels. Final values for the lattice parameters were a = 9.79976(4), b = 12.41163(6), c = 22.86063(11) Å, and V = 2780.561 Å^3. (b) Schematic representation of the 17-sided ($4^6 5^4 6^5 8^2$) 'picnic-basket'-shaped cage.

ulating their X-ray diffraction (XRD) patterns and visually comparing them to the experimental XRD pattern; it also had the overall best (lowest) figure of merit (value of the cost function) of any topology generated. The structure model was then refined by the Rietveld technique from the synchrotron data using the GSAS[9] software package, resulting in the fit to the XRD data shown in Fig. 1. Each Si atom is 4-coordinated. The total number of symmetry-independent oxygens is 14. The range of Si–O bond lengths was 1.573 to 1.623 Å (avg. = 1.595 Å), and the O–Si–O and Si–O–Si bond angle ranges were 105.0° to 111.3° (avg. = 109.5°) and 139.3° to 171.4° (avg. = 155.4°) respectively.

The framework structure of ERS-7, shown in Fig. 2(a), can be described as having a one-dimensional 8-membered ring channel system running along the *b* axis, with large side-pockets along the sides of the channel. The structure can be assembled entirely by 17-sided ($4^6 5^4 6^5 8^2$) picnic-basket-shaped cages (9.0 × 7.6 × 8.2 Å) that share 6 and 8-membered ring faces, such that the channel system runs through the 'basket-handles' while the pockets form the 'basket bottoms' [Fig. 2(b)]. The 8-membered ring channels are consistent with our observations that ERS-7 adsorbs H_2O and methanol, but not *n*-hexane. The cages connected to these channels explain the fact that while *N*,*N*-dimethylpiperidinium is too large to fit into the 8-membered ring channel (7.4 × 6.2 Å), it can still be removed upon decomposition at high temperature without damaging the framework. The ERS-7 framework can also be viewed as consisting of chains of smaller 11-sided cages that share 6-membered ring faces along the *a* axis, but connect in the $b + c$ and $b - c$ directions by additional 4-rings rather than by corners, edges, or faces.

The synthesis of ERS-7 demonstrates that the preparation of new zeolites is related not only to the use of increasingly complex SDAs but also to the systematic screening of the synthesis parameters. The use of simulated annealing to solve the structure of a fairly complex new zeolite demonstrates its importance as an alternative approach when single crystals are unavailable.

We would like to acknowledge Dr. J. C. P. Gabriel (Institut de Materiaux de Nantes, France) and Dr. Clive M. Freeman (MSI, San Diego, CA) for helpful discussions, and Dr. Vojislav Sradanov (Univ. of California at Santa Barbara) for SHG measurements. Work at UCSB was supported by the MRL Program of the National Science Foundation under Award No. DMR96-32716. Work at Brookhaven was supported under Contract No. DE-AC02-98CH10886, Division of Material Sciences, U.S. Department of Energy. The National Synchrotron Light Source is supported by the U.S. Department of Energy, Division of Materials Sciences and Division of Chemical Sciences.

Notes and References

† E-mail: cheetham@mrl.ucsb.edu

‡ Synthesis products were identified by X-ray powder diffraction using a Philips PW1710 vertical diffractometer.

§ Synchrotron XRD data were collected at room temperature over the range $5° \leqslant 2\Theta \leqslant 67.45°$ in steps of 0.005° while the sample (in capillary) was rotated at *ca*. 1 Hz. For data collection, a double-crystal Si[111] monochromator set for λ = 1.1528 Å, a Ge[220] analyzer, horizontal incident and receiving slits of 13 mm and 16 mm respectively, and a sample–detector distance of 700 mm were used. Dehydrated template-free H^+ ERS-7 (SiO_2/Al_2O_3 = 16.7) was prepared by calcining at 550 °C for 5 h under flowing air, repeated ion exchange in an ammonium acetate solution at 60–70 °C, drying at 120 °C, calcining again in air and then under 10^{-5} Torr vacuum, and flame-sealing in a quartz capillary. CCDC 182/932.

1 R. F. Lobo, M. Tsapatsis, C. C. Freyhardt, S. Khodabandeh, P. Wagner, C. Y. Chen, K. J. Balkus Jr., S. I. Zones and M. E. Davis, *J. Am. Chem. Soc.*, 1997, **119**, 8474.
2 P. Wagner, M. Yoshikawa, M. Lovallo, K. Tsuji, M. Tsapatsis and M. E. Davis, *Chem. Commun.*, 1997, 2179.
3 *US Patent* 4 568 654 to Mobil Oil Corp., 1986.
4 *It. Patent Appl.* MI94/A 002037 from Eniricerche S.p.A., 1994.
5 M. W. Deem and J. M. Newsam, *Nature*, 1989, **342**, 260; M. W. Deem and J. M. Newsam, *J. Am. Chem. Soc.*, 1992, **114**, 7189.
6 *Catalysis User Guide*—Release 4.0.0, Sept. 1996, MSI, San Diego, CA, USA.
7 P.-E. Werner, L. Eriksson and M. Westdahl, *J. Appl. Crystallogr.*, 1985, **18**, 367.
8 C. Baerlocher, A. Hepp and W. M. Meier, DLS-76: A Program for Simulation of Crystal Structures by Geometric Refinement, 1977, ETH, Zürich.
9 A. C. Larson and R. B. Von Dreele, GSAS Manual, Los Alamos Report No. LAUR-86-748, 1986, Los Alamos National Laboratory, USA.
10 P. Thompson, D. E. Cox and J. B. Hastings, *J. Appl. Crystallogr.*, 1987, **20**, 79.
11 L. W. Finger, D. E. Cox and A. P. Jephcoat, *J. Appl. Crystallogr.*, 1994, **27**, 892.

Received in Bloomington, IN, USA, 13th May 1998; 8/03572E

Comparison of two means of attachment of an organometallic acid on gold surfaces by combining X-ray photoelectron spectroscopy and IR reflection spectroscopy

Caroline Chavigny,[a] Franck Le Bideau,[a] Claire-Marie Pradier,[a] Serge Palacin,[b] Pierre Brossier[c] and Gérard Jaouen[a]*†

[a] *Ecole Nationale Supérieure de Chimie de Paris, 11 rue Pierre et Marie Curie, 75231 Paris Cedex 05, France*
[b] *Service de Chimie Moléculaire, CEA/Saclay, 91191 Gif sur Yvette, France*
[c] *Faculté de Pharmacie de l'Université de Bourgogne, 7, Boulevard Jeanne d'Arc, 21033 Dijon, France*

Two methods of immobilization of the butyric 4-oxocyclopentadienylmanganese tricarbonyl acid I on gold surface are presented: either through the assembly of a disulfide derived from the acid, or by coupling on a cystamine monolayer; the efficiency of these two ways are evaluated by IR reflection spectroscopy and X-ray photoelectron spectroscopy.

The research of new immunoassay methods avoiding the drawbacks of radioactive tracers appears to be a main line in analysis.[1] We recently demonstrated the possibility to assay drugs, hormones and pesticides by FTIR spectroscopy using organometallic markers.[2] For that purpose, we took advantage of the specific and intense ν_{CO} stretching vibration of the metal carbonyl [$M_y(CO)_x$] within 1900–2150 cm^{-1}. Moreover, this method might be one of the rare realistic approaches to multi-immunoassays thanks to the characteristic positions of the metal carbonyl groups signals.[1]

So far the analysis was performed in solution and required a separation of the free tracer and the antibody-linked tracer. This step was time demanding and turned out to be incompatible with a large scale analytical development. In order to perform this analysis in the solid state, we investigated the immobilization and detectability of organometallic-marked biological molecules. Biological material can be immobilized on a surface as a host in polymer thin films,[3] as a host or an adduct within Langmuir–Blodgett films[4] or can be grafted *via* covalent bonds on a self-assembled monolayer (SAM).[5] We selected the third method because it provides bioactive films with high accessibility for external molecules.

Self-assembled monolayers on gold surfaces are generally prepared from dilute solutions of thiols (or disulfides). Biomolecules can be attached to the surface *via* the terminal functional groups of the assembled thiolate. Before working on the biological matrix, we studied the detectability of manganese tricarbonyl complexes immobilized on the gold surface by IR reflection spectroscopy (IRS). The present study is necessary because the immobilization of metal carbonyl complexes on gold surfaces is a quite new research field.[6,7] We report here a comparison between two means of attachment of an organometallic acid, the butyric 4-oxocyclopentadienylmanganese tricarbonyl **I**, on gold surface. Acid **I** can be prepared following a known synthesis using cymantrene.[8] The attachment of the acid was carried out either in one step with a disulfide derived from the acid **I** (method A) or in two steps *via* the linkage of **I** with a chemically reactive SAM (method B). We used two different and complementary surface spectroscopies to evaluate the efficiency of these two strategies: IR reflection spectroscopy to detect the carbonyl vibrations, and photoelectron X-ray spectroscopy to compare the molecular densities through the S/Au peak area ratio.

To achieve method A, the organometallic acid **I** was transformed into a surface-active molecule. Esterification of **I** was performed with *N*,*N*,*N*′,*N*′-tetramethyl(succinimido)uronium tetrafluoroborate (TSU) and diisopropyl amine in anhydrous DMF[9] to give the *N*-hydroxysuccinimide ester **II**. The disulfide **III** was then formed by overnight reaction of the ester with cystamine in anhydrous DMF in the presence of triethylamine [Scheme 1(*a*)].

SAMs of the disulfide **III** were prepared on gold substrates[10] previously cleaned with UV/ozone treatment. The substrates were then placed in a dilute solution (1.5 mM) of **III** in distilled THF for 20 h.

The IR reflection spectra of the monolayer[11] obtained *via* method A is shown in Fig. 1(*a*). The bands at 2041 and 1968 cm^{-1} are characteristic of the metal carbonyl vibrations, and did not change with reaction time, which indicates that an equilibrium state was reached. A shift to higher frequencies is observed compared to the IR spectrum of the pure compound (the E mode vibration of the pure compound is observed at 1940 cm^{-1}). We believe that this shift is due to hydrogen bonds[12] occurring in the pure compound which lower the frequencies. On the gold surface, such interactions are prevented. The observed frequencies are the same as those in π-acetylcyclopentadienyl manganese tricarbonyl (2040 and 1965 cm^{-1} in KBr disc),[13] which has a similar electron withdrawing substituent on the ring and no possible hydrogen bonds.

In method B, we first prepared the monolayer of cystamine by soaking the gold substrates for 3 h in a solution of cystamine dihydrochloride (0.05 M) in water. Upon removal from the solution, the substrates were rinsed with 20 ml of water, 5 ml of absolute ethanol and then were dried under nitrogen.

The covalent link of the acid **I** was constructed by first activating the acid into the ester **II**. The cystamine monolayer was then immersed for 20 h in the solution, and some diisopropylethylamine added.[14] The protocol is illustrated in Scheme 1(*b*). A 'test slide' was prepared at the same time following the same procedure but without TSU, in order to check the efficiency of the activation. Both were rinsed by two 2 min immersions in DMF, then one in absolute ethanol, dried and analyzed by IRS. The IR reflection spectra obtained *via*

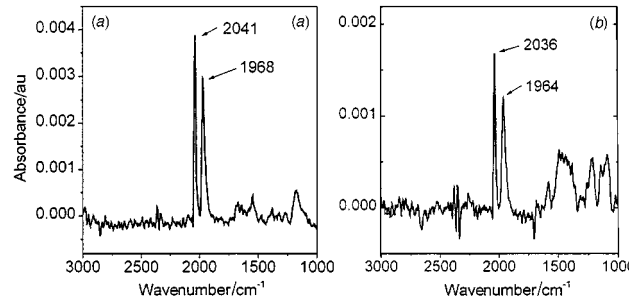

Fig. 1 IR reflection spectra of (*a*) the disulfide **III** monolayer and (*b*) the result of coupling on a cystamine monolayer

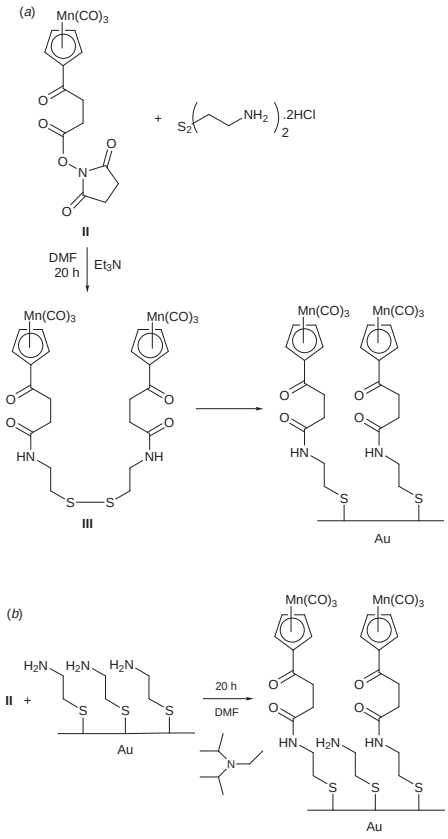

Scheme 1 Methods of attachment of acid **I** onto a gold surface; (*a*) method A and (*b*) method B

method B is shown in Fig. 1(*b*). The covalent coupling of the acid on the surface was proved by the absence of carbonyl vibration bands on the 'test gold slide'.

We now want to compare the two methods of attachment of the organometallic acid **I** on gold. The measurements of the areas of the IR bands at respectively 2041 and 2036 cm^{-1} shows that the carbonyl E vibration band is 48% lower when the attachment was performed *via* method B than *via* method A. Therefore, a discussion of this result requires an evaluation of the density of the sulfur sites within the monolayer built from the disulfide **III** and from cystamine.

We performed XPS analyses at normal incidence on both surfaces and calculated the S/Au ratio. At normal incidence, the thickness of the SAM has a negligible influence on the intensity of the XPS signal.[15] The S 2p photoelectron spectra of the layers of cystamine and disulfide **III** exhibit a peak at 162 eV which is in good agreement with the thiolate moiety on gold.[16] The ratios I_S/I_{Au} are 0.0084 for the disulfide **III** monolayer, and 0.0094 for the cystamine one, which indicates that the molecular density for the cystamine monolayer on the gold surface is a few percent higher than for **III** (considering the experimental error in XPS). We assume that this is not a significant reason for the observed variation in the infrared intensities.

Therefore, the difference in the areas of the carbonyl vibration bands between SAMs prepared *via* method A and B is mainly ascribed to the yield of attachment in the adsorbed phase. Note that the different orientations of the metal carbonyl groups may also account for variations of the IR intensities as the reflection mode is only sensitive to the contribution of the dipole moments normal to the surface. However, considering the roughness of the surface at the molecular scale, and the likely amorphous character of these monolayers constituted by molecules having bulky terminal groups, we assume that the metal carbonyl moieties of C_{3v} symmetry are randomly oriented. The observed IR signal is consequently unaffected by a preferential orientation of the molecules, but essentially determined by the number of attached metal carbonyl moieties. Therefore, the yield of attachment is the main factor for the differences in the IRS spectra. We found that the attachment *via* method B was *ca*. 45% of the attachment *via* method A (average of three experimental values taking into account the slight difference in surface densities shown by XPS).

This value can be compared to the 40% of activated CO_2H obtained after one cycle of activation of the 11-mercaptoundecanoic acid groups by *N*-hydroxysulfosuccinimide (NHSS) with EDC.[17] The limited yield of 40–45% in both cases underlines the importance of the steric effects.

An organometallic acid was covalently attached to a cystamine monolayer on gold. The amount of attachment was evaluated by combining two surface techniques, XPS and IRS, and comparing the signals of the monolayer obtained after coupling into the adsorbed phase with those from the corresponding disulfide layer.

This work allows us to envisage an immunoassay using organometallic markers in the solid phase.

We gratefully acknowledge research grants from CNRS and Region Bourgogne (France) and D.R.E.T., Délégation Générale pour l'Armement (DGA).

Notes and References

† E-mail: jaouen@extjussieu.fr

1 A. Varenne, A. Vessières, M. Salmain, S. Durand, P. Brossier and G. Jaouen, *Anal. Biochem*., 1996, **242**, 172 and references therein.
2 G. Jaouen, A. Vessières and I. S. Butler, *Acc. Chem. Res*., 1993, **26**, 316.
3 G. Bidan, *Sensing effects in electroconducting conjugated polymers* in *Polymer Films in Sensor Applications*, Technomic Publ. Co. Inc., ed. G. Harsani, Basel, 1995.
4 W. M. Reichert, C. J. Bruckner and J. Joseph, *Thin Solid Films*, 1987, **152**, 345.
5 Th. Wink, S. J. van Zuilen, A. Bult and W. P. van Bennekom, *Analyst*, 1997, **122**, 43R.
6 D. Kang and M. S. Wrighton, *Langmuir*, 1991, **7**, 2169.
7 T. T. Ehler, N. Malmberg, K. Carron, B. P. Sullivan and L. J. Noe, *J. Phys. Chem. B*., 1997, **101**, 3174.
8 R. Dabard and M. Le Plouzennec, *Bull. Soc. Chim. Fr*., 1972, **3**, 3594.
9 W. Bannwarth, D. Schmidt, R. L. Stallard, C. Hornung, R. Knorr and F. Müller, *Helv. Chim. Acta*, 1988, **71**, 2085.
10 The gold substrates (1 cm^2) were purchased from EMFCorp. (Evaporated Metal Film Corporation). They consist of glass substrates covered with 50 Å of Ti and 1000 Å of gold.
11 We use the term 'self-assembled monolayer' for this organic film cautiously, as we did not characterize the extent of order of the layer.
12 B. V. Lokshin, S. G. Kazaryan and A. G. Ginzburg, *Bull. Acad. Sci. USSR, Div. Chem. Sci*., 1988, 257.
13 F. A. Cotton and J. R. Leto, *Chem. Ind*., 1958, 1368.
14 The addition of an organic base was necessary in order to deprotonate the cystamine dihydrochloride. Only the NH_2 functionalities actually react with the activated ester.
15 H. A. Biebuyck, C. D. Bain and G. M. Whitesides, *Langmuir*, 1994, **10**, 1825.
16 C. D. Bain, H. A. Biebuyck and G. M. Whitesides, *Langmuir*, 1989, **5**, 723.
17 B. L. Frey and R. M. Corn, *Anal. Chem*., 1996, **68**, 3187.

Received in Cambridge, UK, 3rd April 1998; 8/02551G

Stereoselective α-glycosidation using $FeCl_3$ as a Lewis acid catalyst

Swapan K. Chatterjee and Peter Nuhn*†

FB Pharmazie, Martin Luther Universität, Wolfgang-Langenbeck-Str. 4, 06120 Halle, Germany

A simplified procedure for the stereoselective α-glycosidation of peracetylated sugars, carrying a participating group at C_2, with aliphatic alcohols in the presence of $FeCl_3$ as a Lewis acid is described.

In continuation of our work[1] on the study of cellular response towards liposomes and their cryoprotection through glycolipids and the interaction of phospholipid and glycolipids, we required large amounts of different pure anomers of glycolipids with varying numbers of spacer unit. In spite of a number of methods reported in the literature[2] *cis*-glycosidation is still a problem; in most of the reported syntheses partial or full protection of the sugar moiety is required, *e.g.* protection with Bn[3] or TBDMS.[4] The presence of an anchimeric assistant group, *e.g.* in the case of protection with an acyl group particularly at the C_2 position of the pyranose ring, leads to a cyclic transition state or non-isolable cyclic intermediate[5] (**A** in Scheme 1), thereby resulting in *trans*-glycosidation.

Partial or full protection of the glycosyl donor without a participating group at C_2 is not always easy. In our previous paper[3] we reported such a stereoselective α-glycosidation starting from a 2,3,4,6-tetrabenzyl monosaccharide. Even the most readily available partially-protected monosaccharide, 2,3,4,6-tetrabenzyl glucose, could be prepared by us in only 40–50% overall yield starting from the methyl glucoside.[6] The loss of product is occurring during the hydrolysis of methyl-2,3,4,6-tetrabenzyl glycoside due to the instability of the product to acidic hydrolytic conditions.

We report here for the first time α-glycosidation with a glycosyl derivative having a participating group at the C_2 position. Anomerisation of β-glucopyranosides is already known *via* treatment with titanium chloride,[7a] or mercuric bromide.[7b] Nakanishi[7c] first observed the anomerisation of tetrabenzyl β-methylglucoside to α-methylglucoside in the presence of $FeCl_3$. Srivastava[8] reported stereoselective peracetylation of different monosaccharides to give α-pentaacetyl pyranosides with $FeCl_3$. These observations lead us to try glycosidation with $FeCl_3$ starting directly from readily available peracetylated monosaccharide and aliphatic alcohols. Thus reaction of pentaacetyl sugar with alcohols in the presence of anhydrous $FeCl_3$ in CH_2Cl_2 at room temperature lead stereoselectively to the α-anomer.‡ This is the first observation of stereoselective α-glycosidation occurs inspite of the presence of the anchimeric assistant *O*-acetyl group at the C_2 position of the pyranose ring of glucose, mannose and galactose (Scheme 2, Table 1).

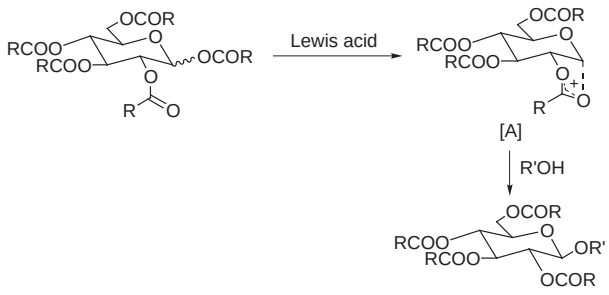

Scheme 1

Disaccharide moieties in which the glycosyl parts are bound α to each other are wide-spread in natural systems, *e.g.* the

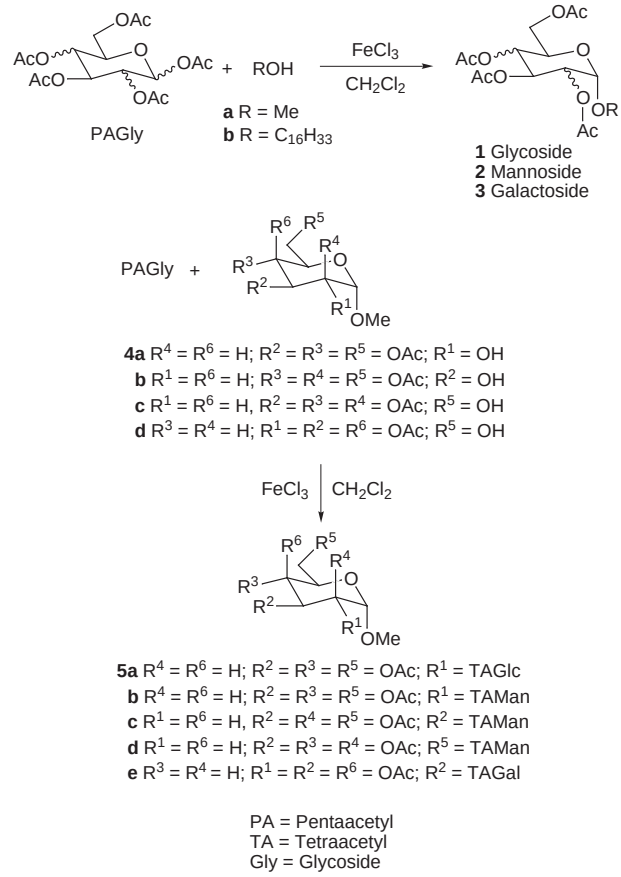

Scheme 2

Table 1 Reactions of alcohols with peracetylated monosaccharides in the presence of $FeCl_3$

No.	Peracetylated sugar	Alcohol	Product	Yield (%)	Anomeric ratio[a] (α : β)
1	PAGlc	MeOH	**1a**	95	98 : 2
2	PAGlc	$C_{16}H_{33}OH$	**1b**	70	93 : 7
3	PAMan	MeOH	**2a**	90	100 : 0
4	PAMan	$C_{16}H_{33}OH$	**2b**	75	100 : 0
5	PAGal	MeOH	**3a**	88	95 : 5
6	PAGal	$C_{16}H_{33}OH$	**3b**	68	92 : 8
7	PAGlc	**4a**	**5a**	75	90 : 10
8	PAMan	**4a**	**5b**	73	100 : 0
9	PAMan	**4b**	**5c**	72	100 : 0
10	PAMan	**4c**	**5d**	70	100 : 0
11	PAGal	**4d**	**5e**	68	90 : 10

[a] The anomeric ratios were determined by GCMS or HPLC analysis.

glycoproteins in cell membranes, the immune system, receptors of different bacterial cells[9] and also the human P blood-group system.[10] They are therefore of great interest for cell-cell recognition. We found that triacetyl-α-methylglycosides **4** react, in the presence of ferric chloride, with different pentaacetyl monosaccharides to give heptaacetyl disaccharides **5** in high yield where the monosaccharide moiety is stereoselectively α-orienteded to the glycosyl donor.

This work was supported by the Deutsche Forschungsgemeinschaft (Sonderforschungsbereich 197).

Notes and References

† E-mail: nuhn@pharmazie.uni-halle.de

‡ *General procedure*: To a solution of pentaacetylmonosaccharide (2 g) in CH_2Cl_2 below 5 °C was added slowly $FeCl_3$ (1 equiv.), and the mixture was stirred for 5 min. An equimolar amount of alcohol was then added to the reaction mixture portionwise over 15 min. and stirred at room temperature. Continuous TLC monitoring showed no significant formation of the β-anomer. After completion of the reaction, indicated by the disappearance of the alcohol by TLC (there is always some transformation of the alcohol to the acetate due to transesterification) the reaction mixture was poured into sat. aq. sodium hydrogen carbonate and extracted with Et_2O. Chromatography of the resultant mixture gave the expected glycoside. GCMS and HPLC analysis showed it to be the α-anomer (Table 1), Pure anomer can be obtained *via* preparative TLC. ^{13}C and ^{1}H NMR and mass spectroscopic and other analytical data are identical to those reported previously (ref. 3).

1 G. Bendas, F. Wilhelm, W. Richter and P. Nuhn, *Eur. J. Pharm. Sci.*, 1996, **4**, 211; P. Nuhn, T. Pfaff, G. Bendas, F. Wilhelm and S. K. Chatterjee, *Arch. Pharm.*, 1994, **327**, 429; A. Engel, G. Bendas, F. Wilhelm, M. Mannova, M. Ausborn and P. Nuhn, *Int. J. Pharm.*, 1994, **107**, 99; A. Engel, K. Augsten, F. Wilhelm, S. K. Chatterjee and P. Nuhn, *Arch. Pharm.*, 1993, **326**, 648; G. Förster, O. de la Cruz Rodriguez, G. Bendas and P. Nuhn, *Prog. Colloid Polym. Sci.*, 1995, **98**, 201.

2 G. Wulff and G. Röhle, *Angew Chem., Int. Ed. Engl.*, 1974, **13**, 157; H. Paulsen, *ibid.*, 1982, **21**, 155; R.R. Schmidt, *ibid.*, 1986, **25**, 212; J. Thiem, *Annu. Rep. Prog. Chem., Sect. B*, 1985, **81**, 311; K. Toshima and K. Tatsuta, *Chem. Rev.*, 1993, **93**, 1503.

3 F. Wilhelm, S. K. Chatterjee, B. Rattay, P. Nuhn, R. Benecke and J. Ortwein, *Liebigs Ann.*, 1995, 1673.

4 M. Tanaka, M. Okita and I. Yamatsu, *Carbohydr. Res.*, 1993, **241**, 81.

5 D. Kahne, D. Yang, J. J. Lim, R. Miller and E. Paguaga, *J. Am. Chem. Soc.*, 1988, **110**, 8716.

6 S. Koto, N. Morishima, Y. Miyata and S. Zen, *Bull. Chem. Soc. Jpn.*, 1976, **49**, 2639.

7 (*a*) S. Koto, N. Morishima. R. Kawahara, K. Ishikawa and S. Zen, *Bull. Chem. Soc. Jpn.*, 1982, **55**, 1092; (*b*) P. Nuhn and G. Wagner, *Z. Chem.*, 1967, **7**, 154; (*c*) N. Ikemoto, O. K. Kim, L.-C. Lo, V. Satyanarayana, M. Chang and K. Nakanishi, *Tetrahedron Lett.*, 1992, **33**, 4295.

8 F. Dasgupta, P. P. Singh and H. C. Srivastava, *Carbohydr. Res.*, 1980, **80**, 346; V. Ferrieres, J.-N. Bertho and D. Plusquellee, *Tetrahedron Lett.*, 1995, **36**, 2753.

9 H. Leffler and C. Svanborg-Eden, *FEMS Microbiol. Lett.*, 1980, **8**, 127; G. Källenius, R. Möllby, S. B. Svenson, J. Winberg, A. Lundblad, S. Svenssen and B. Cedergren, *ibid.*, 1980, **7**, 297.

10 M. Naiki and M. Kato, *Vox Sang.*, 1979, **37**, 30; R. R. Race and R. Sanger, *Blood Groups in Man*, 6th edn., Blackwell, Oxford, 1975.

Received in Cambridge, UK, 22nd April 1998; revised manuscript received, 15th June 1998; 8/04533J

Synthesis of heme–tris(imidazolyl)methane copper complex, the first binuclear complex bearing three imidazole ligands for copper, as an active site model of cytochrome *c* oxidase

Fumito Tani, Yasuhiro Matsumoto, Yoshimitsu Tachi, Takao Sasaki and Yoshinori Naruta*†

Institute for Fundamental Research of Organic Chemistry, Kyushu University, Fukuoka 812-8581, Japan

As an active site model of cytochrome *c* oxidase, a new covalently-linked binuclear complex with three imidazole ligands for copper, heme–tris(imidazolyl)methane copper, was prepared and spectroscopically characterized.

Cytochrome *c* oxidase (CcO) is a terminal respiratory protein complex which catalyzes the four-electron reduction of O_2 to water in aerobic organisms.[1] The structures of bovine heart[2] and *Paracoccus denitrificans*[3] CcOs have been independently revealed by X-ray crystallography. Heme a_3 and Cu_B, which form a unique binuclear center, are directly responsible for dioxgen reduction. The histidinyl imidazole axially ligates to the iron in heme a_3, while Cu_B has the three histidinyl imidazole ligands for the copper. The separations between the iron and the copper atoms in the active site were determined to be 4.5 Å for the bovine heart and 5.2 Å for the bacterial CcO.

A number of heme-based binuclear Fe–Cu complexes have been prepared[4] to elucidate the mechanism of O_2 reduction and/or to reproduce an EPR-silent, antiferromagnetic coupled Fe^{III}–X–Cu^{II} moiety, which are the characteristics of the resting state of CcO. We recently reported that the reduced form (Fe^{II}–Cu^{I}) of the heme–tris(pyridylmethyl)amine copper complex reacted with dioxygen to give a stable oxygenated complex **1** in a μ-1,2-peroxo fashion at ambient temperature.[5] To the best of our knowledge, this is the first well-characterized dioxygen adduct of a CcO modeling complex. Although the coordination to the copper ions is considered to affect the binding and reduction of dioxygen significantly, there have been no examples of a binuclear model complex having three imidazole ligands for the copper ion similar to the native ones. As a close model with a Cu–L_3 moiety, we reported the oxidized form of heme–trispyrazolyl copper complex **2**,[6] which, however, did not exhibit a large enough formation constant with copper ion to allow further study. Therefore, we designed and synthesized a new model complex, heme–tris(imidazolyl)methane copper [**Fe^{III}(TPP)–Cu^{II}(TIMC_2)Cl_3**]. Tris(imidazolyl)methane is a tridendate chelating ligand which can give stable complexes with copper ion.[7] The two components, porphyrin and tris(imidazolyl)methane, are connected through an amide linkage to maintain a suitable geometry and separation of the two metal ions.

The synthetic routes to the desired complex are shown in Scheme 1.‡ (*N*$^{\tau}$-Methylhistamin-2-yl)-bis(*N*-methylimidazol-2-yl)methane **6** (**TIMC_2-NH_2**) could be obtained *via* the coupling between silyl-protected *N*$^{\tau}$-methy-2-bromohistamine **5** and the lithiated anion of bis(*N*-methylimidazol-2-yl)methane[8] under $Pd(PPh_3)_4$-catalyzed conditions.[9] *N*$^{\tau}$-Methylhistamine **3** was prepared from commercially available histamine dihydrochloride in three steps according to the reported methods[10] in 71% overall yield. There were some prerequisites for the protection of the NH_2 group: first, the protecting group should be robust enough under the following strong basic conditions involving BuLi, and second, the group should be removable under mild conditions and should be easily separable from the reaction mixture. Thus, a cyclic disilyl group[11] was chosen as the protecting group. A solution of **3** and DBU§ was treated with 1,1,4,4-tetramethyl-1,4-dichlorosilylethylene to give the cyclic disilazole **4** in 90% yield. Bromination at the C-2 position of **4** was accomplished with BuLi and 1,2-dibromo-1,1,2,2-tetrafluoroethane in 94% yield with conservation of the disilyl protecting group. Litiation of bis(*N*-methylimidazol-2-yl)methane at CH_2 was performed with BuLi in THF, followed by the addition of $Pd(PPh_3)_4$ and **5** . The mixture was

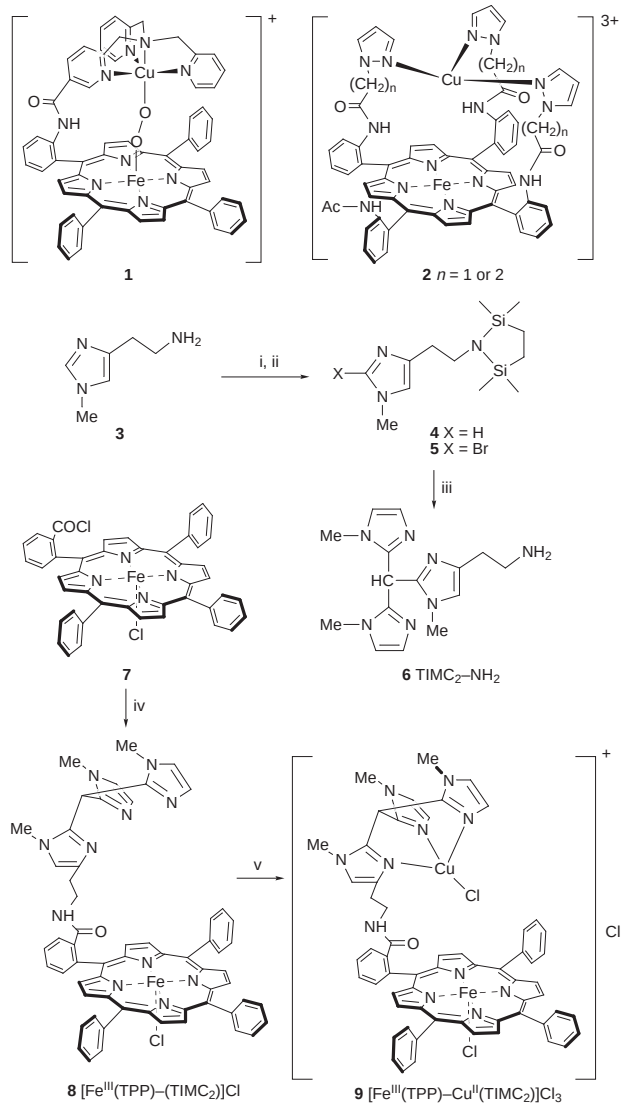

Scheme 1 *Reagents and conditions*: i, DBU, 1,1,4,4-tetramethyl-1,4-dichlorosilylethylene, CH_2Cl_2, 2 h, room temp., 90%; ii, BuLi, Et_2O , 1h, −78 to −35 °C, 1,2-dibromo-1,1,2,2-tetrafluoroethane, −78 to −25 °C; iii, BuLi, bis(*N*-methylimidazol-2-yl)methane, THF, 1 h, −78 to −20 °C, $Pd(PPh_3)_4$, overnight, 50 °C; iv, **6**, Pr^i_2NEt, CH_2Cl_2, 2 h, 0 to 20 °C; v, $CuCl_2·6H_2O$, MeOH–CH_2Cl_2, 1 h, room temp.

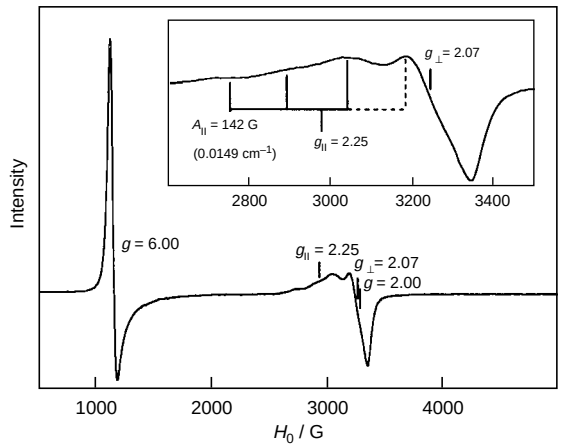

Fig. 1 EPR spectrum of **9** {**[Fe^{III}(TPP)–Cu^{II}(TIMC$_2$)]Cl$_3$**} in CH_2Cl_2 at 6 K, microwave frequncy = 9.3423 GHz, power = 1 mW

heated overnight at 50 °C to enhance the coupling reaction. The removal of the starting compounds by sublimation under high vaccum conditions afforded **TIMC$_2$-NH$_2$ 6** in 25% yield.

5-(2-Carboxyphenyl)-10,15,20-triphenylporphyrin was used as the porphyrin moiety. In order to avoid complications during the insertion of the two different metal ions to two different ligand sites, iron(III) was introduced into the porphyrin ligand prior to coupling with the **TIMC$_2$** moiety. The acid chloride **7**, obtained quantitatively from the free acid, was coupled with **6** in the presence of Pr^i_2NEt in CH_2Cl_2 to give the mononuclear complex **8** {**[Fe^{III}(TPP)–(TIMC$_2$)]Cl**; *m/z* = 993, λ_{max}/nm (ε/M^{-1} cm^{-1}) = 378 (23 200), 417 (46 700), 511 (5170), 576 (2410), 695 (1380), 775 (520)} in 31% yield. The final desired complex **9** {**[Fe^{III}(TPP)–Cu^{II}(TIMC$_2$)]Cl$_3$**} was prepared quantitatively by the addition of $CuCl_2 \cdot 6H_2O$ in MeOH–CH_2Cl_2. Its electronic spectrum [λ_{max}/nm (ε/ M^{-1} cm^{-1}) = 378 (26 900), 417 (44 700), 510 (6560), 577 (2330), 654 (2110), 687 (2110)] was similar to that of the mononuclear heme complex. Its electrospray mass spectrum showed a cluster of peaks at *m/z* 1128 as a base peak, which is assignable to the monocation **[Fe^{III}(TPP)–Cu^{II}(TIMC$_2$)Cl$_2$]$^+$**. The distribution of isotope peaks was in good accord with simulation. The high-resolution mass spectrum (FAB, NBS) also gave an acceptable mass number within 10 mmeu [Calc. for $C_{60}H_{47}N_{11}OFeCuCl_2$ ([M - Cl]$^+$): 1128.4053. Found: 1128.4101]. The EPR spectrum of this complex showed signals at g = 6.00 and 2.00, which are characteristic of typical high spin iron(III) porphyrins, and signals at $g_\parallel$ = 2.25 and $g_\perp$ = 2.07 derived from Cu^{II} (Fig. 1). The lack of a meaningful magnetic interaction in the EPR spectrum indicated a large separation of the two paramagnetic centers . The four-split hyperfine structure of Cu^{II} centered at $g_\parallel$ was observed with $A_\parallel$ = 142 G (0.0149 cm^{-1}). It has been shown that as the coordination geometry of copper in a CuL_4 center is distorted from square planar to teterahedral, $g_\parallel$ increases and $A_\parallel$ decreases with an antiparallel linear correlation.[12] Comparing the present $g_\parallel$ and $A_\parallel$ values with those of the reported Cu^{II} complexes, we conclude that the coordination geometry of the copper is distorted tetragonal rather than planar. This spectroscopic evidence substantiated the designed structure of **[Fe^{III}(TPP)–Cu^{II}(TIMC$_2$)]Cl$_3$**. Of all the CcO models, this is the first binuclear complex bearing three imidazole ligands coordinated to copper.

The reaction between the reduced form (Fe^{II}–Cu^{I}) of the present complex and dioxygen is now under investigation, along with a comparison with our previous binuclear oxygenated complex (**1**).

This research was financially supported by a Grant-in-Aid for COE Research (#08CE2005) and for Scientic Research on Priority Areas (#09235225) from the Ministry of Education, Science and Culture, Japan.

Notes and References

† E-mail: naruta@ms.ifoc.kyushu-u.ac.jp

‡ Experimental details will be reported elsewhere. All new compounds were fully characterized by spectroscopic methods and elemental analyses. Stated yields refer to isolated compounds. Electronic spectra were measured in CH_2Cl_2.

§ Simple tertiary amines like Et_3N were ineffective for this reaction. Since the removal of generated HCl is critical for the completion of the reaction, application of amines more basic than imidazole, such as DBU, is essential.

1 For a review, see; S. Ferguson-Miller and G. T. Babcock, *Chem. Rev*., 1996, **96**, 2889.
2 T. Tsukihara, H. Aoyama, E. Yamashita, T, Tomizaki, H. Yamaguchi, K. Shinzawa-Itoh, R. Nakashima, R. Yaono and S. Yoshikawa, *Science*, 1995, **269**, 1069; T. Tsukihara, H. Aoyama, E. Yamashita, T, Tomizaki, H. Yamaguchi, K. Shinzawa-Itoh, R. Nakashima, R. Yaono and S. Yoshikawa, *Science*, 1996, **272**, 1136.
3 S. Iwata, C. Ostermeier, B. Ludwig and H. Michel, *Nature*, 1995, **376**, 660.
4 J. P. Collman, L. Fu, P. C. Hermann and X. Zhang, *Science*, 1997, **275**, 949; A. Nanthakumar, S. Fox, N. N. Murthy and K. D. Karlin, *J. Am. Chem. Soc*., 1997, **119**, 3898; J.-O. Baeg and R. H. Holm, *Chem. Commun.*, 1998, 571 and references cited therein.
5 T. Sasaki, N. Nakamura and Y. Naruta, *Chem. Lett.*, 1998, 351.
6 T. Sasaki and Y. Naruta, *Chem. Lett.*, 1995, 663.
7 T. N. Sorrell and A. S. Borovik, *J. Am. Chem. Soc.*, 1987, **109**, 4255.
8 P. K. Byers and A. J. Canty, *Organometallics*, 1990, **9**, 210.
9 M. Kumada, *Pure Appl. Chem.*, 1980, **52**, 669 and references cited therein.
10 G. J. Dyrant, J. C. Emmett, C. R. Ganellin, A. M. Roe and R. A. Slater, *J. Med. Chem.*, 1976, **19**, 923; P. G. Potvin and M. H. Wong, *J. Chem. Soc., Chem. Commun.*, 1987, 672.
11 S. Djuric, J. Venit and P. Magnus, *Tetrahedron Lett.*, 1981, **21**, 1787.
12 H. Yokoi, *Bull. Chem. Soc. Jpn.*, 1974, **47**, 3037; U. Sakaguchi and A. W. Addison, *J. Am. Chem. Soc.*, 1977, **99**, 5189; H. Yokoi and A. W. Addison, *Inorg. Chem.*, 1977, **16**, 1341.

Received in Cambridge, UK, 11th May 1998; 8/03498B

Ion pair chromatographic resolution of tris(diimine)ruthenium(II) complexes using TRISPHAT anions as resolving agents

Jérôme Lacour,*† Sonya Torche-Haldimann, Jonathan J. Jodry, Catherine Ginglinger and France Favarger

Département de Chimie Organique, Université de Genève, quai Ernest Ansermet 30, CH-1211 Genève 4, Switzerland

Enantiomers of chiral tris(diimine)ruthenium(II) complexes can be separated on a polar chromatographic phase (SiO_2) when associated with TRISPHAT counterions (2 equivalents).

Chiral tris(diimine)ruthenium(II) complexes have been extensively studied in the fields of photochemistry and photophysics, and as probes in DNA.[1] Many applications require enantiopure complexes (Δ or Λ) and, for those made from achiral ligands, a resolution is usually needed due to the shortage of enantioselective methods of synthesis.[2] Traditionally, resolutions of chiral cationic tris(diimine)ruthenium(II) complexes are realised by the formation of diastereomeric ion pairs (IPs) with anionic chiral resolving agents, and then depend principally on solubility differences.[3] Ion-pair chromatographic resolutions, using cation exchangers and electrolytes with chiral anions in the mobile phase, are possible and lead to efficient separation of diastereomeric IPs.[4] Herein, we report a new chromatographic resolution procedure involving pre-formed diastereomeric mixtures of chiral tris(diimine)ruthenium(II) complexes and TRISPHAT anions (**1**, 2 equiv.). The resulting

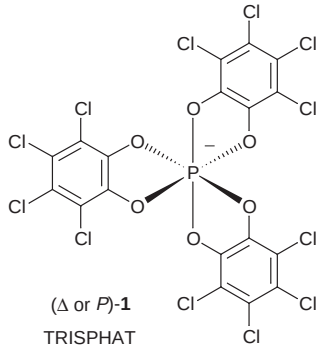

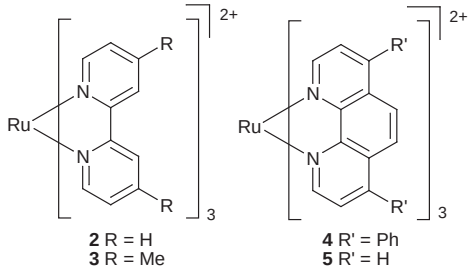

diastereomeric IPs are poorly retained on polar chromatographic phase (SiO_2) and large differences in the retardation factors are observed.

Recently, we have shown that the easily prepared and resolved chiral TRISPHAT anion **1** [tris(tetrachlorobenzenediolato)phosphate(V)] is configurationally stable as an ammonium salt in solution.[5] Anion **1** is an efficient NMR chiral shift agent and a valuable host in molecular recognition studies, conferring unique properties to its IPs.[6] For instance, TRISPHAT modifies profoundly the chromatographic properties of cations associated with it (*e.g.* triarylcarbenium cations) and the resulting IPs are poorly retained on polar chromatographic phases.[6b] This result encouraged us to examine whether enantiopure TRISPHAT anion could be used for the IP chromatographic resolution of configurationally stable chiral cations, such as the tris(diimine)ruthenium(II) complexes. We hypothesised that selective chiral discriminating interactions would occur between these three-bladed propellers (Δ^+–Δ^- *vs.* Λ^+–Δ^-) resulting in a good separation.[6c] We decided to test this hypothesis with $[Ru(bipy)_3]^{2+}$ **2**, $[Ru(4,4'\text{-diMebipy})_3]^{2+}$ **3**, $[Ru(bathophen)_3]^{2+}$ **4** and $[Ru(phen)_3]^{2+}$ **5** complexes using the cinchonidinium-(*P* or Δ)-**1** salt (**1a**) as resolving agent.[5,6a] Complexes **2**-Cl_2 and **3**-Cl_2 were prepared following the description of Broomhead and Young,[7] and salts **3**-$(PF_6)_2$, **4**-$(PF_6)_2$ and **5**-$(PF_6)_2$ in a single step from $Ru(DMSO)_4Cl_2$ and the respective bipyridine or phenanthroline ligands (3 equiv.).[8]

The potential of TRISPHAT **1** to serve as a chromatographic resolving agent was first evaluated by analytical thin layer chromatography (TLC): Solutions of salt **1a** (2.0 equiv.) in acetone and racemic **2**-Cl_2, **3**-Cl_2, **3**-$(PF_6)_2$ or **4**-$(PF_6)_2$ (1.0 equiv.) in CH_2Cl_2 were prepared, mixed together, and the resulting solutions adsorbed on silica gel plates. Development by elution with CH_2Cl_2 or $CHCl_3$ showed the formation of two bands corresponding to the two new diastereomeric IPs, [Δ-(**2**–**4**)](Δ-**1**)$_2$ and [Λ-(**2**–**4**)](Δ-**1**)$_2$. Much reduced affinity for silica gel was exhibited as foreseen, as the (**2**–**4**)(Δ-**1**)$_2$ IPs were retained to a much lower extent (Table 1).

The retention of diastereomeric salts (**2**–**4**)(Δ-**1**)$_2$ depended upon the nature of the cation and the concentration of the salts.[6b] Solutions were thus applied (spotted) as concentrated as possible. Due to the streaking of salts (**2**–**4**)(Δ-**1**)$_2$ on TLC, we have not calculated retardation factors (R_f), but rather measured the distance moved by the analyte band to the *top* (and not to the centre) of the spot: The derived ratios, called just *R*, for the resulting IPs were in the range of 0.45–0.75 for the most eluted diastereomer and 0.35–0.54 for the least (CH_2Cl_2 as eluent). We observed rather large differences between the *R* values of the diastereomeric IPs (max. ΔR = 0.23). More lipophilic cations (**3** and **4**, entries 2–5) were retained less than **2** and **5**. The less polar $CHCl_3$ led to better separation than CH_2Cl_2. The nature of

Table 1 Retardation factors of diastereomeric $[Ru(LL)_3](\Delta\text{-}\mathbf{1})_2$

			R (**2**–**5**)(Δ-**1**)$_2$[a,b]		
Entry	Racemic salt	*R*[a,b] (**2**–**5**)-X_2	Most eluted	Least eluted	Δ*R*
1[c]	**2**$(Cl)_2$	< 0.05	0.45	0.33	0.12
2[c]	**3**$(Cl)_2$	< 0.05	0.75	0.52	0.23
3[c]	**3**$(PF_6)_2$	< 0.05	0.76	0.54	0.22
4[c]	**4**$(PF_6)_2$	0.08	0.75	0.65	0.10
5[d]	**4**$(PF_6)_2$	0.15	0.65	0.46	0.19
6[c]	**5**$(PF_6)_2$[e]	< 0.05	0.42	[f]	[f]

[a] *R* represents the distance moved by the analyte band to the top. [b] Spotted as concentrated as possible. [c] CH_2Cl_2 as eluent. [d] $CHCl_3$ as eluent. [e] TLC done with solution containing partially resolved Δ-**5**. [f] Not applicable.

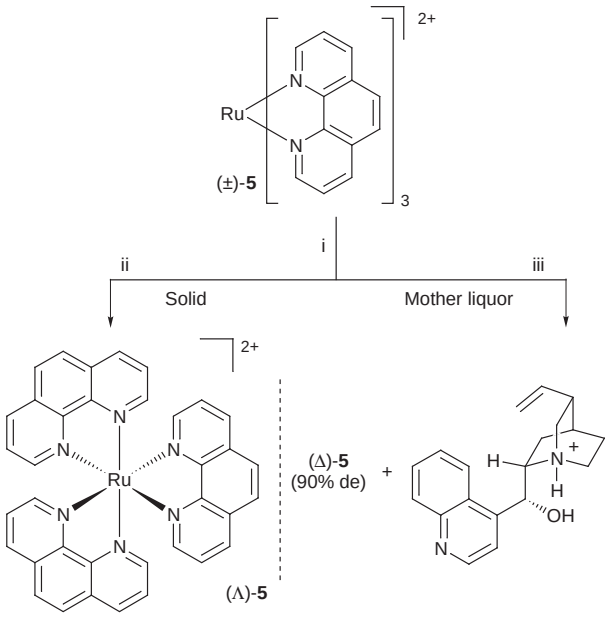

Scheme 1 *Reagents and conditions*: i, 1.0 equiv. of (±)-**5**-$(PF_6)_2$ in CH_2Cl_2, 2.0 equiv. of **1a** in acetone, CH_2Cl_2, 10 min; ii, filtration, essentially Λ-**5**; iii, mother liquor, cinchonidinium:Δ-**5** (4:1), de 90%

the anionic counterion (Cl^-, PF_6^-) in the precursor salt seems to have, within experimental error, no influence (entries 2 and 3). The behaviour of the (**2**–**4**)(Δ-**1**)$_2$ ion pairs is quite remarkable as the precursor salts (**2**–**4**)$(PF_6)_2$ migrate little under these chromatographic conditions.

TLC analysis of racemic salt **5**-$(PF_6)_2$ in the presence of anions Δ-**1** could not be completed as planned: The precipitation of an orange solid containing essentially Λ-**5** was observed in seconds upon the mixing of the solutions of **5**-$(PF_6)_2$ and **1a**.‡ A direct, yet partial, resolution of **5** was thus afforded as the filtration of the solid gave a mother liquor containing the cinchonidinium cation and Δ-**5** (90% de) in a 4:1 ratio (Scheme 1).

Preparative chromatographic resolution was possible for the ruthenium(II) diimine complexes **3** and **4**, exhibiting good solubility in CH_2Cl_2 (or $CHCl_3$) and large Δ*R* values when associated with **1**. From mixtures of **1a** (2.0 equiv.) and racemic salts **3**-$(PF_6)_2$ and **4**-$(PF_6)_2$ (1.0 equiv.), pure separated diastereomeric IPs [Δ-(**3**,**4**)](Δ-**1**)$_2$ and [Λ-(**3**,**4**)](Δ-**1**)$_2$ could be afforded in reasonable yields (Table 2):§

Table 2 Preparative ion pair chromatographic resolution

Entry	Salts	Most eluted[a]	Least eluted[a]	Mixed fraction[a]	Eluents[b]
1	**3**-$(PF_6)_2$	34%[c]	15%[d]	41%	A only
2	**3**-$(PF_6)_2$	40%[c]	—	56%[e]	B then A
3	**4**-$(PF_6)_2$	45%[c]	29%[d]	24%	B then A

[a] Yields for isolated products. [b] A = CH_2Cl_2 and B = $CHCl_3$. [c] Homochiral complex $\Delta^+(\Delta^-)_2$. [d] Heterochiral complex $\Lambda^+(\Delta^-)_2$. [e] The lower solubility of (Δ-**3**)(Δ-**1**)$_2$ in $CHCl_3$ leads to its gradual release in solution and thus to an important contamination of the least eluted fraction.

The enantiomeric excesses of the cations in the various chromatographic fractions were easily assessed by TLC and/or determined precisely by ^1H NMR analysis.¶ Due to the streaking of the IPs on silica gel, the most rapidly eluted diastereomers were always afforded in better yields than the least, and rather large fractions containing both diastereomers were isolated. Circular dichroism (CD) analyses of solutions of the most and least rapidly eluted separated diastereomers indicated that the cationic complexes had absolute Δ and Λ configurations respectively (Fig. 1). Homochiral [Δ-(**3**,**4**)](Δ-**1**)$_2$ complexes were less well retained than heterochiral complexes [Λ-(**3**,**4**)](Δ-**1**)$_2$ on silica gel.

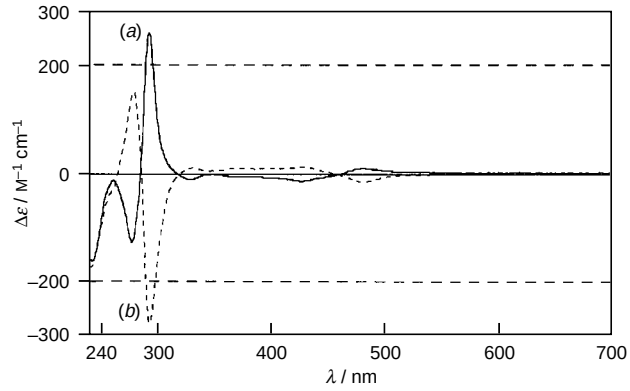

Fig. 1 CD spectra of the most and least eluted diastereomeric complexes (*a*) (Δ-**3**)(Δ-**1**)$_2$ and (*b*) (Λ-**3**)(Δ-**1**)$_2$ in CH_2Cl_2 at 20 °C

In conclusion, we have developed a new chromatographic resolution procedure for rather lipophilic cationic tris(diimine)ruthenium(II) complexes; it requires just 2 equiv. of the resolving agent and a polar chromatographic phase (SiO_2), which thus makes it economical and practical.

We are grateful for financial support of this work by the Swiss National Science Foundation. We thank Mr A. Pinto, Mr J.-P. Saulnier, Mr W. Kloeti and Mrs E. Sandmeyer for NMR and MS measurements.

Notes and References

† E-mail: lacour@sc2a.unige.ch

‡ ^{31}P NMR analyses (20% $[^2H_6]$DMSO–$CDCl_3$) of the solid and the mother liquor reveal the presence of TRISPHAT and PF_6^- in both fractions.

§ *Typical procedure*: To a solution of 67.7 mg of **3**-$(PF_6)_2$ (71.7 μmol, 1.0 equiv.) in CH_2Cl_2 (10 ml) was added a solution of 152.7 mg of **1a** (143.5 μmol, 2.0 equiv.) in acetone (5 ml) and, after 10 min of stirring, 1.0 g of SiO_2 [J. T. Baker silica gel (30–60 μm)]. The resulting mixture was concentrated *in vacuo* affording a fine orange powder, which was placed on the top of a chromatography column (SiO_2, 3 × 18 cm). Elution with CH_2Cl_2 afforded fractions that were collected, analysed by TLC/NMR and gathered according to their enantiomeric purity.

¶ The associated TRISPHAT anions behave as NMR chiral shift agents.

1 A. Von Zelewsky, P. Belser, P. Hayoz, R. Dux, X. Hua, A. Suckling and H. Stoeckli-Evans, *Coord. Chem. Rev.*, 1994, **132**, 75; J. K. Barton, *Science*, 1986, **233**, 727; J. K. Barton, *Pure Appl. Chem.*, 1989, **61**, 563; I. Ortmans, C. Moucheron and A. Kirsch- De Mesmaeker, *Coord. Chem. Rev.*, 1998, **168**, 233.

2 P. Belser, S. Bernhard, E. Jandrasics, A. Von Zelewsky, L. De Cola and V. Balzani, *Coord. Chem. Rev*, 1997, **159**, 1; A. Von Zelewsky, *Stereochemistry of Coordination Compounds*., Wiley, Chichester, UK, 1996.

3 F. P. Dwyer and E. C. Gyarfas, *J. Proc. R. Soc. N. S. W.*, 1949, **83**, 174; 1949, **83**, 170; R. D. Gillard and R. E. E. Hill, *J. Chem. Soc., Dalton Trans.*, 1974, 1217; G. B. Porter and R. H. Sparks, *J. Photochem.*, 1980, **13**, 123.

4 B. T. Patterson and F. R. Keene, *Inorg. Chem.*, 1998, **37**, 645; N. C. Fletcher, P. C. Junk, D. A. Reitsma and F. R. Keene, *J. Chem. Soc., Dalton Trans.*, 1998, 133; T. J. Rutherford, M. G. Quagliotto and F. R. Keene, *Inorg. Chem.*, 1995, **34**, 3857; F. R. Keene, *Coord. Chem. Rev.*, 1997, **166**, 121.

5 J. Lacour, C. Ginglinger, C. Grivet and G. Bernardinelli, *Angew. Chem.*, 1997, **109**, 660; *Angew. Chem., Int. Ed. Engl.*, 1997, **36**, 608.

6 (*a*) J. Lacour, C. Ginglinger, F. Favarger and S. Torche-Haldimann, *Chem. Commun.*, 1997, 2285; (*b*) J. Lacour, S. Barchéchath, J. J. Jodry and C. Ginglinger, *Tetrahedron Lett.*, 1998, **39**, 567; (*c*) J. Lacour, J. J. Jodry, C. Ginglinger and S. Torche-Haldimann, *Angew. Chem., Int. Ed. Engl.*, 1998, in the press.

7 J. A. Broomhead and C. G. Young, *Inorg. Synth.*, 1990, **28**, 338.

8 I. P. Evans, A. Spencer and G. Wilkinson, *J. Chem. Soc., Dalton Trans.*, 1973, 204; L. F. Cooley, C. E. L. Headford, C. M. Elliot and D. F. Kelley, *J. Am. Chem. Soc.*, 1988, **110**, 6673.

Received in Basel, Switzerland, 26th May 1998; 8/03904F

Oxa-bowls: formation of exceptionally stable diozonides with novel, C–H···O hydrogen bond directed, solid state architecture

Goverdhan Mehta*† and R. Uma

Molecular Design and Synthesis Laboratory of JNCASR, School of Chemistry, University of Hyderabad, Hyderabad 500 046, India

Several tetraquinane-based diolefins on ozonization furnish unusually stable diozonides of 'bowl-like' topology and their solid state structure reveals interesting architecture woven through a network of unique C–H···O interactions.

We have been engaged in the synthesis of a range of novel, high symmetry, 'bowl-shaped' molecular entities, composed of a carbocyclic base and hetero-atom speckled rim.[1] In the context of these endeavours, we became interested in an octacyclic, hexaoxa-bowl **1**, $C_{14}H_{14}O_6$, of C_{2v} symmetry, which we planned to access from the hexaaldehyde **2**, through a cascade of intramolecular acetalization protocols.[1] Compound **2**, in turn, was proposed to be prepared from the C_{2v} tetraquinane **3** *via* ozonolysis or equivalent oxidative cleavage of the disubstituted double bonds (Scheme 1). During our studies of **1**, we observed that several derivatives of **3** on ozonization furnish remarkably stable diozonides in a highly stereoselective manner. Two of these tetraquinane derived diozonides readily furnished single crystals and their X-ray crystallographic analysis shows a fascinating packing pattern and supramolecular arrangement, sustained by a network of C–H···O hydrogen bonds.[2] To the best of our knowledge, only one stable diozonide [derived from hexamethyl (Dewar) benzene] is known[3a] so far, although several stable mono-ozonides have been reported recently.[3c,d] The crystal structure[3a,b] of the diozonide from hexamethyl (Dewar) benzene has also been determined, but the authors did not observe any significant intermolecular contacts.

Tetraquinanes **3**, **4** and their oxa-analogues **5**–**8** reported earlier by us,[4] on ozonolysis in CH_2Cl_2 at −78 °C directly furnished the corresponding diozonides **9**–**14** after the removal of the solvent and could be readily crystallized (Scheme 2). All the diozonides were stable at room temperature (for months) and showed little decomposition on either moderate heating or on exposure to Me_2S and triphenylphosphine under standard conditions (stirring in CH_2Cl_2 solution). The gross structures of

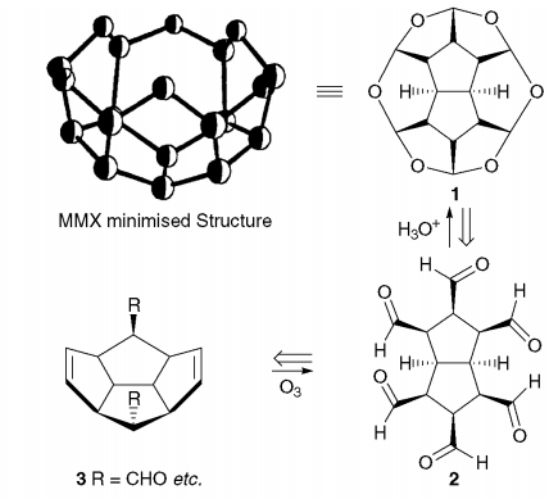

Scheme 1

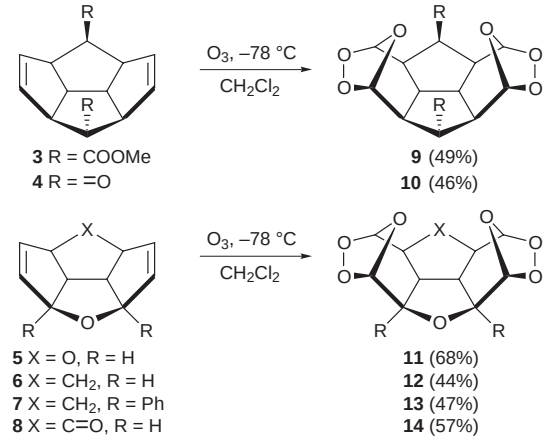

Scheme 2

9–**14** were fully revealed through the incisive analysis of their ^{1}H and ^{13}C NMR data.[5] However, the bowl-like *syn,syn*-stereochemistry present in **9**–**14**, with the two oxa-bridges protruding inwards could not be delineated unambiguously, although the MMX calculations showed this arrangement to be the most stable.‡ Therefore, recourse was taken to X-ray crystallography and two of the diozonides **9** and **14** furnished single crystals suitable for structure determination.

The diozonide **9** crystallized in space group *C*2/*c* and an ORTEP perspective (Fig. 1)§ revealed the stereochemistry as *syn,syn* with the O1 and O1a oxa-bridges tilting significantly inwards (O1 and O1a distance being 2.62 Å), and this orientation is facilitated by intramolecular C–H···O hydrogen bonds[2] between the bridgehead H1 and H1a atoms and the O4a

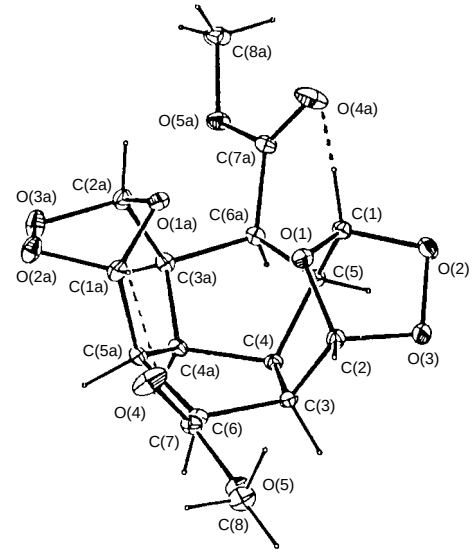

Fig. 1 ORTEP plot of **9**

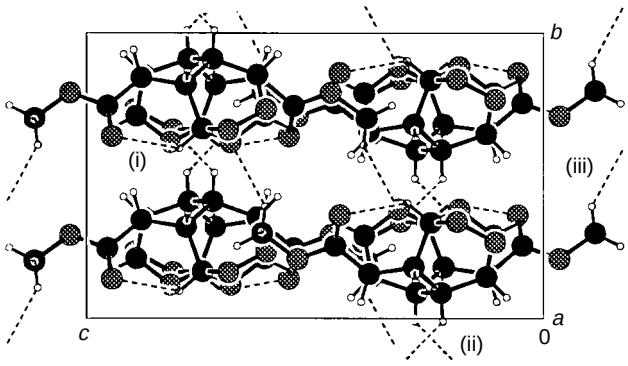

Fig. 2 Crystal packing in **9**, view down *a* axis. Selected C–H···O interactions: [H···O (Å), C(H)···O (Å), CH···O (°)]: (i) (intra, C1–H1···O4) 2.21, 2.93, 129.5; (ii) (inter, C4–H4···O2) 2.58, 3.34, 134.4; (iii) (inter, C8–H8C···O1) 2.60, 3.18, 119.5.

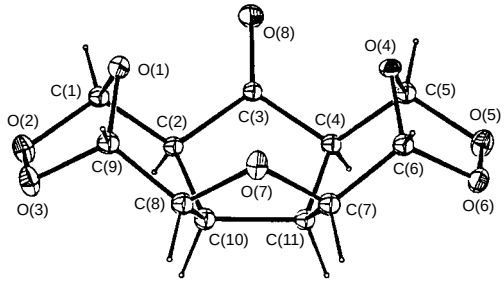

Fig. 3 ORTEP plot of **14**

and O4 carbonyl groups of the ester moieties (H···O distance 2.21 Å, C···O 2.93 Å and C–H···O angle of 129.5°) (Fig. 1). The packing pattern shows that the bowl-like molecules of **9** are stacked one over the other along the *b* axis in a columnar arrangement (Fig. 2). In the *ab* plane there are arrays of uni-directional bowls, each engaged in four C–H···O hydrogen bonds (two below and two above) to nearest neighbours through H4, H4a (ring junction protons on the diquinane moiety) and O2a, O2 oxygens of the peroxo bridge (H···O distance 2.58 Å, C···O 3.34 Å and C–H···O angle of 134.4°) along the *b* axis. The adjacent *ab* planes consist of bowls growing in opposite directions and are held by weak C–H···O contacts between the Hc protons of the ester methyls and O1 oxa-bridges of the inversion related bowls (Fig. 2).

The oxa-bowl **14** crystallizes in space group $Pca2_1$ and the molecules are tightly packed as indicated by its high density (1.681 Mg m^{-3}). An ORTEP diagram (Fig. 3)§ once again revealed the *syn,syn* stereochemistry but the two oxa-bridges are now far apart (O1 to O4 distance is 4.22 Å), perhaps due to repulsion within the congested concave surface with O7. The bowls are held by C–H···O hydrogen bonds (H···O distance 2.36 Å, C···O 3.28 Å and C–H···O angle of 155.1°) between H10 (ring junction proton on the diquinane moiety) and O7 ether oxygen, along the *c* axis, defining a ribbon-like pattern (Fig. 4). There is a bowl inversion pattern along the *a* axis and these bowls are held through a C1–H1···O5 contact. Along the *b* axis the bowls are held by C–H···O hydrogen bonds between the H7 (α to the ether oxygen) and the O8 carbonyl oxygen (H···O distance 2.57 Å, C···O 3.49 Å and C–H···O angle of 156.6°) to generate another ribbon-like pattern (Fig. 4). It is noteworthy that in the structures of both **9** and **14**, the least acidic diquinane ring junction protons are involved in the C–H···O hydrogen bonds and this is perhaps a consequence of the bowl-like topology present in these molecules.

In summary, we have described the characterization of several 'bowl-like' diozonides of exceptional stability and their X-ray structure reveals a novel architecture sustained through a network of C–H···O hydrogen bonds.

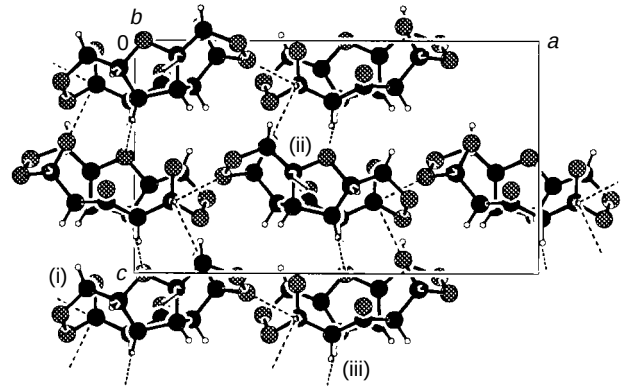

Fig. 4 Crystal packing in **14**, view down *b* axis. Selected C–H···O interactions: [H···O (Å), C(H)···O (Å), CH···O (°)]: (i) (inter, C1–H1···O5) 2.42, 3.05, 121.4; (ii) (inter, C7–H7···O8) 2.57, 3.49, 156.6; (iii) (inter, C10–H10···O7) 2.36, 3.28, 155.1.

We thank DST for the support of National Single Crystal X-Ray Facility at the University of Hyderabad. One of us (R. U.) thanks the CSIR for a Fellowship.

Notes and References

† E-mail: gm@orgchem.iisc.ernet.in

‡ The diozonides **9**–**14** can in principle occur in three diastereoisomeric forms, *viz. syn,syn* (with the two oxa-bridges directed within the diquinane moiety), *anti,anti* (with the two peroxy-bridges directed within the diquinane moiety) and *syn,anti* (with one oxa- and one peroxy-bridge directed within the diquinane moiety).

§ *X-Ray data* for **9**: $C_{16}H_{18}O_{10}$, M = 370.30, colourless crystals from CH_2Cl_2, monoclinic, space group $C2/c$, a = 11.534(6), b = 9.174(9) and c = 14.825(19) Å, β = 101.12(8)°, V = 1539(3) Å^3, Z = 4, D_c = 1.598 Mg m^{-3}, T = 293 K, $F(000)$ = 776, μ(Mo-Kα) = 0.135 mm^{-1}, crystal dimensions 0.23 × 0.11 × 0.15 mm. Data were collected on Enraf–Nonius MACH-3 diffractometer, graphite-monochromated Mo-Kα radiation (λ = 0.71073 Å), by the ω scan method in the range $2 \leqslant \theta \leqslant 25°$, 1351 unique reflections [R_{int} = 0.0379], of which 1211 had $F_o > 4\sigma(F_o)$, were used in all calculations. At final convergence R_1 [$I > 2\sigma(I)$] = 0.0447, wR_2 = 0.1197 for 119 parameters, GOF = 1.074, $\Delta\rho_{max}$ = 0.297 e Å^{-3}, $\Delta\rho_{min}$ = −0.251 e Å^{-3}. The data were reduced using XTAL (ver. 3.4), solved by direct methods, refined by full-matrix least-squares on F^2 with the non-H atoms anisotropic, and H atoms isotropic.[6] For **14**: $C_{11}H_{10}O_8$, M = 270.19, colourless crystals from ethyl acetate–hexane, orthorombic, space group $Pca2_1$ (no. 29), a = 15.547(3), b = 7.584(1) and c = 9.052(10) Å, V = 1067.3(13) Å^3, Z = 4, D_c = 1.681 Mg m^{-3}, T = 293 K, $F(000)$ = 560, μ(Mo-Kα) = 0.147 mm^{-1}, crystal dimensions 0.20 × 0.11 × 0.13 mm. Data were collected as above in the range $2 \leqslant \theta \leqslant 30°$, 1648 unique reflections [R_{int} = 0.0], of which 741 had $F_o > 4\sigma(F_o)$, were used in all calculations. At final convergence $R_1[I > 2\sigma(I)]$ = 0.0672, wR_2 = 0.1724 for 117 parameters, GOF = 1.046, $\Delta\rho_{max}$ = 0.294 e Å^{-3}, $\Delta\rho_{min}$ = −0.283 e Å^{-3}. The structure was solved as above with all O atoms anisotropic, C and H atoms isotropic.[6] CCDC 182/918.

1 G. Mehta and R. Vidya, *Tetrahedron Lett.*, 1997. **38**, 4173; G. Mehta and R. Vidya, *Tetrahedron Lett.*, 1997, **38**, 4177.
2 R. Taylor and O. Kennard, *J. Am. Chem. Soc.*, 1982, **104**, 5063; G. R. Desiraju, *Acc. Chem. Res.*, 1996, **29**, 441; T. Steiner, *Chem. Commun.*, 1997, 727.
3 (*a*) K. J. McCullough, S. Tanaka, K. Teshima and M. Nojima, *Tetrahedron*, 1994, **50**, 7625; (*b*) H. N. Junker, W. Schafer and H. Niedenbruck, *Chem. Ber.*, 1967, **100**, 2508; (*c*) H. Mayr, J. Baran, E. Will, H. Yamakoshi, K. Teshima and M. Nojima, *J. Org. Chem.*, 1994, **59**, 8126; (*d*) J. S. Buckleton, G. R. Clark and C. E. F. Rickard, *Acta Crystallogr., Sect. C*, 1995, **51**, 494.
4 G. Mehta, A. Srikrishna, A. V. Reddy and M. S. Nair, *Tetrahedron*, 1981, **37**, 4543; G. Mehta and M. S. Nair, *J. Am. Chem. Soc.*, 1985, **107**, 7519; G. Mehta and K. Raja Reddy, *J. Org. Chem.*, 1987, **52**, 460; G. Mehta and K. Raja Reddy, *Tetrahedron Lett.*, 1988, **29**, 3607.
5 All compounds were fully characterized on the basis of their spectral and analytical data.
6 G. M. Sheldrick, SHELXL-97, University of Göttingen, Germany, 1997.

Received in Cambridge, UK, 26th May 1998; 8/03915A

Efficient catalytic cleavage of DNA mediated by metalloaminoglycosides†

Alavattam Sreedhara and James A. Cowan*‡

Evans Laboratory of Chemistry, The Ohio State University, 100 West 18th Avenue, Columbus, Ohio, 43210, USA

Metalloaminoglycosides have been synthesized and demonstrated to mediate catalytic cleavage of DNA at physiological pH and temperature.

Antitumor antibiotics such as neocarzinostatin,[1] bleomycin,[2] and elsamicin[3] create single or double strand nicks on duplex DNA. The latter are biologically more significant since they appear to be less readily repaired by natural DNA repair mechanisms.[4] Molecules that demonstrate DNA cleavage activity must possess either a hydrolytic, photoactivatable, or a redox active center, as well as recognition elements that target ds DNA.[5,6] We have explored the chemistry of Cu^{2+} derivatives of the aminoglycosides neomycin B (neo) and kanamycin A (kan) (Scheme 1),§ and demonstrate their ability to linearize DNA by non-random two-strand cleavage under catalytic conditions, and ultimately to effect complete degradation of plasmid DNA. Both hydrolytic and oxidative pathways have been identified.

A variety of first row transition metal ion complexes of kanamycin A were tested to assess their DNA cleavage efficiency; however, only a mixture of Cu^{2+} and kanamycin A was found capable of effecting rapid (< 1 h) degradation of plasmid DNA at 1 μM concentration. A systematic reactivity profile of the isolated and purified Cu(kan), **1**,¶ with plasmid DNA allowed observation of nicked DNA after brief (5 min) exposure to 0.5 μM complex (Fig. 1, lane 3). Both $Cu(kan)_2$, **2**, and Cu(neo), **3**, were also found capable of mediating DNA cleavage at catalytic concentrations as low as 100 nM; however, as a result of the hydrolytic instability of **2** and **3**, further DNA scission studies were focused on complex **1**.¶,‖

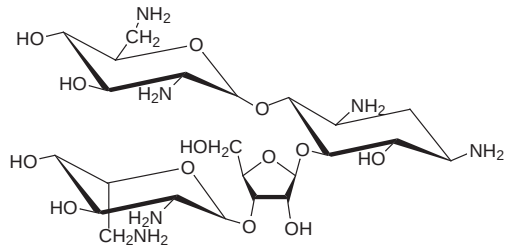

neomycin B

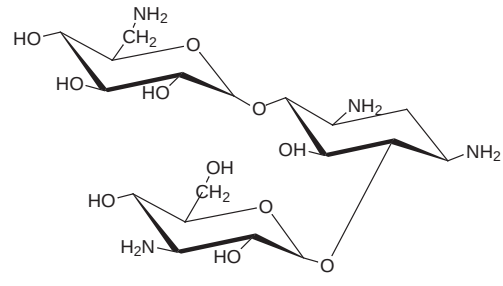

kanamycin A

Scheme 1

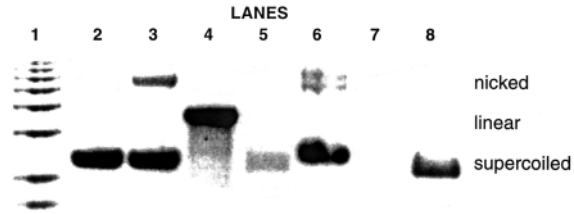

Fig. 1 Agarose gel electrophoresis of the reaction products following T4 ligase treatment of the nicked or linearized plasmid pT7-7†† obtained by reaction with Cu(kan) and BamH1, respectively. The reaction mixture (10 μl) containing plasmid DNA and metal–kanamycin complex was incubated for 1 h at 37 °C, mixed with 2 μl loading buffer (bromophenol blue, xylene cyanole and 50% glycerol) and loaded onto a 0.8% agarose gel containing ethidium bromide. Control experiments were run with plasmid DNA in the presence and absence of 5 μM kanamycin A. The gel was run at a constant voltage of 120 mV for 60–90 min in TAE buffer, washed in distilled water, visualized under a UV transilluminator and photographed on polaroid films. DNA concentrations are 50 μM: lane 1, 1 kb markers; lane 2, DNA + 0.5 μM Cu(kan), followed by treatment of reaction products with 2 units T4 ligase; lane 3, DNA + 0.5 μM Cu(kan); lane 4, DNA + 1 μl BamH1; lane 5, DNA + 0.5 μM Cu(kan) + 0.1 μM H_2O_2; lane 6, DNA + 1 μl BamH1, followed by treatment of reaction products with 2 units T4 ligase; lane 7, DNA + 0.5 μM Cu(kan) + 0.1 μM H_2O_2, followed by treatment of reaction products with 2 units T4 ligase; lane 8, DNA.

A hydrolytic degradative pathway is supported by several experimental criteria. In particular, neither standard inhibitors of reactive oxygen species (azide, superoxide dismutase, DMSO, EtOH), nor anaerobic conditions were found to inhibit DNA cleavage.[8] Further, it was found that plasmid DNA nicked by Cu(kan) (Fig. 1, lane 3) can be circularized by T4 DNA ligase (Fig. 1, lane 2),[9] while the resulting circularized plasmid demonstrates significantly higher transformation efficiencies than the nicked form.** The re-ligation and transformation efficiency indicate that DNA cleavage by Cu(kan) in the absence of external reducing agents is indeed hydrolytic.

A distinct oxidative pathway has also been identified. Addition of a reducing agent such as ascorbic acid or dithiothreitol (DTT) was found to enhance the DNA cleaving ability of **1**, and nicking was observed at nanomolar concentrations (Fig. 2). Interestingly, complete conversion of supercoiled

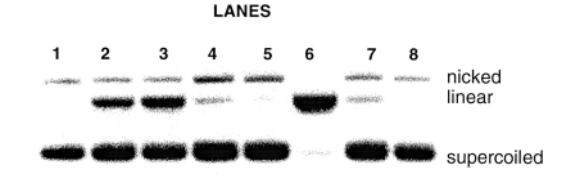

Fig. 2 Agarose gel electrophoresis of the oxidative cleavage reaction of plasmid pT7-7 by Cu(kan) **1** in the presence of ascorbate. Reactions were carried out for 1 h as follows: lane 1, 51 μM DNA; lane 2, + 1 nM **1**/10 μM asc; lane 3, + 1 nM **1**/10 μM asc; lane 4, + 1 nM **1**/1 μM asc; lane 5, + 1 nM **1**/0.1 μM asc; lane 6, + 5 nM **1**/10 μM asc; lane 7, + 5 nM **1**/1 μM asc; lane 8, + 5 nM **1**/0.1 μM asc. For lane 2, Cu^{2+}(kan) and ascorbate were mixed and preincubated at 37 °C for 30 min, to form Cu^{+}(kan), before addition of substrate DNA. The results were similar to those obtained by simultaneous mixing (lane 3). Experimental conditions for gel eletrophoresis are described in the legend to Fig. 1.

DNA (51 μM base pair) to a linear form was observed with a catalytic concentration of **1** (5 nM) in the presence of 10 μM ascorbate (Fig. 2, lane 6), while Cu^{2+}(aq) alone or with added ascorbate did not result in DNA cleavage under similar reaction conditions. This indicates non-random scission of the complementary strand in close proximity to the initial nick site, leading to production of linear DNA, since random cutting should produce a smear of fragment sizes. Complexes **1** to **3** degrade plasmid DNA completely in the presence of 10 μM H_2O_2. Fig. 1 (lane 5) shows extensive degradation of the plasmid over the time of this reaction, relative to control DNA shown in lane 8, with the range of smaller product fragments essentially undetectable. Furthermore, DNA treated with Cu(kan) and H_2O_2 is cleaved into random small and undetectable fragments that could not be ligated using T4 ligase (Fig. 1, lane 7).

In the presence of oxygen donor ligands, copper has been shown to produce a variety of oxidatively active intermediates, including a non-diffusable copper-oxene species,[10] and diffusable hydroxy radicals through Fenton-type chemistry.[11] The presence of DMSO and EtOH, which are hydroxy radical quenchers, do not have inhibitory effects on oxidative DNA cleavage by **1**. However, superoxide dismutase (SOD) and NaN_3 exhibit considerable inhibition of the oxidative DNA cleavage mediated by **1**, indicating that activated oxygen species (such as O_2^- or $^1O_2$) are most likely involved in plasmid cleavage. Also, superoxide generated by ascorbate-reduced copper can dismute to H_2O_2, which then reacts with another equivalent of cuprous ion through a Fenton mechanism to produce hydroxy radical like species, which might be metal bound. These species are analogous to metal-oxo species and are responsible for initiating the oxidative DNA strand scission chemistry. Both metal-oxo and metal-hydroxo species are expected to cleave the DNA backbone, but are not expected to be quenched by hydroxy radical quenchers,[12,13] as was observed in the case of **1**.

To address the issue of hydroxy radical involvement, production of this species was quantified using rhodamine B as a reporter molecule in the presence of **1** and ascorbic acid.[11,12] Substantial quantities of hydroxy radical were generated by Cu(kan) in the presence of ascorbate. However, in the presence of substrate plasmid no hydroxy radicals were trapped by rhodamine B. Furthermore, neither DMSO nor EtOH were able to quench the oxidative DNA scission reactions, indicating that any hydroxy radicals generated are not diffusible. A requirement of dioxygen for the oxidative scission reaction is substantiated by the fact that no hydroxy radical (determined by the rhodamine B test) and no cleavage was observed under anaerobic conditions. A mechanistic model that is consistent with these observations has a diffusible Cu^I-generated superoxide species interacting with another Cu^I center with production of the reactive metal-oxo or metal-hydroxo species.

In summary, we report the first example of catalytic cleavage and linearization of double-strand DNA by a synthetic complex at physiological pH and temperature. Both hydrolytic and oxidative pathways have been identified. Although other workers have described oxidative DNA cleavage by copper complexes,[8a,11,14–19] these are non-catalytic, requiring a large excess of reagent (from 0.1 to 1 mM copper complex with 25 nM to 10 μM DNA) and often extended reaction times of several hours to days. The cleavage efficiency and ease of synthesis of metalloaminoglycosides make them attractive molecules for therapeutic applications.

J. A. C. is a Camille Dreyfus Teacher–Scholar (1994–99). A. S. thanks The Ohio State University for the award of a postdoctoral fellowship.

Notes and References

† Supported in part by the National Science Foundation (CHE-9706904).
‡ E-mail: cowan@chemistry.ohio-state.edu
§ Aminoglycosides carry a large positive charge at physiological pH (from +3 to +6) and bind with high affinity to anions and nucleic acids *via* electrostatic and hydrogen bonding contacts.[7] Interestingly, the antitumor molecules described earlier[1–3] also contain aminated sugars in their framework.
¶ Complex **1** was synthesized by addition of $CuSO_4$ (0.0624 g, 0.25 mmol) to kanamycin A sulfate (0.1455 g, 0.25 mmol), in 5 ml water. After stirring at room temperature for 24 h, ethanol (5 ml) was added to precipitate a blue solid. This was filtered, washed twice by stirring in EtOH for 6 h, dissolved in water, and EtOH precipitated to yield **1**. Complexes **2** and **3** were formed similarly, using 2 equiv. of kan to form **2**. All products have been purified and give satisfactory elemental analysis, EPR, and UV–VIS data.
‖ Also excess metal-free aminoglycoside was found to inhibit cleavage, supporting a requirement for direct DNA binding to effect cleavage. At extreme concentrations, neomycin B alone has also been shown to mediate hydrolysis of a ribodinucleotide substrate (0.1 mM adenylyl-3,5-adenosine, ApA, and 0.3 M neomycin B).[20]
** Ligase treated Cu(kan) nicked plasmid demonstrated more than two-fold higher transformation efficiences than the nicked product itself.
†† A gift from D. R. Dean.[21]

1 I. H. Goldberg, *Acc. Chem. Res.*, 1991, **24**, 191.
2 J. Stubbe and J. W. Kozarich, *Chem. Rev.*, 1987, **87**, 1107.
3 A. Parraga and J. Portugal, *FEBS Lett.*, 1992, **300**, 25.
4 L. F. Povirk, *Mutat. Res.*, 1991, **257**, 127.
5 (*a*) M. A. Billadeau and H. Morrison, *Metal Ions Biol. Syst.*, 1996, **33**, 269 and references therein; (*b*) D. S. Sigman, R. Landgraf, D. M. Perrin and L. Pearson, *Metal Ions Biol. Syst.*, 1996, **33**, 485 and references therein.
6 (*a*) T. C. Bruice, A. Tsubouchi, R. O. Dempcy and L. P. Olson, *J. Am. Chem. Soc.*, 1996, **118**, 9867; (*b*) K. A. Deal, A. C. Hengge and J. N. Burstyn, *J. Am. Chem. Soc.*, 1996, **118**, 1713; (*c*) L. A. Jenkins, J. K. Bashkin and M. E. Autrey, *J. Am. Chem. Soc.*, 1996, **118**, 6882; (*d*) P. Hurst, B. K. Takasaki and J. Chin, *J. Am. Chem. Soc.*, 1996, **118**, 9982; (*e*) C. J. Burrows and S. E. Rokita, *Metal Ions Biol. Syst.*, 1996, **33**, 537; (*f*) J. R. Morrow and V. M. Shelton, *New J. Chem.*, 1994, **18**, 371; (*g*) R. Breslow and D-L. Huang, *Proc. Natl. Acad. Sci. USA*, 1991, **88**, 4080.
7 (*a*) A. G. Gilman, T. W. Rall, A. S. Nies and P. Taylor, in *The Pharmacological Basis for Therapeutics*, ed. L. S. Goodman and A. G. Gilman, MacMillan, London, 1990; (*b*) T. Ohyama, D. Wang and J. A. Cowan, *Chem. Commun.* 1998, 467.
8 (*a*) E. L. Hegg and J. N. Burstyn, *Inorg. Chem.*, 1996, **35**, 7474; (*b*) R. Hettich and H-J. Schneider, *J. Am. Chem. Soc.*, 1997, **119**, 5638.
9 (*a*) L. M. T. Schnaith, R. S. Hanson and L. Que, *Proc. Natl. Acad. Sci. USA*, 1994, **91**, 569; (*b*) L. A. Basile, A. L. Raphael and J. K. Barton, *J. Am. Chem. Soc.*, 1987, **109**, 7550.
10 D. S. Sigman and C. B. Chen, *ACS Symp. Ser.*, 1989, **402**, 24.
11 F. V. Pamatong, C. A. Detmer III and J. R. Bocarsly, *J. Am. Chem. Soc.*, 1996, **118**, 5339.
12 C. A. Detmer III, F. V. Pamatong and J. R. Bocarsly, *Inorg. Chem.*, 1996, **35**, 6292.
13 L. O. Rodriguez and S. M. Hecht, *Biochem. Biophys. Res. Commun.*, 1982, **104**, 1470.
14 S. Routier, J-L. Bernier, J-P. Catteau, P. Colson, C. Houssier, C. Rivalle, E. Bisagni and C. Bailly, *Bioconj. Chem.*, 1997, **8**, 789.
15 S. Oikawa and S. Kawanishi, *Biochemistry*, 1996, **35**, 4584.
16 R. R. Joshi, S. M. Likhite, R. K. Kumar and K. N. Ganesh, *Biochim. Biophys. Acta*, 1994, **119**, 285.
17 W. Bal, J. Lukszo and K. S. Kasprzak, *Chem. Res. Toxicol.*, 1997, **10**, 915.
18 D. S. Sigman, D. R. Graham, V. D. D'Aurora and A. M. Stern, *J. Biol. Chem.*, 1979, **254**, 12 269.
19 T. Itoh, H. Hisada, T. Sumiya, M. Hosono, Y. Usui and Y. Fujii, *Chem. Commun.* 1997, 677.
20 S. Kirk and Y. Tor, *Chem. Commun.*, 1998, 147.
21 S. Chen, L. Zheng, D. R. Dean and H. J. Zalkin *J. Bacteriol.*, 1997, **179**, 7587.

Received in Bloomington, IN, USA, 20th April 1998; 8/02903B

Optimization of neutrocyanine chromophores based on five-membered heterocycles for photorefractive applications

Frank Würthner,*[a]† Christoph Thalacker,[a] Ralf Matschiner,[b] Katarzyna Lukaszuk[b] and Rüdiger Wortmann*[b]‡

[a] *Abteilung Organische Chemie II, Universität Ulm, Albert-Einstein-Allee 11, 89081 Ulm, Germany*
[b] *Institut für Physikalische Chemie, Universität Mainz, Jakob-Welder-Weg 11, 55099 Mainz, Germany*

Exceptionally large photorefractive figures-of-merit are observed for neutrocyanine dyes based on dialkylaminothiophenes and −furans linked to quinoid five-membered heterocyclic acceptor groups by a methine bridge.

Chromophores based on 2-dialkylaminothiophenes with strong acceptor units in the 5-position are among the most interesting developments in dye chemistry of the last few years.[1–6] Showing enhanced electron-donating properties compared to *p*-dialkylaminobenzenes and higher thermal and chemical stability than dialkylaminopolyenes, 2-dialkylaminothiophenes became one of the most useful electron donor units for nonlinear optical (NLO) chromophores.[2–5] Furthermore, 5-dimethylamino-5'-nitro-2,2'-bithiophene is among the best indicator dyes for the study of solvent polaritity because of its outstanding positive solvatochromism.[6] Whereas all these dyes bear a chromophoric system which may be considered as 'polyene-like' with a large change of dipole moment upon optical excitation, we were recently able to polarize 2-dialkylaminothiophenes by a strong heterocyclic acceptor group up to the *cyanine limit*, which is characterized by equal dipole moments in the ground and the excited states, sharp and very intense absorption bands and vanishing solvatochromism.[7] Based on those highly polarizable dipolar dyes photorefractive (PR) materials[8] of unprecedented performance could be devised.[7,9]

Here we present optical, electrooptical and structural properties of a new series of thiophene-based neutrocyanine dyes. Structure–property relationships will be elucidated which lead to general guidelines for the design of highly efficient PR chromophores.

According to Scheme 1, neutrocyanines (top right) are derived from cyanines (top left) by replacement of the iminium unit by non-ionic but very strong acceptor substituents (*e.g.* di- or tri-cyanovinyl). As a result, uncharged but highly dipolar chromophores are obtained. This should also be true if the conjugated chain is part of a heterocyclic system (bottom). However, since the symmetry of the cyanine chromophor is broken and aromaticity comes into play, even the tricyanovinyl acceptor group is not strong enough to polarize 2-dialkylaminothiophene to the cyanine limit.[3b] This goal may be achieved in a quite general way, however, by using heterocyclic acceptor units.

Thiophene dyes **1**−**6** and furan **7** were obtained§ by condensation reactions of the CH-acidic heterocycles with 2-dibutylamino-5-formyl-thiophene and -furan and studied by

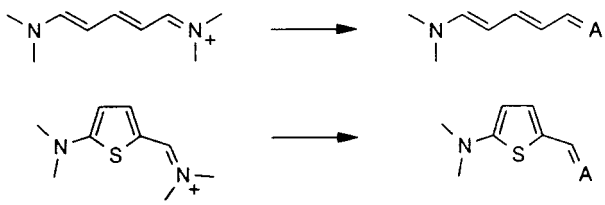

Scheme 1

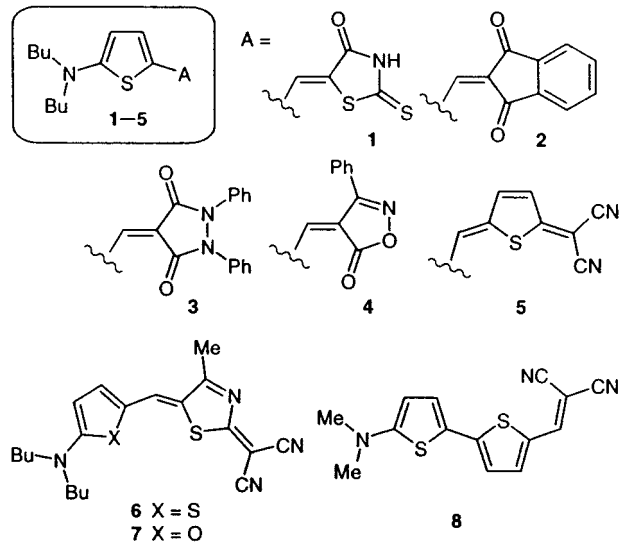

UV–VIS optical and electrooptical absorption measurements (EOAM).[10] EOAM experiments yield the dipole moment of the electronic ground state μ_g as well as the dipole change upon optical excitation $\Delta\mu = (\mu_a - \mu_g)$, whereas optical spectroscopy provides information on the transition dipole moment μ_{ag} and the absorption maximum λ_{ag}. From these data a PR figure-of-merit F_0 and a resonance parameter c^2 may be calculated according to eqns. (1) and (2).¶

$$F_0 = [54\mu_g\mu_{ag}^2\Delta\mu\lambda_{ag}^2/(hc_0)^2 + 4\mu_g^2\mu_{ag}^2\lambda_{ag}/(hc_0kT)]/M \quad (1)$$

$$c^2 = \tfrac{1}{2}[1-\Delta\mu(4\mu_{ag}^2 + \Delta\mu^2)^{-1/2}] \quad (2)$$

The PR figure-of-merit [eqn. (1)] was derived only recently[11] and established by us and others.[7,9] The two terms in eqn. (1) are commonly referred to as the electrooptical and birefringence contributions. It is found that the latter is usually dominant (> 80%).[7,11] Eqn. (2) defines a useful parameter to characterize the charge transfer properties of donor/acceptor-substituted compounds.[11] It is closely related to the BLA-parameter introduced by Marder *et al.*[12a] and the parameter MIX introduced by Barzoukas *et al.*[12b] and can be regarded as a measure of the admixture of the zwitterionic resonance structure (Scheme 2) to the electronic ground state. Thus eqn. (2) allows us to classify donor/acceptor-substituted chain molecules from polyene-type molecules($c^2 \approx 0$) to betaine-type molecules ($c^2 \approx 1$) with the neutrocyanine ('cyanine limit') being located in the middle ($c^2 \approx 0.5$).

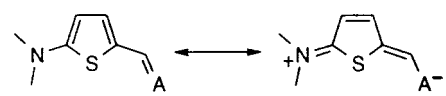

Scheme 2

Table 1 Optical and electrical properties of chromophores **1**–**8** and DANS[a] from UV–VIS and EOAM measurements in dioxane

Compound	λ_{ag}/nm (ε_{max}/l mol^{-1} cm^{-1})	μ_{ag}/D	μ_g/D	$\Delta\mu$/D	c^2	$F_0/10^{-74}$ m^4 C^2 mol V^{-2} kg^{-1}
1	513 (59 100)	8.2	6.7	7.2	0.30	0.32
2	510 (114 600)	9.0	5.7	4.2	0.39	0.24
3	489 (110 900)	9.0	7.0	2.1	0.44	0.26
4	500 (76 800)	8.2	7.9	2.4	0.43	0.35
5	647 (55 400)	9.8	11.2	7.8	0.32	1.44
6	641 (83 250)	9.7	13.6	3.1	0.42	1.84
7	650 (84 920)	9.3	14.6	0.5	0.49	1.98
8[b]	543 (41 000)	8.4	8.7	15.6	0.16	0.60
DANS[a,b]	426 (30 300)	7.7	7.4	21.8	0.09	0.32

[a] 4-Dimethylamino-4'-nitrostilbene. [b] For comparison we used the molar mass of the dibutylamino derivative for the calculation of the F_0 values.

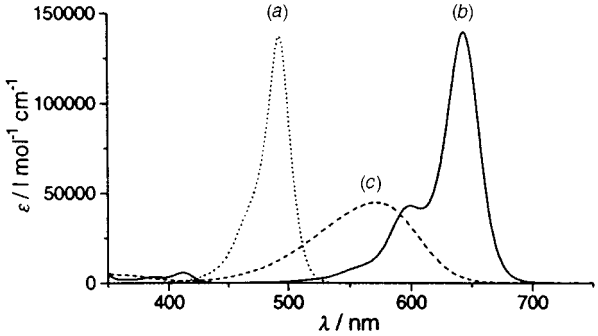

Fig.1 UV–VIS absorption spectra of PR neutrocyanine dyes (*a*) **3** and (*b*) **6** and (*c*) NLO dye **8** in CH_2Cl_2

The optical properties (λ_{ag}, ε_{max}, μ_{ag}) of neutrocyanines **1**–**7** (c^2 = 0.30–0.49) reveal intense transitions with very narrow bandwidths for their main absorption band, which is very favorable for applications in photonics (Table 1, Fig. 1). Thus dyes **1**–**7** may be used at laser frequencies significantly closer to the absorption maximum than for typical NLO chromophores such as **8**,[3] which exhibit very broad absorption bands thus causing absorption problems. Depending on the number of methine groups in the conjugated chain, we observe absorption maxima at *ca.* 500 nm for seven methine groups (**1**–**4**) and *ca.* 650 nm for nine methine groups (**5**–**7**).Whereas the optical properties of **1**–**7** exhibit very similar features, significant differences in the dipolar contributions to F_0 are found. Having about twice the number in their ground-state dipole moments μ_g, compounds **5**–**7** gain a factor of about four [second term in eqn. (1)] to F_0 compared to **1**–**4**. To explain this important point a closer look at the molecular structures and charge distributions in the ground state is helpful.‖ Semiempirical calculations indicate a high degree of charge separation for **5**–**7**. The highest electron density is found at the thiazole nitrogen (**6**,**7**) and the dicyanomethylene functionalities (**5**–**7**) of the heterocyclic acceptor at the *opposite* side of the methine bridge. In this way, a fairly extended chromophore is formed. On the other hand, **1**–**4** have their acceptor carbonyl groups *ortho* to the methine bridge. This limits the conjugated path to a rather short distance. Furthermore, the unfavorable orientation of the carbonyl group dipole moment leads to significant cancellation of the total molecular dipole moment.

Finally we note the successful tuning of the c^2 value from 0.32 in **5** to the perfectly equilibrated cyanine point (c^2 = 0.49) in **7**. Concomitantly, both the extinction coefficient and the PR figure-of-merit F_0 could be substantially increased. This improvement is particularly impressive when compared to NLO chromophore **8** which differs from **5** only by the position of the methine bridge. Moreover, the exocyclic dicyanomethylene moiety in **5**–**7** opens the way for an extension of the conjugated chain to long-wavelength neutrocyanine chromophores, which we will address in the future.

In conclusion we have presented a new series of neutrocyanine chromophores based on five-membered heterocycles. Their photorefractive figures-of-merit range from 0.22 up to 1.98, which is the highest value reported. As their use in optical devices depends on transparency at the applied laser frequency, their narrow-band absorption represents another significant advantage over currently available PR chromophores.[7–9] The possibility of building extended π-systems with alternating aromatic and quinoid moieties as suggested by **5**–**7** might be of relevance for the design of IR dyes and low band-gap polymers as well.[13]

We gratefully acknowledge the financial support of the Fonds der Chemischen Industrie and the BMBF (Liebig grant for new materials for F. W.), the Volkswagen foundation and BASF.

Notes and References

† E-mail: frank.wuerthner@chemie.uni-ulm.de
‡ E-mail: rwortmann@mzdmza.zdv.uni-mainz.de
§ All new compounds had spectral (^{1}H NMR, UV–VIS) and microanalytical properties (C,H,N,S) in agreement with the assigned structures.
¶ M is the molar mass, T is the temperature, c_0 is the speed of light, h is Planck's constant and k isBoltzmann's constant.
‖ According to NMR studies all thiophene chromophores exhibit a conformational preference for the structure shown in Scheme 1. This conformation was used as the input geometry for AM1 calculations (structure, charge distribution).

1 F. A. Mikhailenko, L. I. Shevchuk and I. T. Rozhdestvenskaya, *Khim. Geterotsikl. Soedin*, 1975, **3**, 316.
2 A. K.-Y. Jen, V. P. Rao, K. Y. Wong and K. J. Drost, *Chem. Commun*., 1993, 90.
3 (*a*) F. Würthner, F. Effenberger, R. Wortmann and P. Krämer, *Chem. Phys.*, 1993, **173**, 305; (*b*) F. Steybe, F. Effenberger, S. Beckmann, P. Krämer, C. Glania and R. Wortmann, *Chem Phys.*, 1997, **219**, 317.
4 M. G. Hutchings, I. Ferguson, D. J. McGeein, J. O. Morley, J. Zyss and I. Ledoux, *J. Chem. Soc., Perkin Trans. 2*, 1995, 171.
5 M. Blanchard-Desce, V. Alain, P. V. Bedworth, S. R. Marder, A. Fort, C. Runser, M. Barzoukas, S. Lebus and R. Wortmann, *Chem. Eur. J.*, 1997, **3**, 1091.
6 F. Effenberger and F. Würthner, *Angew. Chem., Int. Ed. Engl.*, 1993, **32**, 719; C. Reichardt, *Chem. Rev*., 1994, **94**, 2324.
7 F. Würthner, R. Wortmann, R. Matschiner, K. Lukaszuk, K. Meerholz, Y. DeNardin, R. Bittner, C. Bräuchle and R. Sens, *Angew. Chem., Int. Ed. Engl*., 1997, **36**, 2765; K. Meerholz, Y. DeNardin, R. Bittner, R. Wortmann and F. Würthner, *Appl. Phys. Lett*., in the press.
8 K. Meerholz, *Angew. Chem., Int. Ed. Engl*., 1997, **36**, 945; W. E. Moerner and S. M. Silence, *Chem. Rev*., 1994, **94**, 127.
9 B. Kippelen, S. R. Marder, E. Hendrickx, J. L. Maldano, G. Guillernet, B. L. Volodin, D. D. Steele, Y. Enami, Sandalphon, Y. J. Yao, J. F. Wang, H. Röckel, L. Erskine and N. Peyghambarian, *Science*, 1998, **279**, 54
10 W. Liptay, in *Excited States*, ed. E. C. Lim, Academic Press, New York, 1974, vol. 1, pp. 129–229
11 R. Wortmann, C. Poga, R. J. Twieg, C. Geletneky, C. R. Moylan, P. M. Lundquist, R. G. DeVoe, P. M. Cotts, H. Horn, J. E. Rice and D. M. Burland, *J. Chem. Phys.*, 1996, **105**, 10 637.
12 (*a*) S. R. Marder, C. B. Gorman, F. Meyers, J. W. Perry, G. Bourhill, J.-L. Brédas and B. M. Pierce, *Science*, 1994, **265**, 632; (*b*) M. Barzoukas, C. Runser, A. Fort and M. Blanchard-Desce, *Chem. Phys. Lett*., 1996, **257**, 531.
13 J. Roncali, *Chem. Rev*., 1997, **97**, 173.

Received in Cambridge, UK, 3rd June 1998; 8/04168G

Synthesis of methylene isosteres of α- and β-D-galactopyranosyl-L-serine

Alessandro Dondoni,*† Alberto Marra and Alessandro Massi

Dipartimento di Chimica, Laboratorio di Chimica Organica, Università, 44100-Ferrara, Italy

The $BF_3{\cdot}Et_2O$ promoted coupling of tetra-*O*-benzyl-α-D-galactopyranosyl trichloroacetimidate with a silyl enol ether carrying an oxazolidine ring leads to the α-*C*-glycosylmethyl ketone (32%, 95% ds) that is converted into the title α-*C*-glycosyl amino acid by carbonyl oxygen removal (Barton–McCombie) and oxidative cleavage (Jones) of the heterocyclic ring, and into the β-isomer by anomerization and the same two-step sequence.

Towards a better understanding and control of the function of sugars in natural glycopeptides,[1] the synthesis of their analogues in which the sugar moieties are linked to the peptide backbone by an all-carbon chain that is resistant to chemical and enzymatic degradation is a topic of increasing importance in glycobiology and medicinal chemistry. Therefore carbon-linked glycosyl amino acids as precursors to glycopeptide mimetics are current synthetic targets in various laboratories.[2] Different syntheses of methylene isosteres of *O*-glycosyl serines have been reported[2a–c,f–h] since these sugar amino acids are the most common constituents of natural glycoproteins. The *C*-glycosylation of a suitable α-amino acid equivalent[2c] appears to be the most direct route to these compounds.[3] Therefore we describe here the synthesis of α- and β-*C*-galactosyl serine **1** (Gal-CH_2-Ser), *i.e.* the methylene isosteres of D-galactose α- and β-linked to L-serine (Gal-*O*-Ser, **2**), employing the silyl enol ether **3** as a novel homoalanine carbanion equivalent. To the best of our knowledge this is the first approach to a pair of α- and β-isomer *C*-glycosyl amino acids *via* a single synthetic scheme.

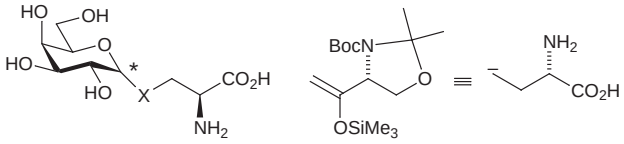

1 X = CH_2
2 X = O
3

The multigram scale synthesis of **3** started from the known[4] methyl L-threoninate **4** which was transformed by a sequence of high yielding reactions into the ketone **6** (Scheme 1).‡ The enantiomeric purity of this key intermediate was established by reduction to the alcohol **5** with sodium borohydride (75% ds) and conversion of the latter into its Mosher ester. Silylation of the oxazolidinyl ketone **6** was readily effected using TMSOTf and Et_3N[5] furnishing exclusively the kinetic trimethylsilyl enol ether **3** in 82% yield.§

The glycosylation of the silyl enol ether **3** was carried out with the readily available electrophilic sugar tetra-*O*-benzyl α-D-galactopyranosyl trichloroacetimidate[6] **7** (Scheme 2). Unoptimized conditions involved the addition *via* syringe pumping of an Et_2O solution of **7** (2 equiv.) to silyl enol ether **3** and $BF_3{\cdot}Et_2O$ (1 equiv.) in Et_2O at −15 °C. The expected[7] major product, α-*C*-glycoside **8,** and the β-anomer **10** were isolated by column chromatography in 32% overall yield and 19:1 ratio.¶ Also isolated was the ketone **6** (45%) arising from the hydrolysis of unreacted **3**, and a mixture of anomeric galactosyl trichloroacetamides (70%). The recovery of the enantiomerically pure ketone **6** demonstrated that the configuration at the

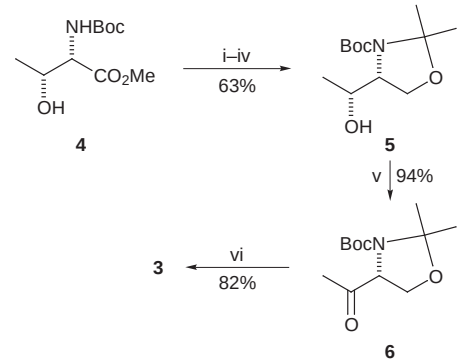

Scheme 1 *Reagents and conditions*: i, TBDMSOTf (1.2 equiv.), Et_3N, DMAP, DMF, 0 °C to room temp., 1.5 h; ii, $LiAlH_4$ (4 equiv.), THF, −50 °C, 50 min; iii, 2-methoxypropene, CSA, CH_2Cl_2, 0 °C to room temp., 1.5 h; iv, Bu_4NF, THF, room temp., 6 h; v, PCC (5 equiv.), CH_2Cl_2, 4 Å MS, room temp., 20 min; vi, TMSOTf (1.4 equiv.), Et_3N (1.6 equiv.), CH_2Cl_2, −15 °C, 1 h

stereocenter of the silyl enol ether **3** was unaffected under the glycosylation conditions. Towards the target *C*-glycosyl amino acid, the deoxygenation of the sugar ketone **8** was first carried out through the classical Barton–McCombie reduction-elimination sequence[8] affording **9** in 60% yield. Treatment of **9** with the Jones reagent induced the cleavage of the oxazolidine ring and oxidation of the alcohol in a single step to give the α-linked tetra-*O*-benzyl-*C*-galactosyl-L-serine **1a** in 96% isolated yield. This compound proved to be contaminated by *ca.* 5% (^1H NMR analysis) of the corresponding α-amino alcohol. Therefore, the amino acid **1a** was fully characterized through its methyl ester.

Guided by earlier work regarding the base-catalyzed equilibration of α-*C*-glycosides bearing a carbonyl group in the side chain,[9] the anomerization of the α-*C*-glycosylmethyl ketone **8** was carried out upon treatment with Bu^tLi in Et_2O (Scheme 3). Under these conditions a mixture of **8** and the β-anomer **10** in a

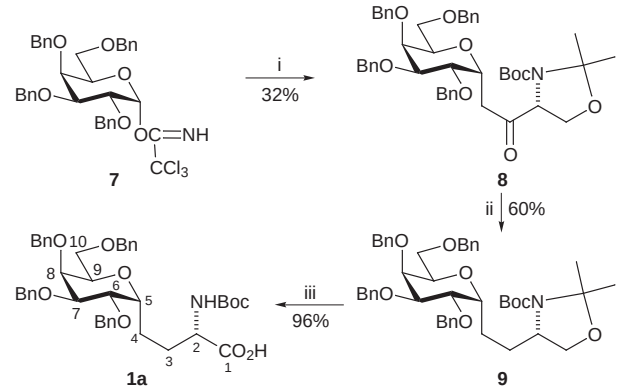

Scheme 2 *Reagents and conditions*: i, **3** (0.5 equiv.), $BF_3{\cdot}Et_2O$ (0.5 equiv.), Et_2O, −15 °C, 2 h; ii, $NaBH_4$, MeOH–Et_2O, −20 °C, 1 h, then 1,1′-thiocarbonyldiimidazole (10 equiv.), DMAP (15 equiv.), THF, reflux, 6 h, then Bu_3SnH (10 equiv.), AIBN (0.1 equiv.), toluene, 85 °C, 2 h; iii, 1 M Jones reagent (3 mol per mol of reactant), acetone, 0 °C to room temp., 3.5 h

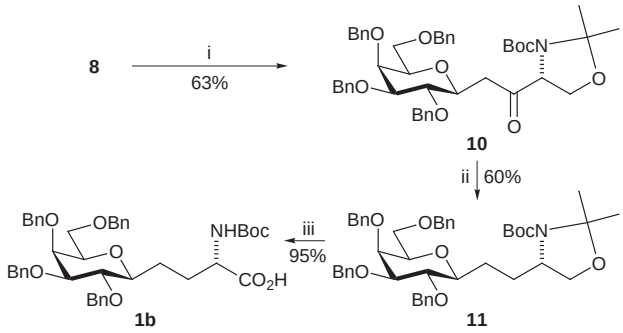

Scheme 3 *Reagents and conditions*: i, Bu^{t}Li (1.2 equiv.), Et_2O, −78 to −20 °C, 2 h, then room temp., 2 h; ii, $NaBH_4$, MeOH–Et_2O, −20 °C, 1 h, then 1,1′-thiocarbonyldiimidazole (10 equiv.), DMAP (15 equiv.), THF, reflux, 6 h, then Bu_3SnH (10 equiv.), AIBN (0.1 equiv.), toluene, 85 °C, 2 h; iii, 1 M Jones reagent (3 mol per mol of reactant), acetone, 0 °C to room temp., 3.5 h

3:7 ratio and 90% overall yield was obtained. The isolated β-*C*-glycosylmethyl ketone **10** was subjected to the radical deoxygenation as described above for **8** to give the β-*C*-alkyl glycoside[2h] **11** (60% isolated yield). The conversion of the oxazolidine ring of this compound into the α-amino acid moiety by treatment with the Jones reagent gave the known[2b,h] β-D-linked tetra-*O*-benzyl-*C*-galactosyl-L-serine **1b** (95%). The synthesis of **1b** highlights the use of the silyl enol ether **3** as the homoalanine carbanion equivalent since a similar approach cannot be developed by using amino acid equivalents[2c,3] lacking the carbonyl group.

In conclusion, the synthesis of **1a** and **1b** demonstrates the viability of a new approach to α- and β-linked *C*-glycosyl amino acids starting from a single carbohydrate precursor. The protected hydroxy and amino groups (as *O*-benzyl and *N*-Boc derivatives) and, by contrast, the free carboxylic group constitute a synthetically convenient structure for the incorporation of these *C*-glycosyl amino acids into a peptide chain. The application of this method for the preparation of pairs of amino acids by glycosylation of the silyl enol ether **3** with other sugars is now of interest.

Notes and References

† E-mail: adn@dns.unife.it

‡ *Selected data* for **3**: $[\alpha]_D$ +23.4 (*c* 0.6); $\delta_H(C_2D_2Cl_4$, 120 °C) 4.26 (d, 1 H, *J* 1.5), 4.24 (dd, 1 H, *J* 3.5, 7.0), 4.21 (d, 1 H, *J* 1.5), 4.04 (dd, 1 H, *J* 7.0, 8.5), 3.95 (dd, 1 H, *J* 3.5, 8.5), 1.63, 1.58 (2 s, 6 H), 1.46 (s, 9 H), 0.30 (s, 9 H). For **5**: mp 87–88 °C (from cyclohexane); $[\alpha]_D$ +24.2 (*c* 0.7); $\delta_H(CDCl_3)$ 4.18–4.11, 4.00–3.77 (2 m, 4 H), 1.58 (s, 3 H), 1.50 (s, 12 H), 1.18 (d, 3 H, *J* 6.5). For **6**: $[\alpha]_D$ +56.9 (*c* 2.1); $\delta_H(C_2D_2Cl_4$, 120 °C) 4.36 (dd, 1 H, *J* 3.1, 7.2), 4.15 (dd, 1 H, *J* 7.2, 9.0), 3.95 (dd, 1 H, *J* 3.1, 9.0), 2.20 (s, 3H), 1.70, 1.57 (2 s, 6 H), 1.51 (s, 9 H). For **8**: $[\alpha]_D$ +53.3 (*c* 0.9); $\delta_H([^2H_6]$DMSO, 120 °C) 4.09 (dd, 1 H, $J_{1a,1b}$ 9.0, $J_{1a,2}$ 7.2, H-1a), 3.86 (dd, 1 H, $J_{1b,2}$ 3.2, H-1b), 2.91 (dd, 1 H, $J_{4a,4b}$ 17.0, $J_{4a,5}$ 8.2, H-4a), 2.68 (dd, 1 H, $J_{4b,5}$ 4.5, H-4b). For **9**: $[\alpha]_D$ +37.1 (*c* 0.8); $\delta_H([^2H_6]$DMSO, 160 °C) 4.02–3.73 (m, 8 H), 3.69 (dd, 1 H, *J* 4.2, 11.3), 3.65 (dd, 1 H, *J* 2.2, 8.1), 1.76–1.50 (m, 4 H). For **1a**: $\delta_H(CDCl_3)$ 5.29 (br d, 1 H, $J_{2,NH}$ 6.5, NH), 4.30–4.24 (m, 1 H, H-2), 1.99–1.84, 1.80–1.51 (2 m, 4 H, 2 H-3, 2 H-4); $\delta_C(CDCl_3)$ 176.3 (CO_2H), 155.8 (CO_2Bu^t), 53.5 (C-2), 28.3 (CH_3). For **1a Me ester**: $[\alpha]_D$ +29.0 (*c* 1.0); $\delta_H([^2H_6]$DMSO, 120 °C) 6.53 (br d, 1 H, $J_{2,NH}$ 7.5, NH), 4.06–3.84 (m, 5 H), 3.79–3.72 (m, 2 H), 3.65 (dd, 1 H, $J_{9,10b}$ 4.4, $J_{10a,10b}$ 10.8, H-10b), 3.61 (s, 3 H, OMe), 1.92–1.57 (m, 4 H). For **10**: $[\alpha]_D$ +22.4 (*c* 0.4); $\delta_H([^2H_6]$DMSO, 120 °C) 4.47 (dd, 1 H, $J_{1a,2}$ 7.8, $J_{1b,2}$ 3.8, H-2), 4.07 (dd, 1 H, $J_{7,8}$ 2.8, $J_{8,9}$ *ca.* 0.5, H-8), 4.05 (dd, 1 H, $J_{1a,1b}$ 9.0, H-1a), 3.81 (dd, 1 H, H-1b), 3.76 (dd, 1 H, $J_{6,7}$ 9.1, H-7), 3.74 (ddd, 1 H, $J_{4a,5}$ 2.5, $J_{4b,5}$ 8.8, $J_{5,6}$ 9.2, H-5), 3.69 (ddd, 1 H, $J_{9,10a}$ 6.0, $J_{9,10b}$ 6.5, H-9), 3.57 (dd, 1 H, $J_{10a,10b}$ 10.0, H-10a), 3.51 (dd, 1 H, H-10b), 2.82 (dd, 1 H, $J_{4a,4b}$ 16.1, H-4a), 2.63 (dd, 1 H, H-4b). $[\alpha]_D$ Values were measured in $CHCl_3$ at 20 ± 2 °C; ^1H and ^{13}C NMR spectra were recorded at 300 and 75 MHz, respectively).

§ TMSOTf and Et_3N were added in three portions to the cooled (-15 °C) CH_2Cl_2 solution of **6** in order to avoid extensive removal of the protecting groups.

¶ The α- and β-D-configuration of *C*-glycosides **7** and **10** was proved by ^1H NMR analysis of the corresponding tetra-*O*-acetyl derivatives ($J_{5,6}$ 4.7 and 9.8, respectively, in $[^2H_6]$DMSO at 120 °C).

1 H. Kunz, *Angew. Chem., Int. Ed. Engl.*, 1987, **26**, 294; *Pure Appl. Chem.*, 1993, **65**, 1223; Y. C. Lee and R. T. Lee, *Acc. Chem. Res.*, 1995, **28**, 321; R. A. Dwek, *Chem. Rev.*, 1996, **96**, 683; G. Arsequell and G. Valencia, *Tetrahedron: Asymmetry*, 1997, **8**, 2839.

2 (*a*) L. Petrus and J. N. BeMiller, *Carbohydr. Res.*, 1992, **230**, 197; (*b*) C. R. Bertozzi, D. G. Cook, W. R. Kobertz, F. Gonzales-Scarano and M. D. Bednarski, *J. Am. Chem. Soc.*, 1992, **114**, 10 639; (*c*) B. J. Dorgan and R. F. W. Jackson, *Synlett*, 1996, 859; (*d*) T. F. Herpin, W. B. Motherwell and J.-M. Weibel, *Chem. Commun.*, 1997, 923; (*e*) F. Burkhart, M. Hoffmann and H. Kessler, *Angew. Chem., Int. Ed. Engl.*, 1997, **36**, 1191; (*f*) L. Lay, M. Meldal, F. Nicotra, L. Panza and G. Russo, *Chem. Commun.*, 1997, 1469; (*g*) S. D. Debenham, J. S. Debenham, M. J. Burk and E. J. Toone, *J. Am. Chem. Soc.*, 1997, **119**, 9897; (*h*) A. Dondoni, A. Marra and A. Massi, *Tetrahedron*, 1998, **54**, 2827; (*i*) T. Fuchss and R. R. Schmidt, *Synthesis*, 1988, 753.

3 After the submission of this paper and during the editorial processing, a paper appeared dealing with the SmI_2-promoted glycosylation of a homoalanine equivalent. See: D. Urban, T. Skrydstrup and J.-M. Beau, *Chem. Commun.*, 1998, 955.

4 P. Garner and J. M. Park, *J. Org. Chem.*, 1987, **52**, 2361.

5 L. Rossi and A. Pecunioso, *Tetrahedron Lett.*, 1994, **35**, 5285.

6 R. R. Schmidt, J. Michel and M. Roos, *Liebigs Ann.*, 1984, 1343.

7 Axial *C*-glycosides are usually formed by coupling electrophilic sugars with various carbon nucleophiles; see D. E. Levy and C. Thang, *The Chemistry of C-Glycosides*, Pergamon, Oxford, 1995; M. H. D. Postema, *C-Glycoside Synthesis*, CRC Press, Boca Raton, 1995.

8 D. H. R. Barton and S. W. McCombie, *J. Chem. Soc., Perkin Trans. 1*, 1975, 1574.

9 H. Ohrui, G. H. Jones, J. G. Moffatt, M. L. Maddox, A. T. Christensen and S. K. Byram, *J. Am. Chem. Soc.*, 1975, **97**, 4602; P. Allevi, M. Anastasia, P. Ciuffreda, A. Fiecchi and A. Scala, *J. Chem. Soc., Perkin Trans. 1*, 1989, 1275; A. Dondoni and A. Marra, *Tetrahedron Lett.*, 1993, **34**, 7327.

Received in Liverpool, UK, 20th January 1998; 8/00571K

Deep-cavity cavitands: synthesis and solid state structure of host molecules possessing large bowl-shaped cavities

Huaping Xi, Corinne L. D. Gibb, E. D. Stevens and Bruce C. Gibb*†

Department of Chemistry, University of New Orleans, New Orleans, LA 70148, USA

A novel family of deep-cavity cavitands is prepared *via* the first examples of the stereoselective bridging of resorcin[4]arenes with carbon electrophiles.

Cavitands, molecules that contain a rigid enforced cavity, have a proven proclivity for a diverse range of applications; as molecular scaffolds,[1] as components in the formation of carceplexes,[2–4] or as host molecules in their own right.[2,5] In this later context, extending the paradigm to enzyme mimicry raises an important question; for a host with a necessarily large cavity, how do we incorporate both structural rigidity to its hydrophobic pocket while simultaneously imparting reasonable solubility on the system? This paper details our initial work towards addressing this question.

The most important factor contributing to the broad repertoire of cavitands as molecular hosts is undoubtedly the ease of synthesis of the corresponding resorcin[4]arenes (octols), *e.g.* **1a**–**d**.[6] Accordingly, attempts to increase the size of a cavitand's

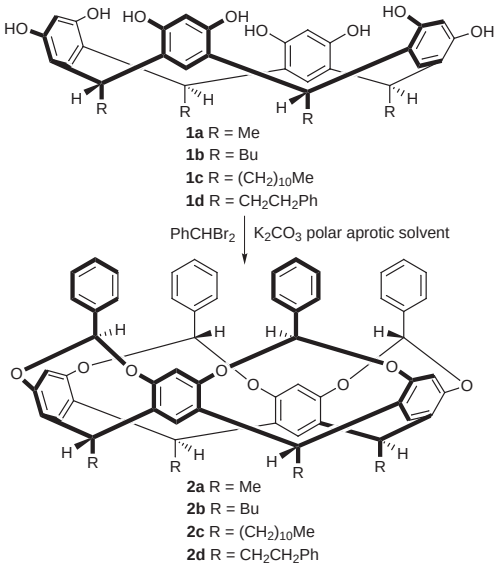

cavity have centered around the bridging of the phenolic pairs of these building blocks with a variety of moieties;[7–9] an early example of cavitands with enlarged cavities being provided by Cram, with the formation of the conformationally flexible velcraplexes.[10] Here we demonstrate an important first step towards large, non-collapsing, hydrophobic pockets; the synthesis of deep-cavity cavitands[11] of the general structure **2**, *via* the stereoselective bridging of octols with benzal bromides. We believe that this procedure will provide access to a significant range of rigid hosts possessing large hydrophobic cavities,[12] as well as a variety of novel molecular building-blocks for self-assembling systems.[13]

In the standard procedure for bridging octols, for example methylene bridging with $BrClCH_2$, there are a considerable number of variables that can be adjusted. Thus, to constrain our investigations, and in an effort to more precisely define influences that may affect bridging reactions in general, we decided to modify arguably the two most influential parameters: the solvent and the rate of addition (*via* syringe pump) of the octol to the reaction. To monitor the influence of the pendent (R) groups of the octols we extended this syntheses matrix by examining the bridging of the four octols **1a**–**d**. Table 1 shows the yields of the deep-cavity cavitands **2a**–**d** from the corresponding octols using $PhCHBr_2$ as the bridging material and K_2CO_3 as base.‡ In all cases, although a total of six diastereomers could potentially be formed, only one isomer was isolated from the varying amounts of polymeric material.

The Me-octol **1a** proved resistant to benzal bridging for each of the solvents investigated;[14] a maximum yield of 10% being obtained from bulk intractable polymer. The four-fold symmetry of the cavitand was evident from the ^1H NMR data, the most characteristic feature of which was a singlet at *ca*. 5.5 ppm for the protons on the bridging carbons. That the product was indeed cavitand **2a**, and not the diastereomer with the phenyl groups pointing into the cavity, was demonstrated by X-ray crystallography.[15] Interestingly, the solid state structure (Fig. 1) also revealed that this cavitand dimerizes in a head to head fashion to generate cavities between the rigid dimers. Furthermore, the contiguous nature of these cavities results in the formation of channels (cross-section = 8.3 × 6.6 Å within a cavity, or 7.4 × 4.2 Å at the mouth of each cavity) that zigzag along a common axis.[16]

Similar low yields were obtained for **1b** in DMA and NMP. However, with the slow addition of the octol in DMPU, the deep-cavity cavitand, **2b**, was isolated in 58% yield; a remarkable yield when compared to either the statistical 6.25%, or the similar yields obtained for methylene bridging with CH_2ClBr.[17] Encouraged by this disparity between **1a** and **1b**, we investigated the bridging of **1c**. For this compound we found that the reaction was successful in either DMA or DMPU, with maximum yields somewhat lower than for **1b**. Finally, we found

Table 1 Yields for the formation of deep-cavity cavitands **2a**–**d**[a]

Entry	Octol	Product	Solvent[b]	Yield (%) *via* 4 h addn. of octol (2 d addn.)
1	**1a**	**2a**	DMA	< 5 (< 5)
2	**1a**	**2a**	NMP	< 5 (< 5)
3	**1a**	**2a**	DMPU	6 (10)
4	**1b**	**2b**	DMA	6 (< 5)
5	**1b**	**2b**	NMP	6 (7)
6	**1b**	**2b**	DMPU	35 (58)
7	**1c**	**2c**	DMA	41[c] (*c*)
8	**1c**	**2c**	NMP	< 5 (< 5)
9	**1c**	**2c**	DMPU	17 (40)
10	**1d**	**2d**	DMA	56 (51)
11	**1d**	**2d**	NMP	57 (55)
12	**1d**	**2d**	DMPU	31 (42)

[a] These results relate to 250 mmol scale reactions. However, yields were essentially identical for multi-gram reactions. [b] See ref. 14. [c] Because of crystallization problems in DMA, octol **1c** was added over a 2 h period.

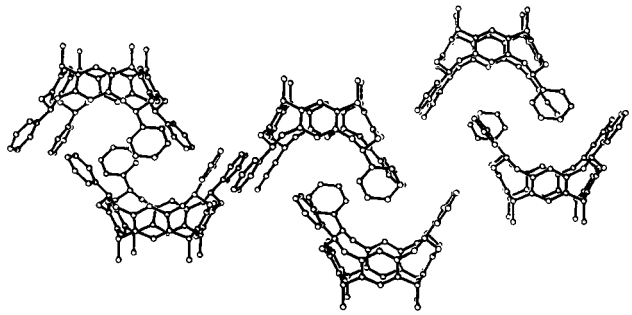

Fig. 1 Ball and stick diagram showing a view perpendicular to the direction of the channel. The central dimeric pair of deep-cavity cavitands is behind the plane formed by its adjacent neighbors. For clarity, the hydrogen atoms and the disordered solvents have been omitted.

benzal bridging of **1d** to be relatively solvent independent, with the highest yields again comparable with methylene bridging.

These results, in conjunction with uniformly poor yields obtained when the octol was added as a solid (data not shown), highlight the importance of a constant, slow rate of addition of the octol to the reaction. Equally as important, the apparently capricious nature of the solvent/R group relationship highlights the need to investigate these reactions in a variety of solvents. To gain more insight into influences that affect benzal bridging, a further series of experiments were undertaken (data not shown). Briefly, for the DMA solvated reaction with **1d**, we observed no significant dependence of the yield on reaction scale or concentration, but that the use of caesium carbonate as base, or $PhCHCl_2$ as bridging material, had a pronounced, detrimental effect on the yield.

The most significant observation from these results is that bridging is more favored for octols with larger pendent groups; a reflection, we believe, of a propensity for large groups to preorganise the octol into a bowl shaped conformation suitable for bridging. In a related issue, we attribute the apparent reduction in solvent-dependent yield with increasing size of the R group to a stronger association between such groups which pushes the equilibrium between favorable and unfavorable conformations towards the former.

Pin-pointing the precise cause of this stereoselective bridging is complicated by a lack of knowledge of the bridging mechanism in general. However, regardless of the pathway, the overall reaction is clearly highly diastereoselective, as steric demands induce a remarkable average of at least 87% stereoselectivity for each bridge.

In conclusion, we have demonstrated an approach to extending the π-surface of cavitands in a manner that should allow formation of a range of host molecules possessing large enforced cavities. With the concept of catalytic machinery preorganized within hydrophobic pockets our long term goal, we are currently extending our studies to the formation of a variety of functionalized deep-cavity cavitands.

We are grateful to John C. Sherman for helpful discussions and Richard B. Cole of the New Orleans Center for Mass Spectrometry Research for mass analyses of the products. This work was partially supported by the Louisiana Board of Regents Support Fund (1997-00)-RD-A-23, and a Research Innovation Award from Research Corporation.

Notes and References

† E-mail: bcgcm@uno.edu

‡ The following general procedure is illustrative: the octol (0.275 mmol) was added as a solution in the respective solvent (5 ml) to a stirred mixture of 450 mg of K_2CO_3 and 200 μl (1.25 mmol) benzal bromide ($PhCHBr_2$) in 12 ml of solvent. After stirring for 2 days at 25 °C, an additional 67 μl (0.42 mmol) of $PhCHBr_2$ was added and the reaction mixture warmed to 40 °C. After 1 day, a further 67 μl (0.42 mmol) of $PhCHBr_2$ was added and the temperature increased to 50 °C. This temperature was maintained for a further day, when an additional 67 μl (0.42 mmol) of $PhCHBr_2$ was added, and the reaction heated to 60 °C for 3 days. The reaction was then cooled, and the solvent removed under reduced pressure. The crude mixture was partitioned between water and $CHCl_3$, the $CHCl_3$ layer separated and the aqueous layer extracted twice with $CHCl_3$. The organic layers were then combined, dried with anhydrous $MgSO_4$, and the solvent removed under reduced pressure. Column chromatography (silica gel, $CHCl_3$–hexane, 1 : 1) afforded the corresponding deep-cavity cavitand which was dried (0.1 mmHg, 110 °C) overnight. All compounds gave satisfactory NMR, MS and elemental analysis (±0.4%).

Selected data for **2a**: mp > 300 °C; δ(300 MHz, $CDCl_3$) 1.86 (d, 12 H, *J* 7.5), 5.20 (q, 4 H, *J* 7.5), 5.50 (s, 4 H), 6.69 (s, 4 H), 7.42 (m, 16 H), 7.68 (d, 8 H, *J* 7.8); *m/z* 897.13 ($M + H^+$), 919.11 ($M + Na^+$) (Calc. for $C_{60}H_{48}O_8$: C, 80.33; H, 5.40. Found: C, 80.05; H, 5.45%).

1 For the isolation of β-unsubstituted enols, see S. Watanabe, K. Goto, T. Kawashima and R. Okazaki, *J. Am. Chem. Soc.*, 1997, **119**, 3195. For the TASP analysis of peptide structure, see B. C. Gibb, A. R. Mezo and J. C. Sherman, *Tetrahedron Lett.*, 1995, **36**, 7587.

2 D. J. Cram and J. M. Cram, *Container Molecules and Their Guests*, Royal Society of Chemistry, Cambridge, 1994.

3 J. C. Sherman, *Tetrahedron*, 1995, **51**, 3395.

4 K. Nakamura, C. Sheu, A. E. Keating, K. N. Houk, J. C. Sherman, R. G. Chapman and W. L. Jorgensen, *J. Am. Chem. Soc.*, 1997, **119**, 4321.

5 P. Timmerman, E. A. Brinks, W. Verboom and D. N. Reinhoudt, *J. Chem. Soc., Chem. Commun.*, 1995, 417; P. Timmerman, K. G. A. Nierop, E. A. Brinks, W. Verboom, F. C. J. M. van Veggel, W. P. van Hoorn and D. N. Reinhoudt, *Chem. Eur. J.*, 1995, **1**, 132; M. Vincenti and E. Dalcanale, *J. Chem. Soc., Perkin Trans. 2*, 1995, 1069; S. Watanabe, K. Goto, T. Kawashima and R. Okazaki, *Tetrahedron Lett.*, 1995, **36**, 7677; P. Soncini, S. Bonsignore, E. Dalcanale and F. Ugozzoli, *J. Org. Chem.*, 1992, **57**, 4608; J. A. Tucker, C. B. Knobler, K. N. Trueblood and D. J. Cram, *J. Am. Chem. Soc.*, 1989, **111**, 3688.

6 A. G. W. Högberg, *J. Org. Chem.*, 1980, **45**, 4498; L. M. Tunstad, J. A. Tucker, E. Dalcanale, J. Weiser, J. A. Bryant, J. C. Sherman, R. C. Helgeson, C. B. Knobler and D. J. Cram, *J. Org. Chem.*, 1989, **54**, 1305.

7 For phosphate bridging, see T. Lippmann, H. Wilde, E. Dalcanale, L. Mavilla, G. Mann, U. Heyer and S. Spera, *J. Org. Chem.*, 1995, **60**, 235; P. Delangle and J.-P. Dutasta, *Tetrahedron Lett.*, 1995, **36**, 9235.

8 For alkyl chain bridging, see D. J. Cram, S. Karbach, H.-E. Kim, C. B. Knobler, E. F. Maverick, J. L. Ericson and R. C. Helgeson, *J. Am. Chem. Soc.*, 1988, **110**, 2229.

9 For silicon bridging, see D. J. Cram, K. D. Stewart, I. Goldberg and K. N. Trueblood, *J. Am. Chem. Soc.*, 1985, **107**, 2574.

10 J. R. Moran, J. L. Ericson, E. Dalcanale, J. A. Bryant, C. B. Knobler and D. J. Cram, *J. Am. Chem. Soc.*, 1991, **113**, 5707. For hydrogen bonding variants, see D. M. Rudkevich, G. Hilmersson and J. Rebek Jr., *J. Am. Chem. Soc.*, 1997, **119**, 9911.

11 For topologically similar systems, see L. R. MacGillivray and J. L. Atwood, *J. Am. Chem. Soc.*, 1997, **119**, 6931; W. Xu, J. J. Vittal and R. J. Puddephatt, *J. Am. Chem. Soc.*, 1995, **117**, 8362.

12 Note that aromatic rings attached to the resorcinol units (C-2) are forced to adopt a conformation orthogonal to the cavity rim: C. von dem Bussche-Hünnefeld, R. C. Helgeson, D. Bühring, C. B. Knobler and D. J. Cram, *Croatia Chem. Acta*, 1996, **69**, 447.

13 For a recent, spectacular example of the self assembly of resorcinarenes, see L. R. MacGillivray and J. L. Atwood, *Nature*, 1997, **389**, 469.

14 Solvents employed were dimethylacetamide (DMA), 1-methyl-2-pyrrolidinone (NMP) and 1,3-dimethyl-3,4,5,6-tetrahydropyrimidin-2(1*H*)-one (DMPU).

15 *Crystal data* for **2a**: $C_{60}H_{48}O_8 \cdot 1.5CHCl_3 \cdot 0.5C_6H_{14} \cdot 0.5H_2O$, *M* 1021, monoclinic, space group $P2_1/c$, a = 15.1106(7), b = 28.6654(14), c = 14.6484(7) Å; β = 109.1515(10)°, V = 5993.8(5) Å^3, Z = 4, T = 113(2) K, μ = 0.275 mm^{-1}. 46 542 reflections measured, 12 707 unique reflections (R_1 = 0.0680), $R(F)$ = 0.0817 and $wR(F^2)$ = 0.1481 and S = 1.197 for 8773 reflections with $I > 6\sigma(I)$. CCDC 182/899.

16 Given distances are atom-to-atom.

17 J. C. Sherman, C. B. Knobler and D. J. Cram, *J. Am. Chem. Soc.*, 1991, **113**, 2194; B. C. Gibb, R. G. Chapman and J. C. Sherman, *J. Org. Chem.*, 1996, **61**, 1505.

Received in Colombia, MO, USA, 12th May 1998; 8/03571G

An efficient semisynthesis of 7-deoxypaclitaxel from taxine

Radomir Matović[a] and Radomir N. Saičić*[b]†

[a] *ICTM, Center for Chemistry, Njegoseva 12, Belgrade, YU-11000 Yugoslavia*
[b] *Faculty of Chemistry, University of Belgrade, Studentski trg 16, PO Box 158, Belgrade, YU-11001 Yugoslavia*

Highly cytotoxic 7-deoxypaclitaxel analogues are obtained by a semisynthesis starting from taxine—the most abundant naturally occurring taxane diterpene fraction.

Owing to its great potential in the successful treatment of many types of cancer, unusual mode of antimitotic action, and complex molecular architecture, paclitaxel has attracted enormous interest from the scientific community.[1] Paclitaxel is currently produced *via* extraction from the bark of the Pacific yew, *Taxus brevifolia*, or by semisynthesis from 10-deacetylbaccatin III, which is in turn isolated, most notably, from the leaves of the European yew, *Taxus baccata*.[2] However, 10-deacetylbaccatin III is not the most abundant secondary metabolite of the yew tree: its variable content in the needles of *Taxus baccata* ranges from 0.05 to 1 g per kg of leaves.[3] In contrast, a mixture of alkaloids collectively referred to as 'Taxine' **2** can be obtained by a simple extraction procedure in yields of 7–12 g kg^{-1},[4] the two major constituents of this fraction (*ca.* 35%) being taxine B **2a** and isotaxine B **2b**;[5] therefore, the development of the procedure that would allow for the efficient use of this starting material for the preparation of biologically active paclitaxel analogues would be of considerable interest.

Earlier reports on 7-deoxypaclitaxel **1**, obtained by radical deoxygenation of paclitaxel, or baccatin derivative, showed this compound to be of comparable, or even superior, cytotoxic activity with respect to paclitaxel,[6] and, given the structural congruence with taxine B, indicated it as a semisynthetic target. The possibility of such a synthetic transformation was investigated by several groups.[7] As the preparative separation of taxine alkaloids is difficult, the crude taxine mixture was hydrolysed in order to obtain a well-defined starting material, *i.e.* tetraol **3**. However, the differentiation between hydroxy groups in tetraol **3** required extensive use of protective groups, leading to long synthetic sequences, and lowering considerably the overall yield.[8] We endeavoured to develop an efficient procedure for the conversion of taxine into 7-deoxypaclitaxel derivatives (Scheme 1). The accomplishment of this task was expected not only to give access to large amounts of 7-deoxypaclitaxel analogues, but also to provide additional information on the reactivity of the taxane system, as well as derivatives suitable for further SAR studies.

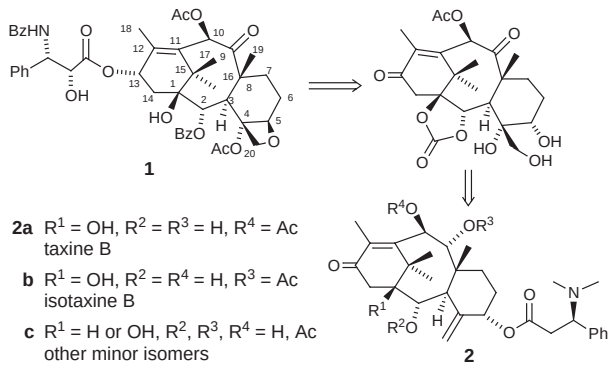

Scheme 1

We first re-examined the possibility of exploiting the favourable arrangement of functional groups in the major constituent of taxine, *i.e.* taxine B **2a** (Scheme 2). Quaternization of the crude taxine,[7a] followed by DBU induced elimination under anhydrous conditions, afforded a mixture of 9- and 10-acetyl-5-cinnamoyltaxicine I (**4** and **5**), which could be separated by a flash chromatography on a SiO_2 column, and were isolated in yields of 1 and 1.7 g kg^{-1} of needles, respectively. The former could be isomerised into the required 10-acetyl derivative **5** by treatment with methanolic KOAc (43% yield at 70% conversion, without optimisation), to afford a total of 2 g of 10-acetyl-5-cinnamoyltaxicine I **5** per 1 kg of dry leaves.

With the suitable starting compound **5** in hand, the synthesis of 7-deoxybaccatin III proceeded as displayed in Scheme 3. Treatment of **5** with phosgene, followed by hydrolytic work-up, furnished the cyclic carbonate **6** (90%), which was further oxidised to diketone **7** (Dess–Martin periodinane, 80%), thus establishing the final functionalization of the 'upper' part of the molecule. The elaboration of the oxetane ring was envisaged to proceed *via* triol **10**.[7a] For that purpose a method for selective removal of the cinnamoyl chain was needed, as the simultaneous cleavage of the C-10 acetate would require additional protective steps. To achieve this, allylic cinnamate **7** was oxidised with OsO_4/NMO, as it was anticipated that intramolecular hydrogen bonding in **8** should activate the dihydroxyphenylpropionate ester towards hydrolysis under very mild conditions. Although some concern existed about the stereochemical outcome of the osmylation, to our pleasure the reaction proceeded in quantitative yield, and with complete stereoselectivity. This structural change brought about the expected modification in the reactivity profile of **8**, as indicated by its proclivity towards spontaneous migration of the ester side chain from O-5 to O-20 on standing in solution at room temperature; treatment of **8** with K_2CO_3 or $NaHCO_3$ in MeOH–H_2O at 0 °C induced very rapid hydrolysis of the dihydroxypropanoate ester, but the hydrolysis of the C-10 acetate also

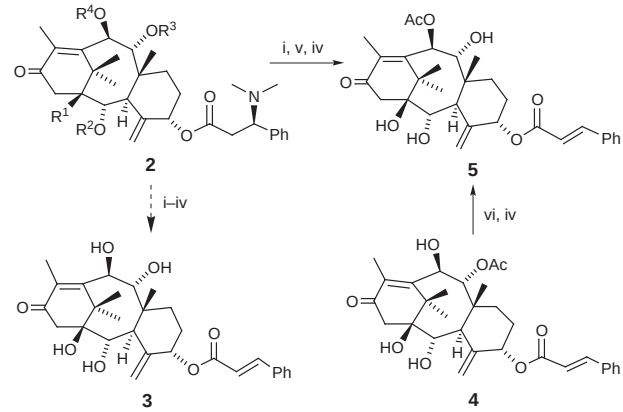

Scheme 2 *Reagents and conditions*: i, MeI, THF, room temp., 5 h; ii, K_2CO_3, H_2O, EtOH, room temp., 3 h; iii, NaOMe, MeOH, 0 °C, 16 h; iv, column chromatography on SiO_2; v, DBU, $CHCl_3$, room temp., 1.5 h; vi, 10% KOAc in MeOH, room temp., 3 h

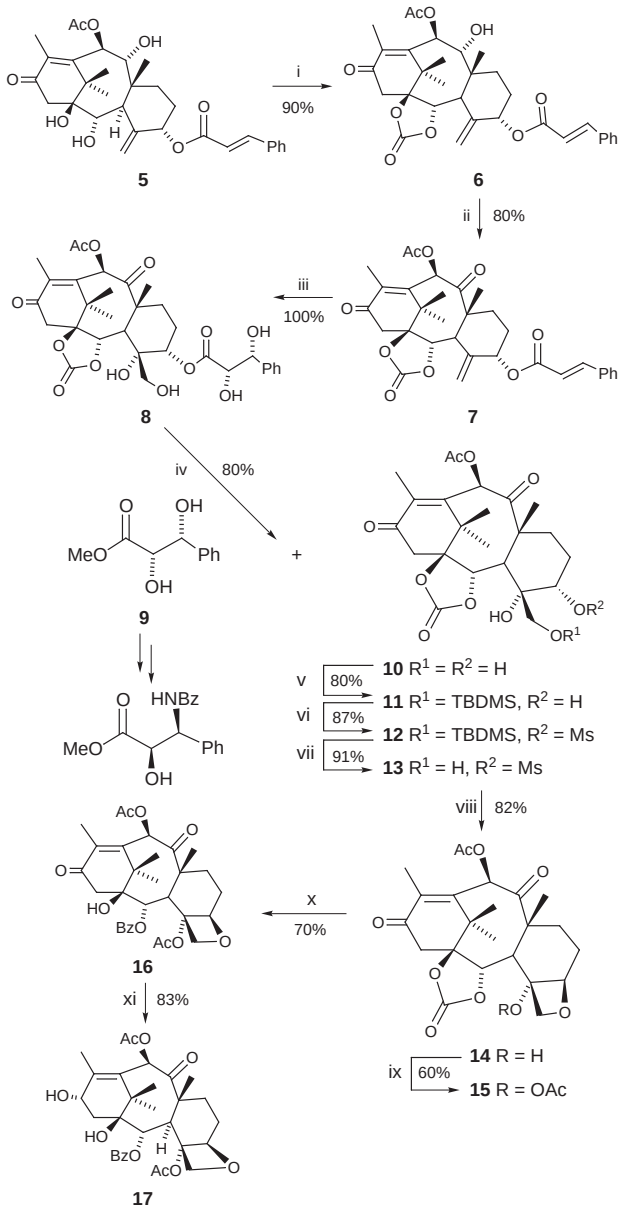

Scheme 3 *Reagents and conditions*: i, $COCl_2$ (20 equiv.), CH_2Cl_2, 0 °C, 20 min; then Et_2O, H_2O, imidazole (cat.), 0 °C, 20 min; ii, Dess–Martin periodinane (2 equiv.), CH_2Cl_2, TFA (cat.), room temp., 12 h; iii, OsO_4 (cat.), NMO, THF, H_2O, room temp., 4 h; iv, 10% KOAc in MeOH, reflux, 30 min; v, TBDMSCl, imidazole, DMF, room temp., 3 h; vi, MsCl, Py, 0 °C to room temp., 24 h; vii, 7% HF in MeCN, room temp., 7 h; viii, Pr^i_2NEt (7 equiv.), toluene, reflux, 30 h; ix, Ac_2O (7 equiv.), DMAP (14 equiv.), CH_2Cl_2, room temp., 4 h; x, PhLi (10 equiv.), THF, −78 °C, 0.5 h; then Ac_2O, DMAP, CH_2Cl_2, room temp., 1 h; xi, $NaBH_4$ (excess), MeOH, room temp., 3 h

occurred under these conditions. Eventually, refluxing **8** with methanolic KOAc afforded the desired triol **10** in 80% yield. Optically pure (*2S*,*3R*)-(-)-methyl 2,3-dihydroxy-3-phenylpropanoate **9** was isolated as the side product of this reaction, and further converted into the paclitaxel side chain according to a previously published procedure.[9] The transformation of the key intermediate **10** into 7-deoxybaccatin III **17** was accomplished by applying a modified methodology previously developed in total syntheses of paclitaxel.[1,7a] In this way, starting from cinnamoyltaxicine I **5**, 7-deoxybaccatin III was obtained in 11.5% overall yield (unoptimized).[10]

7-Deoxybaccatin is a direct precursor of paclitaxel analogues: esterification of **17** with acid **18**,[11] followed by acidic hydrolysis (TsOH in MeOH) afforded 7-deoxypaclitaxel **1** in 75% yield (Scheme 4).[12]

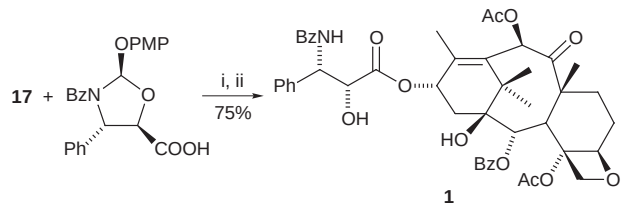

Scheme 4 *Reagents and conditions*: i, DCC, DMAP (cat.), room temp., 3 h; ii, 5% TsOH in MeOH, room temp., 1 h

The described chemistry offers an efficient pathway for the preparation of new paclitaxel derivatives, and points to the naturally abundant taxane diterpene fraction—taxine—as a valuable starting material for further semisynthetic studies.

Notes and References

† E-mail: rsaicic@chem.bg.ac.yu

1 *Taxol®: Science and Applications*, ed. M. Suffness, CRC Press, Boca Raton, 1995, and references cited therein. Isolation and structure elucidation: M. C. Wani, H. L. Taylor, M. E. Wall, P. Coggon and A. T. McPhail, *J. Am. Chem. Soc.*, 1971, **93**, 2325. Total syntheses: K. C. Nicolaou, H. Ueno, J.-J. Liu, P. G. Nantermet, Z. Yang, J. Renaud, K. Paulvannan and R. Chadha, *J. Am. Chem. Soc.*, 1995, **117**, 653; R. A. Holton, H.-B. Kim, C. Somoza, F. Liang, R. J. Biediger, P. D. Boatman, M. Shindo, C. C. Smith, S. Kim, H. Nadizadeh, Y. Suzuki, C. Tao, P. Vu, S. Tang, P. Zhang, K. K. Murthi, L. N. Gentile and J. H. Liu, *J. Am. Chem. Soc.*, 1994, **116**, 1599; S. J. Danishefsky, J. J. Masters, W. B. Young, J. T. Link, L. B. Snyder, T. V. Magee, D. K. Jung, R. C. A. Isaacs, W. G. Bornmann, C. A. Alaimo, C. A. Coburn and M. J. Di Grandi, *J. Am. Chem. Soc.*, 1996, **118**, 2843; P. A. Wender, N. F. Badham, S. P. Conway, P. E. Floreancig, T. E. Glass, J. B. Houze, N. E. Krauss, D. Lae, D. G. Marquess, P. L. McGrane, W. Meng, M. G. Natchus, A. J. Shuker, J. C. Sutton and R. E. Taylor, *J. Am. Chem. Soc.*, 1997, **119**, 2757

2 J.-N. Denis, A. E. Greene, D. Guenard, F. Gueritte-Voegelein, L. Mangatal and P. Potier, *J. Am. Chem. Soc.*, 1998, **110**, 5917

3 G. Chauviere, D. Guenard, F. Picot, V. Senilh and P. Potier, *C. R. Seances Acad. Sci., Ser. 2*, 1981, **293**, 501; K. M. Witherup, S. A. Look, M. W. Stasko, T. J. Ghiorzi, G. M. Mushik and G. M. Cragg, *J. Nat. Prod.*, 1990, **53**, 1249; see also ref. 2.

4 H. Lucas, *Arch. Pharm.*, 1856, **14**, 438; G. Appendino, in *Alkaloids: Chemical and Biological Perspectives*, ed., S. W. Pelletier, Pergamon, Oxford, 1996, vol. 11, p. 237; L. H. D. Jenniskens, E. L. M. van Rosendaal, T. A. van Beek, P. H. G. Wiegerinck and H. W. Scheeren, *J. Nat. Prod.*, 1996, **59**, 117; for an alternative isolation procedure, see ref. 7(*a*).

5 L. Ettouati, A. Ahond, C. Poupat and P. Potier, *J. Nat. Prod.*, 1991, **54**, 1455; in some specimens of *Taxus baccata* a content of taxine as high as 17 g kg^{-1} was found, 10 g being taxine B; the authors are grateful to Dr A. Ahond and Dr C. Poupat for this personal communication.

6 A. G. Chaudhary, J. M. Rimoldi and D. G. I. Kingston, *J. Org. Chem.*, 1993, **58**, 3798; S.-H. Chen, S. Huang, J. Kant, C. Fairchild, J. Wei and V. Farina, *J. Org. Chem.*, 1993, **58**, 5028; V. Farina, S.-H. Chen, D. R. Langley, M. D. Wittman, J. Kant and D. Vyas, *Eur. Pat. Appl.*, EP 590,267/6 apr, **1994** (*Chem. Abstr.*, 1994, **121**, 205747n).

7 (*a*) L. Ettouati, A. Ahond, C. Poupat and P. Potier, *Tetrahedron*, 1991, **47**, 9823; (*b*) P. H. G. Wiegerinck, L. Fluks, J. B. Hammink, S. J. E. Mulders, F. M. H. de Groot, H. L. M. van Rosendaal and H. W. Sheeren, *J. Org. Chem.*, 1996, **61**, 7092; (*c*) I. Fenoglio, G. M. Nano, D. G. V. Velde and G. Appendino, *Tetrahedron Lett.*, 1996, **37**, 3203; (*d*) H. Poujol, A. A. Mourabit, A. Ahond, C. Poupat and P. Potier, *Tetrahedron*, 1997, **53**, 12 575 and references cited therein.

8 While this work was in progress, the first semisynthesis of 7-deoxybaccatin from **3** was reported, in 15 steps and 1.7% overall yield, see ref. 7(*d*).

9 J.-N. Denis, A. Correa and A. E. Greene, *J. Org. Chem.*, 1990, **55**, 1957

10 Spectral data identical to those reported in ref. 7(*d*).

11 A. M. Kanazawa, J.-N. Denis and A. E. Greene, *Chem. Commun.*, 1994, 2591

12 ^{1}H NMR data identical to those reported in ref. 6.

Received in Glasgow, UK, 28th May 1998; 8/03990I

Enantiomeric discrimination of chiral amines with new fluorescent chemosensors

Dong Wang,*[a]† Tian-Jun Liu,[a] Wen-Chun Zhang,[a] William T. Slaven IV[b] and Chao-Jun Li*[b]

[a] *Institute of Chemistry, Chinese Academy of Sciences, Beijing 100080, China*
[b] *Department of Chemistry, Tulane University, New Orleans, LA 70118, USA*

Fluorescent chiral sensors for the enantiomeric recognition of chiral amines have been developed.

Molecular recognition is a fundamental property of various natural systems and has attracted a significant amount of research interest recently.[1] Such recognition plays a key role in biosynthesis and protein folding. Enantiomeric recognition is a characteristic of many enzymatically catalyzed reactions generating optically active biological molecules and is the basis of asymmetric synthesis.[2] Because chiral amines and related compounds are the basic building blocks of biological systems, the study of enantiomeric recognition of these compounds is of particular significance.[3] Such studies, besides providing an understanding of the functions of natural living processes, also provide useful information for the understanding and design of asymmetric catalysis systems, new pharmaceutical agents[4] and separation materials.[5] Optical sensors have been of great interest in the last decade due to their often simple design and ease of handling. These sensors are increasingly important for biological and environmental analysis[6] as well as for pharmaceutical applications.[7] A promising technique is based on fluorescent probes due to their very sensitive detection ability.[8] These sensors are based on the large changes in their fluorescent properties during interaction with analytes. Recently, Shinkai's group developed a fluorescent molecular sensor that can discriminate D- and L-monosaccharides through their fluorescence response to the binding of guest species.[9] Binding of each enantiomer of the monosaccharides alters the fluorescence intensity to differing degrees, enabling them to be distinguished. More recently, Still and co-workers described small organic fluorescent sensors that detect the presence of unlabeled tripeptides in a sequence-selective manner.[10] Here we report the enantiomeric discrimination of chiral amines using designed receptors that act as sensors by changing fluorescence intensity during host–guest interactions.[11]

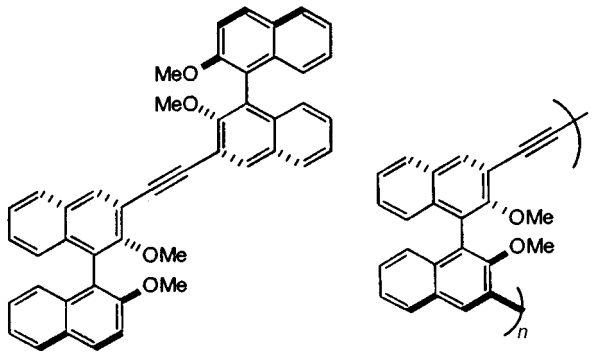

1 **2**

The chiral hosts used in our study are dimeric (**1**) and oligomeric (**2**) binaphthol-derivatives that we have previously developed.[12] For the chiral guest amines, we chose D- and L-α-phenylethylamines (**3**), as well as D- and L-phenylalanine methyl esters (**4**). The ^{1}H NMR studies were carried out in a $CDCl_3$ solution of chiral dimer (−)-**1** and D- or L-phenylethylamine (**3**) (host : guest = 1 : 1). Differences in chemical shifts of D- and L-**3** were observed: $\Delta\delta$(D−L) = 0.04 ppm (12 Hz) at δ 1.37 due to methyl-H, 0.04 ppm (12 Hz) at δ 4.2 due to CH of **3**, and 0.01 ppm (3 Hz) at δ 3.7 due to methoxy-H of the host **1**. The results indicated clearly that the complexation of chiral host **1** and the guest chiral amine, as well as enantio discriminations, occurred in $CDCl_3$ solution.

The fluorescence study was carried out in MeCN with the measurements performed on a Hitachi 850 Fluorescent Spectrometer. The experimental procedure is as follows: a solution of the host in MeCN (c 1.4 × 10^{-5} mol ml^{-1}) was titrated with a solution of the chiral amine in MeCN. The fluorescence intensity was measured and the quantum yields determined.[12] The fluorescence quantum yield of the chiral host was assigned as ϕ_0. Upon addition of the chiral guest, the fluorescence quantum yield ϕ of the solution was measured at various concentrations. ϕ/ϕ_0 was plotted against the concentration of the guest. Because most amines do not have a fluorescence chromaphore, an emission wavelength (λ_{em}) at 410 nm, the typical emission of a naphthalene ring, was used to measure the change in fluorescence intensity. Thus, changes in this wavelength can be attributed to the interaction of the guest chiral amines with the chiral host due to host–guest complexation.

It was found that the interaction of the two enantiomers of chiral amines did not have a substantial effect on the emission wavelength. On the other hand, a strong change in fluorescence response intensity was observed with the use of different enantiomers. As illustrated from the plots (Figs. 1 and 2), the dimer and oligomer hosts have different responses to the concentration changes of the guest molecules. When α-phenylethylamine was used as the chiral guest, the following observations were made: at a concentration of (10–15) × 10^{-5} mol dm^{-3}, $[\phi/\phi_0]_L/[\phi/\phi_0]_D$ has a value of 1.13 for the dimeric host and a value of 1.37 for the oligomeric host; whereas at a concentration of (2–5) × 10^{-5} mol dm^{-3}, the $[\phi/\phi_0]_L/[\phi/\phi_0]_D$ values changed to 0.81 for the dimeric and 1.07 for the oligomeric hosts respectively. Thus, in the case of the dimeric host, a change in the concentration of α-phenylethylamine from (10–15) to (2–5) × 10^{-5} mol dm^{-3} reversed the fluorescence

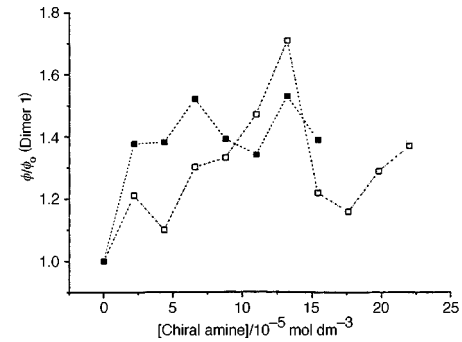

Fig. 1 ϕ/ϕ_0 ratio of fluorescent quantum yield of D- and L-α-phenylethylamine with dimer **1** as the host: (■) D-α-phenylethylamine and (□) D-α-phenylethylamine

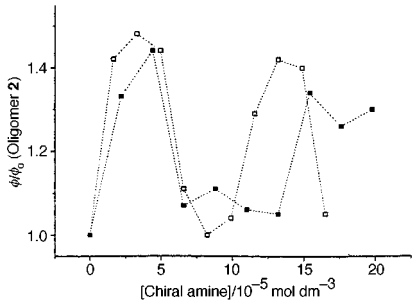

Fig. 2 ϕ/ϕ_0 ratio of fluorescent quantum yield of D- and L-α-phenylethylamine with oligomer **2** as the host: (■) D-α-phenylethylamine and (□) D-α-phenylethylamine

response of the two enantiomers. Such a reversed fluorescence response was also observed during the measurement of phenylalanine methyl ester (Figs. 3 and 4). At a concentration of (7–9) $\times$ 10^{-5} mol dm^{-3}, the $[\phi/\phi_0]_L/[\phi/\phi_0]_D$ has a value of 1.19 for the dimeric host and a vlaue of 1.10 for the oligomeric host; whereas at a concentration of (2–4) $\times$ 10^{-5} mol dm^{-3}, the $[\phi/\phi_0]_L/[\phi/\phi_0]_D$ values changed to 0.97 for the dimeric and 0.98 for the oligomer hosts. Interestingly, the strongest reversal of fluorescence properties for the two enantiomers with the dimeric host was observed at a concentration of 5 $\times$ 10^{-5} mol dm^{-3}, in which the $[\phi/\phi_0]_L/[\phi/\phi_0]_D$ value was measured at 0.86. However, the fluorescence response of the oligomeric host appears relatively constant under the different concentrations of phenylalanine methyl ester. At a concentration of 5 $\times$ 10^{-5} mol dm^{-3}, the $[\phi/\phi_0]_L/[\phi/\phi_0]_D$ value of the oligomeric host was measured at 0.96. As the structure of the hosts has been characterized as having a helical concave structure,[12] we suspect that the chiral amines would clathrate into the chiral host through a π–π interaction between the naphthyl moiety of the host and the phenyl group of the aromatic amine and hydrogen bond. The enantio discrimination could stem from the chiral naphthyl moiety and the main chain chirality of the oligomers. The multiple interacting points and chiral units of the hosts may play different roles during chiral discrimination, which could explain the aberrant response of fluorescence on the concentration of the chiral guest. In conclusion, we have developed two fluorescence sensors for the chiral recognition of chiral amines. The recognition was confirmed by ^{1}H NMR measurement. The fluorescence response of the chiral sensor was found to be markedly influenced by the concentration of chiral amines. Currently, we are developing more selective systems to discrimination among chiral amines on the basis of the present investigation.

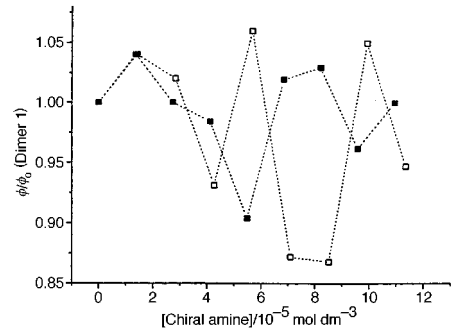

Fig. 3 ϕ/ϕ_0 ratio of fluorescent quantum yield of D- and L-phenylalanine methyl ester with dimer **1** as the host: (□) D-phenylalanine methyl ester and (■) I-α-phenylalanine methyl ester

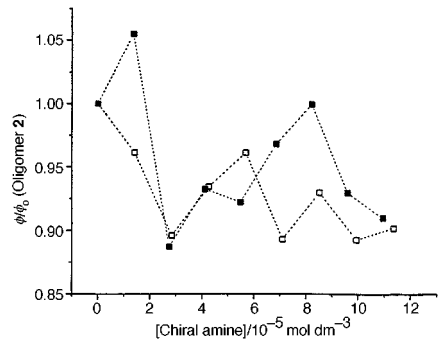

Fig. 4 ϕ/ϕ_0 ratio of fluorescent quantum yield of D- and L-phenylalanine methyl ester with oligomer **1** as the host: (□) D-phenylalanine methyl ester and (■) L-phenylalanine methyl ester

Support of this research was provided by the Natural Science Foundation of China and the Center for Photo-induced Processes (NSF-LEQSF).

Notes and References

† E-mail: g210@mimi.cnc.ac.cn

1 For recent treatises on molecular recognition, see *Inclusion Phenomena and Molecular Recognition*, ed. J. L. Atwood, Plenum, New York, 1990; *Molecular Recognition Mechanisms*, ed. M. Delaage, VCH, New York, 1991; *Molecular Structure and Life: Molecular Recognition of Nucleic Acids*, ed. Y. Kyogoku and Y. Nishimura, Japan Scientific Society Press, Tokyo, 1992; *Principles of Molecular Recognition*, ed. A. D. Buckingham, A. C. Legon and S. M. Roberts, Blackie Academic and Professional, London 1993; S. M. Roberts, *Molecular Recognition: Chemical and Biochemical Problems II*, CRC Press, Boca Raton, 1992; J. M. Lehn, *Supramolecular Chemistry*, VCH, Weinheim, 1995.

2 For recent treatises, see *Supramolecular Chemistry I—Directed Synthesis and Molecular Recognition, Topics in Current Chemistry*, ed. W. Weber, vol. 165, Springer-Verlag, Berlin, 1993; R. Noyori, *Asymmetric Catalysis in Organic Synthesis*, Wiley, New York 1994; J. Seyden-Penne, *Chiral Auxiliaries and Ligands in Asymmetric Synthesis*, Wiley, New York, 1995; G. Procter, *Asymmetric Synthesis*, Oxford University Press, Oxford, 1996; *Catalytic Asymmetric Synthesis*, ed. I. Ojima, VCH, New York, 1993.

3 For an excellent up-to-date review, see X. X. Zhang, J. S. Bradshaw and R. M. Izatt, *Chem. Rev*., 1997, **97**, 3313.

4 For a recent treatise, see *The Design of Drugs to Macromolecular Targets*, ed. C. R. Beddell, Wiley, Chichester, 1992.

5 For recent monograph, see *Chromatographic Separations Based on Molecular Recognition*, ed. K. Jinno, VCH, Weinheim, 1996.

6 For examples, see M. A. Mortellaro and D. G. Nocera, *J. Am. Chem. Soc.*, 1996, **118**, 7414.

7 For a recent monograph, see M. C. Trans, *Biosensors (Sensor Physics and Technology)*, Chapman & Hall, London, 1993; B. R. Eggins, *Biosensors: An Introduction*, Wiley, Chichester, 1996; D. Buerk, *Biosensors: Theory and Applications*, Technomic, Lancaster, 1993.

8 For representitative examples, see T. W. Bell, Z. Hou, Y. Luo, M. G. B. Drew, E. Chapoteau, B. P. Czech and A. Kumar, *Science*, 1995, **269**, 671; Q. Zhou and T. M. Swager, *J. Am. Chem. Soc.*, 1995, **117**, 7017 and refs. cited therein; R. Dagani, *C & EN*, 1995, July 17, 63; For a recent monograph, see *Fluorescent Chemosensors for Ion and Molecular Recognition*, ed. A. W. Czarnik, *ACS Symp. Ser.* 538, American Chemical Society, Washington, DC, 1993.

9 T. D. James, K. R. A. S. Sandanayake and S. Shinkai, *Nature*, 1995, **374**, 345.

10 C. T. Chen, H. Wagner and W. C. Still, *Science*, 1998, **279**, 851.

11 Previously, Irie and co-workers observed a significant difference in the fluorescence quenching rate duing the study of the interaction between simple binaphthyl and chiral amines, see M. Irie, T. Yorozu and K. Hayashi, *J. Am. Chem. Soc.*, 1978, **100**, 2236; T. Yorozu, K. Hayashi and M. J. Irie, *J. Am. Chem. Soc.*, 1981, **103**, 5480.

12 C. J. Li, D. Wang and W. T. Slaven IV, *Tetrahedron Lett.*, 1996, **37**, 4459; C. J. Li, W. T. Slaven IV, V. T. John and S. Banerjee, *Chem. Commun.* 1997, 1569; D. Wang, T. J. Liu, C. J. Li and W. T. Slaven IV, *Polym. Bull.*, 1997, **39**, 265; T. J. Liu, D. Wang, F. L. Bai, C. J. Li and W. T. Slaven IV, *Chin. J. Polym. Sci.*, 1998, **18**, 234.

Received in Columbia, MO, USA, 16th April 1998; 8/02855I

$Co_2(CO)_6$-induced deformation of alkynes as a reversible modulator of supramolecular interactions: controlling the synthesis of catenanes

Darren G. Hamilton and Jeremy K. M. Sanders*†

Cambridge Centre for Molecular Recognition, University Chemical Laboratory, Lensfield Road, Cambridge, UK CB2 1EW

Complexation of $Co_2(CO)_6$ clusters to the alkyne bonds of a hybrid crown macrocycle alters the dimensions of the macrocyclic cavity such that inclusion complexation and catenane formation by catalytic ring closing metathesis is prevented; since removal of the $Co_2(CO)_6$ 'protecting group' is readily achieved, this procedure provides a general method for modulation of supramolecular interactions.

We show here that cobalt carbonyl complexation to alkyne groups provides a simple and reversible method for the modulation of molecular geometry. Since alkynes are popular linker groups that allow the precise spatial positioning of molecular components,[1] this complexation process offers a general approach for the control of supramolecular interactions. We exemplify the principle by controlling the binding properties of macrocycle **1** and hence its ability to act as a template for catenane formation under catalytic ring closing metathesis (RCM) conditions. Complexation of $Co_2(CO)_6$ clusters to the acetylene links of this hybrid crown macrocycle removes its ability to bind electron deficient substrates, while oxidative removal of the clusters restores the macrocycle's original structural form and binding capacity.

The reaction of dicobalt octacarbonyl with acetylene functions has been known for over 40 years (Scheme 1).[2] The complexes were originally of interest as some of the first characterised systems featuring multi-point attachment of an organic molecule to more than one metal atom. Complexation of an acetylene group to a cobalt carbonyl cluster has been used as a protecting group to mask the reactivity of the triple bond,[3] and also as an activating group to promote reactions requiring the stabilisation of an electron-deficient carbon centre.[4]

The complexation process is accompanied by a dramatic change in the geometry of the linear acetylenic carbon backbone. Complexation of $Co_2(CO)_6$ to diphenylacetylene reduces the Ph–C–C bond angles from 180 to around 138°;[5] this observation has been exploited in attempts to prepare *cyclo*-C_{18} by temporarily altering the geometry of precursors to favour cyclisation.[6] Of greatest relevance to the present discussion is the structure of the bis-$Co_2(CO)_6$ complex of diphenylbutadiyne (Ph–C≡C–C≡C–Ph).[7] The C–C–C bond angles at the four nominally sp hybridised centres of this complex fall in the range 139–145°. We predicted that if a butadiyne linker were incorporated into a macrocycle then cluster complexation to this host could induce sufficient structural change to inhibit guest binding. Hybrid macrocycle **1** appeared an ideal candidate with which to test this theory since it forms a weak donor–acceptor complex with π-deficient diimides ($K_a \approx 400$ M^{-1}), and has also been employed as a template for [2]catenane formation under kinetically controlled conditions.[8]

Treatment of a THF solution of **1** with excess $Co_2(CO)_8$ (3 equiv. per triple bond) rapidly affords a single complexed product **2** which may be obtained in near quantitative yield after chromatography on silica gel.‡ The ^{1}H NMR spectrum of **2** closely resembles that of **1** save for an aromatic doublet that shifts upfield from around 6.80 to 6.11 ppm perhaps as a result of the greater proximity of the two aromatic components. The ^{13}C NMR spectrum provides rather more information: the methylene carbons adjacent to the complexed butadiyne link are shifted downfield from around 56 to 68–70 ppm (obscured by OCH_2CH_2 resonances). The complexed acetylenic carbons are found at 96 and 93 ppm, downfield shifted from around 72 ppm in free **1**. These shifts are consistent with the introduction of strongly electron withdrawing substituents and previously reported values.[7] The electrospray ionisation mass spectrum of **2** reveals the sequential loss of CO ligands from the bis-$Co_2(CO)_6$ complexed macrocycle (M_r = 1124). Notably, the ^{1}H NMR spectrum of **2** in $CDCl_3$ was unchanged after standing in solution for several weeks; samples stored as dry solids proved similarly robust. Removal of the cobalt clusters could be achieved by treatment of **2** with iron(III) nitrate[3] in EtOH or, more conveniently, with trimethylamine oxide in THF.§ Regeneration of free **1** could be conveniently monitored by TLC. An intermediate, presumably the mono-$Co_2(CO)_6$ complex, could be discerned prior to complete conversion to **1**. Scheme 2 summarises the structural protection and deprotection steps.

We exemplify the application of this idea by controlling the formation of a π-donor/π-acceptor [2]catenane under catalytic ring closing metathesis conditions. The catalytic RCM reaction has become a familiar synthetic tool[9] and has also been employed in templated macrocycle[10] and catenane syntheses.[11] We anticipate that the reversible nature of the RCM bond-forming reaction will facilitate competition and evolution between related interlocked systems and thus provide the 'error-checking' facility necessary for the reliable assembly of higher

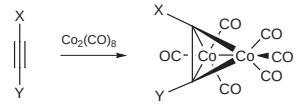

Scheme 1 General reaction of a functionalised acetylene with $Co_2(CO)_8$

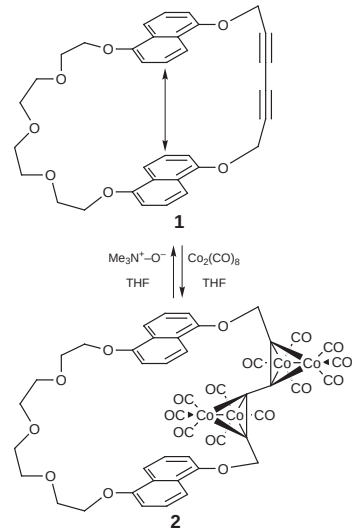

Scheme 2 Blocking of a cyclophane receptor cavity by temporary structural modification

order interlocked molecular systems. The interlocking procedure also provides an ideal means with which to demonstrate the feasibility of our blocking principle.¶

Exposing a 2 : 1 molar ratio of diimide diolefin **3** and hybrid macrocycle **1** to Grubbs' catalyst (DCM, rt, 3 days) afforded the three isomeric forms of the corresponding [2]catenane **4**; direct hydrogenation of the reaction mixture (H_2, Pd–C) gave a single catenane product **5** in 15% overall yield.‖ Under identical reaction conditions a 2 : 1 molar ratio of diolefin **3** and complexed macrocycle **2** did not undergo interlocking, periodic analysis (LC-MS, TLC) revealing only the stubborn persistence of **2**. After three days 1 mol equiv. of free macrocycle **1** was added to the metathesis mixture and production of [2]catenane **4** commenced: this observation proves that under 'live' metathesis conditions macrocycle **2** is indeed blocked to threading by diolefin **3**. Direct hydrogenation (H_2, Pd–C) of the crude reaction mixture yielded the expected [2]catenane **5** and the protected macrocycle **2**.

The significance of the survival of **2** throughout this sequence of events lies in the realisation that this structural tool provides the means by which to prevent binding at one masked recognition site whilst the chosen reaction conditions act on a binding event elsewhere in the system or, potentially, within the same molecule. Both the olefin metathesis and hydrogenation steps are chemically orthogonal to the deprotection of **2**, the cobalt complexed macrocycle being unaffected by two distinct chemical transformations occurring within the system. We intend to exploit these observations in controlled syntheses of linear [*n*]catenanes.[12] There also exists the possibility of inhibiting a supramolecular interaction within a complex by cluster removal; an alternative view of this process is to regard the cluster as an effector for a particular interaction (Fig. 1). We also note that variations in cluster nuclearity and substitution pattern lead to subtle geometry changes in the resulting adducts, providing a means to fine tune molecular geometry.[13] In summary, it appears likely that both the specific, as described in this work, and general concepts of binding modulation through temporary structural modification will be of use in the area of host–guest chemistry.

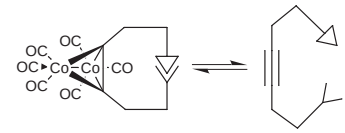

Fig. 1 Inhibition of a supramolecular interaction by cluster removal.

We thank the Engineering and Physical Sciences Research Council (UK) for generous financial support and Professor Phil Parsons (Sussex, UK) for suggesting the use of a trialkylamine oxide as a cluster removal reagent.

Notes and references

† E-mail: jkms@cam.ac.uk

‡ **1→2**: to a solution of **1** (150 mg, 0.3 mmol) in dry THF (5 mL) was added $Co_2(CO)_8$ (560 mg, 1.6 mmol) under argon. After stirring for 30 minutes at room temperature the solvent was evaporated and the residue purified by column chromatography (SiO_2; $CHCl_3$–Et_2O–MeOH, 30 : 69 : 1) to afford **2** (R_f = 0.6) as a red–brown solid (293 mg, 96%): ^{1}H NMR ($CDCl_3$, 400 MHz) δ 7.88 (d, *J* 8 Hz, 2 H), 7.83 (d, *J* 8 Hz, 2 H), 7.30 (t, *J* 8 Hz, 3 H), 6.98 (t, *J* 8 Hz, 3 H), 6.84 (d, *J* 8 Hz, 2 H), 6.11 (d, *J* 8 Hz, 2 H), 5.19 (s, 4 H), 4.32 (m, 4 H), 3.98 (m, 4 H), 3.81 (m, 4 H), 3.74 (m, 4 H): ^{13}C NMR ($CDCl_3$, 100 MHz) δ 239.00, 154.45, 153.36, 125.44, 125.11, 115,16, 114.39, 106.17, 105.60, 71.36, 70.66, 69.73, 68.58, 68.37: ES–MS (positive ion) 1142.65 ($[M + NH_4]^+$, 12%), 1124.61 ($[M]^+$, 18%), 1086.66 ($[M - 2CO + NH_4]^+$, 100%), 1057.65 ($[M - 3CO + NH_4]^+$, 68%).

§ **2→1**: $Fe(NO_3)_3 \cdot 9H_2O$ (6 equiv.)–EtOH, rt, 3 days, or Me_3N^+–O^- (10 equiv.), THF, rt, 45 min; ammonium cerium(IV) nitrate (CAN) effects essentially instantaneous removal of the appended clusters[4] but also rapidly degrades the regenerated free macrocycle **1**.

¶ A preliminary experiment confirmed that **1** is unaffected by exposure to Grubbs' metathesis catalyst.

‖ M_r = 1288.29 ($[M + NH_4]^+$).

1 D. O'Krongly, S. R. Denmeade, M. Y. Chiang and R. Breslow, *J. Am. Chem. Soc.*, 1985, **107**, 5544; S. Anderson and H. L. Anderson, *Angew. Chem., Int. Ed. Engl.*, 1996, **108**, 2075; H. L. Anderson and J. K. M. Sanders, *J. Chem. Soc., Perkin Trans. 1*, 1995, 2223; B. J. Whitlock and H. W. Whitlock, in *Comprehensive Supramolecular Chemistry*, eds. J. L. Atwood, J. E. D. Davies, D. D. MacNicol and F. Vögtle, Elsevier, New York, 1996, vol. 2, p. 309; J. K. M. Sanders, *ibid*., vol. 9, p. 131.

2 H. W. Sternberg, H. Greenfield, R. A. Friedel, J. Wotitz, H. R. Markby and I. Wender, *J. Am. Chem. Soc.*, 1954, **76**, 1457.

3 K. M. Nicholas and R. Pettit, *Tetrahedron Lett.*, 1971, **12**, 3475; P. Magnus and P. A. Carter, *J. Am. Chem. Soc.*, 1988, **110**, 1626; L. R. Milgrom, R. D. Rees and G. Yahioglu, *Tetrahedron Lett.*, 1997, **38**, 4905.

4 D. Seyferth and M. O. Nestle, *J. Am. Chem. Soc.*, 1975, **97**, 7417; S. L. Schreiber, T. Sammakia and W. E. Crowe, *J. Am. Chem. Soc.*, 1986, **108**, 3128.

5 W. G. Sly, *J. Am. Chem. Soc.*, 1959, **81**, 18.

6 F. Diederich, in *Modern Acetylene Chemistry*, eds. P. J. Stang and F. Diederich, VCH, Weinheim, NewYork, Basel, Cambridge, Tokyo, 1995, p. 443.

7 B. F. G. Johnson, J. Lewis, P. R. Raithby and D. A. Wilkinson, *J. Organomet. Chem.*, 1991, **408**, C9.

8 D. G. Hamilton, N. Feeder, L. Prodi, S. J. Teat, W. Clegg and J. K. M. Sanders, *J. Am. Chem. Soc.*, 1998, **120**, 1096.

9 R. H. Grubbs, S. J. Miller and J. C. Fu, *Acc. Chem. Res.*, 1995, **28**, 446.

10 M. J. Marsella, H. D. Maynard and R. H. Grubbs, *Angew. Chem., Int. Ed. Engl.*, 1997, **36**, 1101.

11 B. Mohr, M. Weck, J.-P. Sauvage and R. H. Grubbs, *Angew. Chem., Int. Ed. Engl.*, 1997, **36**, 1308.

12 D. G. Hamilton, J. E. Davies, L. Prodi and J. K. M. Sanders, *Chem. Eur. J.*, 1998, **4**, 608.

13 G. G. Melikyan and K. M. Nicholas, in *Modern Acetylene Chemistry*, eds. P. J. Stang and F. Diederich, VCH, Weinheim, New York, Basel, Cambridge, Tokyo, 1995, p. 99.

Received in Cambridge, UK, 4th June 1998; 8/04208J

Cycloheptyne–cobalt complexes *via* allylation of stabilized γ-carbonyl cations

James R. Green*†

Chemistry and Biochemistry, School of Physical Sciences, University of Windsor, Windsor, Ontario, N9B 3P4, Canada

The Bu_2BOTf mediated reaction of stannylsilanes (5 and 9) with γ-methoxy-alkynoate and -alkynone hexacarbonyldicobalt complexes (8), followed by conversion of the organic carbonyl into an acetate and a $BF_3{\cdot}OEt_2$ mediated intramolecular reaction, affords cycloheptenyne hexacarbonyldicobalt complexes (13 and 15).

Cyclic alkynes are compounds of limited stability.[1] The smallest unsubstituted member of the series which can be isolated under conventional laboratory conditions is cyclooctyne; in the vast majority of cycloheptynes and smaller cycloalkynes, the strain of bending the sp hybridized carbon atoms substantially away from 180° has too great an energetic cost. This situation may be ameliorated by resorting to transition metal complexes of cycloheptynes, particularly the dicobalt hexacarbonyl complexes.[2]Alkyne hexacarbonyldicobalt complexes have bond angles which average *ca*. 140° at the alkynyl carbons; the resultant lower angle strain renders the cycloheptyne and cyclohexyne complexes thermally stable.[3]

In addition to the above reasons, cobalt cycloheptyne complexes are of interest due to the potential for applying the rich synthetic utility of cobalt–alkyne complexes[4–6] to seven membered ring systems. This potential is largely unexplored, however, as these systems have been prepared infrequently,[7,8] and their systematic synthesis and study has escaped report. Notably, the attempt to prepare systems of this type *via* a double Nicholas reaction using allyldimetal equivalent **1** and propargylic ether **2** met with complete failure.[9]

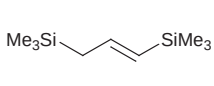

1

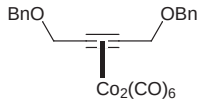

2

During our recent work involving silver mediated reactions of γ-chloro-alkynoate and -alkynone hexacarbonyldicobalt complexes,[10] we observed striking effects of the presence of an additional oxygen based function on the viability of propargyl alcohol or propargyl ether based Nicholas reactions. As a result, we believed that a stepwise reaction of **1** at the carbon bearing the chloride, manipulation of the carbonyl into a leaving group, and intramolecular allylsilane attack would give a cycloheptenyne complex.‡ Therefore, we tested the reaction of chloride **3** with **1** and $AgBF_4$ (0 °C, CH_2Cl_2), and to our surprise obtained a small amount of **4** as the sole condensation product. Compound **4** most probably results from the preferential loss of the internal trimethylsilyl group from the β-silyl cation intermediate, and allyldimetal equivalents with different electrofuges were investigated for their reactivity with **3**. Stannylsilane **5a**[11] gave more satisfactory results, and allylsilane **6a** was obtained as the major product, contaminated with vinylsilane **7a** (55%, **6a** : **7a** = 78 : 22). In this case the source of the isomeric impurity is believed to be Lewis acid mediated allylic rearrangement of the tin moiety in **5a** to give isomeric allyltin **5a′**;[12] despite this, recovered **5a** showed no evidence of **5a′**. Attempts to use systems with more bulky silyl groups gave improved regiochemical ratios in favour of the allylsilane product, at the expense of a satisfactory chemical yield.

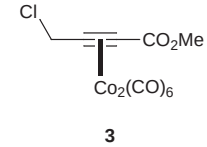

3

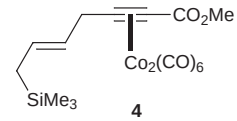

4

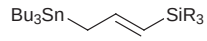

5a R = Me
5b R = Et

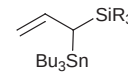

5a′ R = Me
5b′ R = Et

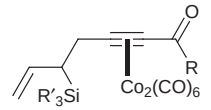

6a R′ = Me, R = OMe
6b R′ = Et, R = OMe
6c R′ = Et, R = Ph
6d R′ = Et, R = Me

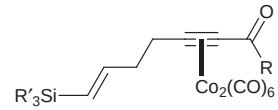

7a R′ = Me, R = OMe
7b R′ = Et, R = OMe
7c R′ = Et, R = Ph
7d R′ = Et, R = Me

Based on the report from Jacobi's laboratory of the condensation of boron enolates with γ-methoxyalkynoate hexacarbonyldicobalt complexes,[13] we found that Bu_2BOTf (0 °C, CH_2Cl_2) was capable of inducing the condensation between propargyl ether **8a** with **5a** to give **6a**/**7a** (84%, **6a** : **7a** = 78 : 22). While regiochemical impurity **7a** was still present, the use of silylstannane **5b**[14] with **8a** was now possible, and allylsilane **6b** could be prepared in good yield with only a trace of **7b** (63%, **6b** : **7b** = 96 : 4; Table 1). Application of this protocol to phenyl ketone **8b** gave **6c** as the major product, with a more substantial amount of vinylsilane **7c** (73%, **6c** : **7c** = 82 : 18). The methyl ketone **8c** would undergo additional reaction of the alkyl ketone function in the presence of >1 equivalents of Bu_2BOTf, and optimum results for the formation of **6d** were obtained by inverting the order of reagent addition, and by conducting the reaction at −60 °C (39%, 77% based on recovered starting material, **6d** : **7d** = 92 : 8). Finally, silylstannane **9**[15] reacted smoothly with **8a** to give **10** in good yield (83%).

The carbonyl functions in **6** and **10** could be converted into a leaving group by low temperature (−78 °C) reduction with Bu^i_2AlH, and trapping of the resultant alkoxide with freshly distilled acetic anhydride at room temperature, affording acetates **11–12** in excellent yields. In the case of phenyl ketone **6c**, the acylation step was very slow, and the addition of sodium acetate with catalytic amounts of DMAP was required to give useful amounts of **11c**.

Table 1 Bu_2BOTf mediated condensations of allyldimetals **5** and **9** with **8**

Substrate	Allyldimetal	Product	Ratio	Yield (%)
8a	**5a**	**6a** + **7a**	78 : 22	84
8a	**5b**	**6b** + **7b**	96 : 4	63
8b	**5b**	**6c** + **7c**	82 : 18	73
8c	**5b**	**6d** + **7d**	92 : 8	39 (77)[a]
8a	**9**	**10**	—	83

[a] Based on recovered starting material.

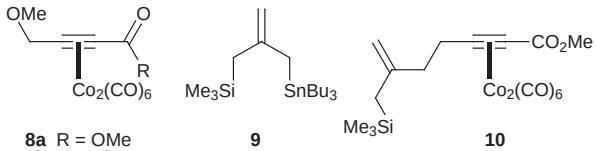

8a R = OMe
8b R = Ph

9

10

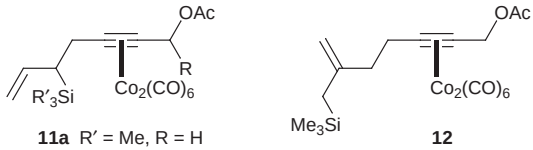

11a R′ = Me, R = H
11b R′ = Et, R = H
11c R′ = Et, R = Ph
11d R′ = Et, R = Me

12

With the appropriately attached allylsilane and propargylic acetate functions in place, the ability of the substrates to form cycloheptyne complexes was investigated. Slow addition of a CH_2Cl_2 solution of **11** to a 0 °C CH_2Cl_2 solution of excess $BF_3{\cdot}Et_2O$ (final substrate concentration = 1 mM) rapidly afforded cycloheptenyne complexes **13**, as red–violet oils of good thermal stability, in excellent yields (Table 2). In the phenyl and methyl substituted cases **11c** and **11d**, trace amounts of fluorocycloheptyne complexes **14b** (8%) and **14c** (6%), respectively, were also isolated. In the case of substrate **12**, cyclization under these conditions afforded methylenecycloheptyne complex **15a** contaminated with a minor amount of the *endo* double bond isomer **15b** (46%, 87 : 13), along with desilylated fluorocycloheptyne complex **16** (44%). An alternative procedure which employed the slow addition of $BF_3{\cdot}Et_2O$ (5 equiv.) to a solution of **12** (1.5 mM) at 0 °C gave slightly enhanced amounts of **15a** + **15b** (55%, 90 : 10) and a small amount of **16** (8%).

The results demonstrate the facility with which the Nicholas reaction chemistry of cobalt stabilized γ-carbonyl cations can be applied to the preparation of cycloheptyne cobalt complexes. Further work in this area, including that on superior allyldimetal equivalents and one pot, [4 + 3] cycloaddition approaches to the

Table 2 Conversion of condensation products **6** and **10** to cycloheptenynes complexes **13** and **15**

Substrate	Acetate (Yield [%])	Cycloheptenyne (Yield [%])	Fluorocycloheptyne (Yield [%])
6a	**11a** (88)	**13a** (89)	—
6b	**11b** (90)	**13a** (87)	—
6c	**11c** (84[a])	**13b** (84)	**14b** (8)
6d	**11d** (88)	**13c** (85)	**14c** (6)
10	**12** (90)	**15a** + **b** (46) [87 : 13][b]	**16** (44)

[a] DMAP (0.2 equiv.) and NaOAc (excess) added during acylation step. [b] Numbers in square brackets represent the **15a** : **b** ratio.

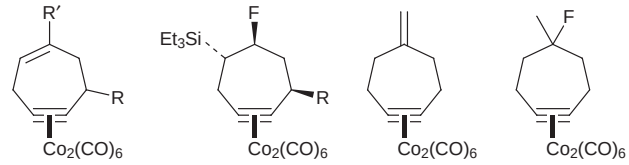

13a R = H, R′ = H
13b R = Ph, R′ = H
13c R = Me, R′ = H
15b R = H, R′ = CH_3

14a R = Ph
14b R = Me

15a

16

complexes, and the synthetic applications of these compounds are in progress and will be reported in due course.

Notes and References

† E-mail: jgreen@uwindsor.ca

‡ This represents an *endo–trig* variant of the Schreiber group ring closure step.[7]

1 A. Krebs and J. Wilke, *Top. Curr. Chem.*, 1983, **109**, 189; H. Meier, *Adv. Strain Org. Chem.*, 1991, **1**, 215.
2 M. J. Went, *Adv. Organomet. Chem.*, 1997, **41**, 69.
3 The stabilization of other strained alkynes also has been accomplished by complexation to the hexacarbonyldicobalt unit; see Y. Rubin, C. B. Knobler and F. Diederich, *J. Am. Chem. Soc.*, 1990, **112**, 4966; M. H. Haley and B. L. Langsdorf, *Chem. Commun.*, 1997, 1121.
4 R. S. Dickson and P. J. Fraser, *Adv. Organomet. Chem.*, 1974, **12**, 323.
5 A. J. M. Caffyn and K. M. Nicholas, in *Comprehensive Organometallic Chemistry II*, ed. E. W. Abel, F. G. A. Stone and G. Wilkinson, ed. L. S. Hegedus, Pergamon, Oxford, 1995, vol. 12, ch. 7.1; K. M. Nicholas, *Acc. Chem. Res.*, 1987, **20**, 207.
6 N. E. Schore, in *Comprehensive Organometallic Chemistry II*, ed. E. W. Abel, F. G. A. Stone and G. Wilkinson, ed. L. S. Hegedus, Pergamon, Oxford, 1995, vol. 12, ch. 7.2; N. E. Schore, *Org. React.*, 1991, **40**, 1; N. E. Schore, in *Comprehensive Organic Synthesis*, ed. B. M. Trost, ed. L. A. Paquette, Pergamon, Oxford, 1991, vol. 5, ch. 9.1; N. E. Schore, *Chem. Rev.*, 1988, **88**, 1081.
7 S. L. Schreiber, M. T. Klimas and T. Sammakia, *J. Am. Chem. Soc.*, 1986, **108**, 3128; T. Nakamura, T. Matsui, K. Tanino and I. Kuwajima, *J. Org. Chem.*, 1997, **62**, 3032.
8 N. E. Schore and S. D. Najdi, *J. Org. Chem.*, 1987, **52**, 5296; M. Isobe, C. Yenjai and S. Tanaka, *Synlett*, 1994, 916; S. Hosokawa and M. Isobe, *Synlett*, 1995, 1179.
9 S. Takano, T. Sugihara and K. Ogasawara, *Synlett*, 1992, 70.
10 C. S. Vizniowski, J. R. Green, T. L. Breen and A. V. Dalacu, *J. Org. Chem.*, 1995, **60**, 7496.
11 G. E. Keck and D. R. Romer, *J. Org. Chem.*, 1993, **58**, 6083.
12 M. Pereyre, J.-P. Quintard and A. Rahm, *Tin in Organic Synthesis*, Butterworths, London, 1987, pp. 216–218; A. Yanagisawa, A. Ishiba, H. Nakashima and H. Yamamoto, *Synlett*, 1997, 88.
13 P. A. Jacobi, S. C. Buddhu, D. Fry and S. Rajeswari, *J. Org. Chem.*, 1997, **62**, 2894.
14 Prepared in 90% yield, as adapted from the procedure of J. M. Muchowski, R. Naef and M. L. Maddox, *Tetrahedron Lett.*, 1985, **26**, 5375.
15 Prepared in 60% yield by the stannylation of 2-chloromethyl-3-trimethylsilylprop-1-ene according to S. Chandrasekhar, S. Latour, J. D. Wuest and B. Zacharie, *J. Org. Chem.*, 1983, **48**, 3810.

Received in Corvallis, OR, USA, 4th May 1998; 8/03316A

A new structural type in iron carboxylate cluster chemistry *via* use of bis-bipyridine ligands: $[Fe_6O_4Cl_4(O_2CPh)_4L_2][FeCl_4]_2$

Craig M. Grant,[a] Michael J. Knapp,[b] John C. Huffman,[a] David N. Hendrickson*[b] and George Christou*[a]

[a] *Department of Chemistry and the Molecular Structure Center, Indiana University, Bloomington, IN 47405-4001, USA. E-mail: christou@indiana.edu*

[b] *Department of Chemistry-0358, University of California at San Diego, La Jolla, CA 92093-0358, USA*

The reaction between $FeCl_3$, NaO_2CPh and L [L = 1,2-bis(2,2′-bipyridyl-6-yl)ethane] in MeCN gives the title complex 1 whose cation contains an unusual $[Fe_6(\mu_3\text{-}O)_4]^{10+}$ core, whereas in MeOH the dinuclear complex $[Fe_2(OMe)_2Cl_2(O_2CPh)L][FeCl_4]$ 2 is obtained; magnetic studies indicate that the cations of 1 and 2 both have $S = 0$ ground states, consistent with the expected antiferromagnetic exchange interactions.

In recent years, the synthesis and study of high-spin molecules (possessing large values of spin S in their ground state) have assumed greater importance as it has been discovered that such molecules represent the source of a new magnetic phenomenon, namely single-molecule magnetism.[1,2] As a result of a large spin and a negative magnetoanisotropy, as reflected in the zero-field splitting parameter D, such a single-molecule magnet (SMM) can be magnetized by an external magnetic field below some critical or blocking temperature. The first SMMs to be identified were $[Mn_{12}O_{12}(O_2CR)_{16}(H_2O)_4]$ (R = Me, Et, Ph, *etc.*) complexes (S = 9 or 10)[1–3] and their one-electron reduced versions in $[Mn_{12}O_{12}(O_2CR)_{16}(H_2O)_4]^-$ salts (S = 19/2).[2] More recently, the $[Mn_4O_3X(O_2CMe)_3(dbm)_3]$ (X = Cl^-, Br^-, F^-, O_2CMe^-, *etc.*; dbm^- is the anion of dibenzoylmethane) complexes with $S = 9/2$[4,5] and $[V_4O_2(O_2CR)_7(L\text{–}L)_2]^z$ salts [L–L = 2,2′-bipyridine (bpy), $z = +1$; L–L = 2-picolinate, $z = -1$] with $S = 3$[6] have also been discovered to be SMMs, as has a $[Fe_8O_2(OH)_{12}(tacn)_6]^{8+}$ salt (tacn = 1,4,7-triazacyclononane) with $S = 10$.[7]

Important to the future of the field of high-spin molecules, and to the possible identification of new SMMs, is the development of synthetic methodologies that can yield new metal clusters, particularly those of Mn^{III} and Fe^{III}. With this in mind, we have been investigating the ability of bis-bipyridine ligands such as L to assemble new cluster types with Mn^{III} and Fe^{III} not available with simpler ligands such as bpy itself. We herein describe access *via* this route to a new Fe_6 structural type, as well as a related Fe_2 species, confirming the potential of this ligand for cluster synthesis in Fe^{III}–Mn^{III} chemistry.

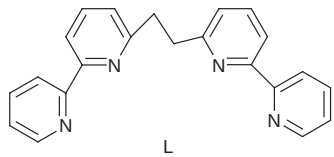

L

The reaction between $FeCl_3$, NaO_2CPh and L (4 : 4 : 1) in MeCN gave a red–brown solution and an off-white solid (NaCl). After 24 h reaction time, the solution was filtered, and the filtrate concentrated under vacuum to half its original volume and layered with Et_2O. Red–brown crystals of $[Fe_6O_4Cl_4(O_2CPh)_4L_2][FeCl_4]_2 \cdot 2MeCN$ **1**·2MeCN slowly grew over 1–2 weeks in 40% yield; dried solid analysed as **1**·MeCN.† The same reaction in a 3 : 3 : 1 ratio carried out in MeOH gave an orange precipitate. This was collected by filtration and recrystallized from warm MeOH–MeCN (1 : 1) to give orange needles of $[Fe_2(OMe)_2Cl_2(O_2CPh)L][FeCl_4]$ **2** in 28% yield.† Note that the use of bpy instead of L in the MeCN reaction gives $[Fe_4O_2(O_2CPh)_7(bpy)_2][FeCl_4]$, the cation of which has been previously reported.[8]

The structures‡ of the cations of **1** and **2** are shown in Figs. 1 and 2, respectively. The centrosymmetric cation of **1** contains an unusual $[Fe_6(\mu_3\text{-}O)_4]^{10+}$ core (6 × Fe^{III}) that can be conveniently described as consisting of three edge-fused $[Fe_2O_2]$ rhombs to which are attached two additional Fe atoms Fe(1) and Fe(1′); the latter are four-coordinate with distorted tetrahedral geometry whereas the other Fe atoms are six-coordinate with distorted octahedral geometry. A side view shows the $[Fe_6O_4]$ core to be nearly planar. The L and central $PhCO_2^-$ groups bridge the Fe(2)/Fe(3) and Fe(2′)/Fe(3′) pairs. An alternative description of the structure is particularly useful: the cation consists of two $[Fe_2O_2(O_2CPh)L]^+$ fragments that are linked by inter-fragment bonds Fe(2)–O(7′) and Fe(2′)–O(7), and this incipient, supramolecular chain formation is terminated by the $[FeCl_2(O_2CPh)]$ caps at each end, whose Fe(1) and O(10) atoms bind to and prevent O(6) and Fe(3) from attaching to another $[Fe_2O_2(O_2CPh)L]^+$ fragment. Note the unusual nearly T-shaped geometry of O(7) and O(7′), with Fe(2′)–O(7)–Fe(3) angles of 159.25(21)°.

The cation of **2** contains a $[Fe_2(\mu\text{-}OMe)_2]^{4+}$ core with bridging L and $PhCO_2^-$ groups, and octahedral geometry at each Fe^{III} completed by terminal Cl^- ions. The dinuclear unit is thus similar to the repeating $[Fe_2O_2(O_2CPh)L]^+$ fragment of **1**, with aggregation blocked by the MeO^--for-O^{2-} substitution at

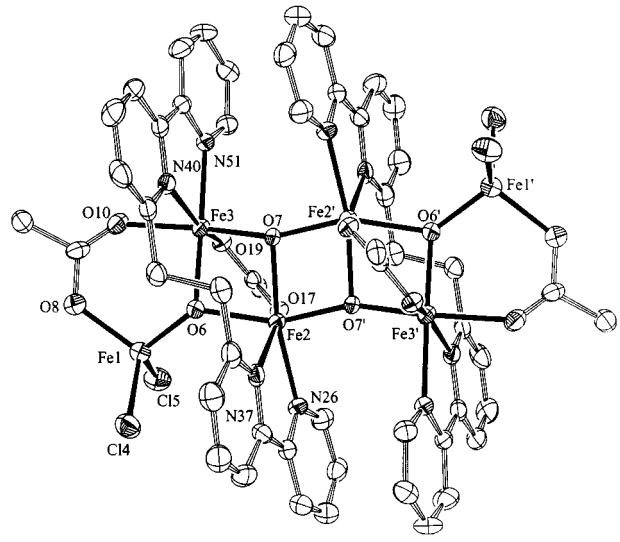

Fig. 1 The structure of the cation of **1**; only the *ipso* C atoms of the Ph rings are shown. Selected interatomic distances (Å) are: Fe(1)···Fe(2) 3.483(2), Fe(1)···Fe(3) 3.357(2), Fe(2)···Fe(3) 2.932(2), Fe(2)···Fe(2′) 3.054(2), Fe(2)···Fe(3′) 3.692(2), Fe(1)–O(6) 1.806(4), Fe(2)–O(6) 1.994(4), Fe(2)–O(7) 2.045(4), Fe(2)–O(7′) 1.889(4), Fe(3)–O(6) 1.965(4), Fe(3)–O(7) 1.864(4). Primed and unprimed atoms are related by the inversion centre.

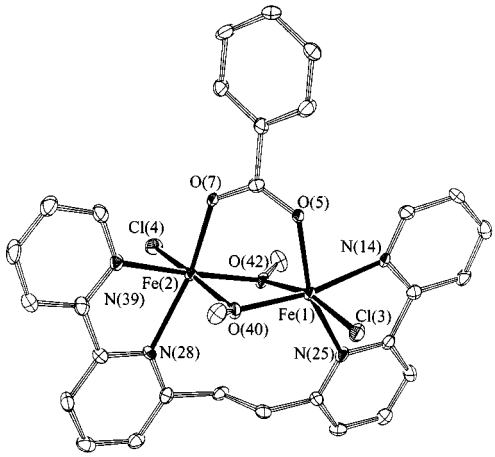

Fig. 2 The structure of the cation of **2**. Selected interatomic distances (Å) and angles (°) are: Fe(1)···Fe(2) 3.088(2), Fe(1)–O(40) 1.981(4), Fe(1)–O(42) 1.993(4), Fe(1)–Cl(3) 2.290(2), Fe(2)–O(40) 2.013(4), Fe(2)–O(42) 1.973(4), Fe(2)–Cl(4) 2.271(2); Fe(1)–O(40)–Fe(2) 101.31(19), Fe(1)–O(42)–Fe(2) 102.29(18).

the bridging position and terminal Cl^- ions on the Fe atoms. The Fe(1)···Fe(2) distance in **2** [3.088(2) Å] is only slightly longer than the Fe(2)···Fe(3) distance in **1** [2.932(2) Å].

Comparison of **1** and **2** shows that L is a binucleating ligand and it adopts the same bridging mode in both complexes with the ethylene bridge forcing the two bpy halves to be essentially parallel. There appears to be no reason why longer chains of $[Fe_2O_2(O_2CPh)L]^+$ repeating units with $[FeCl_2(O_2CPh)]$ caps should not be possible, yielding the supramolecular $[Fe_{2n+2}O_{2n}Cl_4(O_2CPh)_{n+2}L_n]^{n+}$ family of which **1** is the $n = 2$ member. This possibility is currently being investigated by changes in the reagent ratios.

Solid-state magnetic susceptibility data were collected in a 1 Tesla field. The effective magnetic moment μ_{eff} ($\chi_m T$) value for **1** slowly decreases from 10.30 μ_B (13.26 cm^3 K mol^{-1}) at 13.0 K and then decreases rapidly to 6.76 μ_B (5.71 cm^3 K mol^{-1}) at 2.0 K. Subtracting out the expected values for the $[FeCl_4]^-$ anions ($S = 5/2$) shows that μ_{eff} and $\chi_m T$ for the cation decrease to essentially zero at low temperatures, indicating a $S = 0$ ground state. Similarly, μ_{eff} ($\chi_m T$) values for **2** are 9.33 (10.88), 5.90 (4.35) and 5.19 μ_B (3.37 cm^3 K mol^{-1}) at 300, 9.00 and 2.00 K (Fig. 3), respectively. Subtracting out the contribution from the $[FeCl_4]^-$ anion again indicates a $S = 0$ ground state, and fitting of the 13.0–300 K data (lower T data were affected by zero-field splitting in the anion and were omitted) to a Heisenberg exchange model ($\hat{H} = -2JS_1S_2$) gives $J = -10.48$ cm^{-1} with g held at 2.00 (solid line in Fig. 3). This value is as expected from the empirical J *vs.* $2P$ relationship, where $2P$ is the shortest Fe–O–Fe bond distances, which suggests J for **2** should be 10.89 cm^{-1} for $2P = 3.966$ Å.[9] Plots of μ_{eff} *vs.* T and magnetization *vs.* magnetic field for compounds **1** and **2** are available as supplementary information. See http://www.rsc.org/suppdata/cc/1998/1753.

In summary, the use of the bis-bipyridine ligand L has allowed access to a new Fe_6 structural type, as well as an Fe_2 species. The ability of L to provide new high nuclearity Fe and Mn species is under continuing investigation, as is the use of this ligand to access Fe_2 species of biological relevance to the many Fe biomolecules containing a dinuclear oxo-bridged unit.

This work was supported by the National Science Foundation.

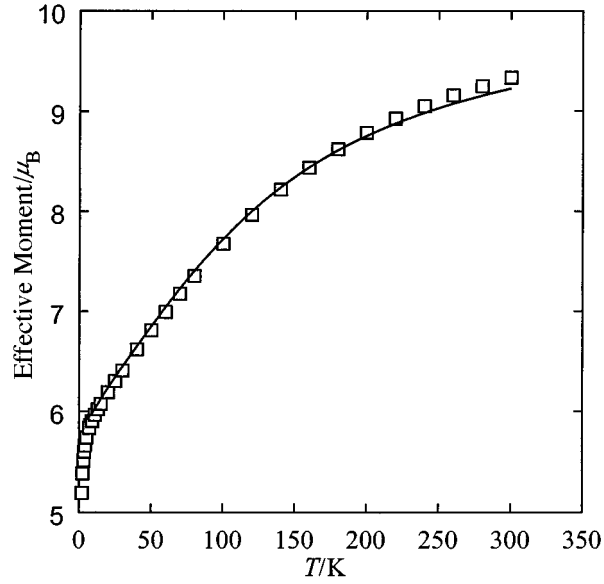

Fig. 3 Plot of effective magnetic moment *vs.* T for complex **2**. The solid line is a fit of the 13.0–300 K data to the appropriate theoretical equation for an exchange-coupled Fe^{III}_2 cation and non-interacting $S = 5/2$ anion. See the text for the fitting parameters.

Notes and References

† The complexes analysed satisfactorily (Complex **1**·MeCN. Found: C, 41.34; H, 2.71; N, 5.68. $C_{74}H_{59}Cl_{12}Fe_8N_9O_{12}$ requires C, 41.56; H, 2.78; N, 5.89%. Complex **2**. Found: C, 41.36; H, 3.28; N, 6.24. $C_{31}H_{29}Cl_6Fe_3N_4O_4$ requires C, 41.29; H, 3.24; N, 6.21%).

‡ *Crystal data* for **1**·2MeCN: $C_{76}H_{62}Cl_{12}Fe_8N_{10}O_{12}$, $M_r = 2179.60$, monoclinic, $P2_1/a$, $a = 15.317(2)$, $b = 18.303(3)$, $c = 16.168(3)$ Å, $\beta = 108.91(1)°$, $U = 4288.1$ Å^3, $Z = 2$, $T = 104$ K. Residuals were $R(F) = 0.0551$ and $R_w(F) = 0.0576$ using 5610 unique reflections; reflections with $F < 3\sigma(F)$ were given zero weight. *Crystal data* for **2**: $C_{31}H_{29}Cl_6Fe_3N_4O_4$, triclinic, $P\bar{1}$, $a = 14.099(6)$, $b = 18.510(7)$, $c = 7.108(3)$ Å, $\alpha = 96.77(2)$, $\beta = 99.45(2)$, $\gamma = 81.16(2)°$, $U = 18.00.0$ Å^3, $Z = 2$, $T = 101$ K. Residuals were $R(F) = 0.0558$ and $R_w(F) = 0.0431$ using 4691 unique reflections; reflections with $F < 2.33\sigma(F)$ were given zero weight. CCDC 182/940.

1 R. Sessoli, H.-L. Tsai, A. R. Schake, S. Wang, J. B. Vincent, K. Folting, D. Gatteschi, G. Christou and D. N. Hendrickson, *J. Am. Chem. Soc.*, 1993, **115**, 1804; R. Sessoli, D. Gatteschi, A. Caneschi and M. Novak, *Nature*, 1993, **365**, 141.
2 H. J. Eppley, H.-L. Tsai, N. Devries, K. Folting, G. Christou and D. N. Hendrickson, *J. Am. Chem. Soc.*, 1995, **117**, 301; S. M. J. Aubin, S. Spagna, H. J. Eppley, R. E. Sager, G. Christou and D. N. Hendrickson, *Chem. Commun.*, 1998, 803.
3 S. M. J. Aubin, H. J. Eppley, I. A. Guzei, K. Folting, P. K. Grantzel, A. L. Rheingold, G. Christou and D. N. Hendrickson, *J. Am. Chem. Soc.*, 1998, submitted for publication.
4 S. M. J. Aubin, M. W. Wemple, D. M. Adams, H.-L. Tsai, G. Christou and D. N. Hendrickson, *J. Am. Chem. Soc.*, 1996, **118**, 7746.
5 S. K. J. Aubin, N. R. Dilley, L. Pardi, J. Krzystek, M. W. Wemple, L.-C. Brunel, M. B. Maple, G. Christou and D. N. Hendrickson, *J. Am. Chem. Soc.*, 1998, **120**, 4991.
6 Z. Sun, C. M. Grant, S. L. Castro, D. N. Hendrickson and G. Christou, *Chem. Commun.*, 1998, 721; S. L. Castro, Z. Sun, C. M. Grant, J. C. Bollinger, D. N. Hendrickson and G. Christou, *J. Am. Chem. Soc.*, 1998, **120**, 2365.
7 A.-L. Barra, P. Debrunner, D. Gatteschi, C. E. Schulz and R. Sessoli, *Europhys. Lett.*, 1996, **35**, 133.
8 J. K. McCusker, J. B. Vincent, E. A. Schmitt, M. L. Mino, K. Shin, D. K. Coggin, P. M. Hagen, J. C. Huffman, G. Christou and D. N. Hendrickson, *J. Am. Chem. Soc.*, 1991, **113**, 3012.
9 S. M. Gorun and S. J. Lippard, *Inorg. Chem.*, 1991, **30**, 1625.

Received in Cambridge, UK, 19th May 1998; 8/03760D

Asymmetric hydrogen transfer protocol for enantiocontrolled synthesis of (−)-chokol G

Regina Mikie Kanada, Takahiko Taniguchi and Kunio Ogasawara*†

Pharmaceutical Institute, Tohoku University, Aobayama, Sendai 980-8578, Japan

An enantiocontrolled route to the (−)-chokol G, a fungitoxic metabolite from stromata of *Epichloe typhia*, has been devised by employing a Ru^{II}-catalyzed asymmetric hydrogen transfer reaction as the key step.

Noyori and co-workers have found that Ru^{II}-complexes of chiral *N*-tosyl-1,2-diphenylethylenediamines are efficient catalysts for the kinetic resolution of racemic aryl and alkenyl alcohols under asymmetric hydrogen transfer conditions in acetone.[1] In general, the reaction proceeds facilely to give highly enantiomerically enriched alcohols with generation of achiral ketones *via* consumption of the enantiomeric alcohols. The reaction, therefore, loses one half of the starting material unless *meso* substrates having a ene-1,4-diol functionality are used. We envisaged that the catalytic asymmetric hydrogen transfer reaction might be carried out without loss of half of the starting material by using substrates having an appropriate structural background. In this regard we chose 2-methylcyclopent-2-enol derivative **1**, having a cyclopentene-3,5-diyl functionality attached to its 4,5-carbons, which does not lose the chirality due to the 4,5-functionality even though its allylic alcohol functionality loses its chirality. We report herein the first example of the asymmetric resolution of racemic allylic alcohol (±)-**1** by asymmetric hydrogen transfer reaction, without formation of an achiral waste product, to give the chiral enone (+)-**2** and the chiral alcohol (+)-**1**, both of which may be converted into (−)-chokol G[2,3] **3**, a fungitoxic metabolite from stromata of *Epichloe typhia*.[2]

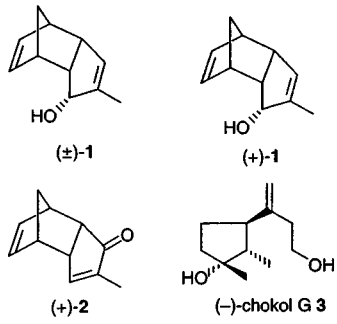

The tricyclic ene-1,2-diol bis-silyl ether[4] **5**, obtained in 90% yield from the diester **4**, was reacted with 1,1-dimethoxyethane in the presence of $BF_3{\cdot}OEt_2$[5,6] to give the aldol product **6**. Without purification, **6** was immediately refluxed in TFA to initiate the ring expansion[5,6] to furnish the β-hydroxy enone **7**,‡ which was treated with Me_2SO_4 in the presence of NaH to give the β-methoxy enone **8** in 56% overall yield from **5**. Treatment of the enone **8** with LAH in refluxing Et_2O afforded in one step the *endo*-allyl alcohol (±)-**1** stereoselectively as a single product in 65% overall yield (Scheme 1).

To carry out the asymmetric hydrogen transfer reaction, the racemic allyl alcohol (±)-**1** was stirred in acetone at room temperature in the presence of a catalytic amount (1 mol%) of the ruthenium catalyst,[1,7] prepared from [{$RuCl_2$(η⁶-mesitylene)}$_2$] and (1*S*,2*S*)-1-*N*-(*p*-tolylsulfonyl)-1,2-diphenylethylenediamine (TsDPEN). The reaction terminated within 5 h to afford the enantiomerically enriched enone (+)-**2**, in 44% yield, leaving the highly enantiomerically enriched allylic alcohol (+)-**1**, $[\alpha]_D^{31}$ +185.4 (*c* 1.1, $CHCl_3$), in 37% yield.§ The enantiomeric purities of the products were determined to be 87 and 98% ee by HPLC using a chiral column (CHIRALCEL OD, elution with 0.1% Pr^iOH–hexane) after converting **1** into the benzoate. When the catalyst, prepared similarly from [{$RuCl_2$(η⁶-cymene)}$_2$] in place of [{$RuCl_2$(η⁶-mesitylene)}$_2$], was used under the same conditions, virtually the same results were obtained to give the enone (+)-**2** in 49% yield with 73% ee and (+)-**1** in 36% yield with >99% ee, although the reaction proceeded at a much faster rate (2 h). The latter alcohol (+)-**1** afforded the enone (−)-**2**, $[\alpha]_D^{27}$ −85.8 (*c* 1.3, $CHCl_3$) [lit.,[8] −85.4 (*c* 1.4, $CHCl_3$)], in 89% yield upon oxidation with manganese(II) dioxide. On the other hand, the former (+)-enone (+)-**2** may be inverted without loss of the original chiral integrity to the enantiomeric (−)-enone **2** in 50% overall yield *via* the epoxide **9** by sequential Wharton rearrangement and oxidation[8] (Scheme 2).

Having established a methodology for the resolution of a particular racemate without losing one enantiomer by employing the asymmetric hydrogen transfer reaction, we next carried out conversion of the resulting enantiomerically pure enone (−)-**2** into (−)-chokol G[3] **3** so as to demonstrate its synthetic potential. The synthesis was commenced by the 1,4-addition reaction of (−)-**2** with 4-*tert*-butyldimethylsiloxybut-2-enyllithium, generated *in situ* by treating 2-bromo-4-*tert*-butyldimethylsiloxybut-2-ene with Bu^tLi,[9] in the presence of lithium 2-thienyl(cyano)cuprate.[9] The reaction furnished the *exo*-addition product **10** in 94% yield as a mixture of the two epimers at the α-methyl center. On thermolysis in refluxing Ph_2O, the mixture afforded the single enone **11**, $[\alpha]_D^{27}$ −97.5 (*c* 1.2, $CHCl_3$), in 87% yield by retro-Diels–Alder reaction and spontaneous α-epimerization to the thermodynamically more stable isomer having *trans*-α,β-configuration. Treatment of **11**

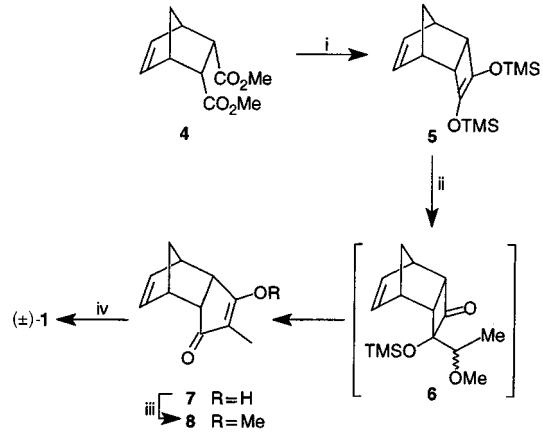

Scheme 1 *Reagents and conditions*: i, Na, TMSCl, toluene, reflux (90%); ii, $MeCH(OMe)_2$, $BF_3{\cdot}OEt_2$, CH_2Cl_2, −78 °C, then TFA, reflux; iii, Me_2SO_4, NaH, DMF–THF (1:1) (56% from **5**); iv, LAH, Et_2O, reflux (65%)

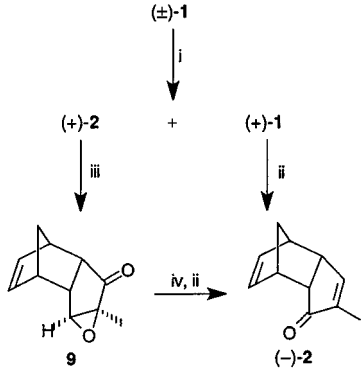

Scheme 2 *Reagents and conditions*: i, [Ru^{II}(η^6-mesitylene)], (1*S*,2*S*)-TsDPEN (1 mol%), acetone, room temp., 4.6 h, [44% and 87% ee for (+)-**2** and 37% and 98% ee for (+)-**1**]; ii, MnO_2, CH_2Cl_2 (89%); iii, 30% H_2O_2, 0.5 M NaOH, MeOH; iv, $NH_2NH_2{\cdot}H_2O$, AcOH (cat.), MeOH, then MnO_2, CH_2Cl_2 [50% from (+)-**2**]

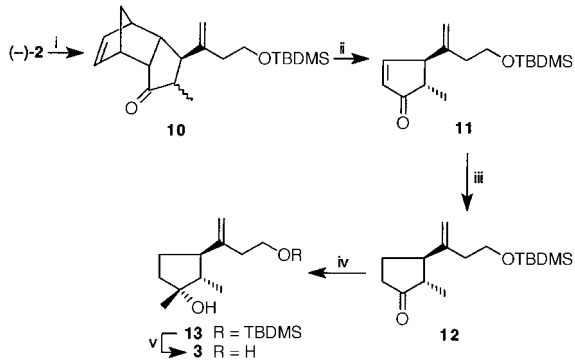

Scheme 3 *Reagents and conditions*: i, CH_2=C(Br)CH_2CH_2OTBDMS, Bu^tLi, 2-thienyl(CN)CuLi, Et_2O, −25 °C (94%); ii, Ph_2O, reflux (87%); iii, DIBAL-H, CuI, HMPA–THF (1:4), −78 °C (92%); iv, MeLi, $CeCl_3$, THF, −78%; v, Bu_4NF, THF [69% from **12** after separation of the epimer (6%)]

with DIBAL-H in the presence of CuI and HMPA[10] in THF allowed 1,4-reduction to give the cyclopentenone **12**, $[\alpha]_D^{29}$ +45.2 (*c* 1.3, $CHCl_3$), in 92% yield. Reaction of **12** with excess MeLi in the presence of $CeCl_3$[3b,11] afforded a mixture consisted of two epimers which, without separation, was exposed to TBAF to give (−)-chokol G[2] **3**, $[\alpha]_D^{29}$ −58.1 (*c* 0.4, MeOH) [natural[2] −43.3 (*c* 0.24, MeOH)], in 69% overall yield as the major product accompanied with the minor epimeric alcohol, $[\alpha]_D^{29}$ −34.2 (*c* 0.3, MeOH), in 6% overall yield. Since the conversion of chokol G **3** into the other congeners, chokols A, B, C, F and K, chokolic acid B, and chokolal A, in the racemic series has been established,[12] the present synthesis formally constitutes the chiral preparation of these natural products.

We thank the Ministry of Education, Science, Sports and Culture of Japan for a scholarship (to R. M. K.).

Notes and References

† E-mail konol@mail.cc.tohoku.ac.jp

‡ All new compounds had spectroscopic [IR, ^{1}H NMR, mass] and analytical (high resolution) data consistent with their assigned structure.

§ When the reaction was terminated after 2 h, the highly enantiomerically enriched enone (+)-**2** was obtained in 30% yield with 98% ee, leaving the enantiomerically enriched alcohol (+)-**1** in 47% yield with 59% ee.

1 S. Hashiguchi, A. Fujii, K.-J. Haack, K. Matsumura, T. Ikariya and R. Noyori, *Angew. Chem., Int. Ed. Engl.*, 1997, **36**, 288. Pertinent reviews, see: S. Hashiguchi, A. Fujii and R. Noyori, *J. Synth. Org. Chem. Jpn.*, 1996, **54**, 818; R. Noyori and S. Hashiguchi, *Acc. Chem. Res.*, 1997, **30**, 97.

2 Isolation: H. Koshino, S. Togiya, S. Terada, T. Yoshihara, S. Sakamura, T. Shimanuki, T. Sato and A. Tajimi, *Agric. Biol. Chem.*, 1989, **53**, 789.

3 Only racemic syntheses have been reported so far: (*a*) N. Yamauchi and K. Kakinuma, *Agric. Biol. Chem.*, 1989, **53**, 3067; (*b*) S. Tanimori, T. Ohashi and M. Nakayama, *Biosci. Biotechnol. Biochem.*, 1992, **56**, 353; (*c*) L. Deloux and M. Srebnik, *Tetrahedron Lett.*, 1996, **37**, 2735.

4 R. D. Miller, D. L. Dolce and V. Y. Merritt, *J. Org. Chem.*, 1976, **41**, 1221.

5 J. Shimada, K. Hashimoto, B. H. Kim, E. Nakamura and I. Kuwajima, *J. Am. Chem. Soc.*, 1984, **106**, 1759.

6 S. N. Crane, T. J. Jenkins and D. J. Burnell, *J. Org. Chem.*, 1997, **62**, 8722.

7 K.-J. Haack, S. Hashiguchi, A. Fujii, T. Ikariya and R. Noyori, *Angew. Chem., Int. Ed. Engl.*, 1997, **36**, 285.

8 An alternative chiral route to the enone **8**: T. Sugahara and K. Ogasawara, *Tetrahedron Lett.*, 1996, **37**, 7403.

9 S. Okamoto, Y. Kobayashi, H. Kato, T. Takahashi, J. Tsuji and F. Sato, *J. Org. Chem.*, 1988, **53**, 5590; I. Shiina, H. Iwadare, H. Sakoh, Y. Tani, M. Hasegawa, K. Saitoh and T. Mukaiyama, *Chem. Lett.*, 1997, 1139; G. Stork, K. Manabe and L. Liu, *J. Am. Chem. Soc.*, 1998, **120**, 1337.

10 S. Takano, K. Inomata and K. Ogasawara, *J. Chem. Soc., Chem. Commun.*, 1992, 169.

11 T. Imamoto, Y. Sugiura and N. Takiyama, *Tetrahedron Lett.*, 1984, **25**, 4233.

12 S. Tanimori, T. Ueda and M. Nakayama, *Biosci. Biotechnol. Biochem.*, 1994, **58**, 1174.

Received in Cambridge, UK, 8th June 1998; 8/04343D

Synthesis of *N*-heterocycles *via* lactam-derived ketene aminal phosphates. Asymmetric synthesis of cyclic amino acids.

K. C. Nicolaou,* Guo-Qiang. Shi, Kenji Namoto and Federico Bernal

Department of Chemistry and The Skaggs Institute for Chemical Biology, The Scripps Research Institute, 10550 North Torrey Pines Road, La Jolla, California 92037, USA and Department of Chemistry and Biochemistry, University of California, San Diego, 9500 Gilman Drive, La Jolla, California 92093, USA

A variety of *N*-heterocycles can be synthesized from lactams *via* Pd^0-catalyzed couplings of their corresponding enol phosphates.

Due to the rich chemistry and biology of nitrogen-containing compounds, the synthesis of *N*-heterocycles has been a central and important theme within organic chemistry. The functionalization of lactams to substituted heterocycles *via* the corresponding enol triflates has been reported.[1] However, the triflate-based methodology has been proven cumbersome due to the rather unstable, difficult-to-isolate nature of the triflates and the necessity to use unconventional and expensive triflating reagents. Here we report the synthesis of lactam-derived ketene aminal phosphates[2] and their utilization for the construction of a variety of *N*-heterocycles, including enantiomerically enriched cyclic amino acids. In contrast to their triflate counterparts, these phosphate intermediates enjoy remarkable stability, efficiency of formation and reactivity, as well as easy access and versatility (Scheme 1).[3]

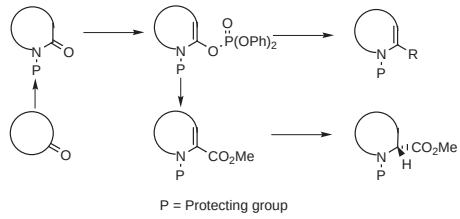

Scheme 1

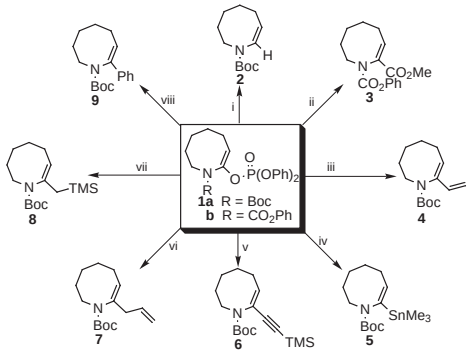

Scheme 2 *Reagents and conditions*: i, Et_3Al (1 M in hexanes, 2.0 equiv.), $Pd(PPh_3)_4$ (0.05 equiv), THF, 6 h, 92%; ii, CO (1 atm), $Pd(OAc)_2$ (0.1 equiv.), PPh_3 (0.2 equiv.), MeOH (3.0 equiv.), Et_3N (3.0 equiv.), DMF, 60 °C, 4 h, 72%; iii, $Bu_3SnCH{=}CH_2$ (2.0 equiv.), $Pd(PPh_3)_4$ (0.05 equiv.), LiCl (3.0 equiv.), THF, heat, 3 h, 85%; iv, $(Me_3Sn)_2$ (2.0 equiv.), $Pd(PPh_3)_4$ (0.05 equiv.), LiCl (3.0 equiv.), THF, heat, 3 h, 77%; v, $Me_3SiC{\equiv}CH$ (3.0 equiv.), $Pd(PPh_3)_4$ (0.1 equiv.), CuI (0.1 equiv.), Et_2NH–THF (2:1), 25 °C, 4 h, 84%; vi, $Bu_3SnCH_2CH{=}CH_2$ (2.0 equiv.), $Pd(PPh_3)_4$ (0.05 equiv.), LiCl (3.0 equiv.), THF, heat, 4 h, 93%; vii, Me_3SiCH_2MgCl (3.0 equiv.), $Ni(acac)_2$ (0.05 equiv.), Et_2O, 25 °C, 1 h, 88%; viii, PhZnCl (2.0 equiv.), $Pd(PPh_3)_4$ (0.05 equiv.), THF, 50 °C, 1 h, 87%

The synthesis of ketene aminal diphenylphosphates **1a**,**b** is accomplished from the eight-membered *N*-Boc or *N*-CO_2Ph protected lactams *via* their potassium enolates. These compounds proved quite stable at ambient temperatures and to silica gel flash chromatography, entering a variety of coupling reactions with appropriate partners under palladium(0) or nickel(0) catalyzed conditions, (Scheme 2). All of these reactions proceeded smoothly in good to excellent yields, furnishing a variety of products capable of further functionalization.

The generality and scope of the present technology was further illustrated by synthesizing ketene aminal phosphates of different ring sizes, as shown in Table 1. Two useful applications of the newly synthesized dienes[4] (Table 1) are shown in Scheme 3. Thus, diene **4**† enters smoothly into a Diels–Alder reaction with benzoquinone affording, after silica gel-induced tautomerization, hydroquinone **22**, while diene **17** reacted with singlet oxygen to afford endoperoxide **23**. The latter compound was reduced to diol **24** in 57% overall yield upon treatment with aluminium amalgam.

Table 1 Preparation and Stille coupling of lactam-derived ketene aminal phosphates

Entry	Phosphate[a]	Yield (%)	Coupling product[b]	Yield (%)
1	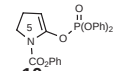 **10**	93	 **16**	65
2	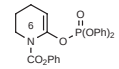 **11**	95	 **17**	80
3	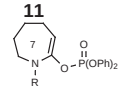 **12a** R = Boc **b** R = CO_2Ph	91	 **18**	76
4	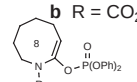 **1a** R = Boc **b** R = CO_2Ph	96	 **4**	85
5	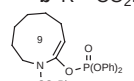 **13**	41[c]	 **19**	94
6	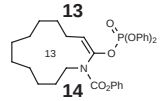 **14**	81	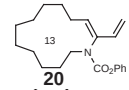 **20**	81
7	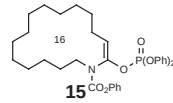 **15**	96	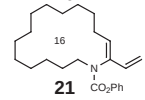 **21**	73

[a] Conditions: $(PhO)_2P(O)Cl$ (1.5 equiv.), KHMDS (1.2 equiv.), THF, −78 °C, 0.5 h; add base to lactam and phosphoryl chloride. [b] Coupling conditions as described in Scheme 2 for compound **1a.** [c] KHMDS (1.0 equiv.) was used.

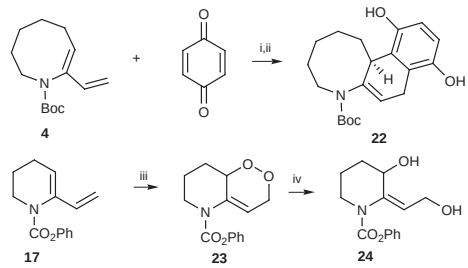

Scheme 3 *Reagents and conditions*: i, benzoquinone (5.0 equiv.), toluene, heat, 24 h; ii, silica gel, Et_2O, 12 h, 86% (2 steps); iii, O_2, tetraphenylporphine (trace), CCl_4, 500 W halogen lamp, 15 min, ; iv, Al-Hg (excess), THF–H_2O (10:1), 1.5 h, 57%

The chemistry of ketene aminal phosphates was explored further through their Pd-catalyzed carbonylation and subsequent asymmetric hydrogenation. Thus, a series of compounds arising from carbonylation of the ketene aminal phosphates were synthesized in good yields (Table 2). They were then subjected to asymmetric hydrogenation[6,7] in the presence of a catalytic amount of [Rh(COD)-(−)-(*R*,*R*)-(Et-DuPHOS)]OTf.[8] This afforded the corresponding cyclic amino acids in excellent yields and with high enantioselectivities except for the five- and six-membered rings, which resisted hydrogenation under standard conditions and gave low enantioselectivities at high pressures. Inspection of the NMR spectra of the compounds with larger ring sizes (7–16) revealed that the unsaturated esters exist as two rotamers, with rotamer **A** being

Table 2 Synthesis of cyclic dehydroamino acids from carbonylation of ketene aminal phosphates and subsequent asymmetric hydrogenation

Phosphate	Carbonylation[a]	Yield (%)	Hydrogenation[b]	Yield (%)	Ee (%)[c]
10	 **25**	70[d]	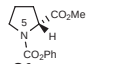 **31**	84	0.4
11	 **26**	78	 **32**	95[e]	26.5
12b	 **27**	82	 **33**	96	94.8
1b	 **3**	72	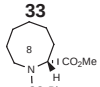 **34**	96	97.0
13	 **28**	79	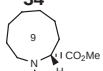 **35**	97	94.5
14	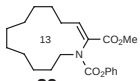 **29**	89[d,f]	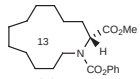 **36**	96	91.3
15	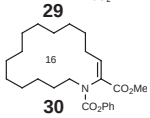 **30**	86[d,f]	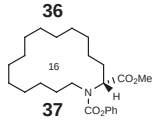 **37**	86	86.0

[a] Conditions: CO (1 atm), $Pd(OAc)_2$ (0.1 equiv.), PPh_3 (0.2 equiv.), MeOH (40 equiv.), Et_3N (2.0 equiv.), DMF, 60 °C, 3–6 h; [b] Conditions: H_2 (90 psi), [Rh(COD)-(−)-(*R*,*R*)- Et-DuPHOS)]OTf (0.06 equiv.), MeOH, room temp., 24 h. [c] Determined by HPLC on a Chiralcel OD using hexanes–Pr^iOH (7:1) as eluent (for compounds **31–33**) or an AD column using hexanes–Pr^iOH (97:3) as eluent (for compounds **34–37**). [d] (*R*)-(+)-BINAP (0.1 equiv.) was used instead of PPh_3 (see ref. 5). [e] Reaction performed under H_2 (400 psi) at 70 °C in EtOH. [f] Yield based on 77% conversion.

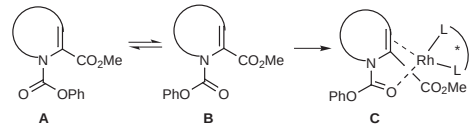

Scheme 4

the preferred one (Scheme 4). However, the five- and six-membered ring compounds **25** and **26** show the presence of only one rotamer, assumed to be rotamer **A**, in their NMR spectra. Through variable temperature NMR experiments, it was found that the rotamer **B** of **26** appears at around 70 °C. It is, however, rotamer **B** that enables the formation of the requisite chelation complex **C** which could result in asymmetric induction during hydrogenation.[6] This phenomenon can also explain the lack of reactivity of **25** and **26** under standard conditions.

The chemistry described herein demonstrates the potential of cyclic ketene aminal phosphates as substrates for the construction of a variety of *N*-heterocycles, including alkaloid structures and unnatural amino acids through transition metal catalyzed reactions. Multiple applications in synthesis are envisioned for this new synthetic technology.

We thank Professor K. B. Sharpless, Dr L. Gooβen, and Dr K. R. Dress for assistance with chiral HPLC and high pressure equipment. This work was financially supported by the National Institutes of Health, USA (G. M.) and The Skaggs Institute for Chemical Biology.

Notes and References

† *Synthetic procedure* for **4**: To a solution of *N*-CO_2Ph protected 2-azacyclooctanone (1.16 g, 4.7 mmol) and $(PhO)_2P(O)Cl$ (1.46 ml, 7.0 mmol) in THF (80 ml) at −78 °C was added KHMDS (0.5 M in toluene, 14.1 ml, 7.0 mmol). After being stirred at −78 °C for 30 min, the reaction mixture was treated with 1 M aq. NH_3 (80 ml) for 10 min. The organic phase was separated and the aqueous layer was extracted with Et_2O (3× 20 ml). The combined organic phases were dried ($MgSO_4$) and concentrated. The residue was subjected to flash column chromatography (silica gel, 1:1 Et_2O–hexanes containing 2% Et_3N) to give phosphate **1b** (2.18 g, 96%). A solution of **1a** (0.24 g, 0.52 mmol), anhydrous LiCl (66 mg, 1.57 mmol), tri-*n*-butyl(vinyl)tin (0.31 ml, 1.05 mmol) and $Pd(PPh_3)_4$ (53 mg, 0.046 mmol) in THF (20 ml) was heated at 70 °C under Ar for 3 h. The solution was then diluted with Et_2O and filtered through silica gel. The filtrate was concentrated and the residue was subjected to flash column chromatography (silica gel, 1:9 Et_2O–hexanes) to give diene **4** (105 mg, 85%).

1 For the use of lactam-derived enol triflates in carbon–carbon bond forming reactions, see: T. Okita and M. Isobe, *Synlett*, 1994, 589; T. Okita, and M. Isobe, *Tetrahedron*, 1995, **51**, 3737; T. Luker, H. Hiemstra and W. N. Speckamp, *Tetrahedron Lett.*, 1996, **37**, 8257; T. Luker, H. Hiemstra and W. N. Speckamp, *J. Org. Chem.*, 1997, **62**, 3592; T. Luker, H. Hiemstra and W. N. Speckamp, *J. Org. Chem.*, 1997, **62**, 8131.

2 For the use of lactone-derived ketene acetal phosphates, see: K. C. Nicolaou, G.-Q. Shi, J. L. Gunzner, P. Gärtner and Z. Yang, *J. Am. Chem. Soc.*, 1997, **119**, 5467.

3 The larger lactams were synthesized from the corresponding ketones *via* a Beckmann rearrangement, see: G. A. Olah and A. P. Fung, *Synthesis*, 1979, 537.

4 W. J. Scott and J. K. Stille, *J. Am. Chem. Soc.*, 1986, **108**, 3033.

5 BINAP has been previously used as a superior ligand to monodentate and other bidentate systems in aromatic amination; see: J. P. Wolfe, S. Wagaw and S. L. Buchwald, *J. Am. Chem. Soc.*, 1996, **118**, 7215.

6 For a catalytic hydrogenation review, see: R. Noyori, *Asymmetric Catalysis In Organic Synthesis*, Wiley-Interscience, New York, 1994, ch. 2.

7 To the best of our knowledge, there is only one example of a catalytic asymmetric hydrogenation of a cyclic dehydroamino acid derivative, see: C. J. Foti and D. L. Comins *J. Org. Chem.*, 1995, **60**, 2656.

8 M. J. Burk, M. F. Gross, T. Gregory, P. Harper, C. S. Kalberg, J. R. Lee and J. P. Martinez, *Pure Appl. Chem.*, 1996, **68**, 37.

Received in Corvallis, OR, USA, 2nd June 1998; 8/04198I

Enantioselectivity *vs.* kinetic resolution in antibody catalysis: formation of the (*S*) product despite preferential binding of the (*R*) intermediate

Doron Shabat,[a,b] Hagit Shulman,[b] Harel Itzhaky,[b] Jean-Louis Reymond*[c] and Ehud Keinan*[a,b]†‡

[a] *The Scripps Research Institute, Department of Molecular Biology and the Skaggs Institute for Chemical Biology, 10550 North Torrey Pines Road, La Jolla, California 92037, USA*
[b] *Department of Chemistry, Technion - Israel Institute of Technology, Technion City, Haifa 32000, Israel*
[c] *Department of Chemistry and Biochemistry, University of Bern, Freiestrasse 3, 3012 Bern, Switzerland*

Antibody 14D9, which catalyzes the stereoselective transformation of achiral enol ethers into the corresponding (*S*)-ketals, resolves a racemic mixture of structurally similar chiral enol ethers by selective conversion of the (*R*)-enol ether into the (*R*)-ketal, raising the possibility that the (*S*) transition state is preferencially stabilized by the antibody despite a better binding of the (*R*) intermediate.

Catalytic antibodies, which are produced by immunization against stable transition state analogs of chemical reactions,[1] offer unique opportunities, not only in expanding the repertoire of synthetic tools available to the organic chemist,[2] but also in studying fundamental aspects of enzymatic catalysis.[3] For example, antibody 14D9, which was raised against the quaternary ammonium hapten **1b**, has taught us a great deal about

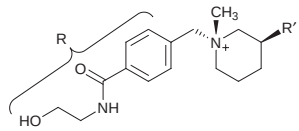

1a R′ = H
b R′ = $CH_2NHCO(CH_2)_3CONH$-carrier protein

synthetic opportunities using catalytic antibodies and also about mechanistic aspects of biocatalysis.[4] This proficient catalyst might be mechanistically related to primordial glycosidase enzymes.[5] Herein we report on a unique property of this catalyst. The antibody catalyzes the enantioselective protonolysis of achiral enol ethers to give the (*S*) product. Yet, evidence from kinetic resolution of chiral enol ethers shows that 14D9 binds the (*R*) oxocarbenium ion intermediate more strongly than the (*S*) intermediate.

The 14D9-catalyzed conversion of enol ether **2** into a mixture of ketone **3** and ketal **4**, which both have an (*S*) configuration (Scheme 1), goes through an intermediate oxocarbenium ion **I**, which is produced in the rate-limiting protonation of enol ether **2**.[6] Partitioning of this intermediate to give the final products **3** and **4** depends on the availability of water molecules in the medium. Ketal **4** does not form in aqueous solutions and is produced exclusively within the antibody binding site. Therefore, the optical purity of **4** provides a direct measure of the enantioselectivity in the antibody-catalyzed reaction. Indeed, the 14D9-catalyzed protonolysis of **2** was found to be highly stereoselective, producing (*S*)-**4** in 99.5% ee.[6]

There is an intriguing question related to the origin of the enantioselectivity in the rate-determining protonation step. Intuitively, one would expect that (*S*) selectivity arises from preferential binding of the antibody to both the (*S*) transition state, (*S*)-TS and the structurally similar (*S*) intermediate, (*S*)-**I** [Fig. 1A]. Nevertheless, we cannot rule out *a priori* the alternative possibility, in which the antibody still binds selectively to (*S*)-TS but binds preferentially to the opposite enantiomeric intermediate (*R*)-**I** [Fig. 1B].

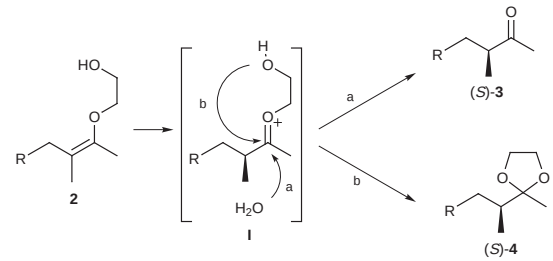

R = $HO(CH_2)_2NHCOC_6H_4$

Scheme 1

This mechanistic issue could be resolved if the affinity of 14D9 to each of the two enantiomeric forms of **I** could be compared. These enantiomeric intermediates occur not only along the reaction pathway leading from **2** to ketal **4**, but also along the similar conversion of the isomeric enol ether **5** to **4** (Scheme 2). Therefore, one could obtain the desired information about the relative stability of (*S*)-**I** and (*R*)-**I** by studying the kinetic resolution of **5** by 14D9. Conversion of (*S*)-**5** and (*R*)-**5** into ketals (*S*)-**4** and (*R*)-**4**, respectively, proceeds *via* the enantiomeric intermediates (*S*)-**I** and (*R*)-**I**. If the antibody catalyzed the protonolysis of (*S*)-**5** preferentially over (*R*)-**5** this would imply that 14D9 binds (*S*)-**I** more tightly than (*R*)-**I**. This would be consistent with the energy diagram shown in Fig. 1(A) for enol ether **2**. Conversely, if catalytic protonolysis of (*R*)-**5** was faster than that of (*S*)-**5**, this would support the alternative energy profile described in Fig. 1(B).

Substrate **5** was prepared from methyl 4-bromomethylbenzoate and ethyl 2-methyl-3-oxobutanoate.[6,7] The initial alkylation product was decarboxylated and the resultant ketone was converted to the corresponding 1,3-dioxolane. The latter was opened with $(Me_3Si)_2NH$ and TMSI to produce a mixture of three isomeric enol ethers in almost equal proportions. These isomers were separated by column chromatography and each was subjected to aminolysis with ethanolamine. The two

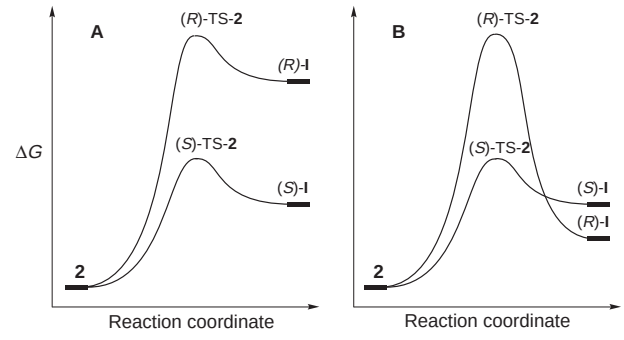

Fig. 1 Alternative free energy diagrams for the antibody-catalyzed enantioselective protonation of enol ether **2**

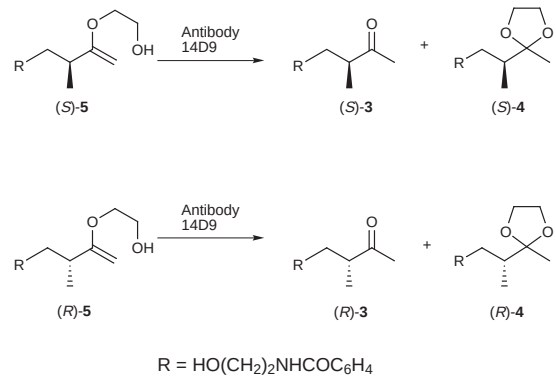

Scheme 2

Table 1 Kinetic parameters for the antibody 14D9-catalyzed hydrolysis of **5**[a]

Substrate	K_M/μM	k_{cat}/min^{-1}	k_{un}/min^{-1}	k_{cat}/k_{un}	K_{TS}/μM
rac-**5**	480 ± 200	(4.3 ±1.9)× 10^{-2}	1.55× 10^{-5}	2760	0.17
(*R*)-**5**	210 ± 70	(4.6 ± 1.5)× 10^{-2}	1.55× 10^{-5}	2990	0.07
(*S*)-**5**	470 ± 230	(3.4 ± 1.7)× 10^{-3}	1.55× 10^{-5}	220	2.14

[a] Reactions were carried out in 100 mM NaCl and 50 mM 1,3-bis[tris-(hydroxymethyl)methylamino]propane (bistris), pH 8.0, 25 °C. Ketal **4** (*ca.* 20%) was formed in all cases.

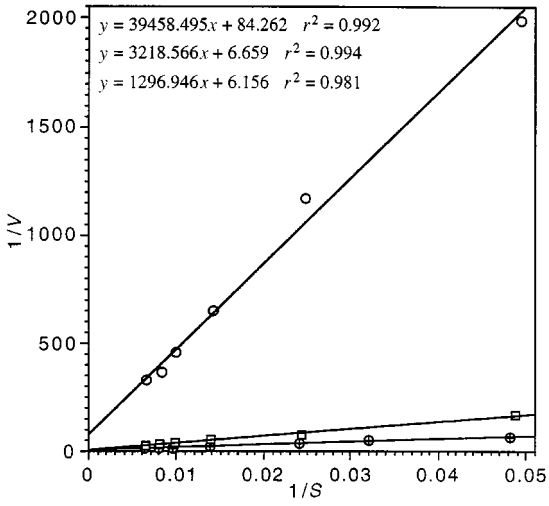

Fig. 2 Lineweaver–Burk plot of reaction rates for the formation of ketone **3** from (□) racemic enol ether **5**, (○) (*S*)-**5** and (⊕) (*R*)-**5**. For the reactions conditions, see Table 1.

enantiomers of **5** were separated by HPLC using a chiral-phase column.[8] Their absolute configurations were determined by converting them to the corresponding ketals and comparing these ketals with authentic samples of (*R*)-**4** and (*S*)-**4**.[6]

Antibody 14D9 catalyzes the protonolysis of racemic **5**, (*R*)-**5** and (*S*)-**5**. In each case catalysis is fully inhibited by the addition of the hapten **1a**, confirming that the reaction occurs within the antibody's combining site. The observation that ketal **4** (approximately 10–20% of the product) is obtained from all three substrates, **2**, (*R*)-**5** and (*S*)-**5**, is consistent with the concept that all of these reactions proceed *via* intermediate **I** within the antibody's combining site.

Interestingly, (*R*)-**5** was found to be a better substrate than (*S*)-**5**, with both a lower K_M and a higher k_{cat} (Table 1 and Fig. 2). A preparative scale experiment with antibody 14D9 using saturating concentrations of racemic **5** (pH 8, 5 μM catalyst and 1 mM racemic **5**) lead to the formation of (*R*)-**4**. Measuring the optical purity of **4**, which is formed exclusively in the antibody-catalyzed process with no background reaction, should allow an unequivocal determination of the degree of kinetic resolution of racemic **5** by 14D9. Under these saturating conditions the enantiomeric purity (63% ee) is consistent with the observed ratio of k_{cat} for each enantiomer of **5**. We calculated the dissociation constants of the transition states,[9] using the equation $K_{TS} = K_M/(k_{cat}/k_{un})$, and found that antibody 14D9 binds the transition state leading from (*R*)-**5** to intermediate (*R*)-**I** ($K_{TS\text{-}5}$ = 7× 10^{-8} M) 31 times more strongly than the transition state leading from (*S*)-**5** to intermediate (*S*)-**I** ($K_{TS\text{-}5}$ = 2.14× 10^{-6} M).

Although this experiment does not measure directly the binding constant of 14D9 to the oxocarbenium ions (*R*)-**I** and (*S*)-**I**, the transition states that lead from (*S*)-**5** to (*S*)-**I** and from (*R*)-**5** to (*R*)-**I** are very closely related to these intermediates. The 31-fold selectivity in the kinetic resolution of **5** suggests that the natural binding selectivity of antibody 14D9 favors intermediate (*R*)-**I**. The (*R*) selectivity in the hydrolysis of **5** stands in stark contrast to the (*S*) selectivity observed in the 14D9-catalyzed hydrolysis of several enol ethers such as **2**, and supports the mechanistic option shown in Scheme 2(*b*).

Earlier experiments indicate that the high catalytic efficiency observed with enol ethers such as **2** (k_{cat}/k_{un} = 10^3–10^4) is caused by a carboxylic acid residue acting as a general acid catalyst within the antibody's binding pocket.[10] Thus, the strong preference for protonation on the *re*-face of enol ether **2** to produce the (*S*) products is the result of the relative positioning of this general acid with respect to the bound substrate.[11] The evidence presented here suggests that 14D9 binds (*R*)-**I** tighter than (*S*)-**I**. It also raises the intriguing possibility that moving the catalytic residue in the antibody binding pocket by mutagenesis could create a new catalyst that will convert prochiral enol ethers to (*R*) products. Moreover, such a modified antibody is expected to be a more efficient catalyst. Future experiments will address this possibility.

This work was supported by the US-Israel Binational Science Foundation (E. K.), the Skaggs Institute for Chemical Biology (E. K.), the Swiss National Science Foundation (J. L. R.) and the Wander Stiftung, Bern, Switzerland (J. L. R.).

Notes and References

† E-Mail: keinan@tx.Technion.ac.il, keinan@scripps.edu
‡ Incumbent of the Benno Gitter and Ilana Ben-Ami Chair of Biotechnology, Technion.

1 P. G. Schultz and R. A. Lerner, *Science*, 1995, **269**, 1835; E. Keinan and R. A. Lerner, *Isr. J. Chem.*, 1996, **36**, 113; R. A. Lerner, S. J. Benkovic and P. G. Schultz, *Science*, 1991, **252**, 659; N. R. Thomas, *Nat. Prod. Rep.*, 1996, 479.
2 T. L. Li, R. A. Lerner and K. D. Janda, *Acc. Chem. Res.*, 1997, **30**, 115.
3 J.-P. Charbonnier, B. Golinelli-Pimpaneau, B. Gigant, D. S. Tawfik, R. Chap, D. G. Schindler, S.-H. Kim, B. S. Green, Z. Eshhar and M. Knossow, *Science*, 1997, **275**, 1140; G. J. Wedemayer, P. A. Patten, L. H. Wang, P. G. Schultz, R. C. Stevens, *Science*, 1997, **276**, 1665.
4 J.-L. Reymond, K. D. Janda, R. A. Lerner, *Angew. Chem., Int. Ed. Engl.*, 1991, **30**, 1711; S. C. Sinha, E. Keinan and J.-L. Reymond, *Proc. Natl. Acad. Sci. U.S.A.*, 1993, **90**, 11 910; S. C. Sinha, E. Keinan and J.-L. Reymond, *J. Am. Chem. Soc.*, 1993, **115**, 4893; J.-L. Reymond, J.-L. Reber and R. A. Lerner, *Angew. Chem., Int. Ed. Engl.*, 1994, **33**, 475; S. C. Sinha and E. Keinan, *J. Am. Chem. Soc.*, 1995, **117**, 3653.
5 D. Shabat, S. C. Sinha, J.-L. Reymond and E. Keinan, *Angew. Chem.*, 1996, **35**, 2628.
6 D. Shabat, H. Itzaky, J.-L. Reymond and E. Keinan, *Nature*, 1995, **374**, 143.
7 S. C. Sinha and E. Keinan, *Isr. J. Chem.*, 1996, **36**, 185.
8 Separation of the enantiomers was carried out using a normal phase chiral column (Chiralcel OD, Chiral Technologies Inc.) with hexane–Pr^{i}OH (80:20) at a flow rate of 1 ml min^{-1}; the retention times of (*S*)-**5** and (*R*)-**5** are 9.13 and 12.23 min, respectively.
9 J. L. Kurz, *J. Am. Chem. Soc.*, 1963, **85**, 987; J. Kraut, *Science*, 1988, **242**, 533; J.-L. Reymond and Y. Chen, *Isr. J. Chem.*, 1996, **36**, 199.
10 J.-L. Reymond, G. K. Jahangiri, C. Stoudt and R. A. Lerner, *J. Am. Chem. Soc.*, 1993, **115**, 3909.
11 G. K. Jahangiri and J.-L. Reymond, *J. Am. Chem. Soc.*, 1994, **116**, 11 264

Received in Glasgow, UK, 25th March 1998; 8/02374C

Competitive formation of η¹-1-phosphaallene and 1*H*-phosphirene complexes

Rainer Streubel,*† Hendrik Wilkens and Peter G. Jones

Institut für Anorganische und Analytische Chemie der TU-Braunschweig, Postfach 3329, D-38023 Braunschweig, Germany

The 2*H*-azaphosphirene complex 1 reacts with triorganostannyl(ethoxy)acetylenes 2a,b to yield bifunctional η¹-1-phosphaallene 5a,b and 1*H*-phosphirene complexes 6a,b; 5a,b and 6a,b are characterized by NMR spectroscopy (^{13}C, ^{31}P) and complex 6b by single crystal X-ray diffraction.

1-Phosphaallenes[1] and their isomers, 1*H*-phosphirenes,[2] and complexes of both,[1,2] have attracted interest because of their synthetic applications in heterocyclic chemistry. At present, there are three main routes to 1-phosphaallenes: elimination of silanolate, reactions of phosphaketenes with phosphoranyl ylides or 1,3-shift reactions of alkinylphosphanes.[1] Despite current research activities, only one example of an η¹-1-phosphaallene complex is known, obtained from a complexation reaction with nickel tetracarbonyl.[3] Furthermore, in contrast to thermally induced rearrangements of cyclopropenes to allenes,[4] related transformations of 1*H*-phosphirene complexes into η¹-1-phosphaallene complexes, or *vice versa*, have not been reported.

We now report the first example of competitive formation of η¹-1-phosphaallene and 1*H*-phosphirene complexes, which has been found to proceed upon thermal decomposition of the 2*H*-azaphosphirene complex **1**[5] in the presence of triorganostannyl(ethoxy)acetylenes **2a**,**b**.[7]

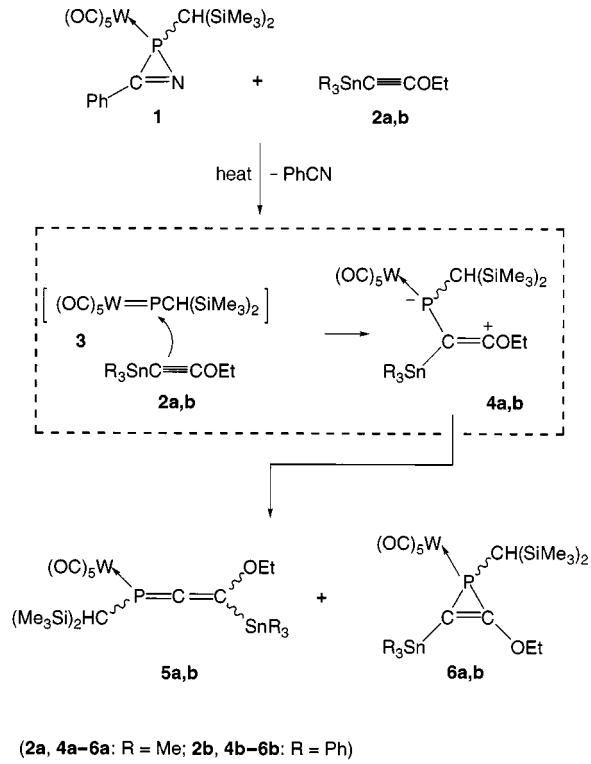

Scheme 1 *Reagents and conditions*: **5a**,**b** and **6a**,**b**: 1 mmol **1** was treated with 2 mmol **2a** at 80 °C for 1.5 h or with 2 mmol **2b** at 70 °C for 2.5 h, respectively. Work-up by column chromatography at low temperature afforded **5a** and **6a** as a mixture, which could not be further separated, and **5b**, **6b**, which have been fully characterized (**5b**: 58%, mp 116 °C; **6b**: 33%, mp 128 °C); the dotted lines indicate the reaction course proposed.

Complex **1** reacts on heating in solution with the acetylene derivatives **2a**,**b** to give the η¹-1-phosphaallene complexes **5a**,**b** and the corresponding 1*H*-phosphirene complexes **6a**,**b** (Scheme 1). The product formation is explained as followed: thermally induced ring-cleavage of the 2*H*-azaphosphirene complex yields benzonitrile, determined by IR spectroscopy, and the phosphanediyl complex [(OC)$_5$W=PCH(SiMe$_3$)$_2$] **3** in the first reaction step. As illustrated in Scheme 1, reaction of **3** with the alkynes **2a**,**b** leads to zwitterionic products **4a**,**b**, which can be regarded as common precursors of the final products **5** and **6**. Furthermore, because the complexes **5b** and **6b** remain unchanged upon heating of pure samples, subsequent rearrangements (**5**–**6** and/or **6**–**5**) can be excluded with reasonable certainty.

The composition and constitution of **5a**,**b** and **6a**,**b** are confirmed by NMR spectroscopic and **5b**, **6b**, additionally, by mass spectrometric investigations.‡ The typical ^{13}C NMR data of **6a**,**b** (**6a**: δ 226.5, $^1J_{PC}$ 90.9 Hz; **6b**: δ 228.2, $^1J_{PC}$ 90.7 Hz) unambigously establish the existence of the 1-phosphaallene moiety in **5a**,**b**. The coordination mode is confirmed by the $^1J_{WP}$ coupling constant values of 262.6 Hz (**5a**) and 265.5 Hz (**5b**), which are in the expected range of η¹-P-coordinated ligands with low-coordinated phosphorus.[7]

In comparison to the related 2-ethoxy substituted 1*H*-phosphirene complex **6c**,[8] the complexes **6a**,**b** show high-field shifted resonances of the phosphorus nuclei at δ −107.4 (**6a**) and −98.2 (**6b**) (*cf.* δ −90.8[8]). Compared to **6c** the carbon-13 resonance values of the three-membered ring in **6a**,**b** are remarkably downfield shifted [C^2: δ 175 ± 3 (*cf.* 158.8), C^3: δ 100 ± 5 (*cf.* 88.1)]. Furthermore, the $^{(1+2)}J_{PC}$ coupling constants of these carbon atoms of **6a**,**b** show greater differences in magnitudes than those observed for 1*H*-phosphirene complex

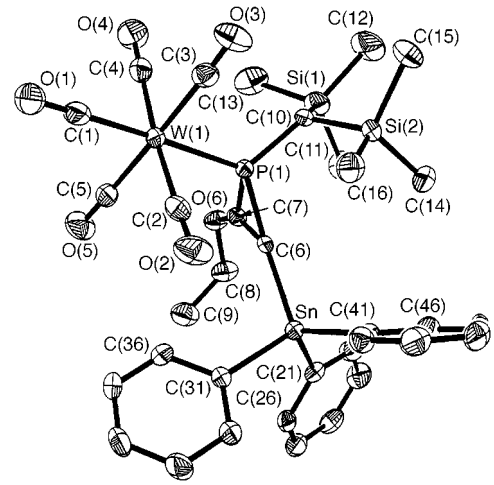

Fig. 1 Molecular structure of complex **6b** in the crystal. Selected bond lengths (pm) and angles (°): W(1)–P(1) 249.83(11), P(1)–C(7) 176.8(4), P(1)–C(6) 182.8(4), P(1)–C(10) 182.2(4), O(6)–C(7) 132.6(5), Sn–C(6) 213.5(4), Sn–C(25) 213.8(4); W(1)–P(1)–C(10) 119.04(14), C(7)–P(1)–C(6) 43.14(19), C(6)–C(7)–P(1) 70.9(3), C(7)–C(6)–P(1) 66.0(2), O(6)–C(7)–C(6) 146.0(4).

6c (**6a**,**b**: C^3: $^{(1+2)}J_{PC}$ 25 ± 3 Hz, C^2: $^{(1+2)}J_{PC}$ ⩽ 3 Hz; **6c**: 4.9 and 2.0 Hz[8]).

The X-ray crystal structure analysis of the complex **6b** confirms the molecular structure (Fig. 1).§ In comparison to the structure [8] of **6c** (values given in square brackets) the endocyclic P–C bond lengths of **6b** are lengthened {P(1)–C(6) 1.828(4) [1.792(8)], P(1)–C(7) 1.768(4) [1.753(8)], C(6)–C(7) 1.323(6) [1.298(11)] Å}, probably because of increased steric strain in **6b**.

We are currently investigating the synthetic potential of this new route to η^1-1-phosphaallene complexes and the reactivity of the complexes **5a**,**b** and **6a**,**b**.

This work was supported by the Fonds der Chemischen Industrie and by the Deutsche Forschungsgemeinschaft. We thank Mr A. Weinkauf for X-ray data collection.

Notes and References

† E-mail: r.streubel@tu-bs.de

‡ Correct elemental analysis were obtained for complexes **5b** and **6b**. NMR data were recorded at room temperature in $CDCl_3$ solution at 50.3 MHz (^{13}C) and 81.0 MHz (^{31}P); *J*/Hz. *Selected spectroscopic data* for **5a**: ^{13}C NMR, δ −8.3 (s, $^1J_{119SnC}$ 356.3, $^1J_{117SnC}$ 339.3, Hz, $SnMe_3$), 156.1 (s, P=C=*C*), 196.4 (d, $^2J_{PC}$ 9.7 Hz, *cis*-CO), 200.2 (d, $^2J_{PC}$ 30.3 Hz, *trans*-CO), 226.5 (d, $^1J_{PC}$ 90.9 Hz, P=*C*=C); ^{31}P NMR, δ 76.4 (s, $^1J_{WP}$ 262.6, $^3J_{119SnP}$ 152.8, $^3J_{117SnP}$ 144.3 Hz). **5b**: ^{13}C NMR, δ 154.5 (d, $^2J_{PC}$ 2.0 Hz, P=C=*C*), 196.2 (d, $^2J_{PC}$ 9.2 Hz, *cis*-CO), 199.8 (d, $^2J_{PC}$ 30.4 Hz, *trans*-CO), 227.8 (d, $^1J_{PC}$ 90.4 Hz, P=*C*=C); ^{31}P NMR, δ 87.4 (s, $^1J_{WP}$ 265.5, $^3J_{119SnP}$ 174.7, $^3J_{117SnP}$ 167.5 Hz). **6a**: ^{13}C NMR, δ −6.8 (s, $^1J_{119SnC}$ 371.4, $^1J_{117SnC}$ 355.1 Hz, $SnMe_3$), 97.2 (d, $^{(1+2)}J_{PC}$ 23.2 Hz, PCSn), 172.5 (s, $^2J_{SnC}$ 53.4 Hz, PCO), 197.6 (d, $^2J_{PC}$ 8.2, $^1J_{WC}$ 126.4 Hz, *cis*-CO), 199.8 (d, $^2J_{WC}$ 29.3 Hz, *trans*-CO); ^{31}P NMR, δ −107.4 (s, $h_{1/2}$ 15 Hz, $^1J_{WP}$ 265.1, $^2J_{SnP}$ 49.6 Hz); MS (EI, ^{120}Sn, ^{184}W): M^+ at *m*/*z* = 934. **6b**: ^{13}C NMR, δ 94.7 (d, $^{(1+2)}J_{PC}$ 21.4 Hz, PCSn), 175.4 (d, $^{(1+2)}J_{PC}$ 3.1 Hz, PCO), 197.2 (d, $^2J_{PC}$ 8.5 Hz, *cis*-CO), 198.7 (d, $^2J_{PC}$ 28.5 Hz, *trans*-CO); ^{31}P NMR, δ −98.2 (s, $h_{1/2}$ 95 Hz); MS (EI, ^{120}Sn, ^{184}W): M^+ at *m*/*z* = 934.

§ *Crystal data* for **6b**: $C_{34}H_{39}O_6PSi_2SnW$, monoclinic, space group $P2_1/c$, a = 21.024(2), b = 9.2419(10), c = 19.619(3) Å, β = 95.753(15)°, U = 3792.8(8) Å^3, Z = 4, μ = 3.8 mm^{-1}, T = −130 °C. Colourless block 0.6 × 0.5 × 0.5 mm, Mo-Kα radiation, Stoe STADI-4 diffractometer, 8387 intensities to $2\theta_{max}$ 50°, 6681 unique (R_{int} 0.021) used for all calculations. Structure solution by heavy-atom method, anisotropic refinement on F^2 (program SHELXL-97, G. M. Sheldrick, Univ. of Göttingen). Treatment of H atoms: rigid methyls, others riding. Final $wR(F^2)$ 0.075, conventional $R(F)$ 0.030 for 412 parameters. CCDC 182/930.

1 Review: R. Appel, in *Multiple Bonds and Low Coordination in Phosphorus Chemistry*, ed. M. Regitz and H. J. Scherer, Georg Thieme Verlag, Stuttgart, New York, 1990, p. 157.
2 Reviews: F. Mathey, *Chem. Rev.*, 1990, **90**, 997; F. Mathey and M. Regitz, in *Comprehensive Heterocyclic Chemistry II*, ed. A. R. Katritzky, C. W. Rees and E. F. V. Scriven, Pergamon, New York, 1997, p. 277.
3 R. Appel, F. Knoch and V. Winkhaus, *J. Organomet. Chem.*, 1986, **307**, 93.
4 M. A. Kirms, H. Primke, M. Stohlmeier and A. de Meijere, *Recl. Trav. Chim. Pays-Bas*, 1986, **105**, 462.
5 R. Streubel, A. Ostrowski, S. Priemer, U. Rohde, J. Jeske and P. G. Jones, *Eur. J. Inorg. Chem.*, 1998, 257.
6 S. V. Ponomarev, S. Y. Pechurina and I. F. Lutsenko, *Zh. Obschch. Khim.*, 1969, **39**, 1171; S. V. Ponomarev, M. B. Erman, S. A. Lebedev, S. Y. Pechurina and I. F. Lutsenko, *Zh. Obshch. Khim.*, 1971, **41**, 127.
7 R. Streubel and H. Wilkens, unpublished work.
8 A. Ostrowski, J. Jeske, P. G. Jones and R. Streubel, *J. Chem. Soc., Chem. Commun.*, 1995, 2507; A. Ostrowski, J. Jeske, F. Ruthe, P. G. Jones and R. Streubel, *Z. Anorg. Allg. Chem.*, 1997, **623**, 1897.

Received in Basel, Switzerland, 9th June 1998; 8/04385J

New ammonium carboxylate host compounds screened by combinatorial chemistry

Kazuki Sada,*† Kei Yoshikawa and Mikiji Miyata*‡

Department of Material and Life Science, Graduate School of Engineering, Osaka University, 2-1 Yamadaoka, Suita, Osaka, 565-0871, Japan

Seventeen new ammonium carboxylate host compounds were screened from a combinatorial library of one hundred ammonium carboxylates formed by mixing ten amines and ten carboxylic acids.

The combinatorial library approach has been widely used in the screening of drugs and biological receptors.[1] More recently, this method has been applied to searching for functional compounds in many fields, such as new synthetic reagents,[2,3] superconducting materials,[4] luminescent materials,[5] polymeric materials,[6] artificial molecular receptors,[7] and so on. However, there has been no application of combinatorial chemistry for screening lattice inclusion compounds.

Design of nanoporous materials using organic compounds is now one of the most interesting topics in organic solid-state chemistry.[8,9] However, it is difficult to design inclusion cavities *via* molecular structure. The most promising method for designing molecular cavities relies upon chemical modification of 'leading' compounds that have been found accidentally.[8] We report here seventeen new host compounds *via* application of combinatorial chemistry to finding lattice inclusion compounds.

Ten commercially available amines (**a–j**) and ten carboxylic acids (**1–10**) were used to form the combinatorial salt library. One hundred salts were prepared by mixing stock solutions of the two components in a 1:1 molar ratio. The resulting salt crystals were obtained by filtration or by removal of the solvents, and characterized by IR and ^{1}H NMR analysis. Pr^{i}OH was chosen as the trial guest due to the moderate solubility of the various salts in this solvent. All salts were subjected to recrystallization from Pr^{i}OH, and the resulting crystals were characterized by ^{1}H NMR analysis and X-ray diffraction. Table 1 summarizes the clathrate formation results. Seventeen salts formed inclusion crystals with Pr^{i}OH, fifty four salts yielded guest-free crystals only and twenty salts did not form crystalline materials at all. In some cases, single components crystallized from Pr^{i}OH solution. This result indicates that at least seventeen ammonium carboxylates have inclusion abilities. Testing other guest compounds will yield inclusion compounds with different compositions.

The salts of small carboxylic acids or small amines did not form inclusion compounds with Pr^{i}OH. They formed guest-free crystals or failed to give crystalline materials. On the other hand, the salts of brucine (**j**) formed Pr^{i}OH clathrates. Its complex shell-like molecular structure with tertiary amino groups allows **j** to form molecular cavities in the crystalline state. The inclusion ability and the crystal structure of **3·j**, one of the seventeen host salts, were further investigated.

Complex **3·j** forms inclusion compounds with various organic solvents such as alcohols, ethers, ketones, aromatic esters and aromatic hydrocarbons. Table 2 summarizes the guest compounds and the host–guest ratios. Fig. 1 shows the crystal structure of **3·j** with Pr^{i}OH (1 : 1 : 1).§ The most striking structural feature is the one-dimensional corrugated monolayer structure of the conjugate anions of **3**, which has been observed in molecular complexes[10] or diastereomeric salts.[11] The conjugate cations of **j** bridge the monolayer *via* the salt bridge

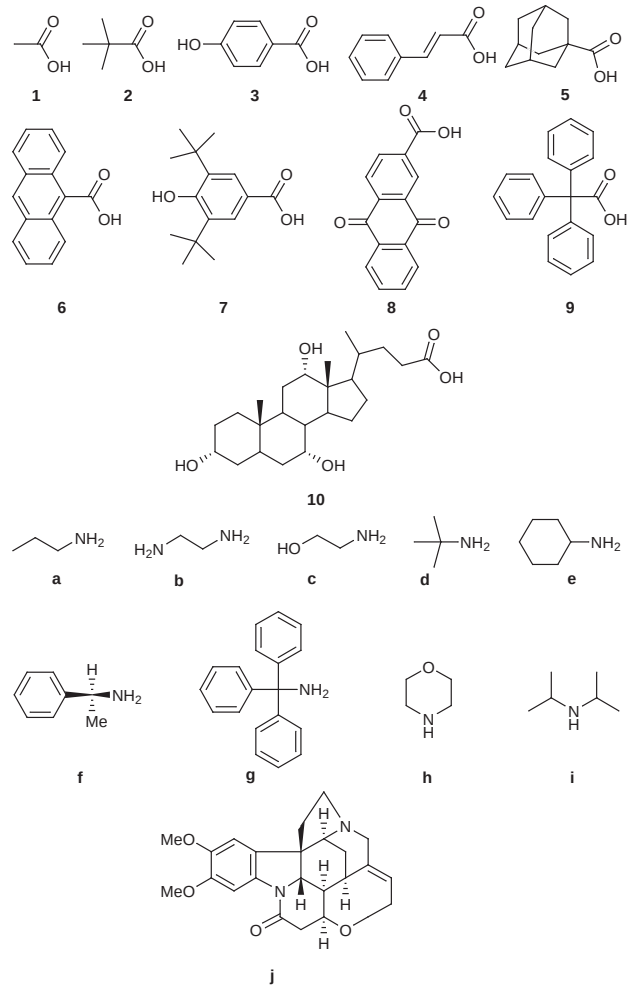

Table 1 Formation of inclusion crystals of one hundred salts with Pr^{i}OH[a]

	1	**2**	**3**	**4**	**5**	**6**	**7**	**8**	**9**	**10**
a	nc	nc	gf	nc	gf	gf	INC	gf	gf	gf
b	gf	acid	INC	gf	acid	gf	nc	nc	gf	gf
c	nc	nc	gf	gf	gf	nc	nc	gf	INC	gf
d	gf	gf	gf	gf	acid	INC	gf	INC	gf	INC
e	gf	gf	gf	gf	nc	INC	gf	gf	nc	nc
f	gf	gf	gf	gf	gf	gf	nc	gf	gf	gf
g	amine	amine	INC	nc	amine	INC	amine	gf	INC	amine
h	gf	nc	gf	gf	gf	INC	gf	gf	gf	gf
i	nc	nc	gf	acid	gf	gf	gf	gf	gf	nc
j	nc	nc	INC	INC	INC	gf	INC	INC	gf	INC

[a] INC = inclusion crystal, gf = guest-free crystal, nc = no crystallization, acid = crystal of acid only, amine = crystal of amine only

Table 2 Guest molecules of **3·j** and molar ratios of **3**, **j** and guest molecules in the inclusion crystals[a]

Guest molecule	Molar ratio	Guest molecule	Molar ratio
MeOH	2:2:3	acetone	2:2:1
EtOH	1:1:1	butan-2-one	1:1:1
Pr^nOH	1:1:1	MeOAc	1:1:1
Pr^iOH	1:1:1	MeCN	2:2:1
Bu^nOH	1:1:1	toluene	2:1:1
Bu^sOH	1:1:1	PhEt	2:1:1
Bu^tOH	1:1:1	*o*-xylene	2:1:1
$C_5H_{11}OH$	1:1:1	*m*-xylene	2:1:1
$PrMeCHCH_2OH$	1:1:2	*p*-xylene	2:2:1
$Pr^i(CH_2)_3OH$	1:1:2	$PhPr^n$	4:2:1
$Bu^t(CH_2)_2OH$	1:1:3	CH_2Cl_2	1:2:4
$MeOCH_2CHMeOH$	1:1:1	$ClCH_2CH_2Cl$	2:2:1
THF	1:1:1		

[a] Molar ratios determined by ^1H NMR analysis.

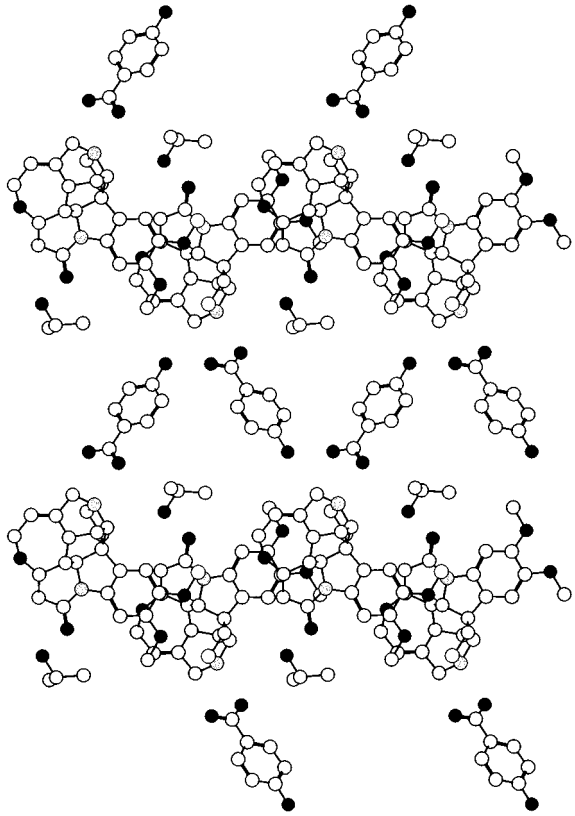

Fig. 1 X-Ray crystal structure of **3·j** with Pr^iOH (1 : 1 : 1)

and the hydrogen bond between them. The corrugated monolayer provides molecular channels that the guest alcohol is included in. The unique shell-like molecular shape of **j** yields the robust monolayer structure *via* van der Waals forces, and the monolayer motif enables **j** to form the Pr^iOH clathrates with various counter carboxylate anions.

In summary, we demonstrated the application of combinatorial chemistry to finding lattice inclusion compounds. Some ammonium carboxylates such as **3·j** form inclusion compounds with various organic compounds. Inclusion compounds of inorganic quaternary salts are already known.[12] However, ammonium carboxylates have been recognized as a source of host compounds.[13] Proper choice of amines and carboxylic acids provides us with various host compounds. Application to chiral recognition by enclathration of salt formation between chiral acid and achiral amines, achiral amine and chiral acid, or chiral acid and chiral amines, is now under investigation.

Notes and References

† E-mail: sadakazu@ap.chem.eng.osaka-u.ac.jp
‡ E-mail: miyata@ap.chem.eng.osaka-u.ac.jp

§ *Crystal data* for **3•j**·Pr^iOH (1:1:1): $C_{23}H_{27}N_2O_4{\cdot}C_7H_5O_3{\cdot}C_3H_8O$ (592.69), orthorhombic, space group $P2_12_12_1$ (#19), a = 13.070(1), b = 18.901(2), c = 12.120(3) Å, V = 2994.2(6) Å^3, −55 °C, Z = 4, m = 0.94 cm^{-1}, 2140 independent reflections, R = 0.040. CCDC 182/931.

1 F. Balkenhohl, C. von dem Bussche-Hünnefeld, A. Lansky and C. Zechel, *Angew. Chem., Int. Ed. Engl.*, 1996, **35**, 2288; L. A. Thompson and J. Ellman, *Chem. Rev.*, 1996, **96**, 555.
2 For examples, K. Burgess, H.-J. Lim, A. M. Porte and G. A. Sulikowski, *Angew. Chem., Int. Ed. Engl.*, 1996, **35**, 220; B. M. Cole, K. D. Shimizu, C. A. Krueger, J. P. A. Harrity, M. L. Snapper and A. H. Hoveyda, *Angew. Chem., Int. Ed. Engl.*, 1996, **35**, 1668.
3 A review of solid-phase organic reactions: P. H. H. Hermkens, H. C. J. Ottenheijm and D. C. Rees, *Tetrahedron*, 1997, **53** , 5643 and references cited therein.
4 X.-D. Xiang, X. Sun, G. Briceno, Y. Lou, K.-A. Wang, H. Chang, W. G. Wallace-Freedman, S.-W. Chen and P. G. Schultz, *Science*, 1995, **268**, 1738; G. Briceno, Y. Lou, H. Chang, X. Sun, P. G. Schultz and X.-D. Xiang, *Science*, 1995, **270**, 273.
5 E. Danielson, J. H. Golden, E. W. McFarland, C. M. Reaves, W. H. Weinberg and X.-D. Wu, *Nature*, 1997, **389**, 944.
6 S. Brocchini, K. James, V. Tangpasuthadol and J. Kohn, *J. Am. Chem. Soc.*, 1997, **119**, 4553.
7 M. S. Goodman, V. Jubian, B. Linton and A. D. Hamilton, *J. Am. Chem. Soc.*, 1995, **117**, 11 610.
8 *Comprehesive Supramolecular Chemistry*, *Solid-state Supramolecular Chemistry: Crystal Engineering*, ed. D. D. MacNicol, F. Toda and R. Bishop, Pergamon, Oxford, 1996, vol. 6.
9 For other examples, see K. Ogura, T. Uchida, M. Noguchi, M. Minoguchi, A. Murata, M. Fujita and K. Ogata, *Tetrahedron Lett.*, 1990, **31**, 3331; T. Suzuki, H. Fujii, Y. Yamashita, C. Kabuto, S. Tanaka, M. Harasawa, T. Mukai and T. Miyashi, *J. Am. Chem. Soc.*, 1992, **114**, 3034; N. Hayashi, Y. Mazaki and K. Kobayashi, *J. Org. Chem.*, 1995, **60**, 6342; V. A. Russell, C. C. Evans, W. Li and M. D. Ward, *Science*, 1997, **276**, 575 and references cited therein.
10 F. Toda, K. Tanaka and H. Ueda, *Tetrahedron Lett.*, 1985, **22**, 4669; F. Toda, K. Tanaka, H. Ueda and T. Oshima, *Isr. J. Chem.* 1985, **25**, 338; S. S. B. Glover, R. O. Gould and M. D. Walkinshaw, *Acta Crystallogr.*, 1985, **C41**, 990; A. A. Pinkerton, P.-A. Carrupt, F. Claret and P. Vogel, *Acta Crystallogr.*, 1993, **C49**, 1636.
11 R. O. Gould and M. D. Walkinshaw, *J. Am. Chem. Soc.*, 1984, **106**, 7840; S. Kuwata, J. Tanaka, N. Onda, T. Yamada, T. Miyazawa, M. Sugiura, Y. In, M. Doi, M. Inoue and T. Ishida, *Bull. Chem. Soc. Jpn.*, 1993, **66**, 1501.
12 Reviews: F. Vögtle, H.-G. Löhr, J. Franke and D. Worsch, *Angew. Chem., Int. Ed. Engl.*, 1985, **24**, 727; K. Tanaka and F. Toda, in ref. 8, p. 517.
13 For an example of the design of a porous organic crystal based on ammonium carboxylate, see R. E. Melendez, C. V. K. Sharma, M. J. Zaworotko, C. Bauer and R. D. Rogers, *Angew. Chem., Int. Ed. Engl.*, 1996, **35** 2213.

Received in Cambrdige, UK, 1st May 1998; 8/03288B

Room temperature ionic liquids as novel media for 'clean' liquid–liquid extraction

Jonathan G. Huddleston, Heather D. Willauer, Richard P. Swatloski, Ann E. Visser and Robin D. Rogers*†

Department of Chemistry, The University of Alabama, Tuscaloosa, AL 35487, USA

The partitioning of simple, substituted-benzene derivatives between water and the room temperature ionic liquid, butylmethylimidazolium hexafluorophosphate, is based on the solutes' charged state or relative hydrophobicity; room temperature ionic liquids thus may be suitable candidates for replacement of volatile organic solvents in liquid–liquid extraction processes.

Liquid–liquid extraction has often been a favored choice of the process engineer for the development of separation processes.[1] Traditional solvent extraction,[2] however, employs an organic solvent and an aqueous solution as the two immiscible phases and the increasing emphasis on the adoption of clean manufacturing processes and environmentally benign technologies may make such processes seem increasingly anachronistic because of their high usage of toxic, flammable, volatile organic compounds (VOCs). The costs of solvents are high and their safe engineering attracts significant capital costs over and above simple containment. Disposal of spent extractants and diluents will also attract increasing costs through the impact of environmental protection regulations. So much are VOCs the normal media for organic synthetic processes, that current worldwide usage of these materials has been estimated at over 5 billion dollars per annum.[3]

The design of safe and environmentally benign separation processes has an increasingly important role in the development of clean manufacturing processes and in the remediation of sites contaminated by an older generation of manufacturing technologies. Recently, considerable interest has been manifest in the use of room temperature ionic liquids as solvents for industrial catalytic reactions, including polymerizations, alkylations, and acylations.[3–6] This approach appears to allow the controlled production of desired products from reactants with a minimum of waste production through side reactions due to the tendency of ionic liquids to suppress conventional solvation and solvolysis phenomena.[3,4]

Room temperature ionic liquids are liquids that are composed entirely of ions, and in this sense alone resemble the ionic melts which may be produced by heating normal metallic salts such as sodium chloride to high temperature (*e.g.* NaCl to over 800 °C).[3] In fact, ionic liquids can now be produced which remain liquid at room temperature and below (even as low as −96 °C) and appear to be undemanding and inexpensive to manufacture.[3–5] Ionic liquids based on methylimidazolium are favorable species for investigation because of their air and water stability, their wide liquidus range, the fact that they remain liquid at room temperature, and their relatively favorable viscosity and density characteristics.[7,8] In addition, the R group of the cation is variable and may be used to fine tune the properties of the ionic liquid. It is reported that such ionic liquids are able to solvate a wide range of species including organic, inorganic, and organometallic compounds. Miscibility with a number of organic solvents such as benzene and toluene has also been reported.[9]

In view of these developments, it seems likely that the design and implementation of separation processes for product recovery from these media will assume increasing importance. Additionally, it may be apparent that *ionic liquids may in themselves be suitable, and indeed favorable, media for the design of novel liquid–liquid extraction systems.* Some features of these ionic liquid systems, the high solubilities of organic species, the prevalence of high coulombic forces resulting in the practical absence of any significant vapor pressure,[3] and the availability of air and moisture stable, water immiscible ionic liquids (*e.g.* imidazolium salts of PF_6^- or BF_4^-) may recommend such systems as being uniquely suited to the development of completely novel liquid–liquid extraction processes. The data presented here indicate that the partitioning of a number of charged and uncharged aryl organic moieties in a biphasic extraction system comprising the phases butylmethylimidazolium hexafluorophosphate ([BMIM][PF_6]) and water is similar to their partitioning in traditional organic solvent–water systems.

[BMIM][PF_6] was prepared by modification of published procedures.‡ Equal volumes of the ionic liquid and distilled deionized water were contacted in the presence of ^{14}C-labelled tracers of several ionizable and nonionizable substituted aryl molecules. The distribution of the solutes between the heavy, ionic liquid phase and the light, water phase was determined radiochemically.

The distribution data provided in Fig. 1 highlight the relationship between the distribution ratios observed here and similar partitioning in octan-1-ol–water systems (an often used empirical hydrophobicity scale).[10] There is a close relationship between the two systems, although there appear to be differences in detail as is usual in comparing partition between different solvent systems having differing solvation properties.[11,12] The values of the distribution coefficients (*P*) in the octan-1-ol–water system are in general an order of magnitude higher than the corresponding distribution ratios (*D*) for the [BMIM][PF_6]–water system. The reasons for this have not yet

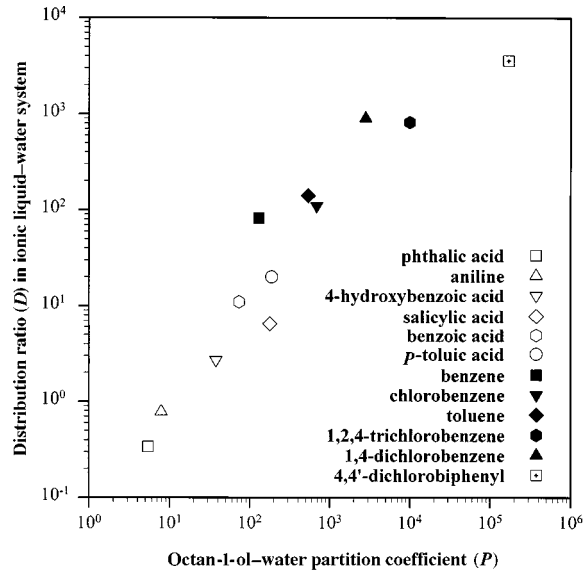

Fig. 1 Correlation of partitioning data between [BMIM][PF_6]–water and octan-1-ol–water biphasic systems

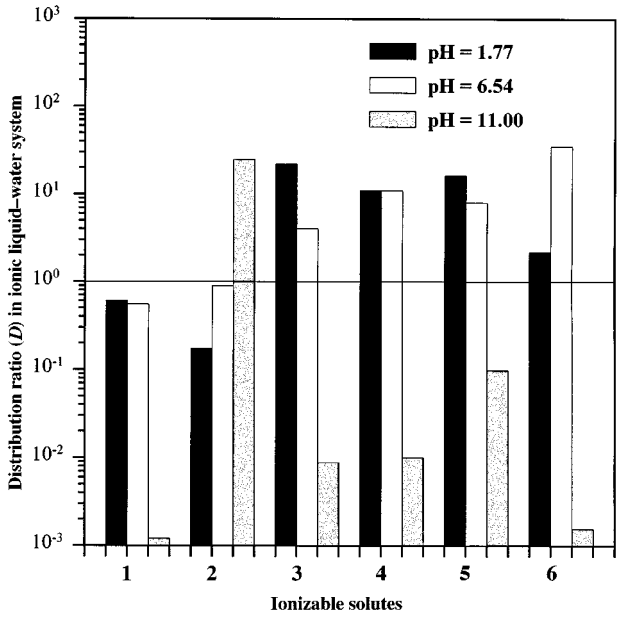

Fig. 2 The solutes studied include: **1** phthalic acid (p*K*1 = 2.89, p*K*2 = 5.51), **2** aniline (pK_b = 9.42), **3** 4-hydroxybenzoic acid (p*K*1 = 4.48, p*K*2 = 9.32), **4** benzoic acid (pK_a = 4.19), **5** salicylic acid (p*K*1 = 2.97, p*K*2 = 13.40), **6** *p*-toluic acid (p*K*1 = 2.27)

been elucidated, but may reflect a generally less hydrophobic character to the [BMIM][PF_6] phase, or may also be due to the strong polar contribution of the relatively high concentration of charged groups present in the ionic liquid compared to the octan-1-ol–water system. These differences do not necessarily imply that ionic liquids represent a 'poorer' extracting phase than octan-1-ol; the distribution values found are adequate for practical applications.[2]

Fig. 1 also shows that for this rather limited set of solute species, those species having charged groups or strong hydrogen bonding moieties (open symbols in Fig. 1) have, in general, much lower partition coefficients than similar neutral or apolar species (filled symbols in Fig. 1). The effect of charge on the distribution of these species was thus investigated further. The ionizable solutes were partitioned in the [BMIM][PF_6]–water system as described above, but with the pH of the aqueous phase adjusted to either pH 1.77 (using concentrated H_2SO_4) or to pH 11 (using concentrated NH_4OH).

The data in Fig. 2 confirm that the distribution coefficient is higher for the uncharged form than for the charged form. For benzoic acid (**4** in Fig. 2) the partition coefficient is higher under acidic or near neutral conditions than in basic solution. For the oppositely charged base, aniline (**2**), the partition coefficient is higher at alkaline pH than in acidified solution. Similar behavior is observed for the other ionizable solutes employed in the study. It is even possible to rationalize differences in solute partitioning at a given pH from the understanding of the predominant charged state in solution (*i.e.* by comparing the pK_a values and the predicted magnitude of the molecule's charge at that pH).

It is worth noting that, in almost all cases, the distribution of these solutes varies from values of *D* greater than 1 to less than 1 depending on the charged state of the solutes. This indicates a change in phase preference between solutes in their charged and uncharged forms. Once again, this is a useful observation and simplification implying that classical techniques of solvent extraction, which are often ideally designed around the fractionating power which may be achieved by the adoption of forward and backward extracting steps,[1,2] may easily be adapted to extractions performed utilizing ionic liquids.

Ionic liquids represent a novel class of solvents and may now also be considered as a novel medium for liquid–liquid extraction. Limited experience with room temperature ionic liquids based on alkylmethylimidazolium hexafluorophosphate suggests that such systems may be easily adapted to conventional liquid–liquid extraction practice.¶ The observation of an approximate correspondence between the distribution of these aryl solutes in the ionic liquid system and their distribution in an octan-1-ol–water system is a useful design criterion. Interestingly, the low vapor pressures of such systems suggest novel methods of solute recovery through evaporative–pervaporative techniques for appropriately volatile solutes. These interesting biphasic systems continue to be actively studied in our laboratories for the development of novel, 'clean' separation technologies.

This research is supported by the Division of Chemical Sciences, Office of Basic Energy Sciences, Office of Energy Research, U.S. Department of Energy (Grant No. DE-FG02-96ER14673).

Notes and References

† E-mail: RDRogers@Bama.ua.edu

‡1-Butyl-3-methylimidazolium chloride was prepared by reaction of equal molar amounts of 1-methylimidazole and chlorobutane in a round-bottomed flask fitted with a reflux condenser by heating and stirring at 70 °C for 48–72 h. The resulting viscous liquid was allowed to cool to room temperature and then was washed three times with 200 mL portions of ethyl acetate. After the last washing, the remaining ethyl acetate was removed by heating to 70 °C under vacuum. To prepare the ionic liquid, hexafluorophosphoric acid (1.3 mol) was added (slowly to prevent the temperature from rising significantly) to a mixture of 1-butyl-3-methylimidazolium chloride (1 mol) in 500 mL of water. After stirring for 12 h, the upper acidic aqueous layer was decanted and the lower ionic liquid portion was washed with water (10 × 500 mL) until the washings were no longer acidic. The ionic liquid was then heated under vacuum at 70 °C to remove any excess water.

§ The procedures used in the standard radiochemical assay utilized are described in ref. 13 for similar work investigating aqueous biphasic systems. Standard radiometric assay of equal volumes of the separated phases allows calculation of the distribution ratio as the ratio of the activity in the ionic liquid phase over the activity in the water phase.

¶ Although we were unable to detect water in the ionic liquid by TGA, NMR does indicate the presence of a small amount of water after contact with an aqueous phase. The exact composition and water content of these potential solvents are under active investigation.

1 T. C. Lo, in *Handbook of Separations Techniques for Chemical Engineers*, ed. P. A. Schwietzer, McGraw-Hill, New York, 1996, pp. 1-450–1-529.
2 J. Rydberg, C. Musikas and G. R. Choppin, *Principles and Practices of Solvent Extraction*, Marcel Dekker, New York, 1992.
3 K. R. Seddon, *J. Chem. Technol. Biotechnol.*, 1997, **68**, 351.
4 Y. Chauvin and H. Olivier-Bourbigou, *CHEMTECH*, 1995, **25**, 26.
5 C. L. Hussey, *Pure Appl. Chem.*, 1988, **60**, 1763.
6 V. R. Koch, C. Nanjundiah and R. T. Carlin, *US Pat.* 95-497310 950630.
7 J. S. Wilkes and M. J. Zaworotko, *J. Chem. Soc., Chem. Commun.*, 1992, 965.
8 J. Fuller, R. T. Carlin, H. C. De Long and D. Haworth, *J. Chem. Soc., Chem. Commun.*, 1994, 299.
9 J. S. Wilkes, J. A. Levisky, R. A. Wilson and C. L. Hussey, *Inorg. Chem.*, 1982, **21**, 1263.
10 C. Hansch, A. Leo and D. Hoekman, *Exploring QSAR Hydrophobic, Electronic and Steric Constants*, American Chemical Society, Washington, DC, 1995.
11 D. E. Leahy, J. J. Morris, P. J. Taylor and A. R. Wait, *J. Chem. Soc., Perkin Trans. 2*, 1992, 723.
12 D. E. Leahy, J. J. Morris, P. J. Taylor and A. R. Wait, *J. Chem. Soc., Perkin Trans. 2*, 1992, 705.
13 J. G. Huddleston, S. T. Griffin, J. Zhang, H. D. Willauer and R. D. Rogers, in *Aqueous Two-Phase Systems*, ed. R. Kaul in *Methods in Biotechnology*, ed. J. M. Walker, Humana Press, Totowa, NJ, 1998, in press.

Received in Columbia, MO, USA, 26th May 1998; 8/03999B

The syntheses of $C_6CH_2^{\bullet -}$ and the corresponding carbenoid cumulene C_6CH_2 in the gas phase

Suresh Dua, Stephen J. Blanksby and John H. Bowie†

Department of Chemistry, The University of Adelaide, South Australia, 5005, Australia

The ion $(C_6CH_2)^{\bullet -}$ is formed in the gas phase by the process –C≡C–C≡C–C≡C–CH_2OEt → $(C_6CH_2)^{\bullet -}$ + EtO•, and charge stripping of the product radical anion yields the carbenoid neutral C_6CH_2; this can be either a singlet (the ground state), which is best represented as the carbene :C=C=C=C=C=C=CH_2, or a triplet; the adiabatic electron affinity and the dipole moment of the carbenoid neutral are calculated to be 2.82 eV and 7.33 D respectively.

Small cumulenes have been detected in circumstellar gas and dust envelopes which surround red giant stars, in particular, the bright carbon-rich star IRC-10216.[1–3] These include C_n (n = 3 and 5), C_nH (n = 2–8) and C_nH_2 (n = 2–4 and 6), with neutrals where n is even generally being more abundant than those where n is odd.[1–5] The high electron affinities of these neutrals suggests the possibility that the corresponding anions may co-occur with the neutrals in circumstellar envelopes.[6–8] We have reported the syntheses of a number of these anions in the source of a VG ZAB 2HF mass spectrometer [*e.g.* C_5H^-[8] and three isomers of $C_5H_2^{\bullet -}$[9]] and have used collision-induced charge stripping of the anions to effect the syntheses of the appropriate neutrals.[9] Both C_5CH_2 and C_6CH have already been detected in circumstellar envelopes,[3] and it has been suggested that C_6CH_2 should also be present,[10] and that it should be an excellent candidate for detection because of its large dipole moment [calculated to be 7.33 D (Table 1)].[5] The proposed pathways *via* which such hydrocarbons can form in the interstellar environment have been reviewed.[11]

We describe the synthesis and structures of both $(C_6CH_2)^{\bullet -}$ and the corresponding carbenoid cumulene neutral.

The radical anion of C_6CH_2 was synthesised in the source of the ZAB 2HF mass spectrometer as summarised in sequence (1). The reaction between HO^- and DC_6CH_2OEt‡ yields the

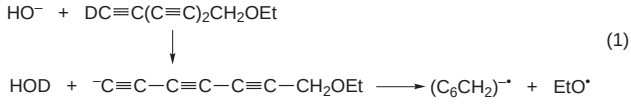

(1)

anion $^-C_6CH_2OEt$ which undergoes facile loss of EtO• to yield $(C_6CH_2)^{\bullet -}$. Source formed $(C_6CH_2)^{\bullet -}$ ions are then fired through a collision cell containing O_2 (at 2×10^{-7} Torr; 1 Torr = *ca.* 133 Pa) to produce a beam of neutral C_6CH_2 which then proceeds into a second collison containing O_2 (at 2×10^{-7} Torr) which effects ionisation of the neutral to form a decomposing C_6CH_2 radical cation. The resultant neutralisation reionisation spectrum of $(C_6CH_2)^{\bullet -}$ ($^-NR^+$)[16] is shown in Fig. 1. The observation of a pronounced recovery signal (at *m/z* 86) in the spectrum indicates that the neutral has a lifetime of at least 10^{-6} s, and the similarities between the $^-NR^+$ spectrum and the corresponding charge reversal (CR) spectrum of $C_6CH_2^{\bullet -}$ (listed in the caption to Fig. 1) suggests that the neutral formed has the same connectivity as the radical anion.[17]

Ab initio calculations for both the neutral and radical anion were carried out at the RCCSD(T)/aug-cc-VDZ//B3LYP/6-31G* level of theory using GAUSSIAN94[19] and MOLPRO 96.4.[20] Details are summarised in Table 1. The radical anion and both the singlet and triplet neutrals are best represented as

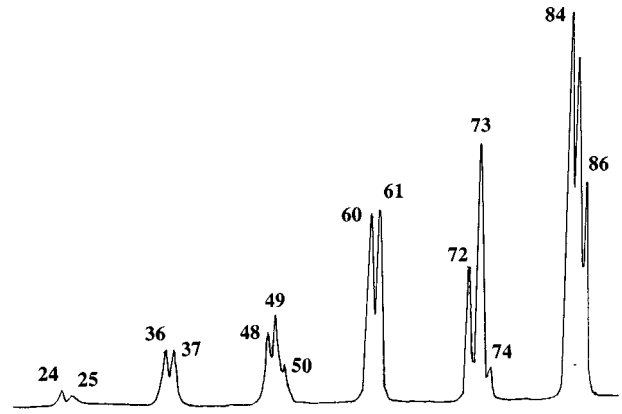

Fig. 1 Neutralisation reionisation ($^-NR^+$) mass spectrum of $C_6CH_2^{\bullet -}$. VG ZAB 2HF mass spectrometer. O_2 in both collision cells (measured pressure outside cells = 2×10^{-7} Torr). CR spectrum of $C_6CH_2^{\bullet -}$ (O_2 in the first collision cell, measured pressure outside cell -2×10^{-7} Torr) as follows [*m/z* (relative abundance)]: 86(49%), 85(88), 84(100), 74(4), 73(57), 72(13), 62(3), 61(43), 60(29), 50(3), 49(19), 48(9), 37(15), 36(9), 25(1), 24(0.5).

Table 1 *Ab initio* calculations for anions and neutrals

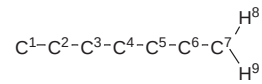

	Anion	Neutral (singlet)	Neutral (triplet)
State	($^2B_1$)	($^1A_1$)	($^3A_2$)
Symmetry	C_{2v}	C_{2v}	C_{2v}
Energy (hartrees)[a]	−266.969928	−266.866186	−266.833462
Rel. energy (kJ mol^{-1})	0	272	358
Adiabatic electron affinity (eV)		2.82	
Dipole moment (Debye)	8.10	7.33	6.40
Bond length (Å)[b]			
C^1C^2	1.272	1.289	1.301
C^2C^3	1.334	1.301	1.301
C^3C^4	1.256	1.270	1.274
C^4C^5	1.323	1.293	1.297
C^5C^6	1.261	1.271	1.272
C^6C^7	1.345	1.320	1.329
C^7H^8	1.090	1.090	1.089
C^7H^9	1.090	1.090	1.089
Bond angles (°)[b]			
$C^1C^2C^{3c}$	180.0	180.0	180.0
$C^6C^7H^8$	121.98	121.61	121.16
$C^6H^7H^9$	121.98	121.61	121.16
$H^8C^7H^9$	116.04	116.78	117.67
$C^6C^7H^8H^9$	180.0	180.0	180.0

[a] RCCSD(T)/aug-cc-p VDZ level of theory including zero point vibrational energy [calculated from vibrational frequencies at the B3LYP/6-31G* level of theory, and scaled by 0.9804 (ref. 18)]. [b] B3LYP/6-31G* level of theory. [c] All other angles along the carbon skeleton are also 180.0°.

simple linear cumulenes. The ground state of neutral C_6CH_2 corresponds to the singlet carbenoid cumulene :C=C=C=C=C=C=CH_2 (*cf.* ref. 21) which has a calculated dipole moment of 7.33 D. The adiabatic electron affinity of this neutral is estimated to be 2.82 eV; thus we propose that $C_6CH_2^{\bullet -}$ as well as the corresponding neutral may be present in the circumstellar environment.

Notes and References

† E-mail: jbowie@chemistry.adelaide.edu.au

‡ 1-Ethoxy-7-deuteriohepta-2,4,6-triyne was formed by desilyation of the corresponding trimethylsilyl triyne with MeOD/DO^- (*cf.* ref. 12). The trimethylsilyl triyne was prepared by coupling between TMS–C≡C–C≡C–Li (ref. 13) and Br–C≡C–CH_2OEt (ref. 14) using CuBr as catalyst (ref. 15).

1 H. Olofsson, in *Molecules in the Stellar Environment, Lecture Notes in Physics*, ed. O. G. Jorgenson, Springer, Heidelberg, 1994, pp. 114–133, and refs. cited therein.
2 P. F. Bernath, K. H. Hinkle and J. J. Keady, *Science*, 1989, **244**, 562; K. H. Hinkle, in *Molecules in the Stellar Environment, Lecture Notes in Physics*, ed. O. G. Jorgensen, Springer, Heidelberg, 1994, pp. 99–114, and refs. cited therein.
3 A. Omont, in *Molecules in the Stellar Environment, Lecture Notes in Physics*, ed. O. G. Jorgenson, Springer, Heidelberg, 1994, pp. 135–138, and refs. cited therein.
4 M. J. Travers, M. C. McCarthy, C. A. Gottlieb and P. Thaddeus, *Astrophys. J.*, 1996, **465**, L77.
5 Cited as unpublished work in, M. C. McCarthy, M. J. Travers, A. Korvacs, W. Chen, S. E. Novick, C. A. Gottlieb and P. Thaddeus, *Science*, 1997, **275**, 518.
6 J. Natterer, W. Koch, D. Schröder, N. Goldberg and H. Schwarz, *Chem. Phys. Lett.*, 1994, **229**, 429.
7 S. Petrie, *Mon. Not. R. Astron. Soc.*, 1996, **281**, 137.
8 S. J. Blanksby, S. Dua, J. H. Bowie and J. C. Sheldon, *Chem. Commun.*, 1997, 1833.
9 S. J. Blanksby, S. Dua, J. H. Bowie, D. Schröder and H. Schwarz, submitted for publication in *J. Phys. Chem.*
10 M. C. McCarthy, M. J. Travers, C. A. Gottlieb and P. Thaddeus, *Astrophys. J.*, 1997, **483**, L139.
11 D. Smith and P. Spanel, *Mass Spectrom. Rev.*, 1995, **14**, 255.
12 B. N. Ghose, *Synth. React. Inorg. Metal-Org. Chem.*, 1994, **24**, 29.
13 A. B. Holmes, C. L. D. Jennings-White, A. H. Shulthess, B. Akinde and D. R. M. Walton, *J. Chem. Soc., Chem. Commun.*, 1979, 840.
14 C. Cai and A. Vasella, *Helv. Chim. Acta*, 1995, **78**, 2053.
15 J. Miller and G. Zweifel, *Synthesis*, 1983, 128.
16 For an account of neutralisation/reionisation of negative ions, and definitions of nomenclature, see N. Goldberg and H. Schwarz, *Acc. Chem. Res.*, 1994, **27**, 347.
17 For an account of the application of the comparison of $^-NR^+$ and CR spectra of an anion, see C. A. Schalley, G. Hornung, D. Schröder and H. Schwarz, *Chem. Soc. Rev.*, 1998, **27**, 91.
18 M. W. Wong, *Chem. Phys. Lett.*, 1996, **256**, 391.
19 GAUSSIAN94, Revision C3, M. J. Frish, G. W. Trucks, H. B. Schlegel, P. M. W. Gill, B. G. Johnson, M. A. Robb, J. R. Cheeseman, T. Keith, G. A. Petersson, J. A. Montgomery, K. Raghavavhari, M. A. Al-Latham, V. G. Zakrzewski, J. V. Ortiz, J. B. Foresman, J. Cioslowski, B. B. Stefanov, A. Nanayakkara, M. Challacombe, C. Y. Peng, P. V. Ayala, W. Chen, M. W. Wong, J. L. Andres, E. S. Replogle, R. Gomperts, R. L. Martin, D. J. Fox, J. S. Binkley, D. J. Defrees, J. Baker, J. P. Stewart, M. Head-Gordon, C. Gonzalez and J. A. Pople, Gaussian Inc., Pittsburgh, PA, 1995.
20 H.-J. Werner, P. J. Knowles, J. Almlf, R. D. Amos, M. J. O. Deegan, S. T. Elbert, C. Hampel, C. Meyer, K. Peterson, R. Pitzer, A. J. Stone and R. Lindh, MOLPRO 96.4.
21 K. Aoki and S. Ikuta, *J. Mol. Struc.*, 1994, **310**, 229.

Received in Cambridge, UK, 1st June 1998; 8/04070B

Synthesis and characterization of the new microporous fluorogallophosphate Mu-2 with a novel framework topology

P. Reinert,[a] B. Marler[b] and J. Patarin*[a]†

[a] *Laboratoire de Matériaux Minéraux, ENSCMu., UPRES-A 7016, 3 rue Alfred Werner, 68093 Mulhouse Cedex, France*
[b] *Institut für Mineralogie, Ruhr Universität Bochum, D-44780 Bochum, Germany*

A new three-dimensional microporous fluorogallophosphate whose structure consists of a cubic arrangement of double-four-ring units (D4R) hosting F^- anions was synthesized from a fluoride-containing aqueous medium in the presence of 4-amino-2,2,6,6-tetramethylpiperidine as organic template.

Since 1985, a large number of gallophosphates with microporous frameworks obtained by hydrothermal synthesis have been reported in the literature.[1] The use of the fluoride method[2] led to the discovery of the large pore cloverite, a structure with a three-dimensional 20-membered-ring channel system,[3] the LTA-type $GaPO_4$[4] and several gallophosphates named ULM-*n*.[5] In fact, it was shown that the fluoride anions play a structural role stabilizing the double-four-ring (D4R) units of the structure.[3] This type of secondary building unit was also observed for the gallophosphate Mu-1,[6] which is constituted of isolated D4R units, and the fluorogallophosphate Mu-3[7] whose structure consists of chains of D4Rs. The specific location of F^- trapped within this type of unit was also previously observed for the gallophosphate ULM-5,[8] but in this case F^- is also a component of the framework as it bridges the gallium atoms. Here we report the synthesis and characterization of a new fluorogallophosphate, Mu-2, which was obtained in an aqueous fluoride-containing medium in the presence of 4-amino-2,2,6,6-tetramethylpiperidine as organic template. This organic species was previously introduced into an aluminosilicate gel and led to the crystallization of the precursor of ferrierite.[9] The chain-like fluorogallophosphate Mu-3 was obtained in a quasi-non-aqueous medium in the presence of the same organic template.[7]

Mu-2 was synthesized from an aqueous fluoride-containing mixture in the presence of 4-amino-2,2,6,6-tetramethylpiperidine (R). Typically, the molar composition of the starting gel was $1Ga_2O_3 : 1P_2O_5 : 0.3HF : 1R : 80H_2O$. The gel was prepared by first mixing 0.56 g of the gallium source [an amorphous gallium oxide hydroxide obtained by heating a gallium nitrate solution (Rhône-Poulenc) at 250 °C for 24 h] with 0.58 g of phosphoric acid solution (85% H_3PO_4, Normapur, Prolabo) and the required amount of distilled water (3.4 g). After homogenization 0.04 g of hydrofluoric acid (40% Normapur, Prolabo) and 0.39 g of 4-amino-2,2,6,6-tetramethylpiperidine (Fluka, purum > 97%) were added successively under stirring. The gel was mixed at room temperature for 1 h and transferred to a Teflon-lined stainless-steel autoclave. After heating at 170 °C for 5 days, the solid obtained was washed with distilled water. Mu-2 was easily isolated from the batch by ultrasonication in the form of large rounded truncated cubes with a size close to 100 μm (Fig. 1). This preparation also gives an unidentified phase (probably a layered material) which does not contain fluoride anions.

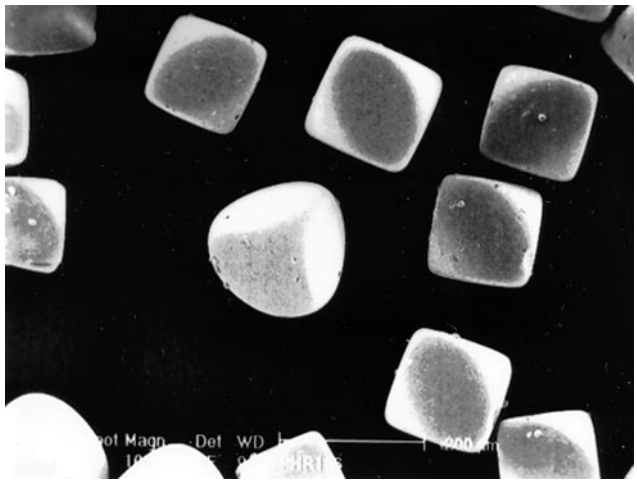

Fig. 1 Scanning electron micrograph of rounded truncated cubes of Mu-2

The X-ray diffraction pattern of Mu-2 was unambiguously indexed with a cubic *I*-centered cell with $a = 16.377(1)$ Å. The elemental analysis of the as-synthesized sample of Mu-2 gave the following composition (wt.%): Ga: 32.9; P: 13.6; F: 1.73; R: 14.4. This analysis is in good agreement with the electron microprobe analysis performed on the rounded truncated cubes. The amount of organic species was confirmed by quantitative ^1H liquid NMR spectroscopy (by dissolution of the sample in 6 M HCl) and 6 molecules were found per unit cell. From the ^{13}C CP-MAS solid-state NMR spectroscopy the amine is occluded in a protonated form (probably monoprotonated according to the structure determination).‡

The TG and DSC curves of as-synthesized Mu-2 were recorded under air on a Setaram TG/DSC111 thermoanalyser.

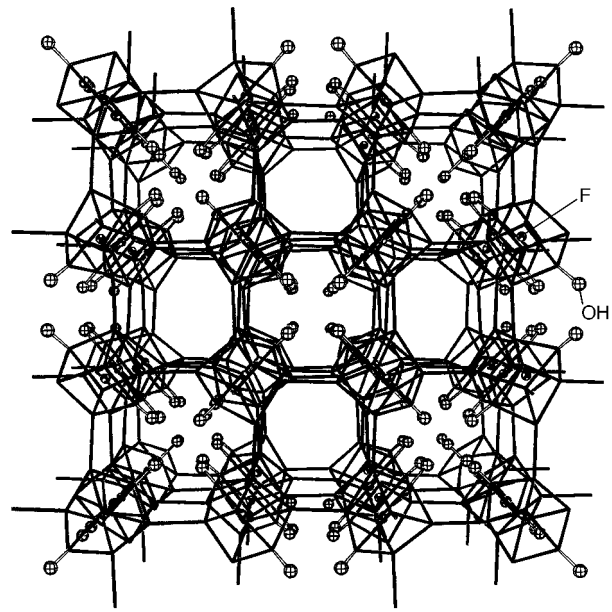

Fig. 2 Perspective view of the framework of the gallophosphate Mu-2 showing the two types of cage-like voids (one without OH group; the other with 8 T-OH groups); the Ga and P atoms are located at the vertices

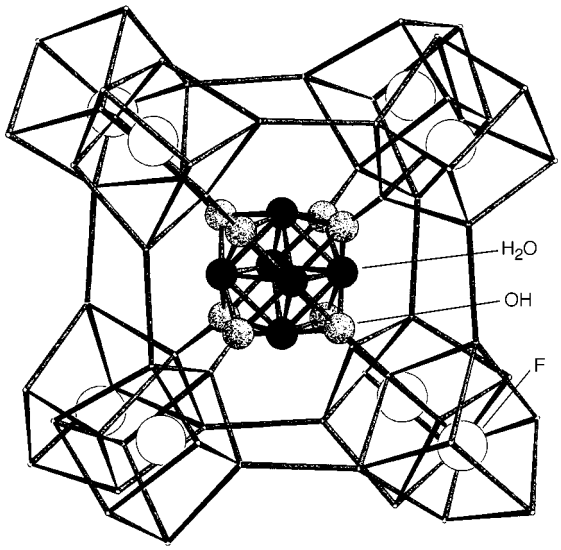

Fig. 3 The $(OH)_8(H_2O)_6$ cluster surrounded by eight D4Rs

Two broad endothermic peaks located at *ca*. 100 and 200 °C are observed. They correspond to the elimination of the physisorbed water molecules, the dehydroxylation of the T-OH groups and the removal of the fluoride anions (mass loss: 7.2%). The second mass loss (*ca*. 14.4%) corresponds to the removal of the organic species (several exothermic peaks on the DSC curve) and is achieved after calcination at 1000 °C. This new gallophosphate shows a low thermal stability. The structure collapses at *ca*. 300 °C and the cristobalite-type gallophosphate crystallizes at 600 °C.

The ^{19}F MAS solid-state NMR spectrum of Mu-2 displays a single signal at −72 ppm (relative to $CFCl_3$). Such a chemical shift value was previously found for the LTA- and CLO-type gallophosphates and is unambiguously assigned to fluoride anions trapped in the D4R units of the structure.

Taking into account all of the results and the density measurement (d_{mes} = 2.48 kg m^{-3}), the unit cell formula of Mu-2 is $Ga_{32}P_{32}O_{120}(OH)_{16}F_6(C_9H_{21}N_2)_6{\cdot}12H_2O$.

The structure analysis based on single crystal and powder X-ray data§ revealed that Mu-2 has a novel framework topology (Fig. 2). The gallophosphate framework of Mu-2 can be completely built from D4Rs as the fundamental building blocks. As observed from ^{19}F NMR spectroscopy, the D4Rs are occupied by a fluoride anion (according to the chemical analysis the occupancy factor is 0.75). Each $[Ga_4P_4O_{15}(OH)_2F]$ building block is interconnected with six other building blocks *via* common oxygen atoms. The remaining two corners of the D4R are T-OH groups (one P-OH and one Ga-OH). The interconnection of the D4Rs forms a three-dimensional but interrupted framework which has a three-dimensional pore system of 8MR pore openings. The framework which shows a strict alternation of phosphorus and gallium atoms at the T sites possesses two types of cage-like voids. The first type of cage (six per unit cell) does not contain any OH groups, whereas the second one (two per unit cell) displays 8 T-OH groups. The protonated 4-amino-2,2,6,6-tetramethylpiperidine occluded into the first type of cage (with a free volume of *ca*. 500 Å^3) is disordered.

An interesting feature of this structure is the $(OH)_8(H_2O)_6$ cluster (Fig. 3) present in the second type of cage. The sixteen T-OH groups of the D4Rs point either to the origin (0, 0, 0) or the center of the unit cell ($\frac{1}{2}$, $\frac{1}{2}$, $\frac{1}{2}$) such that the OH groups are arranged in two $(OH)_8$ cubes [the O–O distance between neighboring hydroxyl groups is 2.85(1) Å]. The six water molecules which are located close to the middle of the cube faces form hydrogen bridges to each other and the hydroxyl groups. The center of the $(OH)_8(H_2O)_6$ cluster, however, is vacant.

Notes and References

† E-mail: j.patarin@univ-mulhouse.fr

‡ For the structure determination 2885 intensities from a twinned single crystal were collected on a four circle Syntex R3 diffractometer in omega scan mode. 1014 reflections remained after merging and were used for the structure analysis based on the SHELXTL program system.[10] The structure was solved by direct methods.

§ The XRD powder data were recorded on a Siemens D5000 diffractometer with a linear 6° position sensitive detector in Debye–Scherrer geometry (Ge monochromator, λ = 1.5406 Å). The Rietveld refinement (2θ range = 7–97°, space group $I23$, number of observations = 3790, number of reflections = 404, number of structural parameters = 40) performed with the XRS-82 program[11] converged to R_F = 0.077, R_{wp} = 0.107 while the statistically expected R_{exp} is 0.113. A detailed description of the structure including the atomic coordinates, displacement parameters, bond lengths and angle of Mu-2 will be published elsewhere.[12] CCDC 182/928.

1 J. B. Parise, *J. Chem. Soc., Chem. Commun.*, 1985, 606.
2 J. L. Guth, H. Kessler, J. M. Higel, J. M. Lamblin, J. Patarin, A. Seive, J. M. Chezeau and R. Wey, in *Zeolite Synthesis*, ed. M. L. Occelli and H. E. Robson, ACS, Washington, DC, 1989, p. 176.
3 M. Estermann, L. B. McCusker, C. Baerlocher, A. Merrouche and H. Kessler, *Nature*, 1991, **352**, 320.
4 A. Merrouche, J. Patarin, M. Soulard, H. Kessler and D. Anglerot, in *Molecular Sieves—Synthesis of Microporous Inorganic Material*, ed. M. L. Occelli and H .E. Robson, Van Nostrand Reinhold, New York, vol. 1, 1992, p.384.
5 G. Férey, *J. Fluorine Chem.*, 1995, **72**, 187.
6 S. Kallus, J. Patarin and B. Marler, *Microporous Mater.*, 1996, **7**, 89.
7 P. Reinert, J. Patarin, T. Loiseau, G. Ferey and H. Kessler, *Microporous Mesoporous Mater.*, in press.
8 T. Loiseau and G. Férey, *J. Solid State Chem.*, 1994, **111**, 407.
9 L. Schreyeck, P. Caullet, J. C. Mougenel, J. L. Guth and B. Marler, *Microporous. Mater.*, 1996, **6**, 259.
10 SHELXTL, Software package for crystal structure determination by Siemens Analytical X-ray Instruments, Inc., 1990.
11 Ch. Baerlocher, X-Ray Rietveld System XRS-82, Institut für Kristallographie und Petrographie, ETH, Zurich, 1982.
12 B. Marler, P. Reinert and J. Patarin, to be published.

Received in Bath, UK, 17th April 1998; 8/03423K

Formation of isocyanate species on the surface of mordenite-type zeolite catalysts for the reduction of NO by hydrocarbons with H_2O

Moon Hyeon Kim, In-Sik Nam*† and Young Gul Kim

Research Center for Catalytic Technology, Department of Chemical Engineering, School of Environmental Engineering, Pohang University of Science and Technology (POSTECH)/Research Institute of Industrial Science and Technology (RIST), P.O. Box 125, Pohang 790-600, Korea

Surface isocyanate species with IR bands at 2274 and 2325 cm^{-1} play a crucial role for the maintenance of the water tolerance of HM, CuHM and CuNZA catalysts for NO reduction by hydrocarbons in the presence of H_2O.

Several reaction intermediates for the selective reduction of NO by hydrocarbons have been suggested.[1–7] However, their significance during the course of the reaction is still under investigation. Surface NO_x species such as nitrosyls (M–NO), dinitrosyls [M–$(NO)_2$], nitrites (M–NO_2 or M–ONO) and nitrates (M–NO_3 or M–ONO_2) have been found upon the adsorption of NO_x on the surface of zeolite catalysts containing transition metal ions[1–4] and have been regarded as plausible intermediates for this reaction system. The role of organic nitro- and nitrito-species on the catalyst surface was also examined by FTIR studies.[1,4,5] The formation of isocyanate species (–NCO) on Al_2O_3-based catalysts was observed during NO removal reaction with hydrocarbons containing C_3H_6, C_2H_2 or *n*-C_7H_{16}.[6] N-containing surface compounds such as C_2N_2, CN and NCO along with organic nitro-groups are observed over Na- and Ce-exchanged ZSM-5 catalysts.[5] Both surface nitrile and isocyanate compounds were also found over Cu-ZrO_2 catalyst for NO reduction by C_3H_6.[7] However, which of the proposed intermediates plays a major role for this reaction system is still controversial.

Kim *et al.*[8a] recently reported a couple of catalytic systems exhibiting high NO removal activity: HM or CuHM catalyst employing C_2H_4 as a reductant and CuNZA catalyst with C_3H_6. The initial NO conversion of 63% of HM and CuHM catalysts immediately dropped to 20% conversion when 7.3% H_2O was present in the feed gas stream, while a loss of NO conversion of $< 10\%$ was observed for the CuNZA catalyst.[8b] In the present study, it was of interest to examine from the viewpoint of reaction intermediates why the latter catalytic system exhibits stable deNO_x activity maintenance in the presence of H_2O in the feed gas stream while the former does not.

The preparation procedures and physicochemical properties of the mordenite-type zeolite catalysts HM, CuHM and CuNZA employed in this study have been previously described in detail elsewhere.[8] The copper contents of CuHM and CuNZA catalysts are 3.5 (Cu/Al = 0.24) and 2.0 wt.% (Cu/Al = 0.22), respectively. When the reaction mixture including 500 ppm of NO, 1000 ppm of C_2H_4 or 2000 ppm of C_3H_6 and 4.2% of O_2 was admitted onto the self-supporting catalyst wafers pretreated at 550 °C for 2 h in a laboratory designed IR cell, the surface species formed on the catalyst surface during the reduction with or without H_2O at 360 or 400 °C were examined by *in situ* FTIR spectroscopy at room temperature.

Fig. 1 shows IR spectra before and after the reaction in the absence of H_2O. The HM catalyst after reaction exhibited a strong absorption band at 2274 cm^{-1} and broad bands between 2200 and 1950 cm^{-1}. A similar peak at 2275 cm^{-1} was also observed for the CuHM catalyst. However, the IR spectra of the catalyst in the absorption range < 2200 cm^{-1} are clearly different compared to those over the HM catalyst, revealing a distinct peak at 1900 cm^{-1}. The CuNZA catalyst also shows the development of three bands in the wavenumber region 2400–1800 cm^{-1}, with maxima at 2325, 2032 and 1903 cm^{-1}. None of these bands are observed for the catalysts before the reaction.

The formation of isocyanate (–NCO) species has been observed for the reaction of NO and CO over supported noble metal catalysts: at 2270–2250 cm^{-1} for Al_2O_3[9] and 2320–2180 cm^{-1} for SiO_2[9,10] as a support. Prominent IR absorptions at 2270–2230 cm^{-1} of isocyanate species were also observed for NO reduction by hydrocarbons over SCR catalysts.[6,7] Hayes *et al.*[4] tentatively assigned the band at 2260 cm^{-1} observed for the reduction of NO with C_3H_6 over CuZSM-5 catalyst to an organic nitrile species, while Hoost *et al.*[3] suggested isocyanate for a similar band at 2295 cm^{-1}. An unassigned N-containing species containing C, N and O in a 1 : 1 : 1 ratio was formed on Na- and Ce-exchanged ZSM-5 catalysts[5] whereas the adsorption of isocyanic acid (HNCO) on CuZSM-5 catalyst led to a strong absorption peak at 2260 cm^{-1}.[11] With the absorption band at 2298 cm^{-1} for a CuZSM-5 catalyst adsorbing acetone oxime, Beutel *et al.*[12] also observed a similar IR peak at 2271 cm^{-1} when the catalyst was treated with an aqueous NaNCO solution. Moreover, HCN and C_2N_2 chemisorbed on SiO_2 as SiCN and SiNC could be easily converted into SiNCO by heating in an oxygen atmosphere, as previously reported by Morrow and Cody.[13]

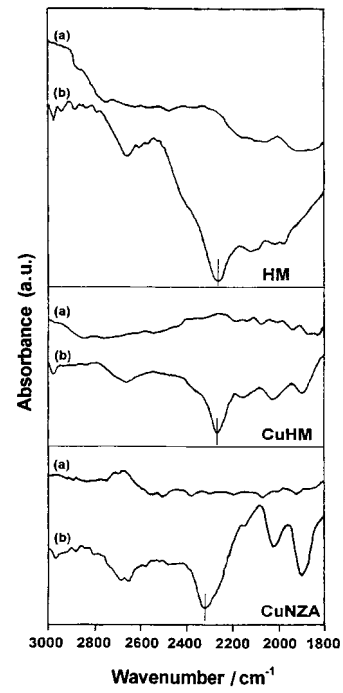

Fig. 1 IR spectra of mordenite-type zeolite catalysts: (a) before reaction; (b) after reaction without H_2O. Reaction conditions: NO 500 ppm, C_2H_4 1000 (HM and CuHM) or C_3H_6 2000 ppm (CuNZA), O_2 4.2% and T = 360 (HM and CuHM) or 400 °C (CuNZA).

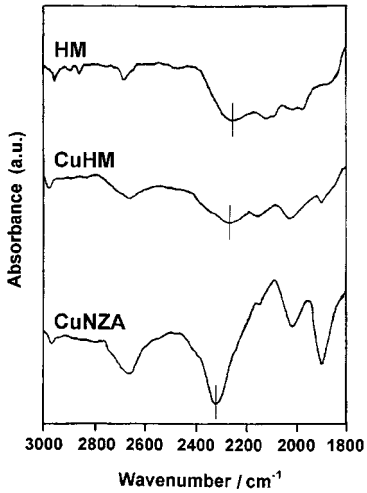

Fig. 2 IR spectra of mordenite-type zeolite catalysts after reaction with H_2O. Reaction conditions: NO 500 ppm, C_2H_4 1000 (HM and CuHM) or C_3H_6 2000 ppm (CuNZA), O_2 4.2%, H_2O 7.3% and T = 360 (HM and CuHM) or 400 °C (CuNZA).

Based upon the previous studies, the absorption bands at 2274 and 2325 cm^{-1} (Fig. 1) may be attributed to isocyanate species formed on the surface of the zeolite catalysts. The same species was also observed over CuZSM-5 catalyst for NO reduction by C_3H_6, but not with C_2H_4.[11] However, its formation on the mordenite-type zeolite catalysts was observed, regardless of the types of reductant employed in the present study, which is also in good agreement with the IR study for NO reduction by C_2H_4 and C_3H_6 over CuZSM-5.[14]

Three major nitrosyl complexes such as Cu^{2+}–NO, Cu^{+}–NO and Cu^{2+}–$(NO)_2$ are commonly observed for Cu-exchanged zeolites upon the adsorption of NO.[2,15] It is generally known that the surface NO_x species on the zeolite catalysts exhibit absorption bands at 1895–1910 cm^{-1}.[2–4,11] Therefore, the peaks at 1900 and 1903 cm^{-1} over CuHM and CuNZA catalysts are primarily due to the formation of NO bonded to isolated Cu^{2+} sites on the catalyst surface. This is clear from the fact that no absorption in this wavenumber region occurred for the copper-free catalyst, HM. The identification of the bands in the region 2200–1950 cm^{-1}, notable at 2148 and 2030 cm^{-1}, is less straightforward; they may arise from carbonyl species formed on the catalyst surface.

To examine the effect of H_2O on the formation of the –NCO species during the reduction of NO by hydrocarbons, the IR spectra of the three catalysts were examined in the presence of 7.3% H_2O, as shown in Fig. 2. The absorption intensity of the –NCO species at *ca*. 2274 cm^{-1} significantly decreased for the synthetic mordenite catalysts, HM and CuHM in the presence of water, while no notable change was found for the CuNZA catalyst. However, the peaks between 2200 and 1950 cm^{-1} still maintain their intensity, regardless of the presence of H_2O in the feed gas stream. Reduction of the –NCO band by H_2O adsorbed on the surface of Al_2O_3-supported Cu–Cs oxide catalyst has also been reported.[6] However, no difference in the peak intensities for the catalyst exposed to gas phase water and for the hydrated catalyst was observed.

HM and CuHM catalysts exhibited a loss of NO removal activity of $>45\%$ with 7.3% of H_2O in the feed gas stream[8b] which is in accord with the dramatic reduction of the absorption band of the –NCO species on the surface of the catalysts. The significant loss of the deNO_x efficiency of the catalysts for the NO removal reaction in the presence of H_2O is primarily due to the competitive adsorption of NO and H_2O on the catalyst surface as well as of hydrocarbons and H_2O.[8b] The alteration of NO removal activity by H_2O however, was apparently negligible for the CuNZA catalyst. It should be noted that the adsorption capacity of NO and hydrocarbons on CuNZA catalyst was also maintained with H_2O in the feed gas stream.[8b] This indicates that the feed of H_2O to the catalyst surface does not suppress the formation of the reaction intermediate on the catalyst surface (see Fig. 2) and may be why the CuNZA catalyst exhibits the strong water tolerance found in the previous study.[8b]

In conclusion, a surface isocyanate species was formed on mordenite-type zeolite catalysts for the reduction of NO by hydrocarbons, regardless of the reductant employed. This indicates that the species plays a crucial role for NO removal reaction with hydrocarbons over the catalysts. The formation of –NCO species on the catalyst surface is also critical for the maintenance of NO removal activity when H_2O is present in the feed gas stream.

Notes and References

† E-mail: isnam@postech.ac.kr

1 Y. Li, T. L. Slager and J. N. Armor, *J. Catal.*, 1994, **150**, 388.
2 J. Valyon and W. K. Hall, *J. Phys. Chem.*, 1993, **97**, 1204.
3 T. E. Hoost, K. A. Laframboise and K. Otto, *Appl. Catal. B*, 1995, **7**, 79.
4 N. W. Hayes, R. W. Joyner and S. Shapiro, *Appl. Catal. B*, 1996, **8**, 343.
5 C. Yokoyama and M. Misono, *J. Catal.*, 1994, **150**, 9 and references therein.
6 Y. Ukisu, S. Sato, A. Abe and K. Yoshida, *Appl. Catal. B*, 1993, **2**, 147.
7 C. Li, K. A. Bethke, H. H. King and M. C. Kung, *J. Chem. Soc., Chem. Commun.*, 1995, 427.
8 M. H. Kim, I.-S. Nam and Y. G. Kim, (*a*) *Appl. Catal. B*, 1995, **6**, 297; (*b*) *Appl. Catal. B*, 1997, **12**, 125.
9 W. C. Hecker and A. T. Bell, *J. Catal.*, 1984, **85**, 389 and references therein.
10 F. Solymosi and J. Rasko, *Appl. Catal.*, 1984, **10**, 19.
11 I. C. Hwang, D. H. Kim and S. I. Woo, *Catal. Lett.*, 1996, **42**, 177.
12 T. Beutel, B. J. Adelman and W. M. H. Sachtler, *Catal. Lett.*, 1996, **37**, 125.
13 B. A. Morrow and I. A. Cody, *J. Chem. Soc., Faraday Trans. 1*, 1975, **71**, 1021.
14 F. Radtke, R. A. Koeppei and A. Baiker, *J. Chem. Soc., Chem. Commun.*, 1995, 427.
15 T. Cheung, S. K. Bhargava, M. Hobday and K. Foger, *J. Catal.*, 1996, **158**, 301.

Received in Cambridge, UK, 2nd June 1998; 8/04133D

A concise stereoselective synthesis of the C-aromatic taxane skeleton: an application of novel sequential transacetalation oxonium ene cyclization

H. R. Sonawane,*† Dilip K. Maji, G. H. Jana and G. Pandey

Division of Organic Chemistry (Technology), National Chemical Laboratory, Pune-411008, India

A three-step sequence for the construction of the C-aromatic taxane nucleus from easily available A-ring unit 2 and C-aromatic unit 3 is reported; $SnCl_4$ promoted reaction of 4, presumably *via* the diastereoselective oxonium ene cyclisation reaction of 6a formed *in situ*, delivers cyclic ether 5a which on treatment with Bu^{n}Li provides C-aromatic taxane skeleton 8.

The remarkable chemotherapeutic potential and the unique molecular framework of taxol[1] **1** have stimulated enormous synthetic efforts towards the synthesis of taxane diterpenoids.[2] Although five different total syntheses of **1** have been reported[3] in recent years, interest towards the development of new synthetic methods to acquire potent taxol analogues continues to grow. In this context, one of the long standing problems has been the construction of the sterically congested central eight-

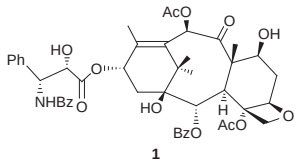

1

membered B-ring. In view of the known difficulties stemming from the high degree of ring strain and the transannular interactions associated with the direct cyclooctane annulation process, a recourse to indirect methods such as fragmentation of bicyclic systems, ring contraction and ring expansion have been developed.[4] For the purposes of construction of the taxane skeleton, particularly *via* C_{10}–C_{11} bond formation as the key step, the methods available are limited to the Heck reaction,[5] the Kishi–Nozaki coupling reaction[6] and the intramolecular nitrile oxide cyclization reaction.[7] Moreover, the application of these methods is severely restricted due to their substrate-specific nature and also the difficulty encountered in deriving the required substrates. In this context, we have initiated a new convergent approach starting with B-*seco*-taxane **A** wherein the critical bond connection between C_{10}–C_{11} was envisioned to arise from the α-alkoxycarbenium ion generated from **B** *via* treatment with a Lewis acid (Scheme 1). This approach was expected to help overcome the known unfavorable entropic and transannular interactions associated with the direct cyclooctane annulation using an acyclic precursor. We report herein our successful preliminary results for the construction of taxane skeleton **8** *via* the oxonium ene cyclisation reaction of **4** as the key step.

The precursor compound **4** was readily assembled by the reaction of aryllithium reagent **3**, prepared *via* the reductive metalation of the diethylacetal of 2-iodophenylacetaldehyde[8] using Bu^{n}Li, with compound **2** (Scheme 2). The utility of chiral A-ring unit **2** derived from α-pinene in the preparation of B-*seco*-taxanes has recently been reported by us.[9] The substrate **4** (75%) was found to be a mixture of **4a** (1*R**,2*R**) and **4b** (1*R**,2*S**) in the ratio of 3.4:1, established from the ^{1}H NMR spectral data.[10] Since the separation of individual diastereomers

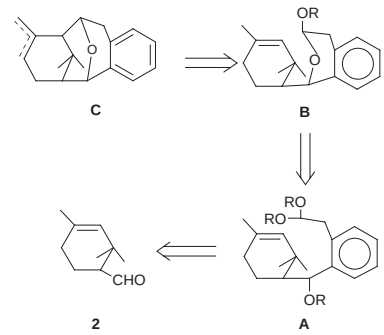

Scheme 1

was found to be difficult, it was decided to use the mixture of isomers for the next step.

Addition of $SnCl_4$ (2.5 equiv.) to a stirring solution of **4** in CH_2Cl_2 at −60 °C for 3 h, followed by quenching of the reaction mixture with saturated aqueous NH_4Cl, usual workup and purification *via* silica gel column chromatography, afforded compound **5a** in 32% yield (Scheme 3). The ^{1}H and ^{13}C NMR spectra of **5a** confirmed its structure and indicated that it possessed a complete taxane core incorporating an *endo*-ether linkage connecting C_2 and C_{10} in the central eight-membered B-ring. The structural assignment was further supported by comparing the ^{1}H NMR data from the structurally related C-aromatic *exo/endo* atropisomeric taxanes reported by Shea.[11]

In order to understand the mode of formation of **5a** from **4**, the reaction was also examined using two more Lewis acids, *i.e.* $TiCl_4$ and $BF_3{\cdot}Et_2O$ (Table 1). It was noticed that these Lewis acids are equally effective in promoting the formation of **5a**. For example, the reaction of 1 equiv. of $SnCl_4$ with **4** provided transacetalation product **6** in good yield (65–74%) as a mixture of diastereomers (suggested on the basis of the ^{1}H NMR spectrum). Interestingly, when **6** was separately treated with $SnCl_4$ (1.5 equiv.), it was readily transformed to compound **5a**, thus, revealing the nature of the overall transformation[12] (Scheme 3). The only other report that deals with a similar type of strategy for the construction of the taxane skeleton is from Hitchcock and Pattenden,[13] who demonstrated the efficacy of a

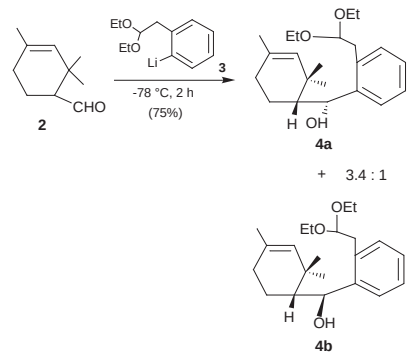

Scheme 2

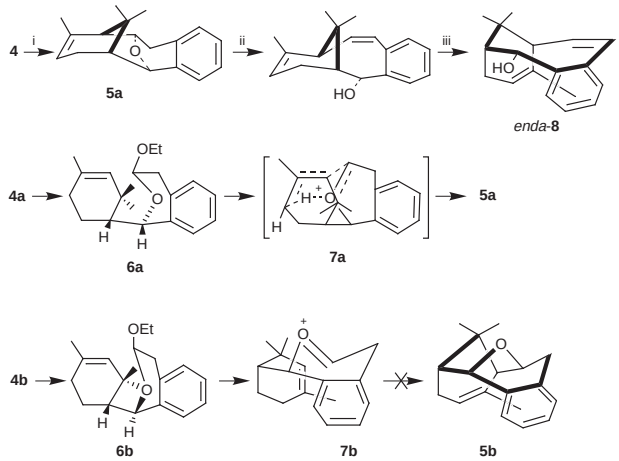

Scheme 3 *Reagents and conditions*: i, $SnCl_4$ (2.5 equiv.), −60 °C, 3 h, CH_2Cl_2; ii, Bu^nLi, THF, room temp., 7 h; iii, heat

Table 1 Results of Lewis acid-promoted cyclisations

Compound	Lewis acid (equiv.)	*T*/°C	Product	Yield (%)
4	$SnCl_4$ (2.5)	−60	**5a**	32
4	$SnCl_4$ (1.1)	−78	**6**	74
6	$SnCl_4$ (1.5)	−60	**5a**	41
4	$TiCl_4$ (1.1)	−78	**6**	72
4	$BF_3{\cdot}Et_2O$ (1.1)	−78	**6**	65

tandem radical macrocyclization–transannular sequence using an appropriately functionalised A-ring unit.

Initially, the high stereoselectivity observed in the overall cyclization process, *viz.* **4**→**5a**, appeared somewhat intriguing. However, mechanistic considerations along with an examination of the molecular models helped us greatly in increasing our understanding. Mechanistically, in analogy with Overman's proposal,[14] a concerted oxonium ion ene cyclization may well be visualized in the formation of *exo*-**5a** from oxonium ion **7a**, derived from the major isomer **6a** involving a favorable six-membered transition state. The lack of the possibility of such a transition state, due to the unfavorable geometry of the oxonium ion **7b**, from the minor isomer **6b** precludes it from undergoing an analogous type of cyclization that would lead to **5b**.

In order to transform **5a** into a molecule having taxane skeleton **8** it was treated with Bu^nLi[15] at room temperature, which furnished crystalline compound *endo*-**8**[16] (78%; mp 141 °C), instead of the corresponding *exo*-**8**. This observation may possibly be explained by considering a thermal *exo* to *endo* atropisomerization[17] during the work-up stage. The structure and stereochemical assignment of *endo*-**8** follows from a detailed ^1H NMR decoupling experiment and selected coupling constants. Finally, the structure was confirmed by a 2D-COSY NMR experiment.

In conclusion, we have described a facile entry into a functionalized C-aromatic taxane ring system employing an oxonium ene cyclization reaction as the key step for the first time. The potential of this method to construct the ABC system of taxol is under investigation.

We are grateful to Dr M. Vairaman, IICT, Hyderabad, for prompt help in providing HRMS data. D. K. M. and G. H. J. thank CSIR and DST, New Delhi, India, for the award of fellowships and financial assistance, respectively.

Notes and References

† E-mail: pandey@ems.ncl.res.in

1 M. C. Wani, H. L. Taylor, M. E. Wall, P. Coggon and A. T. McPhail, *J. Am. Chem. Soc*., 1971, **93**, 2325.
2 K. C. Nicolaou, M-W. Dai and R. K. Guy, *Angew. Chem., Int. Ed. Engl*., 1994, **33**, 15; A. N. Boa, P. R. Jenkins and N. J. Lawrence, *Contemp. Org. Synth.*, 1994**,** 47.
3 I. Shiina, H. Iwadare, H. Sakoh, M. Hasegawa, Y. Tani and T. Mukaiyama, *Chem. Lett*., 1998., 1 and references cited therein.
4 N. A. Petasis and M. A. Patane, *Tetrahedron*, 1992, **48,** 5757.
5 J. J. Masters, J. T. Link, L. B. Snyder, W. B. Young and S. J. Danishefsky, *Angew. Chem., Int. Ed. Engl.*, 1995, **34**, 1723.
6 M. H. Kress, R. Ruel, W. H. Miller and Y. Kishi, *Tetrahedron Lett*., 1993**, 34,** 5999.
7 Y. Hirai and H. Nagaoka, *Tetrahedron Lett.*, 1997, **38**, 1969.
8 J. E. leffler and A. F. Wilson, *J. Org. Chem*., 1960, **25**, 424.
9 H. R. Sonawane, S. G. Sudrik, M. M. Jakkam, A. Ramani and B. Chanda, *Synlett.*, 1996, 175. In the present work the experiment was carried out with (±)-**2** which was prepared by the Diels–Alder reaction of 2,4-dimethylpenta-1,3-diene and acrolein catalysed by $BF_3{\cdot}OEt_2$.
10 Separation of **4a** and **4b** *via* derivatisation and cyclisation is underway. *Selected data* for **4**: $\nu_{max}(CHCl_3)/cm^{-1}$ 3450, 2900, 1360, 1210; $\delta_H(CDCl_3$, 200 MHz) 7.6–7.1 (m, 4H), 5.3 (s, 0.77H), 5.05 (s, 1H), 4.85 (d, *J* 10.8, 0.23H), 4.7–4.55 (m, 1H), 3.8–3.55 (m, 2H), 3.55–3.3 (m, 2H), 3.2–2.9 (m, 2H), 2.0–1.5 (m, 8H), 1.4–1.0 (m, 12H) (Calc. for $C_{22}H_{34}O_3$: C, 76.30; H, 9.82. Found: C,75.99; H, 9.43%).
11 R. W. Jackson, R. G. Higby, J. W. Gilman and K. J. Shea, *Tetrahedron*, 1992, **48**, 7013.
12 L. F.Tietze, *Chem. Rev*., 1996, **96**, 115.
13 S. A. Hitchcock and G. Pattenden, *Tetrahedron Lett*., 1992, **33**, 4843.
14 For an elegant application of this concept in the synthesis of Δ^4-oxocene, see T. A. Blumenkopf, G. C. Look and L. E. Overman, *J. Am. Chem. Soc*., 1990, **112**, 4399.
15 M. E. Jung and S. J. Miller, *J. Am. Chem. Soc*., 1981, **103**, 1984.
16 *Selected data* for **8**: ν_{max}(Nujol)/cm^{-1} 3273, 2950, 2800, 1254, 1021; $\delta_H(CDCl_3$, 200 MHz) 7.55 (d, *J* 7.6, 1H), 7.2 (dt, *J* 6.4, 1.2, 1H); 7.1 (dt, *J* 6,1.2, 1H), 7.0 (d, *J* 7.4, 1H), 6.6 (d, *J* 10.7, 1H), 6.0 (dd, *J* 11.7, 1H), 5.1 (s, 1H), 4.55 (br s, 1H), 2.35 (d, *J* 9.2, 1H), 2.1 (br s, 2H), 1.7 (br s, 1H), 1.3 (s, 3H), 1.2 (d, *J* 1.2, 3H), 1.05 (s, 3H); $\delta_C(CDCl_3$, 50 MHz) 142.8, 135.9, 133.5, 132.1, 129.9, 126.5, 126.1, 125.6, 124.6, 120.5, 70.1, 49.9, 46.7, 32.9, 29.7, 26.1, 24.2, 22.8 (Calc. for $C_{18}H_{22}O$: 254.1670 (M+). Found: 254.1666).
17 M. Seto, K. Morihira, Y. Horiguchi and I. Kuwajima, *J. Org. Chem*., 1994, **59**, 3165.

Received in Cambridge, UK, 1st June 1998; 8/04084B

Direct synthesis of functionalized mesoporous silica by non-ionic alkylpolyethyleneoxide surfactant assembly

Roger Richer and Louis Mercier*†

Department of Chemistry and Biochemistry, Laurentian University, Sudbury, Ontario, Canada P3E 2C6

The co-condensation of tetraethoxysilane (TEOS) and organotrialkoxysilane [$(RO)_3SiR'$] assembled in the presence of structure-directing non-ionic polyethyleneoxide surfactant micelles provides a convenient neutral pH synthesis methodology for the one-step preparation of organically functionalized mesostructured materials.

The surfactant-directed synthesis of mesoporous molecular sieves, high surface area metal oxides (800–1400 $m^2\ g^{-1}$) with uniform pore sizes (20–100 Å in diameter), have in recent years commanded much attention in the field of materials chemistry.[1–4] Organically functionalized derivatives of such materials were produced by the incorporation or grafting of suitable moieties onto the surface of preformed mesostructured oxides,[5] producing highly effective adsorbents[6,7] and catalysts.[8] Subsequently, an alternate functionalization strategy was reported in which organosilane groups were directly incorporated into the mesostructures by a one-step synthesis procedure,[9–12] allowing the preparation of ordered porous materials with controlled chemical composition by stoichiometric adjustment of the synthesis mixture. Since cationic surfactants were used to prepare these materials, acid leaching was required to remove the templating micelles from the electrically charged frameworks, a treatment which sometimes lead to the structural decomposition of the materials.[11] The use of a non-electrostatic assembly strategy to prepare such functionalized mesostructures may therefore produce an electrostatically neutral framework, allowing the non-destructive removal of the structure-directing surfactant by simple solvent extraction.[13] Here, we report a new synthesis strategy for the one-step preparation of organically functionalized charge-neutral mesoporous silica using non-ionic alkylpolyethyleneoxide surfactants as structure-directing agents, namely Tergitol 15-S-12 $[CH_3(CH_2)_{14}(OCH_2CH_2)_{12}OH]$ and Triton-X100 $[(CH_3)_3C(CH_3)_2CCH_2C_6H_4(OCH_2CH_2)_{10}OH]$.

The non-functionalized mesostructured silicas MSU-1 and MSU-2 were prepared according to previously published assembly techniques,[4] using Tergitol 15-S-12 and Triton-X, respectively, as structure-directing surfactants. Functionalized derivatives of MSU-1 and MSU-2 were synthesized by stirring TEOS and mercaptopropyltrimethoxysilane (MPTMS) in solutions of Tergitol 15-S-12 (0.02 mol l^{-1}) or Triton-X100 (0.027 mol l^{-1}) at 308 K until clear mixtures formed, then NaF was added (the molar composition of each mixture was 0.1 surfactant: $1-x$ TEOS: x MPTMS:0.02 NaF, where x = 0, 0.02 or 0.05). After aging for 24 h, the resulting powders were filtered, air dried and washed by Soxhlet extraction over ethanol for 24 h. The functionalized mesostructures assembled using Tergitol-15-S-12 were thus labeled as MP-MSU-1-2% (x = 0.02) and MP-MSU-5% (x = 0.05), while those prepared from Triton-X100 were designated as MP-MSU-2-2% (x = 0.02) and MP-MSU-5% (x = 0.05). The mesostructures were characterized by powder X-ray diffraction (XRD), N_2 sorptometry, elemental analysis (for S), ^{29}Si MAS-NMR and scanning electron microscopy (SEM). The materials' physical properties obtained from these techniques are given in Table 1.

The low angle powder XRD patterns of the MSU-1 and MSU-2 materials featured dominant first order (d_{100}) diffraction peaks (with d-spacings of 51 and 66 Å, respectively, see Table 1) and broad, low intensity second order (d_{200}) peaks at higher incidence angle. These represent features typical of ordered mesostructured oxides with 'wormlike' pore channel structures, as expected of materials assembled using either neutral[2] or non-ionic surfactants.[3,4] As organosilane moieties are incorporated into the mesostructures, the d_{100} peaks of the materials become shifted to higher diffraction angles, indicating progressive contractions of the lattice d-spacings upon functional group loading (Table 1). Although this effect is slight for the MP-MSU-1 mesostructures (a contraction of only 6% from MSU-1 to MP-MSU-1-5%), significant contraction of the MSU-2 lattice is observed (by 39% from MSU-2 to MP-MSU-2-5%). Moreover, the intensities of the (100) peaks for the functionalized materials were lower in intensity compared to their respective parent mesostructures, and the higher order (200) reflections are no longer detected. Lypophilic interactions between the organosilane molecules and the hydrophobic core of the micelles are likely to result in the deeper penetration of the organosilane molecules within the micelle than do the TEOS molecules. This will cause the micelle structure to 'open-up' and allow TEOS molecules to migrate deeper within the micelle, where they subsequently crosslink with the organosilane functionalities. The perturbations thus caused to the micelle organization thus results in the assembly of more disordered materials with shorter lattice spacings.

The N_2 adsorption isotherms of MSU-1 [Fig. 1(a)] and MSU-2 [Fig. 1(b)] both featured well resolved inflexions at partial pressures between 0.3 and 0.6, demonstrating the existence of uniform mesopore channels with diameters of 32 Å [Fig. 1(c)] and 41 Å [Fig. 1(d)], respectively. No appreciable hysteresis loops were observed in any of the isotherms' desorption

Table 1 Physical characteristics of mesostructures and their functionalized derivatives

Sample	d_{100} lattice spacing/Å	BET surface area/$m^2\ g^{-1}$	Pore diameter/Å[a]	S content/ mmol g^{-1}	Organosilane content (%)[b]
MSU-1	51	1225	32	0	0
MP-MSU-1-2%	50	943	26	0.40	2.6
MP-MSU-1-5%	48	858	22	0.87	5.8
MSU-2	66	1018	41	0	0
MP-MSU-2-2%	50	1176	27	0.47	3.0
MP-MSU-2-5%	40	763	—	1.1	7.7

[a] Measured using the Horvath–Kawazoe pore size distribution model.[14] [b] Percentage of Si atoms present as organosilane with respect to total Si content.

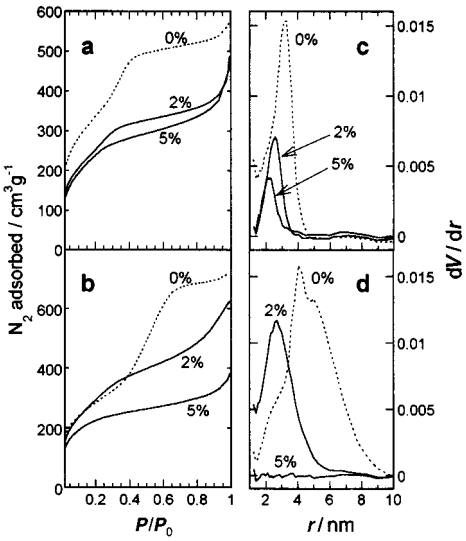

Fig. 1 Left: N_2 adsorption isotherms of (a) MSU-1 (dotted curve) and MP-MSU-1 materials (solid curves), and of (b) MSU-2 (dotted curve) and MP-MSU-2 materials (solid curves). Right: background-substracted Horvath–Kawazoe pore diameter (r) distribution[14] of (c) MSU-1 (dotted curve) and MP-MSU-1 materials (solid curves), and of (d) MSU-2 (dotted curve) and MP-MSU-2 materials (solid curves).

branches, denoting the absence of bottlenecking in the pore channels. The surfactant extraction technique was thus effective in removing the surfactant from the pore channels without damaging the structure of the synthesized materials. The large BET surface areas measured were likewise consistent with the presence of highly porous materials (Table 1). The isotherms of the functionalized derivatives MP-MSU-1-2% [Fig. 1(a)] and MP-MSU-2-2% [Fig. 1(b)] were also indicative of mesoporosity, but the shifts observed in the positions of the inflexions (to between 0.1 and 0.3) show that constrictions in the pore channels have arisen. This can be attributed to both the lattice contractions and to the presence of the mercaptopropyl (MP) moieties which line the pore channel walls, thus reducing the pore diameters and volumes of the mesostructures [Fig. 1(c) and (d)]. Despite pore constriction, the functionalized materials nonetheless retained the very high surface areas characteristic of mesoporous molecular sieves (Table 1). The isotherms of the increasingly loaded MP-MSU-1-5% and MP-MSU-2-5% mesostructures demonstrated an even greater constriction of the pores (Table 1), resulting in further reduction of total pore volume in MP-MSU-1-5% [Fig. 1(c)] and no discernable porosity in MP-MSU-2-5% [Fig. 1(d)]. The significant decreases in surface areas for both of these materials (Table 1) further substantiate these observations. Since all of the functionalized materials are shown to exhibit crystallographic ordering according to their XRD patterns, the incremental featurelessness observed in their N_2 isotherms can be explained by the influence of the increasing amounts of mercaptopropyl groups lining the framework channels, disrupting the uniformity of the pores and reducing their diameters.

The SEM images of the materials revealed aggregates of ultrafine spherical particles with a 'cotton ball'-like morphology. The particles appeared to be quite uniform in size, with diameters averaging about 0.3 μm for all compositions. The minute sizes of these particles creates significant textural porosity within the mesostructure aggregates, resulting in notable sloping of the nitrogen adsorption curves beyond the mesopore inflexions, as well as significant nitrogen uptake observed at relative pressures approaching unity [Fig. 1(a) and 1(b)].

The ^{29}Si MAS NMR spectra of the functionalized mesostructured (recorded with a 600 s pulse delay) denoted the presence of the following Si sites: Q^4 signals at −110 ppm [$(SiO)_4Si$], Q^3 signals at −101 ppm [$(SiO)_3SiOH$] (both corresponding to framework silica derived from hydrolyzed TEOS), and T^2 and T^3 signals (at −60 and −65 ppm, respectively) corresponding to the organosilane (mercaptopropylsilane) silicon atoms.[11] In all cases, the Q^4/Q^3 signal intensity ratios were close to 1.5, while the intensities of the T^2 and T^3 signals increased as a function of organosilane loading in the materials. By comparing the integrations of these NMR signals, in combination with the elemental analysis results (for S content), the functional group content in the mesostructures was deduced and expressed in Table 1 both in terms of S content and organosilane percentage. Although the amount of organosilane incorporated into the MP-MSU-1 materials was found to be close to that expected on the basis of the stoichiometry of the solution reaction mixture, the functional group loading in MP-MSU-2-2% and MP-MSU-2-5% exceeded this content by a factor of *ca*. 1.5 (Table 1). This suggests that preferential assembly of the organosilane molecules has occurred at the interface of the Triton-X micelles, denoting a greater attraction of the organosilane molecules to the surfactant's hydrophobic chain.

The one-step preparation of functionalized mesoporous silica by non-ionic surfactant assembly presents a clear advantage over methodologies involving charged quaternary ammonium surfactants, namely that it does not necessitate the use of potentially destructive acid leaching to remove the framework-bound surfactant from the mesostructures. Moreover, the assembly process described in this paper is achieved under neutral pH conditions, unlike the other direct-synthesis approaches which were performed in alkaline environments.[9–12] This feature connotes the possibility of incorporating organic functionalities that would be unstable or otherwise reactive under non-neutral pH conditions, such as strongly electrophilic functionalities. For example, we have preliminary experimental evidence which demonstrates the successful incorporation of chloroalkyl functionalities into mesostructured frameworks following the synthetic protocol described in this paper.

The authors would like to thank the Ontario Geosciences Centre (Sudbury, Ontario), Dr Allan Palmer (Natural Resources Canada, Nepean, Ontario) and Dr Glenn Facey (University of Ottawa NMR Lab) for providing instrumental support. We also gratefully acknowledge the Laurentian University Research Fund (LURF) for financial support.

Notes and References

† E-mail: lmercier@nickel.laurentian.ca

1 C. T. Kresge, M. E. Leonowicz, W. J. Roth, J. C. Vartuli and J. S. Beck, *Nature*, 1992, **359**, 710.
2 P. T. Tanev and T. J. Pinnavaia, *Science*, 1995, **267**, 865.
3 S. A. Bagshaw, E. Prouzet and T. J. Pinnavaia, *Science*, 1995, **269**, 1242.
4 E. Prouzet and T. J. Pinnavaia, *Angew. Chem., Int. Ed. Engl.*, 1997, **36**, 516.
5 D. Brunel, A. Cauvel, F. Fajula and F. DiRenzo, *Stud. Surf. Sci. Catal.*, 1995, **97**, 173.
6 L. Mercier and T. J. Pinnavaia, *Adv. Mater.*, 1997, **9**, 500.
7 X. Feng, G. E. Fryxell, L.-Q. Wang, A. Y. Kim, J. Liu and K. M. Kemner, *Science*, 1997, **276**, 923.
8 T. Maschmeyer, F. Rey, G. Sankar and J. M. Thomas, *Nature*, 1995, **378**, 159.
9 M. H. Lim, C. F. Blanford and A. Stein, *Chem. Mater.*, 1998, **10**, 467.
10 W. M. Van Rhijn, D. E. DeVos, B. F. Sels, W. D. Bossaert and P. A. Jacobs, *J. Chem. Soc., Chem. Commun.*, 1988, 317.
11 S. L. Burkett, S. D. Sims and S. J. Mann, *Chem. Commun.*, 1996, 1367.
12 C. E. Fowler, S. L. Burkett and S. J. Mann, *Chem. Commun.*, 1997, 1769.
13 D. J. Macquarrie, *Chem. Commun.*, 1996, 1961.
14 G. Horvath and K. J. Kawazoe, *J. Chem. Eng. Jpn.*, 1983, **16**, 470.

Received in Bloomington, IN, USA, 1st May 1998; 8/03285H

Typeset and printed by Black Bear Press Limited, Cambridge, England

ChemComm
FEATURE ARTICLE

Reductive cleavage and related reactions leading to molybdenum–element multiple bonds: new pathways offered by three-coordinate molybdenum(III)

Christopher C. Cummins

Department of Chemistry room 2-227, Massachusetts Institute of Technology, Cambridge, MA, 02139-4307, USA

Three-coordinate molybdenum(III) complexes comprise a new class of reactive-yet-isolable substances. Related to a well known class of metal–metal triple bonded dimers, the monomeric molybdenum(III) complexes supported by sterically-demanding *N-tert*-alkylanilide ligands offer previously unavailable synthetic routes to molybdenum–element multiple bonds. Terminal nitride, phosphide and carbide functionalities have been prepared from reactions with dinitrogen, white phosphorus and carbon monoxide, respectively.

Introduction

Professor Malcolm H. Chisholm of Indiana University has championed the chemistry of compounds containing Mo≡Mo and W≡W triple bonded moieties since the early 1970s.[1] For the most part, the compounds of interest have supporting amide (*e.g.* NMe_2) or alkoxide (*e.g.* OBu^t) ligands. Although chromium(III) does not exhibit a similar tendency to form unbridged metal–metal triple bonds, it was shown in seminal work by Bradley's group that the complex $Cr(NPr^i_2)_3$ **1** exists in discrete monomeric form.[2] Moreover, the compound manifests a trigonal-planar coordination geometry, along with a high-spin (quartet) ground state. Thus an interesting dichotomy arose between the chemistry of chromium(III), on the one hand, and that of molybdenum(III) and tungsten(III) on the other. The successful synthesis of a discrete monomeric molybdenum(III) entity would bridge this gap, and hints that such a species might be accessible *via* implementation of bulky amide ligands can be found in reported attempts at the synthesis of $Mo[N(SiMe_3)_2]_3$ **2**.[3] Note, indeed, that the hexamethyldisilazide ligand is known to support three-coordination for the 3d metals Sc through Co in the 3+ oxidation state, and that the remarkable amide $U[N(SiMe_3)_2]_3$ **3** is a monomer.[4]

Against the foregoing backdrop, we set out to explore complexes of the new amide ligand N(R)Ar [R = $(CD_3)_2CH_3$, Ar = 3,5-$C_6H_3Me_2$], and related derivatives.[5] Use of the $C(CD_3)_2CH_3$ substituent was deemed worthwhile as a ^2H NMR spectroscopic handle, and the choice of substituents was prompted by a desire to (i) avoid β-hydrogens, (ii) combine one roughly spherical substituent with one roughly planar substituent for efficient intramolecular packing, and (iii) use hydrocarbon-only building blocks so as to avoid decomposition pathways to which silylamides are prone, such as cyclometallation or N–Si bond cleavage.[6]

A ready synthesis of deuterated *N-tert*-butylanilides was found to consist of $[^2H_6]$acetone condensation with the desired substituted aniline, followed by treatment of the resulting imine with methyllithium.[5] The most widely successful ligand to date is that derived from deprotonation of *N*-$[^2H_6]$-*tert*-butyl-3,5-dimethylaniline with *n*-butyllithium. Crystallization from ether affords the white etherate $Li[N(R)Ar](OEt_2)$, which is suitable for reaction with transition metal halides.

Synthesis and characterization of three-coordinate complexes

Following the lead of Bradley's synthesis of $Cr(NPr^i_2)_3$ **1** from chromium(III) chloride and lithium diisopropylamide,[2] it was elected to investigate the reaction of $MoCl_3(THF)_3$[7] with $Li[N(R)Ar](OEt_2)$.[5] In this endeavour, the presence of a deuterium label in the ligand led to rapid identification of appropriate conditions for the synthesis of $Mo[N(R)Ar]_3$ **4**, the compound exhibiting a single ^2H NMR peak at δ *ca.* 64.[8] Various conditions were sampled, with the result that a 2 : 1 lithium amide to molybdenum chloride stoichiometry was deemed optimal (ostensibly to speed conversion to products) and that diethyl ether solvent gave the best results. The desired compound, $Mo[N(R)Ar]_3$ **4**, has been obtained in 60–80% isolated yield as a lipophilic orange–red crystalline substance.[9] Other variously substituted anilide ligands including the 'parent' $-N(Bu^t)Ph$,[9] the adamantyl-substituted derivatives –N(1-Ad)Ar and –N(2-Ad)Ar, and the mono-fluorinated derivative –N(R)(4-C_6H_4F)[10] have all provided corresponding three-coordinate tris-anilide complexes of Mo^{III} following the standard protocol developed for **4**.[9]

An important feature of the characterization of **4** is the fact, substantiated by X-ray crystallography,[9] that it exists in the solid as discrete mononuclear complexes with no short intermolecular contacts. As such, **4** and related derivatives constitute the first definitive examples of three-coordinate molybdenum. The geometry at molybdenum is trigonal planar. Thus, although Mo≡Mo triple bonds are known to be *ca.* 80 kcal mol^{-1} (1 cal = 4.184 J),[11] the substituents are sufficiently large in the present case to obviate dimerization.[12] A representative structure[9] is that of $Mo[N(R)Ar]_3$ **4**, shown in Fig. 1.

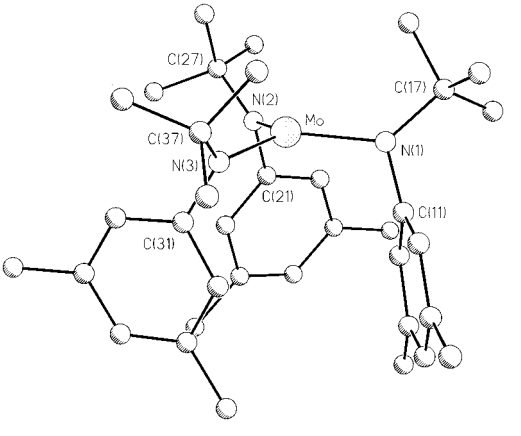

Fig. 1 Ball and stick representation of $Mo[N(R)Ar]_3$ **4**, from X-ray coordinates.[9] The Mo–N distances average 1.967(7) Å, and the sum of N–Mo–N angles is 357.7(3)°.

The X-ray crystallography studies show that the intramolecular packing conformation is one with the three 3,5-$C_6H_3Me_2$ substituents on one side of the trigonal plane and the three Bu^t groups on the other side. Another conformation that would

maximize the in-plane N to Mo π bonding is a 'two-up, one-down' arrangement of substituents; investigation of this alternative by molecular mechanics suggests that it is higher in energy by *ca.* 6 kcal mol^{-1} than the observed conformation.[12] Solution NMR spectra of Mo[N(R)Ar]$_3$ **4** are consistent with preservation of the pseudo-C_3 symmetric structure, with only a single –N(R)Ar environment being observed down to *ca.* −40 °C. EXAFS data collected at 10 K on frozen toluene solutions likewise were consistent with the pseudo-C_3 symmetric conformation.[9]

Also critical to an appreciation of the tris-anilide molybdenum(III) complexes is the fact that they are high spin, with all three d electrons unpaired. This is known from both solution and solid-state magnetic susceptibility studies, with μ_{eff} for the complexes being close to the spin-only value.[9] Symmetry arguments and computational studies[13] agrees that this should be the case, and indicate that the half-occupied orbitals possess σ (d_{x^2}) and π (d_{xz}, d_{yz}) symmetry with respect to the pseudo-C_3 axis. This is an interesting point to be recalled later in the bonding discussion pertaining to very stable nitrido complexes, *e.g.* N≡Mo[N(R)Ar]$_3$ **5**.

With regard to the properties of **4**, it should be noted that despite its coordinative unsaturation no reaction is observed with pyridine, triethylphosphine, or tetrahydrofuran (benzene, 25 °C). Thus, the compound is not a Lewis acid. If this result is to be attributed to electronic effects, then a reluctance to go low-spin (making the d_{z^2} orbital available) can be invoked. Otherwise, it can be suggested that the pyridine, PEt_3, and THF molecules are too large to access the molybdenum center. That more electron-deficient complexes such as Ti[N(R)Ar]$_3$ **6** display an η^3 bonding mode for the N(R)Ar ligand,[14] while the molybdenum complexes display strictly the η^1 bonding mode, can be taken as evidence that the Mo complexes are not overly electron-poor.

Reactions furnishing the nitrido linkage

Theoretical work has placed the N≡Mo bond dissociation enthalpy (BDE) at *ca.* 165 kcal mol^{-1}, nearly 75% of the value for the N≡N triple bond of dinitrogen.[13] This being the case, it is not surprising that many reactions have been found which, in effect, transfer a nitrogen atom to Mo[N(R)Ar]$_3$ **4**, giving rise to N≡Mo[N(R)Ar]$_3$ **5**. Compound **5** can thus be regarded as a thermodynamic sink in systems containing **4** and sources of a nitrogen atom. Also, **4** can be regarded as an example of an 'azophilic' complex, in much the same way that fragments poised to form strong bonds to oxygen [*e.g.* Ta(OSiBu$^t_3$)$_3$] **7** are regarded as oxophilic.[15] The notion of the extreme stability of **5** is further substantiated by electrochemical studies showing that the complex is highly resistant to both oxidation and reduction.

Geometric and electronic structure issues related to diamagnetic **5** are reminiscent of the discussion given above for **4**. A representative structure is that of NMo[N(Bu^t)Ph]$_3$ **8**, shown in Fig. 2.[9] As in the case of **4**, the aryl groups are close-packed on one side of the molecule, while the Bu^t groups now form a protective 'pocket' about the Mo≡N triple bond. The three d electrons unpaired in **4** are involved in **5** in making the σ and π bonds to the nitrido nitrogen, bonds which have the same symmetry as the orbitals (d_{z^2}, d_{xz} and d_{yz}) utilized in **4** for the unpaired electrons. Thus it can be seen that the molybdenum–anilide bonding is essentially unperturbed on going from **4** to **5** (a notion substantiated by bond length considerations), and that the conformation of the Mo[N(R)Ar]$_3$ fragment also remains essentially constant. Little reorganization is required for addition of a nitrogen atom to **4**.

During initial purifications of **4** by recrystallization (OEt_2, −40 °C), it was noted that solutions became purple if under N_2, but retained the orange–red color of **4** if maintained in an argon atmosphere. Solid **4** can be manipulated under N_2 without any observable decompostion, and 0.05 M solutions of **4** stored

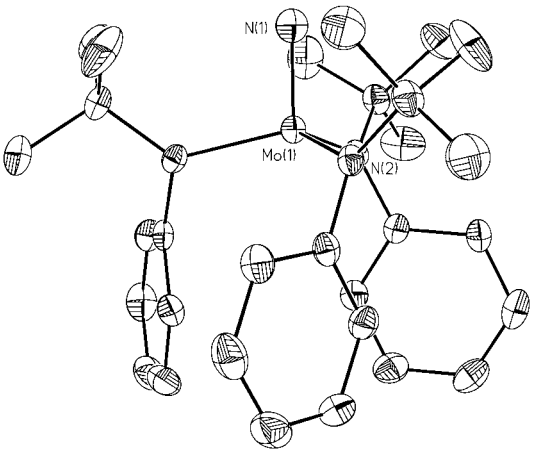

Fig. 2 Thermal ellipsoid representation of N≡Mo[N(Bu^t)Ph]$_3$ **8** from an X-ray study.[9] The Mo–$N_{nitride}$ bond resides on a crystallographic threefold axis. Ellipsoids are at the 35% probability level. The Mo–$N_{nitride}$ bond length is 1.658(5) Å, while the Mo–N_{amide} bond length is 1.979(2) Å.

under N_2 at room temperature degrade only slowly (*ca.* 5% per day). Naturally it was surmised that the purple color was due to N_2 chemistry, favored at low temperature either due to enhanced solubility of N_2 or to other entropic factors. In fact, at the time a purple N_2-bridged dimolybdenum(III) amido complex was already known, namely (μ-N_2)[Mo(Bu^t-Me$_2$SiNCH$_2$CH$_2$)$_3$N]$_2$ **9**.[16] Thus, the purification process for **4** was developed to involve exclusion of N_2. The full details of the reaction of **4** with N_2[9] were not elucidated until after **5** had already been characterized in full in the context of a nitrous oxide N–N cleavage reaction.[8]

Nitrous oxide

The existence of molybdenum(VI) nitrido-tris-amide complexes such as NMo(NPh$_2$)$_3$[17] **10** was an early indicator that **4** should function as an N-atom acceptor. This raised the question: what molecule might serve, with a minimum of reorganization, as a nitrogen-atom donor? One answer that came to mind was nitrous oxide, since loss of its terminal nitrogen atom would yield nitric oxide. The latter, while admittedly reactive, is a viable diatomic gas plausible as a leaving group in an N-atom transfer reaction. A problem with the selection of nitrous oxide as an N-atom donor was that literature precedent showed clearly that reducing metal complexes react with N_2O to give exclusive N–O bond cleavage, liberating N_2 as a stable byproduct.[18] This is why nitrous oxide is sometimes referred to as 'a clean oxidant'. Furthermore, on thermodynamic grounds one expects N–O bond cleavage, given that the N–O bond is the weaker by *ca.* 75 kcal mol^{-1} of the two bonds in the molecule.[19]

Experiments showed that solutions of **4** react smoothly with nitrous oxide (≥4 equiv.), **4** being converted rapidly (≤5 min, 25 °C) to a 1:1 mixture of nitride **5** and the similarly diamagnetic nitrosyl derivative (ON)Mo[N(R)Ar]$_3$ **11** with no observable intermediates [eqn. (1)].[8] Various conditions were

$$\underset{\mathbf{4}}{\text{Mo[N(R)Ar]}_3} \xrightarrow{N_2O} \underset{\mathbf{5}}{\text{N≡Mo[N(R)Ar]}_3} + \underset{\mathbf{11}}{\text{O=N=Mo[N(R)Ar]}_3} \quad (1)$$

sampled, and in no case was the ratio of nitride : nitrosyl perturbed from 1 : 1. Careful analysis of the reaction mixtures ruled out the presence of the (at the time unknown) oxo complex, Mo(O)[N(R)Ar]$_3$ **12**, which would have been produced if **4** has deoxygenated nitrous oxide. (As described below, brown paramagnetic oxo complex **12** can be synthesized independently.[20])

An independent synthesis of nitrosyl **11** was achieved by simple treatment of a solution of **4** with nitric oxide [eqn. (2)].[8]

$$\underset{\mathbf{4}}{\text{Mo[N(R)Ar]}_3} \xrightarrow{NO} \underset{\mathbf{11}}{\text{O=N=Mo[N(R)Ar]}_3} \quad (2)$$

The yellow, diamagnetic compound was produced in high yield, its synthesis being reminiscent of Bradley's classic synthesis of $(ON)Cr[N(SiMe_3)_2]_3$ **13**.[21] The synthesis and characterization of **11** in pure form permitted unambiguous assignment of its contribution to the NMR spectra from the N_2O reactions. Furthermore, the rapid and efficient combination of nitric oxide with **4** raised the possibility that free NO may be involved in the mechanism for nitrous oxide N–N bond cleavage by **4**. A second possibility is that the mechanism involves bimetallic activation of nitrous oxide, an appealing possibility that neatly accounts for the observed 1 : 1 ratio of **5** : **11**. The data in hand, however, are insufficient to pinpoint the mechanism of the splitting reaction. Definitive kinetic data will have to be acquired by stopped-flow techniques in order to settle the issue.

Characterization of nitride **5** was required for a complete interpretation of the data from nitrous oxide reactions with **4**. Interestingly, a clean route to **5** was discovered that involves treatment of **4** with mesityl azide.[8] This reaction, like the N_2O reaction, is unusual in comparison with known reactions of the substrate with reducing metal compounds. Normally, reductants elicit N_2 elimination from organoazides, giving metal imido derivatives.[22] Here, as demonstrated with a ^{15}N-labeling study, abstraction of the terminal nitrogen atom occurred, giving high-yield conversion to pale yellow **5**. As in the case of the N_2O activation reaction, the mechanism of mesityl azide N–N bond cleavage by **4** remains to be elucidated in detail. A key issue here is whether the N–N bond breaks before or after the N–C bond. The issue of a bimetallic activation mechanism is not important for the case of mesityl azide, since no evidence was found for the formation of the putative aryldiazenido complex $MesN{=}NMo[N(R)Ar]_3$. Based on subsequent synthetic studies, the latter is expected to be a stable, diamagnetic complex.

Dinitrogen

Having characterized nitride **5**, $N{\equiv}Mo[(R)Ar]_3$, a more detailed interpretation of the behavior of **4** in the cold under N_2 (1 atm) became possible.[23] Catalina Laplaza noticed that the purple solutions (presumed to contain $(\mu\text{-}N_2)\{Mo[N(R)Ar]_3\}_2$, **14**) lost the purple color upon standing for a couple of hours at 25 °C, and that peaks for nitride **5** were dominant in corresponding NMR spectra. This raised the exciting possibility that **4** was able to directly bind and split N_2, under mild conditions, and in the absence of any added reagents! Accordingly it was found that **4** could be converted in good yield to **14** by storage of a toluene solution under N_2 at −40 °C for 3–5 days. Subsequent warming to room temperature gave quantitative conversion to nitride **5** with the first-order kinetics and a $t_{1/2}$ of *ca.* 30 min.[23]

Subsequent work has included extensive characterization of the intermediate purple dinitrogen complex **14**, with its N–N bond length of 1.19(2) Å (EXAFS) and ν_{NN} of 1630 cm^{-1} (Raman).[9] The dinitrogen ligand bridges the two molybdenum centers in the typical[24] linear, end-on fashion, and the relatively high symmetry of the complex renders it paramagnetic, with a triplet ground state. It exhibits a single ^2H NMR signal at δ *ca.* 14. Isotopic labeling studies with $^{15}N_2$ permitted determination of a temperature-dependent primary kinetic isotope effect on the splitting reaction (conversion of **14** to **5**),[9] the magnitude of which was in accord with predictions based on the observed Raman ν_{NN} of $(\mu\text{-}^{15}N_2)\{Mo[N(R)Ar]_3\}_2$ and the diatomic oscillator approximation.[9]

The mechanism of dinitrogen cleavage by **4** has now also been studied in considerable detail by theoretical methods.[13] The important steps are [eqn.(3)] binding of dinitrogen by **4** to

$$\underset{\mathbf{4}}{Mo[N(R)Ar]_3} + N_2 \rightleftharpoons \underset{\mathbf{15}}{N_2Mo[N(R)Ar]_3} \quad (3)$$

give the low-spin 1 : 1 adduct, $(N_2)Mo[N(R)Ar]_3$ **15**, [eqn. (4)] trapping of **15** by a second equiv. of **4** to give dinuclear **14**, and [eqn. (5)] unimolecular fission of **14** at the N–N bond *via* a

$$\underset{\mathbf{4}}{Mo[N(R)Ar]_3} + \underset{\mathbf{15}}{N_2Mo[N(R)Ar]_3} \longrightarrow \underset{\mathbf{14}}{(\mu\text{-}N_2)[Mo\{N(R)Ar\}_3]_2} \quad (4)$$

$$\underset{\mathbf{14}}{(\mu\text{-}N_2)[Mo\{N(R)Ar\}_3]_2} \longrightarrow 2\ \underset{\mathbf{5}}{N{\equiv}Mo[N(R)Ar]_3} \quad (5)$$

zigzag (not linear) transition state to produce 2 equiv. of nitride **5**.

Experimentally we have not yet been able to observe the 1 : 1 adduct **15** directly, and we postulate that the binding of N_2 by **4** is rapid and reversible with only small equilibrium concentrations of **15** being present under 1 atm of N_2. To observe **15** directly, experiments are currently underway wherein **4** is being monitored by NMR and IR under large dinitrogen pressures. Theoretical studies predict that **15** will feature an end-on interaction between Mo and the N_2, and this is in accord with the structure of recently reported $N_2Mo(Me_3SiNCH_2CH_2)_3N$ **16**,[25] which has been shown (in contrast to **15**) not to be labile.

Although the reductive cleavage of dinitrogen to nitride by well-defined transition metal complexes in homogeneous solution was unprecedented prior to 1995,[23] it can be expected that more examples of this remarkable reaction type will eventually come to light. A very recent example comes from the labs of Floriani,[26] and it involves the use of niobium calixarene complexes. It is reasonable to speculate that the development of robust complexes capable of N_2 reductive cleavage will eventually result in applications in catalysis, the ultimate goal being the development of a homogeneous analog of the Haber–Bosch process.[27] The real obstacle to this type of application, currently, rests in the low reactivity of the very stable metal–nitrido functional group—*e.g. ca.* 165 kcal mol^{-1} for the Mo≡N bond in $NMo[N(R)Ar]_3$.[13]

Nitrogen atom transfer

Intermetal nitrogen atom transfer is a reaction type known for less than a decade, and it has the attractive feature of providing a means for breaking a metal–nitrogen triple bond under mild conditions in homogeneous solution.[28] Although such reactions—in which a neutral N atom passes completely from one metal to another with breaking of one M≡N triple bond and formation of a new one—have been proposed to proceed by μ_2-N atom-bridged intermediate complexes,[29] experimental verification of this has come only recently.[10]

A question one might ask concerns the degree to which the spectator ligands in a nitrido metal complex attenuate the affinity of the metal fragment for the N atom. In an experiment[30] designed to compare alkoxides with anilides, $Mo[N(R)Ar]_3$ was treated with Chisholm's alkoxynitride complex, $NMo(OBu^t)_3$, **17**.[31] Reaction of **4** with **17** [eqn. (6)] led to formation of a blue

$$\underset{\mathbf{4}}{Mo[N(R)Ar]_3} + \underset{\mathbf{17}}{N{\equiv}Mo(OBu^t)_3} \longrightarrow \underset{\mathbf{18}}{(Bu^tO)_3Mo{=}N{=}Mo[N(R)Ar]_3} \quad (6)$$

intermediate, presumed to be $(Bu^tO)_3Mo(\mu\text{-}N)Mo[N(R)Ar]_3$, **18**.[30] Conducting the reaction in benzene at 25 °C in the absence of N_2 led to formation of nitride **5** along with 0.5 equiv. of the well known metal–metal triple-bonded dimer,[11] $Mo_2(OBu^t)_6$, **19** [eqns. (7) and (8)]. Thus, N-atom transfer was sub-

$$\underset{\mathbf{18}}{(Bu^tO)_3Mo{=}N{=}Mo[N(R)Ar]_3} \rightleftharpoons \underset{\mathbf{5}}{N{\equiv}Mo[N(R)Ar]_3} + \underset{\mathbf{20}}{'Mo(OBu^t)_3'} \quad (7)$$

$$2\ \underset{\mathbf{20}}{'Mo(OBu^t)_3'} \longrightarrow \underset{\mathbf{19}}{(Bu^tO)_3Mo{\equiv}Mo(OBu^t)_3} \quad (8)$$

stantiated,[30] and the –N(R)Ar-substituted complex demonstrated a greater affinity for the nitrogen atom than the alkoxide-substituted complex. The reaction is interesting in that it provides precedent for synthesis of a metal–metal multiple bond from a metal nitride, and also in that the observation of a blue

intermediate [eqn. (6)] suggested that more might be learned about the mechanism of this type of N-atom transfer.[30]

An interesting spin on the N-atom transfer reaction occurred when **4** was treated with alkoxynitride **17** under an atmosphere of N_2 (benzene, 25 °C).[30] Under these conditions, formation of the dimer **19** was nearly shut down, while formation of nitride **5** proceeded smoothly. The very slow reaction of **4** directly with N_2,[9] assessed in control experiments to occur to an extent of ⩽5% per day under these conditions,[30] cannot account for the smooth conversion of **4** to **5** in the presence of **17**, suggesting that **17** catalyzes the splitting of N_2 by **4** [eqn. (9)].[30] This

$$\underset{\mathbf{20}}{\text{'Mo(OBu}^t\text{)}_3\text{'}} + \underset{\mathbf{4}}{\text{Mo[N(R)Ar]}_3} \xrightarrow{N_2} \underset{\mathbf{5}}{\text{N}{\equiv}\text{Mo[N(R)Ar]}_3} + \underset{\mathbf{17}}{\text{N}{\equiv}\text{Mo(OBu}^t\text{)}_3} \quad (9)$$

supposition was substantiated by experiments involving reaction of **4** with **17** under an atmosphere of $^{15}N_2$, which resulted in label incorporation into both the alkoxynitride **17** and **5** isolated after the reaction.[30] A mechanistic scenario accommodating the data involves (i) N-atom transfer to generate **5**, (ii) concomitant formation of some form of 'Mo(OBu^t)$_3$', **20**, and N_2 splitting either by **20** alone or *via* a heterodinuclear species such as putative (Bu^{t}O)$_3$Mo(μ-N$_2$)Mo[N(R)Ar]$_3$ **21**. Combining the latter three steps provides a plausible mechanism for the observed result, namely that the splitting of N_2 by **4** is accelerated in the presence of alkoxynitride **17**.[30]

In pursuit of more information regarding the putative N-atom bridged complexes in intermetal nitrogen atom transfer reactions, it was elected to treat **4** and analogues with another nitridomolybdenum amide complex, namely NMo(NMe$_2$)$_3$ **22**.[10] This particular choice was prompted by speculation that an N-atom bridged species might possess greater thermal stability if the two molybdenum fragments involved possess electronically similar ligand sets. Dimethylamide ligands, in addition, were regarded as small enough to permit N-atom transfer. The latter consideration is important in that control experiments[10] showed that no reaction occurs between **4** and NMo[N(Bu^t)Ph]$_3$ **8**, or between **5** and Mo[N(Bu^t)Ph]$_3$ **23**.

A striking teal color was generated upon mixing the three-coordinate complex Mo[N(R)Ar$_{4F}$]$_3$ (**24**, Ar$_{4F}$ = 4-C$_6$H$_4$F) with **22** in toluene or ether [eqn. (10)].[10] The nitride-bridged

$$\underset{\mathbf{24}}{\text{Mo[N(R)Ar}_{4F}\text{]}_3} + \underset{\mathbf{22}}{\text{N}{\equiv}\text{Mo(NMe}_2\text{)}_3} \longrightarrow \underset{\mathbf{25}}{\text{(Me}_2\text{N)}_3\text{Mo}{=}\text{N}{=}\text{Mo[N(R)Ar}_{4F}\text{]}_3} \quad (10)$$

complex (Me$_2$N)$_3$Mo(μ-N)Mo[N(R)Ar$_{4F}$]$_3$ **25** was isolated in good yield and characterized by a variety of techniques including X-ray diffraction (Fig. 3).[10] Although the structure was of marginal quality due to dimethylamide disorder, the nitride nitrogen appeared to be situated equidistant from the two dissimilarly ligated Mo centers.

Although this particular μ-nitride species (**25**) seemed relatively robust, a more fragile analog was generated by treatment of **22** with the 'parent' complex **23** [eqn. (11)].[10] Thus

$$\underset{\mathbf{23}}{\text{Mo[N(Bu}^t\text{)Ph]}_3} + \underset{\mathbf{22}}{\text{N}{\equiv}\text{Mo(NMe}_2\text{)}_3} \longrightarrow \underset{\mathbf{27}}{\text{(Me}_2\text{N)}_3\text{Mo}{=}\text{N}{=}\text{Mo[N(Bu}^t\text{)Ph]}_3} \quad (11)$$

was derived a suitable synthesis of the symmetrical μ-nitride complex (μ-N)[Mo(NMe$_2$)$_3$]$_2$ **26**, by treatment of **23** with 2 equiv. of **22**. The notion is that the unsymmetrical ligated μ-nitride complex (Me$_2$N)$_3$Mo(μ-N)Mo[N(Bu^t)Ph]$_3$ **27** is thermally unstable, and serves as a source of 'Mo(NMe$_2$)$_3$' **28** under the reaction conditions [eqn. (12)]. Trapping of **28** by the second

$$\underset{\mathbf{27}}{\text{(Me}_2\text{N)}_3\text{Mo}{=}\text{N}{=}\text{Mo[N(Bu}^t\text{)Ph]}_3} \rightleftharpoons \underset{\mathbf{28}}{\text{'Mo(NMe}_2\text{)}_3\text{'}} + \underset{\mathbf{22}}{\text{N}{\equiv}\text{Mo[N(Bu}^t\text{)Ph]}_3} \quad (12)$$

equiv. of **22** provides the symmetrically substituted nitride derivative, nitridodimolybdenum–hexadimethylamide [**26**, eqn. (13)]. Using this procedure, thermally sensitive **26** could be

$$\underset{\mathbf{28}}{\text{'Mo(NMe}_2\text{)}_3\text{'}} + \underset{\mathbf{22}}{\text{N}{\equiv}\text{Mo(NMe}_2\text{)}_3} \rightleftharpoons \underset{\mathbf{26}}{\text{(Me}_2\text{N)}_3\text{Mo}{=}\text{N}{=}\text{Mo(NMe}_2\text{)}_3} \quad (13)$$

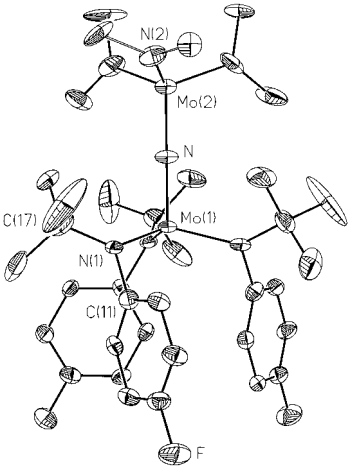

Fig. 3 Thermal ellipsoid representation of (Me$_2$N)$_3$Mo(μ-N)Mo[N(R)Ar$_{4F}$]$_3$ **25**, from an X-ray study.[10] The Mo–N–Mo axis resides on a crystallographic threefold axis; the resulting NMe$_2$ disorder is not shown. Ellipsoids are at the 35% probability level. The Mo(1)=N bond length is 1.82(4) Å, while the Mo(2)=N bond length is 1.83(4) Å.

isolated in pure form by fractional crystallization, and was characterized by X-ray crystallography (Fig. 4). The μ-N atom in **26** resides at a crystallographic center of inversion, with a Mo–N distance of 1.7990(8) Å. This distance is consistent with an Mo–N double bond,[10] the Mo≡N distance in **8** being 1.658(5) Å.[9] A molecular-orbital description of **26** also suggests a bond order of two between both molybdenum atoms and the bridging nitride ligand, the highest-lying three electrons being in a π-symmetry molecular orbital that possesses a node at the bridging nitrogen atom. A compound fascinating in its simplicity, **26** is related to the well known dimer Mo$_2$(NMe$_2$)$_6$ **29**[11] by formal insertion of a neutral nitrogen atom into the metal–metal triple bond. Indeed, thermal decomposition of **26** gives rise to a mixture of **22** and **29**.[10]

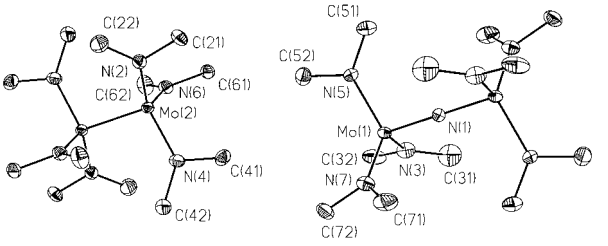

Fig. 4 Thermal ellipsoid representation of (μ-N)[Mo(NMe$_2$)$_3$]$_2$ **26** and Mo$_2$(NMe$_2$)$_6$ **29**, from an X-ray study in which the two occurred together in a 1:1 cocrystal.[10] Ellipsoids are at the 35% probability level. The Mo(1)=N(1) bond length is 1.7990(8) Å, while the Mo(1)–N(5) bond length is 1.953(8) Å.

The molybdenum systems described in this section do much to augment our knowledge of intermetal N-atom transfer reactions. Importantly, as earlier surmised[29] it is now established[10] that N-atom bridged species play an important role as intermediates in the transfer process. Some of the mixed-valence N-atom bridged species have been isolated, such that much can be expected to be gained from a study of their physical properties, decomposition kinetics, and other reaction chemistry. An intriguing aspect of the chemistry is that sources of the reactive, sterically-unhindered fragments 'Mo(OBu^t)$_3$' **20**[30] and 'Mo(NMe$_2$)$_3$' **28**[10] are available *via* N-atom transfer chemistry. Now that N-atom abstractors such as **4** are readily prepared, it is likely that other synthetic applications of N-atom transfer chemistry will result.

Molybdenum–phosphorus chemistry: establishment of the terminal phosphide (M≡P) functionality

The chemistry in this section stemmed from a desire to explore in broad terms the reactivity of **4** and related three-coordinate molybdenum compounds. Having learned about the pronounced stability of the Mo≡N triple bond in **5**,[9] it was of interest to see if the analogy could be pushed to phosphorus, an endeavor which if successful would lead to an unknown functional group: the terminal phosphide, M≡P.[32] As described below, it is indeed possible to draw several analogies between the molybdenum–nitrogen and the molybdenum–phosphorus chemistries.

Activation of white phosphorus

White phosphorus, consisting of tetrahedral P_4 molecules, is the most abundant form of elemental phosphorus.[33] The majority of its transition-metal mediated reactions involve metal carbonyl fragments and cluster chemistry.[34] The closest precedent for the reaction of a three-coordinate molybdenum compound with white phosphorus comes, as so many good things do, from the labs of Malcolm Chisholm. Thus, the dimethylamine adduct of the tungsten dimer $W_2(OCH_2Bu^t)_6$ **30** was treated with P_4 in an attempt to prepare the W≡P functional group.[35] What was obtained instead is the interesting complex, $(\eta^3\text{-}P_3)W(OCH_2Bu^t)_3(HNM_2)$, **31**.[35] The latter can be understood as a P_4 molecule with one vertex replaced by the isolobal tungsten tris-alkoxide fragment.[36]

In contrast to Chisholm's tungsten chemistry, three-coordinate **4** reacts smoothly with P_4 in toluene at 25 °C to afford the desired terminal phosphide derivative P≡Mo[N(R)Ar]$_3$ **32**, [eqn. (14)].[37] The analog stemming from reaction of 'parent'

$$\underset{\mathbf{4}}{Mo[N(R)Ar]_3} \xrightarrow{P_4} \underset{\mathbf{32}}{P{\equiv}Mo[N(R)Ar]_3} \qquad (14)$$

Mo[N(Bu^t)Ph]$_3$ **23** with P_4, namely PMo[N(Bu^t)Ph]$_3$ **33**, was prepared similarly,[10] and both have been characterized by X-ray diffraction. Compounds **32** and **33** are diamagnetic yellow–gold crystalline solids that dissolve readily in standard organic solvents. They, like their three-coordinate precursors, are readily prepared on 5–10 g scales.

A most intriguing feature of the NMR spectra of the terminal phosphide compounds is that their ^{31}P signal appears downfield of 1200 ppm! The latter phenomenon has been studied in detail by solid-state NMR techniques, and by computational methods.[38] The enormous downfield isotropic signal is interpreted[38] as arising from an unusually large chemical shift anisotropy in the system, consonant with field-induced mixing of the ground state with a paramagnetic excited state. The excited state in question is thought to involve promotion of electron density from an M–P σ bonding orbital into an orbital that is M–P π* in character.[38]

Structurally, phosphide compounds **32** and **33** are similar to nitride **8**, and the respective Mo≡P bond distances 2.119(4) and 2.111(2) Å are of interest (Fig. 5). Triple-bond covalent radii can be estimated for both Mo and P using the reference compounds P_2 and $Mo_2(NMe_2)_6$, giving the prediction of 2.055 Å for an Mo≡P triple bond.[37] Agreement with the experimental values is seen to be quite close.

Triamidoamine-supported[39] molybdenum and tungsten phosphide complexes PMo(Me$_3$SiNCH$_2$CH$_2$)$_3$N **34** and PW(Me$_3$SiNCH$_2$CH$_2$)$_3$N **35** were reported close on the heels[40] of **32**; **35** exhibited a W≡P distance of 2.162(4) Å, with an interesting added twist that the tungsten–phosphorus coupling constant had an unanticipated low value of 138 Hz. Organophosphide and phosphinidene complexes of tungsten exhibit much larger values of J_{WP}.[40] The data may be taken as an indication that the phosphorus 3s orbital participates little in the tungsten–phosphorus bonding, but rather accommodates a rather low-lying lone pair of electrons. Interestingly, compounds **35** and **34** were prepared not *via* a reaction with elemental phosphorus, but rather through treatment of precursor chloro complexes with Li[P(H)Ph] in what must involve a complex sequence of steps.[40] Such methodology was later successful for the preparation of the corresponding terminal arsenide complexes, As≡M(Me$_3$SiNCH$_2$CH$_2$)$_3$N (M = Mo **36**, W **37**), which have been the subject of a force-constant study.[41]

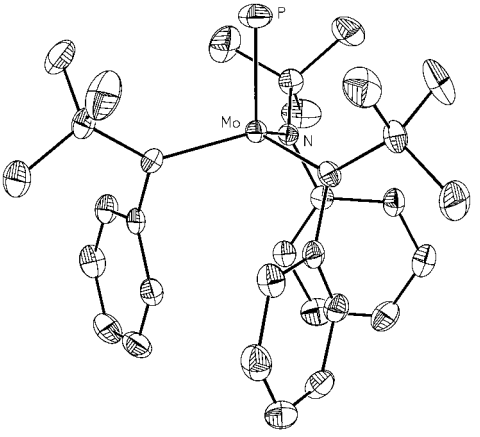

Fig. 5 Thermal ellipsoid representation of P≡Mo[N(Bu^t)Ph]$_3$ **33**, from an X-ray study.[10] The P–Mo bond is coincident with a crystallographic threefold axis. Ellipsoids are at the 35% probability level. The Mo≡P bond length is 2.111(2) Å, while the Mo–N bond length is 1.973(2) Å.

Reactions of terminal phosphide complexes with oxo, sulfur atom, and nitrene donors

First off it should be stated that like nitride **5**, phosphide **32** is not an exceptionally reactive compound. In part, the low reactivity of **32** toward certain reagents (including benzonitrile, benzaldehyde and methyl iodide) can be ascribed to the substantial steric shielding of the M≡P triple bond by *tert*-butyl groups. However, phosphide **32** does undergo some reactions involving addition of a terminal substituent to the phosphorus atom, especially in cases where a cumulene-like moiety Mo=P=X (X = O,[42] S[37] or NMes[37]) with a delocalized π system can arise.

Sulfur atom transfer to the terminal phosphide

The so-called PS complex, S=P=Mo[N(R)Ar]$_3$ **38** was prepared either in 62% yield in a slow reaction of **32** with elemental sulfur [43 h, OEt$_2$, 25 °C, eqn. (15)], or in 50% yield in a rapid reaction with ethylene sulfide [1.5 h, OEt$_2$, 25 °C, eqn. (16)].[37]

$$\underset{\mathbf{32}}{P{\equiv}Mo[N(R)Ar]_3} \xrightarrow{1/8\ S_8} \underset{\mathbf{38}}{S{=}P{=}Mo[N(R)Ar]_3} \qquad (15)$$

$$\underset{\mathbf{32}}{P{\equiv}Mo[N(R)Ar]_3} \xrightarrow{SC_2H_4} \underset{\mathbf{38}}{S{=}P{=}Mo[N(R)Ar]_3} \qquad (16)$$

The purple–red compound exhibits a ^{31}P NMR signal at δ 383, a dramatic upfield shift relative to phosphide **32**. That **38** exists as discrete monomeric units in the solid state was verified by X-ray crystallography (Fig. 6).[42] The Mo–P and P–S bond lengths are respectively 2.100(2) and 1.921(3) Å, and the angle at P is linear. It is a striking observation that the Mo–P distance is not significantly different than in the terminal phosphide species. Since the P–S distance is similar to what has been found for phosphine sulfides, perhaps the best valence-bond description of the 'PS' complex is, in fact, S–P≡Mo[N(R)Ar]$_3$, with appropriate formal charges: positive on P and negative on S. An important point to take into consideration in any analysis of the bonding in the PS complex **38** relative to phosphide **32** is that in the former the phosphorus 3s orbital is necessarily utilized in the σ framework, while in the latter all indications[38] are that it does not participate in the bonding.

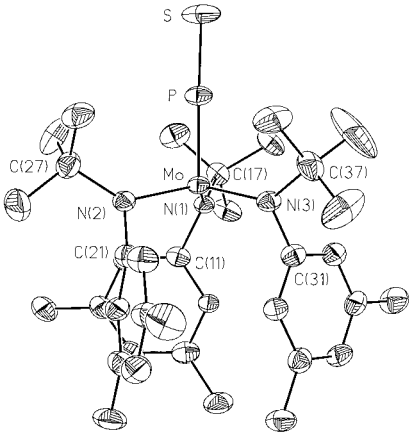

Fig. 6 Thermal ellipsoid representation of $SPMo[N(R)Ar]_3$ **38**, from an X-ray study,[42] Ellipsoids are at the 35% probability level. The P=S bond length is 1.921(3) Å, while the Mo=P bond length is 2.100(2) Å.

Although the importance of the $S{=}P{=}Mo[N(R)Ar]_3$ resonance structure for **38** has not yet been substantiated chemically, the $S{-}P{\equiv}Mo[(R)Ar]_3$ structure being favored by crystallographic data,[42] some support for the former structure comes from reactivity studies on the corresponding oxo derivative.[42] Before leaving the PS complex, however, it should be noted that formation of **38** by sequential addition of the elements phosphorus and sulfur to three-coordinate **4** represents an exceedingly satisfying and simple synthesis of a previously unknown type of cumulene.

Oxo transfer to the terminal phosphide

Underscoring the relatively unreactive nature of **32**, early attempts to synthesize the 'PO' complex, $O{=}P{=}Mo[N(R)Ar]_3$ **39** resulted in no reaction. Reagents employed unsuccessfully include pyridine- and trimethylamine-*N*-oxides and dry oxygen. The harsh and hydrocarbon-insoluble oxidant iodosylbenzene was also treated with **32**, but the reaction resulted in extensive decomposition. Dimethyldioxirane (Me_2CO_2) is a powerful, thermally unstable, hydrocarbon-soluble oxidant that is typically used as 5% solutions in acetone.[43] Treatment of phosphide **32** with the Me_2CO_2 ultimately proved a successful route to the PO complex **39**.[42]

Accordingly, treatment of a gold dichloromethane solution of **32** at −78 °C with the stoichiometric amount of Me_2CO_2 gave rise to an intense purple color [eqn. (17)].[42] It proved necessary

$$\underset{\mathbf{32}}{P{\equiv}Mo[N(R)Ar]_3} + O_2CMe_2 \longrightarrow \underset{\mathbf{39}}{O{=}P{=}Mo[N(R)Ar]_3} + OCMe_2 \qquad (17)$$

to precipitate PO **39** from the reaction mixture by addition of cold acetonitrile. Once pure, the purple, diamagnetic [$\delta(^{31}P)$ 269.8] **39** can be manipulated at 25 °C with minimal decomposition. The most common problem encountered in handling **39** is that, under a variety of conditions, phosphide **32** is regenerated from it.

X-Ray crystallography showed PO **39** to possess an essentially linear angle at P [177.6(8)°], and Mo–P and P–O distances of 2.079(5) and 1.49(2) Å, respectively.[42] Thus, like the phosphorus monosulfide complex **38**, PO **39** exhibits a shorter Mo≡P distance than phosphide **32**! This can indeed be taken as evidence that the $O{-}P{\equiv}[N(R)Ar]_3$ resonance structure is an important contributor, with appropriate formal charges. The P–O distance is essentially the same as for free phosphorus monoxide,[44] tricyclohexylphosphine oxide[45] and some μ_3-PO complexes in clusters.[46]

Some evidence lending credence to the $O{=}P{=}Mo[N(R)Ar]_3$ resonance structure for **39** is available in the form of reaction chemistry.[42] This resonance structure is reminiscent of the resonance structure, $O{=}C{=}ML_n$, invoked for metal carbonyls in describing the classic Fischer carbene synthesis.[47] Thus can be seen the analogy to organic carbonyls, and the fact that nucleophiles add to the complexed CO carbon understood. Likewise, the zirconocene reagent Cp_2ZrMe_2, which possesses nucleophilic methyl groups in conjunction with an oxophilic metal center, reacts with PO **39** with formation of a phosphorus–carbon and a zirconium–oxygen bond.[42] The product, **40**, is the result of insertion of the PO moiety into the Zr–Me bond. Compound **40** is orange–brown and diamagnetic, and structurally can be deemed analogous to $Mo(NMe_2)_4$[48] or $Mo[P(Cyclohexyl)_2]_4$.[49] The Mo–P and P–O bonds in **40** are 2.169(2) and 1.613(5) Å, such that multiple bonding between molybdenum and the trigonal-planar phosphorus center can be invoked.[42] Also, an analogy can be extended to relate compound **40**, with its Zr–O–P–Mo moiety, to 'zirconoxy carbenes' prepared by reaction of zirconocene derivatives with metal carbonyl complexes.[50]

Thus was the first complex containing a terminal PO, or phosphorus monoxide, ligand prepared and characterized.[42] Previous examples of complexes containing PO ligands have involved oxidation of bridging phosphide ligands in multimetallic clusters.[46] The PO molecule has garnered attention as a free species, due to its presence in interstellar space, and as a heavy analog of nitric oxide.[51] It will certainly be of interest to determine the extent of the chemistry of PO as a ligand in coordination chemistry, especially given the analogy with NO. Although information concerning the P–O bond strength in **39** is not yet available, preliminary results show that the complex is readily deoxygenated by triethylphosphine.

Reaction of **32** *with an aryl azide*

In some respects, the reactivity patterns of phosphide **32** are reminiscent of an electron-poor triogranophosphine. One reaction characteristic of triorganophosphines is that with organoazides to produce phosphinimines, a reaction known as the Staudinger reaction.[52] Seeking to push the analogy between **32** and PR_3 compounds, **32** was treated in ether with mesityl azide at 25 °C over a period of *ca.* 22 h [eqn. (18)].[37] The reaction

$$\underset{\mathbf{32}}{P{\equiv}Mo[N(R)Ar]_3} + N_3Mes \xrightarrow{-N_2} \underset{\mathbf{41}}{MesN{=}P{=}Mo[N(R)Ar]_3} \qquad (18)$$

afforded a diamagnetic blue–green product, which turned out to be $(MesNP)Mo[N(R)Ar]_3$ **41**, the product of a Staudinger-like addition of mesitylazide to **32** with loss of dinitrogen. The compound displays a single –N(R)Ar ligand environment according to room-temperature proton and carbon NMR spectroscopies.[37]

X-Ray crystallography showed **41** to possess an essentially linear Mo–P–N angle,[37] and confirmed the molecular connectivity. Interestingly, **41** is a unique phosphorus-monosubstituted aryldiazonium complex; the related 'iminophosphenium' cation $[PNAr^*]^+$ (Ar* = 2,4,6-$C_6H_2Bu^t_3$) is known as a discrete species, having been isolated and characterized as its tetrachloroaluminate salt.[53]

Thus was the reactivity of phosphide **32** confirmed to be related, at least to a degree, to that characteristic of triorganophosphines. It is interesting that, to date, the reactivity of terminal phosphide complexes M≡P is restricted to the addition of groups to the P terminus. No reactions have yet been identified in which the M≡P triple bond engages in cycloaddition reactions, despite the fact that such reactions are prevalent for closely related high-valent terminal phosphinidene complexes.[54] Further developments can be expected for phosphide complexes in this regard, especially if they can be generated in conjunction with a less sterically demanding ancillary ligand coordination sphere.

One-coordinate carbon multiply-bonded to molybdenum: the terminal carbide functionality

Having found that the $Mo[N(R)Ar]_3$ fragment is well suited as a platform for the construction of molybdenum–element multiple bonds, it was only natural to turn attention to some questions in the organometallic genre. A specific question of interest had to do with whether a carbide complex anion, *e.g.* $^{-}[C{\equiv}Mo\{N(R)Ar\}_3]$ **42**, isoelectronic to nitride **5**, could be accessed. Indeed, one-coordinate carbon was known previously only in, for example, carbon monoxide, isocyanides and cyanide ion. The functional group constituted by one-coordinate carbon bonded only to a single metal center was unknown.

To follow the chemistry it was deemed worthwhile to utilize a ^{13}C label for the carbon in question. This was made feasible by the observation that $Mo[N(R)Ar]_3$ **4** readily binds carbon monoxide in an irreversible fashion.[55] Thus, carbonyl $(O^{13}C)$-$Mo[N(R)Ar]_3$ **43** was obtained in 88% yield as a brown paramagnetic species [eqn. (19)].[55] Magnetic susceptibility

$$\underset{\mathbf{4}}{Mo[N(R)Ar]_3} \xrightarrow{CO} \underset{\mathbf{43}}{OCMo[N(R)Ar]_3} \qquad (19)$$

measurements were consistent with assignment of carbonyl **43** as a low-spin complex of molybdenum(III), an IR band at 1797 cm^{-1} was attributed to ν_{CO} for complex **43**, and the ^2H NMR spectrum of **43** revealed a single –N(R)Ar ligand environment.[55]

Now the problem remained of turning the carbonyl oxygen into a leaving group. A strategy was adopted whereby complex **43** would be (i) reduced to its corresponding anion and (ii) treated with a suitable electrophile. In practice it was observed that treatment of **43** with an excess of sodium amalgam in THF provided the desired anion [**44**, eqn. (20)] which is diamagnetic

$$\underset{\mathbf{43}}{OCMo[N(R)Ar]_3} \xrightarrow{Na/Hg} \underset{Na[\mathbf{44}]}{Na^{+}[^{-}O{-}C{\equiv}Mo\{N(R)Ar\}_3]} \qquad (20)$$

and can be written with a molybdenum–carbon triple bond as in $^{-}[O{-}C{\equiv}Mo\{N(R)Ar\}_3]$. The hope was that anion **44** would behave as a nucleophile in a manner analogous to an alkoxide ion. Although **44** could be isolated as its sodium salt, it was simply generated *in situ* for treatment with electrophiles. Pivalyl chloride was identifed as a suitable electrophile and, accordingly, the neutral diamagnetic 'carbido pivalate' complex $Bu^tC(O)O{-}^{13}C{\equiv}Mo[N(R)Ar]_3$ **45**, was obtained in 82% yield as a beige solid, and was fully characterized [eqn. (21)].[55]

$$\underset{Na[\mathbf{44}]}{Na^{+}[^{-}O{-}C{\equiv}Mo\{N(R)Ar\}_3]} + Bu^tC(O)Cl \xrightarrow{-NaCl} \underset{\mathbf{45}}{Bu^tC(O)O{-}C{\equiv}Mo[N(R)Ar]_3} \qquad (21)$$

But for the great stability of the $-C{\equiv}Mo[N(R)Ar]_3$ core under reductive conditions, the synthesis might have reached a dead end with compound **45**. It was hoped that the pivalate moiety would be removed under reductive conditions, with the desired carbide anion $^{-}[C{\equiv}Mo\{N(R)Ar\}_3]$ **42** perhaps to be obtained directly. Although the situation did not prove to be so simple, it was indeed the case that reductive conditions resulted in removal of the $-O_2CBu^t$ group, albeit less than quantitatively. Subjection of **45** to an excess of solid sodium mirror in THF led [eqn. (22)], according to ^{13}C NMR monitoring, to production of

$$\underset{\mathbf{45}}{Bu^tC(O)O{-}C{\equiv}Mo[N(R)Ar]_3} \xrightarrow{i\ Na^0,\ ii\ MeCN} \underset{\mathbf{46}}{HC{\equiv}Mo[N(R)Ar]_3} \qquad (22)$$

a mixture containing the desired 'sodium carbide' (Na[**42**], identified tentatively as several peaks in the vicinity of δ 500), methylidyne $HC{\equiv}Mo[N(R)Ar]_3$ **46**, and the carbonyl anion **44**. Given the complexity of the mixture, it was opted to attempt protonation of **42** to methylidyne **46**, and to attempt separation of the latter from the salt of **44**. Fortunately, addition of the crude mixture to acetonitrile was found to effect the desired transformation. Being relatively insoluble in acetonitrile, methylidyne **46** was easily separated from the soluble salt of **44**. The isolated yield of **46** was 53%, based on the neutral carbonyl precursor **43**.[55] Methylidyne **46** has a characteristic ^{13}C NMR peak at δ 287, accompanied by a J_{CH} of 157 Hz. A recent single-crystal X-ray diffraction study shows **46** to be a pseudo-threefold symmetric species with an Mo≡C triple bond distance of 1.699(5) Å.

Now the task at hand was to deprotonate **46** and to isolate **42** as a salt with a large cation, this in order to sequester a version of **42** having one-coordinate carbon. Given the interpretation that the preceding chemistry had relied upon deprotonation of acetonitrile by **42**, it was evident that a strong base would be required for deprotonation of methylidyne **46**. Benzylpotassium[56] was chosen, as it can conveniently be weighed out as a solid and because potassium, being a heavier alkali metal, should exhibit a decreased tendency to coordinate to a carbanion (compared with Li or Na), especially if complexed with a suitable crown ether or cryptand complement. Reaction in THF of methylidyne **46** with K(benzyl) led, as desired [eqn. (23)], to production of the potassium salt of carbide **42**, isolated

$$\underset{\mathbf{46}}{HC{\equiv}Mo[N(R)Ar]_3} + K(benzyl) \xrightarrow{-toluene} \underset{K[\mathbf{42}]}{K^{+}[^{-}C{\equiv}Mo\{N(R)Ar\}_3]} \qquad (23)$$

in 69% yield as a solvent-free dimer (X-ray, Fig. 7). In C_6D_6, where K[**42**] presumably retains its dimeric structure, a single sharp ^{13}C signal is observed for the carbide carbon at δ 494.5. A closer look (X-ray) at the structure of dimeric K[**42**] reveals a central K_2C_2 square, with the coordination at K complemented by π complexation of two –N(R)Ar aryl groups per potassium. The structure thus incorporates encapsulation of the potassium cations by lipophilic residues, accounting for the observed good solubility of the compound in C_6D_6, and also for the lack of retention of THF.

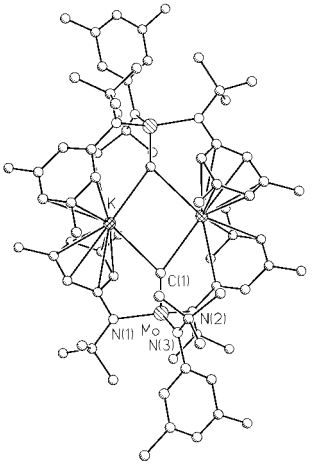

Fig. 7 Ball and stick representation of dimeric potassium carbide $K_2[\mathbf{42}]_2$, from an X-ray study.[55] A crystallographic center of inversion is located at the center of the dimer. The C(1)≡Mo distance is 1.68(3) Å, while the K···C distance is 2.94(2) Å.

Encapsulation of the potassium was achieved in two ways;[55] addition of cryptofix-2,2,2 to a solution of K[**42**] gave [K(2,2,2-crypt)][**42**] [eqn. (24)], whereas when K[**42**] was

$$\underset{K[\mathbf{42}]}{K^{+}[^{-}C{\equiv}Mo\{N(R)Ar\}_3]} \xrightarrow{2,2,2\text{-crypt}} \underset{[K(2,2,2\text{-crypt})][\mathbf{42}]}{[K(2,2,2\text{-crypt})^{+}][^{-}C{\equiv}Mo\{N(R)Ar\}_3]} \qquad (24)$$

treated with 2 equiv. of benzo-15-crown-5, the salt [K(benzo-15-crown-5)$_2$][**42**] was produced [eqn. (25)]. Both salts exhi-

$K^+[^-C{\equiv}Mo\{N(R)Ar\}_3]$ K[**42**] —benzo-15-crown-5→ $[K(benzo\text{-}15\text{-}crown\text{-}5)_2^+][^-C{\equiv}Mo\{N(R)Ar\}_3]$ (25)
$[K(benzo\text{-}15\text{-}crown\text{-}5)_2]$[**42**]

bited low benzene solubility, in contrast to the dimeric precursor K[**42**], suggesting that the new salts consisted of discrete anions and cations. Remarked upon initially as a curious observation was the fact that the carbide ^{13}C signal (THF) for the new salts was rather broad.[55] Thanks in part to a suggestion from Professor Klaus H. Theopold, it has been determined that proton exchange between methylidyne **46** and its conjugate base takes place on the NMR timescale, with rate parameters such that a small percentage of **46** is sufficient to broaden substantially the carbide ^{13}C signal. For [K(2,2,2-crypt)][**42**], the ^{13}C signal in question was reported as δ 482.8, but this parameter is sensitive, of course, to the presence of small quantities of **46**. It is now known that addition of K(benzyl) to a THF solution of [K(2,2,2-crypt)][**42**] results in dramatic sharpening of the carbide ^{13}C signal, presumably due to removal of trace quantities of methylidyne **46**.

X-Ray crystallographic confirmation of the presence of Mo-bound one-coordinate carbon was obtained with the structure of $[K(benzo\text{-}15\text{-}c\text{-}5)_2]$[**42**], which exhibits discrete and separate cations and anions (Fig. 8).[55] An interesting metrical parameter is the Mo≡C distance to the carbido carbon, 1.713(9) Å, which is not significantly different from the corresponding value found for methylidyne **46**. Also noteworthy is the fact that anion **42** displays conformational features very similar to those (described above) for the isoelectronic nitride **5**.[9]

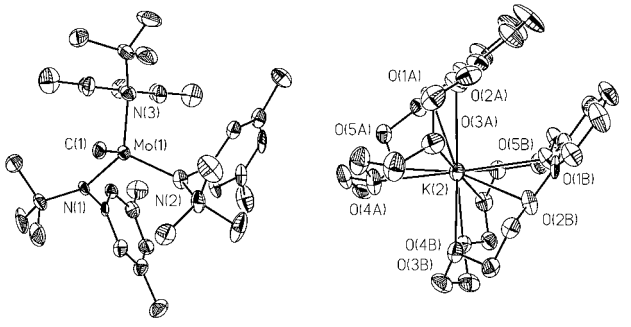

Fig. 8 Thermal ellipsoid representation of carbide salt $[K(benzo\text{-}15\text{-}crown\text{-}5)_2]$[**42**], from an X-ray study.[55] The Mo≡C distance is 1.713(9) Å.

Thus was established one-coordinate carbon as a viable functional group in organometallic chemistry.[55] It is interesting to reflect on the circuitous nature of the compound's synthesis, the carbide carbon arising from carbon monoxide.[57] Much remains to be elucidated with regard to terminal carbide reactivity, and with respect to the issue of synthesis of neutral or even cationic variants. In the present case, anion **42** displays a marked downfield shift for its carbido carbon nucleus, a circumstance likely arising from a large ^{13}C chemical shift anisotropy.[38] More detailed studies should shed light on this interesting finding, in conjunction with information on the M≡C bonding in this unusual species.

Terminal oxo, sulfide, selenide and telluride complexes

In the preceding sections we have seen that $Mo[N(R)Ar]_3$ **4** offers ready synthetic inroads to triple bonds involving Mo and C,[55] N[9] or P.[37] Also, several complexes of the sort Y=X=Mo[N-(R)Ar]$_3$ were described (*e.g.* YX = OP **39**,[42] SP **38**,[42] MesNP **41**[37] and ON **11**[8]) which all are linear cylindrically symmetric 8π systems analogous to CO_2 or N_2O, and thus anticipated to be rather stable. Thus, the triple bonds and the 8π systems can be regarded as the 'sinks' in the chemistry of $Mo[N(R)Ar]_3$ **4**. Especially intriguing in this regard is the observation that the reaction of **4** with N_2O led to exclusive N–N bond cleavage, rather than to formation of the putative oxo species, O=Mo[N-(R)Ar]$_3$ **12**.[8] The latter result runs completely counter to the known chemistry of nitrous oxide, a molecule that prefers to act as an oxo source with liberation of N_2.[18] Our interest piqued by these observations, we set out to prepare oxo **12** by an alternate route. When this endeavor was successful, a further course of action was undertaken involving synthesis of the heavier congeners of **12**, namely E=Mo[N(R)Ar]$_3$ (E = S **47**, Se **48** and Te **49**).[58]

The synthesis of the paramagnetic, chocolate-brown oxo-molybdenum(v) complex **12** proved to be straightforward, involving addition of pyridine-*N*-oxide to an ethereal solution of **4**.[20] Such a procedure [eqn. (26)] led to isolation of **12** in 72%

$$\underset{\mathbf{4}}{Mo[N(R)Ar]_3} + O{\leftarrow}NC_5H_5 \xrightarrow{\text{–pyridine}} \underset{\mathbf{12}}{O{=}Mo[N(R)Ar]_3} \qquad (26)$$

yield. Characterization of **12** included EPR spectroscopy, magnetic susceptibility measurements, ^2H NMR spectroscopy, and X-ray crystallography.[20]

The structure of monomeric **12** is significant in being of low symmetry relative to its threefold symmetric relatives, of which nitride **5** is representative.[9] The low symmetry of **12** arises from three disparate O–Mo–N–C_{tert} dihedral angles: 40, 3 and 62°;[20] a typical value for threefold symmetric analogues being 35°. Electronic structure arguments indicate that the low symmetry of **12** (and its heavier congeners, described below) is a consequence of the d^1 electron configuration. The unpaired electron resides, according to calculations, in an orbital that has π* character with respect to the Mo=O multiple bond. Since there are two such orbitals, but only one electron to populate them, the complex is subject to a Jahn–Teller distortion involving the disposition of the –N(R)Ar ligands. The latter adopt an orientation that minimizes repulsive interactions between the unpaired electron and the Mo–N π bonds. The heavier chalcogenide complexes **47**, **48** and **49**, which have less ionic character to their Mo=E bonds than in the case of oxo complex **12**, likewise exhibit low-symmetry structures, but these are C_s as opposed to the case for **12**, which in the solid state has C_1 symmetry. Despite the low symmetry of all the E=Mo[N(R)Ar]$_3$ complexes, in solution they are fluxional as judged by their ^2H NMR spectra, which show but a single signal at 25 °C.[20]

Whereas the oxo compound **12** was not amenable to preparation by the direct reaction of $Mo[N(R)Ar]_3$ **4** with dioxygen, the heavier chalcogenide derivatives all could be prepared by interaction of **4** with the respective elemental chalcogen.[20] Thus, S=Mo[N(R)Ar]$_3$ **47** was obtained in 63% yield subsequent to treatment of **4** with S_8 [eqn. (27)]. Reaction

$$\underset{\mathbf{4}}{Mo[N(R)Ar]_3} + \underset{E = S, Se \text{ or } Te/PEt_3}{1/n\ E_n} \longrightarrow \underset{E = S\ \mathbf{47},\ Se\ \mathbf{48},\ Te\ \mathbf{49}}{E{=}Mo[N(R)Ar]_3} \qquad (27)$$

of **4** with elemental selenium gave Se=Mo[N(R)Ar]$_3$ **48** in 80% yield after 11 h in ether at 25 °C. Elemental tellurium reacted only sluggishly with **4**, such that catalytic PEt_3 was employed, to catalyze the reaction *via* the phosphine telluride. The result was the isolation in 73% yield of Te=Mo[N(R)Ar]$_3$ **49**, as a dark brown solid. Characterization of the molybdenum(v) chalogenide complexes by EPR spectroscopy provided increasingly well resolved rhombic spectra on going from E = O to E = Te. Density functional calculations indicated that the covalent character of the Mo=E bond increased as O ≪ S < Se < Te. The Mo=E bond lengths, as determined by X-ray crystallography are E = O, 1.706(2); S, 2.1677(12); Se, 2.3115(6) and Te, 2.5353(6) Å (see Fig. 9 for a representative drawing of telluride **49**).[20]

A very telling set of experiments involved thermochemical measurements made on reactions that lead to oxo **12** and sulfide **47**.[20] For instance, the heat of reaction of **4** with pyridine-*N*-oxide was measured, permitting estimation of the bond dissociation enthalpy D(MoO) as 155.6 ± 1.6 kcal mol^{-1}. This

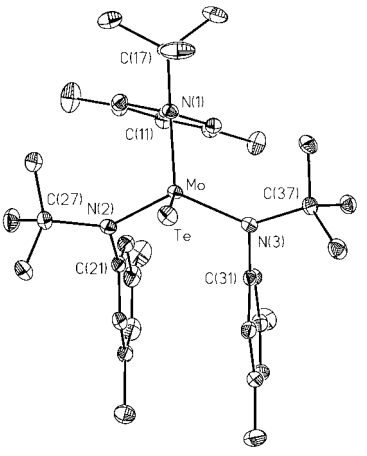

Fig. 9 35% probability level thermal ellipsoid representation of terminal telluride **49**, from an X-ray study.[20] The Te=Mo bond length is 2.5353(6) Å. Reproduced with permission from *J. Am. Chem. Soc.*

measurement indicates that **12** possesses one of the strongest metal–oxo bonds known,[59] and carries the corollary that the result of N_2O reaction with **4** is not a consequence of any thermodynamic bias.[19] Although there is a paucity of data for terminal metal–sulfur bond strengths in the literature, a D(MoS) of 104.4 ± 1.2 kcal mol^{-1} was obtained for **47** from measurement of the heat of reaction of ethylene sulfide with **4**.[20] The latter is an alternative method for preparing **47**, an example of thiirane desulfurization.[60] Although experimental data are not available for the selenide– and telluride–molybdenum bond dissociation enthalpies, density functional theoretical methods predict values of 91 and 71 kcal mol^{-1}, respectively, for **48** and **49**.[20]

Molecular orbital calculations performed for sulfide **47**, as for the other chalcogenide complexes, indicate the SOMO (singly occupied molecular orbital) to be largely Mo–E π* in character. The SOMO is high-lying relative to the highest-lying doubly occupied level, additionally, such that the complexes should be regarded as one-electron reductants.[20] This behavior is manifested both in terms of intermolecular and intramolecular redox chemistry. An example of the former is the ferrocenium triflate or iodine oxidation of **12** to provide salts of the $[O{\equiv}Mo\{N(R)Ar\}_3]^+$ cation. Chalcogenide complexes **12**, **47**, **48** and **49** are all thermally sensitive, with Bu^t radical elimination from the –N(R)Ar ligands occurring at elevated temperatures. Thermolysis (60–80 °C, 5–25 h) of the Mo=E complexes accordingly led to first-order decay, with the products being a new series of diamagnetic molybdenum(VI) chalcogenide complexes, E=Mo(=NAr)[N(R)Ar]$_2$ (E = O **50**, S **51**, Se **52**, Te **53**). The thermal instability of **12** and its heavier molybdenum(V) congeners contrasts sharply with the thermally robust nature of nitride **5**[9] and phosphide **32**.[37] such that although the chalcogenide complexes[20] are isolable and could be characterized, they do not represent 'sinks' in the chemistry of Mo[N(R)Ar]$_3$ **4**.

Concluding remarks

The isolation and characterization of three-coordinate molybdenum(III) complexes has been facilitated by the use of bulky *N-tert*-butylanilide ancillary ligands. The remarkable new complexes, embodied by Mo[N(R)Ar]$_3$ **4**, display a wealth of dramatic new reaction chemistries, and thereby have opened up new areas of inquiry in transition metal chemistry. Accordingly, dinitrogen cleavage to molecular molybdenum nitride **5** has been realized under mild and mechanistically well defined conditions.[9] The same nitride forms in equimolar amounts with nitrosyl **11**, in a highly unusual example of nitrous oxide N–N bond cleavage by **4**.[8] New vistas have opened for intermetal N-atom transfer reactivity; N-atom bridged intermediates have been characterized,[10] and the atom transfer reaction has been coupled with N_2 cleavage and metal–metal bond formation.[30] White phosphorus, with its tetrahedral P_4 molecules, has been harnessed to provide examples of terminal phosphide species,[37] the phosphorus analog of nitride **5**.[9] The sinks in the system have been identified as featuring Mo–element triple bonds or three-membered 8π-electron cumulenes, with Mo[(R)Ar]$_3$ comprising a terminus. These observations have permitted the chemistry to be extended to encompass the terminal carbide functionality (one-coordinate carbon bonded to a single metal),[55] and a molybdenum complex of phosphorus monoxide.[42]

As the reactivity patterns for **4** become more well established, it will be of interest to probe the detailed effects of ligand-induced steric requirements in the system, and to search for routes to related three-coordinate compounds based on other metals, including tungsten. Because Mo[N(R)Ar]$_3$ **4** can be prepared in multigram quantities, and can be prepared inexpensively for synthetic applications without deuterium-enrichment in the –N(R)Ar ligand,[61] it may be expected that the compound will find manifold applications in synthetic chemistry. At the very least, the reaction pathways uncovered in the context of studying **4** and related compounds can serve as a starting point for the mechanism-based design of new reagents or catalyst systems.

Finally, the characterization of Mo[N(R)Ar]$_3$ **4**[8] and the initial elucidation[23] and documentation[9] of its reaction chemistry[37] serve as a striking reminder of the riches that surely do remain to be mined within the realm of exploratory synthetic inorganic chemistry.

Acknowledgments

I am indebted to the coworkers from my group whose names appear in the list of references. The hard work, enthusiasm, and skillful laboratory technique of these individuals has brought to fruition the chemistry reported on in this article. I am grateful to Professors Richard R. Schrock and Peter T. Wolczanski for helpful discussions, and for inspiration to study the chemistry of three-coordinate transition-metal complexes. For financial support I gratefully acknowledge the National Science Foundation (CAREER Award CHE-9501992), the Alfred P. Sloan Foundation, the Packard Foundation, 3M, DuPont, Union Carbide, and Monsanto.

Christopher C. Cummins was educated at Cornell University where he carried out research under the direction of Professor Peter T. Wolczanski and received his A.B. degree in 1989. His PhD work, carried out at the Massachusetts Institute of Technology under the direction of Professor Richard R. Schrock, was in the areas of block copolymer synthesis and coordination chemistry with triamidoamine ligands. In 1993 he graduated from M.I.T. and accepted an Assistant Professorship at the same institution. His research has focused on inorganic radical chemistry, the activation by three-coordinate transition metal complexes of small molecules including dinitrogen and the nitrogen oxides, and the development of new synthetic methods for inorganic chemistry. In 1996 he was promoted to the rank of Professor. In 1997 Dr Cummins received the Phi Lambda Upsilon Fresenius Award, and in 1998 he received the Award in Pure Chemistry from the American Chemical Society and the Alan T. Waterman Award from the National Science Foundation.

Notes and References

† E-mail: ccummins@MIT.EDU

1 M. H. Chisholm, *Acc. Chem. Res.*, 1990, **23**, 419.
2 E. C. Alyea, J. S. Basi, D. C. Bradley and M. H. Chisholm, *Chem. Commun.*, 1968, 495; D. C. Bradley, M. B. Hursthouse and C. W. Newing, *Chem. Commun.*, 1971, 411.

3 D. C. Bradley and M. H. Chisholm, *Acc. Chem. Res.*, 1976, **9**, 273.
4 P. G. Eller, D. C. Bradley, M. B. Hursthouse and D. W. Meek, *Coord. Chem. Rev.*, 1977, **24**, 1; see also C. C. Cummins, *Prog. Inorg. Chem.*, 1998, **47**, 685, and references therein.
5 A. R. Johnson and C. C. Cummins, *Inorg. Synth.*, 1998, **32**, 123.
6 S. J. Simpson and R. A. Andersen, *Inorg. Chem.*, 1981, **20**, 3627; H. Bürger and U. Wannagat, *Monatsh Chem.*, 1963, **94**, 761.
7 J. R. Dilworth and J. Zubieta, *Inorg. Synth.*, 1986, **24**, 193.
8 C. E. Laplaza, A. L. Odom, W. M. Davis, C. C. Cummins and J. D. Protasiewicz, *J. Am. Chem. Soc.*, 1995, **117**, 4999.
9 C. E. Laplaza, M. J. A. Johnson, J. C. Peters, A. L. Odom, E. Kim, C. C. Cummins, G. N. George and I. J. Pickering, *J. Am. Chem. Soc.*, 1996, **118**, 8623.
10 M. J. A. Johnson, P. M. Lee, A. L. Odom, W. M. Davis and C. C. Cummins, *Angew. Chem., Int. Ed. Engl.*, 1997, **36**, 87.
11 F. A. Cotton and R. A. Walton, *Multiple Bonds Between Metal Atoms*, Oxford University Press, New York, 1993.
12 J. Haln, C. R. Landis, V. A. Nasluzov, K. M. Neyman and N. Rösch, *Inorg. Chem.*, 1997, **36**, 3947.
13 Q. Cui, D. G. Musaev, M. Svensson, S. Sieber and K. Morokuma, *J. Am. Chem. Soc.*, 1995, **117**, 12 366; K. M. Neyman, V. A. Nasulzov, J. Hahn, C. R. Landis and N. Rösch, *Organometallics*, 1997, **16**, 995.
14 P. W. Wanandi, W. M. Davis, C. C. Cummins, M. A. Russell and D. E. Wilcox, *J. Am. Chem. Soc.*, 1995, **117**, 2110.
15 D. R. Neithamer, R. E. LaPointe, R. A. Wheeler, D. S. Richeson, G. D. Van Duyne and P. T. Wolczanki, *J. Am. Chem. Soc.*, 1989, **111**, 9056.
16 K.-Y. Shih, R. R. Schrock and R. Kempe, *J. Am. Chem. Soc.*, 1994, **116**, 8804.
17 Z. Gebeyehu, F. Weller, B. Neumüller and K. Dehnicke, *Z. Anorg. Allg. Chem.*, 1991, **593**, 99.
18 G. A. Vaughan, C. D. Sofield, G. L. Hillhouse and A. L. Rheingold, *J. Am. Chem. Soc.*, 1989, **111**, 5491; P. T. Matsunaga, G. L. Hillhouse and A. L. Rheingold, *J. Am. Chem. Soc.*, 1993, **115**, 2075; M. R. Smith, P. T. Matsunaga and R. A. Andersen, *J. Am. Chem. Soc.*, 1993, **115**, 7049; F. Bottomley, *Polyhedron*, 1992, **11**, 1707; C. C. Cummins, R. R. Schrock and W. M. Davis, *Inorg. Chem.*, 1994, **33**, 1448.
19 P. A. Hintz, M. B. Sowa, S. A. Ruatta and S. L. Anderson, *J. Chem. Phys.*, 1991, **94**, 6446.
20 A. R. Johnson, W. M. Davis, C. C. Cummins, S. Serron, S. P. Nolan, D. G. Musaev and K. Morokuma, *J. Am. Chem. Soc.*, 1998, **120**, 2071.
21 D. C. Bradley, M. B. Hursthouse, C. W. Newing and A. J. Welch, *J. Chem. Soc., Chem. Commun.*, 1972, 567.
22 D. E. Wigley, *Prog. Inorg. Chem.*, 1994, **42**, 239.
23 C. E. Laplaza and C. C. Cummins, *Science*, 1995, **268**, 861.
24 M. Hidai and Y. Mizobe, *Chem. Rev.*, 1995, **95**, 1115.
25 M. B. O'Donoghue, N. C. Zanetti, W. M. Davis and R. R. Schrock, *J. Am. Chem. Soc.*, 1997, **119**, 2753.
26 A. Zanotti-Gerosa, E. Solari, L. Giannini, C. Floriani, A. Chiesi-Villa and C. Rizzoli, *J. Am. Chem. Soc.*, 1998, **120**, 437.
27 T. Travis, *Chem. Ind.*, 1993, 581.
28 L. K. Woo, *Chem. Rev.*, 1993, **93**, 1125.
29 L. K. Woo, J. G. Goll, D. J. Czapla and J. A. Hays, *J. Am. Chem. Soc.*, 1991, **113**, 8478.
30 C. E. Laplaza, A. R. Johnson and C. C. Cummins, *J. Am. Chem. Soc.*, 1996, **118**, 709.
31 D. M.-T. Chan, M. H. Chisholm, K. Folting, J. C. Huffman and N. S. Marchant, *Inorg. Chem.*, 1986, **25**, 4170.
32 M. Scheer, K. Schuster, T. A. Budzichowski, M. H. Chisholm and W. E. Streib, *J. Chem. Soc., Chem. Commun.*, 1995, 1671.
33 N. N. Greenwood and A. Earnshaw, *Chemistry of the Elements*, Pergamon, Oxford, 1984.
34 O. J. Scherer, M. Detzel, G. Berg, J. Braun, H. Edinger, T. Mohr, G. Schwarz, P. Walther and G. Wolmerschauser, *Phosphorus Sulfur Silicon Relat. Elem.*, 1996, **110**, 133.
35 M. H. Chisholm, J. C. Huffman and J. W. Pasterczyk, *Inorg. Chim. Acta*, 1987, **133**, 17.
36 R. Hoffmann, *Angew. Chem., Int. Ed. Engl.*, 1982, **21**, 711.
37 C. E. Laplaza, W. M. Davis and C. C. Cummins, *Angew. Chem., Int. Ed. Engl.*, 1995, **34**, 2042.
38 G. Wu, d. Rovnyak, M. J. A. Johnson, N. C. Zanetti, D. G. Musaev, K. Morokuma, R. R. Schrock, R. G. Griffin and C. C. Cummins, *J. Am. Chem. Soc.*, 1996, **118**, 10 654.
39 R. R. Schrock, *Acc. Chem. Res.*, 1997, **30**, 9.
40 N. C. Zanetti, R. R. Schrock and W. M. Davis, *Angew. Chem., Int. Ed. Engl.*, 1995, **34**, 2044.
41 J. A. Johnson-Carr, N. C. Zanetti, R. R. Schrock and M. D. Hopkins, *J. Am. Chem. Soc.*, 1996, **118**, 11 305.
42 M. J. A. Johnson, A. L. Odom and C. C. Cummins, *Chem. Commun.*, 1997, 1523.
43 R. W. Murray, *Chem. Rev.*, 1989, **89**, 1187; W. Adam, J. Bialas and L. Hadjiarapoglou, *Chem. Ber.*, 1991, **124**, 2377; M. Ferrer, M. Gilbert, F. Sanchez Baeza and A. Messeguer, *Tetrahedron Lett.*, 1996, **37**, 3585.
44 H.-B. Qian, *J. Mol. Spectrosc.*, 1995, **174**, 599.
45 J. A. Davies, S. Deutremez and A. A. Pinkerton, *Inorg. Chem.*, 1991, **30**, 2380.
46 O. J. Scherer, J. Braun, P. Walther, G. Heckmann and G. Wolmershuser, *Angew. Chem., Int. Ed. Engl.*, 1991, **30**, 852; J. F. Corrigan, S. Doherty, N. J. Taylor and A. J. Carty, *J. Am. Chem. Soc.*, 1994, **116**, 9799.
47 E. O. Fischer, in *Nobel Lectures in Chemistry*, ed. T. Frängsmyr, World Scientific, Singapore, 1993, p. 105.
48 M. H. Chisholm, F. A. Cotton and M. W. Extine, *Inorg. Chem.*, 1978, **17**, 1329.
49 R. T. Baker, P. J. Krusic, T. H. Tulip, J. C. Calabrese and S. S. Wreford, *J. Am. Chem. Soc.*, 1983, **105**, 6763.
50 P. T. Wolczanski and J. E. Bercaw, *Acc. Chem. Res.*, 1980, **13**, 121.
51 W. A. Herrmann, *Angew. Chem., Int. Ed. Engl.*, 1991, **30**, 818.
52 Y. G. Gololobov and L. F. Kasukhin, *Tetrahedron*, 1992, **48**, 1353.
53 E. Niecke, M. Nieger and F. Reichert, *Angew. Chem., Int. Ed. Engl.*, 1988, **27**, 1715.
54 C. C. Cummins, R. R. Schrock and W. M. Davis, *Angew. Chem., Int. Ed. Engl.*, 1993, **32**, 756; T. L. Breen and D. W. Stephan, *J. Am. Chem. Soc.*, 1995, **117**, 11 914.
55 J. C. Peters, A. L. Odom and C. C. Cummins, *Chem. Commun.*, 1997, 1995.
56 R. R. Schlosser and J. Hartmann, *Angew. Chem., Int. Ed. Engl.*, 1973, **12**, 508.
57 G. M. Jamison, A. E. Bruce, P. S. White and J. L. Templeton, *J. Am. Chem. Soc.*, 1991, **113**, 5057.
58 G. Parkin, *Prog. Inorg. Chem.*, 1998, **47**, 1.
59 R. H. Holm and J. P. Donahue, *Polyhedron*, 1993, **12**, 571.
60 C. P. Gerlach and J. Arnold, *Inorg. Chem.*, 1996, **35**, 5770; C. C. Cummins, R. R. Schrock and W. M. Davis, *Inorg. Chem.*, 1994, **33**, 1448.
61 The natural isotopic abundance amine *N*-*tert*-butyl-3,5-dimethylaniline is conveniently prepared in 50–100 g batches *via* aryne generation from 1-bromo-2,4-dimethylbenzene in *tert*-butylamine solvent. The procedure is analogous to the preparation of the 'parent' *N*-*tert*-butylaniline as reported in the following: E. R. Biehl, S. M. Smith and P. C. Reeves, *J. Org. Chem.*, 1971, **36**, 1841. The desired amine, *N*-*tert*-butyl-3,5-dimethylaniline, is produced in *ca.* 75% crude yield, and is separated from its isomer by recrystallization of the hydrochloride. Manuscript in preparation.

8/02402B

Synthesis and characterization of the nine-atom, rhena- and tungsta-boranes $(Cp^*Re)_2B_7H_7$ and $(Cp^*W)_2B_7H_9$, $Cp^* = \eta^5\text{-}C_5Me_5$. Molecular mimics of hypoelectronic main-group clusters in Zintl phases

Andrew S. Weller, Mayou Shang and Thomas P. Fehlner*

Department of Chemistry and Biochemistry, University of Notre Dame, Notre Dame, Indiana 45665 USA.
E-mail: Fehlner.1@nd.edu

Geometric and molecular orbital analyses of the metallaboranes $(Cp^*Re)_2B_7H_7$ and $(Cp^*W)_2B_7H_9$, which display unusual, but identical, core structures and skeletal electron pair counts of $n - 2$, demonstrate a close connection between these molecular compounds and anionic, hypoelectronic main-group clusters found in the solid state.

The chemistry of metallaborane complexes is dominated by two-valence electron fragments of Group 8 and Group 9 metals[1–3] such as $\{Fe(CO)_3\}$ or $\{CoCp\}$, $Cp = \eta^5\text{-}C_5H_5$, in which the metal fragment replaces a boron vertex in the resulting metallaborane.[4] The fact that transition-metal halides, $[Cp^*MCl_n]_m$, $Cp^* = \eta^5\text{-}C_5Me_5$, react with monoboron reagents to yield metallaboranes[5] permits the synthesis of compounds containing earlier transition metals (M = Ta,[6] Cr,[7] Mo[8] and W[9,10]). We anticipated that the lower number of valence electrons and higher frontier orbital energies of such fragments would lead to unusual behavior. Indeed, in small clusters the metal center introduces unsaturation on the bonding network supported, in part, by the relatively higher energy metal functions.[6–8] Alternatively, when more boron atoms are available, highly capped structures result.[9] Moving to Group 7 transition metals[11,12] we now report the synthesis of the first example of a dirhenaborane, which displays an unprecedented nine-atom molecular structure. For support, the nearly isostructural and isoelectronic tungsten analog is also described.

Addition of BH_3·thf to Cp^*ReCl_4[13] at room temperature and subsequent gentle heating affords the pale yellow rhenaborane $(Cp^*Re)_2B_7H_7$ **1** in good yield after chromatographic workup.† Its red, isostructural and isoelectronic partner, $(Cp^*W)_2B_7H_9$ **2** is formed as a minor product during the pyrolysis of $Cp^*WH_3B_4H_8$ in toluene.‡[9] Both compounds **1** and **2** have been fully characterized by single-crystal X-ray diffraction,[11]B and ^{1}H NMR spectroscopy and high-resolution mass spectrometry. The ^{11}B NMR spectra of **1** and **2** display four signals in the ratio 1 : 2 : 2 : 2, distributed over an unusually large[14] chemical shift range of ≈ 100 ppm. In addition to signals due to Cp* and BH_t groups, the ^{1}H NMR spectrum of **2** displays a broad integral two resonance at δ −8.9 in the region associated with μ or μ_3 B–H–M groups while for **1** the high-field region is featureless.

The solid-state molecular structures of compounds **1** and **2** are shown in Fig. 1.§ Both feature similar structural cores, although the structural motif is not one anticipated for a nine-atom cluster *e.g.* tricapped trigonal prism. Compound **1** has effective C_{2v} symmetry, while the presence of the two μ_3 B–H–W hydrogen atoms affords **2** with approximate C_2 symmetry. The metal–metal distances of 2.7875(6) in **1** and 2.9522(8) Å in **2**, both fall in the range associated with their respective M–M single bonds.[15] The seven skeletal electron pairs (sep) associated with **1** and **2** are three less than expected for a normal nine-vertex *closo* cluster.[16] Hence, we have explored the geometric and electronic factors responsible.

Fenske–Hall calculations[17,18] on the Cp analogs of **1** and **2** show a large HOMO–LUMO gap for both compounds consistent with the observed stability and electron count. The respective HOMOs are metal–metal bonding and their unfilled antibonding partners are found to higher energy. Further confirmation of a metal–metal bond is provided by Mulliken overlap populations of 0.12 and 0.13 for **1** and **2**, respectively. Corbett has described examples of hypoelectronic main-group clusters in Zintl phases[19] with accompanying non-standard deltahedral structures. Distortion of the standard deltahedron for a given *closo n*-atom skeleton to that observed leads to a reduced number of low-energy cluster bonding orbitals thereby supporting the low sep count found. In a similar spirit, we note that the observed geometry of **1** (and **2**) may be generated by a 45° rotation of one of the square pyramidal faces of a tricapped trigonal prism around its C_2 axis thereby converting the four

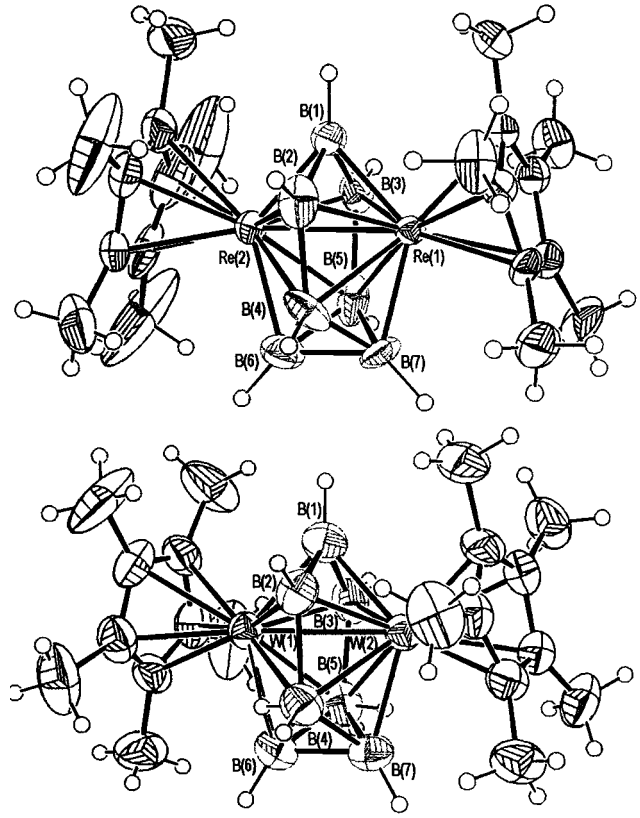

Fig. 1 The molecular structure of $(Cp^*Re)_2B_7H_7$ **1** (top) and $(Cp^*W)_2B_7H_9$ **2** (bottom). Selected bond distances (Å) for **1**: Re(1)–Re(2) 2.7875(6), Re(1)–B(1) 2.053(13), Re(1)–B(2) 2.14(2), Re(1)–B(3) 2.12(2), Re(1)–B(4) 2.231(14), Re(1)–B(5) 2.28(2), Re(1)–B(7) 2.116(14), B(1)–B(2) 1.81(2), B(2)–B(4) 1.80(2), B(3)–B(5) 1.85(3), B(5)–B(6) 1.69(3), B(6)–B(7) 1.70(2). Selected bond distances (Å) for **2**: W(1)–W(2) 2.9522(8), W(1)–B(1) 2.154(14), W(1)–B(3) 2.160(12), W(1)–B(6) 2.209(15), W(1)–B(2) 2.268(14), W(1)–B(5) 2.285(14), W(1)–B(4) 2.441(15), B(1)–B(2) 1.809(19), B(2)–B(4) 1.937(19), B(3)–B(5) 1.89(2), B(5)–B(6) 1.75(2), B(6)–B(7) 1.74(2).

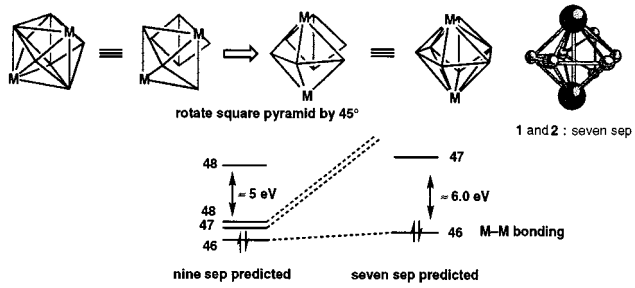

Scheme 1

five-connect vertices of the square base into two four- and two six-connect vertices (Scheme 1). Inclusion of a metal–metal bond generates the observed structure. We have successfully modeled this distortion for **1**. On moving from a hypothetical neutral Re_2B_7 tricapped trigonal prism with a Re–Re bond to the observed structure, two low lying orbitals move to higher energy, thereby accounting for the observed sep count of $n - 2$. Alternatively, the observed structure can be rationalized by inserting a {BH} fragment into a B–B bond of a hypothetical dodecahedral $Cp^*_2Re_2B_6H_6$ cluster. Note that the observed geometry accommodates the electropositive metal centers in high connectivity cluster vertices as well as the propensity for both rhenium and tungsten to form metal–metal bonds.

Compounds **1** and **2** can thus be described as molecular metallaborane counterparts of hypoelectronic main-group cluster Zintl phases. Of course, they possess different properties being neutral (no cations or high cluster charges), molecular (soluble in aliphatic solvents) and modestly air-stable. Full details as well as related chemistry will appear in due course.

The generous support of the National Science Foundation is gratefully acknowledged.

Notes and References

† Reaction of Cp^*ReCl_4 (0.06 g, 0.130 mmol) with BH_3·thf (6 equiv.) for 16 h at 45 °C in toluene, followed by removal of volatiles *in vacuo* and purification by chromatography (toluene–hexane 1 : 2) afforded moderately air-stable, pale yellow, $(Cp^*Re)_2B_7H_7$ **1** (0.036 g, 0.497 mmol, 66% yield based on Re). *Spectroscopic data* for **1**: MS (FAB, NBA matrix), M^+ = 728, 2 Re, 7 B, 20 C atoms, calc. *m/z* 728.2662, obs. 728.2676. ^{11}B NMR (C_6D_6, 21 °C) [$J(^{11}B–^1H)$ in parentheses]: δ 101.7 [d, 1 B (169 Hz)], 85.6 [d, 2 B (164 Hz)], 82.1 [d, 2 B (164 Hz)], 3.6 [d, 2 B (166 Hz)]. ^{1}H NMR (C_6D_6, 21 °C): δ 11.21 [partially collapsed quartet (pcq), 2 H (162 Hz)], 10.12 [pcq, 1 H (167 Hz)], 8.63 [pcq, 2 H (173 Hz)], 1.92 (s, 30 H, Cp*), −0.04 [pcq, 2 H (166 Hz)].

‡ Pyrolysis of $Cp^*WH_3B_4H_8$ in toluene at 110 °C for 20 min afforded $(Cp^*W)_2B_7H_9$ **2** in low yield (5%) after preparative thin-layer chromatography as an inseparable mixture with $(Cp^*W)_3(\mu\text{-}H)B_8H_8$. *Spectroscopic data* for **2**: MS (FAB), M^+ = 723, 2 W, 7 B, 20 C atoms, calc. *m/z* 723.2785, obs. 723.2773. ^{11}B NMR (C_6D_6, 21 °C): δ 99.0 [d, 1 B (147 Hz)], 83.5 [d, 2 B (153 Hz)], 46.6 [d, 2 B (158 Hz)], 17.6 [d, 2 B (136 Hz)]. ^{1}H NMR (C_6D_6, 21 °C): δ 10.40 [pcq, 2 H (146 Hz)], 10.15 [pcq, 1 H (143 Hz)], 5.98 [pcq, 2 H (156 Hz)], 2.23 [pcq, 2 H (136 Hz)], 2.04 (s, 30 H, Cp*), −8.88 (2 H, μ_3-H).

§ *Crystallographic data* for **1**, $C_{20}H_{37}B_7Re_2$, M = 725.57, tetragonal, $P4_2bc$, a = 23.750(3), b = 23.750(3), c = 9.0035(7) Å, U = 5078.7(10) Å^3, Z = 8, μ = 9.530 mm^{-1}. 5079 independent reflections collected (293 K) and 3870 were observed [$I > 2\sigma(I)$]. R_1 = 0.0388, (wR_2 0.0855).

For **2**: $C_{20}H_{39}B_7W_2$, M = 722.88, monoclinic, $P2_1/n$, a = 8.8158(17), b = 18.068(5), c = 16.623(4) Å, β = 101.34(3)°, U = 2596.0(11) Å^3, Z = 4, μ = 8.860 mm^{-1}. 4525 independent reflections collected (293 K) and 3835 were observed [$I > 2\sigma(I)$]. R_1 = 0.0492, (wR_2 0.1337). CCDC 182/941.

1 L. Barton and D. K. Srivastava in *Comprehensive Organometallic Chemistry II*, ed. E. W. Abel, F. G. A. Stone and G. Wilkinson, Pergamon, Oxford, 1995, ch. 8.
2 J. D. Kennedy, *Prog. Inorg. Chem.*, 1984, **32**, 519.
3 J. D. Kennedy, *Prog. Inorg. Chem.*, 1986, **34**, 211.
4 T. P. Fehlner, *Struct. Bonding* (*Berlin*), 1997, **87**, 111.
5 Y. Nishihara, K. J. Deck, M. Shang and T. P. Fehlner, *J. Am. Chem. Soc.*, 1993, **115**, 12 224.
6 S. Aldridge, H. Hashimoto, M. Shang and T. P. Fehlner, *Chem. Commun.*, 1998, 207.
7 S. Aldridge, H. Hashimoto, K. Kawamura, M. Shang and T. P. Fehlner, *Inorg. Chem.*, 1998, **37**, 928.
8 S. Aldridge, M. Shang and T. P. Fehlner, *J. Am. Chem. Soc.*, 1998, **120**, 2586.
9 A. S. Weller, M. Shang and T. P. Fehlner, *J. Am. Chem. Soc.*, in press.
10 H. J.Bullick, P. D. Grebenik, M. L. H. Green, A. K. Hughes, J. B. Leach and P. C. McGowan, *J. Chem. Soc., Dalton Trans.*, 1995, 67.
11 S. J. Hildebrandt, D. F. Gaines and J. C. Calabrese, *Inorg. Chem.*, 1978, **17**, 790; D. F. Gaines and S. J. Hildebrandt, *Inorg. Chem.*, 1978, **17**, 794.
12 P. Kaur, S. D. Perera, T. Jelinek, B. Stibr, J. D. Kennedy, W. Clegg and M. Thornton-Pett, *Chem. Commun.*, 1997, 217; M. A. Beckett, M. Bown, X. L. R. Fontaine, N. N. Greenwood, J. D. Kennedy and M. Thornton-Pett, *J. Chem. Soc., Dalton Trans.*, 1988, 1969; M. A. Beckett, N. N. Greenwood, J. D. Kennedy and M. Thornton-Pett, *J. Chem. Soc., Dalton Trans.*, 1985, 1119.
13 W. A. Herrmann, E. Herdtweck, M. Flöel, J. Kulpe, U. Küsthardt and J. Okuda, *Polyhedron*, 1987, **6**, 1165.
14 C. E. Housecroft, *Adv. Organomet. Chem.*, 1991, **33**, 1.
15 See, for example, R. Poli, G. Wilkinson, M. Motevalli and M. B. Hursthouse, *J. Chem. Soc., Dalton Trans.*, 1985, 931; A. L. Rheingold and J. R. Harper, *Acta Crystallogr., Sect. C*, 1991, **47**, 184.
16 K. Wade, *Adv. Inorg. Chem. Radiochem.*, 1976, **18**, 1.
17 R. F. Fenske, *Pure Appl. Chem.*, 1988, **27**, 61.
18 M. B. Hall and R. F. Fenske, *Inorg. Chem.*, 1972, **11**, 768.
19 J. D. Corbett, *Struct. Bonding* (*Berlin*), 1997, **87**, 157.

Received in Bloomington, IN, USA, 3rd June 1998; 8/05356A

Stereoretentive introduction of (*E*)- and (*Z*)-γ-alkoxyallyl groups into carbonyl compounds *via* light-promoted reaction with γ-alkoxyallylstannanes

Akio Takuwa,*† Yutaka Nishigaichi, Seiji Ebara and Hidetoshi Iwamoto

Department of Material Science, Faculty of Science and Engineering, Shimane University, Matsue, 690-8504, Japan

The light-promoted condensation between carbonyl compounds and (*E*)- or (*Z*)-γ-alkoxyallylstannanes affords predominantly the linear homoallylic alcohols, with retention of the double bond geometry of the γ-alkoxyallyl moieties.

It is well-known that both (*E*)- and (*Z*)-γ-methoxyallylstannanes add to aldehydes at the γ-position in the presence of BF_3•OEt_2 to produce the vicinal diol monomethyl ether (γ-product).[1] The α-ethoxyallylstannane also afforded the γ-product *via* a double allylic shift (one at the reagent level and the second in the addition reaction).[2] In addition, Thomas,[3] Marshall[4] and Gung[5] have reported that α-alkoxy or α-silyloxy substituted crotylstannanes also reacted at the γ-position with aldehydes or ketones under both thermal and Lewis acid-promoted conditions to afford the homoallyl alcohols having an alkoxy or silyloxy group at the terminus of the allylic carbon (*i.e.* vinyl ethers) and that the geometry of the vinyl ether unit in the products is generally *Z* or an *E*/*Z* mixture depending on the reaction conditions and on the substrates. Thus, the stereoretentive introduction of (*E*)- and (*Z*)-γ-alkoxyallyl groups at the α-position of carbonyl compounds has yet to be developed. We[6] and Fukuzumi[7] have found recently that the light-promoted reaction between Group 14 organometallic compounds and electron accepting carbonyl compounds is one of the most useful methodologies for selective carbon–carbon bond forming reactions. In connection with our interest in the light-promoted reaction of allylstannane, we studied the photoallylation of carbonyl compounds with γ-methoxy- and γ-siloxy-allylstannanes. Reported here is the first example of the regioreversed and stereoretentive introduction of (*E*)- and (*Z*)-γ-alkoxyallyl groups *via* light-promoted reaction (Scheme 1).

Irradiation ($h\nu$ > 400 nm) of an MeCN solution containing (*E*)-γ-(methoxyallyl)tributylstannane [(*E*)-**1a**, 24 mmol dm^{-3}] and benzil (**2a**, 20 mmol dm^{-3}) for 2 h at 0 °C gave two addition products. These were identified as the desired α-product (*E*)-**3a** (74%) and the regioisomeric γ-product **4a** (18%) (Table 1, entry 1). Irradiation of the diketone **2a** with the geometrically isomeric tin reagent (*Z*)-**1a** under the same conditions afforded

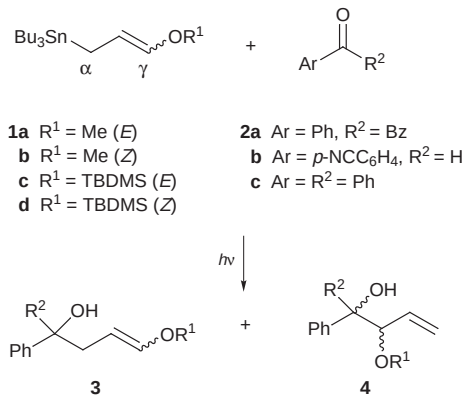

Scheme 1

the α-product (*Z*)-**3a** (66%) and the regioisomer **4a** (23%) (entry 2). The *E*/*Z* olefin geometry of α-product **3a** could be deduced from the 12.7 and 6.3 Hz coupling constants of the vicinal vinyl protons in the ^{1}H NMR spectrum.‡ Double allylation of the two carbonyl groups in the diketone **2a** did not occurred even under prolonged irradiation. The photoallylation also proceeded even in less polar solvents such as benzene and hexane, but slightly less efficiently. (*E*)- and (*Z*)-γ-[(*tert*-Butyldimethylsiloxy)allyl]tributylstannanes [(*E*)- and (*Z*)-**1b**] also reacted photochemically with **2a** to give again the desired α-products predominantly, with complete retention of the double bond geometry of the allylic moiety of the tin reagent **1b** in both cases (entries 3 and 4). When the γ-methoxyallylstannane had a bulky *tert*-butyl group at the β-position (**1c**), it showed complete α-regioselectivity [eqn. (1)]. Thus, the α-regioselectivity depended upon the steric crowding around the γ-position of the allylic stannanes.

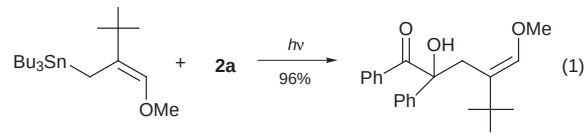

(1)

The photoallylation of *p*-cyanobenzaldehyde **2b** with γ-alkoxyallylstannanes was also examined. Irradiation of the absorption band of aldehyde **2b** in MeCN containing (*E*)- or (*Z*)-**1a** with light of wavelength longer than 320 nm for 5 h at 0 °C gave two regioisomeric homoallylic alcohols in which the γ-methoxyallyl group was again introduced preferentially at the α-position (entries 5 and 7). Similar but higher α-regioselectivity was observed in the photoallyltion with the siloxyallyltin reagents (*E*)- and (*Z*)-**1b**. However, the γ-alkoxyallylic groups in both the tin reagents **1a**,**b** were

Table 1 Light-promoted condensation of (*E*)- and (*Z*)-γ-alkoxyallyltributylstannanes with carbonyl compounds

Entry	1	2	*T*/°C	Products (% yield; *E*:*Z*)[a,b]
1	(*E*)-**1a**	**2a**	0	**3a** (74; 98:2), **4a** (18)
2	(*Z*)-**1a**	**2a**	0	**3a** (66; 2:98), **4a** (21)
3	(*E*)-**1b**	**2a**	0	**3b** (78; 99:1), **4b** (9)
4	(*Z*)-**1b**	**2a**	0	**3b** (74; 1:99), **4b** (14)
5	(*E*)-**1a**	**2b**	0	**3c** (36; 91:9), **4c** (14)
6	(*E*)-**1a**	**2b**	−78	**3c** (37; 96:4), **4c** (13)
7	(*Z*)-**1a**	**2b**	0	**3c** (32; 14:86), **4c** (17)
8	(*Z*)-**1a**	**2b**	−78	**3c** (42; 8:92), **4c** (21)
9	(*E*)-**1b**	**2b**	0	**3d** (39; 88:12), **4d** (8)
10	(*E*)-**1b**	**2b**	−78	**3d** (37; 92:8), **4d** (6)
11	(*Z*)-**1b**	**2b**	0	**3d** (36; 13:87), **4d** (12)
12	(*Z*)-**1b**	**2b**	−78	**3d** (47; 8:92), **4d** (15)
13	(*E*)-**1a**	**2c**	−78	**3e** (52; 96:4), **4e** (15)
14	(*Z*)-**1a**	**2c**	−78	**3e** (46; 9:91), **4e** (19)

[a] *E*:*Z* ratios were determined by ^{1}H NMR analysis of the crude mixture. [b] The γ-products consisted of a 1:1 mixture of *syn* and *anti* diastereomers.

introduced with partial loss of the geometry of the allylic double bond. On the other hand, when the irradiation was carried out at −78 °C in propionitrile, the geometry of the γ-alkoxyallylic group of the tin reagents **1a**,**b** was almost completely maintained in the α-products (entries 6 and 8). Benzophenone **2c** could also be allylated with (*E*)- and (*Z*)-**1a** to give preferentially the α-product with retention of the geometry of the γ-methoxyallyl moiety (entries 13 and 14).

The present allylation is initiated by an electron transfer from the tin reagent **1** to the photoexcited carbonyl compound **2** to give the γ-alkoxyallyltributyltin radical cation (**1**$^{\bullet+}$)-ketyl radical anion pair (**2**$^{\bullet-}$), followed by the dissociation of the (γ-alkoxyallyl) C–Sn bond of **1**$^{\bullet+}$ into a γ-alkoxyallyl radical and a tributyltin cation.[6,7] The resulting γ-alkoxyallyl radical couples with **2**$^{\bullet-}$ preferentially at the less crowded α-position to yield the linear homoallylic alcohol. The configuration of the γ-alkoxyallyl unit is maintained without *E*/*Z*-isomerization during all these processes to give the α-product stereospecifically.

When the $BuSnCl_3$-mediated transmetallation method[8] was employed for the reaction of the tin reagents (*E*)- and (*Z*)-**1a** with aldehyde **2b**, the α-product **3a** was also produced from both the tin reagents, but the olefin geometry of the product **3a** was *Z* regardless of the geometry of the starting tin reagents.§ In addition, it has been reported that alkoxyallyl carbanion reagents (ROCH=CHCH$_2$M: R = alkyl or $SiMe_3$; M = Li) react with electrophiles including carbonyl compounds to afford (*Z*)-linear vinyl ethers.[9]

In conclusion, we have found that the present light-promoted reaction provides the first example of a stereoretentive introduction of (*E*)- and (*Z*)-γ-alkoxyallyl groups from γ-alkoxyallylstannanes into carbonyl compounds at the α-position.

This work was supported by a Grant-in-aid for Scientific Research (No. 09640636) from the Ministry of Education, Science, Sports and Culture, Japan.

Notes and References

† E-mail: takuwa@riko.shimane-u.ac.jp

‡ After irradiation, the products were separated into individual regioisomers (**3a** and **4a**) by TLC (SiO_2, hexane–Et_2O, 1:1, v/v). Each geometrical isomer could be purified by carefully repeating the TLC separation (hexane–CH_2Cl_2, 1:2, v/v). *Selected data* for α-product (*E*)-**3a**: oil; δ_H($CDCl_3$, 270 MHz) 2.7 (dd, *J* 7.7, 15.2, 1H), 3.0 (dd, *J* 7.7, 13.2, 1H), 3.4 (s, 3H), 4.1 (s, 1H), 4.4 (ddd, *J* 12.7, 13.2, 15.2, 1H), 6.2 (d, *J* 12.7, 1H), 7.2–7.8 (m, 10H); ν_{max}($CHCl_3$)/cm^{-1} 3534 (OH), 1679 (C=O). For α-product (*Z*)-**3a**: oil; δ_H($CDCl_3$, 270 MHz) 2.9 (dd, *J* 7.0, 14.4, 1H), 3.2 (dd, *J* 7.0, 15.4, 1H), 3.4 (s, 3H), 4.4 (ddd, *J* 6.3, 14.4, 15.4, 1H), 4.5 (s, 1H), 6.0 (d, *J* 6.3, 1H), 7.2–7.8 (m, 10H); ν_{max}($CHCl_3$)/cm^{-1} 3542 (OH), 1673 (C=O). All other compounds gave satisfactory spectral data. The γ-product **4a** consisted of a 1:1 mixture of *syn* and *anti* diastereomers, which supports the proposed reaction mechanism showing the products being formed by the combination of allylic and ketyl radicals.

§ To a solution of the tin reagent (*E*)- or (*Z*)-**1a** (0.3 mmol) in CH_2Cl_2 (6 ml) under N_2 at −78 °C was added $BuSnCl_3$ (0.3 mmol) in CH_2Cl_2 (3 ml). After stirring the mixture at that temperature for 10 min, the substrate **2b** (0.2 mmol) was added slowly and the resulting mixture was stirred for 2 h at that temperature. The reaction mixture was quenched with a 10% aq. KF and worked up as usual. The (*Z*)-α-product was obtained in 19 and 71% yield, respectively, along with a very small amount of γ-product [(*Z*)-**3a**:**4a** = 91:9 from (*E*)-**1a**; 99:1 from (*Z*)-**1a**].

1 M. Koreeda and Y. Tanaka, *Tetrahedron Lett*., 1987, **28**, 143; V. Gevorgyan and Y. Yamamoto, *J. Chem. Soc*., *Chem. Commun*., 1994, 59.
2 J. P. Quintard, B. Elissondo and M. Pereyre, *J. Org. Chem*., 1983, **48**, 1559.
3 A. J. Pratt and E. J. Thomas, *J. Chem. Soc*., *Perkin Trans. 1*, 1989, 1521; *J. Chem. Soc*., *Chem. Commun*., 1982, 1115.
4 J. A. Marshall and W. Y. Gung, *Tetrahedron*, 1989, **45**, 1043; J. A. Marshall and G. S. Weimaker, *Tetrahedron Lett*., 1991, **32**, 2101.
5 B. W. Gung, D. T. Smith and M. A. Wolf, *Tetrahedron Lett*., 1991, **32**, 13; B. W. Gung, A. J. Peat, B. M. Snook and D. T. Smith, *Tetrahedron Lett*., 1991, **32**, 453.
6 A. Takuwa, Y. Nishigaichi and H. Iwamoto, *Chem. Lett*., 1991, 1013; A. Takuwa, Y. Nishigaichi, T. Yamaoka and K. Iihama, *J. Chem. Soc*., *Chem. Commun*., 1991, 1359; A. Takuwa, J. Shiigi and Y. Nishigaichi, *Tetrahedron Lett*., 1993, **34**, 3457.
7 S. Fukuzumi and T. Okamoto, *J. Am. Chem. Soc*., 1994, **116**, 5503; S. Fukuzumi, *Bull. Chem. Soc. Jpn*., 1997, **70**, 1.
8 H. Miyake and K. Yamamura, *Chem. Lett*., 1992, 1369.
9 W. C. Still and T. L. Macdonald, *J. Org. Chem*., 1976, **41**, 3620; W. C. Still and T. L. Macdonald, *J. Am. Chem. Soc*., 1974, **96**, 5561; D. A. Evans, G. C. Andrews and B. Buckwalter, *J. Am. Chem. Soc*., 1974, **96**, 5560.

Received in Cambridge, UK, 12th June 1998; 8/04459G

Intralayer hydrogen-bond-directed self-assembly of nano-fibers from dicarboxylic valylvaline bolaamphiphiles

Masaki Kogiso,*† Takeshi Hanada, Kiyoshi Yase and Toshimi Shimizu

National Institute of Materials and Chemical Research, 1-1 Higashi, Tsukuba, Ibaraki, 305-8565, Japan

Dicarboxylic L-valyl-L-valine bolaamphiphiles produced nanoscale fibers with widths of 10–30 nm, *via* proton-triggered self-assembly in water, which are dominated by both intralayer, lateral hydrogen-bond networks between end carboxylic acid groups and parallel β-sheet networks between amide groups.

Carboxylic amphiphiles form a variety of self-assemblies such as micelles, vesicles, fibers, and crystals in water. The formation behavior strongly depends upon hydration states, salt concentrations, and pH conditions in aqueous dispersions.[1,2] In particular, the end carboxy groups exist as carboxylate anions (soap), acid–soaps, acids, or a mixture of these. To date it is still uncertain whether inter- or intra-layer carboxy interactions enforce the crystalline order and whether they dominate supramolecular structures or not.[3] A large number of crystal structures have been reported for fatty acids that form an acid-acid cyclic dimer,[3,4] whereas only one crystallization was achieved for potassium palmitate soap.[3,5] This indicates that no specific interlayer interactions are dominant in the soaps. We have recently demonstrated the formation of rod-like micelles, supramolecular microtubes,[6] and needle-shaped crystals[7] in water from dicarboxylic glycylglycine bolaamphiphiles. In addition to hydrophobic interactions between the alkylene spacers, the predominant forces driving these self-assemblies involve anion-anion, intralayer acid-anion, and interlayer acid-acid interactions, respectively.[8] Here we describe proton-triggered nano-fiber formation from valylvaline bolaamphiphiles **1–3**, which is dominated by intralayer acid-acid and amide hydrogen-bond networks. Furthermore, the separate contributions of the inter- and intra-layer interactions on the supramolecular structures was evaluated using FT-IR analysis.

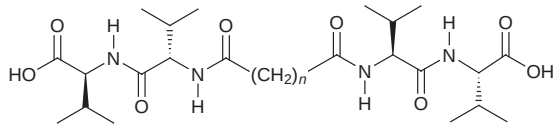

1 $n = 6$
2 $n = 8$
3 $n = 10$

The dicarboxylic bolaamphiphiles **1–3** with an L-valyl-L-valine moiety at each end were synthesized by condensation of alkane-1,*n*-dicarboxylic acid (n = 6, 8 and 10) with 2 equiv. of *C*-protected L-valyl-L-valine benzyl ester, followed by deprotection of the *C*-terminal.‡

The obtained white powders of **1–3** are sparingly soluble in water (< 0.1 mg ml^{-1} at 23 °C), but become highly soluble (> 50 mg ml^{-1} at 23 °C) after neutralization with alkali hydroxides. When alkaline aqueous solutions of **1–3** (10 mM, 2 equiv. NaOH, pH > 7) were slowly acidified by vapor diffusion of 1–5% AcOH into the solution,[7,8] the bolaamphiphiles **2** (n = 8) and **3** (n = 10) produced a hydrogel in 1–2 weeks. In contrast, the bolaamphiphile **1** (n = 6) with a shorter oligomethylene bridge formed a crystalline solid as a precipitate. We obtained these self-assemblies at pH 3.4, 4.3 and 4.9 for **1**, **2** and **3**, respectively. From pH titration results,[8] the original carboxylate anions of **1–3** proved to be fully protonated at these pH values. Elemental analyses of the crystal from **1** and the dehydrated gels from **2** and **3** are also consistent with the protonated state.§

Energy-filtering transmission electron microscopy (EF−TEM) is a useful tool for observing low-contrast organic and biological samples without staining.[9] Furthermore, unstained TEM observations have the advantage of avoiding awkward microscopic artifacts. EF−TEM of the hydrogel revealed that the gels from **2** and **3** are comprised of a number of fibrous assemblies with micrometers lengths [Fig. 1(a)]. High-resolution EF−TEM images clearly show the presence of nanoscale fibers with widths of 10–30 nm [Fig. 1(b)]. No significant intertwisted fibers, observed for organogels made of N-protected bolaform amides,[10] can be seen. Furthermore, small angle X-ray diffraction analysis of the fibers from **2** and **3** displayed no crystalline Bragg reflections. These findings indicate that the proton-triggered self-assembly provides supramolecular fibers made of the fully protonated bolaamphiphiles **2** or **3**.

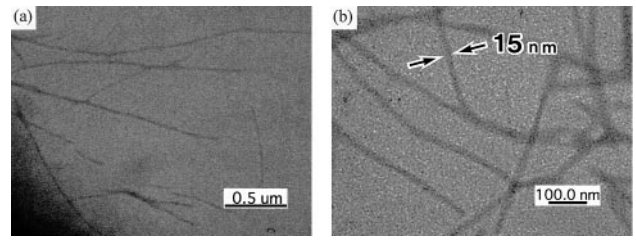

Fig. 1 (a) Energy-filtering transmission electron micrograph of the nano-fibers made of 3. (b) High-resolution image of the same specimen.

FT-IR spectra of the dried self assemblies from **1–3** were measured on a CaF_2 plate. Fig. 2 shows a partial FT-IR spectrum of the dehydrated fibers from **3**. The CH_2 antisymmetric and symmetric stretching bands of **3** appear at 2930 and 2856 cm^{-1}, respectively. The CH_2 scissoring band gives a single sharp peak at 1467 cm^{-1}. These band characteristics

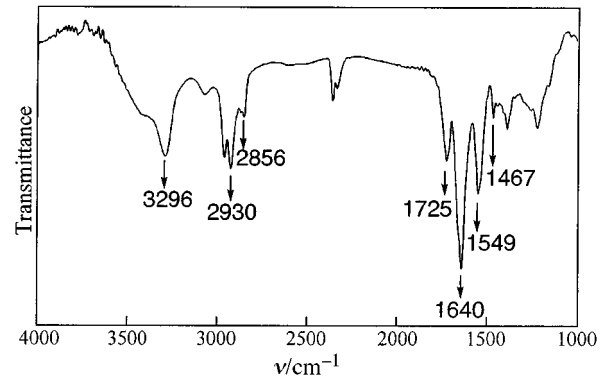

Fig. 2 FT-IR spectrum of the dehydrated fibers from **3** in the region of 1000–4000 cm^{-1}

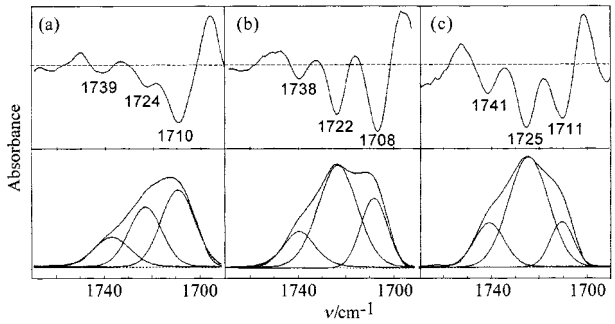

Fig. 3 FT-IR spectra in the CO_2H band region of the dried self-assemblies from (a) **1**, (b) **2** and (c) **3**. Top: second-derivative plots. Bottom: curve-fitting results.

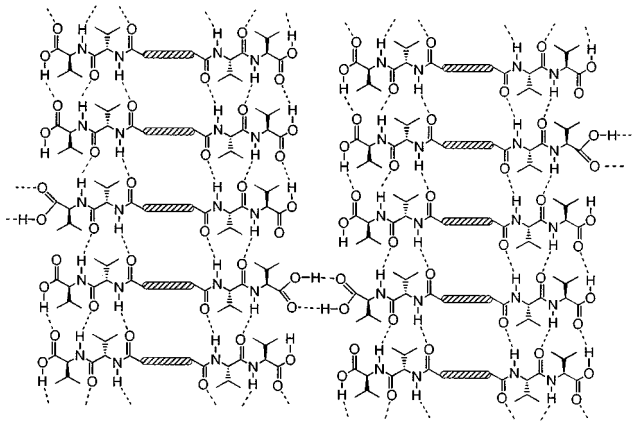

Fig. 4 A possible model for the predominant intralayer hydrogen-bond network within the nano-fibers from **2** or **3**. Interlayer acid-acid hydrogen bonds are partly depicted.

suggest that the alkylene bridge of **3** has a high *trans* conformational population[11] and that its packing mode is triclinic.[12] On the other hand, the presence of a parallel β-sheet network between amide groups can be confirmed by the N–H stretching, with the amide I and II bands at 3296, 1640 and 1549 cm^{-1}, respectively.[13] This is in contrast with the three-dimensional networks of hydrogen bonds found within microtube membranes and crystals of oligoglycine bolaamphiphiles.[7,8] The isopropyl groups of the valine residue enforce two-dimensional hydrogen-bond networks due to steric hindrance.

A broad band due to the carboxylic acids (CO_2H) appears around 1725 cm^{-1}, whereas no carboxylate anion (COO^-) bands can be seen around 1600 cm^{-1}. Fig. 3 shows FT-IR spectra in the CO_2H band region for the dried self-assemblies of **1–3** and their second derivative plots. Curve-fitting analysis also supports the validity of this deconvolution for the CO_2H band. As a result, we found three independent absorption bands at 1741, 1725, and 1711 cm^{-1} for **3**. The absorption bands near 1740 and 1725 cm^{-1} can be assigned to the C=O stretching vibration of the free, non-hydrogen bonded and laterally hydrogen-bonded CO_2H groups, respectively.[14] On the other hand, the bifurcated hydrogen bond of the CO_2H groups, which is commonly observed in the solid state, displays a band around 1710 cm^{-1}. The area ratio of each band for **3** is calculated to be 20:65:15 for the non-hydrogen-bonded:laterally hydrogen-bonded:bifurcated CO_2H groups. The nano-fibers made of **2** also display three FT-IR bands at 1738, 1722, and 1708 cm^{-1} with an area ratio of 15:60:25, respectively. However, the CO_2H band area ratio of **1** is 20:35:45. These results indicate that intralayer, lateral hydrogen-bond networks are of great importance in the nano-fiber formation from **2** and **3**. On the basis of the FT-IR analyses, a possible hydrogen-bond network within the nano-fibers is shown in Fig. 4. Intralayer interactions between the carboxylic peptide head groups enforce an extended molecular sheet. Similar structures were also depicted for the organogel-forming bolaform amides with no interacting end functionalities.[10] On the other hand, interlayer cyclic dimer formation by the CO_2H groups determines the crystalline structure of **1**. The bolaamphiphile **1** probably requires stronger interlayer interactions to compensate for a decrease in hydrophobic interactions.

In conclusion, the FT-IR deconvolution analysis of the CO_2H bands clarified that intra- and inter-layer interactions between the head groups of **1–3** control the formation of supramolecular nano-fibers and the crystalline solid, respectively.

Notes and References

† E-mail: mkogiso@home.nimc.go.jp

‡ *Selected data* for **1**: yield 69 %, mp 193 °C; $[\alpha]_D$ −46.9. For **2**: yield 79%, mp 184 °C; $[\alpha]_D$ −46.1. For **3**: yield 61%, mp 134 °C; $[\alpha]_D$ −39.9; δ_H(270 MHz, [$^2H_6$]DMSO) 0.83 [d, *J* 5.4, 24H, $(CH_3)_2CH\times$ 4], 1.20 [m, 12H, $CH_2(CH_2)_6CH_2$], 1.45 [m, 4H, $CH_2(CH_2)_6CH_2$], 1.99 [m, *J* 5.4, 4H, $(CH_3)_2CH\times$ 4], 2.08 (t, *J* 5.4, 4H, $COCH_2CH_2\times$ 2), 4.08 (t, *J* 5.4, 24H, $NHCHCO\times$ 2), 4.24 (t, *J* 5.4, 2H, $NHCHCOOH\times$ 2); 7.79 (d, *J* 8.1, 2H, $NHCHCO\times$ 2); 7.88 (d, *J* 8.1, 2H, $NHCHCO\times$ 2). These *C*-terminated bolaamphiphiles **1–3** are analogues of the *N*-protected bolaform amides reported by Hanabusa and co-workers (ref. 10).

§ Calc. for the fully protonated state of **3** ($C_{32}H_{58}O_8N_4 0.5H_2O$): C, 60.44; H, 9.35; N, 8.82. Found: C, 60.24; H, 9.27; N, 8.90%.

¶ EF−TEM of the specimens was performed at 80 keV using an analytical electron microscope (Carl Zeiss EM 902) with a Castain-Henry type electron energy filter at room temperature.

1 J.-H. Fuhrhop, H.-H. David, J. Mathieu, U. Liman, H.-J. Winter and E. Boekema, *J. Am. Chem. Soc.*, 1986, **108**, 1785; J.-H. Fuhrhop, C. Demoulin, J. Rosenberg and C. Boettcher, *J. Am. Chem. Soc.*, 1990, **112**, 2827; T. Imae and B. Trend, *Langmuir*, 1991, **7**, 643.
2 T. Imae, Y. Takahashi and H. Muramatsu, *J. Am. Chem. Soc.*, 1992, **114**, 3414; O. Träger, S. Sowade, C. Böttcher and J.-H. Fuhrhop, *J. Am. Chem. Soc.*, 1997, **119**, 9120.
3 J.-H. Fuhrhop and J. Köning, in *Membranes and Molecular Assemblies: The Synkinetic Approach*, The Royal Society of Chemistry, UK, 1994, p.186.
4 L. Leiserowitz, *Acta. Crystallogr.*, 1976, **B32**, 775; F. Kaneko and M. Kobayashi, *Acta. Crystallogr.*, 1990, **C46**, 1490.
5 J. H. Dumbleton and T. R. Lomer, *Acta. Crystallogr.*, 1965, **19**, 301;
6 T. Shimizu, M. Kogiso and M. Masuda, *Nature*, 1996, **383**, 487.
7 T. Shimizu, M. Kogiso and M. Masuda, *J. Am. Chem. Soc.*, 1997, **119**, 6209; M. Kogiso, M. Masuda and T. Shimizu, *Supramol. Chem.*, 1998, **9**, in the press.
8 M. Kogiso, S. Ohnishi, K. Yase, M. Masuda and T. Shimizu, *Langmuir*, 1998, in the press.
9 A. Starosud, D. P. Bazett-Jones and C. H. Langford, *Chem. Commun.*, 1997, 443; A. D. Chesne, B. Gerharz and G. Lieser, *Polym. Int.*, 1997, **43**, 187; L. Reimer, *Energy-Filtering Transmission Electron Microscopy*, Springer-Verlag, Berlin, Heidelberg, 1995.
10 K. Hanabusa, J. Tange, Y. Taguchi, T. Koyama and H. Shirai, *J. Chem. Soc., Chem. Commun.*, 1993, 391; K. Hanabusa, R. Tanaka, M. Suzuki, M. Kimura and H. Shirai, *Adv. Mater.*, 1997, **9**, 1095.
11 R. G. Snyder, H. L. Strauss and C. A. Elliger, *J. Mol. Spectrosc.*, 1961, **7**, 116.
12 V. Vand, *Acta Crystallogr.*, 1951, **4**, 104; R. G. Snyder, *J. Phys. Chem.*, 1982, **86**, 5145.
13 C. Toniolo and M. Palumbo, *Biopolymers*, 1977, **16**, 219.
14 L. Sun, L. J. Kepley and R. M. Crooks, *Langmuir*, 1992, **8**, 2101; J. Dong, Y. Ozaki and K. Nakashima, *Macromolecules*, 1997, **30**, 1111.

Received in Cambridge, UK, 14th May 1998; 8/03606C

An STM–XPS study of ammonia oxidation: the molecular architecture of chemisorbed imide 'strings' at Cu(110) surfaces

Albert F. Carley, Philip R. Davies and M. Wyn Roberts*

Department of Chemistry, Cardiff University, PO Box 912, Cardiff, UK CF1 3TB. E-mail: robertsmw@cardiff.ac.uk

The structural characteristics of imide strings formed when a Cu(110) surface is exposed to an ammonia rich NH_3–O_2 mixture at 325 K have been determined by STM. The spacing of the NH units within a string is 5 Å and at complete coverage the strings are separated by 7.2 Å.

Here we provide a detailed insight into the structure of the imide overlayer that results from the oxidation of ammonia at a Cu(110) surface. The experiment was carried out under dynamic co-adsorption conditions where there is no evidence at the surface of either of the two reactants, ammonia and oxygen, and investigated using X-ray photoelectron spectroscopy (XPS) and scanning tunneling microscopy (STM). The combination of STM with *in situ* XPS provides a unique and powerful approach to the study of the mechanism of surface reactions: STM provides structural information at the atomic level and XPS allows chemical identification of the surface species. The dual function ultra high vacuum spectrometer was supplied by Omicron Vakuumphysik.

The formation of a chemisorbed imide adlayer at a Cu(110) surface exposed to an ammonia-rich (30 : 1) mixture of ammonia and dioxygen was first established by us using XPS and high resolution electron energy loss spectroscopy (HREELS).[1,2] Subsequently, Bradshaw *et al*.[3] showed using photoelectron diffraction that the imide species are adsorbed in the short-bridge site on Cu(110). Previous STM studies by Madix's group[4] have concentrated on the reaction of pre-adsorbed oxygen atoms on Cu(110) by ammonia. Chem-isorptive replacement of oxygen occurs primarily at Cu–O chain ends[4,5] leading to a mixed imide–oxygen adlayer.

An STM image of the Cu(110) surface saturated with imide species (Fig. 1) shows close-packed, broad NH(a) 'strings' with a uniform separation between strings of 7.2 Å, which is close to twice the copper lattice spacing in the $<100>$ direction. Since individual NH species are generally not resolved along the strings, STM alone cannot determine the packing density of the imide moieties in the $<1\bar{1}0>$ direction. However, quantification[6] of the observed XP N(1s) spectrum gives a saturation coverage of 2.6×10^{14} cm^{-2}. Population of all the short bridge sites (*i.e*. a 2×1 structure) would lead to a saturation imide coverage of *ca*. 5×10^{14} cm^{-2}. We conclude that the imide species are adsorbed in alternate short bridge sites, with a NH–NH spacing of *ca*. 5 Å. This is in excellent agreement with recent density functional calculations.[7] Whether the imide species are adsorbed in a $p(2 \times 2)$ or a $c(2 \times 4)$ surface structure cannot be determined from the present data.

Corroboration of the intermolecular spacing of the imide molecules comes from an analysis of the string labelled '6' in Fig. 2, observed during the real-time study of the growth of imide strings on the copper surface at 325 K. Unusually, discrete features within the string are resolved in this case, with a spacing of 5.2 Å. We were able to observe this particular feature develop alongside the already completed NH string labelled '5' at approximately the same rate as other NH strings. The feature was stable (as were all the features recorded in this

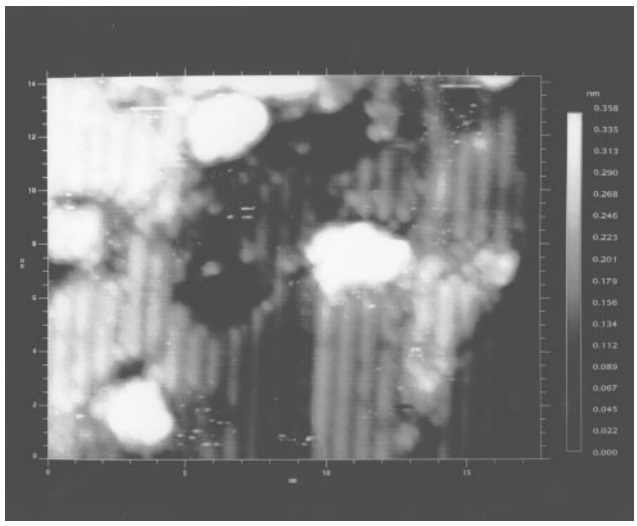

Fig. 1 STM image of a Cu(110) surface saturated with imide species after several hours exposure to the 30 : 1 ammonia–dioxygen mixture. Note the regular spacing of the imide rows. STM imaging conditions: sample bias −0.62 V, tunneling current 0.24 nA, scan speed 215 nm s^{-1}.

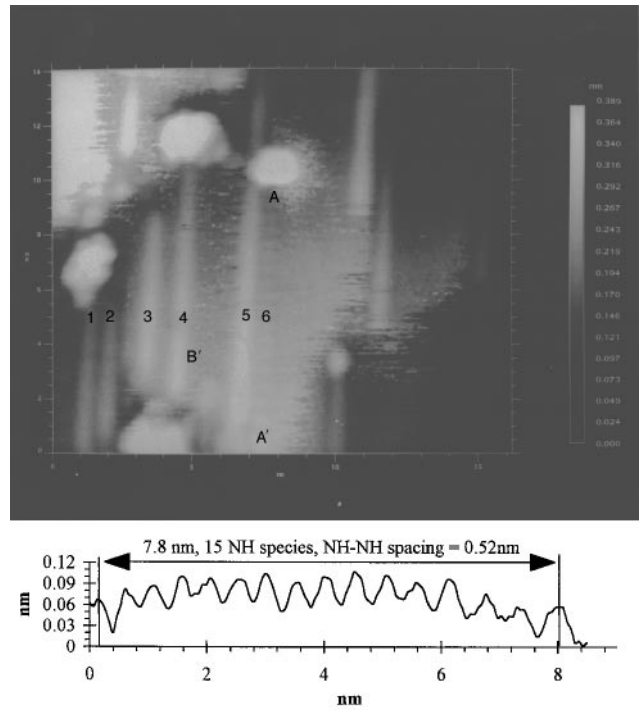

Fig. 2 STM image recorded during exposure of a Cu(110) surface at 325 K to a 30 : 1 ammonia–dioxygen mixture; the image was recorded after 2300 s at a mixture pressure of 1.5×10^{-8} mbar. The characteristically broad imide rows are aligned in the $<1\bar{1}0>$ direction. Selected NH strings are numbered 1–6; the line profile below the image was obtained between the points A and A' and shows a corrugation reflecting the individual imide species in row 6. STM imaging conditions: sample bias −1.00 V, tunneling current 0.25 nA, scan speed 91 nm s^{-1}.

experiment) for at least 40 minutes and was identical in both the forward and the reverse scan. Why the NH molecules should be resolved in this particular feature (and a few others) but not in the majority of cases is not clear. We have already reported[1,2] that XPS shows that only NH is present at the surface, as reflected in an N 1s feature with a binding energy of 397.8 eV, during exposure of Cu(110) to such an ammonia–dioxygen mixture.

It is significant that the NH species form extended strings at the surface, rather than simply adsorbing randomly. We have previously established that under dynamic co-adsorption conditions novel surface chemistry can be observed through the interaction of weakly adsorbed species, possessing a short surface life-time, with reactive co-adsorbates (see the reviews in ref. 8). In this case, NH formation results from the interaction of ammonia molecules (present at immeasurably low coverages under the reaction conditions and undergoing rapid surface diffusion) with transient oxygen species. The NH (possibly radical-like) species then diffuse across the terraces and are trapped at sites adjacent to the ends of NH strings, where they are energetically most stable.[7] We have not however been able to progress further the debate[1,9] as to whether at the Cu(110) surface the reactive oxygen species are atomic [eqns. (1) and (2)] or molecular [eqn. (3)] in nature (s = surface transient; a = chemisorbed species):

$$O_2(g) \rightarrow 2\,O^{\delta-}(s) \quad (1)$$

$$NH_3(s) + O^{\delta-}(s) \rightarrow NH(a) + H_2O(g) \quad (2)$$

$$NH_3(s) + O_2^{\delta-}(s) \rightarrow NH(a) + O(a) + H_2O(g) \quad (3)$$

Both atomic[10] and molecular[11] transient oxygen species have been implicated in the surface chemistry observed at other metal surfaces under dynamic coadsorption conditions.

A further observation that can be made in Fig. 1 is that during the early stages of the development of the NH overlayer, nucleation of NH strings frequently occurs not at the ideal close-packed spacing of 7.2 Å but one lattice spacing further apart giving a spacing of 10.8 Å. (Compare for example the separation between NH strings 1 and 2, and 3 and 4.) This observation is interesting because although these NH strings appear very stable even at 325 K, continual exposure to the ammonia–dioxygen mixture generates a close-packed layer with a uniform 7.2 Å string separation. This can only result from a displacement of some of the NH chains due to lateral interactions between imide species, as newly formed NH groups diffuse to short-bridge sites located between imide chains separated by 10.8 Å.

In summary, the mechanism of the selective oxidation of ammonia at Cu(110), first investigated using X-ray and electron energy loss spectroscopies,[1,2] has been developed through STM to provide a model at the molecular level. Details of the interatomic spacing of the NH units within an imide string and the spacings between the rows of strings have been obtained for the first time.

We are grateful to EPSRC for their generous support of this research.

Notes and References

1 B. Afsin, P. R. Davies, A. Pashuski and M. W. Roberts, *Surf. Sci. Lett*., 1991, **259**, L724.
2 B. Afsin, P. R. Davies, A. Pashuski, M. W. Roberts and D. Vincent, *Surf. Sci*., 1993, **284**, 109.
3 C. J. Hirschmugel, K. M. Schindler, O. Schaff, V. Fernandez, A. Theobald, P. Hofmann, A. Bradshaw, R. Davis, N. A. Booth, D. P. Woodruff and V. Fritzsche, *Surf. Sci.*, 1996, **352**, 232.
4 X-C. Guo and R. J. Madix, *Faraday Discuss.*, 1996, **105**, 139.
5 A. F. Carley, P. R. Davies, M. W. Roberts and D. Vincent, *Top. Catal.*, 1994, **1**, 35.
6 A. F. Carley and M. W. Roberts, *Proc. R. Soc. London A*, 1978, **363,** 403.
7 P. R. Davies and J. Keel, in preparation.
8 M. W. Roberts, *Chem. Soc. Rev.*, 1989, **18**, 451; 1996, **25**, 437; M. W. Roberts, *Appl. Surf. Sci*., 1991, **52**, 133; A. F. Carley, P. R. Davies and M. W. Roberts, *Curr. Opin. Solid State Mater. Sci.*, 1997, **2,** 525.
9 M. Neurock, R. A. van Santen, W. Biemolt and A. P. J. Jansen, *J. Am. Chem. Soc*., 1994, **116**, 6860.
10 C. T. Au and M. W. Roberts, *Nature*, 1986, **319**, 206; *J. Chem. Soc., Faraday Trans. I*, 1987, **83**, 2047. A. F. Carley and M. W. Roberts, *J. Chem. Soc., Chem. Commun*., 1987, 355.
11 A. F. Carley, M. W. Roberts and S. Yan, *J. Chem. Soc., Chem. Commun*., 1988, 267; *J. Chem. Soc., Faraday Trans.*, 1990, **86**, 2701; A. F. Carley, M. W. Roberts and M. Tomellini, *J. Chem. Soc., Faraday Trans.*, 1991, **87,** 3563.

Received in Cambridge, UK, 19th June 1998; 8/04657C

Short and efficient route to substituted linear triquinanes from 2-methoxyphenols

Day-Shin Hsu, Polisetti Dharma Rao and Chun-Chen Liao*†

Department of Chemistry, National Tsing Hua University, Hsinchu, Taiwan 30043

Highly oxygenated and substituted *cis,anti,cis* fused linear triquinanes are prepared from commercially available 2-methoxyphenols and cyclopentadiene.

Extensive efforts by synthetic organic chemists during the last two decades towards the synthesis of polyquinane natural products have resulted in the development of several elegant approaches.[1] However, except for a few, most of these approaches are either target oriented or require fairly long sequences of reactions to arrive at the desired carbon framework. Consequently, the search for new methodologies that provide efficient and rapid access to desired quinane skeletons continues.

Masked *o*-benzoquinones **1** bearing an array of functional groups can be easily generated *in situ* by the oxidation of commercially available 2-methoxyphenols with hypervalent iodine reagents such as (diacetoxy)iodobenzene (DAIB) and [bis(trifluoroacetoxy)]iodobenzene (BTIB) in MeOH.[2] Masked *o*-benzoquinones **1**, being the most easily accessible cyclohexa-2,4-dienones, readily undergo Diels–Alder reactions in various modes, *i.e*. they act as dienes and dienophiles in both inter- and intra-molecular reactions.[2–6] We have already made use of these reactions in the synthesis of highly functionalized bicyclo-[2.2.2]octenones,[2] *cis*-decalins,[3,4] linear and angular triquinanes[5] and in the synthesis of several natural products.[6] We herein report the development of a new and simple approach to facilitate stereoselective synthesis of highly substituted linear triquinanes using Diels–Alder reactions of cyclopentadiene with *in situ* generated masked *o*-benzoquinones and oxa-di-π-methane (ODPM) photorearrangement as the key steps.

Accordingly, we have carried out the Diels–Alder reactions of cyclopentadiene with masked *o*-benzoquinones **1**, generated *in situ* by adding a solution of a 2-methoxyphenol **2** (2 mmol) in MeOH (8 ml) to a mixture of DAIB (3 mmol) and cyclopentadiene (50 mmol) in MeOH (6 ml) at reflux during 1 h. It was observed that products **3** were produced exclusively except in the cases of **1d** and **1f** (Scheme 1, Table 1). Masked *o*-benzoquinones **1d** and **1f** produced both the possible adducts, *i.e.* **3d** and **4d** and **3f** and **4f**, respectively. Compound **4d** was isolated in pure form while the thermally unstable compound **4f** was found to rearrange to **3f** rapidly. Then the adduct **4d** was subjected to rearrangement in mesitylene at 160 °C for 10 min. As expected compound **3d** was produced in almost quantitative yield. To simplify the preparation of compounds **3d** and **3f**, the concentrated reaction mixtures obtained individually from the reactions of **1d** and **1f** with cyclopentadiene were heated, without purification, in mesitylene at 160 °C for 10 min to furnish compounds **3d** and **3f** in 86 and 76% yield, respectively. It was also observed that by extending the Diels–Alder reaction time to 6 h for **1d** and 18 h for **1f** the desired products could also be obtained exclusively (Table 1).

The observation of products **4d** and **4f** and their isomerization to **3d** and **3f** respectively suggests that a tandem process involving a Diels–Alder reaction followed by Cope rearrangement is in operation in the formation of the latter compounds which are secondary products at least in part if not all. However, controlled experiments carried out at 0 °C made it clear that there are two competetive Diels–Alder reactions taking place. Importantly, in both the modes these cycloadditions are regio- and stereo-selective. In such cycloaddition reactions of cyclopentadiene,[7] this is the first time that a stable and thoroughly characterized norbornene-type adduct, **4d**, has been isolated.

For the conversion of compounds **3a–g** into triquinanes, they were irradiated in acetone using light of wavelength centered at 300 nm in a Rayonet reactor. While **3a** provided the desired ODPM rearrangement product **5a** in 68%, **3b** furnished the expected triquinane **6b** in 45% yield. In other cases a complex reaction mixture was a regular feature. These results are not unexpected since only in the cases of **3a** and **3b** does the biradical intermediate enjoy resonance stabilization by the methoxycarbonyl group. Treatment of **5a** with Ac_2O and BF_3•OEt_2[8] resulted in the highly oxygenated linear triquinane **6a** (Scheme 2). The overall yield of compound **6a** from **2a** is *ca*. 42%. The stereochemical assignments of the triquinane **6a** were based on NOE studies.

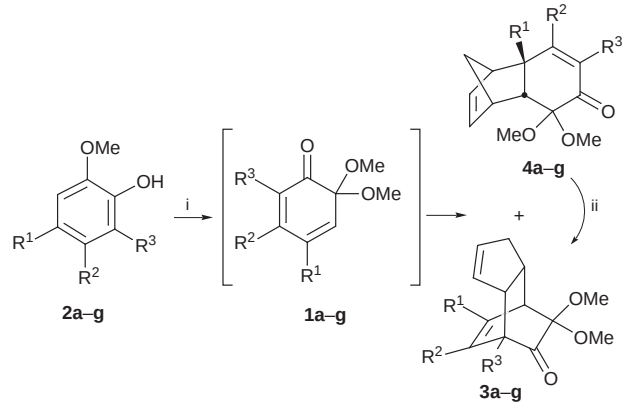

a $R^1 = CO_2Me$, $R^2 = R^3 = H$
b $R^1 = CO_2Me$, $R^2 = H$, $R^3 = OMe$
c $R^1 = H$, $R^2 = CO_2Me$, $R^3 = H$
d $R^1 = R^2 = R^3 = H$
e $R^1 = Me$, $R^2 = R^3 = H$
f $R^1 = R^3 = H$, $R^2 = Me$
g R^1 = 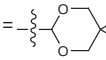 , $R^2 = R^3 = H$

Scheme 1 *Reagents and conditions*: i, cyclopentadiene, DAIB, MeOH, reflux, 1 h; ii, reflux

Table 1 Diels–Alder reactions of masked *o*-benzoquinones (MOBs) with cyclopentadiene

Phenol	MOB	*t*/h	Products	Yield[a] (%)
2a	**1a**	1	**3a**	87
2b	**1b**	1	**3b**	83
2c	**1c**	1	**3c**	80
2d	**1d**	1	**3d** + **4d**	55 + 27
2d	**1d**	6	**3d**	82
2e	**1e**	1	**3e**	91
2f	**1f**	1	**3f** (+**4f**)[b]	
2f	**1f**	18	**3f**	78
2g	**1g**	1	**3g**	85

[a] Yields are of isolated products and are unoptimized. [b] Observed in the ^1H NMR spectrum of the crude reaction mixture.

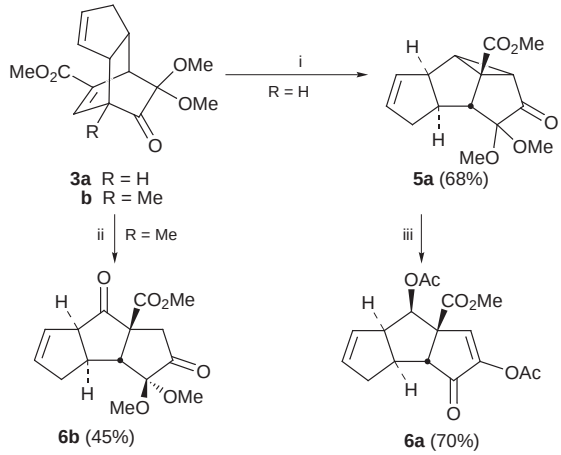

Scheme 2 *Reagents and conditions*: i, *hν* (1% in acetone), 18 h; ii, *hν* (1% in acetone), 10 h; iii, Ac_2O, BF_3•OEt_2, CH_2Cl_2, 60 °C, 3 h

It was anticipated that reductive removal of the ketal group in compounds **3c–f**, which is known to stabilize free radicals, would minimize the undesired photodecarbonylation. Accordingly, the demethoxylation of **3d–g** was achieved by reduction with SmI_2 to produce compounds **7d–g** in excellent yields.[9] Irradiation of compounds **7d–g** in acetone gave the desired products **8d–g** in agreement with our prognostications. Attempted cleavage of the cyclopropane ring of compound **8d** under the conditions previously employed for the transformation of compound **5a** into **6a** proceeded in an undesired fashion. Consequently, the procedure recently developed by Enholm and Jia for the cleavage of analogous compounds was adopted.[10] Thus treatment of compounds **8d–g** with Bu_3SnH and AIBN in refluxing benzene provided the desired linear triquinanes **9d–g** in good yields (Scheme 3, Table 2). A single stereoisomer was obtained in all cases with one exception. Compound **9f** was produced as a 1:10 mixture of epimers.

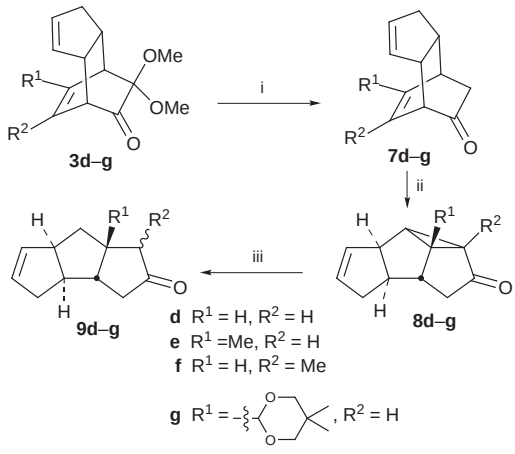

Scheme 3 *Reagents and conditions*: i, SmI_2 (4 equiv.), THF–MeOH, room temp., 10 min; ii, *hν* (1% in acetone), 24 h; iii, Bu_3SnH, AIBN, benzene, reflux

Table 2 Stereoselective synthesis of linear triquinanes (**3**→**7**→**8**→**9**)

Substrate	Product[a]	Yield (%)	Product[b]	Yield (%)	Product[c]	Yield (%)
3d	**7d**	91	**8d**	65	**9e**	70
3e	**7e**	93	**8e**	50	**9f**	81
3f	**7f**	79	**8f**	48	**9g**	83
3g	**7g**	95	**8g**	58	**9h**	93

[a] See ref. 9 for experimental procedure. [b] A 1% solution in acetone was irradiated for 24 h. [c] See ref. 10 for experimental procedure.

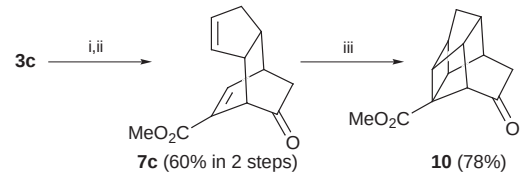

Scheme 4 *Reagents and conditions*: i, $HS(CH_2)_3SH$, BF_3•OEt_2, CH_2Cl_2, room temp.; ii, Raney Ni, EtOH; iv, *hν*, acetone

For the removal of the ketal group in compound **3c**, which cannot be affected by SmI_2, it was subjected to transketalization followed by reduction with partially deactivated Raney nickel,[11] to obtain **7c**. Irradiation of compound **7c** in acetone, however, gave [2+2] photocyclization product **10** instead of the desired ODPM rearrangement product (Scheme 4). This is an undesired result and is probably due to the localization of the triplet excited state energy in the α,β-unsaturated ester moiety to give the [2+2] adduct, rather than localization of the triplet excited state energy in the keto group, which is necessary for ODPM rearrangement to proceed.

The stuctures of all the new compounds **3**, **4d** and **5**–**10** were thoroughly established by IR, ^1H and ^{13}C NMR and mass spectral analysis. In the cases of compounds **3a**,**c–f**, H–H COSY spectra assisted in fixing the position of the double bond in the five-membered ring. The stucture of compound **10** was also unambiguously established with the help of a H–H COSY spectrum.

In conclusion the above methodology provides appropriately oxygenated and variously substituted linear triquinane skeletons with naturally occurring *cis*,*anti*,*cis* stereochemistry making use of inexpensive readily available aromatic compounds as starting materials. The present methodology is complementary to the existing related ones such as Wender's approach based on arene-alkene *meta* photoaddition and Singh's methodology based on ODPM rearrangement.[12,13] Application of this methodology to the total synthesis of *Lycopodium* alkaloids of the magellanane group,[14] using compound **9g** as the key intermediate, is in progress in our laboratory.

We thank the National Science Council (NSC) of the Republic of China for financial support. One of us (P. D. R.) thanks the NSC for a post-doctoral fellowship.

Notes and References

† E-mail: ccliao@faculty.nthu.edu.tw

1 G. Mehta and A. Srikrishna, *Chem. Rev.*, 1997, **97**, 671.
2 C.-S. Chu, T.-H. Lee and C.-C. Liao, *Synlett*, 1994, 635.
3 T.-H. Lee, C.-C. Liao and W.-C. Liu, *Tetrahedron Lett.*, 1996, **37**, 6819.
4 P.-Y. Hsiu and C.-C. Liao, *Chem. Commun.*, 1997, 1086; P. D. Rao, C.-H. Chen and C.-C. Liao, *Chem. Commun.*, 1998, 155; P.-Y. Hsu, Y.-C. Lee and C.-C. Liao, *Tetrahedron Lett.*, 1998, **39**, 659; R. Carlini, K. Higgs, R. Rodrigo and N. Taylor, *Chem. Commun.*, 1998, 65.
5 J.-T. Hwang and C.-C. Liao, *Tetrahedron Lett.*, 1991, **32**, 6583.
6 C.-S. Chu, C.-C. Liao and P. D. Rao, *Chem. Commun.*, 1997, 1537; T.-H. Lee and C.-C. Liao, *Tetrahedron Lett.*, 1996, **37**, 6869; C.-C. Liao and C.-P. Wei, *Tetrahedron Lett.*, 1989, **30**, 2255.
7 D. M. Bratby and G. I. Fray, *J. Chem. Soc. (C)*, 1971, 970; J.-P. Gesson, L. Hervaud and M. Mondon, *Tetrahedron Lett.*, 1993, **34**, 2941.
8 J. H. Rigby and C. Senanayake, *J. Org. Chem.*, 1988, **53**, 440.
9 G. A. Molander and G. Hahn, *J. Org. Chem.*, 1986, **51**, 2596; T. Imamoto and M. Oho, *Chem. Lett.*, 1987, 501.
10 E. J. Enholm and Z. J. Jia, *J. Org. Chem.*, 1997, **62**, 174.
11 D. C. Humber, A. R. Pinder and R. A. Williams, *J. Org. Chem.*, 1967, **32**, 2335.
12 P. A. Wender, L. Siggel and J. M. Nuss, in *Comprehensive Organic Synthesis*, ed. B. M. Trost, I. Flemming and L. A. Paquette, Pergamon, Oxford, 1991, vol. 5, p. 645 and references cited therein.
13 V. Singh and B. Thomas, *J. Org. Chem.*, 1997, **62**, 5310.
14 L. A. Loyola, G. Morales and M. Castillo, *Phytochemistry*, 1979, **18**, 1721.

Received in Cambridge, UK, 11th May 1998; 8/03499K

The triisopropylsilyl effect: exceptional Cram-type selectivity in Mukaiyama aldol reactions of a silyl ketene thioacetal

Anthony P. Davis,*† Stephen J. Plunkett and Jayne E. Muir

Department of Chemistry, Trinity College, Dublin 2, Ireland

The level of 1,2-asymmetric induction in the $BF_3{\cdot}OEt_2$-promoted addition of silyl ketene thioacetals to α-asymmetric aldehydes is affected by the bulk of the silyl group; unprecedented Cram-type selectivity is given by the triisopropylsilyl derivative 8a.

The optimisation of 1,2-asymmetric induction in additions to aldehydes **1** still presents challenges in stereoselective synthesis. Effective methodology is available for substrates with heteroatom-based substituents,[1] while good 'Cram-type' selectivity can now be obtained with α-aryl aldehydes, or where R^1 and R^2 are alkyl groups of greatly differing steric bulk.[2,3] However, in cases where the α-substituents are more subtly differentiated, it is still difficult to achieve acceptable levels of selectivity. We now describe a variant of the Mukaiyama aldol addition which provides useful Cram-type selectivities with even the most 'difficult' of aldehydic substrates.

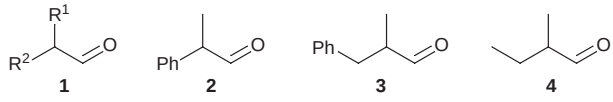

1 **2** **3** **4**

The new method is related to the conventional Mukaiyama addition as explored by Heathcock and Flippin [*e.g.* eqn. (1)],[3a] and to our subsequent development exemplified by eqn. (2).[3f]

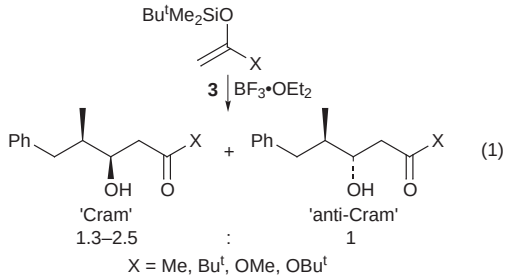

(1)

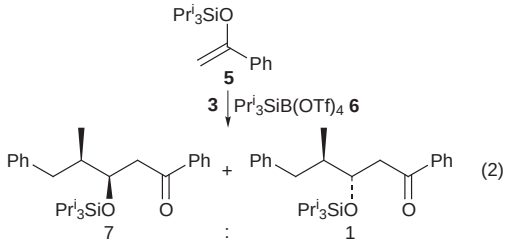

(2)

The Heathcock study yielded good selectivities (up to 36 : 1) with 2-phenylpropanal **2**, but modest results with the more challenging **3**. In our own methodology, use of triisopropylsilyl enol ether **5**, and 'supersilylating agent' **6**[4] gave a selectivity of *ca.* 100 : 1 with **2** and [as shown in eqn. (2)] a useful level of 7 : 1 with **3**. The improvement was thought to be due to the bulk of the Pr^i_3Si group in intermediate **7**, requiring the nucleophile to pass close to the asymmetric centre.[5] Control experiments employing $BF_3{\cdot}OEt_2$ catalysis, and **3** as substrate, gave lower selectivities (*ca.* 3 : 1) that did not depend substantially on the bulk of the silyl group in the enolate.[3f,6]

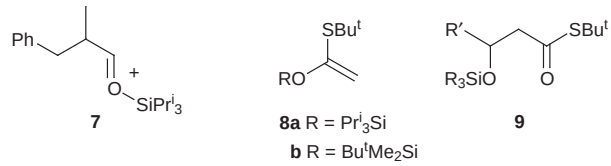

7 **8a** R = Pr^i_3Si **9**
b R = Bu^tMe_2Si

The present work was aimed at extending the scope of our earlier method, specifically by employing a nucleophile of more general utility than **5**. Silyl ketene thioacetals **8** seemed especially attractive due to the versatility of the thioester groups in aldol products **9**.[3e] Accordingly, we prepared the triisopropylsilyl derivative **8a** and, for comparison, the *tert*-butyldimethylsilyl analogue **8b**, by treatment of *tert*-butyl thioacetate with LDA/THF/DMPU followed by Pr^i_3SiOTf and Bu^tMe_2SiCl respectively.‡ Reaction of **8a**/**8b** with aldehydes **2**–**4**, catalysed by the corresponding supersilylating agents under the conditions reported previously,[3f] gave the expected β-silyloxy thioesters **10** and **11** [eqn. (3), R_L = large, R_S = small] with the

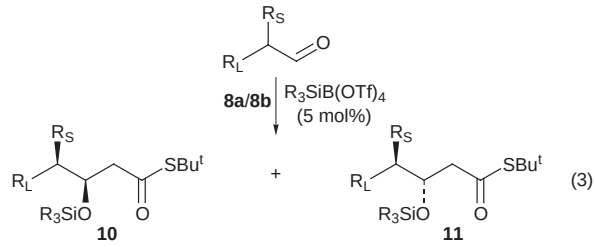

10 **11** (3)

yields and diastereoselectivities shown in Table 1. Although not startling, the results were pleasing in that they generalised the earlier discovery (dependence of selectivity on steric bulk of SiR_3), registered an acceptable selectivity of 5 : 1 for aldehyde **3**, and confirmed that even the exceptionally challenging substrate **4** could be transformed with significant selectivity (3.5 : 1) using reagent **8a**.

Table 1 Additions of silyl ketene thioacetals **8a**/**8b** to α-asymmetric aldehydes **2**–**4** catalysed by $R_3SiB(OTf)$[a]

Aldehyde	Nucleophile	Yield (%)	**12** : **13**[b]
2	**8b**	80	27 : 1
2	**8a**	79	77 : 1
3	**8b**	58	3.6 : 1
3	**8a**	78	5.5 : 1
4	**8a**	88	3.5 : 1

[a] Reaction conditions: $R_3SiB(OTf)_4$ (5 mol%), CH_2Cl_2, −80 °C, 1 h, quenching at low temp. with sat. aq. $NaHCO_3$. [b] Determined by NMR integration. Cram's rule was assumed to hold for all substrates, and was used to assign product stereochemistries.

By contrast, a surprise awaited when, for completeness, we repeated the reactions employing the conventional promoter $BF_3{\cdot}OEt_2$ [eqn. (4)]. On the basis of the earlier results with the

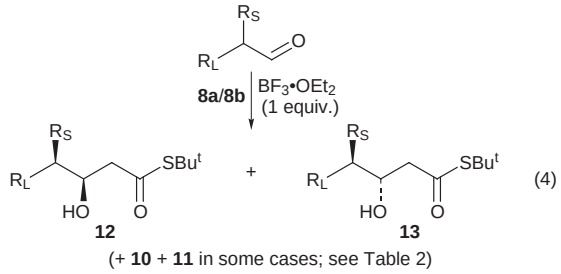

(+ **10** + **11** in some cases; see Table 2)

silyl enol ethers, we expected inferior diastereoselectivity with little dependence on R_3Si. In fact, as shown in Table 2, the method produced *higher* selectivities, which *did* increase with the bulk of the silyl group. The analysis was complicated by small amounts of **10** and **11** which appeared in some cases in addition to the expected products **12** and **13**. However, whether or not these were taken into account, *the discrimination achieved by the triisopropylsilyl reagent* **8a** *was quite outstanding.* For aldehyde **2** the selectivity was raised to the point where the minor isomer was difficult to detect with certainty, while for **3** and **4** the ratios were superior to those achieved in any previously reported additions.[7]

Although some aspects of this behaviour remain mysterious, a partial explanation is possible based on computer-based molecular modelling.[8] Systematic conformational searches on **8a** and **8b** reveal preferred structures in which the bulky Bu^t(S) and R_3Si(O) groups are held above and below the plane of the C=C bond, effectively shielding the nucleophilic carbon from attack by electrophiles (Fig. 1). As both faces are affected, these nucleophiles appear highly hindered and might be expected to react with unusual diastereoselectivity. The R_3Si appears to be the more flexible of the two blocking groups,§ suggesting that attack may occur through the face *anti* to Bu^t(S) and providing an explanation for the sensitivity of the reactions to the steric bulk of R_3Si. In contrast, **5** adopts conformations in which one face of the C=C bond is shielded, but the other is essentially free (Fig. 1). It therefore attacks **3**·BF_3 with moderate selectivity, which does not depend greatly on the bulk of R_3Si. This analysis does *not* explain why catalysis by $R_3SiB(OTf)_4$ does not lead to even greater selectivity with **8**, as it does with **5**. We can only assume that the combination of an exceptionally hindered nucleophile **8** and a similarly hindered electrophile **7** causes a change in mechanism which degrades selectivity.

Table 2 Additions of silyl ketene thioacetals **8a**/**8b** to **2**–**4** catalysed by $BF_3{\cdot}OEt_2$[a]

Aldehyde	Nucleophile	Yield (%)	**12**:**13**[b]
2	**8b**	84	54:1
2	**8a**	76	~130:1
3	**8b**	43 (51)[c]	5.8:1 (5.5:1)[c]
3	**8a**	78 (81)[c]	13:1 (12:1)[c]
4	**8a**	77 (90)[c]	5.4:1 (5.0:1)[c]

[a] Reaction conditions: $BF_3{\cdot}OEt_2$ (1 equiv.), CH_2Cl_2, −80 °C, 30 min, quenching at low temp. with aqueous phosphate buffer (pH 7). [b] NMR integration; see Table 1. [c] Major products **12** and **13** were accompanied by minor quantities of **10** and **11**. Unbracketed figures refer to **12**/**13** only, while bracketed figures include contributions from the silylated products.

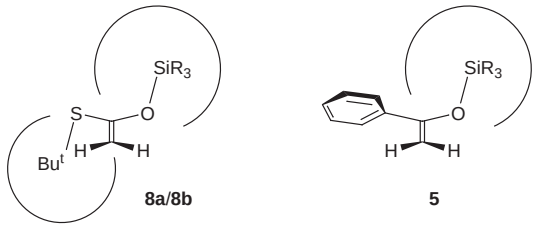

Fig. 1 Schematic views of **8a**/**8b** and **5** in their preferred conformations, as predicted by computer-based molecular modelling

In conclusion, we have discovered an addition to aldehydes which takes place with unprecedented Cram-type selectivity, and gives products which can serve as versatile intermediates for organic synthesis. Our results further highlight the special utility of the triisopropylsilyl group as a tool for directing reactivity through long-range steric intervention.[9]¶

Financial support for this work was provided by Forbairt (the Irish science and technology agency) and the EU Human Capital and Mobility Programme.

Notes and References

† E-mail: adavis@tcd.ie

‡ Conveniently, the Pr^i_3Si derivative **8a** could be purified by flash chromatography (hexane–Et_2O, 40:1). Substantial losses were incurred when the same technique was applied to **8b**.

§ Conformations in which the silicon atom is roughly in the plane of C=C bond appear at energies ⩾11 kJ mol^{-1} above baseline.

¶ An alternative might be the *tert*-butyldiphenylsilyl group. However, a limited series of experiments indicates that, in this system, its effective bulk lies between that of Pr^i_3Si and TBDMS.

1 Leading ref.; R. S. Atkinson, *Stereoselective Synthesis*, Wiley, Chichester, 1995, pp. 300–306.
2 Organometallic reagents: M. T. Reetz, R. Steinbach, J. Westermann, R. Peter and B. Wenderoth, *Chem. Ber.*, 1985, **118**, 1441; M. T. Reetz, N. Harmat and R. Mahrwald, *Angew. Chem., Int. Ed. Engl.*, 1992, **31**, 342; Y. Yamamoto and K. Maruyama, *J. Am. Chem. Soc.*, 1985, **107**, 6411; M. T. Reetz, S. Sanchev and H. Haning, *Tetrahedron*, 1992, **48**, 6813; Y. Yamamoto and J. Yamada, *J. Am. Chem. Soc.*, 1987, **109**, 4395; T. Furuta and Y. Yamamoto, *J. Chem. Soc., Chem. Commun.*, 1992, 863; B. H. Lipshutz, S. H. Dimock and B. James, *J. Am. Chem. Soc.*, 1993, **115**, 9283; S. Fukuzawa, K. Mutoh, T. Tsuchimoto and T. Hiyama, *J. Org. Chem.*, 1996, **61**, 5400; G. Cainelli, D. Giacomini, P. Galletti and A. Marini, *Angew. Chem., Int. Ed. Engl.*, 1996, **35**, 2849.
3 Enolates: (*a*) C. H. Heathcock and L. A. Flippin, *J. Am. Chem. Soc.*, 1983, **105**, 1667; (*b*) A. I. Meyers and R. D. Walkup, *Tetrahedron*, 1985, **41**, 5089; (*c*) L. A. Flippin and M. A. Dombroski, *Tetrahedron Lett.*, 1985, **26**, 2977; (*d*) L. A. Flippin and K. D. Onan, *Tetrahedron Lett.*, 1985, **26**, 973; (*e*) C. Gennari, M. G. Beretta, A. Bernardi, G. Moro, C. Scolastico and R. Todeschini, *Tetrahedron*, 1986, **42**, 893; (*f*) A. P. Davis and S. J. Plunkett, *J. Chem. Soc., Chem. Commun.*, 1995, 2173.
4 A. P. Davis and M. Jaspars, *Angew. Chem., Int. Ed. Engl.*, 1992, **31**, 470; A. P. Davis, J. E. Muir and S. J. Plunkett, *Tetrahedron Lett.*, 1996, **37**, 9401.
5 C. H. Heathcock, *Aldrichim. Acta*, 1990, **23**, 99.
6 S. J. Plunkett, Ph.D. thesis, University of Dublin, 1996.
7 For comparison, additions to **4** usually result in *ca.* 1:1 ratios of diastereomers (recent example: J. J. Eshelby, P. J. Parsons and P. J. Crowley, *J. Chem. Soc., Perkin Trans. 1*, 1996, 191). Even a highly hindered lithium α,α-bis(alkylthio) enolate gave a ratio of just 3.5:1 with this substrate [ref. 3(*c*)]. Only the arylthionation-allylation of Heathcock, which is not a simple addition reaction, gives selectivities comparable with the present method (I. Mori, P. A. Bartlett and C. H. Heathcock, *J. Am. Chem. Soc.*, 1987, **109**, 7199).
8 Macromodel V5.5, MM3* force field. See; F. Mohamadi, N. G. J. Richards, W. C. Guida, R. Liskamp, C. Caufield, G. Chang, T. Hendrickson and W. C. Still, *J. Comput. Chem.*, 1990, **11**, 440.
9 C. Rücker, *Chem. Rev.*, 1995, **95**, 1009.

Received in Cambridge, UK, 3rd June 1998; 8/04153I

Electrochemical synthesis of dialkylsubstituted polystannanes and their properties

Mitsutoshi Okano,* Naoki Matsumoto, Makoto Arakawa, Toshiyuki Tsuruta and Hiroshi Hamano

Department of Photo-Optical Engineering, Tokyo Institute of Polytechnics, 1583 Iiyama, Atsugi, Kanagawa, 243-0297 Japan. E-mail: okano@photo.t-kougei.ac.jp

Poly(dibutylstannane) and poly(dioctylstannane) were obtained by electrochemical polymerization of dibutyldichlorostannane and dioctyldichlorostannane, respectively, in a one-compartment cell equipped with a platinum cathode and a silver anode, using tetrabutylammonium perchlorate and DME as the supporting electrolyte and the solvent, respectively.

Polystannanes have attracted the attention of many researchers,[1–4] because heavier atoms in the backbone of σ-conjugated polymers are expected to give larger σ-conjugation, narrower band gaps, and more metallic character.[5–10]

The most frequently employed synthetic pathways to polysilanes and polygermanes, which have been more extensively studied as σ-conjugated polymers, are Wurtz coupling with alkali metals,[11] electrochemical reduction,[12–15] and dehydrogenative coupling.[16] Among these, electrochemical reduction has been said to be the most important pathway as an industrial method. However, for polystannanes, Wurtz coupling[4,17] and dehydrogenative coupling[1,2] reactions, but no electrochemical reduction, have been reported.

The purpose of this communication is to report the electrochemical syntheses of poly(dibutylstannane), $(Bu_2Sn)_n$, and poly(dioctylstannane), $(Oct_2Sn)_n$, and their basic properties.

Dibutyldichlorostannane and dioctyldichlorostannane were purchased from Tokyo Kasei Kogyo and Gelest, Inc., respectively, and vacuum distilled before use. Electrosynthesis was carried out according to the method reported previously,[12] using a Pt cathode, an Ag anode, and a one-compartment cell equipped with a syringe port. Tetrabutylammonium perchlorate (TBAP), precipitated from ethyl acetate–pentane solution and vacuum dried, was the supporting electrolyte and dry DME was the solvent. A constant voltage of 20 V was applied between the two electrodes. The charge passing through the circuit was monitored by a coulometer. Electrolysis was terminated when the charge reached a previously calculated value based on eqn. (1) and the amount of monomer used. Typically, 95% of the

$$n\mathrm{R_2SnCl_2} \xrightarrow{+\,2ne} (\mathrm{R_2Sn})_n + 2n\mathrm{Cl^-} \qquad (1)$$

R = Bu, Oct

theoretically required charge was passed because it was known from previous work[12] that complete electrolysis (electrolysis with 100% of the theoretically calculated charge) tends to give a lower yield and lower molecular weight as a result of backbiting reactions.

Isolation of the dialkyl-substituted polystannane was carried out as follows. As described in detail below, the polystannanes are extremely sensitive to moisture in air. Therefore, all the isolation procedures were carried out under nitrogen atmosphere and using syringe techniques. After electrolysis, most of the polymer was obtained as a precipitate and the rest of the polymer was dissolved in the electrolyte solution. Firstly, all the contents of the electrolysis cell were transferred to a two-necked flask connected to a vacuum line and equipped with a rubber septum. The supernatant solution in the electrolysis cell was transferred to the two-necked flask by a syringe technique. Then, pentane (50 ml) was introduced into the electrolysis cell and the remaining precipitated polymer was dissolved whilst being stirred magnetically. The polymer solution thus obtained was transferred and added to the previously collected supernatant solution in the two-necked flask. Then, all the solvent was removed from the two-necked flask under reduced pressure. Next, the polymer was separated from the supporting electrolyte and low molecular weight compounds as follows. Pentane (30 ml) was introduced into the two-necked flask to redissolve all the polymer. In order to precipitate polystannane and to dissolve the supporting electrolyte and low molecular weight compounds, dry methanol (100 ml) was added. The polymer was obtained by discarding the supernatant solution. The above procedure for the separation of supporting electrolyte and low molecular weight compounds was repeated. Then, the remaining solvent was removed under reduced pressure to obtain the polymer sample. A pure sample was obtained by Soxhlet extraction using pentane as the solvent. Finally, the collected polymer was dried in vacuum. The resulting polymer was a slightly sticky yellow solid regardless of the substituent groups (butyl or octyl).

Typical synthetic data are summarized in Table 1. Yields were 40–60% for $(Bu_2Sn)_n$ and 30–50% for $(Oct_2Sn)_n$. Syntheses were also successful in tetrahydrofuran. Absorption spectra were measured in pentane because pentane dissolves polystannanes well and also because polystannanes were found to be stable in pentane in the dark. Absorption maxima varied from 378 to 381 nm for $(Bu_2Sn)_n$, and were at slightly shorter wavelengths for $(Oct_2Sn)_n$. Devylder *et al*. reported that λ_{max} of $(Bu_2Sn)_n$ reaches a plateau value of 380 nm as its molecular weight increases.[4] Therefore, electrochemically obtained $(Bu_2Sn)_n$ had λ_{max} values as long as those of $(Bu_2Sn)_n$. Molecular weight values should be handled with care for they were measured using tetrahydrofuran as the eluent, in which the polystannanes degraded slowly because of the moisture remaining in THF. Significant amounts of polystannanes may have decomposed during the analysis. However, the molecular weight values seem reasonable. Molecular weights of *ca*. 10000 are as good as electrochemically synthesized σ-conjugated polymers since under the same electrolysis conditions, the authors obtained a M_w of 10 000–25 000 for $(Bu_2Ge)_n$ and 15 000–35 000 for $(Bu_2Si)_n$.

It has been reported that polystannanes are somewhat sensitive to the air.[2] The authors wished to clarify whether

Table 1 Synthetic results

Polymer	Yield/g (%)	C.E.[b]	λ_{max}[c]/nm	M_w ($\times 10^4$)	M_w/M_n
$(Bu_2Sn)_n$	2.22 (56.1)	59.1	381	1.09	2.6
$(Bu_2Sn)_n$	1.83 (46.6)	49.1	379	1.17	2.1
$(Bu_2Sn)_n$[a]	2.01 (50.8)	53.5	378	0.64	1.3
$(Oct_2Sn)_n$	1.20 (27.9)	29.4	378	0.59	1.7

[a] Synthesized in THF. [b] Current efficiency. [c] Measured in pentane. [d] Measured by GPC using THF as the eluent.

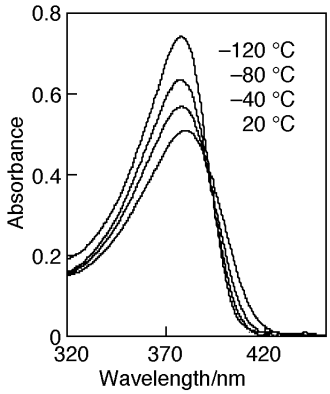

Fig. 1 Absorption spectra of $(Bu_2Sn)_n$ as a function of temperature.

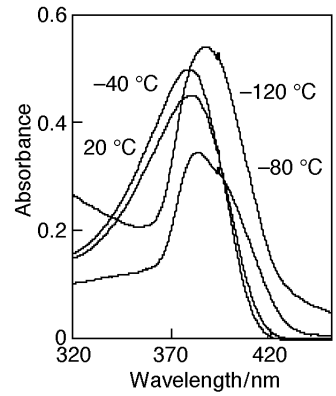

Fig. 2 Absorption spectra of $(Oct_2Sn)_n$ as a function of temperature.

polystannanes are sensitive to oxygen or sensitive to moisture in the air. In order to determine the stability of $(Bu_2Sn)_n$ toward oxygen, oxygen gas was bubbled into the pentane solution of $(Bu_2Sn)_n$. No decomposition was observed. In contrast, it was very difficult to obtain a stable tetrahydrofuran solution of $(Bu_2Sn)_n$. Even in freshly distilled CaH-dried tetrahydrofuran, a $(Bu_2Sn)_n$ solution of a concentration suitable for UV absorption measurements was not stable. Therefore, it was concluded that $(Bu_2Sn)_n$ is stable toward oxygen but extremely reactive to moisture.

The thermochromic behavior of $(Bu_2Sn)_n$ was examined because thermochromic behavior is most frequently discussed as a typical property of σ-conjugated polymers. Polysilanes and polygermanes, which have dialkyl substituent groups larger than butyl, are well known to exhibit so-called discontinuous thermochromic changes. However, $(Bu_2Sn)_n$ did not exhibit discontinuous thermochromic changes in pentane between −120 °C and room temperature (see Fig. 1). It has been said that the thermochromic behavior of σ-conjugated polymers is attributable to conformation changes in the main chains, and that such conformation changes are controlled by side chain interactions. Considering the fact that Sn–Sn bonds are much longer than Si–Si and Ge–Ge bonds, the above-mentioned lack of discontinuous thermochromic changes in $(Bu_2Sn)_n$ is attributable to weak side chain interactions. In contrast to $(Bu_2Sn)_n$, $(Oct_2Sn)_n$ showed discontinuous thermochromic changes (see Fig. 2). The absorption shift was much smaller than those observed for $(Oct_2Ge)_n$ and $(Oct_2Si)_n$. The absorption shift, which can be regarded as a manifestation of changes in effective conjugation length induced by conformation changes, decreased from $(Oct_2Si)_n$ to $(Oct_2Sn)_n$. For further discussions concerning these phenomena, it should be confirmed that the conformation changes of the polymers are of the same kind, *i.e*. all-*trans* and helical-*gauche* conformations.

To conclude, two dialkyl-substituted polystannanes were successfully synthesized by an electrochemical method. Considering the results obtained in the electrochemical syntheses of various polysilanes and polygermanes,[12] syntheses of all kinds of dialkyl-substituted polystannanes are expected to be successful as well. Syntheses of phenyl-substituted polystannanes are the authors' next challenge in this field because syntheses of phenyl-substituted polysilanes and polygermanes are more difficult than the dialkyl-substituted polymers.[12]

Notes and References

1 T. Imori and T. D. Tilley, *J. Chem. Soc., Chem. Commun*., 1993, 1607.
2 T. Imori, V. Lu, H. Cai and T. D. Tilley, *J. Am. Chem. Soc*., 1995, **117**, 9931.
3 Y. Yokoyama, M. Hayakawa, T. Azemi and K. Mochida, *J. Chem. Soc., Chem. Commun*., 1995**,** 2275.
4 N. Devylder, M. Hill, K. C. Molloy and G. J. Price, *Chem. Commun*., 1996, 711.
5 K. Takeda and K. Shiraishi, *Chem. Phys. Lett.*, 1992, **195**, 121.
6 W. Drenth, M. J. Janssen, G. J. M. van der Kerk and J. A. Vliegenhart, *J. Organomet. Chem*., 1964, **2**, 265.
7 W. Drenth, J. G. Noltes, E. J. Bulten and H. M. J. C. Creemers, *J. Organomet. Chem*., 1969, **17**, 173.
8 S. Adams and M. Drager, *Angew. Chem., Int. Ed. Engl*., 1987, **26**, 1255.
9 L. R. Sita, *Organometallics*, 1992, **11**, 1442.
10 L. R. Sita, *Acc. Chem. Res.*, 1994, **27**, 191.
11 R. West, *J. Organomet. Chem*., 1986, **300**, 327.
12 M. Okano, K. Takeda, T. Toriumi and H. Hamano, *Electrochim. Acta*, in press.
13 L. Martins, S. Aeiyach, M. Jouini, P.-C. Lacaze, J. Satge and G. Rima, *Appl. Organomet. Chem.*, 1997, **11**, 583.
14 S. Kashimura, M. Ishifune, H.-B. Bu, M. Takebayashi, S. Kitajima, D. Yoshihara, R. Nishida, S. Kawasaki, H. Murase and T. Shono, *Tetrahedron Lett*., 1997, **38**, 4607.
15 K. Huang and L. A. Vermeulen, *Chem. Commun*., 1998, 247.
16 T. D. Tilley, *Acc. Chem. Res*., 1993, **26**, 22.
17 W. Zou and N.-L. Yang, *Am. Chem. Soc., Div. Polym. Chem*., 1992, **33**, 188.

Received in Cambridge, UK, 8th June 1998; 8/04299C

3_{10}-Helix stabilization *via* side-chain salt bridges[1]

T. Scott Yokum, Matthew G. Bursavich, Ted Gauthier, Robert P. Hammer*† and Mark L. McLaughlin*

Department of Chemistry, Louisiana State University, Baton Rouge, Louisiana, 70803-1804, USA

Decapeptides, Sb-10 (H-Api-Aib-Aib-Glu-Aib-Aib-Glu-Aib-Aib-Api-NH_2) and Ipi-10 (H-Api-Aib-Aib-Lys-Aib-Aib-Lys-Aib-Aib-Api-NH_2), where Aib is α-aminoisobutyric acid and Api is 4-aminopiperidine-4-carboxylic acid, are designed to be amphipathic as 3_{10}-helices; Sb-10 is the first example of a 3_{10}-helical peptide stabilized by side-chain salt bridging or ion pairing.

The 3_{10}-helix (*i*, *i* + 3 hydrogen bonding pattern) comprises 10% of all recognized helical structures in proteins.[2] These helices are commonly found in short stretches of proteins, often as the terminating segment of an α-helix.[2] Interest in the 3_{10}-helix arises because the 3_{10}-helix is thought to participate in receptor binding and may also be a protein folding intermediate to the α-helix.[2,3] *De novo* design studies examining the 3_{10}-helix have primarily focused on peptides rich in α,α-disubstituted amino acids (ααAAs).[4,5] The ααAAs are used extensively because the ϕ and ψ angles of these residues are restricted to those favoring helical structures.[4] Many factors have been reported for the selective formation of the 3_{10}-helix over the α-helix including: placement of ααAAs, percentage of ααAAs, peptide length, and peptide design.[5–7] Unfortunately, most studies exploring these factors have focused on hydrophobic peptides in organic media.[4] The extensive library of methods available for the stabilization of α-helices in aqueous media such as amphipathy, side-chain intra- and inter-peptide salt bridges, and side-chain covalent linkages[8–10] provides an excellent starting point for the stabilization of 3_{10}-helical peptides in aqueous media. The Marqusee–Baldwin peptides cleanly show α-helix stabilization from intra-helical, side-chain ion-pairing that is reduced at high salt concentrations.[9a] The *i*, *i* + 4 positioning of Glu and Lys residues stabilize the α-helix while *i*, *i* + 3 positioning does not. Additional combinations of salt-bridging residues (*i*, *i* + 4) also stabilize α-helical conformations.[9b]

We have reported the synthesis and characterization of a 3_{10}-helical decapeptide with 80% ααAAs (Fig. 1; **Ipi-10**).[7] The high percentage of ααAAs in **Ipi-10** promotes helicity and the peptide was designed to be most amphipathic as a 3_{10}-helix. Herein we report the synthesis and characterization of an analogous amphipathic 3_{10}-helical peptide containing two intra-peptide side-chain salt bridges (**Sb-10**), which are designed to further stabilize the 3_{10}-helix.

Sb-10 has the same sequence as **Ipi-10** with the exception of glutamic acids replacing the lysines. The peptide sequences are: **Sb-10**, H-Api-Aib-Aib-Glu-Aib-Aib-Glu-Aib-Aib-Api-NH_2 and **Ipi-10**, H-Api-Aib-Aib-Lys-Aib-Aib-Lys-Aib-Aib-Api-NH_2, where Aib is α-aminoisobutyric acid and Api is 4-aminopiperidine-4-carboxylic acid. The design results in an amphipathic 3_{10}-helix that places the two Api residues and the two glutamic acids on the same face (*i*, *i* + 3) of the 3_{10}-helix (Fig. 1). The *i*, *i* + 3 placement of the Glu and Api residues potentially introduces ionic interactions that can provide additional 3_{10}-helix stability relative to the alternative α-helix conformations, since *i*, *i* + 3 salt bridges do not stabilize α-helices.[9a]

Sb-10 was synthesized *via* a combination of manual and automated solid-phase peptide synthesis. The first three C-terminal residues were coupled to PAL-PEG-PS (PerSeptive Biosystems) by refluxing the preformed fluoren-9-ylmethoxycarbonyl (Fmoc)-amino acid fluorides (8 equiv.) and Pr^i_2NEt (3 equiv.) in CH_2Cl_2 until quantitative Fmoc cleavage tests[11] showed at least 90% coupling for each step.[12] The remainder of the peptide was synthesized on a PerSeptive Biosystems 9050 peptide synthesizer using preformed Fmoc-acid fluorides.[12] The peptide was purified by RP-HPLC on a C4 column with a H_2O–MeCN–0.5% TFA gradient. Peptide purity was greater than 95% according to an analytical RP-HPLC using C18 column and a similar gradient. Molecular weight was verified by MALDI-MS and amino acid analysis gave the expected amino acid content. Peptide concentrations for circular dichroism (CD) studies were determined by quantitative amino acid analysis.

α- and 3_{10}-Helical peptides have minima centered about 222 (n→π*) and 207 nm (π→π*) in the CD spectra. The ratio, *R*, of the n→π* band over the π→π* band differentiates the α- and 3_{10}-helix.[13] The ratio is near 1 for the α-helix and is approximately 0.4 for a 3_{10}-helix.[13]‡

The CD spectra of **Sb-10** and **Ipi-10** for comparison were taken in 50–100% aqueous–organic solvent mixtures [1:1 MeCN–H_2O, 9:1 MeCN–H_2O, 9:1 MeCN–trifluoroethanol (TFE)]. **Ipi-10** has a CD spectra indicative of a weak 3_{10}-helix only in 100% organic solvent [Fig. 2(A)].§ **Sb-10** exhibits moderate α-helicity in 1:1 MeCN–H_2O and begins to show 3_{10}-helical character in 9:1 MeCN–H_2O. In 9:1 MeCN–TFE,

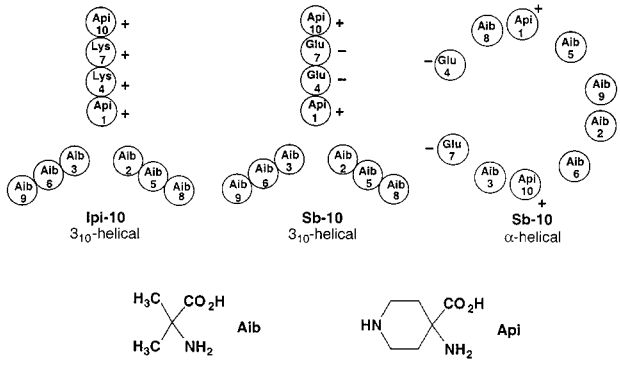

Fig. 1 Helical wheel diagrams of **Ipi-10** and **Sb-10**

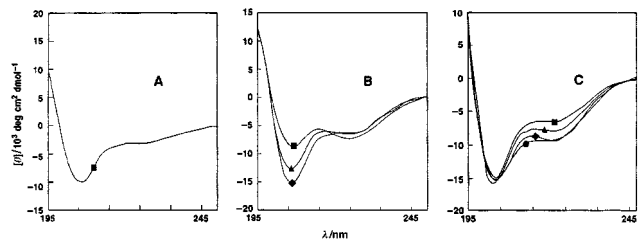

Fig. 2 Circular dichroism spectra with 0.2 mM peptide: (A) **Ipi-10** in 9:1 MeCN–TFE (■); (B) **Sb-10** in 1:1 MeCN–H_2O (■), 9:1 MeCN–H_2O (▲) and 9:1 MeCN–TFE (◆); (C) **Sb-10** with 0.1 M TMAT in 9:1 MeCN–TFE (■), 0.01 M TMAT in 9:1 MeCN–TFE (▲), 0.001 M TMAT in 9:1 MeCN–TFE (●) and 9:1 MeCN–TFE (◆)

Table 1 Circular dichroism data and derived structural parameters for **Sb-10**

Solvent	$[\theta]_{\pi\rightarrow\pi^*}$[a,b]	$[\theta]_{n\rightarrow\pi^*}$[a,c]	*R*	Helicity[d] (%)
9:1 MeCN–TFE	−15230	−6579	0.43	71 (3_{10})
9:1 MeCN–H_2O	−12749	−6461	0.50	*e*
1:1 MeCN–H_2O	−8673	−7433	0.85	31 (α)
0.1 M TMAT in 9:1 MeCN–TFE	−15774	−9576	0.61	*f*
0.01 M TMAT in 9:1 MeCN–TFE	−15038	−9235	0.61	*g*
0.001 M TMAT in 9:1 MeCN–TFE	−15333	−6531	0.43	71 (3_{10})

[a] Units for $[\theta]$ are deg cm^2 dmol^{-1}. [b] The minimum for the $[\theta]_{\pi\rightarrow\pi^*}$ band is in the range from 205–209 nm. [c] The minimum for the $[\theta]_{n\rightarrow\pi^*}$ band is in the range from 222–225 nm. [d] The percentage of α-helix is estimated using the equation: α-helix (%) = $-100([\theta]_{n\rightarrow\pi^*}+ 3000)/33000$ and the percentage of 3_{10}-helix is estimated using the equation: 3_{10}-helix (%) = $-100([\theta]_{\pi\rightarrow\pi^*})/21\ 500]$. [e] This peptide probably forms a mixture of α-helical, 3_{10}-helical and coil structures. The percentage of α-helix is estimated at 29% and the percentage of 3_{10}-helix is estimated at 59%. [f] This peptide probably forms a mixture of α-helical, 3_{10}-helical and coil structures. The percentage of α-helix is estimated at 57% and the percentage of 3_{10}-helix is estimated at 73%. [g] This peptide probably forms a mixture of α-helical, 3_{10}-helical and coil structures. The percentage of α-helix is estimated at 54% and the percentage of 3_{10}-helix is estimated at 70%.

the CD spectrum of **Sb-10** has strong 3_{10}-helical character (71% 3_{10}-helicity). The transition of **Sb-10** from an α-helix to a 3_{10}-helix as the solvent dielectric is decreased agrees with the theoretical calculations of the solvent effects on the 3_{10}/α-helix equilibrium.[14] Marshall's calculations predict Aib-rich peptides should favor the α-helix in water and the 3_{10}-helix in less polar media.[14]

The percent 3_{10}-helicity of **Sb-10** is estimated to be higher than that of **Ipi-10** (71 *vs.* 45%[5]) suggesting that the two salt bridges significantly stabilize the 3_{10}-helical conformation. The CD spectral changes upon titration of **Sb-10** with an organic solution (9:1 MeCN–TFE) of tetramethylammonium trifluoroacetate¶ (TMAT, 0.0 to 0.1 M) are consistent with side-chain ionic interactions stabilizing 3_{10}-helical conformation. **Sb-10** makes a transition from a 3_{10}-helix to a partial α-helical structure as the TMAT concentration is increased. The decreasing 3_{10}-helix stability of **Sb-10** as the salt concentration is increased parallels what has been observed for α-helical peptides stabilized by side chain ionic interactions.[9a]

Ipi-10 and **Sb-10** have the same number of residues, the same percentage of ααAAs, and the same amphipathic design. The α-helix forming propensities of lysine and glutamic acid are similar[15] so the additional 3_{10}-helicity of **Sb-10** compared to **Ipi-10** must result from side-chain interactions. The decreasing stability of the 3_{10}-helical conformation of **Sb-10** as salt concentration is increased also supports the idea that *i*, *i* + 3 salt bridging or ion pairing stabilize 3_{10}-helices.

We thank the National Science Foundation and the National Institutes of Health for support of this research *via* an NSF grant (CHE-9500992 to RPH) and an NIH grant (GM 42101, to Professor Mary D. Barkley and M. L. M). M. G. B. was an undergraduate researcher supported by a grant to the Louisiana State University, College of Basic Sciences, from the Howard Hughes Medical Institute.

Notes and References

† E-mail: chammer@chrs1.chem.lsu.edu

‡ This intrepetation of ratio (*R*) of the n→π* and π→π* bands of the CD spectrum has been disputed by Andersen *et al.* (N. H. Andersen, Z. Liu and K. S. Prickett, *FEBS Lett.*, 1996, **399**, 47). Their study used much longer peptides (22 residues) containing low percentages (1/22–5/22) of Aib, which can form highly amphipathic α-helices (but not amphipathic 3_{10}-helices). They find that comparison of NMR (NOE) and CD evidence suggests that these peptides are a mixture of α-helix, 3_{10}-helix (in one case) and random coil. When the CD was corrected for 'disordered' residues, a peptide containing 5/22 Aib residues had $R > 1$, which they argue goes against the findings of Toniolo (ref. 13). We are confident in the case of **Ipi-10** and **Sb-10** that $R \sim 0.4$ reflects a 3_{10}-helix and not some contribution from a random coil spectrum as the CD of **Ipi-10** and **Sb-10** in water or phosphate buffer are essentially baseline ($-[\theta]_{\pi\rightarrow\pi^*} < 50$). This is apparently due to a very weak random coil ('disordered') spectrum of these peptides resulting from the lack of stereogenic amino acids (only 2 L-Lys or 2 L-Glu resides).

§ **Sb-10** shows no concentration dependence of the CD spectrum in 9:1 MeCN–TFE over a 10-fold concentration range (0.02–0.3 mM): $[\theta]_{\pi\rightarrow\pi^*} = -15\ 000 \pm 750$; $R = 0.42 \pm 0.02$. This suggests that **Sb-10** is monomeric under these conditions.

¶ A highly organic-soluble salt, such as TMAT, is required for titration of the **Sb-10** side-chains because strong 3_{10}-helix character is only present in 100 % organic media.

1 Taken in part from the PhD dissertation of T. Scott Yokum, Louisiana State University, 1998.
2 D. J. Barlow and J. M. Thornton, *J. Mol. Biol.*, 1988, **201**, 601.
3 C. Toniolo and E. Benedetti, *Trends Biochem. Sci.*, 1991, **16**, 350; M. Gerstein and C. Chothia, *J. Mol. Biol.*, 1991, **220**, 133; C. A. McPhalen, M. G. Vincent, D. Picot, J. N. Jansonius, A. M. Lesk and C. Chothia, *J. Mol. Biol.*, 1992, **227**, 197.
4 B. V. V. Prasad and P. Balaram, *CRC Crit. Rev. Biochem.*, 1984, **16**, 307; P. Balaram, *Curr. Opin. Struct. Biol.* 1992, **2**, 845; G. R. Marshall, E. E. Hodgkin, D. A. Langs, G. D. Smith, J. Zabrocki and M. T. Leplawy, *Proc. Natl. Acad. Sci. U.S.A.*, 1990, **87**, 487; J. D. Augspurger, V. A. Bindra, H. A. Scheraga and A. Kuki, *Biochemistry*, 1995, **34**, 2566; E. Benedetti, *Biopolymers*,1996, **40**, 3; G. Hungerford, M. Martinez-Insua, D. J. S. Birch and B. D. Moore, *Angew. Chem., Int. Ed. Engl.*, 1996, **35**, 326.
5 T. S. Yokum, T. J. Gauthier, R. P. Hammer and M. L. McLaughlin, *J. Am. Chem. Soc.*, 1997, **119**, 1167.
6 I. L. Karle, J. L. Flippen-Anderson, R. Gurunath and P. Balaram, *Protein Sci.*, 1994, **3**, 1547.
7 G. Basu, K. Bagchi and A. Kuki, *Biopolymers*, 1991, **31**, 1763; G. Basu and A. Kuki, *Biopolymers*, 1993, **33**, 995.
8 J. M. Stewart, in *The Amphipathic Helix*, ed. R. M. Epand, CRC Press, Boca Raton, FL, 1993, pp. 21–37.
9 (*a*) S. Marqusee and R. L. Baldwin, *Proc. Natl. Acad. Sci. U.S.A.*, 1987, **84**, 8898; (*b*) G. Merutka and E. Stellwagen, *Biochemistry*, 1991, **30**, 1591; (*c*) O. D. Monera, N. E. Zhou, C. M. Kay and R. S. Hodges, *J. Biol. Chem.*, 1993, **268**, 19 218.
10 G. Ospay and J. W. Taylor, *J. Am. Chem. Soc.*, 1990, **112**, 6046.
11 G. B. Fields, Z. Tian and G. Barany, in *Synthetic Peptides: A User's Guide*, ed. G. A. Grant, W. H. Freeman and Co., USA, 1992.
12 C. L. Wysong, T. S. Yokum, G. A. Morales, R. L. Gundry, M. L. McLaughlin and R. P. Hammer, *J. Org. Chem.*, 1996, **61**, 7650.
13 C. Toniolo, A. Polese, F. Formaggio, M. Crisma and J. Kamphuis, *J. Am. Chem. Soc.*, 1996, **118**, 2744.
14 M. L. Smythe, S. E. Huston and G. R. Marshall, *J. Am. Chem. Soc.*, 1995, **117**, 5445.
15 J. M. Scholtz and R. L. Baldwin, *Annu. Rev. Biophys. Biomol. Struct.*, 1992, **21**, 95; K. T. O'Neil and W. F. DeGrado, *Science*, 1990, **250**, 646.

Received in Columbia, MO, USA, 6th February 1998; revised manuscript received 8th July 1998; 8/05458D

Consecutive catalytic hydroformylation-acetalization of glucal derivatives with rhodium–phosphite and pyridinium toluene-*p*-sulfonate as catalysts: the influence of protecting groups.

Elena Fernández,[a] Alfonso Polo,[b] Aurora Ruiz,[a] Carmen Claver[a]* and Sergio Castillón*[a]†

[a] *Departament de Química, Universitat Rovira i Virgili, Pl Imperial Tarraco 1, 43005 Tarragona, Spain*
[b] *Departament de Química, Universitat de Girona, Girona, Spain*

Consecutive catalytic hydroformylation-acetalization of unsaturated carbohydrates (glucals) to give the dimethyl acetal of 2-*C*-formyl-D-alditol derivatives using the catalytic system [Rh(μ-OMe)(cod)]$_2$/P(O-*o*-Bu^{t}C$_6$H$_4$)$_3$/PPTS is strongly dependent on the protecting groups on the carbohydrate.

Sequential reactions have emerged as a direct and economic synthesis procedure, because different reactions can be carried out without isolating any intermediates, which means greater economy in solvents and purification.[1] The most popular sequential reactions are the so-called domino[2] (cascade) or tandem[3] reactions, in which several bonds are formed through different intermediates. In the consecutive 'one-flask' reactions, the product of one reaction is the starting material for a second reaction that occurs in the same flask. Although many examples of this methodology have been published, there are few examples of catalytic consecutive reactions which require different catalysts.[1–3]

We have already reported the synthesis of acetals from alkenes by means of a consecutive hydroformylation-acetalization process with rhodium–phosphine and pyridinium toluene-*p*-sulfonate (PPTS) as hydroformylation and acetalization catalysts respectively.[4] Since the catalyst for the hydroformylation process requires the presence of basic phosphine ligands, and the acetalization reaction requires an acid catalyst, the main goal of that process was to find two compatible catalytic systems. The solution was to use phosphonium or pyridinium salts in the presence of phosphine.

Here we show that the consecutive hydroformylation-acetalization of unsaturated carbohydrates (glucals) using rhodium complexes and PPTS as catalysts, respectively, is strongly dependent on the protecting groups in the carbohydrate.

We have previously reported[5,6] the hydroformylation of 3,4,6-tri-*O*-acetyl-D-glucal **1** using the [Rh(μ-OMe)(cod)]$_2$/P(O-*o*-Bu^{t}C$_6$H$_4$)$_3$[7] catalytic system to give a mixture of aldehydes which are the result of introducing the formyl group at position 2 of the sugar ring (Scheme 1). The low selectivity was due to the elimination of AcOH from **2** to give an α,β-unsaturated aldehyde **3**, under the drastic reaction conditions required. In order to prevent this elimination we intend to convert *in situ* the aldehyde function formed in the hydroformylation reaction into the acetal function (Scheme 2). Moreover, this will enable us to deprotect and transform the hydroxy groups and then to take advantage of the reactivity of the acetal or aldehyde function.

Thus, the hydroformylation of **1** was carried out with the catalytic system [Rh(μ-OMe)(cod)]$_2$/P(O-*o*-Bu^{t}C$_6$H$_4$)$_3$, under

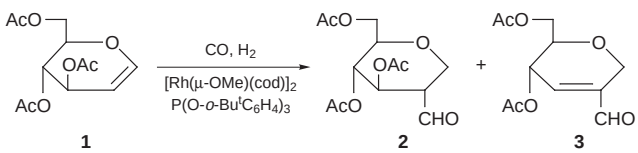

1 **2** **3**

Scheme 1

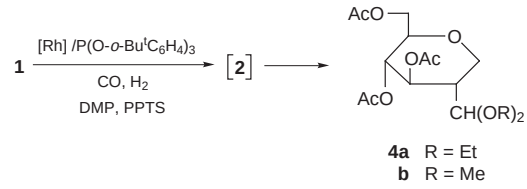

4a R = Et
b R = Me

Scheme 2

standard hydroformylation conditions (50 bar, 100 °C, CH_2Cl_2).[5,6] A mixture of aldehydes **2** and **3** was principally obtained (Table 1, entry 1). When the reaction was performed in $CH(EtO)_3$ under the same reaction conditions, the main compounds obtained were **2** and **3** together with small amounts of several hydroformylation-acetalization products such as the acetal **4a** (entry 2). Adding 60 mg of PPTS per 5 mmol of substrate to the reaction mixture gave a complex mixture, in which the hydroformylation-acetalization product **4a** was predominant, but the aldehydes had not completely disappeared (entry 3). By increasing the amount of PPTS, higher percentages of diethyl acetal **4a** were obtained, although conversion was low (entry 4). When the solvent was $CH(OMe)_3$ conversion decreased, although the selectivity in the dimethoxy derivative **4b**‡ was similar (entry 5). The use of 2,2-dimethoxypropane, another useful reagent for acetal formation, as the solvent did not allow the acetal to form and the elimination product **3** was obtained instead (entry 6). Interestingly, when PPTS was added, acetal **4b** was principally obtained in 66% yield (entry 7). Small quantities of the less reactive α,β-unsaturated aldehyde **3** remained in the mixture.

In the presence of PPTS the acetalization reaction is faster than the elimination of AcOH from **2** to give **3**. Moreover, it is interesting to note that there were fewer secondary reaction products, such as isomeric aldehydes (< 10%) and hydrogenation (< 10%) products, under these slightly acid conditions.

Table 1 Hydroformylation-acetalization of 3,4,6-tri-*O*-acetyl-D-glucal **1** with the catalytic system [Rh(μ-OMe)(cod)]$_2$/P-(O-*o*-Bu^{t}C$_6$H$_4$)$_3$/PPTS[a]

Entry	PPTS/mg	Solvent	Conversion (%)[b]	Products (%)[c] **2**	**3**	**4a**	**4b**
1	—	$Cl_2C_2H_4$	90	54	22	—	—
2	—	$HC(OEt)_3$	87	9	24	27	—
3	60	$HC(OEt)_3$	98	28	10	51	—
4	120	$HC(OEt)_3$	74	6	11	55	—
5	60	$HC(OMe)_3$	75	3	2	—	52
6	—	DMP[d]	94	22	43	—	—
7	60	DMP[d]	92	0	9	—	66

[a] Standard conditions: glucal (5 mmol), [Rh(μ-OMe)(cod)]$_2$ (0.05 mmol), P(O-*o*-Bu^{t}C$_6$H$_4$)$_3$ (0.5 mmol), PPTS, solvent (15 ml), 100 °C, 50 bar, CO/H_2 = 1, 48 h. [b] Percentage of transformed product. [c] Detected by GC. Other minor aldehydes and small amounts of the hydrogenation product were also observed. [d] DMP = 2,2-dimethoxypropane.

Table 2 Hydroformylation-acetalyzation of glucal derivatives[a]

Substrate	Product	Yield (%)[b]
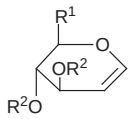	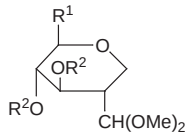	
5 $R^1 = CH_3$, R^2 = Ac	**8** $R^1 = CH_3$, R^2 = Ac	65
6 $R^1 = CH_2OPiv$, R^2 = Piv	**9** $R^1 = CH_2OPiv$, R^2 = Piv	56
7 $R^1 = CH_2OBz$, R^2 = Bz	**10** $R^1 = CH_2OBz$, R^2 = Bz	42
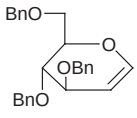	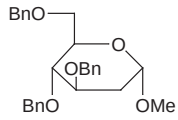	85
11	**12**	

[a] Standard conditions: glucal (5 mmol), $[Rh(\mu\text{-OMe})(cod)]_2$ (0.05 mmol), $P(O\text{-}o\text{-Bu}^tC_6H_4)_3$ (0.5 mmol), PPTS (0.25mmol), solvent (15 ml), 100 °C, 50 bar, CO/H_2 = 1, 48 h. [b] Isolated yield.

The glucal **5** reacted in similar hydroformylation-acetalization conditions to give the acetal **8** in a 65% yield (Table 2).

When the hydroxy groups in the carbohydrates were protected with other acyl derivatives such as pivaloyl (**6**) or benzoyl (**7**), the hydroformylation-acetalization products **9** and **10** were also obtained as the main products although in lower yields. This was probably because the steric hindrance of these bulkier groups decreases the rate of hydroformylation.

Unexpectedly, benzyl protected glycal **11** gave only the methyl α-glycoside **12** under the hydroformylation-acetalization conditions. As a result, both the rhodium complex and the acidic proton compete to attack the double bond so that when the protecting groups in the hydroxy groups are acyls, the double bond is deactivated. Therefore, the electrophilic attack cannot take place and rhodium coordination is preferred. However, when hydroxy groups are converted to ethers (*e.g.* the benzyl derivative **11**) the double bond is relatively activated and the attack of the acidic proton is faster. The fact that the reactivity of the double bond in the glucal depends on the protecting group can be rationalised as an 'armed-disarmed' effect.[8] This effect has been successfully used in disaccharide synthesis with glycals as glycosyl donors,[9] but to the best of our knowledge this is the first example of this effect being observed in competitive catalytic reactions.

In conclusion, the catalytic system $[Rh(\mu\text{-OMe})(cod)]_2/P(O\text{-}o\text{-Bu}^tC_6H_4)_3$ in the presence of PPTS allows the consecutive hydroformylation-acetalization reaction of glucals, depending on the protecting groups present in the carbohydrate ring. Thus, when hydroxy groups are protected as acyl derivatives the hydroformylation-acetalization leads to the dimethyl acetal of 2-*C*-formylalditol derivatives such as **4a**,**b**, **8**, **9** and **10**. However, when the protecting groups are benzyl, the methyl glycosides resulting from the addition of MeOH to the double bond of glucal are observed, but not the hydroformylation products.

This research was supported by DGR (Direcció General de Recerca, de la Generalitat de Catlunya), Grants QFN95-4725-C03-2 and 1995DGR 00528.

Notes and References

† E-mail: sergio@argo.urv.es

‡ *Selected data* for **4b**: $\delta_H(CDCl_3)$ 2.01 (s, 3H, $OCOCH_3$), 2.03 (s, 3H, $OCOCH_3$), 2.09 (s, 3H, $OCOCH_3$), 2.33 (tt, *J* 11, 4.8, 1H, H_2), 3.34 (s, 3H, OCH_3), 3.36 (s, 3H, OCH_3), 3.43 (dd, *J* 11.7, 11, 1H, H_{1a}), 3.53 (ddd, *J* 9.1, 4.9, 2.0, 1H, H_5), 4.09 (dd, *J* 12, 2.0, 1H, H_6), 4.12 (dd, *J* 12, 4.9, 1H, $H_{6'}$), 4.22 (dd, *J* 4.8, 1.9, 1H, H_7), 4.24 (dd, *J* 11.7, 4.8, 1H, H_{1e}), 4.95 (t, *J* 9.1, 1H, H_4), 5.19 (dd, *J* 11, 9.1, 1H, H_3): $\delta_C(CDCl_3)$ 20.5, 20.6, 20.6, 43.6, 54.7, 55.6, 62.5, 65.7, 69.4, 72.1, 76.1, 103.6, 169.7, 170.1, 170.6 (Found: C, 51.42; H, 7.00. Calc.: C, 51.72; H, 6.89%).

1 L. F. Tietze and U. Beifuss, *Angew. Chem., Int. Ed. Engl.*, 1993, **32**, 131.
2 L. F. Tietze, *Chem Rev.*, 1996, **96**, 115.
3 R. B. Bunce, *Tetrahedron*, 1995, **51**, 13 103; P. J. Parsons, C. S. Penkett and A. J. Shell, *Chem. Rev.*, 1996, **96**, 195.
4 E. Fernández and S. Castillón, *Tetrahedron Lett.*, 1994, **35**, 2361.
5 A. Polo, E. Fernández, A. Ruiz, C. Claver and S. Castillón, *J. Chem. Soc., Chem. Commun*., 1992, 639.
6 E. Fernández, A. Ruiz, C. Claver, S. Castillón, A. Polo, J. Piniella and A. Alvarez-Larena, *Organometallics*, 1998, **17**, 2857.
7 P. W. N. M. van Leeuwen and C. F. Robeck, *J. Organomet. Chem.*, 1983, **258**, 343.
8 B. Fraser-Reid, Z. Wu, U. E. Udodong and H. Ottosson, *J. Org. Chem.*, 1990, **55**, 6068.
9 R. W. Friesen and S. J. Danishefsky, *J. Am. Chem. Soc.*, 1989, **111**, 6656.

Received in Cambridge, UK, 4th June 1998; 8/04220I

Reactions of metalloalkynes.‡ The reaction of the ethyne-1,2-diyl complex, $[\{Ru(CO)_2(\eta\text{-}C_5H_5)\}_2(\mu\text{-}C{\equiv}C)]$, with $[Mo_2(CO)_4(\eta\text{-}C_5H_5)_2]$. An example of $\mu_3,\eta^1\text{-}C{\equiv}C$ coordination of a carbide ligand

Christopher S. Griffith, George A. Koutsantonis,*† Brian W. Skelton and Allan H. White

Department of Chemistry, University of Western Australia, Nedlands, Perth, WA, Australia, 6907

Reaction of $[\{Ru(CO)_2(\eta\text{-}C_5H_5)\}_2(\mu\text{-}C{\equiv}C)]$ with $[Mo_2(CO)_4(\eta\text{-}C_5H_5)_2]$ gave $[MoRu_2(\mu_2\text{-}CO)_3[\mu_3\text{-}C{\equiv}C\{Ru(CO)_2(\eta\text{-}C_5H_5)\}](\eta\text{-}C_5H_5)_3]$ as the major product after chromatography and not the expected dimolybdenum 'alkynyl' adduct; this new complex contains a carbide (C_2) ligand bound, in triply bridging mode to the $MoRu_2$ triangle, through one carbon and the other in a monohapto fashion to the other ruthenium atom.

We are interested in the reactivity of metalloalkynes in so far as their reactivity is similar to that of simple organic alkynes.[1] The dimetalloalkynes, or ethyne-1,2-diyl complexes, are a special class of these complexes and their reactivity has been of particular interest to us.[2–14] Ethyne-1,2-diyl complexes contain the C_2 ligand which is often implicated in catalytic CO hydrogenation mechanisms. Multinuclear homo- and hetero-metallic complexes containing the C_2 molecule offer the opportunity to study and observe the reactivity of such species.[15]

Herein we report the unexpected course of the reaction between $[Mo_2(CO)_4(\eta\text{-}C_5H_5)_2]$ **1** and the dimetalloalkyne, $[\{Ru(CO)_2(\eta\text{-}C_5H_5)_2\}_2(\mu\text{-}C{\equiv}C)]$ **2**. We have recently found[16] that metalloalkynes of ruthenium and iron, *viz*. $[M(CO)_2(\eta\text{-}C_5H_5)(C{\equiv}CR)]$, react readily with complex **1**, giving, in the case of ruthenium, the expected 'alkyne' adduct **A**. The analogous

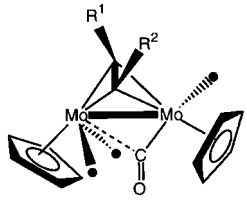

A: $R^1 = Ru(CO)_2(C_5H_5)$, R^2 = Me or Ph
B: R^1 = H; R^2 = Me or Ph
G: $R^1 = R^2 = Ru(CO)_2(C_5H_5)$

iron compounds underwent Fe–C bond cleavage, by a yet to be determined mechanism, and resulted in the formation of complexes **B** in their reaction with **1**. It is of note that the analogous reaction with an iron congener of **2**, *viz*. $[\{Fe(CO)_2(\eta\text{-}C_5Me_5)_2\}(\mu\text{-}C{\equiv}C)]$, resulted in carbonyl transfer to **1** to give $[Mo_2(CO)_6(\eta\text{-}C_5H_5)_2]$ with decomposition.[2b]

The reaction (Scheme 1)§ in refluxing toluene gave a mixture of products and some unreacted starting material that were readily separated using column chromatography. The major red–black fraction provided a good yield of $[MoRu_2(\mu\text{-}CO)_3[\mu_3\text{-}C{\equiv}C\{Ru(CO)_2(\eta\text{-}C_5H_5)\}](\eta\text{-}C_5H_5)_3]$ **3**, an electron deficient 45-electron cluster considering the $\mu_3,\eta^1\text{-}C{\equiv}C\{Ru(CO)_2(\eta\text{-}C_5H_5)\}$ unit as only a two-electron donor. The compound remarkably contains a μ_3-CC fragment bound to the $MoRu_2$ triangle and is, to our knowledge, the only example of this type of coordination to any metal cluster other than those of Cu[17] or Li.[18] Moreover, the bonding mode of the C_2 ligand observed here is also unique in so far as it is surrounded by metals but not 'buried'. The range of bonding modes so far observed for the interaction of four metals with a carbide ligand

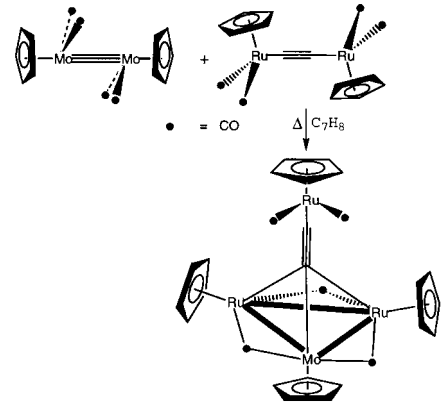

Scheme 1

(Fig. 1) implicates the π system of the triple bond more fully in bonding in multi-metallic systems.

The ^{1}H NMR spectrum of **3** comprises two signals at δ 5.26 and 4.90 in a 1 : 3 ratio which are assigned to the Mo(η-C_5H_5) and Ru(η-C_5H_5) moieties, respectively. These signals remain unchanged in the temperature range 296–233 K. This implies that the Mo(η-C_5H_5) and Ru(η-C_5H_5) vertices are undergoing fluxional motion giving rise to an averaged signal for the three Ru(η-C_5H_5) vertices and a separate signal for the Mo(η-C_5H_5) vertex. This fluxionality is also reflected in the ^{13}C NMR spectrum of **3**. This contains two signals for cyclopentadienyl ligands and two signals are observed at δ 234.2 and 232.4 which are assigned to the terminal and bridging CO ligands. The signals observed at δ 308.4 and 87.2 are assigned to the μ_3-C and η^1-C of the carbide ligand, respectively.

These data and those reported in the footnote were insufficient to unequivocally assign the connectivity and as such a room-temperature single-crystal X-ray structure study¶ was undertaken. The structure determination is of limited utility given that the cell obtained in the tetragonal setting *P*4/*m* contains a pseudo-inversion centre, relating two independent molecules in the asymmetric unit, and with a crystallographic mirror plane coincident with the molecular symmetry plane in each of the independent molecules. In addition, the specimen obtained after many attempts was of marginal suitability for the experiment. However, the results are consistent with the

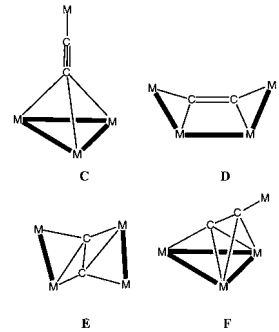

Fig. 1 Bonding modes for a carbide ligand bound to tetrametallic systems

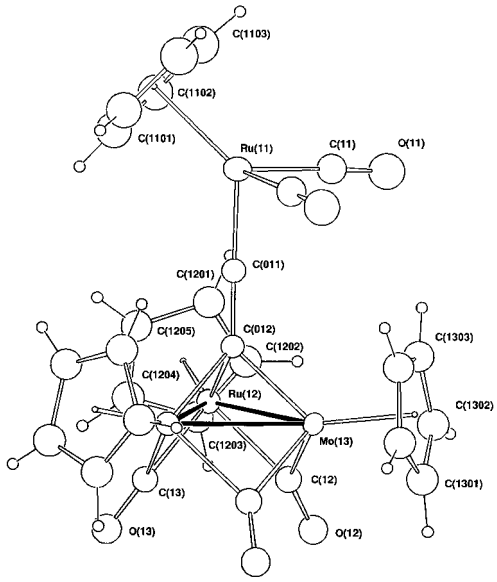

Fig. 2 Projection of one molecule of **3** approximately through the $MoRu_2$ plane. 20% thermal ellipsoids are shown for the metal atoms; other non-hydrogen atoms are shown as isotropic spheres; hydrogen atoms have arbitrary radii of 0.1 Å. Selected bond lengths (Å) and angles (°): Ru(*n*2)–Mo(*n*3) 2.701(2), 2.700(2); Ru(*n*2)–Ru(*n*2′) 2.704(2), 2.710(2); Ru(*n*1)–C(0*n*2) 2.01(1), 1.77(2); C(0*n*2)–C(0*n*1) 1.39(2), 1.46(3); Ru(*n*1)–C(0*n*1)–C(0*n*2) 179(1), 175(2); Ru(*n*2)–Mo(*n*3)–Ru(*n*2′) 60.09(6), 60.24(6); Mo(*n*3)–Ru(*n*2)–Ru(*n*2′) 59.96(4), 59.88(4) for the two molecules (molecule 1, $n = 1$; molecule 2, $n = 2$).

stoichiometry and connectivity as expressed in **3** and Fig. 2, albeit with interatomic parameters of a higher than desired uncertainty. The molecules are best considered as being composed of trinuclear heterometallic $MoRu_2$ triangles with each metal atom coordinated by a pentahapto cyclopentadienyl ligand which is essentially perpendicular to the plane of the triangle. The structure determination cannot rigorously exclude the possibility of scrambling of the molybdenum atom among other metal sites of the triangle in the solid. The metal cores are coordinated from 'above' by the μ_3,η^1-C≡C{$Ru(CO)_2(\eta$-$C_5H_5)$} unit which has its CC axis at right angles to the metal triangles with the μ_3-C symmetrically bridging to each of the metal core atoms. Three bridging carbonyls complete the coordination of the metal core and these are directed 'below' the plane of the core.

The formal electron count gives this substituted triangular cluster 45 cluster valence electrons (CVE) with each Ru atom achieving an 18-electron count and the Mo formally electron deficient with a 16-electron count. In the various bonding modes and their valence bond representations hitherto observed for the carbide ligand bound to four metals (Fig. 1)[19] the CC unit has a formal bond order of three in mode **C** while in mode **D** the bond order is two and in **E** and **F** it is one. Theoretical calculations[19] have been performed that rationalise the bonding observed for **D**–**F** and it is noteworthy that complex **3** (mode **C**) does not adopt mode **F** where the electron deficiency experienced by the Mo atom could be alleviated.

The mechanism operating in this reaction is unclear. However, it is likely that the CC bond of **2** interacts initially with the unsaturated metal–metal bond in **1** to give a structure similar to **G** which presumably undergoes fragmentation, evidenced by the isolation of $[Ru(CO)_2(\eta$-$C_5H_5)]_2$ from the reaction. The reason for this fragmentation is presumably steric.[16] It is possible that **G** undergoes homolytic cleavage of a $Ru(CO)_2(\eta$-$C_5H_5)$ group and that this is the source of the dimer isolated from the mixture; this, however, seems unlikely given the ultimate stoichiometry of the product.

Work is in progress to identify the minor products from the reaction in the hope that they will shed further light on the mechanism operating in this reaction.

We thank the Australian Research Council for supporting this work. C. S. G. is the holder of an Australian Postgraduate Award.

Notes and References

† E-mail: gak@chem.uwa.edu.au

‡ Part 1, Parts 2 and 3 given in ref. 16.

§ *Synthesis* of **3**: an equimolar amount of $[Mo_2(CO)_4(\eta$-$C_5H_5)_2]$ **1** (29 mg, 0.085 mmol) and $[\{Ru(CO)_2(\eta$-$C_5H_5)\}_2(\mu$-C≡C)] **2** (40 mg, 0.085 mmol) in toluene (25 mL) was heated at reflux for 15 h. After cooling the solvent was removed *in vacuo*, and the residue was dissolved in the minimum amount of CH_2Cl_2 and chromatographed on silica [CH_2Cl_2–hexanes (3 : 2)] to resolve four bands. The first band gave unreacted $[Mo_2(CO)_4(\eta$-$C_5H_5)_2]$, the second yellow band yielded $[Ru_2(CO)_4(\eta$-$C_5H_5)_2]$ (2 mg, 6%), the third yellow band remains unidentified and the fourth red–black band gave **3** (45 mg, 84%), mp 145 °C (decomp.). Found: C, 39.34; H, 2.59. FABMS: *m/z* 824 (M^+). $C_{27}H_{20}MoO_5Ru_3$ requires C, 39.34; H, 2.59. *m/z* 824. IR (toluene) ν(CO) 1959m, 1893m, 1823s, 1781m.

¶ *Crystal/refinement data* for **3**: $C_{27}H_{20}MoO_5Ru_3\cdot0.25CH_2Cl_2$, $M = 844.8$, tetragonal space group $P4/m$ (C^1_{4h}, no. 83), $a = 20.996(15)$, $c = 12.632(7)$ Å, $U = 5568(7)$ Å^3, D_c ($Z = 8$) 2.02 g cm^{-3}, 6412 independent, absorption corrected and 3958 observed [$I > 3\sigma(I)$], diffractometer data refined by full matrix least squares to $R = 0.072$, $R_w = 0.082$ (statistical weights). 2θ–θ scan mode, $2\theta_{max}$ 55°; monochromatic Mo-Kα radiation, $\lambda = 0.7107_3$ Å; $T = 295$ K; anisotropic thermal parameter forms were refined for the metal atoms only, $(x, y, z, U_{iso})_H$ being constrained at estimated values.[20] The geometry of the disordered CH_2Cl_2 molecule of solvation was restrained to ideal values. CCDC 182/939.

1 G. A. Koutsantonis, J. P. Selegue and J.-G. Wang, *Organometallics*, 1992, **11**, 2704.
2 (*a*) M. Akita, N. Ishii, A. Takabuchi, M. Tanaka and Y. Morooka, *Organometallics*, 1994, **13**, 258; (*b*) M. Akita, S. Sugimoto, A. Takabuchi, M. Tanaka and Y. Morooka, *Organometallics*, 1993, **12**, 2925.
3 M. Akita, A. Takabuchi, M. Terada, N. Ishii, M. Tanaka and Y. Morooka, *Organometallics*, 1994, **13**, 2516.
4 R. S. Barbieri, C. R. Bellato and A. C. Massabni, *Thermochim. Acta*, 1995, **259**, 277.
5 J. A. Davies, M. El-Ghanam, A. A. Pinkerton and D. A. Smith, *J. Organomet. Chem.*, 1991, **409**, 367.
6 M. P. Gamasa, J. Gimeno, I. Godefroy, E. Lastra, B. M. Martinvaca, S. Garciagranda and A. Gutierrezrodriguez, *J. Chem. Soc., Dalton Trans.*, 1995, 1901.
7 G. Koutsantonis and J. P. Selegue, *J. Am. Chem. Soc.*, 1991, **113**, 2316.
8 H. Lang, *Angew. Chem., Int. Ed. Engl.*, 1994, **33**, 547.
9 T. E. Muller, S. Choi, D. M. P. Mingos, D. Murphy, D. J. Williams and V. Yam, *J. Organomet. Chem.*, 1994, **484**, 209.
10 T. E. Muller, D. M. P. Mingos and D. J. Williams, *J. Chem. Soc., Chem. Commun.*, 1994, 1787.
11 K. Onitsuka, T. Joh and S. R. Takahashi, *J. Organomet. Chem.*, 1994, **464**, 247.
12 K. Onitsuka, K. Yanai, F. Takei, T. Joh and S. Takahashi, *Organometallics*, 1994, **13**, 3862.
13 K. Sunkel, U. Birk and C. Robl, *Organometallics*, 1994, **13**, 1679.
14 F. Takei, K. Yanai, K. Onitsuka and S. Takahashi, *Angew. Chem., Int. Ed. Engl.*, 1996, **35**, 1554.
15 M. Akita and Y. Morooka, *Bull. Chem. Soc. Jpn.*, 1995, **68**, 420.
16 C. S. Griffith, G. A. Koutsantonis, B. W. Skelton and A. H. White, *J. Chem. Soc., Dalton Trans.*, 1998, 1575; L. T. Byrne, C. S. Griffith, J. P. Hos, G. A. Koutsantonis, B. W. Skelton and A. H. White, *J. Organomet. Chem.*, 1998, in press. Parts 2 and 3 of this series, respectively.
17 L. Naldini, F. Demartin, M. Manassero, M. Sansoni, G. Rassu and M. A. Zoroddu, *J. Organomet. Chem.*, 1985, **279**, C42; V. W. Yam, W. K. Lee and T. F. Lai, *Organometallics*, 1993, **12**, 2383; D. M. Knotter, A. L. Spek and G. Van Koten, *J. Chem. Soc., Chem. Commun.*, 1998; 1738; D. M. Knotter, A. L. Spek, D. M. Grove and G. Van Koten, *Organometallics*, 1992, **11**, 4083; J. Diéz, M. P. Gamasa, J. Gimeno, A. Aguirre and S. García-Granda, *Organometallics*, 1991, **10**, 380; F. Olbrich, J. Kopf and E. Weiss, *Angew. Chem., Int. Ed. Engl.*, 1993, **32**, 1077.
18 M. Geissler, J. Kopf, B. Schubert, E. Weiss, W. Neugebauer and P. v. R. Schleyer, *Angew. Chem., Int. Ed. Engl.*, 1987, **26**, 587.
19 G. Frapper and J. F. Halet, *Organometallics*, 1995, **14**, 5044.
20 S. R. Hall, G. S. D. King and J. M. Stewart, *The XTAL 3.4 User's Manual*, University of Western Australia, Perth, 1995.

Received in Columbia, MO, USA, 2nd March 1998; 8/01744A

A mild, efficient and selective oxidation of sulfides to sulfoxides

José M. Fraile, José I. García, Beatriz Lázaro and José A. Mayoral*†

Departamento de Química Orgánica y Química Física, Instituto de Ciencia de Materiales de Aragón, Universidad de Zaragoza-C.S.I.C., E-50009 Zaragoza, Spain

Several titanium derivatives supported on silica have been investigated as catalysts in the sulfide→sulfoxide oxidation; the supported titanium/tartaric acid catalyst is highly suited to reactions carried out with H_2O_2, leading to high yields and high sulfoxide/sulfone selectivities, while small asymmetric inductions (up to 13%) are observed.

The selective oxidation of sulfides to sulfoxides has been a challenge for many years, partly due to the importance of sulfoxides as intermediates in organic synthesis.[1] In recent years selective oxidation of sulfides to sulfoxides has been carried out with a large number of supported reagents.[2] Recently, the use of H_2O_2 has taken on a new importance due to environmental implications, however, a catalyst is necessary to activate this oxidant. TS-1[3,4] and TS-2,[5] promote sulfide oxidation, but the use of bulky sulfides is precluded by their limited access to the Ti active sites. In order to overcome this limitation other molecular sieves have been used.[3–6] Ti-MCM-41 allows the oxidation of bulky sulfides,[6] but with low sulfoxide/sulfone selectivity.

Following a methodology closely related to that used by Shell to prepare $TiCl_4$-modified silica,[7] we have treated silica with $Ti(OPr^i)_4$ and shown[8] that this solid is an efficient catalyst in the epoxidation of alkenes of any size with hydroperoxides. We considered it interesting to test these silica-supported titanium compounds as catalysts in the selective oxidation of sulfides to sulfoxides (Scheme 1).

Firstly we tested the silica treated with $Ti(OPr^i)_4$ (**cat-1**, Ti content: 1.02 mmol g^{-1}) as a catalyst in the oxidation of methyl *p*-tolyl sulfide with TBHP and with H_2O_2 (Table 1, entries 1–4). Although the oxidation is faster with TBHP, a better sulfoxide/sulfone selectivity is obtained with H_2O_2. The recovered catalysts show a similar activity, but the product selectivity increases, mainly in the reaction carried out with H_2O_2, which indicates that the recovered catalyst does not have the same structure. It seems logical that in the presence of a large excess of water (we use 30% H_2O_2), the isopropoxy groups are hydrolysed to hydroxy groups, and that this modification of the Ti environment influences the course of the reaction.

In view of these results we decided to assess the effect of the introduction of polar groups near the titanium and we treated the original catalyst with diethyl (*R*)-tartrate (Scheme 2) to obtain **cat-2** (1.06 mmol Ti g^{-1}). The modification of the catalyst was monitored by IR spectroscopy, which shows the appearance of a broad carbonyl band. The width of this band indicated the presence of several kinds of carbonyl groups, and Scheme 2 shows only one of the possibilities. The catalytic tests (Table 1, entries 4–7) show that the introduction of diethyl tartrate reduces the catalytic activity and increases the sulfoxide/sulfone

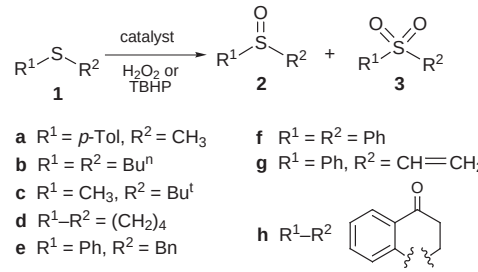

Scheme 1

Table 1 Results obtained in the oxidation of methyl *p*-tolyl sulfide **1a** promoted by different supported titanium catalysts[a]

				Yield (%)				
Entry	Catalyst	Sulfide	Oxidant	*t*/h	Total	sulfoxide **2**	sulfone **3**	**2**:**3**
1	**cat-1**	**1a**	TBHP	0.5	79	59	20	75:25
2	**cat-1**[b]	**1a**	TBHP	2	85	71	14	83:17
3	**cat-1**	**1a**	H_2O_2	3	87	75	12	86:14
4	**cat-1**[b]	**1a**	H_2O_2	3	88	84	4	95:5
5	**cat-2**	**1a**	TBHP	4	90	83[c]	7	92:8
6	**cat-2**	**1a**	H_2O_2	3	89	77[d]	12	87:13
7	**cat-2**[b]	**1a**	H_2O_2	3.5	85	84	1	99:1
8	**cat-3**	**1a**	TBHP	4	91	82[e]	9	90:10
9	**cat-3**	**1a**	H_2O_2	4	96	95[f]	1	99:1
10	**cat-3**[b]	**1a**	H_2O_2	4.5	96	95	1	99:1
11	—	**1a**	H_2O_2	24	49	47	2	96:4
12	**cat-3**	**1a**	H_2O_2	24	97	94	3	97:3
13	**cat-3**	**1b**	H_2O_2	4	100	100	0	—
14	**cat-3**	**1c**	H_2O_2	24	97	94	3	97:3
15	**cat-3**	**1d**	H_2O_2	4	98	96	2	98:2
16	**cat-3**	**1e**	H_2O_2	24	94	93	1	99:1
17	**cat-3**	**1f**	H_2O_2	24	97	95	2	98:2
18	**cat-3**	**1g**	H_2O_2	24	97	94	3	97:3
19	**cat-3**	**1h**	H_2O_2	24	95	92	3	97:3

[a] At 25 °C with 187 mg cat per mmol sulfide and 1 equiv. oxidant, in CH_2Cl_2 (with TBHP) or MeOH (with H_2O_2). The reactions were monitored by GC and the final results determined by ^1H NMR spectroscopy after filtering and washing the catalyst. [b] Catalyst recovered from a reaction with the same oxidant. [c] 7% ee. [d] 2% ee. [e] 8% ee. [f] 13% ee.

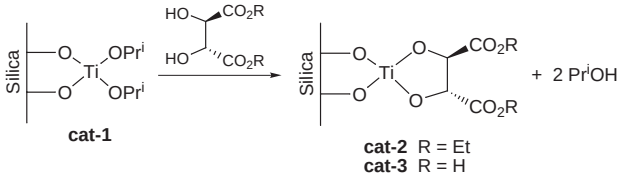

cat-1

cat-2 R = Et
cat-3 R = H

Scheme 2

selectivity in the reaction carried out with TBHP, while the catalytic performance is almost unchanged when H_2O_2 is used. The recovered catalyst gives an exceptional sulfoxide/sulfone selectivity (entry 7), which points to a new structure of the catalytic sites after recovery, as shown by the modification of the IR carbonyl band, which suggests the hydrolysis of the ester groups.

In view of this we decided to treat the initial catalyst with (*R*)-tartaric acid and to test the catalytic activity of this solid (**cat-3**, 0.82 mmol Ti g^{-1}). The results obtained with TBHP (entry 8) are very similar to those obtained using the catalyst containing diethyl (*R*)-tartrate (**cat-2**). However, the reactions carried out with H_2O_2 (entries 9 and 10) lead to an excellent sulfoxide/sulfone ratio and a very high selectivity (97%) with respect to the H_2O_2.

(*R*)-Tartaric acid is strongly adsorbed onto silica, thus it is important to assess the modification of the titanium centres and the catalytic role of these centres. The modification of the environment of titanium can be estimated from the amount of Pr^{i}OH lost during the preparation of the catalyst. Although it is not possible to obtain quantitative conclusions, given that some Pr^{i}OH may remain adsorbed on the silica surface, GC analysis shows that 65 ± 5% of the Pr^{i}O groups present in the original solid are lost during treatment. This result agrees with the modification of most of the titanium atoms. The catalytic role of the titanium was confirmed by adsorbing onto silica gel the same amount of (*R*)-tartaric acid used to modify the catalyst and carrying out the reaction in the presence of this solid. The results obtained are the same as those reached in the absence of catalyst, showing that the catalytic activity is related to the presence of titanium.

Although it was not the aim of the present work, the introduction of chiral centers may produce an asymmetric reaction, and so this possibility was considered. The ee of the sulfoxides was determined as previously described,[9] and the absolute configuration was determined by polarimetry.[10] The low ee obtained for the (*R*)-sulfoxide provides additional evidence for the modification of the catalytic centers.

Given that the catalyst obtained by treatment with (*R*)-tartaric acid (**cat-3**) leads to the best selectivity, we tested the effect of using a smaller amount of catalyst. Very good results were obtained, with a sulfide/titanium ratio = 140, by simply increasing the reaction time. In order to test the general scope of this method it was applied to several other sulfides (Scheme 1, Table 1, entries 12–19).

This solid promotes the reaction with a very small amount of catalyst and leads to high yields and selectivities. The methodology is applicable to bulky sulfides and is compatible with the presence of other oxidisable functions, as shown in the last two examples where epoxidation of the double bond (**1g**) or Baeyer–Villiger oxidation of the ketone (**1h**) were not observed.

As far as the mechanism is concerned, either the H_2O_2 may be the oxidation agent, *via* a Ti–OOH intermediate, or a supported peracid intermediate may be formed.

We tested the recovery of the catalyst in the oxidation of dibutyl sulfide **1b** (Table 2). A gradual leaching of titanium takes place. However, this leaching is very slow given that after five reactions each mmol of titanium has been treated with about 5000 mmol of water. Furthermore, even the fifth reaction takes place with reasonable yield and selectivity. The existence of leaching suggests that the reaction can take place, at least in part, in the homogeneous phase. In order to clarify this point we treated **cat-3** with H_2O_2 for 4 h. The solid was separated by filtration and the filtrate used in the oxidation of a corresponding amount of sulfide **1a**. The filtrate promotes the reaction with a 83:17 sulfoxide/sulfone ratio. In another experiment we carried out the reaction of **1a** until 85% conversion (15 min), then the catalyst was separated by filtration and both the solid and the filtrate were used in a new reaction. The sulfide was consumed in both reactions at almost the same rate.

Table 2 Recovery of the catalyst in the oxidation of **1b** with H_2O_2 promoted by **cat-3**

		Yield (%)			
Run	*t*/h	Total	Sulfoxide **2b**	Sulfone **3b**	Ti/mmol g^{-1}[a]
1	4	100	100	0	0.82
2	5	98	96	2	—
3	8	96	92	4	—
4	8	90	82	8	—
5	9	91	82	9	—
6	—	—	—	—	0.22

[a] Determined by plasma emission spectroscopy.

In our opinion these results indicate the co-existence of the homogeneous and heterogeneous reactions and that a very active homogeneous catalyst is obtained under these conditions. Therefore, it seems that the identification of the homogeneous species and the improvement of the behaviour of the heterogeneous system against leaching are important aims.

These results clearly show that modification of the environment of titanium *via* introduction of organic molecules can modify the performance of the catalysts. This strategy opens the way to the preparation of new families of supported chiral catalysts in which grafting is carried out through the metal instead of through the chiral auxiliary.

This work was made possible by the generous financial support of the C.I.C.Y.T. (Project MAT96-1053).

Notes and References

† E-mail: mayoral@posta.unizar.es

1 J. Drabowski, P. Kielbasinski and M. Mikolajczyk, *Synthesis of Sulfoxides*, Wiley, New York, 1994; M. Madesclaire, *Tetrahedron*, 1986, **42**, 549.
2 G. W. Breton, J. D. Fields and P. J. Kropp, *Tetrahedron Lett.*, 1995, **36**, 3825; P. Kannan, R. Sevvel, S. Rajagopal and K. Pitchumani, *Tetrahedron*, 1997, **53**, 7635; R. S. Varna, R. K. Saini and H. M. Meshram, *Tetrahedron Lett.*, 1997, **38**, 6525; M. H. Ali and W. C. Stevens, *Synthesis*, 1997, 764; M. Hirano, S. Yakabe, S. Itoh, J. H. Clark and T. Morimotoa, *Synthesis*, 1997, 1161; V. Hulea, P. Moreau and F. di Renzo, *J. Mol. Catal. A*, 1996, **111**, 355.
3 R. S. Reddy, J. S. Reddy, R. Kumar and P. Kumar, *J. Chem. Soc., Chem. Commun.*, 1992, 84.
4 P. S. Raglavan, V. Ramaswamy, T. T. Upadhya, A. Sudalai, A. V. Ramaswamy and S. Sivasankar, *J. Mol. Catal. A*, 1997, **122**, 75.
5 S. V. N. Raju, T. T. Upadhya, S. Ponatnam, T. Daniel and A. Sudalai, *Chem. Commun.*, 1996, 1969.
6 A. Corma, M. Iglesias and F. Sánchez, *Catal. Lett.*, 1996, **39**, 153.
7 R. A. Sheldon, in *Aspects of Homogeneous Catalysis*, ed. R. Ugo, Reidel, Dordrecht, 1981, vol. 4, pp. 1–70.
8 C. Cativiela, J. M. Fraile, J. I. García and J. A. Mayoral, *J. Mol. Catal. A*, 1996, **112**, 259.
9 M. Deshmukh, E. Duñach, S. Juge and H. B. Kagan, *Tetrahedron Lett.*, 1984, **25**, 3467.
10 K. Mislow, M. M. Green, P. Laur, J. T. Melillo, T. Simmons and A. L. Ternay Jr., *J. Am. Chem. Soc.*, 1965, **87**, 1958.

Received in Cambridge, UK, 3rd June 1998; 8/04180F

A novel cyclic formal, 1,3,5,7-tetraoxacyclononane, from the direct reaction of 1,3,5-trioxane and ethylene oxide

J. Masamoto,*[a]† N. Yamasaki,[a] W. Sakai,[a] T. Itoh,[a] N. Tsutsumi[a] and H. Nagahara[b]

[a] *Kyoto Institute of Technology, Matsugasaki, Sakyo, Kyoto 606-8585, Japan*
[b] *Asahi Chemical Industry Co., Ltd. Kojimashionasu, Kurashiki 711-8510, Japan*

A new reaction between 1,3,5-trioxane and ethylene oxide has been observed and a novel cyclic formal, which is the reaction product of 1 equiv. of 1,3,5-trioxane and 1 equiv. of ethylene oxide, has been isolated and identified.

Weissermel and co-workers[1,2] proposed the reaction of formaldehyde with ethylene oxide to form 1,3-dioxolane as the initiation mechanism of the copolymerization of 1,3,5-trioxane and ethylene oxide. Collins *et al.*[3] confirmed that ethylene oxide was converted to 1,3-dioxolane and then from 1,3-dioxolane, 1,3,5-trioxepane was formed. They stated that the direct reaction of ethylene oxide with 1,3,5-trioxane was impossible because of the weak basicity of 1,3,5-trioxane. Weissermel and co-workers[1,2] and Collins *et al.*[3] proposed the formation mechanism of 1,3-dioxolane from ethylene oxide and formaldehyde, and for a long time this was thought plausible for the initiation mechanism of copolymerization of trioxane and ethylene oxide.

We have performed the direct reaction of ethylene oxide with 1,3,5-trioxane, which was thought impossible for a long time, and isolated a novel cyclic formal. From this novel cyclic formal, 1,3,5-trioxepane was formed and then 1,3-dioxolane was also generated. This reaction identified the precise initiation mechanism of the copolymerization of 1,3,5-trioxane and ethylene oxide.

Purified 1,3,5-trioxane (30 g) was melted under an N_2 atmosphere in a glass vessel immersed in an oil bath and held at 70 °C. Gaseous ethylene oxide (4.5 mol% with respect to 1,3,5-trioxane) was introduced into the molten 1,3,5-trioxane which was stirred with a magnetic mixer. A cyclohexane solution of $BF_3{\cdot}OBu_2$ (7×10^{-3} mol% with respect to 1,3,5-trioxane) was introduced into the molten mixture of 1,3,5-trioxane and ethylene oxide through the cap of the glass vessel with a microsyringe. The mixture was stirred using a magnetic mixer in an oil bath to maintain the reaction temperature at 70 °C. The reaction mixture was sampled with a syringe and then poured into PrOH containing a small amount of KOH. The reaction mixture was analyzed by gas chromatography. This showed a 33% yield of the novel compound based on the initial amount of ethylene oxide.

The novel compound was separated using a micro-distillation apparatus (bp 180 °C at 1 atm; mp 8.4 °C and bp 95 °C at 25 torr). Its chemical structure was confirmed using ^{1}H NMR, ^{13}C NMR and mass spectral and elemental analysis.

Fig. 1 shows the ^{1}H NMR pattern of the new compound. The ratio of H^a (proton of formal linkage, δ 5.05) to H^b (proton of formal linkage, δ 4.93) and H^c (proton of ether linkage, δ 3.85) is 1:2:2. Fig. 2 shows the ^{13}C NMR pattern of the new compound, and shows three different types of carbon: C^a (formal carbon, δ 96.9), C^b (formal carbon, δ 97.1) and C^c (ether carbon, δ 70.5). Fig. 3 shows the EI mass spectrum of the new compound, which shows the molecular weight of 134 and composition formula of $C_5H_{10}O_4$, which is in accordance with the molecular weight and composition formula of 1,3,5,7-tetraoxacyclononane (TOCN). The observed elemental analyses are in accordance with the theoretical values (Found: C, 44.76; H, 7.75. Calc.: C, 44.78; H, 7.50%).

The reaction concentration profile is shown in Fig. 4. The profile begins when the initiator (a cyclohexane solution of $BF_3{\cdot}OBu_2$) is injected into the molten mixture of 1,3,5-trioxane and ethylene oxide. At first, as the ethylene oxide concentration (4.5 mol% with respect to 1,3,5-trioxane) decreases, the TOCN concentration increases proportionally. Later, as the TOCN

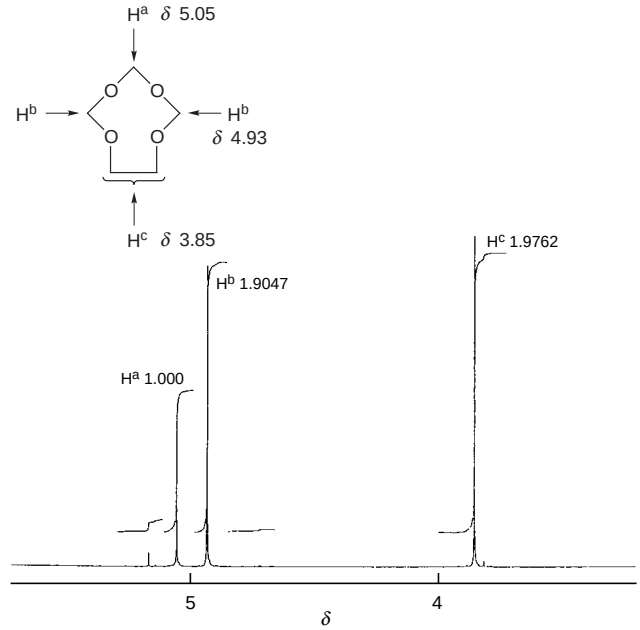

Fig. 1 ^{1}H NMR spectrum of the new compound

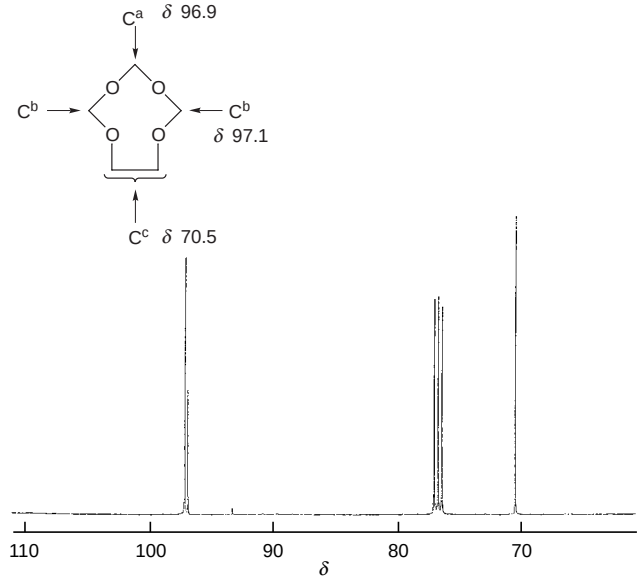

Fig. 2 ^{13}C NMR spectrum of the new compound

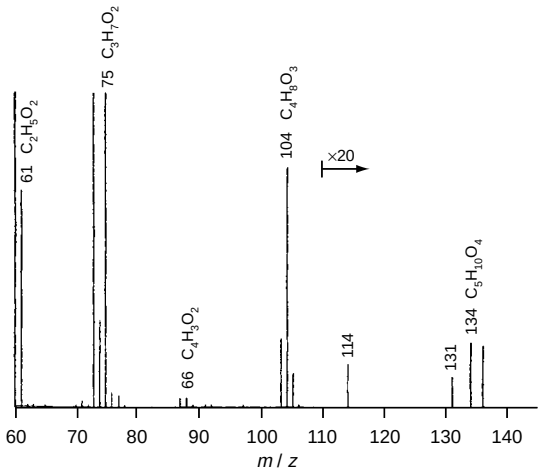

Fig. 3 EI mass spectrum of the new compound

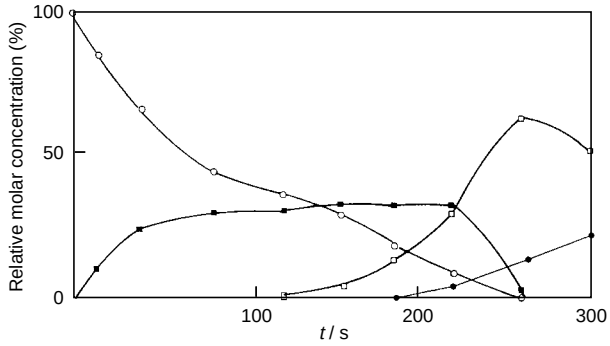

Fig. 4 Profile of reaction of 1,3,5-trioxane and ethylene oxide: (○) ethylene oxide, (■) 1,3,5,7-tetraoxacyclononane, (□) 1,3,5-trioxepane, (●) 1,3-dioxolane. $[EO]_0$ = 4.5 mol% with respect to 1,3,5-trioxane. t = 0 indicates the time at which the initiator is injected into the molten mixture of 1,3,5-trioxane and ethylene oxide. Percentage on the vertical axis indicates the relative molar concentration of ethylene oxide or related compounds to the initial concentration of ethylene oxide.

concentration decreases again, the concentration of 1,3,5-trioxepane increases. Soon after the appearance of 1,3,5-trioxepane, 1,3-dioxolane appeares, and with the decrease in concentration of 1,3,5-trioxepane, the concentration of 1,3-dioxolane increases.

Although the equilibrium concentration of 1,3,5-trioxepane and 1,3-dioxolane exist, there is no equilibrium concentration of TOCN. This might be attributed to the higher ring strain energy

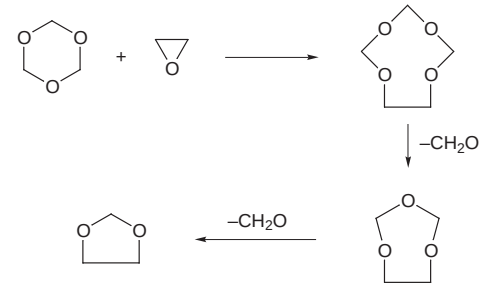

Scheme 1

of the nine-membered ring compound of TOCN compared to those of the seven- and five-membered ring compounds. In the case of the cycloalkane, the ring strain energy of the nine-membered ring compound is 27 kJ mol^{-1} higher compared to those of the seven- and five-membered ring compounds.[4]

The newly isolated intermediate, the novel cyclic compound TOCN, identifies a new direct reaction between 1,3,5-trioxane and ethylene oxide, as well as the precise initiation mechanism of the copolymerization of 1,3,5-trioxane and ethylene oxide. First, ethylene oxide directly reacts with 1,3,5-trioxane to produce TOCN (Scheme 1). The 1,3,5-trioxepane is then formed from TOCN, and 1,3-dioxolane is formed from 1,3,5-trioxepane.

Using gas chromatography, we observed compounds of higher molecular weights than TOCN as minor components, which were presumed to be the addition product of ethylene oxide and TOCN. Confirmation of this point will be discussed in the near future.

Notes and References

† E-mail: masamoto@ipc.kit.ac.jp

1 K. Weissermel, E. Fischer, K. Gutweiler and H. D. Hermann, *Kunststoffe*, 1964, **54**, 410.
2 K. Weissermel, E. Fischer, K. Gutweiler, H. D. Hermann and H. Cherdron, *Angew. Chem., Int. Ed. Engl*., 1967, **6**, 526.
3 G. L. Collins, R. K. Green, F. M. Beradinelle and W. H. Ray, *J. Polym. Sci., Polym. Chem. Ed*., 1981, **19**, 1579.
4 P. Kubisa, in *Cationic Polymerization: Mechanism, Synthesis, and Applications*, ed. K. Matyjaszewski, Dekker, New York, 1995, pp. 437–553.

Received in Cambridge, UK, 27th February 1998; 8/01653D

Enhanced catalytic activity of MCM-41-grafted aluminium isopropoxide in MPV reductions

R. Anwander,*[a]† C. Palm,[b] G. Gerstberger,[a] O. Groeger[b] and G. Engelhardt[b]

[a] *Anorganisch-chemisches Institut, Technische Universität München, Lichtenbergstr. 4, D-85747 Garching, Germany*
[b] *Institut für Technische Chemie I, Universität Stuttgart, Pfaffenwaldring 55, D-70569 Stuttgart, Germany*

Aluminium alkoxide moieties are grafted onto purely siliceous mesoporous MCM-41 *via* siloxide linkages, producing materials which reveal enhanced catalytic activity in the MPV reduction of cyclic ketones; nitrogen physisorption and ^{27}Al MAS NMR spectroscopy are applied to characterise the catalytically active hybrid systems.

The potential of aluminium reagents, in particular 'Al(OPr^i)$_3$', in Meerwein–Ponndorf–Verley (MPV) reductions and Oppenauer oxidations is well documented.[1,2] Although these transformations formally proceed catalytically, an excess of the aluminium compound is commonly required.[3] Heterogeneously performed MPVO reactions utilising, for example, oxidic or zeolitic materials have also been reported to cope better with catalyst separation.[4,5] Recently, we and others envisaged the mesoporous silicate MCM-41 as a versatile support material for metalorganic moieties.[6,7] As part of this program, we present our preliminary findings on the catalytic MPV reduction of 4-*tert*-butylcyclohexanone mediated by grafted aluminium alkoxide species, including a detailed ^{27}Al MAS NMR study.

MCM-41-supported aluminium isopropoxide **2** was initially prepared according to a one-step solution impregnation by contacting Al(OPr^i)$_3$ and MCM-41 **1** in *n*-hexane.‡,§[8,9]

Assuming a monofunctional surface reaction, a ligand/metal ratio of *ca*. 2.0 can be derived for material **2** from elemental analysis (Table 1). Furthermore, an aluminium surface coverage of *ca*. 1.3 Al nm^{-2} can be calculated from the metal content and the BET surface area of material **1** (1059 m^2 g^{-1}). A considerable amount of unreacted isolated silanol groups is still present after the grafting procedure as indicated by the ν(OH) vibration mode at 3695 cm^{-1} in the IR spectrum. Al(OPr^i)$_3$ immobilisation in the mesopores of material **1** drastically decreases the pore volume and pore diameter as revealed by nitrogen physisorption (Table 1). However, the obtained adsorption/desorption isotherm is still of type IV.

We found that careful drying of the solvent isopropanol (= reductant) significantly increased the catalytic activity of Al(OPr^i)$_3$ in this MPV reduction (Table 2, run 1 *vs.* 2). In contrast, material **2** exhibits dramatically enhanced catalytic activity, producing 86% of the 4-*tert*-butyl cyclohexanol isomers after 5 h even at ambient temperature (run 5). At 80 °C material **2** afforded almost quantitative conversion after 30 min (run 6).¶[10] Hybrid material **2** could easily be separated from the reaction mixture of run 5 by centrifugation. After washing with HOPr^i the catalytic activity of the recovered solid material (**2b**) remained unchanged (run 7). The combined HOPr^i fractions showed no further activity upon addition of new substrate. We also found no catalytic activity for parent material **1** (run 3).

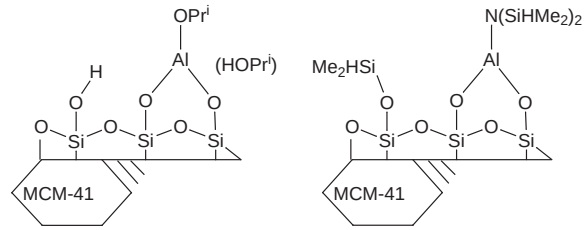

For comparison, recent studies by others revealed that H-MCM-41 and Na-MCM-41 (Si/Al = 15, activation temperature 450 °C) gave only 10% conversion of 4-*tert*-butylcyclohexanone after 6 h at 80 °C.[4] A zirconium hybrid system obtained according to the synthesis sequence: silica + Zr(CH$_2$Bu^t)$_4$ + HOPr^i, showed 75% conversion of cyclohexanone after 20 h at 80 °C.[5]

The efficiency of the MPV reduction is known to depend on the Lewis acidity of the metal center and the ligand exchange ability.[1,2] These factors are markedly affected by the type of (co-)ligand and co-ordination geometry at the metal center. In order to gain further insight into the co-ordination geometry of the catalytically active species, a detailed ^{27}Al MAS NMR study was performed. The ^{27}Al MAS NMR spectrum of Al(OPr^i)$_3$ shows a sharp resonance at 0 ppm typical of octahedral aluminium, accompanied by weak and broad signals

Table 1 Analytical data, pore volume and pore diameter

Sample[a]	Elemental analysis[b] wt.% C	wt.% Al	V_p[c]/cm^3 g^{-1}	$d_{p,max}$[d]/nm
1	—	—	0.89	2.8
2	15.61	6.2	0.33	1.75
2a	8.61	6.6	0.46	2.0
2b[e]	10.39	6.9	0.45	2.0
3	9.97	2.5	0.35	1.7
4	9.89	2.5	0.40	1.85

[a] Pretreatment temperature: 250 °C, 3 h, 10^{-3} Torr for **1**; 100° C, 3 h, 10^{-3} Torr for **2a**, **2b** and **4**; 25 °C, 3 h, 10^{-3} Torr for **2** and **3**. [b] Al by ICP analysis. [c] BJH desorption cumulative pore volume of pores between 1.5 and 4.5 nm diameter. [d] Pore diameter according to the maximum of the BJH pore size distribution calculated form the desorption branch. [e] Recovered material from run 5 (Table 2).

Table 2 Catalytic activities of aluminium isopropoxide species in the MPV reduction of 4 *tert*-butylcyclohexanone[a]

Run	Precatalyst	Conversion (%) (*trans*:*cis*) 5 h	24 h
1[b]	[Al(OPr^i)$_3$]	< 1	7 (4.0)
2	[Al(OPr^i)$_3$]	16 (2.1)	59 (2.1)
3[c]	**1**	—	< 1
4[d]	**1** (silylated)	—	< 1
5	**2**	86 (2.3)	> 99 (2.2)
6[e]	**2**	> 99 (2.1)	> 99 (2.2)
7	**2b**	85 (2.3)	> 99 (2.3)
8	**4**	88 (2.6)	> 99 (2.6)

[a] Conditions: 25 g HOPr^i, 0.1 g *n*-nonane, 0.78 g ketone, *ca.* 5 mol% of precatalyst, 25 °C (mol% = 100 $n_{aluminium}/n_{substrate}$). [b] HOPr^i not predried. [c] 0.20 g mesoporous material. [d] 0.20 g SiMe$_3$-silylated material. [e] 80 °C.

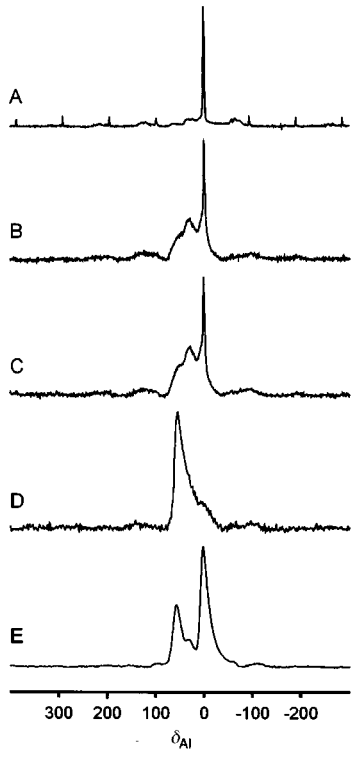

Fig. 1 ^{27}Al NMR spectra: (A) Al(OPr^i)$_3$ as received from Aldrich; (B) material **2**; (C) recovered material **2a**; (D) material **4**; (E) material **2** exposed to air for several days (completely hydrolysed); all hybrid materials were evacuated for 5 h at 25 °C, 10^{-2} Torr prior to measurement

at about 60 and 30 ppm attributable to distorted 4- and 5-co-ordinated aluminium (Fig. 1A).‖[11] In contrast, the spectrum of hybrid material **2** (Fig. 1B) exhibits, besides the sharp resonance at 0 ppm (15%), an intense broad signal pattern in the range of 75 to −25 ppm, clearly indicating the formation of additional aluminium sites. Deconvolution by computer simulation (Bruker WINFIT) yields a Gaussian line at 54 ppm (25%) of regular tetrahedral aluminium sites, and a quadrupolar line shape (δ_{iso} = 49, QCC = 7.5 MHz, 60%), typical of heavily distorted 4-co-ordinated aluminium.[12] Interestingly, this signal pattern did not change after the first catalytic run (material **2a**, Fig. 1C), proving the preservation of the lower-co-ordinated, surface constrained and hence stronger Lewis acidic aluminium centres which are proposed to contribute to the enhanced catalytic activity of material **2**. This is in accord with a previous kinetic study.[13] where the 'melt' form of Al(OPr^i)$_3$ which consists of the predominantly trimeric form with 4- and 5-co-ordinated aluminium centres was found to be 10^3 times more reactive in MPV reductions than the tetrameric form containing 4- and 6-co-ordinated aluminium.

This finding could be corroborated by applying a synthetic approach which exclusively produces lower-co-ordinated aluminium surface species. Novel 4-co-ordinate Al[N(SiHMe$_2$)$_2$]$_3$·thf was reacted with material **1** to yield material **3** *via* a siloxide formation/silylation sequence (*ca.* 0.5 Al nm^{-2}).**[6] Subsequent treatment of hybrid material **3** with a slight excess of HOPr^i afforded material **4** (Table 1). The pore texture of material **4** is roughly comparable to that of material **2**, supporting a disruption of the tetrameric form of Al(OPr^i)$_3$ upon grafting. The ^{27}Al MAS NMR spectrum of material **3** revealed poor signal intensity (not shown in Fig. 1), probably due to the formation of surface-docked alumoxo-silylamide sites in highly distorted co-ordination environments.[14] Upon silylamide/HOPr^i ligand exchange the co-ordination geometry at the aluminium center is markedly relaxed. The resulting ^{27}Al MAS NMR spectrum now features a broad, asymmetric signal with a maximum at 55 ppm, indicating the presence of predominantly 4- and 5-co-ordinated aluminium species (Fig. 1D). Material **4** displayed catalytic activity comparable to that of material **2** (run 8). Although silylated **1** was shown to be catalytically inactive (run 4), the partly silylated surface of material **4** may affect its catalytic performance by hydrophobicity effects.[15] Spectrum E in Fig. 1 shows the ^{27}Al resonances of a completely hydrolysed sample of material **2**. The three overlapping signals of tetrahedral (58 ppm), 5-co-ordinated (34 ppm) and octahedral (0 ppm) aluminium sites are now clearly visible.

We have shown that MCM-41-grafted aluminium isopropoxide is an efficient catalyst in the MPV reduction of 4-*tert*-butylcyclohexanone. A detailed ^{27}Al MAS NMR study revealed that the enhanced catalytic activity can be ascribed to the formation of low-co-ordinated (4-, 5-), geometrically distorted aluminium species. Surface confinement prevents the aluminium alkoxide moieties from self-association, while the silicate material simultaneously acts as an electron-withdrawing matrix.

We thank the Deutsche Forschungsgemeinschaft for generous support.

Notes and References

† E-mail: anwander@arthur.anorg.chemie.tu-muenchen.de

‡ All manipulations were performed in a nitrogen-filled glovebox (MB Braun MB150B-G-II) as described elsewhere.[6] Purely siliceous MCM-41 was prepared according to the literature and dehydrated at 280 °C, 10^{-5} Torr prior to use. All of the resulting hybrid materials were synthesized in *n*-hexane at ambient temperature in 24 h and subsequently washed several times with *n*-hexane to remove unreacted educt compounds.

§ A similar post-synthetic aluminium incorporation was recently applied to produce mesoporous aluminosilicates.[9]

¶ Although it was shown earlier that addition of Al(OPr^i)$_3$ to alumina significantly enhanced its catalytic activity at 80 °C, this phenomenon was not further explained.[10]

‖ The solution spectrum of Al[(μ-OPr^i)$_2$Al(OPr^i)$_3$]$_3$ in toluene at 25 °C gives a similar spectrum with the very broad signal of the 4-co-ordinated Al disappearing into the base line.[11]

** The formation of both surface bonded metal silylamide '[μSiO]$_x$–Al[N(SiHMe$_2$)$_2$]$_y$' [ν(SiH) = 2102 cm^{-1}], silylated species '≡SiO–SiHMe$_2$' [ν(SiH) = 2151 cm^{-1}] and the consumption of all surface silanol groups was revealed by FTIR spectroscopy.

1 A. L. Wilds, *Org. React.*, 1994, **2**, 178.
2 C. F. de Graauw, J. A. Peters, H. van Bekkum and J. Huskens, *Synthesis*, 1994, **10**, 1007.
3 See for recent examples: K. Nishide, Y. Shigeta, K. Obata and M. Node, *J. Am. Chem. Soc.*, 1996, **118**, 13103; M. Fujita, Y. Takarada, T. Sugimura and A. Tai, *Chem. Commun.*, 1997, 1631.
4 E. J. Creyghton, S. D. Ganeshie, R. S. Downing and H. van Bekkum, *J. Mol. Catal. A*, 1997, **115**, 457 and references therein.
5 P. Leyrit, C. McGill, F. Quignard and A. Choplin, *J. Mol. Catal. A*, 1996, **112**, 395.
6 R. Anwander, O. Runte, J. Eppinger, G. Gerstberger, E. Herdtweck and M. Spiegler, *J. Chem. Soc., Dalton Trans.*, 1998, 847.
7 S. O'Brien, J. Tudor, S. Barlow, M. J. Drewitt, S. J. Heyes and D. O'Hare, *Chem. Commun.*, 1997, 641 and references therein.
8 J. S. Beck, J. C. Vartuli, W. J. Roth, M. E. Leonowicz, C. T. Kresge, K. D. Schmitt, C. T.-W. Chu, D. H. Olson, E. W. Sheppard, S. B. McCullen, J. B. Higgins and J. L. Schlenker, *J. Am. Chem. Soc.*, 1992, **114**, 10 834.
9 R. Mokaya and W. Jones, *Chem. Commun.*, 1997, 2185.
10 L. Horner and U. B. Kaps, *Liebigs Ann. Chem.*, 1980, 192.
11 J. W. Akitt and R. H. Duncan, *J. Magn. Reson.*, 1974, **15**, 162.
12 G. Engelhardt and D. Michel, *High resolution solid-state NMR of silicates and zeolites*, Wiley, New York, 1987.
13 V. J. Shiner, Jr. and D. Whittaker, *J. Am. Chem. Soc.*, 1969, **91**, 394.
14 R. Anwander, C. Palm, O. Groeger and G. Engelhardt, *Organometallics*, 1998, **17**, 2027.
15 T. Tatsumi, K. A. Koyano and N. Igarashi, *Chem. Commun.*, 1998, 325.

Received in Bath, UK, 14th April 1998; 8/02996B

New paradigms in cycloaddition face-selectivities: remarkable effect of remote substituents in singlet oxygen addition to hexacyclo[7.5.1.0^{1,6}.0^{6,13}.0^{8,12}.0^{10,14}]pentadeca-2,4-diene system

Goverdhan Mehta,*[a] R. Uma,[a] M. N. Jagadeesh[b] and Jayaraman Chandrasekhar*[b]†

[a] *School of Chemistry, University of Hyderabad, Hyderabad 500046, India*
[b] *Department of Organic Chemistry, Indian Institute of Science, Bangalore 560012, India*

Different modes of direct through-space interactions between remote substituents and an approaching reagent are indicated as important additional controlling factors of face selectivity in singlet oxygen cycloaddition to facially differentiated cyclohexa-1,3-dienes.

Evaluation of stereoelectronic effects that influence π-face selection and control diastereoselectivity in [4+2]-cycloadditions to cyclic dienes continues to be an area of intense scrutiny and new explorations.[1] In this context, substrates in which the 1,3-diene moiety is grafted on to a rigid polycyclic frame to eliminate conformational ambiguities are particularly advantageous, as the facial discrimination and stereoelectronic perturbations can be effected through distal modulation of functionalities.[2,3] In recent years, several polycyclic systems **1**–**4** embodying a cyclic 1,3-diene substructure have been devised and probed for diastereoselection employing a variety of dienophiles, but among these, **4** has been more enduring[3] because of its rigidity, ready accessibility,[4] reactivity and functional group manoeuvrability. In the hexacyclic diene **4**, facial discrimination in the cyclohexadiene moiety is manifested through the interplay of the steric effects of cyclobutyl hydrogens and the electronic interactions of the carbonyl groups. The diastereoselectivities observed in cycloadditions to several derivatives of **4** (obtained through substitutions on the diene moiety as well as modifications of the carbonyl group) have led to the identification of steric effects, filled orbital and electrostatic repulsions, the Cieplak effect and transition state geometrical distortions as the main determinants of face-selectivity.[3] We have now observed that even the simplest derivatisation can lead to a reversal in diastereoselectivity which we interpret in terms of transition state interactions, some of which have not been recognised before as contributors to face selectivity. These subtle effects, though promoted in the present case by the geometry of the hexacyclic system **4** and the relative spatial orientation of the diene unit and the remote functionality, can be operative in other substrates as well and in the absence of other dominant effects, can be the principal determinants of face selectivity; *inter alia* caution must be exercised in extrapolating stereoselectivities, even when seemingly inconsequential functional group changes are effected at distal sites.

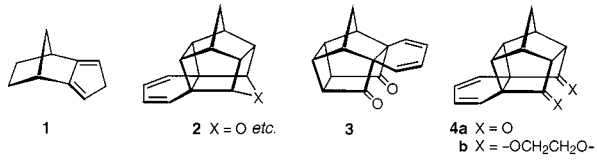

The hexacyclic *endo,endo*-diol **5a**, its diacetate **5b** and dimethyl ether **5c** readily underwent cycloaddition with $^1O_2$ generated in the presence of Methylene Blue (500 W tungsten lamp, O_2, $CHCl_3$, 5–10 °C, 4–5 h) to furnish a diastereomeric mixture of endoperoxides **6a–c** and **7a–c** in 80–85% yield.[5] While the gross structures of both the 'bottom' and 'top' addition endoperoxides **6a**–**c** and **7a**–**c**, respectively, were apparent from the spectral characteristics (^{1}H and ^{13}C NMR), their stereochemistry was unambiguously determined *via* X-ray crystal structure determination‡ of the major endoperoxides **6b** and **7c**. The diastereoselectivities observed in the $^1O_2$ additions (Scheme 1) indicated that while in the *endo,endo*-diol **5a** and diacetate **5b** 'bottom' face addition was preferred, complete reversal occurred in the case of the dimethyl ether **5c** and the 'top' addition product was exclusively obtained. The expectation from earlier studies and interpretations[3] with substrates such as **4b** was that repulsion between *endo*-directed oxygens in **5a**–**c** and the $^1O_2$ reagent should uniformly favour addition from the 'top' face. While the observed selectivity in **5c** was fully in consonance with this reasoning, the unpredicted outcome of diastereoselectivities in the case of **5a,b** suggested intervention of some additional, unrecognized interactions and these needed to be probed through transition state modelling.

The origin of the variations in face selectivities in **5a**–**c** was examined through AM1 calculations[6] on $^1O_2$ addition transition states. Saddle points with vanishing gradients and characterized by a single imaginary vibrational frequency were located for the top and bottom face addition. The possibility of conformational variation in the OR groups was considered by using different initial geometries.

For the methoxy derivative **5c**, two sets of transition structures are obtained, both favoring the top face attack by varying degrees. While the energy preference is marginal (0.2 kJ mol^{-1}) in the structures in which the methyl groups are pointed towards the diene moiety, a strong bias (10.3 kJ mol^{-1}) is predicted when the methyl groups are oriented away from the diene. In the latter, repulsive interactions involving the oxygen lone pairs towards the approaching $^1O_2$ evidently come into play [Fig. 1(*a*)]. Hence the exclusive formation of the top face adduct in **5c** is entirely consistent with electrostatic control of face selection.

For the $^1O_2$ addition to the dihydroxy derivative **5a**, a significant bottom face preference (7.9 kJ mol^{-1}) is computed, qualitatively in accord with the experimental trend. The transition structures for both the top and bottom face approach lack any symmetry (C_1) due to an intramolecular O–H···O hydrogen bond. In the bottom face attack saddle point, an additional hydrogen bonding interaction is evident. The second OH group in the structure interacts with one of the oxygen

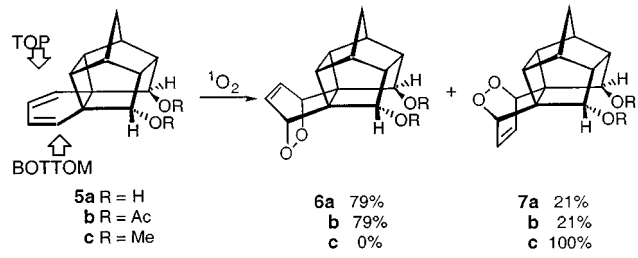

Scheme 1

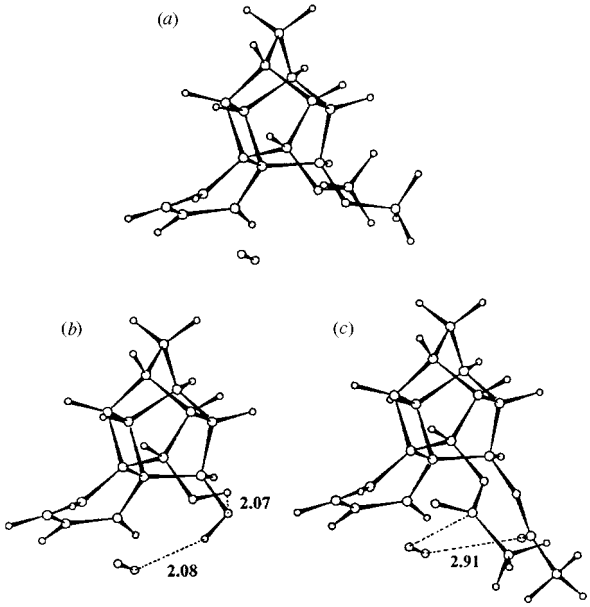

Fig.1 AM1 optimised transition state structures for the bottom face addition of $^1O_2$ to (*a*) **5c**, (*b*) **5a** and (*c*) **5b**

atoms of the approaching dienophile [Fig. 1(*b*)]. The cyclic, cooperative hydrogen bonds seem to provide enough stabilization to overcome electrostatic repulsions noted in **5c**. Additional proof for the role of hydrogen bonding with the singlet oxygen was obtained by computing the energies of transition states with C_s symmetry constraints which led to conformations similar to those of the dimethoxy derivative. The face selectivity calculated in these high energy conformations is revealing. With both the OH groups pointing towards the diene, the bottom face approach of $^1O_2$ is favored by 25.6 kJ mol^{-1}. In this structure, the two OH groups form strong hydrogen bonds with either end of the dienophile. In the alternative transition structures in which the OH groups point away from the diene, an electrostatic preference for top face attack (12.6 kJ mol^{-1}) similar to that calculated for the corresponding conformation of **5c** is obtained.

Transition state energies favoring the bottom face attack for the diacetoxy derivative **5b** are also consistent with experiment. Remarkably, the computed preference (6.9 kJ mol^{-1}) is similar to that obtained in the most stable transition state structures of **5a**. While the latter allows hydrogen bonding between the substituent and $^1O_2$, the origin of the selectivity in **5b** is intriguing. The calculated transition state structure for the bottom face attack suggests a possible mode of stabilisation. The oxygen atoms of the dienophile make fairly short contacts (2.9 Å) with the carbonyl carbon atoms of the symmetrically oriented ester groups [Fig. 1(*c*)]. The O···C=O angles of 91° support the possibility of a favorable interaction between the lone pairs on $^1O_2$ with the π* orbitals on the ester linkages. Similar long range attractive interactions have been recognised,[7] on the basis of several solid state structures, as key factors governing the nature of the reaction coordinate in nucleophilic additions to carbonyl groups. We now propose that such orbital interactions between the reagent and the remote substituent direct the approach of $^1O_2$. The attractive effects are not translated into any reaction at the substituent, but only result in the delivery of the reagent to the nearby diene face. Evidence for this model comes from calculations on a different conformation of the diester groups, with the acyl units pointing away from the diene. While the energy of the transition state for top face addition was virtually unaffected by the conformational change, in the case of the bottom face addition transition state, the ester groups were reorientated to attain the conformation shown in Fig. 1(*c*), implying the stabilizing interactions present in this structure.

In summary, a subtle change of functionality in **5** leads to remarkable variations in the face selectivities of $^1O_2$ additions. Our results indicate that direct through-space interactions between remote substituents and the approaching reagent *via* three distinct modes, *viz.* electrostatic, hydrogen bonding and stabilizing orbital interactions, need to be considered as additional stereoelectronic factors in determining face selectivity.

We thank Mr B. K. Dirghangi and Mr S. Mondal for solving an X-ray structure and DST for support of X-ray facilities at the University of Hyderabad and IACS, Calcutta.

Notes and References

† E-mail: jc@orgchem.iisc.ernet.in

‡ *Crystal data* for **6b**: $C_{19}H_{20}O_6$, M =_344.35, colourless crystals from CH_2Cl_2–hexane, triclinic, space group $P\bar{1}$, a = 8.381(1), b = 8.620(1), c = 12.508(3) Å, α = 87.52(1), β = 85.08(1), γ = 62.32(1)°, V = 797.3(2) Å^3, Z = 2, D_c = 1.434 Mg m^{-3}, T = 293 K, F(000) = 364, μ(Mo-Kα) = 0.107 mm^{-1}, crystal dimensions 0.14× 0.21× 0.16 mm. Data were collected on Enraf-Nonius MACH-3 diffractometer, graphite-monochromated Mo-Kα radiation (λ = 0.71073 Å), by the ω scan method in the range $2 \leqslant \theta \leqslant 25°$, 2804 unique reflections [R_{int} = 0.0], of which 2213 had $F_o > 4\sigma(F_o)$, were used in all calculations. At final convergence $R_1[I > 2\sigma(I)]$ = 0.0497, wR_2 = 0.1936 for 228 parameters, GOF = 1.334, $\Delta\rho_{max}$ = 0.403 e Å^{-3}, $\Delta\rho_{min}$ = -0.357 e Å^{-3}. The data were reduced using XTAL (ver. 3.4), solved by direct methods, refined by full-matrix least-squares on F^2 with the non-H atoms anisotropic, and H atoms isotropic (ref. 8).

For **7c**: $C_{17}H_{20}O_4$, M = 288.3, colourless crystals from CH_2Cl_2–hexane, monoclinic, space group $I2/a$, a = 26.035(8), b = 8.259(3) and c = 26.04(1) Å, β = 90.05(3)°, V = 5599(3) Å^3, Z = 16, D_c = 1.372 Mg m^{-3}, T = 296 K, F(000) = 2464, μ(Mo-Kα) = 0.097 mm^{-1}, crystal dimensions 0.25× 0.20× 0.45 mm. Data were collected on Siemens R3m/V diffractometer, graphite-monochromated Mo-Kα radiation (λ = 0.71073 Å), by the ω scan method in the range $3 \leqslant 2\theta \leqslant 42°$, 3077 unique reflections [R_{int} = 0.03], of which 1961 had $F > 4\sigma(F)$, were used in all calculations. At final convergence R_1 = 0.0564, wR_2 = 0.0588 for 309 parameters, GOF = 1.47, $\Delta\rho_{max}$ = 0.23 e Å^{-3}, $\Delta\rho_{min}$ = −0.22 e Å^{-3}. The structure was solved by direct methods, refined by full-matrix least-squares on F^2 with all non-hydrogen atoms anisotropic, except C4–C9, C17, C25–C30, C38 and H atoms, which were isotropic (ref. 9). CCDC 182/942.

1 J. B. Macaulay and A. G. Fallis, *J. Am. Chem. Soc.*, 1990, **112**, 1136; I. Okamoto, T. Ohwada and K. Shudo, *J. Org. Chem.*, 1996, **61**, 3155 and references cited therein.
2 W. D. Fessner, C. Grund and H. Prinzbach, *Tetrahedron Lett.*, 1991, **32**, 5935; G. Mehta, S. Padma, S. H. K. Reddy and M. Nethaji, *J. Chem. Soc., Perkin Trans. 1*, 1994, 2049.
3 J. M. Coxon, M. J. O'Connell and P. J. Steel, *J. Org. Chem.*, 1987, **52**, 4726; B. Pandey, U. R. Zope and N. R. Ayyangar, *Synth. Commun.*, 1989, **19**, 585; J. M. Coxon, R. G. A. R. Maclagan, D. Q. McDonald and P. J. Steel, *J. Org. Chem.*, 1991, **56**, 2542; J. M. Coxon, S. T. Fong, D. Q. McDonald and P. J. Steel, *Tetrahedron Lett.*, 1993, **34**, 163; J. M. Coxon, S. T. Fong, K. Lundie, D. Q. McDonald, P. J. Steel, A. P. Marchand, F. Zaragoza, U. R. Zope, D. Rajagopal, S. G. Bott, W. H. Watson and R. P. Kashyap, *Tetrahedron*, 1994, **50**, 13037; G. Mehta, R. Uma, A. Pramanik, J. Chandrasekhar and M. Nethaji, *J. Chem. Soc., Chem. Commun.*, 1995, 677; G. Mehta and R. Uma, *Tetrahedron Lett.*, 1995, **36**, 4873.
4 A. S. Kushner, *Tetrahedron Lett.*, 1971, **12**, 3275; G. Mehta, V. Singh and K. S. Rao, *Tetrahedron Lett.*, 1980, **21**, 1369.
5 All new compounds were fully characterized on the basis of spectral and analytical data.
6 J. J. P. Stewart, *J. Comput. Aided Mol. Des.*, 1990, **4**, 1.
7 H. B. Bürgi and J. D. Dunitz, *Acc. Chem. Res.*, 1983, **16**, 153.
8 G. M. Sheldrick, SHELX-97, University of Göttingen, Germany, 1997.
9 G. M. Sheldrick, SHELXTL PLUS, structure determination software program, Siemens Analytical X-Ray instruments Inc., Madison, WI, 1990.

Received in Cambridge, UK, 8th June 1998; 8/04313B

Facile α-β isomerisation of the σ-π phenylethenyl ligand at the diiron centre

Simon Doherty[a] and Graeme Hogarth*[b]†

[a] *Department of Chemistry, University of Newcastle, Bedson Building, Newcastle-upon-Tyne, UK NE1 7RU*
[b] *Department of Chemistry, University College London, 20 Gordon Street, London, UK WC1H 0AJ*

At 110 °C α-substituted $[Fe_2(CO)_6(\mu\text{-}PhC{=}CH_2)(\mu\text{-}PPh_2)]$ 1 is cleanly converted into the β-isomer $[Fe_2(CO)_6(\mu\text{-}HC{=}CHPh)(\mu\text{-}PPh_2)]$ 2, a process which is accelerated in the presence of arylphosphines; with $P(OMe)_3$ mono- and di-substituted adducts of 1 are isolated at 70 °C, which cleanly isomerise at higher temperatures.

The alkenyl ligand has been proposed as a key intermediate for the Fischer–Tropsch process[1] and as a result, the chemistry of this important ligand has been studied at a variety of metal centres, the emphasis of this work being based on carbon–carbon bond forming reactions.[2–4] Monosubstituted alkenyl complexes can adopt isomeric forms **I**–**III** with the substituent

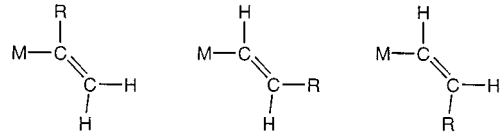

I II III

on either the α- or β-carbon. Interconversion of β-isomers II and III has been noted in a number of instances, and results from rotation about the carbon-carbon bond.[5,6] In contrast, as far as we are aware, and despite the large volume of literature concerning alkenyl complexes, α,β-isomerisation of alkenyl complexes has not been reported. Herein we describe the clean conversion of an α-substituted alkenyl ligand (**I**) to its β-isomer (**II**) at the diiron centre, a process which is accelerated in the presence of arylphosphines.

A convenient route to alkenyl complexes involves the hydrometalation of alkynes, primary alkynes giving both α- and β-substituted isomers depending upon the regioselectivity of the process. Hydrodimetalation of PhC≡CH by $[Fe_2(CO)_7(\mu\text{-}H)(\mu\text{-}PPh_2)]$ is reported to afford a mixture of α-$[Fe_2(CO)_6(\mu\text{-}PhC{=}CH_2)(\mu\text{-}PPh_2)]$ **1** and β-$[Fe_2(CO)_6(\mu\text{-}HC{=}CHPh)(\mu\text{-}PPh_2)]$ **2** substituted isomers in a 4:1 ratio.[7] In our hands, and provided that the temperature is not raised during work-up, the α-isomer **1** is the sole product as shown by ^1H NMR spectroscopy. However, when a toluene solution of **1** was heated at 110 °C for 1 h clean conversion to β-isomer **2** was noted, being isolated in >90% yield after chromatography. Conversion of **1** to **2** is easily followed by ^1H NMR spectroscopy. Under these conditions conversion was quantitative, the appearance of a low-field multiplet being characteristic of the α-proton of an alkenyl ligand. Following the reaction by NMR and IR spectroscopy failed to reveal any intermediates.

In the presence of arylphosphines, alkenyl isomerisation was accelerated. Heating a toluene solution of **1** and PPh_3 to 110 °C for 10 min lead to the quantitative formation of the β-substituted phosphine adduct $[Fe_2(CO)_5(PPh_3)(\mu\text{-}HC{=}CHPh)(\mu\text{-}PPh_2)]$ **3a**.‡ The ^1H NMR spectrum clearly showed that both carbonyl substitution and alkenyl isomerisation had occurred, the α-proton appearing at δ 8.35. Monitoring the reaction by ^{31}P NMR spectroscopy again failed to reveal any intermediates. The acceleration of alkenyl isomerisation was found for other phosphines, including P(*p*-tolyl)$_3$ and P(*m*-tolyl)$_3$ (Scheme 1). In contrast, addition of the more sterically demanding isomer

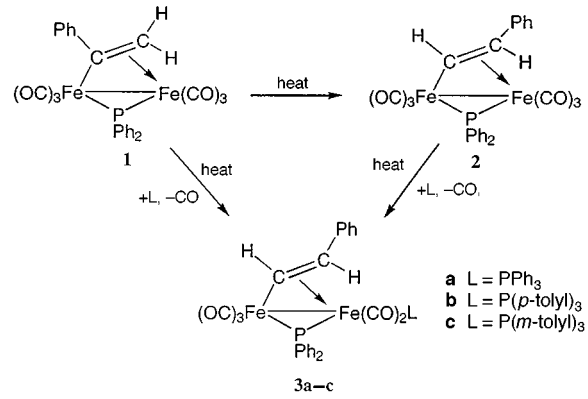

Scheme 1

P(*o*-tolyl)$_3$ did not result in accelerated isomerisation, **2** being the sole product, and suggesting that it is carbonyl substitution which accelerates alkenyl isomerisation.

Further insight was gleaned from the reaction of $P(OMe)_3$ with **1** (Scheme 2). This proceeded rapidly (10 min) at 70 °C and led to a mixture of $[Fe_2(CO)_5\{P(OMe)_3\}(\mu\text{-}PhC{=}CH_2)(\mu\text{-}PPh_2)]$ **4d** and $[Fe_2(CO)_4\{P(OMe)_3\}_2(\mu\text{-}PhC{=}CH_2)(\mu\text{-}PPh_2)]$ **4e**.‡ Pertinently, the α-substituted alkenyl ligand is maintained throughout. Warming both **4d** and **e** to reflux in toluene resulted in their rapid (< 10 min) conversion into the β-substituted isomers $[Fe_2(CO)_5\{P(OMe)_3\}(\mu\text{-}HC{=}CHPh)(\mu\text{-}PPh_2)]$ **3d** and $[Fe_2(CO)_4\{P(OMe)_3\}_2(\mu\text{-}HC{=}CHPh)(\mu\text{-}PPh_2)]$ **3e**, respectively, also obtained from the direct reaction of $P(OMe)_3$ with **2**, while reaction of the latter with PPh_3 afforded **3a** in a similar manner.

Conversion of **3** to **4** involves both carbonyl substitution and alkenyl isomerisation. For the arylphosphines utilised to date, carbonyl substitution is rate-determining, being followed by rapid alkenyl isomerisation. In contrast, with the less sterically demanding $P(OMe)_3$, carbonyl substitution is more facile and alkenyl isomerisation becomes rate-determining. While the

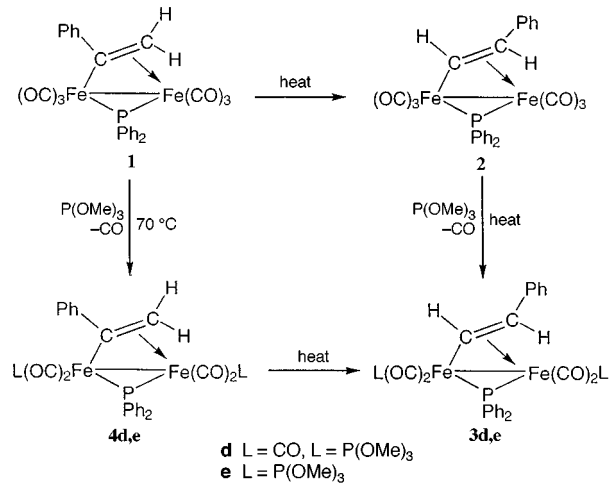

Scheme 2

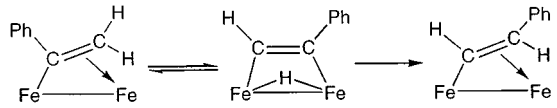

Scheme 3

origin of the rate acceleration of alkenyl isomerisation is not clear, since the β-phenylethenyl ligand is generated in all cases it must be thermodynamically preffered. It is difficult to see how this can be a result of steric effects in the hexacarbonyl complexes and we believe that their must be an electronic preference for the adoption of the β-isomer, while the hydrodimetalation reaction affords the α-isomer preferentially as a result of Markovnikov addition.

The precise manner in which alkenyl isomerisation occurs is as yet unknown. It may simply occur *via* a direct 1,2-proton shift, although it is difficult to see how the rate of such a process would be strongly affected by ligand substitution. A second possibility is that it results from a reversible C–H addition to the diiron centre (Scheme 3). Such a process would afford a hydrido–alkyne intermediate, with the alkyne lying parallel to the diiron vector and acting as a two-electron donor in order to preserve the EAN count of 34. Carbon-hydrogen bond formation from this intermediate would either regenerate the α-isomer or irreversibly afford the thermodynamically favoured β-isomer. Both oxidative addition and reductive elimination are likely to be sensitive to the steric and electronic nature of the other ligands, and this may account for the observed changes in the rate of alkenyl isomerisation.

We are currently investigating whether α–β alkenyl isomerisation is general by studying analogous reactions of other α-substituted complexes $[Fe_2(CO)_6(\mu\text{-}RC{=}CH_2)(\mu\text{-}PPh_2)]$. Further we are trying to gain more mechanistic insight into this transformation *via* reaction of **1** with a wider range of phosphines, phosphites and related reagents, while we are looking for alternative low-temperature routes to phosphine substituted α-alkenyl complexes in order to obtain kinetic information concerning the rate acceleration.

Notes and References

† E-mail: g.hogarth@ucl.ac.uk

‡ All compounds exhibit satisfactory spectroscopic and analytical data. *Selected data* for **3a**: ν(CO)(CH_2Cl_2)/cm^{-1} 2034m, 1983vs, 1947s, 1917m, 1884w; δ_H($CDCl_3$) 8.35 (dd, *J* 27.9, 12.9, 6.5, 1H, H_α), 7.9–6.4 (m, 30H, Ph), 4.12 (dd, *J* 12.9, 5.4, 1H, H_β); δ_P($CDCl_3$) 181.2 (d, *J* 93.4, μ-PPh_2), 73.0 (d, *J* 93.4, PPh_3). For **3b**: ν(CO)(CH_2Cl_2)/cm^{-1} 2030m, 1982vs, 1946s, 1917m, 1885w; δ_H($CDCl_3$) 8.35 (ddd, *J* 27.8, 12.9, 6.5, 1H, H_α), 7.8–7.0 (m, 25H, Ph), 6.62 (d, *J* 7.5, 2H, Ph), 4.13 (dd, *J* 12.9, 5.3, 1H, H_β), 2.36 (s, 9H, Me); δ_P($CDCl_3$) 180.6 (d, *J* 93.9, μ-PPh_2), 72.0 (d, *J* 93.9, PPh_3). For **3c**: ν(CO)(CH_2Cl_2)/cm^{-1} 2033m, 1982vs, 1970sh, 1949m, 1915m; δ_H($CDCl_3$) 8.31 (ddd, *J* 27.8, 12.9, 6.5, 1H, H_α), 7.8–7.0 (m, 25H, Ph), 6.58 (d, *J* 7.1, 2H, Ph), 4.08 (dd, *J* 12.8, 5.4, 1H, H_β), 2.37 (s, 9H, Me); δ_P($CDCl_3$) 180.6 (d, *J* 94.4, μ-PPh_2), 70.6 (d, *J* 94.4, PPh_3). For **3d** (two isomers A:B in 2:1 ratio): ν(CO)(CH_2Cl_2)/cm^{-1} 2035s, 1987vs, 1971m, 1958s; δ_H($CDCl_3$) 7.8–7.1 (m, Ph), 3.65 (d, *J* 11.2, Me, 9H, A), 3.60 (d, *J* 11.2, Me, 9H, B), 3.16 (d, *J* 15.2, 1H, B), 3.01 (dt, *J* 15.4, 3.3, 1H, A), 2.28 (dt, *J* 12.1, 3.3, 1H, A), 2.24 (d, *J* 10.5, 1H, B); δ_P($CDCl_3$, 213 K) 188.1 [d, *J* 52.7, P(OMe_3), B], 186.6 [d, *J* 70.2, P(OMe_3), A], 165.0 (d, *J* 70.2, PPh_2, A), 152.5 (d, *J* 52.7, PPh_2, B). For **3e**: ν(CO)(CH_2Cl_2)/cm^{-1} 1997vs, 1962s, 1932m; δ_H($CDCl_3$) 7.8–7.1 (m, 15H, Ph), 3.55 (d, *J* 11.2, 9H, Me), 3.51 (d, *J* 11.2, 9H, Me), 3.00 (d, *J* 16.1, 1H), 2.15 (d, *J* 10.8, 1H); δ_P($CDCl_3$, 213 K) 189.8 [d, *J* 47.0, P($OMe)_3$], 189.1 (d, *J* 71.6), 145.9 (br, PPh_2). For **4d**: ν(CO)(CH_2Cl_2)/cm^{-1} 2037s, 1989vs, 1976s, 1956s, 1928m; δ_H($CDCl_3$, 223K) 8.73 (ddd, *J* 31.8, 12.7, 8.1, 1H, H_α), 7.8–6.8 (m, 15H, Ph), 3.79 (d, *J* 11.1, 9H, Me), 3.73 (t, *J* 14.0, 1H, H_β); δ_P($CDCl_3$, 223 K) 182.6 [d, *J* 154.7, P($OMe)_3$], 177.7 (d, *J* 154.7, PPh_2). For **4e** (two isomers A:B in 6:1 ratio): ν(CO)(CH_2Cl_2)/cm^{-1} 1995s, 1963vs, 1930s, 1910m; δ_H($CDCl_3$, 223 K) 8.74 (ddd, *J* 30.2, 13.0, 8.1, 1H, H_α, A), 8.63 (br, 1H, H_α, B), 7.85–6.8 (m, Ph), 3.96 (br, 1H, H_β, B), 3.79 (d, *J* 11.2, 9H, A), 3.73 (d, *J* 11.2, 9H, Me, B), 3.50 (d, *J* 11.5, 1H, H_β, A), 3.32 (d, *J* 11.0, 9H, A), 3.28 (br, 9H, Me, B); δ_P($CDCl_3$, 223 K) 196.8 [d, *J* 45.5, μ-P($OMe)_3$, B], 188.6 [d, *J* 145.7, P($OMe)_3$, A], 181.0 [d, *J* 150.7, P($OMe)_3$, B], 180.3 [d, *J* 59.8 P($OMe)_3$, A], 165.4 (dd, *J* 145.7, 59.8, PPh_2, A), 159.0 (dd, *J* 150.7, 45.0, PPh_2, B).

1 P. M. Maitlis, H. C. Long, R. Quyoum, M. L. Turner and Z-Q. Wang, *Chem. Commun.*, 1996, 1.
2 S. A. R. Knox, *J. Cluster Sci*., 1992, **3**, 385; G. C. Bruce, B. Gagnus, S. E. Garner, S. A. R. Knox, A. G. Orpen and A. J. Phillips, *J. Chem. Soc., Chem. Commun.*, 1990, 1360.
3 J. M. Martinez, H. Adams, N. A. Bailey and P. M. Maitlis, *J. Chem. Soc., Chem. Commun.*, 1989, 286; J. Martinez, J. B. Gill, H. Adams, N. A. Bailey, I. M. Saez, G. J. Sunley and P. M. Maitlis, *J. Organomet. Chem.*, 1990, **394**, 583.
4 R. Yanez, J. Ros, X. Solans, M. Font-Altaba and R. Mathieu, *Organometallics*, 1990, **9**, 543; R. Yanez, J. Ros, F. Dahan and R. Mathieu, *Organometallics*, 1990, **9**, 2484.
5 P. O. Nubel and T. L. Brown, *J. Am. Chem. Soc.*, 1984, **106**, 644; P. O. Nubel and T. L. Brown, *J. Am. Chem. Soc.*, 1984, **106**, 3474.
6 D. L. Reger, E. Mintz and L. J. Lebioda, *J. Am. Chem. Soc*., 1986, **108**, 1940; R. H. Philip, Jr., D. L. Reger and A. M. Bond, *Organometallics*, 1989, **8**, 1714.
7 S. A. MacLaughlin, S. Doherty, N. J. Taylor and A. J. Carty, *Organometallics*, 1992, **11**, 4315.

Received in Cambridge, UK, 10th June 1998; 8/04403A

A stereoselective synthesis of a 2-functionalized-methyl-1β-methylcarbapenem key intermediate *via* decarboxylation

Woo-Baeg Choi, Jaemoon Lee, Joseph E. Lynch,*† R. P. Volante, Paul J. Reider and Robert A. Reamer

Process Research, Merck Research Laboratories, PO Box 2000, Rahway, NJ 07065, USA

An efficient synthesis of a key intermediate 2a for the synthesis of 2-functionalized methyl-1β-methylcarbapenem antibiotics 1 has been realized *via* a stereoselective decarboxylation reaction.

The emergence of multiple drug resistant bacteria and the alarming increase in the number of infections resulting from these organisms have clearly demonstrated an urgent need for new antimicrobial agents. Methicillin resistant *Staphylococcus aureus* (MRSA) is one of the more common of these infectious agents and in the early 1990s accounted for about 20% of the bacterial cultures isolated in hospitals.[1] MRSA remains a challenging target of antimicrobial research programs throughout the pharmaceutical industry. 2-Functionalized-methyl-1β-methylcarbapenem antibiotics **1** have drawn much attention due their potent activity against a variety of pathogens including MRSA.[2] However, the lack of an efficient synthesis of these carbapenems has hindered their development as clinical candidates. The 2-hydroxymethyl-1β-methyl ketone **2a** is a key intermediate in the synthesis of **1** and several syntheses of **2a** in variously protected forms have appeared in the literature.[2a,3]

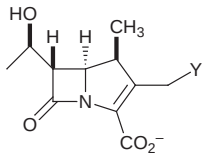

1

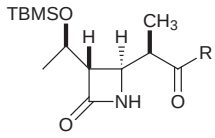

2a R = CH_2OH
b R = OH
c R = CH_2OBn
d R = OCH_3

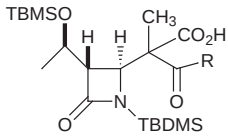

3a R = CH_2OH
b R = OH
c R = CH_2OBn
d R = OCH_3

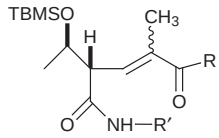

4a R = CH_2OBn, R′ = TBDMS
b R = OCH_3, R′ = TBDMS
c R = CH_2OBn, R′ = H

Some time ago, we (and others) reported that the malonic acid **3b** underwent a highly stereoselective decarboxylation/protonation to give the 1β-methyl carboxylic acid **2b**.[4a,b] We envisioned that the keto acid **3a** or **3c** should undergo a similar decarboxylation to give **2a** or **2c**, respectively.

After several unsuccessful attempts to generate the requisite β-keto acid **3a** *via* aqueous ester saponification, we adjusted our strategy to allow preparation of a β-keto acid in a nonpolar solvent *via* hydrogenolysis of a suitable benzyl ester. Benzyl 4-benzyloxy-2-methyl-3-oxobutyrate **5** was prepared by the Claisen condensation of benzyl propionate (2 equiv. + 2 equiv. LDA) and methyl *O*-benzylglycolate in 80% yield (Scheme 1). The acetoacetate **5** was then coupled with acetoxyazetidinone **6** (K_2CO_3 in DMF at 45 °C, 1 h) to give *ca*. 2:1 diastereomeric mixture **7** in 85–90% yield. *N*-silylation of **7** was carried out using TBDMSOTf and Et_3N in DMF to give **8** in quantitative yield. In our previous work on the malonic acid series we had

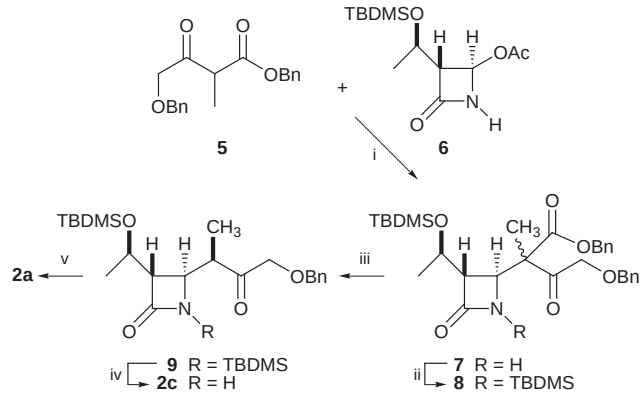

Scheme 1 *Reagents and conditions*: i, K_2CO_3, DMF, 45 °C, 1 h; ii, Et_3N, TBDMSOTf, DMF; iii, HCO_2H, EtOAc, 5% Pd/C, 30 psi H_2, room temp., 1 h; iv, Bu^n_4NF, CH_2Cl_2, 0 °C; v, 10% Pd/C, EtOH, 45 psi H_2

observed a remarkable diastereospecificity in the decarboxylation reaction.[4d] We found that only the (1*R*)-ester **3d** underwent decarboxylation to give **2d**. The (1*S*)-diastereomer underwent decarboxylation only under forcing conditions resulting in ring cleavage and giving **4b** as a major product. We were concerned that such diastereospecificity would be problematic with the 2:1 mixture of diastereomers **8**. We thus separated the two isomers of **8** (silica gel chromatography) and investigated the decarboxylation of each isomer individually. Each benzyl ester **8** was subjected to hydrogenolysis conditions (3 equiv. HCO_2H, 5% Pd/C, 30 psi, room temp., 1 h) in EtOAc. Surprisingly both isomers cleanly gave **9** as a single stereoisomer (> 99:1 β:α).[5] Encouraged by the individual results, the 2:1 mixture of **8** was subjected to hydrogenolysis/decarboxylation to give the desired β-methyl product **9** in 95% yield along with 3–4% of **4a**. *N*-desilylation of **9** was achieved using TBAF in CH_2Cl_2 at 0 °C giving **2c** in 85% yield.[6] Debenzylation of **2c** was accomplished under more vigorous hydrogenolysis conditions in EtOH (10% Pd/C, 45 psi H_2, 1 h) to give **2a** in 90% yield.[7,8]

Although the malonic acid series demonstrated a stereospecific decarboxylation,[4d] this was not an issue in the decarboxylation of **8** (*via* **3c**). This could be due to the greater stability of the enol intermediate and the corresponding lower transition state energy *vs.* the ketene acetal intermediate in the malonic acid series. The greater selectivity in the protonation step may be a result of the lower reaction temperature (20 °C for **2a** *vs.* 80 °C for **2b**) as well as the relative energetics of the two systems.

The Authors thank Dr Mark Greenlee for helpful suggestions during the preparation of this manuscript.

Notes and References

† E-mail: joe_lynch@merck.com

1 A. Tomasz, *New England J. Med.*, 1994, **330**, 1247; F. C. Tenover and J. M. Hughes, *JAMA*, 1996, **275**, 300.

2 (*a*) S. Schmitt, T. N. Salzmann, D. Shih and B. G. Christensen, *J. Antibiot.*, 1988, 780; (*b*) M. Imuta, H. Itani, H. Ona, T. Konoike, S. Uyeo, Y. Kimura, H. Miwa, S. Matsuura and T. Yoshida, *Chem. Pharm.*

Bull., 1991, **39**, 672; (*c*) A. J. Corraz, S. L. Dax, N. K. Dunlap, N. H. Georgopapadakou, D. D. Keith, D. L. Pruess, P. L. Rossman, R. Then, J. Unowsky and C.-C. Wei, *J. Med. Chem.*, 1992, **35**, 1828; (*d*) J. C. Arnould, R. N. Illingworth, W. W. Nichols and R. G. Wilson, *Bioorg. Med. Chem. Lett.*, 1996, **20**, 2449.

3 (*a*) M. Imuta, H. Itani, H. Ona; Y. Hamada, S. Uyeo and T. Yoshida, *Chem. Pharm. Bull.*, 1991, **39**, 663; (*b*) S. Uyeo and H. Itani, *Tetrahedron Lett.*, 1994, **35**, 4377; (*c*) X. E. Hu and T. P. Demuth, Jr., *J. Org. Chem.*, 1998, **63**, 1719.

4 (*a*) W.-B. Choi, H. R. O. Churchill, J. E. Lynch, A. S. Thompson, G. R. Humphrey, R. P. Volante; P. J. Reider and I. Shinkai, *Tetrahedron Lett.*, 1994, **35**, 2275; (*b*) T. Murayama, A. Yoshida, T. Kobayashi and T. Miura, *Tetrahedron Lett.*, 1994, **35**, 2271; (*c*) D. K. Jones, D. C. Liotta, W.-B. Choi, R. P. Volante, P. J. Reider, I. Shinkai, H. R. O. Churchill and J. E. Lynch, *J. Org. Chem.*, 1994, **59**, 3749; (*d*) W.-B. Choi, H. R. O. Churchill, J. E. Lynch, R. P. Volante, P. J. Reider, I. Shinkai, D. K. Jones and D. C. Liotta, *J. Org. Chem.*, 1995, **60**, 8367.

5 The crude product was filtered through Celite, washed with aq. Na_2CO_3 and analyzed by ^{1}H NMR spectroscopy. The major isomer of **8** cleanly gave a >99:1 β:α mixture of **9**, while the minor isomer of **8** gave the same 99:1 β:α mixture of **9** along with 7–10% ring opened by-product **4a**.

6 During the desilylation, 7–10% of **4c** was formed.

7 The C-1 configuration was determined by conversion of **2a** to the known acetate [ref. 3(*a*)]. The spectroscopic data of the acetate were found to be identical to those reported.

8 *Selected data* for **2a**: $\delta_H(CDCl_3)$ 6.43 (br s, 1 H), 4.38 (d, *J* 19.4, 1 H), 4.25 (d, *J* 19.4, 1 H), 4.15 (m, 1 H), 3.85 (dd, *J* 1.9, 5.0, 1 H), 3.25 (br s, 1 H), 2.93 (dd, *J* 1.9, 4.6, 1 H), 2.84 (1 H, m), 1.19 (d, *J* 7.0, 3 H), 1.16 (d, *J* 6.3, 3 H), 0.85 (s, 9 H), 0.06 (s, 3 H), 0.04 (s, 3 H); $\delta_C(CDCl_3)$ 211.8, 168.5, 67.9, 65.3, 61.8, 51.4, 44.7, 25.8, 22.6, 17.9, 12.4, −4.3, −4.9.

Received in Corvallis, OR, USA, 1st June 1998; 8/04125C

Circular dichroism and absolute conformation of Δ⁴-uronate derivatives: a semi-empirical rule for inherent chiral α-alkoxy acrylates

Iontcho R. Vlahov,[a] Hélène G. Bazin[b] and Robert J. Linhardt*[b]†

[a] *Baker Norton Pharmaceuticals, Inc., 4400 Biscayne Boulevard, Miami, Florida 33137, USA*
[b] *Division of Medicinal and Natural Products Chemistry and Department of Chemical and Biochemical Engineering, University of Iowa, Iowa City, Iowa 52242, USA*

The theoretical basis for using CD spectroscopy to predict the conformation of Δ⁴-uronates is reported.

As part of ongoing research into the chemistry of glycosaminoglycans, our laboratory has been exploring the use of Δ⁴-uronate derivatives as building blocks for the synthesis of heparin. Circular dichroism (CD) spectroscopy was used to study the conformation of these Δ⁴-uronate derivatives in an effort to better understand differences in their reactivity.[1]

Qualitative molecular orbital (MO) theory, frequently used to explain molecular properties (*e.g.* geometry,[2] photoelectron spectra[3] or reactivity[4]) can also help in better understanding CD spectra. Rotational strength (*R*),[5] a substance property, can be defined as the area under a CD band multiplied by a factor [eqn. (1)].

$$R = 0.229 \times 10^{-38} \int (\Delta\varepsilon/\lambda \mathrm{d}\lambda \qquad (1)$$

R is theoretically given by the scalar product of the electronic (μ) and the magnetic (*m*) transition moments for the absorption observed [eqn. (2)].

$$R = \mu m = |\mu|\ |m| \cos\beta \qquad (2)$$

When light is absorbed by the electron cloud of a molecule, electron charge can be shifted in the direction of the electric field vector of the light wave, and it may also be rotated. This first phenomenon corresponds to μ, the latter to *m*. The values of μ and *m* can be determined by identifying the molecular orbitals (MOs) at which the electron excitation mainly occurs. From the cosine term of eqn. (2) it follows that the CD is positive if the angle between μ and *m* is acute ($0 < \beta < 90°$), and negative if the angle is obtuse ($90 < \beta < 180°$). In limited cases the vectors μ and *m* are prependicular to each other, so the scalar product is zero ($\cos 90 = 0$) and the Cotton effect vanishes.

Qualitatively μ and *m* can be determined by multiplying together the two MOs between which the transition occurs (Snatzke MO recipe).[6] The absolute directions of μ and *m* depend on the arbitrary choice of the orbital phases and have no physical meaning.[7] However, their relative orientation determines the sign of the CD. This single CD argument only gives information about the absolute conformation of a molecule (*i.e.* the sign of a torsion angle around a bond) and not about the absolute configuration. A second method is required to correlate the absolute conformation with the determined absolute configuration.

The Δ⁴-uronate derivatives as shown in Fig. 1(*a*) are formally α-alkoxy acrylates. Their C=C–O moiety is locked into the chiral conformation of the dihydropyran ring, making this chromophore inherently chiral[8] [Fig. 1(*b*)]. We propose a semi-empirical rule for predicting the absolute conformation of cyclic α-alkoxy acrylates based on the sign of the Cotton effect. Snatzke has already suggested such a semi-empirical rule for chiral dihydropyrans incorporating an enol ether chromophore, present, for example, in glycals and in many iridoids.[6,7,9]

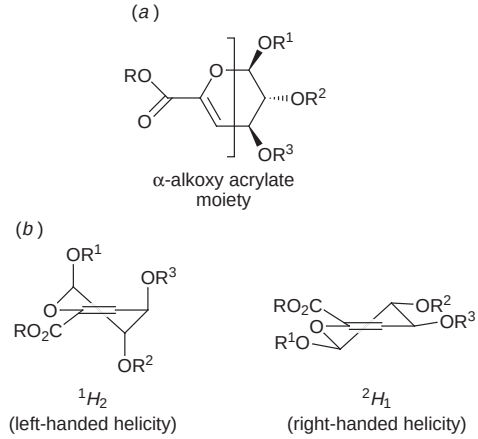

Fig. 1 The structure of (*a*) the α-alkoxyacrylate moiety in Δ⁴-uronate derivatives and (*b*) the half-chair conformers of the Δ⁴-uronate derivatives

The CD spectra of the Δ⁴-uronates (Fig. 2) show a Cotton effect around 235–240 nm. This band is negative for the compounds **1**–**5**, and positive for compounds **6** and **7**. Since this

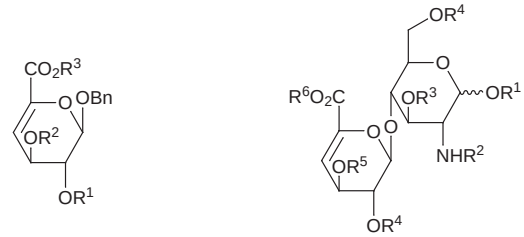

1 $R^1 = R^2 = H$, $R^3 = Me$
2 $R^1 = R^2 = Piv$, $R^3 = Me$
3 $R^1 = R^2 = R^3 = Bn$
4 $R^1 = R^2 = TBDMS$, $R^3 = Me$
5 R^1–$R^2 = (Pr^i_2Si)O(Pr^i_2Si)$
6 $R^1 = R^3 = R^5 = R^6 = H$, $R^2 = R^4 = SO_3H$
7 $R^1 = R^3 = R^4 = R^5 = R^6 = H$, $R^2 = Ac$

CD band corresponds to a strong UV absorption, it must come from a $\pi \rightarrow \pi^*$ transition and not from a forbidden $n \rightarrow \pi^*$ transition. Application of the Snatzke MO recipe to such an α-alkoxy acrylate chromophore is shown in Fig. 3. Here the relevant MOs approximate the two possible HOMOs and the LUMO of the isoelectronic 2,3-dimethylbutadiene dianion, although the LCAO coefficients are not identical. The terminal AOs are twisted to reflect the chirality (left-handed twist chosen). The formal multiplications $\pi_a\pi^*$ and $\pi_b\pi^*$ reveal the generation of an electronic transition moment μ. For the $\pi_a \rightarrow \pi^*$ transition, μ is localized nearly exclusively in the achiral part of the chromophore, so this excitation cannot correspond to the strong Cotton effect measured. The latter must then come from the $\pi_b \rightarrow \pi^*$ transition. The translation of charge during the $\pi_b \rightarrow \pi^*$ excitation generates μ. Part of the charge is transferred

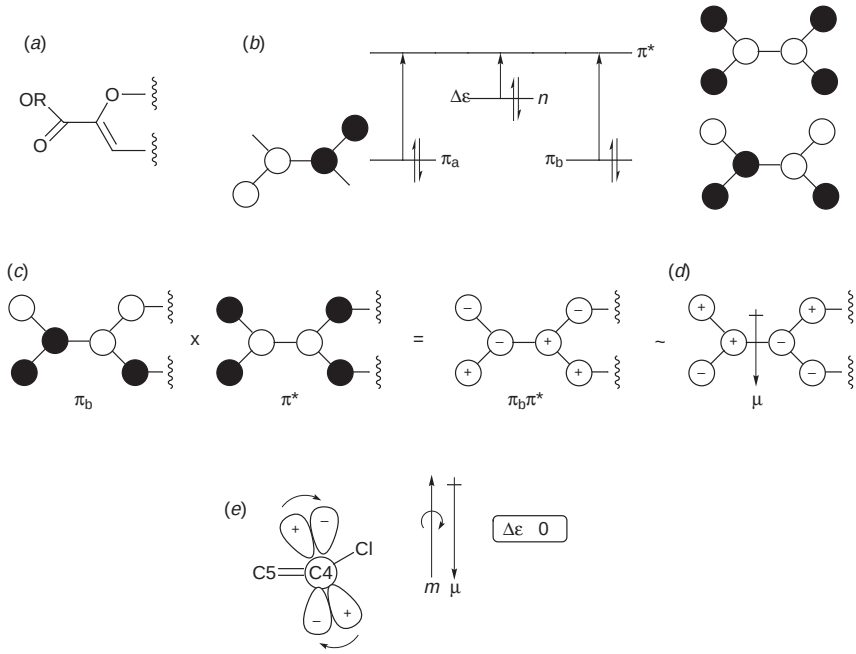

Fig. 3 Application of Snatzke MO formalism to Δ^4-uronates: (*a*) chiral α-alkoxy acrylate chromophore (absolute conformation of the dehydropyran ring is chosen as $^1H_2$; (*b*) relevant MOs of the isoelectronic 2,3-dimethylbutadiene dianion; (*c*) formal multiplication of π_b and π^* giving the electron density; (*d*) charge translation and μ; (*e*) concomitant charge rotation and *m*

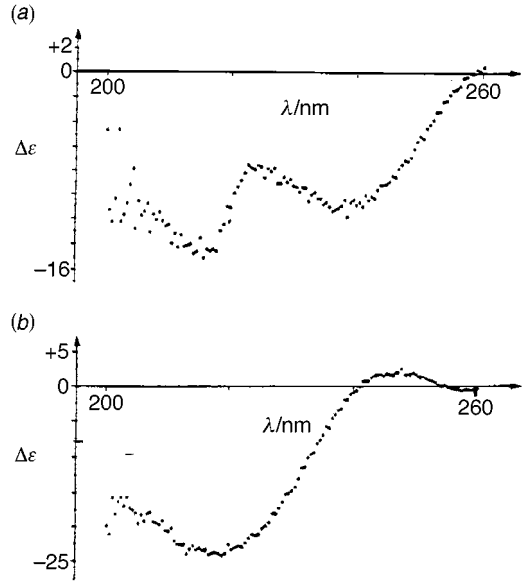

Fig. 2 Superposition of CD curves with (*a*) negative (**1**–**5**) and (*b*) positive Cotton effects (**6** and **7**). These compounds show a single absorption peak at 235–240 nm.

within the dihydropyran ring and this is done for the absolute conformation $^1H_2$ chosen on a left-handed helical path. Such rotation of charge along the line connecting C4–O_{ring} generates *m* which, by the right-hand rule, is oriented antiparallel to μ. The resulting Cotton effect is, therefore, negative and the absolute conformation of the dihydropyran ring in compounds **1**–**5** is $^1H_2$.

For compounds **6** and **7** (a positive Cotton effect measured) the charge is transferred on a right-handed helical trajectory, thus predicting a $^2H_1$ absolute conformation for their ring systems.

The ^{1}H NMR data for the compounds are in full agreement with the prediction of their absolute conformation concluded from this new semi-empirical rule. CD spectroscopy provides the absolute conformation, information that is simply not obtainable using NMR analysis.

We thank Professors Dan Quinn and Lei Geng for their helpful suggestions and the National Institutes of Health (GM38060) for supporting this research.

Notes and References

† E-mail: robert-linhardt@uiowa.edu

1 H. G. Bazin, I. Capila and R. J. Linhardt, *Carbohydr. Res.*, 1998, in the press.
2 B. M. Gimarc, *Acc. Chem. Res.*, 1974, **7**, 384.
3 H. Bock, *Angew. Chem.*, 1977, **89**, 631.
4 R. B. Woodward and R. Hoffmann, *The Conservation of Orbital Symmetry*, 1970, Verlag Chemie, Academic Press, Weinheim.
5 F. Ciardelli and P. Salvadori, *Fundamental Aspects and Recent Developments in ORD and CD*, Heyden, London, 1973; M. Legrand and M. Rougier, in *Stereochemistry, Fundamentals and Methods*, ed. H. Kagan, Thieme, Stuttgart, 1977, vol. 2, p. 33.
6 G. Snatzke, *Angew. Chem., Int. Ed. Engl.*, 1979, **18**, 363.
7 G. Snatzke and H. Kagan, *Pure Appl. Chem.*, 1979, **51**, 769.
8 A. Moscowitz, *Tetrahedron*, 1961, **13**, 48; A. Moscowitz, K. Mislow, A. Glass and C. Djerassi, *J. Am. Chem. Soc.*, 1961, **84**, 1945.
9 A. Konoval, G. Snatzke and P. Thies, *Tetrahedron*, 1978, **34**, 253.

Received in Cambridge, UK, 27th April 1998; 8/03108H

Molecular recognition using β-cyclodextrin-modified dendrimers: novel building blocks for convergent self-assembly

George R. Newkome,*† Luis A. Godínez, and Charles N. Moorefield

Center for Molecular Design and Recognition, University of South Florida, Tampa, FL, 33620, USA

The synthesis of β-cyclodextrin-based dendrimers 3 and 5 is described; using phenolphthalein as a UV–VIS active probe, it is shown that the binding cavities of these modified receptors retain their molecular recognition properties and can be employed as polyfunctional monomers in self-assembly.

Cyclodextrins (CDs) constitute a popular family of cyclic oligosaccharides whose molecular structures resemble truncated cones.[1] These polyhydroxylated materials have been the subject of numerous investigations in the area of molecular recognition due to their combined solubility in aqueous media and their ability to embrace a wide variety of molecular guests in a well-defined cavity.[2] Also, the *n* primary hydroxy groups at the narrow side of the receptor's cavity exhibit greater reactivity with sterically demanding electrophiles than the *2n* secondary OH groups on the wider, bottom side of the molecule.[1] Therefore, using the appropriate reagents, CDs can be selectively modified to incorporate specific functional groups on the narrow side of the receptor's hydrophobic cavity. Many researchers have capitalized on this property and have subsequently reported the synthesis of modified CDs that have been successfully used as catalysts,[3] receptors for nucleotides[4] and ions,[5] molecular tube precursors,[6] modified electrodes[7] and chemical sensors,[8] to mention but a few applications.[9] Recently, a single CD has been attached to a dendritic surface and investigated with respect to ester hydrolysis activity.[10] β-CDs have also been coordinated to ferrocenyl-terminated dendrimers to study redox characteristics.[11]

As a complementary part of our research program, we are exploring the use of non-covalent interactions and molecular recognition concepts[12] to promote the ordered self-assembly of dendritic structures. These concepts have been eloquently employed by Zimmerman and co-workers.[13]

We herein report the synthesis of two water-soluble dendritic β-CD monomers that retain their molecular recognition properties. These materials therefore belong to a new family of modified receptors that can be envisioned as synthons for convergent, molecular recognition-based assembly of more complex structures and, ultimately, dendritic networks.

Recently, we reported the synthesis of isocyanate[14] **1** and its use in the synthesis of combinatorial-based dendrimers.[15] Attempted treatment of β-CD with triester **1**, under different reaction conditions, afforded no addition products, presumably due to combined steric hinderance. To circumvent this inertness, we prepared 6-heptaamino-β-CD heptahydrochloride[16] **3**‡ (Scheme 1) since isocyanate **1** was known to react with amines under mild conditions.[14] Thus, treatment of heptaamine **3** with 7 equiv. of isocyanate **1** (Pr^i_2EtN, DMF, 25 °C, 5 h) afforded (85%) the first tier polyester dendritic CD monomer. Formic acid hydrolysis (12 h) and dialysis afforded (40%) the polycarboxylic acid **4**, as supported by the ^{13}C NMR spectral data [$\delta(D_2O)$ 158.9 (NH*C*ONH), 178.0 (CO_2).

Construction of the second tier was accomplished by treatment of **4** with 21 equiv. of Behera's amine[17] **2** [DCC, HOBT, DMF–DMSO, 2 d, 25 °C]. Formic acid hydrolysis subsequently afforded (25%) the desired dendritic CD polyacid

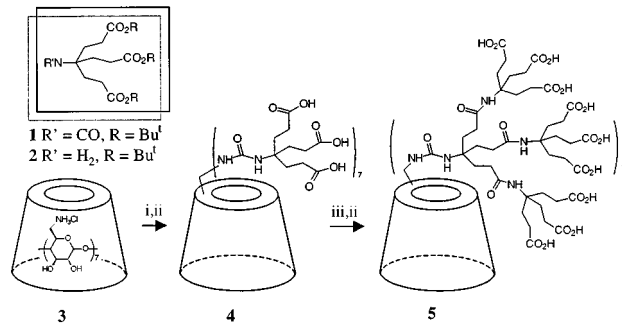

Scheme 1 *Reagents and conditions*: i, **1** (7 equiv.), base, DMF; ii, HCO_2H; iii, **4** (21 equiv.), DCC, HOBT, DMF–DMSO

5, whose spectral data supported the conversion [$\delta(D_2O)$158.6 (NH*C*ONH), 179.6 (CO_2).

An important requirement for the synthesis of 'dendrimerized' CDs, that are to be subsequently used as monomers of more complex structures, is that the complexation site, *i.e.* the hydrophobic cavity of the receptor, must remain basically unchanged. In order to verify that CDs **4** and **5** had retained the critical binding locus, displacement experiments, exploiting the well-known association properties of β-CD, were performed.

In moderately basic aqueous medium, phenolphthalein solutions are characterized by a deep purple color that essentially turns colorless upon addition of β-CD.[2b] This dramatic decrease in the UV absorption of the indicator is not

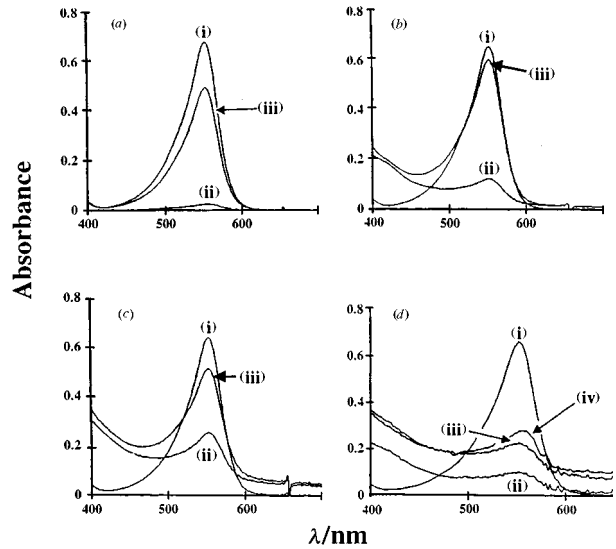

Fig. 1 The effect of CD addition to a 30 μM solution of phenolphthalein pH 10.5 buffer solution (I = 0.6) on the UV spectra for (*a*) β-CD, (*b*) **4** and (*c*) **5**: (i) dye only, (ii) dye and CD (2 mM) and (iii) dye, CD and adamantan-2-amine hydrochloride (5 mM). (*d*) UV spectra of (i) dye, (ii) dye and **4**, (iii) dye, **4** and the bis(adamantane ester) of tetraethylene glycol and (iv) dye, **4**, bis(adamantane ester)and 18-crown-6.

due to a change on the protonation state of the molecule but rather to a specific host–guest inclusion interaction involving hydrogen-bonding, van der Waals forces, and the hydrophobic effect.[18] Complexation of the indicator by inclusion into the β-CD hydrophobic cavity can be thus conveniently followed by UV–VIS spectroscopy. It can be seen in Fig. 1, by comparing spectra (*a*)(i) and (*a*)(ii), that the absorbance at λ = 552 nm of a 30 μM solution of phenolphthalein in a pH 10.5 buffer solution[19] drops dramatically upon the addition of 60 equiv. of β-CD. Consistent with the complexation properties of the unmodified β-CD, spectra (*b*), (*c*) and (*d*) showed similar changes in the absorbance of basic phenolphthalein solutions [spectra (i)] after addition of either CDs **4** or **5** [spectra (iii)]. This decrease in the absorbance of phenolphthalein in the presence of the modified receptors suggests that the indicator is either included in the hydrophobic cavity of the CD or interacting in a similar way with the hyperbranched structure of either **4** or **5**. To rule out the later possibility, we added non-UV-active adamantane derivatives which are known[20] to bind very strongly to β-CD molecules by forming 1:1 inclusion complexes with stability constants on the order of 10^4 M^{-1}.

As observed in Scheme 2, the addition and subsequent inclusion of an adamantane in the CD cavity should promote, if in fact the phenolphthalein is included in the CD cavity, the displacement of the indicator into the bulk of the basic aqueous medium. As a consequence, the solution should become purple

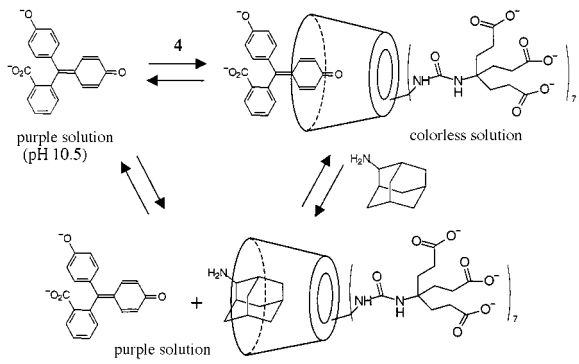

Scheme 2

and the absorbance at λ = 552 nm should increase. Figs. 1(a)(iii), (b)(iii) and (c)(iii), indicate that addition of 2.5 mol of 2-adamantanamine hydrochloride per mol of CD increases the absorption of light of the three aqueous solutions; therefore, as with simple β-CD, the dendritic CDs **4** and **5** retain their binding sites and can incorporate, on the basis of molecular recognition, hydrophobic guests in basic aqueous media. Reappearance of the solution color and absorbance observed in Fig. 1(*d*)(iii), while not as dramatic, was promoted by the addition (0.5 equiv.) of a bis(adamantane ester) of tetraethylene glycol (prepared by the addition of 2 equiv. of adamantanecarbonyl chloride to tetraethylene glycol in the presence of Et_3N). The smaller shift in equilibrium [as compared to Figs. 1(*a*)–(*c*)] to uncomplexed dye in the bulk solution was postulated to arise, at least in part, from Na^+ binding of the polyethylene glycol chain promoting a compact, non-linear structure and thus inhibiting chain elongation and bis-dendrimer assembly. Saturating the solution with 18-crown-6 [Fig. 1(*d*)(iv)] supports this conjecture by further slightly shifting the equilibrium toward displaced absorbing dye and increasing the concentration of the bis-complex (Scheme 3). Another explanation for diminished absorption using the bis(adamantane) could center on other aggregation phenomena as suggested by a heightened spectral baseline. For all cases the percent displacement of dye *via* the addition of adamantane was determined: Fig. 1(*a*), 71.5%; 1(*b*), 89.5%; 1(*c*), 69.5%; 1(*d*), 23%; 1(*d*) with 18-crown-6, 33%.

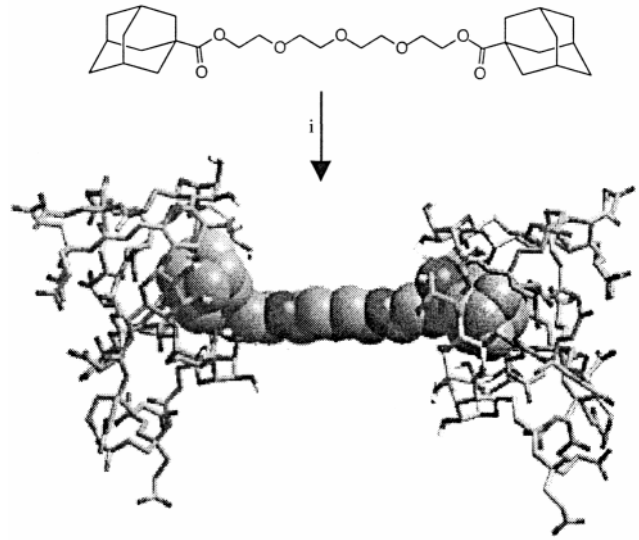

Scheme 3 *Reagents and conditions*: i, **4**, aq. NaOH–$NaHCO_3$ buffer (I = 0.6) (ref. 19).

The National Science Foundation (DMR-96-22609) is gratefully acknowledged for partial financial support of this work.

Notes and References

† E-mail: gnewkome@research.usf.edu

‡ All new compounds exhibited satisfactory spectral and elemental analysis.

1 G. Wenz, *Angew. Chem., Int. Ed. Engl.*, 1994, **33**, 803.
2 (*a*) M. L. Bender and M. Komiyama, *Cyclodextrin Chemistry*, Springer, Berlin, 1978; (*b*) J. Szejtli, *Cyclodextrins and their Inclusion Complexes*, Akadémiai Kiadó, Budapest, 1982.
3 M. T. Reetz and S. R. Waldvogel, *Angew. Chem., Int. Ed. Engl.*, 1997, **36**, 865.
4 A. V. Eliseev and H. J. Schneider, *J. Am. Chem. Soc.*, 1994, **116**, 6081.
5 L. A. Godínez, J. Lin, M. Muñoz, A. W. Coleman and A. E. Kaifer, *Electroanalysis*, 1996, **8**, 1072.
6 A. Harada, J. Li and M. Kamachi, *Nature*, 1993, **364**, 516.
7 M. T. Rojas, R. Königer, J. F. Stoddart and A. E. Kaifer, *J. Am. Chem. Soc.*, 1995, **117**, 336; C. Henke, C. Steinem, A. Janshoff, G. Steffan, H. Luftmann, M. Sieber and H. J. Galla, *Anal. Chem.*, 1996, **68**, 3158.
8 R. Corradini, A. Dossena, G. Galaverna, R. Marchelli, A. Panagia and G. Sartor, *J. Org. Chem.*, 1997, **62**, 6283.
9 H. Asanuma, M. Kakazu, M. Shibata, T. Hishiya and M. Komiyama, *Chem. Commun.*, 1997, 1971.
10 J. Suh, S. S. Hah, and S. H. Lee, *Bioorg. Chem.* 1997, **25**, 63.
11 R. Castro, I. Cusdrado, B. Alonso, C. M. Casado, M. Morán and A. E. Kaifer, *J. Am. Chem. Soc.*, 1997, **119**, 5760.
12 G. R. Newkome, B. D. Woosley, E. He, C. N. Moorefield, R. Güther, G. R. Baker, J. Merrill, G. H. Escamilla and H. Luftmann, *Chem. Commun.* 1996, 2737.
13 F. Zeng and S. C. Zimmerman, *Chem. Rev.*, 1997, **97**, 1681.
14 G. R. Newkome, C. D. Weis, C. N. Moorefield and F. R. Fronczek, *Tetrahedron Lett.*, 1997, **38**, 7053; G. R. Newkome and C. D. Weis, *US Pat.*, 5,703,271 (Dec. 30, 1997).
15 G. R. Newkome, C. D. Weis, C. N. Moorefield, G. R. Baker, B. J. Childs and J. Epperson, *Angew. Chem., Int. Ed. Engl.*, 1998, **37**, 307; *Angew. Chem.*, 1998, **110**, 318.
16 Syntheses of the peraminated CD derivative **3** was accomplished *via* the following procedure: J. Boger, R. J. Corcoran and J.-M. Lehn, *Helv. Chim. Acta*, 1978, **61**, 2190.
17 G. R. Newkome and C. D. Weis, *Org. Prep. Proced. Int.*, 1996, **28**, 485.
18 Á. Buvári and L. Barcza *J. Chem. Soc., Perkin Trans. 2*, 1988, 1687.
19 (HCO_3^-/CO_3^{2-}, I = 0.6). Prepared according to *CRC Handbook of Chemistry and Physics*, 72nd edn., ed. D. R. Lide, CRC Press, Boca Raton, 1991.
20 L. A. Godínez, L. Schwartz, C. M. Criss and A. E. Kaifer, *J. Phys. Chem. B*, 1997, **101**, 3376.

Received in Corvallis, OR, USA, 11th May 1998; 8/03536I

An efficient preparation of ditopic receptors based on polyaza[*n*]paracyclophanes

M. Isabel Burguete,[a] Enrique García-España,*[b] Santiago V. Luis,*[a]† Juan F. Miravet,[a] Lorena Payá,[a] Manuel Querol[a] and Conxa Soriano[b]

[a] *Department of Inorganic and Organic Chemistry, ESTCE, University Jaume I, E-12080 Castellón, Spain*
[b] *Departaments of Inorganic and Organic Chemistry, University of Valencia, c/ Doctor Moliner 50, E-46100, Burjassot, (Valencia), Spain*

Coordination patterns of tetraaza[*n*]paracyclophanes allow for the selective protection of three out of the four nitrogen atoms *via* the use of simple Zn^{2+} salts; accordingly, a simple method for the preparation of ditopic receptors based on polyaza[*n*]paracyclophanes has been devised.

Ditopic polyaza receptors containing two macrocyclic subunits have become a very important synthetic target, in particular since the discovery of the anti-HIV activity associated to some of those systems.[1] Accordingly, a number of different synthetic strategies have been put forward in recent years to achieve this goal. In this way, several families of receptors having the general structure **1** have been recently prepared.[2]

One of the most general synthetic routes for the preparation of this class of compounds is based on the selective protection of the nitrogen atoms in such a way as to leave only one unprotected, reactive nitrogen atom in the macrocycle.[2,3] This intermediate is then reacted with a dihalide to afford, after N-deprotection, the expected ditopic receptor (Scheme 1). As a matter of fact, preparation of ditopic receptors has been one of the central motifs for the development of synthetic strategies for the selective N-functionalization of polyazamacrocycles.

Polyaza[*n*]paracyclophanes **2** represent a very interesting kind of polyaza macrocyclic receptors.[4] One of their most remarkable ligational features is the fact that the presence of the aromatic spacer precludes the simultaneous involvement of all the nitrogen atoms in the coordination to a metal centre (see structure **3**). Thus, for instance, 2,6,9,13-tetraaza[14]paracyclophane **2a** coordinates M^{2+} ions with just three out of its four nitrogen atoms. One of the benzylic nitrogen atoms remains non-coordinated, thus being able to act as a base or as a nucleophile. This property has allowed the development of a simple and novel procedure for selective mono- and di-functionalization of this kind of macrocycle with a variety of reactive alkyl halides, according to the general scheme shown in Scheme 2, to give compounds **4** and **5**.[5] In this way, the otherwise experimentally difficult selective protection of three of the nitrogen atoms can be easily achieved *via* the use of simple metal ions, like Zn^{2+}, without the need of more elaborate reagents or synthetic routes.

This synthetic approach can be further extended to the preparation of ditopic bis-macrocyclic receptors **8** based on

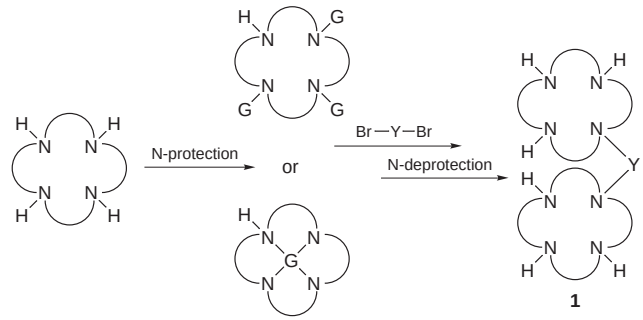

Scheme 1

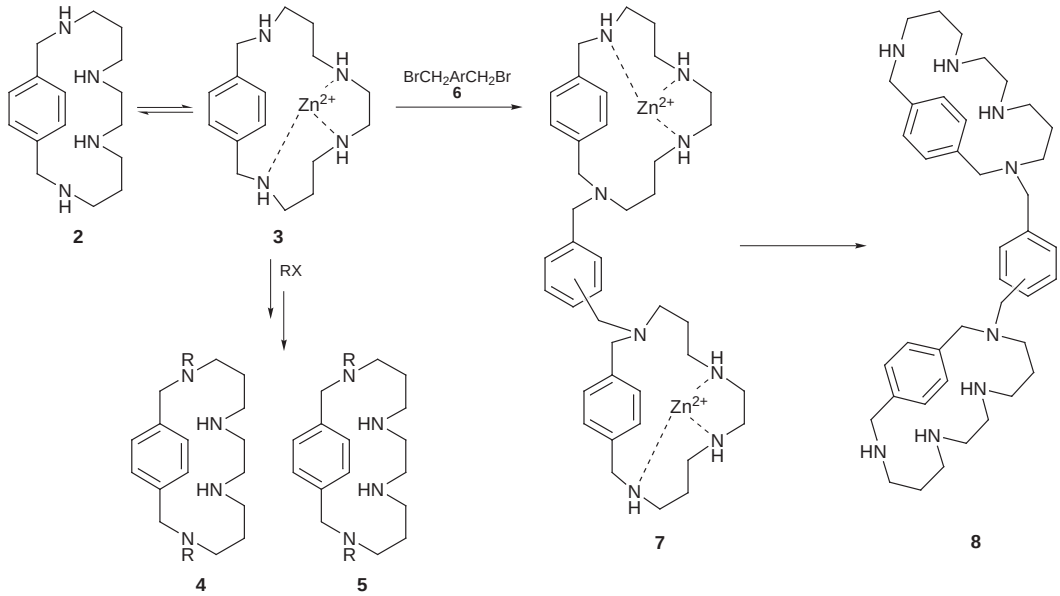

Scheme 2

Table 1 Results obtained in the preparation of ditopic receptors **8** derived from tetraaza[*n*]paracyclophanes

Starting macrocycle[a]	Alkylating agent[b]	Polyamine:base ratio	*t*/days	Yield[c] (%)
2a	**6a**	1:1	1	30
2a	**6a**	1:1	3	37
2a·4HBr	**6a**	1:5	3	40
2a·4HBr	**6a**	1:7	3	87
2b	**6a**	1:7	3	24
2b·4HBr	**6a**	1:7	3	75
2a·4HBr	**6b**	1:7	3	78
2a·4HBr	**6b**	1:7	5	78
2b·4HBr	**6b**	1:7	3	59
2b·4HBr	**6b**	1:7	5	60
2a·4HBr	**6c**	1:7	3–5	< 10[d]
2b·4HBr	**6c**	1:7	3–5	< 10[d]

[a] Compound **2a** (B323): 2,6,9,13-tetraaza[14]paracyclophane; Compound **2b** (D323): 2,6,9,13,tetraaza-16,17,19,20-tetramethyl[14]paracyclophane. [b] Compound **6a**: 1,4-bis(bromomethyl)benzene; Compound **6b**: 1,3-bis(bromomethyl)benzene; Compound **6c**: 1,2-bis(bromomethyl)benzene. [c] Product obtained after chromatographic purification. [d] Estimated from the crude product after the reaction.

polyaza[*n*]paracyclophanes when a bis(halomethyl)benzene is used as the alkylating agent (Scheme 2).

The low coordination of the metal centre in the complexes formed by polyaza[*n*]paracyclophanes **2** has been shown to provide mechanisms for the participation of the coordinated cation in biomimetic catalytic proceses.[4] In this sense, the preparation of ditopic receptors **8** represents an interesting synthetic target.

Results obtained for different macrocycles and aromatic spacers are summarised in Table 1. Careful control of the reaction conditions is required. We used the cyclic polyamines as free bases or as their hydrobromides, and different ratios of macrocycle/base were tested in the range of *ca.* 1 to 10. Best results were obtained when an excess (*ca.* 7:1) of base (anhydrous K_2CO_3) is used and the polyamine is introduced as its hydrobromide. The use of 1,4-bis(halomethyl)arenes gives better yields than the 1,3-substituted analogues. The expected products could not be obtained for 1,2-bis(halomethyl)arenes.‡

The nature of the aliphatic chains between the nitrogen atoms is also very important. Good results were only obtained when propylenic sub-units are present and the expected ditopic receptors could not be prepared starting from cyclophanes containing only ethylenic spacers. This can be related with the different coordination patterns of the macrocycles used.[5b] In this context it is worth mentioning that tetraazacyclophanes containing only ethylenic sub-units have been shown to be able to form dinuclear Cu^{2+} complexes in which all four nitrogen atoms are coordinated.[4b]

Preliminary analyses of the acid-base and coordination tendencies of these compounds have shown some interesting trends. Protonation constants obtained from pH titrations show that in the pH range 2–11 all ligands can take up to seven protons, the eighth protonation not being generally detected under our experimental conditions. At neutral pH values the main species for all ligands are the tetraprotonated ones.§ The high positive charge achieved by these ligands at neutral pH allows us to consider them as potential receptors for anionic species. Thus, for instance, compound **8b** (obtained from **2b** and **6a**) strongly interacts with the barbituric acid derivative 1*H*,3*H*-pyrimidine-2,4,5,6-tetrone 5-oxime (violuric acid) **9** with complexation percentages around 90–100% in a wide pH range (pH < 8).[6]¶

On the other hand, when the interaction with metal cations is considered, compounds **8** revealed the possibility of forming

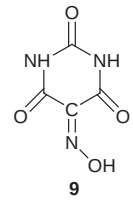

9

mono- as well as di-nuclear complexes. Thus, for instance, **8d** (obtained from **2b** and **6b**) in the presence of Cu^{2+} salts is able to form both CuL and Cu_2L species with stability constants of $\log K_{CuL}$ = 13.46(3) and $\log K_{Cu2L}$ = 8.8(1). These results also open the possibility for the study of those complexes as potential biomimetic catalysts in aqueous media. Such studies are being presently carried out.

Notes and References

† E-mail: luiss@qio.uji.es

‡ All compounds show the expected spectroscopic data. The most distinctive spectroscopic feature of receptors **2** is the presence in their ^{1}H NMR spectra of three well-defined benzylic singlets at δ 3.4–3.5, 3.6 and 3.7–3.9. *Selected data* for **8a**: $\delta_H(CDCl_3)$ 1.47 (m, 4 H), 1.65 (m, 4 H), 2.34 (t, 4 H), 2.52 (s, 8 H), 2.54–2.66 (m, 8 H), 2.73 (t, 4 H), 3.39 (s, 4 H), 3.62 (s, 4 H), 3.77 (s, 4 H), 7.26 (s, 8 H), 7.39 (s, 8 H); δ_C 26.2, 27.1, 45.3, 46.3, 47.2, 48.4, 48.7, 49.7, 52.7, 59.0, 59.3, 128.7, 129.3, 137.9, 138.5, 139.5.

§ For instance, stepwise protonation constants for receptor **8b**, determined by pH fitrations at 298.1 K in 0. 15 mol dm^{-3}, are: $\log K_{HL}$ = 9.9(2), $\log K_{H2L}$ = 9.53(3), $\log K_{H3L}$ = 8.41(4), $\log K_{H4L}$ = 7.77(4), $\log K_{H5L}$ = 5.95(4), $\log K_{H6L}$ = 4.67(4), $\log K_{H7L}$ = 3.64(4) and $\log K_{H8L}$ < 2. Charges are omitted for clarity.

¶ In the pH range 7–5, the predominant species are H_7LA and H_8LA, obtained by the interaction of the monoanion of violuric acid and the pentaprotonated [log*K* = 4.93(4)] or hexaprotonated receptor [log*K* = 6.18(4)], respectively.

1 G. J. Bridger, R. T. Skerlj, D. Thornton, S. Padmanabban, S. A. Martellucci, G. W. Henson, M. J. Abrams, N. Yamamoto, K. De Vreese, R. Pauwels and E. De Clercq, *J. Med. Chem.*, 1995, **38**, 366; G. J. Bridger, R. T. Skerlj, S. Padmanabban, S. A. Martellucci, G. W. Henson, M. J. Abrams, H. C. Joao, M. Witvrouw, K. De Vreese, R. Pauwels and E. De Clercq, *J. Med. Chem.*, 1996, **39**, 109.

2 K. Wieghardt, I. Tolksdorf and W. Herrmann, *Inorg. Chem.*, 1985, **24**, 1230; M. Ciampolini, L. Fabbrizzi, A. Perotti, A. Poggi, B. Seghi and F. Zanobini, *Inorg. Chem.*, 1987, **26**, 3527; J. L. Sessler and J. W. Sibert, *Tetrahedron*, 1993, **49**, 8727; S. Mallik, R. D. Johnson and F. H. Arnold, *J. Am. Chem. Soc.*, 1994, **116**, 8902; D. Xu, P. G. Mattner, K. Prasad, O. Repic and T. J. Blacklock, *Tetrahedron Lett.*, 1996, **37**, 5301; E. Kimura, S. Aoki, T. Koike and M. Shiro, *J. Am. Chem. Soc.*, 1997, **119**, 3068.

3 A. Filali, J.-J. Yaouanc and H. Handel, *Angew. Chem., Int. Ed. Engl.*, 1991, **30**, 560; P. L. Anelli, M. Murru, F. Uggeri and M. Virtuani, *J. Chem. Soc., Chem. Commun.*, 1991, 1317; V. Patinec, J. J. Yaouanc, J. C. Clément, H. Handel and H. des Abbayes, *Tetrahedron Lett.*, 1995, **36**, 79; B. Boitrel, B. Andrioletti, M. Lachkar and R. Guillard, *Tetrahedron Lett.*, 1995, **36**, 4995; D. Parker and J. A. G. Williams, *J. Chem. Soc., Perkin Trans. 2*, 1996, 1581; D. Parker, K. Senanayake and J. A. G. Williams, *Chem. Commun.*, 1997, 1777.

4 (*a*) A. Bencini, M.I. Burguete, E. García-España, S.V. Luis, J.F. Miravet and C. Soriano, *J. Org. Chem.*, 1993, **58**, 4749; (*b*) A. Andrés, C. Bazzicaluppi, A. Bianchi, E. García-España, S.V. Luis, J. F. Miravet and J. A. Ramirez, *J. Chem. Soc., Dalton Trans.*, 1994, 2995; (*c*) E. García-España, J. Latorre, S. V. Luis, J. F. Miravet, P. E. Pozuelo, J. A. Ramírez and C. Soriano, *Inorg. Chem.*, 1996, **35**, 4591; (*d*) B. Altava, M. I. Burguete, S. V. Luis, J. F. Miravet, E. García-España, V. Marcelino and C. Soriano, *Tetrahedron*, 1997, **53**, 4751.

5 (*a*) M. I. Burguete, B. Escuder, S. V. Luis, J. F. Miravet and E. García-España, *Tetrahedron Lett.*, 1994, **35**, 9075; (*b*) M. I. Burguete, B. Escuder, J. C. Frías, E. García-España, S. V. Luis and J. F. Miravet, *J. Org. Chem.*, 1998, **63**, 1810.

6 For the interaction of bis-macrocycles with barbituric derivatives, see: T. Koike, M. Takashige, E. Kimura, H. Fujioka and M. Shiro, *Chem. Eur. J.*, 1996, **2**, 617.

Received in Cambridge, UK, 20th May 1998; 8/03790F

Covalent coupling of an organic chromophore into functionalized MCM-41 mesophases by template-directed co-condensation

Christabel E. Fowler,[a] Bénédicte Lebeau[b] and Stephen Mann*[a]

[a] *Department of Chemistry, University of Bath, Bath, UK BA2 7AY*
[b] *Laboratoire des Matériaux Minéraux, CNRS UPRES-A 7016 - NSCMu, 3 rue Alfred Werner, 68093 Mulhouse Cedex, France*

An ordered organo-silica-surfactant mesophase containing a covalently-linked chromophore was synthesized with MCM-41-type architecture by template-directed co-condensation of tetraethoxysilane and 3-(2,4-dinitrophenylamino)propyl-(triethoxy)silane: a dye-functionalized mesoporous silica with hexagonal order was produced by surfactant extraction of the as-synthesized material prepared under acidic conditions.

The synthesis and properties of ordered mesostructured and mesoporous inorganic-based materials are currently receiving much attention.[1] The ability to prepare these organized materials depends on the use of surfactant,[2,3] block copolymer,[4,5] microemulsion,[6,7] colloidal[8] or bacterial[9] templates which pattern the deposition of the mineral phase by physical and chemical interactions at the inorganic-organic interface. More chemically complex ordered mesophases are being prepared either by post-synthetic grafting[10,11] or *via* direct routes involving the co-condensation of tetraalkoxysilanes and organo-functionalized trialkoxysilanes.[12–16] Such hybrid materials are intrinsically interesting as new forms of organized matter, as well as being of potential technical importance in catalysis[16,17] metal-ion extraction[18] and adsorption processes.[19]

Previously, we have described the synthesis of a range of organo-silica-surfactant mesophases with MCM-41 architectures containing covalently-linked chemically active groups such as alkyl, aryl, allyl, thiol, amino, epoxy, or imidazole moieties.[12,13] Here we extend this approach and show that an intact chromophore can be covalently incorporated into the MCM-41 mesostructure by direct chemical synthesis involving co-condensation of tetraethoxysilane (TEOS) and 3-(2,4-dinitrophenylamino)propyl(triethoxy)silane (DNPTES) in the presence of hexadecyl(trimethyl)ammonium bromide (C_{16}TMABr) micelles. Although a previous report has described the synthesis of phthalocyanine-doped MCM-41, the chromophore was present as an additive within the surfactant micelles.[20] Post-synthetic grafting of a Schiff-base moiety to the surface of MCM-41 silica produced a mesoporous material which showed a characteristic absorption spectrum for the organic ligand.[21] Thus, to the best of our knowledge, the work reported here is the first example of the direct synthesis of an ordered mesoporous silica containing covalently linked organic chromophore functionalities.

A silica-surfactant mesophase was synthesised from either an alkaline or acidic mixture containing the following molar composition, respectively: C_{16}TMABr:NaOH:TEOS:DNPTES:H_2O = 0.12:0.5:0.9:0.1:130 and C_{16}TMABr:HCl:TEOS:DNPTES:H_2O = 0.12:9.2:0.9:0.1:130.‡ In both methods, small-angle X-ray powder diffraction (SAXRD) of the bright yellow as-synthesized materials gave peaks corresponding to hexagonally-ordered organo-silica-surfactant mesophases with unit cell parameters of 4.55 (basic mixture) and 4.31 nm (acidic mixture)§ (Fig. 1). The product prepared under basic conditions showed sharper reflections than the analogous material synthesized at low pH. Acid extraction of the C_{16}TMABr surfactant template from the latter was achieved without loss of the hexagonally ordered MCM-41 structure or contraction in the unit cell parameter (Fig. 1), to produce a dye-functionalized inorganic replica with channel-like mesopores.§ In contrast, similar treatment of the product prepared at high pH resulted in a disordered organo-silica hybrid. TEM images, which showed hexagonal sets of lattice fringes, as well as parallel fringes corresponding to side-on projections of the mesostructure (Fig. 2), were consistent with the long range order parameters determined by SAXRD.

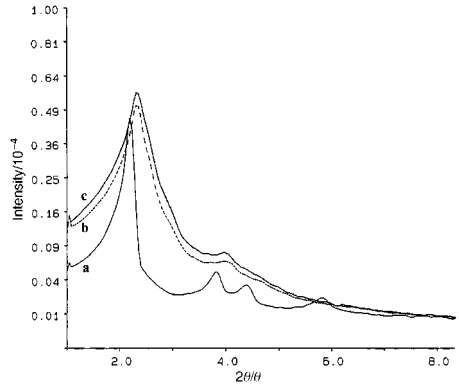

Fig. 1 SAXRD profiles for dye-functionalized ordered silica mesophases: (a) as-synthesized material prepared at high pH, (b) as-synthesized material prepared at low pH, and (c) after surfactant-extraction of material prepared under acidic conditions

Nitrogen adsorption studies confirmed that surfactant extraction of the dye-functionalized material produced under acidic conditions was predominantly mesoporous. A type IV isotherm, with a distinct capillary condensation step that was characteristic of a MCM-41 mesoporous material with a relatively large pore size distribution, was observed. The BET surface area was 760 $m^2\ g^{-1}$, with an average BJH pore diameter of 2 nm. These values are less than those typically reported for pure MCM-41 silicas. As no significant lattice contraction was observed by

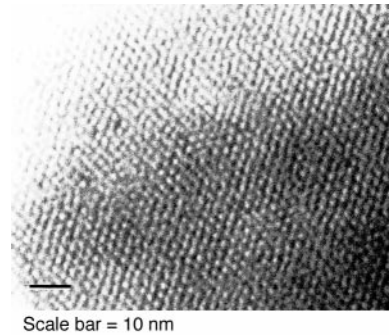

Fig. 2 TEM image of as-synthesized dye-functionalized MCM-41 material showing hexagonally ordered mesostructure. Scale bar = 10 nm.

SAXRD, we attribute this reduced porosity to pendent chromophore moieties that extend into the channel spaces.

^{29}Si DP MAS NMR spectroscopy showed distinct resonances for siloxane [Q^n = $Si(OSi)_n(OH)_{4-n}$, n = 2–4] and organosiloxane [T^m = $RSi(OSi)_m(OH)_{3-m}$, m = 1–3] centres in both the as-synthesized and surfactant-extracted materials.¶ The predominance of T^3 compared with T^2 and T^1 organosiloxane centres indicated that condensation of the organo-functionality in the MCM-41 wall structure was extensive. ^{13}C CP MAS NMR spectroscopy indicated that the dinitrophenylaminopropyl chromophore was covalently linked into the mesophase as an intact unmodified moiety both before and after surfactant extraction.‖ This was consistent with FTIR spectra of the as-synthesised and surfactant-extracted materials which showed characteristic Si–O–Si framework vibrations [1050 (large band), 1200 (shoulder), 480, 750 and 900 cm^{-1}), a Si–C band at 1150 cm^{-1}, as well as vibrations indicative of the chromophore (1338, 1621, 2880–2980, and 3365 cm^{-1}). The intensities of these vibrations were equal in the as-synthesised and surfactant-extracted materials, suggesting no disintegration or loss of the dinitrophenylaminopropyl functionality during the solvent extraction procedure. CHN analysis indicated that *ca*. 20 mol% of the dye functionality was incorporated into the MCM-41 structure.

Diffuse reflectance UV–VIS spectroscopy of the as-synthesised materials showed two broad absorbance bands at 317 and 417nm. These bands were characteristic of the *o*- and *p*-nitro groups, respectively, of the chromophore,[22] and indicated that the optical properties of the dye moiety were maintained when covalently linked into the MCM-41 structure. Extraction of the surfactant resulted in a shift in the position of the band with highest intensity from 317 to 341nm, indicating that the dinitrophenylaminopropyl groups were preferentially located in the pore spaces rather than internalized within the mineral walls. This band was observed at 350 nm for both an acetone solution of non-hydrolysed DNPTES and a sol-gel film of amorphous silica containing hydrolysed DNPTES, suggesting that the blue shift observed for the as-synthesized MCM-41 mesophase was due to specific interactions of the organic moiety with the surfactant micelles. As the infrared spectra of the surfactant-extracted and as-synthesized materials were unchanged, protonation of the chromophore can be ruled out as a cause of the shift in the absorption band.

Our results suggest that it should be possible to incorporate a range of organic chromophores into surfactant-silica mesophases and corresponding mesoporous replicas without extensive modification of the optical properties. Although further work is required, the covalent attachment of dye molecules into ordered or semi-ordered porous MCM-type materials could be of general importance in a number of areas. In principle, the organic moieties can be dispersed and isolated from each other, which for some systems, for example with rhodamine derivatives, should minimize intermolecular quenching of fluorescence properties. Furthermore, the combination of mesoporosity and optical properties should give rise to interesting materials, particularly when host–guest interactions are being examined. Similarly, covalently linked chromophores could be used as sensors in separations technologies to detect molecules within the channel-like pores of MCM-41 phases fabricated in the form of thin membranes. Finally, as the optical properties of the chromophore can be highly sensitive to the local environment, such moieties could be used to probe the internal structure and dynamics of silica mesophases in general.

We thank Dr David C. Apperley at the University of Durham, UK, for solid state NMR data, Dr Christine G. Göltner and Ingrid Zenke at the Max Planck Institute of Colloids and Interfaces, Teltow, Germany, for help with initial SAXRD data, and the University of Bath for financial support.

Notes and References

† E-mail: s.mann@bath.ac.uk

‡ In a typical preparation under alkaline conditions, C_{16}TMABr (0.40 g, Aldrich) was dissolved in a solution containing 1.0 M NaOH (5.0 g) and distilled, deionised H_2O (17.55 g). TEOS (1.5 g, Aldrich) and DNPTES (0.31 g, Apollo Sci. Ltd) were added, and the mixture stirred for 24 h at room temperature. The solid product was filtered, washed with H_2O and dried for 10 h in air. Extraction of the surfactant was performed by stirring a suspension of the solid product (0.99 g dm^{-3}) in 1.0 M HCl in EtOH at 75 °C for 24 h. The extracted material was filtered, washed with EtOH and dried for 10 h at 100 °C *in vacuo*. CHN analysis gave 6.9% (N), 19.2% (C) and 2.8% (H). For preparations under acidic conditions, TEOS (3.43 g) and DNPTES (0.71 g) were added to acetone (1.34 ml) and co-hydrolysed by addition of 3.85 M HCl acid (0.33 ml) (TEOS:DNPTES:acetone:HCl = 0.9:0.1:1.0:1.0). The mixture was stirred for 15 min at room temperature, and the resulting sol added with stirring to 42.8 ml of a solution of C_{16}TMABr (18.7 mg ml^{-1}; 51.3 mM) in 3.85 M HCl. The final solution was stirred and heated at 90 °C overnight (16 h). The yellow precipitate was filtered, washed repeatedly with distilled H_2O and EtOH, and dried in an oven at 70 °C. Surfactant extraction was performed as described above.

§ SAXRD *d* spacings (*hkl*): DNPTES-MCM (as-synthesized, high pH): 3.95 (100), 2.30 (110), 1.99 (200) and 1.51 nm (210); DNPTES-MCM (as-synthesized, low pH): 3.74 (100), 2.15 (110) and 1.98 nm (200); DNPTES-MCM (surfactant-extracted, low pH): 3.76 (100), 2.20 (110) and 2.00 nm (200). Unit cell parameter, $a = 2d_{100}/\sqrt{3}$.

¶ ^{29}Si DP (direct polarization) MAS NMR data (60 MHz, TMS, 20 °C) for DNPTES-MCM (as-synthesized, high pH): δ −50.9 (T^1, 3.1%), −58.1 (T^2, 4.7%), −66.7 (T^3, 12.5%), −90.3 (Q^2, 7.5%), −98.7 (Q^3, 34.4%), −108.6 (Q^4, 37.9%). For DNPTES-MCM (surfactant-extracted, high pH): δ 58.9 (T^2, 5.0%), −66.9 (T^3, 11.4%), −91.5 (Q^2, 5.9%), −100.6 (Q^3, 37.6%), −109.3 (Q^4, 40.1%).

‖ ^{13}C CP MAS NMR data for DNPTES-MCM (as-synthesized, high pH): δ 11.2, 23.0, 46.7, 115.5, 123.1, 129.4, 135.4, 148.6. For DNPTES-MCM (surfactant-extracted, high pH): δ 10.2, 22.6, 46.3, 115.0, 123.4, 129.8 135.5, 148.5.

1 D. Zhao, P. Yang, Q. Huo, B. F. Chmelka and G. D. Stucky, *Curr. Opin. Solid State Mater. Chem.*, 1998, **3**, 111.
2 C. T. Kresge, M. E. Leonowicz, W. J. Roth, J. C. Vartuli and J. S. Beck, *Nature*, 1992, **359**, 710.
3 G. S. Attard, J. C. Glyde and C. G. Göltner, *Nature* 1995, **378**, 366.
4 C. G. Göltner, S. Henke, M. C. Weisenberger and M. Antonietti, *Angew. Chim., Int. Ed. Engl.*, 1998, **37**, 613.
5 D. Zhao, J. Feng, Q. Huo, N. Melosh, G. H. Fredrickson, B. F. Chmelka and G. D. Stucky, *Science*, 1998, **279,** 548.
6 A. Imhof and D. J. Pine, *Nature*, 1997, **389**, 948.
7 D. Walsh and S. Mann, *Nature*, 1995, **377**, 320.
8 M. Antonietti, B. Berton, C. G. Göltner and H.-P. Nentze, *Adv. Mater*., 1998, **10**, 154.
9 S. A. Davis, S. L. Burkett, N. H. Mendelson and S. Mann, *Nature*, 1997, **385**, 420.
10 R. Burch, N. Cruise, D. Gleeson and S. C. Tsang, *Chem. Commun.*, 1996, 951.
11 T. Maschmeyer, F. Rey, G. Sankar and J. M. Thomas, *Nature*, 1995, **378**, 159.
12 S. L. Burkett, S. D. Sims and S. Mann, *Chem. Commun.*, 1996, 1367.
13 C. E. Fowler, S. L. Burkett and S. Mann, *Chem. Commun.*, 1997, 1769.
14 D. J. MacQuarrie, *Chem. Commun.*, 1996, 1961.
15 M. H. Lim, C. F. Blanford and A. Stein, *J. Am. Chem. Soc*., 1997, **119**, 4090.
16 M. H. Lim, C. F. Blanford and A. Stein, *Chem. Mater.*, 1998, **10**, 467.
17 J. H. Clark and D. J. MacQuarrie, *Chem. Commun.*, 1997, 853.
18 X. Feng, G. E. Fryxell, L. Q. Wang, A. Y. Kim, J. Liu and K. M. Kemner, *Science*, 1997, **276**, 923.
19 C. M. Bambrough, R. C. T. Slade, R. T. Williams, S. L. Burkett, S. D. Sims and S. Mann, *J. Colloid. Interface Sci.*, 1998, **201,** 220**.**
20 H. S. Zhou, H. Sasabe and I. Honma, *J. Mater. Chem.*, 1998, **8**, 515.
21 P. Sutra and D. Brunel, *Chem. Commun.*, 1996, 2485.
22 E. P. Bescher, E. Hong, Y. H. Xu and J. D. Mackenzie, *Mater. Res. Soc. Symp*., 1996, **435**, 605.

Received in Cambridge, UK, 19th May 1998; 8/03736A

Formation of triumphene, $C_{60}F_{15}Ph_3$: first member of a new trefoil-shaped class of phenylated [60]fullerenes

Olga V. Boltalina,[a] Joan M. Street[b] and Roger Taylor*[a]†

[a] *The Chemistry Laboratory, CPES School, University of Sussex, Brighton, UK BN1 9QJ*
[b] *Chemistry Department, The University, Southampton, UK SO17 1BJ*

Reaction of $C_{60}F_{18}$ with benzene/$FeCl_3$ during two weeks at room temperature produces the phenylated trefoil-shaped derivative $C_{60}F_{15}Ph_3$; higher reaction temperatures produce $C_{60}Ph_{18}$ from replacement of all fluorines by phenyl groups.

Arylated fullerenes may ultimately constitute the largest class of fullerene derivatives. Many have been made and some fully characterised, *e.g.* $C_{60}Ar_5X$, (X = H, Cl),[1–3] $C_{60}Ph_5OH$ (two isomers),[4] $C_{60}Ph_n$ (n = 2, 4),[5] $C_{70}Ph_n$ (n = 2, 4, 6, 8, 10),[6] $C_{70}Ph_9OH$,[7] $C_{70}Ph_8(OH)_2$,[4] $C_{60}PhH$ and $C_{70}PhH$,[8] a benzo-[*b*]furo[60]fullerene[9] and an isoquinolino[60]fullerene.[10] A number of other derivatives have been identified but so far by mass spectrometry only.[11,12] Most have been made by Friedel–Crafts reactions of fullerenes or halogenofullerenes with the aromatics. They are reasonably soluble and stable, especially towards EI mass spectrometry, and some are luminescent.[6] In $C_{60}Cl_6$, the least accessible chlorine was not readily replaced.[1,2]

Recently we described the formation and characterisation of $C_{60}F_{18}$, a polar crown-shaped molecule, shown in Fig. 1.[13] Fluorofullerenes are very susceptible towards nucleophilic substitution,[14] and fluoroalkanes are the most reactive of the halogenoalkanes in Friedel–Crafts alkylation of aromatics.[15] We now describe the successful isolation and characterisation of the first derivative that results from replacement of fluorine by phenyl, and which shows a unique arylation pattern.

Two samples of $C_{60}F_{18}$ (5 mg) were each added to solutions of anhydrous $FeCl_3$ (*ca.* 5 mg) dissolved in anhydrous benzene (2 ml). One solution was set aside for two weeks, the other was heated to *ca.* 70 °C for 1 h. The mixtures were evaporated to dryness and the resultant solids extracted with CCl_4 (to separate unreacted catalyst). Removal of this solvent under vacuum gave deposits that were dissolved in 1 : 1 hexane–toluene and purified by HPLC using a 4.6 mm × 25 cm Cosmosil Buckyprep column, with a flow rate of 1 ml min^{-1}. From both samples a main fraction of $C_{60}F_{15}Ph_3$ eluted at 49.6 min, and from the heated sample, minor fractions eluted at 14.3 and 17.7 min, these being $C_{60}F_{15}Ph_5$ and $C_{60}F_{15}Ph_7$, respectively. Comparison with the retention time of $C_{60}F_{18}$ (*ca.* 45 min with elution by toluene) shows that replacement of F by Ph reduces the retention time. As in the case of phenylated [60]fullerenes,[12] the retention time is reduced by increasing the phenylation level.

The mass spectrum of the crude extract showed also the presence of $C_{60}Ph_{18}$, but attempted separation resulted in degradation, with a broad peak indicated to be $C_{60}Ph_{18}O(OH)_2$, 2142 amu, eluting at 9.3 min (1 : 1 hexane–toluene, 0.5 ml min^{-1}).

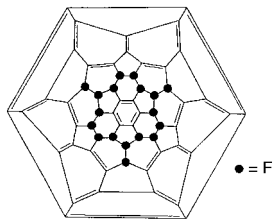

Fig. 1 Schlegel diagram for $C_{60}F_{18}$

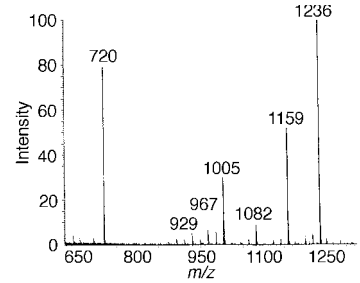

Fig. 2 EI mass spectrum (70 eV) for $C_{60}F_{15}Ph_3$

The mass spectrum (Fig. 2) shows the $C_{60}F_{15}Ph_3$ parent ion at 1236 amu, with peaks at 1159, 1082 and 1005 amu due to successive loss of phenyl groups. The structure of $C_{60}F_{18}$ suggests that the three fluorines which have been replaced by phenyl are the most accessible ones giving a product of C_{3v} symmetry. This is confirmed by the ^{1}H NMR spectrum (Fig. 3) which shows only one set each of the *o*-, *m*- and *p*-hydrogens of the phenyl groups; a spectrum run at −60 °C is identical, proving that the phenyl groups rotate freely and are thus not in a hindered environment.

The structure is further confirmed by the ^{19}F NMR spectrum (Fig. 4) which shows three peaks in a 1 : 2 : 2 intensity ratio at δ −137.22, −138.36 and −145.0, with respective half-height peak widths are *ca.* 12, 12 and 8 Hz respectively. Comparison with the ^{19}F NMR spectrum for $C_{60}F_{18}$ (four peaks in a 2 : 2 : 1 : 1 intensity ratio) shows that it is one of the latter (due to three equivalent fluorine atoms) that is replaced. The 2D-COSY spectrum (inset to Fig. 4), shows that the single intensity fluorine is directly coupled to one of the (adjacent) double intensity peaks. Thus it is the most accessible fluorine that has been replaced, the ease of replacement of the chlorines in $C_{60}Cl_6$.

The structure of $C_{60}F_{15}Ph_3$, which has encouraged us to name it as 'triumphene', is therefore as shown in Fig. 5. The simplicity of preparation suggests that it will be possible to make a large range of other aryl derivatives, the limiting step being only the low availability at present of $C_{60}F_{18}$.

Previously, one of us suggested that nucleophilic replacement of fluorine (in the absence of a catalyst) occurs *via* addition-elimination, because S_N1 substitution (giving a cation on the strongly electron-withdrawing cage) seemed improbable, and S_N2 substitution is impossible.[14] However, if $C_{60}F_{15}Ph_3$

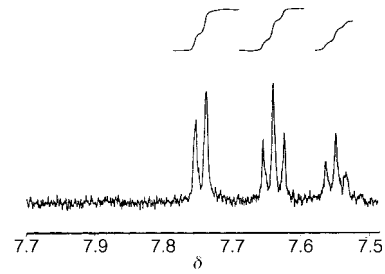

Fig. 3 ^{1}H NMR spectrum for $C_{60}F_{15}Ph_3$

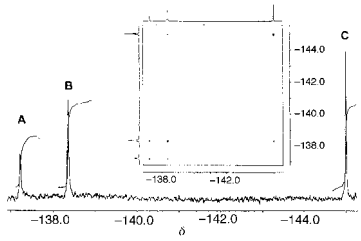

Fig. 4 ^{19}F NMR spectrum for $C_{60}F_{15}Ph_3$ with 2D-COSY spectrum inset. The peak labels correspond to the fluorine atoms identified as in Fig. 5.

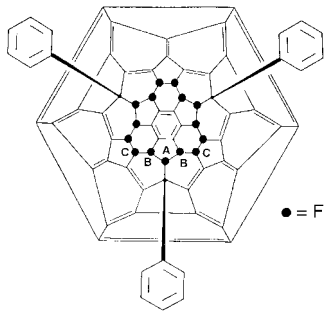

Fig. 5 Schlegel diagram of the structure of $C_{60}F_{15}Ph_3$

was formed by addition-elimination, it could not have C_{3v} symmetry since the phenyl groups would necessarily lie off the symmetry plane of the original $C_{60}F_{18}$. The present work therefore provides unambiguous evidence for direct fluorine replacement in nucleophilic substitution of fluorofullerenes, and is here facilitated by the presence of the Friedel–Crafts catalyst. This reinforces our conclusions concerning replacement of chlorine by phenyl in $C_{60}Cl_6$.[2] Moreover, the reaction of $C_{60}Ph_5Cl$ with $AlCl_3$ produces a free isolable carbocation,[16] and it is clear now that in the presence of these catalysts, substitution in halogenofullerenes takes place *via* an S_N1 mechanism, though necessarily involving frontside attack only.

We have insufficient $C_{60}F_{15}Ph_7$ and $C_{60}F_{15}Ph_5$ at present for full characterisation, but the addition of phenyl groups in pairs suggests that they add across a 6,6-double bond, *e.g.* that which lies on the symmetry plane (the bond across which oxygen adds to give $C_{60}F_{18}O$).[16] One could expect that with longer reaction times, $C_{60}F_{15}Ph_9$ may be observed as a further derivative.

Remarkably, we observed the presence of more volatile $C_{60}Ph_{18}$ (2108 amu) in an early acquisition of the mass spectrum of the crude material (Fig. 6); the mass spectrum shows also the doubly charged $M^+/2$ ions. The spectrum is notable in being less contaminated by the lower phenylated components that we have seen with other phenylation methods.

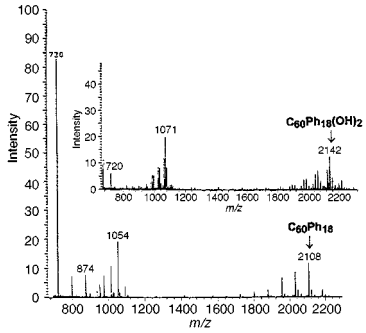

Fig. 6 EI mass spectrum for $C_{60}Ph_{18}$; inset is the mass spectrum for $C_{60}Ph_{18}(OH)_2$ showing also traces of the epoxide derivative

Despite the anticipated steric hindrance, the addition pattern in $C_{60}Ph_{18}$ is likely to be the same as in the fluoro precursor. The mass spectrum shows the presence of a nineteenth phenyl group at much lower intensity. This is due to further phenylation of the cage (well-known to occur with fullerenes and benzene in the presence of Friedel–Crafts catalysts)[11] and indicated in this work by the formation of $C_{60}F_{15}Ph_7$ *etc.* However, the markedly lower intensity of $C_{60}Ph_{19}$ compared to that of $C_{60}Ph_{18}$ provides very strong circumstantial evidence that the eighteen phenyl groups are indeed located at the sites previously occupied by fluorine, giving rise to a fascinating structure of extreme aromaticity.

We have been unable to obtain substitution of F by Ph in $C_{60}F_{36}$ (or in $C_{60}F_{48}$) under the conditions described above.

We attempted also to purify the $C_{60}Ph_{18}$ by HPLC but were unsuccessful because it appeared to oxidise to a diol, $C_{60}Ph_{18}(OH)_2$, and the epoxide derivative, as shown by peaks of 2142 and 2158 amu in the mass spectrum (inset to Fig. 6). Oxygenated derivatives of phenylated fullerenes are prone to form readily.[12]

We thank the Royal Society for a Joint Project Award.

Notes and References

† E-mail: r.taylor@sussex.ac.uk

1 A. G. Avent, P. R. Birkett, J. D. Crane, A. D. Darwish, G. J. Langley, H. W. Kroto, R. Taylor and D. R. M. Walton, *J. Chem. Soc., Chem. Commun.*, 1994, 1463.
2 P. R. Birkett, A. G. Avent, A. D. Darwich, I. Hahn, H. W. Kroto, G. J. Langley, J. O'Loughlin, R. Taylor and D. R. M. Walton, *J. Chem. Soc., Perkin Trans. 2*, 1997, 1121.
3 M. Sawamura, H. Iikura and E. Nakamura, *J. Am. Chem. Soc.*, 1996, **118**, 12850.
4 A. G. Avent, P. R. Birkett, A. D. Darwish and R. Taylor, to be submitted.
5 P. R. Birkett, A. G. Avent, A. D. Darwich, H. W. Kroto, R. Taylor and D. R. M. Walton, *J. Chem. Soc., Perkin Trans 2*, 1997, 457.
6 P. R. Birkett, A. G. Avent, A. D. Darwich, H. W. Kroto, R. Taylor and D. R. M. Walton, *Tetrahedron*, 1996, **52**, 5235 and unpublished work.
7 P. R. Birkett, A. G. Avent, A. D. Darwish, H. W. Kroto, R. Taylor and D. R. M. Walton, *Chem. Commun.*, 1996, 1231.
8 A. Hirsch, T. Grösser, A. Skiebe and A. Soi, *Chem. Ber.*, 1993, **126**, 1061.
9 A. G. Avent, P. R. Birkett, A. D. Darwich, H. W. Kroto, R. Taylor and D. R. Walton, *Chem. Commun.*, 1997, 1579.
10 A. K. Abdul-Sada, A. G. Avent, P. R. Birkett, A. D. Darwich, H. W. Kroto, R. Taylor, D. R. M. Walton and O. B. Woodhouse, *Chem. Commun.*, 1998, 307.
11 R. Taylor, G. J. Langley, M. F. Meidine, J. P. Parsons, A. K. Abdul-Sada, T. J. Dennis, J. P. Hare, H. W. Kroto and D. R. M. Walton, *J. Chem. Soc., Chem. Commun.*, 1992, 667; G. A. Olah, I. Bucsi, C. Lambert, R. Aniszfeld, N. J. Trivedi, D. K. Sensharma and G. K. S. Prakash, *J. Am. Chem. Soc.*, 1991, **113**, 9385, 9387; G. A. Olah, I. Bucsi, D. S. Ha, R. Aniszfeld, C. S. Lee and G. K. S. Prakash, *Fullerene Sci. Technol.*, 1997, **5**, 389.
12 A. D. Darwich, P. R. Birkett, G. J. Langley, H. W. Kroto, R. Taylor and D. R. M. Walton, *Fullerene Sci. Technol.*, 1997, **5**, 705.
13 O. V. Boltalina, V. Yu. Markov, R. Taylor and M. P. Waugh, *Chem. Commun.*, 1996, 2549.
14 R. Taylor, J. H. Holloway, E. G. Hope, G. J. Langley, A. G. Avent, T. J. Dennis, J. P. Hare, H. W. Kroto and D. R. M. Walton, *J. Chem. Soc., Chem. Commun.*, 1992, 665; R. Taylor, G. J. Langley, J. H. Holloway, E. G. Hope, A. K. Brisdon, H. W. Kroto and D. R. M. Walton, *J. Chem. Soc., Perkin Trans. 2*, 1995, 181.
15 G. A. Olah, *Friedel-Crafts and Related Reactions*, Interscience, New York, 1963, vol. 1, p. 40.
16 A. G. Avent, O. V. Boltalina, P. W. Fowler, A. Yu. Lukonin, V. K. Pavlovich, J. B. Sandall, J. M. Street and R. Taylor, *J. Chem. Soc., Perkin Trans. 2*, 1998, 1319.

Received in Cambridge, UK, 23rd March 1998; revised manuscript received, 9th July 1998; 8/05340E

Multiple α-agostic interactions in a metal–methyl complex: the neutron structure of $[Mo(NC_6H_3Pr^i_2\text{-}2,6)_2Me_2]$

Jacqueline M. Cole*[a,b]† Vernon C. Gibson,[c] Judith A. K. Howard,[a] Garry J. McIntyre[b] and Gary L. P. Walker[c]

[a] *Department of Chemistry, University of Durham, South Road, Durham, UK DH1 3LE*
[b] *Institut Laue Langevin, B.P. 156, 38042 Grenoble Cedex 9, France*
[c] *Department of Chemistry, Imperial College, South Kensington, London, UK SW7 2AY*

The neutron structure of $[Mo(NC_6H_3Pr^i_2)\text{-}2,6)_2Me_2]$ reveals two highly distorted methyl ligands; this distortion is due to the presence of multiple C–H···M α-agostic interactions.

Since the formalisation of the three-centre C–H···M 'agostic' interaction by Brookhart and Green in the mid 1980s,[1] these interactions have been found to occur in many coordinatively unsaturated alkyl, aryl and polyhapto hydrocarbon metal complexes.[2] They are relatively readily observed and detected in alkyl derivatives possessing β-hydrogens, either in solution for rapidly averaging agostic hydrogens *via* the effect of isotopic perturbation on C–H coupling constants and chemical shift positions, or in the solid state by X-ray crystallography.‡ Agostic interactions in metal–methyl species have proved more difficult to detect because (1) any isotopic perturbation of the resonance effect is diluted over a greater number of hydrogen environments and (2) in X-ray structure determinations, there are no obvious ligand distortions of the type seen in longer chain alkyls and it is inherently difficult with X-rays to locate the methyl hydrogen atom positions with any accuracy. The only reliable method of establishing the presence of agostic interactions in metal–methyl complexes is *via* diffraction.

To date, the only metal methyl complex to have been characterised by neutron diffraction that shows clear evidence for an α-agostic methyl C–H···M interaction is $[TiMeCl_3(Me_2PCH_2CH_2PMe_2)]$.[3] Here, we describe the neutron structure of the coordinatively unsaturated molybdenum α-agostic dimethyl complex $[Mo(NC_6H_3Pr^i_2\text{-}2,6)_2Me_2]$ which was prepared from the reaction of $[Mo(NC_6H_3Pr^i_2\text{-}2,6)_2Cl_2(dme)]$ with 2 equiv. of methylmagnesium chloride. Full synthetic details will be reported elsewhere.[4] A crystal of dimensions 6.0 × 2.0 × 1.0 mm was grown from a saturated pentane solution at −35 °C. The molecular structure of $[Mo(NC_6H_3Pr^i_2\text{-}2,6)_2Me_2]$ is shown in Fig. 1, along with selected bond lengths and angles.

The geometry about the metal centre is best described as distorted tetrahedral with inter-ligand angles in the range 107–114°. The bond distances for the Mo–N and N–C(*ipso*) bonds [1.756(2) and 1.382(2) Å, respectively] in combination with Mo–N–C angles [159.6(1)°] are consistent with linear imido ligands.[5] The two methyl groups are crystallographically equivalent so the following discussion concentrates on only one methyl group. Each methyl group shows a partial positional disorder amongst the hydrogen atom sites, which can be described as resulting from a slight rocking motion about C(13), the pivot atom for a fluxional rotation which, averaged over all possible sites in all unit cells, gives the 'static average' picture shown. H(13A) can be resolved into two positions [(H13A) and (H13′)] with occupancies in the ratio 2 : 1 and these refine independently both isotropically and anisotropically. The latter tends to a distortion and an overlap in the two density distributions, but with derived molecular parameters very close to those reported herein, which result from an isotropic description of the disordered sites.

A large amount of librational motion therefore exists, thus disguising the precise position of the hydrogen atoms. However, despite the librational effects, the average geometry gives conclusive results. The coordination of each methyl group is markedly distorted from regular tetrahedral geometry and of special note are the particularly small angles Mo(1)–C(13)–H(13A) [103.7(4)°] and Mo(1)–C(13)–H(13B) [104.7(3)°] which are consistent with the hydrogen atoms being drawn towards the metal centre. Consequently, the angles, Mo(1)···H(13A)–C(13) (52.6°) and Mo(1)···H(13B)–C(13) (51.8°) are noticeably larger than those corresponding to the hydrogen atoms H(13C) and H(13′) (43.0 and 43.9° respectively).

The Mo(1)···H(13A) and Mo(1)···H(13B) distances [2.585(8) and 2.598(5) Å, respectively] are also significantly shorter than Mo(1)···H(13C) and Mo(1)···H(13′) [2.755(5) and 2.76(1) Å] and the Mo(1)–C(13) bond length of 2.112(2) Å is very short,

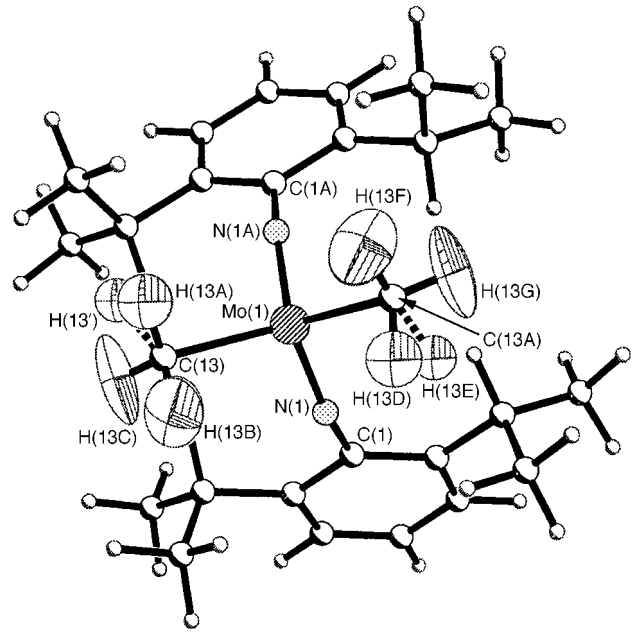

Fig. 1 The molecular structure of $[Mo(NC_6H_3Pr^i_2\text{-}2,6)_2Me_2]$ with 50% probability thermal ellipsoids shown on the methyl hydrogen atoms, thus indicating the extent of libration. Selected bond dimensions (Å and °): Mo(1)–N(1) 1.756(2), Mo(1)–C(13) 2.112(2), Mo(1)···H(13A) 2.585(8), Mo(1)···H(13′) 2.76(1), Mo(1)–H(13B) 2.598(5), Mo(1)···H(13C) 2.755(5), N(1)–C(1) 1.382(2), C(13)–H(13A) 1.07(1), C(13)–H(13′) 1.09(1), C(13)–H(13B) 1.068(7), C(13)–H(13C) 1.049(8); N(1)–Mo(1)–N(1A) 112.5(1), N(1)–Mo(1)–C(13) 107.86(7), C(13)–Mo(1)–C(13A) 114.1(2), C(13)–Mo(1)···H(13A) 23.7(2), C(13)–Mo(1)···H(13′) 21.0(3), C(13)–Mo(1)···H(13B) 23.4(2), C(13)–Mo(1)···H(13C) 19.8(2), Mo(1)–N(1)–C(1) 159.6(1), Mo(1)–C(13)–H(13A) 103.7(4), Mo(1)–C(13)–C(13′) 115.1(6), Mo(1)–C(13)–H(13B) 104.7(3), Mo(1)–C(13)–H013C) 117.2(3).

comparing with literature values of 2.554 Å (mean) and 2.189 Å (lower quartile).[6] This short Mo–C distance is also likely to be a consequence of the agostic interactions. All C–H distances are identical within experimental error. Of the two α-agostic hydrogen atoms per methyl group (therefore, four agostic interactions per molecule) both appear strong and of the same strength, judging by their relative geometries.

More than one agostic interaction in $[Mo(NC_6H_3Pr^i_2\text{-}2,6)_2Me_2]$ is not unreasonable since this molecule is quite severely coordinatively unsaturated. It is not possible to place a precise electron count on the complex since, for symmetry reasons, the two *cis* imido ligands are in direct competition for one of the metal d_π orbitals. This means that the electron count must be below 16 electrons (the count derived from assuming that both imido ligands can form two π bonds) and formally could be as low as 14 electrons (*i.e.* the count arising from three π-bonds between the molybdenum and the two imido groups). In general, the results described here underscore the notion that agostic interactions will occur whenever a metal centre possesses a suitably oriented and energetically accessible vacant orbital, and that multiple interactions of this kind may occur at a single metal centre. The neutron diffraction study described here shows clear evidence for four α-agostic methyl C–H···M interactions within $[Mo(NC_6H_3Pr^i_2\text{-}2,6)_2Me_2]$. It represents the second metal–methyl complex showing α-agostic interactions and the first one to show multiple agostic interactions.

The authors wish to thank the Institut Laue Langevin, Grenoble, France (J. M. C.) and the EPSRC (J. M. C. and G. L. P. W.) for financial support.

Notes and References

† Present address: School of Physical Sciences, University of Kent at Canterbury, Canterbury, Kent, UK CT2 7NR. E-mail: J.M.Cole@ukc.ac.uk

‡ It should be noted that the evidence for β-agostic interactions is often derived from other structural parameters such as a low M–C–C bond angle rather than direct location of the agostic hydrogen atom position.

§ *Crystal data* for $[Mo(NC_6H_3Pr^i_2\text{-}2,6)_2Me_2]$: $C_{26}H_{40}MoN_2$, M_r = 475.94, deep orange–red rectangular crystal (6.0 × 1.8 × 1.0 nm), monoclinic, space group *C*2/*c*, a = 20.240(4), b = 6.550(1), c = 19.910(4) Å, β = 103.99(3)°, V = 2561.2(8) Å^3, Z = 4, T = 150.0(2) K, D_c = 1.234 g cm^{-3}, $F(000)$ = 348, μ = 0.233 mm^{-1}, 2110 unique reflections ($6.56 \leqslant 2\theta \leqslant 60.02°$) were measured on the D9 four circle diffractometer at the Institut Laue Langevin (ILL), Grenoble, France in a beam of wavelength 0.8405(2) Å obtained by reflection from a Cu(220) monochromator. Half-wavelength contamination was removed with an erbium filter. The sample was mounted on the cold head of an Air Products closed-cycle refridgerator. Background corrections following Lehmann and Larsen[7] and Lorentz corrections were applied. Cryostat shield and absorption corrections were made using the local program ABSCAN and the DATAP program[8] respectively (transmission range: 0.6477–0.8045). The structure was refined by full-matrix least-squares refinement using SHELXL-93[9] against 2100 reflections. Refinement of 312 positional and anisotropic displacement parameters for all atoms [except for isotropic H(13A) and H(13′)] converged to $R1$ [$I > 2\sigma(I)$] = 0.0467 and wR_2 [$I > 2\sigma(I)$] = 0.0462 [$w = 1/\sigma^2(F_o)^2$] with S = 1.431.

1 M. Brookhart and M. L. H. Green, *J. Organomet. Chem.*, 1983, **250**, 395.
2 See, for example: A. D. Poole, D. N. Williams, A. M. Kenwright, V. C. Gibson, W. Clegg, D. C. R. Hockless and P. A. O'Neil, *Organometallics*, 1993, **12**, 2549; J. M. Bondcella, M. L. Cajigal and K. A. Abboud, *Organometallics*, 1996, **15**, 1905; R. H. Grubbs and G. W. Coates, *Acc. Chem. Res.*, 1996, **29**, 85; D. Braga, F. Grepioni, K. Biradha and G. R. Desiraju, *J. Chem. Soc., Dalton Trans.*, 1996, 3925; M. Etienne, R. Mathieu and B. Donnadieu, *J. Am. Chem. Soc.*, 1997, **119**, 3218; W. Trakarnpruk, I. HylaKryspin, A. M. Arif, R. Gleiter and R. D. Ernst, *Inorg. Chim. Acta*, 1997, **259**, 197.
3 Z. Dawoodi, M. L. H. Green, V. S. B. Mtetwa, K. Prout, A. J. Schultz, J. M. Williams and T. F. Koetzle, *J. Chem. Soc., Dalton Trans.*, 1986, 1629.
4 V. C. Gibson, C. Redshaw, G. L. P. Walker, J. M. Cole, J. A. K. Howard, V. J. Hoy and L. Kuzmina, *J. Chem. Soc., Dalton Trans.* in preparation.
5 D. E. Wigley, *Prog. Inorg. Chem.*, 1994, **42**, 239; W. A. Nugent and J. M. Mayer, *Metal–Ligand Multiple Bonds*, Wiley Interscience, New York, 1988; A. Bell, W. Clegg, P. W. Dyer, M. R. J. Elsegood, V. C. Gibson and E. L. Marshall, *J. Chem. Soc., Chem. Commun.*, 1994, 2247.
6 F. H. Allen, L. Brammer, O. Kennard, A. G. Orpen, R. Taylor and D. G. Watson, *J. Chem. Soc., Dalton Trans.*, 1989, S1.
7 M. S. Lehmann and F. K. Larsen, *Acta Crystallogr. Sect. A*, 1974, **30**, 580.
8 P. Coppens, in *The Evaluation of Absorption and Extinction in Single-Crystal Structure Analysis* in *Crystallographic Computing*, ed. F. R. Ahmed, Munksgaard, 1970.
9 G. M. Sheldrick, SHELXL-93. *Program for the refinement of crystal structures*, University of Göttingen, Germany, 1993.

Received in Cambridge, UK, 29th April 1998; 8/03221A

First selenide-centered Cu^I_8 cubic clusters containing dialkyl diselenophosphate ligands. X-Ray structure of $\{Cu_8(\mu_8\text{-}Se)[Se_2P(OPr^i)_2]_6\}$

C. W. Liu,*[a] Hsiu-Chih Chen,[a] Ju-Chung Wang*[b] and Tai-Chiun Keng[b]

[a] *Department of Chemistry, Chung Yuan Christian University, Chung-Li, Taiwan 320, R.O.C. E-mail: chenwei@cchp01.cc.cycu.edu.tw*

[b] *Department of Chemistry, Soochow University, Taipei, Taiwan 11102, R.O.C.*

$[Cu_8(\mu_8\text{-}Se)[Se_2P(OPr^i)_2]_6\}$, the first discrete Cu^I_8 cubane in which each face of the cube is bridged by a diselenophosphate ligand and has an interstitial selenide ion (Se^{2-}), is reported.

The interests in combining transition metals and main group elements in clusters stem from two possibilities that these compounds could be useful precursors for the synthesis of new materials and provide a search for new coordinations and geometries.[1] We are interested in the synthesis of molecular cubic clusters having an interstitial main-group atom because they are not only extremely rare[2] but also particularly interesting in view of their unusual bonding characteristics.[3] Although there are several examples of metal carbonyls having μ_8-E (E = C,[4] Si,[5] P,[6] S[7] and As[8]) bridges, the metallic frameworks surrounding the interstitial atom are largely tetragonal (square) antiprisms.

In 1990, Fenske and Krautscheid reported a beautiful mega cluster, $Cu_{20}(\mu_8\text{-}Se)Se_{12}(PEt_3)_{12}$ **1**,[9] which consists of an undistorted, selenide centered Cu_8 cube, each of whose edges is bridged by a peripheral copper atom. The resulting 20 copper atom polyhedron is surrounded by twelve selenium ligands which are arranged in such a fashion as to form a near regular icosahedron. The peripheral copper atom is further coordinated by a PEt_3 ligand. The average formal oxidation state of each copper atom of the cluster is 1.3. In 1995, a sulfide centered Cu^I_8 cube, $\{Cu_8(\mu_8\text{-}S)[S_2P(OPr^i)_2]_6\}$ **2**, whose core geometry is analogous to the central portion of Fenske's compound was reported by Fackler.[1] Unlike compound **1** in which each edge of the cube is bridged by a copper atom, **2** is bridged by a sulfur atom of the dithiophosphate ligand. This brings to our attention as to whether a discrete Cu_8 cube with a selenium atom in its center can be isolated.

In order to synthesize a molecule having a selenide centered Cu^I_8 cube, we focused our attention on the ligand dialkyl diselenophosphate, $Se_2P(OR)_2^-$ (dsep). In sharp contrast to many studies on compositions and structures of phosphor-1,1-dithiolato metal complexes,[10] the chemistry of phosphor-1,1-diselenolato metal compounds has received scant attention. Consequently, there are very few papers referring to this ligand.[11] Among these, are the preparation of various dialkyl diselenophosphates and investigations of the spectroscopic properties of several main group and transition metal complexes. Powder X-ray patterns of some of the compounds are also included. Herein, we report the first discrete Cu^I_8 cubane encapsulating a selenide ion (Se^{2-}), $\{Cu_8(\mu_8\text{-}Se)[Se_2P(OPr^i)_2]_6\}$ **3**. To our surprise this is also the first phosphor-1,1-diselenolato complex of any element studied by single crystal X-ray diffraction.

Treatment of $NH_4Se_2P(OPR^i)_2$ and $Cu(MeCN)_4PF_6$ in a 2 : 1 ratio in diethyl ether at 0 °C for 4 h results in a pale yellow solution. After chromatographic work-up (silica gel, eluent CH_2Cl_2–hexane = 3 : 2), a yellow material identified as **3** can be isolated in 40% yield. Compound **3** was fully characterized by positive FAB mass spectrometry, NMR† (^1H, ^{31}P) and X-ray diffraction.‡ In the positive FAB mass spectrum, a peak at *m/z* 2429 corresponds to the intact selenide-centered diselenolate Cu^I cluster. Also appearing in the mass spectrum is a peak at *m/z* 2122 which can be attributed to loss of a dsep ligand giving $\{Cu_8(\mu_8\text{-}Se)[Se_2P(OPr^i)_2]_5\}^+$. The ^{31}P NMR spectrum displays a singlet with satellites (J_{PSe} 671 Hz) at δ 73. This clearly implies all dsep ligands of **3** are equivalent in solution.

One and a half molecules of **3** exist in the asymmetric unit with the Se(02) atom located at a crystallographic inversion center. Fig. 1 shows a thermal ellipsoid drawing of one of the two independent molecules of **3**. The copper atoms are arranged at the corners of an almost regular cube. Each selenium atom of the dsep ligand bridges two copper atoms. Thus dsep exhibits a 'tetrametallic tetraconnective'[10f] (μ_2, μ_2) coordination pattern and each occupies a square face of the cube. The average 'bite distance' is 3.784(2) Å, which is *ca.* 0.2 Å longer than that observed for the sulfur analogue.[2a] Each copper atom of the cube is coordinated to three selenium atoms of three different ligands. The averaged Cu–Se(dsep) bond length is 2.447 Å and the Se–Cu–Se bond angles range from 113.15(11) to 118.09(11)°. In addition to the distorted trigonal planar geometry around the copper atom, there is a strong interaction to the central selenium atom. The average Cu–Cu distance of **3** is 2.928 Å, which is *ca.* 0.08 Å shorter than that observed for Fenske's compound. Consequently, the bond length between

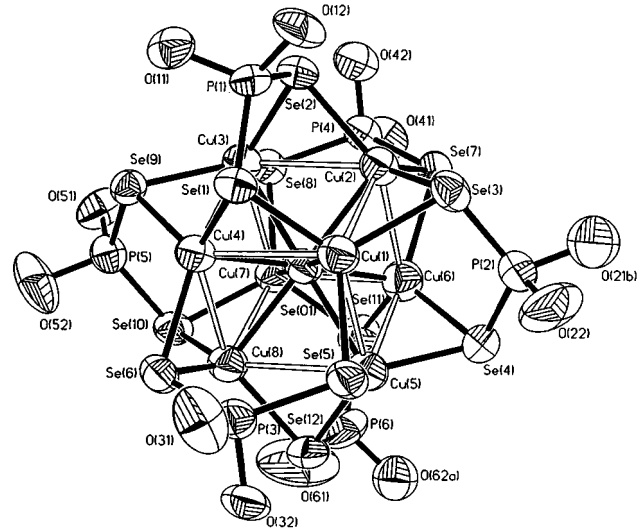

Fig. 1 The thermal ellipsoid drawing (50% probability) of one of the two independent molecules of **3**. The isopropyl groups are omitted for clarity. Selected bond lengths (Å): Se(01)–Cu(1) 2.550(3), Se(01)–Cu(2) 2.524(3), Se(01)–Cu(3) 2.577(3), Se(01)–Cu(4) 2.520(3), Se(01)–Cu(5) 2.546(4), Se(01)–Cu(6) 2.506(3), Se(01)–Cu(7) 2.532(3), Se(01)–Cu(8) 2.532(3), Cu(1)–Cu(2) 2.919(3), Cu(1)–Cu(4) 2.929(3), Cu(1)–Cu(5) 2.921(3), Cu(2)–Cu(6) 2.917(3), Cu(2)–Cu(3) 2.941(3), Cu(3)–Cu(4) 2.974(3), Cu(3)–Cu(7) 2.955(3), Cu(4)–Cu(8) 2.859(3), Cu(5)–Cu(6) 2.920(4), Cu(5)–Cu(8) 2.966(4), Cu(6)–Cu(7) 2.875(4), Cu(7)–Cu(8) 2.966(4).

the central selenide and the peripheral copper atoms ranges from 2.506(3) to 2.577(3) Å and is slightly shorter than that of $[Cu_{20}Se_{13}(PEt_3)_{12}]$, [2.605(3) Å]. Astonishingly the averaged $Cu–Se_{cen}$ bond length, (2.535 Å), in **3** is even shorter than that of the corresponding sulfide analogues (2.694[2a] and 2.585 Å[2b]). Overall owing to the lack of fourfold symmetry, molecule **3** has an idealized T_h point group symmetry. The central selenide atom in conjunction with the twelve selenium atoms of the ligands forms a body-centered icosahedron. Previously this type of geometry has only been observed upon two occasions, for **1** and $Cu_{26}Se_{13}(PEt_2Ph)_{14}$.[12]

Besides Fenske's cluster **1**, compound **3** is the only coordination complex possessing a μ_8-Se bridge. Nevertheless, μ_8-Se bridges do exist in several solid state materials of the type A_2Se (A = Li, Na, and K) with antifluorite structure.[13] It is worth noting that a metal atom in the center of a metallic cube is known for Ni[14] and Pd[15] and a remarkable solid state material, $K_4Cu_8Te_{11}$, in which a potassium ion is encapsulated in the center of a cubic Cu_8 core has also been reported.[16]

The P–Se distances of **3**, [2.144(7)–2.177(6) Å], are slightly shorter than those observed for bridging PSe_2 fragments in the solid state compounds $A_2AuP_2Se_6$ (A = K, Rb) [2.197(6)–2.258(6) Å],[17] $[Cs_2Cu_2P_2Se_6]$ [2.186(4)–2.202(5) Å],[18] and the molecular complexes $[Hg_4(Se_2)_2(PSe_4)_4]^{8-}$ [2.221(5)–2.237(5) Å][19] and $[Fe_2(CO)_4(PSe_5)_2]^{2-}$ [2.214(6)–2.216(6) Å.[20] Observation of a μ_2, μ_2 bridging mode in **3** is unusual and unprecedented for selenophosphate complexes. Three new clusters containing dsep ligands, $Ag_8(\mu_8\text{-}Se)[Se_2P(OPr^i)_2]_6$, $Ag_9(\mu_7\text{-}Se)[Se_2P(OPr^i)_2]_8$ and $Ag_{10}(\mu_7\text{-}Se)[Se_2P(OPr^i)_2]_8$ have also been characterized and details will be reported in due course.

The research grant (NSC 87-2113-M-033-003 to CWL, NSC87-2113-M-031-002 to JCW) from the National Science Council of Taiwan is greatly appreciated.

Notes and References

† $^{31}P\{^1H\}$ NMR ($CDCl_3$), δ 73 (J_{SeP} 671 Hz); ^1H NMR ($CDCl_3$), δ 1.37 [d, 72H, $CH(CH_3)_2$], 4.88 [m, 12H, $CH(CH_3)_2$]; $^{77}Se\{^1H\}$ NMR ($CDCl_3$), δ −59 (J_{SeP} 671 Hz). Unfortunately we were unable to detect the resonance frequency of the central selenide ion in the ^{77}Se NMR which might be caused by the long T_1 value. FAB MS, *m/z* 2429 (M^+), 2122 (M − dsep); Anal. Calc. for $C_{36}H_{84}Cu_8O_{12}P_6Se_{13}$: C, 17.80; H, 3.46. Found: C, 17.66; H, 3.34%.

‡ *Crystal data*: $C_{36}H_{84}Cu_8O_{12}P_6Se_{13}$, M = 2429.65; monoclinic, space group $P2_1/n$, a = 13.8341(8), b = 36.969(2), c = 21.9728(12) Å, β = 93.2630(10)°, V = 11219.3(11) Å^3, Z = 6, D_c = 2.158 Mg m^{-3}, $F(000)$ = 6960, T = 298(2) K.

An orange crystal with dimensions 0.20 × 0.20 × 0.40 mm was used for X-ray structural analysis. Intensity data were collected over one quadrant using the ω scan mode on a Siemens SMART CCD diffractometer equipped with graphite monochromated Mo-Kα radiation (λ = 0.710 73 Å). A total of 11 805 unique reflections were measured. The structure was solved by direct methods using SHELXTL-PLUS software package.[21] All Cu and Se atom positions were revealed on the first refinement. Other non-hydrogen atoms were located from subsequent difference Fourier syntheses. Parts of oxygen and carbon atoms of the isopropyl groups (7 out of 18) were found disordered. These disordered atoms were treated in an equal population model. Bond distances were constrained for disordered atoms and atoms connected to the disordered atoms during the structure refinement. These constraints were: P–O = 1.600 Å, O–C = 1.500 Å and C–C = 1.550 Å. The structure was refined by full-matrix least-squares method on F^2. All but disordered atoms and atoms attached to them were refined anisotropically. H-atoms were not included. Refinement converged to $R1$ = 0.0748 [$I > 2\sigma(I)$], $wR2$ = 0.1664 (all data) and S = 1.143 based on 940 variables, 43 restraints, and 11 805 reflections. CCDC 182/947.

1 D. Fenske, in *Clusters and Colloids-From Theory to Applications*, ed. G. Schmid, VCH, Weinheim, Germany, 1994.
2 C. W. Liu, R. T. Stubbs, R. J. Staples and J. P. Fackler, Jr., *J. Am. Chem. Soc.*, 1995, **117**, 9778; Z. X. Huang, S. F. Lu, J. Q. Huang, D. M. Wu and J. L. Huang, *Jiegou Huaxue* (*J. Struct. Chem.*), 1991, **10**, 213; I. G. Dance, R. Garbutt and D. Craig, *Inorg. Chem.*, 1987, **26**, 3732.
3 R. A. Wheeler, *J. Am. Chem. Soc.*, 1990, **112**, 8737; E. Furet, A. L. Beuze, J.-F. Halet and J.-Y. Saillard, *J. Am. Chem. Soc.*, 1995, **117**, 4936.
4 A. Ceriotti, G. Longoni, M. Manassero, M. Perego and M. Sansoni, *Inorg. Chem.*, 1985, **24**, 117; A. Ceriotti, A. Fait, G. Longoni, G. Piro, F. Demartin, M. Manassero, M. Perego and M. Sansoni, *J. Am. Chem. Soc.*, 1986, **108**, 8091; V. G. Albano, P. Chini, G. Ciani, S. Martinengo and M. Sansoni, *J. Chem. Soc., Dalton Trans.*, 1978, 463; V. G. Albano, M. Sansoni, P. Chini, S. Martinengo and D. Strumolo, *J. Chem. Soc., Dalton Trans.*, 1975, 305.
5 K. M. MacKay, B. N. Nicholson, W. T. Rhobinson and A. W. Sims, *J. Chem. Soc., Chem. Commun.*, 1984, 1276.
6 J. L. Vidal, W. E. Walker, R. L. Pruett and R. C. Schoening, *Inorg. Chem.*, 1979, **18**, 129; J. L. Vidal, W. E. Walker and R. C. Schoening, *Inorg. Chem.*, 1981, **20**, 238; L. M. Bullock, J. S. Field, R. J. Haines, E. Minshall, D. M. Smit and G. M. Sheldrick, *J. Organomet. Chem.*, 1986, **310**, C47.
7 L. Garlaschelli, A. Fumagalli, S. Martinengo, B. T. Heaton, D. O. Smith and L. Strona, *J. Chem. Soc., Dalton Trans.*, 1982, 2265; A. Fumagalli, S. Martinengo and G. Ciani, *J. Organomet. Chem.*, 1984, **273**, C46.
8 B. T. Heaton, L. Strona, R. Della Pergola, J. L. Vidal and R. C. Schoening, *J. Chem. Soc., Dalton Trans.*, 1983, 1941; J. L. Vidal, *Inorg. Chem.*, 1981, **20**, 243.
9 D. Fenske and H. Krautscheid, *Angew. Chem., Int. Ed. Engl.*, 1990, **29**, 1452.
10 J. R. Wasson, G. M. Woltermann and H. J. Stoklosa, *Fortschr. Chem. Forsch.* (*Top. Curr. Chem.*), 1973, **35**, 65; R. C. Mehrotra, G. Srivastava and B. P. S. Chauhan, *Coord. Chem. Rev.*, 1984, **55**, 207; K. C. Molloy and J. J. Zuckerman, *Acc. Chem. Res.*, 1983, **16**, 386; R. T. M. Tiekink, *Main Group Met. Chem.*, 1992, **15**, 161; I. Haiduc, *Rev. Inorg. Chem.*, 1981, **3**, 353; I. Haiduc, D. B. Snowerby and S.-F. Lu, *Polyhedron*, 1995, **14**, 3389.
11 V. Krishnan and R. A. Zingaro, *J. Coord. Chem.*, 1971, **1**, 1; M. V. Kudchadker, R. A. Zingaro and K. J. Irgolic, *Can. J. Chem.*, 1968, **46**, 1415; V. Krishnan and R. A. Zingaro, *Inorg. Chem.*, 1969, **8**, 2337; C. K. Jorgenson, *Mol. Phys.*, 1962, **5**, 485; A. A. G. Tomlinson, *J. Chem. Soc. A*, 1971, 1409; G. M. Larin and M. E. Dyatkina, *Izv. Akad. Nauk SSSR, Ser. Khim.*, 1972, **6**, 1413.
12 A. Deveson, S. Dehnen and d. Fenske, *J. Chem. Soc., Dalton Trans.*, 1997, 4491.
13 A. F. Wells, *Structural Inorganic Chemistry*, Oxford 5th ed., 1984.
14 D. Fenske, J. Ohmer and K. Merzweiler, *Angew. Chem., Int. Ed. Engl.*, 1988, **27**, 1512; J. G. Brennan, T. Siegrist, S. M. Stuczynki and M. L. Steigerwald, *J. Am. Chem. Soc.*, 1989, **111**, 9240; J. P. Zebrowski, R. K. Hayashi, A. Bjarnason and L. F. Dahl, *J. Am. Chem. Soc.*, 1992, **114**, 3121.
15 D. Fenske and C. Persau, *Z. Anorg. Allg. Chem.*, 1991, **593**, 61; D. Fenske, H. Fleischer and C. Persau, *Angew. Chem., Int. Ed. Engl.*, 1989, **28**, 1665.
16 Y. Park and M. G. Kanatzidis, *Chem. Mater.*, 1991, **3**, 781.
17 K. Chondroudis, T. J. McCarthy and M. G. Kanatzidis, *Inorg. Chem.*, 1996, **35**, 3451.
18 T. J. McCarthy and M. G. Kanatzidis, *Inorg. Chem.*, 1995, **34**, 1257.
19 K. Chondroudis and M. G. Kanatzidis, *Chem. Commun.*, 1997, 401.
20 J. Zhao, W. T. Pennington and J. W. Kolis, *J. Chem. Soc., Chem. Commun.*, 1992, 265.
21 SHELXTL-Plus 5.03. Siemens Analytical X-ray Instruments Inc., Karlsruhe, Germany, 1995.

Received in Cambridge, UK, 25th June 1998; 8/04852E

The intercalation compound $Li(Mn_{0.9}Co_{0.1})O_2$ as a positive electrode for rechargeable lithium batteries

A. Robert Armstrong, Robert Gitzendanner, Alastair D. Robertson and Peter G. Bruce*

School of Chemistry, University of St. Andrews, North Haugh, St. Andrews, Fife, UK KY16 9ST

By replacing only 10% of the Mn by Co in the layered lithium intercalation compound $LiMnO_2$ the amount of lithium that can be removed and reinserted is increased by 50% corresponding to an increase in the ability to store charge from 130 to 200 mA h g^{-1} at 100 μ A cm^{-2} and rendering this low cost/toxicity material of potential interest as a positive electrode in rechargeable lithium batteries; furthermore the cooperative Jahn–Teller distortion due to localised high spin $Mn^{3+}(3d^4)$ in $LiMnO_2$ appears to be suppressed for $Li_x(Mn_{0.9}Co_{0.1})O_2$; $x < 0.9$ (80% Mn^{3+} assuming Co^{3+}).

First generation rechargeable lithium batteries are now a major commercial success.[1] They utilise the layered intercalation compound, $LiCoO_2$, as the positive electrode from which lithium is removed on charging the cell and reinserted on discharge.[2,3] Only half the lithium may be removed and reinserted reversibly (Li_xCoO_2; $0.5 < x < 1$) limiting the practical capacity to store charge to *ca.* 130 mA h g^{-1}. In order to develop much needed second generation batteries, new lithium intercalation hosts are essential. The challenge facing solid state chemistry is to synthesise lithium intercalation compounds that possess a higher capacity to cycle lithium in a host which is cheaper and less toxic than $LiCoO_2$.[2] Several systems have been extensively investigated including those based on layered $LiNiO_2$ and the spinel $LiMn_2O_4$.[4–11] The former offers improved capacity of *ca.* 170 mA h g^{-1} while the latter (110 mA h g^{-1}) is cheaper and less toxic than $LiCoO_2$. Recently we reported the first synthesis of layered $LiMnO_2$, isostructural with $LiCoO_2$.[12–14] Key to the preparation was the use of a low temperature ion exchange route. Being a manganese oxide it has the potential to deliver a low cost/toxicity electrode. Most of the lithium may be removed on initial charging (> 200 mA h g^{-1} at 100 μA cm^{-2}) but only a proportion of this can be reinserted (*ca.* 130 mA h g^{-1}) rendering this otherwise attractive cathode of less interest. By replacing only 10% of the Mn by Co, a material is obtained, the cost and toxicity of which remain sufficiently low to be of industrial interest and for which the ability to sustain a high capacity on cycling (200 mA h g^{-1} on cycling at 100 μA cm^{-2}) is enhanced.

Synthesis of $Li(Mn_{0.9}Co_{0.1})O_2$ employed the ion exchange method reported previously.[12] $Na(Mn_{0.9}Co_{0.1})O_2$ was synthesised by mixing Na_2CO_3, $Mn(CH_3CO_2)_2{\cdot}4H_2O$ and $Co(CH_3CO_2)_2{\cdot}4H_2O$ in water, drying by rotary evaporation then heating initially at 250 °C for 3 h then 670 °C for 1 h in air. The resulting solid was subjected to ion exchange by refluxing in a 5–10 fold excess of LiBr in hexanol at 150 °C for 8 h. Rietveld refinement using powder neutron data collected on POLARIS (ISIS, RAL, Oxfordshire) confirmed that the structure is layered and isostructural with $LiCoO_2$ (α-$NaFeO_2$ structure). A good fit was obtained between the observed and calculated powder diffraction profiles [R_{wp} = 0.026, rhombohedral cell with lattice parameters a = 2.8750(2) Å and c = 14.3930(8) Å, c/a = 5.006], Fig. 1. The structure is composed of close packed oxide ion layers stacked to yield a cubic close packed arrangement, a sheet of octahedral sites is located between each pair of oxide layers and alternate sheets are occupied by transition metal and lithium ions. The very different scattering lengths of Mn and Co made it possible to refine their occupancies on the shared transition metal sites. Values for Mn and Co of 0.93(1) and 0.07(1) were obtained. We have also synthesised Co substituted compounds up to $Li(Mn_{0.5}Co_{0.5})O_2$ and refinement with neutrons shows a continuous increase of the Co content on the transition metal sites and an associated contraction of the *a*-axis corresponding to shortening of the TM-O distances (TM = transition metal), as expected for a continuous solid solution. The *a*-axis contracton is consistent with replacement of Mn^{3+} by Co^{3+} rather than Co^{2+}/Mn^{4+}. Atomic emission analysis revealed a slightly lithium deficient composition of $Li_{0.85}(Mn_{0.9}Co_{0.1})O_2$ which agrees well with the amount of lithium that can be removed and inserted electrochemically and with the neutron refinement of the Li site occupancy.

Mn^{3+} is a Jahn–Teller active ion and in pure $LiMnO_2$ it results in a distortion from the ideal rhombohedral structure to monoclinic symmetry.[12] The cooperative Jahn–Teller distortion persists on deintercalation giving rise to a two phase mixture of monoclinic $LiMnO_2$ and rhombohedral $Li_{0.5}MnO_2$ until the $Li_{0.5}MnO_2$ composition is reached at which the structure becomes a single rhombohedral phase. At this point only 50% of the transition metal sites are occupied by the Jahn–Teller active Mn^{3+} ion. It appears that a combination of cobalt substitution and slight lithium deficiency is enough in the case of $Li_{0.85}(Mn_{0.9}Co_{0.1})O_2$ to suppress the cooperative Jahn–Teller distortion despite 75% of the transition metal sites being occupied by Mn^{3+} (assuming Co^{3+}). We have inserted lithium into $Li_{0.85}(Mn_{0.9}Co_{0.1}O_2)$ and find that even for $Li_{0.9}(Mn_{0.9}Co_{0.1}O_2)$ (80% Mn^{3+} if Co^{3+}) there is no evidence for a cooperative distortion in the X-ray or neutron data. The Jahn–Teller distortion in $LiMnO_2$ is driven by the localised high spin $3d^4$ configuration of Mn^{3+}. It is interesting that such a low level of Co^{3+} suppresses the distortion. Understanding the electronic structure in detail and particularly investigating the origin of the suppression of the cooperative Jahn–Teller distortion is beyond the scope of this paper and necessitates a subsequent study,

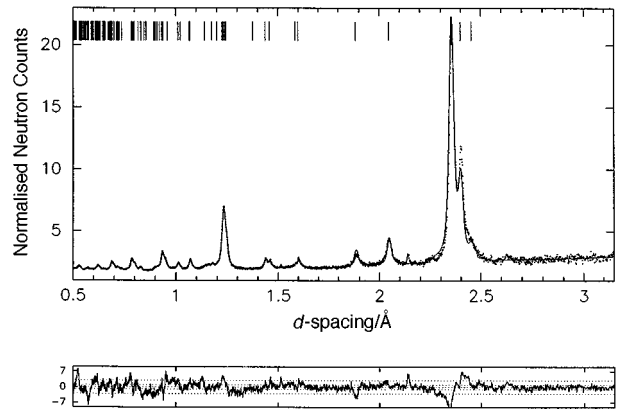

Fig. 1 Powder neutron diffraction data for $Li_{0.85}(Mn_{0.9}Co_{0.1})O_2$. Dots, experimental points points; solid line, fit by a layered structure and lower solid line, difference plot. The peak at d = 2.15 Å arises from the vanadium sample can.

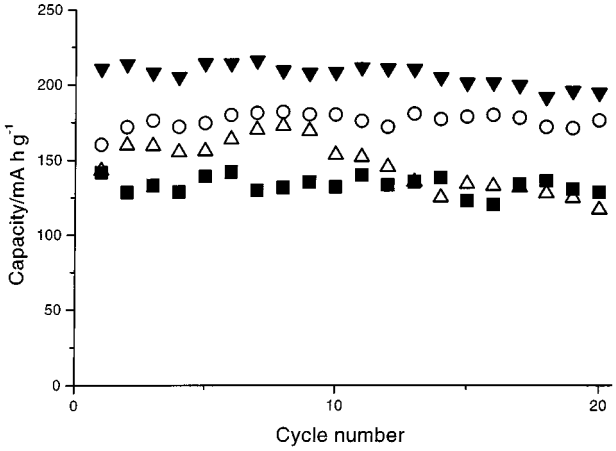

Fig. 2 Variation of specific discharge capacity with cycle number at 100 μA cm^{-2} and 2.6–4.8V; for layered $LiMnO_2$ and three Co doped samples. (△) $Li(Mn_{0.95}Co_{0.05})O_2$, (▼) $Li(Mn_{0.90}Co_{0.10})O_2$, (○) $Li(Mn_{0.85}Co_{0.15})O_2$, (■) $LiMnO_2$.

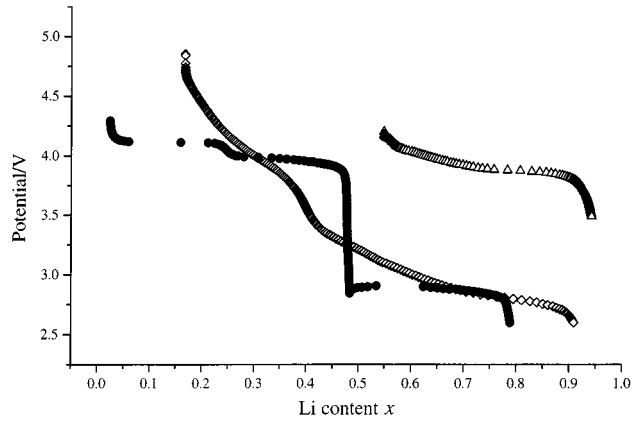

Fig. 3 Discharge curves for: (◇) layered $LiMn_{0.9}Co_{0.1}O_2$, (●) $LiMn_2O_4$ spinel and (△) layered $LiCoO_2$

already underway, which will include establishing the oxidation states of Mn and Co.

The performance of the material as an intercalation electrode in a cell was investigated by forming a composite between the intercalation compound, super S carbon and Kynar Flex 2801 binder (a copolymer based on PVDF) in the weight ratios 85 : 10 : 5. The electrode was cast onto Al foil. Cycling was performed in three-electrode cells (Li counter and reference) in 1 M $LiPF_6$ in EC–DMC (2 : 1) as electrolyte and at a constant current density of 100 μA cm^{-2} (14 mA g^{-1}) within the potential range 2.6–4.8 V, Fig. 2. The discharge capacity on the first cycle is 210 mA h g^{-1} and ranges between this value and 200 mA h g^{-1} up to twenty cycles (the variation between different cells is < 5%), demonstrating a substantial improvement in capacity compared with $LiMnO_2$ and eliminating the capacity loss on the first cycle. Why might this be so?

Cycling lithium in the spinel host $LiMn_2O_4$ over the range $Li_{1+x}Mn_2O_4 (0 < x < 1)$, involves a two phase reaction between cubic $LiMn_2O_4$ and tetragonal $Li_2Mn_2O_4$, arising from the Jahn–Teller distortion which occurs when more that 50% of the octahedral 16d sites in spinel are occupied by Mn^{3+}.[6] As a result, there is an abrupt change in the unit cell volume on Li cycling as one phase converts to the other, leading to disconnection of the particles and the formation of isolated regions in the electrode incapable of storing lithium.[15] A similar first order phase change occurs in the case of layered $LiMnO_2$ within the first cycle. We also know from extensive X-ray and neutron diffraction studies, HREM and electrochemical data that $LiMnO_2$ converts to a spinel phase on cycling.[16] The absence of a Jahn–Teller distortion in $Li_{0.85}(Mn_{0.9}Co_{0.1})O_2$ may be related to the elimination of the abrupt capacity loss suffered by $LiMnO_2$ within the first cycle. Further work will be carried out, including longer term cycling, to better understand the mechanism of intercalation in the Co doped materials and to understanding how a small proportion of Co modifies the process compared with pure $LiMnO_2$.

Results from compositions which neighbour $Li_{0.85}(Mn_{0.9}Co_{0.1})O_2$ are also shown in Fig. 2. The data indicate that the capacity retention is even better for compositions with more than 10% Co, however the overall capacity is somewhat reduced.

Only a proportion of the capacity is delivered above 4 V *vs.* Li^+/Li, Fig. 3. However, the move to 2.3 V electronics in mobile communications and other portable applications coupled with the use of graphite anodes which deliver a large proportion of their capacity at a voltage near that of lithium metal, makes 3 V electrodes attractive for future lithium-ion batteries. The intense current interest in α-MnO_2 and its derivatives, which operate at 3 V, bears witness to this.[17]

P. G. B. is indebted to the EPSRC, the EU and NEDO for financial support and to the staff of the Rutherford–Appleton Laboratory for assistance with neutron data collection.

Notes and References

1 B. Scrosati, *Nature*, 1995, **373**, 557.
2 P. G. Bruce, *Chem. Comm*., 1997, 1817.
3 K Mizushima, P. C. Jones, P. J. Wiseman and J. B. Goodenough, *Mater. Res. Bull*., 1980, **15**, 783.
4 W. Li, J. N. Reimersw and J. R. Dahn, *Solid State Ionics*, 1993, **67**, 123.
5 A. Rougier, P. Gravereau and C. Delmas, *J. Electrochem. Soc*., 1996, **143**, 1168.
6 M. M. Thackeray, W. I. F. David, P. G. Bruce and J. B. Goodenough, *Mater. Res. Bull*., 1993, **18**, 461.
7 J. M. Tarascon, W. R. McKinnon, F. Coowar, T. N. Bowmer, G. Amatucci and D. Guyomard, *J. Electrochem. Soc*., 1994, **141**, 1421.
8 R. J. Gummow, A. de Kock and M. M. Thackeray, *Solid State Ionics*, 1994, **69**, 59.
9 H. Huang and P. G. Bruce, *J. Power Sources*, 1995, **54**, 52.
10 Y. Gao and J. R. Dahn, *J. Electrochem. Soc*., 1996, **143**, 100.
11 G. Pistoia, D. Zane and Y. Zhang, *J. Electrochem. Soc*., 1995, **142**, 2551.
12 A. R. Armstrong and P. G. Bruce, *Nature*, 1966, **381**, 499.
13 F. Capitaine, P. Gravereau and C. Delmas, *Solid State Ionics*, 1996, **89**, 197.
14 G. Vitins and K. West, *J. Electrochem. Soc*., 1997, **144**, 2587.
15 P. G. Bruce, A. R. Armstrong and H. Huang, *J. Power Sources*, 1997, **68**, 19.
16 J. Shao-Horn, S. A. Hackney, A. R. Armstrong, P. G. Bruce, R. Gitzendanner, C. S. Johnson and M. M. Thackeray, *Electrochem. Soc. Abstr*., 1997, **97–2**, 98; *J. Electrochem. Soc*., submitted.
17 M. H. Rossouw, D. C. Liles and M. M. Thackeray, *Prog. Batt. Batt. Mater*., 1996, **15**, 8.

Received in Bath, UK, 14th May 1998; 8/03741H

Synthesis and characterization of an oxasapphyrin-uranyl complex

Jonathan L. Sessler,* Andreas Gebauer, Michael C. Hoehner and Vincent Lynch

Department of Chemistry and Biochemistry, The University of Texas at Austin, Austin, TX 78712, USA. E-mail: sessler@mail.utexas.edu

Reaction of monooxasapphyrin with uranyl diacetate in the presence of triethylamine leads to the formation of a stable, in-plane aromatic uranyl complex.

Sapphyrin (*e.g.* **1**) is an aromatic 22 π-electron expanded

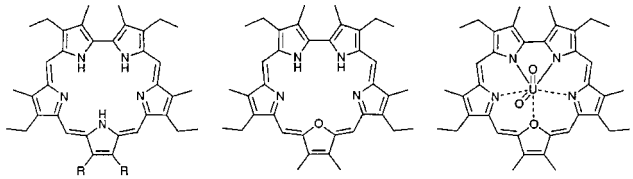

1a R = Me
1b R = Et

2 **3**

porphyrin that has been known for more than 30 years.[1,2] Its pioneering role in expanded porphyrin research[2a–c] and the more recent finding that it[2d] and other related materials[3] bind anions in their protonated forms continues to inspire interest in these pentapyrrolic systems. In spite of this increased attention, the metal coordination chemistry of sapphyrin remains woefully underdeveloped.[2] At first blush this seems surprising since one of the most intuitively appealing aspects of sapphyrin[2a] is that it should act to stabilize complexes with larger cations than those normally coordinated by porphyrins (*e.g.* Gd^{3+}, UO_2^{2+}, *etc.*).

However, efforts to obtain such complexes have so far failed.[2a,4]† Recently, we prepared an organic-soluble, furan-containing analogue of sapphyrin, system **2**,[8] and now wish to report that this monooxa species supports the formation of a stable, in-plane uranyl complex (**3**).

The rationale for using **2** as a possible uranyl chelating ligand derived from an appreciation of what happens when sapphyrin **1b** is treated with UO_2^{2+}. Under most reaction conditions the macrocycle is either returned unchanged or suffers decomposition. However, in the presence of methanol a uranyl complex (**4**) of what is a formally a reduced form of sapphyrin may be isolated.[4] This finding was rationalized in terms of intermediates **I**, **II** and **III** (Scheme 1) playing a critical role in mediating the key nucleophilic attack step leading to the formation of the reduced, methoxy-functionalized product **4**.

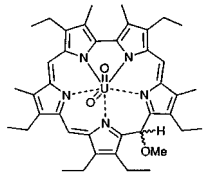

4

This led us to consider that a stable, aromatic uranyl complex might be obtainable were the central pyrrole of the tripyrrane 'replaced' by a furan. Such a replacement would also create a ligand that, once deprotonated, would be dianionic and hence well suited to coordinate the uranyl cation on a charge matching basis.

As it transpired, treatment of the bis-hydrochloride salt of **2**, but not **1**·2HCl,[4] with uranyl diacetate dihydrate in acetonitrile containing triethylamine led, after column chromatographic purification, to the formation of a green metallic solid. This material displays a UV–VIS spectrum typical of a sapphyrin

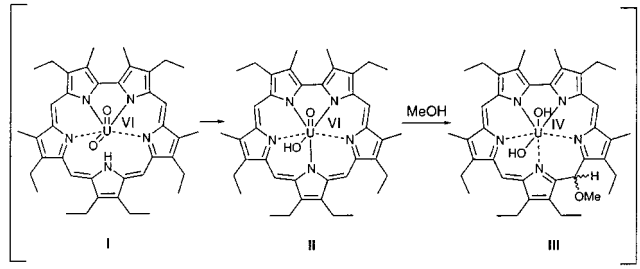

Scheme 1 Proposed intermediates in the formation of **4**

species with one strong Soret band at 483 nm and three weaker Q-type absorption bands at 624, 647 and 708 nm (Fig. 1). The significant bathochromic shift (29 nm) of the Soret band compared to the starting oxasapphyrin bis-HCl salt (Soret band at 454 nm, Q-type bands at 625, 633, 669 and 689 nm), together with the bathochromic shift and different aspect of the Q-type bands (Fig. 1), provided a preliminary 'hint' that (i) the metal insertion process was successful and (ii) the monooxasapphyrin skeleton was still intact.

Proton NMR spectroscopic studies revealed the presence of two sets of peaks at the low field frequencies (*i.e.* 10.37 and 10.78 ppm, respectively) typical of aromatic sapphyrin *meso* protons.[9] On the other hand, no signals ascribable to internal NH protons were observed. Since sapphyrins such as **1** and **2** are known to be quite basic (*i.e.* easily protonated),[2,10] this finding is interpreted as being consistent with the formation of a metal complex wherein the key metal-to-ligand contacts involve, at a minimum, all four of the nitrogens present in the macrocyclic core (*i.e.* structure **3**). The presence of a uranyl moiety was also implied by the identification of a ν(O=U=O) band in the IR spectrum at 936 cm^{-1}. Final proof for the formation of the proposed 1 : 1 uranyl complex then came from an X-ray crystallographic analysis.

Crystals of **3** were grown by allowing a dichloromethane solution of the complex to diffuse slowly into hexanes.‡ As illustrated in Fig. 2(*a*) the uranyl cation is located almost in the center of the sapphyrin. The uranyl-to-nitrogen distances of 2.449(4) Å (U–N1), 2.470(3) Å (U–N5), 2.582(4) Å (U–N2), and 2.587(3) Å (U–N4) are all very similar to one another. By contrast, the oxygen of the sole furan subunit, at a distance of 2.791(3) Å (U–O3), is significantly further away. The ur-

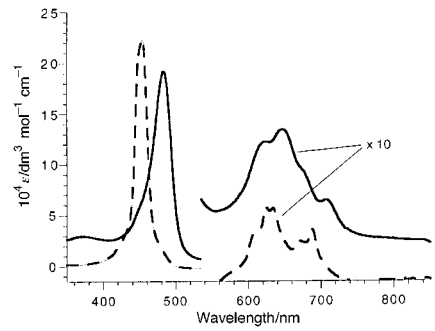

Fig. 1 UV–VIS spectrum of the monooxasapphyrin-uranyl complex **3** (—) as recorded in CH_2Cl_2. Also shown for comparison is the spectrum (---) of the starting monooxasapphyrin macrocycle (**2**·2HCl).

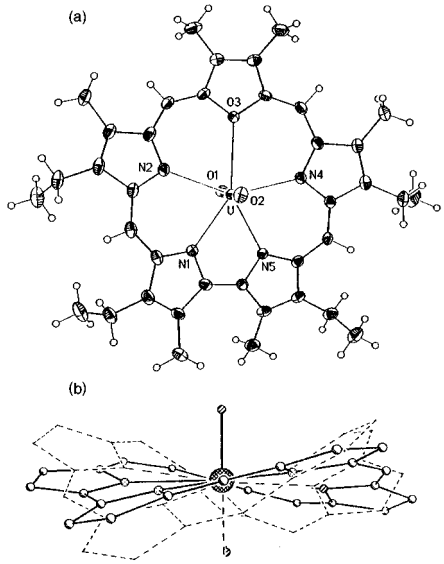

Fig. 2 (*a*) Front view of $C_{38}H_{42}N_4O_3U$ (**3**) showing the heteroatom labeling scheme. Thermal ellipsoids are scaled to the 30% probability level. H atoms are scaled to an arbitrary size. (*b*) Overlay of the side views of **3** (ball-and-stick model) and the pentaphyrin–uranyl complex **5** (dashed lines). The β-substituents of both have been omitted for clarity.

anium(VI) cation is found to sit within a distorted pentagonal bipyramidal ligand environment (the relevant angles are: 75.00(11)° (N1–U–N2), 72.97(10)° (N2–U–O3), 74.18(10)° (O3–U–N4), 74.75(11)° (N4–U–N5), 64.11(12) (N1–U–N5) and 176.29(13) (O1–U–O2), respectively.

Complex **3** possesses a saddle-shaped conformation as illustrated in Fig. 2(*b*). However, the distortion found is much less than that observed in the case of an earlier reported pentaphyrin uranyl complex **5** (*cf.* Fig. 2).[6b] To the extent that

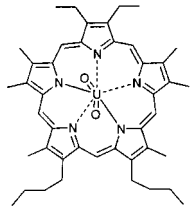

5

the binding core of pentaphyrin is expected to be larger than that of sapphyrin, this comparative finding lead us to suggest that the saddle-shaped distortion of the uranyl pentaphyrin **5**, and to a lesser extent that of the oxasapphyrin complex **3**, is caused by a macrocyclic core that is too big (as opposed to too small) for the uranyl cation. This is reflected in the average N–UO_2^{2+} bond distances; these are 2.522 and 2.541 Å, in the case of **3** and **5**, respectively.

Complex **3** was also studied by cyclic voltammetry.§ Here, one quasi-reversible reduction wave was observed at 0.62 V (100 mV s^{-1}) that most likely belongs to the UO_2^{2+}–UO_2^{+} couple. In addition, one irreversible reduction wave at 1.58 V (100 mV s^{-1}), assignable to a UO_2^{2+} to U^{4+} reduction process, and one irreversible oxidation wave at 0.64 V (100 mV s^{-1}), ascribed to the oxasapphyrin ligand, are also observed. The quasi-reversible wave of the UO_2^{2+}–UO_2^{+} couple is found to fall at a significantly more positive potential than the corresponding uncomplexed UO_2^{2+}–UO_2^{+} couple (E_0 = 0.163 V),[11] as would be expected in light of the favorable bonding interactions present in complex **3**.

Complex **3** was found to be very stable when stored as a solid or in CH_2Cl_2 solution over long periods of time at room temp. in the presence of air. It was also found to be stable, as a CH_2Cl_2 solution, when exposed briefly to aqueous solutions of pH = 2 (70% decomposition after 72 h), or when treated with those of pH = 11 for longer periods (no apparent decomposition after 72 h). By contrast, almost complete decomplexation was observed within a few min when HOAc (10% v/v) was added to a solution of **3** in $CHCl_3$.

In summary, we have described the first example of a stable in-plane metal cation complex of a sapphyrin derivative. It provides a further cogent demonstration of how small changes in ligand structure (in the present instance an O for NH 'replacement') can influence significantly the metal chelation chemistry of a given system.

Support of this research by the National Science Foundation (Grants CHE 9122161 and CHE 9725399 to J. L. S.) is gratefully acknowledged.

Notes and References

† Uranyl complexes of two other pentapyrrolic systems, namely superphthalocyanine[5] and pentaphyrin[6] are known. Also known are sitting-atop η^2-Rh^I and -Ir^I complexes as well as 1 : 1 Zn^{II} and Co^{II} derivatives.[2a,e,7]

‡ *Crystal data* for **3**: dark green crystals, monoclinic, $P2_1/n$, Z = 4, a = 11.990(1), b = 15.351(1), c = 18.954(1) Å, β = 104.53(1)°, V = 3377.1(5) $Å^3$, D_c = 1.65 g cm^{-3}, μ = 48.49 cm^{-1}. 11 387 reflections were measured, of which 9466 were unique [R_{int} (F^2) = 0.021]. The structure was refined on F^2 to a $R_w(F^2)$ = 0.0857 with a goodness of fit = 1.074 for 416 parameters, while the conventinal $R(F)$ = 0.0358. CCDC 182/945.

§ Cyclic voltammetry was carried out (25 ± 2 °C) under dry argon using a Bioanalytic Systems Inc. (BAS) CV-59W version 2 MF9093 voltammetric analyzer. Dry MeCN was the solvent, 0.1 M $NBu^n_4PF_6$ the electrolyte, a 1.6 mm Pt disk the working electrode, and a Pt wire the auxilary electrode. A Ag–AgCl couple, separated from the bulk solution by means of a porous Vycor plug, was used as the reference electrode.

¶ Determined by recording the change in absorption at 455 nm as a function of time.

1 R. B. Woodward, in *Aromaticity: An Internatinal Symposium Sheffield, 1966*, Special Publication no. 21, The Chemical Society, London, 1966.

2 (*a*) V. J. Bauer, D. L. J. Clive, D. Dolphin, J. B. Paine III, F. L. Harris, M. M. King, J. Loder, S.-W. C. Wang and R. B. Woodward, *J. Am. Chem. Soc.*, 1983, **105**, 6429; (*b*) M. J. Broadhurst, R. Grigg and A. W. Johnson, *J. Chem. Soc., Perkin Trans. 1*, 1972, 2111; (*c*) M. J. Broadhurst, R. Grigg and A. W. Johnson, *Chem. Commun.*, 1969, 23; (*d*) J. L. Sessler, M. J. Cyr, V. Lynch, E. McGhee and J. A. Ibers, *J. Am. Chem. Soc.*, 1990, **112**, 2810; (*e*) A. K. Burrell, J. L. Sessler, M. Cyr, E. McGhee and J. A. Ibers, *Angew. Chem.*, 1991, **103**, 83; *Angew. Chem., Int. Ed. Engl.*, 1991, **30**, 91; (*f*) J. L. Sessler, J. Lisowski, K. A. Boudreaux, V. Lynch, J. Barry and T. J. Kodadek, *J. Org. Chem.*, 1995, **60**, 5975; (*g*) L. Latos-Grazynski, K. Rachlewics, *Chem. Eur. J.*, 1995, **1**, 68; (*h*) R. Paolesse, S. Licoccia, M. Spagnoli, T. Boschi, R. G. Khoury and K. M. Smith, *J. Org. Chem.*, 1997, **62**, 5133; (*i*) C. Brückner, E. D. Sternberg, R. W. Boyle and D. Dolphin, *Chem. Commun.*, 1997, 1689.

3 J. L. Sessler and S. J. Weghorn, *Expanded, Contracted and Isomeric Porphyrins*, Elsevier, Oxford, 1997, pp. 453–489 and references therein.

4 A. K. Burrell, M. C. Cyr, V. Lynch and J. L. Sessler, *J. Chem. Soc., Chem. Commun.*, 1991, 1710.

5 V. W. Day, T. J. Marks and W. A. Wachter, *J. Am. Chem. Soc.*, 1975, **97**, 4519; T. J. Marks and D. R. Stojakovic, *J. Am. Chem. Soc.*, 1978, 1695; E. A. Cuellar, D. R. Stojakovic and T. J. Marks, *Inorg. Synth.*, 1980, **20**, 97.

6 (*a*) A. Gossauer, *Bull. Soc. Chim. Belg.*, 1983, **92**, 793; (*b*) A. K.Burrell, G. Hemmi, V. Lynch and J. L. Sessler, *J. Am. Chem. Soc.*, 1991, **113**, 4690.

7 J. L. Sessler, M. J. Cyr and A. K. Burrell, *Synlett*, 1991, 127.

8 J. L. Sessler, M. C. Hoehner, A. Gebauer, A. Andreivsky and V. Lynch, *J. Org. Chem.*, 1997, **62**, 9251.

9 For typical proton NMR chemical shift data for sapphyrin see: J. L. Sessler and S. J. Weghorn, *Expanded, Contracted and Isomeric Porphyrins*, Elsevier, Oxford, 1997, pp. 253–302 and references therein.

10 J. L. Sessler, M. Cyr and A. K. Burrell, *Tetrahedron*, 1992, **48**, 9661.

11 J. R. Brand and J. W. Cobble, *Inorg. Chem.*, 1970, **9**, 912.

Received in Columbia, MO, USA, 21st May 1998; 8/03975E

An unprecedented triply interpenetrated chiral network of 'square-planar' metal centres from the self-assembly of copper(II) nitrate and 1,2-bis(4-pyridyl)ethyne

Lucia Carlucci, Gianfranco Ciani,* Piero Macchi and Davide M. Proserpio

Dipartimento di Chimica Strutturale e Stereochimica Inorganica and Centro CNR, Via G. Venezian 21, 20133 Milano, Italy. E-mail: davide@csmtbo.mi.cnr.it

Copper(II) nitrate reacts with 1,2-bis(4-pyridyl)ethyne (bpethy) in ethanol to yield mixtures containing, beside to a one-dimensional ladder-like polymer, a networked [Cu(bpethy)$_2$] species, with a triply interpenetrated chiral frame based on pseudo-square planar metal centres, showing a topology theoretically predicted but never observed before, and containing uncoordinated ligands as guest molecules.

The crystal engineering of networked coordination polymers, of potential utility as zeolite-like materials, has produced in recent times novel interesting assemblies by using suitable bidentate spacer ligands. Among these an important class is represented by ligands containing two 4-pyridyl donor units interconnected by chains or groups of different types, which can afford variated lengths, linear or non-linear geometries, and conformationally rigid or non-rigid molecular skeletons. With the most simple of these ligands, *i.e.* 4,4′-bipyridyl, a variety of architectures have been obtained in the past years.[1] The use of longer bis(4-pyridyl) spacers has afforded very interesting structural motifs, as double helices,[2] double sheets,[3] interpenetrated ladders[4,5] and brick-wall frames,[4] interpenetrated diamondoid nets[6] and other noteworthy species.[7,8] We have studied the self-assembly process of one of these ligands, the rigid linear 1,2-bis(4-pyridyl)ethyne (bpethy), with copper(II) nitrate.

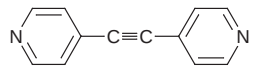

bpethy

The choice of such building elements was performed with the aim to gain some control of the networking process, since the nitrate anions, due to their donor ability, are known to give rise either to T-shaped metal centres (metal to ligand molar ratio 1 : 1.5)[1a,4] or to pseudo-square planar metal centres (metal to ligand molar ratio 1 : 2).[1b] Moreover, in the latter case an array of single sheets of squares, commonly observed with 4,4′-bipyridyl,[1b,9] seemed to us rather unlikely, taking into account the increased length of bpethy (*ca.* 9.8 *vs.* 7.1 Å). Looking, therefore, for a 3D network of square planar centres as the target, besides the prototypical frame of NbO (topology $6^4 8^2$, A in Scheme 1) we have found only two other examples,

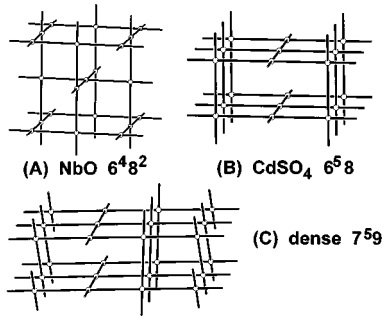

Scheme 1

suggested by O'Keeffe,[10] and referred to as the tetragonal $CdSO_4$ (B)† and the so-called 'dense' net (C). In a very recent communication a product from the self-assembly of copper(II) nitrate and 1,2-bis(4-pyridyl)ethane has been described,[11] containing a (twofold interpenetrated) 3D net based on pseudo-square planar copper centres, which has been erroneously ascribed to the NbO topological type (A) but, indeed, belongs to the $CdSO_4$ one (B). We report here the first example of a (triply interpenetrated) coordination network of the third topological type (C). Again a theoretically anticipated topology, of unlike existence within simple inorganic compounds, can be accomplished in the area of coordination polymers. The reactions of $Cu(NO_3)_2 \cdot 3H_2O$ with bpethy afford mixtures of products. On layering over an ethanolic solution of the salt an ethanolic solution of the ligand (molar ratio 1 : 2) the formation of small elongated blue crystals is observed after few days. The product, investigated by single crystal X-ray analysis,‡ corresponds to $[Cu(bpethy)(NO_3)_2] \cdot 0.5EtOH$ **1**. On allowing the solution to concentrate almost to dryness by evaporation, the reaction further proceeds, giving flat hexagonal blue crystals of a second species **2**, also characterized by X-ray analysis,‡ together with other minor unidentified products. Compound **1** consists of one-dimensional linear chains of Cu^{II} ions linked by bpethy ligands, which run in parallel pairs joined by bridging nitrate anions, in a ladder-like fashion. The metal ions exhibit Jahn–Teller distorted octahedral coordinations (2 N atoms of bpethy, 2 O atoms of a chelating nitrate, and 2 O atoms of two asymmetric μ-η^1-anions, see Fig. 1, top). The ladders propagate in two different directions (rotated by 39.6°) as shown in Fig. 1, bottom. Compound **2** is a more complex and interesting species, formulated as $[\{Cu(bpethy)_2(H_2O)_2\}\{Cu(bpethy)_2(NO_3)(H_2O)\}_2][NO_3]_4 \cdot bpethy \cdot 1.33H_2O$. It contains a fascinating tridimensional polymeric architecture consisting of three interwoven nets, each belonging to the topological type C of Scheme 1. A single net (Fig. 2) presents linear –Cu–bpethy–Cu–bpethy– chains both parallel and perpendicular to the trigonal crystallographic ***c*** axis, joined at the square-planar metal centres (Cu···Cu contacts all *ca.* 13.6 Å). The chains perpendicular to

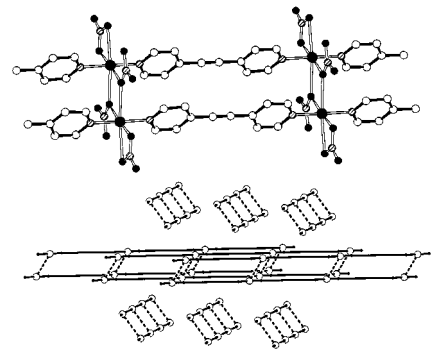

Fig. 1 A view of one mesh of the ladder in **1** (top) and a schematic view of the packing of the ladders (bottom)

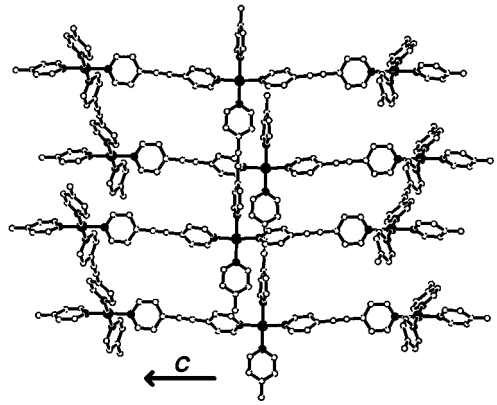

Fig. 2 A view of part of a single dense net C in compound **2**

the ***c*** axis are rotated by 120° about this axis on passing to each successive layer, in a 3_1 helical disposition, thus resulting in a chiral network. The topology of this network exhibits some peculiar features among the known four-connected nets:[10] (i) it is unique in not containing circuits shorter than heptagons; (ii) it has the highest 'topological density'§ (and is thus termed 'dense'); (iii) each metal node is ideally surrounded by eight equidistant neighbours but directly connected only to four of these. The voids present in a single net are too large to be left filled only by the counter ions. Thus three $[Cu(bpethy)_2]$ nets of the same topology interpenetrate as illustrated in Fig. 3.¶ Indeed, the three nets are not identical because of the difference in the coordination of the Cu^{II} ions: the octahedral metal environments show in all cases four equatorial N-bonded pyridyl groups, but the axial (loosely bonded) ligands are two water molecules in one of the three nets (net I, black), and a water molecule and a η^1-nitrate anion in the other two (nets II and III, white and dotted). In spite of the threefold interpenetration there are still voids that contain, besides free nitrate anions, disordered water molecules and uncoordinated bpethy ligands (Fig. 3). These molecules, moreover, form hydrogen

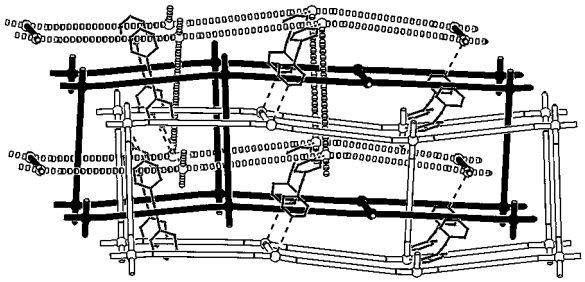

Fig. 3 A schematic view of the three interpenetrated nets C in **2**. Net I (black) is crystallographically independent, while nets II and III (white and dotted) are related by twofold axes. The solvated ligand molecules are also shown with their hydrogen bonds (dashed lines).

bonds involving the two nitrogen atoms and two water molecules coordinated to the copper ions of nets II and III (N···O 2.82 Å), giving rise to hydrogen bond bridges Cu–(H_2O)–bpethy–(H_2O)–Cu, of length 17.59 Å. Taking into accout these interactions nets II and III together can be described as an unique tridimensional five-connected array, interpenetrated by the four-connected net I. Interpenetration phenomena involving different types of nets are quite rare; we have found only one previous example, *i.e*. the interpenetration of two different diamondoid networks in K_2PdSe_{10}.[12] Though the preference of compound **2** for the C type topology, rather than A or B, remains unexplained, the unusual features observed (new topology, interpenetration of different motifs, network chirality, guest molecules anchored to the frame) make this species an interesting solid state rarity, as well as a notewhorty reference structure for the engineering of frames based on square-planar metal centres.

Notes and References

† This net can be sligthly distorted in such a manner to tolerate the presence of tetrahedral centres substituting the square planar centres. This is the case for $CdSO_4$ itself as well as for the coordination polymer $[Ag_2$(hexamethylenetetramine)$][NO_3]_2$; O. M. Yaghi, H. Li and M. O'Keeffe, *Mater. Res. Soc. Symp. Proc.*, 1997, **453**, 127.

‡ *Crystal data*: **1** $[Cu(bpethy)(NO_3)_2]\cdot 0.5EtOH$, monoclinic, space group *C*2/*c* (no. 15), a = 25.540(8), b = 9.186(3), c = 15.482(12) Å, β = 117.08(4)°, V = 3234(3) Å^3, Z = 8, Dc = 1.605 Mg m^{-3}, final R value 0.0933 for 1039 independent absorption corrected (ψ-scan) reflections [$I > 2\sigma(I)$].

2: $[\{Cu(bpethy)_2(H_2O)_2\}\{Cu(bpethy)_2(NO_3)(H_2O)\}_2](NO_3)_4\cdot bpethy\cdot 1.33H_2O$, trigonal, space group $P3_121$ (no. 152), $a = b$ = 13.652(1), c = 40.648(2) Å, V = 6560.9(8) Å^3, Z = 3, D_c = 1.450 Mg m^{-3}, final R value 0.0789 for 3952 independent absorption corrected (SADABS) reflections [$I > 2\sigma(I)$].

The data collections were performed by the ω-scan method, Mo-Kα radiation (λ = 0.710 73 Å), at 293 K on an Enraf-Nonius CAD-4 diffractometer for **1** and at 243 K on a SMART-CCD area-detector diffractometer for **2**, within the limits $3 < \theta < 25°$ (**1**) and $1 < \theta < 26°$ (**2**). The structures were solved by direct methods (SIR97)[13] and refined by full-matrix least squares (SHELX97).[14] Anisotropic thermal factors were assigned in **1** to Cu and the NO_3^- atoms and in **2** to all the non-hydrogen atoms except for a disordered nitrate and a solvated water molecule. The assignment of the absolute structure for **2** was confirmed by the statistics and the refinement of the absolute structure parameter as implemented in SHELX-97, to a value of 0.07(4).[15] All the diagrams were obtained using the SCHAKAL97 program.[16] CCDC 182/953.

§ The topological density has been defined[10] as the cumulative sum of the numbers of topological neighbours for the first ten coordination shells (1186 for A, 1488 for B, 2078 for C and 980 for diamond).

¶ In the one-dimensional helical coordination polymer $[Ag(pytz)](NO_3)$ [pytz = 3,6-di(4-pyridyl)-1,2,4,5-tetrazine][8] the nitrate ions show weak interactions with the metal ions (Ag···O 2.79 Å). We have rationalized that, by assuming these contacts also as bonds, the overall topology is of type C, three-fold interpenetrated; however, given the long Ag···O distances, a one-dimensional chain description is perhaps more appropriate.

1 (*a*) P. Losier and M. J. Zaworotko, *Angew. Chem., Int. Ed. Engl.*, 1996, **35**, 2779; (*b*) M. Fujita, Y. J. Kwon, S. Washizu, and K. Ogura, *J. Am. Chem. Soc.*, 1994, **116**, 1151; (*c*) R. W. Gable, B. F. Hoskins, and R. Robson, *J. Chem. Soc., Chem Commun.*, 1990, 1677; (*d*) L. R. MacGillivray, S. Subramanian, and M. J. Zaworotko, *J. Chem. Soc., Chem Commun.*, 1994, 1325; (*e*) L. Carlucci, G. Ciani, D. M. Proserpio and A. Sironi, *J. Chem. Soc., Chem Commun.*, 1994, 2755; (*f*) O. M. Yaghi and H. Li, *J. Am. Chem. Soc*., 1995, **117**, 10401.

2 L. Carlucci, G. Ciani, D. W, v. Gudenberg and D. M. Proserpio, *Inorg. Chem.*, 1997, **36**, 3812.

3 T. Hennigar, D. C. MacQuarrie, P. Losier, R. D. Rogers and M. J. Zaworotko, *Angew. Chem., Int. Ed. Engl.*, 1997, **36**, 972.

4 M. Fujita, Y. J. Kwon, O. Sasaki, K. Yamaguchi and K. Ogura, *J. Am. Chem. Soc*., 1995, **117**, 7287.

5 A. J. Blake, N. R. Champness, A. Khlobystov, D. A. Lemenovskii, W.-S. Li and M. Schröder, *Chem. Commun*., 1997, 2027.

6 A. J. Blake, N. R. Champness, S. S. M. Chung, W.-S. Li and M. Schröder, *Chem. Commun.*, 1997, 1005.

7 D. Whang and K. Kim, *J. Am.Chem. Soc*., 1997, **119**, 451.

8 M. A. Withersby, A. J. Blake, N. R. Champness, P. Hubberstey, W.-S. Li, and M. Schröder, *Angew.Chem., Int.Ed. Engl.*, 1997, **36**, 2327.

9 J. Lu, T. Paliwala, S. C. Lim, C. Yu, T. Niu and A. J. Jacobson, *Inorg. Chem.*, 1997, **36**, 923.

10 M. O'Keeffe, *Z. Kristallogr.*, 1991, **196**, 21; M. O'Keeffe and B. G. Hyde, *Crystal structures I: patterns and symmetry*, Mineralogical Society of America, Washington, D.C., 1996; see also M. O'Keeffe, *Nature*, 1998, **392**, 879.

11 K. N. Power, T. L. Hennigar and M. J. Zaworotko, *Chem. Commun.*, 1998, 595.

12 K.-W. Kim and M. G. Kanatzidis, *J Am. Chem. Soc.*, 1992, **114**, 4878.

13 A. Altomare, G. Cascarano, C. Giacovazzo, A. Guagliardi, M. C. Burla, G. Polidori and M. Camalli, *J. Appl. Crystallogr*., 1994, **27**, 435.

14 G. M. Sheldrick SHELX-97, University of Göttingen, Germany, 1997.

15 H. D. Flack, *Acta Crystallogr. Sect. A*, 1983, **A39**, 876.

16 E. Keller, SCHAKAL97, University of Freiburg, Germany, 1997.

Received in Cambridge, UK, 15th May 1998; 8/03662D

Aluminosilicate mesoporous molecular sieves with enhanced stability obtained by reacting MCM-41 with aluminium chlorohydrate

Robert Mokaya* and William Jones

Department of Chemistry, University of Cambridge, Lensfield Road, Cambridge, UK CB2 1EW. E-mail: rm140@cus.cam.ac.uk

Aluminosilicate MCM-41 materials prepared by post-synthesis alumination using aqueous aluminium chlorohydrate exhibit remarkably high mechanical and hydrothermal stability and in addition the materials, after steaming at high temperatures, possess stronger Brønsted acid sites compared to the parent material.

Recently, heteroatom substituted mesoporous molecular sieves such as MCM-41 have attracted much interest due to their potential use as hosts, adsorbents or catalysts.[1] Of particular interest are Al-containing materials which may be used as solid acid catalysts.[2,3] The structural stability of such aluminosilicate mesoporous molecular sieves is very important to their application as catalysts. Indeed the thermal and hydrothermal stability of Al-containing MCM-41 has been the focus of much recent research.[3,4] Despite good thermal stability, AlMCM-41 materials generally suffer from poor (and unpredictable) structural ordering and low hydrothermal stability and are easily destroyed by boiling in water or by steaming at high temperatures.[3,4] Studies on the mechanical stability of mesoporous molecular sieves have concentrated on pure silica materials[5] and to the best of our knowledge there is no data on the mechanical stability of silica-alumina materials. The structural stability of mesoporous molecular sieves can be improved by increasing the thickness of the pore walls and/or by enhancing the local ordering of the walls. This may be achieved by post-synthesis treatments such as pore wall grafting[6] or recrystallisation.[7] We have recently discovered that structurally well ordered AlMCM-41 can be prepared by reacting purely siliceous MCM-41 with aluminium chlorohydrate (ACH) solution containing Al polycations. Herein we report on the remarkable stability of the resulting aluminosilicate materials.

The starting material, a purely siliceous MCM-41 (designated PSMCM), was prepared according to ref. 8. AlMCM-41 was prepared by adding 1.0 g of calcined PSMCM to a 50 ml solution of ACH at 80 °C and stirring for 2 h (at 80 °C). The precursor Al-grafted MCM-41 was obtained by filtration and thoroughly washed with distilled water (until free of Cl^- ions), dried at room temperature and calcined in air at 550 °C for 4 h. The physical properties of the purely siliceous material (PSMCM) and AlMCM-41 samples prepared from ACH solutions with Al concentrations of 0.12, 0.30 and 0.48 mol l^{-1} (designated AlMCM2 (Si/Al = 9.7), AlMCM4 (Si/Al = 6.5) and AlMCM5 (Si/Al = 6.1) respectively) are given in Table 1. The *d* spacing of the AlMCM materials is higher than that of the starting PSMCM material and generally increases with the amount of aluminium incorporated. This is consistent with the incorporation of increasing amounts tetrahedral Al into the framework and is in part due to the longer Al–O bond length compared to the Si–O bond. The effect of the incorporation of Al onto the framework is clearly illustrated by the changes in the thickness (calculated by subtracting the pore diameter from the lattice parameter) of the pore walls. At 16 Å the wall thickness of PSMCM is comparable to the largest reported values for MCM-41.[8] On Al incorporation the wall thickness progressively increases up to 23.9 Å (for AlMCM5). The increase in wall thickness is at the expense of pore diameter which reduces from 31.6 Å for PSMCM to 25.8 Å for AlMCM5. The surface area reduces slightly while the pore volume shows a larger decrease. However, the lowest surface area (753 m^2 g^{-1}) and pore volume (0.62 cm^3 g^{-1}) obtained for the most aluminous sample (AlMCM5) is still high.

The mechanical stability of the Al-grafted materials was investigated by pressing the materials in a steel die of diameter 13 mm for 10 min. The effects of compression (external pressures were calculated from the applied force and the die diameter) on the ordering and textural properties of AlMCM4 (Si/Al = 6.5) are shown in Fig. 1 and Table 1. Except for a slight decrease in the *d* spacing, compaction at 185 MPa does not have any significant effect on the XRD pattern of AlMCM4. The retention of structural integrity is confirmed by the minimal decrease in the surface area and pore volume (Table 1). Compaction at 370 MPa resulted in a decrease in XRD peak intensity (with no further decrease in *d* spacing) and was accompanied by a 29% decrease in surface area and 25% decrease in pore volume. After compaction at the higher pressure of 740 MPa the surface area and pore volume reduced by 60%. However, the XRD pattern still indicates retention of some hexagonal symmetry. The mechanical stability exhibited here is remarkable especially in the light of previous studies which have shown that pure silica MCM-41 is essentially destroyed at 224 MPa.[5] It is likely that the stability observed

Table 1 *d* spacing and textural properties of the studied materials

Sample	d_{100}/Å	Surface area/m^2 g^{-1}	Pore volume/cm^3 g^{-1}	APD[a]/Å	a_o[b]/Å	Wall thickness/Å
PSMCM	41.2	887	0.85	31.6	47.6	16.0
AlMCM2	42.0	760	0.69	29.3	48.5	19.2
AlMCM4	42.8	767	0.65	26.5	49.4	22.9
AlMCM4 (185 MPa)[c]		755	0.57	27.4		
AlMCM4 (370 MPa))[c]		547	0.49	28.5		
AlMCM4 (740 MPa))[c]		284	0.26	30.6		
AlMCM5	43.0	753	0.62	25.8	49.7	23.9
ST-AlMCM5)[d]		558	0.45	22.6		
REF-AlMCM5)[e]		834	0.70	24.9		

[a] APD = average pore diameter (determined using BJH analysis). [b] a_0 = Lattice parameter, from the XRD data using the formula $a_0 = 2d_{100}/3$. [c] Sample AlMCM4 compressed at the pressures shown in parentheses. [d] Sample AlMCM5 steamed at 750 °C for 4 h. [e] Sample AlMCM5 refluxed in distilled water for 16 h.

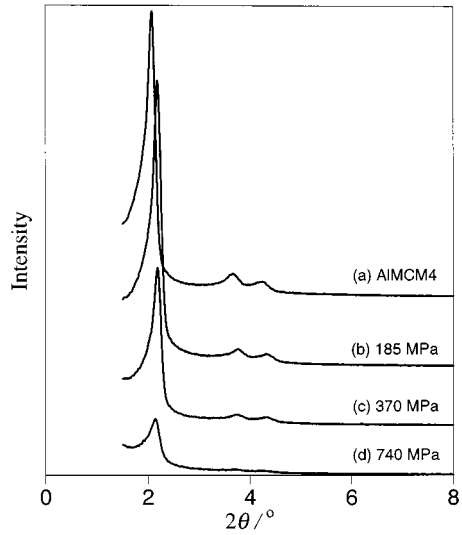

Fig. 1 Powder XRD patterns of sample AlMCM4; (a) original material and after compaction at (b) 185 MPa, (c) 370 MPa and (d) 740 MPa

here is due to the much thicker walls of the Al-grafted sample; a direct (mixed-gel) synthesised Al-MCM-41 material (with a Si/Al ratio of 23 and 11 Å thick walls) was destroyed after compaction at 370 MPa. We also investigated the mechanical stability of the pure silica starting material (PSMCM) and observed good structural integrity (not unlike that of AlMCM4) up to 370 MPa. However, after compaction at 740 MPa the degradation of PSMCM (as indicated by XRD) was much greater than that of AlMCM4.

To investigate hydrothermal stability, the Al-grafted materials were subjected to steaming at 750 °C for 4 h or refluxing in distilled water for 16 h (at a water to sample ratio of 1 l g^{-1}). The effects of these treatments on the ordering and textural properties of AlMCM5 (Si/A/ = 6.1) are shown in Fig. 2 and Table 1. After steaming, the Al-grafted sample exhibits an XRD pattern which indicates retention of structural ordering albeit with reduced peak intensity and lower *d* spacing. This is accompanied by a 3.2 Å reduction in pore diameter and a 25% decrease in both the surface area and pore volume. Previous studies have shown that whereas pure silica MCM-41 is relatively stable to steaming, Al-containing MCM-41 materials

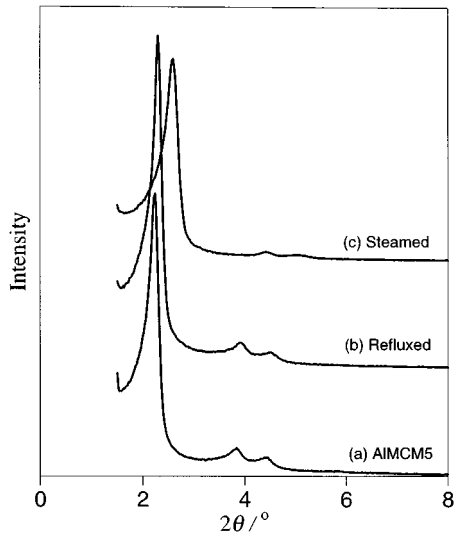

Fig. 2 Powder XRD patterns of sample AlMCM5; (a) original material and after (b) refluxing in water for 16 h and (c) steaming at 750 °C for 4 h

are on the other hand highly unstable.[3] It is therefore noteworthy that the Al-grafted material reported here is able to maintain structural ordering and considerably high surface area and pore volume. To ascertain the effect of steaming on catalytic properties we compared the acid content[2] and activity (for cumene cracking)[2] of AlMCM5 with its steamed analogue (ST-AlMCM5). The acid content of ST-AlMCM5 was 0.257 mmol $H^+ g^{-1}$ compared to 0.605 mmol $H^+ g^{-1}$ for AlMCM5. However, despite a lower acid content, the conversion of cumene was higher for the steamed sample; ST-AlMCM5 had an initial rate (in mmo l g^{-1} h^{-1} and taken at 10 min time on stream) of 1.225 compared to a rate of 0.843 for AlMCM5. This translates to an apparent turnover frequency (TOF) of 4.75 over ST-AlMCM5 and 1.4 over AlMCM5. This results indicate that the acid sites in the steamed sample (though fewer in number due to some dealumination) are stronger than those on AlMCM5. This observations are reminiscent of the behaviour of steam stabilised Y zeolites. To the best of our knowledge, this is the first example of an Al-containing MCM-41 material, which exhibits such stability to high temperature steaming. Indeed a direct (mixed-gel) synthesised Al-MCM-41 material (Si/Al = 23) was destroyed by similar hydrothermal treatment with its surface area decreasing by 75%.

The hydrothermal stability of the Al-grafted materials is further illustrated by their stability in boiling water. Fig. 2 indicates that heating (refluxing) of AlMCM5 in boiling water for 16 h had virtually no deleterious effect on its XRD pattern which suggests excellent retention of structural ordering. This is confirmed by the fact that the surface area and pore volume, far from decreasing, actually increase (Table 1). When subjected to similar treatment the structural ordering of the pure silica starting material (PSMCM) was destroyed and its surface area reduced by 65%. The direct (mixed-gel) synthesised Al-MCM-41 material (Si/Al = 23) was even less stable and was rendered amorphous after refluxing in water for a shorter time of 6 h.

We have demonstrated that Al-containing MCM-41 with good structural stability can be prepared by reacting purely siliceous MCM-41 with aluminium chlorohydrate. The enhanced mechanical and hydrothermal stability of materials reported here may be due to recrystallisation effects, involving the grafted Al, which act to heal defect sites in the structure of the MCM-41 materials. This is likely because the Al is initially grafted onto the pure silica material *via* silanol groups which are known to occur at defect sites. Similar recrystallisation effects are known to occur in zeolites.[9] Stable aluminosilicate MCM-41 materials are expected to find use as solid acid catalysts especially for processes which require catalyst regeneration under severe conditions.

R. M. is grateful to the EPSRC for an Advanced Fellowship.

Notes and References

1 X. S. Zhao, G. Q. Lu and G. J. Millar, *Ind. Eng. Chem. Res.*, 1996, **35**, 2075.
2 R. Mokaya and W. Jones, *J. Catal.*, 1997, **172**, 211.
3 A. Corma, M. S. Grande, V. Gonzalez-Alfaro and A. V. Orchilles, *J. Catal.*, 1996, **159**, 375.
4 J. M. Kim, J. H. Kwak, J. Shinae and R. Ryoo, *J. Phys. Chem.*, 1995, **99**, 16742.
5 V. Y. Gusev, X. Feng, Z. Bu, G. L. Haller and J. A. O'Brien, *J. Phys. Chem.*, 1996, **100**, 1985.
6 R. Mokaya and W. Jones, *Chem. Commun.*, 1997, 2185.
7 K. R. Kloestra, H. van Bekkum and J. C. Jansen, *Chem. Commun.*, 1997, 2281.
8 C-F. Cheng, D. H. Park and J. Klinowski, *J. Chem. Soc. Faraday Trans.*, 1997, **93**, 193.
9 D. W. Breck, *Zeolite Molecular Sieves*, Robert E. Krieger Company, New York, 1974, p. 441.

Received in Bath, UK, 20th June 1998: 8/04805C

A manganese-containing molecular sieve catalyst designed for the terminal oxidation of dodecane in air

Robert Raja and John Meurig Thomas*†

Davy Faraday Research Laboratory, The Royal Institution of Great Britain, 21 Albemarle Street, London, UK W1X 4BS

Mn^{III} ions that replace a few percent of the framework Al^{III} sites in a microporous aluminophosphate—number 18, with a pore aperture of 3.8 Å—function as catalytically active centres for the selective oxidation of dodecane preferentially at C_1 and C_2.

The activation and functionalisation of alkanes are notoriously difficult to execute and control—far more so than the processes involved in their complete oxidation (combustion).[1] Taking cues from the general field of redox metallo-enzymes[2–4] that catalyse shape- and regio-selectively the oxidation of hydrocarbons, but also from framework-substituted, transition-metal-ion-incorporated microporous aluminium phosphates (AlPOs),[5–7] we have designed a heterogeneous catalyst that selectively converts dodecane in air, without the need for stoichiometric donors such as alkyl hydroperoxides or H_2O_2.

The catalyst consists of so-called AlPO-18,[8] in which a small fraction, typically 4 atom%, of the Al^{III} ions has been isomorphously replaced, during synthesis,[9] by Mn^{II} ions. Separate experiments, involving combined *in situ* X-ray absorption spectroscopy and X-ray diffractometry[10,11] plus *ex situ* scanning transmission electron microscopy, have established that, in O_2 or dry air, at temperatures up to *ca*. 550 °C, the Mn^{II} ions (like those of isomorphously substituted Co^{II}) are all converted to the +3 oxidation state while remaining tetrahedrally coordinated (*i.e*. coordinatively unsaturated) without loss of structural integrity of the AlPO host or exsolution from it of its embedded transition-metal ions. EXAFS and other analyses show that the individual Mn^{III} active sites are spatially well separated throughout the three-dimensional internal surface of the catalyst. Whereas all these active centres are accessible to small molecules, because of the structural characteristics of AlPO-18 (see Fig. 1) only those situated at the mouths of the pores that emerge at exterior surfaces are accessible to the extremities of the linear dodecane.

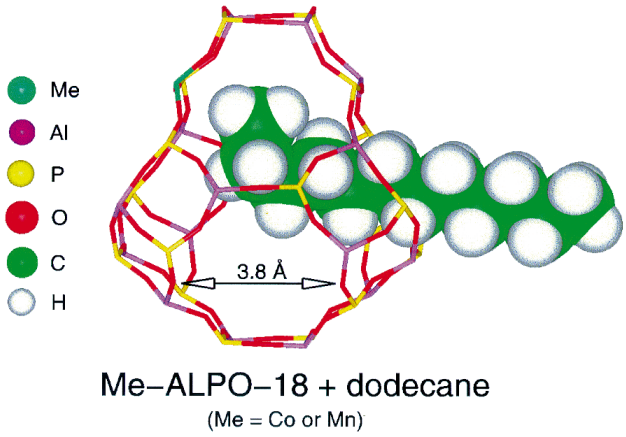

Fig. 1 Energy-minimised configuration adopted by *n*-dodecane at 0 K inside an AlPO-18 framework. The terminal methyl group (C_1) and C_2 of the dodecane are significantly closer to a tetrahedral framework site containing the metal ion (manganese, in this case) than either C_3, C_4 or C_5, implying that the Mn^{III} ions in the framework of the AlPO-18 cage, along with intracage O_2, exert a greater influence on the C_1 and C_2 than on other carbons on the dodecane backbone.

The details of the synthesis of Mn^{II}-containing AlPO-18 are exactly the same as for that of other MeAlPO-18 (Me = Co, Zn, Mg, Mn, *etc*.) catalysts.[6] Briefly, the Mn^{II} ion is introduced to the template-containing precursor gel from which small crystals of phase pure product appear. Upon gentle calcination in O_2, the template (*N*,*N*-diisopropylethylamine) is entirely gasified, leaving the cages of the resulting catalyst empty. In a typical experiment, 0.5 g of catalyst was added to 50 g of dodecane in a stainless steel high pressure catalytic reactor (Cambridge Reactor Design) lined with PEEK (poly ether ether ketone), and equipped with a mechanical stirrer and liquid sampling valve. Removal of samples for analyses during the course of the reaction is possible without perturbing the pressure in the reactor. Dry air was pressurised into the reaction vessel (1.5 MPa) and the reactor was heated to the desired temperature (373 K). Samples were periodically removed, analysed by gas chromatography (GC; Varian 3400 CX} equipped with a BPX5 column (25 m × 0.32 mm) and a flame ionisation detector (FID), and the total conversion and product distribution (estimated in moles and normalised with respect to the GC response factor) were determined as a function of time (using 1,2-dichlorobenzene as internal standard). The acids formed were esterified and analysed as methyl esters.[12] The identity of the products was confirmed by injecting authenticated standard samples. The mass balance was calculated for each run and the estimated error in the analysis arising from handling or sampling loss is less than 6.0 mol%.

Exactly analogous experiments were carried out with another manganese-containing AlPO, MnAlPO-36[13] in which the pore diameter is appreciably larger (6.5 Å × 7.5 Å), thereby permitting much greater access to the dodecane. Fig. 2 and Table 1 summarise the results. It is obvious that the small pore aperture of MnAlPO-18 (and of CoAlPO-18) results in

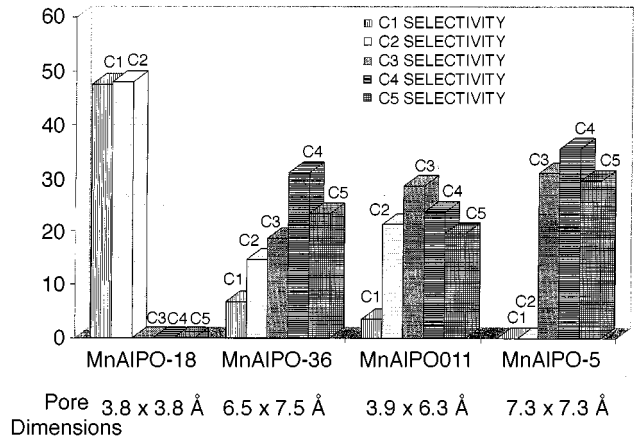

Fig. 2 Bar chart summarising the various degrees of regio-selectivity in the oxidation of dodecane over four microporous MnAlPO catalysts. The regio-selectivity for terminal oxidation with MnAlPO-18 far exceeds that of any of the other three.

Table 1 Oxidation of dodecane[a] in air: comparison of catalysts

Catalyst	Conv./mmol	Product[b] distribution/mmol											
		C_1-ol	C_1-al	Lauric acid	C_2-ol	C_2-one	C_3-ol	C_3-one	C_4-ol	C_4-one	C_5-ol	C_5-one	Others[c]
Mn-ALPO-18 (0.04)	16.08	1.27	4.71	1.65	4.47	3.25	—	—	—	—	—	—	0.73
Mn-ALPO-36 (0.04)	15.20	0.47	—	0.55	0.95	1.27	1.37	1.45	2.63	2.07	1.65	1.89	0.90
Mn-ALPO-5 (0.04)	13.75	—	—	—	—	—	2.28	1.97	2.07	2.83	1.59	2.46	0.55
Mn-ALPO-11 (0.04)	6.82	0.24	—	—	0.91	0.53	0.75	1.19	0.58	1.03	0.43	0.91	0.25

[a] Dodecane = 49.7 g; catalyst = 0.5 g; air = 1.5 MPa; temp. = 373 K; time = 24 h. [b] C_1-ol = dodecan-1-ol; C_1-al = dodecanal; C_2-ol = dodecan-2-ol; C_2-one = dodecan-2-one; C_3-ol = dodecan-3-ol; C_3-one = dodecan-3-one; C_4-ol = dodecan-4-ol; C_4-one = dodecan-4-one; C_5-ol = dodecan-5-ol; C_5-one = dodecan-5-one. [c] Others = mainly CO_2, CO, water and lower olefins/hydrocarbons in the gas phase.

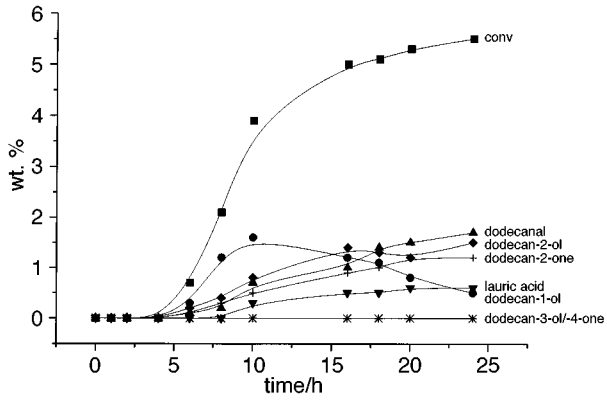

Fig. 3 Typical kinetic plots for the oxidation of dodecane over MnAlPO-18 catalyst under the conditions given in Table 1

oxidation of the dodecane (total conversion = 5.5 wt.%) only at C_1 and C_2, whereas in MnAlPO-36 (possessing essentially the same concentration of the active site) (total conversion = 5.2 wt.%) the oxyfunctionalization occurs at essentially all the carbon atoms of the dodecane backbone, and more predominantly at the C_4 and C_5 positions. The kinetics of oxidation of dodecane using MnAlPO-18 was studied in detail (Fig. 3), and after an initial period of induction (4 h), dodecan-1-ol and dodecan-2-ol were formed simultaneously, and were subsequently oxidised to dodecanal, lauric acid and dodecan-2-one at prolonged contact times. In an identical experiment, the solid catalyst was filtered off (when hot) after 8 h (conversion = 2.4 wt.%) and the reaction was continued for a further 16 h. But, no further conversion was observed, showing that the Mn^{III} ions in the framework of the molecular sieve are solely responsible for the catalysis. (The reaction mixture was independently analysed by ICP analysis and no detectable quantities of Mn or Co were observed.) MnAlPO-18 and CoAlPO-18 (and possibly other transition-metal ion substituted AlPO-18) are therefore good candidates for suitable catalysts in the production of functionalised hydrocarbons required as surfactants and detergents. We know from parallel work[14] that a CoAlPO-18 (total conversion = 7.1 wt.%) catalyst preferentially activates the terminal and secondary methyl groups of *n*-hexane.

We believe that the key to the catalytic activity is the coordinatively unsaturated Mn^{III} ion. Just as with the tetrahedrally coordinated Ti^{IV} ions in TS-1,[15] metallocene derived Ti↑MCM-41[16,17] and especially the Co^{III} ions in CoAlPO-18,[14] expansion of the coordination shell in the transition state is likely to be facile. Moreover, after the departure of the products, the retention of the isolated Mn^{III} ions in the framework of the microporous host favours the regeneration of the catalyst's activity. Its selectivity, however, is solely due to the pore size dimensions that govern access of the hydrocarbon. It should be mentioned that, after the reaction, the catalyst (MnAlPO-18) was washed thoroughly with methanol and activated at 550 °C for 12 h in the presence of dry air. It was then recycled twice without significant loss in catalytic activity (conv. = 15.65 mmol) and selectivity (C_1 = 48% and C_2 = 47.6%).

We thank EPSRC, UK for financial support (rolling grant to J. M. T.), the Royal Commission for the Exhibition of 1851 for a Research Fellowship to R. R., Dr G. Sankar for help in sample preparation and useful discussions and Dr R. G. Bell for computer guidance.

Notes and references

† E-mail: robert@ri.ac.uk, jmt@ri.ac.uk

1 C. L. Hill, in *Activation and functionalisation of alkanes*, Wiley, Chichester, 1989; see also J. M. Thomas, *Nature*, 1985, **314**, 669 and references therein.
2 *Dioxygen Reactions*, ed. I. Bertini, H. B. Grey, S. J. Lippard and J. S. Valentine, Mill Valley, CA, 1994.
3 N. Herron and C. A. Tolman, *J. Am. Chem. Soc*., 1987, **109**, 2837.
4 K. Sauer, V. K. Yachandra, R. D. Britt and M. P. Klein, in *Manganese Redox Enzymes*, ed. V. L. Pecoraro, VCH Publishers, New York, 1992.
5 J. M. Thomas, G. N. Greaves, G. Sankar, P. A. Wright, J. Chen, A. J. Dent and L. Marchese, *Angew. Chem*., 1994, **33**, 1871.
6 J. Chen and J. M. Thomas, *J. Chem. Soc., Chem. Commun*., 1994, 603.
7 P. A. Barrett, G. Sankar, C. R. A. Catlow and J. M. Thomas, *J. Phys. Chem*., 1996, **100**, 8977.
8 A. Simmen, L. B. McCusker, Ch. Baerlocher and W. M. Meier, *Zeolites*, 1991, **11**, 654.
9 J. Chen, P. A. Wright, J. M. Thomas, S. Natarajan, L. Marchese, S. M. Bradley, G. Sankar, C. R. A. Catlow, P. L. Gai-Boyes, R. P. Townsend and C. M. Lok, *J. Phys. Chem*., 1994, **98**, 10216.
10 J. M. Thomas and G. N. Greaves, *Science*, 1994, **265**, 1675.
11 G. Sankar, J. M. Thomas, G. N. Greaves and A. J. Dent, *J. Phys. IV. (France)*, 1997, **7**, C2, 871.
12 R. Raja and P. Ratnasamy, *Catal. Lett*., 1997, **48**, 1.
13 P. A. Wright, S. Natarajan, J. M. Thomas, R. G. Bell, P. L. Gai-Boyes, R. H. Jones and J. S. Chen, *Angew. Chem., Int. Ed. Engl.*, 1992, **31**, 1472.
14 R. Raja, J. M. Thomas, G. Sankar and R. G. Bell, in preparation.
15 C. Lamberti, S. Bordiga, A. Zecchina, G. Vlaic, G. Tozzola, G. Petrini and A. Carati, *J. Phys. IV. (France)*, 1997, **7**, C2, 851.
16 G. Sankar, F. Rey, J. M. Thomas, G. N. Greaves, A. Corma, B. R. Dobson and A. J. Dent, *J. Chem. Soc., Chem. Commun*., 1994, 2279.
17 T. Maschmeyer, F. Rey, G. Sankar and J. M. Thomas, *Nature*, 1995, **378**, 159.

Received in Liverpool, UK, 27th May 1998; 8/03984D

Displacement of a cyclopentadienyl ligand by a crown ether from a lanthanocene(II) [LnCp''$_2$]; crystal structures of the first cationic lanthanoid(II) complexes, [SmCp''([18]-crown-6)][SmCp''$_3$]·0.5C_6H_6 and [YbCp''([18]-crown-6)][Cp'']·3C_6H_6 [Cp'' = η^5-$C_5H_3(SiMe_3)_2$-1,3]

Yurii K. Gun'ko, Peter B. Hitchcock and Michael F. Lappert*†

The Chemistry Laboratory, University of Sussex, Brighton, UK BN1 9QJ

Treatment of [SmCp''$_2$] or [YbCp''$_2$] with [18]-crown-6 in benzene at ambient temperature yields the X-ray characterised, crystalline salts [SmCp''([18]-crown-6)][SmCp''$_3$]·0.5C_6H_6 1 and [YbCp''([18]-crown-6)][Cp'']·3C_6H_6 2; 1 with K in toluene affords [K([18]-crown-6)(η^2-PhMe)$_2$][SmCp''$_3$], also accessible from [SmCp''$_2$], K[Cp''] and [18]-crown-6 in toluene [Cp'' = η^5-$C_5H_3(SiMe_3)_2$-1,3].

The use of crown ethers to solubilise lanthanoid (Ln) halides or nitrates is well documented.[1] By contrast, the chemistry of (crown ether)Ln organometallic complexes is still undeveloped, although we have recently studied the reactions of some tri(cyclopentadienyl)lanthanoid(III) complexes with potassium in the presence of [18]-crown-6 and an arene, which have yielded the crystalline salts [K([18]-crown-6)(C_6H_6)$_2$][{LaCp'$_2$}$_2$(μ,η-C_6H_6)][2a] and [K([18]-crown-6)(η^2-PhMe)$_2$][(LnCp''$_2$)$_2$(μ,η-PhMe)] [Cp' = η^5-$C_5H_3Bu^t_2$-1,3; Cp'' = η^5-$C_5H_3(SiMe_3)_2$-1,3; Ln = Ce or Pr].[2b]

We now report (*a*) two facile, but diverse, cyclopentadienyl displacement reactions from a lanthanocene(II) [LnCp''$_2$] (Ln = Sm or Yb) by a crown ether, affording (Scheme 1) the crystalline [SmCp''([18]-crown-6)][SmCp''$_3$]·0.5C_6H_6 **1** or [YbCp''([18]-crown-6)][Cp'']·3C_6H_6 **2**; (*b*) the partial redistribution of **2** in toluene into **2** and [YbCp''$_2$([18]-crown-6)]; (*c*) the synthesis from a toluene solution of another crystalline tri(cyclopentadienyl)samarate(II) [K([18]-crown-6)(η^2-PhMe)$_2$][SmCp''$_3$]·0.5PhMe **3** from either **1** and K, or [SmCp''$_2$], K[Cp''] and [18]-crown-6 (Scheme 1); and (*d*) the X-ray structures of **1–3**.‡ Further features of interest are that **1** and **2** are the first examples of cationic lanthanoid(II) complexes, **2** the first lanthanoid salt containing a cyclopentadienide counter-ion, and **1** and **3** are new members of the rare family of salts containing a lanthanate(II) anion.[3]

Each of the crystalline salts **1–3** gave satisfactory microanalytical results, as well as IR and NMR§ spectra. The latter in [$^2H_8$]toluene or [$^2H_6$]benzene for **1** and **3** were complicated by the paramagnetism of the f^6 Sm^{II} causing strongly shifted signals, but were substantially temperature-invariant in the range 0 to +50 °C. The ^{29}Si{^{1}H} NMR spectra of **1** at 25 °C showed two signals at δ 98.50 ([SmCp''([18]-crown-6)]$^+$) and δ −58.59 ([SmCp''$_3$]$^-$) in the appropriate 1 : 3 ratio. By contrast, for the case of the diamagnetic f^{14} Yb^{II} salt **2**, there was partial redistribution in toluene solution, readily monitored, especially by ^{171}Yb{^{1}H} and ^{29}Si{^{1}H} (three signals at δ 44.47, −2.49 and −19.68 in a 1 : 1 : 3 ratio at 25 °C), but also ^{1}H NMR spectra in the same temperature regime; cooling below −10 °C led to crystallisation of **2**. The ^{171}Yb{^{1}H} NMR spectra in [$^2H_8$]toluene revealed two signals at 25 °C: δ −82.46, assigned to **2**, and δ 14.44, assigned to [YbCp''$_2$([18]-crown-6)] {*cf.*[4] δ 0 for [Yb(η^5-C_5Me_5)$_2$(thf)$_2$] in thf at 296 K}; whereas at 50 °C a single broad signal at δ −1.77 was observed, indicative of a fast exchange process between the two species but a decrease in the relative contribution of **2**. Lowering the temperature to −10 °C led to a decrease in relative intensity and shift of the higher frequency signal to δ 30.35, and simultaneously an enhancement in relative intensity and shift of the lower frequency signal to δ −32.43. These data show that in toluene or benzene there is an equilibrium between **2** and the neutral complex [YbCp''$_2$([18]-crown-6)], with the latter favoured at higher temperatures.

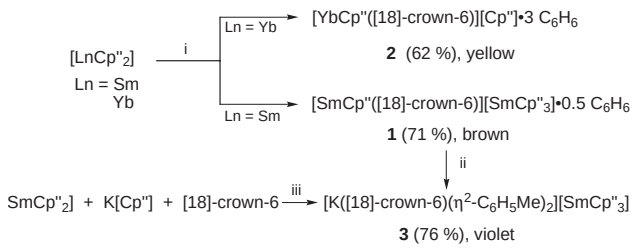

Scheme 1 Synthesis of the crystalline cyclopentadienyllanthanoid(II) salts **1**–**3**. *Reagents and conditions*: i, [18]-crown-6, benzene, 12 h, *ca.* 20 °C; ii, K (mirror), toluene, 3 h, *ca.* −30 °C, iii, toluene, 5 h, *ca.* 20 °C.

Crystalline **1** consists of well separated ions, Fig. 1. The cation [SmCp''([18]-crown-6)]$^+$ has a sandwich-like structure; the Sm is located within the cavity of the quasi-parallel Cp'' and the crown ligand, the latter being distorted due to strong O(6) atom deviation. The centroid of the Cp'' ring and the six oxygen atoms of the crown ether form a strongly distorted pentagonal bipyramidal arrangement around Sm. The crown ether is disordered 0.57 : 0.43 over two orientations, approximately related by mirror symmetry, with two carbon positions in common. The Sm(1)–C_{sp^2} distances are in the range 2.828(6) to 2.913(6) Å [to C(5) shortest, to C(3) longest] with Sm(1)–Cp''(centroid) 2.606(6) Å; this compares with 2.553 Å in [Sm(Cp'')Cp'''(thf)] [Cp''' = η^5-$C_5H_2(SiMe_3)_3$-1,2,4)].[5] The average Sm(1)–O distance of 2.714 Å [ranging from 2.571(9) to 2.829(9) Å, to O(5) shortest, to O(3) longest] is *ca.* 0.15–0.2 Å longer than in Sm^{III} crown ether complexes.[1e] The [SmCp''$_3$]$^-$ anion in **1** has the Sm in an almost trigonal planar arrangement with respect to the centroids of the three Cp'' ligands, as in [SmCp''$_3$].[6] The Sm(2)–C_{sp^2} distances are in the range 2.816(6) to 3.092(6) Å [to C(39) shortest, to C(26) longest], with two Sm–Cp''(centroid) distances of 2.701(6) and one of 2.670(6) Å, compared with 2.698(5) to 2.807(5) Å in [SmCp''$_3$].[6]

Crystalline **2**, likewise, has well separated ions, the nearest Yb contact to the anion being 6.58 Å. The sandwich-like nature of the cation [YbCp''([18]-crown-6)]$^+$ resembles that of **1**. The Yb(1)–C_{sp^2} distances, ranging from 2.739 to 2.814 Å [to C(5) shortest, to C(3) longest], as well as *d*[Yb–Cp''(centroid)] 2.508(7) Å, are significantly longer than in [{YbCp''$_2$}$_\infty$], having Yb–C_{sp^2} from 2.654(5) to 2.684(6) with Yb–Cp''(centroid) 2.382 and 2.366 Å.[7] The Yb–O distances range from 2.519(5) to 2.583(6) Å [to O(4) shortest, to O(1) longest]. The anion is such that two Cp' groups lie across inversion centres with the disorder only partially resolved and hence the dimensions are unreliable.

Crystalline **1** and **3** have identical anions. The asymmetric unit contains two cations and two anions and one toluene solvate molecule. The six K–O bond lengths range from 2.72(2) to 2.83(2) Å and the K···C(from η^2-PhMe) contacts are 3.53(3) Å.

A reaction which has some analogy with the formation of salt **1** from [SmCp"$_2$] is that between MgR_2 or Mg(Br)R and a cryptand or an azacrown ether to yield [MgR(macrocycle)][MgR_3] or [MgR(macrocycle)][Mg(Br)R_2], which show fluxionality in [$^2H_6$]benzene involving exchange of R as between cation and anion (*e.g.* R = Bu^i).[8]

The formation of the [SmCp"$_3$]$^-$ counter anion in **1** contrasts with the [Cp"]$^-$ of **2** in the related ytterbium reaction. We suggest that [SmCp"([18]-crown-6)][Cp"] is first formed, but captures a further molecule of [SmCp"$_2$] to give **1**; the lack of reaction between **2** and [YbCp"$_2$] is attributed to steric hindrance, Yb^{2+} being significantly smaller than Sm^{2+}.

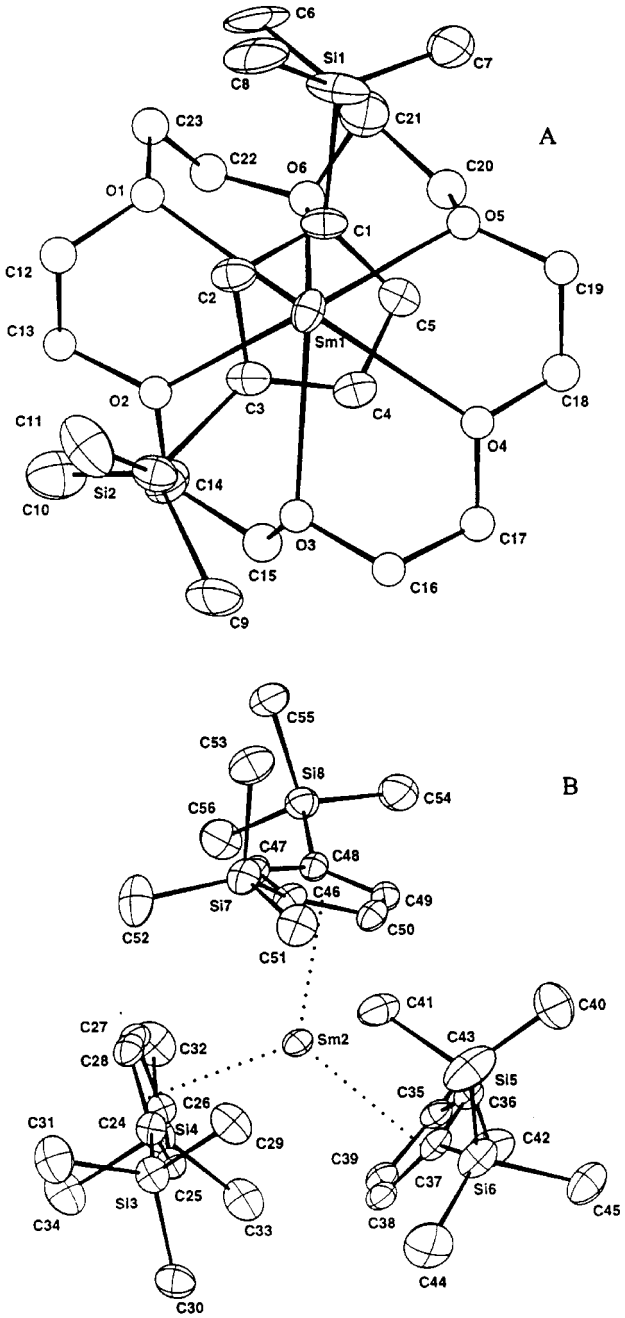

Fig. 1 The structure of cation (**A**) and anion (**B**) in **1**; selected bond lengths and angles are in the text

The results here presented open up a new chapter in organolanthanoid chemistry; the cationic lanthanoid(II) complexes, in particular **1**, are expected to have a rich chemistry. For **2**, we shall replace [Cp]$^-$ by a weakly coordinating anion.

We thank EPSRC for the award of a fellowship to Yu. K. G. and for other support.

Notes and References

† E-mail:M.F.Lappert@sussex.ac.uk

No reprints available.

‡ *Crystal data*: **1**, $C_{59}H_{111}O_6Si_8Sm_2$, M = 1441.9, T = 173(2) K, monoclinic, space group $P2_1/n$ (no. 14), a = 19.902(7), b = 14.610(4), c = 26.89(2) Å, β = 107.10(4)°, U = 7474(6) Å^3, F(000) = 2996, Z = 4, D_c = 1.28 g cm^{-3}, μ(Mo-Kα) = 1.73 mm^{-1}, specimen 0.40 × 0.35 × 0.20 mm^3, 9128 unique reflections for 2 < θ < 22°, R_1 = 0.041 for 7379 reflections with $I > 2\sigma(I)$, wR_2 = 0.109 (all data), S = 1.048; **2**, $C_{52}H_{84}O_6Si_4Yb$, M = 1090.59, T = 173(2) K, monoclinic, space group $P2_1/n$ (no. 14), a = 12.168(5), b = 39.88(2), c = 12.858(6) Å, β = 115.46(4)°, U = 5634(4) Å^3, F(000) = 2280, Z = 4, D_c = 1.29 g cm^{-3}, μ(Mo-Kα) = 1.79 mm^{-1}, specimen 0.30 × 0.30 × 0.10 mm^3, 9935 unique reflections for 2 < θ < 25°, R_1 = 0.058 for 8259 reflections with $I > 2\sigma(I)$, wR_2 = 0.227 (all data), S = 1.134; **3**, $C_{59}H_{103}\underline{K}O_6Si_6Sm\cdot0.5(C_7H_8)$, M = 1312.5, T = 173(2) K, triclinic, space group $P\bar{1}$ (no. 2), a = 11.895(3), b = 17.148(10), c = 37.923(11) Å, α = 87.03(3), β = 84.19(2), γ = 69.87(3)°, U = 7224(5) Å^3, F(000) = 2780, Z = 4, D_c = 1.21 g cm^{-3}, μ(Mo-Kα) = 1.01 mm^{-1}, specimen 0.20 × 0.10 × 0.10 mm^3, 13461 unique reflections for 2 < θ < 20°, R_1 = 0.095 for 7363 reflections with $I > 2\sigma(I)$, wR_2 = 0.289 (all data), S = 1.19. An Enraf-Nonius CAD-4 diffractometer, λ(Mo-Kα) 0.71073 Å, absorption corrections, solution by direct methods, full-matrix least-squares refinement on all F^2. CCDC 182/943.

§ *Selected spectroscopic data*: for **1**: ^{29}Si{^{1}H} NMR (49.7 MHz, 298 K, [$^2H_8$]toluene): δ 98.50, −58.59 (1 : 3); for **2**: ^{1}H NMR (300 MHz, 298 K, C_6D_6): δ 6.71 (br, 3H, Cp-ring, free Cp"$^-$), 6.42 (br, 3H, Cp-ring), 3.16 (br, s, 24H, 18-crown-6), 0.66 (br, 18H, $SiMe_3$), 0.41 (s, 18H, $SiMe_3$, free Cp"$^-$); the ^{1}H NMR spectrum also contains signals assigned to [YbCp"$_2$([18]-crown-6)]: δ 6.58 (br, m, 3H, Cp-ring), 3.44 (br, s, 24H, 18-crown-6), 0.47 (s, 36H, $SiMe_3$); ^{1}H NMR (300 MHz, 323 K, C_6D_6): δ 6.60 (vbr sh, 3H, Cp-ring), 3.47 (br sh, 24H, 18-crown-6), 0.50 (vbr, 36H, $SiMe_3$); ^{29}Si{^{1}H} NMR (49.7 MHz, 298 K, [$^2H_8$]toluene): δ 44.47 ([YbCp"([18]-crown-6)]$^+$), −2.49 (free Cp"$^-$), −19.68 ([YbCp"$_2$([18]-crown-6)]) (rel. ratios: 1 : 1 : 3); ^{171}Yb{^{1}H} NMR (43.77 MHz, 298 K, [$^2H_8$]toluene): δ 14.44 ($\Delta w_{1/2}$ = 45 Hz), −82.46 ($\Delta w_{1/2}$ = 130 Hz); (43.77 MHz, 323 K, [$^2H_8$]toluene): δ −1.77 ($\Delta w_{1/2}$ = 90 Hz); (43.77 MHz, 263 K, [$^2H_8$]toluene): δ 30.35 ($\Delta w_{1/2}$ = 30 Hz), −32.43 ($\Delta w_{1/2}$ = 145 Hz).

1 (*a*) J.-C. G. Bünzli and D. Wessner, *Coord. Chem. Rev*., 1984, **60**, 191 and refs. therein; (*b*) J.-C. G. Bünzli and D. Wessner, *Isr. J. Chem*., 1984, **24**, 313; (*c*) R. D. Rogers and A. N. Rollins, *Inorg. Chim. Acta*, 1995, **230**, 177, and refs. therein; (*d*) G. Crisci and G. Meyer, *Z. Anorg. Allg. Chem*., 1994, **620**, 1023; (*e*) C. Runschke and G. Meyer, *Z. Anorg. Allg. Chem*., 1997, **623**, 981, and refs. therein; (*f*) 1997, **623**, 1017 and refs. therein.

2 (*a*) M. C. Cassani, D. J. Duncalf and M. F. Lappert, *J. Am. Chem. Soc*., submitted; (*b*) Yu. K. Gun'ko, P. B. Hitchcock, M. F. Lappert and C. J. Cardin, *J. Chem. Soc., Dalton Trans.*, submitted.

3 *Cf*. F. T. Edelmann, in *Comprehensive Organometallic Chemistry*, eds. E. W. Abel, F. G. A. Stone and G. Wilkinson, Pergamon, Oxford, 2nd edn., 1995, vol. 4 (ed. M. F. Lappert), p. 11; C. Apostolidis, G. B. Deacon, E. Dornberger, F. T. Edelmann, B. Kanellakopulos, P. MacKinnon and D. Stalke, *Chem. Commun*., 1997, 1047.

4 *Cf*. J. M. Keates and G. A. Lawless, in *Advanced Applications of NMR to Organometallic Chemistry*, eds. M. Gielen, R. Willem and B. Wrackmeyer, Wiley, New York, 1996, p. 357.

5 W. J. Evans, G. Kociok-Köhn, S. E. Foster, J. W. Ziller and R. J. Doedens, *J. Organomet. Chem*., 1993, **444**, 61.

6 W. J. Evans, R. A. Keyer and J. W. Ziller, *J. Organomet. Chem*., 1990, **394**, 87.

7 P. B. Hitchcock, J. A. K. Howard, M. F. Lappert and S. Prashar, *J. Organomet. Chem*., 1992, **437**, 177.

8 R. M. Fabicon, A. D. Pajerski and H. G. Richey, Jr., *J. Am. Chem. Soc*., 1993, **115**, 9333.

Received in Cambridge, UK, 5th May 1998; revised manuscript received 6th July 1998; 8/05544K

Novel intramolecular rearrangement of 3-bromo-3,3-difluoroalanine Schiff bases *via* radical *ipso*-substitution at the aromatic ring

Hideki Amii, Susumu Kondo and Kenji Uneyama*†

Department of Applied Chemistry, Faculty of Engineering, Okayama University, Tsushimanaka 3-1-1, Okayama 700-0082, Japan

3-Bromo-3,3-difluoroalanine Schiff bases are synthesized by bromodifluoromethylation of the corresponding glycine Schiff bases with CF_2Br_2; their intramolecular rearrangement involving radical *ipso*-substitution at the aromatic ring of the imine moiety provides 3,3-difluoro-3-arylpropanoates in good yields.

Organofluorine compounds are receiving increasing attention in the medicinal, agricultural, and material sciences. In particular, interest in fluorine-containing amino acids and their derivatives has existed for many years, since they have potentially unique biological activities and thus are a current synthetic target.[1] Herein we report a new approach to the preparation of 3-bromo-3,3-difluoroalanine Schiff bases **2** and their intramolecular rearrangement *via* radical *ipso*-substitution at the aromatic ring, which provides β,β-difluoroalkanoates.[2,3]

3-Bromo-3,3-difluoroalanine Schiff bases **2** are synthesized using commercially available CF_2Br_2, the simplest CF_2 unit.[4] Appropriate choice of reaction conditions was essential to avoid the decomposition of the bromodifluoromethyl moiety of **2** due to nucleophilic attack of the bases, such as NaH and even LDA. When Schiff base **1** was treated with lithium 2,2,6,6-tetramethylpiperidide (LTMP) in THF at −78 °C followed by CF_2Br_2, difluoromethylene compounds **2** were obtained in good yields [eqn (1)].

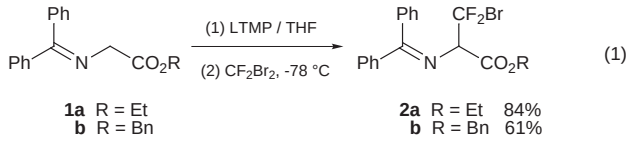

3-Bromo-3,3-difluoroalanine Schiff bases **2** are interesting fluorinated synthetic building blocks, and their transformations were examined next. Firstly, we explored Bu_3SnH/AIBN mediated radical cleavage of the carbon–bromine bond in **2**. Treatment of **2a** with Bu_3SnH/AIBN/benzene at 80 °C for 2.5 h gave not only the reduction product **3a** (10%), but also unexpectedly gave ethyl 3,3-difluoro-3-phenylpropanoate[5] **4a** (60%) as the major product [eqn (2)]. Raising the reaction

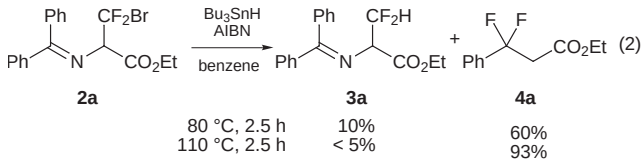

temperature (> 110 °C) favoured the rearrangement (**2a**→**4a**). The formation of **4a** can be explained by assuming the pathway pictured in Scheme 1. Initially, Bu_3SnH/AIBN mediated homolytic fission of the C–Br bond in **2** generates α,α-difluoroalkyl radical species **5**. The resultant α-fluorinated carbon radical **5** undergoes intramolecular *ipso* attack to the aromatic group[6–10] of the imine moiety of **5**, forming the spiro cyclohexadienyl radical **6**. Extrusion of aromatic nitrile **7** from **6** then occurs to furnish the carbon radical **8**.[11] Subsequent hydrogen abstraction gives rise to β,β-difluorocarboxylic acid ester **4** as the final product.

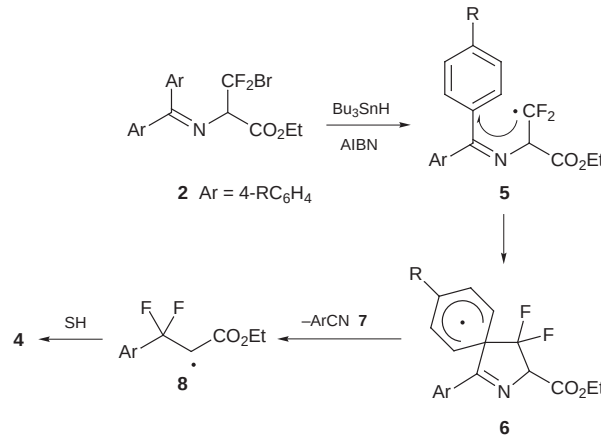

Scheme 1

Other examples of selective formation of **4** are given in Table 1. The Schiff bases **2** which possess either electron-donating or -withdrawing substituents on the aryl ring of the imine moiety provide **4** in high yields. It is noted that the reactions of **2c** and **2d**, which have electron-donating substituents, required more forcing conditions (entries 2 and 3), whereas electron-withdrawing substituents enhanced the reaction rates (entries 4 and 5).

Table 1 Radical rearrangement of Schiff base **2**[a]

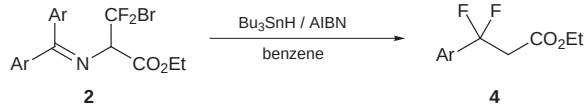

Entry	Ar	*T*/°C	*t*/h	Product	Yield[b] (%)
1	Ph	110	2.5	**4a**	93
2	4-MeC_6H_4	130	7.0	**4c**	90
3	4-$MeOC_6H_4$	130	7.0	**4d**	99
4	4-FC_6H_4	110	1.5	**4e**	80 (99)[c]
5	4-$CF_3C_6H_4$	110	2.0	**4f**	90

[a] All reactions were carried out in sealed glass tubes containing **2**, Bu_3SnH (2 equiv.) and AIBN (0.1 equiv.). After the reactions were completed, an equimolar amount of aromatic nitrile was generated (90–95% isolated yield in each case). [b] Reported yields are isolated yields unless specified. [c] The number in parentheses is the yield determined by ^{19}F NMR analysis.

The Schiff bases **1** are easily synthesized in one pot from the corresponding arylmagnesium bromides, aryl cyanides and glycine ethyl ester hydrochloride [eqn (3)].[12] In the net transformation to **4**, aryl cyanides were regenerated after completion of the intramolecular radical rearrangement, as shown in Scheme 1. Thus, the construction of **4** was formally

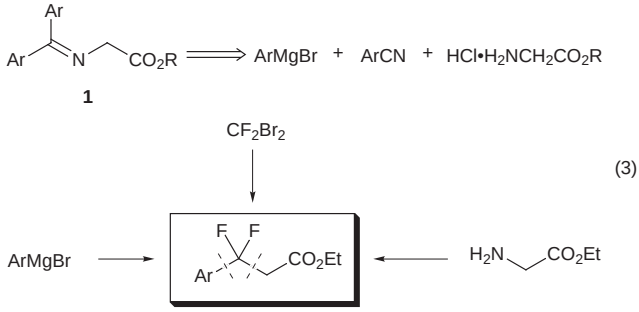

(3)

achieved by the coupling of three components, *i.e.* ArMgBr, CF_2Br_2 and glycine derivatives.

In conclusion, the synthesis and a novel reaction of 3-bromo-3,3-difluoroalanine Schiff bases were developed, which provide a new route to difluoromethylene compounds *via* intramolecular rearrangement involving radical *ipso*-substitution at the aromatic ring.

We thank to the SC NMR laboratory of Okayama University for ^{19}F NMR analyses and the Ministry of Education, Science, Sports and Culture of Japan for financial support (Grant-in-Aid for scientific research, No. 09305058).

Notes and References

† E-mail: uneyamak@cc.okayama-u.ac.jp

‡ Representive experimental procedures. (i) To a solution of 2,2,6,6-tetramethylpiperidine (106 mg, 0.75 mmol) in freshly distilled THF (1 ml) cooled down to 0 °C under argon atmosphere, 1.53 M BuLi in hexane (0.50 ml, 0.75 mmol) was added dropwisely and then stirred for an additional 30 min. The LTMP solution was cooled to −78 °C, and the solution of glycine Schiff base (0.5 mmol) in THF (1 ml) was added dropwisely to the LTMP solution. After 1 h, CF_2Br_2 (525 mg, 2.5 mmol) was added, and the mixture was stirred at −78 °C for a further 5 h. The reaction mixture was quenched with aq. NH_4Cl, and the organic layer was washed with brine and dried over Na_2SO_4. Purification of the products by recrystalization from hexane gave colorless plates. (ii) A solution of **2a** (19.9 mg, 0.05 mmol), Bu_3SnH (34.9 mg, 0.12 mmol) and AIBN (1.0 mg, 6.0 mmol) in benzene (2 ml) was heated at 110 °C in a sealed glass tube for 2.5 h. The reaction mixture was cooled, reduced in volume, and purified by chromatography on silica gel (hexane–EtOAc) to afford **4a** (10.0 mg, 93%) as a colorless oil.

1 V. P. Kukhar' and V. A. Soloshonok, *Fluorine-containing Amino Acids*, Wiley, Chichester, UK, 1995.
2 A [3,3]-sigmatropic rearrangement route to β,β-difluoro-carbonyl compounds has been reported: see S. T. Patel, J. M. Percy and R. D. Wilkes, *Tetrahedron*, 1995, **51**, 11 327.
3 T. Takagi, N. Okikawa, S. Johnoshita, M. Koyama, A. Ando and I. Kumadaki, *Synlett*, 1996, 82.
4 Reaction of an alanine Schiff base with CF_2Br_2 in the presense of LDA has been reported: see P. Bay and J. P. Vevert, *Tetrahedron Lett.*, 1978, **14,** 1215.
5 Compound **4a** was identified by comparison with an authentic sample synthesized by difluorination of ethyl benzoylacetate using DAST, see S. C. Sondej and J. A. Katzenellenbogen, *J. Org. Chem.*, 1986, **51**, 3508.
6 L. Benati, P. Spagnolo, A. Tundo and G. Zanardi, *J. Chem. Soc., Chem. Commun.*, 1979, 141.
7 J. Grimshaw, R. Hamilton and J. Trocha-Grimshaw, *J. Chem. Soc., Perkin Trans. 1*, 1982, 229.
8 J. Aubé, X. Peng, Y. Wang and F. Takusagawa, *J. Am. Chem. Soc.*, 1992, **114**, 5466.
9 E. Lee, H. S. Whang and C. K. Chung, *Tetrahedron Lett.*, 1995, **36**, 913.
10 M. L. E. N. da Mata, W. B. Motherwell and F. Ujjainwalla, *Tetrahedron Lett.*, 1997, **38**, 137 and 141.
11 An equimolar amount of aromatic nitrile was isolated and identified by GC, NMR and IR analysis and comparison with authentic material.
12 M. J. O'Donnell and R. L. Polt, *J. Org. Chem.*, 1982, **47**, 2663.

Received in Cambridge, UK, 27th May 1998; 8/03944E

Photo-induced depolymerization of reversible supramolecular polymers

Brigitte J. B. Folmer, Esther Cavini, Rint P. Sijbesma and E. W. Meijer*†

Laboratory of Macromolecular and Organic Chemistry, Eindhoven University of Technology, PO Box 513, 5600 MB Eindhoven, The Netherlands

The degree of polymerization of supramolecular polymers based on quadruple hydrogen bonding of 2-ureido-4-pyrimidone units is decreased upon the photochemical formation of reversibly interfering end-caps.

Photo-induced processes to control the molecular weight of polymers are well-known and used in many advanced applications, like coatings and photolithography.[1–3] In all of these processes, the photochemical event changes the molecular structure by either polymerization of monomers, the cross-linking of polymers, the depolymerization of polymers or the side-chain modifications of polymers by, for example, the photo-induced formation of initiators or catalysts. The changes in the chemical composition of the material and, hence, in properties like solubility or viscosity, are the result of the breaking or making of covalent bonds of the polymer.

Recently, we introduced the concept of using quadruple hydrogen bonding to prepare reversible supramolecular polymers.[4] Linear polymers **1** (Fig. 1) are formed by the self-assembly of two 2-ureido-4-pyrimidone units, which dimerize strongly in solvents like $CHCl_3$ and in the solid state with dimerization constants (K_{dim}) exceeding 10^6 M^{-1}. The polymers obtained exhibit true polymer properties illustrated by high solution viscosities, shear thinning in the melt and viscoelastic properties of the neat materials. The reversibility of the supramolecular polymers, with degrees of polymerization (DP) of more than 500, is demonstrated by experiments where monofunctional 2-ureido-4-pyrimidone **2** is added as a chain stopper to polymer **1**. A rapid exchange controls the DP, leading to a strong decrease in viscosity upon addition of **2** to **1**. This control of DP resembles the way the DP of condensation polymers is tuned,[5] but now in an unprecedented rapid way under ambient conditions.

Here we report on the photo-induced generation of chain stopper **2**, and how the viscosity of the solution of supramolecular polymer **1** is triggered by a photochemical process (Scheme 1). We designed precursor **3**, being the *o*-nitrobenzyl

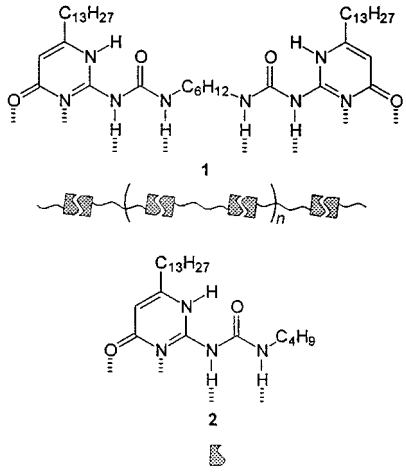

Fig. 1 Difunctional compound **1**, which forms supramolecular polymer chains, and monofunctional compound **2**, which acts as an end-cap

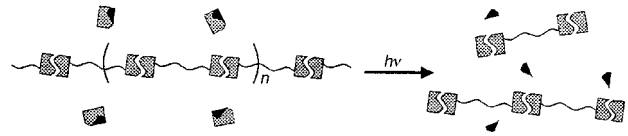

Scheme 1

ether protected derivative of chain stopper **2**. This protecting group is well-known for its clean cleavage upon UV irradiation,[6] by which compound **3** is converted into chain stopper **2** (Scheme 2).

Compound **3** was prepared by the reaction of *o*-nitrobenzyl chloride with **2**, that in turn was made by the reaction of butyl isocyanate with the corresponding isocytosine. Bifunctional compound **1** was prepared by the reaction of the same isocytosine and hexane-1,6-diyl diisocyanate following a procedure published previously.[4] When **1** is more than 99.9% pure, a DP of around 700 is obtained and a 40 mM solution of **1** in $CHCl_3$ exhibits a η_{rel} of 13.16.

The photolability of **3** was investigated by UV irradiation of a 9.9 mM solution of **3** in $CDCl_3$.‡ The progress of the deprotection was readily monitored *via* ^{1}H NMR spectroscopy; the H-5 signal of pyrimidine **3** at δ 6.25 decreased in intensity as the upfield H-5 signal of pyrimidone **2** at δ 5.81 increased. Also the characteristic NH signals of **2**, downfield in comparison to the NH signals of **1** due to dimerization, appear upon formation of **2**.

The photogeneration of **2** (0.1 equiv.) in the presence of polymer **1** was monitored *via* viscosity measurements (η_{rel} in $CDCl_3$), as presented in Fig. 2. The addition of 0.1 equiv. of precursor **3** produced a small decrease in the viscosity (η_{rel} went from 13.16 to 10.79) *versus* the enormous drop in viscosity (η_{rel} went from 13.16 to 1.92) upon the addition of 0.1 equiv. of chain stopper **2**. After 2 h irradiation of the mixture of **1** and **3**, the η_{rel} is similar to the η_{rel} of a solution of **1** and 0.1 equiv. of chain stopper **2**. The shape of the plot of the decrease in η_{rel} with time is consistent with the monoexponential formation of **2** from **3** and the way **2** directly affects the DP of **1**.

In order to check for artefacts in the approach used, we have performed a number of reference experiments. A decrease in

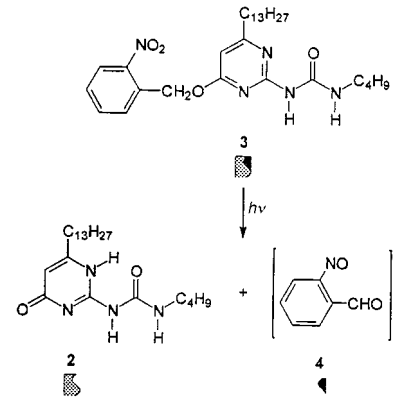

Scheme 2

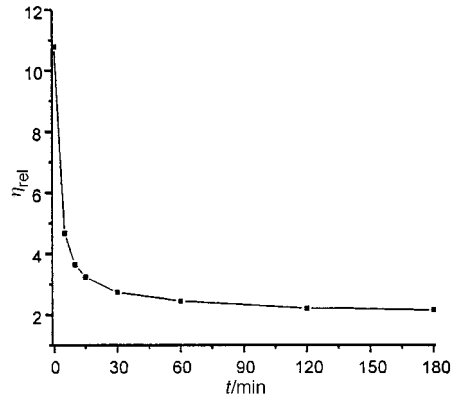

Fig. 2 Relative viscosity of a 40 mM solution of **1** with 0.1 equiv. of **3** in $CHCl_3$ upon UV irradiation

η_{rel} from 13.16 to 12.83 was found after 4 h irradiation of **1** without end-caps. The addition of 0.1 equiv. of *o*-nitrobenzyl ether protected phenol to a solution of **1** in $CDCl_3$ followed by UV irradiation for 3 h resulted in a decrease in η_{rel} from 13.16 to 8.46, while the addition of 0.1 equiv. of phenol to a 40 mM solution **1** in $CDCl_3$, resulted in a relative viscosity of 11.00. Hence, the large decrease in viscosity of the photoactive system is mainly caused by the formation of chain stopper **2**.

In conclusion, we have demonstrated the triggering of the DP of a reversible supramolecular polymer. These experiments also confirm the selectivity and specificity of polymer formation by quadruple hydrogen bonding.

Part of this investigation was supported by The Netherlands Foundation for Chemical Research (SON), with financial aid from The Netherlands Organization for Scientific Research (NWO). E. C. acknowledges the EU for an Erasmus grant.

Notes and References

† E-mail: tgtobm@chem.tue.nl

‡ The equipment used for the deprotection was a 15 W Cosmolux fluorescent UV lamp, and the solution was irradiated in a quartz cuvette at a distance of 10 cm.

1 M. Irie, Y. Hirano, S. Hashimoto and K. Hayashi, *Macromolecules*, 1981, **14**, 262; M. Irie, A. Menju and K. Hayashi, *Macromolecules*, 1979, **12**, 1177.
2 G. S. Kumar, P. DePra, K. Zhang and D. C. Neckers, *Macromolecules*, 1984, **17**, 2463; G. S. Kumar and D. C. Neckers, *Chem. Rev.*, 1989, **89**, 1915.
3 M.-K. Leung, J. M. J. Fréchet, J. F. Cameron and C. G. Wilson, *Macromolecules*, 1995, **28**, 4693.
4 R. P. Sijbesma, F. H. Beijer, L. Brunsveld, B. J. B. Folmer, J. H. K. K. Hirschberg, R. F. M. Lange, J. K. L. Lowe and E. W. Meijer, *Science*, 1997, **278**, 1601.
5 P. J. Flory, *The Principles of Polymer Chemistry*, Cornell University Press, New York, 1986.
6 S. M. Kalbag and R. W. Roeske, *J. Am. Chem. Soc.*, 1975, **97**, 440.

Received in Bath, UK, 20th June 1998; 8/04797I

Novel single molecule precursor routes for the direct synthesis of highly monodispersed quantum dots of cadmium or zinc sulfide or selenide

B. Ludolph, M. A. Malik, P. O'Brien* and N. Revaprasadu

Department of Chemistry, Imperial College of Science, Technology and Medicine, South Kensington, London, SW7 2AY UK. E-mail: p.obrien@ic.ac.uk

Good quality highly mono-dispersed nanoparticles of II–VI binary chalcogenides ME (M = Zn or Cd, E = S or Se) have been prepared in a 'one-pot' synthesis by the thermolysis in tri-*n*-octylphosphine oxide (TOPO, *e.g.* at 200 °C for 45 min, *ca.* 50 Å ± 2.5 Å diameter) of the corresponding bis[methyl(*n*-hexyl)di-thio or -seleno]carbamato {M[E_2CN-Me(C_6H_{13})]$_2$, E = S or Se} complexes; the CdS, CdSe and ZnSe particles have been characterized by electronic spectroscopy, photoluminiscence, X-ray diffraction and electron microscopy (SAED, SEM and TEM).

Compound semiconductors as isolated quantum dots[1–7] are the subject of considerable interest. Cadmium selenide has been extensively studied and is an attractive material because its band gap can be tuned across the visible region by varying the size of the material in the range 400–800 nm. One particularly useful approach to the synthesis of CdSe is the pyrolysis of metal–organic species in tri-*n*-octylphosphine oxide.[8] We have successfully developed a variation of this method in which single molecule precursors, often based on carbamato complexes, have been used. A wide range of quantum dots have been prepared including CdSe, CdS, PbS, PbSe and ZnSe.[9–11]

However, we have now developed some novel air stable precursors based on bis[methyl(*n*-hexyl)diselenocarbamato]-zinc or -cadmium which decompose cleanly in MOCVD to selenides.[12–14] Here, we have used these compounds in a novel 'one pot' synthesis of quantum dots of the II–VI semiconductors ME (M = Zn or Cd and E = S or Se). Highly monodispersed CdSe, CdS, ZnSe, and ZnS with good optical properties can be prepared.

In a typical synthesis,† 1.0 g of the precursor was dissolved in 15 ml trioctylphosphine (TOP). This solution was then injected into hot trioctylphosphine oxide (TOPO) (200 °C) and kept at this temperature for 30–40 min. The resulting solution was cooled to *ca.* 70 °C and an excess of methanol added and a flocculant precipitate formed. The solid was separated by centrifugation and redispersed in toluene. The toluene was removed under vacuum to give TOPO capped ME nanoparticles. The absorption edge of the nanoparticles were calculated using the direct band gap method.[15]‡ The optical absorption edge for CdSe nanoparticles showed a clear blue shift (614 nm, 2.02 eV, fraction 1 to 599 nm, 2.09 eV, fraction 5) as compared to the bulk band gap (716 nm, 1.73 eV). A similar but smaller shift (498 nm, 2.48 eV, fraction 1 to 493 nm, 2.51 eV, fraction 5) was shown by CdS nanoparticles (bulk 512 nm, 2.42 eV).

Accurate measurement of the absorption edge for ZnS nanoparticles (bulk ZnS 340 nm, 3.65 eV) was difficult owing to the overlap with TOPO absorption (300 nm). Different fractions of ZnSe nanoparticles showed a blue shift in the absorption spectra (362 nm, 3.42 eV to 345 nm, 3.59 eV) as compared to the bulk band gap (480 nm, 2.58 eV). The average size of the particles decreases from fraction 1 to 5. The relatively small shift in the absorption edge from fraction 1 to 5 for both CdS and ZnSe samples reflects the relatively narrow size distribution in these samples.

TEM images show well defined, spherical particles with the size range of 53–59 Å (CdS), 54–59 Å (CdSe) (Fig. 1), and 35–42 Å (ZnSe). The XRD patterns for CdSe, CdS (Fig. 1 and 2) and ZnSe show broad peaks typical of small particles. The SAED pattern exhibits broad diffuse rings owing to the small size of the crystallites. The indexing of the lattice parameters patterns of XRD and SAED for CdSe, CdS and ZnSe indicate the formation of the hexagonal phase.§ The EDAX pattern clearly confirmed the presence of the corresponding elements for ME nanoparticles. The strong peak for phosphorus in each case was due to the capping of the particles by TOPO which was further confirmed by shift in the IR band (P=O) for TOPO.

The photoluminescence spectra for CdS nanoparticles show a broad band edge emission from 589 to 504 nm for excitation at 370 nm depending upon the concentration of samples. A shift in luminescence maxima at higher concentration was observed which is due to filtering effects which became important at such concentrations. Near band edge luminescence was observed for CdSe for a excitation wavelength at 465 nm which indicates a fluorescence activation by surface derivation. The maximum of the emission band is gradually blue shifted as the size distribution become weighted with particles of the smaller dimensions. Fig. 3(a) and (b) show the photoluminescence and band edges for CdSe and CdS nanoparticles. The luminescence spectrum of ZnSe nanoparticles showed a broad emission at 440

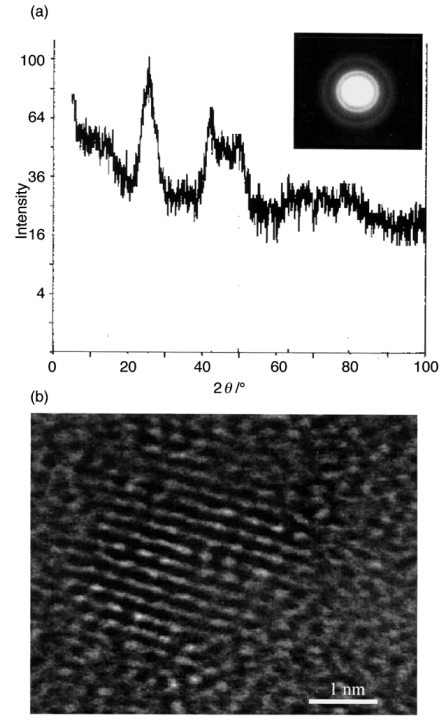

Fig. 1 (a) XRD and SAED pattern for CdSe nanoparticles and (b) HRTEM image of a CdSe Q-dot (diameter: 5 nm)

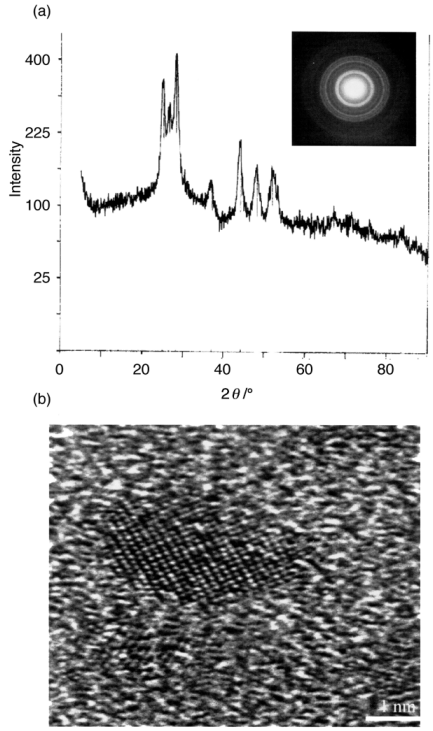

Fig. 2 (a) XRD and SAED pattern for CdS nanoparticles and (b) HRTEM image of a CdS Q-dot (diameter: 5 nm)

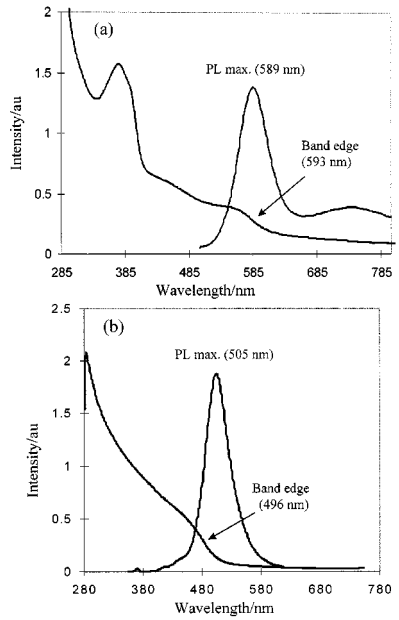

Fig. 3 Optical absorption spectrum and photoluminescence spectrum showing the band edge and emission maximum of (a) CdSe (fraction 3) and (b) CdS (fraction 3)

nm for an excitation wavelength of 345 nm. The emission spectrum is red shifted in relation to the band edge by *ca.* 0.04 eV. As the particle size decreases the surface/volume ratio increases thereby increasing the number of surface traps. These surface states or defects normally associated with semiconductor nanoparticles are passivated by TOPO. Therefore the deep trap emission associated with these states are absent.

In conclusion, good quality highly mono-dispersed nanoparticles of ME have been prepared for the first time by thermolysis in TOPO using $M[E_2CNMe(C_6H_{13})]_2$ type single molecule precursors in a one pot synthesis. These are the first stable, non-air sensitive single molecule precursors which can easily be used to give high yields of TOPO capped quantum dots. The CdS, CdSe and ZnSe particles have been characterized by UV–VIS, PL, EDAX, XRD, SAED and TEM whereas the ZnS particles were characterized by UV–VIS, PL and EDAX only and are being investigated for other properties.

Paul O'Brien is the Royal Society Amersham International Research Fellow (1997/98) and the Sumitomo/STS Professor of Materials Chemistry. We thank the EPSRC for a grant supporting work on single molecule precursors for quantum dots. B. L. was supported by the Socrates program of the EU and N. R. by a Royal Society/FRD development program between ICSTM.

Notes and References

† The compounds were prepared by adaptations of the literature methods[15,16] and fully characterised by NMR, mass spectrometry, microanalysis and IR spectroscopy.

‡ A Philips PU 8710 spectrophotometer was used to carry out the optical measurements, the samples were placed in silica cuvettes (1 cm path length). For photoluminescence spectroscopy a Spex FluoroMax instrument with a xenon lamp (150 W) and a 152 P photomultiplier tube as a detector was used to measure the photoluminescence of the particles. Good spectra were obtained with the slits set at 2 nm and an integration time of 1 s. The samples were placed in quartz cuvettes (1 cm path length). The wavelength of excitation is indicated in the text and was shorter than the onset of absorption of the particular sample being studied. X-Ray diffraction patterns were measured using a Philips PW 1700 series automated powder diffractometer using Cu-Kα radiation at 40 kV and 40 mA with a secondary graphite crystal monochromator. Samples were supported on glass slides (5 cm). A concentrated toluene solution was slowly evaporated at room temperature onto a glass slide to obtain a sample for analysis. A JOEL 2000 FX MK 1 electron microscope operating at 200 kV with an Oxford Instrument AN 10000 EDS analyser was used for the conventional TEM images. Selected area electron diffraction (SAED) patterns were obtained using a JEOL 2000 FX MK2 electron microscope operated at 200 kV. The samples for TEM and SAED were prepared by placing a drop of a dilute solution of sample in toluene on a copper grid (400 mesh, agar). The excess of solvent was wicked away with a paper tip and the sample allowed to dry completely at room temperature. EDAX (energy dispersion analytical X-ray spectroscopy) was performed on the sample deposited by evaporation on glass substrates by using a JEOL JSM35CF scanning electron microscope.

§ The X-ray diffraction pattern of the CdS particles gave peaks with the following observed *d*/Å values (% relative intensity, *hkl*): 3.55 (76, 100), 3.35 (52, 002), 3.16 (100, 101), 2.06 (43, 110) and 1.90 (26, 103) corresponding to hexagonal cadmium sulfide; 3.57 (62, 100), 3.36 (91, 002), 3.16 (100, 101), 2.45 (29, 102), 2.07 (48, 110) and 1.90 (50, 103) (ASTM). CdSe: 3.50 (100, 002), 2.13 (80, 110), 1.84 (50, 112) and 1.48 (10, 211) corresponding to hexagonal phase; 3.51 Å (70, 002), 2.15 (85, 110), 1.83 (50, 112) and 1.38 Å (8, 211) {ASTM}. ZnSe: 3.06 (70, 101), 1.99 (100, 110), 1.24 (35, 105), 1.10 (40, 302) corresponding to hexagonal phase; 3.05 (70, 101), 1.99 (100, 110), 1.22 (40, 105), 1.09 (40, 302){ASTM}.

1 A. Henglein, *Chem. Rev.*, 1989, **89**, 1861.
2 M. L. Steigerwald and L. E. Brus, *Acc. Chem. Rev.*, 1990, **23**, 183.
3 Y. Wang and N. Herron, *J. Phys. Chem.*, 1991, **95**, 525.
4 H. Weller, *Adv. Mater.*, 1993, **5**, 88.
5 X. Li, J. R. Fryer and D. J. Cole-Hamilton, *J. Chem. Soc., Chem. Commun.*, 1994, 1715.
6 S. W. Haggata, D. J. Cole-Hamilton and J. R. Fryer, *J. Mater. Chem.*, 1997, **7**, 1969.
7 M. Green and P. O'Brien, *Adv. Mater. Opt. Electron.*, 1997, **7**, 277.
8 C. B. Murray, D. J. Murray and M. G. Bawendi, *J. Am. Chem. Soc.*, 1993, **115**, 8706.
9 T. Trindade and P. O'Brien, *Adv. Mater.*, 1996, **8**, 161.
10 T. Trindade and P. O'Brien, *Chem. Mater.*,1997, **9**, 523.
11 N. Revaprasadu, M. A. Malik, P. O'Brien, M. M. Zulu and G. Wakefield, *J. Mater. Chem.*, 1998, 1885.
12 M. Chunggaze, J. McAleese, P. O'Brien and D. J. Otway, *Chem. Commun.*, 1998, 833.
13 P. O'Brien, D. J. Otway and J. R. Walsh, *Adv. Mater. CVD*, 1997, **3**, 227.
14 M. Chunggaze, M. A. Malik and P. O'Brien, *Adv. Mater.*, submitted.
15 J. I. Pankove, *Optical Processes in Semiconductors*, Dover Publications, Inc., New York, 1970.

Received in Bath, UK, 1st July 1998; 8/05411H

Chemoenzymatic total synthesis of the sesquiterpene (−)-patchoulenone

Martin Banwell*† and Malcolm McLeod

Research School of Chemistry, Institute of Advanced Studies, The Australian National University, Canberra, ACT 0200, Australia

Monochiral *cis*-1,2-dihydrocatechol 2, obtained by microbial oxidation of toluene, has been converted, *via* intermediate 3, into the cyperene-type sesquiterpene 1.

(−)-Patchoulenone **1** is a prominent member of the cyperene class of sesquiterpenes and was first isolated in 1964 from *Cyperus rotundus* Linné (*Cyperaceae*), a plant common in Sudan, India, China, Thailand and Japan.[1,2] The compound has

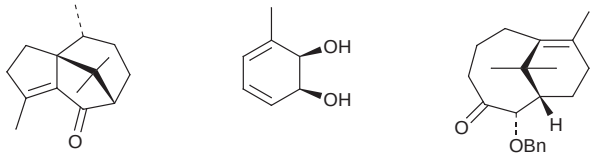

1 **2** **3**

also been identified as a constituent of, *inter alia*, the root bark of *Uvaria narum* Wall. (*Annonaceae*)[3] and *Piptostigma fugax*.[4] Despite a number of the source plants being used in traditional medicines, only a modest amount is known about the biological properties of (−)-patchoulenone. Thus, compound **1** shows[2] *in vitro* activity (EC_{50} 1.08×10^{-4} M) against the malarial parasite *Plasmodium falciparum*, strong anti-fungal activity against *Rhizoctonia solani* and *Saprolegnia asterophora*,[4] and significant toxicity in a brine shrimp bioassay.[4]

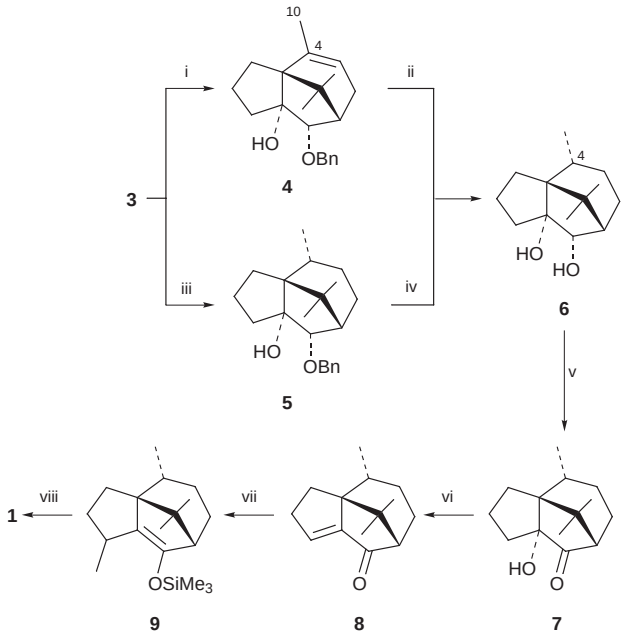

Scheme 1 *Reagents and conditions*: i, $SnCl_2$ (0.25 equiv.), $CHCl_3$, 18 °C, 1 h; ii, H_2 (60 psi), 10% Pd/C, MeOH, 18 °C, 48 h; iii, SmI_2 (1.6 equiv.), HMPA, THF, 0 °C, 0.25 h; iv, H_2 (1 atm), 10% Pd/C, THF, 18 °C, 0.75 h; v, $(COCl)_2$ (3.0 equiv.), DMSO (5.0 equiv.), CH_2Cl_2, −78 °C, 0.25 h, then **6**, 0.25 h then Et_3N (6.0 equiv.) −78 to 0 °C, 0.25 h; vi, $SOCl_2$, pyridine, 40 °C, 1 h; vii, MeLi (10 equiv.), CuBr·DMS (5.0 equiv.), THF, −40 °C, 0.5 h, then **8**, Me_3SiCl (10 equiv.), HMPA, −78 °C, 0.5 h; viii, DDQ (4.0 equiv.), 2,6-lutidine (6.5 equiv.), CH_2Cl_2, 18 °C, 0.1 h

The 1,4,9,9-tetramethyl-2,4,5,6,7,8-hexahydro-3*H*-3a,7-methanoazulene framework associated with the cyperene-type sesquiterpenes has been the subject of a number of synthetic studies[5] and the title compound itself has been synthesised by Hikino *et al*[6] who used (+)-camphor as the starting material. The racemic modification of patchoulenone has also been prepared *via* the Lewis acid catalysed addition of a diazo ketone to a tethered olefin.[7] We now report a quite distinct and chemoenzymatic total synthesis of (−)-patchoulenone which employs the monochiral *cis*-1,2-dihydrocatechol **2**, obtained by microbial oxidation of toluene, as starting material.[8]

In connection with synthetic approaches to taxoids, we have recently described[9] the conversion of compound **2** into the bicyclo[5.3.1]undecenone **3**. As has been observed in a closely related system,[10] the carbon–carbon double-bond and carbonyl group within compound **3** are in close proximity. As a consequence the molecule readily engages in a tin(II) chloride catalysed intramolecular Prins reaction (Scheme 1) to give the tricyclic isomer **4** {97%, $[\alpha]_D$ −32 (*c* 2.0)‡}. Hydrogenation of compound **4** using H_2 at 60 psi and with palladium on carbon as catalyst provided a *ca.* 3:1 mixture of the saturated *cis*-diol **6**§ {59%, mp 209–211 °C (sealed tube), $[\alpha]_D$ −21.4 (*c* 0.6)} and its C4-epimer {21%, mp 207–209 °C (sealed tube), $[\alpha]_D$ +37.2 (*c* 0.7)} which could be separated from one another by flash chromatography. An alternative route to the pivotal compound **6** involved subjecting compound **3** to reductive cyclisation using samarium(II) iodide[11] and a chromatographically separable mixture of **5** {39%, mp 53–54 °C, $[\alpha]_D$ +17.9 (*c* 0.9)} and the $\Delta^{4(10)}$-isomer {54%, $[\alpha]_D$ +65 (*c* 0.4)} of compound **4** was produced. Hydrogenolysis of compound **5** could be achieved under standard conditions and the resulting diol **6** (95%) was oxidised to the acyloin **7** {91%, $[\alpha]_D$ −0.2 (*c* 1.0)} using the Swern reagent. Dehydration of compound **7** to the enone **8** {68%, $[\alpha]_D$ −150 (*c* 0.5)} could be effected using thionyl chloride in pyridine at 40 °C. This latter compound was subjected to reaction with the Gilman reagent derived from methyllithium and copper(I) bromide–dimethyl sulfide (DMS) complex[12] and the ensuing enolate anion trapped with trimethylsilyl chloride to give the unstable silyl enol ether **9**, which was obtained as a single diastereoisomer. Dehydrogenation of compound **9** with DDQ/2,6-lutidine[13] then gave (−)-patchoulenone **1** {77% from **8**, mp 50–51 °C (lit.,[1] 52.5 °C), $[\alpha]_D$ −101 (*c* 0.4) [lit.,[1] −97.1 (*c* 8.0)]}, the ^1H and ^{13}C NMR spectral data for which matched those reported[2] for the natural product.

We thank the Institute of Advanced Studies for financial support including the provision of a Postdoctoral Fellowship to M. M. Drs G. Whited and L. Kwart of Genencor International Inc. (Palo Alto) are thanked for providing generous supplies of the *cis*-1,2-dihydrocatechol **2**.

Notes and References

† E-mail: mgb@rsc.anu.edu.au

‡ All optical rotations were determined in chloroform solution at 20 °C

§ All new and stable compounds had spectroscopic data (IR, NMR, mass spectrum) consistent with the assigned structure. Satisfactory combustion and/or high resolution mass spectral analytical data were obtained for new compounds and/or suitable derivatives.

1 B. Trivedi, O. Motl, V. Herout and F. Sorm, *Collect. Czech. Chem. Commun*., 1964, **29**, 1675.
2 C. Thebtaranonth, Y. Thebtaranonth, S. Wanauppathamkul and Y. Yuthavong, *Phytochemistry*, 1995, **40**, 125.
3 A. Hisham, V. Wray, L. Pieters, M. Claeys, R. Dommisse and A. Vlietinck, *Magn. Reson. Chem*., 1992, **30**, 295.
4 H. Achenbach and A. Schwinn, *Phytochemistry*, 1995, **38**, 1037.
5 G. Büchi, W. D. MacLeod Jr. and J. Padilla O. , *J. Am. Chem. Soc*., 1964, **86**, 4438 and refererences cited therein.
6 H. Hikino, K. Ito, K. Aota and T. Takemoto, *Chem. Pharm. Bull*., 1968, **16**, 43.
7 W. F. Erman and L. C. Stone, *J. Am. Chem. Soc.*, 1971, **93**, 2821.
8 For reviews on the applications of *cis*-1,2-dihydrocatechols in synthesis see: D. A. Widdowson, D. W. Ribbons and S. D. Thomas, *Janssen Chim. Acta*, 1990, **8**, 3; H. A. J. Carless, *Tetrahedron: Asymmetry*, 1992, **3**, 795; S. M. Brown, and T. Hudlicky, in *Organic Synthesis: Theory and Applications*, ed. T. Hudlicky, JAI, Greenwich, CT, 1993, vol. 2, 113; T. Hudlicky and J. W. Reed, in *Advances in Asymmetric Synthesis*, ed. A. Hassner, JAI, Greenwich, CT, 1995, vol. 1, p. 271; T. Hudlicky and A. J. Thorpe, *Chem. Commun*., 1996, 1993.
9 M. G. Banwell, P. Darmos, D. C. R. Hockless and M. D. McLeod, *Synlett*., 1998, 897.
10 R. A. Holton and A. D. Williams, *J. Org. Chem*., 1988, **53**, 5981.
11 G. A. Molander and C. Kenny, *J. Am. Chem. Soc*., 1989, **111**, 8236 and references cited therein.
12 H. O. House, C.-Y. Chu, J. M. Wilkins and M. J. Umen, *J. Org. Chem*., 1975, **40**, 1460.
13 T. L. Fevig, R. L. Elliott and D. P. Curran, *J. Am. Chem. Soc*., 1988, **110**, 5064; I. Fleming and I. Paterson, *Synthesis*, 1979, 736.

Received in Cambridge, UK, 30th June 1998; 8/04980G

Fabrication of a covalently attached multilayer *via* photolysis of layer-by-layer self-assembled films containing diazo-resins

Junqi Sun,[a] Tao Wu,[a] Yipeng Sun,[a] Zhiqiang Wang,[a] Xi Zhang*[a] Jiacong Shen[a] and Weixiao Cao[b]

[a] *Key Lab of Supramolecular Structure and Spectroscopy, Department of Chemistry, Jilin University, Changchun, 130023, China. E-mail: xi@mail.jlu.edu.cn*

[b] *College of Chemistry and Molecular Engineering, Peking University, Beijing, 100871, China*

Construction of highly stable covalently attached multilayer films was achieved by UV irradiation of ionic self-assembled multilayer films of diazo-resins and poly(sodium styrene sulfonate).

A layer-by-layer self-assembly technique based on electrostatic interaction as the driving force has attracted much attention in recent years.[1–3] This technique has proved to be a rapid and experimentally very simple way to produce complex layered structures with precise control of layer composition and thickness. However, the stability of such assembled films depends on the nature of solvent and is not always adequate.[4] How to improve the stability of such films is thus still a challenge. Here, we report on photoreactive multilayer films containing diazo-resins as polycations and poly(sodium 4-styrene sulfonate) as polyanions held together by electrostatic interactions. Upon UV irradiation, the adjacent interfaces of the multilayer films react to form a crosslinking structure which greatly improved the stability of the films. These changes were confirmed by UV–VIS and FTIR spectroscopy.

UV–VIS spectra were obtained using a Shimadzu 3100 UV–VIS-NIR spectrophotometer and IR spectra were obtained using a Bruker IFS66V FTIR instrument. The synthesis of the diazo-

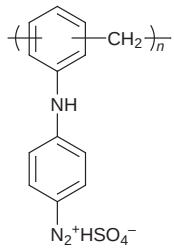

DAR

resin, DAR has been reported elsewhere.[5] The fabrication process of multilayer films containing DAR and PSS was conducted in the dark. The freshly cleaned substrate (quartz or CaF_2 slide) was first immersed in 0.9 vol% aqueous cationic poly(diallyldimethylammonium chloride) (PDDA) solution for 20 min. After rinsing with deionized water, the substrate was alternately dipped into aqueous solutions of PSS (1 mg ml^{-1}) and then DAR (1.5 mg ml^{-1}) for 20 min, with intermediate water washing and N_2 drying. Multilayer films can be formed by repeating the last two steps repeatedly.

UV–VIS spectroscopy was used to follow the fabrication process. Fig. 1 shows the UV–VIS absorption spectra for 2, 4, 6 and 8 bilayers of DAR/PSS assembled on a quartz slide. The absorbance at 380 nm is attributed to the π–π* transition of the diazonium group.[6] The linear increase in absorbance at 380 nm with the number of layers indicates a progressive deposition. The assembled films were immersed in a ternary mixture of H_2O–DMF–$ZnCl_2$ (3 : 5 : 2, w/w/w) to investigate their stability. This ternary system was chosen because of the high solubility of the polyelectrolyte complex of DAR/PSS in this solvent. Nearly 30% of the assembled films were dissolved after 5 min immersion according to the decrease of absorbance at 250 and 380 nm, and indicates that this type of ionic self-assembled film is not adequately stable in the ternary solvent.

Owing to the well known reactivity of diazonium and sulfonate groups, the above assembled films containing 8 bilayers of DAR/PSS were irradiated with a 30 W medium power mercury lamp at a distance of 10 cm. Fig. 2 shows the changes in UV–VIS spectra of the films with different time of irradiation, from which, we can clearly see that the absorbance at 380 nm decreases dramatically due to the decomposition of the diazonium group and within 5 min, the decomposition had proceeded completely. We then immersed the irradiated films into the same ternary solvent as for the untreated film and sonicated it for 0.5 h. No detectable damage of the films was observed, according to the absorbance at 250 nm, indicating a much greater stability.

From the change of the stability of the multilayer films before and after UV irradiation, it is proposed that photoreaction takes place between the diazonium and sulfonate groups. First, DAR is converted into its phenyl cationic form after released N_2 upon UV irradiation, then an S_N1 type of nuclear displacement by sulfonate occurs[7] as shown in Scheme 1.

Photoreaction changes the crosslinking structure of the multilayer film from ionic to covalent so that a three dimensional network forms which covers the whole substrate including four side faces. This can explain, despite the interaction between the substrate and the first layer of multilayer films not being covalent, the stability of the films in

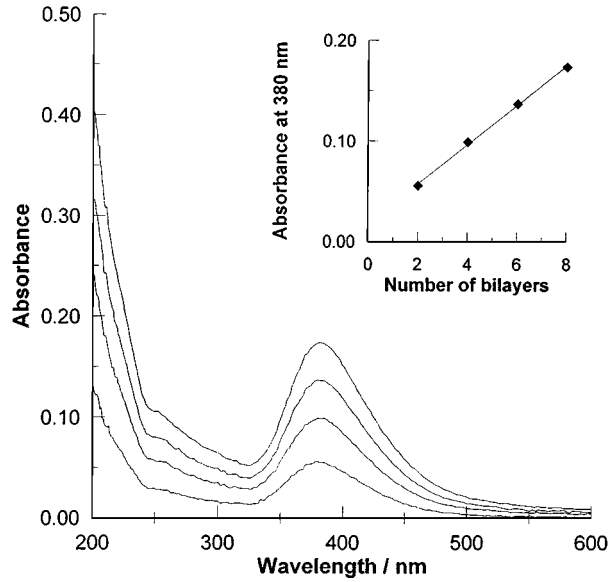

Fig. 1 UV–VIS absorption spectra of multilayer films of DAR/PSS, from the lower to upper, the number of bilayers is 2, 4, 6 and 8. Inset shows the absorption at 380 nm *vs.* the number of bilayers.

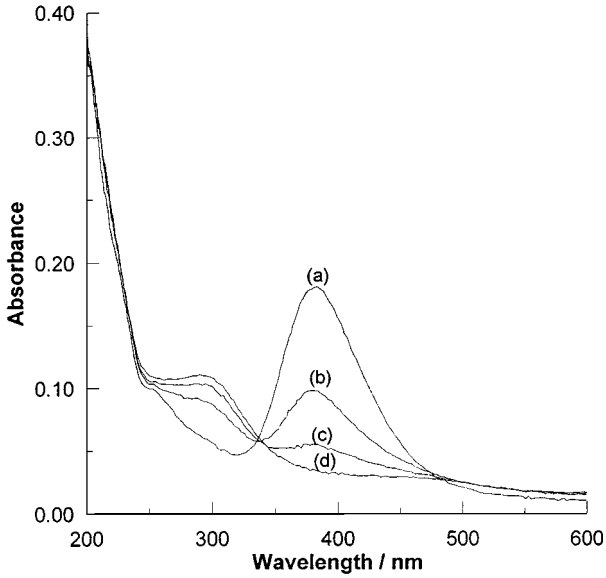

Fig. 2 UV–VIS absorption spectra of eight bilayers of DAR/PSS upon irradiation with UV light for (a) 0, (b) 0.5, (c) 1 and (d) 5 min

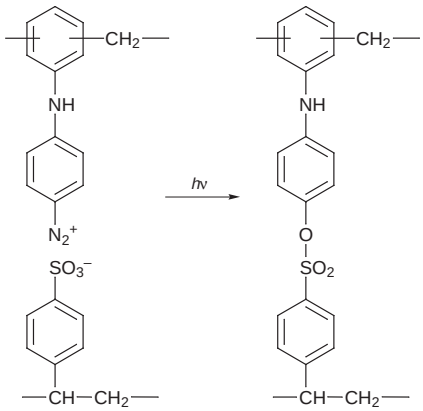

Scheme 1 Photoreaction of DAR and PSS

all solvents, such as MeOH, DMSO, DMF, $CHCl_3$ as well as the ternary solvent described above.

The photoreaction of diazonium and sulfonate groups in multilayer films was further confirmed by IR spectroscopy (for IR spectra see http://www.rsc.org./suppdata/cc/1998/1853). Two absorption peaks at 2166 and 1178 cm^{-1} are observed in the IR spectra of 12 bilayers of DAR/PSS assembled on a CaF_2 substrate before UV irradiation, which originate from the asymmetric stretching of CN_2 and symmetric stretching of SO_3^-, respectively. After UV light irradiation, the absorption at 2166 cm^{-1} disappeared completely, indicating the decomposition of the diazonium group. Meanwhile, a new absorption at 1162 cm^{-1} appears which corresponds to the symmetric stretching of the sulfonate coupled with the phenyl group. In layer-by-layer multilayer films, photoreaction should be facilitated to some extent by the close proximity of the diazonium and sulfonate groups.

In conclusion, a new type of covalently attached multilayer film has been fabricated by exploiting the layer-by-layer technique and then by photoreacting diazonium and sulfonate groups at the interface. Owing to the formation of three-dimensional crosslinking structure based on covalent bonding, the resulting multilayer films are much more stable than those based on ionic interactions. Further studies are in progress to assemble functional semiconductor nanoparticles and organic dye molecules into this covalently attached three-dimensional network.

This work was supported by National Natural Science Foundation of China.

Notes and References

1 G. Decher and J. D. Hong, *Macromol. Chem., Macromol. Symp.*, 1991, **46**, 321.
2 Y. M. Lvov and G. Decher, *Crystallogr. Rep.*, 1994, **39**, 628.
3 Y. P. Sun, E. C. Hao, X. Zhang, B. Yang and J. C. Shen, *Chem. Commun.*, 1996, 2381.
4 G. Z. Mao, Y. Tsao, M. Tirrell and H. T. Davis, *Langmuir*, 1995, **11**, 942.
5 W. X. Cao, S. J. Ye, S. G. Cao and C. Zhao, *Macromol. Rapid Commun.*, 1997, **18**, 983.
6 S. Patai, *The Chemistry of Diazonium and Diazo Groups*, John Wiley and Sons, Chichester–New York–Brisbane–Toronto, 1978, p. 351.
7 B. S. Furniss, A. J. Hannaford, P. W. G. Smith and A. R. Tatchell, *Textbook of Practical Organic Chemistry*, Longman Scientific and Technical, London, 5th edn., 1989, p. 922.

Received in Cambridge, UK, 18th June 1998; 8/04623I

Anionically induced decomposition of 2-ethoxycarbonylprop-2-enyl peroxides

C. Cramay, R. Ferdinando, M. Degueil-Castaing and B. Maillard*†

Laboratoire de Chimie Organique et Organométallique, associé au CNRS UMR 5802, Université Bordeaux 1, F-33405 Talence-Cedex, France

Treatment of 2-ethoxycarbonylprop-2-enyl peroxides with potassium alkylperoxylate, the sodium enolate of diethyl malonate and a primary or secondary amine yields epoxides *via* a two-step process: (i) addition of the nucleophile to the acrylic unsaturated bond and (ii) intramolecular anionic substitution on the peroxidic bond.

2,3-Epoxy esters are useful synthons, in particular for the production of 2-, 3- , 2,3-di-hydroxy and 3-amino-2-hydroxy esters.[1] The general methods of synthesis are the Darzen's condensation[2] and the various epoxidations[2] of 2,3-ethylenic esters. Many years ago the formation of epoxides was identified[3] in the homolytically induced decomposition of allyl *tert*-butyl peroxide. Subsequently, the free radical addition of reactive hydrogen donor solvents to allylic peroxides was used to prepare functionalised epoxides[4,5] (Scheme 1). Such a reaction, applied to acrylic peroxy derivatives, led to the formation of an epoxide with the simultaneous creation of a C–C bond, affording a new method for generation of 2,3-epoxy esters.[6] However, in some cases, synthetic interest in this reaction was limited by the formation of a mixture of several epoxides in low yields. For example, an attempt to prepare 1-ethoxycarbonyl-1-[2,2-bis(methoxycarbonyl)ethyl]oxirane[7] by free radical addition of dimethyl malonate to *tert*-butyl 2-ethoxycarbonylprop-2-enyl peroxide **1** failed mainly for two reasons:[7] (i) both possible radicals were generated from dimethyl malonate by hydrogen abstraction by radicals $Bu^tO\cdot$ and $Me\cdot$ and (ii) inefficient addition of the electrophilic radical $\cdot CH(CO_2Me)_2$ to the electron-poor double bond of the acrylic peroxide.

The selective production of the desired radical from dimethyl malonate was brilliantly solved by Roberts *et al.*[8] by application of reverse polar effects resulting from the addition of an aminoborane to the medium in the induced decomposition of allyl *tert*-butyl peroxide. Following the same approach and considering the existence of an *umpolung* effect on changing from the radical (electrophilic) to the anion (nucleophilic)[9] we designed an anionic-induced decomposition of **1** to produce epoxides **2** (Scheme 2). Indeed, the Michael addition[10] of $^-CH(CO_2Et)_2$ to ethyl acrylate suggested a possible addition of this carbanion to the unsaturation of **1**. The formation of an epoxy peroxide as a by-product in the synthesis of **1**[11] has to be considered as a good argument in favor of the feasibility of the intramolecular attack of the O–O bond, even if Yang and Finnegan[12] identified the adduct peroxide in the addition of Bu^tOOH to ethyl acrylate under basic conditions. The capacity of the *tert*-butoxide anion to abstract a proton from malonate would make this anionic-induced decomposition a chain process. The validity of this proposal was verified *via* the formation of **2** (R = Et, yield 60%) by the addition of 1 equiv. of peroxide **1**, at −10 °C, to a THF solution of diethyl malonate, previously treated with 0.1 equiv. of NaOEt.

The success of this reaction, the first synthetic example of an anionic decomposition of an allylic peroxide, prompted us to extend this work to other nucleophiles with the objective of gaining a better knowledge of its mechanism. The possible existence of either a concerted, or a two-step process must be considered. The simple way to prove that the adduct carbanion was a real intermediate was to offer it a chance to take a pathway other than the S_Ni reaction on the *tert*-butylperoxy group. This was arranged in the anionically induced decompositions of peroxide **1** induced by the potassium cumylperoxide anion, with the formation of two different epoxy peroxides, or by piperidine with the simultaneous production of an amino peroxide and an amino epoxide (Scheme 3). In the addition of potassium *tert*-butylperoxide to peroxide **3** the generation of two peroxy epoxides (Scheme 4) confirmed the existence of a general two-step process for the anionic-induced decomposition of unsaturated peroxides.

These preliminary results showed that allylic peroxides having an electron-poor double bond can suffer an anionically-induced decomposition consisting of two steps: (i) Michael addition of a nucleophile to the unsaturation and (ii) S_Ni reaction on the peroxidic function. Such steps may be part of a chain mechanism if the eliminated alkoxide is sufficiently basic to regenerate the nucleophile by proton abstraction from NuH, as in the reaction using diethyl malonate or an hydroperoxide; then only catalytic amounts of base are necessary. In the case of amines there is no need for a base because the nucleophile is provided by the lone pair of the nitrogen atom. The third case of interest appears to be when the eliminated alkoxide is not efficient enough to produce the nucleophile: it is then necessary to provide a stoichiometric amount of nucleophile to react with the unsaturated peroxide. This last possible induced decomposition was checked using ethyl 2-methylpropanoate as the precursor of the nucleophile,[13] the base being LDA. The addition at −78 °C of a THF solution of $Me_2C^-CO_2Et$[13] to peroxide **1** afforded after classical treatment the expected epoxy diester in a yield of 74%.

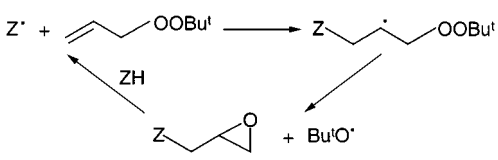

Scheme 1

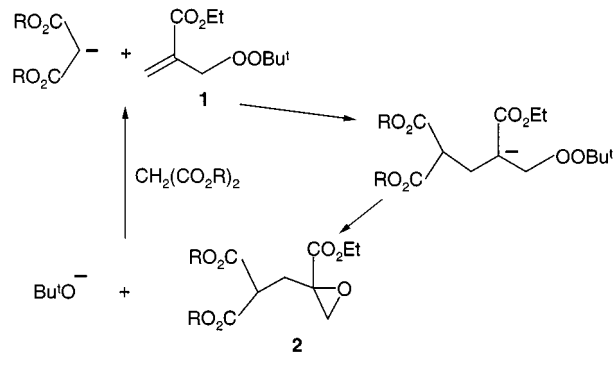

Scheme 2

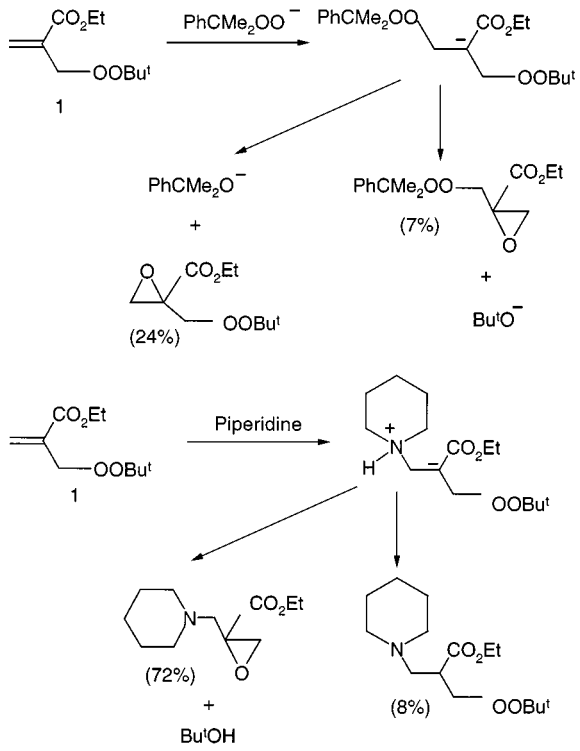

Scheme 3

In conclusion, anionically-induced decomposition of unsaturated peroxides having electron-poor double bonds by an addition-S_Ni process was clearly identified for the first time and appears a promising way to obtain oxygenated heterocycles such as epoxides (these reactions are currently under study in our group). This approach complements the homolytically induced decomposition of such unsaturated peroxides according to the *umpolung* effect identified in the replacement of a radical by the corresponding anion.

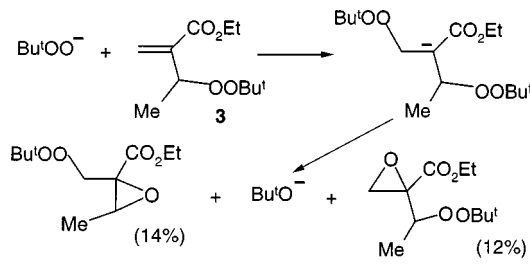

Scheme 4

Notes and References

† E-mail: b.maillard@lcoo.u-bordeaux.fr

1 See *e.g.* W. A. Kleschick, C. S. Lu and S. Thornburgh, *Synthesis*, 1990, 783; J. L. van der Baan, J. W. F. K. Barnick and F. Bickelhaupt, *Synthesis*, 1997, 897; M. Diaz and R. M. Ortuno, *Tetrahedron: Asymmetry*, 1995, **6**, 1845; S. Saito, M. Takashi, T. Ishikawa and T. Morikawa, *Tetrahedron Lett.*, 1991, **32**, 667; R. Nouguier, M. P. Bertrand, P. Picon and P. Perfetti, *Tetrahedron Lett.*, 1994, **35**, 8171.
2 For a review, see G. Berti, *Top. Stereochem.*, 1973, **7**, 93.
3 R. R. Hiatt and V. G. K. Nair, *Can. J. Chem.*, 1980, **58**, 450.
4 E. Montaudon, F. Rakotomanana and B. Maillard, *Bull. Soc. Chim. Fr.*, 1985, 198.
5 E. Montaudon, M. Agorrody, F. Rakotomanana and B. Maillard, *Bull. Soc. Chim. Belg.*, 1987, **96**, 769.
6 C. Navarro, M. Degueil-Castaing, D. Colombani and B. Maillard, *Synlett*, 1992, 587.
7 D. Colombani and B. Maillard, *J. Chem. Soc., Perkin Trans. 2*, 1994, 745.
8 H. S. Dang and B. P. Roberts, *Tetrahedron Lett.*, 1992, **33**, 4621; *J. Chem. Soc., Perkin Trans. 1*, 1993, 891.
9 B. Giese, *Free Radicals in Organic Synthesis: Formation of Carbon-Carbon Bonds*, Pergamon, Oxford, 1986, p. 29.
10 For a recent review, see P. Perlmutter, *Conjugate Addition Reactions in Organic Synthesis*, Pergamon, Oxford, 1992.
11 C. Navarro, M. Degueil-Castaing, D. Colombani and B. Maillard, *Synth. Commun.*, 1993, **23**, 1025.
12 N. C. Yang and R. A. Finnegan, *J. Am. Chem. Soc.*, 1958, **80**, 5845.
13 P. S. Engel and M. A. Schexnayder, *J. Am. Chem. Soc.*, 1975, **97**, 150.

Received in Cambridge, UK, 1st May 1998; 8/03300E

Biosynthesis of isoprenoids in *Escherichia coli*: The fate of the 3-H and 4-H atoms of 1-deoxy-D-xylulose

José-Luis Giner,[a] Bernhard Jaun[b] and Duilio Arigoni*[b]

[a] *Department of Chemistry, State University of New York - ESF, Syracuse, NY 13210, USA*
[b] *Laboratorium für Organische Chemie, Eidgenossische Technische Hochschule, Universitätstr. 16, Zürich, CH-8092, Switzerland*

The ubiquinone obtained from *E. coli* after feeding of 1-deoxy[3-^{2}H]xylulose shows labeling of the *E*-methyl group in the terminal unit and of all other positions derived from the terminal methylene group of isopentenyl pyrophosphate, whilst label from 1-deoxy[4-^{2}H]xylulose is retained exclusively in the double bond corresponding to the dimethylallyl pyrophosphate starter unit.

Recent studies have indicated that in *E. coli* the early steps of isoprenoid biosynthesis, *i.e.* formation of isopentenyl pyrophosphate (IPP) **3** and dimethylallyl pyrophosphate (DMAPP) **4**, occur *via* a mevalonate-independent pathway,[1,2] known to be operative also in other bacteria[1] as well as in green algae[3] and higher plants.[4] This alternative route proceeds *via* the intermediacy of 1-deoxy-D-xylulose **1a** (or the corresponding 5-phosphate **1b**) as first demonstrated for the formation of ubiquinone and menaquinone in *E. coli*,[2] and subsequently confirmed for the formation of a variety of terpenes in higher plants.[5]

The first committed step in the formation of IPP and DMAPP from **1a** or **1b** (Scheme 1) is believed to be a rearrangement to the branched aldehyde **2**, as suggested by the labeling patterns observed for the biosynthesis of the related tetrol **5** in *Corynebacterium ammoniagenes*[6] and the demonstration that **1a** indeed serves as a precursor of **5** in leaves of *Liriodendron tulipifera*.[7] Clearly, the overall conversion of **1a** to IPP and DMAPP requires *inter alia* three reductive steps, but the sequence of events remains unknown. To narrow down the number of mechanistic possibilities we have now investigated the fate of the H-atoms at positions 3 and 4 of 1-deoxyxylulose **1a** during the biosynthesis of ubiquinone in *E. coli* by using specifically deuterated forms of the precursor.

The required labeled substrates were prepared by exploitation of a recently described synthetic route centered on the Sharpless asymmetric dihydroxylation of **8** to **9** (Scheme 2).[8] For the preparation of 1-deoxy[3-^{2}H]xylulose **1c**, 1-triphenylphosphoranylidenepropan-2-one **7** was deuterated at the 1-position by deuterium-exchange in CH_2Cl_2–D_2O–CD_3OD (10:1:1) in the presence of 0.1% TFA. The resulting 1-deoxyxylulose was shown to contain 85% deuterium at C-3 and 5% at C-1 by a combination of ^{1}H and ^{2}H NMR spectroscopy of its 5-benzyl ether. The [4-^{2}H]-labeled 1-deoxyxylulose **1d** was assembled from benzyloxy[1-^{2}H]acetaldehyde, itself available from the unlabeled compound **6** through reduction with $LiAlD_4$ (> 99 atom%) and subsequent Swern oxidation of the resulting deuterated alcohol. A deuterium content of 70% was estimated for **1d** by ^{1}H NMR analysis of the corresponding 5-benzyl ether.

Samples of the labeled precursors (640 mg) were fed to 1 l cultures of *E. coli* (K-12 strain). The cells were grown for 24 h at 37 °C in a minimal medium containing 3.0 g l^{-1} glucose.[9] Ubiquinone **10** was obtained in a yield of 2.5 mg l^{-1}, which is twice as high as normally observed in the absence of the precursor. The biosynthetic samples were analyzed by mass spectrometry and NMR spectroscopy.[10]

The ubiquinone produced in the presence of **1c** was shown by integration of the 500 MHz ^{1}H NMR spectrum to contain 31% CH_3 and 69% CDH_2 in the (*E*)-31'-methyl position (signals at δ 1.679 and 1.661, respectively). In addition, integration of the signal cluster at δ 1.91–2.0 also indicated 69% monodeuteration of the CH_2 groups labeled with a square in formula **10**. These data correspond to a specific incorporation rate of 81% per unit derived from added **1c**.† The location of the deuterium was confirmed by peaks at δ 1.976 and 1.689 in the ^{2}H NMR spectrum in a ratio of approximately 7:1; an additional minor peak at δ 1.608 is due to the labeling of the (*Z*)-methyl groups by the small amount of deuterium present at C-1 of the precursor. The retention of deuterium from the 3-position of 1-deoxyxylulose **1c** in the positions arising from the terminal methylene group of IPP was further verified by ^{13}C NMR

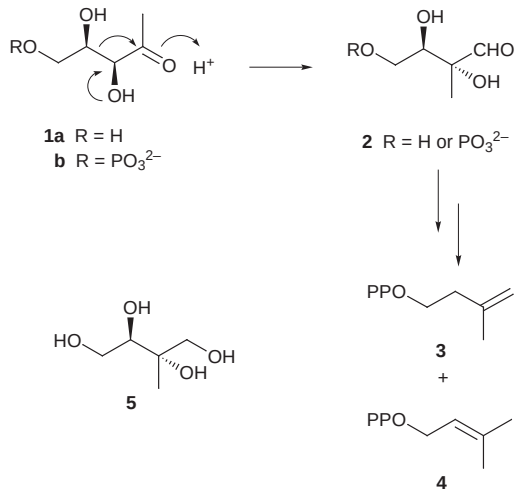

Scheme 1

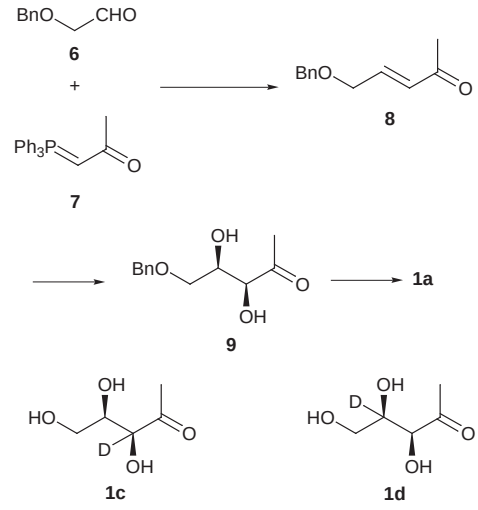

Scheme 2

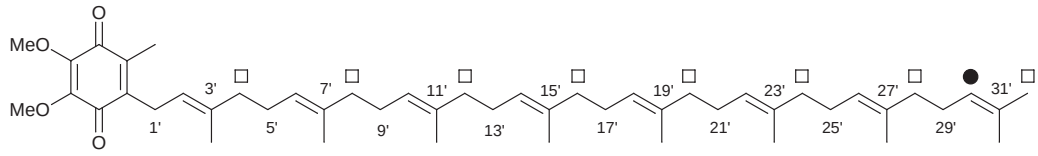

10 □ position of the label from **1c**
● position of the label from **1d**

analysis. The signal for the (*E*)-31'-methyl group bearing one deuterium was observed as a triplet (J_{C-D} = 19.1 Hz) shifted by −288 ppb from the signal of the unlabeled compound at δ 25.672. Monodeuteration of the labeled methylene positions was evidenced by the appearance of a broad triplet (J_{C-D} = 19.5 Hz) with an α-shift of −385 ppb from the normal signals at δ 39.735 and 39.714. The presence of deuterium at the positions indicated in **10** also resulted in β-shifts of −30 ppb for the adjacent quaternary olefinic carbons (δ 137.6–134.8) and of −72 ppb for the adjacent methylene carbons (δ 26.5–26.8). The signals due to the methyl group at C-3' (δ 16.334) and the other internal methyl groups (δ *ca*. 16.0) displayed γ-shifts of −30 ppb, while a γ-shift of −17 ppb was observed for the (*Z*)-methyl group at C-31' (δ 17.660).

Mass spectral analysis (EI) of the ubiquinone sample from the feeding experiment with **1d** disclosed the presence of an amount of d_1 molecular ions corresponding to *ca*. 45% of the total. From this value an approximate 65% specific incorporation of the label from **1d** into a single C_5 unit of **10** can be estimated. As a first indication that the label was localized at C-30' the same proportion of d_1 ions was observed for the $C_5H_9^+$ fragment expected to originate from the terminal C_5 unit of the isoprenyl chain. In keeping with this, the ^{2}H NMR spectrum displayed a single sharp signal at δ 5.138 and the ^{1}H NMR spectrum showed by integration the loss of *ca*. 0.36 H from the olefinic region, but no diminution of the resolved olefinic signals at δ 4.938 (2'-H) and 5.061. Independent proof for the location of the label came from the ^{13}C NMR spectrum which showed a marked diminution of peak intensity for the signal at δ 124.435. This signal must be assigned to C-30' since a β-shift of −99 ppb was observed for C-31' (δ 131.263) and γ-shifts were observed for the (*E*)- and the (*Z*)-methyl groups at C-31' (−63 and −21 ppb, respectively).‡

Thus, the deuterium label from C-4 of the precursor **1d** is retained in the 30'-position, *i.e.* in the double bond corresponding to the DMAPP starter unit, but not in any of the remaining double bonds generated from IPP in the elongation process. This is in striking contrast to the situation observed for the mevalonate pathway in eukaryotic organisms where the same H-atom of IPP (H_{Re}) is lost both in the isomerization to DMAPP and in the elimination step of the elongation process.[11] An IPP isomerase has been partially purified from *E. coli*;[12] if DMAPP is generated in the organism mainly through the action of this enzyme, then one has to conclude that in *E. coli* different H-atoms are lost from IPP in the isomerization and in the elongation process. The alternative that IPP and DMAPP may be formed independently from a common intermediate of the new pathway seems less plausible but cannot be dismissed on the basis of our results.

The difference in the metabolic origin observed in this study for the olefinic hydrogens of ubiquinone may prove relevant in connection with hitherto unexplained reports based on natural abundance ^{2}H NMR analysis of cyclic monoterpenes from higher plants which had disclosed a substantial relative enrichment of deuterium at the carbon atom stemming from C-2 of the starter DMAPP unit with respect to the other vinylic hydrogen atom of the geranyl pyrophosphate precursor.[13]

We thank Dr Linda Thöny-Meyer (Mikrobiologisches Institut der ETH-Z) for the *E. coli* K-12 wild-type strain, and Dr J. Schierle and Dr H. Keller (Hoffmann-La Roche A.G., Basel) for a sample of ubiquinone. Financial support by Novartis International A.G., Basel, is gratefully acknowledged.

Notes and References

† Mass spectral analysis of the sample of **6** derived from **1c** showed a cluster of M^+ ions corresponding to the addition of up to eight deuterium atoms per molecule.

‡ A β-shift of −108 ppb was also observed for the signal at δ 26.795 which can now be assigned to C-29'; additional shifted signals at δ 134.918 ($\Delta\delta$ = +7 ppb) and 124.292 ($\Delta\delta$ = −6 ppb) are most probably due to the two olefinic carbons of the adjacent C_5 unit.

1 M. Rohmer, M. Knani, P. Simonin, B. Sutter and H. Sahm, *Biochem. J.*, 1993, **295**, 517.
2 S. T. J. Broers, ETH Thesis (1994) No. 10978, Zürich.
3 J. Schwender, M. Seemann, H. K. Lichtenthaler and M. Rohmer, *Biochem. J.*, 1996, **316**, 73.
4 A. Cartayrade, M. Schwarz, B. Jaun and D. Arigoni, *Second Symposium of the European Network on Plant Terpenoids*, Strasbourg Bischenberg, France, Jan. 23–27, 1994, Abstr. P1; M. K. Schwarz, ETH Thesis (1994) No. 10951, Zürich; W. Eisenreich, B. Menhard, P. J. Hylands, M. H. Zenk and A. Bacher, *Proc. Natl. Acad. Sci. U.S.A.*, 1996, **93**, 6431; W. Eisenreich, S. Sagner, M. H. Zenk and A. Bacher, *Tetrahedron Lett.*, 1997, **38**, 3889; H. K. Lichtenthaler, J. Schwender, A. Disch and M. Rohmer, *FEBS Lett.*, 1997, **400**, 271; W. Knoss, B. Reuter and J. Zapp, *Biochem. J.*, 1997, **326**, 449.
5 D. Arigoni, S. Sagner, C. Latzel, W. Eisenreich, A. Bacher and M. H. Zenk, *Proc. Natl. Acad. Sci. U.S.A.*, 1997, **94**, 10 600; J. G. Zeidler, H. K. Lichtenthaler, H. U. May and F. W. Lichtenthaler, *Z. Naturforsch., Teil C*, 1997, **52**, 15; J. Schwender, J. Zeidler, R. Groener, C. Mueller, M. Focke, S. Braun, F. W. Lichtenthaler and H. K. Lichtenthaler, *FEBS Lett.*, 1997, **414**, 129; S. Sagner, C. Latzel, W. Eisenreich, A. Bacher and M. H. Zenk, *Chem. Commun*, 1998, 221.
6 T. Duvold, J.-M. Bravo, C. Pale-Grosdemange and M. Rohmer, *Tetrahedron Lett.*, 1997, **38**, 4769.
7 S. Sagner, W. Eisenreich, M. Fellermeier, C. Latzel, A. Bacher and M. H. Zenk, *Tetrahedron Lett.*, 1998, **39**, 2091.
8 J.-L. Giner, *Tetrahedron Lett.*, 1998, **39**, 2479.
9 D. Zhou and R. H. White, *Biochem. J.*, 1991, **273**, 627.
10 S. Terao, K. Kato, M. Shiraishi and H. Morimoto, *J. Chem. Soc., Perkin Trans. 1*, 1978, 1101; Y. Naruta, *J. Org. Chem.*, 1980, **45**, 4097. These assignments were independently confirmed by HMBC and HMQC NMR experiments.
11 For a review, see C. D. Poulter and H. C. Rilling, in *Biosynthesis of Isoprenoid Compounds*, ed. J. W. Porter and S. L. Spurgeon, Wiley, New York, 1981, vol. 1, p. 161.
12 S. Fujisaki, T. Nishino and H. Katsuki, *J. Biochem.*, 1986, **99**, 1327.
13 D. Arigoni, D. E. Cane, J. H. Shim, R. Croteau and K. Wagschal, *Phytochemistry*, 1993, **32**, 623 and references cited therein.

Received in Glasgow, UK, 12th June 1998; 8/04461I

Observation of ^{18}O solvent-induced isotope shifts in ^{19}F NMR signals

John R. P. Arnold*[a]† and Julie Fisher[b]

[a] *School of Biology, University of Leeds, Leeds, UK LS2 9JT*
[b] *School of Chemistry, University of Leeds, Leeds, UK LS2 9JT*

$H_2{}^{18}O$ solvent-induced isotope shifts, which have differing dependence on the level of ^{18}O-enrichment, have been observed in the ^{19}F NMR signals of F^- and 5-fluorouridine, but are absent in 5-fluorouracil.

The chemical shift of an ^{19}F NMR signal is highly sensitive to its environment, and as such it is well-suited to the observation of the solvent-induced isotope shift (SIIS). This is the shift observed when the solvent is changed to a heavier isotope form, usually by an H to D substitution, and most commonly this is a change from H_2O to D_2O.[1] Fluorine-modified amino acids and heterocyclic bases have been incorporated into biomolecules, and subsequent H_2O/D_2O SIIS measurements have enabled evaluation of the solvent exposure of specific residues in proteins[2,3] and nucleic acids.[4–7] An alternative heavy isotope form of water is $H_2{}^{18}O$. Thirty years ago a study of NaF, made without the benefit of today's high magnetic fields and FT techniques, gave the $H_2{}^{16}O/H_2{}^{18}O$ SIIS (herein the ^{18}O-SIIS) as being '< 0.05 ppm' upfield.[8] The origin of the fluorine H_2O/D_2O SIIS has been considered in terms of hydrogen bonding with the solvent and the different vibrational behaviour of H_2O and D_2O.[9] It has been calculated that an OH bending vibration can account for about 30% of the H_2O/D_2O SIIS observed for F^-.[10] Lower frequency librational modes are also potential contributors to the SIIS, but a failure to detect any ^{18}O-SIIS for 50 mM F^- led to the conclusion that these librational modes do not play a significant role in the SIIS of fluorine.[9] Here we report a re-examination of the ^{18}O-SIIS of fluorine.

We investigated the fluoride ion, which has been used in a number of previous studies of ^{19}F SIIS,[1,8–10] together with 5-fluorouridine and 5-fluorouracil, which represent subunits commonly used to incorporate fluorine into nucleic acids to probe structure and function, as well as being important anti-cancer chemotherapy agents.[11] The experimental arrangement placed fluoride, fluorouridine and fluorouracil in the same sample, so that the solution conditions for each were identical.‡ With the ^{18}O enrichment at 86%, the fluoride and fluorouridine resonances both displayed small but distinct upfield shifts, whilst fluorouracil showed no such effect (Fig. 1 and Table 1).§ On reducing the ^{18}O enrichment to 53%, the fluoride SIIS was reduced whilst the fluorouridine SIIS was *downfield*; with fluorouracil still showing no isotope shift. A further decrease in ^{18}O enrichment to 43% reduced the isotope shifts of F^- and of fluorouridine (still downfield). Further significant reduction of the ^{18}O content was impractical due to the difficulty in measuring the diminishing isotope shifts. Thus the effect of ^{18}O enrichment of the solvent water for F^- is an upfield shift proportional to the level of ^{18}O enrichment (within experimental error). For fluorouridine the effect is more complicated, but can be explained by the observed isotope shift being the sum of one term which is upfield and proportional to the ^{18}O content, and a second term which is downfield and non-linear. The change from an upfield to a downfield isotope shift with decreasing ^{18}O enrichment of the solvent meant that at some point the ^{18}O-SIIS would be zero. This behaviour is illustrated by Fig. 2, where at 66% ^{18}O, the ^{18}O-SIIS was not detectable (*i.e.* being less than the linewidth). Both solvent-induced and intra-molecular isotope shifts are generally upfield on heavy atom substitution.[1] However, a few cases of downfield isotope shifts have been reported,[1,12] and other than where noted above, we know of no previous reports of ^{18}O-induced isotope shifts of ^{19}F, nor of ^{18}O-SIIS for any other NMR-active nucleus.

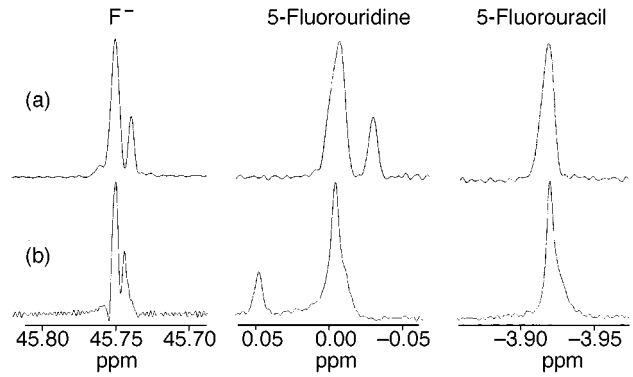

Fig. 1 ^{19}F NMR spectra (^1H-decoupled) of fluoride ion (left), 5-fluorouridine (centre) and 5-fluorouracil (right). Smaller signals are due to ^{18}O-induced shifts. (a) ^{18}O-enrichment in central chamber of concentric tube was 86%, solute concentrations 4 mM fluoride, 1 mM for both fluorouridine and fluorouracil. (b) ^{18}O-enrichment 53%, concentrations 30 mM fluoride, 1 mM for both fluorouridine and fluorouracil.

Table 1 SIIS values for fluoride, 5-fluorouridine and 5-fluorouracil‡§

Solvent system	Concentrations[a]/mM	Enrichment[b] (%)	SIIS[c] (ppm) F^-	5-Fluorouridine	5-Fluorouracil
$H_2{}^{16}O/H_2{}^{18}O$	4, 1, 1	86	−0.0120	−0.0227	0
$H_2{}^{16}O/H_2{}^{18}O$	4, 1, 1	53	−0.0068	+0.0089	0
$H_2{}^{16}O/H_2{}^{18}O$	4, 1, 1	43	−0.0060	+0.0080	0
$H_2{}^{16}O/H_2{}^{18}O$	30, 1, 1	53	−0.0056	+0.050	0
$H_2{}^{16}O/H_2{}^{18}O$	50, 1, 1	53	−0.0040	+0.044	0
H_2O/D_2O	4, 1, 1	100	−2.771	−0.243	−0.199
H_2O/D_2O	50, 1, 1	100	−2.679	−0.255	−0.190

[a] In the order of fluoride ion (as NaF), 5-fluorouridine, 5-fluorouracil, present in the same sample. [b] Enrichment of the heavier-isotope solvent in its chamber of the concentric NMR tubes. [c] Negative values indicate upfield shift for heavier-isotope solvent, positive for downfield shift. ^{18}O-SIIS values have estimated error span of ±0.0005 ppm. H_2O/D_2O SIIS estimated error margin ±0.001 ppm.

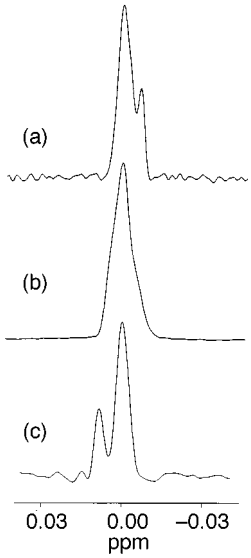

Fig. 2 ^{19}F NMR spectra (^{1}H-decoupled) of 5-fluorouridine (5 mM) with varying ^{18}O-enrichment in the central chamber of concentric tubes: (a) 87, (b) 66 and (c) 44%. ^{18}O-SIIS values are −0.0060, 0 and +0.0084 ppm respectively (all ± 0.0005 ppm).

In order to approach the conditions used in a previously reported study[9] (*i.e.* 50 mM NaF), we increased the flouride ion concentration from 4 to 30 and then 50 mM, whilst using 53% ^{18}O. With this increasing concentration, the SIIS of fluoride ion decreased in an approximately linear fashion so that it was only 0.004 ppm at 50 mM. The combination of lower magnetic field strengths and relatively high fluoride concentration would thus account for the previous negative results.[9] Increasing the fluoride ion concentration also made the SIIS of fluorouridine significantly more pronounced, but did not cause any change to the absence of a perceptible ^{18}O-effect for the resonance of fluorouracil (Table 1 and Fig. 1).

The H_2O/D_2O SIIS values are also given in Table 1; those for F^- are in fair agreement with previous reports.[1,8,10] Values for fluorouridine and fluorouracil have not previously been reported, but 0.39 ppm has been given for closely related 2'-deoxy-5-fluorouridine[6] for 10–100% D_2O (since seperate tubes were used) under different sample conditions. Our value for fluorouridine is some 25% larger than that for fluorouracil. This may be related to the absence of an observable ^{18}O-SIIS for the latter, if the internal vibrations of solvent water make a stronger contribution to the ^{19}F chemical shift of fluorouridine than to that of fluorouracil. Alternatively, for fluorouracil, upfield and downfield contributions to the ^{18}O-SIIS may more consistently balance than would seem to be the case in fluorouridine. Pyrimidine bases have been noted to weakly self-associate in aqueous solution,[13] but with the relatively low concentrations used here the effect of this should be small (*i.e.* in the order of 0.1% of the molecules being associated, based on typical association constants[13]).

We have shown that an ^{18}O-SIIS for ^{19}F is detectable, and can be of relatively significant magnitude. Thus the librational motions within the water molecule cannot be discounted from contributing to the fluorine chemical shift, but clearly other terms are also involved, at least for fluoropyrimidines. The ^{19}F ^{18}O-SIIS may prove to be a useful complement to the H_2O/D_2O SIIS in the study of fluorine-labelled proteins and nucleic acids.

This work was supported by the Wellcome Trust. J. R. P. A. is a Senior Wellcome Fellow.

Notes and references

† E-mail: genjrpa@leeds.ac.uk

‡ Samples for NMR analysis were prepared as follows: a solution of NaF (4 mM), 5-fluorouridine (1 mM), 5-fluorouracil (1 mM), and EDTA (0.1 mM) in 25 mM sodium phosphate buffer, pH 6.8 was divided into portions which were then lyophilised to dryness. The residues were then re-dissolved in appropriate volumes of 90% $H_2{}^{16}O$/10% D_2O or 90% $H_2{}^{18}O$/10% D_2O. In this way the ^{16}O and ^{18}O portions contained identical concentrations of all solutes. The solutions were placed in an NMR tube containing a concentric insert, with typically 80 µl of ^{18}O-enriched sample in the central chamber, and 330 µl of ^{16}O sample in the outer part. An ^{18}O-shifted signal is thus identified by its size compared to the ^{16}O resonance. Reduction of the ^{18}O enrichment was achieved by diluting with the ^{16}O solution. The concentration of NaF was increased by evaporating to dryness appropriate volumes of NaF solution in H_2O, and then redissolving these in the ^{18}O and ^{16}O solutions. For measurements of H_2O/D_2O effects, lyophilised solutions were redissolved in either H_2O or D_2O, and placed in concentric NMR tubes.

§ All ^{19}F NMR spectra were acquired on a GE-Omega 500 spectrometer at 470.5 MHz using a 5 mm ^{19}F/^{1}H probe. Broadband ^{1}H decoupling was applied by waltz-16 modulation of the decoupler. All spectra were acquired with a sample temperature of 25 °C. FIDs were multiplied by Gaussian functions and zero-filled prior to Fourier transformation. The digital resolution of the ^{19}F NMR spectra were at least 0.12 Hz (0.00026 ppm) per point. Chemical shifts are shown with respect to 5-fluorouridine (in the lighter isotope solvent) as the internal reference.

1 P. E. Hansen, *Prog. Nucl. Magn. Reson. Spectrosc.*, 1988, **20**, 207.
2 J. T. Gerig, *Prog. Nucl. Magn. Reson. Spectrosc.*, 1994, **26**, 293.
3 M. A. Danielson and J. J. Falke, *Ann. Rev. Biomol. Struct.*, 1996, **25**, 163.
4 Q. Chen, R. H. Shafer and I. D. Kuntz, *Biochemistry*, 1997, **36**, 11 402.
5 W-C. Chu and J. Horowitz, *Biochemistry*, 1991, **30**, 1655.
6 W. J. Metzler and P. Lu, *J. Mol. Biol.*, 1989, **205**, 149.
7 L. Zhou, M. Rajabzadeh, D. D. Traficante and B. P. Cho, *J. Am. Chem. Soc.*, 1997, **119**, 5384.
8 A. Loewenstein and M. Shroper, *J. Chem. Soc., Chem. Commun.*, 1968, 214.
9 P. E. Hansen, H. D. Dettman and B. D. Sykes, *J. Magn. Reson.*, 1985, **62**, 487.
10 C. Deverell, K. Schaumburg and H. J. Bernstein, *J. Chem. Phys.*, 1968, **49**, 1276.
11 D Machover, *Cancer*, 1997, **80**, 1179.
12 W. Arias and J. M. Risley, *J. Org. Chem.*, 1991, **56**, 3741.
13 F. Aradi, *Magn. Reson. Chem.*, 1990, **28**, 246.

Received in Cambridge, UK, 9th June 1998; 8/04359K

$[Re_9Se_{11}Br_6]^{2-}$: the first example of an Re_9 condensed cluster†

Vladimir E. Fedorov,*[a] Mark R. J. Elsegood,*[b] Spartak S. Yarovoi[a] and Yuri V. Mironov[a]

[a] *The Institute of Inorganic Chemistry, Russian Academy of Sciences, Novosibirsk, 630090, Russia*
[b] *Department of Chemistry, Bedson Building, University of Newcastle-upon-Tyne, Newcastle-upon-Tyne, UK NE1 7RU. E-mail: Mark.Elsegood@ncl.ac.uk*

A new type of rhenium condensed cluster $[Re_9Se_{11}Br_6]^{2-}$ has been synthesized by the reaction of Re_3Br_9 and PbSe at 550 °C and structurally characterised; the structure of $[Re_9Se_{11}Br_6]^{2-}$ contains the bioctahedral rhenium cluster Re_9 which can be considered as the result of progressive uniaxial condensation of three Re_3 clusters.

Condensation of fragments with the formation of polyhedral clusters is one of the most promising methods in synthetic cluster chemistry.[1] The most remarkable examples of the applicability of this method are seen in the syntheses of some octahedral clusters, for example, the zirconium halide cluster $[Zr_6Cl_{12}(PMe_2Ph)_6]$ which is formed from three binuclear complexes $[Zr_2Cl_6(PMe_2Ph)_4]$,[2] or of sulfide and selenide cluster complexes of molybdenum and tungsten $[M_6Y_8(PEt_3)_6]$ by reductive dimerization of two triangular cluster complexes $[M_3S_4Cl_4(PEt_3)_x]$.[3] Recently[4] we have developed a condensation method for the high yield synthesis of the octahedral rhenium cluster chalcobromides $Re_6E_4Br_{10}$ and $Re_6E_8Br_2$ (E = S, Se, Te) using the triangular cluster rhenium bromide Re_3Br_9 and lead or cadmium chalcogenides (PbE or CdE where E = S, Se and Te) as starting compounds. We have found that given condensation reactions can yield not only octahedral clusters but also other cluster complexes.

Here we present the preparation‡ and structural characterisation§ of a new cluster complex $[PPh_4]_2[Re_9Se_{11}Br_6]$ containing the bioctahedral rhenium cluster anion $[Re_9Se_{11}Br_6]^{2-}$. This type of cluster was not known for rhenium previously. It can be considered as the result of progressive uniaxial condensation of three Re_3 clusters.

$[PPh_4]_2[Re_9Se_{11}Br_6]$ crystallises with triclinic symmetry to form dark red prisms. The $[Re_9Se_{11}Br_6]^{2-}$ unit (Fig. 1) is structurally identical to that of $Co_9Se_{11}(PPh_3)_6$[7] and Mo_9E_{11} (E = S, Se) which was found in some ternary molybdenum chalcogenides.[8–14] In the crystal structures of the latter, the metal ion is bonded to six X atoms belonging to the adjacent Mo_9E_{11} cluster units, so $[Mo_9E_{11}X_{6/2}]$ units similar to $[Re_9Se_{11}Br_6]^{2-}$ are formed.

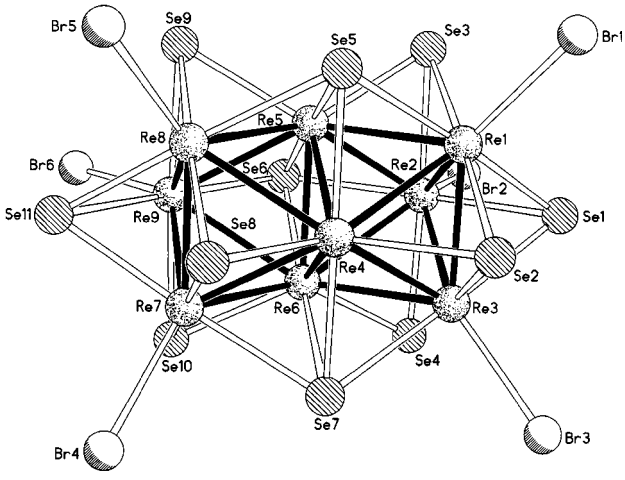

Fig. 1 Structure of the $[Re_9Se_{11}Br_6]^{2-}$ anion showing the atom labelling scheme and highlighting the bioctahedral Re_9 core

The environments of the external Re atoms (Re1–3 and Re7–9) in $[Re_9Se_{11}Br_6]^{2-}$ are similar and consist of four Re atoms, four Se atoms forming a quasi-planar square, and one Br atom. The internal Re atoms Re4–6 are connected to six Re and four Se atoms.

The Re–Re distances within the Re_9 cluster can be classified into three groups. The first corresponds to the distances within the two external Re_3 triangles formed by the Re1–3 and Re7–9 atoms, here the mean distances are 2.596(1) and 2.594(1) Å respectively; these are the shortest Re–Re distances in the Re_9 cluster. The second group is formed by Re4–6 atoms of the internal Re_3 triangle, these Re–Re distances are the longest in the cluster with a mean of 2.687(1) Å. And finally, the third group comprises the Re–Re bonds between these Re_3 triangles (inter-triangle distances) which range from 2.645(1) to 2.663(1) Å. So, in the $[Re_9Se_{11}Br_6]^{2-}$ cluster the two external Re_3Se_3 triangles are compressed whereas the middle Re_3Se_3 triangle is expanded by comparison.

It is well known that the metal–metal distances in octahedral condensed clusters depend on the number of the valence electrons on the metal atom [the so-called valence electron concentration (VEC)], which are available for the metal–metal intracluster bonding.[15] Comparing the Re_9 obtained here and the Mo_9 cluster which is found in some ternary molybdenum selenides,[8–14] we can see that an increased charge on this cluster leads mainly to an increase in the size of the median triangle. For example, going from $In_2Mo_{15}Se_{19}$ to $In_{3.33}Mo_{15}Se_{19}$, the corresponding Mo–Mo distances increase from 2.681 to 2.768 Å[8] showing that the same tendency is found here.

To provide a further strategy for the synthesis of other condensed rhenium clusters, it is interesting to consider the VEC and the stability of related compounds. For example, in the series of condensed clusters $[Mo_9E_{11}]^0$, $[Mo_{12}E_{14}]^{2-}$, $[Mo_{18}E_{20}]^{4-}$, $[Mo_{24}E_{26}]^{6-}$, $[Mo_{30}E_{32}]^{8-}$, $[Mo_{6/2}E_{6/2}]^{2-}$ the number of valence electrons per metal atom (VEC) available for M–M bonding is increased from 3.56, 3.83, 4, 4.08, 4.13 to 4.33, respectively,[16] to allow an increase in the order of the metallic bonding. In other words, the formal oxidation state of metal atoms is lowered. In rhenium cluster chemistry, the situation is the same, namely, the VEC for $[Re_6E_8]^{2+}$ and $[Re_9Se_{11}Br_6]^{2-}$

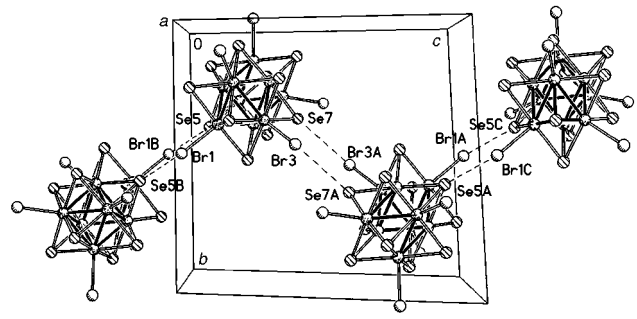

Fig. 2 Intercluster interactions *via* Se···Br short contacts

cluster units is 4 and 4.11, respectively. Here it is interesting to remark that for the hypothetical $[Re_{12}E_{14}Br_6]^{2-}$ dianion (the unknown member from the next step of progressive condensation of Mo_3X_3 units) the VEC would be 4.33, that is the same as in $[Mo_{6/2}E_{6/2}]^{2-}$ clusters.

An interesting feature of the structure is the infinite chains of clusters along the crystallographic *c* axis: each cluster unit $[Re_9Se_{11}Br_6]^{2-}$ exhibits interactions to two neighbours *via* Se···Br short contacts across inversion centres (Fig. 2): Br1–Se5A 3.547 Å, Br3–Se7B 3.840 Å.

We would like to thank the EPSRC for provision of the X-ray equipment and Professor William Clegg for the use of this equipment and associated computing facilities. This work was also supported by Russian Foundation for Basic Research (grant N 96-03-32955).

Notes and References

† Dedicated to Professor Achim Müller on the occasion of his 60th birthday.

‡ *Experimental procedure*: Re_3Br_9, PbSe and KBr in molar ratio 1 : 4 : 6 were heated in an evacuated fused-silica tube at 550 °C for 2 d. The reaction mixture was washed with water and a small amount of boiled HBr. The resulting solid was washed with MeOH to give a dark red solution. An excess of $[PPh_4]Br$ was added to this solution causing precipitation of a brown powder. Recrystallisation from MeCN leads to the formation of two types of crystals, dark red prisms and pyramids. The prism crystals were used for X-ray analysis.

§ *X-Ray structure analysis*: $(PPh_4)_2Re_9Se_{11}Br_6$, dark red prism, crystal dimensions, 0.33 × 0.19 × 0.18 mm, triclinic, space group $P\bar{1}$, a = 13.3335(9), b = 15.3791(11), c = 17.1175(12) Å, α = 84.687(2), β = 73.086(2), γ = 77.672(2)°, Z = 2, V = 3279.1(4) Å^3 [T = 160(2) K]. D_c = 3.750 g cm^{-3}, Bruker SMART CCD diffractometer, $2\theta_{max}$ = 50.00; Mo-Kα radiation, λ(Kα_1) = 0.710 73 Å; ω rotation with narrow frames, 20 611 reflections measured, 11 412 independent reflections (R_{int} = 0.0399) all of which were included in the refinement; data corrected for Lorentz and polarisation effects[5] and for absorption by a semi-empirical method based on high data redundance, μ = 263.8 cm^{-1}, min, max. transmission = 0.0257, 0.0659, solution by direct methods,[6] anisotropic refinement on F^2 by full-matrix least squares[6] to give: $R_w = \{\Sigma[w(F_o^2 - F_c^2)^2/\Sigma[w(F_o^2)^2]\}^{1/2}$ = 0.0901, conventional R = 0.0371 for 8028 reflections having $F_o^2 > 2\sigma(F_o^2)$, goodness of fit on F^2 values = 0.956 for 686 refined parameters. The largest features in the final difference electron density map were within ±2.87 e Å^{-3} close to the Re atoms. CCDC 182/956.

1 T. Saito, in *Early Transition Metal Clusters with π-Donor Ligands*, ed. M. H. Chisholm, VCH, New York, 1995, p. 66.
2 F. A. Cotton, P. A. Kibala and W. J. Roth, *J. Am. Chem. Soc.*, 1988, **110**, 298.
3 T. Saito, A. Yoshikawa, T. Yamagata, H. Imoto and K. Unoura, *Inorg. Chem.*, 1989, **28**, 3588; T. Saito, N. Yamamoto, T. Nagase, T. Tsuboi, K. Kobayashi, T. Yamagata, H. Imoto and K. Unoura, *Inorg. Chem.*, 1990, **29**, 764.
4 V. P. Fedin, H. Imoto, T. Saito, V. E. Fedorov, Yu. V. Mironov and S. S. Yarovoi, *Polyhedron*, 1996, **15**, 1229; V. E. Fedorov, S. S. Yarovoi, Yu. I. Mironov, U.-H. Paek, S. C. Shin and M.-L. Seo, *Abstracts of Fifth Eurasia Conference on Chemical Sciences*, Guangzhou, China, December 10–14, 1996, p. 534; S. S. Yarovoi, Yu. I. Mironov, Yu. V. Mironov, A. V. Virovets, V. E. Fedorov, U.-H. Paek, S. C. Shin and M.-L. Seo, *Mater. Res. Bull.*, 1997, **32**, 1271.
5 Bruker SAINT, program for integration of frame data, Bruker Analytical X-ray Instruments, Madison, WI, 1994.
6 G. M. Sheldrick, SHELXTL manual, version 5, Bruker Analytical X-ray Instruments, Madison, WI, 1994.
7 D. Fenske, J. Ohmer and J. Hachgenei, *Angew. Chem., Int. Ed. Engl.*, 1985, **24**, 993.
8 A. Grüttner, K. Yvon, B. Seeber, R. Chevrel, M. Potel and M. Sergent, *Acta Crystallogr., Sect. B*, 1979, **35**, 285.
9 R. Chevrel, M. Potel, M. Sergent, M. Decroux and O. Fischer, *Mater. Res. Bull.*, 1980, **15**, 867.
10 M. Potel, R. Chevrel and M. Sergent, *Acta Crystallogr., Sect. B*, 1981, **37**, 1007.
11 P. Gougeon, J. Padiou, J. Y. Le Marouille, M. Potel and M. Sergent, *J. Solid State Chem.*, 1984, **51**, 218.
12 P. Gougeon, M. Potel, J. Padiou, M. Sergent, C. Boulanger and J. M. Lecuire, *J. Solid State Chem.*, 1987, **71**, 543.
13 B. D. Davis and W. R. Robinson, *J. Solid State Chem.*, 1990, **85**, 332.
14 P. Gougeon and M. Potel, *Acta Crystallogr., Sect. C*, 1993, **49**, 427.
15 K. Yvon, *Curr. Top. Mater. Sci.*, 1979, **3**, 53.
16 R. Chevrel, P. Gougeon, M. Potel and M. Sergent, *J. Solid State Chem.*, 1985, **57**, 25.

Received in Basel, Switzerland, 29th June 1998; 8/04967J

Chelating diphosphine–palladium(II) dihalides; outstandingly good catalysts for Heck reactions of aryl halides

Bernard L. Shaw* and Sarath D. Perera

School of Chemistry, University of Leeds, Leeds, UK LS2 9JT

Contrary to previously held views, chelating diphosphine–palladium dihalide complexes are excellent catalysts for Heck reactions involving aryl halides; the undesirability of trying to prepare such catalysts *in situ* is discussed.

The Heck vinylation or olefination reaction [eqn. (1)] is very

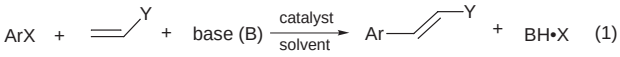

important in organic synthesis.[1a–c] A Heck catalyst is frequently generated *in situ* from $Pd(OAc)_2$ and a tertiary phosphine, L = PPh_3 or P(*o*-tolyl)$_3$; commonly 1–5 mol% of Pd is used which means that the maximum turnover numbers are only 100–20. When discussing arylation with aryl halides[1b] Heck stated that 'chelating diphosphines do not give as good catalysts'; this was in comparison with the catalysts commonly used and mentioned above and which are therefore a benchmark for comparing reactivity and performance. Cabri and co-workers[2a] agreed with this statement of Heck and in a review[2b] wrote that his statement 'Chelating diphosphines...in general do not produce useful catalysts' was valid only because aryl halides were used but also wrote 'with bidentate ligands a decrease in reaction rates or sometimes a complete suppression of the reaction is observed'. Ditertiary phosphine–palladium complexes are effective catalysts for Heck reactions with aryl triflates or with aryl halides in the presence of a halide scavenger (Ag or Tl).[1c,2a–c] Overman and coworkers have demonstrated that diphosphine (*e.g.* BINAP)–Pd catalysts promote intramolecular Heck reactions with aryl iodides, with high ee.[2c] However, very large amounts of catalyst, 3–10 mol%, have been used for these reactions. The prevailing belief is that chelating diphosphine–Pd complexes are not good catalysts for the classical Heck reaction [eqn. (1)].

We have now investigated **2a** and **2c** and ditertiary phosphine–palladium(II) dihalide complexes **3a–d** and **4** and find them to be outstanding as catalysts for Heck olefination reactions with aryl iodides and bromides in several respects. Our results are summarised in Table 1. High yields and very high turnover numbers (TONs; up to 225 000) were obtained, with good rates; catalysts were active over the temperature range 50–150 °C, which could probably be extended; in some cases reaction times could probably be reduced, we left some reactions for prolonged times to show that the catalysts were stable; in no case was any metallic Pd produced. The yields were isolated yields and chromatography was not necessary, the Pd being removed by a simple wash with a very small amount of aqueous sodium cyanide solution and the product was then purified by crystallisation. We have used this very effective isolation procedure for Heck reactions catalysed by palladacycles.[3] The very stable complex **2a** can be easily made in high yield, from **1** and $[PdCl_2(NCPh)_2]$[4] by a transannular reaction; we also reported the crystal structure of **2b** and prepared **2c** by metathesis.[4] Treatment of PhI (2.0 g, 10 mmol), styrene and NBu^n_3 with catalyst **2a** (0.044 mg) in dmf at 95 °C for 12 d gave a pale orange solution. This was taken up in CH_2Cl_2 and after a water wash and then a wash with a solution of NaCN (2 mg) in

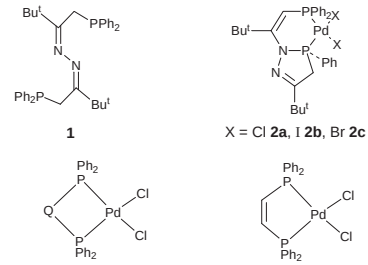

water the organic layer was essentially colourless. The stability constant for $[Pd(CN)_4]^{2-}$ is about 10^{52},[5] and this wash presumably took the Pd into the aqueous layer. Crystallisation from methanol then gave *trans*-stilbene in 67% yield corresponding to a TON of 101 200. The other reaction mixtures summarised in Table 1 were worked up in an analogous manner, except that for reactions with methyl acrylate the work up was done in diethyl ether. In example 2, with 9 days reaction time at 95 °C, the isolated yield of methyl cinnamate was 92%, TON = 139 000. We also studied catalyst **2a** at higher temperatures, 125 and 150 °C, and shorter reaction time (48 h, entries 4 and 5) with very good yields and excellent TONs (110 200 and 60 400) and no sign of decomposition to metallic Pd. Bromide **2c** was a good catalyst for converting methyl acrylate and iodobenzene into methyl cinnamate (example 3). **2a** catalysed the olefination of 4-bromoacetophenone to acetylstilbene; 91% yield, TON = 27 500. Bases other than NBu^n_3 were used, entries 7–10, *viz*. NaOAc, K_2CO_3 with NBu^n_4Cl, K_2CO_3 or $KHCO_3$, in example 8 a reaction temperature of only 50 °C was used. Reaction 11, with 4-bromocyanobenzene was carried out at 125 °C for 12 h. Products were identified by their proton NMR spectra.

The 4-membered ring chelated dppm complex **3a**[6,7] (0.032 mg) converted PhI (1 g) plus styrene into stilbene at 150 °C/48 h in 87% yield with a TON of 76 300 and no sign of decomposition. **3a** also converted 4-bromoacetylbenzene into 4-acetylstilbene at 125 °C in 88% yield. The 5-membered chelate ring complex catalysts **3b**[8] and **4**[9] gave very good yields (76% to 95%) of stilbene derivatives and **4** gave acetylstilbene in 82% yield, using $KHCO_3$ as base. The 6-membered ring chelate **3c** gave a particularly high TON (224 700) and 80% yield for the conversion of iodobenzene/styrene to stilbene, with reaction conditions 3 d/125 °C; the 7-membered chelate dppb complex **3d** under these conditions gave a TON of 170 300. **3c** and **3d** also catalysed reactions of 4-bromoacetylbenzene with styrene in high yields and with good TONs. We favour a mechanism for the syntheses summarised in Table 1 involving a Pd^{II}–Pd^{IV} cycle similar to those we proposed for Heck reactions catalysed by palladacycles or in the phosphine free systems (Jeffery conditions).[3,10]

Typically, in Heck syntheses involving chelating diphosphines, the diphosphine and the equivalent amount of palladium, *e.g.* palladium acetate, has been added to the mixture of reactants in the belief that a compound of type $[(L–L)PdX_2]$[2b] will form *in situ*. However, there are very good reasons for

Table 1 Selected results of the Heck reactions catalysed by P–P palladium chelates[a]

No.	Aryl halide	Olefin	ArX/olefin mmol/mmol	Catalyst (mmol)	Time (T/°C)	Yield (%) (TON)
1	PhI	sty	10/15	**2a** (6.6×10^{-5})	12 d (95 °C)	67 (101000)
2	PhI	mac	10/15	**2a** (6.6×10^{-5})	9 d (95 °C)	92 (139000)
3	PhI	mac	10/15	**2c** (4.6×10^{-3})	24 h (95 °C)	81 (1760)
4	PhI	sty	10/15	**2a** (6.6×10^{-5})	48 h (125 °C)	73 (110200)
5	PhI	sty	5/7.5	**2a** (6.6×10^{-5})	48 h (150 °C)	80 (60400)
6	bab	sty	2/3	**2a** (6.6×10^{-5})	66 h (125 °C)	91 (27500)
7[b]	PhI	sty	2/3	**2a** (1.7×10^{-2})	20 h (95 °C)	69 (81)
8[c]	PhI	mac	10/15	**2a** (5×10^{-2})	42 h (50 °C)	68 (136)
9[d]	bab	sty	10/15	**2a** (1.08×10^{-2})	40 h (125 °C)	85 (787)
10[e]	bab	sty	10/15	**2a** (1.08×10^{-2})	30 h (125 °C)	76 (703)
11	bcb	sty	2/3	**2c** (4.6×10^{-3})	12 h (125 °C)	75 (326)
12	PhI	sty	5/7.5	**3a** (5.7×10^{-5})	48 h (150 °C)	87 (76300)
13	bab	sty	10/15	**3a** (5.8×10^{-3})	24 h (125 °C)	88 (1520)
14	bab	sty	10/15	**3b** (6×10^{-3})	24 h (125 °C)	87 (1450)
15[e]	bab	sty	10/15	**4** (5.2×10^{-3})	24 h (125 °C)	82 (1580)
16	PhI	sty	10/15	**3c** (3.56×10^{-5})	3 d (125 °C)	80 (224700)
17	bab	sty	2/3	**3c** (9.3×10^{-3})	24 h (125 °C)	75 (161)
18	PhI	sty	10/15	**3d** (3.64×10^{-5})	3 d (125 °C)	62 (170300)
19	bab	sty	2/3	**3d** (3×10^{-4})	24 h (125 °C)	79 (5270)

[a] For all except examples 7–10 and 15, 1.2 equiv. NBu^n_3 to the aryl halide were used as base; dmf was used as solvent to dissolve the catalyst, *e.g.* in examples 6, 11, 17 and 19, 1 cm^3 of dmf was used; in examples 1–5, 12, 16 and 18, 2 cm^3; in examples 9, 13, 14 and 15, 5 cm^3; in examples 8 and 10, 10 cm^3. sty = styrene, mac = methyl acrylate, bab = 4-bromoacetylbenzene, bcb = 4-bromocyanobenzene. [b] $NaOAc \cdot 3H_2O$ (2.65 mmol) used as base. [c] K_2CO_3 (25 mmol, base) and Bu^n_4NCl (10 mmol) were used. [d] K_2CO_3 (15 mmol) used as base. [e] $KHCO_3$ (25 mmol) used as base.

thinking that in some cases only a fraction of the Pd will do this. In Pd^{II} and Pt^{II} chemistry, in many cases, on addition of one equivalent of a chelating diphosphine or diarsine to $[MX_4]^{2-}$, half of the Pd^{II} or Pt^{II} is converted into $[M(L–L)_2]^{2+}$, *i.e.* in eqn. (2) half the metal will remain as $[MX_4]^{2-}$.[12a–d] This follows from the very high *trans*-effect (*trans*-labilising effect) of a tertiary phosphine (arsine) compared with a chloride ligand. We showed that a chloride ligand *trans* to a tertiary phosphine such as PEt_3 was substituted by pyridine about 10^4 times faster than chloride *trans* to another chloride ligand,[11] *i.e.* in eqn. (2) the

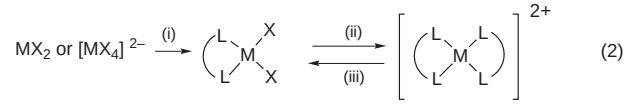

(2)

rate of substitution (ii) will be much greater than that of substitution (i). Thus a Magnus type salt $[M(L–L)_2][MX_4]$ is formed, which is often of very low solubility. Conversion of such a salt to *cis*-$[(L–L)MX_2]$ is often difficult; boiling it in dmf (bp 153 °C) or with a mixture of hydrochloric acid and ethanol will often effect the conversion[12a–c] but in some cases even such extreme conditions are not sufficient or satisfactory.[12c,d] A satisfactory method of synthesising complexes of type $[(L–L)PdX_2]$ is to treat a compound of type $[PdX_2(NCR)_2]$, *e.g.* the well known $[PdCl_2(NCPh)_2]$, with the chelating diphosphine in a suitable solvent system, *e.g.* CH_2Cl_2 or acetone,[12a–d] and this is the method we have used in the present work. Complexes **3a**–**d** and **4** have been studied extensively[6–9,12a–d] and **3a**–**c** have had their crystal structures determined.[7]

As will be gathered from the above, process (iii) in eqn. (2) may be exceedingly slow and it is not known in detail how it occurs. Palladium acetate is a trimer, the acetate ligand is labile and one might expect that on adding a chelating diphosphine and the equivalent amount of palladium acetate to a mixture of reactants for a Heck synthesis, *in situ*, much of the Pd would be converted into $[Pd(L–L)_2]^{2+}$ but not much $[(L–L)PdX_2]$ (X = OAc *etc*.) would be formed. If so it calls into question some arguments which have been put forward when discussing Heck reactions involving Pd–chelating diphosphine catalysts.[2b,c] It is recommended that catalysts for Heck reactions should be preformed and the source of Pd and the phosphine not added separately to the reactants; this could become especially important when very small amounts of Pd and diphosphine are used.

Even when catalysts are generated from a Pd^0 complex, such as $Pd_2(dba)_3$, the resultant complex(es) will oxidatively add aryl halide to give Pd^{II} complexes which could then participate in a catalytic cycle involving Pd^{II}/Pd^{IV}.

Notes and References

* E-mail: b.l.shaw@chem.leeds.ac.uk

1 (*a*) R. F. Heck, *Palladium Reagents in Organic Synthesis*, Academic Press, London, Benchtop Edition, 1990; (*b*) R. F. Heck, *Vinyl Substitution with Organopalladium Intermediates*, in *Comprehensive Organic Synthesis*, ed. B. M. Trost and I. Fleming, Pergamon, Oxford, 1991, vol. 4, p. 833; (*c*) A. de Meijere and F. E. Meyer, *Angew. Chem., Int. Ed. Engl.*, 1994, **33**, 2379.

2 (*a*) W. Cabri, I. Candiani and A. Bedeschi, *J. Org. Chem.*, 1992, **57**, 3558; (*b*) W. Cabri and I. Candiani, *Acc. Chem. Res.*, 1995, **28**, 2; (*c*) L. E. Overman and D. J. Poon, *Angew. Chem.*, 1997, **36**, 518.

3 B. L. Shaw, S. D. Perera and E. A. Staley, *Chem. Commun.*, 1998, 1361.

4 S. D. Perera, B. L. Shaw and M. Thornton-Pett, *J. Chem. Soc., Dalton Trans.*, 1993, 3653.

5 M. T. Beck, *Pure Appl. Chem.*, 1987, **59**, 1703.

6 W. L. Steffen and G. J. Palenik, *Inorg. Chem.*, 1976, **15**, 2432.

7 D. W. Meek, P. E. Nicpon and V. I. Meek, *J. Am. Chem. Soc.*, 1970, **92**, 5351.

8 G. Booth and J. Chatt, *J. Chem. Soc. (A)*, 1966, 634.

9 D. J. Gulliver, W. Levason and K. G. Smith, *J. Chem. Soc., Dalton Trans.*, 1981, 2153.

10 B. L. Shaw, *New J. Chem.*, 1998, **22**, 77.

11 F. Basolo, J. Chatt, H. B. Gray, R. G. Pearson and B. L. Shaw, *J. Chem. Soc.*, 1961, 2207.

12 (*a*) A. T. Hutton and C. P. Murray, in *Comprehensive Coordination Chemistry*, ed. G. Wilkinson, R. D. Gillard and J. A. McCleverty, vol. 5, p. 1162; (*b*) C. A. McAuliffe and W. Levason, *Phosphine, Arsine and Stibine Complexes of the Transition Elements*, Elsevier, Amsterdam, 1979; (*c*) J. Chatt and F. G. Mann, *J. Chem. Soc.*, 1939, 1622; (*d*) M. J. Hudson, R. S. Nyholm and M. H. B. Stiddard, *J. Chem. Soc.*, 1968, 40.

Received in Cambridge, UK, 15th June 1998; 8/04475I

Enzymatic synthesis of a chiral gelator with remarkably low molecular weight

Vassil P. Vassilev, Eric E. Simanek, Malcolm R. Wood and Chi-Huey Wong*†

Department of Chemistry and the Skaggs Institute for Chemical Biology, The Scripps Research Institute, 10550 North Torrey Pines Road, La Jolla, CA 92037, USA

In one enzymatic step, two products of low molecular weight are obtained: one is a gelator of organic solvents, the other crystallizes to form an extended hydrogen-bondednetwork.

One product synthesized during our investigations of the enzymatic synthesis of β-hydroxy-α-amino acids using threonine aldolases was an optically-active, low molecular weight gelator of organic solvents.[1] Compound **1** is remarkably effective: only 0.2–0.4% of **1** is required for gel formation. Herein we report our investigations of **1** and **2** utilizing transmission electron microscopy, single crystal X-ray diffraction, and computation.

The products of the enzymatic aldol reaction between glycine and 2,3-*O*-isopropylideneglyceraldehyde (Scheme 1) are two diasteriomers which differ only in their absolute stereochemistry at C3. While **1** forms a gel in most organic solvents (Table 1), **2** crystallizes. This difference led us to investigate this system further.

While gel formation in aqueous and non-aqueous media by high molecular weight molecules is a well documented phenomenon, the study of low molecular weight gelators is in its infancy.[2] Their potential as nucleating agents for synthetic polymers and in health care products has been recognized.[3–8] All of these molecules contain chiral centers, hydrophobic regions, and groups capable of forming intermolecular interactions such as hydrogen bonds. Beyond such a description, our ability to predict which molecules will form gels in not possible: their discovery occurs serendipitously. In addition to the above cited small molecules, other recently published examples include derivatives of cholesterol,[9] 2,3-bis(*n*-decyloxy)anthracenes,[10] calixarenes,[11] and fluorinated hydrocarbons.[12] A majority of the gelators identified—especially those which give quartenary structure visible in electron micrographs—incorporate large aliphatic (hexadecyl, octadecyl) chains.[13–16]

Due to the low solubility of **1** in organic solvents, a MeOH quench strategy is used to form gels. Gels are obtained by first dissolving **1** in a small volume of MeOH, and then adding the solvent of choice warmed to ~ 40 °C: MeOH is typically present in < 10% v/v. Subsequent cooling of the solution to room or low temperature affords the gel. Excess solvent is removed by allowing the gel to stand at room temperature and decanting. After solvent release is complete, the molar ratio of **1**:solvent can be calculated (Table 1).

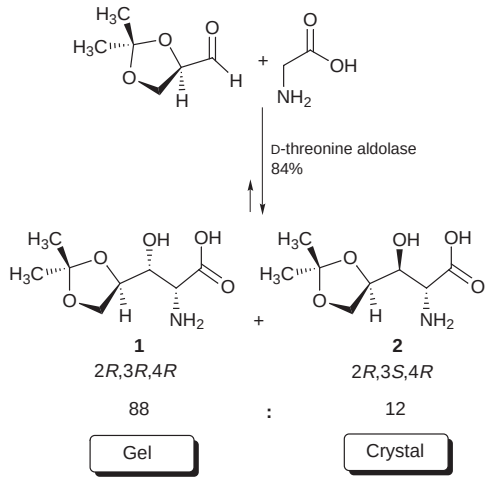

Scheme 1

Table 1 Compound **1** forms gels from a variety of solvents

Solvent	Phase formation	**1**/solvent (mol/mol)	**1**/wt%	*T*/°C[a]
H_2O	solution	—	20.5	—
H_2O–EtOH (1:5)	gel	125	4.5	3
MeOH	solution	—	2.4	—
MeOH	gel	117	4.9	3
THF	gel	702	0.4	room temp.
EtOH	gel	509	0.9	3
Bu^nOH	gel	1456	0.2	3
Pr^iOH	gel	1245	0.3	room temp.
MeCN	gel	1251	0.4	room temp.
Et_2O	gel	443	9	3
$PhCH_2CH_2OH$	gel	723	0.24	3
Bu^sOH	gel	1369	0.2	3
$C_5H_{11}OH$	gel	330	0.7	3
Isoamyl alcohol	solution	—	0.16	0
$C_8H_{17}OH$	gel	630	0.25	3
Solketal	solution	—	0.48	0

[a] Refers to temperature at which the solution of **1** in the indicated solvent was left to stand before gel formation was observed: 3 °C indicates a cold room at *ca.* 3 °C; 0 °C indicates an ice bath.

Compound **1** can be visualized by transmission electron microscopy following staining with OsO_4 vapor. At *ca.* 40 °C the gel becomes a viscous solution which can be transferred *via* pipet to a carbon-coated EM grid. After air drying for 5 min, the grid is placed in a sealed chamber next to a vial containing aq. OsO_4. After sitting overnight, the sample is examined in the EM. We observe fibers that are similar in appearance to those observed in related systems. Fig. 1(A) shows a low magnification image of the fibril network obtained. Fig. 1(B) shows a higher magnification image in which the dimensions of individual fibers can be measured. To our eyes, while the fibers all appear to be greater than 1 μm in length, they appear to terminate by forming a larger diameter fiber. Their widths also

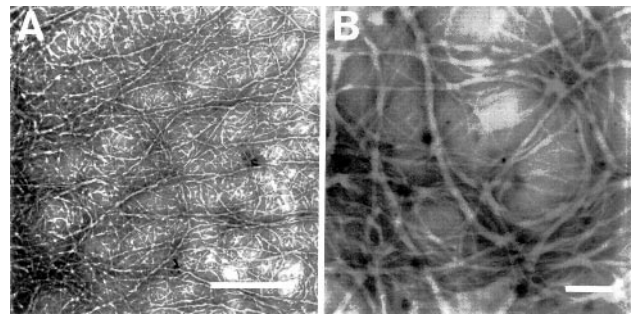

Fig. 1 Transmission electron micrographs of **1**. The scale bars shown represent (A) 2 μm and (B) 200 nm.

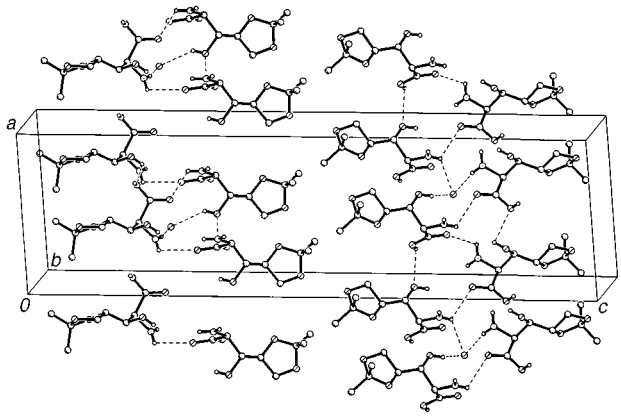

Fig. 2 Packing of **2** occurs with the inclusion of a water molecule (hydrogens omitted). Hydrogen bonds (calculated) are shown as dashed lines.

appear to be well defined. That is, we can identify three distinct sizes: narrow fibers (< 5 nm); medium fibers (20 nm); and wide fibers (> 20 nm). In Fig. 1(A) the wide fibers run from right to left, while medium fibers run between wide fibers. Narrow fibers are difficult to see at this magnification, but are seen in Fig. 1(B). Many of the gel fibers formed by higher molecular weight gelators containing one or more long chain alkanes show quarternary structure within a fibril: they appear woven like a rope. While some of the fibers suggest such a helicity, the images are not as satisfying as those reported by Thierry[3] and Demharter.[16d]

To infer reasonable patterns of intermolecular interactions in **1**, we investigated the crystal structure of **2**, which gave crystals suitable for single-crystal X-ray diffraction from an EtOH–water solution (similar to that in which **1** gives gels).‡ Fig. 2 shows the packing of these molecules in the solid state which contains a hydrophobic domain comprising the isopropylidene ring, and the hydrophilic domain comprising carboxylate, amine, and hydroxy groups. In general, hydrophobic groups of one molecule pack against the hydrophobic groups of neighboring molecules in either an edge-to-edge or face-to-face arrangement.[17] The hydrophilic regions pack to form a 3D network of interactions that are depicted as hydrogen bonds in Fig. 2.[18] Incorporated into the lattice is a highly-coordinated water molecule. All potential hydrogen bonding interactions are satisfied with the exception of the oxygen atoms of the isopropylidene group.

We envisioned that the difference between the gel and crystalline states might arise from the dimensionality of directional intermolecular interactions. That is, in the crystalline state, highly directional hydrogen bonds extend in three dimensions: one dimension is communicated along the hydroxy group at C3. Changing the geometry of this hydroxy group—changing from **2** to **1**—might change directional ordering in the third dimension leading to a gel state. To investigate this possibility we performed Monte Carlo calculations in Macromodel. Unfortunately, we find no conformational preference for the C3 hydroxy group in any of the four diasteriomers.[19]

To better evaluate the structure of the gel, we attempted to prepare gels from acidic or basic solutions of aq. MeOH and *n*-butanol—the solvent which most readily forms gels with **1**.[20]

We observed no gel formation even when *ca.* 10× the amount of **1** required for gel formation from 'pH-neutral' organic solvents was added. It seems very likely that the proton balance must be maintained for hydrogen bonding or ion-pairing to facilitate gel formation.

The molecular basis for the formation of a gel state instead of a crystal state remains unclear. We are pleased, however, that molecules like **1** and **2**—which contain three chiral centers and are available in one enzymatic step—display such interesting properties.

This work was supported by the Division of Materials Sciences of the U.S. Department of Energy under Contract No. DE-AC03-76SF-00098. The authors thank Dr Raj K. Chadha (Scripps) for crystallographic studies.

Notes and References

† E-mail: wong@scripps.edu

‡ *Crystal data* for **2**: $C_8H_{14}NO_5 \cdot 0.5H_2O$, M = 214.22, monoclinic, $C2$ (no. 5), a = 10.272(6), b = 5.795(4), c = 36.215(7) Å, β = 91.20(3)°, V = 2155(2) Å^3, T = 296(2) K, Z = 8, μ = 0.956 mm^{-1}, 3548 reflections collected, 2351 independent reflections (R_{int} = 0.1617), final R [$I > 2\sigma(I)$]: $R1$ = 0.0798, $wR2$ = 0.1875; (all data) $R1$ = 0.1390, $wR2$ = 0.2292. CCDC 182/954.

1 T. Kimura, V. P. Vassilev, G.-J. Shen and C.-H. Wong, *J. Am. Chem. Soc.*, 1997, **119**, 11 734. Compounds **1** and **2** were purified as indicated. Successive recrystallizations from EtOH–water gave **2** in > 97% purity (no impurities were observed by ^{1}H NMR analysis) and **1** in > 95% purity (< 5% of **2** was observed in the ^{1}H NMR spectrum of **1**).
2 J. M. Guenet, *Thermoreversible Gelation of Polymers and Biopolymers*, Academic Press, New York, 1992.
3 A. Thierry, C. Straupe, B. Lotz and J. C. Wittmann, *Polym. Commun.*, 1990, **31**, 299 and references cited therein.
4 F. M. Menger and K. S. Venkatasubban, *J. Am. Chem. Soc.*, 1978, **43**, 3413; F. M. Menger, Y.Yamazaki, K.K. Catlin and T. Nishimi, *Angew. Chem.*, 1995, **107**, 616; *Angew. Chem., Int. Ed. Engl.*, 1995, **34**, 585.
5 M. Jokic, J. Makarevic and M. Zinic, *J .Chem. Soc., Chem. Commun.*, 1995, 1723.
6 K. Hanabusa, Y. Matsumoto, T. Miki, T. Koyama and H. Shirai, *J. Chem. Soc., Chem. Commun.*, 1994, 1401.
7 E. J. De Vries and R. M. Kellog, *J. Chem. Soc., Chem. Commun.*, 1993, 238.
8 H. T. Stock, N. J. Turner and R. McCague, *J. Chem. Soc., Chem. Commun.*, 1995, 2063.
9 Y.-C. Lin, B. Kachar and R. G.Weiss, *J. Am. Chem. Soc.*, 1989, **111**, 5542.
10 T. Brotin, R. Utermohlen, F. Fages, H. Bouas-Laurent and J.-P. Desvergne, *J. Chem. Soc., Chem. Commun.*, 1991, 416.
11 M. Aoki, K. Murata and S. Shinkai, *Chem. Lett.*, 1991, 1751.
12 R. J. Twieg, T. P. Russel, R. Siemens and J. F. Rabolt, *Macromolecules*, 1985, **18**, 1361.
13 For amphiphilic agents, see: H. Hoffmann and G. Ebert, *Angew. Chem.*, 1988, **100**, 933; *Angew. Chem., Int. Ed. Engl.*, 1988, **27**, 902; J.-H. Fuhrhop and W. Helfrich, *Chem. Rev.*, 1993, 1565.
14 For arborols, see: G. R. Newkome, G. R. Baker, S. Arai, M. J. Saunders, P. S. Russo, K. J. Theriot, C. N. Moorefield, L. E. Rogers, J. E. Miller, T. R. Lieux, M. E. Murray, B. Philips and L. Pascal, *J. Am. Chem. Soc.*, 1990, **112**, 8458.
15 For more work from the lab of Hanabusa and colleagues, see: K. Hanabusa, K. Okui, K. Karaki, T. Koyama and H. Shirai, *J. Chem. Soc., Chem. Commun.*, 1992, 1371; K. Hanabusa, J. Tange, Y. Taguchi, T. Koyama and H. Shirai, *J. Chem. Soc., Chem. Commun.*, 1993, 390; K. Hanabusa, Y. Naka, T. Koyama and H. Shirai, *J. Chem. Soc., Chem. Commun.*, 1994, 2683.
16 For other systems, see: (*a*) C. S. Snijder, J. C. de Jong, A. Meetsma, F. van Bolhuis and B. L. Feringa, *Chem. Eur. J.*, 1995, **1**, 594; (*b*) J.-H. Fuhrhop, S. Svenson, C. Boetcher, E. Rossler and H.-M. Vieth, *J. Am. Chem. Soc.*, 1990, **112**, 4307; (*c*) S. Bhattacharya, S. N. Ghanashyam Acharya and A. R. Raju, *J. Am. Chem. Soc.*, 1996, **118**, 2101; (*d*) S. Demharter, H. Frey, M. Dreschler and R. Mulhaupt, *Colloid Polym. Sci.*, 1995, **273**, 661.
17 A similar pattern of packing has been observed by Menger in which the aromatic groups of ditoluoyl-L-cystine stack face-to-face (see ref. 4).
18 The hydrogen atoms are assigned and hydrogen bonds calculated using the SHELX package of programs. We cannot say with certainty that the carboxylate and amino groups exist as CO_2H and NH_2 groups as depicted to form the indicated hydrogen bond, or as an intimate ion pair.
19 The details of the Monte Carlo simulations are available from the authors.
20 When compound **1** (6.0 mg) was dissolved in 1 M NaOH (40 μl) and MeOH (80 μl), addition of 1 ml of *n*-butanol did not produce a gel. Dissolution of **1** (5.6 mg) in 1 M HCl (40 μl) and MeOH (80 μl), and addition of 1 ml of *n*-butanol also failed to produce a gel.

Received in Corvallis, OR, USA, 28th April 1998; 8/03230K

New and efficient selenium reagents for stereoselective selenenylation reactions

Gianfranco Fragale,[a] Markus Neuburger[b] and Thomas Wirth*[a]†

[a] *Institut für Organische Chemie der Universität Basel, St. Johanns-Ring 19, CH-4056 Basel, Switzerland*
[b] *Labor für Kristallographie, Institut für Anorganische Chemie der Universität Basel, Spitalstr. 51, CH-4056 Basel, Switzerland*

The simple substitution of an aryl proton by a methoxy substituent improves the selectivity of the stereoselective selenenylation reaction dramatically, leading to addition products with diastereomeric ratios up to 50 : 1 in the methoxyselenenylation reaction of styrene.

Stereoselective reactions using chiral selenium compounds have been investigated recently by us[1] and other research groups.[2] These reagents can be employed in asymmetric selenenylation reactions or as ligands in metal-catalyzed transformations. For this purpose we have developed readily available chiral diselenides of type **1**. Diselenide **1a** (R' = H),

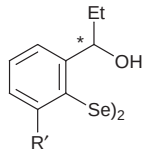

1

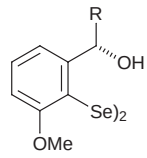

2

which can be synthesized *via* a two-step procedure, has already been used in many stereoselective reactions with good results. We have shown that an oxygen atom in the chiral side chain in close proximity to the selenium is responsible for the efficient transfer of chirality.[3]

C_2-Symmetrical chiral diselenides with an additional chiral side chain at the second *ortho*-position are also very efficient reagents in selenenylation reactions, however, they have to be prepared by multistep synthesis.[2a] Because an additional simple substituent in **1** (R' = Me, CF_3) does not improve the selectivity in the selenenylation reaction,[4] we decided to prepare compounds **2** with heteroatom-containing substituents such as the methoxy group.

Diselenides **2a**,**b** were synthesized from the optically active alcohols **3a**,**b**, respectively (Scheme 1). Alcohol **3a** was obtained by chiral reduction of 3-methoxyacetophenone with (−)-*B*-chlorodiisopinocampheylborane in 97% ee.[5] Through diethylzinc addition to 3-methoxybenzaldehyde catalyzed by (*R*,*R*)-bis{2-[1-(pyrrolidin-1-yl)ethyl]phenyl} diselenide,[6] alcohol **3b** was obtained in 97% ee. The alcohols **3a**,**b** were first deprotonated with Bu^{n}Li in the presence of TMEDA and then lithiated in the *ortho*-position with an excess of PhLi.[7] Successive reaction with selenium and oxidative work-up yields the diselenides **2a**,**b** in 63 and 47% overall yield, respectively.‡

3a R = Me
b R = Et

2a R = Me
b R = Et

Scheme 1 *Reagents and conditions*: i, Bu^{n}Li, TMEDA; ii, PhLi; iii, Se, O_2

From diselenide **2a** crystals suitable for X-ray analysis were obtained. The structure of **2a** (Fig. 1)§ is substantially different from other diselenides bearing heteroatom-containing sidechains. In other structures we found a strong interaction between the heteroatom of the sidechain and the selenium atom. In the structure of **2a** a strong interaction with the oxygen of the methoxy group is observed [Se–O (mean): 2.977 Å] while the distance from the selenium to the oxygen in the side chain (4.22 Å) is clearly greater than the sum of the van der Waals radii (3.40 Å).

As a consequence of these interactions the smallest substituent, namely the hydrogen atom, is placed in the plane of the benzene ring. Because solid state geometries may not be adopted in solution, further structural investigations have been performed.

The structure in solution has been determined through NOE measurements of diselenide **2a** in [$^2H_6$]DMSO. Irradiation at the frequency of the proton in the 5-position (the proton *ortho* to the side chain) showed a strong NOE with the protons of the methyl group and the proton of the hydroxy group. No interaction could be detected with the benzylic proton. Therefore, we suggest that the structure is similar to that in the solid state.

To analyze the substrate efficiency in stereoselective synthesis, we employed these two diselenides in the methoxyselenenylation of styrene. The diselenides **2a**,**b** were transformed *in situ* into the electrophilic triflates **4a**,**b** by bromination and exchange of the bromine ion with AgOTf (Scheme 2). The reaction with **4a** yielded β-methoxy selenide **5a** with a diastereomeric ratio of 50 : 1 in 55% yield.¶ By carrying out the reaction with **4b** bearing an ethyl substituent in the side chain the addition product **5b** was obtained with a diastereomeric ratio of only 11.5 : 1 and 60% yield. This is in

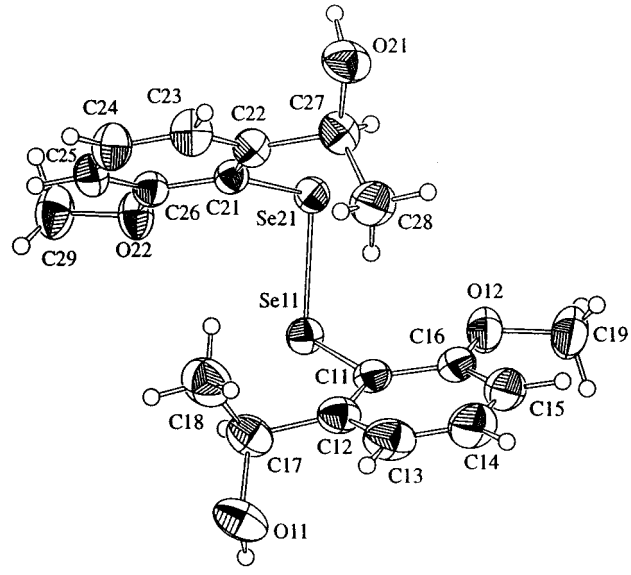

Fig. 1 ORTEP plot of the crystal structure of diselenide **2a**. Thermal ellipsoids are at the 30% probability level.

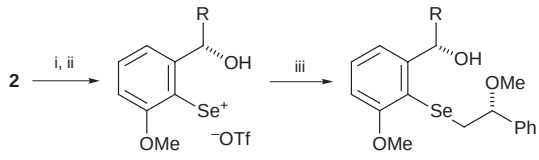

Scheme 2 *Reagents and conditions*: i, Br_2; ii, AgOTf; iii, styrene, MeOH

Table 1 Results of stereoselective reactions with selenium electrophiles generated from diselenides **2a** and **1**

Entry	Alkene	Product	Ratio (% yield) With **4a**	Ratio (% yield) With **6**
1		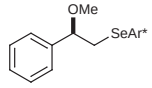	50:1 (55%)	16:1 (81%)
2	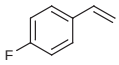	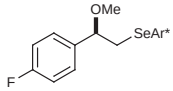	28:1 (45%)	5:1 (49%)
3	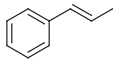	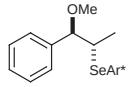	12:1 (51%)	9:1 (45%)
4	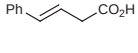	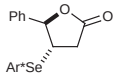	26:1 (54%)	6:1 (41%)
5	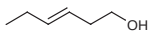		1.5:1 (42%)	1:1 (60%)
6	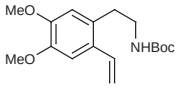	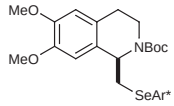	12:1 (66%)	9:1 (66%)

contrast to our previous observations where diselenides bearing ethyl substituents gave better selectivities than those with methyl substituents. Comparison of these results with those obtained using the arylselenenyl triflate **6** generated from diselenide **1a** (16 : 1) showed that selenenyl triflate **4a** represents a more efficient reagent for stereoselective selenenylation reactions (Table 1).

Encouraged by these results, we carried out further investigations with the electrophilic selenenyl triflate **4a** generated from diselenide **2a**. The methoxyselenenylation reaction of 4-fluorostyrene as well as β-methylstyrene showed increased facial selectivity compared to the reaction with the selenenyl triflate **6** derived from diselenide **1a** (entries 2 and 3). The selenolactonization of the unsaturated carboxylic acid (entry 4) was improved to a ratio of 26 : 1 by using the electrophile **4a**. The product of the cyclization of (*E*)-hex-3-enol and electrophile **6** (entry 5) was isolated as a racemate.[8] Cyclization with **4a** showed a modest facial selectivity of 1.5 : 1 in the resulting product. The stereochemistry of the major diastereomer could not be assigned in this case. The product of the cyclization of a carbamate (entry 6) is obtained with a diastereomeric ratio of 12 : 1. After radical removal of the selenium moiety and deprotection, (*S*)-salsolidine is obtained.[9] The absolute stereochemistry is in all cases the same as that observed with diselenide **1a**.

In summary, we present herein a new, readily available organoselenium reagent bearing a methoxy substituent *ortho* to the selenium. The electrophilic methoxyselenenylation of styrene was performed with a diastereomeric excess of 96%. The increased transfer of chirality is due to the forced interaction of the *ortho*-oxygen atom with the selenium. An X-ray diffraction structure and NOE measurements underline this assumption.

Financial support by the Stipendienfonds der Basler Chemischen Industrie (fellowship for G. F.), the Schweizer Nationalfonds and the Treubel-Fonds (fellowship for T. W.) is gratefully acknowledged. We thank Professor B. Giese for his continuing interest and generous support.

Notes and References

† E-mail: wirth@ubaclu.unibas.ch

‡ Alcohol **3a** (1.37 g, 9 mmol) and TMEDA (1.86 g, 9.6 mmol) were dissolved in dry pentane (12 ml) under argon, cooled to 0 °C, treated slowly with Bu^nLi (9 mmol, 1.6 M solution in hexane) and allowed to stir for 15 min. Then PhLi (27 mmol, 3.0 M solution in cyclohexane–Et_2O) was added and the mixture was stirred for 14 h. After cooling to 0 °C, selenium powder (54 mmol, 4.32 g) was added. The mixture was allowed to warm up to room temperature and stirred for an additional 5 h, then 1 M HCl (50 ml) was added. After extraction of the resulting mixture with Bu^tOMe (3 × 50 ml) and drying of the combined organic phases with $MgSO_4$, powdered KOH (100 mg) was added. The solvent was removed under vacuum and the residue purified by flash chromatography (silica gel, Bu^tOMe–pentane 1 : 2) and recrystallized from EtOH to yield **2a** (1.37 g, 66%) as orange crystals: mp 146–148 °C (Calc. for $C_{18}H_{22}O_4Se_2$: C, 46.98; H, 4.82. Found: C, 46.80; H, 4.90%); $[\alpha]$ +914.5 (*c* 0.96, $CHCl_3$); $\delta_H(CDCl_3)$ 1.26 (t, *J* 6.5, 6H), 2.22 (br s, 2H), 3.83 (s, 6H), 5.06 (q, 6.5 Hz, 2H), 6.84 (d, *J* 8.2, 2H), 7.18 (d, *J* 7.8, 2H), 7.36 (t, *J* 8.0, 2H); $\delta_C(CDCl_3)$ 24.2 (q, 2C), 56.3 (q, 2C), 69.3 (d, 2C), 110.0 (d, 2C), 118.0 (d, 2C), 118.7 (s, 2C), 131.3 (d, 2C), 151.4 (s, 2C), 159.7 (s, 2C); $\delta_{Se}(CDCl_3)$ 365.6; *m/z* (EI) 462 ([M^+], 54%), 230 (60), 214 (100), 214 (100), 198 (28), 182 (16), 134 (35), 107 (22), 91 (26), 77 (21); $\nu(CHCl_3)/cm^{-1}$ 3478, 3376, 3005, 2939, 1568, 1464, 1422, 1136, 1051, 1016.

§ *Crystal data* for **2a**: $C_{18}H_{22}O_4Se_2$, M = 460.29, monoclinic, space group $P2_1$, a = 8.1601(5), b = 13.8981(22), c = 16.5883(13) Å, β = 99.903(6)°, U = 1853.2(3) Å^3, Z = 4, T = 293 K, λ = 1.54180 Å^3, D_c = 1.65 g cm^{-3}, μ = 5.28 mm^{-1}, for 7767 observed reflections, R_1 = 0.0258, wR_2 = 0.0313. CCDC 182/957.

¶ The methoxyselenenylations and selenocyclizations were performed as described in refs. 4 and 8. *Selected data* for **5a**: $[\alpha]$ −1.2 (*c* 0.55, $CHCl_3$); $\delta_H(CDCl_3)$ 1.48 (d, *J* 6.5, 3H), 1.65 (br s, 1H), 3.13 (d, *J* 5.3, 1H), 3.14 (d, *J* 8.1, 1H), 3.21 (s, 3H), 3.88 (s, 3H), 4.29 (dd, *J* 8.1, 5.3, 1H), 5.41 (q, *J* 5.8, 1H), 6.79 (d, *J* 8.0, 1H), 7.14 (dd, *J* 7.8, 0.8, 1H), 7.22–7.35 (m, 6H); $\delta_C(CDCl_3)$ 24.1 (q), 34.9 (t), 56.1 (q), 56.8 (q), 69.8 (d), 83.4 (d), 109.9 (d), 117.1 (s), 118.2 (d), 126.6 (d, 2C), 128.0 (d), 128.5 (d, 2C), 129.7 (d), 141.0 (s), 150.0 (s), 162.8 (s). MS(EI): *m/z* (%) 366 (18) [M^+], 230 (37), 184 (30), 151 (27), 135 (21), 121 (100), 103 (14), 91 (18), 77 (15); $\nu(CHCl_3)/cm^{-1}$ 3666, 3382, 3005, 2937, 2838, 1570, 1464, 1431, 1136, 1103, 1052, 1016 (HRMS found: 366.0747. Calc. for $C_{18}H_{22}O_3Se$: 366.0734).

1 Review: T. Wirth, *Liebigs Ann./Recueil*, 1997, 2189 and references cited therein.
2 (*a*) R. Déziel, E. Malenfant, C. Thibault, S. Fréchette and M. Gravel, *Tetrahedron Lett.*, 1997, **38**, 4753; (*b*) Y. Nishibayashi, S. K. Srivastava, H. Takada, S.-I. Fukuzawa and S. Uemura, *J. Chem. Soc., Chem. Commun.*, 1995, 2321; (*c*) K.-I. Fujita, K. Murata, M. Iwaoka and S. Tomoda, *Tetrahedron*, 1997, **53**, 2029; (*d*) T. G. Back and B. P. Dyck, *Chem. Commun.*, 1996, 2567; (*e*) S.-I. Fukuzawa, K. Takahashi, H. Kato and H. Yamazaki, *J. Org. Chem.*, 1997, **62**, 7711.
3 T. Wirth, G. Fragale and M. Spichty, *J. Am. Chem. Soc.*, 1998, **120**, 3376.
4 T. Wirth and G. Fragale, *Chem. Eur. J.*, 1997, **3**, 1894.
5 H. C. Brown, J. Chandrasekharan and P. V. Ramachandran, *J. Am. Chem. Soc.*, 1988, **110**, 1539.
6 T. Wirth, K. J. Kulicke and G. Fragale, *Helv. Chim. Acta*, 1996, **79**, 1957.
7 D. L. Comins and J. D. Brown, *J. Org. Chem.*, 1989, **54**, 3730.
8 G. Fragale and T. Wirth, *Eur. J. Org. Chem.*, 1998, 1361.
9 T. Wirth and G. Fragale, *Synthesis*, 1998, 162.

Received in Cambridge, UK, 5th June 1998; 8/04264K

New branched carbohydrate building block from a tandem elimination-Farvorski rearrangement

Mikael Bols*† and Ib B. Thomsen

Department of Chemistry, University of Aarhus, Langelandsgade 140, DK-8000, Aarhus, Denmark

3-Methoxycarbonyl-1,5-anhydro-β-D-*erythro*-pentofuranose 1 was obtained when 2,3,4-tri-*O*-tosyl-1,6-anhydro-β-D-glucopyranose 2 was treated with NaOMe.

Carbohydrates are a rich and cheap source of chiral compounds for use in stereospecific synthesis.[1] One such popular chiral starting material is 1,6-anhydroglucose **3** (levoglucosan),[2] and its decendants the Cerny epoxides **4** and **5**.[3] Compound **4** is routinely obtained from **3** in two steps: conversion of **3** to 1,6-anhydro-2,4-di-*O*-tosyl-β-D-glucopyranose **6** followed by epoxidation of **6** *via* treatment with NaOMe.[4,5] The tritosylate **2** is sometimes obtained as a byproduct in the tosylation of **3**, but can also be converted to **4** in high yield by treatment with base (Scheme 1).[6]

When recently requiring some **4** we tried to obtain it from **2** using NaOMe as base. However, to our surprise, inspection of the reaction product revealed besides small quantities of **2** and **4** a large amount of another compound. After purification the compound could be isolated in 44% yield and identified by ^{1}H, ^{13}C and COSY NMR and EI mass spectroscopy:[7] a mass peak at *m/z* 159 (M+1) corresponded to $C_7H_{10}O_4$; ^{13}C NMR peaks at δ 52 and 178 identified a methyl ester; ^{13}C NMR peaks at δ 38 and 43 and ^{1}H NMR peaks at δ 2.0 and 2.7 were consistent with deoxygenated CH and CH_2 moieties; and COSY correlations showed anomeric C next to CH_2 next to CH. All were consistent with structure **1**. The stereochemistry at C-3 could be determined by comparison with spectra of the four isomeric acetylated 1,5-anhydropentosides. Only the isomers with the 3 substituent *exo* had a J_{45} value of 0 Hz.

The compound **1** was not formed from epoxide **4**, as **4** was completely stable to prolonged treatment with NaOMe. Formation of compound **1** can be explained by a Farvorski rearrangement of an intermediate ketone **7** (or its regioisomer) as outlined in Scheme 1. The ketone can be formed by elimination of a tosylate. Attack by methoxide and ring opening of the intermediate cyclopropanone **8** apparently occur with high regioselectivity.

Compound **1** is a highly strained compound. On standing in $CDCl_3$ or when subjected to silica gel chromatography under non-basic conditions, **1** was spontaneously and quantitatively transformed to a new crystalline compound. X-Ray crystallographic structure determination revealed it to be the dimer **9** (Scheme 2). This structure determination also confirmed the structure and stereochemistry of **1**. To avoid the conversion of **1** to **9**, chromatography of the former was carried out with 1% Et_3N present.[8]

The tandem elimination-Farvorski rearrangement of a tritosylate is to the best of our knowledge unprecedented. To investigate its generality we also subjected tritosylarabinoside **10** and methyl 2,3,4-tri-*O*-tosyl-α-L-rhamnopyranoside to reaction with NaOMe. From the reaction of **10** Farvorski products **11** and **12** were isolated in 8 and 5% yield, respectively, together with 22% of epoxides **13** (Scheme 3). From the reaction of the tritosylrhamnoside, 29% of a mixture of Farvorski products was formed. Thus the reaction is apparently general but much less favored in these other cases.

Farvorski product **1** is a useful chiral building block. Although the yield of its formation, as is common for many Farvorski rearrangements, is relatively low this is compensated

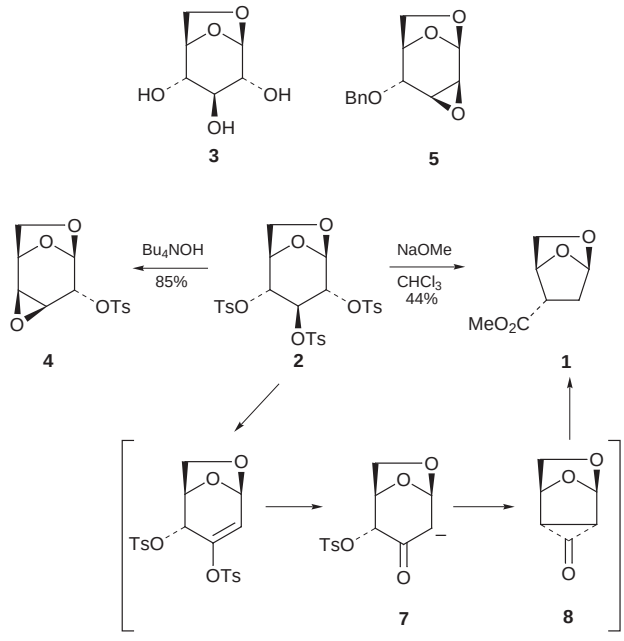

Scheme 1

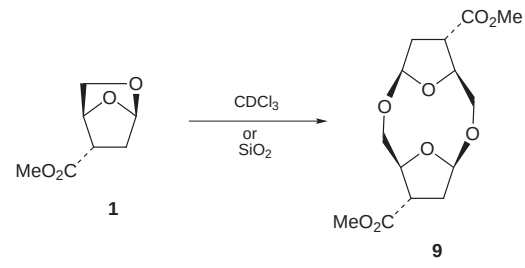

Scheme 2

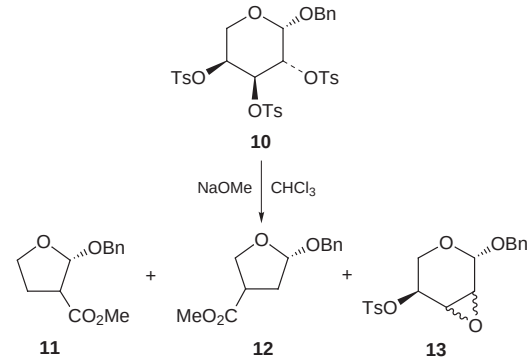

Scheme 3

for by the fact that branched carbohydrate chains are usually synthesised *via* multistep procedures.

We acknowledge financial support from the Danish National Science Research Council (SNF) grant No. 9502986. We also thank B. O. Pedersen for mass spectra and Rita Hazell for X-ray structure determination of **9**.

Notes and References

† E-mail: mb@kemi.aau.dk.

1 M. Bols, *Carbohydrate Building Blocks*, Wiley, New York, 1995; S. Hanessian, *The Chiron Approach*, Pergamon, Oxford, 1983.
2 M. Cerny and J. Stanek, *Adv. Carbohydr. Chem. Biochem.*, 1977, 23.
3 T. Trnka and M. Cerny, *Collect. Czech. Chem. Commun.*, 1971, **36**, 2216.
4 M. Cerny, V. Gut and J. Pacak, *Collect. Czech. Chem. Commun.*, 1961, **26**, 2542.
5 T. B. Grindley, G. J. Reimer, J. Kralovec, R. G. Brown and M. Anderson, *Can. J. Chem.*, 1987, **65**, 1065.
6 W. Szeja, *Carbohydr. Res.*, 1988, **183**, 135.
7 *Selected data* for **1**: $\delta_H(CDCl_3)$ 5.65 (d, 1H, $J_{1,2exo}$ 2.0, H-1), 5.0 (d, 1H, $J_{4,5}$ 2.7, H-4), 3.6 (s, 3H, OMe), 3.5 (m, 2H, H-5a and H-5b), 2.7 (dd, 1H, $J_{2endo,3}$ 8.5, $J_{2exo,3}$ 4.5, H-3), 2.1 (ddd, 1H, $J_{2exo,2endo}$ 12.0, H-2*exo*), 2.0 (dd, 1H, H-2*endo*); $\delta_H(CDCl_3)$ 172.6 (C-3'), 100.4 (C-1), 78.1 (C-4), 68.6 (C-5), 52.2 (OMe), 44.7 (C-3), 36.6 (C-2).
8 *Typical procedure*: To tritosylate **2** (2.35 g) in $CHCl_3$ (25 ml) was added a solution of Na (400 mg) in MeOH (3 ml). The strongly exothermic reaction was left for 30 min. and then water (15 ml) and sat. aq. NH_4Cl (3 ml) was added. The phases were separated and the organic layer dried ($MgSO_4$), concentrated and the content chromatographed in EtOAc–pentane (1:4) with 1% Et_3N to give **1** (261 mg, 44%). In another identical experiment no Et_3N was added to the mobile phase during chromatography. This gave **9** in 49% yield (291 mg).

Received in Glasgow, UK, 5th May 1998; 8/03397H

Remarkable acceleration of dimethyl phosphate hydrolysis by ceric cations

Robert A. Moss*† and Kaliappa G. Ragunathan

Department of Chemistry, Rutgers, The State University of New Jersey, New Brunswick, New Jersey 08903, USA

Ce^{4+} cations in aqueous solution at pH 1.8 and 60 °C reduce the half-life of dimethyl phosphate hydrolysis from 8454 years (pH 7, 60 °C) to 22 min.

Dimethyl phosphate **1** (DMP) strongly resists hydrolysis. A recent meticulous study reports $k = 1.6 \times 10^{-13}$ s^{-1} at 25 °C, equivalent to a half-life of ~137 000 years for the pH 7 uncatalyzed cleavage (by Me–O scission) of DMP by water.[1] This extraordinary stability makes the phosphodiester linkage ideal for its role in the backbone of DNA and RNA.[1,2]

The hydrolysis of DMP can be accelerated; below pH 5, acid catalysis is apparent.[1] Bunton *et al.* reported that at pH 1.24 and 100 °C, the P–O$^-$ of DMP was protonated, and hydrolysis of neutral **1** proceeded with $k = 3.13 \times 10^{-6}$ s^{-1} ($t_{1/2}$ = 2.5 days, 78% Me–O scission).[3] More recently, Kim and Chin found that $[(cyclen)Co(OH_2)_2]^{3+}$ at pD 6.3 and 60 °C catalyzed the hydrolysis of DMP (presumably by P–O scission) with $k = 2 \times 10^{-7}$ s^{-1} ($t_{1/2}$ ~40 days).[2]

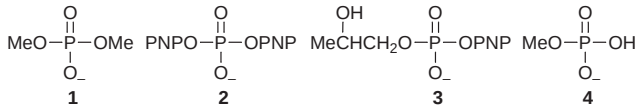

1 **2** **3** **4**

Various transition metal, lanthanide and actinide cations are known to accelerate the hydrolytic cleavage of phosphodiesters.[4] Our own studies of the metal-ion mediated hydrolysis of phosphodiesters have focused on Th^{4+}, Ce^{4+} and Zr^{4+} cleavage of activated substrates such as bis(*p*-nitrophenyl) phosphate **2** (BNPP) and 2-hydroxypropyl (*p*-nitrophenyl) phosphate **3** (HNPP).[5–7] Rate enhancements $>10^9$, relative to the uncatalyzed hydrolyses, were observed in the Th^{4+} or Ce^{4+} cleavage of BNPP.[5,6] A high value of the charge/cation diameter ratio appears necessary for optimal cation reactivity in phosphodiester hydrolysis.[5–8]

In view of our results with substrate **2**,[6] and the known ability of Ce^{4+} to accelerate the cleavage of DNA (at P–O),[9] we have now examined the Ce^{4+} acidic hydrolysis of DMP. The remarkable kinetic results indicate an acceleration of 2×10^8, relative to the uncatalyzed hydrolysis at 60 °C, and a reduction in $t_{1/2}$ from ~8450 years to 22 min.

Hydrolyses of DMP **1** and of methyl phosphate **4** (MP) mediated by ceric ammonium nitrate (CAN) were followed in D_2O at 60 °C by 400 MHz proton NMR spectroscopy, monitoring the disappearance of the Me signals at δ 3.9, relative to an internal pyrazine standard. Solutions of CAN were not buffered, but were adjusted to pH 1.6 or 1.8 (pD 2.0 or 2.2) by addition of pD 13.4 NaOD solution prior to reaction. The pH typically declined by 0.25 during the reaction. Reactions were followed for two half-lives and the infinity titer was obtained after 24 h at 60 °C. Rate constants were duplicated and agreed to ±7%.

With 1 mM DMP at pH 1.6,‡ the measured hydrolytic rate constants varied from 9.3×10^{-5} s^{-1} at [Ce^{4+}] = 2.5 mM to 4.25×10^{-4} s^{-1} at [Ce^{4+}] = 20 mM. A graphical representation of the dependence of k on [Ce^{4+}] appears in Fig. 1, where 'saturation' behavior is apparent. Michaelis–Menten analysis provides K_m ~0.0105 M and a binding constant of ~95 M^{-1}, with k_{cat} ~6.5×10^{-4} s^{-1}.§ Unfortunately, the fit of the data in Fig. 1 to the Michaelis–Menten equation is not very precise. Although saturation (binding of DMP to Ce^{4+}) is observed, the K_m and k_{cat} are approximate.

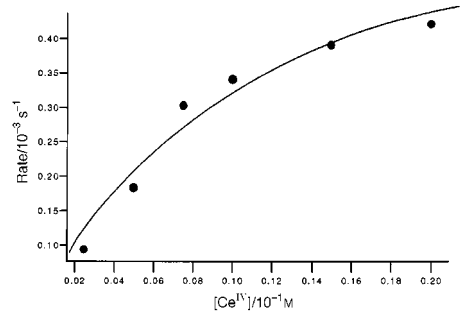

Fig. 1. Pseudo-first order rate constants (s^{-1}) for the hydrolysis of 1 mM DMP by CAN as a function of [Ce^{4+}] at pH 1.6. The points are the experimental values; the solid line is generated from the Michaelis–Menten equation with $K_M = 0.0105$ M and $k_{cat} = 6.48 \times 10^{-4}$ s^{-1}.

Our highest observed rate constant for the cleavage of 1 mM DMP by 10 mM Ce^{4+} was at pH 1.8, 60 °C, where k = $5.28(\pm0.38) \times 10^{-4}$ s^{-1}. At higher pH, precipitation of Ce was apparent.

Comparisons of the hydrolytic kinetics of DMP under neutral,[1] acidic,[3] Co^{3+}-assisted,[2] or Ce^{4+}-mediated conditions appear in Table 1, where the extraordinary acceleration due to Ce^{4+} is manifest. At 200 million, the rate enhancement by acidic Ce^{4+} exceeds those provided by H^+ alone or Co^{3+}-cyclen by factors of 10^3–10^4. The 8454 year 'benchmark' half-life of DMP under neutral conditions at 60 °C is reduced to 22 min by Ce^{4+} at pH 1.8.

The Ce^{4+} cleavage of DMP produces 2 equiv. of MeOH (NMR), so that the reaction is hydrolytic, not oxidative; hydrolysis also occurs in the Ce^{4+} cleavage of deoxyribodinucleotides.[10] Hydrolysis of 1 mM MP **4** by 10 mM CAN at pH 1.8 and 60 °C liberates 1 equiv. of MeOH and proceeds with $k = 6.3 \times 10^{-4}$ s^{-1}, about 1.2 times faster than the corresponding cleavage of DMP. Accordingly, MP does not accumulate during the hydrolysis of DMP. A similar rate ordering prevails during the acid catalyzed hydrolyses of DMP and MP.[3,11]

We briefly examined several other sets of conditions and catalysts for the hydrolysis of DMP. A ten-fold excess of Ce^{3+} at pH 8 (gel) also cleaved DMP at 60 °C, but much more slowly than Ce^{4+} at pH 1.8; the Ce^{3+} hydrolysis was only ~50% complete after 48 h. Surprisingly, Th^{4+} (10 mM) was unreactive toward DMP at pH 3.5 and 60 °C, while Zr^{4+} (10 mM, pH 2.0,

Table 1 Comparison of DMP hydrolyses at 60 °C[a]

Conditions	k_{hydrol}/s^{-1}	k_{rel}	$t_{1/2}$
Neutral[b]	2.6×10^{-12}	1.0	8454 years
H^+, pH 1.24[c]	5.2×10^{-8}	2.0×10^4	154 days
Co^{3+}-cyclen[d]	2.0×10^{-7}	7.7×10^4	40 days
Ce^{4+}, pH 1.8[e]	5.3×10^{-4}	2.0×10^8	22 min

[a] The first two entries are extrapolated to 60 °C from data in the original references. [b] Ref. 1. [c] Ref. 3. [d] Ref. 2; pH 5.9. [e] This work.

60 °C) cleaved DMP slowly ($k \sim 7.6 \times 10^{-6}$ s^{-1}). Addition of 5 mM $PrCl_3$ to 10 mM CAN did not significantly accelerate the cleavage of DMP at pH 2.5, 60 °C; $k = 5.7 \times 10^{-4}$ s^{-1}, comparable to the rate constant with Ce^{4+} alone (Table 1). Rate enhancement due to Pr^{3+}–Ce^{4+} clusters[12] did not occur. Finally, neither added chloride or nitrate ions (120 mM) further enhanced the Ce^{4+} hydrolysis of DMP.

The mechanism of the Ce^{4+}-mediated hydrolysis of DMP is not yet fully defined. The saturation behavior (Fig. 1) implicates binding of substrate P–O$^-$ by Ce^{4+}. The pK_a of the waters of hydration bound to Ce^{4+} is ~0.7,[13] so that the Ce^{4+}-DMP complex will have Ce-bound OH nucleophiles available for attack at the substrate P. One can imagine a P–O(Me) scission mechanistically analogous to that suggested for the Co^{3+}-cyclen/DMP reaction.[2] However, the neutral (> 99.5%)[1] and the acid catalyzed (78%)[3] hydrolyses of DMP occur mainly by O–Me cleavage. Although it seems unlikely that Ce^{4+} complexation of DMP would enhance subsequent H_2O attack at the MeO (rather than the P–O) linkage by the enormous factors observed here, a definitive mechanism requires $H_2{}^{18}O$ studies of the Ce^{4+} hydrolyses of both DMP and MP. These studies, together with comparable examinations of phosphonate monoester hydrolyses, are in progress.

We are grateful to the U.S. Army Research office for financial support.

Notes and References

† E-mail: Moss@Rutchem.Rutgers.Edu

‡ The pK_a of DMP is 1.06 at 60 °C (extrapolated from the data in ref. 3), so that > 77% of the DMP will be in the monoanionic form at pH 1.6, available for binding to Ce^{4+}.

§ From the initial four points of Fig. 1, [Ce^{4+}] = 2.5–10 mM, we can estimate a second order rate constant for the Ce^{4+}/DMP cleavage: $k_2 = 3.5 \times 10^{-2}$ M^{-1} s^{-1} at pH 1.6 and 60 °C. This may be compared with $k_2 = 6.2 \times 10^{-7}$ M^{-1} s^{-1} at pD 6.3 and 60 °C for the Co^{3+}-cyclen/DMP reaction (ref. 2).

1 R. Wolfenden, C. Ridgeway and G. Young, *J. Am. Chem. Soc*., 1998, **120**, 833.
2 J. H. Kim and J. Chin, *J. Am. Chem. Soc*., 1992, **114**, 9792.
3 C. A. Bunton, M. M. Mhala, K. G. Oldham and A. Vernon, *J. Chem. Soc*., 1960, 3293.
4 R. Breslow and D. L. Huang, *Proc. Natl. Acad. Sci. U.S.A.*, 1991, **88**, 4080; J. R. Morrow, L. A. Buttrey and R. A. Berback, *Inorg. Chem*., 1992, **31**, 16; M. Komiyama, K. Matsumura and Y. Matsumoto, *J. Chem. Soc*., *Chem. Commun.*, 1992, 640; H.-J. Schneider, J. Rammo and R. Hettich, *Angew. Chem., Int. Ed. Engl.*, 1993, **32**, 1716; B. K. Takasaki and J. Chin, *J. Am. Chem. Soc.*, 1993, **115**, 9337; R. A. Moss, K. Bracken and J. Zhang, *Chem. Commun.*, 1997, 563.
5 R. A. Moss, J. Zhang and K. Bracken, *Chem. Commun.*, 1997, 1639.
6 K. Bracken, R. A. Moss and K. G. Ragunathan, *J. Am. Chem. Soc*., 1997, **119**, 9323.
7 R. A. Moss, J. Zhang and K. G. Ragunathan, *Tetrahedron Lett.*, 1998, **39**, 1529.
8 A. Roigk, R. Hettich and H.-J. Schneider, *Inorg. Chem.*, 1998, **37**, 751.
9 B. K. Takasaki and J. Chin, *J. Am. Chem. Soc.*, 1994, **116**, 1121; M. Komiyama, T. Kodama, N. Takeda, J. Sumaoka, T. Shiiba, Y. Matsumoto and M. Yashiro, *J. Biochem.*, 1994, **115**, 809; M. Komiyama, T. Shiiba, T. Kodama, N. Takeda, J. Sumaoka and M. Yashiro, *Chem. Lett.*, 1994, 1025; J. Sumaoka, S. Miyama and M. Komiyama, *J. Chem. Soc., Chem. Commun*., 1994, 1755.
10 M. Komiyama, N. Takeda, Y. Takehashi, H. Uchida, T. Shiiba, T. Kodama and M. Yashiro, *J. Chem. Soc., Perkin Trans. 2*, 1995, 269.
11 C. A. Bunton, D. R. Llewellyn, K. G. Oldham and C. A. Vernon, *J. Chem. Soc*., 1958, 3574.
12 N. Takeda, T. Imai, M. Irisawa, J. Sumaoka, M. Yashiro, H. Shigekawa and M. Komiyama, *Chem. Lett.*, 1996, 599.
13 J. Burgess, *Metal Ions in Solution*, Halsted Press, New York, 1978, p. 267.

Received in Corvallis, OR, USA, 22nd June 1998; 8/04860F

A metal-containing synthon for crystal engineering: synthesis of the hydrogen bond ribbon polymer [4,4′-H_2bipy][MCl_4] (M = Pd, Pt)

Gareth R. Lewis and A. Guy Orpen*

School of Chemistry, University of Bristol, Bristol, UK BS8 1TS. E-mail: Guy.Orpen@bristol.ac.uk

The utility of the *cis*-MCl_2···HN^+ chelated hydrogen bond as a synthon in preparation of crystalline [4,4′-H_2bipy][MCl_4] (M = Pd 1, Pt 2) is demonstrated; the structure of 2 contains anions and cations linked by hydrogen bonds to form a ribbon polymer.

Desiraju[1] and others[2] have argued persuasively that crystal engineering or synthesis may be a realistic goal for modern chemistry. The means to this goal is the identification and application of reliable synthons which can control molecular aggregation and lead to crystal structures with (partly) controlled structures, containing sheets, ribbons and other desired motifs in the pattern formed. The synthons listed[1,2] and used to date are drawn in the main from the field of organic chemistry and almost all exploit the directionality of hydrogen bonds to afford the desired control of aggregation. The ability to incorporate metals in the structure offers promise of novel functionalities (chemical, magnetic, optical or electronic) which complement those available in purely organic molecular crystals. Here, we show that the metal assisted hydrogen bond affords a new class of synthon, one which may yield both desirable structures and desirable properties.

Recently,[3] we reported a crystallographic database analysis which demonstrated the ability of metal chloride complexes to act as hydrogen bond acceptors, as others had noted in specific examples.[4] Our study showed that these metal-assisted hydrogen bonds typically showed M–Cl···H angles of between 90 and 120°. The geometry at the hydrogen in these systems is normal[5] with all the shorter M–Cl···HE (E = N, O) bonds having E–H···Cl ⩾140°. These geometric preferences are compatible with the formation of acceptor chelate hydrogen bonds in which a pair of *cis*-chloride ligands at a metal form a chelate hydrogen bond with a single H–N moiety (see **A** in Scheme 1). Indeed, such an interaction in [$HNC_5H_3Ph_2$][$AuCl_4$] has attracted attention.[4a]

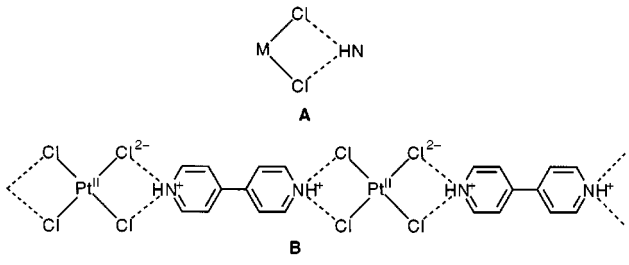

Scheme 1

We therefore sought to establish the utility of the *cis*-MCl_2···HN interaction (**A** in Scheme 1) as a synthon for the preparation of a hydrogen bonded polymer (**B** in Scheme 1) incorporating both inorganic ([MCl_4]$^{2-}$) and organic ([4,4′-H_2bipy]$^{2+}$) components. The planarity and opposite charges of the component ions led us to expect the formation of planar polymeric ribbons of type **B** shown in Scheme 1.

Reaction of aqueous [MCl_4]$^{2-}$ salts (M = Pd or Pt) with [4,4′-H_2bipy][PF_6]$_2$ leads to instantaneous formation of crystalline precipitates [4,4′-H_2bipy][MCl_4] (M = Pd **1**, Pt **2**).† Single crystal structure analysis‡ of **2** shows the desired structure has indeed been formed (Fig. 1). The component ions have normal, planar geometries with exact C_{2h} symmetry. The N–H···Cl bonds are of dimensions (N–H 0.86 Å, H···Cl 2.51 Å, N···Cl 3.219 Å; N–H···Cl 140°, Pt–Cl···H 95°) similar to those typically observed in our database study.[3] The anion···cation··· anion···cation··· ribbons formed are planar (mean atomic deviation 0.038 Å) and all ribbons lie parallel to one another although they are not coplanar. The ribbons lie perpendicular to the crystallographic mirror planes and extend along $2x - z$. Each ribbon lies 5.81 Å above its face-to-face neighbour and is in closer contact with four other ribbons through edge-to-edge interactions (CH···Cl 2.84 Å, Cl···Cl 3.510 Å, Fig. 2). This apparently efficient packing is presumably facilitated by the planarity of the component ions.

That this synthon may have some general applicability is indicated by the similarity of the structure of **2** and those of [4,4′-H_2bipy][$Cu_2(\mu\text{-}X)_2X_4$] (X = Cl **3**;[6] X = Br **4**[7]). In crystalline **3** and **4**, which were prepared for rather different reasons, hydrogen bonded ribbon motifs are present. In contrast, the structure[8] of [4,4′-H_2bipy][$CoCl_4$] is markedly different with the tetrahedral [$CoCl_4$]$^{2-}$ units forming two-centre

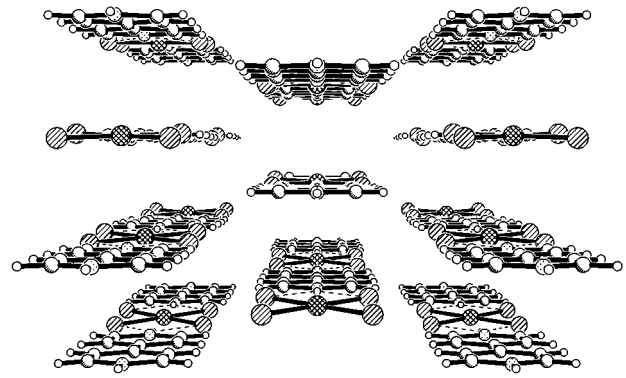

Fig. 2 The crystal structure of [4,4′-H_2bipy][$PtCl_4$] **2**.

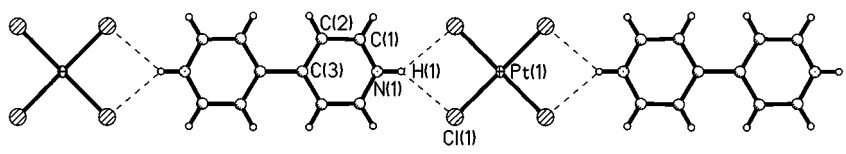

Fig. 1 Structure of one polymeric ribbon in crystalline [4,4′-H_2bipy][$PtCl_4$] **2**.

Cl···HN interactions in a dimeric cyclic $[4,4\text{-}H_2bipy]_2[CoCl_4]_2$ motif.

The utility of the *cis*-MCl_2···HE (E= O, N) synthon, the effect of the charges and geometry of the component species, the consequent structures formed and their properties are under investigation.

Financial support of the EPSRC is gratefully acknowledged. Our thanks go to Professor W. Clegg and Drs S. J. Cole and S. J. Teat and the EPSRC for use of station 9.8 at the Daresbury SRS and assistance in the data collection for compound **2**. We thank Professor N. G. Connelly for helpful discussions and advice.

Notes and References

† *Synthesis* of $[4,4'\text{-}H_2bipy][MCl_4]$ (M = Pd **1**, Pt **2**): addition of a colourless solution of $[4,4'\text{-}H_2bipy][PF_6]_2$ (156 mg, 0.347 mmol) in H_2O (10 cm³) to a brown solution of $Na_2PdCl_4{\cdot}1/3H_2O$ (101 mg, 0.335 mmol) in H_2O (6 cm³) caused the formation of a light brown insoluble precipitate of **1**. The product was washed with H_2O and dried *in vacuo*, yield 121 mg (88%). Orange crystalline compound **2** was prepared similarly from $[4,4'\text{-}H_2bipy][PF_6]_2$ and $K_2[PtCl_4]$, yield 83%. Both complex salts gave satisfactory microanalytical data.

‡ *Crystal structure analysis* of $[4,4'\text{-}H_2bipy][PtCl_4]$ **2**. The crystal structure of **2** was determined from data collected on a Siemens SMART diffractometer (λ = 0.6978 Å) at 160 K on station 9.8 at the Daresbury SRS. The structure was refined by least-squares against all F^2 data corrected for absorption, and hydrogen atoms were located in difference maps. *Crystal data*: $[4,4'\text{-}H_2bipy][PtCl_4]$, $C_{10}H_{10}Cl_4N_2Pt$, M = 495.09, monoclinic, space group $I2/m$ (no. 15), a = 6.6172(3), b = 11.6264(6), c = 8.0962(5) Å, β = 91.266(2)°, U = 622.76(6) Å³, Z = 2, μ = 12.10 mm⁻¹, 512 unique data, $R1$ = 0.034. CCDC 182/946.

1 G. R. Desiraju, *Angew. Chem., Int. Ed. Engl.*, 1995, **34**, 2311; *Chem. Commun.*, 1997, 1475.
2 J. C. MacDonald and G. M. Whitesides, *Chem. Rev.*, 1995, **28**, 37; F. H. Allen, P. R. Raithby, G. P. Shields and R. Taylor, *Chem. Commun.*, 1998, 1043; C. B. Aakeröy and K. R. Seddon, *Chem. Soc. Rev.*, 1993, **22**, 397; I. G. Dance, in *The Crystal as a Supramolecular Entity*, ed. G. R. Desiraju, *Perspectives in Supramolecular Chemistry*, Wiley, Chichester, 1996, vol. 2.
3 G. Aullón, D. Bellamy, L. Brammer, E. A. Bruton and A. G. Orpen, *Chem. Commun.*, 1998, 653.
4 (*a*) G. P. A. Yap, A. L. Rheingold, P. Das and R. H. Crabtree, *Inorg. Chem.*, 1995, **34**, 3474; (*b*) P. J. Davies, N. Veldman, D. M. Grove, A. L. Spek, B. T. G. Lutz and G. van Koten, *Angew. Chem., Int. Ed. Engl.*, 1996, **35**, 1959.
5 G. A. Jeffery, *Introduction to Hydrogen Bonding*, Wiley, Chichester, 1997; G. A. Jeffery and W. Saenger, *Hydrogen Bonding in Biology and Chemistry*, Springer Verlag, Berlin, 1993.
6 M. Bukowska-Strzyzewska and A. Tosik, *Pol. J. Chem.*, 1979, **53**, 2423.
7 A. Tosik, M. Bukowska-Strzyzewska and J. Mrozinski, *J. Coord. Chem.*, 1990, **21**, 253.
8 L. J. Barbour, L. R. MacGillivray and J. L. Atwood, *Supramol. Chem.*, 1996, **7**, 167.

Received in Basel, Switzerland, 2nd June 1998; 8/04128H

Diastereoselective SmI_2-mediated cascade radical cyclisations of methylenecyclopropane derivatives—a synthesis of paeonilactone B

Raymond J. Boffey,[a] Marco Santagostino,[a] William G. Whittingham[b] and Jeremy D. Kilburn*[a]†

[a] *Department of Chemistry, University of Southampton, Southampton, UK SO17 1BJ*
[b] *Zeneca Agrochemicals, Jealott's Hill Research Station, Bracknell, Berkshire, UK RG42 6ET*

The SmI_2-mediated cascade reaction of methylenecyclopropyl ketone 9 proceeds with high diastereoselectivity, which is critically dependent on the presence of HMPA, and provides a short route to paeonilactone B.

Cascade radical cyclisation reactions have proved to be very popular as a synthetic strategy as they allow the construction of several C–C bonds in one step and can provide elegant synthetic routes to complex polycyclic compounds and natural products.[1] Tandem reactions, initiated in particular by the versatile lanthanide reagent SmI_2, have also been a focus of recent attention.[2] We now report that SmI_2-promoted cascade cyclisations of methylenecyclopropyl ketone derivatives lead to bicyclic products in good yield and with excellent diastereoselectivity. This approach provides a short synthetic route to (±)-paeonilactone B **1**, one of several structurally related monoterpenes isolated from paeony roots,[3] all of which feature a highly oxygenated cyclohexane nucleus.[4]

A retrosynthetic analysis of paeonilactone B (Scheme 1) suggested that the *cis*-fused bicyclic methylenecyclohexane **2** could be prepared by a 5-*exo* cyclisation of methylenecyclohexyl radical **3** onto a pendant alkyne, and **3** could, in turn, arise from cyclisation of ketyl radical **5** onto a methylenecyclopropane unit with subsequent '*endo*' ring opening of **4**.[5] Whether such a sequence would prove to be diastereoselective and provide the correct relative stereochemistry of the tertiary alcohol required for the natural product remained to be tested by experiment.

Addition of lithiated methylenecyclopropane to aldehyde **6**,[6] produced the desired alcohols as a readily separable mixture of diastereoisomers **7** and **8** (Scheme 2).[7] The relative stereochemistry for the two diastereoisomers was established by X-ray crystallographic structure analysis of the *p*-nitrobenzoate ester derived from alcohol **8**.[8] Alkylation of the alcohols gave the corresponding prop-2-ynyl ethers, and subsequent ketal deprotection provided the two diastereomeric cyclisation precursors, **9** and **10** respectively, in essentially quantitative yield.

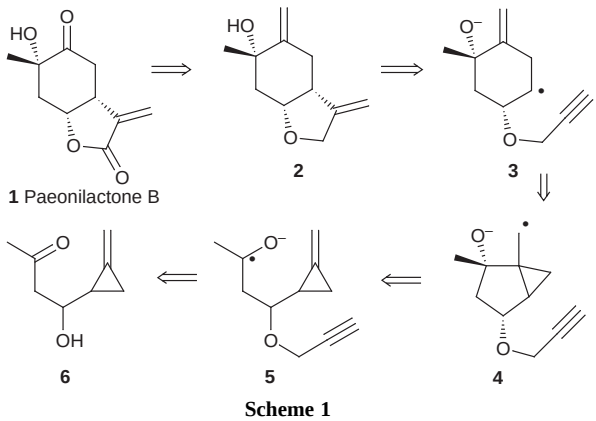

Scheme 1

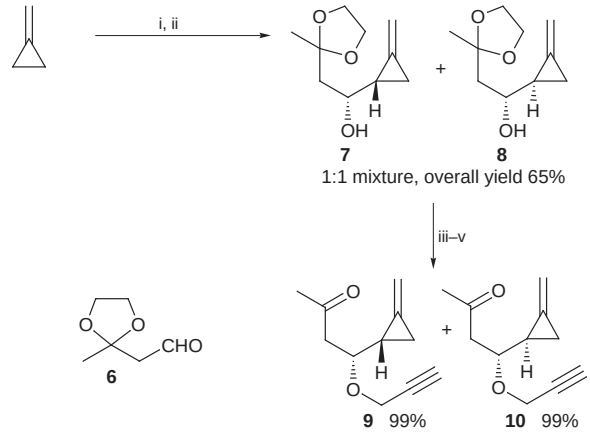

Scheme 2 *Reagents and conditions*: i, BuLi, THF, −78 °C; ii, compound **6**; iii, NaH, DMPU, THF; iv, $HC{\equiv}CCH_2Br$; v, TsOH, acetone, H_2O

Treatment of ketone **9** with SmI_2, under standard conditions[9] (slow addition of **9** to 2.2 equiv. SmI_2, Bu^tOH, HMPA, THF, 0 °C) gave the desired bicyclic products as a readily separable mixture of diastereoisomers, **11** and **12**, in 57 and 6% isolated yields respectively (ratio **11**:**12** = 10 : 1 by analysis of the ^1H NMR spectrum of the crude reaction mixture) (Table 1). In contrast, treatment of diastereoisomeric ketone **10** with SmI_2, under identical conditions, gave the bicyclic product **12** in 73% isolated yield, and only a trace of the diastereoisomer **11** (ratio **12**:**11** > 30 : 1).

In order to rationalise the observed diastereoselectivity we repeated the cyclisations under identical conditions, but replacing HMPA with the less effective chelator DMPU.[10] These cyclisation reactions gave the bicyclic products with reduced overall yields and required a larger excess of SmI_2 (~6 equiv.) for consumption of starting material.[2b] Notably, for the cyclisation of **9**, the diastereoselectivity was reduced (ratio **11**:**12** = 1.5 : 1), whereas for the cyclisation of **10** the

Table 1 Reaction of **9** or **10** with different additives

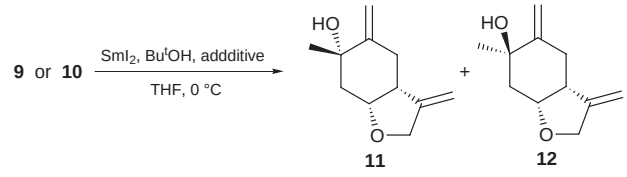

Starting material	Additive	Yield (%)	**11** : **12**
9	HMPA	63	10:1
9	DMPU	40	1.5:1
9	—	~20	1:1.3
10	HMPA	79	< 1:30
10	DMPU	62	< 1:30
10	—	0	—

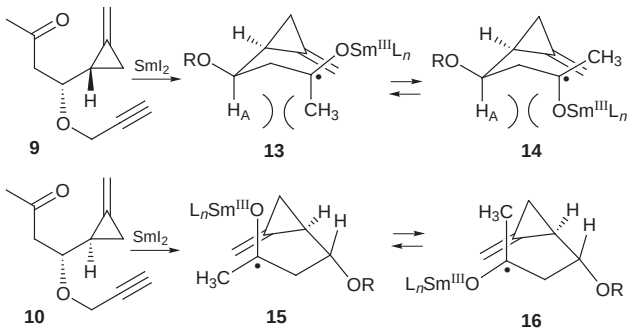

Scheme 3

diastereoselectivity was seemingly unaffected (ratio **12**:**11** > 30 : 1). In the absence of either DMPU or HMPA the cyclisation was, as expected, a poor reaction. Thus **9** gave an overall yield of ~20% of **11** and **12**, but with a reversal of stereoselectivity (ratio **11**:**12** = 1 : 1.3), while cyclisation of **10** yielded none of the desired bicyclic compounds.

The selectivity for the cyclisation of **9** in favour of **11**, in which the tertiary alcohol and ether oxygen are *cis* in the bicyclic product, might be the consequence of chelation control from the weakly basic prop-2-ynylic ether oxygen to the samarium(III) bound to the ketyl radical. However, the decrease in selectivity for the cyclisation of **9** as HMPA is replaced by the weaker chelator DMPU, and reversal of selectivity when neither is present, effectively rules out this possibility. It seems probable that the first step of the cyclisation of **9**, which effectively sets the relative stereochemistry of the product, proceeds through a chair-like transition state, allowing the prop-2-ynyl ether substitutent to adopt a pseudo-equatorial position (Scheme 3). As a consequence of the bond angles of the methylenecyclopropyl group, the alkene appears to be essentially staggered between the ketyl radical oxygen and the ketyl methyl group. Thus the preference for conformer **13** over **14** may largely result from the preference for the bulky $OSm^{III}(HMPA)_n$ moiety to also adopt a pseudo-equatorial position and avoid a 1,3-diaxial interaction with H_A. Replacement of HMPA with DMPU may effectively reduce the steric bulk of the $OSm^{III}L_n$ moiety,[10] leading to a lower selectivity for conformer **13**. In the absence of either HMPA or DMPU the ketyl methyl becomes sterically dominant, leading to a reversal in selectivity.

In contrast, the first step of the cyclisation of **10** may well proceed through a boat-like transition state, since a chair-like transition state would force the prop-2-ynyl ether substituent into a severely hindered axial orientation. In the boat-like transition state the alkene now appears to be largely eclipsed with either the ketyl methyl group (**15**) or the ketyl radical oxygen (**16**). Conformer **15** may now be preferred over **16** since it alleviates the electronic repulsion between the ketyl oxygen functionality and the alkene π-system,[11] and this preference is unaffected by replacing HMPA with DMPU.

Completion of the synthesis of paeonilactone B firstly required protection of the tertiary allylic alcohol as the triethylsilyl ether,[12] followed by oxidation of the allyl ether to the desired α-methylene lactone **17** using CrO_3 and pyridine (Scheme 4).[13] The selective oxidation of the ostensibly more electrophilic cyclohexyl alkene of **17** proved to be impossible with both alkenes reacting rapidly with ozone at −110 °C in EtOH in almost quantitative yield. Even more frustratingly, treatment of **17** with OsO_4 led to dihydroxylation of just the the α-methylene lactone, presumably due to steric congestion around the cyclohexyl alkene. Instead, base-mediated Michael addition of PhSH to **17** gave the thioether which was then successfully ozonolysed to give the desired ketone, with concomitant oxidation of the thioether to the corresponding sulfoxide **18**. Thermal elimination of phenylsulfenic acid[14] then reinstalled the α-methylene lactone and deprotection of the silyl

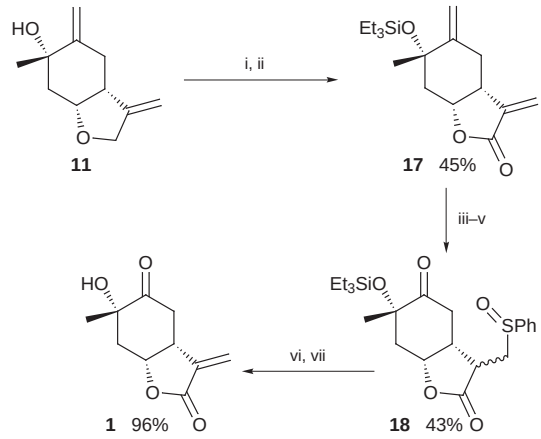

Scheme 4 *Reagents and conditions*: i, Et_3SiOTf, Et_3N, CH_2Cl_2, 0 °C; ii, CrO_3, pyridine, CH_2Cl_2, room temp.; iii, PhSH, Et_3N, MeOH; iv, O_3, MeOH, −78 °C; v, Me_2S; vi, CCl_4, reflux; vii, HF·pyridine, THF

ether was successfully achieved using pyridine·HF,[15] to give (±)-paeonilactone B, whose structure was confirmed by comparison of its NMR and IR spectroscopic data to those reported previously for the natural paeonilactone.[3]

We thank the EPSRC and Zeneca Agrochemicals for a CASE award (R. J. B.) and the EC for a TMR Fellowship (ERBCHBICT930286) (M. S.). We also thank Ms J. Street (Southampton University) and Mr M. Kipps (Zeneca Agrochemicals) for assistance with NMR studies.

Notes and References

† E-mail: jdk1@soton.ac.uk

1 M. Malacria, *Chem. Rev.*, 1996, **96**, 289.
2 (*a*) For a review on SmI_2-initiated tandem reactions, see: G. A. Molander and C. R. Harris, *Tetrahedron*, 1998, **54**, 3321. Surprisingly few cascade *radical* process initiated by SmI_2 have been reported. Two notable examples are: (*b*) T. L. Fevig, R. L. Elliott and D. P. Curran, *J. Am. Chem. Soc*., 1988, **110**, 5064; (*c*) R. A. Batey, J. D. Harling and W. B. Motherwell, *Tetrahedron*, 1996, **52**, 11 421.
3 T. Hayashi, T. Shinbo, M. Shimizu, M. Arisawa, N. Morita, M. Kimura, S. Matsuda and T. Kikuchi, *Tetrahedron Lett*., 1985, **26**, 3699.
4 For previous syntheses of paeonilactones see: M. Rönn, P. G. Andersson and J.-E. Bäckval, *Acta Chem. Scand.*, 1998, **52**, 524; S. Hatakeyama, M. Kawamura, Y. Mukugi and H. Irie, *Tetrahedron Lett.*, 1995, **36**, 267 and references cited therein.
5 For previous studies on cyclisations of methylenecyclopropylalkyl radicals see: C. Destabel, J. D. Kilburn and J. Knight, *Tetrahedron*, 1994, **38**, 11 267; M. Santagostino and J. D. Kilburn, *Tetrahedron Lett*., 1995, **36**, 1365 and references cited therein.
6 T. Oishi, M. Nagai and Y. Ban, *Tetrahedron Lett*., 1968, 491.
7 All compounds were characterised by ^1H and ^{13}C NMR and IR spectroscopy, and by HRMS or microanalysis.
8 We thank Dr M. Webster, University of Southampton, for carrying out the X-ray crystallographic analysis. Details will be published elsewhere.
9 G. A. Molander and J. A. McKie, *J. Org. Chem.*, 1995, **60**, 872.
10 For a study on the effects of HMPA and DMPU as additives in SmI_2-mediated cyclisations of unactivated olefinic ketones, see: G. A. Molander and J. A. McKie, *J. Org. Chem.*, 1992, **57**, 3132. See also ref. 2*b*.
11 Electronic repulsion between the ketyl oxygen functionality and the alkene π-system is generally accepted as being a major factor determining stereoselectivity in SmI_2-mediated cyclisations of unactivated olefinic ketones: see refs. 10 and 2(*b*).
12 C. H. Heathcock, S. D. Young, J. P. Hagen, R. Pilli and U. Badertscher, *J. Org. Chem.*, 1985, **50**, 2095.
13 T. J. Brocksom, R. B. dos Santos, N. A. Varanda and U. Brocksom, *Synth. Commun.*, 1988, **18**, 1403.
14 D. J. Cram and C. A. Kingsbury, *J. Am. Chem. Soc.*, 1960, **82**, 1810.
15 D. Boschelli, T. Takemasa, Y. Nishitani and S. Masamune, *Tetrahedron Lett.*, 1985, **26**, 5239.

Received in Glasgow, UK, 8th June 1998; 8/04297G

The reaction of ketene silyl acetals and silyl enol ethers with CCl_4 without a promoter

Michiharu Mitani*† and Hideo Sakata

Department of Chemistry and Material Engineering, Faculty of Engineering, Shinshu University, Wakasato, Nagano, 380-8553, Japan

The reaction of CCl_4 with ketene silyl acetals and silyl enol ethers in the absence of a promoter at ambient temperature or at reflux, or under photo-irradiation, was performed to form products *via* addition of the trichloromethyl group to those silyl substrates.

The reaction[1] of ketene silyl acetals or silyl enol ethers with a variety of carbon nucleophiles, including carbonyl compounds, conjugated enones or organic halides, with promotion by a Lewis acid or in the presence of a desilylative reagent, such as a fluoride compound, is well known to give α-functionalized carbonyl compounds. As with organic halides, while monohalogen compounds such as tertiary, benzyl and allyl halides afford alkylated products in the presence of a Lewis acid, *e.g.* titanium(IV) chloride,[2] zinc(II) chloride[3] or silver(I) perchlorate,[4] polyhalides such as carbon tetrachloride give β-halo-α,β-unsaturated carbonyl derivatives in the reaction catalyzed with copper(I) chloride,[5] triethylborane[6] or a Ru^{II} complex.[7] We have found that ketene silyl acetals and silyl enol ethers react with CCl_4 at ambient temperature or under reflux, or under photo-irradiation conditions, in the absence of a promoter to form products derived from addition of the trichloromethyl group to the ene moieties of those silyl substrates.

A CCl_4 solution of the ketene silyl acetal **1a**[8] from *N*,*N*-dimethylglycine methyl ester was stirred at ambient temperature for 3 h; VPC analysis of the resulting mixture revealed consumption of **1a** and the appearance of one product (Scheme 1). The product was assigned as *N*,*N*-dimethyl(trichloromethyl)glycine methyl ester **2a** *via* its spectral data after isolation (57% yield). Raising or lowering the reaction temperature resulted in the reduction of the yield of **2a** (18 and 27% at 76 and 0 °C, respectively). The ketene silyl acetal **1b**[9] from methyl methoxyacetate in a CCl_4 solution furnished the α-trichloromethyl ester **2b** in 81% yield under reflux conditions; no reaction occurred at ambient temperature. The ketene silyl acetal **1c** from methyl propionate, which lacks a strongly electron-donating substituent like the amino or alkoxy moieties in **1a** or **1b**, afforded the α-trichloromethyl ester **2c** in a good yield (81%) upon photo-irradiation,‡ while **2c** was formed in only low yield (29%) under reflux conditions. The ketene silyl acetals **1d–g** from linear or branched aliphatic esters also gave α-trichloromethylation products **2d–g** upon photo-irradiation. In the case of **1b**, however, photoreaction diminished the yield of **2b** compared with that obtained *via* thermal reaction.

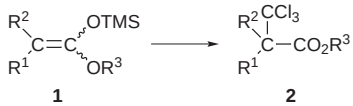

1 **2**

	R^1	R^2	R^3	*E*/*Z*
a	Me_2N	H	Me	50/50
b	MeO	H	Me	0/100
c	Me	H	Me	75/25
d	Et	H	Et	74/26
e	Bu	H	Et	60/40
f	Me	Me	Me	—
g	Bu^t	H	Et	68/32

Scheme 1

Next, the silyl enol ethers were subjected to photoreaction in CCl_4 solution. The silyl enol ethers **3a–c** derived from aliphatic aldehydes formed the aldehydes **4a–c** bearing α-trichloromethyl substituents in good yields (85, 79 and 68%, respectively) (Scheme 2). Photoreaction of the silyl enol ethers

3 **4**

	R^1	*E*/*Z*
a	Et	39/61
b	pentyl	40/60
c	hexyl	42/58

Scheme 2

derived from aliphatic ketones afforded products other than the above-mentioned ones, *i.e.* while 3-trimethylsiloxypent-2-ene **5a** and 4-trimethylsiloxyhept-3-ene **5b**, derived from unbranched ketones, gave the products **6a**,**b** *via* addition of the trichloromethyl group followed by migration of the C=C double bond while retaining the silyl group, 3,3-dimethyl-2-trimethylsiloxybut-1-ene **5c** effected the β,β-dichloro-α,β-unsaturated ketone **7** based on dehydrochlorination after addition of the trichloromethyl group (Scheme 3). These results are collected in Table 1.

Concerning the reaction mechanism, it is postulated that the trichloromethyl radical fragment from CCl_4 attacks the C=C double bond moiety of the silyl substrate to form the product. The spontaneous bond scission of CCl_4 at ambient temperature or under reflux conditions is difficult and thus the formation of **2a**,**b** may be derived from the reaction of the trichloromethyl radical generated *via* single electron transfer (SET) between CCl_4 and the ketene silyl acetals **1a**,**b** bearing strongly electron-donating substituents. Actually, in reactions using either polar (THF) or non-polar (hexane) solvents, the yields of **2a** were better in the former compared with the latter (34 and 2%,

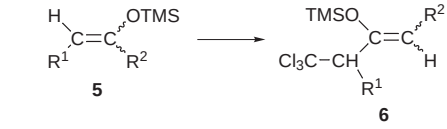

5 **6**

	R^1	R^2	*E*/*Z*
a	Me	Et	45/55
b	Et	Pr	42/58
c	H	Bu^t	

	R^1	R^2	*E*/*Z*
a	Me	Me	50/50
b	Et	Et	50/50

$Cl_2C{=}CHCOBu^t$

7

Scheme 3

Table 1 Reaction of silyl substates **1**,**3** and **5** with CCl_4

Substrate	Conditions	Product	Yield[a] (%)
1a	3 h/room temp.	**2a**	57
1a	3 h/76 °C	**2a**	18
1a	20 h/0 °C	**2a**	27
1b	3 h/76 °C	**2b**	81
1b	4 h/room temp.	**2b**	0
1b	3 h/*hν*	**2b**	65
1c	3 h/76 °C	**2c**	29
1c	1 h/*hν*	**2c**	81
1d	1 h/*hν*	**2d**	73
1e	4 h/*hν*	**2e**	62
1f	1 h/*hν*	**2f**	50
1g	1 h/*hν*	**2g**	18
3a	1 h/*hν*	**4a**	85
3b	1 h/*hν*	**4b**	79 (65)[b]
3c	1 h/*hν*	**4c**	68
5a	1 h/*hν*	**6a**	67
5b	2 h/*hν*	**6b**	61
5c	1 h/*hν*	**7**	69

[a] Determined by VPC analysis. [b] Based on TLC isolation

respectively). The reaction of the ketene silyl acetals upon photo-irradiation should also proceed *via* a SET process, as is suggested by the fact that the formation of **2c** from **1c** was enhanced by addition of $LiClO_4$[10] (Table 2). However, the homolytic scission of the C–Cl bond may preferentially operate in the case of the silyl enol ethers, judging from the fact that the formation of the trichloromethylated product **4b** from **3b** was enhanced in a non-polar solvent compared with a polar solvent (77% in hexane; 68% in THF; 51% in MeCN) and suppressed by addition of $LiClO_4$. The reaction of polyhalides other than CCl_4 with ketene silyl acetals and silyl enol ethers is under way.

Table 2 Effect of $LiClO_4$ on reaction of **1c** with CCl_4 in THF[a]

Conditions	Yield of **2c** (%)
hν/$LiClO_4$	32
hν	14
76 °C/$LiClO_4$	3
76 °C	0

[a] Conditions: **1c** (2 mmol), CCl_4 (4 mmol), $LiClO_4$ (2 mmol) and THF (5 ml), 3.5 h.

Notes and References

† E-mail: mitanim@gipwc.shinshu-u.ac.jp

‡ *Experimental procedure*: A solution consisting of **1c** (0.3200 g, 2 mmol) and CCl_4 (10 ml) was irradiated using a high pressure Hg lamp (500 W) in a quartz tube for 1 h under N_2 atmosphere and then concentrated under reduced pressure. The residue was submitted to preparative VPC.

1 For review articles,see: P. Brownbridge, *Synthesis*, 1983, 1; I. Fleming, *Chimica*, 1980, **34**, 265; T. Mukaiyama, *Angew. Chem., Int. Ed. Engl.*, 1977, **16**, 817; E. W. Colvin, *Silicon Reagents in Organic Synthesis*, Academic press, London, 1981, p. 105.

2 T. H. Chan, I. Paterson and J. Pinsonnault, *Tetrahedron Lett.*, 1977, 4183; M. T. Reetz, I. Chatziiosifidis, U. Lowe and W. F. Maier, *Chem. Ber.*, 1980, **113**, 3741.

3 M. T. Reetz, S. Huttenhain, P. Waltz and U. Lowe, *Tetrahedron Lett.*, 1980, **21**, 2010.

4 H. Takagaki, N. Yasuda, M. Asaoka and H. Takei, *Bull. Chem. Soc. Jpn.*, 1979, **52**, 1241.

5 S. Murai, Y. Kuroki, T. Aya, N. Sonoda and S. Tsutsumi, *J. Chem. Soc., Chem. Commun.*, 1972, 741; T. Okano, T. Uekawa and S. Eguchi, *Bull. Chem. Soc. Jpn.*, 1989, **62**, 2575.

6 J. Sugimoto, K. Miura, K. Oshima and K. Utimoto, *Chem. Lett.*, 1991, 1319.

7 T. Okano, T. Shimizu, K. Sumida and S. Eguchi, *J. Org. Chem.*, 1993, **58**, 5163.

8 Y. Kita, N. Shibata, T. Tohjo and N. Yoshida, *J. Chem. Soc., Perkin Trans. 1*, 1992, 1795.

9 A. Wissner, *J. Org. Chem.*, 1979, **44**, 4617.

10 M. Abe and A. Oku, *J. Org. Chem.*, 1995, **60**, 3065; E. Hasegawa, K. Isshiyama, T. Horaguchi and T. Shimizu, *J. Org. Chem.*, 1991, **56**, 1631.

Received in Cambridge, UK, 29th May 1998; 8/04028A

Three-centre dihydrogen bond with fast interchange between proton and hydride: a very active catalyst for D^+–H_2 exchange†

A. Caballero, F. A. Jalón* and B. R. Manzano

Departamento de Química Inorgánica, Orgánica y Bioquímica, Universidad de Castilla-La Mancha, Avda. Camilo José Cela, 10, 13071 Ciudad Real, Spain. E-mail: fjalon@qino-cr.uclm.es

Protonation of a ruthenium hydride containing the hemilabile ligand PPh_2py gave a complex with a three-centre dihydrogen bond (Ru–H···H–Py_2), and this system exhibits a fast proton/hydride interchange and is a very active catalyst for D^+–H_2 exchange.

The term dihydrogen bond[1] was introduced by Crabtree to designate hydrogen bonds in which the proton acceptor is the σ-electron pair of a transition metal hydride. This type of hydrogen bond has now largely been enlightened by intramolecular examples from Crabtree *et al.*[2] and Morris and coworkers,[3] or by intermolecular cases described by Crabtree and coworkers[4] in the solid state and Epstein and coworkers[5] in solution. The study of such chemical bonds is not only of academic importance, but these types of interaction may also be present in intermediates related to hydrogenation, hydrogen transfer and H–D exchange.[3] We envisaged the synthesis of Ru^{II} complexes possessing several PPh_2py ligands. The affinity of the Ru^{II} centre for phosphorus, and the predicted strain of the resulting four-membered cycles when this phosphine is chelated, anticipates its hemilabile behaviour, the easy accessibility of unsaturated species and the presence of basic pyridine groups near the Ru centre, which could operate as efficient proton abstractors from weak acids such as alcohols or hydrogen, could give rise to interesting catalytic properties. We describe the preparation of PPh_2py–ruthenium complexes including an unprecedented three-centre dihydrogen bond that has special properties.

The reaction of $RuCl_2$(bpzm)(cod) or RuClH(bpzm)(cod)[6] [bpzm = bis(pyrazol-1-yl)methane, cod = cycloocta-1,5-diene] with 3 mol equiv. of PPh_2py gives, after the appropriate work up procedure, the new complexes [RuCl(η^1-PPh_2py)(η^2-PPh_2py)$_2$]Cl **1** and RuClH(η^1-PPh_2py)$_2$(η^2-PPh_2py) **2**, respectively. Two isomers of **2** are present in solution, **2a** and **2b** (Scheme 1), and their ratio depends on the solvent and temperature. This supports the existence of an equilibrium in solution between the two species. The facial structure of **1** and **2a** and the mer for **2b** (Scheme 1) are deduced by considering characteristic J_{PP} couplings for the three observed resonances for each compound.[7] The chelating η^2 coordination of some PPh_2py groups, as proposed in Scheme 1, is supported by the characteristic upfield shift of the corresponding ^{31}P NMR signals with respect to the free phosphine ligand.[8] The hydride resonance in the ^{1}H NMR spectrum of **2a** appears at δ −7.46 and shows a distinctly higher H–P coupling constant with one phosphorus, while that of the *mer* isomer **2b** (δ −11.58) exhibits typical *cis* coupling constants to the three phosphorus centres.[7] This chemical shift is characteristic of a hydride in a *trans* disposition to an N-donor ligand,[9a] as has been found in polyphospine derivatives of Ru, and is in contrast with the values expected for analogous compounds with a Cl^- in a *trans* disposition.[9b] The cationic nature of **1** has been confirmed by conductivity measurements in acetone solution.

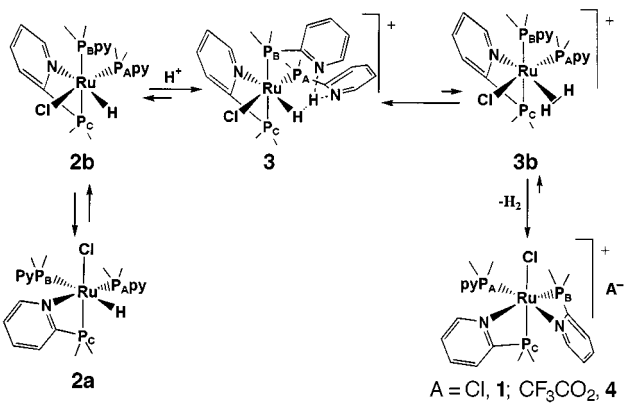

Scheme 1

In order to investigate the ability of complexes **2b** and **2a** to transfer a proton to the hydride with the formation of a dihydrogen bond, 3 equiv. of CF_3CO_2H were added to a **2b** : **2a** (7 : 2 ratio) CD_3CN solution at −40 °C. Under these conditions both isomers were transformed into a unique cationic compound: [RuClH(η^2-PPh_2py){(η^1-PPh_2py)$_2$H}]CF_3CO_2 **3** (Scheme 1). The identical integration of the hydride and proton resonances of **3** indicates that only one proton has been transferred from CF_3CO_2H. The signal of the newly introduced proton was strongly shifted downfield and appeared at δ *ca.* 20. Such a strongly deshielded resonance has been ascribed to acidic protons in very fast exchange between two basic centres.[9a,10] Consequently, this proton must be in fast exchange between the pyridine fragments of the two monodentate phosphines. The resonance of the surplus acid proton appeared separately at δ *ca.* 5. The chemical shifts of the hydride and phosphorus atoms of **3** were only slightly modified with respect to **2b**[7] and therefore the relative disposition of the ligands must be similar in these two complexes. On raising the temperature, both the pyridinium proton and hydride resonances of **3** broadened. The enormous chemical shift difference between the exchanging resonances (> 9000 Hz) prevented the observation of the coalescence. However, kinetic parameters can be calculated by lineshape analysis in the temperature range below the coalescence. This study was undertaken in $(CD_3)_2CO$ (−90 to −10 °C), which allows lower temperatures than CD_3CN. An E_a value of 13.6 ± 2.7 kcal mol^{-1} was obtained (A = 3.8 × 10^{14}). The exchange between the hydride and the pyridinium proton was also confirmed by spin saturation transfer. The irradiation of the hydride resonance of **3** reduced the pyridinium proton integral by *ca.* 50% at −40 °C. Above room temperature, both in $(CD_3)_2CO$ or CD_3CN solution, H_2 was lost and a new product, [RuCl(η^1-PPh_2py)(η^2-PPh_2py)$_2$]CF_3CO_2 **4** (Scheme 1) was formed with an identical structure to **1**, as deduced from its ^{31}P NMR spectrum.[7]

In order to show the existence of a dihydrogen bond in **3**, the T_1(min) of the hydride group both for **2b** and **3** was determined (300 MHz). CD_2Cl_2 was used as the solvent in order to prevent the possible participation of basic or protic solvents in the relaxation rate of the pyridinium proton and, indirectly, over the exchanging hydride. An addition of exactly 1 equiv. of CF_3CO_2H was performed in order to avoid the relaxation rate average with free protons. Under these conditions, the hydride

of **2b** shows a T_1(min) of 217 ms at −35 °C, whereas the T_1(min) for both the hydride and pyridinium proton of **3** is 85 ms at −20 °C. In the latter complex the T_1 values determined are identical for the pyridinium proton and the hydride over the temperature range studied (−90 to −10 °C). This must be a consequence of the observed exchange between these two protons. We have considered that the excess of the hydride relaxation in **3**, as compared to **2b**, is due to the Ru–H···H–py dipole–dipole interaction. In this relaxation the two ^{14}N pyridinium atoms must also participate because the proton, which is bonded to these two groups, is exchanging with the hydride with a half-life of 0.5, according to the aforementioned magnetization transfer experience. The contribution for each ^{14}N has been estimated to be 1.85 s^{-1}.[11] Hence, the relaxation rate due exclusively to the dipole–dipole interaction with the pyridinium proton is deduced to be 5.30 s^{-1}. Using Morris' approximation,[12] a d_{HH} = 1.70 Å has been calculated, a value that is in the range for a dihydrogen bond and demonstrates its existence in **3**.

Although the phenomenon has been previously described,[2b] the proton–hydride exchange already discussed for a dihydrogen bond is very rare, and Crabtree has postulated the participation of non-classical species as intermediates. Neither Crabtree nor our group have detected this intermediate in solution (**3b** in Scheme 1). However, Chaudret and coworkers[13] have recently reported some examples where an intermolecular exchange between coordinated molecular dihydrogen and weak acid protons has been observed.

The loss of H_2 near room temperature shows the lability of the proposed non-classical species **3b** and this opens up the possibility of interchange with free H_2. Besides, the heterolytic cleavage of an H_2 molecule coordinated in this hypothetical complex would be possible considering the observed higher basicity of the pyridine centres with respect to the hydride in **2**. These two characteristics point to a possible activity of **2** toward D^+–H_2 exchange in protic deuterated solvents.

As a consequence of this possibility, H_2 (1 atm) was introduced at room temperature in a sealed NMR tube in contact with a solution of **2** in CD_3OD as a deuteron source. The evolution of the mixture was monitored by ^{1}H NMR spectroscopy during several hours. The change with time of the relative concentration of H_2 and HD observed in this way is depicted in Fig. 1. The relative concentration of D_2 was calculated accepting the constant concentration of the total dihydrogen isotopomers in solution. According to these results, a very efficient catalyst for D^+–H_2 exchange was present in solution. After 33 min, > 90% of H_2 was transformed. In 18 min the HD concentration reached its maximum and afterwards decreased as a consequence of D_2 formation. An increase in the residual CD_3OD OH signal, and not that of the CHD_2 group, was concomitantly observed. **2a** was the major isomer observed in solution and, surprisingly, during the experience the intensity of the hydride signal due to **2a** was scarcely reduced. Only after 7 days did this signal disappear and [$^2H_1$] **2a** was formed. However, very small signals for **2b** were detected at room temperature (**2a** : **2b** = 30 : 1, 20 °C) before the addition of H_2, and these disappeared instantaneously when the gas was present. Therefore, we propose that, although only small amounts of **2b** are present, this is the efficient catalyst for the process. This example shows a dramatic relationship between structure and reactivity.

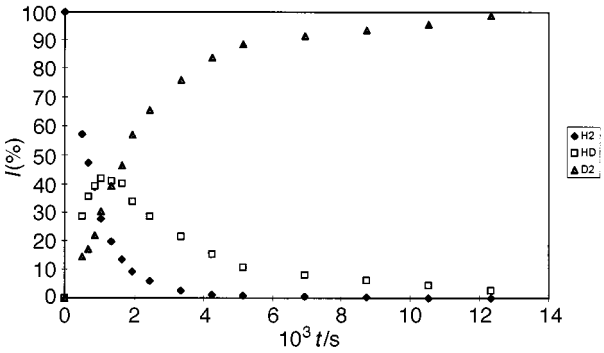

Fig. 1 Relative intensities of the NMR signals of the dihydrogen isotopomers *vs.* time in the D^+–H_2 exchange experiment with **2** CD_3OH; (◆) H_2, (□) HD, (▲) D_2

In conclusion, we present an example where the addition of a proton to the ruthenium monohydrides **2b** and **2a** forms a dihydrogen bond of three centres, and this system shows a fast exchange between the proton and hydride moieties. **2b**, and not **2a**, is extremely active in D^+–H_2 interchange processes. Experiments to assess the catalytic properties of these types of compounds in hydrogen transfer processes are in progress.

We thank to the Dirección General de Investigación Científica y Ténica for financial support (Grant PB95-0901).

Notes and References

† Dedicated to Professor Pascual Royo on his 60th birthday.

1 T. B. Richardson, S. de Gala and R. H. Crabtree, *J. Am. Chem. Soc.*, 1995, **117**, 12 875.

2 (*a*) R. H. Crabtree, P. E. M. Siegbahn, O. Eisentein, A. Rheingold and T. F. Koetzle, *Acc. Chem. Res.*, 1996, **29**, 348 and references therein; (*b*) J. C. Lee, Jr., E. Peris, A. L. Rheingold and R. H. Crabtree, *J. Am. Chem. Soc.*, 1994, **116**, 11014; (*c*) E. Peris, J. Wessel, B. P. Patel and R. H. Crabtree, *J. Chem. Soc., Chem. Commun.*, 1995, 2175; (*d*) W. Yao and R. H. Crabtree, *Inorg. Chem.*, 1996, **35**, 3007.

3 S. Park, A. J. Lough and R. H. Morris, *Inorg. Chem.*, 1996, **35**, 3001 and ref. 2 therein.

4 J. Wessel, J. C. Lee, Jr., E. Peris, G. P. A. Yap, J. B. Fortin, J. S. Ricci, G. Sini, A. Albinati, T. F. Koetzle, O. Eisenstein, A. L. Rheinglod and R. H. Crabtree, *Angew. Chem., Int. Ed. Engl.*, 1995, **34**, 2507; B. P. Patel, W. Yao, G. P. A. Yap, A. L. Rheinglod and R. H. Crabtree, *Chem. Commun.*, 1996, 991.

5 E. S. Shubina, N. V. Belkova, A. N. Krylov, E. V. Vorontsov, L. M. Epstein, D. G. Gusev, M. Niedermann and H. Berke, *J. Am. Chem. Soc.*, 1996, **118**, 1105.

6 M. Fajardo, A. de la Hoz, E. Díez-Barra, F. A. Jalón, A. Otero, A. Rodríguez, J. Tejeda, D. Belletti, M. Lafranchi and A. A. Pellinghelli, *J. Chem. Soc., Dalton Trans.*, 1993, 1937.

7 NMR data (δ, *J* Hz, ^{1}H NMR, ref. TMS; ^{31}P{^{1}H} NMR, ref. 85% H_3PO_4, room temp. unless specified). **1**: $\delta_H(CDCl_3)$, 7–8 (m, 42H, PPh_2py). $\delta_P(CDCl_3)$, 47.10 (dd, $^2J_{PP}$ 33.6, 27.4, P_A), −7.9 (t, $^2J_{PP}$ 27.5, P_B or P_C), −6.35 (dd, $^2J_{PP}$ 33.6, 26.9, P_C or P_B). **2b**: $\delta_H(CD_3CN)$, 7–8 (m, 42H, PPh_2Py), −11.58 (dt, 1H, J_{HP} 26.2, 21.6, Ru–H). **2a**: $\delta_H(CD_3CN)$, 7–8 (m, 42H, PPh_2py), −7.46 (ddd, J_{HP} 115.2, 27.8, 21.8, Ru–H). **2b**: $\delta_P(CD_3CN)$, 69.38 (br, s), 55.53 (dd, J_{PP} 277, 24.4, P_B), −15.05 (br, d J_{PP} 277, P_C). **2a** $\delta_P(CD_3CN)$ 69.28 (br, s P_A), 8.74 (dd, J_{PP} 36.6, 12.8, P_B), −15.13 (br, s P_C). **3**: $\delta_H(CD_3CN, -40\ °C)$, 20 (br, s 1H, pyH), 7–8 (m, 42H, PPh_2Py), −11.85 (dt, 1H, Ru–H). $\delta_P(CD_3CN, -40\ °C)$, 77.55 (qnt, J_{PP} 30.5, P_A), 52.22 (dd, J_{PP} 278.3, 29.9, P_B), −24.33 (dd, J_{PP} 278.3, 32.4, P_C). **4**: δ_H (CD_3CN, 60 °C): 7–8 (m, 42H, PPh_2Py). $\delta_P(CD_3CN, 60\ °C)$, 48.09 (t, J_{PP} 32.4, P_A), −3.96 (t, J_{PP} 27.5, P_B or P_C), −8.96 (t, J_{PP} 32.9, P_C or P_B).

8 G. R. Newkome, *Chem. Rev.*, 1993, **93**, 2067 and references therein.

9 (*a*) M. L. Christ, S. Sabo-Etienne, G. Chung and B. Chaudret, *Inorg. Chem.*, 1994, **33**, 5316; (*b*) K. S. MacFarlane, A. M. Joshi, S. J. Rettig and B. R. James, *Chem. Commun.*, 1997, 1363.

10 S. N. Smirnov, R. S. Golnbev, G. S. Demisov, H. Benedict, P. Schah-Mohamendi and H.-H. Limbach, *J. Am. Chem. Soc.*, 1996, **118**, 4094; F. Carrillo-Hermosilla, F. A. Jalón, A. Otero and E. Villaseñor, *An. Quím. Int. Ed.*, 1996, **92**, 339; K. Wozniak, H.-H. He, J. Klinowski, T. L. Barr and S. E. Hardcastle, *J. Phys. Chem.*, 1996, **100**, 11 408.

11 P. J. Desrosier, L. Cai, Z. Lin, R. Richards and I. Halpern, *J. Am. Chem. Soc.*, 1991, **113**, 173.

12 K. A. Earl, G. Ja, P. A. Maltby and R. H. Morris, *J. Am. Chem. Soc.*, 1991, **113**, 3027.

13 J. A. Ayllón, C. Gervaux, S. Sabo-Etienne and B. Chaudret, *Organometallics*, 1997, **16**, 2000; Y. Guari, J. A. Ayllón, S. Sabo-Etienne, B. Chaudret and B. Hessen, *Inorg. Chem.*, 1998, **37**, 640.

Received in Basel, Switzerland, 27th May 1998; 8/03972K

Synthesis and structure of pure SiO_2 chabazite: the SiO_2 polymorph with the lowest framework density

María-José Díaz-Cabañas, Philip A. Barrett and Miguel A. Camblor*

Instituto de Tecnología Química, Avda. Los Naranjos s/n, 46071 Valencia, Spain. E-mail: macamblo@itq.upv.es

A SiO_2 material with the lowest framework density (15.4 SiO_2 nm^{-3}) and the largest void volume fraction (nearly 50%) ever reported for crystalline silica polymorphs has been synthesised, and its structure solved by direct methods and fully refined using low-resolution powder X-ray diffraction data.

The synthesis of pure silica polymorphs of decreasing density is a scientific challenge which may result in potential applications, including adsorption and separation of organic molecules but also storage of gases such as H_2 and CH_4. Compared to zeolites of the same structure type pure silica polymorphs may in principle offer (1) a larger void space owing to the absence of counter cations in their pores, (2) distinct adsorption properties, characterised by their extreme hydrophobicity,[1] and (3) a far superior thermal stability. Recent calorimetric measurements[2] and theoretical calculations[3] have shown that the enthalpy of formation relative to quartz is very small and increases only slightly with the decreasing framework density (FD, the number of $SiO_{4/2}$ tetrahedra per nm^3). This suggests the synthesis of low-density materials is not thermodynamically hindered and new phases (though normally considered as still metastable with respect to quartz) could be obtained through a kinetic control of the synthesis process. Actually, the synthesis of microporous SiO_2 polymorphs involves a two-step process: the synthesis of a host–guest compound in the presence of a suitable (normally organic) structure-directing agent (SDA), and its calcination to remove the guest organics. Apparently, the use of SDAs affords the required kinetic pathway and/or the additional stabilisation energy that makes the synthesis feasible. However, until recently only silica phases with a relatively high framework density (above 17 $SiO_{4/2}$ nm^{-3}) have been obtained. We have recently found that a modification of a known method for the synthesis of pure silica materials offers new opportunities for decreasing the framework density of the phases obtained.[4] We illustrate here the success of this strategy which has now afforded the synthesis of a new pure silica polymorph isostructural with zeolite chabazite having the lowest ever reported framework density amongst these materials, 15.4 SiO_2 nm^{-3} (14.6 T nm^{-3} for the type material, structure code CHA).[5]

Pure silica chabazite was synthesised hydrothermally using *N*,*N*,*N*-trimethyladamantammonium (TMAda$^+$) in hydroxide form as the structure-directing agent at near to neutral pH in the presence of fluoride. In a typical synthesis 13.00 g of tetraethylorthosilicate were hydrolysed in 31.18 g of a 1.0 M TMAdaOH aqueous solution and the mixture was stirred to allow the ethanol and water to evaporate to a final H_2O/SiO_2 molar ratio of 3.0. Then, 1.33 g of HF (aq., 46.9%) were added and the mixture, which was homogenised by hand, was transferred to Teflon lined stainless steel 60 ml autoclaves. The autoclaves were heated at 150 °C whilst rotated at 60 rpm. After 40 h crystallisation time (pH = 8.5) the solid product was collected, washed and dried, and recognised as chabazite by powder X-ray diffraction (XRD). Its chemical analysis indicates a composition close to $[C_{13}H_{24}NF_{0.5}]_3[Si_{36}O_{72}(OH)_{1.5}]$ [Anal. Found: C, 17.49; H, 2.98; N, 1.56; F, 1.06. The above composition requires: C, 16.78; H, 2.60; N, 1.51; F, 1.02%]. A charge imbalance between F$^-$ and TMAda$^+$ suggests the presence of connectivity defects in this material (see below), and to maintain electrical neutrality we have included 1.5 OH$^-$ per uc in the above idealised composition.

It is interesting that an aluminosilicate isostructural to chabazite (denoted as SSZ-13) may be prepared using the same structure-directing agent in OH$^-$ medium.[6] However, it appears that in the absence of F$^-$ in alkaline medium aluminium is needed for the synthesis of SSZ-13 to succeed.[6] From our experience in OH$^-$ medium using TMAda$^+$ as the structure directing agent an increase in the Si/Al ratio above 50 favours the crystallisation of either ITQ-1[7] or SSZ-23 (depending on the alkali metal cation present) while higher aluminium contents favours SSZ-13 with the CHA topology.[8]

Thermogravimetric analysis in air (10 °C min^{-1}) shows no weight losses below 260 °C, suggesting no water is occluded as a guest in this material, as expected for a pure silica host. The organics and fluorine are removed in the range 300–650 °C through two overlapping exothermic processes (the first centred at 450 °C). Calcination at 580 °C for 3 h is required to prepare the pure silica host, whose adsorption capacity is exceptionally high. From N_2 adsorption experiments at 77 K a micropore volume of 0.30 cm g^{-1} (calculated by the *t*-plot method or by the amount of adsorbed N_2 at any relative pressure between 0.1 and 0.9), a surface area of 602 m^2 g^{-1} (BET method) and a micropore area of 594 m^2 g^{-1} were calculated. The micropore volume of silica chabazite is by far the largest ever reported for a crystalline pure silica polymorph and exceeds by over 30% those of the beta, ITQ-3 and ITQ-4 materials (0.22, 0.23 and 0.22 cm^3 g^{-1} respectively). The void volume fraction of silica Chabazite is almost 50% (0.46 cm^3 cm^{-3}).

The ^{29}Si MAS NMR spectrum of calcined pure silica CHA (Fig. 1) shows two bands at δ −101.4 and −111.4. The first is assigned to $Si(OSi)_3OH$ defect groups and the second to $Si(OSi)_4$ species. Their relative intensities allow us to quantify the amount of defects in pure silica CHA and shows that an appropriate formulation for this material is $[Si_{36}O_{70.5}(OH)_{2.9}]$. The number of defect groups is relatively small compared to silica materials synthesised in OH$^-$ medium, where the Si–OH concentration is typically about four times larger than the

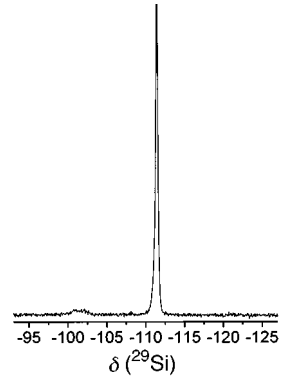

Fig. 1 ^{29}Si MAS NMR spectrum of calcined pure silica chabazite (reference $SiMe_4$ = 0)

Table 1 Data collection and crystallographic parameters for calcined pure silica chabazite

Wavelength		Cu-Kα (graphite monochromated)
Profile range (2θ/°)		5–100
Step size/°		0.01
Step count time/s		2 (5–40° 2θ); 4 (40–100° 2θ)
Number of data points		7740
Number of reflections		609
Profile range used (2θ/°)		22–100
Number of profile parameters		8
Number of structural parameters		14
Number of constraints		0
Unit cell	a/Å	13.52923(8)
	c/Å	14.74828(13)
Space group		$R\bar{3}m$ (no. 166)
Residuals	R_{exp}	7.76
	R_p	8.66
	R_{wp}	11.18
	χ^2	2.083
	R_b	3.96

Table 2 Fractional coordinates and thermal parameters from Rietveld refinement of the pure silica chabasite with esds in parentheses

Atom	x	y	z	U_{ISO}/Å^2
Si(1)	0.22862(10)	0.00002(12)	0.10389(7)	0.0313(7)
O(1)	0.11978(11)	−0.11978(11)	0.12991(18)	0.0308(11)
O(2)	0.33333	0.01978(20)	0.16667	0.0315(10)
O(3)	0.19744(24)	0.09872(12)	0.12173(21)	0.0354(10)
O(4)	0.26344(19)	0	0	0.0335(10)

amount of occluded cations[9] (this would lead in this case to over 30% Si–OH defects with respect to total Si sites). However, it is noticeable that this defect concentration is much larger than expected for a silica material synthesised at near neutral pH in the presence of fluoride.[10] In view of a plausible control of the defect concentration by the synthesis pH and the pK_a of the condensing silicate species,[11] we have tried to reduce the defect concentration of this material by further decreasing the synthesis pH, but with no success. We are currently trying to understand the unexpected behaviour of this system.

The *Si*$(OSi)_4$ resonance in Fig. 1 is noticeable because of its sharpness (26 Hz), which is probably due to a combination of the absence of Al substitution for Si, the presence of a single Si site in the structure (see below) and the relatively low concentration of defects. We have calculated an average Si–O–Si angle of 148.4° for CHA by applying the equation of Thomas *et al.*[12] to the chemical shift of the *Si*$(OSi)_4$ resonance. This is in excellent agreement with the value obtained by Rietveld refinement (148.0°, see below).

Powder X-ray diffraction (XRD) techniques were used to examine the new pure silica Chabazite material. Laboratory Cu-Kα XRD data were recorded on a freshly calcined sample of the title compound. Inspection of the diffraction pattern and refinement of the unit cell parameters taken from Smith *et al.*[13] verified the phase purity and rhombohedral symmetry (space group $R\bar{3}m$). The high crystallinity of the material after calcination enabled the structure to be solved routinely by direct methods in the program Sirpow[14] using Le Bail[15] extracted intensities from the Mprofil[16] program suite. Subsequent Rietveld[17] refinement of the model produced from direct methods was undertaken in the program GSAS[18] using a manually interpolated background together with a pseudo-Voigt[19] function to describe the peak shape. The refinement proceeded smoothly with no constraints used. The crystallographic data are summarised in Table 1, the final atomic positions in Table 2 with the final Rietveld plot depicted in Fig. 2. The average Si–O bond length (1.603 Å) and average O–Si–O and Si–O–Si angles (109.47 and 148.0°, respectively) are in excellent accord with those expected for zeolite materials. These refinement results clearly verify the formation of a highly crystalline chabazitic material.

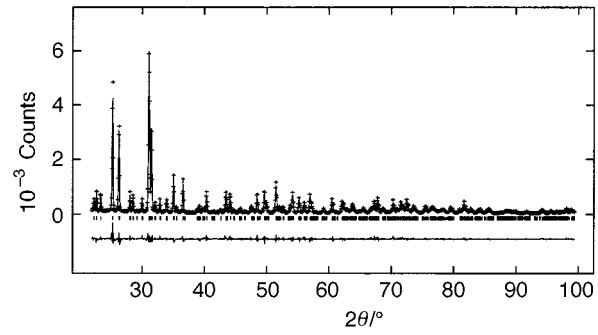

Fig. 2 Rietveld plot for the title compound, observed (+), calculated (solid line) and the difference (lower trace). The tick marks represent the positions of allowed reflections.

The authors greatly acknowledge financial support by the Spanish CICYT (project MAT97-0723). P. A. B. is grateful to the European Union for a postdoctoral fellowship.

Notes and References

1 T. Blasco, M. A. Camblor, A. Corma, P. Esteve, J. M. Guil, A. Martínez, J. A. Perdigón-Melón and S. Valencia, *J. Phys. Chem. A*, 1998, **102**, 75.
2 I. Petrovic, A. Navrotsky, M. E. Davis and S. I. Zones, *Chem. Mater.*, 1993, **5**, 1805.
3 N. J. Henson, A. K. Cheetham and J. D. Gale, *Chem. Mater.*, 1994, **6**, 1647.
4 M. A. Camblor, A. Corma and S. Valencia, *Chem. Commun.*, 1996, 2365; M. A. Camblor, A. Corma and L. A. Villaescusa, *Chem. Commun.*, 1997, 749; M. A. Camblor, A. Corma, P. Lightfoot, L. A. Villaescusa and P. A. Wright, *Angew. Chem., Int. Ed. Engl.*, 1997, **36**, 2659.
5 W. M. Meier, D. H. Olson and Ch. Baerlocher, *Atlas of Zeolite Structure Types*, Elsevier, Amsterdam, 4th edn., 1996.
6 S. I. Zones, R. A. Van Nordstrand, D. S. Santilli, D. M. Wilson, L. Yuen and L. D. Scampavia, *Stud. Surf. Sci. Catal.*, 1989, **49**, 299.
7 M. A. Camblor, C. Corell, A. Corma, M. J. Díaz-Cabañas, S. Nicolopoulos, J. M. González-Calbet and M. Vallet-Regí, *Chem. Mater.*, 1996, **8**, 2415; M. A. Camblor, A. Corma, M. J. Díaz-Cabañas and Ch. Baerlocher, *J.Phys. Chem. B*, 1998, **102**, 44.
8 C. Corell, Ph.D. Thesis, Universidad Politénica de Valencia, 1997.
9 H. Koller, R. F. Lobo, S. L. Burkett and M. E. Davis, *J. Phys. Chem.*, 1995, **99**, 12 588.
10 J. M. Chezeau, L. Delmotte, J. L. Guth and M. Soulard, *Zeolites*, 1989, **9**, 78.
11 P. A. Barrett, M. A. Camblor, A. Corma, R. H. Jones and L. A. Villaescusa, *J. Phys. Chem.*, 1998, **102**, 4147.
12 J. M. Thomas, J. Klinowski, S. Ramdas, B. K. Hunter and D. T. B. Tennakoon, *Chem. Phys. Lett.*, 1983, **102**, 158.
13 L. J. Smith, A. Davidson and A. K. Cheetham, *Catal. Lett.*, 1997, **49**, 142.
14 A. Atomare, C. Burla, C. Cascarano, C. Cascarino, C. Giacovazzo, A. Gualiardi, G. Polidori and R. M. Canalli, *J. Appl. Crystallogr.*, 1994, **27**, 435.
15 A. Le Bail, *Mater. Res. Bull.*, 1988, **23**, 447.
16 A. D. Murray and A. N. Fitch, Mprofil program for Le Bail decomposition and profile refinement, 1990.
17 H. M. Rietveld, *J. Appl. Crystallogr.*, 1969, **2**, 65.
18 A. Larson and R. B. Von Dreele, GSAS Manual, Los Alamos Report No. LA-UR-86-748, 1986.
19 J. B. Hastings, W. Thomlinson and D. E. Cox, *J. Appl. Crystallogr.*, 1984, **17**, 85.

Received in Bath, UK, 20th June 1998; 8/04800B

Supramolecular self-assembling in mesostructured materials through charge tuning in the inorganic phase

Manuel Roca, Jamal El Haskouri, Saúl Cabrera, Aurelio Beltrán-Porter, Jaime Alamo, Daniel Beltrán-Porter, M. Dolores Marcos* and Pedro Amorós*

Institut de Ciència dels Materials de la Universitat de València (ICMUV), Dr. Moliner 50, 46100-Burjassot (València), Spain. E-mail: loles.marcos@uv.es and pedro.amoros@uv.os

Supramolecular self-assembling of organic CTA^+ micelles and inorganic $[VO(H_2O)PO_4]_n^{q-}$ 2D-anions for the isolation of hexagonal mesostructured materials can be reached by charge tuning in the inorganic phase through the adjustment of the vanadium mean oxidation state.

When researchers of the Mobil company reported the discovery of new mesoporous silica based materials denoted MCM-41,[1] the scientific community imagination was newly stimulated and a large amount of related work was published in a very short time.[2] Originally, the synthesis of mesoporous silica materials was related to a liquid-crystal templating mechanism in which surfactant micelles act as supramolecular templates. However, for low surfactant concentrations another model based on the cooperative organisation of inorganic and organic molecular species has been developed. In that case, the most important point in the synthesis of a mesostructured solid is charge density matching at the organic–inorganic interface.[3]

Although much work has been reported on the influence that variation of surfactant characteristics has in the isolation of mesoporous materials,[4] very little has been done regarding the inorganic counterpart. In contrast with silica based materials, other metal oxides show, in general, shorter progression of their hydrolysis and condensation reactions and hence strong limiting problems related with charge matching at the interface appear. In this sense we present here, to the best of our knowledge for the first time, the possibility of controlling the formation of mesostructured solids by tuning the charge density at the inorganic phase through the adjustment of the metal oxidation state in a mixed-valence system.

We have succeeded in the preparation of mesostructured mixed-valence oxovanadium phosphates with different $V^{IV}:V^{V}$ content (ICMUV-2 materials) using CTAB (cetyltrimethylammonium bromide) as a surfactant directing agent in water. A constant $V:H_3PO_4:CTAB:H_2O$ molar ratio of $1:5:0.1:150$ was always used in the starting reactants and the $V^{IV}:V^{V}$ content was adjusted in a continuous way by adding variable amounts of H_2O_2.

Owing to the complexity of the $V–H_3PO_4–CTAB–H_2O$ system our approach has been based on the independent consideration of the organic and inorganic species present in the mother-liquor. Regarding the organic subsystem, we have used low surfactant concentration to favour a cooperative mechanism in which the charge density matching at the interface must be the leading force to the supramolecular organisation for the preparation of ICMUV-2 solids.

In relation to the inorganic moieties, we have carried out our synthesis at very low pH value since under this condition the oxovanadium cations are present as isolated aqua cations[5] and, in the presence of oxophosphorus anions ($H_2PO_4^-$ at the working pH), should lead to successive hydrolysis and condensation reactions which would lead to the formation of the $[VO(H_2O)PO_4]_n^{q-}$ two-dimensional anions.[6] Supramolecular assembling between organic and inorganic species into a mesostructured solid will take place when the charge density of the inorganic moieties matches with that of CTA^+ micelles. We have calculated an approximate charge density at the rod-like micelles surface of $q = +0.014$ e Å^{-2} presuming a hexagonal close packing of surfactant head groups at the micelle surface and using the micelle diameter (37.5 Å) and the van der Waals radius of the head groups (4.5 Å).[7] From this value and taking into account the bond topology of the $[VO(H_2O)PO_4]_n^{q-}$ moieties,[6] the $V^{IV}:V^{V}$ molar ratio which matches the surfactant micelles charge should be $0.54:0.46$. According to this simple calculation we have experimentally found that it is only possible to obtain hexagonal mesostructured solids when the $V^{IV}:V^{V}$ molar ratio lies between $0.20:0.80$ (sample 1) and $0.61:0.39$ (sample 4), the most crystalline solids being those for which the $V^{IV}:V^{V}$ molar ratio has a value around unity ($0.54:0.46$; sample 3) (see Fig. 1). The existence of a $V^{IV}:V^{V}$ range in which charge density matching must somehow occur, is consistent with the ability of the micelle to change its molecular packing and in this way to accommodate its charge density at the surface to the inorganic phase charge. Hence, the highest crystallinity must correspond to the solid with the most ordered micelles, *i.e.* that with close packing of surfactant head groups at the surface. Also, the $V^{IV}:V^{V}$ matching range can be extended to a greater degree below the best calculated value of 0.54 than above since the micelle can easily adopt a looser packing but not a closer one.

In a typical sample preparation, an aqueous suspension (50 ml) containing V metal (0.226 g, 4.44 mmol), V_2O_5 (1.617 g,

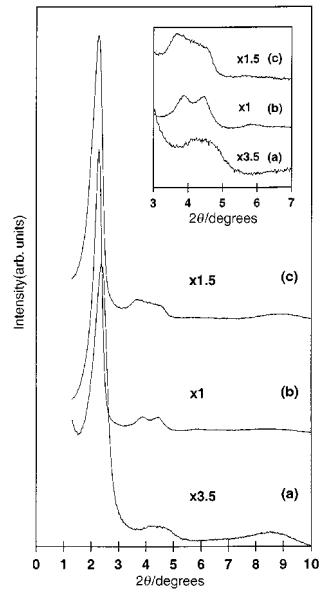

Fig. 1 X-Ray powder diffraction patterns of ICMUV-2 materials having different $V^{IV}:V^{V}$ molar ratios and CTA^+ content; (a) sample 1, (b) sample 3, (c) sample 4

Table 1 Selected synthetic and compositional parameters for ICMUV-2 solids: $[CTA]_x[(V^{IV}O)_y(V^{V}O)_{1-y}PO_4]\cdot zH_2O$

Sample	V^{IV} in solution %	y	x	z
1	35	0.20	0.20	2.01
2	55	0.33	0.33	1.41
3	60	0.54	0.53	1.01
4	85	0.61	0.60	0.65

8.88 mmol) and 7.6 ml of 85% H_3PO_4 was refluxed until complete dissolution. Amounts of V metal and V_2O_5 were adjusted in order to obtain a V^{IV} starting solution and the $V^{IV}:V^{V}$ ratio in the solution was then adjusted by controlled addition of H_2O_2. Subsequently, a 10 ml aqueous solution of CTAB (0.81 g) was added. After stirring for 1 h at room temperature the ICMUV-2 solid was isolated by filtration. Although ICMUV-2 solids can be prepared with slightly higher CTAB concentration (up to $CTAB:H_2O = 0.3:150$) the surfactant concentration used here allows us to obtain the most ordered solids. Table 1 summarises the main synthesis variables and compositional data of selected ICMUV-2 materials. Vanadium oxidation states in the solids were determined by atomic absorption and a redox titration procedure. All the samples were analyzed and characterized by X-ray powder diffraction (Seifert 3000TT diffractometer using Cu-Kα radiation in steps of 0.02° (2θ) for 10 s per step) and TEM on a Philips CM10 instrument operated at 120 kV. Fig. 1 shows the XRD patterns of selected ICMUV-2 materials. Although differences in crystallinity can be observed among solids with different composition, all of them present a similar regular hexagonal array according to TEM analysis and Fig. 2 shows a representative TEM image.

Previously to this work, it was reported the preparation of solids in the V–O–P system which consisted of mixtures of amorphous vanadium and phosphorus oxides[8,9] with a $V:P = 2:1$ molar ratio rather than a genuine vanadyl phosphate. However, in order to obtain an adequate $(VO)_2P_2O_7$ catalyst precursor it is necessary to maintain a $V:P = 1$ molar ratio.[10] In our experiences neither vanadium(V) starting solutions (zero global charged ($[VOPO_4]_n^0$) species, $S^+X^-I^0$ mechanism) nor vanadium(IV) ones ($[VOPO_4]_n^-$ species, S^+I^- mechanism) allowed us to synthesize any kind of solid, only when we reached the necessary charge density matching at the organic-inorganic interface by adjustment of the $V^{IV}:V^{V}$ molar ratio were mesostructured solids obtained. Hence, instead of randomly varying the charge density at the organic phase employed up to now, our approach has allowed us not only a wider range of charge variation when comparing with possible variations offered by changing surfactant characteristics, but a continuous modulation of the charge density at the inorganic phase from $q = 0$ to $q = -1$ per vanadium atom.

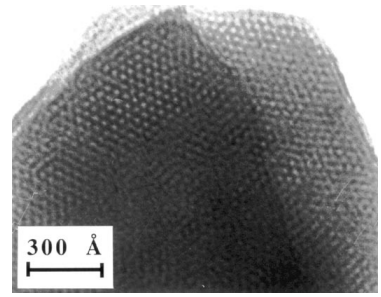

Fig. 2 Representative TEM micrograph of the mesostructured ICMUV-2 materials corresponding to sample 3

The approach reported here suggests that it should be possible to design synthetic strategies for the preparation of hexagonal mesostructured/mesoporous materials for inorganic systems in which different accessible oxidation states are possible for the metallic centre by the simple adjustment of the charge at the inorganic framework.

This work was supported by DGES under grant PB95-1094. J. E. H. and S. C. thank the A.E.C.I. for doctoral grants.

Notes and References

1 C. T. Kresge, M. E. Leonowicz, W. J. Roth, J. C. Vartuli and J. S. Beck, *Nature*, 1992, **359**, 710.
2 A. Corma, *Chem. Rev.*, 1997, **97**, 2373.
3 G. S. Attard, J. C. Glyde and C. G. Göltner, *Nature*, 1995, **378**, 366.
4 S. Manne, T. E. Schäffer, Q. Huo, P. K. Hansma, D. E. Morse, G. D. Stucky and I. A. Aksay, *Langmuir*, 1997, **13**, 6382.
5 C. F. Baes and R. E. Mesmer, *The Hydrolysis of Cations*, John Wiley and Sons, New York, 1976.
6 M. Roca, M. D. Marcos, P. Amorós, J. Alamo, A. Beltrán-Porter and D. Beltrán-Porter, *Inorg. Chem.*, 1997, **36**, 3414.
7 G. G. Warr, R. Sen, D. F. Evans and J. E. Trend, *J. Phys. Chem.*, 1988, **92**, 774.
8 T. Abe, A. Taguchi and M. Iwamoto, *Chem. Mater.*, 1995, **7**, 1429.
9 T. Doi and T. Miyake, *Chem. Commun.*, 1996, 1635.
10 G. Centi, *Catal. Today*, 1993, **16**, 5.

Received in Bath, UK, 14th May 1998; 8/03896A

Carboxylation of methane with CO or CO_2 in aqueous solution catalysed by vanadium complexes

Galina V. Nizova,[a] Georg Süss-Fink,*[b] Sandrine Stanislas[b] and Georgiy B. Shul'pin*[a]

[a] *Semenov Institute of Chemical Physics, Russian Academy of Sciences, ul. Kosygina 4, Moscow 117977, Russia. E-mail: Shulpin@chph.ras.ru*

[b] *Institut de Chimie, Université de Neuchâtel, Avenue de Bellevaux 51, CH-2000, Neuchâtel, Switzerland. E-mail: Georg.Suess-Fink@ich.unine.ch*

Reaction of methane with CO or CO_2 in aqueous solution in the presence of O_2 (catalysed by $NaVO_3$) or H_2O_2 (catalysed by $NaVO_3$–pyrazine-2-carboxylic acid) at 25–100 °C affords acetic acid and in some cases also methanol, methyl hydroperoxide and formaldehyde.

The direct conversion of methane, the least reactive representative of the very inert saturated hydrocarbon family, into valuable chemical products under mild conditions is a challenging problem of metal complex catalysis.[1] A very small number of publications have appeared that describe the homogeneous carboxylation of methane in the absence[2a] or in the presence[2b–e] of soluble metal compounds (see also recent works on theoretical study of carbonylation[3a] and carboxylation with the participation of solid metals[3b]).

We have found that heating an aqueous solution of sodium vanadate in the presence of methane, carbon monoxide and air gives rise to the formation of acetic acid, as well as, in smaller amounts, of methanol and formaldehyde (Table 1).† The yield of acetic acid attains 3700% based on vanadium after 50 h at 100 °C, the total turnover number being 49. In the absence of either V^V or CH_4, no products have been detected. When a larger concentration of vanadate (1.0×10^{-3} mol dm^{-3}) was used, in the absence of air, only 0.2×10^{-3} mol dm^{-3} of $MeCO_2H$ was formed after 16 h at 100 °C. While in the course of the reaction with air the solution remains pale yellow, in the case when air is absent the colour of the solution becomes blue indicating the formation of a V^{IV} derivative. Thus it can be concluded that atmospheric oxygen is capable of reoxidizing the V^{IV} species formed in the reaction between methane, VO_3^- and CO. The yield of acetic acid and its relative content in the mixture of the products increases with the increase of partial CO pressure (Table 2). A comparison to Sen's catalytic system ($RhCl_3$/KI), which gives 790% of acetic acid (based on Rh) after 20 h at 80 °C,[2e] shows that the inexpensive sodium vanadate is more active giving a yield of 3300% of acetic acid (based on V) after 25 h at 100 °C.

Table 1 Carboxylation of methane by carbon monoxide in the presence of air catalysed by $NaVO_3$ in aqueous solution[a]

		Products (concentration/10^3 mol dm^{-3})		
T/°C	*t*/h	$MeCO_2H$	MeOH	HCHO
80	5	0.3	0.2	0.03
	15	0.6	0.4	0.1
	25	1.0	0.6	0.5
100	6	2.0	0.9	0.6
	25	3.3	1.1	1.0
	50	3.7	1.9	1.2

[a] Conditions, see Footnote †. Pressures and concentrations: CH_4, 50 bar; CO, 15 bar; synthetic air, 15 bar; $NaVO_3$, 1.0×10^{-4} mol dm^{-3}; initial pH = 7.30.

Hydrogen peroxide can be used instead of molecular oxygen as reoxidizing agent in the carboxylation using pyrazine-2-carboxylic acid (PCA)[4] as a co-catalyst; no products are detected in the absence of PCA. In this case the selectivity of the reaction depends strongly on temperature and CO pressure (Table 3),‡ the carboxylation at room temperature and relatively high CO pressure yielding acetic acid as a sole product. The initial rate of acetic acid accumulation depends linearly on the initial pressure of methane (when this pressure < 50 bar) and on initial concentration of hydrogen peroxide (when $[H_2O_2] < 0.1$ mol dm^{-3}). The role of PCA in aqueous solution is not completely clear; on the basis of preliminary investigations we can assume that PCA stabilises an active vanadium peroxo species, while the protons from PCA simultaneously facilitate the substitution of coordinated water ligands by H_2O_2 in the coordination sphere of vanadium. The reaction of ethane (20 bar) with CO (5 bar) and H_2O_2 (0.1 mol dm^{-3}) in the presence of $NaVO_3$ (1.0×10^{-4} mol dm^{-3}) gave after 2 h at 40 °C propionic acid (3.0×10^{-4} mol dm^{-3}) and acetic acid (3.3×10^{-3} mol dm^{-3}).

Interestingly, the carboxylation of methane also occurs, when carbon dioxide is used instead of carbon monoxide. Under the conditions described in Table 3, the yield of acetic acid is 2000% based on vanadium after 30 h at 40 °C; methanol was also observed (10^{-4} mol dm^{-3}). No acetic acid can be detected, when the reaction was carried out in the absence of either CH_4 or CO_2.

We believe that the reaction involves hydrogen atom abstraction from methane by a radical or radical-like species. In the case of hydrogen peroxide as an oxidising agent, this species could be a hydroxyl radical or vanadium peroxo complex.[4] The vanadate anion (like permanganate or chromate ions) can also add hydrogen from an alkane to one of oxygen atoms reducing V^V into V^{IV}.[5] The methyl radicals thus formed will react[6] with CO to give the radicals RCO$^\bullet$ and then, after interaction with O_2, produce the radicals RCOOO$^\bullet$ and peroxyacetic acid. If carbon dioxide is used as carboxylating reagent, in the first stage CO_2 is apparently reduced into CO by methyl or/and hydroxyl

Table 2 Carboxylation of methane by carbon monoxide in the presence of air catalysed by $NaVO_3$ in phosphate aqueous buffer solution at various pressures of CO[a]

	Products (concentration/10^3 mol dm^{-3})		
Pressure CO/bar	$MeCO_2H$	MeOH	HCHO
5	0.0	1.3	0.1
10	0.2	1.4	0.3
15	0.4	1.4	0.3
30	0.5	0.6	0.1

[a] Conditions, see Footnote †. Pressures and concentrations: CH_4, 50 bar; synthetic air, 15 bar; $NaVO_3$, 1.0×10^{-4} mol dm^{-3}; pH = 7.01 constant in the course of the reaction; 100 °C; 15 h.

Table 3 Carboxylation of methane by carbon monoxide in the presence of H_2O_2 catalysed by $NaVO_3$ and PCA in aqueous solution[a]

Pressure CO/bar	*T*/ °C	*t*/h	Products (concentration/10^3 mol dm^{-3})	
			$MeCO_2H$	MeOOH
5	25	2	0.9	0.0
		8	1.1	0.0
		16	1.3	0.0
		48	1.6	0.0
	40	2	1.1	0.8
		4	1.3	1.4
		8	1.7	1.7
		16	1.8	2.1
		48	1.9	2.6
	60	2	0.4	0.9
		4	0.5	1.6
		7	0.5	2.3
		16	0.5	2.8
30	25	2	0.4	0.0
		4	0.7	0.0
		8	0.9	0.0
		16	1.1	0.0
		50	1.6	0.0
	40	2	0.5	0.0
		4	0.8	0.0
		8	1.2	0.0
		16	1.4	0.0
		50	2.2	0.0

[a] Conditions, see Footnote ‡. Pressures and concentrations: CH_4, 50 bar; H_2O_2, 0.1 mol dm^{-3}; $NaVO_3$, 1.0×10^{-4} mol dm^{-3}; PCA, 4.0×10^{-4} mol dm^{-3}. Value 0.0 means below detection limit (0.5×10^{-4} mol dm^{-3}).

radicals (dry CO_2 reforming of methane in the presence of solid catalyst at high temperatures is well-known process[7]).

We thank BASF, the Russian Basic Research Foundation, and the Swiss National Science Foundation for support. Authors are indebted to Dr Arthur Höhn, Dr Michael Slany (BASF AG, Ludwigshafen, Germany) and Dr Yuriy N. Kozlov (Institute of Chemical Physics, Moscow) for fruitful discussions.

Notes and References

† The oxidations were carried out in a stainless steel autoclave with intensive stirring (volume of the reaction solution = 30 ml and total volume of autoclave = 100 ml). The autoclave was charged with synthetic air (78% N_2, 21% O_2, 1% Ar), and consecutively with carbon monoxide and methane to the appropriate pressures. The reactions were stopped by cooling with ice, and the reaction solution was analysed for $MeCO_2H$ and MeOH by GC (DANI-86.10; fused silica capillary column 25 m × 0.32 mm × 0.25 μm, CP-WAX52CB; integrator SP-4400), as well as by GC–MS (NERMAG R 30-10, capillary column 25 m × 0.32 mm × 0.25 μm, CP-WAX52CB) and ^{1}H NMR (Varian spectrometer, 200 MHz; in D_2O; in this case GC–MS analysis testified partial H–D exchange in methyl groups of $MeCO_2H$ and MeOH formed). The concentration of formaldehyde was measured spectrophotometrically after its transformation into 2,6-dimethyl-3,5-diacetyl-1,4-dihydropyridine as described previously.[4b]

‡ The reaction was carried out in a glass tube placed into the stainless steel autoclave (100 ml, volume of the solution = 10 ml). (**CAUTION**: the combination of air and H_2O_2 with organic compounds at elevated pressures and temperatures may be explosive!). The resulting solution was analysed by GC (the concentration of MeOOH was measured as concentration of MeOH after reduction of the solution with sodium tetrahydroborate[4]), as well as by GC–MS and ^{1}H NMR.

1 Recent reviews: A. E. Shilov and G. B. Shul'pin, *Chem. Rev.*, 1997, **97**, 2879; Y. Fujiwara, K. Takaki and Y. Taniguchi, *Synlett*, 1996, 591; R. H. Crabtree, *Chem. Rev.*, 1995, **95**, 987. Recent original papers: R. A. Periana, D. J. Taube, E. R. Evitt, D. G. Löffler, P. R. Wentrcek, G. Voss and T. Masuda, *Science*, 1993, **259**, 340; A. Sen, M. A. Benvenuto, M. Lin, A. C. Hutson and N. Basickes, *J. Am. Chem. Soc.*, 1994, **116**, 998; Y. Taniguchi, S. Horie, K. Takaki and Y. Fujiwara, *J. Organomet. Chem.*, 1995, **504**, 137; N. Basickes, T. E. Hogan and A. Sen, *J. Am. Chem. Soc.*, 1996, **118**, 13111; M. Lin, T. Hogan and A. Sen, *J. Am. Chem. Soc.*, 1997, **119**, 6048; N. Mizuno, H. Ishige, Y. Seki, M. Misono, D.-J. Suh, W. Han and T. Kudo, *Chem. Commun.*, 1997, 1295; B. M. Weckhuysen, D. Wang, M. P. Rosynek and J. H. Lunsford, *Angew. Chem., Int. Ed. Engl.*, 1997, **36**, 2374; S. Naito, T. Karaki and T. Iritani, *Chem. Lett.*, 1997, 877; K. Okabe, K. Sayama, H. Kusama and H. Arakawa, *Chem. Lett.*, 1997, 457; Q. Zhang and K. Otsuka, *Chem. Lett.*, 1997, 363; M. Ohmae, K. Miyaji, N. Azuma, K. Takeishi, Y. Morioka, A. Ueno, H. Ohfune, H. Hayashi and Y. Udagawa, *Chem. Lett.*, 1997, 31; T. Kodama, T. Shimizu, A. Aoki and Y. Kitayama, *Energy Fuels*, 1997, **11**, 1257; S. H. Bauer, S. Javanovic, C.-L. Yu and H.-Z. Cheng, *Energy Fuels*, 1997, **11**, 1204; H. Handa, T. Baba and Y. Ono, *J. Chem. Soc., Faraday Trans.*, 1998, **94**, 451; K. Wada, M. Nakashita, A. Yamamoto and T. Mitsudo, *Chem. Commun.*, 1998, 133; N. Muradov, *Energy Fuels*, 1998, **12**, 41.

2 (*a*) M. Lin and A. Sen, *J. Chem. Soc., Chem. Commun.*, 1992, 892; (*b*) T. Nishiguchi, K. Nakata, K. Takaki and Y. Fujiwara, *Chem. Lett.*, 1992, 1141; (*c*) K. Nakata, Y. Yamaoka, T. Miyata, Y. Taniguchi, K. Takaki and Y. Fujiwara, *J. Organomet. Chem.*, 1994, **473**, 329; (*d*) M. Kurioka, K. Nakata, T. Jintoku, Y. Taniguchi, K. Takaki and Y. Fujiwara, *Chem. Lett.*, 1995, 244; (*e*) M. Lin and A. Sen, *Nature*, 1994, **368**, 613; (*f*) M. Lin, T. E. Hogan and A. Sen, *J. Am. Chem. Soc.*, 1996, **118**, 4574.

3 (*a*) P. Margl, T. Ziegler and P. E. Blöchl, *J. Am. Chem. Soc.*, 1996, **118**, 5412; (*b*) H.-J. Freund, J. Wambach, O. Seiferth and B. Dillmann, *Ger. Pat.* DE 44 28 566 C1 (to Hoechst A.G.) 1995.

4 G. B. Shul'pin, D. Attanasio and L. Suber, *J. Catal.*, 1993, **142**, 147; G. V. Nizova and G. B. Shul'pin, *Russ. Chem. Bull.*, 1994, **43**, 1146; G. B. Shul'pin, M. C. Guerreiro and U. Schuchardt, *Tetrahedron*, 1996, **52**, 13 051; G. V. Nizova, G. Süss-Fink and G. B. Shul'pin, *Chem. Commun.*, 1997, 397; *Tetrahedron*, 1997, **53**, 3603; G. Süss-Fink, G. V. Nizova, S. Stanislas and G. B. Shul'pin, *J. Mol. Catal. A*, 1998, **130**, 163.

5 M. M. Kats and G. B. Shul'pin, *Bull. Acad. Sci. USSR, Div. Chem. Sci.*, 1990, **39**, 2233.

6 K. Nagahara, I. Ryu, N. Kambe, M. Komatsu and N. Sonoda, *J. Org. Chem.*, 1995, **60**, 7384; A. P. E. York, J. B. Claridge, A. J. Brungs, S. C. Tsang and M. L. H. Green, *Chem. Commun.*, 1997, 39; J. H. Bitter, K. Seshan and J. A. Lercher, *J. Catal.*, 1997, **171**, 279; Y. Lu, J. Xue, Y. Liu and S. Shen, *Chem. Lett.*, 1997, 515; U. Olsbye, T. Wurzel and L. Mleczko, *Ind. Eng. Chem. Res.*, 1997, **36**, 5180; M. C. J. Bradford and M. A. Vannice, *J. Catal.*, 1998, **173**, 157.

Received in Cambridge, UK, 22nd June 1998; 8/04699I

Synthesis and molecular structure of the first tetranuclear copper(I) silylphosphido cluster $[Cu(CyPSiMe_2PHCy)]_4$

Markus Faulhaber, Matthias Driess*† and Klaus Merz

Lehrstuhl für Anorganische Chemie I, Ruhr-Universität, Universitätsstr. 150, D-44801 Bochum, Germany

The reaction of *N*,*N*-diethylamino(cyclohexylphosphino)dimethylsilane 1 with the benzene solvate of copper(I) trifluoromethylsulfonate furnishes the title complex 2, which has been structurally characterized by X-ray diffraction; the same product results on conversion of bis(cyclohexylphosphino)dimethylsilane 3 with copper(I) trifluoromethylsulfonate in the presence of lithium diisopropylamide as an auxilliary base.

Secondary phosphido anions $[RRP]^-$ are of considerable interest as ligands in the coordination chemistry of transition metals and clusters thereof.[1] Such complexes are also attractive as soft nucleophilic transphosphination reagents for selective synthesis of functionalized phosphane ligands. This has recently been shown for oligomeric copper(I) phosphido complexes.[2] Hitherto knowledge of the structural chemistry and the structure–reactivity relationship of copper phosphido aggregates has been relatively scarce and a silylphosphido cluster has not been described. A convenient method for the preparation of phosphido bridged transition metal complexes and clusters is the electrophilic cleavage of Si–P bonds in silylphosphanes through the corresponding metal halides and alkoxides.[3] However, we recently reported on the template synthesis of the first hexaphosphahexasilacyclododecane by the reaction of a triphosphatrisilacyclohexane with copper(I) or silver(I) trifluoromethylsulfonate, where the building up of new Si–P bonds instead of cleavage was observed.[4] In order to extend this building up method for the preparation of acyclic silylphosphane and −phosphido chelate ligands, we are exploring the reactivity of Si-functionalized silylphosphanes toward coin metal(I) complexes.

Here we report on two preparation routes to the first tetranuclear copper(I) silyl phosphido complex **2** (Fig. 1), containing the $[CyPHSiMe_2CyP]^-$ ligand, and we describe its molecular structure which was elucidated by single-crystal X-ray diffraction.

While it was anticipated that the P–H bond in a secondary silylphosphane of the type R_3Si–PH–R would be metalated by copper(I) trifluoromethylsulfonate ([CuOTf]), surprisingly, transphosphination–silylation reactions were observed, leading to a Cu^I silylphosphidophosphane aggregate. Hence the *N*,*N*-diethylamino(cyclohexylphosphino)dimethylsilane **1** reacts with the benzene solvate of [CuOTf] in toluene to give **2** in the form of dark red crystals in 75% yield (Scheme 1).

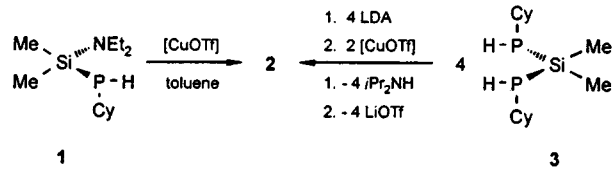

1 3

Scheme 1

Compound **1** (colourless liquid, $bp_{0.01Torr}$ = 85 °C) is readily accessible *via* a procedure analogous to that for the synthesis of *N*,*N*-diethylamino(methylphosphino)dimethylsilane.[5] The reaction mechanism for the formation of **2** is unknown, but we suggest the stepwise process as outlined in Scheme 2.

Apparently, the first step is the electrophilic cleavage of the Si–P bond in **1** to give the corresponding copper phosphide as intermediate and the corresponding silyl(amino)triflate. The copper phosphide intermediate could then co-ordinate another molecule of **1** and subsequent replacement of the NEt_2 group leads to the PSiP chelate moiety in the co-ordination sphere of the Cu^I centre. Compound **2** (Fig. 2) is also accessible starting from bis(cyclohexylphosphino)dimethylsilane **3** and [CuOTf] in the presence of LDA (lithium diisopropylamide) as base in 70% yield. Compound **3** was prepared through phosphination of dimethyldichlorosilane with $LiAl(PHCy)_4$ (Cy = cyclohexyl).[5] The composition of **2** was confirmed by elemental analysis. As expected, the ^{1}H NMR spectrum of **2** shows two signals at δ 0.3 and 0.4 for the diastereomeric methyl groups of the $SiMe_2$ moiety. The cyclohexyl groups exhibit unresolved multiplets between δ 0.7 and 2.9, and the signal of the chemically equivalent P–H protons is observed as a doublet at δ 3.7 ($^1J_{PH}$ = 267 Hz). The ^{31}P NMR spectrum of **2** shows multiplets at δ −100 and −72, which are relatively broad due to the quadrupole moment of the $^{63/65}$Cu nuclei (I = 3/2) . The P–H stretching vibration is observed in the IR spectrum at 2290 cm^{-1}.

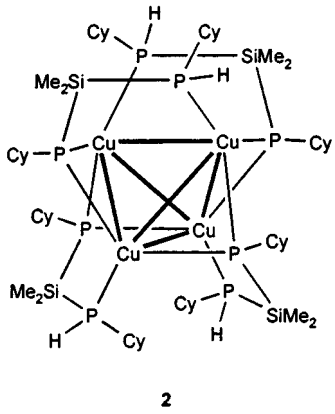

2

Fig. 1 Chelated cluster **2**

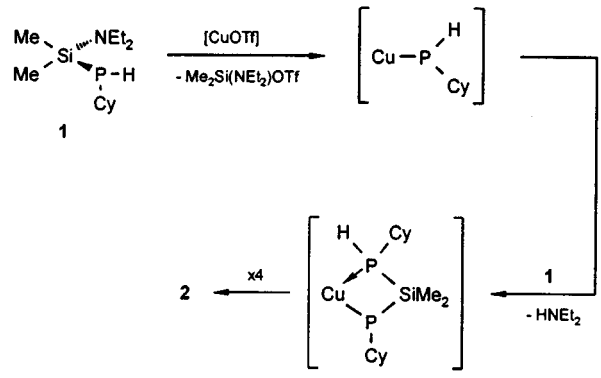

Scheme 2

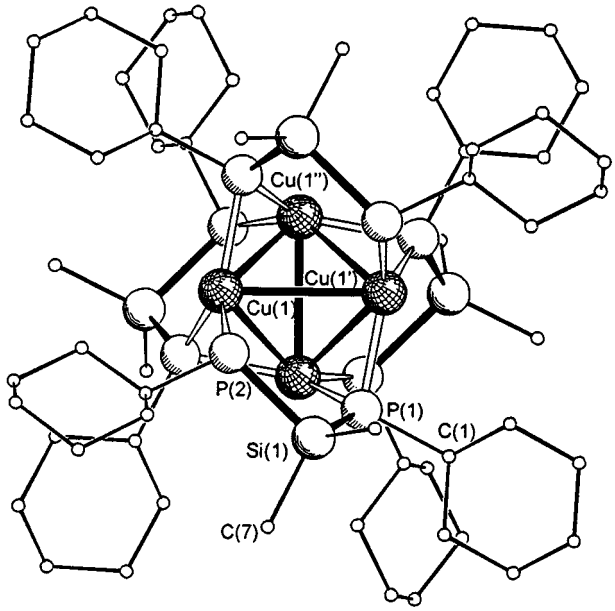

Fig. 2 Molecular structure of **2**. Hydrogen atoms omitted for clarity. Selected distances (Å) and angles (°): P(1)–Si(1) 2.207(5), P(2)–Si(1) 2.263(5), P(1)–C(1) 1.882(9), Si(1)–C(7) 1.890(11), P(2)–Cu(1) 2.261(4), P(1)–Cu(1) 2.270(3), P(1)–Cu(1") 2.235(4), Cu(1)–Cu(1) 3.071(3), Cu(1)–Cu(1") 2.911(2); P(1)–Si(1)–P(2) 98.7(2), Cu(1)–P(1)–Cu(1") 80.5(1), Cu(1")–Cu(1)–Cu(1") 63.67(6).

The X-ray crystallographic analysis‡ proves that **2** exists as a discrete tetramer and its core consists of a distorted Cu_4 tetrahedron. The latter is the result of the chelate property of the ($CyPSiMe_2PHCy$) ligand and, at the same time, of 'metallophilic' dispersion-type interactions between the co-ordinatively unsaturated Cu^I centres. Each phosphane-like P atom is only bonded to one Cu centre while the phosphido-like P atoms are μ_2-co-ordinated. Therefore, two of the six edges of the Cu_4 tetrahedron are not bridged by phosphorus. Accordingly, each Cu center has six neighbouring atoms, three of which are copper and three are phosphorus. The Cu–Cu distances are different: those for the four edges bridged by phosphorus (2.91 Å) are about 0.16 Å shorter than for the two unbridged edges (3.07 Å) of the Cu_4 tetrahedron. Other compounds containing cluster cores of four or more Cu atoms have also been reported. For example, the tetrameric compound $Cu_4I_4[As(C_2H_5)_3]_4$[6] and others with sulfur and nitrogen ligands[7,8] possess a tetrahedral core of Cu^I centres. A structurally related Cu_4 cluster to **2** was reported, where O,O-diisopropyldithiophosphate coordinates *via* η^1 and μ_2 sulfur centres to the Cu centres of the Cu_4 tetrahedron. The Cu–Cu distances in the latter are shorter (2.74 Å for the bridged and 2.95 Å for the unbridged edges of the tetrahedron) than in **2**. The Cu–Cu and Cu–P distances in **2** are within the range observed in other phosphido bridged Cu clusters.[2,7] According to the different co-ordination modes of the phosphino and the phosphido P centres of the ligands, the Si–P distances are not identical: the Si(1)–P(1) distance of the μ_2-coordinating phosphido group (2.207 Å) is about 0.5 Å shorter than the Si(2)–P(1) bond of the η^1-coordinating P atom. The present results underline the value of silylphosphanes for the synthesis of new oligophosphane ligands in the co-ordination sphere of Cu^I centres.

Notes and References

† E-mail: driess@ibm.anch.ruhr-uni-bochum.de

‡ *Crystal data* for **2**: $C_{56}H_{112}Cu_4P_8Si_8$, M = 1399.7, tetragonal, space group $I4_1/a$, a = 23.952(6), c = 12.799(4) Å, U = 7342 Å^3, Z = 4, intensity data were collected on a Siemens P4 diffractometer (Mo-Kα radiation, λ = 0.71707 Å, ω-scan, T = 203 K), $2\theta_{max}$ = 45°, 2381 measured reflections, 164 parameters, μ = 1.414 mm^{-1} $R1$ = 0.070 for 921 observed reflections {$I > 2\sigma(I)$, $wR2$ = 0.206 (all reflections, wR2 = $[\Sigma w(F_o^2 - F_c^2)^2/\Sigma(wF_o^4)]^{-}$}. The structure was solved by direct methods and refined by full-matrix least squares using SHELXL-93.[9] All non-hydrogen atoms were refined using anisotropic thermal parameters; hydrogen atoms were included by use of a riding model and fixed isotropic thermal parameters. CCDC 182/926.

1 A. J. Carty, S. A. McLaughlin and D. Nucciarone, in *Phosphorous-31 NMR Spectroscopy in Stereochemical Analysis*, ed. J. G. Verkade and L. D. Quin, Verlag Chemie, Weinheim, 1987, p. 559.
2 A. H. Cowley, D. M. Giolando, R. A. Jones, C. M. Nunn and J. M. Power, *J. Chem. Soc., Chem. Commun.*, 1988, 208; C. Meyer, H. Grützmacher and H. Pritzkow, *Angew. Chem., Int. Ed. Engl.*, 1997, **36**, 2471.
3 D. Fenske, in *Clusters and Colloids—From Theory to Applications*, ed. G. Schmid, Verlag Chemie, Weinheim, 1994, p. 219; D. J. Brauer, G. Hessler, P. C. Knüppel and O. Stelzer, *Inorg. Chem*., 1990, **29**, 2370.
4 M. Driess, M. Faulhaber and H. Pritzkow, *Angew. Chem., Int. Ed. Engl.*, 1997, **36**, 1892.
5 L. D. Balashova, A. B. Bruker and L. Z. Soborovskii, *J. Gen. Chem. USSR*, 1966, **36**, 76.
6 A. F. Wells, *Z. Kristallogr., Kristallgeom., Kristallphys., Kristallchem.*, 1936, **94**, 447.
7 V. Schramm, *Inorg. Chem.*, 1978, **17**, 714; C. L. Raston and A. H. White, *J. Chem. Soc., Dalton Trans.*, 1976, 2153; J. R. Nicholson, I. L. Abrahams, W. Clegg and C. D. Garner, *Inorg. Chem*., 1985, **24**, 1092; M. Driess, S. Martin, K. Merz, H. Pritzkow, V. Pintchouk, H. Grützmacher and M. Kaupp, *Angew. Chem., Int. Ed. Engl.*, 1997, **9**, 1894.
8 S. L. Lawton, W. J. Rohrbaugh and G. T. Kokotailo, *Inorg. Chem.*, 1972, **11**, 612.
9 G. M. Sheldrick, SHELXL-93, A Program for Crystal Structure Refinement, University of Göttingen, 1990.

Received in Basel, Switzerland, 6th May 1998; 8/03394C

Palladium-catalysed reaction of aryl bromides with metallocenes to produce pentaarylated cyclopentadienes

Masahiro Miura,*[a]† Sommai Pivsa-Art,[a] Gerald Dyker,*[b]‡ Jörg Heiermann,[b] Tetsuya Satoh[a] and Masakatsu Nomura[a]

[a] *Department of Applied Chemistry, Faculty of Engineering, Osaka University, Suita, Osaka 565-0871, Japan*
[b] *Fachbereich 6, Organische/Metallorganische Chemie der Gerhard-Mercator-Universität-GH Duisburg, Lotharstrasse 1, D-47084 Duisburg, Germany*

Aryl bromides can efficiently react with some metallocenes, typically zirconocene dichloride, in the presence of a palladium/phosphine catalyst system and an appropriate base to produce the corresponding pentaarylated cyclopentadienes.

Palladium-catalysed coupling reactions of aryl halides with alkenes, alkynes and organometallic species are now recognized to be highly useful and are widely employed for the preparation of substituted aromatic compounds.[1] It has been recently shown that intermolecular arylation of certain aromatic substrates, such as acenaphthylene,[2a–c] azulene[2a] and 2-phenylphenols,[3a] and a number of five-membered heteroaromatic substrates, including indoles,[4a] furans,[2b,4b] thiophenes[3b,4b] and azoles,[3b,4c] *i.e.* imidazole, oxazole and thiazole derivatives, with aryl halides can also proceed under palladium catalysis without the stoichiometric metalation of the aromatic compounds. In our investigation into the arylation of metallocenes as five-membered aromatic substrates, we observed an unprecedented reaction in which aryl bromides can efficiently react with some of them to produce the corresponding pentaarylated cyclopentadienes in good yields (Schemes 1 and 2), which is reported herein. Note that pentaphenylcyclopentadiene as well as cyclopentadienes having other bulky substituents are known to form stable complexes with various metals, and the synthesis and properties of the complexes have been the subjects of intense study.[5] Recently, the pentaphenyl compound was applied as a ligand of an iron-containing asymmetric catalyst[6] and also as a component of electroluminescent devices.[7] Thus, new, effective methods for the synthesis of its derivatives appear to be of widespread interest. However, only a limited number of the methods have been so far reported.[8–11]

The catalytic reaction was first examined using bromobenzene **1a** (6 mmol) and a number of metallocenes **2** (0.5 mmol) in the presence of $Pd(OAc)_2$ (0.125 mmol), PPh_3 (0.5 mmol), and Cs_2CO_3 (6 mmol) in DMF at 130 °C for 6 h (Scheme 1). From the reaction was obtained pentaphenylcyclopentadiene **3** as the major product; the reaction efficiency was found to be a marked function of the identity of metallocenes: The yields of **3** using **2a**–**e** (M = Fe, Co, Ni, $TiCl_2$, $ZrCl_2$) were < 1, 23, 62, 64 and 70% (based on the cyclopentadiene moiety, *i.e.* 1 mmol = 100%), respectively. Thallium cyclopentadienide was only as effective as **2b**. It should be noted that the use of

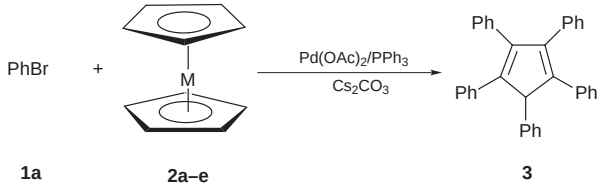

1a **2a–e** **3**

2a: M = Fe, **2b**: M = Co, **2c**: M = Ni, **2d**: M = $TiCl_2$, **2e**: M = $ZrCl_2$

Scheme 1

iodobenzene and K_2CO_3 in place of **1a** and Cs_2CO_3, respectively, in the reaction with **2c** significantly reduced the product yield, giving biphenyl as the major product. Analysis of the reaction mixture with **2c** or **2e** after a reaction time of 3 h by GLC–MS confirmed the formation of tri- and tetra-phenylcyclopentadienes together with **3** in comparable amounts, while the peaks of the tri- and tetra-substituted compounds disappeared after 6 h. From the reaction with **2e** using reduced amounts of **1a** (3 mmol) and of palladium acetate (0.0125 mmol) for 20 h, the intermediary products could also be isolated and identified to be 1,2,4-triphenyl- (21%) and 1,2,3,4-tetraphenylcyclopenta-1,3-diene (9%). These results suggest that phenylpalladium species generated in the medium can react with **2c** or **2e** effectively in the initial stages of the reaction, and the cyclopentadienyl moiety is further phenylated in a stepwise manner to the end product **3**.

When the reaction using 4-fluorobromobenzene **1b** in place of **1a** was carried out, contamination by phenyl groups from PPh_3 in the product was observed.[12] Therefore, the applicability of $Pd(OAc)_2/P(o\text{-Tol})_3$ and $Pd_2(\mu\text{-OAc})_2/(P\text{-}C)_2$ [P-C = $o\text{-}CH_2C_6H_4P(o\text{-Tol})_2$], which would avoid the scrambling of aryl moieties,[12] was examined for the reaction of **1a** with **2e**. The latter complex has recently been proven to be an efficient catalyst for the Heck reaction.[12] However, the use of these catalyst systems considerably retarded the reaction and it could not be completed. Consequently, the reaction of **1b** with **2e** was carried out using $P(4\text{-}FC_6H_4)_3$ as ligand. As expected, the corresponding product **4** could be cleanly isolated, although the yield was only moderate (Scheme 2 and Table 1).

One of the possible ways to promote the reaction could be the use of relatively more basic and sterically hindered phosphines.[13,14] It was found that PBu^t_3 can considerably enhance the reaction of **1a** and **2e**: the reaction was completed within 3 h to give **3** in an isolated yield of 77%. Furthermore, in the reactions of **1b** and 4-methyl-, 4-methoxy-, and 3-methylbromobenzenes **1c–e** using PBu^t_3, no incorporation of *tert*-butyl groups in the products was detected, giving the expected compounds **4**–**7**§ in fair to good isolated yields. The use of this phosphine was essential for the reaction of **1d** to take place. Remarkably, under the optimized conditions the amount of palladium catalyst can be reduced to 0.0125 mmol (0.25 mol% per transferred aryl group) while still achieving an acceptable isolated yield of **5** (60%).

In the reaction of a relatively bulky bromide, 2,5-dimethylbromobenzene **1f**, with **2e**, however, PPh_3 afforded a considerably better yield of product **8**§ (70%) compared with PBu^t_3 (31%). While the analysis of **8** obtained using PPh_3 by MS indicated contamination with $C_5H(Ph)(2,5\text{-}Me_2C_6H_3)_4$ (8%), fortunately the purity could be increased to 98% *via* a single recrystallization from MeOH–C_6H_6. The formation of **8** is of special interest, since it should be sterically very crowded. Compound **8** was found to consist of at least six rotamers at room temperature: its ^1H NMR showed six obvious methine proton peaks (three minor ones at δ 4.85, 5.07 and 5.25 and

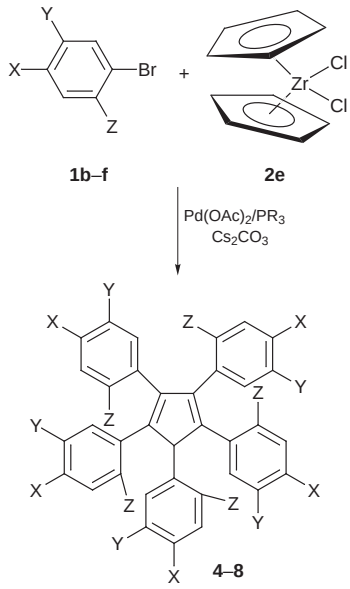

Scheme 2

Table 1 Reaction of **1a**–**f** with **2e**[a]

Bromide							
1	X	Y	Z	R in PR_3	*t*/h	Product	Yield (%)[b]
a	H	H	H	Ph	6	**3**	70
a	H	H	H	Bu^t	3	**3**	77
b	F	H	H	4-FC_6H_4	24	**4**	38
b	F	H	H	Bu^t	1	**4**	60
c	Me	H	H	Bu^t	1	**5**	78
c[c]	Me	H	H	Bu^t	20	**5**	60
d	MeO	H	H	Bu^t	1.5	**6**	45
e	H	Me	H	Bu^t	1	**7**	80
f	H	Me	Me	Bu^t	22	**8**	31
f	H	Me	Me	Ph	24	**8**	70[d]

[a] See also Scheme 2. Reaction conditions: **1** (6 mmol), **2e** (0.5 mmol), $Pd(OAc)_2$ (0.125 mmol), PR_3 (0.5 mmol), Cs_2CO_3 (6 mmol), DMF (10 cm^3), 130 °C. Workup was carried out by adding TsOH (12 mmol) and filtering through a silica gel column, followed by chromatographic purification. [b] Isolated yield based on the amount of cyclopentadiene moiety (1 mmol = 100%). Satisfactory elemental and spectral (^1H and ^{13}C NMR and mass) analyses data were obtained for each compound. [c] Reaction with 0.0125 mmol of $Pd(OAc)_2$ and 0.05 mmol of PBu^t_3. [d] Contaminated with $C_5H(Ph)(2,5\text{-}Me_2C_6H_3)_4$ (8%).

three major ones at δ 5.10, 5.29 and 5.46 in $CDCl_3$) together with more than 20 methyl peaks. This resembles the previously reported spectrum for tetra(2-methylphenyl)cyclopentadienone at a lower temperature of −43 °C.[15] The peaks in the ^1H NMR spectrum of **8** in DMSO-d_6 were still notably sharp even at 100 °C, reflecting its crowded nature, while they were completely broadened at 150 °C.

In summary, we have shown that various homosubstituted pentaarylcyclopentadienes can be prepared *via* the treatment of aryl bromides with metallocenes, typically zirconocene dichloride, under palladium catalysis. This novel synthetic method represents an efficient and straightforward alternative to the rather tedious 'tetracyclone route',[5,8] opening up opportunities for the construction of even extremely sterically crowded pentaarylcyclopentadienes. Its synthetic application as well as the detailed reaction mechanism are currently under investigation.

Notes and References

† E-mail: miura@ap.chem.eng.osaka-u.ac.jp
‡ E-mail: dyker@uni-duisburg.de

§ *Selected data* for **4**: mp 186–187 °C (Found: C, 78.13; H, 3.95. Calc. for $C_{35}H_{21}F_5$: C, 78.35; H, 3.94%); δ_H(400 MHz, $CDCl_3$) 4.90 (s, 1H), 6.73–6.77 (m, 4H), 6.84–6.95 (m, 14H), 7.07–7.10 (m, 2H). For **5**: mp 250 °C (Found: C, 92.56; H, 7.04. Calc. for $C_{40}H_{36}$: C, 92.98; H, 7.02%); δ_H(500 MHz, $CDCl_3$) 2.17 (s, 6H), 2.20 (s, 3H), 2.26 (s, 6H), 4.97 (s, 1H), 6.81–6.95 (m, 18H), 7.07 (d, *J* 7.8, 2H). For **6**: mp 193–194 °C (Found: C, 80.28; H, 6.07. Calc. for $C_{40}H_{36}O_5$: C, 80.51; H, 6.08%); δ_H(500 MHz, $CDCl_3$) 3.68 (s, 6H), 3.71 (s, 3H), 3.75 (s, 6H), 4.89 (s, 1H), 6.56–6.58 (m, 4H), 6.67–6.71 (m, 6H), 6.88–6.92 (m, 8H), 7.08–7.10 (m, 2H). For **7**: mp 163–164 °C (Found: C, 92.94; H, 7.10. Calc. for $C_{40}H_{36}$: C, 92.98; H, 7.02%); δ_H(400 MHz, $CDCl_3$) 2.08 (s, 6H), 2.15 (s, 6H), 2.23 (s, 3H), 5.02 (s, 1H), 6.77–6.93 (m, 15H), 6.99–7.04 (m, 5H). For **8**: mp 194–196 °C (Found: C, 91.92: H, 7.97. Calc. for $C_{45}H_{46}$: C, 92.10; H, 7.90%); δ_H(400 MHz, $CDCl_3$) 1.72–2.46 (m, 30H), 4.86–5.45 (m, 1H), 6.46–7.10 (m, 15H).

1 R. F. Heck, *Palladium Reagents in Organic Syntheses*, Academic Press, New York, 1985; A. de Meijere and F. E. Meyer, *Angew. Chem., Int. Ed. Engl.*, 1994, **33**, 2379; J. Tsuji, *Palladium Reagents and Catalysts*, Wiley, Chichester, 1995.
2 (*a*) Review: G. Dyker, *Chem. Ber./Recueil*, 1997, **130**, 1567; (*b*) G. Dyker, *J. Org. Chem.*, 1993, **58**, 234; (*c*) G. Dyker, J. Körning, P. G. Jones and P. G. Bubenitschek, *Angew. Chem., Int. Ed. Engl.*, 1993, **32**, 1733.
3 (*a*) T. Satoh, Y. Kawamura, M. Miura and M. Nomura, *Angew. Chem., Int. Ed. Engl.*, 1997, **36**, 1740; (*b*) S. Pivsa-Art, T. Satoh, Y. Kawamura, M. Miura and M. Nomura, *Bull. Chem. Soc. Jpn.*, 1998, **71**, 467.
4 (*a*) Y. Akita, Y. Itagaki, S. Takizawa and A. Ohta, *Chem. Pharm. Bull.*, 1989, **37**, 1477; (*b*) A. Ohta, Y. Akita, T. Ohkuwa, M. Chiba, R. Fukunaga, A. Miyafuji, T. Nakata, N. Tani and Y. Aoyagi, *Heterocycles*, 1990, **31**, 1951; (*c*) Y. Aoyagi, A. Inoue, I. Koizumi, R. Hashimoto, K. Tokunaga, K. Gohma, J. Komatsu, K. Sekine, A. Miyafuji, J. Kanoh, R. Honma, Y. Akita and A. Ohta, *Heterocycles*, 1992, **33**, 257.
5 For recent work on complexes using C_5Ph_5: D. Matt, M. Huhn, M. Bonnet, I. Tkatchenko, U. Englert and W. Kläui, *Inorg. Chem.*, 1995, **34**, 1288; S. Barry, A. Kucht, H. Kucht and M. D. Rausch, *J. Organomet. Chem.*, 1995, **489**, 195; I. Kuksis and M. C. Baird, *Organometallics*, 1996, **15**, 4755; D. J. Hammack, M. M. Dillard, M. P. Castellani, A. L. Rheingold, A. L. Rieger and P. H. Rieger, *Organometallics*, 1996, **15**, 4791; I. Kuksis, I. Kovács, M. C. Baird and K. F. Preston, *Organometallics*, 1997, **15**, 4991; A. M. Bond, R. Colton, D. A. Fiedler, L. D. Field, D. Leslie, T. He, P. A. Humphery, C. M. Lindall, F. Marken, A. F. Masters, H. Schumann, K. Suehring and V. Tedesco, *Organometallics*, 1997, **16**, 2787; C. Janiak, R. Weimann and F. Görlitz, *Organometallics*, 1997, **16**, 4933.
6 J. C. Ruble, H. A. Latham and G. C. Fu, *J. Am. Chem. Soc.*, 1997, **119**, 1492.
7 For example: C. Adachi, T. Tsuji and S. Saito, *Appl. Phys. Lett.*, 1990, **56**, 799; Y. Ohmori, Y. Hironaka, M. Yoshida, N. Tada, A. Fujii and K. Yoshino, *Synth. Met.*, 1997, **85**, 1241.
8 W. Broser, P. Siegle and H. Kurreck, *Chem. Ber.*, 1968, **101**, 69; L. D. Field, K. M. Ho, C. M. Lindall, A. F. Masters and A. G. Webb, *Aust. J. Chem.*, 1990, **43**, 281.
9 T. R. Jack, C. J. May and J. Powell, *J. Am. Chem. Soc.*, 1977, **99**, 4707.
10 H. Schumann, H. Kucht and A. Kucht, *Z. Naturforsch.*, **1992**, 47b, 1281; R. H. Lowack and K. P. C. Vollhardt, *J. Organomet. Chem.*, 1994, **476**, 25.
11 Related reaction of iodocyclopentadienyl complexes with tributyl(cyclopentadienyl)stannane to give a mixture of 1,2,4,5- and 1,1,2,4-substituted cyclopentadienes: R. Boese, G. Bräunlich, J.-P. Gottenland, J.-T. Hwang, C. Troll and K. P. C. Vollhardt, *Angew. Chem., Int. Ed. Engl.*, 1996, **35**, 995.
12 W. A. Herrmann, C. Brossmer, C.-P. Reisinger, T. H. Riermeier, K. Öffele and M. Beller, *Chem. Eur. J.*, 1997, **3**, 1357 and references cited therein.
13 V. V. Grushin and H. Alper, *Chem. Rev.*, 1994, **94**, 1047 and references cited therein.
14 M. Nishiyama, T. Yamamoto and Y. Koie, *Tetrahedron Lett.*, 1998, **39**, 617; T. Yamamoto, M. Nishiyama and Y. Koie, *Tetrahedron Lett.*, 1998, **39**, 2367.
15 R. Willem, A. Jans, C. Hoogzand, M. Gielen, G. V. Binst and H. Pepermans, *J. Am. Chem. Soc.* 1985, **107**, 28.

Receieved in Cambridge, UK, 29th May 1998; 8/04026E

Enantioselective sulfoxidation mediated by vanadium-incorporated phytase: a hydrolase acting as a peroxidase

Fred van de Velde, Lars Könemann, Fred van Rantwijk and Roger A. Sheldon*†

Laboratory for Organic Chemistry and Catalysis, Delft University of Technology, Julianalaan 136, 2628 BL Delft, The Netherlands

Phytase (E.C. 3.1.3.8), which *in vivo* mediates the hydrolysis of phosphate esters, catalyses the enantioselective oxidation of thioanisole with H_2O_2, both in the presence and absence of vanadate ion, affording the *S*-sulfoxide in up to 66% ee at 100% conversion.

In the last decade peroxidases, notably chloroperoxidase (CPO; E.C. 1.11.1.10) from *Caldariomyces fumago*, have been shown to catalyse a variety of synthetically useful (enantioselective) oxygen transfer reactions with H_2O_2,[1] including enantioselective oxidation of sulfides.[2] However, a major shortcoming of all heme-dependent peroxidases, such as CPO, is their low operational stability,[3] resulting from facile oxidative degradation of the porphyrin ring. In contrast, vanadium haloperoxidases, such as vanadium chloroperoxidase from *Curvularia inaequalis*[4] are non-heme enzymes and, hence, are much more stable. Unfortunately, the active site of vanadium-dependent haloperoxidases can accommodate only very small substrates, such as halide ion, which severely curtails their utility, although Andersson *et al.*[5] recently found that the vanadium-dependent bromoperoxidase from *Corallina officinalis* mediates the enantioselective oxidation of aromatic sulfides. Recently, it was established[6] that vanadium chloroperoxidases are structurally closely related to the acid phosphatases and the apoenzyme was shown to exhibit phosphatase-like activity. Moreover, vanadate and other transition metal oxoanions are known to be potent inhibitors of acid phosphatases[7] and the related phytases[8] and sulfatases.[9] Hence, we reasoned that incorporation of vanadate ion in these enzymes should produce novel, semi-synthetic peroxidases.

To test this hypothesis we investigated the oxidation of thioanisole with H_2O_2 (Scheme 1) catalysed by vanadium-incorporated phytase (from *Aspergillus ficuum*). At low vanadate concentrations (< 15 μM) we observed quantitative conversion to the sulfoxide, the *S*-enantiomer being preferentially formed in 56% ee. At higher vanadate concentrations (> 25 μM), in contrast, further oxidation to the corresponding sulfone also occurred.

In the standard procedure thioanisole (5 mM) and phytase [30 mg dry weight; 12 mg protein (> 95 % phytase); 0.18 μmol; 1400 U] were dissolved in formate buffer (7 ml; 0.1 M; pH 5.1; containing 0 to 30 μM Na_3VO_4). At this pH vanadate is predominantly present[10] as $H_2VO_4^-$. After 10 min H_2O_2 (5.5 mM) was added and the course of the reaction was followed by chiral HPLC (Chiralcel OD column; Daicel Chemical Industries, Ltd.) using 1,2,3-trimethoxybenzene as an internal standard. Of a wide variety of structurally related enzymes tested (details to be reported elsewhere) only phytase exhibited substantial peroxidase activity.

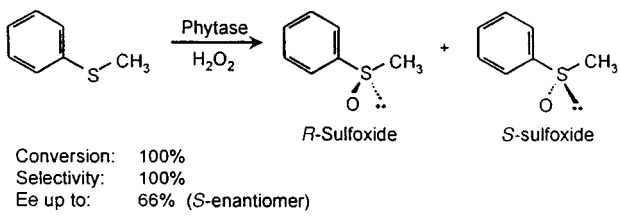

Scheme 1

We studied the influence of the vanadate concentration on the reaction rate and ee of thioanisole oxidation. As shown in Fig. 1 the reaction rate showed saturation kinetics with respect to the vanadate concentration. From these data we calculated a maximum rate of 120 μmol h^{-1} (which represents a turnover frequency of 11 min^{-1}) and a dissociation constant (K_d) for the vanadate ion of 15.4 μM, which is in the same order of magnitude as its reported K_I value for phosphatases and sulfatases.[9] The ee of the formed sulfoxide increased from 47% to a plateau (from 2.5 to 20 μM) of 56% at room temperature. At 4 °C this value was improved to 66% (see Table 1). At a vanadate concentration of 20 μM the rate of the non-enzymatic reaction was 0.5 μmol h^{-1}. Surprisingly, phytase also catalysed the enantioselective sulfoxidation of thioanisole, giving the

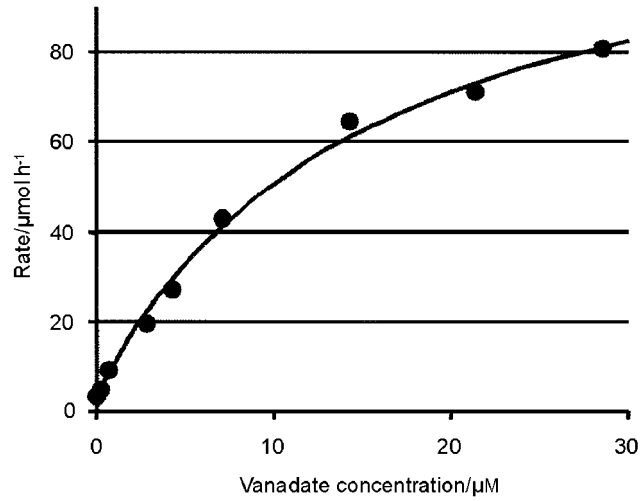

Fig. 1 Influence of the vanadate concentration on the oxidation of thioanisole

Table 1 Sulfoxidation of thioanisole mediated by phytase[a]

Phytase/mg protein	VO_4^{3-}/μM	*T*/°C	*t*/h	Conversion/ mol%	Ee (%)
0	10	25	5	10	0
12	10	25	3	100	56
12	10	4	3	100	66
0	0	25	5	10	0
1.7	0	25	5	15	25
4.2	0	25	5	23	37
12	0	25	5	47	47
16	0	25	5	81	51
12	0	4	23	44	54
12	0	40	5	68	33
0	0	40	5	34	0

[a] For experimental conditions see text.

S-sulfoxide in 47% ee, *even in the complete absence of vanadium*.

We subsequently studied the metal-free phytase-catalysed sulfoxidation in more detail (Table 1). The conversion and ee increased with increasing enzyme concentration, consistent with the reaction being enzyme catalysed. At room temperature the enzyme activity for the two enantiomers was 0.16 μmol h^{-1} (mg protein)$^{-1}$ and 0.04 μmol h^{-1} (mg protein)$^{-1}$ respectively for the *S*- and the *R*-enantiomer. In consequence, the *intrinsic* enantioselectivity of the enzyme is 58% ee (*S*) at room temperature. In the absence of enzyme, a 34% conversion to racemic sulfoxide was observed in 5 h at 40 °C. Decreasing the temperature from 40 to 4 °C reduced the rate of the blank reaction from 9.52 10^{-8} to 3.42 10^{-9} M s^{-1}, resulting in a corresponding increase in enantioselectivity from 33 to 54% ee.

The highest ees were observed in formate buffer, but a carboxylate buffer was not essential. Ammonium chloride and MES‡ were also effective, giving conversions and (ee values) after 5 h of 74% (35%) and 71% (43%), respectively, in experiments performed at 4 mM H_2O_2. This rules out the *in situ* formation of peroxycarboxylic acids (from the carboxylate buffers) as observed with lipases[11] and metal-free bacterial haloperoxidases.[12] The optimum pH was 5.1 which coincides with that of the natural reaction of phytase. The enantioselectivity decreased from 33 to 18% with increasing H_2O_2 concentration from 5.5 to 20 mM, owing to an increased contribution from the blank reaction at higher H_2O_2 concentrations.

A few experiments were performed aimed at providing insights into the origins of the observed metal-free catalysis. Reactions performed under nitrogen showed no difference with the reactions performed under air. When the reaction was performed with $H_2{}^{18}O_2$ (Campro Scientific) analysis of the sulfoxide product by GC–MS showed that the oxygen (100%) is derived from H_2O_2. Addition of the radical scavenger Trolox™-C,§ a water soluble analog of vitamin E, had no influence on the conversion or enantioselectivity, consistent with hydroxyl radicals not being involved in the enantioselective oxidation.

This leaves us with the question of the origin of the observed oxygen transfer catalysis. It is not metal-based as there is no metal ion in the active site. Although the chelating agent EDTA completely inhibited the enantioselective oxidation this is probably due to removal of calcium ions required for the stability of the enzyme. The crystal structure of phytase from *Aspergillus ficuum* was recently resolved to 2.5 Å, showing that an aspartate residue (Asp339) is located in the active site.[13] Similarly, acid phosphatases are also known to contain aspartate in the active site.[7] Hence, it is tempting to speculate that this aspartate plays a key role in the observed catalysis. Reaction of the free carboxylate group with H_2O_2 would give the corresponding peroxycarboxylic acid which could be the active oxidant. When the reaction was performed with *tert*-butyl hydroperoxide (TBHP) no catalysis was observed consistent with the above proposed formation of peroxycarboxylic acids. Appropriate site-directed mutagenesis studies should be able to confirm the key role of Asp339 in the catalytic mechanism.

In conclusion, we have demonstrated the feasibility of rationally designing a semi-synthetic peroxidase *via* incorporation of vanadium into the active site of phytase by exploiting the structural similarity of vanadate to phosphate. Surprisingly, the metal-free phytase also catalyses enantioselective oxidation and further studies are underway aimed at clarifying the mechanism and exploring the scope of this novel oxygen transfer catalysed by a hydrolase.

We gratefully acknowledge a gift of phytase by Gistbrocades N.V. The financial support of the Dutch Innovation Oriented Program on Catalysis (IOP catalysis; IKA94013) is gratefully acknowledged.

Notes and References

† E-mail: Secretariat-OCK@stm.tudelft.nl

‡ 2-(*N*-Morpholino)ethanesulfonic acid

§ 6-Hydroxy-2,5,7,8-tetramethylchromane-2-carboxylic acid

1 M. P. J. van Deurzen, F. van Rantwijk and R. A. Sheldon, *Tetrahedron*, 1997, **53**, 13 183.
2 S. Colonna, N. Gaggero, G. Carrea and P. Pasta, *Chem. Commun.*, 1997, 439; S. Colonna, N. Gaggero, L. Casella, G. Carrea and P. Pasta, *Tetrahedron: Asymmetry*, 1992, **3**, 95; M. P. J. van Deurzen, I. J. Remkes, F. van Rantwijk and R. A. Sheldon, *J. Mol. Catal. A: Chem.*, 1997, **117**, 329.
3 M. P. J. van Deurzen, K. Seelbach, F. van Rantwijk, U. Kragl and R. A. Sheldon, *Biocatal. Biotrans.*, 1997, **15**, 1.
4 J. W. P. M. van Schijndel, E. G. M. Vollenbroek and R. Wever, *Biochim. Biophys. Acta*, 1993, **1161**, 249; J. W. P. M. van Schijndel, P. Barnett, J. Roelse, E. G. M. Vollenbroek and R. Wever, *Eur. J. Biochem.*, 1994, **225**, 151; A. Messerschmidt and R. Wever, *Proc. Natl. Acad. Sci. U.S.A.*, 1996, **93**, 392.
5 M. Andersson, A. Willetts and S. Allenmark, *J. Org. Chem.*, 1997, **62**, 8455.
6 W. Hemrika, R. Renirie, H. L. Dekker, P. Barnett and R. Wever, *Proc. Natl. Acad. Sci. U.S.A.*, 1997, **94**, 2145; A. F. Neuwald, *Protein Sci.*, 1997, **6**, 1764.
7 Y. Lindqvist, G. Schneider and P. Vihko, *Eur. J. Biochem.*, 1994, **221**, 139; C. M. Vescina, V. C. Salice, A. M. Cortizo and S. B. Etcheverry, *Biol. Trace Elem. Res.*, 1996, **53**, 185.
8 A. Mahajan and S. Dua, *J. Agric. Food Chem.*, 1997, **45**, 2504.
9 P. J. Stankiewicz and M. J. Gresser, *Biochemistry*, 1988, **27**, 206.
10 M. T. Pope, *Heteropoly and Isopoly Oxometalates*, Springer-Verlag, Berlin, 1983, p. 34.
11 M. C. de Zoete, F. van Rantwijk, L. Maat and R. A. Sheldon, *Recl. Trav. Chim. Pays-Bas*, 1993, **112**, 462.
12 M. Picard, J. Gross, E. Lübbert, S. Tölzer, S. Krauss, K.-H. van Pée and A. Berkessel, *Angew. Chem., Int. Ed. Engl.*, 1997, **36**, 1196.
13 D. Kostrewa, F. Grüninger-Leitch, A. D'Arcy, C. Broger, D. Mitchell and A. P. G. M. van Loon, *Nat. Struct. Biol.*, 1997, **4**, 185.

Received in Cambridge, UK, 22nd June 1998; 8/04702B

The structure of the ionophoric antibiotic Na-tetronasin (M139603) in solution

Tamas Martinek,[a] Frank G. Riddell,*[b]† Trevor J. Rutherford,[b] Sina Sareth[b] and Charles T. Weller[c]

[a] *Institute of Pharmaceutical Chemistry, Albert Szent Gyorgyi Medical University, Szeged, Hungary*
[b] *School of Chemistry, University of St Andrews, St Andrews, Scotland, UK KY16 9ST*
[c] *School of Biomedical Sciences, University of St Andrews, St Andrews, Scotland, UK KY16 9ST*

The structure of the ionophoric antibiotic sodium tetronasin (M139603) in chloroform solution has been determined using NMR spectroscopic methods and is shown to contain a water molecule bound to the sodium which is hydrogen bonded to oxygens in the molecule.

The ionophoric antibiotics are an intriguing series of compounds that have widespread biological action.[1] In particular they are efficient mediators of the transport of metal ions and H^+ through the limiting membranes of cells. This property is presumed to be responsible for their biological activity through the dissipation of trans-membrane ion concentration gradients. It is believed that in most cases the transport occurs by the ionophore forming a 1 : 1 complex with the metal ion which then diffuses through the membrane.

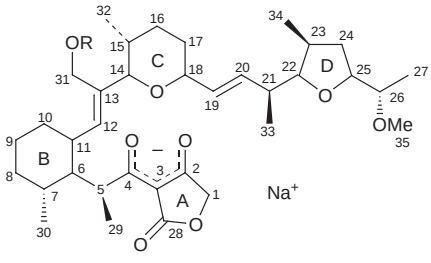

1 R = H [Tetronasin (or M139603)]

2 R = 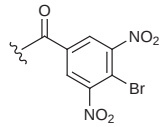

The discovery of M139603 **1** (subsequently called tetronasin) an ionophoric antibiotic from the aerobic fermentation of *Streptomyces longisporoflavus* NCIB 11426, was announced by ICI in 1980.[2] Its structure is rather different from those of the other common acidic ionophoric antibiotics in that it possesses a biosynthetically rare acid group in the form of an acyl tetronic acid moiety. Tetronasin and several of its derivatives have shown useful properties as coccidiostats and as growth promoters in ruminant animals, reducing methane production and increasing the propionate/acetate ratio in the rumen.[2–4]

A substantial amount of experimental work on the biosynthesis[5] *via* a polyketide mechanism and the synthesis[6–9] of tetronasin has been reported in recent years.

Experiments on the transporting ability of tetronasin for Li^+, Na^+ and K^+ through model biological membranes were performed by Riddell and Arumugam.[10] According to this work tetronasin is one of the faster transporting ionophoric antibiotics for the alkali metal ions. Interestingly, tetronasin displays the fastest association and dissociation rates in the membrane surface yet measured for the sodium salt of an ionophoric antibiotic.

The structure of tetronasin has been determined crystallographically from the 4-bromo-3,5-dinitrobenzoyl derivative **2** of the sodium salt.[11] The sodium ion was observed to be six-coordinated in the solid through five oxygen atoms from the molecule, two of which come from the tetronic acid, and a water molecule which occupies the sixth position. The sodium ion was observed to be at the centre of a very distorted octahedron.

An early report of the NMR spectra of tetronasin[12] suggested that the solution conformation of the ionophore is similar to that determined crystallographically. The solution conformation must, however, differ from that of the solid because ester formation at C(31) removes a hydroxy group which would undoubtedly be involved in hydrogen bonding in the original molecule. It seemed to us that modern NMR methods for the determination of the structure of biomolecules in solution would be appropriate to be applied to the sodium salt of tetronasin. The interest in the solution structure is two-fold. First, it would assist in explaining the rapid association and dissociation rates of the sodium salt during the transport process. Secondly, it might be possible to locate the bound water molecule, observed by crystallography, using NMR methods. Water molecules bound to biologically important molecules are potentially of functional importance and an ability to identify bound water molecules is of considerable significance. Other ionophoric antibiotics whose structures in solution have been solved by NMR methods include sodium salinomycin[13] and sodium monensin.[14]

The assignment of the ^1H NMR spectrum of sodium tetronasin[15] in $CDCl_3$ was straightforward. The resonances for H(12), H(19) and H(20) can readily be identified in the 1D ^1H NMR spectrum. Starting from these resonances the use of COSY and DQF COSY connectivities gave most of the assignments. The region between 1 and 2 ppm is rather crowded and so the chemical shifts of geminal hydrogen pairs were determined by a 2D HSQC experiment at natural abundance. Conformationally relevant scalar couplings were obtained from the 1D spectrum, from a *J*-resolved 2D spectrum and from an E. COSY spectrum.

NOESY spectra were obtained with mixing times of 100, 200, 300, 450 and 600 ms and NOE build up rates proved to be essentially linear in the 0–200 ms range. The NOESY cross peak intensities at 200 ms were used to establish distance restraints. The NOESY spectra contained cross peaks due to exchange between C(31)OH and a broad peak at around 1.77 ppm. At ambient temperature no additional NOESY cross peaks were observed from either of these peaks. However, as the temperature is lowered to −20 and −25 °C additional cross peaks of low intensity were observed from the 1.77 ppm peak which had shifted to 2.20 and 2.28 ppm respectively. Importantly, these cross peaks moved with changes in the position of the diagonal peak. At −25 °C these cross peaks are to $C(31)H_2$ (two cross peaks), C(19)H and $C(29)H_3$. The existence of these cross peaks clearly shows that the broad resonance in the 2.0 ppm region is from a bound water molecule. The absence of these cross peaks at ambient temperature is presumably due to rapid exchange of the bound water molecule.

Starting from the structure derived from X-ray crystallography and employing standard methods[16] including simulated annealing with the use of 49 NOE distance constraints, applied as ±7% of the measured NOE distance, a structure of the molecule was derived without the additional bound water

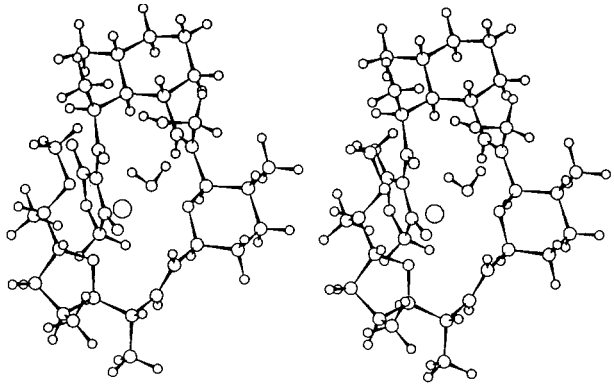

Fig. 1 Stereoview of the finalised structure of sodium tetronasin in solution incorporating the bound water molecule found from molecular modelling and incorporating the NMR distance constraints

molecule. The C(31) hydroxy group is found to hydrogen bond to the C(4) oxygen. The sodium is surrounded by five oxygen atoms. At this point the additional water molecule was introduced which was held close to the sodium with a 5 Å tether. No NOE constraints from the four cross peaks due to the bound water were introduced because the quantification of the NOE intensities was complicated by chemical exchange. The final structure, shown in Fig. 1, emerged after initial minimisation followed by restrained simulated annealing from 400 to 10 K and a final minimisation.

To test the goodness-of-fit a back calculation of the NOE intensities was performed on the model without the bound water molecule, which gave a relative root mean square deviation of 0.16.[17]

Molecular modelling without the NOE constraints led to the molecule unfolding after 100 ps of molecular dynamics at 303 K. A similar calculation on the coupling constants, which had not been used as restraints in the molecular modelling, gave a root mean square deviation of 0.05.[18] The model is thus seen to be in very satisfactory agreement with the experimental data.

The sodium is seen to be at the centre of a distorted octahedron of oxygen atoms with sodium to oxygen distances in the region 2.42 to 2.67 Å. The C(31) hydroxy group remains hydrogen bonded to the C(4) oxygen and the additional water molecule, whose oxygen is 2.67 Å from the sodium, is hydrogen bonded at one end to the C(31) hydroxy group and at the other to the C(26) (methoxy) oxygen.

In contrast to the other ionophoric antibiotics such as monensin, tetronasin has no tail to head hydrogen bond to 'close the circle' within the ligand. The only hydrogen bond involving a hydroxy group occurs across the molecule near the head between the C(31) hydroxy group and the C(4) oxygen. The water forms an additional 'brace' in a 'head to tail' fashion but this is expected to be less strong than a direct hydrogen bond. The C(31) hydroxy group thus has a defined role of structural importance for the sodium tetronasin complex. The design of other ionophoric materials with five oxygen ligands may well require water to be incorporated in the structure in a similar manner to the water in tetronasin. Also, unlike the other ionophoric antibiotics tetronasin takes a water molecule with it into the hydrophobic environment of a chloroform solution and, by implication, into the fatty interior of the membrane. Finally, during the initial series of simulated annealing all of the conformations observed had the acid head group of the molecule close to the sodium ion but in some of these conformations the oxygens remote from the tetronic acid had broken free. These three factors suggest why the on–off rates for sodium with tetronasin are the fastest yet observed for the ionophoric antibiotics. The lack of a direct head to tail hydrogen bond and the presence throughout of one molecule of water will lead to fewer steps in the association/dissociation processes. The lower number of steps in turn could lower the activation energies for these recognition processes.

Notes and References

† E-mail: fgr@st-and.ac.uk

1 F. G. Riddell, *Chem. Br.*, 1992, 533.
2 D. W. Davies and G. L. F Norris, *BP Appl.*, 2, 027, 013 (1980); *Chem. Abstr.*, 1980, **93**, 184292w.
3 D. W. Davies and M. J. Smithers, *EP Appl.*, 70, 622 (1983); *Chem. Abstr.*, 1983, **99**, 158138e.
4 G. L. R. Gordon and M. W. Phillips, *Lett. Appl. Microbiol.*, 1993, **17**, 220.
5 B. J. Rawlings, *Nat. Prod. Rep.*, 1997, **14**, 523.
6 G. J. Boons, I. C. Lennon, S. V. Ley, E. S. E. Owen, J. Staunton and D. J. Wadsworth, *Tetrahedron Lett.*, 1994, **35**, 323.
7 G. J. Boons, D. S. Brown, J. A. Clase, I. C. Lennon and S. V. Ley, *Tetrahedron Lett.*, 1994, **35**, 319.
8 S. V. Ley, J. A. Clase, D. J. Mansfield and H. M. I. Osbourne, *J. Heterocycl. Chem.*, 1996, **33**, 1533.
9 K. Hori, H. Kazuno, K. Nomura and E. Yoshi, *Tetrahedron Lett.*, 1993, **34**, 2183.
10 F. G. Riddell and S. Arumugam, *Biochim. Biophys. Acta*, 1989, **984**, 6.
11 D. H. Davies, W. E. Snape, P. J. Suter, T. J. King and C. P. Falshaw, *J. Chem. Soc., Chem. Commun.*, 1981, 1073.
12 J. Grandjean and P. Laszlo, *Tetrahedron Lett.*, 1983, **24**, 3319.
13 S. Mronga, G. Müller, J. Fischer and F. G. Riddell, *J. Am. Chem. Soc.*, 1993, **115**, 8414.
14 D. L. Turner, *J. Magn. Reson. (B)*, 1995, **108**, 137.
15 All spectra were obtained at 300 K on a Varian Unity-plus 500 spectrometer operating at 500.3 MHz for ^{1}H, using standard pulse sequences unless otherwise stated.
16 All molecular mechanics simulations were carried out on Silicon Graphics O2, Origin 200 and INDY computers using MSI/Biosym's CDiscover (Discover 95) software package in an Insight II environment. For the energy calculation the extensible Systematic Force Field (ESFF) was used with a 9.5 Å cut off for van der Waals and Coulomb interactions. The effect of solvent was taken into account by application of a distance dependent dielectric constant varying from 1 to an upper limit of 4.5. During the molecular dynamics calculations the velocity Verlet integrator and 1 fs timesteps were used. The temperature was controlled by direct velocity scaling with a 10 K temperature window. Minimisation was applied after every simulated annealing in cascade manner; steepest-descent, conjugate gradient (Fletcher algorithm), Newton method (BFGS algorithm). The iteration limit was 1500 steps, and the final convergence criterion was 0.0001 as maximum derivative.
17 No allowance was made in this unweighted calculation for the relatively larger errors that occur with the smaller NOE observations.
18 The root mean square deviation (rmsd) is here defined as:

$$\text{rmsd} = \sqrt{\frac{\sum_n \left(\frac{J_{(obs)} - J_{(calc)}}{J_{(obs)}} \right)^2}{n}}$$

Received in Cambridge, UK, 15th June 1998; 8/04482A

Synthesis of *endo,exo*-furofuranones using a highly diastereoselective C–H insertion reaction

Richard C. D. Brown*† and Jeremy D. Hinks

Department of Chemistry, University of Southampton, Highfield, Southampton, UK SO17 1BJ

A highly stereoselective ring closure of α-diazo-γ-butyrolactones to form the 2,6-diaryl-3,7-dioxabicyclo[3.3.0]octane ring system is reported; a formal synthesis of the furofuran lignan asarinin 1 is also described.

The 2,6-diaryl-3,7-dioxabicyclo[3.3.0]octane ring system is a key structural element in a large sub-class of lignan natural products, the furofuranoids (*i.e.* **1**, **2**, sesamin and aptosimon).[1,2] The electron rich aromatic substituents, which are characteristic of lignans, occupy *endo*- or *exo*-orientations on the 3,7-dioxabicyclo[3.3.0]octane core, which itself may be present at various levels of oxidation. The challenge of correctly establishing the four contiguous stereogenic centres present within the furofuranoids combined with their diverse biological activities has provoked substantial interest in their synthesis.[1–3] Our synthetic interest lay in the possibility of employing a C–H insertion reaction of an α-diazo-γ-lactone to form the 2,6-diaryl-3,7-dioxabicyclo[3.3.0]octane ring system. By targeting a furofuranone such as **4** as an advanced intermediate (Scheme 1), we hoped to develop a versatile route which could also be applied to the synthesis of other furofuranoids like asarinin **1** and cinnamonol **2**.

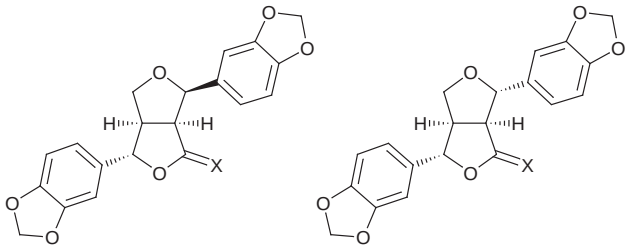

Our retrosynthetic analysis of the furofuranone **4** identified diazolactone **5** as a potential precursor (Scheme 1). Intramolecular C–H insertion into one of the diastereotopic C2–H bonds present in **5** would be expected to provide the furofuranone scaffold. We did not consider that the stereochemistry at the ring junction would be an issue, assuming that the 1,5-*cis*-adduct would be obtained. However, we were more reluctant to predict the stereochemical outcome at C2, hoping that we might control the stereoselectivity at this position through the use of different catalysts and conditions. The *trans*-relationship of the C5 and C6 substituents would be established in the cyclobutanone **6** which would arise from a [2+2] olefin–keteniminium salt cycloaddition reaction between **7** and **8**.

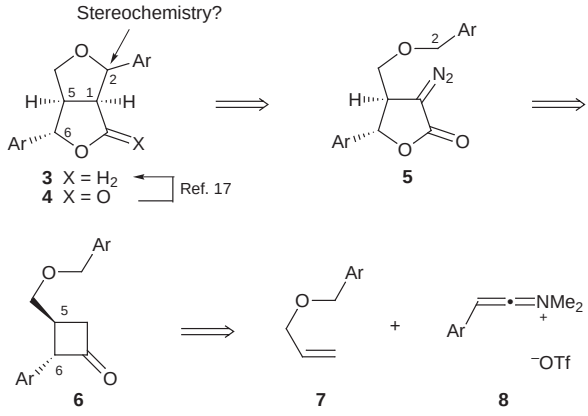

Scheme 1

Initial synthetic studies focused on the synthesis of a simple furofuranone **12a** (Ar = Ph, Scheme 2). According to Ghosez's protocol,[4] amide **9a**[5] was converted *in situ* to the corresponding keteniminium salt which underwent cycloaddition with benzyl allyl ether **7a**.[6] After hydrolysis of the intermediate cyclobutanone iminium salts, a mixture of diastereomeric cyclobutanones **10a** (*trans*:*cis*, 7:1) was obtained which was further enriched in the *trans*-isomer by careful chromatography. Due to the instability of the cyclobutanone **10a** it was immediately oxidised to the γ-lactone **11a**‡ using either MCPBA or H_2O_2 in AcOH.[7]

A search of the literature only revealed one previously reported synthesis of an α-diazo-γ-butyrolactone **13** which does not possess an additional stabilising group adjacent to the diazo functionality.[8] Although the deformylative diazo transfer procedure used to prepare **13** did provide our desired diazolactone **5a**, the yield was very poor, so alternative diazo transfer procedures were investigated. In view of our reluctance to

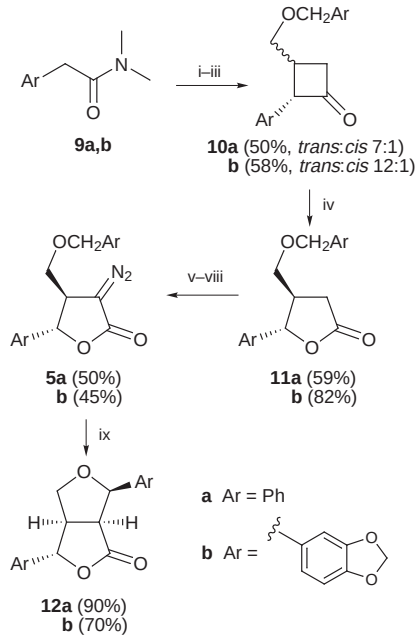

Scheme 2 *Reagents and conditions*: i, Tf_2O, CH_2Cl_2, −20 °C; ii, **7a** or **7b**, 2,6-di-*tert*-butylpyridine, CH_2Cl_2 (followed by 1equiv. K_2CO_3 for **7b**); iii, $NaHCO_3$ (aq.); iv, H_2O_2, AcOH; v, LiHMDS, THF; vi, *p*-$NO_2C_6H_4SO_2N_3$, THF, −78 °C; vii, AcCl; viii, DMAP, THF; ix, 2 mol% $Rh_2(OAc)_4$, CH_2Cl_2, room temp.

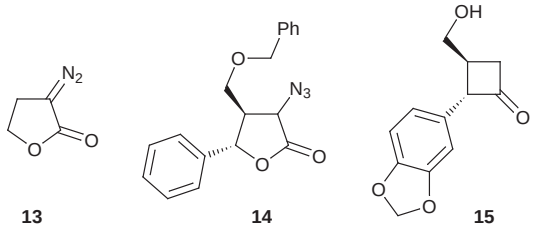

13 **14** **15**

pursue other methods of decarbonylative diazo transfer,[9,10] and the existence of encouraging reports of direct diazo transfer to ester and imide enolates, we focused our efforts on the later approach.[11,12]

The conditions reported for direct diazo transfer to ester enolates failed to give satisfactory yields of the diazo lactone **5a**, with azide **14** isolated as the major product. Although disappointing, the isolation of substantial amounts of azide **14** strongly implied that the intermediate triazine anion **17** was being formed efficiently (Scheme 3). An earlier study of the decomposition of triazines had shown that the relative proportions of diazo transfer and azide transfer were influenced by the reaction conditions.[12] In our case the triazine **18** proved to be too unstable to isolate,§ however, treatment of the reaction mixture with AcCl provided a mixture of isomeric *N*-acetyltriazines **19**.[13]¶ When the acetyl triazines **19** were treated with an equivalent of DMAP smooth conversion to a 1:1 mixture of azide **14** and the desired diazo lactone **5a** was observed. The reason for the increased proportion of diazo lactone **5a** are not clear at present although it is tempting to suggest that generation of a metal-free triazine anion, by the nucleophilic deacylation of **19** with DMAP, is important.

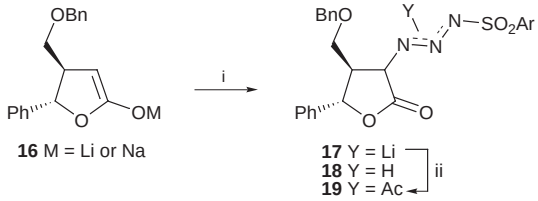

16 M = Li or Na

17 Y = Li
18 Y = H
19 Y = Ac

Scheme 3 *Reagents and conditions*: i, *p*-$NO_2C_6H_4SO_2N_3$, THF, −78 °C; ii, AcCl, −78 °C to room temp.

Gratifyingly, the key C–H insertion reaction required to set up the furofuranone framework proceeded extremely cleanly when diazo lactone **5a** was treated with a catalytic amount of $Rh_2(OAc)_4$, providing a single diastereoisomeric product **12a**. The relative stereochemistry of the furofuranone **12a** was assigned as *endo,exo* on the basis of NOE experiments. We were intrigued by the possibility of conducting the same intramolecular C–H insertion reaction under thermal conditions, which might provide altered stereoselectivity. In fact, heating the diazo lactone **5a** in 1,2-dichloroethane cleanly afforded the same cyclised product **12a**, again in excellent yield and stereoselectivity.

Relatively few of the published approaches to the synthesis of furofuranoid lignans have addressed the stereoselective synthesis of the less common *endo,exo* structures.[14–19] To demonstrate the scope of our approach to the synthesis of furofuranoid containing natural products the synthesis of *epi*-aptosimon **12b** was investigated. The conversion of *epi*-aptosimon **12b** to the furofuran lignan asarinin **1** has been reported previously.[17]
Initial attempts to carry out the [2+2] cycloaddition reaction of allyl ether **7b**[6] (Ar = 3,4-methylenedioxyphenyl) with the keteniminium salt derived from amide **9b**[20] failed to provide **10b**. Instead the major isolated product was the alcohol **15** arising from acid-catalysed cleavage of the benzylic ether bond which was assisted by the electron donating methylenedioxy group. The problem was almost certainly due to the formation of di-*tert*-butylpyridinium triflate under the reaction conditions. Fortunately this problem was easily resolved by the addition of anhydrous K_2CO_3 to the reaction mixture, allowing the desired cycloadduct **10b** to be obtained in good yield.

Baeyer–Villager oxidation of **10b** followed by diazo transfer to the resulting lactone **11b** afforded the cyclisation precursor **5b** in a yield of 37% from ketone **4b**. As was the case for the model diazo lactone **5a**, the C–H insertion reaction of **5b** proceeded cleanly to give the known furofuranone (±)-*epi*-aptosimon **12b** in good yield.

In summary, we have achieved a concise and diastereoselective synthesis of the 2,6-diaryl-3,7-dioxabicyclo[3.3.0]octane ring system. Significant contributions include: the development of conditions for conducting the keteniminium–olefin [2+2] cycloaddition reaction with alkenes bearing acid-sensitive functionality; and a method for effecting diazo transfer on γ-butyrolactones to provide the α-diazo-γ-butyrolactones **5** in acceptable yield. Finally, (±)-*epi*-aptosimon **12b** has been synthesised using this approach, representing a formal synthesis of the natural product (±)-asarinin **1**.

We thank the Royal Society for a University Research Fellowship (R. C. D. B.). We would also like to acknowledge the use of the EPSRC funded Chemical Database Service at Daresbury.[21]

Notes and References

† E-mail: rcb1@soton.ac.uk

‡ Due to the difficult chromatographic separation of the *cis*- and *trans*-diastereoisomers, γ-lactone **11a** was contaminated with a trace of the *cis*-isomer.

§ Protonation of the triazine anion (ref. 17) (AcOH or pH 7 phosphate buffer) followed by warming to ambient temperature afforded predominantly azide **14** along with a small amount of diazo transfer product **5a**.

¶ The *N*-acetyltriazines **19** exhibited very complex ^1H and ^{13}C NMR spectra, probably due to the presence of regio- and diastereo-isomers.

1 R. S. Ward, *Nat. Prod. Rep.*, 1995, **12**, 183.
2 R. S. Ward, *Nat. Prod. Rep.*, 1997, **14**, 43.
3 R. S. Ward, *Chem. Soc. Rev.*, 1982, 75.
4 C. Schmit, J. B. Falmangne, J. Escudero, H. Vanlierde and L. Ghosez, *Org. Synth.*, 1990, **69**, 199.
5 O. Mårtensson and E. Nilsson, *Acta Chem. Scand.*, 1960, 1129.
6 H. C. Arndt and S. A. Carroll, *Synthesis*, 1979, 202.
7 E. J. Corey, Z. Arnold and J. Hutton, *Tetrahedron Lett.*, 1970, 307.
8 A. Schmitz, U. Kraatz and F. Korte, *Chem. Ber.*, 1975, **108**, 1010.
9 M. D. Weingarten and A. Padwa, *Synlett*, 1997, 189.
10 D. F. Taber, K. You and Y. Song, *J. Org. Chem.*, 1995, **60**, 1093.
11 L. Lombardo and L. N. Mander, *Synthesis*, 1980, 368.
12 D. A. Evans, T. C. Britton, J. A. Ellman and R. L. Dorow, *J. Am. Chem. Soc.*, 1990, **112**, 4011.
13 S. E. Denmark, N. Chatani and S. V. Pansare, *Tetrahedron*, 1992, **48**, 2191.
14 S. Takano, K. Samizu and K. Ogasawara, *Synlett*, 1993, 785.
15 K. Samizu and K. Ogasawara, *Chem. Lett.*, 1995, 543.
16 D. R. Stevens and D. A. Whiting, *Tetrahedron Lett.*, 1986, **27**, 4629.
17 D. R. Stevens, C. P. Till and D. A. Whiting, *J. Chem. Soc., Perkin Trans. 1*, 1992, 185.
18 C. P. Till and D. A. Whiting, *J. Chem. Soc., Chem. Commun.*, 1984, 590.
19 A. Pelter, R. S. Ward, P. Collins, R. Venkateswarlu and I. T. Kay, *J. Chem. Soc., Perkin Trans. 1*, 1985, 587.
20 J. S. Buck and W. H. J. Perkin, *J. Chem. Soc.*, 1924, **125**, 1680.
21 D. A. Fletcher, R. F. McMeeking and D. Parkin, *J. Chem. Inf. Comput. Sci.*, 1996, **36**, 746.

Received in Cambridge, UK, 8th July 1998; 8/05296D

Fast oxygen uptake/release over a new CeO_x phase

Daniela Terribile,[a] Jordi Llorca,*[b] Marta Boaro,[a] Carla de Leitenburg,[a] Giuliano Dolcetti[a] and Alessandro Trovarelli*[a]

[a] *Dipartimento di Scienze e Tecnologie Chimiche, Università di Udine, via Cotonificio 108, 33100 Udine, Italy. E-mail: trovarelli@dstc.uniud.it*
[b] *Departament de Química Inorgànica, Universitat de Barcelona, Diagonal 647, 08028 Barcelona, Spain*

High-temperature reduction/oxidation cycles promote the oxygen storage capacity of mesoporous ceria; this is associated with the formation during reduction of a hexagonal CeO_x phase which on reoxidation gives amorphous ceria.

Ceria has long been recognized as a key component of catalysts for the treatment of emissions from automobiles. One of the most important functions that it performs is to act as an oxygen buffer, releasing oxygen for CO and hydrocarbon oxidation in a rich environment (excursion on the reducing side of the stoichiometric point) and storing oxygen from O_2 and NO during lean operations (excursion on the oxidizing side of the stoichiometric point).[1] This fast oxygen release/uptake is a consequence of the ease with which ceria can be reduced/oxidized and shift reversibly from the +4 to the +3 oxidation state in accordance with eqn. (1).

$$CeO_2 \rightleftharpoons CeO_x + 0.5(2 - x)O_2 \; (1.5 < x < 2) \qquad (1)$$

Under conditions typically encountered in auto-exhaust catalysis, this reaction occurs easily and reversibly, and CeO_2 is able to accommodate a large number of oxygen vacancies while maintaining its fluorite-type lattice.

The ability to store and release oxygen under actual operating conditions is affected by several parameters, particularly ageing and the consequent loss of surface area, which strongly influences the ability of ceria to perform its action.[2] To partly overcome these problems, much effort has been devoted to the preparation of ceria with enhanced textural and oxygen storage properties. Several strategies have been adopted, including the use of ceria doped with lanthanide or transition metal and/or the development of novel preparation methodologies.[3,4] We have recently described the preparation of mesoporous ceria with enhanced textural properties, demonstrating that by using surfactants as templating agents, CeO_2 with surface area exceeding 200 $m^2\ g^{-1}$ could be obtained.[5] Here, we report the preliminary results on the redox and oxygen storage behaviour of this high-surface area ceria after study of its structural and morphological evolution under a reducing and oxidizing environment. For the first time, a direct relation between the formation of a new reduced phase and fast oxygen uptake has been established. This adds to the basic understanding of the mechanism of oxygen storage in these materials. In addition, a comparison of mesoporous ceria with conventionally prepared CeO_2 will show the importance of the preparation method in the development of materials with novel properties.

High-surface area ceria was prepared according to the methodology previously described.[5] The sample used in this study had a surface area of 194 $m^2\ g^{-1}$ after calcination at 723 K, which compares favorably with the value of 92 $m^2\ g^{-1}$ obtained with ceria prepared by conventional precipitation.

Fig. 1 shows the X-ray powder diffraction pattern of mesoporous ceria ($MSCeO_2$) treated under H_2 at 1373 K for 1 h. For the purposes of comparison, the XRD pattern of conventionally prepared ceria ($CVCeO_2$) subjected to the same treatment under H_2 is also shown. In contrast to the pattern of $CVCeO_2$, the diffractogram of $MSCeO_2$ reduced at 1373 K clearly shows the presence of more than one phase. Peaks belonging to cubic CeO_2 are indicated with an arrow. All the other signals originate from a single reduced 'CeO_x' phase. Careful analysis of the CeO_x phase diffraction peaks enables us to identify a hexagonal unit cell with $a = 9.626(4)$ and $c = 7.076(3)$ Å. This hexagonal phase, which is isostructural with ternary compounds of the type $Pr_8Si_6O_{24}$ or $Sm_4Si_3O_{12}$, has not previously been reported in the phase diagram of non-stoichiometric cerium oxide at this composition range.

The stability of the new hexagonal phase on reheating under air was followed by *in situ* temperature-programmed XRD experiments. As the treatment temperature increases, the relative intensities of all the peaks attributed to the new hexagonal CeO_x phase progressively decrease while maintaining their relative proportions, providing additional evidence that all the indexed lines correspond to the same phase. Increasing amorphization of the CeO_x phase is observed between 673 and 773 K, whereas at 1073 K reoxidation is complete and the CeO_x phase has been totally transformed to cubic CeO_2. Analysis of the shape of the diffraction signals indicates that during this process small CeO_2 crystallites originate from amorphous ceria. The process is fully reversible and subsequent redox treatments alter neither the structural features and morphology of the observed phase nor the dynamics of its formation. The presence of both cubic and hexagonal phases in reduced mesoporous ceria was confirmed by high-resolution transmission electron microscopy and electron diffraction technqiues. Fig. 2 shows an HREM image and the oriented SAED pattern of a near-discrete hexagonal CeO_x phase particle. From the ED pattern it is inferred that the particle belongs to the hexagonal system with lattice parameters $a = 9.62(4)$ and $c = 7.07(1)$ Å. These values are in excellent agreement with those obtained by XRD. Reduction carried out under temperature-programmed conditions (5% H_2 in Ar, 10 K min^{-1}) indicates that the stoichiometry of this phase is CeO_x with x close to 1.66. Reoxidation of the

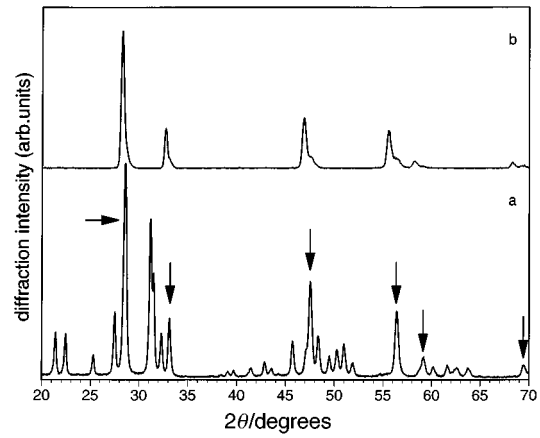

Fig. 1 X-Ray diffraction pattern of $MSCeO_2$ (a) and $CVCeO_2$ (b) treated under hydrogen for 1 h at 1373 K. Before measurements, the samples were cooled at room temperature under hydrogen.

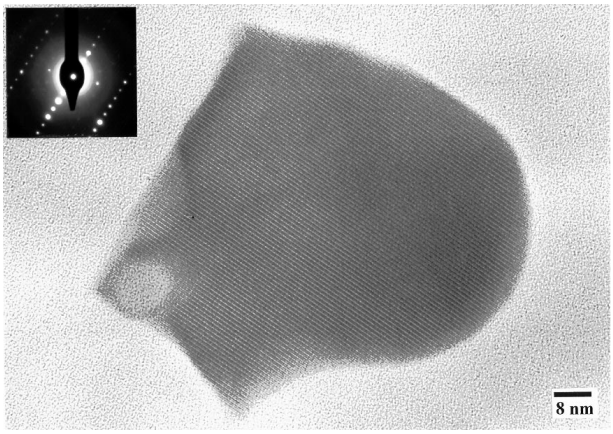

Fig. 2 High-resolution transmission electron microscope image and associated electron diffraction pattern (inset) corresponding to hexagonal CeO_x phase present in reduced mesoporous ceria. The particle is oriented along [$\bar{4}8\bar{4}3$]. Planes close to origin are ($\bar{1}10\bar{4}$) at 1.73 Å and ($\bar{1}010$) at 8.34 Å.

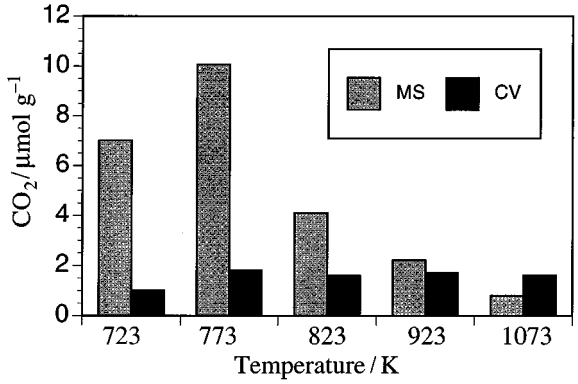

Fig. 3 Oxygen storage capacity of $MSCeO_2$ (gray bar) and $CVCeO_2$ (black bar) measured at 673 K after a redox cycle. Reduction under H_2(5%)–Ar at 1373 K for 1 h and oxidation under air for 1 h at the temperature indicated.

phase (1% O_2 in He, 10 K min^{-1}) occurs slowly at room temperature and complete reoxidation is observed near 800 K. In contrast, oxidation of reduced ceria (obtained from $CVCeO_2$) occurs easily even at room temperature and most of the reoxidation is observed at temperatures lower than 400 K.

The oxygen storage behaviour under dynamic conditions of CeO_2 obtained after oxidation of the CeO_x phase at different temperatures was studied by the method of alternately pulsing O_2 (2% in He) and CO (4% in He) over the catalyst (0.5 ml pulse size) at a temperature of 673 K and following CO_2 evolution.[6] The results, reported in Fig. 3, indicate that there is an optimum temperature for the reoxidation of CeO_x at which the highest conversion to CO_2 occurs. In contrast, reduction and oxidation of $CVCeO_2$ does not produce any variation of oxygen storage capacity. This unique behaviour can be related to the different phases formed in the two samples. Reduction under hydrogen at high temperature causes cubic ceria to lose oxygen and to form non-stoichiometric suboxides which finally give Ce_2O_3. However if the temperature is below 1373 K, only intermediate stoichiometries, which maintain the fluorite structure, are formed from cubic ceria. On reoxidation at room temperature, these oxides easily transform back to CeO_2.[7] In the case of reduced $CVCeO_2$, the fluorite structure is maintained and reoxidation merely fills up the oxygen vacancies. In contrast, the reoxidation of the CeO_x phase to pure CeO_2 in reduced $MSCeO_2$ implies the transformation of a hexagonal phase to a cubic one. This transformation does not occur directly but takes place through the formation of an intermediate amorphous phase whose concentration reaches a maximum in the range 673–773 K. The transformation of amorphous CeO_2 to crystalline ceria originates small CeO_2 crystallites deposited on bulk CeO_2. It is suggested that the presence of this amorphous/crystalline ceria on the top of large CeO_2 crystallites is responsible for enhancement of the oxygen storage capacity in this temperature range for it is known that small CeO_2 crystallites display unusually high defect and transport properties[8] which could enhance surface and bulk ion mobility. consequently increasing the rate of fast oxygen uptake/release over reduced/oxidized ceria. Reoxidation at temperatures higher than 823 K results in the transformation of amorphous or small ceria crystallites into bulk sintered ceria with a loss of oxygen storage. At this point, to recover activity, the material should be subjected to another redox cycle to form hexagonal CeO_x.

Notes and References

1 A. Trovarelli, *Catal. Rev.-Sci. Eng.*, 1996, **38**, 439.
2 S. J. Schmieg and D. N. Belton, *Appl. Catal. B: Environ.*, 1995, **6**, 127.
3 G. Ranga Rao, J. Kaspar, R. Di Monte, S. Meriani and M. Graziani, *Catal Lett.*, 1994, **24**, 107.
4 A. Trovarelli, F. Zamar, J. Llorca, C. de Leitenburg, G. Dolcetti and J. Kiss, *J. Catal.*, 1997, **169**, 490.
5 D. Terribile, A. Trovarelli, C. de Leitenburg, G. Dolcetti and J. Llorca, *Chem. Mater.*, 1997, **9**, 2676.
6 S. Kacimi, J. Barbier Jr., R. Taha and D. Duprez, *Catal. Lett.*, 1993, **22**, 343.
7 V. Perrichon, A. Laachir, G. Bergeret, R. Frety, L. Tournayan and O. Touret, *J. Chem. Soc., Faraday Trans.*, 1994, **90**, 773.
8 Y. M. Chiang, E. B. Lavik, I. Kosachi, H. L. Tuller and J. Y. Ying, *Appl. Phys. Lett.*, 1996, **69**, 185.

Received in Bath, UK, 20th June 1998; 8/04802I

One step synthesis of highly active and selective epoxidation catalysts formed by organic–inorganic Ti containing mesoporous composites

Avelino Corma,* José L. Jordá, Maria T. Navarro and Fernando Rey*

Instituto de Tecnología Química, UPV-CSIC, Universidad Politécnica de Valencia, Avda. de los Naranjos s/n, 46022 Valencia, Spain. E-mail: acorma@itq.upv.es

Ti-MCM-41 materials with methylated silicons have been prepared in one step synthesis; the resultant organic–inorganic composites are highly stable and present the highest activity and selectivity ever reported on Ti containing mesoporous catalysts for the epoxidation of olefins using organic peroxides.

The synthesis of molecular sieve mesoporous materials[1] have expanded the possibilities of zeolites and zeotypes, opening new possibilities in the fields of adsorption and catalysis.[2] Postsynthesis treatments devoted to prepared inorganic–organic composites have been carried out by silylating MCM-41 and MCM-48 materials, and in this way their stability, adsorption and catalytic properties have been improved.[3–7] Following the methodology used in sol–gel chemistry to functionalize amorphous silica, organically functionalized mesoporous silicas have been prepared by the co-condensation of tetraethoxysilane and organoalkoxysilanes in the presence of surfactant templates.[8] This method has been successfully extended to the introduction of thiol, amine, epoxide, imidazole and alkyl functionalities.[9] Taking this into account, and the fact that titanium containing molecular sieves increase their activity and selectivity by a postsynthesis silylation,[5,10] prompted us to prepare by direct synthesis, in one step, organic–inorganic self-assembled Ti-MCM-41 materials. Here, we will show that the process is successful, resulting in epoxidation catalysts much more active and selective than any similar materials reported up to now.

The synthesis of organo-silica containing Ti-MCM-41 materials were carried out with gels having the following molar compositions: $(1 - x)$ $Si(OCH_3)_4 : x$ $CH_3Si(OCH_2CH_3)_3 : 0.26$ TMAOH : 0.15 CTABr : 24.3 $H_2O : y$ $Ti(OCH_2CH_3)_4$ where x was varied from 0.15 to 0.35 and y between 0.0166 and 0.0075 (Table 1). Crystallisation was performed at 135 °C for 24 h in Teflon lined stainsteel autoclaves. The final solids were recovered by filtration, washed with water and dried at 60 °C, overnight. The occluded surfactant was removed by a two step extraction procedure. First, the solid was refluxed in a solution of 0.05 M H_2SO_4 in ethanol for 1 h. Then, the remaining occluded surfactant was extracted by refluxing the solid in a 0.15 M solution of HNO_3 in heptane–ethanol (52 : 48) over 24 h. In both steps, a liquid/solid ratio of 50 was used.

Table 1 Synthesis gel compositions for preparing methyl-tethered-Ti-MCM-41 in a single step synthesis

	Synthesis gel			Elemental analysis (wt.%)		
	Silica source					
Sample	TMOS	MTEOS	Ti/Si	C	N	C/N
1	1[a]	0	0.0075	33.28	2.29	16.95
2	0.75[a]	0.25	0.0075	33.78	2.07	19.04
3	0.85	0.15	0.0075	33.84	1.95	20.25
4	0.75	0.25	0.0075	34.33	1.98	20.23
5	0.65	0.35	0.0075	33.14	1.87	21.16
6	0.5	0.5	0.0075	—	—	—
7	0.75	0.25	0.0111	33.91	2.04	19.39
8	0.75	0.25	0.0166	33.84	1.95	20.25

[a] TEOS.

The materials before and after surfactant extraction were characterized by XRD, ^{29}Si MAS NMR, UV–VIS, IR spectroscopies and elemental analysis. The catalytic epoxidation of cyclohexene with *tert*-butylhydroperoxide (TBHP) on the Ti organosilica containing MCM-41 catalysts was carried out at 60 °C using an olefin/TBHP molar ratio of 4 and a liquid/catalyst ratio fixed at 20 (m/m). Aliquots of the reaction mixture were withdrawn at different reaction times and analysed by GC.

$Si(OCH_3)_4$ (TMOS) was chosen as the silica source because the structural order of the organo-silica MCM-41 samples obtained by using this precursor is superior to those of samples obtained using $Si(OEt)_4$ (TEOS).

The XRD patterns of samples prepared in the presence of different concentrations of $MeSi(OEt)_3$ (MTEOS) shown in Fig. 1, indicate that there is a limit for the incorporation of organosilica entities in the MCM-41 structure. It was found that the maximum MTEOS/Si ratio, for which a well ordered material is obtained, occurs at a value at 0.35.

Elemental analysis of the samples (Table 1) indicates that the C/N ratio is always > 19, which is the expected value if only CTA^+ filled the pores, and consequently this is an indication that CH_3Si groups are also incorporated into the MCM-41 structure. This assumption has been further established by ^{29}Si MAS NMR and IR spectroscopy. The ^{29}Si MAS NMR spectra of the methyl containing Ti-MCM-41 materials show four signals centred at −110, −100, −90, −65 and −55 ppm that can be assigned, respectively, to $Si(OSi)_4$ [Q_4], $HOSi(OSi)_3$ [Q_3], $(HO)_2Si(OSi)_2$ [Q_2], $MeSi(OSi)_3$ [MQ_3] and $MeHOSi(OSi)_2$ [MQ_2] environments around silicon.[11] The integrated intensity of MQ_2 + MQ_3 signals increases as the MTEOS concentration is increased in the synthesis gel, indicating that there is correspondence between the MTEOS concentration in the gel and the incorporation of CH_3Si groups in the final organosilica material. The presence and stability of CH_3Si

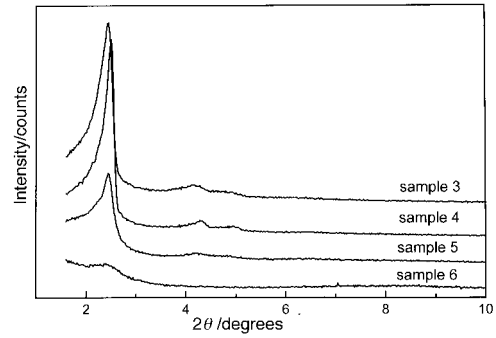

Fig. 1 XRD patterns showing the influence of the concentration of $MeSi(OEt)_3$ on the structural order of the methyl containing Ti-MCM-41 catalysts

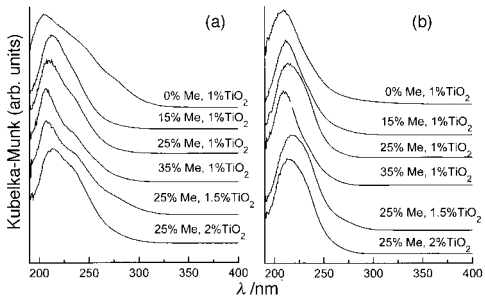

Fig. 2 UV–VIS DRS spectra of the methyl containing Ti-MCM-41 materials of as prepared (b) and extracted (b) samples

groups have been also studied by IR spectroscopy. The IR spectra of the sample heated under vacuum at different temperatures, show bands at 2974 and 1411 cm^{-1}, that can be assigned to methyl groups directly linked to silicon,[12] while, bands appearing at 2956, 2927 and 1464 cm^{-1} can be assigned to the CTA^+ cations located within the pores of the MCM-41 structure.[3] It is observed that the bands attributed to CTA^+ cations decrease in intensity with increased temperature, while bands assigned to methyl groups directly bonded to the silica wall remain nearly unchanged up to temperatures as high as 700 °C, indicating that the Si–C bond in the MCM-41 structure is highly stable to heat.

The UV–VIS spectra of the Ti containing inorganic–organic mesoporous silica materials for the as-prepared and extracted materials containing different methyl group concentrations on the silica walls are shown in Fig. 2(*a*) and (*b*), respectively where a narrow band centred at 220 nm, is taken as proof of Ti incorporation into the silica wall.[14,15] Also, when the UV–VIS spectra of the extracted samples is compared with those of the as-prepared samples, it was found that the 220 nm band is even narrower in the extracted samples than in the as-prepared materials. This indicates that Ti is located in a more distorted tetrahedral environment when the surfactant fills the pores of the MCM-41 structure, similarly to Ti-MCM-41 without any Si–C bonds.

The UV–VIS spectra for samples containing different amounts of Ti [Fig. 2(a) and (b)] in the synthesis gel showed that the 220 nm band becomes broader and a shoulder at 240 nm appears when the Ti content increases. However, after extraction all the samples show a very similar UV–VIS spectra, indicating that during extraction the tetrahedral coordination around the Ti centers becomes more regular.

The catalytic activity of the methyl containing samples for the epoxidation of cyclohexene pass through a maximum when *ca*. 25% of the silicon atoms are methylated. However, the selectivity to the epoxide decreases with increased methyl content, while the efficiency of TBHP increases with level of organic groups on the silica wall [Fig. 3(*a*)–(*c*)].

The production of epoxide calculated after 30 min of reaction was 10.6 mol min^{-1} (mol Ti)$^{-1}$ which gives an initial reaction rate, assuming a pseudo-first order reaction, of 21 mol min^{-1} (mol Ti)$^{-1}$ with a selectivity of 94% to the epoxide at a level of conversion of 98%. These results are, so far, the best ever obtained on Ti-MCM-41 incorporating Ti either by direct synthesis[16] or by anchoring titanocene[17] [0.4 and 2.1 mol min^{-1} (mol Ti)$^{-1}$ respectively], and they are much better than those obtained on titanium–silica cogels[18] [4.7 mol min^{-1} (mol Ti)$^{-1}$].

The inorganic–organic Ti-MCM-41 is highly stable in the presence of water and it represents one step forward in the preparation of epoxidation catalysts.

We gratefully acknowledge CICYT for financial support (MAT 97-1207-C03-01 and MAT 97-1016-C02-01), Ministerio de Educación y Ciencia (doctoral research fellowship to J. L. J.), CSIC and VARIAN IBERICA (postdoctoral fellowship to M. T. N.) and J. A. Gaona for technical assistance.

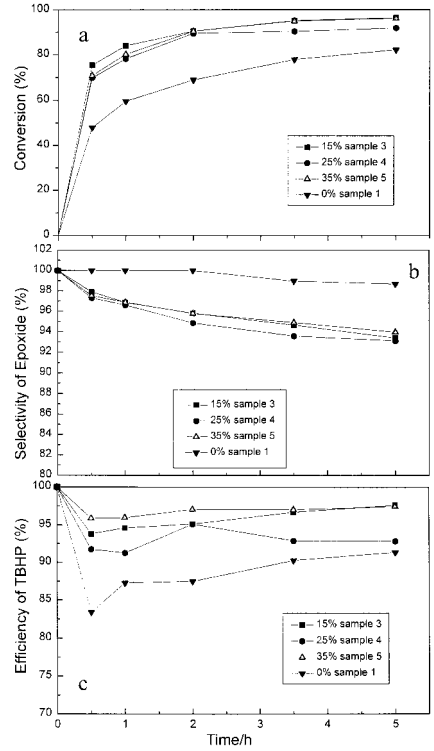

Fig. 3 Influence on the catalytic performance of the methyl concentration on the surface of the methyl containing Ti-MCM-41 catalysts; (a) catalytic activity, (b) selectivity to the epoxide and (c) efficiency of TBHP. *Reaction conditions*: 56.3 mmol of cyclohexene, 14.0 mmol TBHP, reaction temperature = 333 K and 0.3 g catalyst.

Notes and References

1 C. T. Kresge, M. E. Leonowicz, W. J. Roth, J. C. Vartuli and J. S. Beck, *Nature*, 1992, **359**, 710.
2 A. Corma, *Chem. Rev.*, 1997, **97**, 2373.
3 K. A. Koyano, T. Tatsumi, Y. Tanaka and S. Nakata, *J. Phys. Chem.*, 1997, **101**, 9436.
4 W. M. Van Rhijn, D. E. De Vos, B. F. Sels, W. D. Bossaert and P. A. Jacobs, *Chem. Commun.*, 1998, 317.
5 T. Tatsumi, K. A. Koyano and N. Igarashi, *Chem. Commun.*, 1998, 325.
6 X. S. Zhao and G. Q. Lu, *J. Phys. Chem.*, 1998, **102**, 1556.
7 J. Liu, X. Feng, G. E. Fryxell, L. Q. Wang, A. Y. Kim and M. Gong, *Adv. Mater.*, 1998, **10**, 161.
8 S. L. Burkett, S. D. Sims and S. Mann, *Chem. Commun.*, 1996, 1367.
9 C. E. Fowler, S. L. Burkett and S. Mann, *Chem. Commun.*, 1997, 1769.
10 B. Notari, *Adv. Catal.*, 1996, **41**, 253.
11 D. W. Sindorf and G. E. Marciel, *J. Am. Chem. Soc.*, 1983, **105**, 3767.
12 L. J. Bellamy, *The Infrared Spectra of Complex Molecular*, Chapman and Hall, London, 1975, 3rd edn., vol. 1.
13 A. Corma, V. Fornés, M. T. Navarro and J. Pérez-Pariente, *J. Catal.*, 1994, **148**, 569.
14 A. Zechinna, G. Spoto, S. Bordiga, A. Ferrero, G. Petrini, G. Leofanti and M. Padovan, *Stud. Surf. Sci. Catal.*, 1991, **69**, 251.
15 T. Blasco, M. A. Camblor, A. Corma and J. Pérez-Pariente, *J. Am. Chem. Soc.*, 1993, **115**, 11 806.
16 T. Blasco, A. Corma, M. T. Navarro and J. Pérez-Pariente, *J. Am. Chem. Soc.*, 1995, **156**, 65.
17 T. Maschmeyer, F. Rey, G. Sankar and J. M. Thomas, *Nature*, 1995, **378**, 159.
18 R. Hutter, T. Mallat and A. Baiker, *J. Catal.*, 1995, **153**, 177.

Received in Bath, UK, 20th June 1998; 8/04801K

Supramolecular assembly of well-separated, linear columns of closely-spaced C_{60} molecules facilitated by dipole induction

Leonard J. Barbour, G. William Orr and Jerry L. Atwood*

Department of Chemistry, University of Missouri-Columbia, Columbia, MO 65211, USA. E-mail: atwoodj@missouri.edu

Co-crystallization of C_{60} with *p*-bromocalix[4]arene propyl ether results in a remarkably well packed structure; the calixarene molecules pack with their dipole moments aligned unidirectionally and the unusually close van der Waals contact between the C_{60} molecules is most likely a result of an opposing induced dipole.

Solid-state supramolecular systems involving fullerenes are of interest with regard to the development of novel nanostructures with potentially interesting properties.[1] Although the exploitation of non-covalent interactions is an area of especially intense focus in the field of crystal engineering,[2] this approach cannot be applied effectively to the supramolecular manipulation of fullerenes since these molecules simply lack the necessary functionality. Thus, in order to 'engineer' a desired arrangement of C_{60} molecules in the solid state, one needs to consider their size and shape as the principal structure-directing properties. In addition to optimizing their energies of interaction, molecules will tend to arrange in a manner that makes efficient use of the available space and it is because these two mechanisms cooperate in a subtle manner that crystal structures are generally difficult to predict with accuracy.

Pure C_{60} crystallizes in a face centered cubic (fcc) lattice as a cubic close packed (ccp) arrangement of spheres.[3,4] An array of this type results in the formation of large voids in the lattice (the packing efficiency is only *ca* 74 %) and it follows that co-crystallization with small molecules, or even irregularly shaped larger molecules, may lead to more efficiently packed structures of enhanced stability. Indeed, this statement is supported by several crystal structures of supramolecular complexes of C_{60} that have been reported in recent years.[5] In some cases, it appears that the structure entails only a slight modification of the pure C_{60} structure with small molecules or ions occupying the voids between the spheres, while in other cases, the structure bears little or no resemblance to the pure fullerene phase.

We are currently investigating supramolecular systems composed of co-crystals of calixarenes and fullerenes. The structural chemistry of calixarenes is usually focused on exploitation of their intramolecular cavities for molecular inclusion and in this regard we and other workers have recently reported inclusion complexes of calix[5,6]arene derivatives with C_{60} and C_{70}.[6] In contrast, the calix[4]arenes are not suited to the formation of analogous inclusion complexes with fullerenes because their cavities are relatively small. Moreover the well-known C_{4v} cone conformation of these molecules is usually dependent on the presence of hydroxyl groups at the lower rim (*i.e.* the cone is stabilized by a cyclic hydrogen bonded arrangement), and substitution at this position gives rise to the so-called 'pinched-cone' C_{2v} conformation with an even smaller cavity. Despite the reduced possibilities for the formation of true inclusion compounds, simple calix[4]arene derivatives are similar in dimensions to C_{60} (*ca* 10 Å) and thus co-crystallization of these species may result in interesting and efficiently packed arrangements of the molecules in stoichiometric proportions.

As part of our ongoing study of the interactions between calixarenes and fullerenes, we are currently investigating the effects of substitution at both the upper and lower rims of calix[4]arene (compounds **1**–**4**) on solid-state packing arrangements when co-crystallized with fullerenes.

We now present the results of a remarkably interesting packing mode for a co-crystal of C_{60} with **1**.

Slow diffusion of propan-2-ol into a solution of **1** and C_{60} (5:1 molar ratio) in *o*-dichlorobenzene resulted in the formation of crystals suitable for single-crystal X-ray diffraction analysis.† The molecular structure of the final model is shown in Fig. 1 and the overall packing arrangement of the structure is shown in Fig. 2. The structure is acentric and all the calixarene molecules are arranged in one-dimensional strands (in a head-to-tail arrangement) parallel to [001] such that their dipole moments have the same orientation throughout the crystal. One set of distal propyl groups on each calixarene molecule protrudes down into the small voids between the bromine atoms of the calixarene directly below. The remaining two propyl groups flare out to fill lattice voids associated with the packing of adjacent calixarene strands.

The C_{60} molecules are also arranged in one-dimensional strands running parallel to [001] at 0,0,*z* and $\frac{1}{2},\frac{1}{2},z$. Since the space group symmetry is consistent with an orientationally disordered C_{60} molecule manifesting as a sphere of uniform electron density, the exact positions of the fullerene atoms cannot be determined. However, it is fortuitous that the center···center distance of the fullerenes is represented by the crystallographic *c* axis, which it was possible to determine

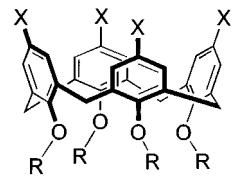

	X	R
1	Br	Pr^n
2	Br	CH_2Ph
3	I	CH_2Ph
4	Br	Me

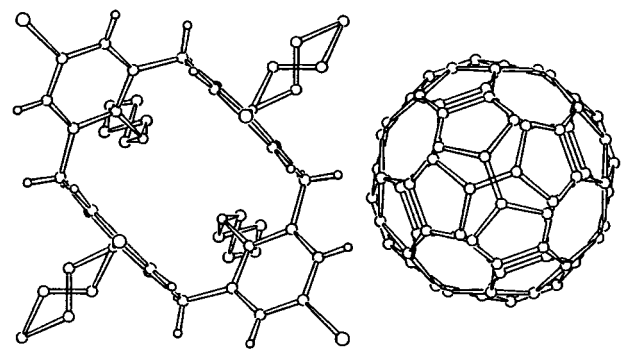

Fig. 1 Projection showing the molecular structure of the calixarene and C_{60} molecules. The calixarene assumes the pinched-cone conformation as a result of substitution at its lower rim. The C_{60} molecule was modeled as being fourfold rotationally disordered with two separate orientations.

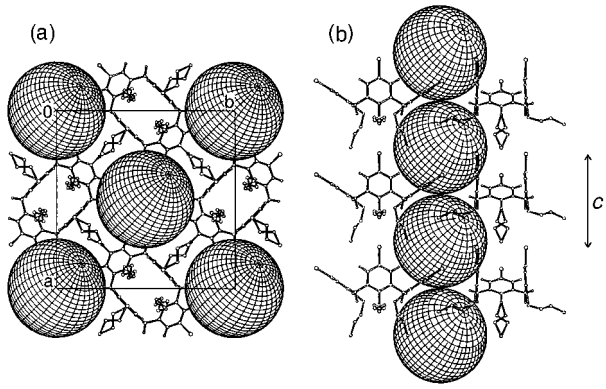

Fig. 2 Packing diagrams (hydrogen atoms omitted) viewed along (a) [001] looking down the linear columns of calixarene and C_{60} molecules, and (b) [−110] showing a side view of the columns and the space-optimization of the calixarene propyl groups.

accurately as 9.8782(5) Å at −100 °C [9.9231(6) Å at room temperature]. In contrast to the close spacing of the C_{60} molecules within the linear strands, the individual nearest-neighbor strands are separated by 12.81 Å (half the diagonal distance of the *ab* unit cell face). Within the linear strands, the $C_{60}\cdots C_{60}$ separation is 0.05 Å shorter than in the structure of pure C_{60}.[3] Taking the mean atom-to-atom diameter of the C_{60} molecule as being approximately 7.07 Å,[3,7] the short $C_{60}\cdots C_{60}$ separation along [001] implies that the shortest possible intermolecular C_{60} C···C distance for a spherically disordered molecule ranges from 2.81 to 3.15 Å. The upper limit compares favorably with previously reported values.[8,9]

The present structure is a striking example of the size–shape complementarity between **1** and C_{60} that allows the formation of an efficiently packed two-component system. This is evidenced by the observation that the crystallographic *c* axis is the repeat distance for both the calixarenes and fullerenes within their respective linear strands as shown schematically in Fig. 3. Although one-dimensional arrangements of C_{60} molecules have been observed in previously reported structures,[10] the complete structural isolation of such strands is unprecedented. Perhaps the most interesting and surprising aspect of the structure is that all the calixarene molecules align themselves in the same direction rather than adopting an overall centrosymmetric arrangement. As a consequence of this polar arrangement, the C_{60} molecules undergo dipole induction and this phenomenon

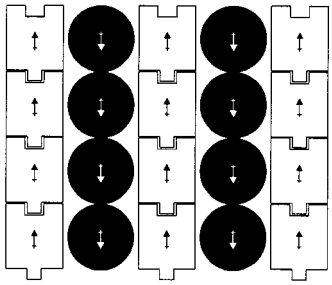

Fig. 3 Schematic representation of the packing arrangement between the calixarene and C_{60} molecules. The view is perpendicular to the *c* axis and the C_{60} molecules are represented by shaded circles. The calixarenes stack in a modular fashion with their dipoles all aligned in the same direction. The calixarene repeat distance exactly matches that for the C_{60} molecules while an opposing polarity is induced in the latter.

satisfactorily accounts for the rather close spacing of the fullerenes within their linear strands.

We are grateful for funding from the National Science Foundation.

Notes and References

† *Crystal data* for $C_{100}H_{44}Br_4O_4$: M = 1628.99, dark red needle-shaped crystal, 0.40 × 0.20 × 0.20 mm, tetragonal, space group *P4bm* (no. 100), $a = b$ = 18.1160(6), c = 9.8782(5) Å, Z = 2, V = 3241.9(2) Å^3, D_c = 1.669 g cm^3, Siemens SMART CCD diffractometer, Mo-Kα radiation, λ = 0.7107 Å, T = −100 °C, $2\theta_{max}$ = 54.3º, 19179 reflections collected, 3735 unique (R_{int} = 0.0327), μ = 2.548 mm^{-1}. SHELX-TL structure solution and refinement software, final *GOF* = 1.179, *R*1 = 0. 1174, *wR*2 = 0.3472, *R* indices based on 3111 reflections with $I > 2\sigma(I)$ (refinement on F^2), L_p and absorption corrections applied, μ = 2.548 mm^{-1}, min. transmission factor = 0.621. The structure was solved by direct methods and expanded by difference electron density synthesis. The asymmetric unit consists of a quarter each of a calixarene and a spherically disordered C_{60} molecule. The calixarene molecule is situated on the intersection of two mutually perpendicular mirror planes running along $x,x + ½,z$ and $\frac{1}{2} - x,x,z$. The propyl groups are disordered across the mirror planes and their hydrogen atoms were not placed. The fullerene molecules are positioned on the fourfold rotation axes at 0,0,z and $\frac{1}{2},\frac{1}{2},z$. CCDC 182/952.

1 J. L. Atwood, M. J. Barnes, R. S. Burkhalter, P. C. Junk, J. W. Steed and C. L. Raston, *J. Am. Chem. Soc*., 1994, **116**, 10346; J. A. Chupa, S. Xu, R. F. Fischetti, R. M. Strongin, J. P. McCauley, A. B. Smith and J. K. Blasie, *J. Am. Chem. Soc*., 1993, **115**, 4383; S. Saito and A. Oshiyama, *Phys. Rev. B*., 1994, **49**, 17413; P. W. Stephens, D. Cox, J. W. Lauher, L. Mihaly, J. B. Wiley, P.-M. Allemand, A. Hirsch, K. Holczer, Q. Li, J. D. Thompson and F. Wudl, *Nature*, 1992, **355**, 331.

2 G. R. Desiraju, *Crystal Engineering: The Design of Organic Solids*, Elsevier, Amsterdam, 1989; G. R. Desiraju and C. V. Krishnamohan Sharma, in *The Crystal as a Supramolecular Entity*, ed. G. R. Desiraju, John Wiley & Sons, New York, 1996.

3 S. Liu, Y. Lu, M. M. Kappes and J. A. Ibers, *Science*, 1991, **254**, 408

4 W. Bensch, H. Werner, H. Bartl and R. J. Schlögl, *J. Chem. Soc., Faraday Trans*., 1994, **90**, 2791.

5 Q. Zhu, O. Zhou, N. Coustel, G. B. M. Vaughan, J. P. McCauley, W. J. Romanow, J. E. Fischer and A. B. Smith, *Science*, 1991, **254**, 545; J. D. Crane, P. B. Hitchcock, H. W. Kroto, R. Taylor and D. R. M. Walton, *J. Chem. Soc. Chem. Commun*., 1992, 1764; A. Izuoka, T. Tachikawa, T. Sugawara, Y. Suzuki, M. Konno, Y. Saito and H. Shinohara, *J. Chem. Soc., Chem. Commun*., 1992, 1472; D. M. Eichhorn, S. Yang, W. Jarrell, T. F. Baumann, L. S. Beall, A. J. P. White, D. J. Williams, A. G. M. Barrett and B. M. Hoffman, *J. Chem. Soc., Chem. Commun*., 1995, 1703; O. Zhou, J. E. Fischer, N. Coustel, S. Kycia, Q. Zhu, A. R. McGhie, W. J. Romanow, J. P. McCauley, A. B. Smith and D. E. Cox, *Nature*, 1991, **351**, 462; M. J. Rosseinsky, *J. Mater. Chem*., 1995, **5**, 1497.

6 J. L. Atwood, L. J. Barbour, I. B. N. Sudria and C. L. Raston, *Angew. Chem., Int Ed. Engl*. 1998, **37**, 981; J. L. Atwood, L. J. Barbour, C. L. Raston and C. Sandoval, *Chem. Eur. J*., in press, T. Haino, M. Yanase and Y. Fukazawa, *Angew. Chem. Int., Ed. Engl*. **1997**, *36*, 259.

7 M. Fedurco, M. M. Olmstead and W. R. Fawcett, *Inorg. Chem*., 1995, **34**, 390.

8 O. Zhou, J. E. Fischer, N. Coustel, S. Kycia, Q. Zhu, A. R. McGhie, W. J. Romanow, J. P. McCauley, A. B. Smith and D. E. Cox, *Nature*, 1991, **351**, 4.

9 H.-B. Bürgi, E. Blanc, D. Schwarzenbach, S. Liu, Y. Lu, M. M. Kappes and J. A. Ibers, *Angew. Chem., Int. Ed. Engl*., 1992, **31**, 640.

10 P. W. Stephens, D. Cox, J. W. Lauher, L. Mihaly, J. B. Wiley, P.-M. Allemand, A. Hirsch, K. Holczer, Q. Li, J. D. Thompson and F. Wuhl, *Nature*, 1992, **355**, 331.

Received in Cambridge, UK, 11th June 1998; 8/04419H

Metal-based chirality and spin state change in 16-electron $CpML_2$ systems: a computational study of $CpW(NO)(PH_3)$

Kevin M. Smith,[a] Rinaldo Poli*[a] and Peter Legzdins[b]

[a] *Laboratoire de Synthèse et d'Electrosynthèse Organometallique, Faculté des Sciences 'Gabriel', Université de Bourgogne, 6 Boulevard Gabriel, 21100 Dijon, France. E-mail: Rinaldo.Poli@u-bourgogne.fr*

[b] *Department of Chemistry, University of British Columbia, Vancouver, British Columbia, Canada V6T 1ZI*

Density functional theory calculations indicate that $CpW(NO)(PH_3)$ possesses a planar triplet ground state, a result with significant implications for the inversion of configuration of 16e, d^6 $CpML_2$ species.

Several highly reactive Cp*W(NO)L intermediates (L = PMe_3,[1] PPh_3,[2] =$CHCMe_3$,[3] HCCPh[4–6]) have previously been shown to be generated by reductive elimination of CMe_4 or $SiMe_4$.† These proposed 16 electron, d^6 Cp*W(NO)L species are not observed as they proceed to activate C–H bonds,[1–4] coordinate weak π-acceptor ligands,[7] or engage in coupling and rearrangement reactions[5,6] with available trapping reagents. Previous theoretical studies[8–10] have demonstrated that the geometries and orbital energies of 16e, d^6 $CpML_2$ species are influenced by the bonding properties of their ligands. For example, π-donor ligands enforce a planar-at-metal conformation (*i.e.* the metal sits on the plane defined by the two ligands L and the Cp center of gravity), while pyramidal geometries are preferred for complexes containing either σ-donor (π-neutral) or π-acceptor ligands. However, these studies were carried out using semiempirical methods and so were confined to the spin singlet energy hypersurface. The computational studies that we report here for the $CpW(NO)(PH_3)$ model system indicate that the spin state can play a previously unsuspected yet critical role in 16e, d^6 $CpML_2$ species.

The optimised geometries and relative energies of the singlet and triplet $CpW(NO)(PH_3)$ complexes are shown in Table 1 and Fig. 1.‡ The singlet is pyramidal at W, as expected for a $CpML_2$ species containing π-acceptor and σ-donor ligands.[9,10] However, triplet $CpW(NO)(PH_3)$ is calculated to possess a planar geometry at W, and to be 3.3 kcal mol^{-1} (1 cal = 4.184 J) more stable than the pyramidal singlet species. No significant variation in W–NO bond distance is observed between the two different spin configurations since the W–NO π-bonding orbitals are fully occupied in both cases.[17] There is, however, the expected[18,19] slight overall extension of all bond lengths in the triplet, as well as an increase in CNT–W–P angle.

Table 1 DFT-B3LYP optimized geometries and energies for $CpW(NO)(PH_3)$

	Energy minima		Spin-crossover point	
Parameter	Singlet	Triplet	Singlet	Triplet
φ (N–W–CNT–P)	125.0	180.0	130.0	130.0
W–CNT	2.018	2.093	2.023	2.107
W–P	2.482	2.522	2.481	2.528
W–N	1.791	1.794	1.792	1.795
N–O	1.251	1.252	1.251	1.253
CNT–W–P	121.38	132.82	122.37	129.37
CNT–W–N	128.55	133.55	128.35	133.48
P–W–N	93.33	93.63	95.36	85.64
W–N–O	175.34	176.71	175.37	176.90
Relative energy/kcal mol	0	−3.3	+0.8	+0.8

While triplet $Cp*W(NO)(PR_3)$ complexes have yet to be detected spectroscopically, the intermediacy of such a species where R = Ph is consistent with kinetic measurements of the reaction between $Cp*W(NO)(\eta^2\text{-}PPh_2C_6H_4)H$ and $CNCMe_3$.[7,20] Replacing the Cp and PH_3 ligands of the model complex with bulkier Cp* and PR_3 groups would be expected to enforce a larger CNT–W–P angle and a planar-at-W geometry, thereby further destabilising the singlet state. The steric shielding of the metal centre coupled with the expected reduced reactivity[21] of the high-spin configuration should impart additional stability, making triplet $Cp*W(NO)(PR_3)$ compounds reasonable synthetic targets.§

In order to explore the role of the triplet spin state in the inversion of pyramidal, diamagnetic $CpML_2$ species, further calculations were performed at various values of ϕ for both spin states (Fig. 1). The highest energy singlet conformation is the planar geometry (ϕ = 180°), leading to an inversion barrier of 7.7 kcal mol^{-1} along the singlet spin surface, which compares well with previous studies on other 16-electron systems.[10] The energy of triplet $CpW(NO)(PH_3)$ increases relatively gradually as the geometry is distorted away from the planar-at-W conformation. As a result, the ϕ angle at which both spin states are equal in energy corresponds to a high degree of pyramidalization ($\phi \approx$ 130°), only 0.8 kcal mol^{-1} higher in energy than the singlet ground state.

The one-dimensional energetic situation illustrated in Fig. 1 would suggest a low-energy inversion mechanism for diamagnetic, pyramidal $CpW(NO)(PH_3)$ *via* the spin triplet surface.¶ However, the two geometries at the spin-crossover point are significantly different (Table 1). According to the Franck–Condon principle, both the geometries and the energies must be very similar for the spin flip process to occur. At the crossover

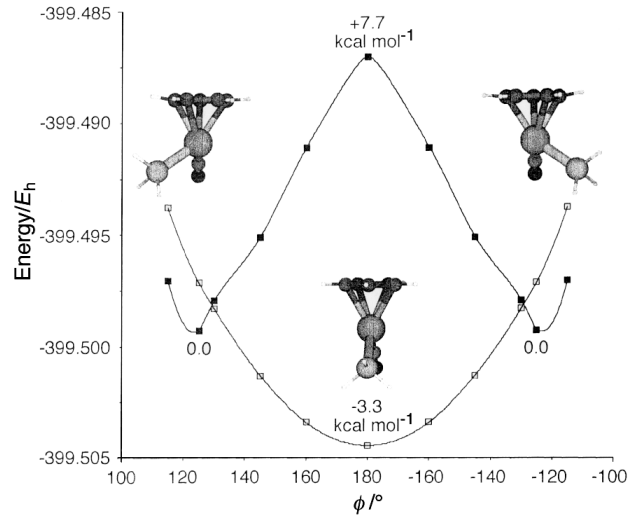

Fig. 1 B3LYP/LANL2DZ energies of optimized singlet (■) and triplet (□) $CpW(NO)(PH_3)$ at various fixed dihedral N–W–CNT–P (ϕ) angles

point (ϕ = 130°), the vertical excitation energies of singlet and triplet geometries (energy of the triplet configuration at the singlet geometry and of the singlet configuration at the triplet geometry) are 6.9 and 8.2 kcal mol^{-1}, respectively. These numbers give an estimate of the upper bound of the spin flip barrier.‖

The energetic proximity of these vertical excitation energies and the inversion barrier along the singlet surface (within *ca.* 1 kcal mol^{-1}) prohibits the definitive identification of the inversion mechanism (two-state *vs.* one-state) for the CpW(NO)(PH_3) species. It is readily apparent, however, that the involvement of the triplet spin state represents a distinct and realistic alternative to a process restricted to the singlet spin surface, the only mechanism which has hitherto been considered for this class of compounds. Further experimental and theoretical work is unquestionably required to explore this possibility for Cp*W(NO)L species, as well as for $CpML_2$ compounds in general.

Several 16e, d^6 Cp*M(PR_3)X species have been invoked in intra- and inter-molecular C–H bond activation reactions (M = Ir, X = CH_3^+;[25] M = Os, X = CH_2SiMe_3;[26] M = Ru, X = CH_2CMe_3;[27] M = Re, X = CO, PMe_3;[28–30] M = W, X = NO[1]). In particular, much recent theoretical, synthetic, and mechanistic work has been focused on the low-temperature alkane C–H bond activation reactions of the Cp*Ir(PMe_3)(CH_3)$^+$ complex,[31–34] but to the best of our knowledge, only one study has addressed the possible involvement of triplet species in this system.[19] The role of the spin state in the reactivity of unsaturated Cp*W(NO)L species is currently under theoretical investigation.[35]

R. P. thanks the Région Bourgogne for supporting this research, and K. M. S. is grateful for a TMR Marie Curie Postdoctoral Fellowship.

Notes and References

† Cp = η^5-C_5H_5; Cp* = η^5-C_5Me_5; CNT = Cp ring centroid.

‡ Calculations were performed using Gaussian 94.[11] The LanL2DZ basis set was employed to perform geometry optimisations with a density functional theory (DFT) approach. The three-parameter form of the Becke, Lee, Yang and Parr functional (B3LYP)[12] was employed. The LanL2DZ basis set includes both Dunning and Hay's D95 sets for H and C[13] and the relativistic electron core potential (ECP) sets of Hay and Wadt for the heavy atoms.[14–16] Electrons outside the core were all those for H, C, N and O, the 5s, 5p, 5d and 6s electrons for W and the 3s and 3p electrons for P. The mean value of the first-order electronic wavefunction, which is not an exact eigenstate of S^2 for unrestricted calculations on open shell systems, was considered suitable for the unambiguous identification of the spin state. Ground state energies are based on complete geometry optimisations. The singlet geometry for ϕ = 180° was optimised with an imposed mirror plane. For all other values of ϕ, the C_5 ring of the Cp ligand was fixed as a regular pentagon, the degree of pyramidalisation was set at a specific N–W–CNT–P dihedral angle (ϕ), and the geometry was optimised with no other constrained parameters.

§ For the use of steric bulky ligands in stabilising Cp*Ru(PR_3)X species, see refs. 9, 22 and 23.

¶ For discussion of similar examples of 'two-state reactivity' see ref. 24 and references therein.

‖ For a discussion of the problems inherent in estimating spin-crossover energies, see refs. 18, 21 and 24.

1 P. Legzdins, J. T. Martin, F. W. B. Einstein and R. H. Jones, *Organometallics*, 1987, **6**, 1826.
2 J. D. Debad, P. Legzdins, S. A. Lumb, R. J. Batchelor and F. W. B. Einstein, *Organometallics*, 1995, **14**, 2543.
3 E. Tran and P. Legzdins, *J. Am. Chem. Soc.*, 1997, **119**, 5071.
4 J. D. Debad, P. Legzdins, S. A. Lumb, R. J. Batchelor and F. W. B. Einstein, *J. Am. Chem. Soc.*, 1995, **117**, 3288.
5 P. Legzdins and S. A. Lumb, *Organometallics*, 1997, **16**, 1825.
6 P. Legzdins, S. A. Lumb and V. G. Young, Jr., *Organometallics*, 1998, **17**, 854.
7 D. J. Burkey, J. D. Debad and P. Legzdins, *J. Am. Chem. Soc.*, 1997, **119**, 1139.
8 C. C. Bickford, T. J. Johnson, E. R. Davidson and K. G. Caulton, *Inorg. Chem.*, 1994, **33**, 1080.
9 T. J. Johnson, K. Folting, W. E. Streib, J. D. Martin, J. C. Huffman, S. A. Jackson, O. Eisenstein and K. G. Caulton, *Inorg. Chem.*, 1995, **34**, 488.
10 T. R. Ward, O. Schafer, C. Daul and P. Hofmann, *Organometallics*, 1997, **16**, 3207.
11 M. J. Frisch, G. W. Trucks, H. B. Schlegel, P. M. W. Gill, B. G. Johnson, M. A. Robb, J. R. Cheeseman, T. A. Keith, G. A. Petersson, J. A. Montgomery, K. Raghavachari, M. A. Al-Laham, V. G. Zakrzewski, J. V. Ortiz, J. B. Foresman, J. Cioslowski, B. B. Stefanov, A. Nanayakkara, M. Challacombe, C. Y. Peng, P. Y. Ayala, W. Chen, M. W. Wong, J. L. Andres, E. S. Replogle, R. Gomperts, R. L. Martin, D. J. Fox, J. S. Binkley, D. J. Defrees, J. Baker, J. P. Stewart, M. Head-Gordon, C. Gonzales and J. A. Pople, Gaussian 94 (Revision E.1). Gaussian Inc., Pittsburgh, PA, 1995.
12 A. D. Becke, *J. Chem. Phys.*, 1993, **98**, 5648.
13 T. H. Dunning, Jr. and P. J. Hay, in *Modern Theoretical Chemistry*, ed. H. F. Schaefer, III, Plenum Press, New York, 1976, p. 1.
14 P. J. Hay and W. R. Wadt, *J. Chem. Phys.*, 1985, **82**, 270.
15 W. R. Wadt and P. J. Hay, *J. Chem. Phys.*, 1985, **82**, 284.
16 P. J. Hay and W. R. Wadt, *J. Chem. Phys.*, 1985, **82**, 299.
17 P. Legzdins, W. S. McNeil, K. M. Smith and R. Poli, *Organometallics*, 1998, **17**, 615.
18 P. E. M. Siegbahn, *J. Am. Chem. Soc.*, 1996, **118**, 1487.
19 M.-D. Su and S.-Y. Chu, *J. Am. Chem. Soc.*, 1997, **119**, 5373.
20 D. J. Burkey and P. Legzdins, manuscript in preparation.
21 R. Poli, *Chem. Rev.*, 1996, **96**, 2135.
22 B. K. Campion, R. H. Heyn and T. D. Tilley, *J. Chem. Soc., Chem., Commun.*, 1988, 278.
23 H. E. Bryndza, P. J. Domaille, R. A. Paciello and J. E. Bercaw, *Organometallics*, 1989, **8**, 379.
24 S. Shaik, M. Filatov, D. Schröder and H. Schwarz, *Chem. Eur. J.*, 1998, **4**, 193.
25 B. A. Arndsten and R. G. Bergman, *Science*, 1995, **270**, 1970.
26 P. W. Wanandi and T. D. Tilley, *Organometallics*, 1997, **16**, 4299.
27 H. Lehmkuhl, M. Bellenbaum, J. Grundke, H. Mauermann and C. Kruger, *Chem. Ber.*, 1988, **121**, 1719.
28 R. G. Bergman, P. F. Seidler and T. T. Wentzel, *J. Am. Chem. Soc.*, 1985, **107**, 4358.
29 J. M. Aramini, F. W. B. Einstein, R. H. Jones, A. H. Klahn-Oliva and D. Sutton, *J. Organomet. Chem.*, 1990, **385**, 73.
30 C. Leiva and D. Sutton, *Organometallics*, 1998, **17**, 1700.
31 D. L. Strout, S. Zaric, S. Niu and M. B. Hall, *J. Am. Chem. Soc.*, 1996, **118**, 6068.
32 C. Hinderling, D. Feichtinger, D. A. Plattner and P. Chen, *J. Am. Chem. Soc.*, 1997, **119**, 10 793.
33 H. F. Luecke and R. G. Bergman, *J. Am. Chem. Soc.*, 1997, **119**, 11 538.
34 S. Niu and M. B. Hall, *J. Am. Chem. Soc.*, 1998, **120**, 6169.
35 R. Poli, P. Legzdins and K. M. Smith, manuscript in preparation.

Received in Cambridge, UK, 6th July 1998; 8/05176C

The effect of substitution of the C–F group for the C–H group in crystal packing as well as thermal behaviour

Naoto Hayashi,*† Takashi Mori and Kiyoshi Matsumoto*

Graduate School of Human and Environmental Studies, Kyoto University, Yoshida, Sakyo-ku, Kyoto, 606-8501, Japan

The packing motif and/or thermal stability of a crystal is controlled by intermolecular C–F···π interactions.

The C–F group is similar to the C–H group in size. However, when the C–F group is substituted for the C–H group, the crystal structure is generally no longer identical.[1] In a few cases, the change in the packing motif has been explained in terms of C–H···F–C interaction,[2] π–π interaction,[3] *etc*. Here we report the first example of an intermolecular C–F··π interaction which controls the packing motif as well as the thermal stability of the crystal, on the basis of comparison of four crystalline complexes which are composed of triphenylmethanol derivatives, *i.e.* triphenylmethanol (**F0**), (4-fluorophenyl)diphenylmethanol (**F1**), bis(4-fluorophenyl)phenylmethanol (**F2**) and tris(4-fluorophenyl)methanol (**F3**), and MeOH.

By slow evaporation from MeOH solution, **F1** and **F2** afforded 1:1 complexes, as **F1**·MeOH‡ and **F2**·MeOH,‡ respectively, their stoichiometric ratios being the same as that of **F0**.[4] Interestingly, an X-ray analysis revealed that both **F1**·MeOH and **F2**·MeOH are isostructural to **F0**·MeOH;[5] one host and one guest molecule exist in an asymmetric unit, and two hosts and two guest molecules comprise a molecular assembly with the aid of a hydrogen bond (Fig. 1). The fact that none of the fluorine atoms take part in hydrogen bonding with the hydroxy groups is consistent with the reports of Dunitz and Taylor.[6] It is noteworthy that the fluorine atom is disordered in **F1**·MeOH. The disordered fluorines are observed only on two phenyl moieties [*i.e.* plane A and B, in Fig. 1(*a*)], occupancy factors of which are evaluated to be 0.69 and 0.31 for F(A) and F(B), respectively. Disorder of the fluorine atoms is also found in **F2**·MeOH, but it is not identical to that in **F1**·MeOH. The fluorine atoms in **F2**·MeOH are observed on all the three phenyl rings; the occupancy factors are 0.95, 0.80, and 0.25 for F(A), F(B), and F(C), respectively [Fig. 1(*b*)].

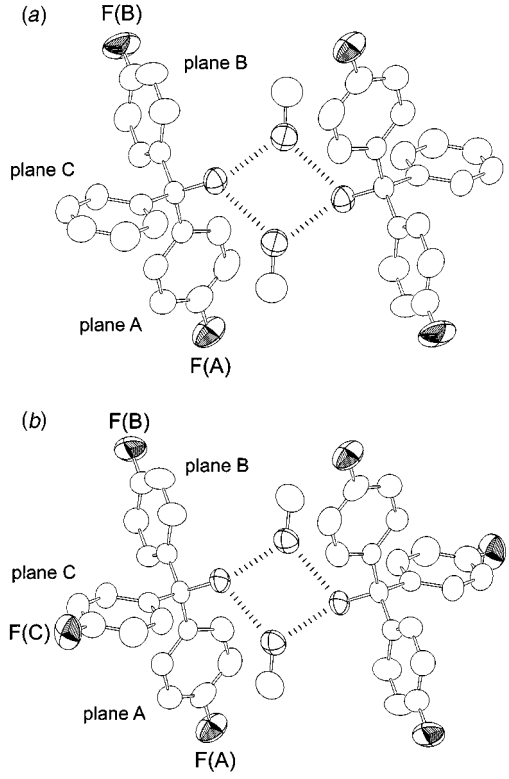

Fig. 1 Perspective views of (*a*) **F1**·MeOH and (*b*) **F2**·MeOH. For clarity, fluorine and oxygen atoms are represented by discriminated ellipsoids, and hydrogen atoms are omitted. Hydrogen bonds are specified by dotted lines.

Despite their isomorphous characteristics, the thermal behaviour of **F0**·MeOH, **F1**·MeOH and **F2**·MeOH upon DSC (differential scanning calorimetry) measurement§ are somewhat different. On heating, the guest molecule in **F0**·MeOH and **F1**·MeOH was lost at very similar temperatures (T_{onset} = 78.5[4] and 76.0 °C, respectively), whereas **F2**·MeOH released the guest at rather lower temperature (T_{onset} = 64.8 °C).

This finding can be explained in terms of C–H··π and C–F··π interactions: Fig. 2 shows that two phenyl rings in **F1**·MeOH, *i.e.* plane C and B, are arranged in an edge-to-face manner. The interplanar angle and centroid-to-centroid distance of the two planes are estimated to be 91.5° and 5.39 Å, respectively. No C–H··π interactions could be observed among the other pairs of phenyl rings. Such a T-shaped arrangement of two benzene rings is known to be energetically favourable.[7] If a fluorine atom is substituted onto plane C in this packing motif, the energetic advantage due to the C–H··π interaction will be lost. This is one of the principal reasons that the disordered fluorine atom in **F1**·MeOH was observed solely on plane A and B. On the other hand, the disordered fluorine atoms, F(A) and F(B), play no role with respect to the thermal stability of the lattice.

In the case of **F2**·MeOH, the disordered fluorine atoms are observed on the plane C as well. It causes the loss of the energetically favorable C–H··π interaction as well as introducing an electrostatic repulsion between the electronegative fluorine atom and the π-electrons. In addition to these, a steric

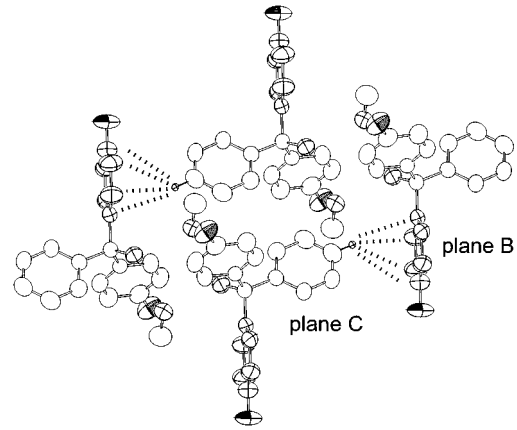

Fig. 2 Projection of the host–guest structure of **F1**·MeOH. Dashed lines represent CH–π interactions.

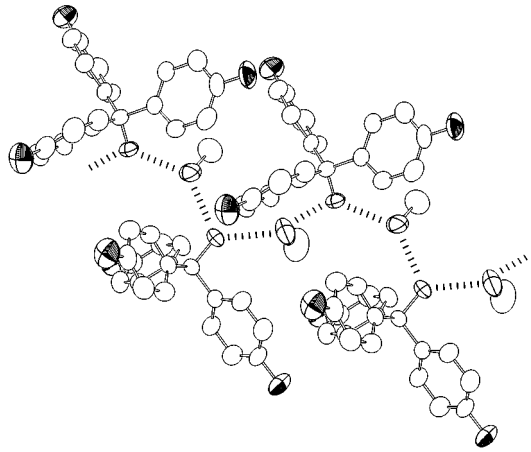

Fig. 3 Perspective view of **F3**·MeOH. For clarity, fluorine and oxygen atoms are represented by discriminated ellipsoids, and hydrogen atoms are omitted. Hydrogen bonds are specified by dotted lines.

repulsion arises, since the distance from the fluorine to the plane B is calculated to be 2.87 Å, which is significantly shorter than the sum of van der Waals radii's of each moiety (F = 1.47, C_{ar} = 1.77 Å).[8] The sum of these factors should lead the instability of the lattice of **F2**·MeOH, so that the guest MeOH is lost more readily than that of **F0**·MeOH and **F1**·MeOH.

Although **F3** also afforded 1:1 complex with MeOH, the crystal structure of **F3**·MeOH‡ is quite different from those of the others. The hydrogen-bonded cyclic network (H–G–H–G) is found in the other complexes, whilst the –H–G–H–G– sequence of an infinite chain of hydrogen bonding is observed in **F3**·MeOH (Fig. 3). Among the four MeOH complexes described here, **F3**·MeOH is thermally most unstable: the guest MeOH was released just at 48.3 °C (onset). The exceptional packing motif of **F3**·MeOH is ascribable to the unfavorable C–F··π interaction again. The C–F··π interaction is not critical in **F2**·MeOH with respect to the packing motif, because only one fourth of the *para* positions of plane C are substituted by fluorine atoms. However, complete occupation would make it too disadvantageous in energy for **F3** to adopt a similar packing motif to the other complexes, so that **F3**·MeOH crystallized in a distinct manner.

These results demonstrate new aspects of a fluorine in crystalline chemistry as well as in medicinal and biological chemistry. Further investigations on the effect of fluorine on crystal structure as well as thermal behaviour are currently underway.

Notes and References

† E-mail: hayashi@alchemy.jinkan.kyoto-u.ac.jp

‡ *Crystal data* for **F1**·MeOH: $C_{20}H_{19}F_1O_2$, M = 310.36, triclinic, $P\bar{1}$ (no.2), a = 9.348(4), b = 11.756(5), c = 8.537(3) Å, α = 98.93(4), β = 114.31(3), γ = 77.66(4)°, V = 832.8(6) Å^3, T = 298 K, Z = 2, μ(Mo-Kα) = 0.86 cm^{-1}, refined using 1438 reflections R = 0.066. For **F2**·MeOH: $C_{20}H_{18}F_2O_2$, M = 328.34, triclinic, $P\bar{1}$ (no.2), a = 9.489(3), b = 11.698(3), c = 8.595(3) Å, α = 99.35(2), β = 113.47(2), γ = 77.68(2)°, V = 851.8(4) Å^3, T = 298 K, Z = 2, μ(Mo-Kα) = 0.96 cm^{-1}, refined using 1427 reflections, R = 0.047. For **F3**·MeOH: $C_{20}H_{17}F_3O_2$, M = 346.32, monoclinic, Cc (no.9), a = 10.402(2), b = 23.251(4), c = 8.170(1) Å, β = 115.79(1)°, V = 1779.1(6) Å^3, T = 288 K, Z = 4, μ(Mo-Kα) = 1.03 cm^{-1}, refined using 1616 reflections, R = 0.045. All the structures were solved by direct methods and refined on teXsan (ref. 9). CCDC 182/948.

§ DSC analysis was performed as follows: crystals were removed from the mother liquor, blotted dry on filter paper and crushed before analysis. Sample weight in each case was 7–10 mg. The temperature range was from ambient temperature to 200 °C at a heating rate of 10 °C min^{-1}.

1 K. Vishnumurthy, T. N. G. Row and K. Venkantesan, *J. Chem. Soc., Perkin Trans. 2*, 1996, 1475; K. Vishnumurthy, T. N. G. Row and K. Venkatesan, *J. Chem. Soc., Perkin Trans. 2*, 1997, 615.
2 T. Hasegawa, K. Inukai, S. Kagoshima, T. Sugawara, T. Mochida, S. Sugiura and Y. Iwasa, *Chem. Commun.*, 1997, 1377.
3 G. W. Chates, A. R. Dunn. L. M. Henling, D. A. Dougherty and R. H. Grubbs, *Angew. Chem., Int. Ed. Engl.*, 1997, **36**, 248; G. W. Chates, A. R. Dunn. L. M. Henling, J. W. Ziller, E. B. Lobkovsky and R. H. Grubbs, *J. Am. Chem. Soc.*, 1998, **120**, 3641.
4 Although the inclusion properties of triphenylmethanol, X-ray crystal structure and thermal release of the guest component of its methanol clathrate have been reported (ref.5), we performed DSC analysis and a re-examination of the X-ray diffraction study (not shown) of it here for comparison.
5 E. Weber, K. Skobridis and I. Goldberg, *J. Chem. Soc., Chem. Commun.*, 1989, 1195.
6 J. D. Dunitz and R. Taylor, *Chem. Eur. J.*, 1997, **3**, 89.
7 J. L. Atwood, S. G. Bott, C. James and C. L. Raston, *J. Chem. Soc., Chem. Commun.*, 1992, 1349; J. L. Atwood, F. Hamada, K. D. Robinson, G. W. Orr and R. L. Vincent, *Nature*, 1991, **349**, 683; S. Apel, M. Czugler, V. J. Griffith, L. R. Nassimbeni and E. Weber, *J. Chem. Soc., Perkin Trans. 2*, 1997, 1949; T. Steiner and W. Saenger, *J. Chem. Soc., Chem. Commun.*, 1995, 2087; M. Nishio, M. Hirota, and Y. Umezawa, *The CH/π Interaction. Evidence, Nature and Consequences*, Wiley, New York, 1998.
8 A. Bondi, *J. Phys. Chem.*, 1964, **68**, 441.
9 TeXsan, Crystal Structure Analysis Package, Molecular Structure Corporation, 1992.

Received in Cambridge, UK, 15th May 1998; 8/03655A

The synthesis of water soluble isoindoline nitroxides and a pronitroxide hydroxylamine hydrochloride UV–VIS probe for free radicals

Damien A. Reid, Steven E. Bottle*† and Aaron S. Micallef

CIDC, School of Physical Sciences, Queensland University of Technology, GPO Box 2434, Brisbane Q 4001, Australia

The novel water soluble nitroxides 5-trimethylammonio-1,1,3,3-tetramethylisoindolin-2-yloxyl iodide 8 and 5-carboxy-1,1,3,3-tetramethylisoindolin-2-yloxyl 10 are prepared by nitration of the parent nitroxide 2 and bromination of its amine precursor 1; the stable ($t_{1/2}$ > 580 h in MeOH; *ca* 72 h in physiological saline) pronitroxide 2-hydroxy-1,1,3,3-tetramethylisoindoline hydrochloride 6 was synthesised by treatment of 2 with HCl gas in dry EtOH and reacts with radicals to form 2; the transformation can be followed by UV–VIS spectroscopy.

Nitroxide radicals have long been used as spin labels and probes in biological systems, where, in some cases, their presence also affords protection from oxidative stress and radiative damage.[1–4] However, the 1,1,3,3-tetramethylisoindolin-2-yloxyl (TMIO) nitroxides **2** (Scheme 1) have been largely overlooked for these applications, their main use to date being in spin trapping experiments.[5,6] The TMIO system enjoys a number of advantages over the commercially available nitroxides, the most significant being its excellent thermal and chemical stability and superior EPR linewidths.[7] However, its use in biological systems has been limited because of the near absence of any water soluble derivatives. The sulfonate has been reported,[8] but has not been fully characterised. We here report the synthesis of two water soluble TMIO derivatives, 5-carboxy-1,1,3,3-tetramethylisoindolin-2-yloxyl **10** and 5-trimethylammonio-1,1,3,3-tetramethylisoindolin-2-yloxyl iodide **8**. We also report an alternative strategy for converting the hydrophobic TMIO into a water soluble derivative, with the synthesis of 2-hydroxy-1,1,3,3-tetramethylisoindoline hydrochloride **6**, the first stable water soluble pronitroxide incorporating the isoindoline system.

Compounds **1** and **2** were prepared according to the literature procedures of Griffiths *et al.*[9] Treatment of **1** with Br_2 (6 equiv.) in the presence of $AlCl_3$ (12 equiv.) resulted in oxidative debenzylation and bromination giving 2,5-dibromo-1,1,3,3-tetramethylisoindoline **5** (40%).[10] The slow addition of Bu^nLi (3.6 equiv.) to a solution of **5** in dry THF and quenching gave 5-carboxy-1,1,3,3-tetramethylisoindoline **9** (not isolated) upon aqueous workup [δ_H([$^2H_6$]DMSO) 1.70 (12H, s, Me), 7.45 (1H, d, ArH), 7.88 (1H, d, ArH), 7.94 (1H, dd, ArH), 9.55 (2H, br, NH_2^+); δ_C([$^2H_6$]DMSO) 28.5 (Me), 68.0 (C1, C3), 122.3 (ArC), 123.3 (ArC), 123.7 (ArC), 130.7 (ArC), 143.0 (ArC), 146.8 (ArC), 166.8 (C=O)]. Tungstate oxidation[9] of **9** gave **10** [23% (based on **5**), mp 214–218 °C; $CHCl_3$, g = 2.00585, a_N = 14.45 G (Found: C, 66.57; H, 6.92; N, 6.28; Calc. for $C_{13}H_{16}NO_3$: C, 66.67; H, 6.84; N, 5.98%); *m/z* (EI) 234, 220, 219, 204, 189].

The synthesis of **3** was achieved *via* the quantitative nitration of **2** according to the method of Bolton *et al.*[11] Hydrogenation of **3** (H_2, Pd/C, 10 psi, 4 h) followed by treatment with PbO_2 (0.5 equiv.) to reoxidise to the nitroxide gave **4** as a yellow solid [98%; mp 195–196 °C (from EtOH) (lit.,[12] 198 °C)]. This material possesses substantial synthetic utility, the amine providing a pathway for coupling to amino acids and proteins as well as incorporating into sugars.[13]

The water soluble ammonium nitroxide **8** was prepared *via* basic methylation of **4** (MeI, 120 equiv.; NaH, 10 equiv.) in a sealed vessel (65 °C, 96 h). The product was isolated *via* extraction into water (**CAUTION**: excess NaH) and recovered

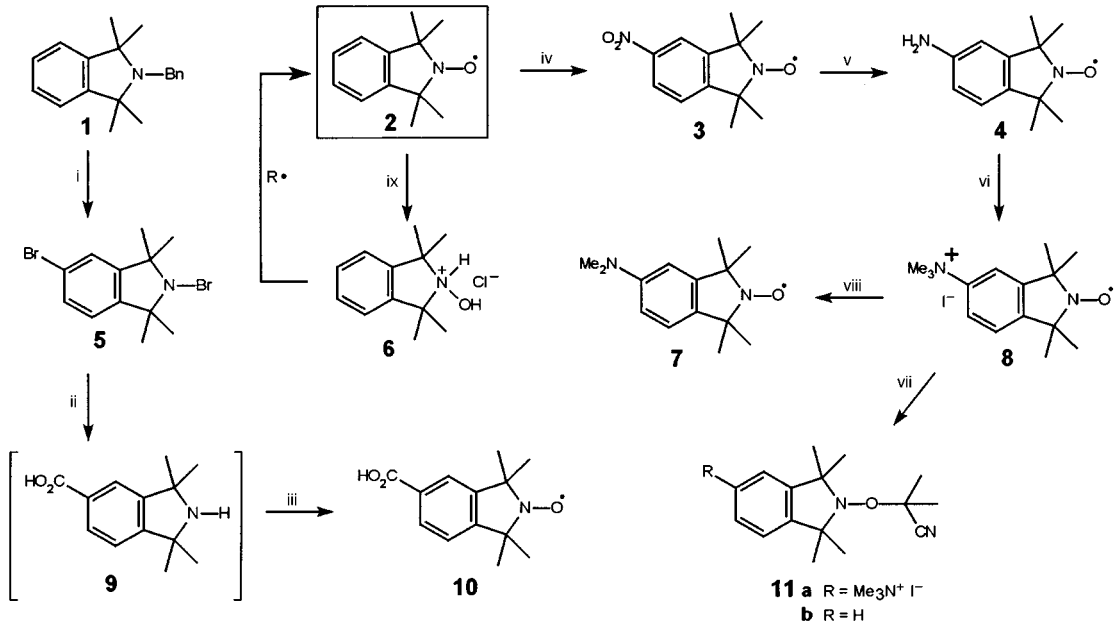

Scheme 1 *Reagents and conditions*: i, Br_2, $AlCl_3$, 0 °C, 40%; ii, Bu^nLi, −78 °C, then CO_2; iii, H_2O_2, Na_2WO_4, 23 (from **5**); iv, HNO_3, H_2SO_4, > 95%; v, H_2, Pd, then PbO_2, > 95%; vi, MeI, NaH, 65 °C, 90%; vii, AIBN, 90 °C, 90%; viii, 170 °C, 0.1 mmHg; ix, HCl, EtOH, > 95%

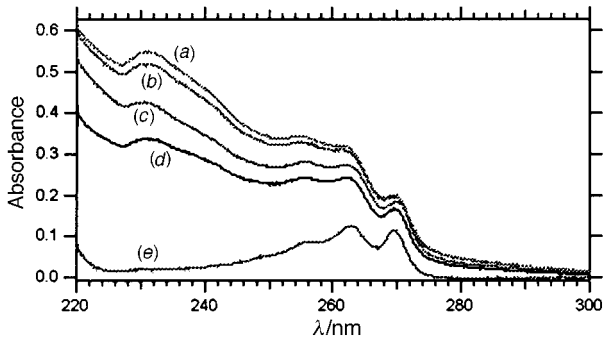

Fig. 1 UV–VIS spectra following the reaction of **6** (2.6×10^{-4} M) with AIBN (0.5 equiv.), 90 °C, in degassed MeOH under N_2 after (*a*) 0.0, (*b*) 1.5, (*c*) 3.0, (*d*) 7.5 and (*e*) 9.0 h. Chromatography confirmed only trace amounts of 2-cyanopropyl adduct **11b**.

by evaporation. The crude solid was taken up in hot EtOH (*ca.* 80 ml) and passed through a short Al_2O_3 column [Al_2O_3 (neutral, act. I), eluent: EtOH–EtOAc (1:4), 700 ml]. Evaporation yielded a yellow crystalline solid **8** [90%; mp 173–174 °C (decomp.) (from H_2O), 175–176 °C (decomp.) (from EtOH, slightly contaminated with inorganics) (Found: C, 46.70; H, 6.58; N, 7.21. Calc. for $(C_{15}H_{24}N_2OI)_2 \cdot H_2O$: C, 46.88; H, 6.56; N, 7.29%); *m/z* (FAB) 248; (EI) 233 ($M - 15$), 142 (MeI^+), 127 (I^+) (accurate to *ca.* 1 ppm)]. The nitroxide **8** has also been characterised by EPR (H_2O, g = 2.00562, a_N = 15.83 G, a_N = 0.204 G), NMR analysis of its 2-cyanopropyl adduct **11a** and by its characteristic thermal decomposition product **7** [mp 126–129 °C (Found: C, 72.10; H, 9.18; N, 11.90. Calc. for $C_{14}H_{21}N_2O$: C, 72.06; H, 9.07; N, 12.01%); *m/z* (EI) 233]. The nitroxide **8** is soluble in water at a concentration of *ca.* 120 mM, exceeding the typical[14,15] solubility requirement for spin probes.

The synthesis of **6** was achieved by bubbling dry HCl into a stirred solution of **2** in EtOH. The reaction was complete when the strong orange colour of the nitroxide had reduced to a faint yellow (*ca.* 0.5 h). Evaporation yielded a white solid **6** [98%; mp 196–198 °C (decomp.) (from MeCN) (Found: C, 63.54; H, 8.05; N, 6.07. Calc. for $C_{12}H_{18}NOCl$: C, 63.29; H, 7.97; N, 6.15%); $\delta_H(CDCl_3)$ 1.79 (12H, s, Me), 7.18 (2H, d, ArH), 7.39 (2H, d, ArH); $\delta_C(CDCl_3)$ 25.5 (Me), 75.9 (C1, C3), 121.9 (ArC), 129.7 (ArC), 139.3(ArC)]. The hydroxylamine hydrochloride **6** is soluble in water at concentrations greater than 1 M.

Hydroxylamines have been used[16] as oxygen sensitive probes in MRI and recently[17] in the determination of reactive oxygen species by EPR analysis with ten-fold greater sensitivities than can be achieved using conventional nitrone spin traps. We have found that the transition from **6** (and its unprotonated equivalent) to **2** can be monitored by UV–VIS spectroscopy and have followed the reaction of **6** with the 2-cyanopropyl radicals generated from the thermolysis of AIBN (see Fig. 1). Blank reactions confirmed this transition did not occur in the absence of AIBN under identical conditions. The ability to observe the formation of a nitroxide spectroscopically, without the use of EPR methods, is quite novel and demonstrates the potential for **6** to act as a UV–VIS probe for free radicals. The hydroxylamine hydrochloride **6** is particulary inert in the solid form and is even stable in solution, having a half life ($t_{1/2}$) > 580 h at 0.26 mM in MeOH exposed to the atmosphere at room temperature (determined by UV–VIS analysis). Treatment with base, however, greatly reduces the stability of **6**, the free hydroxylamine having $t_{1/2}$ < 4 h in MeOH solution. This pronitroxide also possesses significant stability in physiological saline phosphate buffer (pH 6.9) where it has $t_{1/2}$ *ca.* 72 h at 0.26 mM. Notably, when converted to the nitroxide in physiological media this species remains in solution (at this concentration), again demonstrating the potential of **6** as a water soluble radical scavenger.

We thank the CIDC, QUT and the ARC for financial support.

Notes and References

† E-mail: s.bottle@qut.edu.au

1 *Free Radicals in Diagnostic Medicine*, ed. D. Armstrong, Plenum, New York, 1994, p. 241.
2 *Oxygen Free Radicals and Scavengers in the Natural Sciences*, ed. G. Mozsik, I. Emerit, J. Feher, B. Matkovics and A. Vincze, Akademiai Kindo, Budapest, 1993, p. 63.
3 S. M. Hahn, C. M. Krishna, A. Samuni, W. DeGraff, D. O. Cuscela, P. Johnstone and J. B. Mitchell, *Cancer Res. (Suppl.)*, 1994, **54**, 2006s.
4 A. Samuni, D. Godinger, J. Aronovitch, A. Russo and J. B. Mitchell, *Biochemistry*, 1991, **30**, 555.
5 W. K. Busfield, K. Heiland and I. D. Jenkins, *Tetrahedron Lett.*, 1994, **35**, 6541.
6 W. K. Busfield, I. D. Jenkins and P. Van Le, *Polym. Bull.*, 1996, **36**, 435.
7 D. G. Gillies, L. H. Sutcliffe and X. Wu, *J. Chem. Soc., Faraday Trans.*, 1994, **90**, 2345.
8 D. G. Gillies, L. H. Sutcliffe, X. Wu and P. S. Belton, *Food Chem.*, 1996, **55**, 349. Full synthetic details for this species, including yield and characterisation, have not as yet been published.
9 P. G. Griffiths, G. Moad, E. Rizzardo and D. H. Solomon, *Aust. J. Chem.*, 1983, **36**, 397.
10 A. S. Micallef and S. E. Bottle, unpublished work.
11 R. Bolton, D. G. Gillies, L. H. Sutcliffe and X. Wu, *J. Chem. Soc., Perkin Trans. 2*, 1993, 2049.
12 A. M. Giroud and A. Rassat, *Bull. Soc. Chem. Fr.*, 1979, **1–2**, II-48.
13 P. E. James, S. K. Jackson, C. C. Rowlands and B. J. Mile, *J. Chem. Soc., Perkin Trans. 2*, 1992, 1503.
14 J. F. Glockner, H.-C. Chan and H. M. Swartz, *Magn. Reson. Med.*, 1991, **20**, 123.
15 P. D. Morse, II and A. I. Smirnov, *Magn. Reson. Chem.*, 1995, **33**, S46.
16 F. Desmar. M. Kueder, S. Rugeli, A. Blinc, M. Sentjure and S. Pecar, *J. Magn. Reson.*, 1991, **95**, 281.
17 S. Dikalov, M. Skatchkov and E. Bassenge, *Biochem. Biophys. Res. Commun.*, 1997, **230**, 54.

Received in Cambridge, UK, 7th July 1998; 8/05228J

Observation of supramolecular π–π dimerization of a dinuclear ruthenium complex by ^{1}H NMR and ESMS

Eléna Ishow, André Gourdon* and Jean-Pierre Launay

Groupe Electronique Moléculaire, CEMES-CNRS, UPR 8011, BP 4347 29 Rue Jeanne Marvig, 31055 Toulouse, France. E-mail: gourdon@cemes.fr

The dinuclear ruthenium complex of bis{dipyrido[3,2-*f*:2′,3′-*h*]quinoxalo}[2,3-*e*:2′,3′-*l*]pyrene (bqpy) forms dimers in solution maintained only by π–π stacking of the bridging ligand, stable enough to be observed not only by ^{1}H NMR spectroscopy but also by electrospray mass spectrometry at low accelerating cone voltage.

In recent years much attention has been drawn to supramolecular architectures maintained by weak interactions.[1] We report here the first evidence, by ^{1}H NMR and electrospray mass spectrometry, of the supramolecular dimerization of a dinuclear metallic complex only maintained by π-π stacking.

We have recently observed by ^{1}H NMR spectroscopy the supramolecular aggregation in solution of the monometallic complex $[(bpy)_2Ru(tpphz)]^{2+}$ where tpphz is the fully aromatic tetrapyrido[3,2-*a*:2′,3′-*c*:3″,2″-*h*:2‴,3‴-*j*]phenazine.[2] This dimerization by π–π stacking of the tpphz part, was not observed for the dinuclear complex $[(bpy)_2Ru(tpphz)Ru(bpy)_2]^{4+}$. Indeed, the relatively short intermolecular Ru–Ru distance (12.77 Å determined by X-ray diffraction), and therefore the high intermolecular coulombic repulsions, preclude any efficient stacking. Along these lines we have synthesized the dinuclear complex **1** of bis-{dipyrido[3,2-*f*:2′,3′-*h*]quinoxalo}[2,3-*e*:2′,3′-*l*]pyrene (bqpy). In this complex, the calculated intermetallic distance is *ca.* 20 Å, long enough to allow an efficient aggregation of two complexes.

Attempts to synthesize bqpy from 5,6-diamino-1,10-phenanthroline and tetraketopyrene[3] gave only intractable mixtures of insoluble bqpy and by-products. This lack of solubility emphasizes the very important π–π interactions in this type of compound. We have used instead the alternative synthetic route depicted in Scheme 1 which involves successive functionalizations of soluble precursor complexes.† Reaction of 6-amino-5-nitro-1,10-phenanthroline, obtained by nucleophilic amination of 5-nitro-1,10-phenanthroline,[2] with $Ru(bpy)_2Cl_2\cdot 2H_2O$ in refluxing ethanol gave the corresponding amino–nitro complex in 82% yield which was then reduced by hydrazine hydrate over Pd/C to provide the diamino complex **2** in 89% yield. Condensation with tetraketopyrene[3] gave first **3** and then **1** on prolonged heating in acetonitrile–methanol–acetic acid (yield 64%). In contrast to the free ligand bqpy, **1** is soluble in various solvents depending on its counter anions.

As expected by analogy with the mononuclear $[(bpy)_2Ru(tpphz)]^{2+}$ complex, the ^{1}H NMR spectra are very sensitive to concentration.

On one hand, the bqpy protons are clearly the most affected with displacements up to 0.9 ppm between extreme conditions. Their signals are significantly broadened and move upfield with increasing concentration, the most influenced ones being the pyrene protons H^d and H^e; on the other hand, the bpy proton signals are only slightly broadened and move downfield in a smaller extent (maximum 0.1 ppm). We have attributed this concentration effect to the aggregation in solution of dinuclear species by π-stacking of the central bqpy aromatic parts. Consistent with this hypothesis, a temperature increase causes similar effects as dilution. This aggregation, which must be rapid with respect to the NMR timescale, modifies the local electron density and/or the ring current effects in the vicinity of the bqpy ligand. As a matter of fact, the π-stacking localizes the electron density on the central quinoxalopyrene part and decreases the electron density on the ruthenium atoms. These ^{1}H NMR spectra modifications are in agreement with those encountered in some host–guest organic complexes, catenanes and rotaxanes[4] in which inclusion induces shielding and broadening of the aromatic hosts and guest signals. The association constant monomer–dimer has been estimated at 830 M^{-1} by standard curve-fitting to a plot of chemical shift *vs.* concentration (at concentrations below 1.9×10^{-3} M).

This dimerization in solution can also be observed by electrospray mass spectrometry (ESMS). This soft ionisation method[5] has been recently used for the direct characterization of weakly bonded species containing non-covalent interactions such as receptor–ligand,[6] enzyme–substrate,[7] heme–protein complexes,[8] oligonucleotide duplexes[9] and hydrogen-bonded supramolecular assemblies.[10] Moreover, it has also been possible to observe by this technique the formation of multinuclear metal coordination complexes under equilibrium conditions.[11] As low ionisation energies are involved, non-covalent molecular architectures, the stability of which depends on weak interactions, are not destroyed so that ion distributions in the mass spectra reflect with confidence the species arrangement in solution. In our case, we have been able to isolate and discriminate the formation of the supramolecular dimer of **1** only maintained by weak π–π interactions by varying the accelerating cone voltage to control the fragmentation during the ionisation process. The ESMS spectrum recorded at cone voltage of 60 V showed four major peaks at *m/z* 1873, 864, 526 and 359.9 corresponding to pseudomonomolecular ions with the loss of 1, 2, 3, and 4 PF_6^-, and also a fifth intense peak at *m/z* 1200. A state of charge of $\mathbf{3}^+$ was found for this peak by optimizing the resolution of the isotopic pattern. Both values, charge and mass unity, are in total agreement with the formation of the dimeric entity $\{[(bpy)_2Ru^{II}(bqpy)-Ru^{II}(bpy)_2]_2 + 5PF_6^-\}^{3+}$ corresponding to a dimeric neutral

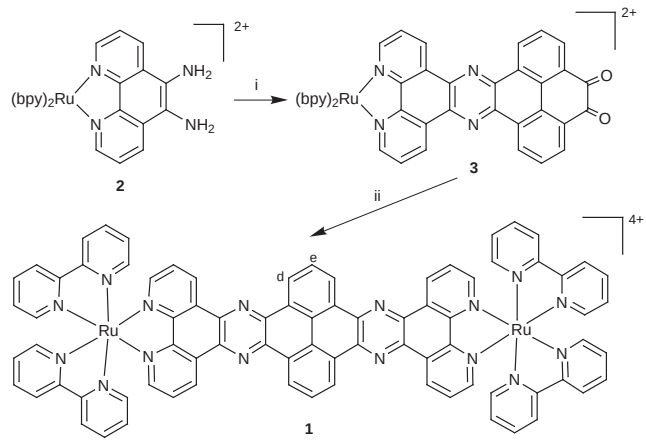

Scheme 1 *Reagents and conditions*: i, ii, tetraketopyrene, MeCN–MeOH–AcOH (20:15:1 v/v), reflux, 4 d, 64%

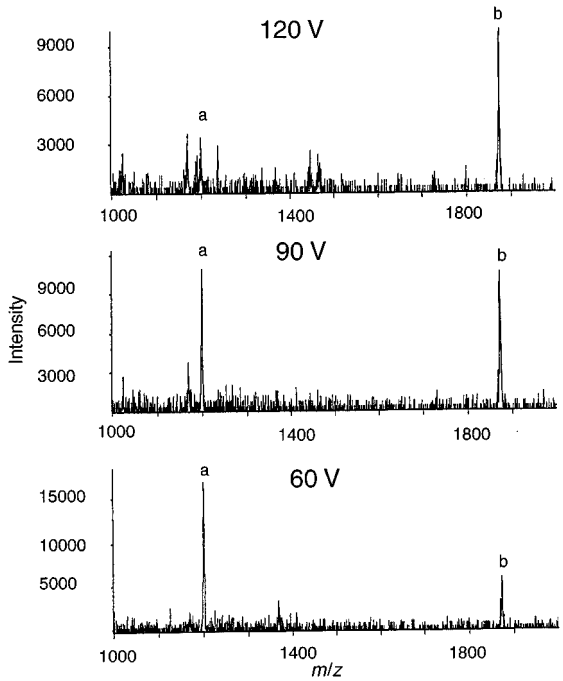

Fig. 1 Detail of the ESMS spectra of **1** in MeCN/H_2O 1 : 1 at cone voltages of 60, 90 and 120 V in the range *m/z* 1000–2000. a refers to the dimeric species $\{[\mathbf{1}_2](PF_6)_5\}^{3+}$ and b to the superimposition of the monomer $\{[\mathbf{1}](PF_6)_3\}^{+}$ and of the dimer $\{[\mathbf{1}_2](PF_6)_6\}^{2+}$. Note the scale change at 60 V.

species $\mathbf{1}_2$ after loss of three PF_6^- counter anions PF_6^-. And likewise, the peak at *m/z* 1873 is also clearly an isotopically resolved overlap of $\{\mathbf{1}\text{-}PF_6\}^+$ and $\{\mathbf{1}_2\text{-}2PF_6\}^{2+}$ species. Moreover, by raising the cone voltage to 90 and 120 V (Fig. 1), this peak intensity decreased and finally vanished, whereas the four other peaks remained nearly unchanged; simultaneously, the voltage increase engendered the partial fragmentation of the dinuclear complex **1** as a novel peak appeared at *m/z* 1169, assigned to the fragmentation product $[(bpy)_2Ru(bpqy)]^{2+}$ with one PF_6^-.

Although the exact geometry of this dimer in solution cannot be determined with accuracy by experimental techniques, some insights can be inferred from theories and experiments on small polyaromatic organic molecules and from molecular mechanics calculations. The steric crowding of the bulky $Ru^{II}(bpy)_2$ extremities imposes a geometry in which the metal–metal axes are more or less perpendicular to each other to allow a quite short bqpy–bqpy distance. In that conformation, both bqpy planes can be either perpendicular (T-shape) or parallel (stacked). On the basis on previous studies,[12] it seems reasonable to assume a stacked geometry for the dimer $\mathbf{1}_2$ in which the ligand bqpy exhibits a large aromatic extension. Stability of such stacked large systems actually results from a compromise between the dominant favourable van der Waals attraction, which seems to be linearly correlated with the number of aromatic moieties, and the repulsive coulombic interactions. In the case of the dimer $\mathbf{1}_2$, these repulsive coulombic interactions are considerably reduced by the strong electron-acceptor ruthenium extremities which decrease the electronic density on the central pyrene-type regions.[13] By positioning two complexes in this perpendicular conformation (Fig. 2), with the bqpy planes parallel at 3.5 Å, the distance between two ruthenium centres belonging to two different molecules is estimated to 14.5 Å which precludes any significant couloumbic repulsion between the metallic moieties.

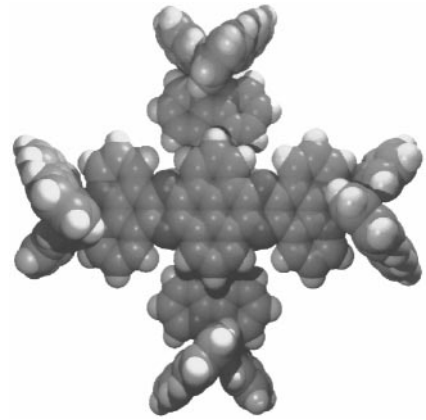

Fig. 2 CPK representation of the dimer $\mathbf{1}_2$

Additionally, such a geometry often exhibits an offset of the aromatic parts from the face-to-face aggregation for the stacked molecules to accommodate with the repulsive coulombic interactions allowed here by the length of the bridging ligand.

This work was supported by the CNRS and the EEC program Electron and Energy Transfer in Model Systems(CHRXCT-94-0538). S. Richelme and C. Claparols are acknowledged for ES–MS experiments.

Notes and References

† Spectroscopic data for **1**: ^{1}H NMR (Bruker WF250, 250 MHz, CD_3CN, 298 K, 2.6×10^{-4} M); δ 9.74 (d, *J* 7.0 Hz, 4H; H^d), 9.63 (d, *J* 8.2 Hz, 4H; H^c), 8.61 (d, *J* 8.3 Hz, 4H; H^3), 8.57 (d, *J* 8.5 Hz, 4H; $H^{3'}$), 8.38 (d, *J* = 7.0 Hz, 2H; H^e), 8.30 (dd, *J* 5.4, 1.3 Hz, 4H; H^a), 8.17 (ddd, *J* 8.0, 7.9, 1.4 Hz, 4H; H^4), 8.06 (ddd, *J* 8.0, 7.9, 1.4 Hz, 4H; $H^{4'}$), 7.99 (dd, *J* 8.2, 5.3 Hz, 4H; H^b), 7.92 (d, *J* 5.1 Hz, 4H; H^6), 7.82 (d, *J* 5.3 Hz, 4H; $H^{6'}$), 7.52 (ddd, J 6.5, 6.5, 1.2 Hz, 4H; H^5), 7.21 (ddd, J 6.2, 6.2, 1.2 Hz, 4H; $H^{5'}$); MS (ESMS, Perkin-Elmer Sciex, solvent: MeCN–H_2O (1:1 v/v), injection 5 µl min^{-1}); *m/z* 1873 $[M - PF_6^-]^+$, 864 $[M - 2PF_6^-]^{2+}$, 526 $[M - 3PF_6^-]^{3+}$, 359.9 $[M - 4PF_6^-]^{4+}$.

1 J.-M. Lehn, *Pure Appl. Chem.*, 1978, **50,** 871; *Supramolecular Chemistry*, VCH, Weinheim, 1995.
2 J. Bolger, A. Gourdon, E. Ishow and J.-P. Launay, *Inorg. Chem.*, 1996, **35**, 2937; *J. Chem. Soc., Chem. Commun.*, 1995, 1799.
3 H. Vollmann, H. Becker, M. Corell and H. Streeck, *Justus Liebigs Anal. Chem.*, 1937, **531**, 2.
4 See for example: D. Philp and J. F. Stoddart, *Angew. Chem., Int. Ed. Engl.*, 1996, **35**, 1154 and references therein; B. J. Whitlock and H. W. Whitlock, *J. Am. Chem. Soc.*, 1990, **112**, 3910.
5 M. Przybylski and M. O. Glocker, *Angew. Chem., Int. Ed. Engl.*, 1996, **35**, 806 and references therein.
6 B. Ganem, Y.-T. Li and J. D. Henion, *J. Am. Chem. Soc.*, 1991, **113**, 6294.
7 M. Baca and S. B. Kent, *J. Am. Chem. Soc.*, 1992, **114**, 3992; B. Ganem, Y.-T. Li and J. D. Henion, *J. Am. Chem. Soc.*, 1991, **113**, 7818.
8 V. Katta and B. T. Chait, *J. Am. Chem. Soc.*, 1991, **113,** 8534.
9 B. Ganem, Y.-T. Li and J. D. Henion, *Tetrahedron Lett.*, 1993, **34**, 1445.
10 K. C. Russel, E. Leize, A. Van Dorsselaer and J.-M. Lehn, *Angew. Chem., Int. Ed. Engl.*, 1995, **34**, 209.
11 E. Leize, A. Van Dorsselaer, R. Krämer and J.-M. Lehn, *J. Chem. Soc., Chem. Commun.*, 1993, 990; A. Marquis-Rigault, A. Dupont-Gervais, P. N. W. Baxter, A. Van Dorsselaer and J.-M. Lehn, *Inorg. Chem.*, 1996, **35**, 2307 and references therein.
12 H.-J. Scheider, T. Schiestel and P. Zimmermann, *J. Am. Chem. Soc.*, 1992, **114**, 7698.
13 F. Cozzi, M. Cinquini, R. Annuziata and J. S. Siegel, *J. Am. Chem. Soc.*, 1993, **115**, 5330.

Received in Basel, Switzerland, 27th April 1998; Revised manuscript received 21st July 1998; 8/05809A

Utility of a diene–tricarbonyliron complex as mobile chiral auxiliary: iterative use for constructing contiguous chiral centers

Yoshiji Takemoto,*[a] Yasutaka Baba,[b] Naoki Yoshikawa,[b] Chuzo Iwata,[b] Tetsuaki Tanaka*[b] and Toshiro Ibuka[a]

[a] *Graduate School of Pharmaceutical Sciences, Kyoto University, Sakyo-ku, Kyoto 606-8501, Japan. E-mail: takemoto@pharm.kyoto-u.ac.jp*

[b] *Graduate School of Pharmaceutical Sciences, Osaka University, 1-6 Yamada-oka, Suita, Osaka 565-0871, Japan*

Three stereogenic centers bearing azide, methoxy, and ethylthio groups, have been constructed stereoselectively using the sole chirality of the $Fe(CO)_3$ group with concurrent 1,2-migration of the $Fe(CO)_3$ group and the obtained product was converted to an *anti*-aminoalcohol derivative to determine the absolute stereochemistry.

Nucleophilic attack on coordinated polyenes is an important reaction in π-organometallic chemistry.[1] If reactions of this type occur with predictable regio- and stereo-selectivity, they can be of synthetic utility. For example, the reactivity of acyclic (pentadienyl)iron(1+) cations has been the subject of recent intense investigations.[2] However, compared with cyclic iron(1+) cation complexes,[3] regio- and stereo-selective nucleophilic addition to the acyclic (pentadienyl)iron(1+) cations seems to be difficult due to their configurational flexibility. Thus far, several efficient methods, which skip the isolation of the acyclic (pentadienyl)iron(1+) cations (*in situ* generation), have been developed and applied to natural product synthesis.[4] Previously, we described the regio- and stereo-selective 1,5-nucleophilic substitution of the cyanophosphate $Fe(CO)_3$ complexes with several heteroatomic nucleophiles, giving the 1,2-migrated products of the $Fe(CO)_3$ group with (*E*,*Z*)-configuration.[5] Here, we wish to describe the regio- and stereoselective synthesis of (*E*,*E*)-1,5-substituted adducts and their novel application to construction of contiguous stereogenic centers in acyclic alkenes (Scheme 1).

During our studies on the 1,5-nucleophilic substitution of the cyanophosphate **1**† with methanol, we found that the 1,5-substitution of **1** into the (*E*,*E*)-adducts was catalyzed by trityl perchlorate ($TrClO_4$) in the presence of various nucleophiles. Indeed, treatment of **1** with 10 equiv. of heteroatomic nucleophiles such as methanol, ethanol, and $TMSN_3$ in the presence of 1.1 equiv. of $TrClO_4$ in THF at room temperature gave the desired products **2a**–**c**‡ in moderate yields in all cases (Scheme 2). Furthermore, $TrClO_4$ also promoted the isomerization of the (*E*,*Z*)-adduct **3**‡ to the (*E*,*E*)-adduct **2a**‡ in 81% yield.

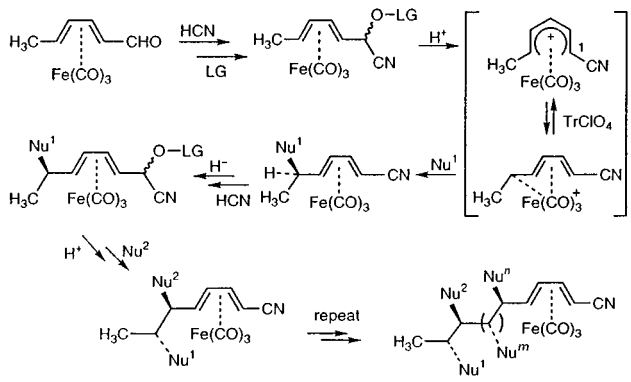

Scheme 1 Utility of an iron–tricarbonyl complex as a mobile chiral ligand

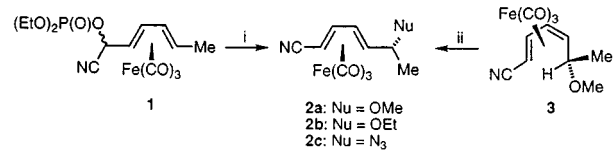

Scheme 2 *Reagents and conditions*: i, NuH (10 equiv.), $TrClO_4$ (1.1 equiv.), THF, r.t., 49% (Nu = MeOH) for **2a**; 41% (Nu = EtOH) for **2b**; 56% (Nu = $TMSN_3$) for **2c**; ii, MeOH (10 equiv.), $TrClO_4$ (1.1 equiv.), THF, r.t., 81%

We next examined the possibility of iterative manipulation of this 1,5-nucleophilic substitution with the obtained azide **2c** (Scheme 3). The requisite cyanophosphate **4** was prepared from **2c** as follows. The reduction of **2c** with diisobutylaluminium hydride (DIBAL-H) was followed by the reaction with diethylphosphoryl cyanide[6] to afford the desired cyanophosphate **4**.† The crude cyanophosphate **4** was subjected to a catalytic amount of $BF_3{\cdot}OEt_2$ in methanol at 0 °C to give rise to the (*E*,*Z*)-1,2-migrated product **5**‡ as a single isomer in 53% yield in two steps (method A).[5] On the other hand, the subjection of **4** to 1.1 equiv. of $TrClO_4$ and 10 equiv. of methanol in THF at room temp. afforded the (*E*,*E*)-1,2-migrated product **6**‡ as a single isomer in 52% yield in two steps (method B). These results indicate that the second nucleophile was introduced regio- and stereo-selectively with the 1,2-migration of the $Fe(CO)_3$ group without influence of the azide group.

In order to determine the absolute stereochemistry of **6** and also to extend this method to the asymmetric synthesis of a natural product such as 2,3-*anti*-aminoalcohol[7] **14** (Scheme 4), we next applied this iterative manipulation to the chiral compound (+)-**2c**. Although we have already reported the efficient asymmetric synthesis of the chiral $Fe(CO)_3$ complexes by the catalytic asymmetric alkylation of *meso*-hexadienal $Fe(CO)_3$ complex **7**, the reaction with dimethylzinc resulted in low yield and poor enantioselectivity.[8] So, we first investigated other reaction conditions to obtain (+)-**2c** enantioselectively. After many experiments, we found that Kobayashi's procedure[9]

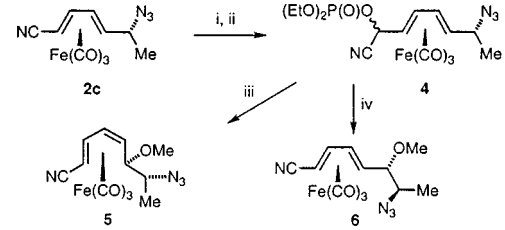

Scheme 3 *Reagents and conditions*: i, DIBAL-H, CH_2Cl_2, −78 °C, 78%; ii, $(EtO)_2P(O)CN$, LiCN, THF, r.t.; iii, $BF_3{\cdot}Et_2O$, MeOH, 0 °C, 53%; iv, $TrClO_4$, MeOH, THF, r.t., 52%

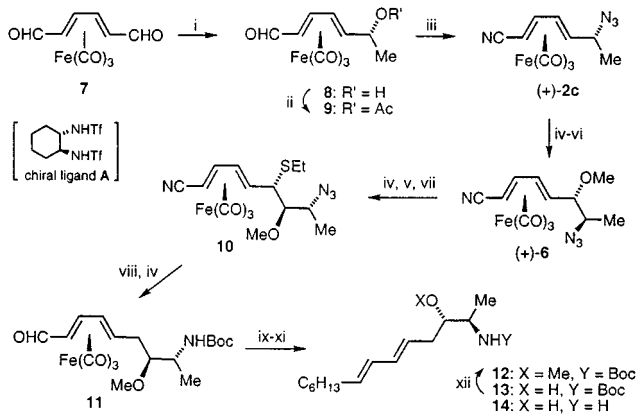

Scheme 4 *Reagents and conditions*: i, Me_2Zn, $Ti(OPr^i)_4$, chiral ligand (A), −20 → 0 °C, toluene, 71%; ii, Ac_2O, pyridine, CH_2Cl_2, r.t., 80%; iii, $TMSN_3$, $Sc(OTf)_3$, CH_2Cl_2, r.t., 90%; iv, DIBAL-H, CH_2Cl_2, −78 °C, 88% for **2c**, 77% for **6a**, 78% for **10**; v, $(EtO)_2P(O)CN$, LiCN, THF, r.t.; vi, $TrClO_4$, MeOH (10 equiv.), THF, r.t., 52%; vii, $TrClO_4$, EtSH (10 equiv.), THF, r.t., 61%; viii, H_2 (5 atm), 10% Pd/C, $(BOC)_2O$, MeOH, r.t., 81%, ix, $C_5H_{11}PPh_3Br$, Bu^nLi, toluene, −78–0 °C, 73%; x, H_2 (3 atm), 10% Pd/C, MeOH, r.t., 81% xi, Me_3NO, benzene, 60 °C, 85%; xii, MeI, Ag_2O, MeCN, reflux, 53%

was suitable for the purpose. The reaction of **7** with 1.8 equiv. of dimethylzinc and 1.8 equiv. of titanium(IV) isopropoxide in the presence of the chiral ligand (**A**) in toluene at 0 °C gave rise to monomethylated complex **8** in 71% yield with 96% ee. After acetylation of **8**, an azide group was introduced stereoselectively by the treatment of **9** with $TMSN_3$ and $Sc(OTf)_3$ in CH_2Cl_2 to afford (+)-**2c**.§ Here we undertook the same manipulation developed above (method B) with (+)-**2c** to obtain the *anti*-adduct (+)-**6**‡ in a comparable yield without any racemization. The further introduction of an ethylthio group into (+)-**6** by a similar procedure using $TrClO_4$ and ethanethiol (method B) also proceeded successfully to give the desired (*E*,*E*)-adduct **10**‡ as a single isomer in 61% yield. The hydrogenation in the presence of di-*tert*-butyl dicarbonate and sequential reduction with DIBAL-H of **10** gave the carbamate **11**, which was converted to **12** by a three-step sequence [Wittig reaction, hydrogenation over 10% Pd/C, and decomplexation]. This compound **12** was identical to the synthetic sample which was prepared from the known (2*R*,3*S*)-aminoalcohol derivative **13**[10] by the methylation (MeI, Ag_2O, MeCN, reflux; 53%) in respect of ^1H NMR, IR, mass, and $[\alpha]_D$. Based on these results, it is revealed that all substituents in **6** and **10** would be introduced from the opposite side of the $Fe(CO)_3$ group to give all *anti*-adducts in this iterative manipulation using method B. In conclusion, we have achieved the highly stereoselective synthesis of **12**, a key compound for the asymmetric synthesis of the natural product **14**, by using the (diene)$Fe(CO)_3$ group as a sole and mobile chiral auxiliary. This is the first example in the π-organometallic chemistry that the π-coordinated metal-group controls the contiguous stereogenic centers in acyclic compounds with concurrent 1,2-migration.

Notes and References

† Owing to the instability of **1** and **4** towards column chromatography, these compounds were used as a diastereomixture (2 : 3) without purification.

‡ The relative and absolute stereochemistry of **2a**–**c**, **3**, **5**, **6** and **10** were elucidated from the reported examples[2] and conversion of **10** and the reported product **13** to **12**.

§ Under these reaction conditions, the aldehyde group was converted to a nitrile group.

1 P. J. Harrington, *Transition Metals in Total Synthesis*, John Wiley & Sons, New York, 1990; J. P. Collman, L. S. Hegedus, J. R. Norton and R. G. Finke, *Principles and Applications of Organotransition Metal Chemistry*, University Science Books, Mill Valley, CA, 1987.

2 W. A. Donaldson, *Aldrichim Acta*, 1997, **30**, 17; A. J. Pearson, *Iron Compounds in Organic Synthesis*, Academic Press, London, 1994; R. Gree, *Synthesis*, 1989, 341.

3 C. Tao, *Encyclopedia of Reagents for Organic Synthesis*, ed. L. A. Paquette, John Wiley & Sons, London, 1995, vol. 7, p. 5043.

4 A. Braun, L. Toupet and J.-P. Lellouche, *J. Org. Chem.*, 1996, **61**, 1914; D. M. Gree, J. T. Martelli, R. L. Gree and L. J. Toupet, *J. Org. Chem.*, 1995, **60**, 2316; W. A. Donaldson, P. T. Bell, Z. Wang and D. W. Bennett, *Tetrahedron Lett.*, 1994, **35**, 5829; C. Quirosa-Guillou and J.-P. Lellouche, *J. Org. Chem.*, 1994, **59**, 4693; W. R. Roush and C. K. Wada, *Tetrahedron Lett.*, 1994, **35**, 7347.

5 Y. Takemoto, N. Yoshikawa and C. Iwata, *J. Chem. Soc., Chem. Commun.*, 1995, 631.

6 S. Harusawa, R. Yoneda, T. Kurihara, Y. Hamada and T. Shioiri, *Tetrahedron Lett.*, 1984, **25**, 427.

7 E. A. Jares-Erijiman, C. P. Bapat, A. Lithgow-Bertelloni, K. L. Rinehart and R. Sakai, *J. Org. Chem.*, 1989, **54**, 366.

8 Y. Takemoto, Y. Baba, I. Noguchi and C. Iwata, *Tetrahedron Lett.*, 1996, **37**, 3345.

9 H. Takhashi, T. Kawakita, M. Ohno, M. Yoshikawa and S. Kobayashi, *Tetrahedron*, 1992, **48**, 5691.

10 K. Mori and H. Matsuda, *Liebigs Ann. Chem.*, 1992, 131.

Received in Cambridge, UK, 6th July 1998; 8/05171B

An alternative interpretation of the HETCOR NMR spectra of poly(lactide)

Khalid A. M. Thakur,*[a]† Robert T. Kean,[a] Mark T. Zell,[b] Brian E. Padden[b] and Eric J. Munson*[b]‡

[a] *Cargill Incorporated, Central Research, PO Box 5699, Minneapolis, MN 55440, USA*
[b] *University of Minnesota, Department of Chemistry, 207 Pleasant St. SE, Minneapolis, MN 55455, USA*

An alternative to the assignments proposed recently by Chisholm *et al.* for the ^{1}H and ^{13}C NMR resonances of poly(lactide) based on their HETCOR spectra is presented; we find that the HETCOR spectra are consistent with older assignments of the tetrad and hexad stereosequence resonances in the ^{1}H and ^{13}C NMR spectra and we believe that the influence of adjacent chiral units on the NMR chemical shift extends asymmetrically and is opposite in the case of ^{1}H and ^{13}C nuclei; this is in contrast to the assumption that the observed chiral repeat unit for any particular stereosequence resonance is the same for ^{1}H and ^{13}C NMR spectra as used by Chisholm *et al.* in their analysis.

NMR spectroscopy has been shown to be an effective method for characterizing the stereosequence distribution in poly(lactide) (PLA) samples.[1,2] Homonuclear decoupled ^{1}H NMR and proton-decoupled ^{13}C NMR spectra have been used to explore the kinetics and predict the stereoisomer composition in PLA.[2–5] Recently, Chisholm *et al* have proposed an alternative set of stereosequence assignments for the ^{1}H and ^{13}C NMR resonances based on heteronuclear correlation (HETCOR) spectra for poly(*rac*-lactide) and poly(*meso*-lactide).[6] The nomenclature for stereosequence assignments of NMR resonances of PLA has been detailed in a number of previous reports.[1,2,6] Fig. 1 reproduces the spectra and assignments obtained for poly(*rac*-lactide) and poly(*meso*-lactide) from one of those reports.[2]

Chisholm *et al.* found cross-peaks between **sis** resonances in the ^{1}H NMR spectra and **isi** and **iss**/**ssi** resonance in the ^{13}C spectra in the HETCOR of poly(*meso*-lactide).[6] In the HETCOR of poly(*rac*-lactide), they found cross-peaks between the **sis** and **iis**/**sii** resonances in the ^{1}H spectra and the **isi** resonance in the ^{13}C spectra. Since these results appeared to contradict the previous assignments, they proposed a new set of stereosequence assignments. However, we believe these are inconsistent with the intensity distribution predicted from simple probability rules. For example, in the ^{13}C NMR spectrum of poly(*meso*-lactide), their assignment of the **isi** and **sis** resonances are reversed such that the **isi** resonance has a higher intensity than the **sis** resonance. The **sis** stereosequence is formed by isotactic addition of two *meso*-lactides, and should have a significantly larger intensity than the **isi** stereosequence, which requires two isotactic additions of three *meso*-lactide monomers. Under polymerization conditions such that no transesterification or epimerization occurs, the **sis** intensity should always be greater than the **isi** intensity.

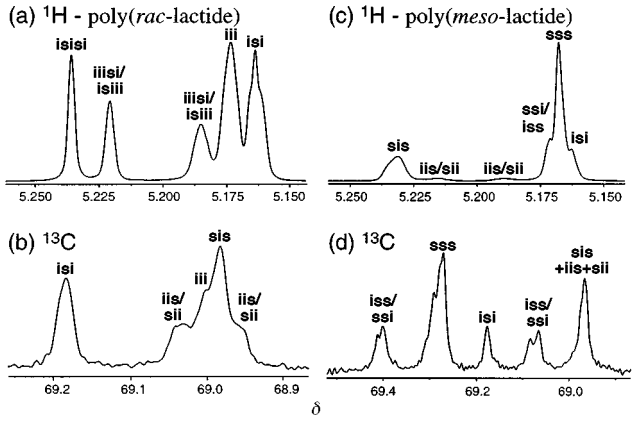

Fig. 1 Methine resonances in ^{1}H and ^{13}C NMR spectra of poly(*rac*-lactide) (a,b), and poly(*meso*-lactide) (c,d). The poly(*meso*-lactide) contained 6% *rac*-lactide as an impurity.

The observed nucleus in a resonance representing a tetrad (or hexad) stereosequence is from one of the two chiral repeat units at the center of the sequence. The tetrad sensitivity arises due to an asymmetrical extent of influence of adjacent chiral repeat units on NMR chemical shifts. If the influence were symmetrical, only triad or pentad stereosequence resonances would be observed in the NMR spectra. The cause of the asymmetrical influence in a tetrad stereosequence resonance in PLA is not known. It may be related to the presence of asymmetric repeat units having a carbonyl on one side and an ester oxygen on the other. It is also possible that the asymmetrical influence on the chemical shift in the ^{1}H NMR spectra is opposite as compared to the ^{13}C NMR spectra. The consequence is that the observed repeat unit for a given stereosequence resonance is not identical in the ^{1}H and ^{13}C NMR spectra, but are adjacent chiral repeat units at the center of the sequence. For example, in the stereosequence –*RRSS*–, represented by **isi**, the observed repeat unit could be either –***R***– or –***S***–. The HETCOR spectra reported by Chisholm *et al*. would result if in case of the ^{1}H NMR spectra the observed nucleus comes from –**R**, and in the case of the ^{13}C NMR spectra, the observed nucleus is from –***S***– (or *vice versa*). Our justification for the analysis of the specific cross peaks present in the HETCOR spectra of poly(*rac*-lactide) and poly(*meso*-lactide), based on the assumption of opposite asymmetrical influence for ^{1}H and ^{13}C NMR, follows.

In poly(*rac*-lactide), –*RR**S**SR*– and –*RR**S**SS*– sequences may be represented as **isi** adjacent to **sis** and **sii**, respectively. If in the ^{13}C spectra the observed repeat unit representing **isi** is –***S***–, this would appear in the ^{1}H NMR spectra as either **sis** or **sii** depending on which repeat unit (*R* or *S*) is adjacent to the **isi** stereosequence. Unfortunately, due to equal probability of occurrence, it is not possible to experimentally distinguish and identify the **iis** resonance from the **sii** resonance.[1,2,6] Hence as observed in the HETCOR, the **isi** resonance in ^{13}C NMR spectrum should have cross peaks with **sis** and one of the **sii**/**iis** resonances in the ^{1}H NMR.

In poly(*meso*-lactide), –*RR**S**SR*– and –*SR**S**SR*– are represented as **isi** and **ssi**, respectively, adjacent to a **sis**. Assuming a similar relationship as above, the –***S***– would appear as a **sis** in the ^{1}H NMR spectrum and either **isi** or **ssi** (not **iss**) in the ^{13}C NMR spectrum. And as observed in the HETCOR, the **sis** resonance in the ^{1}H NMR should have cross peaks with **isi** and one of the **ssi**/**iss** resonances in the ^{13}C NMR spectrum.

Table 1 shows the cross peaks expected to occur if the observed repeat unit in ^{13}C NMR is on the right side and in the ^{1}H NMR it is on the left side of the central two units for poly(*rac*-lactide), and Table 2 shows similar information for poly(*meso*-lactide). It is also possible that the reverse is true, *i.e.* the observed repeat unit in ^{13}C NMR is on the left side and in ^{1}H NMR is on the right side of the central two units. Owing to

Table 1 poly(*rac*-lactide); **ss** not possible

^{13}C	^{1}H
sis	**isi**
isi	**sii/sis**
ssi	**sii/sis**
iis	**isi**
iii	**iii/iis**

Table 2 poly(*meso*-lactide) **ii** not possible

^{13}C	^{1}H
ssi	**sis**
sis	**isi/iss**
iss	**ssi/sss**
sss	**ssi/sss**
isi	**sis**

limitations in the experimental data and equal probability of asymmetric stereosequences,[1,2,6] it is not possible to determine the direction of the asymmetric influence on ^{13}C and ^{1}H NMR chemical shifts. However, we have clearly shown that the asymmetric influence must be opposite in ^{13}C and ^{1}H NMR, and the observed repeat unit for a given stereosequence resonance is not identical in ^{13}C and ^{1}H NMR.

Further work is in progress to uniquely identify the direction of the asymmetric influence with respect to the molecular coordinates. These and other experiments using ^{13}C labeled PLA to conclusively identify the stereosequence resonances are in progress and will be reported in the near future.

Support for this work was provided by a NIST ATP grant to Cargill Incorporated.

Notes and References

† E-mail: kathakur@mmm.com
‡ E-mail: munson@chem.umn.edu

1 H. R. Kricheldorf, C. Boettcher and K. U. Tönnes, *Polymer*, 1992, **33**, 2817.
2 K. A. M. Thakur, R. K. Kean, E. S. Hall, J. J. Kolstad, T. Lindgren, M. A. Doscotch, J. L. Siepmann and E. Munson, *Macromolecules*, 1997, **30**, 2422.
3 K. A. M. Thakur, R. K. Kean, E. S. Hall, M. A. Doscotch and E. J. Munson, *Anal. Chem.*, 1997, **69**, 4303.
4 K. A. M. Thakur, R. T. Kean, E. S. Hall, J. J. Kolstad and E. J. Munson, *Macromolecules*, 1998, **31**, 1487.
5 J. Coudane, C. Ustarizpeyret, G. Scwach and M. Vert, *J.Polym. Sci. A: Polym. Chem.*, 1997, **35**, 1651.
6 M. H. Chisholm, S. S. Iyer, M. E. Matison, D. G. McCollum and M. Pagel, *Chem. Commun.*, 1997, **20**, 1999.

Received in Columbia, MO, USA, 10th December 1998; 7/08911B

Synthesis and crystal structure of an arenesulfenyl iodide with unprecedented stability

Kei Goto,*† Michel Holler and Renji Okazaki*‡

Department of Chemistry, Graduate School of Science, The University of Tokyo, 7-3-1 Hongo, Bunkyo-ku, Tokyo, 113-0033, Japan

An arenesulfenyl iodide with unprecedented stability was synthesized by oxidation of a thiol bearing a novel bowl-type substituent with iodine, whose monomeric structure was determined by X-ray crystallographic analysis.

Sulfenyl iodides (RSI) have been suggested to play decisive roles as reaction intermediates in iodination reactions in the human thyroid gland[1] as well as in iodine oxidation of thiols.[2] Although more information concerning simple well defined sulfenyl iodides is desirable, the study of their chemistry has been hampered by their instability resulting from the ready disproportionation reaction ($2RSI \rightarrow RSSR + I_2$), the ΔH value of which is -4.30 kcal mol^{-1}.[3] In the solid state they are much less stable partly because of the large sublimation energy of solid I_2 (14.9 kcal mol^{-1}). Several aromatic acylsulfenyl iodides have been isolated and shown to be stable at room temperature for several hours, but they decompose below 50 °C.[4] The only structural analysis of a sulfenyl iodide was carried out for Ph_3CSI at -118 °C,[5] which is stable in the solid state at -78 °C and in solution in the dark.[6] Thus, no sulfenyl iodide stable at room temperature has so far been structurally characterized.[7] On the other hand, the reported value of the S–I bond dissociation energy is not so small (49.4 ± 2 kcal mol^{-1} for HS–I),[8] suggesting that this species will be stable if the disproportionation process is suppressed. Recently, we reported that a stable arenesulfenic acid can be obtained by direct oxidation of a thiol by taking advantage of a novel bowl-type

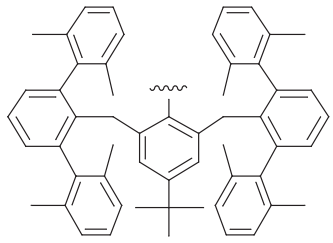

1 ≡ Bmt

substituent **1** (denoted as Bmt hereafter).§[9,10] Here we describe the synthesis of an arenesulfenyl iodide with unprecedented stability by iodine oxidation of the corresponding arenethiol, along with its crystal structure.

The sulfenyl iodides isolated so far have been synthesized mostly by halide exchange reaction of the corresponding sulfenyl chloride[6] or oxidation of the corresponding heavy metal thiolates.[4,11] There has been no example of the synthesis of a stable sulfenyl iodide by iodine oxidation of a thiol although this reaction has been considered to involve a sulfenyl iodide as an intermediate and seems to be the most straightforward synthetic pathway to it. Oxidation of thiol **2**[12] bearing the Bmt group with an equimolar amount of I_2 in the presence of triethylamine in $CDCl_3$ resulted in the quantitative formation of sulfenyl iodide **3**, which was isolated by silica gel chromatography as dark brown crystals in 92% yield (Scheme 1).¶ The stability of **3** was remarkable both in the crystalline state and in solution; it showed a melting point at 257 °C and no decomposition was observed even after heating at 80 °C for 12 h in toluene-d_8. It is stable at room temperature in air for more than several months. In the UV–VIS spectrum, **3** showed an absorption maximum at 328 nm in chloroform.

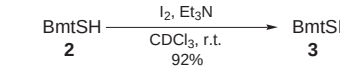

Scheme 1

The structure of **3** was finally established by X-ray crystallographic analysis.‖ An ORTEP drawing of **3** is shown in Fig. 1 with selected bond lengths and angles. The figure clearly shows that the two rigid *m*-terphenyl units surround the S–I functionality like the brim of a bowl, thus preventing the disproportionation process effectively. It was reported that in the crystal structure of Ph_3CSI at -118 °C the molecules are linked *via* short S···I contacts of 3.210(4) Å so that a zig-zag chain is formed.[5] By contrast, the shortest intermolecular S···I distance in **3** is 6.654(2) Å, clearly indicating its monomeric nature. The S–I bond length [2.386(2) Å] is distinctly shorter than that of Ph_3CSI [2.406(4) Å] probably because of the absence of the intermolecular interaction. The S–I moiety is almost perpendicular to the benzene plane [I(1)–S(1)–C(1)–C(2) angle, 87.7(6)°].

In spite of its high thermal stability, sulfenyl iodide **3** undergoes ready reactions with some reagents. Treatment of **3** with butane-1-thiol (8 equiv.) in the presence of triethylamine reduced it to the parent thiol **2** with the formation of a small

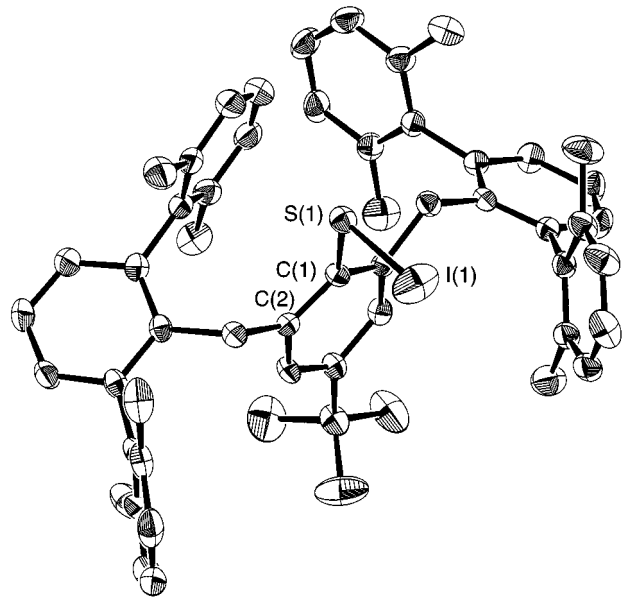

Fig. 1 Crystal structure of **3** (ORTEP drawing; thermal ellipsoids at 30% probability level). Selected bond lengths (Å), bond angles (°), and torsion angle (°): S(1)–I(1), 2.386(2); S(1)–C(1), 1.783(7); I(1)–S(1)–C(1), 101.3(2); I(1)–S(1)–C(1)–C(2), 87.7(6).

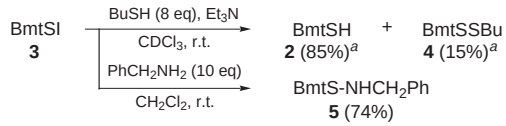

Scheme 2 [a] Estimated by ^{1}H NMR

amount of disulfide **4** (Scheme 2). The reaction of **3** with benzylamine (10 equiv.) readily afforded sulfenamide **5**. On the other hand, **3** was found to be unreactive toward thiol **2** bearing the same substituent. Oxidation of **2** with 0.5 equiv. of I_2 in the presence of triethylamine afforded a 1 : 1 mixture of **2** and **3**, no disulfide formation being detected even after 24 h at room temperature (Scheme 3). These results imply that two species which are otherwise incompatible can be present in the same system with retention of their reactivities toward other reagents when they bear a bowl-type substituent. Under the same conditions, 2,4,6-trimethylbenzenethiol (MesSH) was immediately oxidized to MesSSMes and even 2,4,6-tri-*tert*-butylbenzenethiol (Mes*SH) afforded Mes*SSMes* although the reaction was much slower. Apparently, the bowl-shaped structure of the Bmt group is more effective for prevention of dimerization than a Mes* group, where the functionality is more closely shielded.

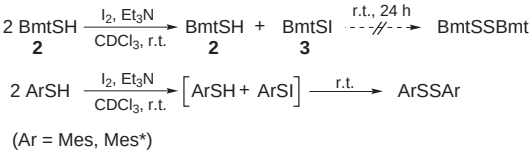

Scheme 3 Mes* = $C_6H_2Bu^t_3$-2,4,6

This work was partly supported by Grants-in-Aid for Scientific Research (No. 07854035 and 94187) from the Ministry of Education, Science, Sports and Culture, Japan. We also thank Tosoh Akzo Co., Ltd. for the generous gift of alkyllithiums. M. H. is grateful to the Japan Society for the Promotion of Science for the Postdoctoral Fellowship for Foreign Researchers.

Notes and References

† Present address: Department of Chemistry, School of Science, Kitasato University, 1-15-1 Kitasato, Sagamihara, Kanagawa 228-8555, Japan. E-mail: goto@jet.sci.kitasato-u.ac.jp

‡ Present address: Department of Chemical and Biological Sciences, Faculty of Science, Japan Women's University, 2-8-1 Mejirodai, Bunkyo-ku, Tokyo 112-8681, Japan. E-mail: okazaki@jwu.ac.jp

§ Bmt denotes 4-*tert*-butyl-2,6-bis[(2,2",6,6"-tetramethyl-*m*-terphenyl-2'-yl)methyl]phenyl.

¶ **3:** mp 252–257 °C; ^{1}H NMR (500 MHz, $CDCl_3$): δ 0.97 (s, 9H), 1.95 (brs, 24H), 3.70 (brs, 4H), 6.46 (s, 2H), 6.84 (brs, 8H), 6.94 (t, ^3J = 7.3 Hz, 4H), 7.03 (d, ^3J = 7.5 Hz, 4H), 7.33 (t, ^3J = 7.5 Hz, 2H); ^{13}C NMR (125 MHz, $CDCl_3$): δ 21.0 (q), 30.8 (q), 34.7 (s), 34.8 (t), 125.0 (d), 126.8 (d), 127.0 (d), 127.5(d), 129.3 (d), 129.4 (s), 136.2 (s), 137.2 (s), 140.8 (s), 142.1 (s), 146.2 (s), 151.1 (s); UV–VIS ($CHCl_3$): $\lambda_{max}(\varepsilon)$ = 328 nm (4000 dm^3 mol^{-1} cm^{-1}).

‖ *Crystal data* for **3**·0.5C_7H_8: $C_{59.5}H_{61}SI$, M = 935.10, monoclinic, space group $P2_1/n$, a = 15.668(8), b = 17.47(1), c = 18.71(1) Å, β = 105.91(4)°, U = 4926(4) Å^3, Z = 4, D_c = 1.261 g cm^{-3}, μ = 7.30 cm^{-1}. The intensity data were collected at 293 K on a Rigaku AFC7R diffractometer with Mo-Kα radiation (λ = 0.71069 Å), and the structure was solved by direct methods and expanded using Fourier techniques. The non-hydrogen atoms were refined anisotropically. Hydrogen atoms were included but not refined. The final cycle of full-matrix least-squares refinement was based on 3789 observed reflections [$I > 3.00\sigma(I)$] and 539 variable parameters with $R(R_w)$ = 0.058(0.045). CCDC 182/944.

1 H. Fraenkel-Conrat, *J. Biol. Chem.*, 1955, **217**, 373; J. P. Danehy, in *Sulfur in Organic and Inorganic Chemistry*, ed. A. Senning, Marcel Dekker, New York, 1971, vol. 1, pp. 327–339; L. Field and C. M. Lukehart, in *Sulfur in Organic and Inorganic Chemistry*, ed. A. Senning, Marcel Dekker, New York, 1982, vol. 4, pp. 327–367.
2 J. P. Danehy, C. P. Egan and J. Switalski, *J. Org. Chem.*, 1971, **36**, 2530.
3 J. P. Johnson, M. P. Murchie, J. Passmore, M. Tajik, P. S. White and C.-M. Wong, *Can. J. Chem.*, 1987, **65**, 2744.
4 S. Kato, E. Hattori, M. Mizuta and M. Ishida, *Angew. Chem., Int. Ed. Engl.*, 1982, **21**, 150.
5 R. Minkwitz, H. Preut and J. Sawatzki, *Z. Naturforsch. Teil B*, 1988, **43**, 399.
6 E. Ciuffarin and G. Guaraldi, *J. Org. Chem.*, 1970, **35**, 2006.
7 The structures of several sulfur and selenium iodine cations have been characterized. For a review, see: T. Klapötke and J. Passmore, *Acc. Chem. Res.*, 1989, **22**, 234.
8 R. J. Hwang and S. W. Benson, *J. Am. Chem. Soc.*, 1979, **101**, 2615.
9 K. Goto, M. Holler and R. Okazaki, *J. Am. Chem. Soc.*, 1997, **119**, 1460.
10 For related compounds, see: K. Goto, N. Tokitoh and R. Okazaki, *Angew. Chem., Int. Ed. Engl.*, 1995, **34**, 1124; T. Saiki, K. Goto, N. Tokitoh and R. Okazaki, *J. Org. Chem.*, 1996, **61**, 2924; T. Saiki, K. Goto and R. Okazaki, *Angew. Chem., Int. Ed. Engl.*, 1997, **36**, 2223.
11 S. Kato, Y. Komatsu, K. Miyagawa and M. Ishida, *Synthesis*, 1983, 552.
12 K. Goto, M. Holler and R. Okazaki, *Tetrahedron Lett.*, 1996, **37**, 3141.

Received in Cambridge, UK, 1st May 1998; revised manuscript received 10th July 1998; 8/05449E

ChemComm
FEATURE ARTICLE

Effects of electron donation into C–F σ* orbitals: explanations, predictions and experimental tests

Weston Thatcher Borden†

Department of Chemistry, Box 351700, University of Washington, Seattle, Washington, 98195-1700, USA

The ability of C–F σ* orbitals to act as electron acceptors is shown to be capable of explaining and predicting a wide variety of apparently unrelated phenomena. Among these are (i) pyramidalization of fluorinated radical centers, (ii) the much weaker π-bond in tetrafluoroethylene (TFE) than in ethylene, (iii) the stepwise reaction of TFE with butadiene to form 2,2,3,3-tetrafluoro-1-vinylcyclobutane, rather than the Diels–Alder adduct, (iv) the thermodynamic favorability of replacing C–H with C–C bonds at fluorinated carbons, (v) the preference for disrotatory ring opening and closure of 1,1-difluorocyclopropanes, and (vi) the change from a triplet to a singlet ground state upon substitution of fluorines for the pair of hydrogens at C-2 of cyclopentane-1,3-diyl.

Over the past ten years my research group at the University of Washington has been carrying out computational research on organic molecules containing geminal fluorines. The unifying principle that has emerged from our research is that C–F σ-bonds have low-lying antibonding σ* orbitals, which are capable of accepting electrons from nonbonding p-π AOs, either on the same carbon or on adjacent carbons, and also from σ- and π-bonds on adjacent carbons. We have applied this understanding to explaining otherwise puzzling results, already in the literature, and to making new predictions that we have subsequently verified experimentally.

There is now good evidence, both computational[1a] and experimental,[1b] that the ability of C–F σ* orbitals to accept unshared electron pairs from adjacent carbons (negative hyperconjugation) stabilizes fluorinated carbanions. However, as will be shown in this article, the electron-accepting ability of C–F σ* orbitals is also capable of explaining and predicting a wide variety of additional and apparently unrelated phenomena. Among these are the following: (i) in contrast to methyl radical, trifluoromethyl radical is non-planar and has a high barrier to inversion;[2] (ii) tetrafluoroethylene (TFE) has a much weaker π-bond than ethylene;[3] and, (iii) unlike ethylene, TFE does not undergo a Diels–Alder reaction with butadiene but, instead, forms 2,2,3,3-tetrafluoro-1-vinylcyclobutane [eqn. (1)];[4] (iv)

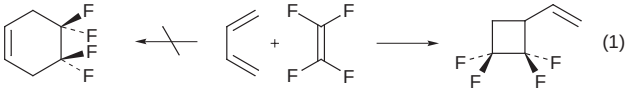

(1)

heats of formation show that transfer of the geminal fluorines from difluoromethane to C-2 of propane [eqn. (2)] is exothermic

$$CH_2F_2 + H_3CCH_2CH_3 \rightarrow CH_4 + H_3CCF_2CH_3 \qquad (2)$$

by 14.5 kcal mol^{-1};[5] (v) although 1-ethyl-2-methylcyclopropane undergoes stereorandom ring opening and closure,[6] replacement of the geminal ring hydrogens by geminal fluorines has been both predicted[7] and found[8] to lead to a very large preference for stereomutation by coupled disrotation of the alkylated ring carbons [eqn. (3)]; and (vi) cyclopentane-1,3-diyl has a triplet ground state;[9] but, as predicted,[10] a derivative of 2,2-difluorocyclopentane-1,3-diyl appears to have a singlet ground state.[11]

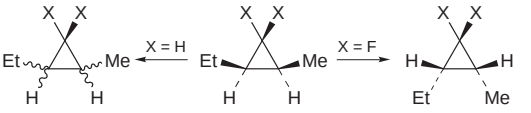

(3)

In showing how these diverse phenomena can all be explained by the electron accepting ability of the σ* orbitals of C–F bonds, I will take advantage of the possibility in a review of this type of revealing the intellectual threads that connect what might otherwise appear to be a collection of unrelated research projects. This review is written from a historical perspective and describes how one research project led to another and how each contributed to our understanding of the effects of geminal fluorines on the structure, energetics, and reactivity of fluorinated alkanes, alkenes, radicals, and diradicals.

Why do some radical centers have significant barriers to planarity?

In 1976 I taught a course on MO theory at the University of Washington. The text for the course[12] used second-order perturbation theory to explain the shapes of simple molecules. Bill Cherry, who was a graduate student in the course, saw how this theoretical framework could be used to explain the greater degree of pyramidalization and much higher barrier to inversion in phosphine, compared to ammonia, and why successive replacement of the hydrogens by fluorines in AH_3 molecules with seven or eight valence electrons also increases the barriers to inversion.[13,14] Subsequent conversations between Bill, his thesis adviser, Nick Epiotis, and myself resulted in the three of us coauthoring an article for *Accounts of Chemical Research* on this subject.[15]

The crucial factor in determining how favorable pyramidalization is in a planar AH_3 molecule is the amount of net stabilization provided by the mixing of the nonbonding p_z AO (a_2'') on A with the antibonding $2a_1'$ MO.[13,15] These orbitals are shown in Fig. 1, which also illustrates how their mixing upon pyramidalization transforms the nonbonding p_z AO in planar AH_3 into an MO that consists of a hybridized AO on A whose smaller lobe interacts in a bonding fashion with the three hydrogens.

According to second-order perturbation theory, the amount of net stabilization that arises from mixing between a_2'' and $2a_1'$ is inversely proportional to the size of the energy gap between these orbitals.[12,13,15] Therefore, in two similar AH_3 molecules (*e.g.* NH_3 and PH_3 or CH_3 and SiH_3), the energy lowering caused by pyramidalization and, hence, the amount of pyramidalization at the equilibrium geometry will both be larger in the molecule with the smaller energy difference between the antibonding $2a_1'$ and the nonbonding a_2'' orbitals.

Calculations find that planar AH_3 molecules have much lower-lying $2a_1'$ antibonding MOs when A is a second-row, rather than a first-row atom.[13,15] Consequently, second-order perturbation theory rationalizes the greater pyramidalization and higher barriers to inversion found in phosphines than in

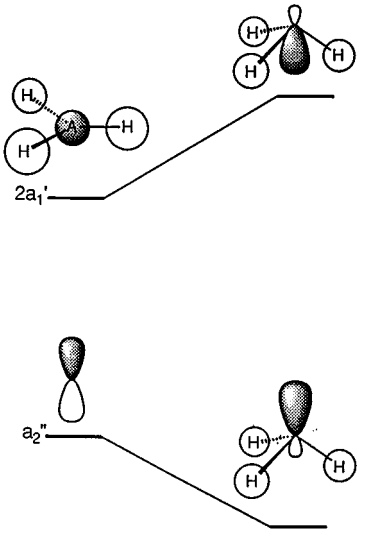

Fig. 1 Effect of mixing the a_2'' nonbonding MO with the $2a_1'$ antibonding MO of planar AH_3 on pyramidalization

amines[16] and in silyl radicals, compared to alkyl radicals.[17] The existence of low-lying $2a_1'$ MOs in planar PH_3 and SiH_3 can be traced to the fact that, unlike the case with 2s and 2p AOs, the maximum density of a 3s AO is significantly closer to the nucleus than that of a 3p AO.[18]

Another way to lessen the energy difference between the nonbonding a_2'' AO on A and the antibonding $2a_1'$ MO in AH_3 is to replace the three hydrogens with more electronegative atoms, such as fluorines.[13,15] The reduction in the energy difference between a_2'' and $2a_1'$ that results from the substitution of fluorine for hydrogen makes mixing of these two orbitals by pyramidalization more energetically favorable.The physical reason that this substitution leads to pyramidalization is that, as shown in Fig. 1, the filled MO that results from mixing of these two orbitals is no longer localized just on A, but is delocalized onto the more electronegative fluorines. Experimentally, it is known that electronegative substituents increase the barriers to inversion at nitrogen[16,19] and, as noted in the Introduction, it has also been found that successive replacement of hydrogens by fluorines results in increased pyramidalizaion and higher barriers to inversion in carbon-centered radicals.[2]

The effect of pyramidalization on the π-bond dissociation energy of tetrafluoroethylene and on the barriers to rotation in fluorinated allyl radicals

In a footnote in our 1977 paper in *Accounts* we pointed out that the favorability of pyramidalization of silyl,[17] cyclopropyl,[20] and fluoroalkyl[2] radical centers should tend to weaken the π-bonds in silenes, methylenecyclopropane, and tetrafluoroethylene (TFE), thus possibly accounting, at least in part, for the high reactivity of these compounds.[15] As illustrated in Fig. 2, if

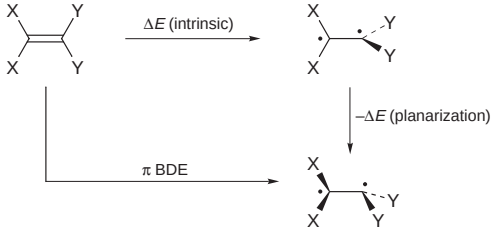

Fig. 2 Thermocycle showing that the π BDE of an alkene is reduced from the intrinsic strength of a π-bond between the planar radical centers by the energy released by their pyramidalization

a π-bond is formed between two radical centers, one or both of which prefer a pyramidal geometry, the π-bond dissociation energy (BDE) will be less than the intrinsic strength of a π-bond formed between the planar radical centers by the amount of energy that is released by their pyramidalization. We have investigated the impact of this effect on the π BDEs of silenes,[21] disilenes,[22] methylenecyclopropane,[23] and tetrafluoroethylene (TFE).[24]

The electronegative substituents attached to each carbon in TFE have a substantial effect on reducing the π-bond strength in TFE from that in ethylene. The strength of the π-bond in ethylene can be obtained experimentally from either the kinetics of *cis–trans* isomerization of 1,2-dideuterioethylene[25] or from the thermodynamics of the reaction shown in eqn. (4).[26] Both methods give a π-bond energy of *ca.* 65 kcal mol^{-1}.

$$H_2C{=}CH_2 + CH_3CH_3 \rightarrow 2\ CH_3CH_2\cdot \qquad (4)$$

Obviously, the kinetics of *cis–trans* isomerization cannot be used to provide an experimental value for the π-bond energy of TFE, but the thermodynamics of the reaction in eqn. (5) with

$$F_2C{=}CF_2 + CF_2XCF_2X \rightarrow 2\ CF_2XCF_2\cdot \qquad (5)$$

X = F has been employed to yield an experimental value of 52 ± 2 kcal mol^{-1} for this quantity.[3]

Computationally, either the barrier to rotation or the energy of the reaction in eqn. (5) can be used. Both types of calculations concur with experiment in finding that the π-bond in TFE is *ca.* 15 kcal mol^{-1}weaker than that in ethylene.[24]

We used *ab initio* calculations to show that the lower π-bond energy in TFE, compared to ethylene, is due entirely to the energetic cost of planarizing the radical centers in TFE. The energy of 18.0 kcal mol^{-1}that is computed to be necessary to planarize the carbons in the singlet diradical transition state for rotation about the double bond[27] is very close to the calculated increase of 18.4 kcal $mol^{-1}$when the energy of the reaction in eqn. (5) is recomputed with the radical center in CF_2XCF_2 (X = H) constrained to planarity.[24] The intrinsic strength of the π-bond in TFE is actually *ca.* 3 kcal mol^{-1} larger than that in ethylene.[27]

Dr Bruce Smart suggested that we investigate whether the much lower barrier to rotation that EPR experiments had found in 1,1,3,3-tetrafluoroallyl radical,[28a] compared to the unfluorinated radical,[28b,c] might have a similar explanation. We found that pyramidalization of the twisted CF_2 group did indeed lower the barrier to rotation in 1,1,3,3-tetrafluoroallyl radical by about 10 kcal mol^{-1}.[29] In the corresponding anion pyramidalization was calculated to provide so much stabilization that a C_s geometry, with one CF_2 group pyramidalized and twisted out of conjugation, was computed to be 17 kcal mol^{-1} *lower* in energy than the planar, conjugated, C_{2v} structure and only 1 kcal mol^{-1} higher in energy than a C_2 structure in which both CF_2 groups are pyramdalized but oriented so that they are in conjugation with the central carbon.[30]

It was known experimentally that 1,1-difluoroallyl radical does not have a particularly low barrier to CF_2 rotation.[28a,b] If CF_2 group pyramidalization were the sole reason for the low barrier to rotation found in 1,1,3,3-tetrafluoroallyl radical, one would have expected 1,1-difluoroallyl to have a similarly low barrier to rotation of the CF_2 group.

In agreement with experiment, our calculations found the barrier to CF_2 rotation to be 6.9 kcal mol^{-1} higher in 1,1-difluoroallyl than in 1,1,3,3-tetrafluoroallyl. The results of our CISD calculations are summarized in Fig. 3.[27]

As shown in Fig. 3, pyramidalization of the rotated CF_2 group actually contributes more to lowering the barrier to rotation in 1,1-difluoroallyl than in 1,1,3,3-tetrafluoroallyl radical. The barrier to CF_2 rotation is higher in difluoro- than in tetrafluoroallyl radical because the intrinsic barrier to rotation of a planar CF_2 group is 9.7 kcal mol^{-1} larger in the former than in the latter radical. The reason for the intrinsically higher barrier to planar CF_2 rotation in difluoroallyl is that, after CF_2 rotation, the $CH{=}CH_2$ π-bond that remains in difluoroallyl is about 10 kcal mol^{-1} weaker than the $CH{=}CF_2$ π-bond that remains in tetrafluoroallyl. A similar difference between the intrinsic

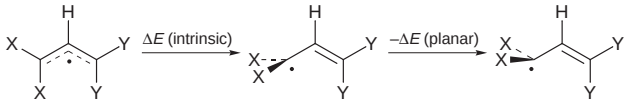

X	Y	ΔE (intrinsic)	ΔE (planar)
H	H	15.4	0.1
F	F	12.6	9.9
H	F	12.3	0.0
F	H	22.3	12.7

Fig. 3 Intrinsic rotation barriers and planarization energies (kcal mol^{-1}) calculated for allyl, difluoroallyl, and tetrafluoroallyl radicals (ref. 27). The net barriers to rotation are given by ΔE (rotation) = ΔE (intrinsic) − ΔE (planarization) − ΔZPE, where the zero-point energy corrections (kcal mol^{-1}) are ΔZPE = −0.9 for X = Y = H, 1.3 for X = Y = F, −0.5 for X = H, Y = F, and 1.3 for X = F, Y = H. The origin of the different signs of the ΔZPE corrections for X = H and X = F resides in the pyramidalization that occurs for X = F in the transition state for rotation (ref. 27).

π-bond energies of ethylene and 1,1-difluoroethylene (DFE) was calculated.[27] This explains why these two molecules have similar π BDEs, despite the fact that the latter contains a CF_2 group, pyramidalization of which is calculated to lower the intrinsic π BDE by 11.4 kcal mol^{-1}.

The origin of the much higher intrinsic π-bond energy in DFE than in either ethylene or TFE is the asymmetric substitution of fluorine on the π-bond in DFE. This allows much better donation of the p-π fluorine lone pairs into the π-bond in DFE than in TFE. The 14.6 ± 1.5 kcal mol^{-1} exothermcity of the reaction in eqn. (6) can be viewed as a specific example of

$$H_2C{=}CH_2 + F_2C{=}CF_2 \rightarrow 2\ F_2C{=}CH_2 \qquad (6)$$

Paulings finding that the reaction, $A_2 + B_2 \rightarrow 2$ AB is always exothermic and that the exothermicity increases with the elecronegativity difference between A and B.[27]

Why does TFE not undergo a Diels–Alder reaction with butadiene?

Although the reaction of ethylene with buta-1,3-diene yields a trace of vinylcyclobutane,[31] by far the major product (99.98%) is cyclohexene, formed by a concerted Diels–Alder reaction. In contrast, as shown in eqn. (1), TFE reacts with buta-1,3-diene to give, as the only isolated product, 2,2,3,3-tetrafluoro-1-vinylcyclobutane,[4] formed *via* a stepwise mechanism involving a diradical intermediate.[32]

Although the π-bond in TFE is considerably weaker than the π-bond in ethylene,[3,27] this fact, by itself, does not explain why a transition state involving formation of a bond to just one carbon of TFE is apparently lower in energy than the transition state for a Diels–Alder reaction, in which bonds are simultaneously formed to both carbons. In fact, our calculations found that, despite the weaker π-bond in TFE, the energy difference between the reactants and the transition state for a concerted Diels–Alder reaction is nearly the same for TFE and ethylene.[33] Moreover, *syn* pyramidalization of TFE to ϕ = 26°, as in the transition state for its Diels–Alder reaction with butadiene, was computed to raise the energy of TFE by 5 kcal mol^{-1} more than the same distortion in ethylene. Presumably, repulsions between the fluorines make pyramidalization of TFE in a *syn* fashion energetically costly, so that CF_2 pyramidalization in the Diels–Alder transition state does not accelerate this reaction.

The prediction that the Diels–Alder reactions of butadiene with both TFE and ethylene have approximately the same activation energy cannot be verified experimentally, because, as noted above, TFE reacts rapidly with butadiene to form a diradical intermediate. The energy of this diradical, relative to the reactants, was calculated to be *ca.* 26 kcal mol^{-1} lower for TFE than for ethylene. Clearly this is why TFE, unlike ethylene, reacts with butadiene by forming just one C–C bond.

As expected, the CF_2 radical center is highly pyramidal (ϕ = 47°) in the diradical; and, of course, the CF_2 group at which the new C–C bond is formed also becomes non-planar. Relief of the 18 kcal mol^{-1} 'strain' that is associated with having two planar CF_2 groups in TFE is obviously the major factor that favors the diradical pathway by 26 kcal mol^{-1} in the reaction of TFE with butadiene. However, this diradical intermediate is apparently stabilized by an additional 8–10 kcal mol^{-1} when it is formed from TFE than from ethylene.

We were able to show that the source of this additional stabilization of the fluorinated, over the unfluorinated, diradical is the greater strength of the C–C bond that is formed in the reaction of butadiene with TFE than with ethylene. This bond is not only stronger, but it is also 0.05 Å shorter in the fluorinated than in the unfluorinated diradical. Our calculations indicated that about 90% of the greater strength of this bond comes from the geminal pair of fluorines on the carbon to which this bond is formed.

Calculations and experimental heats of formation both show the favorability of forming C–C bonds to fluorinated carbons. For example, the reaction in eqn. (7) can be thought of as

$$H_3CCH_2CH_3 + HCF_2CH_3 \rightarrow H_3CCH_3 + CH_3CF_2CH_3 \qquad (7)$$

replacing a hydrogen in 1,1-difluoroethane with a methyl group from propane. Without corrections for ΔZPE, we calculated this reaction to be exothermic by 8.0 kcal mol^{-1} at the MP2 level of theory,[33] which is slightly larger than the value of 6.2 kcal mol^{-1} obtained from experimental heats of formation.[5] An even more dramatic example is provided by the reaction in eqn. (2), in which both hydrogens in difluoromethane are replaced by methyl groups. As noted in the introduction, experimental heats of formation[5] show that this reaction is exothermic by 14.5 kcal mol^{-1}.

Electron delocalization into C–F σ* orbitals in neutral molecules

One possible explanation of the preference for attachment of electronegative elements, such as fluorine[33,34c] and oxygen,[34] to the more highly alkylated of two carbons is that the electrons in the C–H bonds at the β carbons delocalize electrons into the low-lying C–F and C-O σ* orbitals. This would explain not only the energetics of the reactions shown in eqns. (2) and (7), but also why our calculations found that the lengths of C–F bonds increase with increasing alkylation of the carbon to which they are attached, and why the lengths of C–C bonds decrease with the addition of fluorines to one of the carbons.

It is generally accepted that electron delocalization into C–F σ* MOs stabilizes carbanions[1] and is also responsible for the anomeric effect observed when fluorine and a heteroatom with unshared π electrons are attached to the same carbon.[35] However, it is much less clear to what extent delocalization of electrons from C–H bonds into C–F σ* MOs actually is responsible for the energetic preference for attachment of alkyl groups to fluorinated carbons and the accompanying changes in bond lengths. In order to test whether delocalization of electrons into C–F σ* orbitals is of any importance in neutral molecules, we performed additional calculations.[36]

Computational evidence, supporting the delocalization of π-electrons into C–F σ* orbitals, was actually published in 1983 by Greenberg *et al.*[37] Their calculations found the reaction in eqn. (8) to be exothermic by 9.6 kcal mol^{-1}.

(8)

They attributed the exothermicity to electron donation from the π-bonding orbital of 3,3-difluorocyclopropene into the out-of-phase combination of C–F σ* orbitals. This interaction, which can be represented schematically by the ionic resonance structure shown in Fig. 4, confers a degree of aromaticity on 3,3-difluorocyclopropene. The calculated and observed bond

Fig. 4 Resonance structures for 3,3-difluorocyclopropene. The ionic resonance structure schematically depicts the effect of electron donation from the π-bonding orbital into the out-of-phase combination of C–F σ* orbitals.

lengths and dipole moment of this molecule are consistent with the delocalization of electron density from the π-bond into the C–F σ* orbitals that is depicted in Fig. 4.[36]

The differences in symmetry between the HOMO and LUMO of the ethylene π-bond in cyclopropene and the butadiene π-bonds in cyclopentadiene should make hyperconjugative electron donation from the C–H bonds at C-5 of cyclopentadiene much more stabilizing than delocalization of electron density into the C–F σ* orbitals of 5,5-difluorocyclopentadiene. These hyperconjugative interactions should make cyclopentadiene somewhat aromatic and 5,5-difluorocyclopentadiene somewhat anti-aromatic. Therefore, it is not surprising that our calculations found the reaction in eqn. (9) to be endothermic by 14.1 kcal mol^{-1}.[36]

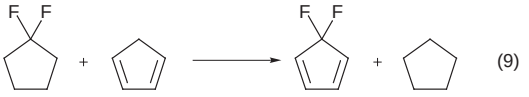

(9)

Hyperconjugative delocalization into C–F σ* orbitals in 1,3-diradicals

If the C–F σ* orbitals in 1,1-difluorocyclopropene can accept electron density from the π-bonding orbital, they should certainly be able to accept electron density from the in-phase combination of non-bonding p-π AOs in 2,2-difluoropropane-1,3-diyl. Similarly, if the C–H bonds at C-5 of cyclopentadiene can donate electron density into the antibonding butadiene LUMO, they certainly ought to be able to donate electron density into the in-phase combination of non-bonding p-π AOs in propane-1,3-diyl. These hyperconjugative interactions are depicted by the resonance structures in Fig. 5.

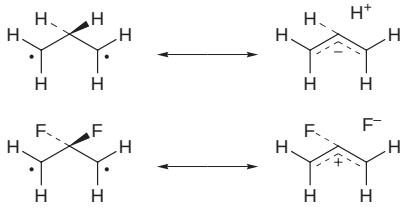

Fig. 5 Resonance structures depicting hyperconjugative electron donation from the C–H bonds of the central CH_2 group into the in-phase combination of p-π AOs at C-1 and C-3 in propane-1,3-diyl and electron donation from the in-phase combination of p-π AOs at C-1 and C-3 into the C–F σ* orbitals at C-2 in 2,2-difluoropropane-1,3-diyl

Thirty years ago Hoffmann analyzed the results of his extended Hückel calculations on propane-1,3-diyl in terms of interaction of the C–H bonds at C-2 with the in-phase combination of p-π AOs at C-1 and C-3.[38] This interaction destabilizes the latter orbital, making it advantageous for the two non-bonding electrons to occupy preferentially the out-of-phase combination of p-π AOs at C-1 and C-3. This combination is the highest occupied MO (HOMO) of the allylic anion in the hyperconjugated resonance structure for propane-1,3-diyl in Fig. 5.

An orbital interaction diagram for 2,2-difluoropropane-1,3-diyl shows that the in-phase combination of p-π AOs at C-1 and C-3 is stabilized by interaction with the C–F σ* orbitals at C-2.[7,36] Therefore, the two non-bonding electrons preferentially occupy the orbital that results from this mixing. This orbital has the same symmetry as the HOMO of the allylic cation in the hyperconjugated resonance structure for 2,2-difluoropropane-1,3-diyl in Fig. 5.

The difference in the symmetry of the HOMO between propane-1,3-diyl and 2,2-difluoropropane-1,3-diyl is predicted to result in a difference in the preferred mode by which these two diradicals are formed from, and undergo closure to, the corresponding cyclopropanes. More specifically, although ring opening and ring closure are predicted to be conrotatory in cyclopropane,[38] they are predicted to be disrotatory in 1,1-difluorocyclopropane.[7,36]

The difference in the symmetry of the HOMOs between unfluorinated and fluorinated diradicals can explain some otherwise puzzling experimental results that were obtained by Dolbier and co-workers[39] and which are summarized in Fig. 6.

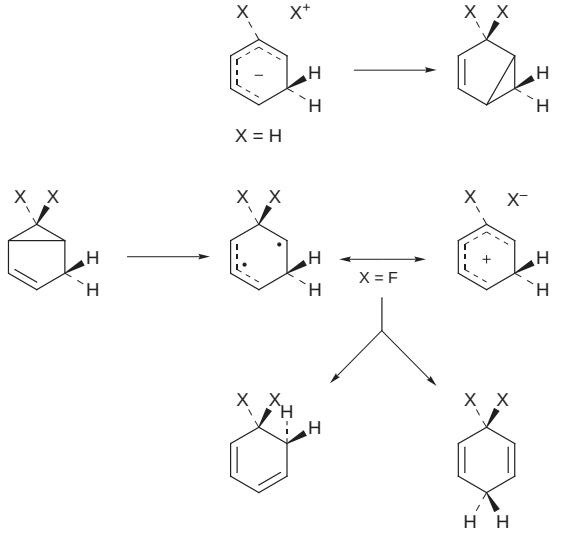

Fig. 6 Rearrangement pathways followed by bicyclo[3.1.0]hex-2-ene and its 6,6-difluoro derivative. The hyperconjugated resonance structure shown for the diradical intermediate formed in each reaction can be used to rationalize the difference between the reaction pathways followed by the hydrocarbon and fluorocarbon (ref. 36).

Derivatives of bicyclo[3.1.0]hex-2-ene (X = H) undergo vinylcyclopropane rearrangements, presumably *via* a diradical intermediate; but Dolbier found that 6,6-difluorobicyclo-[3.1.0]hex-2-ene (X = F) gives no vinylcyclopropane rearrangement product; only the two products of hydrogen shifts in a putative diradical intermediate were detected.

The hyperconjugated resonance structures shown in Fig. 6 can readily account for the different reactions observed for X = H and X = F.[36] Hyperconjugative electron donation from the C–X bonds for X = H gives the diradical intermediate some character of a pentadienyl anion. Disrotation, which is the only stereochemically feasible mode of ring closure in the diradical, is allowed by orbital symmetry for a pentadienyl anion; but the node in the LUMO at the distal CH_2 group makes [1,2]-hydrogen shifts from this carbon symmetry forbidden. In contrast, for X = F, hyperconjugative electron delocalization into a C–X σ* orbital in the diradical confers on it some character of a pentadienyl cation. For such a species disrotatory ring closure is forbidden by orbital symmetry, but the symmetry of the LUMO makes [1,2]-hydrogen shifts allowed.

The hyperconjugated resonance structures for propane-1,3-diyl and 2,2-difluoropropane-1,3-diyl in Fig. 5 also allow one to predict that π-electron donation from alkyl groups at C-1 and C-3 should compete with electron donation from a filled combination of C–H bonding orbitals at C-2. In contrast, it is clear from Fig. 5 that electron donation from alkyl groups at C-1 and C-3 should enhance electron donation into the C–F σ* orbitals of the fluorocarbon. Both predictions have been confirmed by *ab initio* calculations[7,36] and are consistent with the experimental results that are discussed in the next section.

Before discussing the effect on cyclopropane stereomutations of replacing the hyperconjugatively electron-donating CH_2 group in propane-1,3-diyl with the electron-accepting CF_2 group in 2,2-difluoropropane-1,3-diyl, it is important to address the question of whether two hydrogens or two fluorines at C-2 provide more stabilization for the diradical formed by cyclopropane ring opening. After correcting eqn. (10) for the fact that the

$$H_3CCF_2CH_3 + \cdot H_2CCH_2CH_2\cdot \rightarrow \cdot H_2CCF_2CH_2\cdot + H_3CCH_2CH_3 \quad (10)$$

C–H BDE of 2,2-difluoropropane is computed to be 2.4 kcal mol^{-1} larger than that of propane, the CF_2 group in 2,2-difluoropropane-1,3-diyl is calculated to provide 3.2 kcal mol^{-1} more stabilization for this diradical than the CH_2 group at C-2 provides for propane-1,3-diyl.[36]

Stereomutation of cyclopropanes and 1,1-difluorocyclopropanes

The publication of Hoffmann's 1968 paper on propane-1,3-diyl[38] inspired a huge amount of computational and experimental work on the stereomutation of cyclopropane. Our own computational efforts in this area were initially motivated less by an interest in propane-1,3-diyl *per se* than by the desire to have calculations on the hydrocarbon diradical with which we could compare our computational results on 2,2-difluoropropane-1,3-diyl.[7]

The most important results of the computational and experimental studies of the hydrocarbon diradical can be summarized as follows. (i) *Ab initio* calculations predict only a 1–2 kcal mol^{-1} preference for con- over dis- and monorotation,[40] a much smaller preference than was found by Hoffmann's Extended Hückel calculations.[38] (ii) As already noted, *ab initio* calculations also predict that alkyl substituents will greatly reduce the small preference for conrotation that is computed for unsubstituted cyclopropane.[36] (iii) Presumably for this reason, experiments on the stereomutation of substituted cyclopropanes have found no preference for coupled rotation.[6,40]

For cyclopropane substituted only by deuterium, (iv) Berson and co-workers[41a,b] and, later, Baldwin[41c] reported a preference for coupled rotation in their studies of the stereomutation of [1,2-$^2H_2$]cyclopropane. (v) However, Baldwin and co-workers found no evidence for coupled rotation in their subsequent study of the stereomutation of [1,2,3-$^2H_3$, 1-^{13}C]cyclopropane.[41d,e] (vi) Calculations show that isotope effects are incapable of reconciling the results of these two experiments.[40a,b] (vii) The results of reaction dynamics calculations[42] are more consistent with the experimental results for [$^2H_2$]cyclopropane[41a–c] than for [$^2H_3$]cyclopropane.[41d,e]

Since the dynamics calculations predict that the coupled rotation found in [$^2H_2$]cyclopropane consists of not only orbital symmetry-allowed conrotation but also of symmetry-forbidden disrotation, the experimental results on [$^2H_2$]cyclopropane should not be taken as confirmation of Hoffmann's prediction of a preference for coupled *conrotation* in the stereomutation of cyclopropane. There is currently no method available for distinguishing between conrotation and disrotation in the experimental study of the stereomutation of [1,2-$^2H_2$]cyclopropane; so there is no known experimental technique that could disprove the mischievous conjecture of a devil's advocate who asserted that the coupled methylene rotation observed in the stereomutation of [$^2H_2$]cyclopropane consists entirely of disrotation rather than conrotation.

What a difference geminal fluorines make! As already noted, the greater ability of C–F σ* orbitals at C-2 to accept electrons in 1,3-diradicals, compared to the ability of filled C–H orbitals at C-2 to donate electrons, is calculated to make hyperconjugative stabilization of the so-called (0,0) geometry[38] of 2,2-difluoropropane-1,3-diyl larger than that of the same geometry of the hydrocarbon diradical.[36] This should make disrotation much more favorable in the stereomutation of 1,1-difluorocyclopropane than conrotation is in the stereomutation of cyclopropane. The results of *ab initio* calculations on the ring opening of the fluorocarbon show that the transition state for disrotation is, in fact, *ca.* 4 kcal mol^{-1} lower in energy than the transition states for conrotation, monorotation, or cleavage of a ring bond to C-1.[7,36]

As discussed above, 2,3-dialkyl-1,1-difluorocyclopropanes are expected to show an even greater preference for disrotatory ring opening and closure than 1,1-difluorocyclopropanes. As shown in Fig. 7, the calculated preference for ring opening of

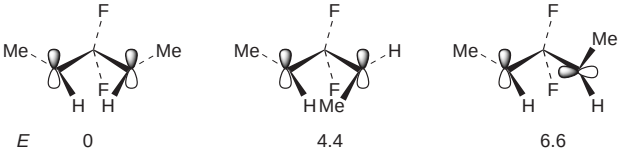

Fig. 7 Relative CASPT2 energies (kcal mol^{-1}) of three conformations of 3,3-difluoropentane-2,4-diyl (ref. 8)

1,1-difluoro-2,3-dimethylcyclopropane to the s-*trans*,s-*trans* (0,0) geometry of 3,3-difluoropentane-2,4-diyl, over rotation of just one methylene group, to form the so-called (0,90) geometry,[38] amounts to 6.6 kcal mol^{-1} when the effects of dynamic electron correlation[43] are included at the CASPT2 level.[8]

As also shown in Fig. 7, ring opening of 2,3-dimethyl-1,1-difluorocyclopropane to the s-*trans*,s-*cis* (0,0) geometry of 3,3-difluoropentane-2,4-diyl is calculated to be more favorable than opening to the (0,90) geometry, but only by 2.2 kcal mol^{-1}.[8] The very large calculated preference of *ca.* 4 kcal mol^{-1} for ring opening to the s-*trans*,s-*trans*, rather than the s-*trans*,s-*cis* geometry of 3,3-difluoropentane-2,4-diyl has been shown to have its origin in the symmetry of the HOMO in this fluorinated diradical.[36]

The large predicted preference for opening of a 2,3-dialkyl-1,1-difluorocyclopropane to an s-*trans*,s-*trans*, rather than an s-*trans*,s-*cis*, geometry can be used to design an experiment to distinguish between conrotatory and disrotatory ring opening.[7,36] If, as predicted, ring opening is disrotatory, the *cis* cyclopropane stereoisomer will open to the preferred s-*trans*, s-*trans* geometry of the 1,3 diradical, whereas the *trans* cyclopropane stereoisomer must open to the s-*trans*,s-*cis* geometry. Therefore, if ring opening is, in fact, disrotatory, an optically active *cis*-2,3-dialkyl-1,1-difluorocyclopropane should racemize faster than its *trans* stereoisomer.

In collaboration with the group of Professor William Dolbier, we prepared optically active *cis*- and *trans*-2-ethyl-3-methyl-1,1-difluorocyclopropane and studied the stereomutations of these two isomers.[8] At 274.5 °C, racemization of the *cis* isomer was found to be 107 times faster than its epimerization to the *trans* isomer by any pathway that effects one-center rotation. At this temperature, racemization was also found to be favored over epimerization in the *trans* isomer, but only by a factor of 6.6. The finding that the ratio of the rate constants for racemization and epimerization is 16.2 times larger for the *cis* cyclopropane than for its *trans* isomer shows that the coupled rotation that is observed in both isomers is disrotation, as predicted.[7,36]

Effect of electron delocalization into C–F σ* orbitals on singlet-triplet energy differences in 1,3-diradicals

Increasing the energy separation between the HOMO and LUMO in a diradical selectively stabilizes the lowest singlet state, relative to the triplet, since in the former state more than one electron can occupy the HOMO, whereas in the latter the HOMO and the LUMO are each occupied by one electron.[44] Thus, either the presence of filled σ orbitals at C-2 that are good hyperconjugative electron donors or unfilled σ* orbitals that are good hyperconjugative electron acceptors can, in principle,

result in singlet ground states for derivatives of propane-1,3-diyl. Therefore, it is not surprising that, although cyclopentane-1,3-diyl has been both calculated[10,45] and found[9] to have a triplet ground state, the ground state of 2,2-difluorocyclopentane-1,3-diyl has been predicted to be a singlet (Fig. 8).[10]

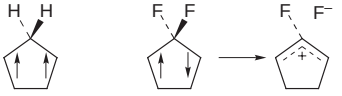

Fig. 8 Cyclopentane-1,3-diyl is known to have a triplet ground state (ref. 9), but electron donation into the C–F σ* orbitals at C-2 is predicted to make 2,2-difluorocyclopentane-1,3-diyl a ground state singlet (ref. 10)

In order to test this prediction, we collaborated with the research groups of Professors Waldemar Adam and Jakob Wirz on the generation and study of the derivative of 1,3-diphenyl-2,2-difluorocyclopentane-1,3-diyl shown in Scheme 1.[11] As

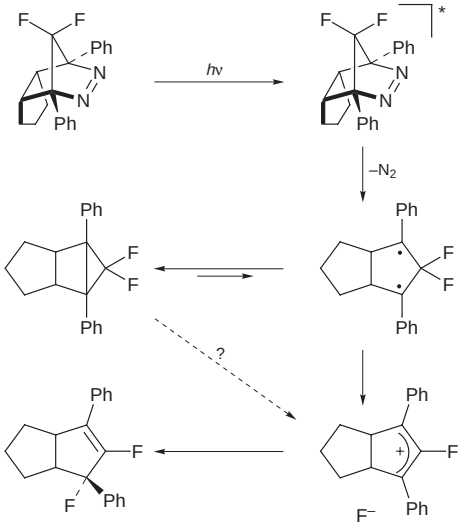

Scheme 1

shown, the diradical was generated by flash photolysis of an azo compound. A strong absorption with λ_{max} = 530 nm appeared with a time constant of τ = 8 ± 1 ps, and in pentane it disappeared with τ = 80 ± 3 ns. In this solvent the diradical reacts to form both the tricyclic difluoride and the bicyclic difluoroalkene. The former was observed by ^{19}F NMR spectroscopy at low temperatures, but at room temperature it rearranges with τ = 225 ± 20 μs to the latter.

The temperature dependence of the rate of disappearance of the diradical was measured and gave log A = 12.8 ± 0.4 and E_a = 7.8 ± 0.5 kcal mol^{-1}. These Arrhenius parameters are very different from those of log A = 6.7 and E_a = 2.6 kcal mol^{-1} measured for disappearance of the hydrocarbon diradical, lacking the geminal fluorines. The fluorocarbon and hydrocarbon diradicals also differ in the rate of their reaction with O_2. The former cannot be trapped by oxygen, making $k_{O2} < 4 \times 10^7$ M^{-1}s^{-1}; whereas, the latter reacts with O_2 with a rate constant of $k_{O2} = 3 \times 10^9$ M^{-1}s^{-1}.

The hydrocarbon diradical gives a triplet EPR spectrum and, like the parent cyclopentane-1,3-diyl, it appears to have a triplet ground state. This accounts for the low values of log A and E_a for the disappearance of the hydrocarbon diradical, since intersystem crossing to a slightly higher energy singlet state is the rate determining step. The reaction of the triplet hydrocarbon diradical with triplet oxygen is fast, because the two triplet species can give a singlet product by forming two C–O bonds in a concerted fashion.

The high E_a for disappearance of the fluorocarbon diradical allowed frozen solutions of it to be studied at low temperatures. At 77 K the red color of the diradical persisted for a day, but no triplet EPR signal was detected. The conclusion that the fluorinated diradical has a singlet ground state is supported by the activation parameters for its disappearance, which are typical of those for a spin-allowed process, and the rate at which it is trapped by oxygen, which was too slow for us to measure. These experimental results[11] are consistent with our prediction that the ability of C–F σ* orbitals to accept electrons is sufficiently large to make the singlet the ground state of 2,2-difluorocyclopentane-1,3-diyls.[10]

Future research

In the course of the theoretical studies described in the previous sections, we moved from explaining phenomena that were already known to predicting new phenomena. Prediction is the ultimate goal of any theory, and the experimental confirmation of our predictions that geminal fluorine substituents should result in disrotatory cyclopropane ring-opening and in singlet ground states for 1,3-diradicals shows that delocalization of electrons into C–F σ* orbitals is a very useful theoretical construct.

If the presence of low-lying empty σ* orbitals at C-2 can stabilize the singlet states of 1,3-diradicals, it follows that high-lying filled σ orbitals at C-2 should have the same effect. Therefore, replacement of the C–H bonds at C-2 of propane-1,3-diyl by weaker bonds to less electronegative elements, for example silicon, should also favor formation of the (0,0) geometries of such diradicals by coupled rotation of the methylene groups in the ring-opening reactions of the corresponding cyclopropanes. The hyperconjugated resonance structure for 2,2-disilylpropane-1,3-diyl in Fig. 9 allows the

Fig. 9 Hyperconjugated resonance structure for 2,2-disilylpropane-1,3-diyl

prediction that ring-opening to form this diradical should be conrotatory.

To the extent that the hyperconjugated resonance structures, like that in Fig. 9, are important, it seems likely that 2,2-disilylcyclopentane-1,3-diyls should, like 2,2-difluorocyclopentane-1,3-dilyls, have singlet ground states. However, since disrotatory closure is expected to be an orbital-symmetry forbidden reaction in 2,2-disilylcyclopentane-1,3-diyls, unlike their difluoro-substituted counterparts, they should be kinetically stabilized against ring closure.

These qualitative predictions have already survived the tests of calculations performed at levels that are deemed to provide quantitatively accurate results.[46,47] It remains to be seen if, as predicted, geminal disilylcyclopropanes will be found experimentally to undergo stereomutation by coupled conrotation[46] and whether 2,2-disilylcyclopentane-1,3-diyls will be found to have singlet ground states and appreciable kinetic barriers to ring closure.[47]

Acknowledgements

I wish to thank my many collaborators, who, over the past twenty years, performed the computational and experimental studies that are described in this article. I am particularly grateful to Dr David A. Hrovat, who was involved to some extent in nearly all the research projects described in this article and who prepared the figure for the cover of this issue. I also thank the National Science Foundation, which generously supported this research. This article is dedicated to the memory of Professor Paul D. Bartlett, in whose physical organic chemistry course at Harvard in 1964 I first learned about the propensity of TFE and other fluorinated alkenes to undergo stepwise cycloaddition reactions.

Weston Thatcher Borden received his undergraduate degree from Harvard in 1964. Following a year spent on a Fullbright Fellowship, studying theoretical chemistry with H. C. Longuet-Higgins, he returned to Harvard and, under the guidance of E. J. Corey, was awarded a PhD in 1968. After another five years on the faculty of the same institution, he joined the Chemistry Department at the University of Washington. His research activities include the synthesis and study of molecules of theoretical interest and the application of qualitative molecular orbital theory and quantitative *ab initio* calculations to the understanding of organic chemistry. He has received fellowships from the Alfred P. Sloan Foundation, the Guggenheim Foundation, and the Japanese Society for the Promotion of Science, and a Humboldt Senior Scientist Award. His non-chemical interests include gardening, hiking, and traditional Japanese arts, such as *chanoyu* and *ikebana*.

Notes and References

† E-mail: borden@chem.washington.edu

1 See, for example, (*a*) D. A. Dixon, T. Fukunaga and B. E. Smart, *J. Am. Chem. Soc*., 1986, **108**, 4027; (*b*) I. A. Koppel, V. Pihl, J. Koppel, F. Anvia and R. W. Taft, *J. Am. Chem. Soc*., 1994, **116**, 8654 and references therein.

2 R. W. Fessenden and R. H. Schuler *J. Chem. Phys.*, 1965, **43**, 2704; K. S. Chen, P. J. Krusic, P. Meakin and J. Kochi, *J. Phys. Chem*., 1974, **78**, 2014.

3 E. C. Wu and A. S. Rogers, *J. Am. Chem. Soc*., 1976, **98**, 6112.

4 D. D. Coffman, P. L. Barrick, R. D. Cramer and M. S. Raasch, *J. Am. Chem. Soc*., 1949, **71**, 490; P. D. Bartlett, *Quart. Rev. Chem. Soc.*, 1970, **24**, 473.

5 B. E. Smart, in *Molecular Structure and Energetics*, ed. J. F. Liebman and A Greenberg, VCH, Deerfield Beach, FL, 1986, vol. 3, pp. 141–191.

6 W. L. Carter and R. G. Bergman, *J. Am. Chem. Soc*., 1968, **90**, 7344; R. G. Bergman and W. L. Carter, *J. Am. Chem. Soc*., 1969, **91**, 7411.

7 S. J. Getty, D. A. Hrovat and W. T. Borden, *J. Am. Chem. Soc*., 1994, 116, 1521.

8 F. Tian, S. B. Lewis, M. D. Bartberger, W. R. Dolbier, Jr. and W. T. Borden, *J. Am. Chem. Soc*., 1998, **120**, 6187.

9 S. L. Buchwalter and G. L. Closs, *J. Am. Chem. Soc*., 1975, **97**, 3857; *J. Am. Chem. Soc*., 1979, **101**, 4688.

10 J. D. Xu, D. A. Hrovat and W. T. Borden, *J. Am. Chem. Soc*., 1994, **116**, 5425.

11 W. Adam, W. Borden, C. Burda, H. Foster, T. Heidenfelder, M. Heubes, D. A. Hrovat, F. Kita, S. B. Lewis, D. Scheutzow and J. Wirz, *J. Am. Chem. Soc*., 1998, **120,** 593.

12 W. T. Borden, *Modern Molecular Orbital Theory for Organic Chemists*, Prentice-Hall, Englewood Cliffs, NJ, 1975.

13 W. R. Cherry and N. D. Epiotis, *J. Am. Chem. Soc*., 1976, **98**, 1135. A similar perspective on the origin of the differences between ammonia and phosphine was published by C. C. Levin, *J. Am. Chem. Soc*., 1975, **97**, 5649.

14 Hybridization arguments can also be used to rationalize the effects of substituents on pyramidalization of AH_3 molecules: H. A. Bent, *Chem. Rev*., 1961, **61**, 275; W. A. Bernett, *J. Org. Chem*., 1969, **34**, 1772.

15 W. Cherry, N. Epiotis and W. T. Borden, *Acc. Chem. Res*., 1977, **10**, 167.

16 Review: J. Lambert, *Top. Stereochem.*, 1971, **6**, 19.

17 P. J. Krusic and J. K. Kochi, *J. Am. Chem. Soc*., 1969, **91**, 3938; H. Sakurai, M. Murakasmi and M. Kumada, *J. Am. Chem. Soc*., 1969, **91**, 519.

18 W. Kutzelnigg, *Angew. Chem., Int. Ed. Engl.*, 1984, **23**, 272.

19 Review: J. M. Lehn, *Fortschr. Chem. Forsch*., 1970, **15**, 1970.

20 S. Deycard, L. Hughes, J. Lusztyk and K. U. Ingold, *J. Am. Chem. Soc*., 1987, **109**, 4954.

21 H. Sun, D. A. Hrovat and W. T. Borden, *J. Am. Chem. Soc*., 1987, **109**, 5275.

22 D. A. Hrovat, H. Sun and W. T. Borden, *J. Mol. Struct. (Theochem)*, 1988, **163**, 51.

23 W. T. G. Johnson and W. T. Borden, *J. Am. Chem. Soc*., 1997, **119**, 5930.

24 S. Y. Wang and W. T. Borden, *J. Am. Chem. Soc*., 1989, **111**, 7282.

25 J. E. Douglas, B. S. Rabinovitch and F. S. Looney, *J. Chem. Phys.*, 1955, **23**, 315.

26 S. Benson, *Thermochemical Kinetics*, 2nd edn., Wiley, New York, 1976, pp. 63–65.

27 A. Nicolaides and W. T. Borden, *J. Am. Chem. Soc*., 1992, **114**, 8682.

28 (*a*) P. J. Krusic, P. Meakin and B. E. Smart, *J. Am. Chem. Soc*., 1974, **96**, 7382; (*b*) B. E. Smart, P. J. Krusic, P. Meakin and R. C. Bingham, *J. Am. Chem. Soc*., 1974, **96**, 6211; (*c*) H. Korth, H. Trill and R. Sustmann, *J. Am. Chem. Soc*., 1981, **103**, 4483.

29 J. H. Hammons, M. B. Coolidge and W. T. Borden, *J. Phys. Chem.*, 1990, **94**, 5468.

30 J. H. Hammons, D. A. Hrovat and W. T. Borden, *J. Phys. Org. Chem*., 1990, **3**, 635; see also D. A. Dixon, T. Fukunaga and B. E. Smart, *J. Phys. Org. Chem*., 1988, **1**, 153.

31 P. D. Bartlett and K. E. Schueller, *J. Am. Chem. Soc*., 1968, **90**, 6071.

32 P. D. Bartlett, K. Hummel, S. P. Elliot and R. A. Minns, *J. Am. Chem. Soc*., 1972, **94**, 2898; P. D. Bartlett, G. M. Cohen, K. H. Elliot, R. A. Minns, C. M. Sharts and J. Y. Fukunaga, *J. Am. Chem. Soc*., 1972, **94**, 2899.

33 S. J. Getty and W. T. Borden, *J. Am. Chem. Soc*., 1991, **113**, 4334.

34 (*a*) C. Rüchardt, *Angew. Chem., Int. Ed. Engl*., 1970, **9,** 830; (*b*) A. E. Dorigo, K. N. Houk and T. Cohen, *J. Am. Chem. Soc*., 1989, **111**, 8976; (*c*) Y. D. Wu, W. Kirmse and K. N. Houk, *J. Am. Chem. Soc*., 1990, **112**, 4557.

35 See, for example, M. M. Rahman, D. M. Lemal and W. P. Dailey, *J. Am. Chem. Soc*., 1988, **110**, 1964 and references cited therein.

36 S. J. Getty, D. A. Hrovat, J. D. Xu, S. A. Barker and W. T. Borden, *J. Chem. Soc., Faraday Trans*., 1994, **90**, 1689.

37 A. Greenberg, J. Liebman, W. R. Dolbier, Jr., K. S. Medinger and A. Skancke, *Tetrahedron*, 1983, **39**, 1533.

38 R. Hoffmann, *J. Am. Chem. Soc*., 1968, **90**, 11475.

39 W. R. Dolbier, Jr., J. J. Keaffaber, C. R. Burkholder, H. Koroniak and J. Pradhan, *Tetrahedron*, 1972, **48**, 9649.

40 (*a*) S. J. Getty, E. R. Davidson and W. T. Borden, *J. Am. Chem. Soc.*, 1992, **114,** 2085; (*b*) J. E. Baldwin, Y. Yamaguchi and H. F. Schaefer III, *J. Phys. Chem.*, 1994, **98**, 7513; (*c*) both of these papers contain references to the extensive computational and experimental literature on the subject of trimethylene stereomutations.

41 (*a*) L. D. Pedersen and J. A. Berson, *J. Am. Chem. Soc.*, 1975, **97**, 238; (*b*) J. A. Berson, L. D. Pedersen and B. K. Carpenter, *J. Am. Chem. Soc.*, 1976, **98**, 122; (*c*) S. J. Cianciosi, N. Ragunathan, T. R. Freedman, L. A. Nafie and J. E. Baldwin *J. Am. Chem. Soc.*, 1990, **112,** 8204; (*d*) S. J. Cianciosi, N. Ragunathan, T. R. Freedman, L. A. Nafie, D. K. Lewis, D. A. Glenar and J. E. Baldwin, *J. Am. Chem. Soc.*, 1991, **113**, 1864; (*e*) J. E. Baldwin, in *The Chemistry of the Cyclopropyl Group*, ed. Z. Rappoport, Wiley, New York, 1995, vol. 2, ch. 9.

42 C. Doubleday, Jr., K. Bolton and W. L. Hase, *J. Am. Chem. Soc.*, 1997, **119**, 5251; D. A. Hrovat, S. Fang, W. T. Borden and B. K. Carpenter, *J. Am. Chem. Soc.*, 1997, **119,** 5253.

43 W. T. Borden and E. R. Davidson, *Acc. Chem. Res.*, 1996, **29**, 87.

44 W. T. Borden, in *Diradicals*, ed. W. T. Borden, Wiley, New York, 1982. pp. 1–72.

45 M. P. Conrad, R. M. Pitzer and H. F. Schaefer III, *J. Am. Chem. Soc.*, 1979, **101**, 2245; C. D. Sherrill, E. T. Seidl and H. F. Schaefer III, *J. Phys. Chem.*, 1992, **96**, 371.

46 A. Skancke, D. A. Hrovat and W. T. Borden, *J. Am. Chem. Soc*., 1998, **120**, 7079.

47 W. T. G. Johnson, D. A. Hrovat, A. Skancke and W. T. Borden, *Theor. Chem. Acc.*, in the press.

8/03750G

Domino reaction of lithiated allenes with nitriles†

Peter Langer,*[a]‡ Manfred Döring[b] and Dietmar Seyferth[c]

[a] *Institut für Organische Chemie der Georg-August-Universität Göttingen, Tammannstrasse 2, 37077 Göttingen, Germany*
[b] *Institut für Anorganische und Analytische Chemie der Universität Jena, August-Bebel-Strasse 2, 07743 Jena, Germany*
[c] *Department of Chemistry, Massachusetts Institute of Technology, Cambridge, Massachusetts 02139, USA*

Addition of nitriles to dilithiated allenes results in a unique domino cyclization which involves the so far highest number of nitrile molecules added to an organolithium reagent to form unambiguously characterized oligomers.

The development of domino reactions is of ongoing interest in organic synthesis.[1] Interestingly, although the base-catalyzed polymerization of nitriles has been followed for a long time and the mixtures obtained were among the first organic polymers, only a few structurally unambiguously characterized oligomers derived from multiple addition reactions of nitriles have been reported so far. In contrast, the palladium-catalyzed oligomerization of six isonitrile molecules has recently been reported.[2] Addition of 2 equiv. of a nitrile to an organometallic reagent has been achieved by reaction of 2,3-bis-lithiated methylbutadiene with PhCN,[3a] by 1,4-addition of nitriles to (butadiene)zirconocene[3b,c] and by base-induced oligomerization of glycolonitrile.[3d] Very recently, a domino reaction initiated by addition of a Grignard reagent to a tris-nitrile has been reported.[4a] Herein we report the addition of up to 4 equiv. of a nitrile to dilithiated allenes, a process which we believe includes a novel type of rearrangement reaction.[5]

1,1-Diphenyl-3,3-dilithioallene **2** was generated in one pot by treatment of the TBDMS enol ether **1** with an excess of LDA in THF, a reaction recently developed by us.[6] This process presumably proceeds *via* a mechanism involving initial lithiation of the allyl system of the silyl enol ether, elimination of lithium silanolate and lithiation of the 1,1-diphenylallene formed (Scheme 1). The elimination could either occur directly (path A) or proceed *via* a O→C silyl migration/Peterson elimination sequence (path B).

Reaction of lithiated allenes with nitriles was expected to result in formation of allenylimines. Selected examples of these compounds have recently been prepared in moderate yields by reaction of allenic aldehydes with amines.[7] Reaction of **2** with 2.2 equiv. of PhCN resulted in a complex reaction mixture from which two products, **3** (9%) and **4** (14%) (Scheme 2), were isolated by column chromatography in low yields. Much to our surprise, FAB-MS suggested that products derived from reaction of the allene with three and four nitriles, respectively, had been formed. The yield of **4** was significantly improved by use of 4.5 equiv. of the nitrile. Yellow-coloured imidazole **3** and colourless 5-imidazol-5-yl-1,4-dihydropyrimidine **4** were isolated in 12 and 51% yield, respectively.§ Similar results were obtained when 10 equiv. of PhCN were employed. Reaction of dilithioallene **2** with pivalonitrile afforded as the sole isolated product the colourless imidazole **5** (66%). The imine group was hydrolyzed during aqueous work-up to generate an α,β-unsaturated keto group. Reaction of **2** with *p*-tolunitrile gave the orange coloured imidazole **6** (28%).

Formation of the sterically crowded imidazoles **3**–**6** can be rationalized by the mechanism shown in Scheme 2. The

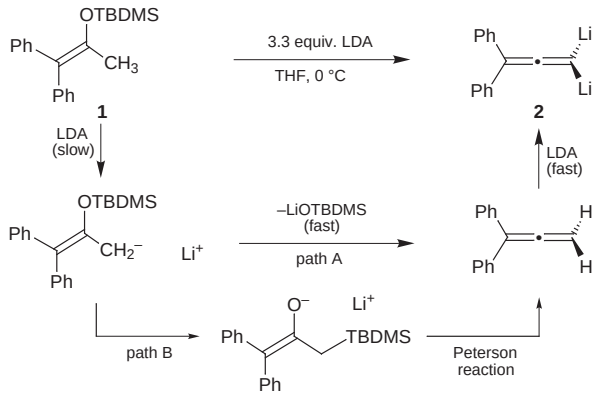

Scheme 1

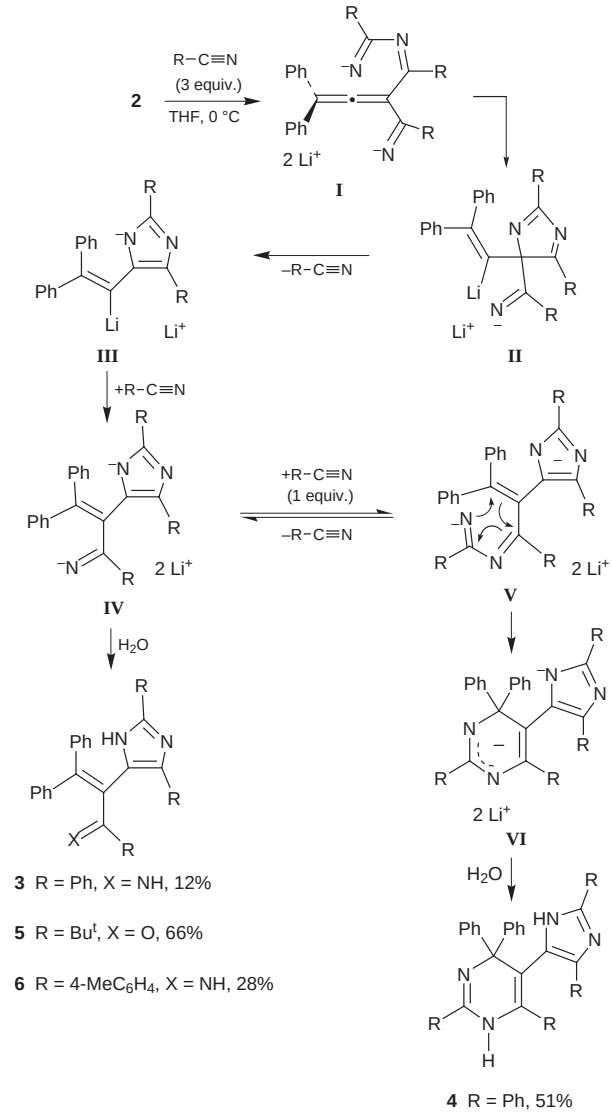

Scheme 2

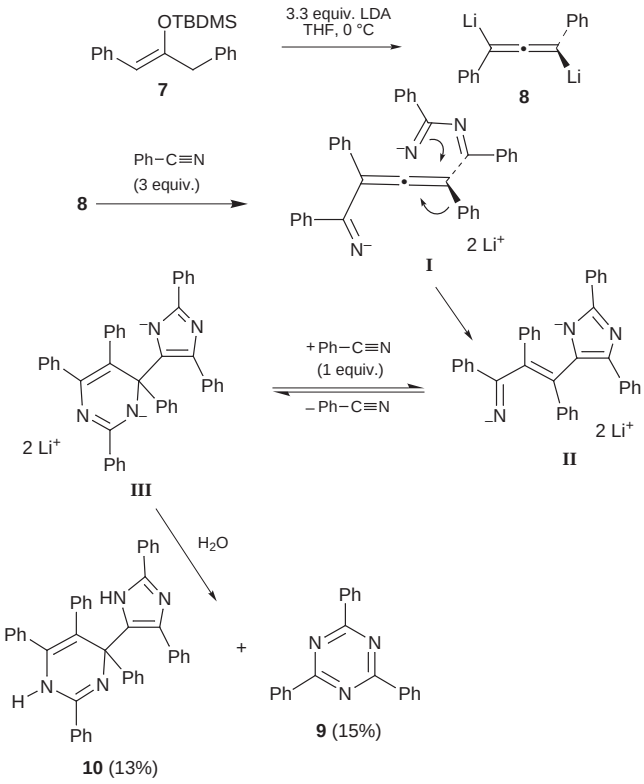

Scheme 3

terminal carbon atom of the allene dianion **2** initially reacts with two molecules of the nitrile. Presumably, the negative charge will mainly be localized at the nitrogen atoms. A third nitrile molecule is attacked (intermediate **I**) and the amidine anion thus formed attacks the terminal allene carbon atom to give intermediate **II** which contains a five-membered ring and a vinyl carbanion function. An aromatic imidazole anion (intermediate **III**) is generated next by elimination of 1 equiv. of the nitrile. The vinyl carbanion subsequently reacts with the nitrile to give intermediate **IV**. The fourth nitrile molecule is attacked by the imine anion of intermediate **IV** to generate an amidine anion (intermediate **V**). The amidine anion attacks the terminal allene carbon atom bearing the phenyl groups to give a dihydropyrimidine anion (intermediate **VI**). Aqueous work-up furnishes heterocycles **4** and **3** derived from intermediates **VI** and **IV**, respectively.

Reaction of PhCN with the dianion of 1,3-diphenyl-1,3-dilithioallene **8** (formed *in situ* by reaction of silyl enol ether **7** with 3.3 equiv. of LDA) afforded after hydrolytic work-up a mixture of 2,4,6-triphenyltriazine **9**[8] (formed by trimerization of the nitrile) and imidazole **10** (a 1:4 product). The formation of **10** can be explained by a reaction sequence similar to that leading to oligonitrile **4** (Scheme 3). This reaction seems to involve migration of a phenyl rather than a phenylimino group.

It is noteworthy that all carbon atoms of the allene system are involved sequentially in the reaction leading to cyclic oligonitrile **4**. The intramolecular attack of the amidine anion on the terminal (rather than on the central) allene carbon atom and the subsequent rearrangement reaction (**I**→**IV**, Scheme 2) are surprising. However, this process can be explained by the stability of the aromatic imidazole anion formed. Steric hindrance seems to be the reason that no addition of a fourth nitrile molecule takes place for **5** and **6**. Interestingly, treatment of the dianion of 2-methylbenzimidazole or of amide derived dianions with 4.5 equiv. of PhCN resulted in addition of only 1 equiv. of the nitrile to the dianion rather than in formation of an open-chained oligonitrile.[9] This striking difference to the reaction of the allene dianion **2** suggests that the addition of the imine anion to the nitrile is a reversible process which becomes irreversible when the amidine anion generated can undergo a consecutive reaction to form a more stable intermediate (such as **IV** and **VI** in Scheme 2).¶ It is noteworthy that the number of nitrile molecules added to the dianion does not depend on the number of equivalents of the nitrile employed in the reaction. Therefore, there is some relationship between the reaction reported and self-assembly processes.

P. L. thanks Professor A. de Meijere for his support. Financial support from the Fonds der Chemischen Industrie e. V. (award of a fellowship to P. L.) is gratefully acknowledged.

Notes and References

† Regioselective reactions of ambident dianions, Part 5. For Part 4, see ref. 5(*d*).

‡ E-mail: planger@uni-goettingen.de

§ *Preparation of imidazole* **4**. To a THF solution (40 ml) of silyl enol ether **1** (1.80 g, 5.6 mmol) was added a THF solution of LDA which was prepared by addition of Bu^{n}Li (1.6 M in hexane) to a THF solution (20 ml) of Pr$^i_2$NH (3.3 equiv.) at 0 °C. The solution was stirred at 20 °C for 6 h during which time the color of the solution became deep red. A THF solution (10 ml) of PhCN (2.58 ml, 4.5 equiv.) was added at 0 °C by syringe. After stirring for 10 h at 20 °C, water (20 ml) was added to the deep purple solution and the colour changed to yellow. The reaction mixture was extracted (Et_2O–THF = 1:1) and the combined organic layers were dried ($MgSO_4$), filtered and the solvent was removed *in vacuo* to give imidazole **4** (1.73 g, 51%) after purification by column chromatography (silica gel, Et_2O–light petroleum = 1:1) as a colorless solid, mp 146–150 °C; δ_H([$^2H_8$]THF, 200 MHz) 6.75–8.20 (m, 30 H, Ar), 8.75 (br, 1 H, NH), 10.68 (br, 1 H, NH); δ_C([$^2H_8$]THF, 50 MHz) 107.20 (C, *C*Ph$_2$), 125.27, 125.76, 125.87, 126.06, 126.26, 127.12, 127.30, 127.50, 128.02, 128.08, 128.17, 128.30, 128.68, 128.90, 129.21, 129.76 129.92, 130.86 (CH, Ph), 132.15, 132.19, 136.43, 136.73, 137.37, 138.19 (C, Ph, =*C*Ph$_2$), 145.67, 148.50, 148.78 (C, C=*C*N), 150.65, 150.78 (C, CN$_2$); ν_{max}(KBr)/cm^{-1} 3495 (br), 3395 (br), 3060 (m), 3029 (m), 2923 (w), 1640 (s), 1598 (m), 1578 (m), 1524 (s), 1496 (m), 1446 (m), 1395 (s), 1370 (m), 1178 (m), 1072 (m), 1028 (m), 697 (s); *m/z* (FAB) 605 (100%, M$^+$+1); Calc. for $C_{43}H_{32}N_4$: C, 85.41; H, 5.33; N, 9.26. Found.: C, 85.17; H, 5.61; N, 9.62%.

¶ The reactions cited in refs. 3(*a*)–(*d*) involve only a single addition of each nucleophilic center to a nitrile molecule since the imine anions formed are intramolecularly trapped to form stable dianionic systems. In contrast, in ref. 4, a second nitrile group is attacked by the initially formed imine anion. Thus, in the third step of the reaction, a stable anion could be formed.

1 For reviews on domino reactions, see: L. F. Tietze and U. Beifuss, *Angew. Chem.*, 1993, **105**, 137; *Angew. Chem., Int. Ed. Engl.*, 1993, **32**, 131; A. de Meijere and F. E. Meyer, *Angew. Chem.*, 1994, **106**, 2473; *Angew. Chem., Int. Ed. Engl.*, 1994, **33**, 2379.

2 T. Tanase, T. Ohizumi, K. Kobayashi and Y. Yamamoto, *J. Chem. Soc., Chem. Commun.*, 1992, 707.

3 (*a*) R. B. Bates, B. Gordon III, P. C. Keller and J. V. Rund, *J. Org. Chem.*, 1980, **45**, 168; (*b*) G. Erker, M. Berlekamp, L. Lopez, M. Grehl, B. Schönecker and R. Krieg, *Synthesis*, 1994, 212; (*c*) M. Riedel and G. Erker, *Synthesis*, 1994, 1039; (*d*) G. Arrhenius, K. K. Baldridge, S. Richards-Gross and J. S. Siegel, *J. Org. Chem.*, 1997, **62**, 5522.

4 (*a*) S. Mathé and A. Rassat, *Tetrahedron Lett.*, 1998, **39**, 383; (*b*) see also: L. N. Cherkasov and K. V. Balyan, *Zh. Org. Khim.*, 1965, **1**, 1811.

5 For domino reactions of dilithio compounds from our laboratory, see: (*a*) P. Langer, M. Döring, H. Görls and R. Beckert, *Liebigs Ann./Receuil*, 1997, 2553; (*b*) P. Langer and M. Döring, *Synlett*, 1998, 396; (*c*) P. Langer and M. Döring, *Synlett*, 1998, 399; (*d*) P. Langer, J. Wuckelt, M. Döring and R. Beckert, *Eur. J. Org. Chem.*, 1998, 1467.

6 D. Seyferth, P. Langer and M. Döring, *Organometallics*, 1995, **14**, 4457.

7 M. S. Sigman and B. E. Eaton, *Tetrahedron Lett.*, 1993, **34**, 5367.

8 Triazines have been previously obtained by base induced cyclotrimerization of aryl nitriles: see C. Grundmann, in *Methoden Org. Chem.* (Houben-Weyl), 4th edn., Thieme, Stuttgart, New York, 1985, vol. E512, 1544.

9 For open-chained oligonitriles see M. Buhmann, M. H. Möller, U. Rodewald and E.-U. Würthwein, *Chem. Ber.*, 1993, **126**, 2467.

Received in Cambridge, UK, 23rd April 1998; 8/03040E

An enantiocontrolled synthesis of a key intermediate to (+)-lactacystin

Sung Ho Kang*† and Hyuk-Sang Jun

Department of Chemistry, Korea Advanced Institute of Science and Technology, Taejon. 305-701, Korea

An asymmetric synthesis of a key intermediate 16 to (+)-lactacystin 1 has been established starting from epoxide 2 *via* intramolecular mercurioamidation of allylic trichloroacetimidate 4 and concomitant addition-reduction of ester 13 by Pr^i MgBr, in which reduction of the intermediate ketone proceeded with complete stereoselectivity.

Since neurotrophic factors are responsible for the survival and function of neurons,[1] they might be useful in the treatment of various nerve diseases.[2] Omura *et al*. screened a number of microbial culture samples to isolate the first non-protein neurotrophic agent (+)-lactacystin **1** from *Streptomyces* sp. OM-6519.[3] Its structure, elucidated by NMR spectroscopy and X-ray crystallographic analysis, is composed of (*R*)-*N*-acetylcysteine and a unique pyroglutamic acid *via* a thioester linkage.[4] (+)-Lactacystin inhibits cell proliferation, induces neuritogenesis and increases the intracellular cAMP level transiently in the Neuro 2A neuroblastoma cell line.[3,5] Its intriguing structural features as well as potential therapeutic utility have engendered considerable interest in the fields of synthetic and medicinal chemistry. Here we describe a stereoselective synthetic route to (+)-lactacystin.[6–9] The key steps of our synthesis comprise tertiary amination of the olefinic double bond in allylic trichloroacetimidate **4** *via* mercurioamidation,[10] facile differentiation of the hydroxymethyl groups in **10** by ring formation and diastereoselective derivatization of ester **13** into alcohol **14**.

The known epoxide **2**,[11] $[\alpha]_D^{20}$ −24.7 (*c* 1.15, $CHCl_3$), was treated with LDA to give allylic alcohol **3**, $[\alpha]_D^{21}$ +10.4 (*c* 1.44, $CHCl_3$), in 91% yield (Scheme 1). Only the primary hydroxy group of **3** was functionalized to a trichloroacetimidate. The crude monoimidate **4** was subjected to intramolecular mercurioamidation using mercuric trifluoroacetate with K_2CO_3 to furnish a 1:1 diastereomeric mixture of oxazolines **5** in 92% overall yield after aqueous KBr work-up. Since oxidative demercuration[12] of **5** using O_2 failed under a variety of reaction conditions, it was attempted by exposing **5** to TEMPO in the presence of $LiBH_4$ to provide the oxidized products **6** in 78% yield. The secondary hydroxy groups of **6** were protected with $MeOCH_2Cl$ (MOMCl) and then the silyl groups were removed to afford the corresponding primary alcohols in 84% overall yield. While PDC oxidation of the alcohols in DMF was sluggish, they were efficiently oxidized to carboxylic acids **8** in 78% yield by Swern oxidation[13] followed by $KMnO_4$ oxidation.[14] Complete hydrolysis and the ensuing cyclization were effected by heating **8** at reflux with ethanolic HCl in AcOH. The 2,2,6,6-tetramethylpiperidyl (TEMP) groups of the generated pyrrolidinones **9** were reductively cleaved *in situ* by adding zinc to the hot reaction mixture to produce trihydroxy pyrrolidinone **10**, $[\alpha]_D^{19}$ +9.5 (*c* 0.95, MeOH), in 72% overall yield from **8**.

For the appropriate elaboration of the α-hydoxymethyl groups in **10**, it was chemoselectively reacted with acetone under acidic conditions to give a 7:1 mixture of acetonides **11** and **12** in 95% combined yield (Scheme 2). After chromatographic separation, the primary alcohol **11**, $[\alpha]_D^{20}$ +31.4 (*c* 1.10, $CHCl_3$), was oxidized under Swern conditions and the resulting aldehyde reacted with Pr^{i}MgBr under various reaction conditions to furnish a 1 : 1 mixture of alcohols **14** and **15** along with an appreciable amount of the reduced starting alcohol **11**. Owing to the inefficient Grignard addition, **11** was converted into ester **13**, $[\alpha]_D^{21}$ +57.1 (*c* 1.70, $CHCl_3$), in 90% yield. Subjection of **13** to 1 equiv. of Pr^{i}MgBr provided the corresponding isopropyl ketone in 80% yield, the stereoselective reduction of which was attempted employing several reducing agents such as oxazaborolidine,[15] Ipc_2Cl,[16] sodium triacetoxyborohydride,[17] $NaBH_4$ in the presence of diethylmethoxyborane,[18] and so forth. However, the best stereoselectivity turned out to be 5 : 1 in favor of **14** with $NaBH_4$ in MeOH at 0 °C. Some experimentation revealed that an excess amount of Pr^{i}MgBr reduced the generated isopropyl ketone to the alcohol **14**. Accordingly, **13** was treated with > 2 equiv. of Pr^{i}MgBr to give selectively only the desired diastereomeric alcohol **14**, $[\alpha]_D^{20}$ +40.5 (*c* 1.20, $CHCl_3$), in 91% yield. Acidic hydrolysis of **14** yielded trihydroxy pyrrolidinone **16**, mp 198–199 °C (decomp.), $[\alpha]_D^{20}$ +16.2 (*c* 0.62, MeOH), quantitatively, the spectroscopic data of which are identical to those reported in the literature and which is a known intermediate to (+)-lactacystin **1**.[8,19]

We have developed an enantioselective synthetic route to (+)-lactacystin **1** *via* several crucial steps, including animo hydroxylation of the olefinic double bond in **3**, the hydrolytic cyclization of **8**, and the regio- and stereo-selective functionalization of one hydroxymethyl group in **10**; these should have versatility in the synthesis of its analogues.

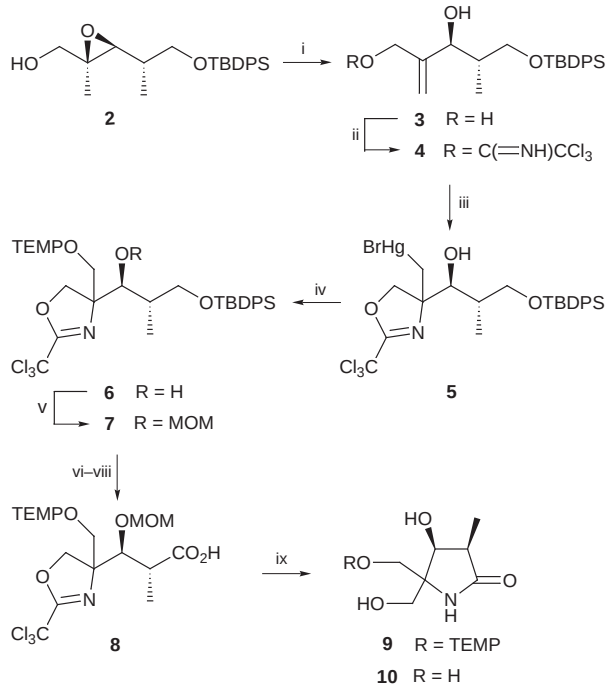

Scheme 1 *Reagents and conditions*: i, LDA, THF, 0–24 °C; ii,Cl_3CCN, DBU, EtCN, −78 °C; iii, $Hg(O_2CCF_3)_2$, K_2CO_3, THF, 0 °C, then aq. KBr; iv, TEMPO, $LiBH_4$, THF, 24 °C; v, MOMCl, Pr$^i_2$NEt, CH_2Cl_2, 0–24 °C; vi, Bu_4NF, H_2O, THF, 45 °C; vii, $(COCl)_2$, DMSO, Et_3N; viii, 1 M $KMnO_4$, 1.25 M NaH_2PO_4, Bu^{t}OH, 24 °C; ix, conc. HCl, EtOH, AcOH, reflux, then Zn, reflux

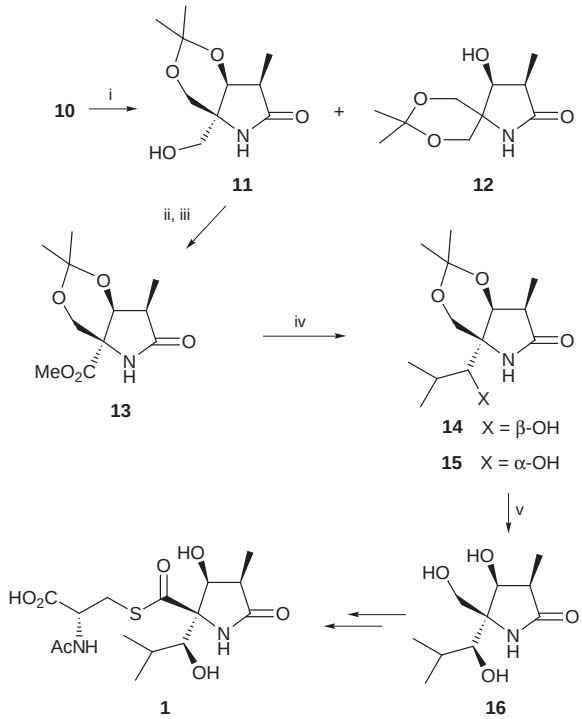

Scheme 2 *Reagents and conditions*: i, TsOH, acetone, 24 °C; ii, Jones' reagent, acetone, 0 °C; iii, CH_2N_2, THF, 0 °C; iv, Pr^iMgBr, THF, −20 to 0 °C; v, TsOH, MeOH, 60 °C

This work was supported by Creative Research Initiatives of the Korean Ministry of Science and Technology.

Notes and References

† E-mail: shkang@kaist.ac.kr

1 F. Hefti and W. J. Weiner, *Ann. Neurol.*, 1986, **20**, 275; Y.-A. Barde, *Neuron*, 1989, **2**, 1525.
2 P. Dohty, J. G. Dickson, T. P. Flanigan and F. S. Walsh, *Neurochem.*, 1985, **44**, 1259; B. A. Sabei, J. Gottlieb and G. E. Schneider, *Brain Res.*, 1988, **459**, 373.
3 S. Omura, T. Fujimoto, K. Otogurro, K. Matsuzaki, R. Moriguchi, H. Tanaka and Y. Sasaki, *J. Antibiot. Chem.*, 1991, **44**, 113.
4 S. Omura, K. Matsuzaki, T. Fujimoto, K. Kosuge, T. Furuya, T. Fujita and A. Nakagawa, *J. Antibiot. Chem.*, 1991, **44**, 117.
5 H. Tanaka, M. Katagiri, S. Arinie, K. Matsuzaki, J. Inokoshi and S. Omura, *Biochem. Biophys. Res. Commun.*, 1995, **216**, 291.
6 E. J. Corey and G. A. Reichard, *J. Am. Chem. Soc.*, 1992, **114**, 10677; E. J. Corey, W. Li and G. A. Reichard, *J. Am. Chem. Soc.*, 1998, **120**, 2330.
7 T. Sunazuka, T. Nagamitsu, K. Matsuzaki, H. Tanaka, S. Omura and A. B. Smith, III, *J. Am. Chem. Soc.*, 1993, **115**, 5302; T. Nagamitsu, T. Sunazuka, H. Tanaka, S. Omura, P. A. Sprengeler and A. B. Smith, III, *J. Am. Chem. Soc.*, 1996, **118**, 3584.
8 H. Uno, J. E. Baldwin and A. T. Russell, *J. Am. Chem. Soc.*, 1994, **116**, 2139.
9 N. Chida, J. Takeoka, N. Tsutsumi and S. Ogawa, *J. Chem. Soc., Chem., Commun.*, 1995, 793.
10 S. H. Kang and S. B. Lee, *Chem. Commun.*, 1998, 761.
11 E. N. Jacobsen, I. Marko, W. S. Mungall, G. Schröder and K. B. Sharpless, *J. Am. Chem. Soc.*, 1988, **110**, 1968; W. P. Griffith and S. V. Ley, *Aldrichim. Acta*, 1990, **23**, 13.
12 C. L. Hill and G. M. Whitesides, *J. Am. Chem. Soc.*, 1974, **96**, 870.
13 A. J. Mancuso and D. Swern, *Synthesis*, 1981, 165.
14 A. Abiko, J. C. Roberts, T. Takemasa and S. Masamune, *Tetrahedron Lett.*, 1986, **27**, 4537.
15 E. J. Corey, R. K. Bakshi and S. Shibata, *J. Am. Chem. Soc.*, 1987, **109**, 5551; E. J. Corey, R. K. Bakshi and S. Shibata, C.-P. Chen and V. K. Singh, *J. Am. Chem.* Soc., 1987, **109**, 7925.
16 J. Chandrasekharan, P. V. Ramachandran and H. C. Brown, *J. Org. Chem.*, 1985, **50**, 5446.
17 A. K. Saksena and P. Mangiaracina, *Tetrahedron Lett.*, 1983, **24**, 273.
18 K.-M. Chen, G. E. Hardtmann, K. Prasad, O. Repic and M. J. Shapiro, *Tetrahedron Lett.*, 1987, **28**, 155.
19 All new compounds showed satisfactory spectral data. *Selected data* for **16:** δ_H(300 MHz, CD_3OD) 0.94 (3H, d, *J* 6.7), 1.02 (3H, d, *J* 6.7), 1.11 (3H, d, *J* 7.5), 1.91–2.00 (1H, m), 2.79 (1H, p, *J* 7.5), 3.49 (1H, d, *J* 3.6), 3.78 (2H, s) and 4.40 (1H, d, *J* 7.5); δ_C(75.5 MHz, CD_3OD) 9.5, 17.6, 22.7, 30.6, 42.6, 63.4, 70.7, 74.4, 79.1 and 181.6.

Received in Cambridge, UK, 29th June 1998; 8/04954H

Generation of cyclobutadiene derivatives from 1-metallo-4-halobuta-1,3-diene derivatives

Haruka Ubayama,[a] Wen-Hua Sun,[a] Zhenfeng Xi[b] and Tamotsu Takahashi*[a]†

[a] *Catalysis Research Center and Graduate School of Pharmaceutical Sciences, Hokkaido University, Sapporo 060, Japan*
[b] *Department of Chemistry, Peking University, Beijing 100871, China*

1-Zircona-4-halobuta-1,3-diene derivatives react in the presence of CuCl to produce cyclobutadiene derivatives which afford their dimers, or Diels–Alder adducts with dimethyl maleate or fumarate.

Cyclobutadiene is one of the most attractive molecules.[1] Several methods have been reported to generate cyclobutadiene derivatives,[1,2] such as (i) irradiation in argon matrix, (ii) preparation from diazo compounds or 3,4-dichlorocyclobutenes or (iii) dimerization of alkynes promoted by metal compounds. A conceptually new and simple method using intramolecular coupling of 1-metallo-4-halobuta-1,3-diene **1** can be considered as a preparative method for cyclobutadiene derivatives, as shown in eqn. (1). However, this simple method has not to the

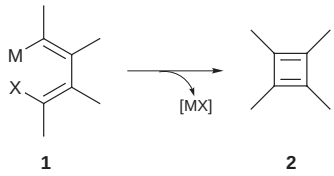

1 **2** (1)

best of our knowledge been reported.

Here we report that 1-zircona-4-halobuta-1,3-diene derivatives afford *in situ* cyclobutadiene derivatives **2** in the presence of CuCl.

Recently, we reported the highly selective monohalogenation reaction of zirconacyclopentadienes **3** giving 1-zircona-4-halobuta-1,3-diene derivatives **4** [eqn. (2)].[3] Addition of 1 equiv. of

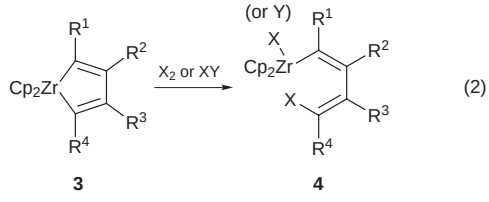

3 **4** (2)

X_2 = I_2; XY = NBS or NCS

CuCl to **4** in THF at room temperature afforded stereodefined tricyclo[4.2.0.0^{2,5}]octa-3,7-diene derivatives **5** within 1 h in good isolated yields (**5a**:‡ R = Et, 72%; **5b**: R = Me, 53%; **5c**:§ R = Pr, 78%) [eqn. (3)]. The ^{1}H and ^{13}C NMR spectra of **5b**

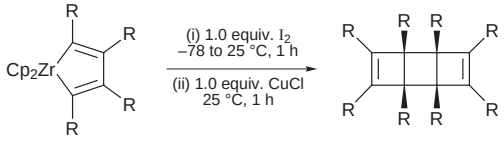

3 (3)

5a R = Et, 72%
b R = Me, 53%
c R = Pr, 78%

were identical with those of authentic *syn*-**5b** prepared according to the literature procedure.[4]

This result indicated that cyclobutadienes were formed *in situ* in this reaction. This reaction can be explained by intramolecular coupling between the 1,4 sp^2 carbon centers of **1** followed by dimerization of cyclobutadienes, as shown in Scheme 2.

Alternatively, addition of 2 equiv. of CuCl to **3a** and monohalogenation of dicopper species **6**[5] formed *in situ* with 1 equiv. of stilbene dibromide also afforded **5a** in 78% yield along with the formation of 98% of stilbene [eqn. (4)].

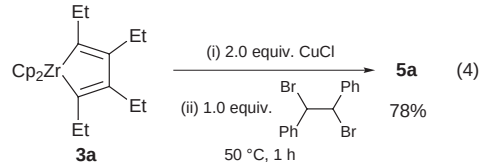

3a (4)

Cyclobutadiene derivatives **2** formed *in situ* by this method were trapped with dimethyl maleate and dimethyl fumarate.[1,2,6] As expected, bicyclic compounds, dimethyl 1,4,5,6-tetraethylbicyclo[2.2.0]hex-5-ene-2-*endo*,3-*endo*-dicarboxylate **7a**[6] and its analogue **7b**, dimethyl 1,4,5,6-tetraethylbicyclo[2.2.0)hex-5-ene-2-*endo*,3-*exo*-dicarboxylate **8a** and its analogues **8b** and **8c**[6] were formed in fairly good yields from dimethyl maleate and dimethyl fumarate, respectively (Scheme 1). The stereochemistry of **7** and **8** was determined by

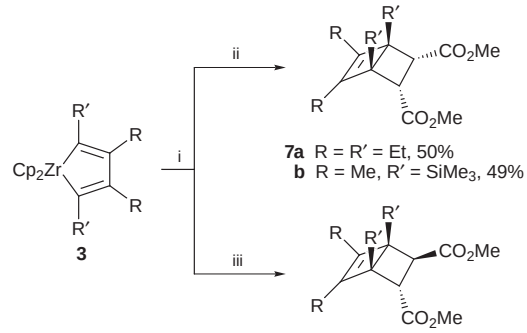

3

Scheme 1 *Reagents and conditions*: i, NBS (1 equiv.), 0 to 25 °C, 1 h; ii, dimethyl maleate (2 equiv.), CuCl (1 equiv.), 0 °C. 12 h; iii, dimethyl fumarate (2 equiv.), CuCl (1 equiv.), 0 °C, 12 h

comparison of their NMR data with those of authentic **7a** and **8c** prepared according to the literature.[6] Other bicyclohexene derivatives **9** were also formed *via* the same procedures as described above.[7]

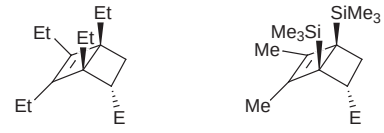

9a E = CO_2Me, 71%
b E = CN, 61%
9c E = CO_2Me, 50%
d E = CN, 55%

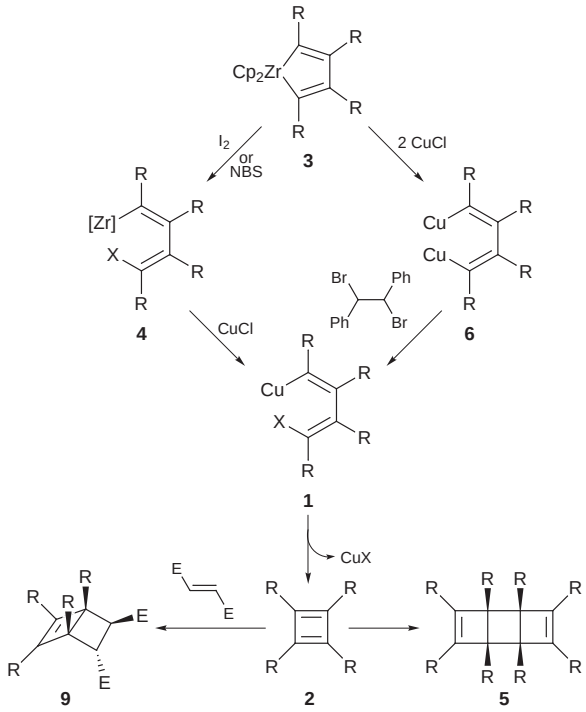

Scheme 2

The formation of **7**, **8** and **9** supports the *in situ* generation of cyclobutadiene derivative **2**.[1,6,7] The reactions described here are summarized in Scheme 2.

Further investigations towards practical application of this simple method in organic synthesis are in progress.

Notes and References

† E-mail: tamotsu@cat.hokudai.ac.jp

‡ *Selected data* for **5a**: δ_H($CDCl_3$, Me_4Si) 0.94 (t, *J* 7.5, 12 H), 1.06 (t, *J* 7.6, 12 H), 1.58–1.66 (m, 4 H), 1.67–1.75 (m, 4 H), 1.83–1.92 (m, 4 H), 2.03–2.17 (m, 4 H); δ_C($CDCl_3$, Me_4Si) 12.06, 13.18, 20.50, 21.89, 53.35, 144.97.

§ *Selected data* for **5c**: δ_H($CDCl_3$, Me_4Si) 0.87–0.91 (m, 24 H), 1.31–1.57 (m, 24 H), 1.72–1.79 (m, 4 H), 1.95–2.02 (m, 4 H); δ_C($CDCl_3$, Me_4Si) 14.95, 15.55, 20.86, 22.01, 31.31, 31.72, 53.04, 144.07.

1 For reviews on cyclobutadiene derivatives, see (*a*) G. Maier, *Angew. Chem., Int. Ed. Engl.*, 1974, **13**, 425; (*b*) T. Bally and S. Masamune, *Tetrahedron*, 1980, **36**, 343; (*c*) G. Maier, *Angew. Chem., Int. Ed. Engl.*, 1988, **27**, 309; (*d*) M. Regitz, H. Heydt and U. Bergstrasser, *Adv. Strain Org. Chem.*, 1996, **5**, 161.

2 For reviews on metal complexes of cyclobutadiene and derivatives, see P. M. Maitlis and K. W. Eberius, in *Non-benzenoid Aromatics*, Academic Press, New York, 1971, vol. II, p. 360; A. Efraty, *Chem. Rev.*, 1977, **77**, 691. See also ref. 1(*d*).

3 H. Ubayama, Z. Xi and T. Takahashi, *Chem. Lett.*, 1998, 517; T. Takahashi, W. Sun, C. Xi, H. Ubayama and Z. Xi, *Tetrahedron*, 1998, **54**, 715.

4 H. M. Rosenberg and E. C. Eimutis, *Can. J. Chem.*, 1967, **45**, 2263.

5 Formation of dicopper species **6**, see T. Takahashi, R. Hara, Y. Nishihara and M. Kotora, *J. Am. Chem. Soc.*, 1996, **118**, 5154; T. Takahashi, Z. Xi, A. Yamazaki, Y. Liu, K. Nakajima and M. Korora, *J. Am. Chem. Soc.*, 1998, **120**, 1672.

6 J. B. Koster, G. J. Timmermans and H. van Bekkum, *Synthesis*, 1971, 139.

7 P. B. J. Driessen and H. Hogeveen, *J. Organomet. Chem.*, 1978, **156**, 265; F. van Rantwijk, R. E. van der Stoel and H. van Bekkum, *Tetrahedron*, 1978, **34**, 569.

Received in Cambridge, UK, 3rd July 1998; 8/05136D

Synthesis and X-ray crystallographic structure of $Ga_4(OH)_6(3\text{-}Bu^tpzH)_{10}I_6\cdot 2MeCN$: a quasi double heterocubane

Paul Hodge and Brian Piggott*

Chemistry Department, University of Hertfordshire, College Lane, Hatfield, Hertfordshire, UK AL10 9AB. E-mail: b.piggott@herts.ac.uk

The reaction of $K[HB(3\text{-}Bu^tpz)_3]$ with GaI_3 resulted in breakdown of the ligand and formation of a novel Ga/O cluster. This compound can be described as four edge-sharing Ga/O,N octahedra or as two face sharing partial Ga/O heterocubanes, *i.e.* a quasi double heterocubane.

In a previous publication we reported the reaction of Na[Me-$Ga(pz)_3$] with $GaCl_3$ to give $Ga_8(pz)_{12}O_4Cl_4\cdot 2THF$, which is based on a Ga_4O_4 core.[1] However, this core contains edge bridging groups and we therefore refer to this and analogous structures as 'non-discrete'. 'Discrete' Ga_4N_4, Ga_4S_4, Ga_4Se_4 and Ga_4Te_4 cubanes are known,[2,3] but to date no 'discrete' Ga_4O_4 cubane has been reported. A similar situation existed in indium chemistry with 'discrete' In_4N_4, In_4S_4, In_4Se_4 and In_4Te_4 cubanes[2,4] and a 'non-discrete' In_4O_4 cubane[5] being known. However, very recently, a 'discrete' In_4O_4 cubane, $In_4O_4(C(SiMe_3))_4$ has been reported.[6]

As an extension of our work on Ga/O cubanes we attempted to synthesise a 'discrete' Ga_4O_4 cubane by replacing Na[Me-$Ga(pz)_3$] with $K[HB(3\text{-}Bu^tpz)_3]$, thus eliminating the possibility of Ga–pz bridging, and $GaCl_3$ with GaI_3, since I^- is a better leaving group than Cl^-. $HB(3\text{-}Bu^tpz)^-$ was chosen in preference to less hindered trispyrazolylborates because of the stabilisation that would be conferred on the cubane by the bulky (3-Bu^tpzH) groups, a known breakdown product of $HB(3\text{-}Bu^tpz)_3^-$.[7] We therefore reacted $K[HB(3\text{-}Bu^tpz)_3]$ with GaI_3 in THF. The clear diamond shaped plate crystals, **1**, isolated from the reaction mixture were subjected to elemental analysis, IR, ^1H and ^{13}C NMR, and mass spectral analysis.† It was not possible to deduce the structure of **1** from this data and so an X-ray crystallographic study was undertaken.‡ The results are shown in Fig. 1 from which the six I^- ions, all the hydrogen atoms and the two molecules of MeCN have been omitted for clarity. From Fig. 1 it is evident that the target compound has not been synthesised but instead $Ga_4(OH)_6(3\text{-}Bu^tpzH)_{10}I_6\cdot 2MeCN$, **1**. The structure of **1** can be described in terms of four, edge sharing, Ga/O,N octahedra. However, given the main thrust of this work we describe it as two face sharing heterocubanes each of which is missing a Ga ion on the long diagonal through the centre of the shared face, an inversion centre. This particular structure is unprecedented in Ga chemistry although $[(CpAl)_6P_4]$[8] and $Al_{10}(OH)_{16}(OSiEt_3)_{14}$[9]

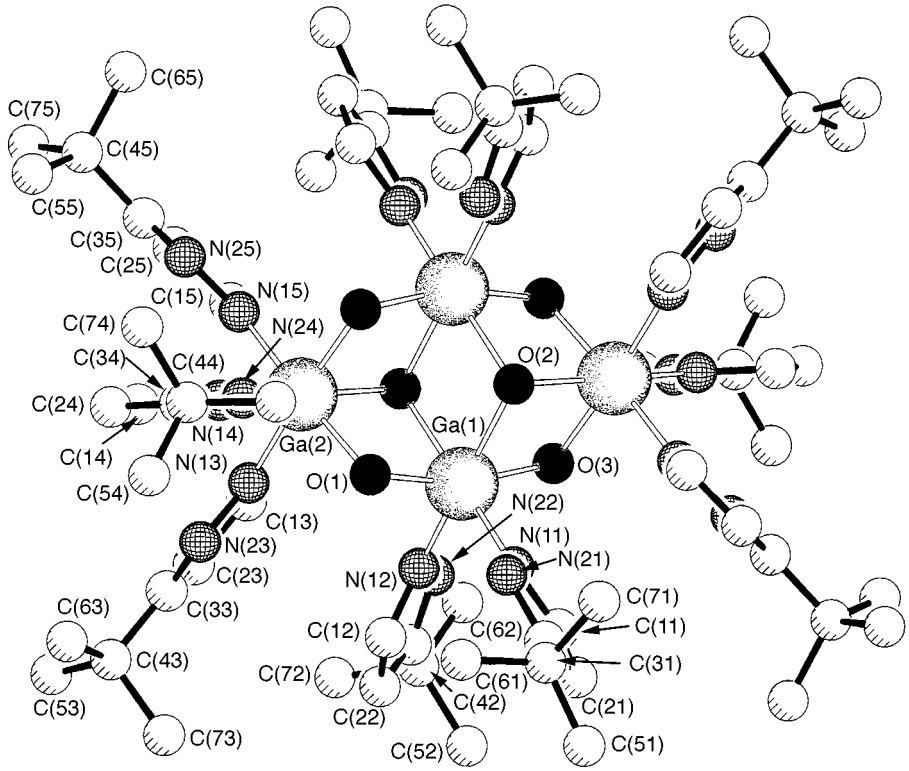

Fig. 1 Structure of **1** with the I^-, H and MeCN removed. Selected bond lengths (Å) and angles (°): Ga(1)–O(1) 1.896(5), Ga(1)–O(2) 2.090(6), Ga(1)–O(3) 1.912(5), Ga(1)–O(2′) 2.106(5), Ga(2)–O(1) 1.963(6), Ga(2)–O(2) 2.021(5), Ga(2)–O(3′) 1.951(5); Ga(1)–O(1)–Ga(2) 106.3(2), Ga(1)–O(2)–Ga(2) 97.4(2), Ga(1)–O(2)–Ga(1′) 101.8(2), Ga(1)–O(3)–Ga(2′) 106.4(2), Ga(2)–O(2)–Ga(1′) 97.1(2), O(1)–Ga(1)–O(2) 77.7(2), O(3)–Ga(1)–O(2) 91.0(2), O(1)–Ga(1)–O(2′) 90.5(2), O(3)–Ga(1)–O(2′) 77.4(2), O(2)–Ga(1)–O(2′) 78.2(2), O(1)–Ga(2)–O(3′) 89.7(2), O(2)–Ga(2)–O(3′) 78.6(2), O(1)–Ga(2)–O(2) 77.0(2). Symmetry transformation used to generate primed atoms: ′ $-x, -y, -z + 1$.

can be claimed to be structurally analogous. Each Ga in **1** attains six coordination by bonding to either two or three 3-Bu^{t}pzH groups and it is thought that the presence of these bulky groups help stabilise the complex. The Ga/O bond lengths and angles that define **1** are given in Fig. 1, from which it can be seen that the corresponding parameters in $Ga_8(pz)_{12}O_4Cl_4\cdot 2THF$ *viz*. Ga_c–O–Ga_c 98.26(6)°, O–Ga_c–O 81.08(6)° and Ga_c–O 2.003(1) Å are within comparable range.[1] Given the reducing properties of HB(3-Bu^{t}pz)$_3^-$,[7] the Ga–Ga distances were examined for evidence of metal–metal bonding. However, since these distances fall within the range 3.089–3.256 Å, whereas the Ga–Ga distances in a series of Ga^I dimers range from 2.34 to 2.54 Å,[8] such bonding is precluded. However, the Ga–Ga distances in **1** are less than the sum of the van der Waals radii of Ga (3.80 Å).[10] Similarly the O–O distances, which are in the range 2.50–2.76 Å, are less than the sum of the van der Waals radii of O (3.00 Å).[10] These observations indicate some degree of strain within the cluster. The corresponding distances in $Ga_8(pz)_{12}O_4Cl_4\cdot 2THF$ are Ga–Ga 3.022 Å and O–O 2.61 Å.[1]

A number of important questions are raised by the structure of **1** with, perhaps, the most important being the origin of the hydroxyl groups. This question was raised in our previous publication with reference to the formation of $Ga_8(pz)_{12}O_4Cl_4\cdot 2THF$, where it was suggested that the source of the oxygen was either air or moisture entering the system on prolonged standing at low temperature.[1] Although dried solvents and Schlenk techniques were used in the synthesis of **1** the conditions for air/moisture exclusion were not the most stringent possible. This was part of the synthetic strategy. However, it is now proposed to repeat this experiment under the most strictly controlled conditions to investigate the method of oxygen inclusion through ^{17}O studies.

Given that, at present, examples of quasi double heterocubanes are extremely rare it would seem that this structural type is an oddity with little relevance to cubane chemistry. However, we do not subscribe to this view and are confident that other examples will be identified thus establishing quasi double heterocubanes as a significant structural type with implications for the synthesis of compounds of higher nuclearity. The reason for this confidence is that we believe the difference between a quasi double cubane and a cubane, in this case $[Ga_4(OH)_6(3\text{-Bu}^t\text{pzH})_{10}]^{6+}$ and $[Ga(OH)_4(3\text{-Bu}^t\text{pzH})_{12}]^{8+}$, is finely balanced sterically and by judicious choice of ligand and control of stoichiometry interconversion can be achieved.

Notes and References

† *Synthesis*: all manipulations were performed under argon using standard Schlenk techniques and all solvents dried prior to use. To a Schlenk tube charged with GaI_3 (1.05 g, 2.33 mmol) was added K[HB(3-Bu^{t}pz)$_3$] (0.98 g, 2.33 mmol) and 60 cm^3 of THF. The pale yellow slurry was stirred for 18 h after which the solvent was removed *in vacuo*. Dichloromethane (60 cm^3) was added to the off-white residue, stirred, and the suspension filtered to remove KI. CH_2Cl_2 was removed *in vacuo* and 60 cm^3 of MeCN was added to the off-white residue. The pale yellow solution was reduced to one third of its original volume and placed in a freezer. After one week clear diamond shaped plates formed which were filtered off and used in the X-ray analysis. Yield: 1.04 g, 75% (Found: C, 33.73; H, 5.35; N, 11.15; Ga, 11.49; I, 34.26. Calc. for $C_{78}H_{132}N_{24}O_6Ga_4I_6$: C, 36.85; H, 5.23; N, 13.22; Ga, 10.97; I, 29.25%). We attribute the poor analysis to solvent dependency. NMR (250 MHz): δ_H 10.42 (br s, NH + OH), 7.70 (br s, H^3), 6.27 (br s, H^4), 5.23 (s, MeCN), 1.38 (s, CMe_3); D_2O addition, δ 7.50 (d, H^3), 6.18 (d, H^4), 4.20 (br s, NH + OH), 1.50 (s, CMe_3); δ_C 156.6 (C^5), 134.9 (C^3), 102.6 (C^4), 30.2 (CMe_3). IR 3197 [ν(NH)], 3100 [ν(CH)], 2966 [ν(CH)], 1495 (ring breathing).

‡ *Crystal data* for **1**: $C_{78}H_{132}N_{24}O_6Ga_4I_6$, M = 2536.31, orthorhombic, space group *Pbca*, a = 16.00(3), b = 25.051(5), c = 26.424(5) Å, U = 10591(4) Å^3, Z = 2, D_c = 1.591 Mg m^{-3}, F(000) = 5008, λ = 0.71069 Å, T = 150 K, μ(Mo-Kα) = 2.811 mm^{-1}. Data were collected on a Delft Instruments FAST TV area detector diffractometer. Of a total of 38 055 collected reflections 8332 were unique. The structure was solved by direct methods. Refinement was by full matrix least squares on F^2. Non hydrogen atoms were refined anisotropically and all hydrogen atoms except those on the hydroxyl groups were included in fixed positions and refined with the riding model. Final R indices [$I > 2\sigma(I)$] $R1$ = 0.0538, $wR2$ = 0.1188. One of the two solvent molecules, MeCN, showed slight disorder but this was not modelled. CCDC 182/951.

1 V. Capparelli, P. Hodge and B. Piggott, *Chem. Commun.*, 1997, 937.
2 T. Belgardt, H. W. Roesky, M. Noltemeyer and H.-G. Schmidt, *Angew. Chem., Int. Ed. Engl.*, 1993, **32**, 1056.
3 A. R. Barron, *Chem. Soc. Rev.*, 1993, **22**, 93.
4 W. Uhl, R. Graupner, M. Layh and V. Schüz, *J. Organomet. Chem.*, 1995, **493**, C1.
5 A. M. Arif and A. R. Barron, *Polyhedron*, 1988, **7**, 2091.
6 W. Uhl and M. Pohlmann, *Chem. Commun.*, 1998, 451.
7 A. Frazer, P. Hodge and B. Piggott, *Chem. Commun.*, 1996, 1727.
8 C. Dohmeier, D. Loos and H. Schnöckel, *Angew. Chem., Int. Engl. Engl.*, 1996, **35**. 129.
9 A. W. Apblett, A. C. Warren and A. R. Barron, *Chem. Mater.*, 1992, **4**, 167.
10 J. E. Huheey, E. A. Keiter and R. L. Keiter, *Inorganic Chemistry*, Harper Collins, New York, 1993.

Received in Cambridge, UK, 12th June 1998; 8/04460K

Heterogeneous transfer hydrogenation involves pairwise hydrogen transfer from the same position of two molecules of formic acid

Jinquan Yu and Jonathan B. Spencer*†

University Chemical Laboratory, Lensfield Road, Cambridge, UK CB2 1EW

Using the reduction of an alkyne to *cis*-alkene as a hydrogen trap, differentially deuterium labelled formic acid is shown to deliver a pair of hydrogen atoms either from the formyl or the carboxy position, which suggests that palladium diformate is a key intermediate in heterogeneous transfer hydrogenation.

The oxidation of formic acid to carbon dioxide has been widely used as a source of hydrogen for the reduction of organic compounds.[1–3] This reaction has been shown to be one of the most effective methods for transfer hydrogenation that could potentially replace traditional hydrogenation conditions, such as asymmetric reduction where high pressure is often required.[4] The reverse reaction involving conversion of carbon dioxide to formic acid using catalytic hydrogenation has attracted much interest in recent years because it offers an environmentally friendly approach to the use of carbon resources as a raw material for the chemical industry.[5–8] The advantage of using heterogeneous catalysts in industrial processes has prompted us to investigate the mechanism of this reversible reaction catalysed by palladium on carbon.

A major effort has already been directed to the understanding of the mechanism of this reaction in homogeneous systems with the formato-(hydrido) metal complex proposed as a key intermediate **1** [Scheme 1(*a*)], based on deuterium labelling studies and *ab initio* calculations.[9–11] Recent studies using NMR spectroscopy have provided evidence for the existence of this intermediate,[12,13] however, as discussed by Halpern,[14] such thermodynamically stable compounds may not be the active species on hydrogenation pathways.

It has been proposed that the formato-(hydrido) metal complex **1** collapses to give a metal dihydrido species **2** [Scheme 1(*a*)] which can then carry out the reduction.[9] If this mechanism is operating in heterogeneous systems then the two hydrogen atoms from the same formic acid molecule will always be transferred as a pair in one catalytic cycle. Correspondingly, when the catalytic cycle proceeds from carbon dioxide to formic acid, one hydrogen molecule will provide both hydrogen atoms for the reduction of one molecule of carbon dioxide to give the same intermediate **1**.

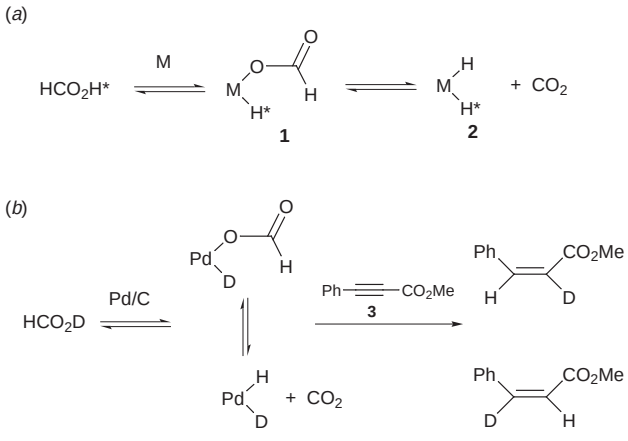

Scheme 1

To investigate whether **1** is the active intermediate that provides the hydrogen on the catalytic cycle, the reduction of the triple bond of phenylpropiolate to the *cis*-double bond was employed to trap the hydrogen liberated by the collapse of **1** [Scheme 1(*b*)]. If differentially deuterium labelled formic acid (HCO_2D or DCO_2H) is used then the distribution of deuterium across the *cis*-double bond can determine the origin of the hydrogen transferred to the triple bond. The reduction of a double bond was not used as a reporter molecule for the hydrogen transfer because of the possible additional incorporation of deuterium through isomerization of the double bond before saturation occurs.[15,16]

When the reduction was carried out with HCO_2D the results show that the major product is the *cis*-double bond containing two hydrogen atoms (Table 1), rather than mono-deuterated *cis*-double bond which would be predicted to dominate if both hydrogen atoms came from the same molecule of formic acid as proposed previously for the homogeneous system.[9] It is possible that the major product containing two hydrogen atoms on the double bond could be formed by the preferential donation of hydrogen from the metal surface (H–Pd–D, intermediate **2,** Scheme 1) owing to a favourable kinetic isotope effect. However, when **3** was reduced with an equal mixture of hydrogen and deuterium the results show that there is no

Table 1 Reduction of methyl phenylpropiolate

	Product distribution (%)[a]		
Hydrogen source	H + H	H(D) + D(H)	D + D
HCO_2D[b]	72	10	18
DCO_2H[b]	25	18	57
XCO_2D[c]	28	37	35
$H_2 + D_2$[d]	25	51	24

[a] Errors for the data are ±5%. [b] Labelled formic acids were prepared by treating sodium formate (either DCO_2Na or HCO_2Na) with 1 M HCl or DCl, extracted with Et_2O and dried over anhydrous Na_2SO_4. Distillation of the extracts gave DCO_2H or HCO_2D (99% atom excess as determined by ^1H NMR analysis and mass spectrometry). Pd/C (10%, 38 mg) was added to a mixture of HCO_2D or DCO_2H (235 mg, 5.0 mmol), Et_3N (2.8 g) and phenylpropiolate **3** (80 mg, 0.5 mmol) and vigorously stirred under a blanket of argon. The progress of the reaction was monitored by TLC and stopped at approximately 40% conversion to avoid formation of the fully saturated product. This precaution was taken because the protons α to the carbonyl group of the saturated product can exchange under these conditions and could potentially lead to scrambling of the label. The reaction mixture was filtered to remove the catalyst and evaporated to give residue (81 mg) which was purified by column chromatography (eluted with hexane–Et_2O, 50:1) to afford 25 mg of *cis*-alkene. The distribution of deuterium across the double bond of the *cis*-alkene was determined by ^1H NMR analysis and mass spectrometry. [c] X = a mixture of D and H (2:1). [d] Pd/C (10%, 19 mg) was added to a mixture of Et_3N (2.8 g) and phenylpropiolate **3** (80 mg, 0.5 mmol) and purged with hydrogen and deuterium (1:1). The reaction mixture was stirred at room temperature and stopped at approximately 40% conversion. The isolation and analysis of the *cis*-alkene was carried out as detailed above.

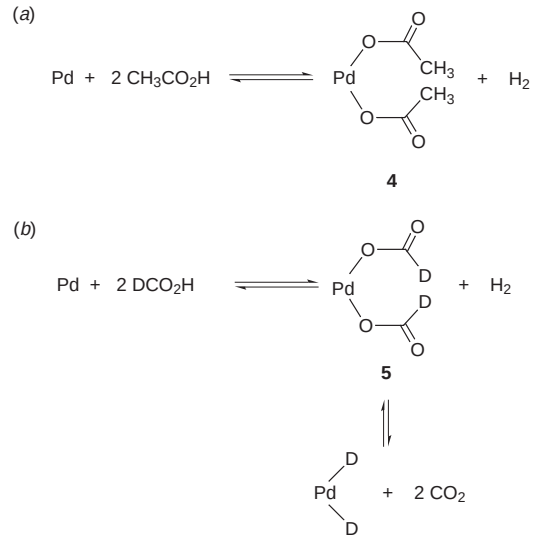

Scheme 2

substantial isotope effect (Table 1), which was also found in an earlier study using a homogeneous catalyst.[17] Furthermore, this mechanism cannot account for the fact that more double deuterated than mono-deuterated *cis*-double bond is formed.

These results would be consistent with a direct pairwise hydrogen transfer from either the formyl or the carboxy position of two different formic acid molecules. It is feasible that two hydro-formato species **1** on the surface of the metal could line up in such a way that the two adjacent formyl groups can donate hydrogen in a pairwise manner. However, palladium is known to react with acetic acid to form palladium diacetate **4** with the liberation of hydrogen from the carboxy position [Scheme 2(*a*)][18] which has prompted us to propose that palladium diformate **5** is formed in a similar manner and is reponsible for pairwise transfer of two formyl hydrogens [Scheme 2(*b*)]. Although palladium diformate has not been isolated, maybe owing to its instability, other metal diformate species have been characterised, such as vanadyl diformate,[19] triarylbismuth diformate[20] and ruthenium diformate.[21] This last example is particularly important because it was identified during the hydrogenation of carbon dioxide using a homogeneous ruthenium catalyst.

The formation of the palladium diformate would give one molecule of hydrogen solely from the carboxy end of the two formic acid molecules that can be used for the reduction of the triple bond (Scheme 3). The palladium diformate can then transfer another pair of hydrogen atoms from the formyl positions to another triple bond. The results with DCO_2H also show that the major *cis*-alkene produced from the alkyne contains two deuterium atoms on the double bond (Table 1). The minor monodeuterated product is probably formed by scrambling of the deuterium label. This could occur either *via* reduction of the carbon dioxide to give formic acid[9] or by collapse of intermediate **5** [Scheme 2(*b*)], if not immediately

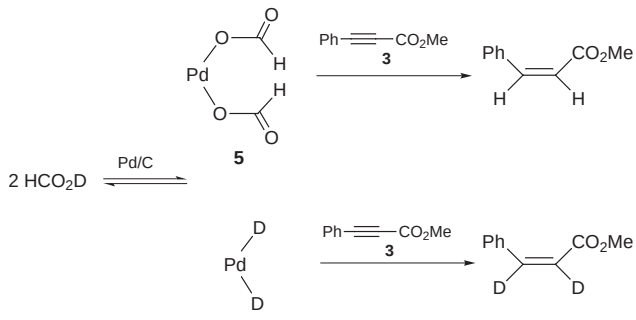

Scheme 3

trapped by the triple bond, to give deuterium which can then mix with the hydrogen from the carboxy end to form HD. The formation of HD from hydrogen and deuterium on the surface of the metal has been shown to readily occur in a control experiment (Table 1).

The combined results with HCO_2D and DCO_2H strongly suggests that the hydrogen comes directly from the palladium diformate intermediate **5** rather than intermediate **1**, since this latter species would give the same distribution of deuterium on the double bond in both cases. The high level of pairwise addition of hydrogen from HCO_2D or deuterium from DCO_2H demonstrates the greater reactivity of the formyl position. It is noteworthy that there is a higher incorporation of hydrogen from the formyl position of HCO_2D than deuterium from the same position of DCO_2H, suggesting an isotope effect is involved in the cleavage of the carbon–hydrogen bond of the palladium diformate (Table 1).

The theory was further tested by using a mixture of DCO_2D and HCO_2D in a ratio of 2:1 to reduce the triple bond. The results show that there is a large increase in product containing one hydrogen and one deuterium compared to the product obtained using soley HCO_2D (Table 1). The increase in monodeuterated *cis*-alkene can only be accounted for by pairwise transfer from the formyl position rather than from the formato-hydride intermediate **1** which would be predicted to produce less of the monodeuterated product with the addition of DCO_2D.

The results clearly show that heterogeneous transfer hydrogenation involves the transfer of a pair of hydrogen atoms either from the formyl or the carboxy position of two molecules of formic acid. This provides evidence that palladium diformate is a key intermediate in this reaction and suggests that the reduction of carbon dioxide must also proceed through the diformate intermediate.

We thank the Royal Society for the award of a Royal Society University Research Fellowship (J. B. S.) and the British Council and the Chinese Government for the award of Sino-British Friendship Scholarship (J. Y.).

Notes and References

† E-mail: jbs20@cam.ac.uk

1 A. Fujii, S. Hashiguchi, N. Uematsu, T. Ikariya and R. Noyori, *J. Am. Chem. Soc.*, 1996, **118**, 2521.
2 N. Uematsu, A. Fujii, S. Hashiguchi, T. Ikariya and R. Noyori, *J. Am. Chem. Soc.*, 1996, **118**, 4916.
3 K. Matsumura, S. Hashiguchi, T. Ikariya and R. Noyori, *J. Am. Chem. Soc.*, 1997, **119**, 8738.
4 R. Noyori and S. Hashiguchi, *Acc. Chem. Res.***,** 1997, **30**, 97.
5 E. T. Sundquist, *Science*, 1993, **259**, 934.
6 P. G. Jessop, I. Takao and R. Noyori, *Nature*, 1994, **368**, 231.
7 P. G. Jessop, I. Takao and R. Noyori, *Chem. Rev.*, 1995, **95**, 259.
8 W. Leitner, *Angew. Chem., Int. Ed. Engl.*, 1995, **34**, 2207.
9 W. Leitner, J. M. Brown and H. Brunner, *J. Am. Chem. Soc.*, 1993, **115**, 152.
10 P. G. Jessop, Y. Hsiao, T. Ikariya and R. Noyori, *J. Am. Chem. Soc.*, 1996, **118**, 344.
11 F. Hutschka, A. Dedieu, M. Eichberger, R. Fornika and W. Leitner, *J. Am. Chem. Soc.*, 1997, **119**, 4432.
12 J. Tsai and K. M. Nicholas, *J. Am. Chem. Soc.*,1992, **114**, 5117.
13 E. Lindner and B. Keppeler, P. Wegner, *Inorg. Chim. Acta*, 1997, **258**, 97.
14 J. Halpern, *Science*, 1982, **217**, 401.
15 J. Yu and J. B. Spencer, *J. Am. Chem. Soc.*, 1997, **119**, 5257.
16 J. Yu and J. B. Spencer, *J. Org. Chem.*, 1997, **62**, 8618.
17 J. A. Osborn, F. H. Jardine, J. F. Young and G. Wilkinson, *J. Chem. Soc. (A)*, 1996, 1711.
18 S. M. Morehouse, A. R. Powell, J. P. Heffer, T. A. Stephenson and G. Wilkinson, *Chem. Ind.*, 1964, 544.
19 D. Mootz and R. Seidel, *Acta Crystallogr., Sect. C*, 1987, **43**, 1218.
20 H. Suzuki, T. Ikegami, Y. Matano and N. Azuma, *J. Chem. Soc., Perkin Trans. 1*, 1993, 2411.
21 M. K. Whittlesey, R. N. Perutz and M. H. Moore, *Organometallics*, 1996, **15**, 5166.

Received in Liverpool, UK, 20th May 1998; 8/03809K

Self-assembly of a novel nanoscale giant cluster: $[Mo_{176}O_{496}(OH)_{32}(H_2O)_{80}]$†

Chang-Chun Jiang, Yong-Ge Wei, Qun Liu, Shi-Wei Zhang,* Mei-Cheng Shao and You-Qi Tang

Department of Chemistry, Peking University, Beijing 100871, PR China. E-mail: zsw@ipc.pku.edu.cn

Reduction of an acidified solution of $Na_2MoO_4{\cdot}2H_2O$ by iron powder results in the formation of the title compound $[Mo_{176}O_{16}O_{480}(OH)_{32}(H_2O)_{80}]$; the compound is tyre shaped and consists of sixteen $\{Mo_8\}$ subunits being linked by forty-eight MoO_6 octahedra; remarkable features are the size and mass (which is of the order of a protein) and its nano-dimensional cavity of *ca.* 3 nm in diameter.

One of the challenges chemists are facing today is how to synthesize larger mesoscopic molecules from molecular fragments. The aim of such research is not only to improve the understanding of the extreme complexity of natural process, but also to synthesize molecular materials with novel properties, *e.g.* electric and magnetic, which may be anticipated for mesoscopic compounds. Indeed, considerable progress has been made in the field of polymetalate chemistry.[1,2] We have evolved the so-called 'reduction–reconstitution' self-assembly process and synthesized a class of large mixed-valent, nanoscale polyoxomolybdate anions[3–7]‡ constructed of $\{Mo_8\}$ or $\{Mo_{17}\}$ fragments:[2] $[Mo_{36}O_{108}(NO)_4(H_2O)_{16}]^{12-}$ **1**,[3] $[Mo_{57}V_6O_{180}(NO)_6(OH)_3(H_2O)_{18}]^{21-}$ **2**,[4] $[Mo_{57}Fe^{III}_6O_{174}(NO)_6(OH)_3(H_2O)_{24}]^{15-}$ **3**,[5] $[Mo_{57}Fe^{II}_6O_{177}(NO)_6(OH)_2(H_2O)_{22}(MoO)_2]^{18-}$ **4**[6] and $\{\{(H_2O)MoO_{2.5}[Mo_{36}O_{108}(NO)_4(H_2O)_{16}]O_{2.5}Mo(H_2O)\}^{12-}\}_n$ **5**[7] and some of them were also obtained later by Müller's group.[2] By slightly changing the reaction conditions in the same system, Müller *et al.* succeeded in isolating a giant cluster $[Mo_{154}(NO)_{14}O_{420}(OH)_{28}(H_2O)_{70}]^{14-}$ **6**.[2,8] Now we have succeeded in synthesizing an even larger nanocompound $[Mo_{176}O_{496}(OH)_{32}(H_2O)_{80}]$ **7** which is also constructed of $\{Mo_8\}$ fragments.

Compound **7** was prepared following the general method leading to 'molybdenum blue'. A solution of $Na_2MoO_4{\cdot}2H_2O$ (5.0 g, 20.7 mmol) in H_2O (50 ml) was adjusted to a pH of *ca.* 1.0 with 36.5% hydrochloric acid. After addition of iron powder (50 mg, 0.9 mmol), the mixture was left to stand for one month to crystallize. The preparation yields blue–black, tetragonal-bipyramidal well defined crystals of **7** in *ca.* 30% yield. Reduction with elemental Al or Zn as well as $N_2H_4{\cdot}2HCl$ yields the same well defined crystals. The compound was characterized by IR and UV–VIS spectroscopy, cerium(IV) sulfate redox titration and elemental analysis,§ as well as by single-crystal X-ray diffraction.¶

The rather intricate single-crystal X-ray structure analysis reveals that the ring-shaped compound **7** consists of 160 MoO_6 octahedral and 16 pentagonal bipyramids of type MoO_7 (Figs. 1 and 2). The structure has approximate D_{8d} symmetry. Sixteen $\{Mo_8\}$ fragments are linked with sixteen Mo atoms in the equatorial plane and another sixteen $\{Mo_2\}$ groups.[2] Each of the sixteen subunits has a pentagonal-bipyramidal MoO_7 center about which seven other MoO_6 octahedral are grouped by corner- and edge-sharing to form an $\{Mo_8\}$ fragment. This $\{Mo_8\}$ fragment also occurs in **1**–**6**, which, however, possess a pentagonal bipyrimidal $Mo(NO)O_6$ centre.

The structure type of **1**–**5** is different from that of **6** and **7**. In **1**–**5** two $\{Mo_8\}$ fragments above and below the equatorial plane are linked through one equatorial Mo atom and are transformed into each other by reflection across the equatorial mirror plane. Thus anion **1** has approximate C_{2h} symmetry and anions **2** and **3** have D_{3h} symmetry. In other words, this kind of linking manner implies that there are $\{Mo_{17}\}$ fragments as building blocks in these anions. By contrast, the arrangement of $\{Mo_8\}$ fragments in **7** (D_{8d} symmetry), which is like that of **6** (D_{7d} symmetry), are twisted relative to each other. This shift means that in **6** and **7** two equatorial Mo atoms are required to link two $\{Mo_8\}$ fragments and so there are sixteen Mo atoms in the equatorial plane in **7** (fourteen in **6**). Two neighbouring $\{Mo_8\}$ fragments on the same side of the equatorial plane are linked

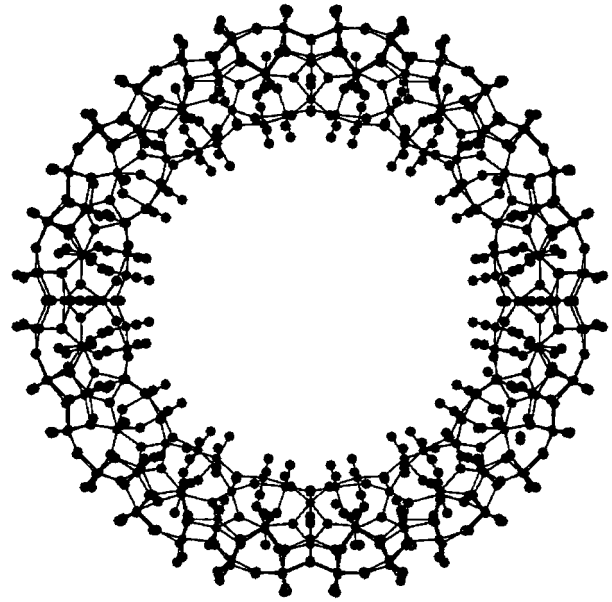

Fig. 1 Ball-and-stick model of the nanoscale cluster (view parallel to the C_8 axis)

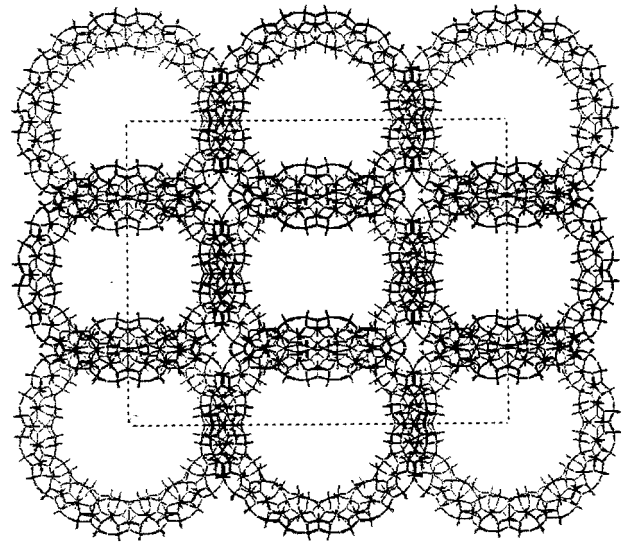

Fig. 2 Packing of the $\{Mo_{176}\}$ molecules in the crystal (view parallel to the *c* axis)

through two Mo atoms (or one $\{MoO_2(H_2O)(\mu_2\text{-}O)\text{-}MoO_2(H_2O)\}$ group) *i.e.* a $\{Mo_2\}$ unit, instead of only one V or Fe center as in **2** and **3**, respectively. However, the central $\{MoNO\}^{3+}$ group of the $\{Mo_8\}$ fragment of **6** is replaced by $\{MoO\}^{4+}$ group in **7**.

Whereas the basic structure of compound can be determined unambiguously, it will probably never be possible to ascertain the exact number of crystallization waters by XRD owing to disorder of the lattice water molecules, the tendency to lose solvent and the weak diffraction of the crystal to X-rays. According to elemental analysis and TGA, the number of water is *ca*. 600 ± 50.

A remarkable feature of **7** is its nanoscale cavity and corresponding host properties. The cavity itself, which is like the inside of a tyre, measures about 3 nm in diameter. A further characteristic of **7** is that it dissolves extremely well in water, ethanol or acetone. This high solubility can be attributed to the large surface built up of a large number of H_2O molecules and OH groups. It is noteworthy that crystals of **7** are obtained from 'molybdenum blue'. 'Molybdenum blue' used to be regarded as amorphous, but recently Müller *et al.* have made some suggestions about its structure[9] and they also succeeded in isolating a compound $Na_{15}\{Mo_{144}O_{409}(OH)_{28}(H_2O)_{56}\}$, *ca.* 250 H_2O **8** from it[10] whose structure resembles **6** apart from some defects in **8**. Now it can be proposed that 'molybdenum blue' is a mixture of compounds which have a similar basic ring-shaped structure.

Polyoxoanions constitute a large class of inorganic compounds,[11] however, the number of different structural types is small. There are indications that **1**–**8** belong to the same kind structural type of compounds as they are all synthesized by a similar method and linked up *via* $\{Mo_8\}$ fragments in different ways. It can be presumed that under suitable reaction conditions, a variety of novel nanoscale clusters with high complexity and multifunctionality could be synthesized by the reduction–reconstruction self-assembly process developed in our laboratory.

Financial support from the National Natural Science Fondation of China No. 29371004 and No. 29733080 is gratefully acknowledged.

Notes and References

† Just before this manuscript was mailed, similar work by Müller *et al.* was published (*Angew. Chem., Int. Ed. Engl.*, 1998, **37**, 1220). However, they prepared their crystals by a different method and solved the structure in space group *Cmcm.*

‡ The charges given here are the values given by Müller *et al.* However, cluster anions with different charges are also obtained in our laboratory.

§ Elemental analysis. Calc. for $[Mo_{176}O_{16}O_{480}(OH)_{32}(H_2O)_{80}]\cdot(600 \pm 50)H_2O$: Mo, 44.9; Found: Mo, 44.0; Na, 0.2; Cl, 0.2%. Characterization of **7**: main IR bands (KBr disc): 1726s, 1618m, 974m, 914w, 668w, 558s cm^{-1}; UV–VIS (H_2O), 750, 220 nm. Cerium sulfate titration: 1 g of **7** reduces 0.830 mmol $Ce(SO_4)_2\cdot2(NH_4)_2SO_4\cdot4H_2O$ corresponding to 32 Mo^V atoms in each molecule.

¶ *Crystal data* for $[Mo_{176}O_{16}O_{480}(H_2O)_{80}(OH)_{32}]\cdot(600 \pm 50)\ H_2O$: M = 36 522.24, orthorhombic, space group *Amm*2 (no. 38), a = 66.628(13), b = 53.760(11), c = 31.775(6) Å, V = 113 816(39) $Å^3$, $F(000)$ = 71 024, Z = 4, D_c = 2.131 g cm^{-3}, Mo-Kα radiation, λ = 0710 69 Å, μ = 1.99 min^{-1}. Intensity data were collected on a Rigaku AFC6S diffractometer at 296 K and a total of 25 975 reflections were collected, of which 12 706 reflections were observed, the structure was solved with direct method and difference Fourier map using SHELXS97 and refined using SHELXL97. Owing to the poor ability of diffraction of the crystal and the limit of the number of reflections, only the Mo atoms are refined anisotropically with $R1$ = 0.1050 for observed reflections and $wR2$ = 0.2685 for all the data.

1 K. Wassermann, M. H. Dickman and M. T. Pope, *Angew. Chem., Int. Ed. Engl.*, 1997, **36**, 1445.
2 A. Müller, F. Peters, M. T. Pope and D. Gatteschi, *Chem. Rev.*, 1998, **98**, 239 and references therein.
3 S.-W. Zhang, D.-Q. Liao, M.-C. Shao and Y.-Q. Tang, *J. Chem. Soc., Chem. Commun.*, 1986, 835.
4 S.-W. Zhang, G.-Q. Huang, M.-C. Shao and Y.-Q. Tang, *J. Chem. Soc., Chem. Commun.*, 1993, 37.
5 G.-Q. Huang, S.-W. Zhang and M.-C. Shao, *Polyhedron*, 1993, **12**, 2067.
6 G.-Q. Huang, S.-W. Zhang and M.-C. Shao, *Chin. Sci. Bull.*, 1995, **40**, 1438.
7 S.-W. Zhang, Y.-G. Wei, Q. Yu, M.-C. Shao and Y.-Q. Tang, *J. Am. Chem. Soc.*, 1997, **119**, 6440.
8 A. Müller, E. Krickmeyer, J. Meyer, H. Bogge, F. Peters, W. Plass, E. Diemann, S. Dillinger, F. Nonnenbruch, M. Randerath and C. Menke, *Angew. Chem., Int. Ed. Engl.*, 1995, **34**, 2122.
9 A. Müller, J. Meyer, E. Krickemeyer and E. Diemann, *Angew. Chem., Int. Ed. Engl.*, 1996, **35**, 1206.
10 A. Müller, E. Krickemeyer, H. Bogge, M. Schmidtmann, F. Peters, C. Menke and J. Meyer, *Angew. Chem., Int. Ed. Engl.*, 1997, **36**, 484.
11 M. T. Pope, *Heteropoly and Isopoly Oxometalates*, Springer-Verlag, New York, 1983.

Received in Cambridge, UK, 9th June 1998; 8/04358D

Preparation and structural characterization of naphtho[2,1-*d*:6,5-*d*′]bis([1,2,3]dithiazole) NT and π-stacked mixed valence salt $[NT]_3[BF_4]_2$

Tosha M. Barclay,[a] Ian J. Burgess,[b] A. Wallace Cordes,[a] Richard T. Oakley[b]† and Robert W. Reed[b]

[a] *Department of Chemistry and Biochemistry, University of Arkansas, Fayetteville, Arkansas, 72701 USA*
[b] *Department of Chemistry, University of Waterloo, Waterloo, Ontario, N2L 3G1 Canada*

Naphtho[2,1-*d*:6,5-*d*′]bis([1,2,3]dithiazole) NT, prepared by a 'double Herz' condensation of 2,6-diaminonaphthalene with S_2Cl_2, can be electrooxidized to the conductive, π-stacked mixed valence salt $[NT]_3[BF_4]_2$.

The bis([1,2,3]dithiazoles) **1**[1] and **2**[2] represent the first members of a new family of redox active heterocycles with potential

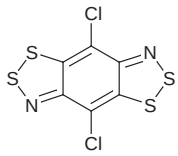

1

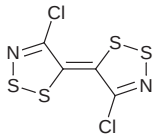

2

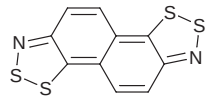

3 NT

applications in the design of molecular conductors.[3] While their oxidation potentials are relatively high, the resulting radical cations are extremely stable, forming crystalline 1:1 salts with inorganic counterions. Compound **1** must be prepared by the condensation of diaminobenzenedithiol with sulfur monochloride, as the use of Herz chemistry,[4] *i.e.* a double ring closure of *p*-phenylenediamine with sulfur monochloride, is not effective; the products of this reaction are largely polymeric.[5] We now report that, in contrast to this behavior, the condensation of 2,6-diaminonaphthalene[6] with sulfur monochloride leads, with remarkable regiospecificity and in good yield, to the 'double Herz' cyclocondensation product naphtho[2,1-*d*-:6,5-*d*′]bis([1,2,3]dithiazole) NT **3**. We also describe the structure and redox chemistry of NT, and its use in the formation of the conductive, π-stacked mixed valence salt $[NT]_3[BF_4]_2$.

In contrast to the complex reaction of 1,5-diaminonaphthalene with S_2Cl_2,[7] the condensation of 2,6-diaminonaphthalene with S_2Cl_2 in the presence of pyridine as auxiliary base proceeds *via* electrophilic ring closure at both *peri*-positions[8] to afford what we presume is an oxidized form (radical cation or dication) of the title compound NT **3**. Chlorination of the remaining C–H positions does not occur. In a typical preparation S_2Cl_2 (30 ml) was added to a slurry of 2,6-diaminonaphthalene (3.00 g, 19.0 mmol) in 20 ml of CH_2Cl_2 and the mixture stirred overnight. Pyridine (9.1 g, 115 mmol) in 15 ml of CH_2Cl_2 was then added dropwise and the mixture stirred for another 2 h. The resulting mixture was filtered, and the solid washed with MeCN (3 × 75 ml) to remove pyridine hydrochloride. The remaining solid was slurried in 100 ml MeCN and reduced with Ph_3Sb (6.8 g, 19.0 mmol) overnight. The resulting red–black precipitate was filtered off, washed with 50 ml of MeCN and dried *in vacuo*. This solid was extracted repeatedly with hot chlorobenzene to give deep blue solutions which yielded golden needles of **3** (NT) (2.5 g, 8.9 mmol, 47%) upon cooling. Further purification by fractional sublimation at 180–130 °C/10^{-2} Torr afforded golden blocks, mp 316–320 °C, UV–VIS ($C_2H_4Cl_2$) λ_{max} (log ε) 622 (4.6) nm.‡

Cyclic voltammetry on solutions of NT in THF (with Pt electrodes and 1 M $Bu^n_4NPF_6$ as supporting electrolyte) reveals two reversible oxidation waves with $E_{1/2}$ = 0.41 and 0.66 V *vs.* SCE. These potentials are significantly lower than those observed for **1** (0.93, 1.5 V) and **2** (0.80, 1.25 V),[1,2] and comparable to those found for TTF.[9] Consistently, the intense π–π transition in NT (622 nm) is to longer wavelength of the corresponding absorption maxima in **1** (522 nm) and **2** (565 nm).[1,2] In order to test the potential of NT as a donor for the formation of charge transfer salts we have explored the use of electrocrystallization methods.[10] To date we have found that electrooxidation of NT in a 2:1 mixture of CS_2:$C_2H_4Cl_2$ containing 0.1 M $Bu^n_4NBF_4$ as supporting electrolyte, and using Pt electrodes, currents of 3–5 μA, and growth periods of 10–14 days, affords lustrous black needles of the mixed valence salt $[NT]_3[BF_4]_2$. When dissolved in liquid SO_2, lilac colored solutions of $[NT]_3[BF_4]_2$ exhibit a strong and persistent EPR signal of the $[NT]^+$ radical cation (Fig. 1), with g = 2.0106 and a hyperfine coupling pattern based on a_N = 0.235 mT. Additional coupling to two pairs of hydrogens with a_H = 0.079 and 0.048 mT is also observed.

The crystal structures of both NT and $[NT]_3[BF_4]_2$ have been determined by X-ray diffraction.§ In the structure of NT itself the molecules lie on a center of inversion; the packing pattern consists of slipped π-stacks of NT molecules running in the *x* direction (Fig. 2). In the asymmetric unit of the mixed valence salt $[NT]_3[BF_4]_2$ one NT molecule (A) lies on a center of inversion, while the other molecule (B), along with the BF_4^- ion, adopt general positions. The molecules are packed in layers (Fig. 3) in which the B molecules form dimer units across a center of inversion. These dimers are linked by S···S contacts of 3.407(2) (S3···S5) and 3.250(2) (S4···S6) Å.[11] The B dimers and A molecules adopt an alternating π-stacked arrangement, in which the unique A molecules are slipped relative to the B dimers (Fig. 3). The BF_4^- anions are located between the stacks, bridging B dimers on one side to A molecules on the other.

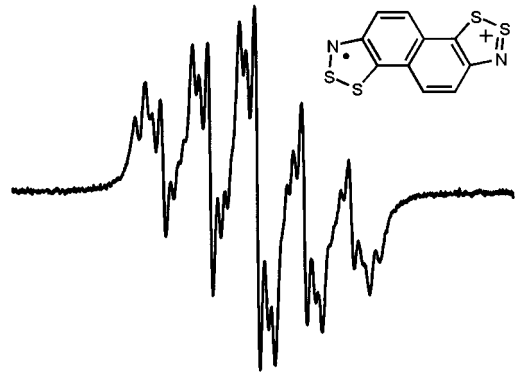

Fig. 1 X-Band EPR spectrum of the $[NT]^+$ radical cation (in liquid SO_2 at 298 K). Sweep width = 2.5 mT.

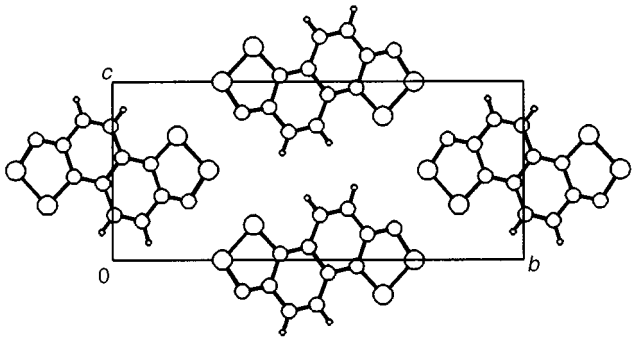

Fig. 2 Crystal packing of NT, viewed along the *x* direction

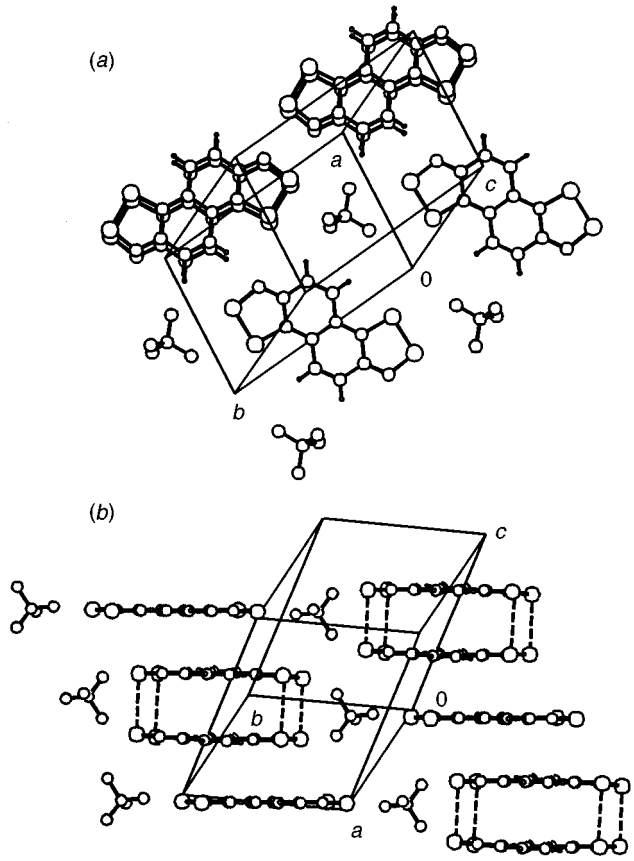

Fig. 3 Crystal packing of $[NT]_3[BF_4]_2$, showing (*a*) layers of neutral molecules and radical cation dimers and (*b*) alternating slipped π-stacks

While the 3:2 stoichiometry of the salt formally implies the presence of a 2/3 positive charge per heterocyclic layer, comparison[12] of the intramolecular distances in NT and $[NT]_3[BF_4]_2$ suggests that the B molecules are nominally oxidized to the radical cation (+1) state, while the A molecules are neutral. The unusual triple-decker[13] stacking pattern found for $[NT]_3[BF_4]_2$ is thus comprised of closed shell ($[NT]_2^{2+}$ and NT) units, and the material is expected to be a semiconductor. Preliminary pressed pellet conductivity measurements on $[NT]_3[BF_4]_2$ nonetheless indicate a relatively high value of σ = *ca.* 10^{-2} S cm^{-1}, indicative of a well developed band structure. More detailed transport property measurements are in progress. Meanwhile, the present results augur well for the use of NT and related bis([1,2,3]dithiazoles) in the design of new conductive charge transfer salts.

We thank the NSERC, the NSF/EPSCoR program and the State of Arkansas for financial support. We also acknowledge the US Department of Education for doctoral fellowship to T. M. B.

Notes and References

† E-mail: oakley@sciborg.uwaterloo.ca

‡ The proposed formula of NT is in agreement with elemental and mass spectrometric analysis.

§ *Crystal data* for NT and $[NT]_3[BF_4]_2$: Data were collected (at 293 K) on an Enraf-Nonius CAD-4 automated diffractometer with graphite-monochromated Mo-Kα radiation (λ = 0.71073 Å) using θ–2θ scans to a $2\theta_{max}$ = 50°. The structures were solved by direct methods and refined by full-matrix least-squares analysis which minimized $\Sigma w(\Delta F)^2$. For NT: $S_4N_2C_{10}H_4$, M = 280.39, monoclinic, space group $P2_1/n$, with a = 3.8784(12), b = 17.2855(14), c = 7.7653(8) Å, β = 102.617 (18)°, V = 508.02(18) Å^3, Z = 2, D_c = 1.83 g cm^{-1}, μ = 0.86 mm^{-1}. 73 Parameters were refined using 901 unique observed reflections [$I > 0.0\ \sigma(I)$] to give R = 0.030, R_w = 0.048. For $[NT]_3[BF_4]_2$: $S_6N_3C_{15}H_6BF_4$, M = 507.39, triclinic, space group $P\bar{1}$, with a = 9.3225(14), b = 10.650(2), c = 11.302(5) Å, α = 108.04(2), β = 117.32(3), γ = 98.175(14)°, V = 892.6(4) Å^3, Z = 2, D_c = 1.89 g cm^{-1}, μ = 0.78 mm^{-1}. 262 Parameters were refined using 2314 unique observed reflections [$I > 1.0\ \sigma(I)$] to give R = 0.049, R_w = 0.059. CCDC 182/963.

1 T. M. Barclay, A. W. Cordes, J. D. Goddard, R. C. Mawhinney, R. T. Oakley, K. E. Preuss and R. W. Reed, *J. Am. Chem. Soc*., 1997, **119**, 12136.
2 T. M. Barclay, A. W. Cordes, R. T. Oakley, K. E. Preuss and R. W. Reed, *Chem. Commun*., 1998, 1039.
3 For recent reviews on molecular conductor design, see M. R. Bryce, *Chem. Soc. Rev.*, 1991, **20**, 355; R. Gomper and H. W. Wagner, *Angew. Chem., Int. Ed.*, 1988, **27**, 1437; M. C. Grossel and S. C. Weston, *Contemp. Org. Synth.*, 1994, **1**, 317.
4 W. K. Warburton, *Chem. Rev.*, 1957, **57**, 1011.
5 O. J. Scherer, G. Wolmershäuser and R. Jotter, *Z. Naturforsch., Teil B*, 1982, **37**, 432.
6 The preparation of 2,6-diaminonaphthalene was adapted from that used for 2-aminonaphthalene: *Org. React.*, 1942, **1**, 120. See also N. Donaldson, in *The Chemistry and Technology of Naphthalene Compounds*, E. Arnold Ltd., London, 1958, p. 224.
7 W. Ried and J. Valentin, *Justus Liebigs Ann. Chem.*, 1966, **699**, 183.
8 R. Mayer, *Phosphorus Sulfur*, 1985, **23**, 277.
9 A. J. Berlinsky, J. F. Carolan and L. Weiler, *Can. J. Chem.*, 1974, **52**, 3373; T. Kobayashi, Z. Yoshida, H. Awaji, T. Kawase and H. Yoneda, *Bull. Chem. Soc. Jpn*., 1984, **56**, 2591; D. L. Lichtenberger, R. L. Johnston, K. Hinkelmann, T. Suzuki and F. Wudl, *J. Am. Chem. Soc.*, 1990, **112**, 3302.
10 J. R. Ferraro and J. M. Williams, in *Introduction to Synthetic Electrical Conductors*, Academic Press, New York, 1987, p. 25; D. A. Stephens, A. E. Rehan, S. J. Compton, R. A. Barkhau and J. M. Williams, *Inorg. Synth*., 1986, **24**, 135.
11 G. Wolmershäuser, G. Wortmann and M. Schnauber, *J. Chem. Res. (S)*, 1988, 358.
12 The S–S and S–N bonds should be shortened, and the C–N bonds lengthened, by oxidation. Thus the S–S, S–N and N–C distances in NT are, respectively, 2.0950(7), 1.6430(18) and 1.310(3) Å. The corresponding mean distances in $[NT]_3[BF_4]_2$ are: molecule A, 2.0854(19), 1.641(4), 1.304(6) Å; molecule B, 2.056(7), 1.603(7), 1.329(6) Å.
13 C. D. Bryan, A. W. Cordes, R. C. Haddon, R. G. Hicks, R. T. Oakley, T. T. M. Palstra, A. S. Perel and S. R. Scott, *Chem. Mater*., 1994, **6**, 508.

Received in Cambridge, UK, 8th July 1998; 8/05299I

Synthesis of porous yttrium aluminium oxide templated by dodecyl sulfate assemblies

Mitsunori Yada,* Masahumi Ohya, Masato Machida and Tsuyoshi Kijima

Department of Materials Science, Faculty of Engineering, Miyazaki University, Miyazaki, 889-2192, Japan.
E-mail: t0a201u@cc.miyazaki-u.ac.jp

An yttrium aluminium oxide dodecyl sulfate mesophase with a hexagonal structure has been synthesized by a homogeneous precipitation method using urea and was converted into a porous material with a specific surface area of 662 m^2 g^{-1} by anion exchange of the surfactant with acetate ion.

Increasing attention has been paid to mesoporous materials, mainly because of their great applicabilities as catalysts, molecular sieves and host materials based on their large internal surface areas and narrow pore size distributions. The first examples of such materials, MCM-41[1] and FSM-16[2] silicas, were synthesized by calcining their mesostructured precursors formed in the presence of a cationic surfactant. This approach has been applied to the preparation of niobium, zirconium and other binary metal oxide-based mesophases.[3,4] Much less study, however, have been reported concerning similar but ternary metal oxide-based materials such as those containing $AlPO_4$[5] and $AlBO_3$[6] as their skeleton.

Our previous studies demonstrated the synthesis of aluminium-based dodecyl sulfate mesophases by the homogeneous precipitation method using urea, in which the surfactant mesophases occurred initially in the layer structure and grew into their hexagonal form with versatile morphologies such as winding-rod, spherical, tubular and funneled shapes depending on the urea concentration.[7,8] A similar observation was made for the gallium-based dodecyl sulfate system.[9] Coincorporation of dodecyl sulfate and alkyl alcohols in the aluminium-based system also led to a lamellar structure with biomimetic surface patterns such as cone-shaped or terraced hollows and domed scales.[10] Recently, we also succeeded in the synthesis of a mesoporous yttrium oxide by the anion exchange method with acetate anion.[11]

Yttrium aluminium oxide is useful as hosts for solid-state lasers such as YAG ($Y_3Al_5O_{12}$) or YALO ($YAlO_3$) and luminescence systems and window materials for a variety of lamps. Therefore, if we could obtain a ordered mesoporous yttrium aluminium mixed oxide, it would be useful not only for adsorbing or separating agents and catalytic bodies but also as a host for the homogeneous dispersion of optically functional species, followed by its post-sintering. The aluminium component combined with yttrium oxide units would also be effective for increasing the solid acidity of the resulting oxide. Here, we report the synthesis of an yttrium aluminium oxide mesophase templated by dodecyl sulfate assemblies with a hexagonal structure and its conversion into a porous material by anion exchange of the surfactant species with acetate ion.

The yttrium aluminium oxide surfactant mesophases with lamellar and hexagonal structures were synthesized by the homogenous precipitation method using urea. Yttrium nitrate hexahydrate [$Y(NO_3)_3{\cdot}6H_2O$] was used as the yttrium source and aluminium nitrate nonahydrate [$Al(NO_3)_3{\cdot}9H_2O$] was used as the aluminium source and sodium dodecyl sulfate [SDS,Me-$(CH_2)_{11}OSO_3Na$] was used as the templating agent. Yttrium nitrate, aluminium nitrate, SDS, urea and water were mixed at a molar ratio of 0.375 : 0.625 : 2 : 30 : 60 and stirred at 40 °C for 1 h to obtain a transparent mixed solution. The nominal Y to Al molar ratio of 3 : 5 corresponds to that for YAG. Urea was used to gradually raise the pH of the reaction mixture since on heating at above 60 °C it is hydrolyzed and releases ammonia. The mixed solution was heated at 80 °C and then kept at that temperature. The pH of the reaction mixture increased from an initial value of 3.6, due to hydrolysis of urea, and precipitation occurred. Immediately after 3 or 20 h, the resulting mixtures were cooled to room temperature to prevent further hydrolysis of urea. After centrifugation, the resulting solids were washed with water a few times and then dried at 60 °C. Powder X-ray diffraction (XRD) measurements were made on a Simadzu XD-D1 diffractometer with Cu-Kα radiation. X-Ray microanalysis (XMA) was conducted with a HORIBA EMAX-5770 instrument. Transmission electron microscopy (TEM) was carried out using a Hitachi H-800MU instrument.

Precipitation at 80 °C commenced when the pH of the reaction mixture reached 6.1 after 1.5 h. Two white solid samples, **1** and **2**, were separated after 3 and 20 h, respectively. The XRD pattern of **1** is characterized by three diffraction peaks at 2θ = 1–7°, along with a halo band near 2θ = 20° [Fig. 1(a)]. The former three peaks are attributable to the 001, 002 and 003 reflections for a lamellar phase with an interlayer spacing of 3.9 nm and the halo band suggests that the short-range arrangement of constituent atoms is completely disordered. According to XMA, the dodecyl sulfate (S) to metal (Al + Y) mole ratio was 0.63, and the Y to Al mole ratio was 0.18. In contrast to the layered mesophase **1**, the XRD pattern of **2** is characterized by a major peak located at $2\theta \approx 2.3°$ and two weak peaks at 2θ = 3–5° along with a halo at $2\theta \approx$ 20°[Fig. 1(b)]. On the basis of a hexagonal unit cell with a = 4.3 nm, these three peaks can be assigned to the 100, 110 and 200 reflections. Thus, these two XRD patterns indicate that the

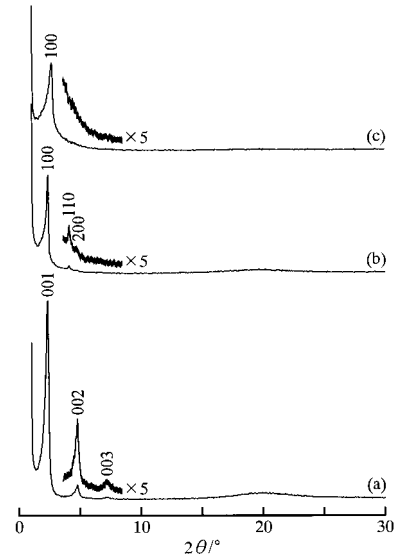

Fig. 1– XRD patterns of yttrium aluminium oxide mesophases templated by dodecyl sulfate assemblies; (a) **1**, (b) **2** and (c) **3**

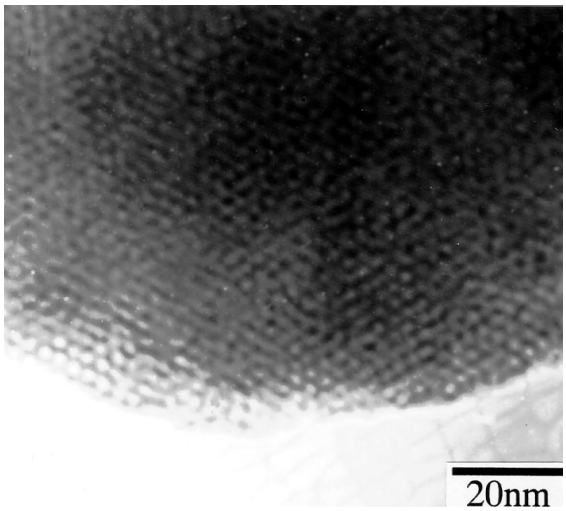

Fig. 2 TEM image of yttrium aluminium oxide mesophase **2** viewed along the axis of the hexagonal channel

yttrium aluminium mixed oxide mesophase undergoes a layer to hexagonal structural transition, as observed in the Al-, Ga- and Y-based systems.[7–11] The unit cell parameter of 4.3 nm for the Y–Al based hexagonal mesophase **2** is equal to that for the Al-based mesophase, but is much less than that for the Y-based mesophase (6.1 nm). A transmission electron micrograph of **2** showed a regular hexagonal array of channels extending for several hundred nanometers or more as shown in Fig. 2. This ordered hexagonal arrangement is similar to the atomic arrangement for the Al-based hexagonal mesophase and MCM-41, but is different from a disordered arrangement observed for the Y-based one. Furthermore, the S to metal mole ratio of 0.31 for the Y–Al based mesophase **2** is close to 0.33 and 0.28 for the Al- and Y-based analogues, indicating that nearly the same amount of surfactant per metal is incorporated in these three mesophases. The Y to Al mole ratio for the Y–Al based mesophase **2** is only 0.34, being nearly half its nominal value. Details for the control of Y to Al mole ratio in the resulting mesophases will be described elsewhere.

A further attempt was made to remove the surfactant species from the hexagonal mesophase **2** by anion exchange with acetate anions in a manner similar to that reported by Holland *et al*. for mesoporous aluminophosphate;[12] the mesophase sample (0.5 g) was mixed with a 0.05 M ethanol solution of sodium acetate (40 ml), and then stirred at 40 °C for 1 h. The centrifuged solid was then washed repeatedly with ethanol. The 100 reflection for the acetate-treated solid **3** shifted slightly to higher angle relative to that of **2**, and the 110 and 200 reflections for the former disappeared, as shown in Fig. 1(c). No sulfur species were detected by XMA of **3**, suggesting the complete removal of dodecyl sulfate species. Since the Y to Al molar ratio of 0.36 for **3** is nearly equal to 0.34 for **2**, the resulting decrease of unit cell parameter *a* from 4.3 to 3.8 nm would be attributable to partial condensation of hydroxide groups induced by the removal of surfactant. Preliminary data suggested that the solid **3** become completely disordered upon calcination at 300 °C for 5 h in air.

Fig. 3 shows an N_2 adsorption isotherm for **3**, measured after heating at 150 °C for 1 h to remove adsorbed water. The rapid adsorption in the range of P/P_0 = 0–0.25 for the sample is due

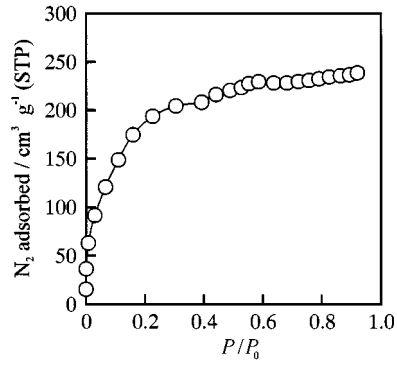

Fig. 3 N_2 adsorption isotherm for **3**

to the monolayer coverage of pores and particle surface and capillary condensation in the pores. The specific surface area determined by the BET method was as large as 662 $m^2\ g^{-1}$ and the pore size determined by Clanston–Inkley method[13] was 1.6 nm. Pre-heating of **3** at 150 °C for dehydration led to a decrease of its crystallinity, as suggested from a slight shift of the 100 reflection from 2.6 to 2.9°. Upon similar acetate-treatment, the Al-based hexagonal mesophase collapsed in structure to yield a specific surface area of only 12 $m^2\ g^{-1}$, whereas the Y-based analogue was converted into a mesoporous solid with a specific surface area of as large as 545 $m^2\ g^{-1}$ without any radial contraction.[11] Thus, the pore structure change observed in the Y–Al mixed system is a result of the stabilization of the inorganic framework due to the combination of yttrium-based species with Al-based structural units.

In conclusion, we have synthesized, for the first time, a hexagonal yttrium aluminium oxide mesophase by a homogeneous precipitation method using urea, and demonstrated its conversion into an acetate-exchanged porous material. The present approach and findings using the homogenous precipitation method will contribute to further development of functional mesostructured ternary or even more complex metal-based oxides.

Notes and References

1 C. T. Kresge, M. E. Leonowicz, W. J. Roth, J. C. Vartuli and J.S.Beck, *Nature*, 1992, **359**, 710.
2 T. Yanagisawa, T. Shimizu, K. Kuroda and C. Kato, *Bull. Chem. Soc. Jpn.*, 1990, **63**, 988.
3 D. M. Antonelli and J. Y. Ying, *Angew. Chem., Int. Ed. Engl.*, 1995, **34**, 2014.
4 U. Ciesla, S. Schacht, G. D. Stucky, K. K. Unger and F. Schüth, *Angew. Chem., Int. Ed. Engl*., 1996, **35**, 541.
5 D. Zhao, Z. Luan and L. Kevan, *Chem. Commun.*, 1997, 1009.
6 S. Ayyappan and C. N. R. Rao, *Chem. Commun.*, 1997, 575.
7 M. Yada, M. Machida and T. Kijima, *Chem.Commun.*, 1996, 769.
8 M. Yada, H. Hiyoshi, K. Ohe, M. Machida and T. Kijima, *Inorg. Chem.*, 1997, **36**, 5565.
9 M. Yada, H. Takenaka, M. Machida and T. Kijima, *J. Chem. Soc., Dalton Trans.*, 1998, 1547.
10 M. Yada, H. Kitamura, M. Machida and T. Kijima, *Langmuir*, 1997, **13**, 5252.
11 M. Yada, H. Kitamura, M. Machida and T. Kijima, to be published.
12 B. T. Holland, P. K. Isbester, C. F. Blanford, E. J. Munson and A. Stein, *J. Am. Chem. Soc.*, 1997, **119**, 6796.
13 R. W. Cranston and F. A. Inkley, *Adv. Catal.*, 1957, **9**, 143.

Received in Cambridge, UK, 12th June 1998; 8/04449J

De novo design of microporous transition metal oxides

Furio Corà,*[a] Dewi W. Lewis[b] and C. Richard A. Catlow[a]

[a] *The Royal Institution of Great Britain, 21 Albemarle Street, London, UK W1X 4BS. E-mail: furio@ri.ac.uk*
[b] *Department of Materials Science and Metallurgy, University of Cambridge, Pembroke Street, Cambridge, UK CB2 3QZ*

***Ab initio* Hartree–Fock calculations are performed on the molybdenum and tungsten trioxides and bronzes, obtained by inserting alkali metal atoms or larger species in the MO_3 framework; we examine four known polymorphs and two new structures with a microporous architecture, and characterise their relative stability; we also explore the synthesis conditions under which the microporous polymorphs may be obtained, by designing potential organic templates.**

The structural chemistry of the Mo and W trioxides and bronzes comprises several known polymorphs, such as the perovskite (PV) structure of WO_3, $NaMoO_3$ and $NaWO_3$, the layered (L) α-MoO_3, hexagonal (Hex) $K_{0.33}WO_3$ and pyrochlore (PY) Cs_xWO_3. The bronzes are obtained by inserting extra species into the empty interstices of the host MO_3 lattice, and can be described as comprising an MO_3 framework, in whose pores are located the inserted, or extra-framework, cations.

In the PV, Hex and PY structures, the framework is built entirely of corner-sharing MO_6 octahedra, which connect into 4-membered rings in the PV, and 6-membered rings in the Hex and PY polymorphs. The 6-membered rings form hexagonal channels, which are parallel in the Hex, and intersect in the PY structure; the dimension of the extra-framework voids increases therefore in the order of PV < Hex < PY. In the L polymorph, the MO_6 octahedra connect corner- and edge-sharing in the *bc* plane, leaving a layered structure along *a*. Interstices are present in the interlayer region.

In recent work, we highlighted the importance of the M–O bonding pattern,[1–2] of Coulomb[2] and structural forces,[3] and of steric constraints[4] in the solid state chemistry of Mo and W oxides and bronzes. We now examine the relative stability of the framework structures in the insertion compounds.

A common feature of transition metal oxides (TMOs) are structural distortions due to off-centerings of the metal ions M in their coordination octahedra. In PV materials, the off-centering of M hybridises a set of levels, which in the cubic phase are of M–O non-bonding character, into π M–O bonding (in the valence band) and antibonding (in the conduction band) combinations.[1] When the metal ion has formal electronic configuration d^0, as in MoO_3 and WO_3, only the M–O bonding level is filled, and the distortion is stable; in the bronzes, the inserted atoms ionise and cede electrons to the host lattice, populating the M–O antibonding level at the bottom of the conduction band, which opposes the distortion. The PV-structured W bronzes are stable in the cubic phase.[1] The M–O bonding pattern in the valence and conduction bands is common to all the polymorphs examined, and a partial population of the conduction band will oppose off-centerings of M. Here, we are interested in the insertion compounds A_xMO_3, in which the metal ion has configuration d^x; we shall therefore consider only framework structures in which the M ions are on-centre in their coordination octahedra. We have optimised, under the above constraint, the structure of the four cited polymorphs of WO_3 and MoO_3, using a periodic restricted Hartree Fock Hamiltonian, as implemented in CRYSTAL95.[5] Basis set, tolerances and computational conditions are the same as described in refs. 2 and 3; a convergence criterion of 10^{-6} E_h was used in the geometry optimisation. From the calculated energies, we have constructed a scale of relative stability for the host MO_3 framework; results are summarised in Table 1. We note that the undistorted L polymorph is highly unstable with respect to the other three structures examined, suggesting that insertion compounds based on L-MoO_3 would not be stable following the cation insertion. The relative stability of the other three polymorphs (PV, Hex and PY) parallels their relative density, as higher electrostatic energies stabilise the densest structures.

Moving from the binary oxides to the insertion compounds, the relative stability of the polymorphs is altered; a balance between the Coulomb and steric effects stabilises the structures whose interstices have dimensions comparable with the size of the inserted ions. The experimentally reported crystal structures, for instance of the W bronzes, on increasing the size of the inserted ion, move from the cubic-PV form of $NaWO_3$ towards the Hex K_xWO_3 and Rb_xWO_3, to the PY structure obtained by insertion of Cs and of primary and secondary ammonium salts.[6] The importance of the short-range repulsion between the inserted ion and the MO_3 framework increases with increasing ionic size of the extraframework ion; in ref. 4 we estimated it as 0.52 eV for the relatively small K^+ ion in the hexagonal channels of Hex-WO_3. The energy arising from the short-range repulsion is therefore sufficient to offset the energy difference between the framework structures examined, shifting the stability towards the polymorphs with interstices of the appropriate dimensions. Extraframework ions present during the synthesis of the host MO_3 framework may therefore effectively act as inorganic templates, or structure-directing agents.

The use of organic cationic templates is a standard procedure in the synthesis of microporous aluminosilicates (zeolites), where the correlation between the shape of the organic cation and that of the pore structure obtained is now recognised.[7] The energy difference between the silica polymorphs is in the range of 0.1–0.2 eV per formula unit, much smaller than that we calculated in the Mo and W trioxides (excluding the L polymorph, the energy range of the PV, Hex and PY structures is of *ca.* 0.5 eV per formula unit). We attribute the higher energy difference in the trioxides to two effects: (i) the higher ionic charges, which increases the Madelung field, and (ii) the rigidity of the octahedral framework of TMOs, compared to the more flexible tetrahedral framework of silicates. We note however that the difference in framework energy is still in the range of the steric repulsion, and can be reversed, as confirmed by the different stable structures of the alkali W bronzes. We believe therefore that a template/host approach, similar to that employed in the synthesis of zeolites, can also be applied to obtain novel TMO frameworks. The advantages of TMOs with larger pores are manyfold: for example, such materials would better satisfy the requirement for high ionic conductivity and

Table 1 Relative energy (in eV per formula unit) of the MO_3 frameworks examined

Material	PV	Hex	PY	L	$H^{2\times1}$	$H^{2\times2}$
MoO_3	0.00	0.238	0.607	4.281	0.943	1.128
WO_3	0.00	0.315	0.725	5.471	0.902	1.393

structural stability, necessary in electro- and photo-chromic applications, and in Li batteries. Furthermore, if the pore sizes reach the dimension of small organic molecules, microporous TMOs would allow heterogeneous catalytic applications, and combine the molecular-sieve characteristics of zeolites with the higher acidic strength and redox properties of early transition metal cations.

Attempts to use organic cations, usually quaternary ammonium salts, to template novel TMO frameworks have been reported,[8] but resulted in the formation of inorganic polyanions, the Keggin structures, rather than extensive M–O frameworks. We now examine the topic with a more analytic approach, exploiting the insight that can be obtained from computer modelling to provide information on the relative stability and on the required synthesis conditions for new, microporous structures of TMOs. In particular, we employ a strategy recently developed for the *de novo* design of structure-directing agents in zeolites:[9] given a target microporous architecture, the organic template is gradually grown within the pores, to design molecules which provide optimal space filling and maximum interaction energy with the selected porous system, thus helping to direct the synthesis towards the target structure.

The method requires the knowledge of the porous TMO structure as starting point. This is a challenging task by itself, since microporous structures built up on MO_6 octahedra have so far never been reported; the only exceptions are the OMS sieves based on edge-sharing of $Mn^{IV}O_6$ units,[10] in which the framework has stoichiometry MO_2 and not MO_3 as required for the MO and W oxides. The first problem to solve is therefore that of designing a suitable target structure.

The PV and Hex structures can be imagined as a 2D arrangement, repeated by corner-sharing of the axial oxygens along the third direction; in the design of new structures we retained this 2D approach, as a useful starting point. If we define a new building block, as a chain of *n* aligned edge-shared octahedra, a series of new structures can be obtained from the same connectivity of the PV and Hex phases, replacing single octahedral units with alternating chains of *m* and *n* edge-shared octahedra. Given the method of construction, we denote the new structures $PV^{m\times n}$ and $H^{m\times n}$ (the 1×1 structures reproduce the PV and Hex polymorphs). All the new structures have an MO_3 framework stoichiometry. We have calculated the electronic distribution, geometry and energy of the first two members of the $H^{m\times n}$ series: $H^{2\times 1}$ and $H^{2\times 2}$ (Fig. 1). The new structures represent local minima in the potential energy surface; hence, if synthesised, they would have a non-zero activation barrier towards phase transformations. The calculated internal energy is compared in Table 1 with that of the known polymorphs. The new structures are unstable, as expected; the energy difference has nonetheless the same order of magnitude as that between the known polymorphs and is within the range of the steric energy. It may therefore be possible to overcome this difference with steric effects; given the relative instability of the framework, the template must be selected carefully, and must fit tightly in the porous structure to stabilise these particular polymorphs; which is probably why previous attempts with 'randomly' selected templates failed.

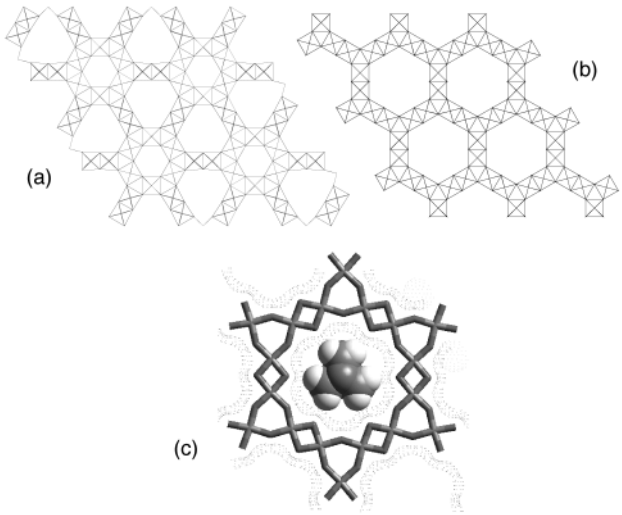

Fig. 1 Disposition of octahedra in the MO_3 framework of the $H^{2\times 1}$ (a) and $H^{2\times 2}$ (b) structures; diazobicyclooctane molecule, as located by the program ZEBEDDE[9] inside the pores of the $H^{2\times 2}$ structure (c)

Finally, we applied the *de novo* method to design templating agents specific for the $H^{2\times 1}$ and $H^{2\times 2}$ structures. The interactions between the framework and the organic template were evaluted *via* interatomic potentials;[11] energy-minimised structures were obtained for each template in a rigid host MO_3 framework, ignoring the M-template terms. Candidate templates are ranked by their calculated binding energy (E_B) with the host lattice: the higher the E_B the more favourable the molecule is considered as a template.[7] The pores of the $H^{2\times 1}$ structure have dimensions comparable to unsubstituted hydrocarbon chains, suggesting that *n*-amines or *n*-diamines, as used in zeolite synthesis may be suitable as templates. The pores of the $H^{2\times 2}$ polymorph have a size comparable to the 12-membered rings in zeotypes, and allow the insertion of more structured organic moieties. Our calculations reveal that adamantane and diazobicyclooctane derivatives are of suitable dimensions, the latter [Fig. 1(c)] having the highest E_B. Future experimental studies will test the prediction of these calculations.

In summary, our computational study has shown the feasibility on energetics grounds of an extensive range of microporous chemistry based on octahedral MoO_3 and WO_3, and has suggested that such structures may be synthesised using a host/guest templating approach.

F. C. thanks ICI Katalco and MSI for funding; the provision of time on the IBM/SP2 computer at the Daresbury Laboratory is gratefully acknowledged. D. W. L. acknowledges funding from the Oppenheimer Trust and the Royal Society.

Notes and References

1 F. Corà, M. Stachiotti, C. O. Rodriguez and C. R. A. Catlow, *J. Phys. Chem. B*, 1997, **101**, 3945; M. Stachiotti, F. Corà, C. O. Rodriguez and C. R. A. Catlow, *Phys. Rev. B*, 1997, **55**, 7508.
2 F. Corà, A. Patel, N. M. Harrison, R. Dovesi and C. R. A. Catlow, *J. Am. Chem. Soc.*, 1996, **118**, 12 174.
3 F. Corà, A. Patel, N. M. Harrison, C. Roetti and C. R. A. Catlow, *J. Mater. Chem.*, 1997, **7**, 959.
4 F. Corà and C. R. A. Catlow, *Solid State Ionics*, in press.
5 R. Dovesi, V. R. Saunders, C. Roetti, M. Causà, N. M. Harrison, R. Orlando and E. Aprà, *CRYSTAL95 User's Manual*, Univ. of Torino, Italy, 1996.
6 P. J. Wiseman and P. G. Dickens, *J. Solid State Chem.*, 1976, **17**, 91; I. Tsuyumoto, A. Kishimoto and T. Kudo, *Solid State Ionics*, 1993, **59**, 211; T. Kudo, J. Oi, A. Kishimoto and M. Hiratami, *Mater. Res. Bulletin*, 1991, **26**, 779; P. Zavalij, J. D. Guo, M. S. Whittingham, R. A. Jacobson, V. Pecharsky, C. K. Bucker and S. J. Hwu, *J. Solid State Chem.*, 1996, **123**, 83.
7 M. E. Davis and R. F. Lobo, *Chem. Mater.*, 1992, **4**, 759; D. W. Lewis, C. M. Freeman and C. R. A. Catlow, *J. Phys. Chem.*, 1995, **99**, 11 194.
8 G. G. Janauer, A. Dobley, J. D. Guo, P. Zavalij and M. S. Whittingham, *Chem. Mater*, 1996, **8**, 2096.
9 D. W. Lewis, D. J. Willock, C. R. A. Catlow, J. M. Thomas and G. J. Hutchings, *Nature*, 1996, **382**, 604.
10 Y. F. Shen, S. L. Suib and C. L. Oyoung, *J. Am. Chem. Soc.*, 1994, **116**, 11 020.
11 cff91_czeo molecular forcefield and Discover 4.0, Molecular Simulations Inc., San Diego, 1997.

Received in Bath, UK, 20th June 1998; 8/04804E

Transformation of cyclohexene to enantiopure cyclitols mediated by sequential oxyselenenylation with (*S*,*S*)-hydrobenzoin: synthesis of D-*chiro*-inositol and *muco*-quercitol

Kwan Soo Kim,*† Jong Il Park, Hoi Kyung Moon and Hann Yi

Department of Chemistry, Yonsei University, Seoul, 120-749, Korea

Oxyselenenylation of cyclohexene with (*S*,*S*)-hydrobenzoin and subsequent oxidation-elimination allows isolation of an allylic ether in which further phenylselenenylation is completely regioselective, thus allowing entry to the cyclitols D-*chiro*-inositol and *muco*-quercitol.

Cyclitols have attracted a great deal of attention from synthetic chemists due to their diverse biological activity and their versatility as synthetic intermediates.[1] Although several methods are available for the synthesis of cyclitol derivatives, there still remains a need for new methodology starting from simple starting materials because the cyclitol derivatives are structurally very diverse and the new methodology could be applied for the synthesis of other highly functionalized cyclic compounds. In this regard, it is noteworthy that cyclohexadiene *cis*-diols obtained from halobenzene by microbial oxidation[2] and from $PhMe_2SiCl$ by reduction and subsequent asymmetric dihydroxylation[3] have been used for the synthesis of cyclitols and other natural products.

Oxyselenenylation of a cycloalkene with an appropriate alcohol and the subsequent oxidation-elimination of the resultant oxyselenide would afford a cyclic allylic alcohol derivative. If a second oxyselenenylation of this cyclic allylic alcohol derivative was followed by oxidation-elimination to give a cycloalk-3-ene-1,2-diol derivative, a correctly protected cyclitol might be efficiently synthesized. However, it has been documented that the oxyselenenylation of both cyclic[4] and acyclic[5] allylic alcohol derivatives usually provides 1,3-diol rather than 1,2-diol derivatives. Therefore, in order to make this serial oxyselenenylation methodology work for the synthesis of enantiopure cyclitols, not only the stereochemistry but also the regiochemistry of the oxyselenenylation must be controlled. We have solved this problem by using a chiral diol, (*S*,*S*)-hydrobenzoin, for the oxyselenenylation of cyclohexene. Herein we report the successful conversion of cyclohexene into various enantiopure cyclitols and the synthesis of important natural cyclitols *muco*-quercitol **1** and D-*chiro*-inositol **2**, which

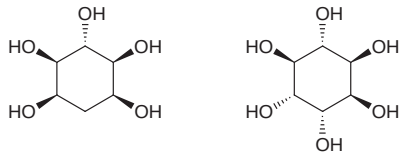

1 **2**

is valuable due to its physiological activity as an insulin mediator[6] and its limited availability.

To a solution of *N*-(phenylseleno)phthalimide (*N*-PSP) (3.44 mmol), (*S*,*S*)-hydrobenzoin (4.13 mmol), and cyclohexene (4.13 mmol) in CH_2Cl_2 (60 ml) was added slowly $BF_3{\cdot}OEt_2$ (0.34 mmol) at 0 °C. Stirring the reaction mixture at room temperature for a further 2 h afforded two diastereomeric oxyselenides [**3** plus the (1*R*,2*R*)-diastereomer; *ca.* 1:1 ratio] in 80% yield (Scheme 1). Although oxyselenenylation with other selenium reagents such as PhSeCl, PhSeBr and PhSeOTf was also possible, they frequently generated the undesired haloselenide or hydroxyselenide. Oxyselenide **3**‡ was separated by column chromatography and converted into olefin **4** {$[\alpha]_D$ −82.3 (*c* 0.7)} by the oxidation with $NaIO_4$ in the presence of $NaHCO_3$ followed by elimination of the resulting selenoxide. Intramolecular oxyselenenylation of **4** using PhSeOTf§ at −78 °C gave only *cis*-fused bicyclic dioxane **5**{$[\alpha]_D$ −34.5 (*c* 0.4)}. Thus, both regiochemistry and stereochemistry were completely controlled in the second oxyselenenylation step. Oxidation of selenide **5** and subsequent elimination provided olefin **6**.

Dihydroxylation of **4** with OsO_4 and NMO and subsequent hydrogenolysis of the resulting **7** afforded triol **8**. The absolute configuration of **8** was assigned on the basis of its ^1H NMR spectrum and by comparison of its specific rotation with that of authentic material {$[\alpha]_D$ +72.8 (*c* 1.0)}.[7] Reduction of selenide **5** with Bu_3SnH gave compound **9**. Dihydroxylation of **6** and subsequent hydrogenolysis of the resulting diol **10** gave tetrol **11**, which, by acetylation, afforded tetraacetate **12**. Examination of ^1H NMR spectrum of **9** and comparison with the ^1H NMR spectra of **12** with that of its known racemate[8] clearly indicated that the relative stereochemistry of compound **6** is *cis*. Consequently, the C1 and C2 configurations of cyclohex-3-ene-

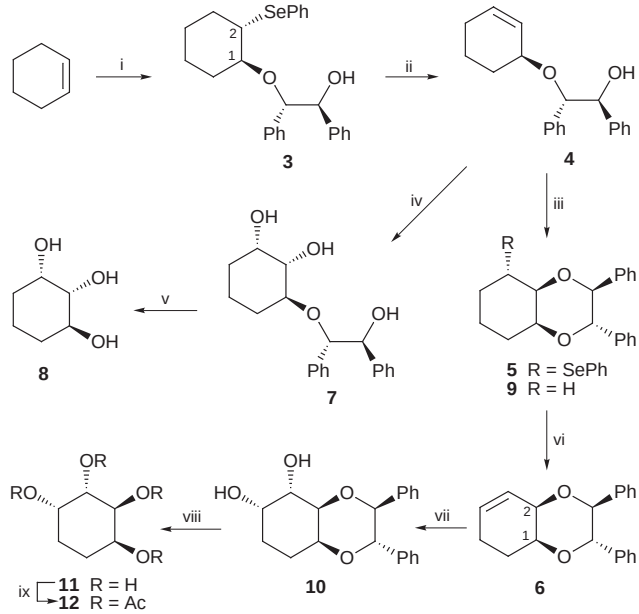

Scheme 1 *Reagents and conditions*: i, (*S*,*S*)-hydrobenzoin, *N*-PSP, $BF_3{\cdot}OEt_2$ (cat.), CH_2Cl_2, room temp., 2 h, 40% of **3** and 40% of its (1*R*,2*R*)-diastereomer; ii, $NaIO_4$, $NaHCO_3$, MeOH–H_2O, room temp., 10 min, then 90 °C 48 h, 92%; iii, PhSeOTf, CH_2Cl_2, −78 °C, 2 h, 68%; iv, OsO_4 (cat.), NMO, acetone–H_2O, room temp., 24 h, 76%; v, H_2, Pd-C (cat.), EtOH, 50 psi, room temp., 12 h, 85%; vi, $NaIO_4$, $NaHCO_3$, MeOH–H_2O, room temp., 10 min, then 90 °C 48 h, 90%; vii, $K_2OsO_4H_2O$ (cat.), NMO, acetone–H_2O, reflux, 20 h, 92%; viii, H_2, Pd-C (cat.), EtOH, 50 psi, room temp., 8 h, 98%; ix, Ac_2O, pyridine, 50 °C, 12 h, 86%

1,2-diol derivative **6** were unambiguously determined to be *S* and *R*, respectively. On the other hand, a ^{1}H NMR decoupling experiment with compound **3** showed *trans* diaxial coupling (8.2 Hz) between H1 and H2 and thus the C1 and C2 configurations of **3** were assigned as *S* and *S*, respectively.

Epoxidation of **6** with MCPBA in CH_2Cl_2 afforded *trans*-epoxide **13** {R_f = 0.30 (silica gel, hexane−EtOAc, 10:1); $[\alpha]_D$ −126.9 (*c* 0.11)} along with its *cis* isomer {R_f = 0.11, $[\alpha]_D$ −112.0 (*c* 0.1)} (*trans*:*cis* = *ca.* 7:3) (Scheme 2). Epoxidation in other solvents gave poorer results. Diaxial opening of the epoxide ring of **13** with PhSeNa gave exclusively hydroxyselenide **14**, whereupon oxidation with 30% H_2O_2 followed by elimination provided allylic alcohol **15** {$[\alpha]_D$ + 3.0 (*c* 0.2)}. Dihydroxylation of **15** occurred on the opposite face to the allylic hydroxy group to afford exclusively triol **16** {$[\alpha]_D$ −50.5 (*c* 0.11)} in 92% yield. Hydrogenolysis of **16** provided *muco*-quercitol **1**, of which the spectroscopic data and physical properties were identical with those of authentic material. Further characterization of **1** was performed *via* transformation to the known pentaacetate **17**.[9]

Protection of the hydroxy group in **15** with the sterically demanding TBDPS group and subsequent epoxidation of the resulting TBDPS ether **18** {$[\alpha]_D$ +17.8 (*c* 1.1)} with MCPBA afforded the desired *trans*-epoxide **19** {R_f = 0.40 (silica gel, hexane–$CHCl_3$–EtOAc, 20:5:1); $[\alpha]_D$ −22.3 (*c* 0.74)} along with *cis*-epoxide {R_f = 0.35; $[\alpha]_D$ −33.2 (*c* 0.80)} (*trans*:*cis* = 3:2). Diaxial opening of the epoxide ring in **19** with PhSeNa afforded exclusively hydroxyselenide **20**, which turned out to be a mixture of two rotational isomers (3:2) about one of the single bonds in the OTBDPS group. The mixture of two stable atropisomers **20** was separated by flash chromatography, and each was converted into allylic alcohol **21,** which was also a stable and separable mixture of atropisomers (3:2). Evidence for the atropisomerism in compounds **20** and **21** could be readily obtained by removal of their TBDPS groups. Thus, treatment of each atropisomer of **20** with TBAF gave the diol **22** which did not show any atropisomerism. Diol **23** {$[\alpha]_D$ +23.0 (*c* 0.10)}, obtained from both atropisomers of **21** by deprotection with TBAF, also showed no atropisomerism.

Dihydroxylation of **23** followed by hydrogenolysis of the resultant **24** {$[\alpha]_D$ − 68.1 (*c* 0.32)} with $Pd(OH)_2$-C (Degussa type) in the presence of a trace amount of conc. HCl gave D-*chiro*-inositol **2**, the physical properties of which are identical with those of authentic **2**.[10] Perbenzoate **25**[11] was prepared for further characterization of **2**. A similar synthesis starting with the (1*R*,2*R*)-diasteromer of **3** would provide L-*chiro*-inositol. The development of the highly diastereoselective oxyselenenylation of cyclohexene with various chiral alcohols including hydrobenzoin derivatives is now in progress.

This work was supported by a grant from Basic Research Institute Program (BSRI-97-3422), Ministry of Education, Korea. Support from OCRC-KOSEF is also acknowledged.

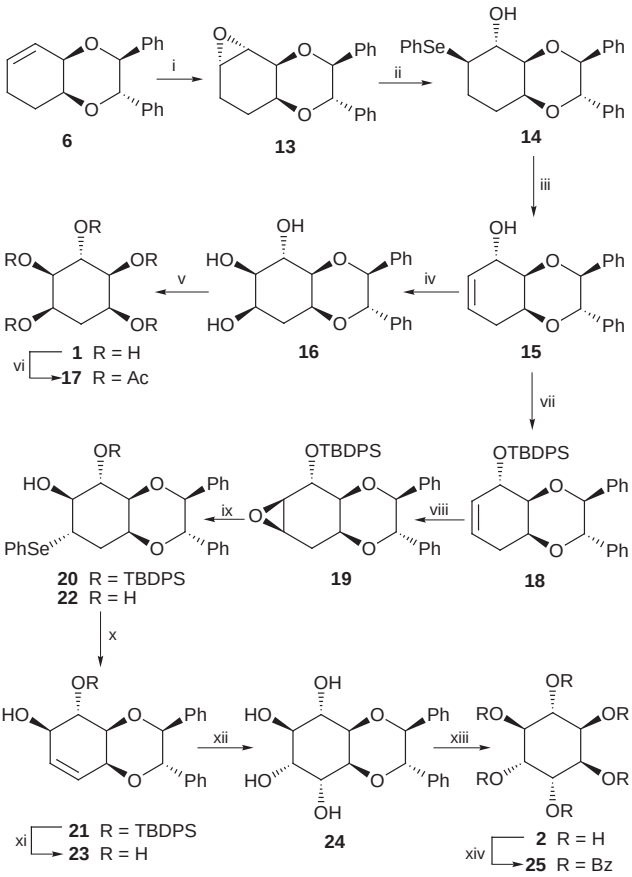

Scheme 2 *Reagents and conditions*: i, MCPBA, $NaHCO_3$, CH_2Cl_2, reflux, 16 h, 60% of **13** and 26% of its *cis* isomer; ii, PhSeSePh, $NaBH_4$, EtOH, reflux, 4 h, 95%; iii, 30% H_2O_2, THF–EtOH, room temp., then reflux, 6 h, 96%; iv, $K_2OsO_4H_2O$ (cat.), NMO, acetone–H_2O, reflux, 20 h, 92%; v, H_2, $Pd(OH)_2$ (cat.), conc. HCl (trace), EtOH, 15 psi, room temp., 1 h, 93%; vi, Ac_2O, pyridine, room temp., 12 h, 85%; vii, TBDPSCl, imidazole, DMF, reflux, 14 h, 87%; viii, MCPBA, $NaHCO_3$, CH_2Cl_2, reflux, 20 h, 51% of **19** and 34% of its *cis* isomer; ix, PhSeSePh, $NaBH_4$, Bu^{n}OH, reflux, 24 h, 83% (a mixture of two atropisomers, 3:2); x, $NaIO_4$, $NaHCO_3$, MeOH–H_2O, room temp., 10 min, then 90 °C, 48 h, 90% (a mixture of two atropisosmers, 3:2); xi, Bu$^n{}_4$NF, THF, room temp., 5 h, 92%; xii, $K_2OsO_4H_2O$ (cat.), NMO, acetone–H_2O, reflux, 18 h, 87%; xiii, H_2, $Pd(OH)_2$ (cat.), conc. HCl (trace), EtOH, 15 psi, room temp., 1 h, 82%; xiv, BzCl, pyridine, 12 h, room temp., 86%

Notes and References

† E-mail: kwan@alchemy.yonsei.ac.kr

‡ *Selected data* for **3**: colourless glass (Found: C, 69.16; H, 6.42. $C_{26}H_{28}O_2Se$ requires C, 69.17; H, 6.25%); R_f = 0.27 (silica gel, hexane–EtOAc, 7:1); $[\alpha]_D$ +4.2 (*c* 0.55, CH_2Cl_2); δ_H(500 MHz; $CDCl_3$) 1.20–1.36 (2 H, m), 1.39–1.52 (2 H, m), 1.53–1.63 (1 H, m), 1.65–1.73 (1 H, m), 2.02–2.10 (1 H, m), 2.12–2.19 (1 H, m), 3.31–3.37 (1 H, m), 3.39–3.45 (2 H, m), 4.37 and 4.62 (2 H, ABq, *J* 8.1), 6.96–7.01 (2 H, m), 7.07–7.22 (11 H, m), 7.36–7.40 (2 H, m). For (1*R*,2*R*)-diastereomer of **3**: white solid, mp 60–62 °C; R_f = 0.37 (silica gel, hexane–EtOAc, 7:1); $[\alpha]_D$ −79.5 (*c* 1.48, CH_2Cl_2); δ_H(500 MHz; $CDCl_3$) 1.02–1.14 (2 H, m), 1.16–1.28 (1 H, m), 1.41–1.62 (3 H, m), 1.64–1.72 (1 H, m), 2.14–2.21 (1 H, m), 3.21–3.28 (1 H, m), 3.44–3.50 (1 H, m), 4.26 and 4.68 (2 H, ABq, *J* 8.7), 4.72–4.80 (1 H, s), 6.92–6.94 (2 H, m), 6.92–7.02 (2 H, m), 7.12–7.19 (6 H, m), 7.29–7.32 (3 H, m), 7.68–7.72 (2 H, m).

§ Unlike the first oxyselenenylation step, the intramolecular oxyselenenylation proceeded in a reasonable yield only with PhSeOTf, possibly because other selenium reagents, including *N*-PSP, are not reactive enough for the intramolecular oxyselenenylation.

1 Reviews: T. Hudlicky, D. A. Entwistle, K. K. Pitzer and A. J. Thorpe, *Chem. Rev.*, 1996, **96**, 1195; J. J. Kiddle, *Chem. Rev.*, 1995, **95**, 2189; T. Hudlicky and M. Cebulak, *Cyclitols and Derivatives*, VCH, New York, 1993; D. C. Billington, *The Inositol Phosphates—Chemical Synthesis and Biological Significance*, VCH, Weinheim, 1993.
2 T. Hudlicky and A. J. Thorpe, *Chem. Commun.*, 1996, 1993.
3 A. Angelaud and Y. Landais, *Tetrahedron Lett.*, 1997, **38**, 1407; *J. Org. Chem.*, 1996, **61**, 5202.
4 D. Liotta, G. Zima and M. Saindane, *J. Org. Chem.*, 1982, **47**, 1258.
5 K. S. Kim, H. B. Park, J. Y. Kim, Y. H. Ahn and I. H. Jeong, *Tetrahedron Lett*., 1996, **37**, 1249.
6 J. M. Mato, K. L. Kelly, A. Alber, L. Jarett, B. E. Corkey, J. A. Cashel and D. Zopf, *Biochem. Biophys. Res. Commun.*, 1987, **146**, 764; J. Larner, L. C. Huang, C. F. W. Schwartz, A. S. Oswald, T. Y. Shen, M. Kinter, G. Tang and K. Zeller, *Biochem. Biophys. Res. Commun.*, 1988, **151**, 1416.
7 H. Paulsen and O. Brauer, *Chem. Ber*., 1977, **110**, 331.
8 H. Z. Sable, K. A. Powell, H. Katchian, C. B. Niewoehner and S. B. Kadlec, *Tetrahedron*, 1970, **26**, 1509.
9 G. E. McCasland, *Adv. Carbohydr. Chem. Biochem.*, 1965, **20**, 11.
10 *Carbohydrates*, ed. P. M. Collins, Chapman and Hall, New York, 1987, p. 289.
11 E. A. Kobat, D. L. McDonald, C. E. Balbu and H. O. L. Fisher, *J. Am. Chem. Soc.*, 1953, **75**, 4507.

Received in Cambridge, UK, 1st June 1998; 8/04072I

Polymer-supported selenium reagents for organic synthesis

K. C. Nicolaou,*† Joaquín Pastor, Sofia Barluenga and Nicolas Winssinger

Department of Chemistry and The Skaggs Institute for Chemical Biology, The Scripps Research Institute, 10550 North Torrey Pines Road, La Jolla, California 92037, USA
Department of Chemistry and Biochemistry, University of California, San Diego, 9500 Gilman Drive, La Jolla, California 92093, USA

Organoselenium resins 1–4 were prepared from polystyrene *via* lithiation and quenching with MeSeSeMe, and shown to react with a variety of substrates, aiding in useful functionalizations.

Combinatorial chemistry and solid phase synthesis have recently emerged as powerful tools for the drug discovery process.[1] The latter technique is particularly useful for combinatorial library construction due to its adaptability to the powerful and elegant split-pool methods[2] and because of the well recognized purification advantages associated with it. The utilization of polymer-bound reagents,[3] in particular, has gained popularity due to the non-requirement for tethering the substrate to the polymer. Here we describe the preparation of a series of solid-supported selenium resins[4,5] **2–4** (Scheme 1) and their application as linkers and reagents for solid phase synthesis. A distinct advantage of the new reagents is the convenience of handling and their totally odorless nature as compared to the non-bound reagents, whose toxicity and foul smell is often problematic.

Scheme 1 summarizes the preparation of the new resins **2–4** from readily available starting materials. Thus, polystyrene beads suspended in cyclohexane were treated with Bu^nLi–TMEDA[6] and the lithiated species was quenched with MeSeSeMe,[7] furnishing selenium reagent **1** as a pale yellow resin (the loading of selenium was controlled by addition of MeSeSeMe in substoichiometric amounts to the lithiated polystyrene). Exposure of **1** to bromine resulted in quantitative conversion[8] to the polymer-supported selenenyl bromide **2**, which was isolated after filtration and washing as a deep red resin. The selenium

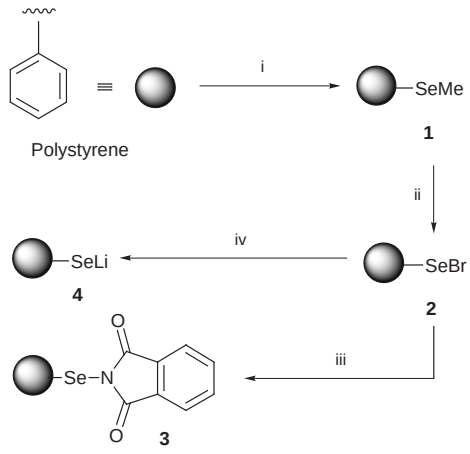

Scheme 1 *Reagents and conditions*: i, Bu^nLi (2.5 M in hexanes, 24 equiv.), TMEDA, cyclohexane, 65 °C, 4 h, then filtration and washing with THF, then dimethyl diselenide (2.0 mmol g^{-1} of polystyrene), THF, 0 °C, 30 min, 100%; ii, Br_2 (0.9 equiv.), $CHCl_3$, 0 °C, 10 min, 100% (based on consumption of Br_2), then filtration and washing, then EtOH, 70 °C, 1 h, > 95%; iii, potassium phthalimide (1.5 equiv.), 18-crown-6 (1.5 equiv.), benzene, 23 °C, 5 h, > 95% yield; iv, $LiBH_4$ (2.0 M in THF, 2.0 equiv.), THF, 23 °C, 1 h, > 95%

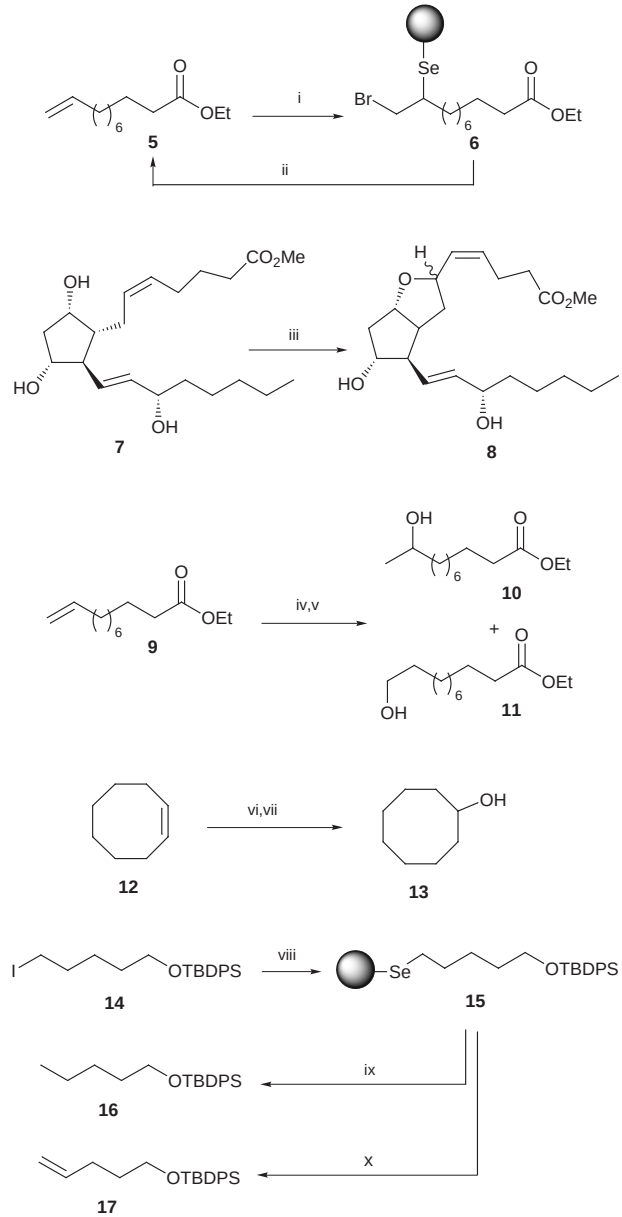

Scheme 2 *Reagents and conditions*: i, **2** (1 equiv.), CH_2Cl_2, 23 °C, 30 min; ii, Bu^n_3SnH (4 equiv.), AIBN (0.01 equiv.), PhMe, 110 °C, 6 h, 92% (2 steps); iii, **2** (1.5 equiv), THF, −78 °C, 30 min, then H_2O_2 (30%, 2 equiv.), −78 → 23 °C, 20 h, 94% (2 steps); iv, **3** (0.5 equiv.), H_2O (1 equiv.), CSA (0.05 equiv.), CH_2Cl_2, 24 h; v, Bu^n_3SnH (2 equiv.), AIBN (0.005 equiv.), PhMe, 110 °C, 6 h, 82% (2 steps), **10** : **11** = 2 : 1; vi, **3** (0.5 equiv.), H_2O (1 equiv.), CSA (0.05 equiv.), CH_2Cl_2, 24 h; vii, Bu^n_3SnH (2 equiv.), AIBN (0.005 equiv.), PhMe, 110 °C, 6 h, 80% (two steps); viii, **4** (0.5 equiv.), THF, 23 °C, 12 h; ix, Bu^n_3SnH (2 equiv.), AIBN (0.005 equiv.), PhMe, 110 °C, 6 h, 89% (2 steps); x, H_2O_2 (30%, 1 equiv), THF, 23 °C, 12 h, 78% (2 steps)

Table 1 Polymer-bound selenium promoted synthesis of 2-deoxyglycosides[a]

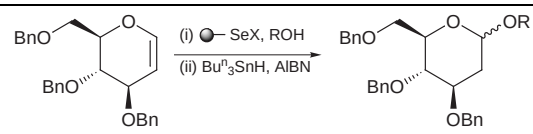

18 **19**

Entry	ROH	Reagent	Solvent	*t*/h	Yield (%)	Ratio α : β
1	BnOH	**2**	CH_2Cl_2	24	87	2 : 1
2	BnOH	**2**	PhMe	24	96	2 : 1
3	BnOH	**2**	MeCN–CH_2Cl_2 (2 : 1)	24	86	5 : 1
4	BnOH	**3**	CH_2Cl_2	48	68	1 : 5
5	BnOH	**3**	PhMe	48	72	1 : 5
6	BnOH	**3**	MeCN–CH_2Cl_2 (2 : 1)	48	23	1 : 1
7	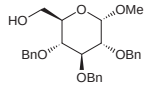	**2**	MeCN–CH_2Cl_2 (2 : 1)	24	61	8 : 1
8	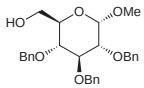	**3**	PhMe	48	45	1 : 1
9	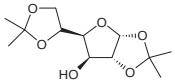	**2**	MeCN–CH_2Cl_2 (2 : 1)	96	50	20 : 1

[a] All reactions were carried out under an atmosphere of argon in the presence of 4 Å molecular sieves. *Reagents and conditions*: i, (for reagent **2)** ROH (1 equiv.), 2,6-di-*tert*-butyl-4-methylpyridine (1 equiv.), **2** (0.5 equiv.); (for reagent **3)** ROH (1 equiv.), CSA (1 equiv.) and **3** (0.5 equiv.); solvent and time as shown in Table; ii, Bu$^n_3$SnH (2 equiv.), AIBN (0.005 equiv.), PhMe, 110 °C, 8 h.

phthalimide reagent **3** was obtained as a yellow resin from **2** by displacement with potassium phthalimide in the presence of 18-crown-6 (> 95% yield),[9] while the lithium selenide **4** (a pale yellow resin) was prepared by $LiBH_4$ reduction of **2** (95% yield). All new reagents appeared to be quite stable in the air at ambient temperature (inert atmosphere is recommended, however, for their storage and use).

Scheme 2 displays chemistry demonstrating the use of resins **2–4** both as solid phase linkers and polymer-bound reagents. Thus, olefin **5** was quantitatively loaded onto the polymer by treatment with the polymer-bound selenium bromide resin **2** and, subsequently, released reductively under the influence of Bu$^n_3$SnH–AIBN (cat.) to recover the starting olefin **5** in 92% overall yield. The polymer-bound selenium bromide **2** was also shown to be as effective as phenylselenium bromide for the known two-step transformation[10] of $PGF_{2\alpha}$ methyl ester **7** to the PGI_2 analogues **8** (94% yield, *ca.* 2 : 1 ratio of C-6 epimers, Scheme 2). Hydration of an olefin was demonstrated to proceed smoothly with the selenium phthalimide resin **3**.[9] Thus, terminal olefin **9** was converted to the regioisomeric alcohols **10** and **11** in 82% overall yield (**10** : **11** *ca.* 2 : 1 ratio) by the action of reagent **3** and CSA in the presence of H_2O, followed by reductive cleavage from the solid support with Bu$^n_3$SnH–AIBN. Furthermore, cyclic olefin **12** was converted to alcohol **13** in 80% overall yield by the same two-step procedure. The use of the resin **4** was demonstrated as follows. Alkyl iodide **14** was efficiently loaded onto the polymer through mild alkylation conditions in THF. The substrate was then released from the polymer (**15**) by either free radical chemistry to obtain the corresponding alkyl compound **16** (89% overall yield) or oxidative conditions leading to olefinic product **17** (78% overall yield).

Table 1 summarizes applications of polymer-bound selenium bromide **2** and selenium phthalimide[11] **3** to the synthesis of 2-deoxyglycosides.[12] Most noteworthy is the inverse glycosidation stereoselectivity obtained under different reaction conditions. Thus, glycosidation of tri-*O*-benzylglucal **18** with BnOH using the polymer-bound selenenyl bromide reagent **2** (X = Br) followed by Bu$^n_3$SnH–AIBN (cat.) cleavage of the newly formed selenium–carbon bond released the 2-deoxy glycosylated product **19** in 86% yield with 5 : 1 selectivity in favor of the α-anomer (entry 3), whereas the same transformation carried out with the polymer-bound selenenyl phthalimide reagent **2** yielded the product in 72% with a 5 : 1 selectivity in favor of the β-anomer (entry 5).

In conclusion, we have successfully prepared a series of polymer-bound selenium reagents/linkers and demonstrated a number of their uses in organic synthesis. These reagents should find useful applications in solid phase and combinatorial synthesis due to their versatility and ease of handling.

We thank Drs Dee H. Huang and Gary Siuzdak for NMR and mass spectroscopic assistance, respectively. This work was financially supported by the Skaggs Institute for Chemical Biology, the National Institutes of Health, USA, and grants from Novartis, Amgen, Pfizer, Merck, DuPont-Merck, Hoffmann LaRoche and Schering-Plough.

Notes and References

† E-mail: kcn@scripps.edu

1 For selected reviews, see: F. Balkenhohl, C. von dem Brussche-Hünnefeld, A. Lansky and C. Zechel, *Angew. Chem., Int. Ed. Engl.*, 1996, **35**, 2288; L. A. Thompson and J. A. Ellman, *Chem. Rev.*, 1996, **96**, 555; M. A. Gallop, R. W. Barret, W. J. Dower, S. P. Foder and E. M. Gorden, *J. Med. Chem.*, 1994, **37**, 1233; E. M. Gorden, R. W. Barret, W. J. Dower, S. P. Foder and M. A. Gallop, *J. Med. Chem.*, 1994, **37**, 1385; W. H. Moos, G. D. Green and M. R. Pavia, *Annu. Rep. Med. Chem.*, 1993, **28**, 315.

2 For general references, see: J. J. Baldwin and I. Henderson, in *Synthesis of Encoded Small Molecule Combinatorial Libraries*, ed. J. P. Delvin, Dekker, New York, NY, 1997; A. W. Czarnick, *Curr. Opin. Chem. Biol.*, 1997, **1**, 60; X. Y. Xiao, C. Zhao, H. Potash and M. P. Nova, *Angew. Chem., Int. Ed. Engl.*, 1997, **37**, 780; P. A. Tempest and R. W. Armstrong, *J Am. Chem. Soc.*, 1997, **119**, 7607.

3 S. W. Kaldor and M. G. Siegel, *Curr. Opin. Chem. Biol.*, 1997, **1**, 101.

4 For reviews of the use of organoselenium reagents in organic synthesis see: K. C. Nicolaou and N. A. Petasis, *Selenium in Natural Product Synthesis*, CIS Inc, Philadelphia, PA, 1984; D. Liotta, *Organoselenium Chemistry*, Wiley, NY, 1986.

5 To the best of our knowledge, this constitutes the first report of the polymer-bound reagents presented herein. For previous preparation of polymer bound selenophenol, phenylselenium chloride and diphenyl selenoxide by copolymerization of 4-vinylselenophenol with divinylbenzene, see: R. Michels, M. Kato and W. Heitz, *Makromol. Chem.*, 1976, **177**, 2311.

6 M. J. Farrall and M. J. Fréchet, *J. Org. Chem.*, 1976, **41**, 3877.

7 For an example of a related reaction, see: C. Lambert, M. Hilbert, L. Christiaens and N. Dereu, *Synth. Commun.*, 1991, **21**, 85.

8 L. Laitem, P. Thibaut and L. Christians, *J. Heterocycl. Chem.*, 1976, **13**, 469.

9 K. C. Nicolaou, D. A. Claremon, W. E. Barnette and S. P. Seitz, *J. Am. Chem. Soc.*, 1979, **101**, 3704.

10 K. C. Nicolaou, W. E. Barnette and R. L. Magolda, *J. Am. Chem. Soc.*, 1981, **103**, 3480.

11 To the best of our knowledge, this is the first example of selenium phthalimide promoted glycosidation.

12 For previous examples of selenium mediated glycosidations, see: G. Jaurand, J.-M. Beau and P. Sinay, *Chem. Commun.*, 1981, 572; M. Peres and J.-M. Beau, *Tetrahedron Lett.*, 1989, **30**, 75; F. Calvani, P. Crotti, C. Gardelli and M. Pineschi, *Tetrahedron Lett.*, 1994, **50**, 12 999; W. R. Roush and X.-F. Lin, *J. Am. Chem. Soc.*, 1995, **117**, 2236.

Received in Corvallis, OR, USA, 23rd June 1998; 8/04795B

Catalytic oxidation of alkyl aromatics using a novel silica supported Schiff base complex

Ian C. Chisem,[a] John Rafelt,[a] M. Tantoh Shieh,[b] Janet Chisem (née Bovey),[a] James H. Clark,*[a]† Roshan Jachuck,[b] Duncan Macquarrie,[a] Colin Ramshaw[b] and Keith Scott[b]

[a] *Department of Chemistry, University of York, Heslington, York, UK YO10 5DD*
[b] *Department of Chemical and Process Engineering, University of Newcastle-upon-Tyne, Newcastle-upon-Tyne, UK NE1 7RU*

A new heterogeneous catalyst based on a chemically modified mesoporous silica gel and possessing immobilised chromium ions has been prepared and successfully applied to the aerial oxidation of alkyl aromatics at atmospheric pressure and in the absence of solvent.

The oxidation of organic substrates provides routes to a wide range of functionalised molecules. Traditional methods involve the use of large quantities of poisonous high oxidation state Cr, Mn and Os reagents.[1] Lower oxidation state metals such as Co^{II}, Mn^{II} and Cu^{II} in AcOH may be used[2] with O_2 as the consumable oxidant. However, the conditions are often harsh, the reagent mixture is corrosive (bromide is used as a promoter), and the chemistry is rarely selective. Environmentally acceptable catalytic oxidations that operate under moderate conditions in the liquid phase with high selectivity are clearly desirable. A range of supported reagents has been used in the liquid phase oxidation of organic substrates. Advantages of supported reagents include ease of handling, use and recovery, low toxicity and the avoidance of solvents. However, in oxidations, supported reagents have generally acted as *stoichiometric* reagents, making their large scale use difficult and expensive. We have proven the possibility of developing genuinely *catalytic* supported reagents which are active in some oxidations.[3,4] More recently, catalysts based on chemically modified silicas, which have higher catalytic site densities, have been prepared.[5,6] We now report a novel heterogeneous catalyst for the liquid phase partial oxidation of alkyl aromatic substrates based on a chemically modified mesoporous silica gel which possesses significantly enhanced activity. The material strongly binds chromium ions and is robust, reusable and active in the oxidation of ethylbenzene and methyl aromatics.

The preparation of the chromium catalyst (CHRISS) is shown in Scheme 1. Salicylaldehyde (1 equiv.) was added to excess absolute EtOH, to which 3-aminopropyl(trimethoxy)silane (1 equiv.) was added. The solution instantly became yellow due to imine formation. Chromium(III) acetate (0.5 equiv.) was then added to the solution, and the mixture stirred for a further 30 min to allow the new ligands to complex the chromium. The silica (Kieselgel 100) was then added and the mixture stirred overnight. The final product was washed with water, EtOH and finally Et_2O until the washings were colourless. Further drying of the solid product was carried out on a rotary evaporator at 70 °C for 2 h. The loading achieved is *ca.* 0.10 mmol g^{-1} [determined by atomic absorption spectroscopy (AAS)]. The catalyst has an average pore size of 100 Å and a particle size of 30–140 μm. The infrared spectrum of the free ligand (*i.e.* prior to complexation with the metal) shows a band at 1642 cm^{-1} attributed to the C=N stretching vibration of the imine. This is reduced to 1593 cm^{-1} upon complexation of Cr^{3+}. Apart from bands in the 250–450 nm region, the diffuse reflectance UV spectrum of the catalyst shows a band at *ca.* 600 nm corresponding to d-d transition for the metal complex. The band is shifted to higher wavelength by about 30 nm from the corresponding band in pure $Cr(OAc)_3$ or $Cr(OAc)_3$ physisorbed on silica, consistent with a change in ligand environment.

The catalytic oxidation of ethylbenzene (used as a model substrate) was carried out in neat substrate using 1.5 g catalyst and air as the consumable source of oxygen. The reaction was performed in a baffled glass reactor with overhead stirring and fitted with a Dean–Stark trap to facilitate the removal of water from the reactor. After a short induction period the conversion rate in the first 5 h of operation was *ca.* 5% h^{-1}, corresponding to a frequency of 1225 turnovers h^{-1} per catalytic site (assuming 0.10 mmol g^{-1} loading of the active site). After the first 5 h, the rate of conversion dropped significantly; this is attributed to the inefficient removal of water from the reaction system, and poor adsorption of ethylbenzene onto the catalyst surface as the acetophenone concentration increases. In addition, catalyst reuse studies were performed by recycling 1.5 g of catalyst twice without any regeneration or conditioning by decanting the liquid from the reactor and adding fresh substrate and then repeating the experiment. The results shown in Fig. 1 demonstrate that the recycled catalyst retains its activity and the catalytic rate is equal to that of the fresh catalyst. Furthermore, the induction period observed with the use of fresh catalyst was eliminated when the catalyst was recycled. This suggests that poor product desorption when the catalyst is not saturated with the product was the cause of the induction periods observed.

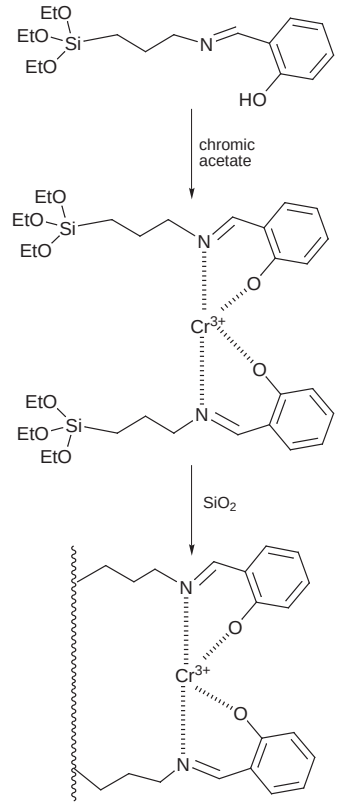

Scheme 1

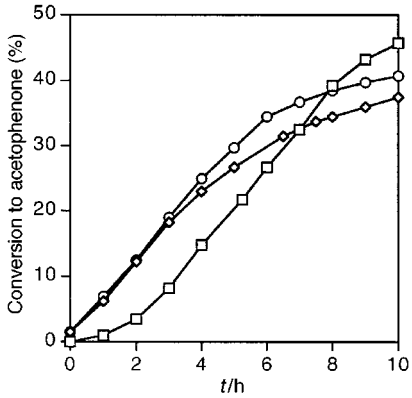

Fig. 1 Production of acetophenone in the oxidation of ethylbenzene using 5 g of the immobilised chromium on silica catalyst: (□) fresh catalyst, (○) first recycle and (◇) second recycle

After 5 h the activity of the recycled catalyst begins to decrease; the effect is more pronounced on the second recycle. The reason for this deactivation is not fully understood. Further reuse studies are in progress, including regeneration and conditioning of spent catalyst.

It is believed that the imprinted method of synthesis allows the chromium to become very tightly bound to the support. To verify that oxidation is occurring due to heterogeneous catalysis, several test reactions were carried out which were designed to encourage the formation of leached chromium. In one test reaction, an unimprinted version of the catalyst was made. Unlike the original catalyst, where the ligands are complexed with the metal and then grafted onto the silica support, the unimprinted version involves the grafting of the ligands before the complexation with the metal ions. This method of production gave a lower loading (0.05 mmol g^{-1} by AAS) and it is likely that the metal–ligand binding is significantly reduced in strength due to the less favourable spatial orientation of the ligands on the surface, leading to a less robust catalyst. In the second experiment, a catalyst based on physisorbed chromium(III) on the silica surface was made. The catalyst was formed by dissolving chromium(III) in EtOH, and stirring with the silica gel. The solvent was then removed by rotary evaporation, leaving a grey solid. The results shown in Fig. 2 indicate that the imprinted version of the CHRISS catalyst is the most active of the species studied. Both the unimprinted and the physisorbed materials show little activity above that of a control reaction, containing no catalyst.

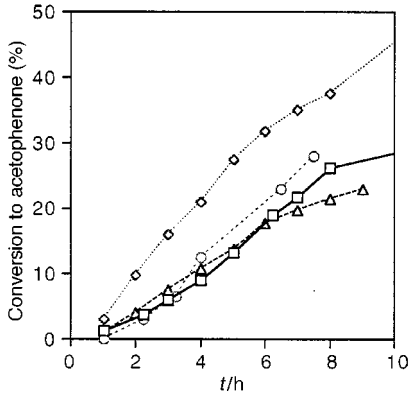

Fig. 2 Production of acetophenone in the oxidation of ethylbenzene using (□) an unimprinted catalyst, (○) a physisorbed chromium(III) catalyst, (◇) the imprinted catalyst and (△) no catalyst

We have successfully extended catalytic chemistry to the commercially important oxidation of methyl aromatics. *p*-Chlorotoluene, *p*-xylene and *o*-xylene all undergo aerial oxidation at atmospheric pressure in neat substrate with the supported chromium catalyst (Table 1). Again it was necessary to prove that the catalysis was not due to leached chromium. Following the method described by Lempers and Sheldon,[7] a *p*-xylene reaction was hot filtered after 1 h (*i.e.* at an early stage of the reaction) to remove the catalyst. The reaction was then restarted without the catalyst, and the product isolated after 24 h. The reaction yielded 15 g of *p*-toluic acid (compared to 166 g from the reaction with CHRISS) which corresponds to the amount formed during an oxidation without the catalyst, *i.e.* the formed product is due to autoxidation. Analysis of the reaction mixture after hot filtration of the catalyst showed < 0.5 ppm of chromium.‡

Table 1 Oxidation reactions using CHRISS[a]

Substrate	*T*/°C	Product(s)	Isolated yield (%)
Ethylbenzene	130	acetophenone	50
p-Xylene	138	*p*-toluic acid	29
		terephthalic acid	5
o-Xylene	145	*o*-toluic acid	7
p-Chlorotoluene	130	*p*-chlorobenzoic acid	12

[a] Reactions were carried out using the supported chromium catalyst (1.5 g) in neat substrate (4.1 mol) with an air feed rate of 800 ml min^{-1} and an agitation rate of 1500 rpm, for a period of 24 h.

The activity of the catalyst is significantly greater than the commercial supported chromium catalyst and other supported reagents based on chemically modified surfaces.[3–6] The fact that we were not able to detect Cr, that experiments with less-robustly held catalysts proceeded at the background rate, and that the reaction after filtration failed to exceed the background rate leads us to believe that the active species is the surface bound Cr complex. The efficiency of the catalytic systems, the use of air as the only consumable source of oxygen and the avoidance of solvent makes them excellent examples of environmentally friendly processes.

The financial support of the EPSRC Clean Technology Unit is gratefully acknowledged. We also thank the Royal Academy of Engineering for a Clean Technology Fellowship (to J. H. C.) and the Royal Society for a University Research Fellowship (to D. J. M.).

Notes and References

† E-mail: jhc1@york.ac.uk

‡ Metal analysis was undertaken by AAS, with a detection limit of 0.5 ppm.

1 J. Muzart, *Chem. Rev.*, 1992, **92**, 113.
2 K. Weissermel and H.-J. Arpe, *Industrial Organic Chemistry*, 2nd edn, VCH, Weinheim, 1993.
3 J. H. Clark, A. P. Landon, D. J. Macquarrie and K. Martin, *J. Chem. Soc., Chem. Commun.*, 1989, 1355.
4 Envirocats, Contract Catalysts, Knowsley Industrial Park, Prescot, Merseyside.
5 J. H.Clark and D. J. Macquarrie, *Chem. Soc. Rev.*, 1996, 303.
6 J. Chisem, I. C. Chisem, J. S. Rafelt, D. J. Macquarrie and J. H. Clark, *Chem. Commun.*, 1997, 2203.
7 H. E. B. Lempers and R. A. Sheldon, *J. Catal.*, 1998, **175**, 62.

Received in Cambridge, UK, 13th July 1998; 8/05420G

The synthesis and aggregation properties of a novel anionic gemini surfactant

Kevin Jennings,[a] Ian Marshall,[a] Helen Birrell,[a] Andrew Edwards,[a] Neville Haskins,[a] Olle Sodermann,[b] Anthony J. Kirby[c] and Patrick Camilleri*[a]†

[a] *SmithKline Beecham Pharmaceuticals, New Frontiers Science Park, Third Avenue, Harlow, Essex, UK CM19 5AW*
[b] *Physical Chemistry 1, University of Lund, PO Box 124, S-221 00, Lund, Sweden*
[c] *University Chemical Laboratory, Lensfield Road, Cambridge, UK CB2 1EW*

The aggregation of a peptide-based anionic gemini surfactant has been found to be highly dependent on the environment in which this property is measured; dimensions of aggregates varied from those generally observed in micellar species to those in fibrillar material.

About 25 years ago a rather unusual type of surfactant molecule consisting of dimeric amphiphiles, made up of two long hydrocarbon chains and two ionic groups linked by a spacer, was reported by Bunton *et al.*[1] The name 'gemini' was used by Menger in 1991 to identify these detergents.[2]

The unusual structures of gemini surfactants result in surface and bulk properties that differ from those observed for more conventional single-chain monomeric surfactants having the same number of carbon atoms per polar 'head' group. Thus whereas monomeric surfactants tend to form spherical micelles in dilute solution, geminis usually form thread-like aggregates. Geminis generally have lower critical micelle concentration (cmc) values; their foaming and wetting properties are excellent, resulting in a more efficient lowering of the surface tension of water; they also show unexpected viscosity changes as their concentration is increased.

Most gemini surfactants synthesised over recent years contained bisphosphate or bis(quaternary ammonium) ionic groups linked by spacers ranging from a rigid aromatic group to a more flexible short aliphatic chain. The length of the saturated hydrocarbon tails has ranged from 8 to 18 carbon atoms. The length, flexibility and polarity of the linker group can have a profound effect on the resulting shapes of aggregates formed by gemini surfactants.[2,3]

We have synthesised a peptide-based gemini surfactant **1,** starting from the reaction of L-cysteine with dibromoethane to form the bisthioether. Reaction of the latter with Boc-protected glycine-*O*-succinimide, followed by deprotection, gave compound **2**. This reacted further as shown in Scheme 1 to give **1** as the dipotassium salt. The structure of **1** was confirmed by its ^{1}H and ^{13}C NMR spectra, measured in D_2O. A FAB mass spectrum of **1** in a glycerol matrix, scanning in negative ion mode, gave an isotopic distribution corresponding to the calculated pattern fitting $C_{40}H_{74}N_{6O}O_{12}S_4K$, as shown in Fig. 1.

Gemini **1** was soluble in aqueous media even at neutral pH. The presence of **1** in solutions of the hydrochloride of 1-(1,3-dichloro-6-trifluoromethyl-9-phenanthryl)-3-dibutylaminopropan-1-ol, an anti-malarial drug known as halofantrine and marketed by SmithKline Beecham,[4] caused a substantial change in the fluorescence spectrum of this compound (Fig. 2). From a plot (not shown) of the increase in the intensity of this drug with the increase of the concentration of **1**, an approximate measurement of the cmc was obtained as 10^{-4} mol dm^{-3}. This value is lower than those reported for single hydrocarbon chain surfactants, such as sodium dodecyl sulphate, where the cmc was measured[5] as 7×10^{-3} mol dm^{-3}. Low cmc values have been reported for other gemini surfactants.[2] Fig. 2(*c*) shows that the intensity of the spectrum of halofantrine increases substantially on standing for 24 h, indicating that the organisation of micelles had changed during this period. Electron micros-

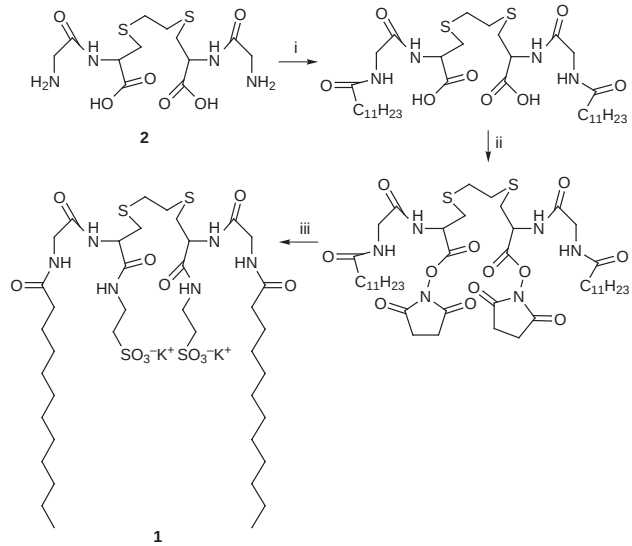

Scheme 1 *Reagents*: i, $C_{11}H_{23}COCl$, NaOH, H_2O; ii, *N*-hydroxysuccinimide, DCC, THF; iii, taurine, K_2CO_3, H_2O, THF

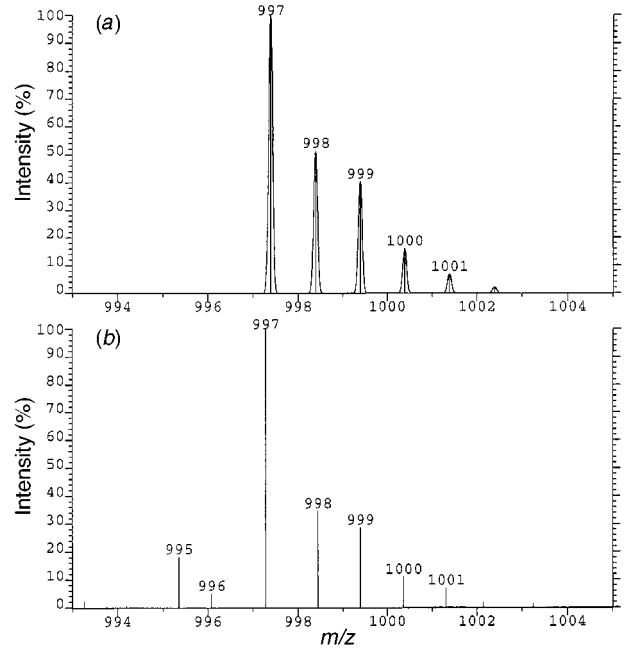

Fig. 1 FAB mass spectrum of **1**: (*a*) calculated and (*b*) experimental isotopic distribution. The spectrum was obtained using a Micromass 70-VSEQ mass spectrometer, negative ionization effected by a primary beam of caesium ions.

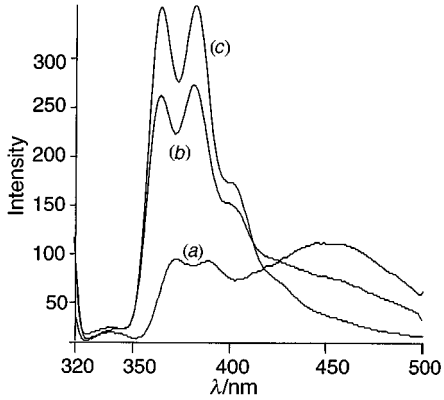

Fig. 2 Emission spectra (λ_{ex} 310 nm) of a 10 μM solution of halofantrine: (*a*) in water, (*b*) in water containing 1 mg ml^{-1} of **1** (fresh solution) and (c) in water containing 1 mg ml^{-1} of **1** (24 h standing). Spectra were recorded on a Perkin-Elmer LS50 spectrofluorimeter.

copy measurements (see later) confirm morphological changes in the organisation of micelles at periods shorter than 24 h.

The diffusion coefficient of **1** was measured as 5.2×10^{-11} m^2 s^{-1} by carrying out diffusion experiments on a sample which was 0.1% (1 mg ml^{-1}) by weight. This value indicated the presence of rather small micelles with a hydrodynamic radius of about 3.5 nm. As the cmc is so low, the diffusion coefficient measured is that of the micelles, with a negligible contribution from the free surfactant.

Attempts to study the morphology of these micelles (1 mg ml^{-1}) in deionised water by transmission electron microscopy (TEM) by negative staining (using 5% w/v ammonium molybdate containing 1% w/v trehalose) at early time points after preparation proved problematic due to surfactant/stain interactions and poor sample spreading; images were obtained that showed discrete globular structures 3 to 5 nm in diameter and globular strings, ~40 nm in length [Fig. 3(A)]. Further analysis of the surfactant solutions after storage at 4 °C for 24 h or longer periods proved easier to prepare by spreading on a grid and staining.

TEM analysis of this aged solution by negative staining gave distinct fibrillar/ribbon structures with periodic 'twist-like' features [Fig. 3(B)]. Fibrils appeared in excess of 10 μm long and ranged between 6 ± 1.5 (n = 23) and 40 ± 13 nm (n = 11) in width. Three populations were identified based on the periodic features exhibited. Low numbers of flat ribbon-like fibrils with irregular spaced twists were seen interspersed among fibrils with 145 ± 23 nm (n = 37) periodicity and a smaller population of shorter 63 ± 8nm (n = 23) period fibrils.

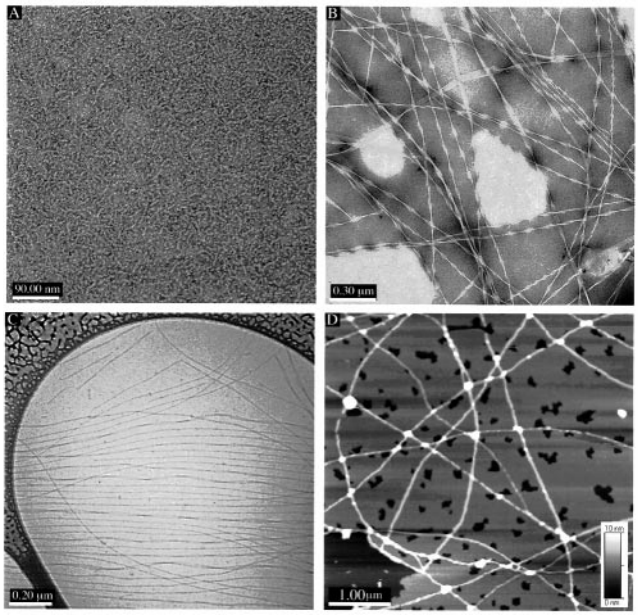

Fig. 3 (A) Negative stained TEM images of **1** immediately after dissolution; (B) negative stained TEM images recorded after 21 h; (C) cryogenic TEM images recorded after 9 days dissolution; and (D) AFM images of surfactant dried onto mica (sample taken from a solution which was 6 h old). TEM and AFM images were obtained using a Hitachi H7100 microscope and a TopoMetrix Explorer microscope, respectively.

Cryogenic transmission electron microscopy (TEM) of samples incubated at 4 °C for 9 days confirmed the presence of fibrils similar to those seen by negative staining after 24 h [Fig. 3(C)]. Fewer fibrils showed periodic features than were seen by negative staining—those present also appeared longer at 211 ± 4 nm (n = 20). Other fibrils (10–20 nm wide) appeared to lack any periodicity. A noticeable inter-fibrillar regular parallel spacing of 20 to 40 nm observed may reflect electrostatic repulsion between surfactant anionic head groups in aqueous solution.

Atomic force microscopy (AFM) images of **1** were also obtained for samples, dried on mica from filtered deionised water, immediately after dissolution and 6 h after dissolution. Images of surfactant immediately after dissolution showed orientated fibrils on top of a relatively flat substructure. Fibrils showed heights of 0.3–0.5 nm above the underlying structure and widths of 37 ± 8 nm. Spreading artefacts due to drying would be expected to result in underestimates of fibril height and overestimates of fibril width (due to tip-sample interactions).

At 6 h after dissolution [Fig. 3(D)] three distinct morphologies were observed by AFM for dried surfactant: sheets, *ca.* 3–4 nm in thickness; globules, 44 nm ± 14 nm (n = 12) in cross-section and 1–5 nm in height; and fibrils, 48 nm ± 10 nm (n = 8) in cross-section and 2–5 nm in height. Fibrils were found to settle predominantly on top of the underlying sheets: areas of exposed mica were largely free of fibrils or contained fibril fragments. This may reflect the strong electrostatic repulsion between the anionic head groups, which would be expected to lie on the outer surface of fibrils in aqueous solution, and the negatively charged mica surface. Approximately 80% of fibrils displayed clear periodicity (mean periodic length = 106 ± 18 nm; n = 8). Periodic features were conserved when the scan direction was rotated through 90° (data not shown) suggesting that it was not caused by a scanning artefact.

The disappearance of smaller fibrils and the appearance of larger, periodic fibrils with time is consistent with a time-dependent aggregation/twisting of early fibrils into larger structures. The fibrilisation phenomena, observed in the TEM and AFM analysis of aggregates of **1,** are reminiscent of those observed in the aggregation of β-amyloid protein (β-AP),[6] which has been implicated in the development of Alzeimer's disease. β-AP contains both hydrophobic and hydrophilic peptide sequences, and has been reported to have micellar properties.[7] Further studies are in progress aimed at identifying the structural features of **1** that lead to the observed aggregation properties.

Notes and References

† E-mail: Patrick_Camilleri@sbphrd.com

1 C. A. Bunton, L. Robinson, J. Schaak and M. F. Stam, *J. Org. Chem.*, 1971, **36**, 2346.
2 F. M. Menger and C. A. Littau, *J. Am. Chem. Soc.*, 1993, **115**, 10 083.
3 M. J. Rosen, *Chemtech*, 1993, **23**, 30.
4 J. P. Coulard, J. Le Bras, S. Matheron, B. Moriniere, M. G. Siamot and J. F. Rossignol, *Trans. R. Soc. Trop. Med. Hyg.*, 1986, **80**, 615.
5 P. Camilleri and G. N. Okafo, *J. Chem. Soc., Chem. Commun.*, 1992, 530.
6 D. D. Howlett, K. H. Jennings, D. C. Lee, M. S. G. Clark, F. Brown, R. B. Wetzel, S. J. Wood, P. Camilleri and G. W. Roberts, *Neurodegeneration*, 1995, **4**, 23.
7 B. Soreghan, J. Kosmoski and C. Glabe, *J. Biol. Chem.*, 1994, **269**, 28 551.

Received in Cambridge, UK, 10th July 1998; 8/05394D

Metal catalyst-free by design. The synthesis of amides from alkyl iodides, carbon monoxide and amines by a hybrid radical/ionic reaction

Ilhyong Ryu,*† Kiyoto Nagahara, Nobuaki Kambe, Noboru Sonoda,‡ Sergio Kreimerman and Mitsuo Komatsu

Department of Applied Chemistry, Faculty of Engineering, Osaka University, Suita, Osaka 565-0871, Japan

Amides can be synthesized from alkyl iodides and amines in the presence of CO (20–25 atm), without using transition metal catalyst; the radical cascade is initiated thermally using AIBN and allyltributyltin.

Transition metal catalysts facilitate many useful synthetic transformations. However, metal catalyst-free procedures, which do not require complicated techniques for recovering the expensive metals and ligands, would have a distinct advantage.[1] We recently discovered that irradiation conditions enable us to synthesize carboxylic acid esters from alkyl iodides, CO, and ROH.[2] This ester synthesis represents an intriguing example of a reaction which was previously possible only in the presence of a catalyst, but can now be carried out under metal catalyst-free conditions. The role of irradiation was unclear, especially as to whether it was generating an alkyl/iodine radical pair in a non-chain process or simply initiated a radical chain process. Here we report the synthesis of amides from alkyl iodides, CO and amines under thermal initiation conditions [eqn. (1)], expanding the utility of the metal catalyst-free approach and demonstrating the involvement of a radical *chain* transfer step in this hybrid radical/ionic reaction.

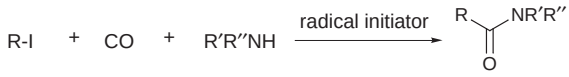

(1)

Thermally initiated conditions for the catalyst-free synthesis of amides were examined for the conversion of 2-iodooctane **1a**, diethylamine, and CO into *N*,*N*-diethyl amide **2** [eqn. (2)]. No reaction took place under thermal conditions without a radical initiator. However, the results with conventional radical initiators, such as AIBN and BPO, were disappointing, since only low yields of the desired **2** were obtained. For example, when a hexane solution of **1a** and Et_2NH was heated under 25 atm of CO at 80 °C for 8 h in the presence of AIBN (30 mol%), **2** was obtained in 10% yield. A dramatic increase in the yield of **2** up to 91% was achieved when both AIBN (25 mol%) and allyltributyltin (10 mol%) were used. The combination of AIBN and tris(trimethylsilyl)silane also gave a good result but AIBN–tributyltin hydride gave inferior results. On the other hand, in the presence of 20 mol% of galvinoxyl, the reaction was inhibited, and 81% of iodide **1a** was recovered. These results convinced us that the pathway by which amide **2** is formed includes a radical *chain* transfer.

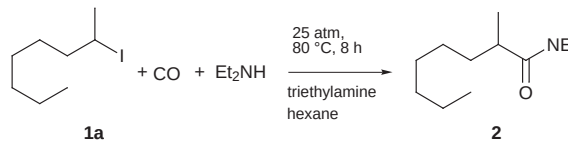

1a **2** (2)

no initiator	0%
AIBN (30 mol%)	10%
BPO (20 mol%)	17%
AIBN (25 mol%), allyltributyltin (10 mol%)	91%
AIBN (25 mol%), allyltributyltin (10 mol%), galvinoxyl (20 mol%)	5%
AIBN (25 mol%), $(TMS)_3SiH$ (20 mol%)	80%
AIBN (30 mol%), Bu_3SnH (30 mol%)	43%

Encouraged by the above results, we then examined the generality of the amide synthesis using AIBN–allyltin as thermal initiator. Table 1 shows that amides can be successfully prepared from RI, medium pressure CO (20–25 atm) and amines.[3] In general triethylamine was added as a base to trap HI, whereas in entry 3, for convenience 2 equiv. of the amine were used as both nucleophile and base. Solvents can be varied, and even in the case where MeOH was used as the solvent, the amide was the only product of the carbonylation reaction (entry 4). Both primary and secondary amines were useful. In general carbonylation of tertiary radicals is relatively inefficient compared with secondary and primary alkyl radicals due to the facile reverse reaction.[4,5] However, the unique radical/ionic cooperation driving the carbonylation/decarbonylation equilibrium in the forward direction could provide an enormous advantage for the carbonylation of tertiary radicals. Using bis(2-ethylhexyl)amine, diamide **8** was prepared (entry 7). On the other hand, when an *o*-aminobenzyl alcohol was treated with **1d**, an *N*-acylated product **10** was obtained (entry 9). In these examples, standard flash chromatography on silica gel was used for the isolation of products, whereas in one case, Renaud's recently reported procedure for removing small amounts of tin residue was tested and found to be convenient (entry 8).[6]

It should be noted that the use of irradiation conditions, which were employed in our previous study,[2] can also be used for the amide synthesis, and are especially useful for the reaction of primary alkyl iodides.[7] Scheme 1 illustrates the three step

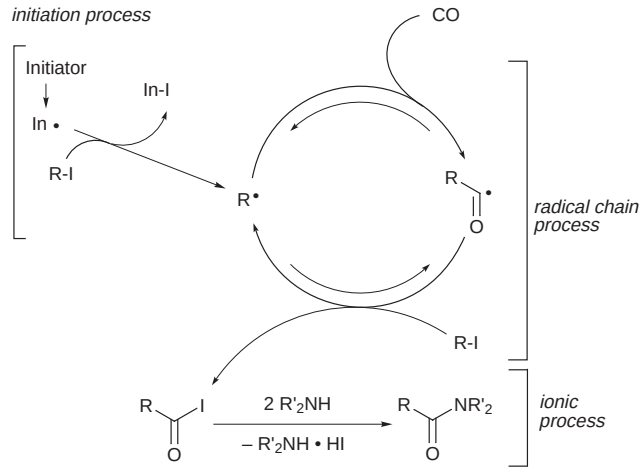

Scheme 1

Table 1 Amide synthesis *via* catalyst-free carbonylation of alkyl iodides[a]

Entry	Alkyl iodide	Amine (equiv.)/ solvent/conditions	Product	Yield (%)[b]
1	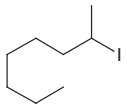 **1a**	Et_2NH (0.9) Et_3N (1.3) hexane (0.5 ml) 80 °C, 8 h CO (25 atm)	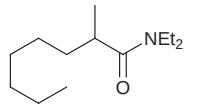 **2**	89
2	**1a**	n-$C_6H_{13}NH_2$ (1.1) Et_3N (1.1) hexane (0.5 ml) 80 °C, 8 h CO (20 atm)	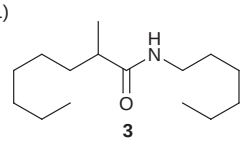 **3**	60[c]
3	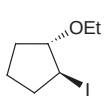 **1b**	Et_2NH (2.3) hexane (0.5 ml) 80 °C, 8 h CO (20 atm)	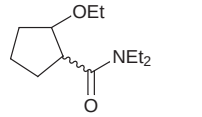 **4** (*trans*:*cis* = 85:15)	82
4[d]	 **1c**	piperazine Et_3N (3.0) MeOH (1 ml) 80 °C, 10h CO (20 atm)	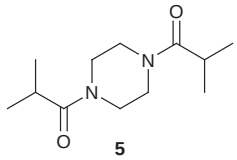 **5**	57
5	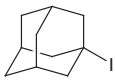 **1d**	$PhNH_2$ (1.0) Et_3N (1.3) MeCN (0.5 ml) 80 °C, 8 h CO (20 atm)	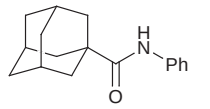 **6**	96
6	**1d**	Et_2NH (0.9) Et_3N (1.5) hexane (0.5 ml) 80 °C, 8 h CO (20 atm)	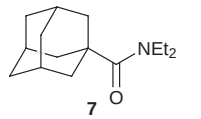 **7**	80
7	 **1e**	bis(2-ethylhexyl)-amine (0.5) Et_3N (1.5) hexane (0.5 ml) 80 °C, 8 h CO (20 atm)	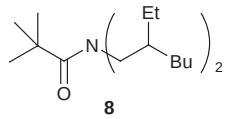 **8**	97
8	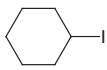 **1f**	Bu_2NH (1.0) Et_3N (1.3) hexane (0.5 ml) 90 °C, 8 h CO (20 atm)	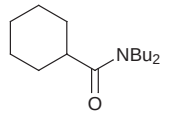 **9**	74[e]
9	**1d**	*o*-amino benzyl-alcohol(1.0) Et_3N (1.3) MeCN (0.5 ml) 80 °C, 10 h CO (25 atm)	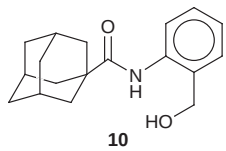 **10**	52

[a] In general reactions were conducted on 1 mmol scale with AIBN (20–30 mol%)–allyltributyltin (10%) as initiator. For typical procedure: see ref. 3. [b] Yields after isolation by chromatography on silica gel. [c] *N*-Hexyl-*N*-(1-methylheptyl)amine was formed as a by-product by direct aminolysis. [d] Molar ratio: **1c**:piperazine:Et_3N = 2.5:1.0:3.0. [e] Renaud's NaOH workup (ref. 6) was performed to eliminate tin residues.

mechanism: (i) radical initiation *via* either irradiation or thermal initiator, (ii) radical chain propagation, composed of two reversible type radical reactions (carbonylation and iodine atom transfer), and (iii) ionic quenching to shift the equilibria of the reversible radical reactions.

In this study, we have achieved a new metal-free synthesis of amides from organic iodides, CO and amines using AIBN and allyltributyltin, which previously could only be accomplished in the presence of a transition metal catalyst.[8] We are now examining the applications of this approach to bifunctional substrates which hold promise for the synthesis of a variety of nitrogen heterocycles and designed polyamides.

This work was supported by a Grant-in Aid for Scientific Research on Priority Areas (No. 09238232) from the Ministry of Education, Science, Sports and Culture of Japan. Thanks are due to the Instrumental Analysis Center, Faculty of Engineering, Osaka University, for assistance in obtaining 600 MHz NMR, HRMS and elemental analyses. I. R. thanks the Sumitomo Foundation for financial support. K. N. is grateful to JSPS Research Fellowships for Young Scientists. S. K. thanks the Ministry of Education, Science, Sports and Culture of Japan for the scholarship.

Notes and References

† E-mail: ryu@chem.eng.osaka-u.ac.jp
‡ Present Address: Department of Applied Chemistry, Faculty of Engineering, Kansai University, Suita, Osaka 564-0073, Japan

1 For recent progress in the efficient recovery of catalysts including fluorous biphasic systems, see J. A. Gladysz, *Science*, 1994, **266**, 55; I. T. Horváth and J. Rábai, *Science*, 1994, **266**, 72; J. J. J. Juliette, I. T. Horváth and J. A. Gladysz, *Angew. Chem., Int. Ed. Engl.*, 1997, **36**, 1610. Also see a related review: D. P. Curran, *Angew. Chem., Int. Ed.*, 1998, **37**, 1174.
2 K. Nagahara, I. Ryu, M. Komatsu and N. Sonoda, *J. Am. Chem. Soc.*, 1997, **119**, 5465.
3 General procedure: A magnetic stirring bar, AIBN (0.3 mmol), hexane (0.5 ml), allyltributyltin (0.1 mmol), alkyl iodide **1a** (1 mmol), triethylamine (1.3 mmol) and amine (1.2 mmol) were placed in a 50 ml stainless steel autoclave with a glass liner. The autoclave was closed, purged twice with CO, pressurized with 25 atm of CO and then heated with stirring at 80 °C for 8 h. Excess CO was discharged at room temperature. Washing the crude mixture with MeCN (10 ml) followed by precipitation of ammonium salts in Et_2O (40 ml), filtration, evaporation of filtrate and column chromatography on silica gel gave pure amide **2**.
4 Rapid decarbonylation rates (10^5 to 10^6 s^{-1} at room temp.) of pivaloyl radical are known, see: Y. P. Tsentalovich and H. Fischer, *J. Chem. Soc., Perkin Trans. 2*, 1994, 729; C. E. Brown, A. G. Neville, D. M. Rayner, K. U. Ingold and L. Lusztyk, *Aust. J. Chem.*, 1995, **48**, 363; C. Chatgilialoglu, C. Ferreri, M. Lucarini, P. Pedrielli and G. F. Pedulli, *Organometallics*, 1995, **14**, 2672.
5 I. Ryu and N. Sonoda, *Angew. Chem., Int. Ed. Engl.*, 1996, **35**, 1050.
6 P. Renaud, E. Lacôte and L. Quaranta, *Tetrahedron Lett.*, 1998, **39**, 2123.
7 Reaction of primary alkyl iodides under thermal initiation conditions suffers from direct aminolysis.
8 For examples of amide synthesis by catalytic carbonylation, see A. Schoenberg and R. F. Heck, *J. Org. Chem.*, 1974, **39**, 3327; T. Kobayashi and M. Tanaka, *J. Organomet. Chem.*, 1982, **231**, C12; T. Kobayashi and M. Tanaka, *J. Organomet. Chem.*, 1982, **233**, C64; F. Ozawa, H. Soyama, T. Yamamoto and A. Yamamoto, *Tetrahedron Lett.*,1982, **23**, 3383; T. Kondo, Y. Sone, Y. Tsuji and Y. Watanabe, *J. Organomet. Chem.*, 1994, **473**, 163. Also see a related review: A. Yamamoto, *Bull. Chem. Soc. Jpn.*, 1995, **68**, 433.

Received in Cambridge, UK, 27th July 1998; 8/05815F

Serinal-derived vinyl oxiranes as novel and versatile building blocks for the stereoselective synthesis of D- and L-*erythro*-sphingosines

Christian Hertweck,[a] Helmar Goerls[b] and Wilhelm Boland*[a]†

[a] *Max-Planck-Institute for Chemical Ecology, Tatzendpromenade 1a, D-07745 Jena, Germany*
[b] *Institute for Inorganic and Analytical Chemistry, Friedrich-Schiller-University, Jena, Germany*

Oxazolidine vinyl oxirane 1, a novel and highly versatile building block for the preparation of enantiopure D-(+)-*erythro*-sphingosine and analogues, has been prepared by chloroallylboration of the Garner aldehyde with absolute stereocontrol and in good yield.

Over the last decade, interest in the biological functions of sphingosine, and its derivatives, has increased dramatically. While ceramide has been shown to be an important regulatory component of programmed cell death,[1] sphingosine-1-phosphate (SPP) has been implicated as a secondary messenger in cell proliferation and survival.[2] In addition, sphingosine and its N-methylated derivatives were found to be involved in cell signalling,[3] the induction of cancer cell apoptosis[4] and in the regulation of inflammatory processes.[5] Since the biological activity of these molecules varies substantially with structural modifications of the alkyl side chain,[6] unnatural and functionalized sphingosines are an inviting target for synthesis.

Many protocols for sphingoid base synthesis have been reported.[7] However, a versatile building block, easily accessible in high optical purity, that may be linked to a large variety of functionalized residues has not been available to date. Here, we report the synthesis of such a precursor, vinyl oxirane **1**, that leads directly to isomerically pure protected sphingoid bases, without the need for further synthetic manipulations of the side chain (Scheme 1).

Following the protocol of Oehlschlager, readily available and configurationally stable L-Garner aldehyde **3**[8] was alkylated with an *in situ* formed γ-(*Z*)-chloroallyl-(+)-diisopinocampheylborane **5**[9] to give chlorohydrin **4** in good yield (72% after cleavage of the borinic ester with 8-hydroxyquinoline,[10] 68% after buffered oxidative work-up[11]) (Scheme 2). Subsequent treatment of **4** with a sterically hindered base (DBU) provided vinyl oxirane **1** in high yield under mild conditions.[12] Analyses of ^{1}H and ^{13}C NMR spectra of the crude reaction mixture showed the relative diastereoselectivity to be higher than 97:3 (*anti*:*syn*), which clearly resulted from matched stereochemical bias of the double diastereoselection. With achiral γ-chloroallyl-BBN,[9] similar diastereospecificity was observed, resulting from substrate controlled *si*-facial attack of the allylation reagent. Thus, use of 9-MeO-9-BBN is an inexpensive alternative to the pinene-based borane, provided that a slightly lower degree of diastereoselection (*anti*:*syn* = 95:5), and the formation of *trans*-**1** (4%) as a by-product, is acceptable. Irrespective of the borane used, the entire sequence could be conducted as a 'one-pot' synthesis with an overall yield of 48–57% starting from **3**. Moreover, the protocol does not require tedious purification of any of the intermediates between commercially available serine and the vinyl oxirane building block **1**, and is suitable for multigram synthesis.[8] Upon recrystallisation of the crude product, colourless needles [mp 49–50.5 °C (pentane–Et_2O = 1:1 v/v)]; $[\alpha]_D^{25}$ +40.37 (*c* 1.08, $CHCl_3$)] were obtained and, in all cases, only a single isomer could be detected by NMR spectroscopy. The ORTEP plot (Fig. 1) shows the X-ray structure‡ of vinyl oxirane **1**. The crystal structure shown and semiempirical calculations of the energy minimised conformation of **1** (data not shown) proved to be in good agreement. Both the ORTEP and energy minimised plots

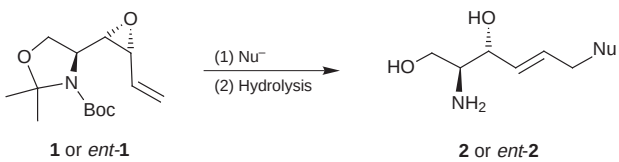

1 or *ent*-**1** **2** or *ent*-**2**

Scheme 1

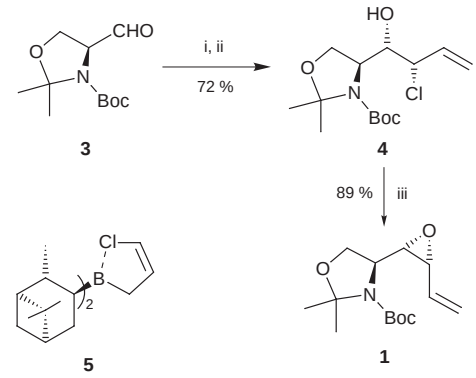

Scheme 2 *Reagents and conditions*: i, (+)-Ipc_2BOMe (or 9-MeO-9-BBN), allyl chloride, Et_2O, Cy_2NLi, THF, $BF_3{\cdot}OEt_2$, −100 °C; ii, 8-hydroxyquinoline, MeOH or H_2O_2, $NaHCO_3$ buffer; iii, DBU, CH_2Cl_2, 0 °C

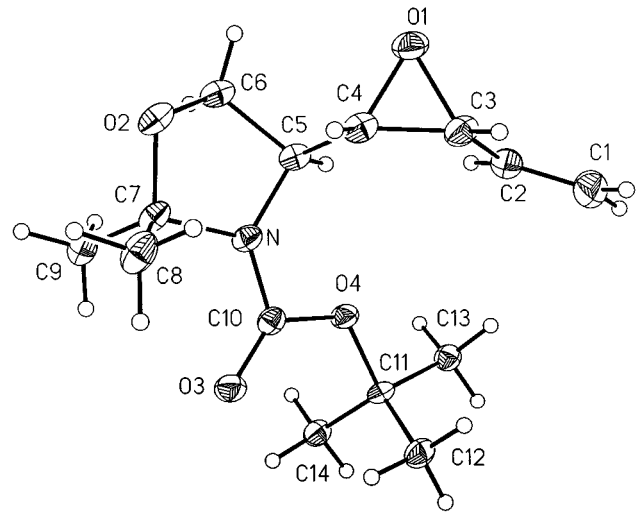

Fig. 1 The molecular structure of vinyl oxirane **1** (ORTEP plot) showing the absolute stereochemistry. Selected bond lengths (Å) and angles (°): C(2)–C(3) 1.472(3), C(3)–C(4) 1.478(3), O(1)–C(4) 1.444(2), O(1)–C(3) 1.461(2); C(4)–O(1)–C(3) 61.1(1), O(1)–C(3)–C(2) 116.0(2), O(1)–C(3)–C(4) 58.8(1), O(1)–C(4)–C(3) 60.0(1), O(1)–C(4)–C(5) 115.3(2); C(1)–C(2)–C(3)–C(4) −159.2(1).

demonstrated that the vinyl oxirane moiety is exposed in such a fashion that nucleophiles, for example lower order or hetero-cuprate reagents, would be predicted to react preferentially *via* a S_N2' type nucleophilic substitution. Electronic and steric factors are expected to determine the initial cuprate–olefin complex, leading to an *anti*-γ σ-allyl cuprate intermediate that suffers reductive elimination to yield the desired S_N2' *E*-configured product.[13]

In fact, excellent selectivity was observed upon treatment of **1** with an *in situ* prepared organocuprate as depicted in general in Scheme 1. Introduction of the alkyl side chain occurred smoothly and proceeded with exclusive formation of the (*E*)-double bond according to ^{13}C and ^{1}H NMR analysis. For the synthesis of native C_{18}-sphingosine,[7] dodecyl bromide was subjected to Br–Li exchange with Bu^{t}Li in Et_2O at −100 °C, followed by transmetallation with CuCN. Coupling of the resulting cuprate with vinyl oxirane **1** provided the protected sphingosine as a single diastereomer in high yield (82%).[14] The free sphingoid base was liberated by mild acid hydrolysis.§ Since cuprates containing sensitive functional groups are readily available by transmetallation of organozinc precursors, this approach promises to be a particularly simple route to a wide range of native and modified sphingosines, under exceptionally mild conditions (*e.g.* for the introduction of isotopes or their attachment on stationary phases for affinity chromatography).

In conclusion, the isomerically pure key intermediate **1** (or *ent*-**1**) is readily available from D- or L-serine on a large scale. This versatile reagent should find general use in the stereoselective synthesis of natural products with special emphasis on D- and L- sphingoid bases and nitrogen heterocycles,[15] which are often difficult and time-consuming to prepare *via* published protocols. Methods for the *syn*-selective chloroallylation of **3** are also under investigation with a view to making the *threo*-series of sphingoid bases equally accessible.

Financial support by the Deutsche Forschungsgemeinschaft, Bonn, and the Fonds der Chemischen Industrie, Frankfurt, is gratefully acknowledged. We thank the BASF AG, Ludwigshafen, and the Bayer AG, Leverkusen, for generous supplies of chemicals and solvents.

Notes and References

† E-mail: boland@ice.mpg.de

‡ *Crystal Data* for **1**: $C_{14}H_{23}NO_4$, M = 269.33 g mol^{-1}, colourless prism, size 0.30 × 0.28 × 0.24 mm^3, orthorhombic, space group $P2_12_12_1$, a = 5.7136(2), b = 9.9806(5), c = 26.526(1) Å, V = 1512.6(1) Å^3, T = −90 °C, Z = 4, ρ_{calc} = 1.183 g cm^{-3}, μ(Mo-Kα) = .86 cm^{-1}, F(000) = 584, 4084 reflections in h (−6/6), k (−11/11), l (−29/29), measured in the range $2.18 \leqslant \theta \leqslant 23.25°$, 2136 independent reflections, R_{int} = 0.0347, 2004 reflections with $F_o > 4\sigma(F_o)$, 265 parameters, R_{obs} = 0.0315, wR^2_{obs} = 0.0785, GOOF = 1.043, Flack-parameter 2(1), largest difference peak and hole: 0.123/−0.143 e Å^{-3}. For the data collection, a Nonius KappaCCD using graphite-monochromated Mo-Kα radiation was used. Data were corrected for Lorentz and polarisation effects. The structure was solved by direct methods (SHELXS) and refined by full-matrix least-squares techniques against F_o^2 (SHELXL-93). All hydrogen atoms were located by difference Fourier synthesis and refined isotropically. The non-hydrogen atoms were refined anisotropically. XP (SIEMENS Analytical X-ray Instruments, Inc.) was used for structure representations. The absolute stereochemistry was not determined crystallographically. CCDC 182/961.

§ *Reagents and conditions*: i, $C_{12}H_{25}Br$, Et_2O, Bu^{t}Li, −100 °C, then CuCN, −40 °C; ii, 1 M HCl, THF, room temperature.

1 T. Ariga, W. D. Jarvis and R. K. Yu, *J. Lipid Res.*, 1998. **39**, 1.
2 H. Zhang, N. N. Desai, A. Olivera, T. Seki, G. Brooker and S. Spiegel, *J. Cell Biol.*, 1991, **114**, 155.
3 S. Pyne, D. G. Tolan, A. M. Conway and N. Pyne, *Biochem. Soc. Trans.*, 1997, **25**, 549.
4 E. A. Sweeney, C. Sakakura, T. Shirahama, A. Masamune, H. Ohta, S. Hakomori and Y. Igarashi, *Int. J. Cancer*, 1996**, 66**, 358.
5 Y. Igarashi, *J. Biochem.*, 1997, **122**, 1080.
6 A. Karrenbauer, D. Jeckel, W. Just, R. Birk, R. R. Schmidt, J. E. Rotham and F. T. Wieland, *Cell*, 1990, **63**, 259; I. Ansorge, D. Jeckel, F. Wieland and K. Lingelbach, *Biochem. J.*, 1995, **308**, 335.
7 For some examples, see: P. Garner, J. M. Park and E. Malecki, *J. Org. Chem.*, 1988, **53**, 4395; P. Herold, *Helv. Chim. Acta*, 1988, **71**, 354; H.-E. Radunz, R. M. Devant and V. Eiermann, *Liebigs Ann. Chem.*, 1988, 1103; A. Dondoni, G. Fantin, M. Fogagnolo and P. Pedrini, *J. Org. Chem.*, 1990, **55**, 1439.
8 P. Garner and J. M. Park, *J. Org. Chem.*, 1987, **52**, 2361; A. McKillop, R. J. K. Taylor, R. J. Watson and N. Lewis, *Synthesis*, 1994, 31; P. Meffre, P. Durand, E. Branquet and F. Le Goffic, *Synth. Commun.*, 1994, **24**, 2147.
9 S. Jayaraman, S. Hu and A. C. Oehlschlager, *Tetrahedron Lett.*, 1995, **36**, 4765; S. Hu, S. Jayaraman and A. C. Oehlschlager, *J. Org. Chem.*, 1996, **61**, 7513.
10 H. C. Brown, U. S. Racherla, Y. Liao and V. V. Khanna, *J. Org. Chem.*, 1992, **57**, 6608.
11 A. G. M. Barrett, J. J. Edmunds, J. A. Hendrix, J. W. Malecha and C. J. Parkinson, *J. Chem. Soc., Chem. Commun.*, 1992, 1240.
12 C. Hertweck and W. Boland, *Tetrahedron*, 1997, **53**, 14 651.
13 J. A. Marshall, *Chem. Rev.*, 1989, **89**, 1503 and references cited herein.
14 A similar transformation of a structurally related vinyl oxirane, prepared in eight steps from D-glucosamine, has been reported recently: T. Murakami and M. Hato, *J. Chem. Soc., Perkin Trans. 1*, 1996, **8**, 823.
15 B. M. Trost and T. S. Scanlan, *J. Am. Chem. Soc.*, 1989, **111**, 4988.

Received in Cambridge, UK, 10th June 1998; 8/04415C

Synthesis of 1,4-bis(1,3,4-oxadiazol-2-yl)-2,5-dialkoxybenzene–oligothiophene copolymers with different emissive colors: synthetically tuning the photoluminescence of conjugated polymers

Wang-Lin Yu,[a] Hong Meng,[a] Jian Pei,[a] Yee-Hing Lai,[b] Soo-Jin Chua[a] and Wei Huang*[a]†

[a] *Institute of Materials Research and Engineering, National University of Singapore, Singapore 119260, Republic of Singapore*
[b] *Department of Chemistry, National University of Singapore, Singapore 119260, Republic of Singapore*

The copolymers of oligothiophenes and 1,4-bis(1,3,4-oxadiazol-2-yl)-2,5-dialkoxybenzene were synthesized with blue, green and orange emissive light depending on the length of the oligothiophene.

In the past few years, π-conjugated polymers have been intensively studied for applications in polymer light-emitting diodes (PLEDs).[1–3] One of the significant advantages of polymer electroluminescent materials is the ease with which the emissive wavelength can be tuned, especially for the realization of blue light.[1] The emissive spectrum of a conjugated polymer basically depends on its π–π* band gap, which can be tailored using different backbone structures.[1,2] For polymers with the same backbone structure, the emissive spectra could also be tuned by attaching different functional groups or/and by controlling the steric conformation of the backbone through synthetic methodology.[4,5] Another effective approach to tuning emissive color is to block the extension of conjugation by inserting non-conjugated groups or other conjugation-blocking groups into the backbone of a conjugated polymer.[6–10] For the conjugation-interrupted approach, thiophene-based polymers have attracted special attention because of the environmental stability of polythiophenes and the ease of synthesis and modification of oligothiophenes. It has been proven that oligothiophenes with different numbers of thiophene rings can emit from blue to red fluorescence.[11] We present here a new synthetic approach to tune the emissive spectra of totally conjugated polymers based on oligothiophenes.

Our new approach incorporates two types of conjugated blocks together to construct a conjugated polymer backbone. One of the two conjugated blocks has a small band gap, while the other has a relatively large band gap. With the fact that head-to-tail regioregular poly(3-alkylthiophenes) may emit light with λ_{max} at around 725 nm,[12] oligomers of 3-alkylthiophene can therefore be used as the smaller band gap blocks in our design. On the other hand, most 1,3,4-oxadiazole-containing conjugated polymers and molecular materials exhibit quite large band gaps (larger than 3.0 eV).[13] Therefore 1,4-bis(1,3,4-oxadiazol-2-yl)benzene was chosen as the larger band gap block in the newly designed polymers **1**–**3**. These polymers may be seen as polythiophene-based polymers, in which the 1,4-bis(1,3,4-oxadiazol-2-yl)benzene group is inserted into the backbone. The extension of conjugation along the backbone of polythiophene is limited or changed, but not interrupted, due to the existence of the 1,4-bis(1,3,4-oxadiazol-2-yl)benzene groups. The conjugated length of the oligothiophenes can be controlled and different functional groups can be attached to the thiophene ring and the benzene ring in the 1,4-bis(1,3,4-oxadiazol-2-yl)benzene moiety, which will result in variation of the emission spectra of the resultant polymers and enhance the solubility of the polymers.

The general synthetic procedure for polymers **1**–**3** is displayed in Scheme 1. The dicarbonyl chlorides **4**–**6** were prepared from the corresponding monomer, dimer and trimer of 3-alkylthiophene, which were synthesized as described in the literature,[14,15] by carboxylation at the α-positions of the thiophene rings with Bu^nLi and dry ice and subsequent reaction with $SOCl_2$.[15] The dihydrazide **7** was prepared from diethyl 2,5-dioctyloxyterephthalate, which was obtained from diethyl 2,5-dihydroxyterephthalate *via* reaction with 1-bromooctane, through a reaction with excess hydrazine monohydrate. The chemical structures and purity of all the compounds were identified by ^1H and ^{13}C NMR, mass and elemental analyses. The polycondensation between the dicarbonyl chlorides and the dihydrazide in *N*-methylpyrrolidinone (NMP) in the presence of LiCl and pyridine afforded the polyhydrazides **1′**–**3′**. The polyhydrazides were isolated by pouring the reaction mixtures into water and then filtering and washing with water and EtOH. The polyhydrazides were converted to the final polymers **1**–**3** by refluxing in $POCl_3$. Pouring the reaction mixtures into water

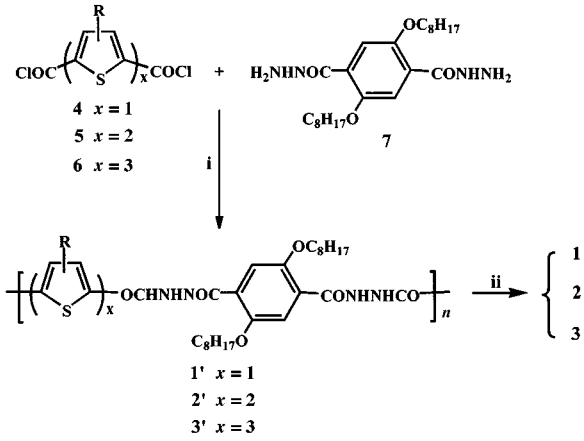

Scheme 1 *Reagents and conditions*: i, LiCl, pyridine, NMP, 4 h; ii, $POCl_3$, reflux, 6 h

precipitated the final polymers. Polymers **1**–**3** were obtained as gray, yellow and orange powders, respectively, after being washed with water, EtOH and Et_2O and dried under reduced pressure at room temperature. Polymers **1** and **3** are partially soluble in both $CHCl_3$ and THF. Polymer **2** is completely soluble in $CHCl_3$ and partially soluble in THF. However, all the three polymers readily dissolve in a mixture of $CHCl_3$ with a small amount of TFA to give clear solutions. By means of gel permeation chromatography (GPC) using THF as eluent and polystyrene as standard, the molecular weights of the THF soluble parts of the polymers were measured to be M_n = 5419 (M_w/M_n = 1.9) for polymer **1**, 7574 (2.0) for polymer **2**, and 2814 (1.4) for polymer **3**. The actual molecular weights of the polymers should be much higher than these measured values because of the insolubility of the parts with higher molecular weights. The structures of the polymers were confirmed by ^1H and ^{13}C NMR and elemental analyses.‡

The absorption and fluorescence spectra of polymers **1**–**3** as films are shown in Fig. 1. The films were prepared *via* spin-coating on a quartz plate using solutions of the polymers in $CHCl_3$ with a small amount of TFA. The expected gradual bathochromic shift of the absorption spectra is exhibited with the increasing length of oligothiophenes in the polymers. The absorption maximum increases from **1** (λ_{max} = 420 nm) to **2** (λ_{max} = 441 nm) to **3** (λ_{max} = 461 nm). The absorption spectra of all the three polymers are structured, as indicated by the well-defined sub-peaks or shoulders at 360 and 443 nm for **1**, 419 and 471 nm for **2**, and 439 and 494 nm for **3**. It is worth noting that the structures in the spectra become less defined on going from **1** to **3**. This phenomenon implies that the polymers with shorter oligothiophenes have a more regular structure in the solid state. Polymers **1**–**3** in the solid state emit intense blue, green and orange light, respectively, upon UV–VIS excitation (λ > 350 nm). The peak wavelengths in the emission are 489 nm for **1**, 530 nm for **2**, and 579 nm for **3,** respectively. The emissive spectra are much less structured than the absorption spectra. The Stokes shifts were determined to be 69 nm for **1**, 89 nm for **2**, and 118 nm for **3**. The spectral difference among the three polymers could be further ascribed to differences in the internal charge transfer along the backbones of the polymers in their excited states.

Comparing the spectral data with those of alkyl-substituted oligothiophenes and conjugation-interrupted polymers based on oligothiophenes,[8–10, 16–18] polymers **1**–**3** correspond to the effective conjugated length of about three, four to five, and five to six extended thiophene rings, respectively. It is evident that the 1,4-bis(1,3,4-oxadiazol-2-yl)benzene moiety does not play a role as a conjugation-interrupting block in the polymers, but is a part of the whole conjugated structure. Its contribution to conjugation is equivalent to about two to three extended thiophene rings.

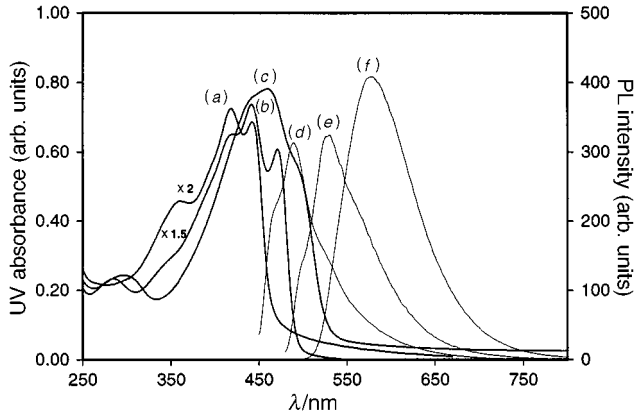

Fig. 1 Absorption [(*a*) 1, (*b*) **2** and (*c*) **3**]and fluorescence [(*d*) **1**, (*e*) **2** and (*f*) **3**] spectra of polymers **1**–**3** in films at room temperature

In conclusion, we have synthesized a new series of totally conjugated copolymers consisting of oligothiophenes and 1,4-bis(1,3,4-oxadiazol-2-yl)-2,5-dioctyloxybenzene. The emissive color of the copolymers could be tuned from blue to green to orange by increasing the number of thiophene ring in the oligothiophene blocks from one to three. The 1,4-bis(1,3,4-oxadiazol-2-yl)-2,5-dioctyloxybenzene block acts as part of the whole conjugated structure and is equivalent to about two to three thiophene rings. Another important aspect of this contribution to electroluminescent polymeric materials is that it might provide an effective approach to the synthesis of n-doped type electroluminescent materials with different emissive colors due to the high electron affinity of 1,3,4-oxadiazole.

Notes and References

† E-mail: wei-huang@imre.org.sg

‡ *Selected data* for Polymer **1**: δ_H($CDCl_3$–CF_3CO_2D, 20:1) 7.93 (s, 1H), 7.74 (d, 2H), 4.23 (s, 4H), 3.20 (t, 2H), 2.00–1.60 (br, 6H), 1.60–1.15 (br, 30H), 0.83 (m, 9H) (Calc. for $C_{38}H_{54}N_4SO_4$: C, 68.85; H, 8.21; N, 8.46; S, 4.84. Found: C, 68.01; H, 8.20; N, 8.94; S, 4.33%). For Polymer **2**: δ_H($CDCl_3$) 7.84 (s, 2H), 7.75 (s, 2H), 4.19 (t, 4H), 2.62 (t, 4H), 1.93 (br, 4H), 1.59 (br, 8H), 1.23 (br, 44H), 0.84 (t, 12); δ_C($CDCl_3$) 162.71, 160.99, 150.84, 144.39, 132.19, 131.09, 125.30, 116.36, 114.57, 69.65, 31.78, 30.50, 29.52, 29.48, 29.30, 29.23, 28.88, 26.05, 22.56, 13.99 (Calc. for $C_{54}H_{80}N_4S_2O_4$: C, 71.01; H, 8.83; N, 6.13; S, 7.02. Found: C, 70.46; H, 9.14; N, 6.11; S, 7.13%). For Polymer **3**: δ_H($CDCl_3$–CF_3CO_2D, 20:1) 7.92 (s, 2H), 7.76 (s, 2H), 7.38 (s, 2H), 4.28 (t, 4H), 2.94 (br, 4H), 1.97 (br, 4H), 1.78 (br, 4H), 1.65–1.00 (br, 34H), 0.87 (br, 12 H); δ_C($CDCl_3$) 162.42, 160.92, 150.84, 140.86, 135.82, 135.14, 132.38, 127.20, 122.49, 116.40, 114.56, 69.72, 31.79, 30.37, 29.60, 29.38, 29.21, 26.11, 22.58, 14.00 (Calc. for $C_{54}H_{74}N_4S_3O_4$: C, 69.04; H, 7.94; N, 5.96; S, 10.24. Found: C, 67.54; H, 8.83; N, 6.08; S, 10.29%).

1 N. C. Greenham and R. H. Friend, in *Solid State Physics*, ed. H. Ehrenreich and F. Spaepen, Academic Press, London, 1995, vol. 49, p. 2.
2 F. Hide, M. A. Díaz-García, B. J. Schwartz and A. J. Heeger, *Acc. Chem. Res.*, 1997, **30**, 430.
3 A. Kraft, A. C. Grimsdale and A. B. Holmes, *Angew. Chem., Int. Ed.*, 1998, **37**, 402.
4 B. Xu and S. Holdcroft, *Macromolecules*, 1993, **26**, 4457.
5 M. Berggren, O. Inganäs, G. Gustafsson, J. Rasmusson, M. R. Anderson, T. Hjeertberg and O. Wennerström, *Nature*, 1994, **372**, 444; M. R. Anderson, M. Berggren, O. Inganäs, G. Gustafsson, J. C. Gustafsson-Carlberg, D. Selse, T. Hjeertberg and O. Wennerström, *Macromolecules*, 1995, **28**, 7525.
6 B. L. Burn, A. B. Holmes, A. Kraft, D. D. C. Bradley, A. R. Brown, R. H. Friend and R. W. Gymer, *Nature*, 1992, **356**, 47.
7 M. Hay and F. L. Klavetter, *J. Am. Chem. Soc.*, 1995, **117**, 7112.
8 W. Li, T. Maddux and L. Yu, *Macromolecules*, 1996, **29**, 7329.
9 B. S. Kang, M.-L. Seo, Y. S. Jun, C. K. Lee and S. C. Shin, *Chem. Commun.*, 1996, 1167.
10 Y. Kunugi, L. L. Miller, T. Maki and A. Canavesi, *Chem. Mater.*, 1997, **9**, 1061.
11 D. Fichou, M.-P. Teulade-Fichou, G. Horowitz and F. Demanze, *Adv. Mater.*, 1997, **9**, 75.
12 K. A. Murray, S. C. Moratti, D. R. Baigent, N. C. Greenham, K. Pichler, A. B. Holmes and R. H. Friend, *Synth. Met.*, 1995, **69**, 395.
13 X.-C. Li, A. Kraft, R. Cervini, G. C. W. Spencer, F. Cacialli, R. H. Friend, J. Gruener, A. B. Holmes, J. C. De Mello and S. C. Moratti, *Mater. Res. Soc. Symp. Proc.*, 1996, **413**, 13**.**
14 R. D. McCullough, R. D. Lowe, M. Jayaraman and D. L. Anderson, *J. Org. Chem.*, 1993, **58**, 904.
15 W.-L. Yu, H. Meng, J. Pei, W. Huang, Y. F. Li and A. J. Heeger, *Macromolecules*, 1998, **31**, 4838.
16 A. Yassar, D. Delabouglise, M. Hmyene, B. Nessak, G. Horowitz and F. Garnier, *Adv. Mater.*, 1992, **4**, 490.
17 R. A. J. Janssen, L. Smilowitz, N. S. Sariciftci and D. Doses, *J. Chem. Phys.*, 1994, **101**, 1787.
18 P. F. van Hutten, R. E. Gill, J. K. Herrema and G. Hadziioannou, *J. Phys. Chem.*, 1995, **99**, 3218.

Received in Cambridge, UK, 3rd June 1998; 8/04159H

Inter-anion O–H$^-$···O$^-$ hydrogen bond like interactions: the breakdown of the strength–length analogy

Dario Braga,[a] Fabrizia Grepioni[a] and Juan J. Novoa[b]

[a] *Department of Chemistry G. Ciamician, University of Bologna, 40126 Bologna, Italy.*
E-mail: dbraga@ciam.unibo.it and grepioni@ciam.unibo.it
[b] *Departament de Química Física, Facultat de Química, Universitat de Barcelona, 08028 Barcelona, Spain.*
E-mail: novoa@zas.qf.ub.es

It is demonstrated that inter-anion O–H$^-$···O$^-$ interactions, commonly regarded as strong hydrogen bonds, are not associated with energetically stable anion–anion interactions; inter-anion O–H$^-$···O$^-$ act as a tugboat interaction that control anion aggregation and minimise anion–anion repulsions.

Strength and directionality render the hydrogen bond[1] (HB) the masterkey interaction in supramolecular chemistry[2] and in crystal engineering.[3] Commonly the HB is defined as a stable interaction between an A–H donor and a B acceptor, being A and B electronegative atoms or electron rich groups.[1,4,5] Strong HB are recognised in the solid state by the presence of H···B and A···B separations shorter than van der Waals contact distances and by A–H···B angles that tend to linearity. In these cases the length–strength analogy is believed to hold, *i.e.* the shorter the acceptor–donor distance the stronger the bond. It is customary to distinguish between neutral HB, when both A–H and B belong to neutral fragments, and ionic HB when ions are involved as donors and/or acceptors.[1,4] The case in which both donor and acceptor belong to negatively charged systems, *i.e.* A–H$^-$···B$^-$, falls in this latter category.

In the following we demonstrate, in the prototypical case of inter-ionic O–H$^-$···O$^-$ interactions commonly found in salts of polyprotic acids [such as $KHCO_3$ and KHC_2O_4 (*vide infra*)], that ionic HB are not energetically stable because they are associated with inter-anion electrostatic repulsions.

Experimentally, O–H$^-$···O$^-$ interactions possess the same geometrical properties as neutral O–H···O bonds. The distribution of inter-molecular/ionic O···O distances for neutral O–H···O and O–H$^-$···O$^-$ interactions, as obtained from a search of systems containing carboxylic–carboxylate groups within the Cambridge Structural Database[6] (CSD), are compared in Fig. 1. Inter-anion O–H$^-$···O$^-$ interactions constitute a very well defined subset and are distinct from neutral O–H···O bonds. O$^-$···O$^-$ separations are significantly shorter, both as mean values and as lowest deciles, than O···O distances. Such a decrease in length is traditionally taken as indicative of a substantial increase in HB strength. This observation is in apparent contradiction with another seemingly simple argument: when the charge is delocalised the electrostatic interaction between small anions is repulsive. We face the intriguing question: how possibly the interaction between anions, which are supposed to repel each other electrostatically, can lead to shorter O···O separations than in the corresponding neutral aggregates?

In order to tackle this problem we have used the HF and B3LYP methods with the 6-31 + G (2d,2p) basis set[8] to compute at the *ab initio* level the first-neighbour inter-anion energies[7] for several crystals taken from the CSD sample.[9a–d] Both methods are well suited to deal with the type of ionic interactions discussed herein.[9a,e]

We have chosen to discuss the representative case of potassium hydrogen oxalate, KHC_2O_4.[10] An analysis of the charge distribution on the $[HC_2O_4]^-$ anion shows that the negative charge is delocalised over the whole anion, with a slightly more negative charge on the deprotonated oxygen atom.[11] Fig. 2 allows to rationalise the ion packing in crystalline KHC_2O_4. The $[HC_2O_4)]^-$ anions form chains separated by O···O distances of 2.522 Å. The crystal can be described as a stacking sequence of corrugated layers formed by K^+ cations and by $[HC_2O_4]^-$ chains, respectively (Fig. 2b).

The presence of short O···O separations along the $[HC_2O_4]^-$ chains is the first point to address. The interaction energy computed for two consecutive $[HC_2O_4]^-$ units in the experimental orientation is repulsive [+39 and +46 k cal mol^{-1} (1 cal = 4.184 J) at the HF and B3LYP levels, respectively]. The molecular electrostatic (MEP) map[12] of the isolated anion (Fig. 3) shows that a +1 charge always experiences an attractive interaction except at very short distance from the nuclei. The most negative regions in the $[HC_2O_4]^-$ MEP map are on the oxygens of the deprotonated group, whereas the least negative ones are on the OH region of the protonated group. The absence of positive regions in the MEP map indicates that, irrespective of the relative orientation, two $[HC_2O_4]^-$ anions repel each other electrostatically. The stability of the anionic chain arises from the presence of the K^+ cations. This can be demonstrated by calculating[8] the interaction energy within the subunit $K_2(HC_2O_4)_2$ which is stable against its dissociation into two K^+ and two $[HC_2O_4]^-$ ions (−232 and −334 k cal mol^{-1} at the HF and B3LYP levels, respectively). This indicates that K^+···$[HC_2O_4]^-$ attractive interactions largely predominate over repulsive K^+···K^+ and $[HC_2O_4]^-$···$[HC_2O_4]^-$ terms. In accord with the observed packing, the geometry of the subunit does not

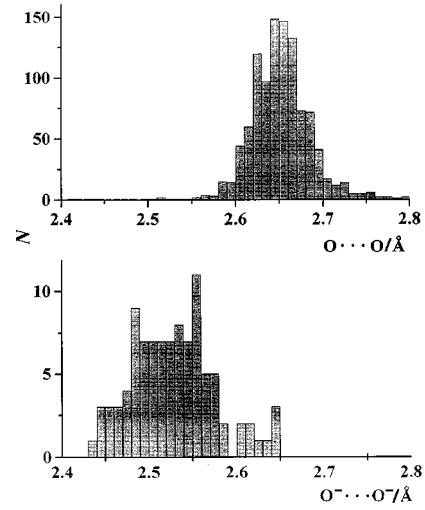

Fig. 1 Histograms of the two populations of O···O separations for neutral O–H···O (top) and inter-anion O–H$^-$···O$^-$ (bottom). Mean values for the O···O separations are 2.652(1) and 2.528(5) and lowest deciles are 2.615 and 2.462 Å, respectively. Intermolecular search on systems containing carboxylic/carboxylate groups based on a cut-off distance of 2.8 Å; duplicate hits manually removed.

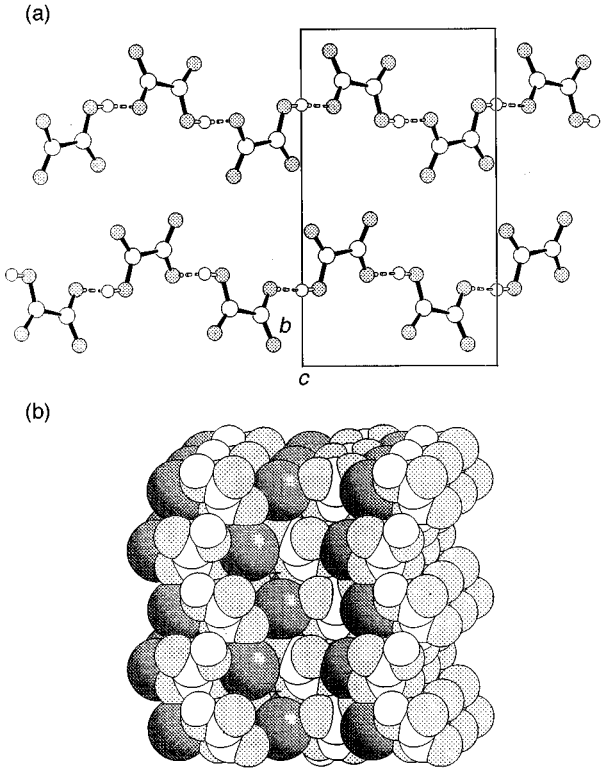

Fig. 2 The experimental packing in crystalline KHC_2O_4. (a) Chains of $[HC_2O_4]^-$ anions. (b) Space filling representation of the ion organisation.

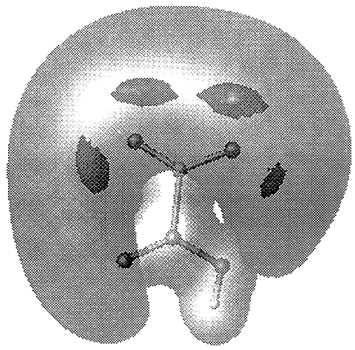

Fig. 3 Molecular electrostatic (MEP) map of an isolated $[HC_2O_4]^-$ anion computed at the HF/6-31 + G (2d,2p) level. Dark regions correspond to -170 kcal mol^{-1}, light grey to -100 kcal mol^{-1}, and light regions around the nuclei to +10 kcal mol^{-1}.

change significantly when fully optimised. To understand why hydrogen bond-like short distances and geometry are maintained on packing $[HC_2O_4]^-$ anions we computed the interaction energy by varying systematically the relative orientation of two $[HC_2O_4]^-$ anions at a fixed distance of 7 Å between the centres of mass. The two most stable (*i.e.* least repulsive) orientations correspond to the chain present in crystalline KHC_2O_4 and to the dimer found in other salts, respectively. Thus the inter-anion HB corresponds to the orientations that favour overlap of the least repulsive MEP regions on the anions. It is important to emphasise that, since $[HC_2O_4]^-\cdots[HC_2O_4]^-$ repulsions are much smaller than $K^+\cdots[HC_2O_4]^-$ attractions, the inter-anion O···O equilibrium distance along the chain is attained at a shorter O···O separation than in neutral HBs. This is a manifest break-down of the widely accepted length–strength relationship in hydrogen bonded solids.

If a bond between two atoms/molecules/ions is taken as anything that requires energy to be broken (whether large or small amount of energy does not matter) then the O–H$^-\cdots$O$^-$ interaction cannot be considered a bond because the ionic chains (or dimers) would 'fall apart' if the cations were removed. Therefore, the O–H$^-\cdots$O$^-$ interaction should be regarded as a *pseudo*-HB because it minimises inter-anion repulsions, but it is not stabilising on an absolute scale.

What is it, then? It is a tugboat interaction, that does not link ions (as an intermolecular chemical bond would do) but rather organises the ions in space, hence conferring directionality to anion–anion electrostatic interactions. The OH group on the anion becomes a probe capable, in the process of crystal nucleation and construction, of exploring the potential energy hypersurface of another anion to find the site of higher nucleophilicity even within the 'thick fog' of a negative field. This understanding has enormous implications in crystal engineering studies, mainly when ionic building blocks are involved,[13] as in organic conductors and superconductors,[14] and in the devise of new synthetic strategies to obtain robust materials.[15] Ionic solids are much more stable than most molecular solids, including those formed of hydrogen bond connected molecules. The inter-anion HB allows the utilisation of molecular synthons within strong ionic fields.

DB and FG acknowledge financial support by MURST (project 'Dispositivi Supramoleculari') and University of Bologna (project 'Materiali Innovativi'). J. J. N. thanks DIGES (project PB95-0848-C02-02) and CIRIT for their support, and CESCA-CEPBA for the allocation of computer time.

Notes and References

1 G. A. Jeffrey and W. Saenger, *Hydrogen Bonding in Biological Structures*, Springer-Verlag, Berlin, 1991.
2 J. M. Lehn, *Supramolecular Chemistry: Concepts and Perspectives*, VCH, Weinheim, 1995.
3 *Perspectives in Supramolecular Chemistry. The Crystal as a Supramolecular Entity*, ed. G. R. Desiraju, Wiley, Chichester, 1996.
4 C. B. Aakeröy and K. R. Seddon, *Chem. Soc. Rev.*, 1993, 397.
5 P. A. Kollman and L. C. Allen, *Chem. Rev.*, 1972, **72**, 283.
6 F. H. Allen and O. Kennard, *Chem. Des. Automat. News*, 1993, **8**, 31.
7 M. Deumal, J. Cirujeda, J. Veciana, M. Kinoshita, Y. Hosokoshi and J. J. Novoa, *Chem. Phys. Lett.*, 1997, **265**, 190.
8 Hereafter identified as HF/6-31 + G (2d,2p) level. The computations were done using Gaussian 94, Revision C.3, 1994: M. J. Frisch, G. W. Trucks, H. B. Schlegel, P. M. W. Gill, B. G. Johnson, M. A. Robb, J. R. Cheeseman, T. Keith, G. A. Peterson, J. A. Montgomery, K. Raghavachari, M. A. Al-Laham, V. G. Zakrzewski, J. V. Ortiz, J. B. Foresman, J. Ciolowski, B. B. Stefanov, A. Nanayakkara, M. Challacombe, C. Y. Peng, P. Y. Ayala, W. Chen, M. W. Wong, J. L. Andres, E. S. Replogle, R. Gomperts, R. L. Martin, D. J. Fox, J. S. Binkley, D. J. Defrees, J. Baker, J. J. P. Stewart, M. Head-Gordon, C. Gonzalez and J. A. Pople, Gaussian Inc., Pittsburgh PA, 1995. Note that a complete computational treatment of the crystal is beyond the scope of this article.
9 (*a*) W. J. Hehre, L. Radom, P. v. R. Schleyer and J. A. Pople, *Ab. initio Molecular Orbital Theory*, Wiley, New York, 1986; (*b*) The B3LYP method is a nonlocal formulation of the DEFT functional made by combining the three parameter Becke exchange functional and the Lee–Yang–Parr correlation functional, which is known to give good results for ionic clusters; (*c*) A. D. Becke, *Phys. Rev. A*, 1988, **38**, 3098; (*d*) C. Lee, W. Yang and R. G. Parr, *Phys. Rev. B*, 1988, **37**, 785; (*e*) C. Lee, G. Fitzgerald, M. Planas and J. J. Novoa, *J. Phys. Chem.*, 1996, **100**, 7398.
10 H. Einspar, R. E. Marsh and J. Donohue, *Acta Crystallogr., Sect. B*, 1972, **28**, 2194.
11 The HF/6-31 + G (2d,2p) charges from a Mulliken population analysis are -0.65 *e* on the deprotonated oxygen, -0.70 *e* on the other oxygen within the same COO group, and 0.55 *e* on its carbon atom. The charges on the other atoms of the molecule are 0.0 on the H, -0.19 on the O(OH), -0.51 on the O(C=O) and 0.51 on the C(C=O).
12 P. Politzer and J. S. Murray, *Rev. Comput. Chem.*, 1991, **2**, 273.
13 D. Braga and F. Grepioni, *Chem. Commun.*, 1998, 911.
14 J. M. Williams, J. R. Ferraro, R. J. Thorn, K. D. Carlson, U. Geiser, H. H. Wang, A. M. Kini and M.-H. Whangbo, *Organic Superconductors* (*Including Fullerenes*). *Synthesis, Structure, Properties, and Theory*, Prentice Hall, Englewood Cliffs, 1992.
15 D. Braga, F. Grepioni and G. R. Desiraju, *Chem. Rev.*, 1998, **98**, 1375.

Received in Basel, Switzerland, 10th June 1998; 8/04392B

Sonoelectrochemical production of hydrogen peroxide at polished boron-doped diamond electrodes

Richard G. Compton,[a] Frank Marken,*[a] Christiaan H. Goeting,[a] Ross A. J. McKeown,[a] John S. Foord,[a] G. Scarsbrook,[b] R. S. Sussmann[b] and A. J. Whitehead[b]

[a] *Physical and Theoretical Chemistry Laboratory, Oxford University, Oxford, UK OX1 3QZ. E-mail: Frank@physchem.ox.ac.uk*
[b] *DeBeers Industrial Diamond Division (UK) Ltd., Charters, Sunninghill, Ascot, Berkshire, UK SL5 9PX*

Power ultrasound applied to erosion resistant and mechanically stable free standing highly boron-doped diamond electrodes allows the electrochemical reduction of dioxygen to hydrogen peroxide under conditions of extremely high rates of mass transport and in the presence of cavitation.

The ability to manufacture boron-doped CVD (chemical vapour deposited) diamond routinely is opening the way to the use of this material for technically demanding applications such as a novel electrode material.[1] Advantages of CVD diamond in this new application include its extreme hardness, chemical inertness, and dimensional stability.[2] The electrode material used in this study is in the form of a 5 × 5 × 0.6 mm diamond square with a typical boron-doping level of 10^{20} cm^{-3} corresponding to a B/C atom ratio of 1/1000 which allows a resistivity of 3×10^{-4} Ω m to be achieved. The use of the free standing diamond plate allows problems with substrate interference and adhesion[3] to be overcome. Further, polishing of the electrode surface produces an essentially flat (surface roughness 20–30 nm R_A) and therefore, in the electrochemical sense, ideal electrode surface with properties which are likely to be different to those reported for 'as grown' diamond electrodes.

In sonoelectrochemistry[4] electrode materials are exposed to extreme conditions with mechanical strain induced by pressure waves of some 10 bar amplitude and cavitation induced liquid jets[5] strong enough to cause severe erosion.[6] As an extremely hard material diamond has been extensively characterised *e.g.* for its resistance to water jet erosion.[7] In this test a diamond surface withstands a 0.8 mm diameter water jet with a velocity in excess of 500 m s^{-1}. This compares to a value of 150 m s^{-1} for the erosion of soda lime glass and to jets caused by cavitation in aqueous media with a velocity in the order of 200 m s^{-1}. Therefore diamond appears to be a promising alternative replacing especially the commonly employed carbon based materials graphite and glassy carbon.

An AFM image of the surface of a highly boron-doped and polished diamond plate electrode is shown in Fig. 1. Owing to the polishing the surface is flat down to the nanometer scale and the characteristic faceting typically observed on a 10–100 μm scale for the polycrystalline material has been removed. Raman spectroscopy (excitation wavelength 632.8 nm) reveals this material to be high quality diamond with a strong and sharp signal at 1331 cm^{-1} (FWHM 4.4 cm^{-1}) characteristic for diamond sp^3-carbon.

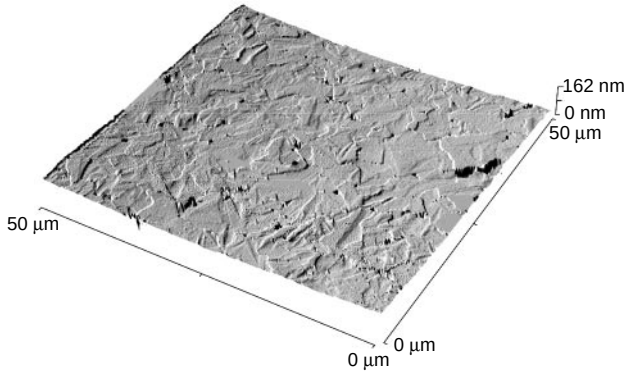

Fig. 1 AFM image of the surface topography of a polished highly boron-doped diamond electrode.

In Fig. 2(a) a cyclic voltammogram† for the one electron reduction of 1 mM $Ru(NH_3)_6^{3+}$ in aqueous 0.1 M KCl is shown [eqn.(1)].

$$Ru(NH_3)_6^{3+} + e^- \leftrightarrow Ru(NH_3)_6^{2+} \quad (1)$$

The well defined voltammetric responses remain symmetric even at fast potential scan rates of up to 1 V s^{-1}. The separation between the peak potentials for the cathodic and the anodic

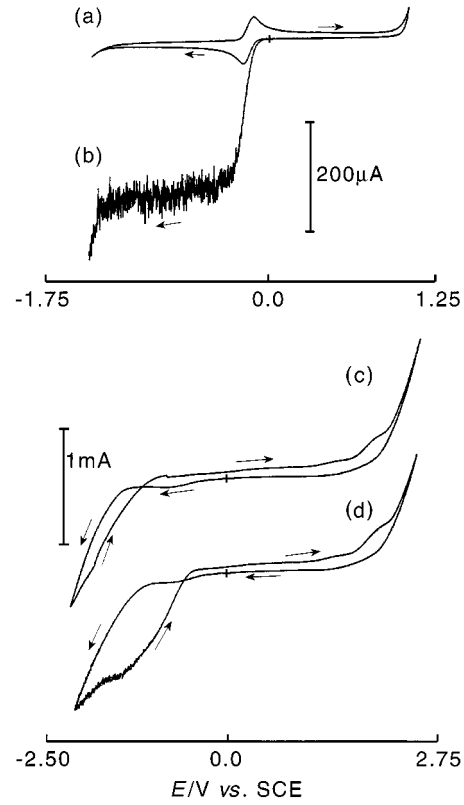

Fig. 2 (a) Cyclic voltammogram obtained for the reduction of 1 mM $Ru(NH_3)_6^{3+}$ in 0.1 M KCl at a polished 5 × 5 mm diamond electrode with a scan rate of 0.1 V s^{-1}. (b) Sonovoltammogram obtained under the same conditions with 90 W cm^{-2} ultrasound intensity and 10 mm electrode to horn distance. Cyclic sonovoltammograms obtained in 0.1 M phosphate buffer at pH = 2 (c) in the absence and (d) in the presence of *ca.* 0.87 mM dioxygen.

Table 1 Electrochemical data obtained from cyclic voltammograms for the reduction of 1 mM $Ru(NH_3)_6^{3+}$ in 0.1 M KCl at a polished highly boron-doped diamond electrode at $T = 20 \pm 2$ °C

Scan rate/ V s^{-1}	$E_{1/2}$[a]/V *vs.* SCE	ΔE_p/mV	$I_{p,cath.}$/ 10^{-6} A	k^{ob}[b]/cm s^{-1}
0.02	−0.18	72	22	9.5×10^{-3}
0.05	−0.18	81	34	9.4×10^{-3}
0.10	−0.18	84	47	11×10^{-3}
0.20	−0.18	96	66	10×10^{-3}

[a] Obtained as mid potential $E_{1/2} = 0.5(E_{p,cath.} + E_{p,anod.})$. [b] Standard rate constant for heterogeneous electron transfer calculated from ΔE_p.[10]

current responses increases with scan rate from 66 mV at a scan rate of 10 mV s^{-1} in agreement with a quasi-reversible electron transfer process with $k° = 0.01 \pm 0.003$ cm s^{-1} similar to standard rate constants for electron transfer observed on other diamond and glassy carbon type materials.[9] Data are summarised in Table 1.

In the presence of power ultrasound the current observed for the reduction of 1 mM $Ru(NH_3)_6^{3+}$ in aqueous 0.1 M KCl is considerably enhanced [Fig. 2(b)]. This mass transport enhanced current response now exhibits 'steady-state' characteristics and the limiting current which can be controlled by changing the ultrasound intensity or the horn to electrode distance may be described by eqn. (2):

$$I_{lim} = n F A D [\text{substrate}] / \delta(D) \quad (2)$$

In this expression the limiting current, I_{lim}, is related to the number of electrons transferred per substrate molecule, *n*, the Faraday constant, *F*, the electrode area, *A*, the diffusion coefficient, *D*, and the diffusion layer thickness, $\delta(D)$, which in aqueous media has been shown[8] to be proportional to $D^{1/3}$. The resulting limiting currents from the sonovoltammetric measurements for the reduction of $Ru(NH_3)_6^{3+}$ with $D = 0.91 \times 10^{-9}$ m^2 s^{-1} may therefore be used for the calibration of the diffusion layer thickness at constant ultrasound intensity and over a range of different electrode to horn distances.

It has recently been shown that the sonoelectrochemical reduction of oxygen at Ni–Cu alloy materials[11] (also known to be very hard and erosion resistant) and at Ti alloy sonotrodes[12] predominantly leads to the 4-electron reduction from dioxygen to water. Sonovoltammograms obtained by scanning the potential over a wide range in the absence [Fig. 2(c)] and in the presence [Fig. 2(d)] of dioxygen in 0.1 M phosphate buffer at pH = 2 at a highly boron doped diamond electrode show some characteristic features different to those previously observed at metal alloy electrodes. A wide solvent window with dioxygen evolution beginning to occur at a potential of +2.2 V *vs*. SCE is observed. Hydrogen evolution commences at a very negative potential of −1.5 V *vs*. SCE. However, after scanning the potential negative and reversing the scan direction the current appears to be increased and a 'crossing' occurs at −1.2 V *vs*. SCE. This feature is a 'tell-tale' sign for a chemical change at the electrode/solution interface, *e.g*. the reduction of surface functional groups of the polished diamond which then cause an increase in the rate of the proton reduction process.

This chemical change on the surface of the polished diamond electrode causes even more pronounced changes in the kinetics for the reduction of *ca*. 0.87 mM dioxygen in aqueous 0.1 M phosphate buffer at pH = 2 [Fig. 2(d)]. After the onset of the reduction process at a potential of −1.2 V *vs*. SCE and reversing the scan direction at −2.1 V *vs*. SCE a sustained limiting current with $I_{lim} = -0.86$ mA can be detected which finally decays with a half wave potential of −0.8 V *vs*. SCE. The calculation of the number of transferred electrons, *n*, per dioxygen molecule based on eqn. (2) and the above calibration procedure with a diffusion coefficient[14] for dioxygen of $D = 1.65 \times 10^{-9}$ m^2 s^{-1} gives $n = 2.1 \pm 0.1$ consistent with the two electron reduction of oxygen to hydrogen peroxide [eqn. (3)].

$$O_2 + 2\,e^- + 2\,H^+ \rightarrow H_2O_2 \quad (3)$$

A colorimetric test reaction with iodide[13] was used to confirm the formation of hydrogen peroxide after a period of 20 minutes electrolysis at an applied potential of −2.0 V *vs*. SCE. In contrast, under the same experimental conditions but without electrolysis the sonolytic formation of H_2O_2 was found to be negligible. The change of the surface properties of the boron-doped diamond electrode which has been reported to be present to a much smaller extent for 'as grown' boron-doped diamond[14] was found to be reversed by scanning into the region of positive potentials and the nature and mechanistic significance of the surface functional groups on the surface of the polished highly boron-doped diamond is currently the topic of a more detailed study by both electrochemical and spectroscopic techniques.

F. M. thanks the Royal Society for the award of a University Research Fellowship and New College (Oxford) for a Stipendiary Lectureship.

Notes and References

† In electrochemical experiments an Autolab PGSTAT 20 system (Eco Chemie, NL) was used for recording voltammetric data in conjunction with a special thermostated three-electrode cell of 25 cm^3 volume which has been described recently.[8] Experimental details for Raman and AFM measurements have been published.[3] Industrially polished boron-doped diamond was treated with oxidising acid in order to remove sp^2 type carbon from the polished surface and has been used as received from De Beers Industrial Diamond Division. Experiments were carried out after degassing with pure argon or dioxygen (BOC) at a temperature thermostated to 20 ± 2 °C.

1 J. S. Xu, M. C. Granger, Q. Y. Chen, J. W. Strojek, T. E. Lister and G. M. Swain, *Anal. Chem.*, 1997, **69**, A591.
2 Q. Y. Chen, M. C. Granger, T. E. Lister and G. M. Swain, *J. Electrochem. Soc.*, 1997, **144**, 3806.
3 C. H. Goeting, F. Jones, J. S. Foord, J. C. Eklund, F. Marken, R. G. Compton, P. R. Chalker and C. Johnston, *J. Electroanal. Chem.*, 1998, **442**, 207.
4 (*a*) D. J. Walton and S. S. Phull, *Adv. Sonochem.*, 1996, **4**, 205; (*b*) R. G. Compton, J. C. Eklund and F. Marken, *Electroanalysis*, 1997, **9**, 509.
5 P. R. Birkin and S. SilvaMartinez, *Anal. Chem.*, 1997, **69**, 2055.
6 N. A. Madigan, C. R. S. Hagan, H. Zhang and L. A. Coury, Jr., *Ultrasonics Sonochem.*, 1996, **3**, S239.
7 (*a*) C. R. Seward, E. J. Coad, C. S. J. Pickles and J. E. Field, *Wear*, 1995, **186**–**187**, 375; (*b*) C. S. J. Pickles, PhD Thesis, Cambridge, August 1991.
8 H. A. O. Hill, Y. Nakagawa, F. Marken and R. G. Compton, *J. Phys. Chem.*, 1996, **100**, 17395.
9 (*a*) R. DeClements, G. M. Swain, T. Dallas, M. W. Holtz, R. D. Herrick II and J. L. Stickney, *Langmuir*, 1996, **12**, 6578; (*b*) M. R. Deakin, K. J. Stutts and R. M. Wightman, *J. Electroanal. Chem.*, 1985, **182**, 113.
10 R. S. Nicholson, *Anal. Chem.*, 1965, **37**, 1351.
11 L. Nei, F. Marken, Q. Hong and R. G. Compton, *J. Electrochem. Soc.*, 1997, **144**, 3019.
12 H. N. McMurray, D. A. Worsley and B. P. Wilson, *Chem. Commun.*, 1998, 887.
13 *Practical Sonochemistry*, ed. T. J. Mason, Ellis Horwood, Chichester, 1991, p. 46.
14 T. Yano, D. A. Tryk, K. Hashimoto and A. Fujishima, *J. Electrochem. Soc.*, 1998, **145**, 1870.

Received in Cambridge, UK, 13th July 1998; 8/05418E

A highly ordered ferrocene system regulated by podand peptide chains

Akihiro Nomoto, Toshiyuki Moriuchi, Shuhei Yamazaki, Akiya Ogawa and Toshikazu Hirao*†

Department of Applied Chemistry, Faculty of Engineering, Osaka University, Yamada-oka, Suita, Osaka 565-0871, Japan

The ferrocene bearing the podand dipeptide chains, Ala-Pro-OEt, which are aligned parallel in solution by the two rigid intramolecular hydrogen bonds, manifests a novel helically ordered arrangement with one turn of 14.70 Å pitch height in the crystal packing possibly due to the intramolecular hydrogen bonds (the N–H···O=C distance is 2.06 Å) and the hydrophobic interaction of the podand dipeptide chains (the distance between the nearest ferrocene units is 4.54 Å).

Architectural control of molecular assemblies utilizing specific interactions as observed in biological systems is considered to be one of the most convenient approaches to highly ordered supramolecular systems, most of which are expected to exhibit novel functions.[1] In particular, hydrogen bonding has been exploited for the elaboration of regulated supramolecules such as dendrimers[2] and artificial peptides.[3] Crystal engineering has also contributed to a key technique for this purpose.[4] The incorporation of transition metal complexes into such highly structured biomolecules is envisioned to provide new biomaterials and efficient redox systems.[5] Ferrocenes, which possess a reversible redox couple and rotatory cyclopentadienyl moieties, have been regarded as useful organometallic scaffolds for molecular receptors[6] and peptide mimetic models.[7] We have already focused on such properties to demonstrate a unique coordination behavior of the ferrocenes bearing podand *N*-heterocyclic pendant groups.[8] Our system design described here is addressed by an efficient communication of podand peptide chains both intramolecularly and intermolecularly to order the redox-active ferrocene system.

A chiral dipeptide, L-alanyl-L-proline, which is considered to consist of a hydrogen bonding site (Ala) and a hydrophobic moiety (Pro), is incorporated into a redox-active ferrocene scaffold.‡ Ferrocene derivatives **1** and **2** bearing two and one Ala-Pro-OEt chains, respectively, exhibited a reversible oxidation/reduction wave attributable to the Fe(III)/Fe(II) couple at 740 mV and 567 mV *vs.* SCE, respectively, which are indicative of the electron-withdrawing amide function.

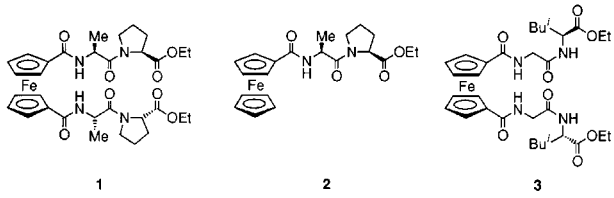

1 **2** **3**

X-Ray crystallography studies revealed several interesting structural features. The X-ray crystal structure of **1**§ is depicted in Fig. 1. Surprisingly, the two dipeptide chains of **1**, which have C_2 symmetry, are oriented in the same direction despite the free rotary cyclopentadienyl rings and sterically bulky proline moieites. This structure is considered to be stabilized by two C_2-symmetrical intramolecular hydrogen bonds between CO (Ala) and NH (another Ala) of each podand peptide chain. The N–H···O=C distance of the hydrogen bonds is 2.06 Å. Intermolecular hydrogen bonding was not observed even in the molecular packing. In contrast to the structure of **1**, each molecule of **2**¶ is connected by an intermolecular hydrogen-bonding network, in which the peptide chain is not arranged parallel to the chain of the next molecule. It is also noteworthy that the β-angle of **2** (defined as the angle between the plane of the cyclopentadienyl ring and C(ipso)–CO(bridging) bond) is 24.6° or 23.3°. This value is unexpectedly large compared with those of **1** (5.6°), probably due to the intermolecular hydrogen bonding. The conjugation between the cyclopentadienyl ring and carbonyl group of **2** is disturbed to some extent.

A striking feature is that **1** is found to be packed in a helical molecular arrangement with one turn of 14.70 Å pitch height [Fig. 1(b)], within which the distance between the closest ferrocene units is 4.54 Å. The proline rings and ethyl groups individually form the hydrophobic cores, which are considered to be one of the factors that control the crystal packing and permit the helical assembly. Such an assembly was not observed in the crystal structure of ferrocene **3**‖ bearing podand glycyl-L-leucine chains although the isobutyl group is expected to form

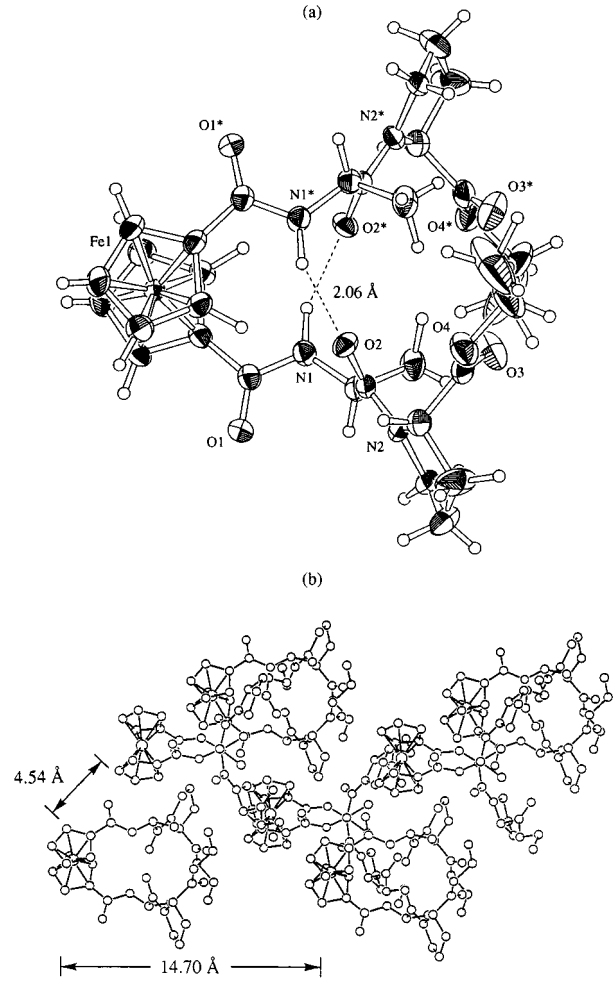

Fig. 1 (a) X-Ray crystal structure of ferrocene **1**. The hydrogen bonds are shown as dotted lines. (b) Crystal packing of ferrocene **1**.

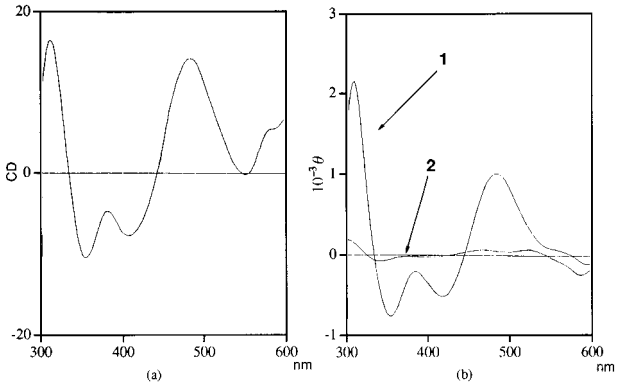

Fig. 2 (a) CD spectrum of ferrocene **1** in the solid state (KBr pellet) and (b) CD spectra of ferrocenes **1** and **2** in CH_3CN (5.0×10^{-4} M)

a hydrophobic core. A helical molecular arrangement is only characteristic of **1**.

The CD spectrum of **1** in the solid state (KBr pellet) showed Cotton effects corresponding to the absorbances of the ferrocene moiety in the UV–VIS spectrum [Fig. 2(a)]. The Cotton effects seem to be caused by the reflection of chirality of the regulated podand peptide chains possessing two rigid intramolecular hydrogen bonds. Furthermore, a similar CD spectrum for **1** was obtained in acetonitrile [Fig. 2(b)] in sharp contrast with the finding that such effects were not observed with **2** in both solid and solution states. This result suggests that the podand peptide chains of **1** are also regulated even in solution by the intramolecular hydrogen bonds.

The ^{1}H NMR spectrum of **1** exhibited only one kind of NH peak at lower field (δ = 8.95, 5.0 mM) as compared with **2** (δ = 6.58, 10.0 mM). These results indicate that the intramolecular hydrogen bonds of **1** are identical in CD_2Cl_2 solution.[7b] Such bonding is also confirmed by the IR spectrum (CH_2Cl_2, ν_{N-H} **1**: 3301 cm^{-1}; **2** 3418 cm^{-1}).[7b]

The oxidation of **1** to a ferrocenium species **1**$^+$ was achieved with CAN [cerium(IV) diammonium nitrate] to show the broad absorption around 657 nm in the UV–VIS spectrum. Interestingly, the Cotton effects were observed even in the CD spectrum of **1**$^+$. A similar oxidative transformation was performed electrochemically, and monitored by *in situ* CD measurement at 1.2 V *vs.* SCE. The Cotton effects of the above-mentioned ferrocenium species are independent of the presence of CAN. These results suggest that the rigid structure of **1** is maintained even in the oxidized form, presumably by the intramolecular hydrogen bonding.

In conclusion, we have designed and synthesized the novel peptide **1** containing a ferrocene unit, in which the podand dipeptide chains (Ala-Pro-OEt) are regulated in both solid and solution states by the two rigid intramolecular hydrogen bonds. Also, a novel helically ordered arrangement is achieved in the crystal packing, where the proline rings and ethyl groups individually form the hydrophobic cores. The present system is likely to be related to helical electron hopping. Studies on the effects of peptide chains and redox-switching properties are now in progress to disclose the scope of an ordered system based on peptide interactions.

This work was financially supported in part by a Grant-in-Aid for Exploratory Research from the Ministry of Education, Science and Culture, Japan and the Shorai Foundation for Science and Technology.

Notes and References

† E-mail: hirao@chem.eng.osaka-u.ac.jp

‡ Typical procedure for the synthesis of **1**. To a stirred mixture of 1,1′-ferrocenedicarboxylic acid chloride (0.10 mmol) and H-Ala-Pro-OEt·HCl (0.22 mmol) in dichloromethane (2 mL) was dropwise added triethylamine (0.50 mmol) under argon at 0 °C. After stirring at room temperature for 1 h, water (20 mL) was added to the mixture. Extraction with dichloromethane (3×10 mL) followed by evaporation gave the crude ferrocene **1**. Chromatography on an alumina column eluting with dichloromethane and recrystallization from dichloromethane afforded an orange solid in 58% yield. **1**: IR (KBr) 3315, 2991, 1740, 1632, 1544, 1434, 1372, 1336, 1292, 1186, 1026 cm^{-1}; IR (CH_2Cl_2, 1.0 mM) 3301 (N–H) cm^{-1}; ^{1}H NMR (600 MHz, CD_2Cl_2) δ 8.77 (d, 2H, J = 7.6 Hz), 4.85–4.78 (m, 6H), 4.59 (dd, 2H, J = 4.6, 4.3 Hz), 4.45–4.44 (m, 2H), 4.27–4.26 (m, 2H), 4.14–4.05 (m, 4H), 3.89–3.85 (m, 2H), 3.69–3.66 (m, 2H), 2.33–2.27 (m, 2H), 2.12–2.07 (m, 4H), 2.01–1.96 (m, 2H), 1.32 (d, 6H, J = 7.3 Hz), 1.26 (q, 6H, J = 7.0 Hz). **2**: IR (KBr) 3312, 2982, 1743, 1652, 1626, 1535, 1436, 1298, 1183 cm^{-1}; IR (CH_2Cl_2, 1.0 mM) 3418 (N–H) cm^{-1}; ^{1}H NMR (600 MHz, CD_2Cl_2) δ 6.60 (d, 1H, J = 6.9 Hz), 4.83 (quint. 1H, J = 6.9 Hz), 4.69–4.63 (m, 2H), 4.47 (dd, 1H, J = 8.6, 8.2 Hz), 4.35–4.33 (m, 2H), 4.21–4.10 (m, 7H), 3.77–3.73 (m, 1H), 3.66–3.62 (m, 1H), 2.27–2.22 (m, 1H), 2.12–1.94 (m, 3H), 1.42 (d, 3H, J = 6.9 Hz), 1.26 (t, 3H, J = 7.2 Hz). **3**: IR (KBr) 3283, 2959, 1745, 1634, 1552, 1454, 1371, 1304, 1197, 1028 cm^{-1}; IR (CH_2Cl_2, 1.0 mM) 3415, 3320 (N–H) cm^{-1}; ^{1}H NMR (600 MHz, CD_2Cl_2) δ 8.49 (t, 2H, J = 6.1 Hz), 6.48 (d, 2H, J = 10.8 Hz), 4.81–4.79 (m, 4H), 4.63–4.59 (m, 2H), 4.43–4.39 (m, 4H), 4.19 (q, 4H, J = 6.6 Hz), 3.95 (dd, 2H, J = 16.2, 6.1 Hz), 3.87 (dd, 2H, J = 16.2, 6.1 Hz), 1.74–1.57 (m, 6H), 1.28 (t, 6H, J = 6.6 Hz), 1.02–0.97 (m, 12H).

§ *Crystal data* for **1**: $C_{32}H_{42}N_4O_8Fe$, M = 666.55, tetragonal, space group $I4_1$, a = 14.978(4), c = 14.699(7) Å, V = 3297(1) Å^3, Z = 4, T = 23.0 °C, D_{calc} = 1.343 g cm^{-3}, μ(Mo-Kα) = 5.12 cm^{-1}, R = 0.048, R_w = 0.048 for 1975 independent observed reflections ($2\theta_{max}$ = 55.0°).

¶ *Crystal data* for **2**: $C_{21}H_{26}N_2O_4Fe$, M = 426.29, orthorhombic, space group $P2_12_12_1$, a = 17.834(3), b = 18.012(2), c = 12.623(2) Å, V = 4054.8(8) Å^3, Z = 8, T = 23.0 °C, D_{calc} = 1.397 g cm^{-3}, μ(Mo-Kα) = 7.72 cm^{-1}, R = 0.058, R_w = 0.056 for 5222 observed reflections ($2\theta_{max}$ = 55.1°).

‖ *Crystal data* for **3**: $C_{32}H_{46}N_4O_8Fe$, M = 670.58, triclinic, space group $P1$, a = 9.294(1), b = 11.783(1), c = 8.924(1) Å, α = 98.65(1), β = 116.481(9), γ = 81.41(1)°, V = 861.0(2) Å^3, Z = 1, T = 23.0 °C, D_{calc} = 1.293 g cm^{-3}, μ(Mo-Kα) = 4.90 cm^{-1}, R = 0.045, R_w = 0.040 for 3991 independent observed reflections ($2\theta_{max}$ = 55.1°). CCDC 182/965.

1 M. Engels, D. Bashford and M. R. Ghadiri, *J. Am. Chem. Soc.*, 1995, **117**, 9151; H. Mihara, Y. Haruta, S. Sakamoto, N. Nishino and H. Aoyagi, *Chem. Lett.*, 1996, 1; C. A. Mirkin, R. L. Letsinger, R. C. Mucic and J. J. Storhoff, *Nature*, 1996, **382**, 607; A. P. Alivisatos, K. P. Johnsson, X. Peng, T. E. Wilson, C. J. Loweth, M. P. Bruchez Jr. and P. G. Schultz, *Nature*, 1996, **382**, 609.

2 W. T. S. Huck, R. Hulst, P. Timmerman, F. C. J. M. van Veggel and D. N. Reinhoudt, *Angew. Chem., Int. Ed. Engl.*, 1997, **36**, 1006.

3 J. P. Schneider and J. W. Kelly, *Chem. Rev.*, 1995, **95**, 2169; J. S. Nowick, E. M. Smith and M. Pairish, *Chem. Soc. Rev.*, 1996, **25**, 401; D. A. Leigh, A. Murphy, J. P. Smart and A. M. Z. Slawin, *Angew. Chem., Int. Ed. Engl.*, 1997, **36**, 728.

4 A. D. Burrows, C.-W. Chan, M. M. Chowdhry, J. E. McGrady and D. M. P. Mingos, *Chem. Soc. Rev.*, 1995, **24**, 329; F. D. Lewis, J.-S. Yang and C. L. Stern, *J. Am. Chem. Soc.*, 1996, **118**, 12 029.

5 D. G. McCafferty, B. M. Bishop, C. G. Wall, S. G. Hughes, S. L. Mecklenberg, T. J. Meyer and B. W. Erickson, *Tetrahedron*, 1995, **51**, 1093; R. C. Mucic, M. K. Herrlein, C. A. Mirkin and R. L. Letsinger, *Chem. Commun.*, 1996, 555; A. B. Gretchikhine and M. Y. Ogawa, *J. Am. Chem. Soc.*, 1996, **118**, 1543; P. J. Dandliker, R. E. Holmlin and J. K. Barton, *Science*, 1997, **275**, 1465; P. A. Arnold, W. R. Shelton and D. R. Benson, *J. Am. Chem. Soc.*, 1997, **119**, 3181.

6 J. C. Medina, T. T. Goodnow, M. T. Rojas, J. L. Atwood, B. C. Lynn, A. E. Kaifer and G. W. Gokel, *J. Am. Chem. Soc.*, 1992, **114**, 10 583; P. D. Beer, *Chem. Commun.*, 1996, 689.

7 (*a*) H. Eckert and C. Seidel, *Angew. Chem., Int. Ed. Engl.*, 1986, **25**, 159; (*b*) R. S. Herrick, R. M. Jarret, T. P. Curran, D. R. Dragoli, M. B. Flaherty, S. E. Lindyberg, R. A. Slate and L. C. Thornton, *Tetrahedron Lett.*, 1996, **37**, 5289; (*c*) M. Kira, T. Matsubara, H. Shinohara and M. Sisido, *Chem. Lett.*, 1997, 89.

8 T. Moriuchi, I. Ikeda and T. Hirao, *Inorg. Chim. Acta*, 1996, **248**, 129; T. Moriuchi, I. Ikeda and T. Hirao, *J. Organomet. Chem.*, 1996, **514**, 153.

Received in Columbia, MO, USA, 13th November 1997; revised manuscript received 13th July 1998; 8/05780J

Solid-state solvolysis induced *via* charge-transfer complexation by solid-phase grinding followed by contact with solvent vapor

Motoko Tanaka and Keiji Kobayashi*†

Department of Chemistry, Graduate School of Arts and Sciences, The University of Tokyo, Komaba, Meguro-ku, Tokyo 153-8902, Japan

When 9-thienothienylfluoren-9-ol derivatives were ground together with DDQ then exposed to methanol vapor, solvolysis occurred to yield 9-methoxyfluorenes *via* the generation of a radical cation by solid-state single-electron transfer.

While organic reactions are usually carried out in solvents, solid-state reactions have also been extensively investigated.[1] The solid-state reactions between two different compounds have been realized by grinding a mixture of powdered reactant and reagent[2] or by using co-crystals in which two reactant molecules are preorganized in reactive positions.[3] Both of these methodologies, however, cannot be applied to solvolysis, for which dissolution of substrates in solvents is inevitable. We have recently achieved solid-state photosolvolysis[4] in the crystalline host–guest inclusion complexes with EtOH as a guest component.[5] We now report here on novel solid-state solvolysis by solvent vapor induced by solid–solid contact followed by gas–solid contact, from which a new consequence of solid-state grinding can be deduced.

In a typical run, an equimolar mixture of 9-thienothienylfluoren-9-ol **1a** and dichlorodicyanoquinone (DDQ) was ground in a mortal and pestle and the resulting dark green solids were exposed to MeOH vapor below 5 °C for 6 h (Scheme 1). The resulting solids were shown to include a methoxy-substituted product **2a** in 42% yield. DDQ was recovered quantitatively. When substrate **1a** was ground alone and then exposed to MeOH vapor, the reaction did not occur at all, indicating that DDQ acts as a catalyst.[6]

Similarly, ethanolysis and propanolysis were accomplished for **1a** as well as for naphthyl-substituted **1b** and diols **1c** and **1d** to give the corresponding alkoxy derivatives in 5–32% yields. For **1a** and **1d**, tetracyanoethylene (TCNE) also promoted the solvolysis to give the methyl ethers in 70 and 51% yields, respectively, along with 16% of the dimethyl ether in the latter.

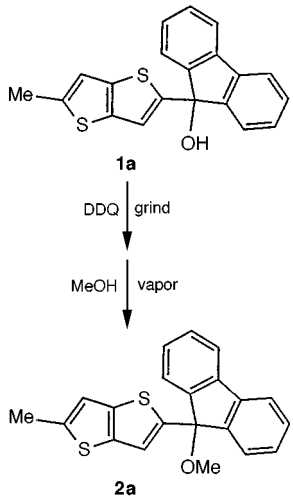

Scheme 1

On the other hand, tetracyanoquinodimethane (TCNQ) and *p*-chloranil caused no solvolysis. In all cases, the solid states were retained throughout the procedure of grinding and exposure.

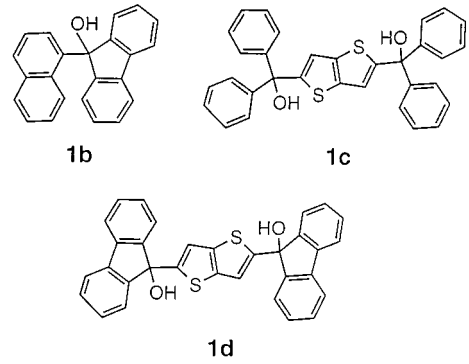

The colored solids obtained by solid-state grinding of **1a** with DDQ exhibited an absorption maximum at 650 nm ascribed to a CT band, as measured by solid-state reflectance spectroscopy. EPR signals were observed for these solid samples.‡ Crystalline charge-transfer complexes were not obtained *via* recrystallization of **1a** and DDQ from MeCN solution. This was also the case for **1b** and **1c**; the charge-transfer complexation was realized only by grinding these compounds with the electron acceptor in the solid-state. The resulting solids exhibited EPR signals and solvolysis occurred upon solid–vapor contact.

For **1d**, a crystalline 1:1 charge-transfer complex was obtained from a highly concentrated colored solution of **1d** and DDQ in MeCN. In sharp contrast to the solids obtained by solid-state grinding, those obtained by recrystallization exhibited no EPR signals and did not undergo solvolysis upon exposure to solvent vapor. Furthermore, the ground mixture of **1d** and DDQ exhibited a charge-transfer band maximum (653 nm) at longer wavelength than the complex obtained by recrystallization (629 nm). All the above observations indicate that the solid-state grinding generates radical ions and that these species are essential to promote the solvolysis by vapor.

Catalytic effects of π-donors in the acetolysis of 2,4,7-trinitro-9-fluorenyl *p*-toluenesulfonate has been reported,[7] in which the π-donors are assumed to polarize the C-O bond leading to easy heterolytic bond cleavage. The present results appear to be different from such type of catalytic solvolysis in a solution. It has been quite often observed that radical cations generated *via* single-electron transfer undergo the cleavage of a σ-bond.[8] In order to see if such reaction occurs in the radical cation of **1a**, we have carried out the electrochemical oxidation of **1a** in MeOH and ascertained the formation of **2a**. This finding, however, does not settle the mechanism, because the precursor species to **2a** are only slightly generated in the ground solids; the spin concentration of the ground solids is estimated to be only 2% at most from the EPR signal intensity and furthermore **2a** is formed in mear trace amounts when the ground mixture is dissolved in MeOH. Thus the carbocation

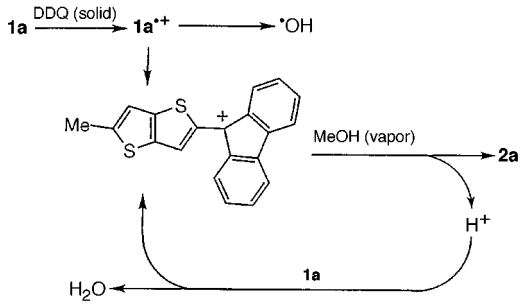

Scheme 2

species should be propagated in the solid phase upon gas-solid contact.

As a most plausible mechanism at this stage, we assume that the methoxy substitution occurs in a catalytic chain process initiated by a small amount of the cation generated from the radical cation of **1a**, as depicted in Scheme 2.§ The acid-catalysed ether formation in the solid state was supported by the occurrence of the ethoxy substitution in a crystalline inclusion complex[9] **1d**·$(EtOH)_2$ upon grinding with toluene-*p*-sulfonic acid without solvent.

The reasons why only the ground mixtures of the substrates and acceptors show EPR signals and hence undergo the solvolysis by vapor should be discussed. The substrates used in this work are not planar molecules, and have irregular shape and conformational freedom. For such molecules, close packing in a periodic donor–acceptor arrangement is not easily attained upon recrystallization,¶ as noted already. On the other hand, solid-state grinding would force some of the molecules closer together while still being free from lattice control, and hence permit much stronger charge-transfer interactions than those in crystalline charge-transfer complexes derived from a solution.

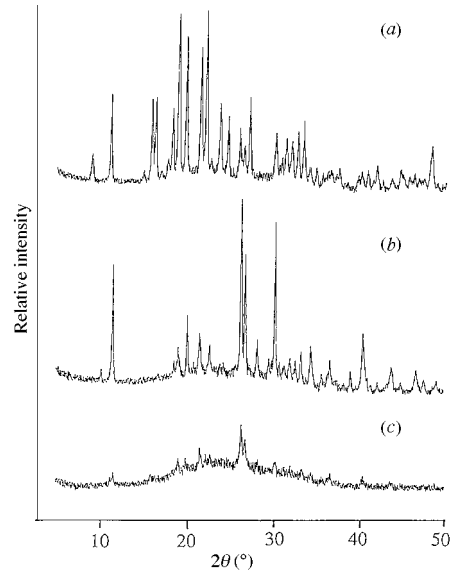

Fig. 1 Powder X-ray diffraction patterns of (*a*) **1a**, (*b*) DDQ and (*c*) a ground mixture of **1a** and DDQ

The above explanation is in line with the results of a powder X-ray diffraction study. The diffraction intensities of the ground solids of **1a** with DDQ decrease significantly as compared with those of each component (Fig. 1), indicating the collapse of the crystalline phase without reorganization into a new charge-transfer crystal phase. Despite the inability of the mixtures to give co-crystal packing, the charge-transfer contacts are strong enough to induce single-electron transfer, which could be partially due to the use of the planar moieties on **1a**. It has been reported that crystalline charge-transfer complexes can be formed by grinding together solid donor and acceptor components.[10] Such behavior has also been encountered for planar donor and acceptor molecules that can also co-crystallize from solution. Thus, it seems reasonable that the reactivity of the present solvolysis system using solvent vapor depends not only on the electron accepting and donating abilities, but also on the molecular shape, of the substrates and electron acceptors.

Notes and References

† E-mail: ckobak@komaba.ecc.u-tokyo.ac.jp

‡ For the ground solids of **1a** and DDQ, an EPR signal occurs at $g = 2.0043$ with a simple profile of a type usually observed for monoradical species.

§ Alternatively the collapse of the radical cation to form H^+ and an alkoxy radical would be possible. In this case also H^+ would give the cation which enters into the chain process.

¶ Most of the substrates in this work act as host species for clathrate crystals, indicating that it is difficult for these compounds to crystallized without incorporation of other guest molecules. See also ref. 9.

1 *Reactivity in Molecular Crystals*, ed. Y. Ohashi, VCH, Weinheim, 1993; W. Jones, in *Oranic Molecular Solids, Properties and Applications*, ed. W. Jones, CRN Press, NY, 1997, p. 149.
2 For a recent example, see: B. Goud and G. R. Desiraju, *J. Chem. Res. (S)*, 1995, 244.
3 For recent examples, see: M. Kudoh. K. Naruchi, F. Akutsu and M. Miura, *J. Chem. Soc., Perkin Trans. 2*, 1993, 555; N. B. Singh, N. P. Singh, V. A. Kumar and M. Nethaji, *J. Chem. Soc., Perkin. Trans. 2*, 1994, 361.
4 The photosolvolysis of fluorenols has been studied in detail. See for examples: P. Wan and E. Krogh, *J. Am. Chem. Soc*., 1989, **111**, 4887; R. A. McClelland, N. Mathivanan and S. Steenken, *J. Am. Chem. Soc*., 1990, **112**, 4857; A. K. Kolter and S. S. Wang, *J. Am. Chem. Soc.*, 1963, **85**, 114.
5 N. Hayashi, Y. Mazaki and K. Kobayashi, *Terahedron Lett.*, 1994, **35**, 5883.
6 DDQ has been known to catalyse the C–O bond cleavage of ethers and acetals. See for examples: A. Oku, M. Kinugasa and T. Kamada, *Chem. Lett.*, 1993, 165; K. Tanemura, T. Suzuki and T. Horaguchi, *Bull. Chem. Soc. Jpn*., 1994, **67**, 290; J. H. Penn and D.-L. Deng, *Tetrahedron*, 1992, **48**, 4823.
7 A. K. Colter and S. S. Wang, *J. Am. Chem. Soc*., 1963, **85**, 114.
8 M. Schmittel and A. Burghart, *Angew. Chem., Int. Ed. Engl.*, 1997, **36**, 2550.
9 For properties of **1c** and **1d** as a host compound, see: N. Hayashi, Y. Mazaki and K. Kobayashi, *J. Org. Chem*., 1995, **60**, 6342; N. Hayashi, K. Kuruma, Y. Mazaki, T. Imakubo and K. Kobayashi, *J. Am. Chem. Soc*., 1998, **120**, 3799 and references cited therein.
10 M. J. S. Dewar and A. Lepley, *J. Am. Chem. Soc*., 1961, **83**, 4560; F. Toda and H. Miyamoto, *Chem. Lett*., 1995, 861.

Received in Cambridge, UK, 11th May 1998; 8/03496F

Alkane oxidation with manganese substituted polyoxometalates in aqueous media with ozone and the intermediacy of manganese ozonide species

Ronny Neumann*† and Alexander M. Khenkin

Casali Institute of Applied Chemistry, Graduate School of Applied Science, The Hebrew University of Jerusalem, Jerusalem 91904, Israel

Manganese substituted polyoxometalates (POMs), such as $Li_{12}[Mn^{II}_2ZnW(ZnW_9O_{34})_2]$ were effective catalysts for the oxidation of alkanes to ketones with ozone in an aqueous reaction medium; a green intermediate compound observable by UV–VIS and ESR at −78 °C was postulated to be a reactive manganese ozonide species.

Transition metal substituted polyoxometalates have been studied as oxidatively resistant analogues of metalloporphyrins. The difference between the porphyrin ligand and the oxotungstate ligands when using peroxygen compounds is considerable because with polyoxometalates reaction can occur both at the transition metal center and the tungstate sites.[1] However, 'metalloporphyrin type' formation of stable Cr(v)=O species[2] and manganese catalyzed oxidation of alkenes has been observed using iodosylbenzene as oxidant.[3] A ruthenium substituted polyoxometalate has also been shown to activate dioxygen in a manner similar to a ruthenium porphyrin system.[4] Ozone is an environmentally benign (dioxygen is the co-product), single oxygen donor. The bond cleavage of alkenes with ozone[5] and the facile deactivation of organic ligands such as porphyrins[6] preclude the use of ozone for catalytic epoxidation of alkenes. The oxidative stability of polyoxometalates now presents an ideal opportunity for investigating the oxidation of alkanes with ozone catalyzed by manganese substituted polyoxometalates.

Catalysis with transition metal substituted polyoxometalates is commonly practiced by transferring the polyoxoanion into an organic solvent using a quaternary ammonium cation. With ozone such an approach is unacceptable due to self-oxidation of the counter cation. Use of lithium cations and 40–50% *t*-butyl alcohol–water allows formation of a neutral homogeneous reaction medium. Typically, 10 μmol $Li_{12}[Mn^{II}_2ZnW(ZnW_9O_{34})_2]$ was dissolved in 2.5 mL 40% *t*-BuOH–water and 1 mmol substrate was added. The mixture was cooled to ≈2 °C and ozone as 2.5 mol% O_3/O_2 was bubbled at 30 mmol $O_3\ h^{-1}$ through the solution for 45 min. Ethylbenzene, 82 mol% conversion, yielded acetophenone (major product, ≈85 mol%) and 1-phenylethanol (minor product, ≈15 mol%). Conversion for a control reaction without catalyst was 15 mol% with similar selectivities. Other manganese containing polyoxometalates such as $K_5PMn^{II}W_{11}O_{39}$, $K_6SiMn^{II}W_{11}O_{39}$, $K_6H_6Si-Mn^{II}_2W_{10}O_{40}$ and $K_{10}[Mn_4(PW_9O_{34})_2]$ gave (based on manganese equivalents) similar (±3 mol%) conversions in 50% *t*-BuOH–water. All other polyoxometalates, $K_x[M_2ZnW(ZnW_9O_{34})_2]$ or $K_xSiMW_{11}O_{39}$, with M = Zn^{2+}, Co^{2+}, Cu^{2+}, Ru^{3+}, Cr^{3+} or Fe^{3+} showed essentially *no* catalytic activity. The reaction was general for alkylaromatics, and cyclic and acyclic alkanes as may be observed in Table 1. The reactivity was as expected, *i.e.* alkylaromatics > cyclic alkanes > acyclic alkanes. The selectivity of the oxidation to ketones as the major product is contrary to what has been observed in manganese porphyrin hydroxylations with ozone where 1-phenylethanol is the major product in ethylbenzene oxidation.[6,7] Also notable is the carbon–carbon bond scission in cumene. Oxidation of cyclohexanol yielded only 20% cyclohexanone under identical reaction conditions and both cumyl alcohol and *tert*-butyl alcohol were (< 1% conversion) inert. These results indicate that alcohols were not intermediate products.

Table 1 Oxidation of alkanes with ozone catalyzed by $Li_{12}[Mn^{II}_2ZnW(ZnW_9O_{34})_2]$ in 40% *t*-BuOH–water[a]

Substrate	Product, mol%	Conversion, mol%
Ethylbenzene	Acetophenone, 85 1-Phenylethanol, 15	82 (15)
Diphenylmethane	Benzophenone, > 98	62
Tetrahydronapthalene	α and β-Tetralone,[b] > 98	56
Cumene	Acetophenone, > 98	38
Cyclohexane	Cyclohexanone, > 98	41
Cyclooctane	Cyclooctanone, > 98	38
n-Decane	2-, 3-, 4- and 5-Decanone,[b] > 98	28

[a] Reaction conditions: 1 mmol substrate, 10 μmol $Li_{12}[Mn^{II}_2ZnW(ZnW_9O_{34})_2]$, 2.5 mL 40% *t*-BuOH–water, 45 min, 2 °C. [b] The amounts of ketone were not quantified.

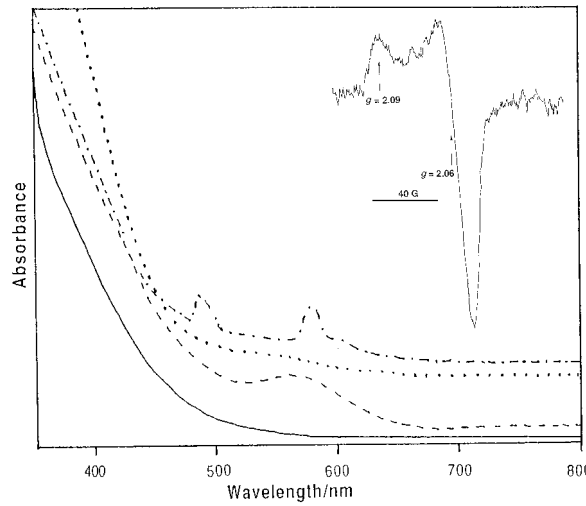

Fig. 1 UV–VIS spectra of various $[Mn_2ZnW(ZnW_9O_{34})_2]^{q-}$ species and the ESR spectrum of the active species. (a) —— $[Mn^{II}_2ZnW(ZnW_9O_{34})_2]^{12-}$, (b) - - - - $[Mn^{III}_2ZnW(ZnW_9O_{34})_2]^{10-}$, (c) ····· brown manganese(v) species, (d) -·-·- green manganese(v)–oxo species. The concentration of $[Mn_2ZnW(ZnW_9O_{34})_2]^{q-}$ was 5×10^{-4} M and the UV–VIS spectra are slightly offset for clarity. Spectra (a) and (b) were taken at ambient temperature, (c) was taken at 2 °C and (d) was taken immediately after removal from −78 °C using a diode array spectrometer. In (d), the optical density is a superposition of the light scattering because of condensation of water on the cuvette and the absorption from the manganese polyoxometalate. The peaks are distorted resulting in a truncated (from the bottom) appearance and with narrow peak widths. The ESR spectrum was taken at 120 K after purging the ozone with N_2.

The reactivity of alkanes was further probed by oxidation of *cis*-decalin. Oxidation at the tertiary position yielded a *trans*-decalol–*cis*-decalol ratio of ≈4 : 1 for both the catalysed and non-catalysed reaction.[8] Oxidation of 1 : 1 cyclohexane–cyclo-

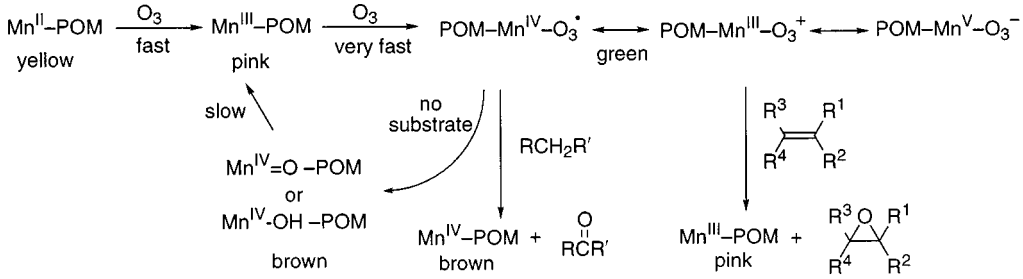

Scheme 1

hexane-d_{12} gave a low kinetic isotope effect (KIE), k_H/k_D = 1.2.[9] The findings that cumene selectively formed acetophenone, *cis*-decalin gave *trans*-decalol as the major product and the low KIE in the oxidation of C_6H_{12}–C_6D_{12} all point to an alkyl radical intermediate in the oxidation of alkanes.

The reaction mechanism was further studied by UV–VIS, Fig. 1. The original catalyst, $Li_{12}[Mn^{II}{}_2ZnW(ZnW_9O_{34})_2]$, is yellow. Upon addition of ozone at 2 °C, the solution within a minute turns pink, (Mn^{III}) λ_{max} = 560 nm, as is known for $[Mn^{III}{}_2ZnW(ZnW_9O_{34})_2]$.[9–10] Further addition of ozone turns the solution brown forming a Mn^{IV}–oxo compound.[11] The later was inactive in a stoichiometric reaction with alkenes.[11] The brown compound was not stable slowly reverting within an hour to the pink manganese(III). In a further experiment, a solution of $Q_{12}[Mn^{II}{}_2ZnW(ZnW_9O_{34})_2]$ (Q = trioctylmethyl ammonium) in acetone was cooled to −78 °C and ozone was passed through the solution yielding a green solution, λ_{max} = 486, 580 nm, Fig. 1(d). Further characterization of the green solution by ESR, Fig. 1 (inset), showed an anisotropic spectrum with peaks at $g_{\|}$ = 2.09 and $g_{\perp}$ = 2.06.

After purging the solution of excess ozone with N_2, stoichiometric amounts of alkenes were added. The solution was brought to −40 °C and turned pink after a few minutes. 2,3-Dimethyl-2-butene and cyclooctene, 80 and 63% conversion respectively, reacted selectively to give epoxides as sole products whereas norbornene (74% conversion) gave 94% *exo* epoxide and 6% 2-norbornanone. *cis*-Stilbene was epoxidized 95% stereoselectively with no formation of the cleavage product, benzaldehyde. An identical experiment carried out with stoichiometric addition of ethylbenzene gave a darkish brown solution and yielded (28 mol% based on manganese) acetophenone–1-phenylethanol, ≈20 : 1.

Our interpretation of the results of the catalytic and stoichiometric oxidation reactions, and the UV–VIS and ESR spectra is summarized in Scheme 1. The initial yellow Mn^{II}–POM is first oxidized to the pink Mn^{III}–POM. The catalytic cycle begins by reaction of Mn^{III}–POM with ozone to give the stipulated active intermediate, the green manganese species. Based on the spectra and the reactivity profile, we assign the green compound as a manganese ozonide complex. The ESR spectrum is attributable to an anisotropic oxygen centered radical species[12] formulated here as POM–Mn^{IV}–O–O–O$^{\cdot}$, formed by reaction of Mn^{III}–POM and O_3. Other canonical forms, POM–Mn^{III}–O–O–O^+ or POM–Mn^{V}–O–O–O^- are possible. The UV–VIS spectrum is supportive of this assignment, since peaks at 450–480 nm are typically observed for ozonides.[12] In the absence of a substrate and/or at higher temperatures the compound quickly decays by reduction or disproportionation to a brown manganese(IV) oxo or hydroxy species (a typical ESR spectrum with peaks at g = 2 and 4 was also observed)[11] and then more slowly to Mn^{III}–POM. The formulation of the green species as an ozonide is consistent with the oxidation reaction profiles observed. In alkane oxidation non-catalytic and catalytic reactions showed practically identical selectivity with a preponderance of the ketones as products, a low KIE, formation of acetophenone from cumene and the formation of an equilibrium mixture of *trans*-decalol–*cis*-decalol from *cis*-decalin. This reactivity clearly supports a reaction occuring through a free alkyl radical intermediate[13] as opposed to a oxygen-rebound mechanism often invoked in metalloporphyrin oxidation.[14] Epoxidation of alkenes with retention of stereochemistry is explainable through reaction of the ozonide, POM–Mn^{III}–O–O–O^+ canonical form, as an electrophile with the nucleophilic alkene with co-formation of molecular oxygen and Mn^{III}–POM.

This research was supported by the Basic Research Foundation administered by the Israel Academy of Sciences and Humanities.

Notes and References

† E-mail: ronny@vms.huji.ac.il

1 R. Neumann and M. Gara, *J. Am. Chem. Soc.*, 1995, **117**, 5066.
2 D. E. Katsoulis and M. T. Pope, *J. Chem. Soc., Chem. Commun.*, 1986, 1186; A. M. Khenkin and C. L. Hill, *J. Am. Chem. Soc.*, 1993, **115**, 8178.
3 C. L. Hill and R. B. Brown, *J. Am. Chem. Soc.*, 1986, **108**, 536; D. Mansuy, J.-F. Bartoli, P. Battioni, D. K. Lyon and R. G. Finke, *J. Am. Chem. Soc.*, 1991, **113**, 7222.
4 R. Neumann and M. Dahan, *Nature*, 1997, **388**, 353.
5 P. S. Bailey, *Ozonation in Organic Chemistry*, Academic Press, New York, 1978.
6 S. Camperstrini, A. Robert and B. Meunier, *J. Org. Chem.*, 1991, **56**, 3725; Z. Gross, S. Nimri and L. Simkhovich, *J. Mol. Catal. A: Chem.*, 1996, **113**, 231; Z. Gross and L. Simkhovich, *J. Mol. Catal. A: Chem.*, 1997, **117**, 243.
7 B. Meunier, *Chem. Rev.*, 1992, **92**, 1411.
8 J. R. Lindsay Smith and P. R. Sleath, *J. Chem. Soc., Perkin Trans. 2*, 1983, 1165.
9 J. T. Groves and T. E. Nemo, *J. Am. Chem. Soc.*, 1983, **105**, 6243.
10 C. M. Tourné, G. F. Tourné and F. Zonnevijlle, *J. Chem. Soc., Dalton Trans.*, 1991, 143.
11 X. Zhang, M. T. Pope, M. R. Chance and G. B. Jameson, *Polyhedron*, 1995, **14**, 1381; X. Zhang, G. B. Jameson, C. J. O'Connor and M. T. Pope, *Polyhedron*, 1996, **15**, 917; X. Zhang, C. J. O'Connor, J. B. Jameson and M. T. Pope, *Inorg. Chem.*, 1996, **35**, 30; X. Zhang and M. T. Pope, *J. Mol. Catal. A: Chem.*, 1996, **114**, 201.
12 S. Schlick, *J. Chem. Phys.*, 1972, **56**, 654; J. Steffen, W. Hesse, M. Jansen and D. Reinen, *Inorg. Chem.*, 1991, **30**, 1923; W. Hesse, M. Jansen and W. Schnick, *Prog. Solid State Chem.*, 1989, **19**, 47.
13 E. T. Denisov and T. G. Denisova, *Kinet. Catal.* (*Engl. Transl.*), 1996, **37**, 46.
14 J. T. Groves, *J. Chem. Educ.*, 1985, **62**, 928.

Received in Cambridge, UK, 10th June 1998; 8/04396E

Supramolecular metallocalixarene chemistry: linking metallocalixarenes through imido bridges

Vernon C. Gibson,*[a]† Carl Redshaw,[a] William Clegg[b] and Mark R. J. Elsegood[b]

[a] *Department of Chemistry, Imperial College, South Kensington, London, UK SW7 2AY*
[b] *Department of Chemistry, University of Newcastle upon Tyne, Newcastle upon Tyne, UK NE1 7RU*

The synthesis and structures of two novel extended-array metallocalixarenes, derived from the ring-opening of imido–molybdenum precursors, are described.

The ability of calixarenes to act as receptors for a variety of guest molecules is a feature of central importance to their chemistry.[1] The development of supramolecular structures incorporating calixarenes offers an opportunity to extend calixarene host–guest interactions to two- and possibly three-dimensional lattices. Although supramolecular structures have been seen as a result of guest–host interactions,[2] and metal–oxo bridges,[3] clear methodologies for covalently linking metallocalixarenes have not, to our knowledge, been described. Here, we report the synthesis and solid state structures of two novel metallocalixarenes derived from the ring-opening of imido–molybdenum precursors. In one case the metallocalixarenes are linked by hydrogen bonding between pendant amino groups and in the other by a covalent linkage between imido ligands that gives rise to a two-dimensional array of 'cup-to-cup' metallocalixarene units.

Treatment of the tetraimido dimolybdenum complex **1**[4] with two molar equivalents of H_4L (H_4L = calix[4]arene) in refluxing toluene affords, after work-up, the bridged complex {[Mo(NCMe)L]$_2$[3,5-Pr$^i_2$-4-NC$_6$H$_2$)$_2$CH$_2$]} **2** according to Scheme 1.‡ Complex **2** is presumed to form *via* initial displacement of two chloride ligands (per molybdenum), followed by proton transfer to one of the imido ligands to release the *para*-bridged dianiline. Crystals suitable for X-ray diffraction§ were grown from acetonitrile at room temperature. The molecular structure is shown in Fig. 1(a) and selected bond lengths and angles are given in the caption. Each molybdenum possesses a pseudo-octahedral geometry similar to that found in the monometallocalix[4]arene analogue of **1**.[5] The molybdenum atoms are displaced from the O_4 mean planes towards the imido nitrogens of the bridging ligand by 0.246 and 0.247 Å. The molecule has approximate C_2 symmetry, the rotation axis running through the C(13) atom. Significantly, the metallocalixarenes are organised in a 'cup-to-cup' arrangement which gives rise to a calixarene 'socket' [Fig. 1(b)], thus offering the potential for hosting guest molecules in the cooperatively aligned calixarene cavities.

In an extension of this work, we then targetted metallocalixarene species with pendant amino functionalities which we envisaged would allow the linking of metallocalixarene units *via*, for example, amide bonds. Treatment of the chelating bis(imido)molybdenum complex {Mo(OBu^t)$_2$[(2-NC$_6$H$_4$)$_2$-CH$_2$CH$_2$]} **3** with H_4L (one equivalent) in toluene affords, after work-up, the monoimido calixarene complex {[Mo(N-CMe)L][2-NC$_6$H$_4$CH$_2$CH$_2$C$_6$H$_4$NH$_2$-2′]} **4** in which the imido ligand contains a 'free' amino functionality (Scheme 1). Complex **4** is presumed to form *via* loss of two *tert*-butanol ligands followed by transfer of two protons to one of the imido ligands to release the pendant amino group.[5] The IR spectrum of **4** has a strong ν(N–H) stretch at 3165 cm^{-1}, indicative of an

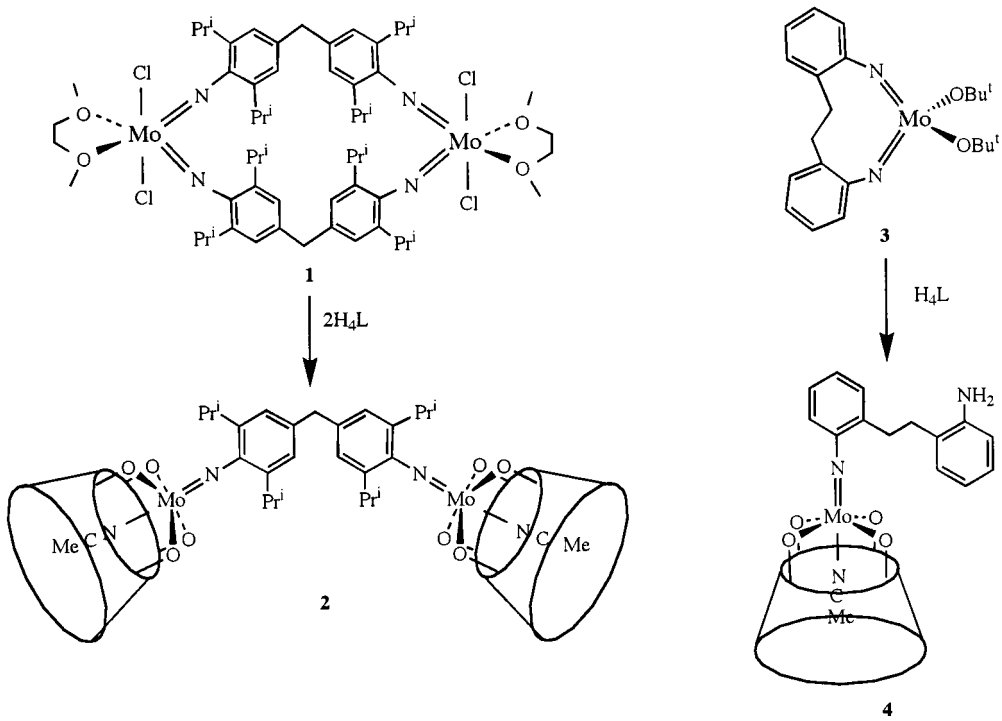

Scheme 1

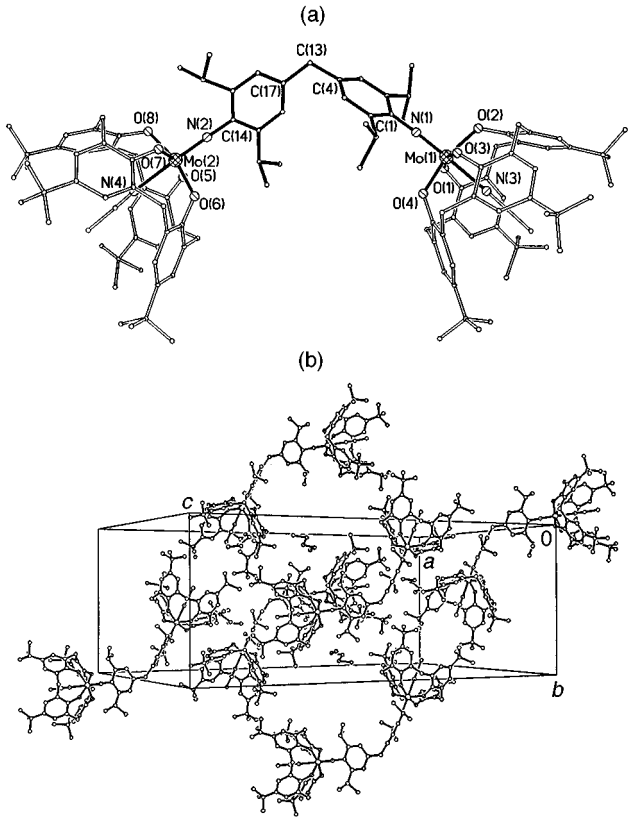

Fig. 1 Molecular structure of **2** without H atoms: (a) showing the atom labelling; (b) the crystal packing diagram showing the 'cup-to-cup' alignment of the metallocalixarene units. Selected bond lengths (Å) and angles (°): Mo(1)–N(1) 1.735(5), Mo(1)–O(1) 1.936(5), Mo(1)–O(2) 1.941(4), Mo(1)–O(3) 1.936(5), Mo(1)–O(4) 1.949(5), Mo(1)–N(3) 2.304(6), Mo(2)–N(2) 1.716(5), Mo(2)–O(5) 1.948(5), Mo(2)–O(6) 1.942(4), Mo(2)–O(7) 1.920(4), Mo(2)–O(8) 1.953(5); Mo(1)–N(1)–C(1) 176.7(5), Mo(2)–N(2)–C(14) 178.8(5), C(4)–C(13)–C(17) 112.2(5) (a colour version is provided at: http://www.rsc.org./suppdata/cc/1998/1969.

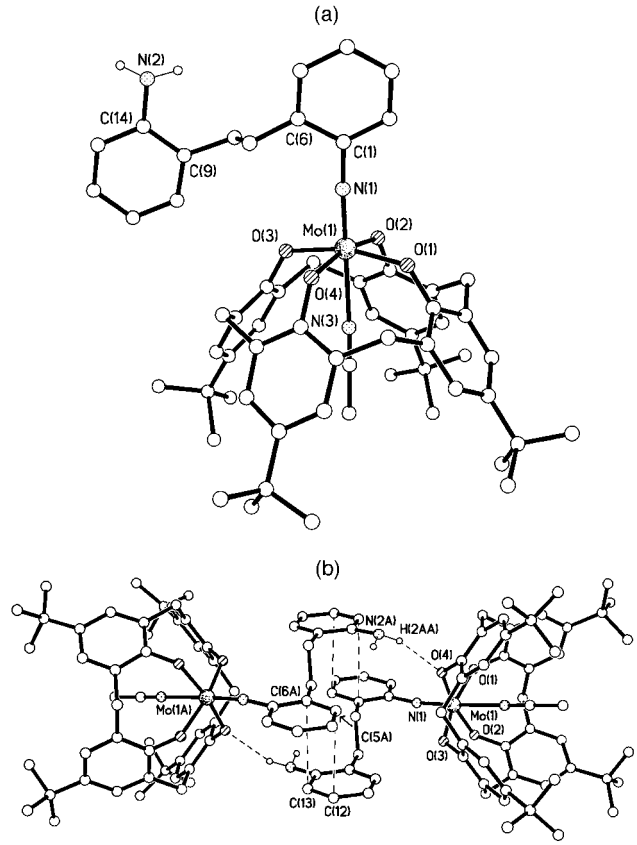

Fig. 2 Molecular structure of **4** without hydrogen atoms: (a) showing the atom labelling; (b) showing the intermolecular interactions between adjacent metallocalixarene units. Selected bond lengths (Å) and angles (°): Mo(1)–N(1) 1.729(2), Mo(1)–O(1) 1.9419(18), Mo(1)–O(2) 1.9334(16), Mo(1)–O(3) 1.9323(18), Mo(1)–O(4) 1.9713(16), Mo(1)–N(3) 2.326(2); Mo(1)–N(1)–C(1) 171.60(19).

uncoordinated NH_2 group, together with a strong ν(C–N) stretch at 1287 cm^{-1}. The structure was confirmed by an X-ray crystallographic study and is shown in Fig. 2(a). Each of the two aromatic rings of the imido ligand interact weakly with two aromatic carbons on an adjacent imido ligand [C(5)···C(12A) 3.449, C(6)···C(13A) 3.561 Å], and there is a hydrogen-bonding interaction between one of the amine hydrogens and a calixarene oxygen atom [O(4)···H(2AA) 2.188 Å] [Fig. 2(b)].

The complexes described here represent the first steps towards the covalent linking of metallocalixarene units and the development of tailored supramolecular metallocalixarene arrays.

The Engineering and Physical Sciences Research Council is thanked for financial aupport.

Notes and References

† E-mail: v.gibson@ic.ac.uk

‡ Satisfactory elemental analyses have been obtained on **2** and **4**. Selected spectroscopic data for **2**: ^{1}H NMR ($CDCl_3$, 300 MHz, 298 K) δ 7.12 (m, 20H, aromatic H), 4.68 [spt, 4H, $^3J_{HH}$ 6.8, C*H*$(CH_3)_2$], 4.43 (d, 8H, $^2J_{HH}$ 12.2, CH_2), 4.26 (s, 2H, ArC*H*$_2$Ar), 3.23 (d, 8H, $^2J_{HH}$ 12.2, CH_2), 1.53 [d, 24H, $^3J_{HH}$ 6.8 Hz, (C*H*$_3$)$_2$CH], 1.21 [m, 72H, $(CH_3)_3$C], −0.08 (s, 6H, MeCN). For **4**: ^{1}H NMR ($CDCl_3$, 300 MHz, 298 K) δ 8.05–6.50 (overlapping m, 16H, aromatic H), 4.42 (d, 4H, $^2J_{HH}$ 12.2, CH_{2calix}), 3.95 (br s, 2H, NH_2), 3.67 (t, 2H, $^2J_{HH}$ 7.4, ArC*H*$_2$), 3.36 (t, 2H, $^2J_{HH}$ 7.4, ArC*H*$_2$), 3.32 (d, 4H, $^2J_{HH}$ 12.2 Hz, CH_{2calix}), 2.03 (s, 3H, MeCN), 1.21 [s, 36H, (C*H*$_3$)$_2$CH], −0.08 (s, 3H, MeCN).

§ *Crystal data* for **2**·2C_5H_{12}: $C_{117}H_{144}Mo_2N_4O_8$·2C_5H_{12}, M = 2070.5, monoclinic, space group *I*2/*a* (non-standard setting of *C*2/*c* avoiding large β angle), a = 34.891(2), b = 16.2235(11), c = 45.318(3) Å, β = 101.303(2)°, U = 25155(3) Å^3, Z = 8, D_c = 1.093 g cm^{-3}, μ = 0.251 mm^{-1} (Mo-Kα, λ = 0.71073 Å), T = 160 K. 51852 Reflections were measured on a Siemens SMART CCD area-detector diffractometer and corrected for absorption. The structure was solved by direct methods and refined by full-matrix least-squares on F^2 values of all 16446 unique data (R_{int} = 0.1135) with restraints on disordered substituents and solvent molecules; $R' = \{\Sigma[w(F_o^2 - F_c^2)^2]/\Sigma[w(F_o^2)^2]\}^{1/2}$ = 0.2589 for all data, conventional R = 0.0779 on F values of 11304 reflections with $F_o^2 > 2\sigma(F_o^2)$; goodness of fit = 1.086 on F^2 for 1432 parameters and 423 restraints. Largest peak in final difference map 1.224 e Å^{-3} (> 3.2 Å from all atoms, possibly further unresolved disordered solvent). Programs: Siemens SMART (control), SAINT (integration), SHELXTL and local programs.

Crystal data for **4**: $C_{60}H_{69}MoN_3O_4$, M = 992.12, triclinic, space group $P\bar{1}$, a = 12.5913(8), (b) = 14.5121(9), c = 14.5797(8) Å, α = 81.253(2), β = 84.564(2), γ = 84.657(2)°, U = 2612.9(3) Å^3, Z = 2, D_c = 1.261 g cm^{-3}, μ = 0.300 mm^{-1} (Mo-Kα, λ = 0.71073 Å), T = 160 K. 16442 Reflections were measured as for **2** yielding 11367 unique data (R_{int} = 0.0193). The structure was solved by Patterson synthesis and refined as for **2** with restraints on one disordered *tert*-butyl group; R' = 0.1004 for all data, R = 0.0412 on F values of 9626 reflections with $F_o^2 > 2\sigma(F_o^2)$; goodness of fit = 1.061 on F^2 for 658 parameters and 139 restraints. Largest peak in final difference map 0.686 e Å^{-3}. CCDC 182/971.

1 *Calixarenes* by C. D. Gutsche, Royal Society of Chemistry, Cambridge, 1989.
2 A. Zanotti-Gerosa, E. Solari, L. Giannini, C. Floriani, A. Chiesi-Villa and C. Rizzoli, *Chem. Commun.*, 1996, 119; J. A. Acho, T. Ren, J. W. Yuu and S. J. Lippard, *Inorg. Chem.*, 1995, **34**, 5226.
3 B. Xu and T. M. Swager, *J. Am. Chem. Soc.*, 1993, **115**, 1159.
4 V. C. Gibson, C. Redshaw, W. Clegg, M. R. J. Elsegood, U. Siemeling and T. Turk, *J. Chem. Soc., Dalton Trans.*, 1996, 4513.
5 V. C. Gibson, C. Redshaw, W. Clegg and M. R. J. Elsegood, *J. Chem. Soc., Chem. Commun.*, 1995, 2371.

Received in Basel, Switzerland, 5th March 1998; 8/01808A

Dediazoniation reactions of arenediazonium ions under solvolytic conditions: fluoride anion abstraction from trifluoroethanol and α-hydrogen atom abstraction from ethanol

Peter S. J. Canning, Katharine McCrudden, Howard Maskill*† and Brian Sexton

Chemistry Department, University of Newcastle upon Tyne, Newcastle upon Tyne, UK NE1 7RU

Arenediazonium salts decompose thermally and photochemically in trifluoroethanol to yield trifluoroethyl ethers and (in part by fluoride abstraction from the solvent) fluoroarenes; the less reactive compounds in trifluoroethanol decompose readily in ethanol to give arenes in a radical reaction involving abstraction of the α-hydrogen from the ethanol.

Dediazoniation reactions are amongst the oldest known industrial organic chemical reactions, and their mechanisms are also amongst the earliest to have been investigated.[1] For some years, thermal decomposition of arenediazonium tetrafluoroborates has been used as a route for making fluoroarenes—compounds of increasing importance for the production of pharmaceuticals and agrochemicals. The Balz–Schiemann reaction is one method which involves isolation of the salt and its subsequent thermal decomposition,[2] a potentially hazardous process. Other methods involve decomposition of diazonium salts in liquid hydrogen fluoride,[3] but these also have obvious potential for danger. We have been investigating alternative procedures for decomposing diazonium salts with a view to (i) understanding better the mechanisms involved, and (ii) developing a method more environmentally acceptable and less hazardous than ones currently available. In the course of these investigations, we have discovered that aryl cations (generated by loss of dinitrogen from the arenediazonium ions) are able to abstract fluoride from fluoro alcohols in competition with being captured by the hydroxylic residue of the alcohol. We have also shown that the intermediates involved in the decomposition in ethanol of arenediazonium cations with electron-withdrawing substituents abstract an α-hydrogen from the ethanol. Additionally, we have demonstrated that, under photolysis in trifluoroethanol (TFE), otherwise very unreactive arenediazonium ions react very readily. This product analytical evidence, and the attendant kinetics studies, contribute further to ongoing investigations world-wide of the chemistry of exceedingly short-lived reactive intermediates.

Table 1 Kinetics results[a] for the solvolysis of arenediazonium tetrafluoroborates $XC_6H_4N_2^+ BF_4^-$

Solvent	X	$k_{25}/10^{-6}s^{-1}$	$\Delta H^{\ddagger}$/kJ mol^{-1}	$\Delta S^{\ddagger}$/J K^{-1} mol^{-1}
TFE	*m*-NO_2	0.60	124	54
TFE	*m*-F	1.18	124	59
TFE[b]	H	92.1	114	62
TFE	*m*-OMe	873	103	42
EtOH	*m*-OMe	409	97	14
EtOH	*m*-F	941	64	−87
EtOH	H	232	75	−64

[a] Rate constants at 25 °C were extrapolated using the Eyring equation from average values obtained at other temperatures. Standard deviations on individual rate constants were generally about 1% and reproducibility was better than about 5%. The estimated uncertainty on $\Delta H^{\ddagger}$ is *ca.* 6 kJ mol^{-1} and 12 J K^{-1} mol^{-1} on $\Delta S^{\ddagger}$. [b] Previously reported values (ref. 5): k_{25} = 68.3 × 10^{-6} s^{-1}, $\Delta H^{\ddagger}$ = 114 kJ mol^{-1} and $\Delta S^{\ddagger}$ = 58 J K^{-1} mol^{-1}.

Table 1 gives kinetics results for arenediazonium tetrafluoroborates investigated by our normal UV method.[4,5] In TFE, a solvent which generally promotes heterolytic reactions, we observe high enthalpies of activation and appreciably positive entropies of activation in agreement with previous results.[5,6] Such findings are accommodated by the Zollinger heterolytic mechanism[7] [Scheme 1, where Nu = nucleophile

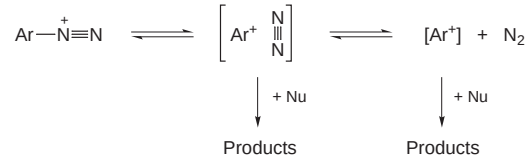

Scheme 1

(*e.g.* solvent)] except that under our reaction conditions, the first two steps will be essentially irreversible. In accord with earlier workers, we also observe that electron-withdrawing substituents decrease reactivity,[5,6,8] an effect brought about principally through increases in the enthalpy of activation (Table 1). For the *m*-methoxy compound, the most reactive of these compounds in TFE, we note comparable reactivity in ethanol. However, for the much less reactive *m*-fluoro analogue in TFE, we note unexpectedly high reactivity in ethanol, and quite different activation parameters; $\Delta H^{\ddagger}$ is now much lower and $\Delta S^{\ddagger}$ strongly negative, signalling a different mechanism.

In TFE, the products of the thermally induced solvolyses are principally the aryl trifluoroethyl ethers, but between 10 and 35% of aryl fluorides are observed (Table 2). These compounds

Table 2 Product analyses[a] from solvolytic decompositions of arenediazonium salts $XC_6H_4N_2^+ Z^-$ Products (%)

Solvent/ROH	X	Z^-	Mode	ArOR	ArF	ArH
TFE	H	BF_4^-	thermal	72	28	< 0.1
TFE	H	Cl^-	thermal	90	10	—
TFE[b]	H	BF_4^-	thermal	66	34	—
TFE	H	BF_4^-	*hν*	57	43	—
TFE	*m*-F	BF_4^-	thermal	65	35	< 0.1
TFE	*m*-F	BF_4^-	*hν*	67	33	< 0.1
TFE	*m*-NO_2	BF_4^-	*hν*[c]	57	43	—
EtOH	H	BF_4^-	thermal	96	4	< 1
EtOH	*m*-F	BF_4^-	thermal	20	< 0.1	80
EtOH	*m*-F	BF_4^-	*hν*	15	< 0.1	85
EtOH	*m*-NO_2	BF_4^-	thermal	8	< 1	92[d]

[a] Analyses were carried out by GLC, usually with undecane as internal standard. Each reaction was carried out at least twice, and up to *ca.* six chromatograms were obtained for each reaction. Yields quoted are normalised (total = 100%), absolute recoveries being variable between *ca.* 80–100%. [b] Reaction contained 0.63 mol dm^{-3} $NaBF_4$. [c] This reaction was too slow thermally for a reliable product analysis to be obtained. [d] When the reaction was carried out in CH_3CD_2OH, *m*-$DC_6H_4NO_2$ was isolated by preparative GLC, and characterised by mass spectrometry and ^{1}H NMR spectroscopy.

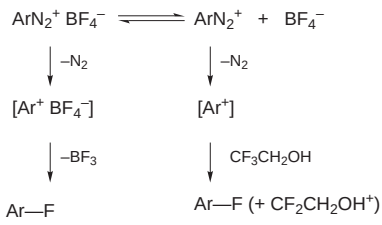

Scheme 2

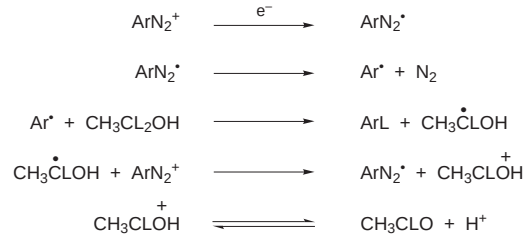

Scheme 3

were identified by comparison with authentic samples, and in some cases were isolated by preparative GLC and characterised. If aryl radical intermediates are the source of this fluorine transfer, the same intermediates would also be expected to give some degree of hydrogen transfer. No appreciable yields of reduction product were detected in reactions in TFE, so aryl cations are implicated as the source of fluorine abstraction. Aryl fluorides had previously been detected from reactions of very dilute arenediazonium tetrafluoroborates in aqueous TFE in which the reactants will have been fully dissociated. Since aryl cations are exceedingly short lived,[9] they cannot diffuse through the medium and select very dilute tetrafluoroborate as a reaction partner. Consequently, the TFE component of the solvent was implicated as the source of the fluorine in the product aryl fluorides. This was confirmed by solvolysing benzenediazonium chloride in TFE and obtaining 10% fluorobenzene (compared with 28% from the tetrafluoroborate). We conclude that the fluoroarenes generated from arenediazonium tetrafluoroborates in TFE arise from fluoride abstraction by the aryl cation in part from the solvent and in part from the tetrafluoroborate anion within undissociated ion-pairs (Scheme 2) (where possible involvement of ion-molecule pair intermediates, as in Scheme 1, has been omitted for clarity). In agreement with this proposal, addition of sodium tetrafluoroborate (which will increase the degree of ion-pair association) led to a modest increase in the yield of fluoroarene in TFE. We have no evidence yet regarding the identity of the species remaining after fluoride abstraction from the trifluoroethanol, $(CF_2CH_2OH)^+$, or about whether the fluoride abstractions are concerted or stepwise.

Strongly electron-withdrawing substituents decrease the reactivity of benzenediazonium tetrafluoroborate in TFE, and high temperatures or long times are required for their reactions (Table 1). However, we observed that photolysis using a low wattage UV source at room temperature of a dilute solution in TFE effected complete reaction within minutes; similar observations in liquid hydrogen fluoride have already been reported.[3] Analysis by GLC confirmed that the products (aryl fluoride and aryl trifluoroethyl ether) are the same as in the very slow thermal reaction, and that the yields are rather similar (Table 2). It appears, therefore, that photolysis in TFE involves the same aryl cation intermediates as the much slower thermal reaction.

Analytical results using ethanol as solvent confirmed the kinetics results—the reaction is qualitatively different from that in TFE for compounds with electron-withdrawing substituents. It was already known that ethanol can act as a reducing agent for some arenediazonium ions,[10] and that analogous reactions in methanol involve radical intermediates.[11] Additionally, there is a report that the reaction in methanol involves abstraction of the α-hydrogen.[12] Ethanolysis of *m*-fluoro- and *m*-nitro-benzenediazonium tetrafluoroborates gives high yields of the reduction product, and the former gives a very similar product analysis under photolysis at room temperature. The parent compound (X = H) gives very little reduction and (not surprisingly) very little fluorobenzene under these reaction conditions. The product analysis of the parent compound, therefore, does not provide evidence of a change in mechanism upon transfer from TFE to ethanol intimated by the changed kinetics parameters; at the present we have no ready explanation of this. When *m*-nitrobenzenediazonium tetrafluoroborate was solvolysed in [1,1-$^2H_2$]ethanol (CH_3CD_2OH), [3-^{2}H]nitrobenzene was isolated by preparative GLC and identified by ^{1}H NMR spectroscopy and mass spectrometry. Given the characteristically different kinetics parameters for these arenediazonium salts deactivated in the heterolytic pathway by electron-withdrawing substituents and the different product analytical profiles in ethanol, a different mechanism must be involved. Taking into account the previous evidence for reactions in methanol,[11] and proof that the intermediate abstracts an α-hydrogen from the ethanol, we propose the radical chain mechanism in Scheme 3 based upon earlier proposals by DeTar[13] and Bunnett.[11] The reductant in the initiating step has not yet been identified, but is almost certainly ethanol itself.

We thank the EPSRC for studentships to P. S. J. C., K. M. and B. S., and Zeneca (formerly ICI) for financial support; we also thank Drs J. H. Atherton and D. J. Moody of Zeneca for helpful and stimulating discussions.

Notes and References

† E-mail: h.maskill@ncl.ac.uk

1 H. Zollinger, *Diazo and Azo Chemistry; aliphatic and aromatic compounds*, Interscience, New York, 1961; W. Ando, *The Chemistry of Diazonium and Diazo Groups*, ed. S. Patai, Interscience, New York, 1978.
2 G. Balz and G. Schiemann, *Chem. Ber.*, 1927, **60**, 1186.
3 N. Yoneda and T. Fukuhara, *Tetrahedron*, 1996, **52,** 23.
4 R. M. Banks, H. Maskill, R. Natarajan and A. A. Wilson, *J. Chem. Soc., Perkin Trans. 2*, 1980, 427; I. M. Gordon and H. Maskill, *J. Chem. Soc., Perkin Trans. 2*, 1991, 1951.
5 H. Maskill and K. McCrudden, *Croat. Chem. Acta*, 1992, **65,** 567.
6 D. F. DeTar and A. R. Ballentine, *J. Am. Chem. Soc.*, 1956, **78,** 3916; C. G. Swain, J. E. Sheats and K. G. Harbison, *J. Am. Chem. Soc.*, 1975, **97,** 783.
7 R. G. Bergstrom, R. G. M. Landells, G. H. Wahl and H. Zollinger, *J. Am. Chem. Soc.*, 1976, **98**, 3301; R. G. Bergstrom, G. H. Wahl and H. Zollinger, *Tetrahedron Lett.*, 1974, 2975; I. Szele and H. Zollinger, *J. Am. Chem. Soc.*, 1978, **100**, 2811; Y. Hashida, R. G. M. Landells, G. E. Lewis, I. Szele and H. Zollinger, *J. Am. Chem. Soc*., 1978, **100**, 2816.
8 M. L. Crossley, R. H. Kienle and C. H. Benbrook, *J. Am. Chem. Soc.*, 1940, **62,** 1400.
9 R. A. McClelland, V. M. Kanagasabapathy, N. S. Banait and S. Steenken, *J. Am. Chem. Soc.*, 1992, **114,** 1816.
10 N Kornblum, *Org. React.*, 1944, **2**, 262.
11 (*a*) J. F. Bunnett and C. Yijima, *J. Org. Chem.*, 1977 **42**, 639; (*b*) T. J. Broxton, J. F. Bunnett and C. H. Paik, *J. Org. Chem.*, 1977 **42**, 643.
12 L. Melander, *Ark. Kemi*, 1951, **3,** 525 [cited in ref. 11(*b*)].
13 D. F. DeTar and T. Kosuge, *J. Am. Chem. Soc.*, 1958, **80,** 6072; D. F. DeTar and M. N. Turetzky, *J. Am. Chem. Soc.*, 1955, **77,** 1745.

Received in Cambridge, UK, 22nd June 1998; 8/04686G

Multiple pathways in the cleavage of benzyl groups from phosphonium salts by lithium aluminium hydride

Neil Donoghue and Michael J Gallagher*†

School of Chemistry, University of New South Wales, Sydney 2052, Australia

Reduction of benzylphosphonium salts by $LiAlD_4$ affords a phosphine and $PhCH_2D$, 2-$DC_6H_4CH_3$ and $PhCH_3$; pathways involving P^V and P^{VI} intermediates are proposed to account for these products.

Benzyl groups are readily removed from benzylphosphonium salts by $LiAlH_4$ in THF to give a phosphine and toluene in good yields.[1,2] The reaction forms the basis of a general method for the preparation of unsymmetrical phosphines[1b] and has found use in the synthesis of cyclic phosphines,[3] but attempts to extend the utility of the reaction to the cleavage of phenyl groups from the more readily accessible arylphosphonium salts have met with limited success,[4] loss of either alkyl or aryl groups or both occurring in an apparently inconsistent way. Reduction of ylides from alkyltriphenylphosphonium salts proceeds exclusively with loss of phenyl[4,5] even when the ylidic carbon is benzylic, establishing that reduction of salts does not proceed *via* ylide formation. Reduction of resolved chiral benzylic salts occurs with partial or complete racemisation at phosphorus,[6] implying that the reaction proceeds *via* a configurationally mobile phosphorane of the type R_4PH. Such compounds have only been observed to form from phosphonium salts in the specialised case of the spirobisbiphenylyl system **1**.[7]

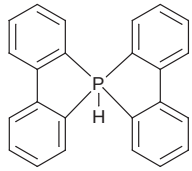

1

Theoretical considerations[8] suggest that the decomposition, shown in eqn. (1), is an allowed concerted process for two

$$R_5P \rightarrow R_3P + RR \quad (1)$$

substituents in the equatorial plane of a trigonal bipyramid, suggesting a reasonable pathway for the overall reduction, but it is not obvious why benzyl groups are a favoured leaving group if ionic stability of the leaving group were not an important factor, as had been generally supposed.[2] A possible reason could be a cheleotropic rearrangement of an intermediate phosphorane **2** with transfer of hydrogen from phosphorus to the *ortho* carbon of the benzyl group, followed by aromatisation of the methylenecyclohexa-2,4-diene thus expelled (Scheme 1).

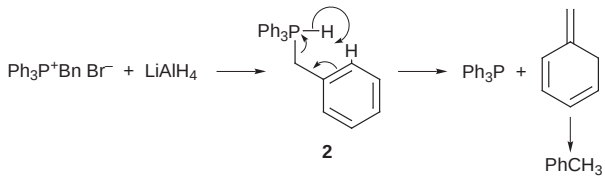

2

Scheme 1

A similar pathway (Scheme 2) can be visualised for allylphosphonium salts and reported reductions of these by

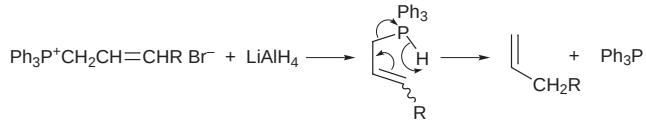

3

Scheme 2

$LiAlH_4$ appear to proceed exclusively with allylic inversion ('S_N2' substitution').[2b] Thus, reduction of (*E*)-cinnamyltriphenylphosphonium bromide with $LiAlD_4$ yields triphenylphosphine and 1-phenyl[1-^{2}H]but-2-ene. Further, these allylic cleavages proceed more rapidly with phosphonium salts than they do with the analogous ammonium salts, which are similarly cleaved but largely without allylic inversion.[9]

We now report that reduction of benzyltriphenylphosphonium bromide with $LiAlD_4$ in refluxing THF (5 h) affords toluene, [α-^{2}H]toluene and [*o*-^{2}H]toluene in a ratio of approximately 1:1:1 as determined by ^{1}H, ^{2}H and ^{13}C NMR spectroscopy; the other product, Ph_3P, showed no deuterium incorporation. The identity of the *o*-deuterated toluene was further confirmed by HSQC 2D ^{1}H/^{13}C{^{1}H} NMR and by comparison with authentic material obtained by quenching 2-$CH_3C_6H_4MgBr$ with D_2O. Analogous comparisons confirmed the absence of detectable amounts of *m*- or *p*-deuterated toluene in the salt reduction. No exchange is observed when toluene is refluxed with $LiAlD_4$ in THF or when the product mixture of toluenes is treated with $LiAlH_4$, indicating that the three hydrocarbons all arise in the reduction process.

We extended the examination to the products from the $LiAlD_4$ reduction of all the phosphonium salts, $Bn_nP^+Ph_{4-n}$ Br^- (n = 0–4) and the results are summarised in Table 1. Ph_4P^+ Br^- cannot, of course, give toluene but under the same conditions it affords a mixture of PhH (21%) and PhD (79%) measured by mass spectrometry.

We have elsewhere presented evidence that the reduction of phosphonium salts with metal hydrides proceeds *via* a number of intermediates,[10] **4–6** (Scheme 3). Clearly, formation of R^-, which subsequently abstracts a proton from THF, could account for the formation of undeuterated hydrocarbon and decomposition of **2** by concerted processes could lead to either α- or *o*-deuterated toluene. Part of the [α-^{2}H]toluene will arise during the conversion of the 6-[^{2}H]methylenecyclohexa-1,3-diene to

Table 1 Yields of toluenes formed by reduction of $Bn_nP^+Ph_{4-n}$ Br^- with $LiAlD_4$

	Yield (%)		
n	$PhCH_3$	$PhCH_2D$	2-$DC_6H_4CH_3$
4	9	86	5
3	7	84	9
2	11	62	27
1	31	31	38
0	21[a]		79[b]

[a] C_6H_6. [b] C_6H_5D.

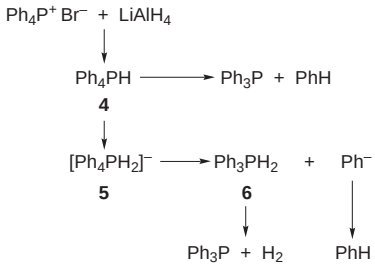

Scheme 3

toluene but there is too much deuterium on the benzylic carbon to be all accounted for in this way, since the ^{1}H–^{2}H isotope effect should ensure that the bulk of the deuterium originally in the *ortho* position, remains there. Therefore, most of the deuterium in $PhCH_2D$ arises by other processes of which there seem to be two, either a concerted loss of deuterium and $PhCH_2$ from **4**, or S_N2 type displacement at the benzylic carbon by hydride ion equivalent. We are unable to determine the relative contributions of these two pathways but we have observed that benzyldimethylphenylammonium bromide exclusively loses $PhCH_2D$ when refluxed in THF with $LiAlD_4$ [eqn. (2)], and,

$$Ph(CH_3)_2N^+CH_2Ph\ Br^- + LiAlD_4 \rightarrow PhNMe_2 + PhCH_2D \quad (2)$$

since an N^V intermediate is very improbable, this presumably goes *via* an S_N2 related process. Also, thermal decomposition of R_5P has resulted in products understandable in terms of concerted loss of two groups [eqn. (1)], *e.g.* the dissociation of PCl_5 to PCl_3 and Cl_2.[11] The exclusive *ortho* selectivity is, we believe, best explained by a concerted intramolecular hydride transfer since an S_N2' attack on the ring might reasonably be expected to give some of the [4-^{2}H]toluene. An alternative process involving radicals, formed by homolysis of P–C (or P–H) bonds, has not been excluded but the exclusive *ortho* deuterium transfer and the absence of the coupling product, 1,2-diphenylethane, lead us to favour a concerted pathway.

We thank the Australian Research Council for support.

Notes and References

† E-mail: m.gallagher@unsw.edu.au

1 (*a*) W. J. Bailey and S. A. Buckler, *J. Am. Chem. Soc.*, 1957, **79**, 3567; (*b*) W. J. Bailey, S. A. Buckler and F. Marktscheffel, *J. Org. Chem.*, 1960, **25**, 1996.
2 (*a*) H. J. Cristeau and F. Plénat, *The Chemistry of Organophhosphorus Compounds*, Interscience, Chichester, 1994, vol. 3, pp. 138–140; (*b*) J. Seyden-Penne, *Reductions by the Alumino- and Borohydrides in Organic Synthesis*, 2nd edn., Wiley-VCH, New York, 1997, pp. 34–36.
3 R. C. Hinton and F. G. Mann, *J. Chem. Soc.*, 1959, 2835.
4 S. T. D. Gough and S. Trippett, *J. Chem. Soc.*, 1961, 4263.
5 V. D. Makhaev and P. Borisova, *Zh. Obsch. Khim.*, 1984, **54**, 2550.
6 L. Horner, L. Hoffmann and P. Beck, *Chem.Ber.*, 1958, **91**, 1583; W. E. McEwen, K. F. Kumli, A. Blade-Font, M. Zanger and C. A. Vander Werf, *J. Am. Chem. Soc.*, 1964, **86**, 2378; P. D. Henson, K. Nauman and K. Mislow, *J. Am. Chem. Soc.*, 1969, **91**, 5645; L. Horner and M. Ernst, *Chem.Ber.*, 1970, **103**, 318.
7 D. Hellwinkel, *Angew. Chem., Int. Ed. Engl.*, 1966, **5**, 968.
8 R. Hoffmann, J. M. Howell and E. L. Muetterties, *J. Am. Chem. Soc.*, 1972, **94**, 3047; F. Keil and W. Kutzelnigg, *J. Am. Chem. Soc.*, 1975, **97**, 3623; J. M. Howell, *J. Am. Chem. Soc.*, 1977, **99**, 7447; W. Kutzelnigg and J. Wasilewski, *J. Am. Chem. Soc.*, 1982, **104**, 953; G. Trinquier, J.-P. Daudey, G. Cariana and Y. Madaule, *J. Am. Chem. Soc.*, 1984, **106**, 4794; C. S. Ewig and J. R. Van Wazer, *J. Am. Chem. Soc.*, 1989, **111**, 1552; H. Wasada and K. Hirao, *J. Am. Chem. Soc.*, 1992, **114**, 16; I. Lee, C. K. Kim, B.-S. Lee and T.-K. Ha, *J. Mol. Struct. (Theochem)*, 1993, **279**, 191; J. Moc and K. Morokuma, *J. Am. Chem. Soc.*, 1995, **117**, 11 790.
9 T. Hirabe, M. Nojima and S. Kusabayashi, *J. Org. Chem.* 1984, **49**, 4084.
10 N. Donoghue and M. J. Gallagher, *Phosphorus Sulfur Silicon*, 1997, **123**, 169.
11 D. Hellwinkel, *Top. Curr. Chem.*, 1983, **109**, 2.

Received in Cambridge, UK, 6th July 1998; 8/05179H

Chemical recycling of poly(ethylene) by catalytic degradation into aromatic hydrocarbons using H-Ga-silicate

Yoshio Uemichi,*† Kazuhiko Takuma and Akimi Ayame

Department of Applied Chemistry, Muroran Institute of Technology, Mizumoto, Muroran, 050-8585, Japan

H-Ga-silicate exhibits excellent catalytic activity towards the formation of aromatic hydrocarbons, mainly benzene, toluene and xylenes (BTX), in the degradation of poly(ethylene), indicating its high potential as a catalyst for the advanced chemical recycling of polyolefins.

It is currently very important to recycle waste plastics from the standpoints of environmental protection and conservation of energy. A chemical method that converts plastics into valuable chemical feedstocks or fuels is of great interest because it provides a viable means to contributing to the solution of problems caused by waste disposal. The conversion of plastics can be achieved thermally or catalytically. Since thermal degradation of polyolefins, the main components of waste plastics, is a low selectivity reaction, successful application of catalysts to these conversion processes would be a key step towards the development of the plastic recycling technologies.

Catalytic degradation of polyolefins has mostly been carried out with a view to obtaining valuable hydrocarbon mixtures as fuels.[1–4] There have been only a few reported studies on chemical recycling (otherwise termed feedstock recycling, raw material recycling or tertiary recycling) which aims to yield chemical feedstocks.[5–7] To achieve chemical recycling, polyolefins must be decomposed in high yield into useful feedstocks. This step is usually more difficult than conversion into fuels. In other words, chemical recycling requires cracking catalysts with selectivities much higher than those required for fuel recovery. This is the reason why catalytic chemical recycling of polyolefins has not been developed. Here we report that H-Ga-silicate is highly effective as a catalyst for producing aromatic hydrocarbons selectively in the degradation of poly(ethylene). This successful result means that chemical recycling of polyolefins is now a feasible operation.

Catalytic degradation of low-density poly(ethylene) (Aldrich LDPE, density 0.915 g cm^{-3}) has been carried out using a flow reactor at 400–525 °C, at atmospheric pressure and under a He stream (10 cm^3 min^{-1}). The poly(ethylene) melt, heated at 270 °C, was fed at a feed rate of 0.02 g min^{-1} into the reactor loaded with 0.2 g of catalyst for 15 min. The degradation products were classified into gas (C_1 to C_4), liquid ($>C_5$) and coke (carbonaceous deposit on the catalyst surface). The composition of the gaseous and liquid products was analysed by gas chromatography. The details of the reaction procedures have been given elsewhere.[1] A commercially available H-Ga-silicate (Si/Ga = 25, N. E. CHEMCAT) was pressed into a disk, crushed and sieved to 16–32 mesh granules, and finally calcined at 500 °C for 3 h in air. The Ga catalyst was compared with H-ZSM-5 (Si/Al = 15, N. E. CHEMCAT) and amorphous silica–alumina (Si/Al = 5.4, Nikki Chemical N631L). These alternatives have been extensively used for the conversion of polyolefins into liquid fuels. The acidic properties of the catalysts were evaluated from their catalytic activities for three model reactions: *n*-hexadecane cracking was carried out at 400 °C, using 1 mg of catalyst, cumene dealkylation at 250 °C and 10 mg, and propan-2-ol dehydration at 175 °C and 3 mg. In each case, a pulse reactor loaded with the powdered catalyst was operated under flowing He (30 cm^3 min^{-1}).

Fig. 1 shows the activities of the catalysts for the acid-catalysed model reactions. The highest conversions were shown by H-ZSM-5, followed by H-Ga-silicate. The Ga catalyst was much more active than silica–alumina for the cracking of cumene and *n*-hexadecane, which occurs on strong acid sites, while both catalysts showed almost the same activity for the dehydration of propan-2-ol, which proceeds on weakly acidic sites. It is suggested from these results that H-Ga-silicate is less acidic than H-ZSM-5, but has acid sites that are significantly stronger than those on silica–alumina, which exhibited low cracking activities.

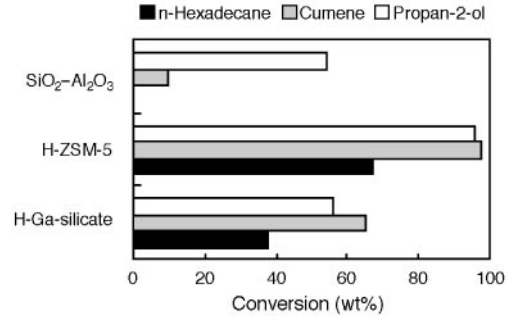

Fig. 1 Catalytic activities for model reactions

The catalysts thus characterised showed quite different activities and selectivities in the degradation of poly(ethylene). The results are summarised in Table 1. H-Ga-silicate is highly effective as a catalyst for the production of aromatic hydrocarbons. A high temperature was favourable to producing the aromatics selectively. A yield of more than 70 wt% was obtained at 525 °C and the liquid product substantially consisted of aromatic hydrocarbons. Benzene, toluene and xylenes (BTX), important raw materials, accounted for most of the aromatics produced. H-ZSM-5 also produced considerable amounts of aromatics at 525 °C. However, the yield was lower than that obtained over H-Ga-silicate at 400 °C. On the other hand, silica–alumina was not suitable for producing aromatics. About 40 wt% yield of aromatics has also been reported in the degradation of poly(ethylene) over metal/carbon catalysts at 526 °C with longer contact times.[5] H-Ga-silicate gives superior results.

Fig. 2 shows the product distributions as a function of carbon number. The products obtained over H-Ga-silicate were distributed over carbon numbers 1–13. The proportion of C_6–C_8

Table 1 Yields of products from degradation of poly(ethylene)

		Yield/wt%				
Catalyst	*T*/°C	Gas	Liquid	Aromatics	BTX	Coke
H-Ga-silicate	400	40.3	59.4	44.1	30.1	0.3
H-Ga-silicate	525	28.0	72.0	71.6	61.8	—[a]
H-ZSM-5	525	58.0	42.0	40.8	33.5	—[a]
SiO_2–Al_2O_3	525	57.2	42.1	9.5	3.7	0.4

[a] Less than 0.05%.

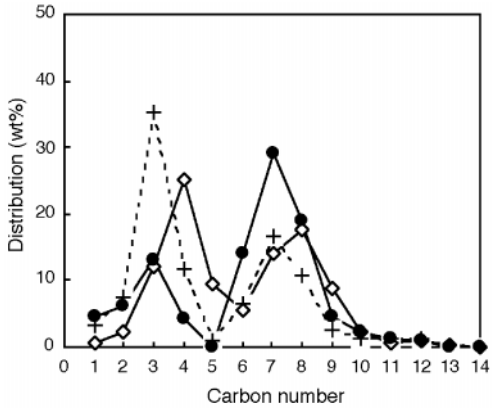

Fig. 2 Carbon number distributions of the products: (+) H-ZSM-5 (525 °C), (◇) H-Ga-Si (400 °C) and (●) H-Ga-Si (525 °C)

components, mostly BTX, increased with reaction temperature, probably indicating greater aromatisation of the gaseous fractions at higher temperatures. The Ga catalyst showed good stability when reused, as expected from the very small amount of coke deposited on the catalyst surface (Table 1). The ZSM-5-type structure of H-Ga-silicate is likely to resist coke formation.

Ishihara *et al.*[8] reported that the degradation of poly(ethylene) over silica–alumina proceeds as follows: polymer→oligomer→liquid→gas. We believe the consecutive degradation mechanism is applicable to the present work and the aromatics are formed from the oligomer, liquid and/or gas, not directly from the polymer itself. That is, the aromatisation and cracking proceed competitively, and their relative contributions determine the product distributions. Cracking is probably a predominant reaction with H-ZSM-5, over which the liquid hydrocarbons corresponding to the aromatic precursors were converted into gaseous fractions. Thus, the cracking activity of H-ZSM-5 with strong acidity seems to be too high to give a good yield of aromatics. On the other hand, H-Ga-silicate has moderate cracking ability, whilst greatly enhancing aromatisation *via* the catalytic action of Ga species on the catalyst surface.[9,10] Aromatisation would predominate over cracking at high temperature and, hence, the yield of aromatics greatly increased with reaction temperature. It is therefore reasonable to consider that a good balance between cracking and aromatisation activities is the origin of the excellent catalytic performance of H-Ga-silicate. Both aromatisation routes, by direct dehydrocyclisation of the liquid intermediates and by oligomerisation of gaseous fractions and subsequent cyclisation, must be involved in the degradation over the Ga catalyst. The latter should be important at high temperature.

Notes and References

† E-mail: uemichi@muroran-it.ac.jp

1 Y. Uemichi, M. Hattori, T. Itoh, J. Nakamura and M. Sugioka, *Ind. Eng. Chem. Res.*, 1998, **37**, 867.
2 J. Aguado, D. P. Serrano, M. D. Romero and J. M. Escola, *Chem. Commun*., 1996, 725.
3 A. R. Songip, T. Masuda, H. Kuwahara and K. Hashimoto, *Energy Fuels*, 1994, **8**, 136.
4 W. Ding, J. Liang and L. L. Anderson, *Energy Fuels*, 1997, **11**, 1219.
5 Y. Uemichi, Y. Makino and T. Kanazuka, *J. Anal. Appl. Pyrolysis*, 1989, **14**, 331.
6 A. A. Garforth, Y.-H. Lin, P. N. Sharratt and J. Dwyer, *Appl. Catal. A*, 1998, **169**, 331.
7 W. Kaminsky, B. Schlesselmann and C. M. Simon, *Polym. Degrad. Stab*., 1996, **53**, 189.
8 Y. Ishihara, H. Nanbu, T. Ikemura and T. Takesue, *Fuel*, 1990, **69**, 978.
9 H. Kitagawa, Y. Sendoda and Y. Ono, *J. Catal*., 1986, **101**, 12.
10 Y. Ono, *Catal. Rev. Sci. Eng*., 1992, **34**, 179.

Received in Cambridge, UK, 29th June 1998; 8/04927K

Stabilisation of β-hairpin conformations in a protein surface mimetic using a bicyclic template derived from (2*S*,3*R*,4*R*)-diaminoproline

Marc E. Pfeifer and John A. Robinson*†

Institute of Organic Chemistry, University of Zurich, Winterthurerstrasse 190, 8057 Zurich, Switzerland

A trifunctional template, derived by formal coupling of (*S*)-aspartic acid and (2*S*,3*R*,4*R*)-diaminoproline (available from vitamin C) as a diketopiperazine, was incorporated by solid-phase peptide synthesis into a protein loop mimetic containing the sequence -Ala-Asn-Pro-Asn-Ala-Ala-; this was shown by NMR analysis to adopt a stable β-hairpin conformation in DMSO.

Many proteins exert their biological activity through interactions involving relatively small regions of their exposed surfaces. Small synthetic molecules that mimic surface features of proteins are therefore of potential interest in the design of novel drug candidates. Unlike folded proteins, however, short linear peptides are inherently flexible molecules. To overcome this problem, much attention has been focused recently on the design of templates to constrain peptide chains into biologically relevant secondary and tertiary structures.[1,2] We report here a novel bicyclic template, comprising a diketopiperazine derived from aspartic acid and (2*S*,3*R*,4*R*)-diaminoproline, which was designed to stabilize β-hairpin conformations, as typically found in protein loops connecting adjacent antiparallel β-strands.

In previous work,[3,4] we described the synthesis of template **1**, and its incorporation into the loop mimetic **2**, containing the NPNA (Asn.Pro.Asn.Ala) motif found in a tandemly repeated form in the circumsporozoite protein of *Plasmodium falciparum*.[5] Based on NMR and MD studies, we could show that **2** adopts a stable β-turn conformation within the NPNA motif, while the 4-amido N-atom in the 4-aminoproline moiety of the template prefers a pseudo-equatorial position,[3,6] as depicted in Fig. 1. Here, we set out to introduce an additional amino group in an axial position at the 3-position of the pyrrolidine ring, as in **3**, which could then be used as an anchoring group to more accurately position a peptide loop in a β-hairpin geometry, as in **4**.

A convenient gram-scale synthesis of (2*S*,3*R*,4*R*)-diaminoproline was established by exploiting a known route to the bicyclic β-lactam **5** from vitamin C, which has been implemented already on a multi-kilogram scale in a commercial synthesis of β-lactamase inhibitors.[7] As shown in Scheme 1, **5**

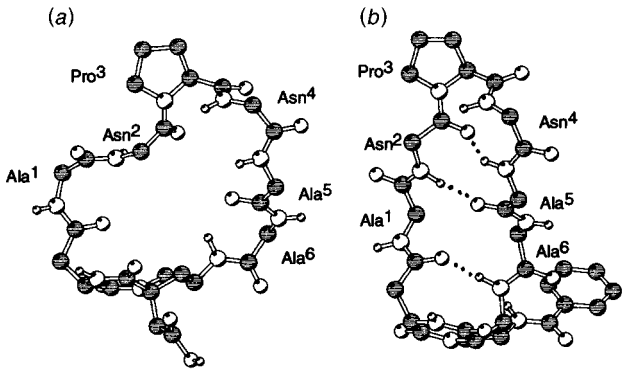

Fig. 1 Average solution structures of (*a*) **2** and (*b*) **4** deduced by SA (see text). The side-chains of Ala and Asn, and all hydrogen atoms apart from peptide NHs, are omitted for clarity. N, O and amide H atoms = white, C atoms = grey.

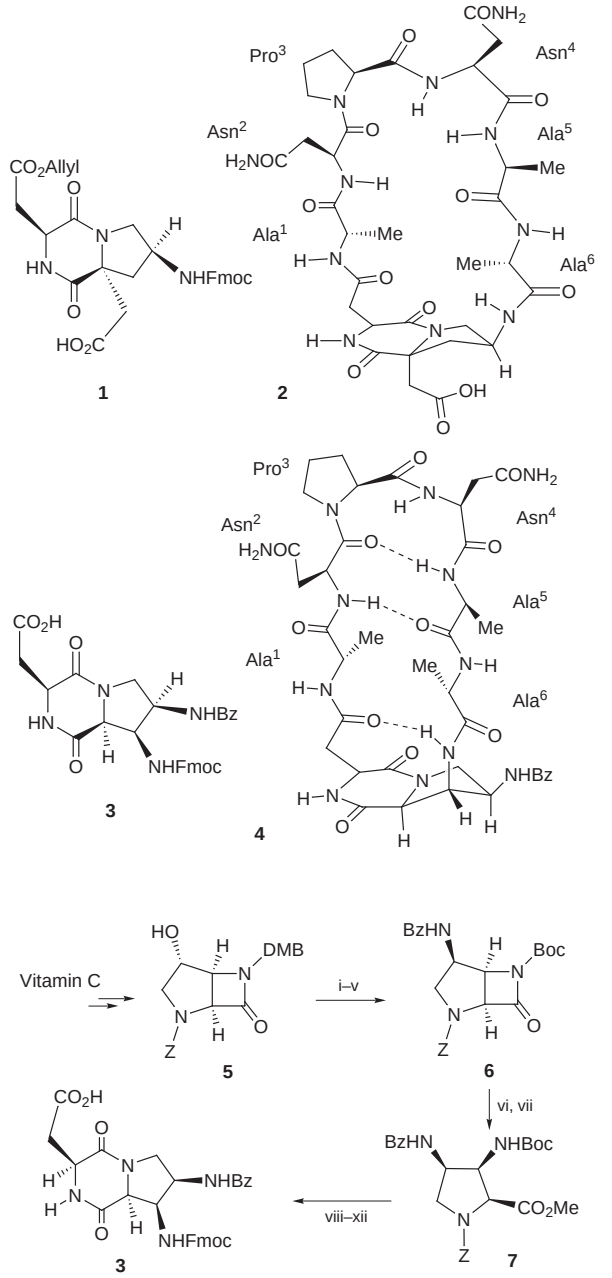

Scheme 1 *Reagents and conditions*: i, PhthH, Ph_3P, THF, DEAD (61%); ii, $MeNHNH_2$, DMF, 80 °C; iii, Bz_2O, Et_3N, CH_2Cl_2 (66% over 2 steps); iv, $K_2S_2O_8$, Na_2HPO_4, aq. MeCN, 78 °C (77%); v, Boc_2O, Et_3N, DMAP, CH_2Cl_2 (60%); vi, Na_2CO_3, aq. THF; vii, CH_2N_2, Et_2O (98% over 2 steps); viii, H_2, Pd/C, DMF (96%); ix, Z-Asp(OBu^t)-OH, HATU, HOAt, Pr^i_2EtN, CH_2Cl_2 (80%); x, H_2, Pd/C, DMF (100%); xi, TFA, CH_2Cl_2 (89%); xii, Fmoc-OSucc, Pr^i_2EtN, CH_2Cl_2 (60%)

Table 1 Temperature coefficients[a] ($-\Delta\delta/T$), H/D exchange rates[b] ($t_{1/2}$) for amide protons, and ^3J coupling constants[c] measured for **4**

			^3J/Hz			
Residue	$-(\Delta\delta/T)$/ppb K^{-1}	$t_{1/2}$/min	$^3J_{\alpha,NH}$	$^3J_{\alpha,\beta}$	$^3J_{\beta,\gamma}$	$^3J_{\gamma,\delta}$
Ala[1]	6.0	33	7.5	6.9	—	—
Asn[2]	3.2	280	7.6	5.0, 4.1	—	—
Asn[4]	1.4	350	9.4	10.3, 3.9	—	—
Ala[5]	0.0	260	7.0	6.8	—	—
Ala[6]	5.1	23	9.1	6.9	—	—
dApro[7]	1.9[d] 4.2[e]	$>10^4$ [d] 240[e]	8.9[d] 7.0[e]	3.5	4.3	10.1, 9.6
Asp[8]	5.1	4.5	<2.0	3.1, 4.1	—	—

[a] The temperature coefficients for the peptide amides are given; dApro[7] refers to the diaminoproline and Asp[8] to the aspartate moieties, respectively, of the template. Measurements were made in d_6-DMSO in the range 295–320 K. [b] The half-lifes ($t_{1/2}$) of amide resonances were determined by fitting residual peak intensities after dissolution in d_6-DMSO + 10% d_4-methanol to an exponential function. The exchange rates may be classified as: fast [Asp[8] NH and Asn[2]/Asn[4] side chain NHs (data not shown)]; medium (Ala[1], Ala[6]); slow [Asn[2], Asn[4], Ala[5], dApro[7] C(γ)-NH]; and very slow [dApro[7] C(β)-NH]. [c] Measured using 1D and/or E.COSY spectra. [d] For C(β)-NH. [e] For C(γ)-NH

was converted into **6** by a Mitsunobu reaction[8] and exchange of protecting groups, and the β-lactam ring was then opened to yield after esterification the orthogonally protected (2*S*,3*R*,4*R*)-diaminoproline derivative **7**. Thereafter, coupling to Z-Asp(OtBu)-OH, cyclisation to afford the diketopiperazine, and further manipulation of the protecting groups gave **3** in good overall yield.

The template **3** could be incorporated into the cyclic peptide **4** using standard solid-phase methods and Fmoc chemistry.[9] For example, **3** was coupled to Tentagel S-AC resin, and the peptide chain was then elaborated to afford H-Ala-Asn(Mtt)-Pro-Asn(Mtt)-Ala-Ala-Template-Resin. After cleavage from the resin with 1% TFA in CH_2Cl_2, the linear precursor was cyclized using HATU/HOAt‡ in DMF, and all side-chain protecting groups were then removed with TFA in CH_2Cl_2 (35:60) and TIPS (5% v/v). After purification by HPLC, the cyclic peptide **4** was obtained from **3** in 11% yield.

The preferred conformation of **4** was studied in d_6-DMSO (**4** has low solubility in water at pH 5) at 305 K, a temperature at which the amide NH protons are optimally resolved in 1D ^{1}H NMR spectra. A relatively stable β-hairpin conformation in the peptide backbone was indicated in NOESY spectra of **4** by NOEs connecting Ala[1] H(α) as well as Asn[2] NH with Ala[5] NH, which were not observed in earlier studies[3,6] of **2**. A β-turn in the NPNA motif was also indicated, in particular, by a relatively strong Asn[4] to Ala[5] d_{NN} NOE, as well as NOEs between Asn[2] H(β)s and Ala[5] NH, as observed in earlier studies[3,4,6] of **2**. Average solution structures were determined by dynamic simulated annealing§ (SA) using distance restraints derived from NOE build-up curves in a series of NOESY spectra with increasing mixing times. The SA structures showed no major distance restraint violations (*e.g.* >0.2 Å) and revealed a well defined β-hairpin backbone conformation, including a βI turn in the NPNA motif, as in the representative structure **4** shown in Fig. 1.

A critical test of the accuracy of the SA structures is to examine how well they also account for other experimental data, in particular, ^3J coupling constants, relative H/D exchange rates of amide protons, and amide proton chemical shift temperature coefficients. Structure **4** predicts intramolecular hydrogen-bonding across the hairpin, involving the C(β)-NH with O(δ) of the template, as well as Asn[2] NH with Ala[5] CO (indicated by dotted lines in **4** and in Fig. 1). We observe very low amide proton temperature coefficients for these two amide NH groups, as well as relatively slow amide NH exchange rates, measured in d_6-DMSO with 10% v/v d_4-methanol (Table 1), data which indicate the involvement of these NH groups in intramolecular hydrogen-bonding. In addition, the ^3J values for protons in the template, in particular within the diaminoproline moiety, show values consistent with the geometry found in the SA structures, with the C(β)-NH axial, and the C(γ)-NH equatorial. To a first approximation, therefore, the experimental data are interlocking and consistent with the derived SA structures, which indicate a significantly populated β-hairpin conformation in the backbone of **4**. The molecule should not be viewed as rigid, however, and MD simulations may provide a more detailed description of allowed conformational dynamics on the MD time-scale in this system.

Studies are now underway to determine how general this approach is to the construction of conformationally defined β-hairpin loop mimetics of diverse size and sequence. The amino functionality at C(γ) in the template may be useful in this context to allow its attachment to a solid-support for solid-phase syntheses, as well as for coupling to other carrier molecules.

The authors thank the Swiss National Science Foundation for financial support, and Dr Pflieger, F. Hoffmann-La Roche, Basel, for a generous gift of compound **5**.

Notes and References

† E-mail: robinson@oci.unizh.ch

‡ Abbreviations: HATU = *O*-(7-azabenzotriazol-1-yl)-*N*,*N*,*N*',*N*'-tetramethyluronium hexafluorophosphate; HOAt = 1-hydroxy-7-azabenzotriazole; TIPS = triisopropylsilane.

§ The method used for SA calculations has been described in detail elsewhere (refs. 3 and 6).

1 D. P. Fairlie, M. L. West and A. K. Wong, *Curr. Med. Chem.*, 1998, **5**, 29.
2 S. Hanessian, G. McNaughton-Smith, H.-G. Lombart and W. D. Lubell, *Tetrahedron*, 1997, **53**, 12 789.
3 C. Bisang, L. Jiang, E. Freund, F. Emery, C. Bauch, H. Matile, G. Pluschke and J. A. Robinson, *J. Am. Chem. Soc.*, 1998, **120**, 7439.
4 F. Emery, C. Bisang, M. Favre, L. Jiang and J. A. Robinson, *Chem. Commun.*, 1996, 2155.
5 C. Bisang, C. Weber, J. Inglis, C. A. Schiffer, W. F. van Gunsteren, I. Jelesarov, H. R. Bosshard and J. A. Robinson, *J. Am. Chem. Soc.*, 1995, **117**, 7904.
6 C. Bisang, C. Weber and J. A. Robinson, *Helv. Chim. Acta.*, 1996, **79**, 1825.
7 C. Hubschwerlen, *Synthesis*, 1986, 961-962; R. Charnas, K. Gubernator, I. Heinze, C. Hubschwerlen, EP 0 508 234 A2, 1991.
8 O. Mitsunobu, M. Wada and T. Sano, *J. Am. Chem. Soc.*, 1972, **94**, 679.
9 E. Atherton and R. C. Sheppard, *Solid Phase Peptide Synthesis - a Practical Approach*, IRL Press, Oxford, 1989.

Received in Cambridge, UK, 10th June 1998; 8/04412K

Unsymmetric dipnictenes—synthesis and characterization of MesP=EC$_6$H$_3$-2,6-Trip$_2$ (E = As or Sb; Mes = C$_6$H$_2$-2,4,6-Me$_3$, Trip = C$_6$H$_2$-2,4,6-Pr$^i_3$)

Brendan Twamley and Philip P. Power*

Department of Chemistry, University of California, Davis, California 95616, USA

The use of terphenyl substituents enables the isolation of unsymmetrical dipnictenes with P=As or P=Sb double bonds by a new synthetic route.

The first stable diphosphene Mes*P=PMes* (Mes* = C$_6$H$_2$-2,4,6-Bu$^t_3$) was synthesized by Yoshifuji and coworkers in 1981, *via* the magnesium reduction of Mes*PCl$_2$ in THF.[1] Since that report many further examples of diphosphenes[2] have been synthesized. In contrast, the number of analogous compounds involving double bonds to the heavier pnictogens has remained quite small. For example, there are only two structurally characterized molecules with As–As double bonds,[3] and just one with a P–As double bond.[4] Stable compounds with Sb–Sb[5a] and Bi–Bi[5b] double bonds have only been reported recently. The latter were synthesized by a novel synthetic method involving the deselenation of 1,3,5,2,4,6-triselenatrispnictane (ArESe)$_3$ (Ar = 2,4,6-tris[bis(trimethylsilyl)methyl]phenyl, E = Sb or Bi), whereas the related phosphorus or arsenic species, *i.e.* diphosphenes, diarsenes and phosphaarsenes, have usually been prepared *via* reduction with magnesium or sodium naphthalenide or in the case of the unsymmetrical compounds, by the coupling of ArECl$_2$ and Ar′E′H$_2$ in the presence of DBU (1,8-diazabicyclo[5.4.0]undec-7-ene).[4,6,7a] Other methods for synthesizing phosphaarsenes have used Me$_3$SiCl elimination[7b–d] or coupling of the RECl$_2$ (E = P, As) precursors in the presence of Bu^{t}Li.[7e] Currently, there is only one report of a phosphastibene, Mes*P=SbCH(SiMe$_3$)$_2$,[4,6] which was synthesized by the coupling of Mes*PH$_2$ with (Me$_3$Si)$_2$CHSbCl$_2$. However this compound is unstable under ambient conditions and it was characterized by high resolution mass spectrometry and ^{31}P NMR. Using a novel direct elimination method, we now report the isolation of the stable unsymmetric phosphastibene MesP=SbC$_6$H$_3$-2,6-Trip$_2$ (**1**) and phosphaarsene MesP=AsC$_6$H$_3$-2,6-Trip$_2$ (**2**) (Trip = 2,4,6-Pr$^i_3$).

Reaction of the dilithiophosphide Li$_2$PMes[8] in a 1:1 stoichiometry with 2,6-Trip$_2$H$_3$C$_6$ECl$_2$ (E = Sb, As) in Et$_2$O at −78 °C affords the corresponding phosphastibene MesP=SbC$_6$H$_3$-2,6-Trip$_2$ (**1**) and phosphaarsene MesP=AsC$_6$H$_3$-2,6-Trip$_2$ (**2**) (see Scheme 1). Both **1** and **2** were isolated† in low but reproducible yields of 1% and 7% respectively, and their structures were determined by X-ray crystallography (see Figs. 1 and 2).‡

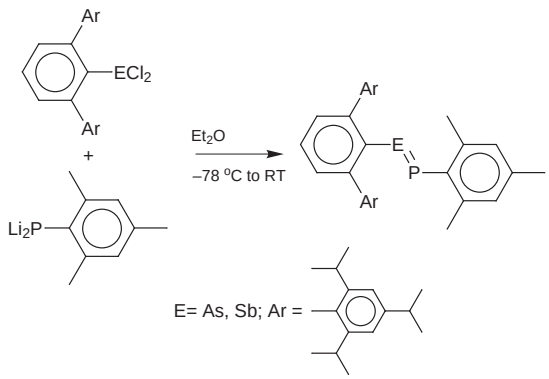

Scheme 1 Synthesis route to unsymmetric dipnictenes

Compound **1** is the first example of a stable species with a P–Sb double bond [P–Sb = 2.335(2) Å]. The molecule has a *trans* configuration with a Sb–C bond distance of 2.174(7) Å and C–Sb–P and C–P–Sb angles of 100.9(2) and 95.7(3)°. There is a torsion angle of 4.2° in the C(37)–P(1)–Sb(1)–C(1) array. The ^{31}P NMR spectrum displays a singlet at 543 ppm which is 77 ppm upfield from Mes*P=SbCH(SiMe$_3$)$_2$ (620 ppm),[4,6] which demonstrates the shielding effect of the bulky terphenyl substituent. In the solid state **2**, which also has a *trans* conformation, has an As–P bond distance of 2.134(2) Å. The As–C bond distance is 1.975(6) and C–As–P and C–P–As angles are 101.4(2)° and 96.7(2)° respectively. These parameters are in reasonable agreement with the only other structurally characterized analogue Mes*P=AsCH(SiMe$_3$)$_2$[4,6] which has an

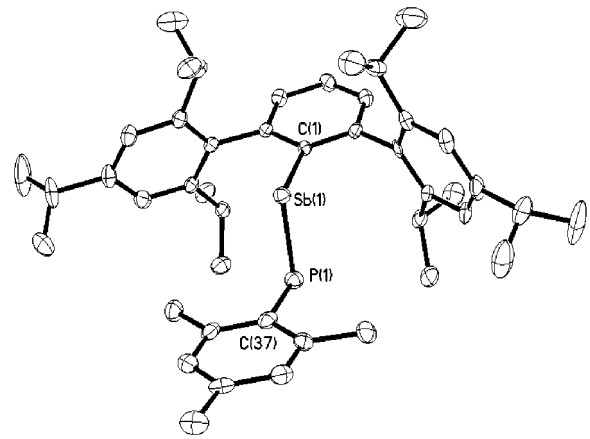

Fig. 1 ORTEP diagram of the structure of **1** (30% probability). H atoms omitted for clarity.

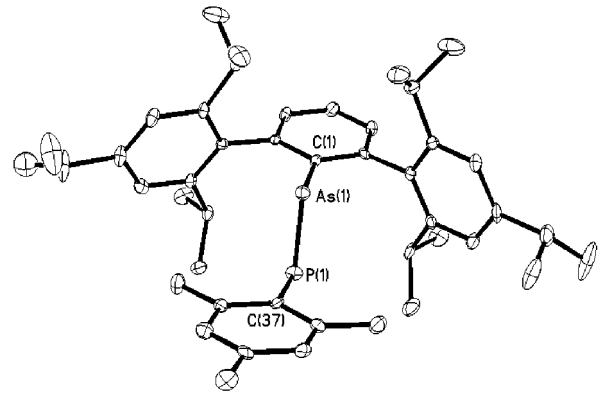

Fig. 2 ORTEP diagram of the structure of **2** (30% probability). H atoms omitted for clarity.

As–P distance of 2.125(1) Å, and C–As–P, C–P–As angles of 101.35(9)°, 96.37(9)°. **2** has a torsion angle of 3.2° for the array C(37)–P(1)–As(1)–C(1). The ^{31}P NMR spectrum of **2** shows a sharp singlet at 534 ppm which is 41 ppm upfield from that of Mes*P=AsCH(SiMe$_3$)$_2$ (575 ppm) and is almost identical to those of (Me$_3$Si)$_2$CHP=AsMes* (533 ppm),[6] and ArP=AsAr (537 ppm) Ar = 2,6-dimesityl-4-methylphenyl.[7a]

The As–P and Sb–P bonds are *ca.* 8% shorter than the calculated covalent single bond distances (2.33 and 2.54 Å)[9] which indicates considerable double bond character. The percentage shortening is comparable to that seen in symmetrical double bonded compounds.[2] In addition **1** and **2** display bond angles of 100.9(2) and 101.35(9)° at antimony and arsenic and narrow angles of 95.7(3) and 96.7(2)° at the phosphorus atoms. The wider angles at arsenic and antimony are somewhat surprising but are probably due to the larger size of the aryl substituents at these atoms. It may be noted that the angles at all the pnictogens are considerably smaller than would be expected for approximately sp^2 hybridization, indicating a concentration of s-character in the lone pair orbitals.

The electronic spectra for **1** and **2** each exhibit two absorption maxima, 512 nm (ε 373), 397 nm (ε 3417) and 467 nm (ε 216), 356 nm (ε 2477) respectively. The spectrum of **2** closely matches those of Mes*P=AsCH(SiMe$_3$)$_2$ [454 nm (ε 280), 353 nm (ε 7500],[4] and ArP=AsAr [463 nm (ε 870), 385 nm (ε 9549) (Ar = 2,6-dimesityl-4-methylphenyl)], [7a] whereas the spectrum of **1** shows a characteristic red-shift for double-bond systems of heavier group 15 elements as seen in *e.g.* ArSb=SbAr,[5a] 599 nm (ε 170), 466 nm (ε 5200) and ArBi=BiAr,[5b] 660 nm (ε 100), 525 nm (ε 4000), where Ar = C$_6$H$_2$-2,4,6-{CH(SiMe$_3$)$_2$}$_3$.

The reaction of 2,6-Trip$_2$H$_3$C$_6$BiCl$_2$ with either Li$_2$PMes or H$_2$PMes with DBU does not lead to the formation of the bismuth analogue MesP=BiC$_6$H$_3$-2,6-Trip$_2$. Instead, the purple symmetrical dibismuthene 2,6-Trip$_2$H$_3$C$_6$Bi=BiC$_6$H$_3$-2,6-Trip$_2$ is formed. The details of this structure as well as those of the corresponding distibenes, diarsenes, and diphosphenes will be reported in the near future.

We thank the National Science Foundation for financial support.

Notes and References

† *Experimental:* **1**: under anaerobic and anhydrous conditions, a solution of 2,6-Trip$_2$H$_3$C$_6$SbCl$_2$ (0.5 g, 0.74 mmol), in Et$_2$O (40 mL) was added to a suspension of MesPLi$_2$ (0.122 g, 0.74 mmol) in Et$_2$O (20 mL) at −78 °C, dropwise (10 min). The mixture was stirred at −78 °C (1 h) before warming to room temperature and stirred overnight. The solvent was removed *in vacuo* and the orange residue was extracted with hexane (40 mL) and filtered through Celite to give a deep orange solution. Concentration of the solution and prolonged cooling at −25 °C for 15 days yielded orange crystalline **1**, 62 mg, 1%. Mp 184–188 °C. ^{1}H NMR (300 MHz, C$_6$D$_6$) δ 1.15 [d, 12H, *o*-CH(C*H*$_3$)$_2$, $^3J_{HH}$ = 6.9 Hz], 1.23 [d, 12H, *p*-CH(C*H*$_3$)$_2$, $^3J_{HH}$ = 6.9 Hz], 1.36 [d, 12H, *o*-CH(C*H*$_3$)$_2$, $^3J_{HH}$ = 6.9 Hz], 1.97 (s, 6H *o*-Me), 2.18 (s, 3H, *p*-Me), 2.798 [sept., 2H, *p*-C*H*(CH$_3$)$_2$, $^3J_{HH}$ = 6.9 Hz], 3.20 [sept., 4H, *o*-C*H*(CH$_3$)$_2$, $^3J_{HH}$ = 6.9 Hz], 6.73 (s, 2H, *m*-Mes), 7.13 (s, 4H, *m*-Trip), 7.32 [t, 1H, *p*-C$_6$H$_3$, $^3J_{HH}$ = 7.4 Hz], 7.46 (d, 2H, *m*-C$_6$H$_3$, $^3J_{HH}$ = 7.2 Hz). ^{13}C{^{1}H} NMR (75 MHz, C$_6$D$_6$) δ 20.66 (Mes-*C*H$_3$), 22.3 [*o*-CH(*C*H$_3$)$_2$], 24.29 [*p*-CH(*C*H$_3$)$_2$], 26.53 [*o*-CH(*C*H$_3$)$_2$], 31.33 [*o*-*C*H(CH$_3$)$_2$], 34.78 [*p*-*C*H(CH$_3$)$_2$], 121.14 (*m*-Trip), 128.28 (*p*-C$_6$H$_3$), 129.27 (*m*-C$_6$H$_3$), 130.02 (*m*-Mes), 137.43 (*i*-Trip), 137.73 (*o*-C$_6$H$_3$), 138.69 (*o*-Mes), 146.78 (*p*-Trip, *p*-Mes), 147.19 (*o*-Trip), 149.32 (d, *i*-Mes-P, J_{CP} = 5.7 Hz), 201.56 (*i*-C$_6$H$_3$). ^{31}P{^{1}H} NMR (121.7 MHz C$_6$D$_6$) δ 543. UV–VIS. (λ_{max}, ε) 512 nm, 373; 398 nm, 3417. **2**: this compound was prepared in a similar manner to that described for **1**; 2,6-Trip$_2$H$_3$C$_6$AsCl$_2$ (0.5 g. 0.79 mmol) and MesPLi$_2$ (0.131 g. 0.79 mmol) were reacted in Et$_2$O and **2** was isolated as pale orange crystals 40 mg, 7%. Mp 239–241 °C. ^{1}H NMR (300 MHz, C$_6$D$_6$) δ 1.16 [d, 12H, *o*-CH(C*H*$_3$)$_2$, $^3J_{HH}$ = 6.6 Hz], 1.25 [d, 12H, *p*-CH(C*H*$_3$)$_2$, $^3J_{HH}$ = 6.9 Hz], 1.32 [d, 12H, *o*-CH(C*H*$_3$)$_2$, $^3J_{HH}$ = 6.9 Hz], 1.82 (s, 6H, *o*-Me), 2.04 (s, 3H, *p*-Me), 2.82 [sept., 2H, *p*-C*H*(CH$_3$)$_2$, $^3J_{HH}$ = 6.9 Hz], 3.16 [sept., 4H, *o*-C*H*(CH$_3$)$_2$, $^3J_{HH}$ = 6.9 Hz], 6.62 (s, 2H, *m*-Mes), 7.13 (s, 4H, *m*-Trip), 7.28 (t, 1H, *p*-C$_6$H$_3$, $^3J_{HH}$ = 7.35 Hz), 7.38 (d, 2H, *m*-C$_6$H$_3$, $^3J_{HH}$ = 7.35 Hz). ^{13}C{^{1}H} NMR (75 MHz, C$_6$D$_6$) δ 20.86 (Mes-CH$_3$), 22.6 [*o*-CH(*C*H$_3$)$_2$], 24.37 [*p*-CH(*C*H$_3$)$_2$], 26.4 [*o*-CH(*C*H$_3$)$_2$], 31.43 [*o*-*C*H(CH$_3$)$_2$], 34.783 [*p*-*C*H(CH$_3$)$_2$], 121.06 (*m*-Trip), 128.15 (*p*-C$_6$H$_3$), 128.85 (*m*-C$_6$H$_3$), 130.03 (*m*-Mes), 137.63 (*i*-Trip), 137.99 (*o*-C$_6$H$_3$), 138.4 (*o*-Mes), 146.68 (*p*-Trip, *p*-Mes), 147.07 (*o*-Trip), 144.59 (d, *i*-Mes-P, J_{CP} = 4.3 Hz). ^{31}P{^{1}H} NMR (121.7 MHz C$_6$D$_6$) δ 534. UV–VIS. (λ_{max}, ε) 467 nm, 216; 356 nm, 2477.

‡ *Crystal data* at 130 K with Cu-Kα (λ = 1.54170 Å) radiation: **1** C$_{45}$H$_{60}$PSb, M = 753.65, triclinic, space group $P\bar{1}$, a = 12.848(3), b = 13.095(3), c = 13.642(3) Å, α = 102.97(3), β = 112.31(3), γ = 96.31(3)°, V = 2020.2(7) Å^3, Z = 2, D_c = 1.239 Mg m^{-3}, μ = 5.986 mm^{-1}, scan type 2θ, θ range 3.55 to 56.25°. GoF on F^2 1.027 for 5307 unique observed data and 434 parameters, R_1 6.04%, wR_2 13.46%; **2** C$_{45}$H$_{60}$PAs, M = 706.82, triclinic, space group $P\bar{1}$, a = 12.846(2), b = 12.918(3), c = 13.806(4) Å, α = 114.606(16), β = 102.508(17), γ = 93.932(16)°, V = 2000.7(8) Å^3, Z = 2, D_c = 1.173 Mg m^{-3}, μ = 1.725 mm^{-1}, scan type 2θ, θ range 3.58 to 56.45°. GoF on F^2 1.017 for 5272 unique observed data and 439 parameters, R_1 6.96%, wR_2 13.31%. Solution and refinement (full matrix least-squares on F^2) were performed using SHELXTL Plus 1994. CCDC 182/967.

1 M. Yoshifuji, I. Shima, N. Inamoto, K. Hirotsu and T. Higuchi, *J. Am. Chem. Soc.*, 1981, **103**, 4587.

2 (*a*) A. H. Cowley, *Polyhedron*, 1984, **3**, 389; (*b*) A. H. Cowley and N. C. Norman, *Prog. Inorg. Chem.*, 1986, **34**, 1; (*c*) M. Yoshifuji, in *Multiple Bonds and Low Coordination in Phosphorus Chemistry*, ed. M. Regitz and O. J. Scherer, Georg Thieme Verlag, Stuttgart, 1990; (*d*) L. Weber, *Chem. Rev.*, 1992, **92**, 1839; (*e*) N. C. Norman, *Polyhedron*, 1993, **12**, 2431.

3 A. H. Cowley, J. G. Lasch, N. C. Norman and M. Pakulski, *J. Am. Chem. Soc.*, 1983, **105**, 5506; (*b*) C. Couret, J. Escudie, Y. Madaule, H. Ranaivonjatovo and J.-G. Wolf, *Tetrahedron Lett.*, 1983, **24**, 2769; (*c*) A. H. Cowley, N. C. Norman and M. Pakulski, *J. Chem. Soc., Dalton Trans.*, 1985, 383.

4 A. H. Cowley, J. G. Lasch, N. C. Norman, M. Pakulski and B. R. Whittlesey, *J. Chem. Soc., Chem. Commun.*, 1983, 881.

5 (*a*) N. Tokitoh, Y. Arai, T. Sasamori, R. Okazaki, S. Nagase, H. Uekusa and Y. Ohashi, *J. Am. Chem. Soc.*, 1998, **120**, 443; (*b*) N. Tokitoh, Y. Arai, R. Okazaki and S. Nagase, *Science*, 1997, **277**, 78.

6 A. H. Cowley, J. E. Kilduff, J. G. Lasch, S. K. Mehrotra, N. C. Norman, M. Pakulski, B. R. Whittlesey, J. L. Atwood and W. E. Hunter, *Inorg. Chem.*, 1984, **23**, 2582.

7 (*a*) K. Tsuji, Y. Fuji, S. Sasaki and M. Yoshifuji, *Chem. Lett.*, 1997, 855; (*b*) P. Jutzi and U. Meyer, *J. Organomet. Chem.*, 1987, **326**, C6; (*c*) L. Weber, D. Bungardt, U. Sonneberg and R. Boese, *Angew. Chem., Int. Ed. Engl.*, 1988, **27**, 1537; (*d*) L. Weber and U. Sonnenberg, *Chem. Ber.*, 1989, **122**, 1809; (*e*) J. Escudie, C. Couret, H. Ranaivonjatovo and J.-G. Wolf, *Tetrahedron Lett.*, 1983, **24**, 3625.

8 K. Niedeik and B. Neumuller, *Z. Anorg. Allg. Chem.*, 1993, **619**, 885.

9 N. N. Greenwood and A. Earnshaw, *Chemistry of the Elements*, 2nd edn, Butterworth-Heinemann, London, 1997, ch. 13, p. 547.

Received in Bloomington, IN, USA, 22nd June 1998; 8/04722G

A macrocyclic [60]fullerene–porphyrin dyad involving π–π stacking interactions

Elke Dietel,[a] Andreas Hirsch,*[a] Emerich Eichhorn,[b] Anton Rieker,[b] Steffen Hackbarth[c] and Beate Röder[c]

[a] *Institut für Organische Chemie, Universität Erlangen-Nürnberg, Henkestraße 42, D-91054 Erlangen, Germany*
[b] *Institut für Organische Chemie, Universität Tübingen, Auf der Morgenstelle 18, D-72076 Tübingen, Germany*
[c] *Institut für Physik, Humboldt Universität Berlin, Invalidenstraße 110, D-10115 Berlin, Germany*

The very regioselective twofold cyclopropanation of C_{60} with a porphyrin bismalonate leads to a C_2 symmetrical [60]fullerene–porphyrin dyad with pronounced electronic interactions between the two π–π stacked chromophores.

In a project aimed at the synthesis of stereochemically defined architectures involving fullerene and porphyrin building blocks[1] we became interested in the development of a model compound with a face-to-face arrangement of the two π-systems and an electronic interaction between the two chromophores. In order to achieve this goal, we decided to restrict the conformational freedom within a dyad by introducing two covalent linkages *via* a tether controlled synthesis[2] with the porphyrin itself being an integral part of the tether.

For this purpose we synthesized the bifunctionalized porphyrin **1** using a mixed aldehyde approach (Scheme 1).[3] Benzaldehyde, 3-[2-(methoxymalonyloxy)ethoxy]benzaldehyde and pyrrole were stirred with $BF_3{\cdot}Et_2O$ as catalyst and Ph_4PCl in CH_2Cl_2 for one hour. After the addition of chloranil the mixture was refluxed for another hour. Separation of **1** from other reaction products required repeated purification with column chromatography (silica gel, CH_2Cl_2–ethyl acetate 20 : 1). The free base porphyrin was converted into the metallated compound **2**† by stirring with $ZnCl_2$ in refluxing acetone. **2** was attached to C_{60} *via* a twofold cyclopropanation achieved by the action of iodine and DBU.[4] This bisaddition proceeds with outstanding regioselectivity, since next to uncharacterized oligomeric material, bisadduct **3** with a *trans*-2 addition pattern (out–out isomer[2]) was formed as the only regioisomer (HPLC) and isolated in 41% yield by flash chromatography (silica gel, toluene–ethyl acetate 9 : 1).

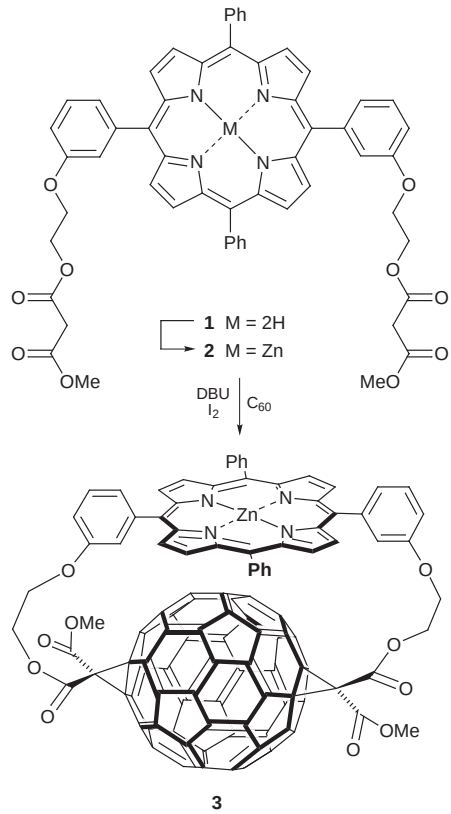

3

Scheme 1

The dyad **3** was completely characterized‡ allowing for an unambiguous structure assignment. The symmetry of **3** is C_2. This is clearly reflected by the splitting of the porphyrin signals to a doublet, for example four signals instead of two observed in **2** for the β-pyrrole C atoms at 131.74, 131.79, 132.03 and 132.08 ppm. Moreover, the C_2 symmetric binding of the tether is revealed by only one signal for the equivalent methoxy protons at 53.87 ppm, two signals for the two different carbonyl groups at 163.49 and 163.53 ppm, two signals for the two different sp^3-C atoms at 70.06 and 70.72 ppm and 26 resolved signals for the 28 different sp^2-C atoms of the fullerene core. Next to the *cis*-**3** and *trans*-**3** adducts (with in–in or out–out bridging and C_2 symmetry) the depicted structure of **3** is the only one consistent with the NMR spectra. The correct structure assignment of **3** as the *trans*-**2** out–out isomer was provided by a combination of molecular mechanics calculations and UV/VIS spectroscopy: (1) the other C_2 symmetric isomers are inaccessible for this tether (MM+ force field), since their strain energy is considerably higher; (2) each addition pattern gives rise to a characteristic electronic absorption spectrum in both the visible and the UV part.[5] The latter is not covered by the absorptions of the porphyrin moiety and therefore the presence of a *trans*-2 addition pattern within **3** is unambiguously revealed by the comparison with the UV/VIS spectra of a variety of series of corresponding bisadducts.[5]

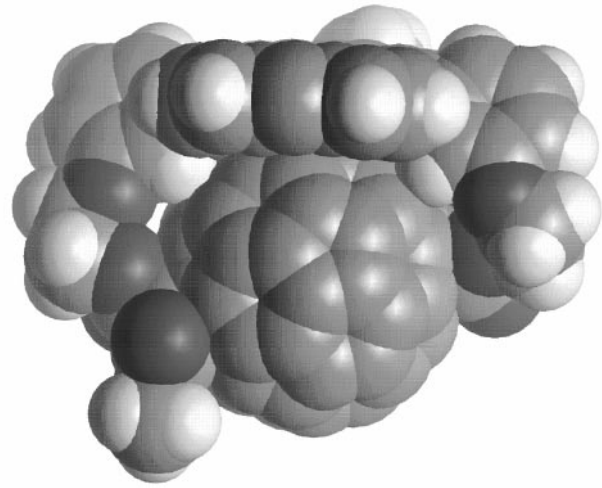

Fig. 1 Space-filling model of the PM3 (Spartan 4.1) calculated structure of **3**. The *meso*-phenyl ring in the front is omitted for clarity.

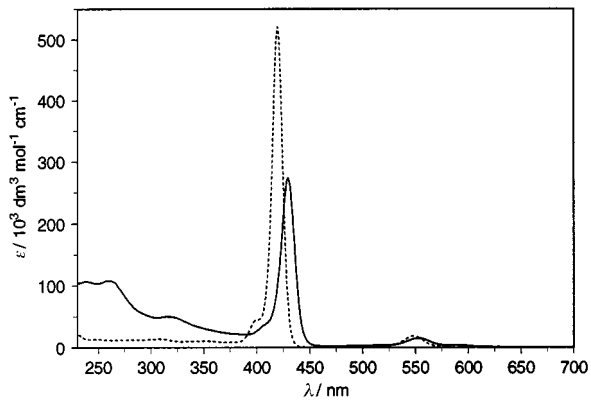

Fig. 2 Electronic absorption spectra of **2** (dashed line) and **3** in CH_2Cl_2 at $c = 3.5 \times 10^{-6}$ mol dm^{-3}.

In the MM+ minimized structure of **3** (Fig. 1) the average distance between the four pyrrole N atoms and the Zn atom of the macrocycle and their nearest neighbours on the fullerene moiety is 3.4 Å. The shortest distance between the Zn atom and a fullerene C atom is only 3.0 Å and therefore even shorter than the interplanar distance in graphite.

Electroanalytical investigations on **3** using cyclic voltammetry and differential pulse voltammetry reveal two oxidative and six reductive electron transfer processes which are also present in either the parent porphyrin **2** or the *trans*-2-bis(diethylmalonate) **4**.[5] Only slight shifts, for example of 16 mV, to a more negative potential for the first porphyrin oxidation are detected.§ Compared with **2** the Soret- and Q-bands of **3** show a bathochromic shift and decrease of the molar absorption coefficients indicating a considerable photoinduced interaction between the two chromophores (Fig. 2). Also photophysical analyses of **3** reflect the close proximity and stacking interaction between the corresponding π-systems. Time-dependent luminescence measurements reveal a complete quenching of the typical porphyrin fluorescence with a maximum at about 500 nm which is present in the monoadduct dyad **5**.[1] However, a

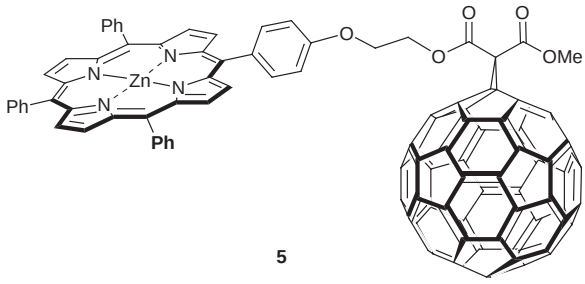

5

new luminescence band at 850 nm was found. The luminescence intensity increases with decreasing temperature. The luminescence decay can be fitted double exponentially with the decay times $\tau_1 = 2.84$ ns and $\tau_2 = 0.42$ ns. The relative amplitudes of the decay times were calculated to be 2.12 : 1. This, together with a complete lack of photosensitized $^1O_2$ generation typical for porphyrins,[6] C_{60} and many of its derivatives,[7] suggests an efficient photoinduced energy transfer from the porphyrin to the fullerene.

Detailed comparative investigations on electron and energy transfer processes of **3** and related systems including those with different central metals and additional addends like electron acceptors and dendrimers are currently under way.

We thank the 'Volkswagen Stiftung' for financial support.

Notes and references

† Detailed procedures for the synthesis and spectroscopic data of **1** and **2** will be reported elsewhere.

‡ *Spectroscopic data* for **3**: ^{1}H NMR (400 MHz, $CDCl_3$, 25 °C) δ 8.82–8.75 (8 H, m), 8.27 (2 H, d), 8.19 (2 H, d), 7.93 (2 H, d), 7.80–7.64 (10 H, m), 7.37 (2 H, d), 5.15 (2 H, dt), 4.77 (2 H, dt), 4.49 (4 H, t), 3.93 (6 H, s); ^{13}C NMR (100.5 MHz, $CDCl_3$, 25 °C) δ 163.53, 163.49, 156.57, 150.19, 150.08, 150.04, 147.91, 145.07, 144.98, 144.67, 144.60, 144.03, 143.47, 143.43, 142.81, 142.74, 142.63, 142.33, 142.08, 142.00, 141.82, 141.62, 141.51, 141.44, 141.38, 141.33, 141.16, 140.85, 140.74, 139.96, 139.59, 138.44, 138.41, 138.00, 137.95, 137.91, 134.40, 134.15, 132.08, 132.03, 131.79, 131.74, 127.72, 127.41, 126.77, 126.55, 126.42, 125.27, 121.40, 120.43, 115.17, 70.72, 70.06, 67.30, 65.11, 53.87, 49.16; UV/VIS $\lambda_{max}(CH_2Cl_2)$/nm (ε/dm^3 mol^{-1} cm^{-1}) 240 (109000), 260 (110200), 315 (50900), 407 (sh, 38400), 429 (273900), 552 (26200); FT-IR (KBr) ν/cm^{-1} 3053, 3021, 2950, 2922, 2867, 1750, 1596, 1576, 1480, 1433, 1237, 1108, 1069, 1003, 796, 702, 527; FAB-MS *m*/*z* 1714 (M^+).

§ Formal potentials ($E°$/V): **2** $E_{ox}^1 = 0.273$, $E_{ox}^2 = 0.712$, $E_{red}^1 = -1.898$, $E_{red}^2 = -2.234$; **3** $E_{ox}^1 = 0.257$, $E_{ox}^2 = 0.712$, $E_{red}^1 = -1.156$, $E_{red}^2 = -1.487$, $E_{red}^3 = -1.741$, $E_{red}^4 = -1.898$, $E_{red}^5 = -2.085$, $E_{red}^6 = -2.300$; **4** $E_{red}^1 = -1.102$, $E_{red}^2 = -1.467$, $E_{red}^3 = -1.910$, $E_{red}^4 = -1.987$, $E_{red}^5 = -2.325$. The redox potentials $E°$ were determined from cyclic voltammograms (mean value of corresponding E_p^r and $E_p°$) and differential pulse voltammograms in 0.22 mmolar solutions of **3** in CH_2Cl_2–NBu_4PF_6 (0.1 M) at Pt/Ir using a Ag–$AgClO_4$ (0.01 M)/NBu_4PF_6 (0.01 M)/acetonitrile reference electrode and were recalculated against internal Fc/Fc^+ ($\Delta V = 0.21$ V).

Note added in proof. A macrocyclic *trans*-1 fullerene–porphyrin conjugate was recently obtained by F. Diederich (personal communication).

1 E. Dietel, A. Hirsch, J. Zhou and A. Rieker, *J. Chem. Soc., Perkin Trans. 2*, 1998, 1357.
2 J.-F. Nierengarten, V. Gramlich, F. Cardullo and F. Diederich, *Angew. Chem.*, 1996, **108**, 2242.
3 F. Li, K. Yang, J. S. Tyhonas, K. A. MacCrum and J. S. Lindsey, *Tetrahedron*, 1997, **53**, 12339.
4 (*a*) C. Bingel, *Chem. Ber.*, 1993, **126**, 1957; (*b*) C. Bingel, presentation at the meeting 'New Perspectives in Fullerene Chemistry and Physics', October 10–12, 1994, Rome.
5 F. Djojo, A. Herzog, I. Lamparth, F. Hampel and A. Hirsch, *Chem. Eur. J.*, 1996, **2**, 1537.
6 (*a*) B. Röder, *Biophys. Chem.*, 1990, **35**, 303; (*b*) S. Oelkers, *SPIE Proc.*, 1994, **2325**, 116; (*c*) B. Röder, C. Zimmermann and R. Herter, *SPIE Proc.*, 1994, **2325**, 80; (*d*) W. Spiller and S. Hackbarth, *J. Porphyrins Phthalocyanines*, 1998, **2**, 145.
7 J. W. Arbogast, A. P. Darmanyan, C. S. Foote, Y. Rubin, F. Diederich, M. M. Alvarez, S. J. Anz and R. L. Whetten, *J. Phys. Chem.*, 1991, **95**, 11.

Received in Cambridge, UK, 29th May 1998; 8/04047H

Rhodium catalysed diboration of unstrained internal alkenes and a new and general route to zwitterionic [$L_2Rh(\eta^6$-catBcat)] (cat = 1,2-$O_2C_6H_4$) complexes†

Chaoyang Dai,[a] Edward G. Robins,[b] Andrew J. Scott,[c] William Clegg,[c] Dmitri S. Yufit,[b] Judith A. K. Howard[b] and Todd B. Marder*[a,b]

[a] *Department of Chemistry, University of Waterloo, Waterloo, Ontario, N2L 3G1, Canada*
[b] *Department of Chemistry, University of Durham, Durham, UK DH1 3LE. E-mail: Todd.Marder@durham.ac.uk*
[c] *Department of Chemistry, University of Newcastle upon Tyne, Newcastle upon Tyne, UK NE1 7RU*

Reactions of [L_2Rh(acac)] (L = alkene or phosphine) with B_2cat_3 yield the zwitterionic complexes [$L_2Rh(\eta^6$-catBcat)] and [(acac)Bcat] cleanly; [(dppm)Rh(η^6-catBcat)], the X-ray structure of which is reported, is an excellent catalyst for the diboration of vinylarenes and unstrained internal alkenes *cis*- and *trans*-stilbene and *trans*-β-methylstyrene.

Catalysed 1,2-diborations of alkynes, 1,4-diboration of 1,3-dienes and α,β-unsaturated ketones, as well as additions of B–Si and B–Sn bonds to alkynes, α,ω-diynes and enynes have been the subject of a recent review.[1] These reactions are catalysed by platinum or palladium complexes and usually a single catalytic pathway leads to a single product. In contrast, the catalysed diboration of alkenes can lead to up to nine products owing to the competition between B–C reductive elimination and β-hydride elimination from the L_nM(Bcat)[CHRCHR′(Bcat)] intermediate formed by alkene insertion into the M–B bond. Initially, we examined[2] [(dppb)Rh(η^6-catBcat)], [dppb = $Ph_2P(CH_2)_4PPh_2$] an outstanding hydroboration catalyst,[3] for the addition of B_2cat_2 to 4-vinylanisole and obtained the desired 1,2-diboration product 4-$MeOC_6H_4CH$(Bcat)CH_2(Bcat) in 44% yield. The remaining products included 23% of 4-$MeOC_6H_4CH$(Bcat)CH_3 and 22% of the unusual 2,2,2-tris(boronate) ester 4-$MeOC_6H_4CH_2C$(Bcat)$_3$, both arising from intermediates generated by the β-hydride elimination process. A catalyst system composed of [$AuCl(PEt_3)$] + $Cy_2P(CH_2)_2PCy_2$ gave exclusive formation of the 1,2-bis(boronate) ester; however, catalyst activity and stability were lower than desired. Miyaura and coworkers[4] reported the addition of B_2pin_2 (pin = $OCMe_2CMe_2O$) to terminal alkenes and cyclic alkenes having internal ring strain using a catalytic amount of $Pt(dba)_2$ at 50 °C, but attempts to diborate internal alkenes such as stilbene were unsuccessful. Iverson and Smith[5] reported similar results using $Pt(cod)_2$ or $Pt(norbornene)_3$ as catalyst precursors at ambient temperatures. Clean diboration was observed for norbornene and norbornadiene, but not for other internal alkenes, apparently as a result of complications arising from β-hydride elimination. In addition, neither of the base-free Pt systems is appropriate for modification with chiral ligands. We report herein the first catalyst system capable of diborating internal alkenes including *cis*- and *trans*-stilbene, and *trans*-β-methylstyrene without significant by-products.

Several zwitterionic [$L_2Rh(\eta^6$-catBcat)] complexes had been prepared previously[3] by addition of HBcat to either [$L_2Rh(\eta^3$-2-Me-allyl)] or [L_2Rh(acac)] precursors; however, with L = arylphosphine the reaction had to be carried out under hydroboration conditions (*i.e.* in the presence of excess alkene and HBcat) in order to isolate the [(dppb)Rh(η^6-catBcat)] cleanly. In addition, this approach is obviously inappropriate for L_2 = $(alkene)_2$ or diene. We have now found that reactions (Scheme 1) of [L_2Rh(acac)] with B_2cat_3 yield quantitatively the zwitterionic complexes [$L_2Rh(\eta^6$-catBcat)] [L_2 = $(C_2H_4)_2$ **1a**, $(C_8H_{14})_2$ **1b**, cod **1c**, $(PPh_2Me)_2$ **1d**, dppm **1e**, dppe **1f**, dppp = $Ph_2P(CH_2)_3PPh_2$ **1g**, dppb **1h**, dppf = 1,1-bis(diphenylphosphino)ferrocene **1i**] and (acac)Bcat **2** as evidenced by ^1H, ^{11}B, and ^{31}P NMR spectroscopy, full details of which will be reported elsewhere.

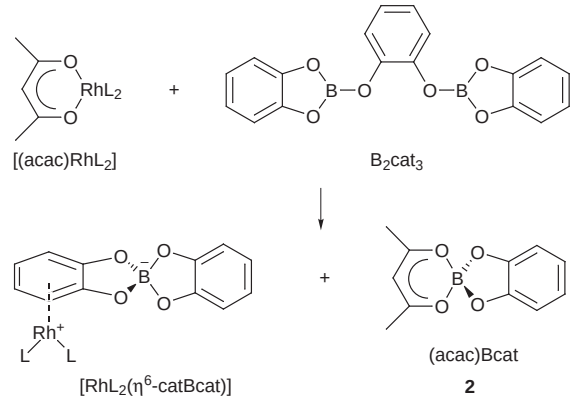

1a $L_2 = (C_2H_4)_2$ **f** L_2 = dppe
b $L_2 = (C_8H_{14})_2$ **g** L_2 = dppp
c L_2 = cod **h** L_2 = dppb
d $L_2 = (PPh_2Me)_2$ **i** L_2 = dppf
e L_2 = dppm

Scheme 1 Synthesis of zwitterionic rhodium complexes

Of particular interest is the fact that 4 mol% of [(dppm)Rh(η^6-catBcat)] **1e**,‡ prepared *in situ* from [(dppm)Rh(acac)] and B_2cat_3 in THF, and whose molecular structure§ is shown in Fig. 1, catalyses the diboration of (addition of B_2cat_2 to) vinylarenes, norbornene and the

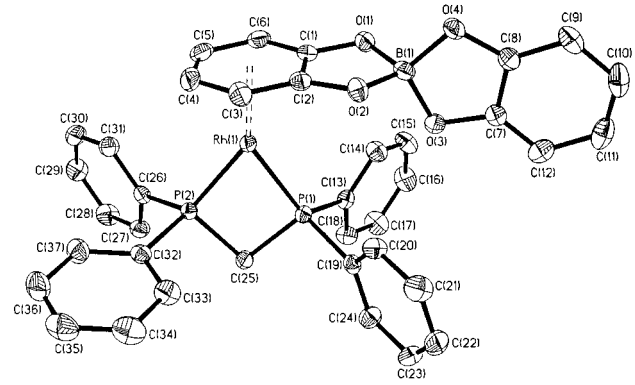

Fig. 1 View of the molecular structure of [(dppm)Rh(η^6-catBcat)] **1e** with ellipsoids shown at 50% probability and H atoms omitted for clarity. Selected distances (Å) and angles (°) Rh(1)–P(1) 2.2332(5), Rh(1)–P(2) 2.2134(5); P(1)–Rh(1)–P(2) 72.938(17).

Table 1 [(acac)Rh(dppm)]/B_2cat_3-catalyzed diboration of alkenes[a]

Entry	Alkene	Product	Time/h	Yield(%)
a		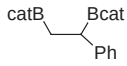	2	87
b	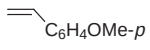	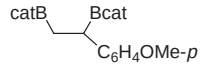	2.5	77
c	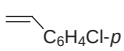	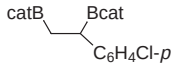	1	79
d		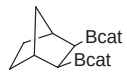	6	>99
e	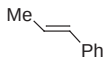	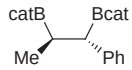	30	>99
f	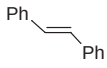	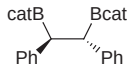	<72	92
g		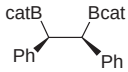	<72	>99

[a] All reactions were carried out in THF or [$^2H_8$]THF at room temp. in the presence of 4 mol% catalyst [(acac)Rh(dppm)]/B_2cat_3, and alkene : B_2cat_2 = 1:1; product yields determined by ^1H and ^{13}C NMR spectroscopy.

unstrained internal alkenes *cis* and *trans*-stilbene and *trans*-β-methylstyrene at room temp. (Table 1).¶ *Syn*-addition of the B_2 unit to the alkene was evident in the NMR spectra of the norbornene diboration product (entry d). A crystal structure§ of the *trans*-stilbene diboration product (entry f) is also consistent with *syn*-addition. The disorder observed in the crystal structure results from the apparent superposition in space of the two enantiomers of the racemic compound; attempts to solve the structure based on the *meso*-model gave an unreasonable central C–C bond length. Likewise, in CD_2Cl_2, the signal for the unique benzylic C–H proton at δ 3.71 is distinct from that for the *cis*-stilbene diboration product (entry g) which occurs at δ 3.78 the latter thus being assigned to the *meso* compound. Diboration of *trans*-β-methylstyrene (entry e) proceeds in >99% yield,¶ generating two adjacent and distinct chiral carbon centres.

Significantly reduced hapticity of the π-coordinated catecholate must be required in order to generate vacant sites for alkene and B–B activation. Although reaction times were found to be somewhat longer than in THF, the diborations can also be carried out in less polar C_6D_6 suggesting that complete dissociation into L_2Rh^+ and $[Bcat_2]^-$ is unlikely. The success of the dppm based catalyst system compared with the dppb system indicates that the relative rates of B–C reductive elimination *vs*. β-hydride elimination are a sensitive function of the bite angle of the chelating phosphine ligand.

This is the first report of the catalysed diboration of unstrained internal alkenes and of an efficient phosphine-containing catalyst system for alkene diboration. Further work will examine the mechanism of the reaction, the diboration of other unsaturated substrates and the use of chiral bis(phosphine)-containing zwitterionic Rh complexes for asymmetric diboration reactions.

T. B. M. acknowledges support from NSERC of Canada, the University of Durham for Special Equipment and Special Projects Grants, the University of Newcastle upon Tyne through a Senior Visiting Research Fellowship, and the NSERC/Royal Society (London) Bilateral Exchange Program, W. C. thanks EPSRC for an equipment grant, A. J. S. thanks EPSRC for a studentship, and J. A. K. H. thanks the University of Durham for a Sir Derman Christopherson Fellowship.

Notes and References

† Dedicated to Professor Warren Roper on the occasion of his 60th birthday. Preliminary results were presented at the Fifth Chemical Congress of North America, Cancun, Mexico, November 1997, Abstract No. 1493.

‡ *NMR spectroscopic data* for **1e** in C_6D_6: $^{31}P\{^1H\}$, δ −22.97 (d, $^1J_{RhP}$ 184.6 Hz); $^{11}B\{^1H\}$, δ 15.76; ^1H, δ 3.62 (td, $^3J_{RhH}$ 2.0, $^2J_{PH}$ 10.8 Hz, 2 H, CH_2), 4.74 (m, 2 H, η^6-C$_6H_4O_2$), 6.28 (m, 2 H, η^6-C$_6H_4O_2$), 6.60 (m, 1 H, C$_6H_4O_2$), 6.76 (overlapping m, 2 H, C$_6H_4O_2$), 6.87–7.13 (overlapping m, 13 H, C$_6H_4O_2$ and C$_6H_5$), 7.65 (m, 8 H, C$_6H_5$).

§ *Crystal data*: for **1e** from C_6D_6: $C_{37}H_{30}BO_4P_2Rh{\cdot}C_6D_6$, M = 798.42, orthorhombic, space group $P2_12_12_1$, a = 13.2932(7), b = 15.2327(8), c = 17.8046(10)Å, U = 3605.3(3)Å^3, Z = 4, D_c = 1.471 g cm^{-3}, μ(Mo-Kα) = 0.606 mm^{-1}, T = 160 K. Full-matrix least-squares refinement on F^2 (G. M. Sheldrick, SHELXTL manual, Bruker AXS Inc., Madison, WI, USA, 1994, version 5) anisotropic for all non-H atoms and isotropic for H (461 parameters) using 8415 unique data (including 3634 Friedel pairs; 26 554 total collected; R_{int} = 0.0251) from a Bruker AXS SMART CCD diffractometer (θ < 28.46°) gave $R1$ [$I > 2\sigma(I)$] = 0.0212, $wR2$ (all data) = 0.0473. Residual electron density within ± 0.28 e Å^{-3}.

For *rac*-PhCH(Bcat)CH(Ph)(Bcat) from [$^2H_8$]THF: $C_{26}H_{20}B_2O_4{\cdot}C_4D_8O$, M = 498.16, monoclinic, space group $P2_1/m$, a = 6.1548(5), b = 19.853(2), c = 10.4004(9)Å, β = 95.933(3)°, U = 1264.1(2) Å^3, Z = 2, D_c = 1.309 g cm^{-3}, μ(Mo-Kα) = 0.085 mm^{-1}, T = 100 K. Full-matrix least-squares refinement on F^2 as above, anisotropic for all non-disordered non-H atoms, isotropic for H and disordered atoms with disordered H atoms not included in the refinement (198 parameters) using 2970 unique data (14 317 total collected; R_{int} = 0.060) (θ < 27.50°) gave $R1$ [$I > 2\sigma$(I)] = 0.0827, $wR2$ (all data) = 0.1931. Residual electron density within ± 0.572 e Å^{-3}. CCDC 182/949.

¶ *A representative procedure for* the diboration of *trans*-β-methylstyrene: in a N_2-filled glove-box, [(acac)Rh(dppm)] (0.010 mmol) and B_2cat_3 (0.010 mmol) were charged into a 20 ml vial and dissolved in THF (0.5 ml). The solution was stirred rapidly for *ca*. 5 min and then a solution of *trans*-β-methylstyrene (0.250 mmol) in THF (0.5 ml) was added. Finally, B_2cat_2 (0.250 mmol) was added portionwise and the resulting reaction mixture allowed to stir rapidly at room temperature. Aliquots (1 μl) were removed regularly to monitor the disappearance of alkene *via* GC–MS. Crude product was isolated by reduction of the THF volume by *ca*. 50% followed by addition of *n*-hexane (2–3 ml). *Spectroscopic data* for PhCH(Bcat)CH(Me)(Bcat) in C_6D_6: ^1H NMR, δ 1.12 (d, 3 H, J 7.5 Hz), 2.39 (dq, 1 H, J 11.4, 7.5 Hz), 3.05 (d, 1 H, J 11.4 Hz), 6.69 (m, 4 H), 6.88 (m, 4 H), 7.02 (m, 1 H), 7.14 (m, 2 H), 7.29 (m, 2 H). $^{11}B\{^1H\}$ NMR, δ 35.6 (br s, 2B). HRMS. Calc. for $C_{21}H_{18}B_2O_4$: m/z 356.1391. Found m/z 356.1391.

1 T. B. Marder and N. C. Norman, *Top. Catal.*, 1998, **5**, 63.
2 R. T. Baker, P. Nguyen, T. B. Marder and S. A. Westcott, *Angew. Chem., Int. Ed. Engl.*, 1995, **34**, 1336; *Angew. Chem.*, 1995, **107**, 1451.
3 S. A. Westcott, H. P. Blom, T. B. Marder and R. T. Baker, *J. Am. Chem. Soc.*, 1992, **114**, 8863.
4 T. Ishiyama, M. Yamamoto and N. Miyaura, *Chem. Commun.*, 1997, 689.
5 C. N. Iverson and M. R. Smith III, *Organometallics*, 1997, **16**, 2757.

Received in Cambridge, UK, 22nd June 1998; 8/04710C

Catalytic asymmetric Diels–Alder reactions of α-thioacrylates for the preparation of norbornenone

Varinder K. Aggarwal,*[a]† Emma S. Anderson,[a] D. Elfyn Jones,[a] Kerstin B. Obierey[a] and Robert Giles[b]

[a] *Department of Chemistry, University of Sheffield, Sheffield, UK S3 7HF*
[b] *SmithKline Beecham, Old Powder Mills, Tonbridge, Kent, UK TN11 9AN*

Cu^{II}–bisoxazoline complexes catalyse the asymmetric Diels–Alder cycloaddition of α-thioacrylates with cyclopentadiene to give the cycloadducts in up to 92% yield, 88% de and >95% ee for the *endo* product; deprotection gives good yields of (1*S*,4*S*)-norbornenone with high enantioselectivity.

The catalytic asymmetric Diels–Alder reaction has been an area of considerable interest over the last two decades and a large number of metals, ligands and dienophiles have been studied.[1–4] The most successful systems have common features associated with them: a bidentate ligand which complexes to the metal and a dienophile which acts as a two point binder to the ligand–metal complex.[5–7] Two point binding of both the ligand to the metal and dienophile to the complex results in limiting the number of accessible conformations of the dienophile bound to the Lewis acid and can result in high enantioselectivity.

We have been interested in developing ketene equivalents for Diels–Alder reactions[8] and have therefore sought dienophiles that could be easily converted to carbonyl compounds. To achieve good levels of enantioselectivity we also needed dienophiles that could act as two point binders to appropriate metals. α-Thioacrylates seemed ideal for our purpose as it was known that α-methylthioacrylates underwent Diels–Alder reactions with cyclopentadiene, for example, and that the adducts could be readily converted into norbornenones.[9–11] Such dienophiles may also act as two point binders to appropriate metals through carbonyl and sulfur coordination. We therefore prepared a range of α-thioacrylates.[12] We chose copper as the metal due to its known propensity to bind to both the sulfide and ester moieties and as ligands we chose bisoxazolines[13,14] due to the success of copper–bisoxazoline complexes in Diels–Alder reactions.[15–25]

Diels–Alder reactions were conducted between cyclopentadiene and the various acrylates[26] using the copper bisoxazoline complex **8**[27] (Scheme 1) and the results are shown in Table 1.

It was found that the selectivity of the Diels–Alder reaction was highly dependent on the nature of the ester and thio substituent. Higher selectivity was obtained with phenylthio- compared to methylthio-acrylates (entries 1 and 3) and higher selectivity was obtained with small or moderately sized ester substituents [Me, Et, Pr^i >> Bu^t (entries 2, 3, 6, 8 and 9)]. The Bu^t ester was much less reactive than the other esters and the reaction had to be conducted at 0 °C (entry 8). This presumably was the cause of the reduction in enantioselectivity. Higher selectivity was obtained at lower temperature (compare entries 3 and 4) and the use of cationic complexes[16] led to high reactivity even at −78 °C (entries 5 and 7) and high *exo*/*endo* selectivity as well as high enantioselectivity. The optimum reagents and conditions required ethyl α-phenylthioacrylate as dienophile, the cationic phenyl-substituted bisoxazoline–cop-

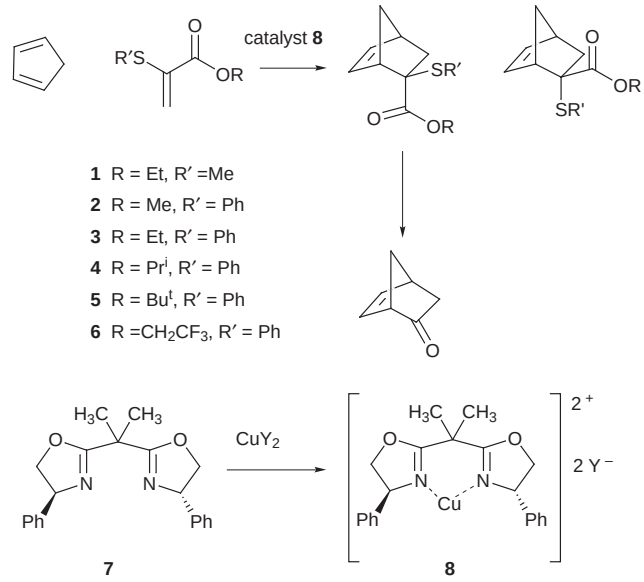

7 **8**

Scheme 1

Table 1 Diels–Alder reactions of α-thioacrylates with cyclopentadiene catalysed by Cu–bisoxazoline complexes

	Dienophile								
Entry		R	R′	Catalyst[a]	*t*/h	*T*/°C	Yield (%)	*exo*:*endo*[b]	Ee[c] (%)
1	**1**	Et	Me	$Cu(OTf)_2$	6	−40	53	1:2.4	40
2	**2**	Me	Ph	$Cu(OTf)_2$	6	−40	44	1:3.7	84
3	**3**	Et	Ph	$Cu(OTf)_2$	6	−40	50	1:4	80
4	**3**	Et	Ph	$Cu(OTf)_2$	9	−78	76	1:7	>95
5	**3**	Et	Ph	$CuBr_2/AgSbF_6$[d]	1	−78	92	1:15	>95
6	**4**	Pr^i	Ph	$Cu(OTf)_2$	4	−40	70	1:2.3	85
7	**4**	Pr^i	Ph	$CuBr_2/AgSbF_6$[d]	2.5	−78	90	1:5	81
8	**5**	Bu^t	Ph	$Cu(OTf)_2$	5.5	0	91	1:2.5	26
9	**6**	CF_3CH_2	Ph	$CuBr_2/AgSbF_6$[d]	1.5	−78	92	1:13	>95

[a] 20 mol% $Cu(OTf)_2$, 30 mol% bisoxazoline **7**, 1 equiv. dienophile and 4 equiv. cylopentadiene. [b] Determined by NMR integration of crude reaction mixtures. [c] Determined by NMR integration in the presence of Pirkle's reagent, (*R*)-(−)-2,2,2-trifluoro-1-(9-anthryl)ethanol. [d] 10 mol% of $CuBr_2/AgSbF_6$, 10 mol% bisoxazoline **7**, 1 equiv. dienophile and 4 equiv. cylopentadiene.

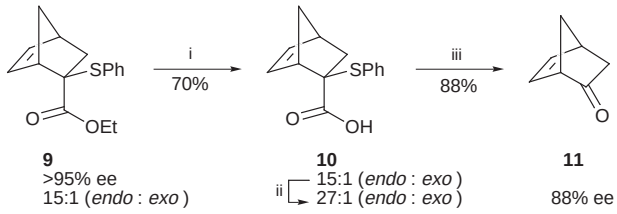

Scheme 2 *Reagents and conditions*: i, KOH, Bu^{i}OH, H_2O; ii, recrystallisation (light petroleum); iii, $(PhO)_2P(O)N_3$, Et_3N, MeCN, H_2O

per complex, and reaction at −78 °C in CH_2Cl_2 (entry 5); under these conditions good diastereoselectivity and essentially complete enantioselectivity was observed.

Conversion of the α-phenylthio ester to a carbonyl group was initially problematic. Hydrolysis of the ester to the acid occurred efficiently but attempts to convert the α-phenylthio acid **10** to the carbonyl group using NCS was unsuccessful. This reagent had previously been used to convert an α-methylthio acid to a carbonyl group.[9] We were eventually successful using a different strategy: instead of activating the sulfide we activated the acid and reacted the α-phenylthio acid with diphenylphosphoryl azide[28] and obtained the corresponding ketone **11** directly in high yield and with 88% ee[29] (Scheme 2). The lower enantioselectivity observed for **11** is due to the presence of the *exo* isomer in **10**.

A transition state involving bidentate binding of the dienophile *via* sulfur and the carbonyl oxygen to a square planar Cu^{II} complex[15,16,21,23,24,30,31] may be used to rationalise the enantio- and diastereo-selectivities. However, the high enantioselectivity observed is perhaps surprising as the alkene of the dienophile lies close to the C_2 axis of the metal catalyst where it encounters the minimum steric influence from the phenyl groups of the oxazoline moiety. Indeed, all successful dienophile–metal–oxazoline combinations place the alkene moiety directly over one of the oxazoline substituents where it has maximum influence on the enantioselectivity of the reaction.[32] In our case we believe that the substituent on sulfur plays a major role in controlling enantioselectivity. We believe there is very high diastereoselectivity in formation of the dieneophile–metal–oxazoline complex (only one of the two enantiotopic lone pairs binds to the copper) and it is the orientation of the sulfur substituent which controls the facial attack on the dienophile (Fig. 1). This substituent is forced below the plane of the complex and when this group is large it effectively blocks the *Si* face of the dienophile and therefore forces the diene onto the *Re* face. From analysis of molecular models, the opposite enantiomer would be expected if the dienophile was bound to Cu in a tetrahedral arrangement. This provides further circumstantial evidence for a square planar complex.

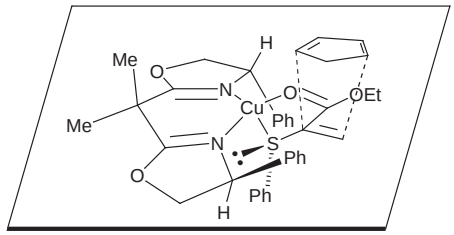

Fig. 1 The dienophile–metal–oxazoline complex

The size of the ester group of the dienophile is critical; an excessively bulky group may prevent the essential two-point binding, as seems to be the case with *tert*-butyl. Equally, the substituent on sulfur of the dienophile is also critical. Although the same discrimination between the lone pairs on sulfur may be observed with the *S*-methyl substituted dienophile, the methyl group is not sufficiently sterically hindering to effectively block the *Si* face to approach of the diene component, resulting in significantly reduced enantioselectivity in this case.

We thank the EPSRC and SB for a CASE award (E. A.), the European Union and Sheffield University for additional support. We thank Ian Davies (Merck) for valuable discussions.

Notes and References

† E-mail: v.aggarwal@sheffield.ac.uk

1 W. Oppolzer, *Angew. Chem., Int. Ed. Engl.*, 1984, **23**, 876.
2 H. B. Kagan and O. Riant, *Chem. Rev.*, 1992, **92**, 1007.
3 T. Oh and M. Reilly, *Org. Prep. Proced. Int.*, 1994, **26**, 129.
4 L. C. Dias, *J. Braz. Chem. Soc.*, 1997, **8**, 289.
5 E. J. Corey and J. J. Rohde, *Tetrahedron Lett.*, 1997, **38**, 37.
6 E. J. Corey, D. BarnesSeeman and T. W. Lee, *Tetrahedron Lett.*, 1997, **38**, 1699.
7 E. J. Corey, D. BarnesSeeman and T. W. Lee, *Tetrahedron Lett.*, 1997, **38**, 4351.
8 V. K. Aggarwal, J. Drabowicz, R. S. Grainger, Z. Gultekin, M. Lightowler and P. L. Spargo, *J. Org. Chem.*, 1995, **60**, 4962.
9 B. M. Trost and Y. Tamaru, *J. Am. Chem. Soc.*, 1977, **99**, 3101.
10 J. L. Boucher and L. Stella, *Tetrahedron*, 1988, **44**, 3595.
11 J. L. Boucher and L. Stella, *Tetrahedron*, 1988, **44**, 3607.
12 J. Durman, J. I. Grayson, P. G. Hunt and S. Warren, *J. Chem. Soc., Perkin Trans. 1*, 1986, 1939.
13 A. Pfaltz, *Acc. Chem. Res.*, 1993, **26**, 339.
14 A. V. Bedekar, E. B. Koroleva and P. G. Andersson, *J. Org. Chem.*, 1997, **62**, 2518.
15 D. A. Evans, S. J. Miller and T. Lectka, *J. Am. Chem. Soc.*, 1993, **115**, 6460.
16 D. A. Evans, J. A. Murry, P. Vonmatt, R. D. Norcross and S. J. Miller, *Angew. Chem., Int. Ed. Engl.*, 1995, **34**, 798.
17 D. A. Evans, M. C. Kozlowski and J. S. Tedrow, *Tetrahedron Lett.*, 1996, **37**, 7481.
18 D. A. Evans and D. M. Barnes, *Tetrahedron Lett.*, 1997, **38**, 57.
19 D. A. Evans and J. S. Johnson, *J. Org. Chem.*, 1997, **62**, 786.
20 D. A. Evans, E. A. Shaughnessy and D. M. Barnes, *Tetrahedron Lett.*, 1997, **38**, 3193.
21 I. W. Davies, C. H. Senanayake, R. D. Larsen, T. R. Verhoeven and P. J. Reider, *Tetrahedron Lett.*, 1996, **37**, 1725.
22 I. W. Davies, L. Gerena, L. Castonguay, C. H. Senanayake, R. D. Larsen, T. R. Verhoeven and P. J. Reider, *Chem. Commun.*, 1996, 1753.
23 I. W. Davies, L. Gerena, D. W. Cai, R. D. Larsen, T. R. Verhoeven and P. J. Reider, *Tetrahedron Lett.*, 1997, **38**, 1145.
24 M. Johannsen and K. A. Jorgensen, *J. Org. Chem.*, 1995, **60**, 5757.
25 M. Johannsen, S. Yao and K. A. Jorgensen, *Chem. Commun.*, 1997, 2169.
26 The acrylates were prepared from the corresponding sulfoxides by a Pummerer reaction. See: J. Durman, J. I. Grayson, P. G. Hunt and S. Warren, *J. Chem. Soc., Perkin Trans. 1*, 1986, 1939; H. J. Monteiro and A. L. Gemal, *Synthesis*, 1975, 437.
27 The catalyst formed from the phenyl-substituted bisoaxazoline with $Cu(OTf)_2$ was found to be much more reactive at room temperature than catalysts incorporating Bu^i-, Bn- or Bu^t-substituted bisoxazolines which required up to eight days to go to completion. Studies were therefore concentrated on the phenyl-substituted bisoaxazoline.
28 K. Ninomiya, T. Shioiri and S. Yamada, *Tetrahedron*, 1974, **30**, 2151.
29 Chiral GC analysis of **(±)-9** was carried out on a Chiral cyclodextrin α column (30 m, 0.25 mm i.d.), using hydrogen as the carrier gas at 16 psi, 70 °C isothermal, flame ionisation detection. **(**1*R*,4*R***)-(+)-9** had a retention time of 10.50 min while **(**1*S*,4*S***)-(−)-9** had a retention time of 10.04 min. From GC analysis, **(**1*S*,4*S***)-(−)-9** was obtained with 88% ee.
30 D. A. Evans, M. C. Kozlowski, C. S. Burgey and D. W. C. MacMillan, *J. Am. Chem. Soc.*, 1997, **119**, 7893.
31 Jorgensen has suggested that reactions occur *via* square planar and tetrahedral Cu complexes depending on the substitution of the oxazoline (ref. 24).
32 For an exception, see: Y. Honda, T. Date, H. Hiramatsu and M. Yamauchi, *Chem. Commun.*, 1997, 1411. They carried out a cycloaddition between a benzoylacrylate and cyclopentadiene using MgI_2–bisoxazoline complex. No comment was made on the origin of the enantioselectivity.

Received in Liverpool, UK, 10th July 1998; 8/05366I

Stereoselective and N-terminal selective α-alkylation of peptides using a pyridoxal model compound as a chiral N-terminal activator

Kazuyuki Miyashita, Hiroshi Iwaki, Kuninori Tai, Hidenobu Murafuji and Takeshi Imanishi*†

Graduate School of Pharamceutical Sciences, Osaka University, 1-6 Yamadaoka, Suita, Osaka 565-0871, Japan

Stereoselective and N-terminal selective α-alkylation of peptides is achieved using a pyridoxal model compound as an N-terminal activator which also functions as a chiral auxiliary.

Peptides containing unnatural amino acid(s) are gathering much attention because of their biochemical and medicinal properties. Although such peptides are generally synthesized by sequential coupling of the respective amido acids prepared independently,[1] several methods for the direct modification of peptides have also been reported.[2–4] Most of these methods, however, deal with the alkylation of peptides at sites other than the N-terminal position and seem to lack generality. In addition, their stereoselectivities depend on the stereochemistries of the peptides employed and are not always sufficient.[2,3] In contrast, direct N-terminal modification of peptides appears to be of great utility for the synthesis of peptides including unnatural amino acids, particularly where applied to combinatorial chemistry, as both liquid- and solid-phase peptide syntheses are generally achieved by sequential coupling from a C-terminal amino acid. O'Donnell and co-workers recently reported an interesting method utilizing this idea: direct N-terminal selective α-alkyltion of peptides *via* imine formation.[4] The only serious problem with their method is the lack of stereoselectivity. If the α-alkylation takes place with predictable stereoselectivity, this method would be more useful and versatile. In order for this method to be applicable to the synthesis of various peptides with predictable stereochemistry, it is desirable that the stereoselectivity of the α-alkylation is induced only by an external chiral auxiliary, and is not influenced by the neighbouring chiral centre on the peptide sequence. Here we report a useful method for N-terminal selective and stereoselective α-alkylation of peptides using a chiral pyridoxal model compound bearing an ionophore function.

Taking into account the application of the reaction not only to liquid-phase synthesis but also to solid-phase synthesis, we investigated the benzylation of the aldimines prepared from L-Ala-NHBn and some chiral pyridoxal models under various conditions.‡ As a consequence, we found that the reaction with pyridoxal model **1** having a chiral ansa-structure§ in the presence of $LiClO_4$[5] and DBU was the most effective for the present purpose and stereoselectively afforded the α-benzylated product (*R*)-**4** (X = NHBn) and recovered **1** (79%) after an acidic treatment (run 1 in Table 1 and Scheme 1).

These conditions were employed for the alkylation of peptides **2** (X = AA-OBn) and the results are summarized in Table 1.¶ The peptide-aldimine **3** (X = L-Ala-OBn) prepared from L-Ala-L-Ala-OBn and **1** was also stereoselectively benzylated at the N-terminal position without any detectable racemisation at the C-terminal α-position *via* these sequential reactions (run 2).‖ As expected, the stereochemistry at the N-terminal α-position was not related to the stereoselectivity at all (run 3). In order to examine the influence of the stereogenic centre at the neighbouring C-terminal α-position on the stereoselectivity of the alkylation, dipeptides L-Ala-Gly-OBn, L-Ala-L-Val-OBn, L-Ala-D-Ala-OBn, and L-Ala-D-Val-OBn were chosen as substrates. The reaction of peptides without a stereogenic centre or with a bulkier alkyl group at the C-terminal position similarly gave good *R*-stereoselectivity (runs 4 and 5). Moreover, in the reactions of the peptides having a D-amino acid at the C-terminal position, the same predominantly *R*-configuration was gained with slightly lower stereoselectivity (runs 2 *vs.* 6 and 5 *vs.* 7). It is noteworthy and quite significant that neither the stereochemistry nor the size of the

Table 1 Alkylation of aldimines **3** with RBr

	Substrate **2**						Product **4**	
Run	R^1	R^2	X	R	M^+	*t*/h	Yield (%)[a]	*R*:*S*[b]
1	Me	H	NHBn	Bn	Li	2.5	60	83:17
2	Me	H	L-Ala-OBn	Bn	Li	4	51	86:14
3	H	Me	L-Ala-OBn	Bn	Li	4	53	86:14
4	Me	H	Gly-OBn	Bn	Li	4	46	83:17
5	Me	H	L-Val-OBn	Bn	Li	4.5	50	88:12
6	Me	H	D-Ala-OBn	Bn	Li	4	49	74:26
7	Me	H	D-Val-OBn	Bn	Li	5	51	73:27
8	Me	H	L-Ala-OBn	4-$O_2NC_6H_4CH_2$	Li	4	50	85:15
9	Me	H	L-Ala-OBn	CH_2=$CHCH_2$	Li	4.5	48	73:27
10	Me	H	L-Ala-OBn	CH≡CCH_2	Li	4.5	56	84:16
11	Me	H	L-Ala-L-Ala-OBn	Bn	Li	5	48	86:14
12	Me	H	L-Ala-OBn	Bn	none	7	38	21:79
13	Me	H	L-Ala-OBn	Bn	Na	5	38	26:74
14	Me	H	L-Ala-OBn	Bn	K	7	32	23:77

[a] Isolated yield based on substrate **2**. [b] The stereochemistries of the products (*R*)- and (*S*)-**4** (X = L-Ala-OBn) were confirmed by comparing with an authentic sample (*S*)-**4** (X = L-Ala-OBn) prepared from L-Ala and (*S*)-(α-Bn) Ala-OBn, which had been obtained using our previous method (ref. 5). The stereochemistries of other products **4** were assigned as shown from their (*R*)-MTPA amides by comparing their ^1H and ^{19}F NMR data with those of the (*R*)-MTPA amide of authentic (*S*)-(α-Bn)Ala-L-Ala-OBn and (*S*)-(α-Bn)Ala-OBn. Excepting runs 1 and 4, the ratio was determined from the ^1H NMR spectra. In the runs 1 and 4, the ratios were determined from the ^1H and ^{19}F NMR spectra of the corresponding (*R*)-MTPA amides.

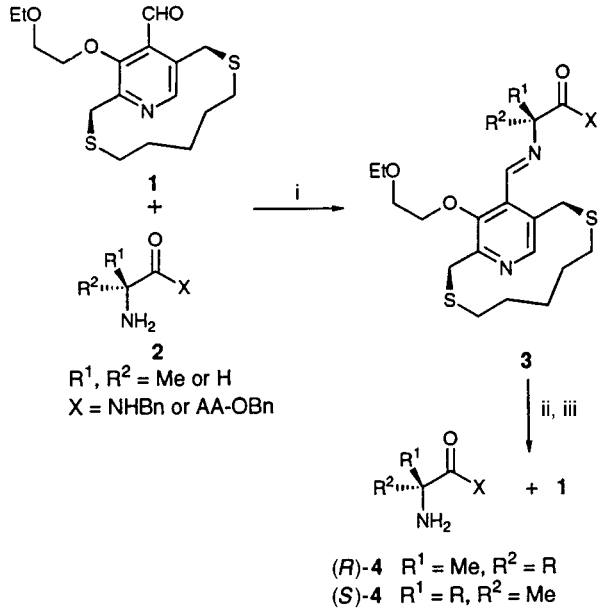

Scheme 1 *Reagents and conditions*: i, CH_2Cl_2, room temp.; ii, RBr, $MClO_4$, DBU, MeCN, 0 °C; iii, $TsOH·H_2O$, AcOEt, room temp., 30 min

substituent at the C-terminal α-position of the peptides affected the stereoselectivity. In addition, alkylation with other alkyl bromides proceeded successfully with similar stereoselectivities (runs 8–10). Tripeptide L-Ala-L-Ala-L-Ala-OBn was also stereoselectively benzylated under the same conditions (run 11). These findings show that compound **1** can work as an external chiral auxiliary as well as an N-terminal activator, at least in the synthesis of peptides with neutral amino acids at the neighbouring position.

Interestingly, the reaction without Li^+ or with other alkali metal ions was found to show the reverse stereoselectivity (runs 12–14). Concerning the reaction mechanism, ^1H NMR analysis of the peptide-aldimine **3** in the absence and presence of Li^+ revealed that the rotation of the C4–C4′ bond shown in Fig. 1 was induced only by the addition of Li^+.[5] The stereoselectivities obtained in the absence and presence of Li^+ appear to be attributable to these preferred conformations. Although the detailed mechanism has yet to be determined, predominant attack of the electrophile on the enolates from the side of the ansa-loop (*i.e.* upper side in Fig. 1) in the respective conformations could explain the stereoselectivities.**

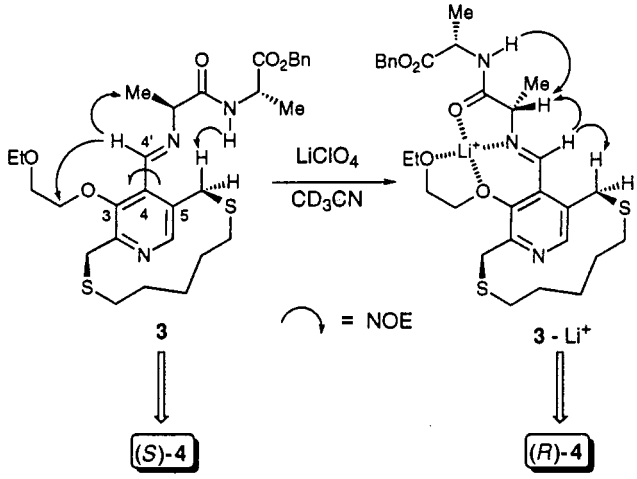

Fig. 1 Selected NOE data for **3** in the absence and presence of Li^+

In the present study, we have demonstrated the first example of stereoselective and N-terminal selective α-alkylation of peptides using a chiral pyridoxal model as an N-terminal activator which also functions as a chiral auxiliary. This α-alkylation reaction could be incorporated into standard sequential peptide syntheses, and could provide a novel method for the stereoselective synthesis of unnatural peptides, in particular, for construction of unnatural peptide libraries.††

This research was financially supported in part by the Houansha Foundation (HOUANSHA) and by a Grant-in-Aid for General Scientific Research (09672282) from the Ministry of Education, Science, Sports and Culture of Japan.

Notes and References

† E-mail: imanish@phs.osaka-u.ac.jp

‡ Although we first applied the pyridoxal model compound and the reaction conditions which had previously been effective for the asymmetric alkylation of α-amino esters (ref. 6) to this reaction, the desired stereoselectivity was not obtained. Hence, reactions with pyridoxal models having a chiral ionophore chain at C-3 and/or a chiral ansa-structure in the presence of various organic bases and metal ions were examined. Details will be reported in a full article.

§ The pyridoxal derivative **1** was synthesized from the 3-hydroxy derivative (ref. 7) according to the literature procedure (refs. 5, 6).

¶ *General procedure*: The peptide-aldimine was prepared according to the previously described procedure (ref. 5). To a stirred solution of peptide-aldimine **3** (0.10 mmol) and $LiClO_4$ (32.2 mg, 0.30 mmol) in MeCN (1 ml) was added DBU (29.9 μl, 0.20 mmol) at 0 °C. After stirring for 5 min at the same temperature, BnBr (13.2 μl, 0.11 mmol) was added and the mixture was stirred at 0 °C for the period indicated in Table 1. The reaction mixture was diluted with AcOEt (10 ml) and washed with cold water and cold brine. To the organic layer, $TsOH·H_2O$ (38.6 mg, 0.20 mmol) was added and the mixture was stirred for 30 min at room temperature and partitioned with Et_2O and water. The Et_2O phase was worked-up as usual and the residue was purified by SiO_2 column chromatography (AcOEt–hexane = 1 : 2) to give recovered **1** (70–80%). The aqueous phase was basified with $NaHCO_3$ and extracted with AcOEt. Usual work-up and purification with SiO_2 column chromatography (AcOEt) yielded the benzylated peptide **4**.

‖ This was confirmed by the fact that the (*R*)-MTPA amide derived from the benzylated dipeptide was shown to be a mixture of only two diastereomers based on the N-terminal α-position by ^1H and ^{19}F NMR analyses.

** The ansa-loop could push the other substituents out of the side of the ansa-loop and consequently make the other side crowded, which might allow the electrophile to approach from the same side of the ansa-loop. See also ref. 8.

†† Further extensions to the synthesis of longer peptides and to solid-phase synthesis are in progress.

1 R. M. Williams, *Synthesis of Optically Active α-Amino Acids*, Pergamon, Oxford, 1989; H. Heimgartner, *Angew. Chem., Int. Ed. Engl.*, 1991, **30**, 238; T. Wirth, *Angew. Chem., Int. Ed. Engl.*, 1997, **36**, 225.

2 R. Polt and D. Seebach, *J. Am. Chem. Soc.*, 1989, **111**, 2622; S. A. Miller, S. L. Griffiths and D. Seebach, *Helv. Chim. Acta*, 1993, **76**, 563; D. Seebach, A. K. Beck, H. G. Bossler, C. Gerber, S. Y. Ko, C. W. Murtiashaw, R. Naef, S. Shoda, A. Thaler, M. Krieger and R. Wenger, *Helv. Chim. Acta*, 1993, **76**, 1564; H. G. Bossler and D. Seebach, *Helv. Chim. Acta*, 1994, **77**, 1124; H. G. Bossler, P. Waldmeier and D. Seebach, *Angew. Chem., Int. Ed. Engl.*, 1994, **33**, 439.

3 U. Kazmaier, *J. Org. Chem.*, 1994, **59**, 6667.

4 M. J. O'Donnell, C. Zhou and W. L. Scott, *J. Am. Chem. Soc.*, 1996, **118**, 6070; W. L. Scott, C. Zhou, Z. Fang and M. J. O'Donnell, *Tetrahedron Lett.*, 1997, **38**, 3695.

5 K. Miyashita, H. Miyabe, C. Kurozumi and T. Imanishi, *Chem. Lett.*, 1995, 487; K. Miyashita, H. Miyabe, C. Kurozumi, K. Tai and T. Imanishi, *Tetrahedron*, 1996, **52**, 12 125.

6 K. Miyashita, H. Miyabe, K. Tai, C. Kurozumi and T. Imanishi, *Chem. Commun.*, 1996, 1073.

7 H. Kuzuhara, M. Iwata and S. Emoto, *J. Am. Chem. Soc.*, 1977, **99**, 4173; M. Ando, Y. Tachibana and H. Kuzuhara, *Bull. Chem. Soc. Jpn.*, 1982, **55**, 829.

8 H. Kuzuhara, N. Watanabe and M. Ando, *J. Chem. Soc., Chem. Commun.*, 1987, 95.

Received in Cambridge, UK, 20th July 1998; 8/05596C

Zirconocene-catalysed cyclobutene formation by reaction of alkynyl halides with EtMgBr

Kayoko Kasai,[a] Yuanhong Liu,[b] Ryuichiro Hara[b] and Tamotsu Takahashi*[b]†

[a] *Department of Chemistry, Miyagi University of Education, Sendai 980, Japan*
[b] *Catalysis Research Center and Graduate School of Pharmaceutical Sciences, Hokkaido University, Sapporo 060, Japan*

Zirconium-catalysed reaction of alkynyl halides with EtMgBr produced cyclobutene derivatives in which two carbon–carbon bonds were formed on the ethyl moiety of EtMgBr *via* an ethylene group in a catalytic cycle.

The zirconium-catalysed reaction of olefins with EtMgBr was first reported as an ethylmagnesation reaction by Dzhemilev.[1] Recently, we found that the reaction proceeds *via* a zirconocene–ethylene complex and a zirconacycle.[2,3] However, so far the ethyl moiety of EtMgBr has only been incorporated in products as an ethyl group in the catalytic reaction with olefins[1–4] or acetylenes.[5] There has been no example in which two carbon–carbon bonds were formed on the ethyl moiety in the catalytic cycle in the strict sense, even though it is converted into an ethylene group in the cycle. We report here the first example of the formation of two carbon–carbon bonds to the ethyl moiety of EtMgBr in a catalytic cycle.

Typically, when 1 mmol of 1-chlorooct-1-yne **1a** was treated with a catalytic amount of $(C_5H_5)_2ZrCl_2$ (10 mol%) and 3 equiv. of EtMgBr in THF (5 ml) at room temperature for 24 h, 1-hexylcyclobutene **2a** was formed in 61% yield [eqn. (1)].

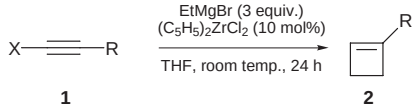

1 **2** (1)

Table 1 shows the results of cyclobutene formation reactions under the catalytic conditions. The choice of halogen on the terminal carbon of the alkynes was important. 1-Bromo- and 1-iodo-alkynes did not give cyclobutenes under these conditions; only metal–halogen exchange products were formed. The yields were also dependent on the amount of EtMgBr, and the use of 3 equiv. was found to be suitable in all the cases for the catalytic reactions. Interestingly, when a diyne dichloride **1c** was treated under similar conditions, a bridged dicyclobutenyl product **2c** was obtained.

This reaction was interesting due to the fact that an alkynyl chloride and ethylene derived from EtMgBr reacted formally in a [2 + 2] cycloaddition with the loss of halogen. In order to understand this catalytic reaction, we also carried out stoichiometric reactions.[6] The results are shown in Table 2. A typical procedure is as follows. To a solution of $(C_5H_5)_2ZrCl_2$ (0.37 g, 1.25 mmol) in THF (6 ml) was added EtMgBr (1.0 M THF solution, 2.5 mmol) at −78 °C. The reaction mixture was warmed up to −40 °C and stirred for 1 h. To the mixture was added 1-chlorooct-1-yne at −78 °C. The mixture was stirred for 1 h at room temperature. After stirring for 1 h, the reaction mixture was quenched with 3 M HCl and the usual workup gave 1-hexylcylobutene in 80% yield. The same products were obtained under both catalytic and stoichiometric conditions; however, under the latter conditions the reaction proceeded much faster. It is noteworthy that the intermolecular coupling of the chloroalkyne moieties with ethylene derived from EtMgBr

Table 1 Formation of cyclobutenes under catalytic conditions[a]

XC≡CR	Product	Yield[b] (%)
1a	 **2a**	61
1b	 **2b**	51
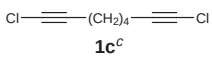 **1c**[c]	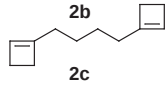 **2c**	54
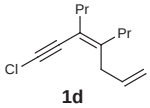 **1d**	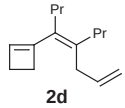 **2d**	50

[a] Unless otherwise noted, $(C_5H_5)_2ZrCl_2$ (10 mol%) and EtMgBr (3 equiv.) were used for the catalytic reactions. Conditions: room temperature, 24 h. [b] Yields were determined *via* GC using hydrocarbons as internal standards. [c] $(C_5H_5)_2ZrCl_2$ (20 mol%) and EtMgBr (6 equiv.) were used.

Table 2 Formation of cyclobutenes under stoichiometric conditions[a]

XC≡CR	Product	Yield[b] (%)
1a	**2a**	80 (80)
	**2a**	66
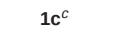	**2a**	60
1b	**2b**	83
1c[c]	**2c**	89[d] (60)
1d	**2d**	80[d] (50)
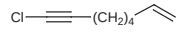 **1e**	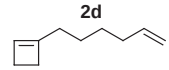 **2e**	40

[a] Unless otherwise noted, $(C_5H_5)_2ZrCl_2$ (1.25 equiv.) and EtMgBr (2.5 equiv.) were used for the stoichiometric reactions. Conditions: room temperature, 1 h. [b] Unless otherwise noted, yields were determined *via* GC using hydrocarbons as internal standards. [c] $(C_5H_5)_2ZrCl_2$ (2.5 equiv.) and EtMgBr (5 equiv.) were used. [d] Yield was determined by NMR analysis. Isolated yields are given in parentheses.

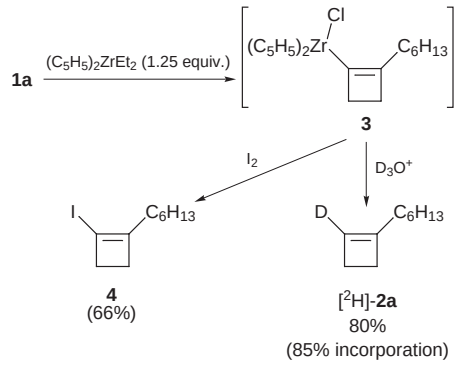

Scheme 1

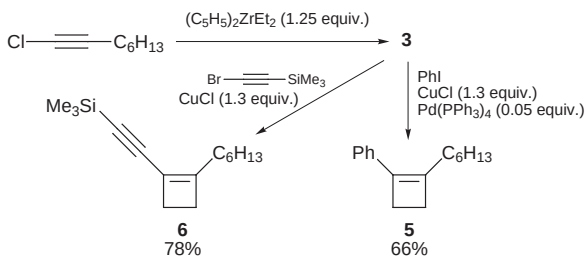

Scheme 2

predominated over the intramolecular coupling of an alkynyl group with an olefin moiety, or the second alkynyl group when **1c**–**e** were used.

Deuterolysis of the stoichiometric reaction mixture gave [^{2}H]-**2a** in 80% yield with 85% deuterium incorporation. Iodinolysis gave a 66% yield of iodocylobutene **4**. These results suggest that the intermediate is cyclobutenylzirconium **3** (Scheme 1).

Since the intermediate **3** contains a zirconium–carbon bond, the further carbon–carbon bond formation reactions of alkenylzirconium compounds were examined (Scheme 2). To a stoichiometric reaction mixture of **1a** and $(C_5H_5)_2ZrEt_2$ prepared *in situ* from $(C_5H_5)_2ZrCl_2$ and 2 equiv. of EtMgBr were added iodobenzene, CuCl (1.3 equiv.) and $Pd(PPh_3)_4$ (0.05 equiv.). The mixture was stirred at 50 °C, and 1-hexyl-2-phenylcyclobutene **5** was obtained in 66% overall yield based on **1a**. Similarly, treatment of **3** with 1-bromo-2-trimethylsilylacetylene and CuCl (1.3 equiv.) gave alkynylcyclobutene **6** in 78% yield. This procedure is a convenient preparative method for various 1,2-disubstituted cyclobutenes.

Introducing ethylene gas to a solution of the Negishi reagent (Cp_2ZrBu_2)[7] and subsequent addition of a 1-chloroalkyne also gave cyclobutene **2a** in good yield as expected [eqn. (2)]. This

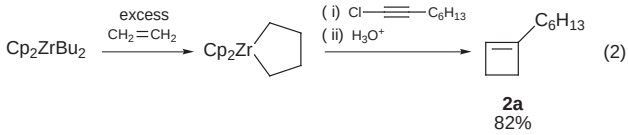

(2)

clearly showed that ethylene and the ethyl moiety of EtMgBr are equivalent in the carbon–carbon bond formation described above.

A plausible mechanism of the catalytic cyclobutene ring formation is shown in Scheme 3. The zirconocene–ethylene complex reacts with haloalkyne **1** to form α-halozirconacyclopentene **7**, which undergoes a ring-closing reaction to give cyclobutenyl–zirconocene complex **3**. This ring-closing reaction might proceed *via* reductive elimination of

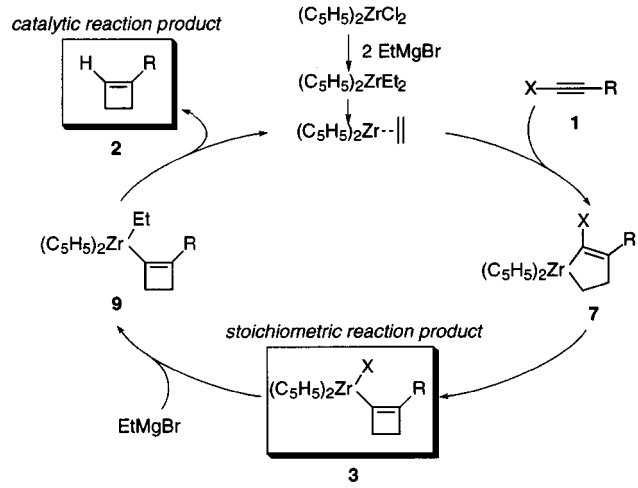

Scheme 3

zirconacyclopentenes[6] and oxidative addition of the alkenyl chloride moiety to zirconocene.[8] The ethylene complex is regenerated by the reaction of **3** with EtMgBr to complete the catalytic cycle.

Notes and References

† E-mail: tamotsu@cat.hokudai.ac.jp

1 U. M. Dzhemilev and O. S. Vostrikova, *J. Organomet. Chem.*, 1985, **285**, 43.
2 T. Takahashi, T. Seki, Y. Nitto, M. Saburi, C. J. Rousset and E. Negishi, *J. Am. Chem. Soc.*, 1991, **113**, 6266.
3 For related Zr-catalyzed reactions of olefins with EtMgBr, see also A. H. Hoveyda and Z. Xu, *J. Am. Chem. Soc.*, 1991, **113**, 5079; K. S. Knight and R. M. Waymouth, *J. Am. Chem. Soc.*, 1991, **113**, 6268; D. P. Lewis, P. M. Muller and R. J. Whitby, *Tetrahedron Lett.*, 1991, **32**, 6797.
4 N. Suzuki, D. Y. Kondakov and T. Takahashi, *J. Am. Chem. Soc.*, 1993, **115**, 8485. For a related study, see J. P. Morken, M. T. Didiuk and A. H. Hoveyda, *J. Am. Chem. Soc.*, 1993, **115**, 6997.
5 For related Zr-catalyzed reactions of alkynes with EtMgBr, see also T. Takahashi, K. Aoyagi, V. Denisov, N. Suzuki, D. Choueiry, C. J. Rousset and E. Negishi, *Tetrahedron Lett.*, 1993, **34**, 1145.
6 For stoichiometric cyclobutene formation from zirconacycles, see T. Takahashi, Z. Xi, R. Fischer, S. Huo, C. Xi and K. Nakajima, *J. Am. Chem. Soc.*, 1997, **119**, 4561; Y. Liu, W. Sun and T. Takahashi, *Chem. Commun.*, 1998, 1133.
7 E. Negishi, D. R. Swanson, F. E. Cederbaum and T. Takahashi, *Tetrahedron Lett.*, 1986, **27**, 2829.
8 T. Takahashi, M. Kotora, R. Fischer, Y. Nishihara and K. Nakajima, *J. Am. Chem. Soc.*, 1995, **117**, 11039.

Received in Cambridge, UK, 22nd June 1998; 8/04697B

Sulfone-linked paracyclophanes

Ian Baxter,[a] Howard M. Colquhoun,[b]*† Philip Hodge,[c]*‡ Franz H. Kohnke*[c]§¶ and David J. Williams*[a]‖

[a] *Department of Chemistry, Imperial College, South Kensington, London, UK SW7 2AY*
[b] *Department of Chemistry, University of Salford, Salford, UK M5 4WT*
[c] *Department of Chemistry, University of Manchester, Manchester, UK M13 9PL*

Oxidation of the macrocyclic thioether sulfones $(S\phi SO_2\phi)_n$ (ϕ = 1,4-phenylene; n = 2 or 3) affords sulfone-linked paracyclophanes $(\phi SO_2)_4$ and $(\phi SO_2)_6$; single crystal X-ray analysis reveals the tetramer, $(\phi SO_2)_4$, to be a near-perfect square box, whilst the hexamer, $(\phi SO_2)_6$, adopts a much more irregular conformation; exhaustive oxidation of $(S\phi SO_2\phi)_4$, leads not to the expected octamer, $(\phi SO_2)_8$, but to the heptasulfone sulfoxide $[(\phi SO_2)_7(\phi SO)]$.

The recent discovery of a route to macrocyclic aromatic thioether sulfones containing from four to (at least) 24 aromatic rings has opened up the possibility of converting these, by oxidation, to their all-sulfone analogues (Scheme 1).[1] The strongly electron-withdrawing nature of the sulfone group compared to the electron-donating thioether linkage offers the potential to create a new family of π-electron deficient receptors which, unlike those based on bipyridinium systems,[2] would obviate the need for counterions. Moreover, the exceptionally rigid nature of the diphenyl sulfone unit, coupled with its preferred 'open-book' conformation,[3] should provide a high degree of pre-organisation in any non-covalent complexation process. From a materials perspective, these all-sulfone macrocycles could provide a new approach (ring-opening polymerisation)[4] to the extremely stable but very high-melting and currently unprocessable linear poly(1,4-phenylene sulfone).[5]

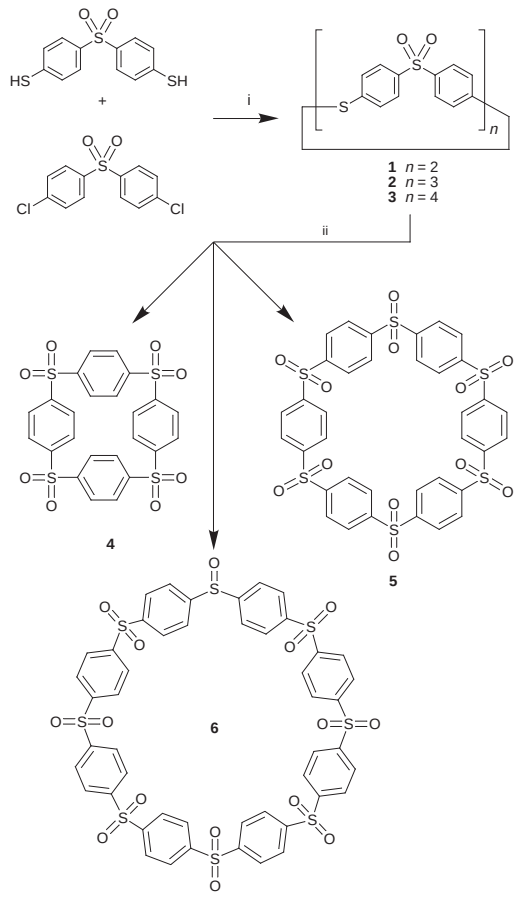

Scheme 1 *Reagents and conditions*: i, K_2CO_3, DMA, 150 °C, 48 h; ii, H_2O_2, AcOH, 60 °C

Here we report that peroxide oxidation of the macrocyclic thioethersulfones **1** and **2** in glacial acetic acid does indeed afford the sulfone-linked paracyclophanes **4** and **5** (sulfur analogues of the known [1.1.1.1]paracyclophane and [1.1.1.1.1.1]paracyclophane, respectively).[6] Oxidation of **3** cannot however be driven to completion under these conditions,** the reaction ceasing at the heptasulfone sulfoxide stage (**6**) rather than affording the expected cyclic octasulfone.

The symmetrical aromatic substitution pattern in macrocycles **4** and **5** results in the observation of only a *single* ^{1}H NMR resonance (δ 8.21) for each compound, replacing the AA′BB′ pattern associated with the 1,4 sulfide sulfone substitution patterns of **1** and **2**. However, in keeping with the presence of a sulfoxide linkage in **6**, the ^{1}H NMR spectrum of this material comprises an AA′BB′ system integrating as two aromatic rings, together with a single resonance representing the remaining six rings, at δ 8.21, superimposed on the lower field component. Confirmation that compound **6** is a single oxidation product (rather than a mixture) was provided by the unchanging ratio of the integration values in its ^{1}H NMR spectrum on repeated recrystallisation from DMA, and by MALDI-TOF mass spectrometry of **6** (anthracene-1,8,9-triol matrix, LiBr as cationising agent) which showed a strong parent ion at *m/z* 1111, corresponding to $[(C_6H_4SO_2)_7(C_6H_4SO)Li]^+$.

The solubilities of macrocycles **4** and **6** in conventional organic solvents are very low indeed and, although ^{1}H and ^{13}C NMR spectra of **4** were obtained (with some difficulty) in [$^2H_6$]DMSO solution, a solvent mixture of TFA and CD_2Cl_2 was required to obtain NMR spectra of compound **6**. The cyclic hexamer **5**, in contrast, was easily soluble in a wide range of organic solvents including $CHCl_3$ and acetone.

In order to establish the conformational characteristics of the diaryl sulfone unit as a function of ring size, single crystal X-ray structures were determined for **4** (DMSO solvate), **5** (acetone

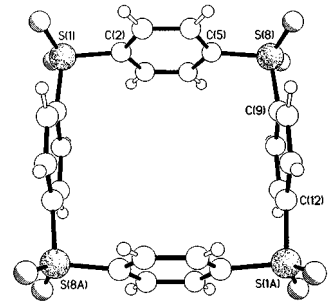

Fig. 1 Molecular structure of the cyclic tetrasulfone **4**. There is a very slight tilting from orthogonality of the aromatic rings with respect to the S_4 plane; the C(2)–C(7) ring is inclined at 86° and the C(9)–C(14) ring at 89° to this plane.

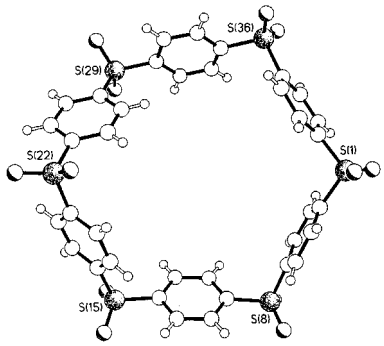

Fig. 2 Molecular structure of the cyclic hexasulfone **5**. Torsion angles about the S–phenyl linkages are in the range 45–88°, with the exception of an 8° torsion angle at S(29).

solvate) and **6** (DMSO solvate).†† The C–S–C bond angles in **5** and **6** lie very close to the conventional unstrained value[3] of 105° but in the effectively *square* cyclic tetramer **4** (Fig. 1) these angles are sharply reduced to an average value of 99.5°. Commensurate distortions are evident in the aromatic ring systems, which in **4** undergo a distinct outward bowing such that 1,4-related C–S bonds, which would normally be co-linear, here subtend angles averaging 10°. In contrast, the aromatic rings of oligomer **5** (Fig. 2) are bowed *inwards*, with the corresponding angle averaging −7.5°.

Remarkably, the structure of compound **6** in fact represents that of the originally-expected octasulfone [(1,4-$C_6H_4SO_2)_8$]. It thus appears that, when oxidation reaches the heptasulfone sulfoxide stage, this compound is able to crystallise *as though it were* the octasulfone, with the 'missing' oxygen atom being disordered over all sixteen possible sites. In keeping with the identification of macrocycle **6** as a *pseudo*-octasulfone, the average crystallographic occupancy of the oxygen atoms in the molecule refined to a value significantly less than one (*ca.* 0.96; *cf.* a calculated value of 0.94 for 15/16 occupancy). Macrocycle **6** adopts a 'figure-of-eight' conformation (Fig. 3) which is essentially strain-free, the two halves of the molecule each approximating the box-like structure of oligomer **4**. Contacts between the sulfone oxygen atoms at S(22) and S(22A) are avoided by a relative shearing of the two sides of the macrocycle, though there is evidence for weak but co-operative C–H···O hydrogen bonding interactions between these sulfone oxygens and transannular C–H groups (Fig. 3).

The cyclic tetramer **4** provides a rare example of a structurally characterised organic molecular square.[7] The mutually orthogonal orientation of the four aromatic rings results in a cylindrical free pathway through the macrocycle (based on van der Waals surfaces) of diameter *ca.* 3.3 Å. The presence of this electrophilic binding site suggests the possibility of complexation with first-row anions such as fluoride or cyanide, and of rotaxane formation with linear, electron-rich species such as the polyalkynes. Complexation studies with **4** are currently in progress.

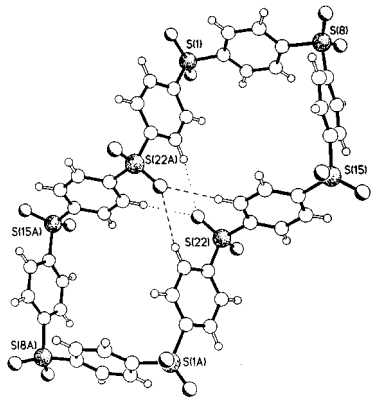

Fig. 3 Molecular structure of the cyclic *pseudo*-octasulfone **6** showing the transannular C–H···O interactions; the two independent sets of C–O and H–O distances and C–H···O angles are: 3.46 and 2.53 Å, 176°; 3.58 and 2.65 Å, 170°

We wish to thank Mr P. R. Ashton of the University of Birmingham for the MALDI-TOF mass spectrometric analysis, and the EPSRC for financial support.

Notes and References

† E-mail: h.m.colquhoun@chemistry.salford.ac.uk
‡ E-mail: philip.hodge@man.ac.uk
§ On leave from the Department of Organic and Biological Chemistry, University of Messina, I-98166, Messina, Italy.
¶ E-mail: franz@scirocco.unime.it
‖ E-mail: djw@ic.ac.uk

** The macrocyclic sulfide sulfone **1**, **2** or **3** (ref. 1) **(**0.30 g) was suspended in a mixture of glacial AcOH (15 cm^3) and 30% aq. H_2O_2 (7.5 cm^3) and heated at 60 °C for 8 h with continuous sonication. For macrocycle **3**, further 30% H_2O_2 (7.5 cm^3) was then added to the reaction mixture and oxidation continued at 85 °C for 16 h. Yields were essentially quantitative. *Selected data* for **4**: δ_H([$^2H_6$]DMSO) 8.21 (s); δ_C([$^2H_6$]DMSO) 130.0, 145.1 (Found: 559.9730. Calc.for $C_{24}H_{16}S_4O_8$: 559.9728). For **5**: δ_H([$^2H_6$]DMSO) 8.21 (s); δ_C([$^2H_6$]DMSO) 129.6, 144.5; *m/z* (ES-MS, −ve) 874–877 ([M+Cl]$^-$). For **6**: δ_H(CD_2Cl_2–TFA) 8.21 (s+m, 28H), 7.94 (m, 4H); *m/z* (LiBr-doped MALDI-TOF) 1011 [$(C_6H_4SO_2)_7(C_6H_4SO)Li]^+$ and 1027 [$(C_6H_4SO_2)_7(C_6H_4SO)Na]^+$.

†† *Crystal data* for **4**: [$C_{24}H_{16}O_8S_4$·2DMSO]: M = 716.86, monoclinic, a = 9.966(5), b = 18.003(5), c = 10.391(4) Å, β = 118.22(2)°, V = 1643(1) Å^3, space group $P2_1/c$, Z = 2, ρ_{calc} = 1.449 g cm^{-3}, μ(Cu-Kα) = 43.1 cm^{-1}, F(000) = 744, T = 293 K, 2419 unique reflections ($2\theta \leqslant 124°$), of which 1461 were observed [$I_o > 2\sigma(I_o)$]. R_1 = 0.0793, wR_2 = 0.1968. For **5**: [$C_{36}H_{24}O_{12}S_6$·2.5($CH_3)_2CO$)]: M = 986.11, orthorhombic, a = 11.220(3), b = 29.432(3), c = 29.860(4) Å, V = 9861(3) Å^3, space group $Pbca$, Z = 8, ρ_{calc} = 1.328 g cm^{-3}, μ(Cu-Kα) = 31.0 cm^{-1}, F(000) = 4096, T = 293K, 7741 unique reflections ($2\theta \leqslant 124°$), of which 3718 were observed [$I_o > 2\sigma(I_o)$]. R_1 = 0.0778, wR_2 = 0.2037. For **6**: [$C_{48}H_{32}O_{15}S_8$·6DMSO]: M = 1573.98, triclinic, a = 11.479(2), b = 11.583(2), c = 15.936(3) Å, α = 80.34(2), β = 78.63(2), γ = 62.78(1)°, V = 1840(1) Å^3, space group $P\bar{1}$, Z = 1, ρ_{calc} = 1.421 g cm^{-3}, μ(Cu-Kα) = 44.2 cm^{-1}, F(000) = 820, T = 203 K, 5401 unique reflections ($2\theta \leqslant 120°$), of which 3969 were observed [$I_o > 2\sigma(I_o)$]. R_1 = 0.0821, wR_2 = 0.2156.

Data for all structures were collected on Siemens P4 diffractometers using graphite monochromated Cu-Kα radiation (λ = 1.54178 Å; rotating anode source for **6**) and ω-scans. The data were corrected for Lorentz and polarisation effects and for absorption (using ψ-scans). The structures were solved by direct methods and refined by least-squares based on F^2. All computations were carried out using the SHELXTL 5.03 package. CCDC 182/970.

1 I. Baxter, H. M. Colquhoun, P. Hodge, F. H. Kohnke, and D. J. Williams, *Chem. Commun.*, 1998, 283.
2 M. Asakawa, P. R. Ashton, S. Menzer, F. M. Raymo, J. F. Stoddart, A. J. P. White and D. J. Williams, *Chem. Eur. J.*, 1996, **2**, 877.
3 H. M. Colquhoun, *Polymer* 1997, **38**, 991, and references cited therein.
4 Recent reviews of macrocyclic ring-opening polymerisation: D. J. Brunelle, in *New Methods of Polymer Synthesis*, ed. J. R. Ebdon and G. C. Eastmond, Blackie, London, 1995, p. 197. Y. F. Wang, K. P. Chan and A. S. Hay, *React. Funct. Polym.*, 1996, **30**, 205; P. Hodge, H. M. Colquhoun and D. J. Williams, *Chem. Ind. (London)*, 1998, 162.
5 D. R. Robello, A. Ulman and E. J. Urankar, *Macromolecules*, 1993, **26**, 6718.
6 Y. Miyahara, T. Iazu and T. Yoshino, *Tetrahedron Lett*., 1983, **24**, 5277; G. W. Gribble and C. F. Nutaitis, *Tetrahedron Lett*., 1985, **26**, 6023.
7 M. Asakawa, P. R. Ashton, S. Menzer, F. M. Raymo, J. F. Stoddart, A. J. P. White and D. J. Williams, *Chem. Eur. J.*, 1996, **2**, 877 and references cited therein.

Received in Cambridge, UK, 17th July 1998; 8/05549A

Synthesis of a biotin functionalized pyrrole and its electropolymerization: toward a versatile avidin biosensor

L. M. Torres-Rodriguez,[a] A. Roget,[a]* M. Billon,[a] T. Livache[b] and G. Bidan[a]†

[a] *Laboratoire d'électrochimie moléculaire et de structures des interfaces, UMR 5819 (CNRS-CEA-Université J.Fourier), Département de Recherches Fondamentales sur la Matière Condensée/CEA-Grenoble 17, avenue des Martyrs, 38054 Grenoble, France*

[b] *CIS Bio international. DIVT, BP 175, 30203, Bagnols sur Cèze Cedex, France*

The synthesis of a biotinylated pyrrole and its copolymerization with pyrrole for the purpose of constructing an electronic conducting polymer (ECP) avidin sensor is reported, using fluorescence detection to determine the efficiency of the sensing process.

Electronic conducting polymers (ECP) have many interesting features that make them ideal candidates for sensing devices, and have thus became the subject of many investigations. In addition to their ease of electrodeposition, these polymers can be functionalized by insertion of specific moieties[1] that provide desirable features such as the selective recognition of alkaline cations.[2] The application of ECP in the field of sensors has also been extended to biological species,[3–5] including DNA, peptides and enzymes. The detection of these species is based on the specific recognition between a biological moiety that is inserted in the ECP film, and its complementary target in solution. The subsequent recognition is detected either by radioactive labels,[5] or by a significant change in the electrochemical[3,4] or spectrochemical response[6] of the ECP.

An important aspect of these biosensors is the immobilization of desired biological species in the ECP film. This has been accomplished by the entrapment of the species in the polymer matrix during electrodeposition, and by the use of grafted monomers which are then copolymerized with ungrafted monomers. In the case of the former, the electropolymerization conditions must be compatible with the stability of the biomolecule; in addition for the latter case, specific conditions must be developed for each of the grafted species. These approaches were successfully carried out for the construction of DNA biochips.[7]

A recent approach for immobilization is postpolymerization functionalization. In this case, a two-step chemical procedure is needed. First, starting monomers with an activated ester are grafted onto the polymer that will form the ECP film. Secondly, after electrodeposition the biological species is covalently coupled to the hanging ester *via* a reactive amino group.[8]

Here we report an original approach for the insertion of biochemical entities in the ECP film *via* the synthesis of a biotinylated polypyrrole. Because of the biotin–avidin affinity, biochemical entities bearing avidin units can bind to the biotin units grafted on the polypyrrole network. This approach allows immobilization of biomolecules on the ECP surface in an easy one-step process, without the use of harsh chemical reagents, since the biotin–avidin system requires only mild immobilization conditions.

The biotinylated polypyrrole film described here is a copolymer electrosynthesized from pyrrole and biotinylated pyrrole, in which the biotin is linked to the nitrogen atom of a pyrrole unit by a hydrophilic spacer arm. The choice of this spacer arm is crucial. It has to be long enough to ensure unrestricted recognition of the biotin by avidin, and a length of eleven atoms or more is deemed necessary.[9] In addition, its chemical composition is important in order to guarantee solubility during the preparation of the active layer, and to achieve good solvation of biotin in order to optimize the recognition. We thus selected a spacer with a hydrophobic/hydrophilic balance originating from three oxygen atoms and ten methylene groups.

The synthesis of the biotinylated pyrrole (Scheme 1) is achieved by coupling an aminoalkylpyrrole and a biotin entity. The aminoalkylpyrrole synthesis was carried out using the reaction pathway described by Jirkowsky and Baudy.[10] While the yields we obtained were consistent with the reported values for the ethanediamine, the equivalents of diamine and the reflux time were increased from 1 to 3 equiv. and 1 to 5 h, respectively. In the second step, the amino group was reacted with the activated ester of biotin to produce the biotinylated pyrrole in 54% yield after purification by column chromatography.

The copolymerization of the film was carried out on microelectrodes (50×50 μm) arrayed on a silicon chip, using different ratios of biotinylated pyrrole to pyrrole monomers (from 5×10^{-3} to 5×10^{-7}). The presence and activity of biotin to avidin was verified by incubating the film with streptavidin–phycoerythrin (Aldrich) and measuring the fluorescence using a microscope equipped with a DCC camera. We used a conjugate between streptavidin and a fluorescent phycobiliprotein, namely R-phycoerythrin, in order to maximize fluorescence and to minimize quenching. The support was previously washed by a phosphate buffer then blocked by Denhardt's reagent‡ in order to avoid non-specific adsorption of the avidin; proteins[11,12] are readily adsorbed onto polypyrrole surfaces without this pretreatment.

The results of these measurements on the microelectrode array are summarized in Fig. 1. The intensity of the fluorescence

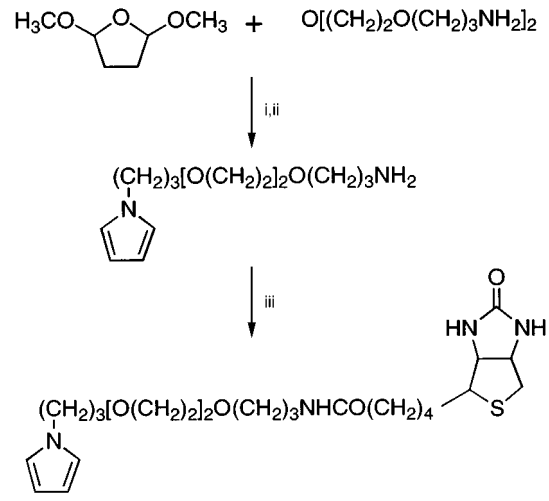

Scheme 1 *Reagents and conditions*: i, 4,7,10-trioxatridecane-1,13-diamine (3 equiv.), AcOH, dioxane, reflux, 5 h, 32%; ii, 10% KOH, reflux, 5 h, 65%; iii, D-biotin *N*-hydroxysuccinimide ester (1equiv.), DMF, room temp., 16 h, 54%

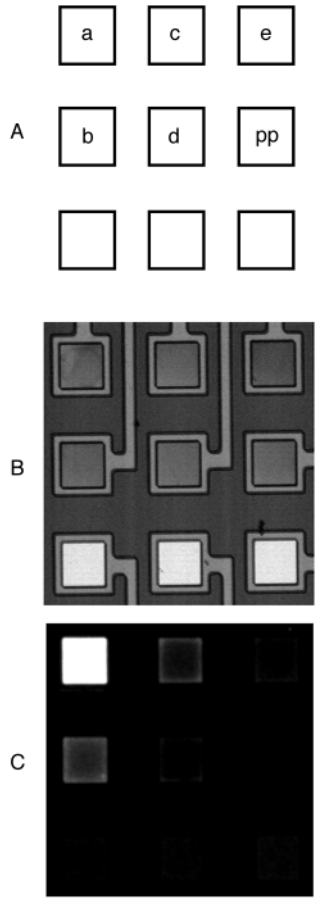

Fig. 1 (A) Pattern of the biotin repartition on the microelectrode array. Electrosyntheses were carried out at 100 mV s^{-1} by repetitive potential scans between −0.35 and 0.85 V *vs.* SCE of 20 mM pyrrole and a decreasing amount of biotin pyrrole with a synthesis charge of 18 mC cm^{-2} (about 60 nm thickness) in 0.1 M $LiClO_4/H_2O$ containing 3% of MeCN on microelectrodes (50 × 50 μm^2) arrayed on a silicon chip. Biotinylated polypyrrole synthesized in presence of (a) 100, (b) 10, (c) 1, (d) 0.1 and (e) 0.01 μM of biotin pyrrole respectively; (pp) = polypyrrole. Each electropolymerization was followed by a thorough washing step and blocking step (see text). (B) Differential interference contrast view of microelectrodes to check the effective deposition of a biotinylated polypyrrole film on the plots. (C) Fluorescence results after a revelation process using a solution of streptavidin–R-phycoerythrin followed by washing in a phosphate buffer.

is related to the amount of biotin involved in the copolymerization reaction and yields the amount of accessible biotin at the surface of the film. The measured fluorescence intensity decreased with a decreasing biotinylated pyrrole to pyrrole ratio. Taking the area marked (a) as the standard, the intensity decreased to 18 and 10.5% of this value when the ratio was decreased to 1:10 and 1:100 [areas (b) and (c)], respectively. In the case of the pure polypyrrole film [without biotin, indicated by region (pp) in Fig. 1(A)], a weak fluorescence was still observed, but only about 2% of the value for (a) and noticeably weaker than the thousand-fold dilution. This indicates that the immobilization of the avidin conjugate on the different dots is specific of the biotin–avidin interaction.

In conclusion, we have reported a simple way of preparing an ECP active layer that is capable of the recognition of avidin conjugates, which would facilitate study of the behavior of many commercial biomolecules. Indeed, this system is very versatile due to the availability of a wide variety of avidin conjugates, which would allow for the elaboration of a large number of biosensors. However, in order to use this sensor on real biological samples, the signal/noise ratio should be increased. In addition, this method has the advantage of miniaturization *via* the use of electrochemical addressing of the electrodeposition.

L. M. T.-R. thanks CONACYT (Mexico) for a scholarship.

Notes and References

† E-mail: gbidan@cea.fr

‡ The microelectrodes were dipped for 10 min at room temperature in Denhardt's reagent, composed of 0.02% Ficoll, 0.02% polyvinylpyrrolidone and 0.02% BSA. The dots were then rinsed with a buffer solution and incubated for 5 min in the dark in a solution of 5% streptavidin–R-phycoerythrin. After washing, the fluorescence was recorded for 1 s with a microscope equipped with a CDD camera.

1 G. Bidan, in *Polymer Films in Sensor Applications*, ed. G. Harsanyi, Technomic, Pennsylvania, 1995, pp. 206–260.
2 H. K. Youssoufi, M. Hmyene, F. Garnier and D. Delabouglise, *J. Chem. Soc., Chem. Commun.*, 1993, 1550.
3 F. Garnier, H. K. Youssoufi, P. Srivastava and A. Yassar, *J. Am. Chem. Soc.*, 1994, **116**, 8813.
4 A. Emge and P. Bäuerle, *Synth. Met.*, 1997, **84**, 213.
5 T. Livache, A. Roget, E. Dejean, C. Barthet, G. Bidan and R. Téoule, *Nucleic Acids Res.*, 1994, **22**, 2915.
6 K. Faïd and M. Leclerc, *Chem. Commun.*, 1996, 2761.
7 T. Livache, B. Fouque, A. Roget, J. Marchand, G. Bidan, R. Téoule and G. Mathis, *Anal. Biochem.*, 1998, **255**, 188.
8 H. K. Youssoufi, F. Garnier, P. Srivastava, P. Godillot and A. Yassar, *J. Am. Chem. Soc.*, 1997, **119**, 7388.
9 D. J. Brigati, D. Myerson, J. J. Leary, B. Spalholz, S. Z. Travis, C. K. Y. Fong, G. D. Hsiung and D. C. Ward, *Virology*, 1983, **126**, 32.
10 I. Jirkowsky and R. Baudy, *Synthesis*, 1981, 481.
11 H. Ge and G. G. Wallace, *J. Liq. Chromatogr.*, 1990, **13**, 3260.
12 A. Hodgson, M. Spencer and G. G. Wallace, *React. Polym.*, 1992, **18**, 77.

Received in Cambridge, UK, 17th June 1998; 8/04611E

A new route to functionalised π-allyltricarbonyliron lactam complexes from aziridines and their use in stereoselective synthesis and oxidative conversion to β-lactams

Steven V. Ley*† and Ben Middleton

Department of Chemistry, University of Cambridge, Lensfield Road, Cambridge, UK CB2 1EW

Aziridinyl enones can be converted in good yield into π-allyltricarbonyliron lactam complexes bearing ketone functionality in the side chain; addition of a variety of nucleophiles into the side chains of these complexes proceeds in good yield and excellent (> 95%) de to afford secondary and tertiary alcohols which on treatment with trimethylamine *N*-oxide form the corresponding β-lactams in good yield.

π-Allyltricarbonyliron lactam complexes have been previously investigated as precursors to stereodefined β- and δ-lactams,[1] and have been utilised in the synthesis of several natural products in our laboratory.[2] Previous preparation of these complexes involved the treatment of π-allyltricarbonyliron lactone complexes with a primary amine[3] or the sonochemical reaction of an alkenyl carbamate with $Fe_2(CO)_9$.[2a] In an isolated example, Aumann has also shown that UV irradiation of the vinyl aziridine **1** in the presence of $Fe(CO)_5$ leads to the formation of a π-allyltricarbonyliron lactam complex **2** in 71% yield (Scheme 1).[4]

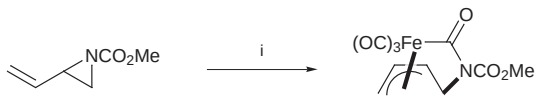

1 **2**

Scheme 1 *Reagents and conditions*: i, $Fe(CO)_5$, benzene, *hν*, 71%

We have additionally demonstrated that ketone functionalised π-allyltricarbonyliron lactone complexes, available from epoxy enone precursors, are versatile chiral templates for organic synthesis.[5] Here we show that the corresponding π-allyltricarbonyliron lactam complexes may be prepared from functionalised alkenyl aziridines by treatment with $Fe_2(CO)_9$ under ultrasonication.[6] This allows the rapid, large scale synthesis of π-allyltricarbonyliron lactam complexes bearing carbonyl functionality in the side chains and facilitates investigation into the potential of these lactam-tethered π-allyltricarbonyliron units as chiral templates. We also show that oxidative decomplexation of the stereodefined alcohols generated by diastereoselective addition of nucleophiles to ketone-bearing π-allyltricarbonyliron lactam complexes can be effected by treatment with trimethylamine *N*-oxide, providing an efficient route to highly functionalised β-lactams.

Racemic enones **6a**,**b** were synthesised in a four step sequence from a known common precursor, dibromo ester **3**[7] (Scheme 2). Treatment of **3** with excess $BnNH_2$ in boiling benzene[8] afforded a 1:1 mixture of methyl esters **4a**,**b** which were separated by flash column chromatography. Reduction with $LiAlH_4$ and Swern oxidation[9] of the crude product yielded the aldehydes **5a**,**b**. Horner–Wadsworth–Emmons coupling with diethyl (2-oxopropyl)phosphonate[10] afforded **6a**,**b** respectively in good yield. Sonication of **6a** in benzene in the presence of nonacarbonyldiiron afforded the *exo*-lactam complex **7a** in good yield, with only a small proportion of the chromatographically separable isomeric *endo* complex **7b** being formed (dr 14:1). Similarly, treatment of enone **6b** under the same conditions yielded a 10:1 ratio of **7b** and **7a** in 77% yield.

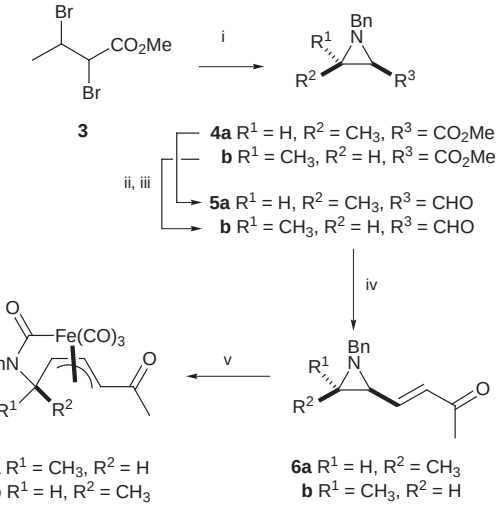

Scheme 2 *Reagents and conditions*: i, $BnNH_2$, benzene, reflux, 16 h, then chromatographic separation, 35% (**4a**), 35% (**4b**); ii, $LiAlH_4$, Et_2O, 0 °C, 2 h; iii, $(COCl)_2$, Me_2SO, NEt_3, CH_2Cl_2, −70 °C, 3 h, 63% (**5a**), 56% (**5b**) (over 2 steps); iv, $(EtO)_2P(O)CH_2COMe$, NaH, THF, 0 °C, 10 min, 91% (**6a**), 83% (**6b**); v, $Fe_2(CO)_9$, benzene, sonication, 30 °C, 3 h, 68% (dr 14:1) (**7a**), 77% (dr 10:1) (**7b**)

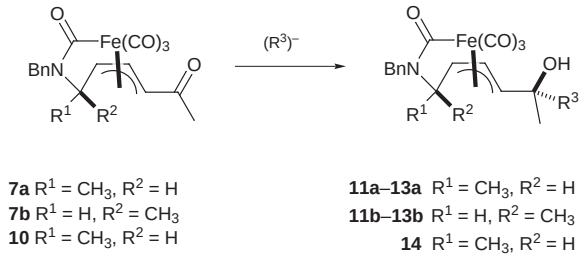

Enantiomerically enriched *exo* complex **10** could be synthesised in five steps from enantiomerically enriched methyl ester **9** (Scheme 3), accessible *via* cyclisation of the known L-threonine derivative **8**.[11] Reaction as above afforded *exo*

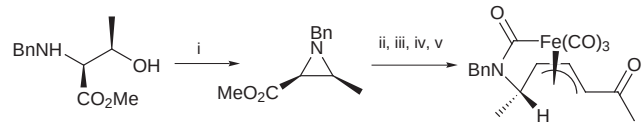

Scheme 3 *Reagents and conditions*: i, PPh_3, CCl_4, MeCN, 25 °C, 16 h, 83%; ii, $LiAlH_4$, Et_2O, 0 °C, 2 h; iii, $(COCl)_2$, Me_2SO, NEt_3, CH_2Cl_2, −70 °C, 3 h, 59% (over 2 steps); iv, $(EtO)_2P(O)CH_2COMe$, NaH, THF, 0 °C, 10 min, 83%; v, $Fe_2(CO)_9$, benzene, sonication, 30 °C, 3 h, 68% (dr 18:1)

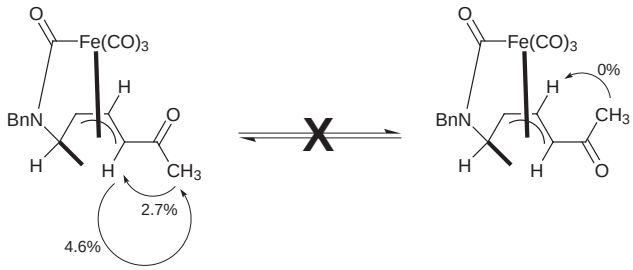

Figure 1 Selected NOE enhancements of complex **7b**

Table 1 Reaction of nucleophiles with π-allyltricarbonyliron lactam complexes bearing methyl ketone functionality in the side chain

Starting material	Conditions	R^3	Product[a]	Yield (%)[b]
7a	$NaBH_4$, MeOH–CH_2Cl_2, −70 °C	H	**11a**	77
7b	$NaBH_4$, MeOH–CH_2Cl_2, −70 °C	H	**11b**	65
10[c]	$NaBH_4$, MeOH–CH_2Cl_2, −70 °C	H	**14**[d]	76
7a	$AlBu^i_3$, CH_2Cl_2, 0 °C	H	**11a**	77
7b	$AlBu^i_3$, CH_2Cl_2, 0 °C	H	**11b**	70
7a	$AlEt_3$, CH_2Cl_2, 0 °C	Et	**12a (11a)**	52 (26)
7b	$AlEt_3$, CH_2Cl_2, 0 °C	Et	**12b (11b)**	62 (32)
7a	Allyltributyltin, $BF_3{\cdot}OEt_2$, CH_2Cl_2, 0 °C	allyl	**13a**	86
7b	Allyltributyltin, $BF_3{\cdot}OEt_2$, CH_2Cl_2, 0 °C	allyl	**13b**	89

[a] De determined by 600 MHz ^{1}H NMR, determined to be > 95%. [b] Figures in parentheses refer to isolated yield of reduction side product. [c] Ee > 95% [determined by 200 MHz ^{1}H NMR analysis in the presence of Pr(hfc)$_3$]. [d] Ee > 95% [determined by 600 MHz ^{1}H NMR analysis of the corresponding (*S*)-(+)-α-methoxy-α-(trifluoromethyl)phenylacetyl ester].

complex **10** in > 95% ee [determined by 200 MHz ^{1}H NMR spectroscopy in the presence of the chiral shift reagent (+)-Pr(hfc)$_3$].[12]

In order that the addition of nucleophiles to the ketone group in the sidechain proceeds with high diastereocontrol, it is necessary that the tricarbonyliron group blocks one face of the carbonyl group, thus forcing approach of the nucleophile to occur from the opposite side, and that the ketone adopts only one reactive conformation. The solution conformation of complex **7b** was investigated by the use of NOE experiments. These results clearly show that the s-*cis* conformation is adopted preferentially (Fig. 1). These results are consistent with earlier studies carried out on π-allyltricarbonyliron lactone complexes.[5a] Reaction of complexes **7a**,**b** with a variety of nucleophiles (Table 1) afforded the addition products **11a–13a** and **11b–13b** in good yield and excellent diastereoselectivity (de > 95%).[13] Reduction of enantiomerically enriched **10** with $NaBH_4$ to form alcohol **14** proceeded in 76% yield without loss of enantiopurity, as determined by 600 MHz ^{1}H NMR analysis of the ester formed with (*S*)-(+)-α-methoxy-α-(trifluoromethyl)phenylacetyl chloride.[14]

Furthermore, it was discovered that treatment of complexes **11–13** with excess Me_3NO in THF at room temperature affords the functionalised β-lactams **15–17** in good yield (Table 2). This result is an improvement over the published method of oxidative decomplexation with ceric ammonium nitrate[3] which

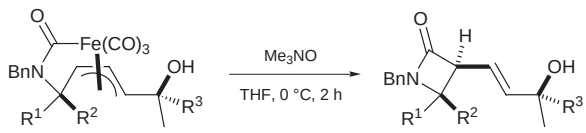

11–13 **15–17**

Table 2 Decomplexation of functionalised π-allyltricarbonyliron lactam complexes to β-lactams

Starting material	R^1	R^2	R^3	Product	Yield (%)[a]
11a	Me	H	H	**15a**	63
11b	H	Me	H	**15b**	65
12a	Me	H	Et	**16a**	61
12b	H	Me	Et	**16b**	65
13a	Me	H	allyl	**17a**	54
13b	H	Me	allyl	**17b**	69

[a] Isolated yield after treatment with excess Me_3NO in THF at 0 °C for 2 h, followed by chromatography on Florisil.

has given markedly lower yields of β-lactams with this type of substrate.[15]

In summary, a convenient route to racemic and homochiral π-allyltricarbonyliron lactam complexes bearing ketone functionality in the side chain has been developed. It has been shown that the tethered tricarbonyliron moiety is able to direct nucleophilic attack on an appended methyl ketone group, affording complexes bearing secondary and tertiary alcohol functionality in good yield and with excellent diastereoselectivity. A novel oxidative decomplexation method allows the generation of highly functionalised β-lactams bearing stereodefined secondary and tertiary alcohol centres. These results should extend further the utility of π-allyltricarbonyliron complexes for natural product synthesis.

We gratefully acknowledge financial support from the EPSRC, the Isaac Newton Trust and Zeneca Pharmaceuticals (to B. M.) and the BP Endowment and the Novartis Research Fellowship (to S. V. L.).

Notes and References

† E-mail: svl1000@cus.cam.ac.uk

1 For a general review on the synthetic utility of π-allyltricarbonyliron lactone complexes see: S. V. Ley, L. R. Cox and G. Meek, *Chem. Rev.*, 1996, **96**, 423 and references cited therein.
2 (*a*) S. V. Ley and J. G. Knight, *Tetrahedron Lett.*, 1991, 7119; (*b*) S. V. Ley, S. T. Hodgson and D. M. Hollinshead, *Tetrahedron*, 1985, 5871; (*c*) S. V. Ley, S. T. Hodgson, D. M. Hollinshead, C. M. R. Low and D. J. Williams, *J. Chem. Soc., Perkin Trans. 1*, 1985, 2375.
3 S. V. Ley, G. D. Annis, E. M. Hebblethwaite, S. T. Hodgson and D. M. Hollinshead, *J. Chem. Soc., Perkin Trans. 1*, 1983, 2851.
4 R. Aumann, K. Fröhlich and H. Ring, *Angew. Chem., Int. Ed. Engl.*, 1974, **13**, 275.
5 (*a*) S. V. Ley, L. R. Cox, G. Meek, K.-H. Metten, C. Piqué and J. M. Worral, *J. Chem. Soc., Perkin Trans. 1*, 1997, 3299; (*b*) S. V. Ley and L. R. Cox, *J. Chem. Soc., Perkin Trans. 1*, 1997, 3315; (*c*) S. V. Ley and L. R. Cox, *Chem. Commun.*, 1998, 227
6 S. V. Ley, A. M. Horton and D. M. Hollinshead, *Tetrahedron*, 1984, 1737.
7 T. Hudlicky, L. Radesca and H. L. Rigby, *J. Org. Chem.*, 1987, **52**, 4397.
8 M. Prostetnik, N. P. Salzman and H. E. Carter, *J. Am. Chem. Soc.*, 1955, **77**, 1856.
9 D. Swern and K. Omura, *Tetrahedron*, 1978, 1651.
10 W. S. Wadsworth Jr., *Org. React.*, 1977, **25**, 73.
11 H. Rapoport, K. J. Shaw and J. R. Luly, *J. Org. Chem.*, 1985, **50**, 4521.
12 D. Parker, *Chem. Rev*. 1991, **91**, 1441.
13 Only one diastereoisomeric product could be observed *via* 600 MHz ^{1}H NMR analysis, thus the quoted 95% de is a conservative estimate of selectivity.
14 H. S. Mosher and J. A. Dale, *J. Am. Chem. Soc.*, 1973, **95**, 512.
15 Treatment of a solution of complex **11a** in MeCN with CAN (6.5 equiv.) at −20 °C in the dark for 2 h afforded β-lactam **15a** in 31% isolated yield after chromatography on Florisil.

Received in Liverpool, UK, 8th July 1998; 8/06236F

UV-induced strand break damage in single stranded bromodeoxyuridine-containing DNA oligonucleotides

Zara A. Doddridge, Jane L. Warner, Paul M. Cullis* and George D. D. Jones*†

Centre for Mechanisms of Human Toxicity and the Department of Chemistry, University of Leicester, Leicester, UK LE1 7RH

Aerobic UVB photolysis of single stranded bromodeoxyuridine (BrdU)-containing DNA oligonucleotides produces immediate and latent strand break products consistent with a specific BrdU base radical-mediated abstraction of the C1′ hydrogen atom from the 5′ neighbouring deoxyribose.

Substitution of genomic thymidine with bromodeoxyuridine (BrdU) renders aerobic cell cultures more sensitive towards the lethal effects of UV and γ-radiation.[1,2] One mechanism proposed to contribute to sensitisation is an increase in the yield of radiation-induced strand breaks caused by the presence of BrdU in DNA.[1,2] From examinations of the duplex structure it was initially proposed that the additional radiation-induced BrdU-mediated strand breakage occurs *via* the formation of reactive uracil(U)-5-yl base radicals, which in turn abstract hydrogen atoms from the 5′ neighbouring deoxyribose.[2,3] Subsequent molecular studies have indeed demonstrated that under anaerobic conditions UV photolysis of BrdU-containing DNA yields both immediate and latent (alkali labile) breaks at the nucleosides 5′ to the site of BrdU.[4–7] To date, however, there have been few definitive molecular studies of BrdU-mediated DNA strand breakage in the presence of oxygen[8] (conditions under which cellular sensitisation is observed) and none in single-stranded DNA.

Here we have examined immediate and alkali-induced strand break products from a 5′- or 3′-^{32}P-end labelled single stranded (*ss*) BrdU-containing DNA oligonucleotide upon UVB photolysis (*ca*. 0.41 mW cm^{-2}), using high resolution denaturing polyacrylamide gel electrophoresis (PAGE). The strand break products were assigned by reference to the products of Maxam and Gilbert reactions,[9] and by enzymatic end-group analysis. Aerobic UVB photolysis of 5′-GCTAGCTATT-BrdU-TTATC-GATCG-3′ **1** results in specific strand cleavage at the nucleoside situated immediately 5′ to BrdU and proceeds with the loss of this 5′-nucleoside. Thus, photolysis of **1** yields a strand break product **6** nine nucleotides in length [Fig. 1(*a*)] together with a strand break product **7** eleven nucleotides in length [Fig. 2(*a*)] (Scheme 1). Co-migration of the photo-induced fragments with products of Maxam and Gilbert reactions implies the presence of phosphate moieties at both termini of the induced breaks. This was confirmed by demonstrating that **6** was a substrate for the 3′-phosphatase activity (+3′P) of T4 polynucleotide kinase (T4PNK), yielding **8** [Fig. 1(*b*)], and that **7** was a substrate for the 5′-phosphatase activity of shrimp alkaline phosphatase (SAP), yielding **9** [Fig. 2(*b*)] (see also Scheme 1).

Piperidine treatment of photolysed **1** yields an approximate five-fold increase in the yield of **6** [Fig. 1(*c*)] suggesting that the majority of BrdU-mediated damage induced at the 5′-nucleotide are alkali labile lesions and not immediate strand breaks.[2,10] This observation of the majority of piperidine-induced breaks occurring at exactly the same location as immediate breaks, and yielding the same 3′-termini, implies a common mechanistic route for both types of strand break at this site. This is consistent with H-atom abstraction occurring from C1′ of the 5′-deoxyribose leading the formation of a deoxyribolactone lesion within the oligonucleotide (**5**)[11] and a small number of direct breaks possessing phosphate termini,[12,13] although the precise mechanism for the direct strand break pathway remains to be elucidated. Structure **5** is sensitive to the strand cleaving effects of alkali and subsequent piperidine treatment would yield further breaks possessing phosphate termini.[11] Interestingly, piperidine treatment of photolysed **1** also appears to produce minor fragmentation about the BrdU moiety possibly the consequence of an induced diffusible species giving rise to piperidine sensitive lesions.

UV illumination under anaerobic conditions yields higher levels of strand breakage plus a markedly different pattern of 3′-termini damage, consisting of both phosphates and other unidentified moieties [Fig. 2(*c*)]. It is known from other studies that generation of a C1′ radical under both oxic and anoxic conditions leads to immediate and latent strand breaks possessing phosphate termini, with release of the undamaged base and the damaged sugar (probably as methylenefuranone **10**).[11–13] The present observation of different end groups following anaerobic photolysis of *ss* BrdU-containing oligonucleotides indicates that, in the absence of oxygen, H-atom abstraction must occur from a site other than (or in addition to) C1′, presumably C2′. These observations are similar to those of Cook and Greenberg[7] for duplexed BrdU-oligonucleotides. On the basis of kinetic isotope measurements these workers

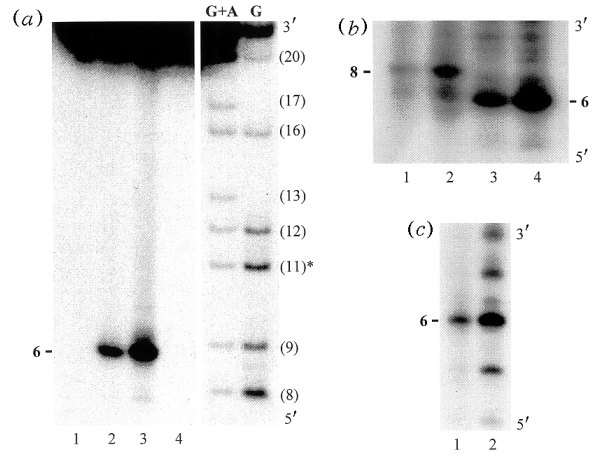

Fig. 1 Autoradiograms of the strand break products of 5′-^{32}P-labelled **1** upon aerobic photolysis and PAGE analysis. (*a*) Photolysis of **1** showing the specific formation of **6** (lane 1: no UV exposure; lane 2: 15 min UV; lane 3: 45 min UV; lane 4: nascent **1** (containing T in place of BrdU), 45 min UV); also shown are the fragment products of Maxam and Gilbert reactions specific for cleavage at G and G+A in 5′-GCTAGCTAGGTGGATCGATCG-3′; the bracketed numbers indicate fragment length with (*) indicating the location of BrdU in the BrdU-oligonucleotides. **(*b*)** Susceptibilty of **6** towards the 3′-phosphatase activity of T4 polynucleotide kinase (T4PNK) to give **8**. In these experiments the released strand break products were 5′-^{32}P-end labelled *after* photolysis using [γ-^{32}P]ATP plus T4PNK either possessing 3′-phosphatase activitity (+ 3′P) (from USB) or T4PNK lacking 3′-phosphatase activity (− 3′P) (from Boehringer Mannheim). {lane 1: 20 min UV + (+ 3′P); lane 2: 45 min UV + (+ 3′P); lane 3: 20 min UV + (− 3′P); lane 4: 45 min UV + (− 3′P)}. **(*c*)** Alkali lability of photolysed **1** revealing an enhanced formation of **6** upon piperidine treatment [lane 1: 15 min UV; lane 2: 15 min UV + piperidine (1 M, 90 °C, 30 min)].

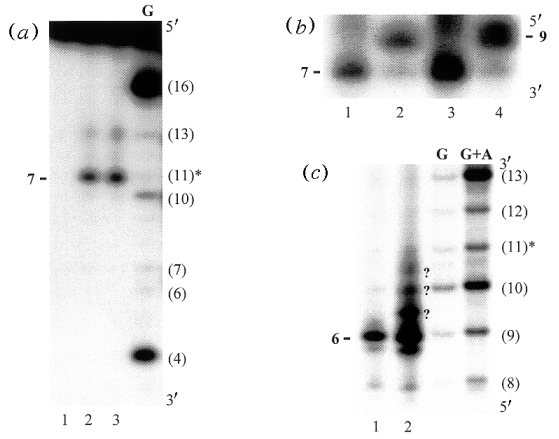

Fig. 2 (*a*),(*b*) Autoradiograms of the strand break products of 3′-^{32}P-ddA-labelled **1** upon aerobic photolysis and PAGE analysis. (*a*) Photolysis of **1** showing the specific formation of **7** (lane 1: no UV exposure; lane 2: 30 min UV; lane 3: 60 min UV); also shown are the fragment products of Maxam and Gilbert reactions specific for cleavage at G in **1**; the bracketed numbers indicate fragment nucleotide length (excluding 3′-ddA) with (*) indicating the location of BrdU. **(*b*)** Susceptibilty of **7** towards the phosphatase activity of SAP to give **9** (lane 1: 30 min UV; lane 2: 30 min UV + SAP; lane 3: 60 min UV; lane 4: 60 min + SAP). (*c*). Autoradiogram of the strand break products of 5′-^{32}P-labelled **1** upon aerobic or anaerobic photolysis and PAGE analysis. Photolysis of **1** showing the specific formation of **6** plus other unidentified products (denoted as **?**) (lane 1: 45 min UV, aerobic; lane 2: 45 min UV, anaerobic); also shown are the fragment products of Maxam and Gilbert reactions specific for cleavage at G and G+A in **1**; the bracketed numbers indicate fragment nucleotide length with (*) indicating the location of BrdU.

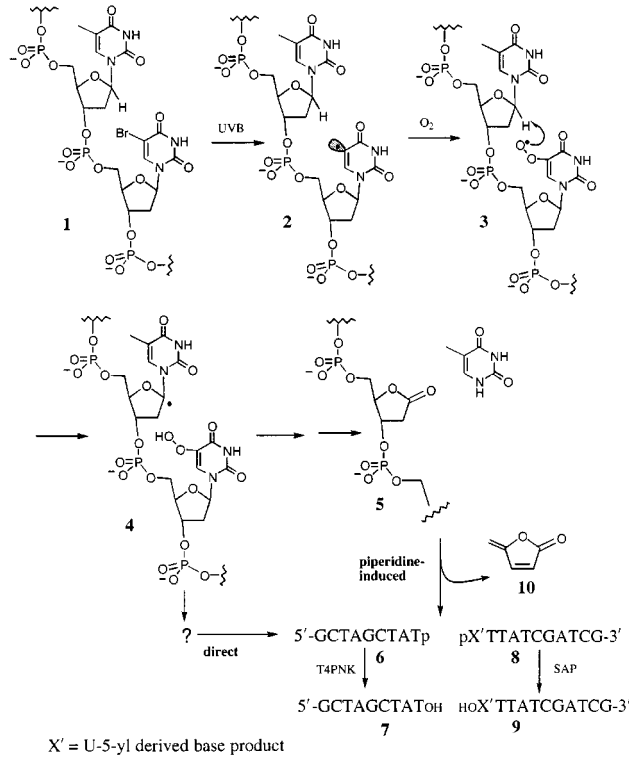

Scheme 1

conclude that under anaerobic conditions U-5-yl radicals abstract the C2′ hydrogen atom of the 5′-deoxyribose, ultimately yielding cleavage products containing 3′-phosphate and a labile 2′-deoxy-3′-ketonucleotide.[7] Clearly, if the anaerobic U-5-yl-mediated abstraction of C2′–H is occuring in our system then specific C2′ abstraction in duplexed BrdU-DNA is not simply a result of conformational effects imposed by the double helix, as it persists in *ss* systems under anaerobic conditions.

It is difficult to rationalise the aerobic abstraction of C1′–H and the anaerobic abstraction of C2′–H by simply evoking U-5-yl as being the sole abstracting species. We therefore propose that under anaerobic conditions it is the initial U-5-yl base radical that abstracts from a site other than C1′ (or a number of different sites), whilst under aerobic conditions the U-5-yl base peroxyl radical (U-5-yl-OO·), formed by the addition of oxygen to the 5-yl radical centre, mediates abstraction specifically from C1′ (Scheme 1).

Support for the above proposal, that in the presence of oxygen abstraction is from C1′, comes from the recent published observation of Greenberg *et al.* that direct strand breaks, mediated by the 5,6-dihydrothymid-5-yl radical in *ss* oligonucleotides in the presence of oxygen, proceed *via* the specific abstraction of the C1′ hydrogen atom by the corresponding base peroxyl radical species.[14] These authors also refer to their preliminary unpublished observations of C1′–H abstraction on photolysis of *ss* BrdU-oligonucleotides under aerobic conditions which directly supports our present observations.[14] Additional support for the specific abstraction of C1′–H by a peroxyl radical comes from calculations of enthalpies for H-atom abstraction in deoxyribose[15] which suggests that the C1′ may be the sole position from which a peroxyl radical could abstract.

Our observations are in broad agreement with those of Sugiyama *et al.*[8] who have demonstrated that under aerobic conditions it is the C1′ hydrogen atom which is predominatly abstracted in duplexed BrdU-containing oligonucleotides; however, they do not propose the base peroxyl radical intermediate as being formed and they propose some abstraction from C2′, both possibly resulting from constraints imposed by the more rigid duplex structure. Our present studies are continuing with examinations of duplexed BrdU-containing oligonucleotides, to investigate the effect of strandidness on BrdU-mediated radical reactions, and to allow for the examination of possible bi-strand lesions leading to double strand breaks and multiply damaged sites.[16]

The authors acknowledge funding from the MRC [project grant to G. D. D. J. (G95277655MA), studentship stipend to Z. A. D. (G609/1490), and Fellowship to G. D. D. J.] and the University of Leicester (Fellowship to G. D. D. J.).

Notes and References

† E-mail gdj2@leicester.ac.uk

1 C. F. Webb, G. D. D. Jones, J. F. Ward, D. J. Moyer, J. A. Aguilera and L. L. Ling, *Int. J. Radiat. Biol.*, 1993, **64**, 695.
2 F. Hutchinson, *Quart. Rev. Biophys.*, 1973, **6**, 201.
3 J. D. Zimbrick, J. F. Ward and L. S. Myers Jr., *Int. J. Radiat. Biol.*, 1969, **16**, 525.
4 J. Cadet and P. Vigney, in *Bioorganic Photochemistry*, ed. H. Morrisn, Wiley-Interscience, New York, 1990, vol 1, pp. 3–229.
5 I. Saito, *Pure Appl. Chem.*, 1992, **64**, 1305.
6 H. Sugiyama, Y. Tsutumi and I. Saito, *J. Am. Chem. Soc.*, 1990, **112**, 6720.
7 G. P. Cook and M. M. Greenberg, *J. Am. Chem. Soc.*, 1996, **118**, 10 025.
8 H. Suigiyama, K. Fujimoto and I. Saito, *Tetrahedron Lett.*, 1996, **37**, 1805.
9 A. M. Maxam and W. Gilbert, *Methods Enzymol.*, 1980, **65**, 499.
10 R. O. Rahn and H. G. Sellin, *Photochem. Photobiol.*, 1983, **37**, 661.
11 A. P. Breen and J. A. Murphy, *Free Radical Biol. Med.*, 1995, **18**, 1033.
12 B. K. Goodman and M. M. Greenberg, *J. Org. Chem.*, 1996, **61**, 2.
13 M. M. Meijler, O. Zelenko and D. S. Sigman, *J. Am. Chem. Soc.*, 1997, **119**, 1135.
14 M. M. Greenberg, M. R. Barvian, G. P. Cook, B. K. Goodman, T. J. Matray, C. Tronche and H. Venkatesan, *J. Am. Chem. Soc.*, 1997, **119**, 1828.
15 K. Miaskiewicz and R. Osman, *J. Am. Chem. Soc.*, 1994, **116**, 232.
16 J. F. Ward, *Int. J. Radiat. Biol.*, 1994, **66**, 427.

Received in Glasgow, UK, 10th June 1998; 8/04416C

Unusual results in the liquid phase alkylation of naphthalene with isopropyl alcohol over zeolite H-beta

Changqing He,[a] Zhongmin Liu,[a] François Fajula[b] and Patrice Moreau[b]*†

[a] *Dalian Institute of Chemical Physics, 457 Zhongshan Road, PO 110, Dalian, 116023, PR China*
[b] *Laboratoire de Matériaux Catalytiques et Catalyse en Chimie Organique, UMR 5618 CNRS, ENSCM, 8 rue de l'Ecole Normale, 34296 Montpellier, Cedex 5, France*

Unexpected compounds are formed with high selectivity in the liquid phase alkylation of naphthalene with isopropyl alcohol over large pore zeolite H-beta; these have been confirmed to be cyclized products from naphthalene derivatives.

2,6-Dialkylnaphthalenes are valuable compounds for the production of high-quality polyester fibres, plastics and thermotropic liquid crystal polymers.[1] Taking into account that these compounds are manufactured inefficiently by the nonselective alkylation of naphthalene over conventional Friedel–Crafts catalysts[2] or solid silica–alumina catalysts,[3] considerable attention has recently been paid to the development of new processes for the selective preparation of 2,6-dialkylnaphthalenes using environment-friendly zeolite catalysts. Owing to the steric hindrance of naphthalene, medium pore zeolites, such as HZSM-5, show moderate activity in naphthalene alkylation.[4,5] Large pore zeolites, such as Mordenite, beta, Y, and more recently mesoporous aluminosilicates, have been investigated. Alkylating agents bulkier than MeOH, such as isopropyl[5–9] or cyclohexyl derivatives[7,10] and butanol,[11,12] have been also applied successfully to the selective formation of 2,6-dialkylnaphthalenes. Among these studies, substantial advances have been made in naphthalene isopropylation for both the understanding of the alkylation mechanism and the design of catalysts leading to high selectivity in forming 2,6-diisopropylnaphthalenes.[5–9] H-beta has been shown to be more active and selective than HY in the alkylation of benzene with propylene[13] but did not demonstrate selectivity in the alkylation of polyaromatics until recently.[5,9,11,12] Nevertheless, it has been reported that H-beta shows an unexpected high selectivity for *sec*-butylbenzene in the alkylation of benzene with isobutyl alcohol.[14] In our search for suitable catalysts for the selective synthesis of 2,6-dialkylnaphthalenes, we have recently found another peculiar characteristic of H-beta zeolite in the liquid phase alkylation of naphthalene with isopropyl alcohol, in which a series of unexpected compounds were formed with high yield under given conditions. Here we report on the unusual results thus obtained and the identification of the new compounds.

Zeolite catalyst H-beta (Si/Al = 12.5) was obtained from PQ Corporation (CP 810 B-25). HY (Si/Al = 15) was prepared by standard ion-exchange, calcination, steam dealumination and acid leaching procedures from a parent synthetic zeolite. Activation of H forms was achieved by calcination at 773 K for 5 h with a heating rate of 60 K h^{-1} in a flow of dry air. The isopropylation of naphthalene was carried out in a 0.16 dm^3 stirred autoclave reactor (Parr Instrument Company). Under standard reaction conditions, 10 mmol of naphthalene, 20 mmol of Pr^iOH, 10 mmol of undecane as an internal standard sample and 0.1 dm^3 of cyclohexane as solvent were mixed together in the autoclave, and then freshly calcined zeolite (0.5 g) was added. The reaction temperature was set at 473 K and the pressure was maintained at 2 MPa with nitrogen. Samples were withdrawn periodically and analysed on a Varian Series 30 gas chromatography equipped with HP-5 capillary column (25 m) and a FID detector. GC–MS (HP5970) with an OV1 capillary column (25 m) and NMR (Brücker AC200) analysis were used for the identification of the new compounds.

Typical reaction results are listed in Table 1. The activity of H-beta is much lower than that of HY, as shown by the naphthalene conversion which reaches a maximum of 30% under standard reaction conditions, compared with 90% for HY. GC–MS analysis indicates that the new compounds have molecular mass (*m/z*) of 210, 252 and 292, respectively, different from the products usually obtained in naphthalene isopropylation over large pore zeolite catalysts[5–9] which are isopropylnaphthalene (IPN), diisopropylnaphthalene (DIPN), triisopropylnaphthalene (TIPN) and tetraisopropylnaphthalene (TetIPN) with molecular mass of 170, 212, 254 and 296, respectively. As shown in Table 1, H-beta possesses a peculiar catalytic function for the production of the new compounds. After 2 h, the selectivity (around 50 mol%) of total new compounds is higher than that of alkylated derivatives, mainly IPN (43 mol%). DIPN selectivity is unexpectedly low and no TIPN is detected. Such a result is totally different from those obtained by Chu and Chen[5] who used continuous fixed-bed reactor conditions. In agreement with previous results, HY zeolite shows a higher activity and selectivity for DIPN and TIPN than H-beta. It is observed that the new compounds are also formed over HY, but in much smaller amounts than over H-beta. Moreover, the distribution of the new compounds produced over the two zeolites are different. H-beta gives more than 80 mol% of '210' and less '252' or '292', while HY

Table 1 Reaction results of isopropylation of naphthalene over different zeolites at 473 K[a]

			Product distribution (mol%)					New compound distribution (mol%)			
Catalyst	*t*/h	Conv. (%)	IPN	DIPN	TIPN	New	Others[b]	'210'	'252'	'292'	'294'
H-beta	1	18.7	49.6	2.6	0	46.3	1.5	86.2	10.8	2.8	0.0
	7	28.5	42.6	3.1	0	48.1	6.2	84.0	10.2	6.0	0.0
HY	1	92.3	36.9	41.1	14.7	5.9	1.4	0.0	88.9	0.0	11.1
	7	94.6	31.1	46.2	14.2	7.1	1.4	0.0	91.7	0.0	8.3

[a] Reactions conditions: catalyst (0.5g), naphthalene (10 mmol), Pr^iOH (20 mmol), undecane (10 mmol), cyclohexane (100 ml), 2.0 MPa. [b] Others include methyl(isopropyl)naphthalene and ethyl(isopropyl)naphthalene

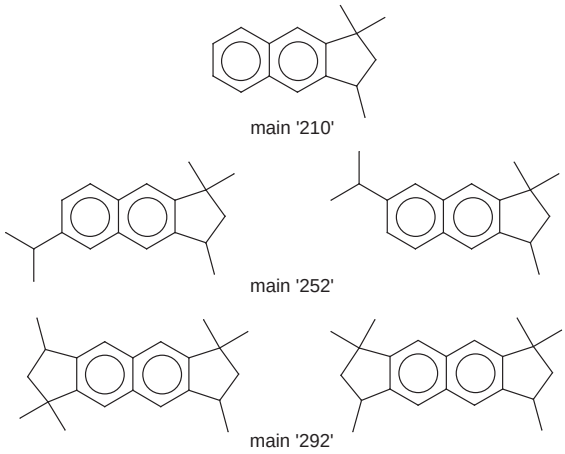

Fig. 1 Proposed structures for the main isomers in new compounds

produces mainly '252' and almost no '210'. There were also many isomers among the new compounds. In fact, there were at least five isomers of '210' and seven isomers of '252' and '292'.

The identification of these new compounds has been made possible by GC-MS and ^{13}C NMR analysis. First, a simple conclusion can be drawn from GC–MS results. Products '210' and '252' could be derived from DIPN and TIPN respectively by removing H_2, and '292' could be produced from TetIPN by removing two equiv. of H_2, suggesting that in a '210' molecule, for example, a branched double bond or an additional hydrocarbon ring might be formed. Second, no dehydrogenated derivative (*e.g. m/z* 168) from IPN (*m/z* 170) is detected, implying that dehydrogenation takes place only between two isopropyl groups, resulting in the cyclization. Therefore, the new compounds are most likely the cyclized products from DIPN, TIPN and TetIPN. That is, one or two additional rings have been formed on naphthalene in the reaction process.

A mixture of the new compounds was isolated by distillation from the products of naphthalene isopropylation over H-beta with the following composition: 79 mol% of '210' (which contains 72% of the main '210' isomer), 9.5 mol% of '252' and 10.6 mol% of '292'. ^{13}C NMR measurements have been applied to this mixture and the obtained spectrum has been compared to those of methyl styrene, indane and tetralin, selected as possible comparable samples, and those of related compounds such as benzocyclobutane, octamethylcyclobutane and dimethylcyclobutanes.[15] The characteristic signals near δ 145.8 in the ^{13}C NMR spectrum of this enriched mixture are similar to those of benzocyclobutane (δ 145.2)[15] or indane (δ 144.3), possibly due to the quaternary carbon atoms of a four- or five-membered ring fused to a benzene ring. This signal position is different in tetralin, where the chemical shift of the corresponding quaternary carbon is at δ 137.4. Therefore, the new additional ring cannot be six-membered. Moreover, the two other signals near δ 45.1 given by the enriched mixture are similar to those obtained with octamethylcyclobutane or 1,1-dimethylcyclopentane for the corresponding quaternary carbon atom.[15] Accordingly, the new ring formed on naphthalene might be five- or four-member. Furthermore, the GC analysis of the products of naphthalene isopropylation over H-beta indicates

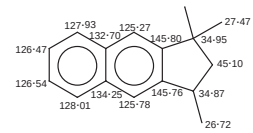

Fig. 2 ^{13}C NMR chemical shifts of the main '210' isomer

that there is one main isomer (72%) among the five '210' species and two main isomers (> 90%) among the seven '252' and '292' species. Such a distribution suggests that the new ring formed in naphthalene is a five-member ring substituted by methyl groups at positions 2',2' and 4', which is the only structure able to give one '210' and two '252' isomers.

Thus, according to the mass, ^{13}C NMR and GC analyses of the new compounds, the structures of the main isomers of '210', '252' and '292' might be consistent with those depicted in Fig. 1, minor isomers possibly resulting from methyl migration and/or ring contraction. The assignment of the ^{13}C NMR chemical shifts of the main '210' isomer (as an example) is indicated in Fig. 2.

Further studies are in progress to elucidate the mechanism and driving force leading to the formation of the new compounds.

The authors thank the France-China PICS-program (No.299) for financial support.

Notes and References

† E-mail: pmoreau@cit.enscm.fr

1 R. M. Gaydos, in *Kirk Othmer Encyclopaedia of Chemical Technology*, ed. R. E. Kirk and D. F. Othmer,Wiley, New York, 1981, vol. 15, p. 698; C. Song and H. H. Schobert, *Fuel Proc. Tech*., 1993, **34,** 157.
2 G. A. Olah and J. A. Olah, *J. Am. Chem. Soc.*, 1976, **98**, 1839.
3 W. M. Kutz and B. B. Corson, *J. Am. Chem. Soc.*, 1945, **67**, 1312.
4 D. Fraenkel, M. Cherniavsky, B. Ittah and M. Levy, *J. Catal*., 1986, **101**, 273.
5 S.-J. Chu, and Y.-W. Chen, *Appl. Catal. A*., 1995, **123**, 51.
6 A. Katayama, M. Toba, G. Takeuchi, F. Mizukami, S. Niwa and S. Mitamura, *J. Chem. Soc., Chem. Commun*., 1991, 39.
7 P. Moreau, A. Finiels, P. Geneste and J. Solofo, *J. Catal.*, 1992, **136,** 487; P. Moreau, A. Finiels, P. Geneste, J. Joffre, F. Moreau and J. Solofo, *Catal. Today*, 1996, **31**, 11.
8 C. Song and S. Kirby, *Microporous Mater*., 1994, **2**, 467; J.-H. Kim, Y. Sugi, T. Matsuzaki, T. Hanaoka, Y. Kubota, X. Tu, M. Matsumoto, S. Nakata, A. Kato, G. Seo and C. Pak, *Appl. Catal. A*, 1995, 131, 15.
9 S.-B. Pu and T. Inui, *Appl. Catal. A.*, 1996, **146**, 305; S.-B. Pu, J. B. Kim, M. Seno, T. Inui, *Microporous Mater*., 1997, **10**, 25.
10 P. Moreau, A. Finiels, P. Geneste, F. Moreau and J. Solofo, *J. Org. Chem.*, 1992, **57**, 5040; D. Mravec, M. Michvocik, M. Hronec, P. Moreau, A. Finiels and P. Geneste, *Catal. Lett.*, 1996, **38**, 267.
11 Z. Liu, P. Moreau and F. Fajula, *Chem. Commun*., 1996, 2653; *Appl. Catal. A*, 1997, **159,** 305.
12 E. Armengol, A. Corma, H. Garcia and J. Primo, *Appl. Catal. A*, 1997, **149**, 411.
13 G. Bellussi, G. Pazzuconi, C. Perego, G. Girotti and G. Terzoni, *J. Catal*., 1995, **157**, 227.
14 A. Mitra, S. Subramanian, D. Das, S. V. V. Chilukuri and D. K. Chakraborty, *Appl. Catal. A*, 1997, **153**, 233.
15 *Carbon-13 NMR Spectroscopy*, ed. H.-O. Kalinowski, S. Berger and S. Braun, Wiley, Chichester, New York, Brisbane, Toronto, Singapore, 1984, p 120.

Received in Cambridge, UK, 15th June 1998; 8/04508I

Vesicle–enzyme communication

Fredric M. Menger,* Kingsley H. Nelson and Yingbo Guo

Department of Chemistry, Emory University, Atlanta, Georgia, 30322, USA

Acetylcholinesterase and chymotrypsin are able to catalyze hydrolyses of vesicle-bound substrates at rates that depend upon the ability of the substrates to project beyond the membrane surface.

Pathogenic cells have been identified that produce specific enzymes in excessive amounts. For example, bone cancer has been shown to exude unusually large quantities of alkaline phosphatase,[1] while neuroblastomas generate high levels of acetylcholinesterase.[2] Earlier investigations from our laboratory have exploited this phenomenon in connection with a new and potentially specific mode of drug delivery involving compound **1**.[3] There were two key reasons for synthesizing **1**:

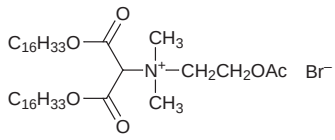

1

(i) It possesses a pair of hydrophobic tails plus a charged headgroup, the components essential for vesicle formation; (ii) It is a substrate for acetylcholinesterase, an enzyme that removes the acetate from the acetylcholine-like moiety. When enzymatic hydrolysis occurs on the 'vesiclized' compound, the freed hydroxy group reacts with one of the ester groups to form a six-membered lactone, thereby eliminating a hydrocarbon tail. But since amphiphiles with a single tail are generally unable to maintain a bilayer structure, the vesicle ruptures and releases its internal contents. The process is enzyme-specific, leading to the possibility of selective release near a cancer cell that overproduces the particular enzyme.

The preceding mechanism presupposes a reaction between a water-soluble enzyme and a vesicle-bound substrate. Somehow, in a manner not yet understood, the substrate within the bilayer membrane is able to find its way to the active site. It seems unlikely that, prior to enzyme binding, a substrate migrates *in toto* from the membrane into the aqueous domain. If this were possible, vesicles would lose and exchange their water-insoluble lipids rapidly, which they do not.[4] A reasonable alternative is that substrates only partially extend themselves beyond the membrane surface. Thus, a lipid molecule might transiently expose its polar moiety (and even portions of its hydrocarbon chains) to the bulk solvent. In this way an enzyme would have an opportunity to grasp the substrate.

An X-ray structure of acetylcholinesterase *(Torpedo californica)* shows that the active site (containing a Ser-His-Glu triad) lies at the bottom of a 'deep and narrow gorge'.[5] Hence, a membrane-bound substrate must seemingly endure a tortuous journey as it leaves the membrane and travels down the cleft to the active site. In actual fact, the journey may not be as difficult as it appears. The cleft is lined with aromatic amino acids that are believed to guide into the active site a substrate molecule reaching the outer rim of the cleft. If this is correct, then one could visualize the escorting of a substrate molecule, which happens to protrude from the membrane, to the active site as soon as a vesicle and a properly oriented enzyme come into contact. It was the purpose of the work reported herein to learn more about such enzyme–vesicle communication.

Substrates in our study consisted of acylated *N*-methyl-7-hydroxyquinolinium iodide derivatives **2**.[6] Acetylcholinester-

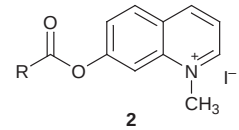

2

ase-catalyzed ester hydrolysis leads to a highly fluorescent 7-hydroxyquinolinium salt (λ_{ex} = 400 and 500 nm), allowing kinetics to be carried out spectrofluorimetrically at substrate concentrations of only 5 μM (phosphate buffer; pH 6.0; 25.0 °C), a concentration far too low to cause membrane disruption. Substrates with hydrophobic R groups were incorporated into the vesicle bilayers during their formation. Vesicles, consisting of dilauroylphosphatidyl choline plus 5% dimyristoyl phosphatidic acid (to inhibit floculation),[7] were prepared with the aid of a LiposoFast low-pressure extruder equipped with a 0.1 μm polycarbonate filter.[8] Monodisperse unilamellar vesicles of about 100 nm diameter (dynamic light scattering) at a total lipid concentration of 1.7 mM were thereby achieved. The concentration of acetylcholinesterase (Sigma electric eel, type V-5) added to the vesicular substrates was about 0.7 μM as determined by enzyme titration.[9]

In the absence of vesicles, but otherwise under the conditions specified above, the acetyl form of **2** (called 'C_2') reacts instantly with acetylcholinesterase. Longer-tailed derivatives are slower: the octanoyl, dodecanoyl, and tetradecanoyl esters ('C_8', 'C_{12}' and 'C_{14}') have half-lives varying from 20–60 s. The hexadecanoyl ester ('C_{16}') is not completely hydrolyzed even after half an hour. Although micellization of C_{16} is not a factor in the slow rate (its concentration lies well below the critical micelle concentration), it is quite possible that chain-coiling, as discussed in another context,[10] sterically impedes access to the headgroup by the enzyme.

Introducing vesicles into the system had no effect upon the fluorescence *vs*. time plots for C_2 even at elevated phospholipid concentrations (Fig. 1). Apparently, the hydrophilic substrate fails to bind to the lipid bilayers. C_8 also displays little rate change when co-mixed with phospholipid, a result explainable by either an absence of vesicle binding or by an efficient enzyme catalysis on bound ester. NMR data, given below, strongly favor the latter. In contrast, vesicular substrates C_{10}–C_{16} experience substantial rate inhibitions, the magnitude of which depend on the length of the chain (Fig. 1). Thus, C_{10} has a half-life of 300 s, whereas C_{14} and C_{16} are, for all practical purposes, inert. The C_{14} and C_{16} tails likely serve to anchor the substrates, *i.e.* to impede the ability of the headgroups to project beyond the membrane surface where reactive encounters with the enzyme's cleft become possible. Note that the data in Fig. 1 have practical implications for prodrug design because release of a membrane-bound moiety depends critically upon the structure of the disposable addendum.[11]

NMR spectra in the absence and presence of vesicles leave no doubt that C_8 (and, by inference, all substrate with chains longer

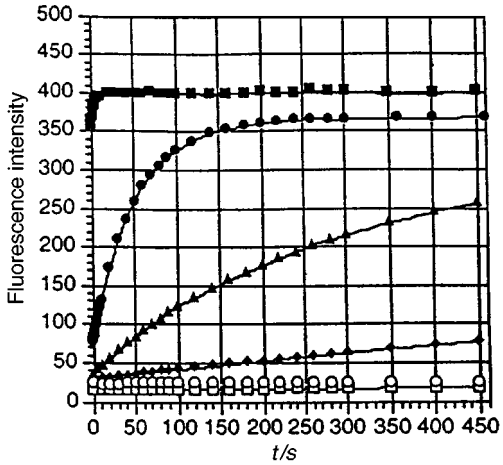

Fig. 1 Change in fluorescence intensity at 500 nm as a function of time in the acetylcholinesterase-catalyzed hydrolysis of vesicular substrates (■) C_2, (●) C_8, (▲) C_{10}, (◆) C_{12}, (□) C_{14} and (○) C_{16} under conditions specified in the text. Note how the reaction rate under standard conditions diminishes with the length of the acyl group.

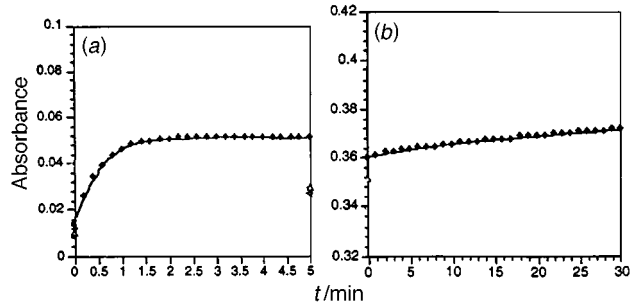

Fig. 2 Change in absorbance at 400 nm as a function of time in the α-chymotrypsin-catalyzed hydrolysis of **3** under conditions specified in the text. (*a*) with no vesicles and (*b*) with vesicles. Absorbance values are higher for the vesicular system owing to scattering by the vesicles.

than eight) is substantially vesicle-bound under the experimental conditions.[12] It was found that the sharp aromatic peaks in free solution are obliterated by the vesicles, an observation consistent with substrate immobilization due to bilayer interactions. As would be expected, hydrophilic C_2 was shown to preserve its sharp signals in the presence of vesicles. The results with C_8 prove that an enzyme can maintain a normal rate despite membrane adsorption of its substrate. In terms of our 'protrusion model', the octanoyl group, but not the more hydrophobic tetradecanoyl or hexadecanoyl group, permits escape of the headgroup from the membrane surface into the clutches of the enzyme. The term 'escape' could signify either a dynamic process (in which C_8 rapidly relocates itself in the presence of an enzyme) or a static process (in which C_8 exists in equilibrium among multiple sites regardless of enzyme).

Two additional experiments are relevant to the above conclusions. (i) Tripling the vesicle concentration at a constant 5 μM substrate had little impact on the kinetics. Total binding of the C_{12} and higher substrates is thus assured. (ii) Instead of mixing C_{10} with the phospholipid prior to vesicle formation, C_{10} was added after substrate-free vesicles had been extruded. Since no difference in the kinetics was observed, the substrate in solution must associate with the vesicles rapidly.

To obtain additional information on enzyme–vesicle interactions, we examined a second water-soluble enzyme, chymotrypsin, operating on substrates **3** and **4**. Fig. 2 compares the

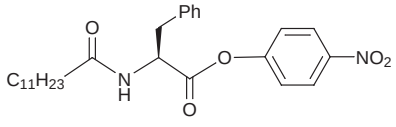

3

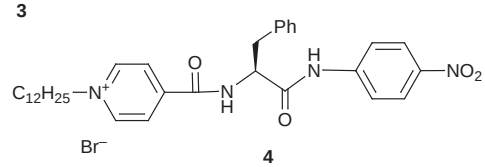

4

hydrolysis of **3** in the absence of vesicles (phosphate buffer; pH 7.0; 25.0 °C; [substrate] = 5.5 μM; [enzyme] = 0.46 μM) with the hydrolysis of **3** in the presence of vesicles (5.3 mM total phospholipid). A two-order-of-magnitude inhibition by the vesicles is evident. With the goal of further modifying vesicular rates, the 'spacer' between the chain and ester group was extended *via* additional amino acids (*e.g.* dodecanoyl-Gly-Gly-Phe-COOAr) or *via* oxyethylene units (*e.g.* dodecyl-$(OCH_2CH_2)_8$OCO-Phe-COOAr).[13] Unfortunately, the non-vesicular rates were too slow to allow the dependency of rate on spacer length to be systematically examined. Compound **4** behaved well, however, and showed actually a 2.5-fold *faster* initial rate when incorporated into vesicles under our standard conditions. The cationic charge on the pyridinium ring likely positions the ester group into the water away from the membrane surface. Both electric charge (to prevent burying of the reactive headgroup) and spacer rigidity (to prevent looping back of headgroups onto the membrane surface) should favor enzyme–vesicle reactions. These features will be incorporated into future prodrug design.

Vesicle membranes clearly offer an attractive means of controlling enzymatic rates and specificities.

We thank the Army Research Office for supporting this work.

Notes and References

1 O. Bodansky, *Biochemistry of Human Cancer*, Academic Press, New York, 1975, p. 80
2 Y. Kimhi, A. Mahler and D. Saya, *J. Neurochem.*, 1980**, 34,** 554.
3 F. M. Menger and D. E. Johnston, *J. Am. Chem. Soc.*, 1991, **113,** 5467.
4 M. A. Roseman and T. E. Thompson, *Biochemistry*, 1980, **19,** 439.
5 J. L. Sussman, M. Harel, F. Frolow, C. Oefner, A. Goldman, L. Toker and I. Silman, *Science*, 1991, **253,** 872.
6 Substrates described here are new compounds that were characterized by NMR, HRMS and elemental analysis. Compound **2** was prepared by acylating 7-hydroxyquinoline with a carboxylic acid in the presence of equimolar DCC (DMF–THF, 24 °C, several days). The resulting ester was treated with MeI (Et_2O, 24 °C, several days).
7 F. M. Menger, J. J. Lee, P. Aikens and S. Davis, *J. Colloid Interface Sci.*, 1989, **129,** 185.
8 M. J. Hope, M. B. Bally, G. Webb and P. R. Cullis, *Biochim. Biophys. Acta* 1985, **812,** 55.
9 T. L. Rosenbury and S. A. Bernhard, *Biochem.*, 1971, **10,** 4114.
10 F. M. Menger and K. H. Nelson, *Tetrahedron Lett.*, 1994, **35,** 1347.
11 R. B. Silverman, *The Organic Chemistry of Drug Design and Drug Action*, Academic Press, San Diego, 1992, pp. 352–401.
12 C. H. A. Seiter and S. I. Chan, *J. Am. Chem. Soc.*, 1973, **95,** 7541.
13 B. Frisch, C. Boeckler and F. Schuber, *Bioconj. Chem.*, 1996, **7,** 180.

Received in Corvallis, OR, USA, 26th June 1998; 8/04914I

How to circumvent plastic phases: the single crystal X-ray analysis of norbornadiene

Jordi Benet-Buchholz, Thomas Haumann and Roland Boese*†

Institut für Anorganische Chemie der Universität Essen, Universtätsstraße 5-7, D-45117 Essen, Germany

The single crystal structure of the ordered phase of norbornadiene was determined using a new method of growing crystals at low temperatures, *via* an *in situ* technique utilising IR light from a CO_2 laser focused on a capillary filled with an organic solution of a sample that usually forms plastic crystals.

The properties of norbornadiene (bicyclo[2.2.1]hepta-2,5-diene), have been discussed extensively with respect to strain, conjugation and reactivity. The molecular structure has been investigated using spectroscopy,[1] gas electron diffraction[2] and theoretical calculations.[3] However, structural parameters from an X-ray analysis are hithero unknown.

Norbornadiene is a molecule of globular shape[4] and thus tends to form plastic crystals which have in general unusually high melting points and very low entropies of melting (< 21 J K^{-1} mol^{-1}).[4] Such plastic phases are orientationally disordered and do not permit acquisition of detailed structural data. Transitions to ordered low temperature phases are often observed upon further cooling; however, in most of the cases, the plastic crystals shatter during the phase transition. In these cases there are only a few methods available for obtaining a single crystal in the ordered low-temperature phase: (i) sublimation of the sample onto a cold finger cooled below the transition point; (ii) crystallization from a solution of the correct concentration such that saturation is reached at a temperature below the transition point; and (iii) using the shattered crystals of the low temperature phase as seeds and thus grow a single crystal by applying a high temperature gradient in a zone melting procedure. In order to circumvent the above problems, we report here a technique of crystal growth that allows direct access to low-temperature phases.

A DSC[5] investigation of norbornadiene revealed a melting point at −16.02 °C (lit.,[6] −19.1 °C) and a transition temperature at −64.23 °C. In the cooling diagram it solidifies at −19.66 °C and exhibits the phase transformation at −92.79 °C. According to the characteristics of plastic phases, the energy of melting is *ca.* five times lower than that of the phase transition.[7]

X-ray powder diffractograms, taken at different temperatures covering the range of the phase transition,[8] show the characteristics of the high temperature (HT) and low temperature (LT) phases (Fig. 1). The hexagonal lattice symmetry of the HT phase [$a = b = 6.056(7)$, $c = 9.711(12)$ Å, −33 °C] agrees with literature data.[9] The LT phase was indexed for a monoclinic cell [$a = 6.291(2)$, $b = 17.873(7)$, $c = 5.157(3)$, $\beta = 113.95(5)$, −163 °C], in contrast to reported data which assumed a tetragonal cell.[10] The calculated densities for the HT and LT phases are 0.993 and 1.154 g cm^{-3}, respectively. The density of the liquid, 0.906 g cm^{-3}, is close to that of the HT phase and is in agreement with the expected properties for plastic phases.

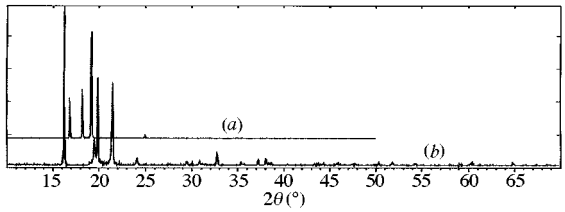

Fig. 1 X-Ray powder diffractograms of norbornadiene at (*a*) −33 and (*b*) −163 °C

In order to evade the HT phase, we modified the *in situ* technique utilizing a focused CO_2 laser beam on a capillary[11] such that, instead of filling the capillary with the neat material, we used an almost saturated solution. The main problems were to find an adequate solvent and an appropriate concentration in order to keep the point of saturation below the transition temperature. A wide variety of different solvents possessing very low melting points and/or low crystallization tendencies as well as good solubility properties were examined. Experiments with common solvents such as pentane failed; however, previous trials to crystallize 1,1-diethenylcyclopropane[12] (mp −131 °C) suggested that this liquid had the desired properties as it remained metastable (oily) down to −193 °C.

Gratifyingly, a 2:1 mixture of norbornadiene–1,1-diethenylcyclopropane produced a single crystal at −163 °C after a few refinement cycles, *i.e.* moving the CO_2 laser beam focus along the capillary over 12 h. The structure was determined by standard procedures.[13]

The most important geometrical parameters are given as mean values, based on the molecular symmetry C_{2v}, in Fig. 2(*a*). Librational corrected data[14] together with a comparison of the experimental structural data and theoretical calculations are given in Table 1. The best agreement with the X-ray data is found for the MP2/6-31G(d) *ab initio* level[15] and the MW data.[1] Most remarkable are the lengths of the single bonds C1–C2, C1–C6, C3–C4 and C4–C5 [1.536(1) Å]; a value of 1.510 Å[16] would be expected for an sp^2–sp^3 carbon bond. The same holds

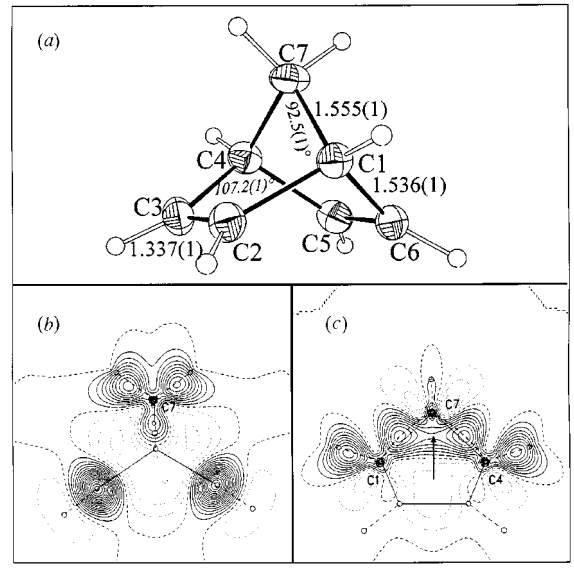

Fig. 2 (*a*) Molecular structure of norbornadiene with the most important bonding parameters. Probability plots 50%. (*b*) Static difference isoelectron density maps based on multipole refinements in the plane of (midpoint of C2–C3)–C7–(midpoint of C5–C6) and (*c*) in the plane of C1–C7–C4, distances at 0.05 e $Å^{-3}$; zero line = broken, negative = dotted.

Table 1 Comparison of experimental and calculated bond lengths and angles for norbornadiene; mean values according to C_{2v} symmetry (XRD: X-ray diffraction, this study; MW: microwave; GED: gas electron diffraction)

	Length/Å			Angle (°)		
Method	C1–C2	C1–C7	C2=C3	C1–C2–C3	C1–C7–C4	β^a
XRD	1.536(1)	1.555(1)	1.337(1)	107.2(1)	92.5(1)	4.5(2)
XRD[b]	1.542(1)	1.560(1)	1.342(1)			
MW[c]	1.530(3)	1.557(3)	1.336(3)	107.1(1)	91.9(2)	4.0(3)
NMR[c]	1.533	1.571	1.339	107.0	92.2	4
GED[d]	1.535(7)	1.573(14)	1.343(3)		94.1(30)	0
HF/						
6-31G(d)	1.539	1.550	1.319	107.7	92.3	2.7
MP2/						
6-31G(d)	1.533	1.552	1.345	107.0	92.3	3.7

[a] Interplanar angle between C1–C2–C3–C4 and H2–C2–C3–H3. [b] Librational corrected data, see ref. 14. [c] Ref. 1. [d] Ref. 2.

for the sp^3–sp^3 bonds between C1–C7 and C4–C7 [1.555(1) Å]; the expected value is 1.544 Å.[16]

In norbornadiene two different types of intramolecular interactions are assumed: homoconjugation, as a through space interaction between the two π-systems, and hyperconjugation, as a through bond interaction between the π-systems and the σ-frame.[17] The latter effect may explain the elongation of the single bonds because the filled π-orbitals of the double bonds have a destabilizing effect on the filled σ-orbitals of the opposite positioned single bonds. The double bonds [1.337(1) Å], however, are close to standard bond lengths (1.335 Å).[16]

Multipole refinements[18] with this data set permitted the production of two-dimensional experimental static electron density maps [Fig. 2(*b*) and (*c*)]. The double bond region in the plane intercepting the double bonds and C7 [Fig. 2(*b*)] shows the typical elliptic distortion. The section through the atoms C1, C7 and C4 [Fig. 3(*c*)] demonstrates the strain produced by the small angle at the bridgehead atom (see Table 1) as the maxima of the electron density of the bent bonds at C1–C7 and C4–C7 are clearly shifted from the internuclear lines. This is emphasized by the dashed interconnective lines [Fig. 2(*c*)]. Another interesting feature in Fig. 2(*c*) is the residual electron density at the internal part of the molecule (marked with an arrow). This electron density is similar to that found in the center of a cyclopropane molecule and which is attributed to σ-aromaticity and rehybridization by angular strain.[19]

Over the last 30+ years various theories have been introduced to describe the high reactivity and the *exo*-selectivity of bicyclo[2.2.1]alkenes compared to similar non-cyclic molecules. A reasonable explanation is the pyramidalisation of the double bonds.[20] The amount of pyramidalisation is described by the interplanar angle β between planes C1–C2–C3–C4 and H2–C2–C3–H3 H. The atoms at the double bonds are displaced to the *endo*-region of the molecule. The X-ray analysis gives β = 4.5(2)° (Table 1). This value agrees well with the theoretically calculated (3.7°) and experimentally determined (4.0°, by microwave and NMR spectroscopy) values.

Houk *et al.*[21] suggested the high frame strain as a cause for the pyramidalisation. An explanation for the direction of the pyramidalisation is not only strain alone, but also a contribution from a torsional interaction.[21] The results from our investigation suggest an additional repulsive effect of the hyperconjugation as the main cause for the pyramidalisation of the double bonds in the direction of the '*exo*' area. The effect of the pyramidalisation is expected to be even stronger for norbornene for which the *ab initio* calculations [MP2/6-31G(d)] predict an angle β of 7.9°.

In summary, molecular and crystal structures for a wide range of orientationally disordered materials should now be accessible with this new method. Crystal growth of the low temperature phase of similar molecules which form plastic crystals in the high temperature phases are in progress.

We thank Dr Sergei Kozhushkov (Universität Göttingen) for the preparation of 1,1-diethenylcyclopropane.

Notes and References

† E-mail: boese@structchem.uni-essen.de

1 G. Knuchel, G. Grassi, B. Vogelsanger and A. Bauder, *J. Am. Chem. Soc.*, 1993, **115**, 10 845.
2 G. Dallinga and L. H. Toneman, *Recl. Trav. Chim. Pays-Bas*, 1968, **87**, 805; A. Yokozeki and K. Kuchitsu, *Bull. Chem. Soc. Jpn.*, 1971, **44**, 2356; E. E. Burnell and P. Diehl, *Can. J. Chem.*, 1972, **50**, 3566; J. W. Emsley and J. C. Lindon, *Mol. Phys.*, 1975, **29**, 531; K. C. Cole and D. R. Gilson, *J. Mol. Struct.*, 1982, **82**, 71.
3 M. Z. Zgierski and F. Zerbetto, *J. Chem. Phys.*, 1992, **98**, 14; C. R. Castro, R. Dutler, A. Rauk and H. Wieser, *J. Mol. Struct.*, 1987, **152**, 241 and references cited therein.
4 J. Timmermans, *J. Phys. Chem. Solids*, 1961, **18**, 1.
5 The DSC investigation was performed with a DuPont 9900 and the programm General V2.2A, heating and cooling rate 2 °C min^{-1}.
6 *CRC Handbook of Chemistry and Physics*, 77th edn., ed. R. David, CRC Press, Boca Raton, New York, London, Tokyo, 1996–1997.
7 E. F. Westrum, in *Molecular Dynamics and Structure of Solid*, ed. R. S. Carter and J. J. Rush, National Bureau of Standards, Washington, DC, 1969, p. 459.
8 Siemens D5000 diffractometer, capillary platform transition technique, Cu-Kα1 = 1.54090 Å, 7° position sentitive detector and LT device of our own design. For indexing, the programs WIN-INDEX and WIN-METRIC Ver. 1.2 from Sigma-C company was used.
9 R. I. Jackson and J. H. Strange, *Acta Crystallogr., Sect. B.*, 1972, **28**, 1645.
10 N. T. Kawai, D. F. R. Gilson and I. S. Butler, *J. Phys. Chem.*, 1990, **94**, 5729.
11 R. Boese and M. Nussbaumer, in *Organic Crystal Chemistry*, ed. E. W. Jones, Oxford University Press, Oxford, UK, 1994, p. 20.
12 T. Haumann, R. Boese, S. I. Kozhushkov, K. Rauch and A. de Meijere, *Liebigs Ann./Recl.*, 1997, 2047.
13 *Crystal data* for norbornadiene: C_7H_8, cylindric crystal with 0.3 mm diameter and *ca*. 10 mm long, Nicolet R3 four circle diffractometer with Mo-Kα radiation at −163 °C, a = 6.2822(12), b = 17.889(3), c = 5.1608(13) Å, β = 113.725(16)°, V = 531.34(19) $Å^3$; Z = 4, D_c = 1.152 g cm^{-3}, μ = 0.06 mm^{-1}, $P2_1/c$, 5865 intensities ($2\theta_{max}$ = 80°), 2727 independent (R_{merg} = 0.0433), 2116 observed [$F_o \geqslant 4\sigma(F)$], correction for cylindrical crystal; structure solution with Siemens SHELXS and refinement on F^2 (Siemens SHELXTL ver. 5.03) (96 parameters), the hydrogen atom positions were taken from a difference Fourier map and refined without constraints, *R1* = 0.0504 (observed data, whole 2θ range), *wR*2 (all data) = 0.1543, $w^{-1} = \sigma^2(F_o^2) + (0.0717P)^2 + (0.050P)$, where $P = [\max F_o^2) + (2F_c^2)]/3$, maximum residual electron density 0.52 e $Å^{-3}$, GOF = 1.144. Multipole refinements (see ref. 21) up to hexadecapole level for C atoms, and dipoles for H atoms, C_{2v} symmetry, fixed hydrogen positions at C–H distances = 1.08 Å, parameter-to-observation ratio 15.87, R = 0.0371, R_w = 0.0275. CCDC 182/962.
14 V. Schomaker and K. N. Trueblood, *Acta Crystallogr., Sect. B*, 1968, **24**, 63.
15 The molecular structures of norbornadiene and norbornene were optimized based on C_{2v} and C_S symmetry, respectively, with GAUSSIAN 92: GAUSIAN 92, C. M. J. Frisch, G. W. Trucks, M. Head-Gordon, P. M. W. Gill, M. W. Wong, J. B. Foresman, B. G. Johnson, H. B. Schlegel, M. A. Robb, E. S. Replogle, R. Gomperts, J. L. Andres, K. Raghavachari, J. S. Binkley, C. Gonzalez, R. L. Martin, D. J. Fox, D. J. Defrees, J. Bakes, J. J. P. Stewart and J. A. Pople, Gaussian Inc., Pittsburg PA, 1992; MP2: C. Møller and M. S. Plesset, *Phys. Rev.*, 1934, **46**, 618.
16 K. Nag and A. Chakravorty, *Coord. Chem. Rev.*, 1980, **33**, 87.
17 T. Haumann, J. Benet-Buchholz, F.-G. Klärner and R Boese, *Liebigs Ann./Recl.*, 1997, 1429.
18 *XD*, Programme Package for Multipole Refinement, T. Koritsanszky, S. Howard, P. R. Mallison, Z. Su, T. Richter and N. K. Hansen, Universität Berlin, beta test ver. 1.1, April 1995.
19 D. Cremer, *Tetrahedron*, 1988, **44**, 7427; M. J. S. Dewar and M. L. McKee, *Pure Appl. Chem.*, 1980, **52**, 1431.
20 R. Huisgen, P. H. J. Ooms, M. Mingin and N. L. Allinger, *J. Am. Chem. Soc., 1980*, **102**, 3951; R. Huisgen, *Pure Appl. Chem.*, 1981, **53**, 171.
21 K. N. Houk, N. G. Rondan, F. K. Brown, W. L. Jorgensen, J. D. Madura and D. C. Spellmeyer, *J. Am. Chem. Soc.*, 1983, **105**, 5980.

Received in Cambridge, UK, 25th June 1998; 8/04842H

Organic–inorganic composite oxide phases: one-dimensional molybdenum oxide chains entrained within a three-dimensional coordination complex cationic framework in [{Cu_2(triazolate)$_2$(H_2O)$_2$}Mo_4O_{13}]

Douglas Hagrman and Jon Zubieta

Department of Chemistry, Syracuse University, Syracuse, NY 13244, USA. E-mail: jazubiet@syr.edu

The hydrothermal reaction of MoO_3, $CuSO_4{\cdot}5H_2O$, 1,2,4-triazole and H_2O produces a 50% yield of [{Cu_2(triazolate)$_2$(H_2O)$_2$}Mo_4O_{13}], a material constructed from {Mo_4O_{13}}$_n^{2n-}$ chains entrained within the three dimensional framework provided by the {Cu_2(triazolate)$_2$(H_2O)$_2$}$_n^{2n+}$ polymeric complex.

Inorganic oxides constitute a vast family of materials which are ubiquitous as both naturally occurring and synthetic materials[1] and are endowed with a range of physical properties giving rise to applications in areas as diverse as heavy construction, sorption, catalysis, biomineralization and microelectronics.[2,3] The recent elaboration of the chemistries of zeolites,[4] mesoporous materials of the MCM-41 class,[5] biomineralized materials,[6] and organically templated transition metal phosphates[7] has led to an appreciation of the dramatic influence of organic components on the microstructures of inorganic oxides.

We have recently described a fifth major class in which organic materials exert a significant structural role in controlling the architecture of the inorganic oxide: the organically templated molybdenum oxides.[8–13] A subclass of these new materials was inspired by the diversity of topologies adopted by metal–dipodal organonitrogen ligand complexes,[14] whose variability of channel dimensions suggested that metal oxide anionic units could be incorporated into the void space of the cationic skeleton. This strategy has provided a variety of novel molybdenum oxides coexisting with mononuclear, binuclear, trinuclear, and one- and two-dimensional coordination complex cations, of which [{Cu(4,4′-bpy)}$_4$$Mo_{15}O_{47}$],[8] [Cu(4,4′-bipyridylamine)$_{0.5}$$MoO_4$], and [Cu{1,2-*trans*-(4-pyridyl)ethene}-MoO_4][15] are representative examples. However, in no instance of a dipodal ligand was a three-dimensional cationic framework observed for the molybdate family of composites, despite introduction of M^{II} sites with octahedral coordination preferences. Recent studies on crystal engineering of three-dimensional frameworks[16] suggested that tripodal or higher denticity ligands with appropriate donor group orientation may favor three-dimensional architectures, although the coordination preferences of the M^{II} site and interactions with the oxide substructure may also influence the structure. Inspired by these results, 1,2,4-triazole was introduced as the organic component for a copper molybdate phase. The expectation of a three-dimensional cationic framework was realized in the isolation of [{Cu_2(triazolate)$_2$(H_2O)$_2$}Mo_4O_{13}] **1**.

The hydrothermal reaction of MoO_3, $CuSO_4{\cdot}5H_2O$, 1,2,4-triazole and H_2O in the mole ratio 1 : 1 : 1 : 1817 for 72 h at 200 °C yielded blue crystals of **1** as a monophasic material in *ca*. 50% yield. The IR spectrum of **1** exhibited a strong band at 954 cm^{-1} ascribed to ν(Mo=O) and a series of bands in the 720–920 cm^{-1} region characteristic of ν(Mo–O–Mo).

As shown in Fig. 1, the structure† of $\mathbf{1}^+$ consists of one-dimensional {Mo_4O_{13}}$_n^{2n-}$ chains entrained within the three-dimensional framework of the {Cu_2(triazolate)$_2$(H_2O)$_2$}$_n^{2n+}$ polymeric coordination cation. There are two unique copper sites in the cationic framework. One site Cu(A) is effectively square pyramidal {CuN_4O} through ligation to four triazolate nitrogen donors, one from each of four triazolate ligands and to a terminal oxo-group of the molybdate chain. The second site Cu(B) is octahedral {CuN_2O_4}, exhibiting coordination to two *trans* disposed triazolate nitrogen donors, two aquo ligands, and two terminal oxo-groups of the molybdate chains. The organic moiety adopts the anionic triazolate form in a three connect ligation mode. The resulting cationic framework is constructed from undulating chains of Cu(A) sites bridged through the 1,2-nitrogen donors of the triazolate ligands and linked to adjacent chains through the Cu(B) centers which coordinate to the remaining 4-nitrogen donors of the triazolate ligands (Fig. 2). This connectivity pattern produces a honeycomb network when viewed along the crystallographic *c* axis. Furthermore, the disposition of bridging triazolate ligands about a chain results in linkage to four adjacent parallel chains (Fig. 1) giving rise to large tunnels which are occupied by the molybdate chains.

The undulating molybdate chain, Fig. 3, is constructed from edge-sharing molybdenum octahedra and tetrahedra. It is noteworthy that the polyhedral connectivity within these {Mo_4O_{13}}$_n^{2n-}$ chains is distinct from that reported for other one-dimensional molybdenum oxides: $K_2Mo_3O_{10}$, $(NH_4)_2Mo_3O_{10}$, $(H_3NCH_2CH_2NH_3)Mo_3O_{10}$, $[H_3N(CH_2)_6NH_3]$-Mo_3O_{10}, $Na(NH_4)Mo_3O_{10}$ and [{Cu(4,4′-bpy)}$_4$$Mo_{15}O_{47}$].[8] The chain structure conforms to the constraints imposed by the copper–triazolate framework and the coordination requirements of the Cu^{II} sites of the framework.

The title compound demonstrates that the structural variability of the cationic scaffolding constructed from appropriately linked transition metal sites extends to 3-D coordination polymers as well as 1-D and 2-D types, with tunable void volumes, providing a domain for the formation of low dimensional metal oxides. The synthetic approach appears to provide a facile method for modification of the structures of metal oxides, employing a 'ship in the bottle' approach, and

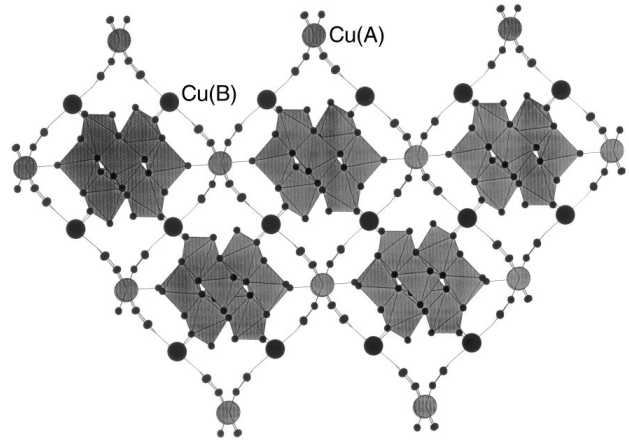

Fig. 1 A view parallel to the crystallographic *b* axis and to the molybdenum oxide chain of the structure of **1**. The molybdate chain is depicted in polyhedral form. The large lighter spheres are the Cu(A) sites, the smaller darker spheres are the Cu(B) sites.

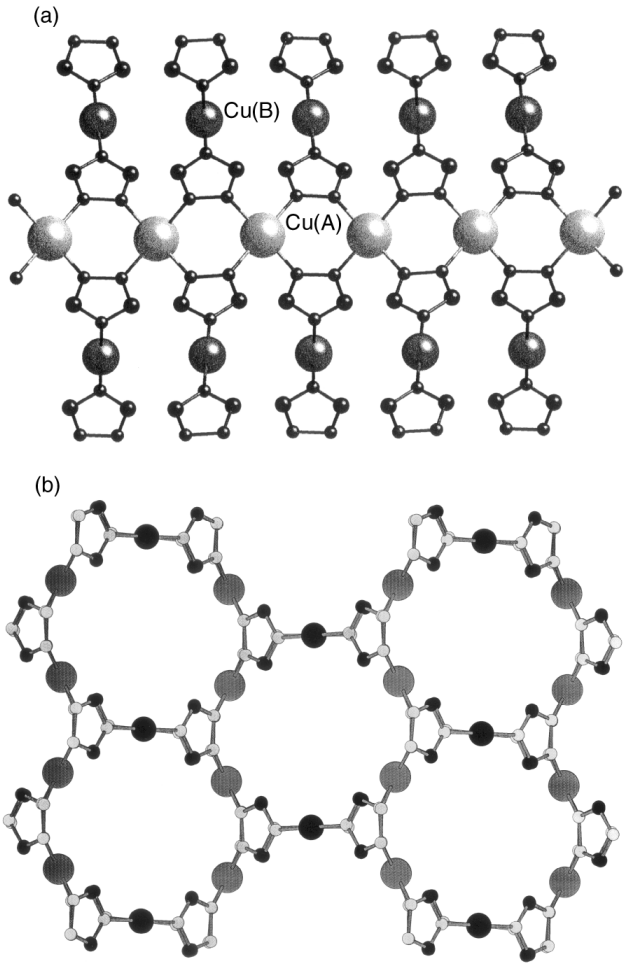

Fig. 2 (a) A view parallel to the crystallographic *a* axis of the chain formed by triazolate bridged Cu(A) sites (large, lighter spheres) and the linkage through Cu(B) centers (large, darker spheres) to adjacent chains. (b) The honeycomb pattern of the $\{Cu_2(triazolate)_2(H_2O)_2\}_n^{2n+}$ framework when viewed parallel to the crystallographic *c* axis. The bonding of the copper sites to the oxide substructure has been omitted for clarity. Selected bond lengths (Å): Cu(A)–N(×4) 1.993(5), Cu(A)–O(10) 2.343(4), Cu(B)–N(×2) 1.947(5), Cu(B)–O 2.000(5)(×2) 2.328(4)(×2).

ultimately for tuning of electronic, magnetic and optical properties of these phases.

This work was supported by NSF Grant CHE 961723.

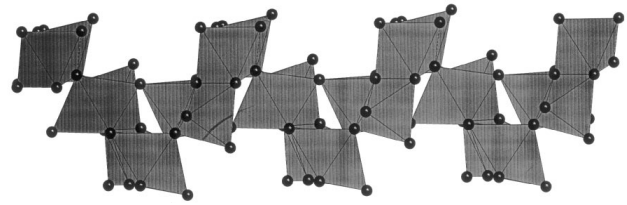

Fig. 3 A polyhedral view of the molybdenum oxide $\{Mo_4O_{13}\}_n^{2n-}$ chain

Notes and References

† *Crystal data* for $C_4H_8Cu_2Mo_4N_6O_{15}$ **1**: M = 891.00, monoclinic, space group $P2_1/n$, a = 13.6939(3), b = 7.7967(1), c = 17.2311(4) Å, β = 89.8570(9)°, V = 1839.71(6) Å^3, Z = 4, D_c = 3.206 g cm^{-3}, T = 243(2) K, μ = 5.004 cm^{-1}, $F(000)$ = 1680; solution and refinement based on 4364 reflections converged at $R1$ = 0.0356 and $wR2$ = 0.0772. CCDC 182/958.

1 N. N. Greenwood and A. Earnshaw, *Chemistry of the Elements*, Pergamon, New York, 1984.
2 D. W. Bruce and D. O'Hare, *Inorganic Materials*, Wiley, Chichester, 1992.
3 A. J. Cheetham, *Science*, 1994, **264**, 794 and references therein.
4 M. L. Occelli and H. C. Robson, *Zeolite Synthesis*, American Chemical Society, Washington, DC, 1989.
5 C. T. Kresge, M. E. Leonowicz, W. J. Roth, J. C. Vartuli and J. S. Beck, *Nature*, 1992, **359**, 710.
6 L. L. Hench, *Inorganic Biomaterials, in Materials Chemistry, and Emerging Discipline*, ed. L. V. Interrante, L. A. Casper and A. B. Ellis, ACS Symp. Ser. 245, 1995, ch. 21, pp. 523–547.
7 M. I. Khan, L. M. Meyer, R. C. Haushalter, C. L. Schweitzer, J. Zubieta and J. L. Dye, *Chem. Mater.*, 1996, **8**, 43.
8 D. Hagrman, C. Zubieta, D. J. Rose, J. Zubieta and R. C. Haushalter, *Angew. Chem., Int. Ed. Engl.*, 1997, **36**, 873 and references therein.
9 P. J. Zapf, R. C. Haushalter and J. Zubieta, *Chem. Commun.*, 1997, 321.
10 P. J. Zapf, R. C. Haushalter and J. Zubieta, *Chem. Mater.*, 1997, **9**, 2019.
11 P. J. Zapf, C. J. Warren, R. C. Haushalter and J. Zubieta, *Chem. Commun.*, 1997, 1543.
12 P. J. Zapf, R. P. Hammond, R. C. Haushalter and J. Zubieta, *Chem. Mater.*, 1998, **10**, 1366.
13 D. Hagrman, P. J. Zapf and J. Zubieta, *Chem. Commun.*, 1998, 1283.
14 See for example K. N. Power, T. L. Hennigar and M. J. Zaworotko, *Chem. Commun.*, 1998, 595.
15 D. Hagrman, R. C. Haushalter and J. Zubieta, *Chem. Mater.*, 1998, **10**, 361.
16 See for example B. F. Hoskins, R. Robson and D. A. Slizys, *Angew. Chem., Int. Ed. Engl.*, 1997, **36**, 2752.

Received in Columbia, MO, USA, 17th June 1998; 8/04689A

First synthesis of sterically hindered cofacial bis(corroles) and their bis(cobalt) complexes

François Jérôme, Claude P. Gros, Catherine Tardieux, Jean-Michel Barbe and Roger Guilard*†

Laboratoire d'Ingénierie Moléculaire pour la Séparation et les Applications des Gaz (L.I.M.S.A.G.), U.M.R. 5633, Faculté des Sciences 'Gabriel', 6, boulevard Gabriel, 21000 Dijon, France. E-mail: Roger.Guilard@u-bourgogne.fr

Syntheses of face-to-face bis(corroles) exhibiting electronic interactions between the two chromophores.

During the past few decades, numerous research has been devoted to the synthesis of dimeric and higher order porphyrins and, to a lesser extent, other macrocyclic tetrapyrroles covalently linked by rigid linkers.[1,2] Bis(porphyrins) with a gable or face-to-face spatial arrangement are effective catalysts for the four-electron reduction of dioxygen to water[3] and the oxidation of organic substrates.[4] A few years ago, 'Pacman' porphyrins achieved the microscopic reverse of dinitrogen fixation.[5] As a result of these significant data, many bisporphyrins and higher oligomers have been prepared with a wide variety of linking units.[6] Except for a few examples,[7] most of these rigidly linked dimeric and higher order oligomeric systems have consisted of porphyrin subunits. At the same time, corrole macrocycles were gaining considerable attention due, in part, to their very rich chemistry and to their ability, compared to porphyrins, to stabilize higher oxidation states of certain coordinated metals.[8] Very recently, symmetrical and unsymmetrical linear bis(corrole) and porphyrin–corrole dyads possessing *para*-phenyl linking units have been described.[7b] Herein, we wish to report the first synthesis of cofacial bis(corroles) **H_6BCA** and **H_6BCB**[9] as well as their bis(cobalt) complexes in order to study metal–metal interactions.

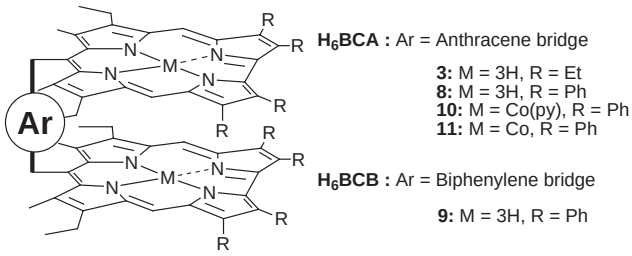

In the course of our work on the syntheses of cofacial bis(porphyrins),[10] it occurred to us that the conjugate addition of a 3,4-disubstituted-2-formylpyrrole to a face-to-face bis(dipyrromethane) followed by a cyclization step should represent a versatile method for new cofacial bis(corroles) formation. Indeed, reaction of compound **1A**[10] with 4 equivalents of **2** in methanol and in the presence of 30% hydrobromic acid in acetic acid led in a first step to the bis(*a*,*c*-biladiene) salt **3a** (Scheme 1), the progress of the reaction being monitored by UV–VIS spectroscopy. *In-situ* addition of sodium hydrogencarbonate and *p*-chloranil followed by addition of 50% hydrazine in water gave **3** as a crude compound after solvent removal. Final purification by chromatography on basic alumina afforded **3** in 5.5% yield. The proton NMR spectrum of the C_2 symmetric derivative **3** exhibits the characteristic patterns of two corrole units cofacially linked by an anthracenyl bridge.[11a] Compound **3** displays a pseudo-molecular peak at *m/z* = 1163 $[M + H]^+$, a Soret band at 402 nm and three Q bands at 510, 548 and 598 nm. Unfortunately, the free-base bis(corrole) **3** was found to be too

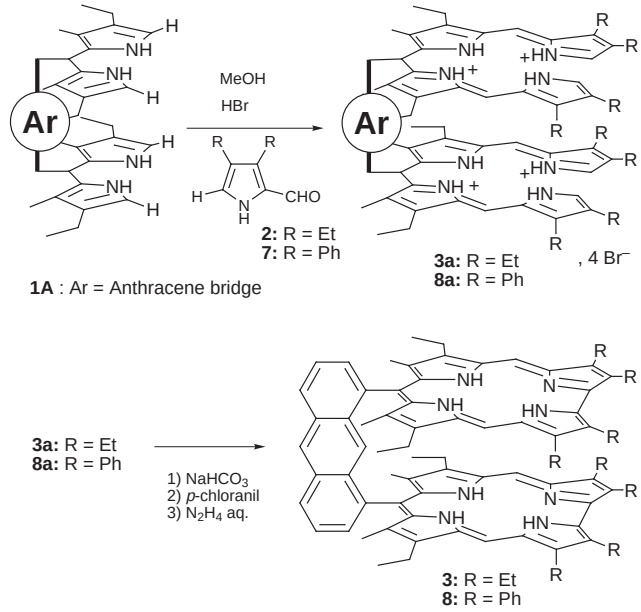

Scheme 1

unstable for a full characterization. Indeed, when left in solution in the presence of air and light, **3** readily decomposed over a period of a few minutes into a small amount of less-polar compounds, along with a large amount of base-line materials presumably due to the decomposition reaction with dioxygen of the free-base bis(corrole) which acts as a sensitizer. Such an instability has been pointed out for 10-monophenyl corrole **4** (Scheme 2).[11b] Indeed, compound **4** (as a free-base) was found to be air-sensitive when left in solution and one of its

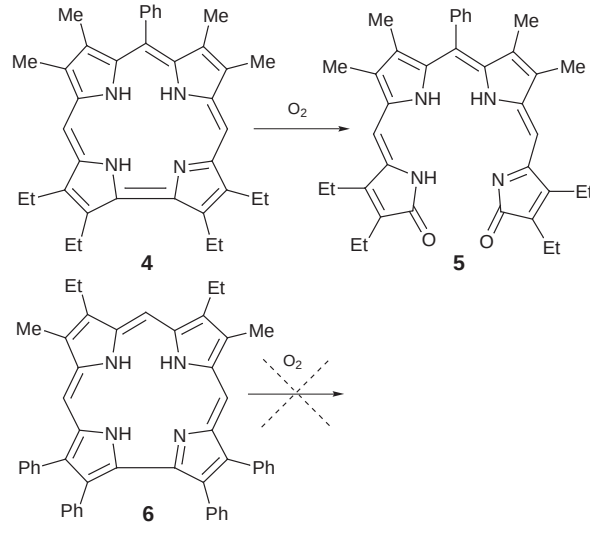

Scheme 2

decomposition products was identified as an open chain tetrapyrrole structure **5**.[11b] To our knowledge, this is the first example of molecular oxygen oxidation of a corrole macrocycle to a biliverdin structure. Our data led to a possible reaction mechanism involving addition of dioxygen at the 1,19-double bond of the corrole derivative followed by bond cleavage giving two amide groups as terminal functions. In order to prevent oxidative attack of the corrole ring and cleavage of the 1,19-double bond, the four β-pyrrole positions (positions 2,3,17 and 18) were substituted by phenyl groups. As expected, free-base corrole **6**[11b,12] is far more stable than its alkyl-substituted counterpart **4** as the presence of the bulky phenyl groups prevent dioxygen oxidation of the 1,19-double-bond. Indeed, the decomposition of **6** in solution in the presence of air and light only occurred over a period of a few days.

According to these results, we were able to synthesize a stable free-base bis(corrole) **8** (Scheme 1) by reacting first **1A**[10] with **7**,[13] and then by cyclizing the bis(*a*,*c*-biladiene) intermediate **8a**, using *p*-chloranil as an oxidant. The free-base derivative **8**[14] was isolated in 12.5% yield. Starting from 1,8-diformylbiphenylene as a spacer and using the same experimental procedure, compound **9**[15] was obtained in 12% yield. LSIMS mass spectra confirms the dimeric structure of **8** and **9** (*m/z* 1549 $[M + H]^+$ and 1523 $[M + H]^+$, respectively). Cofacial bis(corroles) **8** and **9**, containing phenyl rings at eight β-pyrrole positions, are really more stable than the unprotected one **3**. Indeed, when **8** and **9** are exposed in solution to air and light, no major decomposition is observed after a period of 48 h. Interestingly, the UV–VIS absorptions of **8** and **9** show that the spectra are not simply superpositions of the absorptions of the two corrole chromophores. In particular, the Soret bands of **8** and **9** are red-shifted with respect to those of the simple corrole possessing the same substitution patterns due to the electronic interactions occurring between the two corrole units in **8** and **9**. It is also worthy to note that no electronic interaction has been observed in the recently published linear dimers.[7b]

Standard procedures were employed to metallate the corrole core with cobalt acetate.[16] Compound **8** was heated at 80 °C in pyridine with 2.5 equivalents of $Co(OAc)_2$, the metallation reaction being monitored by UV–VIS spectroscopy. Completion of the reaction occurring within 1–2 h was indicated by the complete disappearance of the absorption at 607 nm and the appearance of a Q band at 597 nm; the Soret band being simultaneously slightly red-shifted (λ_{max} 414 and 435 nm). After purification, the homobimetallic $BCA(Co)_2(py)_2$ derivative **10** was isolated in 23% yield. Interestingly, the two axial pyridine ligands can easily be removed under vacuum (20 mmHg, 50 °C) to yield quantitatively **11**. The electronic absorption spectra of **11** shows a 37 nm blue-shift of the Soret band [λ_{max} (ε/dm^3 mol^{-1} cm^{-1}) = 377 (117 000), 398 (144 000), 529 (47 900) nm] compared to **10**. In LSIMS mode, the molecular peak for the **BCA** complex is observed at *m/z* = 1660 $[M + H]^+$ (100%). It is also worthy to note that **11** decomposes rapidly in the absence of coordinated axial ligands.

In conclusion, these cofacial bis(corroles) can be easily prepared in four steps (starting from the bridging unit) and on a large scale. Moreover, the synthesis of **8** and **9** described here integrate well for the development of coordination chemistry of cofacial bis(corroles) on a broad basis; work is currently underway in these directions.

Notes and References

1 L. R. Milgrom, in *The Colours of Life*, ed. L. R. Milgrom, Oxford University Press, New York, 1997, p. 191.

2 J. L. Sessler and S. J. Weghorn, *Expanded, Contracted and Isomeric Porphyrins*, Pergamon, Oxford, 1997.

3 C. K. Chang, H.-Y. Liu and I. Abdalmuhdi, *J. Am. Chem. Soc.*, 1984, **106**, 2725; J. P. Collman, F. C. Anson, C. E. Barnes, C. S. Bencosme, T. Geiger, E. R. Evitt, R. P. Kreh, K. Meier and R. B. Pettman, *J. Am. Chem. Soc.*, 1983, **105**, 2694; J. P. Collman, J. E. Hutchison, M. A. Lopez, A. Tabard, R. Guilard, W. K. Seok, J. A. Ibers and M. L'Her, *J. Am. Chem. Soc.*, 1992, **114**, 9869.

4 Y. Naruta, M. Sasayama and K. Maruyama, *Chem. Lett.*, 1992, 1267.

5 J. P. Collman, J. E. Hutchison, M. S. Ennis, M. A. Lopez and R. Guilard, *J. Am. Chem. Soc.*, 1992, **114**, 5654; J. P. Collman, J. E. Hutchinson, M. A. Lopez and R. Guilard, *J. Am. Chem. Soc.*, 1992, **114**, 8066.

6 J. L. Sessler, M. R. Johnson, T. Y. Lin and S. E. Creager, *J. Am. Chem. Soc.*, 1990, **112**, 9310; R. Cosmo, C. Kautz, K. Meerholz, J. Heinze and K. Mullen, *Angew. Chem. Int. Ed. Engl.*, 1989, **28**, 604; N. Ono, H. Tomita and K. Maruyama, *J. Chem. Soc., Perkin Trans. 1*, 1992, 2453; C. K. Chang and I. Abdalmuhdi, *J. Org. Chem.*, 1983, **48**, 5388; S. Chardon-Noblat and J.-P. Sauvage, *Tetrahedron Lett.*, 1991, **47**, 5123.

7 (*a*) A. Osuka, S. Marumo, K. Maruyama and N. Mataga, *Bull. Chem. Soc. Jpn.*, 1995, **68**, 262; (*b*) R. Paolesse, R. K. Pandey, T. P. Forsyth, L. Jaquinod, K. R. Gerzevske, D. J. Nurco, M. O. Senge, S. Licoccia, T. Boschi and K. M. Smith, *J. Am. Chem. Soc.*, 1996, **118**, 3869.

8 S. Licoccia and R. Paolesse, in *Metal Complexes with Tetrapyrrole Ligands III*, ed. J. W. Buchler, Springer-Verlag, Berlin and Heidelger, 1995, p. 71; T. A. Melenteva, *Russ. Chem. Rev.* (*Engl. Transl.*), 1983, **52**, 641; J. L. Sessler and S. J. Weghorn, in *Expanded, Contracted and Isomeric Porphyrins*, Pergamon, Oxford, 1997, p. 11; E. Vogel, S. Will, A. S. Tilling, L. Neumann, J. Lex, E. Bill, A. X. Trautwein and K. Wieghardt, *Angew. Chem., Int. Ed. Engl.*, 1994, **33**, 731; S. Will, J. Lex, E. Vogel, V. A. Adamian, E. Van Caemelbecke and K. M. Kadish, *Inorg. Chem.*, 1996, **35**, 5577; E. Van Caemelbeck, S. Will, M. Autret, V. A. Adamian, J. Lex, J.-P. Gisselbrecht, M. Gross, E. Vogel and K. M. Kadish, *Inorg. Chem.*, 1995, **34**, 184.

9 **H_6BC** for free-base biscorrole, **A** for anthracene bridge, **B** for biphenylene bridge.

10 M. Lachkar, A. Tabard, S. Brandès, R. Guilard, A. Atmani, A. De Cian, J. Fischer and R. Weiss, *Inorg. Chem.*, 1997, **36**, 4141; R. Guilard, S. Brandès, A. Tabard, N. Bouhmaida, C. Lecomte, P. Richard and J. M. Latour, *J. Am. Chem. Soc.*, 1994, **116**, 10 202; R. Guilard, M. A. Lopez, A. Tabard, P. Richard, C. Lecomte, S. Brandès, J. E. Hutchison and J. P. Collman, *J. Am. Chem. Soc.*, 1992, **114**, 9877; J. P. Collman, Y. Ha, R. Guilard and M. A. Lopez, *Inorg. Chem.*, 1993, **32**, 1788.

11 (*a*) ^{1}H NMR ($CDCl_3$) for **3**: δ 8.84 (s, 4 H, *meso* H), [10.27 (s, 1 H), 8.40 (s, 1 H), 7.65 (d, 2 H), 7.54 (d, 2 H), 6.94 (dd, 2 H) anthracene H], 3.91 (m, 24 H, CH_2CH$_3$), 2.15 (s, 12 H, Me), 1.44 (m, 36 H, CH$_2$CH_3), −2.61 (s br, 6 H, NH); (*b*) C. Tardieux, C. P. Gros and R. Guilard, *J. Heterocycl. Chem.*, 1998, in press.

12 Elemental analysis: Calc. for **6**, $C_{49}H_{42}N_4$: C, 85.68; H, 6.16; N, 8.16. Found: C, 85.77; H, 6.21; N 7.80%. ^{1}H NMR ($CDCl_3$): δ 9.76 (s, 2 H, *meso* H^5, H^{15}), 9.50 (s, 1 H, *meso* H^{10}), 7.88–6.96 (m, 20 H, Ph), 3.95 (q, 4 H, CH_2CH$_3$), 3.33 (s, 6 H, Me), 1.68 (t, 6 H, CH$_2$CH_3), −0.73 (s, NH), −1.47 (s, NH). IR : ν 3350 (NH), 2960 (CH), 2928 (CH), 2868 (CH) cm^{-1}. UV–VIS (CH_2Cl_2): λ_{max} (ε/dm^3 mol^{-1} cm^{-1}) 400 (83 400), 413 (74 700), 564 (19 400), 599 nm (20 900); UV–VIS (after HCl bubbling): λ_{max} (ε/dm^3 mol^{-1} cm^{-1}) 414 (95 900), 475 (15 000), 593 (39 500). MS (EI): *m/z* (%) 686 (100) $[M]^+$, 343 $[M]^{2+}$.

13 M. Friedman, *J. Org. Chem.*, 1965, **30**, 859.

14 Elemental analysis: Calc. for **8**, $C_{112}H_{90}N_8\cdot 3H_2O$: C, 83.96; H, 6.04; N, 7.00. Found: C, 83.96; H, 6.00; N 6.78%. ^{1}H NMR (C_6D_6): δ 8.86 (s, 4 H, *meso* H), [8.79 (s, 1 H), 8.36 (d, $^3J_{H-H}$ = 6.5, 2 H), 7.98 (s, 1 H) anthracene H], 7.80 (m, 8 H, Ph), [7.65 (d, $^3J_{H-H}$ = 6.5, 2 H), 7.57 (dd, $^3J_{H-H}$ = 6.5, 2 H) anthracene H], 7.52 (m, 8 H, Ph), 7.29 (m, 24 H, Ph), 3.27 (qd, $^2J_{H-H}$ = 14.7, $^3J_{H-H}$ = 7.5, 4 H, CH_AH$_B$CH$_3$), 3.22 (qd, $^2J_{H-H}$ = 14.7 Hz, $^3J_{H-H}$ = 7.5 Hz, 4 H, CH_AH$_B$CH$_3$), 1.95 (s, 12 H, Me), 1.31 (t, $^3J_{H-H}$ = 7.5 Hz, 12 H, CH$_2$CH_3), −2.83 (s, 3 H, NH), −3.00 (s, 3 H, NH). IR : ν 3482 (NH), 3401 (NH), 2961 (CH), 2923 (CH), 2870 (CH) cm^{-1}. UV–VIS (CH_2Cl_2): λ_{max} (ε/dm^3 mol^{-1} cm^{-1}) 406 (171 000), 578 (44 500), 607 nm (37 000). MS (LSIMS): *m/z* 1549 $[M + H]^+$.

15 Elemental analysis: Calc. for **9**, $C_{110}H_{88}N_8\cdot 2H_2O$: C, 84.79; H, 5.96; N, 7.20. Found: C, 84.44; H, 5.98; N, 7.45%. ^{1}H NMR (C_6D_6): δ 9.59 (s, 4 H, *meso* H), [7.98 (d, 2 H), 7.61 (dd, 2 H), 7.47 (d, 2 H)] biphenylene H], 7.10 (m, 40 H, Ph), 3.54 (m, 8 H, Et), 3.07 (s, 12 H, Me), 1.52 (t, 12 H, Et), −2.80 (s, 3 H, NH), −3.00 (s, 3 H, NH). UV–VIS (CH_2Cl_2): λ_{max} (ε/dm^3 mol^{-1} cm^{-1}) 412 (142 000), 572 (34 000), 608 nm (33 000). MS (LSIMS): *m/z* 1523 $[M + H]^+$.

16 M. Conlon, A. W. Johnson, W. R. Overend, D. Rajapaksa and C. M. Elson, *J. Chem. Soc., Perkin Trans. 1*, 1973, 2281.

Received in Basel, Switzerland, 1st July 1998; 8/05078C

Stabilisation of an endiolate by co-ordination to vanadium(IV)

Mahin Farahbakhsh, Hauke Schmidt and Dieter Rehder*

Chemistry Department, University of Hamburg, D-20146 Hamburg, Germany. E-mail: rehder@Xray.chemie.uni-hamburg.de

The redox reaction between $[VCl_2(tmeda)_2]$ (tmeda = *N,N,N′,N′*-tetramethylenediamine) and benzil yielded the non-oxo V^{IV} benzoin complex $[V(tmeda)\{Ph(O)C{=}C(O)Ph\}_2]\cdot thf$ (C_2 symmetry), the first structurally characterised vanadium–endiolate complex.

V^{II} is a versatile reducing agent which has been used to effectively reduce, *inter alia*, nitrogen to ammonia,[1] protons to hydrogen,[2] bromoalkanes to alkanes[3] or sulfidophenylsulfanylethane to ethylene and thiocatecholate.[4] V^{II} is also the active intermediate in many reductive hydrogenation and C–C coupling reactions carried out in the presence of the catalyst system VCl_n–H^+–Zn.[5–8] In an effort to establish general pathways leading to non-oxo vanadium-(IV) and -(V) complexes, we have now exploited the reducing potential of V^{II}, stabilised in the form of $[VCl_2(tmeda)_2]$, to reduce benzil to 1,2-dihydroxyethylene and to concomitantly coordinate this tautomeric form of benzoin to vanadium. The use of $[VCl_2(tmeda)_2]$[9] allows the reaction to be carried out in solvents which, unlike water or alcohols, do not straight away provide an oxo group which would otherwise give rise to the formation of the favoured vanadyl [oxovanadium(IV)] moiety. Non-oxo (sometimes also termed 'bare') complexes of high-valent vanadium are of interest in the context of amavadin, a molecular compound of V^{IV} isolated from mushrooms of the genus *Amanita*,[10] and of vanadium nitrogenase, which presumably contains a $\{V(\mu\text{-}S)_3(his)(homocitrate)\}$ coordination site.[11]

Non-oxo complexes of vanadium in its oxophilic oxidation states +IV and +V are still scarce. Examples include [V(salen)(benzilate)],[12] [V(tben)] [H_4tben = *N,N,N′,N′*-tetrakis(2-hydroxybenzyl)ethylenediamine],[13] and [V(salhan)] [H_2salhan = bis(salicylaldehyde-2-hydroxyanil)].[14] Nor has the chemistry of vanadium complexes containing 1,2-diolates as ligands[15–18] yet been developed to a great extent, although this class of complexes is of some interest with respect to model compounds for the physiologically relevant interaction of vanadium with sugars and sugar derivatives such as nucleotides and nucleosides. One such complex, a dimeric adenosyldioxovanadate, has recently been structurally characterised.[19] In contrast to simple α-hydroxycarbonyl compounds, the equilibrium between enediol and the α-hydroxycarbonyl form may be in favour of the former in the case of sugars. Complexes containing the enediol tautomeric form of an α-diketone bound to a vanadium centre have so far not been described. They are known in the dinuclear systems $[W_2X_6(O_2C_2R_2)_2]$ (X = Cl, OR′)[20] and $[Mo_2O_5(O_2C_2Ph_2)_2]$.[21] Vanadium coordination to enolate[22a] and ynolate[22b] has also been reported.

$[V(tmeda)\{Ph(O)C{=}C(O)Ph\}_2]$ forms on addition of benzil to $[VCl_2(tmeda)_2]$ (molar ratio 1:1) dissolved in refluxing, absolute thf. Black, crystalline material of $[V(tmeda)\{Ph(O)C{=}C(O)Ph\}_2]\cdot thf$,† suitable for the X-ray structure determination, is obtained as *n*-pentane is allowed to diffuse into the saturated thf solution within a few days. Since the conversion of benzil to benzoin is a two-electron reduction, half of the vanadium is lost in a side-reaction, the nature of which has not yet been revealed. The exclusive formation of the *Z* isomer of the enediol tautomeric form of benzoin hints at a reaction mechanism where benzil is associated with and thus activated by the V^{II} centre prior to reduction. The coordination of bidentate oxo-functional ligands such as β-diketonates[23] and β-diolates[24] to V^{II} has been noted before (*cf.* also ref. 9).

An ORTEP drawing of $[V(tmeda)\{Ph(O)C{=}C(O)Ph\}_2]\cdot thf$‡ is shown in Fig. 1. The overall geometry is distorted octahedral. V, N1, N1A, O2 and O2A form an approximate plane (deviations: V 0.000, O2 +0.240, O2A −0.240, N1 −0.265, N1A +0.265 Å), O1 and O1A are in the axis, which is slightly bent; the angle O1–O1A amounts to 169.77(8)°. The point symmetry is C_2, with the twofold axis bisecting the angles O2–V–O2A, N1–V–N1A, and the ethylene backbone of the tmeda ligand. Distorted octahedral geometries have also been reported for other non-oxo vanadium complexes,[12–14] while the trigonal-prismatic or distorted trigonal-prismatic arrangements are realised in $[V(hazb)_2]$ [H_2hazb = bis(2,2′-dihydroxyazobenzene],[25] and in non-oxo vanadium(IV) complexes containing ONS donor sets.[26] The carbon–carbon bond length [1.369(3) Å] and the bond angles (average 120°) at the carbons forming the benzoin backbone clearly indicate that the enediol form (sp^2 hybridisation at both carbons) prevails. The V–O bond lengths [1.896(1) and 1.922(1) Å] exceed those of V–O(alkoxide) with a sp^3 hybridised carbon of the alkoxo group (typically 1.77–1.81 Å[12,15a,16–18]); they compare to V–O(phenolate) (1.87–1.91 Å) and V–O(enolate)[22a] [1.928(2) Å], and also to the V–O bond lengths to the non-bridging sugar alkoxides in $[VO_2(\mu\text{-adenosine})_2]^{2-}$ [1.939(2) and 1.916(2) Å];[19] but they are exceeded by V–O(β-diketonate) bond lengths (1.98–2.02 Å).[27]

The +IV state of vanadium has further been established by EPR spectroscopy and cyclic voltammetry.§ The CV exhibits a reversible one-electron reduction step ($V^{IV} \leftrightarrows V^{III}$) at $E_{1/2}$ = −1.080 V, and an irreversible oxidation ($V^{IV} \rightarrow V^{V}$) at +0.27 V *vs.* SCE. The EPR parameters (g_0 = 1.962 , A_0 = 89.0 G; in thf) compare to those commonly found for V^{IV} complexes with a coordination environment dominated by oxygen functionali-

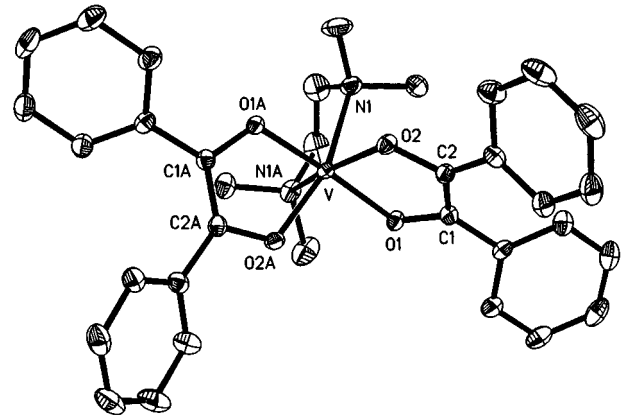

Fig. 1 ORTEP drawing, showing the 50% probability ellipsoids, and numbering scheme for $[V(tmeda)\{Ph(O)C{=}C(O)Ph\}_2]$. Selected bond distances (Å) and bond angles (°): V–N1 2.204(2), V–O1 1.896(2), V–O2 1.921(2), C1–C2 1.369(3), O1–C1 1.342(2), O2–C2 1.354(2), C1–C10 1.474(3), C2–C20 1.472(3); N1–V–N1A 80.35(11), O1–V–O2 79.19(6), O1–V–O1A 169.80(9), O2–V–O2A 108.93(9), N1–V–O1 100.29(7), N1–V–O2 87.10(7) O1–C1–C2 113.3(2), O1–C1–C10 116.4(2), C2–C1–C10 130.3(2).

ties.[28] The BVS analysis, using the parameters provided by Carrano *et al*.,[29] leads to a valence state for vanadium of 3.9.

We are presently expanding this novel route to non-oxo V^{IV} complexes by redox-interaction between a low-valent vanadium centre and a 'pre-ligand' system that serves as the oxidising agent and, in its reduced form, a ligand to the oxidised vanadium.

Notes and References

† [V(tmeda){Ph(O)C=C(O)Ph}$_2$]·thf was prepared in 44% yield. A satisfactory microanalysis was obtained. The ν(C=O) bands are at 1610 and 1588 cm^{-1} (KBr pellet).

‡ *Crystal data* for [V(tmeda){Ph(O)C=C(O)Ph}$_2$]·thf, $C_{38}H_{44}N_2O_5V$, M = 659.69, orthorhombic, space group *Pccn*, a=27.887(10), b = 8.916(2), c = 14.154(6) Å, Z = 4, V = 3519(2) Å^3, D_c = 1.245 g cm^{-3}, μ = 2.71 mm^{-1}, an absorption correction (DIFABS) was applied. Data were collected at 173(2) K on an Enraf Nonius CAD4 diffractometer (Cu-Kα irradiation, λ = 1.541 78 Å, graphite monochromator) in the 2θ scan mode, θ = 3.17–76.35°. Measured reflections 3716, independent reflections 3680 (R_{int} = 0.0152); refined parameters 234. The solution of the structure (SHELXS 97) and refinement (SHELXL 97) converged to a conventional [*i.e.* based on the $I > 2\sigma(I_0)$ criterion] $R1$ = 0.0454 and $wR2$ = 0.1284. Non-hydrogen atoms were refined anisotropically, hydrogen atoms were calculated into ideal positions and included in the final FMLS refinement. Maximum and minimum residual electron densities were 0.540 and −0.637 e Å^{-3}. Only one half of the structure, including one complete enediolate ligand, is crystallographically unique. The thf of crystallisation was treated with a 1:1 disorder model, as required by the crystallographic C_2 axis (symmetry transformation $-x + 1, -y, -z + 1$). CCDC 182/955.

§ X-Band EPR spectra (Bruker ESP 300E) were obtained at 9.74 GHz in *ca.* 1 mM solutions. CV measurements (Princeton Applied Research potentiostat 273A; working electrode: Pt foil, counter electrode: Pt wire) were carried out in *ca.* 1 mM DMF solution with 0.2 M TBAP as conductance salt. The potentials are referenced against SCE. The same crystalline material used for the X-ray structure determination was employed for the EPR and CV studies.

1 N. T. Denisov, N. I. Shuvalova and A. E. Shilov, *Kinet. Catal*., 1994, **35**, 700; G. J. Leigh, R. Prieto-Alcón and J. R. Sanders, *J. Chem. Soc., Chem. Commun*., 1991, 921; B. Folkesson and R. Larsson, *Acta Chem. Scand., Sect. A*, 1979, **33**, 347.

2 N. P. Luneva, S. A. Mironova, A. E. Shilov, M. Yu. Antipin and Y. T. Struchkov, *Angew. Chem., Int. Ed. Engl*., 1993, **32**, 1178.

3 T. Hirao, K. Hirao, T. Hasegawa, Y. Oshiro and I. Ikeda, *J. Org. Chem.*, 1993, **58**, 6529.

4 W. Tsagkalidis, D. Rodewald and D. Rehder, *J. Chem. Soc., Chem. Commun*., 1995, 165.

5 For a review see: D. Rehder and H. Gailus, *Trends Organomet. Chem*., 1994, **1**, 397.

6 T. Hirao, T. Hasegawa, Y. Maguruma and I. Ikeda, *J. Org. Chem*., 1996, **61**, 366.

7 M. Kang, J. Park, A. W. Konradi and S. F. Pedersen, *J. Org. Chem*., 1996, **61**, 5528.

8 B. Kammermeier, G. Beck, W. Hola, D. Jacobi, B. Napierski and H. Jendralla, *Chem. Eur. J*., 1996, **3**, 307.

9 The particular role of this V^{II} complex, and other V^{II} systems are reviewed in: G. J. Leigh and J. S. de Souza, *Coord. Chem. Rev*., 1996, **154**, 71.

10 E. M. Armstrong, R. L. Beddoes, L. J. Calviou, J. M. Charnock, D. Collison, N. Ertok, J. H. Naismith and C. D. Garner, *J. Am. Chem. Soc*., 1993, **115**, 807.

11 J. Chen, J. Christiansen, R. C. Tittsworth, B. J. Hales, S. J. George, D. Coucouvanis and S. P. Cramer, *J. Am. Chem. Soc*., 1993, **115**, 5509.

12 V. Vergopoulos, S. Jantzen, D. Rodewald and D. Rehder, *J. Chem. Soc., Chem. Commun*., 1995, 377.

13 A. Neves, A. S. Ceccato, I. Vencato, Y. P. Mascarenhas and C. Erasmus-Buhr, *J. Chem. Soc., Chem. Commun.*, 1992, 652.

14 H. Hefele, E. Ludwig, E. Uhlemann and F. Weller, *Z. Anorg. Allg. Chem*., 1995, **621**, 1973.

15 (*a*) W. Priebsch and D. Rehder, *Inorg. Chem*., 1990, **29**, 3013; (*b*) D. C. Crans, R. A. Felty, H. Chen, H. Eckert and N. Das, *Inorg. Chem*., 1994, **33**, 2427; W. J. Ray, Jr., D. C. Crans, J. Zheng, J. W. Burgner, II, H. Deng and M. Mahroof-Tahir, *J. Am. Chem. Soc.*, 1995, **117**, 6015.

16 D. C. Crans, R. A. Felty and M. M. Miller, *J. Am. Chem. Soc*., 1991, **113**, 265.

17 D. C. Crans, R. A. Felty, O. P. Anderson and M. M. Miller, *Inorg. Chem*., 1993, **32**, 247.

18 S. P. Rath, S. Mondal, A. Chakravorty, *Inorg. Chim. Acta*, 1997, **263**, 247; S. Mondal, S. P. Rath, S. Dutta and A. Chakravorty, *J. Chem. Soc., Dalton Trans*., 1996, 99.

19 S. J. Angus-Dunne, R. J. Batchelor, A. S. Tracey and F. W. B. Einstein, *J. Am. Chem. Soc*., 1995, **117**, 5292.

20 M. H. Chisholm, J. C. Huffman and A. L. Raterman, *Inorg. Chem*., 1983, **22**, 4100.

21 Q. Chen, S. Liu, H. Zhu and J. Zubieta, *Polyhedron*, 1989, **8**, 2915.

22 (*a*) N. Julien-Cailhol, E. Rose, J. Vaisserman and D. Rehder, *J. Chem. Soc., Dalton Trans*., 1996, 2111; (*b*) J. Jubb and S. Gambarotta, *J. Am. Chem. Soc*., 1993, **115**, 10 410.

23 M. Döring, H. Görls, E. Uhlig, K. Brodersen, L. Dahlenburg and A. Wolski, *Z. Anorg. Allg. Chem.*, 1992, **614**, 65.

24 E. Solari, S. de Angelis, C. Floriani, A. Chiesi-Villa and C. Guastini, *Inorg. Chem*., 1992, **31**, 141.

25 E. Ludwig, H. Hefele, E. Uhlemann, F. Weller and W. Kläui, *Z. Anorg. Allg. Chem*., 1995, **621**, 23.

26 W. Bansse, E. Ludwig, E. Uhlemann, F. Weller, K. Dehnicke and W. Herrmann, *Z. Anorg. Allg. Chem.*, 1992, **613**, 36; M. Farahbakhsh, H. Nekola, H. Schmidt and D. Rehder, *Chem. Ber./Recueil*, 1997, **130**, 129.

27 M. Mikuriya, T. Kotera, F. Adachi and S. Bandow, *Chem. Lett*., 1993, 945; H. Schmidt, M. Bashirpoor and D. Rehder, *J. Chem. Soc., Dalton Trans*., 1996, 3865; M. Bashirpoor, H. Schmidt, C. Schulzke and D. Rehder, *Chem. Ber./Recueil*, 1997, **130**, 651.

28 A. Jezierski and J. B. Raynor, *J. Chem. Soc., Dalton Trans.*, 1981, 1.

29 C. J. Carrano, M. Mohan, S. H. Holmes, R. de la Rosa, A. Butler, J. M. Charnock and C. D. Garner, *Inorg. Chem.*, 1994, **33**, 646.

Received in Basel, Switzerland, 6th May 1998; 8/03393E

Observing and modelling energetically close α- and β-carbon–hydrogen agostic interactions in an isopropyl tris(pyrazolyl)boratoniobium complex

Joëlle Jaffart,[a] René Mathieu,[a] Michel Etienne,*[a]† John E. McGrady,[b] Odile Eisenstein*[b]‡ and Feliu Maseras*[b]

[a] *Laboratoire de Chimie de Coordination du CNRS, UPR 8241, 205 Route de Narbonne, 31077 Toulouse Cedex 4, France*
[b] *Laboratoire de Structure et Dynamique des Systèmes Moléculaires et Solides, UMR 5636, Université de Montpellier II, 34095 Montpellier Cedex 5, France*

An equilibrium between α- and β-agostic interactions has been observed in Tp*Nb(Cl)(CHMe$_2$)(PhC≡CMe) 1 [Tp* = hydridotris(3,5-dimethylpyrazolyl)borate] while only α-agostic interactions have been observed for the analogous ethyl complex; calculations using the hybrid QM/MM method IMOMM (B3LYP:mm3) methodology properly account for the experimental results, and suggest that steric effects are responsible for the presence of distinct minima in the isopropyl complex.

Agostic interactions have been found to play an important role in the olefin polymerization reactions and also in the isomerization and dynamics of alkyl groups.[1–5] One of the central issues has been the competition between α- and β-agostic interactions. While theoretical studies have suggested that the two situations could correspond to stable minima, the β-agostic interaction has always been calculated to be energetically favored.[6] To our knowledge, the two types of agostic interactions have never been observed in any single system, since fast rotation of alkyl chain makes characterization of secondary minima unlikely on the NMR time scale. We report here the first observation of an equilibrium between α-C–H and β-C–H agostic forms of an isopropyl group in the formally d^2 complex Tp*Nb(Cl)(CHMe$_2$)(PhC≡CMe) **1** [Tp* = hydridotris(3,5-dimethylpyrazolyl)borate]. We have previously shown that *n*-alkyl complexes such as Tp*Nb(Cl)(CH$_2$R)(PhC≡CMe) exhibit only α-agostic interaction.[7]

The isopropyl complex Tp*Nb(Cl)(CHMe$_2$)(PhC≡CMe) **1** has been isolated in 75% yield from the reaction of Tp*NbCl$_2$(PhC≡CMe)[8] with 1 equiv. of (CHMe$_2$)MgCl.[9] X-Ray diffraction[10] on a single crystal at 160 K reveals a β-agostic structure as shown in Fig. 1. Interaction of one β-H with Nb results in a pronounced distortion of both the alkyl ligand and the metal coordination sphere. An acute Nb–Cα–Cβ angle, a shortened Cα–Cβ bond, a close Nb–Hβ contact and a markedly obtuse Cα–Nb–Cl angle are noteworthy data.[1] The conformation of the isopropyl group is such that the non-agostic Me sits in the wedge formed by two *cis*-pyrazole rings, as do the R groups in Tp*Nb(Cl)(CH$_2$R)(PhC≡CMe) complexes, all of which exhibit α-agostic structures.[7] NMR studies on **1**, however, reveal a more complex situation in solution.

The ^{1}H NMR spectra of **1** in CD$_2$Cl$_2$ indicate dynamic behavior due to an unprecedented equilibrium between a β- and an α-agostic form, **1β** and **1α** respectively (Scheme 1). In the slow exchange regime (193 K), the equilibrium constant measured as the ratio **1β** : **1α** is 3.9 ($\Delta G°_{193}$ = −2.2 kJ mol^{-1}). **1β** is characterized by isopropyl methyls at δ 1.29 and 0.05 (both d, *J* 7 Hz) and a methine proton at δ 2.10. The 'in-plane' rotation of the agostic Me is not frozen out as observed in other β-agostic complexes of the early transition metals. Evidence for the β-agostic interaction thus comes from the ^{13}C NMR data which are consistent with the rehybridization of Cα towards sp^2(δ 72.0, $^1J_{CH}$ 141 Hz). Spectroscopic data for **1α**, including a shielded Hα at δ −1.13 and a broad deshielded Cα at δ 126.4

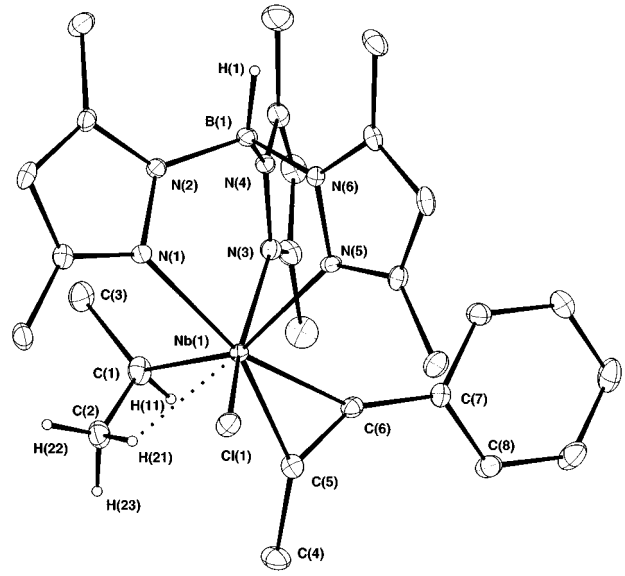

Fig. 1 Plot of the molecular structure of **1**. Located and refined H are shown. Selected bond lengths (Å): Nb(1)–C(1), 2.228(4); Nb(1)···C(2), 2.608(4); C(1)–C(2), 1.476(7); C(1)–C(3), 1.535(6); Nb(1)–H(21), 2.17(5). Selected bond angles (°): Nb(1)–C(1)–C(2), 87.0(3); Nb(1)–C(1)–C(3), 121.2(3); Cl(1)–Nb(1)–C(1), 122.1(1); C(2)–C(1)–C(3), 115.3(4); Cl(1)–Nb(1)–C(1)–C(2), 5.3; Nb(1)–C(1)–C(2)–H(21), 2.4.

with a reduced $^1J_{CH}$ (100 ± 5 Hz), testify to the α-agostic interaction. Significantly, there is no NMR evidence for a putative third Nb–C rotamer, which might or might not have a β-agostic interaction, namely that with Hα in the wedge formed by the two *cis* pyrazole rings (see discussion of the X-ray data).

The synthesis of Tp*Nb(Cl)[CH(CD$_3$)$_2$](PhC≡CMe) (**1**-d_6), selectively deuterated at the isopropyl methyls, has been achieved.[9] Owing to the preference for H rather than D to occupy an agostic position,[1,11] a thermodynamic isotope effect

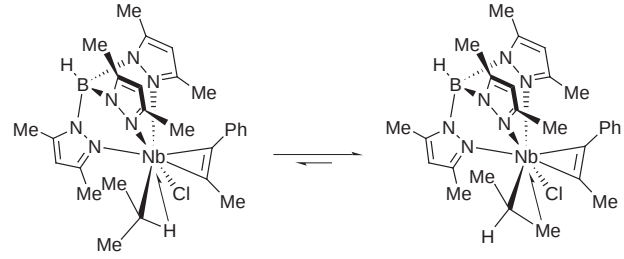

Scheme 1

should lead to an equilibrium shift towards the formation of **1α**-d_6, *i.e.* to a smaller equilibrium constant. An isotopic perturbation of the equilibrium is indeed observed. At 193 K the ratio **1β**-d_6 : **1α**-d_6 is 3.2 ($\Delta G°_{193}$ = −1.9 kJ mol^{-1}), which translates to a $\Delta\Delta G°_{193}$ of 0.3 kJ mol^{-1} in favor of **1α**, giving further evidence for the proposed equilibrium between β- and α-agostic forms of the isopropyl group.

The electronic structure of the isopropyl complex **1**, along with that of the ethyl complex,[7b] were examined using the integrated molecular orbitals and molecular mechanics (IMOMM) methodology,[12,13] which has recently been used successfully to model agostic interactions.[15] Only one minimum was located for the ethyl complex, corresponding to the structurally characterized α-agostic isomer.[7b] In contrast, two minima are obtained for the isopropyl complex, one corresponding to the β-agostic structure described above, and the other, 9.3 kJ mol^{-1} higher in energy, to an α-agostic isomer related to the first by rotation of 120° about the Nb–CH(CH$_3$)$_2$ bond. All three minima show features typical of agostic interactions, namely short Nb···H distances (2.35–2.58 Å), long agostic C–H bonds (1.112–1.116 Å), obtuse Cl–Nb–Cα angles (110.8–126.9°) and angles substantially less than 109.5° (86.3–92.4°) between the Nb–Cα bond and the agostic group (H or CH$_3$).

The location of two distinct minima for the isopropyl system, lying very close in energy, raises the question of the origin of the barrier to rotation about the Nb–C bond. The absence of a β-agostic minimum for the ethyl complex suggests that the barrier is not caused by the intrinsic stability of the agostic interactions themselves. The hindered rotation may be thus caused by the steric constraints of the Tp* ligand. The most sterically favorable conformation for the alkyl chain places one Me group along a wedge defined by two *cis*-pyrazole rings, where the pendant methyl groups of Tp* present a significant barrier to rotation about the Nb–C bond. This 'locking' of the non-agostic Me group leaves an α-C–H bond and a Me group to compete for the electron deficient Nb centre in the isopropyl complex, but only two α-C–H groups in the ethyl analogue, thereby accounting for the presence of two distinct isomers in the former, but only one in the latter.

Thanks are due to Bruno Donnadieu and Francis Lacassin for collecting the X-ray data and operating the AMX 400 NMR machine, respectively. J. J. is grateful to the Ministère de l'Enseignement Supérieur et de la Recherche for a fellowship, J. E. M to the European Community for a Marie Curie Fellowship (Grant number ERBFMBICT 971985) and F. M. to the C.N.R.S for a position of Research Associate.

Notes and References

† E-mail: etienne@lcc-toulouse.fr
‡ E-mail: odile.eisenstein@lsd.univ-montp2.fr

1 For a review on agostic interactions, see: M. Brookhart, M. L. H. Green and L.-L. Wong, *Prog. Inorg. Chem.*,1988, **36**, 1.
2 For olefin polymerization at d^6 centers, see: (*a*) W. E. Piers and J. E. Bercaw, *J. Am. Chem. Soc.*, 1990, **112**, 9406; (*b*) H. Krauledat and H.-H. Brintzinger, *Angew. Chem., Int. Ed Engl.*, 1990, **29**, 1412; (*c*) N. Barta, B. A. Kirk and J. R. Stille, *J. Am. Chem. Soc.*, 1994, **116**, 8912; (*d*) R. H. Grubbs and G. W. Coates, *Acc. Chem. Res.*, 1996, **29**, 85
3 For olefin polymerization at d^6 centers, see: M. J. Tanner, M. Brookhart and J. M. DeSimone, *J. Am. Chem. Soc.*, 1997, **119**, 7617.
4 For isomerization and dynamics of alkyl groups, see: (*a*) M. L. H. Green, A. Sella and L.-L. Wong, *Organometallics*, 1992, **11**, 2650; (*b*) M. Brookhart, E. Hauptman and D. M. Lincoln, *J. Am. Chem. Soc.*, 1992, **114**, 10394; (*c*) M. Brookhart, D. M. Lincoln, A. F. Volpe and G. F. Schmidt, *Organometallics*, 1989, **8**, 1212; (*d*) C. P. Casey and C. S. Yi, *Organometallics*, 1991, **10**, 33; (*e*) B. J. Burger, M. E. Thompson, W. D. Cotter and J. E. Bercaw, *J. Am. Chem. Soc.*, 1990, **112**, 1566; (*f*) D. J. Tempel and M. Brookhart, *Organometallics*, 1998, **17**, 2290.
5 For multiple agostic interactions, see: (*a*) A. D. Poole, D. N. Williams, A. M. Kenwright, V. C. Gibson, D. C. R. Hockless and P. A. O'Neil, *Organometallics*, 1993, **12**, 2549; (*b*) K. H. den Hann, L. J. de Boer, J. H. Teuben, A. L. Spek, B. Kojic-Prodic, G. H. Hays and R. Huis, *Organometallics* 1986, **5**, 1726.
6 (*a*) Y. Han, L. Deng and T. Ziegler, *J. Am. Chem. Soc.*, 1997, **119**, 5939; (*b*) T. K. Woo, L. Fan and T. Ziegler, *Organometallics*, 1994, **13**, 2252; (*c*) D. G. Musaev, M. Svensson, K. Morokuma, S. Strömberg, K. Zetterberg and P. E. M. Siegbahn, *Organometallics*, 1997, **16**, 1933; (*d*) D. G. Musaev, R. D. J. Froese, M. Svensson and K. Morokuma, *J. Am. Chem. Soc.*, 1997, **119**, 367; (*e*) A. Haaland, W. Scherer, K. Ruud, G. S. McGrady, A. J. Downs and O. Swang, *J. Am. Chem. Soc.*, 1998, **120**, 3762.
7 (*a*) M. Etienne, R. Mathieu and B. Donnadieu, *J. Am. Chem. Soc.*, 1997, **119**, 3218; (*b*) M. Etienne, *Organometallics*, 1994, **13**, 410.
8 M. Etienne, F. Biasotto, R. Mathieu and J. L. Templeton, *Organometallics*, 1996, **15**, 1106.
9 Complex **1** like its dichloro precursor[8] exists as a mixture of discrete rotamers depending on the orientation of PhC≡CMe with respect to the organometallic moiety. Data are discussed and depicted for the major alkyne rotamer but all conclusions are valid for the other rotamer. Full analytical and spectroscopic data are available from the authors.
10 *Crystal data* for **1**: $C_{27}H_{37}BClN_6Nb$, M = 584.8, monoclinic, $P2_1/n$, a = 15.169(2), b = 10.7604(7), c = 16.886(2) Å, β = 98.43(1)°, V = 2726(1) Å^3, Z = 4, T = 160 K, μ = 5.47 cm^{-1}, R = 0.0289, Rw = 0.0281 for 2412 reflections [$I > 2\sigma(I)$] and 342 parameters. CCDC 182/966.
11 (*a*) M. Brookhart, W. Lamanna and M. B. Humphrey, *J. Am. Chem. Soc.*, 1982, **104**, 2117; (*b*) R. B. Calvert and J. R. Shapley, *J. Am. Chem. Soc.*, 1978, **100**, 7726.
12 F. Maseras and K. Morokuma, *J. Comput. Chem.*, 1995, **16**, 1170.
13 IMOMM calculations were performed on the experimental complex replacing Ph of alkyne by H. The QM part of the calculation was performed on the model system [Nb(NH=CH$_2$)$_3$Cl{CH(CH$_3$)$_2$}(HCCH)]$^+$ with Gaussian 92/DFT,[14a] using the B3LYP density functional. A pseudopotential was used for the internal electrons of niobium, and a valence double-ζ basis set for all atoms, with the addition of a polarisation d shell on Cl. The positive charge in the QM part, which arises because the negatively charged Tp* ligand is replaced by three neutral NH=CH$_2$ groups, should not influence the relative energies of the two minima. The molecular mechanics (MM) part was performed using mm3(92).[14b]
14 (*a*) M. J. Frisch, G. W. Trucks, H. B. Schlegel, P. W. M. Gill, B. G. Johnson, M. W. Wong, J. B. Foresman, M. A. Robb, M. Head-Gordon, E. S. Replogle, R. Gomperts, J. L. Andres, K. Raghavachari, J. S. Binkley, C. Gonzalez, R. L. Martin, D. J. Fox, D. J. Defrees, J. Baker, J. J. P. Stewart and J. A. Pople, *Gaussian 92/DFT*, Gaussian, Inc., Pittsburgh, Pennsylvania, 1993; (*b*) N. L. Allinger, mm3(92), QCPE, Bloomington, Indiana, 1992.
15 (*a*) G. Ujaque, A. C. Cooper, F. Maseras, O. Eisenstein and K. G. Caulton, *J. Am. Chem. Soc.*, 1998, **120**, 361; (*b*) F. Maseras and O. Eisenstein, *New. J. Chem.*, 1998, **22**, 5.

Received in Cambridge, UK, 30th July 1998; 8/05993D

Synthesis and characterization of a chelating 2-dimethylsilylpyridine complex of titanocene(III)

Leijun Hao,[a] Hee-Gweon Woo,[b] Anne-Marie Lebuis,[a] Edmond Samuel[c] and John F. Harrod*[a]

[a] *Department of Chemistry, McGill University, Montreal, Canada H3A 2K6. E-mail: harrod@omc.lan.mcgill.ca*
[b] *Department of Chemistry, Chonnam University, Kwangju 50-757, Korea*
[c] *Laboratoire de Chimie Organométallique de l'ENSCP (URA 403 CNRS), 11 rue P. et M. Curie, 75005 Paris, France*

The complex $Cp_2Ti[2\text{-}SiMe_2(C_5H_4N)]$ 1, the first example of a chelating silyl, and a tertiary silyl complex of Cp_2Ti(III), is prepared by reaction of $2\text{-}SiHMe_2(C_5H_4N)$ with Cp_2TiMe_2, and its X-ray structure, EPR spectrum and reactions with C_5H_5N and PMe_3 are reported.

Titanocene silyl complexes have been implicated as intermediates in a number of catalytic reactions of hydrosilanes.[1–3] Although several such complexes with primary, secondary and unsubstituted silyl ligands have been synthesised and characterised, they still remain quite rare.[4–8] To our knowledge, only two titanocene complexes with tertiary silyl ligands have been reported, both of which are titanocene(IV) compounds.[9,10] We report here the first example of a tertiary silyl titanocene(III) complex in which the silyl group is part of a chelating ligand.

Reaction of Cp_2TiMe_2 with 2-(dimethylhydrosilyl)pyridine (2.2 equiv.) in hexane resulted in a slow evolution of CH_4, identified by the characteristic rotational fine structure in its gas phase infrared spectrum, and a color change of the solution from orange to purple over a period of 2 to 3 days. Upon cooling to −20 °C for 24 h, deep purple crystals of **1** precipitated and were isolated in 63% yield. In solution ([$^2H_8$]toluene), **1** gave no discernible ^1H or ^{29}Si NMR resonances, as is often the case with strongly paramagnetic Ti(III) complexes. The EPR spectra of **1** (Fig. 1) in solution at both low (−20 °C) and room temperature exhibit a well resolved triplet at g = 1.9872 with a_N = 1.9 G, due to coupling of a single unpaired electron to the ^{14}N nucleus (I = 1) in the pyridine, and satellites due to hyperfine interactions with Ti nuclei [I = 7/2, ^{49}Ti (5.5%); I = 5/2, ^{47}Ti (7.75%)] with a_{Ti} = 8.8 G.

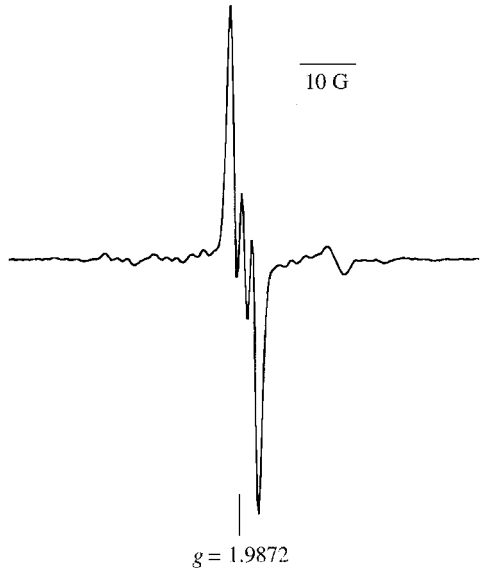

Fig. 1 EPR spectrum of **1** (−20 °C; toluene)

The single crystal X-ray structure of a molecule of **1** shows that this complex is mononuclear (Fig. 2).† The geometry about the titanium center is very similar to those found in the analogous non-chelating silyl(tertiaryphosphine) complexes with the exception of the very acute N–Ti–Si angle of 64.72(7)° compared to the P–Ti–Si angles [84.8(1) to 86.2(2)°] in the latter complexes.[4] The bonding parameters are close to those observed for other titanocene(III) silyl complexes.[4]

Solutions of **1** are air sensitive, but relatively stable at room temperature under inert atmosphere. They decompose slowly over a period of days to give an unidentified paramagnetic product (broad single EPR resonance; g = 1.9778). Such a signal is often observed in the decomposition products of titanocene(III) complexes.[1] The enhanced thermal stability of the chelating tertiary silylpyridine complex **1** is in sharp contrast to the analogous non-chelating silyl(tertiarylphosphine) complexes $Cp_2Ti(PMe_3)(SiHRR')$ (R = H or Ph, R′ = Ph) which are stable only for minutes at ambient temperature.[4,5] We attribute the unusual stability of **1** to the absence of the Si–H hydrogens for further dehydrocoupling reactions.[5]

The pyridine ligand in **1** is labile and can be replaced by other donor ligands as shown in eqn. (1). Solutions of **1** treated with excess PMe_3 in toluene give **2a** [eqn. (1)] identified by its characteristic EPR spectrum which displayed a simple doublet at g = 1.9936 with a_P = 29.3 G, a_{Ti} = 7.7 G (*cf.* ref. 4) and observed by a color change of the solution from purple to bright violet. This reaction is reversible. Removal of the solvent along with the volatile PMe_3 by pumping, followed by redissolution of the residue, gave the starting complex **1**. Similarly, reaction of **1** with excess pyridine gave the silyl(pyridine)titanocene complex **2b**.‡

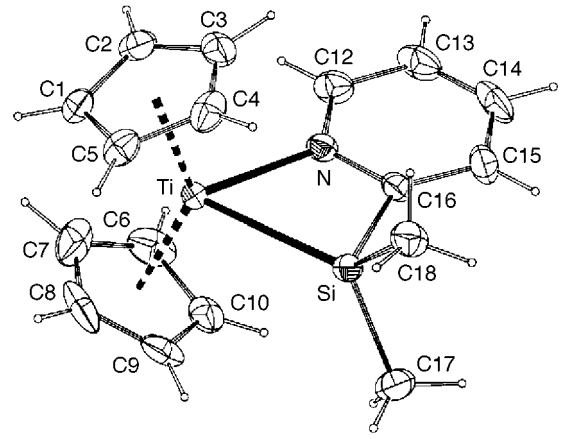

Fig. 2 A view of the structure of **1** (30% probability ellipsoids). Selected bond lengths (Å) and bond angles (°): Ti–N 2.229(2), Ti–Si 2.651(2), N–C(12) 1.340(4), N–C(16) 1.360(4), Si–C(16) 1.922(3), Si–C(17) 1.901(3); N–Ti–Si 64.72(7), Cp(cent)–Ti–Cp(cent) 137.2(1), Ti–N–C(16) 110.0(2), Ti–Si–C(16) 79.64(9), N–C(16)–Si 105.6(2).

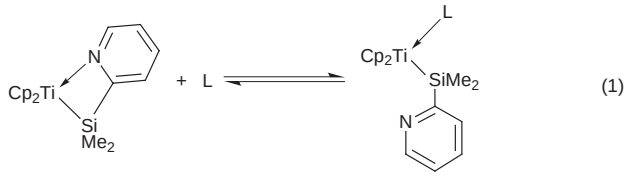

(1)

1 **2**

(**2a**, L = PMe_3; **2b**, L = pyridine)

We are continuing to explore the reactions with group 4 metallocenes by modifying the chelating ligand and preparing other novel group 14/15 chelating ligands.

Support for this work from NSERC Canada and the Fonds FCAR du Québec is gratefully acknowledged.

Notes and References

† *Crystal data* for **1**: $C_{17}H_{20}NSiTi$, M = 314.33, monoclinic, space group $P2_1/c$, a = 14.786(9), b = 7.814(3), c = 14.488(4) Å, β = 106.48(4)°, V = 1605(1) Å^3, Z = 4, D_c = 1.301 g cm^{-3}, F(000) = 660, μ = 5.130 mm^{-1}, crystal size: 0.49 × 0.36 × 0.05 mm. Data were collected at 220 K on an Enraf Nonius CAD4 diffractometer using Cu-Kα radiation (λ = 1.54056 Å) in the $\omega/2\theta$ scan mode. A total of 11485 reflections were measured in the range 3.11° < θ < 69.96° of which 2638 with $I > 2\sigma(I)$ were considered observed. The structure was solved by direct methods using SHELXS96 and refined by full-matrix least-squares on F^2 using SHELXL-96.[11] R = 0.0599 [for $I > 2\sigma(I)$] and $wR2$ = 0.1695 (for all data). CCDC 182/982.

Elemental analysis of **1**: Calc. for $C_{17}H_{20}NSiTi$: C: 64.97; H: 6.37; N: 4.46. Found C: 65.25; H: 7.08; N: 4.42%.

‡ EPR data for **2b** in toluene at 20 °C: g = 1.9878, a_{Ti} = 9.5 G, a_N = 2.0 G.

1 C. Aitken, J. F. Harrod and E. Samuel, *J. Am. Chem. Soc.*, 1986, **108**, 4059.
2 J. F. Harrod and S. S. Yun, *Organometallics*, 1987, **6**, 1381.
3 S. Xin, C. Aitken, J. F. Harrod, Y. Mu and E. Samuel, *Can. J. Chem.*, 1990, **68**, 471.
4 E. Samuel, Y. Mu, J. F. Harrod, Y. Dromzee and Y. Jeannin, *J. Am. Chem. Soc.*, 1990, **112**, 3435
5 H.-G. Woo, J. F. Harrod, J. Hénique and E. Samuel, *Organometallics*, 1993, **12**, 2883.
6 L. Hao, A.-M. Lebuis, J. F. Harrod and E. Samuel, *Chem. Commun.*, 1997, 2193.
7 L. Hao, A.-M. Lebuis and J. F. Harrod, *Chem. Commun.*, 1998, in press.
8 E. Spaltenstein, P. Palma, K. A. Kreutzer, C. A. Willoughby, W. M. Davis and S. L. Buchwald, *J. Am. Chem. Soc*., 1994, **116**, 10308.
9 L. Rösch, G. Altnau, J. Pickardt and N. Bruncks, *J. Organomet. Chem*., 1980, **197**, 51.
10 V. A. Igonin, Yu. E. Ovchinnikov, V. V. Dement'ev, V. E. Shklover, T. M. Timofeeva, T. M. Frunze and Yu. T. Struchkov, *J. Organomet. Chem*., 1989, **371**, 187.
11 G. M. Sheldrick, SHELXL-96, Program for Structure Analysis, University of Göttingen, Germany, 1996.

Received in Bloomington, IN, USA, 15th May 1998; revised manuscript received 27th July 1998; 8/06556J

2,6-Bis(2,4,6-triisopropylphenyl)phenyl as an extraordinarily bulky ligand in organometallic chemistry. Synthesis and molecular structure of $[(Mes^*_2C_6H_3)MCl_2]_2$ (M = Ga, In; Mes* = $C_6H_2Pr^i_3$-2,4,6)

Jianrui Su, Xiao-Wang Li and Gregory H. Robinson*

Department of Chemistry, The University of Georgia, Athens, GA 30602-2556, USA. E-mail: robinson@sunchem.chem.uga.edu

Gallium chloride or indium chloride interacts with 2,6-bis(2,4,6-triisopropylphenyl)phenyllithium, $(Mes^*_2C_6H_3)Li$ (Mes* = $C_6H_2Pr^i_3$-2,4,6), affording $[(Mes^*_2C_6H_3)MCl_2]_2$ (M = Ga 1, In 2), interesting group 13 organometallic crystalline dimers, characterized by elemental analyses, ^1H and ^{13}C NMR spectroscopy, and single-crystal X-ray diffraction.

The utilization of bulky ligands in organometallic chemistry is a proven means to compounds which may be particularly sensitive, reactive, or otherwise unstable. This practice has achieved great prominence in the organometallic chemistry of the heavier group 13 elements, particularly where aryl ligands are concerned. The simplest aryl derivatives, triphenylaluminium and triphenylgallium, have been known for decades while the bulkier trimesityl derivatives of aluminium[1] and gallium[2] were first reported in 1986. Herein we report the synthesis† and molecular structure‡ of gallium (**1**) and indium (**2**) derivatives of the very sterically demanding 2,6-bis(2,4,6-triisopropylphenyl)phenyl ligand, $Mes^*_2C_6H_3$ (Mes* = $C_6H_2Pr^i_3$-2,4,6),[3] $[(Mes^*_2C_6H_3)MCl_2]_2$, isolated from reaction of $(Mes^*_2C_6H_3)Li$ with the respective metal chloride [eqn. (1)].

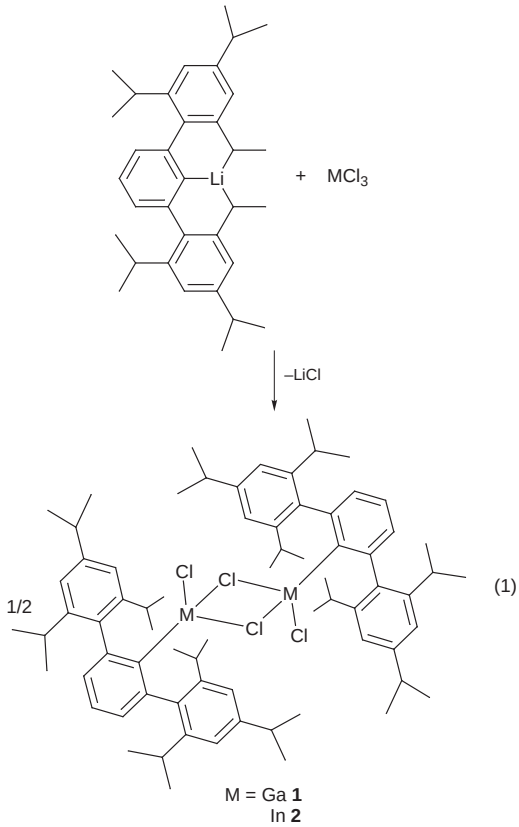

The title compounds, characterized by elemental analyses, ^1H and ^{13}C NMR spectroscopy and single-crystal X-ray diffraction, are noteworthy as they represent interesting organometallic group 13 halide derivatives of the sterically demanding 2,6-bis(2,4,6-triisopropylphenyl)phenyl ligand. The molecular structure of $[(Mes^*_2C_6H_3)MCl_2]_2$ (M = Ga **1**, In **2**) is shown in Fig. 1.

Sterically demanding arylgallium dihalides have been shown to play a critical role in the preparation of novel low-valent organometallic gallanes containing Ga–Ga bonds. For example, 2,6-dimesitylphenylgallium dichloride, upon alkali metal reduction, has been shown to afford Ga_3^{2-} three-membered dianionic metalloaromatic rings.[4–7] Conversely, the gallium dichloride of 2,6-bis(2,4,6-triisopropylphenyl)phenyl, $(Mes^*_2C_6H_3)_2GaCl_2$, prepared *in situ* and allowed to interact with sodium, has recently been shown by this laboratory to give an unprecedented gallium–gallium triple bond in $Na_2[Mes^*_2C_6H_3Ga{\equiv}GaC_6H_3Mes^*_2]$—the first gallyne, a dianionic organogallium congener of acetylene.[8,9] That adjusting the steric demands of an arylgallium halide may afford such interestingly

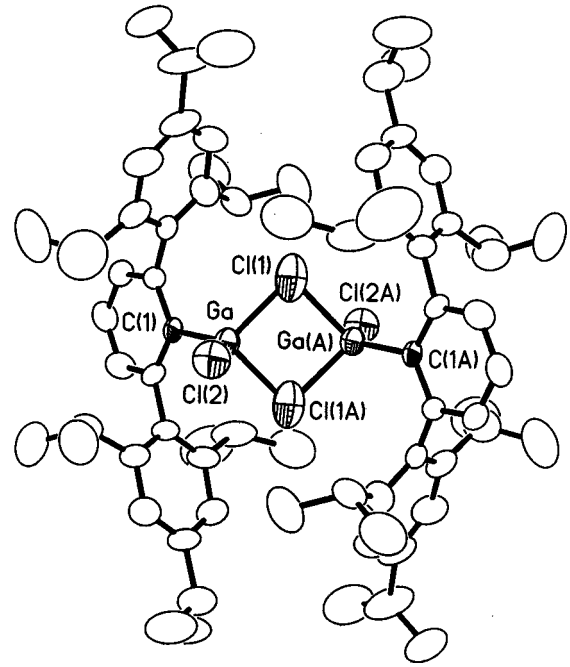

Fig. 1 Molecular structure of **1**. Selected bond distances (Å) and angles (°): for **1**: Ga–C(1) 1.949(8), Ga–Cl(1) 2.196(5), Ga–Cl(1A) 2.201(5), Ga–Cl(2) 2.230(3), Ga(A)–Cl(1) 2.201(5); C(1)–Ga–Cl(1) 112.3(3), C(1)–Ga–Cl(1A) 114.0(3), Cl(1)–Ga–Cl(1A) 90.3(2), C(1)–Ga–Cl(2) 127.3(3), Cl(1)–Ga–Cl(2) 104.0(2), Cl(1A)–Ga–Cl(2) 102.3(2), Ga–Cl(1)–Ga(A) 89.7(2). For **2** (the atom numbering scheme is the same as that for **1**): In–C(1) 2.129(5), In–Cl(1A) 2.233(4), In–Cl(1) 2.236(4). In(A)–Cl(1) 2.233(4); C(1)–In–Cl(1A) 115.3(2), C(1)–In–Cl(1) 114.0(2), Cl(1A)–In–Cl(1) 81.6(2), C(1)–In–Cl(2) 130.7(3), Cl(1A)–In–Cl(2) 103.2(2), Cl(1)–In–Cl(2) 100.7(2), In–Cl(1)–In(A) 98.4(2).

diverse products is sufficiently intriguing to warrant examination of the structural dynamics of this sterically demanding aryl with group 13 metal halides.

Compounds **1** and **2**, soluble in diethyl ether, hexane, and aromatics, assume isostructural dimeric structures possessing two μ_2-bridging chlorine atoms. The bridging chlorine atoms and the metal atoms constitute a planar four-membered M_2Cl_2 ring about a center of symmetry with the two aryl ligands and the two terminal chlorine atoms residing alternately above and below this ring. The environment about the metal centers may be described as distorted tetrahedral as the bond angles about gallium range from 90.3(2) to 127.3(3)°. Considering the steric bulk of the given ligand it is somewhat surprising that these complexes are not monomeric. The most convenient comparison relative to the title compounds concerns the respective 2,6-dimesitylphenyl derivatives. Although the structure of **1** compares with the bis[(dimesitylphenyl)gallium dichloride] derivative, $[(Mes_2C_6H_3)GaCl_2]_2$,[10] it is noteworthy that in **1** the $Ga–Cl_{bridging}$ bond distances [2.196(5) and 2.201(5) Å] are shorter than the $Ga–Cl_{terminal}$ bond distance [2.230(3) Å]. By contrast, for $[(Mes_2C_6H_3)GaCl_2]_2$, the $Ga–Cl_{bridging}$ bond distance [2.334(5) Å] is considerably longer than the $Ga–Cl_{terminal}$ distance [2.172(5) Å]. This trend is also observed for **2** wherein the $In–Cl_{bridging}$ distances [2.236(4) and 2.233(4) Å] are shorter than the $In–Cl_{terminal}$ bond distance [2.448(7) Å]. In $[(Mes_2C_6H_3)InCl_2]_2$[11] the situation is just the opposite with the $In–Cl_{bridging}$ bond distances [2.519(2) and 2.514(2) Å] being considerably longer than the $In–Cl_{terminal}$ bond distances [2.344(3) Å]. Thus, it is interesting to note that for both gallium and indium the bridging M–Cl bonds are shorter than the terminal M–Cl bonds where the sterically more demanding ligand is involved. Indeed, it is noteworthy that the bridging In–Cl distance in **2** of 2.233(4) Å appears to be the shortest In–Cl distance on record. Lastly, it is significant that **2** represents only the third example of a dimeric organoindium halide: $[(Mes_2C_6H_3)InCl_2]_2$ and $[Mes_2InCl]_2$[12] being the other two examples.

We are grateful to the National Science Foundation (G. H. R.: CHE 9520162) and to the donors of The Petroleum Research Fund, administered by the American Chemical Society, for support of this work.

Notes and References

† *Syntheses*: in a dry box a 100 ml flask was charged with $GaCl_3$ (0.88 g, 5 mmol) or $InCl_3$ (1.11 g, 5 mmol) and ether (30 ml). To this solution at −78 °C a diethyl ether solution (30 ml) of $(Mes^*_2C_6H_3)Li·OEt_2$ (2.81 g, 5 mmol) was added dropwise with vigorous stirring. The mixture was stirred for 3 h at this temperature and then allowed to warm slowly to room temp. After stirring for one day the solvent was removed from the mixture *in vacuo*. The residue was extracted with hexane (60 ml) and the white precipitate (LiCl) was separated by filtration. The volume of the colorless filtrate was reduced and placed in a freezer (−20 °C) for 2 days to give cubic colorless crystals. Both **1** and **2** crystallize with one unit of hexane in the unit cell. For **1**: 2.2 g, 65% yield; melting point, 256 °C; Anal. Calc. (found) for $C_{72}H_{98}Cl_4Ga_2$ (E + R Microanalytical Laboratories, Corona, NY): C, 69.50 (68.69); H, 7.90 (8.43%). ^{1}H NMR (300 MHz, 297 K, C_4D_8O), δ 0.89 [d, 12H, CH_3 (Pr^i)], 1.03 [d, 12H, CH_3 (Pr^i)], 1.09 [d, 12H, CH_3 (Pr^i)], 1.22 [d, 12H, CH_3(Pr^i)], 1.26 [d, 12H, CH_3 (Pr^i)], 1.42 [d, 12H, CH_3 (Pr^i)], 2.81 [m, 12H, CH(Pr^i)], 6.61–7.37 [m, 6H, CH (aromatic)], 6.94 [s, 4H, CH (aromatic)], 6.99 [s, 4H, CH (aromatic)]. ^{13}C NMR (300 MHz, 297 K, C_4D_8O), δ 27.67, 33.58, 33.98, 34.12, 37.85, 38.29 (Pr^i); 123.3, 123.9, 130.1, 131.2, 131.6, 150.2, 150.3, 151.7 (aromatic). For **2**: 2.66 g, 75% yield; melting point, 233 °C; Anal. Calc. (found) for $C_{72}H_{98}Cl_4In_2$: C, 64.80 (62.20); H, 7.40 (7.87%). ^{1}H NMR (300 MHz, 297 K, C_4D_8O), δ 0.90 [d, 12H, CH_3(Pr^i)], 1.04 [d, 12H, CH_3(Pr^i)], 1.09 [d, 12H, CH_3(Pr^i)], 1.22 [d, 12H, CH_3 (Pr^i)], 1.27 [d, 12H, CH_3(Pr^i)], 1.43 [d, 12H, CH_3(Pr^i)], 2.82 [m, 12H, CH(Pr^i)], 6.63–7.39 [m, 6H, CH (aromatic)], 6.96 [s, 4H, CH (aromatic)], 7.01 [s, 4H, CH (aromatic)]. ^{13}C NMR (300 MHz, 297 K, C_4D_8O), δ 28.15, 34.03, 34.46, 34.59, 38.31, 38.77 (Pr^i); 123.8, 124.4, 130.5, 131.8, 132.1, 150.6, 150.8, 152.3 (aromatic). The solvent present in the crystal lattice contributes to the less than ideal elemental analyses.

‡ *Molecular structures*: crystals were mounted in glass capillaries under an atmosphere of nitrogen and sealed. X-Ray intensity data were collected at 22 °C on a Siemens P4 diffractometer (Mo-Kα radiation; λ = 0.710 73 Å) using ω-scan technique to a maximum 2θ value of 45°. Both structures were solved by direct methods using the SHELXTL 5.0[13] system of programs. Non-hydrogen atoms were refined anisotropically while the hydrogen atoms were placed in ideal positions with their coordinates and thermal parameters riding on the attached carbon atoms. These two crystalline compounds are isostructural: monoclinic, space group $P2_1/c$ (no. 14). The asymmetric unit contains one half $[(Mes^*_2C_6H_3)MCl_2]_2$ (M = Ga, In) and one half hexane molecule situated on inversion centers, thereby generating the other half molecules.

Crystallographic data: $[(Mes^*_2C_6H_3)GaCl_2]_2$ **1**: a = 13.863(8), b = 15.775(9), c = 18.02(1) Å, β = 106.04(4)°, V = 3789(4) Å^3, Z = 2, R = 0.077, $wR2$ = 0.235 for 2613 [$I > 2\sigma(I)$]. $[(Mes^*_2C_6H_3)InCl_2]_2$, **2**: a = 14.273(3), b = 15.671(3), c = 18.048(3) Å, β = 106.45(1)°, V = 3872(1) Å^3, Z = 2, R = 0.039, $wR2$ = 0.122 for 3226 [$I > 2\sigma(I)$]. A slight disorder was observed for the terminal chlorine [Cl(2)] atom in **2**. CDCC 182/959.

1 J. J. Jerius, J. M. Hahn, A. F. M. M. Rahman, O. Mols, W. H. Isley and J. P. Oliver, *Organometallics*, 1986, **5**, 1812.
2 O. T. Beachley, Jr., M. R. Churchill, J. C. Pazik and J. W. Ziller, *Organometallics*, 1986, **5**, 1814.
3 B. Schiemenz and P. P. Power, *Organometallics*, 1996, **15**, 958.
4 X.-W. Li, W. T. Pennington and G. H. Robinson, *J. Am. Chem. Soc.*, 1995, **117**, 7578.
5 Y. Xie, P. R. Schreiner, H. F. Schaefer, III, X.-W. Li and G. H. Robinson, *J. Am. Chem. Soc.*, 1996, **118**, 10 635.
6 X.-W. Li, Y. Xie, P. R. Schreiner, K. D. Gripper, R. C. Crittendon, C. F. Campana, H. F. Schaefer, III and G. H. Robinson, *Organometallics*, 1996, **15**, 3798.
7 Y. Xie, P. R. Schreiner, H. F. Schaefer, III, X.-W. Li and G. H. Robinson, *Organometallics*, 1998, **17**, 114.
8 J. Su, X.-W. Li, R. C. Crittendon and G. H. Robinson, *J. Am. Chem. Soc.*, 1997, **119**, 5471.
9 Y. Xie, R. S. Grev, J. Gu, H. F. Schaefer, III, P. v. R. Schleyer, J. Su, X.-W. Li and G. H. Robinson, *J. Am. Chem. Soc.*, 1998, **120**, 3773.
10 R. C. Crittendon, X.-W. Li, J. Su and G. H. Robinson, *Organometallics*, 1997, **16**, 2443.
11 G. H. Robinson, X.-W. Li and W. T. Pennington, *J. Organomet. Chem.*, 1995, **501**, 399.
12 J. T. Leman and A. R. Barron, *Orgnometallics*, 1989, **8**, 2214.
13 G. M. Sheldrick, SHELXTL 5.0, Crystallographic Computing System, Siemens Analytical X-Ray Instruments, Madison, WI, 1995.

Received in Columbia, MO, USA, 22nd January 1998; Revised manuscript received 20th July 1998; 8/05875J

Stabilisation of duplex DNA by 7-halogenated 8-aza-7-deazaguanines

Frank Seela*† and Georg Becher

Laboratorium für Organische und Bioorganische Chemie, Institut für Chemie, Universität Osnabrück, Barbarastr.7, D-49069 Osnabrück, Germany

Oligonucleotides containing 7-halogenated 8-aza-7-deaza-2′-deoxyguanosine ($c^7z^8G_d$) derivatives such as d($Br^7c^7z^8$ G-C)$_4$ 8 (T_m = 88 °C) and d($I^7c^7z^8$ G-C)$_4$ 9 (T_m = 84 °C) are significantly more stable than d(G-C)$_4$ 5 (T_m = 59 °C).

The introduction of 7-halogenated 7-deazapurines (pyrrolo-[2,3-*d*]pyrimidines **A**) into oligonucleotides reveals that these residues are well accommodated in the major groove of the duplex DNA. Furthermore, this modified DNA is stabilised and the particular DNA structure is retained.[1,2] Consequently, the 7 position of 7-deazapurines is an ideal site for the introduction of functional residues into the DNA which can serve later as reporter groups, cleaving agents or residues useful in sequencing by mass spectrometry or by atomic force microscopy.[3] In the series of modified nucleobases related to purines, the 8-aza-7-deazapurines (pyrazolo[3,4-*d*]pyrimidines **B**) depict another heterocyclic system which can be derivatised at the same position while retaining the Watson–Crick recognition site of a purine base (**C**), but not showing the unfavourable properties of 8-substituted purine residues.[4]

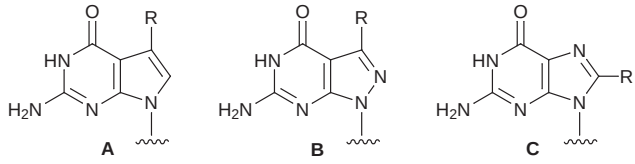

Regular pyrazolo[3,4-*d*]pyrimidine nucleosides have already been incorporated into oligonucleotides.[5–7] Also, the monomeric 7-bromo and 7-iodo derivatives of 8-aza-7-deaza-2′-deoxyguanosines (**1a**,**b**) have been synthesised.[8] As we wanted to prove whether compounds **1a**,**b** show the same favourable properties as the corresponding 7-deazapurines, building blocks for oligonucleotide solid-phase synthesis were prepared. For this purpose the isobutyryl residue was introduced as an amino protecting group yielding the protected nucleosides **2a** (64%) and **2b** (66%) (Scheme 1). The protecting group stability was determined UV spectrophotometrically at 300 nm in conc. NH_3 at 40 °C. The half-lives of 7-bromo-8-aza-7-deaza-2′-deoxyguanosine **2a** ($Br^7c^7z^8G_d$; 38 min) and 7-iodo-8-aza-7-deaza-2′-deoxyguanosine **2b** ($I^7c^7z^8G_d$;41 min) were similar to that of the parent 8-aza-7-deaza-2′-deoxyguanosine ($c^7z^8G_d$; 37 min).[7] Subsequently, 4,4′-dimethoxytrityl (DMT) groups were introduced under standard conditions furnishing the 5′-protected compounds **3a** and **3b** (74 and 71% yield), respectively. They were then converted into the phosphoramidites **4a** and **4b** (80 and 76%). All monomeric compounds were characterised by ^{1}H, ^{13}C and ^{31}P NMR spectra as well as by elemental analyses.[9]

Next, the self-complementary hexanucleotides d($Br^7c^7z^8$G-C)$_3$ **13** and d($I^7c^7z^8$G-C)$_3$ **14** as well as the octamers d($Br^7c^7z^8$G-C)$_4$ **8** and d($I^7c^7z^8$G-C)$_4$ **9** were prepared using the building blocks **4a**,**b**. The oligonucleotides were removed from the solid support (conc. aq. NH_3), deprotected and purified on OPC cartridges.[10] Their purity was proven by ion-exchange chromatography on a 4 × 50 mm NucleoPac PA-100 column (DIONEX), and MALDI-TOF mass spectra[11] were obtained. Their base composition was confirmed by enzymatic hydrolysis. Furthermore, their thermodynamic stability was determined by temperature dependent UV–melting profiles. Table 1 summarises T_m values as well as thermodynamic data (MeltWin[12]) of the duplex formation of the self-complementary oligonucleotides **5**, **7**–**9** and **12**–**14** as well as of the corresponding oligomers containing 7-deazaguanine (c^7G_d) (**6**, **10** and **11**).[2]

According to Table 1 it is apparent that the 8-aza-7-deazaguanine moiety which has no 7-substituent stabilises the oligonucleotide duplex [d(c^7z^8G-C)$_4$] **7** (T_m = 72 °C) compared to the parent 2′-deoxyguanosine [d(G-C)$_4$] **5** (T_m = 59 °C, ΔT_m = 13 °C), while the 7-deaza-2′-deoxyguanosine in [d(c^7G-C)$_4$] **6** shows a destabilisation (T_m = 53 °C, ΔT_m = −6 °C).[2] These findings are in agreement with earlier observations made on other oligonucleotides as well as on polynucleotides.[13–15] The octanucleotides with halogenated 8-aza-7-deazaguanine residues [d($Br^7c^7z^8$G-C)$_4$] **8** (T_m = 88 °C) and [d($I^7c^7z^8$G-C)$_4$] **9** (T_m = 84 °C) show considerable duplex stabilisation. The stability of these duplexes was even higher than those of the related oligomers with the 7-halogenated 7-deazaguanine residues (**10** and **11**). Due to the high T_m values of **8** and **9** it was not possible to obtain a complete melting profile, which is necessary to determine the thermodynamic data. Therefore, a set of hexanucleotides was measured showing *ca*. 15 °C lower T_m values. Again, the iodo compound **14**

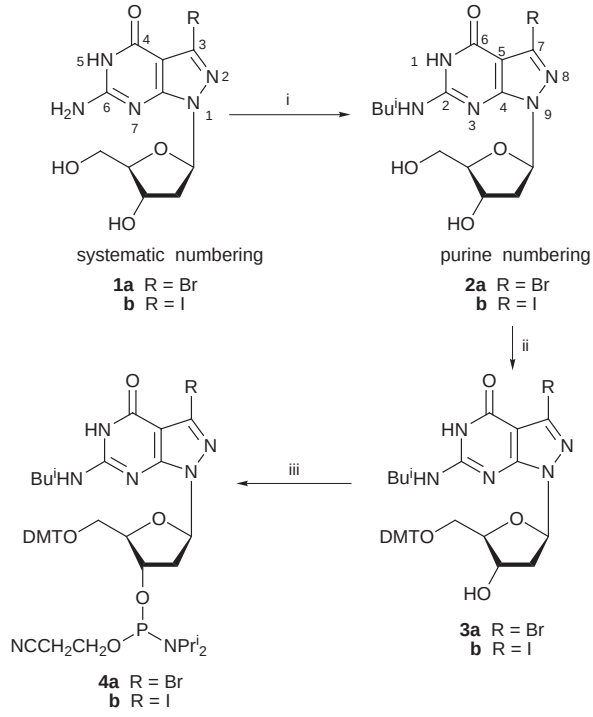

Scheme 1 *Reagents and conditions*: i, HMDS, Bu^i_2O, DMF, room temp., 13 h, 64% (**2a**), 66% (**2b**); ii, DMTCl, py, room temp., 4 h, 74% (**3a**), 71% (**3b**); iii, (Pr^i_2N)($NCCH_2CH_2O$)PCl, THF, room temp., 30 min, 80% (**4a**), 76% (**4b**)

Table 1 T_m values and thermodynamic data of duplex formation of oligonucleotides[a,b]

Compound	T_m/°C	ΔH/kcal mol^{-1}	ΔS/cal K^{-1} mol^{-1}	ΔG_{298}/kcal mol^{-1}
d(G-C)$_4$·d(G-C)$_4$ **5·5**	59	−67	−179	−11.9
d(c^{7}G-C)$_4$·d(c^{7}G-C)$_4$ **6·6**	53	−65	−178	−10.2
d(c^{7}z^{8}G-C)$_4$·d(c^{7}z^{8}G-C)$_4$ **7·7**	72	−74	−193	−14.5
d(Br^{7}c^{7}z^{8}GC)$_4$·d(Br^{7}c^{7}z^{8}GC)$_4$ **8·8**	88	[c]	[c]	[c]
d(I^{7}c^{7}z^{8}G-C)$_4$·d(I^{7}c^{7}z^{8}G-C)$_4$ **9·9**	84	[c]	[c]	[c]
d(Br^{7}c^{7}G-C)$_4$·d(Br^{7}c^{7}G-C)$_4$ **10·10**	67	−71	−188	−13.0
d(I^{7}c^{7}G-C)$_4$·d(I^{7}c^{7}G-C)$_4$ **11·11**	67	−66	−171	−12.6
d(G-C)$_3$·d(G-C)$_3$ **12·12**	47	−55	−150	−8.4
d(Br^{7}c^{7}z^{8}G-C)$_3$·d(Br^{7}c^{7}z^{8}G-C)$_3$**13·13**	73	−70	−181	−14.3
d(I^{7}c^{7}z^{8}G-C)$_3$·d(I^{7}c^{7}z^{8}G-C)$_3$ **14·14**	71	−63	−162	−12.9

[a] Oligonucleotide conc. is 10 μM. [b] Measured in 10 mM Na cacodylate, 10 mM $MgCl_2$, 0.1 M NaCl. [c] Not measurable.

exhibits a somewhat lower T_m value than the bromo derivative **13** (Table 1). When comparing the thermodynamic data of the duplexes **13·13** and **14·14** with the unmodified duplex **12·12** it is apparent that a more favourable enthalpy term leads to duplex stabilisation. This effect was much more pronounced in the series of oligonucleotides containing 7-halogenated 8-aza-7-deazaguanine than in those containing halogenated 7-deazaguanine.

From the chromatographic behaviour of the 7-halogenated nucleosides **1a**,**b** on RP-18 HPLC (Fig. 1) as well as of the corresponding oligonucleotides **8**, **9**, **13** and **14** it is apparent that the halogen substituents make the compounds more hydrophobic. Thus, the major grooves of such DNA duplexes become hydrophobic and water molecules, normally being present in these grooves, are expelled. This can influence both the enthalpy and the entropy of duplex formation. However, enthalpic changes play the major role.

Another difference which is observed for the 7-halogenated 8-aza-7-deazaguanine nucleosides compared to the non-halogenated compounds is the change of the pK values of deprotonation (7-deaza-8-aza-2′-deoxyguanosine = 9.3; compounds **1a**,**b** = 9.0). This effect also increases the N-glycosylic bond stability[8] and is most likely explained by the electron-withdrawing effect caused by the 7-substituents. As a result, the hydrogen bonds within the G-C base-pair are strengthened and the duplex becomes stabilised. It was also shown that the triphosphates of 8-aza-7-deazaguanine nucleosides are efficiently incorporated into DNA using DNA polymerases;[16] they are useful for introducing reporter groups into a sterically unproblematic position of the DNA molecule.

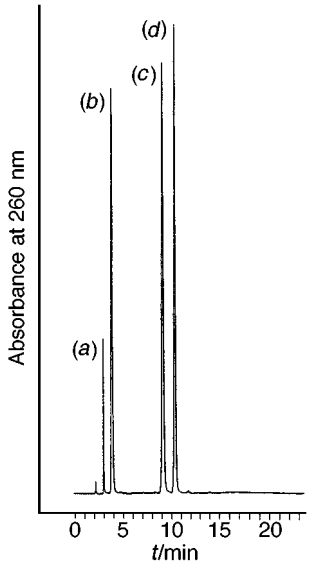

Fig. 1 HPLC profile of (*a*) 6-amino-1*H*-pyrazolo[3,4-*d*]pyrimidin-4(5*H*)-one, (*b*) 8-aza-7-deaza-2′-deoxyguanosine, (*c*) **1a** and (*d*) **1b** on a RP-18 (200 × 10 mm) column. The following solvent systems were used: 0.1 M (Et_3NH)OAc (pH 7.0)–MeCN (95:5) (A) and MeCN (B). They were used according to the following profile: 20 min 5–20% B in A, 35 min 20–50% B in A, 35 min 5% B in A.

We thank Dr N. Ramzaeva for helpful discussions. Financial support by the Bundesministerium für Bildung, Forschung und Technologie (BMBF) is gratefully acknowledged.

Notes and References

† E-mail: Fraseela@rz.uni-Osnabrueck.de

1 F. Seela and H. Thomas, *Helv. Chim., Acta*, 1995, **78**, 94.
2 N. Ramzaeva and F. Seela, *Helv. Chim. Acta*, 1996, **79**, 1549.
3 C. W. Siegert, A. Jacob and H. Köster, *Anal. Biochem.*, 1996, **243**, 55.
4 S. N. Rao and P. A. Koliman, *J. Am. Chem. Soc.*, 1986, **108**, 3048.
5 F. Seela, N. Ramzaeva and M. Zulauf, *Nucleosides Nucleotides*, 1997, **16**, 963.
6 C. R. Petrie, A. D. Adams, M. Stamm, J. Van Ness, S. M. Watanabe and R. B. Meyer, *Bioconjugate Chem.*, 1991, **2**, 441.
7 F. Seela and H. Driller, *Helv. Chim. Acta*, 1988, **71**, 1191.
8 F. Seela and G. Becher, *Synthesis*, 1998, 207.
9 *Selected data* for **3a**: δ_H([$^2H_6$]DMSO) 1.03 [d, *J* 6.7, $(CH_3)_2$], 2.25 [m, H_β-C(2′)], 2.75 [m, H_α-C(2′)], 3.05 [m, H_2-C(5′)], 3.70 (s, 2 CH_3O), 3.95 [m, H-C(4′)], 4.44 [m, H-C(3′)], 5.30 [d, *J* 4.5, HO-C(3′)], 6.37 [t, *J* 6.5, H-C(1′)], 6.77–7.16 (2m, 13 arom. H), 11.86 (s, NH), 11.97 (s, NH). For **4a**: δ_P($CDCl_3$) 148.4, 148.5. For **3b**: δ_H([$^2H_6$]DMSO) 1.12 [d, *J* 6.7, $(CH_3)_2$], 2.25 [m, H_β-C(2′)], 2.77 [m, H_α-C(2′)], 3.03 [m, H_2-C(5′)], 3.70 (s, 2 CH_3O), 3.92 [m, H-C(4′)], 4.44 [m, H- C(3′)], 5.29 [d, *J* 4.2, HO-C(3′)], 6.37 [t, *J* 5.5, H-C(1′)], 6.76–7.33 (2m, 13 arom. H), 11.83 (s, NH), 11.92 (s, NH). For **4b**: δ_P($CDCl_3$) 148.4, 148.5.
10 Oligonucleotide Purification Cartridges, Applied Biosystems, Weiterstadt, Germany.
11 *Selected data* for d(c^{7}z^{8}GC)$_4$ **7**: Calc.: 2412. Found (M^+): 2412. For d(Br^{7}c^{7}z^{8}GC)$_4$ **8**: Calc.: 2727. Found (M^+): 2728. For d(I^{7}c^{7}z^{8}GC)$_4$ **9**: Calc. 2918. Found (M^+) 2915.
12 J. A. McDowell and D. H. Turner, *Biochemistry*, 1996, **35**, 14 077.
13 F. Seela and H. Driller, *Nucleic Acids Res.*, 1989, **17**, 901.
14 F. Seela and S. Lampe, *Helv. Chim. Acta*, 1994, **77**, 1003.
15 L. J. P. Latimer and J. S. Lee, *J. Biol. Chem.*, 1991, **266**, 13 849.
16 K. Mersmann and F. Seela, unpublished results.

Received in Glasgow, UK, 10th June 1998; 8/04414G

Chameleon catches in combinatorial chemistry: Tebbe olefination of polymer supported esters and the synthesis of amines, cyclohexanones, enones, methyl ketones and thiazoles

Christopher P. Ball,[a] Anthony G. M. Barrett,*[a]† Alain Commerçon,*[b] Delphine Compère,[a] Cyrille Kuhn,[a] Richard S. Roberts,[a] Marie L. Smith*[a] and Olivier Venier[a]

[a] *Department of Chemistry, Imperial College of Science, Technology and Medicine, London, UK SW7 2AY*
[b] *New Lead Generation, Rhône-Poulenc Rorer, Vitry, France*

Tebbe olefination of supported esters $R^1CO_2CH_2$–polymer gave the corresponding vinyl ethers $R^1C(=CH_2)OCH_2$–polymer which were released, under acidic conditions, to produce methyl ketones R^1COMe; by reductive amination, to produce amines $R^1CH(Me)NHR^2$; by bromination and reaction of $R^1CBr(CH_2Br)OCH_2$-polymer with thioureas to produce thiazoles; or, for supported dienyl ethers derived from α,β-unsaturated esters, by Diels–Alder reaction and acid mediated cleavage to produce cyclohexanone derivatives.

Solid phase synthesis is invaluable for the construction of libraries of small organic compounds for biological evaluation.[1] Such bioassay is frequently carried out in solution using an appropriate enzyme or receptor. The method of attachment and detachment of the requisite substrates to the resin is critical. In many solid phase syntheses, the substrates are conveniently attached to the polymer support through a carboxylic acid function. This is readily achieved using supports including Merrifield, Wang and Tentagel resins *etc*.[2] Following substrate modification, cleavage affords a carboxylic acid, ester, amide or, *via* reductive cleavage, a primary alcohol. Methods that allow for the cleavage of resin bound carboxylate derivatives yet which access alternative and variable functionality would be extremely desirable. Herein we report the conversion of supported esters into enol ethers,[3] with subsequent on-resin functionalisation and detachment with amplification of diversity.

Methylenation of the resin bound esters **1**‡ with the Tebbe reagent[4] **12** (PhMe–THF 25 °C, 12 h) gave the corresponding vinyl ethers **2** (Scheme 1). The reaction mixtures were quenched with 15% aq. NaOH and the resin washed consecutively with THF, H_2O, EtOAc, EtOAc–MeOH (1:1) and MeOH followed by removal of solvent *in vacuo*. In this reaction, commercial Tebbe reagent (Aldrich) proved to be superior to either **12** generated *in situ*,[5] where premature cleavage from the support was a problem, or the Petasis reagent (Cp_2TiMe_2).[6] Hydrolysis (1 M H_2SO_4 in DMF or 1% TFA in CH_2Cl_2) of ethers **2** brought about cleavage from the resin and gave the corresponding ketones **3**§ (41–92%). Alternatively, acid mediated hydrolysis and reductive amination[7] using amine **13** and $NaBH(OAc)_3$ gave the corresponding amines **4**¶ (13–89%).

The ethers **2** were found to be useful intermediates for further transformations prior to detachment from the resin. Thiazoles, important pharmacophores with diverse biological activities,[8] are available from α-bromo ketones *via* the Hantzsch thiazole synthesis. Thus reaction of the vinyl ether **2** (R = Bn) with Br_2 (1 M in CH_2Cl_2, 2 equiv., 1 h) and washing (CH_2Cl_2) gave the corresponding supported dibromide **5** as indicated by the disappearance of the enol ether (IR), gel phase magic angle spinning ^1H NMR [400 MHz; $CDCl_3$: δ 4.25(CH_2Br)] and elemental analysis (loading 0.65 mmol g^{-1}). Reaction of the dibromide **5** (R = Bn) with thiourea (4 equiv., MeOH at reflux, 12 h), neutralisation (K_2CO_3), filtration with MeOH and evaporation gave thiazole **6** (R = Bn) contaminated with excess thiourea. This impurity was removed by reverse phase HPLC or, more simply, using the polymer supported α-bromo ketone scavenger **14**[9] (200–400 mesh, 0.96 mequiv.g^{-1}, 2 equiv.). Using either of these purification methods, thiazole **6** (R = Bn) was obtained in 40% yield based on the loading of the Merrifield resin (1.0 mmol g^{-1}) to which the phenylacetic acid had been attached. This methodology, which has been extended to a range of thiazoles **6**,‖ has the major advantage of starting from readily available carboxylic acids rather than less diverse commercial α-bromo ketones.

Tebbe methylenation of the resin bound α,β-unsaturated esters **7**[10]‡ (ν_{max}/cm^{-1} 1720–1740) gave the corresponding supported dienyl ethers **8** (1635–1650 cm^{-1}) which could be either hydrolysed (1% TFA in $CDCl_3$) to provide the enones **9**** or converted into the Diels–Alder adducts **10**. The diene

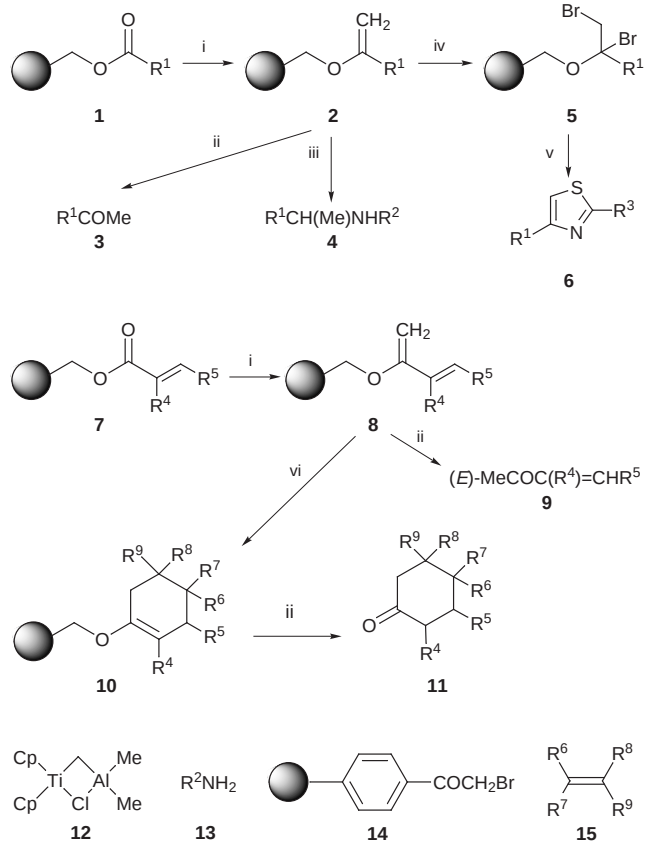

Scheme 1 *Reagents and conditions*: i, **12**, PhMe, THF, 25 °C; ii, 1% TFA, CH_2Cl_2, 25 °C; iii, 1 M H_2SO_4, DMF, then **13**, $NaBH(OAc)_3$, 25 °C; iv, Br_2, CH_2Cl_2 (1 M, 2 equiv.), 25 °C; v, R^3CSNH_2 (4 equiv.), MeOH, reflux, then **14** (2 equiv.), MeOH, reflux; vi, **15**, PhMe, 25 °C (maleimide) or 80–100 °C (other dienophiles)

resins **8** may be stored for up to six months without loss of activity but were generally used directly. Diels–Alder reaction with *N*-methylmaleimide (PhMe, 25 °C) or 2-chloroacrylonitrile, methyl vinyl ketone, dimethyl fumarate or 2-ethylacrolein (PhMe, 80–100 °C) gave the immobilised cyclohexene derivatives **10**. Subsequent cleavage from the resin (1% TFA in CH_2Cl_2) gave the corresponding cyclohexanone derivatives **11**.†† We observed high *endo*-selectivity with *N*-methylmaleimide consistent with the solution phase reactions of 2-silyloxy dienes with maleimides[11] and in contrast with Diels–Alder reactions of resin bound 4-substituted 2-aminobutadienes.[12]

In summary, we have developed a novel detachment method for the removal of substrates from a solid support which allows for the concomitant introduction of further diversity. This strategy using chameleon‡‡ catches should be applicable to the generation of diverse libraries from polymer supported carboxylic esters. Further reactions of the supported enol ethers will be reported in due course.

We thank Rhône-Poulenc Rorer for the most generous support of our programmes on parallel and combinatorial syntheses under the auspices of the TeknoMed project. In addition we thank GlaxoWellcome Research Ltd. for their endowment (to A. G. M. B.), the Royal Society for a Dorothy Hodgkin fellowship (to M. L. S) and the Wolfson Foundation for establishing the Wolfson Centre for Organic Chemistry in Medical Science at Imperial College.

Notes and References

† E-mail: m.stow@ic.ac.uk

‡ The supported esters **1** and **7** were prepared from Merrifield resin (200–400 mesh, 1.0–1.7 mequiv. g^{-1}) (Cs_2CO_3, KI, DMF, 80 °C) [the Tebbe olefination chemistry in this paper has also been carried out on Wang resin (200–400 mesh, 0.7–1.13 mequiv. g^{-1})]. For an alternative synthesis of supported α,β-unsaturated esters see ref. 12. All syntheses in this paper were carried out both manually, using single bead FT-IR spectroscopy to follow reactions (**1** 1720–1740, **2** 1635–1645, **7** 1720–1740, **8** 1635–1650 cm^{-1}) and in a parallel fashion on a Nautilus™ 2400 Organic Synthesizer (Argonaut Technologies, Inc.). All the products were at least 90% pure (HPLC, GC–MS). All yields were determined with respect to the original loading of chloride for Merrifield resin.

§ The ketones **3** [R^1 (%)] were isolated by filtration and evaporation: $Me(CH_2)_6$ (87%); Ph (62%); 4-BrC_6H_4 (41%); 4-IC_6H_4 (71%); 4-$MeOC_6H_4$ (92%); 3-$MeOC_6H_4$ (56%); 2,4,6-$(MeO)_3C_6H_2$ (47%); 4-$MeOC_6H_4CH_2$ (74%); 4-PhC_6H_4 (65%) and 3-indolyl–CH_2CH_2 (74%).

¶ The amines **4** [R^1, R^2 (%)] were isolated by filtration, partition between Et_2O and 1 M NaOH, drying ($MgSO_4$) and evaporation: $Me(CH_2)_6$, Pr (13%); $Me(CH_2)_6$, cyclopropyl (19%); $Me(CH_2)_6$, allyl (27%); 4-$MeOC_6H_4CH_2$, Pr (89%); 4-$MeOC_6H_4CH_2$, cyclopropyl (85%); 4-$MeOC_6H_4CH_2$, allyl (89%); 3-indolyl–CH_2CH_2, Pr (65%); 3-indolyl–CH_2CH_2, cyclopropyl (61%); 3-indolyl–CH_2CH_2, allyl (79%).

‖ The thiazoles **6** [R^1, R^3 (%)] were isolated following purification using scavenger **14**: Ph, NH_2 (40%); Ph, NHMe (15%); Ph, NHBn (10%); Ph, Me (14%); 3-$MeOC_6H_4$, NH_2 (23%); 3-$MeOC_6H_4$, NHMe (15%); 3-$MeOC_6H_4$, NHBn (13%); $Me(CH_2)_6$, NH_2 (15%); $Me(CH_2)_6$, NHMe (10%); $Me(CH_2)_6$, NHBn (12%).

** The enones **9** [R^4, R^5 (%)] were quantified by cleavage (1% TFA in $CDCl_3$) and ^1H NMR with a $(Me_3Si)_2O$ reference: H, Ph (50%); H, Me (28%); H, Et (31%); H, Pr (33%); H, $Me(CH_2)_6$ (48%); $(CH_2)_4$ (53%).

†† The cyclohexanones **11** [R^4, R^5, dienophile, (%, diastereoselectivity)] were quantified by cleavage (1% TFA in $CDCl_3$) and ^1H NMR with a $(Me_3Si)_2O$ reference: H, Ph, *N*-methylmaleimide (30%, 97:3); H, Me, *N*-methylmaleimide (30%, 97:3); H, Et, *N*-methylmaleimide (18%, 97:3); H, Pr, *N*-methylmaleimide (27%, 97:3); H, $Me(CH_2)_6$, *N*-methylmaleimide (35%, 7:3); $(CH_2)_4$, *N*-methylmaleimide (51%, 97:3); H, Ph, (*E*)-$MeO_2CCH{=}CHCO_2Me$ (17%, 1:1); H, Ph, $H_2C{=}CClCN$ (23%, 7:3); H, Ph, $H_2C{=}CEtCHO$ (21%, 5:3); H, Ph, $H_2C{=}CHAc$ (44%, 7:3); H, Me, $H_2C{=}CHAc$ (11%, 5:3); H, $Me(CH_2)_6$, $H_2C{=}CEtCHO$ (19%, 3:1); H, $Me(CH_2)_6$, $H_2C{=}CEtAc$ (22%, 4:1); $(CH_2)_4$, $H_2C{=}CEtCHO$ (20%, 2:2:1:1); $(CH_2)_4$, $H_2C{=}CHAc$ (43%, 3:2).

‡‡ For other chameleons see refs. 13 and 14. Petasis has mentioned the possibility of the olefination of polymer supported peptides using Cp_2TiMe_2 but has yet to report any details: *Fifth Chemical Congress of North America*, Cancun, Mexico, November 13, 1997.

1 For examples see: P. H. H. Hermkens, H. C. J. Ottenheijm and D. C. Rees, *Tetrahedron*, 1997, **53**, 5643; S. H. D. J. Gravert and K. D. Janda, *Chem. Rev.*, 1997, **97**, 489; L. A. Thompson and J. A. Ellman, *Chem. Rev.*, 1996, **96**, 555.
2 J.-P. Montheard, M. Chatzopoulos and M. Camps, *J. Macromol. Sci., Rev. Macromol. Chem. Phys.*, 1988, **C28**, 503; V. Krchnak, D. Cabel, A. Weichsel and Z. Flegelova, *Lett. Pept. Sci.*, 1995, **1**, 27; M. Bodanszky and D. T. Fagan, *Int. J. Pept. Protein Res.*, 1977, **10**, 375.
3 F. Effenberger, *Angew. Chem., Int. Ed. Engl.*, 1969, **8**, 295.
4 S. H. Pine, R. Zahler, D. A. Evans and R. H. Grubbs, *J. Am. Chem. Soc.*, 1980, **102**, 3270.
5 L. F. Cannizzo and R. H. Grubbs, *J. Org. Chem.*, 1985, **50**, 2386.
6 N. Petasis and E. I. Bzowej, *J. Am. Chem. Soc.*, 1990, **112**, 6392.
7 A. F. Abdel-Magid, K. G. Carson, B. D. Harris, C. A. Maryanoff and R. D. Shah, *J. Org. Chem.*, 1996, **61**, 3849; C. G. Boojamra, K. M. Burow and J. A. Ellman, *J. Org. Chem.*, 1995, **60**, 5742.
8 P. C. Kearney, M. Fernandez and J. A. Flygare, *J. Org. Chem.*, 1998, **63**, 196 and references cited therein.
9 S. Kobayashi and M. Moriwaki, *Tetrahedron Lett.*, 1997, **38**, 4251.
10 C. R. Johnson and B. Zhang, *Tetrahedron Lett.*, 1995, **36**, 9253; P. Wipf and T. C. Henninger, *J. Org. Chem.*, 1997, **62**, 1586.
11 M. Adeva, E. Caballero, F. Garcia, M. Medarde, H. Sahagun and F. Tome, *Tetrahedron Lett.*, 1997, **38**, 6893.
12 M. Crawshaw, N. W. Hird, K. Irie and K. Nagai, *Tetrahedron Lett.*, 1997, **38**, 7115.
13 G. H. Posner, T. D. Nelson, C. M. Kinter and K. Afarinkia, *Tetrahedron Lett.*, 1991, **32**, 5295; B. M. Trost and G. K. Mikhail, *J. Am. Chem. Soc.*, 1987, **109**, 4124; E. Schaumann, and A. Kirschning, *Tetrahedron Lett.*, 1988, **29**, 4281; D. H. R. Barton, L. Bohe and X. Lusinchi, *Tetrahedron Lett.*, 1987, **28**, 6609; A. Padwa, W. Dent and P. E. Yeske, *J. Org. Chem.*, 1987, **52**, 3944; A. G. M. Barrett, *Chimica*, 1982, **36**, 248.
14 M. R. Gowravaram and M. A. Gallop, *Tetrahedron Lett.*, 1997, **38**, 6973.

Received in Liverpool, UK, 26th March 1998; revised manuscript received, 27th July 1998; 8/05874A

A tailor-made hexagonal system in a molecular conductor

Tatsuro Imakubo,*[a] Takahisa Maruyama,[a] Hiroshi Sawa[b] and Keiji Kobayashi*[a]

[a] *Department of Chemistry, Graduate School of Arts and Sciences, The University of Tokyo, Komaba, Meguro-ku, Tokyo 153-8902, Japan. E-mail: cimax@komaba.ecc.u-tokyo.ac.jp*
[b] *Department of Physics, Faculty of Science, Chiba University, Yayoi, Inage-ku, Chiba 263-8522, Japan*

A unique hexagonal system based on an organic π-donor has been tailored by the *strong* and *directional* I···N intermolecular interaction, and its highly symmetrical structure including two types of channels and high conductivity are reported.

The development of highly symmetrical systems is always of interest in materials science as in the cases of molecular conductors based on fullerenes,[1,2] and the introduction of a characteristic intermolecular interaction is necessary to construct a unique molecular-based crystal system. One of the major techniques for controlling solid-state molecular assemblies is the use of the hydrogen bond,[3] however, it is not always enough to fix the direction of the interaction. Recently, we have found that the *strong* and *directional* I···X (X = CN, S or halogen atoms) type cation···anion interaction is useful to control the molecular arrangement of organic conductors.[4] An example of the above I···N interaction is the impressive one-dimensional chain structure in the crystal of *p*-iodobenzonitrile.[5] In the course of our study to extend and generalize the new I···N architecture for molecular-based materials, we have designed diiodo(pyrazino)diselenadithiafulvalene (DIPS, **1**; Scheme 1) which contains two interaction sites, the iodine atom and the nitrogen atom on the edges of the skeleton. Here we report the synthesis, structure and physical properties of a unique hexagonal system with high conductivity and two types of channels tailored by the strong and directional I···N intermolecular interactions.

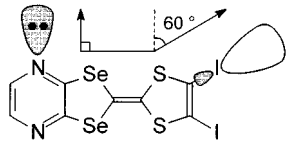

1

Scheme 1 Schematic view of molecular structure of a new iodine-bonded π-donor **1** and directions of lone pair on the pyrazine ring and σp LUMO on the C–I bond (see text)

Synthesis of **1**† was achieved by the cross-coupling reaction of 4,5-diiodo-1,3-dithiole-2-one[6] and pyrazine-fused 1,3-diselenole-2-one.[7] Long rod-like single crystals (average size 1 mm long, 0.1 mm diameter) of $(\mathbf{1})_3(PF_6)(solv.)_x$ [solv. = chlorobenzene, dichloromethane or trichloroethane] were obtained by the galvanostatic oxidation (1.0 μA) of a solution (20 ml) containing **1** (*ca.* 8 mg) and tetrabutylammonium hexafluorophosphate (*ca.* 20 mg) as a supporting electrolyte. Single crystals were grown on the anode within a few days and the hexagonal section of the rod is in accordance with the hexagonal crystal system (Fig. 1). Elemental analyses indicate that the donor-anion ratios of the salts are 3 : 1 and the solvent used in the crystallization is included in the crystal.‡

Temperature dependences of the conductivity for the salts were measured by the standard four-probe method. They are all semiconductive from room temperature, however, the room temperature conductivity is rather high ($\sigma_{rt} \approx 10$ S cm^{-1}) and the activation energy is small (*ca.* 50 meV).

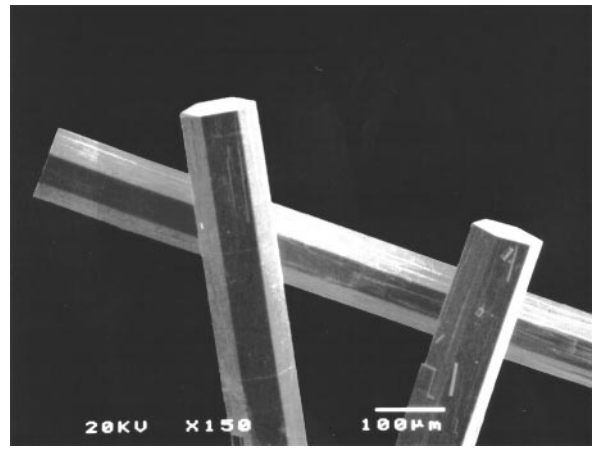

Fig. 1 Photographic SEM image of single crystals for $(\mathbf{1})_3(PF_6)(chlorobenzene)_{1.15}$

X-Ray structural analyses were performed on the single crystals and all salts crystallize into a hexagonal $P6_3/mcm$ space group and are isostructural.§ Fig. 2 shows the unit cell of the PF_6–chlorobenzene salt and there are two types of triangular units of the donor molecules within the *ab* plane, ordered clockwise and anticlockwise, respectively. The hexagonal lattice is constructed by the alternating repetition of these triangular units. The shortest intermolecular I···N distance is 2.879(6) Å and it is almost 20% shorter than the sum of the van der Waals radii (3.53 Å; Bondi[8]). This characteristic I···N contact is much shorter than that of the above-mentioned *p*-iodobenzonitrile crystal (3.18 Å)[5a] and indicates the existence of a very strong intermolecular I···N interaction. The value of the C–I···N angle is almost linear [178.3(2)°] and it is in good agreement with the direction of the pσ LUMO along the carbon–iodine single bond and the lone pair on the pyrazine ring

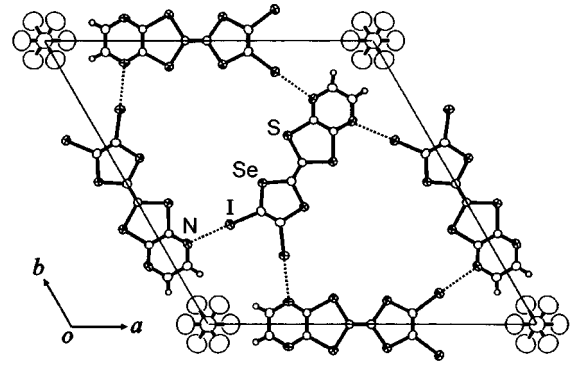

Fig. 2 Crystral structure of $(\mathbf{1})_3(PF_6)(chlorobenzene)_{1.15}$ viewed along the crystallographic *c* axis. Chlorobenzene molecules are omitted for clarity. The shortest I···N intermolecular distance (dotted line) is 2.879(6) Å.

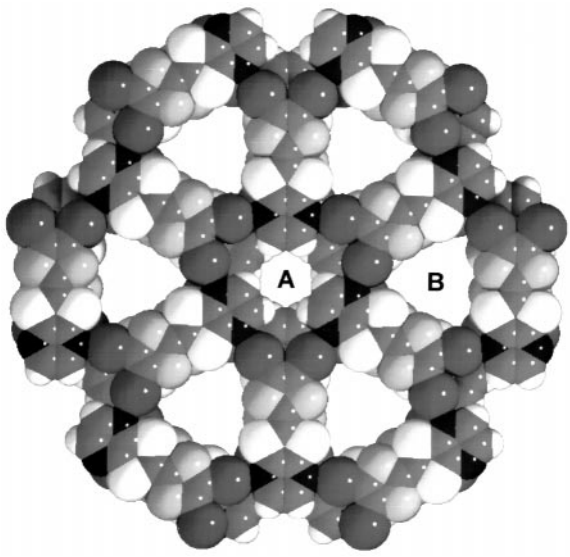

Fig. 3 Extended hexagonal donor-column arrangement of the $(\mathbf{1})_3$(anion)-(solv.)$_x$ crystal system

(Scheme 1). The donor molecule also forms a one-dimensional column along the *c* axis within the head-to-tail mode, this is the regular manner for unsymmetrical π-donors. The topology of the donor network should be recognized as the combination of: (i) characteristic I···N intermolecular interaction parallel to the molecular plane, and (ii) columnar stack perpendicular to the molecular plane.

Fig. 3 shows the extended donor network projected onto the *ab* plane and we can see that there are two types of channels along the *c* axis. One is hexagonal and surrounded by the edges of donor molecules (channel site A, *ca.* 4 Å diameter) and the other is an equilateral triangle surrounded by the sides of donor molecules (channel site B, side length *ca.* 7.5 Å). The PF_6 anion is in channel site A and the phosphorus atom is on the crystallographic special position. The included solvent is in channel site B and is highly disordered due to the low symmetry of the molecule compared with the crystallographic symmetry. Comparing the structures of the salts including different solvent molecules, the whole crystal system is not affected by changing of the solvent and the hexagonal arrangement is identical. The guest-independent channel structure is similar to those of the inorganic 'zeolite' systems[9] and it would be promising to introduce functionalized guest molecules to obtain multi-functionalized materials. Preliminary thermogravimetric experiments indicated that the PF_6–dichloromethane single crystals began to release the included solvent around 80 °C. The decrease in the sample weight had stopped after annealing at 110 °C for 5 days in the case of the powdered sample and the amount of weight loss (*ca.* 6% *vs.* initial weight) is in accordance with the calculated weight percent of dichloromethane included in the crystal.

We thank Professor R. Kato for the use of his conductivity measurement apparatus, and the Material Design and Characterization Laboratory of ISSP (University of Tokyo) for the use of their X-ray diffractometers and SEM-EPMA. This work was partially supported by Grant-in-Aids for Scientific Research from the Ministry of Education, Science, Sports and Culture, Japan.

Notes and References

† Selected data for **1**: orange–red wool; mp > 250 °C (decomp.); ^{1}H NMR ($CDCl_3$, 500 MHz); δ 8.12 (s, 2H); MS (EI, 70 eV): 602 ($C_8H_2N_2I_2S_2{}^{80}Se_2$, M^+), 475 ($M^+ - I$), 348 ($M^+ - I_2$); Calc. for $C_8H_2N_2I_2S_2Se_2$: C, 15.96; H, 0.33; N, 4.65. Found: C, 16.05; H, 0.48; N, 4.66%.

‡ Contents of the solvent molecules based on elemental analyses are: chlorobenzene *ca.* 1.15, dichloromethane *ca.* 1.66, trichloroethane *ca.* 1.30.

§ X-Ray diffraction data were collected on a Mac Science four-circle diffractometer (solv. = chlorobenzene) or a Rigaku AFC6S automatic four-circle diffractometer (solv. = dichloromethane, trichloroethane) with monochromated Mo-Kα(λ = 0.71069 Å) radiation up to 2θ = 60° at 293 K. The structures were solved by direct methods and refined with full-matrix least-squares methods using reflections with $I \geqslant 3\sigma(I)$. The data were corrected for Lorentz and polarization effects. Anisotropic thermal parameters were used for non-hydrogen atoms except disordered solvent molecules. All calculations were performed with use of the 'teXsan' program package of MSC. *Crystal data* for $(\mathbf{1})_3(PF_6)(chlorobenzene)_{1.15}$: $(C_{24}H_6N_6I_6S_6Se_6)(PF_6)(C_6H_5Cl)_{1.15}$, M = 2080.30, hexagonal, space group $P6_3/mcm$ (no. 193), a = 20.242(2), c = 7.274(2) Å, V = 2581.2(6) Å^3, μ = 82.32 cm^{-1}, D_c = 2.676 g cm^{-3}, $F(000)$ = 1891.40, Z = 2, R = 0.031, R_w = 0.021, GOF = 1.70 for 912 observed reflections out of 2647 unique reflections. $(\mathbf{1})_3(PF_6)(dichloromethane)_{1.66}$: $(C_{24}H_6N_6I_6S_6Se_6)(PF_6)(CH_2Cl_2)_{1.66}$, M = 2091.85, hexagonal, space group $P6_3/mcm$ (no. 193), a = 20.165(5), c = 7.28(1) Å, V = 2562(2) Å^3, μ = 84.02 cm^{-1}, D_c = 2.711 g cm^{-3}, $F(000)$ = 1897.44, Z = 2, R = 0.050, R_w = 0.036, GOF = 2.28 for 721 observed reflections out of 1513 unique reflections. $(\mathbf{1})_3(PF_6)(trichloroethane)_{1.30}$: $(C_{24}H_6N_6I_6S_6Se_6)(PF_6)(C_2H_3Cl_3)_{1.30}$, M = 2124.29, hexagonal, space group $P6_3/mcm$ (no. 193), a = 20.20(2), c = 7.263(8) Å, V = 2565(3) Å^3, μ = 84.23 cm^{-1}, D_c = 2.750 g cm^{-3}, $F(000)$ = 1929.60, Z = 2, R = 0.044, R_w = 0.023, GOF = 1.33 for 547 observed reflections out of 1512 unique reflections. CCDC 182/978.

1 For recent progress of molecular conductors, see Z. V. Vardeny and A. J. Epstein, ed., *Synth. Met.*, 1997, **86** (the latest proceedings of the international conference on science and technology of synthetic metals, ICSM'96).
2 For recent progress of fullerenes, see H. W. Kroto, J. E. Fischer and D. E. Cox, *The Fullerenes*, Pergamon, Oxford, 1993; *Acc. Chem. Res.* (special issue on buckminsterfullerenes), 1992, **25**, 97.
3 (*a*) G. R. Desiraju, *Crystal engineering: the design of organic solids*, Elsevier, Amsterdam, 1989; (*b*) G. R. Desiraju, *Angew. Chem., Int. Ed. Engl.*, 1995, **34**, 2311 and references therein.
4 (*a*) T. Imakubo, H. Sawa and R. Kato, *Synth. Met.*, 1995, **73**, 117; (*b*) T. Imakubo, H. Sawa and R. Kato, *J. Chem. Soc., Chem. Commun.*, 1995, 1097; (*c*) T. Imakubo, H. Sawa and R. Kato, *J. Chem. Soc., Chem. Commun.*, 1995, 1668; (*d*) T. Imakubo, H. Sawa and R. Kato, *Mol. Cryst. Liq. Cryst.*, 1996, **285**, 27.
5 (*a*) E. O. Schlemper and D. Britton, *Acta Crystallogr.*, 1965, **18**, 419; (*b*) G. R. Desiraju and R. L. Harlow, *J. Am. Chem. Soc.*, 1989, **111**, 6757.
6 (*a*) R. Gompper, J. Hock, K. Polborn, E. Dormann and H. Winter, *Adv. Mater.*, 1995, **7**, 41; (*b*) T. Imakubo, H. Sawa and R. Kato, *Synth. Met.*, 1997, **86**, 1883.
7 G. C. Papavassiliou, S. Y. Yiannopoulos, J. S. Zambounis, K. Kobayashi and K. Umemoto, *Chem. Lett.*, 1987, 1279.
8 A. Bondi, *J. Phys. Chem.*, 1964, **68**, 441.
9 W. M. Meier and D. H. Olson, *Atlas of zeolite structure types*, Butterworth-Heinemann, London, 1992.

Received in Cambridge, UK, 29th June 1998; 8/04958K

Ozone-cleavable gemini surfactants, a new candidate for an environmentally friendly surfactant

Araki Masuyama,*† Chikara Endo, Shin-ya Takeda and Masatomo Nojima

Department of Materials Chemistry, Faculty of Engineering, Osaka University, Suita, Osaka 565-0871, Japan

Three types of gemini surfactants bearing carbon–carbon double bond(s) showed excellent surface-active properties, and readily decomposed into non-surface-active fragments and/or single-chain surfactants with different surface-active properties upon exposure to ozone in water.

Surfactants are one of the representative chemical products which are consumed in large quantities every day on a world-wide scale. Special regard concerning environmental safe-guards should be paid to the development of the next generation of new surfactants. Application of ozone in waste water treatment is noted as a modern key technology for the environmental protection of rivers and lakes.[1] Many sewage treatment plants in which an ozonation process is incorporated are operating around the world.

We herein propose a new design of novel surfactant featuring 'environmentally-friendly' characteristics. The concept is based on the following two points: (i) lowering the quantity of surfactant used will contribute greatly to reducing the load on the natural purification system, and (ii) breaking down the original surfactant molecules into smaller fragments after they have fulfilled their original applications will assist the waste water treatment process. Concerning the first point, double-chain surfactants bearing two hydrophilic ionic head groups, generally called 'gemini surfactants',[2] are an attractive motif

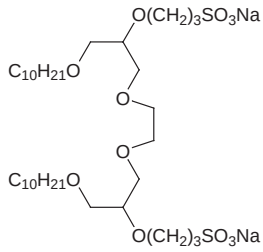

1

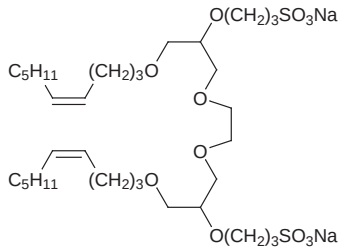

2

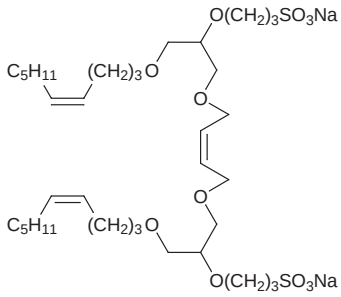

3

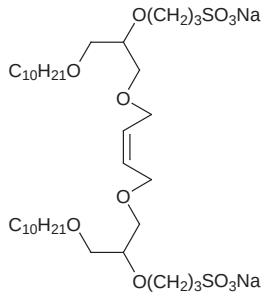

4

because many types of gemini surfactants, such as **1**,[3] have very small CMC (critical micelle concentration) values and have the ability to significantly lower surface tension, both of which properties cannot be achieved *via* simple modification of the structure of conventional single-chain monoionic surfactants.[4] The second point is connected with 'chemocleavable' or 'destructive' surfactants, which are one of the stimulating targets of research in the chemistry of amphiphilic compounds.[5] Taking into account these backgrounds, we have recently designed and prepared three types of gemini surfactants bearing carbon–carbon double bond(s) in their lipophilic chains and/or the connecting part (**2**–**4**). Ozonation is applied as a trigger for the destruction of these unsaturated gemini surfactants in water. In connection with our latter approach, Piasecki and co-workers have investigated the reactivity of long-chain alkyl-substituted cyclic acetals toward ozone in water.[6]

Preparation of the target compounds **2**–**4** was achieved according to the established method.[3] Thus they were synthesised by the reaction of 1,2:9,10-diepoxy-4,7-dioxadecane (for preparation of **2**) or (*Z*)-1,2:11,12-diepoxy-4,9-dioxadodec-6-ene (for **3** and **4**) with (*Z*)-dec-4-en-1-ol (for **2** and **3**) or decan-1-ol (for **4**) in the presence of base, followed by sulfopropylation of the resulting double-chain diols with propane-1,3-sultone.‡ Table 1 summarises the data for their CMC, γ_{CMC} (the surface tension at CMC, as an indication of the effectiveness of adsorption at the air/water interface)[7] and pC_{20} (the efficiency of adsorption)[7] values, which were obtained from respective surface tension *vs*. concentration (on a log scale) curves measured by the Wilhelmy method. The corresponding data for the gemini surfactant **1**[3] and the single-chain sulfonate $[C_{10}H_{21}O(CH_2)_2SO_3Na]$ **5**[7] are also included in Table 1 as reference amphiphiles.

The CMC of a surfactant bearing carbon–carbon double bond(s) in its lipophilic chain is generally higher than that of the corresponding saturated compound.[7] This is also the case for the CMC of gemini surfactants **1**–**3**. It should be noted, however, that the CMC values of **2** and **3** are two orders lower than that of the conventional single-chain analogue **5**. Interestingly, the CMC of the gemini surfactant **4** is very similar to that of the corresponding saturated gemini surfactant **1**, indicating that the CMC is not affected by an unsaturated bond in the connecting part of these gemini surfactants. In summary, both effectiveness and efficiency of adsorption on the surface for a series of gemini surfactants **1**–**4**, regardless of the presence or the absence of double bond(s) in the molecule, are much higher than those for the single-chain surfactant **5**.

Ozonolysis of gemini surfactants **2**–**4** was easily accomplished by passing ozone through their micellar aqueous solutions (1×10^{-2} mol dm^{-3}) at room temperature. Subsequent treatment of the reaction mixture with $NaBH_4$ afforded

Table 1 Interfacial properties of surfactants **1–5** measured by the Wilhelmy method at 20 °C in water

Surfactant	CMC/mol dm^{-3}	γ_{CMC}/mN m^{-1}	pC_{20}
1[a]	3.2×10^{-5}	30.0	5.2
2	9.0×10^{-5}	34.0	5.1
3	1.0×10^{-4}	33.5	5.2
4	2.5×10^{-5}	33.0	5.7
5[b]	1.6×10^{-2}	41.0	2.1

[a] Ref. 3. [b] Ref. 7.

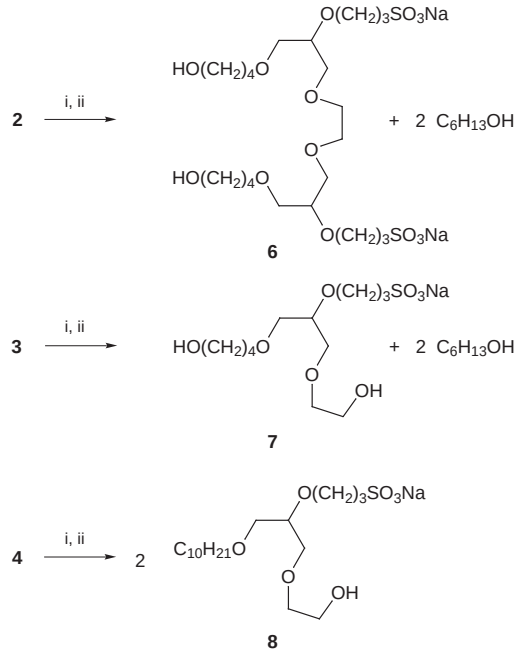

Scheme 1 *Reagents and conditions*: i, **2**, **3** or **4** in water (1×10^{-2} mol dm^{-3}), O_3 (10 equiv.), room temp.; ii, $NaBH_4$ (1.5 equiv.), 5 min., room temp.

the corresponding degradation products, as shown in Scheme 1.§ These products could be extracted as a mixture in each case with $CHCl_3$–MeOH (3:1, v/v). Their structures were confirmed by comparison of their ^1H and ^{13}C NMR data with those of hexan-1-ol and authentic samples of **6**–**8**.¶ Judging from the TLC results of the extracted mixtures and their ^1H NMR spectra in D_2O, other degradation products were not observed and compounds **6**–**8** were found to be produced almost quantitatively.

After ozonolysis and successive reduction of micellar solutions of gemini surfactants **2** and **3**, oil droplets (*i.e*. hexan-1-ol) appeared in the solutions; stable foams were not observed, even immediately after shaking the solutions. Stable foams were generated, however, by shaking solutions containing ozonolysis product **8**. Compound **8** was still surface-active and its surface-active properties were: CMC = 8.0×10^{-4} mol dm^{-3}; γ_{CMC} = 35 mN m^{-1}; pC_{20} = 3.8. Thus the interfacial properties of the parent gemini surfactant **4** and the single-chain surfactant **8** are quite different. Thus, surfactant **4** is categorised as a second generation type of cleavable surfactant.[8]

In summary, the readily accessible gemini surfactants **2**–**4** possess considerable potential as high-performance surfactants. Fragmentation of **2**–**4** in water smoothly takes place on exposure to ozone, followed by reduction with $NaBH_4$ under mild conditions. Studies on various surface-active properties of a homologous series of gemini surfactants and their biodegradability are now in progress.

This work was supported in part by the Fund for Environmental Protection Research from the Nihon-Seimei Foundation.

Note and References

† E-mail: toratora@chem.eng.osaka-u.ac.jp

‡ All new compounds gave satisfactory spectroscopic and microanalytical data.

§ A suitable reductant is required to give stable degradation products in water because the corresponding unstable α,α′-dihydroxy peroxides are formed by ozonolysis of the substrates. $NaBH_4$ was chosen because it is an inexpensive industrial reductant and can be used in water.

¶ Authentic compound **6** was prepared by the reaction of $THPO(CH_2)_4OH$ (THP = tetrahydropyranyl) with ethylene glycol diglycidyl ether, followed by sulfopropylation with propane-1,3-sultone and successive deprotection of the THP group by treatment with sulfuric acid. The reaction of $THPO(CH_2)_4OH$ with mono-THP-protected ethylene glycol glycidyl ether, or the reaction of decyl glycidyl ether with mono-THP-protected ethylene glycol, followed by sulfopropylation and successive deprotection afforded authentic compounds **7** and **8**, respectively.

1 E. D. Schroeder, in *Water and Wastewater Treatment*, 5th edn., McGraw-Hill Kodansha, Tokyo, 1979, ch. 11; *Water Treatment Plant Design*, McGraw-Hill, N. Y., ch. 8; S. J. Masten and S. H. R. Davies, *Adv. Environ. Sci. Technol.*, 1994, **28**, 517; R. G. Rice, *Ozone: Sci. Eng.*, 1997, **18**, 477; V. Brenna, *Acqua Aria*, 1997, 30; H. Gulyas, *Water Sci. Technol.*, 1997, **36**, 9.

2 M. J. Rosen, in *New Horizons. An AOCS/CSMA Detergent Industry Conference*, ed. R. T. Coffey, AOCS Press, Champaign, 1996, ch. 8.

3 Y.-P. Zhu, A. Masuyama, T. Nagata and M. Okahara, *J. Jpn. Oil Chem. Soc.*, 1991, **40**, 473.

4 M. Okahara, A. Masuyama, Y. Sumida and Y.-P. Zhu, *J. Jpn. Oil Chem. Soc.*, 1988, **37**, 746; F. M. Menger and C. A. Littau, *J. Am. Chem. Soc.*, 1991, **113**, 1451; Y.-P. Zhu, A. Masuyama, Y. Kobata, Y. Nakatsuji, M. Okahara and M. J. Rosen, *J. Colloid Interface Sci.*, 1993, **158**, 40; R. Zana and Y. Talmon, *Nature*, 1993, **362**, 228; A. Masuyama, M. Yokota, Y.-P. Zhu, T. Kida and Y. Nakatsuji, *J.Chem. Soc. Chem. Commun.*, 1994, 1435.

5 B. Burczyk and L. Weclas, *Tenside Deterg*., 1980, **17**, 21; D. A. Jaeger and M. R. Frey, *J. Org. Chem.*, 1982, **47**, 311; S. Yamamura, M. Nakamura and T. Takeda, *J. Am. Oil Chem. Soc.*, 1989, **66**, 1165; D. Ono, A. Masuyama and M. Okahara, *J. Org. Chem.*, 1990, **55**, 4461; A. Sokolowski, A. Piasecki and B. Burczyk, *J. Am. Oil. Chem. Soc.*, 1992, **69**, 633; D. Ono, A. Masuyama, Y. Nakatsuji, M. Okahara, S. Yamamura and T. Takeda, *J. Am. Oil Chem. Soc.*, 1993, **70**, 29; D. A. Jaeger, *Supramol. Chem.*, 1995, **5**, 27.

6 A. Piasecki, A. Sokolowski, B. Burczyk and K. Piasecka, *J. Am. Oil Chem. Soc.*, 1986, **63**, 557.

7 M. J. Rosen, in *Surfactants and Interfacial Phenomena*, 2nd edn., Wiley, N. Y., 1989, ch. 2, 3 and 5.

8 D. A. Jaeger, Y. M. Sayed and A. K. Dutta, *Tetrahedron Lett*., 1990, **31**, 449.

Received in Cambridge, UK, 27th July 1998; 8/05825C

Carbonyl propargylation or allenylation by 3-haloprop-1-yne with tin(II) halides and tetrabutylammonium halides

Yoshiro Masuyama,*† Akihiro Ito, Mamiko Fukuzawa, Kohji Terada and Yasuhiko Kurusu

Department of Chemistry, Sophia University, 7-1 Kioicho, Chiyoda-ku, Tokyo 102-8554, Japan

3-Bromoprop-1-yne causes carbonyl propargylation with tin(II) chloride and tetrabutylammonium bromide in water to produce 1-substituted but-3-yn-1-ols, while 3-chloroprop-1-yne causes carbonyl allenylation with tin(II) iodide and tetrabutylammonium iodide in 1,3-dimethylimidazolidin-2-one to produce 1-substituted buta-2,3-dien-1-ols.

Carbonyl propargylation or allenylation by 3-haloprop-1-yne with tin(II) chloride is one of the most convenient methods for introduction of propargyl (prop-2-ynyl) or allenyl functions.[1–3] The propargylation or allenylation is promoted by NaI or LiI; it has been presumed that the actual starting material, which reacts with tin(II) chloride, is 3-iodoprop-1-yne derived from the *in situ* reaction 3-bromoprop-1-yne with NaI or LiI.[1,3] We have found that carbonyl allylation by allylic acetates, allylic bromides, allylic chlorides and vinyl epoxides with rin(II) halide can be promoted by tetrabutylammonium bromide (TBABr).[4–8] A lack of reaction with TBABr might suggest that LiI is required to form the intermediate 3-iodoprop-1-yne.[3] Tetrabutylammonium halide (TBAX‴) probably reacts with tin(II) halide (SnX''_2) to form tetrabutylammonium trihalostannate, which is more nucleophilic than SnX''_2. We thus envisioned that TBAX‴ would promote carbonyl propargylation or allenylation by 3-haloprop-1-yne with SnX''_2.[9,10] We here report that using different halogens in SnX''_2 and TBAX‴ affects the selectivity between carbonyl propargylation and allenylation by 3-haloprop-1-yne; carbonyl propargylation occurs with $SnCl_2$ and TBABr, while carbonyl allenylation occurs with SnI_2 and TBAI.

The reaction of 3-haloprop-1-yne **1** and benzaldehyde (**2**, R = Ph) with SnX''_2 and TBAX‴ was investigated under various conditions. The results are summarized in Table 1. The reaction of 3-bromoprop-1-yne (**1**, X′ = Br) with $SnCl_2$ and TBABr at 50 °C in water led to carbonyl propargylation to produce 1-phenylbut-3-yn-1-ol (**3**, R = Ph) (entry 7, Method A), while the reaction of 3-chloroprop-1-yne (**1**, X′ = Cl) with SnI_2 and TBAI at 25 °C in 1,3-dimethylimidazolidin-2-one (DMI) led to carbonyl allenylation to produce 1-phenylbuta-2,3-dien-1-ol (**4**, R = Ph) (entry 13, Method B) [eqn. (1)]. TBAX‴ accelerated

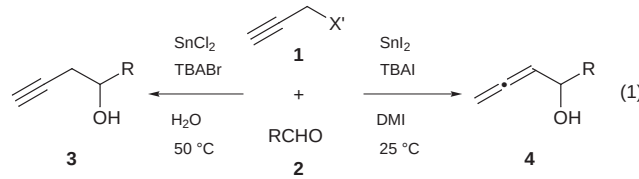

(1)

the carbonyl propargylation or allenylation; > 0.1 equiv. of TBAX‴ was required (entries 5–8). In the propargylation the use of $SnCl_2$ and TBABr (or TBACl) is superior to other combinations of reagents, while SnI_2–TBAI is the best combination of reagents for the allenylation. 3-Chloroprop-1-yne (**1**, X′ = Cl) did not react under the same conditions as those of the propargylation with **1** (X′ = Br). Water is a more effective solvent in the propargylation than some organic polar solvents, such as DMI and THF, in which both organic substrates and $SnCl_2$ are soluble (entries 1, 2 and 8). The by-product produced during the propargylation, 4-phenylbut-3-en-2-one (**5**, R = Ph), was probably formed by the hydration of allenylated product **4** (R = Ph).[3] The reaction of **1** (X′ = Cl) and **2** (R = Ph) with SnI_2–TBAI did not occur in water, and proceeded with lower selectivity for the allenylation in DMI–water (entry 14). Thus, water is unsuitable for the allenylation, in which DMI is a better solvent than DMF or THF (entries 11–13).

Table 1 Propargylation and allenylation of **2** (R = Ph) with SnX''_2 and TBAX‴ [a]

Entry	X′	X″	TBA X‴ (mmol)	Solvent	*t*/h	Yield (%) **3** + **4**[b]	**5**[c]
1	Br	Cl	Br (1)	DMI	24	25 (100:0)	4
2	Br	Cl	Br (1)	THF	10	60 (100:0)	9
3	Br	Cl	Br (1)	THF–H_2O[d]	8	70 (100:0)	8
4	Br	Cl	Br (1)	CH_2Cl_2–H_2O[d]	8	58 (100:0)	12
5	Br	Cl	—	H_2O	24	17 (100:0)	0
6	Br	Cl	Br (0.1)	H_2O	8	61 (100:0)	13
7[e]	Br	Cl	Br (0.3)	H_2O	8	70 (100:0)	9
8	Br	Cl	Br (1)	H_2O	7	72 (100:0)	10
9[f]	Br	Cl	Br (1)	H_2O	70	44 (100:0)	9
10	Br	Br	Br (1)	H_2O	10	58 (100:0)	15
11[f,g]	Cl	I	I (0.1)	THF	70	91 (31:69)	0
12[f,g]	Cl	I	I (0.1)	DMF	28	91 (19:81)	0
13[f,g,h]	Cl	I	I (0.1)	DMI	23	78 (4:96)	0
14[f,g]	Cl	I	I (0.1)	DMI–H_2O[d]	47	57 (33:67)	11

[a] The reaction of 3-haloprop-1-yne (1.5 mmol) and benzaldehyde (1.0 mmol) was carried out with SnX''_2 (1.5 mmol) and TBA in solvent (3 ml) at 50 °C. [b] Yields of a mixture of **3** (R = Ph) and **4** (R = Ph). The ratio in parentheses was determined by ^{1}H NMR analysis (JEOL GX-270 or Λ–500). [c] Isolated yields of **5** (R = Ph). [d] Organic solvent–H_2O = 1:1. [e] Method A. [f] The reaction was carried out at 25 °C. [g] NaI (1.5 mmol) was added. [h] Method B.

Table 2 Either propargylation or allenylation with SnX''_2 and TBAX‴

R	Method[a]	*t*/h	Yield (%) **3** + **4**[b]	**5**[c]
4-$MeO_2CC_6H_4$	A	7	75 (100:0)	14
4-$MeO_2CC_6H_4$	B	24	80 (17:83)	0
4-NCC_6H_4	A	16	77 (100:0)	4
4-NCC_6H_4	B	23	62 (2:98)	0
4-MeC_6H_4	A	20	70 (100:0)	4
4-MeC_6H_4	B	23	53 (7:93)	0
4-$MeOC_6H_4$	A	16	62 (100:0)	4
4-$MeOC_6H_4$	B	25	50 (5:95)	0
$Me(CH_2)_6$	A	12	63 (100:0)	0
$Me(CH_2)_6$	B	90[d]	50 (7:93)	0
c-C_6H_{11}	A	12	48 (100:0)	7
c-C_6H_{11}	B	88[d]	71 (20:80)	0

[a] Method A: Entry 7 in Table 1. Method B: Entry 13 in Table 1. [b] Yields of a mixture of **3** and **4**. The ratio in parentheses was determined by ^{1}H NMR analysis (JEOL GX-270 or Λ–500). [c] Isolated yields. [d] The reaction was carried out at 0 °C.

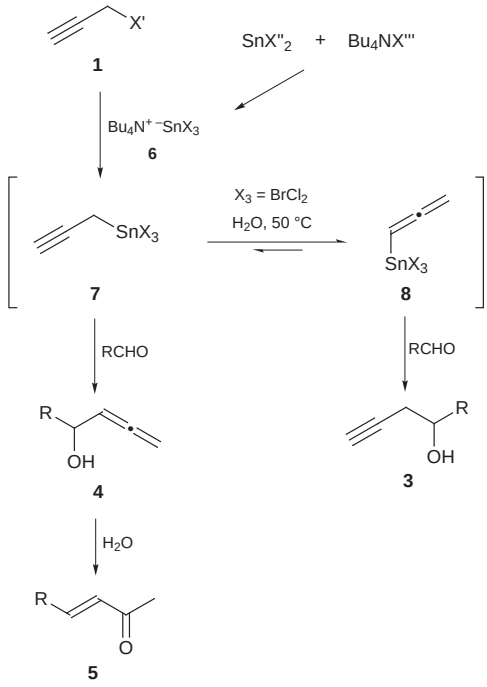

Scheme 1

The propargylation (Method A) and allenylation (Method B) of various aldehydes by 3-haloprop-1-yne **1** was carried out under the conditions which gave the best results for benzaldehyde, as summarized in Table 2. Aromatic aldehydes bearing an electron-donating or −withdrawing group and aliphatic aldehydes can be used to afford the corresponding 1-substituted but-3-yn-1-ols **3** using the $SnCl_2$–TBABr/water system or the corresponding 1-substituted buta-2,3-dien-1-ols **4** with the SnI_2–TBAI/DMI system in moderate yields.

A plausible mechanism was illustrated with Scheme 1. The difference between propargylation using the $SnCl_2$–TBABr/water system and allenylation using the SnI_2–TBAI/DMI system may be due to the Lewis acidity of the tin, reaction temperature and reaction medium. ^{1}H NMR (JEOL Λ–500) observation in [$^2H_7$]DMF at 25 °C revealed that prop-2-ynyltriiodotin (**7**, X = I) was first formed *via* the reaction of 3-chloroprop-1-yne (**1**, X′ = Cl) with SnI_2 and NaI. Prop-2-ynyltriiodotin (**7**, X = I) probably proceeded *via* γ-addition to the aldehyde (carbonyl allenylation), without isomerizing to propa-1,2-dienyltriiodotin (**8**, X = I), in dry polar solvents such as DMI and DMF to produce buta-2,3-dien-1-ols **4**.‡ In contrast, the isomerization of prop-2-ynylbromodichlorotin (**7**, X_3 = $BrCl_2$), derived from reaction of 3-bromoprop-1-yne (**1**, X′ = Br) with $SnCl_2$ and TBABr at the organic–aqueous interface, to propa-1,2-dienylbromodichlorotin (**8**, X_3 = $BrCl_2$) probably occurred more rapidly at 50 °C than carbonyl allenylation by **7** (X_3 = $BrCl_2$).§ The carbonyl propargylation by **8** (X_3 = $BrCl_2$) at 50 °C in water thus produced but-3-yn-1-ols **3**.¶

Notes and References

† E-mail: y-masuya@hoffman.cc.sophia.ac.jp

‡ The carbonyl allenylation by **7** (X = I) seems to have proceeded *via* an acyclic antiperiplanar transition state, because of the weakly Lewis acidic tin in **7** (X = I). See ref. 7 and 8.

§ It was shown by ^{1}H NMR analysis (JEOL Λ–500) that prop-2-ynyltriiodotin (**7**, X = I), derived from 3-chloroprop-1-yne (**1**, X′ = Cl) *via* reaction with SnI_2 and NaI in [$^2H_7$]DMF, isomerized easily to propa-1,2-dienyltriiodotin (**8**, X = I) at 50 °C; J. A. Marshall, R. H. Yu and J. F. Perkins, *J. Org. Chem*., 1995, **60**, 5550.

¶ The carbonyl propargylation by **8** (X_3 = $BrCl_2$), which has a strongly Lewis acidic tin, seems to have proceeded *via* a usual six-membered cyclic transition state.

1 T. Mukaiyama and T. Harada, *Chem. Lett*., 1981, 621.
2 G. P. Boldrini, E. Tagliavini, C. Trombini and A. Umani-Ronchi, *J. Chem. Soc., Chem. Commun*., 1986, 685.
3 M. Iyoda, Y. Kanao, M. Nishizaki and M. Oda, *Bull. Chem. Soc. Jpn*., 1989, **62**, 3380.
4 Y. Masuyama, in *Advances in Metal-Organic Chemistry*, ed L. S. Liebeskind, JAI, Greenwich, 1994, vol. 3, p. 255.
5 Y. Masuyama, J. Nakata and Y. Kurusu, *J. Chem. Soc., Perkin Trans. 1*, 1991, 2598.
6 Y. Masuyama, M. Kishida and Y. Kurusu, *J. Chem. Soc., Chem. Commun*., 1995, 1405.
7 Y. Masuyama, M. Kishida and Y. Kurusu, *Tetrahedron Lett*., 1996, **37**, 7103.
8 Y. Masuyama, A. Ito and Y. Kurusu, *Chem. Commun*., 1998, 315.
9 For selective carbonyl propargylation in Barbier-type procedures, see: H. Tanaka, T. Hamatani, S. Yamashita and S. Torii, *Chem. Lett*., 1986, 1461 and references cited therein.
10 For carbonyl propargylation and allenylation, see: H. Yamamoto, in *Comprehensive Organic Synthesis*, ed B. M. Trost, Pergamon, Oxford, 1991, vol. 2, p. 81.

Received in Cambridge, UK, 6th August 1998; 8/06206D

Unexpected regioselectivity in the coupling of π-coordinated tritylallene with an amido ligand in molybdenum complex

Bor-Chen Huang, Ying-Chih Lin,* Yi-Hong Liu and Yu Wang

Department of Chemistry, National Taiwan University Taipei, Taiwan 106, Republic of China. E-mail: yclin@mail.ch.ntu.edu.tw

Coupling of π-coordinated tritylallene with an amido ligand was unexpectedly found to take place at the terminal carbon in the reaction of $[Cp(CO)_3Mo(\eta^2\text{-}CH_2{=}C{=}CHCPh_3)][BF_4]$ 1, with three secondary amines (dimethylamine, piperidine, morpholine).

The synthesis and reactivity of organometallic complexes containing η^3-allyl,[1] η^1-allenyl[2] and η^1-propargyl[3] ligands have attracted a great deal of attention owing to their wide applications in organic synthesis. We recently reported distinctive regiospecificity of C–C bond formation in the reactions of tungsten allenyl and propargyl complexes. In the allenyl system,[4] reactions with amines and with alcohols afforded high yields of azametallacycles and oxametallacycles, respectively. The C–C bond formation takes place solely at C_α of the allenyl ligand in both cases. By contrast, the corresponding propargyl complex afforded exclusively the β-coupled allylic complex, the latter regiospecificity was assumed to proceed *via* a η^2-allene intermediate.[5] In a particular system, the η^2-tritylallene complex $[Cp(CO)_3M(\eta^2\text{-}CH_2{=}C{=}CHCPh_3)][BF_4]$, (M = Mo **1**, M = W **1′**, Cp = η^5-C_5H_5) could be isolated and displays coupling reactivity with the expected regiospecificity in reactions with alcohols and some amines.[6] However, when we studied more reactions of **1** with amines, three amines were found to display different regioselectivity. Herein we report the unexpected regioselectivity in the reaction of **1** with these three amines, yielding the α-amido substituted allylic complex as the major product and the β-amido allylic complex as the minor product.

Reaction of **1** with neat piperidine at room temperature for 1 h afforded two amido-substituted allylic products. The major product $Cp(CO)_2Mo[\eta^3\text{-}CH(CONC_5H_{10})CHCHCPh_3]$ **2a**,† has a surprising α-amido-substituted geometry, and the minor product $Cp(CO)_2Mo[\eta^3\text{-}CH_2C(CONC_5H_{10})CHCPh_3]$ **3a**, a normal β-amido-substituted geometry (Scheme 1). The two isomers can be separated by chromatography over silica gel. Complexes **2a** and **3a** were collected as orange–yellow and light-yellow microcrystalline powders upon re-crystallization from hexane–CH_2Cl_2 in *ca.* 65 and 17% yields, respectively. Similar results were found with morpholine and dimethylamine to yield the α-amido-allylic complexes **2b**, **c**† respectively as the major product and the β-amido-allylic complexes **3b**, **c** as the minor product and an X-ray analysis was carried out on a crystal of **2b**.‡ An ORTEP drawing of **2b** is shown in Fig. 1. The most salient feature of the molecule is the presence of an amido-substituted tritylallyl ligand. The amido substituent is attached to the α-carbon C(5) of the allyl ligand with a geometry *syn* to the central hydrogen and the trityl moiety is in an *anti* configuration.

Two possible mechanisms are proposed to account for the formation of **2a**. In both cases, it is necessary to consider nucleophilic attack of amine to the terminal carbonyl giving the amido ligand. Deprotonation[7] of the tritylallene ligand in the presence of amine may result in formation of an allenyl ligand and coupling of the amido ligand with the α-carbon of the σ-allenyl followed by protonation would give the major product.[8] Alternatively, coupling of the amido group with allene leading to C–C bond formation may precede hydrogen migration and the selectivity would be controlled by the presence of the trityl group. To better understand the detail and with the hope to see an intermediate the reaction was monitored

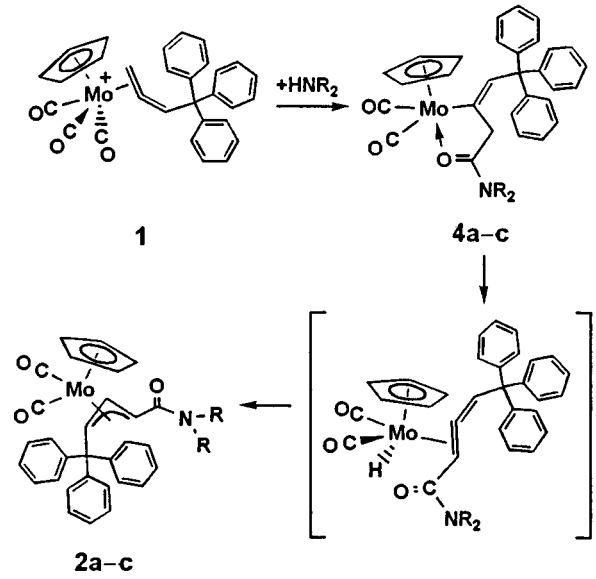

Scheme 1 HNR_2 = piperidine **a**, morpholine **b** or dimethylamine **c**

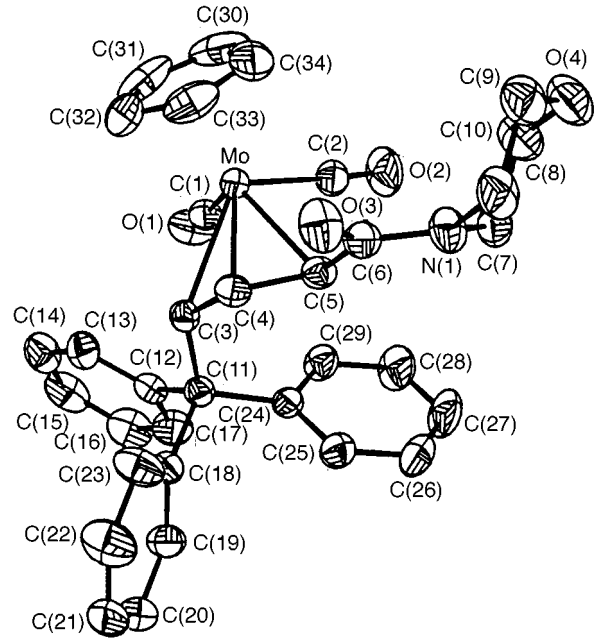

Fig. 1 ORTEP drawing of **2b** with thermal ellipsoids shown at the 50% probability level. Selected bond distances (Å) and angles (°): Mo–C(3) 2.379(2), Mo–C(4) 2.212(2), Mo–C(5) 2.359(2), C(3)–C(4) 1.417(3), C(4)–C(5) 1.409(3), C(5)–C(6) 1.500(3), C(6)–N(1) 1.356(3), C(6)–O(3) 1.228(3); C(4)–C(3)–C(11) 125.1(2), C(4)–C(5)–C(6) 115.4(2), C(1)–Mo–C(2) 77.13(11).

spectroscopically. When the reaction was carried out at −60 °C, an intermediate was indeed observed. Upon addition of piperidine at −60 °C, the light yellow complex **1** dissolved and the solution turned deep red, to give a mixture of an unstable intermediate **4a** as well as **3a**. In the IR spectrum of the mixture the intermediate displays two peaks at 1927 and 1828 cm^{-1} as well as one amido CO stretching absorption at 1577 cm^{-1}. The latter suggested the presence of O-coordinated amido carbonyl.[9] Complex **4a**† transforms to **2a** in 1 h at room temperature but at lower temperature this process is slowed and the structure of **4a** can be assigned on the basis of the spectroscopic data of the mixture obtained at −60 °C. In the ^{1}H NMR spectrum, two doublet resonances at δ 2.28 and 2.74 with J_{HH} 22.4 Hz indicate the presence of a CH_2 group while a singlet resonance at δ 6.55 is assigned to the =CH– group for **4a**. Two-dimensional HSQC[10] data confirms the CH_2 ^{13}C resonance at δ 47.2 and ^{13}CH group at δ 147.5. In the HMBC[11] spectrum, the cross-peak between the CH_2 (δ_H 2.28, 2.74) and the CON (δ_C 180) groups[12] indicate C–C bond formation at the terminal CH_2 group. These observations imply that the intermediate could be a vinyl[13] complex, (Scheme 1) and the first mechanism is thus ruled out. Hydrogen migration of **4a** may proceed through β-elimination to give the metal hydride allene followed by coupling of the hydride at C_β of the allene to give the final product **2a**.

Reactions of **1** with other amines such as methylamine, ethylamine, propylamine, phenylamine, benzylamine, diethylamine, diisopropyl amine, di-*sec*-butylamine, diisobutyl amine and hydrazine gave only the β-coupled product. The p*K*a values of the three unique amines (8.30 for morpholine, 10.90 for Me_2NH and 11.20 for piperidine) giving the α-coupled product are in the range of regular amines (4.69 for aniline to 11.1 for diisopropyl amine) while no striking steric effect is seen for these three amines. While we cannot explain their different reactivity, this is the first case where coupling at the α-position of a η^2-allene has been found. A detailed mechanism for this unusual coupling, the reactivity of compound **1** with other nucleophiles and the corresponding reaction for the tungsten system is currently under investigation.

We are grateful for support of this work by the National Science Council, Taiwan, the Republic of China.

Notes and References

† *Selected spectroscopic data*: ^{1}H and ^{13}C{^{1}H} NMR were recorded in $CDCl_3$ relative to $SiMe_4$ and IR in CH_2Cl_2. **2a**: IR, 1954s, 1873s, 1605m cm^{-1}. ^{1}H NMR, δ 7.28–7.11 (m, 15H, aromatic H), 5.39 (t, J_{HH} 10.0 Hz, 1H, H_{centre}), 5.28 (5H, s, Cp), 5.06 (d, J_{HH} 10.0 Hz, 1H, CH_{syn}), 3.60, 3.24, 2.83 (m, 4H, H_2CNCH_2), 1.52 (m, 6H, $CH_2CNCH_2C_3H_6$), 0.99 [1H, d, J_{HH} 10.0 Hz, HCC(O)N]. ^{13}C{^{1}H} NMR, δ 241.4, 238.4 (CO), 169.9 (C=O), 130.3, 127.2, 126.1 (Ph), 94.1 (Cp), 70.1 (CH_{centre}), 68.6 (CH_{syn}), 61.2 (CPh_3), 50.2 (CH_{anti}), 46.3, 43.3 (CH_2NC_2H), 26.8, 25.7, 24.7 ($NC_2H_4C_3H_6$). FAB MS: *m/z* 614 (M^+ + 1), 585 (M^+ − CO), 557 (M^+ − 2CO). **2b**: IR (KBr), 1937s, 1858s, 1623m cm^{-1}. ^{1}H NMR, δ 7.29–7.15 (m, Ph), 5.40 (t, J_{HH} 10.2 Hz, 1H, H_{centre}), 5.29 (s, 5H, C_5H_5), 5.07 (d, J_{HH} 10.2 Hz, 1H, H_{syn}), 3.57–2.73 (m, 8H, NC_4H_8O), 0.88 (d, J_{HH} 10.2 Hz, 1H, H_{anti}); ^{13}C{^{1}H} NMR, δ 241.6, 237.8 (CO), 170.5 (C=O), 130.3–126.1 (Ph), 94.2 (Cp), 69.9 (CH_{centre}), 68.8 (CH_{syn}), 66.9 (CH_2OCH_2), 61.2 (CPh_3), 49.0 (CH_{anti}), 45.8, 42.5 (CH_2NC_2H). FAB MS: *m/z* 616 (M^+ + 1), 587 (M^+ − CO), 559 (M^+ − 2CO). **2c**: IR (KBr), 1939s, 1855s, 1611m cm^{-1}. ^{1}H NMR, δ 7.28–7.15 (m, Ph), 5.36 (t, J_{HH} 10.2 Hz, 1H, H_{centre}), 5.29 (s, 5H, C_5H_5), 5.05 (d, J_{HH} 10.2 Hz, 1H, H_{syn}), 2.81, 2.46 (s, 2H, NCH_3), 1.12 (d, J_{HH} 10.2 Hz, 1H, H_{anti}). ^{13}C{^{1}H} NMR, δ 241.8, 238.3 (CO), 171.8 (C=O), 130.3–126.2 (Ph), 94.2 (Cp), 70.3 (CH_{centre}), 61.1 (CPh_3), 50.8 (CH_{syn}), 37.1, 36.1 (NCH_3). FAB MS: *m/z* 574 (M^+ + 1), 545 (M^+ − CO), 515 (M^+ − 2CO). **4a**: ^{1}H NMR ($CDCl_3$): δ 7.27–7.08 (m, Ph), 6.55 (s, 1H, =CH), 5.33 (s, 5H, C_5H_5), 2.74 (d, J_{HH} 22.4 Hz, 1H, CH*H*), 2.28 (d, J_{HH} 22.4 Hz, 1H, C*H*H), 3.26–2.66 (m, 4H, CH_2NCH_2), 1.96 (m, 6H, $CH_2NCH_2CH_2CH_2CH_2$). ^{13}C NMR [$(CD_3)_2CO$], δ 180 (CON), 162.5 (Mo–C), 147.5 (=CH–), 47.2 (CH_2).

‡ *Crystal data* for **2b**: $C_{34}H_{31}O_4NMo$, M = 613.54, monoclinic, space group $P2_1/c$, a = 13.6809(4), b = 9.8539(3), c = 21.6322(7) Å, β = 104.061(1), V = 2828.9(2) Å^3, Z = 4, D_C = 1.441 g cm^{-3}, μ = 5.03 cm^{-1}, F(000) = 1264, 20 869 reflections collected on Smart CCD [T = 295(2) K], 6481 independent reflections (R_{int} = 0.0436) observed with $I > 2\sigma(I)$, 362 parameters, no restraints. The final discrepancy indices R_1 and wR_2 were 0.0357 and 0.0734 respectively. CCDC 182/980.

1 C.-C. Su, J.-T. Chen, G.-H. Lee and Y. Wang, *J. Am. Chem. Soc.*, 1994, **116**, 4999; J.-C. Choi and T. Yamamoto, *J. Am. Chem. Soc*., 1997, **119**, 12 390; R.-H. Hsu, J.-T. Chen, G.-H. Lee and Y. Wang, *Organometallics*, 1997, **16**, 1159; K. Okuro and H. Alper, *J. Org. Chem.*, 1997, **62**, 1566.

2 K.-W. Liang, G.-H. Lee, S.-M. Peng and R.-S. Liu, *Organometallics*, 1995, **14**, 2353; P. Blenkiron, J. F. Corrigan, N. J. Taylor and A. J. Carty, *Organometallics*, 1997, **16**, 297; S. Doherty, M. R. J. Elsegood, W. Clegg, N. H. Rees, T. H. Scanlan and M. Waugh, *Organometallics*, 1997, **16**, 3221; S. Doherty, M. R. J. Elsegood, W. Clegg, M. F. Ward and M. Waugh, *Organometallics*, 1997, **16**, 4251; M. A. Esteruelas, F. J. Lahoz, M. Martin, E. Onate and L. A. Oro, *Organometallics*, 1997, **16**, 4572.

3 M.-C. Chen, R.-S. Keng, Y.-C. Lin, Y. Wang, M.-C. Cheng and G. H. Lee, *J. Chem. Soc., Chem. Commun*., 1990, 1138.

4 T.-W. Tseng, I.-Y. Wu, J.-H. Tsai, Y.-C. Lin, D.-J. Chen, G.-H. Lee, M.-C. Cheng and Y. Wang, *Organometallics*, 1994, **13**, 3963.

5 T.-W. Tseng, I.-W. Wu, Y.-C. Lin, C.-T. Chen, M.-C. Chen, Y.-J. Tsai, M.-C. Chen and Y. Wang, *Organometallics*, 1991, **10**, 43; I.-Y. Wu, T.-W. Tseng, Y.-C. Lin, M.-C. Cheng and Y. Wang, *Organometallics*, 1993, **12**, 478.

6 L. Lee, I.-Y. Wu, Y.-C. Lin, G.-H. Lee and Y. Wang, *Organometallics*, 1994, **13**, 2521.

7 H. A. Brune, W. Eberius and H. P. Wolff, *J. Organomet. Chem.*, 1968, **12**, 485.

8 K. Hiraki, N. Ochi, Y. Sasada, H. Hayashida, Y. Fuchita and S. Yamanaka, *J. Chem. Soc., Dalton Trans.*, 1985, 873; E. Hernandez and H. Hoberg, *J. Organomet. Chem.*, 1986, **315**, 245; R. Vac, J. H. Nelson, E. B. Milosavljevic, L. Solujic and J. Fischer, *Inorg. Chem.*, 1989, **28**, 4132.

9 D. Hedden, D. M. Roundhill, W. C. Fultz and A. L. Rheingold, *Organometallics*, 1986, **5**, 336; R. D. Adams and S. Wang, *Organometallics*, 1987, **6**, 45; M. Shakij, S. P. Varkey and P. S. Hameed, *Polyhedron*, 1994, **13**, 1355.

10 G. Bodenhausen and D. J. Ruben, *Chem. Phys. Lett.*, 1980, **69**, 185.

11 W. Adam, J. Rutterlik, R.-M. Schuhmann and J. Sundermeyer, *Organometallics*, 1996, **15**, 4586; G. Jia, W.-F. Wu, R. C. Y. Yeung and H.-P. Xia, *J. Organomet. Chem.*, 1997, **539**, 53.

12 A. Bax and M. F. Summers, *J. Am. Chem. Soc.*, 1986, **108**, 2093; A. Bax and D. Marion, *J. Magn. Reson.*, 1988, **78**, 186.

13 F. Muller, G. van Koten, K. Vrieze and D. Heijdenrijk, *Organometallics*, 1989, **8**, 33.

Received in Cambridge, UK, 21st July 1998; 8/05689G

Electrospray mass spectrometric studies of the rhenium hydroxy and methoxy carbonyl complexes $[Re_2(\mu\text{-}OR)_3(CO)_6]^-$ (R = H, Me)

Chenghua Jiang,[a] William Henderson,*[b] T. S. Andy Hor,*[a] Louise J. McCaffrey[b] and Yaw Kai Yan*[c]

[a] *Department of Chemistry, Faculty of Science, National University of Singapore, Kent Ridge, Singapore 119260*
[b] *Department of Chemistry, University of Waikato, Private Bag 3105, Hamilton, New Zealand*
[c] *Division of Chemistry, National Institute of Education, Nanyang Technological University, 469 Bukit Timah Road, Singapore 259756. E-mail: yanyk@nievax.nie.ac.sg*

Exchange reactions of $[Re_2(\mu\text{-}OR)_3(CO)_6]^-$ (R = H, Me) with alcohols and phenol have been established by electrospray mass spectrometry (ESMS); dehydration of $[Re_2(\mu\text{-}OH)_3(CO)_6]^-$ and the β-hydride elimination reaction of $[Re_2(\mu\text{-}OMe)_3(CO)_6]^-$ have also been observed under ESMS conditions.

Transition-metal carbonyl hydroxides and alkoxides have been proposed as intermediates in a number of important reactions, such as metal-catalysed hydrogenation of CO,[1] the water–gas shift reaction,[2] and carboalkoxylation of alkenes.[3] Although the syntheses of the complexes $[Re_2(\mu\text{-}OR)_3(CO)_6]^-$ (R = H, Me, Et, Pr^i) were reported more than two decades ago,[4] the chemistry of these complexes have received relatively little attention.[5] This is perhaps due to the perceived limited scope of reactivity of these compounds. Simpson and Bergman recently reported the facile alkoxide-exchange reactions of the terminal-alkoxo complexes *fac*-$[Re(\eta^1\text{-}OR)(L)_2(CO)_3]$ (L = phosphine or arsine, R = Me, Et, Pr^i) with alcohols and phenols.[6] It is of interest to investigate the feasibility of analogous exchange reactions involving the bridging-alkoxo complexes $[Re_2(\mu\text{-}OR)_3(CO)_6]^-$, which have in principle three exchangeable alkoxide or hydroxide ligands. Such exchange reactions have been briefly alluded to in the literature[4b,7] but no systematic study has been carried out on them.

The study of the alkoxide exchange reactions of the tris-alkoxo-bridged complexes is expected to be complicated by the formation of singly, doubly and triply-exchanged species which exist in equilibrium with each other (Scheme 1). Identification of these inter-converting species in solution by IR or NMR spectroscopy is expected to be very difficult, especially when the R group (*e.g. n*-octyl) gives a complex ^{1}H NMR spectrum.

We wish to report here that electrospray mass spectrometry (ESMS) is a very convenient yet informative technique that is appropriate for the study of the exchange reactions of the complexes $[Re_2(\mu\text{-}OH)_3(CO)_6]^-$ **1** and $[Re_2(\mu\text{-}OMe)_3(CO)_6]^-$ **2**.† Ionic species existing in equilibrium in solution are transferred intact into the gas phase in the spectrometer and can be directly identified by their *m/z* values, regardless of their rate of inter-conversion on the NMR timescale. Thus, the various exchanged species arising from the reactions of **1** and **2** with different alcohols can be unambiguously identified in the mass spectra and the relative abundance of these species at different times after addition of alcohol can be monitored.

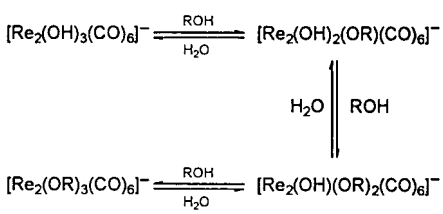

Scheme 1

At a cone voltage of 5 V, solutions of complex **1** in MeCN (typically 0.1 mg ml^{-1}) give a clean strong signal of the parent ion at *m/z* 591/593, together with a weak ion signal at *m/z* 879 corresponding to $[Re_3(OH)_4(CO)_9]^-$.[8] The latter ion is most probably a side product during the synthesis of **1**.[5] This impurity can be converted to **1** simply by adding a drop of aqueous NaOH to the ESMS solution.[9]

About 1 min after addition of a few drops of methanol to the ESMS solution of **1**, the spectrum showed low intensity peaks at *m/z* 605/607, 619/621 and 633/635, corresponding respectively to the singly, doubly and triply (OH → OMe) exchanged species. The peaks of the exchanged species rapidly grew in intensity with respect to that of the parent ion $[Re_2(\mu\text{-}OH)_3(CO)_6]^-$ over 10 min. (Fig. 1), although the exact relative intensities of these peaks at 10 min showed some variability between experiments. On standing the solution overnight (16 h) the main ion observed was $[Re_2(\mu\text{-}OMe)_3(CO)_6]^-$, with the bis- and mono-methoxy ions still present in successively lower abundance, and no parent ion remaining. A clean intense peak of the permethoxylated ion was obtained on letting the solution stand for two weeks, with trace peaks of only the bis-methoxy species remaining. It is also noteworthy that throughout the experiment, the trirhenium ion $[Re_3(OH)_4(CO)_9]^-$ appeared to be unaffected by methanol. These results indicate that (OH → OMe) exchange is quite facile on complex **1**, with all three hydroxy ligands being replaceable.

The (OH → OMe) exchange is readily reversible, as indicated by the ESMS detection of small amounts of $[Re_2(\mu\text{-}$

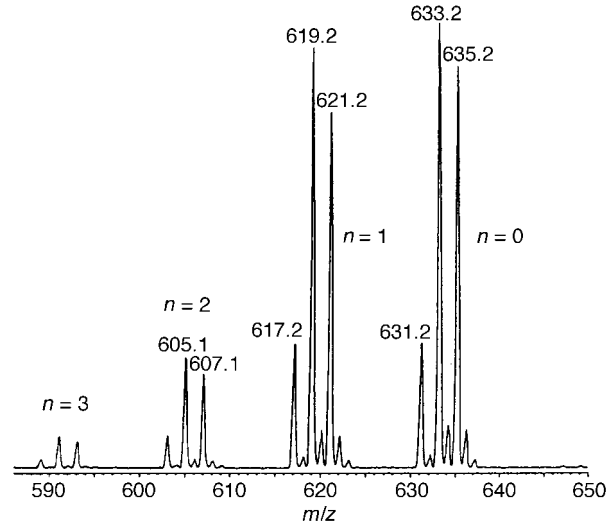

Fig. 1 High-resolution negative ion electrospray mass spectrum of a solution of complex **1** in MeCN, 10 min after addition of MeOH (cone voltage 5 V), showing the presence of the ions $[Re_2(OH)_n(OMe)_{3-n}(CO)_6]^-$ (n = 0–3)

Table 1 Exchange reactions of complexes **1** and **2** with various reagents

Complex	Reagent	Maximum number of OH/OMe groups exchanged
1	*tert*-Butanol	1
1	Methanol	3
1	Ethanol	3
1	*n*-Octanol	3
1	Phenol	3
1	*p*-Toluenethiol, MeC_6H_4SH	3
1	Benzeneselenol, PhSeH	2
1	$FcCH_2PH_2$ (Fc = ferrocenyl)	0
1	$H_2C(CN)_2$	0
2	Water	3
2	Ethanol	3
2	Phenol	3

$OMe)_2(\mu\text{-}OH)(CO)_6]^-$ even in a freshly made solution of complex **2** in MeCN (not rigorously dried). Other than this hydrolysis product, the spectrum contained only the strong signal of the intact **2** ion at *m/z* 633/635. On adding two drops of water to the ESMS solution, hydrolysis occured over a period of minutes to generate a mixture of mono-, bis- and tris-hydroxy complexes, and after 35 min the dominant ion was $[Re_2(\mu\text{-}OH)_3(CO)_6]^-$. Addition of four drops of methanol to this solution quickly (within 1 min) removed $[Re_2(\mu\text{-}OH)_3(CO)_6]^-$ and regenerated $[Re_2(\mu\text{-}OMe)_3(CO)_6]^-$ as the most abundant ion. These results suggest that (OH → OMe) exchange is more facile than (OMe → OH) exchange, possibly due to the greater steric accessibility of the {Re(μ-OH)Re} unit compared to its methoxy analogue.

Exchange reactions of **1** and **2** with other protic compounds have also been investigated by ESMS, as summarised in Table 1. The results are consistent with an exchange mechanism that involves proton transfer to the hydroxy or methoxy ligands as the first step, since compounds with very weakly acidic protons such as malononitrile and ferrocenylmethylphosphine[10] do not displace the OH and OMe ligands. In this context, it is noteworthy that the electrospary mass spectrum of a solution of a 1 : 1 mixture of **1** and **2** in alcohol-free MeCN showed no OH/OMe scrambled species even after 24 h. Steric factors also play an important role in determining facility of reaction, as indicated by the ability of complex **1** to exchange for only one *tert*-butoxide group.

By themselves, complexes **1** and **2** also exhibit interesting fragmentation behaviour at higher cone voltages. Dehydration of **1** begins to occur at 20 V, when a low abundance peak due to $[Re_2(O)(OH)(CO)_6]^-$ (*m/z* 573/575) appears in the mass spectrum. At 40 V, this is the most abundant ion, with very little parent ion remaining. Decarbonylation of the dehydrated species begins to occur at a cone voltage of 60 V, as indicated by the presence of the ions $[Re_2(O)(OH)(CO)_n]^-$ (n = 3–5). Decarbonylation without dehydration apparently does not occur, since ions such as $[Re_2(\mu\text{-}OH)_3(CO)_n]^-$ (n = 3–5) are not detected throughout. This result clearly indicates that dehydration of complex **1** is energetically much more favourable than decarbonylation.

Dehydration does not occur with complex **2**, which fragments *via* β-hydride elimination instead, at a cone voltage of 50 V. The parent ion eliminates formaldehyde to form $[Re_2(H)(OMe)_2(CO)_6]^-$ (*m/z* 603/605), $[Re_2(H)_2(OMe)(CO)_6]^-$ (*m/z* 573/575), and finally the known species[4b] $[Re_2(H)_3(CO)_6]^-$ (*m/z* 543/545). Decarbonylation of the β-eliminated species also occur at 50 V to give $[Re_2(H)(OMe)_2(CO)_5]^-$ (*m/z* 575/577) and $[Re_2(H)_2(OMe)(CO)_5]^-$ (*m/z* 545/547). The peaks of these decarbonylated ions overlap with the peaks at *m/z* 573/575 and 543/545 respectively to give characteristic 'triplet' patterns. Confirmation of these ions was achieved by deuterium labelling, the species $[Re_2(OCD_3)_3(CO)_6]^-$ being generated by addition of excess CD_3OD to **1**. At high cone voltages, the expected mass shifts corresponding to the ions $[Re_2(D)_n(OCD_3)_{3-n}(CO)_6]^-$ (n = 0–3) were observed. Elimination of acetaldehyde also occurs in an analogous fashion from the ion $[Re_2(OEt)_3(CO)_6]^-$, which was generated by addition of ethanol to **1**. As far as we are aware, β-hydride elimination from coordinated alkoxide ligands has not been observed by ESMS previously.

In conclusion, this study has shown that the complex anions $[Re_2(\mu\text{-}OH)_3(CO)_6]^-$ **1** and $[Re_2(\mu\text{-}OMe)_3(CO)_6]^-$ **2** undergo facile exchange reactions with alcohols and phenol. The feasibility and extent of these reactions can be conveniently and unambiguously determined by electrospray mass spectrometry. The results also suggest that complex **1** can be used as a versatile starting material for the synthesis of a wide range of analogous $[Re_2(\mu\text{-}OR)_3(CO)_6]^-$ and $[Re_2(\mu\text{-}SR)_3(CO)_6]^-$ complexes, by simple reaction of **1** with an excess of the appropriate alcohol or thiol. Other protic or electrophilic compounds can also be investigated for their reactivity with **1**, simply by adding the compound to a solution of **1** and recording the electrospray mass spectrum of the solution. Thus, ESMS can be used as a quick but accurate technique to screen for potentially useful reactions. The prospect of **1** showing interesting biological activity *via* interaction with the OH, SH and NH functional groups of biomolecules is also attractive and is currently being investigated in our laboratories.[11]

We thank the National University of Singapore (NUS) (RP 950695), the University of Waikato, the National Institute of Education, Singapore (RP 15/95 YYK) and the New Zealand Lottery Grants Board for financial support. The award of an NUS research scholarship to C. J. is also gratefully acknowledged, together with a travel grant (to W. H. and L. McC.) from the Asia 2000 Foundation.

Notes and References

† Electrospray mass spectra were obtained in the negative-ion mode with a VG Platform II quadrupole mass spectrometer using HPLC-grade MeCN as the mobile phase. The samples (in MeCN solution) were injected *via* a Rheodyne injector fitted with a 10 μl sample loop, and delivered to the spectrometer source (60 °C) at 0.01 ml min^{-1}. Nitrogen was used as the drying and nebulising gas, and the capillary voltage was 3.5 kV. Cone voltages were typically varied between 5 and 80 V in order to investigate the formation of fragment ions.

1 D. Milstein, *J. Am. Chem. Soc.*, 1986, **108**, 3525.
2 M. A. Bennett and T. W. Matheson, in *Comprehensive Organometallic Chemistry*, ed. G. Wilkinson, F. G. A. Stone and E. W. Abel, Pergamon, Oxford, 1st edn., 1982, vol. 4.
3 H. E.Bryndza and W. Tam, *Chem. Rev.*, 1988, **88**, 1163.
4 (*a*) A. A. Ioganson, B. V. Lokshin, E. E. Kolobova and K. N. Anisimov, *J. General Chem.*, 1974, **20**, 20 (Translated from *Zh. Obshch. Khim.*, 1974, **44**, 23); (*b*) A. P. Ginsberg and M. J. Hawkes, *J. Am. Chem. Soc.*, 1968, **90**, 5930; (*c*) G. Ciani, G. D'Alfonso, M. Freni, P. Romiti and A. Sironi, *J. Organomet. Chem.*, 1978, **152**, 85; (*d*) M. Freni and P. Romiti, *Atti Accad. Naz. Lincei, Mem. Cl. Sci. Fis. Mat. Nat. Rend.*, 1973, **55**, 515.
5 C. Jiang, Y.-S. Wen, L.-K. Liu, T. S. A. Hor and Y. K. Yan, *Organometallics*, 1998, **17**, 173.
6 R. D. Simpson and R. G. Bergman, *Organometallics*, 1993, **12**, 781.
7 G. Ciani and A. Sironi, *Gazz. Chim. Ital.*, 1979, **109**, 615.
8 There is excellent agreement between observed and calculated isotope patterns (L. J. Arnold, *J. Chem. Ed.*, 1992, **69**, 811).
9 Consistent with the equation: 2 $[Re_3(OH)_4(CO)_9]^-$ + OH^- → 3 $[Re_2(OH)_3(CO)_6]^-$. See also Ref. 11(*a*).
10 N. J. Goodwin, W. Henderson and B. K. Nicholson, *Chem. Commun.*, 1997, 31.
11 Water-soluble, low-valent rhenium compounds have received much attention recently due to their potential application in radioimmunotherapy and protein labelling. See: (*a*) R. Alberto, A. Egli, U. Abram, K. Hegetschweiler, V. Gramlich and P. A. Schubiger, *J. Chem. Soc., Dalton Trans.*, 1994, 2815 and references therein; (*b*) U. Abram, S. Abram, R. Alberto and R. Schibli, *Inorg. Chim. Acta*, 1996, **248**, 193 and references therein.

Received in Cambridge UK, 21st July 1998; 8/05684F

Multimetallic porphyrin monomers

Scott L. Darling,[a] Peter K. Y. Goh,[a] Nick Bampos,[a] Neil Feeder,[a] Marco Montalti,[b] Luca Prodi,[b] Brian F. G. Johnson[a] and Jeremy K. M. Sanders*[a]

[a] *University Chemical Laboratory, Lensfield Road, Cambridge, UK CB2 1EW. E-mail: jkms@cam.ac.uk*
[b] *Dipartimento di Chimica 'G. Ciamician', Università degli Studi di Bologna, I-40126 Bologna, Italy*

Complexation of triosmium clusters to pyridyl functionalised metalloporphyrins gives heterometallic derivatives that possess the overall recognition and spectroscopic properties of the porphyrin fragment, while incorporating the electronic and structural characteristics of the cluster.

In recent years a range of porphyrin complexes incorporating numerous metal centres have been prepared as components for molecular-scale devices,[1] conjugated porphyrin polymers,[2] supramolecular systems[3] and light harvesting models.[4] These designs exploit the ability of the metal centre to control the manner in which a supramolecular assembly is constructed, and therefore dictate the properties of the final arrangement. Here we report on the preparation and characterisation of a series of triosmium cluster zinc porphyrin derivatives.

The porphyrin monomers **1**–**3** were synthesised by routes analogous to those previously reported.[5] Their key feature is the incorporation of one or more peripheral pyridyl groups available for metallation by an osmium cluster.[6] The pyridyl ring nitrogen is situated in either the 3-position, from which we might expect two cluster substitution products, or the 4-position from which only one product is possible. Treatment of **1** or **2** with $Os_3(CO)_{10}(NCMe)_2$ (1.1 equiv.) in dichloromethane at room temperature affords, after purification by preparative TLC (SiO_2, hexane : chloroform : ethyl acetate, 20 : 1 : 1), the metallated products **4** and **5** in 42% (R_f = 0.28) and 31% (R_f = 0.32) yields respectively (Scheme 1). Under similar reaction conditions, the bis-coordinated cluster compound **6** was isolated in 35% yield from the reaction of $Os_3(CO)_{10}(NCMe)_2$ (2.2 equiv.) with **3** after preparative TLC (SiO_2, hexane : chloroform : ethyl acetate, 10 : 1 : 1, R_f = 0.29).†

Single crystals of **4** and **5** suitable for X-ray crystallographic analysis were obtained by slow solvent diffusion of methanol into a toluene solution at room temperature.‡ The molecular structure of **4** is as expected: the pyridyl ring of the porphyrin is orthometallated and bridges one edge of the Os_3 triangle to afford a four membered ring containing Os, Os, C and N with the hydride ligand bridging one Os–Os edge. This is consistent with the structure of $[(\mu\text{-H})Os_3(CO)_{10}(\mu\text{-}NC_5H_4)]$.[6] The molecular structure of **5** is isostructural with **4**, the Os_3 unit residing on the 3- and 4-positions on the pyridyl ring (Scheme 1). The unoccupied site nearest to the porphyrin ring (2-position) is presumably inhibited to metallation on steric grounds.

The ^{1}H NMR spectra of **4** and **5** are consistent with the unsymmetrical nature of the molecule: in the spectrum of **4** we observe the porphyrin ring methyl groups as three singlets in a 1 : 2 : 1 intensity ratio. The peripheral methyl groups nearest to the appended cluster are inequivalent, appearing as two singlets because the cluster is not symmetrically disposed about the pyridine ring. However, the furthest methyl groups are unaffected by the presence of the cluster and are effectively equivalent, giving rise to one singlet. The protons of the first methylene group of the hexyl side chains are diastereotopic; additionally two equal intensity *meso* proton resonances are observed. Both of these observations are consistent with the expected slow rotation on the NMR chemical shift timescale about the cluster substituted aryl–porphyrin bond. Since complex **5** follows the same cluster coordination mode as **4**, the spectrum of **5** exhibits similar resonances to **4**.

For **6** the coordinated clusters can be *cis* or *trans* to one another (relative to the porphyrin plane) as shown in Scheme 2.§ At ambient temperature the ^{1}H NMR spectrum of **6** exhibits one

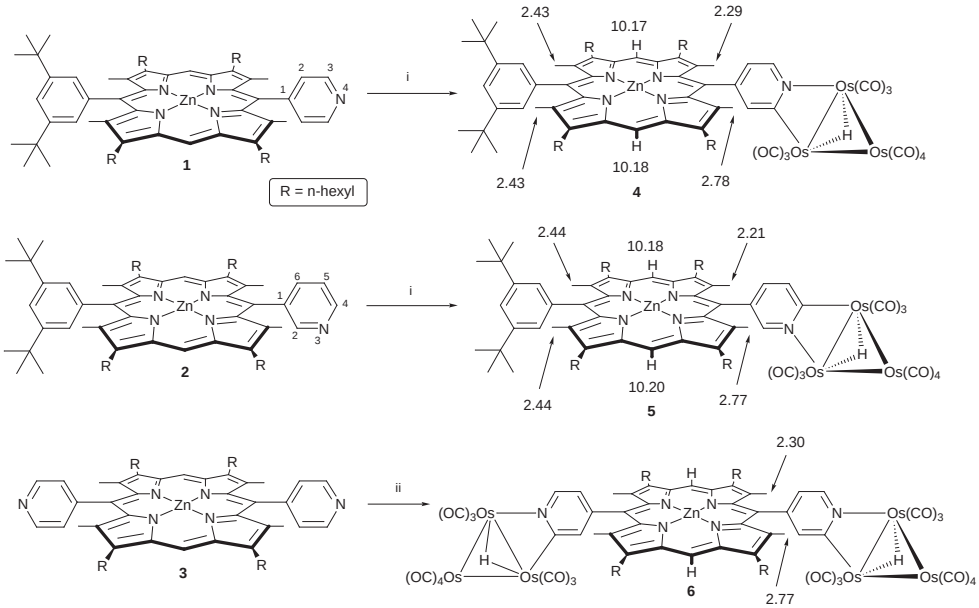

Scheme 1 *Reagents and conditions*: i, 1.1 equiv. $Os_3(CO)_{10}(NCMe)_2$, CH_2Cl_2, RT, 3 h; ii, 2.2 equiv. $Os_3(CO)_{10}(NCMe)_2$, CH_2Cl_2, RT, 4 h. Selected chemical shifts for complexes **4**–**6**.

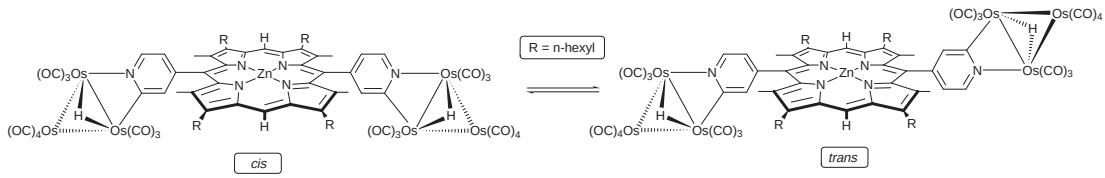

Scheme 2 Exchange between the *cis* and *trans* isomeric forms of **6**

meso resonance which splits into a 1 : 2 : 1 multiplet at 280 K indicating the presence of at least two species (*cis* and *trans* isomers). A NOESY experiment at 280 K shows NOE cross-peaks for the outer signals, H_a and H_b, of the 1 : 2 : 1 multiplet only with the central resonance, H_c indicating that the *cis* and *trans* isomers are interconverting on the NOESY timescale. For the methyl groups at room temperature two equal intensity resonances are observed, which remain essentially unchanged at 280 K. The NOESY spectrum at 280 K reveals that these methyl resonances exhibit exchange cross-peaks with each other; in addition the bridging hydride shows a strong NOE cross-peak to the methyl resonance at 2.30 ppm, and a weak NOE cross-peak to the resonance at 2.77 ppm due to magnetisation transfer (Fig. 1). The above observations show that the *meso* protons are sensitive to the overall symmetry of the molecule, while the methyl resonances are only sensitive to the local environment dominated by the orientation of the clusters.[7]

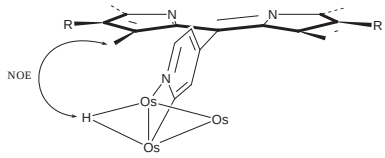

Fig. 1 The orientation of the coordinated cluster relative to the peripheral methyl groups. The CO ligands of the cluster have been omitted.

The absorption spectra of **4**–**6** were similar to **1**–**3**, except for a hypochromic shift of 4, 3, and 7 nm of the Soret band respectively and an increase in absorption between 220 and 420 nm where the cluster absorption bands are evident. More pronounced changes were observed in the luminescence spectra of **4**–**6**. At both room temperature and 77 K the fluorescence spectra intensities and excited state lifetimes of **4**–**6** were somewhat quenched compared to **1**–**3**.¶ Excitation spectra acquired at room temperature at 590 nm, where the fluorescence of the porphyrin is observed, indicate the absence of the cluster bands. In addition, the phosphorescence bands of **4**–**6** compared to **1**–**3** at 77 K show an increase in intensity and a decrease in the triplet lifetime. Collectively, these observations suggest that the quenching observed can be ascribed to a heavy atom effect arising from the cluster rather than to energy- or electron-transfer processes between the cluster and the porphyrin.

The mild preparation and spectroscopic eloquence of complexes **4**–**6** provide potential for the development of functional and structural derivatives. Variation in the nature of the appended cluster, and the porphyrin periphery can be envisaged.

We thank the Engineering and Physical Sciences Research Council, Singapore Government and Università di Bologna (Funds for Selected Research Topics) for financial support.

Notes and References

† *Selected spectroscopic data* for **4**: ^{1}H NMR ($CDCl_3$, 400 MHz) δ 10.18 (s, 1 H), 10.17 (s, 1 H), 8.56 (d, *J* 5.6 Hz, 1 H), 8.26 (d, *J* 1.5 Hz, 1 H), 7.92 (br s, 2 H), 7.82 (t, *J* 1.8 Hz, 1 H), 7.53 (dd, *J* 2.0, 5.8 Hz, 1 H), 3.94 (m, 8 H), 2.78 (s, 3 H), 2.43 (s, 6 H), 2.29 (s, 3 H), 2.16 (m, 8 H), 1.74 (m, 8 H), 1.51 (s, 18 H), 1.48 (m, 8 H), 1.38 (m, 8 H), 0.89 (m, 12 H), −14.83 (s, 1 H); FAB *m*/*z* 1884.5 (M^+); IR (CH_2Cl_2) ν_{CO}/cm^{-1} 2103 (m), 2063 (s), 2052 (s), 2018 (br, s), 2010 (br, s), 1989 (br, m), 1969 (br, w); λ_{max} (CH_2Cl_2)/nm 414, 540, 575 (log [ε/M^{-1} cm^{-1}] 5.3, 4.1, 3.8). For **5**: ^{1}H NMR ($CDCl_3$, 400 MHz) 10.20 (s, 1 H), 10.18 (s, 1 H), 8.92 (d, *J* 1.4 Hz, 1 H), 7.97 (dd, *J* 2.0, 7.9 Hz, 1 H), 7.92 (br s, 2H), 7.83 (t, *J* 1.7 Hz, 1 H), 7.80 (d, *J* 7.6 Hz, 1 H), 3.96 (m, 8 H), 2.77 (s, 3 H), 2.44 (s, 6 H), 2.21 (s, 3 H), 2.19 (m, 8 H), 1.74 (m, 8 H), 1.51 (s, 18 H), 1.46 (m, 8 H), 1.41 (m, 8 H), 0.92 (m, 12 H), −14.74 (s, 1 H); FAB *m*/*z* 2621.1 (M^+); IR (CH_2Cl_2) ν_{CO}/cm^{-1} 2103 (m), 2063 (vs), 2052 (s), 2017 (vs), 2008 (sh), 1998 (sh), 1970 (sh). λ_{max} (CH_2Cl_2)/nm 414, 540, 575 (log [ε/M^{-1} cm^{-1}] 5.2, 4.0, 3.7). For **6**: ^{1}H NMR ($CDCl_3$, 400 MHz) 10.17 (s, 2 H), 8.57 (d, *J* 5.6 Hz, 2 H), 8.23 (d, *J* 1.0 Hz, 2 H), 7.48 (dd, *J* 1.7, 4.7 Hz, 2 H), 3.95 (m, 8 H), 2.77 (s, 6 H), 2.30 (s, 6 H), 2.17 (m, 8 H), 1.72 (m, 8 H), 1.49 (m, 8 H), 1.35 (m, 8 H), 0.91 (m, 12 H), −14.83 (s, 2 H); FAB *m*/*z* 2621.1 (M^+); IR (CH_2Cl_2) ν_{CO}/cm^{-1} 2103 (m), 2063 (vs), 2052 (s), 2017 (br, s), 2008 (br, s), 1998 (br, m), 1970 (br, w); λ_{max} (CH_2Cl_2)/nm 417, 541, 578 (log [ε/M^{-1} cm^{-1}] 5.3, 4.1, 3.8).

‡ *Crystal data* for **4**: $C_{77}H_{91}N_5O_{10}Os_3Zn$, 0.35 × 0.25 × 0.20 mm, T = 180(2) K, M = 1882.5, triclinic, space group $P\bar{1}$, a = 18.139(5), b = 19.184(7), c = 12.811(5) Å, α = 103.81(3), β = 108.47(3), γ = 102.88(3)°, U = 3884(2) Å^3, Z = 2, D_c = 1.60 Mg m^{-3}, λ = 0.71069 Å, F(000) = 1852, μ = 5.253 mm^{-1}, R_1 = 0.0672 [18337 reflections with $I > 2\sigma(I)$], wR_2 = 0.1580 for 17790 independent reflections and 810 parameters. The crystal data for **4** were collected on a Rigaku AFC7r diffractometer. For **5**: $C_{77}H_{91}N_5O_{10}Os_3Zn$, 0.12 × 0.10 × 0.10 mm, T = 180(2) K, M = 1882.5, triclinic, space group $P\bar{1}$, a = 18.135(5), b = 19.048(6), c = 12.739(5) Å, α = 103.55(3), β = 108.74(3), γ = 102.88(3)°, U = 3833(2) Å^3, Z = 2, D_c = 1.63 Mg m^{-3}, λ = 0.71069 Å, F(000) = 1852, μ = 5.324 mm^{-1}, R_1 = 0.0615 [36807 reflections with $I > 2\sigma(I)$], wR_2 = 0.1624 for 13666 independent reflections and 832 parameters. The crystal data for **5** were collected on a R-Axis IIc diffractometer. All non-hydrogen atoms except the disordered carbons of the hexyl chains are anisotropic in both crystals. CCDC 182/989.

§ Each cluster has the possibility of the hydride bridges being *cis* (*i.e.* both at the back or front) or *trans*, with one at the front and one at the back (Scheme 2). Presumably both the *cis* and *trans* isomers of **6** consist of a mixture of front/front and front/back forms, but the distance between the clusters is so great that the two isomers are spectroscopically indistinguishable.

¶ The fluorescence lifetimes at 298 K were 0.76, 0.70, 0.76, 0.30, 0.37 and 0.21 ns for **1**–**6** respectively.

1 R. W. Wagner, J. S. Lindsey, J. Seth, V. Palaniappan and D. F. Bocian, *J. Am. Chem. Soc.*, 1996, **118**, 3996; L. Jaquinod, O. Siri, R. G. Khoury and K. M. Smith, *Chem. Commun.*, 1998, 1261 and references therein.

2 P. N. Taylor, J. Huuskonen, G. Rumbles, R. T. Aplin, E. Williams and H. L. Anderson, *Chem. Commun.*, 1998, 909.

3 N. Kariya, T. Imamura and Y. Sasaki, *Inorg. Chem.*, 1998, **37**, 1658; K. Funatsu, A. Kimura, T. Imamura, A. Ichimura and Y. Sasaki, *Inorg. Chem.*, 1997, **36**, 1625; A. Vidal-Ferran, N. Bampos and J. K. M. Sanders, *Inorg. Chem.*, 1997, **36**, 6117; K. M. Kadish, N. Guo, E. Van Caemelbecke, A. Froiio, R. Paolesse, D. Monti, P. Tagliatesta, T. Boschi, L. Prodi, F. Bolletta and N. Zaccheroni, *Inorg. Chem.*, 1998, **37**, 2358.

4 R. W. Wagner, T. E. Johnson and J. S. Lindsey, *J. Am. Chem. Soc.*, 1996, **118**, 11166; J.-S. Hsiao, B. P. Krueger, R. W. Wagner, T. E. Johnson, J. K. Delaney, D. C. Mauzerall, G. R. Fleming, D. F. Bocian and R. J. Donohoe, *J. Am. Chem. Soc.*, 1996, **118**, 11181; J. Seth, V. Palaniappan, R. W. Wagner, T. E. Johnson, J. S. Lindsey and D. F. Bocian, *J. Am. Chem. Soc.*, 1996, **118**, 11194.

5 H. L. Anderson and J. K. M. Sanders, *J. Chem. Soc., Perkin Trans. 1*, 1995, 2223; L. J. Twyman, unpublished results; C. C. Mak, N. Bampos and J. K. M. Sanders, *Angew. Chem., Int. Ed. Engl.*, in press.

6 C. C. Yin and A. J. Deeming, *J. Chem. Soc., Dalton Trans.*, 1975, 2091; K. Burgess, B. F. G. Johnson and J. Lewis, *J. Organomet. Chem.*, 1982, **233**, C55.

7 For a similar isomerism see: J.-F. Nierengarten, L. Oswald and J.-F. Nicoud, *Chem. Commun.*, 1998, 1545.

Received in Cambridge, UK, 31st July 1998; 8/06020G

A concise enantio- and diastereo-controlled synthesis of (−)-quinic acid and (−)-shikimic acid

Kou Hiroya and Kunio Ogasawara*†

Pharmaceutical Institute, Tohoku University, Aobayama, Sendai 980-8578: Japan

(−)-Quinic acid and (−)-shikimic acid, both recognized as the key intermediates in the shikimate pathway in plants and microorganisms, have been synthesized concisely in an enantio- and diastereo-controlled manner starting from a synthetic equivalent of (*R*)-4-hydroxycyclohex-2-enone.

Both (−)-quinic acid **1** and (−)-shikimic acid **2** occur widely in both plants and microorganisms in which they have been recognized as the pivotal biogenetic precursors in the biosynthesis of a variety of aromatic natural products in the biogenetic pathway known as the shikimate pathway.[1] Since the shikimate pathway is only operative in plants and microorganisms, development of a flexible synthetic procedure for both (−)-quinic acid **1** and (−)-shikimic acid **2** as well as a variety of their derivatives is of great importance in biogenetic studies as well as in the search for herbicidal, antifungal or antibacterial agents that do not affect mammals.[1,2] Although a number of procedures including enantiocontrolled approaches have been developed for the construction of (−)-shikimic acid[3,4] **2**, only three racemic[5] and one chiral[6] procedures have been reported for the synthesis of (−)-quinic acid **1** to date. To explore a unified enantiocontrolled route to both (−)-quinic acid **1** and (−)-shikimic acid **2**, we selected the enantiomerically pure tricyclic ketol silyl ether[7] **3**, obtained from the catalytic asymmetrization[7,8] of the *meso* tricyclic ene-1,4-diol bis-silyl ether **4** and which serves as a synthetic equivalent of (*R*)-4-hydroxycyclohex-2-enone,[9] as the starting material. We describe here a diastereoselective conversion of (−)-**3** into both (−)-quinic acid **1** and (−)-shikimic acid **2** in a concise manner in good overall yields (Scheme 1).

Ketol silyl ether[7,8] (−)-**3** (>99% ee) was treated with $OC(OMe)_2$ in THF in the presence of NaH to afford in good yield the β-keto ester which existed in the single enol form‡ **5**, $[\alpha]_D^{29}$ −191.0 (*c* 1.71, $CHCl_3$). On hydroxylation in DMSO containing KF and $P(OEt)_3$,[10,11] the enol **5** gave diastereoselectively the α-hydroxy-β-keto ester **6**, $[\alpha]_D^{30}$ −59.8 (*c* 1.09, $CHCl_3$), as a single stereoisomer. As expected, NOE experiments indicated the *exo*-stereochemistry of the hydroxy functionality, which was confirmed by the later conversion.

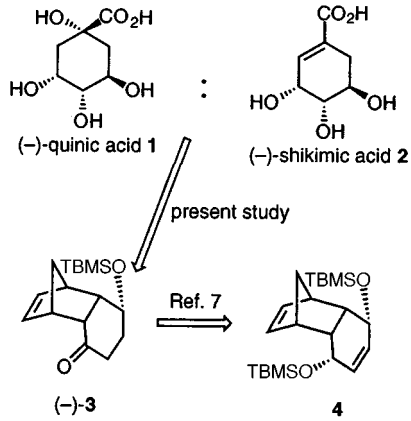

Scheme 1

After acetylation, the resulting tertiary acetate **7**, $[\alpha]_D^{30}$ −61.3 (*c* 1.17, $CHCl_3$), was subjected to thermolysis in Ph_2O (*ca.* 280 °C) to give the cyclohexenone **8**, $[\alpha]_D^{29}$ +83.5 (*c* 0.53, $CHCl_3$), by retro-Diels–Alder reaction.

Although the stereochemistry of the catalytic osmylation of (+)-**8** could not be predicted, the reaction gave a readily separable 15 : 1 mixture from which the *cis*-diol **9**, $[\alpha]_D^{28}$ +82.8 (*c* 1.22, $CHCl_3$), having *syn* configuration to the acetoxy group, was obtained in 86% yield as the major product. The observed high diastereoselectivity may be due to the axially disposed acetoxy group in the molecule, which directs the stereochemistry of the dihydroxylation by interaction with OsO_4 forming a complex such as **8a**. After protection of the *cis*-diol functionality of **9** *via* reaction with $(MeO)_2CMe_2$ in the presence of PPTS,[12] the resulting acetonide **10** was reduced with $NaBH_4$ in MeOH at low temperature to give diastereoselectively the single alcohol **11**, $[\alpha]_D^{30}$ −15.5 (*c* 1.23, $CHCl_3$), which served as the common intermediate for (−)-quinic acid **1** and (−)-shikimic acid **2**. The overall yield of **11** from (−)-**3** was 57% (Scheme 2).

To obtain (−)-quinic acid **1**, **11** was first transformed into the imidazo-1-ylthiocarbonate[13] **12**, which then was treated with Bu_3SnH[13] to give the deoxygenated product **13**, $[\alpha]_D^{30}$ −23.2 (*c* 1.39, $CHCl_3$). Removal of the three oxygen protecting groups

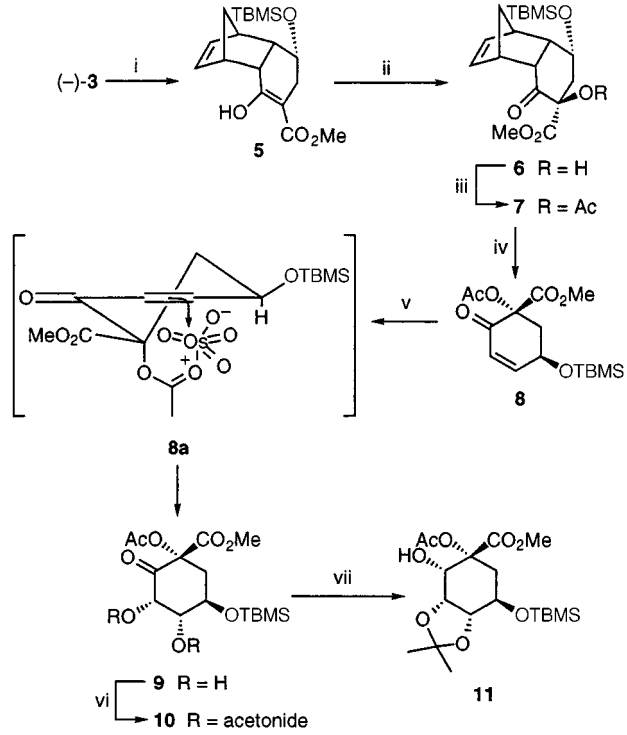

Scheme 2 *Reagents and conditions*: i, NaH, $OC(OMe)_2$, THF, room temp., 23 h (86%); ii, O_2, KF, $P(OEt)_3$, DMSO, room temp., 22 h (90%); iii, Ac_2O, pyridine, room temp., 38 h (100%); iv, Ph_2O, reflux, 1 h (100%); v, OsO_4 (cat.), NMO, THF–H_2O (2 : 1), 0 °C, 72 h (86% 15 : 1 de); vi, $Me_2C(OMe)_2$, PPTS (cat.), 65 h; vii, $NaBH_4$, MeOH, −78 °C, 1.5 h (85% from **9**)

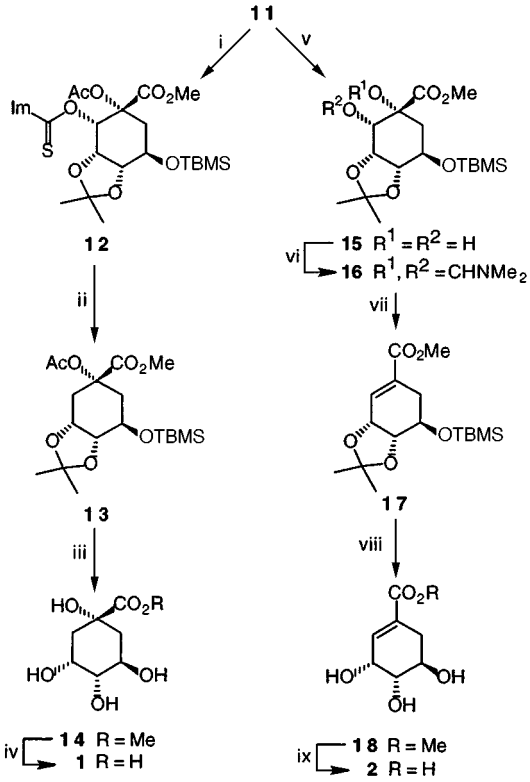

Scheme 3 *Reagens and conditions*: i, thiocarbonyl-1,1′-diimidazole, 50 °C, 14 h (100%); ii, Bu_3SnH, toluene, reflux, 9 h (80%); iii, CBr_4, MeOH, reflux, 19 h (86%); iv, NaOH, H_2O, roo temp., 13 h (100%); v, DBU, MeOH, −20 °C, 20 h; vi, $(MeO)_2CHNMe_2$, room temp., 23 h; vii, Tf_2O, Pr^i_2NEt, toluene, 50 °C, 1 h (80% from **11**); viii, 2% HCl–MeOH, room temp., 40 h (95%); ix, NaOH, THF–H_2O (1 : 1), room temp., 1 h (96%)

was carried out in one step by refluxing **13** with CBr_4 in MeOH[14] to give methyl quinate **14**, $[\alpha]_D^{30}$ −31.6 (*c* 1.45, MeOH), which was identical with authentic material derived from natural (−)-quinic acid **1**. Finally, **14** was hydrolyzed with NaOH to give (−)-quinic acid **1**, mp 167–168 °C, $[\alpha]_D^{30}$ −43.6 (*c* 2.03, H_2O) {lit.,[15] 162–163 °C, −42 to −44 (H_2O)}.

On the other hand, to obtain (−)-shikimic acid **2**, **11** was first deacetylated to give the *cis*-1,2-diol **15**, which afforded the cyclohexene **17**, $[\alpha]_D^{29}$ −19.7 (*c* 1.12, $CHCl_3$), *via* the cyclic amino acetal **16** on treatment with *N*,*N*-dimethylformamide dimethyl acetal followed by Tf_2O.[16] Exposure of **17** with dilute HCl in MeOH allowed spontaneous desilylation and removal of the acetonide group to give methyl shikimate **18**, $[\alpha]_D^{29}$ −130.0 (*c* 0.91, EtOH), which was identical with authentic material.[4] Finally, **18** was hydrolyzed with NaOH to give (−)-shikimic acid **2**, mp 184–185 °C, $[\alpha]_D^{25}$ −164.0 (*c* 0.59, H_2O) {lit.,[4] 184–186 °C, −163.7 (*c* 0.59, H_2O); lit.,[17] 184–186 °C, −170 (*c* 0.86, H_2O)} (Scheme 3).

We thank the Takeda Science Foundation for financial support.

Notes and References

† E-mail: konol@mail.cc.tohoku.ac.jp

‡ All new compounds had spectroscopic (IR, ^1H NMR, ^{13}C NMR, Mass) and analytical (combustion and/or high resolution mass) data consistent with the assigned structure.

1 For example: E. Haslam, *Progress in the Chemistry of Organic Natural Products*, ed. W. Herz, G. W. Kirby, R. E. Moore, W. Steglich and C. Tamm, Springer-Verlag, Wien, New York, 1996, vol. 69, p. 158; P. M. Dewick, *Nat. Prod. Rep.*, 1998, **15**, 17 and previous reports.
2 For example, M. C. Kozlowski, N. J. Tom, C. T. Seto, A. M. Sefler and P. A. Bartlett, *J. Am. Chem. Soc.*, 1995, **117**, 2128; C. U. Kim, W. Lew, M. A. Williams, H. Liu, L. Zhang, S. Swaminathan, N. Bischofberger, M. S. Chen, D. B. Mendl, C. Y. Tai, W. G. Laver and R. C. Stevens, *J. Am. Chem. Soc.*, 1997, **119**, 681.
3 Pertinent reviews for the synthesis of shikimic acid, see: M. M. Campbell, M. Sainsbury and P. A. Seavle, *Synthesis*, 1993, 179; S. Jiang and G. Singh, *Tetrahedron*, 1998, **54**, 4697; Natural (−)-quinic acid has been used as a versatile chiral building block: A. Barco, S. Benetti, C. D. Risi, P. Marchetti, G. P. Pollini and V. Zanirato, *Tetrahedron: Asymmetry*, 1997, **8**, 3515.
4 An alternative enantiocontrolled synthesis developed by the present group: T. Kamikubo and K. Ogasawara, *Chem. Lett.*, 1996, 987.
5 R. Grewe, W. Lorenzen and L. Vining, *Chem. Ber.*, 1954, **87**, 793; E. E. Smissman and M. A. Oxman, *J. Am. Chem. Soc.*, 1963, **85**, 2184; J. Wolinsky, R. Novak and R. Vasileff, *J. Org. Chem.*, 1964, **29**, 3596.
6 Conversion from D-arabinose, H. J. Bestmann and H. A. Heid, *Angew. Chem., Int. Ed. Engl.*, 1971, **10**, 336; see also R.-M. Meier and C. Tamm, *Helv. Chim. Acta.*, 1991, **79**, 807; H. Suemune, K. Matsuno, M. Uchida and K. Sakai, *Tetrahedron: Asymmetry*, 1992, **3**, 297.
7 K. Hiroya, Y. Kurihara and K. Ogasawara, *Angew. Chem., Int. Ed. Engl.*, 1995, **34**, 2287.
8 S. Otsuka and K. Tani, *Synthesis*, 1991, 665.
9 K. Ogasawara, *Pure Appl. Chem.*, 1994, **66**, 2119.
10 G. Büchi, R. Kulsa, K. Ogasawara and R. Rosati, *J. Am. Chem. Soc.*, 1970, **92**, 999.
11 H. Irie, J. Katakawa, M. Tomita and Y. Mizuno, *Chem. Lett.*, 1981, 637.
12 M. Miyashita, A. Yoshikoshi and P. A. Grieco, *J. Org. Chem.*, 1977, **42**, 3772.
13 D. H. R. Barton, W. B. Motherwell and A. Stange, *Synthesis*, 1981, 743; J. R. Rasmussen, C. J. Slinger, R. J. Kordish and D. D. Newman-Evans, *J. Org. Chem.*, 1981, **46**, 4843.
14 A. S.-Y. Lee, H.-C. Yeh and J.-J. Shie, *Tetrahedron Lett.*, 1998, **39**, 5249.
15 *Merck Index*, 1996, **12**, 8243.
16 J. L. King, B. A. Posner, K.-T. Mak and N. C. Yang, *Tetrahedron Lett.*, 1987, **34**, 3919.
17 G. W. Fleet, T. K. M. Shing and S. M. Warr, *J. Chem. Soc., Perkin Trans. 1*, 1984, 905.

Received in Cambridge, UK, 23rd July 1998; 8/05775C

Spermine and thermine conjugates of cholic acid condense DNA, but lithocholic acid polyamine conjugates do so more efficiently

Andrew J. Geall, Dima Al-Hadithi and Ian S. Blagbrough*†

Department of Pharmacy and Pharmacology, University of Bath, Claverton Down, Bath, UK BA2 7AY

Polyamine amides have been prepared from cholic and lithocholic acid by acylation of tri-Boc protected spermine and thermine and their binding affinities for calf thymus DNA were determined using an ethidium bromide fluorescence quenching assay; these polyamine amides are models for lipoplex formation with respect to gene delivery (lipofection), a key first step in gene therapy.

Amongst polyamine-containing natural products,[1] polyaminosteroids form a novel, small group whose members and their analogues display a variety of interesting biological activities. Following DNA binding studies with synthetic polyaminosteroids such as dimer **1**, up to four structural features contribute to the strength and type of DNA interactions: total number of positive charges, cation type, regiochemical distribution of the ammonium groups, and steroid hydrophobicity.[2–4] Recently, a so-called molecular umbrella **2** has been constructed from cholic acid **3** and spermidine, creating structures that can mask an attached agent (dansyl as a drug mimetic) from the surrounding environment.[5] Polyamino-steroid squalamine, isolated from liver and gallbladder tissues of the dogfish shark, *Squalus acanthias*, is a spermidine-containing sterol sulfate which displays antimicrobial and fungicidal properties, and induces osmotic lysis of protozoa.[6–8] Walker and co-workers have recently reported the DNA binding affinity and *in vitro* gene delivery potential of various polyamines conjugated to cholic and lithocholic acids **3** and **4**.[9] Although most of their transfection agents contained a cationic head group attached to a hydrophobic tail (*e.g.* cholic and lithocholic acid derivatives **5** and **6**), the more hydrophilic bile acid conjugate **7** had the greatest transfection activity.[9]

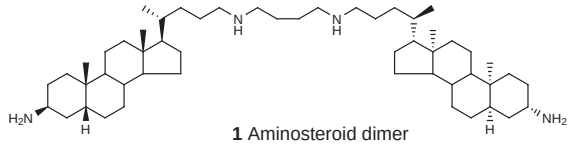

1 Aminosteroid dimer

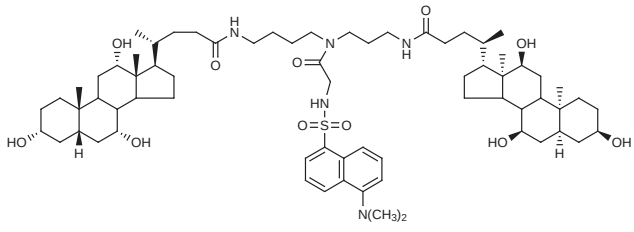

2 Aminosteroid dimer

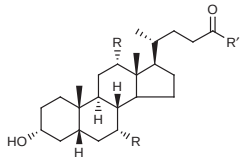

3 R = OH R′ = OH
4 R = H R′ = OH
5 R = OH R′ = pentaethylenehexamine
6 R = H R′ = pentaethylenehexamine
7 R = α-glucoside R′ = pentaethylenehexamine
8 R = H R′ = thermine
9 R = H R′ = spermine
10 R = OH R′ = thermine
11 R = OH R′ = spermine

As part of our continuing studies on polyamine-mediated DNA condensation,[10–12] we have synthesized polyamine conjugates of cholic and lithocholic acids **3** and **4** in order to investigate the effects of changes in hydrophobicity on their binding affinity to DNA. Cholic acid **3** is a sterol nucleus with a hydroxylated hydrophilic surface and an all-hydrocarbon hydrophobic surface, possessing the 5β-cholane ring structure (a *cis*-fused A,B-bicycle). The binding of polyamines to DNA is not a trivial process,[2–4,11–13] spermine and spermidine may bind preferentially to GC-rich major groove and to AT-rich minor groove regions.[11] Structure-activity relationships for the binding of polyamines to DNA, and the subsequent condensation of DNA, indicate that polyammonium ions are suitable for use as gene delivery systems.[10–14] Covalent attachment of a lipid moiety, such as an aliphatic chain or a steroid, further enhances polyamine-mediated DNA condensation. The mechanism by which these compounds cause lipofection is poorly understood.[12–15] Therefore, it is important to determine their physicochemical properties for the design of lipoplexes capable of efficient lipofection.[12,16]

Herein we report the design and synthesis of polyamine amides of lithocholic acid **4**, using our orthogonal protection strategy with polyamines thermine (1,11-diamino-4,8-diazaundecane, norspermine, 3.3.3) and spermine (1,12-diamino-4,9-diazadodecane, 3.4.3) affording **8**‡ and **9** respectively, and the corresponding cholic acid amides **10** and **11**.[10–12] The ^{1}H NMR spectra ([$^2H_6$]DMSO) of their poly-TFA salts all displayed broad ammonium signals at δ 8.00, 8.79 and 8.98 (exchanged with ^2H_2O). In addition, signals at δ 7.20 (1:1:1 t, ^1J = 51 Hz, ^{14}N-^{1}H) were observed for these ammonium ions which we interpret as due to the symmetry of the $R^{14}NH_3^+$ cations.[17] The DNA binding affinities of these polyamine bile acid conjugates were determined using calf thymus DNA and a fluorescence quenching assay based upon ethidium bromide exclusion.[18] The pK_a values of these compounds were assumed to be similar to their 3-cholesteryl carbamate analogues.[12] In our hands, all members of this series of polyamine amides **8–11** were water soluble (at 1 mg ml^{-1}).[9] The binding affinities of these polyamine conjugates have been critically compared as a function of the charge ratio at which 50% (CR_{50}) of the ethidium bromide fluorescence was quenched (measured in 20 mM NaCl). Lithocholic acid conjugates **8** and **9** displayed CR_{50} values of 0.5 and 0.7 respectively (Fig. 1), and these results compare favourably with those obtained using the 3-cholesteryl carbamate of spermine (CR_{50} = 0.62).[12] However, cholic acid conjugates **10** and **11** have significantly weaker binding affinities, displaying CR_{50} values of 5.4 and 5.9 respectively, comparable with spermine (> 4.0) (Fig. 1). Applying the calculation of Burrows and co-workers,[2] and using 330 Da as the mean weight per nucleotide,[16] the C_{50} values of **8**, **9**, **10** and **11** are 3.5, 5.4, 42.0 and 45.9 μM respectively. The poly-

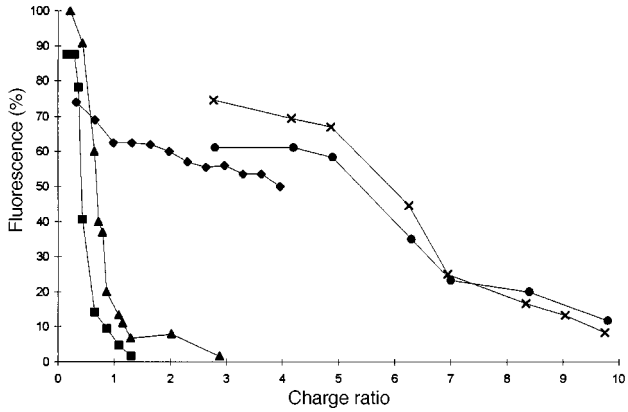

Fig. 1 Ethidium bromide exclusion assay results (calf thymus DNA, [DNA base-pair] = 3.0 μM, 1.3 μM ethidium bromide, 20 mM NaCl, excitation λ = 260 nm, emission λ = 600 nm) showing (◆) spermine, (■) lithocholic acid-thermine conjugate **8**, (▲) lithocholic acid-spermine conjugate **9**, (●) cholic acid-thermine conjugate **10** and (×) cholic acid-spermine conjugate **11**

electrolyte theory of Manning[19] predicts that when 90% of the charge on the DNA is neutralized, condensation will occur.[13] DNA condensation is clearly an efficient process with lithocholic acid polyamine amides **8** and **9** and with 3-cholesteryl carbamates (CR_{50} < 1.0), however an excess of positive charges is required for cholic acid polyamine amides **10** and **11** and for free spermine (CR_{50} > 4.0) to condense calf thymus DNA, reflecting their significantly weaker binding affinities for DNA. Whilst hydrophobicity is important for minor groove recognition,[20] DNA condensation is dependent upon hydrophobicity and distance between positive charges,[21] as well as total number of charges.[13] These data give support to our hypotheses that DNA binding and DNA condensation are also a sensitive function of the lipid attached to the polyamine, as well as a function of the positively charged polyamine moiety.

We thank the EPSRC and Celltech Therapeutics Ltd, for a CASE studentship (to A. J. G.). We acknowledge useful discussions with Dr Richard J. Taylor and Dr Michael A. W. Eaton (Celltech Therapeutics Ltd), and with Dr Ian S. Haworth (University of Southern California). I. S. B. and I. S. H. are recipients of a NATO grant (CRG 970290).

Notes and References

† E-mail: prsisb@bath.ac.uk

‡ Synthesis of **8**: Formation of the monotrifluoroacetamide of thermine, followed by immediate *in situ* Boc-protection of the remaining three amino functional groups with di-*tert*-butyl dicarbonate (4 equiv., 0 to 25 °C over 1 h, then 14 h) afforded the fully protected polyamine. The trifluoroacetyl protecting group was then removed (pH 11, conc. aq. NH_3, 25 °C, 15 h) to afford, after chromatography (flash silica gel, CH_2Cl_2–MeOH–conc. NH_3, 100:10:1 to 50:10:1 v/v/v), tri-Boc protected thermine (50%). *N*-Acylation of the primary amine with lithocholic acid (1.0 equiv., 1.5 equiv. DCC, 0.2 equiv. HOBt, CH_2Cl_2, N_2, 25 °C, 24 h) afforded, after purification (silica gel, CH_2Cl_2–MeOH, 25:1 v/v), tri-Boc protected polyamine amide (86%). Deprotection (CH_2Cl_2–TFA, 10:90 v/v, 0 °C, 2 h) and purification (semi-prep. RP-HPLC, 10 mm × 25 cm, 5 μm, ABZ+Plus, Supelcosil, MeCN–0.1% aq. TFA, 25:75 v/v, 4.0 ml min^{-1}, λ = 220 nm), afforded the poly-TFA salt of polyamine amide **8**, the title compound (34%), which was lyophilized to afford a white powder. Found (FAB +ve ion): 547.5 (M^{++}1) (100%). $C_{33}H_{62}N_4O_2$ requires: M^+, 546. HRMS (FAB +ve ion): Found: 547.4955 (M^{+}+1). $C_{33}H_{63}N_4O_2$ requires: 547.4951.

1 For selected reviews on polyamines, see: B. Ganem, *Acc. Chem. Res.*, 1982, **15**, 290; R. J. Bergeron, *Acc. Chem. Res.*, 1986, **19**, 105; I. S. Blagbrough, S. Carrington and A. J. Geall, *Pharm. Sci.*, 1997, **3**, 223 and references cited therein.
2 H.-P. Hsieh, J. G. Muller and C. J. Burrows, *J. Am. Chem. Soc.*, 1994, **116**, 12 077.
3 H.-P. Hsieh, J. G. Muller and C. J. Burrows, *Bioorg. Med. Chem.*, 1995, **3**, 823.
4 J. G. Muller, M. M. P. Ng and C. J. Burrows, *J. Mol. Recognit.*, 1996, **9**, 143.
5 V. Janout, M. Lanier and S. L. Regen, *J. Am. Chem. Soc.*, 1996, **118**, 1573; V. Janout, M. Lanier and S. L. Regen, *J. Am. Chem. Soc.*, 1997, **119**, 640.
6 K. S. Moore, S. Wehrli, H. Roder, M. Rogers, J. N. Forrest, D. McCrimmon and M. Zasloff, *Proc. Natl. Acad. Sci. U.S.A.*, 1993, **90**, 1354.
7 R. M. Moriarty, S. M. Tuladhar, L. Guo and S. Wehrli, *Tetrahedron Lett.*, 1994, **35**, 8103; R. M. Moriarty, L. A. Enache, W. A. Kinney, C. S. Allen, J. W. Canary, S. M. Tuladhar and L. Guo, *Tetrahedron Lett.*, 1995, **36**, 5139.
8 A. Sadownik, G. Deng, V. Janout and S. L. Regen, *J. Am. Chem. Soc.*, 1995, **117**, 6138.
9 S. Walker, M. J. Sofia, R. Kakarla, N. A. Kogan, L. Wierichs, C. B. Longley, K. Bruker, H. R. Axelrod, S. Midha, S. Babu and D. Kahne, *Proc. Natl. Acad. Sci. U.S.A.*, 1996, **93**, 1585; S. Walker, M. J. Sofia and H. R. Axelrod, *Adv. Drug Delivery Rev.*, 1998, **30**, 61.
10 I. S. Blagbrough and A. J. Geall, *Tetrahedron Lett.*, 1998, **39**, 439; A. J. Geall and I. S. Blagbrough, *Tetrahedron Lett.*, 1998, **39**, 443.
11 I. S. Blagbrough, S. Taylor, M. L. Carpenter, V. Novoselskiy, T. Shamma and I. S. Haworth, *Chem. Commun.*, 1998, 929 and references cited therein.
12 A. J. Geall, R. J. Taylor, M. E. Earll, M. A. W. Eaton and I. S. Blagbrough, *Chem. Commun.*, 1998, 1403.
13 S. C. Tam and R. J. P. Williams, *Struct. Bonding*, 1985, **63**, 103; E. Rowatt and R. J. P. Williams, *J. Inorg. Biochem.*, 1992, **46**, 87; V. A. Bloomfield, *Curr. Opin. Struct. Biol.*, 1996, **6**, 334 and references cited therein.
14 R. Bischoff, Y. Cordier, F. Perraud, C. Thioudellet, S. Braun and A. Pavirani, *Anal. Biochem.*, 1997, **254**, 69; G. Byk, C. Dubertret, V. Escriou, M. Frederic, G. Jaslin, R. Rangara, B. Pitard, J. Crouzet, P. Wils, B. Schwartz and D. Scherman, *J. Med. Chem.*, 1998, **41**, 224; J.-S. Remy, B. Abdallah, M. A. Zanta, O. Boussif, J.-P. Behr and B. Demeneix, *Adv. Drug Delivery Rev.*, 1998, **30**, 85.
15 C. Böttcher, C. Endisch, J.-H. Fuhrhop, C. Catterall and M. Eaton, *J. Am. Chem. Soc.*, 1998, **120**, 12.
16 P. L. Felgner, Y. Barenholz, J. P. Behr, S. H. Cheng, P. Cullis, L. Huang, J. A. Jessee, L. Seymour, F. Szoka, A. R. Thierry, E. Wagner and G. Wu, *Human Gene Ther.*, 1997, **8**, 511.
17 *Tables of Spectral Data for Structure Determination of Organic Compounds*, 2nd edn., Springer-Verlag, Berlin, 1989, H75-H80.
18 H. Gershon, R. Ghirlando, S. B. Guttman and A. Minsky, *Biochemistry*, 1993, **32**, 7143.
19 G. S. Manning, *Quart. Rev. Biophys.*, 1978, **11**, 179.
20 I. Haq, J. E. Ladbury, B. Z. Chowdhry, T. C. Jenkins and J. B. Chaires, *J. Mol. Biol.*, 1997, **271**, 244.
21 Y. Yoshikawa and K. Yoshikawa, *FEBS Lett.*, 1995, **361**, 277.

Received in Cambridge, UK, 29th June 1998; 8/04924F

Oxygenation of alkynes to α,β-acetylenic ketones with dioxygen catalyzed by *N*-hydroxyphthalimide combined with a transition metal

Satoshi Sakaguchi, Tomoyuki Takase, Takahiro Iwahama and Yasutaka Ishii*†

Department of Applied Chemistry, Faculty of Engineering and High Technology Research Center, Kansai University, Suita, Osaka 564-8680, Japan

Alkynes were successfully converted into α,β-acetylenic carbonyl compounds through radical-catalyzed aerobic oxidation using *N*-hydroxyphthalimide (NHPI) combined with a transion metal under mild conditions.

α,β-Acetylenic carbonyl compounds, ynones, are highly valuable precursors in the preparation of a variety of heterocyclic compounds,[1] α,β-unsaturated ketones,[2] cyclopentenones,[3] *C*-nuclosides[4] and chiral pheromones.[5] The conjugated ynones are usually prepared by a coupling reaction of acetylenides with activated acylating reagents such as acid chloride[6b] or anhydrides.[6c,d] Although the oxygenation of prop-2-ynylic C–H bonds is straightforward in the preparation of ynones, only a limited number of methods are available for this purpose. For instance, some chromium complexes are reported to oxidize internal alkynes to conjugated ynones in moderate yields,[7] while the oxidation of alkynes by $Th(NO_3)_2$,[8a] OsO_4,[8b] permaganates[8c] or RuO_4[8d] results in ketones and/or cleaved products such as carboxylic acids as major products. Using electrophilic oxidants such as dimethyldioxirane[9a,b] or H_2O_2,[9c] alkynes are converted into conjugated enones or diketones rather than ynones.

For the synthesis of ynones, one candidate methodology is thought to be the direct introduction of oxygen into a prop-2-ynylic C–H bond *via* a free-radical process, since the abstraction of the hydrogen atom from alkynes by a radical would occur at the energetically favorable prop-2-ynylic position. Recently, we have developed a mild generation method of an active radical species, phthalimide *N*-oxyl radical (PINO), which can readily abstract a benzylic hydrogen atom from toluene, from *N*-hydroxyphthalimide (NHPI) under the influence of dioxygen. Thus, toluene and ethylbenzene could be oxidized to benzoic acid and acetophenone, respectively, under a dioxygen atmosphere (1 atm) at room temperature.[10] Since the bond dissociation energy of the prop-2-ynylic C–H bonds of alkynes (87.3 ± 2 kcal mol^{-1} for pent-2-yne) is approximately equal to that of the benzylic C–H bond of alkylbenzenes (88.0 ± 1 kcal mol^{-1} for toluene),[11] our interest was directed toward the NHPI-catalyzed oxidation of alkynes.

Here we report the first successful catalytic aerobic oxidation of alkynes to conjugated ynones under mild conditions.

Oct-4-yne **1a** was chosen as a model substrate and allowed to react with dioxygen in the presence of a catalytic amount of NHPI and a transition metal [eqn. (1), Table 1]. Surprisingly, the oxidation of **1a** with molecular oxygen (1 atm) under the influence of NHPI (10 mol%) at room temperature produced oct-4-yn-3-one **3a** (69%) along with oct-4-yn-3-ol **2a** (23%) at 34% conversion (run 1). In analogy with the aerobic oxidation of alkylbenzenes by NHPI,[10b] the oxidation of **1a** was found to be significantly accelerated by adding a transition metal such as $Co(acac)_2$. Thus, the oxidation of **1a** catalyzed by NHPI (10 mol%) in the presence of $Co(acac)_2$ (0.5 mol%) gave **3a** (75%) and **2a** (20%) with 70% conversion (run 2).‡ The same oxidation using $Cu(acac)_2$ (0.5 mol%) in place of $Co(acac)_2$ (0.5 mol%) afforded **3a** with 77% selectivity together with **2a** (22%) at 69% conversion (run 3). However, no reaction took place when $Mn(acac)_2$ was employed in place of $Co(acac)_2$ under these conditions. When the reaction of **1a** with NHPI/$Co(acac)_2$ was carried out at elevated temperature (50 °C), the oxidation was almost complete after 6 h to give **3a** with 72% selectivity along with a small amount of a cleaved product, butanoic acid **5a** (run 6). Similar results were also obtained in the oxidation with NHPI/$Cu(acac)_2$. In the oxidation of **1a** using the NHPI/$Mn(acac)_2$ system at 50 °C, **3a** was formed with 62% selectivity at 63% conversion.

It is reported that dodec-5-yne, upon treatment with Bu^tOOH in the presence of SeO_2 catalyst, leads to the acetylenic alcohol dodec-5-yn-4-ol rather than the ynone dodec-5-yn-4-one.[12] However, the present aerobic oxidation of **1a** by the NHPI catalyst formed ynone **3a** in preference to ynol **2a**. In a previous paper, we showed that the NHPI-catalyzed oxidation of alcohols affords ketones in good yields.[10d] In fact, treatment of oct-1-yn-3-ol under dioxygen in the presence of NHPI and $Cu(acac)_2$ gave oct-1-yn-3-one, with 95% selectivity at 57%

Table 1 Aerobic oxidation of **1a** catalyzed by NHPI under selected conditions[a]

			Selectivity (%)[b]			
Run	Metal	Conversion (%)	**2a**	**3a**	**4a**	**5a**
1	–	34	23	69	< 1	< 1
2	$Co(acac)_2$	70	20	75	< 1	< 1
3	$Cu(acac)_2$	69	22	77	< 1	< 1
4	$Mn(acac)_2$	no reaction				
5[c]	–	48	18	63	< 1	< 1
6[c]	$Co(acac)_2$	85	2	72	2	2
7[c]	$Cu(acac)_2$	83	5	70	2	3
8[c]	$Mn(acac)_2$	63	4	62	3	5

[a] Compound **1a** (2 mmol) was allowed to react under O_2 atmosphere (1 atm) in the presence of NHPI (10 mol%) and a metal species (0.5 mol%) in MeCN (5 cm^3) at room temperature (25 °C) for 30 h. [b] Selectivity of the products was determined by GC analysis using an internal standard. [c] The reaction was carried out at 50 °C for 6 h.

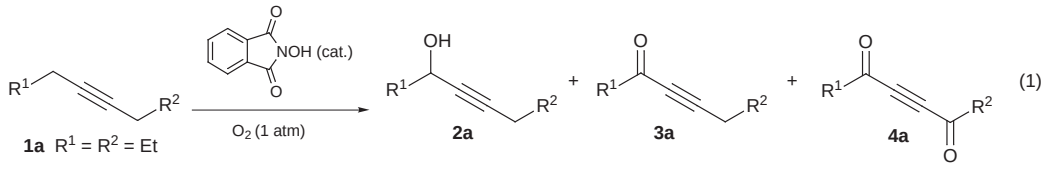

conversion, but in the absence of $Cu(acac)_2$ oct-1-yn-2-ol was converted into the ynone in low yield [eqn. (2)]. This shows that

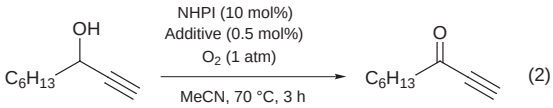

(2)

$Cu(acac)_2$ plays an important role in the conversion of ynol into ynone.

Conventionally, oxidation of alkynes with molecular oxygen is carried out at higher temperatures, *i.e.* 110–150 °C. Under such conditions the reaction results in undesired over-oxidation products such as oxidatively cleaved carboxylic acids.[13] For instance, the oxidation of dodec-6-yne under 70 atm of air at 110 °C is reported to lead to cleaved products such as hexanoic acid and pentanoic acid as principal products.

It is noteworthy that the NHPI-catalyzed oxidation of alkynes with molecular oxygen could be achieved at room temperature, since undesired side reactions arising from high reaction temperatures could be suppressed.

The present successful conversion of alkynes into ynones is believed to result from the fact that the phthalimide *N*-oxyl radical (PINO) can be generated from NHPI under the influence of dioxygen and **1a** at room temperature. Thus, EPR analysis of PINO formed from NHPI under atmospheric dioxygen in the presence or absence of alkyne **1a** at room temperature was performed. As expected, the EPR signal attributed to PINO was observed in the presence of **1a** after 14 h, but in the absence of **1a** no EPR signal was observed. At this stage, we cannot make an accurate assessment of the interaction between NHPI and the alkyne **1a**. The generation of PINO from NHPI in the presence of alkyne **1a** may be facilitated by the weak coordination of NHPI, which is a weak acid having pK_a = 7.0,[14] to the acelylenic π-bond of the alkyne.

Table 2 summarizes the results for the NHPI-catalyzed oxidation of a variety of alkynes in the presence of $Co(acac)_2$ or $Cu(acac)_2$ under oxygen atmosphere. The conversions of substrates were generally high except for terminal alkynes, and the corresponding α,β-acetylenic carbonyl compounds were obtained in moderate to good yields. Symmetric alkynes such as hex-3-yne **1b** and dodec-6-yne **1c** were oxidized into conjugated ynones hex-3-yn-2-one **3b** and dodec-6-yn-5-one **3c**, respectively, in good yields, (runs 1–3). Unsymmetrical alkyne, oct-3-yne **1d** gave a 1:1 mixture of the corresponding conjugated ynones, **3d** and **3d′** (run 4), although the oxidation of dec-3-yne with Bu^tOOH catalyzed by CrO_3 produced only dec-3-yn-2-one.[7c] Under the same conditions, oct-2-yne **1e** afforded oct-2-yn-4-one **3e** with high regioselectivity (run 5). The terminal alkyne oct-1-yne **1f** was oxidized to oct-1-yn-3-one **3f** with high selectivity, although the conversion was moderate (50%) (run 6). On the other hand, for oct-2-yn-1-al **1g**, the aldehyde moiety was selectively oxidized rather than the prop-2-ynylic C–H bond, giving oct-2-ynoic acid **6g** (run 7).

Table 2 Aerobic oxidation of several alkynes catalyzed by NHPI combined with $Co(acac)_2$ or $Cu(acac)_2$[a]

Run	Substrate	Product	Conversion (%)	Selectivity (%)[b]
1[c]	EtC≡CEt **1b**	AcC≡CEt **3b**	93	81
2[d,e]	EtC≡CEt **1b**	AcC≡CEt **3b**	96	75
3[e]	$C_5H_{11}C{\equiv}CC_5H_{11}$ **1c**	BuC(O)C≡CC_5H_{11} **3c**	89	75
4[c]	BuC≡CEt **1d**	PrC(O)C≡CEt **3d** BuC≡CAc **3d′**	92	70[f]
5[e]	$C_5H_{11}C{\equiv}CMe$ **1e**	BuC(O)C≡CMe **3e**	94	70
6[c,e]	$C_6H_{13}C{\equiv}CH$ **1f**	$C_5H_{11}C(O)C{\equiv}CH$ **3f**	50	80
7[c,e]	$C_5H_{11}C{\equiv}CCHO$ **1g**	$C_5H_{11}C{\equiv}CCO_2H$ **6g**	43	74[g]

[a] Substrate (2 mmol) was allowed to react under O_2 atmosphere (1 atm) in the presence of NHPI (10 mol%) and $Cu(acac)_2$ (0.5 mol%) in MeCN (5 cm^3) at 50 °C for 6 h. [b] Yields of the products were determined by GC analysis using an internal standard. Other products were α-alkynyl alcohols (~5%) and cleaved products such as carboxylic acids (~3%) except for run 7. [c] 20 h. [d] $Co(acac)_2$ was used instead of $Cu(acac)_2$. [e] 70 °C. [f] A 1:1 regioisomeric mixure was obtained. [g] Isolated yield.

In conclusion, various alkynes were converted into α,β-acetylenic carbonyl compounds by aerobic oxidation using NHPI combined with Co^{II} or Cu^{II} complexes. The present method provides a facile method for preparing conjugated ynones from alkynes.

This work was financially supported by the Research for the Future program JSPS.

Notes and References

† E-mail: ishii@ipcku.kansai-u.ac.jp

‡ *Typical procedure* for the aerobic oxidation of alkyne: To a solution of NHPI (0.2 mmol, 10 mol%) and a transion metal complex (0.01 mmol, 0.5 mol%) in MeCN (5 cm^3) was added alkyne (2 mmol), then the flask was flushed with oxygen and equipped with a balloon filled with O_2. The reaction mixture was stirred at 25 °C for 30 h. The solvent was evaporated under reduced pressure. The products were purified by column chromatography on silica gel [hexane–EtOAc (10:1 to 3:1)], and characterised by ^1H and ^{13}C NMR, GC–MS and IR spectroscopy.

1 K. Utimoto, M. Miwa and H. Nozaki, *Tetrahedron Lett*., 1981, **22**, 4277.
2 A. B. Smith, III, P. A. Levenberg and J. Z. Suits, *Synthesis*, 1986, 184.
3 M. Karpf, J. Huguet and A. S. Dreiding, *Helv. Chim. Act*., 1986, **65**, 13.
4 S. T-K. Tam, R. S. Klein, F. G. de las Heras and J. J. Fox, *J. Org. Chem*., 1979, **44**, 4854 and references cited therein; C. M. Gupta, G. H. Jones and J. G. Moffatt, *J. Org. Chem*., 1976, **41**, 3000.
5 N. Sayo, K.-I. Azuma, K. Mikawa and T. Nakai, *Tetrahedron Lett*., 1984, **25**, 565; K. Midland and N. H. Nguyen, *J. Org. Chem*., 1981, **46**, 4107.
6 (*a*) M. Yamaguchi, K. Shibata, S. Fujiwara and I. Hirao, *Synthesis*, 1986, 421; (*b*) H. C. Brown, U. S. Racherla and S. M. Singh, *Tetrahedron Lett*., 1984, **25**, 2411; (*c*) J. F. Normant and M. Bourgan, *Tetrahedron Lett*., 1970, **11**, 2659; (*d*) A. G. Davies and R. J. Puddephatt, *Tetrahedron Lett*., 1967, **8**, 2265.
7 (*a*) W. B. Sheats, L. K. Olli, R. Stout, J. T. Lundzen, R. Justus and W. G. Nigh, *J. Org. Chem*., 1979, **44**, 4075; (*b*) J. E. Shaw and J. J. Sherry, *Tetrahedron Lett*., 1971, **12**, 4379; (*c*) J. Muzart and O. Piva, *Tetrahedron Lett*., 1988, **29**, 2321.
8 (*a*) A. Mckilklop, O. H. Oldenziel, B. P. Swann, E. C. Taylor and R. L. Robey, *J. Am. Chem. Soc*., 1973, **95**, 1296; (*b*) M. Schroder and W. P. Griffith, *J. Chem. Soc*., *Dalton Trans*., 1978, 1599; (*c*) D. G. Lee and V. S. Chang, *J. Org. Chem*., 1979, **44**, 2726; (*d*) P. Muller and A. J. Godoy, *Helv. Chem. Acta*. 1981, **64**, 2531.
9 (*a*) R. Curci, M. Fiorentino, C. Fusco, R. Mello, F. P. Ballistreri, S. Failla and G. A. Tomaselli, *Tetrahedron Lett*., 1992, **33**, 7929; (*b*) R. W. Murray and M. Singh, *J. Org. Chem*., 1993, **58**, 5076; (*c*) S. Sakaguchi, S. Watase, Y. Katayama, Y. Sakata, Y. Nishiyama and Y. Ishii, *J. Org. Chem*., 1994, **59**, 5681.
10 (*a*) S. Sakaguchi, S. Kato, T. Iwahama and Y. Ishii, *Bull. Chem. Soc. Jpn*., 1998, **71**, 1237; (*b*) Y. Yoshino, Y. Hayashi, T. Iwahama, S. Sakaguchi and Y. Ishii, *J. Org. Chem*., 1997, **62**, 6810; (*c*) Y. Ishii, T. Iwahama, S. Sakaguchi, K. Nakayama and Y. Nishiyama, *J. Org. Chem*., 1996, **61**, 4520; (*d*) T. Iwahama, S. Sakaguchi, Y. Nishiyama and Y. Ishii, *Tetrahedron Lett*., 1995, **36**, 6923.
11 D. M. Golden, *Annu. Rev. Phys. Chem*., 1982, **33**, 493.
12 M. A. Umbreit and K. B. Sharpless, *J. Am. Chem. Soc*., 1977, **99**, 5527.
13 P. E. Correa, G. Hardy and D. P. Riley, *J. Org. Chem*., 1988, **53**, 1695.
14 D. E. Ames and T. F. Grey, *J. Chem. Soc*., 1955, 3521.

Received in Cambridge, UK, 29th June 1998; 8/04956D

Synthesis of oligomers of tetrahydrofuran amino acids: furanose carbopeptoids

Martin D. Smith,[a] Daniel D. Long,[a] Daniel G. Marquess,[b,c] Timothy D. W. Claridge and George W. J. Fleet*[a]†

[a] *Dyson Perrins Laboratory, University of Oxford, South Parks Road, Oxford, UK OX1 3QY*
[b] *Glaxo Wellcome Ltd., Gunnels Wood Road, Stevenage, Herts, UK SG1 2NY*
[c] *Advanced Medicine Inc., 270 Littlefield Avenue, Suite B, South San Francisco, CA 94080, USA*

An acid catalysed ring rearrangement of a triflate derivative of D-mannono-γ-lactone 6 is the key step in the synthesis of the *C*-glycosyl sugar amino acid derivatives 3 and 4, examples of carbohydrate amino acid building blocks with specific conformational preferences suitable for incorporation into combinatorial amide libraries; homo-oligomerisation *via* solution phase coupling procedures affords furanose carbopeptoids 1 which adopt novel solution state secondary structures.

Carbohydrate amino acids are attractive building blocks for the routine incorporation of carbohydrate moieties into combinatorial libraries by standard peptide coupling techniques.[1] The conformational influence of the sugar backbone on peptide chains has been exploited in the rational design of non-peptide peptidomimetics.[2] Homo-oligomeric sugar amino acids ('carbopeptoids'[3]) based upon a pyranose template have been prepared by solution[4] and solid[5] phase approaches, though to date there are no furanose[6] analogues. Here we describe the synthesis of a *C*-glycofuranosyl sugar amino acid analogue and its oligomerisation to materials which adopt a well-defined secondary structure.

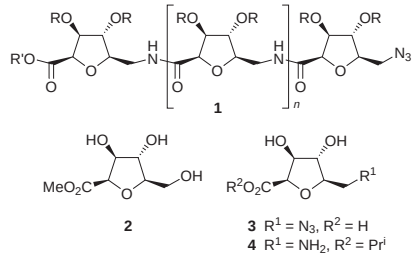

2-*O*-Triflates (trifluoromethanesulfonates) of γ- and δ-lactones in basic[7] or acidic[8] MeOH give good to excellent yields of highly substituted tetrahydrofurancarboxylates. Such a procedure has recently been utilised for the synthesis of *C*-glycosides of glucofuranose,[9] which have provided scaffolds for the generation of glucofuranose libraries. For the synthesis of the *C*-arabinosyl derivative **2**, the triflate **6** is required; in order to effect esterification at C-2, it is necessary to protect the primary hydroxy group at C-6 in D-mannonolactone as its kinetic monoacetonide **5**, easily accessible in 74% yield from the diacetonide of D-mannose.[10] Treatment of the diol **5** with Tf_2O in CH_2Cl_2 in the presence of pyridine caused highly regioselective esterification of the hydroxy group at C-2 to give the stable triflate **6**, which may be isolated in 85% yield; **6** has previously been described but in a significantly poorer yield.[11] Treatment of the crude triflate **6** with HCl in MeOH gave the required ester **2** in 84% yield from **5**, providing multigram quantities of **2** in an overall yield of 62% from D-mannose. The key transformation of **6** to **2** by treatment with acidic MeOH involves hydrolysis of the side chain acetonide, methanolysis of the lactone, followed by intramolecular S_N2-like closure of the resulting open chain hydroxy triflate **7** with inversion of configuration at C-2 (Scheme 1). Although it is possible that intermediates such as **7** could undergo alternative closure to a tetrahydropyran, resulting from attack by the C-6 rather than the C-5 hydroxy group, no *C*-glycopyranosides were isolated; ring closures to *C*-glycopyranoses by nucleophilic displacement at C-2 of a sugar are rare.[12]

The strategy adopted for the synthesis of carbopeptoids **1** utilises well-established peptide bond forming methodology. For the synthesis of sugar amino acid building blocks **3** and **4**, it is necessary to introduce nitrogen at C-6. Selective esterification of **2** with toluene-*p*-sulfonyl chloride in pyridine (to give the 6-*O*-tosyl derivative **8**) and subsequent displacement of the sulfonate ester with NaN_3 in DMF at 90 °C gave the azide **9** in 72% yield over two steps.[13] Hydrolysis of the methyl ester with aq. NaOH and purification by ion exchange chromatography afforded the carboxylic acid **3** in quantitative yield. Catalytic hydrogenation of the methyl ester **9** gave the bicyclic lactam **10** *via* a non-isolable amine; a more hindered ester is required to enable isolation of the required 6-amino component **4**. Accordingly, transesterification of the methyl ester **9** with K_2CO_3 in Pr^iOH gave the isopropyl derivative **11** in 79% yield.[14] Hydrogenation of the azide **11** in the presence of Pd-C in Pr^iOH afforded the amine **4** as the major product together with an unidentified and inseparable minor component; the highly polar amine **4**, characterised as its triacetate **12**, (90% yield from **11**),was used without purification in all further reactions.

Coupling of **4** and **3** was then performed using 1-(3-dimethylaminopropyl)-3-ethylcarbodiimide hydrochloride (EDCI) in DMF in the presence of 1-hydroxybenzotriazole (HOBt). This reaction allowed the isolation of the dimeric compound **13** in 74% yield (from the azide **11**) as an easily handled solid (Scheme 2). No protection of the secondary hydroxy groups is necessary during the coupling procedure. Iteration of the coupling procedure gave ready access to the tetramer **1** (n = 2) and the hexamer **1** (n = 4). The dimer **13** was treated with aq. NaOH and purified by ion exchange chromatography to afford

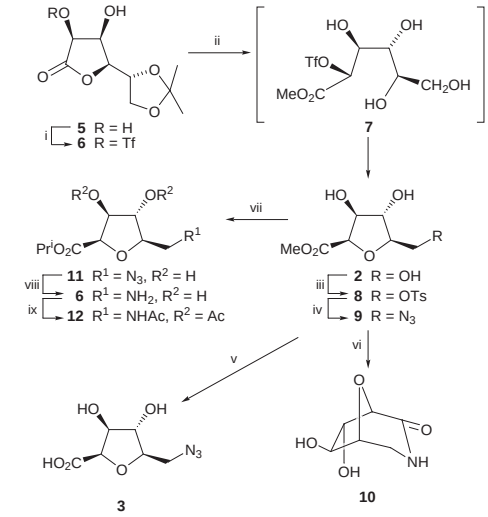

Scheme 1 *Reagents and conditions*: i, Tf_2O, Py, CH_2Cl_2; ii, 1% HCl in MeOH; iii, TsCl, Py; iv, NaN_3, DMF; v, 0.5 M aq. NaOH, dioxane, ion exchange; vi, H_2, Pd, EtOH; vii, K_2CO_3, Pr^iOH; viii, H_2, Pd, Pr^iOH; ix, Ac_2O, Py

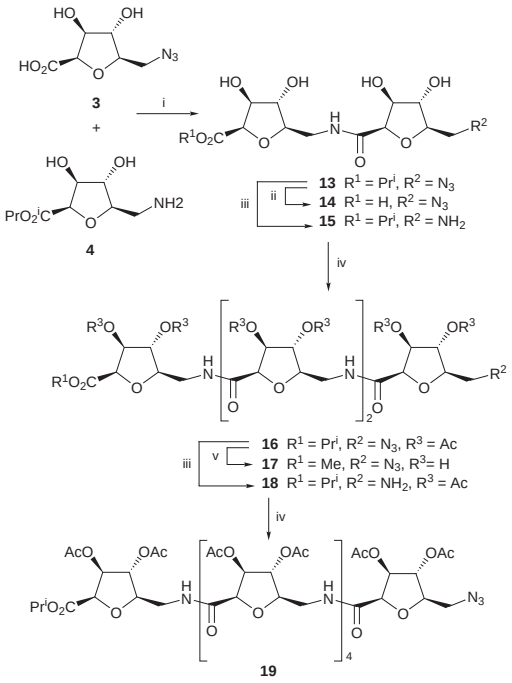

Scheme 2 *Reagents and conditions*: i, EDCI, HOBt, Pr^i_2NEt, DMF; ii, 0.5 M aq. NaOH, dioxane, then Amberlite IR-120 (H^+); iii, H_2, Pd, Pr^iOH; iv, **14** (1 equiv.), EDCI, HOBt, Pr^i_2NEt, DMF, then Ac_2O, Py; v, NaOMe, MeOH, then Amberlite IR-120 (H^+)

the free acid **14** in quantitative yield. Additionally the *N*-terminal azide in **13** was reduced with H_2 in the presence of Pd-C to afford the amine **15**. Coupling of the dimeric building blocks **14** and **15** was performed using EDCI in DMF in the presence of HOBt. The reaction mixture was treated with Ac_2O in pyridine to facilitate isolation of the tetramer **16**[15] (55% from **13**) from which the acetate groups can be removed with NaOMe in MeOH to afford the deprotected carbopeptoid **17** in quantitative yield. Hydrogenation of the tetramer **16** in the presence of Pd gave the *N*-terminal amine **18** which was coupled crude to the dimeric acid **14** using EDCI in DMF in the presence of HOBt. Treatment of the reaction mixture with Ac_2O in pyridine gave the hexamer **19** in 68% yield from the tetramer **16**.

The ease with which highly functionalised tetrahydrofurans, such as **4**, can be synthesised is likely to offer opportunities for the production of a range of carbohydrate amino acid building blocks with specific conformational preferences suitable for incorporation into combinatorial amide libraries. The diversity of possible structures afforded by a carbohydrate template in terms of backbone stereochemistries and protecting group manipulations allows formation of hydrophobic or hydrophilic—and thus water soluble—derivatives. Efficient unprotected oligomerisation to give compounds with well-defined secondary structure emphasizes the versatility of the sugar amino acid building block and alludes to the possibility of a more rational design tailored to specific applications. The following paper provides evidence for conformational preferences of the hexamer **19** and the tetramer **16**; NMR and molecular dynamics indicate that both adopt a well-defined secondary structure based around a repeating β-turn mimic stabilised by intramolecular hydrogen bonds.[16]

The support of the EPSRC and GlaxoWellcome in the form of a CASE studentship (to D. D. L.) is gratefully acknowledged.

Notes and References

† E-mail: george.fleet@chem.ox.ac.uk

1 J. P. McDevitt and P. T. Lansbury, *J. Am. Chem. Soc*., 1996, **118**, 3818; P.S. Ramamoorthy and J. Gervay, *J. Org. Chem*., 1997, **62**, 7801; M. J. Sofia, R. Hunter, T. Y. Chan, A. Vaughan, R. Dulina, H. Wang and D. Gange, *J. Org. Chem*., 1998, **63**, 2802.

2 E. G. von Roedern, E. Lohof, G. Hessler, M. Hoffmann and H. Kessler, *J. Am Chem. Soc*., 1996, **118**, 10 156.

3 K. C. Nicolaou, H. Florke, M. G. Egan, T. Barth and V. A. Estevez, *Tetrahedron Lett*., 1995, **36**, 1775.

4 J. Gervay, T. M. Flaherty and C. Nguyen, *Tetrahedron Lett*., 1997, **38**, 1493 and references cited therein.

5 C. Muller, E. Kitas and H. P. Wessel, *J. Chem. Soc. Chem. Commun*., 1995, 2425; B. Drouillat, B. Kellam, G. Dekany, M. S. Starr and I. Toth, *Bioorg. Med. Chem. Lett*., 1997, **7**, 2247.

6 L. Poitout, Y. le Merrer and J.-C. Depazay, *Tetrahedron Lett*., 1995, **36**, 6887.

7 S. S. Choi, P. M. Myerscough, A. J. Fairbanks, B. M. Skead, C. J. F. Bichard, S. J. Mantell, J. C. Son, G. W. J. Fleet, J. Saunders and D. Brown, *J. Chem. Soc*., *Chem. Commun*., 1992, 1605.

8 J. R. Wheatley, C. J. F. Bichard, S. J. Mantell, J. C. Son, D. J. Hughes, G. W. J. Fleet and D. Brown, *J. Chem. Soc*., *Chem. Commun*., 1993, 1065.

9 C. J. F. Bichard, T. W. Brandstetter, J. C. Estevez, G. W. J. Fleet, D. J. Hughes and J. R. Wheatley, *J. Chem. Soc*., *Perkin Trans. 1*, 1996, 2151.

10 O. T. Schmidt, *Methods Carbohydr. Chem*., 1963, **2**, 319; A. R. Beacham, I. Bruce, S. Choi, O. Doherty, A. J. Fairbanks, G. W. J. Fleet, B. M. Skead, J. M. Peach, J. Saunders and D. J. Watkin, *Tetrahedron: Asymmetry*, 1991, **2**, 883; S. Morgenlie, *Acta Chem. Scand*., 1972, **26**, 2518; D. Horton and J. S. Jewel, *Carbohydr. Res*., 1966, **2**, 251; J. A. J. M. Vekemans, J. Boerekamp, E. F. Godefroi and G. J. F. Chittenden, *Recl. Trav. Chim. Pays-Bas*, 1985, **104**, 266.

11 I. Kalwinsh, K-H. Metten, and R. Brückner, *Heterocycles*, 1995, **409**, 939.

12 J. C. Estevez, A. J. Fairbanks, K. Y. Hsia, P. Ward and G. W. J. Fleet, *Tetrahedron Lett*., 1994, **35**, 3361.

13 *Selected data* for **2**: δ_H(500 MHz, CD_3CN) 3.58 (1H, d, *J* 3.7, OH-4), 3.64–3.74 (3H, m, H-6, H-6′, OH-6), 3.70 (3H, s, CO_2Me), 3.88 (1H, q, *J* 3.2, H-5), 4.03–4.05 (1H, m, H-4), 4.12 (1H, ddd, *J* 4.3, 1.9, 8.4, H-3), 4.33 (1H, d, *J* 8.4, OH-3), 4.59 (1H, d, *J* 4.3, H-2).

14 *Selected data* for **11**: δ_H(500 MHz, CD_3OD) 1.27 (6H, t, *J* 6.2, Me_2CH), 3.38 (1H, dd, *J* 4.7, 12.7, H-6′), 3.62, (1H, dd, *J* 7.5, 12.7, H-6′), 3.91–3.94 (1H, m, H-5), 3.95 (1H, dd, *J* 2.8, 5.7, H-4), 4.26 (1H, dd, *J* 2.8, 5.1, H-3), 4.61 (1H, d, *J* 5.1, H-2), 5.07 (1H, septet, *J* 6.2, Me_2CH).

15 *Selected data* for **16** (500 MHz, $CDCl_3$, 298 K):

	Ring **A**	Ring **B**	Ring **C**	Ring **D**
$\delta_C(C^1)$	167.81	168.11	167.68	167.15
$\delta_H(C^2)$	4.669	4.692	4.708	4.687
$\delta_C(C^2)$	81.02	81.74	81.38	78.93
$\delta_H(C^3)$	5.646	5.559	5.495	5.475
$\delta_C(C^3)$	76.08	75.57	76.01	76.66
$\delta_H(C^4)$	4.904	4.837	5.003	5.250
$\delta_C(C^4)$	78.40	78.06	77.68	77.57
$\delta_H(C^5)$	4.153	4.027	4.123	4.055
$\delta_C(C^5)$	85.00	85.18	85.00	83.19
$\delta_H(C^6)$	3.708/ 3.461	4.027/ 3.224	3.861/ 3.228	3.781/ 3.481
$\delta_C(C^6)$	51.43	41.28	41.28	40.48
δ_H(NH)	—	6.910	8.025	8.191

Carbopeptoids are identified alphabetically from the N- to the C-terminus; protons on each ring are numbered according to IUPAC recommendations on carbohydrate nomenclature.

16 M. D. Smith, T. D. W. Claridge, G. E. Tranter, M. S. P. Sansom and G. W. J. Fleet, *Chem. Commun*., 1998, 2041.

Received in Liverpool, UK, 10th July 1998; 8/05364B

Secondary structure in oligomers of carbohydrate amino acids

Martin D. Smith,[a] Timothy D. W. Claridge,[a] George E. Tranter,[b] Mark S. P. Sansom[c] and George W. J. Fleet*[a]†

[a] *Dyson Perrins Laboratory, University of Oxford, South Parks Road, Oxford, UK OX1 3QY*
[b] *GlaxoWellcome Ltd., Gunnels Wood Road, Stevenage, Herts, UK SG1 2NY*
[c] *Laboratory of Molecular Biophysics, University of Oxford, The Rex Richards Building, South Parks Road, Oxford, UK OX1 3QU*

Short oligomeric chains of tetrahydrofuran amino acids exhibit a novel repeating β-turn type secondary structure in solution stabilised by hydrogen bonds and provide clear evidence that carbopeptoids will allow control of conformation in peptidomimetics.

Secondary structural elements such as α-helices and β-sheets are involved in the processes leading to the folding of proteins into functional conformations. The design and synthesis of novel materials which are predisposed to fold into these ordered structures has been an area of intense interest in recent[1] years as they may have interesting catalytic or selective recognition properties. Oligomers[2] based upon a range of templates have been shown to form helices in solution and the solid state. Our approach involves the use of carbohydrate-like frameworks bearing both an amino and a carboxylic acid functionality[3] which have been proposed as non-peptide peptidomimetics[4] by virtue of their rigidity and conformational influence on peptide backbones. Oligomers of pyranose sugar amino acids[5] ('carbopeptoids'[6]) have been synthesised by solution[7] and solid phase[8] methods, but there are few reports of their conformational preferences.[9] Here we describe oligomers of sugar amino acid derivatives based upon a β-D-*arabino*-furanose scaffold which adopt a novel repeating β-turn type structure stabilised by intramolecular hydrogen bonds in solution.

An efficient synthesis of the tetrameric **2** and hexameric **3** carbopeptoids utilising solution phase coupling procedures is reported in the previous paper.[10]

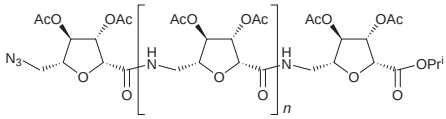

1 *n* = 0, dimer
2 *n* = 2, tetramer
3 *n* = 4, hexamer

Solution conformations in $CDCl_3$ were investigated by ^1H NMR spectroscopy. All resonances were unambiguously assigned by a combination of 2D NMR techniques. Proton spin systems within each residue were identified *via* DQF-COSY and T-ROESY[11] spectra, with the configuration within each sugar ring being confirmed by the observed NOE correlations (cross peaks in NOESY spectra were positive but rather weak, indicating the molecular correlation time, τ_c, to approach the $\omega_o\tau_c$ = *ca*. 1 condition). NOE data also allowed the sequential placement of each residue from the observation of $H2^i$ to HN^{i+1} interactions. To confirm that these were indeed sequential, rather than longer-range correlations brought about by folding of the molecule, semi-selective gradient-enhanced HMBC experiments[12] of the carbonyl region were used to establish unambiguous through-bond ^1H–^{13}C connectivities between adjacent residues *via* correlations with the carbonyl carbons (in particular, $H2^i$ to CO^i and CO^i to $H6^{i+1}$). Finally, the NOE data were further used to establish the solution conformation of the molecule in which tetramer **2** appears to adopt a novel repeating 'β-turn' type structure stabilised by (*i*, *i* − 2) inter-residue hydrogen bonds (Fig. 1). Each repeating tetrahydrofuran unit can be considered as a dipeptide isostere with each H-bond

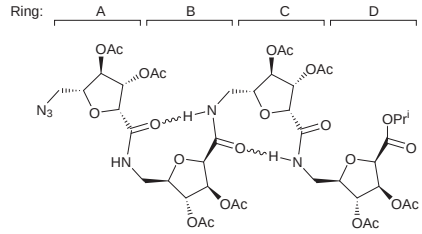

Fig. 1 Representation of the observed solution secondary structure of the tetramer **2** indicating ring labelling. Rings are identified by labelling each residue alphabetically from 'A' at the N-terminus.

completing a turn that is structurally reminiscent of a conventional peptide β-turn.[13]

Proton chemical shift dispersion of **2** is high despite the repeating unit, which is itself suggestive of a well defined solution structure. The ^1H NMR spectrum of the amide region for tetramer **2** and its hexameric homologue **3** is shown in Fig. 2. The chemical shifts of amide protons are sensitive to the presence of hydrogen bonding; a decrease in diamagnetic shielding due to the population of hydrogen bonded states should result in a high-frequency δ_{NH} shift:

For the tetramer **2**, such a shift is observed for two of the three amide protons (δ_H 8.19 and 8.03), subsequently identified as NH^D and NH^C, whose shifts are therefore indicative of involvement in hydrogen-bond formation. The remaining amide (NH^B) resonates at significantly lower frequency (δ_H 6.91), characteristic of an amide which experiences little or no hydrogen-bonding. This shift is similar to that observed for the dimeric unit **1** (δ_H 7.18) which is itself unable to form the inter-residue hydrogen-bond proposed herein for the higher homologues. An equivalent pattern is observed in the hexameric analogue **3** which exhibits four high-frequency amide protons and one again at lower frequency (Fig. 2). The chemical shifts of all three amide protons of the tetramer are, in contrast, similar in DMSO (Table 1), indicating similar solvent hydrogen-bonding interactions for all three. However, temperature coefficients of the amide protons of the tetramer **2** in DMSO indicate that NH^D and NH^C experience greater shielding from these solvent interactions than does NH^B (Table 1) and correlates with the higher chemical shifts of NH^D and NH^C observed in $CDCl_3$.

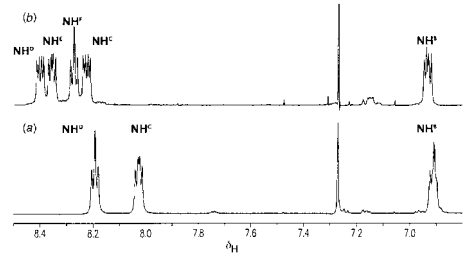

Fig. 2 Amide regions of the ^1H NMR (500 MHz) spectrum of (*a*) tetramer **2** and (*b*) hexamer **3**. Proton assignments are indicated. The spectra were recorded on a Bruker AMX-500 spectrometer at 298 K in $CDCl_3$ and referenced to residual solvent at δ 7.27.

Table 1 Amide proton temperature coefficients and chemical shifts for the tetramer **2**

	$\Delta\delta$([$^2H_6$]DMSO)/ ppb K^{-1}	δ_H([$^2H_6$]DMSO)/ ppm	δ_H($CDCl_3$)/ ppm
NH^D	4.3	8.20	8.19
NH^C	3.9	8.29	8.03
NH^B	5.3	8.12	6.91
H_2O	5.1	—	—

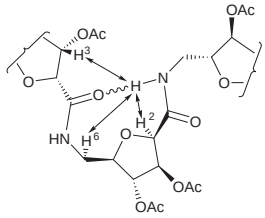

Fig. 3 Representation of the significant inter-residue NOE enhancements observed for each 'turn'. Relevant protons are numbered individually.

The pattern of deshielded *vs.* shielded amide protons for **1–3** is consistent with a repeating structural unit, rather than simply the formation of hydrogen bonds between amide protons and acetate groups on the same or adjacent residues, as is further supported by the NOE data. With only one exception ($H3^A$ to $H6^C$-*pro-S*), all NOEs that were observed *between* residues involved the amide protons and no inter-residue ring–ring interactions could be detected. Significant inter-residue NOEs were NH^i to $H2^{i-1}$, NH^i to $H6^{i-1}$ (stereospecifically) and NH^i to $H3^{i-2}$ (Fig. 3) as observed from both NH^D and NH^C, and are suggestive of the proposed (i, $i-2$) inter-residue hydrogen bonds.

Using these data, molecular dynamics simulations[14] utilising NOE derived distance constraints were performed for the tetramer (Fig. 4). This resulted in the generation of five low energy structures, all of which exhibit the anticipated geometry (backbone atom RMS deviation between the five structures is 0.6 Å). Superposition of these structures [Fig. 4(A)] shows the expected fraying at the C-terminus, which does not participate in hydrogen bonding. The conformer which most satisfies the distance restraints is shown in Fig. 4(B)). This structure is consistent with the lack of ring–ring NOEs and reflects the strong conformational preferences from each sugar ring stereochemistry.

In conclusion, we have shown that short oligomeric furanose sugar amino acid chains—even a tetramer—can adopt well-defined novel secondary structures stabilised by intramolecular hydrogen bonds; this is the first example of a 'carbopeptoid' of *any* length in which secondary structure has been experimentally demonstrated. The ease of synthesis of a wide range of structures such as the tetrahydrofuran **4** is likely to give flexibility and control in the design and applications of peptidomimetics with well-defined secondary structure, low molecular weights and thus good bioavailablity.

The support of the EPSRC is gratefully acknowledged.

Notes and References

† E-mail: george.fleet@chem.ox.ac.uk

1 B. Iverson, *Nature*, 1997, **385**, 114; S. Borman, *Chem. Eng. News*, 1997, 32; S. H. Gellmann, *Acc. Chem. Res.*, 1998, **31**, 173.

2 D. Seebach and J. L. Matthews, *Chem. Commun.*, 1997, 2015; D. W. Appella, L. A. Christianson, I. L. Karla, D. R. Powell and S. H. Gellman, *J. Am. Chem. Soc.*, 1996, **118**, 13 071; D. W. Appella, L. A. Christianson, D. A. Klein, D. R. Powell, X. Huang, J. J. Barchi and S. H. Gellman, *Nature*, 1997, **387**, 381; Y. Hamuro, S. J. Geig and A. D. Hamilton, *J. Am. Chem. Soc.*, 1997, **119**, 10 587; D. M. Bassani, J. M. Lehn, G. Baum and D. Fenske, *Angew. Chem., Int. Ed. Engl.*, 1997, **118**, 1845; J. C. Nelson, J. G. Saver, J. S. Moore and P. G. Wolynes, *Science*, 1997, **277**, 1793.

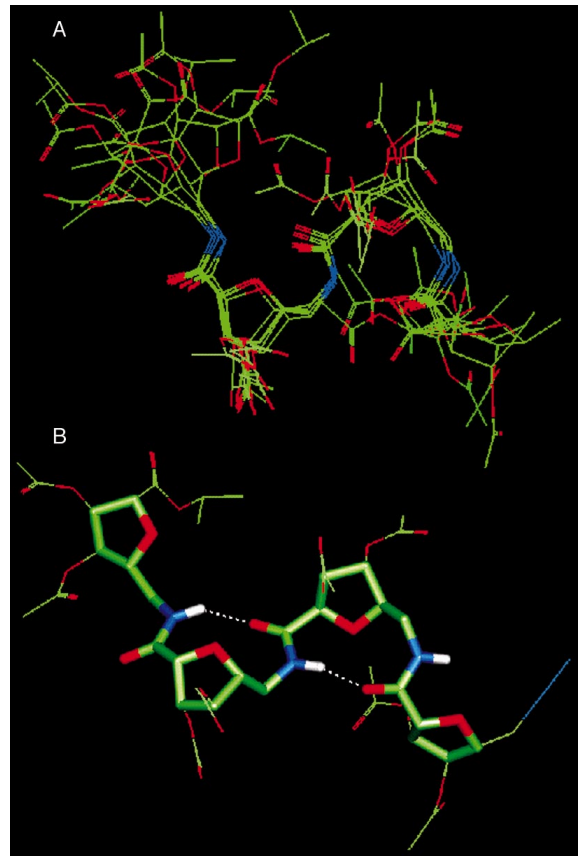

Fig. 4 (A) Five lowest energy structures of the tetramer **2** generated by restrained molecular dynamics simulations performed using the program QUANTA with the CHARMM forcefield. (B) The conformer in best agreement with the experimental restraints from the five structures of the tetramer **2** illustrated in (A). The two hydrogen bonds are indicated by broken lines.

3 K. Heyns and H. Paulsen, *Chem. Ber.*, 1955, **88**, 188; E. G. von Roedern and H. Kessler, *Angew. Chem., Int. Ed. Engl.*, 1994, **334**, 687; E. G. von Roedern, E. Lohof, G. Hessler, M. Hoffmann and H. Kessler, *J. Am Chem. Soc.*, 1996, **118**, 10 156; J. P. McDevitt and P. T. Lansbury, *J. Am. Chem. Soc.*, 1996, **118**, 3818; R. A. Goodnow, A-R. Richou and S. Tam, *Tetrahedron Lett.*, 1997, **38**, 3195.

4 L. Poitout, Y. le Merrer and J-C. Depazay, *Tetrahedron Lett.*, 1995, **36**, 6887.

5 E. F Fuchs and J. Lehmann, *Chem. Ber.*, 1975, **108**, 2254.

6 K. C. Nicolaou, H. M. Florke, G. Egan, T. Barth and V. A. Estevez, *Tetrahedron Lett.*, 1995, **36**, 1775.

7 Y. Suhara, J. E. K. Hildreth and Y. Ichikawa, *Tetrahedron Lett.*, 1996, **37**, 1575; Y. Suhara, M. Izumi, M. Ichikawa, M. B. Penno and Y. Ichikawa, *Tetrahedron Lett.*, 1997, **38**, 7167; H. P. Wessel, C. M. Mitchell, C. M. Lobato and G. Schmidt, *Angew. Chem., Int. Ed. Engl.*, 1995, **34**, 2712; S. Sabesan, *Tetrahedron Lett.*, 1997, **38**, 3127; C. M. Timmers, J. J. Turner, C. M. Ward, G. A. van der Marcel, M. L. C. E. Kouwijzer, P. D. J Grootenhuis and J. H. van Boom, *Chem. Eur. J.*, 1997, **6**, 920.

8 C. Muller, E. Kitas and H. P. Wessel, *J. Chem. Soc., Chem. Commun.*, 1995, 2425; B. Drouillat, B. Kellam, G. Dekany, M. S. Starr and I. Toth, *Bioorg. Med. Chem. Lett.*, 1997, **17**, 2247; R. A. Goodnow, D. L. Preuss, S. Tam and W. W. McComas, *Tetrahedron Lett.*, 1997, **38**, 3199.

9 L.Szabo, B. L. Smith, K. D. McReynolds, A. L. Parill, E. R. Morris and J. Gervay, *J. Org. Chem.*, 1998, **63**, 1074.

10 M. D. Smith, D. D. Long, D. G. Marquess, T. D. W. Claridge and G. W. J. Fleet, *Chem. Commun.*, 1998, 2039.

11 T-L. Hwang and J. L. Shaka, *J. Magn. Reson. (B)*, 1993, **102**, 155.

12 H., Kessler, P. Schmeider, M. Köck and M. Kurz, *J. Magn. Reson.*, 1990, **88**, 615.

13 J. A. Smith and L. G. Pease, *C. R. C. Crit. Rev. Biochem.*, 1980, **8**, 315.

14 B. R. Brooks, *J. Comput. Chem.*, 1983, **4**, 187.

Received in Liverpool, UK, 10th July 1998; 8/05401K

The cyanate ion as a bridging ligand between lanthanide and transition metals. Formation of one-dimensional extended arrays $\{(DMF)_6Ln_2Ni(NCO)_8\}_\infty$ (Ln = Sm, Eu) and monomeric complexes $(DMF)_8Ln_2Ni(NCO)_8$ (Ln = Sm, Eu) with three bridging cyanate ligands

Jianping Liu, Edward A. Meyers, James A. Cowan* and Sheldon G. Shore*

Department of Chemistry, The Ohio State University, Columbus, Ohio 43210, USA. E-mail: shore1@osu.edu

Syntheses and molecular structures of the first cyanate bridged lanthanide-transition metal complexes, $(DMF)_8Ln_2Ni(NCO)_8$ and $\{(DMF)_6Ln_2Ni(NCO)_8\}_\infty$ (Ln = Sm, Eu) with three bridging cyanate ligands are reported; magnetic properties of $(DMF)_8Ln_2Ni(NCO)_8$ (Ln = Sm, Eu) complexes are described.

The cyanate ion[1] $[NCO]^-$ offers features as a bridging ligand that have not yet been adequately exploited by linking metal ions through two types of bonding modes: terminal N-bonding, 1,1-μ-N (**I**)[2–7] and both ends-bonding, 1,3-μ (**II**).[8–10] Complexes that have been reported, with two exceptions, are molecular entities that form a single cyanate or a double cyanate bridge between two metals. Exceptions are a silver cyanate complex, a chain-like array with single cyanate bridges[4] and a copper 2,4-lutidine cyanate complex, a chain-like array with two cyanate bridges.[5]

I

II

Here we report syntheses and molecular structures of the first examples of cyanate bridged complexes with three bridging cyanate ligands between a lanthanide and a transition metal. These are the monomeric complexes $(DMF)_8Ln_2Ni(NCO)_8$ (Ln = Sm **1**, Eu **2**) that can be converted into one-dimensional, extended arrays $\{(DMF)_6Ln_2Ni(NCO)_8\}_\infty$ (Ln = Sm **3**, Eu **4**).

The complexes $(DMF)_xLn_2Ni(NCO)_8$ (x = 6 or 8; Ln = Sm, Eu) were synthesized quantitatively by the reaction of 2 : 1 : 8 molar ratios of $LnCl_3$, $NiCl_2$, and K(NCO) in DMF at ambient temperature over a two day period.† Under slightly different crystallization conditions, two unique types of crystals, monomeric complexes $(DMF)_8Ln_2Ni(NCO)_8$ (Ln = Sm **1**, Eu **2**) and one-dimensional, extended arrays $\{(DMF)_6Ln_2Ni(NCO)_8\}_\infty$ (Ln = Sm **3**, Eu **4**) were obtained.† Both **1** and **2** as well as **3** and **4** are isomorphous. The molecular structures of **2** and **4** are shown in Figs. 1 and 2.‡

In complex **2**, the formula is $[(DMF)_8Eu_2Ni(NCO)_8]$. Since the Ni^{2+} ion is located on the crystallographic inversion center, the formula of the asymmetric unit is one-half the molecular formula. The Eu^{3+} and Ni^{2+} ions are linked together by three bridging cyanate ligands to form a slightly distorted trigonal bipyramidal $Eu(\mu\text{-}N)_3Ni$ unit. Interestingly, the distance between Ni^{2+}–Eu^{3+} [3.256(1) Å] is approximately equal to the sum of their atomic radii (3.20 Å),[11] which is probably a result of the three bridging $[NCO]^-$ groups. The forth cyanate ion is a terminal ligand bonded to an Eu^{3+} center. In addition, four DMF molecules are coordinated to the Eu^{3+} ion through their oxygen atoms. Compound **4** is very similar to compound **2**, except that in complex **2** one DMF molecule around Eu^{3+} is replaced by a cyanate ion thereby resulting in the formation of the extended array complex **4**. In complex **4** two cyanate ions form two cyanate bridges to link another Eu^{3+} and a one-dimensional infinite array is formed. The distance between the two adjacent $Eu(1)^{3+}$ and $Eu(2)^{3+}$ centers is 4.081(1) Å. The distances of Ni^{2+}–$Eu(1)^{3+}$ [3.231(1) Å] and Ni^{2+}–$Eu(2)^{3+}$ [3.235(1) Å] are similar to that observed in complex **2**.

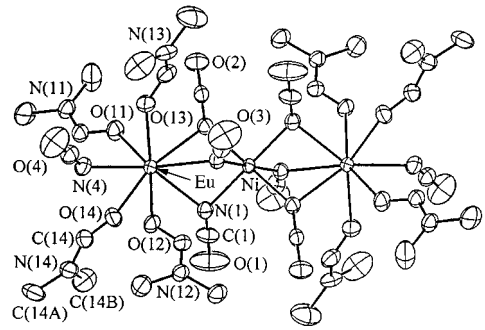

Fig. 1 Molecular structure of $(DMF)_8Eu_2Ni(NCO)_8$ with 50% thermal ellipsoids showing the atomic labelling scheme. DMF hydrogen atoms were omitted for clarity. Selected bond lengths (Å) and angles (°): Eu–O 2.384(5)–2.435(5), Eu–N 2.422(6)–2.563(6), Ni–N 2.081(6)–2.114(6); N–C 1.14(1)–1.18(1) Å, C–O 1.18(1)–1.20(1); N–Ni–N 84.1(2)–85.4(2), Ni–N–Eu 88.4(2)–89.5(2), C–N–Ni, 127.5(6)–142.3(6), C–N–Eu, 127.4(5)–137.8(6), N–C–O 177(1)–179(1).

In complexes **1**–**4**, only nitrogen atoms in the cyanate ligands are coordinated to the metal centers; oxygen atoms remain free. During the structure refinements assignments for N and O peaks on the difference map were interchanged. Assignments shown in Fig. 1 and 2 gave the lowest wR_2 which provides support that nitrogen and oxygen atoms in the $[NCO]^-$ groups are properly identified. Infrared studies of these complexes in the $\nu_{CN} + \nu_{CO}$, ν_{CN} and δ_{NCO} regions are consistent with those observed in complexes[2,3,12,13] for which only M–NCO bonding is claimed.

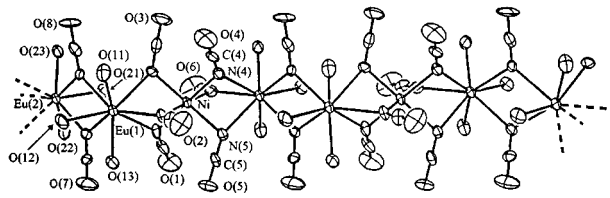

Fig. 2 Molecular structure of $\{(DMF)_6Eu_2Ni(NCO)_8\}_\infty$ with 50% thermal ellipsoids showing the atomic labelling scheme. Only oxygen atoms in DMF were shown for clarity. Selected bond lengths (Å) and angles (°): Eu–O 2.366(9)–2.411(9), Eu–N 2.476(10)–2.517(9), Ni–N 2.096(10)–2.139(9) N–C 1.15(2)–1.20(2) C–O, 1.17(2)–1.21(2); N(7)–Eu–N(8) 69.6(3)–69.8(3), N–Ni–N 178.1(4)–179.2(5), N–Ni–N 82.8(4)–97.4(4), Ni–N–Eu, 88.3(4)–89.5(4), Eu–N–Eu 110.3(4)–110.3(4), C–N–Ni 118.3(8)–129.0(9), C(1,6)–N(1,6)–Eu 142.0(9)–151.4(9), C(7,8)–N(7,8)–Eu 121.0(9)–128.7(9), N–C–O 177(2)–179(2)°.

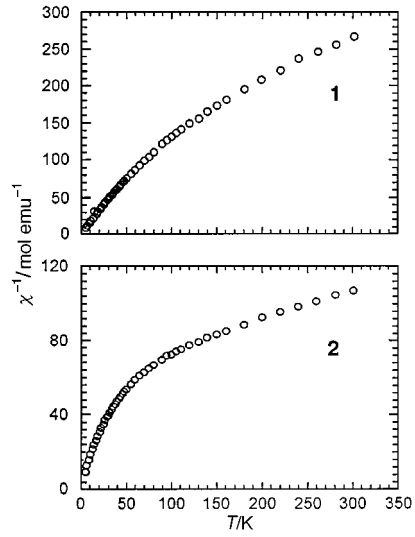

Fig. 3 Plot of $1/\chi$ *vs.* T for complexes $(DMF)_8Sm_2Ni(NCO)_8$ **1** and $(DMF)_8Eu_2Ni(NCO)_8$ **2** at 500 G

Six $[NCO]^-$ groups coordinate to a Ni^{2+} ion through the nitrogen atoms to form an approximately octahedral geometry around Ni^{2+} in both **2** and **4**. The coordination geometry around the Eu^{3+} center is a slightly distorted square antiprism in both **2** and **4**. In **2**, four nitrogen atoms from the $[NCO]^-$ groups and four oxygen atoms from the DMF molecules are coordinated to Eu^{3+}. In **4**, five nitrogen atoms from the $[NCO]^-$ groups and three oxygen atoms from the DMF molecules are coordinated to Eu^{3+}. Bridging $[NCO]^-$ groups between $Eu(1)^{3+}$ and $Eu(2)^{3+}$ ions share an edge of one antiprism base which is the cornerstone for the formation of the one-dimensional infinite chain.

Magnetic properties of **1** and **2** were studied.§ The complexity of the magnetic systems precludes a detailed theoretical analysis at this time, however, several significant observations were made. Both complexes show approximately Curie behavior below 30 K, and deviations at higher temperatures that are manifest as increased susceptibilities (Fig. 3). The deviations normally expected from Curie behavior at low temperature are small relative to the deviations shown at higher temperature for these compounds. Therefore it is the larger effect at higher temperature on which we focus our attention. Ground terms of $^6H_{5/2}$ and $^3F_4$ are assumed for the Sm^{3+} and Ni^{2+} centers in complex **1**, respectively.[14] For Sm^{3+} the first electronic excited state is typically too high in energy to contribute to the magnetic behavior, and so the magnetic properties may arise from antiferromagnetic coupling of the Ln^{3+} and Ni^{2+} ions with population of higher magnetic states at elevated temperature. For Eu^{3+} in complex **2**, a ground state term of $^7F_0$ is assumed. Since the ground state of Eu^{3+} is diamagnetic, the deviation from Curie behavior above 30 K requires a significant contribution from antiferromagnetic coupling of the low lying first excited electronic state of Eu^{3+} to be considered, although the coupling phenomenon may be more complex than the case of Sm^{3+}. Consistent with such a scheme, the low temperature magnetic moment of the europium complex **2** is approximately that of the free Ni^{2+} ion.

We thank the National Science Foundation to support this work through Grant CHE94-09123 and CHE97-00394. We thank Professor Susan M. Kauzlarich and Julia Y. Chan of the University of California at Davis for collecting SQUID data and Professor Samaresh Mitra for helpful comments.

Notes and References

† Preparation of **2** and **4** are described here. Complexes **1** and **3** were prepared in a similar manner. In a dry box, $EuCl_3$ (258.3 mg, 1.0 mmol), $NiCl_2$ (64.8 mg, 0.50 mmol), K(NCO) (324.5 mg, 4.0 mmol), and DMF (*ca.* 15 ml) were placed in a flask and the mixture was stirred for 2 days at ambient temperature under N_2. Filtration separated the KCl precipitate from the deep blue solution. DMF was removed from the filtrate under dynamic vacuum. After 12 h, colorless crystals of $(DMF)_8Eu_2Ni(NCO)_8$ were collected. Yield: nearly quantitative. IR (KBr pellet, cm^{-1}): $\nu_{CN} + \nu_{CO}$: 3518w, 3487w, 3463w, 3397w, 3391w; ν_{CN}: 2188vs, 2180vs, sh, 2122m, (unresolved), δ_{NCO}: 679s, 645w, 631m, 625m, sh, 621m; the remainder of absorption bands belong to DMF: 2940w, 2813vw, 1649s, 1500w, 1440m, 1420w, sh, 1376m, 1251w, 1115m, 1066w, 1015vw, 866vw, 661m. IR (DMF solution, cm^{-1}): $\nu_{CN} + \nu_{CO}$: 3516w, 3491w, 3369w, ν_{CN}: 2194s, sh, 2177vs, ν_{CO}: 1326w, 1260w, δ_{NCO}: 677s, 632m, 619m. Anal: Calc. for $C_{32}H_{56}N_{16}O_8Eu_2Ni$: C, 29.94; H, 4.40; N, 17.46. Found: C, 29.93; H, 4.30; N, 17.50%.

When the filtrate was pumped on for a longer period of time, a viscous oil was formed. After 12 h, colorless crystals consisting of both $(DMF)_8Eu_2Ni(NCO)_8$ and $\{(DMF)_6Eu_2Ni(NCO)_8\}_\infty$ were collected.

‡ Diffraction data were collected with an Enraf-Nonius CAD4 diffractometer using Mo-Kα radiation. All data were corrected for Lorentz and polarization and empirical absorption effects. Crystallographic computations were carried out using SHELXTL program,[15] with trial structures obtained by direct method.

Crystal data: $(DMF)_8Eu_2Ni(NCO)_8$ **2** (−60 °C), monoclinic, space group $P2_1/c$, a = 11.199(2), b = 17.581(7), c = 13.492(6) Å, β = 110.34(2)°, V = 2490.6 Å^3, M = 1283.56, Z = 4, D_c = 1.712 g cm^{-3}, μ = 2.940 mm^{-1}, $F(000)$ = 1284.0, R_1 [3569 independent reflections with $I > 2\sigma(I)$] = 0.0484 ($R_1 = \Sigma||F_o|-|F_c||/\Sigma|F_o|$), wR_2 (4684 reflections measured) = 0.1496 [$wR_2 = \{\Sigma[w(F_o^2 - F_c^2)^2]/\Sigma[w(F_o^2)^2]\}^{1/2}$). $\{(DMF)_6Eu_2Ni(NCO)_8\}_\infty$ **3** (−60 °C), monoclinic, space group $P2_1$, a = 9.404(2), b = 21.060(8), c = 10.915(5) Å, β = 96.41(3)°, V = 2148.1(3) Å^3, M = 1137.37, Z = 2, D_c = 1.758 g cm^{-3}, μ = 3.391 mm^{-1}, $F(000)$ = 1124.0, R_1 [3486 independent reflections with $I > 2\sigma(I)$] = 0.0340 ($R_1 = \Sigma||F_o| - |F_c||/\Sigma|F_o|$), wR_2, (4209 reflections measured) = 0.0886 [$wR_2 = \{\Sigma[w(F_o^2 - F_c^2)^2]/\Sigma[w(F_o^2)^2]\}^{1/2}$). CCDC 979.

§ DC magnetization data were obtained with Quantum Design MPMS Superconducting Quantum Interference Device (SQUID) magnetometer with a 5.5 Tesla superconducting magnet. Data were collected and analyzed with the Magnetic Property Measurement System (MPMS) software supplied by Quantum Design. All samples were measured in zero field and then field cooled. Temperature dependent magnetization data were obtained by first measuring the zero field cooled (ZFC) magnetization in the field while warming from 5 to 300 K, then measuring magnetization while cooling back to 5 K with the field applied to obtain the field cooled (FC) data.

1 A. M. Golub, H. Köhler and V. V. Skopenko, *Chemistry of Pseudohalides*, Elsevier, Amsterdam, 1986, ch. 4, p. 186.
2 D. J. Brauer, H. Bürger, G. Pawelke, K. H. Flegler and A. Hass, *J. Organomet. Chem.*, 1978, **160**, 389.
3 J. Nelson and S. M. Nelson, *J. Chem. Soc. A*, 1969, 1597.
4 D. Britton and J. D. Dunitz, *Acta Crystallogr.*, 1965, **18**, 424.
5 F. Valach, M. Dunaj-Jurčo, J. Garaj and M. Havstijova, *Collect. Czech. Chem. Commun.*, 1974, **39**, 380.
6 W. Beck and K. Werner, *Chem. Ber.*, 1971, **104**, 2901.
7 A. Yu. Tsivadze, G. V. Tsintsadze, Yu. Ya. Kharitonov, A. M. Golub and A. M. Mamulashvili, *Russ. J. Inorg. Chem.*, 1970, **15**, 934.
8 D. M. Duggan and D. N. Hendrickson, *J. Chem. Soc., Chem. Commun.*, 1973, 411.
9 D. M. Duggan and D. N. Hendrickson, *Inorg. Chem.*, 1974, **13**, 2056.
10 T. Schönherr, *Inorg. Chem.*, 1986, **25**, 171.
11 J. C. Slater, *J. Chem. Phys.*, 1964, **41**, 3199.
12 R. A. Bailey, S. L. Kozak, T. W. Michelsen and W. N. Mills, *Coord. Chem. Rev.*, 1971, **6**, 407 and references therein.
13 A. H. Norbury, *Adv. Inorg. Chem. Radiochem.*, 1975, **17**, 231 and references therein.
14 R. S. Drago, *Physical Methods for Chemists*, Saunders, New York, 2nd Edn., 1992, p. 469.
15 SHELXTL (version 5), used to solve and refine crystal structures from diffraction data. Siemens Energy and Automation, Inc. 1994.

Received in Bloomington, IN, USA, 8th June 1998; 8/04348E

Glow discharge synthesis and molecular structures of perchlorofluoranthene and other perchlorinated fragments of buckminsterfullerene

Su-Yuan Xie, Rong-Bin Huang,*† Li-Hua Chen, Wei-Jie Huang and Lan-Sun Zheng

State Key Laboratory for Physical Chemistry of Solid Surfaces, Department of Chemistry, Xiamen University, Xiamen 361005, China

A series of perchlorinated fragments of buckminsterfullerene were prepared by glow discharge using chloroform vapor; their structural features are of significance in understanding the formation mechanism of fullerenes.

Although there have been a great many achievements in the experimental and theoretical investigation of fullerenes, their formation mechanism is still a puzzle to chemists and physicists.[1] Various schemes have been put forward to explain the formation of fullerenes.[2–7] Each of these schemes rationalise the available experimental evidence. None of them, however, can explain the formation process of the mid-sized intermediates (about 20–30 carbon atoms) and none show the formation of five-membered carbon rings that is known to be critical for fullerene formation. In order to understand the process, there has also been tremendous interest in the trapping of intermediates.[8,9] In our laboratory, a series of perchlorinated polycyclic compounds with a five-member ring and various six-member rings, such as perchloroacenaphthylene ($C_{12}Cl_8$), perchlorofluoranthene ($C_{16}Cl_{10}$) and perchlorocorannulene ($C_{20}Cl_{10}$), have been synthesized *via* discharge in liquid $CHCl_3$ rather than *via* conventional organic synthesis. These compounds were characterized as perchlorinated fragments of fullerene, so the work is helpful in understanding the formation mechanism of fullerenes.[10] Recently, we extended the discharge reaction to the vapor phase, and detected fullerenes and other larger perchlorinated fragments among the products. We were able to obtain single crystals of perchloroacenaphthylene and perchlorofluoranthene, and their structures, determined by X-ray diffraction, may provide more information about the formation mechanism.

The synthesis‡ described here was carried out using a typical procedure developed by this group in recent years. After separation procedures, the pure products were collected, and single crystals of high enough quality for X-ray diffraction analysis were obtained after four months growing in solution. The crystals were characterized as perchloroacenaphthylene ($C_{12}Cl_8$) and perchlorofluoranthene ($C_{16}Cl_{10}$) by X-ray diffraction.§ As shown in Fig. 1, octachloroacenaphthylene is a flat molecule, with all its carbon and chlorine atoms effectively located in the same plane. In contrast, perchlorofluoranthene is a very crowded molecule. If it were planar, some of the intramolecular Cl···Cl distances between neighboring chlorine atoms would be about 2.5 Å, whereas the sum of their van der Waals radii is 3.6 Å; the shortest Cl···Cl distances found in similar compounds are about 3.0 Å, as in perchloronaphthalene (3.032 Å),[11] perchloropyrene (3.003 Å),[12] perchlorophenanthrene (3.037 Å)[13] and 1,10-dichloro-3,8-dimethyl-4,7-phenanthroline (3.082 Å).[14] Thus, 3 Å is likely to be the shortest possible distance between chlorine atoms in this kind of overcrowded perchlorinated polycyclic compound. The structural data§ shows that the mean planes of the benzene and naphthalene rings are not in a same plane, and the dihedral angle between the planes is 26.09(5)°. Distortion of the molecule is due to the steric effects of its component chlorine atoms and mainly involves its five-member ring, so the molecule bends with the axis through its five-membered ring. Compared with the sandal structure of perchloropyrene,[12] one isomer of perchlorofluoranthene which has four six-membered rings but no five-membered ring, the twisted structure of perchlorofluoranthene is distorted more severely. The difference can also be found from comparison of another pair of isomers, fluoranthene and pyrene. The structure of the former is non-planar,[15] but the latter is nearly planar.[16] Obviously, formation of the five-membered ring makes the molecule more flexible, so that it can relieve the strain caused by the steric effect of the chlorine atoms. In fact, the five-membered ring is also found in the structures of other perchlorinated polycyclic compounds synthesized in the experiment.

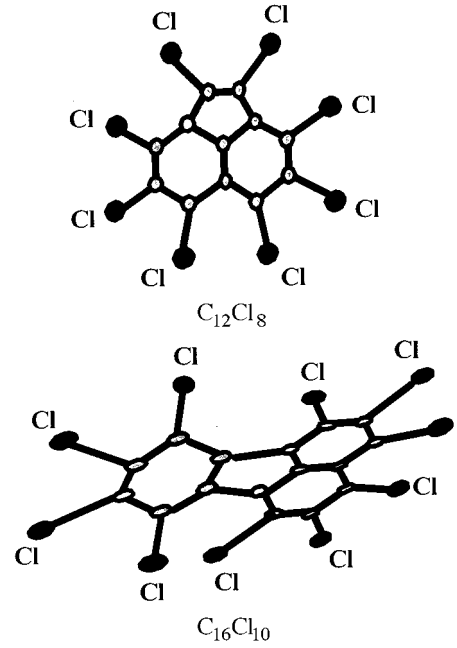

Fig. 1 Molecular structures of perchloroacenaphthylene and perchlorofluoranthene

Formation of the cage structure of the fullerenes also involves the five-membered rings. In fact, C_{60} and other fullerenes were also produced in the glow discharge experiment and were detected by laser-desorption mass spectrometry (Fig. 2). In the mass spectrum, in addition of various fullerene products, some larger perchlorined fragments, such as $C_{22}Cl_{10}$ and $C_{24}Cl_{10}$, are also observed. Although the fullerene products were not seperated, they can be characterized by their particular size distribution.

Products from discharge reactions were expected to be very complicated. However, the products from the discharge reaction of $CHCl_3$ are quite selective: The products were either fullerenes or their perchlorinated fragments. The distorted structure of perchlorofluoranthene suggests that it is the steric effects of the chlorine atoms that limits the possible number of the products and favors the formation of the five-membered ring. Although $CHCl_3$ only contains a single carbon atom, in the

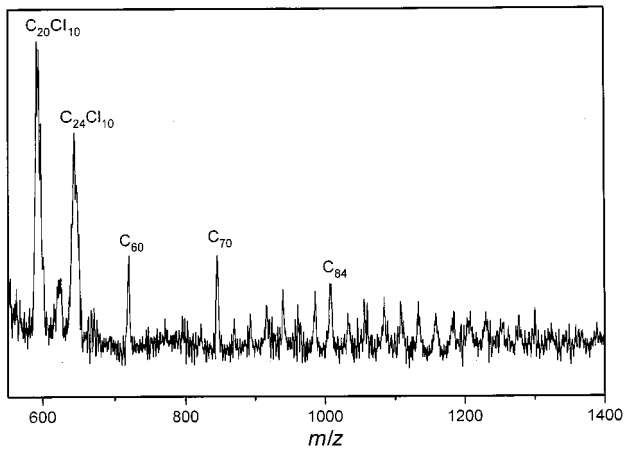

Fig. 2 Laser desorption mass spectrum of fullerenes and other products synthesized from the glow-discharge reaction of $CHCl_3$

discharging reaction it serves as a C1 building block for aggregation into fullerenes or their perchlorinated fragments.

This work was supported by the National Natural Science Foundation of China and by the State Educational Commission of China.

Notes and References

† E-mail: rbhuang@xmu.edu.cn

‡ *Typical procedure*: $CHCl_3$ was evaporated from a flask containing 100 ml liquid $CHCl_3$ into a quartz tube with a diameter of *ca*. 40 mm and a length of *ca.* 250 mm; a pair of copper pipes, which acted as both electrodes and a gas passageway, were mounted at the two ends of the tube. When the vacuum pressure of the tube was reduced to less than 300 Pa and an ac voltage of > 10 kV with 25 kHz frequency was applied to the electrodes, a stable glow discharge emerged in the gap between the two electrodes which could be maintained by adjusting the gap. After reacting for several hours, *ca*. 5 g of black deposit was collected, followed by sublimating at 160 °C to separate hexachlorobenzene and the other volatile matter. The residue was extracted with toluene and separated *via* chromatography (Al_2O_3, light petroleum); the third (yellow) component part was perchlorofluoranthene, the fourth (red) component part was perchloroacenaphthylene, and the remainder were other larger perchlorined fragments, C_{60} and other fullerenes products.

§ *Crystal data* for perchloroacenaphthylene: $C_{12}Cl_8$, M = 428, monoclinic, $P2_1/a$, a = 7.079(5), b = 22.396(5), c = 10.661(5) Å, β = 93.046(5)°, U = 1687.8(15) Å^3, T = 298 K, Z = 4, λ = 105418 Å, μ(Cu-Kα) = 24.687 cm^{-1}, $F(000)$ = 532, red crystals with dimensions 0.16 × 0.17 × 0.79 mm. Data were collected on a Enraf-Nonius CAD-4 diffractometer in the ω–2θ scan mode, and corrected for absorption by ψ. A total of 3768 independant reflections were collected in the range 4 < 2θ < 75°, of which 1628 reflections with $I > 2\sigma(I)$ are considered observed.The SIR92 and SHELXL93 program packages were used to solve and refine the structure, respectively. The final deviation factor R_w = 0.0749, wR = 0.1955.

Crystal data for perchlorofluoranthene: $C_{16}H_{10}$, M = 546.66, triclinic, space group $P\bar{1}$, a = 7.4590(7), b = 11.4920(7), c = 11.8800(8) Å, α = 112.346(5), β = 90.858(6), γ = 106.277(6)°, U = 895.60(12) Å^3, T = 298 K, Z = 2, D_c = 2.02 Mg cm^{-3}, λ = 1.5418 Å, μ(Cu-Kα) = 24.68 cm^{-1}, $F(000)$ = 532, orange crystals with dimensions 0.04 × 0.07 × 0.075 mm. Data were collected on an Enraf-Nonius CAD-4 diffractometer in the ω–2θ scan mode, and corrected for absorption by ψ. A total of 3889 independent reflections were collected in the range 4 < 2θ < 75°, of which 2111 reflections with $I = 2\sigma$ were considered observed. The SIR92 and SHELXL93 programme packages were used to solve and refine the structure, respectively. The final deviation factor R_w = 0.064, wR = 0.1362. CCDC 182/981.

1 S. G. Nancy, *Acc. Chem. Res*., 1996, **29**, 77.
2 R. F. Curl and R. E. Smalley, *Sci. Am*., 1991, **265**, 54.
3 R. E. Haufler, Y. Chai, L. P. E. Chibante, J. Conceicao, C. Jin, L. S. Wang, S. Maruyama and R. E. Smalley, *Mater. Res. Soc. Symp. Proc*., 1991, **206**, 627.
4 R. E. Smalley, *Acc. Chem. Res*., 1992, **25**, 98.
5 J. R. Heath, *ACS Symp. Ser*., 1991, **481**, 1.
6 J. M. Hunter, J. L. Fye, E. J. Roskamp and M. F. Jarrold, *J. Phy. Chem*., 1994, **98**,1810.
7 K. B. Shelimov, J. M. Hunter and M. F. Jarrold, *Int. J. Mass Spectrom. Ion. Processes*, 1994, **138**, 17.
8 T. Grösser and A. Hirsch, *Angew. Chem*., 1993, **105**, 1390; *Angew. Chem., Int. Ed. Engl*., 1993, **32**, 1340.
9 T.-M. Chang, A. Naim, S. N. Ahmed, G. Goodloe and P. B. Shevlin, *J. Am. Chem. Soc*., 1992, **114**, 7603.
10 Rongbin Huang, Weijie Huang, Yuhuang Wang, Zichao Tang and Lansun Zheng, *J. Am. Chem. Soc*., 1997, **119**, 5954.
11 G. Gafner and F. H. Herbstein, *Nature (London)*, 1963, **200**, 130.
12 A. C. Hazell and S. Jagner, *Acta. Crystallogr., Sect. B*, 1976, **32**, 682.
13 F. H. Herbstein, M. Kapon and R. Merksamer, *Acta. Crystallogr., Sect. B*, 1976, **32**, 2205.
14 F. H. Herbstein, M. Kapon and D. Rabinovich, *Isr. J. Chem*., 1972, **10**, 537.
15 A. C. Hazell, D. W. Jones and J. M. Sowden, *Acta. Crystallogr., Sect. B*, 1977, **33**, 1516.
16 A. Camerman and J. Trotter, *Acta. Crystallogr*., 1965, **18**, 636.

Received in Columbia, MO, USA, 12th January 1998; revised manuscript received, 29th July 1998; 8/06160B

Is Ti(η⁸-pentalene)$_2$ a 20-electron complex? A theoretical investigation of a pseudo electron-rich molecule

Karine Costuas and Jean-Yves Saillard*

LCSIM-UMR 6511, Université de Rennes 1, 35042 Rennes Cedex, France. E-mail: saillard@univ-rennes1.fr

DFT calculations confirm the D_{2d} conformation of the title compound proposed by Jonas *et al*; only 9 of the 10 combinations of the π-type ligand orbitals interact with the metal atom: the remaining one, of a_2 symmetry, does not match with any metal orbital and therefore the title compound is not a 20-electron system, but a regular 18-electron complex; calculations predict that the 18-electron [Ti(η⁸-pentalene)$_2$]$^{2+}$ cation should also be attainable.

Jonas and coworkers recently synthesised and characterised a very interesting series of transition metal complexes of V, Ti, Zr and Hf which exhibit a new type of coordination mode of pentalene (C_8H_6).[1–3] In these compounds, exemplified below

1 **2**

by CpV(C_8H_6) **1** and Ti(C_8H_6)$_2$ **2**, the pentalene ligand is folded in such a way that all its carbon atoms are bonded to the metal. Considering the η⁸-bonded pentalene ligand in **1** as being formally a dianion, it is expected to provide the metal centre with its 10 π electrons, leading to a V^{III} 18-electron complex. A similar reasoning leads to the surprising count of 20 electrons in the case of **2**. Such an electron-rich situation generally corresponds to a Jahn–Teller instability due to the presence of two electrons in one (or two) antibonding orbital(s). Unlike **1** and other CpV systems, there is no X-ray characterisation published so far for **2** or related complexes. Its D_{2d} conformation was established on the basis of NMR data.[2] Simple symmetry considerations are fully consistent with the 18-electron count of **1**. Indeed, there is a perfect match between the five empty frontier orbitals of the CpV fragment (four of d-type and one sp-type hybrid)[4] and the five occupied π-type orbitals of $(C_8H_6)^{2-}$,[5] leaving two electrons in a dσ non-bonding level. On the other hand, of the ten occupied π-type combinations of the two $(C_8H_6)^{2-}$ ligands in the D_{2d} complex **2**, only nine have the correct symmetry to match with the nine vacant orbitals of the Ti^{IV} atom. The remaining one, being of a_2 symmetry, cannot overlap with the metal and should remain non-bonding. Thus, symmetry and frontier orbital theory predict an 18-electron count for the D_{2d} conformation of **2**.

Our current interest in transition metal sandwich complexes which do not obey the 18-electron rule[6] as well as in the coordination variability of pentalene with respect to electron count[5] prompted us to perform density functional theory (DFT) calculations[7] on **2**, in order to predict its structure (D_{2d} or less symmetrical), rationalise its electron count and understand its bonding. A full geometry optimisation carried out without any symmetry constraint confirmed the D_{2d} structure (see Fig. 1). The pentalene optimised folding angle is 149°, a value larger than that reported in **1** and related V and Ti complexes (119–127°).[1,2] As a consequence, the Ti–C(pentalene) distances are somewhat larger than those reported for the CpTi(pentalene)

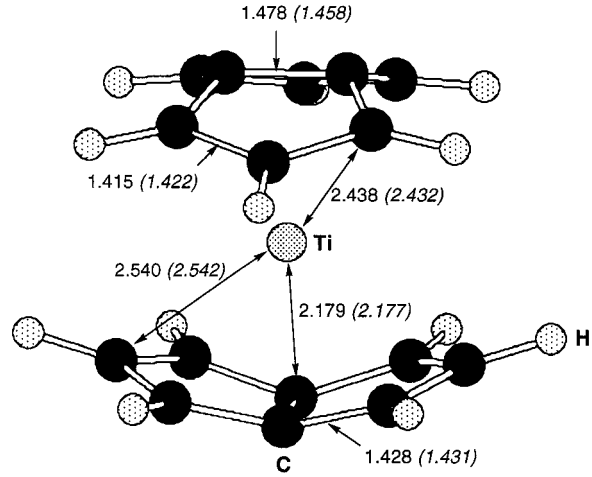

Fig. 1 DFT optimised molecular structure of **2** and **2**$^{2+}$. The values in parentheses correspond to **2**$^{2+}$.

derivatives.[1,2] The MO diagram of **2** is shown in Fig. 2, based on the interaction of the $(C_8H_6)^{2-}$ ligands with the Ti^{IV} center. With an a_2 HOMO deriving from the π-type orbitals of pentalene, it shows clearly that the symmetry-based predictions are correct.[11] The significant HOMO–LUMO gap computed agrees with the stability of these diamagnetic species. The existence of an even larger energy gap below the HOMO suggest that **2**$^{2+}$ or isoelectronic species should also be stable diamagnetic compounds.[12] The optimised geometry of **2**$^{2+}$, for which a HOMO–LUMO gap of 1.93 eV was computed, is very similar to that of **2**. The major metrical data are given in Fig. 1. The folding angle of pentalene is also 149°. Since the a_2 HOMO of **2** has no metal participation, its depopulation in **2**$^{2+}$ has no effect on the Ti–C separations. Since this a_2 orbital derives from

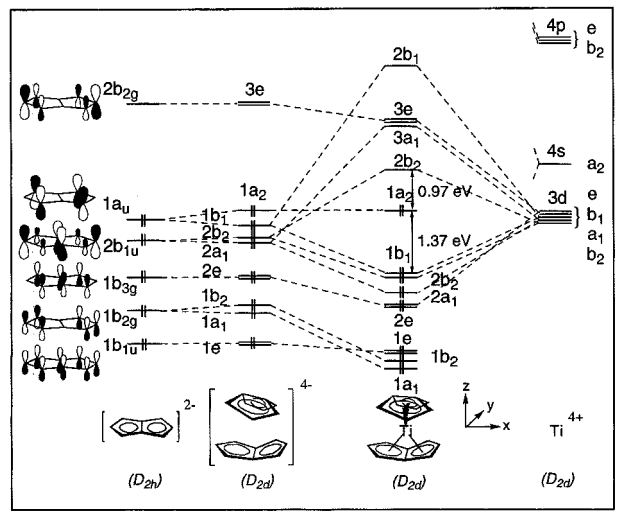

Fig. 2 MO interaction diagram of **2**

the C–C non-bonding $1a_u$ HOMO of $(C_8H_6)^{2-}$ (Fig. 2), there is also little difference between the ligand geometries of **2** and $\mathbf{2}^{2+}$. The shortening by *ca.* 0.02 Å of the central C–C bond upon oxidation is probably due to the σ/π mixing within the non-planar ligands. The smaller folding of pentalene in **2** and $\mathbf{2}^{2+}$, as compared to **1**, is consistent with the fact that in the bis-pentalene systems each ligand [$(C_8H_6)^{2-}$ in **2** and $(C_8H_6)^{-}$ in $\mathbf{2}^{2+}$] is a 9-electron donor whereas in **1** $(C_8H_6)^{2-}$ is a 10-electron donor.

In order to check the possibility of extending the peculiar bonding mode of pentalene in **2** to other ligands, we are currently investigating the electronic structure of hypothetical sandwich complexes of fused conjugated rings such as indacene and naphthalene.

The authors thank the Centre de Ressources Informatiques (CRI) of Rennes and the Institut de Développement et de Ressources en Informatique Scientifique (IDRIS-CNRS) of Orsay for computing facilities.

Notes and References

1 K. Jonas, B. Gabor, R. Mynott, K. Angermund, O. Heinemann and C. Krüger, *Angew. Chem., Int. Ed. Engl.*, 1997, **36**, 1712.

2 K. Jonas, P. Kobl, G. Kollbach, B. Gabor, R. Mynott, K. Angermund, O. Heinemann and C. Krüger, *Angew. Chem., Int. Ed. Engl.*, 1997, **36**, 1714.

3 H. Butenschön, *Angew. Chem., Int. Ed. Engl.*, 1997, **36**, 1695.

4 (*a*) R. Hoffmann, *Angew. Chem., Int. Ed. Engl.*, 1982, **21**, 711; (*b*) T. A. Albright, J. K. Burdett and M.-H. Whangbo, *Orbital Interactions in Chemistry*, John Wiley and Sons, New York, 1984.

5 M. T. Garland, J.-Y. Saillard, I. Chávez, B. Oëclkers and J.-M. Manríquez, *J. Mol. Struct. (THEOCHEM)*, 1997, **390**, 199.

6 (*a*) M. Lacoste, H. Rabaâ, D. Astruc, F. Varret, N. Ardoin, J.-Y. Saillard and A. Le Beuze, *J. Am. Chem. Soc*., 1990, **112**, 9548; (*b*) H. Rabaâ, M. Lacoste, M.-H. Delville-Desbois, J. Ruiz, B. Gloaguen, N. Ardoin, D. Astruc, A. Le Beuze, J.-Y. Saillard, J. Linares, F. Varret, J.-M. Dance and E. Marquestaut, *Organometallics*, 1995, **14**, 5078; (*c*) M.-H. Delville-Desbois, S. Mross, D. Astruc, J. Linares, F. Varret, H. Rabaâ, A. Le Beuze, J.-Y. Saillard, R. D. Culp, D. A. Atwood and A. H. Cowley, *J. Am. Chem. Soc.*, 1996, **118**, 4133; (*d*) M. T. Garland, J.-Y. Saillard, F. Ogliaro, M. Otero and E. Román, *Inorg. Chim. Acta*, 1997, **257**, 253; (*e*) F. Ogliaro, Thèse de Doctorat de l'Université de Rennes 1, 1997; (*f*) J. Ruiz, F. Ogliaro, J.-Y. Saillard, J.-F. Halet, F. Varret and D. Astruc, *J. Am. Chem. Soc.*, submitted.

7 The calculations were carried out with the ADF program[8] developed by Baerends and coworkers,[9] using non-local exchange and correlation corrections.[10] The standard ADF STO basis set IV, of triple-ζ quality for the valence orbitals (except for the single-ζ 4p orbitals), was used for Ti. The other atoms were treated with the standard basis set III, of double-ζ quality for the valence orbitals. The frozen-core approximation was considered.

8 Amsterdam Density Functional (ADF) program, release 2.3.0, Vrije Universiteit, Amsterdam, Netherlands, 1996.

9 (*a*) E. J. Baerends, D. E. Ellis and P. Ros, *Chem. Phys.*, 1973, **2**, 41; (*b*) E. J. Baerends and P. Ros, *Int. J. Quantum Chem.*, 1978, **S12**, 169; (*c*) P. M. Boerringter, G. te Velde and E. J. Baerends, *Int. J. Quantum Chem.*, 1988, **33**, 87; (*d*) G. te Velde and E. J. Baerends, *Int. J. Quantum Chem.*, 1992, **99**, 84.

10 D. A. Becke, *Phys. Rev. A*, 1988, **38**, 3098; (*b*) J. P. Perdew, *Phys. Rev. B*, 1986, **34**, 8822.

11 Situations somewhat related of pseudo electron-rich complexes with a pure non-bonding ligand HOMO have been reported. See for example (and references therein): (*a*) D. L. Morrison and D. E. Wigley, *Inorg. Chem.*, 1995, **34**, 2610; (*b*) D. L. Morrison, P. M. Rodgers, Y.-W. Chao, M. A. Bruck, C. Grittiny, T. L. Tajima, S. J. Alexander, A. L. Rheingold and D. E. Wigley, *Organometallics*, 1995, **14**, 2435; (*c*) H. Tang, D. M. Hoffman, T. A. Albright, H. Deng and R. Hoffmann, *Angew. Chem., Int. Ed. Engl.*, 1993, **32**, 1616.

12 Extended Hückel calculations give a similar situation, with large gaps above (1.82 eV) and below (1.82 eV) the a_2 HOMO.

Received in Cambridge, UK, 21st July 1998; 8/05682J

The first synthesis of promothiocin A

Christopher J. Moody*† and Mark C. Bagley

School of Chemistry, University of Exeter, Stocker Road, Exeter, UK EX4 4QD

The first total synthesis of the naturally occurring macrocyclic thiopeptide promothiocin A 1 is described.

Promothiocin A **1**, isolated from *Streptomyces* sp. SF2741, is a member of the thiopeptide family of antibiotics.[1] These natural products, which inhibit protein synthesis in bacteria, are characterised by their complex structure in which an array of heterocyclic rings is incorporated into a macrocyclic peptide framework. Despite the fascinating biological activity of the thiopeptide antibiotics, little synthetic work has been carried out to date, although the synthesis of the pyridine fragments of the micrococcins, sulfomycin and nosiheptide has been addressed,[2–5] and very recently micrococcin P has yielded to synthesis.[6] In continuation of our interest in the synthesis of heterocyclic natural products,[7] we now report the first total synthesis of promothiocin A **1**, thereby confirming the structure and stereochemistry.

The structure of promothiocin A **1** was established by NMR spectroscopy, although the stereochemistry of the natural product was not reported.[1] Therefore we have assumed that the three stereocentres result from natural amino acids (see Fig. 1) and could be incorporated from suitable derivatives of (*S*)-alanine and (*S*)-valine. The overall plan, indicated by the arrows in Fig. 1, was to form the macrocycle by two peptide coupling reactions (1 and 2), followed by introduction of the dehydroalanine side chain (3).

The starting point was the synthesis of the two oxazoles **2** and **3** from (*S*)-alanine and glycine, respectively. This was readily achieved using our previously published method;[8] thus rhodium(II) acetate catalysed reaction of the *N*-protected amino acid amides with methyl 2-diazo-3-oxobutanoate resulted in clean insertion of the metallocarbenoid into the amide N–H bond. Cyclodehydration of the resulting keto amides using the Wipf protocol (Ph_3P, I_2, Et_3N)[9] gave the required oxazoles **2** and **3** in 56 and 49% overall yield respectively (Scheme 1). The glycine derived oxazole **3** was deprotected to give the 2-aminomethyloxazole **4** for subsequent coupling, whereas the alanine derived oxazole **2** was converted into the oxazole-thiazole-pyridine fragment **5** using our previously developed method,[10] based on the Bohlmann–Rahtz pyridine synthesis.[11]

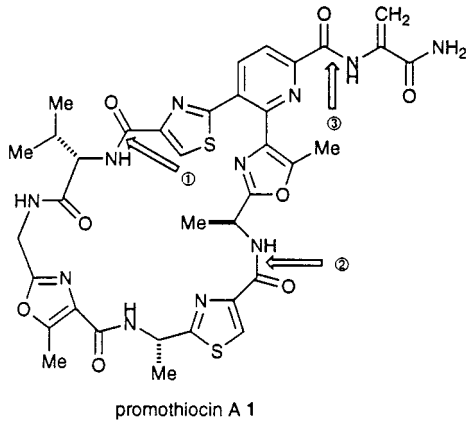

Fig. 1 Promothiocin A **1** and proposed disconnections

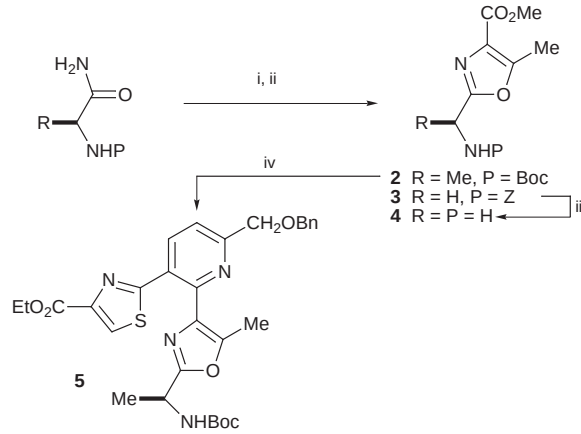

Scheme 1 *Reagents and conditions*: i, methyl 2-diazo-3-oxobutanoate cat. $Rh_2(OAc)_4$, $CHCl_3$, heat (80% for **2**, 76% for **3**); ii, Ph_3P, I_2, Et_3N, CH_2Cl_2 (70% for **2**, 64% for **3**); iii, H_2, Pd-C, MeOH (100%); iv, see ref. 10

The lower valine-oxazole-thiazole fragment **9** was obtained as shown in Scheme 2. Thus *N*-Boc-valine was coupled to the aminomethyloxazole **4** in high yield by mixed anhydride methodology using isobutyl chloroformate and *N*-methylmorpholine (NMM) to give the oxazole **6**. The alanine derived thiazole **7** was obtained from the known *N*-Boc derivative, prepared using the modified Hantzsch reaction,[12] the standard conditions leading to extensive racemisation, and coupled to the carboxylic acid derived by hydrolysis of the ester **6** to give the valine-oxazole-thiazole **8** in excellent yield (Scheme 2). Finally

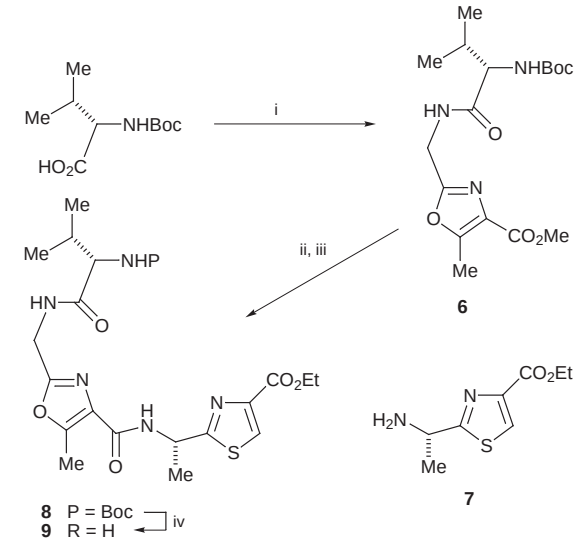

Scheme 2 *Reagents and conditions*: i, Bu^iO_2CCl, NMM, THF, then **4** (87%); ii, LiOH, aq. THF (93%); iii, Bu^iO_2CCl, NMM, THF then **7** (84%); iv, AcCl, EtOH (100%)

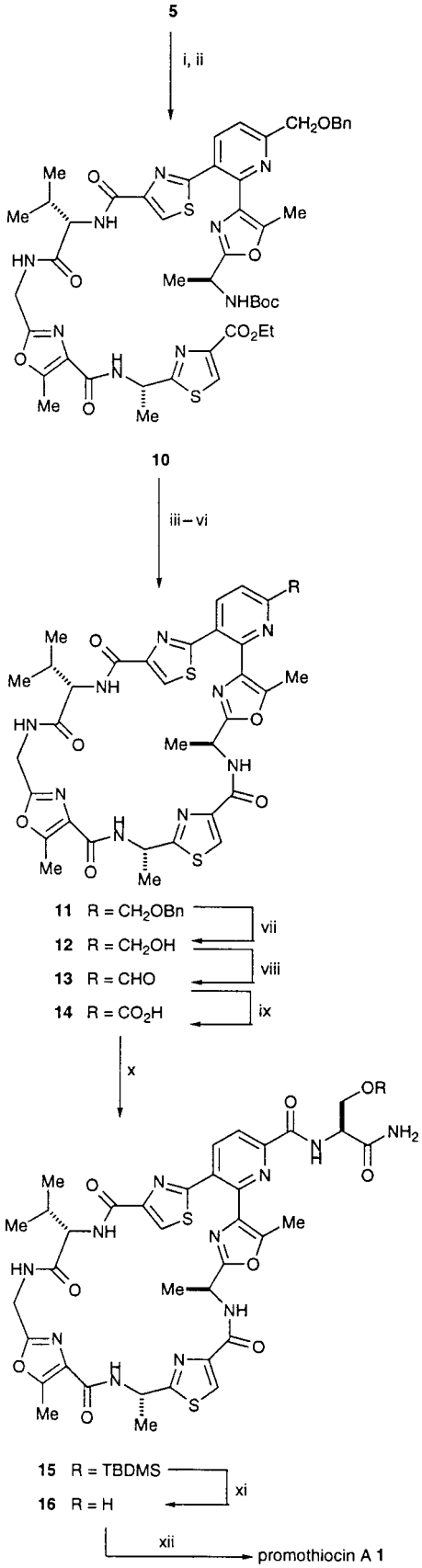

Scheme 3 *Reagents and conditions*: i, LiOH, aq. THF (94%); ii, Bu^iO_2CCl, NMM, THF, then **9** (69%); iii, LiOH, aq. THF (97%); iv, C_6F_5OH, EDCI, CH_2Cl_2 (100%); v, 4 M HCl in dioxane, then aq. $KHCO_3$; vi, Et_3N, $CHCl_3$ (55% over 2 steps); vii, $BCl_3{\cdot}SMe_2$, CH_2Cl_2 (39%); viii, IBX, DMSO (81%); ix, $NaClO_2$, KH_2PO_4, 2-methylbut-2-ene, aq. Bu^tOH (70%); x, *O*-TBDMS-serinamide, EDCI, CH_2Cl_2 (50%); xi, TBAF, THF (57%); xii, MsCl, Et_3N, CH_2Cl_2, then Et_3N (59%)

deprotection of the *N*-terminal Boc group with ethanolic HCl gave the free amine **9** for subsequent coupling.

The coupling of the lower and upper fragments of the promothiocin macrocycle was achieved using mixed anhydride methodology (Scheme 3). Hydrolysis of the ester group in the oxazole-thiazole-pyridine **5** was followed by activation with isobutyl chloroformate/NMM and coupling with the amine **9** to give the terminally protected 'linear peptide' **10** in good yield. Although there are several methods available for macrolactamisation, we have found the Schmidt protocol,[13] used in our recent synthesis of nostocyclamide,[7] to be particularly reliable. Hence the ester group in **10** was hydrolysed and converted into the corresponding pentafluorophenyl ester by coupling with pentafluorophenol in the presence of 1-(3-dimethylaminopropyl)-3-ethylcarbodiimide hydrochloride (EDCI). The pentafluorophenyl ester was not purified but underwent deprotection at the *N*-terminus on treatment with HCl in dioxane. Work-up and treatment with triethylamine resulted in lactamisation to give the promothiocin macrocycle **11** in 55% yield. The synthesis was completed by elaboration of the dehydroalaninamide side chain, although these final steps proved far from trivial. Deprotection of the benzyl ether to give the pyridine-2-methanol derivative **12** was followed by conversion to the aldehyde **13** using *o*-iodoxybenzoic acid (IBX) in DMSO,[14] and further oxidation with sodium chlorite[15] to give the desired acid **14**. Coupling of the acid **14** with the *tert*-butyldimethylsilyl ether of (*S*)-serinamide using EDCI gave the amide **15**; deprotection of the serine side-chain with TBAF was followed by dehydration (MsCl, Et_3N) to give promothiocin A **1** (Scheme 3). The synthetic material had 400 MHz ^1H and 100 MHz ^{13}C NMR spectra identical to those reported for the natural product,[1] and its specific rotation of $[\alpha]_D^{23}$ + 87.3 (*c* 0.34, $CHCl_3$–MeOH, 1 : 1) [lit.,[1] +79.2 (*c* 0.69, $CHCl_3$–MeOH, 1 : 1)] strongly implies that the natural product does indeed have the stereochemistry indicated in Fig. 1. Thus we have completed the first total synthesis of the thiopeptide promothiocin A **1**, and established the stereostructure of the natural product.

We thank the EPSRC and the Leverhulme Trust for support of our research, Claire Hesketh for preliminary experiments, and Dr Vladimir Sik for detailed NMR experiments.

Notes and References

† E-mail: c.j.moody@ex.ac.uk

1 B.-S. Yun, T. Hidaka, K. Furihata and H. Seto, *J. Antibiot.*, 1994, **47**, 510.
2 T. R. Kelly, C. T. Jagoe and Z. Gu, *Tetrahedron Lett.*, 1991, **32**, 4263; T. R. Kelly and F. Lang, *J. Org. Chem.*, 1996, **61**, 4623.
3 K. Okumura, M. Shigekuni, Y. Nakamura and C.-G. Shin, *Chem. Lett.*, 1996, 1025.
4 M. A. Ciufolini and Y. C. Shen, *J. Org. Chem.*, 1997, **62**, 3804.
5 K. Umemura, H. Noda, J. Yoshimura, A. Konn, Y. Yonezawa and C.-G. Shin, *Tetrahedron Lett.*, 1997, **38**, 3539.
6 C.-G. Shin, K. Okumura, M. Shigekuni and Y. Nakamura, *Chem. Lett.*, 1998, 139.
7 C. J. Moody and M. C. Bagley, *J. Chem. Soc., Perkin Trans. 1*, 1998, 601.
8 M. C. Bagley, R. T. Buck, S. L. Hind and C. J. Moody, *J. Chem. Soc., Perkin Trans. 1*, 1998, 591.
9 P. Wipf and C. P. Miller, *J. Org. Chem.*, 1993, **58**, 3604.
10 C. J. Moody and M. C. Bagley, *Synlett*, 1998, 361.
11 F. Bohlmann and D. Rahtz, *Chem. Ber.*, 1957, **90**, 2265.
12 M. W. Bredenkamp, C. W. Holzapfel, R. M. Snyman and W. J. vanZyl, *Synth. Commun.*, 1992, **22**, 3029; E. Aguilar and A. I. Meyers, *Tetrahedron Lett.*, 1994, **35**, 2473.
13 U. Schmidt and F. Stäbler, *J. Chem. Soc., Chem. Commun.*, 1992, 1353.
14 M. Frigerio and M. Santagostino, *Tetrahedron Lett.*, 1994, **35**, 8019.
15 G. A. Kraus and M. J. Taschner, *J. Org. Chem.*, 1980, **45**, 1175.

Received in Cambridge, UK, 23rd July 1998; 8/05762A

Enamine-assisted facile generation of trifluoroacetaldehyde from trifluoroacetaldehyde ethyl hemiacetal and its carbon–carbon bond forming reaction leading to β-hydroxy-β-trifluoromethyl ketones

Kazumasa Funabiki,*† Miwa Nojiri, Masaki Matsui and Katsuyoshi Shibata*

Department of Chemistry, Faculty of Engineering, Gifu University, Yanagido, Gifu, 501-1193, Japan

Trifluoroacetaldehyde ethyl hemiacetal 1 readily reacts with various enamines 2 in hexane at room temperature for 1 h to give the corresponding β-hydroxy-β-trifluoromethyl ketones in good yields.

Much attention has been recently addressed to trifluoromethylated compounds, since they are widely used for the construction of new types of biologically active compounds and liquid crystals. In connection with these circumstances, the development of new strategies and methodologies for the efficient synthesis of trifluoromethylated molecules has become the subject of growing interest.[1] Among the many approaches to such compounds, trifluoroacetaldehyde is one of the most useful compounds, and is employed for the construction of functionalized trifluoromethylated components *via* reaction with a number of reagents, such as metal enolates,[2] ketene silyl acetals[3] (phenylthio)bis(trimethylsilyl)methyllithium,[4] aromatic compounds,[5] olefins[3,6] and dienes.[7] In previous methods for the generation of trifluoroacetaldehyde, however, there exist serious disadvantages, including high reaction temperatures and the use of an excess amount of concentrated H_2SO_4.[8] In addition, trifluoroacetaldehyde is gaseous (bp −18 °C) and very miscible with water, and therefore it must be carefully handled.

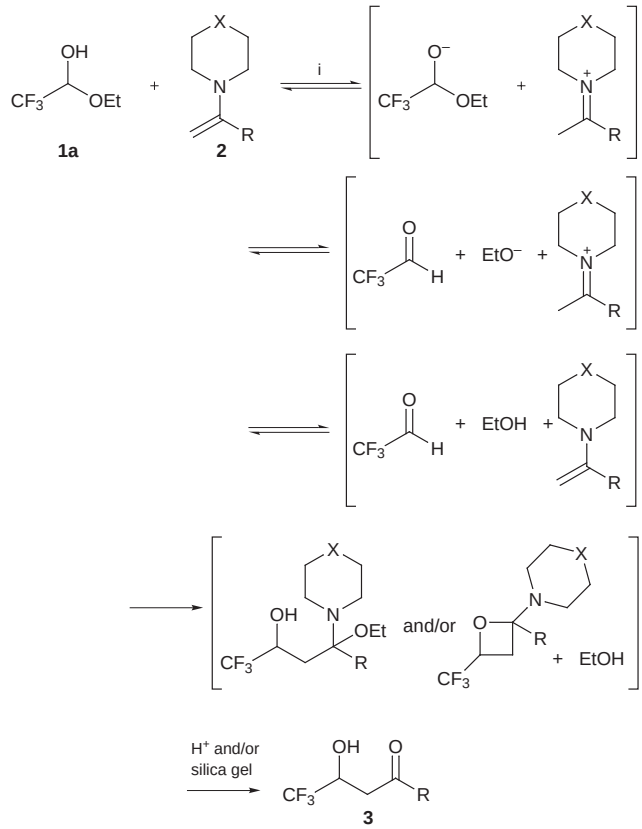

Scheme 1 *Reagents and conditions:* i, room temp., 1 h

Here we describe for the first time the enamine-assisted facile generation of trifluoroacetaldehyde under extremely mild conditions from trifluoroacetaldehyde ethyl hemiacetal,‡ and its carbon–carbon bond forming reaction with enamines in the absence of additives, which permits highly efficient and convenient access to β-hydroxy-β-trifluoromethyl ketones.

When hemiacetal **1a** was allowed to react with an equimolar amount of enamine **2a**, prepared from acetophenone with morpholine, in hexane at room temperature for 1 h, the corresponding β-hydroxy-β-trifluoromethyl ketone **3a** was obtained in 88% yield (Scheme 1 and Table 1, entry 1).

The use of other solvents, such as dichloroethane, THF, PhMe and MeCN, gave comparable yields of **3a**, irrespective of their polarities (entries 2–5). It is noteworthy that the reaction of **1a** proceeded smoothly to furnish the product **3a** in satisfactory yield in the presence of water (entry 6). The substituents on the nitrogen atom of the enamines did not influence the yields of **3a** (entries 1 and 7). Various enamines bearing aromatic and heteroaromatic substituents could successfully participate in the reaction to afford the corresponding β-hydroxy-β-trifluoromethyl ketones **3** in good to excellent yields (entries 8–11, 14–15). The reaction with enamine **2f** carrying a nitro group on the aromatic ring was very sluggish, producing **3e** in only 13% yield because of the lower solubility of **2f**, which could be improved by replacing hexane with toluene as solvent (entries 12 and 13). The electronic character of the aromatic ring has little influence on the rate of the reaction, according to the yields of **2** for the same reaction time (*p*-NO_2 < 2-thienyl =

Table 1 Reactions of trifluoroacetaldehyde ethyl hemiacetal with enamines[a]

Entry	Enamine	X	R	Solvent	Product	Yield (%)[b]
1	**2a**	O	Ph	hexane	**3a**	88
2	**2a**	O	Ph	$ClCH_2CH_2Cl$	**3a**	78
3	**2a**	O	Ph	THF	**3a**	73
4	**2a**	O	Ph	PhMe	**3a**	88
5	**2a**	O	Ph	MeCN	**3a**	75
6	**2a**	O	Ph	hexane–H_2O (40:1)	**3a**	68
7	**2b**	CH_2	Ph	hexane	**3a**	86
8	**2c**	O	*p*-MeC_6H_4	hexane	**3b**	87
9	**2c**	O	*p*-MeC_6H_4	PhMe	**3b**	87
10	**2d**	O	*p*-$MeOC_6H_4$	hexane	**3c**	72
11	**2e**	O	*p*-ClC_6H_4	hexane	**3d**	86
12	**2f**	O	*p*-$O_2NC_6H_4$	hexane	**3e**	13
13	**2f**	O	*p*-$O_2NC_6H_4$	PhMe	**3e**	52
14	**2g**	O	*o*-MeC_6H_4	hexane	**3f**	87
15	**2h**	O	2-thienyl	hexane	**3g**	75
16[c]	**2i**	O	Pr^i	hexane	**3h**	25

[a] All the reactions were carried out with trifluoroacetaldehyde ethyl hemiacetal (1 mmol) and enamine (1 mmol) in solvent (4 ml) at room temperature for 1 h. [b] Isolated yields of analytical pure products. [c] A mixture of enamines **2i** and **4** (29:71) was employed.

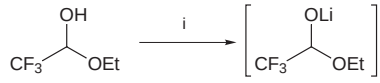

1a **1b**

Scheme 2 *Reagents and conditions:* i, Bu^{n}Li (1.5 equiv.), hexane, 0 °C, 15 min

p-Cl = *p*-H = *p*-Me = *p*-MeO). The reaction of **1a** with the mixture of aliphatic enamines **2i** and 4-(3-methylbut-2-en-2-yl)morphorine **4** (29:71) (1 equiv.) resulted in the exclusive formation of **3h** in 25% yield, and none of the product derived from enamine **4** was detected in the reaction mixture (entry 16). According to these results, the steric effect of the substituents at the β-carbon of the enamines is more important for the the reaction than the electronic effect of the substituents at the α-carbon.

The formation of **3** can be explained by assuming the mechanism shown in Scheme 1. It is significant that the reaction requires only an equimolar amount of enamine, which may act as a base, counter ammonium cation and carbon nucleophile.

More significantly, the reaction of lithium alcoholate **1b**§ with the enamine **2a** did not proceed at all; the acetophenone was recovered in quantitative yield (Scheme 2). According to this result, the ammonium cation, which is generated *via* protonation of the enamine, plays a very important role in the effective generation of trifluoroacetaldehyde in the reaction.

In conclusion, we have demonstrated the enamine-assisted *in situ* generation of trifluoroacetaldehyde and its reaction with enamines, producing the corresponding β-hydroxy-β-trifluoromethyl ketones **3** in high yields. The present method can serve as a synthetically useful entry to β-hydroxy-β-trifluoromethyl ketones, with simple manipulations and high yields of the products. Application of the present methodology to stereoselective synthesis using asymmetric secondary amines or β-monosubstituted enamines is currently in progress in our laboratory.

We thank Dr H. Muramatsu for valuable discussions.

Notes and References

† E-mail kfunabik@apchem.gifu-u.ac.jp

‡ Recent reports have presented the coupling reaction of trifluoroacetaldehyde ethyl hemiacetal, which is considered as an equivalent of trifluoroacetaldehyde. These methods, however, require the use of an excess amount of reagents and/or of limited solvents, the formation of by-products, and relatively low yields of the products, see ref. 9.

§ Kitazume and Yamazaki reported that the tetrahedral form of **1b** is too stable to be converted to trifluoroacetaldehyde due to the strong electron-withdrawing effect of a trifluoromethyl group, see ref 10.

1 For recent examples, see: K. Uneyama, J. Hao and H. Amii, *Tetrahedron Lett.*, 1998, **39**, 4079; A. Ishii, F. Miyamoto, K. Higashiyama and K. Mikami, *Tetrahedron Lett.*, 1998, **39**, 1199; T.-P. Loh and X.-R. Li, *Angew. Chem., Int. Ed. Engl.*, 1997, **36**, 980; G. Foulard, T. Brigaud and C. Portella, *J. Org. Chem.*, 1997, **62**, 9107; A. Abouabdellah, J.-P. Bégué, D. Bonnet-Delpon and T. T. T. Nga, *J. Org. Chem.*, 1997, **62**, 8826; P. Bravo, A. Farina, V. P. Kukhar, A. L. Markovsky, S. V. Meille, V. A. Soloshonok, A. E. Sorochinsky, F. Viani, M. Zanda and C. Zappalá, *J. Org. Chem.*, 1997, **62**, 3424; V. A. Soloshonok and T. Ono, *J. Org. Chem.*, 1997, **62**, 3030; S. Hiraoka, T. Yamazaki and T. Kitazume, *Chem. Commun.*, 1997, 1497; V. A. Soloshonok, D. V. Avilov, V. P. Kukhar, L. V. Meervelt and N. Mischenko, *Tetrahedron Lett.*, 1997, **38**, 4671; Y. Yokoyama and K. Mochida, *Tetrahedron Lett.*, 1997, **38**, 3443; T. Katagiri, H. Ihara, M. Takahashi, S. Kashino, K. Furuhashi and K. Uneyama, *Tetrahedron: Asymmetry*, 1997, **8**, 2933.

2 For boron enolates, see: K. Iseki, S. Oishi and Y. Kobayashi, *Chem. Pharm. Bull.*, 1996, **44**, 2003; K. Iseki, S. Oishi and Y. Kobayashi, *Tetrahedron*, 1996, **52**, 71; Y. Makino, K. Iseki, K. Fujii, S. Oishi, T. Hirano and Y. Kobayashi, *Tetrahedron Lett.*, 1995, **36**, 6527; K. Iseki, S. Oishi and Y. Kobayashi, *Chem. Lett.*, 1994, 1135. For a lithium enolate, see: D. V. Patel, K. Rielly-Gauvin and D. E. Ryono, *Tetrahedron Lett.*, 1988, **29**, 4665.

3 (*a*) K. Mikami, T. Yajima, T. Takasaki, S. Matsukawa, M. Terada, T. Uchimaru and M. Maruta, *Tetrahedron*, 1996, **52**, 85; (*b*) K. Mikami, T. Takasaki, S. Matsukawa and M. Maruta, *Synlett*, 1995, 1057.

4 T. Yamazaki, K. Takita and N. Ishikawa, *J. Fluorine Chem.*, 1985, **30**, 357.

5 For an asymmetric Friedel–Crafts reaction, see: A. Ishii, V. A. Soloshonok and K. Mikami, *74th National Meeting of the Chemical Society of Japan*, Kyoto, March, 1998, Abstr. No. 1D641.

6 R. Pautrat, J. Marteau and R. Cheritat, *Bull. Soc. Chim. Fr.*, 1968, 1182; K. Ogawa, T. Nagai, M. Nonomura, T. Takagi, M. Koyama, A. Ando, T. Miki and I. Kumadaki, *Chem. Pharm. Bull.*, 1991, 39, 1707. For an asymmetric reaction, see: K. Mikami, T. Yazima, N. Siree, M. Terada, Y. Suzuki and I. Kobayashi, *Synlett*, 1996, 837; K. Mikami, T. Yajima, M. Terada, E. Kato and M. Maruta, *Tetrahedron: Asymmetry*, 1994, **5**, 1087; K. Mikami, T. Yajima, M. Terada and T. Uchimaru, *Tetrahedron Lett.*, 1993, **34**, 7591 and ref. 3(*a*).

7 L. Lévêque, M. L. Blanc and R. Pastor, *Tetrahedron Lett.*, 1997, **38**, 6001. For an asymmetric reaction, see: K. Mikami, T. Takasaki, T. Yazima, S. Matsukawa and M. Terada, *72nd National Meeting of the Chemical Society of Japan*, Tokyo, March, 1997, Abstr. No. 4H332.

8 M. Braid, H. Isersone and F. Lawlore, *J. Am. Chem. Soc.*, 1954, **76**, 4027; A. Henne, R. Pelley and R. Alm, *J. Am. Chem. Soc.*, 1950, **72**, 3370; H. Shechter and F. Conrad, *J. Am. Chem. Soc.*, 1950, **72**, 3371.

9 For carbon nucleophiles, see: A. Ishii, K. Higashiyama and K. Mikami, *Synlett*, 1997, 1381; T.-P. Loh and X.-R. Li, *Chem. Commun.*, 1996, 1929; T. Ishihara, H. Hayashi and H. Yamanaka, *Tetrahedron Lett.*, 1993, **34**, 5777; T. Kubota, M. Iijima and T. Tanaka, *Tetrahedron Lett.*, 1992, **33**, 1351; B. Imperiali and R. H. Abeles, *Tetrahedron Lett.*, 1986, **27**, 135; A. Guy, A. Lobgeois and M. Lemaire, *J. Fluorine Chem.*, 1986, **32** 361; D. J. Cook, O. R. Pierce and E. T. McBee, *J. Am. Chem. Soc.*, 1954, **76**, 83. For phosphorus nucleophiles, see: Y. Shen and M. Qi, *J. Chem. Soc., Perkin Trans. 1*, 1994, 1179. For amino acids and nucleotides, see: H. Yin, R. J. Crowder, J. P. Jones and M. W. Anders, *Chem. Res. Toxicol.*, 1996, **9**, 140.

10 S. Kaneko, T. Yamazaki and T. Kitazume, *J. Org. Chem.*, 1993, **58**, 2302.

Received in Cambridge, UK, 29th June 1998; 8/04922J

Synthesis of fluorine-containing cyclic amino acid derivatives *via* ring closing olefin metathesis

Sergey N. Osipov,*[a] Christian Bruneau,[b] Michel Picquet,[b] Alexey F. Kolomiets[a] and Pierre H. Dixneuf*[b]†

[a] *A. N. Nesmeyanov Institut of Organoelement Compounds, Vavilov st. 28, Moscow, V334, GSP-1, 117813, Russia*
[b] *UMR 6509 CNRS Université de Rennes, Laboratoire de Chimie de Coordination et Catalyse, Campus de Beaulieu, 35042 Rennes, France*

New N-protected α-CF_3 amino esters with two alkene chains (1,7-dienes 3 and 1,6-dienes 5) were reacted with the ring closing metathesis catalyst Ru=CHPh$(Cl)_2(PCy_3)_2$ to give the α-CF_3 dehydropipecolinate and prolinate derivatives 6 and 7.

Among various classes of fluorine-containing biologically active compounds, fluorinated amino acids attract considerable attention. They are especially useful candidates for peptide modification, and β-fluoro-containing amino acids offer potential as irreversible inhibitors of pyridoxal phosphate dependent enzymes.[1] A major drawback of peptide drugs is their rapid degradation by proteases, low lipophilicity and high conformational flexibility and the lack of transport systems to direct peptides into cells.[2] The incorporation of α,α-disubstituted amino acids into key positions in peptides is an efficient strategy to retard proteolytic degradation and to stabilize secondary structures.[3,4] Due to the unique properties of the CF_3 group (high electronegativity, lipophilicity and steric hindrance), α-trifluoromethyl amino acids are a special class of α,α-disubstituted amino acids that can profoundly improve the above mentioned characteristics of peptides.[5]

The preparation of rigidified α-amino acids to effect conformational constraints in peptides has played an important role in drug design and development.[6] An efficient access to α-difluoromethyl and α-trifluoromethyl substituted α-amino acids from electrophilic imines of type $XF_2CC(=NPG)CO_2R$ has recently been reported.[7,8] This reaction enabled the direct synthesis of α-fluoromethyl α-amino acids, but the restriction of their conformational flexibility by incorporation into an N-heterocycle was necessary. However, one possible approach is based on intramolecular Ring Closing Metathesis (RCM). The use of olefin metathesis has expanded tremendously in recent years, with applications including the construction of carbo- and hetero-cycles, macrocycles in peptides and other systems.[9] Especially useful are metathesis catalysts based on ruthenium, which have demonstrated remarkable tolerance towards oxygen, protic solvents, and a variety of functional groups.[10]

We now disclose a new effective synthesis of α-trifluoromethyl substituted derivatives of dehydropipecolinic acid and dehydroproline, from α-trifluoromethyl α-amino esters containing two terminal alkene chains, using ring closing olefin metathesis (RCM), according to Scheme 1.

Several imines with different protecting groups on nitrogen, including $PhSO_2$, Boc and Z groups, were successfully applied for the synthesis of α-CF_3 containing α-amino acid derivatives.[11,12] Thus, the preparation of α-CF_3 amino acid derivatives **3** and **5** with two alkene chains was achieved *via* a two-step

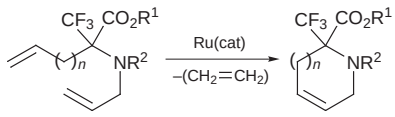

Scheme 1

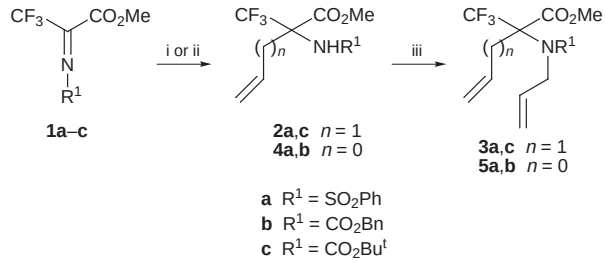

Scheme 2 *Reagents and conditions*: i, CH_2=$CHCH_2MgBr$, THF, −100 °C (1 h) to room temp. (2 h), then aq. HCl (1 M); ii, CH_2=$CHMgBr$, THF, −90 °C to room temp., then aq. HCl (1 M); iii, NaH, DMF, 0 °C, then allyl bromide, 10 h, room temp., then H_2O

procedure starting from the electrophilic imine **1**. The imine **1a** smoothly reacts with allylmagnesium bromide in THF to give the amino acid derivative **2a** in 75% yield. The latter is transformed on deprotonation with NaH and subsequent reaction with allyl bromide into the 1,7-diene derivative **3a** (72%). Similarly, imine **1a** reacts with vinylmagnesium bromide at −90 °C to give **4a** (69%). *N*-Allylation of **4a** *via* successive treatment with NaH and allyl bromide affords the 1,6-diene **5a** (81%) (Scheme 2).

Following the same procedure but starting from the Z and Boc N-protected imines **1b**,**c**, it was possible to isolate in two steps the 1,6-diene **5b** (65%) and the 1,7-diene **3c** (55%) *via* **4b** and **2c**, respectively.

The intramolecular ring closing metathesis reaction was attempted from the 1,7-diene **3a** in CH_2Cl_2 at room temperature in the presence of 10 mol% of the Grubbs catalyst Ru=CHPh$(Cl)_2(PCy_3)_2$ **A**.[9a] The cyclisation of **3a** took place and was completed within 10 h to give the dehydropipecolinate derivative **6a**[13] in high yield (93%) (Scheme 3). The RCM reaction with catalyst **A** (10 mol%) applied to **3c** led to the formation of the six-membered heterocycle **6c** which, after 10 h of reaction, was isolated in 98% yield.

Special interest in α-CF_3 proline derivatives is connected with the fact that proline is known to be unique among the natural amino acids in its abilities to induce β-turns and initiate the folding of an α-helix. Because of these structurally important properties, proline is often suggested as the primary contributor to the biological activity of several proteins, as well as having a key role in biological recognition phenomena.[14]

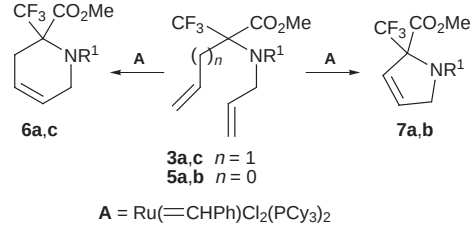

Scheme 3

Dehydroproline derivatives have also found use as starting materials for kanic acid derivatives.[15]

Recently, attempts to prepare dehydroproline derivatives *via* ring closing metathesis from a $BocN(CH_2CH{=}CH_2)CH(CO_2Me)CH{=}CH_2$ precursor have been made and failed. In the presence of $Ru{=}CHCH{=}CPh_2(Cl)_2(PCy_3)_2$ **B** as catalyst, the acyclic α,β-unsaturated ester $\{BocN[C(CO_2Me){=}CHMe]CH_2CH{=}\}_2$ has been obtained.[9a] This is likely due to the high lability of the vinylglycine α-proton of the precursor.

The absence of an acidic α-proton in the vinylglycine structure of compounds **5** was crucial to the suucessful first formation of the desired dehydroprolinates **7**. Under standard RCM conditions in the presence of 11 mol% of catalyst **A**, at room temperature, **5a** (0.23 mmol) was slowly cyclised into **7a**.[13] However, full conversion of **5a** could not be achieved even after 60 h (conversion ~55%) and derivative **7a** was separated from the starting product **5a** by chromatography over silica gel and isolated in 46% yield.

The benzyloxycarbonyl derivative **5b** (0.2 mmol) was also reacted with 10 mol% of catalyst **A** and after 50 h at room temperature the separation of the starting material **5b** by chromatography led to the isolation of 50% of **7b**.

To the best of our knowledge, the above results show the first use of ruthenium-based RCM catalysts for access to α-CF_3 containing heterocycles (the six- and five-membered cyclic α-CF_3 substituted α-amino acid derivatives). Based on known transformations of amino acid derivatives this direct access should open a route to a variety of fluorine-containing substrates.

The authors thank the E.U. INTAS Programme No. 96-1176 for financial support.

Notes and References

† E-mail: pierre.dixneuf@univ-rennes1.fr

1 J. T. Welch and S. Eswarakvishnan, *Fluorine in Bioorganic Chemistry*, Wiley, New York, 1991, 54 and references cited therein.
2 A. Giannis and T. Kolter, *Angew. Chem., Int. Ed. Engl.*, 1993, **32**, 1244.
3 C. Toniolo and E. Benedetti, *Macromolecules*, 1991, **24**, 4004.
4 G. R. Marshal, J. D. Clarc, J. B. Dunbar, G. D. Smith, Y. Zabrocki, A. S. Redlinski and M. T. Leplawy, *Int. J. Pept. Protein Res.*, 1988, **32**, 544.
5 K. Burger, K. Mütze, W. Hollweck and B. Koksch, *Tetrahedron*, 1998, **54**, 5915.
6 M. Goodman and H. Shao, *Pure Appl. Chem.*, 1996, **68**, 1303; W. F. Degrado, *Adv. Protein Chem.*, 1988, **39**, 53 and references cited therein.
7 S. N. Osipov, A. S. Golubev, N. Sewald, T. Michel, A. F. Kolomiets, A. V. Fokin and K. Burger, *J. Org. Chem.*, 1996, **61**, 7521.
8 K. Burger and N. Sewald, *Synthesis* 1990, 115.
9 (*a*) S. J. Miller, M. E. Blackwell and R. H. Grubbs, *J. Am. Chem. Soc.*, 1996, **118**, 9606; (*b*) A. Fürstner and K. Langemann, *J. Org. Chem.*, 1996, **61**, 3942; (*c*) F. P. J. Rutjes and H. E. Schoemaker, *Tetrahedron Lett.*, 1997, **38**, 677; (*d*) M. A. McKenvey and M. Pitarch, *Chem. Commun.*, 1996, 1689.
10 B. Mohr, D. M. Lynn and R. H. Grubbs, *Organometallics*, 1996, **15**, 4317; (*b*) P. Schwab, R. H. Grubbs and J. W. Ziller, *J. Am. Chem. Soc.*, 1996, **118**, 100.
11 S. N. Osipov, N. D. Chkanikov, A. F. Kolomiets and A. V. Fokin, *Bull. Acad. Sci. USSR, Chem. Sect. (Eng.)*, 1986, 1256.
12 N. Sewald and K. Burger, in *Fluorine-containing Amino Acids: Synthesis and Properties*, ed. V. P. Kukhar and V. A. Soloshonok, Wiley, Chichester, 1995, 139 and references cited therein.
13 Satisfactory spectroscopic data and elemental analyses were obtained for compounds **3–7**. *Selected data* for **6a**: $\delta_H(CDCl_3)$ 2.71 (m, 1 H, CH_2), 2.92 (m, 1 H, CH_2), 3.65 (m, 1 H, NCH_2), 3.83 (m, 1 H, NCH_2), 3.88 (s, 3 H, OCH_3), 5.72 (m, 2 H, HC=CH), 7.51(m, 3 H, Ph), 7.95 (m, 2 H, Ph); $\delta_F(CDCl_3)$ −71.1 (s, 3 F, CF_3). For **6c**: $\delta_H(CDCl_3)$ 1.52 [s, 9 H, $(CH_3)_3$], 2.77 (m, 2 H, CH_2), 3.82 (m, 1 H, NCH_2), 3.85 (s, 3 H, OCH_3), 4.25 (m, 1 H, NCH_2), 5.75–6.00 (br m, 2 H, HC=CH); $\delta_F(CDCl_3)$ −71.9 (s, 3 F, CF_3). For **7a**: $\delta_H(CDCl_3)$ 3.89 (s, 3 H, OCH_3), 4.07 (m, 1 H, CH_2), 4.62 (m, 1 H, CH_2), 5.63 (m, 1 H, HC=CH), 6.22 (m, 1 H, HC=CH), 7.51 (m, 3 H, Ph), 7.85 (m, 2 H, Ph); $\delta_F(CDCl_3)$ −72.1 (s, 3 F, CF_3). For **7b** (two conformers): $\delta_H(CDCl_3)$ 3.39 and 3.74 (2 s, 3 H, OMe), 4.27 (dm, 1 H, *J* 15.9, NCH_2), 4.41–4.61 (m, 1 H, NCH_2), 4.93–5.41 (m, 2 H, OCH_2), 5.59–5.76 and 5.83–6.00 (2 m, 1 H, =CH), 6.16–6.35 (m, 1 H, =CH), 7.24–7.40 (m, 5 H, Ph); $\delta_F(CDCl_3)$ −71.91, −71.89 (2 s, CF_3).
14 D. J. Barlow and J. M. Thornton, *J. Mol. Biol.*, 1988, **201**, 601; A. M. P. Koskinen and H. Rapoport, *J. Org. Chem.*, 1989, **54**, 1859; H. H. Ibrahim and W. D. Lubell, *J. Org. Chem.*, 1993, **58**, 6438.
15 M. Horikawa and M. Shirahama, *Synlett*, 1996, 95.

Received in Liverpool, UK, 22nd June 1998; 8/04792H

New sulfide-bridged heterocubanes $[M^{VI}(S)Re^{I}_3(CO)_9(\mu_3\text{-}S)_4]^-$, M = Mo or W, with transition metals in very different oxidation states

Fridmann M. Hornung, Karl Wilhelm Klinkhammer and Wolfgang Kaim*†

Institut für Anorganische Chemie, Universität Stuttgart, Pfaffenwaldring 55, D-70550 Stuttgart, Germany

The cluster anions $[M^{VI}(S)Re^{I}_3(CO)_9(\mu_3\text{-}S)_4]^-$, M = Mo or W, contain three six-coordinate tricarbonylrhenium(I) fragments, held together by one μ_3-sulfide ion and by one reducible and charge transfer-active μ_3-$M^{VI}S_4^{2-}$ unit.

The coordinative versatility of the tetrathiometallates has given rise to a vast number of oligonuclear cluster compounds with intact or altered MS_4^{n-} units (*e.g.* M = Mo or W, *n* = 2; M = Re, *n* = 1) as essential constituents.[1–4] However, there are not many kinds of heterocubanes containing the MS_4^{n-} motif except for species $[MS(M'L)_3(\mu_3\text{-}S)_4]^{n-}$ with four-coordinate centres M′ = Cu^I or Ag^I and L = PR_3 or halogen.[4,5] Heterocubanes with the $MM'_3(\mu_3\text{-}S)_4$ core are generally of interest because of their relevance as models for cluster sites in proteins or on surfaces of industrial catalysts.[6–8]

Herein we present first examples of organometallic heterocubanes with a tetrathiometallate (Mo or W) corner and three six-coordinate low-valent metal centres, *i.e.* rhenium(I) stabilized by three facially arranged carbonyl ligands. The compounds $[M(S)Re_3(CO)_9(\mu_3\text{-}S)_4](NEt_4)$, M = Mo **1** or W **2** were obtained from $Re(CO)_5(CF_3SO_3)$,[9] Li_2S and $(NEt_4)_2MoS_4$ or $(NEt_4)_2WS_4$.‡ Both compounds were crystallised and analysed by X-ray diffraction.§ Fig. 1 illustrates the molecular structure of the cluster anion by example of compound **2**.

Compounds **1** and **2** crystallise in isomorphous fashion with channel structures (Fig. 1). The molecular anions show heterocubane arrangements with fairly ideal tetrahedral MoS_4 or WS_4 and approximately octahedral $ReS_3(CO)_3$ entities. The rigidity of the tetrahedral MS_4 core has been demonstrated recently in the species $(CH_3CN)(OC)_3M'(S_2WS_2)M'(CO)_3(NCCH_3)$, M = Mn or Re.[10] The main differences between **1** and **2** concern the M–S bond lengths in an otherwise qualitatively similar C_{3v} symmetric setting (Fig. 1). Apart from the distortion brought upon the heterocubane by the close to tetrahedral μ_3-MS_4 units (*ca.* 109° angles for S–M–S) there are slightly widened angles of about 95° for Re–S–Re and (μ_3-S1–S3)–Re–(μ_3-S1–S3) but generally compressed bond angles M–S–Re and (μ-S1–S3)–Re–S5 (Fig. 1). All Re···Re distances lie above 3.74 Å whereas the M···Re distances are significantly smaller between 2.93 and 2.97 Å.

The combination between three $(OC)_3Re^+$ groups and a tetrathiometallate(VI) acceptor[2,10–12] function causes a narrowing of the frontier orbital gap as evident from electrochemistry and absorption spectroscopy (Fig. 2). Whereas even the first oxidation occurs irreversibly at +0.48 V (**1**) and +0.45 V (**2**) *vs.* ferrocenium–ferrocene in acetonitrile–0.1 mol dm^{-3} Bu_4NPF_6, cyclic voltammetry at 200 mV s^{-1} revealed reversible first one-electron reduction processes at −1.24 V (**1**) and −1.61 V (**2**). The corresponding values for $(NEt_4)_2MS_4$ at −2.94 V (M = Mo) and −3.16 V (M = W)[10–12] illustrate the effect of tetrathiometallate coordination by $\{(\mu_3\text{-}S)[Re(CO)_3]_3\}^+$.¶ Accordingly, the long-wavelength ligand-to-metal charge transfer $(LMCT_1)^2$ absorption bands ($t_1 \rightarrow 2e$) at 562 nm (**1**, Fig. 2) and 458 nm (**2**) in acetonitrile are lower in energy when compared to the 472 nm for $(NEt_4)_2MoS_4$ and 397 nm for $(NEt_4)WS_4$. Similar shifts were observed for the $LMCT_2$ transitions ($3t_2 \rightarrow 2e$) at 331 nm (**1**, Fig. 2) and 310 nm (**2**). Additional long-wavelength absorption bands at 408 nm (**1**,

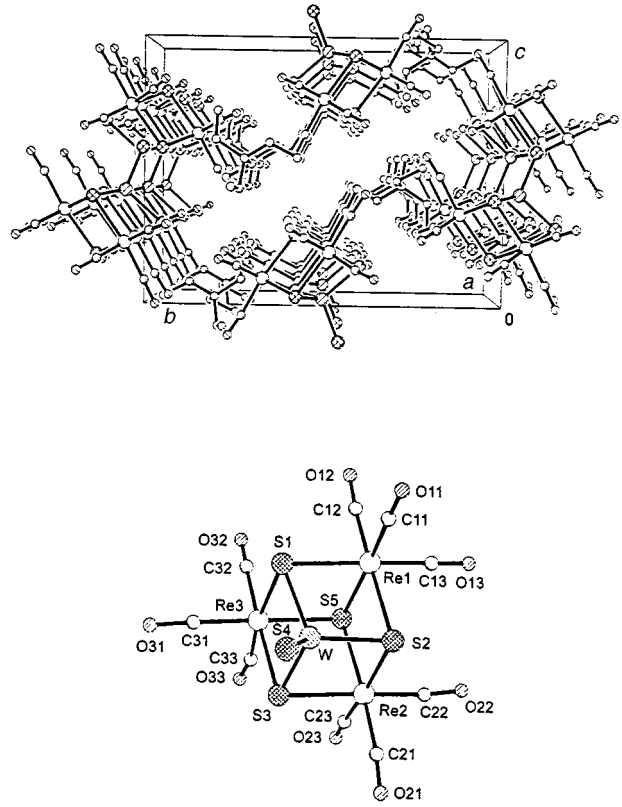

Fig. 1 Crystal structure (top, view along *a* axis) of **2** and molecular structure of the cluster anion. Selected bond lengths (Å) and angles (°) for isomorphous **1** and **2** (in parentheses): M–S4 2.131(8) [2.110(5)], M–(μ_3-S) 2.262(7)–2.285(7) [2.258(5)–2.263(4)], Re–(μ_3-S) 2.502(7)–2.515(7) [2.502(5)–2.522(5)]; S4–M–(μ_3-S) 107.4(3)–110.3(3) [107.3(2)–110.1(2)]. (μ_3-S)–M–(μ_3-S) 109.5(3)–111.2(3) [109.6(2)–111.4(2)], M–(μ_3-S)–Re 75.5(2)–76.4(2) [75.6(2)–76.7(1)], (μ_3-S1–S3)–Re–(μ_3-S1–S3) 96.0(2)–96.5(2) [94.9(2)–95.9(2)], (μ_3-S1–S3)–Re–S5 81.8(2)–83.5(2) [81.3(2)–82.802)], Re–(μ_3-S)–Re 96.3(2)–98.2(2) [96.8(2)–98.8(2)], C–Re–(μ_3-S) 171.6(8)–176.4(9) [171.4(6)–176.5(6)].

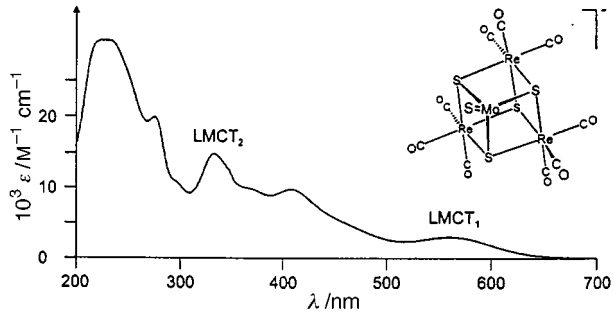

Fig. 2 Absorption spectrum of **1** in acetonitrile solution

Fig. 2) and 362 nm (**2**) may tentatively be attributed to metal-to-metal intracluster charge transfer from the electron-rich rhenium(I) centres to molybdenum(VI) (**1**) or tungsten(VI) (**2**).

Notes and References

† E-mail: kaim@iac.uni-stuttgart.de

‡ *Synthesis (general procedure)*: 1 equivalent of lithium sulfide and 3 molar equivalents of $Re(CO)_5(CF_3SO_3)$[9] were reacted under argon in dichloromethane–THF (5 : 1) for 6 h at room temperature. After filtration and removal of the solvent from the filtrate the remaining residue were redissolved in CH_2Cl_2 and treated with 1 equivalent of $(NEt_4)_2MS_4$ (M = Mo or W), dissolved in acetonitrile. After brief reflux the dark-brown solutions were reduced to dryness, the residue redissolved in CH_2Cl_2–CH_3CN (9 : 1) and chromatographed on a silica gel column. The eluted dark brown (**1**) or red fraction (**2**) was collected, the solvent removed under vacuum, and the dark purple (**1**, 10%) or orange–red (**2**, 34%) product crystallised from acetonitrile at −20 °C. Correct C, H, N analyses. ^{13}C NMR ([$^2H_8$]THF): δ = 7.4 (CH_3), 52.8 (NCH_2), 193.0 (CO_{ax}), 197.6 (CO_{eq}). IR (CH_3CN): ν_{CO} = 2049, 2017, 1961, 1926 cm^{-1} (**1**); ν_{CO} = 2050, 2017, 1961, 1926 cm^{-1} (**2**).

§ *Crystallography*: single crystals were obtained from acetonitrile solutions at −25 °C. Crystals were poured into degassed Nujol and transferred into a capillary. This was sealed and immediately brought into the cold gas stream of a Siemens P4 diffractometer (graphite monochromator, Mo-Kα radiation (λ = 0.71 073 Å)) equipped with low temperature device (183 K). Unit cell dimensions were derived from the least-squares fit of the angular settings of 25 reflections. Crystal and refinement data for **1** (**2**): $C_{17}H_{20}MoNO_9Re_3S_5$ ($C_{17}H_{20}NO_9Re_3S_5W$), M = 1197.18 (1285.09), crystal size 0.30 × 0.25 × 0.25 (0.30 × 0.30 × 0.20) mm, monoclinic, space group $P2_1/n$ (no. 14), a = 11.595(4) [11.593(3)], b = 18.226(5) [18.188(3)], c = 13.527(4) [13.460(3)] Å, β = 95.80(2) [95.89(2)]°, U = 2844.1(14) [2823.1(11)] $Å^3$, D_c = 2.796 (3.024) g cm^{-3}, μ(Mo-Kα) = 13.569 (17.297) mm^{-1}, F(000) = 2192 (2320), ω scans, 5836 (8269) measured reflections, 5569 (6814) independent reflections, $wR2$ = 0.194 (0.164) for 5323 (6437) reflections with $I > -\sigma(I)$, $R1$ = 0.090 (0.068) for reflections with $I > 2\sigma(I)$. Due to the failure of finding appropriate reflection for ψ scans, the data were corrected in both cases using the DIFABS program. The structures were solved using direct methods (SHELXS 86). Site and displacement parameters were refined by full-matrix least-squares techniques (SHELXL 93) based on F_o^2 values. All non-hydrogen atoms were treated anisotropically. The hydrogen atoms were treated isotropically, their sites riding on the appropriate carbon atom with fixed C–H lengths and H–C–H angles. CCDC 182/969.

¶ A second reversible reduction occurs at −1.86 V (**1**) and −1.82 V (**2**), respectively. Attempts to characterise the one-electron reduced forms by EPR were unsuccessful even at 3.5 K, probably due to rapid relaxation. Anodic peak potentials for the second irreversible oxidation are at +0.66 V (**1**) and +0.74 V (**2**), respectively.

1 A. Müller, H. Bögge, H.-G. Tölle, R. Jostes, U. Schimanski and M. Dartmann, *Angew. Chem.*, 1980, **92**, 665; *Angew. Chem., Int. Ed. Engl.*, 1980, **19**, 654; A. Müller, W. Jaegermann and W. Hellmann, *J. Mol. Struc.*, 1983, **100**, 559.

2 A. Müller, E. Diemann, R. Josts and H. Bögge, *Angew. Chem.*, 1981, **93**, 957; *Angew. Chem., Int. Ed. Engl.*, 1981, **20**, 934.

3 K. E. Howard, T. B. Rauchfuss and S. R. Wilson, *Inorg. Chem.*, 1988, **27**, 3561; M. Draganjac and T. B. Rauchfuss, *Angew. Chem.*, 1985, **97**, 745; *Angew. Chem., Int. Ed. Engl.*, 1985, **24**, 742.

4 Y. Jeannin, F. Secheresse, S. Bernes and F. Robert, *Inorg. Chim. Acta*, 1992, **198**, 493.

5 A. Müller, E. Krickemeyer and H. Bögge, *Z. Anorg. Allg. Chem.*, 1987, **61**, 554; Z. Nianyong, W. Jianhui, D. Shaowu, W. Xintao and L. Jiaxi, *Inorg. Chim. Acta*, 1992, **191**, 65; C. D. Scattergood, C. D. Garner and W. Clegg, *Inorg. Chim. Acta*, 1987, **132**, 161.

6 R. H. Holm, *Adv. Inorg. Chem.*, 1992, **38**, 1; D. Coucouvanis, *Acc. Chem. Res.*, 1991, **24**, 1; M. K. Johnson, D. C. Rees and M. W. W. Adams, *Chem. Rev.*, 1996, **96**, 2817; D. C. Rees, Y. Hju, C. Kisker and H. Schindelin, *J. Chem. Soc., Dalton Trans.*, 1997, 3909.

7 E. I. Stiefel and K. Matsumoto, eds., *Transition Metal Sulfur Chemistry*, American Chemical Society, Washington, 1996; T. Weber, ed., *Challenges for Sulfides in Material Sciences and Catalysis*, NATO ASI Series, Kluwer Academic, Dordrecht, in press.

8 C. S. Bahn, A. Tan and S. Harris, *Inorg. Chem.*, 1998, **37**, 2770; M. A. Mansour, M. D. Curtis and J. W. Kampf, *Organometallics*, 1997, **16**, 275; T. Murata, Y. Mizobe, H. Gao, Y. Ishii, T. Wakabayashi, F. Nakano, T. Tanase, S. Yano, M. Hidai, I. Echizen, H. Nanikawa and S. Motomura, *J. Am. Chem. Soc.*, 1994, **116**, 3389.

9 R. J. Shaver and D. P. Rillema, *Inorg. Chem.*, 1992, **31**, 4101.

10 W. Kaim, F. M. Hornung, R. Schäfer, B. Schwederski and J. Fiedler, *Z. Anorg. Allg. Chem.*, 1998, **624**, 1211.

11 R. Schäfer, W. Kaim and J. Fiedler, *Inorg. Chem.*, 1993, **32**, 3199.

12 R. Schäfer, J. Fiedler, M. Moscherosch and W. Kaim, *J. Chem. Soc., Chem. Commun.*, 1993, 896.

Received in Cambridge, UK, 8th July 1998; 8/05295F

Typeset and printed by Black Bear Press Limited, Cambridge, England

ChemComm
FEATURE ARTICLE

Liquid crystals with restricted molecular topologies: supermolecules and supramolecular assemblies

John W. Goodby,*[a]† Georg H. Mehl,[a] Isabel M. Saez,[a] Rachel P. Tuffin,[a] Grahame Mackenzie,[a] Rachel Auzély-Velty,[b] Thierry Benvegnu[b] and Daniel Plusquellec[b]

[a] *The Department of Chemistry, The Faculty of Science and the Environment, The University of Hull, Hull, UK HU6 7RX*
[b] *Ecole Nationale Supérieure de Chimie de Rennes, Laboratoire de Synthèses et Activations de Biomolécules, associé au CNRS, Avenue du Général Leclerc, 35700 Rennes, France*

The term liquid crystal is often associated with fascinating compounds that exhibit unusual melting or solubilisation properties, however, it also represents a unique collection of mesophases that exist between the solid state and the amorphous liquid. As such, this unique state of matter can be accessed by a wide variety of materials from low molar mass to polymeric systems. In this Feature Article we describe some recent studies concerning the liquid-crystalline behaviour of 'in-between' materials that have discrete molecular structures, and which are oligomeric but not low molar mass or polymeric systems. Thus, these materials could be described as having supermolecular architectures. We examine some of their mesophase properties and their abilities to form supramolecular assemblies. The development of liquid crystals that have large molecular structures or consist of large scale assemblies is one step towards creating novel self-organising systems which are of a similar dimension to certain biological materials, such as proteins.

Introduction

Over the past two and a half decades low molar mass liquid crystals (LMMLCs) have been the quintessential molecular electronic materials. The invention of the twisted nematic display (TNLCD) in the early 1970s coupled with Gray and Harrison's development of stable room temperature nematogens based on cyanobiphenyls, **1**, ensured that liquid crystals would be synonymous, across the world, with flat-panel, low voltage visual display units (VDUs).[1] This association has continued with the invention and development of surface stabilised ferroelectric smectic C* displays (SSFLCDs)[2,3] which are near to commercialisation, and the recent extension of this work to device configurations utilising antiferroelectric materials.[4] All devices based on liquid crystal technology are, of course, non-emissive and depend on the reflection of incident light or an artificial light source for viewing. As a consequence, however, materials designed for, and utilised in, LCDs are not usually subject to optical damage. In addition, in-plane switching devices such as SSFLCDs, AFLCDs and bistable nematic displays possess wide viewing angles making them ideal candidates for exploitation in large area, high pixel density devices.

Ever more so, therefore, has the development of materials for use in display devices become a challenge of 'precision' molecular engineering.[1,5] Materials, thus, need to be designed to be chemically and optically stable, possess wide temperature ranges for their liquid crystal phases, have low melting points, low viscosities, suitable birefringences, desirable dielectric properties, low conductivities—in fact the demands on the quality and properties of organic liquid crystals approach those placed on conventional inorganic and semi-conductor materials used in the electronics industry. As a consequence, the design of nematogens is now focused on creating materials based on fluorinated systems because they have low conductivities and viscosities, and suitable positioning of fluoro-substituents allows them to have appropriate dielectric anisotropies for applications,[1,5] see **2**. Similarly, the development of ferroelectric materials is centred on the creation of materials with low viscosities, wide mesophase temperature ranges and low melting points.[6] The design of fast switching low viscosity materials has therefore become akin to the utilisation of aerodynamics in the design of fast sports cars, *i.e.* narrow, stiff, rod-like molecules being the most suitable, *cf.* the phenyl

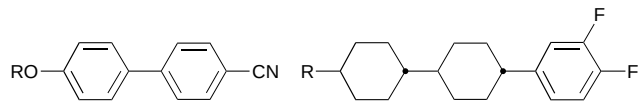

1 **2**

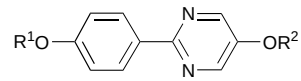

3

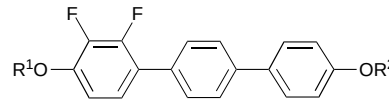

4

pyrimidines **3** and the difluoroterphenyls **4**.[7] Although high technology applications of liquid crystals tend to catch the eye, it should be noted that by far and away the highest consumption of liquid crystals is by the soap and detergents industry,[8] followed by that of companies involved in the production of structural polymers (PLCs), for example, poly(*p*-phenylene terephthalamide) is used commercially as the basis for spinning fibres such as Kevlar® (Du Pont) and Twaron® (Akzo).[9] Cationic, anionic, and non-ionic surfactants (*e.g.* **5**–**7**) have been shown to be capable of exhibiting either thermotropic[10] or lyotropic mesophases,[11] and in some cases materials have been shown to exhibit both forms of mesophase, thereby making them amphotropic. Glyco- and phospho-lipids, akin to those found in cell membranes, provide numerous examples of compounds that self-assemble to form lyotropic liquid crystals and self-organise to form thermotropic phases. Octyl 1-*O*-β-D-glucopyranoside, **8**, which is a commercially available non-ionic detergent (Sigma) exhibits a smectic A* phase upon heating, and lamellar, cubic and hexagonal lyotropic phases on progressive addition of water,[12] for example see Fig. 1.

Liquid crystals thus have many wide and varied applications apart from high profile uses in displays. However, because there is such a short amount of time between discovery/innovation

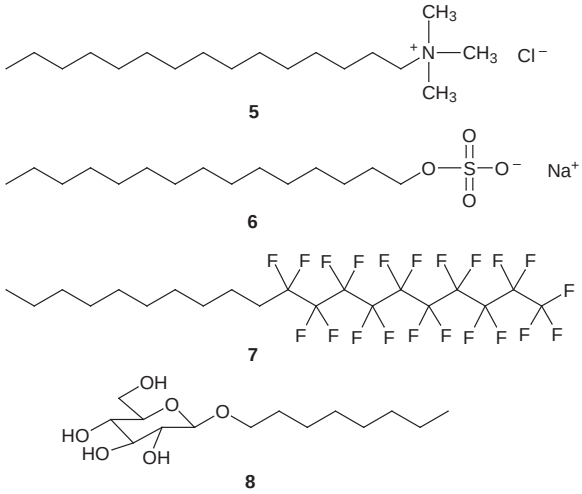

and application in this field there is an impression that liquid crystals are primarily of technological importance. Conversely, the prevalence of many applications of liquid crystals is mainly due to the fact that liquid crystals offer a unique and delicate collection of phases of matter that are precariously balanced between the organised solid state and the amorphous liquid, and which can be accessed by all types of materials, and not just organic compounds. Thus, inorganic, ionic, metal–organic complexed, organic complexed, zwitterionic, elastomeric, dendrimeric, and oligomeric systems, to name a few, have been shown to exhibit mesomorphism.[13]

However, given that much of the research into liquid crystals has been concerned with their potential applications, there still remain two large windows of opportunity for innovation and design of novel materials. Firstly, the gap between conventional low molar mass systems and polymers is relatively unexplored. Little has been reported on large, but discrete, molecular systems, *i.e.* from dimers to trimers to oligomers and dendrimers. When the molecular structures of such systems are well defined, then the materials can be classed as supermolecular entities with clearly defined and unique physical properties. Secondly, the self-assembly of materials to form clusters, aggregates, and complexes *etc*., and then their self-organisation to give mesophases has scarcely been investigated.[14] Both super- and supra-molecular systems are scientifically intriguing and challenging because they involve the rational design and development of large scale structures leading on towards molecular materials of similar dimensions to those of complex systems found in nature, *e.g.* proteins, enzymes, *etc*.

Molecular shape dependency

A primary factor in the formation of liquid crystal phases is the overall, or gross, molecular shape of a compound.[15] Three separate species can be defined where the molecules have the following rotational volumes; spheroid, ellipsoid and discoid. Spheroid mesomorphic materials generally give rise to plastic crystals, ellipsoid or rod-like molecules give rise to calamitic liquid crystals, which include nematic and smectic liquid crystals, and discoid molecules produce nematic–discotic and columnar liquid crystals. Molecules with combinations of these shapes can also be mesomorphic. For instance molecules that possess both disc- and rod-like attributes can exhibit nematic, smectic and columnar phases. Such materials often have polycatenar structures, *i.e.* they possess more than two terminal aliphatic chains (usually four, five or six). Depending on the relative proportion of aliphatic to non-aliphatic regions in the molecular structure, tetracatenar materials can exhibit both

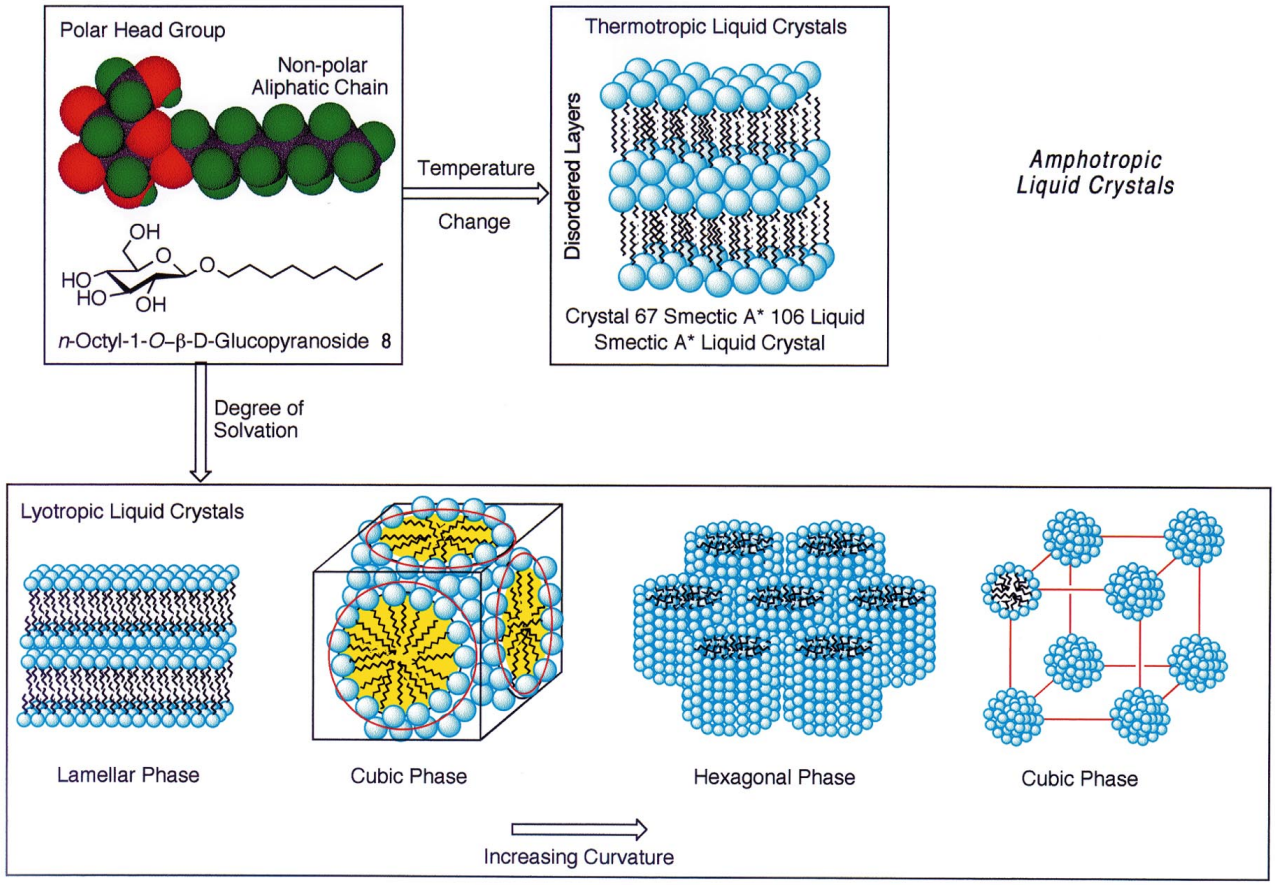

Fig. 1 The phase behaviour of octyl 1-*O*-β-D-glucopyranoside, **8**, when heated to give a thermotropic smectic A* phase, and on addition of water to give lyotropic lamellar, cubic and hexagonal phases. Compound **8** is therefore amphotropic.

smectic/nematic and columnar phases, whereas hexacatenar materials tend to exhibit columnar phases.[16] Similarly molecular structures that combine the features of both discs and spheres can have bowl-like shapes and can produce bowlic or pyramidal mesophases. In most cases, the lowest energy static molecular shape defines mesophase type/formation, however, dynamical variations in molecular structure, such as conformational and geometrical changes, can also impinge on mesomorphic behaviour, particularly if the changes occur as a function of temperature or concentration of solvent.

When a large number of mesogenic units, be they spheroid, ellipsoid or discoid in shape, are linked together they form polymeric liquid crystals. Polymer systems, however, usually have associated problems of dispersity (γ) and degree of polymerization (DP) which impinge on their physical properties. A material that possesses more than one mesogenic unit but with a defined DP and a dispersity of one, *i.e.* a discrete molecular system, could be considered as a supermolecular system. The simplest architectural form of a supermolecular liquid crystal then is a dimer. Dimers may have a number of structural variants, for example the mesogenic units may be joined end to end, side to side, or they may be joined together as Siamese twins.[17] Luckhurst and Imrie,[18] in particular, have made many detailed investigations of dimeric systems, but principally of those where the mesogenic units are linked end to end. Trimers on the other hand can have their mesogenic units joined together in a linear chain, or they may be tethered to a central point, or they may be part of a cyclic system. From these simple examples it can be seen for a system which has available a defined number of structural moieties/units to be used in molecular construction, that a limited variety of molecular topologies are possible, see Fig. 2. However, once a supermolecular architecture has been defined, conformational, geometrical, and configurational factors have to be taken into account in the way a mesophase is formed and stabilised. In this Feature Article, the mesomorphic behaviour for systems that possess restricted molecular topologies and limited molecular flexibilities will be discussed; the first examples involve supermolecular mesogens where the mesogenic units are linked to a central focal point thereby limiting the molecular geometry and conformational structure.

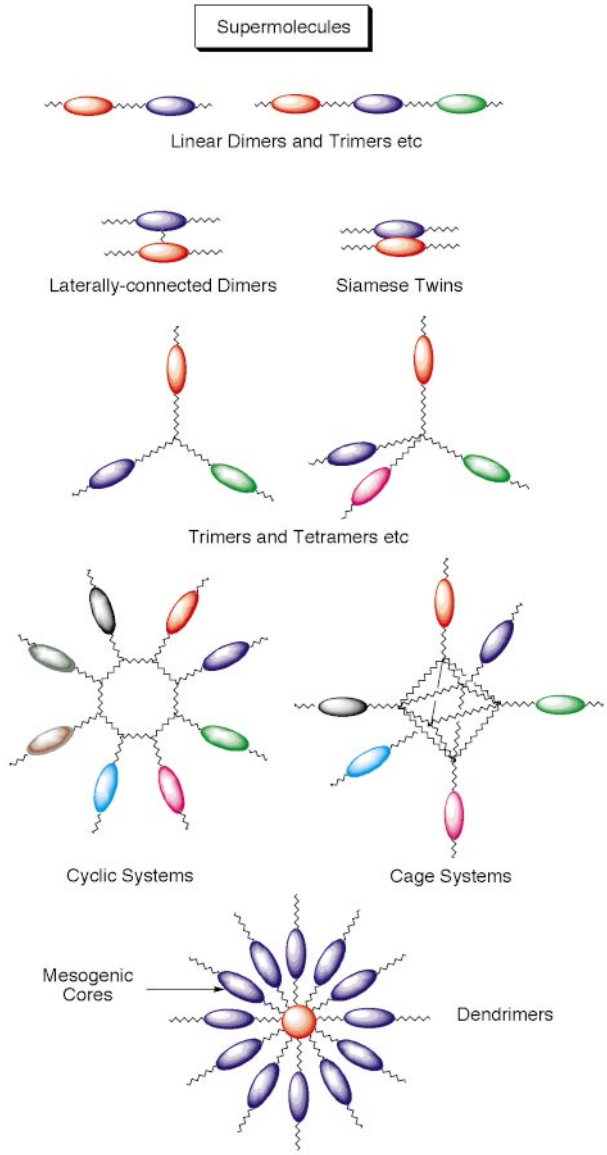

Fig. 2 Various molecular scaffolds for the design of large discrete supermolecules

Materials with defined molecular topologies

The possibility of creating liquid crystals that have large discrete molecular structures with defined molecular topologies is an intriguing prospect because the materials might be expected to exhibit unusual physical properties. For example, on paper an oligomeric material possessing mesogens tethered to a central point could be designed to have a spherical shape with its mesogenic units spread symmetrically about that point. However, if such a material were constrained in a liquid crystal environment, molecular distortion would be expected to occur in order to allow the mesogenic units to pack together.

Examples of simple model tetrahedral systems with cubic symmetry were created by reacting tetrakis(dimethylsiloxy)silane with a variety of alkenyloxy-cyanobiphenyls,[19] thereby generating a set of tetrahedrally substituted mesogenic supermolecules, *e.g.* **9a**–**c**, where four mesogenic units are tethered to a central point. Although such a molecular shape would be expected to disfavour mesophase formation, Table 1 shows that the tetramers exhibit smectic A liquid crystal phases. It is also interesting to note that smectic A phases are preferred over the nematic phase exhibited by the mesogenic monomers themselves. In this sense, these supermolecules are similar in

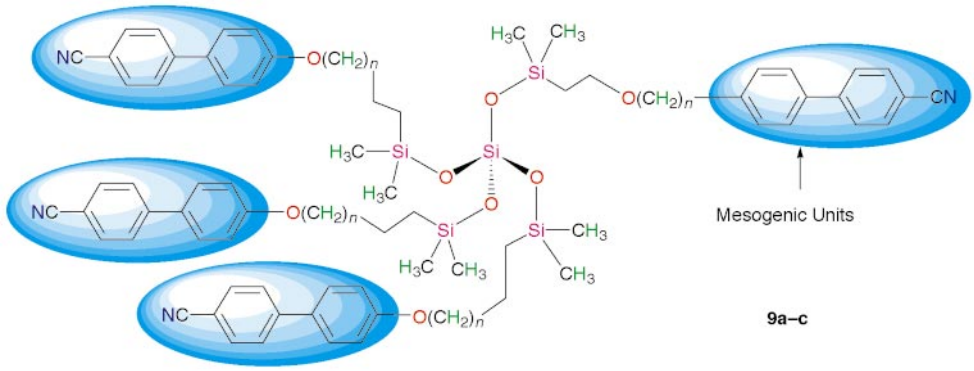

Table 1 Transition temperatures (°C) for the tetramers of structure **9a–c**

Compound	*n*	tg	SmX–SmA	SmA–Iso Liq
9a	2	−9.6	—	88.7
9b	4	−14.7	—	118.7
9c	9	−6.3	38.7	129.7
Cyclic	6	57	—	118.0

mesophase behaviour to conventional side-chain liquid crystal polysiloxanes which have cyanobiphenyl moieties as the mesogenic side group.

In general the smectic A phase has a structure where rod-like molecules pack in diffuse layers where there is no positional ordering of the molecules in the plane and out of the plane of the layers.[15] The only way in which the tetramers can form such a phase is by molecular distortion away from a spherical shape

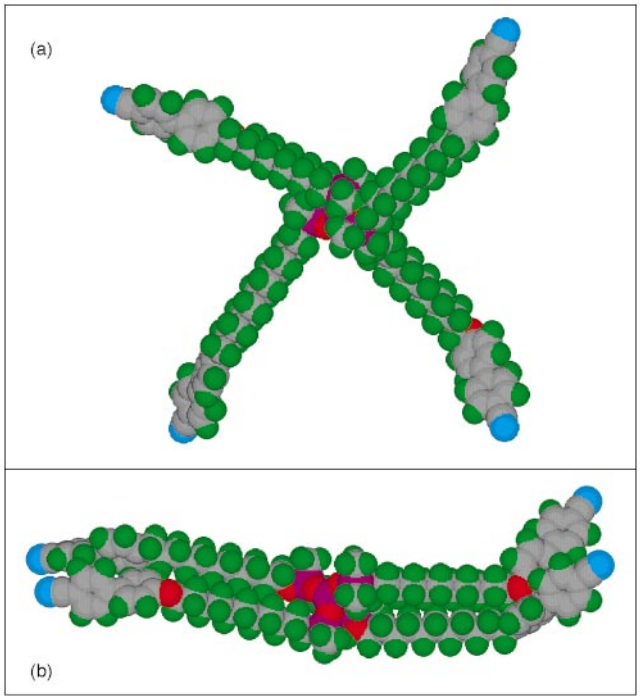

Fig. 3 The molecular shape of tetramer **9c**, (a) shows the shape of the molecule where the four arms were symmetrically positioned about the core; (b) shows the minimised structure in the gas phase at absolute zero using a Silicon Graphics system operating with Quanta and CHARMm software

[see Fig. 3(a)] to give a rod-like conformational structuring. Molecular modelling studies reveal that, even in the gas phase at absolute zero, the conformation where the mesogenic side-chains are aligned is the more energetically favoured conformation [Fig. 3(b)], thereby allowing the supermolecules to achieve rod-like molecular shapes.

Materials **9a** and **9b** exhibit only a smectic A phase, whereas **9c** shows, upon heating, a transition to an additional unidentified phase at 38.7 °C. When the number of methylene units is increased, the isotropization temperatures increase accordingly. Furthermore, the isotropization temperatures of the materials were found to be comparable with those of cyclic siloxanes bearing four side-chains of a similar structure.[20] However, the solidification temperatures of the tetrahedrally substituted systems were found to be much lower. For example, the cyclic analogue of compound **9b** exhibits a glass transition or recrystallisation well above room temperature (*ca.* 50–60 °C), whereas the tetrahedrally substituted equivalent material produces a non-crystalline material that has a low solidification temperature (−14.7 °C). Thus the symmetrically substituted systems show low melting behaviour and primarily glass formation on cooling. This effectively widens the relative temperature ranges of the liquid crystal mesophases.

X-Ray diffraction shows that the trichotomous nature of the tetramers allows for different packing characteristics to exist for the molecules in the smectic A phase. Thus, the separate interactions of the mesogenic units, the alkyl spacers and the silicon cores have to be considered in the formation of the A phase. For the shorter methylene spacer lengths, **9a** and **b**, internal phase separation leads to the smectic A phase being described as a smectic A_d phase with respect to the mesogens and a monolayer smectic A_1 phase with respect to the silicon cores, see Fig. 4. In the smectic A_d phase the mesogenic units are partially interdigitated giving a layer spacing d, where $l < d < 2l$, and l is the molecular length. The smectic A_1 phase is a disordered layered phase where the layer spacing is approximately equal to the molecular length. For the longer methylene spacer lengths, **9c**, the co-existence of smectic A_d and smectic A_2 phases is probable (the smectic A_2 phase is a bilayer system where the layer periodicity is twice the molecular length). The occurrence of these structures can be explained by the presence of biphasic or incommensurate smectic A phases, or even a smectic A anti-phase.

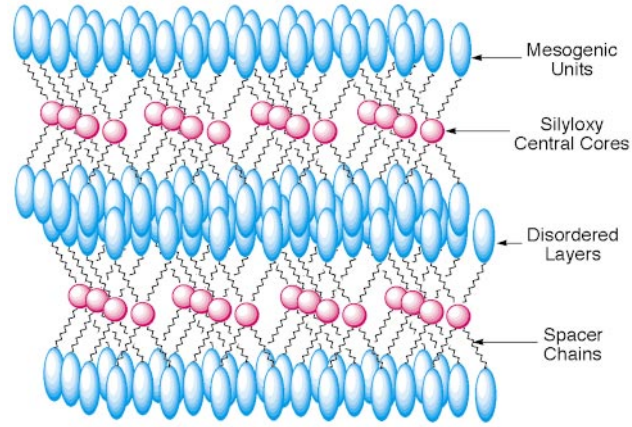

Fig. 4 The structure of the interdigitated smectic A_d phase of tetramers **9a** and **b**. The mesogenic units form an interdigitated bilayer, whereas the silyloxy cores have a monolayer arrangement.

For the tetramers there is adequate free volume for the cyanobiphenyl 'mesogenic arms' to rotate so as to give a distorted rod-like molecular shape. Increasing the number of mesogenic units attached to the central point, however, has the effect of reducing the free volume for the packing of the mesogenic groups, which in turn reduces their freedom of movement and suppresses the ability of the supermolecular system to generate a rod-like conformational form. Increasing the number of mesogens attached to a central point is difficult to achieve without moving in the direction of dendrimer formation, but the substitution of polyhedral core units with mesogenic groups can provide an alternative route to packing a larger number of mesogenic units about a central focal point. The use of various polyhedral siloxane-substituted systems as the central cores of the supermolecular systems allows for meaningful comparisons to be made as the free volume available to the mesogens is reduced as the degree of substitution about the polyhedral core is increased.[21]

The hexakis(dimethylsiloxy)silsesquioxane, **10**, and octasilsesquioxane, **11**, core systems are caged polyhedral units, where silicon atoms are situated at the corners of the cage and oxygen atoms in between. The hexakis-core can be substituted with up to six mesogenic units, whereas the octasilsesquioxane core can be substituted with up to eight mesogenic groups. Comparative materials with similar mesogenic cyanobiphenyl side chains have been prepared. In both cases the cores are not much different in size to the tetrakis(dimethylsiloxy)silane core discussed in the synthesis of the tetramers, optical microscopy shows that, on cooling from the amorphous liquid, smectic A

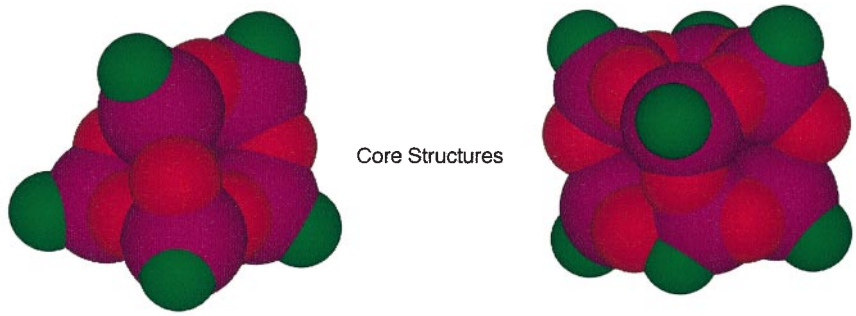

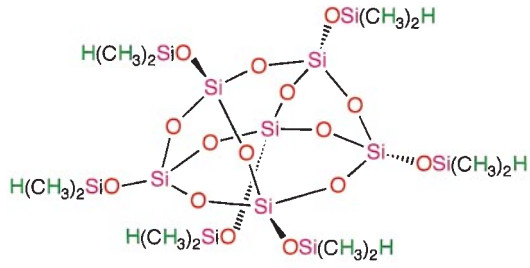

10

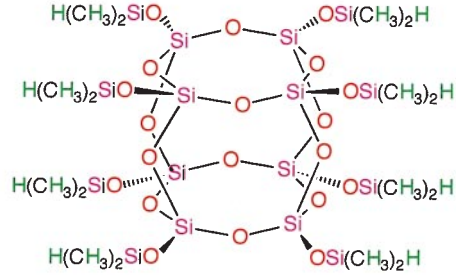

11

liquid crystal phases are formed for the hexakis(dimethylsiloxy)silsesquioxane and octasilsesquioxane systems. Table 2 shows that for the octasilsesquioxane based systems, compounds **12a**–**c**, the clearing temperatures are in a similar temperature regime to those found for the tetrahedrally substituted materials **9a**–**c**. However, the rise in the clearing temperatures, with increasing spacer length, was less steep.[22]

Table 2 Transition temperatures (°C) for the octamers **12a**–**c** based on the octasilsesquioxane core unit

Compound	*n*	tg	Cryst–Sm3	Sm2–Sm3	Sm3–SmA	Sm1–SmA	SmA–Iso Liq
12a	4	11.0	—	—	—	—	93.9
12b	6	3.0	—	—	—	22.5	116.5
12c	11	−7.5	34.4	54.6	64.5	—	128.5

As with the tetramers, the mesogenic arms of the octasilsesquioxane based materials again rotate so that they lie parallel to one another. This creates a rod-like structure where the supermolecules can pack together in layers to form a smectic A phase. Molecular simulations in the gas phase at absolute zero serve to reinforce this point of view. Fig. 5 shows the minimised structure of the cyanobiphenyl substituted octasilsesquioxane

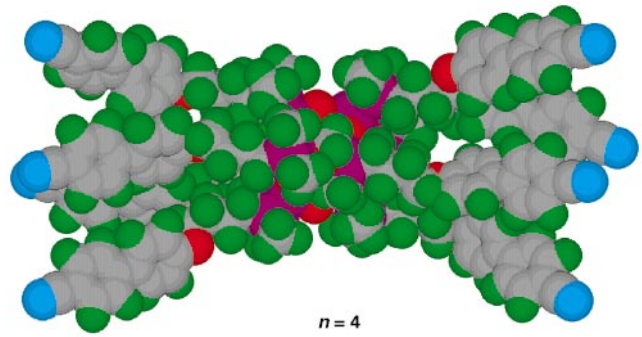

Fig. 5 The minimised structure of the octamer **12a** in the gas phase at absolute zero using a Silicon Graphics system operating with Quanta and CHARMm software

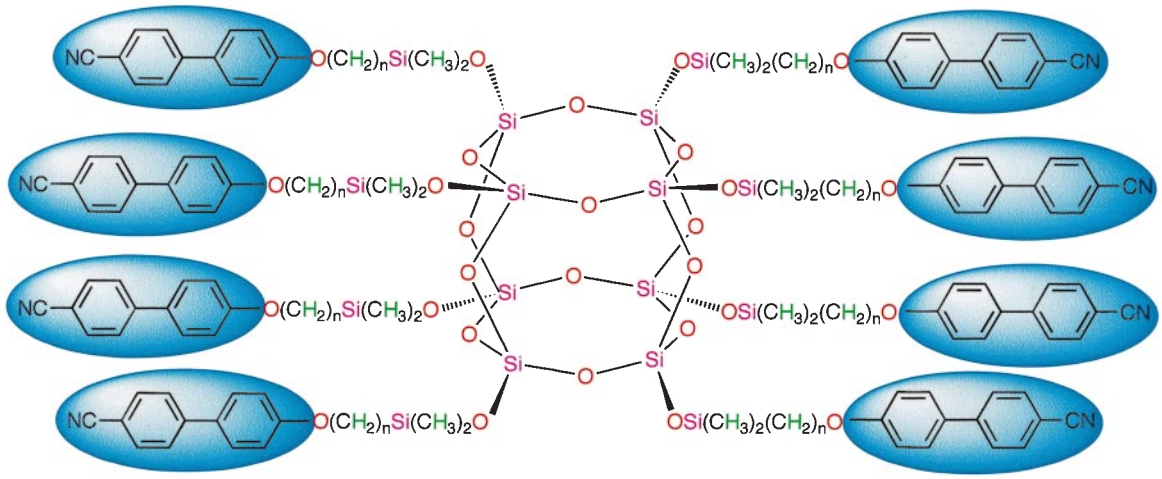

12a-c

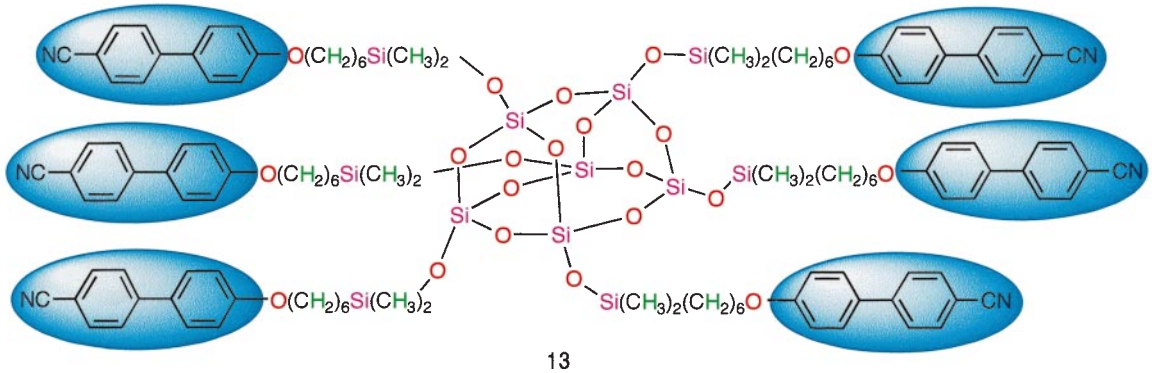

13

with a tetramethylene spacer unit. In this structure the cyanobiphenyl 'mesogenic arms' pack together in a parallel arrangement thereby producing a supermolecular system that has a rod-like gross shape which is conducive to the formation of smectic A phases.

Similar results are obtained for systems based on the hexakis(dimethylsiloxy)silsesquioxane core system, **13**. Again smectic A phases are formed indicating that the molecules must adopt a rod-like structure. Mehl and Saez[21] have reported several other variants of liquid crystals based on polyhedral core units, and where cyanobiphenyl moieties were used as the source of mesogenic units smectic A phases were found. Kreuzer *et al*.[23] have reported that silsesquioxane cores with six, eight and ten mesogenic units, with structures based on that of cholesterol, still appear to exhibit smectic A phases, thus demonstrating the power of the mesogenic environment to inflict conformational changes on the supermolecules so as to distort their shapes from being spherical to being tactoidal, and preventing the formation of nematic, or in the last example from Kreuzer *et al*.[23] chiral nematic phases.

Table 3 Transition temperatures (°C) and enthalpies (in parentheses, J g^{-1}) of transition for a variety of materials that combine the 4′-(2-methylbutylbenzoyloxy)biphenyl-4-carboxylate mesogenic unit, **A**, with siloxy moieties based on the tetramer, **B**, octasilsesquioxane, **E**, cyclic siloxanes, **C** and **D**, and polysiloxane, **F**, systems

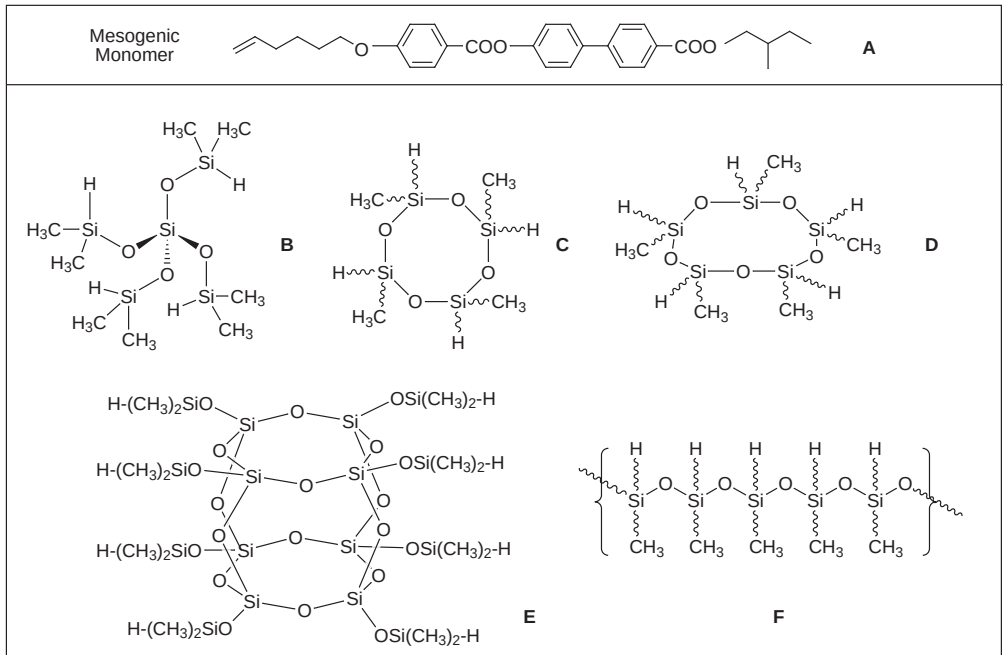

Reactants	Transition temperatures and calorimetric data
A (Monomer)	cryst 78.5 SmC 106.1 (0.7) SmA 157.2 (2.9) N 168.9 (1.51) Iso Liq
A + **B** (Tetramer)	tg -8.4 (0.5) SmCa 125.0 (0.1) SmC 154.4 (0.1) SmA 164.4 (-) Iso Liq
A + **C** (Cyclic Tetramer)	tg 10.3 (0.5) SmX 69.5 (1.0) SmC 184.2 N 193.3 (8.0) Iso Liq
A + **D** (Cyclic Pentamer)	tg 11.2 (0.4) SmC 182.5 (-) SmA 188.7 (6.8) Iso Liq
A + **E** (Caged Octamer)	cryst 143.0 (21.1) SmC 208.0 (0.2) SmA 214.0 (6.4) Iso Liq
A + **F** (Linear Polymer)	tg 19.0 (0.2) SmC 223.5 (0.1) SmA 234.3 (5.3) Iso Liq

Substitution of the silsesquioxane cores with mesogenic groups that are more conducive to smectic mesophase formation, as with the other systems described above, yields supermolecular materials that as expected exhibit smectic phases. However, for the many cases studied, the formation of smectic phases and mesophase temperature ranges are considerably enhanced. For example the use of the 4′-(2-methylbutylbenzoyloxy)biphenyl-4-carboxylate mesogenic unit, which favours the formation of orthogonal smectic A and tilted smectic C, I and F phases, results in the preference for tilted smectic C phases, see compounds **14** and **15**. For compound **14** the smectic C phase is present from 11.5 to 191.5 °C, *i.e.* a temperature range of over 180 °C, whereas it is only present over a temperature range of 22–23 °C for the mesogenic monomer unit. The coupling of the potential stability of the smectic C phase with chirality built into the mesogenic units allows for the possibility of synthesising supermolecular ferroelectric materials which may have interesting non-linear physical properties, *e.g.* antiferroelectric, pyroelectric and piezoelectric properties.

Table 3 shows a comparison of the mesomorphic behaviour for a variety of materials that combine the 4′-(2-methylbutylbenzoyloxy)biphenyl-4-carboxylate mesogenic unit with siloxy moieties based on the tetramer, octasilsesquioxane, cyclic siloxane and polysiloxane systems. It can be seen from the table that in all cases for the supermolecules and the side chain polymer, considerable stabilisation of the liquid crystal properties, and in particular the tilted smectic C phase, is found. However, although the polymer version exhibits similar phase behaviour to the supermolecular systems, its viscosity is very much higher. Conversely, the viscosities of the supermolecular materials are similar to low molar mass liquid crystals.

Further increase in the number of mesogenic units positioned around a central core unit can be achieved only *via* the synthesis of dendrimers. Examples of liquid crystalline dendrimers, however, are surprisingly scarce. The first thermochromic liquid crystalline dendrimer was reported by Percec and Kawasumi for a hyperbranched polyether structure that consists of an AB_2 monomer.[24] Recently, however, the groups of Shivaev and Frey reported simultaneously the synthesis of liquid crystalline carbosilane dendrimers,[25,26] which are similar in structure to the silsesquioxane liquid crystals described above. Some of the reported dendrimers combine a flexible, dendritic carbosilane inner core with an outer region that is functionalised on the surface with cyanobiphenyl mesogenic groups, see Fig. 6. As discussed previously this structural concept appears to be at odds with the formation of liquid crystal phases at first sight, because the rod-like mesogenic units are attached to a molecular scaffolding of globular geometry. Thus, it might be expected that the densely packed mesogenic groups in the outer shell of the dendrimer would ensure a spherical disposition of the supermolecule. However, the dendrimers formed exhibit smectic A phases which again requires that the giant molecules must have conformational rod-like shapes which pack in disordered layers. This suggests that the shapes of the dendritic molecules must be deformed by being in a liquid crystal environment. The possibility of being able to control molecular deformation could lead towards novel applications.

Supermolecules with reduced molecular flexibility

So far the materials discussed have had structures where there is reduced flexibility caused by the tethering of the mesogens to a central point and filling the space about this point with mesogenic groups. Internal flexibility, however, can also be reduced by increasing the number of bridging chains between the mesogenic units; which have so far been limited to one in the above discussion. Fig. 7 for example shows the architectural situation for dimers. When one flexible chain links two mesogenic units together, the odd or even parity of the chain can affect the orientation of the mesogenic units relative to one

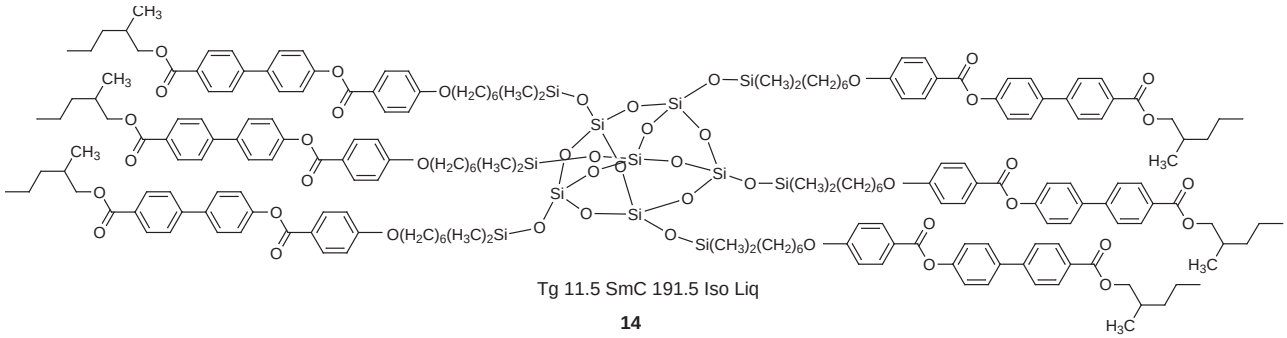

Tg 11.5 SmC 191.5 Iso Liq

14

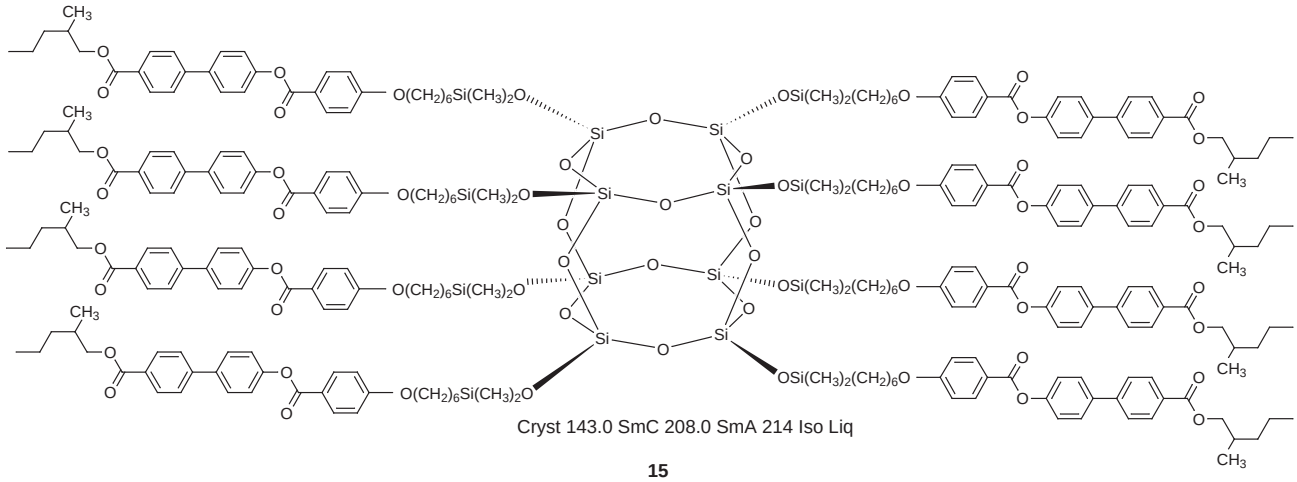

Cryst 143.0 SmC 208.0 SmA 214 Iso Liq

15

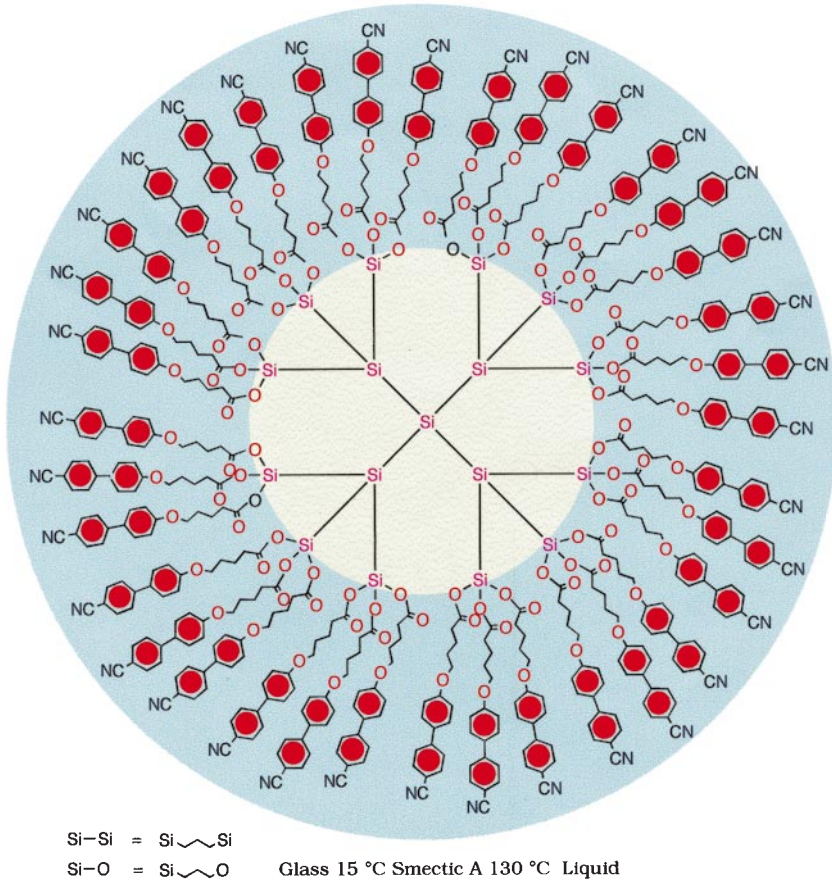

Fig. 6 The structure of a dendrimer that possesses 32 cyanobiphenyl units. The dendrimer exhibits a smectic A phase.

another. For an odd number of methylene units the mesogenic groups will lie at an angle to one another, whereas for an even number of methylene units they will be in line with one another. Thus, the transition temperatures for the even members will be much higher than those of the odd because the even members will have approximately a linear shape rather than a bent one.[18] This effect on molecular shape is particularly important for shorter spacer lengths where the flexibility of the spacer chain is less and the dependency of liquid crystal properties on shape is more pronounced. For dimers where two bridging chains are used to link the mesogenic groups together the degree of flexibility around the centre of the supermolecular structure is further reduced. For instance, if carbocyclic ring systems are introduced between the mesogenic groups, as shown in the middle part of Fig. 7, they will be able to bend in and out of the page, but not so easily in the plane of the page. Carbocyclic rings that are appropriately substituted with mesogenic groups are difficult to synthesise, however, for the purposes of producing model systems it is easier to prepare liquid crystals where two mesogenic groups are attached to a macrocyclic aza-crown ether ring as shown in Fig. 7. Tuffin has taken this approach forward in such a way that she has been able to replicate all forms of liquid crystal behaviour in materials that possess a macrocyclic ring.[27]

When a macrocyclic ring is inserted between two mesogenic units, then the liquid crystal groups do not need necessarily to be symmetrically positioned on the ring, and they can be located asymmetrically. This allows control of molecular shape so that bent or linear systems can be produced. Materials with bent structures will of course exhibit different mesophase properties to those of linear systems.[28] For example compounds **16** and **17** have identical mesogenic groups, but linear compound **16** exhibits a nematic phase, whereas **17** has an additional smectic C phase, and interestingly, because **17** is bent ferroelectric or antiferroelectric properties become a possibility.

Not only can the position of the substituents be varied on the central ring, but so too can the flexibilty of the aza-crown ring. For instance, by increasing the size of the aza-crown ring the degree of flexibility can increased, and as a consequence the mesogenic units become increasingly decoupled from one another.[29] Table 4 clearly demonstrates the effect of increasing the size of the macrocyclic ring. For small ring sizes, nematic phases predominate because the macrocyclic ring acts as part of the rigid central core of the mesogen. As the material 'thinks' it is a 'seven ring' mesogen, high transition temperatures are obtained. When the ring is increased in size the aromatic mesogenic groups start to become decoupled, and smectic phases are introduced. As the ring size is increased further to the extent that the macrocyclic ring can flex and bend more easily, and the mesogenic groups become further decoupled from one another, the smectic phases become destabilised. At this point the motions and orientations of the mesogenic units are relatively independent of one another and the material 'thinks' it is now a quasi-dimer. The flexibility was increased further by substituting oxygen for sulfur in the macrocyclic ring unit, and slightly lower clearing points were obtained and further destabilisation of the smectic state occurred. NMR studies in dilute solution as a function of temperature confirm that the macrocyclic moiety can bend and flex easily about its middle. At low temperatures the molecules were shown to have linear rod-like structures, however when the temperature was raised the population of molecules with hair-pin shaped conformational structures grew.[27] Preliminary X-ray diffraction experiments on the neat mesophases exhibited by a selection of the

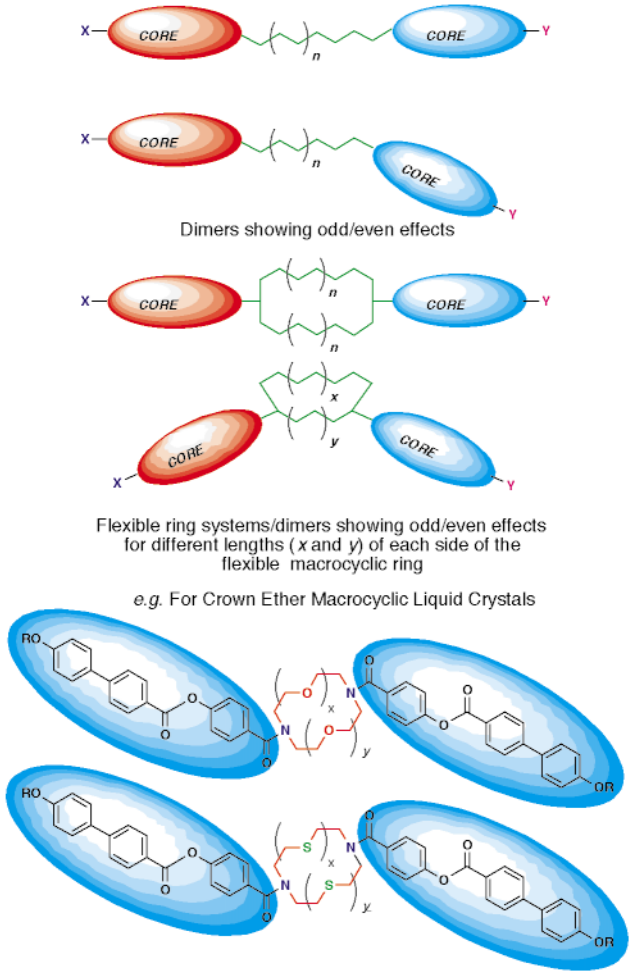

Fig. 7 Schematic representation of mesogenic dimers containing either identical or different mesogenic groups. The linking units between the mesogenic moieties can be either single methylene chains or macrocyclic units. The macrocyclic ring can be an aza-crown *etc*., and the mesogenic groups need not be positioned symmetrically on the ring, *i.e.* $x \neq y$.

materials confirm the presence of a number of sub-phases which have structures based on either linear or bent molecular conformations. Bilayer phases based on molecules that have bent conformational structures, and monolayer phases where the molecules have fully extended rod-like structures were observed, see Fig. 8. In addition, phases where the long axes of the molecules are either orthogonal (SmA_1 and SmA_2) or tilted (SmC_1 and SmC_2) with respect to the layer planes were found, and in the case of bent molecular conformations even 'antiferroelectric-like' phases (SmCalt) were detected.

Supramolecular assemblies of supermolecules

The shapes of the above systems can be varied further by increasing the number and lengths of terminal aliphatic chains attached to the mesogenic aromatic cores. By varying the number and the length of the peripheral aliphatic chains, hair-pin shaped molecular structures can be advantaged over stretched-out conformational structures. Table 5 shows the transition temperatures for a series of compounds based on the tetracatenar macrocyclic liquid crystal structure **18**.[30] It can be seen from the table that as the terminal aliphatic chain length is increased lamellar smectic phases give way to disordered columnar mesophases, and for the hexadecyl homologue, at least, both calamitic and columnar phases are exhibited by the

Table 4 Dependency of the transition temperatures (°C) on macrocyclic ring type **G**, monotropic phase transition given in parentheses

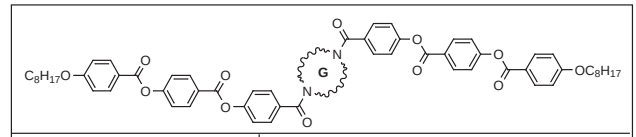

Macrocyclic Core G	Transition Temperatures (°C)
	Cryst 215 N 323 Iso Liq
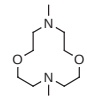	Cryst 195 (SmA 142 N 172.6) Iso Liq
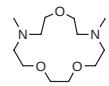	Cryst 151 (SmC 140.2) N 171.6 Iso Liq
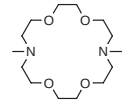	Cryst 194 (N 186.3) Iso Liq
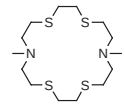	Cryst 199 (N 174) Iso Liq

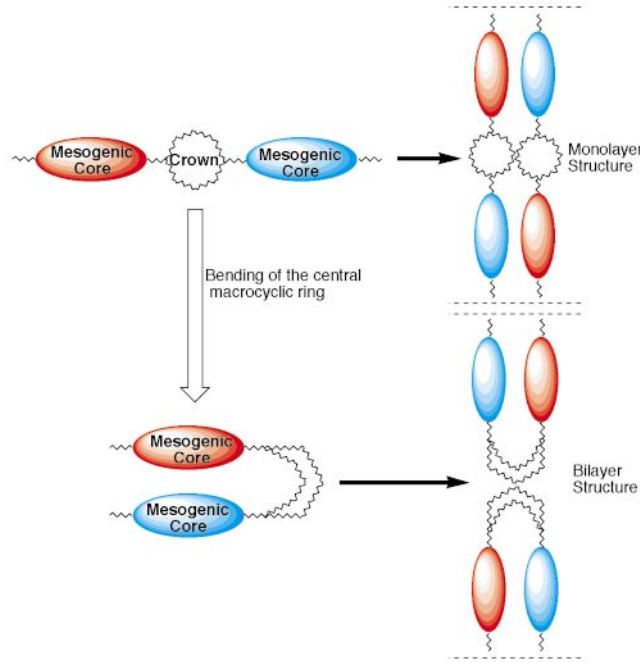

Fig. 8 Packing of the fully extended molecules produces a layered smectic phase, whereas molecular folding about the macrocyclic ring can produce a smectic bilayer structure. As the layer spacing is approximately the same for both conformers mixtures of both structures probably exist.

same material. How then can this be rationalised in terms of molecular shape? One possibility is that clusters of rod-like molecules in their most extended conformations come together, usually in numbers of three, to form disc-like clusters, as postulated for hexacatenar materials.[16] The supramolecular disc-like clusters aggregate and stack in a disordered way to form a columnar architecture. Alternatively, as noted earlier, it is possible that compounds of general structure **18** bend to give hair-pin gross molecular shapes. The bent molecules can

Table 5 Transition temperatures (°C) for the tetracatenar compounds **18a–d**, monotropic phase transition given in parentheses

Compound	Cryst–Liq Cryst	SmC–Iso Liq	SmC–Col	Col–Iso Liq
18a	137.8	(88.0)	—	—
18b	134.9	(129.8)	—	—
18c	134.0	—	(114.0)	(119.0)
18d	120.0	—	—	(90.0)

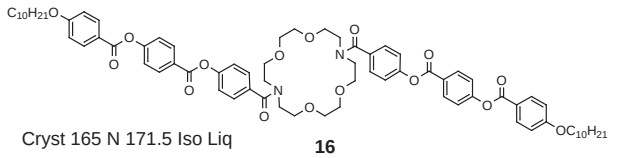

Cryst 165 N 171.5 Iso Liq

16

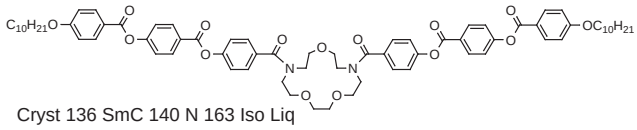

Cryst 136 SmC 140 N 163 Iso Liq

17

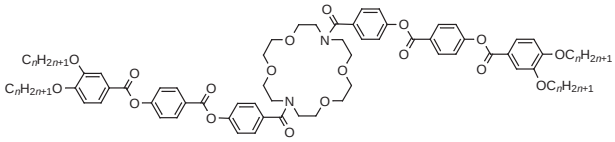

18a–d

effectively assemble together in clusters to give quasi-discs which are the basis for column formation. Thus, in this case we have a supermolecular system, where the conformational structure can change from being linear to being bent in order to support the formation of supramolecular assemblies, which in turn generate a columnar mesophase,[30] as shown in Fig. 9. It is not necessary that the molecules cluster to form flat discs, and in fact the molecules probably remain disordered along the column axes. In this arrangement of the molecules there will be 'pores' running down the column axes, thereby indicating the possibility that such systems might act as ion channels. This arrangement is not too dissimilar to the one proposed previously by Percec *et al*. for synthetic mimics of tobacco mosaic virus.[31]

At the centre of each supermolecular mesogen, of course, is a cavity associated with the aza-crown macrocyclic unit. This cavity is capable of accepting a guest ion, and such resulting guest–host systems have remarkably different phase behaviour to the host system. The guests tested included various metal ions associated with a number of different counter ions.[27] From these studies it is possible to compare the effects produced on sequentially changing the metal ions, *e.g.* Li^+, Na^+, K^+ *etc*., with respect to a common counter ion, such as triflate. Similarly it is also possible to maintain the same metal ion but vary the counter ion. Table 6 shows the variation in mesophase types and transition temperatures for 1 : 1 mixtures obtained in doping studies on the tetradecyloxy tetracatenar material **18b**, and Fig. 10 shows a schematic representation of the structure of the self-assembled columnar phase of **18b** when doped with K^+. The results for the transition temperatures show a strong dependency on the metal ion (and although not shown here, the counter ion). The transition temperatures are markedly affected by the addition of guests, and in some cases mesophases were found to be introduced where other phases exist for the pure host material. The full phase diagrams show there is a strong dependency of phase type and transition temperatures on concentration of the dopant, and therefore these systems could be used as qualitative or quantitative sensors for certain dopants.

Table 6 Dependency of the transition temperatures (°C) on the nature of the metal ion in 1 : 1 mixtures of compound **19a** with the listed metal triflates

Metal salt	Phase behaviour on cooling
None	Iso liq 129.8 SmC 120.0 Cryst
Lithium triflate	Glassy
Sodium triflate	Iso liq 156.0 col 147.0 lamellar 119.0 glass
Potassium triflate	Iso liq 138.0 col 93.0 lamellar 93.0 glass

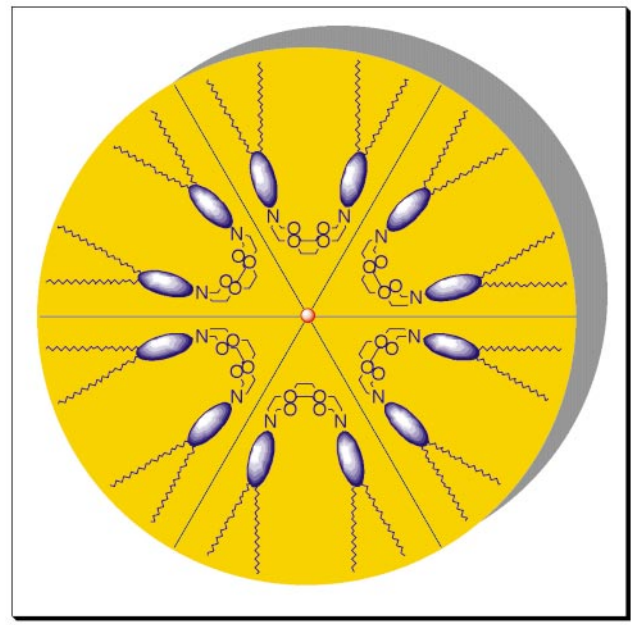

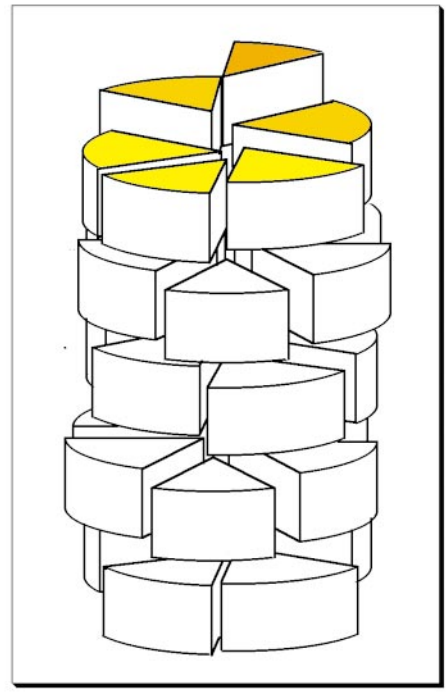

Packing of V-shaped molecules into disc-shaped aggregates and columns

Fig. 9 Self-assembly of folded macrocyclic materials can lead to the formation of disc-like structures which in turn self-organise to give columns. The molecules are disordered along the column axes.

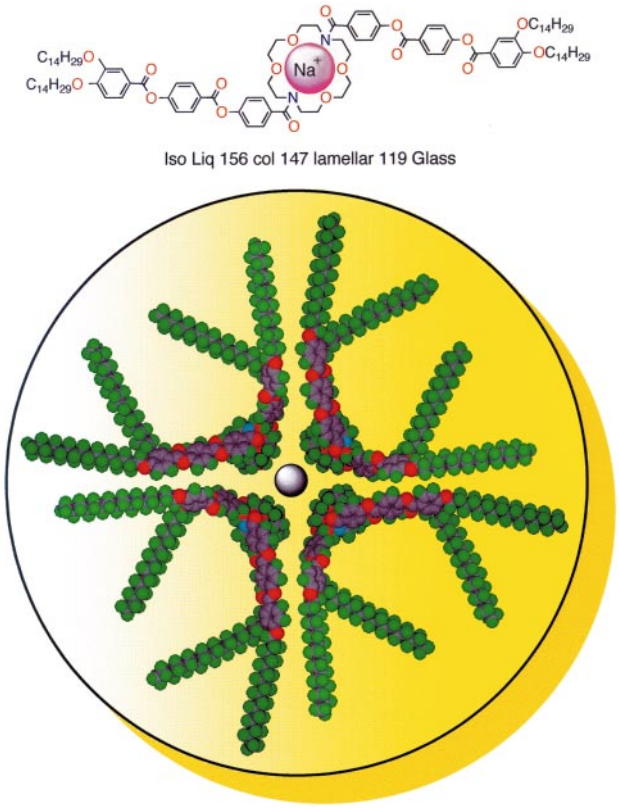

Fig. 10 The self-assembly and self-organisation of folded macrocyclic materials into columns. The inclusion of metal ions stabilises the structure and increases the clearing point of the mesophase.

For some macrocyclic systems mesomorphic properties can be injected into guest–host systems where for the host material alone no liquid crystal properties are found. Tetracatenar compound **19a** exhibits no liquid crystal phases because the aromatic groups responsible for inducing mesomorphic properties are too short, however the material will still have latent tendencies to produce liquid crystal phases. Upon the addition of potassium triflate, the resulting guest–host supramolecular system, **19b**, exhibits a nematic phase.[27] One explanation for such remarkable behaviour is that the host tetracatenar material has a folded or globular structure that is not conducive to mesophase formation because the rigid aromatic cores are too short. However, upon inclusion of potassium ions into the cavities of the macrocyclic unit the molecular structure of the host either unfolds to give a combined guest–host assembly which is much longer and narrower than that of host, or else it forms a rod-like hair-pin complex, see Fig. 11. Either way, the guest–host assembly is now much more rod-like in shape and now more capable of supporting mesomorphic phase behaviour. Thus, as with the other systems described above, this potential guest–host assembly could be used as a sensor because the introduction of liquid crystal properties are sensitive to the concentration of the ionic guest species.

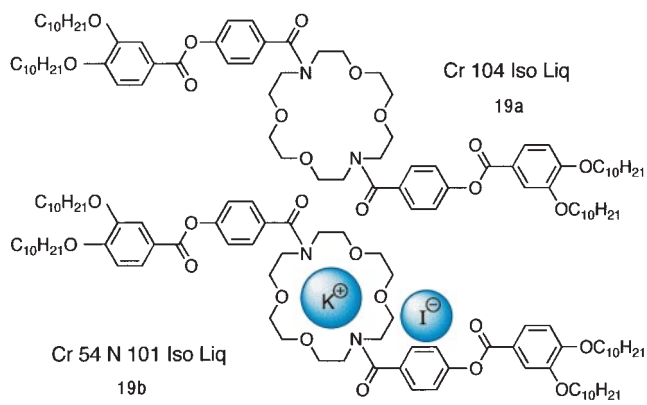

Chiral macrocyclic systems which exhibit chiral nematic phases have also been investigated. The resulting chiral nematic liquid crystals have the property of being able to selectively reflect light of a relatively narrow wave band, *c.f.* non-invasive LC thermometers,[5] and it has been found that when chiral macrocyclic hosts are doped with chiral ionic species, such as amino acids, the wavelength of the reflected light and the degree of circular polarization is dependent on the concentration and spatial configuration of the dopant. Hence the macrocyclic liquid crystal is capable of distinguishing qualitatively and quantitatively between certain types of enantiomers.

Biological systems

Molecular self-assembly and self-organization are becoming increasingly significant in the elucidation of life processes, and to the generation of new supramolecular structures/ensembles and molecular materials.[32–40] As a consequence, the most important inspirations for the conceptual development of such structures and materials are those provided by biological cells, which exemplify the assembly of a variety of microstructures of different sizes and functions. Archaebacteria, with their resistance to extreme conditions, are one class of organisms that have been found to provide a rich source of inspiration. Of particular interest to our studies on molecular topology are lipids derived from thermophilic Archaea. These molecules are characterized by a bipolar architecture with two polar heads linked together by two C_{40} polyisoprenoid chains which are thought to span the membrane, and therefore determine the lipid layer thickness. Although such lipids are classified as bolaphiles, in relation to the glycolipids discussed earlier (and shown in Fig. 1) they are essentially dimers. A unique feature of tetraether-based lipids lies with (i) the high proportion of glycosylated lipids in the membranes of both methanogenous and sulfur depending thermophiles and (ii) the occurrence of unusual carbohydrate moieties, *i.e.* β-D-galactofuranosyl units.[41–43] These structural units may further stabilise the membrane structure through cooperative inter-glycosyl hydrogen bonding, *i.e. via* the formation of supramolecular assemblies.[44,45]

However, in spite of growing attention to archaeal glycolipid structure and function, very few studies have been performed so far to elucidate the relationships between the molecular structure of the glycolipids and the architecture of their supramolecular aggregates. This is in part due to the difficulty of obtaining sufficient amounts of chemically pure compounds from natural sources or by synthetic methods. Some synthetic mimics, however, have been prepared[46] and their self-assembling properties investigated. For instance, compound **20** is a typical representative member of a number of quasi-macrocyclic bolaphiles that have prepared by Auzély-Velty.[47] This material is very similar in structural design to those found in the membranes of archaebacteria and in essence it is an amphotropic dimer.

When the thermal properties of compound **20** were investi-

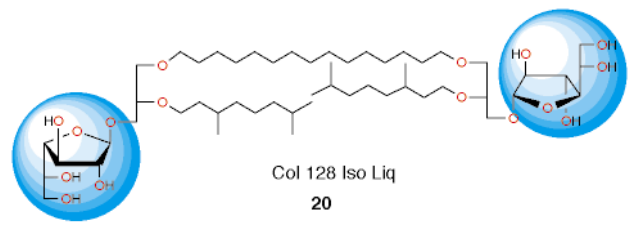

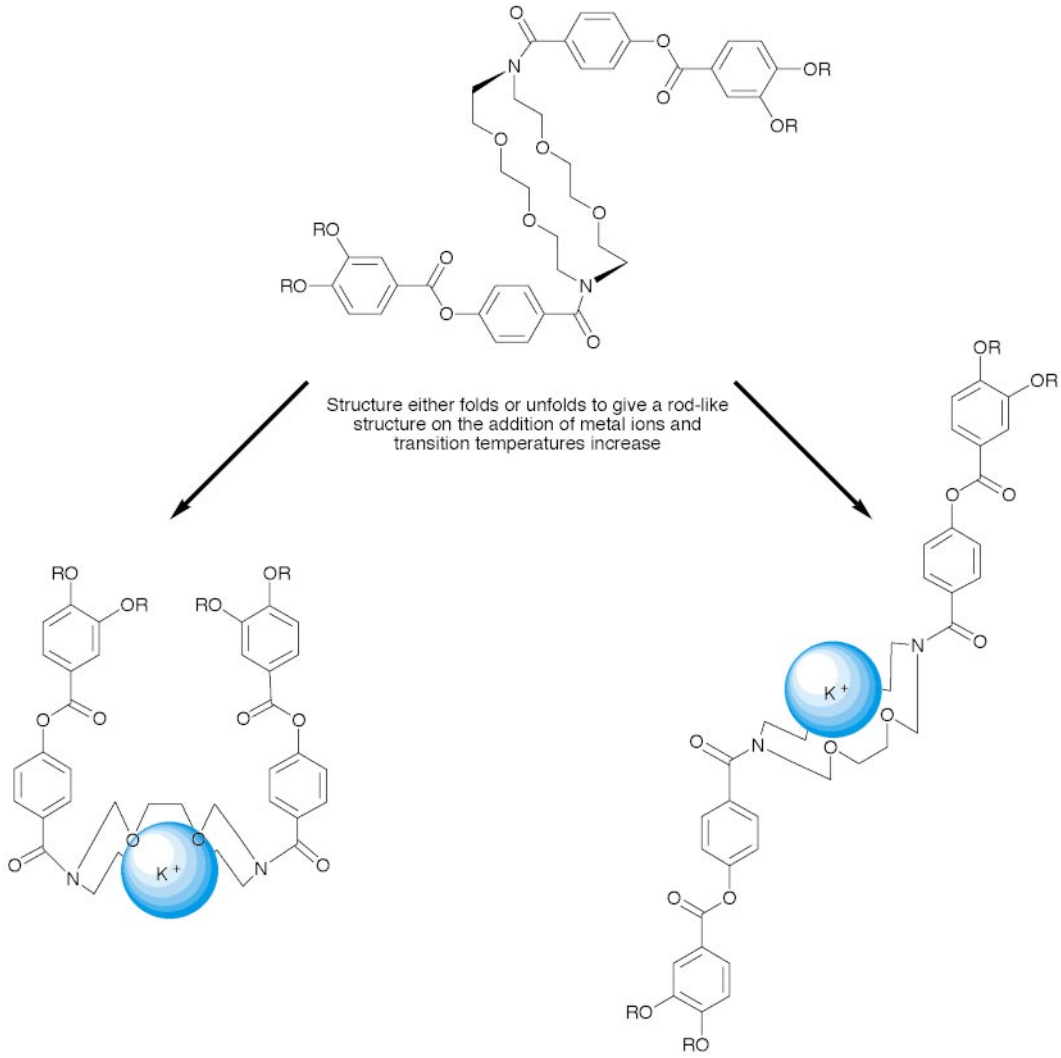

Fig. 11 A globular shaped macrocyclic system undergoes conformational changes upon inclusion of a metal ion. The resulting complex is rod-like in shape and hence the complex is mesomorphic and exhibits a nematic phase.

gated, the material was found to melt just above room temperature from a glassy state directly into a liquid crystal phase which persisted up to a temperature of 128 °C before the isotropic liquid was formed. Upon cooling from the liquid state, the liquid crystal phase was retained *via* supercooling to temperatures well below 0 °C (and under certain conditions down to −50 °C). Thermal cycling served to demonstrate the stability of the mesophase. Thermal optical microscopy showed that the mesophase formed had a columnar structure, Fig. 12(a). The addition of water to the material, plus heating from room temperature, revealed the formation of a lyotropic hexagonal mesophase, Fig. 12(b). The fact that the hexagonal columnar thermotropic phase was found not to be continuously miscible with the hexagonal lyotropic phase indicates that the two columnar structures are not the same. A model for the thermotropic phase based on mixture studies is shown in Fig. 13. In this model the aliphatic chains are on the outside of the columns and the polar head groups are on the inside. This implies that the bolaphiles, just like the macrocycles described earlier, must bend in the centre so that the polar head groups of each end of the glycolipid can interact with one another through hydrogen bonding. Again the hair-pin shaped molecules, just like those shown in Fig. 9 for the macrocyclic systems, cluster together to form quasi-discs which pack in columns (in fact Figs. 9 and 13 could be easily interchanged). In addition, the molecules have no positional order along the column axis. Much the same situation applies for the lyotropic phase structure except for the probability that the columns are composed of double layers with head groups positioned on the outside and on the inside of the columns in order to allow access of water through the system.

In addition to forming thermotropic and lyotropic liquid crystals these bolaphiles also form large scale aggregates on sonication in water, *i.e.* they form vesicles and tubules. These structures are on a much larger scale than those of the columnar structures of lyotropic and thermotropic liquid crystals, however, their existence serves to demonstrate that the process of self-assembly can extend far beyond the level of simple one on one intermolecular interactions.

Conclusions

In conclusion, we have shown that oligomeric materials with unusual discrete large scale molecular structures can exhibit mesomorphic phase behaviour. In order to exhibit such properties molecular deformation takes place. In certain

(a)

(b)

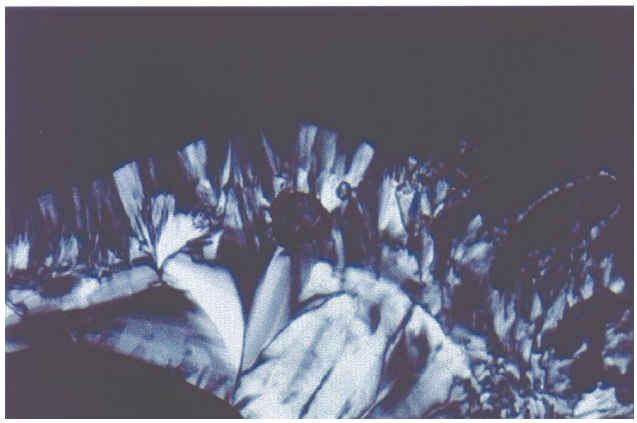

Fig. 12 The defect texture of (a) the thermotropic columnar mesophase and (b) the hexagonal lyotropic mesophase formed by compound **18** (×100)

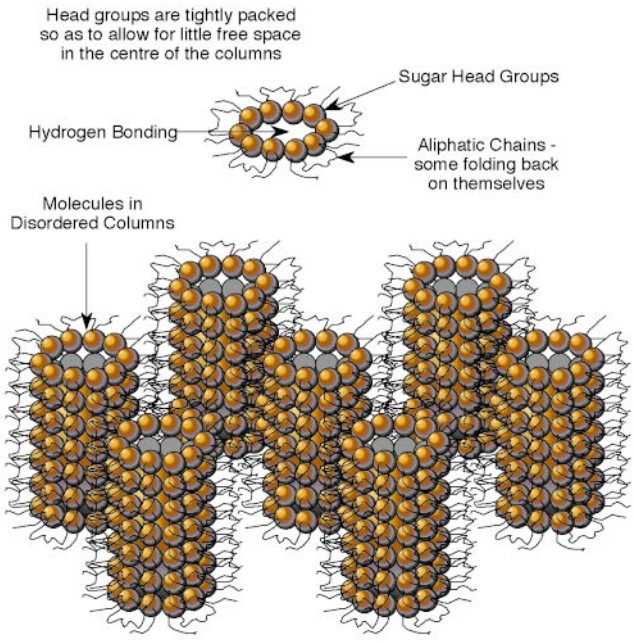

Fig. 13 The disordered hexagonal columnar structure formed by bolaphiles that mimic those found in archaebacteria. The bolaphiles fold in half so that the sugar residues can hydrogen bond. Clustering leads to the formation of disc-like complexes which then self-organise to give a columnar mesophase.

circumstances molecular deformation stabilises the formation of mesophases through a clustering process where the molecules form supramolecular assemblies. The so-formed assemblies self-organise to give mesophases of various types, for example molecules with rod-like molecular structures can fold in the middle to give wedge-shaped conformers which in turn can self-assemble into discs that self-organise into columns. Thus it is possible that materials of this type will have unique properties and hence applications.

Acknowledgements

We thank the following agencies and companies for their financial support; EPSRC, The Leverhulme Trust, E. Merck Ltd (UK), the Defence Research Agency (Malvern), the Alliance Programme of the British Council and the Ministere des Affaires Etrangeres, and the CNRS Région Bretagne.

Professor Goodby is Head of Organic Chemistry and The Liquid Crystals and Advanced Organic Materials Research Group at the University of Hull. Professor Goodby studied chemistry to the Bachelors level at the University of Hull, and then for the PhD in Liquid Crystals under the guidance of Professor Gray CBE, FRS. After two years post-doctoral research in collaboration with Professors Gray and Leadbetter CBE, he joined AT&T Bell Laboratories in the USA. After nine years at Bell Labs, and promotion to Research Supervisor he returned to the UK to become the STL/Thorn EMI Reader in Organic Chemistry. He became Professor and Head of the Liquid Crystal Group in 1990. Professor Goodby was an Amersham International Senior Research Fellow of the Royal Society and the first to be awarded the GW Gray Medal of the British Liquid Crystal Society. Currently, he is the Vice President of the International Liquid Crystal Society.

Notes and References

† E-mail: J.W.Goodby@chem.hull.ac.uk

1 See, for example: H. Hirschmann and V. Reiffenrath, TN, STN Displays, in the *Handbook of Liquid Crystals Vol 2B: Low Molecular Weight Liquid Crystals*, ed. D. Demus, J. W. Goodby, G. W. Gray, H.-W. Spiess and V. Vill, Wiley-VCH, Weinheim, 1998, ch. III, 3.1, pp. 199–229 and references therein.

2 See, for example: S. T. Lagerwall, Ferroelectric Liquid Crystals, in the *Handbook of Liquid Crystals Vol 2B: Low Molecular Weight Liquid Crystals*, ed. D. Demus, J. W. Goodby, G. W. Gray, H.-W. Spiess and V. Vill, Wiley-VCH, Weinheim, 1998, ch. VI, pp. 515–664 and references therein.

3 See, for example: J. S. Patel, Sin-Doo Lee and J. W. Goodby, Physical Properties of Smectic Liquid Crystals and Novel Electro-optic Effects, in *Spatial Light Modulator Technology, Materials, Devices, and Applications*, ed. Uzi Efron, Marcel Dekker, New York, 1995, pp. 33–83 and references therein.

4 See, for example: K. Miyachi and A. Fukuda, Antiferroelectric Liquid Crystals, in the *Handbook of Liquid Crystals Vol 2B: Low Molecular Weight Liquid Crystals*, ed. D. Demus, J. W. Goodby, G. W. Gray, H.-W. Spiess and V. Vill, Wiley-VCH, Weinheim, 1998, ch. VI, pp. 665–692 and references therein.

5 A. W. Hall, J. Hollingshurst and J. W. Goodby, Chiral and Achiral Calamitic Liquid Crystals for Display Applications, in *Handbook of Liquid Crystal Research*, ed. P. J. Collings and J. S. Patel, Oxford University Press, New York and Oxford, 1997, pp. 17–70 and references therein.

6 See, for example: S. M. Kelly, Synthesis of Chiral Smectic Liquid Crystals, in the *Handbook of Liquid Crystals Vol 2B: Low Molecular Weight Liquid Crystals I*, ed. D. Demus, J. W. Goodby, G. W. Gray, H.-W. Spiess and V. Vill, Wiley-VCH, Weinheim, 1998, ch. VI, pp. 493–514 and references therein.

7 G. W. Gray, M. Hird and K. J. Toyne, *Mol. Cryst. Liq. Cryst.*, 1991, **204**, 43; G. W. Gray, M. Hird, D. Lacey and K. J. Toyne, *J. Chem. Soc., Perkin Trans. 2*, 1989, 2041.
8 See, for example: C. Fairhurst, S. Fuller, J. Gray, M. C. Holmes and G. J. T. Tiddy, Lyotropic Surfactant Liquid Crystals, in the *Handbook of Liquid Crystals Vol 3: High Molecular Weight Liquid Crystals*, ed. D. Demus, J. W. Goodby, G. W. Gray, H.-W. Spiess and V. Vill, Wiley-VCH, Weinheim, 1998, ch. VII, pp. 341–392 and references therein.
9 See, for example: E. Chiellini and M. Laus, Main Chain Liquid Crystalline Semiflexible Polymers, in the *Handbook of Liquid Crystals Vol 3: High Molecular Weight Liquid Crystals*, ed. D. Demus, J. W. Goodby, G. W. Gray, H.-W. Spiess and V. Vill, Wiley-VCH, Weinheim, 1998, ch. I, 2, pp. 26–51 and references therein.
10 See, for example: D. Blunk, K. Praefcke and V. Vill, Amphotropic Liquid Crystals, in the *Handbook of Liquid Crystals Vol 3: High Molecular Weight Liquid Crystals*, ed. D. Demus, J. W. Goodby, G. W. Gray, H.-W. Spiess and V. Vill, Wiley-VCH, Weinheim, 1998, ch. VI, 305–340 and references therein.
11 See, for example: P. Ekwall, in *Advances in Liquid Crystals*, ed. G. H. Brown, Academic Press, 1975; C. Fairhurst, S. Fuller, J. Gray, M. C. Holmes and G. J. T. Tiddy, Lyotropic Surfactant Liquid Crystals, in the *Handbook of Liquid Crystals Vol 3: High Molecular Weight Liquid Crystals*, ed. D. Demus, J. W. Goodby, G. W. Gray, H.-W. Spiess and V. Vill, Wiley-VCH, Weinheim, 1998, ch. VII, pp. 341–392 and references therein.
12 C. R. Noller and W. C. Rockwell, *J. Am. Chem. Soc.*, 1938, **60**, 2076; G. A. Jeffrey and S. Bahattacharjee, *Carbohydr. Res.*, 1983, **115**, 53.
13 See, for example: K. Praefcke and D. Singer, Charge Transfer Systems, in the *Handbook of Liquid Crystals Vol 2B: Low Molecular Weight Liquid Crystals*, ed. D. Demus, J. W. Goodby, G. W. Gray, H.-W. Spiess and V. Vill, Wiley-VCH, Weinheim, 1998, ch. XVI, pp. 945–968; J. E. Lydon, Chromonics, *ibid*, ch. XVIII, pp. 981–1008; T. Kato, Hydrogen Bonded Systems, *ibid.*, ch. XVII, pp. 969–980; Ferrocene-containing Thermotropic Liquid Crystals, R. Deschenaux and J. W. Goodby, in *Ferrocenes*, ed. A. Togni and T. Hayashi, VCH, New York, 1995, ch. 9, pp. 471–495.
14 See, for example: T. Kato, Hydrogen Bonded Systems, in the *Handbook of Liquid Crystals Vol 2B: Low Molecular Weight Liquid Crystals*, ed. D. Demus, J. W. Goodby, G. W. Gray, H.-W. Spiess and V. Vill, Wiley-VCH, Weinheim, 1998, ch. XVII, pp. 969–980.
15 J. W. Goodby, Phase Structures of Calamitic Liquid Crystals, in the *Handbook of Liquid Crystals Vol 2A: Low Molecular Weight Liquid Crystals*, ed. D. Demus, J. W. Goodby, G. W. Gray, H.-W. Spiess and V. Vill, Wiley-VCH, Weinheim, 1998, ch. 1, pp. 3–21.
16 H.-T. Nguyen, C. Destrade and J. Malthête, Phasmids and Polycatenar Mesogens, in the *Handbook of Liquid Crystals Vol 2B: Low Molecular Weight Liquid Crystals*, ed. D. Demus, J. W. Goodby, G. W. Gray, H.-W. Spiess and V. Vill, Wiley-VCH, Weinheim, 1998, ch. XII, pp. 865–886; J. Malthête, A.-M. Levelut and H. T. Nguyen, *J. Phys.* (*Paris*), 1986, **46**, L-875; J. Malthête, H. T. Nguyen and C. Destrade, *Liq. Cryst.*, 1993, **13**, 171; D. Guillon, A. Skoulios and J. Malthête, *Europhys Lett.*, 1987, **3**, 67; J. Malthête, A. Collet and A.-M. Levelut, *Liq. Cryst.*, 1989, **5**, 129; A.-M. Levelut, J. Malthête, C. Destrade and H. T. Nguyen, *Liq. Cryst.*, 1987, **2**, 877.
17 D. Demus, *Liq. Cryst.*, 1989, **5**, 75.
18 C. T. Imrie and G. R. Luckhurst, Liquid Crystal Dimers and Oligomers, in the *Handbook of Liquid Crystals Vol 2B: Low Molecular Weight Liquid Crystals*, ed. D. Demus, J. W. Goodby, G. W. Gray, H.-W. Spiess and V. Vill, Wiley-VCH, Weinheim, 1998, ch. X, pp. 801–834.
19 G. H. Mehl and J. W. Goodby, *Chem. Ber.*, 1996, **129**, 521.
20 H. J. Coles and E. A. Corsellis, *Mol. Cryst. Liq. Cryst.*, 1995, **261**, 71; M. Ibn-Elhaj, A. Skoulios, D. Guillon, J. Newton, P. Hodge and H. J. Coles, *Liq. Cryst.*, 1993, **14**, 131.
21 G. H. Mehl and I. M. Saez, *Appl. Organomet. Chem.*, in press.
22 G. H. Mehl and J. W. Goodby, *Angew. Chem.*, 1996, **108**, 279.
23 F.-H. Kreuzer, R. Mauerer and P. Spes, *Makromol. Chem. Macromol. Symp.*, 1991, **30**, 215.
24 S. Bauer, H. Fischer and H. Ringsdorf, *Angew. Chem., Int. Ed. Engl.*, 1993, **32**, 1589.
25 S. A. Ponomarenko, E. A. Rebrov, A. Y. Bobrovsky, N. I. Boiko, A. M. Muzafarov and V. P. Shivaev, *Liq. Cryst.*, 1996, **21**, 1.
26 K. Lorenz, D. Hölter, B. Stühn, R. Mülhaupt and H. Frey, *Adv. Mater.*, 1996, **8**, 414.
27 R. P. Tuffin, PhD Thesis, University of Hull, 1995.
28 R. P. Tuffin, G. H. Mehl, K. J. Toyne and J. W. Goodby, *Mol. Cryst. Liq. Cryst.*, 1997, **304**, 223.
29 R. P. Tuffin, K. J. Toyne and J. W. Goodby, *J. Mater. Chem.*, 1995, **5**, 2093.
30 R. P. Tuffin, G. J. Cross, K. J. Toyne and J. W. Goodby, *J. Mater. Chem.*, 1996, **6**, 1271.
31 V. Percec, D. Schlueter, G. Johansson, J. C. Ronda and G. Ungar, *Polym. Prepr. ACS*, 1996, **37**(**2**), 477; V. Percec, P. Chu, G. Johansson, D. Schlueter, J. C. Ronda and G. Ungar, *Polym. Prepr. ACS*, 1996, **37**(**1**), 68; V. Percec, D. Schlueter, G. Ungar, S. Z. D. Cheng and A. Zhang, *Macromolecules*, 1998, **31**, 1745; V. Percec, *Macromol. Symp.*, 1997, **117**, 267; V. Percec, G. Johansson, G. Ungar and J. P. Zhou, *J. Am. Chem. Soc.*, 1996, **118**, 9855.
32 J. M. Lehn, *Angew. Chem., Int. Ed. Engl.*, 1990, **29**, 1304.
33 P. Ball, *Nature*, 1994, **371**, 202.
34 M. T. Krejchi, E. D. T. Atkins, A. J. Waddon, M. J. Fournier, T. L. Mason and D. A. Tirrell, *Science*, 1994, **265**, 1427.
35 R. S. Lokey and B. L. Iverson, *Nature*, 1995, **375**, 303.
36 D. Philp and J. E. Stoddart, *Angew. Chem., Int. Ed. Engl.*, 1996, **35**, 1155.
37 R. H. Berg, S. Hvilsted and P. S. Ramanujam, *Nature*, 1996, **383**, 505.
38 A. Muller and C. Bengholt, *Nature*, 1996, **383**, 296.
39 D. Me Rosa and A. Morana, in *Neural Networks and Biomolecular Engineering to Bioelectronics*, ed. C. Nicolini, Plenum Press, New York, 1995.
40 C. M. Niemeyer, *Angew. Chem., Int. Ed. Engl.*, 1997, **36**, 585.
41 G. D. Sprott, *J. Bioenerg. Biomembr.*, 1992, **24**, 555.
42 M. Kates, in *The Biochemistry of Archaea (Archaebacteria)*, ed. M. Kates, D. J. Kushner and A. T. Matheson, Elsevier, Amsterdam, 1993.
43 A. Gambacorca, A. Gliozzi and M. De Rosa, *World J. Microbiol. Biotechnol.*, 1995, **11**, 115.
44 M. De Rosa, *Thin Solid Films*, 1996, **284**–**285**, 13.
45 K. Yamauchi and M. Kinoshita, *Prog. Polym. Sci.*, 1993, **18**, 763.
46 R. Auzély-Velty, T. Benvegnu, D. Plusquellec, G. Mackenzie, J. A. Haley and J. W. Goodby, *Angew. Chem.*, in press.
47 R. Auzély-Velty, PhD Thesis, Universite de Rennes, 1997.

8/02762E

Visualising intermolecular interactions in crystals: naphthalene *vs*. terephthalic acid

Joshua J. McKinnon, Anthony S. Mitchell and Mark A. Spackman*†

Division of Chemistry, University of New England, Armidale NSW 2351, Australia

A recently-devised scheme for partitioning crystal space into smooth molecular volumes is used to visualise intermolecular interactions in the crystal structures of naphthalene and terephthalic acid.

The detailed description and classification of intermolecular interactions in molecular crystals is of considerable current interest in crystal engineering,[1] *ab initio* crystal structure prediction,[2] and studies of polymorphism.[3] We have recently described[4] a remarkable new way of exploring molecular crystals by isosurface rendering of smooth, non-overlapping molecular surfaces arising from a partitioning of crystal space based on Hirshfeld's stockholder scheme.[5] These molecular Hirshfeld surfaces partition space in the crystal into regions where the contribution from the sum of spherically-symmetric electron distributions for atoms in the molecule (the promolecule) exceeds the contribution from the corresponding sum over the crystal (the procrystal). Following Hirshfeld, a weighting function $w(\mathbf{r})$ is defined by eqn. (1).

$$w(\mathbf{r}) = \sum_{a\varepsilon molecule} \rho_a(\mathbf{r}) / \sum_{a\varepsilon crystal} \rho_a(\mathbf{r}) = \rho_{promolecule}(\mathbf{r}) / \rho_{procrystal}(\mathbf{r}) \quad (1)$$

The Hirshfeld surface for the particular molecule is defined by $w(\mathbf{r}) = 0.5$, and the volume occupied by the molecule in the crystal is that region where $w(\mathbf{r}) \geqslant 0.5$. For a given crystal structure and set of spherical atomic electron densities, the isosurface defined by $w(\mathbf{r}) = 0.5$ is unique. The first quantitative applications of this partitioning scheme, including measures of molecular size and shape as well as 3D isosurface pictures of these Hirshfeld surfaces, have recently been reported[6] for a variety of van der Waals and hydrogen-bonded crystals.

In a recent article[1a] Desiraju highlighted the way in which crystal engineering is presently at 'an exciting intersection of structural and supramolecular chemistry' and outlined three broad areas in which progress is needed if designer crystals are to become a reality. One of these is the visualisation of a crystal structure in its entirety, rather than focusing on assumed important interactions. This objective recognises the increasingly evident one-upmanship of nature in thwarting attempts to engineer structures for specific purposes,[7] and points to a compelling need for new tools to explore and analyse molecular crystals, taking into account all manner of forces and interactions, strong and directional as well as weak and isotropic. Desiraju gave an example of such a tool, NIPMAT,[8] an interaction display program which produces a pictorial grey-scale matrix from the deviation between all close intermolecular atom-atom contacts in the crystal and the sum of their van der Waals radii, thereby summarising all of the intermolecular interactions simultaneously. In that work, Desiraju demonstrated the application of NIPMAT to two dissimilar molecular crystals: naphthalene and terephthalic acid [see Fig. 6 of ref. 1(*d*)]. Inspired by this example, we decided to apply our Hirshfeld surface partitioning to the same molecular crystals, in the process demonstrating the potential for Hirshfeld surfaces to provide detailed information on all intermolecular interactions at the same time, as well as the relationship between Hirshfeld surfaces in crystals and more conventional representations of molecular surfaces: fused van der Waals spheres and surfaces of constant electron density.

Fig. 1 shows Hirshfeld surfaces for the two molecules, and close examination of them confirms how elegantly and beautifully these surfaces summarise the utter difference between intermolecular packing patterns in these two crystals.‡ The Hirshfeld surface for naphthalene reflects the weak and largely non-directional forces in the crystal, with smoothly varying curvature over the entire surface, and the edge-to-face C–H··π interaction evident as a broad depression above the plane of one ring, in much the same way as seen for benzene.[6] In contrast to this, the Hirshfeld surface of terephthalic acid is characterised by abrupt changes of curvature, especially in the vicinity of the O–H···O hydrogen bonds where the surface is extremely flat, and above and below the molecular plane, where the surface is essentially flat, but with subtle undulations which echo the packing of neighbouring molecules. From Fig. 1 it is evident that naphthalene does not pack in a planar arrangement, while terephthalic acid utilises hydrogen-bonded ribbons which pack slightly offset to, and on top of, one-another.

Fig. 2 illustrates the relationship between the Hirshfeld surfaces in the crystal (mesh in this case) and space-filling representations of the isolated molecules as fused van der Waals spheres. The van der Waals representation of naphthalene fits snugly within the Hirshfeld surface, leaving ample room within this volume in all directions. The same pattern is also seen for terephthalic acid in the vicinity of the phenyl C–H bonds, but the regions around the carboxy groups are dramatically different. Here, as expected, the van der Waals spheres for O and H clearly protrude well beyond the Hirshfeld mesh surface at the ends of the molecule. More subtle is the way in which the oxygen spheres and one H sphere just protrude beyond the Hirshfeld surface on the side of the molecule, corresponding to close C–H···O contacts in the crystal.

Fig. 3 superimposes the Hirshfeld surfaces of these two molecules (mesh) on surfaces of constant electron density on which the molecular electrostatic potential has been colour

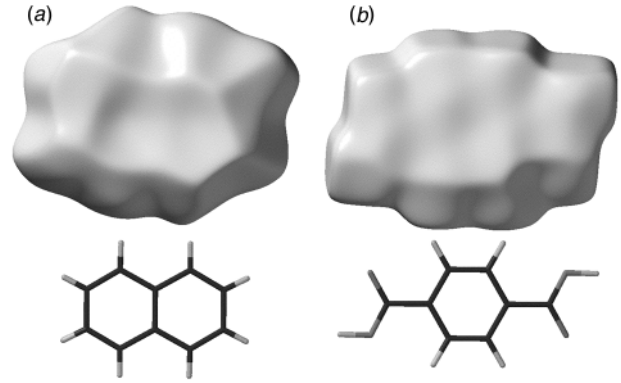

Fig. 1 Hirshfeld surfaces for (*a*) naphthalene and (*b*) terephthalic acid beside stick molecular models. Models and surfaces are all drawn to the same scale.

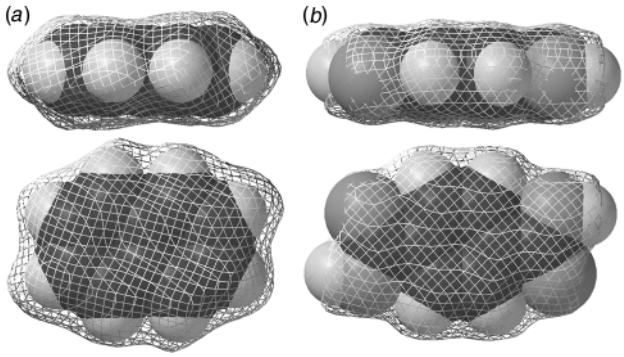

Fig. 2 Front and side views of Hirshfeld surfaces (mesh) for (*a*) naphthalene and (*b*) terephthalic acid superimposed on fused van der Waals sphere representations [van der Waals radii: 1.40 (H), 1.70 (C) and 1.50 Å (O)]

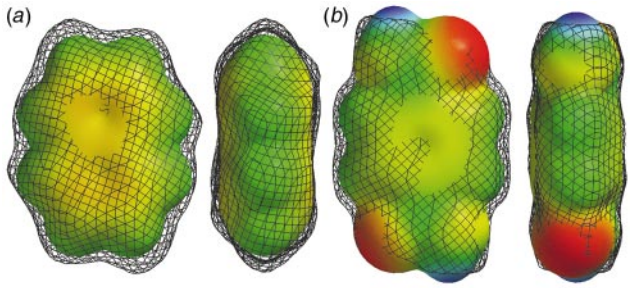

Fig. 3 Front and side views of Hirshfeld surfaces (mesh) for (*a*) naphthalene and (*b*) terephthalic acid superimposed on surfaces of constant electron density (0.002 au) for the isolated molecules, upon which the molecular electrostatic potential has been colour-coded. Colours range from red (–190 kJ mol^{-1} for a unit charge) to blue (+370 kJ mol^{-1}); the same colour range has been used for both molecules.

coded.§ The slightly polar nature of naphthalene (green around the C–H bonds, yellow above the rings) contrasts with the highly localised nature of polarity in the carboxy group of terephthalic acid, and the protrusion of O and H atoms in the latter is evident. A new feature seen in Fig. 3 is the way in which the Hirshfeld surface dips below the surface of constant electron density above the benzene rings for the isolated molecules, just perceptibly in the case of terephthalic acid, but far more so for naphthalene, where it is strikingly evident that, whereas the two rings are essentially equivalent in the electron density surface for the isolated molecule, there is a much closer C–H$\cdots\pi$ contact to one ring than the other in the crystal structure. The C–H$\cdots$O contacts on the edge of the terephthalic acid molecule are also more obvious here than in Fig. 2

We believe that the information on intermolecular interactions which is implicitly contained in an accurate crystal structure analysis is reliably encoded on these Hirshfeld surfaces. The illustrations in this article show how, in a very qualitative manner, this appears to be the case, while at the same time highlighting how the Hirshfeld surfaces, defined as they are for molecules in the crystal, differ fundamentally from representations of isolated molecules. Curvature of the Hirshfeld surface seems to be intimately related to the nature and strength of intermolecular interactions for all examples we have investigated so far, and our future lines of inquiry with these intriguing surfaces will explore this connection further.

Notes and References

† E-mail: mspackma@metz.une.edu.au

‡ Our calculations used the same crystal structures as Desiraju (CSD: NAPHTA10, TEPHTH) with details of the computational method given in ref. 6. Global descriptors of size indicate that the Hirshfeld surfaces of these two molecules are surprisingly similar, with similar volumes (V_H = 172.3 and 169.3 Å^3 for naphthalene and terephthalic acid, respectively), surface areas (S_H = 176.0 and 179.3 Å^2) and packing ratios (P_H = 0.970 and 0.969). As for shape, results for globularity (G = 0.851 and 0.825), a measure of the degree to which the surface area differs from that of a sphere of the same volume, suggest that naphthalene is marginally more spherical than terephthalic acid, while anisotropy ($\sqrt{\Omega}$ = 0.354 and 0.435) confirms that the surface for naphthalene is markedly more isotropic than that for terephthalic acid.

§ These results obtained with the SPARTAN package (see ref. 9); electron density surfaces are at ρ(r) = 0.002 au, from a Hartree–Fock SCF calculation on the isolated molecule with a 6-31G* basis set, at the same geometry as the molecule in the crystal; electrostatic potentials for both molecules utilise the same gradation of colour, with red electronegative and blue electropositive.

1 (*a*) G. R. Desiraju, *Angew. Chem., Int. Ed. Engl.*, 1995, **34**, 2311; (*b*) J. D. Dunitz, in *The crystal as a supramolecular entity*, ed. G. R. Desiraju, Wiley, Chichester, 1996, p. 1; (*c*) C. B. Aakeröy, *Acta Crystallogr., Sect. B*, 1997, **53**, 569; (*d*) G. R. Desiraju, *Chem. Commun.*, 1997, 1475.

2 (*a*) S. L. Price, *J. Chem. Soc., Faraday Trans.*, 1996, **92**, 2997; (*b*) S. L. Price, in *Molecular interactions. From van der Waals to strongly bound complexes*, ed. S. Scheiner, Wiley, Chichester, 1996, p. 297; (*c*) S. L. Price and K. S. Wibley, *J. Phys. Chem. A*, 1997, **101**, 2198; (*d*) A. Gavezzotti, *Acc. Chem. Res.*, 1994, **27**, 309; (*e*) H. R. Karfunkel and R. J. Gdanitz, *J. Comput. Chem.*, 1992, **13**, 1171; (*f*) See articles in *Theoretical aspects and computer modeling of the molecular solid state*, ed. A. Gavezzotti, Wiley, Chichester, 1997.

3 J. Bernstein, *J. Phys. D: Appl. Phys.*, 1993, **26**, B66; J. D. Dunitz and J. Bernstein, *Acc. Chem. Res.*, 1995, **28**, 193; A. Gavezzotti, *J. Am. Chem. Soc.*, 1995, **117**, 12299; G. R. Desiraju, *Science*, 1997, **278**, 404.

4 M. A. Spackman and P. G. Byrom, *Chem. Phys. Lett.*, 1997, **267**, 215.

5 F. L. Hirshfeld, *Theor. Chim. Acta*, 1977, **44**, 129.

6 J. J. McKinnon, A. S. Mitchell, and M. A. Spackman, *Chem. Eur. J.*, 1998, **4**, in the press.

7 See, for example: F. H. Allen, V. J. Hoy, J. A. K. Howard, V. R. Thalladi, G. R. Desiraju, C. C. Wilson, and G. J. McIntyre, *J. Am. Chem. Soc.*, 1997, **119**, 3477; J. A. Swift, R. Pal and J. M. McBride, *J. Am. Chem. Soc.*, 1998, **120**, 96. In the latter work the authors remark that 'This work demonstrates again the current superiority of molecules over chemists in discovering stable crystal packing patterns'.

8 R. S. Rowland, *Am. Crystallgr. Assoc. Abstr.*, 1995, **23**, 63. See also the description and use of NIPMAT in ref. 2(*c*).

9 SPARTAN version 4.0, Wavefunction Inc., 18401 Von Karman Ave., #370, Irvine, CA 92715, USA.

Received in Cambridge, UK, 22nd June 1998; 8/04691C

Synthesis of novel α-functionalized phosphinic acid derivatives of thiophene and the first crystal structure of an α-hydroxyalkylphosphinate

S. W. Annie Bligh,*[a]† Carlos F. G. C. Geraldes,[b] Mary McPartlin,[a] Mahesh J. Sanganee[a] and Thomas M. Woodroffe[a]

[a] *School of Biological and Applied Sciences, University of North London, Holloway Road, London, UK N7 8DB*
[b] *Department of Biochemistry and Centre of Neurosciences, University of Coimbra, 3000 Coimbra, Portugal*

Reaction of 2,5-diformylthiophene with Ph_2CHNH_2 and hypophosphorus acid yields novel α-hydroxy- or α-aminomethylphosphinic acid derivatives depending on reaction conditions; the X-ray structure analysis of diphenylmethylammonium 5-formyl-2-thienyl(hydroxy)methylphosphinate provides the first direct structural information on the α-hydroxyalkylphosphinate class of compounds.

Compounds containing an α-aminoalkylphosphinic acid functional group are of considerable importance because of their anti-bacterial,[1] herbicidal[2] and fungicidal[3] activities. Protonation studies of α-aminomethylphosphinic acids [$R_2NCH_2P(H)O_2H$] have shown that the nitrogen atom is very weakly basic compared to those of α-aminomethylphosphonic acids ($R_2NCH_2PO_3H_2$) and α-aminocarboxylic acids ($R_2NCH_2CO_2H$), and that the phosphinic acid group is strongly acidic.[4] In contrast to the widely studied α-aminoalkylphosphinic acid derivatives, relatively few papers have been reported on the chemistry of α-hydroxyalkylphosphinic acids, although there is evidence that α-hydroxyalkylphosphinate esters are pharmaceutically active.[5] Many effective methods for the preparation of α-aminoalkylphosphinic acids have been developed,[6] but few synthetic routes to α-hydroxyalkylphosphinic acids have been reported and these involve prolonged heating of hypophosphorous acids with aldehydes or ketones,[7] or reaction of ketones with bis(trimethylsilyloxy)phosphine.[8] Here we have successfully prepared both types of α-functionalised phosphinates (Scheme 1); of particular importance is the isolation for the first time of the α-hydroxyalkylphosphinate compound using relatively mild reaction conditions, and the first characterisation by X-ray crystallography of this class of compound.

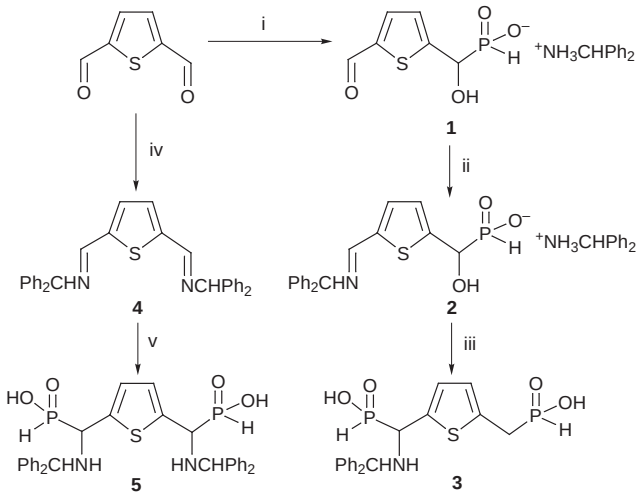

Scheme 1 *Reagents and conditions*: i, Ph_2CHNH_2, 50% aq H_3PO_2, 30%; ii, Ph_2CHNH_2, DMSO, 88%; iii, H_3PO_2, 1,4-dioxane, 26%; iv, Ph_2CHNH_2, MeOH, 51%; v, H_3PO_2, 1,4-dioxane, 72%

The reaction of 2,5-diformylthiophene (prepared as described in ref. 9) with Ph_2CHNH_2 and aqueous hypophosphorous acid (50%) gives an unexpected mono(α-hydroxyalkylphosphinate) derivative **1** rather than the bis(α-aminoalkylphosphinate) derivative **5**. The remaining thiophene carbonyl group is not electrophilic towards the addition of a second water molecule to form the intermediate *gem*-diol; all attempts to prepare the bis(α-hydroxyalkylphosphinate) derivative proved unsuccessful.

The presence of the α-hydroxy group in **1** was confirmed by X-ray structure analysis‡ of the (diphenylmethyl)ammonium salt and the structure of the ions, linked by a hydrogen bond between one of the phosphinate oxygen atoms and a proton of the ammonium cation [O(2)···H(1N) = 1.86 Å] is shown in Fig. 1(*a*). The remaining two protons of the (diphenylmethyl)-ammonium counterion are also involved in hydrogen-bonding to phosphinate oxygen atoms of adjacent symmetry related anions [O···H(N) = 1.72–1.90 Å], resulting in a complicated spiral hydrogen bonded chain of alternating cations and anions running parallel to the *b* axis of the crystal [Fig. 1(*b*)]. Along this helix, adjacent anions (separated by the *b* axis length) are linked by hydrogen-bonding between the α-hydroxy group of one and a phosphinate oxygen of the next [H(1O)···O(3) = 1.98 Å] as can also be seen in Fig. 1(*b*).

In order to prepare the bis(α-aminoalkylphosphinate) derivative **5** from the dialdehyde a two stage process was required. The carbonyl groups were first converted to the imine functions by condensing the dialdehyde and Ph_2CHNH_2 in MeOH to give **4**, and addition of hypophosphorous acid (100%) to **4** in 1,4-dioxane gives a diastereoisomeric mixture of **5** in good yield. However, the addition of hypophosphorous acid (100%) to the mono-imine derivative **2** readily converts the imine to the α-aminoalkylphosphinate, and the presence of excess hypophosphorous acid reduces the α-hydroxy functional group to yield **3**. Attempts to remove the Ph_2CH protecting groups have proved difficult. The new compounds **1–5** give satisfactory elemental analysis and their ^1H, ^{13}C and ^{31}P NMR data§ agree with the structures proposed. Both compounds **1** and **2** have been tested in the antibacterial screen and showed no activity.

Compound **1** is the first example of an α-hydroxyalkylphosphinate as a substituent of a heterocyclic ring. The ability to derivatize only one of the two aldehyde groups to afford the mono(α-hydroxyalkylphosphinate) opens up the possibility that the remaining carbonyl can be used in further reaction with an amine [*e.g.* Scheme 1(ii)]. This availability of an additional active carbonyl in an α-hydroxyalkylphosphinate derivative is thus potentially beneficial for its coupling to biological macromolecules or to polymers for selective metal complexation applications.

We thank GlaxoWellcome (to M. J. S.) for financial support, the EPSRC for a studentship (to T. M. W.) and for use of the Chemical Database Service at Daresbury. S. W. A. B. thanks The Royal Society (European Science Exchange Programme)

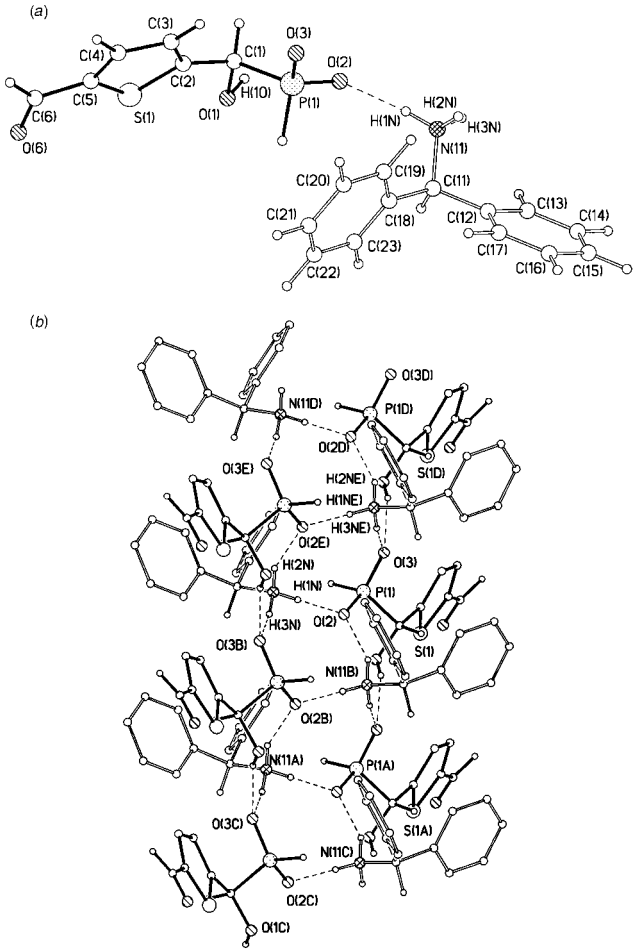

Fig. 1 The structure of **1**: (*a*) the anion and cation linked by one of the H-bonds (only the major component of the rotationally disorder formyl group is shown); (*b*) part of the helical H-bonded chain generated by the 2_1 screw axis parallel to *b* (the symmetry related ions are at A: *x*, −1 + *y*, *z*; B: 0.5 − *x*, −0.5 + *y*, 0.5 − *z*; C: 0.5 − *x*, −1.5 + *y*, 0.5 − *z*; D: *x*, 1 + *y*, *z*; E: 0.5 − *x*, 0.5 + *y*, 0.5 − *z*)

for financial support. C.F.G.C.G. thanks Junta Nacional de Investigaç:o Cientifica e Technológic, Portugal for financial support.

Notes and References

† E-mail: a.bligh@unl.ac.uk

‡ *Crystal data* for **1**: $C_{19}H_{20}NO_4PS$, M = 389.2, pale brown crystal (0.50 × 0.38 × 0.34 mm³), monoclinic, space group $P2_1/n$ (No. 14), a = 15.773(3), b = 5.894(2), c = 21.404(4) Å, β = 104.06(4)°, U = 1930.2 Å³, Z = 4, $F(000)$ = 776, D_c = 1.278 g cm^{-3}, μ(Mo-Kα) = 0.26 mm^{-1}, λ = 0.71069 Å (graphite monochromator). Data were collected on a Philips PW1100 diffractometer in the θ range 3–23° with a scan width of 0.90°. The structure was solved by direct methods (ref. 10); the H-atoms of the ammonium and hydroxy group were located from difference-Fourier syntheses, but were not refined, and the remaining H-atoms were included at idealised positions. Anisotropic displacement parameters were assigned to all non-hydrogen atoms (apart from the phenyl C-atoms, which were constrained to idealised hexagons, C–C 1.395 Å) in the final cycles of full-matrix refinement based on F (ref. 11) which converged at R = 0.0561 (R_w = 0.0581, $w = 1/\sigma^2F_o$) for 1259 unique reflections having $I/\sigma(I) \geqslant 3.0$ and 174 variables. CCDC 182/972.

§ *Selected data* for **1**: δ_H(250 MHz, [$^2H_6$]DMSO) 9.81 (s, 1H, CHO), 9.37 (s, NH), 7.64 (m, 1H, thiophene), 7.35 (m, 10H, Ph), 7.10, (m, 1H, thiophene), 6.77 (d, 1H, J_{PH} 552, PH), 5.51 (s, 1H, $CHPh_2$), 4.70 (d, 1H, $^2J_{P–CH}$ 10.0, CH); δ_P 19.35; δ_C 183.6 (HCO), 147.2, 137.2, 132.4, 124.5, 134.6 (thiophene), 138.2, 128.6, 128.1, 127.1 (Ph), 69.1 (d, J_{PC} 107, CP), 56.9 ($CHPh_2$). For **2**: δ_H(250 MHz, [$^2H_6$]DMSO) 8.87 (s, NH), 8.55 (s, 1H, HCN), 7.25 (m, 21H, Ph and thiophene), 6.90 (m, 1H, thiophene), 6.64 (d, 1H, J_{PH} 489, PH), 5.62, 5.47 (s, 2H, $CHPh_2$), 4.49 (d, 1H, $^2J_{P–CH}$ 11.8, CH); δ_P 20.49; δ_C 1854.8 (HCN), 150.0, 139.5, 131.4, 123.4 (thiophene), 144.2, 139.2, 128.5, 128.1, 127.8, 127.1, 126.6 (Ph), 71.2 (d, J_{PC} 149, CP), 75.7, 56.9 ($CHPh_2$). For **3**: δ_H(250 MHz, [$^2H_6$]DMSO) 7.46–7.19 (m, 11H, Ph and thiophene), 6.84 (s, 1H, thiophene), 6.91 (d, 2H, J_{PH} 530, PH), 6.82 (d, 2H, J_{PH} 510, PH), 5.05 (s, 1H, $CHPh_2$), 3.78 (d, 1H, $^2J_{P–CH}$ 16.5, CH), 3.26 (d, 1H, $^2J_{P–CH}$ 17.5, CH_2); δ_P 27.76, 27.00; δ_C 146.6, 145.5, 141.5, 137.0,132.5, 131.3, 131.1, 130.7 (thiophene and Ph), 67.4 ($CHPh_2$), 60.1 (d, J_{PC} 101, HCP), 36.2 (d, J_{PC} 88.2, H_2CP). For **4**: δ_H(250 MHz, [$^2H_6$]DMSO) 8.66 (s, 2H, HCN), 7.52 (s, 2H, thiophene), 7.41–7.19 (m, 20H, Ph), 5.70 (s, 2H, $CHPh_2$); δ_C 154.9 (HCN), 144.5, 132.1 (thiophene), 143.9, 128.4, 127.1, 126.8 (Ph), 75.8 ($CHPh_2$). For **5**: diastereoisomers (*) δ_H(250 MHz, [$^2H_6$]DMSO) 7.35 (m, 21H, Ph and thiophene), 6.95, 6.88* (s, 1H, thiophene), 6.92 (d, 1H, J_{PH} 546, PH), 5.07, 5.04* (s, 1H, $CHPh_2$), 3.89, 3.83* (d, 1H, $^2J_{P–CH}$ 17.0, CH); δ_P; 27.26, 27.01*; δ_C 146.6, 146.3*, 145.3, 145.1*, 142.6, 142.0, 132.7, 132.5, 132.2, 131.4, 131.0 (Ph and thiophene), 67.5, 67.4* ($CHPh_2$), 60.3, 60.1* (d, J_{PC} 101, CP).

1 J. G. Dingwall, C. D. Campell and E. K. Baylis, *UK Pat. Appl.*, 1 542 938, 1979.
2 P. Kafarski, B. Lejczak, R. Tyka, L. Koba, E. Pliszczak and P. Wieczorek, *J. Plant Growth Regulation*, 1995, **14**, 199.
3 Y. Ishiguri, Y. Yamada, T. Kato, M. Sasaki and K. Mukai, *Eur. Pat. Appl.*, EP 82-301905, 1982.
4 T. Kiss, M. Jezowska-Bojczuk, H. Kozlowski, P. Kafarski and K. Antczak, *J. Chem. Soc., Dalton Trans.*, 1991, 2275; R. J. Motekaitis, I. Murase and A. E. Martell, *J. Inorg. Nucl. Chem.*, 1971, **33**, 3353.
5 E. K. Baylis, *Eur. Pat. Appl.*, EP-614900, 1994.
6 E. K. Baylis, C. D. Campbell and J. G. Dingwall, *J. Chem. Soc., Perkin Trans., 1*, 1984, 2845; D. Grobelny, *Synthesis*, 1987, 94; X. Jiao, C. Verbraggen, M. Borloo, W. Bollaert, A. De Groot, R. Dommisse and A. Haemers, *Synthesis*, 1994, 23.
7 M. C. Marie, *Compt. Rend.*, 1904, **138**, 1707.
8 V. I. Vysotskii and S. V. Levan'kov, *Zh. Obshch. Khim.*, 1991, **61**, 1315.
9 T. Mitsumori, K. Inoue, N. Koya and H. Iwamura, *J. Am. Chem. Soc.*, 1995, **117**, 2467.
10 G. M. Sheldrick, SHELX 86, Program for Crystal Structure Solution, Göttingen, 1986.
11 G. M. Sheldrick, SHELX 76, Program for Crystal Structure Determination, Cambridge, 1976.

Received in Cambridge, UK, 6th July 1998; 8/05189E

Preparation of novel HIV-protease inhibitors

Manfred T. Reetz,*† Claudia Merk and Gerlinde Mehler

Max-Planck-Institut für Kohlenforschung, Kaiser-Wilhelm-Platz 1, D-45470 Mülheim/Ruhr, Germany

The synthesis and biological properties of new HIV-1-protease inhibitors involving amino acids or dipeptides attached to binaphthol, biphenol or embonic acid are described.

Inspite of recent progress in the development of therapeutics for the treatment of AIDS, a number of problems persist.[1] A well-known approach concerns the design and synthesis of HIV-protease inhibitors. The HIV-protease is a well characterized viral enzyme consisting of two units, each composed of 99 amino acids, which join together to form the C_2-symmetric active homo-dimer. Consequently, one strategy has been to prepare C_2-symmetric inhibitors in the form of peptide mimetics, one family of active compounds being C_2-symmetric 1,2-diols flanked by short peptide units.[2] The hydroxy moities have been shown to participate in the interaction with the HIV-protease *via* H-bonding, the configuration at the two stereogenic centers of the diol playing an important role with respect to the degree of binding. We speculated that similar compounds based on chiral binaphthol or biphenol units in place of the traditional diols could constitute a new class of HIV-1-protease inhibitors, specifically because the enhanced acidity of such moieties would be expected to lead to stronger H-bonding. Here we present the initial results of this strategy.

We first envisioned peptides of the type **2b** and **5b** based on racemic 2,2′-dihydroxy-1,1′-binaphthyl-3,3′-dicarboxylic acid **1**. Direct coupling with valine methyl ester resulted in a 14% yield of the desired diastereomeric dipeptide esters **2a**, which were hydrolyzed to the acids **2b**. In order to improve the synthesis, the hydroxy functions of **1** were first protected by benzyl groups (Scheme 1). The diastereomeric mixture of **2b** was separated by HPLC to provide analytically pure (*R,S,S*)-**2b** and (*S,S,S*)-**2b**. In the case of the dipeptide **5b** with two vinylogous amino acid residues, only direct coupling was carried out (Scheme 2).

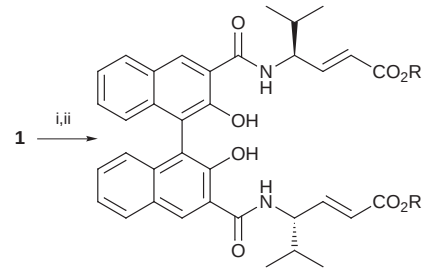

5a R = Et (17%)
b R = H (65%)

Scheme 2 *Reagents*: i, NaOH, NHS, DCC; NEt_3, L-$HCl{\cdot}H_2NCHPr^iCH{=}CHCO_2Et$; ii, LiOH, H_2O

Although there is a limited degree of rotational freedom with respect to the axis going through the two naphthyl units, the C_2-symmetric dipeptides **2b** and **5b** are in fact fairly rigid. In order to introduce more conformational flexibility, we prepared dipeptide **7b** based on embonic acid **6** (Scheme 3). Although the

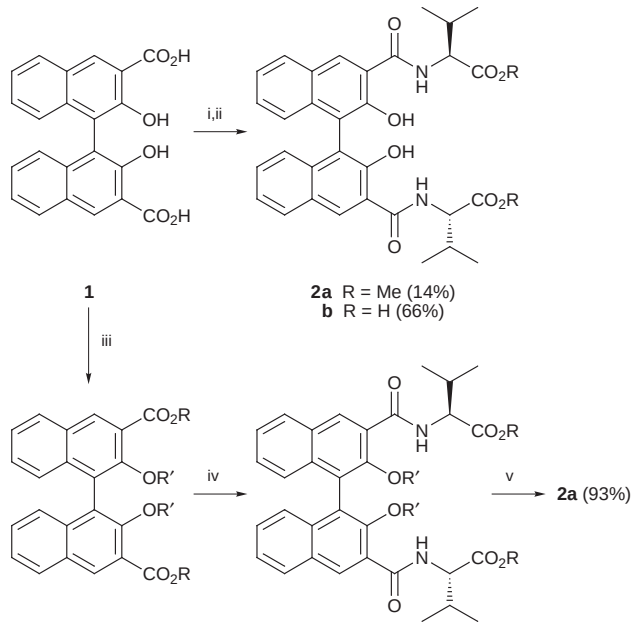

Scheme 1 *Reagents*: i, NaOH, *N*-hydroxysuccinimide (NHS), DCC, L-$H_2NCHPr^iCO_2Me$; ii, LiOH, H_2O; iii, BnBr, K_2CO_3; iv, NHS, DCC, L-$H_2NCHPr^iCO_2Me$; v, $Pd(OH)_2$, cyclohexene

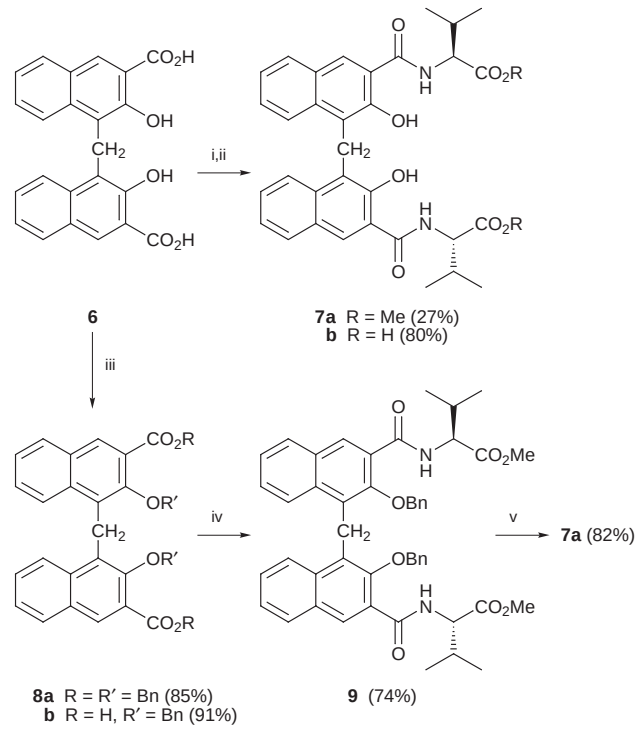

Scheme 3 *Reagents*: i, NaOH, NHS, DCC, L-$H_2NCHPr^iCO_2Me$; ii, LiOH, H_2O; iii, BnBr, K_2CO_3, KOH, H_2O; iv, NHS, DCC, L-$H_2NCHPr^iCO_2Me$; v, $Pd(OH)_2$, cyclohexene

latter is achiral, conformational enantiomers (or diastereomers in the case of **7b**) are likely, especially upon binding to the C_2-symmetric HIV-protease. The dipeptide **10b** incorporating vinylogous valine was synthesized analogously.

In order to test the biological effect of extending the peptidic side-arms, the tetrapeptide **11b** was prepared in a direct manner by NHS–DCC-mediated coupling of **6** with L-valinyl-L-valine ethyl ester. Here, as in all previous cases, the compounds were purified by HPLC and characterized by standard spectroscopic and analytical means.

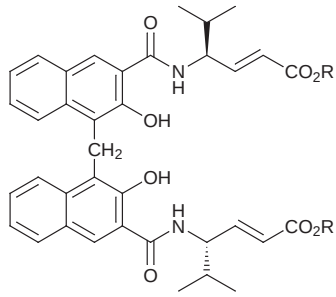

10a R = Me (32%)
b R = H (80%)

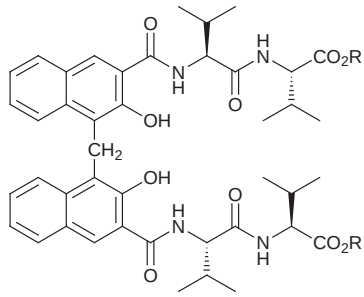

11a R = Et (46%)
b R = H (16%)

Finally, the biphenol derivative **13** was prepared by oxidative coupling[3] of *N*-benzyloxycarbonyl-L-tyrosine methyl ester **12**. Deprotection delivered the dipeptide **14** (Scheme 4).

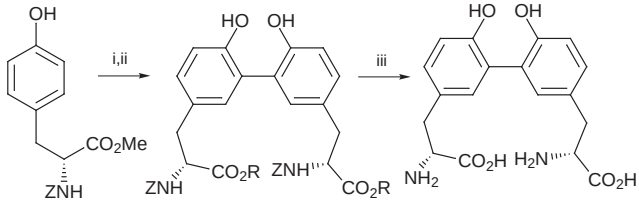

12 (Z = benzyloxycarbonyl) **13a** R = Me (52%) **b** R = H (94%) **14** (90%)

Scheme 4 *Reagents*: i, VOF_3; ii, LiOH, H_2O; iii, H_2, Pd-C

In order to screen the ability of the compounds to inhibit the HIV-1-protease, the IC_{50} values were measured using standard procedures.[4] Table 1 shows that several compounds have activities similar to a number of other HIV-protease inhibitors which have been reported in recent years.[2] It is interesting to note that in the case of **5b** (but not **2b**) the absolute configuration of the binaphthol backbone plays a significant role in the degree of HIV-protease inhibition. Specifically, the (*R*,*S*,*S*)-compound is considerably more active than the (*S*,*S*,*S*)-diastereomer. However, the conformationally more flexible compounds based on embonic acid **6** are more active, especially the tetrapeptide **11b**.

Theoretically, the mode of action of the above compounds can either be due to active-site inhibition of the HIV-protease or to a possible inhibition of dimerization of the two 99-amino acid

Table 1 Properties of synthesized compounds

Compound	Solubility/μM	IC_{50}/μM
(*R*,*S*,*S*)-**2b**	> 65	47
(*S*,*S*,*S*)-**2b**	> 65	48
(*R*,*S*,*S*)-**5b**	> 50	46
(*S*,*S*,*S*)-**5b**	> 50	13
7b	> 100	40
10b	~ 30	8
11b	> 10	2.8
13b	> 100	24
14	> 100	240

units (*i.e*. prevention of homo-dimer formation). In order to shed some light on these aspects, kinetic studies using the model of Zhang were carried out on select compounds, *i.e*. dissociative inhibition constants (K_i) and competitive inhibition constants (K_c) were measured.[5] Accordingly, in the case of the most active compound **11b**, the K_i and K_c values turned out to be 6.9 and 2.0 μM, respectively. This means that active site (competitive) inhibition dominates, although dissociative inhibition plays some role. Mixed inhibition also pertains to the related dipeptide **7b** (K_i = 15.8 μM; K_c = 6.2 μM). In contrast, the mechanism of action of the tyrosin derivative **13b** appears to be based primarily on the inhibition of dimerization of the monomeric HIV-protease units (K_i = 6.8 μM; K_c = 229 μM). This still needs to be studied more closely, *e.g*. using light scattering. However, preliminary molecular modelling is in line with these conclusions.

In summary, we have designed and prepared new HIV-1-protease inhibitors based on naphtholic and phenolic units to which amino acids or dipeptides are attached. Although the respective activities are lower than those of the most potent drugs currently known,[1,2] the discovery of these new lead structures allows for the (combinatorial) synthesis of analogs which may show improved performance.

We thank H.-J. Schramm, J. Büttner and T. Wenger (group of R. Huber at Max-Planck-Institut für Biochemie, Martinsried) for help in the determination of IC_{50} values and kinetic data and for stimulating discussions.

Notes and References

† E-mail: reetz@mpi-muelheim.mpg.de

1 Reviews: G. Moyle and B. Gazzard, *Drugs*, 1996, **51**, 701; J. W. Erickson, *Nat. Struct. Biol*., 1995, **2**, 523; E. K. Wilson, *Chem. Eng. News*, July 29, 1996, p. 42; C. Perez, M. Pastor, A. R. Ortiz and F. Gago, *J. Med. Chem*., 1998, **41**, 836.

2 See for example: M. V. Hosur, T. N. Bhat, D. J. Kempf, E. T. Baldwin, B. Lui, S. Gulnik, N. E. Wideburg, D. W. Norbeck, K. Appelt and J. W. Erickson, *J. Am. Chem. Soc*., 1994, **116**, 847; G. T. Wang, S. Li, N. Wideburg, G. A. Krafft and D. J. Kempf, *J. Med. Chem*., 1995, **38**, 2995; T. N. Bhat, E. T. Baldwin, B. Liu, Y.-S. E. Cheng and J. W. Erickson, *Struct. Biol*., 1994, **1**, 552; C. N. Hodge, P. Y. S. Lam, C. J. Eyermann, P. K. Jadhav, Y. Ru, C. H. Fernandez, G. V. De Lucca, C.-H. Chang, R. F. Kaltenbach III, E. R. Holler, F. Woerner, W. F. Danecker, G. Emmett, J. C. Calabrese and P. E. Aldrich, *J. Am. Chem. Soc*., 1998, **120**, 4570; W. W. Wilkerson, S. Dax and W. W. Cheatham, *J. Med. Chem*., 1997, **40**, 4079; P. K. Jadhav, P. Ala, F. J. Woerner, C. H. Chang, S. S. Garber, E. D. Anton and L. T. Bacheler, *J. Med. Chem*., 1997, **40**, 181.

3 A. G. Brown and P. D. Edwards, *Tetrahedron Lett*., 1990, **31**, 6581; S. M. Kupchan, O. P. Dhingra and C.-K. Kim, *J. Org. Chem*., 1978, **43**, 4076.

4 H.-J. Schramm, J. Boetzel, J. Büttner, E. Fritsche, W. Göhring, E. Jaeger, S. König, O. Thumfart, T. Wenger, N. E. Nagel and W. Schramm, *Antiviral Res*., 1996, **30**, 155.

5 Z.-Y. Zhang, R. A. Poorman, L. L. Maggioria, R. L. Heinrikson and F. J. Kézdy, *J. Biol. Chem*., 1991, **266**, 15 591.

Received in Cambridge, UK, 15th July 1998; 8/05489D

Diphosphonites as highly efficient ligands for enantioselective rhodium-catalyzed hydrogenation

Manfred T. Reetz,*† Andreas Gosberg, Richard Goddard and Suk-Hun Kyung

Max-Planck-Institut für Kohlenforschung, Kaiser-Wilhelm-Platz 1, D-45470 Mülheim/Ruhr, Germany

Chiral ligands with achiral backbones such as ethano- or ferroceno-bridges linking two phosphonites derived from chiral diols such as binaphthol (BINOL) have been prepared; the corresponding Rh complexes are excellent catalysts in the hydrogenation of prochiral olefins such as itaconic acid dimethyl ester or 2-acetamido methyl acrylate, the ee values being 90–99.5%.

Although a number of chiral diphosphanes and diphosphinites have been shown to be effective ligands in transition metal catalyzed asymmetric reactions,[1] the search for new types of chiral auxiliaries continues.[2] Surprisingly, very little is known concerning chiral diphosphonites as ligands in these reactions.[3] Perhaps this is due to the fact that in all cases reported so far the enantioselectivity is poor (ee = 0–32%).[3] We speculated that chelating diphosphonites derived from a proper combination of an achiral backbone and a chiral diol might constitute useful and easily accessible ligands.[4]

Using ferrocene and (*R*)- or (*S*)-BINOL as cheap building blocks,[5] the diphosphonite **1** was easily assembled in three steps (Scheme 1).[6] **1** is an orange–brown crystalline compound, which in the solid state‡ shows some interesting features (Fig. 1). In spite of their different environments, the two independent molecules in the unit cell have almost identical conformations [P1–Cp1–Cp2–P2 −9(1)°, P3–Cp3–Cp4–P4 −7(1)°; Cp, centroid], with the two P atoms in each molecule situated close to one another [P1···P2 3.506(3), P3···P4 3.428(3) Å].

The ethano-bridged analog **2** was also readily synthesized (Scheme 2).

In order to prepare hydrogenation catalysts, the ligands were treated with $Rh(cod)_2BF_4$ under standard conditions,[7] affording the corresponding complexes (*R*,*R*)-(**1**)Rh(cod)BF_4 or (*R*,*R*)-(**2**)Rh(cod)BF_4, which were characterized by NMR, ESI-MS and IR spectroscopy. Thus far it has not been possible to obtain crystals suitable for crystallographic investigations. Two different types of olefins were chosen as substrates for asymmetric

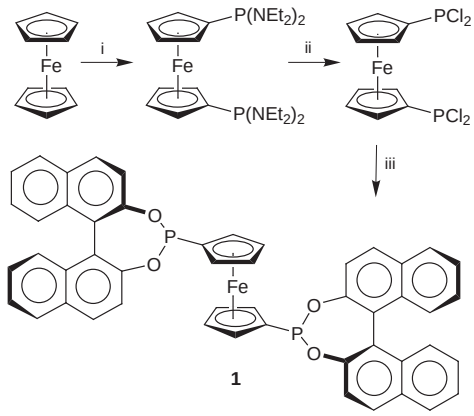

Scheme 1 *Reagents and conditions*: i (*a*) 2.2 equiv. BuLi–TMEDA, hexane, r.t., 12 h; (*b*) 2.2 equiv. $ClP(NEt_2)_2$, THF, −78 °C, 67%; ii, excess HCl, Et_2O, −78 °C, 95%; iii, 2 equiv. (*R*)-(+)-BINOL, toluene, heat, 36 h, 90%

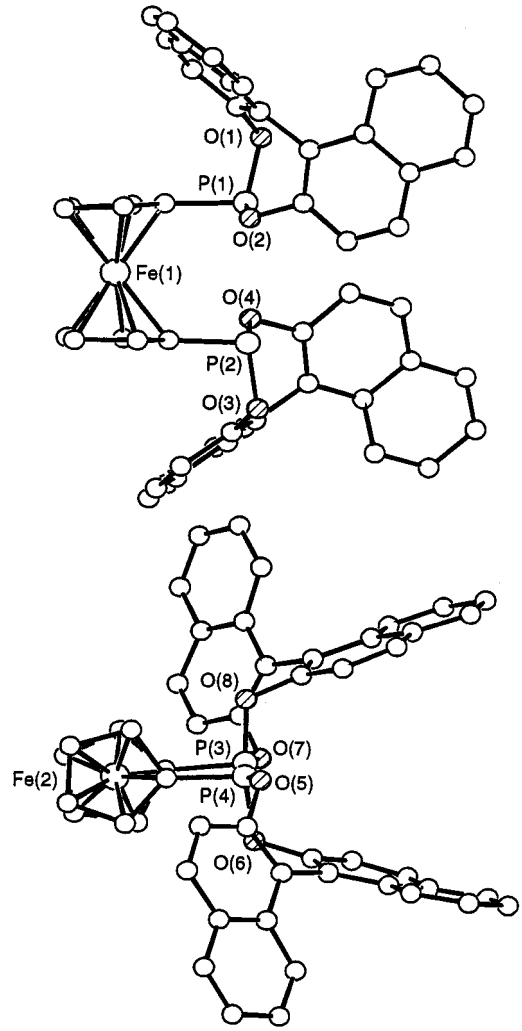

Fig. 1 Molecular structures of the two independent molecules of **1**. Side (upper structure, molecule 1) and top views (the toluene solvent of crystallization has been omitted for clarity).

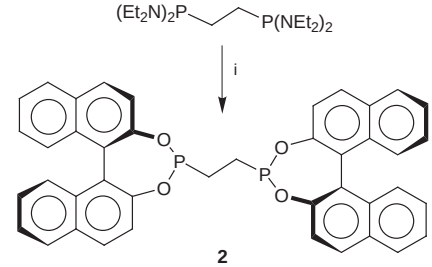

Scheme 2 *Reagents and conditions*: i, 1.95 equiv. (*R*)-(+)-BINOL, THF, heat, 48 h, (70–85%)

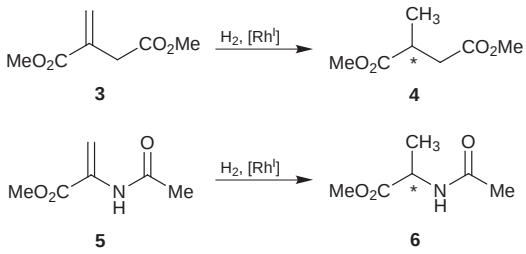

hydrogenation, namely itaconic acid dimethyl ester **3** and 2-acetamido methyl acrylate **5**, leading to the products **4** and **6**, respectively. The results of the hydrogenation experiments with formation of the *R*-configurated products **4** and **6** are remarkable in several ways (Table 1).

Table 1 Enantioselective hydrogenation of dimethyl itaconate (**3**) and 2-acetamido methyl acrylate (**5**)[a]

Entry	Ligand	Substrate	S/C[d]	Yield (%)[e]	ee (%)[e]
1	**1**	**3**	1000	100	> 99.5
2	**1**	**3**	2000	100	> 99.5
3[b]	**1**	**3**	5380	100	> 99.5
4	**2**	**3**	1000	100	97–99
5	**2**	**3**	2000	100	97–99
6[c]	**1**	**5**	1000	100	99.5
7[c]	**2**	**5**	1000	100	90

[a] Hydrogenations were carried out under the following general conditions: 1.3 bar H_2, dichloromethane, r.t., 20 h, *c*(substrate) = 0.1 mol l^{-1}, catalysts prepared *in situ* with Lig/Rh = 1.1 (4 runs each). [b] Using preformed (*R*,*R*)-(**1**)Rh(cod)BF_4. [c] Lig/Rh = 1.0. [d] Substrate to catalyst ratio. [e] Determined by GC analysis.

In the case of substrate **3** both catalysts afford essentially enantiomerically pure product **4**. However, in the hydrogenation of **5** pronounced differences in enantioselectivity were observed (Table 1). Thus, the ferrocene-based catalyst (*R*,*R*)-(**1**)Rh(cod)BF_4 leads to complete enantioselectivity for both substrates (ee > 99.5%). Although experiments directed towards elucidating mechanistic and structural aspects need to be carried out, the present study shows that catalyst (*R*,*R*)-(**1**)Rh(cod)BF_4 is not only readily accessible, but also highly effective. It remains to be seen how well ligand **1** performs in other hydrogenation reactions and in C–C bond forming processes, metals other than rhodium constituting further possibilities.

Notes and References

E-mail: reetz@scmpi-muelheim.mpg.de

‡ *Crystal data for* **1**: $C_{50}H_{32}FeO_4P_2{\cdot}C_7H_8$, M_r = 906.7, orange–brown plate, crystal size 0.08 × 0.59 × 0.66 mm, a = 9.7235(3), b = 16.5610(4), c = 27.5239(7) Å, β = 97.765(1)°, U = 4391.6(2) Å^3, T = 100 K, monoclinic, space group $P2_1$ (no. 4), Z = 4, D_c = 1.37 g cm^{-3}, μ = 0.47 mm^{-1}. Siemens SMART diffractometer, Mo-Kα X-radiation, λ = 0.71073 Å. 39615 measured reflections, analytical absorption correction (T_{min} 0.7343, T_{max} 0.9626), 15179 unique, 11532 observed [$I > 2.0\sigma(F_o^2)$]. The structure was solved by direct methods (SHELXS-97) and refined by full-matrix least-squares (SHELXL-97) on F^2 for all data (C atoms of toluene solvate, isotropic) with Chebyshev weights to R = 0.089 (obs.), wR = 0.232 (all data), absolute stereochemistry determined [Flack parameter 0.00(3)], S = 1.17, H atoms riding, max. shift/error 0.001, residual ρ_{max} = 1.039 e Å^{-3}. CCDC 182/964.

1 See for example: R. Noyori, *Asymmetric Catalysis in Organic Synthesis*, Wiley, New York, 1994, 1st edn. *Catalytic Asymmetric Synthesis*, ed. I. Ojima, VCH, New York, 1993.
2 Recent examples are: M. J. Burk, J. E. Feaster, W. A. Nugent and R. L. Harlow, *J. Am. Chem. Soc*., 1993, **115**, 10125; A. S. C. Chan, W. Hu, C.-C. Pai and C.-P. Lau, *J. Am. Chem. Soc*., 1997, **119**, 9570; P. J. Pye, K. Rossen, R. A. Reamer, N. N. Tsou, R. P. Volante and P. J. Reider, *J. Am. Chem. Soc*., 1997, **119**, 6207; G. Zhu, P. Cao, Q. Jiang and X. Zhang, *J. Am. Chem. Soc*., 1997, **119**, 1799; V. Enev, C. L. J. Ewers, M. Harre, K. Nickisch and J. T. Mohr, *J. Org. Chem*., 1997, **62**, 7092; T. V. RajanBabu, T. A. Ayers, G. A. Halliday, K. K. You and J. C. Calabrese, *J. Org. Chem*., 1997, **62**, 6012; G. Zhu and X. Zhang, *J. Org. Chem.*, 1998, **63**, 3133; F.-Y. Zhang, C.-C. Pai and A. S. C. Chan, *J. Am. Chem. Soc*., 1998, **120**, 5808; Q. Jiang, Y. Jiang, D. Xiao, P. Cao and X. Zhang, *Angew. Chem*., 1998, **110**, 1203; *Angew. Chem., Int. Ed. Engl*., 1998, **37**, 1100; H. Doucet and J. M. Brown, *Tetrahedron: Asymmetry*, 1997, **8**, 3775; C. Pasquier, S. Naili, L. Pelinski, J. Brocard, A. Mortraux and J. Agbassou, *Tetrahedron: Asymmetry*, 1998, **9** 193.
3 I. E. Nifantev, L. F. Manzhukova, M. Y. Antipin, Y. T. Struchkov and E. E. Nifant'ev, *Russ. J. Gen. Chem*., 1995, **65**, 682; recent examples of chiral monophosphinates: D. Haag, J. Runsink and H. D. Scharf, *Organometallics*, 1998, **17**, 398; J. Sakaki, W. B. Schweizer and D. Seebach, *Helv. Chim. Acta*, 1993, **76**, 2654.
4 M. T. Reetz and A. Gosberg, patent applied for 1998.
5 Enantiomerically pure (*R*)- and (*S*)-BINOL are commercially available from Kankyo Kagaku Center (Japan) at a price of about $1300 per kilo.
6 We thank A. Meiswinkel for performing some of the experiments.
7 R. R. Schrock and J. A. Osborn, *J. Am. Chem. Soc*., 1971, **93**, 2397.

Received in Cambridge, UK, 16th July 1998; 8/05524F

A well-defined metallocene catalyst supported on polystyrene beads

Anthony G. M. Barrett* and Yolanda R. de Miguel

Department of Chemistry, Imperial College of Science, Technology and Medicine, London, UK SW7 2AY

A spacer-modified polystyrene support with alcohol functionality was prepared using solid-phase organic reactions, and this resin was further derivatised to give a supported peralkylated titanocene which was active in ethylene polymerisation.

The rapid growth in combinatorial chemistry[1] has generated interest in the development of novel polymers, spacers and linkers for the adaptation of well-known solution methodologies to the solid phase. Transition metal catalysts anchored onto insoluble supports have also received much attention[2] as they are of great use in industrial scale processes, facilitating purification and catalyst recycling. So far, the use of supports for the latest generation of olefin polymerisation catalysts has mainly involved preadsorption of metallocenes on MAO-coated silica[3] or MCM-41.[4] The silica-based catalysts have been successfully used in large scale processes and the polymers obtained appear to be enlarged replicas of the original grains. However catalyst leaching can occur and neither are ideal supports for these unstable catalysts which are subject to facile deactivation. New ways to covalently attach metallocenes and to characterise the resulting complexes are needed, so that superior catalysts may be developed. The recent report by Frechet *et al.*[5] on the preparation of polyolefin spheres and related earlier studies prompts us to report our own work on supported metallocene catalysts.

The objectives of our investigations were to develop a new support **3** for solid-phase chemistry (Scheme 1) that would contain a spacer covalently attached to the resin *via* a stable C–C bond, with an alcohol end group, and to convert it into a well-defined supported titanocene **7**. Grubbs *et al.* have previously reported[6] polymer immobilised Ti-centred metallocene species, but have used these only as the basis of alkene hydrogenation catalysts.

The synthesis of the spacer unit was carried out in solution by sequential monoprotection of tetraethylene glycol (TEG) and monoalkylation with excess 1,5-dibromopentane (Scheme 1). The resulting bromide was attached onto the gel polystyrene support, by alkylation with polystyryllithium, prepared from *p*-bromopolystyrene (Fluka; 1.2–1.3 mmol g^{-1}, 100–400 mesh, 2% DVB) and *n*-butyllithium.[7] The loading level of the desired alcohol resin **3** was estimated during removal of the protecting group from **2b** using UV spectroscopy. FT-IR microspectroscopy, microanalysis and gel phase MAS NMR spectroscopy were used to fully characterise the alcohol resin product **3**.† The derivatisation of this alcohol support **3** was also studied and compared to that of some commercial supports. The nosylate derivative **4** was successfully prepared by treatment with excess 4-nitrobenzenesulfonyl chloride twice. Single bead FT-IR microspectroscopy and microanalysis (%N) were used to determine the extent of conversion. The reaction of the nosylate resin **4** with the tetraalkyl cyclopentadienyl anion was easily monitored by FT-IR and microanalysis (0%N), and gave the peralkylated cyclopentadienyl ligand **5**. The loading level of the cyclopentadienyl resin **5** was estimated by derivatisation with Cookson's reagent,[8] and %N analysis and FT-IR microspectroscopy of the resulting Diels–Alder adduct **6**.

The polymer-supported ligand **5** was converted into the titanocene complex **7** by deprotonation and reaction with cyclopentadienyltitanium trichloride. The titanium content of the beads was determined using inductively coupled plasma-atomic emission spectroscopy. The diffuse reflectance far-IR spectrum of the resin-bound catalyst **7** showed new sharp peaks in the region of 200–400 cm^{-1}, which are typical for Ti–Cl

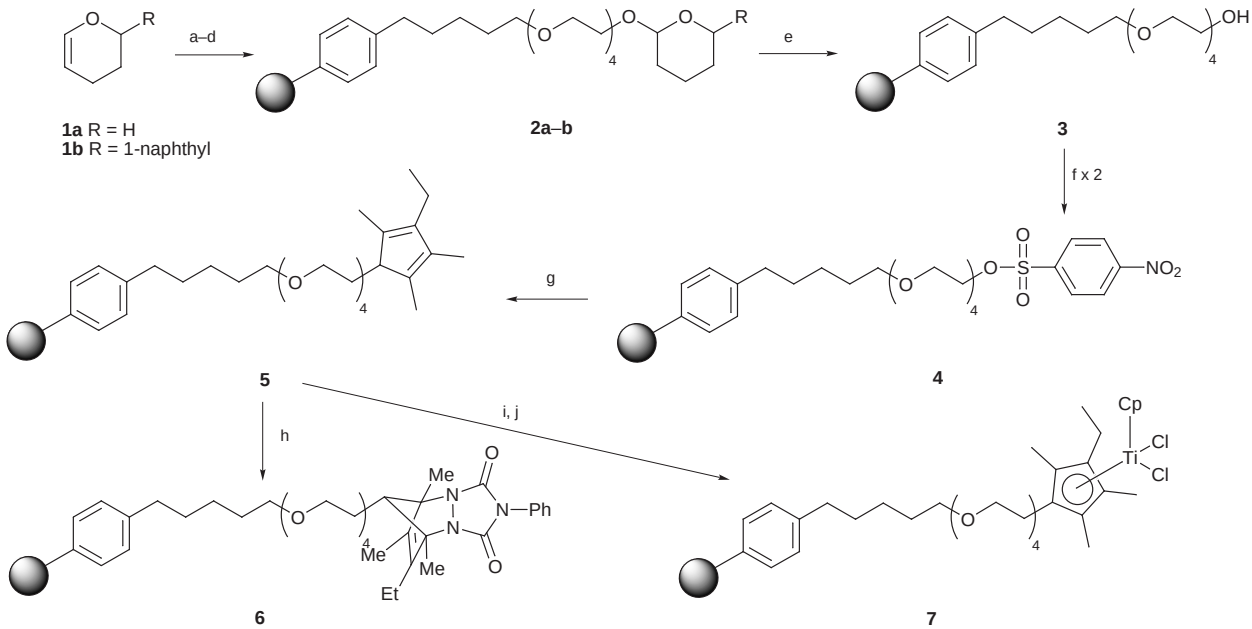

Scheme 1 *Reagents and conditions*: a, TEG, CSA, CH_2Cl_2; b, NaH, THF; c, $Br(CH_2)_5Br$; d, polystyryllithium, toluene, 65 °C, 24 h; e, CSA, THF–H_2O, Δ; f, *p*-O_2NPhSO_2Cl, pyridine, DCM; g, $NaCpMe_3Et$, THF; h, Cookson's reagent, −78 °C, CH_2Cl_2; i, MeLi, THF; j, $CpTiCl_3$, toluene

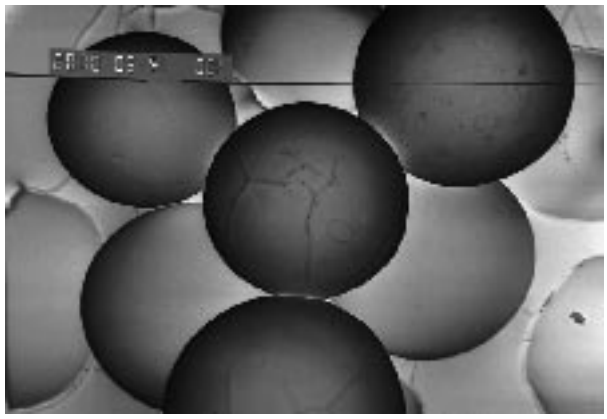

Fig. 1 SEM image of catalyst-containing beads **7**

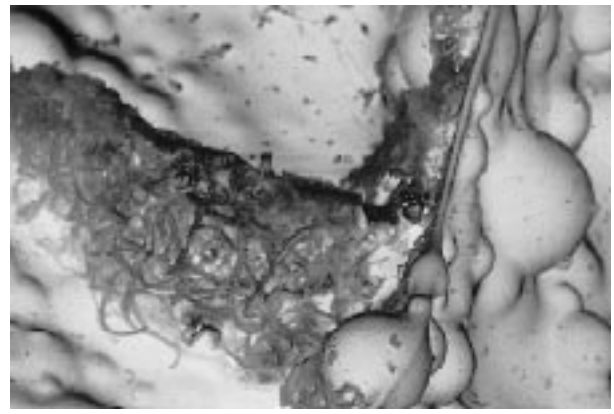

Fig. 2 SEM image of noodle-like polyethylene

stretches.[6] X-Ray photoelectron spectroscopy of a single bead gave a peak for the Ti 2p binding energy (at 457.5 eV) which is identical to that reported for other titanocene dichloride complexes.[9] This was good evidence that the structure of the species on the polymer was indeed analogous to that of the homogeneous catalyst. Scanning electron microscopy showed that the overall condition of the beads **7** (Fig. 1) was excellent. The chemical composition of the beads was also confirmed by X-EDS (X-ray energy dispersive spectroscopy) of clusters of beads. Analysis of the sample showed the presence of chlorine (Cl-Kα line = 2.6 keV) and titanium (Ti-Kα line = 4.5 keV) and the Cl : Ti ratio was roughly 2 : 1; in agreement with the catalyst structure.

This resin-bound complex **7** was tested for polymerisation activity by treatment with MAO (10^3 equiv.) and ethylene gas. The activity per bar per hour was estimated to be 41 g polyethylene per mmol catalyst, which was not as high as expected, probably due to diffusion problems into the active sites within the bead. The resulting noodle-like polyethylene chains emanating from the beads could be directly observed by scanning electron microscopy (SEM; see Fig. 2).‡ Kaminsky's work[10] on the coating of cellulose also described noodle-like morphology and it has been suggested that this only formed on very active catalytic centres. The high local activity of these centres on the polystyrene beads **7** could be due to site-isolation of the active species.

In conclusion, we have successfully prepared an active polymer-bound metallocene catalyst for olefin polymerisation. The full characterisation of this catalyst was made possible by the use of many new analytical techniques for on-the-bead characterisation as well as some novel monitoring methods for solid-phase reactions.§

We thank Professor Vernon C. Gibson and Brian Kimberley for carrying out the catalytic assay of **7** in their laboratories. We would also like to thank BP for financial support (fully-funded PhD studentship).

Note added at proof: Subsequent to the submission of this manuscript, Gibson and co-workers have reported the use of a polystyrene imidovanadium catalyst system for the polymerisation of ethylene: M. C. W. Chan, K. C. Chew, C. I. Dalby, V. C. Gibson, A. Kohlmann, I. R. Little and W. Reed, *Chem. Commun.*, 1998, 1673.

Notes and References

† Selected data for **3**: δ_C 71, υ_{max} 3300–3600 cm^{-1}, 0.5–0.8 mmol g^{-1}; for **4**: υ_{max} 1534, 1349 cm^{-1}, 0.21 mmol g^{-1}; for **5**: 0% N, 0.21 mmol g^{-1}; for **6**: υ_{max} 1718 cm^{-1}, 0.28 mmol g^{-1}; for **7**: see above, 0.07 mmol g^{-1}.
‡ GPC of the polymer was also performed (by extracting PE with trichlorobenzene at 160 °C) and showed a molecular weight peak at 734000 [M_n 358000, M_w 872000] and a polydispersity value (M_w/M_n) of 2.4. The M_n and polydispersity values were similar to those obtained from the soluble titanocene dichloride catalyst[10] [M_n 400000; M_w/M_n 2].
§ Taken from the PhD Thesis of Yolanda R. de Miguel, Imperial College, London 1997.

1 (*a*) B. J. Backes and J. A. Ellman, *Curr. Opin. Chem. Biol.*, 1997, **1**, 86; (*b*) P. H. H. Hermkens, H. C. J. Ottenheijm and D. C. Rees, *Tetrahedron*, 1997, **53**, 5643; (*c*) K. S. Lam, M. Lebl and V. Krchnak, *Chem. Rev.*, 1997, **97**, 411.
2 C. U. Pittman, in *Polymer-Supported Reactions in Organic Synthesis*, ed. P. Hodge and D. C. Sherrington, Wiley, New York, 1980, p. 249.
3 F. Ciardelli, A. Altomare and G. Conti, *Macromol. Symp.*, 1994, **80**, 29.
4 L. K. Van Looveren, D. F. Geysen, K. A. Vercruysse, B. H. Wouters, P. J. Grobet and P. A. Jacobs, *Angew. Chem.*, 1998, **37**, 517.
5 S. B. Roscoe, J. M. J. Frechet, J. F. Walzer and A. J. Dias, *Science*, 1998, **280**, 270; H. Nishida, T. Uozami, T. Arai and K. Soga, *Macromol. Rapid. Commun.*, 1995, **16**, 821.
6 E. S. Chandresakaran, R. H. Grubbs and C. H. Brubaker, Jr., *J. Organomet. Chem.*, 1976, **120**, 49.
7 M. J. Farrall and J. M. J. Frechet, *J. Org. Chem.*, 1976, **41**, 3877.
8 W. Werinckx, P. J. De Clerq, C. Couwenhoven, W. R. M. Overbeek and S. J. Halkes, *Tetrahedron*, 1991, **47**, 9419.
9 J. Cermak, M. Kvicalova, V. Bletcha, M. Capka and Z. Bastl, *J. Organomet. Chem.*, 1996, **509**, 77.
10 W. Kaminsky, *Macromol. Chem. Phys.*, 1996, **197**, 3907.

Received in Liverpool, UK, 30th June 1998; 8/05014G

Electrogenerated poly(thiophenes) with extremely narrow bandgap and high stability under n-doping cycling

Said Akoudad and Jean Roncali*†

Ingénierie Moléculaire et Matériaux Organiques, CNRS UMR 6501, Université d'Angers, 2 Bd Lavoisier, 49045 Angers Cedex, France

The synthesis of a poly(thiophene) polymer with an extremely narrow bandgap is described.

The synthesis of narrow bandgap (E_g) conjugated polymers[1] has been a focus of considerable interest, motivated by their high visible transparency, their ability to be p- and n-doped, allowing their use in electrolytic supercapacitors[2] or dual polymer electrochromic devices,[3] and by the ultimate aim of synthesizing zero bandgap polymers with metallic conduction.

Various routes have been developed to synthesize low bandgap polymers with increased quinoid character in the conjugated backbone,[4] alternating electron-releasing and electron-withdrawing groups[5] or covalent rigidification of the conjugated backbone.[6] Based on a combination of the two first strategies, Yamashita *et al*. have synthesized polymers with the smallest bandgaps known to date ($E_g \approx 0.50$ eV) by electropolymerization of precursors based on three-ring systems with a median pro-quinoid acceptor such as thieno[3,4-*b*]pyrazine (TP) or benzo[1,2-*c*:4,5-*c*′]bis[1,2,5]thiadiazole and two external thiophene or pyrrole rings.[7]

We report here preliminary results on a new electrogenerated small bandgap polymer derived from a bithiophenic precursor involving 3,4-ethylenedioxythiophene (EDOT) and TP. This precursor structure combines the superior polymerizability of bithiophenic structures over more conjugated ones,[8] the solubility imparted by dihexyl chains on the TP system,[9] the high HOMO level of EDOT and the well-known stability of its polymers,[10] and the possibility of achieving an alternating sequence of EDOT and TP units in the polymer.

The synthesis of **1** is depicted in Scheme 1. A Stille coupling between 2,5-dibromo-3,4-dinitrothiophene **5**[11] and 2-tributylstannyl-3,4-ethylenedioxythiophene **4** gave the bromodinitro compound **3** in 17% yield. Reduction of **3** with concomittant dehalogenation using $SnCl_2$ in HCl afforded diamine **2** (33% yield) which was then condensed with tetradecane-7,8-dione to give the target compound **1** in 57% yield.‡

Compound **1** has its absorption maximum at $\lambda_{max} = 456$ nm; the 237 nm red shift compared to the EDOT dimer[12] underlines the effect of the TP moiety on the HOMO–LUMO gap of the molecule.

The cyclic voltammogram of **1** shows an anodic peak potential at 0.72 V. This low oxidation potential results from the incorporation of EDOT in the structure. Consequently electropolymerization can be readily achieved at unusually low applied potential, under either potentiostatic or potentiodynamic conditions. Another interesting point is the very low substrate concentration needed for electropolymerization. Thus; application of recurrent potential scans between −0.50 and +0.60 V to a 5×10^{-4} M solution of **1** in MeCN leads to rapid growth of a new redox system centered at −0.10 V (Fig. 1). The CV of the polymer in a monomer-free electrolytic medium shows a redox system corresponding to the doping process with anodic and cathodic peak potentials at 0.10 and −0.16 V. These values lead to a redox potential *ca*. 0.60 V lower than that of the parent polymer derived from a thiophene–TP–thiophene precursor.[7b] The n-doping system shows cathodic and anodic peaks at −1.12 and −1.30 V (Fig. 1). The potential difference between the onset for oxidation and reduction leads to an estimated bandgap of *ca*. 0.50–0.60 V.

Preliminary stability tests under redox cycling in an oxygen-free medium shows that poly(**1**) retains 80% of its electroactivity after 1000 reduction cycles between −0.20 and −1.50 V at a scan rate of 500 mV s^{-1}, or after 250 full cycles of both oxidation and reduction at 100 mV s^{-1} between +0.60 and −1.50 V. These results contrast with the limited cyclability generally observed for small bandgap polymers.[7a,13]

Electrodeposition of poly(**1**) on indium-tin oxide (ITO) coated glass electrodes gave free-standing films which were

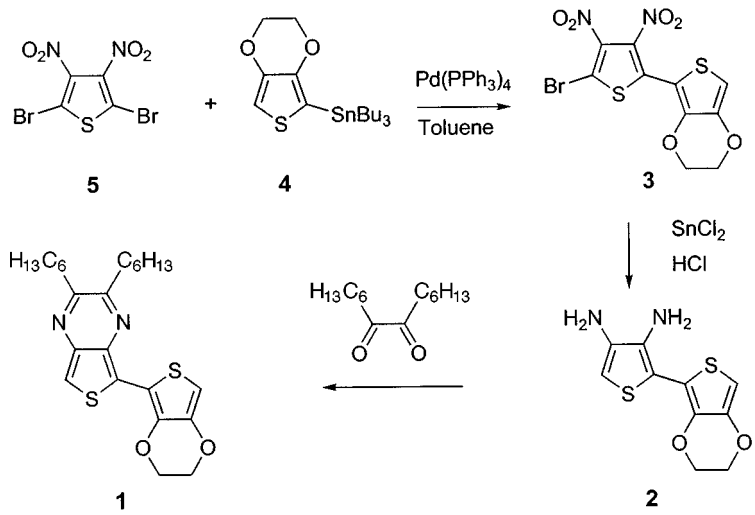

Scheme 1

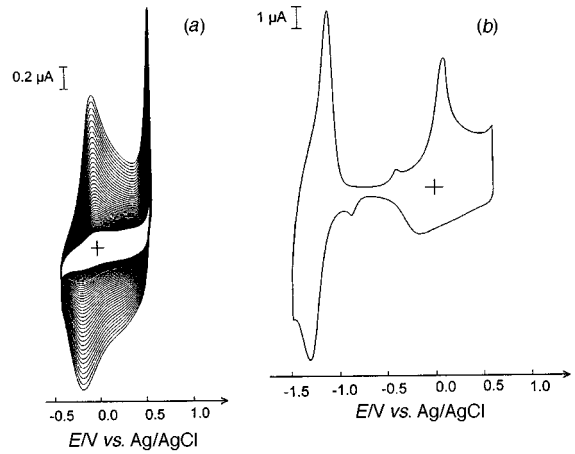

Fig. 1 (*a*) Potentiodynamic electropolymerization of **1** on Pt, t × 10^{-4} M substrate in 0.10 M Bu_4NPF_6–MeCN, scan rate 100 mV s^{-1}. (*b*) Cyclic voltammogram of poly(**1**) in 0.10 M Bu_4NPF_6–MeCN, Pt electrodes, scan rate 100 mV s^{-1}.

submitted to electrochemical reduction followed by immersion in aqueous ammonia over two days. The optical spectrum of neutral poly(**1**) on ITO shows a single absorption band with a maximum at 0.86 eV (1430 nm) and a weak shoulder at *ca*. 1.25 eV (Fig. 2). Unlike the spectra of most of the known small bandgap polymers, this spectrum exhibits a small width at half maximum of the absorption band (0.72 eV) and low absorbance in the whole visible range. These characteristics are consistent with a well-defined polymer structure with a narrow distribution of conjugated chain lengths. Extrapolation to the baseline of the low energy absorption edge crosses the ITO absorption wall and leads to an optical bandgap of 0.36 eV, which is to the best of our knowledge the lowest ever reported for a conjugated polymer. Poly(**1**) shows negligible solubility in CH_2Cl_2 and in hot chlorobenzene it is limited to a few percent. The resulting

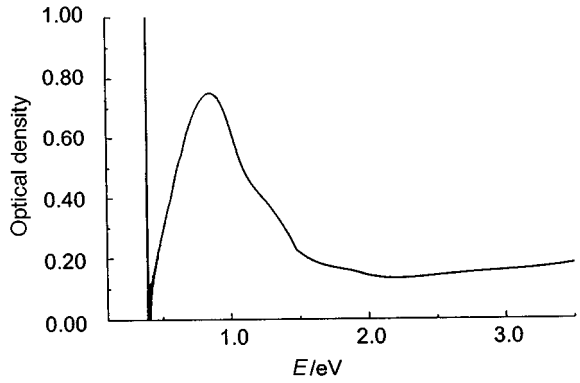

Fig. 2 Optical spectrum of neutral poly(**1**) on ITO (the straight line at 0.40 eV is due to ITO absorption)

solutions show λ_{max} at 800 and 1000 nm, respectively. While this limited solubility might be due to insufficient length in the alkyl substituents, the expected rigid quinonoid structure of the neutral polymer[14] probably contributes to limit the solubility. The improvement of solubility by attachment of longer alkyl chains on both components is presently under investigation.

To summarize, we have shown that a dimeric precursor combining dihexyl-TP and EDOT allows the efficient electrosynthesis of a well-defined polymer with extremely narrow bandgap and excellent stability under n-doping redox cycling. These attractive properties make poly(**1**) an interesting electrode material for various applications, in particular in electrolytic supercapacitors, and work in this direction is now underway.

Notes and References

† E-mail: jean.roncali@univ-angers.fr

‡ *Selected data* for **1**: Brown solid, mp 119 °C; δ_H ($CDCl_3$) 7.57 (1s, 1H), 6.42 (1s, 1H), 4.44 (t, 2H), 4.31 (t, 1H), 2.93 (t, 4H), 2.87 (t, 2H), 1.99 (q, 2H), 1.77 (q, 2H), 1.5–1.2 (m, 12H), 0.9 (m, 6H); δ_C ($CDCl_3$) 156.8, 154.7, 141.3, 141.2, 138.2, 136.8, 125.3, 111.5, 111.3, 100.5, 65.4, 64.7, 35.7, 35.0, 31.9, 31.7, 29.5, 29.2, 28.2, 26.9, 22.7, 22.6, 14.2, 14.1; *m/z* (EI) 444 (M^+ 100%), [found (calc.): C, 64.40 (64.63); H, 7.29 (7.25); N, 6.05 (6.30); S, 14.25 (14.42)].

1 J. Roncali, *Chem. Rev.*, 1997, **97**, 173.
2 A. Rudge, J. Davey, I. Raistrick, S. Gottesfeld and J. P. Ferraris, *J. Power Sources*, 1994, **47**, 89; C. Arbizzani, M. Catellani, M. Mastragostino and C. Mingazzini, *Electrochim. Acta*, 1995, **40**, 1871.
3 S. A. Sapp, G. A. Sotzing, J. L. Reddinger and J. R. Reynolds, *Adv. Mater.*, 1996, **8**, 208.
4 F. Wudl, M. Kobayashi and A. J. Heeger, *J. Org. Chem.*, 1984, **49**, 3382; S. A. Jenekhe, *Nature*, 1986, **322**, 345.
5 J. P. Ferraris and T. L. Lambert, *J. Chem. Soc., Chem. Commun.*, 1991, 1268; E. E.Havinga, W. ten Hoeve and H. Wynberg, *Synth. Met.*, 1993, **55**–**57**, 299; H. A. Ho, H. Brisset, P. Frère and J. Roncali, *J. Chem. Soc., Chem. Commun.*, 1995, 2309.
6 J. Roncali, C. Thobie-Gautier, E. Elandaloussi and P. Frère, *J. Chem. Soc., Chem. Commun.*, 1994, 2249; H. Brisset, P. Blanchard, B. Illien, A. Riou and J. Roncali, *Chem. Commun.*, 1997, 569.
7 (*a*) S. Tanaka and Y. Yamashita, *Synth. Met.*, 1995, **69**, 599; (*b*) S. Tanaka and Y. Yamashita, *Chem. Mater.*, 1996, **8**, 570.
8 P. Bäuerle and S. Scheib, *Adv. Mater*, 1993, **5**, 848; L. Huchet, S. Akoudad and J. Roncali, *Adv. Mater.*, 1998, **10**, 541.
9 M. Pomerantz, B. Chalonger-Gill, L. O. Harding, J. J. Tseng and W. Pomerantz, *J. Chem. Soc., Chem. Commun.*, 1992, 1672.
10 F. Jonas and L. Schrader, *Synth. Met.*, 1991, **41**–**43**, 831; G. Heywang and F. Jonas, *Adv. Mater.*, 1992, **4**, 116.
11 R. Mozingo, S. A. Harris, D. E. Wolf, C. E. Hoffhine, Jr., N. R. Easton and K. Folkers, *J. Am. Chem. Soc.*, 1945, **67**, 2092.
12 S. Akoudad and J. Roncali, *Synth. Met.*, 1998, **93**, 111.
13 M. Kobayashi, N. Colaneri, M. Boysel, F. Wudl and A. J. Heeger, *J. Chem. Phys.*, 1985, **82**, 5717.
14 J. Kastner, H. Kuzmany, D. Vegh, M. Landl, L. Cuff and M. Kertesz, *Macromolecules*, 1995, **28**, 2922; L. Cuff and M. Kertesz, *J. Chem. Phys.*, 1997, **106**, 5541.

Received in Cambridge, UK, 30th June 1998; 8/04992K

A novel polynuclear palladium(II) complex with asymmetric coordination of palladium atoms

Rong Cao,*[a] Weiping Su,[a] Maochun Hong,*[a] Wenjian Zhang,[a] Wing-Tak Wong[b] and Jiaxi Lu[a]

[a] *State Key Laboratory of Structural Chemistry, Fujian Institute of Research on the Structure of Matter, Fuzhou, Fujian 350002, PR China. E-mail hmc@ms.fjirsm.ac.cn or rcao@ms.fjirsm.ac.cn*

[b] *Department of Chemistry, The University of Hong Kong, Pokfulan Road, Hong Kong*

The oxidation of $[Pd_2(dppm)_2Cl_2]$ with selenium in the presence of $NaSCH_2Ph$ in DMF gives rise to a novel polynuclear complex $[Pd_4(\mu_3\text{-}Se)_2(\mu\text{-}SCH_2Ph)_2(\mu\text{-}dppm)_2Cl_2]$; a single crystal X-ray diffraction analysis shows that all the palladium atoms in the compound are tetra-coordinated with distorted square-planar geometry, of which two are asymmetrically coordinated with selenium, sulfur, chlorine, and phosphorus atoms.

Bis(diphenylphosphine)methane (dppm), as a constraining ligand, prefers to lock together two metal atoms in close proximity and favors unusual oxidation states; thus, most palladium complexes containing dppm are binuclear complexes doubly bridged by dppm and related ligands, such as $[Pd_2(\mu\text{-}dppm)_2X_2]$ (X = halogen, **1**),[1–4] and the oxidation state of palladium is mainly +1. Many studies have been carried out on the insertion of small molecules, such as CO, SO_2, RCN *etc*., into the Pd–Pd bond in **1** to yield the so-called A-frame complexes with the maintenance of the oxidation state of palladium.[5] Studies on the insertion of an S or Se bridge into **1** to give rise to complexes $[Pd_2(\mu\text{-}E)(\mu\text{-}dppm)_2X_2]$ (E = S, Se; X = halogen) with a change of the oxidation state of palladium from +1 to +2 have also been reported,[6] whilst reports on the palladium complexes with mixed thiolate and diphosphine ligands, especially those having a palladium formal oxidation state of +2 and containing both dppm and thiolate ligands, are very scare. Very recently, Usón and co-workers have characterised octanuclear $\{[Pd(\mu\text{-}SC_6F_5)(\mu\text{-}dppm)Pd](\mu\text{-}SC_6F_5)\}_4$, in which the oxidation state of palladium remains +1.[7] We have been interested in the chemistry of metal–thiolate–diphosphine complexes and a series of complexes, such as $[Co\{Ph_2P(CH_2)_3PPh_2\}(SPh)_2]$,[8a] $[Co_2(SPh)_4(dppx)]$,[8b,c] and $[Pd(SR)_2(dppx)]$ [dppx = $Ph_2PCH_2PPh_2$, $Ph_2P(CH_2)_2PPh_2$][9] have been isolated. Herein we report the synthesis, crystal structure, and properties of a novel tetranuclear palladium(II) complex with asymmetric coordination of palladium atoms, $[Pd_4(\mu_3\text{-}Se)_2(\mu\text{-}SCH_2Ph)_2(\mu\text{-}dppm)_2Cl_2]\cdot 2DMF$ **2**.

In DMF solution, $[Pd_2(dppm)_2Cl_2]$ was reacted with Se and $NaSCH_2Ph$ giving rise to **2**.† In this reaction, Pd(I) was oxidised to Pd(II) and an Se atom was inserted into the binuclear complex to form the A-frame complex $[Pd_2(dppm)_2Cl_2(\mu\text{-}Se)]$; one of the dppm ligands in the A-frame complex was oxidised to dppmSe by excess Se and was cleaved in the presence of $NaSCH_2Ph$, one of the Cl^- ligands was removed and the A-frame complex was then condensed into the tetranuclear complex **2** through forming μ_3-Se and μ-SCH_2Ph.

$$[Pd_2(dppm)_2Cl_2] \xrightarrow{Se} [Pd_2Se(dppm)_2Cl_2] \xrightarrow[NaSCH_2Ph]{Se} [Pd_4Se_2(SCH_2Ph)_2(dppm)_2Cl_2] + dppmSe + NaCl$$

A crystallographic analysis‡ reveals that the complex is a tetranuclear neutral complex. As shown in Fig. 1, two kinds of palladium environments are present: two of the four palladium atoms are each surrounded by two selenium, one sulfur, and one phosphorus atom forming a distorted square-planar arrangement; the other two are each asymmetrically surrounded by one selenium, one phosphorus, one sulfur, and one chlorine atoms in a highly distorted square-planar arrangement. The sulfur atom of each thiolate ligand is shared by two Pd atoms forming a μ-bridge, while each selenium acts as μ_3-bridge linking three palladium centres. The four palladiums form a zigzag chain with a Pd–Pd distance of 3.191(3) Å, much longer than that in $Pd_2(SCH_2CH_2S)_2(PPh_3)_2$ [3.038(2) Å],[10a] but shorter than that

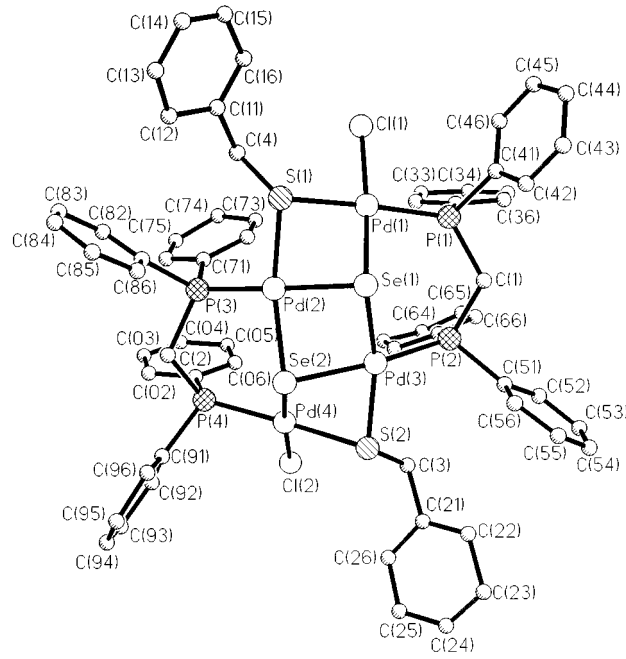

Fig. 1 Molecular structure of $[Pd_4(\mu_3\text{-}Se)_2(\mu\text{-}SCH_2Ph)_2(\mu\text{-}dppm)_2Cl_2]\cdot 2DMF$ with solvent molecules and H atoms omitted. Selected bond lengths (Å) and bond angles (°): Pd(1)–Pd(2), 3.181(3), Pd(2)–Pd(3) 3.228(3), Pd(3)–Pd(4) 3.166(3), Pd(1)–Se(1) 2.387(3), Pd(1)–Cl(1) 2.339(7), Pd(1)–P(1) 2.261(7), Pd(1)–S(1) 2.374(6), Pd(2)–Se(1) 2.432(4), Pd(2)–Se(2) 2.397(3) Pd(2)–P(3) 2.263(7), Pd(2)–S(1) 2.331(6), Pd(3)–Se(1) 2.383(4), Pd(3)–Se(2) 2.446(3), Pd(3)–P(2) 2.262(6), Pd(3)–S(2) 2.326(7) Pd(4)–Se(2) 2.393(4), Pd(4)–Cl(2) 2.345(8), Pd(4)–P(4) 2.264(7), Pd(4)–S(2) 2.381(8); Pd(1)–Pd(2)–Pd(3) 77.9(1), Pd(2)–Pd(3)–Pd(4) 77.0(1), Se(1)–Pd(1)–Cl(1) 173.1(2), Se(1)–Pd(1)–P(1) 94.7(2), Cl(1)–Pd(1)–P(1) 91.1(2), Se(1)–Pd(1)–S(1) 79.5(2), Cl(1)–Pd(1)–S(1) 94.5(2), P(1)–Pd(1)–S(1) 173.3(2), Se(1)–Pd(2)–Se(2) 83.7(1), Se(1)–Pd(2)–P(3) 171.7(2), Se(2)–Pd(2)–P(3) 97.8(2), Se(1)–Pd(2)–S(1) 79.4(2), Se(2)–Pd(2)–S(1) 157.4(2), P(3)–Pd(2)–S(1) 101.1(2), Se(1)–Pd(3)–Se(2) 83.7(1), Se(1)–Pd(3)–P(2) 96.8(2), Se(2)–Pd(3)–P(2) 169.6(2), Se(1)–Pd(3)–S(2) 159.1(2), Se(2)–Pd(3)–S(2) 79.8(2), P(2)–Pd(3)–S(2) 101.7(2), Se(2)–Pd(4)–Cl(2) 174.6(2), Se(2)–Pd(4)–P(4) 95.5(2), Cl(2)–Pd(4)–P(4) 89.4(3), Se(2)–Pd(4)–S(2) 79.8(2), Cl(2)–Pd(4)–S(2) 95.2(3), P(4)–Pd(4)–S(2) 173.8(2), Pd(1)–Se(1)–Pd(2) 82.6(1), Pd(1)–Se(1)–Pd(3) 115.2(1), Pd(2)–Se(1)–Pd(3) 84.2(1), Pd(2)–Se(2)–Pd(3) 83.6(1), Pd(2)–Se(2)–Pd(4) 112.5(1) Pd(3)–Se(2)–Pd(4) 81.7(1), Pd(1)–S(1)–Pd(2) 85.1(2), Pd(3)–S(2)–Pd(4) 84.5(2).

in $Pt_2\{SCH_2CH_2C(CH_3)=CH_2\}_2(PPh_3)_2I_2$ [3.539(1) Å].[11] The average Pd–S–Pd angle [98.6(2)°] is much more obtuse than that in $Pd_2(SCH_2CH_2S)_2(PPh_3)_2$ [80.63(6)°][10*a*] and the average Ni–S–Ni angles in $Ni_2(SCH_2CH_2S)_2(PPh_3)_2$ (82.41°)[10*b*] and $Ni_2\{SCH(CH_3)CH_2S\}_2(PPh_3)_2$ (81.11°).[10*c*] The average Pd–P bond length of 2.291(6) Å is similar to those reported in the Pd–S–P complexes.

^{31}P NMR spectra of the complex show two peaks at 18.595 and 14.493 ppm. It is clear that the P nucleus is deshielded to downfield, indicating that the electrons are transferred from phosphorus atoms to the metal atoms to cause the P nucleus to be deshielded to downfield and the chemical shifts increased.

The authors acknowledge the National Natural Science Foundation of China, the Natural Science Foundation of Fujian Province and the Youth Fund of Chinese Academy of Sciences for financial support.

Notes and References

† *Synthesis* of $[Pd_4(\mu_3\text{-}Se)_2(\mu\text{-}SCH_2Ph)_2(\mu\text{-}dppm)_2Cl_2]\cdot 2DMF$: $NaSCH_2Ph$ (0.42 g, 3 mmol) and selenium powder were dissolved in 15 cm^3 of DMF and the solution was stirred for 12 h. A suspension of $[Pd_2(dppm)_2Cl_2]$ (1.52 g, 6 mmol) in 15 ml of DMF was then added to the solution which turned gradually red-brown with a small amount of black precipitate. The final reaction solution was filtered and the dark-red filtrate was kept at 4 °C. After two weeks, red plate crystals of **2** were collected and washed with distilled water and acetone(yield 22%). Found: C, 45.90; H, 4.12; N, 1.58. Calc. for $C_{70}H_{72}N_2O_2P_4S_2Cl_2Se_2Pd_4$: C, 46.30; H, 4.00; N, 1.54%. IR(KBr): 445(m), 426(m), 375(w), 340(w), 318(w), 300(w), 270(w) cm^{-1}.

‡ *Crystallographic data:* crystal dimensions: 0.25 × 0.30 × 0.30 mm, $C_{70}H_{72}N_2O_2P_4S_2Cl_2Se_2Pd_4$, M = 1815.7, space group $P\bar{1}$ (no. 2), a = 11.203(2), b = 14.928(2), c = 22.354(3) Å, α = 82.27(2), β = 86.86(2), γ = 74.62(2)°, V = 3890(1) $Å^3$, μ = 2.091 mm^{-1}, Z = 2, $R(R_w)$ = 0.086(0.097). Cell dimension measurements and data collections were performed on a Siemens Smart CCD diffractometer with graphite-monochromated Mo-Kα radiation at 23 ± 1 °C. Intensity data were obtained in the range $3.0 \leqslant 2\theta \leqslant 50.0°$ by using the ω scan technique. The data reductions were performed on a Silicon Graphics computer station with Smart CCD software. For the structural analyses, all calculations were performed on an HP/586 computer using SHELXL-PC. The positions of all the palladium, selenium, sulfur, and phosphorus atoms were determined by direct methods, and successive difference electron density maps located the remaining non-hydrogen atoms. All non-hydrogen atoms were refined anisotropically. The positions of all hydrogen atoms were generated geometrically (C–H bond fixed at 0.96 Å), assigned isotropic thermal parameters, and allowed to ride on their respective parent C atoms before the final cycle of least-squares refinement. One phenyl ring exhibiting disorder was fixed as an idealized rigid group. The final anisotropic refinement of all non-hydrogen atoms on F_o for 5438 observations [$F \geqslant 4.0\sigma(F)$] and 593 variables led to convergence. CCDC 182/985.

1 (*a*) M. J. H. Russel and C. F. J. Barnard, *Comprehensive Coordination Chemistry*, ed. G. Wilkinson, R. D. Gillard and J. A. McCleverty, Pergamon, Oxford, 1987, vol. 5, p. 1103; (*b*) A. L. Balch, *Reactivity of Metal–Metal Bonds*, ed. M. H. Chisholm, *ACS Symp. Ser.*, 1981, **155**, 167.
2 (*a*) R. J. Puddephatt, *Chem. Soc. Rev.*, 1983, **12**, 99; (*b*) R. Poilblanc, *Coord. Chem. Rev.*, 1988, **86**, 191.
3 A. L. Balch, in *Homogeneous Catalysis with Metal Phosphine Complexes*, ed. L. H. Pignolet, Plenum, New York, 1983, p. 167.
4 P. M. Maitlis, P. Espinet and M. J. H. Russel, *Comprehensive Organometallic Chemistry*, ed. G. Wilkinson, F. G. A. Stone and E. W. Abel, Pergamon, Oxford, 1982, vol. 6, p. 265.
5 (*a*) P. Braunstein, J.-M. Jud, Y. Dusausou and J. Fisher, *Organometallics*, 1983, **2**, 180; (*b*) P. Braunstein, J.-M. Jud, Y. Dusausou and J. Fisher, *J. Chem. Soc., Chem. Commun*., 1983, 5; (*c*) M. C. Grossel, R. P. Moulding and K. R. Seddon, *J. Organomet. Chem.*, 1983, **253**, C52; (*d*) P. Braunstein, C. de Meric de Bellefon and M. Ries, *ibid*., 1984, **262**, C14; (*e*) P. Braunstein, J. Kervennal and J.-L. Richert, *Angew. Chem., Int. Ed. Engl*., 1985, **24**, 768.
6 (*a*) A. L. Balch, L. S. Benner and M. M. Olmstead, *Inorg. Chem*., 1979, **18**, 2996; (*b*) G. Besenyei, C. L. Lee, J. Gulinski, S. J. Retting, B. R. James, D. A. Nelson and M. A. Lilga, *ibid*., 1987, **26**, 3622; (*d*) G. Besenyei, L. Pàrkànyi, L. I. Simàndi and B. R. James, *ibid*., 1995, **34**, 6118.
7 (*a*) R. Usón, J. Forniés, L. R. Falvello, I. Usón and S. Herrero, *Inorg. Chem.*, 1993, **32**, 1066; (*b*) R. Usón, J. Forniés, S. Fernandez, M. A. Usón, I. Usón and S. Herrero, *Inorg. Chem.*, 1997, **36**, 1912.
8 (*a*) G. W. Wei, M. C. Hong, Z. Y. Huang and H. Q. Liu, *J. Chem. Soc., Dalton Trans.*, 1991, 3145; (*b*) G. W. Wei, H. Q. Liu, Z. Y. Huang, M. C. Hong, L. R. Huang and B. S. Kang, *Polyhedron*, 1991, **10**, 553; (*c*) G. W. Wei, H. Q. Liu, Z. Y. Huang, L. R. Huang and B. S. Kang, *J. Chem. Soc., Chem. Commun.*, 1989, 1839.
9 (*a*) W. P. Su, M. C. Hong, Z. Y. Zhou, F. Xue, H. Q. Liu and T. C. W. Mak, *Acta Crystallogr., Sect. C*, 1996, **52**, 2691; (*b*) W. P. Su, M. C. Hong, R. Cao and H. Q. Liu, *Acta Crystallogr., Sect. C*, 1997, **53**, 66; (*c*) W. P. Su, R. Cao, M. C. Hong, Z. Y. Zhou, F. Xue, H. Q. Liu and T. C. W. Mak, *Polyhedron*, 1997, **16**, 2531.
10 (*a*) R. Cao, M. C. Hong, F. L. Jiang and H. Q. Liu, *Acta Crystallogr., Sect. C*, 1995, **51**, 1280; (*b*) R. Cao, Z. Y. Huang, X. J. Lei, M. C. Hong and H. Q. Liu, *Chin. J. Chem.*, 1992, **10**, 227; (*c*) R. Cao, Z. Y. Huang, X. J. Lei, M. C. Hong and H.Q. Liu, *Acta Crystallogr., Sect. C*, 1992, **48**, 1654.
11 E. W. Abel, D. E. Evans, J. R. Koe, M. B. Hursthouse, M. Mazid, M. F. Mahon and K. C. Molloy, *J. Chem. Soc., Dalton Trans.*, 1990, 1697.

Received in Cambridge, UK, 28th July 1998; 8/05899G

Octakis[4-(2-phenylpropan-2-yl)phenylthio]naphthalene: a conformationally unique host allowing direct observation of a well-defined solid-state acetone conformation

Gary A. Downing,[a] Christopher S. Frampton[b] and David D. MacNicol*[a]†

[a] *Department of Chemistry, University of Glasgow, Glasgow, UK G12 8QQ*
[b] *Roche Discovery Welwyn, Broadwater Road, Welwyn Garden City, Herefordshire, UK AL7 3AY*

In its stoichiometric 1:1 clathrate with acetone, studied by X-ray diffraction at 123 K, the title host molecule possesses a unique abbbabbb conformation with six side-chain units anti-parallel to the other two; the guest acetone's conformation exhibits non-crystallographic C_2 symmetry, and the observed lowering in symmetry from C_{2v} in the vapour is accompanied by a significant opening of the guest's C–C–C angle, in accord with a key theoretical prediction in the literature (*J. Chem. Phys.*, 1993, 98, 2754).

In the design of new spider host molecules, suitably per-substituted naphthalenes, a challenging goal is to establish the precise way in which the structure of the side-chain unit of a given host controls its ability to form crystalline inclusion compounds.[1] For this host series we have stressed the critical role of the host's molecule conformation; this is well illustrated in the case of octakis(3,4-dimethylphenylthio)naphthalene which, in the course of its self-assembly to form nano-scale cavities capable of trapping diverse guest species,[2] adopts an exactly D_2-symmetric **aabbaabb** conformation, (**a** and **b** denoting side-chain units projecting, respectively, above and below the aromatic core). We now report the synthesis of the new spider host octakis[4-(2-phenylpropan-2-yl)phenylthio]-napthalene **1**, possessing a more extended side-chain unit,

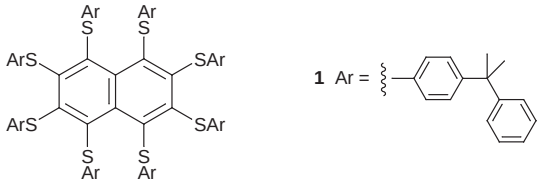

which was initially characterised by ^{1}H NMR, ^{13}C NMR and microanalytical data.‡ The new host **1**, contrasting with the broad inclusion spectrum found for its above-mentioned counterpart, appears to be specific[3] to acetone alone, suggesting the efficiency with which this guest is embedded in the host lattice of **1**. A strictly 1:1 crystalline inclusion compound was formed on recrystallisation of unsolvated **1** from neat acetone.

A low-temperature (123 K) X-ray diffraction analysis was undertaken to determine the host conformation, the conformation of the acetone guest, and the nature of host–guest interactions in this unique adduct of **1**. The 1:1 acetone adduct of **1** is triclinic, space group *P*1, with two host and two acetone guest molecules per unit cell.§ The striking host conformation of **1**, illustrated in Fig. 1(*b*) (the enantiomeric form is also present in the centrosymmetric crystal), is of the previously unknown **abbbabbb** type, with six of the eight side chain units projecting in the opposite direction to the other two. The conformation is close to C_2-symmetric, with the non-crystallographic two-fold axis running normal to the mean plane of the naphthalene core, and bisecting its central carbon–carbon bond. The naphthalene core is markedly non-planar, but almost exactly C_2 in character; corresponding displacements form the ten-carbon mean plane are C(1), C(5), −0.22, −0.23; C(2), C(6), −0.25, −0.25; C(3), C(7), 0.07, 0.08; C(4), C(8), 0.31,

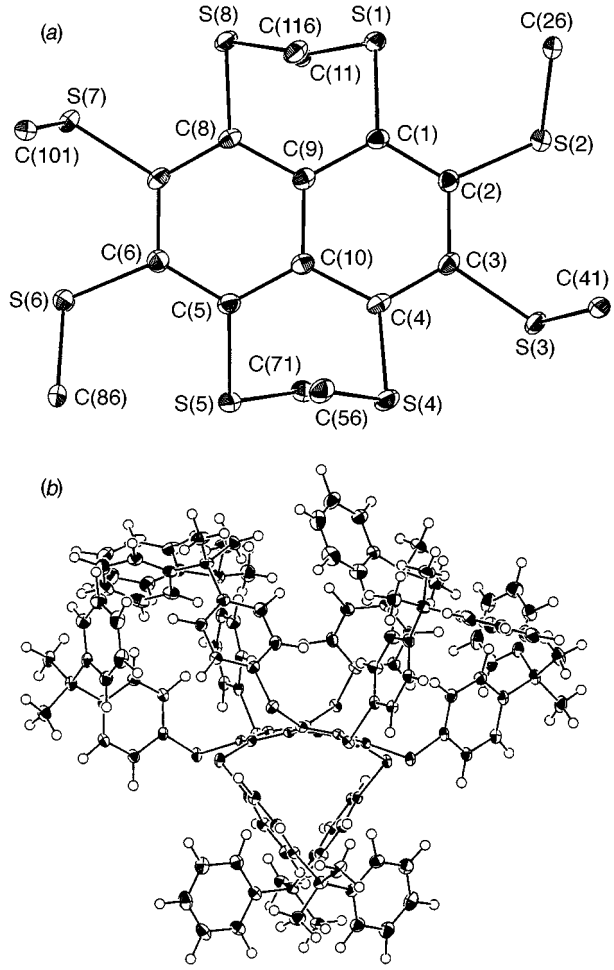

Fig. 1 (*a*) Atomic numbering scheme for the central region of **1** in its acetone clathrate; (*b*) a view illustrating the structure and conformation of the host molecule **1** in its 1 : 1 triclinic adduct with acetone. The host molecule's non-crystallographic C_2 axis is vertical in this view. The distribution of bond lengths (Å) about the naphthalene core is: C(1)–C(2), 1.386(3); C(3)–C(4), 1.386(3); C(5)–C(6), 1.393(3); C(7)–C(8), 1.388(3); C(2)–C(3), 1.424(3); C(6)–C(7), 1.424(3); C(1)–C(9), 1.442(3); C(4)–C(10), 1.439(3); C(5)–C(10), 1.444(3); C(8)–C(9), 1.439(3); C(9)–C(10), 1.427(3). The core bond angles (°) are C(9)–C(1)–C(2), 120.4(2); C(1)–C(2)–C(3), 119.3(2); C(2)–C(3)–C(4), 120.9(2); C(3)–C(4)–C(10), 119.8(2), C(10)–C(5)–C(6), 120.0(2); C(5)–C(6)–C(7), 119.5(2); C(6)–C(7)–C(8), 120.7(2); C(7)–C(8)–C(9), 120.0(2); C(10)–C(9)–C(1), 118.7(2); C(8)–C(9)–C(10), 117.0(2); C(8)–C(9)–C(1), 124.2(2); C(9)–C(10)–C(5), 118.4(2); C(4)–C(10)–C(9), 116.8(2); C(4)–C(10)–C(5), 124.5(2).

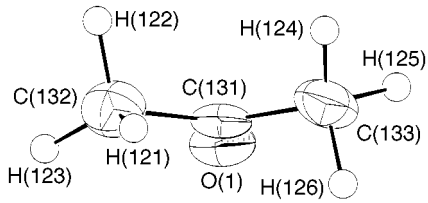

Fig. 2 The near C_2-symmetric conformation of acetone in its 1:1 adduct with host **1** as viewed at a narrow angle to the C=O bond direction

0.30 Å. The average esd for the carbon displacements is 0.002 Å. The corresponding displacements for S(1), S(5); S(2), S(6); S(3), S(7); S(4), S(8): −0.92, −0.89; −0.78, −0.76; 0.18, −0.05; 1.03, 1.00 Å [for other structural data, see caption to Fig. 1(*b*)].

The acetone guest molecule, which also occupies a general position in the unit cell, is shown in Fig. 2. As for the host molecule **1**, all hydrogen atoms were located and, again, the molecule possesses non-crystallographic C_2 symmetry. The non-hydrogen atoms of the guest are exactly coplanar, the angles being C(132)–C(131)–C(133) = 118.3(3), O(1)–C(131)–C(132) = 120.7(3) and O(1)–C(131)–C(133) = 121.0(3)°. The bond lengths are similar to those found for acetone in the vapour phase from a combined analysis of microwave and electron diffraction data[4] [given in parenthesis, for comparison]: O(1)–C(131) = 1.211(3) [1.210(4)], C(131)–C(132) = 1.499(4) [1.517(3)] and C(131)–C(133) = 1.498(4) [1.517(3) Å].

The acetone *conformation* in host **1**, subject to a number of weak host–guest hydrogen–hydrogen interactions (*vide infra)*, is distinct from the C_{2v} equilibrium symmetry situation in the vapour phase, where the in-plane methyl hydrogens eclipse the oxygen atom. It is interesting to note that Smeyers and coworkers[5] have predicted that methyl group rotation, away from the above C_{2v} conformation, will lead to an increase in the C–C–C bond angle. This is in keeping with observation; the C–C–C bond angle for the C_2 guest conformation, 118.2(3)°, is indeed significantly opened compared to the value, 116.0(3)°, for this angle in the C_{2v} vapour phase conformation of acetone. It must be said, of course, that the guest acetone's skeletal geometry may be subject to other host–guest influences, in addition to conformational control by the host lattice.[6] The acetone guest molecule experiences no strong host–guest interactions, and is present in an environment of low polarity. There are no fewer than 17 hydrogen–hydrogen host–guest contacts in the range 2.340–2.959 Å. The closest contact between the host molecule **1** and acetone is of the C–H···O type[7] and has length 2.320 Å. In all, there are five intermolecular contacts between O(1) and hydrogen atoms of **1** and these span the distance range 2.320–2.912 Å.

We thank the EPSRC (UK) for support (to G. A. D.).

Notes and References

† E-mail: D.MacNicol@chem.gla.ac.uk

‡ Compound **1** was prepared by persubstitution of perfluoronaphthalene with an excess of the appropriate thiolate nucleophile in dipolar aprotic solvent, the required thiol, 4-(2-phenylpropan-2-yl)benzenethiol, being prepared from the corresponding phenol by a general literature method (M.S. Newman and H.A. Karnes, *J. Org. Chem*., 1966, **31**, 3980), and having mp 43–44 °C (Calc. for $C_{15}H_{16}S$: C, 78.90; H, 7.02. Found: C, 78.78; H, 7.15%). Perfluoronaphthalene (0.26g, 0.96 mmol) and sodium 4-(2-phenylpropan-2-yl)benzenethiolate (3.74g, 15.3 mmol), prepared from the above thiol and sodium in absolute ethanol, were stirred in dry, degassed 1,3-dimethylimidazolidin-2-one (DMEU) (40 ml) for 3 h at ambient temperature, under N_2. The red–orange reaction mixture was then added to toluene (200 ml), washed with water (10 × 250 ml), and evaporation of the solvent gave a red oil, from which compound **1** was obtained by column chromatography (silica, hexane–EtOAc) as a orange–red microcrystalline material, 1.51g (81%), mp 161–162 °C. *Selected data* for **1**: δ_H(200 MHz, $CDCl_3$) 1.51 (s, 24H), 1.54 (s, 24H), *ca*. 6.6–6.9 (two AA′BB′ spectra, 32H), *ca*. 7.0–7.3 (m, 40H); δ_C(50 MHz, $CDCl_3$) 30.6, 30.7, 42.6, 42.7, 125.6, 125.7, 126.6, 126.7, 126.9, 127.4, 127.5, 128.0, 128.1, 128.9, 134.8, 135.7, 139.6 (overlapping resonances), 143.7, 148.4, 148.9, 150.1, 150.5 (Calc. for $C_{130}H_{120}S_8$: C, 80.57; H, 6.20. Found: C, 80.52; H, 6.29%).

§ *Crystal data* for **1**·$(CH_3)_2CO$: $C_{133}H_{126}O_1S_8$, M_r = 1996.82, triclinic, space group *P*1, a = 19.299(9), b = 20.235(11), c = 16.338(5) Å, α = 92.15(4), β = 104.71(3), γ = 118.47(4)°, U = 5330(4) Å^3, Z = 2, ρ_{calc} = 1.244 Mg m^{-3}, $F(000)$ = 2120, μ = 0.221 mm^{-1}, T = 123(1) K. Crystal dimensions, orange prism, 0.80 × 0.38 × 0.22 mm. Mo-Kα radiation (0.71069 Å), θ_{max} = 25.02°, 19 349 reflections collected, 18 743 unique reflections R_{int} = 0.0216, 15 294 reflections observed [> 2$\sigma(I)$]. Final R (on F using observed data) a *wR*2 (on F^2 using all data) were 0.0372 and 0.1044 respectively for 1279 parameters. Final GOF = 1.002. Maximum and minimum residual density 0.416 and −0.415 e Å^{-3} respectively. Data were collected on a Rigaku AFC7R diffractometer equipped with an Oxford Cryosystems cryostream cooler (ref. 8). The structure was solved using direct methods (SHELXS-86) (ref. 9) and refined on F^2 using all unique data by full-matrix least-squares (SHELXL-93) (ref. 10). All non-hydrogen atoms have anisotropic displacement parameters. All hydrogen atoms were located in difference syntheses, these were assigned a common temperature factor and included in the model but not refined. CCDC 182/983.

1 For a review see, D. D. MacNicol and G. A. Downing, in *Comprehensive Supramolecular Chemistry*, ed. D. D. MacNicol, F. Toda and R. Bishop, Pergamon, Oxford, 1996, vol. 6, ch. 14, pp. 434–444.
2 G. A. Downing, C. S. Frampton, J. H. Gall and D. D. MacNicol, *Angew. Chem., Int. Ed. Engl*., 1996, **35**, 1547.
3 Unsolvated crystals of **1** were obtained on recrystallisation of **1** from neat DMF, DMSO, CH_2Cl_2, 1,4-dioxane, and other solvents.
4 T. Iijima, *Bull. Chem. Soc. Jpn*., 1972, **45**, 3526; see also J. M. Vacherand, B. P. Van Eijck, J. Burie and J. Demaison, *J. Mol. Spectosc*., 1986, **118**, 355.
5 Y. G. Smeyers, M. L. Senent, V. Botella and D. C. Moule, *J. Chem. Phys*., 1993, **98**, 2754 and references cited therein.
6 With regard to the crystalline state, 1109 X-ray crystal structure analyses have been reported for systems in which acetone is present as a ligand component coordinated to a metal (*e.g*. R. Amstutz, J. D. Dunitz, T. Laube, W. B. Schweizer and D. Seebach, *Chem. Ber*., 1986, **119**, 434; M. Hoyer and H. Hartl, *Z. Anorg. Allg. Chem*., 1992, 612) or is 'anchored' in the lattice by one or more hydrogen bonds (*e.g*. C. P. Brock and G. L. Morelan, *J. Phys. Chem*., 1986, **90**, 5631). Both these situations tend to attenuate thermal motion, favouring direct observation of the acetone's hydrogen atoms, but represent relatively strong host–guest interactions. When such motion-reducing interactions are absent, the acetone molecule normally exhibits high thermal motion and/or disorder, however, see for example, A. Dietrich, K. A. Fidelis, D. R. Powell, D. van der Helm and D. L. Eng-Wilmot, *J. Chem. Soc., Dalton Trans*., 1991, 231; A. Avdeef and W. P. Scheafer, *J. Am. Chem. Soc*., 1976, **98**, 5153. Interestingly, no X-ray results from the molecular crystal of acetone itself have yet appeared in the literature.
7 For a recent review of C–H···O interactions see, T. Steiner, *Chem. Commun*., 1997, 727.
8 J. Cosier and A. M. Glazer, *J. Appl. Crystallogr*., 1986, **19**, 105.
9 G. M. Sheldrick, *Acta Crystallogr., Sect. A*., 1990, **46**, 467.
10 G. M. Sheldrick, SHELXL-93, program for the refinement of crystal structures, University of Göttingen, Germany, 1993.

Received in Liverpool, UK, 29th July 1998; 8/05967E

A new and easy method for making micrometer-sized carbon tubes

Chien-Chung Han,*† Jyh-Tsung Lee, Reen-Woei Yang, Hua Chang and Chein-Hwa Han‡

Department of Chemistry, National Tsing Hua University, Hsinchu, Taiwan, ROC

Highly crystalline and single-walled micrometer-sized carbon tubes several centimeters in length have been prepared *via* the pyrolysis of composite fibers consisting of a thermally stable polypyrrole skin layer and a thermally degradable PET core fiber.

Studies on the formation and growth mechanism[1] of nano-size carbon tubes have attracted a lot of research interest in recent years, due to their potential in applications like electron field emitters,[2] nanowires,[3] catalytic micro-reactors and natural gas storage. Various methods have been reported for the preparation of carbon tubes; these include carbon-arc discharge,[4] laser ablation,[5] condensed-phase electrolysis,[6] and the catalytic pyrolysis of hydrocarbons on various substrates such as porous anodic aluminium oxide,[7] fine metal particles[8] and patterned cobalt layers.[9] Regarding nano-tubes, their potential as micro-reactors might be significantly limited due to their relatively small inner diameters, which could preclude the entry of large reactive species or reactants. However, for micrometer-sized carbon tubes, with their relatively larger inner diameter, it would be easier to perform inner surface modifications *via* treatment with various chemicals and render the inner surface active, thus enabling selective separation (or extraction) of interested compounds. Likewise, it would also be easier to embed desired transition metal complexes (with sizes often larger than 2–3 nm) on the inner surface of micrometer-sized tubes, to impart specific catalytic functions. It is envisaged that, with their larger inner tube diameter, the throughput of micrometer-sized tube micro-reactors should be acceptable for practical applications. Similarly, it should also be relatively easier to activate chemically both the inner and outer surfaces of micrometer-sized tubes to facilitate the formation of micro- or meso-porous features, making them suitable for natural gas storage. Although hollow carbon fibers of sub-millimeter size, with 0.4 mm inner diameter and 0.6 mm outer diameter, had been prepared *via* the carbonization of spun poly(acrylonitrile) hollow fibers,[10] there is still a lack of a feasible and reliable method for making thin-walled carbon tubes with diameters in the range of 1–100 μm.

Here, a new and feasible method for the preparation of micrometer-sized single-walled carbon tubes is proposed. The method also enables convenient control of both the diameter and wall thickness of the resultant carbon tubes. Tubes several centimeters in length and pre-organized in one- or two-dimensional matrices have been obtained experimentally.

These carbon tubes were prepared from polypyrrole (PPy)-coated poly(ethylene terephthalate) (PET) fibers by heating the composite fibers at 1000 °C for 3–6 h under an N_2 atmosphere. The PPy coatings were applied *via* a typical reaction-coating approach,[11] by suspending commercially available PET fibers in an aqueous pyrrole solution that contained 2 equiv. of toluene-*p*-sulfonic acid, followed by the addition of oxidants to initiate the polymerization of pyrrole. The resulting PPy thus formed presented itself as a homogeneous black coating on the surface of the PET fibers. The thickness of such PPy coatings could be controlled by altering the pyrrole concentration of the reaction solution, and by the number of reaction-coating treatments conducted. The resulting PPy-coated PET fibers were then slurry-washed with copious amounts of de-ionized water and air-dried for 48 h. The PPy/PET composite fibers, as shown in Fig. 1(*a*), were then placed in a quartz oven and heated from room temperature to 1000 °C at a heating rate of 10 °C min^{-1} under an N_2 atmosphere. An annealing time of between 3 to 6 h was employed after the temperature reached 1000 °C. During the heating and annealing process, some white solid sublimed out of the oven and was identified as a mixture of terephthalic acid and 4-(vinyloxycarbonyl)benzoic acid.§ Most of this solid was collected at between 400 and 500 °C, consistent with the decomposition temperature of the PET fibers. All the carbon fibers obtained after the thermal treatment were found to be hollow tubes with uniform diameters and wall thicknesses, as illustrated by the SEM micrographs in Fig. 1. The wall thickness of such carbon tubes was found to be directly proportional to the thickness of the original PPy coating layer. For example, composite fibers with PPy layer thicknesses of 1.2 (±0.2), 1.5 (±0.3) and 2.0 (±0.3) μm yielded carbon tubes with an average wall thicknesses of 0.38 (±0.05), 0.63 (±0.08) and 1.3 (±0.2) μm, respectively. The electron micrographs of these carbon tubes are illustrated in Fig. 1(*b*)–(*d*). Thermogravimetric analysis of the same composite fibers also showed similar trends on mass retention, with composite fibers having thicker PPy layers displaying higher mass retention after annealing at

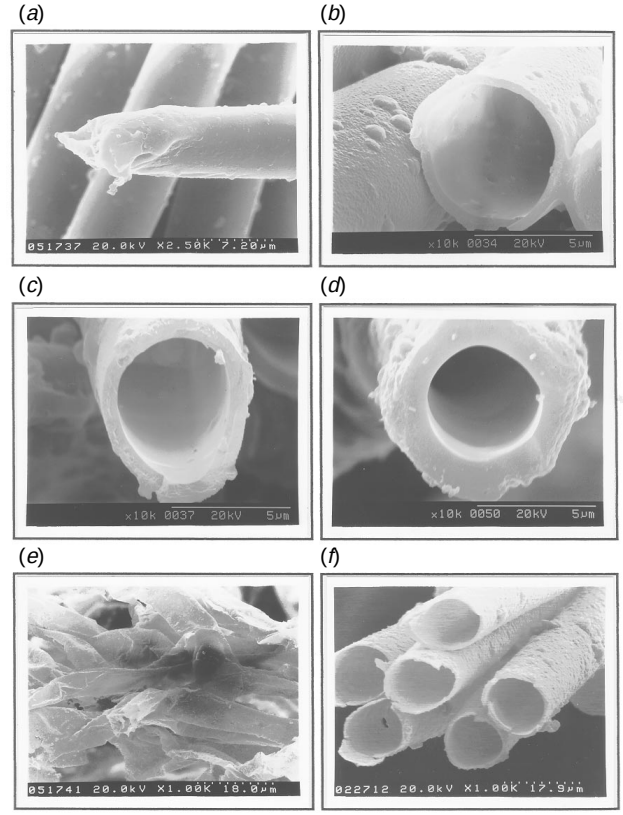

Fig. 1 SEM micrographs for (*a*) PPy/PET composite fibers, (*b*)–(*d*) resultant carbon-tubes of similar diameter (*ca.* 7.5 μm), but with different wall thickness, (*e*) collapsed thin-walled carbon tubes and (*f*) carbon tubes of *ca.* 15 μm diameter

1000 °C. Interestingly, it was found that a minimum thickness of the PPy layer was required to provide sufficient mechanical strength to keep the tubes intact and maintain their round shape during the carbonization process. Fig. 1(*e*) illustrates that, when the PPy layer was less than *ca*. 100 nm in thickness, all the resulted carbon tubes collapsed. Carbon tubes of different sizes can also be prepared from PET fibers with different diameters. For example, carbon tubes with 15 μm in inner diameter [Fig. 1(*f*)] were prepared from PET fibers with a diameter of 16 μm.

All the carbon tubes prepared by the present method were found to be rich in carbon. Elemental analysis results indicated that these tubes consisted essentially of pure carbon, accompanied by small amount of N (< 3 wt%) and H (< 1 wt%). Similar results were obtained by scanning auger microscopy (SAM). A typical SAM spectrum for the outer wall of the carbon tubes clearly reveals that only the C peak at 275 eV is present. The N peak of the original PPy layer at 388 eV had almost completely disappeared. The reduction in N was probably caused by de-nitrogenation of the PPy coating during thermal treatment. Similar de-nitrogenation phenomena had also been reported for the thermal carbonization treatment of poly(acrylonitrile) at *ca.* 800 °C.[12] The de-nitrogenation reaction for the carbon tubes in this study appeared to have taken place throughout the entire tube, as indicated by the SAM spectra for the cross-section and the inner wall of the tubes. Furthermore, the SAM spectrum for the inner wall of the tubes showed hardly any sign of the O peak at 514 eV due to PET core fiber. This suggested that the PET core fiber had decomposed completely, and the tube wall was essentially converted from the original PPy skin layer of the composite fiber.

The use of single-pulse magic-angle-spinning solid-state ^{13}C NMR showed that the carbon of these tubes was unsaturated in nature, with its spectrum showing a complicated broad band between δ 70–160 and a maximum at *ca.* δ 120. The unusual peak broadening may be attributed to the slightly different chemical environment of each carbon atom in the network and its corresponding pair of spinning side-bands. No saturated sp^3 carbons in the range δ 0–70 nor any significant amount of carbonyl carbons between δ 160–300 were observed. The infrared spectra of ground-up carbon tubes as KBr pellets were completely featureless, probably due to the highly symmetric bonding nature of the tubes, as in the case of a carbon matrix with an extensive network. The Raman spectrum for the ground-up carbon tubes showed two bands at *ca.* 1354 and 1584 cm^{-1}, similar to those bands for graphite.

The most intriguing finding in the present study is that, although the carbonized product of PPy powder [annealed at 1000 °C for 3 h] was totally amorphous, the carbon tubes prepared in this study from PPy/PET composite fibers were highly crystalline. The X-ray diffraction spectrum for the ground-up carbon tubes, obtained using a Shimadzu X-ray diffractometer XD-5 with a Cu-Kα radiation source, showed two rather strong and sharp peaks at 2θ = 21.4 and 23.8°, equivalent to a *d*-spacing of 4.15 and 3.74 Å, respectively. Although the X-ray diffraction results indicated the presence of highly crystalline carbons in the tube wall, the lattice structure appeared to be different from the sheet-like morphology of graphite,¶ as the strongest diffraction peak for graphite is at 2θ = 26.6°. Further exploration of the crystalline nature of these carbon tubes with high resolution transmission electron microscopy (TEM) is in progress. It is believed that the surface of the highly stretch-oriented PET fibers might have acted as a template for the arrangement of deposited PPy chains during the polymerization coating process. The formation of more ordered and pre-arranged PPy matrices could increase the possibility of crystalline carbon formation during the carbonization process. The formation of induced structural order in carbon layers on fibres has also been observed for resin-based matrices in carbon–carbon composites.[13]

Using the present new method, carbon tube bundles several centimeters in length have been prepared with little difficulty, and SEM inspection of tubes thus prepared confirmed that they were completely hollow. Similarly, a two-dimensional matrix of carbon tubes has also been successfully prepared for the first time *via* the carbonization of a PPy-coated PET cloth.

A possible carbon tube formation mechanism is suggested as follows. The core PET fibers first melt at *ca.* 254 °C when the crystalline melting point of PET is reached. The PET then decomposes into terephthalic acid and 4-(vinyloxycarbonyl)-benzoic acid by-products *via* intra-chain β-elimination of the ester group between 400 to 500 °C.‖ The resultant by-products then sublime at these elevated temperatures, forming the hollow cores.** Meanwhile, the PPy skin layer also starts to decompose at its decomposition on-set temperature (*i.e.* 310 °C for undoped PPy powder), with the resulting active intermediate species very likely to induce efficient cross-linking of the highly π-bond-conjugated PPy, thus setting up the three-dimensional network of carbon tubes.

We acknowledge financial support from the National Science Council of ROC.

Notes and References

† E-mail: cchan@chem.nthu.edu.tw
‡ Current address: Department of Pharmacy, Chia-Nan College of Pharmacy and Science, Tainan, Taiwan.

§ *Selected data* for terephthalic acid: δ_H (300 MHz, [$^2H_6$]DMSO) 13.4 (s, 2H), 8.15 (s, 4H); δ_c (75 MHz, [$^2H_6$]DMSO) 166.82, 134.62, 129.62. For 4-(vinyloxycarbonyl)benzoic acid: δ_H (300 MHz, $CDCl_3$) 13.4 (s, 1H), 8.20 (s, 4H), 7.50 (dd, 1H, J_{ab} 13.9, J_{ac} 6.3), 5.11 (dd, 1H, J_{ba} 13.9, J_{bc} 1.96), 4.75 (dd, 1H, J_{ca} 6.3, J_{cb} 1.96); δ_C (75 MHz, $CDCl_3$) 170.08, 162.76, 141.23, 133.55, 133.44, 130.27, 130.03, 99.00.

¶ The carbon fibers prepared from poly(acrylonitrile) also did not form the graphitic structure until the annealing temperature was raised up to 2500 °C (ref. 12).

‖ The melting point of the PET fibers was measured by DSC (differential scanning calorimetry) to be 254 °C, and their decomposition on-set temperature was measured by TGA to be at 407 °C.

** The sublimation point for terephthalic acid is 402 °C, as reported in the Merck index (12th edn. 1996, Merck and Co., Inc.).

1 S. Iijima, T. Ichihashi and Y. Ando, *Nature*, 1992, **356**, 776; S. Amelinckx, X. B. Zhang, D. Bernaerts, X. F. Zhang, V. Ivanov and J. B. Nagy, *Science*, 1994, **265**, 635.
2 W. A. d. Heer, A. Chatelain and D. Ugarte, *Science*, 1995, **270**, 1179; W. A. d. Heer, J.-M. Bonard, K. Fauth, A. Chatelain, L. Forro and D. Ugarte, *Adv. Mater.*, 1997, **9**, 87.
3 T. W. Ebbesen, H. J. Lezec, H. Hiura, J. W. Bennett, H. F. Ghaemi and T. Thio, *Nature*, 1996, **382**, 54.
4 S. Iijima, *Nature*, 1991, **354**, 56; T. W. Ebbesen and P. M. Ajayan, *Nature*, 1992, **358**, 220.
5 A. Thess, R. Lee, P. Nikolaev, H. Dai, P. Petit, J. Robert, C. Xu, Y. H. Lee, S. G. Kim, A. G. Rinzler, D. T. Colbert, G. E. Scuseria, D. Tomanek, J. E. Fischer and R. E. Smalley, *Science*, 1996, **273**, 483.
6 W. K. Hsu, J. P. Hare, M. Terrones, H. W. Kroto, D. R. M. Walton and P. J. F. Harris, *Nature*, 1995, **377**, 687.
7 T. Kyotani, L. F. Tsai and A. Tomita, *Chem. Mater.*, 1995, **7**, 1427.
8 M. Endo, *Chemtech.*, 1988, 568.
9 M. Terrones, N. Grobert, J. Olivares, J. P. Zhang, H. Terrones, K. Kordatos, W. K. Hsu, J. P. Hare, P. D. Townsend, K. Prassides, A. K. Cheetham, H. W. Kroto and D. R. M. Walton, *Nature*, 1997, **388**, 52.
10 M. C. Yang and D. G. Yu, *J. Appl. Polym. Sci.*, 1998, **68**, 1331.
11 H. H. Kuhn, A. D. Child and W. C. Kimbrell, *Synth. Met.*, 1995, **71**, 2139; R. Gregory, W. Kimbrell and H. Kuhn, *Synth. Met.*, 1989, **28**, C823.
12 W. Kowbel, E. Hippo and N. Murdie, *Carbon*, 1989, **27**, 219.
13 B. McEnaney and T. J. Mays, in *Essentials of Carbon–Carbon Composites*, ed. C. R. Thomas, The Royal Society of Chemistry, Cambridge, 1993, ch. 6, p. 143.

Received in Cambridge, UK, 1st July 1998; 8/05057K

Valence tautomeric cobalt *o*-quinone complexes in a dual-mode switching array

Daniel Ruiz,[a] Jae Yoo,[a] Ilia A. Guzei,[b] Arnold L. Rheingold[b] and David N. Hendrickson*[a]

[a] *Department of Chemistry-0358, University of California at San Diego, La Jolla, CA 92093-0358, USA. E-mail: dhendrickson@ucsd.edu*

[b] *Department of Chemistry, University of Delaware, Newark, Delaware 19716, USA*

The characterization of valence tautomeric cobalt complexes with an array of four states, each with different optical and magnetic properties, is reported and it is shown that they can interconvert reversibly between the four states either thermally or by redox processes.

Complexes of the composition [Co(3,5-DTBCat)(3,5-DTBSQ)(NN)], where 3,5-DTBCat^{2-} and 3,5-DTBSQ^{-} refer, respectively, to the catecholate (Cat^{2-}) and semiquinonate (SQ^{-}) forms of 3,5-di-*tert*-butyl-*o*-quinone, and NN is a chelating diiminium ligand such as 2,2′-bipyridine (bpy, complex **1**) or 1,10-phenanthroline (phen, complex **2**), exhibit valence tautomerism.[1,2] These complexes can be interconverted in solution or in the solid state by means of different external stimuli such as temperature, pressure or irradiation between a high-spin [Co^{II}(SQ)$_2$(NN)] (*hs*-Co^{II}) or a low-spin [Co^{III}-(Cat)(SQ)(NN)] (*ls*-Co^{III}) form with appreciable changes in their electronic absorption spectra and magnetic ground states.[3–6] In solution, the equilibrium in eqn. (1) can be induced by variations of temperature and monitored by UV–VIS spectroscopy.

$$[Co^{III}(SQ)(Cat)(NN)]\ (ls\text{-}Co^{III}) \rightleftharpoons [Co^{II}(SQ)_2(NN)]\ (hs\text{-}Co^{II}) \quad (1)$$

At low temperatures, there is a band at ≈600 nm characteristic of the *ls*-Co^{III} tautomer. As the temperature of the solution is increased the intensity of the 600 nm band decreases and a band at ≈770 nm characteristic of the *hs*-Co^{II} tautomer increases in intensity. Here we report how this valence tautomerism equilibrium may be converted into an array of four states with different magnetic and optical properties that interconvert reversibly between them, where the additional switching capacity results from an electrochemical process.

The reversible redox characteristics of complexes **1** and **2** were employed to develop the square array shown in Fig. 1. A CH_2Cl_2 solution of complex **1** at 273 K with 0.1 M $NBu^n_4PF_6$ as a supporting electrolyte is mostly in the **1**,*ls*-Co^{III} form, as determined by UV–VIS spectroscopy. The CV of **1**,*ls*-Co^{III} under these conditions exhibits a reversible reduction at E_0 = −0.34 and a reversible oxidation at +0.25 V *vs*. a Ag wire (E_0 of ferrocene under the same experimental conditions is +0.36 V). Previous studies of different *o*-quinone metal complexes have shown that the redox processes occur at the quinone ligands.[7] Therefore, the first process at −0.34 V for complex **1**,*ls*-Co^{III} involves the reduction of the semiquinonate ligand to the catecholate form, whereas the second process involves the oxidation of the catecholate ligand of **1**,*ls*-Co^{III} to the semiquinonate ligand form. A CH_2Cl_2 solution of complex **2** at 305 K with 0.1 M $NBu^n_4PF_6$ as a supporting electrolyte is mostly in the **2**,*hs*-Co^{II} form. The CV of **2**,*hs*-Co^{II} exhibits a reduction process at E_0 = −0.2 V *vs*. a Ag wire. This process corresponds to the reduction of both semiquinonate ligands to catecholate ligands. Examination of the scan rate (υ) dependences for the processes observed for both tautomers showed a linear dependence of the peak current with respect to $\upsilon^{1/2}$, indicating that these redox processes are diffusive. Constant-potential electrolysis experiments have confirmed the reversibility of the different processes. Thus, both of the valence tautomers in eqn. (1) can be reduced reversibly. This allowed us to establish the square array shown in Fig. 1.

Treatment of complex **1**,*ls*-Co^{III} in CH_2Cl_2 at 273 K with 1 equivalent of $Co(Cp)_2$ yielded [Co(Cp)$_2$][Co^{III}(3,5-DTBCat)$_2$(bpy)] (**3**,*ls*-Co^{III}) as a dark-green polycrystalline solid (70% yield).† The S = 0 ground state was confirmed by variable-field magnetization data collected at 2.3 and 5.0 K. The presence of two catecholate ligands was also confirmed by an increase (relative to complex **1**) in the intensity of the characteristic catecholate C–O IR bands seen at ≈1250 cm^{-1}. Our interest in complex **3** was considerably enhanced when it was found that the electronic absorption spectrum of this complex in acetone exhibited a temperature dependence consistent with the following valence-tautomeric equilibrium:

$$[Co^{III}(Cat)_2(bpy)]^-\ (\mathbf{3},ls\text{-}Co^{III}) \rightleftharpoons [Co^{II}(SQ)(Cat)(bpy)]^-\ (\mathbf{3},hs\text{-}Co^{II}) \quad (2)$$

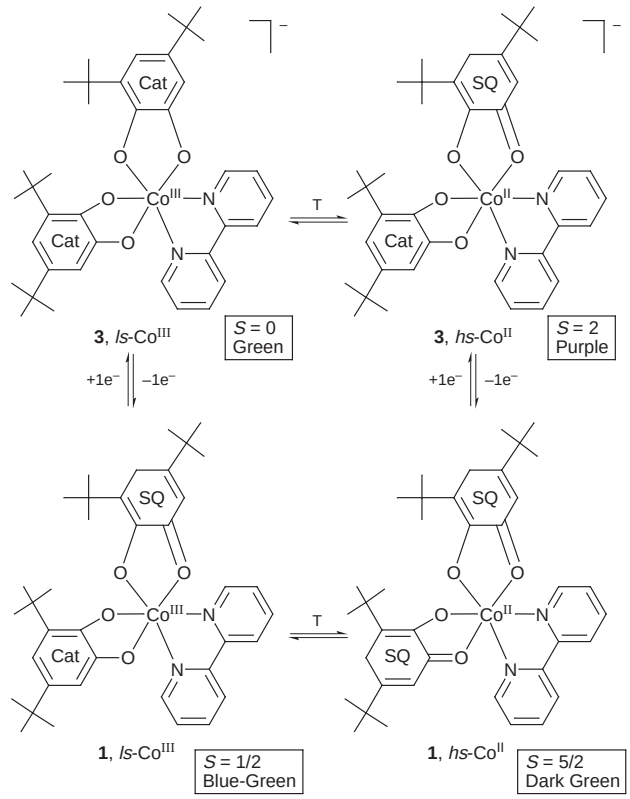

Fig. 1 Diagram of a dual-mode switching array. Complexes **1** and **3** each undergo a valence tautomeric interconversion and the tautomers of complex **3** are obtained reversibly by one-electron reduction of the tautomers of complex **1**. An array of four different states with different optical and magnetic ground states is then obtained.

As shown in Fig. 2, at low temperatures there is an intense band at 405 nm and a second less intense transition at 610 nm, where both bands are characteristic of the (**3**,*ls*-Co^{III})$^-$ isomer. Increasing the temperature converts this *ls*-Co^{III} tautomer to the [Co^{II}(3,5-DTBSQ)(3,5-DTBCat)(bpy)]$^-$ tautomer, identified as (**3**,*hs*-Co^{II})$^-$. The acetone solution changes from green at low temperatures to purple at higher temperatures. Two isosbestic points are seen at 360 and 470 nm, indicating that there are two species in equilibrium. When the sample was cooled, the spectrum characteristic of the (**3**,*ls*-Co^{III})$^-$ form was recovered. The cycle was repeated several times, confirming the reversibility of the interconversion although a gradual decrease of the absorbance was observed due to decomposition of the *hs*-Co^{II} form that reacts even with traces of oxygen. A toluene solution of complex **1** at high temperatures is mostly in the **1**,*hs*-Co^{II} form as confirmed by UV–VIS spectroscopy. Therefore, direct reaction of a toluene solution of complex **1** with 1 equivalent of $Co(Cp)_2$ was used to directly give [$Co(Cp)_2$][Co^{II}(3,5-DTBSQ)(3,5-DTBCat)(bpy)] (**3**,*hs*-Co^{II}) as a purple precipitate obtained after filtration from the solution (20% yield).† This solid is highly air-sensitive, however, it was characterized by variable-temperature magnetic susceptibility, electronic absorption and EPR spectroscopies. The value of μ_{eff} varies gradually from 4.24 μ_B at 320 K to 4.04 μ_B at 70.0 K, whereupon there is an increase to 5.14 μ_B at 20.0 K, followed by a decrease to 3.07 μ_B at 3.0 K. These results are consistent with a *hs*-Co^{II}(S = 3/2) complex with one S = 1/2 semiquinonate ligand, where there is a weak ferromagnetic exchange interaction between the ligand and the metal. Dissolution of **3**,*hs*-Co^{II} in acetone gave the same reversible temperature dependence in the UV–VIS electronic spectrum as shown in Fig. 2 for (**3**,*ls*-Co^{III})$^-$, confirming the existence of the valence tautomeric equilibrium **3**,*ls*-Co^{III-} ⇌ **3**,*hs*-Co^{II-}. X-Band EPR spectra showed the eight-line cobalt hyperfine splitting characteristic of Co–quinone systems [A(Co) ≈ 12 G]. Finally, it must be emphasized that additional constant-potential electrolysis experiments confirmed the reoxidation of the anionic complexes to the neutral species demonstrating the validity of the array detailed in Fig. 1. Thus, an array of four states is controlled by two temperature-controlled valence tautomeric equilibria and two reversible redox processes. The possibility of entering the cycle at each state and advancing through the square array in a clockwise and counter-clockwise direction was also established.

Reduction of complex **2** with 1 equivalent of $Co(Cp)_2$ in CH_2Cl_2 and toluene gave the tautomers [$Co(Cp)_2$][Co^{III}(3,5-DTBCat)$_2$(phen)] (**4**,*ls*-Co^{III}) and [$Co(Cp)_2$][Co^{III}(3,5-DTBSQ)(3,5-DTBCat)(phen)] (**4**,*hs*-Co^{II}).† The magnetic and spectroscopic characterization as well as the variable-temperature UV–VIS spectra of acetone solutions of these two phen $Co(Cp)_2^+$ salts were also found to be similar to those obtained for the corresponding bpy complexes. In short, the neutral phen complex **2** can be reduced and the reduced Co^{III} and Co^{II} species are involved in a valence-tautomeric equilibrium, *i.e.* **4**,*ls*-Co^{III-} ⇌ **4**,*hs*-Co^{II-}, establishing a similar array of four states for the phen complex.

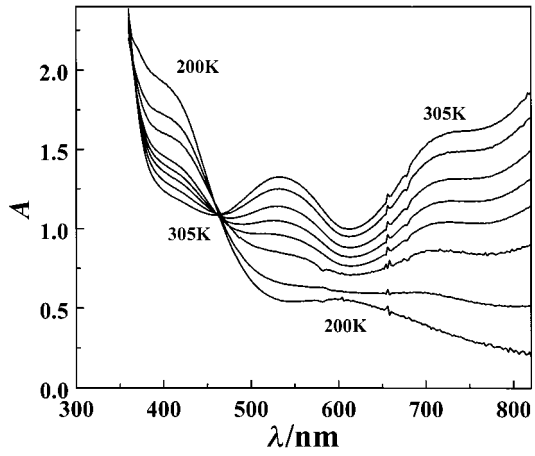

Fig. 2 Temperature dependence of the electronic absorption spectrum of an acetone solution of complex **3**

Oxidation of complex **1** could also establish another valence-tautomeric equilibrium, in addition to the two pictured in Fig. 1. Toward this goal, complex **1** was oxidized in 95% ethanol at 273 K (where complex **1** is mostly in the **1**,*ls*-Co^{III} form) by a H_2O_2–HCl mixture, following a procedure described by Wicklund *et al*.[8] for the oxidation of catecholate ligands. This oxidation gave [Co^{III}(3,5-DTBSQ)$_2$(bpy)]Cl, the Cl^- salt of (**5**,*ls*-Co^{III})$^+$.† Variable-temperature UV–VIS spectroscopy provides convincing evidence of the presence of a valence-tautomeric equilibrium for the oxidized form of the bpy complex in EtOH, *i.e*. for the equilibrium of **5**,*ls*-Co^{III+} ⇌ **5**,*hs*-Co^{II+}. At low temperatures (200 K) an intense band at 570 nm is seen that is characteristic of the (**5**,*ls*-Co^{III})$^+$ tautomer. An increase in temperature to 300 K leads to a decrease in the intensity of this band as a band at 720 nm, that is characteristic of (**5**,*hs*-Co^{II})$^+$, grows in. Two isosbestic points are seen. However, we must emphasize that when the temperature of the EtOH solution of (**5**,*hs*-Co^{II})$^+$ is increased above 300 K, the intensity of the 720 nm band does not increase. Instead, the intensities of both the 720 and 570 nm bands decreased as the temperature was increased above 300 K. We attribute this thermal instability of (**5**,*hs*-Co^{II})$^+$ to loss of the quinone ligand.

In summary, complexes of the composition [$Co(Cp_2)$]-[Co^{III}(3,5-DTBCat)$_2$(NN)] have been shown to undergo valence tautomerism. In addition, the reversibility of the tautomeric equilibria permitted the establishment of an array of four states with different magnetic and optical properties, reversibly interconvertible by means of electrochemical and thermal switching. Such an array of states is suitable to be used in the future as a building block for molecular electronic devices.

Notes and References

† The complex [$Co(Cp)_2$][Co^{III}(3,5-DTBCat)$_2$(bpy)] (**3**,*ls*-Co^{III}) analyzed satisfactorily (C,H,N). [Found: C, 68.07; H, 7.04; N, 3.63. $C_{48}H_{58}N_2O_4Co_2$ requires C, 68.23; H, 6.93; N, 3.31%]. The complex [$Co(Cp)_2$][Co^{II}(3,5-DTBSQ)(3,5-DTBCat)(bpy)] (**3**,*hs*-Co^{II}) analyzed satisfactorily (C,H,N). [Found: C, 56.86; H, 6.91; N, 3.12. $C_{48}H_{58}N_2O_4Co_2$ requires C, 68.23; H, 6.93; N, 3.31%]. The complex [$Co(Cp)_2$][Co^{III}(3,5-DTBCat)$_2$(phen)] (**4**,*ls*-Co^{III}) analyzed satisfactorily (C,H,N). [Found: C, 69.90; H, 6.55; N, 2.88. $C_{50}H_{58}N_2O_4Co_2$ requires C, 69.10; H, 6.70; N, 3.20%]. The complex [Co^{III}(3,5-DTBSQ)$_2$(bpy)]Cl (**5**,*ls*-Co^{III}) analyzed satisfactorily (C,H,N). [Found: C, 65.35; H, 7.18; N, 4.28. $C_{38}H_{48}N_2O_4CoCl$ requires C, 65.80; H, 7.00; N, 4.04%]. The complex [Co(3,5-DTBCat)(bpy)$_2$](BF_4)·$2CH_2Cl_2$ (**6**) analyzed satisfactorily (C, H, N). [Found: C, 59.00; H, 5.60; N, 7.90. $C_{34}H_{40}N_4O_2CoBF_4$ requires C, 59.80; H, 5.80; N, 8.20%].

1 R. M. Buchanan and C. G. Pierpont, *J. Am. Chem. Soc*., 1980, **102**, 4951.

2 P. Gutlich and A. Dei, *Angew. Chem., Int. Ed. Engl*., 1997, **36**, 2734; C. G. Pierpont and C. W. Lange, *Prog. Inorg. Chem*., 1994, **41**, 331.

3 C. Roux, D. M. Adams, J. P. Itie, A. Polian, D. N. Hendrickson and M. Verdaguer, *Inorg. Chem*., 1996, **35**, 2846; D. M. Adams, B. Li, J. D. Simon and D. N. Hendrickson, *Angew. Chem., Int. Ed. Engl*., 1995, **34**, 1881; D. M. Adams, A. Dei, A. L. Rheingold and D. N. Hendrickson, *J. Am. Chem. Soc*., 1993, **115**, 8221.

4 O. S. Jung, D. H. Jo, Y. A. Lee, B. J. Conklin and C. G. Pierpont, *Inorg. Chem*., 1997, **36**, 19; O. S. Jung, D. H. Jo, Y. A. Lee, Y. S. Sohn and C. G. Pierpont, *Angew. Chem., Int. Ed. Engl*., 1996, **35**, 1694.

5 K. Heinze, G. Huttner, L. Zsolnai, A. Jacobi and P. Schober, *Chem. Eur. J*., 1997, **3**, 732.

6 G. A. Abakumov, V. K. Cherkasov, M. P. Bubnov, O. G. Ellert, Z. B. Dobrokhotova, L. N. Zakaharov and Y. T. Struchov, *Dokl. Akad. Nauk SSSR*, 1993, **328**, 12.

7 A. B. P. Lever, P. R. Auburn, E. S. Dodsworth, M. Haga, W. Liu, M. Melnik and W. A. Nervin, *J. Am. Chem. Soc*., 1988, **110**, 8076.

8 P. A. Wicklund, L. S. Beckman and D. G. Brown, *Inorg. Chem*., 1976, **15**, 1996.

Received in Bloomington, IN, USA, 14th April 1998; 8/02803F

Phosphazene P_4-Bu^t base for the Ullmann biaryl ether synthesis

Claudio Palomo,*† Mikel Oiarbide, Rosa López and Enrique Gómez-Bengoa

Departamento de Química Orgánica, Facultad de Química, Universidad del País Vasco, Apdo. 1072, 20080 San Sebastián, Spain

In the presence of phosphazene P_4-Bu^t base and CuBr, aryl halides couple with phenols to give biaryl ethers at *ca.* 100 °C

The reaction of aryl halides with sodium or potassium aryloxides promoted by copper additives results in the formation of aryl ethers, the classical Ullmann biaryl ether synthesis.[1] The major problems of this reaction are the competitive reduction of the aryl halide to the dehalogenated arene[2] and the requirement for extremely harsh conditions, *i.e.* 200–300 °C, long reaction times and strong polar and often toxic solvents.[3] These reaction conditions probably account for an additional problem, namely the formation of isomeric biaryl compounds *via* substitution through an elimination-addition mechanism. On the other hand, the reductive homocoupling of the aryl halide component is also another inherent problem of this reaction.[4] Despite considerable success to date, these efforts have identified the same solution to these problems, namely, the preactivation of the aryl halide component *via*, for instance, the use of transition metals[5] or by placing an electron-withdrawing substituent *ortho* or *para* to the leaving group.[6] Although these variants have a prevalent position in the synthesis of complex macrocyclic peptides,[6,7] there exists no general solution for the direct coupling of aryl halides with phenols.[8]

Recently Buchwald *et al.*[9] described the first case of biaryl ether synthesis with unactivated aryl halides. The reaction occurs at *ca.* 110 °C using Cs_2CO_3 as the key reaction element.

We describe here an efficient method for the direct coupling of aryl halides with phenols that is based on the so-called 'naked anion' phenomenon.[10] Our procedure‡ combines this concept with the use of Schwesinger's phosphazene bases.[11] The synthesis and properties of these bases have been described recently.[12] We have found that P_4-Bu^t base in combination with Cu^I salts in either dioxane or toluene effects the Ullmann reaction of electron-rich, electron-neutral and electron-poor aryl halides with a variety of phenols (Scheme 1). For example, iodobenzene reacted with 2,4-dimethylphenol to produce the corresponding biaryl ether in 81% isolated yield under conditions where the use of other conceptually different bases produced only traces of the expected product, if at all.§ Other copper salts such as CuCl, CuI and $(CuOTf)_2$–benzene were also effective, but Cu^{II} salts did not give the coupling product. As shown in Table 1, the best results were attained using stoichiometric quantities of CuBr, although in some cases the reaction also proceeded well under CuBr catalysis (entries 1, 4, 5 and 8). The method is particularly suitable for electron-neutral aryl halides and *ortho*-substituted phenols. For example 2,6-dimethylphenol (entry 2) provided the corresponding biaryl ether in good yield and even the *o*-*tert*-butyl phenol (entry 3) coupled with *p*-iodotoluene to give the desired biaryl ether in 56% yield. The coupling reaction of *o*-iodotoluene and *o*-cresol (entry 4) also proceeded well to afford the corresponding biaryl ether in 69% yield. In these two latter cases, once again, no coupling reaction was observed when either DBU or TBD§ were used. Under the established reaction conditions, both electron-rich (entry 6) and electron-poor (entries 7–9) aryl halides also were effective in their coupling with phenols.

On the other hand, from the examples in Table 1 it also seems that the reaction conditions used are compatible with various functional groups. Nevertheless, neither the amino or the amido functionalities were inert under these reaction conditions. In fact, treatment of 3,5-dimethyliodobenzene with both aniline and *p*-toluidine afforded, under the above reaction conditions, the corresponding biaryl amines in 78 and 71% yield,

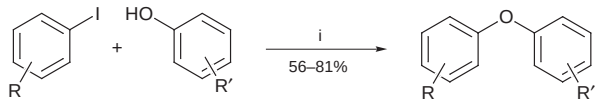

Scheme 1 *Reagents and conditions:* i, P_4-Bu^t, CuBr, toluene, reflux

Table 1 The Ullmann reaction promoted by P_4-Bu^t base in combination with CuBr[a]

Entry	Halide	Phenol	Product	Yield (%)[b]
1	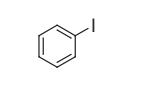			81[c] (73)
2	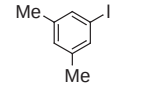			72[d] (54)
3	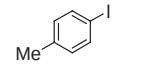			56
4	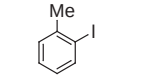			69 (69)
5	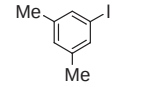			81[c] (72)[e]
6	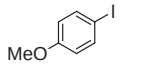			70[e] (25)
7	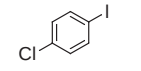			80[f]
8	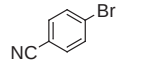			76 (80)
9	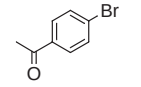			61

[a] Reactions conducted on a 1 mmol scale; aryl halide:phenol:CuBr = 1:2:2 in toluene as solvent unless otherwise stated. [b] Yields in parentheses refer to the reaction under catalytic conditions for Cu^I (20 mol% of CuBr). [c] Dioxane as solvent. [d] Reaction carried out in the presence of DMF (10% v/v). [e] Reaction carried out in the presence of galvinoxyl radical (10 mol%); in the absence of this radical inhibitor undesired byproducts were dominant. [f] Under catalytic conditions a mixture of isomeric biaryl ethers was formed.

respectively.[13] Although the precise role played by the phosphazene P_4-Bu^t base in the outcome of the reaction is not clear at present, two observations may give some clue: (i) the well-known ability of such a base to form highly nucleophilic 'naked' anions and, (ii) the complete solubility that the otherwise insoluble CuBr exhibits in the presence of P_4-Bu^t. Both factors may facilitate the formation of the reactive intermediate aryloxycopper species,[14] which can then react with the aryl halide under essentially homogeneous conditions. In any case, the use of this phosphazene base appears to be critical for performing the coupling reaction under reaction conditions that are unsuitable for conventional bases.

This work was financially supported by the Basque Government (Project EX-1997-108). A grant from the Basque Government to R. L. is gratefully acknowledged.

Notes and References

† E-mail: goppanic@sc.ehu.es

‡ General procedure: A mixture of the aryl halide (1 mmol), the corresponding phenol (2 mmol), P_4-Bu^t (2 mmol) and CuBr (2 mmol or 0.2 mmol for the catalytic version) in dry, deoxygenated toluene or dioxane (3 ml) was refluxed under a nitrogen atmosphere until the aryl halide was consumed as determined by GC analysis (typically 16–20 h). The reaction mixture was then allowed to cool to room temperature, diluted with EtOAc and washed sequentially with saturated aq. NH_4Cl (25 ml), 0.1 M NaOH (25 ml) and water (25 ml). The organic layer was dried over Na_2SO_4 and concentrated *in vacuo*. Purification by flash chromatography on silica gel using hexane afforded the analytically pure product.

§ Among the bases tested, Na_2CO_3, K_2CO_3 and 3,3,6,9,9-pentamethyl-2,10-diazabicyclo[4.4.0]dec-1-ene (PMDBD) were completely uneffective; 1,8-diazabicyclo[5.4.0]undec-7-ene (DBU) and 1,5,7-triazabicyclo[4.4.0]-dec-5-ene (TBD) afforded the coupling product in less than 20% yield along with the starting material and unidentified side products.

1 F. Ullmann, *Chem. Ber.*, 1904, **37**, 853.
2 T. Cohen, J. Wood and A. G. Dietz, Jr., *Tetrahedron Lett.*, 1974, 3555.
3 For reviews on this subject, see: (*a*) A. A. Moroz and M. S. Shvartsberg, *Russ. Chem. Rev.*, 1974, **43**, 679; (*b*) J. Lindley, *Tetrahedron*, 1984, **40**, 1433.
4 T. Cohen and I. Cristea, *J. Am. Chem. Soc.*, 1976, **98**, 748.
5 For a review, see: L. Balas, D. Jhurry, L. Latxague, S. Grelier, Y. Morel, M. Hamdani, N. Ardoin and D. Astruc, *Bull. Soc. Chim. Fr.*, 1990, **127**, 401.
6 For reviews, see: A. V. R. Rao, M. K. Gurjar, K. L. Reddy and A. S. Rao, *Chem. Rev.*, 1995, **95**, 2135; J. Zhu, *Synlett*, 1997, 133.
7 K. Burguess, D. Lim and C. I. Martinez, *Angew. Chem., Int. Ed. Engl.*, 1996, **35**, 1077; K. C. Nicolaou, C. N. C. Boddy, S. Natarajan, T.-Y. Yuee, H. Li, S. Bräse and J. M. Ramanjulu, *J. Am. Chem. Soc.*, 1997, **119**, 3421.
8 For some recent methods, see: G. W. Yeager and D. N. Schissel, *Synthesis*, 1991, 63; K. Smith and D. Jones, *J. Chem. Soc., Perkin Trans. 1*, 1992, 407; E. A. Schmittling and J. S. Sawyer, *J. Org. Chem.*, 1993, **58**, 3229; M. E. Jung and L. S. Starkey, *Tetrahedron*, 1997, **53**, 8815; D. M. T. Chan, K. L. Monaco, R.-P. Wang and M. P. Winters *Tetrahedron Lett.*, 1998, **39**, 2933; D. A. Evans, J. L. Katz and T. R. West, *Tetrahedron Lett.*, 1998, **39**, 2937.
9 J.-F. Marcoux, S. Doye and S. L. Buchwald, *J. Am. Chem. Soc.*, 1997, **119**, 10 539.
10 For a definition of this concept, see for example: L. F. Lindoy, *The Chemistry of Macrocyclic Ligand Complexes*, Cambridge University Press, Cambridge, 1989, p. 107.
11 R. Schwesinger, *Chimia*, 1985, **39**, 269; R. Schwesinger, *Nachr. Chem. Tech. Lab.*, 1990, **38**, 1214; R. Schwesinger, in *Encyclopedia of Reagents for Organic Synthesis*, ed. L. Paquette, Wiley, New York, 1995, vol. 6, p. 4110.
12 R. Schwesinger, H. Schlemper, C. Hasenfratz, J. Willaredt, T. Dambacher, T. Breuer, C. Ottaway, M. Fletschinger, J. Boele, H. Fritz, D. Putzas, H. W. Rotter, F. G. Bordwell, A. V. Satish, G.-Z. Ji, E.-M. Peters, K. Peters, H. Georg von Schnering and L. Walz, *Liebigs Ann.*, 1996, 1055.
13 For recent methods for the synthesis of biaryl amines, see: J. F. Hartwig, *Synthesis*, 1997, 329.
14 For mechanistic considerations, see: H. L. Aalten, G. van Koten, D. M. Grove, T. Kuilman, O. G. Piekstra, L. A. Hulshof and R. A. Sheldon, *Tetrahedron*, 1989, **45**, 5565; Also, see refs. 2 and 3(*b*).

Received in Liverpool, UK, 23rd July 1998; 8/05783D

Control of reaction course of the excited state of charge-transfer complexes by the free energy of backward electron transfer

Naoki Haga,*[a] Hiroaki Takayanagi[a] and Katsumi Tokumaru[b]

[a] *School of Pharmaceutical Sciences, Kitasato University, Minato-ku, Tokyo 108, Japan. E-mail: hagan@pharm.kitasato-u.ac.jp*
[b] *University of Tsukuba, Tsukuba, Ibaraki 305, Japan*

Selective excitation of charge-transfer (CT) complexes between acenaphthylene and various electron acceptors gives net reaction products when the resulting radical ion pairs lie at sufficiently higher energy than the ground state (large $-\Delta G_{BET}$); however, with decrease of $-\Delta G_{BET}$, these tend to become less reactive and finally non-reactive.

During active works on photoinduced electron transfer reactions, attention has been paid to the behavior of the excited states of charge-transfer complexes.[1–9] It was found that, for the combination of aromatic hydrocarbons with electron acceptors, contact radical ion pairs (CIPs) produced on excitation of their charge-transfer complexes facilely undergo backward electron-transfer (BET), the rate constant of which, k_{BET}, increases with decrease of the net free energy difference, $-\Delta G_{BET}$, between the ground state and the radical ion pair, whereas solvent separated radical ion pairs (SSIPs) resulting from encounters of excited states of either donors or acceptors with counterparts follow a bell-shaped k_{BET} *versus* $-\Delta G_{BET}$ relationship.[1–5] The above difference in behavior between CIPs and SSIPs might reflect a much smaller reorganization energy for BET from the former than from the latter.[8] However, the above energy gap effect on the reactivity of CT complexes has been investigated mostly by means of transient absorption spectroscopy, therefore whether the excited states of the CT complexes do or do not give the final reaction products remains unclear. Previously, we found that selective excitation of the CT complex of acenaphthylene (ACN) and TCNE with 546.1 nm light in acetonitrile or dichloroethane did not give any product, whereas excitation of ACN with 435.8 nm light in the presence of TCNE afforded products by way of electron transfer.[10,11]

This finding has led us to examine how $-\Delta G_{BET}$ affects the net chemical reactivity of the excited states of CT complexes between ACN and a series of electron acceptors such as nitriles, acid anhydrides, and quinones,† and we found that the $-\Delta G_{BET}$ value very dramatically controls the net reactivity of the excited state as reported below. The CT complexes‡ were selectively excited in dichloromethane with 546.1 nm light to determine the quantum yields of the reaction, or with >500 nm light to investigate the reaction products, since the CT complexes show absorption at wavelengths longer than 500 nm but ACN shows absorption at wavelengths shorter than 500 nm.

Fig. 1 plots the quantum yields of reaction, Φ_R, against $-\Delta G_{BET}$.§ This indicates that CT complexes with large $-\Delta G_{BET}$ values give net products; however, with lowering of $-\Delta G_{BET}$, Φ_R tends to decrease and finally reaches zero when $-\Delta G_{BET}$ is lower than 1.7 eV.¶ When $-\Delta G_{BET}$ is lower than the threshold, excitation of the CT complexes of ACN with acceptors did not result in any reaction products but excitation of ACN in the presence of the same acceptors afforded reaction products. In these cases, for the same combination of ACN and an acceptor, the SSIP resulting from excitation of ACN is reactive but either the excited state of the CT complex or the CIP resulting therefrom is unreactive. On the other hand, the CIP resulting from the excited CT complex, when lying with $-\Delta G_{BET}$ larger than the threshold, can undergo charge separation to give definite products *via* SSIPs competing with BET.

The Φ_R is composed of efficiencies for charge separation from the excited CT complex, Φ_{CS}, and for the generation of products from the dissociated radical ions, Φ'_R, according to $\Phi_R = \Phi_{CS} \times \Phi'_R$. Therefore, the above results certainly indicate that charge separation practically does not occur when $-\Delta G_{BET}$ is smaller than the above threshold, and the efficiency for charge separation tends to increase with increase of $-\Delta G_{BET}$ as shown in Scheme 1, since the radical ions, once produced from the SSIP, can give reaction products; *i.e.* Φ'_R is always > 0. In fact, excitation of ACN in the presence of the electron acceptors examined afforded reaction products and these were essentially the same as those resulting from excitation of CT complexes when they gave net reaction products.‖ In Scheme 1, A and A′ represent, for example, TCNB and TCNE, respectively.

When the CT complexes afford net reaction products, the resulting products are classified into two classes, *i.e.* those derived from benzoquinones (BQs) and those from non-BQs as shown in Scheme 2. Selective excitation of the CT complexes between ACN and non-BQs, namely acid anhydrides or nitriles, gave mainly two isomeric dimers of ACN, *cisoid*-**1** and *transoid*-**1**, in a ratio of 3–7 : 1, as observed in the excitation of ACN in the presence of electron acceptors such as TCNE which results in electron transfer from the excited ACN to the acceptors followed by the formation of a dimeric radical cation of ACN ($ACN_2^{+\cdot}$) affording *cisoid*- and *transoid*-**1** in the same ratio as above (Scheme 2).[10]

Excitation of the CT complexes of BQs, when affording products, gave addition products (**2**, **3**, and **4**), together with *cisoid*-**1** and *transoid*-**1** (Scheme 2), but no reduction products of BQs such as hydroquinones. For example, selective excitation of the CT complex between ACN and 2-CBQ gave **2**, **3**, and **4** in 13, 32, 7% yields, respectively, together with 20% of **1** with a *cisoid* : *transoid* ratio of 4.0 : 1 on consumption of 21% of

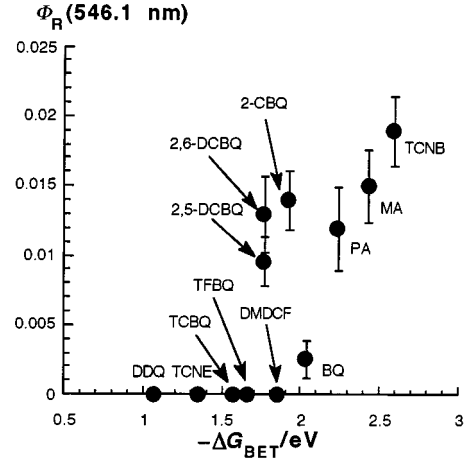

Fig. 1 Plots of quantum yield (Φ_R) at 546.1 nm for the reaction of ACN with various acceptors *versus* the energy gap between the ground state and the CIP ($-\Delta G_{BET}$)

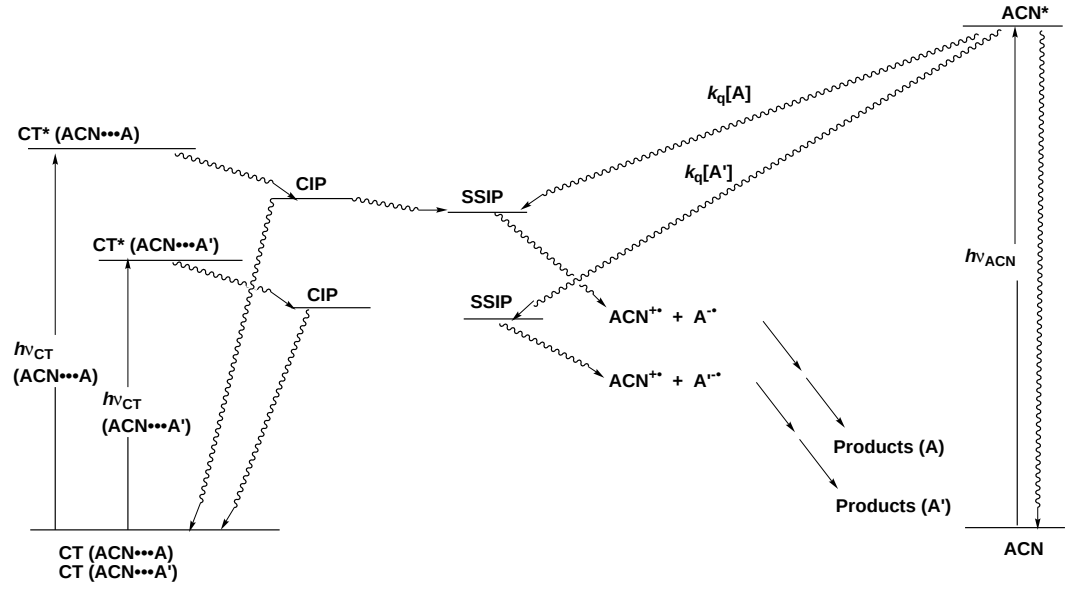

Scheme 1

(1) Acceptors: non-benzoquinones (nitriles and acid anhydrides)

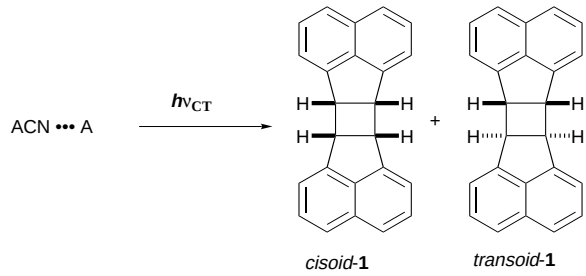

(2) Acceptors: benzoquinones

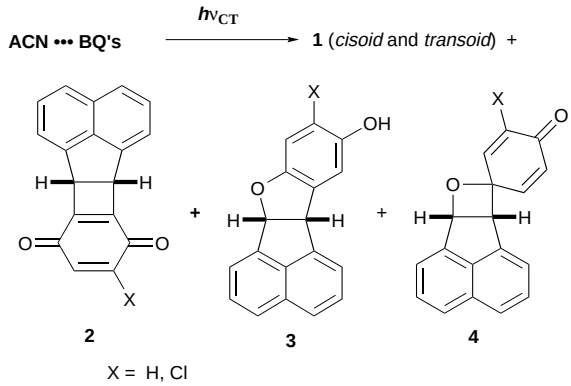

Scheme 2

ACN. Similarly, direct excitation of ACN with > 400 nm light gave *cisoid*-**1**, *transoid*-**1**, **2**, **3**, and **4** in 9, 4, 18, 36, 8% yields, respectively, on consumption of 94% of ACN.

In conclusion, $-\Delta G_{BET}$ clearly controls the reactivity of excited CT complexes by affecting the BET rate from the resulting CIP as schematically drawn in Scheme 1. Details of the present study will be published elsewhere.

To our knowledge, this is the first report to show, in a series of CT complexes between an electron donor with various acceptors, $-\Delta G_{BET}$ dramatically controls the course of reaction leading to final isolable products.

This work was partly supported by a Grant-in Aid for Scientific Research (No. 08640696) from the Ministry of Education, Science, and Culture, Japan, and Kitasato University Research Grant for Young Researchers (N. H.).

Notes and References

† Abbreviations of acceptors in this study: TCNB, tetracyanobenzene; DMDCF, dimethyl dicyanofumarate; MA, maleic anhydride; PA, pyromellitic dianhydride; BQ, 1,4-benzoquinone; 2-CBQ, 2-chloro-1,4-benzoquinone; 2,5-DCBQ, 2,5-dichloro-1,4-benzoquinone; 2,6-DCBQ, 2,6-dichloro-1,4-benzoquinone; TCBQ, chloranil; TFBQ, fluoranil.

‡ The CT complexes show absorptions extending to 400–700 nm in organic solvents depending on the acceptors. The equilibrium constants, K_{eq}, for formation of the 1 : 1 CT complex were spectrophotometrically[12] determined in DCE in the range 1.6–6.2 M^{-1} depending on the acceptors.

§ The quantum yields, Φ_R, for reaction on selective excitation of the CT complexes were determined based on the amount of converted ACN under irradiation by 546.1 nm monochromatic light in DCE.[13]

¶ In the threshold region, 2-CBQ ($-\Delta G_{BET}$ 1.92 eV) showed higher Φ_R than BQ (2.03 eV), and moreover 2,6-DCBQ (1.76 eV) and 2,5-DCBQ (1.76 eV) exhibited much larger Φ_R values than DMDCF (1.85 eV). This fact might be attributed to the heavy atom effect of the chlorine atom in these chloroquinones to enhance conversion of the initially resulting singlet radical ion pair (RIP) to a triplet RIP which will more effectively lead to separation of free radical ions.

‖ An equimolar mixture (0.005–0.02 M) of ACN and an acceptor in DCE was irradiated using a 400 W high pressure mercury lamp in a merry-go-round apparatus at 20 °C as described for TCNE.[10] The products were isolated by flash column chromatography and identified by spectral properties and/or elemental analysis.

1 T. Asahi, M. Ohkohchi and N. Mataga, *J. Phys. Chem.*, 1993, **97**, 13 132.
2 H. Miyasaka, S. Ojima and N. Mataga, *J. Phys. Chem.*, 1989, **93**, 3380, and references therein.
3 S. Ojima, H. Miyasaka and N. Mataga, *J. Phys. Chem.*, 1990, **94**, 5834.
4 N. Mataga and H. Miyasaka, *Prog. React. Kinet.*, 1994, **19**, 317.
5 N. Mataga, *Pure. Appl. Chem.*, 1997, **69**, 729.
6 G. Jones, II, W. A. Haney and X. T. Phan, *J. Am. Chem. Soc.*, 1988, **110**, 1922.
7 G. Jones, II, N. Mouli, W. A. Haney and W. R. Bergmark, *J. Am. Chem. Soc.*, 1997, **119**, 8788.
8 I. R. Gould and S. J. Farid, *Acc. Chem. Res.*, 1996, **29**, 522.
9 Y. Takahashi and J. K. Kochi, *Chem. Ber.*, 1988, **121**, 253.
10 N. Haga, H. Takayanagi and K. Tokumaru, *J. Org. Chem.*, 1998, **63**, 5572.
11 N. Haga, H. Nakajima, H. Takayanagi and K. Tokumaru, *Chem. Commun.*, 1997, 1171.
12 H. A. Benesi and J. H. Hildebrand, *J. Am. Chem. Soc.*, 1949, **71**, 2703.
13 J. G. Calvert and J. N. Pitts, Jr., *Photochemistry*, John Wiley & Sons, Inc, New York, 1966, p. 739.

Received in Cambridge, UK, 14th July 1998; 8/05461D

Orthopalladated triaryl phosphite complexes as highly active catalysts in biaryl coupling reactions

David A. Albisson,[a] Robin B. Bedford,*[a]†‡ Simon E. Lawrence[b] and P. Noelle Scully[a]

[a] *Department of Chemistry, Trinity College Dublin, Dublin 2, Ireland*
[b] *Department of Chemistry, University College Cork, Cork, Ireland*

Orthopalladation of inexpensive, commercially available tris(2,4-di-*tert*-butylphenyl) phosphite gives a dimeric complex 3 which proves to be an extremely active catalyst in biaryl coupling reactions, giving unprecedented turnover numbers of up to 1 000 000 [mol product (mol Pd)$^{-1}$] and turnover frequencies of nearly 900 000 [mol product (mol Pd)$^{-1}$ h^{-1}] in the Suzuki reaction and turnover numbers of up to 830 000 in the Stille reaction.

The use of triaryl phosphite complexes in catalysis has recently enjoyed a renaissance as a result of the activity they show in hydroformylation,[1] asymmetric hydrocyanation[2] and enantioselective alternating co-polymerisation of CO and propene.[3] Our interest lies in the synthesis and catalytic behaviour of orthometallated triaryl phosphite complexes and the role that the metallation plays in their activities.[4] So far the exploitation of such systems has been limited to a few catalytic reductions[4b,5] and only one example of catalytic C–C bond formation.[6]

One particularly important class of C–C coupling reaction is the catalytic formation of non-symmetric biaryls (Scheme 1) by the coupling of aryl halides with either arylboronic acids (the Suzuki reaction) or aryltin reagents (the Stille reaction). In general, catalyst loadings in such reactions are high (1–10 mol%) which imposes financial constraints on scaling up reactions and problems associated with catalyst removal. Therefore the synthesis of high activity catalysts which can be used in low concentrations is a desirable goal. Recently, Beller and co-workers reported the use of the metallated tris(2-

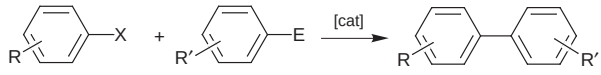

Scheme 1 Suzuki [E = $B(OH)_2$] and Stille (E = SnR_3) biaryl coupling reactions

methylphenyl)phosphinepalladium(II) complex **1** as an efficient catalyst for the Suzuki reaction.[7] The ready ability of triaryl phosphites to undergo analogous metallation reactions as well as their ease of synthesis, commercial availability and very low cost prompted us to examine the possibility of designing well-defined orthometallated Pd^{II}–triaryl phosphite complexes capable of catalysing biaryl coupling reactions.

The reaction of bulky tris(2,4-di-*tert*-butylphenyl)phosphite **2** with $PdCl_2$ gives the orthometallated dimer **3** in 96% yield. Compound **3** has been characterised by satisfactory elemental analysis, ^{1}H and ^{31}P NMR spectroscopy and by single crystal X-ray analysis (Fig. 1).§ Compound **3** shows remarkable stability to air and moisture—in solution it shows no sign of decomposition after several weeks, whilst solid samples can be kept in air for at least six months. No decomposition is observed when **3** is heated at 130 °C in toluene for 24 h, demonstrating that the catalyst also shows good thermal stability.

The coupling of aryl halides and phenylboronic acid catalysed by **3** was investigated and representative results are summarised in Table 1. With 4-bromoacetophenone as substrate, extraordinarily high turnover numbers (TONs) of up to 1 000 000 [mol product (mol Pd)$^{-1}$] and turnover frequencies (TOFs) of nearly 900 000 [mol product (mol Pd)$^{-1}$ h^{-1}] were obtained at 110 °C. The previous highest activity with this substrate was achieved with complex **1** which gave a TON of 74 000 at the higher temperature of 130 °C over 16 h.[7] In the present reaction, lowering the temperature to 70 °C leads to a reduction in activity, but even at 20 °C high levels of activity are observed relative to previous reports of ambient temperature reactions.[8] The reaction is strongly influenced by a change of solvent or base, thus replacing toluene with THF at 70 °C leads to a substantial drop in rate. Similarly, with NaOAc as the base in DMA lower rates are observed.

With 4-bromobenzophenone as substrate high rates and ultimate conversions are also seen. As expected, activity decreases with increasing electron density on the aryl bromide. For instance, when 4-bromoanisole is employed TOFs are about two orders of magnitude lower than with 4-bromoacetophenone, however the ultimate TONs—up to 30 000—are, we believe, without precedent.

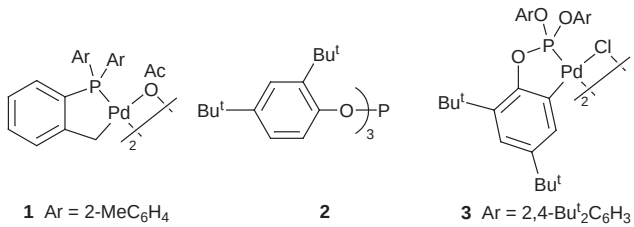

1 Ar = 2-MeC_6H_4 **2** **3** Ar = 2,4-$Bu^t_2C_6H_3$

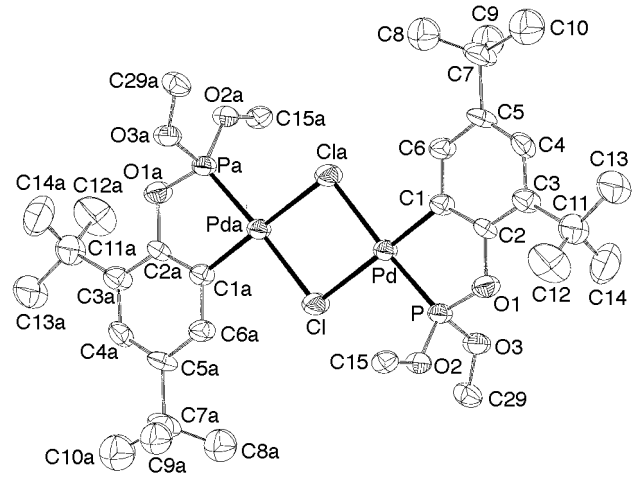

Fig. 1 Molecular structure of **3**. Thermal ellipsoids set at 50% probability. All H-atoms omitted for clarity, as are all but the *ipso*-carbons of the non-metallated aryl rings. Three Bu^t groups are disordered, only major orientation of C7–10 shown. Selected distances (Å) and angles (°): Pd–C1 1.998(6), Pd–Cl 2.4180(16), Pd–Cla 2.4073(17), Pd-P 2.1668(17), P–O1 1.592(4), P–O2 1.585(4), P–O3 1.584(4), C1–Pd–P 80.7(2), P–Pd–Cl 100.35(6), Cl–Pd–Cla 83.92(6), Cla–Pd–C1 95.0(2), Pd–P–O1 108.3(2), Pd–P–O2 120.4(2), Pd–P–O3 120.6(2).

Table 1 Suzuki coupling of aryl bromides with phenylboronic acid catalysed by **3**. Reaction conditions: 10 mmol aryl bromide, 15 mmol $PhB(OH)_2$, 20 mmol base in 30 ml solvent

Aryl bromide	Solvent	[Pd]/mol%	Base	*T*/°C	*t*/h	Conversion (%)[a]	TON/mol product (mol Pd)$^{-1}$
4-bromoacetophenone	DMA	0.1	NaOAc	130	18	66	660
4-bromoacetophenone	DMA	0.1	K_2CO_3	130	1	19	190
4-bromoacetophenone	DMA	0.1	K_2CO_3	130	15	98	980
4-bromoacetophenone	toluene	0.1	K_2CO_3	110	1	100	1000
4-bromoacetophenone	toluene	0.0001	K_2CO_3	110	1	87	870 000
4-bromoacetophenone	toluene	0.0001	K_2CO_3	110	2.25	100	1 000 000
4-bromobenzophenone	toluene	0.0001	K_2CO_3	110	1	33	330 000
4-bromobenzophenone	toluene	0.0001	K_2CO_3	110	15	60	600 000
4-bromoacetophenone	toluene	0.1	K_2CO_3	70	2	100	1000
4-bromoacetophenone	THF	0.1	K_2CO_3	70	2	20	200
4-bromoacetophenone	toluene	0.1	K_2CO_3	20	2	95	950
4-bromoanisole	toluene	0.1	K_2CO_3	110	1	97.5	975
4-bromoanisole	toluene	0.001	K_2CO_3	110	1	5	5000
4-bromoanisole	toluene	0.001	K_2CO_3	110	15	16	16 000
4-bromoanisole	toluene	0.001	K_2CO_3	130	15	30	30 000

[a] Determined by GC and/or ^{1}H NMR analysis of reaction mixture samples, based on aryl bromide.

Table 2 Stille coupling of aryl bromides with $PhSnBu_3$ catalysed by **3**. Reaction conditions: 4 mmol aryl bromide, 5 mmol $PhSnBu_3$ in 20 ml toluene

Aryl bromide	[Pd]/mol%	*T*/°C	*t*/h	Conversion (%)[a]	TON/mol product (mol Pd)$^{-1}$
4-bromoacetophenone	0.2	100	17.5	54	270
4-bromoacetophenone	0.2	120	15	100	500
4-bromoacetophenone	0.0001	120	18	83	830 000
4-bromoanisole	0.1	120	15	84	840

[a] Determined by GC and/or ^{1}H NMR analysis of reaction mixture samples, based on aryl halide.

In the coupling reactions with higher catalyst concentrations ($\geqslant$0.1 mol% Pd) deposition of palladium is observed in the later stages of the reaction. Similarly, reaction of **3** with 1 equiv. of $PhB(OH)_2$ and K_2CO_3 in the absence of an aryl bromide leads to deposition. When this reaction was repeated with 1 equiv. of **2** included, decomposition was inhibited and it was possible to monitor the reaction by ^{31}P NMR spectroscopy. The spectrum after 30 min showed the mixture to be predominantly **2** and **3** but amongst other minor peaks two relatively major low field double doublets were apparent.¶ We have tentatively assigned these to the two isomers of [Pd(Ph){P(OC$_6$H$_2$-2,4-Bu$^t_2$)-(OC$_6$H$_3$-2,4-Bu$^t_2$)$_2$}{P(OC$_6$H$_3$-2,4-Bu$^t_2$)$_3$}] in which the P atoms are disposed *trans* (major) or *cis* (minor). Also apparent is a small peak at δ −18.3. Such a high field shift is consistent with the formation of a Pd^0–phosphite complex. We postulate that reductive elimination of the orthometallated phosphite aryl and a phenyl groups occurs, yielding a catalytically active zero valent palladium species. This is in accord with findings for the use of **1** in the Stille reaction.[9] However, a Pd^{II}/Pd^{IV} couple has recently been suggested to be active in the Heck arylation of alkenes catalysed by **1** and related complexes[10] and at this stage we cannot rule out a related pathway.

Encouraged by the results obtained in the Suzuki reaction we decided to investigate the application of **3** to the Stille reaction. Representative results for the coupling of tributylphenyltin with aryl bromides are summarised in Table 2. With 4-bromoacetophenone as substrate TONs of up to 840 000 were achieved within 18 h at 120 °C. To the best of our knowledge this is the highest reported activity to date, comparing well with that obtained with **1** which gives a TON of 1650 in the coupling of 4-bromoacetophenone with $PhSnMe_3$ at the same temperature.[9] The reaction is again somewhat more sluggish with 4-bromoanisole, but useful conversions are still obtained.

In summary the complex **3** is extremely active in biaryl coupling reactions under both Suzuki and Stille conditions and consequently can be used in very low concentrations. In view of this unprecedented activity and the low cost of **2**—at least two orders of magnitude cheaper than tris(2-methylphenyl)phosphine—we believe that it will be the catalyst of choice in such reactions. We are currently investigating its application to further catalytic processes. Preliminary investigations show it to be extremely active in the Heck arylation of alkenes, showing TONs of up to 5.75 million for activated aryl bromides, and these findings will be published elsewhere.

This work was supported by Forbairt and the Trinity Trust Foundation. We thank Johnson-Matthey for the generous loan of palladium salts and Cork University Foundation for the purchase of an X-ray diffractometer.

Notes and References

† E-mail: bedfordr@tcd.ie
‡ New address: Department of Chemistry, University of Exeter, Exeter, UK EX4 4QD

§ *Crystal data* for **3**: $C_{84}H_{124}Cl_2O_6P_2Pd_2$, M = 1575.47, triclinic, space group $P\bar{1}$, Z = 1, a = 11.957(1), b = 12.911(3), c = 15.300(3) Å, α = 81.08(2), β = 69.46(1), γ = 76.45(1)°, V = 2143.3(6) Å^3, T = 293(2) K, μ = 0.566 mm^{-1}, the final R-factor was 0.057 for 4257 reflections with $I > 2\sigma(I)$. CCDC 182/978.

¶ NMR data: δ_P 155.2 and 118.1 ($^2J_{PP}$ = 29.8 Hz) (minor isomer) and 141.4 and 117.3 ($^2J_{PP}$ = 868.4 Hz) (major isomer).

1 K. Nozaki, N. Sakai, T. Nanno, T. Higashijima, S. Mano, T. Horiuchi and H. Takaya, *J. Am. Chem. Soc.*, 1997, **119**, 4413 and references cited therein; A. van Rooy, E. N. Orij, P. C. J. Kamer, F. van den Aardweg and P. W. M. N. van Leeuwen, *J. Chem. Soc., Chem. Commun.*, 1991, 1096; A. Polo, C. Claver, S. Castillón, A. Ruiz, J. C. Bayon, J. Real, C. Mealli and D. Massi, *Organometallics*, 1992, **11**, 3525; N. Sakai, K. Nozaki and H. Takaya, *J. Chem. Soc., Chem. Commun.*, 1994, 395.
2 T. Horiuchi, E. Shirakawa, K. Nozaki and H. Takaya, *Tetrahedron: Asymmetry*, 1997, **8**, 57.
3 K. Nozaki, N. Sato and H. Takaya, *J. Am. Chem. Soc.*, 1995, **117**, 9911.
4 (*a*) R. B. Bedford, P. A. Chaloner and P. B. Hitchcock, *J. Chem. Soc., Chem. Commun.*, 1995, 2049; (*b*) R. B. Bedford, S. Castillon, P. A. Chaloner, C. Claver, E. Fernandez, P. B. Hitchcock and A. Ruiz, *Organometallics*, 1996, **15**, 3990.
5 L. N. Lewis, *J. Am. Chem. Soc.*, 1986, **108**, 743; L. N. Lewis, *Inorg. Chem.*, 1985, **24**, 4433.
6 L. N. Lewis and J. F. Smith, *J. Am. Chem. Soc.*, 1986, **108**, 2728
7 M. Beller, H. Fischer, W. A. Herrmann, K Öfele and C. Brossmer, *Angew.Chem. Int. Ed. Engl.*, 1995, **34**, 1848.
8 J. C. Anderson, H. Namli and C. A. Roberts, *Tetrahedron*, 1997, **53**, 15 123; J. C. Anderson and H. Namli, *Synlett*, 1995, 765.
9 J. Louie and J. F. Hartwig, *Angew. Chem., Int. Ed. Engl.*, 1996, **35**, 2359.
10 B. L. Shaw, *New J. Chem.*, 1998, 77; B. L. Shaw, S. D. Perera and E. A. Staley, *Chem. Commun.*, 1998, 1361.

Received in Cambridge, UK, 3rd August 1998; 8/06041J

Friedel–Crafts reactions in room temperature ionic liquids

Christopher J. Adams,[b] Martyn J. Earle,[a]† Glyn Roberts[b] and Kenneth R. Seddon[a]

[a] *School of Chemistry, The Queen's University of Belfast, Stranmillis Road, Belfast, Northern Ireland, UK BT9 5AG*
[b] *Unilever Research Laboratories, Port Sunlight, Bebington, Wirral, England, UK L63 3JW*

Friedel–Crafts reactions in the ionic liquid system 1-methyl-3-ethylimidazolium chloride–aluminium(III) chloride can be performed with excellent yields and selectivities, and in the case of anthracene, have been found to be reversible.

The possibility of carrying out chemical transformations in low temperature ionic liquids has, to date, received little attention.[1] Ionic liquids such as the [emim]Cl–$AlCl_3$ ([emim]$^+$ = 1-methyl-3-ethylimidazolium cation) system have been shown to demonstrate catalytic activity in reactions such as Friedel–Crafts acylations,[2,3] alkylation reactions,[4] isomerisation of alkanes,[5] and the alkylation of isobutane with butene.[6] Here, we present a series of reactions of AcCl with carbocyclic aromatic compounds in acidic compositions (X = 0.67)‡ of [emim]Cl–$AlCl_3$ (Fig. 1) and compare their performance with similar reactions in 'conventional' molecular solvents.

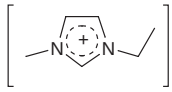

Fig. 1 The structure of the [emim]$^+$ cation

To date, there have been very few publications detailing reactive chemistry in ionic liquids.[1] With the development of ambient temperature ionic liquids, the possibility of investigating chemical processes in these new solvents provides an interesting challenge. One of the most studied ionic liquids is the [emim]Cl–$AlCl_3$ system.[7,8] An investigation of the Friedel–Crafts reactions of simple benzene derivatives in this medium has been performed by Wilkes.[3] With a view towards developing reactions for clean synthesis in ionic liquids, a number of Friedel–Crafts acetylation reactions have now been performed. The Friedel–Crafts reactions of five simple aromatic compounds has been investigated and are shown in Table 1.

The reactions work efficiently, giving the stereoelectronically-favoured product. In the acetylation reaction of naphthalene **1**, the major product was the thermodynamically unfavoured 1-isomer, with a 2% yield of the 2-isomer. This is in accordance with best literature yield and selectivity.[9,10] It has been suggested that the position of attack on naphthalene is determined to a large extent by steric factors.[11] For example, if the reaction is carried out in nitrobenzene or nitromethane,[11] the 2-isomer is the major product and the acylating agent is thought to be an AcCl–$AlCl_3$–nitrobenzene complex. In the ionic liquid, the acylation agent is thought to be the free acylium ion.[3,12,13] Since the acylium ion is much smaller than the adduct, attack at sterically more hindered positions can occur.[3,13] In the ionic liquid, subsequent rearrangement of 1- or 2-acetylnaphthalene was not observed to occur. This was confirmed when the products were heated to 100 °C and in the presence of added hydrogen chloride,[14] and no further reaction was observed. In the acetylations of toluene **2**, chlorobenzene **3** and anisole **4**, all the major products were the 4-isomers. In these cases, the 2-isomers were present, but at levels less than 2%. These yields and selectivities were as good as the best published results.[15–17] With the reaction of 1,1,2,6-tetramethyl-3-isopropylindane **5**, the fragrance traseolide (5-acetyl-1,1,2,6-tetramethyl-3-isopropylindane) was obtained in 99% yield as a single isomer. The stereochemical arrangement of the indane ring was unaffected by the reaction.

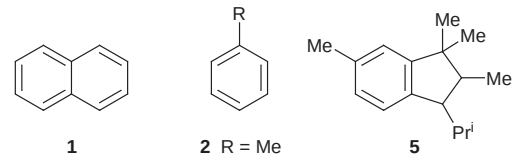

1 **2** R = Me, **3** R = Cl, **4** R = OMe, **5**

The acetylation reactions of anthracene were found to behave in a different manner to those of simpler aromatic compounds. Anthracene is generally considered to undergo acetylation reactions primarily at the 9-position.[18] Furthermore, the possibility of diacetylation exists, and deacetylation reactions complicate the chemistry, leading to a complex mixture of products. Owing to the complexity of the reaction, it was decided to monitor the variation of composition of the reaction mixture with time by gas chromatographic analysis.

It can be seen from Table 2 that 9-acetylanthracene **7** is the initial product in the reaction, formed rapidly in under 5 min, but this subsequently undergoes a slow disproportionation to anthracene and the two isomers of diacetylanthracene, **10** and **11**. Also, small amounts of 1- and 2-acetylanthracene are formed transiently. This implies that the monoacetylation of anthracene is reversible. Since the 1,5- and 1,8-diacetylanthracenes are the only isomers found in the final products, only the 1-acetylacthracene intermediate can undergo diacetylation. A plausible mechanistic scheme for this reaction is given in Scheme 1.

Table 1 Friedel–Crafts acylation of aromatic compounds **1–5** with AcCl in [emim]Cl–$AlCl_3$ (X = 0.67)

Aromatic compound	T/°C	t/h	Products (% yield)
1	0	1	1-AcAr (89), 2-AcAr (2)
2	20	1	4-AcAr (98), 2-AcAr (1)
3	20	24	4-AcAr (97), 2-AcAr (2)
4	−10	0.25	4-AcAr (99)
5	0	1	5-AcAr (99)

Table 2 The acetylation of anthracene **6** in [emim]Cl–$AlCl_3$ (X = 0.67) at 0 °C

		Composition (%)			
Reaction time	AcCl/equiv.	**6**	**7**	**10**	**11**
5 min	1.1	23	69	0	0
24 h	1.1	34	0	32	24
5 min	1.5	15	73	3	1
24 h	1.5	25	0	42	33
5 min	2.1	13	69	5	3
24 h	2.1	1	1	57	42

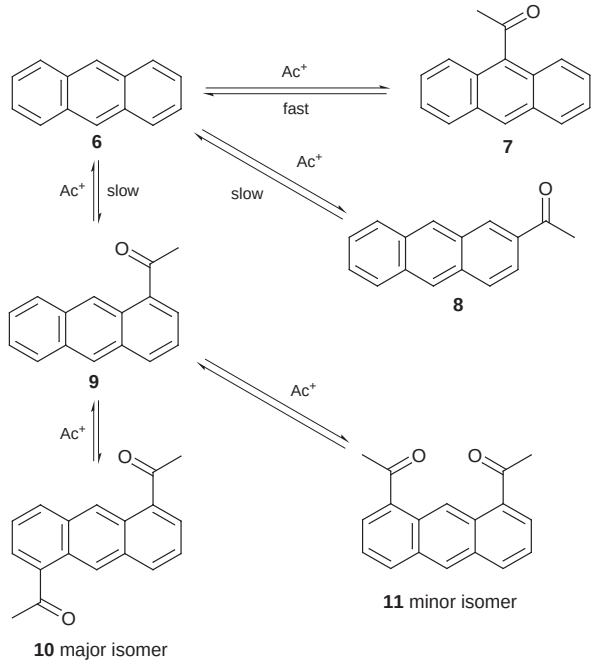

Scheme 1

It was decided to investigate the behaviour of 9-acetylanthracene in the ionic liquid. 9-Acetylanthracene dissolves in the [emim]Cl–$AlCl_3$ (X = 0.67) ionic liquid at 0 °C, and undergoes a slow conversion to anthracene (33%), **8** (12%), **10** (31%) and **11** (22%) (Scheme 1). Initially, a very slow reaction was observed. When a proton source (water) was introduced to the reaction vessel, a more rapid reaction occurred suggesting a proton-catalysed mechanism. The addition of small quantities of water to the reaction vessel leads to the formation of hydrogen chloride, which in chloroaluminate ionic liquids behaves in a superacidic manner.[14]

From these observations, it is possible to propose a plausible mechanism for the behaviour of 9-acetylanthracene in [emim]Cl–$AlCl_3$ (X = 0.67). It behaves in a manner that is very similar to that shown in Scheme 1. The key initial step must involve the protonation of **7** followed by loss of the acylium ion.

The acetylation reactions of pyrene and phenanthrene were also investigated (Table 3). The reaction of pyrene with AcCl in the ionic liquid appeared to behave in a similar manner to that of anthracene. The major products were the 1,6- and 1,8-isomers of diacetylpyrene, **12** and **13**, and the minor product was identified as 1-acetylpyrene **14**. This behaviour has not been reported in previous acetylation studies.[19] In the acetylation of phenanthrene, the mono-acetyl derivatives are the major products, with very little of the diacetyl products formed. As expected, 9-acetylphenanthrene **15** is the major product, and the minor products are the 1- and 2-isomers, **16** and **17**. This is very similar to conventional $AlCl_3$ catalysed reactions of AcCl with phenanthrene.[20]

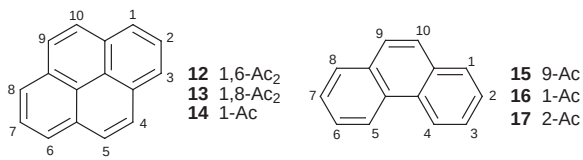

Based on these initial results, ionic liquids appear to provide an excellent medium for performing Friedel–Crafts reactions. Simple aromatic compounds, such as toluene, anisole or chlorobenzene are easily acetylated in yields that are equal to the best literature yields.[9–14] In addition, the regiochemical control of these reactions is excellent. In the acetylation of electron-rich polyaromatics, there is evidence that the reaction is reversible and that deacetylation reactions are proton catalysed. As for the mechanism of these reactions, the reaction of naphthalene appears to show that the acetylating agent is sterically small, and is probably the free acylium ion. It should also be noted that carbocyclic aromatics, such as naphthalene, phenanthrene and pyrene, form highly coloured compounds in acidic [emim]Cl–$AlCl_3$, probably π-complexes as they are paramagnetic.[21,22] The fact that paramagnetic species are present, and that protons play a significant part in these reactions, suggests that the classical mechanisms proposed for the Friedel–Crafts reaction may need modification.

Table 3 The acetylation of pyrene and phenanthrene in [emim]Cl–$AlCl_3$

Aromatic compound	T/°C	Time	AcCl/ equiv.	Starting material	Composition (%) Products
Pyrene	20	2 h	1.2	32	13 (**14**), 55 (**12** + **13**)
Phenanthrene	−10	5 min	1.5	0	55 (**15**), < 5 (**17**), 30 (**16**)

We are indebted to Unilever Research Laboratories, Port Sunlight, for financial support, and wish to thank James Travers for conducting preliminary studies and the EPSRC and the Royal Academy of Engineering for the award of a Clean Technology Fellowship (to K. R. S.).

Notes and References

† E-mail: m.earle@qub.ac.uk

‡ The composition of a tetrachloroaluminate(III) ionic liquid is best described by the apparent mole fraction of $AlCl_3$ [$X(AlCl_3)$] present. Ionic liquids with $X(AlCl_3) < 0.5$ contain an excess of Cl^- ions over $[Al_2Cl_7]^-$ ions, and are called 'basic'; those with $X(AlCl_3) > 0.5$ contain an excess of $[Al_2Cl_7]^-$ ions over Cl^-, and are called 'acidic'; melts with $X(AlCl_3) = 0.5$ are called 'neutral'.

1 R. M. Pagni, *Adv. Molten Salt Chem.*, 1987, **6**, 211.
2 J. K. D. Surette, L. Green and R. D. Singer, *Chem. Commun.*, 1996, 2753.
3 J. A. Boon, J. A. Levisky, J. L. Pflug and J. S. Wilkes, *J. Org. Chem.*, 1986, **51**, 480.
4 V. R. Koch, L. L. Miller and R. A. Osteryoung, *J. Am. Chem. Soc.*, 1976, **98**, 5277.
5 Y. Chauvin, B. Gilbert and I. Guibard, *Chem. Commun.*, 1990, 1715.
6 Y. Chauvin, A. Hirschauer and H. Olivier, *J. Mol. Catal.*, 1994, **92**, 155.
7 J. S. Wilkes, J. A. Levisky, R. A. Wilson and C. L. Hussey, *Inorg. Chem.*, 1982, **21**, 1263.
8 K. R. Seddon, in *Molten Salt Forum*: *Proceedings of 5th International Conference on Molten Salt Chemistry and Technology*, ed. H. Wendt, Trans Tech Publications, Switzerland, 1998, vol. 5-6, p. 53.
9 T. Immediata and A. R. Day, *J. Org. Chem.*, 1940, **5**, 512.
10 D. D. Dowdy, P. H. Gore and D. N. Waters, *J. Chem. Soc., Perkin Trans. 2*, 1991, 1149.
11 G. A. Olah, *Friedel–Crafts Chemistry*, Wiley-Interscience, New York, 1973.
12 B. Chevrier and R. Weiss, *Angew. Chem., Int. Ed. Engl.*, 1974, **13**, 1.
13 J. A. Levisky, J. L. Pflug and J. S. Wilkes, in *Proceedings of the Fourth International Symposium on Molten Salts*, The Electrochemical Society Inc., 1984, vol. 84-2, p. 174.
14 G. P. Smith, A. S. Dworkin, R. M. Pagni and S. P. Zingg, *J. Am. Chem. Soc.*, 1989, **111**, 525, 5075.
15 H. C. Brown, G. Marino and L. M. Stock, *J. Am. Chem. Soc.*, 1959, **81**, 3310.
16 P. M. Baranger, *Bull. Soc. Chim. Fr.*, 1931, 1213.
17 W. L. Judefind and E, E. Reid, *J. Am. Chem. Soc.*, 1920, **42**, 4993.
18 P. H. Gore, *J. Org. Chem.*, 1957, **22**, 135.
19 W. E. Bachmann and M. Carmack, *J. Am. Chem. Soc.*, 1941, **63**, 2494.
20 P. M. G. Bavin and M. J. S. Dewar, *J. Chem. Soc.*, 1956, 164.
21 D. F. Evans, *J. Chem. Soc.*, 1959, 2003.
22 P. Tarakeshwar, J. Y. Lee and K. S. Kim, *J. Phys. Chem.*, 1998, **102**, 2253.

Received in Cambridge, UK, 20th July 1998; 8/05599H

Characterization of chlorine atom adducts of dimethyl and diphenyl sulfide in CCl_4

John E. Chateauneuf

Department of Chemistry, Western Michigan University, Kalamazoo, MI 49008, USA and the Radiation Laboratory, University of Notre Dame, Notre Dame, IN 46556, USA. E-mail: chateauneuf@wmich.edu

The equilibrium constants for the association of chlorine atom with dimethyl and diphenyl sulfide to form chlorine atom adducts have been determined spectroscopically and indicate that both adducts should be considered three electron bond complexes.

Dimethyl sulfide (Me_2S) is known to be the major natural source of sulfur in the atmosphere.[1] Removal of Me_2S from the atmosphere is believed to occur by the reaction of Me_2S with photolytically generated free radicals and halogen atoms. Therefore, there has been considerable interest recently in kinetic and mechanistic investigations of halogen atom reactivity with sulfur containing species.[2–6] An important aspect of these investigations is the possibility of forming chlorine atom adducts to sulfides. It is also important to understand the physiochemical nature of the chlorine adducts in differing physical environments, *e.g.* gas, interfacial and liquid phases. This report presents a spectroscopic and kinetic methodology for the determination of equilibrium constants (K_{eq}) for the formation of chlorine atom molecular complexes in carbon tetrachloride solution. The equilibrium constants determined in this work were compared to values of K_{eq} for known π- and σ-chlorine atom complexes to determine the bonding nature of the dimethyl sulfide and diphenyl sulfide chlorine atom adducts.

The reason it is important to understand the strength of interaction of chlorine atom adducts is that K_{eq} will influence subsequent reactivity of the individual components of the system. Recently, in reports describing the photochemistry of the diphenyl sulfide/chlorine atom adduct ($Ph_2S/Cl^{\bullet}$), the complex was assigned to a π-molecular complex[7] owing to similarities in its absorption spectrum to $Cl^{\bullet}$/arene π-complexes.[8] The assignment is extremely intriguing in that the dimethyl sulfide/chlorine adduct ($Me_2S\therefore Cl$) has been characterized as a sulfur–chlorine three electron bond (2c–3e) adduct by matrix isolation EPR spectroscopy,[9] and in aqueous solution by pulse radiolysis.[10] Therefore, the question arises as to whether $Ph_2S/Cl^{\bullet}$ may demonstrate dual complexation, that is, π-interaction of $Cl^{\bullet}$ with the aromatic rings and σ-bond formation with the sulfur center. This question may be addressed by measuring the apparent reactivity of the $Ph_2S/Cl^{\bullet}$ adduct with 2,3-dimethylbutane (DMB) at low concentrations of complexing agent,[11,12] and in turn determining K_{eq}. The results obtained then may be compared with the reactivity of the known $Cl^{\bullet}$/benzene π-complex[8] and the $Cl^{\bullet}$/pyridine σ-complex.[11,12]

Chlorine atoms, and in turn $Ph_2S/Cl^{\bullet}$, were independently generated by both pulse radiolysis† and 266 nm laser flash photolysis (LFP) of CCl_4‡ containing 1×10^{-3} M Ph_2S. Each method of generation produced the same result, namely absorption spectra containing two absorption bands (λ_{max} = 340 nm, 500 nm; see graphical abstract) that were consistent with the absorption spectrum of $Ph_2S/Cl^{\bullet}$ previously reported.[7] Also consistent with the previous report was 1×10^{10} M^{-1} s^{-1} rate of formation of the $Ph_2S/Cl^{\bullet}$ complex and the 340 nm and 500 nm absorption bands of the $Ph_2S/Cl^{\bullet}$ complex demonstrated identical kinetic behavior. From a detailed kinetic analysis of selectivity in the photochlorination of DMB in the presence and absence of benzene, Ingold and coworkers[8] determined K_{eq} = 200 M^{-1} for the $Cl^{\bullet}$/benzene π-complex, *i.e.* $K_{benzene}$ = 200 M^{-1}. It has been demonstrated[11,12] that K_{eq} of other $Cl^{\bullet}$ complexes ($Cl^{\bullet}$/M) may then be determined by monitoring the apparent reactivity ($k_{apparent}$) of the complex with DMB using time resolved spectroscopy and the relationship, $K_M = K_{benzene} \times k_{apparent}(benzene)/k_{apparent}(M)$. By directly monitoring the formed complex, $Cl^{\bullet}$/M, the apparent reactivity reflects the extent of reversible dissociation§ to free $Cl^{\bullet}$, which then may be scavenged by DMB. The $Ph_2S/Cl^{\bullet}$ complex demonstrated little reactivity towards DMB, $k_{apparent} = 9.9 \times 10^4$ M^{-1} s^{-1}. This results in K_{eq} for formation of the adduct (K_{Ph_2S}) to be 3.2×10^{-5} M^{-1} according to Scheme 1 and the equation above with $K_{benzene}$ and $k_{apparent}$(benzene), see Scheme 2, being 200 M^{-1} and 1.6×10^8 M^{-1} s^{-1}, respectively. For comparison, K_{eq} for formation of the $Cl^{\bullet}$/pyridine σ-complex is 1.2×10^5 M^{-1} and $k_{apparent}$(pyridine) = 2.6×10^5 M^{-1} s^{-1}.[11] The $Me_2S/Cl^{\bullet}$ adduct was also generated by both pulse radiolysis and LFP of CCl_4 (λ_{max} = 365 nm, see graphical abstract). Similar to the $Ph_2S/Cl^{\bullet}$ results, $Me_2S/Cl^{\bullet}$ also demonstrted little reactivity toward DMB, $k_{apparent} = 1.8 \times 10^{-5}$ M^{-1} s^{-1}, yielding $K_{eq} = 1.73 \times 10^5$ M^{-1}, Scheme 3. This is true even at $[Me_2S] = 5 \times 10^{-4}$ M. It should also be noted that in aqueous solution K for neutral disssociation of $Me_2S\therefore Cl \rightarrow Me_2S + Cl^{\bullet}$ is $\ll 10^{-10}$ M^{-1}, whereas $K \approx 4$ M^{-1} for the ionic dissociation to $Me_2S^{\bullet+} + Cl^-$.[10] In CCl_4 there was no spectroscopic evidence of $Me_2S^{\bullet+}$

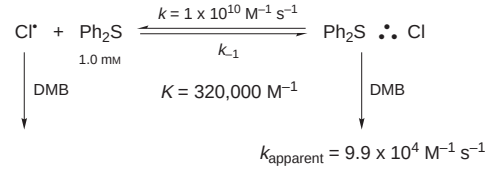

Scheme 1

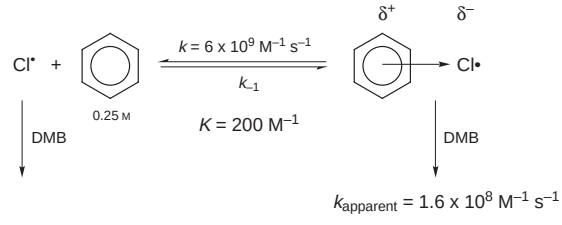

Scheme 2

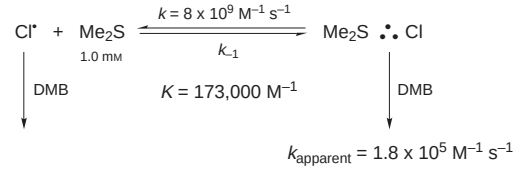

Scheme 3

formation, owing to the lack of solvating power of this solvent.

In summary, the values of K_{eq} for the Cl$^{\bullet}$ adducts with benzene, pyridine, Me_2S and Ph_2S in CCl_4 are: 200 M^{-1}, 120000 M^{-1}, 173000 M^{-1} and 320000 M^{-1}, respectively. Gratifyingly, these results are in accordance with recent theoretical determinations of the 0 *K* binding energies[5,6] of 11.4 kcal mol^{-1} for the Cl$^{\bullet}$/pyridine complex [Table 2 in ref 5; method used G2 (MP2, SVP)] and 12.32 kcal mol^{-1} for the $Me_2S^{\therefore}Cl$ complex [Table 5 in ref. 6; method used QCISD (T)/DZP + ZPC]. The results presented demonstrate that the bonding nature of the Ph_2S/Cl adduct is not consistent with a loosely bound π-molecular complex, and should be considered a three-electron bond $Ph_2S^{\therefore}Cl$ adduct, as is the $Me_2S^{\therefore}Cl$ complex. The methodology presented may prove useful in future characterizations of $R_2S^{\therefore}Cl$ complexes in interfacial and mixed-solvent systems.

The work described herein was supported in part by the Office of Basic Energy Sciences of the U.S. Department of Energy (Contribution No. NDRL-4075) and by Western Michigan University. I would also like to thank Professor Yi-Ping Liu for helpful discussions.

Notes and References

† Pulse radiolysis experiments were performed using a 10 ns pulse of 8 MeV electrons from the Notre Dame Radiation Laboratory linear accelerator (LINAC). The pulse radiolysis apparatus has been described elsewhere.[13]

‡ CCl_4 (Fisher Spectranalyzed) was distilled from K_2CO_3 (35 cm Vigreux column) prior to use.

§ This methodology is only valid in the absence of radical chain regeneration of Cl$^{\bullet}$ which is not possible in the present experiments.

1 M. O. Andreae, in *The Role of Air–Sea Exchange in Geochemical Cycling*, ed. P. Buat-Menard, D. Reidel, Hingam, MA, 1986, pp. 331–362; T. S. Bates, J. D. Cline, R. H. Gammon and S. R. Kelly-Hansen, *J. Geophys. Res.*, 1987, **92**, 2930.
2 N. I. Butkovskaya, G. Poulet and G. LeBras, *J. Phys. Chem.*, 1995, **99**, 4536.
3 M. L. McKee, *J. Phys. Chem.*, 1993, **97**, 10971.
4 R. E. Stickel, J. M. Nicovich, S. Wang, Z. Xhao and P. H. Wine, *J. Phys. Chem.*, 1992, **96**, 9875.
5 M. L. McKee, A. Nicolaides and L. Radom, *J. Am. Chem. Soc.*, 1996, **118**, 10571.
6 S. M. Rsende and W. B. de Almeida, *J. Phys. Chem. A*, 1997, **101**, 9738.
7 T. Sumiyoshi, M. Kawasaki and M. Katayama, *Bull. Chem. Soc. Jpn.*, 1993, **66**, 2510; T. Sumiyoshi, H. Sakai, M. Kawasaki and M. Katayama, *Chem. Lett.*, 1992, 617.
8 N. J. Bunce, K. U. Ingold, J. P. Landers, J. Lusztyk and J. C. Scaiano, *J. Am. Chem. Soc.*, 1985, **107**, 5464, K. U. Ingold, J. Lusztyk, K. D. Raner, *Acc. Chem. Res.*, 1990, **23**, 219.
9 A. Abu-Raqabash and M. C. R. Symons, *J. Am. Chem. Soc.*, 1990, **112**, 8614; M. C. R. Symons and R. L. Petersen, *J. Chem. Soc., Faraday Trans. 2*, 1979, 210.
10 M. Gobl, M. Bonifacic and K.-D. Asmus, *J. Am. Chem. Soc.*, 1984, **106**, 5984; M. Bonifacic and K.-D. Asmus, *J. Chem. Soc., Perkin Trans. 2*, 1980, 758.
11 J. E. Chateauneuf, *J. Am. Chem. Soc.*, 1993, **115**, 1915.
12 R. Breslow, M. Brandl, J. Hunger, N. Turro, K. Cassidy, K. Krogh-Jespersen and J. D. Westbrook, *J. Am. Chem. Soc.*, 1987, **109**, 7204.
13 E. Janata and R. H. Schuler, *J. Phys. Chem.*, 1982, **86**, 2078.

Received in Columbia, MO, USA, 17th June 1998; 8/04622K

A blue photoluminescent $[Zn(L)(CN)_2]$ (L = 2,2′-dipyridylamine) material with a supramolecular one-dimensional chain structure

Kin-Ying Ho, Wing-Yiu Yu, Kung-Kai Cheung and Chi-Ming Che*

Department of Chemistry, The University of Hong Kong, Pokfulam Road, Hong Kong

A novel blue luminescent $[Zn(L)(CN)_2]$ complex (L = 2,2′-dipyridylamine) is synthesized and characterized by an X-ray diffraction study; the crystal packing in the Zn complex reveals that the molecules self-assemble by intermolecular hydrogen bonds [N–H···N≡C distance = 2.965(7) Å] and face-to-face π–π aromatic stacking interactions to form two-dimensional sheets.

Cyanometallates are useful motifs for the construction of supramolecular structures having novel photoelectronic properties; the superstructure formation is usually achieved through bridging linear covalent M–C≡N–M bonding interactions.[1] There have been relatively few attempts to harness terminal cyanide ligand as a binding site for hydrogen bonding in the synthesis of supramolecular assemblies. As part of our endeavour to explore the potential application of some blue luminescent metal complexes for molecular light-emitting diode device fabrications,[2] we are interested in the coordination chemistry of zinc(II) cyanides,[3] the luminescence properties of which have been little studied. Herein is decribed a blue luminescent cyanozinc(II) complex with 2,2′-dipyridylamine ligand L, $[Zn(L)(CN)_2]$, and the solid state structure of which shows cooperative N–H···N≡C hydrogen bonding and π–π stacking interactions.

The zinc(II) complex was prepared by prolonged reflux of a methanolic suspension of $Zn(CN)_2$ with L.† Using hot methanol the product was isolated as pale yellow crystals suitable for an X-ray crystallographic study.‡ Fig. 1 depicts a perspective view with atom numbering of the molecule. The Zn atom adopts a distorted tetrahedral coordination geometry and the measured Zn–N(1)/(3) distances are 2.037(4) and 2.046(4) Å, and the Zn–C(1)/(2) distances are found to be 1.987(6) and 2.007(6) Å. The observed Zn–N distances are comparable to the corresponding bond distances [2.148(9) and 2.082(9) Å] found for a related

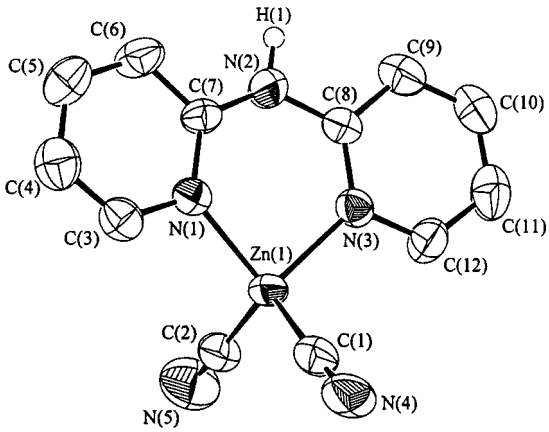

Fig. 1 Perspective view of $[Zn(L)(CN)_2]$ [50% thermal ellipsoids except for H(1)] and atom-numbering scheme. Significant bond distances (Å) and angles (°): Zn(1)–N(1) 2.037(4); Zn(1)–N(3) 2.046(4); Zn(1)–C(1) 1.987(6); Zn(1)–C(2) 2.007(6); N(2)–H(1) 0.91(6). N(1)–Zn(1)–N(3) 92.3(2); N(1)–Zn(1)–C(1) 116.3(2), N(1)–Zn(1)–C(2) 108.4(2); N(3)–Zn(1)–C(1) 108.4(2); N(3)–Zn(1)–C(2) 110.0(2); C(1)–Zn(1)–C(2) 118.3(2).

$[Zn(L)(dien)](NO_3)_2$ complex [dien = bis(2-aminoethyl)-amine].[4] The C(1)–Zn–C(2) bond angle is 108.3(2)°, whereas the N(1)–Zn–N(3) angle is 92.3(2)°.

As shown by the crystal packing (Fig. 2), the molecules are self-organized by extensive intermolecular hydrogen bonds between the amino and the cyano groups (N–H···N≡C) of the adjacent molecules, with obvious directionality and short intermolecular contact between successive nitrogen atoms [N···N distance = 2.965(7) Å]. The N(2)–H(1)···N(4) bond angle is 154(5)°, therefore a polymeric one-dimensional zigzag chain results. A related report by Cotton and co-workers[5] also revealed that the pseudo-tetrahedral $[Co(L)_2]$ molecules stack together to form a one-dimensional ribbon with molecules linked through intermolecular hydrogen bonding. In the present $[Zn(L)(CN)_2]$ complex face-to-face π–π stacking interactions between the aromatic rings of the 2,2′-dipyridylamine ligand are also evident, the interplanar separations are in the range 3.5–3.7 Å, and the glide-related complexes are linked in a head-to-head fashion to generate a supramolecular architecture of an infinite two-dimensional sheet. Inspection of the crystal packing shows that there are two kinds of two-dimensional sheets constituted by the same array of intermolecular forces but having the π–π stacking interactions aligning along different directions, hence a herringbone-type pattern is created.[6]

The spectroscopic and emission data of $[Zn(L)(CN)_2]$ complex are listed in Table 1. In MeOH, the absorption spectrum of the complex is dominated by intraligand π–π* transitions at 255 and 315 nm. In solution, the complex displays a high energy emission with λ_{max} = 359 nm and τ = 10 ns at 298 K. Because there is no significant shift in emission energy for the related $[Zn(L)X_2]$ (X = CN, OAc, Cl) complexes,† the emission is neither MLCT (metal-to-ligand charge transfer) nor LMCT (ligand-to-metal charge transfer) in nature. We tentatively assign it to the intraligand $^1(\pi–\pi^*)$ fluoresence since a similar emission with λ_{max} at 357 nm is also observed for the free ligand. Interestingly, in both solid state and in 77 K MeOH–EtOH glassy solution, the corresponding intraligand $^3(\pi–\pi^*)$

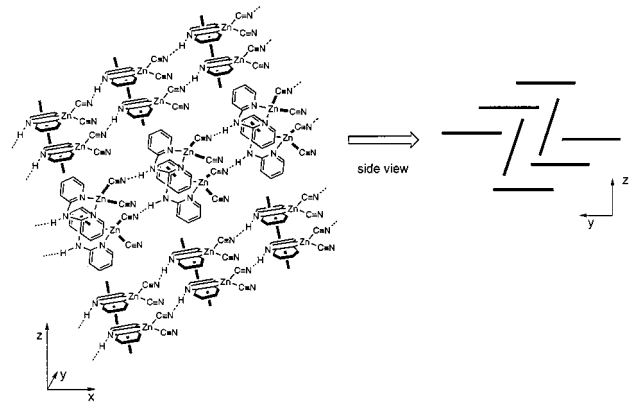

Fig. 2 Herringbone-type crystal packing pattern of $[Zn(L)(CN)_2]$ molecules. The molecules are self-assembled to form extended 2-D sheets by cooperative π–π stacking interactions and extensive intermolecular hydrogen (N–H···N≡C) bonds.

Table 1 Photophysical data for $[Zn(L)(CN)_2]$ and derivatives

Complex	UV–VIS λ/nm (ε/dm^3 mol^{-1} cm^{-1})[a]	Emission λ/nm		
		298 K[b]	77 K[c]	Solid state[d]
$[Zn(L)(CN)_2]$	257 (18000), 316 (16000)	359	351, 392	363, 418
$[Zn(L)(OAc)_2]$	257 (20000), 315 (18000)	359	349, 389	378
$[Zn(L)Cl_2]$	255 (18000), 315 (17000)	360	348, 390	378

[a] In MeOH at 298 K. [b] In degassed MeOH. [c] In MeOH–EtOH (1 : 2). [d] At 298 K.

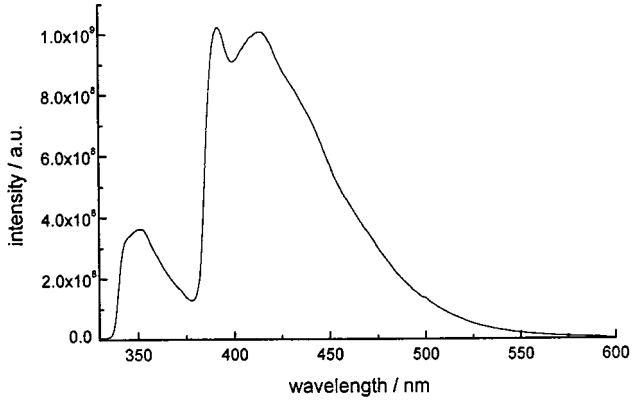

Fig. 3 Emission spectrum of $[Zn(L)(CN)_2]$ (excited at 315 nm) in MeOH–EtOH (1 : 2) glassy solution at 77 K.

phosphorescence has also been observed. As shown in Fig. 3, the lower energy $^3(\pi$–$\pi^*)$ emission at 392 nm (lifetime = 0.33 μs) shows a well resolved vibronic structure with a vibrational spacing of *ca.* 1350 cm^{-1} that is assigned to the skeletal stretching of the ligand.

The $[Zn(L)(CN)_2]$ complex shows an extended two-dimensional structure through cooperative hydrogen bonding and π–π stacking interactions. Its polymeric structure and the blue photoluminescence highlight the potential application of the zinc(II) cyanide complex as an advanced material for blue-light emitting diode devices.

We acknowledge the support from The University of Hong Kong and The Hong Kong Research Grants Council.

Notes and References

† *Preparation* of $[Zn(L)(CN)_2]$. A methanolic solution (20 cm^3) of L (0.17 g, 1 mmol) was added to a refluxing suspension of $Zn(CN)_2$ (0.12 g, 1 mmol) in MeOH (30 cm^3). The mixture was refluxed overnight. After cooling to room temperature, the white solid was collected by filtration. The product complex was extracted from the white solid into boiling methanol, and pale yellow crystals were obtained on cooling of the hot methanolic extract (overall yield: 60%). FT-Raman: 2164, 2153, 1619, 1587 and 1436 cm^{-1}. ^{1}H NMR (270 MHz, CD_3OD, TMS): δ 10.11 (s, 1H), 8.20 (d, 2H, ^3J = 4.3 Hz), 781 (t, 2H, ^3J = 7.3 Hz), 7.56 (d, 2H, ^3J = 7.2 Hz), 7.02 (t, 2H, ^3J = 6.0). FAB-MS: *m*/*z* 289 $[M]^+$, 261 $[M - CN]^+$. Anal. Calc. for $C_{12}H_9N_5Zn$ (M_r = 288.62): C, 49.94; H, 3.14; N, 24.27. Found: C, 49.99; H, 3.02; N, 24.41%.

Preparation of $[Zn(L)(OAc)_2]$. A methanolic solution (20 cm^3) of L (0.17 g, 1 mmol) was added to a refluxing solution of $Zn(OAc)_2 \cdot 2H_2O$ (0.22 g, 1 mmol) in MeOH (30 cm^3). The mixture was refluxed overnight. After cooling to room temperature, the solvent was removed by rotary evaporation, and the white residue was recrystallized by slow diffusion of diethyl ether into methanolic solution to afford colorless crystals (overall yield: 85%). ^{1}H NMR (270 MHz, CD_3OD, TMS): δ 8.38 (dd, 2H, ^4J = 1.2 Hz, ^3J = 5.6 Hz), 7.93 (td, 2H, ^4J = 1.9 Hz, ^3J = 7.9 Hz), 7.20 (d, 2H, ^3J = 8.6 Hz), 7.16 (td, 2H, ^3J = 6.5, ^4J = 1.0 Hz). FAB-MS: *m*/*z*: 294 $[M - OAc]^+$. Anal. Calc. for $C_{14}H_{15}N_3O_4Zn$ (M_r = 354.67): C, 47.41; H, 4.26; N, 11.85. Found: C, 47.25; H, 4.21; N, 11.92%.

Preparation of $[Zn(L)Cl_2]$. A similar procedure as for $[Zn(L)(OAc)_2]$ was employed, except that hot DMF was used for recrystallization (overall yield: 80%). ^{1}H NMR (270 MHz, CD_3OD, TMS): δ 8.20 (d, 2H, ^3J = 2.6 Hz), 7.80 (m, 2H), 7.58 (d, 2H, ^3J = 8.4 Hz), 7.01 (t, 2H, ^3J = 6.3 Hz). FAB-MS: *m*/*z* = 270 $[M - Cl]^+$. Anal. Calc. for $C_{10}H_9Cl_2N_3Zn$ (M_r = 307.49): C, 39.06; H, 2.95; N, 13.67. Found: C, 38.93; H, 2.99; N, 13.75%.

‡ *Crystal data* for $[Zn(L)(CN)_2]$: M_r = 288.62, monoclinic, space group *Cc* (no. 9), *a* = 16.305(1), *b* = 6.445(2), *c* = 13.166(3) Å, β = 115.24(1)°, *U* = 1251.5(5) Å^3, *Z* = 4, D_c = 1.532 g cm^{-3}, μ(Mo-Kα) = 19.51 cm^{-1}, *F*(000) = 584, *T* = 301 K, 1084 unique reflections (2θ < 48°, R_{int} = 0.012) were measured and 931 with $I > 3\sigma(I)$ were used in the refinement. *R* = 0.024, R_w = 0.030 with a goodness-of-fit of 1.62. CCDC 182/974.

1 (*a*) K. R. Dunbar and R. A. Heintz, in *Progress in Inorganic Chemistry*, ed. K. D. Karlin, John Wiley, New York, 1997, vol. 45, p. 283.
2 (*a*) C.-F. Lee, K.-F. Chin, S.-M. Peng and C.-M. Che, *J. Chem. Soc., Dalton Trans*., 1993, 467; (*b*) Y. Ma, H.-Y Chao, Y. Wu, W.-Y. Yu and C.-M. Che, *Chem. Commun.*, 1998, in press.
3 (*a*) B. F. Hoskins and R. Robson, *J. Am. Chem. Soc.*, 1990, **112**, 1546 and references therein; (*b*) M. Uchiyama, Y. Kondo, T. Miura and T. Sakamoto, *J. Am. Chem. Soc*., 1997, **119**, 12372.
4 N. Ray and B. Hathaway, *J. Chem. Soc., Dalton Trans*., 1980, 1150.
5 F. A. Cotton, L. M. Daniels, G. T. Jordan IV and C. A. Murillo, *Chem. Commun*., 1997, 1673.
6 J. J. Wolff, *Angew. Chem., Int. Ed. Engl.*, 1996, **35**, 2195.

Received in Cambridge, UK, 27th July 1998; 8/05814H

Synthesis and characterisation of a pair of azo anion radicals bonded to ruthenium(II)

Maya Shivakumar, Kausikisankar Pramanik, Prasanta Ghosh and Animesh Chakravorty*

Department of Inorganic Chemistry, Indian Association for the Cultivation of Science, Calcutta 700 032, India. E-mail: icac@iacs.ernet.in

The reactions of 1-methyl-2-(*p*-chlorophenylazo)imidazole (L^1) and 2-(phenylazo)pyridine (L^2) with [Ru(H)(X)(CO)(PPh_3)$_3$] (X = Cl, Br) have afforded the green paramagnetic (S = ½) and EPR-active ($g \approx 2.00$) title anion radical complexes [Ru($L^{1\cdot-}$)(Cl)(CO)(PPh_3)$_2$] **1 and [Ru($L^{2\cdot-}$)(Br)(CO)(PPh_3)$_2$] **2** in which the N–N bond lengths lie near 1.35 Å.**

Familiar systems with nitrogen–nitrogen single and double bonds are hydrazines and azobenzenes. One-electron reduction[1–3] of the azo group can lead to a bond order of 1.5 due to population of the azo π* orbital, but no such species have so far been isolated in pure form. Herein we describe the successful synthesis and structural characterisation of a pair of azo anion radicals bonded to bivalent ruthenium. The specific azo ligands used are the 2-(arylazo)heterocycles L^1 [3] and L^2 (general

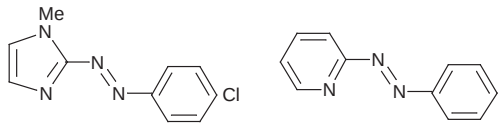

L^1 L^2

abbreviation, L).[4,5] The corresponding radical anions will be represented as $L^{1\cdot-}$ and $L^{2\cdot-}$ respectively.

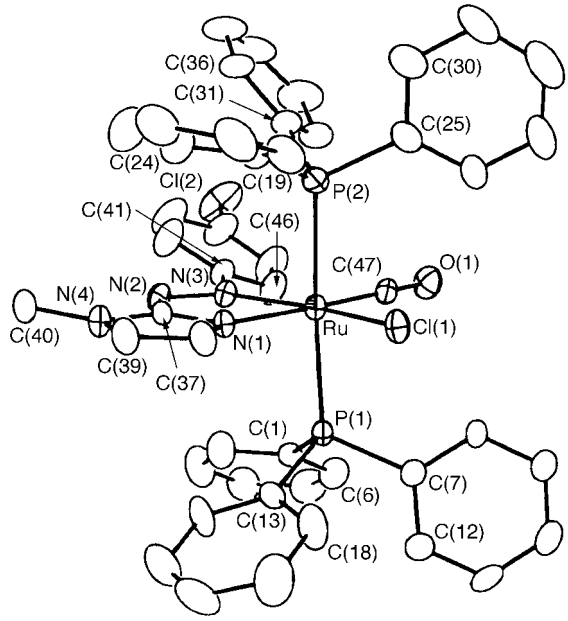

Fig. 1 ORTEP diagram of [Ru($L^{1\cdot-}$)(Cl)(CO)(PPh_3)$_2$] **1** (hydrogen atoms are omitted for clarity). Selected bond distances (Å) and angles (°): Ru–Cl(1) 2.416(2), Ru–P(1) 2.385(2), Ru–P(2) 2.393(2), Ru–N(1) 2.093(6), Ru–N(3) 2.107(6), Ru–C(47) 1.854(8), N(2)–N(3) 1.369(8), O(1)–C(47) 1.116(8), P(1)–Ru–P(2) 175.25(8), Cl(1)–Ru–N(3) 162.6(2), N(1)–Ru–C(47) 175.8(3), N(1)–Ru–N(3) 76.0(2), Ru–C(47)–O(1) 179.5(8).

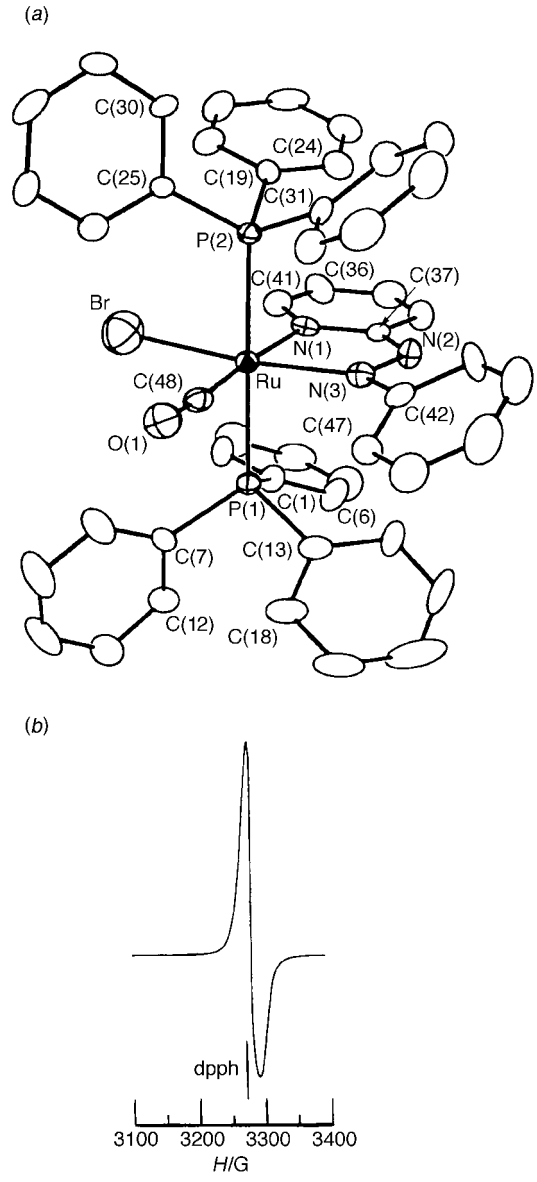

Fig. 2 (*a*) ORTEP diagram of [Ru($L^{2\cdot-}$)(Br)(CO)(PPh_3)$_2$] **2** (hydrogen atoms are omitted for clarity). Selected bond distances (Å) and angles (°): Ru–Br 2.521(3), Ru–P(1) 2.415(4), Ru–P(2) 2.399(4), Ru–N(1) 2.111(13), Ru–N(3) 2.069(13), Ru–C(48) 1.843(17), N(2)–N(3) 1.341(17), O(1)–C(48) 1.125(18), P(1)–Ru–P(2) 176.3(2), Br–Ru–N(3) 168.8(3), N(1)–Ru–C(48) 175.5(6), N(1)–Ru–N(3) 76.3(5), Ru–C(48)–O(1) 175.3(14). (*b*) Powder EPR spectrum of **2** in the X-band (9.11 GHz) at 298 K. Instrument settings: power, 28 dB; modulation, 100 kHz; sweep center, 3200 G; sweep width, 1000 G; sweep time 240 s.

Addition of [Ru(H)(Cl)(CO)(PPh_3)$_3$][6] (0.1 mmol) to a solution of L^1 (0.26 mmol) in dry benzene (10 ml) followed by heating

to reflux for 1 h and subsequent cooling afforded the deep green crystalline complex $[Ru(L^{1\cdot-})(Cl)(CO)(PPh_3)_2]$ **1** in 85% yield (all operations were carried out in an oxygen free environment).† A similar reaction of L^2 with $[Ru(H)(Br)(CO)(PPh_3)_3]$ [6] in dry heptane furnished $[Ru(L^{2\cdot-})(Br)(CO)(PPh_3)_2]$ **2**.† The key to our success is the use of hydridic starting materials which provide the reducing equivalent that is necessary for anion radical generation, eqn. (1), *via* Ru–H bond cleavage.

$$[Ru(H)(X)(CO)(PPh_3)_3] + L \rightarrow [Ru(L^{\cdot-})(X)(CO)(PPh_3)_2] + \tfrac{1}{2} H_2 + PPh_3 \quad (1)$$

The solid complexes which are quite stable in dry air behave as one-electron paramagnets (μ_{eff}: **1**, 1.80 μ_B and **2**, 1.78 μ_B) and display a single-line strong powder EPR signal (298 K) with g = 2.000 for **1** and g = 1.999 for **2**, the respective peak-to-peak line-widths being 9 G and 18 G. This is consistent with the azo anion radical description. The expected small ^{14}N hyperfine splitting is not resolved probably due to dominant anisotropic contributions.[2,7]

The X-ray structures‡ of **1** and **2** are shown in Fig. 1 and 2; Fig. 2 also displays the EPR spectrum of **2**. In each case the L ligand forms a planar five-membered chelate ring to which the *trans*-$Ru^{II}(PPh_3)_2$ fragment lies nearly orthogonally. The halide and carbon monoxide ligands are positioned *trans* to the azo and heterocyclic nitrogen atoms respectively. The N–N distances, 1.369(8) Å in **1** and 1.341(17) Å in **2**, are intermediate between those of double (≈1.25 Å[8]) and single (≈1.45 Å[9]) bonds as expected for the radical anion description.

Aerial oxidation of **1** and **2** in polar solvents gives $[Ru(L^1)(Cl)(CO)(PPh_3)_2]^+$ $\mathbf{1}^+$ and $[Ru(L^2)(Br)(CO)(PPh_3)_2]^+$ $\mathbf{2}^+$ which have been isolated as diamagnetic PF_6^- salts.† In dichloromethane solutions the $E_{\frac{1}{2}}$ values of the $\mathbf{1}^+/\mathbf{1}$ and $\mathbf{2}^+/\mathbf{2}$ couples are respectively −0.47 V and −0.39 V *vs.* SCE. Reversible coulometric recycling between **1** and $\mathbf{1}^+$ and between **2** and $\mathbf{2}^+$ can be repeatedly performed in an inert atmosphere. A wider application of our synthetic procedure for anion radical generation is under scrutiny.

We thank the Indian National Science Academy, Department of Science and Technology and the Council of Scientific and Industrial Research, New Delhi for financial support. Affiliation with the Jawaharlal Nehru Centre for Advanced Scientific Research, Bangalore, India, is acknowledged.

Notes and References

† Satisfactory elemental analyses were obtained. *Selected spectral data*: **1**, UV–VIS (C_6H_6): λ_{max}/nm (ε/dm^3 mol^{-1} cm^{-1}) 568 (5000), 507 (4500), 390 (16400); IR (KBr, cm^{-1}) 1287m (N=N), 1918s (C≡O). **2,** UV–VIS (C_6H_6): λ_{max}/nm (ε/dm^3 mol^{-1} cm^{-1}) 570 (2300), 540 (2200), 380 (7800); IR (KBr, cm^{-1}) 1288m (N=N), 1925s (C≡O). $\mathbf{1}^+PF_6^-$, UV–VIS (CH_2Cl_2): λ_{max}/nm (ε/dm^3 mol^{-1} cm^{-1}) 524 (2940), 415 (12500), 294 (18500); IR (KBr, cm^{-1}) 1312m (N=N), 1945s (C≡O); δ_H ($CDCl_3$; 300 MHz), 7.05 (s, 1H), 6.91 (d, *J* 8.9, 2H), 6.66 (d, *J* 8.9, 2H), 6.32 (s, 1H), 4.13 (s, C*H*$_3$, 3H). $\mathbf{2}^+PF_6^-$, UV–VIS (CH_2Cl_2): λ_{max}/nm (ε/dm^3 mol^{-1} cm^{-1}) 515 (1970), 450 (2070), 380 (6600); IR (KBr, cm^{-1}) 1320m (N=N), 1960s (C≡O); δ_H ($CDCl_3$; 300 MHz) 8.73 (d, *J* 7.8, 1H), 8.25 (t, *J* 7.9, 1H), 7.80 (d, *J* 5.4, 1H), 6.92 (t, *J* 8.1, 2H), 6.77 (t, *J* 6.0, 1H), 6.73 (d, *J* 8.4, 2H).

‡ *Crystal data* for **1**: $C_{47}H_{39}N_4OP_2Cl_2Ru$, M = 909.73, monoclinic, space group $P2_1/n$, a = 10.029(2), b = 33.984(7), c = 12.386(3) Å, β = 97.15(3)°, U = 4189(2) Å^3, Z = 4, μ = 0.620 mm^{-1}, total reflections collected 6866, unique reflections 6218, final R indices for 4109 observed [$I > 2\sigma(I)$] reflections: $R1$ = 0.0547, $wR2$ = 0.1015; **2**: $C_{48}H_{39}N_3OP_2BrRu$, M = 916.74, monoclinic, space group $P2_1/c$, a = 10.226(5), b = 17.443(7), c = 22.760(8) Å, β = 97.75(3)°, U = 4023(3) Å^3, Z = 4, μ = 1.506 mm^{-1}, total reflections collected 6186, unique reflections 5703, final R indices for 3402 observed [$I > 2\sigma(I)$] reflections: $R1$ = 0.1010, $wR2$ = 0.2591. All crystallographic measurements were performed using a Siemens R3m/V four-circle diffractometer and data were collected by the ω-scan method. The structures were solved by the Patterson heavy-atom method (SHELXTL-Ver. 5.03) and refined on F^2 by full matrix least squares using all unique data.[10] All nonhydrogen atoms for **1** and **2** are anisotropic with H-atoms included in calculated positions (riding model). Empirical absorption corrections for both cases were carried out on the basis of azimuthal scans.[11] One phenyl ring of $P(1)Ph_3$ and one of $P(2)Ph_3$ displayed two-fold disorder around C(13)–C(16) and C(31)–C(34) axes respectively in **1**. The crystal of **2** was relatively poorly diffracting and the peaks were broad. CCDC 182/977.

1 J. L. Sadler and A. J. Bard, *J. Am. Chem. Soc.*, 1968, **90**, 1979; B. K. Ghosh and A. Chakravorty, *Coord. Chem. Rev.*, 1989, **95**, 239.
2 C. K. Pal, S. Chattopadhyay, C. R. Sinha and A. Chakravorty, *Inorg. Chem.*, 1996, **35**, 2442.
3 T. K. Misra, D. Das, C. R. Sinha, P. Ghosh and C. K. Pal, *Inorg. Chem.*, 1998, **37**, 1672 and references therein.
4 S. Goswami, R. Mukherjee and A. Chakravorty, *Inorg. Chem.*, 1983, **22**, 2825.
5 R. A. Krause and K. Krause, *Inorg. Chem.*, 1984, **23**, 2195.
6 N. Ahmad, J. J. Levison, S. D. Robinson and M. F. Uttley, *Inorg. Synth.*, 1975, **15**, 45; J. M. Jenkins, M. S. Lupin and B. L. Shaw, *J. Chem. Soc. A*, 1966, 1787.
7 C. K. Pal, S. Chattopadhyay, C. R. Sinha and A. Chakravorty, *Inorg. Chem.*, 1994, **33**, 6140.
8 A. Mostad and C. Romming, *Acta Chem. Scand.*, 1971, **25**, 3561; C. H. Chang, R. F. Porter and S. H. Brauer, *J. Am. Chem. Soc.*, 1970, **92**, 5313; T. Roy and S. P. Sengupta, *Cryst. Struct. Commun.*, 1980, **9**, 965.
9 Y. Morino, T. Iijima and Y. Murata, *Bull. Chem. Soc. Jpn.*, 1960, **33**, 46.
10 G. M. Sheldrick, SHELXTL, Version 5.03, Siemens Analytical X-ray Instruments Inc., Madison, WI, 1994.
11 A. C. T. North, D. C. Phillips and F. S. Mathews, *Acta Crystallogr., Sect. A*, 1968, **24,** 351.

Received in Cambridge, UK, 15th June 1998; 8/04480E

Selective synthesis of MeCHO by C_2H_4–(O_2+NO) cell system

I. Yamanaka,† A. Nishi and K. Otsuka

Department of Chemical Engineering, Tokyo Institute of Technology, Ookayama, Meguro-ku, Tokyo 152-8552, Japan

The formation rate of MeCHO and current for the C_2H_4 | Pd | H_3PO_4 | graphite | O_2 + NO (NO_2) cell are ten times higher than those for the C_2H_4 | Pd | H_3PO_4 | Pt | O_2 cell.

The selective synthesis of MeCHO has been demonstrated by a C_2H_4–O_2 cell system that was assembled as [C_2H_4, H_2O(g) | Pd-black/graphite/PTFE anode | aq. H_3PO_4 in silica wool | Pt-black/graphite/PTFE cathode | O_2].[1] Oxidation of C_2H_4 to MeCHO at the anode [eqn. (1)] and reduction of O_2 to H_2O at the cathode [eqn. (2)] proceeded respectively.

$$C_2H_4 + H_2O \rightarrow MeCHO + 2\,H^+ + 2e^- \quad (1)$$

$$1/2\,O_2 + 2\,H^+ + 2\,e^- \rightarrow H_2O \quad (2)$$

The cell system has several advantages compared with the current Wacker process using a mixture of C_2H_4 and O_2 catalysed by $PdCl_2$ and $CuCl_2$ in HCl solution.[2] For example, (i) the cell system is chloride free, and (ii) no separation processes for products and catalysts are required. Recent attractive heterogeneous catalytic systems have the same advantages.[3,4] The cell system has additional advantages, (iii) the reaction rate and the current are easily controlled by variable resistance, and (iv) the danger of explosion is reduced because C_2H_4 and O_2 are separated by the membrane.[1,5–7] However, the rate of MeCHO formation attained in this C_2H_4–O_2 cell system (1 ~ 2 TON per Pd atom in 1 h)[1] has to be improved dramatically. The TON obtained in the current Wacker process is greater than 10.[2] Therefore, the purpose of this work is to demonstrate the enhancement of the formation rate of MeCHO by one order of magnitude for the C_2H_4–O_2 cell system.

First, the potentials at the anode and the cathode for the C_2H_4–O_2 cell were measured at 353 K. The details of electrochemical measurement have been described elsewhere.[8] The potentials at the anode and the cathode were +0.26 V (*vs.* Ag | AgCl) and +0.86 V respectively under open circuit conditions: the electromotive force (EMF) was 0.60 V. The potentials were changed to +0.65 and +0.67 V under short circuit conditions. The difference in the anode and the cathode potentials under short circuit conditions is due to an Ohm resistance. Thus, the over-potential at the anode was larger than that at the cathode. However, it should be noted that a considerable over-potential existed at the cathode, 32% of the EMF, for the electrochemical reduction of O_2.

If the over-potential at the cathode could be decreased by some means, an additional electrochemical potential could be applied at the anode which should increase the formation rate of MeCHO and the current. On the basis of this concept, many trials were performed for improving the rate of MeCHO formation. In conclusion, it is found that the addition of nitric oxide in a stream of O_2 dramatically enhances the current and the formation rate of MeCHO.

Fig. 1 shows a time profile for the formations of MeCHO and CO_2 [Fig. 1(*a*)] and for the current [Fig. 1(*b*)] with and without addition of NO into an O_2 stream. The apparent surface areas of the electrodes were 2 cm^2. The content of Pd in the anode was 120 μmol. When the circuit was shorted, a current of 3 mA cm^{-2} flowed and MeCHO was selectively produced (> 97%). When NO was added to the stream of O_2, a drastic increase in the current (35 mA cm^{-2}) and the formation rate of MeCHO were observed. When the NO addition was stopped, the current and the formation rate of MeCHO immediately decreased. Then, the current and the formation rate of MeCHO increased again with the addition of NO. It is clear that the addition of NO to the O_2 stream reversibly accelerates both the current and the formation rate of MeCHO. Although the formation rate of CO_2 was also increased by the addition of NO, the selectivity to MeCHO was still quite high (> 95%).

The cathode and anode potentials for the C_2H_4–(O_2+NO) cell system were measured. The cathode potential under open circuit conditions is 1.0 V, which was considerably higher than the value (0.86 V) for the C_2H_4–O_2 cell. A separate experiment showed that the cathode potential for the C_2H_4–NO cell was 0.85 V. When NO was added to the O_2 stream in the cathode compartment, formation of a dark brown gas was observed, indicating the formation of NO_2 [eqn. (3)]. The increase in the cathode potential by the addition of NO and O_2 must be due to the formation of NO_2, which could be a stronger oxidant than O_2 or NO.

$$NO + 1/2\,O_2 \rightarrow NO_2 \quad (3)$$

The anode potential under open circuit conditions is 0.26 V. The EMF for the C_2H_4–(O_2+NO) cell is 0.74 V, which is larger than the value (0.60 V) for the C_2H_4–O_2 cell. When the circuit was shorted, the potentials of the anode and the cathode were changing to 0.88 and 0.93 V, respectively. The over-potentials at the anode and cathode were 0.62 and 0.07 V. The over-potential of 0.07 V at the cathode was smaller than that of 0.19 V for the C_2H_4–O_2 cell, although the current was one order of

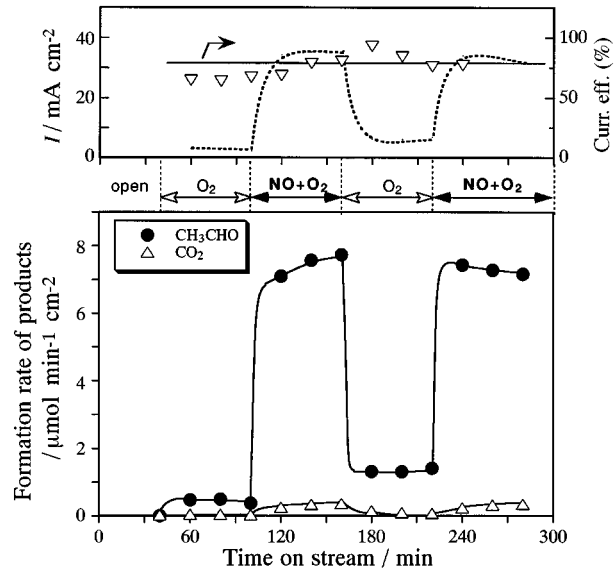

Fig. 1 Effects of NO addition into the O_2 stream at the cathode on the formation of MeCHO with the C_2H_4–O_2 cell: (●) MeCHO and (△) CO_2. C_2H_4 (39 kPa), H_2O (13 kPa), anode | aq. H_3PO_4 in silica wool | cathode, O_2 (51 kPa), He (50 kPa) or NO (50 kPa). T = 353 K. Anode: Pd-black/CF/PTFE, total flow rate = 32 ml min^{-1}. Cathode: Pt-black/graphite/PTFE, total flow rate = 32 ml min^{-1}.

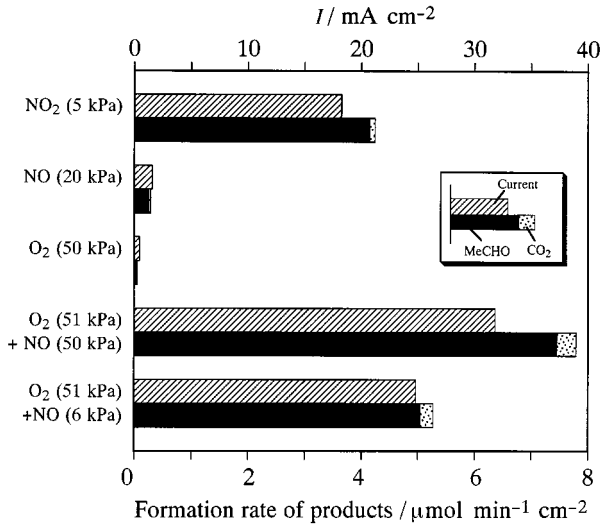

Fig. 2 Effects of some oxidants of the C_2H_4–oxidant cell with graphite/PTFE cathode on the Wacker oxidation. C_2H_4 (39 kPa), H_2O (13 kPa), anode | aq. H_3PO_4 in silica wool | cathode, oxidants. Oxidants: NO_2 (5 kPa), NO (20 kPa), O_2 (50 kPa), NO (50 kPa) + O_2 (51 kPa), and NO (6 kPa) + O_2 (51 kPa). T = 353 K.

magnitude larger than that for the C_2H_4–O_2 cell. This fact suggests that the electrochemical reduction of NO_2 is very easy compared with that of O_2.

The cathode used so far in this work was Pt-black/graphite/PTFE. If the reduction of NO_2 occurs quite easily, we may exclude Pt-black from the cathode. In fact, a cathode without Pt-black (graphite/PTFE cathode) showed very good electrocatalytic performance; a high current of 40 mA cm^{-2} and selective MeCHO formation (3% yield and 8 TON in 1 h). The optimum reaction conditions were studied for the C_2H_4–(O_2+NO) cell using the graphite/PTFE cathode. Then, a maximum yield of 15% and 31 TON in 1 h were obtained, which is fairly good productivity for MeCHO formation.

The results for the oxidation of C_2H_4 using different oxidants are compared in Fig. 2. The cathode in these experiments was graphite/PTFE. A current of 18.5 mA cm^{-2} flowed and MeCHO was selectively produced with the C_2H_4–NO_2 cell, although the pressure of NO_2 was only 5 kPa. A mixture of O_2 and NO was an excellent oxidant but O_2 or NO alone were not effective oxidant at the graphite cathode. When P_{NO} was reduced from 50 to 6 kPa for the C_2H_4–(O_2+NO) cell, the formation rate of MeCHO and the current were slightly decreased. The influences of P_{NO} on the formation rate and the current were small. When NO_2 (5 kPa) was introduced into the anode compartment, catalytic oxidation of C_2H_4 to CO_2 (1.2 μmol min^{-1} cm^{-2}) and MeCHO (0.4 μmol min^{-1} cm^{-2}) proceeded under open circuit conditions. The selective synthesis of MeCHO from C_2H_4 with NO_2 catalysed by the Pd anode does not proceeed. No enhancing effects due to the addition of NO_2 into the anode compartment on the formation of MeCHO and the current were observed under short circuit conditions. These facts confirm that NO_2 produced from a mixture of O_2 and NO works as a strong oxidant at the cathode.

The products for the reduction of NO_2 and NO at the cathode were trace formation of N_2 and N_2O in the gas phase and a small amount of NH_2OH or NH_3 (< 4% current efficiency) in the diaphragm. There are no other products containing nitrogen. These observations suggest that NO_2 is being reduced to NO and H_2O [eqn. (4)].

$$NO_2 + 2\ H^+ + 2\ e^- \rightarrow NO + H_2O \qquad (4)$$

The NO produced here would regenerate NO_2 according to [eqn. (3)]. Thus, NO works as a mediator (or catalyst) for the electrochemical reduction of O_2.

Notes and References

† E-mail: yamanaka@o.cc.titech.ac.jp

1 K. Otsuka, Y. Shimizu and I. Yamanaka, *J. Electrochem. Soc*., 1990, **137**, 2076; *Chem. Commun*., 1988, 1272.
2 J. Smidt, W. Hafner, R. Jira J. Sedlmeier, R. Sieber and H. Kojer, *Angew. Chem*., 1959, **71**, 176.
3 A. W. Stobbe-Kreemers, R. B. Dielis, M. Makkee and J. J. F. Scholten, *J. Catal*., 1995, **154**, 175.
4 K. Nowinska and D. Dudko, *Appl. Catal. A*, 1997, **159**, 75.
5 J. D. Tran, I. Londer and S. H. Langer, *Electrochim. Acta*., 1992, **38**, 221; S. H. Langer and J. A. Colucci-Rios, *Chemtech.*, 1985, 226
6 G. A. Stafford, *Electrochem. Acta*, 1987, **32**, 1137.
7 S. Molhatra and R. Datta, *J. Electrochem. Soc*., 1996, **145**, 3058.
8 I. Yamanaka, T. Akimoto and K. Otsuka, *Electrochim. Acta*, 1994, **39**, 2545.

Received in Cambridge, UK, 2nd July 1998; 8/05092I

Simultaneous determination of dopamine, uric acid and ascorbic acid at an ultrathin film modified gold electrode

Zhiqiang Gao*† and Hai Huang

Department of Chemistry, National University of Singapore, Kent Ridge, Singapore 119260, Republic of Singapore

Well-separated square wave voltammetric peaks for uric acid, dopamine and ascorbic acid were observed at an ultrathin polypyrrole–tetradecyl sulfate film modified gold electrode, which can be used for simultaneous determination of these species in the range of 1 to 500 μM with good reproducibility.

Recently there has been a considerable effort in the development of voltammetric methods for the determination of uric acid (UA), dopamine (DA) and ascorbic acid (AA) in biological samples. It is generally believed that direct redox reactions of these species at bare electrodes are irreversible and therefore require high overpotentials.[1] Moreover the direct redox reactions of these species at the bare electrodes take place at very similar potentials and often suffer from a pronounced fouling effect, which results in rather poor selectivity and reproducibility. The ability to determine UA, DA and AA selectively has been a major goal of electroanalytical research.[2] Since the basal concentrations of UA, DA and AA in biological samples vary from species to species in an extremely wide range, from 1.0×10^{-7} to 1.0×10^{-3} M,[3] both sensitivity and selectivity are of equal importance in developing voltammetric procedures. Various approaches, mainly based on ion-exchange membrane coated electrodes, have been attempted to solve the UA, DA and AA determination problems.[4–8] Ion exchange membranes of both anionic and cationic nature have been developed to electrostatically accumulate/trap oppositely charged analyte molecules. Among them are Nafion,[5] poly(ester sulfonic acid),[6] poly(4-vinylpyridine)[7] *etc*. However, the drawbacks of these ion exchange membrane modified electrodes are their memory effect, non-uniform thickness and poor reproducibility arising from the solvent evaporation method used in the film preparation. Moreover, some of the valuable information is lost when working with these ion exchange membrane modified electrodes because the membranes only allow oppositely charged species access to the electrode.

The electropolymerization of conducting polymers generally results in polymer films which are uniform and strongly adherent to the electrode surface. In addition the polymer films can be deposited onto a small area with a high degree of geometrical conformity and controllable thickness; this aspect is particularly important in the manufacture of microsensors. In short, fabrication of conducting polymer films is flexible and easily controlled, hence provides an attractive means of overcoming the problems caused by the solvent evaporation method.

In this work, the feasibility of modifying gold electrodes in an attempt to develop a sensitive voltammetric procedure for UA, DA and AA was studied. A remarkable improvement in square wave voltammetric responses of UA, DA and AA (voltammetric peaks were separated by about 150 mV from each other) and a noticeable enhancement of voltammetric sensitivity were observed at the polypyrrole–tetradecyl sulfate (PPy–TDS) film modified gold electrode. All of these were brought about by the combined catalytic function of the PPy–TDS film and the minimized background current in square wave voltammetry.

The PPy–TDS film was deposited onto the gold electrode galvanostatically in a deaerated solution saturated with pyrrole and sodium tetradecyl sulfate. The film thickness was controlled in the range of 20–25 nm by measuring the charge passed during electrodeposition. The electrode was then rinsed thoroughly with water and conditioned by cycling the potential for 2 min between –0.20 and 0.50 V at a scan rate of 50 mV s^{-1} (*vs.* Ag/AgCl) in a 0.10 M pH 7.0 phosphate buffer solution. The electrode was ready after a final rinse with water. Under optimum experimental conditions for the deposition of PPy–TDS film, the gold electrode was perfectly covered with an ultrathin PPy–TDS film, confirmed by surface coverage measurement using the copper under potential deposition method.[9]

Fig. 1 shows square wave voltammograms of 0.50 mM DA, UA and AA at both bare gold and the PPy–TDS film coated gold electrodes. As can be seen in Fig. 1(*a*), a rather broad oxidation peak appeared at about 0.32V at the bare gold electrode and the peak potentials for UA, DA and AA were indistinguishable. It is impossible to deduce any conclusive information from the broad voltammetric peak. Depending on the history of the electrode surface and the concentration ratios of UA, DA and AA, the peak potential could vary from 0.30 to 0.5 V. As shown in Fig. 1(*b*), the presence of the PPy–TDS film at the electrode surface resolved the mixed voltammetric response into three well-defined voltammetric peaks at potentials of 0.32, 0.17 and 0.015 V, corresponding to the oxidations of UA, DA and AA, respectively. Furthermore, as indicated in Fig. 1(*b*), substantial increases in peak currents were observed due to the improvements in the reversibilities of the electron transfer processes.[10] This suggests an efficient catalytic reaction between the modified electrode and the three species in solution. When cyclic voltammetry was conducted with the modified gold electrode at different scan rates, good linearities between the peak currents and the square roots of the scan rates for UA, DA and AA were obtained, indicating diffusion-controlled processes in solution. Rotating disk electrode experiments also reached the same conclusions as those obtained by voltammetry for all modified electrodes. No

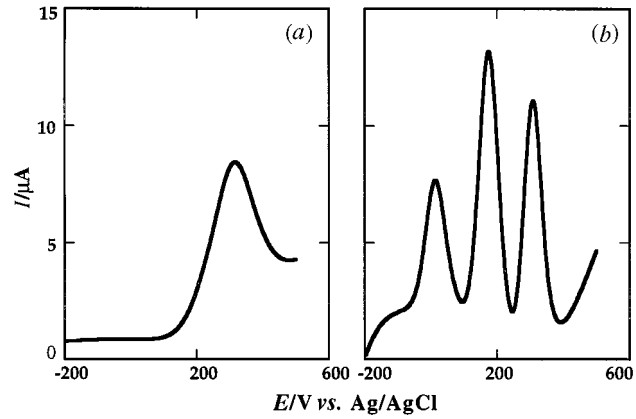

Fig. 1 Square wave voltammograms of 0.50 mM UA, DA and AA at (*a*) a bare gold and (b) a PPy–TDS film modified gold electrode (0.10 M pH 7.0 phosphate buffer, initial potential = −0.2 V, SW amplitude = 25 mV, SW frequency = 15 Hz, SW step = 2 mV)

obvious changes in the peak currents were observed when increasing the film thickness from 20 nm to 1.0 μm, suggesting that the PPy–TDS film has genuine catalytic function towards the oxidation of UA, DA and AA, and that the electron transfer processes within the film and at the film–solution interface are sufficiently fast that they do not affect the catalytic currents of UA, DA and AA. However, the charging current increased with increasing film thickness, thus preventing us from determining UA, DA and AA at micromolar levels. A similar catalytic effect was also observed at PPy films doped with other anions, but large charging currents were observed at PPy films doped with small anions such as chloride, nitrate and sulfate.[11] For practical purpose, in order to minimize the charging current, the PPy–TDS film should be kept as thin as possible, as long as the electrode is completely covered by the PPy–TDS film. Moreover, there is no memory effect at all since analytes cannot penetrate into the highly compact and conductive PPy–TDS film and the electron exchange process takes places at the PPy–TDS film–solution interface.

The overall facility of the modified electrode for simultaneous determinations of UA, DA and AA was demonstrated in solutions with simultaneous changes of concentrations. The peak currents obtained increased linearly with increasing UA, DA and AA concentrations in the range of 1.0 to 500 μM with a correlation coefficient of 0.997–0.998. The detection limits (signal-to-noise ratio = 3.0) for UA, DA and AA were found to be 0.4, 0.4 and 0.6 μM respectively. The modified electrode showed excellent anti-fouling properties. A series of 50 repetitive voltammetric determinations of sample solutions containing 25 μM UA, DA and AA were used to evaluate the stability of the modified electrode. The coefficient of variation was found to be 5.5%, indicating that the modified electrode is not subject to surface fouling by the oxidation products, which are notorious for their surface fouling effects at the bare electrodes.[12] High stability was also observed in phosphate buffer solutions containing high concentrations of chloride. For example, no obvious deterioration was observed after 50 repetitive voltammetric runs in a 0.10 M pH 7.0 phosphate buffer solution containing 0.15 M NaCl. The advantages accruing from the catalytic function of the film improved the selectivity of the voltammetric measurement of UA, DA or AA in the presence of the other two. As demonstrated in Table 1, the peak current obtained for a 25 μM of UA, DA or AA sample solution was practically constant in the presence of a wide range of concentrations of the other two species. In addition the slopes of the calibration curves were almost the same as those obtained with simultaneously changing concentrations of UA, DA and AA.

Table 1 Square wave voltammetric data (SW amplitude = 25 mV, SW frequency = 15 Hz, SW step = 2 mV) for 25 μM UA, DA and AA in mixed solutions at the PPy–TDS film modified gold electrode

AA		DA		UA	
DA + UA/ μM	ip_{AA}/μA	UA + AA/ μM	ip_{DA}/μA	DA + AA/ μM	ip_{UA}/ μA
0.0 + 0.0	0.250	0.0 + 0.0	0.600	0.0 + 0.0	0.510
10 + 10	0.247	10 + 10	0.590	10 + 10	0.512
50 + 50	0.248	50 + 50	0.608	50 + 50	0.505
200 + 200	0.247	200 + 200	0.575	200 + 200	0.498
500 + 500	0.245	500 + 500	0.580	500 + 500	0.490
1000 + 500	0.225	500 + 1000	0.535	1000 + 1000	0.445

In conclusion, we have demonstrated the possibility of using the PPy–TDS film modified electrode for the simultaneous determination of UA, DA and AA. The modified electrode showed excellent sensitivity, selectivity and anti-fouling properties. The high selectivity was proved to be mainly attributed to the catalytic function of the PPy–TDS film.

Notes and References

† E-mail: chmgaoz@nus.edu.sg

1 R. N. Adams, *Anal. Chem*., 1976, **48**, 1126A.
2 J. A. Stamford and J. B. Justice, Jr, *Anal. Chem*., 1996, **69**, 359A.
3 P. Capella, B. Ghasemzadeh, K. Mitchell and R. N. Adams, *Electroanalysis*, 1990, **2**, 175.
4 Z. Gao, K. S. Siow A. Ng and Y. Zhang, *Anal. Chim. Acta*, 1997, **343**, 49 and references cited therein.
5 G. A. Gerhardt, A. F. Oke, F. Nagy, B. Moghaddam and R. N. Adams, *Brain Res*., 1984, **290**, 390.
6 J. Wang and M. S. Lin, *Electroanalysis*, 1990, **2**, 861.
7 J. M. Zen, Y. J. Chen, C. T. Hsu and Y. S. Ting, *Electroanalysis*, 1997, **9**, 1009.
8 J. M. Zen and P. J. Chen, *Anal. Chem*., 1997, **69**, 5087.
9 Z. Gao, K. S. Siow and H. Chan, *Synth. Met*., 1995, **75**, 5.
10 J. Osteryoung and J. J. O'Dea, in *Electroanalytical Chemistry*, ed. A. J. Bard, Marcel Dekker, 1988, vol. 14.
11 Z. Gao, B. Chen and M. Zi, *J. Electroanal. Chem*., 1994, **365**, 197.
12 R. F. Lane and A. T. Hubbard, *Anal. Chem*., 1976, **48**, 1287.

Received in Cambridge, UK, 28th July 1998; 8/05915B

Deep cavity [CpFe(arene)]$^+$ derivatized cyclotriveratrylenes as anion hosts

K. Travis Holman,[a] G. William Orr,[a] Jonathan W. Steed[b] and Jerry L. Atwood*[a]

[a] *Department of Chemistry, University of Missouri-Columbia, Columbia, MO, 65211, USA. E-mail: atwoodj@missouri.edu*
[b] *Department of Chemistry, King's College London, Strand, London, UK WC2R 2LS*

Even in the absence of hydrogen bonding functionality, [CpFe(arene)]$^+$ derivatized cyclotriveratrylenes 5 will bind anionic substrates (*i.e.* [PF_6]$^-$, halides) deep within their preorganized molecular cavities. The crystal structure of 5b[PF_6]$_3$·($CH_3CH_2OCH_2CH_3$)$_{1.5}$·(H_2O) demonstrates the [5b⊂(PF_6)]$^{2+}$ complex and solution halide binding is monitored by ^{1}H NMR spectroscopy.

The development of receptor molecules for the specific complexation and/or detection of anions has over the years proven to be a formidable task. In consequence, a rather large and diverse array of supramolecular anion hosts has appeared.[1] Currently, work in our group is aimed at designing anion hosts by arranging positively charged organometallic moieties around the bowl shaped cavities of polyaromatic macrocycles such as calix[*n*]arenes and cyclotriveratrylene (CTV).[2] Similar organometallic anion receptors, including an amide functionalized [CpFe(arene)]$^+$ host,[3c] have been used extensively by Beer *et al.* for the sensing of anionic species with remarkable selectivity, although these hosts typically couple the function of charge pairing interactions with hydrogen bonding residues.[3] We have found that the tetrametallated calixarene [{(*p*-cymene)Ru}$_4$(calix[4]arene − 2H)]$^{6+}$ **1**, the dimetallated CTV [{(*p*-cymene)Ru}$_2$CTV]$^{4+}$ **2**, and related derivatives can function as anion receptors, despite the absence of hydrogen bonding functionality. The solution anion binding properties of hosts such as **1** and **2**, however, are typically complicated by the ability of the host to bind anions at sites exterior to the host cavity, as well as within.[2] We herein report new deep-cavity [CpFe(arene)]$^+$-based anion hosts whose upper rim charge preorganization allows binding of anions exclusively within the host cavity, and without the use of hydrogen bonding residues.

Racemic cyclotriveratrylene-based hosts **5** were synthesized as their [PF_6]$^-$ salts in good yield (75–85%) by S_NAr substitution of the respective [CpFe(chloroarene)][PF_6]**3a–c** complex with *rac*-cyclotriguaiacylene (CTG)[4] **4** in DMF containing excess K_2CO_3 (Scheme 1).[5] Neutralization of the reaction mixture with 2 M HCl(aq.) followed by addition of NH_4PF_6(aq.) and precipitation with water led to the products, which were further purified by passing through a short column of neutral alumina with acetone and reprecipitating with diethyl ether.

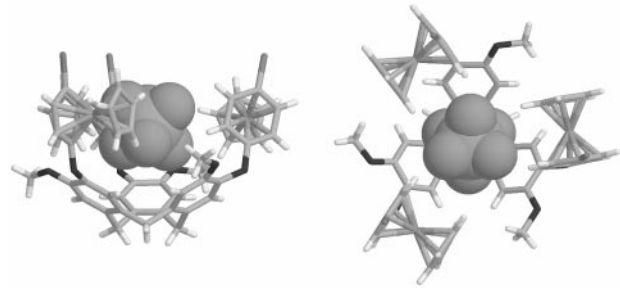

Fig. 1 X-Ray crystal structure of **5b**[PF_6]$_3$·($CH_3CH_2OCH_2CH_3$)$_{1.5}$·(H_2O)† depicting side and top views of [**5b**⊂(PF_6)]$^{2+}$ (see http://www.rsc.org/suppdata/cc/1998/2109 for full colour version of this figure)

The crystal structure of **5b** [PF_6]$_3$·($CH_3CH_2OCH_2CH_3$)$_{1.5}$·(H_2O)† demonstrates an approximate C_3 symmetric host conformation, with all of the [CpFe(arene)]$^+$ substituents directed up from the rim of the CTG moiety, and exemplifies the ability of these new hosts to complex large anions deep within their cavities (Fig. 1). One [PF_6]$^-$ ion is located central to the host cavity with its three-fold symmetry axis matching that of the pseudo three-fold axis of the host cation. The depth of cavity penetration is highlighted by the fact that the phosphorus atom lies approximately 0.6 Å below the plane defined by the iron atoms. Short P···Fe distances of 5.16, 5.14, and 5.08 Å to the three iron atoms of the host are representative of significant charge pairing interactions between the included [PF_6]$^-$ anion and all three metal centers of the host, whereas the other two [PF_6]$^-$ anions each only exhibit similar close contacts to one iron atom at 5.09 and 5.12 Å respectively.

The solution anion binding properties of hosts **5** become evident upon examination of the ^{1}H NMR spectrum of [**5b**][PF_6]$_3$. In NO_2CD_3 the *para* substituted aromatic rings of the upper rim [CpFe(arene)]$^+$ moieties appear as a typical AB pattern, indicative of fast rotation of this group on the NMR timescale. Addition of [NBu_4]Br results in the concomitant splitting of this AB pattern into two separate patterns as the rotation of the [CpFe(arene)]$^+$ moieties is slowed as a consequence of bromide binding. Thus, separate signals are observed for sets of protons on the inside and outside of the molecular cavity of **5b**. In acetone-d_6,‡ **5b** displays inhibited [CpFe(arene)]$^+$ rotation even in the absence of bromide,

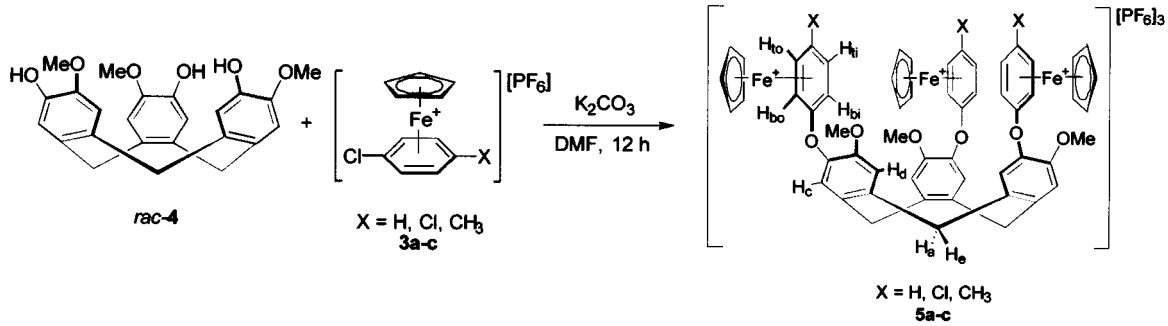

Scheme 1 Synthesis of deep cavity [CpFe(arene)]$^+$-based hosts **5**

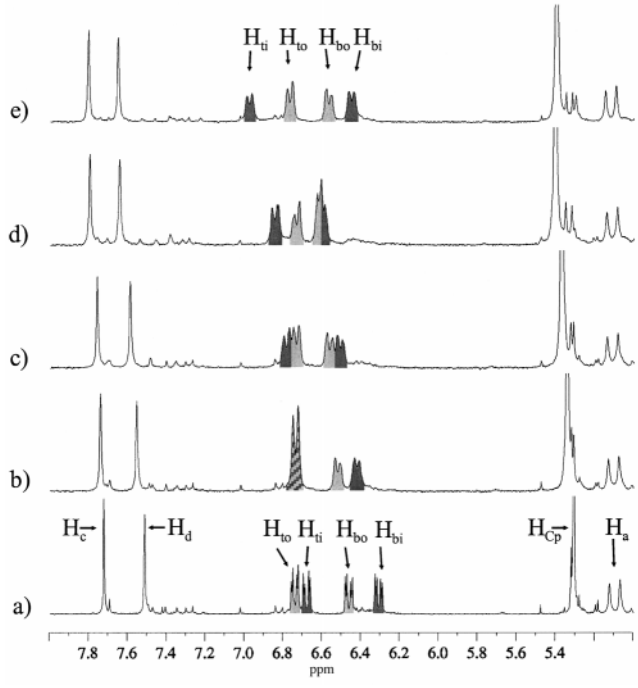

Fig. 2. ^{1}H NMR spectrum of **5b**$[PF_6]_3$ (acetone-d_6, 2.5 mM) with: (a) 0; (b) 0.35; (c) 0.60; (d) 1.00 equivalent of added NBu_4Br; (e) 1.00 equivalent of added NBu_4Cl

probably indicating binding of the $[PF_6]^-$ anion in a fashion similar to that observed in the crystal structure. A ^{1}H–^{1}H NOESY experiment allows assignment of the four unique protons according to Scheme 1 (*e.g.* $H_{top,inside} = H_{ti}$). Although, from this experiment, it is not possible to determine which set of top ($H_{t\_}$) and bottom ($H_{b\_}$) protons (dark or light shaded) correspond to the inside ($H_{\_i}$) of the cavity and which correspond to the outside ($H_{\_o}$), ^{1}H NMR titration experiments with $[NBu_4]Br$ make this apparent. Fig. 2 shows that as up to one equivalent of bromide is added, the chemical shifts of one top/bottom set (dark shaded) of protons are more dramatically affected than the other ($\Delta\delta_{max}$ = 0.17, 0.29 ppm for H_{ti} and H_{bi}). This behavior is indicative of the difference in $[PF_6]^-$ and bromide binding and these protons are thus assigned as those corresponding to the inside of the molecular cavity (H_{ti} and H_{bi}). Similar effects are observed with the addition of NBu_4Cl ($\Delta\delta_{max}$ = 0.30, 0.14 ppm for H_{ti} and H_{bi}) although the magnitude of the chemical shift change is larger for H_{ti} than H_{bi}. Conversely, addition of iodide affects H_{bi} more than H_{ti} and also more than the addition of bromide ($\Delta\delta_{max} \geqslant 0.07$, 0.35 ppm for H_{ti} and H_{bi}). No changes in chemical shifts are observed with the addition of $[NBu_4][PF_6]$.

In all instances precipitation of **5b**$[X]_3$ onsets when any amount greater than one equivalent of halide is added and association constants could not be determined due to these constraints. This in itself is a significant feature of hosts **5**, however, since typical non-preorganized $[CpFe(arene)]^+$ cations are acetone soluble and display essentially no ^{1}H chemical shift changes even in the presence of a large excess of halide. Furthermore, the near linear dependence of the chemical shifts of $H_{\_i}$ on the amount of added halide suggests large association constants and extremely efficient complexation of halides (*vs.* $[PF_6]^-$) by the host in this solvent. That precipitation onsets when more than one equivalent of halide is present is indicative of a soluble $[\mathbf{5b}\subset X]^{2+}$ (X = Cl^-, Br^-, I^-) species which will precipitate in the presence of significant concentrations of unbound halide. It is difficult to interpret the differences in chemical shift behavior of H_{ti} and H_{bi} with the different halides but it is likely an artifact of the relative differences in host conformations of $[\mathbf{5b}\subset(PF_6)]^{2+}$ and the $[\mathbf{5b}\subset X]^{2+}$ species. On the basis of these data, the relative preference of **5b** for the different sized halides cannot be definitively established, but the overall greater changes in chemical shift for iodide complexation may suggest a preference for the larger halide.

The new anion hosts reported represent a new class of anion receptor molecules whose binding properties are a direct consequence of only appropriately arranged sites of positive charge in the molecule. **5a**–**c** have distinct advantages over molecules such as **1** and **2** in that they do not possess significant binding sites exterior to the molecular cavity. We anticipate that the reactive chlorine substituents at the upper rim of **5b** will allow extension of the host cavity. Moreover, we are currently investigating the distinct possibility of synthesizing new metallated cryptophane[6] host molecules by capping off **5b** with another cyclotriguaiacylene moiety. Finally, the chiral nature of **4**, which can be resolved into its two optically active forms,[4] may provide a unique opportunity to investigate enantioselective binding of anionic species using chiral hosts similar to **5**.

We are grateful to the U.S. National Science Foundation for support and NATO for the award of a Collaborative Research Grant (ref. CRG 960320).

Notes and References

† *Crystal data* (173 K, Siemens SMART CCD diffractometer): $[C_{57}H_{48}O_6Cl_3Fe_3][PF_6]_3\cdot(CH_3CH_2OCH_2CH_3)_{1.5}\cdot(H_2O)$, orange–brown, M = 1667.02, monoclinic, $P2_1/c$ (no. 14), a = 17.791(1), b = 21.858(1), c = 18.178(1) Å, β = 103.456(1)°, V = 6874.8(7) Å^3, Z = 4, D_c = 1.61 g cm^{-3}, μ(Mo-Kα) = 9.14 cm^{-1}, G.O.F. = 1.05, wR_2(all data) = 0.199, $R_1[I > 2\sigma(I)]$ = 0.0652, 9468 independent reflections. Manipulations were performed using the program RES2INS.[13] CCDC 182/975.

‡ ^{1}H NMR data (acetone-d_6, 250 MHz, J/Hz) for **5a**: δ 7.73 (s, 3H, H_c), 7.53 (s, 3H, H_d), 6.29–6.39 (m, 9H, $[CpFe(arene)]^+$), 6.23 (t, 6H, ^3J = 5.4, $[CpFe(arene)]^+$), 5.18 (s, 15H, Cp), 5.10 (d, 3H, ^2J = 13.8, H_a), 3.93 (d, 3H, ^2J = 13.8, H_e), 3.79 (s, 9H, OMe); for **5b**: δ 7.72 (s, 3H, H_c), 7.52 (s, 3H, H_d), 6.74 (dd, 3H, ^4J = 1.9, ^3J = 6.9, H_{to}), 6.68 (dd, 3H, ^4J = 12.3, ^3J = 6.9, H_{ti}), 6.46 (dd, 3H, ^4J = 1.9, ^3J = 6.9, H_{bo}), 6.31 (dd, 3H, ^4J = 2.3, ^3J = 6.9, H_{bi}), 5.31 (s, 15H, Cp), 5.10 (d, 3H, ^2J = 13.8, H_a), 3.91 (d, 3H, ^2J = 13.8, H_e), 3.78 (s, 9H, OMe); for **5c**: δ 7.71 (s, 3H, H_c), 7.51 (s, 3H, H_d), 6.22–6.31 (m, 9H, $[CpFe(arene)]^+$), 6.11 (dd, 3H, ^4J = 2.0, ^3J = 5.8, $[CpFe(arene)]^+$), 5.13 (s, 15H, Cp), 5.09 (d, 3H, ^2J = ???, H_a) 3.82 (d, 3H, ^2J = 13.9, H_e), 3.78 (s, 9H, OMe), 2.44 (s, 9H, CH_3).

1 (*a*) C. Seel and J. de Mendoza, *Comprehensive Supramolecular Chemistry*, ed. J. L. Atwood, J. E. D. Davies, D. D. MacNicol and F. Vögtle, Elsevier, New York, 1996, vol. 2, ch. 17, pp. 519–552; (*b*) *Supramolecular Chemistry of Anions*, ed. A. Bianchi, K. Bowman-James and E. García-España, Wiley-VCH, New York, 1997; (*c*) K. T. Holman, J. L. Atwood and J. W. Steed, *Advances in Supramolecular Chemistry*, ed. G. W. Gokel, JAI Press, Greenwich, CT, 1997, vol. 4, ch. 7, pp. 287–330.

2 (*a*) K. T. Holman, M. M. Halihan, J. W. Steed, S. S. Jurisson and J. L. Atwood, *J. Am. Chem. Soc.*, 1995, **117**, 7848; (*b*) J. L. Atwood, K. T. Holman and J. W. Steed, *Chem. Commun.*, 1996, 1401; (*c*) K. T. Holman, M. M. Halihan, S. S. Jurisson, J. L. Atwood, R. S. Burkhalter, A. R. Mitchell and J. W. Steed, *J. Am. Chem. Soc.*, 1996, **118**, 9567; (*d*) M. Staffilani, K. S. B. Hancock, J. W. Steed, K. T. Holman, J. L. Atwood, R. K. Juneja and R. S. Burkhalter, *J. Am. Chem. Soc.*, 1997, **119**, 6324; (*e*) M. Staffilani, G. Bonvicini, J. W. Steed, K. T. Holman, J. L. Atwood and M. R. J. Elsegood, *Organometallics*, 1998, **17**, 1732.

3 (*a*) P. D. Beer, *Chem Commun.*, 1996, 689, and references therein; (*b*) P. D. Beer, *Acc. Chem. Res.*, 1998, **31**, 71, and references therein; (*c*) P. D. Beer, C. A. P. Dickson, N. Fletcher, A. J. Goulden, J. Hodacova and T. Wear, *J. Chem. Soc., Chem. Commun.*, 1993, 828.

4 J. Canceill, A. Collet, J. Gabard, G. Gotarelli and G. P. Spada, *J. Am. Chem. Soc.*, 1985, **107**, 1299.

5 For general methods, see: A. S. Abd-El-Aziz, C. R. de Denus, M. J. Zaworotko and L. R. MacGillivray, *J. Chem. Soc., Dalton Trans.*, 1995, 3375.

6 A. Collet, *Comprehensive Supramolecular Chemistry*, ed. J. L. Atwood, J. E. D. Davies, D. D. MacNicol and F. Vögtle, Elsevier, New York, 1996, vol. 2, ch. 11, pp. 325–365.

7 L. J. Barbour and J. L. Atwood, *J. Appl. Crystallogr.*, 1998, in press.

Received in Cambridge, UK, 10th July 1998; 8/05397I

Large interlayer repeat distances observed for montmorillonites treated by mixed Al–Fe and Fe pillaring solutions

T. Mandalia, M. Crespin, D. Messad and F. Bergaya*

CRMD-CNRS, 1b Rue de la Férollerie, 45 071 Orléans Cedex 2, France. E-mail: f.bergaya@cnrs-orleans.fr

Raw montmorillonites treated with mixed Al–Fe pillaring solutions, with Fe/(Al + Fe) molar ratio between 0.1 and 1, and heated at 300 °C lead to large *d*-spacings according to XRD which increase from 52 Å for the sample with the lowest iron content to 76 Å for the pure Fe-treated clay sample.

Pillared clay minerals (PILCs) are usually obtained by intercalation of large inorganic polymeric cations which exchange the compensating cations from the clay, then dehydration and dehydroxylation occur upon calcination to give metal oxide clusters which act as pillars. These pillars separate adjacent silicate layers which then increases the interlayer distance and creates a permanent porosity between them.[1]

The synthesis of pillared clays has been investigated extensively in the past two decades as a function of the nature of the clays, the nature of the pillars and the conditions of pillaring. Usually, polyoxo-cations of Al, Zr, Ti, Fe, *etc*. are incorporated as pillars. Many reviews have been published.[2,3] The synthesis of pillared clays from mixed pillaring species is less common and the formation of truly mixed pillars is not easy to confirm when two cationic species are simultaneously intercalated.[4]

In most of the pillared clays reported to date the free height is comparable to the van der Waals thickness of the host layers. The term 'supergallery' has been used previously to describe some pillared clays having high basal spacing and where the thickness of the layer ($\approx$10 Å) is smaller than the free interlamellar heights. For example, iron-pillared clays are obtained with basal spacing of *ca.* 23–27 Å[5] and free heights of *ca.* 13–17 Å. In an international patent, McCauley claimed larger basal spacings (>40 Å) of pillared clays obtained by incorporation of various rare earth metals in the trivalent state with aluminium polycations in the clay layers.[6] However claims for gallery heights have never exceeded 40 Å.

In the present work, addition of Al and Fe pillaring solutions, with Fe/(Al + Fe) molar ratio of 0–1 leads to a series of modified Al–Fe-clays with very high distances according to XRD. The products were obtained without incorporation of any non-ionic surfactant or other organic polymeric compounds. The nature of the iron pillaring oligomers is still not well known. In addition, methods for preparing thermally stable Fe-PILCs have not been established.

To study the diffraction patterns of the materials having peaks at very low 2θ angle, proper alignment and calibration of the diffraction instrument is necessary to obtain a good accuracy in the diffraction analysis. To verify that the following obtained results are not an artefact, a low-angle diffraction calibration standard product[7] (silver behenate), considered as a standard which has a set of well-defined (00*l*) diffraction peaks at 2θ angles down to 1.5° with Cu-Kα radiation, was used to calibrate the XRD Siemens D 500 instrument (Fig. 1). The raw Wyoming montmorillonite was received from Comptoir des Minéraux (France). The elemental analyses of this crude montmorillonite obtained by XRF, and corrected by the weight loss which is *ca.* 15%, are: 66.35% SiO_2, 21.61% Al_2O_3, 4.29% Fe_2O_3, 2.70% MgO, 0.02% MnO, 0.21% TiO_2, 2.23% Na_2O, 1.58% CaO, 0.61% K_2O and 0.09% P_2O_5. The cation exchange capacity of this clay was *ca.* 80 mequiv. per 100 g of calcined clay. This material was used without further purification.

The oligomeric pillaring solutions were prepared by the following methods: (i) Al_{13} oligomer: a solution containing hydroxy-Al oligocations with OH : Al ratio of 2.2, was prepared from 0.4 M $AlCl_3 \cdot 6H_2O$ and 0.4 M NaOH. Seven days ageing was carried out at room temperature before use. (ii) Fe oligomer: following the procedure of Rightor *et al.*,[5] Na_2CO_3 powder was added gradually to an aqueous solution of 0.2 M $FeCl_3$, up to a base : Fe ratio of 2. The freshly resulting oligomer was used immediately without ageing.

A 2% suspension of raw clay was prepared by dispersing 2 g of montmorillonite in deionized water. Different amounts of Al and Fe oligomers (Al + Fe = 100%), prepared by the methods described above, were then added simultaneously to this clay slurry to give the ratio of M : clay = 10 mmol (g of clay)$^{-1}$. The suspension was aged for one day at room temperature. The clay products were centrifuged and then washed by successive agitations/centrifugations with deionized water until Cl^- free. Specimens of the clay suspensions were dried on glass slides at room temp. The samples were heated at 300 °C for 3 h. XRD patterns were recorded using Ni-filtered Cu-Kα radiation.

XRD patterns of the various clay samples are shown in Fig. 2. The *d*(001) spacing of the Al-sample is nearly 18 Å [Fig. 2(a)]. This value is similar to those generally reported for Al-PILCs and indicates the success of pillaring. The mixed Al–Fe sample [Fe/(Al + Fe) = 0.1] shows an additional peak at 52 Å which is lower in intensity than the peak at 18 Å. The *d*(004) of this first peak which must appear at nearly 13 Å, could be the origin of the assymetrical behaviour of this reflection [Fig. 2(b)]. The Al–Fe sample [Fe/(Al + Fe) = 0.2] gives two better defined peaks, one at *ca.* 64 Å which indicates that increasing the amount of Fe results in an increase in the *d*-value for the peak appearing at low angle and the other at 16.7 Å with high intensity [Fig. 2(c)]. The position of this second peak coincides with the fourth order (*ca.* 16 Å) of the 64 Å reflection, this again could explain the high intensity of this second peak. The mixed Al : Fe sample [Fe/(Al + Fe) = 0.5] has one peak at 72 Å and a second less intense broad peak centered at *ca.* 15.7 Å [Fig. 2(d)]. In the pure

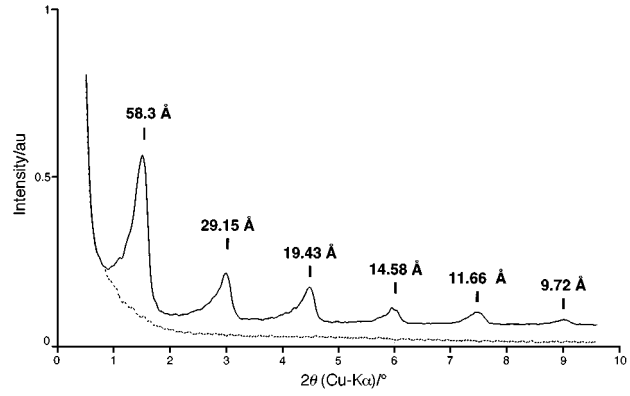

Fig. 1 Low angle XRD pattern of silver behenate powder deposited on glass slide (——) and the glass slide support without sample (- - - -)

Table 1 XRD spacings and textural properties: surface area, porous (V_P) and microporous ($V_{\mu P}$) volumes of the treated montmorillonites (Mt) as a function of Fe/(Al + Fe) molar ratio in the initial solutions, and of the starting raw clay heated at 300 °C. Mesoporous volume (V_{mP}) is obtained by subtracting microporous volume from total porous volume

Clay sample	Fe/(Al + Fe) initial molar ratio	First peak *d*/Å	Specific surface area/ $m^2\ g^{-1}$	$V_P/cm^3\ g^{-1}$	$V_{\mu P}/cm^3\ g^{-1}$	$V_{mP}/cm^3\ g^{-1}$
Mt.Al	0	18.3	246	0.18	0.104	0.076
Mt.Al-Fe	0.1	52	230	0.22	0.082	0.138
Mt.Al-Fe	0.2	64	210	0.23	0.047	0.183
Mt.Al-Fe	0.5	72	202	0.24	0.034	0.206
Mt.Fe	1	76	148	0.22	0.002	0.218
raw Mt heated at 300 °C	0	~10	18.5	0.06	0.004	0.056

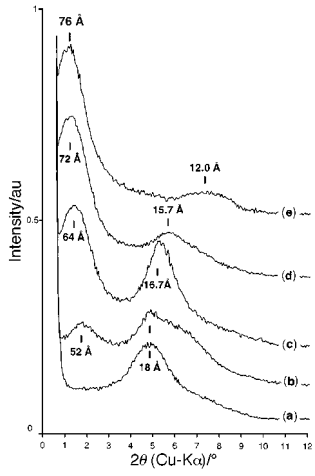

Fig. 2 XRD patterns with oriented specimen, heated at 300 °C, of the clays initially treated by the Al and Fe oligomer solutions in different ratios: (a) Fe/(Al + Fe) = 0; (b) Fe/(Al + Fe) = 0.1; (c) Fe/(Al + Fe) = 0.2; (d) Fe/(Al + Fe) = 0.5 and (e) Fe/(Al + Fe) = 1

Fe sample, the distance of the first peak reaches its maximum at *ca.* 76 Å and the second very broad peak position shifts to a lower distance of *ca.* 12 Å [Fig. 2(e)]. The general observation in all these spectra is that increasing the amount of iron in the initial solutions leads to (i) a shift of the first peak to lower angle and (ii) to a shift of the second peak in the opposite direction with an almost linear decrease in this case of the corresponding basal spacing from 18 to 12 Å.

The high distance observed here for the iron pillared sample was previously suspected by Yamanaka and Hattori,[8] but not shown by XRD. In fact, these authors comparing the adsorption isotherms of different molecules by Al-, Zr- and Fe-PILCs noticed that even though the basal spacings were similar in all these pillared samples, a BET isotherm (presumably, type IV or II) was observed for Fe whereas Langmuir isotherms (type I) were obtained for Zr and Al. From this, they concluded that the pore dimensions of the iron oxide pillared clay are probably larger than those expected from the 16.7 Å obtained basal spacing. They suggested that XRD analysis only reflects the partial well-ordered stacking of the silicate layers, since the remaining disordered parts are not revealed by XRD.

At this stage, the questions are what kind of iron species lead to these high distances of the peaks and do these increasing distances correspond to the interlamellar spaces between the layers? TEM studies are in progress to answer to these questions. In a study on partial hydrolysis of $FeCl_3$, Tchoubar *et al.*[9] have shown in similar experimental conditions that the sizes, which varied with time, of the obtained iron polymers, were centered around 100 Å: thus our *d* values are perhaps not so surprising. However, it is the first time, to our knowledge, that the synthesis of montmorillonites treated by pillaring solutions leading to such unexpectedly large distances of *ca.* 70 Å (XRD) is reported from a regular smectite clay.

The N_2 BET specific surface areas, pore, mesopore and micropore volumes of the treated clays are presented in Table 1. The starting raw montmorillonite clay, heated at 300 °C, exhibits a low surface area of 18.5 $m^2\ g^{-1}$, a low pore volume of 0.06 $cm^3\ g^{-1}$ and a microporosity of 0.004 $cm^3\ g^{-1}$. Al-PILC has, as expected, a surface area of 246 $m^2\ g^{-1}$, a pore volume of 0.18 $cm^3\ g^{-1}$ and a microporosity of 0.104 $cm^3\ g^{-1}$. With increasing Fe/(Al + Fe) initial ratio, the surface areas of the mixed treated clays decrease and reach 148 $m^2\ g^{-1}$ for the pure Fe sample which is still 7 times higher than the surface area of the heated starting clay. Here, the situation is very complex because as shown in our previous studies,[10] some precipitated oxyhydroxide Fe species are retained by the clay outside the interlamellar spaces and the intrinsic surface area is difficult to define. Rather, a comparative global evolution has to be taken into account in these clay materials. Moreover, the total pore volumes of the mixed treated clays remain almost constant, *ca.* 0.23 ± 0.01 $cm^3\ g^{-1}$, while the microporosity of these clays decreases with increased iron content and the residual microporosity value of the iron clay is very low. This indicates that montmorillonite treated with Al–Fe pillared species, creates essentially some mesoporosity between the clay particles, which could be at the origin of these high distances. The pillars may prevent access to the interlamellar spaces and the microporosity decreases to zero, and other unknown species of Al and Fe compounds could be obtained. All these possibilities have to be quantitatively analysed and interpreted from TEM images.

In conclusion, in this work unexpectedly large interlayer distances for montmorillonites treated by mixed Al–Fe and Fe-pillaring solutions are observed by XRD. These distances vary from 52 to 72 Å and reach a maximum at 76 Å in the pure Fe sample. Nevertheless, increasing the amount of iron leads to an increase of mesoporosity instead of microporosity.

This work was supported by an Avicenne European Programme No. 83. We thank D. Tchoubar and B. Jones for helpful discussion.

Notes and References

1 F. Bergaya, *CEA/PLS Newslett.*, 1994, **7**, 11.
2 D. E. W. Vaughan, *Am. Chem. Soc. Symp. Ser.*, 1988, **368**, 308.
3 F. Bergaya, in *Matériaux argileux, Structures, propriétés et applications*, 1990, ed. A. Decarreau, SFMC and GFA, ch. II, pp. 513–537.
4 F. Bergaya, N. Hassoun, J. Barrault and L. Gatineau, *Clay Miner.*, 1993, **28**, 109.
5 E. G. Rightor, M.-S. Tzou and T. J. Pinnavaia, *J. Catal.*, 1991, **130**, 29.
6 J. R. McCauley, *Int. Pat.* WO 88/06488, 1988.
7 T. N. Blanton, T. C. Haung, H. Toraya, C. R. Hubbard, S. B. Robie, D. Louér, H. E. Gobel, G. Will, R. Gilles and T. Raftery, *Powder Diffraction*, 1995, **10**, 91.
8 S. Yamanaka and M. Hattori, *Catal. Today*, 1988, **2**, 261.
9 D. Tchoubar, J. Y. Bottero, P. Quienne and M. Arnaud, *Langmuir*, 1991, **7**, 398.
10 F. Bergaya, *J. Porous Mater.*, 1995, **2**, 91.

Received in Bath, UK, 14th May 1998; 8/03746I

Stereoselective debromination of aryl-substituted *vic*-dibromide with indium metal

Brindaban C. Ranu,*† Sankar K. Guchhait and Arunkanti Sarkar

Department of Organic Chemistry, Indian Association for the Cultivation of Science, Jadavpur, Calcutta 700 032, India

Debromination of both *meso* and *dl* (*erythro* and *threo*) aryl-substituted *vic*-dibromides with indium metal in MeOH leads to *trans*-alkenes exclusively.

The protection-deprotection of olefins *via* bromination-debromination is an important process in organic synthesis. Although bromination generally proceeds smoothly and stereospecifically to give high yields of dibromides, debromination at a later stage in the synthesis often proves more difficult. This is primarily because the efficiency of this process greatly depends upon the stereoselectivity in the debromination step and compatibility of the reagent with the carbon–carbon double bond formed and other functionalities present in the substrates. Many reagents[1] including metals like Zn,[1d] Mg[1d] and Sm,[1h] have been reported in the literature for this reaction, but most of them are also associated with the limitations regarding selectivity and compatibility. Thus, an efficient and selective procedure for debromination of *vic*-dibromides is needed.

In recent times there has been increasing interest in indium-mediated transformations because of certain unique properties inherent to indium.[2] However, although indium has been used extensively in carbonyl addition reactions,[2,3] its potential in other domains has not been explored to any great extent.[4] Because of the close resemblance of indium to magnesium and zinc in several respects, including first ionization potential, indium could also be a potential reducing agent. This prompted us to initiate an investigation of indium-promoted reductive debromination of *vic*-dibromides. We have observed that aryl-substituted *vic*-dibromides undergo smooth debromination to produce the corresponding (*E*)-alkenes when treated with indium metal in MeOH (Scheme 1).

The experimental procedure is very simple. A mixture of *vic*-dibromide (1 mmol) and indium metal (1 mmol,‡ cut into small pieces) in dry MeOH (10 ml) was refluxed for a certain period of time (Table 1) until completion of the reaction (TLC). MeOH was removed and the residue was extracted with Et_2O. Evaporation of solvent followed by purification by silica gel chromatography furnished the pure alkene in high yields.

A wide range of structurally varied aryl-substituted *vic*-dibromides underwent debrominations by this procedure to provide the corresponding alkenes. The results are summarised in Table 1. Very interestingly, only *trans* olefins are obtained from all the substrates, whether they are *meso*/*erythro* or *dl*/*threo* (entries 1, 2, 4, 5, 8, 9). If debromination occurs by the usual *trans*-elimination, *meso*/*erythro*- or *dl*/*threo*-*vic*-dibromides would give *trans*- or *cis*-alkenes, respectively. It is therefore suggested that the reaction occurs *via* a common, relatively stable radical or anion intermediate which directly collapses to (*E*)-alkene. This speculation gains support from the observations that *cis*-stilbene does not undergo isomerisation to the *trans* isomer upon reflux with indium metal or oxidised indium products§ from debromonation of *erythro*-1,2-dibromo-1-phenyl-2-benzoylethane in MeOH, even after 8 h. The presence of *cis*-stilbene was also not detected upon quenching the debromination reaction of *vic*-dibromides of stilbene at an intermediate stage.

In general, the reactions are very clean and high-yielding. MeOH has been found to be the best solvent for this reaction; in pure MeCN the debromination does not proceed at all. Several sensitive functional groups, such as ketone carbonyl, carboxylic ester, hydroxy, methoxy and chloro groups on aromatic rings, remained unaffected under the present reaction conditions. No over-reduction of the produced alkene was observed with any

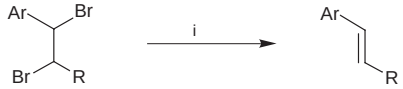

Scheme 1 *Reagents and conditions*: i, In, MeOH, reflux

Table 1 Debromination of aryl-substituted *vic*-dibromides with indium metal in MeOH

Entry	Substrate	*t*/h	Product	Yield (%)[a]
1	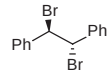	2	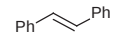	88
2	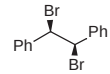	8	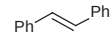	85
3	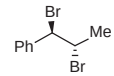	7	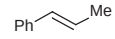	94
4	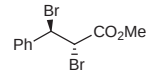	4[b]	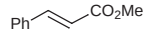	90
5	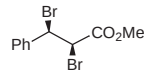	9	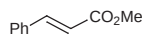	92
6	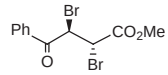	12[b]	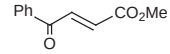	90
7	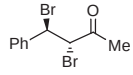	12	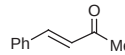	89
8	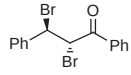	2	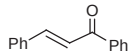	85
9	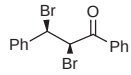	1[c]	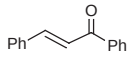	88
10	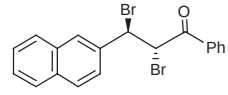	2[d]	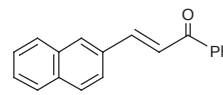	91

[a] Yields refer to pure isolated products fully characterised by spectral and analytical methods. [b] The reaction was performed at room temperature (30 °C) with stirring. [c] MeOH–MeCN (1:1) was used as solvent instead of MeOH to dissolve the *vic*-dibromide. [d] MeOH–MeCN (10:1) was used. [e] 2 equiv. of indium were used.

Table 1 (cont.) Debromination of aryl-substituted *vic*-dibromides with indium metal in MeOH

Entry	Substrate	*t*/h	Product	Yield (%)[a]
11	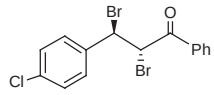	9[c]	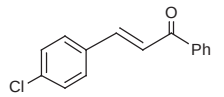	92
12	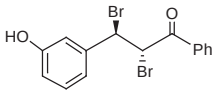	9[c]	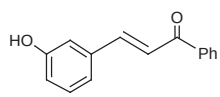	86
13	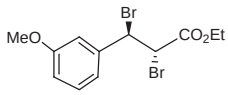	19	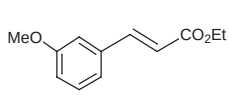	90
14		12	No reaction	
15	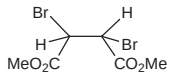	12	No reaction	
16	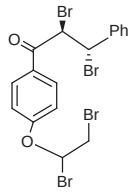	3.5[e]	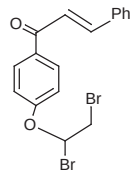	86
17	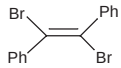	8.5	Ph—C≡C—Ph	88
18	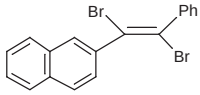	7	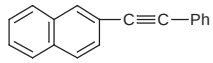	82

[a] Yields refer to pure isolated products fully characterised by spectral and analytical methods. [b] The reaction was performed at room temperature (30 °C) with stirring. [c] MeOH–MeCN (1:1) was used as solvent instead of MeOH to dissolve the *vic*-dibromide. [d] MeOH–MeCN (10:1) was used. [e] 2 equiv. of indium were used.

substrate, unlike those reactions reported using Sm[1h] and Mg.[5] As this reagent is inert to alkyl-substituted dibromides (entries 14, 15), selective debromination of aryl-substituted *vic*-dibromide moieties is achieved in the presence of alkyl-substituted dibromide moieties (entry 16). This procedure is also effective for the debromination of *vic*-dibromoalkenes to the corresponding alkynes (entries 17, 18).

In conclusion, the present procedure provides an efficient and general methodology for reductive debromination of aryl-substituted *vic*-dibromides to the corresponding (*E*)-alkenes; to the best of our knowledge this is the first report of indium-promoted debromination of *vic*-dibromides.[6] The significant improvements offered by this method over other existing debromination procedures[1] are: no overreduction of the double or triple bond formed, tolerance to several reducible functionalities, exclusive formation of (*E*)-alkenes from *cis*- as well as *trans*-dibromides, selective debromination of aryl-substituted dibromide moieties in presence of alkyl-substituted ones, and the easy availability and apparently nontoxic nature of indium metal.¶ Thus, this reaction is endowed with considerable synthetic potential and may provide a new method for reductive debromination and conversion of a *cis*-alkene to its *trans*-isomer. Further investigations of more useful applications are in progress.

We gratefully acknowledge financial support from CSIR, New Delhi [Grant No. 01(1504)/98] for this investigation. S. K. G. and A. S. are also thankful to CSIR for their fellowships. We thank Mr A. Som for his help with this work during his tenure as a summer project student in this laboratory from IIT, Kanpur.

Notes and References

† E-mail: ocbcr@iacs.ernet.in

‡ Debromination also proceeds in the presence of < 1 equiv. of indium; however, the reaction is very slow, *e.g. erythro*-1,2-dibromo-1-phenyl-2-benzoylethane (entry 8) takes 9 h with 0.5 equiv of In compared to 1 h with 1 equiv under identical reaction conditions.

§ We thank one of the referees for this suggestion.

¶ Indium metal is not affected by air and moisture and thus does not require any activation before reaction. Indium can be handled easily without any special precautionary measures and is relatively inexpensive.

1 (*a*) E. L. Allred, B. R. Beck and K.J. Voorhees, *J. Org. Chem.*, 1974, **39**, 1426; (*b*) D. Landini, S. Quici and F. Rolla, *Synthesis*, 1975, 397; (*c*) D. Savoia, E. Tagliavini, C. Trombini and A. U. Ronchi, *J. Org. Chem.*, 1982, **47**, 876; (*d*) E. Baciocchi, in *Chemistry of Functional Groups, Supplement D, Part 1*, ed. S. Patai and H. Rappoport, Wiley, New York, 1983; (*e*) S. G. Davies and S. E. Thomas, *Synthesis*, 1984, 1027; (*f*) K. Yanada, R. Yanada and H. Meguri, *J. Chem. Soc., Chem. Commun.*, 1990, 730; (*g*) J. M. Khurana and G. C. Maikap, *J. Org. Chem.*, 1991, **56**, 2582; (*h*) R. Yanada and N. Negoro, K. Yanada and T. Fujita, *Tetrahedron Lett.*, 1996, **37**, 9313; (*i*) C. Malanga, S. Mannucci and L. Lardicci, *Tetrahedron*, 1998, **54**, 1021; (*j*) T. S. Butcher and M. R. Detty, *J. Org. Chem.*, 1998, **63**, 177.

2 P. Cintas, *Synlett*, 1995, 1087.

3 C. J. Li, D. L. Chen, Y. Q. Lu, J.-X. Haberman and J. T. Mague, *J. Am. Chem. Soc.*, 1996, **118**, 4216; V. J. Bryan and T. H. Chan, *Tetrahedron Lett.*, 1996, **37**, 5341; T.-P. Loh and X. R. Li, *Tetrahedron Lett.*, 1997, **38**, 869; M. B. Isaac and L. A. Paquette, *J. Org. Chem.*, 1997, **62**, 5333; X.-H. Yi, Y. Meng and C.-J. Li, *Chem. Commun.*, 1998, 449.

4 S. Araki, A. Imai, K. Shimizu, M. Yamada, A. Mori and Y. Butsugan, *J. Org. Chem.*, 1995, 60, 1841; B.C. Ranu and A. Majee, *Chem. Commun.*, 1997, 1225; N. Fujiwara and Y. Yamamoto, *J. Org. Chem.*, 1997, **62**, 2318; T. P. Loh, D. S.-C. Ho, K.-C. Xu and K.-Y. Sim, *Tetrahedron Lett.*, 1997, **38**, 865.

5 T. Hudlicky, G. Sinai-Zingde and M. G. Natchus, *Tetrahedron Lett.*, 1987, **28**, 5287.

6 For indium promoted debromination of geminal dibromides, see: S. Araki and Y. Butsugan, *J. Chem. Soc., Chem. Commun.*, 1989, 1286.

Received in Cambridge, UK, 19th August 1998; 8/06530F

A copper(I)-catalysed template synthesis of solvatochromic aryl-arsonium and -stibonium systems and a synchrotron structural study of a tetraarylstibonium di-iodocuprate

David W. Allen,*[a] Joanne P. L. Mifflin[a] and Simon Coles[b]†

[a] *Division of Chemistry, Sheffield Hallam University, Sheffield, UK S1 1WB*
[b] *Department of Chemistry, University of Wales, Cardiff, Cardiff, UK CF1 3TB*

A route to solvatochromic tetraaryl-arsonium and -stibonium phenolate betaines is described, together with a synchrotron structural study of a precursor arylstibonium di-iodocuprate salt in which both cation and anion have unusual geometries.

Methods for the synthesis of aryl-arsonium or -stibonium salts from tertiary arsines or stibines and aryl halides are limited, the usual route being the reaction of the tertiary arsine or stibine, commonly the triphenyl derivative, and an aryl halide, in the presence of aluminium chloride at > 200 °C.[1] We have shown that tertiary phosphines react with aryl halides bearing appropriate donor atoms in the *ortho* position to the halogen in the presence of catalytic quantities of nickel(II) or copper(II) compounds under mild conditions in refluxing ethanol,[2] and were interested in exploring similar template-assisted reactions of triaryl-arsines and -stibines. As triaryl-arsines and -stibines coordinate readily to copper(I) halides to form complexes which are labile in solution,[3] we have investigated their reactions with a series of template aryl halides in the presence of copper(I) iodide, in acetonitrile, and wish to report the formation of tetraaryl-arsonium and -stibonium systems in high yield under these remarkably mild conditions. We have also applied this procedure in the synthesis of the first solvatochromic tetraaryl-arsonium and -stibonium iminophenolate betaines, the properties of which are compared with those of the related phosphonium system. A synchrotron structural study of one tetraarylstibonium salt is also reported, which reveals a significant intramolecular coordinative interaction between the onium centre and the donor atom in the *ortho* position of the template system, and also the presence of a di-iodocuprate(I) anion which interacts with a second di-iodocuprate anion *via* a short copper–copper interaction to give a dinuclear anion.

The reaction of the aryl halides **1** (X = H, Z = OMe; X = Cl, Br, or Ph, Z = OH) with triphenylarsine and copper(I) iodide in acetonitrile under reflux for several hours gave, after pouring into aqueous potassium iodide solution and solvent extraction into dichloromethane, the tetraarylarsonium salts **2** (E = As, Y = I or CuI_2) as yellow-brown crystalline solids. ^1H and ^{13}C NMR spectra were consistent with the proposed structures. Under FABMS conditions, the arsonium salts gave a characteristic molecular ion for the cation present. The structure of the salt **2** (X = H, Z = OMe, E = As, Ar = Ph, Y = I) was also confirmed by a full X-ray crystallographic study.[4] Similarly, treatment of the aryl halides **1** (X = H, Z = OMe; X = Cl, Br, or Ph, Z = OH) and **3** with triphenyl- or tri-*p*-tolyl-stibine and copper(I) iodide in acetonitrile under reflux gave the related arylstibonium salts **2** (E = Sb; Ar = Ph or *p*-tolyl, Y = CuI_2) and **4** (Ar = Ph or *p*-tolyl, Y = CuI_2). Again, ^1H and ^{13}C NMR spectra were consistent with the proposed structures, and under FABMS conditions, each stibonium salt gave a characteristic molecular ion for the cation present. The nature of the anion present was confirmed by negative ion mass spectrometry. The stibonium salts formed more quickly than the related arsonium salts under the same conditions. Attempts to prepare the related phosphonium salts using copper(I) iodide as catalyst in acetonitrile were unsuccessful. Clearly, the group 15 ligand must influence crucial stages of the reaction, for which the mechanism is uncertain. A kinetic study of related nickel(II)-catalysed reactions of phosphines with template aryl halides supported a mechanism in which oxidative insertion of an intermediate phosphine–nickel complex into the carbon–halogen bond was the key step, followed by reductive elimination of the arylphosphonium salt and regeneration of the effective catalyst.[5] It is likely that a similar mechanism applies in the above reactions, perhaps involving a copper(I)–copper(III) redox cycle, in which the triaryl-arsine and -stibine ligands are able to stabilise intermediate organometallic species more effectively than the related triarylphosphines.

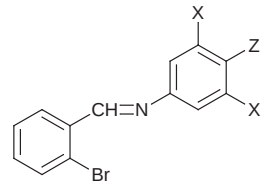

1

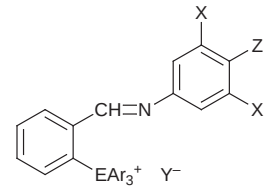

2

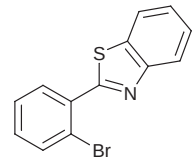

3

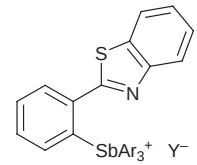

4

A structural study‡ has been made of the stibonium salt **2** (E = Sb; Ar = Ph; X = Br; Z = OH, Y = CuI_2). Routine investigations, using a rotating anode X-ray source, failed to provide data of sufficient intensity to produce a fully refinable structure. Data were therefore collected, upon a crystal of dimensions 200 × 20 × 20 μm, using station 9.8 of the Daresbury SRS.[6] The cation of the observed structure is displayed in Fig. 1 (together with selected bond lengths and angles for both cation and anion). Significant points of interest are the close intramolecular approach of the imino nitrogen to the stibonium centre, the antimony–nitrogen distance (2.65 Å), lying well within the sum of the van der Waals' radii (3.75 Å),[7] and the consequent distortion of the bond angles at antimony from the idealised tetrahedral angle towards a five-coordinate arrangement, consistent with an intramolecular coordinative interaction from nitrogen to antimony to form a five-membered ring. Tetraarylstibonium halides also show considerable distortion from idealised tetrahedral geometry as a result of weak interactions of the stibonium centre with the halide ion, resulting in essentially trigonal bipyramidal structures in which the antimony–halogen bond is unusually long.[8,9] The structure co-crystallises with a 50% occupied CH_2Cl_2 solvent and the counter-ion, which was found to be di-iodocuprate(I). The CuI_2

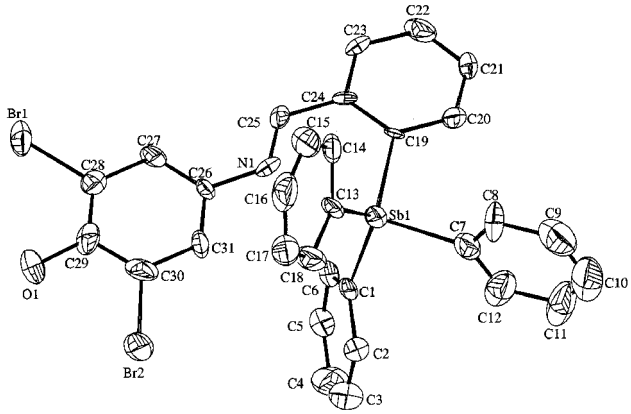

Fig. 1 Structure of the tetraarylstibonium cation with selected bond lengths (Å) and angles (°) for cation and di-iodocuprate anion: Sb–N1 2.65(4), Sb–C1 2.09(2), Sb–C7 2.13(2), Sb–C13 2.13(2), Sb–C19 2.114(14), C25–N1 1.28(2), Cu1–I1 2.508(2), Cu1–I2 2.576(2), Cu–Cu 2.732(4); C1–Sb–C7 106.7(7), C1–Sb–C13 119.2(6), C1–Sb–C19 113.6(6), C7–Sb–C13 102.0(7), C7–Sb–C19 101.4(6), C13–Sb–C19 115.9(6), C19–C24–C25 121.2(14), N1–C25–C24 118.9(13), N1–Sb–C1 83.9(7).

moiety shows a considerable distortion from the expected linear arrangement as a result of a very short copper–copper interaction (2.73 Å) with a second di-iodocuprate anion in the lattice. The stabilisation of poly[dihalocuprate(I)] anions by large phosphonium cations has been documented,[10,11] but the only stibonium salt involving a related anion is that of the copper(II) complex, $(SbPh_4)_2{\cdot}Cu_2Cl_6$.[12] However the Cu–Cu separation in this structure is much greater (3.394 Å) than that in the di-iodocuprate(I) counter-ion discussed here. Comparison with other di-iodocuprate(I) anions crystallizing in the same manner shows the Cu–Cu separation to be somewhat greater than in our example (average = 2.95 Å).[13,14]

Treatment of the salts **2** (E = As or Sb; Ar = Ph; X = Cl, Br, or Ph), dissolved in dichloromethane, with aqueous sodium hydroxide solution, resulted in a marked colour change from yellow to red-purple with formation of the related betaines **5**,

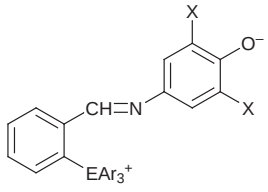

5

which were subsequently isolated and purified by trituration with diethyl ether. Again, ^1H and ^{13}C NMR spectra were consistent with the proposed structures, showing some significant chemical shift changes compared to the parent salts. Under FABMS conditions, cationic molecular ions were again observed. Conversion to the betaines resulted in a significant shift of the visible absorption maximum to longer wavelength. Thus, *e.g.* λ_{max} for the salt **2** (E = Sb; Ar = Ph; X = Cl, Y = CuI_2) in dichloromethane was observed at 358 nm, whereas for the related betaine **5** in the same solvent, λ_{max} = 536 nm. Significantly, in view of the potential link with non-linear optical properties, the betaines exhibited negative solvatochromism, the visible absorption maximum moving to longer wavelength on moving to a solvent of lower polarity. In the case of the above betaine, λ_{max} moved from 536 nm in dichloromethane to 576 nm in THF. The solvatochromic behaviour of the arsonium and stibonium betaines is almost identical to that of the related phosphonium betaines **5** (E = P, Ar = Ph; X = Cl, Br, or Ph) which we reported recently.[15] There is currently growing interest in the optical properties of organic derivatives of the main group 15 elements.[16,17]

We thank the EPSRC National Mass Spectrometry Service Centre, University of Wales, Swansea, for high resolution FABMS determinations, and also Neotronics Scientific Ltd for financial support.

Notes and References

† Author to whom crystallographic enquiries should be addressed.

‡ *Crystal data*: $C_{31.5}H_{23}NOClSbBr_2{\cdot}CuI_2$, M_r = 1065.87, monoclinic, space group $P2_1/n$, a = 9.259(5), b = 24.785(11), c = 15.100(7) Å, β = 98.998(2)°, U = 3422.6(3) Å^3, Z = 4, D_c = 2.069 g cm^{-3}, μ = 5.653 mm^{-1}, $F(000)$ = 2000, crystal size 0.2 × 0.02 × 0.02 mm. Data were collected at 160 K, with a wavelength of 0.6875 Å, on a Bruker (formerly Siemens) SMART CCD area detector diffractometer, equipped with a silicon(111) crystal monochromator and a palladium coated focussing mirror on station 9.8 of the Daresbury SRS. ω scans, with a frame increment of 0.3°, were used to cover a hemisphere of reciprocal space, giving θ_{min} = 1.54° and θ_{max} = 20.00° (index ranges $-11 \leqslant h \leqslant 12$, $-26 \leqslant k \leqslant 32$, $-18 \leqslant l \leqslant 19$). Corrections were applied to account for incident beam decay and absorption effects. A solution was obtained *via* direct methods and refined by full-matrix least-squares on F^2. 3520 unique data were produced from 11707 measured reflections (R_{int} = 0.0882). 389 parameters refined to R_1 = 0.0573 and wR_2 = 0.1253 [$I > 2\sigma(I)$] with s = 1.057 and residual electron densities of 0.967 and −1.124 e Å^{-3}. CCDC 182/984.

1 J. Chatt and F. G. Mann, *J. Chem. Soc.*, 1940, 1192; G. Doak and L. D. Freedman, *Organometallic Compounds of Arsenic, Antimony, and Bismuth*, Wiley Interscience, 1970, and references therein.

2 D. W. Allen, P. E. Cropper, P. G. Smithurst, P. R. Ashton and B. F. Taylor, *J. Chem. Soc., Perkin Trans. 1*, 1986, 1989; D. W. Allen, I. W. Nowell, L. A. March and B. F. Taylor, *J. Chem. Soc., Perkin Trans. 1*, 1984, 2523; D. W. Allen and P. E. Cropper, *Polyhedron*, 1990, **9**, 129.

3 N. R. Champness and W. Levason, *Coord. Chem. Rev.*, 1994, **133**, 115; G. A. Bowmaker, R. D. Hart, E. N. de Silva, B. W. Skelton and A. H. White, *Aust. J. Chem.*, 1997, **50**, 553; G. A. Bowmaker, R. D. Hart and A. H. White, *Aust. J. Chem.*, 1997, **50**, 567.

4 D. W. Allen, J. P. L. Mifflin, M. B. Hursthouse and K. M. A. Malik, to be published.

5 D. W. Allen and P. E. Cropper, *J. Organomet. Chem.*, 1992, **435**, 203.

6 R. J. Cernik, W. Clegg, C. R. A. Catlow, G. Bushnell-Wye, J. V. Flaherty, G. N. Greaves, I. D. Burrows, D. J. Taylor, S. J. Teat and M. Hamichi, *J. Synchrotron Rad.*, 1997, **4**, 279.

7 A. Bondi, *J. Phys. Chem.*, 1964, **68**, 441.

8 G. Ferguson, C. Glidewell, D. Lloyd and S. Metcalfe, *J. Chem. Soc., Perkin Trans. 2*, 1988, 731.

9 L-J. Baker, C. E. F. Rickard and M. J. Taylor, *J. Chem. Soc., Dalton Trans.*, 1995, 2895.

10 S. Andersson, M. Hakansson and S. Jagner, *Inorg. Chim. Acta*, 1993, **209**, 195.

11 A. Pfitzner and D. Schmitz, *Z. Anorg. Allg. Chem.*, 1997, **623**, 1555.

12 A. Bencini, D. Gatteschi and C. Zanchini, *Inorg. Chem.*, 1985, **24**, 704.

13 H. Hartl, I. Brudgam and F. Mahdjour-Hassan-Abadi, *Z. Naturforsch., Teil B*, 1985, **40**, 1032.

14 M. Hofer and H. Hartl, *Z. Anorg. Allg. Chem.*, 1992, **45**, 612.

15 D. W. Allen and X. Li, *J. Chem. Soc., Perkin Trans. 2*, 1997, 1099

16 C. Lambert, S. Stadler, G. Bourhill and C. Brauchle, *Angew. Chem., Int. Ed. Engl.*, 1996, **35,** 644.

17 C. Lambert, E. Schmalzlin, K. Meerholz and C. Brauchle, *Chem. Eur. J.*, 1998, **4**, 512.

Received in Cambridge, UK, 23rd July 1998; 8/05759A

New and improved catalysts for transition metal catalysed radical reactions

Floryan de Campo, Dominique Lastécouères and Jean-Baptiste Verlhac*†

Laboratoire de Chimie Organique et Organométallique (UMR 5802 CNRS), Université Bordeaux I, 351 cours de la Libération, 33405 Talence Cedex, France

New Cu^{I} and Fe^{II} complexes displayed considerable improvements in atom transfer radical addition reactions.

Inter- and intra-molecular radical addition reactions are powerful tools for synthetic organic chemistry. In particular, those reactions initiated by reductive methods such as organotin hydride reduction of ω-haloolefins are well-known processes for the promotion of carbon–carbon bond formation for intramolecular addition and ring construction.[1,2] In contrast, atom transfer radical addition (ATRA) reactions make use of the redox properties of transition metal complexes in order to initiate the reaction by homolytic cleavage of a carbon–halogen bond. As a result, and in contrast to the Kharash addition, the termination step introduces a versatile halogen atom into the product which is then useful for further functionalisation. Thus, a new class of catalysts, most commonly transition metal complexes such as $RuCl_2(PPh_3)_2$,[3] $FeCl_2(P(OEt)_3)_3$,[4] Co(Di-Meglyoxime)$_2$,[5] CuCl(bpy)[3] or a mixture of iron metal and copper bromide,[6] can be used in ATRA reactions. However, only limited success has been reported and only a few examples have appeared which describe cyclisations of allylic trichloroacetates[7] or trichloroacetamides[8] to produce γ-lactones and lactams, respectively, or additions of trihalo compounds such as CCl_4,[9] trichloroacetic acid or esters[10] to olefins. Competing telomerisation is often considered to be a drawback.

Here we report that the use of new copper and iron complexes, for such reactions as the addition of CCl_4 to oct-1-ene and the cyclization of unsaturated trichloroacetates, which lead to a considerable improvement in terms of catalytic activity.

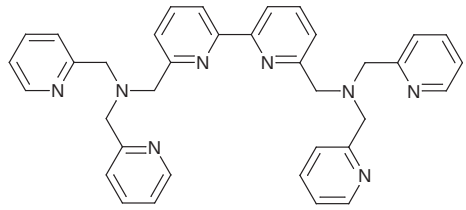

L1

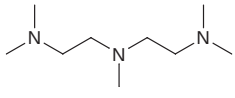

L2

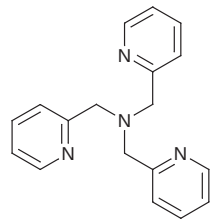

L3

Ligands **L1**, **L2** and **L3** were synthesised according to literature procedures.[11] The catalyst was prepared *in situ* by reacting copper(I) or iron(II) chloride with 1 equiv. of ligand. Whatever the ligand used, the addition of CCl_4 to oct-1-ene proceeds smoothly and affords the corresponding 1:1 adduct. In a typical procedure, oct-1-ene (0.2 M in 1,2-dichloroethane) and CCl_4 (1.1 equiv.) were allowed to react under argon with various amounts of complex (from 30 to 3%) at 80 °C for 18–48 h. Flash chromatography through a short silica gel column and distillation under reduce pressure afforded 1,1,1,3-tetrachlorononane in almost quantitative yield (Scheme 1).

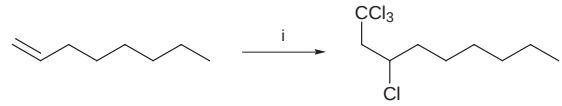

94% [**L1** or **L3** (0.03 mol%, 48 h)]
75% [bpy (0.3 mol%, 48 h)]
70% [**L2** (0.003 mol%, 18 h)]

Scheme 1 *Reagents and conditions*: i, CuCl–ligand, CCl_4

The remarkable solubility of the catalysts, even in concentrated mixtures, and the low quantity of catalyst required in order to complete the reaction represent the major improvement. Thus, even with only 0.003 equiv. of an equimolar mixture of CuCl and ligand **L2**, the tetrachloro adduct is formed in 70% yield, making these systems truly catalytic.

The most significant result was the possibility of using a simple tridentate polyamine (**L2**). This ligand is obtained in a one step procedure from a very cheap starting material. These new complexes induce a faster addition reaction than the widely used Cu(I)Cl/bpy complex. In order to find a catalyst which is less oxygen and water sensitive, we have also investigated the activity of the corresponding iron(II) complexes. Although the iron(II)(bpy) complex was almost inactive, those obtained with **L1** and **L2** exhibit good catalytic activity.‡

Emboldened by these results, we then studied the ability of these catalysts to induce the cyclisation of unsaturated trichloroacetates and particularly pent-4-enyl trichloroacetate **1a** and hex-5-enyl trichloroacetate **2a**. We report herein the synthesis of the eight- and higher-membered lactones by a cyclisation process *via* an *endo* mechanism (Scheme 2). The trichloroacetates were treated at 80 °C (0.1 M in 1,2-dichloroethane) with various amounts of catalyst under argon.

The complexes reported herein are far better catalysts than the previously described CuCl–bpy system.[3] For instance, ligand **L1** in the presence of copper(I) (0.1 mol%) converted quantitatively pent-4-enyl trichloroacetate **1a** into lactone **1b**. Using the same conditions the yield reached only 47% with CuCl–bpy. The CuCl–**L2** system proved to be not as effective in the catalysis of intramolecular reactions, but when $FeCl_2$ was used instead of CuCl, it was possible to obtain a good yield of cyclisation product.§ In all of the experiments described, no significant amount of telomers could be detected. It has been previously reported that with a high stoichiometric ratio of $Cu^{I}Cl$–bpy (30%), significant telomer formation occurs. The lactone formation yield remains average (60%), but all the ester is consumed. The same phenomena could be observed when more that 10% catalyst was used, whatever the final concentration. These results indicate that the concentration of radicals (free or metal-bonded) remains high during the reaction and that the kinetic constant of cyclisation might be smaller than the telomerisation constant.

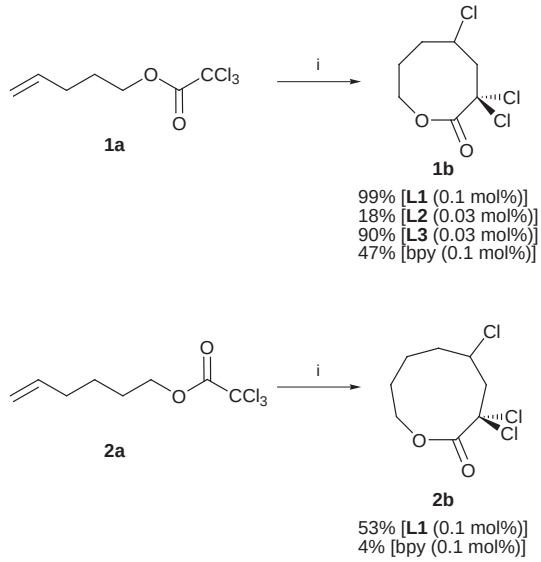

Scheme 2 *Reagents and conditions*: i, CuCl–ligand, 1,2-dichloroethane, 80 °C

The cyclisation of hex-5-enyl trichloroacetate **2a** gave only a low yield of lactone **2b** in the presence of CuCl–bpy (0.1 mol%), but this yield is subsequently improved by the use of either the CuCl–L1 or the $FeCl_2$–L2 systems.¶ In the cyclisation experiments with **2a**, a substantial difference between the yield of cyclisation products and the total conversion, based on the disappearance of **2a**, was noted. The difference in mass balance is probably due to the tendency for **2a** to give oligomers and particularly dimers, which have been characterised by mass spectrometry, because of the increase in ring size.

We have also observed reactions which were impossible to perform with CuCl–bpy;[7] for instance the cyclisation of hept-6-enyl trichloroacetate **3a** afforded the cyclic *endo* lactone **3b** in 70% yield in the presence of CuCl–**L3** (Scheme 3). It was also possible to catalyse the *exo* cyclisation of prop-2-enyl trichloroacetate **4a** with 48% yield in the presence of the same catalyst. In the latter case the $FeCl_2$–**L2** system also proved to be effective.

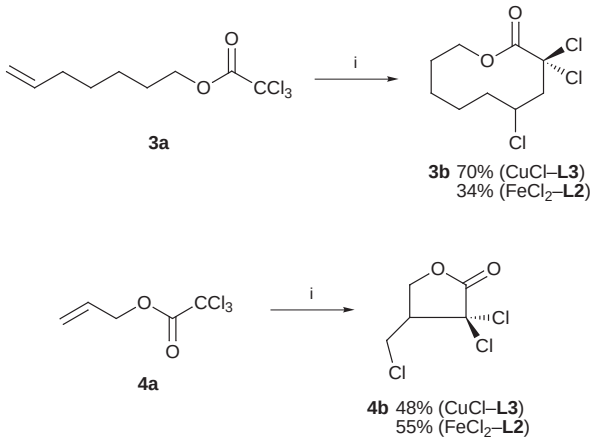

Scheme 3 *Reagents and conditions*: 1,2-dichloroethane, 80 °C, CuCl–**L3** or $FeCl_2$–**L2** catalysts (0.1 mol%)

As previously observed,[3,12] the cyclisation of esters with long unsaturated chains (**1a**, **2a**, **3a**) proceeds *via* an *endo* pathway. This is due to the fact that the most stable conformation for the ester function (s-*trans*) does not impede the cyclisation process if the carbon chain is long enough. With the unsaturated ester **4a**, only the less favourable conformation (s-*cis*) can give rise to the cyclisation product. In this case the formation of a five-membered ring *via* an *exo* pathway is preferred. The but-3-enyl trichloroacetate lies in an intermediate position. It was impossible for us to obtain cyclisation products, we could only detect cyclic dimers and telomers by mass spectrometry. The formation of a six-membered ring lactone *via* the s-*cis* conformation is not favourable and the butenyl chain is not long enough to allow a cyclisation process *via* the s-*trans* conformation. These results are consistent with those reported by O-Yang in the case of α-iodo esters.[12]

As a conclusion, the use of new ligands represents a significant improvement for the catalytic activity of copper(I) and iron(II) complexes in ATRA reactions by reducing the required amount of complex by a factor of 10 to 100. Moreover, they are soluble in the reaction mixture and catalyse reactions which are impossible to perform with the $Cu^{I}Cl$–bpy complex. The metal could also act as a template and allow the notoriously difficult cyclisation of eight- and nine-membered ring lactone precursors as suggested previously.[7] We are currently trying to relate the redox potentials of these complexes to their catalytic activity.

We are indebted to Dr B. Maillard for fruitful discussion and to the Région Aquitaine for financial support.

Notes and References

† E-mail: j-b.verlhac@lcoo.u-bordeaux.fr

‡ In the presence of an 1:1 mixture of $FeCl_2$–ligand (0.03 mol%), the yields were respectively: **L1**, 65% (48 h); **L2**, 75% (18 h); bpy, 4% (18 h).

§ Replacement of CuCl–**L2** by $FeCl_2$–**L2** allowed us to obtain **1b** in 62% yield.

¶ A 50% yield of **2b** was obtained by using the $FeCl_2$–**L2** mixture (0.03 mol%)

1 B. Giese, *Radicals in Organic Synthesis: Formation of Carbon-Carbon Bonds*, Pergamon, New York, 1986.
2 D. P. Curran, *Synthesis*, 1988, **417**, 489.
3 F. O. H. Pirrung, H. Hiemstra and W. N. Speckamp, *Tetrahedron*, 1994, **50**, 12 415. N. Baldovini, M.-P. Bertrand, A. Carrière, R. Nougier and J.-M. Plancher, *J. Org. Chem*., 1996, **61**, 3205
4 G. M. Lee, M. Parvez and S. M. Weinreb, *Tetrahedron*, 1988, **44**, 4671
5 B. P. Branchaud and G. X. Yu, *Organometallics*, 1993, **12**, 4262
6 L. Forti, F. Ghelti and U. M. Pagnoni, *Tetrahedron Lett*., 1996, **37**, 2077
7 F. O. H. Pirrung, H. Hiemstra, W. N. Speckamp, B. Kaptein and H. E. Schoemaker, *Synthesis*, 1995, 458; F. O. H. Pirrung, H. Hiemstra, B. Kaptein, M. E. Martinez Sobrino, D. G. Petra, H. E. Schoemaker and W. N. Speckamp, *Synlett*, 1993, 739
8 H. Nagashima, N. Ozaki, M. Ishii, K. Seki, M. Washiyama and K. Itoh, *J. Org. Chem*., 1993, **58**, 464
9 H. Matsumoto, T. Nakano and Y. Nagai, *Tetrahedron Lett*., 1973, 5147
10 J. C. Phelps and D. E. Bergbreiter, *Tetrahedron Lett*., 1989, **30**, 3915
11 A. Dossing, A. Hazell and H. Toftlund, *Acta Chem. Scand*., 1996, **50**, 95; G. Anderegg and F. Wenk, *Helv. Chim. Acta*, 1967, **50**, 2330. Ligand **L2** was obtained by permethylation of 1,4,7-triazaheptane with a formic acid–formaldehyde mixture
12 F. Barth and C. O-Yang, *Tetrahedron Lett*., 1990, **38**, 1121; J. E. Baldwin, R. M. Adlington, M. B. Mitchell and J. Robertson, *J. Chem. Soc., Chem. Commun*., 1990, 1574.

Received in Cambridge, UK, 14th April 1998; revised manuscript received, 29th June 1998; 8/04915G

A highly cytotoxic L-rhamnose analogue of the antitumour agent spicamycin

Angeles Martín,[a] Terry D. Butters[b] and George W. J. Fleet*[a]†

[a] *Dyson Perrins Laboratory, University of Oxford, South Parks Road, Oxford, UK OX1 3QY*
[b] *Oxford Glycobiology Institute, Department of Biochemistry, University of Oxford, South Parks Road, Oxford, UK OX1 3QU*

Rhamnospicamycin 2, a rhamnose analogue (containing adenine, a carbohydrate, an amino acid and a fatty acid) of the naturally occurring combinatorial library spicamycin 1, is prepared from L-rhamnose and shown to be highly cytotoxic towards human myeloma cells (IC_{50} = 120 nM).

Nucleoside analogues linked to a sugar through the NH_2 group of adenine are very rare.[1] Spicamycin **1**, an antitumour

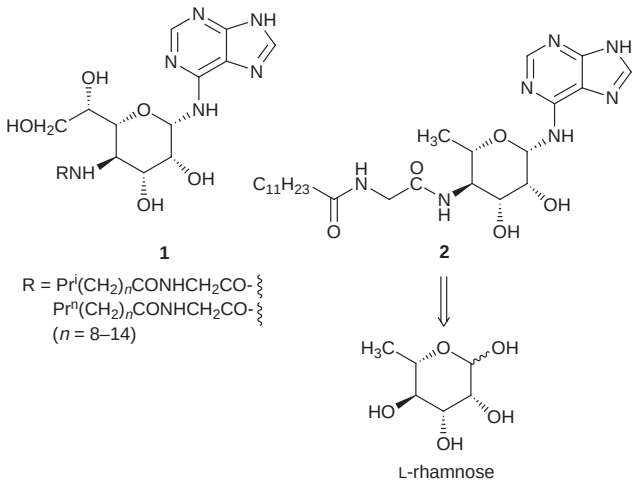

antibiotic isolated from *Streptomyces alanosinicus*,[2] is a naturally occurring combinatorial library of fatty acids linked through glycine to a seven carbon sugar and then through the anomeric position of the carbohydrate to the amino group of adenine.[3] The potential of spicamycin as a new class of antitumour agent[4] stimulated structure activity studies[5] that found that the dodecanoyl derivative **1** (R = decanoyl) had antitumour activity against human gastric cancer SC-9 superior to that of mitomycin C, which is clinically used for many kinds of tumours.[6] A semi-synthetic analogue of spicamycin **1** with a tetradecadienoyl side chain[7] potently inhibits the growth of certain human tumour lines *in vitro* and displays marked *in vivo* activity in Colo 205 colon carcinoma xenografts;[8] it will shortly be available for Phase 1 clinical trials in the USA. Exposure of cells to spicamycin at low concentrations of the drug alters glycoprotein processing and induces some accumulation of oligomannosides; while the molecular mechanism for the activity of spicamycin needs to be clarified, the effects of the compound are consistent with a prominent early effect on the enzymatic machinery or organelles important for proper glycoprotein processing and emphasise the novelty of this agent's likely mechanism of action.[9]

Spicamycin **1** contains a nucleoside base, a carbohydrate, an amino acid and a lipid fragment and thus provides an interesting target for synthesis, and for constructing a wide range of combinatorial libraries from suitable building blocks in which of these components may be varied. No studies on the total synthesis of spicamycin have been reported, all modifications to the structure arising from semi-synthetic procedures from degradation of the natural material. The absolute configuration of the carbohydrate component in **1** was determined by X-ray crystallographic analysis;[10] **1** is a seven carbon sugar analogue of L-mannose, and is thus closely related to L-rhamnose. The total synthesis of closely related carbohydrate analogues of spicamycin would allow the importance of structural features of the carbohydrate to be determined and provide materials for the elucidation of the mechanism of activity of this class of antitumour agent.

Here we report the synthesis of the spicamycin analogue **2** from L-rhamnose and its cytotoxicity against human myeloma cells. The synthesis of rhamnospicamycin **2** requires introduction of nitrogen with retention of configuration at C-4 of L-rhamnose, following by elaboration at the anomeric position of the sugar and at the nitrogen group in C-4. Introduction of the nitrogen as an azide at C-4 permits flexibility in the approach to spicamycin analogues by allowing development of the amino acid side chain or the introduction of the adenine moiety at the anomeric position of rhamnose in either order. Here, the purine is introduced first, but there are clearly many approaches with opportunities for the development of libraries at different stages of the synthesis.

The acetonide **3**, prepared from L-rhamnose in 87% overall yield as previously described,[11] has only the hydroxy group at C-4 of rhamnose unprotected. Oxidation of **3** with PCC in CH_2Cl_2 and subsequent reduction of the resulting ketone with $NaBH_4$ afforded the inverted alcohol **4** in 95% yield over the two steps. Esterification of **4** with Tf_2O and pyridine in CH_2Cl_2 gave the triflate **5** in 82% as a relatively unstable oil. Treatment of **5** with NaN_3 in DMF, followed by cleavage of the acetonide with aqueous TFA, gave the 4-azidorhamnose derivative **6** [mp 81–82 °C (acetone–hexane) $[\alpha]_D^{21}$ −123.5 (*c* 0.72, MeOH)] in 60% yield over two steps (40% from rhamnose). More vigorous hydrolysis of **6** with aqueous TFA at reflux yielded the azido lactols **7**[12] in 86% as a mixture of anomers (α:β, 2:1).

The anomeric amine **8** was obtained from treatment of **7** with aqueous NH_3. All attempts to introduce the adenine moiety directly by addition of 6-chloropurine to **8** were unsuccessful; the principal products were dimeric amines derived from **8**. Accordingly, **8** was reacted with the more electrophilic 4,6-dichloro-5-nitropyrimidine (in the presence of Et_3N as base) to afford the pyrimidine derivative **9** [mp 142–144 °C; $[\alpha]_D^{21}$ +23.2 (*c* 0.59, MeOH)] in 20% yield from **7**, which was converted into the more easily manipulated acetonide **10** [mp 127–129 °C; $[\alpha]_D^{21}$ +50.9 (*c* 0.55, Me_2CO)] in 70% yield. Studies to improve the yield of this key step are in progress.

Reaction of **10** with aqueous NH_3 resulted in nucleophilic displacement of the chloride to give the corresponding amine **11** [mp 180–182 °C, $[\alpha]_D^{21}$ +3.5 (*c* 0.60, Me_2CO)] in 97% yield. Investigation of the activity of a range of reducing agents with the nitro azide **11** failed to identify any reagent with significant selectivity for the nitro group over the azide. Accordingly, the additional carbon necessary for purine formation was added to the free amino group in **11** prior to reduction; treatment of **11** with triethyl orthoformate gave, after work-up in the presence of MeOH, a mixture of the compounds **12** and **13** in a ratio of 1:1 in 65% yield. Hydrogenation of the azides **12** and **13** in MeOH in the presence of Pd/C effected the reduction of the azide and nitro groups to the corresponding diamines which sponta-

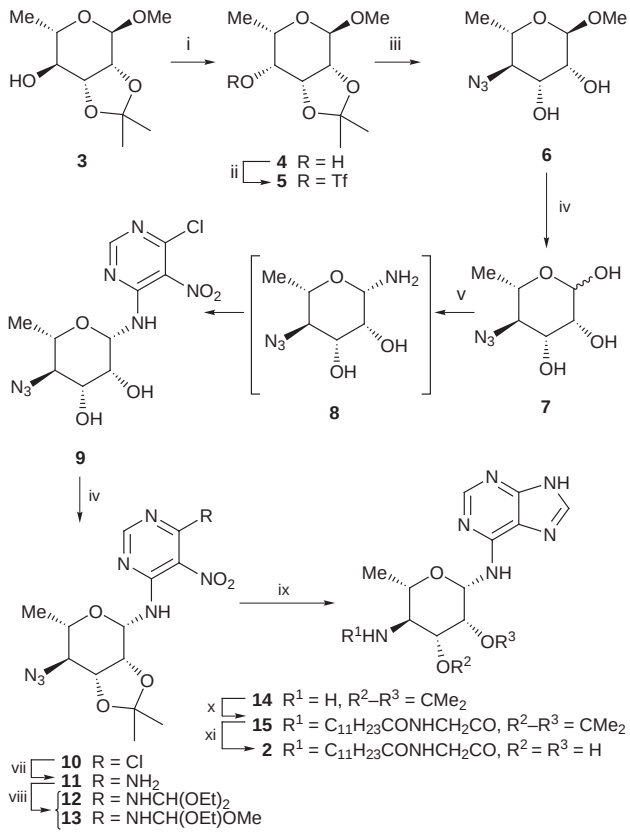

Scheme 1 *Reagents and conditions:* i, PCC, molecular sieves 3Å, CH_2Cl_2, then $NaBH_4$, EtOH–H_2O, 0 °C; ii, Tf_2O, Py, CH_2Cl_2, −10 °C; iii, NaN_3, DMF, then TFA–H_2O 3:7; iv, TFA–H_2O 1:1, 1,4-dioxane, reflux; v, NH_3 (aq), then 4,6-dichloro-5-nitropyrimidine, Et_3N, DMF; vi, $Me_2C(OMe)_2$, CSA, acetone; vii, NH_3 (aq), MeOH, 60 °C; viii, $HC(OEt)_3$, 140 °C, then MeOH, silica; ix, H_2, Pd/C, MeOH; x, dodecanoylglycine, DMF, *N*-hydroxysuccinimide, WSC·HCl; xi, 70% AcOH (aq), 60 °C

neously cyclised to give the purine **14**[13] [oil; $[\alpha]_D^{21}$ +25.4 (*c* 0.22, MeOH)] in 53% yield.

Condensation of the amine **14** with dodecanoylglycine[5] in DMF in the presence of *N*-hydroxysuccinimide and 1-(3-dimethylaminopropyl)-3-ethylcarbodiimide hydrochloride (WSC·HCl) gave the glycopeptide **15** in 71% yield.[14] Finally, removal of the acetonide in **14** with aq. AcOH gave rhamnospicamycin **2**, mp 224–226 °C (decomp.) $[\alpha]_D^{21}$ +9.71 (*c* 0.35 MeOH) in 82% yield; rhamnospicamycin is columnable in organic solvents and easy to purify. The NMR of **2** in DMSO is temperature dependent (in contrast to the NMR in CD_3OD) and may indicate some propensity for intramolecular hydrogen bonding between the carbohydrate hydroxy protons and the adenine nucleus.[15]

In a preliminary study rhamnospicamycin **2** was found to be highly cytotoxic with an IC_{50} value for cell growth (assessed over 15 h in culture using human myeloma cells, HL60 cells) is 120 nM; thus **2** displays much the same potency as that reported for the dodecanoyl derivative of spicamycin **1**.

While there are a number of steps in the synthesis that have yet to be optimised, we have shown that variation in the carbohydrate fragment of spicamycin may allow a wide range of novel materials with cytotoxic activity to be prepared. Spicamycin incorporates a nucleoside, a fatty acid, a sugar and an amino acid all into one component; the potent cytotoxicity with the possibility of a novel mode of action as an anti-cancer agent in regard to modification of glycoprotein processing, together with the opportunity to generate combinatorial libraries, makes this class of compound an attractive one for further synthetic study and biological evaluation of the mechanism.

Financial support from the European Community for a post-doctoral fellowship (Programme Training and Mobility Research) to A. M. (contract no. ERBFMBICT961664) is gratefully acknowledged.

Notes and References

† E-mail: george.fleet@chem.ox.ac.uk

1 E. M. Acton, K. J. Ryan and A. E. Luetzow, *J. Med. Chem.*, 1977, **20**, 1362.
2 Y. Hayakawa, M. Nakagawa, H. Kawai, K. Tanabe, H. Nakayama, A. Shimazu, H. Seto and N. Õtake, *J. Antibiot.*, 1983, **36**, 934.
3 Y. Hayakawa, M. Nakagawa, H. Kawai, K. Tanabe, H. Nakayama, A. Shimazu, H. Seto and N. Õtake, *Agric. Biol. Chem.*, 1985, **49**, 2685.
4 M. Kamishohara, H. Kawai, T. Sakai, T. Isoe, K. Hasegawa, J. Mochizuki, T. Uchida, S. Kataoka, H. Yamaki, T. Tsuruo and N. Õtake, *Oncology Res.*, 1994, **6**, 383; Y. S. Lee, K. Nishio, H. Ogasawara, Y. Funayama, T. Ohira and N. Saijo, *Cancer Res.*, 1995, **55**, 1075.
5 M. Kamishohara, H. Kawai, A. Odagawa, T. Isoe, J. Mochizuki, T. Uchida, Y. Hayakawa, H. Seto, T. Tsuruo and N. Õtake, *J. Antibiot.*, 1993, **46**, 1439.
6 M. Kamishohara, H. Kawai, A. Odagawa, T. Isoe, J. Mochizuki, T. Uchida, Y. Hayakawa, H. Seto, T. Tsuruo and N. Õtake, *J. Antibiot.*, 1994, **47**, 1305.
7 M. Kamishohara, A. Odagawa, A. Suzuki, T. Uchida, T. Kawasaki, T. Tsuruo and N. Õtake, *J. Antibiot.*, 1995, **48**, 1467.
8 M. Kamishohara, H. Kawai, T. Uchida, T. Tsuruo and N. Õtake, *Chemother. Pharmacol.*, 1996, **38**, 495.
9 A. M. Burger, G. Kaur, M. Hollingshead, R. T. Fischer, K. Nagashima, L. Malspiels, K. L. K. Duncan and E. A. Sausville, *Clinical Cancer Res.*, 1997, **3**, 455.
10 T. Sakai, K. Shindo, A. Odagawa, A. Suzuki, H. Kawai, K. Kobayashi, Y. Hayakawa, H. Seto and N. Õtake, *J. Antibiot.*, 1995, **48**, 899.
11 J. Jary, K. Capek and J. Kovár, *Collect. Czech. Chem., Commun.*, 1963, **28**, 217.
12 B. Davis, A. A. Bell, R. J. Nash, A. A. Watson, R. C. Griffiths, M. G. Jones, C. Smith and G. W. J. Fleet, *Tetrahedron Lett.*, 1996, **37**, 8565.
13 All new compounds have satisfactory HRMS or CHN microanalytical data; the anticipated β-stereochemistry at the anomeric position of **14** was confirmed by NOE enhancements between H-1 and the protons at H-2 (11.2%), H-3 (2%) and H-5 (13.8%).
14 The structure of **15** in terms of the anomeric configuration and of the site of attachment to the adenine nucleus was assigned on the basis of COSY, HMQC and HMBC experiments.
15 *Selected data* for **2**: δ_H(500 MHz, CD_3OD) 0.91 [3H, t, *J* 6.8, $CH_3(CH_2)_{10}CO$], 1.22 (3H, d, *J* 6.1, H_3-6′) 1.28–1.34 [16H, m, $CH_3(CH_2)_8CH_2$], 1.65 [2H, m, $CH_3(CH_2)_8CH_2CH_2CO$], 2.30 [2H, t, *J* 7.6, $CH_3(CH_2)_8CH_2CH_2CO$], 3.62 (1H, dq, *J* 6.1, 9.9, H-5′), 3.74 (1H, dd, *J* 3.5, 10.5, H-3′), 3.90 (2H, s, $RNHCH_2CONH$), 3.95 (1H, t, *J* 10.2, H-4′), 4.02 (1H, d, *J* 2.2, H-2′), 5.70 (1H, br s, H-1′), 8.19 (1H, s), 8.35 (1H, s); δ_H(500 MHz, [$^2H_6$]DMSO, 25 °C) 0.83 [3H, t, *J* 6.9, $CH_3(CH_2)_{10}CO$], 0.99 (3H, m, H_3-6′) 1.20–1.25 [16H, m, $CH_3(CH_2)_8CH_2$], 1.48 [2H, t, *J* 6.8, $CH_3(CH_2)_8CH_2CH_2CO$], 2.12 [2H, t, *J* 7.4, $CH_3(CH_2)_8CH_2CH_2CO$], 3.50–3.71 (4H, m), 3.68 (2H, d, *J* 5.7, $RNHCH_2CONH$), 3.80 (1H, s), 4.75 (1H, br s), 5.44, 5.55 (1H, 2 × br s), 7.15 (1H, br. s), 7.60 (1H, d, *J* 9.3), 7.99, 8.00 (1H, 2 × d, *J* 5.7), 8.21, 8.22 (1H, 2 × s), 8.27, 8.29 (1H, 2 × s); δ_H(500 MHz, [$^2H_6$]DMSO, 80 °C) 0.86 [3H, t, *J* 7.0, $CH_3(CH_2)_{10}CO$], 1.05 (3H, d, *J* 6.1, H_3-6′) 1.25–1.31 [16H, m, $CH_3(CH_2)_8CH_2$], 1.53 [2H, t, *J* 7.2, $CH_3(CH_2)_8CH_2CH_2CO$], 2.16 [2H, t, *J* 7.5, $CH_3(CH_2)_8CH_2CH_2CO$], 3.48 (1H, dq, *J* 6.1, 9.4, H-5′), 3.65 (1H, dd, *J* 2.9, 10.3, H-3′), 3.70 (1H, m), 3.72 (2H, d, *J* 5.5, $RNHCH_2CONH$), 3.86 (1H, d, *J* 2.1, H-2′), 5.00 (1H, br s), 5.73 (1H, br s, H-1′), 6.90 (1H, br s), 7.27 (1H, d, *J* 8.6), 7.60 (1H, br s), 8.11 (1H, s), 8.27 (1H, s); δ_C(125 MHz, [$^2H_6$]DMSO, 80 °C) 13.51 (q), 17.82 (q, C-6′), 21.74, 24.92, 28.37, 28.49, 28.54, 28.66, 28.71, 28.73, 31.01, 35.19 [10 × t, $CH_3(CH_2)_{10}CONHCH_2CONH$], 52.89, 70.00, 71.44, 71.86, 78.40 (5 × d, C-1′, C-2′, C-3′, C-4′, C-5′), 118.60 (s), 140.36 (d), 151.89 (d), 151.89 (s), 152.36 (s), 169.45, 172.55 (2 × s, 2 × C=O)

Received in Liverpool, UK, 27th July 1998; 8/05878D

Synthesis and luminescence behaviour of rhenium(I) diynyl complexes. X-Ray crystal structures of [Re(CO)$_3$(^{t}Bu$_2$bpy)(C≡C–C≡CH)] and [Re(CO)$_3$(^{t}Bu$_2$bpy)(C≡C–C≡CPh)]

Vivian Wing-Wah Yam,* Samuel Hung-Fai Chong and Kung-Kai Cheung

Department of Chemistry, The University of Hong Kong, Pokfulam Road, Hong Kong SAR, People's Republic of China. E-mail: wwyam@hkucc.hku.hk

Luminescent rhenium(I) diynyl complexes [Re(CO)$_3$(^{t}Bu$_2$bpy)(C≡C–C≡CH)] and [Re(CO)$_3$(^{t}Bu$_2$bpy)(C≡C–C≡CPh)] were synthesized and their photophysical properties studied; the crystal structures have also been determined.

There has been a rapidly growing interest in the chemical and physical properties of C$_n$-bridged metal-containing materials,[1] in view of their potential applications as nonlinear optical materials, molecular wires, and molecular electronics. With the recent reports on the successful isolation of acetylide-bridged rhenium(I) organometallics[1a–g,2] and our recent efforts in incorporating metal-to-ligand charge transfer (MLCT) excited states into rhenium(I) acetylide units to make luminescent rigid-rod materials,[3] we have extended our work to employ the diynyl unit as the ligand to extend the carbon chain. Herein are reported the synthesis, structure and luminescence behaviour of two rhenium(I) diynyl complexes, [Re(CO)$_3$(^{t}Bu$_2$bpy)(C≡C–C≡CH)] **1** and [Re(CO)$_3$(^{t}Bu$_2$bpy)(C≡C–C≡CPh)] **2**.

Reaction of a mixture of [Re(CO)$_3$(^{t}Bu$_2$bpy)Cl],[4] KF, AgOTf and Me$_3$SiC≡C–C≡CSiMe$_3$ in a 1 : 1 : 1 : 3 ratio in MeOH under reflux conditions in an inert atmosphere of nitrogen for 24 h afforded [Re(CO)$_3$(^{t}Bu$_2$bpy)(C≡C–C≡CH)], which was isolated as orange crystals after purification by column chromatography on silica gel using dichloromethane as eluent, followed by recrystallization from dichloromethane–diethyl ether. On the other hand, reaction of a mixture of [Re(CO)$_3$(^{t}Bu$_2$bpy)Cl], AgOTf, NEt$_3$ and PhC≡C–C≡CH[5] in a 1 : 1 : 2 : 1.5 ratio in refluxing THF under nitrogen for 24 h afforded [Re(CO)$_3$(^{t}Bu$_2$bpy)(C≡C–C≡CPh)]. Purification by column chromatography on silica gel using dichloromethane–light petroleum (1 : 1 v/v) as eluent, followed by subsequent recrystallization from dichloromethane–light petroleum yielded [Re(CO)$_3$(^{t}Bu$_2$bpy)(C≡C–C≡CPh)] as yellow crystals. The identities of both complexes **1** and **2** have been confirmed by satisfactory elemental analyses, ^{1}H NMR spectroscopy, FAB-MS,† and X-ray crystallography.‡

Fig. 1 and 2 depict the perspective drawings of complexes **1** and **2** with atomic numbering, respectively. Both structures show a slightly distorted octahedral geometry about Re with the three carbonyl ligands arranged in a facial fashion. The N–Re–N bond angles of 74.6(2) and 73.9(1)° for **1** and **2**, respectively, are less than 90°, as required by the bite distance exerted by the steric demand of the chelating bipyridine ligand. The two C≡C bond lengths are 1.199(10) and 1.19(1) Å for **1** and 1.198(7) and 1.189(7) Å for **2**, which are comparable to those found for diynyl systems.[1d,6] The Re–C≡C–C≡C units are essentially linear with bond angles of 175.2(6)–179.8(10) and 175.7(5)–178.6(6)° for **1** and **2**, respectively.

The electronic absorption spectra of **1** and **2** show intense absorption bands at *ca.* 404 and 416 nm, respectively, in tetrahydrofuran. With reference to previous spectroscopic work on rhenium(I) diimine systems,[3,4,7] the intense low energy absorption is tentatively assigned as the dπ(Re) → π*(^{t}Bu$_2$bpy) MLCT transition. The lower MLCT absorption energy for **2** than **1** is consistent with the better σ- and π-donating abilities of PhC≡C–C≡C than HC≡C–C≡C,[1j,8,9] which render the Re(I) centre more electron rich, and raise the Re dπ orbital energy. Similar trends have been observed in the related alkynyl system [Re(CO)$_3$(^{t}Bu$_2$bpy)X],[3] in which the MLCT absorption band occurs at higher energy for X = HC≡C than when X = PhC≡C.

Excitation of **1** and **2** both in the solid state and in fluid solutions at room temperature at λ > 400 nm resulted in strong orange luminescence, attributed to the ^{3}MLCT phosphorescence. The excitation spectra of **1** and **2** in THF show excitation bands at *ca.* 400 nm and 410 nm, respectively, which closely resemble those of the MLCT absorption maxima. The photophysical data are summarized in Table 1. The slightly lower MLCT emission energy of **2** than **1** in THF is in line with the stronger σ- and π-donating abilities of the phenyldiynyl unit than the butadiynyl ligand, *i.e.* PhC≡C–C≡C (625 nm) < HC≡C–C≡C (620 nm). Similar trends have been observed in the monoacetylide analogues [PhC≡C (688 nm) < HC≡C (670 nm)].[3] It is interesting to note that both **1** and **2** emit at higher energies than their respective monoacetylide counterparts, *i.e.* in the [Re(CO)$_3$(^{t}Bu$_2$bpy)X] system, the emission energies in THF follow the order: HC≡C–C≡C (620 nm) > HC≡C (670 nm); PhC≡C–C≡C (625 nm) > PhC≡C (688 nm). The observation of a blue shift in emission energies upon increasing

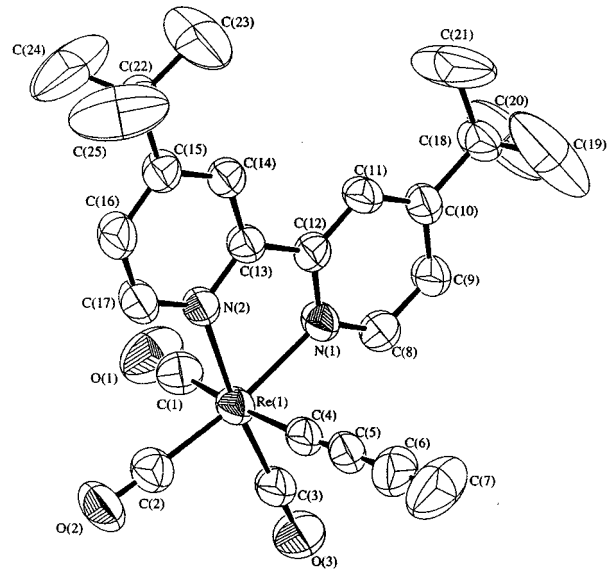

Fig. 1 Perspective drawing of complex **1** with atomic numbering. Hydrogen atoms have been omitted for clarity. Thermal ellipsoids are shown at the 50% probability level. Selected bond distances (Å) and bond angles (°): Re(1)–C(1) 1.946(9), Re(1)–N(1) 2.168(5), Re(1)–N(2) 2.183(4), Re(1)–C(4) 2.114(8), C(4)–C(5) 1.199(10), C(6)–C(7) 1.19(1), N(1)–Re(1)–N(2) 74.6(2), N(1)–Re(1)–C(2) 171.1(2), C(1)–Re(1)–C(4) 174.4(3), C(4)–C(5)–C(6) 178.3(8), C(5)–C(6)–C(7) 179.8(10).

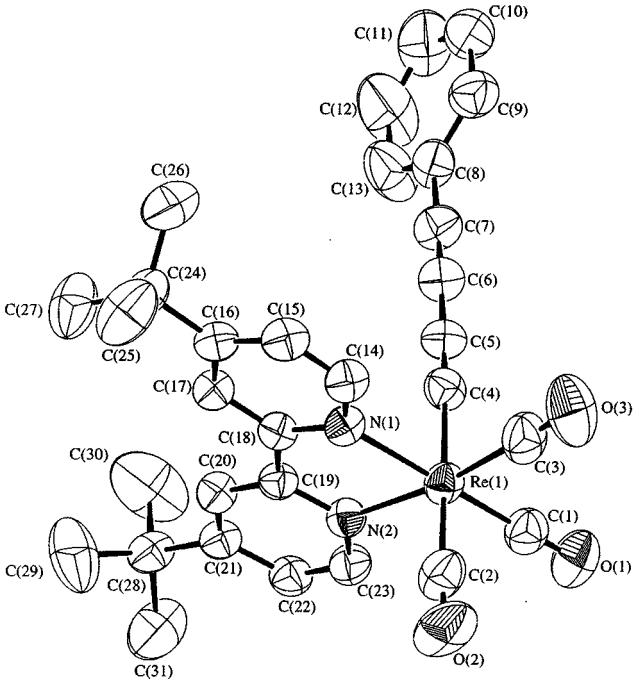

Fig. 2 Perspective drawing of complex **2** with atomic numbering. Hydrogen atoms have been omitted for clarity. Thermal ellipsoids were shown at the 50% probability level. Selected bond distances (Å) and bond angles (°): Re(1)–C(1) 1.913(6), Re(1)–N(1) 2.188(4), Re(1)–N(2) 2.175(4), Re(1)–C(4) 2.126(5), C(4)–C(5) 1.198(7), C(6)–C(7) 1.189(7), N(1)–Re(1)–N(2) 73.9(1), N(1)–Re(1)–C(1) 171.8(2), C(2)–Re(1)–C(4) 176.3(2), C(4)–C(5)–C(6) 177.4(6), C(5)–C(6)–C(7) 178.6(6).

Table 1 Photophysical data for complexes **1** and **2**

Complex	Medium (T/K)	Emission, λ_{em}/nm (τ_o/μs)
1	THF (298)	620 (< 0.1)
	CH_2Cl_2 (298)	604 (< 0.1)
	Solid (298)	565 (< 0.1)
	Solid (77)	580
	EtOH–MeOH glass (4 : 1 v/v) (77)	540
2	THF (298)	625 (< 0.1)
	Solid (298)	570 (< 0.1)
	Solid (77)	570

the C≡C unit is in line with the assignment of a ^{3}MLCT [dπ(Re) → π*(^{t}Bu$_2$bpy)] origin and disfavours the assignment of a ^{3}MLCT [dπ(Re) → π*(C≡C–C≡CR)] or a metal-perturbed ^{3}IL [π(C≡C–C≡CR) → π*(C≡C–C≡CR)] origin. Given the similar σ-donating properties of the monoacetylide *versus* the diynyl unit,[9] the much better π-accepting ability of RC≡C–C≡C than RC≡C would become the dominating factor, stabilizing the Re dπ orbitals to a greater extent, and hence give rise to a higher energy ^{3}MLCT emission.

V. W.-W. Y. acknowledges financial support from the Research Grants Council and The University of Hong Kong, and S. H.-F. C. the receipt of a postgraduate studentship, administered by The University of Hong Kong.

Notes and References

† **1**: ^{1}H NMR (300 MHz, acetone-d_6, 298 K, relative to TMS): δ 1.40 (s, 18H, ^{t}Bu), 1.75 (s, 1H, C≡CH), 7.70 (dd, 2H, 5- and 5′-pyridyl Hs), 8.60 (d, 2H, 3- and 3′-pyridyl Hs), 8.80 (d, 2H, 6- and 6′-pyridyl Hs). Positive FAB-MS: ion clusters at m/z 588 {M}$^+$, 560 {M − CO}$^+$, 539 {M − [C≡C–C≡CH]}$^+$. UV–VIS [λ/nm (ε/dm^{3}mol^{-1}cm^{-1})]: THF, 248(16410), 284(17130), 404(3470); CH_2Cl_2, 310(6100), 396(2690). Elemental analyses. Found: C 50.44, H 4.31, N 4.31. Calc. for **1**·0.5H_2O: C 50.29, H 4.36, N 4.69%. **2**: ^{1}H NMR (300 MHz, acetone-d_6, 298 K, relative to TMS): δ 1.50 (s, 18H, ^{t}Bu), 7.25 (s, 5H, Ph Hs), 7.80 (dd, 2H, 5- and 5′-pyridyl Hs), 8.70 (d, 2H, 3- and 3′-pyridyl Hs), 8.90 (d, 2H, 6- and 6′-pyridyl Hs). Positive FAB-MS: ion clusters at m/z 665 {M}$^+$, 636 {M − CO}$^+$, 539 {M − [C≡C–C≡CPh]}$^+$. UV–VIS [λ/nm (ε/dm^{3}mol^{-1}cm^{-1})]: THF, 298(48570), 340(14610), 416(3220).

‡ *Crystal data* for **1**: [$C_{25}H_{25}O_3N_2Re$], M = 587.69, monoclinic, space group $P2_1/n$ (no. 14), a = 11.273(3), b = 12.748(1), c = 17.168(2) Å, β = 97.60(4)°, V = 2445.7(7) Å^3, Z = 4, D_c = 1.596 g cm^{-3}, μ(Mo-Kα) = 49.97 cm^{-1}, F(000) = 1152, T = 301 K. Convergence for 280 variable parameters by least-squares refinement on F with $w = 4F_o^2/\sigma^2(F_o^2)$, where $\sigma^2(F_o^2) = [\sigma^2(I) + (0.025F_o^2)^2]$ for 2847 reflections with $I > 3\sigma(I)$ was reached at R = 0.028 and wR = 0.034 with a goodness-of-fit of 1.22. For **2**: [$C_{31}H_{29}O_3N_2Re$], M = 663.79, monoclinic, space group $P2_1/c$ (no. 14), a = 11.048(2), b = 11.795(2), c = 21.935(3) Å, β = 94.23(2)°, V = 2859.9(7) Å^3, Z = 4, D_c = 1.542 g cm^{-3}, μ(Mo-Kα) = 42.83 cm^{-1}, F(000) = 1312, T = 301 K. Convergence for 334 variable parameters by least-squares refinement on F with $w = 4F_o^2/\sigma^2(F_o^2)$, where $\sigma^2(F_o^2) = [\sigma^2(I) + (0.030F_o^2)^2]$ for 3876 reflections with $I > 3\sigma(I)$ was reached at R = 0.031 and wR = 0.040 with a goodness-of-fit of 1.40. CCDC 182/995.

1 (*a*) M. Appel, J. Heidrich and W. Beck, *Chem. Ber*., 1987, **120**, 1087; (*b*) J. Heidrich, M. Steimann, M. Appel and W. Beck, *Organometallics*, 1990, **9**, 1296; (*c*) T. Weidmann, V. Weinrich, B. Wagner, C. Robl and W. Beck, *Chem. Ber*., 1991, **124**, 1363; (*d*) Y. Zhou, J. W. Seyler, W. Weng, A. M. Arif and J. A. Gladysz, *J. Am. Chem. Soc*., 1993, **115**, 8509; (*e*) J. W. Seyler, W. Weng, Y. Zhou and J. A. Gladysz, *Organometallics*, 1993, **12**, 3802; (*f*) M. Brady, W. Weng and J. A. Gladysz, *J. Chem. Soc., Chem. Commun*., 1994, 2655; (*g*) U. H. F. Bunz, *Angew. Chem., Int. Ed. Engl*., 1996, **35**, 969; (*h*) T. Weyland, C. Lapinte, G. Frapper, M. J. Calhorda, J-F. Halet and L. Toupet, *Organometallics*, 1997, **16**, 2024; (*i*) H. Schimanke and R. Gleiter, *Organometallics*, 1998, **17**, 275; (*j*) J. Manna, K. D. John and M. D. Hopkins, *Adv. Organomet. Chem*., 1995, **38**, 79; (*k*) N. L. Narvor, L. Toupet and C. Lapinte, *J. Am. Chem. Soc*., 1995, **117**, 7129.

2 (*a*) W. Weng, T. Bartik and J. A. Gladysz, *Angew. Chem., Int. Ed. Engl*., 1994, **33**, 2199; (*b*) W. Weng, T. Bartik, M. T. Johnson, A. M. Arif and J. A. Gladysz, *Organometallics*, 1995, **14**, 889; (*c*) W. Weng, T. Bartik, M. Brady, B. Bartik, J. A. Ramsden, A. M. Arif and J. A. Gladysz, *J. Am. Chem. Soc*., 1995, **117**, 11922.

3 (*a*) V. W. W. Yam, V. C. Y. Lau and K. K. Cheung, *Organometallics*, 1995, **14**, 2749; (*b*) V. W. W. Yam, V. C. Y. Lau and K. K. Cheung, *Organometallics*, 1996, **15**, 1740.

4 (*a*) M. S. Wrighton and D. L. Morse, *J. Am. Chem. Soc*., 1974, **96**, 998; (*b*) M. S. Wrighton, D. L. Morse and L. Pdungsap, *J. Am. Chem. Soc*., 1975, **97**, 2073.

5 R. Eastmond and D. R. M. Walton, *Tetrahedron*, 1972, **28**, 4591.

6 (*a*) M. Akita, M-C. Chung, A. Sakurai, S. Sugimoto, M. Terada, M. Tanaka and Y. Moro-oka, *Organometallics*, 1997, **16**, 4882; (*b*) J. Gil-Rubio, M. Laubender and H. Werner, *Organometallics*, 1998, **17,** 1202.

7 (*a*) G. Tapolsky, R. Duesing and T. J. Meyer, *Inorg. Chem*., 1990, **29**, 2285; (*b*) J. K. Hino, L. D. Ciana, W. J. Dressick and B. P. Sullivan, *Inorg. Chem*., 1992, **31**, 1072.

8 J. Manna, S. J. Geib and M. D. Hopkins, *J. Am. Chem. Soc*., 1992, **114**, 9199.

9 (*a*) D. L. Lichtenberger and S. K. Renshaw, *Organometallics*, 1993, **12**, 3522; (*b*) D. L. Lichtenberger, S. K. Renshaw and R. M. Bullock, *J. Am. Chem. Soc*., 1993, **115**, 3276.

Received in Cambridge, UK, 23rd June 1998; 8/04775H

Atomic nitrogen adduct formation at sp³ carbon in the electrospray ionization process

Kentaro Yamaguchi,*[a]† Shigeru Sakamoto,[a] Hideyuki Tsuruta[b] and Tsuneo Imamoto*[b]

[a] *Chemical Analysis Center, Chiba University, Yayoicho, Inage-ku, Chiba 2638522, Japan*
[b] *Faculty of Science, Chiba University, Yayoicho, Inage-ku, Chiba 2638522, Japan*

Atomic nitrogen attachment to an sp³ carbon during the electrospray ionization process was proved by experiments using $^{15}N_2$ and other evidence.

Electrospray ionization (ESI) has been adopted for the study of various small organic compounds as well as large biomolecules in recent years.[1–5] In the course of our mass spectrometric studies of unstable organic compounds in solution, we have found some unexpected mass shifts of 14 atomic mass units (u).‡ This phenomenon was observed in some aliphatic and aliphatic ether compounds containing sp³ carbons (Fig. 1). Since this shift was found in compounds that mainly consisted of aliphatic moieties, the participation of a CH_2 unit was the most promising hypothesis to explain this mass difference. However, we propose here that atomic nitrogen attachment in the ESI process is the reason for this shift, based on several electrospray mass spectrometric studies including an $^{15}N_2$ experiment.

An electrospray is produced under atmospheric pressure using a strong electric field. This field induces a charge accumulation at the liquid surface located at the end of the nebulizing capillary, which will break to form highly charged droplets.[6–8] In this process, N_2 is frequently used as a sheath gas and sometimes as a drying gas to evaporate the droplets. Ionspray (IS), a form of electrospray using the sheath gas as a pneumatic nebulizer, made it possible to introduce relatively large amounts of solution.[9] The ionization of non-polar compounds is also possible using IS. This method was adopted for our study using N_2 as the sheath gas. A double focus tandem mass spectrometer equipped with an atmospheric ESI source was used for this experiment in order to obtain detailed characteristics of the single charged ion species to be discussed here. Typical conditions for the ESI measurement were as follows: acceleration voltage; 5 kV, resolution; 2000–5000, needle voltage (current); 2.5–5.0 kV (700 to > 20000 nA), desolvation chamber temperature; 100 °C, sample flow; 7 mL h^{-1} and sheath gas flow; 1.5 l min^{-1} (JEOL, JMS–700T). The neat chemicals were sprayed without dilution. In the case of THF, for instance, the $[M + 14]^+$ ion is clearly detected using molecular nitrogen as a pneumatic nebulizing gas in the atmospheric ESI source, as can be seen in Fig. 1(*b*). The ions of *m/z* 71 $[THF - H]^+$ and 145 $[(THF)_2 + H]^+$ are also observed[10] in this spectrum. The results from ESI-MS experiments using $[^2H_{12}]$cyclohexane proved that the mass shift is not ascribed to the elimination and intermolecular attachment of CH_2 (14u) in cyclohexane itself [Fig. 2(*a*)]. A similar result was obtained from the experiment using $[^2H_8]$THF [Fig. 2(*b*)]. We could not help but consider that this shift might be caused by a nitrogen atom at this point.

It is strongly suggested that the attached nitrogen atom comes from the nebulizing gas because no ion signals corresponding to the atomic nitrogen adducts were observed in the experiment using Ar as a nebulizing gas. Moreover, using $^{15}N_2$ as the nebulizing gas (99.7 atom% ^{15}N), a clear mass shift of 15u was observed based on the generation of the $[THF + {}^{15}N]^+$ ion [Fig. 3(*b*)]. The ions assigned as monomeric and dimeric THF were not interfered with. The $^{15}N_2$ experiments for cyclohexane, Et_2O and n-hexane are also shown in Fig. 3.

These results prove the formation of an atomic nitrogen adduct during the ESI process. How does it happen? Does the generation of atomic nitrogen species under atmospheric electric discharge[11] constantly occur? Although this behavior is

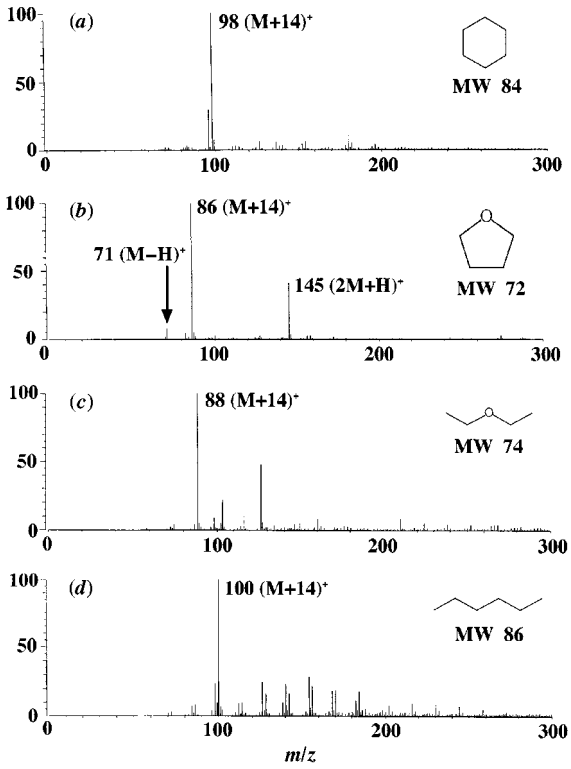

Fig. 1 Electrospray ionization mass spectra exhibiting mass shift of 14u; (*a*) cyclohexane, (*b*) THF, (*c*) Et_2O and (*d*) n-hexane

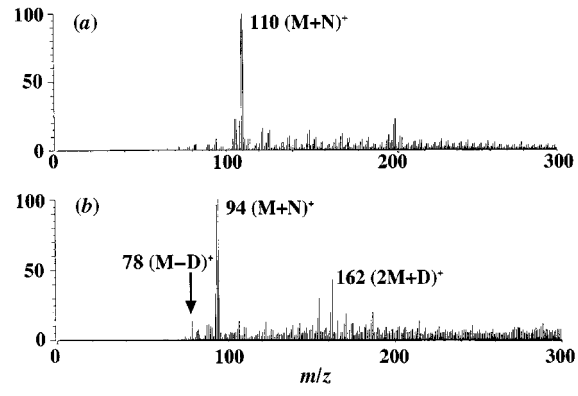

Fig. 2 Electrospray ionization mass spectum of (*a*) $[^2H_{12}]$cyclohexane and (*b*) $[^2H_8]$THF

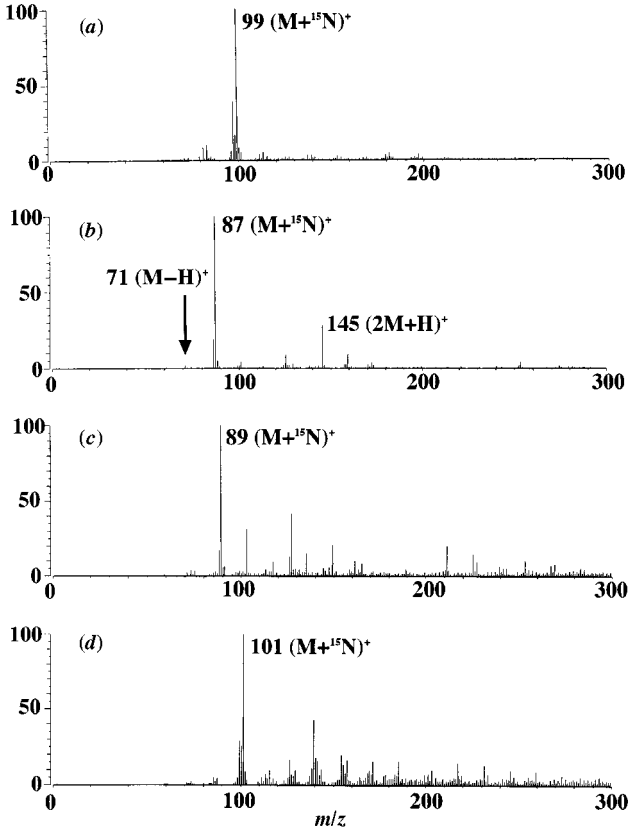

Fig. 3 Electrospray ionization mass spectra exhibiting mass shift of 15u using $^{15}N_2$; (*a*) cyclohexane, (*b*) THF, (*c*) Et_2O and (*d*) n-hexane

thought to be similar to that of the singlet nitrene,[12] a detailed mechanism and the structures of the products are unknown. A methoscopic cluster ion generated from an associative ionization is one of the possible adducts obtained from this process. However, this species is thought to contain a covalently bonded nitrogen because of the potent reactivity of absolute atomic nitrogen. Our result that atomic nitrogen attachment isn't observed in similar compounds that do not contain sp^3 carbons, such as furan and benzene, suggests particular reactivity of this species. In addition, we obtained an ESI mass spectrum of cyclohexylamine, which is identical to the spectrum of nitrogen-attached cyclohexane [Fig. 1(*a*)]. Thus, one of the probable structures of the nitrogen adduct in the case of cyclohexane is cyclohexylamine (Scheme 1).

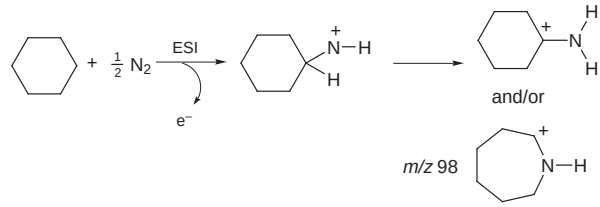

Scheme 1

Detailed structure determination of this cation generated from the nitrogen attachment is our current task. We believe that the interpretation of various mass spectra displaying the unexpected mass shift of 14u will be made easier if the participation of atomic nitrogen attachment is taken into account.

In summary, atomic nitrogen attachment to sp^3 carbons in positive electrospray ionization mass spectrometry was observed. Experiments using $^{15}N_2$ and other evidence definitely suggest that the mass shift of 14u comes from an absolute nitrogen atom. This result points to a facile nitrogen fixation which will be useful in synthetic organic chemistry.[13]

Notes and References

† E-mail: yamaguchi@crystal.cac.chiba-u.ac.jp

‡ The ion assigned as $[M - H]^+$ was observed together with $[2M + H]^+$. Constitution of a 14u shifted species was confirmed by exact mass measurements using these two peaks as the reference ions, *m/z* 86.0604 (C_4H_8NO requires 86.0606, $[THF + N]^+$).

1 J. B. Fenn, M. Mann, C. K. Meng, S. F. Wong and C. M. Whitehouse, *Science*, 1989, **246**, 64.
2 A. P. Bruins, *Trends Anal. Chem.*, 1994, **13**, 81.
3 R. D. Smith, J. A. Loo, R. R. O. Loo, M. Busman and H. R. Udesth, *Mass Spectrom. Rev*., 1991, **10**, 359.
4 R. Colton, A. D'Agostino and J. C. Traeger, *Mass Spectrom. Rev*., 1995, **14**, 79; M. Mann, *Org. Mass Spectrom*., 1990, **25**, 575.
5 B. Chait and S. B. H. Kent, *Science*, 1992, **257**, 1885.
6 A. T. Balades, M. G. Ikonomou and P. Kebarle, *Anal. Chem*., 1991, **63**, 2109.
7 P. Kebarle and L. Tang, *Anal. Chem*., 1993, **65**, 972A.
8 C. G. Enke, *Anal. Chem*., 1997, **69**, 4885.
9 A. P. Bruins, T. R. Covey and J. D. Henion, *Anal. Chem*., 1989, **59**, 2642.
10 R. Arakawa, S. Tachiyashiki and T. Matuso, *Anal. Chem*., 1996 **67**, 4133.
11 D. P. Shoemaker, in *Experiments in Physical Chemistry*, 5th edn., McGraw Hill, Singapore, 1989, Experimental 41.
12 C. Wentrup, in *Advances in Heterocyclic Chemistry*, ed. A. R. Katritzky and A. J. Boulton, Academic Press, New York, 1981, vol. 28, ch. 5.
13 M. Hori and M. Mori, *J. Org. Chem*., 1995, **60**, 1480.

Received in Cambridge, UK, 15th May 1998; 8/03653E

Polymers containing backbone acetylene, anthracene and tetra-, penta- or hexa-coordinate silicon units: UV–visible, photoluminescence and solution $\chi^{(3)}$ non-linear optical properties

William E. Douglas,*[a]† Daniel M. H. Guy,[a] Ajoy K. Kar*[b] and Changhai Wang[b]

[a] *CNRS UMR 5637, Université Montpellier II, 34095 Montpellier cedex 5, France*
[b] *Department of Physics, Heriot-Watt University, Riccarton, Edinburgh, Scotland, UK EH14 4AS*

Poly(aryleneethynylenesilylene)s of general structure $(C{\equiv}CSiR_2C{\equiv}CX)_n$ (X = 9,10-anthrylene) containing tetra-, penta- or hexa-coordinate silicon exhibit high $\chi^{(3)}$ values, the absorbance and emission spectra being red-shifted with respect to those for the corresponding monomers $R_2Si(C{\equiv}CAr)_2$ (Ar = 9-anthryl); these properties are consistent with extensive through-Si conjugation along the backbone.

As recently reviewed, conjugated poly(aryleneethynylene)s are of current interest on account of their photo- and electroluminescent properties and large third order harmonic generation, the $\chi^{(3)}$ values being similar to those for poly(diacetylene)s.[1] The incorporation of electron-rich anthracene units into poly(aryleneethynylene)s has been found to have a marked influence on the luminescence properties,[2] and is particularly effective in π-electron delocalisation along the backbone of such polymers containing Pt.[3] The silicon-containing analogues $(C{\equiv}CSiR_2C{\equiv}CX)_n$ [poly(aryleneethynylenesilylene)s] have been known for some years,[4] those where X is phenylene exhibiting blue photoluminescence[5] with a solution Re($\chi^{(3)}$) value of -9.3×10^{-13} esu.[6] Few polymers containing hypercoordinate silicon are known although the latter exhibits very different chemical and electronic behaviour from tetracoordinate silicon.[7] Recently we prepared poly(aryleneethynylenesilylene)s containing backbone hexacoordinate silicon groups,[8] and the series has now been extended to the corresponding polymers with pentacoordinate silicon incorporating the 8-dimethylamino-1-naphthyl (NpN) ligand known to give stable hypercoordinate species.[9]

The pentacoordinate compounds were obtained from the previously characterized[10] dichlorosilane **1** which was treated with monoethynyl Grignard reagent (Scheme 1) to give the new (4 + 1)-coordinate[11] diethynylsilane **2**.‡ Likewise, tetracoordinate monomer **5** with two 1-naphthyl groups was prepared from dichlorosilane **4** (Scheme 2), the spectral data being similar to those for $Ph_2Si(C{\equiv}CH)_2$.[4,12]

Monomers **2** and **5** undergo palladium-catalysed cross-coupling polymerization with 9,10-dibromoanthracene affording, respectively, **3** containing pentacoordinate Si (Scheme 1) and **6** with tetracoordinate $(1\text{-Np})_2Si$ groups (Scheme 2), the latter being similar to the Ph_2Si analogue **7**.[13] Size exclusion chromatography (SEC) showed both materials to be low molecular weight polymers (Table 1) similar to previously

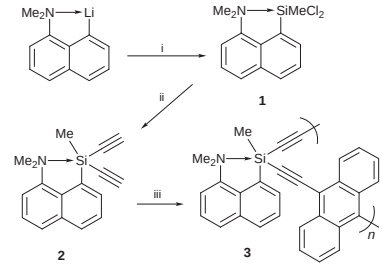

Scheme 1 *Reagents and conditions*: i, excess $MeSiCl_3$, Et_2O, room temp., 5 h; ii, HC≡CMgBr, THF, −78 °C to room temp.; iii, 9,10-dibromoanthracene, $(PPh_3)_2PdCl_2$, CuI, PPh_3, Et_3N, PhMe, 4 h, 89 °C

reported polymer **8** containing hexacoordinate Si.[8] Reflecting the change in the electronic environment, the Si*C*≡C ^{13}C and ^{29}Si NMR resonances are shifted upfield with increasing coordination number, there being little effect on the $\nu_{C\equiv C}$ IR absorbance (Table 1).

Model monomers **9** and **10** containing tetracoordinate Si were prepared by palladium-catalysed cross-coupling with 9-bromoanthracene (Scheme 2, Table 2). The spectral data are similar to those for the analogous polymers (Table 1), the second IR $\nu_{C\equiv C}$ band in the polymers appearing in the monomers as an ill-defined shoulder around 2150 cm^{-1}.

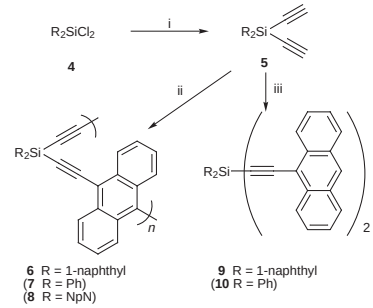

Scheme 2 *Reagents and conditions*: i, HC≡CMgBr, THF, −78 °C to room temp.; ii, 9,10-dibromoanthracene, $(PPh_3)_2PdCl_2$, CuI, PPh_3, Et_3N, PhMe, 16 h, 89 °C; iii, 9-bromoanthracene, $(PPh_3)_2PdCl_2$, CuI, PPh_3, Et_3N, PhMe, 4 d, 89 °C

Table 1 Properties of polymers

Si Coord. no.	Polymer	Colour	M_w[a]	M_w/M_n[a]	n[b]	$\nu_{C\equiv C}$/cm^{-1} [c]	δ_{Si}[d]	δ_C[d] Si*C*≡C[e]	δ_C[d] SiC≡*C*[e]	Φ_f[f]
4	**7**	red	23 500	3.2	56	2124	−47.4	102.2	106.1	0.15
4	**6**	orange	8 800	2.8	17	2130	−48.0	103.1	107.3	0.41
5	**3**	red	12 400	2.7	28	2129	−54.9	102.2	110.1	0.01
6	**8**	orange	20 000	3.2	34	2128	−61.0	90.8	103.1	0.02

[a] Determined by SEC with reference to polystyrene standards. [b] Number of units calculated from value of M_w. [c] In Nujol mull. [d] In $CDCl_3$ solution. [e] Assigned by analogy with results of ^{13}C–^1H coupling experiments on $(1\text{-Np})_2Si(C{\equiv}CPh)_2$. [f] Quantum yield, Φ_f, determined in THF solution with an excitation wavelength of 370 nm and with reference to 9,10-diphenylanthracene standard.

Table 2 Properties of model monomers

Monomer	Colour	$\nu_{C\equiv C}$/cm^{-1} [a]	δ_{Si} [b]	δ_C [b] SiC≡C [c]	δ_C [b] SiC≡C [c]	Φ_f [d]
9	red	2122, 2142	−48.1	101.1	107.7	0.65
10	orange–red	2122, 2148	−47.2	100.1	106.6	0.88

[a] In Nujol mull. [b] In $CDCl_3$ solution. [c] Assigned by analogy with results of ^{13}C–^1H coupling experiments on $(1\text{-Np})_2Si(C\equiv CPh)_2$. [d] Quantum yield, Φ_f, determined in THF solution at an excitation wavelength of 370 nm with reference to 9,10-diphenylanthracene standard.

The UV–VIS spectra in CH_2Cl_2 solution [Fig. 1(A)] show intense absorption bands with fine structure most probably arising from transitions similar to those for anthracene. With respect to the bands in anthracene, those for **9** and **10** are red-shifted with increased extinction coefficients, the bathochromic shift being greater than for 9-ethynylanthracene.[14,15] The corresponding bands in the polymers are further red-shifted with respect to those in (i) **9** and **10**, (ii) 9,10-diethynylanthracene (λ_{max}, 356, 377, 423 nm),[16] and (iii) 9,10-bis(trimethylsilylethynyl)anthracene (λ_{max}, 391, 414, 439 nm). In addition, the polymers (except **6**) show a new broad absorption peak around 520 nm tailing off towards 575 nm, corresponding to an optical gap of *ca.* 2.2 eV. Monomers **9** and **10** show a similar new absorption occurring at lower wavelength than for the polymers (*e.g.* **9**: λ_{max} 451 nm). These properties suggest the presence of through-Si conjugation.

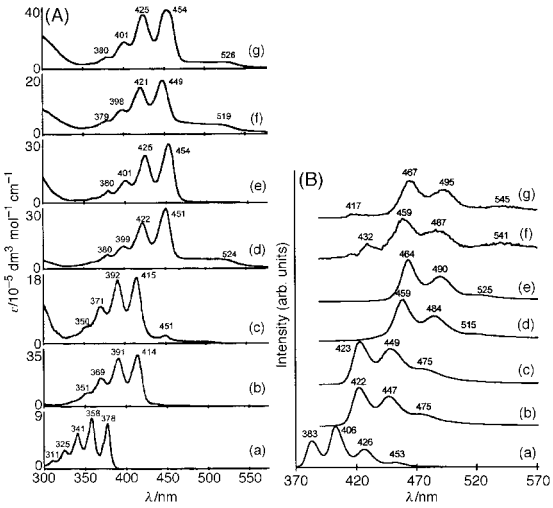

Fig. 1 (A) UV–VIS spectra in CH_2Cl_2 solution and (B) fluorescence spectra in THF solution at an excitation wavelength of 370 nm of (*a*) anthracene, (*b*) **10**, (*c*) **9**, (*d*) **7**, (*e*) **6**, (*f*) **3** and (*g*) **8**

Likewise, the fluorescence spectra [Fig. 1(B)] show a red-shift on going from anthracene to **9** and **10** and then a further such shift on going to the polymers, the apparent Stokes shifts[17] lying in the range 8–13 nm (*cf.* anthracene 5 nm). For the polymers, the low energy band at *ca.* 540 nm is probably due to excimer formation since (i) the relative intensity is concentration dependent, and (ii) anthracene compounds are known to dimerize on absorbing 320–400 nm light.[18] A picosecond time-resolved photoluminescence study of **7** (1 g l^{-1} in THF) at 532 nm showed maximum emission at 470 nm and a decay time constant of *ca.* 6 ns. Unlike polymers **3**, **7**, **8** and poly(*p*-phenyleneanthryleneethynylene)s,[19] **9** and **10** are highly emissive (*cf.* anthracene: Φ_f = 0.32[20]).

The sign and the magnitude of the real and imaginary parts of $\chi^{(3)}$ were determined for polymers **3**, **7** and **8** by solution Z-scan measurements[21] in the near-resonant region at 1064 nm (Table 3),§ the polymers being of sufficient chain length for the $\chi^{(3)}$ effects to be at a maximum.[22] High activity was found [in particular Im($\chi^{(3)}$) for **3** containing pentacoordinate Si], the value of Re($\chi^{(3)}$) being comparable to that determined in the resonant region at 590 nm for poly(phenyleneethynylenesilylene).[6] At 595 nm, a rather fast dominant relaxation time of *ca.* 20 ps was observed for the three polymers;¶ under non-resonant conditions the materials are expected to be considerably faster.

Table 3 Solution $\chi^{(3)}$ properties[a]

Si Coord. no.	Polymer	β/cm GW^{-1}	Im($\chi^{(3)}$)/esu	n_2/cm^2 W^{-1}	Re($\chi^{(3)}$)/esu
4	**7**	0.27	1.8×10^{-13}	5.0×10^{-15}	4.0×10^{-13}
5	**3**	1.20	8.0×10^{-13}	—	—
6	**8**	0.27	1.8×10^{-13}	5.0×10^{-15}	4.0×10^{-13}

[a] Z-scan measurements in $CHCl_3$ solution (50 g l^{-1}) at 1064 nm, pulse duration 140 ps, intensity 20 GW cm^{-2}.

In conclusion, the UV–VIS, photoluminescence and high $\chi^{(3)}$ properties of the polymers are consistent with extensive through-Si conjugation along the backbone.

Notes and References

† E-mail: douglas@crit.univ-montp2.fr

‡ *Selected data* for **2**: 76%; mp 102.4–104.3 °C; $\delta_{Si}(CDCl_3)$ −56.6; $\delta_C(CDCl_3)$ 91.3 (SiC≡*C*), 93.0 (Si*C*≡C); $\nu_{C\equiv C}$(Nujol)/cm^{-1} 2036, 2021.

§ The values of n_2 were extracted from the Z-scan results with large uncertainties since the data could not be fitted well (no satisfactory result could be obtained for **3**).

¶ Excite-probe experiments on dilute polymer solutions with 0.6 ps pulses at 595 nm showed appreciable linear absorption and bleaching nonlinearity or saturable absorption. The relaxation dynamics could not be described with a single excited-state lifetime.

1 R. Giesa, *J. Macromol. Sci., Rev. Macromol. Chem. Phys.*, 1996, **C36**, 631.
2 K. Tada, M. Onoda, M. Hirohata, T. Kawai and K. Yoshino, *Jpn. J. Appl. Phys.*, 1996, **35**, L251.
3 M. S. Khan, A. K. Kakkar, N. J. Long, J. Lewis, P. Raithby, P. Nguyen, T. B. Marder, F. Wittmann and R. H. Friend, *J. Mater. Chem.*, 1994, **4**, 1227.
4 R. J. P. Corriu, W. E. Douglas and Z.-X. Yang, *J. Polym. Sci., Polym. Lett. Ed.*, 1990, **28**, 431.
5 S. P. Huang, S. Jeglinski, X. Wei, Z. V. Vardeny, Y. W. Ding and T. J. Barton, *Mol. Cryst. Liq. Cryst.*, 1994, **256**, 513.
6 R. K. Meyer, R. E. Bender, Z. V. Vardeny, Y. Ding and T. Barton, *Mol. Cryst. Liq. Cryst.*, 1994, **256**, 597.
7 C. Chuit, R. J. P. Corriu, C. Reyé and J. C. Young, *Chem. Rev.*, 1993, **93**, 1371.
8 K. Boyer-Elma, F. H. Carré, R. J.-P. Corriu and W. E. Douglas, *J. Chem. Soc., Chem. Commun.*, 1995, 725.
9 J. T. B. H. Jastrzebski, C. T. Knaap and G. van Koten, *J. Organomet. Chem.*, 1983, **255**, 287.
10 F. Carré, R. J. P. Corriu, A. Kpoton, M. Poirier, G. Royo and J. C. Young, *J. Organomet. Chem.*, 1994, **470**, 43.
11 F. Carré, C. Chuit, R. J. P. Corriu, A. Mehdi and C. Reyé, *Angew. Chem., Int. Ed. Engl.*, 1994, **33**, 1097.
12 C. S. Kraihanzel and M. L. Losee, *J. Organomet. Chem.*, 1967, **10**, 427.
13 R. J. P. Corriu, W. E. Douglas, Z.-X. Yang, Y. Karakus, G. H. Cross and D. Bloor, *J. Organomet. Chem.*, 1993, **455**, 69.
14 S. Akiyama, F. Ogura and M. Nakagawa, *Bull. Chem. Soc. Jpn.*, 1971, **44**, 3443.
15 Z. Rappoport, P. Shulman and M. Thuval, *J. Am. Chem. Soc.*, 1978, **100**, 7041.
16 W. Chodkiewicz, P. Cadiot and A. Willemart, *Compt. Rend.*, 1957, **245**, 2061.
17 J.-L. Brédas, J. Cornil and A. J. Heeger, *Adv. Mater.*, 1996, **8**, 447.
18 H. Bouas-Laurent, A. Castellan and J. P. Desvergne, *Pure Appl. Chem.*, 1980, **52**, 2633.
19 T. M. Swager, C. J. Gil and M. S. Wrighton, *J. Phys. Chem.*, 1995, **99**, 4886.
20 S. Kyushin, M. Ikarugi, M. Goto, H. Hiratsuka and H. Matsumoto, *Organometallics*, 1996, **15**, 1067.
21 M. Sheik Bahae, A. A. Said, T. H. Wei, D. J. Hagan and E. W. van Stryland, *IEEE J. Quantum Electron.*, 1990, **26**, 760.
22 I. D. W. Samuel, I. Ledoux, C. Delporte, D. L. Pearson and J. M. Tour, *Chem. Mater.*, 1996, **8**, 819.

Received in Cambridge, UK, 16th July 1998; 8/05518A

Stereoselective radical aryl migrations from sulfur to carbon

Armido Studer*† and Martin Bossart

Laboratorium für Organische Chemie, Eidgenössische Technische Hochschule, ETH-Zentrum, Universitätstrasse 16, CH-8092 Zürich, Switzerland

Stereoselective radical 1,5 aryl migrations from sulfur (in arenesulfonates) to carbon with diastereoselectivities of up to 14:1 are presented.

$C(sp^2)$–$C(sp^3)$ bonds occur in many natural products and new methods for their stereoselective formation are important. In the literature, there are only a very few methods for stereoselective $C(sp^3)$–aryl bond formation. The Heck[1] and Michael[2] reactions have to be mentioned at this point. Numerous examples of radical aryl transfers (C→C,[3] N→C,[4] O→C[5] and S→C[6]) have been published, however, we were surprised to find only three reports of stereoselective radical aryl migrations.[7] Herein we describe highly diastereoselective 1,5 aryl migrations from sulfur to carbon.

Motherwell, in his pioneering studies, has shown that intramolecular *ipso* substitution in arenesulfonates by aryl radicals is an efficient method for biaryl synthesis.[6] Based on our work on the stereoselective phenyl migration from Si to C[8] we decided to test arenesulfonates as possible 'arene sources' in the intramolecular stereoselective radical *ipso* substitution reaction. To this end, arenesulfonates **1–5** were prepared in moderate to good yields (50–90%) from (*like*)-4-iodopentan-2-ol and the corresponding commercially available sulfonyl chlorides in pyridine.[9] The racemic‡ iodo alcohol was easily prepared from (*meso*)-pentan-2,4-diol according to established procedures.[10] We were pleased to find that *ipso* substitution occurs smoothly (Scheme 1, Table 1). Slow addition of tin hydride to **1** in refluxing benzene under optimized conditions§ afforded the known[11] alcohol **6** in 76% yield with high selectivity (*u*:*l* = 13:1, entry 1). Both electron poor and electron rich arenes can be stereoselectively transferred. Thus, the *p*-fluorophenyl derivative **7** was obtained in 59% yield with a slightly lower selectivity (10:1, entry 2).¶ In the case of the electron rich anisyl and dansyl derivatives a lower yield was observed (**8**, 50%, 9:1; **10**, 52%, 11:1, entries 3 and 5). Even heteroarenes can be used in the *ipso* substitution as shown for the thienyl transfer (**9**, 74%, 9:1, entry 4). As a side product, the corresponding reduced (dehalogenated) sulfonate was always observed in these aryl migration reactions.

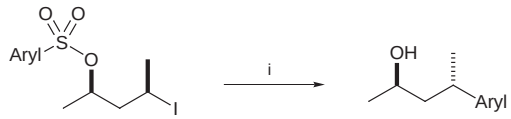

1–5 **6–10**

Scheme 1 *Reagents and conditions*: i, Bu_3SnH, AIBN, syringe pump, benzene (0.03 M)

Table 1 Stereoselective aryl transfer from sulfur to carbon

Entry	Sulfonate	Aryl	Product	Yield (%)	Ratio (*u*:*l*)[a]
1	**1**	Ph	**6**	76	13:1
2	**2**	4-FC_6H_4	**7**	59	10:1
3	**3**	4-$MeOC_6H_4$	**8**	50	9:1
4	**4**	thienyl	**9**	74	9:1
5	**5**	5-Me_2N-naphthyl	**10**	52	11:1[b]

[a] Determined by GC analysis. [b] Determined by ^1H NMR spectroscopy.

In order to study the 1,2-stereoinduction, sulfonate **11** was prepared as a 1:1 mixture of diastereoisomers. Aryl migration under analoguous conditions provided alcohol **12** in 49% yield (*l*:*u* = 7:1, Scheme 2). The relative configuration of the major isomer was assigned after oxidation (Swern) to the corresponding known[12] aldehyde.

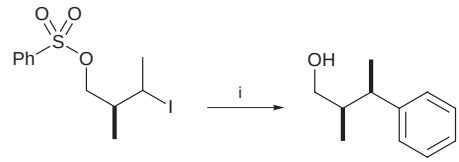

11 **12** (49%, *l* : *u* = 7 : 1)

Scheme 2 *Reagents and conditions*: i, Bu_3SnH, AIBN, syringe pump, benzene (0.05 M)

From the stereochemical outcome of the reactions discussed above, we suggest the following model to explain the observed selectivities: radical **13** undergoes intramolecular *ipso* attack at the aryl group of the sulfonate to form cyclohexadienyl radical **14**. Products derived from 1,7 addition were not observed. We assume that the low energy transition state for the formation of **14** resembles a chair with the substituents in equatorial positions. Fragmentation (re-aromatization) then affords radical **15** which after SO_2 extrusion and reduction leads to the corresponding alcohol. It is not clear how fast the SO_2 extrusion process is by which the corresponding alkoxyl radical is formed. However, in the crude product mixture of the aryl migration reactions, we never observed sulfur-containing products derived from **15**; therefore, we assume that the SO_2 extrusion is faster than trapping of the intermediate radical **15** with Bu_3SnH.‖ According to this model, the observed 1,3- (→ *unlike* products) and 1,2-selectivity (→ *like* product) can be readily understood.

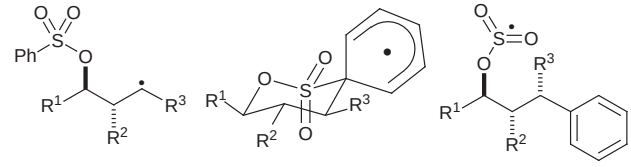

13 **14** **15**

As a first application of this method we studied a one pot reaction sequence where a radical addition reaction is followed by a stereoselective phenyl migration. Sulfonate **16** was prepared from the corresponding homoallylic alcohol and benzenesulfonyl chloride as described above (43%).[9] Radical acceptor **16** and ethyl iodoacetate (1.5 equiv.) were reacted under atom transfer conditions[13] in benzene [$Bu_3SnSnBu_3$ (10%), *hν*, 300 W sun lamp, 0.1 M] to afford iodide **17**, which after dilution (→ 0.05 M) was directly transformed upon slow addition of Bu_3SnH (1.8 equiv. over 7 h) and AIBN (0.25

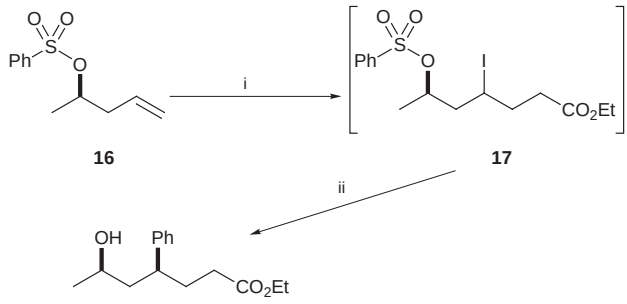

18 (24%, *u* : *l* = 14 : 1)

Scheme 3 *Reagents and conditions*: i, $Bu_3SnSnBu_3$ (10%), *hν*, ICH_2CO_2Et, benzene (0.1 M); ii, Bu_3SnH, AIBN, syringe pump, benzene (0.05 M)

equiv.) to **18** (Scheme 3). Hydroxy ester **18** was isolated in 24% yield (unoptimized) as a 14:1 (*u*:*l*) mixture of diastereoisomers. The intermediate iodide **17** was formed with no selectivity, as shown in a separate experiment by ^{1}H NMR analysis of a sample taken after the iodine transfer reaction.

In summary, we have shown that the intramolecular *ipso* substitution is an efficient method for the stereoselective C(sp^2)–C(sp^3) bond formation. Since many sulfonyl chlorides are commercially available, a variety of aryl groups can be stereoselectively transferred to form products which are difficult to prepare by any other method.

We are grateful to Professor Dr D. Seebach for generous financial support and to Professor Dr D. P. Curran for helpful discussions.

Notes and References

† E-mail: studer@org.chem.ethz.ch

‡ All the compounds described herein were prepared as racemic mixtures. In the schemes only one enantiomer is shown.

§ *General procedure*: Bu_3SnH (1.5 equiv.) and AIBN (0.3 equiv.) in benzene (0.8–1.2 M) were added over 7 h (syringe pump) to a refluxing solution of the iodide in benzene (0.03 M). After complete addition the reaction mixture was stirred under reflux for additional 30 min. The mixture was then allowed to cool to room temperature and MeLi (5 equiv.) was slowly added. After stirring for 30 min the reaction mixture was hydrolyzed with saturated aq. NH_4Cl. Extraction with Et_2O and washing of the organic phase with brine afforded, after drying ($MgSO_4$) and purification by flash column chromatography (SiO_2, pentane–Et_2O), the corresponding alcohol. (MeLi treatment is not neccessary but advantageous since the tin halide formed is transformed to the corresponding methylated compound which is easily removed.)

¶ The relative configurations of the alcohols **7–10**, and **18** were assigned by analogy to **6** based on the characteristic chemical shift of the hydrogen atom (of the major isomer) at the newly formed stereogenic center.

‖ We believe that the products are formed under kinetic control; however, Motherwell has shown that SO_2 extrusion is rather slow in his systems and that in the biaryl synthesis the entire process is probably reversible [ref. 6(*c*)]. Experiments to elucidate the mechanism are planned.

1 M. Shibasaki, in *Advances in Metal-Organic Chemistry*, ed. L. S. Liebeskind, JAI, Greenwich, 1996, vol. 5, p. 119.
2 R. E. Gawley and J. Aubé, in *Principles of Asymmetric Synthesis*, ed. J. E. Baldwin FRS and P. D. Magnus FRS, Pergamon, 1996, p. 145; N. Krause, *Angew. Chem., Int. Ed.*, 1998, **37**, 283.
3 L. Giraud, E. Lacôte and P. Renaud, *Helv. Chim. Acta*, 1997, **80**, 2148 and references cited therein.
4 E. Lee, H. S. Whang and C. K. Chung, *Tetrahedron Lett.*, 1995, **36**, 913.
5 E. Lee, C. Lee, J. S. Tae, H. S. Wang and K. S. Li, *Tetrahedron Lett.*, 1993, **34**, 2343; D. Crich and J.-T. Hwang, *J. Org. Chem.*, 1998, **63**, 2765.
6 (*a*) S. Caddick, K. Aboutayab, K. Jenkins and R. I. West, *J. Chem. Soc., Perkin Trans. 1*, 1996, 675; F. Aldabbagh and W. R. Bowmann, *Tetrahedron Lett.*, 1997, **38**, 3793; (*b*) W. B. Motherwell and A. M. K. Pennell, *J. Chem. Soc., Chem. Commun.*, 1991, 877; M. L. E. N. da Mata, W. B. Motherwell and F. Ujjainwalla, *Tetrahedron Lett.*, 1997, **38**, 137; (*c*) M. L. E. N. da Mata, W. B. Motherwell and F. Ujjainwalla, *Tetrahedron Lett.*, 1997, **38**, 141; E. Bonfand, W. B. Motherwell, A. M. K. Pennell, M. K. Uddin and F. Ujjainwalla, *Heterocycles*, 1997, **46**, 523.
7 H. J. Köhler and W. N. Speckamp, *J. Chem. Soc., Chem. Commun.*, 1980, 142; D. L. Clive and T. L. B. Boivin, *J. Org. Chem.*, 1989, **54**, 1997; J. Aubé, X. Peng, Y. Wang and F. Takusagawa, *J. Am. Chem. Soc.*, 1992, **114**, 5466.
8 A. Studer, M. Bossart and H. Steen, submitted for publication.
9 R. S. Tipson, *J. Org. Chem.*, 1944, **9**, 235.
10 P. Place, M.-L. Roumestant and J. Goré, *Bull. Soc. Chim. Fr.*, 1976, 169.
11 J. M. Brown and R. G. Naik, *J. Chem. Soc., Chem. Commun.*, 1982, 348.
12 I. Fleming and J. J. Lewis, *J. Chem. Soc., Perkin Trans. 1*, 1992, 3257.
13 D. P. Curran, M-H. Chen and D. Kim, *J. Am. Chem. Soc.*, 1989, **111**, 6265.

Received in Cambridge, UK, 27th August 1998; 8/06718I

Stereoselective *O*-glycosylation reactions employing diphenylphosphinate and propane-1,3-diyl phosphate as anomeric leaving groups

Vankayalapati Hariprasad, Gurdial Singh*† and Isabelle Tranoy

Department of Chemistry, University of Sunderland, Sunderland, UK SR1 3SD

Glycosidation of tetra-*O*-benzyl-D-glucose using diphenylphosphinate as the leaving group afforded β-*O*-linked glycosides as the major products, whilst the use of propane-1,3-diyl phosphate as the leaving group resulted in the exclusive formation of β-*O*-linked glycoside.

The essential role that glycoconjugates play in a large number of molecular processes is now well recognised. The impact of these complex molecules in biological processes such as neuronal development, fertilisation, proliferation of cells and the organisation into specific tissues is truly remarkable.[1] Furthermore in tumours there are changes in the carbohydrate structures found at the cell surface and these appear to be intimately involved with metastasis.[2] Carbohydrates are also important in inducing protective antibody response which is responsible for the protection of the organism during infection.[3] As a direct consequence of these properties there has been a resurgence of interest in the chemistry of carbohydrates by both chemists and biologists and thus an enormous amount of methodology has been developed for *O*-glycosylation.[4] In particular there have been a number of reports regarding glycosyl donors that have a phosphorus atom in the leaving group at the anomeric centre. Interest in this has arisen due to the fact that phosphorus compounds can be readily modified by several other atoms allowing the preparation of a range of leaving groups. The coupling reactions of glycosyl diphenyl phosphates, glycosyl diphenylphosphinimidates and glycosyl phosphoramidates have received much attention;[5] in all of these reports 1,2-*trans*-β-linked glycosides are formed with a stereoselectivity of *ca.* 3 : 1 in favour of the β-isomer. The employment of *S*-glycosyl phosphorodimidothioates has also been reported and affords 1,2-*cis*-glycosidic linkages,[6] and the use of dimethylphosphinothioate as glycosyl donors has also been investigated.[7]

In order to extend the scope of this methodology we decided to investigate the possibility of using the diphenylphosphinyl group for coupling of sugars with peptides/amino acids. Our attraction to this approach was derived from the fact that its use had been elegantly demonstrated for the coupling and *N*-protection of amino acids.[8] One of the major considerations in adopting this approach was the principle that one should be able to utilise the same coupling reagent for the synthesis of oligosaccharides and peptides, although in the former case we are forming a glycosidic bond rather than an amide bond; however the leaving group is the same in both reactions. In addition the employment of the diphenylphosphinate and propane-1,3-diyl phosphate groups[9] should result in the preparation of *O*-glycosides with improved stability, enabling ready isolation and storage of these compounds. Additionally we chose to study propane-1,3-diyl phosphate as the leaving group as this would provide a comparison of the effect of pK_a on leaving group ability. Furthermore the introduction of the cyclic phosphate group would allow us to assess the influence of steric requirements at the anomeric centre.

We chose to investigate the coupling at the anomeric centre of tetra-*O*-benzyl-D-glucopyranose. Our attraction to this was multi-faceted, with the major consideration being that there would be no participation by the C-2 substituent in the coupling reaction; furthermore, these processes had received scant attention in the literature and in addition we would have a flexible method that would allow the synthesis of *O*-glycopyranosides.

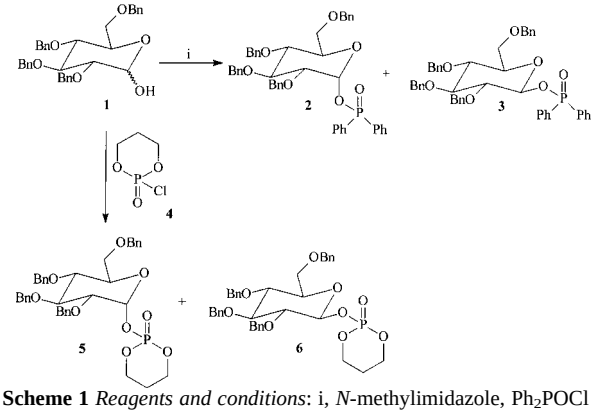

Scheme 1 *Reagents and conditions*: i, *N*-methylimidazole, Ph_2POCl

Treatment of tetra-*O*-benzyl-D-glucopyranose **1** with diphenylphosphinyl chloride and *N*-methylimidazole resulted in the formation of the phosphinates **2**‡ and **3** (ratio 10 : 1) in 95% yield (Scheme 1), which could be separated by column chromatography. However for ease we conducted all of our reactions with this anomeric mixture, which could be stored at −20 °C for 3–4 months without decomposition.[10] Similar treatment of **1** with the cyclic phosphoryl chloride **4** resulted in formation of the phosphates **5**‡ and **6**, which were inseparable by chromatography, in 65% yield, (ratio *ca.* 10 : 1).

We thus proceeded to study the reactions of the phosphinates **2** and **3** and also of the cyclic phosphates **5** and **6** with a range of nucleophiles (Scheme 2, Table 1). In the case of the reaction of n-butanol with pure **2** there was little difference in the stereochemical outcome of the reaction to that found using the anomeric mixture. In general the chemical yield was excellent, however the observed stereoselectivity in these cases was poor, being in the order of 3 : 1 in favour of the desired β-isomer. The stereochemistry of products was established by ^{1}H and ^{13}C NMR analysis. The ^{13}C NMR spectra were particularly useful as the β-isomers **7** had chemical shifts above δ 100 whilst the α-isomers **8** had a resonance at *ca.* δ 96,[11] allowing assignment of the newly formed stereocentre.

In the case where we employed propane-1,3-diyl phosphate as the leaving group the stereoselectivity was improved, with the β-isomer being the major compound in the case of oxygen nucleophiles. To our surprise the use of serine- and thereonine-derived nucleophiles resulted in the formation of **8** as the major isomer; this may be as a result of a hydrogen bonding interaction with the N–H, resulting in delivery from the α-face of the

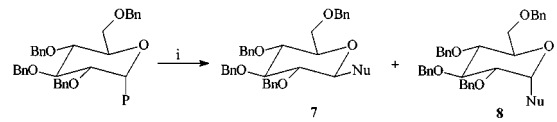

Scheme 2 *Reagents and conditions*: i, nucleophile (1 equiv.), TMSOTf (1 equiv.), −78 °C, 25 min

Table 1 Results of reaction of **2**, **3**, **5** and **6** with nucleophiles

Phosphinate/ phosphate	Nucleophile	Yield (%)[a]	Ratio **7** : **8**
2	Bu^{n}OH	89	2 : 1
2 and **3**	Bu^{n}OH	90	2 : 1
2 and **3**	MeOH	94	4 : 1
2 and **3**	Pr^{i}OH	93	3.5 : 1
2 and **3**	**9**	88	2.5 : 1
2 and **3**	**10**	94	1 : 2
2 and **3**	**11**	85	2 : 1
2 and **3**	**12**	92	2 : 1
2 and **3**	**13**	84	3 : 1
5 and **6**	Bu^{n}OH	99	7 only
5 and **6**	MeOH	96	7 : 3
5 and **6**	Pr^{i}OH	98	7 : 3
5 and **6**	**9**	91	1 : 2
5 and **6**	**10**	83	1 : 2
5 and **6**	**11**	88	4 : 1
5 and **6**	**12**	68	7 only
5 and **6**	**13**	72	7 only

[a] All yields are for isolated products.

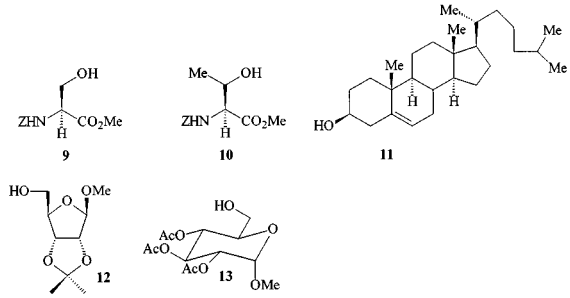

glucose. We were gratified to observe that we had attained our goal of excellent selectivity in the formation of **7** in the cases where we employed sugar-derived nucleophiles. This is particularly encouraing as we have a 2-*O*-benzyl protecting group which is non-participating in glycosylation reactions and would be expected to result in the formation of the α-glycosides. As a result of these findings one could, in principle, use *O*-benzyl protected sugars as starting materials and by changing the activating group of the glycosyl donor either desired stereoisomer can be obtained, thus alleviating the need for differentially protected starting sugars.

We have thus established that tetra-*O*-benzyl-D-glucopyranose can be converted into *O*-linked glycosides with high stereoselectivity in the cases where we employed propane-1,3-diyl phosphate as the leaving group, adding to the methodology available for the synthesis of complex carbohydrates.

We thank Professor R. Ramage (Edinburgh University) for helpful discussions and encouragement. We also thank the EPSRC for access to the mass spectrometry service at the University of Wales, Swansea (Director, Dr J. A. Ballantine).

Notes and References

† E-mail: gurdial.singh@sunderland.ac.uk

‡ All compounds gave satisfactory spectral and microanalytical data. *Selected data* for **2**:[10] $[\alpha]_D$ +83.3 (*c* 4.3, $CHCl_3$); δ_H(400 MHz, $CDCl_3$) 3.62–3.77 (4H, m), 3.86–4.07 (2H, m), 4.36 (1H, d, *J* 11.87), 4.47 (1H, d, *J* 10.50), 4.51 (1H, d, *J* 11.87), 4.60 (1H, d, *J* 11.22), 4.73 (1H, d, *J* 11.22), 4.80 (1H, d, *J* 10.56), 4.85 (1H, d, *J* 10.56), 4.96 (1H, d, *J* 11.21), 5.99 (1H, dd, *J* 3.3, 11.9), 7.10–7.84 (m, 30H); δ_C(100.40 MHz, $CDCl_3$) 68.08 (C-6), 72.10, 73.21, 74.64, 76.67, 79.14 (C-4), 79.20 (C-2), 81.13 (C-3), 84.28 (C-5), 92.79 (C-1), 127.41–128.24 (Ar-C), 130.31–132.40 (Ar-C), 137.57–138.40 (Ar-C); δ_P(161.70 MHz, $CDCl_3$) 32.50. For **5**: mp 101–103 °C; $[\alpha]_D$ +65.7 (*c* 1.4, $CHCl_3$); δ_H(270 MHz, $CDCl_3$) 1.55–1.63 (1H, m, J_{PH} 15.2), 2.14–2.28 (1H, m, J_{PH} 15.2), 3.61–3.78 (4H, m), 3.89–3.99 (2H, m), 4.15–4.41 (4H, m), 4.44 (1H, d, *J* 11.87), 4.52 (1H, d, *J* 11.87), 4.56 (1H, d, *J* 11.87), 4.63 (1H, d, *J* 11.21), 4.71 (1H, d, *J* 11.87), 4.80 (1H, d, *J* 10.56), 4.84 (1H, d, *J* 11.22), 4.94 (1H, d, *J* 11.22), 5.85 (1H, dd, *J* 10.56, 3.30), 7.13–7.37 (20H, m); δ_C(67.8 MHz, $CDCl_3$) 25.84 (1C, d, *J* 7.01), 68.14, 68.65 (d, *J* 7.01), 68.86 (d, *J* 7.01), 75.51, 76.94, 79.03, 94.78, 127.60–128.09 (Ar-C), 137.50–138.47 (Ar-C); δ_P(109.25 MHz, $CDCl_3$) −10.99; *m/z* (EI) 660.6 (M^+) (Found: C, 67.4; H, 6.3; P, 4.7. $C_{37}H_{41}O_9P$ requires C, 67.3; H, 6.3; P, 4.7%). For **6**: (selected features) δ_H(270 MHz, $CDCl_3$) 5.24 (1H, app t, *J* 13.19, 7.26); δ_C(67.8 MHz, $CDCl_3$) 98.44; δ_P(109.25 MHz, $CDCl_3$) −10.60. For **7** (Nu = OBu): mp 69–71 °C; $[\alpha]_D$ +16.5 (*c* 1.3, $CHCl_3$); δ_H(270 MHz, $CDCl_3$) 0.91 (3H, t, *J* 7.26), 1.35–1.71 (4H, m), 3.41–3.50 (2H, m), 3.52–3.69 (4H, m), 3.73 (1H, dd, *J* 10.55, 1.98), 3.97 (1H, dt, *J* 12.53, 5.93), 4.39 (1H, d, *J* 7.91, H-1), 4.51 (1H, d, *J* 11.21), 4.55 (1H, d, *J* 11.87), 4.61 (1H, d, *J* 12.54), 4.71 (1H, d, *J* 10.55), 4.76 (1H, d, *J* 11.21), 4.80 (1H, d, *J* 10.56), 4.91 (1H, d, *J* 10.55), 4.93 (1H, d, *J* 10.56), 7.10–7.37 (20H, m); δ_C(67.8 MHz, $CDCl_3$) 13.85, 19.29, 31.82, 67.88, 69.02, 69.78, 73.45, 74.85, 74.98, 75.66, 77.96, 82.29, 84.72, 103.60 (C-1), 127.58–128.37 (Ar-C), 138.23, 138.32, 138.61, 138.74 (Found M^+, 596.3138. $C_{38}H_{44}O_6$ requires 596.3138). For **7** (Nu = **13**):[12] $[\alpha]_D$ +65.5 (*c* 3.3, $CHCl_3$); δ_H(270 MHz, $CDCl_3$) 1.99 (3H, s), 2.02 (3H, s), 2.08 (3H, s), 3.29 (3H, s), 3.41–3.55 (3H, m), 3.64–3.80 (2H, m), 3.84–3.97 (4H, m), 4.38 (1H, d, *J* 8.57), 4.46 (1H, d, *J* 11.87), 4.49 (1H, d, *J* 11.87), 4.56 (1H, d, *J* 11.87), 4.58 (1H, d, *J* 10.55), 4.64 (1H, d, *J* 11.21), 4.74 (1H, d, *J* 11.22), 4.81–4.85 (3H, m), 4.89 (1H, d, *J* 10.55), 4.91 (1H, d, *J* 11.21), 5.36 (1H, app t, *J* 4.62), 7.03–7.27 (20H, m); δ_C(67.8 MHz, $CDCl_3$) 20.68, 20.70, 29.59, 66.83, 68.43, 69.51, 70.24, 70.82, 73.15, 74.67, 74.82, 75.12, 75.47, 80.21, 81.27, 82.49, 84.71, 96.61 (C-1′), 102.93 (C-1), 127.52–128.51 (Ar-C), 137.72, 138.06, 138.34, 138.50, 170.10, 170.29, 170.40.

1 A. Varki, *Glycobiology*, 1993, **3**, 97.
2 J. Kellerman, F. Lottspeich, A. Henschen and W. Muller-Esterl, *Eur. J. Biochem.*, 1986, **154**, 471; S. Hakomori, *Cancer Res.*, 1985, **45**, 2405; J. Montreuil, *Adv. Carbohydr. Chem. Biochem.*, 1980, **37**, 157.
3 N. Sharon, *Trends Biochem. Sci.*, 1984, **9**, 198.
4 G. J. Boons, *Tetrahedron*, 1996, **52**, 1095; K. Toshima and K. Tatsuta, *Chem. Rev.*, 1993, **93**, 1503; K. J. Hale and A. C. Richardson, *Carbohydrates*, in *The Chemistry of Natural Products*, ed. K. H. Thomson, Blackie, 1993, ch. 1, p. 1.
5 S. Hashimoto, T. Honda and S. Ikegami, *Tetrahedron Lett.*, 1991, **32**, 1653; S. Hashimoto, T. Honda and S. Ikegami, *Heterocycles*, 1990, **30**, 775; S. Hashimoto, T. Honda and S. Ikegami, *Chem. Pharm. Bull.*, 1990, **38**, 2323; S. Hashimoto, T. Honda and S. Ikegami, *J. Chem. Soc., Chem. Commun.*, 1989, 685.
6 H. Harada, S. Hashimoto, T. Honda and S. Ikegami, *Tetrahedron Lett.*, 1992, **33**, 3523; S. Hashimoto, T. Honda and S. Ikegami, *Tetrahedron Lett.*, 1990, **31**, 4769.
7 T. Inazu and T. Yamanoi, *Chem. Lett.*, 1990, 849; T. Inazu and T. Yamanoi, *Chem. Lett.*, 1989, 69; T. Inazu, H. Hosokawa and Y. Satoh, *Chem. Lett.*, 1985, 297.
8 R. Ramage, D. Hopton, M. J. Parrott, G. W. Kenner and G. A. Moore, *J. Chem. Soc., Perkin Trans. 1*, 1984, 1357 and references cited therein.
9 T. R. Fukuto and R. L. Metcalf, *J. Med. Chem.*, 1965, **8**, 759; F. Ramirez, H. Tsuboi, H. Okazaki and R. F. Marecek, *Tetrahedron Lett.*, 1982, **23**, 5375; R. N. Hunston, S. A. Jones, C. McGuigan, T. Richard, J. Balzarini and E. De Clercq, *J. Med. Chem.*, 1984, **27**, 440; E. L. Eliel, S. Chandraserkaran, L. E. Carpenter II and J. G. Verkade, *J. Am. Chem. Soc.*, 1986, **108**, 6651.
10 A. Esswein and R. R. Schmidt, *Liebigs Ann. Chem.*, 1988, 675.
11 K. Bock and C. Pedersen, *Adv. Carbohydr. Chem. Biochem.*, 1983, **41**, 27.
12 S. Houdier and P. J. A. Vottéro, *Tetrahedron Lett.*, 1993, **34**, 3283; for the α-isomer of this compound, see: P. G. Garegg, J.-L. Maloisel and S. Oscarson, *Synthesis*, 1995, 409.

Received in Liverpool, UK, 6th July 1998; 8/05206I

First of a new family of tetraamine bis(μ-thiolate)-containing macrocycles: structure and stepwise oxidations and reductions of the dinickel(II) complex

Sally Brooker,[a]* Paul D. Croucher,[a] Tony C. Davidson,[a] Geoffrey S. Dunbar,[a] A. James McQuillan[a] and Geoffrey B. Jameson[b]

[a] *Department of Chemistry, University of Otago, PO Box 56, Dunedin, New Zealand. E-mail: sbrooker@alkali.otago.ac.nz*
[b] *Institute of Fundamental Sciences, Chemistry, Massey University, Palmerston North, New Zealand*

Reduction of a dinickel(II) dithiolate Schiff-base macrocyclic complex with sodium borohydride results in a 'bowl'-shaped dinickel(II) dithiolate amine macrocyclic complex which exhibits four separate one-electron redox processes.

The active site of the [Ni,Fe]-hydrogenases, metalloenzymes which catalyse $H_2 = 2H^+ + 2e^-$, has only recently been established to be dimetallic.[1] There has been considerable debate as to the oxidation state(s) of the nickel centre during the catalytic cycle.[2] As the overall reaction is a redox process it seems likely that either one or both of the doubly cysteinate-bridged metal ions, nickel and iron, change oxidation state during the catalytic cycle, although a third possibility, of the thiolate residues being non-innocent, has yet to be ruled out. Early studies of mononickel thiolate model compounds established many important chemical and electrochemical points,[2] and indicated that interactions with species such as carbon monoxide and hydrogen occur in the Ni(I) oxidation state.[2,3] In order to better mimic the dimetallic active site, studies are now probing the impact of the presence of a second metal ion, doubly bridged to the nickel ion by thiolate residues, on the properties of the complexes.[4–8] We have prepared a family of dinickel thiolate model complexes in which the two incorporated nickel(II) ions are bridged by thiolate(s): the polydentate ligands employed supply N_2S_2 or $N_2X_1S_1$ (X = O or N) coordination to each nickel ion.[5–7] Here we present the substantial effects on structure and electrochemistry of varying the nature of the nitrogen donors from imine to amine in a dinucleating macrocycle which provides N_2S_2 coordination environments to each of the pair of bound nickel(II) ions.

The red, diamagnetic, tetraimine macrocyclic complex **2** was prepared as reported (**CAUTION**: Perchlorate salts are potentially explosive and should therefore be handled with appropriate care).[6] The first of this new generation of tetraamine macrocyclic complexes, complex **1**, was prepared from **2** by sodium borohydride reduction in MeOH in air followed by an acid workup.[9] Red single crystals of **1** were obtained in 60–80% yield by recrystallisation of the crude product from MeCN by vapour diffusion of diethyl ether and an X-ray structure determination carried out.†‡ The nickel(II) ions in **1** have an N_2S_2 square planar environment (Fig. 1) as observed in the tetraimine complex **2**.[6] However, in complex **1** the overall shape of the complex is very different to that of **2**. Specifically, in addition to the folding of the two phenyl planes, which is observed in both complexes (angles between phenyl planes: 98.8 and 105.9° in **2** *vs.* 111.5° in **1**), the ligand in complex **1** exhibits a second folding at right angles to the first, which leads to a 'bowl'-shaped complex overall (Fig. 1) rather than the 'bowed' shape observed for **2**.[6] This additional fold is possible in **1** because of the change from conjugated trigonal imine groups in **2** to flexible tetrahedral amine groups in **1**, and this is readily seen by comparison of the distances of the nitrogen atoms from the plane of the respective phenyl rings (**2**, N 0.25–0.52 Å out-of-plane; **1**, N 1.10 and 1.11 Å oop). This leads

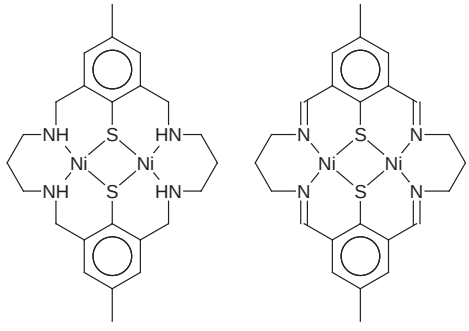

as $[Ni_2L1][ClO_4]_2$ **1** as $[Ni_2L2][ClO_4]_2$ **2**

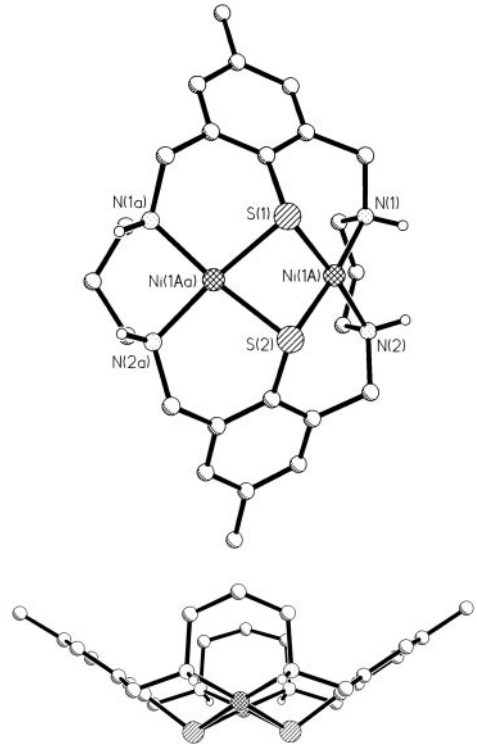

Fig. 1 Perspective diagrams of the cation of **1**, $[Ni_2L1]^{2+}$. No hydrogen atoms, except those on the amine nitrogen atoms, are shown. Selected bond lengths (Å) and angles (°): Ni(1A)–N(2) 1.951(4), Ni(1A)–N(1) 1.951(4), Ni(1A)–S(1) 2.1685(18), Ni(1A)–S(2) 2.177(2), N(2)–Ni(1A)–N(1) 88.72(18), N(2)–Ni(1A)–S(1) 174.37(14), N(1)–Ni(1A)–S(1) 96.45(14), N(2)–Ni(1A)–S(2) 96.62(14), N(1)–Ni(1A)–S(2) 174.22(14), S(1)–Ni(1A)–S(2) 78.13(8), C(15)–S(1)–Ni(1A) 107.3(2), C(15)–S(1)–Ni(1Aa) 107.3(2), Ni(1A)–S(1)–Ni(1Aa) 88.19(9), C(25)–S(2)–Ni(1Aa) 106.8(2), C(25)–S(2)–Ni(1A) 106.8(2), Ni(1Aa)–S(2)–Ni(1A) 87.76(12), where symmetry transformation a is $x, -y - 1/2, z$.

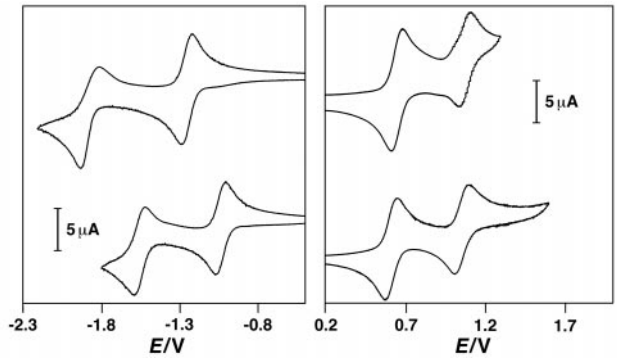

Fig. 2 Cyclic voltammograms of **1** (top) and **2** (bottom). Conditions: 1 mM complex in MeCN, 200 mV s^{-1}, 0.1 M NBu_4ClO_4 electrolyte, referenced to Ag/0.01 M $AgNO_3$ (the Fc/Fc^+ couple occurred at +0.13 V). Reduction potentials (V) for the dinickel complexes **1** (L*n* = L1) and **2** (L*n* = L2) respectively: $E_{1/2}$ $[Ni_2Ln]^{3+/4+}$ $+1.10^{QR}$, $+1.07^{QR}$; $E_{1/2}$ $[Ni_2Ln]^{2+/3+}$ $+0.69^{R}$, $+0.63^{R}$; $E_{1/2}$ $[Ni_2Ln]^{+/2+}$ -1.18^{R}, -1.01^{R}; $E_{1/2}$ $[Ni_2Ln]^{0/+}$ -1.86^{QR}, -1.46^{R}. K_d (**1**, ox) = 1.2×10^{-7}, K_d (**1**, red) = 1.1×10^{-11}, K_d (**2**, ox) = 3.6×10^{-8}, K_d (**2**, red) = 2.5×10^{-8}; ^{R} reversible, ^{QR} quasi-reversible.[14]

to the N_2S_2 mean planes of the two encircled nickel atoms intersecting at an angle much closer to 90° in **1** (124°) than is observed in **2** (146.3 and 146.4°), which in turn results in shorter Ni···Ni separations in **1** (3.14 and 3.15 Å in **2** *vs.* 3.02 Å in **1**): a shortening of the S···S separations (2.84 and 2.85 Å in **2** *vs.* 2.74 Å in **1**) is also observed in **1**, along with changes in the angles at sulfur (Fig. 1 caption).[6] The 'bowl' created by this new macrocyclic ligand distinguishes the two axial sites on the nickel atoms, producing an 'inside' and 'outside' surface which may lead to interesting features when reactivity studies are carried out. All of the amine hydrogen atoms point in the same direction (*cis*) with respect to the macrocyclic 'bowl'.

The cyclic voltammograms obtained for complexes **1** and **2** are shown in Fig. 2. In both cases a series consisting of four separate one-electron steps is readily identified: the dinickel(II) complexes can be oxidised in two steps or reduced in two steps. From EPR studies and comparisons with related $N_2X_1S_1$ (X = O or N) square planar dinickel thiolate complexes and dizinc complexes these processes are believed to be largely metal-centred (*i.e.* $Ni^{I}_2 \leftrightarrow Ni^{I}Ni^{II} \leftrightarrow Ni^{II}_2 \leftrightarrow Ni^{II}Ni^{III} \leftrightarrow Ni^{III}_2$).[6,7] The mixed valent forms of the complexes prepared by electrochemical oxidation or reduction exhibit axial EPR spectra consistent with metal-based Ni(III) or Ni(I) species respectively. In the former, *g* values are of the order of $g_{\|}$ 2.02 and $g_{\perp}$ 2.20 and in the latter, $g_{\|}$ 2.01 and $g_{\perp}$ 2.08. These values are consistent with those derived for the oxidised and reduced forms of the metal with equatorial tetraaza-donors. Precise data will be reported elsewhere.[7] Interestingly the potentials at which the two sequential oxidation processes of $[Ni^{II}_2Ln]^{2+}$ (*n* = 1 or 2) occur do not vary much with the change from imine to amine nitrogen donors. In contrast the potentials of the two sequential reduction processes of $[Ni^{II}_2Ln]^{2+}$ (*n* = 1 or 2) differ significantly: there is a substantial shift to more negative potentials on changing from imine to amine nitrogen donors, as expected given that this equates to a reduction of π-acceptor ability.[10] A second feature is that the two waves have a greater ΔE, corresponding to the mixed valent species $[Ni_2L1]^{+}$ being more stable with respect to disproportionation. It is curious that the dramatic differences in the reductive processes of **1** when compared with **2** are not reflected in the oxidative processes and we are further investigating this point.[7]

The successful synthesis of this tetraamine complex, **1**, represents a major step towards the production of stable dimetallic species suitable for redox and binding studies as the macrocycle is hydrolytically stable in contrast to the parent Schiff base. The nature and reactivity of the redox products are of considerable interest both in their own right and due to their relevance to the redox process catalysed by [Ni,Fe]-hydrogenases.[11] Further work is under way to explore these exciting aspects of our dinickel thiolates.[7]

This work was supported by grants from the University of Otago. We thank Professor W. T. Robinson (University of Canterbury) for the X-ray data collections and C. Beck (University of Sydney), Professor A. McAuley and Dr S. Subramanian (University of Victoria) for the EPR spectra.[7] This work is dedicated to Professor W. Roper on the occasion of his 60th birthday.

Notes and References

† Satisfactory C,H,N,S analyses were obtained for **1** and **2**. NMR (300 MHz, CD_3CN, ref. ext. TMS): **1** δ_H (298 K) 7.18 (4H, s), 3.64 (8H, d), 3.47 (4H, d), 2.92 (4H, dd), 2.47 (4H, d), 2.27 (6H, s); **2** δ_H (343 K) 9.48 (4H, s, br), 7.54 (4H, s), *ca*. 4.50 (4H, br), *ca*. 4.31 (4H, br), 2.46 (6H, s), 2.24 (2H, d, br), 1.64 (2H, br).

‡ *Crystal data* for **1**: $C_{28}H_{40}Cl_2N_6Ni_2O_{10}S_2$, dark red square block, crystal dimensions 0.40 × 0.35 × 0.13 mm, orthorhombic, *Pnma*, a = 16.825(3), b = 11.190(2), c = 19.160(4) Å, U = 3607.3(12) $Å^3$, μ = 1.37 mm^{-1}. Data were collected at 149 K on a Bruker SMART diffractometer using graphite-monochromated Mo-Kα, λ = 0.71073 Å. A total of 26349 reflections were collected in the range $3 < 2\theta < 53°$ and the 3900 independent reflections were used in the structural analysis after a semi-empirical absorption correction had been applied. The structure was solved by direct methods (SHELXS-86),[12] and after resolution of severe disorder problems (electronic supplementary information: see http://www.rsc.org/suppdata/cc/1998/2131) the refinement on F^2 against all data (SHELXL-97)[13] converged satisfactorily to $R1$ = 0.068 [for $3036F > 4\sigma(F)$; $wR2$ = 0.191 and goodness of fit = 1.14 for all 3900 F^2; 390 parameters; 230 restraints; +0.70/−0.57 $eÅ^{-3}$]. CCDC 182/993.

1 A. Volbeda, M-H. Charon, C. Piras, E. C. Hatchikian, M. Frey and J. C. Fontecilla-Camps, *Nature*, 1995, **373**, 580.
2 See for example: A. F. Kolodziej, *Prog. Inorg. Chem.*, 1994, **41**, 493; M. A. Halcrow and G. Christou, *Chem. Rev.*, 1994, **94**, 2421; C. M. Goldman and P. K. Mascharak, *Comments Inorg. Chem.*, 1995, **18**, 1; J. C. Fontecilla, *J. Biol. Inorg. Chem.*, 1996, 91; M. Frey, *Struct. Bonding*, 1998, **90**, 97.
3 C. A. Marganian, H. Vazir, N. Baidya, M. M. Olmstead and P. K. Mascharak, *J. Am. Chem. Soc.*, 1995, **117**, 1584.
4 See for example: G. Musie, P. J. Farmer, T. Tuntulani, J. H. Reibenspies and M. Y. Darensbourg, *Inorg. Chem.*, 1996, **35**, 2176; C.-H. Lai, J. H. Reibenspies and M. Y. Darensbourg, *Angew. Chem., Int. Ed. Engl.*, 1996, **35**, 2390.
5 S. Brooker and P. D. Croucher, *J. Chem. Soc., Chem. Commun.*, 1995, 1493; 2075; *Chem. Commun.*, 1997, 459; S. Brooker and T. C. Davidson, *Chem. Commun.*, 1997, 2007.
6 S. Brooker, P. D. Croucher and F. M. Roxburgh, *J. Chem. Soc., Dalton Trans.*, 1996, 3031.
7 S. Brooker, P. D. Croucher, T. C. Davidson, G. S. Dunbar, P. D. Smith, S. P. Cramer, C. Y. Ralston, C. Coates, J. J. McGarvey, C. Beck and S. Subramanian, unpublished results.
8 See for example: A. M. Bond, M. Haga, I. S. Creece, R. Robson and J. C. Wilson, *Inorg. Chem.*, 1988, **27**, 712; G. A. Lawrance, M. Maeda, T. M. Manning, M. A. O'Leary, B. W. Skelton and A. H. White, *J. Chem. Soc., Dalton Trans.*, 1990, 2491; N. D. J. Branscombe, A. J. Blake, A. Marin-Becerra, W.-S. Li, S. Parsons, L. Ruiz-Ramirez and M. Schröder, *Chem. Commun.*, 1996, 2573.
9 N. F. Curtis, *J. Chem. Soc. A.*, 1965, 925.
10 F. V. Lovecchio, E. S. Gore and D. H. Busch, *J. Am. Chem. Soc.*, 1974, **96**, 3109; A. G. Lappin and A. McAuley, *Adv. Inorg. Chem.*, 1988, **32**, 241; T. Yamamura, M. Tadokoro, K. Tanaka and R. Kuroda, *Bull. Chem. Soc. Jpn.*, 1993, **66**, 1984.
11 'Green energy', see for example: T. Newton, *Chem. in Brit.*, 1997, January, 29; J. C. Fontecilla-Camps, A. Volbeda and M. Frey, *Trends Biotechnol.*, 1996, **14**, 417; A. Coghlan, *New Scientist*, 1996, January, 14; L. L. Efros, H. H. Thorp, G. W. Brudvig and R. H. Crabtree, *Inorg. Chem.*, 1992, **31**, 1722.
12 G. M. Sheldrick, *Acta Crystallogr., Sect. A*, 1990, **46**, 467.
13 G. M. Sheldrick, manuscript in preparation.
14 R. Greef, R. Peat, L. M. Peter, D. Pletcher and J. Robinson, *Instrumental Methods in Electrochemistry*, Ellis Horwood, UK, 1985, ch. 6, p. 178.

Received in Cambridge, UK, 13th July 1998; 8/05443F

Organisation of long aliphatic monocarboxylic acids in β-cyclodextrin channels: crystal structures of the inclusion complexes of tridecanoic acid and (*Z*)-tetradec-7-enoic acid in β-cyclodextrin

Stella Makedonopoulou,[a] Irene M. Mavridis,*[a]† Konstantina Yannakopoulou[a] and John Papaioannou[b]

[a] *Institute of Physical Chemistry, National Centre for Scientific Research 'Demokritos', Aghia Paraskevi 153 10, Athens, Greece*
[b] *Laboratory of Physical Chemistry, University of Athens, Panepistimiopolis 157 71, Greece*

In the crystalline state, infinite channels of β-cyclodextrin dimers host infinite arrays of self associated linear aliphatic monocarboxylic acids, thus enclosing the hydrophilic carboxy ends inside the hydrophobic channels.

Non-bonding interactions like H-bonds and hydrophobic interactions comprise the main routes for the assembly of supermolecules,[1a,b] entities detectable as distinct from the constituent molecules. Since the non-covalent bonding interactions are at least an order of magnitude weaker than covalent bonds, stable supermolecules require a large number of such interactions, *i.e.* the presence of a large area of complementary surface[1c,d] in order to compensate for the entropic loss due to organisation. This requirement is fulfilled in the formation of host–guest assemblies. Moreover, if the supermolecules possess groups capable of aggregation *via* non-covalent bonds, it is possible to synthesise supramolecular assemblies. Thus the latter can be generated by introducing groups with a tendency for specific interactions into strategic parts of the supermolecules.[2]

The systems reported here, which involve inclusion of one molecule of a long aliphatic mono-carboxylic acid (tridecanoic acid **1** and (*Z*)-tetradec-7-enoic acid **2**) into two molecules of β-cyclodextrin (β-CD), combine host–guest interactions and supramolecular synthon association of both host and guest to form supramolecular assemblies. They were designed to form three-component pseudo-rotaxanes and subsequent stacking of those into infinite channels. Indeed, such systems were prepared through precipitation from aqueous solutions of β-CD after the addition of a two-fold excess of the aliphatic acids at room temperature. The crystallographic analyses‡ revealed that the above simple process allowed the formation of systems exhibiting many levels of supramolecular organisation.

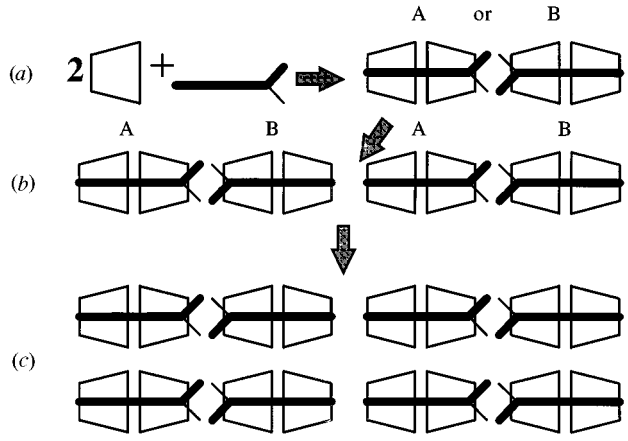

Scheme 1 Schematic representation of (*a*) the self-assembly of two β-cyclodextrin molecules and an aliphatic acid molecule into [3]pseudorotaxanes, (*b*) the formation of a channel supramolecular array and (*c*) supramolecular arrays of higher order by channel association

Firstly, β-CD forms dimers *via* H-bonds between the O3 secondary hydroxy groups of the two monomers, as is common in β-CD inclusion complexes.[3] Each molecule of aliphatic acid threads into the long cavity of a β-CD dimer to form a [3]pseudorotaxane [Scheme 1(*a*)]. The aliphatic guests span the entire length of the β-CD dimer with the carboxylic groups slightly protruding from one primary face and the terminal methyl groups protected at the other end. Threading of two cyclodextrin units (α-CD, permethylated α-CD) onto one long aliphatic molecule has also been observed[4] in aqueous solutions and inter-cyclodextrin H-bonds have been invoked to account for the thermodynamic parameter measurements in solution studies of polypseudorotaxanes.[5]

At a second level, the supramolecular units align along the crystallographic *c* axis to form channels (Fig. 1). The crystallographic asymmetric unit contains one [3]pseudorotaxane in

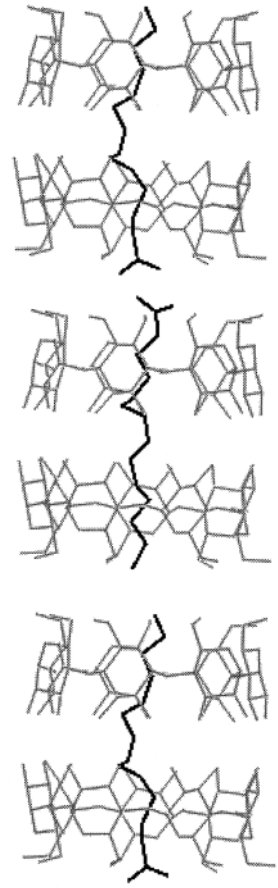

Fig. 1 Channel formation in the β-cyclodextrin complex of (*Z*)-tetradec-7-enoic acid. The two terminal guest molecules have the A orientation and the middle one the B orientation.

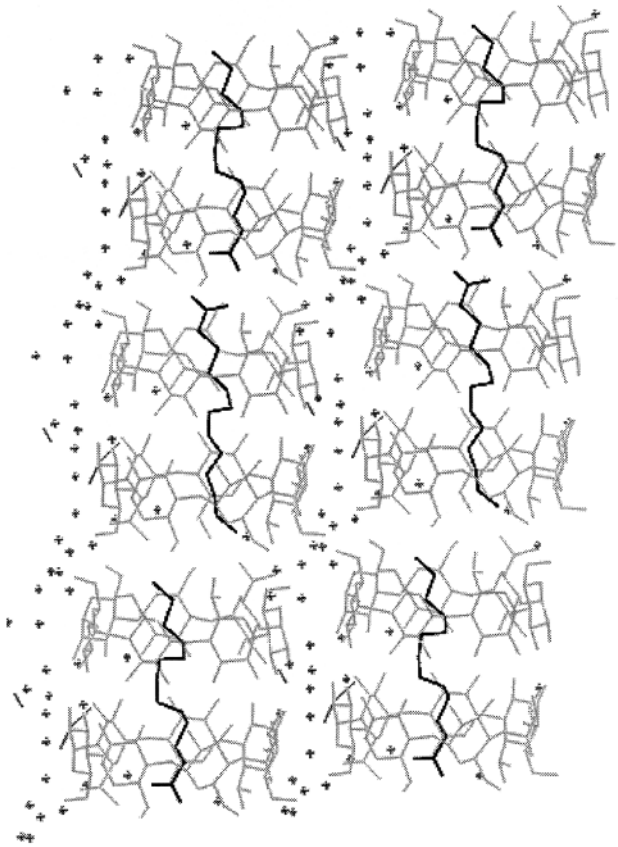

Fig. 2 Organisation in three-dimensions of channels of β-cyclodextrin–tridecanoic acid complexes

which the aliphatic acid is disordered over two orientations (A and B) of almost equal probability (occupation factors for orientations A and B refined to: A = 52%, B = 48% for **1**, and A = 51%, B = 49% for **2**; considered as 50% each from the accuracy of the present data). Therefore, a β-CD dimer encloses one molecule of the acid in orientation A and the adjacent dimer along the channel in orientation B in order to form conventional carboxylic dimers [Scheme 1(*b*)]. The observed distances between the adjacent carboxylic oxygen atoms of orientations A and B are O1A···O1B = 2.50 and OA2···OB2 = 2.74 Å for **1** and OA1···OB1 = 2.70 and O2A···O2B 2.71 Å for **2**. The overall formation of the channel resembles an infinite poly-pseudorotaxane where the β-CD molecules are not threaded onto a polymer chain but onto an linear assembly of aliphatic carboxylic acids held together by intermolecular interactions. In addition, the β-CD host assists in the formation of the supramolecular assembly *via* H-bonds between two primary hydroxy groups of consecutive dimers (O···O distances 2.93 and 2.98 Å for **1** and **2** respectively) that further strengthen the channel.

The supramolecular organisation extends to a third level, since the channels associate *via* H-bonds along the **a** and **b** axes [Scheme 1(c), Fig. 2]. The H-bonding interactions are either through direct association of primary and secondary hydroxy groups (five H-bonds at O···O distances 2.77–2.89 and 2.76–2.91 Å for **1** and **2** respectively) or through intervening water molecules.

Determination of the unit cells of crystals of β-CD complexes of aliphatic mono-acids with 12–16 carbon atoms show that they are isomorphous with the complexes reported here, showing that they also form [3]pseudorotaxanes aligned in channels. In contrast, β-CD complexes of aliphatic di-acids with 10–16 carbon atoms also form [3]pseudorotaxanes but they do not align in channels,[6] preferring to interact with the polar environment. Therefore, in the case of the monocarboxylic acids we observe the remarkable fact that the carboxylic groups prefer to be enclosed inside the hydrophobic environment of the channel rather than interact with the aqueous environment in the periphery of the β-CD dimers, as in the case of the di-acids. We believe that what forces them inside the channel is the presence of the terminal methyl groups of the guest in the other primary face of the β-CD dimers. Due to the presence of the solvent in the lattice, these methyl groups would be exposed to the aqueous environment if channels were not formed. On the other hand, although the carboxylic groups prefer the polar environment, they can be stabilised by self-association into carboxylic dimers. The formation of the latter corresponds to an overall non-polar moiety[7] that can stay inside the hydrophobic channel.

Summarising, we have achieved the construction of an infinite channel structure, based on specific features of simple building blocks, with aliphatic mono-carboxylic acids threaded through two β-CD molecules. The tendency of cyclodextrins to form inclusion complexes and simultaneously to self-associate and form dimers is combined with the tendency of the guest molecules for self association through a very well known synthon, the carboxylic dimer. It is shown that the channel forming ability of similar systems is directly related to the degree of hydrophobicity/hydrophilicity of the end groups of the guest emerging from the primary faces, due to one more variable, the solvent, that influences the packing of the building blocks. Currently, we are exploiting the properties of the systems in order to design transitions between the packing modes[8] of dimeric β-CD complexes *via* the interplay of the aliphatic chain length and the nature of the end groups.

I. M. M. and K. Y. acknowledge the support of the EU program VALUE CTT 472. This work was partially supported by the General Secretariat of Research and Technology of Greece, Program PENED.

Notes and References

† E-mail: mavridi@cyclades.nrcps.ariadne-t.gr

‡ *Crystal data* for **1** $(C_{42}H_{70}O_{35})_2\cdot(C_{13}H_{26}O_2)\cdot(H_2O)_{19.5}$: triclinic, *P*1 a = 15.654(6), b = 15.650(6), c = 15.937(6) Å, α = 101.585(12), β = 101.596(14), γ = 103.585(13)°, V = 3589(2) Å^3, Z = 1, ρ_{calc} = 1.286 g cm^{-3}, $2\theta_{max}$ = 41°, μ(Mo-Kα) = 0.1 mm^{-1}, T = 293 K, $R1$ = 0.0862 for 5862 $F_o > 4\sigma(F_o)$, $wR2$ = 0.2702 for 7565 independent reflections. 19.5 water molecules were located, distributed over 28 positions. For **2** $(C_{42}H_{70}O_{35})_2\cdot(C_{14}H_{26}O_2)\cdot(H_2O)_{14.6}$: triclinic, *P*1, a = 15.6259(9), b = 15.6226(10), c = 15.9349(10) Å, α = 101.547(2), β = 101.555(2), γ = 103.642(2)°, V = 3576.4(4) Å^3, Z = 1, ρ_{calc} = 1.283 g cm^{-3}, μ(Mo-Kα) = 0.1 mm^{-1}, T = 293 K, $R1$ = 0.0862 for 6784 $F_o > 4\sigma(F_o)$, $wR2$ = 0.2505 for 8004 independent reflections. 14.6 water molecules were located, distributed over 32 positions. A full description of the structures will be published elsewhere. CCDC 182/991.

1 (*a*) J.-M. Lehn, *Supramolecular Chemistry*, VCH, 1995; (*b*) F. Vögtle, *Supramolecular Chemistry*, Wiley, 1993; (*c*) D. Philip and J. F. Stoddart, *Angew. Chem., Int. Ed. Engl.*, 1996, **35**, 1154; (*d*) M. C. T. Fyfe and J. F. Stoddart, *Acc. Chem. Res.*, 1997, **30**, 393.
2 (*a*) G. R. Desiraju, *Angew. Chem., Int. Ed. Engl.*, 1995, **34**, 2311; (*b*) G. R. Desiraju, *Chem. Commun.*, 1997, 1475.
3 I. M. Mavridis and E. Hadjoudis, *Carbohydr. Res.*, 1992, **229**, 1.
4 (*a*) A. Botsi, K. Yannakopoulou, B. Perly and E. Hadjoudis, *J. Org. Chem.*, 1995, **60**, 4017; (*b*) K. Eliadou, K. Yannakopoulou, A. Rontoyianni and I. M. Mavridis, unpublished work.
5 A. Harada, J. Li and M. Kamachi, *Macromolecules*, 1994, **27**, 4538.
6 S. Makedonopoulou and I. M. Mavridis, unpublished work.
7 R. K. R. Jetti, S. S. Kuduva, D. S. Reddy, F. Xue, T. C. W. Mak, A. Nangia and G. R. Desiraju, *Tetrahedron Lett.*, 1998, **39**, 913.
8 D. Mentzafos, I. M. Mavridis, G. Le Bas and G. Tsoucaris, *Acta Crystallogr.*, 1991, **B47**, 746.

Received in Columbia, MO, USA, 28th May 1998; 8/04057E

Synthesis of a novel supported solid acid BF_3 catalyst

Karen Wilson and James H. Clark*

Green Chemistry Group, Department of Chemistry, University of York, Heslington, York, UK YO1 5DD. E-mail: jhc1@york.ac.uk

A novel and active form of supported boron trifluoride has been prepared and the active sites identified.

Tightening environmental legislation on the production of waste during homogeneously acid catalysed reactions has led to a demand for heterogenised systems that will aid recovery of the catalyst and minimise pollution. BF_3 is widely used as a Lewis acid catalyst in many organic reactions, including alkylation, acylation, polymerisation, isomerisation and addition reactions,[1] and may be used directly from the gas phase, or complexed with an organic or inorganic ligand (*e.g.* $BF_3{\cdot}OEt_2$ or $BF_3{\cdot}H_3PO_4$). Recovery of boron from the reaction however results in the formation of large amounts of waste, which on an industrial scale is environmentally unacceptable.

The use of a heterogeneous BF_3 system would offer ease of catalyst recovery and reuse, and minimise the production of waste currently formed during BF_3 recovery. However a suitable replacement supported system must also exhibit activities/selectivities comparable to the existing homogeneous route. To date previous attempts to produce oxide supported BF_3 has focused on the use of gaseous BF_3.[2–4] In this paper we report the synthesis, characterisation and reactive properties of a novel mesoporous SiO_2 supported solid acid catalyst prepared using liquid BF_3 precursors. The activity of the catalyst towards the alkylation of phenol with oct-1-ene to form octyl phenyl ether or octylphenol (important in the production of lubricants) was examined.

A range of SiO_2 supported BF_3 catalysts (4 mmol g^{-1} loading) were prepared from $BF_3(H_2O)_2$ (Aldrich 96%) and $BF_3{\cdot}OEt_2$ (Aldrich 99%) precursors. Mesoporous SiO_2 (K100-Merck) of surface area 310 m^2 g^{-1} was dried for 24 hours at 300 °C, then stirred under a N_2 atmosphere with a mixture of the precursor diluted in 100 ml of ethanol or toluene at 20 °C or reflux respectively. The catalyst slurry was stirred for 2 hours, then dried slowly on a rotary evaporator at 50 °C.

Characterisation of the acid sites present on the surface was performed by recording DRIFT spectra following titration of the supported BF_3 catalysts with pyridine as shown in Fig. 1.

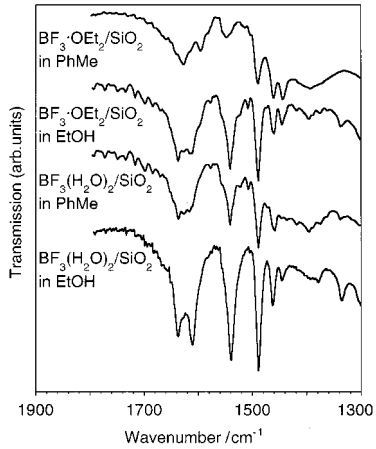

Fig. 1 DRIFTS following pyridine titration of 4 mmol g^{-1} BF_3/SiO_2 catalysts prepared using $BF_3(H_2O)_2$ and $BF_3{\cdot}OEt_2$ precursors in ethanol or toluene

These show that all the catalysts exhibit both Lewis and Brønsted acidity, as indicated by the absorption bands at 1445 and 1461 cm^{-1}, (Lewis sites), and those at 1638 and 1539 cm^{-1} (Brønsted sites). The remaining bands at 1611 and 1489 cm^{-1} are assigned to pyridine bound at either Lewis or Brønsted sites. There is a striking difference in the nature of the acid sites depending on catalyst preparation, with the catalyst prepared from the $BF_3(H_2O)_2$ precursor in ethanol exhibiting the most intense Brønsted bands. Brønsted acidity in solid acid catalysts normally arises from polarised $^{\delta-}O–H^{\delta+}$ sites. The observation of strong Brønsted acidity following attachment of a Lewis acid centre to an oxide support has been reported in other systems,[4,5] and might be attributed to polarisation of surface hydroxyl groups *via* an inductive effect of the electronegative F atoms on BF_3. However what is remarkable in this instance is how the Brønsted acidity varies with catalyst preparation, with the catalysts prepared in ethanol exhibiting higher concentrations of Brønsted acid sites than those prepared in toluene.

The origin of the acid sites on the ethanol prepared $BF_3(H_2O)_2/SiO_2$ catalyst was investigated using thermogravimetric analysis coupled with evolved gas FTIR (TGIR), which allows molecules desorbing from the catalyst during thermal analysis to be identifed by their vibrational spectrum. Fig. 2 shows the thermal analysis results for supported $BF_3(H_2O)_2$ and $BF_3{\cdot}OEt_2$ catalysts which had been prepared in ethanol. Heating both catalysts above 100 °C results in significant weight loss and the observation of ethanol desorption in the IR. However the differential mass lost indicates that the ethanol desorption temperature from $BF_3(H_2O)_2/SiO_2$ is 10 °C higher than from $BF_3{\cdot}OEt_2/SiO_2$, and approximately twice the amount of ethanol is evolved. This corresponds to approximately 4 and 2.5 mmol g^{-1} of ethanol present on each catalyst respectively. The uptake of short chain alcohols has been used as an indication of the strength and concentration of Brønsted acid sites on zeolites.[6] These results therefore suggest that $BF_3(H_2O)_2/SiO_2$ possesses a higher coverage of stronger Brønsted acid sites compared to $BF_3{\cdot}OEt_2/SiO_2$.

Further heating beyond 400 °C results in an additional weight loss which is accompanied by the evolution of HF from the

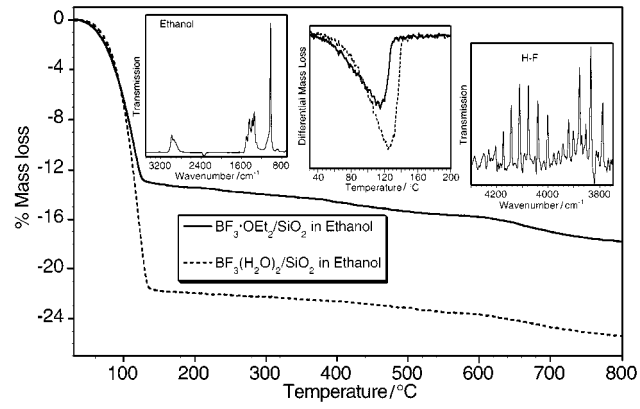

Fig. 2 TGIR comparing 4 mmol g^{-1} $BF_3(H_2O)_2/SiO_2$ and $BF_3{\cdot}OEt_2/SiO_2$. IR spectra recorded during decomposition reveal the evolution of ethanol and HF. The differential mass loss is also shown to indicate the peak ethanol desorption temperature.

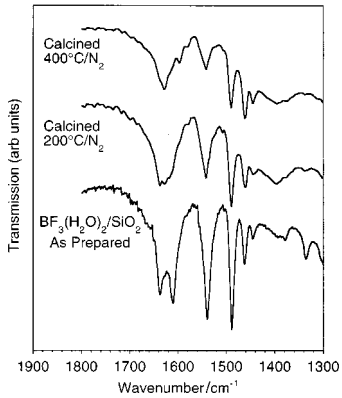

Fig. 3 DRIFTS following pyridine titration of 4 mmol g^{-1} $BF_3(H_2O)_2/SiO_2$ after calcination to 200 °C and 400 °C under N_2. All spectra were recorded at 20 °C.

catalyst. Corresponding DRIFTS/pyridine titrations of catalysts calcined to 200 and 400 °C under N_2, shown in Fig. 3**,** indicate that the Brønsted sites are gradually lost as the calcination temperature is increased.

While BF_3 alone is a Lewis acid, it is often used catalytically when bound to organic ligands to form strong proton donating complexes.[1] The evolution of ethanol at 120 °C coupled with the loss of Brønsted acidity indicates that Brønsted acid sites in the $BF_3(H_2O)_2/SiO_2$ catalyst may arise from the binding of ethanol to supported BF_3 centres resulting in the formation of a $[SiOBF_3]^-[EtOH_2]^+$ complex. Further evidence in support of this model comes from ^1H MAS NMR of the as prepared catalyst which show resonances at 1.343, 4.009 and 8.160 ppm which are consistent with CH_3, CH_2 and OH_2^+ of protonated ethanol respectively.[6] Previous studies have reported that ligand exchange between $BF_3{\cdot}OEt_2$ and ethanol results in the formation of $H^+[BF_3OEt]^-$ complexes.[7] However, to form the protonated ethanol complex proposed in this model interaction with a more protic BF_3 complex is required, *e.g.* $BF_3(H_2O)_2$, which can exist as $[H_3O]^+[BF_3OH]^-$.[1] The trend in Brønsted acidity observed between $BF_3{\cdot}OEt_2$ and $BF_3(H_2O)_2$ precursors can thus be understood in these terms.

Desorption of ethanol from the $BF_3(H_2O)_2/SiO_2$ catalyst following 200 °C calcination lowers the number of Brønsted sites titratable by pyridine (Fig. 3). We atttribute those remaining to the polarisation of surface hydroxyl groups on the support by the BF_x centres. By 400 °C dehydroxylation of the support further reduces the number of Brønsted sites leaving predominantly Lewis acid character, as evidenced by the DRIFTS bands at 1627 and 1462 cm^{-1} which are attributed to the BF_x sites. The evolution of HF above 400 °C observed by TGIR indicates that these BF_x groups start to decompose above this temperature, and by 600 °C no titratable acid sites remain indicating complete decomposition of the BF_x centres. Likewise BET measurements on calcined $BF_3(H_2O)_2/SiO_2$ catalysts reveal the surface area is maintained at 258 m^2 g^{-1} up to 200 °C, indicating that the BF_3 sites are stable to this temperature. An increase in surface area to 266 m^2 g^{-1} is observed on calcining to 400 °C, consistent with the decomposition of BF_3. It should be noted that due to outgassing procedures prior to BET measurements changes in surface area due to ethanol desorption cannot be observed. We believe that these spectroscopic results can be summarised by the model presented in Scheme 1.

The catalytic activity of these supported BF_3 samples was tested using the reaction of oct-1-ene with phenol (performed at 85 °C using 0.05 M of each reactant, in 100 ml of 1,2-dichloroethane with 1 g of supported BF_3 catalyst). Table 1 shows the phenol conversion and selectivities towards octyl phenyl ether obtained after 23 hours reaction time. It is clear that the activity of the $BF_3(H_2O)_2/SiO_2$ catalyst prepared in ethanol is superior to the other samples. The activity can thus be correlated with the

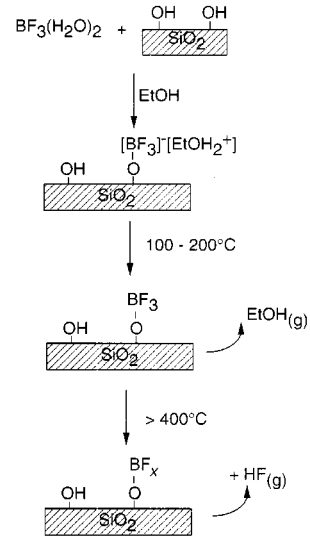

Scheme 1

Table 1 Phenol conversion and selectivities towards octyl phenyl ether after 23 h reaction for the different catalysts

Catalyst	Phenol conversion (%)	Ether selectivity (%)
$BF_3(H_2O)_2/SiO_2$ (EtOH)	30	61
$BF_3(H_2O)_2/SiO_2$ recycled	6	97
$BF_3(H_2O)_2/SiO_2$ ($PhCH_3$)	4	78
$BF_3{\cdot}OEt_2/SiO_2$ (EtOH)	3	85
$BF_3{\cdot}OEt_2/SiO_2$ ($PhCH_3$)	< 1	92

number and strength of Brønsted acid sites identified on these catalysts using TGIR.

Following reuse of $BF_3(H_2O)_2/SiO_2$ samples, a decrease in conversion and selectivity towards ring alkylation products is observed relative to the fresh catalyst. Preliminary characterisation of used catalyst, by DRIFTS and pyridine titration, indicates the nature of the acid sites remains essentially unchanged. The loss of activity on recycling the catalyst may result from organic residue deposited on the catalyst during reaction causing pore blocking and/or poisoning of active sites.

In conclusion, we have synthesised a novel form of supported boron trifluoride which is easy to prepare and handle, shows unusually high Brønsted acidity which can be controlled by activation temperature, and exhibits considerable catalytic activity.

We thank the EPSRC for funding the project, EPSRC/RAEng for a Clean Technology Fellowship (to J. H. C.), and colleagues at York and the University of Newcastle Chemical and Process Engineering Department for helpful discussions.

Notes and References

1 A. V. Topchiev, S. V. Zavgorodnii and Ya. M. Paushkin, *Boron fluoride and its compounds as catalysts in organic chemistry*, Pergamon Press, London, 1958.
2 C. Guo, S. Liao, Z. Qian and K. Tanabe, *Appl. Catal. A*, 1994, **107**, 239.
3 B. A. Morrow and A. Devi, *J. Chem. Soc., Faraday Trans.*, 1972, **68**, 403.
4 M. Marczewski, H. Marczewska and K. Witoslawski, *Bull. Soc. Chim. Fr.*, 1991, 366.
5 E. E. Getty and R. S. Drago, *Inorg. Chem.*, 1990, **29**, 1186.
6 A. Thursfield and M. W. Anderson, *J. Phys. Chem.*, 1996, **100**, 6698.
7 V. A. Tkach, V. A. Gruznykh, N. A. Murasheva, G. Myagmarsuren, T. V. Dmitrieva, G. V. Ratovskii, S. V. Zinchenko and F. K. Shmidt, *React. Kinet. Catal. Lett.*, 1991, **43**, 431.

Received in Cambridge, UK, 3rd August 1998; 8/06060F

Syntheses and structures of $W_2(\mu\text{-}Cl)_3Cl_6^-$ and $W_2(\mu\text{-}Cl)_2Cl_8^{2-}$, new d^2–d^2 confacial and edge-sharing bioctahedral ditungsten compounds, and a convenient synthesis of $W_2(\mu\text{-}Cl)_3Cl_6^{2-}$

Vladimir Kolesnichenko, Dale C. Swenson and Louis Messerle*

Department of Chemistry, The University of Iowa, Iowa City, IA 52242, USA. E-mail: lou-messerle@uiowa.edu

$(NR_4)W_2Cl_9$ and $(NR_4)_2W_2Cl_{10}$, prepared by addition of NR_4Cl (R = alkyl) to $(WCl_4)_x$ powder in CH_2Cl_2, have confacial [W=W, 2.689(1) Å] and edge-sharing bioctahedral [W=W, 2.792(1) Å] structures, respectively, as $NBnEt_3^+$ salts, and convert with added NR_4Cl to $(NR_4)_2W_2Cl_9$ and $(NR_4)WCl_6$ and eventually $(NR_4)_2WCl_6$; $(NR_4)W_2Cl_9$ can be converted to $(NR_4)_2W_2Cl_{10}$ by NR_4Cl at −30 °C.

High symmetry confacial [$M_2(\mu\text{-}L)_3L_6$, D_{3h}; L = ligand] and edge-sharing [$M_2(\mu\text{-}L)_2L_8$, D_{2h}] bioctahedral complexes are known for many transition metals and are of considerable importance for understanding metal–metal single and multiple bonding.[1] The effect of orbital population on M–M distance can be understood by studying isostructural compounds with various d-electron counts. Confacial bioctahedral congeners with differing d-electron counts are known for few metals (*e.g.* Re,[2] W). For tungsten, $W_2(\mu\text{-}Cl)_3Cl_6^{3-}$ (d^3–d^3; one of the first[3] metal–metal bonded compounds to be recognized[4] as such) and d^2–d^3 $W_2(\mu\text{-}Cl)_3Cl_6^{2-}$ have been reported.[5,6] The W–W distance in the former, which has been studied theoretically,[7] is a short 2.409(7)–2.4329(6) Å,[6,8,9] (depending on cation), and increases[6] by 0.12 Å upon oxidation to $W_2(\mu\text{-}Cl)_3Cl_6^{2-}$. While there are many preparations[10] of $W_2(\mu\text{-}Cl)_3Cl_6^{3-}$, few are known for the dianion;[5,6,11] $W_2(\mu\text{-}Br)_3Br_6^{2-}$ is also known.[12]

We recently developed new syntheses of powdered and crystalline $(WCl_4)_x$ and showed that its structure was a linear polymer of edge-sharing bioctahedra with alternating short (double bond) and long (no bond) W···W separations![13] The unusually reactive powder form, prepared from Sn reduction of WCl_6 in $ClCH_2CH_2Cl$, reacts with NR_4Cl to give the new chloroditungstates $W_2(\mu\text{-}Cl)_2Cl_8^{2-}$ **1** and $W_2(\mu\text{-}Cl)_3Cl_6^-$ **2** as well as $W_2(\mu\text{-}Cl)_3Cl_6^{2-}$ **3**. We report synthetic and structural details.

The reaction of NR_4Cl (R_4 = $BnEt_3$, $BnBu_3$, Bu_4) with $(WCl_4)_x$ leads to scission of dinuclear fragments, disproportionation, and then comproportionation depending on stoichiometry and temperature. At 25 °C, reaction of $(WCl_4)_x$ with one equiv. of $NBnEt_3Cl$ (a cation which facilitates product separation) in CH_2Cl_2 leads to $(NBnEt_3)_2(W_2Cl_9)$ [**3**; 96% isolated yield, eqn. (1)]† and $(NBnEt_3)WCl_6$. The mixture is comproportionated by $NBnEt_3Cl$ to $(NBnEt_3)_2WCl_6$ [94% yield, eqn. (1)]. UV–VIS spectra of products matched literature data.[11,14]

$$3\ WCl_4 \xrightarrow[-(NR_4)WCl_6]{3\ NR_4Cl} \underset{\mathbf{3}}{(NR_4)_2[W_2(\mu\text{-}Cl)_3Cl_6]} \xrightarrow{3\ NR_4Cl} 3\ (NR_4)_2WCl_6 \quad (1)$$

The reaction between $(WCl_4)_x$ and $NBnEt_3Cl$ in CH_2Cl_2 at −30 °C yields $(NBnEt_3)_2[W_2(\mu\text{-}Cl)_2Cl_8]$ **1** which crystallizes along with undissolved $(WCl_4)_x$. Upon warming to 25 °C, **1** redissolves and disproportionates to **3** and $(NBnEt_3)WCl_6$ [eqn. (2)], thus establishing that **1** is an intermediate in eqn. (1). With additional $(WCl_4)_x$, **3** and $(NR_4)WCl_6$ comproportionate to emerald green $(NBnEt_3)[W_2(\mu\text{-}Cl)_3Cl_6]$ [**2**; eqn. (2)]. Compound **2** can be prepared conveniently‡ in one step (90% isolated yield) by combining $(WCl_4)_x$ with 0.5 equiv. $NBnEt_3Cl$ in CH_2Cl_2 at 25 °C, and can be converted§ back to **1** (95% isolated yield) at −30 °C by $NBnEt_3Cl$ in CH_2Cl_2; isolation is possible because of the low solubility of the $NBnEt_3^+$ salt. We believe that **1** and **2** have not been observed in previous studies[5,6,14] because they disproportionate in solution (**1**) or in the presence of Cl^- (**2**). Compound **2** is reduced to **3** by either $(NBnEt_3)_2WCl_6$ or Cp_2Fe in CH_2Cl_2. Scheme 1 summarizes the principal transformations.

$$3\ \underset{\mathbf{1}}{(NR_4)_2[W_2(\mu\text{-}Cl)_2Cl_8]} \longrightarrow 2\ \underset{\mathbf{3}}{(NR_4)_2[W_2(\mu\text{-}Cl)_3Cl_6]} + 2\ (NR_4)WCl_6$$

$$\downarrow 6\ WCl_4$$

$$6\ (NR_4)[W_2(\mu\text{-}Cl)_3Cl_6] \quad (2)$$

$$\underset{\mathbf{2}}{}$$

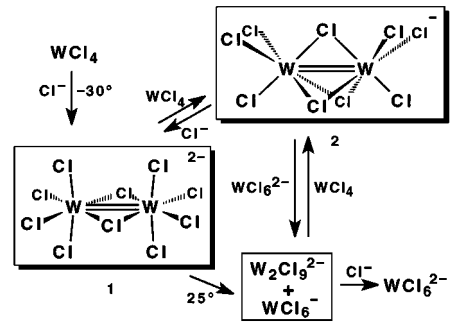

Scheme 1

The syntheses of **1**, **2**, and **3** are facilitated by the use of $(WCl_4)_x$ powder.[13] Reactions of $(WCl_4)_x$, as prepared by reduction of WCl_6 with red phosphorus, $W(CO)_6$, or Sb,[13] with NR_4Cl proceed more slowly and lead to lower purity materials because the lower solubility of these $(WCl_4)_x$ materials results in an excess of NR_4Cl in the early stages of the reactions.

Single crystals of $(NBnEt_3)_2[W_2(\mu\text{-}Cl)_2Cl_8]\cdot 3CH_2Cl_2$ **1** were obtained from −35 °C CH_2Cl_2 solution. The solid-state structure¶ of the centrosymmetric ditungstate portion of **1** (Fig. 1) consists of an edge-sharing bioctahedron with a W(1)–W(1A) distance of 2.792(1) Å, a W(1)–Cl(1)–W(1A) angle of 71.88(6)°, and a Cl(1)–W(1)–Cl(1A) angle of 108.12(6)°. The crystallographically independent axial Cl(2) and Cl(3) in each bioctahedral hemisphere are bent away from Cl(3A) and Cl(2A) with Cl(2)–W(1)–W(1A) and Cl(3)–W(1)–W(1A) angles of

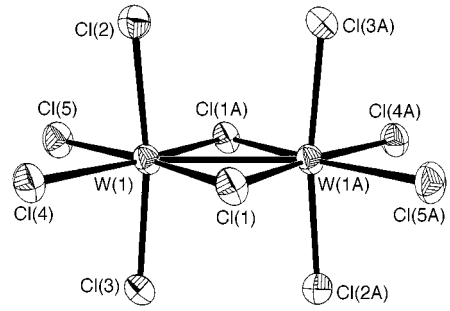

Fig. 1 Thermal ellipsoid plot of the molecular structure of the ditungsten anion portion of **1**

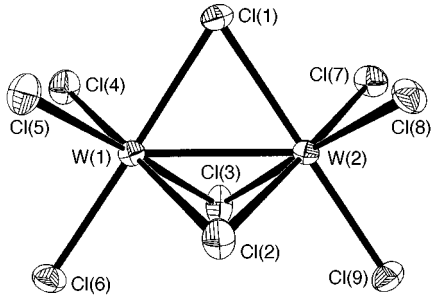

Fig. 2 Thermal ellipsoid plot of the molecular structure of the ditungsten anion portion of **2**

94.38(6)° and 93.98(6)°, respectively, and a Cl(2)···Cl(3A) nonbonded distance which is appreciably closer [3.131(3) Å] than twice the Cl van der Waals (VDW) radius of 1.70–1.90 Å.[15]

The anion in **1** is similar to that of the W≡W bonded portion of $(WCl_4)_x$, and can be formally viewed as the scission of that edge-sharing bioctahedral portion of the polymeric structure[13] and addition of two Cl^- endcaps. The W≡W distance in crystalline $(WCl_4)_x$ is 2.688(2) Å, with W–Cl–W bridge angles of 69.4(2)° and bent-back axial Cl [W–W–Cl(axial), 94.99(12)°]. The axial Cl in each bioctahedral hemisphere of $(WCl_4)_x$ are also closer [3.085(10) Å] than twice the Cl VDW radius. There is no similarity between the structures of **1** and W_2Cl_{10} [*i.e*. $W_2(\mu\text{-}Cl)_2Cl_8$] which has a long W···W separation of 3.814(2) Å and a Cl_μ–W–Cl_μ angle of 81.5(1)°.[16]

The only other Group 6 $M_2(\mu\text{-}Cl)_2Cl_8^{2-}$ compound is edge-sharing bioctahedral $(PPh_4)_2[Mo_2Cl_{10}]$,[17] with no Mo–Mo bond (Mo···Mo, 3.80 Å). The reason(s) for the substantial differences between $Mo_2(\mu\text{-}Cl)_2Cl_8^{2-}$ and $W_2(\mu\text{-}Cl)_2Cl_8^{2-}$ **1** are presently unknown, though the difference in degree of metal–metal bonding parallels that for $Mo_2(\mu\text{-}Cl)_3Cl_6^{3-}$ and $W_2(\mu\text{-}Cl)_3Cl_6^{3-}$.

Single crystals of $(NBnEt_3)[W_2(\mu\text{-}Cl)_3Cl_6]$ **2** were obtained from cooled (−35 °C) $CH_2Cl_2/CHCl_3$ solutions. Single-crystal X-ray diffractometry‖ confirmed that the anion portion of **2** possesses a confacial bioctahedral structure (Fig. 2) with a W(1)–W(2) distance of 2.696(3) Å and an acute W(1)–Cl(μ)–W(2) average angle of 66.6(1)° which is smaller than the bridge angle of 70.53° for an idealized confacial bioctahedron. The W–W distance and W–Cl_μ–W angles are consistent with a formal W(1)–W(2) double-bonding ($a_1'^2e'^2$) interaction.

The W–W distance in $W_2(\mu\text{-}Cl)_3Cl_6^{n-}$ (n = 3, 2, 1) thus increases from 2.409(7) to 2.4329(6) Å for n = 3, to 2.540(1) Å for n = 2, and to 2.696(3) Å for n = 1 (compound **2**), as would be expected from σ-bond weakening with increasing nuclear charge and/or the decrease in formal bond order from 3 to 2.5 to 2.[6] The UV–VIS data for **2** correspond to those reported[11] for $(Bu_4N)_2(W_4Cl_{17})$, whose structure was not determined. The analytical accuracy, as the authors noted, did not rule out an alternative formulation such as $NBu_4(W_2Cl_9)$. It is interesting that $W_4Cl_{17}^{2-}$ was reported[11] to react with excess Cl^- to give products including $W_2Cl_9^{2-}$, as does **2**.

The mechanism of formation of **1**, **2**, and **3** from chloride attack on $(WCl_4)_x$, the solid-state and solution magnetochemistry of **1** and **2** (which exhibits a surprisingly low moment of ⩽ 1.3 μ_B in solution by the Evans method), theoretical studies using the GAMESS program,[18] and the reactivity of the new ditungsten(IV) perchloroanions are under investigation.

The support of Nycomed, Inc. and the University of Iowa Biosciences Initiative Research Program is gratefully acknowledged, as are the useful comments of a reviewer.

Notes and References

† Synthesis of **3**: a stirred mixture of 0.500 g (1.535 mmol) WCl_4 and 0.350 g (1.537 mmol) $NBnEt_3Cl$ in 10 mL CH_2Cl_2 converted in 10 min from a gray suspension to a deep purple-brown suspension with microcrystals, and eventually to a deep blue-purple precipitate in a green-brown solution. After several days, the precipitate was filtered off, washed with CH_2Cl_2 until the wash became light blue-purple, and dried *in vacuo*. Weight = 0.525 g (96% yield). The UV–VIS spectrum (CH_2Cl_2) matched those of known $W_2Cl_9^{2-}$ salts. Anal: W, 33.7; Cl, 29.01. Calc. for $(NBnEt_3)_2W_2Cl_9$: W, 34.32; Cl, 29.78%. The supernatant was cooled to −30 °C for one day and a first crop of the brown crystalline product was isolated by filtration for analysis and dried *in vacuo*; weight 0.110 g (37% yield) $(NBnEt_3)WCl_6$. Anal: W, 31.2; Cl, 36.43. Calc. for $(NBnEt_3)WCl_6$: W, 31.22; Cl, 36.12%.

‡ Synthesis of **2**: a stirred mixture of WCl_4 (1.00 g, 3.07 mmol), $NBnEt_3Cl$ (0.350 g, 1.54 mmol), and CH_2Cl_2 (15 mL) gave a deep blue-green solution after 10–30 min. After one day, the deep blue-green solution was filtered and rotary-evaporated to a viscous oil, which crystallized to 1.218 g dark emerald-green product (90% yield). Anal: W, 41.1; Cl, 35.58. Calc. for $(NBnEt_3)W_2Cl_9$: W, 41.83; Cl, 36.29%. UV–VIS, λ/nm (ε/dm^3 mol^{-1} cm^{-1}): 650 (825), 530 (370), 360 (shoulder), and 305 (22600). MS (FAB, negative ion mode, m/z): 687 (M^+, base peak for $W_2Cl_9^-$ isotope pattern).

§ Synthesis of **1** *via* Cl^- addition to $W_2Cl_9^-$: pre-cooled (−30 °C) solutions of 0.052 g (0.228 mmol) $NBnEt_3Cl$ in 2 mL of CH_2Cl_2 and 0.200 g (0.228 mmol) $(NBnEt_3)(W_2Cl_9)$ in 4 mL of CH_2Cl_2 were mixed. Deep purple-brown microcrystals formed immediately. After aging at −30 °C for 1 day, the crystals were filtered off cold, washed with cold CH_2Cl_2 (*ca*. 5 mL) and dried *in vacuo*. Weight = 0.257 g (95% yield). Anal: W, 30.8. Calc. for $(NBnEt_3)_2W_2Cl_{10}\cdot CH_2Cl_2$: W, 30.85%.

¶ Crystallographic data for **1**: $C_{29}H_{50}Cl_{16}N_2W_2$, $[(NBnEt_3)_2(W_2Cl_{10})\text{-}(CH_2Cl_2)_3]$, M = 680.81, monoclinic, a = 14.620(3), b = 15.430(3), c = 10.860(2) Å, β = 108.38(3)°, V = 2324.9(8) Å^3, T = 213 K, space group $P2_1/n$, Z = 2, μ = 5.889 mm^{-1}, 5553 reflections measured, 4053 independent reflections, $R1$ = 0.0451, $wR2$ = 0.0918.

‖ Crystallographic data for **2**: $C_{13}H_{22}Cl_9NW_2$, M = 879.07, monoclinic, a = 8.910(2), b = 15.350(3), c = 17.920(4) Å, β = 94.80(3)°, V = 2442.3(9) Å^3, T = 213 K, space group $P2_1/c$, Z = 4, μ = 10.398 mm^{-1}, 4672 reflections measured, 3819 independent reflections, $R1$ = 0.0500, $wR2$ = 0.0987. CCDC 182/968.

1 (*a*) F. A. Cotton and R. A. Walton, *Multiple Bonds Between Metal Atoms*, 2nd edn. Clarendon Press, Oxford, 1993, p. 3; (*b*) F. A. Cotton and D. A. Ucko, *Inorg. Chim. Acta*, 1972, **6**, 161; (*c*) R. H. Summerville and R. Hoffmann, *J. Am. Chem. Soc.*, 1979, **101**, 3821; (*d*) S. Shaik, R. Hoffmann, C. R. Fisel and R. H. Summerville, *J. Am. Chem. Soc.*, 1980, **102**, 4555; (*e*) W. C. Trogler, *Inorg. Chem.*, 1980, **19**, 697; (*f*) F. A. Cotton and X. Feng, *Int. J. Quantum Chem.*, 1996, **58**, 671.

2 G. A. Heath, J. E. McGrady, R. G. Raptis and A. C. Willis, *Inorg. Chem.*, 1996, **35**, 6838.

3 (*a*) O. Olsson, *Ber. Dtsch. Chem. Ges.*, 1913, **46**, 566; (*b*) O. Olsson, *Z. Anorg. Allg. Chem*., 1914, **88**, 1914.

4 (*a*) C. Brosset, *Ark. Chem., Miner. Geol. A*, 1935, **12**, no. 4; (*b*) C. Brosset, *Nature*, 1935, **135**, 874.

5 R. Saillant and R. A. D. Wentworth, *J. Am. Chem. Soc.*, 1969, **91**, 2174.

6 F. A. Cotton, L. R. Falvello, G. N. Mott, R. R. Schrock and L. G. Sturgeoff, *Inorg. Chem.*, 1983, **22**, 2621.

7 (*a*) R. Stranger, S. A. Macgregor, T. Lovell, J. E. McGrady and G. A. Heath, *J. Chem. Soc., Dalton Trans.*, 1996, 4485; (*b*) J. E. McGrady, T. Lovell and R. Stranger, *Inorg. Chem.*, 1997, **36**, 3242.

8 W. H. Watson, Jr. and J. Waser, *Acta Crystallogr.*, 1958, **11**, 689.

9 K. R. Dunbar and L. E. Pence, *Acta Crystallogr., Sect. C*, 1991, **47**, 23.

10 (*a*) H. B. Jonassen, A. R. Tarsey, S. Cantor and G. F. Helfrich, *Inorg. Synth.*, 1957, **5**, 139; (*b*) R. A. Laudise and R. C. Young, *Inorg. Synth.*, 1960, **6**, 149; (*c*) E. A. Heintz, *Inorg. Synth.*, 1963, **7**, 142; (*d*) R. C. Young, *J. Am. Chem. Soc.*, 1932, **54**, 4515; (*e*) R. Uzel and R. Pribil, *Coll. Czech. Chem. Commun.*, 1938, **10**, 330; (*f*) O. Collenberg and J. Backer, *Z. Electrochem.*, 1924, **30**, 230; (*g*) R. Saillant, J. L. Hayden and R. A. D. Wentworth, *Inorg. Chem.*, 1967, 6, 1497.

11 W. H. Delphin and R. A. D. Wentworth, *Inorg. Chem.*, 1973, **12**, 1914.

12 J. L. Templeton, R. A. Jacobsen and R. E. McCarley, *Inorg. Chem.*, 1977, **16**, 3320.

13 V. Kolesnichenko, D. C. Swenson and L. Messerle, *Inorg. Chem*., 1998, **37**, 3257.

14 T. B. Scheffler and C. L. Hussey, *Inorg. Chem.*, 1984, **23**, 1926.

15 A. Bondi, *J. Phys. Chem.*, 1964, **68**, 441.

16 F. A. Cotton and C. E. Rice, *Acta Crystallogr., Sect. B*, 1978, **34**, 2833.

17 E. Hey, F. Weller and K. Dehnicke, *Z. Anorg. Allg. Chem*., 1984, **508**, 86.

18 J. Jensen and L. Messerle, unpublished results.

Received in Bloomington, IN, USA, 26th May 1998; 8/03903H

Colloid-roughened surfaces as templates for the heterogeneous nucleation of lepidocrocite γ-FeO(OH) nanoparticles

Marc Nagtegaal, Ram Seshadri and Wolfgang Tremel*

Institut für Anorganische und Analytische Chemie, Johannes Gutenberg-Universität Mainz, Becher Weg 24 D-55099 Mainz, Germany. E-mail: tremel@indigotrem1.chemie.uni-mainz.de

Lepidocrocite γ-FeO(OH) crystals can be specifically nucleated by sulfonate-terminated SAM/gold surfaces from solutions at room temperature; previously 'roughening' the gold surface through the tethering of gold colloids increases yields.

Extensive studies by Rieke and coworkers[1] have established the propensity of sulfonate modified surfaces (of polymers and of self-assembled monolayers (SAMs) of alkylsilyl compounds on silicon) to heterogeneously nucleate the formation of FeO(OH) crystallites from Fe^{III} solutions. We have been interested in extending this chemistry to the use of SAMs of ω-substituted alkylthiols on gold as substrates for such heterogeneous nucleation. This would simultaneously permit greater freedom for manipulation of the surface chemistry of the nucleating substrate, facilitate atomic force microscopic (AFM) investigations and most importantly, permit the use of surface plasmon spectroscopy (SPS) to monitor *in situ*, the accretion of material on the substrate. In the course of these investigations, we have been able to unambiguously confirm that only on sulfonate-terminated substrates is there significant nucleation of FeO(OH) (in the γ modification) at room temperature from Fe^{III} solutions that are otherwise stable to hydrolysis.

Primarily the influence of the sulfonate head-group on the nucleation of FeO(OH) is acidity; nucleation usually being carried out from acidic solutions at pH < 3. Under these conditions, of the typical ω substituents used by us (carboxylates, phosphonates, *etc*.) only the sulfonate group is ionised, permitting its binding to Fe^{III} ions. Size is not a consideration since the O–O distances in SO_3 groups are about 20% smaller than O–O distances in the FeO_6 octahedra that are the principal structural motifs in the different FeO(OH). These points have been discussed extensively by Reeves and Mann who have examined binding between different tetrahedral anions and the iron oxides.[2] Epitaxis between substrate and crystallite is thus not an issue. A strategem to increase the number of nucleation sites on the substrate would then be to chemically tether (using alkyl dithiols) nanometre-sized gold colloids to the substrates in order to microscopically roughen their surfaces. This has previously proved useful in stabilising aragonite.[3]

Gold-coated glass substrates were placed overnight in 1 mM solutions of 1,12-dodecanedithiol (DDDT) in ethanol. After this, they were dipped in toluene sols of gold colloids† for 2 min. Placing these substrates in solutions of iron(III) nitrate resulted in nearly no deposition of material. FeO(OH) does in fact nucleate heterogeneously on bare gold substrates (because the high conductivity and surface energy of gold permits ions that attach initially to be discharged) so we could conclude that the lack of a deposit on the untreated colloid-tethered surface arises from the continued presence of amphiphiles (left over from the colloid preparation). Further treatment of the colloid-covered gold surfaces through exposure to 1 mM ethanolic solutions of the sodium salt of 3-mercaptopropane sulfonic acid (MPS) results in their being able to nucleate the deposition of thin films of orange–brown powders from the Fe^{III} solutions.‡ The use of MPS/colloid/DDDT/gold architectures resulted in significantly greater amounts of the orange–brown powders being deposited than when only MPS/gold substrates are used.

As at least eighteen different crystalline compounds are formed in the Fe–O–H system,[4] it is important to unambiguously establish the nature of the orange brown powders. This could be achieved using grazing-incidence X-ray diffraction, combined with Rietveld profile fitting. Fig. 1 displays experimental and fitted X-ray diffraction profiles,§ acquired with a fixed grazing angle of $\Omega = 0.5°$. The lepidocrocite structure[5] was used in the fit, refining scale, profile and preferred orientation parameters. The various parameters of gold (peaks indicated using asterisks) as a second phase were also refined. Below the fitted profile is a simulation of crystalline lepidocrocite with the *hkl* indices marked.

Fig. 2(a) displays tapping mode AFM images¶ of the gold substrate to which colloids were tethered with DDT. The image is displayed at a magnification wherein it is difficult to distinguish the individual colloid particles, but is necessary for comparison with the other images. The crystals were nucleated under identical conditions on two different substrates, (b) MPS/gold and (c) MPS/colloid/DDDT/gold. The crystals are lath-like. On the MPS/gold substrate, they have typical dimensions of 100 nm × 20 nm in the plane of the substrate. On the colloid modified surface (c) the density of crystals is larger presumably as a result of a greater nucleation,‖ and the crystals are simultaneously bigger, extending to about 200 nm. The

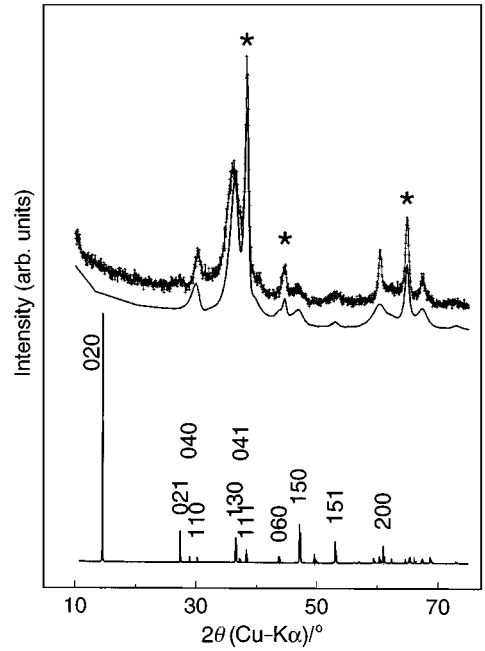

Fig. 1 Experimental and fitted grazing incidence xrd pattern of the FeO(OH) crystals on the MPS/colloid/DDDT/gold assembly. The two profiles have been slightly offset for clarity. The asterisks mark the peaks due to the gold substrate. At the bottom is a simulation of isotropic crystalline lepidocrocite with the *hkl* indices marked.

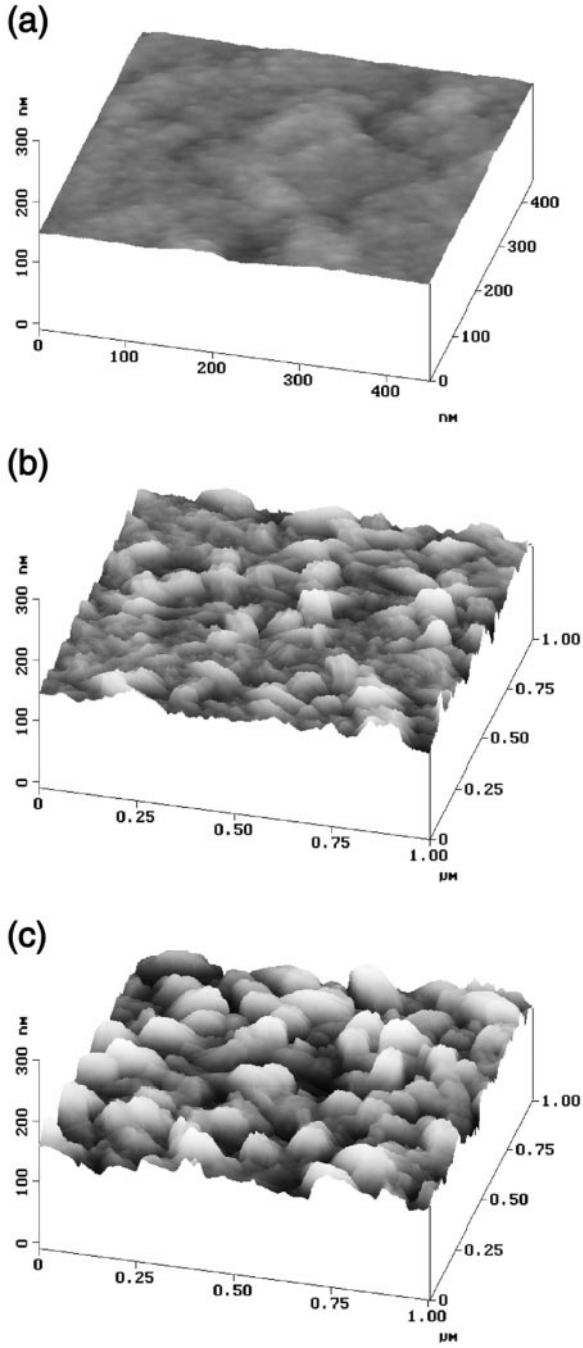

Fig. 2 AFM images of (a) the colloid/DDDT/gold substrate, (b) lepidocrocite crystals grown on MPS/gold and (c) on MPS/colloid/DDDT/gold. The shading is indicative of the height with black referring to the bottom of the scanned image, through gray to white referring to a relative height of 150 nm.

morphology is slightly altered, being a little more rounded. Lepidocrocite is layered,[4] and possesses sheets of FeO_6 double octahedra. An analysis of the structure does not reveal any mode of epitaxy between the O atoms in the structure and a model sulfonate terminated thiol SAM. The layering however suggests that the expected growth direction of the crystals with reference to the substrate would be the direction normal to the sheets namely [010]. The 0*k*0 lines are supressed in the XRD pattern, rather than being enhanced, as one would expect in this case. This arises from two causes. The first is that employing the small grazing Ω angles used in the measurements, one would expect that the incident X-ray will not sample very many 0*k*0 layers. The other is that the pattern clearly displays crystalline correlation lengths that are *hkl* dependent; the peaks with a finite *h* index are more narrow while along those with finite *k*, the peaks are broad, reflecting the poor crystallinity along this direction.

We thank Dr B. Baumgartner of STOE & Cie., Darmstadt for the grazing incidence X-ray diffraction data, and Professor H.-J. Butt for providing access to his AFM facilities. The gold used here was part of a generous gift from Degussa, Hanau, and the dithiol was provided by Mr J. Küther.

Notes and References

† Gold colloids were prepared in two-phase toluene/water systems following the procedure of Brust *et al*.[6] Details on the formation and nature of colloid-tethered gold surfaces can be found in ref. 3.

‡ FeO(OH) crystallisations were performed by placing the substrates in polypropylene flasks containing 2 mM solutions (freshly prepared) of iron(III) nitrate for a period of 48 h at room temperature.

§ X-Ray diffraction data were acquired on a STOE θ–2θ diffractometer and were treated using the XND Rietveld program (version 1.16, J.-F. Bérar, ESRF, Grenoble, France, 1997).

¶ Tapping mode AFM images were acquired using a Nanoscope IIIa, employing Si cantilevers.

‖ From the present data, we infer that higher initial nucleation results in greater deposition on the colloid-roughened surfaces. That the FeO(OH) crystals are simultaneously larger suggests that the small crystals formed initially could anneal into larger ones. Initial X-ray measurements indeed suggest that crystallinity increases (linewidths narrow) with time even on keeping deposited Fe oxides and oxide–hydroxides at room temperature.

1 B. J. Tarasevitch, P. C. Rieke and J. Liu, *Chem. Mater.*, 1996, **8**, 292; P. C. Rieke, B. D. Marsh, L. L. Wood, B. J. Tarasevitch, J. Liu, L. Song and G. E. Fryxell, *Langmuir*, 1995, **11**, 31; P. C. Rieke, B. Tarasevitch, L. Wood, M. Engelhard, D. Baer, G. E. Fryxell, C. John, D. Laeken and M. Jaehning, *Langmuir*, 1994, **10**, 619.

2 N. J. Reeves and S. Mann, *J. Chem. Soc., Faraday Trans.*, 1991, **87**, 3875.

3 J. Küther, R. Seshadri, G. Nelles, H.-J. Butt, W. Knoll and W. Tremel, *Adv. Mater.*, 1998, **10**, 401.

4 R. M. Cornell and U. Schwertmann, *The iron oxides*, VCH, Weinheim, 1996.

5 H. Christensen and A. N. Christensen, *Acta Chem. Scand.*, 1978, **32**, 87.

6 M. Brust, M. Walker, D. Bethell, D. J. Schiffrin and R. Whyman, *J. Chem. Soc., Chem. Commun.*, 1994, 801.

Received in Bath, UK, 14th May 1998; 8/03899F

Enantioselective synthesis of an axially chiral 1,7-naphthyridine-6-carboxamide derivative having potent antagonist activity at the NK_1 receptor

Yoshinori Ikeura,[a] Takenori Ishimaru,[b] Takayuki Doi,[a] Mitsuru Kawada,[c] Akira Fujishima[a] and Hideaki Natsugari*[a]†

[a] Pharmaceutical Research Division, [b] Discovery Research Division and [c] Technology Development Department, Takeda Chemical Industries, Ltd., 2-17-85, Jusohonmachi, Yodogawa-ku, Osaka 532-8686, Japan

A new and highly potent NK_1 antagonist, (*aR*,9*R*)-3 [(*aR*,9*R*)-7-[3,5-bis(trifluoromethyl)benzyl]-8,9,10,11-tetrahydro-9-methyl-5-(4-methylphenyl)-7*H*-[1,4]diazocino[2,1-*g*][1,7]naphthyridine-6,13-dione], was atropdiastereoselectively synthesized in good yield by cyclization of the chiral intermediate 6b.

In our preceding papers,[1] we described the discovery[1a,b] and stereochemical characterization[1c] of the potent NK_1 antagonist[2] **1** {*N*-[3,5-bis(trifluoromethyl)benzyl]-7,8-dihydro-*N*,7-dimethyl-5-(4-methylphenyl)-8-oxo-1,7-naphthyridine-6-carboxamide}. Since **1** has a tertiary carboxamide group at the sterically hindered C_6-position, it exhibits two notable stereochemical properties (Fig. 1). First, the *trans* and *cis* amide conformational isomers (rotamers) of **1** are separable at room temperature;[1a] the compound isolated by conventional work-up is the *trans*-isomer (*trans*-**1**), while the thermodynamically unstable *cis*-isomer (*cis*-**1**) can also be isolated as a minor product by careful separation procedures. Both isomers interconvert and reach an equilibrium state of a *ca.* 7:1 ratio in solution. Second, *trans*-**1** and *cis*-**1** exist as a mixture of two separable and stable enantiomers [(*trans*,*aR*)-**1**, (*trans*,*aS*)-**1** and (*cis*,*aR*)-**1**, (*cis*,*aS*)-**1**, respectively][3] arising from restricted rotation around the C_6–C(O) bond (Fig. 1).[1c] Such stereoisomerism due to restricted rotation is known as atropisomerism among biaryl compounds and some sterically hindered aromatic carboxamides.[4] The atropisomers, (*trans*,*aR*)-**1** and (*trans*,*aS*)-**1**, which were separated by preparative high performance liquid chromatography (HPLC) using a chiral column,‡ have significant stability in solution; *e.g.* they were not interconverted in DMSO at 37 °C for 16 h and underwent racemization only after storage at 50 °C for *ca.* 70 h. Among these four isomers of **1**, the active isomer was shown to be (*trans*,*aR*)-**1**. From a practical perspective, however, separation of the active isomer (*trans*,*aR*)-**1** is difficult, and further studies using *trans*-**1** as a racemate would encounter difficulties, especially at the stage of pharmaceutical development.

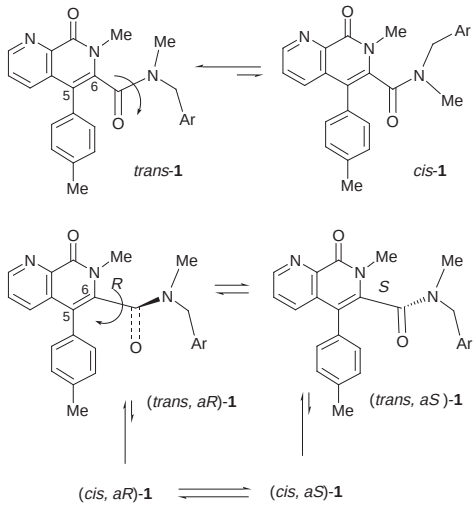

Fig. 1 The stereoisomers of **1**

Thus, in the search for new compounds with an improved stereochemical profile, we designed cyclic analogues of **1**, and analogues with an eight-membered ring (*e.g.* **2** and **3**) (Scheme 2) became target molecules based on the results of conformational studies on *trans*-**1**. Here we describe the atropdiastereoselective synthesis of the potent NK_1 receptor antagonist (*aR*,9*R*)-**3** {(*aR*,9*R*)-7-[3,5-bis(trifluoromethyl)benzyl]-8,9,10,11-tetrahydro-9-methyl-5-(4-methylphenyl)-7*H*-[1,4]-diazocino[2,1-*g*][1,7]naphthyridine-6,13-dione} by cyclization of the chiral intermediate **6b**.

General synthesis of tricyclic analogues of **1** (**2** and **3**) is outlined in Schemes 1 and 2. The key intermediates **6a–c** [7-(hydroxyalkyl)-1,7-naphthyridine-6-carboxamide derivatives] were prepared from the pyrano[3,4-*b*]pyridine-6-carboxylic acid **4**.[5] First, the acid **4** was amidated with 3,5-bis(trifluoromethyl)benzylamine *via* the acid chloride to provide the amide. Treatment of the amide with the appropriate amines **5a–c**,[6] followed by deprotection with TsOH and dehydration with DBU gave **6a–c** (Scheme 1). Cyclization of **6a–c** was accomplished by mesylation followed by treatment with NaH in THF to give **2** and **3** in good yields (Scheme 2).

For the atropisomers in the cyclic analogues of **1** (**2** and **3**), we initially supposed that the flipping of this new ring would be too rapid to enable the separation of stable isomers at room temperature.[7] However, chiral HPLC analysis of **2** showed two peaks at room temperature, and **2** was separated by preparative HPLC using a chiral column to give the atropisomers (*aR*)-**2** and (*aS*)-**2**, which have opposite $[\alpha]_D$ values (+45.6 and −41.3, respectively) and show considerable stability in solution; *e.g.* they are gradually interconverted in DMSO to *ca*. 70% ee at 37 °C over 40 h and undergo racemization after storage at 50 °C for *ca.* 60 h. These results indicate that **2** exists as a racemate, making development as a clinical candidate difficult. Thus, we

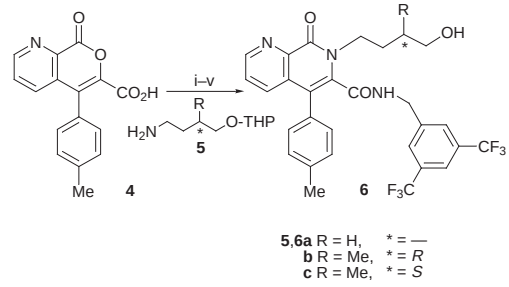

Scheme 1 *Reagents and conditions*: i, $SOCl_2$, THF, reflux, 1.5 h; ii, 3,5-bis(trifluoromethyl)benzylamine, Et_3N, THF, room temp., 0.5 h (71% from **4**); iii, **5**, THF–MeOH, room temp., 16 h ; iv, DBU, toluene–MeCN, reflux, 1 h; v, TsOH, MeOH, room temp., 0.5 h

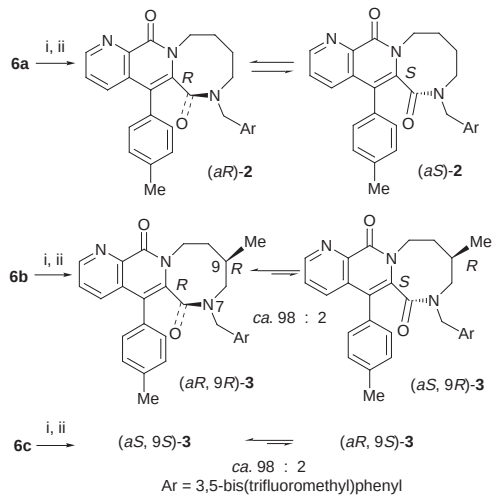

Scheme 2 *Reagents and conditions*: i, MsCl, Et_3N, THF, 0 °C, 0.5 h; ii, NaH, THF, reflux, 1 h [isolated yields from **6**: 79% for **2**, 69% for (*aR*,9*R*)-**3** and 66% for (*aS*,9*S*)-**3**]

next designed the C_9 methyl analogues of **2** (*i.e.* **3**) as target compounds, expecting asymmetric induction from the C_9 chiral center to obtain the desirable chirality arising from atropisomerism, and achieved the stereoselective synthesis of the atropisomer by cyclization of an intermediate with a chiral methyl group, **6b** (Scheme 2). The product ratio of the atropisomer (*aR*,9*R*)-**3** to its isomer (*aS*,9*R*)-**3** was *ca.* 98:2, and a single recrystallization step gave (*aR*,9*R*)-**3** with > 99% de. The minor isomer (*aS*,9*R*)-**3**, with 98.6% de, was isolated as a powdery substance by repeated preparative HPLC at 0 °C using the mother liquor. Both atropisomers, (*aR*,9*R*)-**3** and (*aS*,9*R*)-**3**, were found to be gradually interconverted in solution to reach the same equilibrium state [(*aR*,9*R*)-**3**:(*aS*,9*R*)-**3** = *ca.* 98:2] (*e.g.* in EtOH at 37 °C in *ca.* 60 h).

Single crystal X-ray analysis of (*aR*,9*R*)-**3**[8] revealed that the N_7–C_8–C_9–C_{10} moiety in the eight-membered ring is disposed above the plane of the adjacent 1,7-naphthyridine ring, while the amide oxygen (C_6=O) is below the ring (*i.e. aR* stereochemistry). The relative spatial orientation of the C_9 methyl group and the *N*-[3,5-bis(trifluoromethyl)benzyl] group in (*aR*,9*R*)-**3** was shown to be such that the two groups are disposed in opposite directions. This is presumed to be a thermodynamically stable form which is important for the high atropdiastereoselectivity in the cyclization of **6b**.

The enantiomer of (*aR*,9*R*)-**3** [*i.e.* (*aS*,9*S*)-**3**], with > 99% de, was similarly obtained by the cyclization of the corresponding enantiomeric intermediate **6c** followed by a single recrystallization step (Scheme 2).

Compound (*aR*,9*R*)-**3** exhibited excellent NK_1 antagonistic activities§ both *in vitro* (IC_{50} = 0.45 nM) and *in vivo* (ED_{50} = 4.3 μg kg^{-1}). The structure–activity relationships in the isomers of **3** [for the atropisomer (*aS*,9*R*)-**3**: IC_{50} = 20 nM and ED_{50} = 26 μg kg^{-1}¶ and for the enantiomer (*aS*,9*S*)-**3**: IC_{50} = 340 nM and ED_{50} = > 300 μg kg^{-1}] indicate that the stereochemistry around C_{5a}–C_6(O)–N_7–CH_2Ar is the important factor for receptor recognition.

In summary, the axially chiral compound (*aR*,9*R*)-**3** and its enantiomer (*aS*,9*S*)-**3** were atropdiastereoselectively synthesized by cyclization of the chiral intermediates **6b** and **6c**, respectively. Compound (*aR*,9*R*)-**3** exhibited excellent NK_1 antagonistic activities both *in vitro* and *in vivo*.

The authors thank Mr T. Tanaka for conformational analysis, Ms F. Kasahara for NMR analysis, Mr I. Kamo for *in vivo* screening and Mr Y. Tajima for *in vitro* screening.

Notes and References

† E-mail: natsugari_hideaki@takeda.co.jp
‡ Chiralpack AD, DAICEL Chemical Industries, Ltd., Japan.
§ The NK_1 antagonistic activities were measured *in vitro* for inhibition of [^{125}I] Bolton-Hunter-SP binding in human IM-9 cells (ref. 9) and *in vivo* for inhibition of capsaicin-induced plasma extravasation in the trachea of guinea pigs (ref. 10).
¶ Since the purity of (*aS*,9*R*)-**3** is 98.6% de [*i.e.* it contains *ca.*1% of the active isomer (*aR*,9*R*)-**3**], its intrinsic antagonistic activities may be lower than those observed.

1 (*a*) H. Natsugari, Y. Ikeura, Y. Kiyota, Y. Ishichi, T. Ishimaru, O. Saga, H. Shirafuji, T. Tanaka, I. Kamo, T. Doi and M. Otsuka, *J. Med. Chem.*, 1995, **38**, 3106; (*b*) Y. Ikeura, T. Tanaka, Y. Kiyota, S. Morimoto, M. Ogino, T. Ishimaru, I. Kamo, T. Doi and H. Natsugari, *Chem. Pharm. Bull.*, 1997, **45**, 1642; (*c*) Y. Ikeura, Y. Ishichi, T. Tanaka, A. Fujishima, M. Murabayashi, M. Kawada, T. Ishimaru, I. Kamo, T. Doi and H. Natsugari, *J. Med. Chem.*, in the press.
2 Recent review articles for tachykinin antagonists: S. MacLean, *Med. Res. Rev.*, 1996, **16**, 297; J. A. Lowe III, *Med. Res. Rev.*, 1996, **16**, 527.
3 The italic letter *a* before the corresponding *R* and *S* denotes an axial chirality as suggested by Cahn *et.al.*; R. S. Cahn, C. Ingold and V. Prelog, *Angew. Chem., Int. Ed. Engl.*, 1966, **5**, 385.
4 As for synthesis and separation of atropisomers of some aromatic carboxamides, see S. Thayumanavan, P. Beak and D. P. Curran, *Tetrahedron Lett.*, 1996, **37**, 2899; J. Clayden, N. Westlund and F. X. Wilson, *Tetrahedron Lett.*, 1996, **37**, 577; J. Clayden, J. H. Pink and S. A. Yasin, *Tetrahedron Lett.*, 1998, **39**, 105; A. Ohno, M. Kashiwagi, Y. Ishihara, S. Ushida and S. Oka, *Tetrahedron*, 1986, **42**, 961.
5 H. Natsugari, T. Ishimaru, T. Doi, Y. Ikeura and C. Kimura, *Eur. Pat. Appl.*, EP733632, 1996 (*Chem. Abst.*, 1997, **126**, 8145).
6 K. Mori, *Tetrahedron*, 1983, **39**, 3107; H. Mattes, K. Hamada and C. Benezra, *J. Med. Chem.*, 1987, **30**, 1948.
7 As for atropisomerism in seven-membered heterocycles, see N. W. Gilman, P. Rosen, J. V. Earley, C. Cook and L. J. Todaro, *J. Am. Chem. Soc.*, 1990, **112**, 3969.
8 *Crystal data* for (*aR*, 9*R*)-**3**: $C_{30}H_{25}F_6N_3O_2$, M = 573.54, orthorhombic, 0.80 × 0.50 × 0.20 mm, a = 15.727(3), b = 22.972, c = 7.672(3) Å, V = 2771.6(10) Å^3, T = 298 K, $P2_12_12_1$ (#19), Z = 4, μ(Cu-Kα) = 9.59 cm^{-1}, reflections measured = 2386, R = 0.068. CCDC 182/988.
9 M. A. Cascieri, E. Ber, T. N. Fong, S. Sadowski, A. Basal, C. Swain, E. Seward, B. Frances, D. Burns and C. D. Strader, *Mol. Pharmacol.*, 1992, **42**, 458.
10 A. Eglezos, S. Giuliani, G. Viti and C. A. Maggi, *Eur. J. Pharmacol.*, 1991, **209**, 277.

Received in Cambridge, UK, 9th July 1998; 8/05333B

Dramatic rate acceleration in titanocene catalyzed epoxide openings: cofactors and Lewis acid cocatalysis

Andreas Gansäuer*† and Harald Bluhm

Institut für Organische Chemie der Georg-August-Universität, Tammannstr. 2, D-37077 Göttingen, Germany

High synthetic efficiency concerning yield and catalytic turn-over in intermolecular C–C bond forming reactions of radicals derived from epoxides can be achieved by means of hydrogen bonding with cofactors or by Lewis acid cocatalysis.

Catalytic reactions emerging from stoichiometric transformations have become increasingly important over the last three years.[1,2] We have developed protonation of carbon–titanium and oxygen–titanium bonds as an alternative to silylation for achieving catalytic turnover.[3] This has allowed highly diastereoselective pinacol couplings and chemo- and regioselective reductive openings of epoxides. Here we describe an efficient method for the addition of radicals derived from epoxides to α,β-unsaturated carbonyl compounds yielding synthetically important δ-lactones, hydroxy esters and hydroxy nitriles in high yield, with low catalyst loading in short times.

Under the standard conditions for the reductive opening of epoxides with hydrogen atom donors[3a] dodec-1-ene oxide gives only 21 and 40% yield of the addition products to methyl acrylate (**7**) and acrylonitrile (**6**), respectively, after 72 h in the presence of 5 mol% Cp_2TiCl_2 (Scheme 1). Moreover, the products are contaminated with polymeric material derived from the radical acceptor. We reasoned that low yields and turnovers are due to product inhibition. Compound **6** and MeOH formed after lactonization seemed to be able to efficiently complex at least one of the titanocene species in the catalytic cycle. Similar problems were noticed in reactions of higher substituted epoxides as well as in addition reactions to *tert*-butyl acrylate. Since this type of product inhibition could be a general problem in the *de novo* design of catalytic electron transfer reactions with densely functionalized molecules, a widely applicable solution is of interest for this rapidly expanding field.

Two conceptually different and novel approaches towards binding of the reaction products and thus catalyst activation seemed to be at hand. Since alcohols are formed during the course of the reaction, complexation of the products by hydrogen bond formation with a suitable acceptor, *e.g.* a sterically demanding amine, should be possible.[4] On the other hand a Lewis acid stronger than Cp_2TiCl_2[5] should be complexed by the reaction products and thus allow for catalyst activation and thus higher turnover.[6] Table 1 summarizes the results of our initial optimization studies. Other Lewis acids not included, *e.g.* $AlCl_3$, gave vastly inferior results.

Gratifyingly, using Zn as stoichiometric reductant[7] led to a distinct acceleration of the reaction. It seems that $ZnCl_2$ formed during the course of the reduction of Cp_2TiCl_2 acts as a Lewis acid strong enough to bind MeOH and restore catalyst activity. This effect is even more pronounced when 1 equiv of $ZnCl_2$ is added to the reaction mixture. The same effect could be observed in addition reactions to *tert*-butyl acrylate. Interestingly in the reaction of **1** with **3**, lactone **7** is isolated as the sole product of the reaction in high yield after aqueous work-up when Zn is used as stoichiometric reductant. A detailed kinetic analysis reveals formation of 85% of **6** after 3 h. Subsequently, $ZnCl_2$-initiated cyclization occurs. Thus, it seems that $ZnCl_2$ first allows for efficient formation of **6** and then activates the nitrile strongly towards intramolecular attack by the hydroxy group. The resulting imino ester is hydrolyzed during work-up. Compared to other methods of lactone formation from hydroxy nitriles[8,9] our reaction conditions are clearly milder and a wider variety of functional groups is tolerated. Also the product is formed in a one step procedure without the necessity of isolating and purifing any intermediates.[10] However, with Mn as reductant and $ZnCl_2$ as an additional Lewis acid only **6** is formed after 8 h. Thus, $MnCl_2$ seems to coordinate the nitrile group without allowing activation towards cyclization. Accordingly, the beneficial role of $ZnCl_2$ involves prevention of product inhibition by complexation of the hydroxy group. The utility of our approach was further demonstrated by the fact that catalyst loading in these reactions can be reduced to 1 mol% without significant decrease in yields when reaction times are prolonged.

Table 2 summarizes some of the examples conducted under the optimized reaction conditions. While sterically more

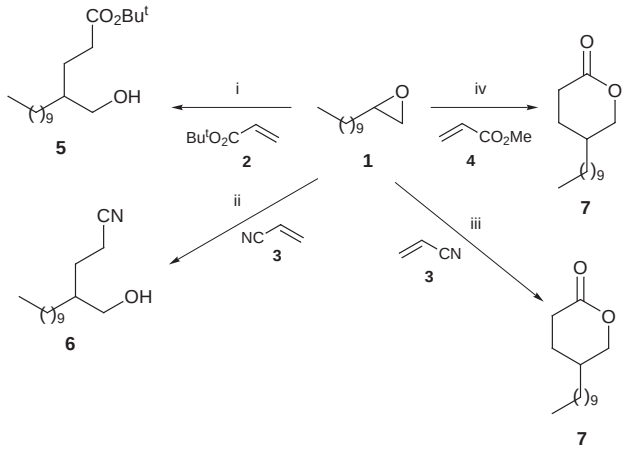

Scheme 1 *Reagents and conditions*: i, $ZnCl_2$, Zn, collidine·HCl; ii, $ZnCl_2$, Mn, collidine·HCl; iii, $ZnCl_2$, Zn, collidine·HCl, or collidine, collidine·HCl; iv, $ZnCl_2$, Zn, collidine·HCl, or collidine, collidine·HCl

Table 1 Optimization of the addition of 1-dodecene oxide to α,β-unsaturated carbonyl compounds

Acceptor	Reductant	Additive	*t*/h	Product	Yield (%)[a]
2	Mn	—	66	**5**	68
2	Zn	$ZnCl_2$	16	**5**	81
2	Zn[b]	—	44	**5**	73
3	Zn	—	16	**7**	83
3	Zn[b]	—	43	**7**	73
3	Zn	$ZnCl_2$	12	**7**	88
3	Mn	$ZnCl_2$	14	**6**	80
4	Mn	—	65	**7**	21
4	Zn	$ZnCl_2$	16	**7**	72

[a] As 94:6 mixture of 5-substituted pyran-2-one **7** and 6-substituted pyranone or 94:6 mixture of 4-hydroxymethyltetradecanenitrile or ester **6** or **5** and 5-hydroxypentadecanenitrile or ester. [b] 1 mol% of catalyst employed.

Table 2 Addition reactions of other epoxides to α,β-unsaturated carbonyl compounds with Lewis acid cocatalysis

Substrate	Reductant/ additive	*t*/h	Product	Yield (%)
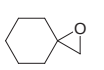	$Zn/ZnCl_2$	24	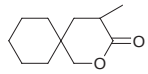	86
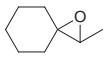	$Zn/ZnCl_2$	16	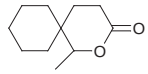	78
	Zn	64	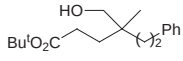	93[a]
	$Zn/ZnCl_2$	12	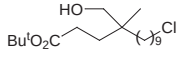	91
	Zn	10	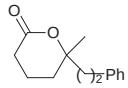	65[b]

[a] Reaction performed in the presence of 4-phenyl-2-butanone (95% recovery). [b] Compound **3** as acceptor, 12 h reflux to complete the reaction.

demanding hydroxy nitriles can be readily obtained in the presence of $ZnCl_2$, refluxing of the reaction mixture yields the lactones in good yields. The reaction conditions tolerate a number of functional groups, *e.g.* ketones and halides, sensitive to stronger SET reagents, *e.g.* SmI_2.[11]

Lewis acid cocatalysis thus offers an attractive means for catalyst activation and alteration of selectivity in titanocene-catalyzed addition reactions of radicals derived from epoxides to α,β-unsaturated carbonyl compounds. Compared to the stoichiometric parent system[12] the amount of Cp_2TiCl_2 to be utilized is reduced by a factor of 200 and only 1.2 equiv. of radical acceptor have to be used compared to the 10 equiv. usually employed under stoichiometric conditions. No significant reduction in isolated yields is observed. Also deoxygenation, constituting a major side reaction under stoichiometric conditions especially for monosubstituted epoxides, was never observed.[12] Our catalytic conditions are therefore clearly superior to the stoichiometric conditions.

Hydrogen bonding also constitutes a convenient way to achieve catalyst activation and to obtain the desired products under mild conditions. However, care has to be taken in choosing the appropriate hydrogen bond acceptor. If the acceptor represents a powerful ligand, *e.g.* DMPU, catalyst deactivation was observed. If a base is chosen as acceptor instead, it should not constitute a sterically accessible ligand and its hydrochloride must not have a higher pK_a[13] than collidine hydrochloride. Otherwise proton transfer precludes catalytic turnover.[3]

Accordingly we decided to test collidine and ran the reaction under buffered protic conditions. Table 3 summarizes the results of our investigations. Clearly collidine has a beneficial role on both catalytic activity and yields of the products.

Table 3 Collidine as cofactor in addition reactions

Substrate	*t*/h	Product	Yield (%)
1	36	**6**	75
	36	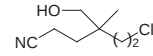	73
	36	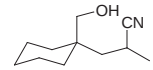	73

Addition to **3** proceeded smoothly to give the desired product **6** in good yields and in reasonable reaction times. It seems that collidine is indeed able to bind hydroxy groups of the reaction products *via* hydrogen bonding. Thus, collidine acts as a cofactor to restore catalytic activity *via* hydrogen bonding.

Notes and References

† E-mail: agansae@gwdg.de

1 For a recent review see A. Fürstner, *Chem. Eur. J.* 1998, **4**, 567.
2 A. Fürstner and A. Hupperts, *J. Am. Chem. Soc.*, 1995, **117**, 4468; A. Fürstner and N. Shi, *J. Am. Chem. Soc.*, 1996, **118**, 2533; 1996, **118**, 12 349; T. Hirao, T. Hasegawa, Y. Muguruma and I. Ikeda, *J. Org. Chem.*, 1996, **61**, 366; R. Nomura, T. Matsuno and T. Endo, *J. Am. Chem. Soc.*, 1996, **118**, 11 666; A. Gansäuer, *Chem. Commun.*, 1997, 457; A. Gansäuer, *Synlett*, 1997, 363; E. J. Corey and G. Z. Zheng, *Tetrahedron Lett.*, 1997, **38**, 1045; T. A. Lipski, M. A. Hilfiker and S. G. Nelson, *J. Org. Chem.*, 1997, **62**, 4566; A. Svatos and W. Boland, *Synlett*, 1998, 549.
3 (*a*) A. Gansäuer, M. Pierobon and H. Bluhm, *Angew. Chem.*, 1998, **110**, 107; *Angew. Chem., Int. Ed.*, 1998, **37**, 101; (*b*) A. Gansäuer and D. Bauer, *J. Org. Chem.*, 1998, **63**, 2070.
4 J.-M. Lehn, *Supramolecular Chemistry*, VCH, Weinheim, 1995.
5 M. T. Reetz, in *Organometallics in Synthesis, A Manual*, ed. M. Schlosser, Wiley, New York, 1994, p. 195.
6 S. Shamyati and S. L. Schreiber, in *Comprehensive Organic Synthesis*, ed. B. M. Trost, I. Fleming and G. Pattenden, Pergamon, Oxford, 1991, vol. 1, p. 283.
7 M. L. H. Green and C. R. Lucas, *J. Chem. Soc., Dalton Trans.*, 1972, 1000; R. S. P. Coutts, P. C. Wailes and R. L. Martin, *J. Organomet. Chem.*, 1973, **47**, 375; D. Sekutowski, R. Jungst and G. D. Stucky, *Inorg. Chem.*, 1978, **17**, 1848.
8 T. Naota, Y. Shichigo and S.-I. Murahashi, *Chem. Commun.*, 1994, 1359.
9 P. Breuilles, R. Leclerc and D. Uguen, *Tetrahedron Lett.*, 1994, **35**, 1401.
10 D. L. J. Clive, P. L. Beaulieu and L. Lu, *J. Org. Chem.*, 1984, **49**, 1313.
11 G. A. Molander, *Chem. Rev.*, 1992, **92**, 29.
12 W. A. Nugent and T. V. RajanBabu, *J. Am. Chem. Soc.*, 1988, **110**, 8561; T. V. RajanBabu and W. A. Nugent, *J. Am. Chem. Soc.*, 1989, **111**, 4525; T. V. RajanBabu, W. A. Nugent and M. S. Beattie, *J. Am. Chem. Soc.*, 1990, **112**, 6408; T. V. RajanBabu and W. A. Nugent, *J. Am. Chem. Soc.*, 1994, **116**, 986.
13 J. March, *Advanced Organic Chemistry*, 4th edn., Wiley, New York, 1992, p. 248; *Handbook of Chemistry and Physics*, 78th edn., ed. D. R. Lide, CRC Press, Boca Raton, 1997, pp. 8–45.

Received in Cambridge, UK, 7th July 1998; 8/05246H

MTO catalyzed oxidation of aldehyde *N*,*N*-dimethylhydrazones with hydrogen peroxide: high yield formation of nitriles and *N*-methylene-*N*-methyl *N*-oxide

Henri Rudler*† and Bernard Denise

Laboratoire de Synthèse Organique et Organométallique, UMR 7311, Université Pierre et Marie Curie, Tour 44-45, 4 Place Jussieu, 75252 Paris Cedex 5, France

***N*,*N*-Dimethylhydrazones of aldehydes react with hydrogen peroxide at −50 °C in the presence of catalytic amounts of methyltrioxorhenium (MTO) to give in high yield the corresponding nitriles and *N*-methylene-*N*-methyl *N*-oxide.**

The transformation of aldehydes into nitriles is an important process in organic synthesis.[1,2] Several procedures are available for that purpose and very recently the oxidative conversion of *N*,*N*-dimethylhydrazones of aldehydes using dimethyldioxirane has been described.[3] Such a transformation has also been achieved by the use of peracids.[4] Both methods suffer from serious drawbacks: they both use stoichiometric amounts of oxidants which are either expensive (low yield formation of dimethyldioxirane from potassium peroxysulfate) and/or are waste-forming processes (acids from peracids). The use of hydrogen peroxide alone[2] or associated with a catalyst (either phosphomolybdic acid or sodium tungstate)[5] has also drawbacks: in the first case satisfactory yields were observed only in the case of hydrazones derived from aromatic aldehydes, whereas in the second case side reactions took place.

During our search for new applications of MTO[6] in organic synthesis, mainly based on the analogy which exists between dimethyldioxirane and the peroxo derivatives obtained upon oxidation of MTO with hydrogen peroxide (*e.g.* the epoxidation of olefins, Scheme 1),[7–11] we surmised that this system might be a good and efficient candidate for the catalytic transformation of *N*,*N*-dimethylhydrazones of aldehydes into nitriles.

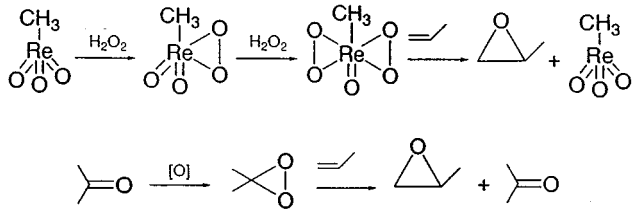

Scheme 1

Indeed, the mechanism which was suggested for the oxidative cleavage of dimethylhydrazones involved an electrophilic oxygen transfer from dioxirane to the terminal nitrogen atom leading to an *N*-oxide.[3] An intramolecular elimination of dimethylhydroxylamine was then supposed to lead to the nitrile (Scheme 2).

It is known that MTO catalyzes the oxidation of tertiary amines to *N*-oxides (Scheme 3).[12] Moreover, hydroxylamines

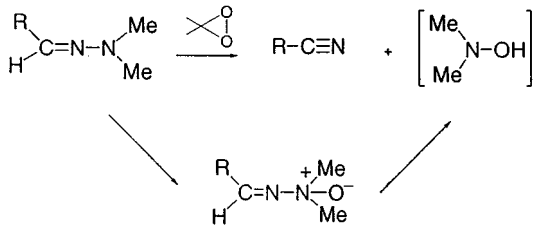

Scheme 2

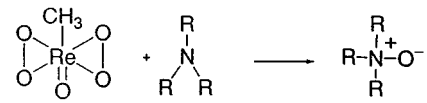

Scheme 3

are also catalytically converted into nitrones by the same system (Scheme 4).[13,14] Taken together, these two reactions would imply the formation of nitriles and *N*-methylene-*N*-methyl *N*-oxide from *N*,*N*-dimethylhydrazones of aldehydes. This indeed turned out to be the case (Scheme 5).

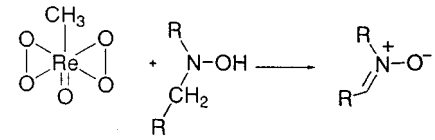

Scheme 4

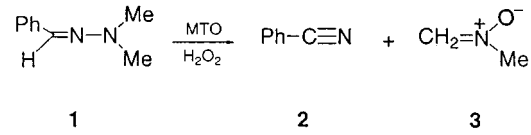

1 **2** **3**

Scheme 5

Thus, an ethanolic solution of the *N*,*N*-dimethylhydrazone of heptanal[15] (0.45 g, 2 ml of EtOH) was added dropwise to a yellow solution of MTO and H_2O_2 (1.5%, 2 equiv. of 35% H_2O_2) in EtOH at −50 °C. The solution was then allowed to warm to room temperature over 1 h. Evaporation of most of the solvent followed by the addition of water and extraction with Et_2O gave, after evaporation of the organic solvent, the expected nitrile (0.29 g, 90%). The aqueous layer was also evaporated *in vacuo* to give an oily yellow liquid, which was also soluble in CH_2Cl_2. The mass spectrum of this product confirmed the molecular formula C_2H_5NO (*m*/*z* 59). The ^{1}H NMR spectrum disclosed two signals: a singlet at δ 3.60 for the NMe group and an AB system for two hydrogens at δ 6.67. The ^{13}C NMR spectrum confirmed the presence of a methyl and a methylene group (DEPT experiment), respectively, at δ 132.5 and 50.85.[11]

An NMR experiment with stoichiometric amounts of preformed MTO diperoxide[9] and the *N*,*N*-dimethylhydrazone of benzaldehyde clearly demonstrated the formation of the expected nitrone. It appears therefore that the transformation of the hydrazones into a mixture of nitriles and nitrone **3**‡ *via* dimethylhydroxylamine requires indeed 2 equiv. of H_2O_2.

Similar results, shown in Table 1, were observed under the same experimental conditions, starting from a series of hydrazones, and giving high yields of the expected nitriles.

Interestingly, epoxidation of the carbon–carbon double bonds of the hydrazones **4**–**7** was not observed under these precise reaction conditions. However, addition of an excess of H_2O_2 (3–4 equiv.) led, in the case of **6**, to the expected epoxy-nitrile

Table 1 Synthesis of nitriles *via* oxidation of *N*,*N*-dimethylhydrazones with MTO and H_2O_2 yield (%)[a]

Entry	Hydrazone	Nitrile	Yield (%)[a]
1	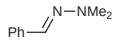		93
2	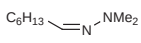		90
3	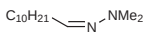		98
4	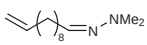	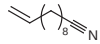	83
5	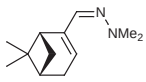	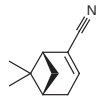	83
6	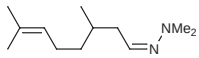	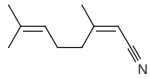	96
7	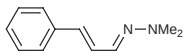	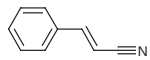	99

[a] Isolated yield.

arising from the oxidation of the non-conjugated double bond. Thus, the low temperature formation of the nitriles in the presence of stoichiometric amounts of H_2O_2 is compatible with the presence of less reactive functional groups.

Under the same conditions, *N*,*N*-dimethylhydrazones of ketones (*e.g.* phenyl ethyl ketone) led to the corresponding ketones, whereas imines derived from aldehydes (*e.g.* *N*-benzylidenemethylamine) gave essentially the corresponding amides (55%) and those derived from ketones (*e.g.* *N*-cyclohexylidenepropylamine), mixtures of oxaziridines and nitrones. Work is in progress to assess the scope of these latter transformations.

Notes and References

† E-mail: rudler@ccr.jussieu.fr

‡ All new compounds exhibited appropriate ^{1}H and ^{13}C NMR spectra and elemental analyses. *Selected data* for **3**: δ_H (200 MHz, D_2O, $SiMe_4$) 6.71 (d, J_{HH} 6, N=C*H*), 6.63 (d, J_{HH} 6, N=C*H*), 3.60 (s, NCH_3); δ_c (50 MHz, D_2O) 132.50 (N=*C*), 50.85 (N*C*H_3).

1 D. Barton and W. D. Ollis, in *Comprehensive Organic Chemistry*, Pergamon, Oxford, UK, 1979, vol. 2, ch. 8, pp. 534–535.
2 R. F. Smith, J. A. Albright and A. M. Waring, *J. Org. Chem.*, 1966, **31**, 4100.
3 A. Altamura, L. D'Accolti, A. Detomaso, A. Dinoi, M. Fiorentino, C. Fusco and R. Curci, *Tetrahedron Lett.*, 1998, **39**, 2009.
4 R. Fernandez, C. Gasch, J. M. Lassaletta, J. M. Llera and J. Vazquez, *Tetrahedron Lett.*, 1993, **34**, 141.
5 S. I. Murahashi, T. Shiota and Y. Imada, in *Organic Synthesis*, Wiley, New York, 1991, vol. 70, pp. 265–271.
6 W. A. Herrmann and F. Kühn, *Acc. Chem. Res.*, 1997, **30**, 169.
7 H. Rudler, J. Ribeiro Gregorio, B. Denise and J. Vaissermann, *J. Organomet. Chem.*, 1997, **548**, 295.
8 H. Rudler, J. Ribeiro Gregorio, Bernard Denise, J. M. Brégeault and A. Deloffre, *J. Mol. Catal. A, Chem.*, 1998, in the press.
9 W. A. Herrmann, R. W. Fischer, W. Scherer and M. U. Rauch, *Angew. Chem., Int. Ed. Engl.*, 1993, **32**, 1157.
10 A. M. Al-Ajlouni and J. H. Espenson, *J. Org. Chem.*, 1996, **61**, 3969.
11 T. H. Zauche and J. H. Espenson, *Inorg. Chem.*, 1997, **36**, 5257.
12 Z. Zhu and J. H. Espenson, *J. Org. Chem.*, 1995, **60**, 1326.
13 R. W. Murray, K. Iyanar, J. Chen and J. T. Wearing, *Tetrahedron Lett.*, 1996, **37**, 805.
14 A. Goti and L. Nannelli, *Tetrahedron Lett.*, 1996, **37**, 6025.
15 M. Yamashita, K. Matsumiya and K. Nakano, *Bull. Chem. Soc. Jpn.*, 1993, **66**, 4100.

Received in Liverpool, UK, 23rd June 1998; 8/04839H

Mesoporous MCM-48 membrane synthesized on a porous stainless steel support

Norikazu Nishiyama,* Akihiro Koide, Yasuyuki Egashira and Korekazu Ueyama

Department of Chemical Engineering, Faculty of Engineering Science, Osaka University, 1-3 Machikaneyama, Toyonaka, Osaka 560-8531, Japan. E-mail: nisiyama@cheng.es.osaka-u.ac.jp

A mesoporous MCM-48 membrane with high thermal stability has been synthesized on a porous stainless steel support by hydrothermal treatment.

Inorganic membranes made of ceramics or metals have been of interest for separation processes owing to their superior characteristics of thermal stability, structural stability and chemical resistance. Mesoporous inorganic membranes with an average pore diameter of 2–10 nm have been studied, mainly with respect to γ-alumina, titania and zirconia membranes prepared by the sol–gel method. However, since they have a wide pore size distribution, other inorganic membranes possessing uniform pore channels have been in demand for high performance applications in nanofiltration, ultrafiltration, pervaporation and membrane reactors.

Mobil scientists discovered a new family of mesoporous molecular sieves designated as M41S in 1992.[1,2] The M41S family includes members having uniform pore structures of hexagonal (MCM-41), cubic (MCM-48) and lamellar (MCM-50) symmetry. In their method, surfactant liquid-crystal structures serve as an organic template for the polymerization of silicates. Parallel to the discovery of M41S materials, Yanagisawa *et al.*[3] and Inagaki *et al.*[4] treated a layered kanemite polysilicate in an aqueous solution of a quaternary ammonium bromide surfactant and prepared a mesoporous silicate designated as FSM-16.

Recently, Ogawa[5,6] developed a rapid synthesis route for mesoporous films under acidic conditions using a mixture of tetramethoxysilane and an aqueous solution of a trimethylammonium salt. The products were transparent films of the hexagonal phase of periodic silica–surfactant composites with a unidimensional pore structure parallel to the surface of a glass substrate. Yang *et al.*[7] fabricated continuous mesoporous silica films on mica under acid conditions. They stated that the surface structure and reactivity of the mica surface controls the orientation of the micellar precursor species.

Straight pores should be oriented perpendicularly to the membrane surface in order to utilize the materials with unidimensional pores for separations. Tolbert *et al.*[8] have synthesized mesostructured silica (MCM-41) particles with orientated hexagonal pores from a hexagonal silicate–surfactant liquid crystal in a high magnetic field. This method has promise for the production of oriented mesopores in thin membranes for use in separations and in chemical sensors. On the other hand, MCM-48 has a three-dimensionally ordered pore structure. Therefore, the MCM-48 membrane is a promising material showing great potential applications such as in filtration, pervaporation and membrane reactors. In this study, a mesoporous membrane made of MCM-48 was synthesized on a porous stainless steel support by hydrothermal treatment.

The MCM-48 membrane was prepared as follows: a stainless steel support with an average pore diameter of 1 μm was placed in tetraethylorthosilicate (TEOS). Then, a solution which consisted of the quaternary ammonium surfactant $C_{16}H_{33}(CH_3)_3NBr$, NaOH and deionized water was added to the TEOS. The molar composition of the mixture was 0.6 $C_{16}H_{33}(CH_3)_3NBr$: 1.0 TEOS : 0.5 NaOH : 60 H_2O. Although a clear solution was obtained after mixing, the solution became inhomogeneous after 30 min of stirring. After the mixture was stirred for 90 more minutes, the mixture and support were transferred to an autoclave. The stainless steel support was placed horizontally in the bottom of the autoclave. The reaction was carried out without stirring at 363 K for 96 h. The product was rinsed with deionized water and calcined at 773 K for 4 h. Powder and a membrane were simultaneously obtained after the reaction. The BET surface area of the powder was measured by nitrogen adsorption at 77 K.

With respect to the mechanical strength of the membrane, it is preferable that the MCM-48 grows in the pores of the support. When the support was covered with a silica layer *ca*. 0.5 mm thick, the layer was removed from the surface of the support by polishing with a spatula until the surface of the stainless steel support appeared. Fig. 1 shows the SEM images for the surface

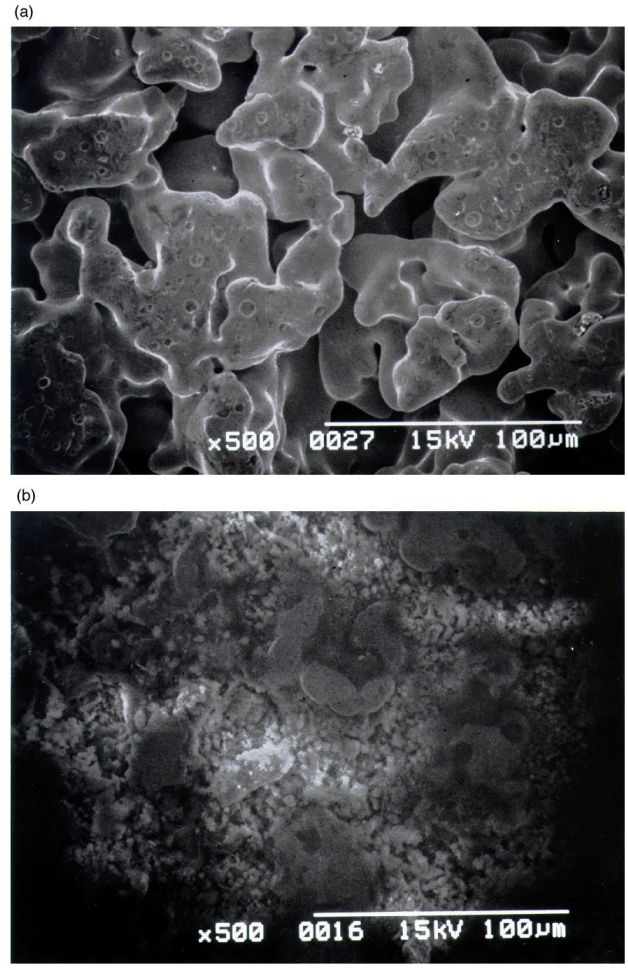

Fig. 1 Scanning electron micrographs of (a) the stainless steel support and (b) the MCM-48 membrane

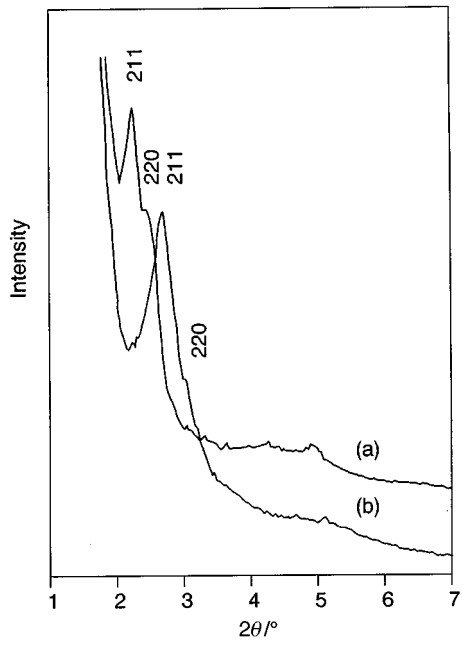

Fig. 2 X-Ray diffraction patterns of MCM-48 membranes (a) before calcination and (b) after calcination

of the original stainless steel support and the polished membrane before calcination. Particles with diameters of about 1 μm can be observed in the pores of the stainless steel.

The X-ray diffraction pattern of the polished membrane before calcination is shown in Fig. 2(a). The peaks for MCM-48 were found in the X-ray diffraction pattern even after the removal of the MCM-48 layer on the support, which indicates that MCM-48 grew in the pores of the stainless steel support. Fig. 2(b) shows the X-ray diffraction pattern of the polished membrane after calcination. The d_{211} values decreased from 3.9 nm to 3.3 nm after calcination because of the shrinkage of the structure. However, the peak intensity was not reduced even after calcination, showing that the ordered structure was maintained even after the removal of the surfactant. This result shows that the MCM-48 membrane prepared in this study has high thermal stability up to 773 K. The powder formed in the solution was MCM-48 with a BET surface area of 1025 $m^2\ g^{-1}$, showing its high quality.

We performed gas permeation tests using the MCM-48 membrane before and after calcination. The tests were carried out using a pressure drop of 100 kPa at room temperature. The permeances of nitrogen are shown in Table 1. Only pinholes and cracks between the MCM-48 particles can be gas permeable before calcination because the mesopores of MCM-48 are blocked by surfactant molecules. The MCM-48 membrane before calcination was impermeable to nitrogen gas. This result shows that MCM-48 particles were densely packed in the pores of the support and formed a compact composite membrane before calcination. The calcined membrane was permeable to nitrogen gas. The compactness of the MCM-48 membrane and the effect of the shrinkage of the structure by calcination on permeation properties will be reported in the near future.

Table 1 The permeance of N_2 through MCM-48 membranes

	Permeance/10^{-5} mol $m^{-2}\ s^{-1}\ Pa^{-1}$
Before calcination	0.0
After calcination	1.5

In conclusion, we have prepared a mesoporous inorganic membrane made of MCM-48 which has a three-dimensionally ordered pore system. A composite layer of stainless steel/MCM-48 was obtained in a compact form.

We thank GHAS at the Department of Chemical Engineering at Osaka University for SEM and XRD measurements. This study was partly supported by the Shimadzu Science Foundation.

Notes and References

1 C. T. Kresge, M. E. Leonowicz, W. J. Roth, J. C. Vartuli and J. S. Beck, *Nature*, 1992, **359**, 710.
2 J. S. Beck, J. C. Vartuli, W. J. Roth, M. E. Leonowicz, C. T. Kresge, K. D. Schmidtt, C. T-W. Chu, D. H. Olson, E. W. Sheppard, S. B. McCullen, J. B. Higgins and J. L. Schlenker, *J. Am. Chem. Soc*., 1992, **114**, 10 834.
3 T. Yanagisawa, T. Shimizu, K. Kuroda and C. Kato, *Bull. Chem. Soc. Jpn.*, 1990, **63**, 988.
4 S. Inagaki, Y. Fukushima and K. Kuroda, *J. Chem. Soc., Chem. Commun.*, 1993, 680.
5 M. Ogawa, *J. Am. Chem. Soc.*, 1994, **116**, 7941.
6 M. Ogawa, *Chem. Commun.*, 1996, 1149
7 H. Yang, A. Kuperman, N. Coombs, S. Mamich-Afara and G. A. Ozin, *Nature*, 1996, **379**, 703.
8 S. H. Tolbert, A. Firouzi and G. D. Stucky, *Science*, 1997, **278**, 265.

Received in Cambridge, UK, 13th July 1998; 8/05419C

Formation of separated *versus* contact ion triples in heavy alkaline-earth thiolates

Scott Chadwick, Ulrich Englich and Karin Ruhlandt-Senge*

Department of Chemistry, 1-014 Center for Science and Technology, Syracuse University, Syracuse NY 13244-4100, USA. E-mail. Kruhland@syr.edu.

The synthesis and structural characterization of the alkaline-earth thiolates [Sr(18-crown-6)(hmpa)$_2$][SMes*]$_2$ and [Ba(18-crown-6)(hmpa)(SMes*)][SMes*], displaying rare ion association modes with only one or no cation–thiolate linkages are presented.

In contrast to the well explored chemistry of separated organometallic lithium and sodium derivatives, little is known about the ionic association in heteroatomic systems. To date no separated alkoxide or aryloxide ion pairs have been described, and, to the best of our knowledge, only one thiolate, [Li(12-crown-4)$_2$][SMes*] (Mes* = $C_6H_2Bu^t_3$-2,4,6), has been reported.[1] The ion association chemistry of alkaline-earth derivatives is even less explored, which might be explained by the potentially more complex chemistry with three different types of ion association: contact triples with two cation–anion linkages, separated ion triples with no contacts between cation and anions, and semi-separated ion triples displaying one cation–anion contact, while the second anion does not interact with the metal center.

Only few examples of separated heteroatomic alkaline-earth derivatives such as [Mg(12-crown-4)$_2$][TeSi(SiMe$_3$)$_3$]$_2$,[2] and [Ca(18-crown-6)(NH$_3$)$_3$][SMes*]$_2$ have been reported.[3] All known strontium and barium chalcogenolates are contract triples, as observed in [Sr(thf)$_4$(=EMes*)$_2$] (E = S, Se),[4] [Sr(NH$_3$)(Py)(μ-SCEt$_3$)$_2$]$_\infty$,[5] [Sr(tmen)$_2$\{SeSi(SiMe$_3$)$_3$\}$_2$],[2] and [Ba(Py)$_5$\{TeSi(SiMe$_3$)$_3$\}$_2$].[2] We present herein the synthesis and structural characterization of the separated [Sr(18-crown-6)(hmpa)$_2$][SMes*]$_2$ **1** (Fig. 1), and the semi-separated [Ba(18-crown-6)(hmpa)(SMes*)][SMes*] **2** (Fig. 2). Compounds **1** and **2** represent examples of the least known association modes for alkaline-earth derivatives.

Several synthetic routes can be utilized for the synthesis of heavy alkaline-earth chalcogenolates, the most efficient of which is the treatment of the ammonia solvated metals with thiol. The insoluble powders, obtained after evaporation of ammonia and addition of thf can be transferred into soluble species by addition of a slight excess of hmpa.†

The Sr center in **1** is eight coordinate, with two strong hmpa donor interactions [2.420(2) Å] in addition to six crown-ether linkages in the range of 2.712(1)–2.736(1) Å. Both, the Sr–hmpa and the crown-ether connections compare well with literature data.[10] The S–C bond length in **1** is observed at 1.771(2) Å, which is slightly shorter than in [Sr(thf)$_4$(SMes*)$_2$],[4] but compares well with Li(12-crown-4)$_2$][SMes*][1] and [Ca(18-crown-6)(NH$_3$)$_3$][SMes*]$_2$.[3]

The comparison of **1** with [Sr(thf)$_4$(SMes*)$_2$] and [Sr(NH$_3$)(Py)(μ-SCEt$_3$)$_2$]$_\infty$ clearly shows that the presence of a multidentate donor (18-crown-6) in combination with a very strong donor (hmpa) greatly affects the ionic association of the resulting complexes. To make the rupture of a Sr–S bond thermodynamically favorable, a significant amount of solvation energy must be provided. Apparently, the donors thf, pyridine or NH$_3$ which are present in the reaction mixtures resulting in the contact triples, do not provide sufficient solvation energy to stabilize a separated Sr cation.

The Ba derivative **2**, which crystallizes with two independent molecules per asymmetric unit, consists of a monocation [Ba(18-crown-6)(hmpa)(SMes*)], and a separated SMes* anion. The Ba centers are eight coordinate with one thiolate [Ba–S 3.012(2) and 3.025(2) Å] and one hmpa contact [Ba–O 2.592(5), 2.594(5) Å], in addition to six crown-ether linkages [2.772(5)–2.807(5) Å]. The Ba atom is slightly displaced from the plane of the six crown-ether oxygen atoms [0.256 and 0.264 Å] towards the hmpa donor, indicating a strong Ba–hmpa interaction. The Ba–S–C angles are observed at 150.8(2) and 153.7(3)°, S–C distances in the contact thiolate are observed at 1.792(7) and 1.805(7); those for the separated anion are identified at 1.777(7) and 1.753(7) Å. The shortest Ba–S distance for the non-coordinating anion is observed at 6.533 Å.

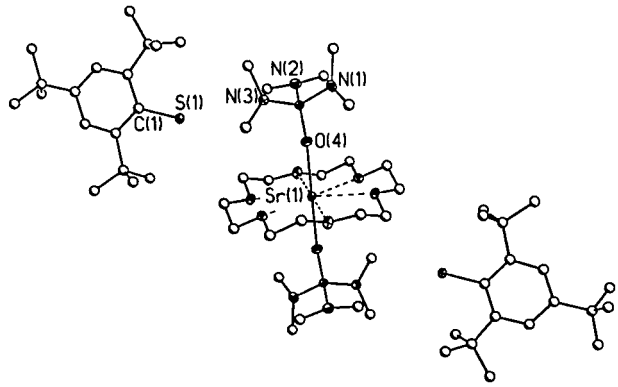

Fig. 1 Computer generated plot of [Sr(18-crown-6)(hmpa)$_2$][SMes*]$_2$ **1**. H atoms have been eliminated for clarity. Sr–O(hmpa) 2.420(2) Å; Sr–O(crown) 2.712(1), 2.718(1), 2.736(1) Å; S–C 1.771(2) Å.

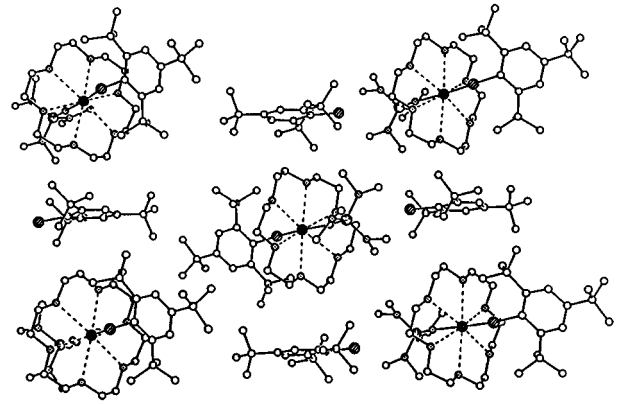

Fig. 2 Computer generated plot showing part of the unit cell in **2**. Ba–S 3.012(2), 3.025(2) Å; Ba–O(hmpa) 2.592(5), 2.594(5) Å; Ba–O(crown) 2.772(5)–2.807(5) Å; S–C (contact) 1.792(7), 1.805(7) Å; S–C (separated) 1.777(7), 1.753(7) Å; Ba–S–C 153.7(3), 150.8(2)°; O(hmpa)–Ba–S 172.8(1), 174.1(1)°.

Several complexes containing Ba–S moieties, where the S atom is part of a S–C–N resonance delocalized system are available for structural comparison to **2**.[6] While the Ba–crown-ether or –hmpa interactions fall in expected ranges,[7] significant differences are observed in the Ba–S distances. The Ba–S lengths in a series of seven-coordinate compounds bearing the 2-mercaptobenzoxazole ligand were observed at a mean value of 3.31(1) Å,[8] while Ba–S interactions in a ten-coordinate trimercaptotriazine derivative are displayed over a range of 3.396(2)–3.692(2) Å.[9] The shorter Ba–S bonds in **2** can be attributed in part to the absence of a second thiolate ligand in the coordination environment of the cation. In addition, the chelating nature of both the mercaptotriazine and the 2-mercaptobenzoxazole ligands might result in the lengthening of the Ba–S bond. The strong Ba–S bond in **2** is further demonstrated by the repeated isolation of **2**, even if very large excesses (up to 12 fold) of hmpa was added to the reaction mixture. The unusually wide Ba–S–C angles of 150.8(2) and 153.7(3)° compare well with those observed in [Ca(18-crown-6)(SMes*)$_2$], where one strong [2.785(2) Å] and one weaker [2.859(2) Å] Ca–S interaction was observed.[7] The environment at the S atom involved in the stronger bond is very similar to that in **2** [Ca–S–C 154.1(2)°].

Several factors affect the ion association in alkali and alkaline-earth chalcogenolates. The balance between steric congestion about the cation and tendency towards maximization of cation–anion interactions is nicely demonstrated in the ion triples [Sr(18-crown-6)(hmpa)$_2$][SMes*]$_2$ **1** and [Ba(18-crown-6)(hmpa)(SMes*)][SMes*] **2**. The smaller Sr cation (CN 8: 1.40 Å)[10] is unable to accommodate one SMes* ligand while maintaining strong crown ether coordination. In the presence of the strong donor hmpa, the Sr–S bond is ruptured (shortest resulting Sr–S 6.301 and 7.252 Å), and hmpa donor molecules occupy the coordination sites perpendicular to the crown ether plane. Ligation by hmpa provides the needed cation coordination while being sterically less demanding than the thiolate anions. This result might be compared to [Ca(18-crown-6)(SMes*)$_2$],[3] isolated in the absence of hmpa. This reaction was carried out in thf, which is apparently unable to provide the necessary solvation energy for the stabilization of a separated cation. The addition of hmpa to the corresponding Ba reaction, results in **2**: the larger Ba cation (CN 8: 1.56 Å)[10] enables the close approach of one thiolate ligand and one hmpa donor.

The synthesis and characterization of the first Sr separated ion triple, **1**, and the novel, unusual intermediate between a contact and a separated ion triple **2**, contributes significantly to the understanding of the association chemistry of the alkaline-earth elements. The detailed analysis of structural parameters gives important insight into the nature and strength of alkaline-earth metal–ligand and –donor interactions, while providing information about the preferred alkaline-earth metal environment. Our work in this area of chemistry is continuing and will be subject of forthcoming publications.

This work was supported by the National Science Foundation (CHE-9702246) and the Deutsche Forschungsgemeinschaft (Postdoctoral stipend for U. E.). Purchase of the X-ray diffractometer was made possible with grants from NSF (CHE-95-27898), the W. M. Keck Foundation and Syracuse University.

Notes and References

† *Synthetic procedures*: all reactions were performed under anaerobic and anhydrous conditions. HSMes* was prepared by published procedures.[11] **CAUTION**: hmpa [hexamethylphosphoramide, P(O)(NMe$_2$)$_3$] is a suspected carcinogen and should be handled in a well ventilated fumehood using gloves. *General procedure* for **1** and **2**: a 100 ml Schlenk flask was charged with 1.0 mmol of metal, 0.26 g (1.0 mmol) of 18-crown-6 and 0.56 g (2.0 mmol) of HSMes*. Approximately 25 ml of predried $NH_{3(l)}$ was condensed into the flask. The deep-blue solution was stirred at −78 °C for 1 h and then warmed up to room temp. 25 ml of thf was added. A heavy yellow–white suspension persisted even after brief heating. As hmpa was added dropwise (0.70 ml, 4.0 mmol), the reaction gradually cleared then became cloudy-white once again. The solution was heated briefly to reflux and immediately filtered through a Celite padded frit. **1**: colorless blocks formed on cooling to room temperature in 16% yield (0.20 g). Mp: shrinking at approximately 215 °C and an irreversible melt at 245–250 °C. ^{1}H NMR ([$^2H_8$]thf), δ 7.06 (s, 4H), 3.83 (s, 24H), 2.62 (d, 36H), 1.74 (s, 36H), 1.24 (s, 18H); ^{13}C{^{1}H}NMR ([$^2H_8$]thf), δ 150.16, 150.10, 120.77, 71.01, 39.15, 37.34, 32.44, 32.03; IR (Nujol), 2920s, 1592w, 1461s, 1377s, 1354m, 1285s, 1190m, 1155s, 1095s, 1024m, 981s, 966s, 876w, 839w, 757s, 616w, 483m cm^{-1}. **2**: colorless crystals formed almost instantly out of a yellow filtrate in 19% yield (0.21 g). Melting to an oily residue at 175–180 °C, decomposition above 200 °C. ^{1}H NMR ([$^2H_5$]py) δ 7.59 (s, 4H), 3.82 (s, 24H), 2.58 (d, 18H), 2.19 (s, 36H), 1.46 (s, 18H); ^{13}C{^{1}H}NMR ([$^2H_5$]py), δ 139.37, 121.37, 70.98, 39.52, 37.31, 34.80, 32.61, 32.03; IR (Nujol), 2854s, 1593w, 1462s, 1377s, 1349w, 1283w, 1246w, 1195w, 1166w, 1087m, 1042w, 979w, 957m, 875w, 833w, 723m, 480w cm^{-1}.

‡ The crystals were mounted as described earlier.[12a] Crystal data for **1** and **2**·0.5C$_7$H$_8$ were collected at 150 K with Mo-Kα radiation (λ = 0.710 73 Å), Bruker SMART CCD diffractometer, graphite monochromator, Oxford Instruments Cryojet low temperature device. Both structures were solved and refined using the SHELXTL program package.[12b] An absorption correction was applied using the program system SADABS.[12c] **1**: M = 632.64, crystal dimensions 0.20 × 0.15 × 0.15 mm, μ = 0.882 mm^{-1}, scan range 3° < 2θ < 57°, monoclinic, space group $P2_1/n$, a = 10.5771(3), b = 17.5403(5), c = 19.8293(7) Å, β = 91.152(1)°, V = 3678.1(2) Å^3, Z = 2, D_c = 1.142 g cm^{-3}, 22232 measured, 8569 independent reflections (R_{int} = 0.0329), 358 refined parameters. R_1 [$I > 2\sigma(I)$] = 0.0441, R_1 (all data) = 0.0667. **2**·0.5C$_7$H$_8$: M = 2363.73, crystal dimensions 0.30 × 0.30 × 0.30 mm, μ = 0.744 mm^{-1}, scan range 2 < 2θ < 50°, monoclinic, space group $P2_1/n$, two independent molecules per asymmetric unit, one disordered solvent toluene molecule, a = 21.2127(3), b = 14.2323(2), c = 43.2258(1) Å, β = 90.613(1)°, V = 13049.4(3) Å^3, Z = 4, D_c = 1.203 g cm^{-3}, 63 151 measured, 22 564 independent reflections (R_{int} = 0.0681), 1222 refined parameters, R_1[$I > 2\sigma(I)$] = 0.0855, R_1 (all data) = 0.1436. Some of the hmpa donors and Bu^t groups in **2** are disordered and have been refined utilizing split positions and a set of restraints. CCDC 182/1005.

1 K. Ruhlandt-Senge, U. Englich, M. O. Senge and S. Chadwick, *Inorg. Chem.*, 1996, **35**, 5820.
2 D. E. Gindelberger and J. Arnold, *Inorg. Chem.*, 1994, **33**, 6293.
3 S. T. Chadwick, U. Englich, B. Noll and K. Ruhlandt-Senge, *Inorg. Chem.*, in press.
4 K. Ruhlandt-Senge, K. Davis, S. Dalal, U. Englich and M. O. Senge, *Inorg. Chem.*, 1995, **34**, 2587.
5 A. P. Purdy, A. D. Berry and C. F. George, *Inorg. Chem.*, 1997, **36**, 3370.
6 D. Barr, A. T. Brooker, M. J. Doyle, S. R. Drake, P. R. Raithby, R. Snaith and D. Wright, *J. Chem. Soc., Chem. Commun.*, 1989, 893; J. H. Burns and R. M. Kessler, *Inorg. Chem.*, 1987, **26**, 1370.
7 A. L. Rheingold, C. B. White and B. S. Haggerty, *Acta Crystallogr., Sect. C*, 1993, **49**, 808; J. A. T. Norman and G. P. Pez, *J. Chem. Soc., Chem. Commun.*, 1991, 971.
8 P. Mikulcik, P. R. Raithby, R. Snaith and D. S. Wright, *Angew. Chem. Int. Ed. Engl.*, 1991, **30**, 428; F. A. Banbury, M. G. Davidson, A. Martin, P. R. Raithby, R. Snaith, R. K. L. Verhorevoot and D. S. Wright, *J. Chem. Soc., Chem. Commun.*, 1992, 1152.
9 K. Henke and D. A. Atwood, *Inorg. Chem.*, 1998, **37**, 224.
10 R. D. Shannon, *Acta Crystallogr., Sect. A*, 1976, **32**, 751.
11 J. M. A. Baas, H. van Bekkum, M. A. Hofnagel and B. M. Wepster, *Recl. Trav. Chim. Pays-Bas*, 1969, **88**, 1110; W. Rundel, *Chem. Ber.*, 1968, **101**, 2956.
12 (*a*) H. Hope, *Prog. Inorg. Chem.*, 1994, **41**, 1; (*b*) G. M. Sheldrick, SHELXTL-PLUS, Program Package for Structure Solution and Refinement, Siemens, Madison, Wisconsin, 1996; (*c*) G. M. Sheldrick, SADABS, Program for Absorption Correction Using Area Detector Data, University of Göttingen, Germany, 1996.

Received in Columbia, MO, USA, 1st July 1998; 8/05122D

Characterization of poly(carbon monofluoride) by ^{19}F and ^{19}F to ^{13}C cross polarization MAS NMR spectroscopy

Thomas R. Krawietz and James F. Haw*†

Department of Chemistry, Texas A&M University, PO Box 300012, College Station, TX 77842-3012, USA

High speed ^{19}F MAS NMR and ^{13}C MAS NMR with ^{19}F to ^{13}C cross polarization allows spectroscopic identification of monofluorinated and geminally difluorinated carbon species in poly(carbon monofluoride).

Poly(carbon monofluoride), $(CF_x)_n$, is a stable, hydrophobic material prepared from graphite and elemental fluorine at high temperatures.[1] $(CF_x)_n$ materials, where x is greater than 0.60, are currently being produced on an industrial scale for use in Li/$(CF_x)_n$ batteries, and these are characterized by high energy density, wide operating temperatures and long storage life.[2] Poly(carbon monofluoride) is also used as a solid lubricant with wear performance better than that of graphite or MoS_2, especially in high temperature or oxidizing environments.[3,4] It is agreed that covalent incorporation of fluorine results in a puckering of the graphite structure into extended sheets of fused cyclohexane rings,[5–8] but other details of the structure of $(CF_x)_n$, including defect sites, are more poorly understood. Previous applications of NMR to this material have been wide-line ^{19}F investigations. One such study concluded that $(CF_x)_n$ is an array of *cis-trans*-linked boats, with all fluorine in axial positions. A more recent student used similar methods to support a *trans-trans*-linked chair structure, and that conclusion is supported by the available X-ray data.[6–9] The availability of technology for very rapid sample rotation has made possible high resolution NMR analysis of solids,[10,11] and several such ^{19}F magic angle spinning (MAS) NMR investigations have appeared in the literature.[12–15] Here we have used high speed MAS to obtain ^{19}F NMR spectra of $(CF_x)_n$ materials that are dominated by the isotropic chemical shifts of bulk and defect structures. Furthermore, we have confirmed our assignments by acquiring ^{13}C NMR spectra of the same materials using cross polarization from ^{19}F and fluorine decoupling.

Two samples of carbon monofluoride were obtained from Aldrich. Fast neutron activation determined the empirical formulae to be $(CF_{0.87})_n$ and $(CF_{1.12})_n$. Samples for NMR investigation were loaded and sealed under an inert nitrogen atmosphere in 4.0 and 5.0 mm zirconia MAS rotors using Delrin [poly(oxymethylene)] endcaps. High speed ^{19}F MAS NMR was performed on a home built spectrometer operating at a fluorine resonance of 188.8 MHz utilizing a 4.0 mm spinning module from Otsuka Electronics. The fluorine chemical shift was externally referenced to an ampoule of trichlorofluoromethane at 0 ppm. $\pi/2$ pulses of 3 μs or less were used. Reported spectra are the result of 1024 transients, utilizing a composite Bloch decay sequence[16] for probe background suppression and a 1 s recycle delay. ^{19}F to ^{13}C CP MAS NMR spectra were acquired on a Chemagnetics CMX-360 operating at 337.8 (^{19}F) and 90.5 MHz (^{13}C) using a probe from Otsuka Electronics spinning 5.0 mm rotors. The magic angle was optimized using the ^{79}Br resonance of KBr.[17] The ^{13}C chemical shift was referenced (17.4 ppm) and the ^{1}H–^{13}C Hartmann–Hahn matching condition was set using hexamethylbenzene. The ^{19}F–^{13}C match was then optimized on polytetrafluoroethylene (PTFE) by adjustment of the ^{19}F power level to coincide with the previously determined ^{13}C $\pi/2$ pulse width. The double-resonance NMR probe contained sufficient fluoropolymer that ^{13}C Bloch decay spectra obtained with ^{19}F decoupling were dominated by background signals, even with background-suppression pulse sequences. Fortunately, probe background was greatly diminished with ^{19}F–^{13}C cross polarization, and background was negligible when the ^{13}C magnetization was generated using composite CP sequences. We optimized the CP contact time by measuring the important relaxation rates. For a sample of $(CF_{0.87})_n$ we measured a ^{19}F $T_{1\rho}$ of 33.4 ± 5.0 ms and 147 ± 18 μs for T_{FC}.[18] We selected a 1.5 ms contact time to provide excellent CP efficiency without unnecessary radio-frequency heating. The ^{13}C $\pi/2$ pulse width was 4.3 μs and high-power ^{19}F decoupling was used. Each ^{13}C NMR spectrum is the result of 2048 transients and a 3 s recycle delay.

Fig. 1 reports ^{19}F MAS NMR spectra of samples of $(CF_{0.87})_n$ and $(CF_{1.12})_n$ obtained with a spinning speed of 18 kHz. This spinning speed was necessary to average the ^{19}F–^{19}F homonuclear dipolar interaction as well as to place spinning sidebands away from spectral regions of interest. The most intense peak in both spectra, at −187 ppm, is assigned by comparison to the fluorines on C9 and C10 of either *trans*- or *cis*-perfluorodecalin, each at −186 ppm. Therefore, the −187 ppm resonance in Fig. 1 is confidently assigned to C–F groups.[19] A second isotropic peak, at −116 ppm, is present in both samples but is clearly larger for the sample with the higher fluorine content. This signal can also be assigned by comparison to perfluorodecalins, for which both the axial and equatorial fluorines in CF_2 groups in the 1, 4, 5, and 8 positions have shifts of −124 ppm.[19] The line widths of both ^{19}F resonances are likely due to chemical heterogeneity, as modest variations in sample temperature or spinning speed suggested no further line narrowing.

Further evidence for these assignments came from the ^{19}F to ^{13}C CP MAS spectra (Fig. 2). Both spectra have a majority resonance at 89 ppm and a shoulder that spectral deconvolution shows to be centered at 111 ppm. The latter feature is distinctly larger in the sample with the higher fluorine content. We assign the ^{13}C resonances by comparison to an earlier study of graphite hydrofluoride, $C_xF_{1-\delta}(HF)_\delta$, by Mallouk and co-workers.[20] $C_xF_{1-\delta}(HF)_\delta$ has a resonance at 88 ppm that was assigned to

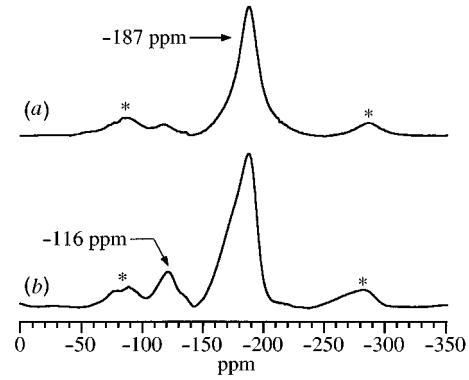

Fig. 1 188.8 MHz ^{19}F MAS NMR spectra of graphite monofluoride having empirical stoichiometries of (*a*) $(CF_{0.87})_n$ and (*b*) $(CF_{1.12})_n$. Spectra were acquired at 298 K using a spinning speed of 18 kHz. Asterisks denote spinning sidebands.

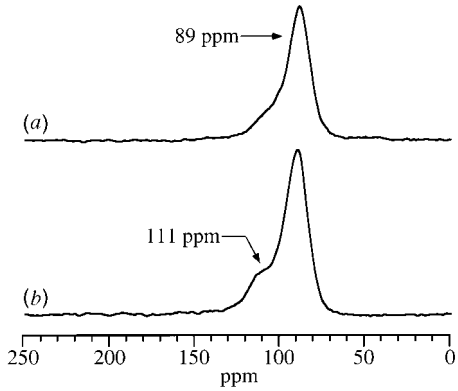

Fig. 2 90.5 MHz ^{13}C MAS NMR spectra of graphite monofluoride obtained with ^{19}F to ^{13}C cross polarization and high power ^{19}F decoupling. Spectra were acquired at 298 K with a spinning speed of 8 kHz. (*a*) $(CF_{0.87})_n$ and (*b*) $(CF_{1.12})_n$.

monofluorinated carbons, and this strongly supports a similar assignment for $(CF_x)_n$. $C_xF_{1-\delta}(HF)_\delta$ also showed a small ^{13}C signal at 112 ppm which Mallouk and co-workers assigned to CF_2 groups at the edge of grains. This supports assignment of the 111 ppm shoulder in Fig. 2 to the carbons in CF_2 groups. Our spectra clearly show that CF_2 groups are enhanced at higher fluorine incorporation, in agreement with Lagow's proposal for the fluorine siting in 'superstoichiometric' poly(carbon monofluoride).[21] However, we have also demonstrated the presence of smaller amounts of CF_2 in a sub-stoichiometric material. In this case, CF_2 groups are still reasonable as peripheral groups at sheet edges or in other defected structures. In principal, we should be able to establish a quantitative relationship between the levels of CF_2 in the ^{19}F and ^{13}C spectra, but the use of cross polarization in the latter case prevents such a comparison.

In conclusion, ^{19}F high speed MAS NMR analysis has permitted resolution of majority and defect sites in highly fluorinated graphite derivatives, and the interpretation of these experiments is supported by ^{13}C MAS NMR with ^{19}F to ^{13}C cross polarization and high power ^{19}F decoupling.

This work was supported by the National Science Foundation (Grant No. CHE-9528959). We would also like to thank Judith A. Sharp and R. Malcolm Brown, Jr. at the University of Texas in Austin for providing transmission electron microscopy and discussions of sample morphology.

Notes and References

† E-mail: haw@chemvx.tamu.edu

1 R. J. Lagow, R. B. Badachhape, J. L. Wood and J. L. Margrave, *J. Chem. Soc., Dalton Trans.*, 1974, 1268.
2 N. Watanabe, H. Touhara, T. Nakajima, N. Bartlett, T. Mallouk and H. Selig, *Inorganic Solid Fluorides*, ed. P. Hagenmuller, Academic Press, Orlando, FL, 1982.
3 T. Nakajima and N. Watanabe, *Graphite Fluorides and Carbon-Fluorine Compounds*, CRC Press, Boston, 1991.
4 R. L. Fusaro and H. E. Sliney, NASA Technical Note, NASA TND-5097, 1969.
5 W. Rüdorff, *Adv. Inorg. Chem. Radiochem.*, 1959, **1**, 320.
6 Y. Kita, N. Watanabe and Y. Fujii, *J. Am. Chem. Soc.*, 1979, **101**, 3832.
7 H. Touhara, K. Kadono, Y. Fujii and N. Watanabe, *Z. Anorg. Allg. Chem.*, 1987, **544**, 7.
8 H. Touhara, K. Kadono, N. Watanabe and J.-J. Braconnier, *J. Electrochem. Soc.*, 1987, **134**, 1071.
9 L. B. Ebert, J. I. Brauman and R. A. Huggins, *J. Am. Chem. Soc.*, 1974, **96**, 7841.
10 S. F. Dec, R. A. Wind and G. E. Maciel, *J. Magn. Reson.*, 1986, **70**, 355.
11 R. K. Harris and P. Jackson, *Chem. Rev.*, 1991, **91**, 1427.
12 S. A. Carss, R. K. Harris, P. Holstein, B. J. Say and R. A. Fletton, *J. Chem. Soc., Chem. Commun.*, 1994, 2407.
13 D. B. Ferguson, T. R. Krawietz and J. F. Haw, *J. Chem. Soc., Chem. Commun.*, 1995, 1795.
14 J. B. Nicholas, J. F. Haw, L. W. Beck, T. R. Krawietz and D. B. Ferguson, *J. Am. Chem. Soc.*, 1995, **117**, 12 350.
15 A. Simon, L. Delmotte, J.-M. Chezeau and L. Huve, *Chem. Commun.*, 1997, 263.
16 J. L. White, L. W. Beck, D. B. Ferguson and J. F. Haw, *J. Magn. Reson.*, 1992, **100**, 336.
17 J. S. Frye and G. E. Maciel, *J. Magn. Reson.*, 1982, **48**, 125.
18 J. Kümmerlen, L. H. Merwin, A. Sebald and H. Keppler, *J. Phys. Chem.*, 1992, **96**, 6405.
19 J. Homer and L. F. Thomas, *Proc. Chem. Soc.*, 1961, 139.
20 T. Mallouk, B. L. Hawkins, M. P. Conrad, K. Zilm, G. E. Maciel and N. Bartlett, *Phil. Trans. R. Soc. Lond. A*, 1985, **314**, 179.
21 R. J. Lagow, R. B. Badachhape, J. L. Wood and J. L. Margrave, *J. Am. Chem. Soc.*, 1974, **96**, 2628.

Received in Corvallis, OR, USA, 29th April 1998; 8/03252A

Stable [60]fullerene carbocations

Anthony G. Avent, Paul R. Birkett,*† Harold W. Kroto, Roger Taylor and David R. M. Walton

The Fullerene Science Centre, School of Chemistry, Physics and Environmental Science, University of Sussex, Brighton, Sussex, UK BN1 9QJ

[60]Fullerene derivatives, $C_{60}Ar_5Cl$ (Ar = Ph or 4-FC_6H_4), react with $AlCl_3$ in solution at room temperature to form C_s symmetrical pentaaryl[60]fullerene carbocations, $C_{60}(Ar)_5^+$.

A number of stable [60]fullerene derivatives which are anions have been synthesised and characterised in solution.[1] In contrast no carbocationic [60]fullerene derivatives have been described to date. However, the non-functionalised [60]fullerene radical carbocation, $C_{60}^{+\cdot}$, has been identified by *in situ* EPR and NMR spectroscopy in super acid media[2] and the fullerene cationic salt $[C_{76}^+][CB_{11}H_6Br_6^-]$ has been fully characterised.[3] Photo-induced electron transfer (PET) has recently been used to generate $C_{60}^{+\cdot}$ which was functionalised *in situ* by reaction with hydrogen donor molecules, such as alcohols, resulting in the formation of 1-substituted 1,2-dihydro[60]fullerene derivatives.[4] Our studies of Friedel–Crafts reactions between chlorofullerenes and aromatic compounds with $FeCl_3$,[5] a moderately strong Lewis acid, imply the formation of either fullerene carbocation intermediates (or of donor–acceptor complexes which subsequently undergo front-side displacement by an aromatic group, which is unlikely). We have now prepared and characterised the first examples of [60]fullerene derivative carbocations, $C_{60}Ar_5^+$ (Ar = Ph or 4-FC_6H_4), which are formed by cleaving the fullerene–Cl bond of $C_{60}Ar_5Cl$ (Ar = Ph **1**;[5a] 4-FC_6H_4 **2**[5c]) using a strong Lewis acid, $AlCl_3$.

The reaction of either **1** or **2** in CH_2Cl_2, $CHCl_3$ or CS_2 with $AlCl_3$ at room temperature over 30 min results in a change from an orange solution to an intense purple–red indicating the formation of new [60]fullerene derivatives. *In situ* ^{1}H NMR spectra (CS_2–CD_2Cl_2) of the above reactions showed that, in each case, complete conversion to a new C_s symmetric pentaarylated [60]fullerene derivative occurs as each spectrum has the same number and intensities of signals as the C_s symmetric starting material; however, the chemical shifts of the signals are significantly different. For example, in the reaction of **2** with $AlCl_3$ the two multiplets due to the Hs of the unique aryl ring (A) are shifted downfield in the reaction product (Fig. 1). Unequivocal assignments for the signals of the pairs of aryl rings (BC and DE) are not possible as NOE experiments result in equal saturation transfer to all similar signals in the spectrum. Irradiation of the highest field 3-H multiplet of the spectrum in Fig. 1(*a*), which is due to one of the two pairs of aryl rings of the reaction product from **2**, results in the equal collapse of the two other 3-H signals (including that of the unique aryl ring). The foregoing data is consistent with the proposal that the $AlCl_3$ is able to abstract the chlorine atom from **1** or **2** generating the carbocations **3** or **4** which are expected to have considerable anti-aromatic character due to their 4π electron systems (Scheme 1). 1,2-Phenyl migration then occurs producing the carbocations **7**‡ and **8**.§ The fact that the NOE data shows equal saturation transfer to all five aryl rings in both of the reaction products implies that there is a dynamic equilibrium between the initial carbocation formed, which can be viewed as the C_5 symmetric anti-aromatic cyclopentadienyl carbocations, **5** and **6**, and the subsequent major reaction products, **7** and **8**, respectively. However, variable temperature NMR spectra of both reaction products to 233 K failed to produce any evidence for the presence of **5** or **6**.

The *in situ* ^{13}C NMR spectra of both **7** and **8** have the required number of signals due to the fullerene carbon atoms [28 sp^2 (26 × 2C and 2 × 1C), three sp^3 (2 × 2C and 1 × 1C) and one carbocationic carbon (1 × 1C$^+$)] in addition to those of the aryl carbons. The signal due to the *ipso*-carbon attached to the fullerene cage of the unique aryl ring A is not observed in the spectrum of **8** and is most probably masked by one of the other *ipso*-signals. The formation of donor–acceptor type complexes can be ruled out as the chemical shifts, δ 173.74 and 171.67, of the signals due to the carbon atoms bearing the positive charge in **7** and **8** respectively are much too low field. However, these values are relatively high-field for carbocationic centres and reflect the exchange of the aryl groups detected by ^{1}H NMR spectroscopy. Other factors, such as the positively charged carbon atom having an empty sp^3-like orbital due to the strained ring system being unable to rehybridise to form a planar sp^2 orbital, should however also be considered. The positive charge is localised mostly at or near to the site of its generation in both **7** and **8**. Consequently the carbon atoms immediately adjacent to the carbon atom bearing the positive charge undergo a large downfield shift (> δ 4) compared with those more remote to the positive centre. This situation is analagous to the observed localisation of either the negative charge in the monoaddended fullerene anions[1a–e] or to the radical electron in mono-radical addition to fullerenes.[7] The signals due to the readily identifi-

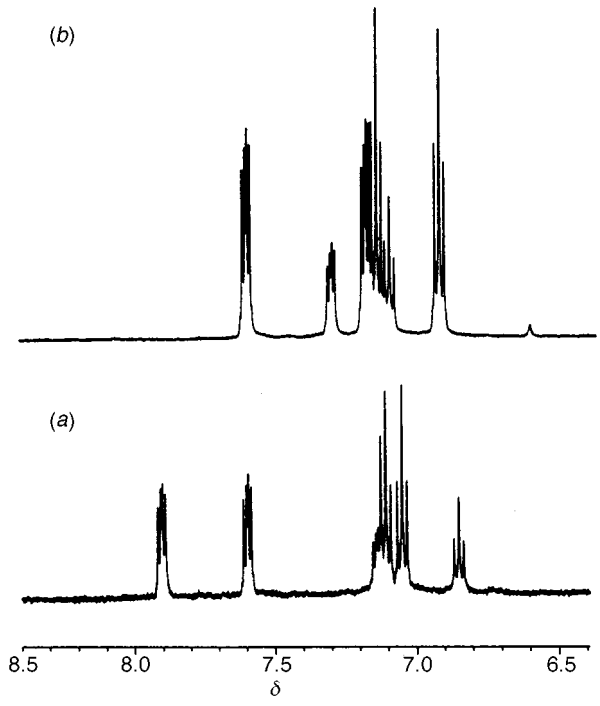

Fig. 1 The ^{1}H NMR spectra of (*a*) **2** and (*b*) the reaction product **8** from the *in situ* reaction of **2** with $AlCl_3$

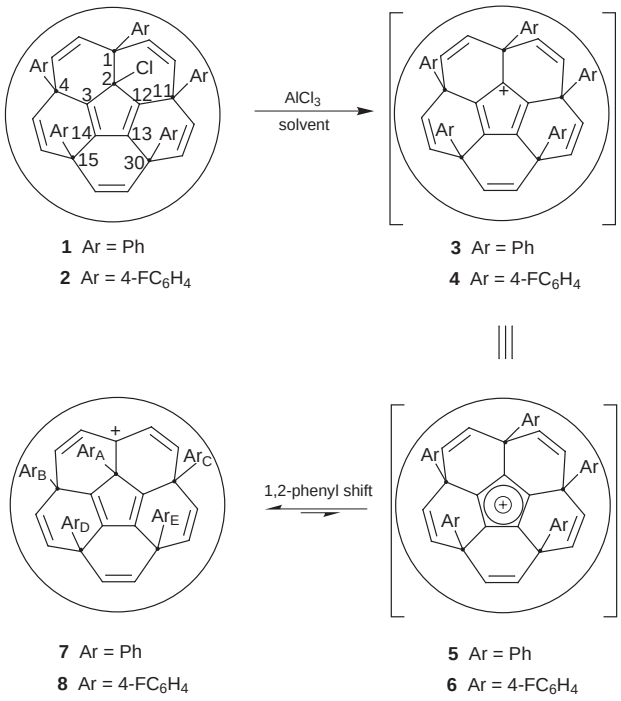

Scheme 1 The proposed reaction sequence for the formation of the carbocations **7** and **8**. Only the five-membered ring around which the phenyl groups are situated in [60]fullerene is shown; the C atoms are numbered using the IUPAC system[6] and the aromatic labels, *e.g.* Ar_A, in **7** and **8** correspond to those used in the text.

able (single intensity) symmetry plane sp^2 carbon atoms (C55/C60 carbons), which are located at the opposite pole of the [60]fullerene cage, undergo anomalously large downfield shifts of δ 2.67 and 2.66 in **7** and δ 1.86 and 1.72 in **8** probably due to the presence of endohedral homoconjugation, *i.e.* overlap of the rear nodes of the orbitals of the sp^2 carbons C55 and C60 with those of the carbocationic carbon C1 and the sp^3 carbon C2 through the interior of the cage. A transannular interaction of this type was first suggested by Olah *et al*. to explain the observed downfield shift of the bridgehead Hs in the ^{1}H NMR spectrum of the 1-adamantyl carbocation.[8] Moreover, endohedral homoconjugation has recently been observed by cyclic voltammetry in the pentaphenylcyclopentadienyl[60]fullerene anion, $C_{60}Ph_5^-$.[9]

Further studies to examine the scope, nature, properties, spectroscopy and chemical reactivity of this new fullerene species are in progress.

We thank the EPSRC (for an Advanced Fellowship to P. R. B.) and the Royal Society for financial support.

Notes and References

† E-mail: p.r.birkett@sussex.ac.uk

‡ *Selected data* for **7**: δ_H[500 MHz; CS_2–CD_2Cl_2 (lock)] 7.14 (t, *J* 7.3, 4 H, H-3 and H-5 aryl BC/DE), 7.19 (d, *J* 7.0, 4 H, H-2 and H-6 aryl BC/DE), 7.28 (t, *J* 7.2, 2 H, H-4 aryl BC/DE), 7.32 (t, 2 H, H-3 and H-5 aryl A), 7.36 (d, 2 H, H-2 and H-6 aryl A), 7.30–7.38 (1 H, H-4 aryl A), 7.39 (t, *J* 7.2, 4 H, H-3 and H-5 aryl BC/DE), 7.46 (t, *J* 7.3, 2H, H-4 aryl BC/DE), 7.66 (t, *J* 7.1 *J* 7.3,, 4 H, H-2 and H-6 aryl BC/DE); δ_C[125.76 MHz; $CDCl_3$ (lock)] (number of carbon atoms) 58.56 (2 C), 63.06 (2 C), 66.77 (1 C), 127.50 (2 C, Ar), 127.71 (3 C, Ar), 128.84 (1 C, Ar), 129.11 (4 C, Ar), 129.32 (2 C, Ar), 129.46 (2 C, Ar), 129.69 (2 C, Ar), 133.61 (2 C, Ar), 134.31 (1 C, *ipso*-Ar A), 136.03 (2 C, *ipso*-Ar BCDE), 137.42 (2 C, *ipso*-Ar BCDE), 139.39 (2 C), 141.46 (2 C), 141.52 (2 C), 141.94 (2 C), 142.25 (2 C), 142.58 (2 C), 142.80 (2 C), 144.18 (2 C), 145.03 (2 C), 145.09 (2 C), 145.48 (2 C), 145.69 (2 C), 146.06 (2 C), 146.11 (2 C), 146.71 (2 C), 146.80 (2 C), 147.64 (2 C), 147.69 (2 C), 148.36 (2 C), 148.86 (2 C), 148.89 (2 C), 149.14 (2 C), 149.53 (1 C, C55/C60), 150.45 (1 C, C55/C60), 152.15 (2 C), 153.91 (2 C), 154.81 (2 C), 163.54 (2 C), 173.74 (1 C, C1); λ(cyclohexane)/nm 429, 562.

§ *Selected data* for **8**: δ_H[500 MHz; CS_2–CD_2Cl_2 (lock)] 6.89–6.93 (m, 4 H, H-3 and H-5 aryl BC/DE), 7.06–7.11 (m, 2 H, H-3 and H-5 aryl BC/DE), 7.11–7.15 (m, 4 H, H-3 and H-5 aryl BC/DE), 7.16–7.19 (m, 4 H, H-2 and H-6 aryl BC/DE), 7.28–7.31 (m, 2 H, H-2 and H-6 aryl A), 7.57–7.61 (m, 4 H, H-2 and H-6 aryl BC/DE); δ_C[125.76 MHz; CS_2–CD_2Cl_2 (lock)] (number of carbon atoms) 57.81 (2 C), 62.26 (2 C), 65.70 (1 C), 116.95 (4 C, d, C-3,5 aryl BC/DE, $^2J_{CF}$ 22), 116.90 (4 C, d, C-3,5 aryl BC/DE, $^2J_{CF}$ 22), 117.99 (2 C, d, C-3,5 aryl A, $^2J_{CF}$ 22), 128.00 (2 C, d, C-2,6 aryl A, $^3J_{CF}$ 9), 129.42 (4 C, d, C-2,6 aryl BC/DE, $^3J_{CF}$ 8), 129.57 (4 C, d, C-2,6 aryl BC/DE, $^3J_{CF}$ 9), 131.83 (2 C, d, C-1 aryl BC/DE, $^4J_{CF}$ 3), 133.08 (2 C, d, C-1 aryl BC/DE, $^4J_{CF}$ 3), 139.31 (2 C), 140.89 (2 C), 141.69 (2 C), 141.72 (2 C), 142.41 (2 C), 142.48 (2 C), 142.76 (2 C), 144.08 (2 C), 144.83 (2 C), 145.24 (2 C), 145.40 (2 C), 145.72 (2 C), 146.21 (2 C), 146.29 (2 C), 146.65 (2 C), 146.77 (2 C), 147.15 (2 C), 147.73 (2 C), 148.40 (2 C), 148.95 (2 C), 149.04 (2 C), 149.32 (2 C), 149.73 (1 C), 150.43 (1 C), 152.44 (2 C), 153.95 (2 C), 154.46 (2 C), 162.32 (2 C), 163.00 (2 C, d, C4 aryl BC/DE, $^1J_{CF}$ 251), 163.05 (2 C, d, C-4 aryl BC/DE, $^1J_{CF}$ 252), 163.35 (1 C, d, C-4 aryl A, $^1J_{CF}$ 253), 171.66 (1 C); δ_F[282.2 MHz; CS_2–CD_2Cl_2 (lock)] −113.77 (septet, 2 F, aryl BC/DE), −112.95 (septet, 2 F, aryl BC/DE), −111.12 (septet, 1 F, aryl A); λ(cyclohexane)/nm 429, 562.

1 (*a*) P. J. Fagan, P. J. Krusic, D. H. Evans, S. A. Lerke and E. Johnston, *J. Am. Chem. Soc*., 1992, **114**, 9697; (*b*) A. Hirsch, A. Soi and H. R. Karfunkel, *Angew. Chem., Int. Ed. Engl*., 1992, **31**, 766; (*c*) A. Hirsch, T. Grösser, A. Skiebe and A. Soi, *Chem. Ber*., 1993, **126**, 1061; (*d*) A. Skiebe, A. Hirsch, H. Klos and B. Gotschy, *Chem. Phys. Lett*., 1994, **220**, 138; (*e*) M. Keshavarz, K. B. Knight, G. Srdanov and F. Wudl, *J. Am. Chem. Soc*., 1995, **117**, 11 371; (*f*) K. Komatsu, Y. Murata, N. Takimoto, S. Mori, N. Sugita and T. S. M. Wan, *J. Org. Chem*., 1994, **59**, 6101; (*g*) M. Sawamura, H. Iikura and E. Nakamura, *J. Am. Chem. Soc*., 1996, **118**, 12 850.

2 S. G. Kukolich and D. R. Huffman, *Chem. Phys. Lett*., 1991, **182**, 263; G. A. Olah, I. Busci, R. Aniszfeld and G. K. S. Prakash, *Carbon*, 1992, **30**, 1203; G. P. Miller, C. S. Hsu, H. Thomann, L. Y. Chiang and M. Bernardo, *Mater. Res. Soc. Symp. Proc*., 1992, **247**, 293; H. Thomann, M. Bernardo and G. P. Miller, *J. Am. Chem. Soc*., 1992, **114**, 6593; L. Y. Chiang, J. W. Swirczewski, C. S. Hsu, S. K. Chowdhury, S. Cameron and K. Creegan, *J. Chem. Soc., Chem. Commun*., 1992, 1791.

3 R. D. Bolskar, R. S. Mathur and C. A. Reed, *J. Am. Chem. Soc*., 1996, **118**, 13 093.

4 C. Siedschlag, H. Luffman, C. Wolff and J. Mattay, *Tetrahedron*, 1997, **53**, 3587.

5 (*a*) A. G. Avent, P. R. Birkett, J. D. Crane, A. D. Darwish, G. J. Langley, H. W. Kroto, R. Taylor and D. R. M. Walton, *J. Chem. Soc., Chem. Commun*., 1994, 1463; (*b*) P. R. Birkett, A. G. Avent, A. D. Darwish, H. W. Kroto, R. Taylor and D. R. M. Walton, *Tetrahedron*, 1996, **52**, 5235; (*c*) P. R. Birkett, A. G. Avent, A. D. Darwish, I. Hahn, H. W. Kroto, G. J. Langley, J. O'Loughlin, R. Taylor and D. R. M. Walton, *J. Chem. Soc., Perkin Trans. 2*, 1997, 1121

6 E. W. Godly and R. Taylor, *Pure Appl. Chem*., 1997, **69**, 1411.

7 J. R. Morton, K. F. Preston, P. J. Krusic, S. A. Hill and E. Wasserman, *J. Phys. Chem*., 1992, **96**, 3576.

8 P. von R. Schleyer, R. C. Fort, Jr., W. E. Watts, M. B. Comisarow and G. A. Olah, *J. Am. Chem. Soc*., 1964, **84**, 4195.

9 H. Ikura, S. Mori, M. Sawamura and E. Nakamura, *J. Org. Chem*., 1997, **62**, 7912.

Received in Liverpool, UK, 10th August 1998; 8/06336B

Anomalous rearrangements in the reaction of acylpolysilanes with $TMSNTf_2$

Malcolm B. Berry,[b] Russell. J. Griffiths,[a] Dmitrii S. Yufit[a] and Patrick G. Steel*[a]†

[a] *Department of Chemistry, University of Durham, Science Laboratories, South Road, Durham, UK DH1 3LE*
[b] *GlaxoWellcome Research and Development, Gunnels Wood Road, Stevenage, Herts, UK SG1 2NY*

Reaction of acylpolysilanes with silylbistriflimides (R_3SiNTf_2) leads to novel silanols *via* a pathway involving two 1,2-migrations of Me_3Si groups from silicon to carbon and one migration of a R_3SiO unit from carbon to silicon; the X-ray structure of one example is reported.

In the course of an investigation of the use of silenes as reagents for novel transformations in organic synthesis we had need to generate silenes from acylpolysilanes in what is effectively a 1,3 silyl migration.[1] This is normally achieved through either thermal (T = *ca*. 180 °C) or photochemical initiation.[1,2] Neither of these methods is compatible with the range of functionality which we wished to explore. Consequently, in order to determine whether it was possible to generate silenes through the Lewis acid promoted 1,3-silyl shift of acylpolysilanes, we investigated the reaction of benzoylpolysilane with silyl based Lewis acids (TMSOTf, $TMSNTf_2$). Here we report that there is no evidence for the formation of silenes in this process (neither silene adducts nor silene dimers are detected) but rather a series of 1,2-migrations occurs to generate a silenium ion intermediate which subsequently undergoes nucleophilic capture.

Initial experiments involved the addition of trimethylsilyl triflate (TMSOTf) to a mixture of the polysilane and piperylene. However, these reactions were complicated by extensive diene polymerisation. Consequently we turned to the use of the corresponding silylbistriflimides (R_3SiNTf_2), readily available from the corresponding allylsilane and bis(trifluoromethylsulfonyl)imide, which has been reported to be more tolerant with respect to alkene polymerisation.[3] Whilst this strategy proved to be no more successful than TMSOTf in inhibiting diene degradation, addition of $TMSNTf_2$ to a solution of the polysilane in CH_2Cl_2 at −78 °C afforded a deep red colour. After stirring at this temperature for 12 h, aqueous workup followed by flash column chromatography afforded a colourless crystalline material in near quantitative yield. Infra-red spectroscopy revealed the presence of an OH group, whilst mass spectroscopy showed a molecular ion at *m/z* 442 which corresponded to the starting material plus Me_3SiOH. Chemical analysis confirmed this formula. However it proved difficult to fit this data with the NMR spectra which showed four $SiMe_3$ units and five different silicon signals. Fortunately it proved possible to grow crystals suitable for X-ray diffraction,‡ which revealed the structure as the silanol **2a** (Fig. 1).§

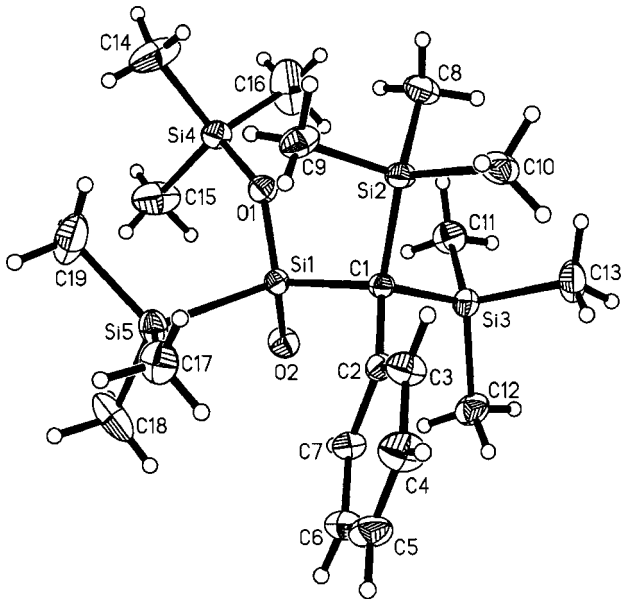

Fig. 1 Molecular structure of **2a**

In order to verify that this was a general procedure we then repeated this experiment with various other acylpolysilanes (Table 1). Whilst 4-trifluoromethylbenzoylpolysilane **1b** and acetylpolysilane **1d** gave similar products, pivaloylpolysilane **1e** failed to react and the 4-methoxyphenyl analogue **2c** underwent rapid decomposition on attempted isolation. To account for these observations we suggest that the reaction follows the pathway outlined in Scheme 1. Initial activation of the carbonyl group by the Lewis acid generates the oxacarbenium ion **5** which is stabilised by three β-Me_3Si units and R^1. In the situation in which the neighbouring alkyl group provides no stabilisation there is no reaction (R = Bu^t). Two successive 1,2 migrations of a trimethylsilyl group from silicon to carbon accompanied by a 1,2 shift of a trimethylsilyloxy group from carbon to silicon then occur. Similar migrations of trimethylsilyl groups from silicon to an adjacent cationic centre are precedented.[4–7] The precise order of these events is not clear and these may be either concerted or stepwise pathways. Whilst a silyl cation may be invoked as an intermediate in this process we have obtained no evidence for this and Lewis base coordinated species **6** and **8** (X = NTf_2^- or $RCOSiR'_3$) are probably more plausible. The resultant 'silenium ion' complex **8** is then hydrolysed by water on aqueous workup to produce the observed silanol. Use of MeOH in this final step leads to the

Table 1 Reaction of acylpolysilanes **1** with trialkylsilylbistriflimides

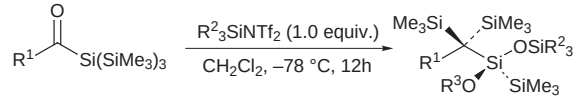

2 $R^2{}_3Si$ = Me_3Si, R^3 = H
3 $R^2{}_3Si$ = Me_3Si, R^3 = Me
4 $R^2{}_3Si$ = Bu^tMe_2Si, R^3 = H

Entry	**1**	R^1	$R^2{}_3Si$	Product	Yield (%)[a,b]
1	**1a**	Ph	Me_3Si	**2a**	93
2	**1a**	Ph	Me_3Si[c]	**2a**	9
3	**1a**	Ph	Me_3Si	**3a**	89[d]
4	**1a**	Ph	Bu^tMe_2Si	**4a**	84
5	**1b**	*p*-$CF_3C_6H_4$	Me_3Si	**2b**	82
6	**1c**	*p*-$MeOC_6H_4$	Me_3Si	**2c**	—[e]
7	**1d**	Me	Me_3Si	**2d**	77
8	**1e**	Bu^t	Me_3Si	**2e**	n.r.

[a] Yields refer to purified isolated compounds. [b] All products gave satisfactory spectroscopic and analytical data. [c] 10 mol% of $TMSNTf_2$ was used. [d] MeOH was added as the quenching agent. [e] Product decomposed on attempted isolation.

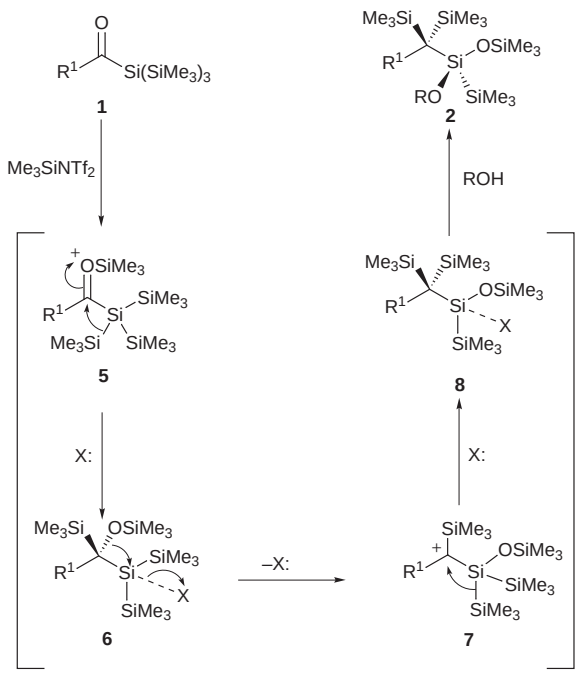

Scheme 1 Mechanistic pathway for the reaction of acylpolysilanes **1** with trialkylsilylbistriflimides

corresponding methoxide analogue **3a** in equally good yield (Table 1, entry 3). Further evidence in support of this pathway come from the use of TBMSOTf as the Lewis acid. As predicted this leads to complete incorporation of the TBDMS group at the silyloxy position (Table 1, entry 4) as confimed by ^{29}Si NMR spectroscopy (**4a**: OSiBu^{t}Me$_2$ δ 9.48; **2a**: OSiMe$_3$ δ 5.44). Furthermore, use of substoichiometric quantities of the initiator produces the same product in a corresponding yield together with recovered starting material (Table 1, entry 2).

Similar structures have been reported by Brook in the reaction of tertiary alkyl acylpolysilanes (R = Bu^t, adamantyl and bicyclo[2.2.2]octyl) with $TiCl_4$.[4] This was accounted for by a similar mechanistic pathway although, in this latter case, a 1,3 methyl shift from one of the trimethylsilyl groups to the 'silenium ion' also occurs. The reason for this difference between the $TiCl_4$ and the bistriflimide promoted pathways is not obvious at the present time.

In conclusion we report a novel rearrangement of acylpolysilanes on reaction with silyl triflates. Attempts to tune this reactivity to generate silenes in a convenient fashion are in progress and will be reported in due course.

We thank GlaxoWellcome and the EPSRC for financial support of this work (studentship to R. J. G. and funding for D. S. Y., repectively), the EPSRC mass spectrometry service at Swansea for accurate mass determinations, Dr A. M. Kenwright and Mr I. H. McKeag for assistance with NMR experiments and Dr M. Jones for mass spectra. The referees are thanked for helpful comments regarding the mechanism of this transformation.

Notes and References

† E-mail: p.g.steel@durham.ac.uk

‡ *Crystal data* for **2a**: $C_{19}H_{42}O_2Si_5$, M = 442.98, monoclinic, space group $P2_1/n$, a = 15.3270(1), b = 10.6851(1), c = 16.8596(1) Å, β = 105.50(1)°, U = 2659.5(9) Å^3, $F(000)$ = 968, Z = 4, D_c = 1.106 mg m^{-3}, μ = 0.28 mm^{-1} (Mo-Kα, λ = 0.71073 Å), T = 120(1) K, 33156 reflections (1.60 ≤ θ ≤ 30.5°) were collected on a Siemens SMART-CCD diffractometer (ω-scan, 0.3° per frame) yielding 7534 unique data (R_{merg} = 0.047). The structure was solved by direct-methods and refined by full-matrix least-squares on F^2 for all data using SHELXL software. All non-hydrogen atoms were refined with anisotropic displacement parameters, H-atoms were located on the difference map and refined isotropically. The H-atom of the OH group could not be located reliably and was not included in the refinement. Final $wR_2(F^2)$ = 0.1095 for all data (399 refined parameters), conventional $R(F)$ = 0.0411 for 5539 reflections with $I \geqslant 2\sigma$, GOF = 1.119. The largest peak on the residual map (0.62 e Å^{-3}) is located on the middle of one of the Si–Si bonds. CCDC 182/1000.

§ Attempts to achieve this transformation using TMSOTf afford a viscous oil which has similar spectroscopic properties to **2a** but whose structure is currently undefined. Details will be given in a full paper.

1 A. S. Batsanov, I. M. Clarkson, J. A. K. Howard and P. G. Steel, *Tetrahedron Lett*., 1996, **37**, 2491.
2 A. G. Brook, J. W. Harris, J. Lennon and M. El Sheikh, *J. Am. Chem. Soc*., 1979, **101**, 83.
3 B. Mathieu and L. Ghosez, *Tetrahedron Lett*., 1997, **38**, 5497.
4 A. G. Brook, M. Hesse, K. M. Baines, R. Kumarathasan and A. J. Lough, *Organometallics*, 1993, **12**, 4259.
5 M. Kumada, J. Nakajima, M. Ishikawa and Y. Yamamoto, *J. Org. Chem*., 1958, **23**, 292.
6 K. Sternberg, M. Michalik and H. Oehme, *J. Organomet. Chem*., 1997, **533**, 265.
7 K. Sternberg and H. Oehme, *Eur. J. Inorg. Chem*., 1998, 177.

Received in Liverpool, UK, 29th July 1998; 8/05966G

Electrorheological behaviour at low applied electric fields of microcrystalline cellulose in BP oils

Jayne L. Davies, Ian S. Blagbrough*† and John N. Staniforth

Department of Pharmacy and Pharmacology, University of Bath, Bath, UK BA2 7AY

Electrorheological fluids have been prepared at low applied electric fields from BP oils containing microcrystalline cellulose (MCC); even at a low applied electric field of 500 V mm^{-1}, 10% MCC in oils rich in linoleic or oleic acids behave as electrorheological fluids with the latter displaying significantly higher yield stresses.

Electrorheology describes the rapid and reversible change in viscosity exhibited by certain suspensions of solid particles in electrically non-conducting liquids upon application of an electric field. Electrorheological (ER) fluids can run freely like water, ooze like honey or solidify like gelatine, depending upon the applied electric field. Winslow pioneered the use of ER fluids in the 1940s, with mechanical engineering applications ranging from a simple hydraulic valve[1] to a complex tracking device for copying machines.[2] The appeal of ER fluids is the rapid response, usually on the millisecond time scale, upon application of an electric field,[3–5] and this response is completely reversible upon removal of the electric field.[5,6] Although typically the electric fields necessary to provide an ER effect are in the region of 1–5 kV mm^{-1}, the power consumption is small (mW).[7]

Traditionally, ER fluids are composed of a dispersed particulate phase,[7,8] in the size range 0.5 to 100 μm, in an insulating base fluid.[9–11] In the absence of an electric field, most ER fluids behave, to a first approximation, as Newtonian fluids. When a continuous DC electric field E is applied to an ER fluid and the fluid is sheared in a direction perpendicular to the field, the relationship between the stress τ and the shear rate γ can be described by the Bingham model. According to this equation, flow only occurs once the applied stress exceeds the static yield stress $\tau_\gamma(E)$. The flow equation is given in eqn. (1), where η_B is

$$\tau(E) = \tau_\gamma(E) + \eta_B\gamma \quad (1)$$

termed the Bingham viscosity. We are investigating the feasibility of using ER fluids as controllable drug delivery systems. In the absence of an electric field, a basal level of drug release will occur by diffusion across a mesh electrode. It is envisaged that upon application of an electric field, drug release will be controlled (hindered or halted).

We initially selected the pharmaceutically acceptable tablet excipient microcrystalline cellulose (MCC) in silicone oil as our ER fluid. This ER fluid has been recently reported, but only under high electric fields (in the range 1–3 kV mm^{-1}).[12,13] This project encompasses the search for pharmaceutically acceptable alternatives to traditional (engineering based) ER base fluid components. Thus, silicone oil (100 cS) or an alternative oil was used as the base fluid, together with sieved MCC (size fraction below 45 μm).‡ We have investigated the use of super refined BP oils as substitutes for silicone oil.‡ Oleic acid [(*Z*)-octadec-9-enoic acid] is the major constituent of apricot kernel (68%),[14] safflower (63%),‡ peanut (56%),[15] and sesame seed oils (45%).[15] Linoleic acid [(*Z*,*Z*)-octadeca-9,12-dienoic acid) is the primary constituent of sweet almond oil (75%)[16] and soyabean oil (50%).[15] In pharmaceutics, peanut and sesame seed oils find their uses as vehicles for sustained-release intramuscular injections.[16] Almond oil is also used as a vehicle for injections[17] and soyabean oil has replaced peanut oil in total parenteral nutrition regimens.[15]

A CSL^2 rheometer (TA Instruments, Leatherhead, UK) has been specially modified to allow the application of an electric field across the test fluid. A small electrolyte reservoir (approximately 0.5 ml) containing a 0.1% w/v solution of aq. KCl was used to form the electrical connection between the power supply (Model PS350 High Voltage Power Supply, Stanford Research Systems, Sunnyvale, CA, USA) and the rheometer geometry. The draw rod is insulated except for the threaded portion at the tip which makes contact with the geometry. In our experiments, we used a small volume (*ca*. 3.5 ml) concentric cylinder where the diameters of the cup and bob were 9.33 and 8.60 mm, respectively, resulting in a gap of 730 μm. All ER fluids were prepared using 10% w/w MCC (sieve fraction below 45 μm) in the appropriate oil, then sonicated (Decon FS300b) for two periods of 15 min prior to analysis. Temperature equilibration (37 ± 0.1 °C) of the sample was carried out for 15 min under the influence of an applied electric field (500 V mm^{-1}) prior to measurement. A continuous ramp of shear stresses from 0 to 50 Pa at a rate of 0.1 Pa s^{-1} was applied to each ER fluid with the resultant shear rate measured. A flow curve was plotted (Fig. 1) and the yield stress was determined by extrapolation of the experimental shear stress–shear rate data to zero shear rate using the Bingham model. Five measurements from each sample were taken and the associated mean and standard deviation were calculated (see Table 1).

In these studies, we have shown that, at a low applied electric field of 500 V mm^{-1}, suspensions of 10% w/w MCC in a range of BP oils behave as ER fluids. Furthermore, in general, BP oils afforded a higher Bingham yield stress than silicone oil (see Table 1), typically 12 Pa compared to 9 Pa. Using the ANOVA

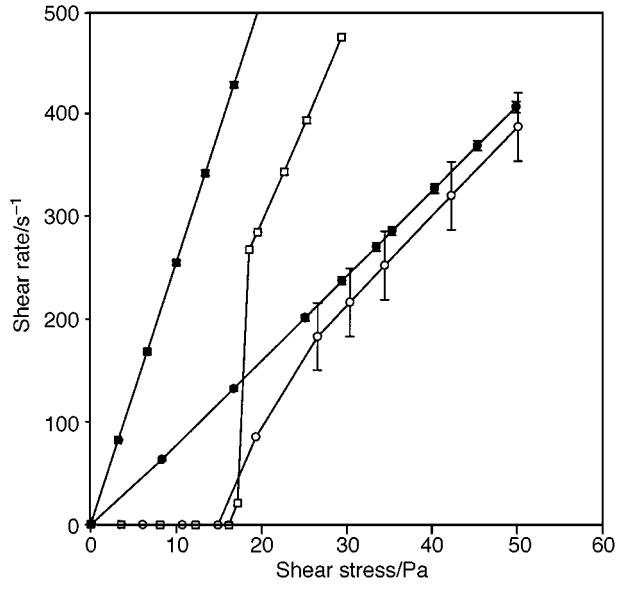

Fig. 1 Comparison of the flow behaviour at 0 V mm^{-1} [(●) silicone oil; (■) sesame seed oil] and 500 V mm^{-1} [(○) silicone oil; (□) sesame seed oil]

Table 1 The Bingham yield stress values for 10% w/w MCC in various oils at 500 V mm^{-1} (n = 5)

Oil	Bingham yield stress/Pa	Standard deviation
Almond	8.79	0.29
Apricot	12.54	0.39
Peanut	12.78	0.33
Safflower	12.17	0.47
Sesame seed	12.27	0.12
Silicone	8.94	0.26
Soyabean	10.53	0.37

test (one way), it was found that there were statistical differences ($p < 0.05$) between the oils. A Fisher analysis was carried out to highlight where differences were present. No significant difference ($p < 0.05$) was found between almond oil and silicone oil. Apricot oil, peanut oil, safflower oil, and sesame seed oils were also found not to be significantly different. In the light of these findings, we conclude that the BP oils which have oleic acid as the major constituent have significantly higher yield stress values compared with the BP oils having linoleic acid as their major constituent. Preliminary studies, using a parallel plate geometry, with 10% MCC in oleic and linoleic acids (*ca.* 95%)‡ also exhibited an ER response at 250 V mm^{-1}. This demonstration of ER responses below 1 kV mm^{-1}, using pharmaceutically acceptable oils, should find ready applications.[18–22]

We thank Hoechst Marion Roussel (Swindon, UK, and Kansas City, USA) for funding this studentship (to J. L. D.). We gratefully acknowledge the support and interest of Dr David Jordan (HMR, Swindon) in our studies.

Notes and References

† E-mail: prsisb@bath.ac.uk

‡ *Reagents*: Microcrystalline cellulose (MCC) (Lot No: E5D7C21, Emcocel 50M, Mendell, Patterson, NY, USA); 100 cS silicone oil, oleic and linoleic acids (Aldrich, Gillingham, UK); super refined BP oils (Croda Oleochemicals, Goole, UK).

1 W. M. Winslow, *U.S. Pat.* 2,417,850 (1947); W. M. Winslow, *J. Appl. Phys*., 1949, **20**, 1137.
2 Z. P. Schulman, R. G. Gorodkin, E. V. Korobko and V. K. Gleb, *J. Non-Newtonian Fluid Mech*., 1981, **8**, 29.
3 J. E. Stangroom, *Phys. Technol*., 1983, **14**, 290.
4 T. C. Halsey, *Science*, 1992, **258**, 761.
5 K. D. Weiss and J. D. Carlson, *Int. J. Mod. Phys. B*, 1992, **6**, 2609.
6 N. Webb, *Chem. Br*., 1990, **26**, 338.
7 H. Block and J. P. Kelly, *J. Phys. D., Appl. Phys*., 1988, **21**, 1661.
8 T. C. Jordan and M. T. Shaw, *IEEE Trans. Electr. Insul*., 1989, **24**, 849.
9 F. Pool, *Science*, 1990, **247**, 1180.
10 F. Filisko, *Chem. Ind*., 1992, **10**, 370.
11 K. O. Havelka and J. W. Pialet, *Chemtech*, 1996, **26**, 36.
12 K. Yatsuzuka, K. Miura, N. Kuramoto and K. Asano, *IEEE Trans. Ind. Gen. Appl*., 1995, **31**, 457.
13 A. Kawai, K. Uchida, K. Kamiya, A. Gotoh, K. Urabe and F. Ikazaki, *Int. J. Mod. Phys. B*, 1996, **10**, 2849.
14 A. Femenia, C. Rossello, A. Mulet and J. Canellas, *J. Agric. Food Chem*., 1995, **43**, 356.
15 *Handbook of Pharmaceutical Excipients*, a joint publication of the American Pharmaceutical Association and the Royal Pharmaceutical Society of Great Britain, Pharmaceutical Press, London, UK, 1994.
16 *British Pharmacopoeia*, Her Majesty's Stationery Office, London, UK, 1993.
17 *Pharmaceutical Codex*, 11th edn, The Pharmaceutical Press, London, 1983.
18 L. Marshall, C. F. Zukoski and J. W. Goodwin, *J. Chem. Soc., Faraday Trans*., 1989, **85**, 2785.
19 M. V. Gandhi and B. S. Thompson, *Electrorheological Fluids*, in *Smart Materials and Structures*, Chapman and Hall, London, UK, 1992.
20 M. Parathasarathy and D. J. Klingenberg, *Mater. Sci. Eng*., 1996, **17**, 57.
21 T. Hao, *Appl. Phys. Lett*., 1997, **70**, 1956.
22 K. Bohon and S. Krause, *J. Polym. Sci*., 1998, **36**, 1091.

Received in Cambridge, UK, 19th August 1998; 8/06533K

Bismuth(III) thioether chemistry: the synthesis and structure of $[Bi_4Cl_{12}(MeSCH_2CH_2CH_2SMe)_4]_n{\cdot}nH_2O$, a highly unusual network involving Bi_4Cl_4 rings and bridging dithioether ligands

Anthony R. J. Genge, William Levason and Gillian Reid*

Department of Chemistry, University of Southampton, Highfield, Southampton, UK SO17 1BJ. E-mail: gr@soton.ac.uk

The structure of $[Bi_4Cl_{12}(MeSCH_2CH_2CH_2SMe)_4]_n{\cdot}nH_2O$ involves $Bi_4Cl_{12}(\eta^1\text{-}MeSCH_2CH_2CH_2SMe)_4$ tetrameric units which are linked by bridging dithioether ligands to give a three-dimensional polymeric network; the Bi_4Cl_4 core is an eight-membered heterocycle which adopts an open cradle conformation.

With the exception of complexes with phosphine and amine ligands,[1,2] the coordination chemistry of the heavier p-block elements such as bismuth is rather poorly developed. A small number of Bi^{III} complexes involving macrocyclic thioethers has been described, including $[BiCl_3([9]aneS_3)]$ ([9]aneS$_3$ = 1,4,7-trithiacyclononane),[3] $[BiCl_3([12]aneS_4)]$ ([12]aneS$_4$ = 1,4,7,10-tetrathiacyclododecane)[4] and $[BiCl_3([18]aneS_6)]$ ([18]aneS$_6$ = 1,4,7,10,13,16-hexathiacyclooctadecane).[5] Macrocyclic ligands however offer enhanced binding properties over acyclic ligands, are conformationally less flexible than their acyclic counterparts and often exhibit different binding modes. Structural studies have shown that these macrocyclic Bi species are discrete molecular entities, with coordination numbers varying from six to nine. As part of our investigation into thio-, seleno- and telluro-ether complexes with p-block elements we report here the preparation and structure of a very unusual Bi^{III} compound $[Bi_4Cl_{12}(MeSCH_2CH_2CH_2SMe)_4]_n{\cdot}nH_2O$. Other than the macrocyclic compounds described above, the only structurally characterised Bi^{III} thioether complex is $[Bi_2I_8(SMe_2)_2][SMe_3]_2$.[6]

Reaction of $BiCl_3$ with 1 mol equiv. of $MeSCH_2CH_2CH_2SMe$ in CH_2Cl_2 affords a light yellow solution. Following filtration and concentration of the solution, the flask was left to stand for several days during which yellow crystals of a compound with the formula $[BiCl_3(MeSCH_2CH_2CH_2SMe)]{\cdot}H_2O$ were isolated in *ca.* 20% yield. The IR spectrum shows the presence of the dithioether, as well as several peaks in the range 300–230 cm^{-1} assigned to Bi–Cl stretching vibrations. Microanalyses are also consistent with the above formulation. Traces of moisture in the CH_2Cl_2 probably account for the associated water. A single crystal X-ray structure determination† revealed a three-dimensional polymeric network with the structural formula $[Bi_4Cl_{12}(MeSCH_2CH_2CH_2SMe)_4]_n{\cdot}nH_2O$. The structure involves $Bi_4Cl_{12}(MeSCH_2CH_2CH_2SMe)_4$ tetrameric units (related by crystallographic $\bar{4}$ symmetry) which are linked by bridging dithioether ligands to give a three-dimensional polymeric network [Fig. 1(a) and (b)]. Each Bi^{III} ion is therefore coordinated to two terminal Cl atoms, Bi–Cl(2) 2.538(7), Bi–Cl(3) 2.533(7) Å, two μ_2 bridging Cl atoms, Bi–Cl(1) 2.913(7), Bi–Cl(1*) 2.969(6) Å, and two S-donors from different bridging dithioether ligands, Bi–S(1) 2.857(7), Bi–S(2*) 2.977(7) Å. The geometry at each Bi atom therefore approximates to a severely distorted octahedron, with an open triangular face which we assume is occupied by the Bi lone pair. The μ_2-bridging Bi–Cl distances are much longer than the terminal distances and are themselves only slightly different, hence an alternative description is that the structure comprises of $[BiCl_2(\eta^1\text{-}MeSCH_2CH_2CH_2SMe)_2]^+$ cations loosely associated into tetramers through interactions with chloride anions, Cl(1) and Cl(1*). There are additional long range, weak interactions which link the μ_2-bridging Cl atoms to Bi centres across the Bi_4Cl_4 ring, forming a pseudo-cuboid arrangement, Bi···Cl(1*) 3.268(7) Å. This interaction is significantly longer than one would expect for a genuine μ_3-bridging Cl.[7] The

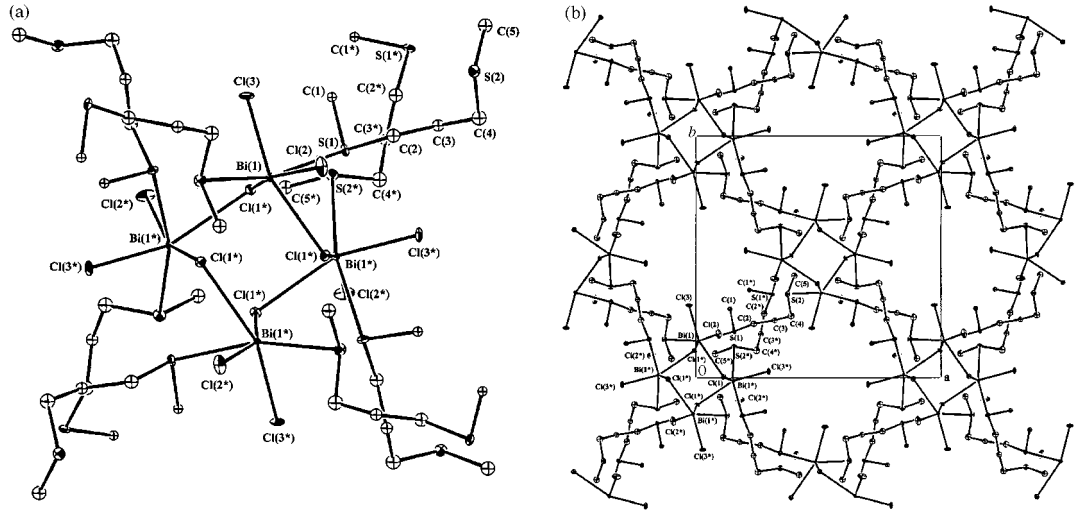

Fig. 1 (*a*) View of a portion of the $[Bi_4Cl_{12}(MeSCH_2CH_2CH_2SMe)_4]_n$ structure with the numbering scheme adopted (H atoms are omitted for clarity and atoms marked with an asterisk are related by a crystallographic $\bar{4}$ operation). Selected bond lengths (Å): Bi–Cl(1) 2.913(7), Bi–Cl(2) 2.538(7), Bi–Cl(3) 2.533(7), Bi–S(1) 2.857(7), Bi–S(2*) 2.977(7) Å. (*b*) View down the *c*-axis of the three-dimensional polymer, illustrating the channels running through the structure.

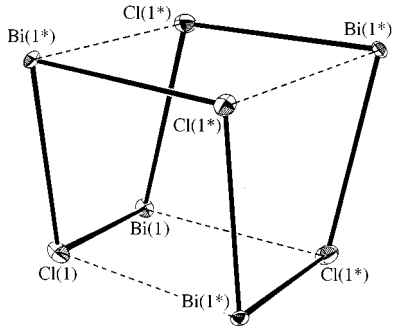

Fig. 2 View of the Bi_4Cl_4 core, illustrating the open cradle conformation. The dashed lines indicate the secondary Bi···Cl interactions.

Bi_4Cl_4 core forms an eight-membered heterocyclic ring which, as a result of the weak Bi···Cl interactions adopts an open cradle conformation (Fig. 2). The secondary Bi···Cl(1*) interaction is in the general direction of the void assumed to be occupied by the lone pair, but not in the direction of the maximum electron density. This behaviour is commonly observed in Bi^{III} and Sb^{III} chemistry.[8]

Bismuth halides often form compounds incorporating partially condensed Bi_4X_4 polyhedra,[7] however, the open cradle or pseudo-cuboid arrangement adopted in the title compound is very unusual. The Bi–S and $Bi–Cl_{terminal}$ bond lengths are similar to those observed in the reported macrocyclic thioether complexes of Bi^{III}, *e.g.* seven-coordinate $[BiCl_3([12]aneS_4)]$ [Bi–S 2.987(3)–3.072(3), Bi–Cl 2.569(4)–2.575(3) Å] and nine-coordinate $[BiCl_3([18]aneS_6)]$ [Bi–S 3.146(4)–3.225(4), Bi–Cl 2.607(4) Å]. The polymeric network arises due to incorporation of bridging $MeSCH_2CH_2CH_2SMe$ ligands. We have shown previously that this and other related group 16 donor ligands can bind to Cu^{I} and Ag^{I} centres and in a small number of cases also yield complex polymeric arrays, although quite different in detail from the title compound.[9]

Further work is underway to establish whether this highly unexpected structural motif is replicated in other Bi^{III} complexes with group 16 donor ligands, and to understand the factors which influence the assembly of supramolecular arrays of this type.

We thank the University of Southampton and the EPSRC for support and thank one of the referees for helpful comments on the structural description.

Notes and References

† *Crystal data* for $C_5H_{12}BiCl_3S_2·H_2O$, M = 469.62, tetragonal, space group $P\bar{4}2_1c$, a = 16.440(10), c = 11.843(7) Å, V = 3200 Å^3, Z = 8, D_c = 1.949 g cm^{-3}, μ(Mo-Kα) = 117.26 cm^{-1}. A pale yellow block (0.40 × 0.35 × 0.10 mm) grown by slow evaporation of a solution of the compound in CH_2Cl_2 was mounted on a Rigaku AFC7S four-circle diffractometer. Data collection at 150 K using Mo-Kα X-radiation (λ = 0.710 73 Å), gave 1668 unique reflections of which 1183 with $F \geqslant 4\sigma(F)$ were used in all calculations. The structure was solved using direct methods[10] and developed by iterative cycles of least-squares refinement[11] and difference Fourier synthesis which revealed a $BiCl_3(MeSCH_2CH_2CH_2SMe)$ unit and a water molecule in the asymmetric unit. Crystallographic $\bar{4}$ symmetry generates the tetrameric unit and the three-dimensional array. The data were corrected for absorption using DIFABS[12] with the model at isotropic convergence (max., min. transmission factors = 1.000, 0.309, respectively). Some of the C atoms in the ligand backbone show quite high thermal motion, although alternative sites could not be identified, hence these were refined isotropically. Anisotropic thermal parameters were refined for the Bi, Cl and S atoms and H atoms associated with the dithioether were included in fixed, calculated positions (the H atoms associated with the H_2O solvent molecule were not located). At final convergence, R = 0.050, R_w = 0.066, S = 1.80 for 79 parameters. CCDC 182/1002.

Satisfactory spectroscopic and analytical data were obtained.

1 N. C. Norman and N. L. Pickett, *Coord. Chem. Rev.*, 1995, **145**, 27.
2 See: C. A. McAuliffe, in *Comprehensive Coordination Chemistry*, ed. G. Wilkinson, R. D. Gillard and J. A. McCleverty, Pergamon, New York 1987, vol. 3, ch. 28.
3 G. R. Willey, M. T. Lakin, M. Ravindran and N. W. Alcock, *J. Chem. Soc., Chem. Commun.*, 1991, 271.
4 G. R. Willey, M. T. Lakin and N. W. Alcock, *J. Chem. Soc., Dalton Trans.*, 1992, 591.
5 G. R. Willey, M. T. Lakin and N. W. Alcock, *J. Chem. Soc., Dalton Trans.*, 1992, 1339.
6 W. Clegg, N. C. Norman and N. L. Pickett, *Polyhedron*, 1993, **12**, 1251.
7 For examples see: A. L. Rheingold, A. D. Uhler and A. G. Landers, *Inorg. Chem.*, 1983, **22**, 3255; G. R. Willey, H. Collins and M. G. B. Drew, *J. Chem. Soc., Dalton Trans.*, 1991, 961.
8 J. F. Sawyer and R. J. Gillespie, *Prog. Inorg. Chem.*, 1986, **34**, 65.
9 J. R. Black, N. R. Champness, W. Levason and G. Reid, *J. Chem. Soc., Dalton Trans.*, 1995, 3439; J. R. Black, N. R. Champness, W. Levason and G. Reid, *Inorg. Chem.*, 1996, **35**, 1820; 1996, **35**, 4432.
10 SHELXS86, Program for Crystal Structure Solution, G. M. Sheldrick, University of Cambridge, 1986.
11 TeXsan: Crystal Structure Analysis Package, Molecular Structure Corporation, Texas, 1995.
12 N. Walker and D. Stuart, *Acta Crystallogr., Sect. A*, 1983, **39**, 158.

Received in Basel, Switzerland, 21st July 1998; 8/05674I

On the efficacy of propeller-shaped, C_3-symmetric triarylphosphines in asymmetric catalysis

Mark T. Powell, Alexander M. Porte and Kevin Burgess*

Department of Chemistry, Texas A & M University, PO Box 300012, College Station, TX 77842-3012, USA.
E-mail: burgess@chemvx.tamu.edu

Ligand sets 1 and 2 were prepared and examined for evidence of C_3-symmetric propeller-shaped conformations in solution, and for their ability to induce enantioselectivity in an allylation reaction.

There are conflicting arguments with regard to the potential of optically pure, C_3-symmetric triarylphosphines in asymmetric syntheses. Some researchers may correctly point to the value of C_2-ligands[1] and claim that application of C_3-ligands is a logical extrapolation of the field. C_3-Symmetric arrangements of three aromatic groups around a central atom can adopt stable enantiomeric propeller-shaped conformations that might provide chiral pockets to facilitate enantiodiscrimination.[2] However, the contrary argument is also convincing. Asymmetric induction cannot increase indefinitely with the symmetry of the chiral directing group because a perfectly spherical object would be useless for inducing a chiral environment.

Experimentally, the value of optically active, propeller-shaped, C_3-symmetric phosphines is hard to assess. This is because of synthetic difficulties associated with obtaining the requisite ligands, and due to a lack of techniques to recognize rigid propeller conformations in solution. Sharpless and co-workers, for instance, prepared triarylphosphine cage structures (an example is shown below) by relatively difficult synthetic routes.[3,4] They then found that in an optically active complex, this ligand stereomutates between enantiomeric propeller-shaped conformations at room temperature. This ligand design therefore did not facilitate a test of the efficacy of propeller-shaped C_3-symmetric ligands, hence their value remained questionable. The work described in this manuscript deals with attempts to address this issue using phosphines **1** and **2**. The tenet of this project is that a chiral substituent on the aromatic rings could be easily installed, and may lead to stable C_3-symmetric propeller-shaped aryl arrays in the ligand.

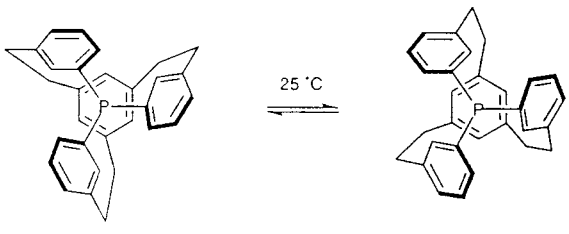

an easily racemized C_3 ligand from Sharpless

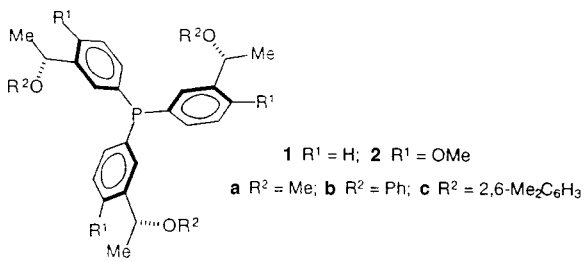

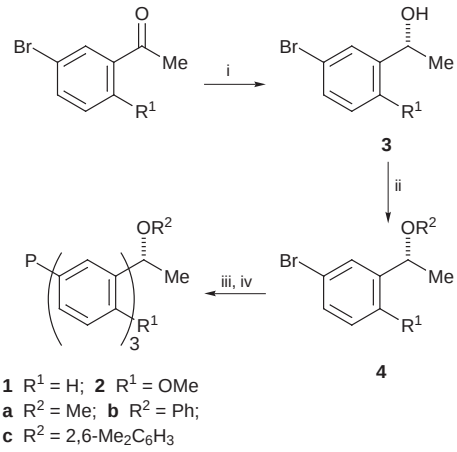

Scheme 1 *Reagents and conditions*: i, $BH_3{\cdot}SMe_2$, 5 mol% 4,5,6,7-tetrahydro-1-methyl-3,3-diphenyl-1*H*,3*H*-pyrrolo[1,2]-[1,3,2]oxazaborolebornane (CBS),[8] CH_2Cl_2, −25 °C, 12 h (94% and 96.2% ee for **1**; 85%, 99% ee for **2**); ii, alkylation (yields range from 70 to 99%, *e.g.* MeI, NaH, DMF for **1a**); iii, ^{t}BuLi, Et_2O, −30 °C, 1 h; iv, PCl_3, Et_2O, −30 to 25 °C (yields typically 30–50% for steps iii and iv)

Scheme 1 outlines the route by which the ligand set **1a–1c** (and later **2a–2c**) was obtained. The route diverges from the common chiral alcohol intermediate **3** hence this strategy is more efficient than ones that rely on different starting materials for each phosphine prepared.

Evidence for preferred stereoisomeric propeller-shaped conformations in solution is hard to obtain. Crystallographic studies of derivatives such as complex **5a** (Fig. 1) indicated the desired conformations exist in the solid state, but these observations can give no indication of their dynamic behavior in solution. Consequently, a set of circular dichroism (CD) spectra was recorded to elucidate solution state conformations. Chiral ordering of the aromatic groups should be accompanied by

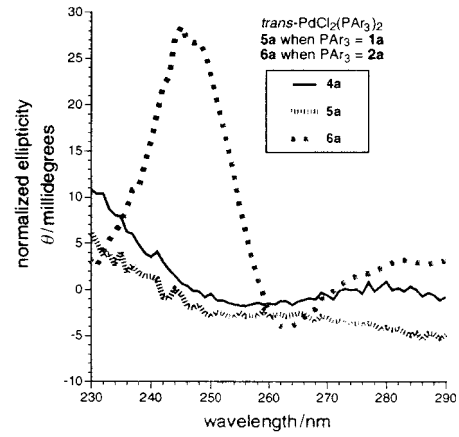

Fig. 1 Comparison of normalized ellipticities (*i.e.* ellipticities per mole of aromatic ring) for compounds **4a**, **5a** and **6a**

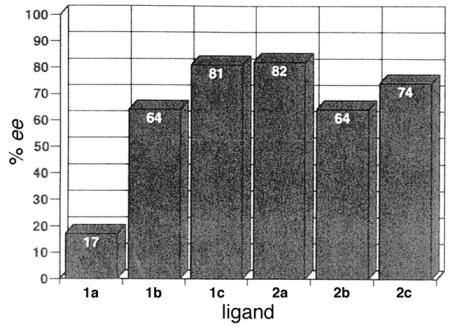

Fig. 2 Phosphines **1** and **2** in an allylation reaction (unoptimized yields, measured by GC using an internal standard: **1a**, 72%; **1b**, 33%; **1c**, 54%; **2a**, 50%; **2b**, 51%; **2c**, 47%)

increased molar ellipticities at wavelengths corresponding to aromatic absorptions for palladium complex **5a** relative to the aryl bromide starting material **4a**.[5] Fig. 1 shows that an increased ellipticity was not observed for complex **5a** derived from ligand **1a**. This led us to suppose that conformational rigidity could be increased by incorporation of a *para*-substituent to disfavor free rotation about the bond to the *meta*-chiral center. Consequently, ligand set **2** was prepared and selected derivatives were examined by CD. Fig. 1 indicates that complex **6a** derived from ligand **2a** does indeed show an enhanced ellipticity relative to intermediate **4a**.

High throughput parallel screens[6] were used to test ligands **1** and **2** in the palladium mediated allylation reaction illustrated below. Thus reactions were run simultaneously in wells contained in a cooled aluminium block, then analyzed using an autosampler/chiral HPLC apparatus. Details of this approach applied in other studies from our group have been documented.[7] Fig. 2 shows the data obtained. The enantioselectivities reached an optimum value of 82%. We think that this level of induction by the distal chiral *meta*-substituents would not be possible unless ordering of the aromatic rings were operative. Enhanced ellipticities when a *para*-substituent is present (*i.e.* **2a** *vs.* **1a**) correlates with dramatically increased enantioselectivities. On average, higher enantioselectivities tend to be observed for the ligands **2** than for series **1**.

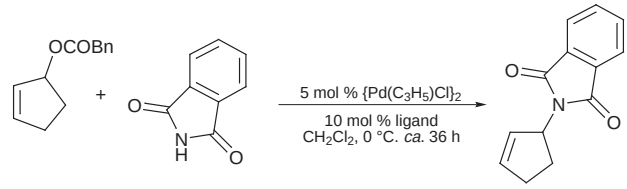

The data presented here suggest that phosphines **2** can exist in conformations in which the aromatic groups are ordered in propeller-shaped arrays, and that these same phosphines give significant induction in an allylation reaction. However, it is unlikely that perfectly C_3-symmetric conformations predominate for ligand **2** in complexes because the *meta*-substituent can adopt orientations that are *exo* and *endo* with respect to the metal. Work now in progress concerns a ligand system for which this is not a possibility.

We thank Marcel Jaspars for some informative preliminary experiments. Support for this work was provided by The Petroleum Research Fund administered by The American Chemical Society, and by The Robert A. Welch Foundation. K. B. thanks the NIH Research Career Development Award, and The Alfred P. Sloan Foundation for a fellowship.

Notes and References

1 J. K. Whitesell, *Chem. Rev.*, 1989, **89**, 1581.
2 C. Moberg, *Angew. Chem., Int. Ed. Engl.*, 1998, **37**, 248.
3 C. Bolm and K. B. Sharpless, *Tetrahedron Lett.*, 1988, **29**, 5101.
4 C. Bolm, W. D. Davis, R. L. Haltermann and K. B. Sharpless, *Angew. Chem., Int. Ed. Engl.*, 1988, **27**, 835.
5 J. W. Canary, C. S. Allen, J. M. Castagnetto and Y. Wang, *J. Am. Chem. Soc.*, 1995, **117**, 8484.
6 K. Burgess, D. Moye-Sherman and A. M. Porte, *Molecular Diversity and Combinatorial Chemistry*, American Chemical Society, Washington DC, 1996, pp. 128–136.
7 A. M. Porte, J. Reibenspies and K. Burgess, *J. Am. Chem. Soc.*, in press.
8 D. J. Mathre, A. S. Thompson, A. W. Douglas, K. Hoogsteen, J. D. Carroll, E. G. Corley and E. J. J. Grabowski, *J. Org. Chem.*, 1993, **58**, 2880.

Received in Bloomington, IN, USA, 24th April 1998; 8/06811I

Formation of oligomers of methyl- and phenyl-pyrrole at an electrified liquid/liquid interface

Vincent J. Cunnane*† and Una Evans

Advanced Sensors Research Unit, Department of Chemical and Environmental Sciences, University of Limerick, Limerick, Ireland

The formation of oligomers of 1-methylpyrrole and 1-phenylpyrrole has been initiated by a heterogeneous electron transfer (HET) step at the interface of two immiscible electrolyte solutions; the HET leads to the formation of a radical cation of the monomer in the organic phase.

In 1975 Guainazzi *et al.*[1] reported that a direct current applied across the liquid/liquid interface of a heterogeneous, unreactive $Cu^{2+}/[V(CO)_6]^-$ redox system, with $CuSO_4$ in the aqueous phase and tetrabutylammonium hexacarbonylvanadate in a 1,2-dichloroethane (DCE) phase, led to the deposition of a copper layer at the interface. More recently electrochemical–chemical (EC) type mechanisms have been reported for such liquid/liquid interfaces.[2,3] Here we report on a novel EC type reaction between an aqueous redox couple and a monomer in DCE leading to oligomer formation in the organic phase, where for the first time the electrochemical step is an electron transfer.

A general scheme for the equilibrium condition for the two phase electron transfer reaction [eqn. (1)] where a reducible

$$n^2O^{1(w)} + n^1R^{2(o)} \leftrightarrow n^1O^{2(o)} + n^2R^{1(w)} \quad (1)$$

species O^1 in the aqueous phase reacts with an oxidisable species R^2 in the organic phase can be expressed in terms of individual ionic activities and the Galvani potential of each phase, leading to a Nernst type equation of the form shown in eqn. (2), where $E°_i$ is the standard potential of the couples in

$$\Delta^w{}_o\phi = E°_{R^2/O^2} - E°_{R^1/O^1} + (RT/n^1n^2F)\ln J_a \quad (2)$$

each phase, R is the gas constant, T is the absolute temperature, F the Faraday constant and J_a is given by eqn. (3), where a is the

$$J_a = a^{n^2}{}_{R^1}a^{n^1}{}_{O^2}/a^{n^2}{}_{O^1}a^{n^1}{}_{R^2} \quad (3)$$

activity of the species in each phase. As such, the position of equilibrium in a two phase redox system is dependent on the values of the standard potentials and also on the interfacial Galvani potential difference.[4] Hence for a given system the position of equilibrium can be determined by an externally imposed Galvani potential difference, using standard electrochemical instrumentation. A HET reaction can thus be observed in the available potential window by careful matching of the standard potentials of the redox couples in each phase.

Cyclic voltammetry (CV) was the main technique used. A flat water/1,2-DCE interface with an area of 0.125 cm^2 was formed in a four electrode cell. The potential difference at the interface was controlled using a four electrode potentiostat (Model 2000, Sycopel Scientific Ltd., Boldon).

DCE (Fluka 99.5% GC grade) was used as received as the organic solvent in all experiments. 18.2 MΩ water used throughout and was prepared using the Maxima ultra pure water system. Li_2SO_4 (Fluka > 98.0%) was used as received as the aqueous supporting electrolyte. Tetraphenylarsonium chloride (TPAsCl) (Fluka, 95%) was used as received in the organic reference phase. Tetraphenylarsonium tetrakis(4-chlorophenyl)borate (TPAsTCPB) was the supporting electrolyte in the organic phase and was prepared using TPAsCl and sodium tetrakis(4-chlorophenyl)borate (NaTCPB) (Fluka > 98.0%). Ferrous sulfate·$7H_2O$(Aldrich 99+%), ferric sulfate·$5H_2O$(Aldrich 97%), 1-methylpyrrole (MPy, Aldrich 99%) and 1-phenylpyrrole (PPy, Aldrich 99%) were also used as received.

To measure the half-wave potentials ($E_{1/2}$) of the aqueous redox couples and the oxidation potentials of the monomers in DCE a 10 μm platinum microelectrode was used. The $E_{1/2}$ of oxidation of 1-methylpyrrole and 1-phenylpyrrole, in the organic electrolyte system, were found to be 750 and 720 mV *vs.* SCE, respectively. Fe^{2+}/Fe^{3+} in the form of $Fe_2(SO_4)_3$/$Fe(SO_4)$ was chosen as the aqueous redox couple as it has a closely matching halfwave potential, with an $E_{1/2}$ of 650 mV *vs.* SCE in the aqueous electrolyte system.

The cell used to observe the electron transfer is shown in Scheme 1,where the monomer is 1-methylpyrrole or 1-phenylpyrrole and δ represents the interface.

Pt/10 mmol Li_2SO_4 + 10 mmol $Fe_2(SO_4)_3$ and 10 mmol $FeSO_4$ (aq)/δ/1 mmol TPAsTCPB + 0.5 mmol monomer (DCE)/1 mmol TPAsCl (aq)/AgCl/Ag

Scheme 1

When the aqueous redox couple is present and in the absence of monomer in the organic phase no charge transfer is observed in the potential window of interest and also no charge transfer is observed when the monomer is present but in the absence of the aqueous redox couple.

When both the aqueous redox couple and monomer are present a charge transfer reaction occurs, this is shown in Fig. 1(*a*). It was found that on continuous cycling the shape of the CV trace changes to give a characteristic S-shaped curve [Fig 1 (*b*)].

From eqn. (2) it can be seen that for a HET reaction, changing the ratio of concentrations of the aqueous redox couple should change the $E_{1/2}$ of the electron transfer reaction and, as can be seen from Tables 1 and 2, this is indeed the case.

Table 1 shows the variation of $E_{1/2}$ for the charge transfer reaction with varying Fe^{III}:Fe^{II} when the cell is: Pt/10 mmol Li_2SO_4 + *x* mmol $Fe_2(SO_4)_3$ and *y* mmol $FeSO_4$ (aq)/δ/1 mmol TPAsTCPB + 0.5 mmol MPy (DCE)/1 mmol TPAsCl (aq)/AgCl/Ag.

Table 2 shows the variation of $E_{1/2}$ for the electron transfer reaction with varying Fe^{III}:Fe^{II} when the cell is: Pt/10 mmol Li_2SO_4 + *x* mmol $Fe_2(SO_4)_3$ and *y* mmol $FeSO_4$ (aq)/δ/1 mmol TPAsTCPB + 0.5 mmol PPy (DCE)/1 mmol TPAsCl (aq)/AgCl/Ag.

Table 1 Variation of $E_{1/2}$ with varying Fe^{III}:Fe^{II} for the charge transfer reaction with MPy

Ratio Fe^{3+}:Fe^{2+}	$Fe_2(SO_4)_3$/ mmol	$Fe(SO_4)$/ mmol	$E_{1/2}$/mV
1:5	1	10	565
2:1	10	10	640
4:1	10	5	660
10:1	10	2	No e-transfer

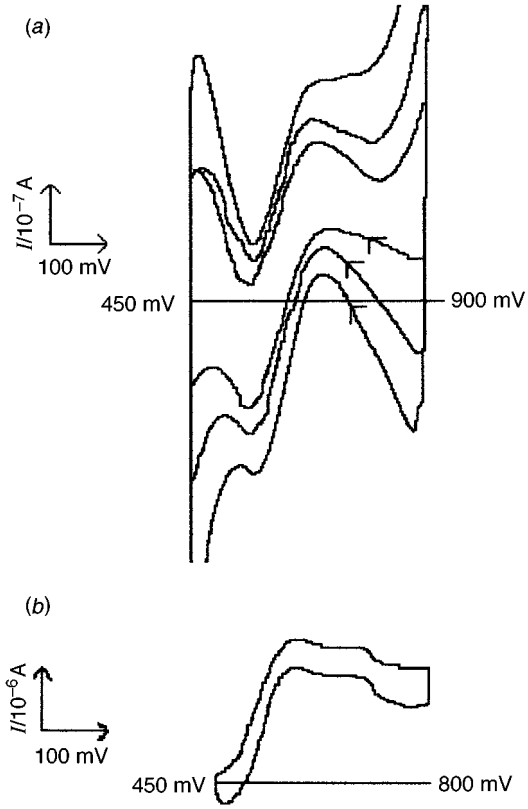

Fig. 1 (*a*) Cyclic voltammograms of the system: Pt/10 mmol Li_2SO_4 + 10 mmol $Fe_2(SO_4)_3$ and 10 mmol $FeSO_4$ (aq)/δ/1 mmol TPAsTCPB + 0.5 mmol MP (DCE)/1 mmol TPAsCl (aq)/AgCl/Ag. Sweep rates: 10, 25 and 50 mV s^{-1}. (*b*) Cyclic voltammogram of the system: Pt/10 mmol Li_2SO_4 + 10 mmol $Fe_2(SO_4)_3$ and 10 mmol $FeSO_4$ (aq)/δ/1 mmol TPAsTCPB + 5 mmol MP (DCE)/1 mmol TPAsCl (aq)/AgCl/Ag after cycling for 30 min at a sweep rate of 100 mV s^{-1}.

The changing shape of the cyclic voltammogram suggested that the electron transfer reaction is not reversible and that the organic phase changes throughout the experiment. UV–VIS spectroscopy was used to study the organic phase. The organic phase was removed from the cell and transferred to a quartz cuvette.

The 1-methylpyrrole monomer shows a characteristic peak at 247 nm when dissolved in DCE. On addition of the base electrolyte salt TPAsTCPB this characteristic monomer peak disappears and a new peak is detected at 271 nm. The disappearance of the monomer peak is probably due to the fact that this sample is blanked using 10 mmol TPAsTCPB, which absorbs in the region below 300 nm. After cycling for 10 min a peak is detected at 293 nm and after 20 min of cycling a peak is detected at 309 nm.

Table 2 Variation of $E_{1/2}$ with varying Fe^{III}:Fe^{II} for the electron transfer reaction with PPy

Fe^{3+}:Fe^{2+}	$Fe_2(SO_4)_3$/ mmol	$Fe(SO_4)$/ mmol	$E_{1/2}$/mV
1:5	1	10	No e-transfer
2:1	10	10	630
20:1	10	1	690

The 1-phenylpyrrole monomer shows a characteristic peak at 260 nm when dissolved in DCE. On addition of the base electrolyte salt TPAsTCPB a peak is observed at 292 nm. After cycling for 10 min a peak is detected at 304 nm, which does not change significantly with further cycling.

Rohde *et al*.[5] reported that the absorbtion maxima of oligomers of 1-methylpyrrole increase with increasing chain length. They found that 1-methylpyrrole monomer has a λ_{max} value of 250 nm increasing to λ_{max} of 290 nm for oligomers with eight methylpyrrole units. They extrapolated the λ_{max} of the insulating polymer, an oligomer of infinite chain length, to be 310 nm.

This change in λ_{max} is observed here for 1-methylpyrrole (and 1-phenylpyrrole) with increasing cycling time. This is an indication that oligomers are being formed in the organic phase.

We have shown for the first time that an electron transfer reaction can be brought about between an aqueous-based redox system and an organic-based monomer unit at an electrified liquid/liquid interface. It is presumed that the electron transfer results in the formation of a radical cation in the organic phase. This radical cation will then undergo various chemical steps leading to the formation of oligomers in the organic phase. Further research is investigating the nature of the oligomers formed and their conducting properties. The system is being expanded to look at other electroactive monomer and organic systems.

This work was supported by Forbairt Scientific Programme (SC/95/255) and by the EU-TMR Network, ODRELLI (ERBFMRXCT960078).

Notes and References

† E-mail: vincent.cunnane@ul.ie

1 M. Guainazzi, G. Silvestri and G. Serravale, *J. Chem. Soc., Chem. Commun*., 1975, 201.
2 E. Wang and Y. Liu, *Electrochim. Acta*, 1990, **35**, 1965.
3 A. K. Kontturi, K. Kontturi, L. Murtomaki and D. J. Schiffrin, *Electrochim. Acta*, 1995, **91**, 3433.
4 V. J. Cunnane, D. J. Schiffrin, C. Beltran, G. Geblewicz and T. Solomon, *J. Electroanal. Chem*., 1988, **247**, 203.
5 N. Rohde, M. Eh, U. Geiβler, M. L. Hallensleben, B. Voigt and M. Voigt, *Adv. Mater*., 1995, **7**, 401–404.

Received in Cambridge, UK, 5th August 1998; 8/06365F

ChemComm
FEATURE ARTICLE

‘Oxo-hydroxo tautomerism’ as useful mechanistic tool in oxygenation reactions catalysed by water-soluble metalloporphyrins

Jean Bernadou*† and Bernard Meunier*†

Laboratoire de Chimie de Coordination du CNRS, 205 route de Narbonne, 31077 Toulouse cedex 4, France

High valent metal–oxo species have been evoked as active intermediates in many different oxidation reactions using manganese or iron porphyrin complexes as catalysts and oxygen atom donors (H_2O_2, PhIO, NaOCl, $KHSO_5$, ... *etc*.) or dioxygen associated to a reductant as oxygen atom source. When these metalloporphyrin-catalysed oxidations are performed in water, such metal–oxo species are able to transfer an oxygen atom coming from either the oxygen source or from bulk water. This fact has been explained by the so-called oxo–hydroxo tautomerism, a mechanism involving a rapid shift of two electrons and one proton from a hydroxo ligand (electron-rich ligand formed by deprotonation of an aqua ligand) to the trans oxo species (electron-poor ligand) leading to the transformation of the hydroxo ligand into an electrophilic oxo entity on the opposite side of the initial oxo. This ‘oxo–hydroxo tautomerism’, evidenced by using ^{18}O-labelled water, has been used as mechanistic tool to unambiguously characterize oxygen atom transfer mechanisms mediated by metal–oxo species in opposition to mechanisms related to free radical oxidation reactions.

Introduction

High-valent metal–oxo intermediates play an important role in catalytic processes involving dioxygen activation and O-atom transfer reactions performed by hemoproteins such as cytochromes P-450 and some peroxidases.[1,2] For example, the so-called Compound I of peroxidases (Cpd I), with two oxidizing equivalents above the ferric state, has been characterised in horseradish peroxidase as an iron(IV)–oxo porphyrin π cation radical, and the great reactivity of P-450 is believed to derive from a formal iron(V)–oxo porphyrin species acting as ultimate oxidant.[3–6] Compound II (Cpd II), the second catalytic intermediate of peroxidases, is an iron(IV)–oxo with only one oxidizing equivalent above the resting state of the corresponding native heme–enzyme. There is no Cpd II intermediate in the catalytic cycle of cytochrome P-450.

$Por\text{-}Fe^{III}$
native state of P-450 or peroxidase

$Por\text{-}Fe^{V}{=}O$ or $(Por^{\bullet+})Fe^{IV}{=}O$ — P-450 active species or Cpd I

$Por\text{-}Fe^{IV}{=}O$ — Cpd II

The recent discovery of oxo–hydroxo tautomerism can contribute to a better characterisation and an improved understanding of chemical reactivities of these high-valent metal–oxo species, not only important for the knowledge of heme-enzymes catalyzing oxidations, but also in the design of efficient biomimetic or bioinspired oxidation catalysts. After a short survey on the characteristics of high-valent metal–oxo complexes, this Feature Article will be focused on the oxo–hydroxo tautomerism.

High-valent metal–oxo species in heme-enzymes and related chemical models

The oxidative reactions mediated by cytochrome P-450 are better described with an iron(V)–oxo as active entity than with any other putative species. Taking in consideration all the different experimental data accumulated for the last three decades on cytochrome P-450, it is reasonable to assume that hydroxylation of alkanes, epoxidation of electron-rich alkenes and formation of *N*-oxides are performed by an electrophilic high-valent iron(V)–oxo rather than by a nucleophilic Fe^{III}–OOH intermediate. The high oxidation state of iron in the perferryl $Fe^{V}{=}O$ species might be reduced by transfering one electron from the sulfur atom of the cysteinato proximal ligand, or from the porphyrin ligand like in peroxidases [ferryl is used for an iron(IV)–oxo species; perferryl is used for an iron(V)–oxo species or an iron(IV)–oxo with a radical cation on the macrocyclic ligand, like in Cpd I of peroxidases].[5b,7] This audacious hypothesis has been supported by establishing in 1975 that a single oxygen atom donor, namely iodosylbenzene PhIO, was a suitable co-factor for a P-450 mediated O-dealkylation reaction.[8] Then, the modeling of peroxide shunt in the catalytic cycle of cytochrome P-450 (short cycle in Scheme 1)

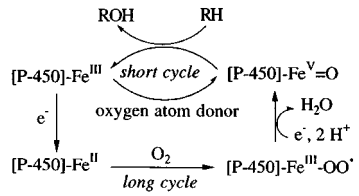

Scheme 1 Catalytic cycle of cytochrome P-450 with the formation of an iron(V)–oxo species (or an iron(IV) radical-cation as in Cpd I of peroxidases) *via* a ‘long catalytic cycle’ with dioxygen, two electrons and two protons or *via* a ‘short cycle’ (peroxide shunt) with oxygen atom donors (PhIO, NaOCl, $KHSO_5$, H_2O_2)

was demonstrated with synthetic metalloporphyrins using PhIO, NaOCl, $KHSO_5$ or H_2O_2.[2,5b,9–12] There is no physical characterisation of the putative iron(V)–oxo for cytochrome P-450 itself because of its very short lifetime, but its orbital diagram based on different calculations has been described by several groups.[13,14] The reactive high-valent iron or manganese–oxo species are usually depicted with a double-bond between the metal and the oxygen atom [complex **A** in Scheme 2, case of an iron(V)–oxo species]. This classical way to represent a metal–oxo bond is convenient to describe the oxidation state of the metal, but one drawback is that the same formalism is used for the non-labile $Ti^{IV}{=}O$ derivative as for the highly reactive $Fe^{V}{=}O$ or $Mn^{V}{=}O$ complex. In fact, the electronic structure of the form **A** with a metal–oxygen double bond is probably higher in energy than the diradical form **B**, an iron(IV)–oxoid species, in a similar way as singlet dioxygen, with a double bond, is higher in energy by 23 kcal mol^{-1} (1 cal = 4.184 J) compared to the triplet ground state, with a single O–O bond and two unpaired electrons (the name ‘oxoid’ underlines the reduction of the bond order between the metal

Form **A** ('singlet state') Form **B** ('triplet state')
d^3 iron(V)–oxo d^4 iron(IV)–oxoid

Scheme 2 Different representations of high-valent iron–oxo entities: form **A** with a double Fe–O bond and form **B** with a diradical and a single Fe–O bond (for a discussion on these two different electronic configurations of iron–oxo species, see ref. 13). X = anionic axial ligand.

center and the oxygen atom). So, the ground state of the high-valent iron–oxo species of cytochrome P-450 will ressemble the diradical Fe^{IV}–O· (for **B**) whereas Fe^{V}=O with a formal double bond (form **A**) represents an excited state. However, Schwarz and coworkers have recently proposed that both states of the perferryl entity will be involved in catalytic hydroxylations, with a spin inversion during the reaction.[13]

The high-valent iron–oxo species of Cpd I of peroxidases (horseradish peroxidase HRP, ligninase, . . . *etc.*) has a lifetime which is long enough to allow the collection of physical data by different methods: UV–VIS, EPR, magnetism, resonance Raman, X-ray absorption and Mössbauer.[2] All these different methods confirmed that Cpd I of horseradish peroxidase is a perferryl species with a radical-cation on the porphyrin ligand $(Por^{\cdot+})Fe^{IV}$=O. X-Ray absorption[15] and resonance Raman[16] studies respectively indicated that the Fe=O bond distance was 1.6 Å with a vibration at 737 cm^{-1}. The π-radical-cation of Cpd I has a predominant $^2A_{2u}$ character, indicative of an electron abstraction from the a_{2u} orbital of the porphyrin ligand.[17] This porphyrin radical is weackly ferromagnetically coupled with the spin $S = 1$ of the ferryl state.[18] It should be noted that HRP is unable to catalyze O-atom transfer reactions, in contrast to chloroperoxidase, suggesting that the lability of the high-valent iron–oxo is mainly controlled by the axial ligand (both chloroperoxidase and cytochrome P-450 have a cysteine as proximal ligand, instead of a histidine for a horseradish peroxidase).[19,20] The reduced accessibility for substrates in HRP can not be the only factor to explain the absence of oxygenation activity for this enzyme, since the amino acids of the distal site responsible for the heterolytic cleavage of the peroxidic O–O bond are not oxidized during the catalytic cycle of HRP despite their close interactions with the active site.

Since the pioneering work of Groves *et al.*[3] on the characterisation of an iron(IV)–oxo radical-cation porphyrin complex, many groups have focused their efforts on the isolation and the description of chemical models of heme-enzymes. In all these model systems, the exchange between the spin $S = 1$ of the ferryl group with the spin $S' = 1/2$ of the porphyrin radical-cation was found to be strongly ferromagnetic in contrast to the weak ferromagnetic coupling usually observed with Cpd I derivatives.[21] The one-electron reduced complex, namely $(Por)Fe^{IV}$=O equivalent to a peroxidase Cpd II, which was described early in the cases of six-coordinate[22*a*] and five-coordinate[22*b*] porphyrin complexes, can be isolated by a reductive chromatography of $(Por^{\cdot+})Fe^{IV}$=O over basic alumina and is stable at room temperature.[22*c*] A $(Por)Mn^{IV}$=O complex has been characterised by X-ray absorption spectroscopy.[23] The Mn–O bond distance is 1.69 Å and the complex has a $S = 3/2$ spin state corresponding to a high spin d^3 configuration. Recently, it has been reported the detection and the characterization of a manganese(V)–oxo porphyrin complex by rapid-mixing stopped-flow spectrophotometry.[24]

High-valent iron–oxo complexes can be prepared with peracids *via* the intermediate formation of a acylperoxo–iron(III) porphyrin complex. This latter compound undergoes a heterolytic cleavage of the O–O bond in dichloromethane to provide the iron–oxo or a homolytic cleavage in toluene to give rise to a bridged *N*-oxide porphyrin.[25] It must be noted that all the high-valent metal–oxo porphyrin complexes are highly electrophilic and as such react with alkanes, alkenes or heteroatoms in contrast to the nucleophilic $(Por)Fe^{III}$–OOH complexes[26] (see also ref. 27 for the use of thianthrene-5-oxide as a probe to distinguish between electrophilic and nucleophilic oxidants).

The stability of high-valent iron– or manganese–oxo species is highly dependent on the nature of the ligands. An inert d^2 square-pyramidal manganese(V)–oxo stable at room temperature has been prepared with a diamido ligand[28] (see also ref. 29 for the design of robust ligands for oxidizing complexes). An additional example of lability *versus* stability of high-valent species is the case of nitrido–manganese(V) porphyrin complexes which is kinetically inert with organic substrates, but able to transfer the nitrido motif to chromium(III) porphyrin *via* a two-electron redox process mediated by a heterobimetallic μ-nitrido intermediate.[30] The same nitrido–manganese(V) porphyrin complexes can be transformed into nitrogen atom-transfer agents after acylation of the nitrido ligand to generate a labile acylimido–manganese(V) porphyrin complex.[31]

At the present stage of knowledge, the design of metal–oxo complexes able to efficiently catalyse oxygenations is still challenging, since all the parameters involved in the different O-atom transfer steps are not fully understood.

A new type of tautomerism: the oxo–hydroxo tautomerism

After the above reminders on high-valent metal-oxo porphyrin complexes, we wish now to report the recent discovery of an oxo–hydroxo tautomerism[32,33] and its utilisation as mechanistic tool in oxygenation reactions catalysed by water-soluble metalloporphyrins.

Using isotopically labelled oxidants or labelled water, it has been shown that the oxygen of the metal–oxo porphyrin complex can be quickly exchanged with water *via* the axial hydroxo ligand with reaction rates depending on the experimental conditions (pH, temperature, composition of the medium, nature of the axial ligands, . . .). We shall see that, using the label distribution in oxidation products modulated by this oxo–hydroxo tautomerism, it is possible to unambiguously distinguish between oxygenation reactions occurring *via* an oxygen transfer from a high-valent metal–oxo complex or *via* an autoxidation mechanism (see ref. 34 for a review on this controversial debate) in metalloporphyrin-catalysed oxygenations carried out in the presence of $H_2{}^{18}O$. For short, the phenomenon termed oxo–hydroxo tautomerism corresponds to a rapid shift of two electrons and one proton from a hydroxo ligand (electron-rich ligand) to the *trans* oxo species (electron-poor ligand) leading to the transformation of the hydroxo ligand into an electrophilic oxo entity on the opposite side of the initial oxo (Scheme 3). The main consequence of this tautomerism is the incorporation within the substrate of an oxygen atom coming from either the oxidant or from bulk water, respectively in the ratio 1 : 1. the degree of ^{18}O-exchange observed into the product (epoxide, alcohol, . . .) is then mechanistically informative.

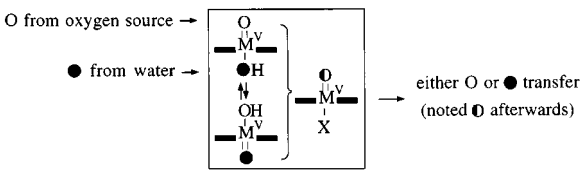

Scheme 3 The oxo–hydroxo tautomerism mediates the incorporation into the oxidation product of 50% of oxygen coming from the primary oxidant and 50% from water. X = hydroxo ligand.

Some previous data on O-exchange of metal–oxo species with bulk water

In the last fifteen years, several reports mentioned the use of ^{18}O-labelling experiments in order to characterize high-valent

metal–oxo species or to elucidate the mechanism of O-transfer by these reactive species. For reactions performed in the presence of water, results varied from 0 to 100% of O-incorporation form water, depending on the experimental conditions. Most of these results can be understood by reference to the oxo–hydroxo tautomerism (for detailed comments, see the paragraph on required conditions to observe oxo–hydroxo tautomerism) or on the basis of a direct O-exchange of the oxo ligand with the bulk water.

Most of the studies to determine the origin of the incorporated oxygen atom in alkene epoxidations or alkane hydroxylation catalysed by metalloporphyrins have been performed in organic solvents or biphasic media with hydrophobic complexes. From these data, it has been concluded that the oxygen atom originated from the primary oxidant (PhIO,[35] LiOCl,[36] $KHSO_5$[37]). When experiments are performed in water or in an organic solvent containing a sufficient amount of water, several reports suggested that high-valent metal–oxo complexes exchanged the coordinated oxygen atom with water (using either labelled water or labelled oxygen atom donor). As indicated in Scheme 4 for a theoretical 100% O-exchange with water, these

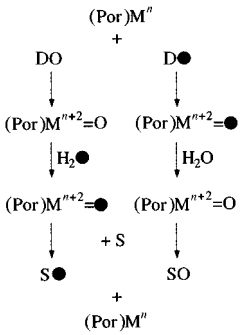

Scheme 4 Principle of labelling studies: case of theoretical 100% O-exchange with water. Unlabelled or ^{18}O-labelled water (H_2O and H_2●) and oxygen atom donor (DO and D●). [Por] = porphyrin ligand; S = substrate.

experiments were usually based on generating the active species with ^{18}O-labelled activating agent [H_2O_2; *m*-chloroperoxybenzoic acid (*m*-CPBA); O_2 in the presence of a reductant] and washing the label in the presence of unlabelled water, or at the reverse, using unlabelled oxidant and performing the reaction in ^{18}O-labelled water.

Resonance Raman investigations on Cpd II of HRP at pH 7, based on isotopic shift of the Fe^{IV}=O stretching mode of Cpd II ($\nu_{Fe=O}$ was observed at 774 cm^{-1} after activation with either $H_2{}^{16}O_2$ or $H_2{}^{18}O_2$ in $H_2{}^{16}O$, at 740 cm^{-1} for activation with either $H_2{}^{16}O_2$ or $H_2{}^{18}O_2$ in $H_2{}^{18}O$), provided evidence for the oxygen atom exchange between the heme-Fe^{IV}=O and bulk water (Table 1).[38] In a controversial manner, this exchange was

Table 1 Resonance Raman data on the possible exchange of the oxygen atom of high-valent metal–oxo species with bulk water

	$\nu_{M=^{16}O}$/ cm^{-1}	$\nu_{M=^{18}O}$/ cm^{-1}	Exchange	Ref.
Fe^{IV}=O (HRP Cpd II)	774	740	Yes	38
Fe^{IV}=O (diacetylheme HRP Cpd II)	781	745	No	39
Mn^{IV}=O (Mn subst HRP Cpd II)	626	596	No	39
$(Por^{\cdot+})Fe^{IV}$=O (TMP)	828	792	No	40

not observed in the case of stable species of diacetylheme or manganese substituted HRP: the Raman spectrum of Cpd II generated with $H_2{}^{16}O_2$ or $H2^{18}O_2$ presented lines at 781 or 745 cm^{-1} (diacetylheme HRP), at 626 or 596 cm^{-1} (Mn–HRP), respectively. No isotope-induced change was observed at neutral pH for 1 h at 4 °C in the presence of $H_2{}^{16}O$ or $H_2{}^{18}O$, indicating no appreciable exchange of the oxo entity with bulk water.[39] In studies performed at −80 °C on a ferryl porphyrin π-cation-radical derived from the synthetic (*meso*-tetramesitylporphyrinato)iron(III) chloride [(TMP)Fe^{III}Cl], the $\nu_{Fe=O}$ band was observed at 828 cm^{-1} (activation with [^{16}O]*m*-CPBA) or 792 cm^{-1} (activation with [^{18}O]*m*-CPBA), the first one remaining unshifted in the presence of $H_2{}^{18}O$; therefore the oxo oxygen atom was not easily exchanged with water under these conditions (Table 1).[40]

The O-exchange of metal–oxo with bulk water can also be monitored by analysing the label content of oxygenation products of reactions catalysed by synthetic metalloporphyrins. Groves *et al.*[3] reported that the high-valent iron–oxo complex generated in a first step from (TMP)Fe^{III}Cl with *m*-CPBA in an organic medium containing 1% $H_2{}^{18}O$ was able, in a second step, to epoxidize norbornene with a 99% ^{18}O-incorporation. This result allowed to discard the hypothesis of either free or metal coordinated peroxyacid as the oxygen transfer agent and support an high-valent iron–oxo intermediate with an oxygen exchangeable with added $H_2{}^{18}O_2$. Incorporation of ^{18}O from bulk water was further noticed[41] in the course of epoxidation of β-methylstyrene by manganese(V)–oxo porphyrin in CH_2Cl_2 saturated in $H_2{}^{18}O$, indicating here also a rather fast exchange of the oxo ligand with water. This ^{18}O-exchange was clearly slower in the case of manganese(IV) species and was inhibited by the presence of pyridine as axial ligand.[41,42]

Oxo-hydroxo tautomerism with water-soluble metalloporphyrins

Epoxidation reaction

We initially reported oxo–hydroxo tautomerism to explain isotopic results observed in aqueous phase during $KHSO_5$ epoxidation of carbamazepine (CBZ), an analgesic and anticonvulsivant drug, catalysed by a cationic water-soluble manganese porphyrin.[33] In such reaction performed at pH 5 in aqueous solution with various contents of $H_2{}^{18}O$, it was shown that half of the oxygen atoms incorporated in the epoxide came from the solvent (Fig. 1(*a*)]. It was checked that neither CBZ-

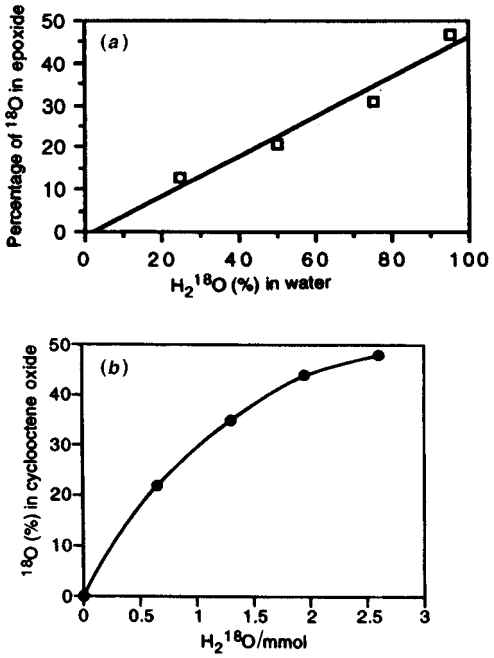

Fig. 1 (*a*) The amount of labelled oxygen found in CBZ oxide correlates with half the content of ^{18}O-label of water present in the reaction mixture. In abscisse: content (%) of $H_2{}^{18}O$ in water (from ref. 33 with permission from the American Chemical Society; see also ref. 44 for a similar correlation). (*b*) Dependence on a sufficient concentration of water in non-aqueous solvent to observe oxo-hydroxo tautomerism. In abscisse: 0.5, 1.0, 1.5, 2.0 and 2.5 mmol of $H_2{}^{18}O$ correspond to 1, 2, 3, 4 and 5 M $H_2{}^{18}O$ concentration, respectively; substrate concentration was 20 mM (from ref. 44 with permission from the American Chemical Society).

oxide[33] nor $KHSO_5$[37,43] exchanged oxygen atoms with water in the reaction conditions.

To explain the constant ratio of 0.5 for the incorporation of oxygen from the solvent, we proposed an oxo–hydroxo tautomerism mechanism[32] (formerly named 'redox tautomerism' in refs. 33, 43–47) involving a coordinated water molecule on the manganese(III) porphyrin precursor **1** (Scheme 5). It must

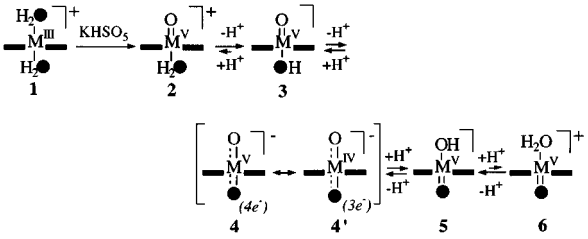

Scheme 5 General scheme for the oxo–hydroxo tautomerism

be noted that a 50% O-exchange corresponds only to the oxo–hydroxo tautomerism involving the hydroxo ligand *trans* to the high-valent metal–oxo complex, but not to a direct exchange of the oxo ligand with bulk water.

Mn(TMPyP), the pentaacetate of the diaquamanganese(III) derivative of *meso*-tetrakis(1-methyl-pyridinium-4-yl)porphyrin, can exist in aqueous medium with one or two metal-bound water molecules as axial ligands (**1** in Scheme 5; see ref. 48 for a X-ray structure of the bis-aqua-MnTMPyP complex). Increasing the metal oxidation state from III to V (going from the Mn^{III} complex **1** to the Mn^{V}=O **2**) should lower sufficiently the pK_a value of the ligated water to allow, at the pH of the reaction, its conversion into a hydroxo ligand (**3**; see ref. 49 for a discussion on the pK_a values of aqua and hydroxo ligands in high-valent metalloporphyrins). Removal of a proton from this hydroxo ligands results in the formation of the stabilized anion **4** with four electrons delocalized on both metal–oxygen bonds (**4′** is a mesomeric form with three delocalized electrons and manganese in the formal oxidation state IV). This anion can be protonated with the same probability at the end of one of the two metal–oxo-like bonds, giving rise to either form **3** or **5**, which reacts with CBZ to produce CBZ-oxide containing either ^{16}O or ^{18}O, respectively, in the ratio 1 : 1. The conversion of **3** to **5** does not necessarily involve **4** and **4′** as discrete deprotonated intermediates but might also proceed *via* a hydrogen-bonded water molecule in a more concerted fashion (Scheme 6).

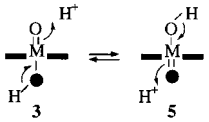

Scheme 6 Key step of the oxo–hydroxo tautomerism

Other recent reports support the concept of oxo–hydroxo tautomerism.[24,44,47] Groves *et al.*[24] reported also the ^{18}O-incorporation in CBZ-oxide in a Mn(TMPyP)-catalysed oxidation of CBZ *via* an oxo–hydroxo interconversion. Lee and Nam described similar ^{18}O-incorporation in cyclooctene epoxidation by either *m*-CPBA, H_2O_2 or Bu^tOOH catalysed by [*meso*-tetrakis(pentafluorophenyl)porphyrinato]iron(III) chloride $Fe^{III}(F_{20}TPP)Cl$, the reaction being performed in a MeOH–CH_2Cl_2 mixture containing 10% H_2O.[44] Even at low pH values, CBZ epoxidation data obtained in aqueous solutions by H_2O_2, Bu^tOOH or $KHSO_5$ in the presence of [*meso*-tetrakis(2,6-dichloro-3-sulfonatophenyl)porphyrinato]iron(III) chloride indicated that the oxo–hydroxo tautomerism was involved.[47] In these latter cases, the experiment strongly supported that a common high-valent iron–oxo species was generated from the different oxidants and was the reactive intermediate responsible for alkene epoxidation.

Hydroxylation reactions (Scheme 7)

The oxo–hydroxo tautomerism was further characterized in the oxidation of deoxyribose C–H bonds of DNA by the Mn(TMPyP)–$KHSO_5$ system.[45] Hydroxylation at carbon-1′ of

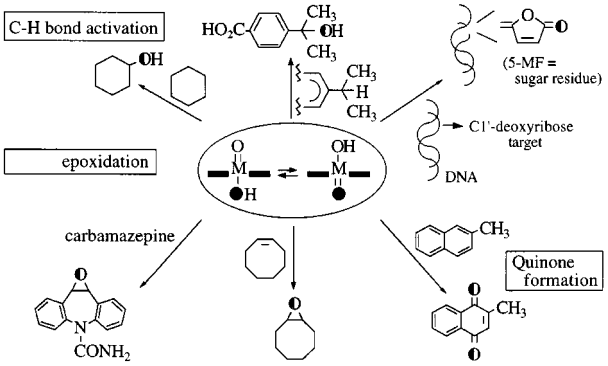

Scheme 7 Examples of oxo–hydroxo tautomerism from literature data. ○: unlabelled oxygen; ●: labelled oxygen; ◐: mixed labelled oxygen.

deoxyribose gave in several steps 5-methylene-2-furanone (5-MF), as final sugar residue. In the presence of labelled $H_2{}^{18}O$, 50% of oxygen coming from the primary oxidant (^{16}O from $KHSO_5$) and 50% from the solvent (^{18}O from $H_2{}^{18}O$) were incorporated in 5-MF, strongly supporting a metal–oxo mediated DNA cleavage with an oxo–hydroxo tautomerism to explain the ^{18}O-incorporation in the desoxyribose oxidation product. Another example came from the monopersulfate oxidation of 4-isopropylbenzoic acid performed in $H_2{}^{18}O$ and catalysed by the same water-soluble metalloporphyrin Mn(TMPyP).[43] In the primary hydroxylation product, 4-(1-hydroxy-1-methylethyl)benzoic acid, nearly half of the oxygen atoms incorporated in the alcohol function came from water. In the cyclohexane hydroxylation by *m*-CPBA catalysed by $Fe(F_{20}TPP)Cl$, the percentage of ^{18}O incorporated in cyclohexanol was also found to be close to 50%, with a reaction mixture containing only 10% of water.[44]

Quinone formation (Scheme 7)

In an aqueous solution the metalloporphyrin-catalysed oxidation of 2-methylnaphthalene to *p*-quinones involves two consecutive oxygen transfers from an intermediate metal–oxo entity responsible for 30 to 55% indirect incorporation of ^{18}O from water into the generated quinones.[46]

Required conditions to observed oxo-hydroxo tautomerism

An axial ligand competitive to the hydroxo ligand inhibits oxo–hydroxo tautomerism

In heme-enzymes, the presence of a cysteinato ligand (cytochrome P-450 or chloroperoxidase) or an imidazole from an histidine (peroxidase) prevents water from coordinating to iron. This implies that there is no possible exchange between high valent metal–oxo intermediates and water through an oxo–hydroxo tautomerism. From this point of view, the experimental data presented above in Table 1 on Cpd II of HRP is rather controversial and suggests that an exchange of the oxygen of the metal-oxo with bulk water on the distal side may occur in some conditions (probably *via* a *cis*-dihydroxo complex and not *via* a prototropy betwen the metal–oxo oxygen and the hydroxo ligand as in the oxo–hydroxo tautomerism).

With synthetic metalloporphyrins the situation is different. Iron and manganese porphyrins are known to form imidazole and pyridine complexes when these heterocycles are present in reaction mixtures. In the epoxidation of *cis*-β-methylstyrene with *m*-CPBA catalysed by $Mn^{III}(TMP)Cl$, the presence of pyridine completely prevents isotopic enrichment of epoxide products when the reaction is performed in the presence of

$H_2{}^{18}O$.[41] In the epoxidation of cyclooctene by Fe(F_{20}TPP)Cl and H_2O_2, it was found that effectively the ^{18}O-incorporation into the product diminished as the amount of 5-chloro-1-methylimidazole added to the reaction mixture increased.[44] So when the axial position opposition to the oxo group is blocked by a ligand (not derived from water), the oxo–hydroxo tautomerism cannot occur and consequently the oxygen incorporated in the oxidation product is 100% from the oxidant, instead of 50% from the oxidant and 50% from water (Scheme 8).

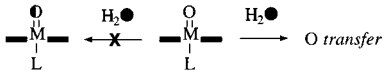

Scheme 8 Inhibition of the oxo–hydroxo tautomerism equilibrium in the presence of strong axial ligands. L = neutral ligand, *e.g.* pyridine or imidazole.

When there is no *trans* ligand, evidently the oxo–hydroxo tautomerism does not occur. But, when the *trans* ligand is a water molecule instead of an hydroxo ligand [see hereafter for a discussion on the case of metal(IV)–oxo species], the tautomerism is largely reduced. This may be an explanation why the oxo–hydroxo tautomerism was not observed during the oxidation of polycyclic aromatic hydrocarbons catalysed by iron tetrasulfophthalocyanine performed in the presence of $H_2{}^{18}O$ (the reactive species was shown to be Fe^{IV}=O)[50] or in cobalt-mediated alkene epoxidations with potassium monopersulfate[51] where the oxygen atom was coming only from the oxidant.

Competitive autoxidation route lowers incorporation of oxygen from water

Groves *et al.* noticed that during cyclooctene[41] or *cis*-β-methylstyrene[42] epoxidation by manganese(IV)–oxo porphyrin under aerobic conditions, dioxygen was intimately involved in the oxidation process with oxidation products partially resulting from an autoxidation process. Evidently, the consequence is a lowering in isotopic enrichment from solvent. During the monopersulfate oxidation of ketoprofen catalysed by Mn(TMPyP),[43] trapping of radical intermediates by molecular oxygen (route i, Scheme 9) was shown to compete with the oxygen rebound mechanism (route ii), explaining the observed reduction of ^{18}O-incorporation from solvent in the final product when ketoprofen was oxidised under air by the system Mn(TMPyP)–$KHSO_5$–$H_2{}^{18}O$ system.

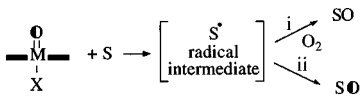

Scheme 9 Diverted autoxidation route lowers the oxygen incorporation rate. Route i: radical escaping from the solvent cage (autoxidation route); route ii: recombination within solvent cage (oxygen rebound mechanism).

Temperature effect

In order to characterize the high-valent reactive species formed by oxidative activation of metalloporphyrins, many experiments have been performed at low temperature with some of them concerning ^{18}O-incorporation into the products in the presence of $H_2{}^{18}O$. In the more extensive study, Lee and Nam[44] described the cyclooctene epoxidation by H_2O_2 or *m*-CPBA in the presence of Fe(F_{20}TPP)Cl at different temperatures. The ^{18}O-enrichment in the epoxide gradually increased as the reaction temperature raised from −78 to 45 °C. The authors suggested that an Fe^{III}–OOR species was involved at low temperature, with a rate of the O–O bond cleavage (leading to the high-valent iron–oxo porphyrin complex) lower than the oxygen atom transfer rate ($k_1 < k_3$ in Scheme 10). At higher

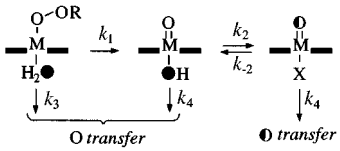

Scheme 10 Kinetic parameters depending on temperature. X = hydroxo ligand.

temperature the formation of the high-valent iron oxo porphyrin should be favored (increase of k_1). However, since tautomerism is a phenomenon highly dependent on temperature, the present results might alternatively be re-interpreted as a fast formation of the iron–oxo species ($k_1 > k_3$), even at low temperature, but with a slow prototropy ($k_2 < k_4$) at this teperature and a faster one ($k_2 > k_4$) at higher temperature (k_3 and k_4 = oxygen atom transfer rates; the best conditions to observe the oxo–hydroxo tautomerism correspond to $k_1 > k_3$ and $k_2 > k_4$). We must note that even at low temperature (−78 °C) iron–oxo porphyrin species have been detected and characterized.[3,21,22]

Differences in exchange kinetics for metal(IV)–oxo and metal(V)–oxo

From experiments conducted on *cis*-β-methylstyrene with manganese(V)–oxo and manganese(IV)–oxo porphyrin complexes, Groves *et al.* concluded from the ^{18}O results that, in addition to differences in oxygen transfer occurring with retention or loss of the stereochemistry, the manganese(IV)–oxo slowly exchanged its oxo ligand with $H_2{}^{18}O$, while the exchange was very fast for the manganese(V)–oxo complex.[41] These data are consistent with Schemes 5 and 11 and with

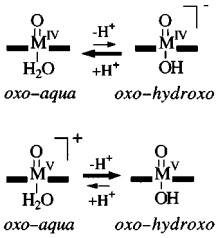

Scheme 11 Equilibria between oxo–aqua and oxo–hydroxo forms depending on the oxidation state of the metal center

literature data on the proton acidity of coordinated water in high-valent species:[49,52,53] going from **3** to **5** only needs a prototropy in the case of a manganese(V)–oxo species (Scheme 5 and 11; the oxo–hydroxo is the major form), whereas in the case of manganese(IV)–oxo (Scheme 11) the ligand *trans* to the oxo is mainly a water molecule owing to the lower acidity of the ligated water when the metal oxidation state is reduced. So, for manganese(IV)–oxo complexes, the oxo–hydroxo tautomerism can only affect the small fraction of metal–oxo species with an hydroxo ligand, the oxo–aqua form being dominant in this case.

Role of the ratio water/substrate concentrations

The percentage of ^{18}O incorporated in oxidation products might be governed by the relative rate to reach the tautomerism equilibrium (k_2 in Scheme 10) which is a function of the water concentration, and the rate of oxygen transfer (k_4) which depends on the substrate concentration. For reaction performed in an essentially aqueous medium (a 90% aqueous solution is 50 M in water) and a substrate rather diluted (*e.g.* 1 mM), the competition between the tautomerism and the oxygen transfer was not observed: the water/substrate molar ratio ($\approx 5 \times 10^4$) was largely in favor of the oxo–hydroxo tautomerism.[33] In an organic medium containing only a small amount of water and at high substrate concentrations, the situation is opposite and can affect the tautomerism equilibrium and consequently the level of ^{18}O-incorporation.[44] An example of such an extreme

condition concerns the epoxidation of 1 M cyclohexene solution in CH_2Cl_2–MeOH containing 5% of $H_2{}^{18}O$ with a metalloporphyrin catalyst and H_2O_2, Bu^{t}OOH or *m*-CPBA as oxygen donor. In these conditions, no ^{18}O-incorporation was observed in the epoxide (water/substrate molar ratio ≈ 3).[35] In intermediate conditions, such as in epoxidation of 20 mM cyclooctene with H_2O_2 catalysed by Fe(F_{20}TPP)Cl in an organic medium containing increasing amounts of water, the 50% O-incorporation from water was observed for a reaction mixture containing at least 10% of water [water/substrate molar ratio above 250; Fig. 1(*b*)].[44] In the rare case of a very small concentration of substrate, then the reaction becomes very slow and the aqua ligand (form **2** or **6** in Scheme 5) can exchange with water from solvent and the ^{18}O incorporation from solvent can raise above 50%.[44]

Other parameters to take into account

Probably several other parameters may influence the oxo–hydroxo tautomerism but no systematic study has been done up to now. Among them, the pH value of the reaction mixture plays surely a key role in this prototropy mechanism as also the nature of the metal and the ligand in the metalloporphyrins through their capacity to form differently coordinated complexes. In addition, some reported variations of the ^{18}O rate of incorporation around 50% suggest that the oxo-hydroxo tautomerism equilibrium is probably tuned by small variations of kinetic parameters, including solvent effect or differences in the kinetic parameters of the oxygen transfer from the metal–oxo to the substrate.

Conclusion

Among the different methods to study the mechanism of oxidation mediated by high-valent metal–oxo complexes, the recent discovery of the 'oxo–hydroxo tautomerism' provides an additional useful tool to discuss the mechanism of catalytic O-atom transfer reactions, the nature of the axial ligand *trans* to the oxo species and the oxidation state of these metal–oxo entities. In particular, when the required conditions to observe the oxo–hydroxo tautomerism are respected, it appears that the incorporation into the oxidation product of 50% of oxygen coming from water constitutes a strong evidence of an oxygen atom transfer involving an high-valent metal–oxo intermediate.

In the future, it might be possible to generalize this oxo–hydroxo tautomerism to other complexes having both the oxo and hydroxo ligands in a *trans* configuration as reported in the present survey for water-soluble metalloporphyrins but also for complexes having these two ligands in a *cis* configuration.

Acknowledgements

The authors are deeply indepted to the work of collaborators and co-workers whose names are listed in the reference list of this review article.

Jean Bernadou was born in Villefranche-de-Rouergue (France) in 1947, and studied Chemistry, Pharmacy (Doctorate in Pharmaceutical Sciences in 1975) and Medicine (Doctorate in 1985) at the University Paul Sabatier of Toulouse, where he was appointed Professor of Medicinal Chemistry in 1987. His collaboration with the group of Bernard Meunier started in 1980 with his research interests in the mechanism of action of antitumor drugs. He is currently working on biological applications of metalloporphyrins, in particular oxidative DNA cleavage, biomimetic oxidation of drugs and characterization of reactive metal–oxo intermediates.

Bernard Meunier was born in 1947 and educated at the Universities of Poitiers (BSc), Montpellier (with R. J. P. Corriu) and Orsay (with H. Felkin, ICSN-CNRS). After a post-doctorate at the University of Oxford, he joined the Laboratoire de Chimie de Coordination du CNRS in Toulouse in 1979. His current research interests include catalytic oxidations, oxidative DNA cleavage, oxidation of pollutants and the mechanism of action of artemisinin derivatives. He is the author of more than 210 publications and patents.

Notes and References

† E-mail: bernadou@lcc-toulouse.fr or bmeunier@lcc-toulouse.fr

1 *Cytochrome P-450: Structure, Mechanism and Biochemistry*, ed. P. R. Ortiz de Montellano, Plenum Press, New York, 2nd edn., 1995.
2 *Peroxidases in Chemistry and Biology*, ed. J. Everse, K. E. Everse and M. B. Grisham, CRC Press, Boca Raton, FL, 1991, vol. I and II.
3 J. T. Groves, R. C. Haushalter, M. Nakamura, T. E. Nemo and B. J. Evans, *J. Am. Chem. Soc.*, 1981, **103**, 2884.
4 O. Bortolini, M. Ricci, B. Meunier, P. Friant, I. Ascone and J. Goulon, *New J. Chem.*, 1986, **10**, 39.
5 (*a*) B. Meunier, *Chem. Rev.*, 1992, **92**, 1411; (*b*) J. T. Groves and Y. Z. Han, in ref. 1, pp. 3–48.
6 T. C. Bruice, *Acc. Chem. Res.*, 1991, **24**, 243; T. G. Traylor, *Pure Appl. Chem.*, 1991, **63**, 265; D. Mansuy, *Coord. Chem. Rev.*, 1993, **125**, 129.
7 P. M. Champion, *J. Am. Chem. Soc.*, 1989, **111**, 3433.
8 F. Lichtenberger, W. Nastainczyk and V. Ullrich, *Biochem. Biophys. Res. Commun.*, 1976, **70**, 936.
9 J. T. Groves, T. E. Nemo and R. S. Myers, *J. Am. Chem. Soc.*, 1979, **101**, 1032.
10 E. Guilmet and B. Meunier, *Tetrahedron Lett.*, 1980, **21**, 4449.
11 B. De Poorter and B. Meunier, *J. Chem. Soc., Perkin Trans. 2*, 1985, 1735.
12 J. P. Renaud, P. Battioni, J. F. Bartoli and D. Mansuy, *J. Chem. Soc., Chem. Commun.*, 1985, 888.
13 S. Shaik, M. Filatov, D. Schröder and H. Schwarz, *Chem. Eur. J.*, 1998, **4**, 193.
14 A. Ghosh, J. Almlöf and L. Que, *J. Phys. Chem.*, 1994, **98**, 5576.
15 J. E. Penner-Hahn, K. S. Eble, T. J. McMurry, M. Renner, A. L. Balch, J. T. Groves, J. H. Dawson and K. O. Hodgson, *J. Am. Chem. Soc.*, 1986, **108**, 7819.
16 K. J. Paeng and J. R. Kincaid, *J. Am. Chem. Soc.*, 1988, **110**, 7913.
17 W. J. Chuang and H. E. Wart, *J. Biol. Chem.*, 1992, **267**, 13 293.
18 M. J. Benecky, J. E. Frew, N. Scowen, P. Jones and B. M. Hoffman, *Biochemistry*, 1993, **32**, 11 929.
19 P. R. Ortiz de Montellano, Y. S. Choe, G. DePillis and C. E. Catalano, *J. Biol. Chem.*, 1987, **262**, 11 641.
20 P. R. Ortiz de Montellano and L. A. Grab, *Biochemistry*, 1987, **26**, 5310.
21 K. Ayougou, D. Mandon, J. Fisher, R. Weiss, M. Müther, V. Schünemann, A. X. Trautwein, E. Bill, J. Terner, K. Jayaraj, A. Gold and R. N. Austin, *Chem. Eur. J.*, 1996, **2**, 1159.
22 (*a*) D-H. Chin, A. L. Balch and G. N. La Mar, *J. Am. Chem. Soc.*, 1980, **102**, 1446; (*b*) A. L. Balch, Y-W. Chan, R-J. Cheng, G. N. La Mar, L. Latos-Grazynski and M. W. Renner, *J. Am. Chem. Soc.*, 1984, **106**, 7779; (*c*) J. T. Groves, Z. Gross and M. Stern, *Inorg. Chem.*, 1994, **33**, 5065.
23 K. Ayougou, E. Bill, J. M. Charnock, C. D. Garner, D. Mandon, A. X. Trautwein, R. Weiss and H. Winkler, *Angew. Chem., Int. Ed. Engl.*, 1995, **34**, 343.
24 J. T. Groves, J. Lee and S. S. Marla, *J. Am. Chem. Soc.*, 1997, **119**, 6269.
25 K. Machii, Y. Watanabe and I. Morishima, *J. Am. Chem. Soc.*, 1995, **117**, 6691.
26 M. F. Sisemore, J. N. Burstyn and J. S. Valentine, *Angew. Chem., Int. Ed. Engl.*, 1996, **35**, 206.
27 W. Adam, D. Golsch and F. C. Görth, *Chem. Eur. J.*, 1996, **2**, 255.
28 T. J. Collins and S. W. Gordon-Wylie, *J. Am. Chem. Soc.*, 1989, **111**, 4511.
29 T. J. Collins, *Acc. Chem. Res.*, 1994, **27**, 279.
30 L. A. Bottomley and F. L. Neely, *Inorg. Chem.*, 1997, **36**, 5435.
31 J. Du Bois, C. S. Tomooka, J. Hason and E. M. Carreira, *Acc. Chem. Res.*, 1997, **30**, 364.
32 The denomination 'oxo–hydroxo tautomerism' which is reminiscent of the keto-enol tautomerism appears to be more precise than 'redox tautomerism' that we initially proposed.[33]
33 J. Bernadou, A. S. Fabiano, A. Robert and B. Meunier, *J. Am. Chem. Soc.*, 1994, **116**, 9375.

34 K. U. Ingold and P. A. MacFaul, in *Biomimetic Oxidations Catalysed by Transition Metals*, ed. B. Meunier, World Scientific Publishing, Singapore, 1998, ch. 2, in press.
35 W. Nam and J. S. Valentine, *J. Am. Chem. Soc.*, 1993, **115**, 1772 and references therein.
36 B. Meunier, E. Guilmet, M. E. De Carvalho and R. Poilblanc, *J. Am. Chem. Soc.*, 1984, **106**, 6668.
37 A. Robert and B. Meunier, *New J. Chem.*, 1988, **12**, 885.
38 S. Hashimoto, Y. Tatsuno and T. Kitagawa, *Proc. Natl. Acad. Sci. USA*, 1986, **83**, 2417.
39 R. Makino, T. Uno, Y. Nishimura, T. Iizuka, M. Tsuboi and Y. Ishimura, *J. Biol. Chem.*, 1986, **261**, 8376.
40 S. Hashimoto, Y. Tatsuno and T. Kitagawa, *J. Am. Chem. Soc.*, 1987, **109**, 8096.
41 J. T. Groves and M. K. Stern, *J. Am. Chem. Soc.*, 1987, **109**, 3812.
42 J. T. Groves and M. K. Stern, *J. Am. Chem. Soc.*, 1988, **110**, 8628.
43 R. J. Balahura, A. Sorokin, J. Bernadou and B. Meunier, *Inorg. Chem.*, 1997, **36**, 3488.
44 K. A. Lee and W. Nam, *J. Am. Chem. Soc.*, 1997, **119**, 1916.
45 M. Pitié, J. Bernadou and B. Meunier, *J. Am. Chem. Soc.*, 1995, **117**, 2935.
46 R. Song, A. Sorokin, J. Bernadou and B. Meunier, *J. Org. Chem.*, 1997, **62**, 673.
47 S. J. Yang and W. Nam, *Inorg. Chem.*, 1998, **37**, 606.
48 S. Prince, F. Körber, P. R. Cooke, J. R. Lindsay Smith and M. A. Mazid, *Acta Crystallogr., Sect. C*, 1993, **49**, 1158.
49 S. Jeon and T. C. Bruice, *Inorg. Chem.*, 1992, **31**, 4843.
50 A. Sorokin and B. Meunier, *Eur. J. Inorg. Chem.*, in press.
51 W. Nam, W. Hwang, J. M. Ahn, S.-Y. Yi and G.-J. Jhon, *Bull. Korean Chem. Soc.*, 1996, **17**, 414.
52 T. W. Kaaret, G. H. Zhang and T. C. Bruice, *J. Am. Chem. Soc.*, 1991, **113**, 4652.
53 K. Rachlewicz and L. Latos-Grazynski, *Inorg. Chem.*, 1996, **35**, 1136.

8/02734J

Systematic analysis of metal coordination sphere geometry from crystallographic data: a general method for detecting geometrical preferences, deformations and interconversion pathways

Judith A. K. Howard,*[a] Royston C. B. Copley,[a] Jing Wen Yao[a] and Frank H. Allen*[b]

[a] *Department of Chemistry, University of Durham, South Road, Durham, UK DH1 3LE. E-mail: J.A.K.Howard@durham.ac.uk*
[b] *Cambridge Crystallographic Data Centre, 12 Union Road, Cambridge, UK CB2 1EZ. E-mail: allen@ccdc.cam.ac.uk*

A simple and general computational procedure using the L–M–L angles for all crystallographic observations of an ML_n coordination sphere generates mappings which reveal geometrical preferences, deformations from standard polyhedral geometries, and interconversions between polyhedral forms; a systematic analysis of the geometry of seven-coordination is described.

Systematic knowledge about geometries, deformations and interconversion pathways of metal coordination spheres is fundamental to inorganic chemistry.[1] For ML_n coordination, where L is any ligand, much knowledge is implicit in the $N_a = n(n-1)/2$ values of the L–M–L valence angles. This has been demonstrated[2] for the lower coordination numbers, $n = 3$, 4, using crystallographic data retrieved from the Cambridge Structural Database (CSD),[3] and using data analysis methods analogous to those applied to conformational studies of organic systems based on torsional metrics.[4]

However, the high topological symmetry of generalised ML_n systems having $n \geqslant 5$ has so far prevented routine systematic studies of the associated angular data sets. For a given system, the topological symmetry gives rise to $n!$ possible enumerations of the chemically equivalent L atoms, hence to $n!$ permutations of the valence angle sequence. There are two ways of addressing this problem so that we can properly visualise and analyse a data matrix of N_a valence angles for N_f occurrences of an ML_n substructure in the CSD, *viz.*: (*a*) By completely filling the parameter space spanned by the valence angles, *i.e.* by including all $n!N_f$ permutationally equivalent angular sequences in the data matrix. This method has frequently been used in the conformational (torsional) analysis of *k*-membered cyclic systems where topological symmetry requires a maximum $2k$-fold data expansion.[4] Given that $n! = 120, 720, 5040, 40320$ for $n = 5, 6, 7, 8$-coordination, visualisation and analysis of permutationally complete valence angle matrices for ML_n systems becomes increasingly intractable.

(*b*) By placing each angular sequence into a single asymmetric unit of the valence angle parameter space. This can be effected by comparing all permutations of each angular sequence with some predefined set of standard values, so as to locate the permuted sequence that provides the best numerical fit to the standard sequence. The numerical overlay therefore assigns a unique atomic enumeration of the L-atoms to each example of ML_n coordination retrieved from the CSD with respect to the atomic enumeration chosen for the standard. The resulting data matrix comprises the N_a valence angles for the basic number (N_f) of fragments retrieved from the database: a much more tractable proposition for visual display and numerical analysis.

In this communication, we describe a general computational procedure in which the topological problem is dealt with according to method (*b*), and which also addresses the problems of data analysis inherent in the dimensionality of the angular description, *i.e.* the fact that $n(n-1)/2$ angles are needed to provide a full description of each coordination sphere. We illustrate the application of the method to a systematic study of the geometrical characteristics of the 372 examples of 7-coordination available in the CSD.

Standard and symmetric *n*-polyhedra [*e.g.* the tetrahedron (T), octahedron (O), pentagonal bipyramid (PBP), capped trigonal prism (CTP), *etc.*] are archetypal reference frames that are used to describe coordination sphere geometries. In many cases, the N_a valence angles for the standard are fixed by symmetry, irrespective of the M–L (or L–L edge) distances. In others, and notably some of the higher-coordination archetypes, valence angle sequences may vary under the symmetry of the archetype. Here, it is necessary to select a set of angles for use as a standard. This does not obviate our method in any way, since the purpose of the standard is to provide a fixed origin in valence angle space that represents an idealised *n*-polyhedron appropriate to the problem under investigation.

We denote the standard set of L–M–L angles as $\theta_{k(\mathrm{std})}$ [$k = 1 \rightarrow N_a$], and determine how far an observed geometry, defined by angles $\theta_{k(\mathrm{obs})}$ derived from the CSD, is distorted from an appropriate archetype, by computing the Euclidean dissimilarity:

$$\mathrm{Rc}(x) = 100 \min_p \left\{ \frac{\Sigma_k [\theta_{k(\mathrm{obs})} - \theta_{k(\mathrm{std})}]^2}{\Sigma_k \theta_{k(\mathrm{std})}^2} \right\}^{\frac{1}{2}} \qquad (1)$$

in which (x) identifies the archetypal standard, and the subscript p indicates that Rc(x) is the minimum value obtained through application of eqn. (1) to all possible sequences of the $\theta_{k(\mathrm{obs})}$ that arise from the $n!$ permutational ligand enumerations. Local FORTRAN77 code derives and applies the permuted L–M–L angle sequences and, for each CSD observation, identifies the specific permutation that is closest to the standard angular description used for archetype (x). Thus, the procedure implicitly identifies the specific labelling of the CSD atoms, L, that best matches the labelling used for the standard.

For 7-coordination, the three common archetypal polyhedra (Scheme 1) are the pentagonal bipyramid (PBP), capped

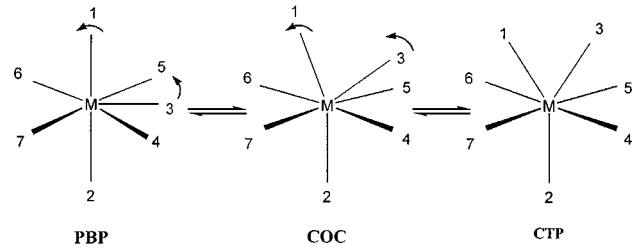

Scheme 1 The PBP ⇔ COC ⇔ CTP interconversion path: atomic movements in 7-coordination. The unique standard angles (°) for CTP: L^1–M–L^2 141.8, L^1–M–L^3 76.4, L^1–M–L^4 127.3, L^1–M–L^5 127.3, L^1–M–L^6 76.4, L^1–M–L^7 76.4, L^2–M–L^4 76.4, L^2–M–L^5 76.4, L^4–M–L^5 87.7, L^4–M–L^6 152.7, L^4–M–L^7 85.9.

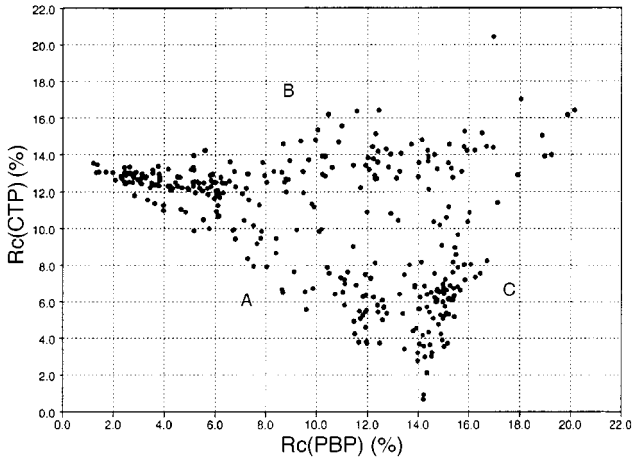

Fig. 1 Rc(CTP) *vs.* Rc(PBP) for all 372 fragments having 7-coordination

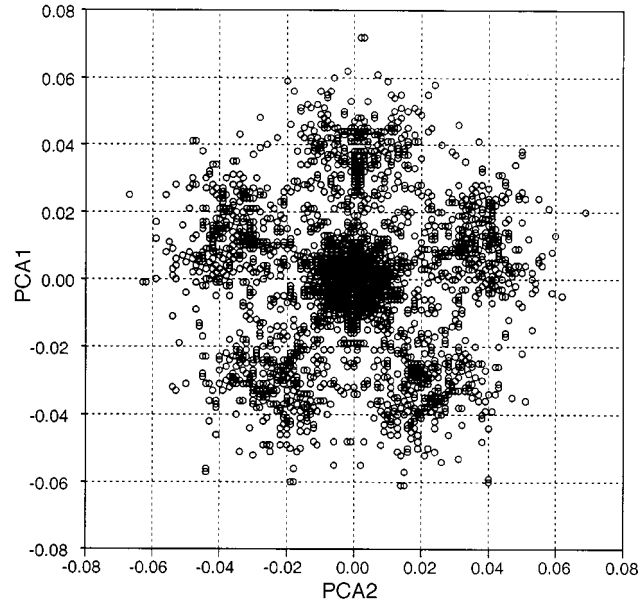

Fig. 2 D_{5h} expanded PCA: PC_1 *vs.* PC_2 for all 372 fragments (7440 observations after expansion)

octahedron (COC), and the capped trigonal prism (CTP). The COC can be considered as an intermediate form on the PBP ⇔ CTP interconversion pathway.[1] Starting from PBP, one of the five equatorial ligands (3 in Scheme 1) moves out of the plane towards apical ligand 1, which then moves away from its apical position. Small relocations of equatorial ligands 4–7 then generate the COC geometry, and further small movements of atoms 3 and 1 generate the CTP polyhedron. The standard CTP angles used in the present report are given in Scheme 1. In practice, users may choose their own standard (origin) angles for the CTP case.

The CSD System program QUEST3D[3] was used to locate 372 examples of ML_7 coordination (L = any non-H atom), and to output the (permutationally random) sequence of 21 L–M–L valence angles for each example. The local code was used to minimise both Rc(PBP) and Rc(CTP) over the 5040 possible permutations using eqn. (1). The dataset was visualised by plotting Rc(PBP) *vs.* Rc(CTP), and Fig. 1 immediately reveals a number of significant features: (*a*) a well populated cluster of PBP geometries having Rc(PBP) up to *ca.* 7%, (*b*) a linear PBP ⇔ CTP interconversion pathway (A in Fig. 1) that passes through a populated COC area, and (*c*) interconversion pathways B and C that connect the PBP and CTP examples with a loose cluster of observations for which both Rc(*x*) values are *ca.* 15% or higher. Examination of individual structures in these areas shows that they arise almost entirely from ML_7 fragments having small ligand bite angles. Conversely, the PBP area is dominated by ML_7 species having either seven or two unidentate ligands. The COC/CTP area is structurally diverse and requires further detailed study.

Because the Rc(*x*) minimisation process does assign standard atomic labels to the seven equivalent ligands in ML_7 systems, we can use this information as a basis for more detailed multivariate data analyses, *e.g.* the principal component analysis (PCA) technique[5] that is commonly applied to conformational problems.[4] In the ML_7 case however, we are now starting with data that defines a single asymmetric unit of parameter space. Thus, we can expand the data set in a controlled manner to reflect full or partial topological symmetries in the resultant PCA plots. Based on previous PCA studies of the conformations of five-membered rings,[4] we may treat the five ligands that most closely map to their coplanar equatorial counterparts in the PBP standard as a cyclic system, which would have exact D_{5h} symmetry in the planar form (a perfect PBP form). To examine the deformations in this system exhibited in real structures, we apply a D_{5h}-expansion to the angular dataset prior to application of PCA. The analysis generates PC_1 and PC_2 as a degenerate pair and Fig. 2, which shows a plot of the PC scores along these orthogonal axes for the expanded dataset, is a readily interpretable visualisation of the dataset: the central cluster of Fig. 2 maps the PBP examples (five equatorial ligands closely coplanar), while the five symmetric 'spokes' map the PBP ⇔ COC ⇔ CTP pathways that arise from each of the equatorial atoms of the PBP standard being designated, in turn and according to the D_{5h} topology, as the mobile ligand 3 in Scheme 1.

An extraordinary richness of information is immediately apparent in the simple two-dimensional visual representation of a 21-dimensional parameter space shown in Fig. 1, while Fig. 2 shows how the analysis can be further enhanced through use of standard multivariate techniques. We stress that any interpretation of structural diversity, in terms of geometrical arrangements, distortions from symmetrical forms, and interconversion pathways, is wholly dependent on the investigator and, as in most structural data mining experiments, a full interpretation (currently in preparation) involves a close examination of individual structures. The technique reported here provides the essential underpinning for such data mining experiments by treating the most difficult problem of atomic permutational symmetry that has, until now, presented a serious disincentive to knowledge discovery in coordination chemistry. Further, the fact that eqn. (1) generates a one-dimensional metric, Rc(*x*), that quantifies how far the shape of an observed coordination sphere deviates from some idealised standard (*x*), raises the possibility of including such metrics in the CSD itself, to form the basis for simple and rapid searches for coordination sphere geometries that are close to (or even far from) a particular reference frame.

Notes and References

1 D. L. Kepert, in *Comprehensive Coordination Chemistry*, Editor-in-Chief G. Wilkinson, 1987, vol. 1, p. 31; M. G. B. Drew, *Prog. Inorg. Chem.*, 1977, **23**, 1.
2 G. Klebe and F. Weber, *Acta Crystallogr., Sect. B*, 1994, **50**, 50; R. Taylor and F. H. Allen, in *Structure Correlation*, ed. H.-B. Bürgi and J. D. Dunitz, VCH, Weinheim, 1994, p. 111.
3 F. H. Allen and O. Kennard, *Chem. Des.-Automat. News*, 1993, **8**, 31.
4 F. H. Allen, M. J. Doyle and T. P. E. Auf der Heyde, *Acta Crystallogr., Sect. B*, 1991, **47**, 412.
5 C. Chatfield and A. J. Collins, *Introduction to Multivariate Analysis*, Chapman and Hall, London, 1980.

Received in Cambridge, UK, 2nd September 1998; 8/06820H

Is the metallocene (3-THF-CH_2-Cp)$_2ZrCl_2$ a better catalyst than the corresponding 2-THF derivative for olefin polymerisation? A molecular modelling study

Edward A. H. Griffiths, Ian R. Gould and Subramaniam Ramdas*

Department of Chemistry, Imperial College of Science, Technology and Medicine, South Kensington, London, UK SW7 2AY. E-mail: s.ramdas@ic.ac.ukur

Semi-empirical, *ab initio* and density functional calculations performed on the active intermediates (2-THF-CH_2-Cp)$_2Zr^+$-CH_3 and (3-THF-CH_2-Cp)$_2Zr^+$-CH_3 indicate that the former is more stable as an intra-molecular complex by up to 21.6 kcal mol^{-1} and is, therefore, a less efficient catalyst for olefin polymerisation.

Incorporating metallocenes onto inorganic supports ($TiCl_3$ on $MgCl_2$) for industrial polymerisation of olefins is a major technical challenge. Anchoring traditional Group IV metallic catalysts, *e.g.* Cp_2ZrCl_2, to the support by mono-substitution of each Cp ring with an appropriate 'tethering' group containing a Lewis base is an attractive strategy. Experimentally, in the homogeneous polymerisation of ethylene[1] by (2-THF-CH_2-Cp)$_2ZrCl_2$ (Fig. 1), the activity was found to be low compared

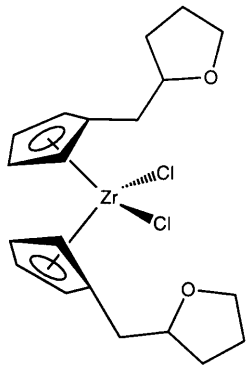

Fig. 1 The structure of (2-THF-CH_2-Cp)$_2ZrCl_2$

to the parent Kaminsky[2,3] catalyst. This was rather surprising in view of the fact that any C-substitution in the Cp rings usually gives rise to a marginal increase in the activity of the catalyst. It was, therefore, suspected that the active catalytic site (2-THF-CH_2-Cp)$_2Zr^+$-CH_3 (generated by MAO alkylation and Cl^- abstraction from the dichloride derivative), could suffer from an intra-molecular complexation of the ether group to the electrophilic Zr centre (see Fig. 2). Ether co-ordination would, of course, compete with ethylene insertion and result in slow polymerisation.

To verify this hypothesis, we have carried out semi-empirical,† *ab initio*‡ and density functional (DFT)§ calculation on the proposed catalytically active intermediate (Fig. 2). Since the evidence for or against internal complexation is unlikely from the study of a single intermediate, we have carried out these calculations on both the 2-THF and 3-THF (see Fig. 3) complexes. The results on the optimised energies and geometries are shown in Tables 1 and 2 respectively.

Semi-empirical calculations yielded on geometry optimisation an energy difference of only 2.9 kcal mol^{-1} between the 2-THF and 3-THF complexes. This is too small a difference to preclude the formation of an internal complex by one of the

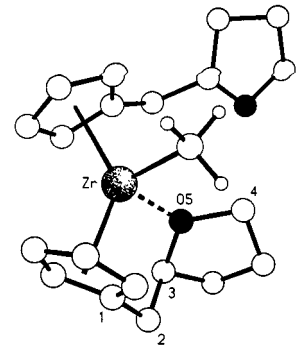

Fig. 2 The structure of the 2-THF cation

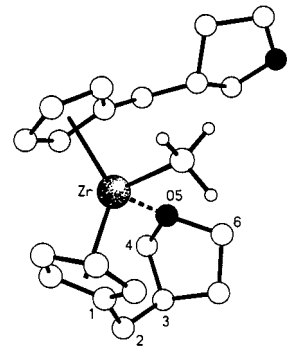

Fig. 3 The structure of the 3-THF cation

Table 1 Energies (kcal mol^{-1}) of the two cations at the semi-empirical (PM3), uncorrelated (HF) and correlated (DFT) levels. The bottom row shows the energy differences

Cation	PM3	HF	DFT
2-THF	-68.5	-629093.9	-677570.5
3-THF	-65.4	-629074.5	-677548.9
ΔE	2.9	19.4	21.6

Table 2 Selected geometry values for the two cations: angles shown in degrees and distances in Å. The figures in brackets refer to the corresponding results from semi-empirical (PM3) calculations. Atom numbering as shown in Fig. 2 and 3

Cation	$Zr–O_5$	$C_1–C_3–C_5$	Angle between $Zr–O_5$ and plane $C_3–C_5–C_4$ (2-THF), $C_4–C_5–C_6$ (3-THF)
2-THF	2.18 (2.27)	110.5 (112.9)	10.9 (50.8)
3-THF	2.19 (2.29)	117.2 (113.0)	30.8 (65.0)

systems. On the other hand, the *ab initio* HF calculations (with geometry optimisation) carried out gave rise to an energy difference of 19.4 kcal mol^{-1}, clearly indicating that the 3-THF complex cation is less stable and, therefore, should remain an active catalytic site. To examine the effects of electron correlation, non-local single-point DFT calculations were undertaken on the optimised geometries obtained above. These DFT calculations indicated a further increase in the energy difference to 21.6 kcal mol^{-1} between the two cations. Thus all the above levels of theory and calculations show that the 2-THF cationic complex is more stable than the 3-THF complex—clearly predicting that the (3-THF-CH_2-Cp)$_2ZrCl_2$ is a better choice between the catalysts. The 3-THF derivative has now been synthesised and its activity for ethylene polymerisation was found to be 9.25 g h^{-1} compared to zero activity for the 2-THF complex.[1]

The results (Table 2) on the optimised geometries reveal the origin of the relative stabilities of the two cationic complexes. In both the systems the Zr and O atoms are within bonding distances of 2.18–2.19 Å. Inspection of the frontier orbitals of both the systems, particularly the LUMO, shows very little difference, indicating the same degree of overlap between the lone pairs of the O and the orbitals of the Zr. We, therefore, conclude that in the 3-THF complex, the increased internal strain is steric in origin and arises from the required distortions in the bond angle between C_1–C_2–C_3 atoms as well as in the angle between the Zr–O bond and the plane of the THF ring.¶

In summary, we have successfully rationalised the poorer activity of the (2-THF-CH_2-Cp)$_2ZrCl_2$ catalyst for ethylene polymerisation compared to the 3-THF variant (not a common experimental choice).

We thank Dr Peter Maddox and Dr John McNally for useful discussions and their contribution to this paper. We thank the EPSRC for a grant (E. A. H. G.) and BP Chemicals for support and permission to publish this work.

Notes and References

† Semi-empirical: The MNDO[4] module provided within SPARTAN[5] employs PM3 parameters, including PM3™ that incorporates d functions for transition metals. The optimised geometries of several organometallic molecules have reproduced the X-ray structures of zirconocenes to within 0.04–0.05 Å on bond lengths and 3–5° on bond angles around the metal atom. Though the optimum energies are unreliable for the purposes of ligand design, the method does provide a useful starting geometry for subsequent *ab initio*/DFT studies.

‡ *Ab initio*: All *ab initio*/DFT calculations were carried out using the GAUSSIAN94 package.[6] Geometry optimisations of the two cationic species were performed at the HF level of theory using the 3-21G basis set.[7] The LanL2DZ effective core potential[8] was placed upon the zirconium atom.

§ DFT: Single point DFT calculations using B3LYP[9,10] were performed with the same basis sets as used for the HF optimisations described above.

¶ It is interesting to note that the crystal structure of the stable tetrahydrofurylcyclopentadienyltitanium trichloride[11] (Fig. 4) is in line with our results from the *ab initio*/DFT methods. The results from the semi-empirical calculations are, however, less reliable for predicting the geometries of such cationic complexes.

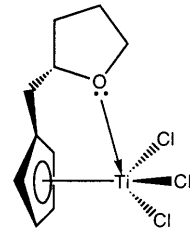

Fig. 4 The structure of tetrahydrofurylcyclopentadienyltitanium trichloride

1 BP Patent No: EP 608054. In a laboratory scale experiment it was found that 1.9 mg (4.1×10^{-3} mmol) of the catalyst (2-THF-CH_2-Cp)$_2ZrCl_2$ in the presence of MAO in toluene (100 ml, 0.41 M) at an ethylene pressure of 4 psig shows no polymerisation activity at room temperature—addition of Cp_2ZrCl_2 to the mixture, however, restored immediate polymerisation activity. In comparison, the catalyst (3-THF-CH_2-Cp)$_2ZrCl_2$ gave 9.25 g h^{-1} of the polymer, under similar experimental conditions.
2 A. Anderson, H. G. Cordes, J. Herwig, W. Kaminsky, A. Merk, R. Mottweiler, J. H. Sinn and H. J. Vollmer, *Angew. Chem., Int. Ed. Engl.*, 1976, **15**, 630.
3 P. C. Mohring and N. J. Colville, *J. Organomet. Chem.*, 1994, **479**, 1.
4 M. J. S. Dewar and W. Thiel, *J. Am. Chem. Soc.*, 1977, **99**, 4899.
5 SPARTAN version 5.0, Wavefunction Inc., 18401 Von Karman Ave., Suite 370, Irvine, CA 92612, USA.
6 GAUSSIAN94 Revision D.3, M. J.Frisch *et al.*, Gaussian Inc., Pittsburgh, PA, 1995.
7 J. S. Binkley, J. A. Pople and W. J. Hehre, *J. Am. Chem. Soc.*, 1980, **102**, 939.
8 P. J. Hay and W. R. Wadt, *J. Chem. Phys.*, 1985, **82**, 270.
9 A. D. Becke, *Phys. Rev. A*, 1988, **38**, 3098.
10 C. Lee, W. Yang and R. G. Parr, *Phys. Rev. B*, 1988, **37**, 785.
11 Y. Qian, G. Li, W. Chen, B. Li and X. Lin, *J. Organomet. Chem.*, 1989, **373,** 185.

Received in Liverpool, UK, 27th February 1998; 8/01673I

Novel lithium 3-sila- and 3-germa-β-diketiminates†‡

Peter B. Hitchcock, Michael F. Lappert* and Marcus Layh

The Chemistry Laboratory, University of Sussex, Brighton, UK BN1 9QJ. E-mail: m.f.lappert@sussex.ac.uk

The novel 3-sila- and 3-germa-β-diketiminates [Li{N(R)-C(Ar)E(R)C(Ar)N(R)}(D)$_n$] (R = SiMe$_3$, Ar = C$_6$H$_3$Me$_2$-2,6 or Ph, E = Si or Ge, D = thf or ArCN and n = 1 or 2) were obtained from the reaction of [Li(ER$_3$)(thf)$_3$] with PhCN or ArCN; the X-ray crystal structures of two representatives of this new class of compounds were determined and shown to have, in contrast to related carbon analogues, the anionic charge localised at Si or Ge.

We have recently reported on the diverse outcome of the reaction of a trimethylsilylmethyllithium reagent, *e.g.* Li(CHR$_2$) or Li(CR$_3$), with an α-H-free nitrile (R = SiMe$_3$).[1] *E.g.* from Li(CHR$_2$) and PhCN, depending on stoichiometry and conditions the product was the crystalline lithium 1-azaallyl **1**,[2] β-diketiminate **2**[3] or **3**,[4] or the isomeric 1,3-diazaallyl **4**.[2]

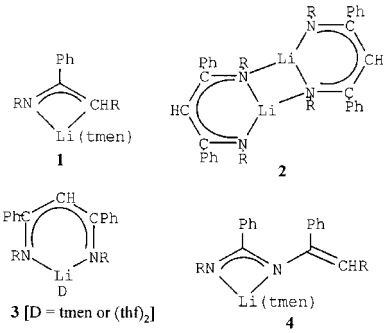

We now focus on the behaviour of the silicon or germanium congener Li(ER$_3$) of Li(CR$_3$) towards PhCN or ArCN (E = Si or Ge, Ar = 2,6-Me$_2$C$_6$H$_3$). This study has led to the isolation (Scheme 1) and characterisation of the novel crystalline compounds **5a**–**c** and **6**, which are 3-sila (**5a**–**c**) or 3-germa (**6**) analogues of the ketiminates **3** or **2**, respectively. Whereas the anionic ligands in **2** and **3** are N,N′-centred, in **5** and **6** they are E-centred.

While [Li(SiR$_3$)(thf)$_3$][5] in pentane with 1 or 2 equiv. of PhCN yielded a mixture, using the bulkier and less reactive ArCN afforded (i in Scheme 1) the red, crystalline lithium 3-sila-β-diketiminate [Li{N(R)C(Ar)Si(R)C(Ar)N(R)}(D)$_n$] **5a** or **5b** in high yield. The exact nature of the product was strongly influenced by the choice of starting material and work-up procedure. When thf-free LiSiR$_3$ was treated with 3.5 equiv. of ArCN, **5c** [(D)$_n$ = (ArCN)$_2$] was isolated, whereas [Li(SiR$_3$)(thf)$_3$] with 2 equiv. of ArCN gave either **5b** [(D)$_n$ = ArCN; removal of volatiles prior to recrystallisation] or **5a** [(D)$_n$ = thf; product directly crystallised from the reaction mixture].

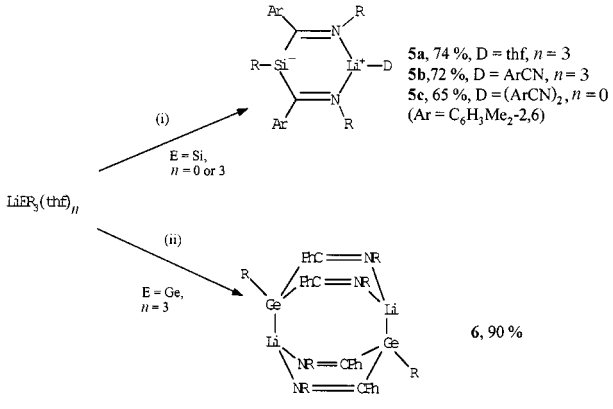

Scheme 1 Some reactions of LiER$_3$ with aryl nitriles (R = SiMe$_3$). *Reagents* (ArCN for i or PhCN for ii) *and conditions*: reagents were mixed in C$_5$H$_{12}$ at −78 °C (i) or −50 °C (ii) and the mixture was then warmed to *ca*. 25 °C and stirred for 12 h.

The germyllithium compound [Li(GeR$_3$)(thf)$_3$][6] was less reactive than its silicon analogue, as evident from its different behaviour towards the two nitriles. Treatment with ArCN gave a stable Lewis acid/base adduct by partial replacement of thf by ArCN. The more reactive PhCN yielded (ii in Scheme 1) bright yellow, crystalline [LiGe(R){C(Ph)=NR}$_2$]$_2$ **6**.

Each of **5a**, **5b**, **5c** and **6** gave satisfactory microanalytical and NMR spectroscopic data.§ In order to investigate the nature of the bonding, and make comparisons with carbon analogues such as the β-diketiminates **2** and **3** and a series of alkali metal cyclopentadienyls M[η^5-C$_4$Me$_4$(ER)] (M = Na or K, E = Si or Ge),[7] the X-ray crystal structures of **5b** (which is structurally similar to **5c**, to be described in the full paper), **5c** (Fig. 1)¶ and **6** (Fig. 2)¶ were determined.

Crystalline **5c** is a monomer; the Li atom is surrounded in an approximately tetrahedral fashion by two nitrogens N(1) and N(2) from the ligand and two from the coordinated nitriles. The atoms Li, N(1), C(1), Si(3), C(2) and N(2) are arranged in a six-membered ring of boat conformation [the angles between the planes N(1)N(2)C(1)C(2) and LiN(1)N(2) or C(1)Si(3)C(2) are 44.3(3) or 28.2(3)°, respectively]. The negative charge is probably mainly localised at the silicon Si(3) [see also δ(^{29}Si{^{1}H}) −15.5 in **5b**], as is indicated by its pyramidal configuration [Σ°Si(3) 336.4(2)°] and the Si(3)–C(1) [1.874(4)

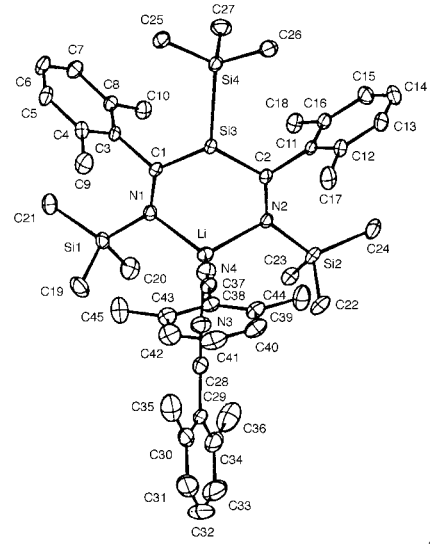

Fig. 1 Molecular structure of **5c** with selected bond distances (Å): Li–N(1) 2.000(7), Li–N(2) 1.995(7), Li–N(3) 2.106(8), Li–N(4) 2.106(9), Si(3)–Si(4) 2.334(5), Si(3)–C(1) 1.874(4), Si(3)–C(2) 1.878(5), N(1)–C(1) 1.303(5), N(2)–C(2) 1.308(5)

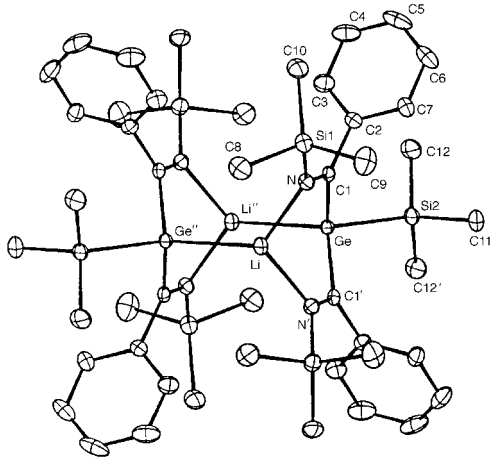

Fig. 2 Molecular structure of **6** with selected bond distances (Å): Li–N 1.954(5), Li–Ge″ 2.657(8), Ge–Si(2) 2.401(1), Ge–C(1) 2.008(3), N–C(1) 1.288(4)

Å], Si(3)–C(2) [1.878(5) Å], C(1)–N(1) [1.303(5) Å] and C(2)–N(2) [1.308(5) Å] bond lengths which are appropriate for SiC single and CN double bonds. The distance between Si(3) and Li of 3.125 Å is much longer than the Si–Li bond in, for example, $[LiSiMe_3)(tmen)_{1.5}]$ [2.70(1) Å],[8] $[\{Li(\mu\text{-}SiMe_3)\}_6]$ [2.62(1)–2.78(1) Å],[9] $[Li(SiR_3)(thf)_3]$ [2.67(1) Å],[5] $[Li(SiR_3)(dme)_{1.5}\}$ [2.630(5) Å],[10] or $[(Li\{\mu\text{-}Si(Me)(SiMe_2Ph)_2\}\})_2]$ [2.664(5), 2.778(7) Å].[11] We conclude that **5c** has a zwitterionic structure with only a weak (hence boat) interaction between the anionic Si(3) and the cationic Li.

The germanium derivative **6**, in contrast to **5c**, is neutral donor-free. Crystalline **6** is a dimer, Fig. 2, in which two six-membered $\overline{LiNC(1)GeC(1')N'}$ rings in boat conformation are connected by a direct Ge–Li bond of 2.657(8) Å. Similar values are reported for $[Li(GeR_3)(thf)_3]$ [2.666(6) Å] and $[Li(GeR_3)(pmdeta)]$ [2.653(9) Å].[6] The Ge atoms are in an approximately tetrahedral environment and the Ge–C(1) and C(1)–N bond distances of 2.008(3) and 1.288(4) Å are typical for Ge^{II}–C single (*e.g.*[12] 2.042(8) Å in $\{Ge(CHR_2)_2\}_2$ or 1.961(8) and 2.007(9) Å in $[Li(12\text{-crown-}4)_2][C_4Me_4\text{-}GeC_6H_2Me_5\text{-}2,4,6]$[7]) and C=N double bonds.

The presence of distinct E–C single and C=N double bonds in crystalline **5c** (E = Si) and **6** (E = Ge) contrasts with the situation in the carbon analogues such as **3**, which have an essentially planar central carbon [E(H), E = C]; this, and the E⋯C (E = C) and C⋯N distances of *ca*. 1.40 and 1.33 Å, respectively,[4] indicates that in **3** there is significant delocalisation in the β-diketiminate ligand.

Whereas studies on the Si and Ge analogues of cyclopentadienyls $[E(R')C_4Me_4]^-$ in $M\{E(R')C_4Me_4\}$ (crown ether) (M = Li, Na or K; E = Si or Ge; R′ = Me, SiR_3 or $C_6H_2Me_3$-2,4,6) showed that in these systems Si and Ge are similarly reluctant to form delocalised aromatic anions, the monoanion of $[Si(Bu^t)C_4Ph_4]^-$ [13*a*] and the dianion $[GeC_4Ph_4]^{2-}$ [13*b*] are aromatic.

The $^{13}C\{^1H\}$ NMR chemical shifts of the skeletal carbon [E*C*(Ph)N] in **5c** (δ 219.4) and **6** (δ 238.0) differ considerably from those in the carbon analogues **2** (δ 177.5)[2] and **3** (D = tmen, δ 174.9),[4] which indicates that the bonding in the crystalline molecules is retained in solution. This is further supported by δ [$^{29}Si\{^1H\}$] −15.5 in **5b** [*cf.* refs. 7 and 13(*a*)].

Compounds **5**, unlike **6**, were soluble in aliphatic hydrocarbons. Attempts to convert the dimer **6** into a monomeric Lewis base (*e.g.* thf or py) adduct have not provided isolable products, but colour changes (red) indicated that reactions had occurred.

It is evident that in the formation of compounds **5** and **6** two successive E–C couplings, followed by unprecedented 1,3-Me_3Si migrations from E to N, are implicated. We propose that the reactions involve intermediates **7**–**10** of Scheme 2.

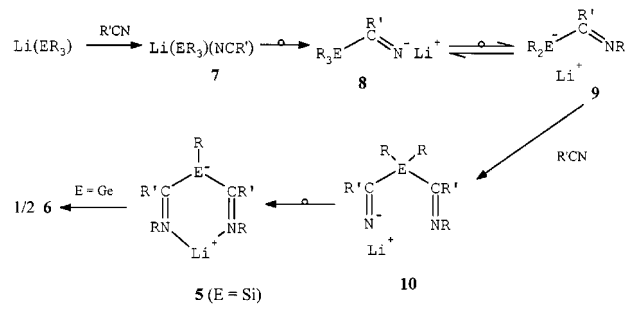

Scheme 2

Anionic 1,3-Me_3Si shifts from N → N,[14] C → N,[1–3] and P → N[15] in reactions with nitriles were previously documented.

Complexes **5** and **6** are of interest for the novelty of their formation and their structures and have potential as ligand transfer reagents.

We thank EPSRC for a fellowship for M. L.

Notes and References

† No reprints available.

‡ Dedicated to Professor Warren Roper as a mark of respect (by M. S. L.) and friendship.

§ *Selected spectroscopic data* [$^7Li\{^1H\}$ at 116.6, $^{13}C\{^1H\}$ at 75.5 and ^{29}Si at 99.4 MHz]. **5b** (C_6D_6): $^7Li\{^1H\}$ δ 1.65; $^{13}C\{^1H\}$ δ 219.5 (CN, s), $^{29}Si\{^1H\}$ δ −15.5 (SiR, s). **5c** (C_6D_6): $^7Li\{^1H\}$ δ 1.64; $^{13}C\{^1H\}$ δ 219.4 (CN, s). **6** (C_6D_6, C_5D_5N): $^7Li\{^1H\}$ δ 0.73; $^{13}C\{^1H\}$ δ 238.0 (CN, s).

¶ *Crystallographic data* for **5c**/**6**: $C_{45}H_{63}LiN_4Si_4/C_{46}H_{74}Ge_2Li_2N_2Si_6(C_5H_{12})_2$, M = 779.3/1127.0, triclinic, space group $P\bar{1}$ (no. 2), a = 11.78(2), b = 12.90(2), c = 16.82(2) Å, α = 82.8(2), β = 72.8(2), γ = 88.9(2)°/monoclinic, space group $C2/m$ (no. 12), a = 18.482(2), b = 16.552(2), c = 12.221(1) Å, β = 112.31(1)°, U = 2423(6)/3460.7(6) Å^3, Z = 2/2, D_c = 1.07/1.08 Mg m^{-3}, F(000) = 840/1204, λ(Mo-Kα) = 0.71073 Å, μ = 0.16/1.00 mm^{-1}. Data were collected at 173(2) K on a Enraf Nonius CAD4 diffractometer in the ω–2θ mode for the range of 2 < θ < 23° (**5c**) or 2 < θ < 25° (**6**). The structures were solved by direct methods (SHELXS86) and refined with full matrix least-squares on all F^2 (SHELXL93). Final residuals for 6738/3160 independent reflections were R_1 = 0.079/0.059, wR_2 = 0.153/0.119 and for the 5083/2590 with $I > 2\sigma(I)$, R_1 = 0.056/0.044, wR_2 = 0.136/0.110. CCDC 182/999.

1 M. F. Lappert and D.-S. Liu, *J. Organomet. Chem.*, 1995, **500**, 203; M. F. Lappert and M. Layh, *Tetrahedron Lett.*, 1998, **39**, 4745.
2 P. B. Hitchcock, M. F. Lappert and M. Layh, *Chem. Commun.*, 1998, 201.
3 P. B. Hitchcock, M. F. Lappert and D.-S. Liu, *J. Chem. Soc., Chem. Commun.*, 1994, 1699.
4 P. B. Hitchcock, M. F. Lappert and R. Sablong, unpublished work; P. B. Hitchcock, M. F. Lappert and S. Tian, unpublished work.
5 K. W. Klinkhammer, *Chem. Eur. J.*, 1997, **3**, 1418; and refs. therein.
6 S. Freitag, R. Herbst-Irmer, L. Lameyer and D. Stalke, *Organometallics*, 1996, **15**, 2839.
7 W. P. Freeman, T. D. Tilley, L. M. Liable-Sands and A. L. Rheingold, *J. Am. Chem. Soc.*, 1996, **118**, 10 457.
8 B. Teclé, W. H. Ilsley and J. P. Oliver, *Organometallics*, 1982, **1**, 875.
9 W. H. Ilsley, T. F. Schaaf, M. D. Glick and J. P. Oliver, *J. Am. Chem. Soc.*, 1980, **102**, 3769.
10 G. Becker, H.-M. Hartmann, A. Münch and H. Riffel, *Z. Anorg. Allg. Chem.*, 1985, **530**, 29.
11 A. Sekiguchi, M. Nanjo, C. Kabuto and H. Sakurai, *Angew. Chem., Int. Ed. Engl.*, 1997, **36**, 113.
12 D. E. Goldberg, P. B. Hitchcock, M. F. Lappert, K. M. Thomas, A. J. Thorne, T. Fjeldberg, A. Haaland and B. E. R. Schilling, *J. Chem. Soc., Dalton Trans.*, 1986, 2387.
13 (*a*) J.-H. Hong and P. Boudjouk, *J. Am. Chem. Soc.*, 1993, **115**, 5883; (*b*) R. West, H. Sohn, D. R. Powell, T. Müller and Y. Apeloig, *Angew. Chem., Int. Ed. Engl.*, 1996, **35**, 1002.
14 D. Stalke, M. Wedler and F. T. Edelmann, *J. Organomet. Chem.*, 1992, **431**, C1 and refs. therein.
15 G. Becker, G. Ditten, K. Hübler, K. Merz, M. Niemeyer, N. Seidler, M. Westerhausen and Z. Zheng, in *Organosilicon Chemistry II: From Molecules to Materials*, ed. N. Auner and J. Weis, Verlag Chemie, Weinheim, 1996, p. 161.

Received in Basel, Switzerland, 27th July 1998; 8/05864D

A simple ladder tin phosphate and its layered relative

S. Ayyappan,[a] X. Bu,[a] Anthony K. Cheetham,*[a] Srinivasan Natarajan[b] and C. N. R. Rao*[b]

[a] *Materials Research Laboratory, University of California, Santa Barbara, CA 93106, USA*
[b] *Chemistry and Physics of Materials Unit, Jawaharlal Nehru Centre for Advanced Scientific Research, Jakkur P.O., Bangalore 560 064, India. E-mail: cnrrao@jncasr.ac.in*

A simple ladder tin phosphate built up of the 4-membered cyclic tecton, $[Sn_2P_2O_4]$, is described along with a related layered material.

A variety of open-framework metal phosphate materials have been synthesized and their structures elucidated in the last few years. Of particular interest to us are the recently-discovered open-framework tin(II) phosphates containing trigonal-pyramidal SnO_3 and or square-pyramidal SnO_4 units linked to tetrahedral PO_4 units.[1–4] The tin phosphates reported so far possess three-dimensional,[1,2] layered[3] or monomeric structures[4] and the Sn/P ratios in these materials are generally greater than unity. To our knowledge, a pure tin(II) phosphate with a chain structure has not yet been discovered, although a tin(II) phosphanate with a chain structure is known.[5] Based on a study of a tin phosphate monomer unit stabilized by hydrogen bonding with the template amine,[4] we suggested recently that the basic building unit present in all the tin(II) phosphate materials is the $[Sn_2P_2O_4]$ moiety, forming a four-membered ring. We, therefore, considered it important to explore the possibility of synthesizing a simple chain tin(II) phosphate formed by the $[Sn_2P_2O_4]$ tecton. A systematic study of Sn(II) phosphates prepared hydrothermally in the presence of various structure-directing agents has enabled us to obtain two very simple materials with a Sn/P ratio of unity. One of the tin(II) phosphates, **I**, containing only four- and eight-membered rings forms a layered structure, whereas the second material, **II**, contains only four-membered rings forming a ladder structure. We can, however, show how **I** can be generated from **II**, by a mere shifting of Sn–O–P bonds. Furthermore, the ladder structure, **II**, fills the gap left by the absence of one-dimensional chain structures in the tin phosphate family.

Compounds **I** and **II** were synthesized hydrothermally by employing DABCO (1,4-diazobicyclo[2,2,2]octane) and DEED (*N*,*N*′-diethylethylenediamine) as the structure-directing agents[6a,b] and characterized by single crystal X-ray diffraction studies,[7a,b] using the Siemens SMART system. The structure of **I**, $[C_6N_2H_{14}]^{2+}2[SnPO_4]^-\cdot H_2O$, is made up of layers constructed by the networking of SnO_3 and PO_4 units. The connectivity between these units creates 4- and 8-membered rings, forming a layer along the *bc* plane (Fig. 1). The individual layers are held together by the protonated DABCO molecules which occupy spaces in between the layers [Fig. 1(b)] along with a water molecule. This is clearly a simple structure compared to the known Sn(II) phosphates.[1–4] The tin(II) phosphate, **II**, $[C_6N_2H_{18}]^{2+}2[SnPO_4]^-$ formed by DEED, however, is even simpler in that its structure involves edge sharing of 4-membered $Sn_2P_2O_4$ rings, forming one-dimensional chains in the form of ladders (Fig. 2). The amine molecule is situated between the ladders. Indeed, **II** can be considered to be an inorganic ladderane, not unlike the organic counterpart.[8] In both **I** and **II**, there are strong hydrogen bond interactions between the anionic framework (layer in the case of **I**, and chain in the case of **II**) and the protonated amine molecules. The Sn–O distances and angles in both the phosphates are as expected for 3-coordinated tin(II) atoms, and the P–O distances and angles are in agreement with those in the previously reported phosphate structures. The P–O [P(1)–O(4) for **I** and P(1)–O(1) for **II**] distance of *ca.*1.5 Å corresponds to the P=O double bond which takes part in hydrogen bonding with the amine.

The two structures formed by the $Sn_2P_2O_4$ tecton described here are the simplest open-framework tin phosphate structures known so far. The layered structure of **I** can be made from the chain structure of **II** by the scheme shown in Fig. 3 [compare this with Fig. 1(a)]. In the proposed transformation, every second alternate 4-membered ring of **II** is broken (Sn–O–P bond—forming a new P=O), accompanied by a simple rotation of the existing P=O group about a P–O single bond giving rise to a Sn–O–P bond and new 4- and 8-membered rings. The broken line in Fig. 3 represents the new Sn–O–P bond formed. Such a formulation is consistent with the doubling of the *b* axis in **I** compared to **II**. In general, *n*-edge-sharing 4-membered rings can give rise to a ring with $4n - 2(n - 1)$ atoms. Or, if we add *n* 4-membered rings to a *m*-membered ring, we get a ring with $m + 2n$ atoms (*m* and *n* represent T atoms; T = Si, P in aluminosilicate zeolites and Sn, P in the present case). We thus

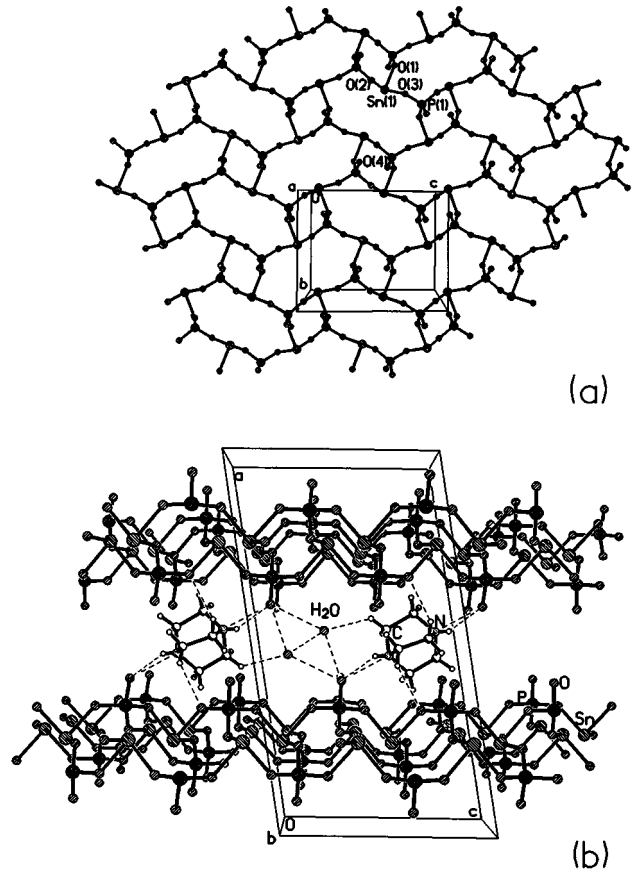

Fig. 1 Structure of **I**, $[C_6N_2H_{14}]^{2+}2[SnPO_4]^-\cdot H_2O$ showing (a) the 4- and 8-membered rings and the connectivity within the layer, and (b) the arrangement of anionic layers, the amine and the water molecules

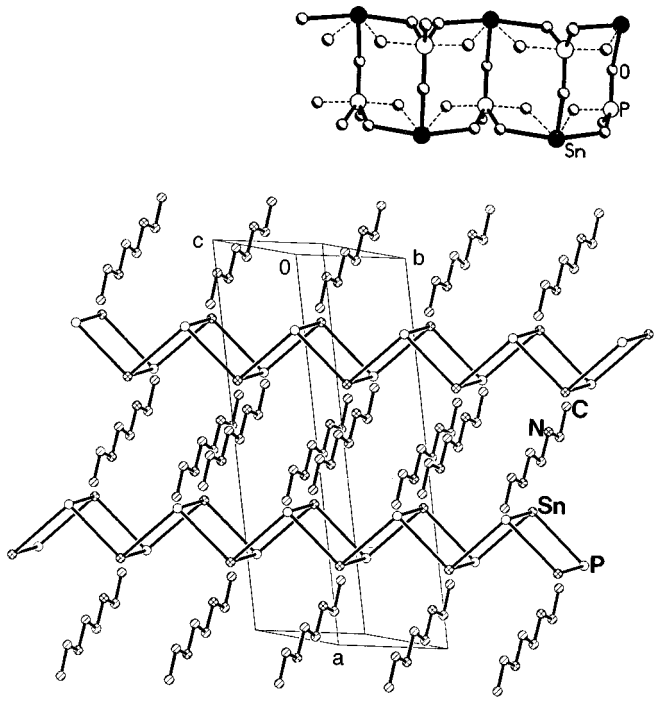

Fig. 2 Structure of **II**, $[C_6N_2H_{18}]^{2+}2[SnPO_4]^-$ showing the ladders and the amine (inset shows oxygen positions and the dotted lines represent the bonding with the disordered oxygens)

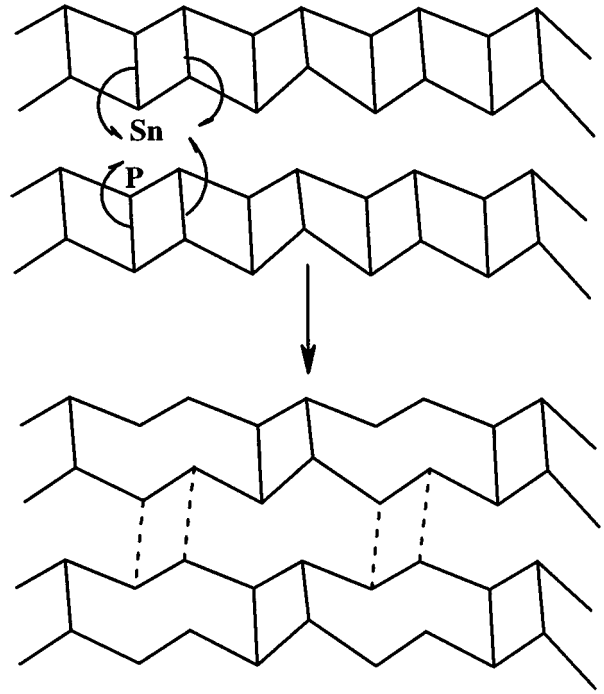

Fig. 3 Conversion of the chain (**II**) into the layered structure shown schematically. Note that the 4-membered rings are broken to form the 8-membered rings. The dotted lines represent the new 4- and 8-membered rings that are formed due to the Sn–O–P bonding and subsequently the layer (oxygens are not shown).

see how 6-, 8-, 10- and 12-membered rings can be formed from the 4-membered units.

The authors thank Unilever Plc for support of a joint research project between MRL, UCSB and JNCASR.

Notes and References

1 S. Natarajan, M. P. Attfield and A. K. Cheetham, *Angew. Chem., Int. Ed. Engl*., 1997, **36**, 978; S. Natarajan and A. K. Cheetham, *Chem. Commun*., 1997, 1089.

2 S. Natarajan, S. Ayyappan, A. K. Cheetham and C. N. R. Rao, *Chem. Mater*., 1998, **10**, 1627; S. Natarajan, M. Eswaramoorthy, A. K. Cheetham and C. N. R. Rao, *Chem. Commun*., 1998, 1561.

3 S. Natarajan and A. K. Cheetham, *J. Solid State Chem*., 1998, in press.

4 S. Ayyappan, A. K. Cheetham, S. Natarajan and C. N. R. Rao, *J. Solid State Chem*., 1998, **139**, 207.

5 P. J. Zapf, D. J. Rose, R. C. Haushalter and J. Zubieta, *J. Solid State Chem*., 1996, **125**, 182.

6 (*a*) 2.06 g of tin(II) oxalate were dispersed in 10 ml of water and 1.8 g of 85 wt% H_3PO_4 were added to the mixture under continuous stirring. 2 g of DABCO were added to the above and stirred until homogeneous. The composition of the mixture was SnC_2O_4 : $1.5H_3PO_4$: 1.8DABCO : $45H_2O$. The mixture was heated initially at 150 °C for 2 days and finally at 180 °C for 2 days and the product contained large quantities of plate-like single crystals. (*b*) 2.06 g of tin(II) oxalate, 2.81 ml of DEED, 5 ml of water and 5 ml of ethylene glycol were mixed together and stirred for 10 min. To this mixture 1.53 g of 85 wt% H_3PO_4 were added and the mixture homogenized and heated at 150 °C for 2 days. The final composition of the mixture was SnC_2O_4 : 1.95DEED : $27.5H_2O$: 8glycol : $1.3H_3PO_4$.

7 (*a*) Crystal data for **I**: $[C_6N_2H_{14}]^{2+}2[SnPO_4]^-\cdot H_2O$, M = 559.4, monoclinic, space group $C2/c$, a = 18.539(2), b = 8.105(1), c = 10.203(1) Å, β = 98.9(2)°, V = 1514.4(1) Å^3, Z = 4, D_c = 2.52 g cm^{-3}, T = 298 K, μ(Mo-Kα) = 3.57 mm^{-1}, R = 0.068, R_w = 0.076 for 717 data with $F \geqslant 3\sigma(F)$. (*b*) Crystal data for **II**: $[C_6N_2H_{18}]^{2+}2[SnPO_4]^-$, M = 271.4, monoclinic, space group $C2/m$, a = 17.938(1), b = 4.883(1), c = 10.814(1) Å, β = 116.9(1)°, V = 844.3(1) Å^3, Z = 2, D_c = 2.15 g cm^{-3}, T = 298 K, μ(Mo-Kα) = 3.2 mm^{-1}, R = 0.057, R_w = 0.14 for 834 data with $F \geqslant 2\sigma(F)$; two of the oxygens bonded to the phosphorous are disordered with a site occupancy factor of 0.5. CCDC 182/1004.

8 G. Mehta, M. B. Viswanath and A. C. Kunwar, *J. Org. Chem*., 1994, **54**, 6131.

Received in Cambridge, UK, 14th August 1998; 8/06417B

First three-component addition reaction in a series of 1,5-bis(dialkylamino)pentamethinium salts: a simple and efficient approach to tridentate chelating ligand systems

Vadim D. Romanenko,*[a,b] Jean-François Colom Toro,[a] François Rivière,[a] Jean-Gérard Wolf[a] and Michel Sanchez*[a]†

[a] *Université Paul Sabatier, Synthèse et Physicochimie Organique, UPR ESA 5068, 118 Route de Narbonne F-31062, Toulouse Cedex 4, France*
[b] *Institute of Biochemistry and Petrochemistry, Academy of Sciences of the Ukraine, Kiev-94, 253660, Ukraine*

A new approach to tridentate chelating NPN, NPO and OPO ligand systems is described *via* a tandem reaction of easily available 1,5-bis(dialkylamino)pentamethinium salts (streptocyanine dyes) with diphenylphosphine in the presence of TfOH.

The role of polymethine dyes as components of industrially important technologies has long been acknowledged.[1] It is surprising, therefore, that the reported chemistry of polymethine salts is rather sparse.[2,3] This is due to the relatively high thermodynamic stability of the polymethine chain and its tendency to be regenerated after reaction. In the pentamethinium series this enables introduction of nucleophilic or electrophilic groups into the chain by substitution rather than addition to the double bonds.

To exploit the synthetic potential of easily available pentamethinium salts[2,4] we now report the application of tandem methodology in the preparation of chelating polyheteroatomic compounds,[5] starting from 1,5-diaryl-substituted pentamethinium salts **1**.

Since non-ionic protic nucleophiles are not capable of direct addition to pentamethinium salts, activation of the latter towards the addition of phosphines might be achieved in the presence of strong protic acid, thus facilitating nucleophilic attack on the intermediate dicationic species.

Treatment of the pentamethinium salts **1** with the Ph_2PH and TfOH in the molar ratio 1:1:1 in a CH_2Cl_2 solution at −35 °C resulted in the quantitative formation of the diiminium salts **3** (Scheme 1). We obtained **3**‡ as colorless crystals in 83–95% yield. NMR signals at *ca.* δ 1.9 (HCP) and 3.2 (CH_2CHP, d, $^3J_{HH}$ 7 Hz) in the ^{1}H NMR spectra and *ca.* δ 187 (C=N$^+$), 35 (C3, $^1J_{CP}$ 22 Hz) and 39 (C2, C4, $^2J_{CP}$ 9 Hz) in the ^{13}C NMR spectra are diagnostic for structure **3**. The ^{31}P NMR signal is observed as a singlet in the range expected for alkyldiphenylphosphines (δ_P *ca.* 3).

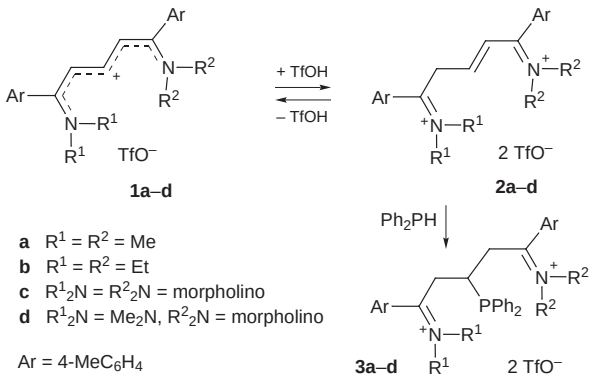

Scheme 1

Single crystals of salt **3b** were obtained from MeCN at 20 °C and X-ray data were collected at 160 K.§ The compound crystallizes along with 1 equiv. of MeCN in space group *P*1 Fig. 1. The C(3) atom in **3b** displays a slightly distorted tetrahedral geometry. The P–C(3) bond length [1.873(2) Å] lies at the higher limit of the normal P–C(sp^3) range, as in the sterically overcrowded compound $HC(PPh_2)_3$ (av. 1.872 Å).[6] Iminium nitrogens are sp^2-hybridized. The distances between the C(sp^2) atoms and nitrogen atoms [C(1)–N(1) and C(5)–N(2), av. 1.294 Å] are considerably shorter than in 1,5-diaryl-substituted pentamethinium salts (*ca.* 1.325 Å)[7] but comparable with those observed in other iminium salts.[8] The C(1)–C(2) and C(4)–C(5) distances are 1.498(3) and 1.507(3) Å, approximately 0.035 Å shorter than the C(2)–C(3) and C(3)–C(4) bonds. This may imply hyperconjugation in the $[HCC(Ar)N]^+$ bond system.

To gain some insight into possible intermediates leading to **3**, we treated **1b** with TfOH in CH_2Cl_2 at −50 °C. Monitoring the reaction *via* ^{13}C NMR spectroscopy clearly showed the reversible build-up of **2b** [δ 186.7 and 176.3 (C^1, C^5), 155.8 (C^3), 128.3 (C^4), 40.1 (C^2)]. The protonation of **1b** was achieved when 1.5-fold molar excess of TfOH was added. Subsequent warming of the solution in the NMR probe resulted in the disappearance of the signals due to **2b** due to its degradation with the loss of the $[Et_2NH_2^+TfO^-]$ salt. The yield of **3** sharply decreased if Ph_2PH was not added to the pentamethinium salt at the same time as the TfOH. The reaction pathway begins with an attack of the proton at the C^2 methine carbon of the substrate. The non-isolable dicationic intermediate **2** allows the efficient trapping of Ph_2PH in the subsequent nucleophilic addition.

An important aspect of salts **3** is their ability to release Ph_2PH. According a variable-temperature ^{31}P NMR study, the reversible cleavage of **3** in MeCN occurs above 50 °C. The

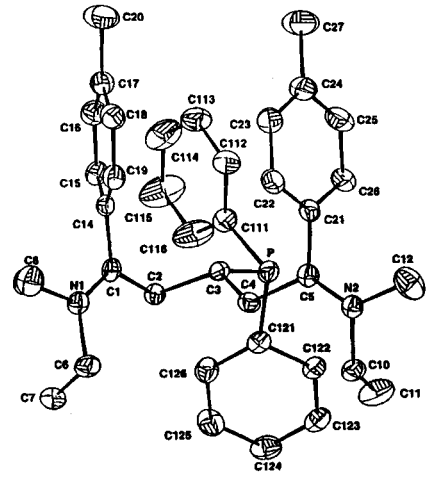

Fig. 1 Molecular structure of **3b** with atomic numbering scheme

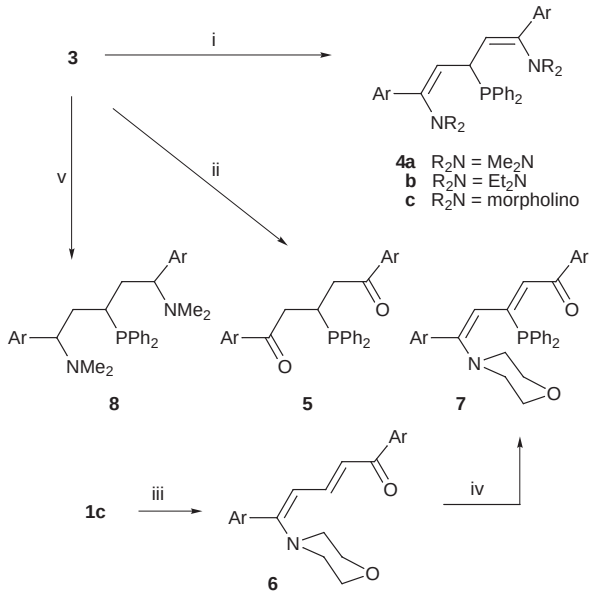

Scheme 2 *Reagents and conditions*: i, KOH, EtOH, 20 °C, 1 h; ii, KOH, EtOH–H_2O (5:1), 70 °C; iii, KOH EtOH–H_2O (5:1), 20 °C, 1 h; iv, Ph_2PH, KOH (cat.), MeCN, 20 °C, 24 h; v, $NaBH_4$, EtOH, −20 °C

addition of 3 mol% TfOH or an equimolar amount of pyridine to a CH_2Cl_2 solution of **3** promotes rupture of the C–P bond and the appearance of a broadened singlet at δ_P −38, indicating a fast proton exchange for the three-component system (**1**/Ph_2PH/TfOH). The cleavage of **3** proceeds slowly at 20 °C in alcohols and very fast in highly polar basic solvents such as HMPA, DMF or NMP. Evaporation of the solvent allows the recovery of **3**. Strong acids (catalytically) and weak bases tend to cleave the P–C(3) bond in **3** due to reversible protonation at the P centre and deprotonation of the chain methylene group. The treatment of **3** in EtOH at 20 °C with 2 equiv. of KOH affords the neutral compounds **4**¶ (Scheme 2). The deprotonation of the dication **3** and the formation of **4** is a highly regioselective reaction if the alternative pathway including protonation of the P atom and subsequent splitting up Ph_2PH is blocked or inhibited. The products **4** were isolated as crystalline materials and, in the case of **4c**, characterised by single-crystal X-ray structure determination.§ The most interesting difference between **3b** and **4c** is a lengthening of the P–C(3) bond [1.892(2) Å for **4c** *vs*. 1.873(2) Å for **3b**]. Meanwhile, compounds **4** do not display evidence for structural lability. Thus factors favouring P–C bond scission in **3** are of electronic rather than steric character.

When **3** was allowed to react with 2 equiv. of KOH in aq. EtOH at 60 °C for 2 h (Scheme 2) the dicarbonyl derivative **5**¶ was obtained. The conversion includes the intermediate formation of **4** and its subsequent hydrolysis. Efforts to synthesize **7** under similar conditions (1 equiv. of KOH, EtOH–H_2O, 60 °C) were not successful. However, reaction of **1c** with 1 equiv. of KOH in EtOH gave a yellow microcrystalline precipitate **6** (78%). Compound **7** was then constructed *via* treatment of **6** with Ph_2PH.¶ Finally, the reduction of **3a** with $NaBH_4$ proceeded smoothly in EtOH at −20 °C to give **8** (62%).¶

In summary, these results illustrate the ability of strong electrophiles to interact with the electron deficient pentamethinium chain, leading to the formation of adducts which are stabilised by addition of proton-donor nucleophiles. Polymethine salts are prospective starting materials for organoelement and coordination chemistry.

V. D. R. acknowledges fellowship support of the University Paul Sabatier (France) and the authors thank Dr B. Donnadieu for crystallographic data collection.

Notes and References

† E-mail: sanchez@ramses.ups-tlse.fr

‡ *Selected data* for **3b**: δ_C(100 MHz, CD_3CN) 13.7 (s, H_3CCH_2), 21.6 (s, 4-$H_3CC_6H_4$), 34.8 (d, $^1J_{CP}$ 22, C³), 40.0 (d, $^2J_{CP}$ 9, C² and C⁴), 51.5 and 54.0 (s, CH_2N), 188.9 (s, C¹ and C⁵); δ_P(81 MHz, CD_3CN) 3.0; *m/z* (FAB +ve, MNBA) 725 ([$M^{2+}TfO^-$]⁺).

§ *Crystal data* for **3b**: $[C_{39}H_{49}N_2P][CF_3SO_3]_2$[MeCN], M = 916.00, triclinic, crystal dimensions 0.50 × 0.40 × 0.20 mm³, space group $P1$, a = 11.379(2), b = 11.464(2), c = 19.099(3) Å, α = 74.06(2), β = 81.82(2), γ = 71.56(2)°, U = 2268(2) Å³, Z = 2, ρ_{calc} = 1.34 g cm^{-3}, μ = 2.17 cm^{-1}, F000 = 962.96. A total 17841 reflections were measured (6649 independent) with R_m = 0.03. The final R (R_w) values were 0.038 (0.039) for 5455 reflections [$I > 2\sigma(I)$] and 567 variables. For **4c**: $[C_{39}H_{43}N_20_2P][CH_3CN]$, M = 643.82, monoclinic, crystal dimensions 0.60 × 0.30 × 0.10 mm³, space group *Ia*, a = 9.445(1), b = 23.713(4), c = 23.305(4) Å, β = 103.64(2)°, U = 3554(3) Å³, Z = 4, ρ_{calc} = 1.11 g cm^{-3}, μ = 1.20 cm^{-1}, F000 = 1376.6. A total 11211 reflections were measured (5254 independent) with R_m = 0.03. The final R (R_w) values were 0.032 (0.037) for 4586 reflections [$I > 2\sigma(I)$] and 461 variables. CCDC 182–976.

¶ *Selected data* for **4–8**. For **4c**: δ_C[100 MHz, $(CD_3)_2CO$] 21.3 (s, 4-$H_3CC_6H_4$), 38.3 (d, $^1J_{CP}$ 13, C³), 51.0 (s, H_2CN), 67.4 (s, H_2CO), 107.2 (s, $^2J_{CP}$ 11, C² and C⁴), 137.7 (d, $^3J_{CP}$ 20, C¹ and C⁵); δ_P(81 MHz) 6.3; *m/z* (FAB +ve, MNBA) 603 $(MH)^+$. For **5**: δ_C(100 MHz, $CDCl_3$) 21.8 (s, 4-$H_3CC_6H_4$), 27.9 (d, $^1J_{CP}$ 13, CP), 40.2 (d, $^2J_{CP}$ 15, C² and C⁴), 198.6 (d, $^3J_{CP}$ 8, C¹ and C⁵); δ_P(81 MHz) −2.0; *m/z* (FAB +ve, MNBA) 465 $(MH)^+$. For **6**: δ_C(100 MHz, CD_3CN) 21.13 (s, 4-$H_3CC_6H_4$), 21.28 (s, 4-$H_3CC_6H_4$), 49.2 (s, CH_2N), 66.8 (s, CH_2O), 102.6 (s, CH), 116.6 (s, CH), 146.8 (s, CH), 161.9 (s, =CN), 189.0 (s, C=O); *m/z* (FAB +ve, GLY) 348 $(MH)^+$. For **7**: δ_C(100 MHz, $CDCl_3$) 21.4 (s, 4-$H_3CC_6H_4$), 21.8 (s, 4-$H_3CC_6H_4$), 34.4 (d, $^1J_{CP}$ 12, CP), 42.5 [d, $^2J_{CP}$ 19, $CH_2C(O)$], 49.5 (s, CH_2N), 67.0 (s, CH_2O), 103.9 (d, $^2J_{CP}$ 11, CH), 199.0 (d, $^3J_{CP}$ 12, CO); δ_P(81 MHz) 1.5; *m/z* (DCI/NH_3) 534 $(MH)^+$. For **8**: δ_C(75.47 MHz, $CDCl_3$) 21.2 (s, 4-$H_3CC_6H_4$), 29.9 (d, $^1J_{CP}$ 15.6, CHP), 35.3 (d, $^2J_{CP}$ 9, CH_2), 42.3 (s, H_3CN), 67.1 (s, C¹ and C⁵); δ_P(81 MHz) −0.1; *m/z* (DCI/NH_3) 523 $(MH)^+$.

1 Recent reviews on polymethine dyes: R. Raue, *Methine Dyes and Pigments* in *Ullmann's Encyclopedia of Industrial Chemistry*, VCH, Weinheim, 5th edn., 1990, vol. A16, pp. 487–534; N. Tyutyulkov, J. Fabian, A. Mehlhorn, F. Dietz and A. Tadjer, *Polymethine Dyes. Structure and Properties*, St. Kliment Ohridski University Press, Sofia, 1991.
2 D. M. Sturmer, in *The Chemistry of Heterocyclic Compounds*, ed. A. Weissberger and E. C. Taylor, Wiley, New York, 1977, vol. 30, p. 441.
3 C. Reichardt, K. Harms, M. Kinzel, G. Schäfer, J. Stein and S. Wocadlo, *Liebigs Ann.*, 1995, 317 and references cited therein; M. P. Fialon, A. Chernega, V. Romanenko, M.-R. Mazières and J.-G. Wolf, *Eur. J. Org. Chem.*, 1998, 329.
4 A. L. Pikus, V. M. Feigel'mann and V. V. Mezheritzkii, *Zh. Org. Khim.*, 1989, 25, 2603; Y. Madaule, M. Ramarohetra, J. G. Wolf, J. P. Declerq and A. Dubourg, *Angew Chem., Int. Ed. Engl.*, 1991, 30, 994.
5 See for example: M. Gandelman, A. Vigalok, L. J. W. Shimon and D. Milstein, *Organometallics*, 1997, **16**, 3981 and references cited therein.
6 H. Schmidbaur, A. Stutzer and E. Herdtweck, *Chem. Ber.*, 1991, **124**, 1095.
7 J.-P. Declerq, A. Dubourg, C. Payrastre, M.-R. Mazières, Y. Madaule and J.-G. Wolf, *Acta Crystallogr. Sect B*, 1996, **52**, 500.
8 D.E. Zacharias, *Acta Crystallogr., Sect B*, 1970, **26**, 1455; T. Barth, C. Krieger, H. A. Staab and F. A. Neugebauer, *Chem. Commun.*, 1993, 1129.

Received in Cambridge, UK, 27th July 1998; 8/05834B

Mechano-catalytic overall water splitting

Shigeru Ikeda,[a] Tsuyoshi Takata,[a] Takeshi Kondo,[a] Go Hitoki,[a] Michikazu Hara,[a] Junko N. Kondo,[a] Kazunari Domen,*[a] Hideo Hosono,[b] Hiroshi Kawazoe[b] and Akira Tanaka[c]

[a] *Research Laboratory of Resources Utilization, Tokyo Institute of Technology, 4259 Nagatsuta, Midori-ku, Yokohama 226-8503, Japan. E-mail: kdomen@res.titech.ac.jp*
[b] *Materials and Structures Laboratory, Tokyo Institute of Technology, 4259 Nagatsuta, Midori-ku, Yokohama 226-8503, Japan*
[c] *Nikon Corp., 1-10-1 Asamizodai, Sagamihara 228-0828, Japan*

Mechano-catalysis, a novel and simple method to decompose water into H_2 and O_2 in which mechanical energy is directly converted into chemical energy, is demonstrated.

H_2 production from water decomposition is one of the most attractive candidates for future clean energy resources. Electrolysis of water is a familiar way to accomplish overall water splitting. Photoelectrochemical and/or photocatalytic decomposition of water have also been pursued from the viewpoint of solar energy utilization.[1–4] Recently, the authors have been studying the decomposition of water on magnetically stirred Cu_2O powder under visible light irradiation.[5] At the stage when H_2 and O_2 evolved steadily in a stoichiometric ratio, we tentatively concluded that the reaction proceeded 'photocatalytically'.[5] In the subsequent study of the system, however, we found several characteristics of the reaction which are unusual for conventional photocatalytic ones. The most striking aspect of the reaction was the continuous evolution of H_2 and O_2 even after the light was turned off. This cannot be understood by the model of a semiconductor photocatalyst in which photoexcited electrons and holes are postulated to directly react with reactant water molecules (or H^+ and OH^- ions).[1] The lifetime of the photoexcited electronic states is at most of the order of milliseconds. We then hypothesized that photon energy was stored in the Cu_2O particle as some chemical species and the excess energy was gradually released to decompose water. To our surprise, however, the evolution of H_2 and O_2 in the dark continued for several hundred hours, and eventually the amounts of evolved H_2 and O_2 exceeded that of Cu_2O used. Another noticeable feature of this reaction is the marked dependence of the H_2 and O_2 evolution rates on the rate of stirring, *i.e.* the rate of H_2O decomposition increases monotonically with the rate of rotation. Without stirring, no H_2 and O_2 evolution occurred.

From these observations, we ended up with the following working hypothesis: the mechanical energy supplied by stirring was converted to chemical energy of H_2 and O_2 with Cu_2O functioning as a mediator or a catalyst. To work out this hypothesis, we have carried out rather extensive experiments by using various binary oxides. Here we report some phenomenological results which seem to be enough to prove our hypothesis. The detailed and atomic scale mechanism is an open question.

The reaction was carried out in a flat-bottomed reaction vessel made of Pyrex glass. Typically 0.1 g of oxide powder was suspended by magnetic stirring (F205, Tokyo Garasu Kikai) in 200 cm^3 of distilled water. The stirring rod was sealed by PTFE (polytetrafluoroethylene, Teflon®). The reaction vessel was attached to a closed gas circulation system (about 800 cm^3) equipped with an evacuation line. Before the reaction, the gas phase was completely evacuated and only water vapor remained. The evolved gas was accumulated and was analyzed by gas chromatography (TCD, Ar carrier, MS 5A column). When performing reactions in the dark, the reaction vessel was completely covered with aluminium foil, and when performing the reaction under photoirradiation, a 500 W Xe lamp placed at the side of the reaction vessel was used. The reaction temperature was at or somewhat lower than room temperature.

Various kinds of binary metal oxides which are stable in water were surveyed in the dark reaction. Cu_2O, NiO, Co_3O_4, and Fe_3O_4 exhibited H_2 and O_2 evolution. Much lower yet definite activity was also exhibited by RuO_2 and IrO_2. Specifically, CuO and Fe_2O_3 did not show activity for the reaction. Typical photocatalysts such as TiO_2, ZnO and WO_3 were also completely inert.

Fig. 1 shows a typical time course of H_2 and O_2 evolution on NiO in the dark. The NiO sample used was a yellow green powder with a BET surface area of about 1 $m^2\ g^{-1}$ and the particle size was about 0.5 μm [purchased from Kanto Chemical, high purity reagent (3 N)]. H_2 and O_2 kept evolving exactly in the stoichiometric ratio of water decomposition. The rate of H_2 and O_2 evolution gradually decreased with the accumulation of the evolved gas probably due to the effect of O_2 pressure. A similar effect was observed for the other three active oxides, *i.e.* Cu_2O, Co_3O_4 and Fe_3O_4. Almost the same time course was reproduced in the second run after evacuation. The total amount of evolved H_2 after the second run was 1.7 mmol, which exceeded the amount of NiO used, *i.e.* 1.3 mmol (0.1 g). No appreciable degradation of the activity was observed even after the second run. It was thus confirmed that this dark reaction proceeds catalytically.

Another point worth noting is the effect of the shape of the stirring rod: when a stirring rod with a flat bottom was used, the rate of H_2 and O_2 evolution was increased by more than an order of magnitude compared with that obtained when a round bottomed rod was used. This indicates that a mechanical effect such as the rubbing of the catalyst powder by the stirring rod is essential for the decomposition of water.

Two further experiments were conducted. First, double-sided adhesive tape was stuck to the flat bottom of the stirring rod and

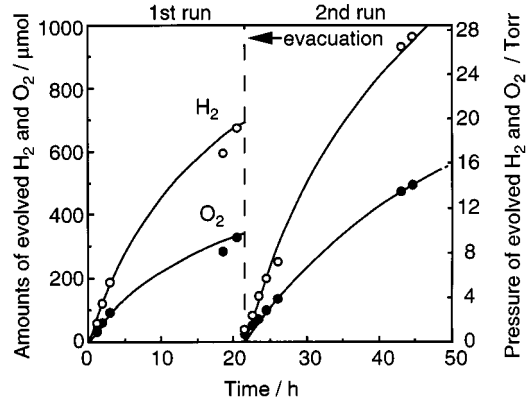

Fig. 1 Time course of H_2 (open circles) and O_2 (filled circles) evolution on NiO in the dark. The gas phase was evacuated at a reaction time of 22 h. Catalyst (NiO): 0.1 g, H_2O: 200 cm^3.

ca. 0.01 g of NiO powder was stuck onto the other side of the tape. The stirring rod was rotated in distilled water without any suspended NiO powder in it, and almost the same rate of H_2 and O_2 evolution as seen in Fig. 1 was achieved. This indicates that at least the major part of the water splitting reaction proceeded in between the stirring rod and the bottom of the glass reaction vessel. This result also excluded the possibility that the Teflon which coated the stirring rod took part in the reaction. Second, a Ni metal foil (35 mm × 9 mm × 0.2 mm) was oxidized at 800 °C for 1 h in air and was rotated in distilled water at the bottom of the reaction vessel by using a stirring rod attached on top of the foil. Again H_2 and O_2 evolution was observed with a rate of about half that obtained in the above experiment using adhesive tape. These results suggest that the rubbing of the oxide materials against the bottom wall of the glass reaction vessel is essential, but the collisions between the oxide particles or at the stirrer surface are not.

In the above experiments, we did not pay much attention to the influence of magnetic fields generated by the stirring device. To avoid magnetic field effects, a motor driven mechanical stirrer was used for the abrasive stirring. The motor rotated the catalyst powder (NiO) stuck on the tip of the driving shaft, which was pressed on the bottom of the reaction vessel. Even in the reaction cell, stoichiometric H_2 and O_2 evolution was observed. Therefore, the magnetic field exerted by the stirrer has nothing to do with the present phenomenon.

From all the above experimental results, we conclude that the H_2 and O_2 evolution is regarded as 'mechano-catalytic' overall water splitting. Because of the first and second laws of thermodynamics, it is not probable that heat of friction leads to the observed water decomposition. We, therefore, consider that these catalysts directly convert mechanical energy to chemical energy.

We now turn to the influence of photoirradiation. When the reaction vessel containing a suspended powder catalyst was irradiated with a Xe lamp, essentially no appreciable change in H_2 and O_2 evolution rate was observed for NiO, Co_3O_4, and Fe_3O_4. However, in the case of Cu_2O, a difference of the rate of H_2 and O_2 evolution was observed as shown in Fig. 2. During the first 50 h, the reaction was carried out under irradiation (> 460 nm) and then the reaction was continued in the dark for another 50 h after the evacuation of the gas phase. The rate of H_2 and O_2 evolution under the irradiation was faster by about 3 times than that in the dark. Because of the difference of the activity between reaction in the dark and under photoirradiation, we previously concluded the observed phenomenon as photocatalysis, which should be corrected. At present, we do not have a satisfactory explanation for the effect of photoirradiation on Cu_2O.

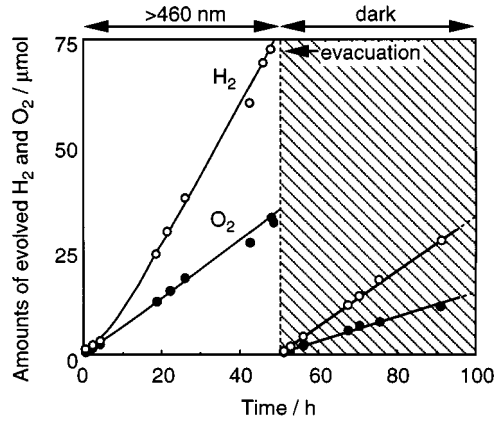

Fig. 2 Time course of H_2 (open circles) and O_2 (filled circles) evolution on Cu_2O under visible light (> 460 nm) irradiation and in the dark. The reaction system was evacuated at a reaction time of 50 h. Catalyst (Cu_2O): 0.1 g, H_2O: 200 cm^3.

As we have shown, the rate of H_2 and O_2 evolution strongly depends on the rubbing method of the catalytic materials, and thus much more efficient systems could be constructed by a suitable reactor design.

This work was partly supported by the Research Institute of Innovative Technology for the Earth (RITE), and also by a Grant-in-Aid for Scientific Research on Priority Area of 'Catalytic Chemistry of Unique Reaction Fields-Extreme Environment Catalysts' from the Ministry of Education, Science, Sports and Culture, Japan, and also by the Research for the Future Program, the Japan Society for the Promotion of Science.

Notes and References

1 M. Grätzel, in *Energy Resources through Photochemistry and Catalysis*, Academic Press, New York, 1983, p. 71.
2 E. Amouyal, in *Homogeneous Photocatalysts*, Wiley Series in Photoscience and Photoengineering, vol. 2, John Wiley & Sons, Chichester, 1997, p. 263.
3 A. Kudo, A.Tanaka, K. Domen, K. Maruya, K. Aika and T. Onishi, *J. Catal*., 1988, **111**, 67.
4 T. Takata, A. Tanaka, K. Shinohara, M. Hara, J. N. Kondo and K. Domen, *Chem. Mater*., 1997, **9**, 1063.
5 M. Hara, T. Kondo, M. Komoda, S. Ikeda, K. Shinohara, A. Tanaka, J. N. Kondo and K. Domen, *Chem. Commun.*, 1998, 357.

Received in Cambridge, UK, 16th June 1998; 8/04549F

Hydrothermal synthesis and structural characterization of a tubular oxovanadium organophosphonate, $(H_3O)[(V_3O_4)(H_2O)(PhPO_3)_3]\cdot xH_2O$ (x = 2.33)

Grant Bonavia,[a] Robert C. Haushalter,[b] Charles J. O'Connor,[c] Claudio Sangregorio[c] and Jon Zubieta*[a]

[a] *Department of Chemistry, Syracuse University, Syracuse, New York 13244, USA. E-mail: jazubiet@syr.edu*
[b] *Symyx Technologies, 3100 Central Expressway, Santa Clara, California 95051, USA*
[c] *Department of Chemistry, University of New Orleans, New Orleans, LA 70148, USA*

The hydrothermal reaction of KVO_3, $PhPO_3H_2$ and water at 180 °C for 116 h yields the tubular mixed valence V^V/V^{IV} polymer $(H_3O)[(V_3O_4)(H_2O)(PhPO_3)_3]\cdot xH_2O$ (x = 2.33).

The widespread contemporary interest in metal phosphonate materials[1–3] reflects their potential applications as sorbents, ion exchangers,[4] ionic conductors,[5] nonlinear optical materials,[6] sensors[7] and catalysts.[8] The vanadyl organophosphonate system has proved particularly fruitful and is represented by molecular clusters of various nuclearities, and one-, two- and three-dimensional phases.[9–11] In common with metal organophosphonates in general, lamellar structures predominate for the vanadyl organophosphonate subclass, with $[(VO)(H_2O)(PhPO_3)]$[12] providing the structural prototype. Lamellar vanadyl organophosphonates possess structurally well defined internal void spaces and coordination sites which allow intercalation of substrate molecules. Modifications of organic substituents, introduction of templating reagents, and variations in metal–phosphonate compositions can be exploited to change substrate-specific recognition and to design novel phases. It is also apparent that variations in reaction conditions can result in significant structural reorganization.[13–15] Thus, the novel tubular material $(H_3O)[(V_3O_4)(H_2O)(PhPO_3)_3]\cdot xH_2O$ **1** (x = 2.33) was prepared by relatively minor modification of the synthetic procedure employed in the isolation of the lamellar $[(VO)(H_2O)(PhPO_3)]$.[12]

The reaction of MVO_3 (M = NH_4^+, Na^+, K^+), $PhPO_3H_2$ and water in the mole ratio 1 : 2.33 : 340 at 180 °C for 116 h yielded dark green hexagonal rods of $(H_3O)[(V_3O_4)(H_2O)(PhPO_3)_3]\cdot xH_2O$ **1** (x = 2.33)† in 75% yield. Although the inorganic cation of the vanadate starting material does not appear in the product, it is absolutely required for the synthesis of **1**, an observation which highlights the often critical role of sacrificial cations in hydrothermal synthesis. Consequently, the reaction of V_2O_5 with $PhPO_3H_2$ under identical conditions yields only $[VO(H_2O)(PhPO_3)]$. It is noteworthy that hydrothermal treatment of $[VO(H_2O)(PhPO_3)]$ with Na^+ at pH 2 results in quantitative conversion to **1**. However, compound **1** was not isolated in more basic environments, where an undefinable powder was observed to form. Attempts to prepare **1** from oxovanadium phenylphosphonate clusters such as $[V_5O_7(OMe)_2(PhPO_3)_5]^-$,[16] and Na^+ in nonaqueous solvents proved fruitless. However, such clusters proved perfectly adequate for synthesis under hydrothermal conditions, suggesting that a solvent of a high dielectric constant is required and that the synthesis of **1** occurs through disassembly of oxovanadium phosphonate units rather than fusion of discrete clusters or unzipping of layered structures into infinite chains which subsequently fuse into the tubular form.

As illustrated in Fig. 1, the structure of **1**‡ consists of $[(V_3O_4)(H_2O)(PhPO_3)_3]_n^{n-}$ tubes running parallel to the *c*-axis. The phenyl groups extend outward from the periphery of the tube, while the vanadyl oxo groups are directed both to the interior and exterior of the cavity. The hydronium cation and the water molecules are contained within the hydrophilic interior of the tube, while the phenyl groups of the tube interdigitate with phenyl groups from adjacent tubes to provide a hydrophobic exterior.

The walls of the tube are constructed from three independent oxovanadium centers, an aqua group and three phosphonate bridging ligands, shown in Fig. 2. Two of the vanadium sites

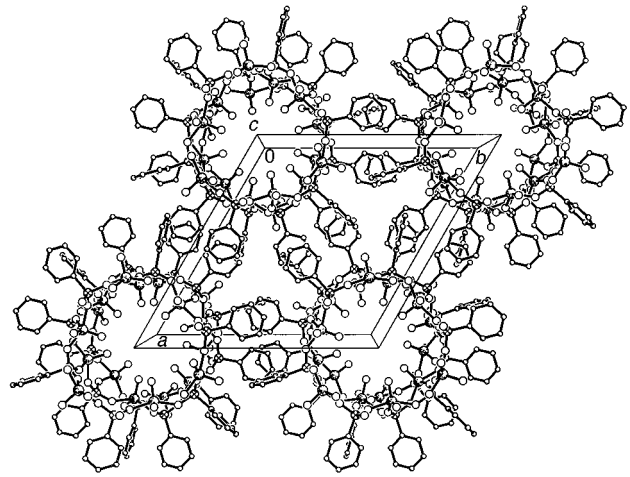

Fig. 1 A view along the crystallographic *c* axis of the tubular structure of the anions of **1**. The hydronium cations and water molecules of crystallization occupy the hydrophilic interior of the tube. The phenyl groups project outward from the tubes and interdigitate in the hydrophobic domains outside the tubes.

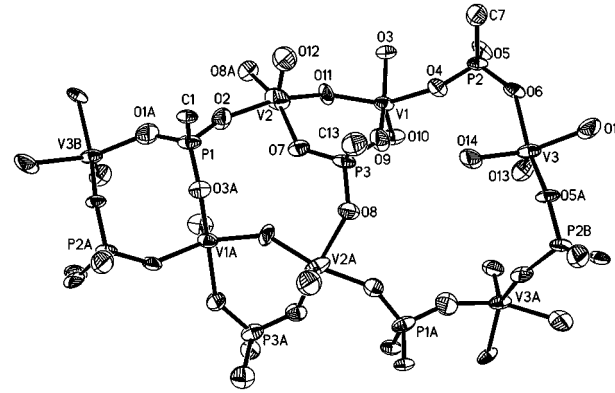

Fig. 2 A view of the V–O–P building blocks of the tube walls, showing the atom-labeling scheme and 50% probability ellipsoids. Selected bond lengths (Å): V1–O10 1.563(3), V1–O11 1.928(3), V1–O3 1.946(3), V1–O9 1.974(3), V1–O4 1.979(3), V2–O12 1.621(4), V2–O11 1.880(3), V2–O7 1.905(3), V2–O2 1.929(3), V2–O8 1.987(3), V3–O13 1.596(4), V3–O5 1.902(3), V3–O6 1.955(3), V3–O1 1.970(4), V3–O14 2.005(4).

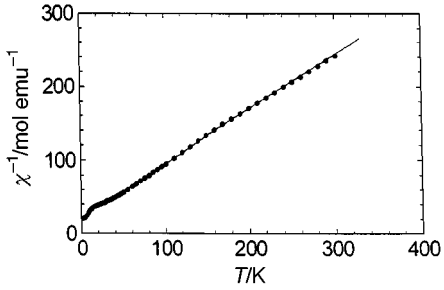

Fig. 3 A plot of $1/\chi$ *vs*. temperature, showing the Curie fit to the data

form a binuclear unit of corner-sharing square pyramids with the terminal oxo-groups in *anti*-orientation with respect to the V–O–V bridge. The remaining three coordination sites on each vanadium center are occupied by oxygen donors from the phosphonate ligands. The third vanadium site V3 is an isolated square pyramid (no V–O–V interactions). The oxo-group is directed toward the interior of the tube, while the coordinated aqua ligand forms parts of the tube wall. The complex pattern of phosphonate bridging of metal centers provides four distinct heteronuclear ring motifs as fundamental building blocks[18] of the tube wall: six atom (VOVOPO), eight atom $(VOPO)_2$, ten atom (VOVOPOVOPO) and sixteen atom $(VOPO)_4$ cycles.

The temperature dependence of the magnetic susceptibility of **1** is shown in Fig. 3. Above 40 K, the magnetic susceptibility conforms to the Curie–Weiss law with a Curie constant corresponding to 3.27 μ_B and a Θ value of −27 K. The effective moment for each of two V^{IV} ions is 2.33 μ_B, indicating a significant orbital contribution to the moment as anticipated for the $^2T_{2g}$ ground state. The negative Θ value indicates the presence of antiferromagnetic spin interactions, and the deviation from Curie–Weiss behavior below 40 K can be ascribed to the coupling of the spins of the d^1 V^{IV} sites. These observations are consistent with charge balance and valence sum calculations[17] which give an average oxidation state of 4.33 per vanadium site, or 1 V^V and 2 V^{IV} centers.

Thermogravimetric analysis of **1** shows weight losses corresponding to 1 and *ca*. 1.5 water molecules of crystallization at 50–60 and 120–140 °C, respectively. A weight loss corresponding to two additional water molecules occurs between 245 and 275 °C. The material decomposes sharply at 305 °C with an additional 30% weight loss to produce a blue amorphous material.

While **1** represents the first example of a tubular structure for the vanadium–organophosphonate system, tubular uranyl phosphonates have been reported recently.[13–15] However, the structure of the wall of **1** is quite distinct from the uranyl species which do not form U–O–U bonds. When viewed down the tube axis, the structure of **1** presents the circular projection also observed for $(UO_2)(PhPO_3)\cdot 0.7H_2O$, whereas $[(UO_2)_3(PhPO_3H)_2]\cdot H_2O$ exhibits a rectangular profile. Although the uranyl materials exhibit neutral tubes, the tube in **1** is anionic with charge compensation provided by hydroxonium cations, which occupy the interior of the tube and hydrogen bond to oxo-groups of the tube wall and water molecules which stuff the tube interior. Furthermore, the vanadyl sites of **1** are five coordinate, a geometry achieved through coordination to terminal and bridging oxo-groups and η^3,μ_3-phosphonate ligation. In contrast, the uranyl centers of the circular tubular material $(UO_2)(PhPO_3)\cdot 0.7H_2O$ are seven coordinate, exhibiting the common *trans* dioxo unit and requiring that the phosphonate adopt the η^3, μ_5-coordination mode. The structure of **1** exhibits two of the phenomena that critically influence the organization of organic–inorganic composite materials, namely, multipoint hydrogen bonding and hydrophilic–hydrophobic interactions.[18]

The research was supported by NSF grant CHE9617232.

Notes and References

† The value of 2.33 for the water of crystallization was estimated from elemental analyses, TGA (*vide infra*) and refinement of the population parameters of the water oxygen atoms in the X-ray crystal structure refinement.

‡ *Crystal data* for $C_{18}H_{24.67}O_{17.33}P_3V_3$ **1**; $P\bar{3}$, a = 18.6754(4), c = 13.8500(4) Å, V = 4183.3(2) Å^3, Z = 6, D_c = 1.820 g cm^{-3}; solution and refinement based on 4932 independent reflections converged at $R1$ = 0.0582, $wR2$ = 0.1627. CCDC 182/986.

1 A. Clearfield, *Prog. Inorg. Chem.*, 1998, **40**, 371.
2 G. Alberti, *Layered Metalphosphonates and Covalently Pillared Diphosphonates*, in *Comprehensive Supramolecular Chemistry*, ed. J. M. Lehn (Chairman), J. L. Atwood, J. E. D. Davies, D. D. McNicol and F. Vögtle, Pergamon, New York, vol. 7 (ed. G. Alberti and T. Bein), 1996, p. 151.
3 D. M. Poojary, B. Zhang, P. Bellinghausen and A. Clearfield, *Inorg. Chem.*, 1996, **35**, 4942 and references therein.
4 A. Clearfield, *Chem. Rev.*, 1988, **88**, 125.
5 G. Alberti and M. Casciola, *Solid State Ionics*, 1997, **97**, 177; G. Alberti, U. Constantino, M. Casciola and R. Vivani, *Solid State Ionics*, 1991, **46**, 61.
6 M. E. Thompson, *Chem. Mater.*, 1994, **6**, 1168.
7 J. L. Snover, H. Byrd, E. P. Suponeva, E. Vicenzi and M. E. Thompson, *Chem. Mater.*, 1996, **8**, 1490.
8 G. Alberti, U. Constantino, M. Casciola and R. Vivani, *Adv. Mater.*, 1996, **8**, 291; G. Alberti and U. Constantino, *J. Mol. Catal.*, 1994, **27**, 235.
9 M. I. Khan and J. Zubieta, *Prog. Inorg. Chem.*, 1995, **43**, 1 and references therein.
10 V. Soghomonian, Q. Chen, R. C. Haushalter and J. Zubieta, *Angew. Chem., Int. Ed. Engl.*, 1995, **34**, 223.
11 G. Bonavia, R. C. Haushalter, C. J. O'Connor and J. Zubieta, *Inorg. Chem.*, 1996, **35**, 5603.
12 G. Huan, A. J. Jacobson, J. W. Johnson and G. W. Corcoran, Jr., *Chem. Mater.*, 1990, **2**, 91.
13 D. M. Poojary, D. Grohol and A. Clearfield, *Angew. Chem., Int. Ed. Engl.*, 1995, **34**, 1508.
14 D. Grohol and A. Clearfield, *J. Am. Chem. Soc.*, 1997, **119**, 9301.
15 D. M. Poojary, A. Cabeza, M. A. G. Aranda, S. Bruque and A. Clearfield, *Inorg. Chem.*, 1996, **35**, 1468.
16 Q. Chen and J. Zubieta, *Angew. Chem., Int. Ed. Engl.*, 1993, **32**, 261.
17 I. D. Brown, in *Structure and Bonding*, ed. M. O'Keefe and A. Navrotsky, Academic Press, New York, 1981, vol. 2, ch. 1.
18 C. J. Warren, R. C. Haushalter and J. Zubieta, unpublished work.

Received in Columbia, MO, USA, 24th June 1998; 8/04864I

Structure and phosphodiesterase activity of Bis-Tris coordinated lanthanide(III) complexes

Soon Jin Oh, Young-Seo Choi, Seok Hwangbo, Sung Chul Bae, Ja Kang Ku, and Joon Won Park*

Department of Chemistry, Center for Biofunctional Molecules, Pohang University of Science and Technology, San 31 Hyoja-dong, Pohang, 790-784, Korea. E-mail: jwpark@vision.postech.ac.kr

A commonly used buffer, 2,2-bis(hydroxymethyl)-2,2′,2″-nitrilotriethanol (Bis-Tris) coordinates lanthanide(III) ion strongly in water to form molecular species that are highly active for the hydrolysis of a phosphate diester, bis(4-nitrophenyl) phosphate.

Ligand free lanthanide ions have been shown to be highly reactive for hydrolyzing phosphate esters including RNA and DNA.[1] There has been considerable interest in developing organic ligands that bind tightly around lanthanide ions in order to increase the solubility of the metal ions, and to develop artificial restriction enzymes by covalently anchoring the metal to molecules that bind nucleic acids sequence specifically.[2] Over the last several years, many elegant ligands (**1**–**7**) that bind

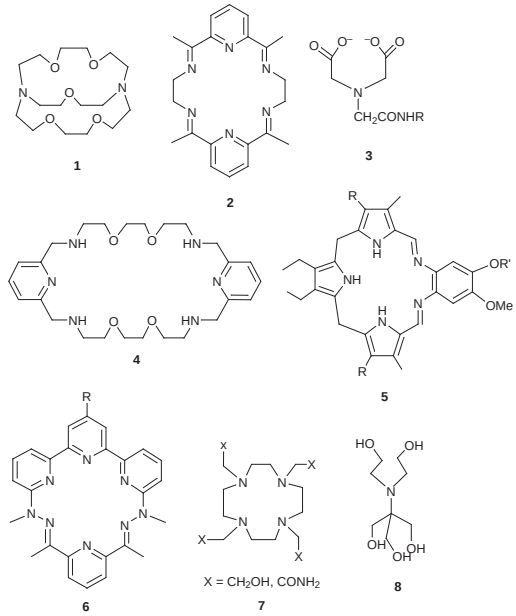

lanthanide ions have been developed for the purpose of hydrolyzing phosphates.[2–5] Negatively charged ligands tend to bind tightly to lanthanide ions but greatly lower the reactivity of the metal ions for hydrolyzing phosphates.† On the other hand, neutral ligands tend to release the lanthanide ions by deligation (**1**, **2**).[3,4] Here we report a remarkably simple neutral ligand (**8**)[6]‡ that binds tightly around lanthanide ions without lowering their reactivity for hydrolyzing phosphates.

Compound **8** is a commonly used buffer 2,2-bis(hydroxymethyl)-2,2′,2″-nitrilotriethanol (Bis-Tris). An equimolar mixture of $LaCl_3$ and Bis-Tris in methanol yielded white crystals. The structure of $[La(\mathbf{8})_2]Cl_3$ (Fig. 1) reveals that the metal has ten coordination sites occupied by two molecules of Bis-Tris.§ Each molecule of Bis-Tris acts as a pentacoordinate ligand with four of its oxygen atoms and its nitrogen atom. The remaining oxygen of Bis-Tris cannot coordinate due to its structural position. Although the crystal structure is that of a 2 : 1 ligand to metal complex, other data shown below indicate that the major species in aqueous solution of an equimolar mixture of $LaCl_3$ and Bis-Tris is a 1 : 1 ligand to metal complex.

Potentiometric titration of an equimolar mixture of $LaCl_3$ and Bis-Tris in water showed that there is no ligand-free La(III) ion or metal-free Bis-Tris. The pK_a of Bis-Tris shifts from 6.5 to 4.0 in the presence of an equivalent of $LaCl_3$ (24 mM), indicating that the formation of the complex is quite favorable in the aqueous solution ($K_f = 5 \times 10^4$ M^{-1}).¶ It is rather surprising to observe such a large binding constant for the neutral ligand, given that the formation constant of the europium(III) cryptand 221 complex is smaller than 0.5 M^{-1}.[3a]‖ Other buffers of the similar structure such as Tris, Bis-Tris Propane, Taps, Tapso, and Tes do not bind to lanthanide ions as well as Bis-Tris. In particular, a binding constant of 2.75×10^2 M^{-1} for Tris has been reported.[7]

In the titration of the equimolar mixture, consumption of 2 equiv. OH^- is observed at around pH 9.8. The low steepness of the titration curve suggest that a dimer **9** is formed at the pH. In the absence of any organic ligands, $LaCl_3$ itself also gives a curve of the similar shape. Based on the slope of the titration curve, it has been suggested that ligand-free lanthanide ions also form dimers or higher order aggregates under alkaline conditions. Thus lanthanide ions tend to form gels under alkaline conditions (pH > 9) even at low concentrations (0.5 mM). Interestingly, equimolar mixtures of $LaCl_3$ and Bis-Tris remain in solution even at 40 mM $LaCl_3$ and pH 11.5. It may be that Bis-Tris prevents aggregation of La(III) ions and enhances solubility by capping the two ends of the dimer **9** (Scheme 1).

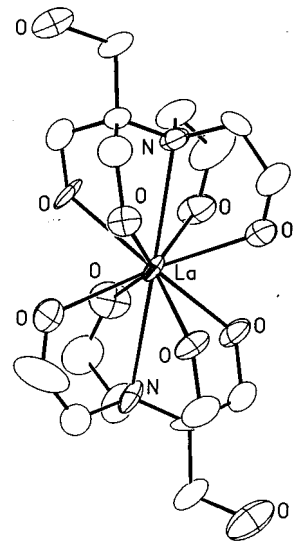

Fig. 1 ORTEP diagram of the lanthanum(III) complex coordinating two molecules of Bis-Tris. Distances between the coordinated oxygen atoms and the metal center are between 2.515(14) and 2.622(13) Å. Distances between the nitrogen atoms and the metal center are between 2.863(14) and 2.948(13) Å. Hydrogen atoms and non-coordinating chloride anions are removed for clarity.

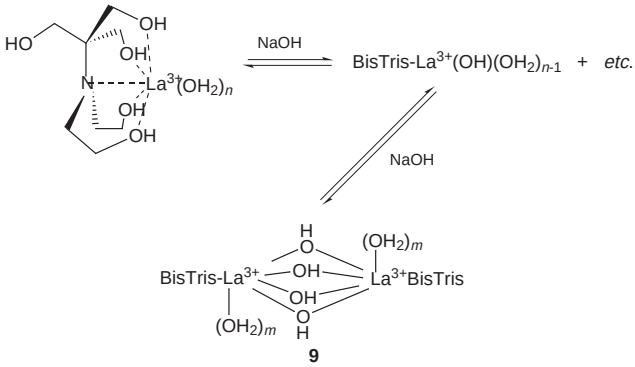

9

Scheme 1

Time-resolved luminescence spectroscopy is a valuable method for investigating Eu(III) complexes in aqueous solution.[8] The number of coordinating waters (q) per Eu(III) center in solution can be obtained by measuring the luminescence lifetimes of each species in water and deuterated water. Fig. 2 shows the excitation spectra of an equimolar mixture of $EuCl_3$ and Bis-Tris in water with 0–2.5 equiv. NaOH added. In the absence of any added NaOH, a single sharp peak at 579.7 nm with the q value of 6 suggests an 1 : 1 Eu to Bis-Tris complex with less than six coordinating water molecules. When two equiv. OH^- is added, a major peak at 580.4 nm with a significantly reduced q (2.5) value appears, which is consistent with structure **9**.

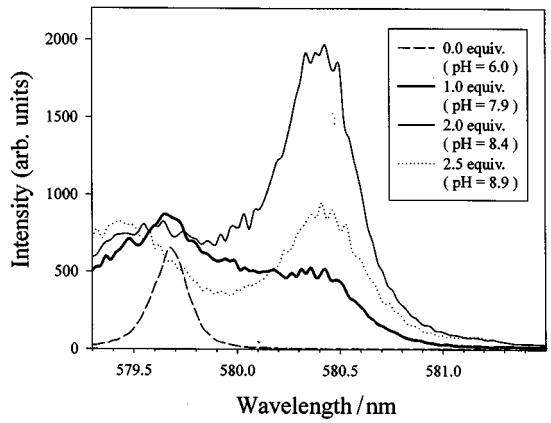

Fig. 2 Excitation spectra of the europium(III) complex in the presence of 1 equiv. of Bis-Tris. Spectra were recorded in water upon addition of (a) 0, (b) 1.0, (c) 2.0 and (d) 2.5 equiv. NaOH.

The reactivity of a 1 : 1 $LaCl_3$ to Bis-Tris solution for hydrolyzing bis(4-nitrophenyl)phosphate (BNPP) initially increases with added NaOH but reaches a maximum at 2 equiv. NaOH. Therefore, complex **9** or its kinetic equivalent is the active species for hydrolyzing BNPP. The phenomenon is observed at a wide range of concentration (0.5–20 mM). Although Bis-Tris increases the solubility of lanthanide ions by tightly complexing them, it does not reduce the reactivity of the metal center for hydrolyzing BNPP. For comparison, the activities were measured at low concentration, where precipitation of free lanthanide ions is not problematic. The hydrolytic activity of a 1 : 1 $LaCl_3$ to Bis-Tris solution (0.5 mM) with 2 equiv. NaOH ($k = 7.3 \times 10^{-3}$ s^{-1}) is comparable to a solution of $LaCl_3$ (0.5 mM) with 2 equiv. NaOH ($k = 8.2 \times 10^{-3}$ s^{-1}). We propose that the hydrolytic mechanism involves nucleophilic attack of the phosphate bridging the two metal centers by one of the bridging hydroxides (**10**).[9]

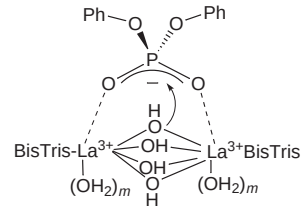

10

We are grateful to the Basic Science Research Fund of Pohang University of Science and Technology and the Korea Foundation of Science and Engineering (96-0501-01-01-3). The authors thank Professor J. Chin for his helpful discussion, and also Dr Ki-Min Park and Dr Dongmok Whang for the X-ray crystallographic analysis.

Notes and References

† Anionic chelates such as EDTA and maleic acid significantly reduce the hydrolytic activity of lanthanide ions.

‡ Polyalcohols such as glycerol and cyclodextrin have been used for effective chelating ligands for lanthanide ions.

§ *Crystal data* for $[La(\mathbf{8})_2]Cl_3$: Colorless crystals of $C_{16}H_{38}N_2O_{10}LaCl_3$; triclinic, space group $P\bar{1}$, $a = 13.9502(2)$, $b = 14.4812(2)$, $c = 21.5698(2)$, $\alpha = 84.5980(10)$, $\beta = 71.707(10)$, $\gamma = 71.6110(10)°$, $V = 3925.91(9)$ Å^3, $Z = 6$, $\mu = 19.9$ cm^{-1}, $D_c = 1.684$ g cm^{-3}, $M = 663.74$. There are two asymmetric units in the unit cell and three independent molecules per unit. The final $R_w(F^2) = 0.2326$ with a goodness of fit = 1.152, while the conventional $R(F) = 0.1034$ for 11 239 reflections with $F_o > 4[\sigma(F_o)]$. The high R value is mostly due to the large formula weight, unavoidable disorder of the unbound hydroxyl groups, and abnormally large thermal vibrations of C13, C21, C56, C58, N11 and O23 atoms. See Fig. S4 in electronic supplementary information section for a numbering scheme (http://www.rsc.org./suppdata/cc/1998/2189).

¶ A commercially available program, BEST, was employed for the data fitting. See A. E. Martell and R. J. Motekraitis, *Determination and Use of Stability Constants*, 2nd edn., VCH, New York, 1992.

‖ A larger formation constant has been reported by Burns *et al*. (*Inorg. Chem.*, 1981, **20**, 616). Uncertainty in interpreting the q values arises from the ill defined influence of the bound OH^- groups.

1 R. Breslow and D.-L. Huang, *Proc. Natl. Acad. Sci. USA*, 1991, **88**, 4080; K. Bracken, R. A. Moss and K. G. Ragunathan, *J. Am. Chem. Soc.* 1997, **119**, 9323; A. Roigk, R. Hettich and H.-J. Schneider, *Inorg. Chem.*, 1998, **37**, 751.

2 D. Magda, S. Crofts, A. Lin, D. Miles, M. Wright and J. L. Sessler, *J. Am. Chem. Soc.*, 1997, **119**, 2293; K. M. Matsumura, M. Endo and M. Komiyama, *J. Chem. Soc., Chem. Commun.*, 1994, 2019; J. Hall, D. Hüsken and R. Häner, *Nucleosides Nucleotides*, 1997, **16**, 1357; S. Hashimoto and Y. Nakamura, *J. Chem. Soc., Chem. Commun.*, 1995, 1413.

3 (*a*) S. J. Oh and J. W. Park, *J. Chem. Soc., Dalton Trans.*, 1997, 753; (*b*) S. J. Oh, K. H. Song, D. Whang, K. Kim, T. H. Yoon, H. Moon and J. W. Park, *Inorg. Chem.*, 1996, **35**, 3780; (*c*) S. J. Oh, C. W. Yoon and J. W. Park, *J. Chem. Soc., Perkin Trans. 2*, 1996, 329; (*d*) S. J. Oh, K. H. Song and J. W. Park, *J. Chem. Soc., Chem. Commun.*, 1995, 575.

4 B. F. Baker, H. Khalili, N. Wei and J. R. Morrow, *J. Am. Chem. Soc.*, 1997, **119**, 8749; S. Amin, D. A. Voss, Jr., W. DeW. Horrcks, Jr. and J. R. Morrow, *Inorg. Chem.*, 1996, **35**, 7466; S. Amin, J. R. Morrow, C. H. Lake and M. R. Churchill, *Angew. Chem. Int. Ed. Engl.*, 1994, **33**, 773; J. R. Morrow, L. A. Buttrey, V. M. Shelton and K. A. Berback, *J. Am. Chem. Soc.*, 1992, **114**, 1903.

5 K. G. Ragunathan and H.-J. Schneider, *Angew. Chem., Int. Ed. Engl.*, 1996, **35**, 1219.

6 J. Rammo, R. Hettich, A. Roigk and H.-J. Schneider, *Chem. Commun.*, 1996, 105; M. Yashiro, T. Takarada, S. Miyama and M. Komiyama, *J. Chem. Soc., Chem. Commun.*, 1994, 1757.

7 J.-M. Pfefferlé and J.-C. G. Bünzli, *Helv. Chim. Acta*, 1989, **72**, 1487.

8 (a) W. D. Horrock and D. R. Sudnick, *J. Am. Chem. Soc.*, 1979, **101**, 334; (b) F. S. Richardson, *Chem. Rev.*, 1982, **82**, 541.

9 B. K. Takasaki and J. Chin, *J. Am. Chem. Soc.*, 1995, **117**, 8582; 1994, **116**, 1121; 1993, **115**, 9337.

Received in Cambridge, UK, 31st July 1998; 8/06021E

The generation and trapping of organozinc carbenoids from orthoformates: a novel alkoxycyclopropanation reaction

Rodney J. Fletcher, William B. Motherwell* and Matthew E. Popkin

Department of Chemistry, Christopher Ingold Laboratories, University College London, 20 Gordon Street, London, UK WC1H OAJ

Alkoxycyclopropanes are readily prepared by reaction of an orthoformate with an alkene in the presence of Me_3SiCl and zinc.

We have previously shown that a useful range of organozinc carbenoids[1] can be generated from the reaction of simple carbonyl compounds with zinc in the presence of a silicon electrophile and that these intermediates can then undergo a variety of reactions including C–H insertion to give alkenes,[2] dicarbonyl coupling[3] and cyclopropanation.[4] More recently, in the light of reports on the preparation of isolable organochromium[5] and organoiron[6] carbenoids *via* two-electron delivery from a metal salt to a preformed carboxonium salt, we have demonstrated that acetals and ketals may be used as precursors for the formation of related organozinc carbenoids *via* reduction of their derived oxonium ions, once again with zinc in the presence of Me_3SiCl.[7]

As a logical consequence of the above sequence, and in view of the proven versatility of alkoxycyclopropanes as highly useful intermediates for organic synthesis,[8] we therefore reasoned, as outlined in Scheme 1, that the Lewis acid assisted cleavage of an orthoformate **1** could give rise, in similar fashion, to hitherto unknown α-alkoxy and α-aryloxy organozinc carbenoids **2**.

A preliminary study using allylbenzene and trimethyl orthoformate as a convenient methoxycarbenoid source served to confirm the above hypothesis (Table 1, entry 1) and also allowed us to develop a convenient experimental method. Thus, a typical experimental procedure would involve slow addition over 24 h of two separate portions of trimethyl orthoformate (1.4 ml, 8 mmol) and Me_3SiCl (1.0 ml, 8 mmol) in Et_2O to a vigorously stirred mixture of the alkene (2 mmol), Me_3SiCl (1.2 ml, 0.9 mmol) and zinc amalgam (2.5 g, 50 mmol) in refluxing Et_2O, each completed addition being followed by a 24 h reflux.

Further inspection of the results in Table 1 using a series of simple alkenes not only emphasises that preparatively useful yields of methoxycyclopropanes can be obtained under mild conditions, but also confirms that cyclopropanation occurs with retention of the original stereochemistry of the alkene (entries 3 and 4), that mono-, di- and tri-substituted alkenes can be used (entries 1–5) and that, as for other organozinc carbenoids,[1,4] there is a distinct stereochemical preference for formation of the more hindered *cis* (or *endo*) isomer (entries 1, 3 and 5).

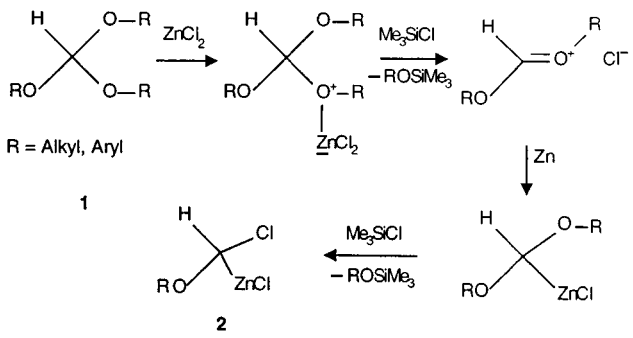

Scheme 1

Our attention was then directed towards the use of a variety of readily available orthoformates in order to assess their relative efficiencies for alkoxy- and aryloxy-carbenoid generation. Comparison of the results in Table 2 using allylbenzene as the standard alkene trap reveals several features of interest. Thus, the selection of tripropyl orthoformate (entry 1) led to a significant decrease in the isolated yield when compared with its trimethyl congener (Table 1, entry 1), presumably as a result of increased steric hindrance for incipient oxonium ion formation and/or electron delivery. However, the ability to preselect an unsymmetrical orthoformate with improved leaving group ability can be advantageous, as in the case of diethyl phenyl orthoformate (entry 2) which afforded only the ethoxycyclopropane in good yield. Furthermore, the obvious parallel which can be drawn in terms of the relative contributions of relief of ring strain and entropic factors involved in the

Table 1 Methoxycyclopropanation of alkenes using trimethyl orthoformate

Entry	Alkene	Products	Isomer ratio[a]	Yield (%)
1	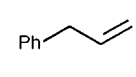	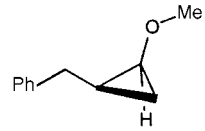	2 : 1	64
2	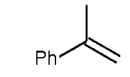	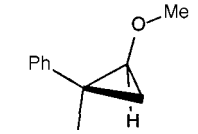	2 : 1	56
3	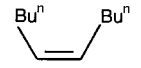	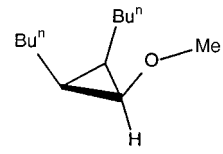	10 : 1	53
4	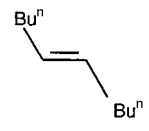	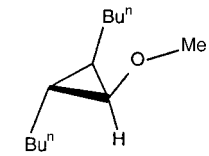	—	56
5	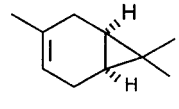	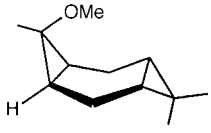	5 : 2	65

[a] Determined using NMR spectroscopy. For convenience, the major *cis* isomer is shown.

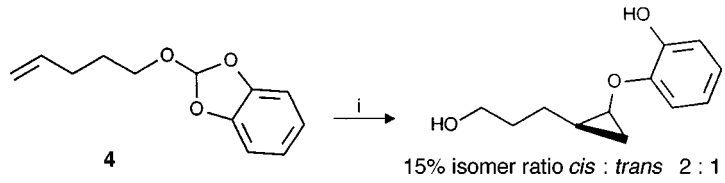

Scheme 2 *Reagents and conditions*: i, Zn/Hg (34 equiv.), Me_3SiCl (5 equiv.) Et_2O, reflux

Table 2 Alkoxy- and aryloxy-cyclopropanation of allylbenzene using orthoformates

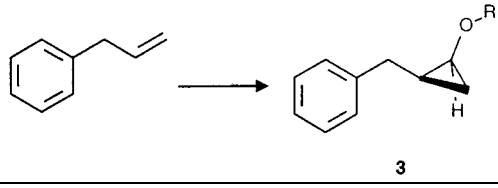

3

Entry	Orthoformate	R	Isomer ratio[a]	Yield (%)
1	$(PrO)_3CH$	Pr	2 : 1	43
2	$(EtO)_2CH(OPh)$	Et	2 : 1	67
3	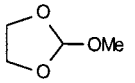	$CH_2CH_2OSiMe_3$	3 : 1	55
4	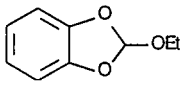	2-hydroxyphenyl	5 : 2	23

[a] Determined using NMR spectroscopy. For convenience, the major *cis* isomer is shown in **3**.

hydrolysis of acetals, ketals and orthoesters[9] can be used to exercise some degree of predictive power, as evidenced by the selective transfers involved in the use of the 2-methoxydioxolane (entry 3) and the catechol derivative (entry 4).

Clearly a useful range of functionalised alkoxy- and aryloxycyclopropanes can now be constructed in this way.

Finally, we have also carried out a preliminary study in order to probe the electronic character of α-alkoxyorganozinc carbenoids. *A priori* it might be argued that such species could be more nucleophilic, and exhibit a chemoselective preference for an electron-deficient alkene. In the event however, as shown by some representative examples in Table 3, the enol ester (entry 1) and the acrylate (entry 2) give comparable yields of cyclopropanated product. However, the result of a direct competition experiment using the monoterpene ester (entry 3) clearly demonstrates that the more electron-rich alkene is favoured over the acrylate.

From a practical standpoint, as in the classical Simmons–Smith reaction,[10] the above method clearly requires the use of an excess of reagents for efficient organozinc carbenoid generation and trapping. This is reflected in the (potentially intramolecular) aryloxycyclopropanation of the unsaturated orthoformate **4** (Scheme 2), where of course only 1 equiv. of alkoxycarbenoid can be produced.

In summary, the above results exemplify a simple and inexpensive method for the preparation of alkoxy- and aryloxycyclopropanes under mild neutral conditions *via* a novel class of organozinc carbenoids. Furthermore, in comparison to traditional methods for the generation of alkoxycarbenoids, the present method obviates the necessity for handling toxic α-halo

Table 3 Alkoxycyclopropanation of various alkenes with orthoformates

Entry	Orthoformate	Substrate	Product	Isomer ratio[a]	Yield (%)
1	$(MeO)_3CH$	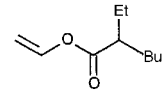	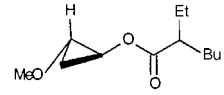	3 : 1	46
2	$(MeO)_3CH$	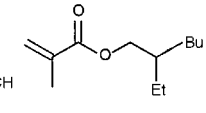	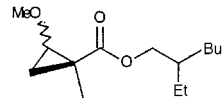	3 : 1[b]	43
3	$(EtO)_3CH$	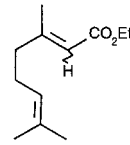	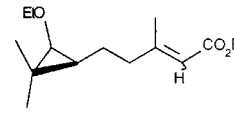	2 : 1[c]	44

[a] Determined using NMR spectroscopy. For convenience, the major isomer is shown. [b] In this case the major isomer was not assigned. [c] 3 : 1 (*E*/*Z*) mixture of isomers was employed as substrate.

and α,α-dihalo ether precursors,[11] or the multistep procedures involved in the preparation of stoichiometric Fischer carbenoids.[12]

We thank the EPSRC for the award of a postdoctoral fellowship (to R. J. F.) and University College, London, for the provision of a postgraduate studentship (to M. E. P.).

Notes and References

1 For a review, see C. J. Nutley and W. B. Motherwell, *Contemp. Org. Synth.*, 1994, 219.
2 W. B. Motherwell, *J. Chem. Soc., Chem. Commun.*, 1973, 935.
3 A. K. Banerjee, M. C. S. Carrasco, C. S. V. Frydrych-Houge and W. B. Motherwell, *J. Chem. Soc., Chem. Commun.*, 1986, 803; C. A. M. Afonso, W. B. Motherwell, D. M. O'Shea and L. R. Roberts, *Tetrahedron Lett.*, 1992, **33**, 3899.
4 W. B. Motherwell and L. R. Roberts, *J. Chem. Soc., Chem. Commun.*, 1992, 1582; W. B. Motherwell and L. R. Roberts, *Tetrahedron Lett.*, 1995, **36**, 1121.
5 R. Imwinkelried and L. S. Hegedus, *Organometallics*, 1988, **7**, 702.
6 R. D. Theys and M. M. Hossain, *Tetrahedron Lett.*, 1992, **33**, 3447; H. Dy. F. Yang and M. M. Hossain, *Synth. Commun.*, 1996, **26**, 1371.
7 W. B. Motherwell, D. J. R. O'Mahony and M. E. Popkin, *Tetrahedron Lett.*, 1998, **39**, 5285.
8 E. Wenkert, *Acc. Chem. Res.*, 1980, **30**, 27.
9 S. W. Smith and M. S. Newman, *J. Am. Chem. Soc.*, 1968, **90**, 1249; R. M. Hahn and C. S. Hudson, *J. Am. Chem. Soc.*, 1944, **66**, 1909; S. A. Barker and E. D. Bourne, *Adv. Carbohydr. Chem.*, 1952, **7**, 137; M. S. Newman and R. S. Harper Jr., *J. Am. Chem. Soc.*, 1958, **80**, 6350.
10 H. E. Simmons, T. L. Cairns, S. A. Vladuchick and C. H. Hoiness, *Org. React.*, 1973, **20**, 1.
11 U. Schöllkopf and G. J. Lehmann, *Tetrahedron Lett.*, 1962, **4**, 165; U. Schöllkopf, J. Paust, A. Ali-Azrak and H. Schumacher, *Chem. Ber.*, 1966, **99**, 3391.
12 M. Brookhart and W. B. Studabaker, *Chem. Rev.*, 1987, **87**, 411.

Received in Cambridge, UK, 6th August 1998; 8/06208K

A new type of tricolor electrochromic system based on the dynamic redox properties of hexaarylethane derivatives

Takanori Suzuki,*† Jun-ichi Nishida and Takashi Tsuji

Division of Chemistry, Graduate School of Science, Hokkaido University, Sapporo 060-0810, Japan

Electrochemical interconversion between 9,9,10,10-tetraaryldihydrophenanthrene 1 and 2,2′-bis(triarylmethylium) 2^{2+} has been proven to proceed *via* open form cation radical $2^{+\cdot}$ as a stable intermediate; using these three species, a novel tricolor electrochromic system that exhibits hysteretic color change (color 1 → color 2 → color 3 → color 1) is formed.

Molecular systems whose properties can be controlled electrochemically are attracting much attention because they might be applicable to the construction of molecular devices such as redox switches.[1] From this point of view the redox couples of hexaarylethanes **1d**,**e** and bis(triarylmethane) dyes **2d**,**e**$^{2+}$ are

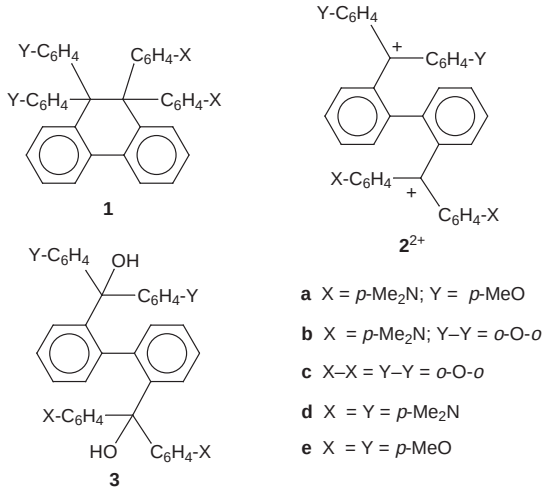

interesting;[2] their noteworthy features include electrochromic behaviour with vivid changes in color and very high bistability due to reversible C–C bond making/breaking[3] upon two-electron transfer (dynamic redox properties). During the course of our mechanistic investigation on the interconversion between **1** and $\mathbf{2}^{2+}$, we have found that a unique tricolor electrochromic system could be achieved using **1a**,**b** and **2a**,**b**$^{2+}$ possessing two different triarylmethane moieties, whose properties are reported herein. Although several multi-color electrochromic systems have been reported (color 1 ↔ color 2 ↔ color 3 ↔ *etc*.),[4] the hysteretic chromicity of the present systems (color 1 → color 2 → color 3 → color 1) is unprecedented.

Unsymmetric diols **3a**‡ and **3b**‡ were prepared in 12 and 8% yield, respectively, by the reaction of 2,2′-dilithiobiphenyl[5] with a mixture of the corresponding two ketones followed by chromatographic separation on SiO_2 from the symmetric diols **3c–e**. Deeply colored dication salts **2a**$^{2+}(BF_4^-)_2$‡ [λ_{max}(MeCN)/nm (log ε) 632 (4.93), 519 (4.72), 319 (4.25), 272 (4.24)] and **2b**$^{2+}(BF_4^-)_2$‡ [632 (4.92), 488 sh (3.76), 425 (4.22), 377 (4.46), 321 (4.23), 261 (4.63)] were obtained in 91 and 93% yield, respectively, by treating these diols with 42% HBF_4–$(EtCO)_2O$. Reduction of the dication salts with SmI_2 in THF gave colorless ethanes **1a**‡ [λ_{max}(MeCN)/nm (log ε) 268 (4.61)] and **1b**‡ [270 (4.58)] in 97 and 78% yield. X-Ray analysis§ has

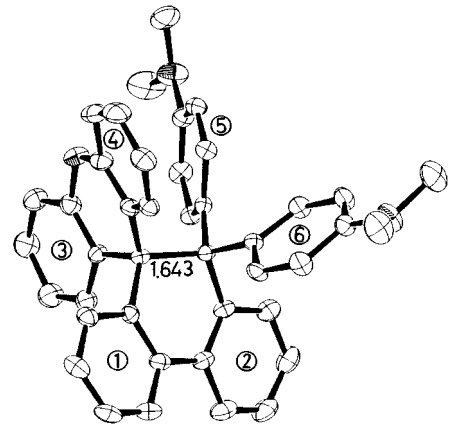

Fig. 1 Molecular geometry of ethane **1b** determined by X-ray analysis. The bipheny skeleton is nearly planar (the dihedral angle between planes 1 and 2: 16.2°), and the central six-membered ring adopts a pseudo-half chair conformation (planes 3 and 6: axial; 4 and 5: equatorial). The xanthene moiety is deformed slightly into the butterfly shape (the dihedral angle between planes 3 and 4: 15.2°). There is no disorder around the ethane bond in **1b**, unlike the symmetric ethane **1e** (ref. 2).

revealed that **1b** has a very long C–C bond [1.643(6) Å] (Fig. 1).¶ Thus, oxidation of **1a**,**b** with 2 equiv. of $(p\text{-}BrC_6H_4)_3N^{+\cdot}SbCl_6^-$ in CH_2Cl_2 led to the fission of the weak bonds to regenerate the dications **2a**,**b**$^{2+}$, which were isolated as $SbCl_6^-$ salts‡ in 82 and 79% yield, respectively. C_2-Symmetric ethane **1c**‡ [λ_{max}(MeCN)/nm (log ε) 282 (4.27), 230 sh (4.71)] and orange-colored **2c**$^{2+}(BF_4^-)_2$‡ [495 sh (3.62), 460 (3.79), 382 (4.56), 263 (4.82)] containing two xanthene moieties were also prepared from diol **3c**‡ for comparisons.

The cyclic voltammogram of **1c** is quite similar to those of **1d**,**e**; it shows irreversible 2e oxidation peak at +1.42 V, and the corresponding cathodic peak is largely shifted to +0.50 V, which was assigned to the 2e reduction peak of **2c**$^{2+}$ (Table 1). In contrast, unsymmetric ethanes **1a**,**b** behave rather differently from **1c–e**. Although their oxidation potentials are close to that of the tetrakis(dimethylamino) derivative **1d**, in the return cycle of the voltammograms there appeared two cathodic peaks (Fig. 2). From independent measurements on **2a**,**b**$^{2+}$ it was confirmed that these peaks are due to two-stage 1e reduction

Table 1 Redox potentials of ethanes **1** and dications $\mathbf{2}^{2+}$ in CH_2Cl_2[a]

	E/V *vs.* SCE		
Compound	E^{ox} (**1**)	E_1^{red} ($\mathbf{2}^{2+}$)	E_2^{red}($\mathbf{2}^{2+}$)
a X = *p*-Me_2N, Y = *p*-MeO	+0.83[b,c]	+0.10	−0.45[c]
b X = *p*-Me_2N, Y–Y = *o*-O-*o*	+0.76[b,c]	+0.24	−0.19[c]
c X–X = Y–Y = *o*-O-*o*	+1.39[b,c]	+0.53[b,c]	
d[d] X = Y = *p*-Me_2N	+0.74[b,c]	−0.42[b,c]	
e[d] X = Y = *p*-MeO	+1.44[b,c]	+0.21[b,c]	

[a] 0.1 mol dm^{-3} $Bu^n_4NBF_4$, Pt electrode, scan rate 100 mV s^{-1}. [b] Two-electron process. [c] Irreversible wave, values were calculated as $E^{ox} = E_{peak} - 0.03$ and $E^{red} = E_{peak} + 0.03$, respectively. [d] Ref. 2.

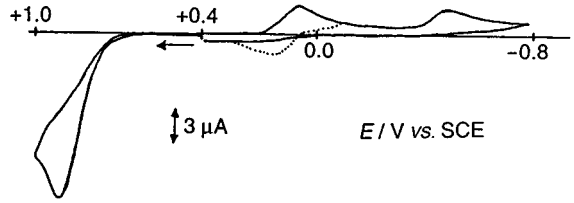

Fig. 2 Cyclic voltammogram of ethane **1a** (10^{-3} mol dm^{-3}) in CH_2Cl_2 (*E*/V *vs.* SCE 0.1 mol dm^{-3} $Bu^n_4NBF_4$, Pt electrode, scan rate 500 mV s^{-1}). The reduction peaks are absent when the voltammogram is first scanned cathodically. As shown by the dotted line, the first reduction wave at +0.07 V is reversible when the scanning was reversed at −0.10 V.

processes of the dications; the first one corresponding to the Y-C_6H_4-C^+-C_6H_4-Y moiety is completely reversible. Furthermore, the anodic peak due to the oxidation of **1a**,**b** appears in the voltammograms of **2a**,**b**$^{2+}$ after scanning the irreversible second 1e reduction wave. Such redox properties can be accounted for only by assuming the reaction mechanism shown in Scheme 1, in which the weakened C–C bond of hexaarylethane **1** is cleaved after 1e oxidation‖ to **1**$^{+\cdot}$ whereas two-fold 1e reduction of **2**$^{2+}$ to **2**$^{2\cdot}$ is necessary before the ring closure to **1**. It should be noted that **2**$^{+\cdot}$ produced from **1**$^{+\cdot}$ is more easily oxidized than **1** [E^{ox}(**1a**,**b**) is much more positive than E^{ox}(**2a**,**b**$^{+\cdot}$) = E_1^{red}(**2a**,**b**$^{2+}$)], thus the steady-state concentration of **2**$^{+\cdot}$ is negligible during the electrochemical oxidation of **1**, although the same specimen is a long-lived intermediate in the reduction process of **2**$^{2+}$.

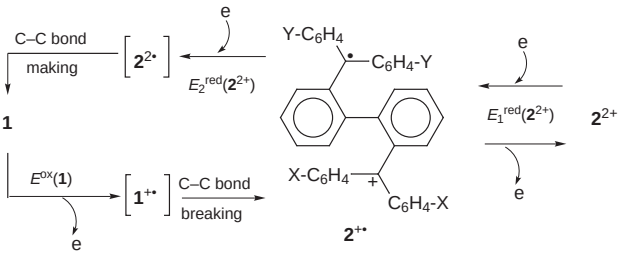

Scheme 1

Thanks to the hysteretic interconversion between **1**, **2**$^{+\cdot}$ and **2**$^{2+}$, novel tricolor electrochromic systems could be constructed using the unsymmetric derivatives. Thus, upon electrochemical oxidation of colorless **1a**, both the blue (X = *p*-Me_2N) and red (Y = *p*-MeO) triarylmethylium chromophores grow simultaneously to develop the violet color of **2a**$^{2+}$ [Fig. 3(*a*)]. On the other hand, the red chromophore disappears first upon reduction of **2a**$^{2+}$ [Fig. 3(*b*), stage 1], and next the blue cation radical **2a**$^{+\cdot}$ is converted to colorless **1a** [Fig. 3(*c*), stage 2] even under the constant-current electrolytic conditions. Similar behaviour but with a different color was observed for the interconversion of **2b**$^{2+}$ (green) (isosbestic points: 248, 270, 300 nm) → **2b**$^{+\cdot}$ (blue) (296 nm) → **1b** (colorless) (309 nm) → **2b**$^{2+}$ (green), showing the generality of the unprecedented pattern of color change.

This work was supported by the Ministry of Education, Science, and Culture, Japan (No. 08640664 and 10146101). We thank Professor Tamotsu Inabe (Hokkaido University) for the use of X-ray analytical facilities. Elemental analyses were carried out by Ms Akiko Maeda at the Center for Instrumental Analysis (Hokkaido University).

Notes and References

† E-mail: tak@science.hokudai.ac.jp

‡ All new compounds gave satisfactory spectral data and analytical values.

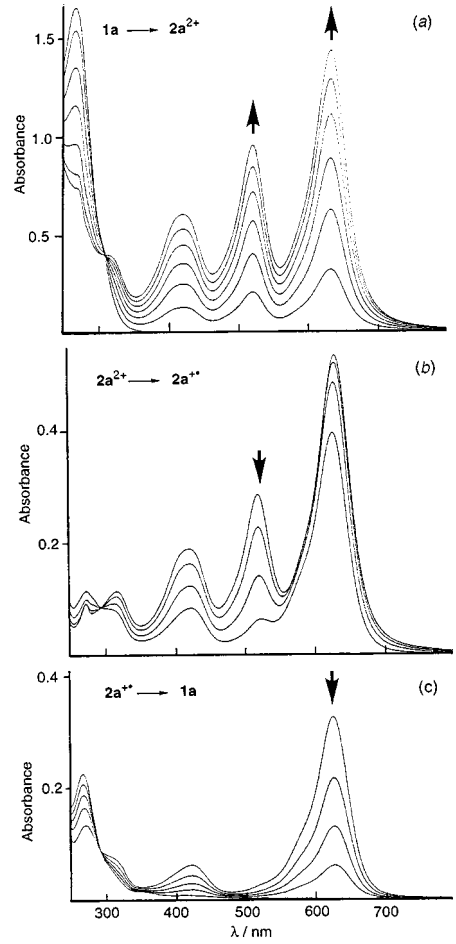

Fig. 3 Changes in the UV–VIS spectra of (*a*) **1a** (3.6 ml; 4.1 × 10^{-5} mol dm^{-3} in MeCN containing 0.04 mol dm^{-3} $Bu^n_4NBF_4$) upon electrochemical oxidation (15 μA) at 10 min intervals, and **2a**$^{2+}$ (3.6 ml soln; 6.6 × 10^{-6} mol dm^{-3} in MeCN containing 0.05 mol dm^{-3} $Bu^n_4NBF_4$) upon electrochemical reduction (70 μA): (b) stage 1, at 0.5 min intervals; (c) stage 2, at 1 min intervals

§ *Crystal Data* for **1b**: $C_{42}H_{36}N_2O$, *M* 584.76, *P*212121, *a* = 14.216(4), *b* = 20.806(6), *c* = 10.483(3) Å, *V* = 3100(1) Å^3, D_c (Z = 4) = 1.253 g cm^{-1}, *Rw* = 0.025. CCDC 182/1003.

¶ Hexaphenylethanes of [3.3.*n*]propellane-type were recently reported to have long C–C bonds [1.611(3)–1.621(3) Å]: G. Dyker, J. Körning, P. Bubenitschek and P. G. Jones, *Liebigs Ann./Recl.*, 1997, 203.

‖ Activation energies for the mesolytic C–C bond fission of diarylethane cation radicals were reported to be lowered by an average of 23 kcal mol^{-1} with respect to homolysis: P. Maslak, W. H. Chapman, Jr., T. M. Vallombroso, Jr. and B. A. Watson, *J. Am. Chem. Soc.*, 1995, **117**, 12380.

1 P. L. Boulas, M. Gómez-Kaifer and L. Echegoyen, *Angew. Chem., Int. Ed.*, 1998, **37**, 216.
2 T. Suzuki, J. Nishida and T. Tsuji, *Angew. Chem., Int. Ed. Engl.*, 1997, **36**, 1329.
3 M. Horner and S. Hünig, *J. Am. Chem. Soc.*, 1977, **99**, 6122; W. Freund and S. Hünig, *J. Org. Chem.*, 1987, **52**, 2154; T. Suzuki, M. Kondo, T. Nakamura, T. Fukushima and T. Miyashi, *Chem. Commun.*, 1997, 2325; T. Suzuki, H. Takahashi, J. Nishida and T. Tsuji, *Chem. Commun.*, 1998, 1331.
4 P. M. S. Monk, R. J. Mortimer and D. R. Rosseinsky, *Electrochromism: Fundamentals and Applications*, VCH, Weinheim, 1995, p. 185.
5 N. Neugebauer, A. J. Kos and P. von R. Schleyer, *J. Organomet. Chem.*, 1982, **228**, 107.

Received in Cambridge, UK, 3rd August 1998; 8/06037A

Novel reductive olefination mediated by Ti(O-i-Pr)$_4$ and Ph$_3$P. One-pot synthesis of trifluoromethylated *trans*-allylic alcohols

Yanchang Shen,*† Yuming Zhang and Yuefen Zhou

Shanghai Institute of Organic Chemistry, Academia Sinica, 354 Fenglin Lu, Shanghai 200032, China

A novel reductive olefination mediated by Ti(O-i-Pr)$_4$ and Ph$_3$P and its application to the 'one-pot' synthesis of perfluoroalkylated *trans*-allylic alcohols are described.

One-pot synthesis has attracted much interest in recent years because it provides a simple and efficient route to compounds by including two or more transformations in a single operation to increase the complexity of a substrate starting from commercially available, relatively simple precusors.[1] In our laboratory 'one-pot' carbon–carbon double bond formation has been observed between α-bromo carboxylic derivatives (esters, amides and nitriles) and aldehydes in the presence of n-Bu$_3$P(As) and catalyst (Pd, Zn, Cd) forming α,β-unsaturated esters, amides and nitriles.[2] This reaction greatly simplifies the traditional Wittig reaction into a stereospecific alkenylation methodology and compresses the three steps of a Wittig reaction to a one-step, one-pot synthesis.[3] Allylic alcohols are employed as useful building blocks in many synthetic applications, particularly in the synthesis of biologically active compounds.[4] Therefore there has been much interest in the development of an effective 'one-pot' method for the preparation of allylic alcohols, especially fluoro species. Numerous methods by which to prepare allylic alcohols are known,[5] but either multiple steps are necessary or the starting materials are not commercially available. Very recently a new stereoselective method for the preparation of allylic alcohols using nickel catalyzed alkylative cyclization of ynals or coupling of aldehydes, alkynes and organozincs has been reported.[6] However, the syntheses of trifluoromethylated allylic alcohols[7a–d] and difluoro species[7e–h] are still limited. Herein we report a novel reductive olefination mediated by Ti(O-i-Pr)$_4$ and Ph$_3$P and its application to the 'one-pot' synthesis of trifluoromethylated *trans*-allylic alcohols (Scheme 1). The results are summarized in Table 1.

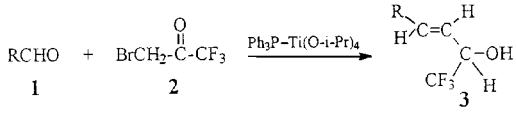

Scheme 1

At present, the tentative hypothesis shown in Schemes 2–4 appears to be consistent with the information currently available. The reaction is postulated to be initiated by the Meerwein–Pondorf–Verley-like reduction of 3-bromo-1,1,1-trifluoroacetone with Ti(O-i-Pr)$_4$ (Scheme 2).[8]

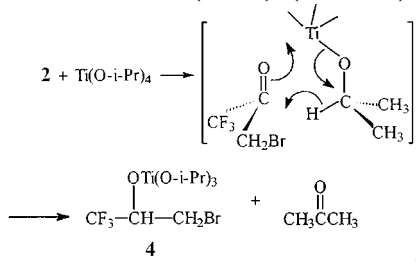

Scheme 2

The halophilic reaction occurred between intermediate **4** and the Ph$_3$P forming ion pair **5** and **6** as reported in the literature (Scheme 3).[9] Compound **6** might be stabilized by a strong electron-withdrawing trifluoromethyl group. Subsequently the active species **5** and **6** reacted with the aldehyde forming the six-membered intermediate **7**. After elimination of triphenylphosphine oxide and HBr the intermediate **8** was formed which was hydrolysed to give the product **3** (Scheme 4).[10]

Table 1 Preparation of perfluoroalkylated allylic alcohols[a] mediated by Ti(O-i-Pr)$_4$ and Ph$_3$P

Compound	R	(Bp/°C)/(*p*/torr)	Yield (%)[b]
3a	C_6H_5	114–115/2.5[c]	90
3b	4-$CH_3C_6H_4$	110/2.5	99
3c	4-FC_6H_4	102–104/2.6	87
3d	4-ClC_6H_4	112/2.5	77
3e	4-$CH_3OC_6H_4$	120/2.5	54
3f	4-$NO_2C_6H_4$	103–104[d]	55
3g	3-BrC_6H_4	105/2.0	71
3h	3-ClC_6H_4	110/2.0	78
3i	2-BrC_6H_4	81/2.5	95
3j	(*E*)-C_6H_5CH=CH	118/2.5	81

[a] All reactions were carried out neat at 80 °C for 24 h, using 1.0 equiv. of Ti(O-i-Pr)$_4$, Ph$_3$P, 3-bromo-1,1,1-trifluoroacetone and aldehyde. [b] Isolated yields. All new compounds were characterized by microanalyses, IR, NMR and mass spectroscopy. [c] Lit.[7a] data 76–77 °C/1 torr. [d] Mp.

3-Bromo-1,1,1-trifluoroacetone was proved to be able to react with Ti(O-i-Pr)$_4$ by independent experiment. When **2** was reacted with Ti(O-i-Pr)$_4$ at 80 °C for 2 h, **4** was isolated and characterized, [11] and further reacted with 4-chlorobenzaldehyde in the presence of Ph$_3$P giving the desired product **3d**.‡

A possible mechanism involving Ph$_3$P attack on 3-bromo-1,1,1-trifluoroacetone to give the enolate, followed by an aldol condensation, transferring the Ph$_3$PBr onto the hydroxylic oxygen, followed by elimination of HBr from **7,** and a Merrwein–Pondorf–Verley 1,2-reduction of the enone product, seems to be discounted, since in the absence of Ti(O-i-Pr)$_4$, no olefination occurred under the same conditions. If the above mentioned mechanism does occur, the olefination product

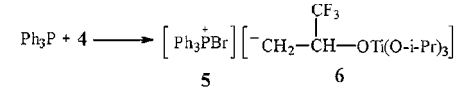

Scheme 3

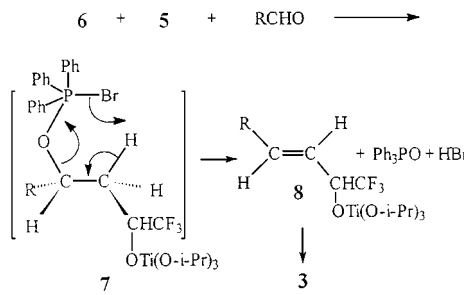

Scheme 4

should be obtained in the absence of $Ti(O\text{-}i\text{-}Pr)_4$. The detailed mechanism is being pursued.

These studies provide, to our knowledge, the first example of organotitanium compounds combined with Ph_3P mediated reductive olefination giving trifluoromethylated *trans*-allylic alcohols efficiently and stereoselectively. This 'one-pot' synthesis is a very convenient starting point using commercially available substances for the preparation of trifluoromethylated allylic alcohols, and the widespread use of these allylic alcohols is quite important in organic synthesis. They are interesting fluorinated building blocks, not easily available by existing synthetic methods.

Notes and References

† E-mail: shenyc@pub.sioc.ac.cn

‡ General experimental procedure: To a mixture of 3-bromo-1,1,1-trifluoroacetone (1 mmol), aldehyde (1 mmol) and Ph_3P (1 mmol) in a capped vessel under nitrogen was injected $Ti(O\text{-}i\text{-}Pr)_4$ (1 mmol). After stirring at 80 °C for 24 h, the reaction mixture was treated with 5% HCl (10 ml) and extracted with Et_2O (3 × 20 ml). The organic layer was washed with water (3 × 10 ml), dried and evaporated to remove the solvent. The residue was chromatographed on silica gel, and eluted with petroleum ether (60–90 °C)–ethyl acetate (95:5) to give the product.

1 L. F. Tietze and U. Beifuss, *Angew. Chem., Int. Ed. Engl.*, 1993, **32**, 131; L. F. Tietze, *Chem. Rev*., 1996, **96**, 115.
2 Y. Shen, *Acc. Chem. Res*., 1998, **31**, in press.
3 BST, *Chemtech*, 1990, May, 260.
4 W. F. Berkowitz and A. S. Amarasekara, *Tetrahedron Lett*., 1985, **26**, 3663; Y. Tamura, H. Annoura and H. Fujioka, *Tetrahedron Lett*., 1987, **28**, 5681; C. Singh, *Tetrahedron Lett*., 1990, **31**, 6901; J. Barluenga, L. Llavona, P. L. Bernad and J. M. Concellon, *Tetrahedron Lett*., 1993, **34**, 3173 and refs. cited therein.
5 N. Ono, A. Kamimura and A. Kaji, *Tetrahedron Lett*., 1984, **25**, 5319; H. Jin, J. Uenishi, W. J. Christ and Y. Kishi, *J. Am. Chem. Soc*., 1986, **108**, 5644; K. Takai, M. Tagashira, T. Kuroda, K. Oshima, K. Utimoto and H. Nozaki, *J. Am. Chem. Soc*., 1986, **108**, 6048; M. Srebnik, *Tetrahedron Lett*., 1991, **32**, 2449; J. C. Fuller, E. L. Stangeland, C. T. Goralski and B. Singaram, *Tetrahedron Lett*., 1993, **34**, 257; V. A. Khripach, V. N. Zhabinskii and E. V. Zhernosek, *Tetrahedron Lett*., 1995, **36**, 607.
6 E. Oblinger and J. Montgomery, *J. Am. Chem. Soc*., 1997, **119**, 9065.
7 (*a*) N. Ishikawa, M. G. Koh, T. Kitazume and S. K. Choi, *J. Fluorine Chem.*, 1984, **24**, 419: (*b*) Y. Shen and T. Wang, *Tetrahedron Lett*., 1989, **30**, 7203; (*c*) T. Kitazume, J. T. Lin and T. Yamazaki, *J. Fluorine Chem*.,1989, **43**, 177; (*d*) T. Kubota and M. Yamamoto, *Tetrahedron Lett*., 1992, **33**, 2603; (*e*) K. Funabiki, Y. Fukushima, T. Inagaki, E. Murata, M. Matsui and K. Shibata, *Tetrahedron Lett*., 1998, **39**, 1913; (*f*) M. J. Broadhurst, J. M. Percy and M. E. Prime, *Tetrahedron Lett*., 1997, **38**, 5903; (*g*) F. Tellier, M. Baudry and R. Sauvetre, *Tetrahedron Lett*., 1997, **38**, 5989; (*h*) M. Omote, A. Ando, T. Takagi, M. Koyama and I. Kumadaki, *Heterocycles*, 1997, **44**, 89.
8 J. March, *Advanced Organic Chemistry*, 4th edn., John Wiley & Sons, New York, 1992, p. 917.
9 R. K. Mackie, in *Organophosphorus Reagents in Organic Synthesis*, ed. J. I. G. Cadogen, Academic Press, London, 1979, p.542.
10 Y. Shen and B. Yang, *J. Organomet. Chem*., 1989, **375**, 45.
11 After fractional distillation under vacuum, a colorless oil **4** was obtained which was sensitive to moisture. Bp 110 °C/0.1 torr; δ_H(300 MHz, $CDCl_3$, TMS) 5.00–4.20 (m, 4H), 3.58 [dd, ^2J(H,H) 10.9, ^3J(H,H) 3.2, 1H], 3.10 [dd, ^2J(H,H) 10.6, ^3J(H,H) 8.8, 1H], 1.28 [d, ^3J(H,H) 6.1, 18H]; δ_F(60 MHz, $CDCl_3$, TFA) 0.3 [d, ^3J(H,F) 5.4].

Received in Cambridge, UK, 10th August 1998; 8/06271D

Novel highly extended and sulfur rich tetrathiafulvalene (TTF) derivatives through an unprecedented TTF core building process

C. Boulle,[a,b] O. Desmars,[b] N. Gautier,[b] P. Hudhomme,*[a,b]† M. Cariou[a] and A. Gorgues*[a]

[a] *Ingénierie Moléculaire et Matériaux Organiques, UMR-CNRS 6501, 2 Boulevard Lavoisier, 49045 Angers Cedex, France*
[b] *Laboratoire de Synthèse Organique, UMR-CNRS 6513, 2 rue de la Houssinière, 44322 Nantes Cedex 03, France*

A new and unexpected tetrathiafulvalene (TTF) core building process is observed *via* reaction of a 1,3-dithiole phosphonate anion with a 2-oxo-1,3-dithiole functionality.

Since their discovery, the transport properties of the charge-transfer salts related to the TTF series have been improved.[1] In particular, chemical modifications[2] of the donor have allowed enhancement of the dimensionality of the related materials, thus preventing metal-to-insulator transitions (Peierls distorsions). With this aim, space extended and sulfur-rich analogs of TTF as the donors constitute very good candidates.[3] Thus, bis(1,4-dithiafulven-6-yl)TTFs were found able to afford interesting 2D electroconductive materials thanks to intermolecular intra- and inter-chain S···S contacts. Unfortunately, under acidic or oxidative conditions, these donors may undergo unwanted internal cyclization reactions when R^1 = H (Scheme 1).[4]

Following our efforts to suppress such side reactions, which have a spoiling effect during the slow electrooxidation process,[3c,d] we have designed new donors **1** related to benzoTTF, bearing no hydrogen atom in the R^1 position, in which the 1,3-dithiol-2-ylidene moieties are connected *via* the R^1–R^1 vinylene substituent. We report here on their straightforward synthesis and on their electrochemical properties.

As outlined in Scheme 2, our synthetic strategy was based on three main steps: (i) a Diels–Alder cycloaddition between 2-oxo-4,5-bis(methylene)-1,3-dithiole **2** and paraquinonic dienophiles with further aromatization of the cycloadduct, (ii) a bis-Horner–Wadsworth–Emmons olefination of the quinonic carbonyl functionalities of **3** with Akiba's reagents,[5] and (iii) a final coupling reaction of the resulting compound **4** with 2-(thi)oxo-1,3-dithioles.

Thus, in the first step, diene **2** was generated *via* two independent routes,[6] either by an annulating reaction involving the thermal decomposition of *S*-propargyl xanthate[7] (Route **A**), or by an iodide induced reductive elimination on 2-oxo-4,5-bis(bromomethyl)-1,3-dithiole[8] (Route **B**). This diene was trapped with a quinone (*p*-benzoquinone or 1,4-naphthoquinone) and further addition of DDQ[9] to perform the aromatization, furnished the corresponding target compounds **3a** and **3b** (Scheme 3).

For the second step, we checked the behaviour of **3a** and **3b** with the anion of **5** generated upon treatment of the corresponding phosphonate with BuLi in THF at −78 °C. From **3a**, the olefination was unsuccessful, this failure being interpreted as resulting from an electron transfer between the quinonic compound acting as the π-acceptor (Ep^1_{red} = −0.56 V *vs.* SCE)[10] and the phosphonate anion acting as the donor.[3d] From

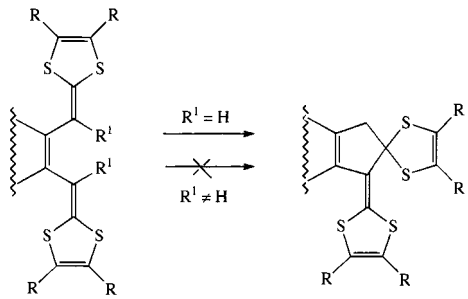

Scheme 1

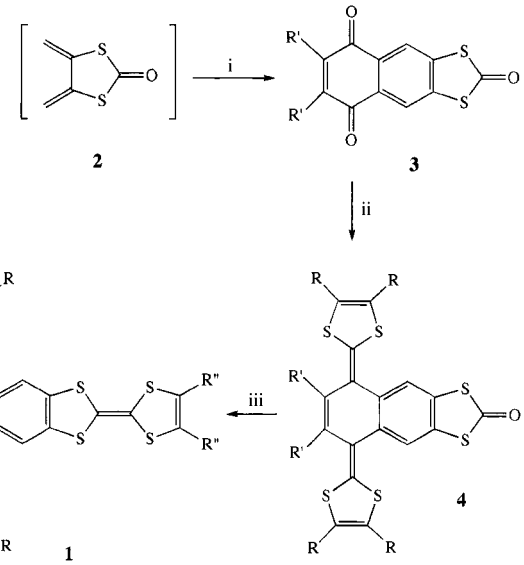

Scheme 2 *Reagents and conditions*: i, Diels–Alder cycloaddition with further aromatization; ii, bis-Horner–Wadsworth–Emmons olefination; iii, coupling reaction

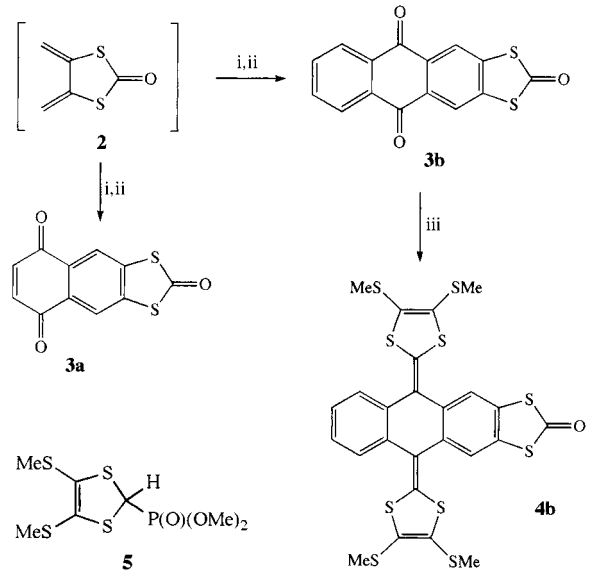

Scheme 3 *Reagents and conditions*: (Route **A**): i, reflux, chlorobenzene, *p*-benzoquinone or 1,4-naphthoquinone; ii, DDQ (**3a**: 30%, **3b**: 46%); (Route **B**): i, $Et_4N^+I^-$, MeCN, *p*-benzoquinone or 1,4-naphthoquinone; ii, DDQ (**3a**: 83%, **3b**: 54%); iii, **5**, BuLi, THF, −78 °C

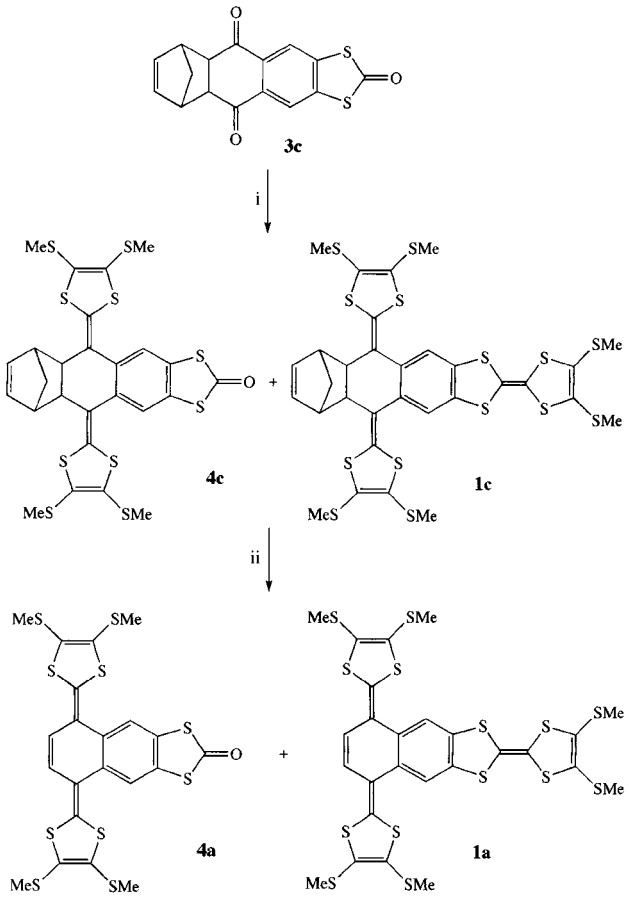

Scheme 4 *Reagents and conditions*: i, **5**, BuLi, THF, −78 °C; ii, thermal treatment

the less oxidizing compound **3b** (Ep^1_{red} = −0.84 V *vs.* SCE), upon treatment with a large excess of the anion of **5**, the bis-olefinated product **4b** could be isolated in 28% yield after silica gel column chromatography (hexane–CH_2Cl_2 1 : 1).

In order to perform the required olefination of **3a**, we decided to suppress the accepting quinonic character thanks to a prior Diels–Alder cycloaddition of cyclopentadiene, this latter being possibly subsequently removed (Yamashita's methodology[11]). Thus, cyclic voltammetry confirmed that the corresponding cycloadduct **3c** is a poor π-acceptor (Ep^1_{red} = −1.42 V *vs.* SCE). Unexpectedly, after reaction of **3c** (0.33 mmol) with a large excess of the anion of **5** (1.98 mmol) in THF (35 ml) and silica gel column chromatography (CS_2–CH_2Cl_2 8 : 1), we observed that the bis-olefinated compound **4c** appearing as the main product (50% yield) was accompanied by the tris-olefinated compound **1c** (25% yield), this latter corresponding to a TTF core building through an unprecedented Horner–Wadsworth–Emmons olefination of the 2-oxo-1,3-dithiole functionality with Akiba's reagent (Scheme 4). We also noted the partial decomposition of the phosphonate anion of **5** to tetrakis(methylsulfanyl)TTF and elimination of dimethyl phosphite.[12] The yield of **1c** was increased to 43% by using 10 equiv. of Akiba's reagent and BuLi. Cyclic voltammetry of **1c** exhibited an irreversible process, suggesting the possible loss of cyclopentadiene which obviously could be induced electrochemically. Nevertheless, this reaction was more readily performed by classical thermal treatment of **1c** in *o*-dichlorobenzene or, directly, in the dry state, in a Kugelrohr apparatus[13] in quantitative yield.

Cyclic voltammetry of **1a** exhibited three reversible oxidation peaks (Table 1), the first one corresponding to a 2e$^-$ process arising from the π-extended *p*-quinodimethane analog of TTF (by analogy with the voltammogram of **4a** and similar observations on such conjugated quinonic systems[3g,11a]) followed by two 1e$^-$ oxidation peaks related to the TTF moiety. These features are in agreement with the sequence: **1a** ⇌ $\mathbf{1a}^{2+}$ ⇌ $\mathbf{1a}^{3+\cdot}$ ⇌ $\mathbf{1a}^{4+}$.

Table 1 Cyclic voltammetry of compounds **1a** and **4a**[a]

	E/V *vs.* SCE					
	In CH_2Cl_2			In *o*-dichlorobenze		
	E_{ox}^1	E_{ox}^2	E_{ox}^3	E_{ox}^1	E_{ox}^2	E_{ox}^3
1a	0.27	0.71	1.12	0.39	0.76	1.15
4a	0.28			0.49		

[a] 1.5 mM in solvent–Bu_4NPF_6 (0.1 M), v = 100 mV s^{-1}.

Given the good π-donor ability of **1a**, efforts are now in progress to generalize this methodology to the synthesis of varied compounds **1** and formation of their corresponding cation radical salts.

Notes and References

† E-mail: pietrick.hudhomme@univ-angers.fr

‡ All new compounds gave satisfactory spectroscopic data. *Selected data* for **1a**: δ_H(*o*-$C_6D_4Cl_2$) 2.51 (s, 18H, SMe), 7.14 (s, 2H, CH quinone), 7.40 (s, 2H, CH arom) (Calc: C, 39.86; H, 2.83. Found: C, 39.05; H, 2.85%). For **4a**: δ_H($CDCl_3$) 2.45 (s, 12H, SMe). 6.32 (br s, 2H, CH quinone), 7.71 (s, 2H, CH arom); *m/z* (EI) 604 (M^+, 1%), 94 (100). For **1c**: δ_H($CDCl_3$) 1.54 (s, 2H, CH_2), 2.36 (s, 6H, SMe), 2.44 (s, 6H, SMe), 2.45 (s, 6H, SMe), 3.03 (br s, 2H, CH), 3.35 (br s, 2H, CH), 5.43 (t, *J* 1.7, 2H, HC=CH), 7.09 (s, 2H, CH arom); *m/z* [FAB (+, m-NBA)] 848 (M^+, 36%), 782 (100), 632 (28).

1 J. M. Williams, J. R. Ferraro, R. J. Thorn, K. D. Carlson, U. Geiser, H. H. Wang, A. M. Kini and M. H. Whangbo, *Organic Superconductors* (*including fullerenes*), Prentice Hall, Englewood Cliffs, New Jersey, 1992; *Organic conductors. Fundamentals and Applications*, ed. J. P. Farges, Marcel Dekker, New York, 1994; M. R. Bryce, *J. Mater. Chem.*, 1995, **5**, 1481.

2 G. Schukat and E. Fanghänel, *Sulfur Rep.*, 1993, **14**, 245; J. Garín, *Adv. Heterocycl. Chem.*, 1995, **62**, 249 and references cited therein.

3 (*a*) M. Sallé, M. Jubault, A. Gorgues, K. Boubekeur, M. Fourmigué, P. Batail and E. Canadell, *Chem. Mater.*, 1993, **5**, 1196; (*b*) A. Gorgues, M. Jubault, A. Belyasmine, M. Sallé, P. Frère, V. Morisson and Y. Gouriou, *Phosphorus Sulfur Silicon*, 1994, **95–96**, 235; (*c*) P. Leriche, A. Belyasmine, M. Sallé, A. Gorgues, M. Jubault, J. Garín and J. Orduna, *Tetrahedron Lett.*, 1997, **38**, 1399; (*d*) A. Gorgues, M. Sallé, P. Hudhomme, P. Leriche, C. Boulle, C. Durand, F. Le Derf, M. Cariou, M. Jubault and P. Blanchard, *Supramolecular Engineering of Synthetic Metallic Materials: Conductors and Magnets*, ed. J. Veciana and C. Rovira, NATO ASI Series, Kluwer, Dordrecht, 1998, in the press. For other highly extended and sulfur rich π-donors see, for example: (*e*) T. Sugimoto, H. Awaji, I. Sugimoto, Y. Misaki, T. Kawase, S. Yoneda and Z. I. Yoshida, *Chem. Mater.*, 1989, **1**, 535; (*f*) Y. Misaki, N. Higuchi, H. Fujiwara, T. Yamabe, T. Mori, H. Mori and S. Tanaka, *Angew. Chem., Int. Ed. Engl.*, 1995, **34**, 1222; (*g*) N. Martín, L. Sánchez, C. Seoane, E. Ortí, P. M. Viruela and R. Viruela, *J. Org. Chem.*, 1998, **63**, 1268.

4 A. Benhamed-Gasmi, P. Frère, A. Belyasmine, K. M. A. Malik, M. B. Hursthouse, A. J. Moore, M. R. Bryce, M. Jubault and A. Gorgues, *Tetrahedron Lett.*, 1993, **34**, 2131.

5 K. Akiba, K. Ishikawa and N. Inamoto, *Bull. Chem. Soc. Jpn.*, 1978, **51**, 2674; A. J. Moore and M. R. Bryce, *Synthesis*, 1991, **26.**

6 C. Boulle, M. Cariou, M. Bainville, A. Gorgues, P. Hudhomme, J. Orduna and J. Garín, *Tetrahedron Lett.*, 1997, **38**, 81.

7 J. Boivin, C. Tailhan and S. Z. Zard, *Tetrahedron Lett.*, 1992, **33**, 7853.

8 R. M. Renner and G. R. Burns, *Tetrahedron Lett.*, 1994, **35**, 269.

9 D. Walker and R. G. Harvey, *Chem. Rev.*, 1967, 153; P. P. Fu and R. G. Harvey, *Chem. Rev.*, 1978, 317.

10 Conditions of cyclic voltammetry: 1.5 mM in CH_2Cl_2–$Bu^n_4NPF_6$ (0.1 M), v = 100 mV s^{-1}, Ep_{red} in V *vs.* SCE.

11 (*a*) Y. Yamashita, T. Suzuki and T. Miyashi, *Chem. Lett.*, 1989, 1607; (*b*) K. Saito, C. Sugiura, E. Tanimoto, K. Saito and Y. Yamashita, *Heterocycles*, 1994, **38**, 2153.

12 E. D. Bergmann and A. Solomonovici, *Synthesis*, 1970, 183.

13 A. Merz and M. Rauschel, *Synthesis*, 1993, 797.

Received in Liverpool, UK, 20th July 1998; 8/05653F

Synthesis and structural characterisation of a novel 2,3-distibene-1,4-dione complex, $[Pt(PEt_3)_2\{\eta^2\text{-}Bu^tC(O)Sb{=}SbC(O)Bu^t\}]$

Steven J. Black,[a] David E. Hibbs,[b] Michael B. Hursthouse,[b] Cameron Jones*[a] and Jonathan W. Steed[c]

[a] *Department of Chemistry, University of Wales, Swansea, Singleton Park, Swansea, UK SA2 8PP. E-mail: c.a.jones@swansea.ac.uk*

[b] *EPSRC X-ray Crystallography Service, Department of Chemistry, University of Wales, Cardiff, PO Box 912, Park Place, Cardiff, UK CF1 3TB*

[c] *Department of Chemistry, King's College London, Strand, London, UK WC2R 2LS*

The reaction of *cis*-$[PtCl_2(PEt_3)_2]$ with 2 equiv. of $[\{[Li\{\eta^2\text{-}OC(Bu^t)EC(Bu^t)O\}(DME)_{0.5}]_2\}_\infty]$, E = Sb or As, affords either the first distibene-dione complex, *cis*-$[Pt(PEt_3)_2\{\eta^2\text{-}Bu^tC(O)Sb{=}SbC(O)Bu^t\}]$, or the related diarsenide-dione bridged complex, *trans*-$[\{Pt(PEt_3)Cl\}_2\{\mu\text{-}\eta^1,\eta^1\text{-}Bu^tC(O)AsAsC(O)Bu^t\}]$, the X-ray crystal structures of which are described.

Since the preparation of the first diphosphene, Mes*P=PMes*, Mes* = $C_6H_2Bu^t_3$-2,4,6; by Yoshifuji in 1981[1] the chemistry of these species has developed into a well explored field.[2] By contrast, the heavier Group 15 analogues of diphosphenes have remained scarce and in the case of distibenes can be confined to one very sterically protected example, (Tbt)Sb=Sb(Tbt) **1** {Tbt = $C_6H_2[CH(SiMe_3)_2]_3$-2,4,6}.[3] In addition, three structurally characterised distibene complexes have been reported, *viz.* $[Fe(CO)_4\{\eta^2\text{-}[(SiMe_3)_2CHSb]_2\}]$ **2**[4] and $[\{W(CO)_5\}_3(\eta^2\text{-},\eta^1\text{-},\eta^1\text{-}RSb{=}SbR)]$ R = Ph,[5] Bu^t;[6] none of which contain functionalised distibene substituents. Our interest in low co-ordination antimony chemistry has recently led to us reporting the first example of a 2-stiba-1,3-dionatolithium complex **3** (E = Sb),[7] which we have begun to investigate as a possible transfer reagent in the formation of transition metal–stibadionate complexes (*cf.* β-diketonate chemistry). This work has led to some unexpected results which include the metal mediated synthesis of the first distibene-dione complex which is reported herein. Several related complexes are also described.

Treatment of *cis*-$[PtCl_2(PEt_3)_2]$ with 2 equiv. of **3** (E = Sb) in DME led to a moderate yield (39%) of **4** after recrystallisation from hexane (Scheme 1). Following this reaction by ^{31}P NMR revealed that the formation of **4** occurs over 5 h without any observable intermediate in the process. The orange crystalline material is air stable, thermally robust in the solid state (mp 112–114 °C decomp.) and stable in solution for days at 25 °C. If the reaction is carried out in a 1 : 1 stoichiometry, compound **4** is the only observable product, and *ca.* 50% of the platinum starting material remains unreacted. Interestingly, when the analogous 2 : 1 reactions of **3** (E = Sb) with *cis*-$[MCl_2(PEt_3)_2]$ (M = Ni, Pd) were carried out antimony mirrors were deposited from the reaction mixtures and the mono-acyl nickel or palladium complexes were isolated in moderate yields, **5** (39%) and **6** (56%), respectively.[8] It is noteworthy that none of the platinum analogue of **5** and **6** was found in the preparation of **4**, and similarly no distibene-dione complexes were identified in the preparations of **5** and **6**. Finally, in an attempt to form the arsenic counterpart of **4** the 2 : 1 reaction of **3** (E = As) with *cis*-$[PtCl_2(PEt_3)_2]$ was carried out but in this case the only tractable product was the diarsenide-dione bridged complex, **7**, which was formed in a low yield (5%, mp 124–126 °C decomp.).

The spectroscopic data† for **4** and **7** support their proposed structures. Of note are the ^{31}P NMR spectra of each complex which display one signal with $^1J_{PtP}$ satellites in the normal coupling range, thus suggesting the equivalence of all phosphine ligands in both complexes in solution. No molecular ions were seen in the mass spectra of **4** and **7**, but in the case of **4** a cluster of signals corresponding to the free distibene-dione ligand was observed. In contrast, the base peak in the mass spectrum of **7** coincides with the loss of a chloride ligand, while a signal relating to the cleavage of the As–As bond (monomer formation) was also detected.

The molecular structures‡ of **4** and **7** are depicted in Figs 1 and 2, respectively. The Pt centres in each have a distorted square planar coordination environment with the PEt_3 ligands *cis*- in **4** and *trans*- in **7**. Not surprisingly, the acyl substituents are *trans*- to each other in both compounds. The Sb–Sb distance in **4** lies almost midway between those for uncoordinated Sb–Sb double and single bonds [*e.g.* 2.642(1) Å in **1**[3] and 2.837 Å in Ph_4Sb_2,[9] respectively] and is slightly shorter than in the only other η^2-distibene complex **2**, 2.774(1) Å.[4] As has been described for **2** and closely related diphosphene complexes, *e.g.* *cis*-$[Pt(dppe)(\eta^2\text{-}PhP{=}PPh)]$,[10] the bonding in **4** can be thought of as lying somewhere between two canonical forms, one an η^2-distibene-Pt(0) complex and the other a three membered σ-bonded metallacycle containing a Pt(II) centre. Consistent with this description is the CSbSbC torsion angle of 173° (*cf.* 153° in **2**) which shows the ligand to be slightly distorted from planarity. In contrast to the distibene-dione ligand in **4**, the ligand in **7** can be thought of as a diarsenide-dione, the As centres of which have distorted trigonal pyramidal geometries (Σ angles = 311.8°). The As–As distance is in the expected region for single bonds and compares well with that in the only other structurally characterised example of a dinuclear complex containing a bridging diarsenide ligand, 2.456(2) Å in *trans*-

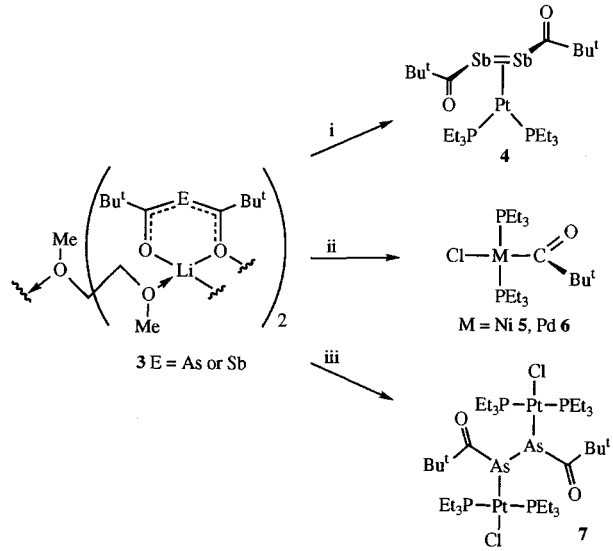

Scheme 1 *Reagents and conditions*: i, E = Sb, 1/2 *cis*-$[PtCl_2(PEt_3)_2]$, – LiCl, – $\{Bu^tC(O)\}_2$; ii, E = Sb, 1/2 *cis*-$[MCl_2(PEt_3)_2]$ (M = Ni or Pd); iii E = As, 1/2 *cis*-$[PtCl_2(PEt_3)_2]$

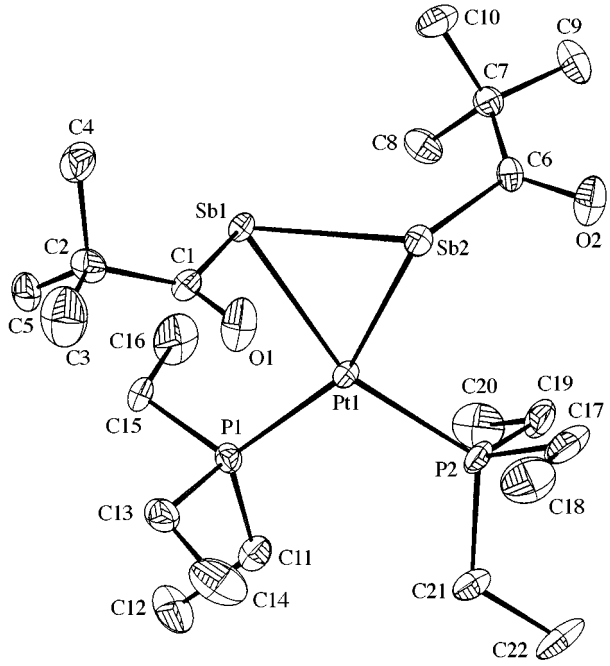

Fig. 1 Molecular structure of *cis*-[Pt(PEt$_3$)$_2${η^2-Bu^{t}C(O)Sb=SbC(O)Bu^t}] **4**. Selected bond lengths (Å) and angles (°): Sb(1)–Sb(2) 2.7551(12), Sb(1)–Pt(1) 2.6667(9), Sb(2)–Pt(1) 2.6501(10), Sb(1)–C(1) 2.279(12), Sb(2)–C(6) 2.224(12), Pt(1)–P(1) 2.281(3), Pt(1)–P(2) 2.286(3), C(1)–O(1) 1.205(13), O(2)–C(6) 1.235(13); C(1)–Sb(1)–Sb(2) 90.8(3), C(6)–Sb(2)–Sb(1) 108.0(3), Pt(1)–Sb(1)–Sb(2) 58.50(3), Pt(1)–Sb(2)–Sb(1) 59.08(2), O(1)–C(1)–Sb(1) 119.0(9), O(2)–C(6)–Sb(2) 112.6(9).

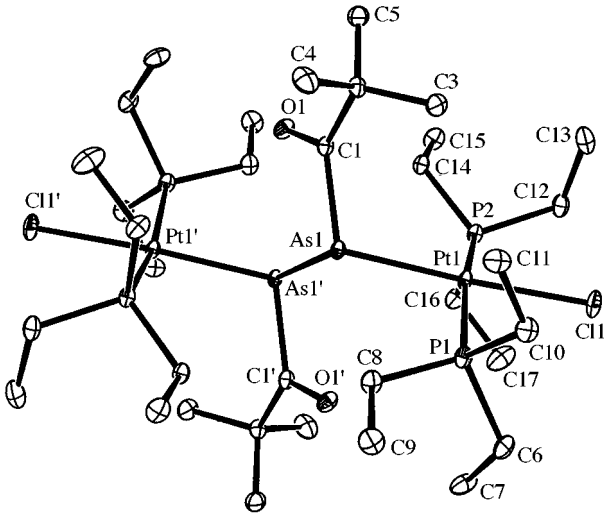

Fig. 2 Molecular structure of *trans*-[{Pt(PEt$_3$)Cl}$_2${μ-η^1,η^1-Bu^{t}C(O)As-AsC(O)Bu^t}] **7**. Selected bond lengths (Å) and angles (°): As(1)–As(1′) 2.4595(9), Pt(1)–As(1) 2.4425(5), As(1)–C(1) 2.010(5), Pt(1)–P(1) 2.3320(13), Pt(1)–P(2) 2.3078(13), Pt(1)–Cl(1) 2.4003(13); C(1)–As(1)–As(1′) 91.86(14), O(1)–C(1)–As(1) 119.3(4), Pt(1)–As(1)–As(1′) 110.63(3), C(1)–As(1)–Pt(1) 109.23(14), Cl(1)–Pt(1)–As(1) 170.95(4), P(1)–Pt(1)–P(2) 166.49(5).

[{CpFe(CO)$_2$}$_2$(μ-η^1,η^1-Ph$_2$As$_2$)].[11] All other bond lengths and angles in **4** and **7** lie in the expected regions.

At present the mechanism of formation of **4** can only be speculated upon but it seems that the likely intermediate is *cis*-[Pt(PEt$_3$)$_2${η^1-Sb[C(O)Bu^t]$_2$}$_2$] **8**, from which each η^1-Sb coordinated stibadionate ligand eliminates an acyl fragment, ·C(O)Bu^t, in a homolytic process. This would leave two coordinated [·SbC(O)Bu^t]$^-$ fragments which could couple, with an accompanying electron transfer to the Pt(II) centre, to give **4**. Although there is no spectroscopic evidence for the Sb-coordinated intermediate, **8**, its existence seems feasible considering that related 2-arsa-1,3-dionato ligands generally prefer η^1-As coordination over η^2-O,O-chelation in late transition metal complexes.[12] The fate of the acyl fragment is also a coupling reaction to give the known diketone, Bu^{t}C(O)C(O)-Bu^t, which was detected as the major product in the GC–MS analysis of the reaction volatiles.

We are currently investigating the mechanisms of formation of **4**–**7** which, when elucidated, should shed light on why such a variety of products result from supposedly similar reactions. These studies will form the basis of a forthcoming publication.

We acknowledge funding from the Leverhulme Trust (for S. J. B.), and King's College London and the EPSRC for provision of the diffractometer systems.

Notes and References

† *Spectroscopic data* **4**: ^{1}H NMR (400 MHz, C$_6$D$_6$, 298 K) δ 0.89 [dt, 18H, $^3J_{PH}$ 17.2 Hz, $^3J_{HH}$ 7.1 Hz, P(CH$_2$C*H*$_3$)$_3$], 1.22 (s, 18H, Bu^t), 1.95 [dq, 12H, $^2J_{PH}$ 22.4, $^3J_{HH}$ 7.1 Hz, P(C*H*$_2$CH$_3$)$_3$]; ^{13}C NMR (100.6 MHz, C$_6$D$_6$, 298 K) δ 9.3 [d, $^2J_{PC}$ 2.0, $^3J_{PtC}$ 25.0 Hz, P(CH$_2$*C*H$_3$)$_3$], 24.6 [d, $^1J_{PC}$ 27.6 Hz, $^2J_{PtC}$ 43.1 Hz, P(*C*H$_2$CH$_3$)$_3$], 27.25 [s, C(*C*H$_3$)$_3$], 53.26 [s, *C*(CH$_3$)$_3$], 242.0 (s, Sb*C*OBu^t); ^{31}P NMR (101.4 MHz, C$_6$D$_6$, 298 K) δ 12.75 (s, $^1J_{PtP}$ 3251.5 Hz, PEt$_3$); IR (Nujol) ν/cm^{-1} 1689m), 1641m; FABMS (NBA matrix) *m*/*z* 431 [M$^+$ − (SbCOBu^t)$_2$, 100%], 414 [M$^+$ − Pt(PEt$_3$)$_2$, 5%]; Found C 31.42; H 5.47; Calc. for C$_{22}$H$_{48}$P$_2$O$_2$Sb$_2$Pt: C, 31.44; H, 5.76. **7**: ^{1}H NMR (400 MHz, C$_6$D$_6$, 298 K) δ 1.12 [dt, 36H, $^3J_{PH}$ 16.1, $^3J_{HH}$ 7.4 Hz, P(CH$_2$C*H*$_3$)$_3$], 1.26 [dq, 24H, $^2J_{PH}$ 25.2 Hz, $^3J_{HH}$ 7.4 Hz, P(C*H*$_2$CH$_3$)$_3$], 1.55 (s, 18H, Bu^t); ^{31}P NMR (101.4 MHz, C$_6$D$_6$, 298 K) δ 10.15 (s, $^1J_{PtP}$ 2401.1 Hz, *P*Et$_3$; IR (Nujol) ν/cm^{-1} 1675m FABMS (NBA matrix) *m*/*z* 1217 (M$^+$ − Cl, 100%), 626 [M$^+$ − PtCl(PEt$_3$)$_2$AsCOBu^t, 20%].

‡ *Crystal data:* **4**, C$_{22}$H$_{48}$O$_2$P$_2$PtSb$_2$, *M* = 845.13, monoclinic, space group *P*2$_1$/*n*, *a* = 19.919(2), *b* = 16.062(4), *c* = 20.132(2) Å, β = 108.48(1), *V* = 6109(2) Å^3, *Z* = 8, *D*$_c$ = 1.838 g cm^{-3}, *F*(000) = 3248, μ = 64.44 cm^{-1}, crystal 0.30 × 0.25 × 0.15 mm, radiation Mo-Kα (λ = 0.71069 Å), 150(2) K, 8946 data, 547 parameters, $R_1[F^2 > 2\sigma(F^2)]$ = 0.0377, wR_2 = 0.0826 (all data). **7**: C$_{34}$H$_{78}$As$_2$Cl$_2$O$_2$P$_4$Pt$_2$, *M* = 1253.76, monoclinic, space group *P*2$_1$/*n*, *a* = 11.2307(4), *b* = 18.2118(7), *c* = 11.6766(5) Å, *V* = 2353.3(2) Å^3, *Z* = 2, *D*$_c$ = 1.769 g cm^{-3}, *F*(000) = 1228, μ = 76.10 cm^{-1}, crystal 0.10 × 0.10 × 0.10 mm, radiation Mo-Kα (λ = 0.71070 Å), 100(2) K, 4621 data, 209 parameters, $R_1[F^2 > 2\sigma(F^2)]$ = 0.0374, wR_2 = 0.0928 (all data). Full details of data collections and solution and refinement of both structures are included as supplementary material, CCDC 182/1008.

1 M. Yoshifuji, I. Shima, N. Inamoto, K. Hirutsu and T. Higuchi, *J. Am. Chem. Soc.*, 1981, **103**, 4587.
2 L. Weber, *Chem. Rev.*, 1992, **92**, 1839 and references therein.
3 N. Tokitoh, Y. Arai, T. Sasamori, R. Okazaki, S. Nagase, H. Uekusa and Y. Ohashi, *J. Am. Chem. Soc.*, 1998, **120**, 433.
4 A. H. Cowley, N. C. Norman, M. Pakulski, D. L. Bricker and D. H. Russell, *J. Am. Chem. Soc.*, 1985, **107**, 8211.
5 G. Huttner, U. Weber, B. Sigwarth and O. Scheidsteger, *Angew. Chem., Int. Ed. Engl.*, 1982, **21**, 215.
6 U. Weber, G. Huttner, O. Scheidsteger and L. Zsolnai, *J. Organomet. Chem.*, 1985, **289**, 357.
7 J. Durkin, D. E. Hibbs, P. B. Hitchcock, M. B. Hursthouse, C. Jones, J. Jones, K. M. A. Malik, J. F. Nixon and G. Parry, *J. Chem. Soc., Dalton Trans.*, 1996, 3277.
8 Full synthetic, spectroscopic and crystallographic data for **5** and **6** have been submitted as supplementary material.
9 K. van Deuter and D. Rehder, *Cryst. Struct. Commun.*, 1980, **9**, 167.
10 J. Chatt, P. B. Hitchcock, A. Pidcock, C. P. Warrens and K. R. Dixon, *J. Chem. Soc., Chem. Commun.*, 1982, 932.
11 A. L. Rheingold, M. J. Foley and P. J. Sullivan, *Organometallics*, 1982, **1**, 1429.
12 S. J. Black, C. Jones and R. C. Thomas, unpublished work.

Received in Cambridge, UK, 27th August 1998; 8/06712K

Naphthalene intercalation into molybdenum disulfide

Laura Kosidowski and Anthony V. Powell*

Department of Chemistry, Heriot-Watt University, Edinburgh, UK EH14 4AS. E-mail: a.v.powell@hw.ac.uk

Exfoliation of $LiMoS_2$ followed by reflocculation permits the intercalation of naphthalene guest molecules into the van der Waals gap of MoS_2.

Layered transition-metal disulfides are versatile intercalation hosts which can accommodate the steric demands of a wide variety of guest species.[1] Their ability to form intercalation compounds is known to be strongly dependent on the electronic structure of the dichalcogenide.[2] This may be traced to the requirement for the host structure to possess low-lying empty electronic states, as a result of the redox process which accompanies the intercalation reaction. Hence, dichalcogenides of group 4 and group 5 transition metals readily form intercalation compounds with a wide variety of guest species. This may be achieved electrochemically or chemically, either by direct reaction with electron donors such as organic Lewis bases or with chemical reducing agents. In contrast, the presence of a low-lying d_{z^2} band in the group 6 materials results in a more limited intercalation chemistry, mainly restricted to alkali metals as guest species.[3]

An alternative route to intercalation compounds of transition-metal disulfides *via* 'single' molecular layers, involving reaction of a colloidal dispersion of the layered host with a solution containing the guest species, has been described.[4] This has successfully been applied to the insertion of sterically disfavoured molecules[5] and those which are poor electron donors including substituted aromatics,[6] polymers[7] and ferrocene.[8] This route potentially provides access to a wide range of intercalation compounds of layered materials and in particular, affords a means of extending the intercalation chemistry of group 6 dichalcogenides to encompass novel guest species. In this work, by describing the synthesis and initial characterisation of a novel naphthalene intercalation compound of MoS_2, we illustrate that guest molecules which are both poor electron donors and non-polar may be introduced by this method.

$LiMoS_2$ was prepared by adding three equivalents of standardised 1.6 M *n*-butyllithium to a dispersion of 2H-MoS_2 in distilled light petroleum (bp 60–80 °C) and stirring for 48 h under N_2. The product, Li_xMoS_2, was washed with several 20 ml portions of light petroleum and dried under vacuum. Powder X-ray diffraction showed it to be single phase with a hexagonal unit cell; a = 3.312(45), c = 6.394(18) Å. The lithium content, x, was determined to be 1.02(2), by flame emission spectroscopy.

All further stages of the reaction were carried out in air. Sufficient de-ionized water was added to $LiMoS_2$ to produce a suspension of 0.08 g ml^{-1} exfoliated MoS_2 (denoted $\{MoS_2\}_{exf}$). The suspension was sonicated for 30 min, a saturated solution of naphthalene in dichloromethane added (in the molar ratio of $C_{10}H_8$: $\{MoS_2\}_{exf}$ = 5 : 1) and the mixture stirred for 24 h. The single layer dispersion reflocculated after acidification to pH = 2 using concentrated HCl. Stirring was then continued for periods between one day and three weeks, after which the solid was separated, washed with water and dichloromethane and vacuum dried. The degree of intercalation was found to vary with the length of stirring time following acidification. It was found that repetition of this method consistently led to intercalation providing the reaction was stirred for 7 days or more following acidification.

Upon exposure of $LiMoS_2$ to water, gas evolution was observed together with the formation of a black opaque suspension. This is consistent with a proposed mechanism for exfoliation.[9] Spontaneous movement of the exfoliated material up the walls of the reaction vessel was also seen to occur.

The powder X-ray diffraction pattern of the intercalated material [Fig. 1(a)] shows two strong lines corresponding to the 001 and 002 reflections, whose shift to lower angle indicates an increase in interlayer spacing. It exhibits a characteristic saw-tooth shape comprising asymmetrically broadened peaks. This is a consequence of the Warren effect[10] which arises from the fact that for a two-dimensional layer, the reciprocal lattice becomes a line perpendicular to the layer and so, for higher diffraction angles, a continuous distribution of diffraction intensity appears. The broadness of the Bragg peaks results from the small particle size, estimated from the degree of broadening to be < 150 Å. Omission of naphthalene from the final preparative step produced a material whose powder X-ray diffraction pattern [Fig. 1(b)] is consistent with the formation of poorly crystalline restacked MoS_2.

The content of the intercalated naphthalene in all product materials was determined by C, H elemental microanalysis and by thermogravimetry. A hydrogen content slightly in excess of that required for a C : H ratio corresponding to naphthalene, was found by C, H analysis. This suggested that some residual water was present. An initial low-temperature mass loss observed in thermogravimetric analysis was consistent with this conclusion, and was used to determine the water content independently. This residual water appears to be on the surface of the product

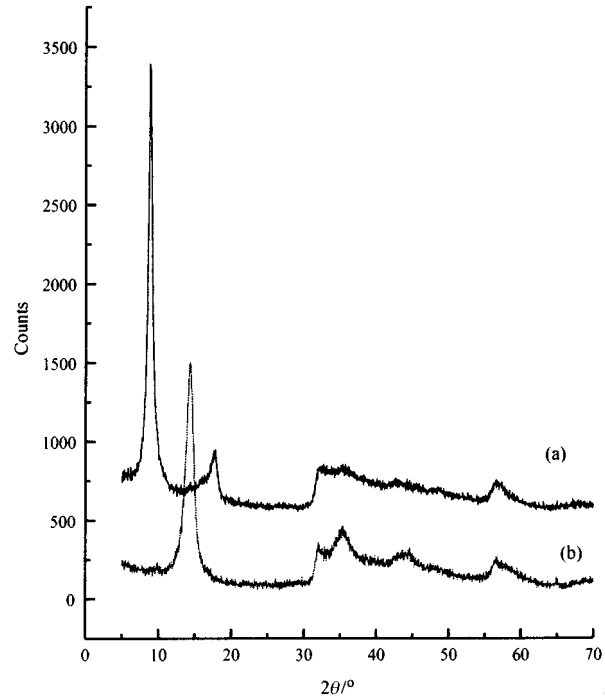

Fig. 1 Powder X-ray diffraction patterns for (a) $(C_{10}H_8)_{0.130}(H_2O)_{0.05}MoS_2$ and (b) restacked MoS_2

Table 1 Characterisation of intercalation compounds

Stirring time/days	Δc/Å	Empirical formula (C, H analysis)	Empirical formula (TG)
1	2.43	$(C_{10}H_8)_{0.07}(H_2O)_{0.11}MoS_2$	$(C_{10}H_8)_{0.07}(H_2O)_{0.06}MoS_2$
7	2.91	$(C_{10}H_8)_{0.08}(H_2O)_{0.33}MoS_2$	$(C_{10}H_8)_{0.08}(H_2O)_{0.28}MoS_2$
9	3.74	$(C_{10}H_8)_{0.11}(H_2O)_{0.26}MoS_2$	$(C_{10}H_8)_{0.11}(H_2O)_{0.20}MoS_2$
13	3.53	$(C_{10}H_8)_{0.13}(H_2O)_{0.19}MoS_2$	$(C_{10}H_8)_{0.13}(H_2O)_{0.14}MoS_2$
14	3.81	$(C_{10}H_8)_{0.13}(H_2O)_{0.05}MoS_2$	$(C_{10}H_8)_{0.13}(H_2O)_{0.05}MoS_2$
14	4.26	$(C_{10}H_8)_{0.20}(H_2O)_{0.19}MoS_2$	$(C_{10}H_8)_{0.20}(H_2O)_{0.12}MoS_2$

material since repeated preparation of samples indicated that there was no relationship between the interlayer expansion and the water content of the sample (Table 1). DSC measurements showed an endothermic transition at 100 °C, again consistent with surface water. It is also unlikely that naphthalene, a hydrophobic molecule, would co-intercalate with water. Atomic absorption analysis of the intercalation product showed it to be free of significant amounts of lithium (< 0.005 moles of Li per mole of MoS_2).

Table 1 shows repeated preparations, only varying in the period of stirring following acidification; their corresponding final interlayer expansion and composition. The length of stirring was found to affect the degree of intercalation observed such that no significant change in the extent of intercalation was observed for stirring times of less than seven days. Beyond this, the extent of intercalation of naphthalene increased with stirring time up to a maximum of 0.20 mole of naphthalene per mole of MoS_2 at 14 days stirring. Longer stirring times did not lead to any increase in the degree of intercalation beyond this value.

The interlayer expansion with respect to MoS_2 is *ca.* 3.8 Å. Molecular modelling calculations[11] indicate the van der Waals size of naphthalene to be *ca.* 6.8 × 5.1 Å. Hence the observed Δc value would suggest that the plane of the aromatic species is parallel to the MoS_2 layers. The smaller values of Δ_c observed at short reaction times may indicate the occurrence of staging. Further evidence for naphthalene intercalation with this orientation is provided by the fact that the p_z orbitals in naphthalene project above and below the plane of the ring in such a way as to give the ring an effective thickness of *ca.* 3.7 Å[12] which is consistent with the interlayer expansion observed in the product reported here. The area of a naphthalene molecule is *ca.* 35 Å^2 which compares with an interlayer area of *ca.* 8.6 Å^2 per molybdenum atom in MoS_2. Such a geometric constraint suggests that the maximum uptake of naphthalene is approximately 0.25 per molybdenum atom: the maximum guest content observed is 0.20. Steric repulsion between neighbouring naphthalene molecules is likely to prevent maximum occupancy of the interlayer spacing from being attained.

Insertion of a non-polar species into a group 6 disulfide has been achieved using the synthetic method reported here. An organic/inorganic composite material is obtained with a limiting content of 0.20 moles of naphthalene per molybdenum atom. The interaction of the organic and inorganic fragments of this material would be expected to lead to changes in the physical properties of the host. Studies of the structural, transport and magnetic properties of the material are currently in progress and will be reported in due course.

Notes and References

1 A. V. Powell, *Annu. Rep. Prog. Chem. Sect C*, 1993, **90**, 177.
2 R. H. Friend and A. D. Yoffe, *Adv. Phys.*, 1987, **36**, 1.
3 J. Rouxel, *Intercalated Layered Materials*, ed. F. Lévy, Dordrecht, 1979, p. 201.
4 A. J. Jacobson, *Mater. Sci. Forum*, 1994, **152**–**153**, 1.
5 L. F. Nazar and A. J. Jacobson, *J. Mater. Chem.*, 1994, **4**, 1419.
6 H. Tagaya, T. Hashimoto, M. Karasu, T. Izumi and K. Chiba, *Chem. Lett.*, 1991, **12**, 2113.
7 M. G. Kanatzidis, R. Bissessur, D. C. DeGroot, J. L. Schindler and C. R. Kannewurf, *Chem. Mater.*, 1993, **5**, 595.
8 W. M. R. Divigalpitiya, R. F. Frindt and S. R. Morrison, *Science*, 1989, **246**, 369.
9 M. Danot, J. L. Mansot, A. S. Golub, G. A. Protzenko, P. B. Fabritchnyi, Yu. N. Novikov and J. Rouxel, *Mater. Res. Bull.*, 1994, **29**, 833.
10 D. Yang, S. Jiménez Sandoval, W. M. R. Divigalpitiya, J. C. Irwin and R. F. Frindt, *Phys. Rev. B*, 1991, **43**, 12 053.
11 'CS Chem 3D Pro' carried out by Dr K. Morgan, Heriot-Watt University.
12 E. Mack, *J. Phys. Chem.*, 1937, **41**, 221.

Received in Bath, UK, 24th July 1998; 8/05984E

Ozone treatment for the removal of surfactant to form MCM-41 type materials

Matthew T. J. Keene, Renaud Denoyel and Philip L. Llewellyn*

Centre de Thermodynamique et de Microcalorimétrie du CNRS, 26 rue du 141ème RIA, 13331 Marseilles, cedex 3, France. E-mail: pllew@ctm.cnrs-mrs.fr

Ozone has been used to remove the organic surfactant species at 250 °C from as synthesised organic/inorganic composite (or mesophase) materials to form mesoporous MCM-41 type solids with higher surface area, larger pores and narrower pore size distribution than those obtained by conventional calcination at 550 °C.

The relatively large interest of MCM-type mesoporous materials that has arisen since 1992[1,2] lies in the fact that they can be tailored to form pores of narrow distribution, from 2 to 10 nm. This opens up a field of fundamental and applied science where a narrow mesopore size distribution and high surface area could be required. Surprisingly for these tailor-made materials where a control of the pore size can be important, a limited number of studies have been published concerning the specific removal of organic material from the as synthesised organic/inorganic composite or mesophase.[3–6] In effect, the removal of the 'templating' surfactant molecules, occluded within this material during the synthesis, is quite often carried out by thermal methods. Commonly, a heating ramp of 1 °C min^{-1} up to a plateau temperature of 550 °C in air is used.[1,2] However, methods such as plasma and supercritical fluid extraction[3] are other possible means to remove this organic material. Several studies have also used washing or ionic exchange of the surfactant.[4–7]

Ozone, is commonly used as a treatment in numerous applications ranging from environmental technology (*e.g.* ozone in water treatment[8]) to physics (*e.g.* cleaning of polished flat surfaces). To date, however, ozone treatment has not been used to eliminate organic species from porous materials. For microporous materials such as zeolites, the elimination of the organic template could be hampered by the steric hindrance of the micropores themselves. This is not the case for slightly larger pores where the elimination of the organic moieties from the pores is hindered to a far lesser extent. The present preliminary study has used ozone at room temperature to remove the organic surfactant to form mesoporous MCM-41 type materials.

The silica mesophase was prepared using the synthesis outlined by Grün *et al.*[9] This particular synthesis route uses tetraethoxysilicate as the silica source and is carried out at 25 °C. The surfactant used was cetyltrimethylammonium bromide (CTABr). After filtering and washing in distilled water, the sample was dried in air at 20 °C overnight. For comparison, part of the sample was calcined under a nitrogen flow, at a heating rate of 1 °C min^{-1}, up to a 550 °C plateau for 4 h. For the ozone treatment, around 0.1 g of sample was placed on a watch glass which was then placed for 24 h under a UV lamp (electrical power 20W : UV power 6.8 W at 254 and 180 nm) whose wavelength is known to create ozone from atmospheric oxygen. To verify the effect of the UV light on the sample, a separate sample was treated by a flow of gaseous ozone produced by an electric arc. Both samples showed similar results on further characterisation. The sample was characterised by X-ray diffraction (Fig. 1), DRIFT (Fig. 2) and argon adsorption manometry at 77 K (Fig. 3). The ozone treated sample was also treated by thermogravimetry up to 1000 °C that showed a 1% weight loss, essentially from silanol condensation forming water.

The XRD patterns shown in Fig. 1 are typical for hexagonal mesoporous materials. For the ozone treated sample, the d_{100} spacing of 4.15 nm is surprising in that it is the same as that found in the initial mesophase. Normally, thermal extraction and ion exchange of the template leads to an appreciable shrinkage of the structure of up to 25%.[4] This is illustrated in the lower pattern obtained for a traditionally calcined sample with a d_{100} spacing of 3.67 nm.

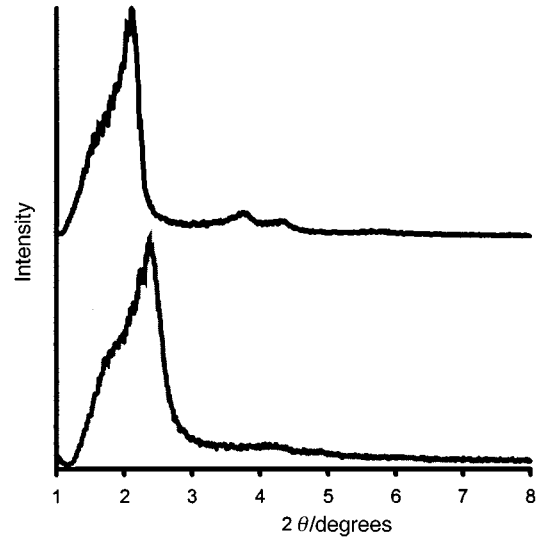

Fig. 1 X-Ray powder diffraction patterns of an ozone treated sample (upper curve) and a sample calcined to 550 °C (lower curve)

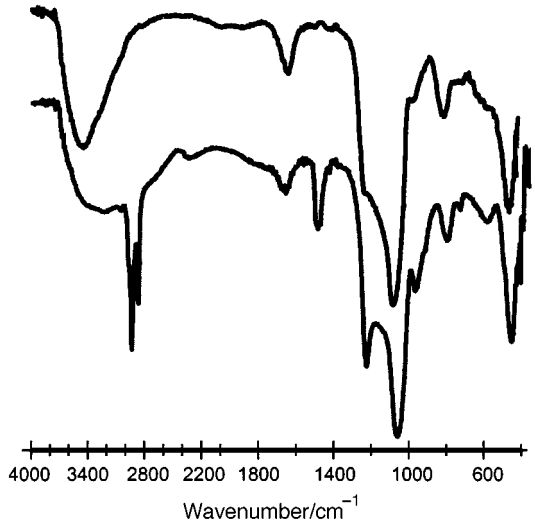

Fig. 2 DRIFT spectra of an ozone treated sample (upper curve) and original mesophase (lower curve)

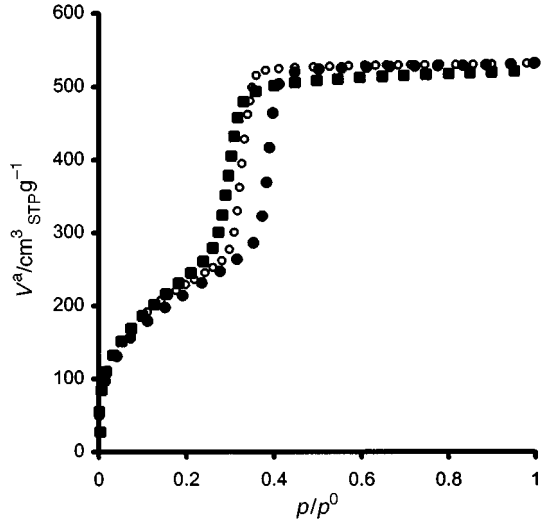

Fig. 3 Argon adsorption–desorption isotherm obtained at 77 K for (i) an ozone treated sample: (●) adsorption, (○) desorption, and (ii) a sample calcined at 550 °C: (■) adsorption

The IR spectrum of the silica mesophase before ozone treatment (lower curve, Fig. 2) clearly shows the peaks resulting from C–H stretching (2924 and 2854 cm^{-1}) as well as a broad signal (3600–3200 cm^{-1}) assigned to hydrogen bonded Si–OH groups.[10] After ozone treatment (upper spectrum, Fig. 2), the C–H peaks are no longer observed whereas a large signal assigned to hydrogen bonded Si–OH persists.

The argon adsorption isotherms at 77 K obtained with the ozone treated sample (circles) and a traditionally calcined sample (squares) (Fig. 3) are both of type IV character[11] and show distinct capillary condensation steps. The capillary condensation step obtained with the ozone treated sample is in reality sharper and slightly higher in relative pressure (p/p^0 = 0.37 compared with 0.30) than that obtained for a sample calcined using a standard thermal treatment. This would seem to indicate that a larger pore size and a narrower pore size distribution can be obtained for MCM41 using ozone treatment. The *t*-plot analysis shows that there are no micropores and relatively little external surface area (*ca.* 25 $m^2\ g^{-1}$) when compared to the calcined sample (*ca.* 40 $m^2\ g^{-1}$). The argon BET surface area obtained is 710 $m^2\ g^{-1}$ for the ozone treated sample, which is similar for the same sample calcined using a standard treatment. Using the geometric formula for the diameter $d = 4V/A$, leads to a pore diameter of 3.6 nm for the ozone treated material.

These results highlight that for mesoporous materials, such as MCM-41, treating by ozone could prove interesting from several points of view. First of all, such treatment is relatively strightforward, as a simple UV lamp can be used. Secondly, it could be envisaged that samples *in situ* can be treated after the synthesis of the mesophase. That is to say that, the elimination of the organic template can be possible within the synthesis medium limiting the total number of synthesis steps required. Thirdly, the ozone treatment is carried out at room temperature, although the temperature reached within the pores themselves could be higher. For this reason ozone treatment could prove well adapted to materials with a fragile structure where, for example, the nature of metal species occluded within the walls during synthesis could be altered on thermal treatment. Finally, this ozone treatment is a clean technology for the removal of organic species as the majority of products formed are thought only to be water and carbon dioxide. However, questions remain of in what forms the nitrogen and bromine are eliminated from the pores. From these points of view ozone treatment could prove more cost effective with respect to thermal treatment for the removal of organic species from these materials.

The authors would like to thank Dr J. Blanchard at the University of Frankfurt for the XRD spectra and the EC TMR program (ERB FM RX CT 960084) for financial support of M. T. J. K.

Notes and References

1 C. T. Kresge, M. E. Leonowicz, W. J. Roth, J. C. Vartuli and J. S. Beck, *Nature*, 1992, **359**, 710.
2 J. S. Beck, J. C. Vartulli, W. J. Roth, M. E. Leonowicz, C. T. Kresge, K. D. Schmitt, C. T.-W. Chu, D. H. Olson, E. W. Sheppard, S. B. McCullen, J. B. Higgins and J. L. Schlenker, *J. Am. Chem. Soc.*, 1992, **114**, 10 834.
3 S. Kawi and M. W. Lai, *Chem. Commun.*, 1998, 1407.
4 C.-Y. Chen, H.-X. Li and M. E. Davis, *Microporous Mater.*, 1993, **2**, 17.
5 R. Schmidt, D. Akporiaye, M. Stöcker and O. H. Ellestad, *Stud. Surf. Sci. Catal. A*, 1994, **84**, 61.
6 S. Hitz and R. Prins, *J. Catal.*, 1997, **168**, 194.
7 P. T. Tanev and T. J. Pinnavaia, *Chem. Mater.*, 1996, **8**, 2068.
8 S. E. Manahon, *Environmental Chemistry*, Willard Grant Press, Boston, 3rd edn., 1979, ch. 8.
9 M. Grün, I. Lauer and K. Unger, *Adv. Mater.*, 1997, **9**, 254.
10 X. S. Zhao, G. Q. Lu, A. K. Whittaker, G. J. Millar and H. Y. Zhu, *J. Phys. Chem. B*, 1997, **101**, 6525.
11 K. S. W. Sing, D. H. Everett, R. A. W. Haul, L. Moscou, R. A. Pierotti, J. Rouquerol and T. Siemieniewska, *Pure Appl. Chem.*, 1985, **57**, 603.

Received in Bath, UK, 4th August 1998; 8/06118A

Unusual reactivity and isomerisation in dicobalt *s*-indacene complexes

Paul Roussel, Mark J. Drewitt, Douglas R. Cary, Catherine G. Webster and Dermot O'Hare*

Inorganic Chemistry Laboratory, South Parks Road, Oxford, UK OX1 3QR. E-mail: dermot.ohare@chem.ox.ac.uk

Di-{Co(Cp)} derivatives of Bu^t_4-*s*-indacene (Ic′) have been prepared, they exist as both *cis* and *trans* isomers which can interconvert in solution; the solution electrochemistry of these complexes show that these bimetallic complexes can exhibit up to four redox events; unusually, attempted oxidation by a protic oxidising agent of $(CoCp)_2$Ic results in attack at the central carbons of the indacene rings.

Organometallic polymers are known to show interesting magnetic and electronic properties arising from the communication of adjacent metal centres. For example, polyferrocenophanes exhibit two oxidation waves for the alternate iron sites.[1] Manriquez *et al*. have reported substantial intramolecular metal–metal communication for bimetallic complexes containing bridging indacene and pentalene ligands,[2] however attempts at synthesis of oligo- and poly-meric transition metal complexes incorporating these ligands have met with limited success owing to their insolubility.

We have been investigating the organometallic chemistry of Ic′ (Ic′ = 1,3,5,7-tetra-*tert*-butyl-*s*-indacene)[3] with the view of making soluble oligomeric complexes with significant intramolecular electron–electron correlation.[4] So far, bimetallic transition metal complexes of Ic′ have only exhibited *cis* coordination of the two metal centres to the planar ligand, however, the transition metal starting materials were dimeric thus favouring this geometry. Thus, syntheses involving suitable monomeric transition metal starting materials should afford a mixture of both *cis* and *trans* bimetallic Ic′ complexes.

Reaction of Ic′ and 2 equiv. of monomeric $[CoCp(C_2H_4)_2]$ gave a brown solution, from which analytically pure $[(CoCp)_2Ic']$ **1**† can be isolated (Scheme 1). The room temperature ^1H NMR spectrum of a solution of **1** in $[^2H_8]$toluene shows two sets of uncorrelated resonances in the ratio 8 : 1, upon cooling the solution to 233 K this ratio changes to 5 : 1. We believe the resonances attributable to the major species are due to the *cis* isomer of **1** (Scheme 1) *vide infra*. In fact, on warming a solution of **1** in $[^2H_8]$toluene we can observe exchange broadening and eventual coalescence of some of the proton resonances due to the *cis* and *trans* isomers for **1** indicating rapid interconversion on the NMR timescale. The mechanism for this interconversion is presently under investigation. The fact that compound **1** is diamagnetic suggests that we should consider the Ic ligand as an L_4 donor in this case coordinated to two monovalent CoCp moieties.[5]

The cyclic voltammetric response of a tetrahydrofuran solution of **1** and tetrabutylammonium hexafluorophosphate (0.1 M) gave four quasi reversible waves at −0.12, −0.75, −1.18 and −1.49 V *vs* F_c–F_c^+.[6] $[Fv(CoCp^*)_2]$[7] (Fv = fulvalene) is reported to give a cyclic voltammogram containing four waves, attributable to the mono- and di-anionic, neutral, mono- and di-cationic species. The fact that we observe stepwise redox events indicates significant intramolecular interaction between the cobalt centres. Astruc and coworkers have demonstrated that $[Fv(CoCp^*)_2]$ may be conveniently oxidised to the dication with HPF_6.[7] We therefore employed a similar approach to the synthesis of the dication of **1**.

Reaction of **1** with 2 equiv. of ammonium tetrafluoroborate at room temperature, after work up, afforded a yellow air stable crystalline powder characterised as $[(CoCp)_2(Ic'H_2)][BF_4]_2$ **2**. The ^1H and ^{13}C NMR spectra of **2** showed that the Ic′ ligand has been protonated at the 4,8 carbon positions (Scheme 1) giving a mixture of *cis* and *trans* isomers. However, in this case the ^1H NMR does allow us to assign the resonances due to the *cis* isomer, since the two protons on each of the 4,8 carbon atoms are now chemically inequivalent. We observe no evidence for any interconversion on the ^1H NMR timescale between the *cis* and *trans* isomers in the temperature range 223–322 K. When the reaction is carried out at room temperature the *cis* : *trans* ratio of **2** is 8 : 1, which reduces to 5 : 1 when the reaction temperature is lowered to 233 K. The reaction of **1** with ND_4BF_4 affords $[^2H_2]$**2**, the ^1H NMR spectrum of the *cis* isomer indicates exclusive deuteration at one site. Geiger has showed that the protonation of $[CoCp_2]^-$ proceeds exclusively at the *exo* position, implying that it does not occur *via* the metal centre.[8]

Suitable crystals for single crystal X-ray diffraction analysis of *trans*-**2** were grown from a concentrated mixture of dichloromethane and acetonitrile. The molecular structure of *trans*-**2** (Fig. 1)‡ contains a crystallographic inversion centre at the middle of the six membered ring of the $Ic'H_2$ ligand and cocrystallised with one molecule of each of acetonitrile, dichloromethane and tetrafluoroborate in the asymmetric unit. The Cp moiety is only slightly staggered with respect to the

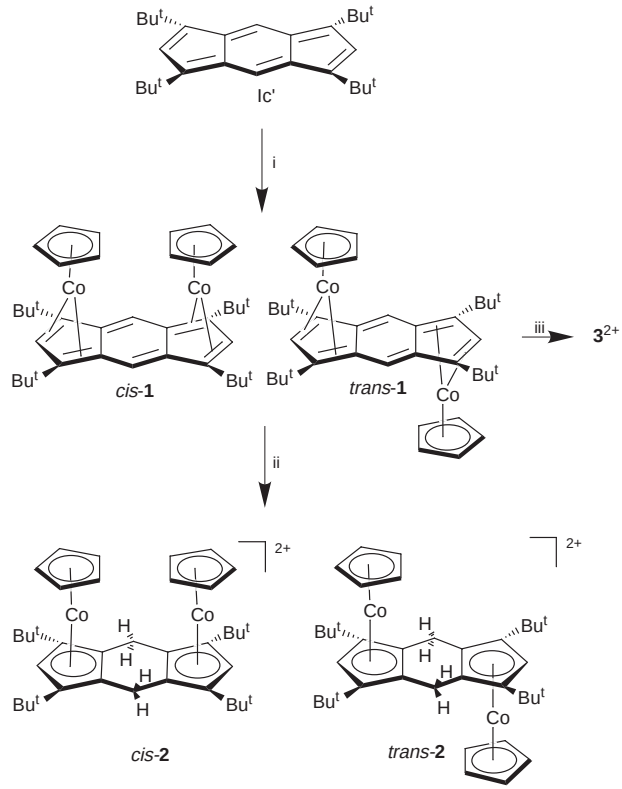

Scheme 1. *Reagents and conditions*: i, $[CoCp(C_2H_4)_2]$ (2.2 mol. equiv.), THF, 24 h, room temp.; ii, NH_4BF_4 (2 mol. equiv.), THF, room temp.; iii, Ag(OTf) (2 mol. equiv.), THF, room temp.

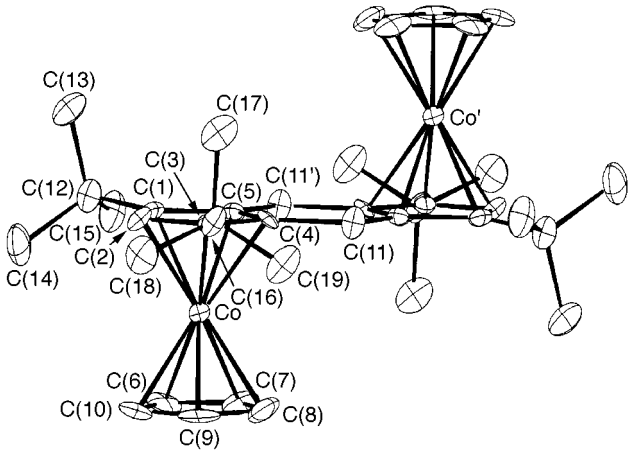

Fig. 1. Molecular structure of the *trans* isomer of **2** (CH_2Cl_2, MeCN, BF_4^- and H atoms have been omitted for clarity). Selected bond lengths (Å): Co–Ic′(centroid) 1.647(1), Co–Cp(centroid) 1.633(1), Co–C(1) 2.055(7), Co–C(2) 2.018(8), Co–C(3) 2.035(8), Co–C(4) 2.028(7), Co–C(5) 2.035(7), Co–C(6) 2.034(9), Co–C(7) 2.028(8), Co–C(8) 2.022(8), Co–C(9) 2.025(8), Co–C(10) 2.022(9).

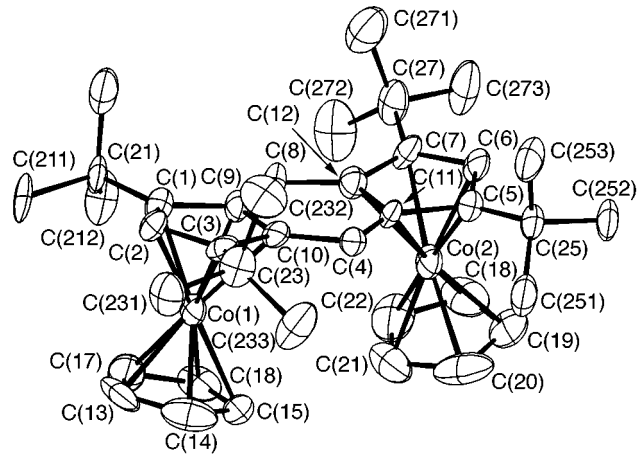

Fig. 2. Molecular structure of the *cis*-isomer of **3** (CH_2Cl_2, $CF_3SO_3^-$ and H atoms have been omitted for clarity). Selected bond lengths (Å): Co(2)–Cp(centroid) 1.66(1), Co(1)–C(1) 2.05(1), Co(1)–C(2) 2.03(1), Co(1)–C(3) 2.04(1), Co(1)–C(9) 2.15(1), Co(1)–C(10) 2.11(1), Co(1)–C(13) 2.04(1), Co(2)–C(5) 2.05(1), Co(2)–C(6) 2.01(1), Co(2)–C(7) 2.06(1), Co(2)–C(11) 2.18(1), Co(2)–C(12) 2.14(1), C(4)–C(10) 2.03(1).

IcH_2 ligand being out of phase by 7.8°, compared to cobaltocene and cobaltocenium cation which are staggered by 30°.[9] Thus **2** can be considered as two doubly bridged cobaltocenium cations. In contrast to the reported dimethyl silyl doubly bridged cyclopentadienyl complexes which are bent, the $Ic'H_2$ fragment is planar.[10] The cyclic voltammetric response of a tetrahydrofuran solution of **2** and tetrabutylammonium hexafluorophosphate (0.1 M) gave an irreversible oxidation wave at 0.65 V and an irreversible reduction wave at −1.31 V *vs* F_c–Fc^+.

Typically, electrophilic addition of a proton to cobaltocene occurs with a one electron reduction to afford the monovalent complex [Co(η^5-Cp)(η^4-C_5H_6)].[11] However the synthesis of **2** proceeds with a two electron oxidation at the cobalt atom. This is possible as the Ic′ undergoes electrophilic addition at the 4,8 carbon positions, which appear to be more reactive than the carbon atoms in the five membered rings.

The successful synthesis of the dication of **1** was achieved by employing aprotic oxidising reagents. Reaction of **1** with 2 equiv. of silver triflate afforded dark red crystalline [$(CoCp)_2$-Ic′]$^{2+}$[OTf]$_2$ **3**. We presume that compound exists as both *cis* and *trans* isomers. Compound **3** is paramagnetic, solutions in CD_3CN give a magnetic moment of 2.1 μ_B per cobalt atom. The molecular structure of *cis*-**3** (Fig. 2) shows the Ic′ ligand is slightly distorted to a convex structure with respect to the two CoCp fragments, thus reducing their steric interaction. The Co–C(Cp) bond lengths are all essentially equivalent [2.02(1)–2.05(1) Å], however, the Co–Ic′ bond lengths vary slightly, shifting the cobalt atoms towards the outside carbon atoms [*cf.* Co(1)–C(1–3) 2.03–2.05 Å, Co(1)–C(9,10) 2.11–2.15 Å]. This is similar to that found in *trans*-[(CoCp*)$_2$(*s*-indacene)]. The Cp(centroid)–Co–Ic′ bond angle of 175° further reducing the steric interaction between the CoCp moieties.

The *cis* isomer of **1** displays greater thermodynamic stability in solution over the *trans* isomer as indicated by the NMR experiments. The prevalence of the *cis* isomer seems somewhat strange from the distortion observed of the Ic ligand in the molecular structure of **3** and that only *trans* isomers are observed in unsubstituted *s*-indacene bimetallic transition metal complexes. We are presently undertaking density functional theory calculations on **1** in an effort to explain this unusual phenomenon.

We thank the EPSRC for financial support and a studentship (M. J. D.).

Notes and References

† *Characterisation data*: **1**: Anal. Calc. for $C_{38}H_{50}Co_2$: C, 73.06; H, 8.07. Found C, 72.19; H, 8.21%. ^{1}H NMR (293 K, C_6D_6) *cis*-**1**, δ 5.14 (s, 2H, CH), 4.95 (s, 2H, CH), 4.47 (s, 10H, Cp), 1.33 (s, 36H, Bu^t). *trans*-**2**, δ 6.36 (s, 2H, CH), 5.18 (s, 2H, CH), 4.47 (s, 10H, Cp), 1.33 (s, 36H, Bu^t). For **2**: Anal. Calc. for $C_{38}H_{40}B_2F_8Co_2$: C, 57.03; H, 6.55. Found C, 57.45; H, 6.44%. ^{1}H NMR (293 K, CD_3CN) *cis*-**2**, δ 5.81 (s, 10H, Cp), 5.49 (s, 2H, CH), 4.11 (d, *J* 20.5 Hz, 2H), 3.65 (d, *J* 20.5 Hz, 2H), 1.41 (s, 36H, Bu^t). *trans*-**2**, δ 5.55 (s, 10H, Cp), 5.34 (s, 2H, CH), 3.95 (s, 2H, CH), 1.47 (s, 36H, Bu^t). For **3**: Anal. Calc. for $C_{40}H_{50}O_6F_6S_2Co_2$: C, 52.06; H, 5.46%. Found: C, 52.29; H, 5.42.

‡ *X-Ray crystal structure analysis*: **2** monoclinic, space group $P2_1/c$, a = 10.564(7), b = 12.721(9), c = 18.019(6) Å, β = 90.578(4)°, U = 2421.35(5) Å^3, Z = 4, D_c = 1.44 g cm^{-3}, μ = 0.97 mm^{-1}, crystal size 0.3 × 0.25 × 0.05 mm, T = 150 K, 90 frames, 31 054 total (5256 independent) reflections, R = 0.08 and R_w = 0.095 for 4749 reflections with $I > 5\sigma(I)$; **3**: monoclinic, space group $P2_1/n$, a = 11.166(1), b = 14.461(1), c = 27.361(2) Å, β = 86.167(4)°, U = 4408.14(5) Å^3, Z = 4, D_c = 1.52 g cm^{-3}, μ = 1.03 mm^{-1}, crystal size 0.3 × 0.2 × 0.05 mm, T = 150 K, 90 frames, 30 179 total (5533 independent) reflections, R = 0.068 and R_w = 0.073 for 3257 reflections with $I > 5\sigma(I)$. CCDC 182/1013.

1 I. Manners, *Adv. Organomet. Chem*., 1995, **37**, 131.
2 J. M. Manriquez, M. D. Ward, W. M. Reiff, J. C. Calabrese, N. L. Jones, P. J. Carroll, E. E. Bunel and J. S. Miller, *J. Am. Chem. Soc*., 1995, **117**, 6182.
3 K. Hafner, B. Stowasser, H. P. Krimmer, S. Fischer, M. C. Bohm and H. J. Linder, *Angew. Chem., Int. Ed. Engl*., 1986, **25**, 630.
4 D. R. Cary, C. G. Webster, M. J. Drewitt, S. Barlow, J. C. Green and D. O'Hare, *Chem. Commun*., 1997, 953.
5 M. L. H. Green, *J. Organomet. Chem*., 1995, **500**, 127.
6 ΔE = 150 mV at 200 mV s^{-1} with $i_{pa}/i_{pc} \approx 1.0$.
7 S. Rigginger, D. Buchholz, M. Delville-Desbois, J. Linares, F. Varret, R. Boese, L. Zsolnai, G. Hutter and D. Astruc, *Organometallics*, 1992, **11**, 1454.
8 W. E. Geiger, W. L. Bowden and N. El Murr, *Inorg. Chem.*, 1979, **18**, 2358.
9 D. Barga, L. Scaccianoce, F. Grepioni and S. M. Draper, *Organometallics*, 1996, **15**, 4675; W. Bunder and E. Weiss, *J. Organomet. Chem.*, 1975, **92**, 65.
10 U. Siemeling, P. Jutzi, B. Neumann and H. Stammier, *Organometallics*, 1992, **11**, 1328.
11 N. El Murr, *J. Organomet. Chem.*, 1981, **208**, C9.

Received in Cambridge, UK, 13th August 1998; 8/06391E

5-*endo-dig* Cyclisations of homopropargylic sulfonamides: a new route to 2,3-dihydropyrroles and β-iodopyrroles

David W. Knight,*[a]† Adele L. Redfern[a] and Jeremy Gilmore[b]

[a] *Chemistry Department, Cardiff University, PO Box 912, Cardiff, UK CF1 3TB*
[b] *Eli Lilly and Co. Ltd., Lilly Research Centre, Erl Wood Manor, Windlesham, Surrey, UK GU20 6PH*

5-*endo-dig* Iodocyclisations of the homopropargylic sulfonamides 12a–c and 13 give excellent yields of the iododihydropyrroles 14a–d and thence the β-iodopyrroles 15a–d, following base-catalysed elimination of sulfinic acid.

We have recently reported that (*E*)-homoallylic tosylamides **1** (R^1, R^2 = alkyl, aryl) undergo highly efficient and stereoselective iodocyclisations to give the 2,5-*trans* iodopyrrolidines **2** in the presence of a base such as K_2CO_3, seemingly *via* a well-defined chair-like transition state conformation. In contrast, in the absence of a base, the corresponding 2,5-*cis* diastereoisomers **3** are obtained exclusively by acid-catalysed isomerization of the initial products **2** (Scheme 1).[1] Although apparently

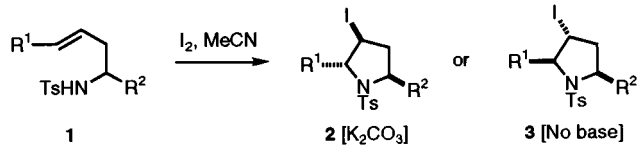

Scheme 1

5-*endo-trig* cyclisations, we do not regard these as exceptions to Baldwin's rules[2] as the process is electrophile- rather than nucleophile-driven; other aspects of our own studies and those of other research groups appear to substantiate this principle.[3] More recently, we have found that the method can be readily extended to include preparations of both 2,5-*trans* and 2,5-*cis* isomers of the substituted prolines **4** and that these undergo a double elimination of both HI and toluene-*p*-sulfinic acid upon warming with DBU in DMF, giving excellent yields of the pyrrole-2-carboxylates **5** (Scheme 2).[4]

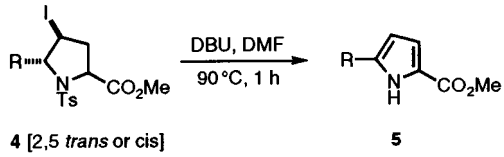

Scheme 2

While this is a useful route to such pyrroles and is related to the established Kenner method, we felt that it was something of a backward step to lose this degree of functionality during the elimination, especially the iodine atom which could otherwise provide a handle for further elaboration. It was with this in mind that we wondered if it might be possible to effect similar cyclisations of related *homopropargylic* amine derivatives, inspired by our recent success in an approach to highly substituted furans.[5] The idea of working at this higher oxidation state is outlined in Scheme 3. If a suitably protected propargylic (prop-2-ynylic) amine **6** were to undergo a 5-*endo-dig* cyclisation, the resulting dihydropyrroles **7** might then be amenable to elimination of the protecting group, leading to pyrroles **8**, in which the electrophilic species used to trigger cyclisation is retained and hence would be available for additional reactions. Further, the dihydropyrrole species **7** might well be useful for

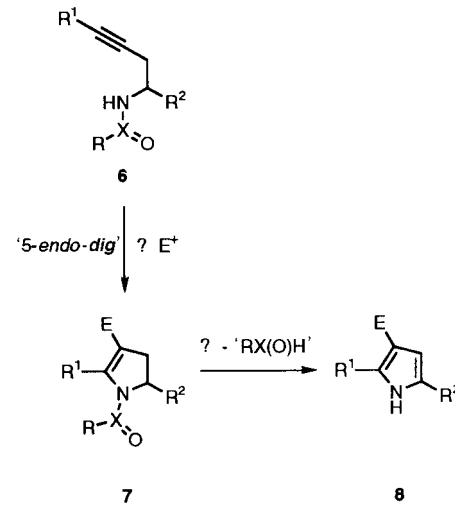

Scheme 3

further elaboration; however, at the outset, we had no idea whether these would be stable compounds. We were encouraged by the fact that, perhaps at first sight surprisingly and in direct contrast to the 5-*endo-trig* mode, 5-*endo-dig* cyclisations are favoured under Baldwin's rules.[2] Herein, we report on a first successful implementation of the approach shown in Scheme 3.

The success of the pyrrolidine and pyrrole syntheses (Schemes 1 and 2) naturally led us to choose as a first option the toluene-*p*-sulfonyl (tosyl) group to mask the amine nitrogen; the routes used to obtain representative substrates are shown in Scheme 4. The benzophenone imine of methyl glycinate **9**[6] was

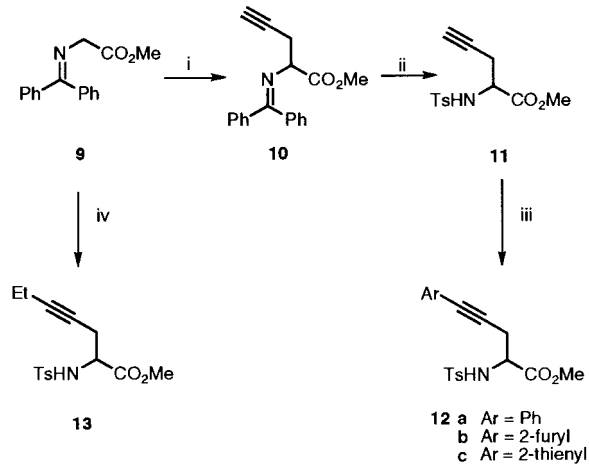

Scheme 4 *Reagents and conditions*: i, propargyl bromide, K_2CO_3, Bu_4NI, MeCN, reflux, 7 h; ii, 2 M aq. HCl, Et_2O, 20 °C, *ca.* 1 h, then TsCl, Et_3N, DMAP (cat.), CH_2Cl_2, 20 °C, 15 h; iii, ArI, CuI (cat.), $Pd(PPh_3)_4$ (cat.), Et_2NH, 20 °C, *ca.* 3 h (TLC monitoring); iv, as i, using 1-bromopent-2-yne

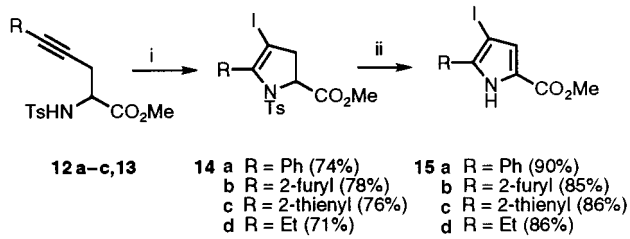

12a–c,13 **14** a R = Ph (74%) b R = 2-furyl (78%) c R = 2-thienyl (76%) d R = Et (71%) **15** a R = Ph (90%) b R = 2-furyl (85%) c R = 2-thienyl (86%) d R = Et (86%)

Scheme 5 *Reagents and conditions*: i, I_2, K_2CO_3 (3 equiv. each), dry MeCN, 0–20 °C, 14 h; ii, DBU (2.1 equiv.), DMF, 20 °C, 14 h

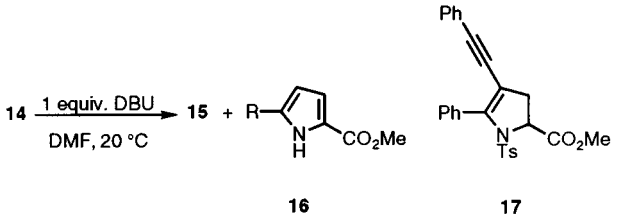

16 **17**

Scheme 6

alkylated[7] with propargyl bromide and the *N*-protecting group of the resulting propargyl glycine **10** exchanged for a tosyl group. Sonogashira coupling[8] of the sulfonamide **11** so obtained with representative iodides provided excellent yields of the cyclisation substrates **12**. An alkyl derivative **13** was obtained using 1-bromopent-2-yne as the alkylating agent, followed by protecting group exchange.‡ An alternative strategy involving couplings between aryl iodides and the imine **10** was unsuccessful. We were delighted to find that exposure of the sulfonamides **12** and **13** to 3 equiv. of I_2 and K_2CO_3 in dry MeCN at ambient temperature resulted in slow but clean cyclisation to give excellent isolated yields of the iododihydropyrroles **14** (Scheme 5).[9] The aryl derivatives **14a–c** turned out to be stable crystalline solids with sharp melting points, whereas the alkyl derivative **14d** was a somewhat sensitive oil which nevertheless could be fully characterized.‡ Further, by stirring these dihydropyrroles **14** with DBU in DMF at ambient temperature, excellent yields of the corresponding iodopyrroles **15** were obtained by elimination of toluene-*p*-sulfinic acid (Scheme 5).‡ It was important to use 2 equiv. of the base; if only 1 equiv. was used, then approximately 50% of the product was the deiodopyrrole **16**, along with the expected product **15** (Scheme 6). We assume that the released sulfinic acid is responsible for this deiodination, perhaps by attack at iodine by sulfur, leading to the sulfonyl iodide, a process greatly reduced by the presence of an additional equivalent of base. Proton-catalysed cycloreversion, with loss of iodine, cyclisation and elimination is another possibility.

Both iodinated species **14** and **15** have potential for further elaboration, especially using one of the many transition metal-catalysed coupling procedures currently available. β-Iodopyrroles have recently been shown to undergo both Stille[10] and Sonogashira couplings.[11] In the present work we have established that the iododihydropyrroles **14** are compatible with palladium catalysts. Thus, a rapid Sonogashira coupling between dihydropyrrole **14a** and phenylacetylene [CuI (0.2 equiv.), $Pd(PPh_3)_4$ (0.1 equiv.), Et_2NH, 20 °C, 2 h] delivered an 82% isolated yield of the enyne **17**, suggesting that they will prove to be useful synthetic intermediates. These aspects and further studies of the scope and limitations of this chemistry are currently being pursued.

We thank the EPSRC Mass Spectrometry Centre, Swansea University, for the provision of high resolution MS data and Eli Lilly and Co. Ltd and the EPSRC for financial support through the CASE Scheme.

Notes and References

† E-mail: knightdw@cf.ac.uk

‡ All compounds reported herein gave satisfactory microanalytical and spectroscopic data.

1 A. D. Jones and D. W. Knight, *Chem. Commun.*, 1996, 915.
2 J. E. Baldwin, *J. Chem. Soc., Chem. Commun.*, 1976, 734 and 738.
3 S. H. Kang and S. B. Lee, *Tetrahedron Lett.*, 1993, **34**, 1955, 7579; J. M. Barks, D. W. Knight, C. J. Seaman and G. G. Weingarten, *Tetrahedron Lett.*, 1994, **35**, 7259; B. H. Lipshutz and T. Gross, *J. Org. Chem.*, 1995, **60**, 3572; K. Chibale and S. Warren, *J. Chem. Soc., Perkin Trans. 1*, 1996, 1935; M. B. Berry, D. Craig, P. S. Jones and G. J. Rowlands, *Chem. Commun.*, 1997, 2141; O. Andrey, L. Ducry, Y. Landais, D. Planchenault and V. Weber, *Tetrahedron*, 1997, **53**, 4339; B. H. Lipshutz and T. Gross, *J. Org. Chem.*, 1995, **60**, 3572 and references cited therein in each.
4 D. W. Knight, A. L. Redfern and J. Gilmore, *Synlett*, 1998, 731.
5 S. P. Bew and D. W. Knight, *Chem. Commun.*, 1996, 1007.
6 M. J. O'Donnell and R. L. Polt, *J. Org. Chem.*, 1982, **47**, 2663.
7 A. Lopez, M. Moreno-Manas, R. Pleixats, A. Roglans, J. Ezquerra and C. Pedregal, *Tetrahedron*, 1996, **52**, 8365.
8 K. Sonogashira, *Comp. Org. Synth.*, 1991, **3**, 521.
9 *Typical experimental procedure* for **14b**: The tosylamide **12b** (70 mg, 0.20 mmol) was stirred in dry MeCN (1 ml) containing anhydrous K_2CO_3 (84 mg, 0.61 mmol) and cooled in an ice bath. I_2 (153 mg, 0.61 mmol) in MeCN (0.6 ml) was added dropwise and the resulting suspension stirred overnight without the addition of further coolant. Saturated aq. sodium thiosulfate was then added until the excess I_2 was decolourized and the organic layer separated. The aqueous layer was extracted with CH_2Cl_2 (2 × 5 ml) and the combined organic solutions dried ($MgSO_4$) and evaporated. Column chromatography of the residue (6 : 1 hexane–EtOAc) gave **14b** (74 mg, 78%) as a pale yellow solid, mp 88–92 °C, ν_{max}/cm^{-1} 2953, 1742, 1597, 1437, 1361, 1212, 1170, 1089, 1017; $\delta_H(CDCl_3$; 400 MHz) 2.45 (3H, s, Ar-CH_3), 2.59 (1H, dd, *J* 17.1 and 9.7, 3-H_a), 2.85 (1H, dd, *J* 17.1 and 2.4, 3-H_b), 3.82 (3H, s, OCH_3), 4.83 (1H, dd, *J* 9.7 and 2.4, 2-H), 6.50 (1H, dd, *J* 3.4 and 1.8, 4′-H), 6.89 (1H, d, *J* 3.4, 3′-H), 7.31 (2H, d, *J* 8.2, 2 × Ar-H), 7.47 (1H, app. br s, 5′-H), 7.60 (2H, d, *J* 8.2, 2 × Ar-H); $\delta_C(CDCl_3$; 100 MHz) 21.6 (Ar-CH_3), 43.5 (3-CH_2), 53.1 (OCH_3), 62.2 (2-CH), 77.6 (4-C), 111.0 (4′-CH), 113.9 (3′-CH), 127.8 (2 × Ar-CH), 129.6 (2 × Ar-CH), 133.5 (C), 135.8 (C), 143.1 (5′-CH), 144.6 (C), 144.8 (C) and 170.6 (CO); *m*/*z* (EI) 473 (M^+, 27%), 318 (17), 191 (88), 159 (51), 132 (56), 104 (55), 91 (100) [Found: C, 42.8; H, 3.4; N, 3.1. $C_{17}H_{16}INO_5S$ requires C, 43.1; H, 3.4; N, 3.0%]. For elimination of toluene-*p*-sulfinic acid: To a stirred solution of the **14** (1 mmol) in dry DMF (5 ml) at ambient temperature, DBU (0.3 ml, 2.1 mmol) was added dropwise and the elimination followed by TLC. Upon completion (*ca.* 12 h), 2 M HCl (5 ml) was added and the resulting mixture extracted with hexane (4 × 20 ml). The combined extracts were dried ($MgSO_4$) and concentrated, then passed through a short silica plug; evaporation of the filtrate left the pure iodopyrrole **15**. *Selected data* for **15b**: pale yellow solid, mp 120–124 °C; ν_{max}/cm^{-1} 3282, 2951, 1697, 1508, 1437, 1395, 1317, 1262, 1203; $\delta_H(CDCl_3$; 400 MHz) 3.88 (3H, s, OCH_3), 6.53 (1H, dd, *J* 3.5 and 1.6, 4′-H), 7.07 (1H, d, *J* 2.7, 3-H), 7.21 (1H, d, *J* 3.5, 3′-H), 7.47 (1H, d, *J* 1.6, 5′-H), 9.45 (1H, br s, NH); $\delta_C(CDCl_3$; 100 MHz) 5.19 (OCH_3), 65.2 (4-C), 107.8, 111.8, 124.5 (all Ar-CH), 129.0, 136.0, 140.5 (all Ar-C), 142.0 (Ar-CH), 162.5 (CO); *m*/*z* (EI) 317 (M^+, 79%), 285 (59), 130 (70), 76 (79), 57 (100) [Found: M^+, 316.9551. $C_{10}H_8INO_3$ requires *M*, 316.9551].
10 J. J. Wang and A. I. Scott, *Tetrahedron Lett.*, 1995, **36**, 7043. See also J. J. Wang and A. I. Scott, *Tetrahedron Lett.*, 1996, **37**, 3247.
11 A. Alvarez, A. Guzman, A. Ruiz, E. Velarde and J. M. Muchowski, *J. Org. Chem.*, 1992, **57**, 1653; P. A. Jacobi, J. S. Guo, S. Rajeswari and W. J. Zheng, *J. Org. Chem.*, 1997, **62**, 2907 and references cited therein.

Received in Liverpool, UK, 2nd August 1998; 8/06386I

A Ru-allenylidene complex with an appended redox-active substituent: spectroscopic characterization of three oxidation states†

Rainer F. Winter*

Institut für Anorganische Chemie der Universität Stuttgart, Pfaffenwaldring 55, D-70569 Stuttgart, Germany. E-mail: winter@iac.uni-stuttgart.de

A Ru allenylidene complex with a ferrocenyl substituent in the aliphatic side chain has been prepared and the effects of the consecutive oxidations of the ferrocenyl group and the Ru have been probed by IR and UV/VIS spectroelectrochemistry.

The reactivity of metal-vinylidene and −allenylidene complexes is now well established and may be employed in a variety of useful transformations.[1,2] In contrast, it is only recently that a similar chemistry of the butatrienylidene ligand has begun to emerge. The reactions of the C_4H_2 ligand present in cationic $[Ru]=C=C=C=CH_2^+$ intermediates include the addition of aprotic nucleophiles to the electrophilic C_γ[3,4] and the addition of protic nucleophiles to the terminal double bond generating methyl substituted allenylidene complexes. Some interesting cycloaddition/cycloreversion chemistry[5] as well as an unusual Aza-Cope rearrangement following the addition of allyl substituted tertiary amines were also reported.[4]

We have initiated a program aimed at synthesizing novel heteroatom substituted Ru-allenylidene complexes $[Ru]=C=C=C(ER_n)R'^+$ from butatrienylidene precursors *trans*-$[ClRu(L_2)_2=C=C=C=CH_2]^+$ (L_2 = chelating diphosphine) and investigating their spectroscopic and electrochemical properties as a function of the heteroatom and the oxidation state of Ru. In this context we are striving for model compounds which allow us to reversibly alter the electronic properties of the unsaturated ligand by attaching redox active substituents to the allenylidene side chain. Here we report our findings on *trans*-$[ClRu(dppm)_2=C=C=C(NMe_2)C_2H_4Fc]^+$ SbF_6^-, **2** [dppm = bis(diphenylphosphino)methane; Fc = ferrocenyl, $(C_5H_4)Fe(C_5H_5)$], which constitutes the first example of such compounds. **2** was prepared in good yield by trapping the *in situ* generated $[ClRu(dppm)_2=C=C=C=CH_2]^+$ with ferrocenylmethyldimethylamine, $FcCH_2NMe_2$. Due to the inherent reactivity of the organometallic amine toward dichloromethane,[6] chlorobenzene had to be employed as solvent. As to the formation of **2**, we assume that the initially generated addition product **1** evolves to the title compound by migration of the resonance stabilized ferrocenylcarbenium ion[7] from the quaternary nitrogen to the neighbouring nucleophilic C_δ (Scheme 1). Thus, the overall reaction closely resembles that observed for Ph_2NH with $FcCH_2^+$ instead of a proton. In the crude reaction mixture, **1** was identified as a minor product along with a third, as yet unidentified component.‡ Although numerous attempts to obtain X-ray quality crystals failed the spectroscopic data leave no doubt as to the identity of **2**.‡ The most characteristic features are the intense allenylidene IR stretch at 1992 cm^{-1} (KBr pellet), the low field quintet in the ^{13}C NMR spectrum at δ 201.8 with a $^2J_{P\text{-}C}$ coupling of 13.6 Hz and the two triplets for the ethylene spacer as well as the signals of a monosubstituted ferrocenyl unit in the ^1H NMR spectrum. The methyl groups attached to the nitrogen give rise to two separate resonance signals in the ^1H and ^{13}C NMR spectra, indicating a double bond character of the C=N bond. Even at 368 K these signals remain separate without any indication of exchange broadening. The energy barrier for rotation must therefore well exceed 73 kJ mol^{-1}. These data are in agreement with the iminiumalkynyl resonance form **B** being the predominant contributor to the electronic structure of **2** as was noted before for other aminoallenylidene complexes.[4,8]

Cyclic and square wave voltammetry of **2** in CH_3CN§ reveal three electrochemical processes within the solvent window, one reduction and two oxidations. At room temperature the reduction is essentially irreversible. At lower temperatures, just above the melting point of the solvent, the chemical decomposition is slowed to a degree that allows us to determine the $E_{1/2}$ of this couple as −2.13 V *vs.* the ferrocene/ferrocenium standard. The first oxidation is a chemically and electrochemically reversible Nernstian process with an $E_{1/2}$ of + 0.02 V, *i.e.* close to that of ferrocene itself. We attribute this feature to the oxidation of the appended ferrocenyl substituent, which is further supported by spectroelectrochemistry (*vide infra*). The second oxidation occurs on the Ru fragment. Under appropriate experimental conditions, the Ru(II/III) couple constitutes a chemically reversible one electron step at $E_{1/2}$ = + 0.62 V which suffers, however, from somewhat slow electron transfer kinetics. Quasireversible behavior has been observed for the Ru(II/III) couples in similar systems.[9] Most significantly, the $E_{1/2}$ of this couple is shifted anodically by 50 mV with respect to otherwise identical complexes but containing a butenyl[4] or $CHEtC=CH_2$ side chain[10] instead of the ferrocenylethyl group. We attribute this shift to the increasing electron withdrawing ability of the allenylidene side chain as the appended ferrocenyl substituent is oxidized.

This effect is also evident from following the stepwise *in situ* oxidation of **2** by UV/VIS and IR spectroscopy. The first oxidation is accompanied by the growth of an absorption band at 642 nm, a region which is characteristic of the ferrocenium chromophore (see insert of Fig. 1). At the same time the intense metal-to-ligand charge transfer absorption band of the [Ru]=C

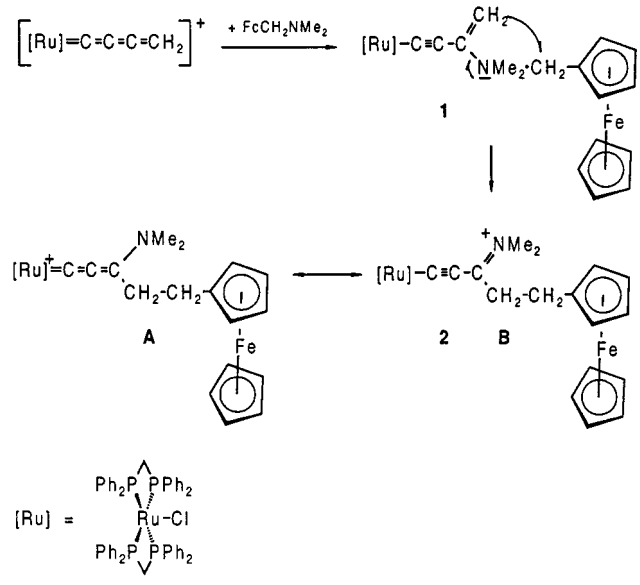

Scheme 1

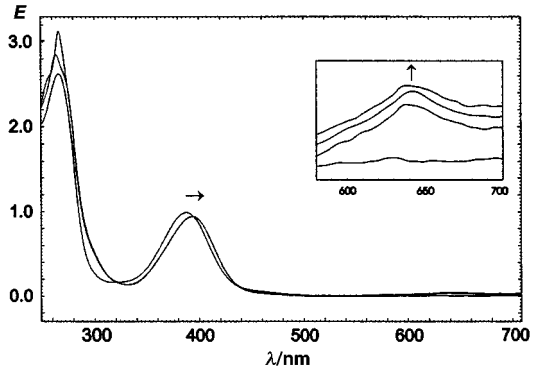

Fig. 1 Spectroscopic changes during the first electrochemical oxidation (Fc/Fc$^+$) of **2** in the UV/VIS region

=C=C(NR$_2$)R′$^{+}$ chromophore experiences a bathochromic shift from 386 nm to 394 nm (Fig. 1). A similar, albeit smaller effect just above the resolution power of our spectrometer is seen during IR monitoring of the first oxidation. Here, the intense allenylidene absorption band moves from 1999 cm^{-1} to 1997 cm^{-1}. Essentially no metal–metal coupling is observed over the partially saturated carbon spacer in the formally mixed valent heterobimetallic monooxidation product as shown by the absence of any absorption in the near IR region.

A larger effect is obtained when **2** is further oxidized. Both the UV/VIS and IR absorption bands exhibit a shift in the opposite direction to that found for the first oxidation process. In the fully oxidized trication the visible band is now positioned at 348 nm (Fig. 2). Another weak, broad band centered at 580 nm does also appear, which we attribute to a d–d transition within the Ru(III) fragment (insert of Fig. 2). The ferrocenium band remains essentially unchanged. In IR spectroelectrochemical experiments the intense absorption of the dication is replaced by a much weaker band at 2022 cm^{-1} as the oxidation of Ru(II) proceeds. We wish to emphasize that under our *in situ* conditions all oxidized species are reasonably stable. In fact, rereducing **2**$^{2+}$ reproduced the starting material in near quantitative (UV/VIS) and about 80% yields (IR). The lesser reversibility in the IR experiment is due to the longer electrolysis time required to convert the higher concentrated samples. We can therefore exclude that the loss of intensity in the IR experiment is caused by extensive decomposition rather than being an intrinsic characteristic of our system. Both the decrease in absorptivity of the IR band as well as its blue shift upon oxidation have also been observed in Ru(II)-cyanide complexes[11] thus emphasizing that, in this special situation, there may indeed be an analogy between the CN$^-$ and an electron poor acetylide ligand.[12] The shifts of the visible and the infrared bands do also point to an increase in bond order of the C$_\alpha$–C$_\beta$ entity as the ruthenium is oxidized.

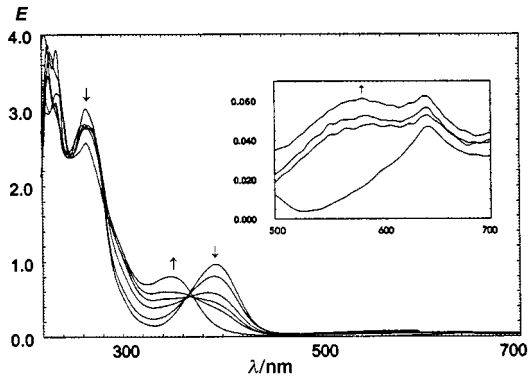

Fig. 2 Spectroscopic changes during the second electrochemical oxidation [Ru(II/III)] of **2** in the UV/VIS region

In summary, we have generated a novel functionalized aminoallenylidene complex by trapping a still elusive [Ru]=C=C=C=CH$_2^+$ intermediate with a suitable tertiary amine. The appended ferrocenyl substituent allows us to reversibly alter the electronic properties of the allenylidene ligand. Ferrocenyl oxidation influences both the Ru(II/III) oxidation potential and the spectroscopic properties of the allenylidene chromophore despite the rather remoteness of the ferrocenyl group and the saturated nature of the connecting bridge. Much larger effects are to be expected if the redox-active tag is attached directly to the delocalized allenylidene system. Work along these lines is in progress.

I am indebted to the Deutsche Forschungsgemeinschaft, DFG, for financial support of this work. The contributions of Stephan Hartmann are also gratefully acknowledged.

Notes and references

† Dedicated to Professor Dr Peter Jutzi on the occasion of his 60th birthday in mid-October.

‡ Selected spectroscopic data: compound **1**: IR (PhCl) 2032; ^{31}P NMR (CDCl$_3$) δ −6.3 (s). Compound **2**: ^{1}H NMR (250 MHz, 298 K, CDCl$_3$), δ 5.12 [2H, d of virtual quint, CH$_2$ (dppm), $^1J_{H\text{-}H}$ = 10.25, $^2J_{P\text{-}H}$ = $^3J_{P\text{-}H}$ = 4.52 Hz], 4.73 [2H, d of virtual quint, CH$_2$ (dppm), $^1J_{H\text{-}H}$ = 10.25, $^2J_{P\text{-}H}$ = $^3J_{P\text{-}H}$ = 4.05 Hz], 4.06 (5H, s, Cp), 4.00 (2H, t, C$_5$H$_4$, $^3J_{H\text{-}H}$ = 1.75 Hz), 3.69 (2H, t, C$_5$H$_4$, $^3J_{H\text{-}H}$ = 1.75 Hz), 2.78 (3H, s, NMe), 2.15 (3H, s, NMe), 1.77 [2H, t (br), CH$_2$, $^3J_{H\text{-}H}$ = 6.9 Hz], 1.63 [2H, t (br), CH$_2$, $^3J_{H\text{-}H}$ = 6.9 Hz]. ^{13}C NMR (62.9 MHz, 298 K, CDCl$_3$, assignments aided by a DEPT-135 experiment) δ 201.8 (quint, C$_\alpha$, $J_{P\text{-}C}$ = 13.6 Hz), 156,7 (br, C$_\gamma$), 119.4 (br, C$_\beta$), 85.5 (C$_{ipso}$, C$_5$H$_4$), 68.5 (Cp), 67.94 (C$_5$H$_4$), 67.87 (C$_5$H$_4$), 49.4 [quint, CH$_2$ (dppm), $J_{P\text{-}C}$ = 10.5 Hz], 43.9 (NMe), 41.7 (NMe), 38.8 (CH$_2$), 27.6 (CH$_2$). ^{31}P NMR (101.26 MHz, 298 K, CDCl$_3$) δ −8.2 (s). UV/VIS λ_{max} ($10^{-3}\varepsilon_{max}$): solvent: CH$_3$OH: 388 (19), 265 (47), 214 (79); CH$_3$CN: 386 (23), 265 (57); CH$_2$Cl$_2$: 397 (20), 267 (49), 234 (60); 1,4-dioxane: 377 (19), 266 (53), 234 (54).

§ Electrochemistry was conducted in a vacuum tight one compartment cell in CH$_3$CN with 0.2 M NBu$_4$PF$_6$ as the supporting electrolyte. Potentials were referenced to internal decamethylferrocene. Conversion to the Cp$_2$Fe$^{0/+}$ scale was done by comparing the $E_{1/2}$ values of both standards in a separate experiment. Spectro-electrochemistry was performed in a modified thin layer IR cell at room temperature. For more details see ref. 6.

1 M. I. Bruce and A. Swincer, *Chem. Rev.*, 1991, **91,** 197.
2 H. Werner, *Chem. Commun.*, 1997, 903; A. Fürstner, M. Picquet, C. Bruneau and P. H. Dixneuf, *Chem. Commun.*, 1998, 1315.
3 M. I. Bruce, P. Hinterding, P. J. Low, B. W. Skelton and A. H. White, *Chem. Commun.*, 1996, 1009; M. I. Bruce, P. Hinterding, P. J. Low, B. W. Skelton and A. H. White, *J. Chem. Soc., Dalton Trans.*, 1998, 467.
4 R. F. Winter and F. M. Hornung, *Organometallics*, 1997, **16,** 4248.
5 M. I. Bruce, P. Hinterding, M. Ke, P. J. Low, B. W. Skelton and A. H. White, *Chem. Commun.*, 1997, 715.
6 R. F. Winter and G. Wolmershäuser, *J. Organomet. Chem.*, in press.
7 A. A. Korizde, N. M. Astakhova and P. V. Petrowskii, *J. Organomet. Chem.*, 1983, **254,** 345; A. Houlton, J. R. Miller, R. M. G. Roberts and J. Silver, *J. Chem. Soc., Dalton Trans.*, 1986, 2345.
8 M. Duetsch, F. Stein, R. Lackmann, E. Pohl, R. Herbst-Irmer and A. de Meijere, *Chem. Ber.*, 1992, **125,** 2051; F. Stein, M. Duetsch, E. Pohl, R. Herbst-Irmer and A. de Meijere, *Organometallics*, 1993, **12,** 2556.
9 M. C. B. Colbert, J. Lewis, N. J. Long, P. R. Raithby, A. J. P. White and D. J. Williams, *J. Chem. Soc., Dalton Trans.*, 1997, 99.
10 R. F. Winter, manuscript in preparation.
11 C. A. Bignozzi, R. Argazzi, J. R. Schoonover, K. C. Gordon, R. B. Dyer and F. Scandola, *Inorg. Chem.*, 1992**,** **31**, 5260.
12 A comprehensive discussion of this topic is given in: J. Manna, K. D. John and M. D. Hopkins, *Adv. Organomet. Chem.*, 1995, **38**, 79.

Received in Cambridge, UK, 7th September 1998; 8/06934D

Strategies to improve the epoxidation activity and selectivity of Ti-MCM-41

Avelino Corma,*[a] Marcelo Domine,[a] José A. Gaona,[a] José L. Jordá,[a] María T. Navarro,[a] Fernando Rey,[a] Joaquin Pérez-Pariente,[b] Junpei Tsuji,[c] Beth McCulloch[d] and Laszlo T. Nemeth[d]

[a] *Instituto de Tecnología Química, (CSIC-UPV), Universidad Politécnica de Valencia, Avenida de los Naranjos s/n. 46022—Valencia, Spain. E-mail: acorma@itq.upv.es*
[b] *Instituto de Catálisis y Petroleoquímica (CSIC), Campus Universitario de Cantoblanco, 28049—Madrid, Spain*
[c] *Sumitomo Chemical Co., Ltd., Petrochemicals Research Laboratory, 2-1 Kitasode Sodegaura City, Chiba Pref., Japan*
[d] *UOP LLC, 50 East Algonquin Road, Des Plaines, IL 60017-5016, USA*

Two strategies to improve the catalytic activity of Ti-MCM-41 materials in the epoxidation of olefins are described; the first approach involves silylation of the surface of Ti-MCM-41 which produces a very hydrophobic catalyst whereas the second approach is based on removal of water from the reaction media; the increase in activity is not due to a change in the intrinsic activity of the Ti sites, but rather to a decrease of the catalyst deactivation by reducing the formation of diols produced by ring opening of the epoxide.

The discovery of TS-1,[1] and its extension to Ti-beta[2] and Ti-MCM-41[3] have broadened the scope of these interesting catalysts to include the oxidation of large hydrocarbon molecules.[3–6] It has been shown with these catalytic systems that the hydrophobic/hydrophilic properties of the surface are just as important as the number of active sites. Control of the hydrophobicity of the molecular sieve allows the optimization of the adsorption of reactants and products.[7,8] This is especially true for the epoxidation of olefins where, irrespective of the nature of the oxidant, the epoxide has higher polarity than the olefinic substrate. Consequently, the epoxide competes more favorably for adsorption on the hydroxylated surfaces of the Ti-silicates.[5] In this respect, the presence of silanol groups as well as the presence of =Ti–OH groups allows adsorption of the epoxide and results in ring opening of the epoxide and the formation of diols. As discussed later, the diols tend to strongly adsorb on the Ti sites and lead to partial deactivation of the catalyst.

We have shown that by decreasing the concentration of the internal silanol groups in Ti-beta, it is possible to significantly increase the selectivity to the epoxide.[7] In the case of materials such as Ti-silica and Ti-MCM-41, which contain a large number of silanol groups, the silanol content can be reduced by reaction with organosilanes[9,10] or by introducing organosilanes directly to the synthesis gel of mesoporous materials,[11–13] and this modification is reflected in the final properties of the catalyst.[13,14] In this manner it has recently been shown that silylated Ti-MCM-41 gives better selectivity to the epoxide when hydrogen peroxide is used as an oxidant.[14] However, the cyclohexene conversion was 13% of the maximum conversion achievable and the selectivity to the epoxide was only 13%. Thus, as shown previously by us,[15] hydrogen peroxide is not an appropriate oxidant for Ti-MCM-41 and consequently the poor performance is not surprising.

It appears that Ti-MCM-41 has the greatest potential as an epoxidation catalyst when organic hydroperoxides are used as the oxidant.[16] Here we will describe two different strategies that give results superior to those that have been reported up to now. In this way, two different samples of Ti-MCM-41 were prepared. The first sample was obtained from a gel having the following molar composition: $SiO_2 : 0.015\ Ti(OEt)_4 : 0.26$ CTABr : 0.26 TMAOH : 24.3 H_2O where CTABr is cetyltrimethylammonium bromide and TMAOH is tetramethylammonium hydroxide. The silica source, Aerosil-200, was obtained from Degussa. The crystallization was performed at 100 °C for 48 h in Teflon lined stainless steel autoclaves. The occluded surfactant was completely removed following a two step extraction procedure.

Ti-MCM-41 was silylated with hexamethyldisilazane (HMDS) as the silylating agent. The silylated samples are referred to as Ti-MCM-41S. The silylation was carried out at 120 °C with a solution of HMDS in toluene under inert atmosphere.

The MCM-41 structure was preserved after silylation and the surface area of the silylated sample was close to 1000 $m^2\ g^{-1}$.

Samples with different levels of silylation were obtained by changing the HDMS/Ti-MCM-41 ratio as shown in Table 1. The carbon content, determined by elemental analysis, was used to calculate the degree of surface coverage (Table 1).

The catalytic activity of these materials was measured in the epoxidation reaction of cyclohexene with *tert*-butylhydroperoxide (TBHP) at 60 °C. The olefin/TBHP ratio was to 4 mol mol^{-1} and the liquid/catalyst ratio was 20 g g^{-1}.

The results shown in Fig. 1 clearly indicate that the catalyst activity and selectivity increase with the level of silylation and much higher conversions and selectivities than those reported up to now have been achieved in this work. It is of interest that relatively low levels of silylation significantly improve the catalyst selectivity to the epoxide, but that over the range of silylation there is very little influence on the catalytic conversion. On the other hand, a significant improvement in catalytic activity is observed when the silylation gives rise to a surface coverage of > 40%. In this case, the selectivity to the epoxide is close to 100%.

The hydrophobicity of Ti-MCM-41S materials was estimated from the weight loss of the fully hydrated sample at 150 °C. We found that there is a linear correlation between the hydrophobicity and the surface coverage with trimethylsilyl groups as shown in Fig. 2. Therefore, one can conclude from Figs. 1 and 2 that in order to obtain a highly active and selective catalyst for epoxidation it is necessary to silylate Ti-MCM-41 above 40% or preferably close to 100%.

Table 1 Silylation conditions and degree of silylation achieved on Ti-MCM-41 catalysts

Sample	Ti content (wt.% TiO_2)	HMDS/ sample	C content (wt.%)	Surface coverage[a] (%)
Ti-MCM-41	1.9	—	—	0
Ti-MCM-41S1	1.9	0.026	4.2	33
Ti-MCM-41S2	1.8	0.034	7.9	63
Ti-MCM-41S3	2.1	0.123	10.3	82
Ti-MCM-41S4	2.0	0.260	11.9	95

[a] The calculated surface coverage per trimethylsilyl group is 47.6 $Å^2$ $molecule^{-1}$.[17]

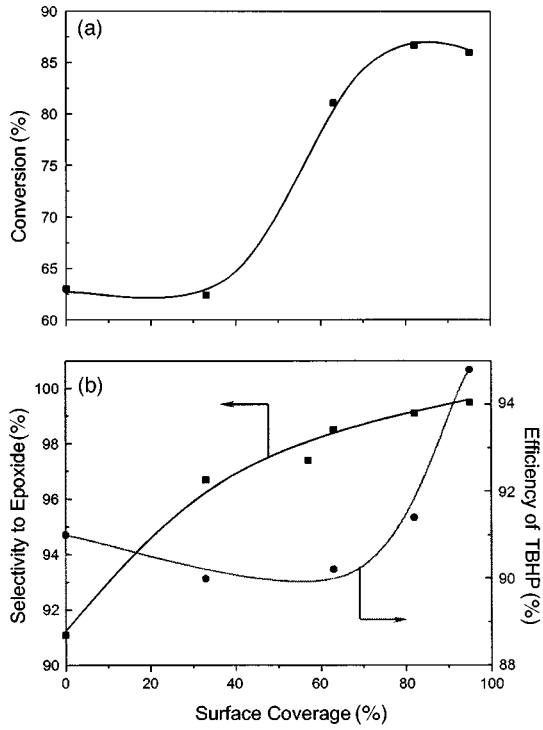

Fig. 1 Catalytic activity in the epoxidation of cyclohexene with TBHP of silylated Ti-MCM-41 at different degrees of surface coverage; (a) catalytic conversion after 30 min of reaction, (b) selectivity to epoxide and efficiency of TBHP at 85% cyclohexene conversion

Nevertheless, it was surprising to find that every hydrophobic Ti-MCM-41 catalysts were required in order to have highly active and selective epoxidation catalysts even when only organic reactants were used. This motivated us to analyze the amount of water contained in the reactants, and it was found by means of ^{1}H NMR that the TBHP contained 8 wt.% water. Then, we carried out the epoxidation of cyclohexene with TBHP which was dried using 4 Å molecular sieves. With ^{1}H NMR we determined that no decomposition of TBHP occurred and the remaining amount of water was below the detection limit of ^{1}H NMR. Under these conditions and using the non-silylated catalyst Ti-MCM-41, which contains 13.5 wt.% water adsorbed on the catalyst, the total conversion and selectivity to the epoxide obtained after 30 min of reaction were 85 and 97%, respectively. These results are very similar to those obtained with the completely silylated sample Ti-MCM-41S4 when using the as-received commercial TBHP.

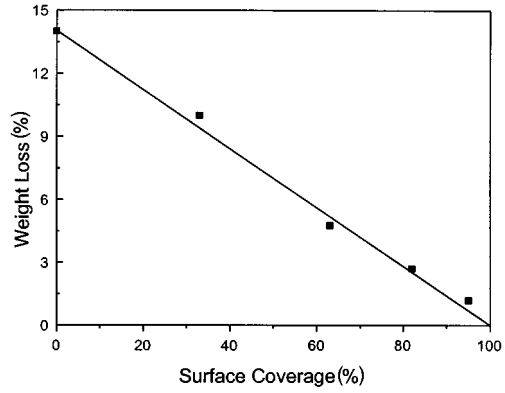

Fig. 2 Variation of the hydrophobicity, calculated as the weight loss at 150 °C by thermogravimetry, with the degree of silylation of Ti-MCM-41 catalysts

An additional experiment was carried out with dry TBHP and dry catalyst Ti-MCM-41. After 30 min the conversion was 91% and the selectivity was 100%. These results are the best conversion and selectivity to epoxide ever reported using Ti-based catalysts for epoxidation processes.

We conclude that the presence of water is responsible for the ring opening of the epoxide. However, its influence goes beyond the selectivity effect, since the diols resulting from the ring opening of the epoxide strongly decrease the catalytic conversion. We have seen this effect by performing the epoxidation reaction using dried TBHP, but adding 3.07 mmol of cyclohexanediol which corresponds to a typical amount of the diol formed during the catalytic experiments when non-dried TBHP is used. Under these conditions, the conversion is significantly reduced to 13% after 30 min of reaction. This result suggests that the increase in activity observed when using either silylated Ti-MCM-41 or non silylated Ti-MCM-41 with dry reactants is due to the significant decrease in the formation of diols which act as catalyst poisons for the Ti sites.

In conclusion we have presented two different strategies that can be used to obtain remarkably active and selective epoxidation catalysts based on Ti-MCM-41. The first strategy relies on the use of highly silylated samples and greater than 40% silylation coverage is required. In this case water can be present in the reaction media up to levels of 3 wt.%. On the other hand, one can use non-silylated catalysts, but in this case water must be removed from the reaction media.

It is also concluded in this work that the increase in activity observed with the silylated hydrophobic catalyst or with the absence of water in the reaction medium, is probably not due to a change of the intrinsic activity of the Ti catalytic sites but rather to a decrease in catalyst deactivation. An increase in catalyst stability is obtained by reducing the formation of diols that are produced by ring opening of the epoxide in the above conditions.

Financial support by the Spanish MAT97-1016-CO2-01 and MAT97-1207-CO3-01 is gratefully acknowledged. J. L. J. and M. D. thank the M.E.C. and M.E.A., respectively, for supporting their doctoral fellowships. M. T. N. thanks the CSIC for the postdoctoral grant. B. M. C. and L. T. N. acknowledge UOP for financial support.

Notes and References

1 M. Taramasso, G. Perego and B. Notari, *US Pat.*, 4 410 501, 1983.
2 M. A. Camblor, A. Corma, A. Martínez and J. Pérez-Pariente, *J. Chem. Soc., Chem. Commun.*, 1992, 589.
3 A. Corma, M. T. Navarro and J. Pérez-Pariente, *J. Chem. Soc., Chem. Commun.*, 1994, 197.
4 T. J. Pinnavaia and W. Zhang, *Stud. Surf. Sci. Catal.*, 1998, **117**, 23.
5 S. Gontier and A. Tuel, *J. Catal.*, 1995, **157**, 124.
6 A. Corma, M. T. Navarro, J. Pérez-Pariente and F. Sánchez, *Stud. Surf. Sci. Catal.*, 1995, **84**, 69.
7 T. Blasco, M. A. Camblor, A. Corma, P. Esteve, J. M. Guil, A. Martínez, J. A. Perdigón and S. Valencia, *J. Phys. Chem. B*, 1998, **102**, 75.
8 M. A. Camblor, A. Corma, P. Esteve, A. Martínez and S. Valencia, *Chem. Commun.*, 1997, 795.
9 H. P. Wulff, *US Pat.*, 3 923 843, 1975.
10 K. A. Koyano, T. Tastumi, Y. Tanaka and S. Nakata, *J. Phys. Chem.*, 1997, **101**, 9436.
11 S. L. Burkett, S. D. Simis and S. Mann, *Chem. Commun.*, 1996, 1367.
12 C. E. Fowler, S. L. Burkett and S. Mann, *Chem. Commun.*, 1997, 1769.
13 A. Corma, J. L. Jordá, M. T. Navarro and F. Rey, *Chem. Commun.*, 1998, 1899.
14 T. Tatsumi, K. A. Koyano and N. Igarashi, *Chem. Commun.*, 1998, 325.
15 T. Blasco, A. Corma, M. T. Navarro and J. Pérez-Pariente, *J. Catal.*, 1995, **156**, 65.
16 A. Corma, *Chem. Rev.*, 1997, **97**, 2373.
17 Insight II Molecular User Guide, San Diego, Biosym/MSI, 1995.

Received in Bath, UK, 20th August 1998; 8/06702C

Cyclodepolymerisation of bisphenol A polysulfone: evidence for self-complementarity in macrocyclic poly(ether sulfones)

Ian Baxter,[a] Abderrazak Ben-Haida,[b] Howard M. Colquhoun,*[c]† Philip Hodge,*[b]‡ Franz H. Kohnke[b]§ and David J. Williams*[a]¶

[a] *Department of Chemistry, Imperial College, South Kensington, London, UK SW7 2AY*
[b] *Department of Chemistry, University of Manchester, Manchester, UK M13 9PL*
[c] *Department of Chemistry, University of Salford, Salford, UK M5 4WT*

The engineering thermoplastic generally referred to as 'bisphenol A polysulfone' undergoes fluoride-promoted cyclodepolymerisation; high molar mass polymer is thus transformed into a series of macrocyclic oligomers containing up to at least 72 aromatic rings; those containing up to 24 rings have been isolated as pure compounds, and single-crystal X-ray studies of the cyclotrimer and cyclotetramer reveal shape-complementary pairs and chains of macrocyles, respectively.

Polycondensation reactions generally afford not only high molar mass linear polymers, but also (in amounts depending on reaction conditions) homologous series of macrocyclic oligomers.[1] As a result, significant quantities of cyclic materials are found in many important commercial polymers. Under equilibrium conditions, linear and cyclic species can interconvert *via* ring-opening polymerisation of macrocyclic oligomers and/or ring-closing depolymerisation (cyclodepolymerisation) of linear chains. Such interconversions have recently been demonstrated for polyesters,[2] polycarbonates,[3] and certain aromatic polyethers.[4] A theoretical framework for ring–chain equilibria in dilute solution has been developed by Mandolini and coworkers, indicating the existence of a threshold concentration below which *only* cyclic species should be present.[5]

Here we report that the high-performance engineering thermoplastic **1**, generally referred to as 'bisphenol A polysulfone' (formed by polycondensation of bisphenol A with 4,4′-dichlorodiphenyl sulfone, and trademarked as *Udel* by the Amoco Corporation and *Ultrason-S* by BASF) undergoes clean cyclodepolymerisation at high temperatures in the presence of fluoride ion. The polymer is transformed, *via* fluoride-promoted ether interchange reactions,[6] into a series of macrocyclic oligomers, ranging from the [2+2] cyclodimer to the [18+18] cyclooctadecamer (Scheme 1).

Heating a 0.5 wt% solution of bisphenol A polysulfone at reflux in DMA with 0.5 equiv. of CsF per polymer repeat unit leads to the disappearance of high molar mass polymer and formation (as evidenced by GPC and HPLC) of a well-defined series of oligomeric compounds.‖ Analysis of the isolated products by MALDI-TOF mass spectrometry (Fig. 1) demonstrates that the oligomers comprise exclusively *macrocyclic* species, with molar masses in the range *m/z* 906 (cyclodimer) to 7980 (cyclooctadecamer). Chromatographic fractionation yielded a series of pure, monodisperse oligomers from cyclodimer (**2**) to cyclohexamer, characterised by elemental analysis, ^{1}H and ^{13}C NMR spectroscopy, mass spectrometry and, in the cases of the cyclotrimer (**3**) and cyclotetramer (**4**), by single crystal X-ray diffraction.**

The cyclodimer (**2**), which crystallises spontaneously from solutions of the commercial polymer, has already been characterised in some detail;[7] the higher macrocycles were however previously unknown. The macrocyclic oligomers from cyclotrimer to cyclohexamer may be isolated as crystalline solvates from solvents such as $CHCl_3$ and CH_2Cl_2, but these

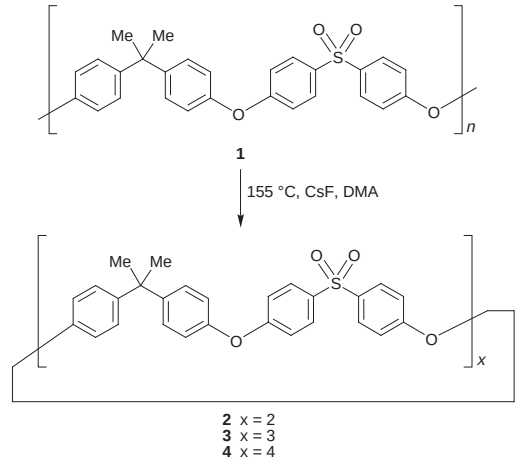

Scheme 1

readily lose solvent on heating to give amorphous, glassy materials. Single crystal X-ray analysis of the cyclotrimer **3**, as its MeCN solvate, shows the molecule to adopt a folded geometry, reminiscent of a tennis ball seam (Fig. 2). As with the cyclodimer,[7] the diphenyl sulfone units adopt 'open book' type conformations, while the diphenylisopropylidene rings are skewed. The diphenyl ether linkages on the other hand appear to be conformationally rather flexible, here adopting both near-orthogonal *and* skewed geometries.

Remarkably, it appears that centrosymmetrically-related pairs of cyclotrimers have self-complementary surfaces, since these interact in the solid state to create supramolecular 'dimers' as shown in Fig. 3. Isopropylidene groups centred on C(71) mutually insert through the loops of complementary oligomer chains between O(8) and S(57). Residual clefts in the surface of the dimer are populated by included MeCN solvent molecules. Dimer stabilisation appears to be achieved through a combination of electronically-complementary face-to-face π-stacking

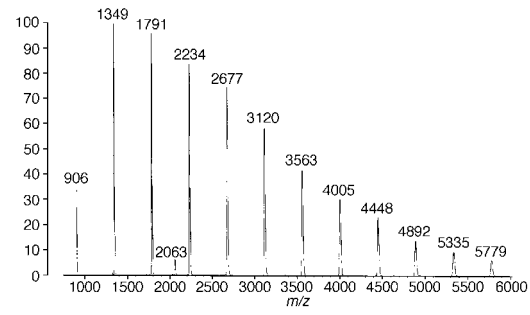

Fig. 1 Partial MALDI-TOF mass spectrum of the macrocyclic products (M + Na^+) formed by cyclodepolymerisation of bisphenol A polysulfone (the small peak at *m/z* 2063 is due to an impurity in the dithranol matrix.)

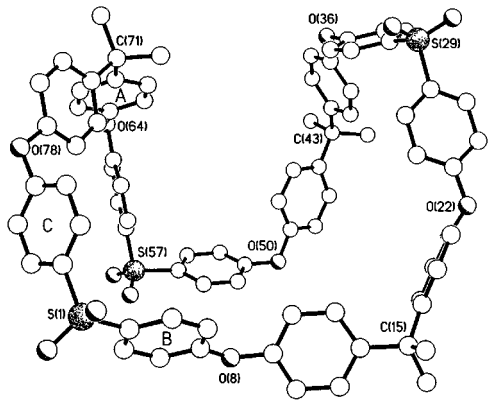

Fig. 2 Structure of **3**, illustrating the tennis ball seam-like conformation adopted in the solid state. Ring torsion angles relative to the plane of the C–X–C bridge (X = S, C, or O) are: at S(1), 86 and 86°; at S(29), 85 and 81°; at S(57), 84 and 79°; at C(15), 76 and 19°; at C(43), 62 and 31°; at C(71), 49 and 46°; at O(8), 79 and 7°; at O(22), 64 and 13°; at O(36), 73 and 4°; at O(50), 60 and 29°; at O(64), 85 and 3°; at O(78), 74 and 28°.

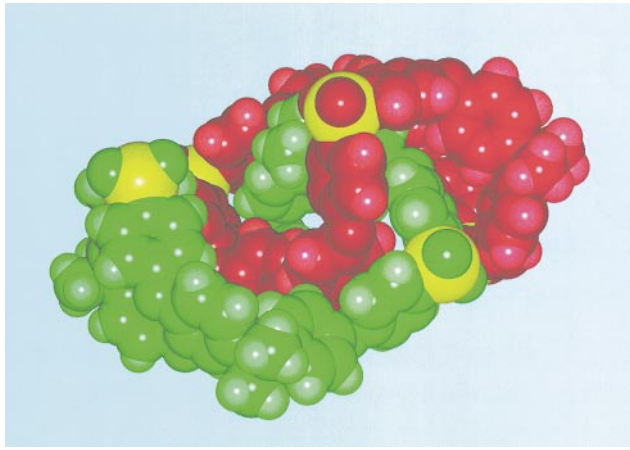

Fig. 3 Space-filling representation of **3**, showing the mutual interpenetration of enantiomeric macrocycles. The centroid···centroid and mean interplanar spacings between rings 'A' and 'B' in centrosymmetrically related molecules of the cyclotrimer are 3.96 and 3.57 Å respectively; the H··π distance and C–H··π angle are 2.71 Å and 175°, respectively; and the H···centroid vector is inclined by 82° to the 'C' ring plane.

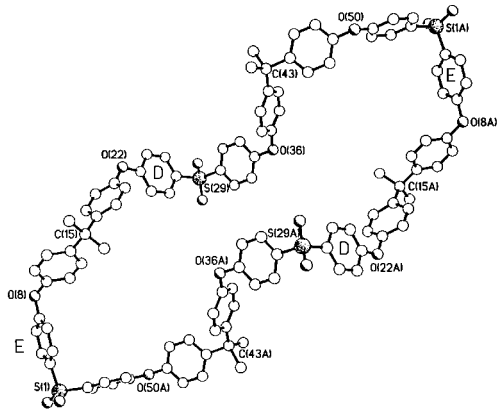

Fig. 4 Structure of **4**. Ring torsion angles relative to the plane of the C–X–C bridge (X = S, C, or O) are: at S(1), 89 and 84°; at S(29), 89 and 76°; at C(15), 57 and 26°; at C(43), 62 and 34°; at O(8), 70 and 27°; at O(22), 76 and 1°; at O(36), 79 and 33°; at O(50), 79 and 2°.

between ring 'A' of one molecule and ring 'B' of another, as well as a C–H··π interaction between the *ortho*-hydrogen *syn* to O(64) and the 'C' ring of an adjacent molecule.

The X-ray structure of the cyclo-tetramer **4** (Fig. 4) shows it to possess crystallographic inversion symmetry. The individual conformational features closely resemble those of the cyclotrimer and generate an elongated macrocycle, of approximately 33.6 × 15.5 Å, containing two distinct cavities. Again there is significant interpenetration of the isopropylidene unit of one macrocycle into the cavity of an adjacent molecule but here, instead of generating isolated pairs of cyclic oligomers, continuous chains of intertwined macrocycles are created.

A valuable new approach to the structural characterisation of non-crystalline polymers emerges from the present work, as it is becoming clear that even *very large* cyclic oligomers of such materials, *when monodisperse*, can afford single crystals of a size and morphology suitable for X-ray analysis. The position is somewhat analogous to that in protein crystallography, where macromolecules are monodisperse for genetic reasons and where strong intramolecular interactions lead to the adoption of compact conformations, allowing macroscopic single crystals to be obtained.

We wish to thank Mr P. R. Ashton of the University of Birmingham for the MALDI-TOF mass spectrometric analysis, and the EPSRC for financial support.

Notes and references

† E-mail: h.m.colquhoun@chemistry.salford.ac.uk
‡ E-mail: philip.hodge@man.ac.uk
§ On leave from the Department Of Organic and Biological Chemistry, University of Messina, I–98166, Messina, Italy.
¶ E-mail: djw@ic.ac.uk

‖ Fractionation of the recovered solid by gradient chromatography on silica (CH_2Cl_2–trichloroethene–EtOAc) afforded the cyclodimer **2** (6%), cyclotrimer **3** (6.5%), cyclotetramer **4** (5.5%), cyclopentamer (4.5%) and cyclohexamer (2.5% yield). Satisfactory elemental analyses, NMR and mass spectra have been obtained. MALDI-TOF mass spectrometry used 1,8,9-trihydroxyanthracene as matrix and sodium trifluoroacetate as cationising agent. Solvated single crystals of **3** and **4** were obtained by slow evaporation of solutions in $CHCl_3$–MeCN and benzene–MeOH respectively.

** *Crystal data* for **3**: $C_{81}H_{66}O_{12}S_3 \cdot 4MeCN$, M_r = 1491.73, triclinic, space group *P*1, a = 14.608(2), b = 16.356(1), c = 17.368 (1) Å, α = 89.17(1), β = 85.49(1), γ = 67.60(1)°, V = 3823.8(7) Å^3, T = 183 K, Z = 2, D_o = 1.296 g cm^{-3}, μ(Cu-Kα) = 14.28 cm^{-1}, F(000) = 1712. R_1 = 0.050, wR_2 = 0.126 for 9088 independent observed reflections [$2\theta \leqslant 120°$, $I > 2\sigma(I)$]. For **4**: $C_{108}H_{88}O_{16}S_4 \cdot 6.6C_6H_6 \cdot 1.4MeOH$, M_r = 2330.40, triclinic, space group *P*1, a = 10.541(1), b = 15.432(1), c = 21.602 (1) Å, α = 105.10(1), β = 91.03(1), γ = 109.71(1)°, V = 3172.2(4) Å^3, T = 203 K, Z = 1, D_o = 1.220 g cm^{-3}, μ(Cu-Kα) = 12.18 mm^{-1}, F (000) = 1230. R_1 = 0.083, wR_2 = 0.206 for 5470 independent observed reflections [$2\theta \leqslant 124°$, $I > 2\sigma(I)$]. Data for both compounds were measured on a Siemens P4/RA diffractometer with graphite-monochromated Cu-Kα radiation using ω-scans. Both sets of data were corrected for Lorentz and polarisation effects, and semi-empirical absorption corrections (from ψ-scans) were applied. The structures were solved by direct methods and non-hydrogen atoms were refined anisotropically using the SHELXTL program package. CCDC 182/992.

1 H. Jacobson and W. H. Stockmeyer, *J. Chem. Phys.*, 1950, **18**, 1600. Recent reviews: D. J. Brunelle, in *New Methods of Polymer Synthesis*, ed. J. R. Ebdon and G. C. Eastmond, Blackie, London, 1995, p. 197; Y. F. Wang, K. P. Chan and A. S. Hay, *React. Funct. Polyms.*, 1996, **30**, 205; P. Hodge, H. M. Colquhoun and D.J. Williams, *Chem. Ind.* (*London*), 1998, 162.
2 B. R. Wood, J. A. Semlyen and P. Hodge, *Polymer*, 1997, **38**, 191.
3 H. O. Krabbenhoft, D. J. Brunelle and E. J. Pearce, *J. Appl. Polym. Sci.*, 1997, **66**, 2251.
4 A. Ben-Haida, I. Baxter, H. M. Colquhoun, P. Hodge, F. H. Kohnke and D. J. Williams, *Chem. Commun.*, 1997, 1533.
5 G. Ercolani, L. Mandolini, P. Mencarelli and S. Roelens, *J. Am. Chem. Soc.*, 1993, **115**, 3901.
6 T. E. Attwood, A. B. Newton, and J. B. Rose, *Br. Polym. J.*, 1972, **4**, 391.
7 H. M. Colquhoun and D. J. Williams, *Macromolecules*, 1996, **29**, 3311.

Received in Cambridge, UK, 17th July 1998; 8/05556D

Effective biocatalytic transgalactosylation in a supercritical fluid using a lipid-coated enzyme

Toshiaki Mori and Yoshio Okahata*†

Department of Biomolecular Engineering, Tokyo Institute of Technology, Nagatsuda, Midori-ku, Yokohama 226-8501, Japan

A lipid-coated β-D-galactosidase is soluble and acts as an efficient trangalactosylation catalyst (the reverse hydrolysis reaction) in supercritical carbon dioxide ($scCO_2$).

Supercritical fluids (scFs) have become attractive as media for chemical reactions, as well as for extraction and chromatography, in the last decade;[1] their physical properties can be manipulated by small changes in pressure or temperature, and several of these properties (*e.g.* density, diffusion and viscosity) are intermediate between those of gases and liquids.[2] The larger diffusion rate in a scF compared to a liquid can be expected to increase the reaction rate.

Several organic reactions in scF have been achieved using homogeneously soluble organometallic complexes as catalysts.[3] Application of scFs for enzymatic reactions has also been reported using immobilized enzymes, as well as native enzymes.[4] However, since the immobilized and native enzymes are not soluble or particularly not stable in scFs, results comparable to those found in aqueous or organic solvents have not been obtained.[4] We have reported that the lipid-coated enzymes such as lipases,[5] phospholipases[6] and glycosidases[7] are soluble in most organic solvents and can catalyze reverse hydrolysis reactions such as esterification and transglycosylation in homogeneous organic media. We expected that lipid-coated enzymes would be homogeneously soluble in scFs as well as organic media, and would show efficient catalytic activity due to the high diffusion rates and the low viscosity found in scFs.

Here we report the high catalytic activity of transgalactosylation using a lipid-coated β-D-galactosidase in supercritical carbon dioxide ($scCO_2$). The reasons carbon dioxide was chosen as the scF are as follows: (i) CO_2 becomes a scF above 31.0 °C and 73.8 atm, conditions which are easily accomplished with gentle heating from ambient temperature and a commercial liquid chromatography pump, (ii) the solvent properties of $scCO_2$ can be continuously varied by changing the pressure or temperature, and (iii) CO_2 is non-toxic and the medium is easily removed by decompression to atmospheric pressure.

A lipid-coated β-D-galactosidase (from *Bacillus circulans*) was prepared by mixing aqueous solutions of enzyme and lipid molecules in the same way as reported previously.[5–7] It was confirmed from elemental analysis, UV absorption, and gel chromatography in CH_2Cl_2 that one enzyme is covered by about 200 ± 50 lipid molecules as a monolayer and that the protein content in the complex is 7 ± 1 wt%.[5–7] The lipid-coated enzyme was also found to be soluble (*ca.* 0.1 mg ml^{-1}) in $scCO_2$ in the range of 32–60 °C and 74–200 atm, by the observation using a pressure-resistant glass vessel (Taiatsu Techno, Co., Tokyo, volume: 10 ml), but not very soluble in liquid CO_2 (at 20 °C and 100 atm) and insoluble in gaseous CO_2 (at 40 °C and 40 atm).

Transgalactosylation reactions were carried out as follows. In a stainless steel or pressure-resistant glass vessel, both the substrates (1-*O*-*p*-nitrophenyl-β-D-galactopyranoside and 5-phenylpentan-1-ol) and a lipid-coated β-D-galactosidase were added, then liquid CO_2 was injected at 100–150 atm using a LC pump (Jasco PU-980 HPLC pump) connected to a CO_2 gas cylinder. The vessel was warmed with magnetic stirring above 40 °C to create the supercritical state, and the pressure was kept constant (±0.1 atm) by a back pressure regulator (JASCO 880–81). At the appointed time, the vessel was degassed carefully under cooling at 0 °C. The residual powder was solubilized in MeCN and analyzed by a HPLC.

Fig. 1 shows typical time courses of the transgalactosylation from 1-*O*-*p*-nitrophenyl-β-D-galactopyranoside (0.1 mM) to 5-phenylpentan-1-ol (1.0 mM) catalyzed by a lipid-coated β-D-galactosidase at 40 °C both in $scCO_2$ at 150 atm and in isopropyl ether at atmospheric pressure. In $scCO_2$, 1-*O*-(5-phenylpentyl)-β-D-galactopyranoside was obtained as the only transgalactosylated product in 72% yield after 3 h, at which point the reaction reached equilibrium. We have reported that the lipid-coated β-D-galactosidase can catalyze the same transgalactosylation in conventional organic solvents such as isopropyl ether.[7] The transgalactosylation in $scCO_2$ was 15-fold faster than in isopropyl ether. In this case, both the enzyme and the substrate

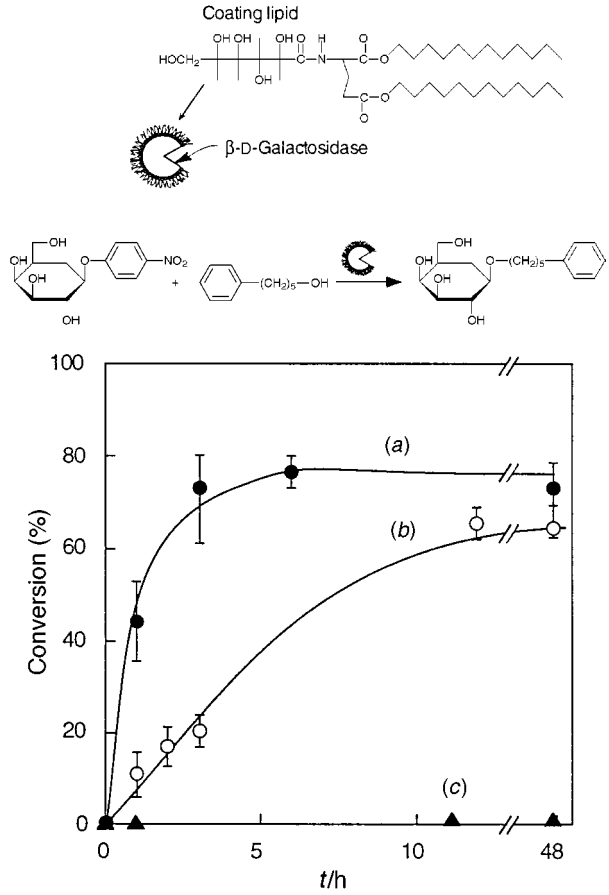

Fig. 1 A schematic illustration of a lipid-coated β-D-galactosidase and time-courses of transgalactosylation from 1-*O*-*p*-nitrophenyl-β-D-galactopyranoside (0.1 mM) to 5-phenylpentan-1-ol (1 mM) at 40 °C catalyzed by β-D-galactosidase (1 mg of protein) in 10 ml: (*a*) a lipid-coated enzyme in $scCO_2$ with 150 atm, (*b*) a lipid-coated enzyme in isopropyl ether, and (*c*) a native enzyme in $scCO_2$ with 150 atm

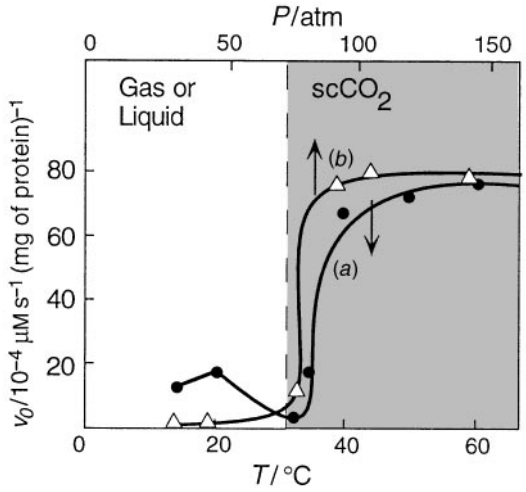

Fig. 2 Effect of (*a*) changing temperature at 150 atm and (*b*) changing pressure at 40 °C on the initial rate of transgalactosylation

were soluble in $scCO_2$, so the increase in the rate may be due to a decrease in the degree of solvation of the substrate. Transgalactosylations also occurred rapidly with acceptor alcohols having large alkyl groups, such as 1,2-*O*-bis(dodecyl)glycerol (conversion 45%) and cholesterol (conversion 15%).

When a lipid-coated lipase (from *Rhizopus delemar*) was prepared and applied as an esterification catalyst for monolaurin and lauric acid, the esterification rate increased 10-fold in $scCO_2$ over that in atmospheric isooctane (data not shown).[8] Although several studies on enzyme reactions in $scCO_2$ using native or immobilized enzymes have been performed, an improvement of reactivity over the reaction in atmospheric liquid media has not been reported.[4] Actually, the native β-D-galactosidase was observed to hardly catalyze the transglycosylation in $scCO_2$, as shown in Fig. 1(*c*). This is due to the insolubility and instability of native enzymes in $scCO_2$.

FT-IR spectra usually provide information about secondary structures, such as the content of α-helix and β-sheet domains in proteins.[9] FT-IR spectra were taken of the lipid-coated β-D-galactosidase in $scCO_2$[10] and a native β-D-galactosidase in D_2O solution. It was indicated from the peak strength of the amide I band at 1600–1700 cm^{-1} that the content of α-helix (21%) and β-sheet (26%) structures of the lipid-coated enzyme in $scCO_2$ agreed reasonably well with those (α-helix: 19%; β-sheet: 30%) of a native enzyme in D_2O solution. Thus, the structure of the lipid-coated enzyme in $scCO_2$ is not significantly changed from that in aqueous buffer solution.

One of the advantages of scFs as reaction media is that their physicochemical properties, such as diffusiion rate, density, polarity and viscosity, can be continuously changed by varying the temperature or pressure of the $scCO_2$ state.[2] The effects of changing temperature and pressure on the initial rates of the transgalactosylation catalyzed by a lipid-coated enzyme are shown in Fig. 2.[11] When the temperature was changed at a constant pressure of 150 atm [Fig. 2(*a*)], galactosylations were very slow below 31 °C, where the medium exists as liquid CO_2 and the lipid-coated enzyme is barely solubilized. The reactivity increased above 31 °C, where the lipid-coated enzyme is solubilized. Since the enzyme activity in aqueous buffer solution increased gradually with increasing temperature from 20 to 60 °C, this activity change depending on temperature is explained by the special physical property changes of $scCO_2$. A similar tendency was observed when the pressure was changed from 50 to 150 atm at 40 °C [Fig. 2(*b*)]. Gaseous CO_2 could not solubilize the lipid-coated enzyme below 72.9 atm (the critical pressure) and the enzyme activity drastically increased in $scCO_2$ depending on the pressure. When the temperature and pressure were changed repeatedly in the region in Fig. 2, the enzyme activity could be controlled reversibly over at least 10 cycles.

In conclusion, lipid-coated enzymes such as β-D-galactosidase and lipase are soluble and can catalyze transgalactosylation and esterification in supercritical CO_2. The enzyme activity was 10–15 times larger than that in conventional organic media. We could switch the enzyme activity on and off by adjusting the pressure or temperature of the CO_2 media across or within the $scCO_2$. In addition, compared with organic solvents $scCO_2$ is non-toxic and easily removed by decompression to atmospheric pressure, and thus is suitable for the biotransformation of food products and drugs. We believe that the combination of a lipid-coated enzyme and a $scCO_2$ reaction medium will form a versatile new system for biotransformation studies.

Notes and References

† E-mail: yokahata@bio.titech.ac.jp

1 A. A. Clifford, *Supercritical Fluids, Fundamentals for Applications, NATO ASI Ser. E*, Kluwer Academic, Netherlands, 1994, vol. 273, pp. 449–479.
2 S. Angus, B. Armstrong and K. M. de Reuck, *Carbon Dioxide, International Thermodynamic Tables of the Fluid State*, 3rd edn., Pergamon, New York, 1976, pp. 13–23.
3 P. G. Jessop, T. Ikariya and R. Noyori, *Nature*, 1994, **368**, 231.
4 K. Nakamura, Y. M. Chi, Y. Yamada and T. Yano, *Chem. Eng. Commun*., 1986, **45**, 207; J. C. Erickson, P. Schyns and C. L. Cooney, *AIChE J*., 1990, **36**, 299; S. V. Kamat, B. Iwaskewycz, E. J. Beckman and A. J. Russell, *Proc. Natl. Acad. Sci. U.S.A*., 1993, **90**, 2940; Y. Ikushima, N. Saito, T. Yokoyama, K. Hatakeda, S. Ito, M. Arai and H. W. Blanch, *Chem. Lett*., 1993, 109.
5 Y. Okahata, Y. Fujimoto and K. Ijiro, *J. Org. Chem*., 1995, **60**, 2244.
6 Y. Okahata, K. Niikura and K. Ijiro, *J. Chem. Soc*., *Perkin Trans. 1*, 1995, 919.
7 T. Mori, S. Fujita and Y. Okahata, *Carbohydr. Res*., 1997, **298**, 65.
8 T. Mori, A. Kobayashi and Y. Okahata, *Chem. Lett*., 1998, 921.
9 K. Griebenow and A. M. Klibanov, *J. Am. Chem. Soc*., 1996, **118**, 11 695.
10 The FT-IR spectrum in $scCO_2$ fluid was recorded in a special stainless steel vessel with ZnSe windows.
11 A phase diagram for CO_2 is available on the RSC's web server, http://www.rsc.org/suppdata/cc/1998/2215

Received in Cambridge, UK, 5th August 1998; 8/06168H

Si–O–based inorganic ring systems containing f-elements: structural characterization of novel siloxanediolates of the lanthanides and actinides†

Volker Lorenz,[a] Axel Fischer,[a] Klaus Jacob,[b] Wolfgang Brüser,[a] Thomas Gelbrich,[c] Peter G. Jones[d] and Frank T. Edelmann*[a]

[a] *Chemisches Institut, Otto-von-Guericke-Universität Magdeburg, Universitätsplatz 2, D-39106 Magdeburg, Germany. E-mail: Frank.Edelmann@Chemie.Uni-Magdeburg.de*
[b] *Institut für Anorganische Chemie, Martin-Luther-Universität Halle-Wittenberg, Geusaer Str., D-06217 Merseburg, Germany*
[c] *Institut für Anorganische Chemie, Universität Leipzig, Linnestr. 3, D-04103 Leipzig, Germany*
[d] *Institut für Anorganische und Analytische Chemie, Technische Universität Braunschweig, Postfach 3329, D-38023 Braunschweig, Germany*

Depending on the reaction conditions and the ionic radius of the lanthanide ion, tetraphenyldisiloxanediol, $(Ph_2SiOH)_2O$, reacts with $[Ln\{N(SiMe_3)_2\}_3\{LiCl(thf)_3\}_3]$ (Ln = Eu, Gd, Sm) to afford novel heterobimetallic rare earth disiloxanediolates, some of which can be regarded as 'inorganic lanthanide metallocenes'; a ring expanded uranium(VI) derivative, $[U\{Ph_2Si(OSiPh_2O)_2\}_2\{(Ph_2SiO)_2O\}]$ 4, is formed upon treatment of uranocene, $[U(\eta^8\text{-}C_8H_8)_2]$, with $(Ph_2SiOH)_2O$.

The chemistry of metallasiloxanes derived from silanediols, disiloxanediols and related Si–OH species is an area of active research[1] because such compounds are valuable precursors for metal oxides and silicates[2,3] as well as models for silica-supported heterogeneous catalysts.[1,4,5] A particularly useful ligand is the tetraphenyldisiloxanediolate dianion, $[(Ph_2SiO)_2O]^{2-}$, which gives rise to a variety of unusual and unexpected structures especially when combined with alkali metals[6] and early transition metals.[2b,6,7] Apparently this ligand has not yet been employed in f-element chemistry, with $[(C_5Me_5)_2Sm(thf)(\mu\text{-}OSiMe_2OSiMe_2O)Sm(C_5Me_5)_2(thf)]$[8] being the only closely related rare earth siloxane derivative. We report here the synthesis of novel lanthanide and uranium complexes derived from $[(Ph_2SiO)_2O]^{2-}$.

Treatment of $[Ln\{N(SiMe_3)_2\}_3\{LiCl(thf)_3\}_3]$ (Ln = Eu, Gd, Sm) (prepared from $LnCl_3$ and 3 equiv. of $LiN(SiMe_3)_2$ in thf solution[9]) with $(Ph_2SiOH)_2O$[10] in different stoichiometries afforded the new lanthanide disiloxanediolates **1**–**3** (Scheme 1). The use of *in situ* prepared lanthanide silylamide reagents in order to maintain the necessary high Li ion concentration is essential for the success of the preparations. The colorless crystalline solids have been fully characterized by elemental analyses, spectroscopic data and X-ray crystallography.§

The X-ray structure of **1** (Fig. 1) shows a heterobimetallic metallasiloxane, in which the central Eu ion is octahedrally surrounded by three mono-anionic chelating $(Et_2O)Li\{Ph_2SiO)_2O\}^-$ units.

The molecular structures of **2** and **3** (Figs. 2 and 3) are especially remarkable. Both complexes are disubstituted lanthanide metallasiloxanes comprising two lithium disiloxanediolate ligands while retaining one functional ligand [Cl or $N(SiMe_3)_2$, respectively]. The latter should make these compounds susceptible for further reactions. It is noteworthy that the outcome of these preparations depends not only on the stoichiometry but also on the size of the Ln^{3+} ion (Gd *vs.* Sm). In each case the coordination sphere of lithium is completed by addition of solvent molecules. The most striking feature of the gadolinium and samarium complexes, however, is their similarity with certain lanthanide metallocenes such as $(C_5Me_5)_2LnN(SiMe_3)_2$[11] (*cf.* **2**) or $(C_5Me_5)_2LnCl(thf)$[12] (*cf.* **3**). There is only one other report on Li-containing anionic ligands formally replacing the cyclopentadienyls in lanthanide metallocenes, *i.e.* the $[(dad)Li]^-$ units (dad = 1,4-diazadiene dianion).[13] It can be anticipated that the lithium disiloxanediolate units in the 'inorganic lanthanide metallocenes' **1**–**3** are quite robust spectator ligands owing to the presence of only Ln–O bonds.

For the synthesis of a related uranium cyclometallasiloxane the long-known sandwich complex uranocene, $[U(\eta^8\text{-}C_8H_8)_2]$,[14] was chosen as soluble starting material. Replacement of both cyclooctatetraenyl ligands upon treatment with an excess of $[(Ph_2SiOH)_2O]$ (an unprecedented reaction pathway

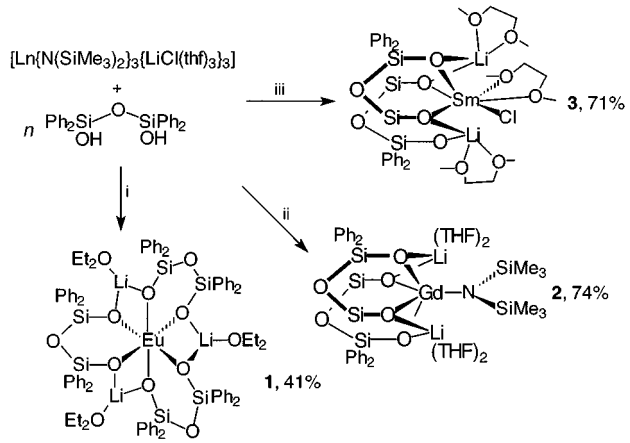

Scheme 1 Synthesis of complexes **1**–**3**. *Reagents and conditions*: i, Ln = Eu, n = 3, toluene–Et_2O; ii, Ln = Gd, n = 2, thf; iii, Ln = Sm, n = 2, DME (four phenyl groups in **2** and **3** have been omitted for clarity).

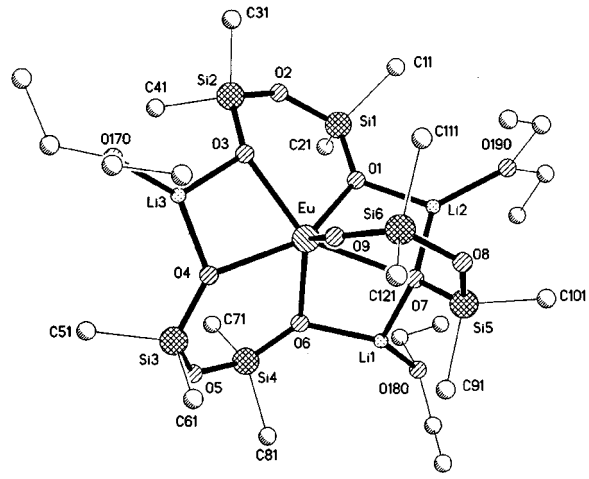

Fig. 1 Molecular structure of complex **1**

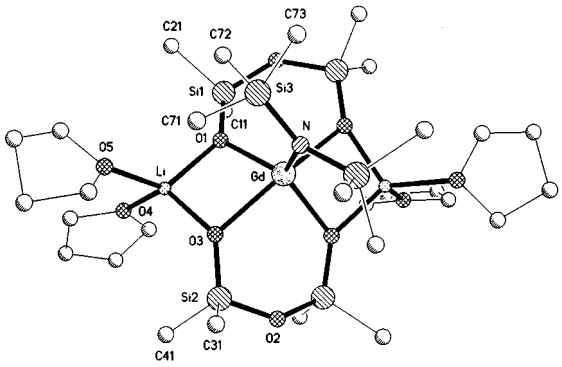

Fig. 2 Molecular structure of complex **2**

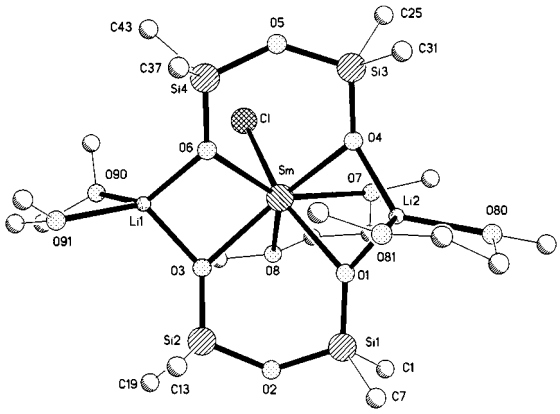

Fig. 3 Molecular structure of complex **3**

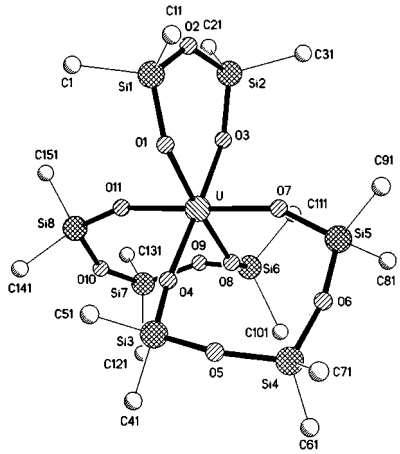

Fig. 4 Molecular structure of complex **4**

for uranocene) resulted in the formation of colorless [U{Ph_2-Si($OSiPh_2O$)$_2$}$_2${(Ph_2SiO)$_2$O}] **4** in 80% yield.

An X-ray structure analysis (Fig. 4) revealed the presence of a hexacoordinated uranium(VI) cyclometallasiloxane containing expanded trisiloxanediolate chelating ligands. This type of ring expansion has been reported earlier and studied in detail by Sullivan and coworkers.[7c] However, compound **4** represents the first example of a mixed-ligand complex containing both the ring expanded ligand and the original tetraphenyldisiloxanediolate dianion.

We conclude that siloxanediolate ligands derived from ($Ph_2SiOH)_2O$ are interesting new spectator ligands for f-elements which in the case of the lanthanides make inorganic analogues of synthetically useful lanthanide metallocenes available.

We thank the Deutsche Forschungsgemeinschaft (Schwerpunktprogramm Siliciumchemie) and the Otto-von-Guericke-Universität Magdeburg for financial support.

Notes and References

† Dedicated to Professor Michael F. Lappert, as a mark of friendship and respect, on the occasion of his 70th birthday.

§ Crystal data: The measurements on **1**, **3** and **4** were performed at −100 °C using a Siemens SMART CCD diffractometer with Mo-Kα X-radiation (λ = 0.710 73 Å). The data on **2** were collected on a Siemens P4 diffractometer at −100 °C.

1: $C_{84}H_{90}EuLi_3O_{12}Si_6$, M = 1632.88, triclinic, space group $P\bar{1}$, a = 13.6639(2), b = 14.5015(2), c = 24.234(2) Å, α = 83.541(2), β = 86.713(2), γ = 61.980(2)°, U = 4222.28(7) Å^3, Z = 2, D_c = 1.284 Mg m^{-3}, F(000) = 1692, μ(Mo-Kα) = 0.885 mm^{-1}. 51 321 reflections, of which 20 536 were independent (R_{int} = 0.039). $R1$ = 0.0394 (conventional) and $wR2$ = 0.0939 (all data), with goodness of fit = 1.065 (SHELXTL software.[15]

2: $C_{70}H_{90}GdLi_2NO_{10}Si_6$, M = 1445.10, monoclinic, space group $C2/c$, a = 22.2584(12), b = 14.4469(8), c = 23.486(2) Å, β = 106.427(6)°, U = 7244.0(7) Å^3, Z = 4, D_c = 1.325 Mg m^{-3}, F(000) = 3004, μ (Mo-Kα) = 1.070 mm^{-1}. 13 420 reflections, of which 6377 were independent (R_{int} = 0.035). $R1$ = 0.0295 (conventional) and $wR2$ = 0.0726 (all data), with goodness of fit = 0.980 (SHELXTL software).[15]

3: $C_{60}H_{70}ClLi_2O_{12}Si_4Sm$, M = 1295.20, monoclinic, space group $P2_1/c$, a = 17.34960(10), b = 17.3002(2), c = 21.2440(3) Å, β = 98.133(1)°, U = 6312.29(12) Å^3, Z = 4, D_c = 1.363 Mg m^{-3}, F(000) = 2668, μ(Mo-Kα) = 1.106 mm^{-1}. 36 094 reflections, of which 12 814 were independent (R_{int} = 0.040). $R1$ = 0.0564 (conventional) and $wR2$ = 0.1450 (all data), with goodness of fit = 1.118 (SHELXTL software).[15]

4: $C_{106}H_{106}N_2O_{12}Si_8U$, M = 2062.68, monoclinic, space group Cc, a = 25.0349(5), b = 14.6569(2), c = 29.4351(5) Å, β = 109.869(1)°, U = 10157.8(3) Å^3, Z = 4, D_c = 1.349 Mg m^{-3}, F(000) = 4224, μ(Mo-Kα) = 1.752 mm^{-1}. 34 298 reflections, of which 16 973 were independent (R_{int} = 0.023). $R1$ = 0.0258 (conventional) and $wR2$ = 0.0597 (all data), with goodness of fit = 1.07 (SHELXTL software).[15] CCDC 182/998.

1 R. Murugavel, A. Voigt, M. G. Walawalkar and H. W. Roesky, *Chem. Rev.*, 1996, **96**, 2205.

2 (*a*) F. Chaput, A. Lecomte, A. Dauger and J. P. Boilot, *J. Mater. Chem.*, 1989, **8**, 1001; (*b*) M. Lazell, M. Motevalli, S. A. A. Shah and A. C. Sullivan, *J. Chem. Soc., Dalton Trans.*, 1997, 3363.

3 A. R. Barron, C. C. Landry, L. K. Cheatham and A. N. MacInnes, *J. Mater. Chem.*, 1991, **10**, 143.

4 Y. I. Yermakov, B. N. Kuznetsov and V. A. Zakharov, *Catalysis by Supported Complexes*, Elsevier, New York, 1981; F. R. Hartley, *Supported Metal Complexes*, Reidel, Boston, 1985; *Tailored Metal Catalysts*, ed. Y. Iwasawa, Reidel, Boston, 1986.

5 F. J. Feher and T. A. Budzichowski, *Polyhedron*, 1995, **14**, 3239; F. T. Edelmann, *Angew. Chem.*, 1992, **104**, 600; *Angew. Chem., Int. Ed. Engl.*, 1992, **31**, 586.

6 M. Motevalli, D. Shah and A. C. Sullivan, *J. Chem. Soc., Dalton Trans.*, 1993, 1849; M. B. Hursthouse, M. A. Hossain, M. Motevalli, M. Sanganee and A. C. Sullivan, *J. Organomet. Chem.*, 1990, **381**, 293; M. Motevalli, D. Shah and A. C. Sullivan, *J. Organomet. Chem.*, 1996, **513**, 239.

7 (*a*) M. A. Hossain, M. B. Hursthouse, A. Ibrahim, M. Mazid and A. C. Sullivan, *J. Chem. Soc., Dalton Trans.*, 1989, 1347; (*b*) M. Motevalli, D. Shah, S. A. A. Shah and A. C. Sullivan, *J. Chem. Soc., Chem. Commun.*, 1994, 2427; (*c*) M. Lazell, M. Motevalli, S. A. A. Shah, C. K. S. Simon and A. C. Sullivan, *J. Chem. Soc., Dalton Trans.*, 1996, 1449.

8 W. J. Evans, T. A. Ulibarri and J. W. Ziller, *Organometallics*, 1991, **10**, 134.

9 D. C. Bradley, J. S. Gothra and F. A. Hart, *J. Chem. Soc., Dalton Trans.*, 1973, 1021.

10 G. I. Harris, *J. Chem. Soc.*, 1963, 5978.

11 K. den Haan, L. L. de Boer, J. H. Teuben, A. L. Spek, B. Kojic-Prodic, G. R. Hays and R. Huis, *Organometallics*, 1986, **5**, 1726; W. J. Evans, R. A. Keyer and J. W. Ziller, *Organometallics*, 1993, **12**, 2618.

12 R. G. Finke, S. R. Keenan, D. F. A. Schiraldi and P. L. Watson, *Organometallics*, 1987, **6**, 1356; H. Yasuda, H. Yamamoto, K. Yokota and A. Nakamura, *Chem. Lett.*, 1989, 1309.

13 H. Görls, B. Neumüller, A. Scholz and J. Scholz, *Angew. Chem.*, 1995, **107**, 732; *Angew. Chem., Int. Ed. Engl.*, 1995, **34**, 673.

14 A. Streitwieser, Jr. and U. Müller-Westerhoff, *J. Am. Chem. Soc.*, 1968, **90**, 7364.

15 G. M. Sheldrick, SHELXTL, Structure Determination Software Programs, Version 5.03 (PC), Siemens Analytical X-Ray Instruments, Madison, WI, 1995.

Received in Cambridge, UK, 2nd July 1998; 8/05095C

Infinite linear chains of Sb atoms in the novel metal-rich polyantimonides $Zr_{7.5}V_{5.5}Sb_{10}$ and $Zr_{6.5}V_{6.5}Sb_{10}$

Holger Kleinke*

FB Chemie, Philipps-Universität Marburg, D-35032 Marburg, Germany. E-mail: kleinke@mailer.uni-marburg.de

The structures of the title compounds exhibit short Sb–Sb bonds besides a multitude of bonding M–M interactions, *i.e.* the M atoms (Zr and V) in low valent states.

Partial electron transfer from the anionic to the cationic component has been used for a variety of so-called '*chimie-douce*' reactions.[1] Whereas the distances between the tellurium atoms decrease in the structures of the ditellurides from $ZrTe_2$ to $PdTe_2$ with increasing electronegativity of the metal atoms, the systematics of the Sb–Sb distances of the monoantimonides is less clear.

No Sb–Sb contacts < 350 pm occur in the structures of many monoantimonides of valence-electron poor transition metals like ScSb[2] and YSb[3] (both NaCl type), TiSb,[4] VSb[5] and NbSb[6] (all NiAs type). This may be considered as a hint to completely reduced Sb(-III). On the other hand, the structure of ZrSb[7] consists in part of puckered layers containing Sb_6 units with Sb–Sb distances of *ca*. 325 pm, which point to weak bonding interactions. This was the motivation to study Zr-rich antimonides. Here, the most metal-rich polyantimonides are presented, whose structures exhibit Sb–Sb bonds besides bonding metal–metal interactions. This observation is in contrast to related metal-rich tellurides[8] and arsenides[9] where neither Te–Te nor As–As bonds were found.

The isostructural pnictides $Zr_{7.5}V_{5.5}Sb_{10}$ and $Zr_{6.5}V_{6.5}Sb_{10}$[10] were synthesized by arc-melting of stoichiometric cold-pressed mixtures of Zr, V, and previously prepared $ZrSb_2$.[11] The metal sites are in part statistically mixed occupied by Zr and V in different ratios. The configurational entropy provides a significant contribution to the stability of these phases, which decompose during annealing at lower temperatures, namely at 900 and 1100 °C. The metal sites may be devided into two classes: the seven independent sites of the first class (white circles in Fig. 1) consist mainly of Zr atoms and form alternating triangles and rectangles parallel to the *b* axis. Five of these positions are surrounded by seven Sb atoms forming distorted pentagonal bipyramides, whereas the other two are located in pentagonal Sb_6 pyramides. The three independent positions of the second class (black circles in Fig. 1, mainly V atoms) are situated in distorted Sb_6 octahedra and Sb_5 square prisms, respectively.

Considering to a first approximation the sites of the first class solely as Zr sites and those of the second class as V sites, corresponding to a hypothetical '$Zr_7V_6Sb_{10}$', the Zr/V ratio per metal site decreases with increasing total M–Sb Pauling bond order, calculated with r_{Zr} = 145 pm, r_V = 122 pm.[12] It is concluded that the site preferences of Zr and V are mainly dominated by the different radii of the M atoms rather than by the different number of valence electrons which should influence basically only the metal–metal interactions.[13] Given the fact that $Zr_{7.7}V_{5.3}Sb_{10}$ and $Zr_{6.5}V_{6.5}Sb_{10}$ crystallize in a new structure type in addition to the occurrence of differential fractional site occupancies, these phases may be classified as typical DFSO stabilized materials,[14] being the first with the very different metal atoms, Zr and V. However, only three ($Zr_{6.5}V_{6.5}Sb_{10}$) or four ($Zr_{7.5}V_{5.5}Sb_{10}$) of the ten M sites show mixed Zr/V occupancies. On the other hand, complete ordering of the Zr and V atoms is observed in the structure of $Zr_2V_6Sb_9$.[15]

The metal atoms are interconnected *via* short metal–metal bonds with lengths between 260 and 310 pm. The majority of these interactions are found between atoms of class II parallel to [010] and between the atoms of the classes I and II, whereas only one of these relatively short bonds connects two atoms of class I, being situated in the *ac* plane [thick line in Fig. 2(a)]. The atoms of the first class form channels which include linear chains of Sb atoms with short alternating Sb–Sb distances of 280 and 288 pm for $Zr_{7.5}V_{5.5}Sb_{10}$ ($Zr_{6.5}V_{6.5}Sb_{10}$: 281 and 288 pm). It is interesting that the surrounding electropositive Zr

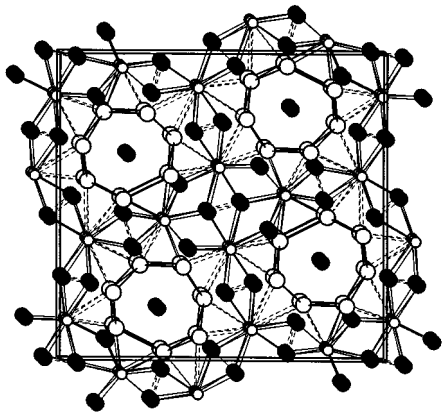

Fig. 1 Projection of the structure of $Zr_{7.5}V_{5.5}Sb_{10}$ along [010]. Large white circles: M atoms of class I (mainly Zr); small white: M atoms of class II (mainly V); medium black: Sb.

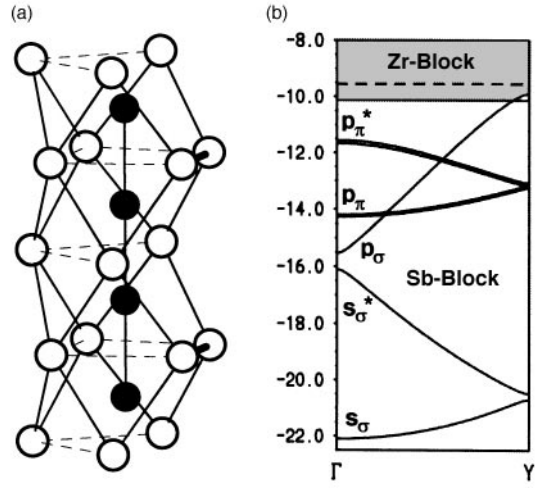

Fig. 2 (a) Part of the infinite $(Zr, V)_7Sb_2$ chain. Thick solid line between M atoms: distance d = 305 pm, thinner lines: 350 pm < d < 370 pm; dashed lines: 380 pm < d < 430 pm. (b) Schematic band structure of an infinite Zr_7Sb_2 unit.

atoms use some electrons for Zr–Zr bonds instead of reducing antimony to Sb(-III). Other Sb–Sb distances in this structure range from 330 to 350 pm (dashed lines in Fig. 1) which is comparable to the second shortest Sb–Sb bonds in elemental antimony (336 pm). Whereas the bonding character of these interactions remains questionable, the shorter distances, being shorter than in elemental antimony (291 pm), may be compared to the lengths of two-electron–two-center bonds found in other polyantimonides, namely in KSb (283 and 285 pm),[16] cyclo-Sb_5^{5-} (between 281 and 291 pm),[17] and Sb_{11}^{3-} (between 276 and 285 pm).[18]

However, the linearity of the Sb chain stands against two-electron–two-center bonds, as can be derived from a comparison with the zigzag Sb(-I) chains in KSb or the Te chains in elemental tellurium. In order to obtain more information about bonding in the Sb chain, the band structure of an infinite Zr_7Sb_2 chain with the atomic positions of the structure of $Zr_{7.5}V_{5.5}Sb_{10}$ (Fig. 2) was calculated using an extended Hückel approximation[19] with parameters listed previously.[15] As a consequence of the Peierls distortion, a gap occurs between the highly disperse p_σ and the p_σ* band of the Sb atoms. With the exception of the p_σ* band, all p states of the Sb atoms are located well below the Zr centered states [Fig. 2(b)]. Since the Zr states are partially occupied because of the bonding Zr–Zr interactions, seven bands of the two Sb atoms of the unit are completely filled, *i.e.* with two electrons per band. This leads to a formal consideration of these Sb atoms being Sb^{2-} which form (delocalized) one-electron–two-center Sb–Sb σ bonds. The latter gives a straightforward explanation for the linearity of the $^1_\infty[Sb^{2-}]$ chain, but not for the short bond lengths. The shortness of the Sb–Sb bonds is most likely a consequence of matrix effects, enabling a relatively short *b* axis and thus strong bonding metal–metal interactions parallel to the *b* axis. In a crude approximation, the formal electron counting schemes (ignoring the Sb–Sb interactions > 330 pm) of $(Zr^{4+})_{7.5}(V^{5+})_{5.5}(Sb^{2-})_2(Sb^{3-})_8(e^-)_{29.5}$ and $(Zr^{4+})_{6.5}(V^{5+})_{6.5}(Sb^{2-})_2(Sb^{3-})_8(e^-)_{30.5}$ show a multitude of electrons (*ca.* 2.3 per M atom) being available for (delocalized) M–M bonds and result in a reasonable averaged oxidation state of −2.8 for the Sb atoms.

This work was financially supported by the Bundesministerium für Bildung, Wissenschaft, Forschung und Technologie, the Deutsche Forschungsgemeinschaft, and the Fonds der Chemischen Industrie. I am grateful to Professor Dr B. Harbrecht for his interest and support.

Notes and References

1 J.-M. Rouxel, *Chem. Eur. J.*, 1996, **2**, 1053.
2 L. H. Brixner, *J. Inorg. Nucl. Chem.*, 1960, **15**, 199.
3 B. Frick, J. Schoenes, F. Hulliger and O. Vogt, *Solid State Commun.*, 1984, **49**, 1133.
4 H. Nowotny and J. Peal, *Monatsh. Chem.*, 1951, **82**, 336.
5 J. Bouwma, C. F. van Bruggen and C. Haas, *J. Solid State Chem.*, 1973, **7**, 255.
6 L. F. Myzenkova, V. V. Baron and Y. M. Savitsky, *Russ. Metall.* (*transl. Izvest. Akad. Nauk SSR, Met.*), 1966, **2**, 89.
7 E. Garcia and J. D. Corbett, *J. Solid State Chem.*, 1988, **73**, 452.
8 R. L. Abdon and T. Hughbanks, *J. Am. Chem. Soc.*, 1995, **117**, 10 035.
9 H. Kleinke and H. F. Franzen, *J. Alloys Compd.*, 1998, **266**, 139.
10 *Crystal data* (IPDS, Stoe, T = 293 K): $Zr_{7.5}V_{5.5}Sb_{10}$: M = 2182 orthorhombic, space group *Pnma*; a = 1871.6(2), b = 567.22(6), c = 1764.9(2) pm; Z = 4, μ = 20.7 mm^{-1}, 2681 independent reflections; $R(F)$ = 0.036, $R_w(F^2)$ = 0.074 for 1069 observed reflections [$I > 2\sigma(I)$]. $Zr_{6.5}V_{6.5}Sb_{10}$: M = 2142 orthorhombic, space group *Pnma*, a = 1866.7(3), b = 569.09(7), c = 1753.7(2) pm, Z = 4, μ = 20.7 mm^{-1}, 2433 independent reflections; $R(F)$ = 0.060, $R_w(F^2)$ = 0.111 for 575 observed reflections [$I > 2\sigma(I)$]. CCDC 182/1007.
11 D. Eberle and K. Schubert, *Z. Metallk.*, 1968, **59**, 306.
12 L. Pauling, *The Nature of the Chemical Bond*, Cornell University Press, Ithaca, NY, 3rd edn., 1948.
13 H. Kleinke and H. F. Franzen, *J. Am. Chem. Soc.*, 1997, **119**, 12 824.
14 M. Köckerling and H. F. Franzen, *Croat. Chem. Acta*, 1995, **68**, 709.
15 H. Kleinke, *Eur. J. Inorg. Chem.*, 1998, **9**, 1369.
16 W. Hönle and H.-G. von Schnering, *Z. Kristallogr.*, 1981, **155**, 307.
17 N. Korber and F. Richter, *Angew. Chem.*, 1997, **109**, 1575.
18 U. Bolle and W. Tremel, *J. Chem. Soc., Chem. Commun.*, 1992, 91.
19 R. Hoffmann, *J. Chem. Phys.*, 1963, **39**, 1397; Program EHMACC, adapted for use on a PC by M. Köckerling, Gesamthochschule Duisburg, 1997.

Received in Bath, UK, 1st July 1998; 8/05410J

Unexpected formation of a sterically protected nitrogen pentasulfide $ArNS_5$ (Ar = 2,6-dimesityl-4-methylphenyl) and the X-ray crystallographic analysis

Shigeru Sasaki, Hiroya Hatsushiba and Masaaki Yoshifuji*

Department of Chemistry, Graduate School of Science, Tohoku University, Aoba, Sendai 980-8578, Japan.
E-mail: yoshifj@mail.cc.tohoku.ac.jp

A stable cyclic nitrogen pentasulfide $ArNS_5$ (Ar = 2,6-dimesityl-4-methylphenyl) was unexpectedly obtained by passing the corresponding *N*-thiosulfinylaniline through a silica gel column and the chair form of the six-membered ring was revealed by X-ray crystallographic analysis.

Cyclic nitrogen polysulfides NS_x other than the eight-membered ring were not known for many years due to the lack of an appropriate method of preparation and their instability. Recently, Steudel *et al*. discovered a route to NS_x heterocycles (x = 5, 6, 8, 9, 11)[1] by using titanocene complexes, but most of them turned out to be unstable materials. On the other hand, introduction of sterically demanding groups has played an important role in the isolation of several cyclic polysulfides such as CS_x,[2] but such an attempt at kinetic stabilization of cyclic nitrogen polysulfides has not been reported. Recently, we[3] and Protasiewicz[4] have reported the synthesis of group15 element compounds such as diphosphenes and phosphaarsene possessing sterically protecting groups of the 2,6-diarylphenyl type, which have been successfully used by Power *et al.* for the stabilization of a wide range of compounds from low valent transition metals to main-group element compounds.[5] One of the noteworthy points of the 2,6-dimesityl-4-methylphenyl group is the difference of reactivity of the *ortho* substituents as compared with the widely used 2,4,6-tri-*tert*-butylphenyl group, in spite of the comparable sterically protecting effect.[3] During our systematic study on group 15 compounds possessing the 2,6-dimesityl-4-methylphenyl group, we became interested in *N*-thiosulfinylaniline **3**, since the 2,4,6-tri-*tert*-butylphenyl derivative cyclizes to form a five membered heterocycle despite the bulkiness of the *tert*-butyl group.[6] However, **3** was not so stable as expected and we obtained the stable cyclic nitrogen pentasulfide $ArNS_5$ **1** unexpectedly (Scheme 1).

2,6-Dimesityl-4-methylaniline (**2**) was prepared by $LiAlH_4$ reduction of the corresponding phenyl azide in 96%, which was synthesized from the corresponding iodobenzene by lithiation followed by quenching with *p*-toluenesulfonyl azide in 95%. Oxidation of **2** with MCPBA afforded the corresponding nitrosobenzene‡ as a stable pale green solid in 72% yield similarly to other sterically protected anilines.[7] Sulfurization of **2**† with S_2Cl_2 in the presence of triethylamine[6,8] gave a reddish purple oil, which was assigned as *N*-thiosulfinylaniline **3**. Almost quantitative formation of **3** was confirmed by ^1H NMR. However, **3** decomposed during attempted purification by column chromatography (SiO_2–*n*-hexane) and cyclic nitrogen pentasulfide **1** was isolated in 21% as a yellow solid. *N*,*N*′-Bis(2,6-dimesityl-4-methylphenyl)sulfurdiimide **4** (10%) was another identified product and 61% of aniline **2** was recovered. Pale yellow prisms suitable for X-ray crystallographic analysis were obtained after recrystallization from *n*-hexane.§

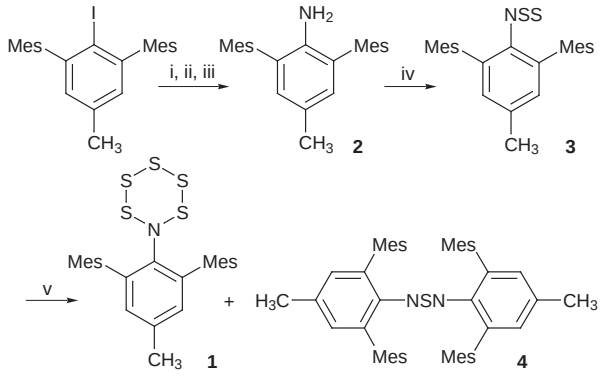

Scheme 1 *Reagents and conditions*: i, *n*-BuLi, THF; ii, TsN_3; iii, $LiAlH_4$, diethyl ether; iv, S_2Cl_2, Et_3N, diethyl ether; v, SiO_2

Fig. 1 shows the molecular structure of **1**. The NS_5 ring takes a chair form like CS_5,[9] S_6,[10] and TiS_5[11] heterocycles and the torsion angles within the six-membered ring range from 67.42(5) to 74.88(8)°, which deviate markedly from values of *ca.* 100° of the stable eight-membered rings such as HNS_7[12] and S_8.[13] On the other hand, the bond lengths and angles do not differ greatly from those for HNS_7.[12] The nitrogen atom takes almost planar geometry with the sum of the bond angles around N(1) as 359.57°, and the dihedral angle between the plane

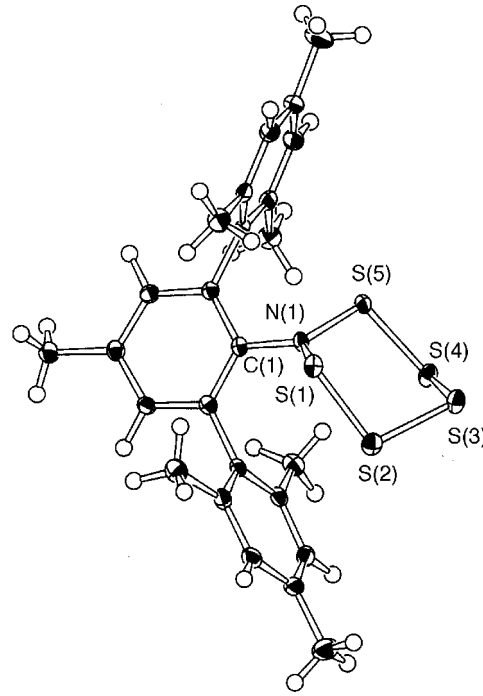

Fig. 1 Molecular structure of **1** in the crystal. ORTEP drawing with 50% probability ellipsoids. Selected bond lengths (Å), bond angles (°), and torsion angles (°): S(1)–N(1) 1.699(1), S(1)–S(2) 2.0612(7), S(2)–S(3) 2.0803(6), S(3)–S(4) 2.0718(6), S(4)–S(5) 2.0704(7), S(5)–N(1) 1.700(1), N(1)–C(1) 1.442(2), S(2)–S(1)–N(1) 104.40(5), S(1)–S(2)–S(3) 100.89(3), S(2)–S(3)–S(4) 99.14(2), S(3)–S(4)–S(5) 102.12(2), S(4)–S(5)–N(1) 104.01(5), S(1)–N(1)–S(5) 116.01(8), S(1)–N(1)–C(1) 121.61(10), S(5)–N(1)–C(1) 121.95(10), S(1)–S(2)–S(3)–S(4) –70.01(3), S(1)–N(1)–S(5)–S(4) 73.29(8), S(2)–S(1)–N(1)–S(5) –74.88(8), S(2)–S(3)–S(4)–S(5) 69.64(3), S(3)–S(2)–S(1)–N(1) 69.20(5), S(3)–S(4)–S(5)–N(1) 69.20(5).

defined by N(1), S(1), S(5), and C(1) and the central benzene ring is 55.07°. The NS_5 ring aligns in the direction of the *b* axis with the short contact less than the sum of van der Waals radii between S(2) and S(5*), S(1) and S(4*) of the neighboring molecules (marked with*), being 3.4102(6) and 3.6219(6) Å, respectively. Although the mechanism of the formation of **1** is not clear at present, oligomerization (stoichiometrically trimerization) of *N*-thiosulfinylaniline **3** followed by elimination of a stable sulfurdiimide **4** might afford **1**, since the electrophilicity of **3** might be enhanced by an acid on the silica gel surface. The ring size could depend on the steric demand or the cavity size made by the two mesityl groups.

The authors are grateful for financial support in part from The Japan Securities Scholarship Foundation and Grants-in-Aid for Scientific Research from the Ministry of Education, Science, Sports and Culture (Nos. 08454193 and 09239101). Shin-Etsu Chemical Co. is also gratefully appreciated for donation of silicon chemicals. The authors also thank Instrumental Analysis Center for Chemistry, Graduate School of Science, Tohoku University for the measurement of mass spectra.

Notes and References

† To a solution of **2** (300 mg, 0.873 mmol) in a mixture of triethylamine (0.3 ml, 2.15 mmol) and diethyl ether (15 ml), a solution of disulfur dichloride (0.09 ml, 1.13 mmol) in diethyl ether (10 ml) was added dropwise at 0 °C to give a red mixture. After being stirred for 1 h at 0 °C, the reaction mixture was poured into ice-water, extracted with diethyl ether, dried over $MgSO_4$, and concentrated to give crude **3** as a red oil almost quantitatively. The oil was submitted to silica-gel column chromatography (gradient elution with *n*-hexane and chloroform) to give **1** (21%) and **4** (10%), together with recovery of **2** (61%). Further recrystallization of **1** from *n*-hexane afforded pure **1** as yellow prisms. **3**: reddish brown oil; ^{1}H NMR (200 MHz, $CDCl_3$) δ 7.05 (2H, s, arom.), 6.87 (4H, s, Mes-arom.), 2.43 (3H, s, CH_3), 2.28 (6H, s, Mes-*p*-CH_3), 2.10 (12H, s, Mes-*o*-CH_3); LRMS (EI, 70 eV) *m/z* 405 (M^+, 8), 341 ($M^+ - 2S$, 62), 326 ($M^+ - 2S - CH_3$, 100), 311 ($M^+ - 2S - 2CH_3$, 25); UV–VIS (CH_2Cl_2) λ_{max} 465 nm. **1**: yellow prisms; mp 133.0–134.0 °C; ^{1}H NMR (200 MHz, $CDCl_3$) δ 7.04 (4H, s, Mes-arom.), 6.84 (2H, s, arom.), 2.37 (6H, s, Mes-*p*-CH_3), 2.34 (3H, s, CH_3), 2.10 (12H, s, Mes-*o*-CH_3); ^{13}C NMR (50 MHz, $CDCl_3$) δ 145.3, 137.6, 137.5, 137.5, 136.4 , 130.7, 128.7, 21.3, 21.2, 20.9 (one quarternary carbon peak was missing at 295 and 323 K, probably due to dynamic behavior); IR (KBr) 3016, 2947, 2916, 2854, 1612, 1452, 1444, 1423, 1375, 1205, 1182, 1039, 1030, 870, 849, 758 cm^{-1}; UV–VIS (hexanes) $\lambda_{max}(\varepsilon)$ 246.4 (17900) nm ; LRMS (EI, 70 eV) *m/z* 501 (M^+, 0.4), 405 ($M^+ - 3S$, 6), 373 ($M^+ - 4S$, 5), 341 ($M^+ - 5S$, 58), 326 ($M^+ - 5S - CH_3$, 100), 311 ($M^+ - 5S - 2CH_3$, 24), 296 ($M^+ - 5S - 3CH_3$, 11); HRMS (EI, 70 eV) Found: *m/z* 501.0757, calc. for $C_{25}H_{27}NS_5$: *M* 501.0748.

‡ 2,6-Dimesityl-4-methylphenylnitrosobenzene: light green crystals; mp 195.0–196.0 °C; ^{1}H NMR (200 MHz, $CDCl_3$) δ 7.03 (2H, s, arom.), 6.93 (4H, s, Mes-arom.), 2.44 (3H, s, CH_3), 2.34 (6H, s, Mes-*p*-CH_3), 1.87 (12H, s, Mes-*o*-CH_3); ^{13}C NMR (50 MHz, $CDCl_3$) δ 162.6, 146.0 , 136.6, 135.6, 135.5, 133.8, 131.0, 128.7, 21.7, 21.1, 20.6; LRMS (EI, 70 eV) *m/z* 357 (M^+, 100), 340 ($M^+ - CH_3$, 87); UV–VIS (CH_2Cl_2) λ_{max} 810 nm.

§ *Crystal data* for **1**: $C_{25}H_{27}NS_5$, M = 501.79, pale yellow prisms, crystal dimensions 0.60 × 0.50 × 0.40 mm^3, monoclinic, space group *C*2/*c* (no. 15), a = 28.445(7), b = 12.653(2), c = 17.078(2) Å, β = 125.79(1)°, U = 4985(1) $Å^3$, Z = 8, D_c = 1.337 g cm^{-3}, μ = 0.479 mm^{-1}, T = 112(1) K, F(000) = 2112.00. Rigaku RAXIS-IV imaging plate area detector with graphite monochromated Mo-Kα radiation, λ = 0.71070 Å. No. of reflections measured 4405. No. of observations [$I > 3.00\sigma(I)$] 4060. The structure was solved by direct method (SAPI91[14]), expanded using Fourier techniques (DIRDIF94[15]), and refined by full matrix least squares on F for 389 variable parameters. The non-hydrogen atoms were refined anisotropically. Hydrogen atoms were refined isotropically. R = 0.031 R_w = 0.054 for observed reflections [$I > 3.00\sigma(I)$] and R = 0.034, R_w = 0.058 for all. Goodness of fit S = 1.42. The maximum and minimum peaks on the final difference Fourier map corresponded to 0.26 and −0.29 e $Å^{-3}$, respectively. Structure solution, refinement, and graphical representation were carried out using teXsan package.[16] CCDC 182/994.

1 For x = 8, 9: K. Bergemann, M. Kustos, P. Krüger and R. Steudel, *Angew. Chem., Int. Ed. Engl.*, 1995, **34,** 1330; for x = 8, 9, 11: R. Steudel, K. Bergemann, J. Buschmann and P. Luger, *Angew. Chem., Int. Ed. Engl.*, 1996, **35**, 2537; for x = 5, 6: R. Steudel, O. Schmann, J. Buschmann and P. Luger, *Angew. Chem., Int. Ed. Engl.*, 1998, **37,** 492.

2 N. Takeda, N. Tokitoh, T. Imakubo, M. Goto and R. Okazaki, *Bull. Chem. Soc. Jpn.*, 1995, **68**, 2757.

3 K. Tsuji, Y. Fujii, S. Sasaki and M. Yoshifuji, *Chem. Lett.*, 1997, 855.

4 E. Urnezius and J. D. Protasiewicz, *Main Group Chemistry*, 1996, **1**, 369; S. Shah, S. C. Burdette, S. Swavey, F. L. Urbach and J. D. Protasiewicz, *Organometallics*, 1997, **16**, 3395.

5 X. He, M. M. Olmstead and P. P. Power, *J. Am. Chem. Soc.*, 1992, **114**, 9668; J. J. Ellison, K. Ruhlandt-Senge and P. P. Power, *Angew. Chem., Int. Ed. Engl.*, 1994, **33**, 1178; S. Simons, L. Pu, M. M. Olmstead and P. P. Power, *Organometallics*, 1997, **16**, 1920.

6 Y. Inagaki, R. Okazaki and N. Inamoto, *Bull. Chem. Soc. Jpn.*, 1979, **52**, 1998.

7 R. Okazaki, T. Hosogai, E. Iwadare, M. Hashimoto and N. Inamoto, *Bull. Chem. Soc. Jpn.*, 1969, **42**, 3611.

8 Y. Inagaki, R. Okazaki and N. Inamoto, *Bull. Chem. Soc. Jpn.*, 1979, **52**, 1998.

9 F. Von Fehér and J. Lex, *Z. Anorg. Allg. Chem.*, 1976, **423**, 103.

10 J. Donohue, A. Caron and E. Goldish, *J. Am. Chem. Soc.*, 1961, **83**, 3748.

11 E. F. Epstein, I. Bernal and H. Köpf, *J. Organomet. Chem.*, 1971, **26**, 229.

12 H.-J. Von Hecht, R. Reinhardt, R. Steudel and H. Bradaczek, *Z. Anorg. Allg. Chem.*, 1976, **426**, 43.

13 A. S. Cooper, W. L. Bond and S. C. Abrahams, *Acta. Crystallogr.*, 1961, **14**, 1008; A. Caron and J. Donohue, *ibid.*, 1965, **18**, 562; S. C. Abrahams, *ibid.*, 1965, **18**, 566.

14 H.-F. Fan, 1991, Structure Analysis Programs with Intelligent Control, Rigaku Corporation, Tokyo, Japan.

15 P. T. Beurskens, G. Admiraal, G. Beurskens, W. P. Bosman, R. de Gelder, R. Israel and J. M. M. Smits, 1994, The DIRDIF94 program system, Technical Report of the Crystallography Laboratory, University of Nijmegen, The Netherlands.

16 Crystal Structure Analysis Package, Molecular Structure Corporation, 1985 and 1992.

Received in Cambridge, UK, 7th July 1998; 8/05235B

Cleavage of a phosphorus carbon triple bond in the reaction of 2,2-dimethylpropylidynephosphine with $[Os_3(CO)_{10}(\mu_3\text{-}\eta^1:\eta^2:\eta^1\text{-}C_2Me)]$

Mathias Nowotny,[a] Brian F. G. Johnson,*[a] John F. Nixon[b] and Simon Parsons[c]

[a] *University Chemical Laboratories, Lensfield Road, Cambridge, UK CB2 1EW. E-mail: bfgj1@cam.ac.uk*
[b] *School of Chemistry, Physics and Environmental Sciences, University of Sussex, Brighton, UK BN1 9QJ*
[c] *Department of Chemistry, University of Edinburgh, West Mains Road, Edinburgh, UK EH9 3JJ*

The reaction of 2,2-dimethylpropylidynephosphine with the cluster $[Os_3(CO)_{10}(\mu_3\text{-}\eta^1:\eta^2:\eta^1\text{-}C_2Me)]$ 1 results in P–C bond cleavage and an insertion of the precoordinated but-2-yne ligand into the phosphorus carbon triple bond of the incoming phosphaalkyne with formation of a novel bridging C_3P-moiety in the structurally characterised complex $[Os_3(CO)_8(\mu_2\text{-}PCBu^t)\{\mu_3\text{-}PC(Me)C(Me)C(Bu^t)\}]$ 2, together with a second $\mu_2\text{-}\eta^2,\eta^2$-ligated phosphaalkyne.

The coordination chemistry of phosphaalkynes RC≡P is of current interest and its similarity to the coordination behaviour of alkynes has been summarised in several recent reviews.[1] In particular, the use of phosphaalkynes as alkyne-like building blocks in the formation of phosphorus containing unsaturated ring systems is of considerable synthetic use.[1,2] Despite several examples of controlled alkyne–alkyne coupling reactions at polynuclear carbonyl clusters,[3] in all our previous attempts to achieve an oligomerisation of phosphaalkynes in the coordination sphere of triruthenium and triosmium carbonyl clusters, we isolated products exclusively resulting from a carbonylation of the incoming $Bu^tC{\equiv}P$ to afford the phosphinidene ligand μ_3-PC(CO)Bu^t, *e.g.* in the complexes $[M_3(CO)_9\{\mu_3\text{-}PC(CO)Bu^t\}_2]$ (M = Ru, Os) and their derivatives.[4] The thermodynamic sink represented by the formation of these complexes is apparently efficient enough to prevent any phosphaalkyne oligomerisation. In an attempt to avoid this dominating pathway and also to facilitate alkyne-like reactions, we decided to modify the reaction system by introducing a precoordinated alkyne unit, a strategy that also proved to be successful in case of an Ir_4 carbonyl cluster system.[5] Here, we wish to present the results of the reaction between 2,2-dimethylpropylidynephosphine and the alkyne cluster $[Os_3(CO)_{10}(\mu_3\text{-}\eta^1,\eta^2,\eta^1\text{-}C_2Me_2)]$ **1**.

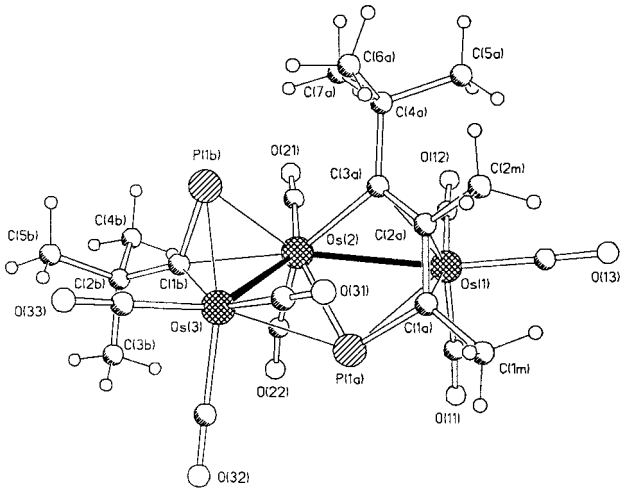

Fig. 1 Molecular structure of $[Os_3(CO)_8(\mu_2\text{-}PCBu^t)\{\mu_3\text{-}PC(Me)C(Me)C(Bu^t)\}]$ **2** with atom numbering scheme. The carbonyl carbon atoms bear the same numbers as the respective oxygen atoms. Selected bond lengths (Å) and angles (°): Os(1)–Os(2) 2.8130(8), Os(2)–Os(3) 2.8217(7), Os(1)–P(1A) 2.701(3), Os(2)–P(1A) 2.368(3), Os(3)–P(1A) 2.666(3), Os(1)–C(1A) 2.227(11), Os(1)–C(2A) 2.271(12), Os(1)–C(3A) 2.283(12), Os(2)–C(3A) 2.209(12), P(1A)–C(1A) 1.790(12), C(1A)–C(2A) 1.42(2), C(2A)–C(3A) 1.43(2), C(1A)–C(1M) 1.501(14), C(2A)–C(2M) 1.53(2), C(3A)–C(4A) 1.56(2), Os(2)–P(1B) 2.423(3), Os(2)–C(1B) 2.257(12), Os(3)–P(1B) 2.424(3), Os(3)–C(1B) 2.111(11), P(1B)–C(1B) 1.731(12), C(1B)–C(2B) 1.53(2), mean Os–C(CO) 1.929(25), mean C(CO)–O(CO) 1.141(18); Os(1)–Os(2)–Os(3) 117.09(2), P(1A)–Os(2)–Os(1) 62.14(8), P(1A)–Os(2)–Os(3) 61.08(8), C(3A)–Os(2)–P(1A) 83.8(3), C(3A)–Os(2)–Os(1) 52.4(3), C(1A)–P(1A)–Os(1) 55.1(4), C(1A)–P(1A)–Os(2) 99.8(4), C(1A)–P(1A)–Os(3) 108.8(4), P(1A)–C(1A)–C(2A) 118.4(8), P(1A)–C(1A)–C(1M) 116.8(8), C(2A)–C(1A)–C(1M) 123.6(11), C(1A)–C(2A)–C(3A) 120.8(11), C(1A)–C(2A)–C(2M) 114.0(10), C(3A)–C(2A)–C(2M) 125.2(10), C(2A)–C(3A)–C(4A) 119.6(11), C(1B)–Os(2)–Os(3) 47.5(3), C(1B)–Os(2)–P(1B) 43.2(3), P(1B)–Os(2)–Os(3) 54.41(7), C(2B)–C(1B)–P(1B) 132.3(9).

The reaction of cluster **1** with 1 equiv. of $Bu^tC{\equiv}P$ in refluxing CH_2Cl_2 resulted in the formation of cluster $[Os_3(CO)_8(\mu_2\text{-}PCBu^t)\{\mu_3\text{-}PC(Me)C(Me)C(Bu^t)\}]$ **2**, which was formulated on the basis of spectroscopic data† and the results of a single crystal structure analysis.‡

In addition to an edge-bridging $\mu_2\text{-}\eta^2:\eta^2$-coordinated phosphaalkyne moiety, this unusual complex bears an additional ligand formed by the coupling of the initial $\mu_3\text{-}\eta^1:\eta^2:\eta^1$-butyne ligand with a second phosphaalkyne molecule. The insertion of this ligand into the bond between Os(1) and Os(3) opens the metal triangle forming a bent three metal chain, with the phosphorus atom P(1a) bridging all three osmium atoms.

Together with the central osmium atom Os(2), this ligand forms a 1-osma-2-phosphacyclopentadiene ring which binds to the terminal osmium atom Os(1) in the η^5-coordination mode. This central five membered ring is essentially planar with the atoms deviating from the best plane by ±0.0579 Å.

It is of special significance, that it is not the ring carbon atom C(1a) vicinal to the phosphorus atom P(1a) which bears the Bu^t substituent of the former phosphaalkyne moiety but carbon atom C(3a). Therefore, the phosphorus carbon triple bond of this precursor is completely cleaved during the course of the reaction leading to the formation of **2**, and a plausible explanation for this finding is represented in Scheme 1. The insertion of the osmium atom Os(2) into a phosphorus carbon bond of an intermediate phosphacyclobutadiene ligand, formed in a [2 + 2]-cycloaddition of the but-2-yne and the phosphaalkyne, leads to the formation of the observed 1-osma-2-phospha-

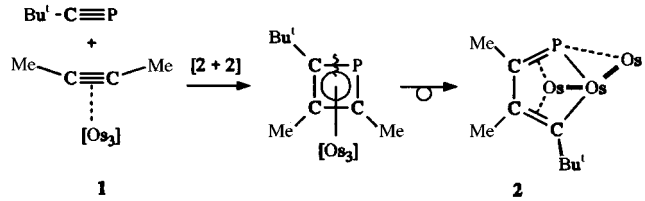

Scheme 1 Hypothetical mechanism for the formation of the $\{\mu_3\text{-}PC(Me)C(Me)C(Bu^t)\}$-subunit in **2**

cyclopentadiene ring. There are relatively few examples of co-cyclodimerization reactions of alkynes and phosphaalkynes at transition metal centres resulting in phosphacyclobutadiene metal complexes that are comparable to the proposed intermediate.[6] Although no information regarding the detailed mechanism outlined in Scheme 1 is available, it is interesting to note that, since only one regioisomer is isolated, insertion into the proposed phosphacyclobutadiene intermediate occurs exclusively at the bond between the phosphorus and the carbon atom bearing the Bu^t substituent.

The fact that the basic open Os_3-triangle in the framework of **2** requires a total of 50 valence electrons with a contribution of four valence electrons from the second μ_2-η^2,η^2-coordinated phosphaalkyne ligand indicates that the central ligand formed by the coupling of butyne and Bu^{t}C≡P acts as a six electron donor. Therefore, it can be concluded that the lone pair centred on P(1a) does not contribute to the cluster framework. The coordination around phosphorus atom P(1a) can be described as a distorted square based pyramid with the three osmium atoms forming the base together with the carbon atom C(1a), while the lone pair of P(1a) points into the direction of the apex.

While the distances between Os(2) and either P(1a) or C(3a) are 2.368(3) and 2.209(12) Å, respectively, lying within the range of normal Os–P and Os–C single bonds,[7] the distances between P(1a) and either Os(1) or Os(3) are *ca.* 30 pm longer than the average [2.701(3) and 2.666(3) Å, respectively]. This indicates a very unusual bonding situation because steric reasons for the observed bond lengthening can be excluded at least in the case of the interaction between Os(3) and P(1a).

The second phosphaalkyne ligand in **2** bridges Os(2) and Os(3) in the μ_2-η^2,η^2-coordination mode with the participation of both P–C π-MOs. The P–C distance of the side on coordinated phosphaalkyne is 1.731(12) Å, which is too short for the expected single bond but easily fits the range of typical P–C double bonds.[7] The Bu^t substituent on the methylidyne carbon atom C(1b) bends away from the osmium atoms as a result of a rehybridisation caused by the coordination, thereby reducing the angle P(1b)–C(1b)–C(2b) from 180° in the free phosphaalkyne to 132.3(9)°. Similar features have been reported for the only other structurally characterized example of a side on-coordinated phosphaalkyne ligand, [$Mo_2Cp_2(CO)_4$(μ_2-η^2 : η^2-PCBu^t)],[8] where the P–C distance is 1.719(3) Å and the P–C–C angle 127.9(3)°.

We thank the Deutsche Forschungsgemeinschaft (Bonn, Bad Godesberg) for a postdoctoral fellowship (M. N.) and the EPSRC for support.

Notes and References

† *Synthesis of* **2**: A mixture of 37.9 mg (0.042 mmol) [$Os_3(CO)_{10}$(μ_3-η^1 : η^2 : η^1-C_2Me_2)] **1**[9] and 4.2 mg (0.042 mmol) 2,2-dimethyl-propylidyne-phosphine[10] in 50 ml of dry CH_2Cl_2 was heated under reflux for 24 h under an inert atmosphere. After filtration and concentration *in vacuo*, **2** was separated from unreacted starting material by thin layer chromatography [silica gel, CH_2Cl_2–hexane (3 : 7)] as the only major product (6%). Yellow crystals suitable for X-ray crystallography were grown by vapor diffusion of hexane into a CH_2Cl_2 solution. ^{1}H NMR [$(CD_3)_2CO$], δ 1.43 (s, 9H, Bu$^{t(b)}$), 1.60 (s, 9H, Bu$^{t(a)}$), 2.41 (s, 3H, Me^{2m}), 2.68 (s, 3H, Me^{1m}); ^{31}P NMR ($CDCl_3$), δ −118.0 (P^{1b}), 229.7 (P^{1a}); IR (CH_2Cl_2), ν_{CO} 2080s, 2050vs, 2023s, 2014s, 1993m, 1970m cm^{-1}; FABMS (MeCN/3-noba), *m/z* 1054 − 28*n*, 0 ≤ *n* ≤ 8, [M − *n* CO]$^+$.

‡ *Crystal data* for **2**·0.5 CH_2Cl_2: $C_{22}H_{24}O_8Os_3P_2$ + 0.5 CH_2Cl_2, M_w = 1091.41, monoclinic, space group *C*2/*c*, *a* = 31.052(4), *b* = 11.315(2), *c* = 17.258(2) Å, β = 108.394(10)°, *U* = 5753.9(13) Å^3, *Z* = 8, D_c = 2.520 Mg m^{-3}, *T* = 150 ± 2 K, *F*(000) = 3992, μ(Mo-Kα) = 13.463 mm^{-1}, yellow needle, 0.23 × 0.08 × 0.06 mm. Intensities of 5861 reflections were collected between 2.73 ≤ θ ≤ 25.06° on a STOE Stadi 4 diffractometer using Mo-Kα radiation (graphite monochromator, ω scan mode). Absorption corrections were applied using ψ-scan data: T_{min} = 0.136, T_{max} = 0.224. The structure was solved by direct methods[11] and refined by full-matrix least-squares on F^2. A molecule of CH_2Cl_2 lies disordered over four positions about the crystallographic two-fold axes (two unique orienations plus their symmetry equivalents; *Z* for the CH_2Cl_2 is thus 4, compared to 8 for the Os cluster and hence this is the hemidichloromethane solvate). The occupancy ratio of the unique molecules refined to 0.29 : 0.21(1), with two common isotropic displacement parameters being respectively refined for the C and Cl atoms. The positional parameters were refined subject to explicit geometry restraints [C–Cl 1.80(2), Cl–Cl 2.93(2) Å]. All other non-H atoms were refined freely with anisotropic displacement parameters.[12] Final *R* values: R_1 = 0.0418 and wR_2 = 0.0805 [based on F^2 and 5082 data with $I > 2\sigma(I)$ and 345 parameters]. The final Fourier difference map showed no residual density outside of −1.378 and 1.303 e Å^{-3}. CCDC 182/1010.

1 J. F. Nixon, *Chem. Rev.*, 1988, **88**, 1327; *Coord. Chem. Rev.*, 1995, **145**, 201; *Chem. Soc. Rev.*, 1995, 319; *Phosphorus: The Carbon Copy*, ed. K. B. Dillon, F. Mathey and J. F. Nixon, Wiley, 1998.
2 D. Böhm, F. Knoch, S. Kummer, U. Schmidt and U. Zenneck, *Angew. Chem., Int. Ed. Engl.*, 1995, **34**, 198.
3 E. Sappa, A. Tiripicchio and P. Braunstein, *Chem. Rev.*, 1983, **83**, 203; J. R. Shapley, C. H. McAteer, R. M. Churchill and L. V. Biondi, *Organometallics*, 1984, **3**, 1595; V. Riaz, M. D. Curtis, A. Rheingold and B. S. Haggerty, *Organometallics*, 1990, **9**; H. Matsuzaka, Y. Mizobe, M. Nisho and M. Hidai, *J. Chem. Soc., Chem. Commun.*, 1991, 1011.
4 R. Bartsch, A. J. Blake, B. F. G. Johnson, P. G. Jones, C. Müller, J. F. Nixon, M. Nowotny, R. Schmutzler and D. S. Shephard, *Phosphorus Sulfur Silicon*, 1996, **115**, 201; P. Escarpa-Gaede, B. F. G. Johnson, J. F. Nixon, M. Nowotny and S. Parsons, *Chem. Commun.*, 1996, 1455.
5 M. H. A. Benvenutti, P. B. Hitchcock, J. F. Nixon and M. D. Vargas, *J. Chem. Soc., Chem. Commun.*, 1994, 1869.
6 P. Binger, R. Milczarek, R. Mynott and M. Regitz, *J. Organomet. Chem.*, 1987, **323**, C35; P. Binger, J. Haas, A. T. Herrmann, F. Langshauser and C. Krüger, *Angew. Chem., Int. Ed. Engl.*, 1989, **28**, 210.
7 *International Tables for Crystallography*, ed. A. J. C. Wilson, Kluwer Academic Publishers, Dordrecht, vol. C.
8 G. Becker, W. A. Hermann, W. Kalcher, G. W. Kriechbaum, C. Pahl, C. T. Wagner and M. L. Ziegler, *Angew. Chem., Int. Ed. Engl.*, 1983, **22**, 413.
9 A. J. Deeming, S. Hasso and M. Underhill, *J. Chem. Soc., Dalton Trans.*, 1975, 1614.
10 G. Becker, G. Gresser and W. Uhl, *Z. Naturforsch., Teil B*, 1981, **36**, 16.
11 SIR92: A. Altomeni, M. C. Burla, M. Camalli, G. Cascarano, C. Giacovazzo, A. Guagliali and G. Polidori, *J. Appl. Crystallogr.*, 1994, **27**, 435.
12 SHELXL-93: G. M. Sheldrick, University of Göttingen, Germany, 1993.

Received in Cambridge, UK, 10th July 1998; 8/05382K

Synthesis and electrochemical properties of new star-shaped thiophene oligomers and their polymers

Frédéric Cherioux,*† Laurent Guyard and Pierre Audebert‡

Laboratoire de Chimie et Electrochimie Moléculaire, Université de Franche-Comté, UFR Sciences, 16, route de Gray, F-25030 BESANCON Cedex, France

The efficient synthesis of some 2,4,6-tris[5-(2,2′-bithienyl)]-1,3,5-triazines and 1,3,5-tris[5-(2,2′-bithienyl)]benzenes and their electrochemical properties are discussed.

Branched conducting polymers with electronically connected nodes are excellent candidates among the family of super-structured conducting polymers. In fact, with such polymers, there should be no need for interchain coupling or interchain electronic transfer in order to insure high electronic conductivity.[1] Moreover, this type of material possesses a three dimensional structure which could also assist the conductivity.

There are few previous reports of this type of conducting polymer because the starting precursors are difficult to synthesise. Previous approaches[2] were made to reticulated conducting polymers, but electronic conjugation was only weakly, or not at all, insured through the nodes. Also, star-shaped oligomers were used but in low proportions to prepare polythiophene gels which were no longer soluble in classical solvents and had high degrees of swelling.[3]

Here we present an efficient method for the synthesis of some 2,4,6-tris[5-(2,2′-bithienyl)]-1,3,5-triazine or 1,3,5-tris[5-(2,2′-bithienyl)]benzene derivatives which are precursor of two-dimensional conducting polymers. Their electrochemical properties have been investigated. A new polymer has been synthesised *via* chemical or electrochemical oxidation of 1,3,5-tris[5-(2,2′-bithienyl)]benzene and the charge transfer kinetics inside has been determined by chronoamperometry experiments.

The 2,4,6-tris[5-(2,2′-bithienyl)]-1,3,5-triazine derivatives **2** were obtained by a triple aromatic nucleophilic substitution of 2,2′-dithienyllithium salts on cyanuric chloride (see Scheme 1). This reaction is very efficient[4] because such substitutions are activated by the mesomer attractive power of the nitrogen atoms, which stabilises the intermediate species. So, 3 equiv. of 2,2′-dithienyllithium salt were added in one portion to 1 equiv. of cyanuric chloride in THF. The crude products were purified by column chromatography with light petroleum–CH_2Cl_2 (1 : 1) as eluent. Only the tri-substituted products **2**§ were formed with yields close to 90% (**2a**: 95%, **2b**: 90%).

However, the tris(2,2′-bithienyl)benzene derivatives **4** were synthesised *via* an another route, as aromatic nucleophilic substitution on an inactivated benzene is very difficult. Moreover, there is only one report in the literature of 1,3,5-trisubstitution on a tri-substituted benzene.[5] Therefore, we adapted a recently described procedure based on a triple ketolisation and dehydration of an aromatic methyl ketone with tetrachlorosilane (TCS)–EtOH.[6] However, this method was developed to afford β-methylchalcone stereoselectively, without polymer formation. The authors obtained some 1,3,5-triarylbenzene derivatives as side products. We modified this reaction so that the major products were the 1,3,5-triarylbenzene derivatives. This was achieved using 5 rather than 1 equiv. of TCS, and increasing the reaction time from the 2–4 h given in the original paper to 18 h. Thus the more general character of this method is demonstrated.

The 5-(2,2′-bithienyl) methyl ketone **3** is made *via* the action of 2,2′-dithienyllithium salts on *N*,*N*-dimethylacetanilide (see Scheme 2). TCS–EtOH (5 equiv.) was added to 5-(2,2′-bithienyl) methyl ketone in anhydrous toluene under nitrogen atmosphere. The mixture was stirring of 18 h at room temperature (see Scheme 2). It was then poured in water, extracted with CH_2Cl_2, and the organic phase was separated, dried, and the solvent removed under reduced pressure. The residue was purified by column chromatography with light petroleum–CH_2Cl_2 (1:1) as eluent. The pure products **4**§ were obtained with good yield (**4a**: 65%, **4b**: 55%).

All the thiophene oligomers described are electrochemically oxidizable. In the cases of the oligomers **2a** and **4a** (with unblocked α-positions), entirely irreversible voltamograms are obtained whatever the scan rate up to 1000 V s^{-1} (peak

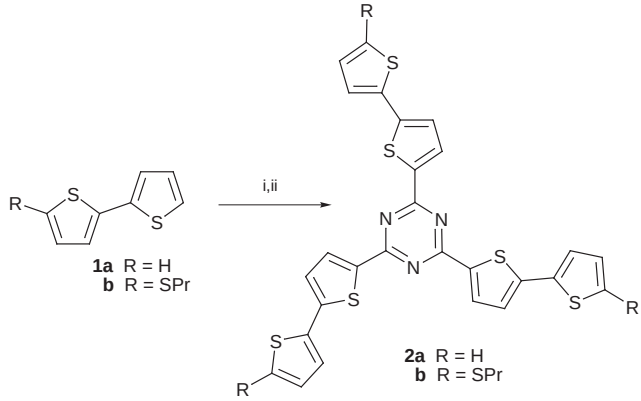

Scheme 1 *Reagents and conditions*: i, Bu^{n}Li; ii, 2,4,6-trichloro-1,3,5-triazine

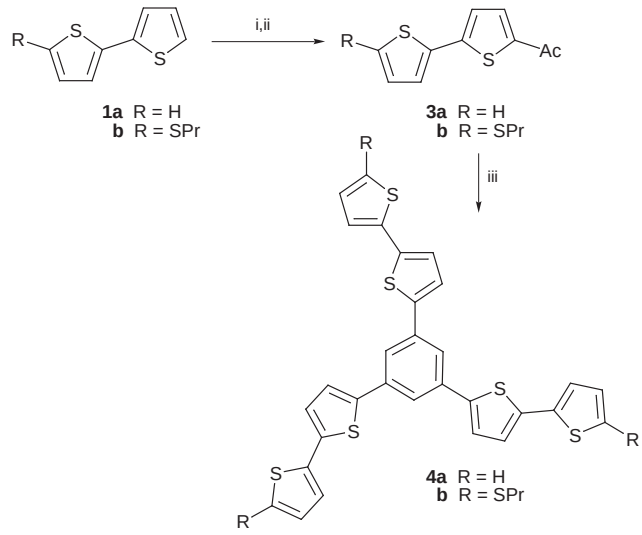

Scheme 2 *Reagents and conditions*: i, Bu^{n}Li; ii, DMA; iii, TCS, EtOH, 18 h, room temp.

potentials at 1 V s^{-1} are 1.41 and 1.02 V *vs*. SCE for **2a** and **4a**, respectively). This demonstrates the very high reactivity of the electrogenerated cation radicals despite the presence of seven aromatic rings. On the other hand, as expected with oligomers **2b** (oxidation peak potential 1.27 V *vs*. SCE at 1 V s^{-1}) and **4b** [redox potentiel $E°$ (half sum of reversible peaks in CH_2Cl_2) of 1.00 V *vs*. SCE is obtained], a return peak is obtained in all cases. As a consequence of the presence of the propylthio group blocking the α-positions, the cation radicals cannot undergo either coupling nor nucleophilic attack due to the steric hindrance of the substituents. It is possible to obtain a standard reversible voltamogram with the benzenic derivative **4b** in CH_2Cl_2. However, in the case of the triazine **2b**, the return peak always features the oxidation of an adsorbed species whatever the solvent, showing that the propyl chains on sulfur are not sufficient in this case to insure sufficient solubility of the electrogenerated cation radical. Similarly in MeCN the cation radical of **4b** also precipitates. The irreversible dication formation is also observable at potentials of 2.13 and 1.97 V *vs*. SCE for **2b** and **4b**, respectively.

Upon oxidation of **2a**, no polymer formation was observed whatever the conditions, therefore probably the cation radicals favour nucleophilic attack on the s-triazine nitrogen atoms to coupling. Conversely the oxidation of **4a** gives an electrodeposited polymer, which displays electroactive characteristics analogous to polythiophene, with a broad reversible peak at an average potential of 0.9 V *vs*. SCE. Chronoamperometry was performed on average thickness films (300 nm) and the diffusion coefficient of the charge transfer is equal to 2×10^{-8} cm^2 s^{-1} (on the basis of one electron for every four thiophene units and a density of 1.5 g cm^{-3}) which is in accordance with values obtained with other conducting polymers.[7] Owing to the ease of the monomer synthesis, larger quantities of polymer can be made by chemical polymerisation with iron(III) chloride. The electrochemical behaviour of the blocked oligomers, especially π-dimer formation, is also being studied.

Notes and References

† E-mail: bernard.laude@univ-fcomte.fr
‡ Permanent address: PPSM-Departement de Chimie, Ecole normale Supérieure, 61 Avenue du President Wilson, F-94235 CACHAN Cedex, France.
§ HRMS analysis **2a**: M^+ = 573, **2b**: M^+ = 795, **4a**: M^+ = 570, **4b**: M^+ = 792. All NMR data are in agreement with the proposed structures.

1 J. M. Tour, *Chem. Rev*., 1996, **96**, 537; W. J. Feast, J. Tsiboulis, K. L. Pouwer, L. Groenendaal and E. W. Meijer, *Polymer*, 1996, **37**, 5017.
2 J. Roncali, P. Marque, A. Yassar, R. Garreau and M. Lemaire, *J. Phys. Chem*., 1987, **91**, 6706; J. Roncali, R. Garreau and M. Lemaire, *J. Electroanal. Chem*., 1990, **278**, 373; S. Courric, Y. Gache and J. Simonet, *J. Electroanal. Chem*., 1993, **362**, 291; Y. Gache and J. Simonet, *J. Phys. Chem*., 1992, **89**, 1027; J. Rault-Berthelot, M. Massaoudi, H. Le Deit and J. Simonet, *Synth. Met*., 1995, **75**, 11.
3 E. Rebourt, B. Pépin-Donat and E. Dinh, *Polymer*, 1995, **36**, 399; B. Sixou, B. Pépin-Donat and M. Nechtschein, *Polymer*, 1997, **38**, 1581; K. Yoshino, S. Morita and K. Nakao, *Synth. Met*., 1991, **41-43**, 1039; K. Yoshino, K. Nakao, M. Onoda and R-I Sugimoto, *Solid State Commun*., 1989, **70**, 609.
4 A. R. Katrisky and B. Nowak-Wydra, *Chem. Scr*., 1984, **24**; F. Cherioux, P. Audebert and P. Hapiot, *Chem. Mater*., 1998, **10**, 1984.
5 R. Weiss, B. Pohmrehn, F. Hampel and W. Bauer, *Angew. Chem., Int. Ed. Engl*., 1995, **34**, 1319.
6 S. S. Elmorsy, A. G. M. Khalil, M. M. Girges, and T. A. Salama, *J. Chem. Res*. 1997, (S) 232; (M) 1537.
7 P. Audebert, M. Maumy and P. Capdevielle, *New J. Chem*., 1992, **16**, 697 and references cited therein.

Received in Cambridge, UK, 26th August 1998; 8/06691D

Diferrocenyl diselenides: excellent thiol peroxidase-like antioxidants

G. Mugesh,[a] Arunashree Panda,[a] Harkesh B. Singh,*[a] Narayan S. Punekar[b] and Ray J. Butcher[c]

[a] *Department of Chemistry, Indian Institute of Technology, Powai, Bombay 400 076, India. E-mail: chhbsia@chem.iitb.ernet.in*
[b] *Biotechnology Centre, Indian Institute of Technology, Powai, Bombay 400 076, India*
[c] *Department of Chemistry, Howard University, Washington DC, 20059, USA*

Synthesis, structure and thiol peroxidase-like antioxidant activity of several diaryl diselenides having intramolecularly coordinating amino groups are described; the diselenides having both tertiary amino groups and redox-active ferrocenyl units show excellent peroxidase activity.

Glutathione peroxidase (GPX) is a well known selenoenzyme which functions as an antioxidant.[1] This selenoprotein catalyses the reduction of harmful peroxides by glutathione and protects the cell membrane from oxidative damage. Recently, much attention has been devoted to the synthesis of simple organoselenium compounds that mimic the action of GPX. After the discovery of Ebselen **1**,[2] several other mimetics have been reported which include the Ebselen homologue,[3] benzoselenazolinones,[4] selenenamide **2**[5a] and related derivatives,[5b] diaryl diselenides,[6] various tellurides and ditellurides,[7] and the enzyme selenosubtilisin.[8]

Recently, diaryl diselenides **3**–**5** with basic amino groups have attracted much attention as GPX mimics because the Se···N intramolecular non-bonded interactions, (i) activate the Se–Se bond towards the oxidative cleavage and, (ii) stabilize the resulting selenenic acid intermediate against further oxidation.[6] In continuation of our work on intramolecularly coordinated organochalcogens,[9] we report here the synthesis, structure and thiol peroxidase activity of a series of closely related novel diselenides **7**–**12**.

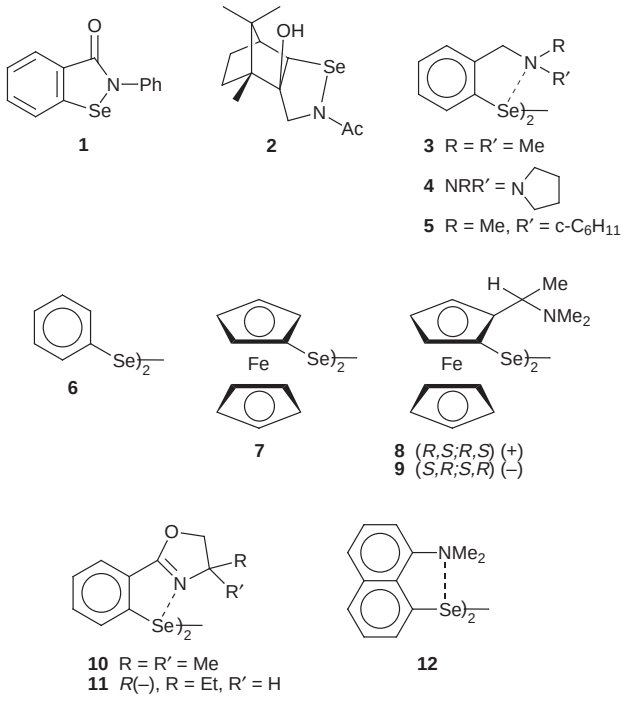

Diselenides **3**,[9a] **7**,[10] **8**,[11] and **9**[11] used in the present study were prepared by the methods indicated. Novel diselenides **10**–**12** were prepared by the ortholithiation method.† The structures of **8**, **10**, **11** and **12** were determined by X-ray diffraction.‡ The catalytic activity was studied according to the method reported by Tomoda and coworkers[6b] using benzenethiol (PhSH) as a glutathione alternative. The initial rates (v_0) for the reduction of H_2O_2 (3.75 mM) by thiol (1 mM) in the presence of various catalysts (0.01 mM) [eqn. (1)] were determined in methanol medium by monitoring the UV absorption at 305 nm due to the formation of diphenyl disulfide (PhSSPh).

$$H_2O_2 + 2PhSH \xrightarrow{\text{Catalyst}} 2H_2O + PhSSPh \qquad (1)$$

Diselenide **6** showed a slight enhancement in the rate (v_0 = 0.55 ± 0.18 μmol dm^{-3} min^{-1}) as compared with the uncatalyzed rate (v_0 = 0.15 ± 0.04 μmol dm^{-3} min^{-1}). Ferrocene was inactive, however, *N*,*N*-dimethyl(ferrocenylethyl)amine, a ferrocene compound containing a basic amino group showed a much better activity (v_0 = 3.16 ± 0.52 μmol dm^{-3} min^{-1}). The rate (v_0 = 3.83 ± 0.32 μmol dm^{-3} min^{-1}) observed for **6** together with *N*,*N*-dimethyl(ferrocenylethyl)amine was equal to the sum of the rates observed for the individual cases (v_0 = 3.71 ± 0.70 μmol dm^{-3} min^{-1}). There was a significant improvement in the activity when the phenyl groups in **6** were replaced by redox active ferrocenyl groups, **7** (v_0 = 3.39 ± 0.37 μmol dm^{-3} min^{-1}). The activity of **7** could not be enhanced by the addition of *N*,*N*-dimethyl(ferrocenylethyl)amine as the rate of the mixed case (v_0 = 5.78 ± 0.79 μmol dm^{-3} min^{-1}) was almost equal to the sum of their rates in the individual cases (v_0 = 6.55 ± 0.45 μmol dm^{-3} min^{-1}). The initial rate in the presence of crystalline Wilson's catalyst (**3**), which has been previously used as liquid or HCl salt,[6a] was 28.38 ± 3.88 μmol dm^{-3} min^{-1}. Surprisingly, under similar conditions, the initial rates for the redox-active diselenides **8** and **9** were 574.01 ± 23.98 and 466.49 ± 28.26 μmol dm^{-3} min^{-1}, respectively. Diselenides **10**, **11** and **12** did not show any noticeable activity under identical conditions.

Almost 18 fold enhancement in the initial reduction rate of **8** and **9** compared with the Wilson's catalyst and *ca*. 900 fold enhancement compared with PhSeSePh under identical experimental conditions was observed. Although compounds **3**, **8** and **9** have similar amino groups, the large increase in the activities of **8** and **9** as compared with **3** indicates that the presence of redox-active group is crucial for high peroxidase activity of **8** and **9**. On the other hand, while compound **7** is much more reactive than **6**, the observation that **7**, whose redox potential§ is as low as those of **8** and **9**, is much less reactive than **8** or **9** clearly suggests that the nearby nitrogen moiety should be equally responsible for activity enhancement of **8** and **9**. In other words, these two functionalities (tertiary amino and redox-active) individually show moderate effects on the activity, however, when present together (**8** and **9**), the effect is synergistic.

The Se···N interaction of an intermediate strength (2.856 and 2.863 Å) in **3** shows moderate effect on the activity whereas, the most active compounds **8** and **9** do not have any such interactions in the solid state as the Se···N bond lengths (3.697 and 4.296 Å for **8**; 3.98 and 4.12 Å for **9**[11b]) are greater than the

sum of their van der Waals radii (3.54 Å). However, the activity of **8** and **9** cannot be regarded as evidence for unimportance of nearby nitrogen since the nitrogen atoms present in the compounds may come closer to the selenium in solution. The inactivity of **10**, **11** and **12** [in which the Se···N interactions are quite strong; **10** (2.705, 2.891 Å), **11** (2.778, 2.794 Å) and **12** (2.628, 2.652 Å)], may be ascribed not only to steric effect, but also to the nature of the nitrogen lone pairs which are either imine lone pair (**10**, **11**) or a lone pair in π-conjugation (**12**), suggesting that they are not basic enough to incorporate in the redox cycle.

In conclusion, we observe that the diselenides which have quite strong Se···N intramolecular interactions do not show any noticeable activity whereas the diselenides which have in-built coordinating basic amino group but do not have Se···N interaction show excellent activity. Secondly, the diselenides in which the selenium atom is directly bonded to a redox active group (ferrocenyl) show a dramatic increase in the peroxidase activity thus supports the supposition made by Back and Dyck.[5a]

We are grateful to the Royal Society of Chemistry, London for funding this work. R. J. B. wishes to acknowledge the DoD-ONR program for funds to upgrade the diffractometer.

Notes and References

† Compound **10**: yield: 60%, mp 158–160 °C. Compound **11**: yield: 40%, mp 120–122 °C. Compound **12**: yield: 60%, mp 136 °C (decomp.). Satisfactory elemental analyses were obtained for all new compounds.

‡ *Crystallographic data*: **8**: $C_{28}H_{36}Fe_2N_2O_2Se_2$, M = 670.21, orthorhombic space group $P2_12_12_1$, a = 10.7903(11), b = 15.1341(12), c = 17.7815(14) Å, V = 2903.7(4) Å^3, Z = 4, D_c = 1.533 Mg m^{-3}, $R(R_w)$ = 0.0511(0.0870), T = 293(2) K, μ = 3.524 mm^{-1}, observed reflections = 4597. **10**: $C_{22}H_{24}N_2O_2Se_2$, M = 506.36, rhombohedral, space group $R\bar{3}$ a = 33.198(4), c = 10.564(2) Å, V = 10083(2) Å^3, Z = 18, D_c = 1.501 Mg m^{-3}, $R(R_w)$ = 0.0500(0.0837), T = 293(2) K, μ = 3.319 mm^{-1}, observed reflections = 4884. **11**: $C_{22}H_{24}N_2O_2Se_2$, M = 506.35, orthorhombic, space group $P2_12_12_1$, a = 8.778(3), b = 12.643(3), c = 20.268(4) Å, V = 2249.2(11) Å^3, Z = 4, D_c = 1.495 Mg m^{-3}, $R(R_w)$ = 0.0456(0.0869), T = 293(2), μ = 3.306 mm^{-1}, observed reflections = 2167. **12**: $C_{24}H_{24}N_2Se_2$, M = 498.37, orthorhombic, space group $P2_12_12_1$, a = 7.6738(10), b = 11.0274(11), c = 26.127(3) Å, V = 2210.9(4) Å^3, Z = 4, D_c = 1.497 Mg m^{-3}, $R(R_w)$ = 0.0564(0.1015), T = 293(2) K, μ = 3.356 mm^{-1}, observed reflections = 2839. CCDC 182/1016.

§ Supporting electrolyte 0.1 M Et_4NClO_4 in MeCN, SCE reference electrode, scan rate 50 mV s^{-1}. Compounds **7**–**9** undergo two quasi-reversible one-electron oxidations at relatively low potentials (**7**: 0.60, 0.79 V; **8**: 0.44, 1.02 V; **9**: 0.45, 1.08 V) whereas the other diselenides undergo irreversible oxidations at higher potentials (**3**: 1.02 V; **6**: 1.82 V; **10**: 0.97 V; **11**: 1.04 V; **12**: 0.95 V); ferrocene: 0.45 V.

1 L. Flohé, G. Loschen, W. A. Günzler and E. Eichele, *Hoppe-Seyler's Z. Physiol Chem.*, 1972, **353**, 987; *Selenium in Biology and Human Health*, ed. R. F. Burk, Springer-Verlag, New York, 1994; L. Flohe, *Curr. Top. Cell. Regul.*, 1985, **27**, 473; A. L. Tappel, *Curr. Top. Cell. Regul.*, 1984, **24**, 87; O. Epp, R. Ladenstein and A. Wendel, *Eur. J. Biochem.*, 1983, **133**, 51.

2 A. Müller, E. Cadenas, P. Graf and H. Sies, *Biochem. Pharmacol.*, 1984, **33**, 3235; A. Wendel, M. Fausel, H. Safayhi, G. Tiegs and R. Otter, *Biochem. Pharmacol.*, 1984, **33**, 3241; M. J. Parnham and S. Kindt, *Biochem. Pharmacol.*, 1984, **33**, 3247; A. Wendel, *Eur. Pat.*, 0,165,534, 1985.

3 P. V. Jacquemin, L. E. Christiaens, M. J. Renson, M. J. Evers and N. Dereu, *Tetrahedron Lett.*, 1992, **33**, 3863.

4 V. Galet, J.-L. Bernier, J.-P. Hénichart, D. Lesieur, C. Abadie, L. Rochette, A. Lindenbaum, J. Chalas, J.-F. Renaud de la Faverie, B. Pfeiffer and P. Renard, *J. Med. Chem.*, 1994, **37**, 2903.

5 (*a*) T. G. Back and B. P. Dyck, *J. Am. Chem. Soc.*, 1997, **119**, 2079; (*b*) H. J. Reich, C. P. Jasperse, *J. Am. Chem. Soc.*, 1987, **109**, 5549.

6 (*a*) S. R. Wilson, P. A. Zucker, R.-R. C. Huang and A. Spector, *J. Am. Chem. Soc.*, 1989, **111**, 5936; (*b*) M. Iwaoka and S. Tomoda, *J. Am. Chem. Soc.*, 1994, **116**, 2557; (*c*) A. Spector, S. R. Wilson and P. A. Zucker, *US Pat.*, 321,138 (C1.546-224; C07C37/02) 1994; (*Chem. Abstr.*, 1994, **121**, P256039r); (*d*) M. Iwaoka and S. Tomoda, *J. Am. Chem. Soc.*, 1996, **118**, 8077.

7 L. Engman, D. Stern, I. A. Cotgreave and C. M. Andersson, *J. Am. Chem. Soc.*, 1992, **114**, 9737; L. Engman, D. Stern, M. Pelcman and C. M. Andersson, *J. Org. Chem.*, 1994, **59**, 1973; K. Vessman, M. Ekström, M. Berglund, C. M. Andersson and L. Engman, *J. Org. Chem.*, 1995, **60**, 4461.

8 Z.-P. Wu and D.Hilvert, *J. Am. Chem. Soc.*, 1989, **111**, 4513; Z.-P. Wu and D. Hilvert, *J. Am. Chem. Soc.*, 1990, **112**, 5647.

9 (*a*) R. Kaur, H. B. Singh and R. P. Patel, *J. Chem. Soc., Dalton Trans.*, 1996, 2719; (*b*) R. Kaur, H.B. Singh and R. J. Butcher, *Organometallics*, 1995, **14**, 4755; (*c*) S. C. Menon, H. B. Singh, J. M. Jasinski, J. P. Jasinski and R. J. Butcher, *Organometallics*, 1996, **15**, 1707; (*d*) S. C. Menon, H. B. Singh, R. P. Patel, K. Das and R. J. Butcher, *Organometallics*, 1997, **18**, 563.

10 M. Herberhold and P. Leitner, *J. Organomet. Chem.*, 1987, **336**, 153.

11 (*a*) Y. Nishibayashi, J. D. Singh, S. Uemura and S. Fukuzawa, *Tetrahedron Lett.*, 1994, **35**, 3115; (*b*) Y. Nishibayashi, J. D. Singh, S. Uemura and S. Fukuzawa, *J. Org. Chem.*, 1995, **60**, 4114.

Received in Cambridge, UK, 29th July 1998; 8/05941A

Observation of a photochemical reaction on the TiO_2 (110) surface by atomic force microscopy

Phillip Sawunyama,[a] Akira Fujishima*[a,b] and Kazuhito Hashimoto*[a,c]

[a] *Kanagawa Academy of Science and Technology, 1583 Iiyama, Atsugi, Kanagawa 243-0297, Japan*
[b] *Department of Applied Chemistry, University of Tokyo, 7-3-1 Hongo, Bunkyo-ku, Tokyo 113-8656, Japan*
[c] *Research Center for Advanced Science and Technology, University of Tokyo, Komaba, Meguro-Ku, Tokyo 153-8904, Japan.*
E-mail: kazuhito@fchem.t.u-tokyo.ac.jp

A photocatalytic surface reaction—the decomposition of a submonolayer of stearic acid mediated by a rutile TiO_2 (110) single crystal—is examined by atomic force microscopy and the results reveal that the reaction occurs at substantially distinct rates at randomly distributed nanoscale surface sites.

The photocatalytic properties of TiO_2 are very interesting and are utilised in many situations. For example, ultraviolet irradiation of TiO_2 produces an amphiphilic surface with both antifogging and self-cleaning properties.[1–3] TiO_2 photocatalytic reactions, like many other surface reactions, have been studied for many years by macroscopic techniques such as vibrational spectroscopy. However, in the last decade, scanning probe techniques such as atomic force microscopy (AFM) have brought new insight on the morphology and molecular structure and periodicity of surfaces. In the present study, we examine the surface reactivity of rutile TiO_2 (110) during the photodecomposition of monolayer islands of stearic acid ($C_{17}H_{35}COOH$) using the AFM.

The submonolayer film of stearic acid was deposited onto a clean and polished rutile TiO_2 (110) single crystal substrate by way of the Langmuir–Blodgett (LB) technique. Film transfer was performed at 15 mN m^{-1} (area ≈ 0.201 nm^2 $molecule^{-1}$) at 20 °C in a clean room. The obtained film was imaged by contact-mode AFM (Seiko Instruments: SPA300 AFM system with a SPI3700 controller) under ambient conditions (T ≈ 20 °C, relative humidity = 40%) using a commercially available triangular Si_3N_4 sharpened cantilever. The force between the tip and sample was typically 1 nN. The UV light source was a Hypercure 200 UV lamp (Yamashita Denso, long wave UV λ_{max} ≈ 365 nm) equipped with a light guide. Incident UV light intensity (measured using a UV radiometer: Topcon UVR-1) at the sample surface was *ca*. 2.5 mW cm^{-2}. In a typical experiment, the tip was withdrawn from the sample before UV light irradiation. After irradiating for a predetermined period, the light was switched off and the tip reengaged for image recording. A representative AFM image before irradiation is shown in Fig. 1(a). A notable feature is the perfectly circular nature of the islands. In two-dimensional phase separated systems, circular domains are thermodynamically favourable and are formed as a result of the minimisation of surface energy through a reduction in interfacial length and curvature.[4,5]

The surface morphological changes upon UV light irradiation are depicted in Fig. 1(b)–(e). The reactivity pattern and reaction trends are very intriguing. Fig. 1(b) imaged at 5 min reaction shows the inhomogeneous pitting or etching of the island as stearic acid molecules photodecomposed. Typical hole diameters were in the range of 24 nm to 100 nm, with an average depth of *ca*. 0.9 nm (hole-depth range ≈0.0–2.25 nm, *cf.* a fully extended stearic acid molecule[6] has a chain length of ≈2.5 nm), corresponding to an estimated 2250 to 40000 stearic acid molecules having undergone photodecomposition, respectively. It should be noted that at this stage of the reaction the organic film comprises a mixture of adsorbed stearic acid as well as possible oxygenated alkyl intermediate molecules.[7] Likewise, we note that imaging of the island edges at higher resolutions revealed no clear trends in bulk island contraction. An island

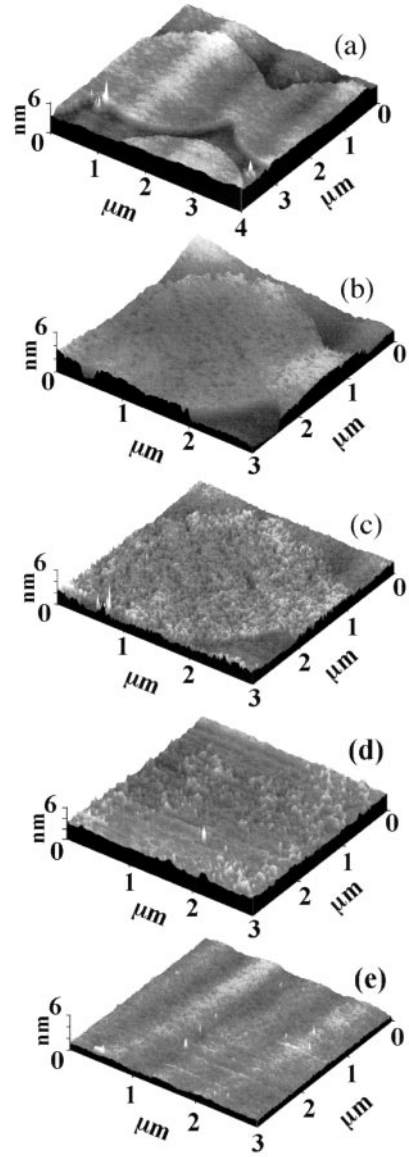

Fig. 1 Sequential 3-D AFM images of the rutile TiO_2 (110) mediated photodecomposition of stearic acid islands. Image (a) is 4 × 4 μm in size whereas all the other images are 3 × 3 μm. The images were obtained after: (a) 0, (b) 5, (c) 10, (d) 20, and (e) 60 min of UV light irradiation, respectively. Incident light intensity at the sample surface ≈2.5 mW cm^{-2}.

contraction scenario would arise if molecules at the edges photodecomposed at a faster rate than those in the interior. However, inhomogeneous decomposition at the edges as well as the interior suggests that the distribution of surface active sites governs surface reactivity. On analysing numerous other islands, we obtained the same randomisation phenomenon. With further irradiation, an even more peculiar reactivity pattern unfolds as depicted in Fig. 1(c) and (d). The surface morphology after irradiating for 10 min reveals a startling merging of holes to generate a mosaic, which eventually disappears with progress of reaction. At 20 min reaction [Fig. 1(d)], the island structure is no longer discernible. Prolonged irradiation resulted in the complete photodecomposition of the stearic acid molecules to CO_2 and H_2O.[8,9] That the reaction goes to completion was corroborated by parallel FT-IR experiments. Further control experiments in which monolayers of stearic acid were deposited onto CaF_2 substrates revealed that TiO_2 is essential for the photodecomposition of stearic acid.

The photodecomposition process is considered to proceed *via* two main oxidative routes, direct hole oxidation and $^{\cdot}OH$ oxidation.[10–12] The observed inhomogeneous reactivity pattern appears to mirror the momentary distribution of the surface active sites. Thus, the spatial localisation of the reaction appears to be largely influenced by the nature and composition of the photocatalyst. Spatially localised electrochemical reactions on TiO_2 surfaces have also been observed by scanning electrochemical microscopy.[13,14] In conclusion, this study reveals that a TiO_2 photocatalytic reaction is spatially localised and occurs at different rates at randomly distributed surface sites.

P. S. gratefully acknowledges financial support from the Science and Technology Agency. We thank Dr L. Jiang for assistance with the AFM measurements.

Notes and References

1 R. Wang, K. Hashimoto, A. Fujishima, M. Chikuni, E. Kojima, A. Kitamura, M. Shimoshigoi and T. Watanabe, *Nature*, 1997, **388**, 431.
2 R. Wang, K. Hashimoto, A. Fujishima, M. Chikuni, E. Kojima, A. Kitamura, M. Shimoshigoi and T. Watanabe, *Adv. Mater*., 1998, **10**, 135.
3 A. Heller, *Acc. Chem. Res*., 1995, **28**, 503.
4 C. M. Knobler, *Science*, 1990, **249**, 870.
5 W. H. Mulder, *J. Phys. Chem. B*, 1997, **101**, 7744.
6 A. Ulman, *An Introduction to Ultrathin Organic Films from Langmuir–Blodgett to Self-Assembly*, Academic Press, Boston, 1991.
7 K. Ikeda, H. Sakai, R. Baba, K. Hashimoto and A. Fujishima, *J. Phys. Chem. B*, 1997, **101**, 2617.
8 S. Sitkiewitz and A. Heller, *New J. Chem*., 1996, **20**, 233.
9 P. Sawunyama, L. Jiang, A. Fujishima and K. Hashimoto, *J. Phys. Chem. B*, 1997, **101**, 11 000.
10 U. Stafford, K. A. Gray, P. V. Kamat and A. Varma, *Chem. Phys. Lett*., 1993, **205**, 55.
11 E. R. Carraway, A. J. Hoffmann and M. R. Hoffmann, *Environ. Sci. Technol*., 1994, **28**, 786.
12 K. Hashimoto, T. Kawai and T. Sakata, *J. Phys. Chem*., 1984, **88**, 4083.
13 N. Casillas, S. J. Charlebois, W. H. Smyrl and H. S. White, *J. Electrochem. Soc*., 1994, **141**, 636.
14 S. B. Basame and H. S. White, *J. Phys. Chem.*, 1995, **99**, 16 430.

Received in Cambridge, UK, 27th July 1998; 8/05848B

A new strategy for the elaboration of pyrrolidine *N*-oxides using the reverse-Cope elimination

Jane R. Hanrahan and David W. Knight*†

Chemistry Department, Cardiff University, PO Box 912, Cardiff, UK CF1 3TB

Condensations of the unsaturated nitrones 13 with lithiated methyl phenyl sulfone provide excellent yields of the unsaturated hydroxylamines 14 as single stereoisomers, which undergo rapid reverse-Cope elimination at ambient temperature, assisted by the constraint of the acetonide ring, leading to the pyrrolidine *N*-oxides 15 as single enantiomers.

As its name suggests, the reverse-Cope elimination is a reaction wherein a hydroxylamine and an alkene contained within the same molecule **1** undergo an addition reaction to give a cyclic *N*-oxide **2**. Originally discovered by the groups of House,[1] Black[2] and Oppolzer,[3] it is only relatively recently that the method has come to prominence, particularly due to the pioneering studies of Ciganek[4] who defined much of its scope and limitations as a useful approach to pyrrolidine *N*-oxides. Despite some earlier speculation,[1] results reported in a seminal paper by Oppolzer's group[5] provide excellent evidence that the transformation is a thermal pericyclic process related to the ene reaction. Subsequently, the latter group applied the reaction as a key step in a synthesis of the alkaloids lycorane and trianthine;[5] other neat applications by the Holmes group have further served to demonstrate the synthetic potential of the reverse-Cope process in the formation of pyrrolidines and also of cyclic nitrones, by related intramolecular additions of hydroxylamines to acetylene groups.[6] Our own contributions (Scheme 1) to this area have been centred around the use of condensation reactions between various unsaturated nucleophiles **3** and aldonitrones **4** to generate suitable hydroxylamines **5** which then undergo the reverse-Cope reaction to give a variety of five-membered heterocycles **6** [Nu = NMe, S, $PhSO_2CH$] and derivatives thereof.[7] With a view to extending the flexibility of the latter pyrrolidine *N*-oxide synthesis, we wondered whether suitable unsaturated hydroxylamines **8** could be generated by nucleophilic additions to molecules **7** containing both nitrone and alkene functions, with the idea of obtaining *N*-oxides **9** (Scheme 2). This idea also gave us an opportunity to test another speculation regarding the reverse-Cope elimination: would the rate of the reaction be increased if the two

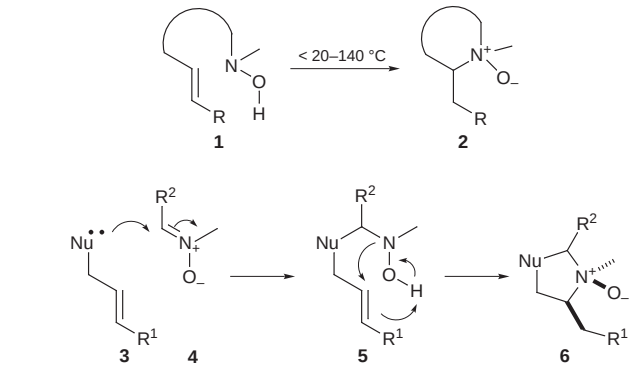

Scheme 1

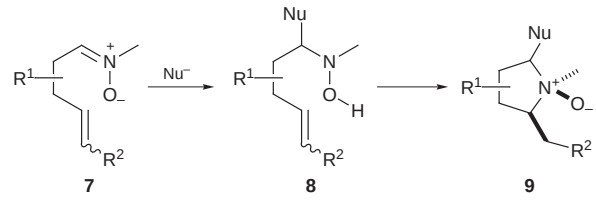

Scheme 2

reacting groups were held together by a second ring? In general, when a substituent is present on the terminus of the alkene group [*i.e.* **7**: $R^2 \neq H$], the rate of the reaction is slowed substantially, which can be a serious constraint when the sensitivity of the product precludes significant heating to induce cyclisation.[2,7] Ciganek in particular[4] has demonstrated the value of remote geminal substituents in aiding reverse-Cope cyclisations, presumably by a Thorp–Ingold effect, and we therefore felt that incorporation of a second ring would prove at least as effective. Herein, we report our first experiments in this area which have resulted in a new and highly stereoselective approach to pyrrolidine *N*-oxides and a somewhat unexpected stereochemical outcome.

We reasoned that an ideal starting material to test these ideas was D-ribose; protection of the primary hydroxy group as a silyl ether and acetonide formation[8] provided derivative **10** in which the acetonide ring provided the required constraint and the residual functionality the opportunity to incorporate the nitrone and alkene groups (Scheme 3). Subsequent Wittig homologation, crucially using potassium *tert*-butoxide as the base, led to good yields of the alkenes **11**, with the *E*/*Z* ratios shown. As the distal stereocentre would be removed if the reverse-Cope cyclisations were to be successful, we made no attempt to separate these isomers. Desilylation and diol cleavage then delivered the aldehydes **12** which were smoothly converted into the corresponding nitrones **13** under standard conditions.

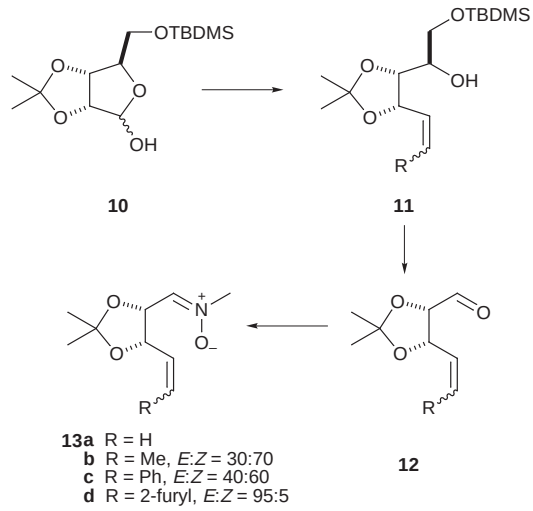

Scheme 3

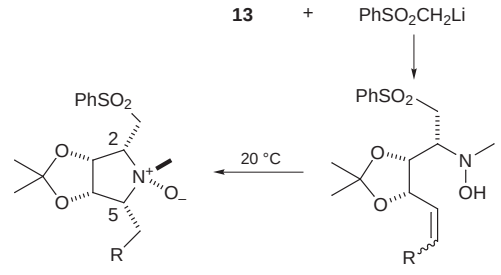

15a R = H, 1 h, 83%
b R = Me, 1 h, 83%
c R = Ph, 5 h, 65%
d R = 2-furyl, 2 h, 88%

Scheme 4

Addition of lithiated methyl phenyl sulfone (Scheme 4) to the nitrones **13** at −78 °C in THF, followed by warming to ambient temperature, quenching with aq. NH_4Cl and extractive work-up, delivered the expected[7] hydroxylamines **14**, essentially as single stereoisomers, according to ^1H and ^{13}C NMR analyses. At this stage, we did not know the configuration of the newly created stereocentre, although comparative spectroscopic data not unreasonably indicated that this was the same sense in each example. However, we suspected that the isomers shown (**14**) were formed, based on the work of the Dondoni group and the associated Houk model for such additions.[9] Further meaningful measurements was precluded when we were pleased to observe that the desired reverse-Cope elimination was already taking place as these analyses were being carried out. As indicated in Scheme 4, the cyclisations proceeded to completion remarkably quickly at ambient temperature in $CHCl_3$ solution, the slowest being the phenyl substituted analogue **14c** which, even so, only required 5 h. The final products **15** were purified by rapid column chromatography; following a brief elution with 5% MeOH–CH_2Cl_2, the rather polar *N*-oxides **15** were eluted as pure compounds using neat MeOH in the isolated yields shown (Scheme 4).

Each product was isolated as a single enantiomer, according to ^1H and ^{13}C NMR data. Detailed NMR analysis, in particular NOE measurements,[10] supported the all-*cis* structures **15** shown and was also consistent with the Dondoni–Houk conclusions concerning the initial carbanion addition.[9] This, perhaps at first, surprising result can be explained by the transition state conformation **16** wherein the alkene and hydroxylamine functions can line up in such a way as to allow for maximum orbital overlap, as indicated in the alternative view **17**. Molecular models indicate that such overlap is less favourable in the alternative chair-like conformation; attempts to quantify this argument are in progress. Such a transition state conformation is similar to one we have previously deduced to explain the stereochemical outcome of the reverse-Cope cyclisations summarized in Scheme 1.[7]

The remarkable ease with which the present cyclisations occur, presumably due to the additional ring constraint, together with the fact that this allows for the incorporation of additional functionality, suggests that this route should find many applications in the stereoselective synthesis of highly substituted pyrrolidines and derivatives thereof, in particular, the more difficult to obtain all-*cis* isomers. Studies aimed at exploiting this are in progress.

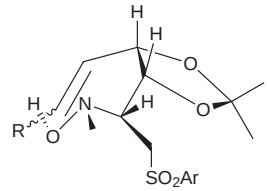

16

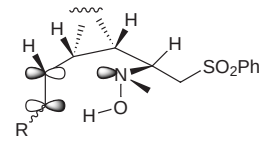

17

We are very grateful the EPSRC for generous support of this work (PDRA to J. R. H.) and to the EPSRC Mass Spectrometry service at Swansea University for the provision of high resolution mass spectral data..

Notes and References

† E-mail: knightdw@cf.ac.uk

1 H. O. House, D. T. Manning, D. G. Melillo, L. F. Lee, O. R. Haynes and B. E. Wilkes, *J. Org. Chem*., 1976, **41**, 855; H. O. House and L. F. Lee, *J. Org. Chem*., 1976, **41**, 863.
2 D. St. C. Black and J. E. Doyle, *Aust. J. Chem*., 1978, **31**, 2317.
3 W. Oppolzer, S. Siles, R. L. Snowden, B. H. Bakker and M. Petrzilka, *Tetrahedron Lett*., 1979, 4391.
4 E. Ciganek, *J. Org. Chem*., 1995, **60**, 5803; E. Ciganek, J. M. Read and J. C. Calabrese, *J. Org. Chem*., 1995, **60**, 5795.
5 W. Oppolzer, A. C. Spivey and C. G. Bochet, *J. Am. Chem. Soc*., 1994, **116**, 3139. For a theoretical study of the reverse-Cope elimination, see I. Komaromi and J. M. J. Tronchet, *J. Phys. Chem. A*., 1997, **101**, 3554.
6 A. B. Holmes, J. Collins, E. C. Davison, A. J. Rudge, T. C. Stork and J. A. Warner, *Pure Appl. Chem*., 1997, **69**, 531; E. C. Davison, I. T. Forbes, A. B. Holmes and J. A. Warner, *Tetrahedron*, 1996, **52**, 11601 and references cited therein.
7 K. E. Bell, M. P. Coogan, M. B. Gravestock, D. W. Knight and S. R. Thornton, *Tetrahedron Lett*., 1997, **38**, 8545; M. P. Coogan, M. B. Gravestock, D. W. Knight and S. R. Thornton, *Tetrahedron Lett*., 1997, **38**, 8549; D. W. Knight, M. P. Leese and A. R. Wheildon, *Tetrahedron Lett*., 1997, **38**, 8553.
8 T. V. RajanBabu, W. A. Nujent, D. F. Taber and P. J. Fagan, *J. Am. Chem. Soc*., 1988, **110**, 7128.
9 A. Dondoni, F. Junquera, F. L. Merchán, P. Merino and T. Tejero, *Tetrahedron Lett*., 1992, **33**, 4221; A. Dondoni, F. Junquera, F. L. Merchán, P. Merino, M.-C. Scherrmann and T. Tejero, *J. Org. Chem*., 1997, **62**, 5484.
10 *Selected data* for **15a**: $[\alpha]_D^{20}$ +16.1 (*c* 0.51, CH_2Cl_2), $\delta_H(CDCl_3)$ 1.18 (3H, s, CH_3), 1.41 (3H, s, CH_3), 1.48, (3H, d, *J* 6.5, 5-CH_3), 2.95 (3H, s, N-CH_3), 3.25 (1H, dq, *J* 6.5 and 6.5, 5-H), 3.52 (1H, dd, *J* 15.0 and 6.5, CH_aH$_b$SO$_2$), 3.85 (1H, ddd, *J* 9.0, 6.5 and 4.0, 2-H), 4.05 (1H, dd, *J* 15.0 and 4.0, CH$_a$*H*$_b$SO$_2$), 4.50 (2H, m, 3- and 4-H), 7.35–7.50 (3H, m, ArH) and 7.80 (2H, m, ArH); $\delta_C(CDCl_3)$ 11.4 (5-CH_3), 25.1 (CH_3), 27.4 (CH_3), 53.1 (N-CH_3), 55.0 (CH_2SO_2), 77.0 (2-CH), 78.4 (5-CH), 83.1 [3(4)-CH], 83.4 [4(3)-CH], 115.5 (OCO), 128.6 and 129.8 (both 2 × ArCH), 134.7 (ArCH) and 139.5 (ArC); *m/z* [ES] 342 (M^+ + H, 100%) [Found: M^+ + H, 342.1375. $C_{16}H_{23}NO_5S$ requires *M*, 342.1375]. Selected NOE data: 2-H/5-H (5.9%); 2-H/N-Me (2.6%); 5-H/N-Me (2.3%); 5- Me/N-Me (< 1%); N-Me/CH_2SO_2 (< 1%).

Received in Liverpool, UK, 10th August 1998; 8/06335D

$[Tl(OPPh_3)_2][Au(C_6F_5)_2]$: the first extended unsupported gold–thallium linear chain

Olga Crespo,[a] Eduardo J. Fernández,[b] Peter G. Jones,[c] Antonio Laguna,*[a] José M. López-de-Luzuriaga,[b] Aránzazu Mendía,[b] Miguel Monge[b] and Elena Olmos[b]

[a] *Departamento de Química Inorgánica, Instituto de Ciencia de Materiales de Aragón, Universidad de Zaragoza-CSIC, E-50009 Zaragoza, Spain. E-mail: alaguna@posta.unizar.es*

[b] *Departamento de Química, Universidad de La Rioja, Obispo Bustamante 3, E-26001 Logroño, Spain*

[c] *Institüt für Anorganische und Analytische Chemie der Technischen Universität, Postfach 3329, D-38023 Braunschweig, Germany*

$Li[Au(C_6F_5)_2]$ reacts with $TlNO_3$ in the presence of $OPPh_3$ affording a complex of stoichiometry $[AuTl(C_6F_5)_2(OPPh_3)_2]_n$, which presents different luminescence properties depending on the conditions and whose crystal structure reveals the existence of unsupported Au–Tl bonds forming a polymeric linear chain.

There is a renewed interest in mixed gold–transition metal compounds because of their fascinating and unique chemical and physical properties. A central issue in their chemistry is the study of closed-shell metal–metal interactions, which have been attributed to correlation effects that are strengthened by the relativistic effects for gold.[1] Structural and theoretical evidence has been accumulated for an entire family of cation–cation interactions between d^8–d^{10}–s^2 systems.[2] Particularly interesting are extended linear chain compounds, because the rationalization of the bonding of these structures still remains as a challenge.[3,4] For instance, $Tl_2Pt(CN)_4$,[5] with a Tl–Pt distance of 3.14 Å, was expected to be ionic with some covalent character[6] although correlation effects and the crystal-field contributions seem to be also important.[7] In contrast, $[AuTl\{Ph_2P(S)CH_2\}_2]$,[3,8] with a shorter Tl–Au distance (3.003 Å), displays mainly ionic bonds between Tl^+ and $[AuX_2]^-$ moieties.[2] This latter unit is also present in the polymeric species $[AgAuX_2L_2]$,[9,10] where X is a pentafluorophenyl group, thus avoiding any bridging effect. Mössbauer spectroscopic studies of such species indicate that $[Au(C_6F_5)_2]^-$ groups act as Lewis bases; the presence of perfluorophenyl groups seems to be the key for their donor properties,[11] which are similar to those postulated for dinuclear units of the form $[Au(ylide)]_2$.[12–14]

Despite the results previously reported, $[Au(C_6F_5)_2]^-$ has not hitherto been employed in the synthesis of other heterometallic compounds. We report here the synthesis and characterization of $[Tl(OPPh_3)_2][Au(C_6F_5)_2]$ (**1**), the first extended unsupported gold–thallium linear chain. This material is formed by reacting a mixture of triphenylphosphine oxide and a solution of $TlNO_3$ in MeOH with a freshly prepared solution of $Li[Au(C_6F_5)_2]$ in diethyl ether at −78 °C. The $LiNO_3$ formed is filtered off and the colourless solution is layered with pentane. Yellow-green crystals of complex **1** are collected after three days in a 40% yield. Compound **1** shows analytical and spectroscopic data in accordance with the proposed structure† and behaves as a 1 : 1 electrolyte in acetone. The absence of colour in ether or acetone solution implies that the interactions between the metal centres are restricted to the solid state.

In contrast, when the same reaction is carried out with the NBu_4^+ instead of the lithium salt, the complex is not formed and the gold(I) starting material is recovered unaltered. However, treatment of $[Au(C_6F_5)_2Cl(PPh_3)]$ with equimolecular amounts of thallium acetylacetonate surprisingly affords complex **1**. The mechanism of such a reaction is not clear, but it involves the reduction of the gold(III) centre and the oxidation of the triphenylphosphine.

The structure of **1** was determined by single-crystal X-ray diffraction[15]‡ (Fig. 1). The two independent gold atoms lie on inversion centres and thus display exact linear co-ordination by the C_6F_5 groups with Au–C distances of 2.058(5), 2.053(6) Å, whereas the thallium centre is bonded to two $OPPh_3$ ligands [O(1)–Tl–O(2) = 80.61(3)°] with typical Tl–O distances of 2.483(3) and 2.550(4) Å. The compound forms a one-dimensional polymer parallel to the crystallographic *x* axis. Including the metal–metal interactions, the geometry at gold is almost square planar and that at thallium is distorted trigonal bipyramidal with a vacant equatorial co-ordination site, presumably associated with the stereochemically active lone pair. The Tl–Au distances [Au(1)–Tl = 3.0358(8), Au(2)–Tl = 3.0862(8) Å] are nearly equal and similar to the sum of thallium and gold metallic radii (3.034 Å). They are similar to those found in $[AuTl(Ph_2P(S)CH_2)_2]_n$ [Tl–Au(intramolecular) = 2.959(2), Tl–Au(intermolecular) = 3.003(2) Å],[3,8] where two 'supporting', $Ph_2P(S)CH_2$ ligands are C-bonded to each gold centre and S-bonded to each thallium atom of a linear chain in which the metallic centres exhibit similar geometries as in **1**. Complex **1** may be considered as containing $[Au(C_6F_5)_2]^-$ and

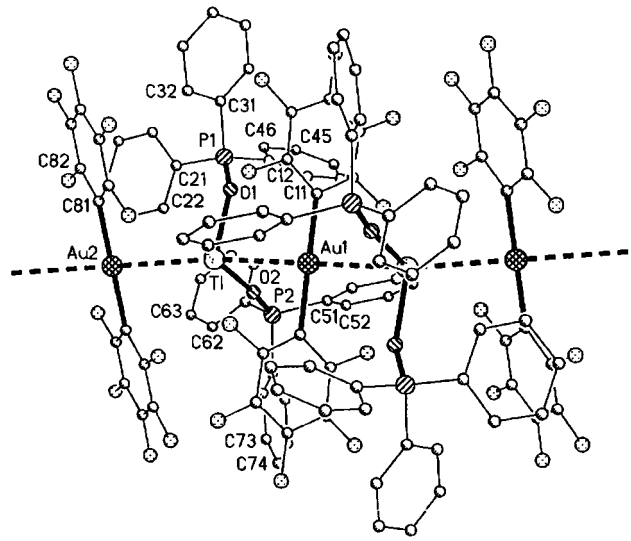

Fig. 1 Molecular structure of complex **1**. Selected distances (Å) and angles (°): Au(1)–C 2.058(5), Au(2)–C 2.053(6), Au(1)–Tl 3.0358(8), Au(2)–Tl 3.0862(8), Tl–O(1) 2.483(3), Tl–O(2) 2.550(4), C(11)–Au(1)–Tl 90.8(2), $C(11)^i$–Au(1)–Tl 89.2(2), C(81)–Au(2)–Tl^{ii} 88.0(2), C(81)–Au(2)–Tl 92.0(2), O–Tl–O 80.61(13), O(1)–Tl–Au(1) 94.73(11), O(2)–Tl–Au(1) 86.16(11), O(1)–Tl–Au(2) 99.04(11), O(2)–Tl–Au(2) 105.55(11), Au(1)–Tl–Au(2) 163.163(8). Symmetry operators: i $-x, -y+1, -z$; ii $-x+1, -y+1, -z$.

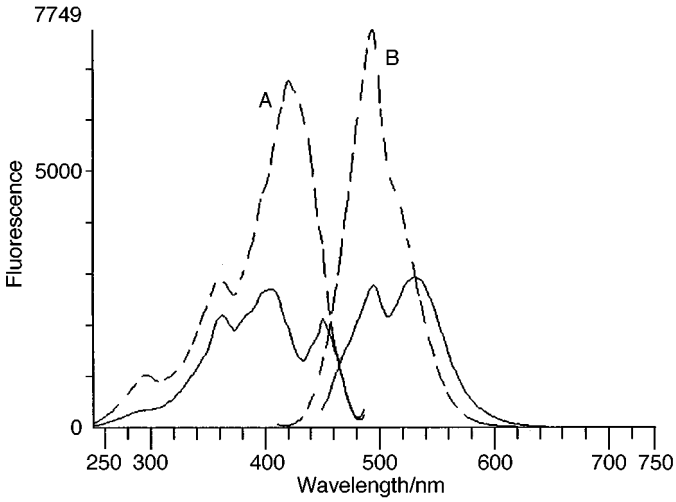

Fig. 2 Excitation and emission spectra of complex **1** in the solid state at 293 K (dashed line) and at 77 K (solid line) (excitation in curve **A**, emission in curve **B**)

$[Tl(OPPh_3)_2]^+$ ions, which are linked by weak M–M′ bonds thus forming the first unsupported Au–Tl linear chain. Four weak Tl···F contacts (3.313–3.488 Å) may also contribute to the stability of the system.

Furthermore, the heteronuclear complexes $[AuTl(Ph_2P(S)CH_2)_2]$ and $[Au_2Pb(Ph_2P(S)CH_2)_4]$[3,8] with d^{10} and s^2 electronic configurations are luminescent and also form linear Au–M linear chains. Similarly, complex **1** luminesces both at room temperature (293 K) (excitation at 421 nm, emission at 494 nm) and at 77 K (maximum excitation at 403 nm, emission at 494 and 530 nm) in the solid state (Fig. 2). The excitation and emission spectra for **1** are virtually mirror images of each other with only a small separation between excitation and emission peaks, suggesting that the dominant emission in this complex is perhaps fluorescence.

Previous Fenske–Hall molecular orbital calculations for a gold–thallium complex[3,8] indicated that although no formal metal–metal single bond is present, the HOMO is a σ* orbital mainly of Tl(I) and the LUMO is a σ orbital of both Au(I) and Tl(I) orbitals. Thus, a feature of this excited state is that the transfer of an electron from an antibonding orbital to a bonding orbital results in a net increase of intermetallic bonding in the excited state, but the luminescence spectrum suggests that there is no change in the Au–Tl distances in this linear chain species.

Neither the gold(I) nor Tl(I) precursor complexes are luminescent under similar conditions suggesting that the emission is a result of interactions between the metals. Moreover, when the product is dissolved in non-halogen solvents the green colour of the solid disappears and the resultant colourless solution is non-emissive. Evaporation of the solvents regenerates the colour and its optical properties. Another interesting feature is when **1** is saturated with halogenated solvents and irradiated with UV light, the emission is also quenched but, upon evaporation of the solvent, it does not regenerate the green product, but instead an uncharacterized grey solid appears which shows an emission at higher energy (476 nm). If the process of dissolution in CH_2Cl_2 is carried out in the dark, the green product is recovered without any change. This promising result seems to indicate that under UV radiation the excited state is able to react with halocarbons in an electron transfer reaction, perhaps making this product appropriate for practical applications.

We are grateful to Professor J. P. Fackler, Jr. for his helpful discussions and the facilities for using his laboratory material. This work was supported by the D.G.E.S. (PB97-1010-C02-02), the University of La Rioja (API-98/B09) and the Fonds der Chemischen Industrie.

Notes and References

† Selected data for **1**: (Calc. for $C_{48}H_{30}AuF_{10}O_2P_2Tl$: C, 44.51; H, 2.33. Found: C, 44.14; H, 2.00%). IR: ν(P=O): 1178 (vs); C_6F_5: 1503 (vs), 957 (vs), 784 (m) cm^{-1}. $^{31}P\{^1H\}$ NMR ($CDCl_3$): δ 30.0 (s, $OPPh_3$); ^{19}F NMR ($CDCl_3$): δ −115.4 (m, F_o), −158.6 (t, J 20 Hz, F_p), −161.8 (m, F_m). MS (FAB+): m/z(%) = 761(5) $[M]^+$; MS (ES): m/z(%) = 531(100) $[M]^-$. Λ (5.0×10^{-4} M, acetone): 113 Ω^{-1} cm^2 mol^{-1}.

‡ *Crystal data* for **1**: $C_{48}H_{30}AuF_{10}O_2P_2Tl$, T = −100 °C, M = 1292.00, monoclinic, space group $P2_1/n$, a = 12.112(3), b = 27.006(3), c = 13.515(2) Å, β = 91.891(12)°, V = 4418.2(14) $Å^3$, Z = 4, μ = 7.11 mm^{-1}, 10486 reflections (Siemens P4 diffractometer, Mo-Kα radiation, $2\theta_{max}$ 50°, ω-scans), 7764 unique. Refinement on F^2 using all reflections; program system SHELXL-93. Final R = 0.0305, R_w = 0.0456, for 581 parameters and 544 restraints; max. $\Delta\rho$ 0.6 e $Å^{-3}$. CCDC 182/1021.

1 P. Pyykkö and F. Mendizabal, *Inorg. Chem.*, 1998, **37**, 3018.
2 P. Pyykkö, *Chem. Rev.*, 1997, **97**, 597.
3 S. Wang, G. Garzón, C. King, J.-C. Wang and J. P. Fackler, Jr., *Inorg. Chem.*, 1989, **28**, 4623.
4 J. S. Miller, *Extended Linear Chain Compounds*, Plenum, New York and London, 1981–1983, vol. 1–3.
5 J. K. Nagle, A. L. Balch and M. M. Olmstead, *J. Am. Chem. Soc.*, 1988, **110**, 319.
6 T. Ziegler, J. K. Nagle, J. G. Snijders and E. J. Baerends, *J. Am. Chem. Soc.*, 1989, **111**, 5631.
7 M. Dolg, P. Pyykkö and N. Runeberg, *Inorg. Chem.*, 1996, **35**, 7450.
8 S. Wang, J. P. Fackler, Jr., C. King and J.-C. Wang, *J. Am. Chem. Soc.*, 1988, **110**, 3308.
9 R. Usón, A. Laguna, M. Laguna, P. G. Jones and G. M. Sheldrick, *J. Chem. Soc., Chem. Commun.*, 1981, 1097.
10 R. Usón, A. Laguna, M. Laguna, B. R. Manzano, P. G. Jones and G. M. Sheldrick, *J. Chem. Soc., Dalton Trans.*, 1984, 285.
11 K. Moss, R. V. Parish, A. Laguna, M. Laguna and R. Usón, *J. Chem. Soc., Dalton Trans.*, 1983, 2071.
12 J. D. Basil, H. H. Murray, J. P. Fackler, Jr., J. Tocher, A. M. Mazany, B. Trzcinska-Bancroft, H. Knachel, D. Dudis, T. J. Delord and D. O. Marler, *J. Am. Chem. Soc.*, 1985, **107**, 6908.
13 H. Schmidbaur, C. Hartmann, J. Riede, B. Huber and G. Müller, *Organometallics*, 1986, **5**, 1652.
14 R. Usón, A. Laguna, M. Laguna, M. T. Tartón and P. G. Jones, *J. Chem. Soc., Chem. Commun.*, 1988, 740.
15 SHELX-93, A Program for Refining Crystal Structures, G. M. Sheldrick, University of Göttingen, Germany.

Received in Basel, Switzerland, 3rd August 1998; 8/06077K

A novel [2,3] intramolecular rearrangement of *N*-benzyl-*O*-allylhydroxylamines

Stephen G. Davies,*† Simon Jones, Miguel A. Sanz, Fátima C. Teixeira and John F. Fox

The Dyson Perrins Laboratory, University of Oxford, South Parks Road, Oxford, UK OX1 3QY

A novel [2,3]-sigmatropic rearrangement whereby *N*-benzyl-*O*-allylhydroxylamines undergo transformation to the corresponding *N*-allylhydroxylamines, which can subsequently be reduced to the corresponding allylamines, is described and evidence for the intramolecular nature of this process presented.

Intramolecular sigmatropic rearrangements have found widespread use in synthetic organic chemistry primarily due to the high selectivities observed in these transformations. In particular, effective use has been made of a variety of [2,3] processes, such as the Meisenheimer[1] and Stevens rearrangements[2] to control stereochemistry as they tend to proceed at significantly lower temperatures than [3,3] processes[3] and thus lead to better observed selectivities. For example, Anderson *et al.* have recently developed an aza-[2,3]-Wittig rearrangement which proceeds with excellent stereocontrol.[4]

During continuation of our lithium amide studies[5] we discovered that *N*-benzyl-*O*-allylhydroxylamine gives *N*-allyl-*N*-benzylhydroxylamine when treated with n-BuLi, a process which may be attributed to a novel [2,3] sigmatropic rearrangement analogous to the [2,3] Wittig rearrangement.[6] We now report our initial investigations into the nature of this rearrangement and demonstrate its synthetic use.

The substrates for all of the rearrangements were easily prepared in two steps and high yield starting from *syn*-benzaldehyde oxime **1** (Scheme 1). *O*-Allylation was achieved by formation of the potassium salt of the oxime and subsequent quenching by treatment with the appropriate allyl bromide.[7] The *O*-allyl oximes **2a**–**d** were reduced with pyridine–borane complex in EtOH–10% HCl to give the desired substrates **3a**–**d** in excellent overall yield.[8] In most cases purification of the intermediates and substrates was achieved by distillation.

The rearrangement was carried out by treatment of the simple *N*-benzyl-*O*-allylhydroxylamine **3a** in dry THF with 1 equiv. of n-BuLi at −78 °C for 1 h, followed by warming to room temperature for 30 min before quenching with water. This afforded the [2,3] rearrangement product **4a** in essentially quantitative yield by examination of the crude ^{1}H NMR spectrum. Purification of this compound proved to be difficult due to decomposition, although it was finally achieved by chromatography on previously deactivated silica gel (1% Et_3N). The hydroxylamine thus obtained as an oil was isolated in 61% yield and the structure confirmed by ^{1}H and ^{13}C NMR spectroscopy and HRMS. With conditions for the rearrangement identified,‡ it was repeated for the other substrates (Scheme 2). All gave the [2,3] rearrangement product, although in the case of the rearrangement to a trisubstituted centre (**3c** → **4c**), the reaction was found to be only 10% complete by ^{1}H NMR spectroscopy after 48 h. However, by heating the reaction mixture to reflux for 2 h after the initial addition of n-BuLi at −78 °C, the reaction proceeded to completion and the [2,3] product was obtained in 60% isolated yield. The hydroxylamines formed in all of these reactions were all very prone to decomposition during purification. Thus, isolated yields of the allylhydroxylamines were always considerably lower than the quantitative yields for the crude reaction observed by ^{1}H NMR spectroscopy. Attempted thermal rearrangement of **3a** by heating under reflux in xylene for 7 h led to only a trace amount of the desired rearrangement product in the ^{1}H NMR spectrum (< 5%).

The rearrangement of the crotylhydroxylamine **3b** rules out the possibility of a 1,2 anionic shift which would have given rise to the *N*-benzyl-*N*-crotylhydroxylamine instead of the observed product. However the possibility still existed that the reaction was intermolecular and not intramolecular. In order to demonstrate that the process was indeed intramolecular the rearrangement was carried out with two different substrates **3b** and **5** with 2 equiv. of n-BuLi (Scheme 3). If an intermolecular process was being observed then the mixed products **4a** and **7** from this rearrangement would be observed. All four of the possible products that could arise from this reaction were prepared in an analogous manner to the hydroxylamines prepared earlier. When the crude ^{1}H NMR spectrum of the mixed reaction was analysed, only peaks due to the respective intramolecular rearrangement products **4b** and **6** were present, and not the crossover products **4a** and **7** confirming that this reaction was indeed an intramolecular process.

Based on these results the reaction is comparable to a [2,3]-Wittig rearrangement, and thus reasonably proceeds *via* a transition state which is similar to that suggested for this process (Scheme 4).[6] Deprotonation of the N–H proton affords the

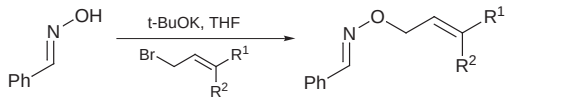

1

Compound	Yield
2a $R^1 = R^2 = H$	91%
2b $R^1 = H$, Me; $R^2 = Me$, H	86%
2c $R^1 = R^2 = Me$	89%
2d $R^1 = Ph$; $R^2 = H$	95%

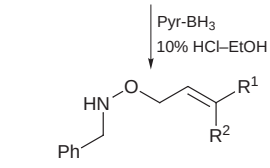

Compound	Yield
3a $R^1 = R^2 = H$	94%
3b $R^1 = H$, Me; $R^2 = Me$,H	85%
3c $R^1 = R^2 = Me$	80%
3d $R^1 = Ph$; $R^2 = H$	84%

Scheme 1

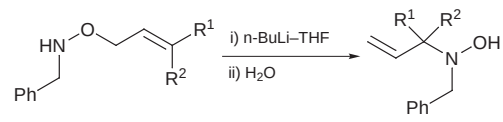

Compound	Compound	Yield[a]
3a $R^1 = R^2 = H$	**4a** $R^1 = R^2 = H$	61%
3b $R^1 = H$, Me; $R^2 = Me$, H	**4b** $R^1 = H$, Me; $R^2 = Me$, H	59%
3c $R^1 = R^2 = Me$	**4c** $R^1 = R^2 = M$ e	60%
3d $R^1 = Ph$; $R^2 = H$	**4d** $R^1 = Ph$; $R^2 = H$	40%

[a]Refers to isolated yields

Scheme 2

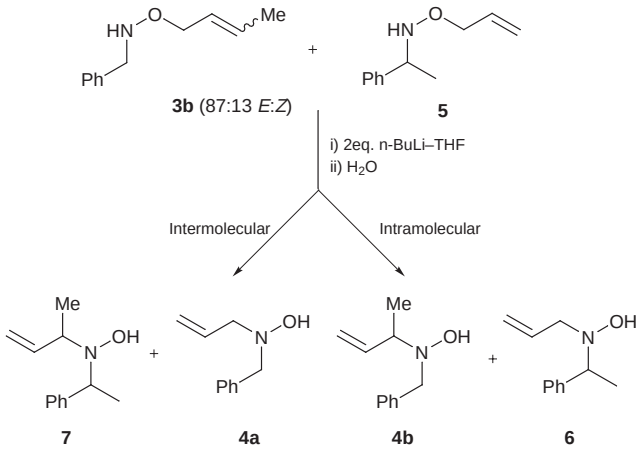

Scheme 3

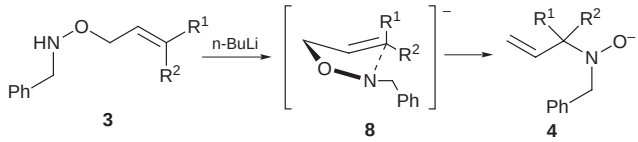

Scheme 4

lithium amide which rearranges through an envelope transition state **8**. The driving force for this reaction lies in the relative stability of the lithium oxy-anion **4** formed compared to the lithium amide precursor **8**, which is illustrated in the pK_a values of the corresponding alcohol and amine (pK_a EtOH = 15.9, pK_a $EtNH_2$ = 35). A similar [1,2] anionic process has been previously reported in which the anion derived from *N*,*O*-bis(trimethylsilyl)hydroxylamine rearranges to *N*,*N*-bis(trimethylsilyl)hydroxylamine.[9]

As already eluded to, the hydroxylamines produced were relatively unstable and were thus difficult to isolate or store for prolonged periods of time. However, the allylamines from which the hydroxylamines are derived are stable and are also useful synthons.[10] Thus, reduction of the hydroxylamines **4a**–**d** with Zn/2 M HCl at 80 °C for 1 h followed by neutralisation (NaOH) and extraction with Et_2O gave the respective amines **9a**–**d** in excellent yields (Scheme 5).

The versatility of this method for the synthesis of allylamines was demonstrated in the synthesis of *N*-allyl-*N*-benzylamine **9a**

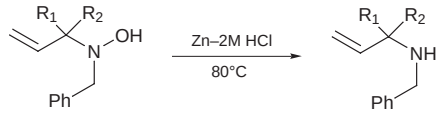

Compound	Compound	Yield
4a $R^1 = R^2 = H$	**9a** $R^1 = R^2 = H$	90%
4b $R^1 = H, Me$; $R^2 = Me, H$	**9b** $R^1 = H, Me$; $R^2 = Me, H$	94%
4c $R^1 = R^2 = Me$	**9c** $R^1 = R^2 = Me$	92%
4d $R^1 = Ph$; $R^2 = H$	**9d** $R^1 = Ph$; $R^2 = H$	91%

Scheme 5

which was prepared in a two step process by rearrangement of the parent hydroxylamine **3a** and subsequent reduction of the crude material to afford the desired allylamine **9a** in excellent overall yield (91%).§ In a similar manner the crotyl- and cinnamyl-hydroxylamines **3b** and **3d** were rearranged then immediately reduced to give the allylic amines **9b** and **9d** in 93 and 92% overall yield respectively.

In conclusion we report a novel [2,3] rearrangement of *N*-benzyl-*O*-allylhydroxylamines to give the corresponding *N*-allyl-*N*-benzylhydroxylamines, which may be reduced to the *N*-benzylallylamines with Zn/HCl. This provides a novel approach to the synthesis of allyl substituted hydroxylamines and amines.

We would like to thank the Ministerio de Educación y Ciência (M. A. S.) and J.N.I.C.T. (Programa Ciência and Praxis XXI) (F. C. T.) for provision of funding and Oxford Asymmetry for technical and financial support.

Notes and References

† E-mail: steve.davies@dpl.ox.ac.uk

‡ *Typical experimental procedure:* n-BuLi (1.66 M, 0.81 mL, 1.35 mmol) was added to a solution of **3a** (200 mg, 1.23 mmol) in anhydrous THF (15 mL) at −78 °C under N_2. After stirring for 1 h the reaction was allowed to warm to room temp. and stirred for a further 30 min. The reaction was quenched with distilled water (25 mL) and extracted with Et_2O (3 × 25 mL). The combined organic extracts were dried ($MgSO_4$) and concentrated *in vacuo*. The residue was purified by column chromatography on deactivated silica gel (1% Et_3N–petroleum ether) eluting with petroleum ether–Et_2O (6:1) to give the desired hydroxylamine **4a** as a clear yellow oil (122 mg, 61%).

§ *Typical proceedure for the reduction of the hydroxylamines*: **4a** (0.100 g, 0.61 mmol) was dissolved in 2 M HCl (5 mL) and zinc dust (0.200 g, 3.1 mmol) added cautiously. The reaction was heated at 80 °C for 1 h, cooled and neutralised with 2 M NaOH. The white suspension was extracted with Et_2O (3 × 15 mL) and dried ($MgSO_4$). Evaporation afforded **9a** (0.081 g, 90%).

Alternatively, the crude product **4a** obtained from rearrangement of **3a** was directly reduced by addition of 2 M HCl (3 mL) and zinc dust (0.200 g, 3.065 mmol) and heating at 80 °C. After 1 h the reaction was cooled, neutralised with 2 M NaOH, extracted with Et_2O (3 × 20 mL) and dried ($MgSO_4$). Evaporation afforded **9a** (0.082 g, 91% overall yield).

1 S. G. Davies and G. D. Smyth, *Tetrahedron: Asymmetry*, 1996, **7**, 1001.
2 P. A. Grieco, D. Boxler and K. Hirori, *J. Org. Chem.*, 1973, **38**, 2572.
3 R. W. Hoffmann, *Angew. Chem., Int. Ed. Engl.*, 1979, **18**, 563.
4 J. C. Anderson, D. C. Siddons, S. C. Smith and M. E. Swarbrick, *J. Chem. Soc., Chem. Commun.*, 1995, 1835.
5 S. G. Davies and O. Ichihara, *Tetrahedron: Asymmetry*, 1991, **2**, 183.
6 K. Mikami and T. Nakai, *Synthesis*, 1991, 594.
7 E. Buehler, *J. Org. Chem.*, 1967, **32**, 261.
8 M. Kawase and Y. Kikugawa, *J. Chem. Soc., Perkin Trans. 1*, 1979, 643.
9 R. West, P. Boudjouk and T. A. Matuszko, *J. Am. Chem. Soc.*, 1969, **91**, 5184.
10 For example, K. Burgess and M. J. Ohlmeyer, *J. Org. Chem.*, 1991, **56**, 1027; G. R. Cook and J. R. Stille, *J. Org. Chem.*, 1991, **56**, 5578.

Received in Liverpool, UK, 5th August 1998; 8/06200E

Highly selective chiral recognition on polymer supports: preparation of a combinatorial library of dihydropyrimidines and its screening for novel chiral HPLC ligands

Kevin Lewandowski, Peter Murer, Frantisek Svec and Jean M. J. Fréchet*†

Department of Chemistry, University of California, Berkeley, California, 94720-1460, USA

A library of more than 140 racemic 4-aryl-1,4-dihydropyrimidines has been synthesized using the single step Biginelli multicomponent condensation; the individual compounds were screened for enantiomer resolution, and the best candidate attached to a solid macroporous polymer support to afford a highly selective separation medium for chiral HPLC.

Combinatorial chemistry is a powerful tool for the rapid preparation of large numbers of different compounds that may be used in the development of new drug candidates and drugs,[1] metal complexing ligands,[2] polymers,[3] materials for electronics,[4] sensors,[5] peptidic ligands for affinity chromatography,[6] and in supramolecular chemistry.[7] The increasing awareness that individual enantiomers of drugs, agrochemicals, pheromones, flavors, fragrances and some other compounds have different interactions with biological systems drive both industry and academia to find means to replace racemates with their single enantiomers. Although the liquid chromatographic separation of enantiomers using chiral stationary phases (CSPs) has emerged only recently, a large number of chiral stationary phases (CSPs) are now commercially available.[8] Despite the variety of CSPs, none of these is universal and new chiral separation media must often be developed for the separation of specific compounds. The well-defined small molecule selectors pioneered by Pirkle[9] using chiral blocks derived from natural sources (amino acids) and porous silica as a support afford the most flexibility in the development of many different chiral stationary phases.

We have now designed an approach that uses combinatorial chemistry as a tool for the *rapid* development of novel, highly selective, chiral stationary phases for HPLC. Our approach applies the so-called principle of reciprocity, which has been introduced by Pirkle for the development of CSPs capable of separating important classes of pharmaceuticals. This principle states that if a single molecule of a chiral selector has different affinities for the enantiomers of another substance, then a single enantiomer of the latter will have different affinities for the enantiomers of the initial selector molecule.[10]

The reciprocal method is especially suitable for situations in which the target enantiomer is known and its separation from a racemate is required. Since chromatographic techniques are readily automated, a broad variety of novel chiral ligands may be considered. Scheme 1 illustrates the general concept of our approach. In the first step, a single enantiomer (+)-T of the target racemate is immobilized onto a suitable polymeric support[11] and the resulting CSP is used for the HPLC screening of a library of racemic compounds (potential selectors) that have been prepared using parallel combinatorial synthesis. The best separated member of this library (±)-S is then prepared as the single enantiomer [*e.g.* (−)-S], coupled to an optimized solid support,[11,12] and used in the second step for the required separation of the racemic target. While only two columns are required in this technique, the tradeoff for the simplicity of this approach is that the developed CSP is optimized for the enantioseparation of only one compound. In reality, this column may well separate other racemates as a result of cross selectivity, however, the α values may be lower.

We have demonstrated the feasibility of this concept with a parallel library of racemic 4-aryl-1,4-dihydropyrimidines (DHPMs) (±)-**1** [Scheme 2(A)]. The DHPM scaffold resulted from our search for novel chiral selectors that do not rely on chiral starting materials from natural sources. DHPMs are easily accessible by the Biginelli multicomponent cyclocondensation developed more than 100 years ago.[13] This simple one-pot reaction combines a β-keto ester or β-keto amide, with an aldehyde and a urea or thiourea. Since a large number of components for the condensation are commercially available, over 140 various DHPMs have been prepared using combinations of 25 aldehydes with six ureas or thioureas, and seven acetoacetates or acetoamides and tested in this initial study.

The library was screened with a chiral stationary phase that contains (*S*)-(3,5-dinitrobenzoyl)leucine (model target) attached to poly[(*N*-methyl)aminoethyl methacrylate-*co*-methyl methacrylate-*co*-ethylene dimethacrylate] beads[12] [Scheme 2(B)] using normal-phase mode HPLC conditions. The separation factor $\alpha = (t_2 - t_0)/(t_1 - t_0)$, where t_0 is the retention time of an unretained compound or column void volume determined using 1,3,5-tri-*tert*-butylbenzene as a marker and t_1 and t_2 are the retention times of the individual enantiomers, was calculated to measure the selectivity of the separation.

While some racemic DHPMs in the library are not resolved at all ($\alpha = 1.0$), α values of 5.2 and 11.7 were achieved for the top candidates 4-(9-phenanthryl)-2-oxo-DHPM (±)-**2** and its thioxo analogue (±)-**3** [Scheme 2(C)], respectively. A single crystal X-ray structure analysis of the 2-oxo compound reveals a cleft-like conformation of the aromatic and heterocyclic ring systems

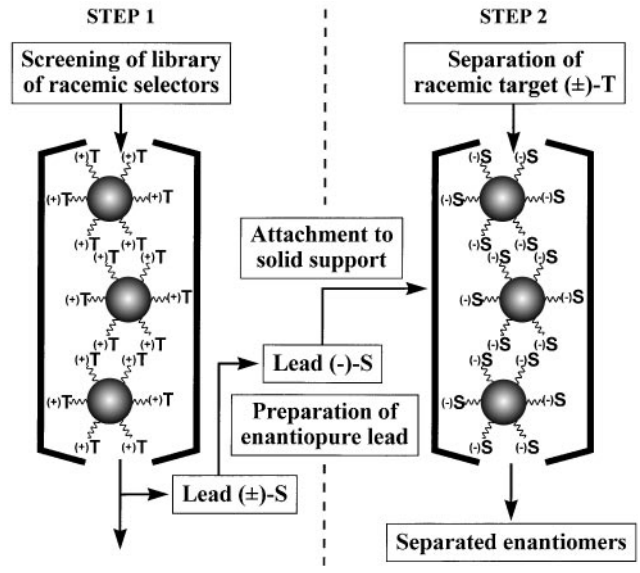

Scheme 1

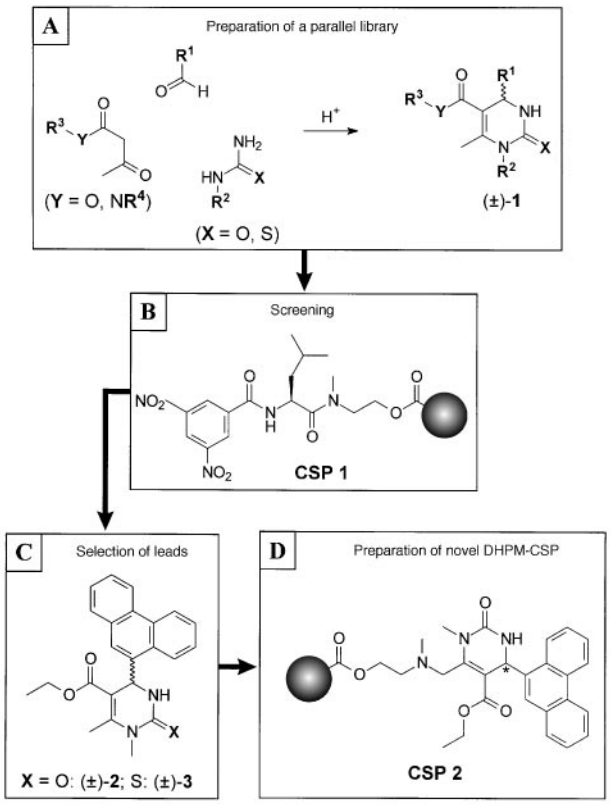

Scheme 2

that appears particularly well suited for sterically controlled interactions.

For the next step, the preparation of the actual CSP requires the preparation of one of the lead compounds in enantiomerically pure form, followed by attachment to a support. Although different routes to the desired single enantiomer can be designed, we simply separated it from the racemate using a semi-preparative column packed with CSP 1 used previously for the screening process. Attachment of the enantiopure selector to the amino functionalized macroporous polymethacrylate support requires its modification to include a suitable coupling site. Although hydrolysis of the ester group to a free carboxy group seems to be attractive, rather harsh conditions have to be used resulting in decomposition of the DHPM. Therefore, a more convenient route—bromination of the methyl group at the C6 position—was applied instead. Since the bromination step is not well suited for the 2-thioxo-DHPM, we used the best 2-oxo-DHPM compound from the library: 4-(9-phenanthryl)-2-oxo-DHPM (−)-**2**. Coupling of the brominated DHPM to the amino functionalized support affords CSP 2 [Scheme 2(D)] which contains 0.20 mmol g^{-1} of the selector. A variety of racemates including amino acid and non-steroid anti-inflammatory drug (profens) derivatives, and dihydropyrimidines were separated on CSP 2 with α values up to 8. These α values are rather high, especially if one considers that the unoptimized methodology used in this demonstration leads to a CSP with a loading of only 0.20 mmol g^{-1}. Although the selectivity may not always be a linear function of loading, the specific selectivity of DHMP selectors is actually higher than that of amino acid based selectors. Since dihydropyrimidines possess well-established pharmacological potential,[8] the ability of CSPs with DHPM selectors to separate these drugs is a very promising tool for the development of these and similar drugs in their single enantiomeric form.

Funding of this research by the National Institute of General Medical Sciences, National Institutes of Health (GM-44885) is gratefully acknowledged. P. M. thanks the Swiss National Science Foundation for a postdoctoral fellowship.

Notes and References

† E-mail: frechet@cchem.berkeley.edu

1 *Combinatorial Chemistry, Synthesis and Application*, ed. S. R. Wilson and A. W. Czarnik, Wiley, New York, 1997.
2 B. M. Cole, K. D. Shimizu, C. A. Krueger, J. P. A. Harrity, M. L. Snapper and A. H. Hoveyda, *Angew. Chem., Int. Ed. Engl.*, 1996, **35**, 1668.
3 S. Brocchini, K. James, V. Tangpasuthadol and J. Kohn, *J. Am. Chem. Soc.*, 1997, **119**, 4553.
4 L. C. Hsieh-Wilson, X. D. Xiang and P. G. Schultz, *Acc. Chem. Res.*, 1996, **29**, 164.
5 T. A. Dickinson and D. R. Walt, *Anal. Chem.*, 1997, **69**, 3413.
6 P. Y. Huang and R. G. Carbonell, *Biotechnol. Bioeng.*, 1995, **47**, 288.
7 Y. Cheng, T. Suenaga and W. C. Still, *J. Am. Chem. Soc.*, 1996, **118**, 1813.
8 *Chiral Separations, Applications and Technology*, ed. S. Ahuja, ACS, Washington D.C., 1997.
9 W. H. Pirkle and T. C. Pochapsky, *Chem. Rev.*, 1989, **89**, 347.
10 W. H. Pirkle, D. W. House and J. M. Finn, *J. Chromatogr.*, 1980, **192**, 143.
11 K. Lewandowski, F. Svec and J. M. J. Fréchet, *Chem. Mater.*, 1998, **10**, 385.
12 K. Lewandowski, P. Murer, F. Svec and J. M. J. Fréchet, *Anal. Chem.*, 1998, **10**, 1629.
13 P. Biginelli, *Gazz. Chim. Ital.*, 1893, **23**, 360.

Received in Corvallis, OR, USA, 11th August 1998; 8/06395H

One step transformation of tricyclopentabenzene (trindane) [$C_{15}H_{18}$] to 4-[1*R*,2*S*,4*R*,5*S*)-1,2,5-trihydroxy-3-oxabicyclo[3.3.0]octane-4 spiro-1′-(2′-oxocyclopentan)-2-yl]butanoic acid [$C_{15}H_{22}O_7$]

Subramania Ranganathan,*[a]† K. M. Muraleedharan,[a] Parimal Bharadwaj*[b] and K. P. Madhusudanan[c]

[a] *Biomolecular Research Unit, Regional Research Laboratory, Trivandrum 695019, India*
[b] *Department of Chemistry, Indian Institute of Technology, Kanpur 208016, India*
[c] *Medicinal Chemistry Division, Central Drug Research Institute, Lucknow 226001, India*

The complete, Ru(VIII) mediated oxidation of the benzene ring of trindane 1 is contained within the framework of peripheral methylenes to yield the unfragmented product 2.

This communication reports the formation of **2** on oxidation of trindane **1** with *in situ* generated Ru(VIII) species.

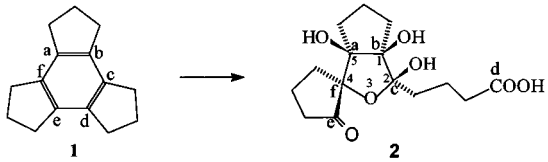

Trindane **1**, despite its ready availability,[1]‡ and being endowed with a three-fold symmetry, has hitherto attracted little synthetic interest.[2]§ In connection with the synthesis of benzene anchored three-fold symmetric systems, having pairs of donors and acceptors, that could lead to surfaces by self assembly, **1** was reacted with Ru(VIII) species, in anticipation of the oxidation of the six benzylic positions.§ The reaction gave no product from benzylic oxidation, but consistently afforded ~15% yields of a crystalline compound, mp 148–150 °C. The ^{13}C NMR spectrum coupled with DEPT studies suggested that the methylenes were intact and showed the presence of two types of carbonyls. The FAB (normal and negative ion) mass spectrum showed a molecular weight of 314. Elemental analysis was consistent with a molecular formula $C_{15}H_{22}O_7$ which when compared to the starting trindane ($C_{15}H_{18}$) amounts to the introduction of seven oxygens. The FTIR indicated the presence of hydroxy groups, cyclopentanone and another carbonyl peak at 1709 cm^{-1}.¶

Single crystal X-ray analysis‖ revealed the structure of the oxidation product as **2**. The crystal structure of **2** and selected interatomic parameters are presented in Fig. 1. All the bond distances and angles are within normal statistical bounds. The three five-membered rings are puckered.

A plausible reationalization of the **1** → **2** conversion, where oxidation is contained by the peripheral methylenes, is presented in Scheme 1.**

The basic framework of **2** is similar to that of ginkgolides,[3] a class of cytotoxic substances having therapeutic value. The one step transformation of hydrocarbon trindane to such condensed, highly oxygenated systems is noteworthy.

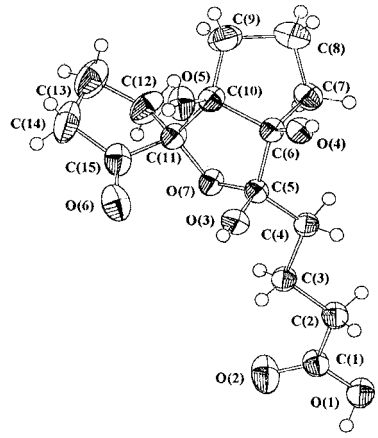

Fig. 1 The single-crystal X-ray structure of **2** with ellipsoids shown at 50% probability. For clarity the hydrogen atoms are not labelled. Selected bond lengths (Å) and angles (°): O(1)–C(1) 1.314(7), O(2)–C(1) 1.20(1), O(3)–C(5) 1.385(7), O(4)–C(6) 1.426(7), O(5)–C(10) 1.435(8), O(6)–C(15) 1.201(8), O(7)–C(5) 1.419(7), O(7)–C(11) 1.435(6); O(1)–C(1)–O(2) 122.6(6), O(1)–C(1)–C(2) 112.9(6), O(2)–C(1)–C(2) 124.5(5), O(3)–C(5)–O(7) 110.9(5), O(3)–C(5)–C(4) 108.1(4), O(3)–C(5)–C(6) 110.5(5), O(4)–C(6)–C(5) 110.0(4), O(4)–C(6)–C(7) 109.3(5), O(4)–C(6)–C(10) 112.7(5), O(5)–C(10)–C(6) 112.9(4), O(5)–C(10)–C(9) 112.9(5), O(5)–C(10)–C(11) 104.9(5), O(6)–C(15)–C(11) 124.6(5), O(6)–C(15)–C(14) 107.2(6), O(7)–C(11)–C(10) 106.3(4), O(7)–C(11)–C(12) 110.5(5), O(7)–C(11)–C(15) 110.2(5).

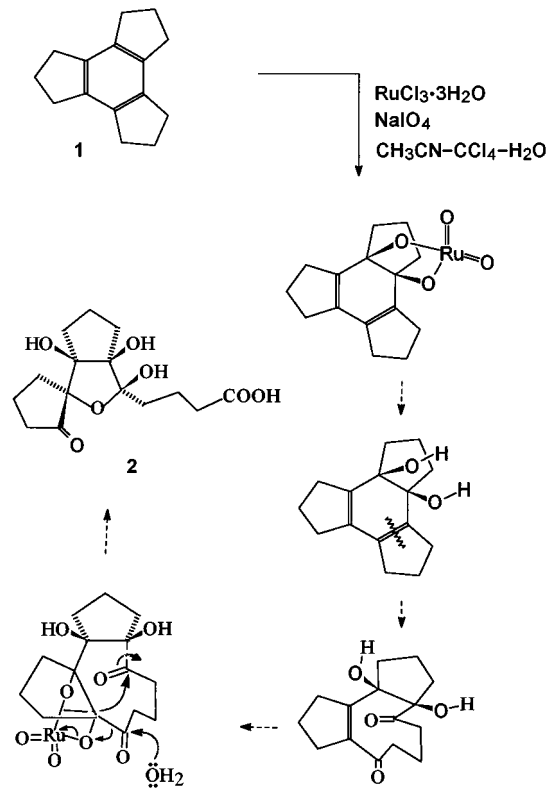

Scheme 1

The resemblance of **2** to sugars was highlighted by simultaneous isolation of **3**, by replacement of the anomeric hydroxy group during workup.††

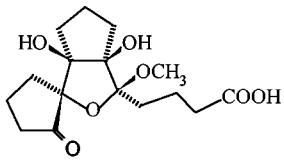

3

The formation of highly functionalized complex condensed systems in one step, by the containment of aromatic ring oxidation within peripheral, methylene groups should be a general reaction. The unpredictable course of such reactions coupled with the delineation of their structures, largely by X-ray crystallography, should provide incentives for exploration along these lines, and which are currently being pursued.‡‡

We are grateful to Indian National Science Academy, New Delhi for support.

Notes and References

† E-mail: ranga@csrrltrd.ren.nic.in

‡ A standardized procedure for **1** based on early reports (ref. 1) is given below:

Cyclopentanone (16 ml, 0.18 mol) in dry EtOH (18 ml) was mixed with conc. H_2SO_4 (8 ml dropwise), refluxed for 15 h, poured on to ice (~70 g), neutralised with sodium carbonate and extracted with CH_2Cl_2 (3 × 30 ml), washed with water, dried ($MgSO_4$), evaporated and chromatographed on a silica gel column using petroleum ether to get 4.0 g (33%) of **1** [mp 92 °C (lit.[1] 95–97 °C)].

§ To the best of our knowledge, the only report (ref. 2) pertains to benzylic hexabromination followed by zinc reduction to afford mixtures of dehydrogenated tricyclopentabenzenes.

¶ A mixture of trindane (0.495 g, 2.5 mmol), CH_3CN–CCl_4–H_2O (10 : 10 : 20 ml), $NaIO_4$ (9.63 g, 45 mmol), $RuCl_3{\cdot}3H_2O$ (2.2 mol%, ~0.015 g) was sealed, shaken for 3 h, cautiously opened, filtered, the residue washed with EtOAc (3 × 20 ml), the organic layers washed with water, dried, evaporated and chromatographed on a silica gel column. Elution with EtOAc–hexane (1 : 1) gave fractions containing **2** (TLC: R_f 0.25, $CHCl_3$–MeOH 9 : 1) which on concentration deposited crystals, mp 148–150 °C (0.120 g, ~15%), Anal. Found: C, 57.55; H, 7.33%. Calc. for $C_{15}H_{22}O_7$: C, 57.32; H, 7.00. ν(KBr, cm^{-1}) 3396, 2972, 1736, 1709, 1432, 1143; δ_H(300 MHz, $CDCl_3$–DMSO-d_6) 1.6–2.5 (m, CH_2), 4.4 (br, OH × 2), 5.9 (br, OH × 1), 7.7 (s, COOH); δ_C($CDCl_3$–DMSO-d_6) 16.19–34.66 (9 × CH_2), 85.99, 87.32, 93.04, 103.78 (4 × C-O), 174.40 (CO), 221.01 (CO); *m/z* (FAB) (neg) 313 (78%), *m/z* (FAB) (pos) + Na^+ 337 (77%).

‖ *Crystal data*: $C_{15}H_{22}O_7$, M_r = 314.332, triclinic, $P\bar{1}$, a = 7.510(4), b = 10.465(1), c = 10.624(4) Å, α = 110.62(4), β = 99.42(8), γ = 91.12(4)°, U = 768.2(6) $Å^3$, Z = 2, D_x = 1.359 g cm^{-3}, μ(Mo-Kα) 0.11 mm^{-1}. Data were collected at 298(1) K, for a crystal of dimensions 0.20 × 0.20 × 0.30 mm, on an Enraf–Nonius CAD4-mach 2 diffractometer. A total of 2939 unique data were collected. The data were corrected for Lorentz polarisation and decay. The structure was solved by the direct method and refined on F using the full matrix least-squares technique using XTAL 3.2 program package and a total of 2195 reflections [$I \geqslant 3\,\sigma(I)$]. The final R,R_w indices were 0.061 and 0.067 for 205 parameters (non-hydrogen atoms, anisotropic hydrogen atoms in idealized positions, C–H 0.96 Å, O–H 0.87 Å with a fixed U_{iso} of 0.10. CCDC 182/1018.

** The nature of **2** would need the oxidation of each carbon centre of the aromatic ring. However, the sequence of events envisaged in Scheme 1 is largely notional. The step leading to *cis* hydroxylation, envisaged as the first step, is required to control the stereochemical outcome of the reaction. Preference, if any, of the reagent addition in the second step is obliterated since the process leads to oxidative C–C scission. Molecular models clearly show that the critical third step requires addition of the reagent from the side *anti* to the *cis* hydroxy grouping—which seem to be dictated by steric factors—to enable the generation of the oxabicyclooctane unit in **2** by transannular addition with correct stereochemical disposition at centres 2 and 4 (Scheme 1).

†† The formation of **3**, which was isolated as a gum, in ~7% yield has been traced to the use of small amounts of MeOH as the co-eluent. A spectral comparison of **2** with this compound indicated a simple replacement of a HO group by MeO, which was confirmed by analytical and detailed spectral studies. ν (neat)/cm^{-1} 3434, 1735, 1445, 1175; δ_H(300 MHz, $CDCl_3$) 1.4–2.4 (m, CH_2), 3.48, 4.21 (s, s, OH × 2, exchangeable), 6.42 (s, COOH, exchangeable), 3.66 (OMe); δ_C($CDCl_3$) 17.05–38.05 (9 × CH_2), 51.48 (CH_3O), 85.95, 88.35, 95.17, 105.00 (4 × C-O), 174.00, 222.90 (2 × CO) (DEPT studies showed 9 × CH_2 and 1 × CH_3]; *m/z* (FAB) (neg) 327.

‡‡ The immediate higher homologues of trindane can be readily prepared from the cyclanones (ref. 1). They would be the natural targets of further studies.

1 R. Mayer, *Chem. Ber.*, 1956, **89**, 1443; F. Petru and V. Galik, *Chem. Listy*, 1957, **51**, 2371.
2 T. J. Katz and W. Slusarek, *J. Am. Chem. Soc.*, 1980, **102**, 1058.
3 P. Braquet, *Ginkgolides-Chemistry, Biology, Pharmacology and Clinical Perspectives*, J. R. Prous Science Publishers, Barcelona, 1988, vol. 1, p. xv; E. J. Corey and A. Y. Gavai, *Tetrahedron Lett.*, 1989, **30**, 6959; E. J. Corey, M.-C. Kang, M. C. Desai, A. K. Ghosh and I. N. Houpis, *J. Am. Chem. Soc.*, 1988, **110**, 649; D. Luca and P. Magnus, *J. Chem. Soc., Perkin Trans. 1*, 1991, 2661.

Received in Cambridge, UK, 1st August 1998; 8/05906C

The first fluoroalkylation of amino acids and peptides in water utilizing the novel iodonium salt $(CF_3SO_2)_2NI(Ph)CH_2CF_3$

Darryl D. DesMarteau*† and Vittorio Montanari

Department of Chemistry, Box 341905, Clemson University, Clemson, SC 29634-1905, USA

The novel iodonium salt $(CF_3SO_2)_2NI(Ph)CH_2CF_3$ is a powerful alkylating reagent which can be utilized in water to trifluoroethylate amino acids and peptides.

Fluorine-containing amino acids have been actively investigated in view of their high potential for biological studies and medical applications.[1] In particular, the use of ^{19}F NMR as a sensitive mechanistic probe has been intensively studied.[2] Synthetic routes to fluorinated amino acids normally involve several steps using fluorinated building blocks, mostly obtained by the conversion of carbon–heteroatom bonds to C–F bonds. A more direct approach to the introduction of fluorine into biochemically significant substrates might involve fluoroalkylations.[3] Cysteine and related amino acids and peptides can be alkylated by alkyl halides or esters if both the substrate and alkylating reagent can be solubilized in mixed water–organic solvents or in liquid ammonia.[4] However, simple fluorine containing alkyl halides and esters are of low reactivity in analogous alkylations. Increasing the reactivity by incorporation of fluoroalkyl groups into iodonium salts such as $CF_3CH_2I(Ph)O_3SCF_3$ is successful[3] but until now such compounds could not be employed in aqueous media or basic solvents since they are instantly destroyed under these conditions.

In contrast the novel iodonium salt $(CF_3SO_2)_2NI(Ph)CH_2CF_3$ (**1**) is unexpectedly stable to water. Herein we report the first fluoroalkylations in aqueous media and the application of **1** to the alkylation of representative biochemically significant substrates (Scheme 1).

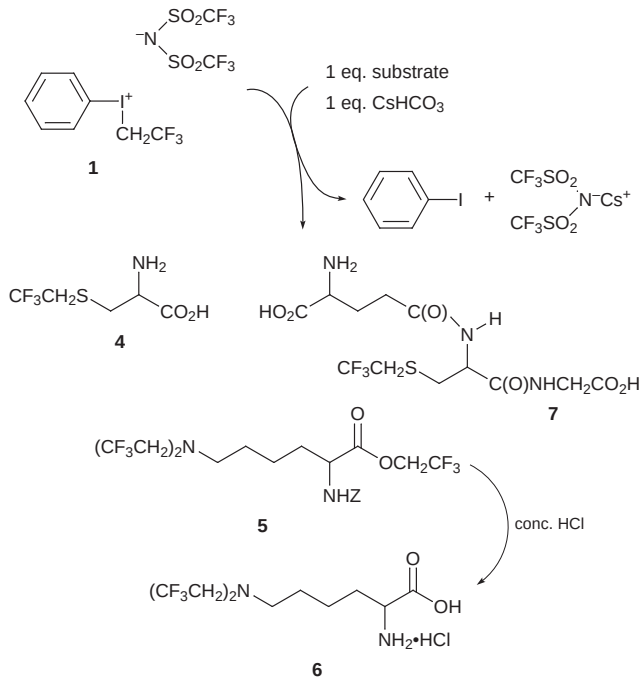

Scheme 1 Reaction of **1** with cysteine N^{α}-Z-lysine and glutathione and the trifluoroethylated products obtained

Bis(trifluoromethylsulfonyl)imide, $(CF_3SO_2)_2NH$ (**2**), originally devised for establishing the existence of Xe–N bonds,[5] is one of the strongest acids known in the gas phase.[6] Derivatives of the acid typically have unusual properties as exemplified by the *N*-fluoro compound which is a powerful fluorinating reagent.[7,8] Perfluoroionomers and ionene polymers made in this laboratory, containing the repeating $(R_fSO_2NXSO_2R'_f)$ unit (X = H or other cation) have high potential in solid polymer electrolyte fuel cells and polymer lithium batteries, and are promising superacid catalysts.[9] In connection with this research, it is useful to synthesize novel salts of **2** as model compounds for structure and reactivity studies. The first iodine(III) compound we prepared, $[Ph_2I]^+[N(SO_2CF_3)_2]^-$ (**3**), is a stable, low-melting compound (67 °C) and a strong arylating agent.[10] Encouraged by this result, a high-yield synthesis of **1** was developed.‡ We found that **1** immediately transfers the trifluoroethyl group to nucleophiles, such as aniline, in organic solvents. Surprisingly **1**, which is very slightly soluble in water, is hydrolyzed only slowly. This fact led us to investigate fluoroalkylation reactions in water as a solvent. Using simple amines as model compounds, we observed high yields of trifluoroethylamines from 1 equiv. each of **1**, substrate, and $NaHCO_3$.

Based on this novel result, our goal became the alkylation of amino acids. The reactive side-chain of cysteine and lysine were considered, anticipating that the products would be of interest for biochemical studies. *S*-Trifluoroethyl-L-cysteine (**4**) was readily obtained in 60–90% isolated yields.§ Fig. 1 shows the X-ray crystal structure of **4**.¶

Under the same conditions the commercially available N^{α}-Z-protected L-lysine unexpectedly reacted with 3 equiv. of **1** to give the ester $(CF_3CH_2)_2N(CH_2)_4CH(NH\text{-}Z)COOCH_2CF_3$ (**5**). Hydrolysis of **5** in 37% HCl gave N^{ε}-bis(trifluoroethyl)-L-lysine hydrochloride (**6**) in 60% overall yield.

Compounds **4** and **6** are modified in the side-chains but are otherwise normal amino acids: they can be converted into the Fmoc-protected acyl fluorides in good overall yield. This form of protection–activation is very useful in the assembly of peptides of any size according to many literature examples.[11] By means of these acyl fluorides the unlikely event of extensive racemization under our alkylation conditions could be easily ruled out: reaction with (*R*)- or (*S*)-phenethylamine gave

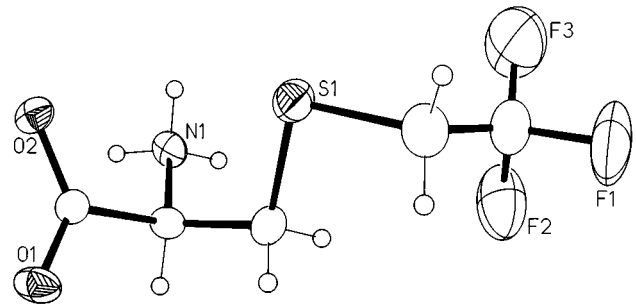

Fig. 1 Crystal structure of *S*-trifluoroethylcysteine **4** showing one of the two unique molecules in the unit cell

diastereoisomeric amides that are clearly distinguishable by ^{1}H and ^{19}F NMR.[12]

A different approach to the use of **1** is the direct reaction with a peptide having unprotected side-chains. We tested the reaction on glutathione (GSH, γ-Glu-Cys-Gly) because of its biochemical relevance and commercial availability in preparative amounts. Under the same conditions used for the preparation of **4**, we obtained complete conversion to a mixture of the desired *S*-trifluoroethylglutathione (**7**) and oxidized glutathione (**8**) in an 8:2 ratio. Compound **7** was separated from **8** by precipitation from water–ethanol.

In summary, we have reported that **1** reacts rapidly in water, under mildly alkaline conditions, with unprotected cysteine and glutathione, and with N^{α}-protected lysine, to give the novel amino acids **4** and **6**, and tripeptide **7**.

The covalent polar residue CF_3CH_2 can now be readily introduced into a variety of peptide building blocks or into suitable preassembled peptides. These results provide interesting potential for modifying the bioactivity of peptides and as probes for biochemical reactions.

The promise of **1** for the synthesis of other useful compounds, such as fluorine-tagged ligands for metal complexes,[13] is obvious, considering that the successful reactions described above were those with the greatest potential for failure, in our view. In fact, recent results show that the bis-fluoroalkylation observed with lysine is a general and facile reaction.[14]

Financial support of this research by the National Science Foundation is gratefully acknowledged. Crystallographic data were supplied by W. T. Pennington and G. Schimek.

Notes and References

† E-mail: fluorin@clemson.edu

‡ Bis(trifluoromethylsulfonyl)imide was obtained from its lithium salt (HQ-115™, 3M Co., St. Paul, MN) by vacuum sublimation from H_2SO_4 (see ref. 7). The other starting material $CF_3CH_2I(OCOCF_3)_2$, a hygroscopic solid that melts at 39–40 °C without decomposition, was prepared by oxidation of CF_3CH_2I with 50% H_2O_2 (available from Aldrich, Inc.) in TFAA under N_2 (3–5 d, RT). The preparation of **1** is simple, but anhydrous conditions must be maintained throughout the reaction. In a typical small-scale reaction, **2** (1.40 g, 5 mmol) was added under N_2, in one portion, into a solution of $CF_3CH_2(OCOCF_3)_2$ (2.16 g, 5 mmol) in CFC 113 (20 mL). This addition is endothermic. After 10 min, benzene (0.43 ml, 5 mmol) was rapidly added with ice–water cooling. The reaction mixture was allowed to return to 25 °C during 30 min and then stirred at 25 °C for 6 h. The volatiles were removed under vacuum and the residue was stirred with ice–water (50 ml) for 15 min. The precipitate was collected on a glass frit and freeze-dried to yield **1**, 1.28 g (46%) as a white powder, mp 77–79 °C. On a larger scale (up to 30 g of **1**) we have routinely obtained yields greater than 70%.

All other materials are commercially available and were used as received. The novel products **4–7** were fully characterized by ^{1}H, ^{19}F and ^{13}C NMR and elemental analysis.

§ Typical procedure. Cysteine (606 mg, 5 mmol), $CsHCO_3$ (968 mg, 5 mmol), and **1** (3.2 g, 5.6 mmol) were added into a degassed mixture of pH 10 buffer (Hydrion, Na_2CO_3–$NaHCO_3$, 20 mL) and CH_2Cl_2 (10 mL) at 5 °C under nitrogen with rapid stirring. The reaction mixture was allowed to return to 23 °C during 30 min. The aqueous phase was separated, neutralized and evaporated to a crystalline solid. This solid was refluxed twice in 30 mL CH_3CN to extract the Cs salt of **2**. The resulting powder was suspended in 10 mL water at pH 7, filtered through a syringe filter to remove insoluble cysteine and slowly evaporated to yield crystalline **4** (874 mg, 82%), $[\alpha]_D^{25}$ −15 (*c* 0.37, 4 M HCl).

¶ Crystal data of **4**: formula, $C_5H_8F_3NO_2S$; M = 203.2; monoclinic; $P2_1$(#4); T = 25 °C; a = 9.503(3), b = 5.166(3), c = 16.957(3) Å, β = 91.45(2)°; V = 832.2(6) Å^3; D_{calc} = 1.622 g cm^{-3}; Z = 4 (2 unique); μ = 0.40 mm^{-1}; empirical absorption correction (0.94–1.00); Mo-Kα radiation with graphite monochromator, λ = 0.71073 Å; Rigaku AFC7R diffractometer; 2119 measured reflections (R_{int} = 1.61%); 1676 reflections used with $F > 2\sigma(F)$; $2\theta_{max}$ = 55°; 217 parameters; non-H atoms refined anisotropically; H atoms fixed in calculated positions (C–H = 0.96 Å); full-matrix least-squares refinement; R = 4.68%/R_w = 5.93%. CCDC 182/1019.

1 *Biomedical Frontiers of Fluorine Chemistry*, ed. I. Ojima, J. R. McCarthy and J. T. Welch, ACS Symposium Series 639, 1996; *Fluorine-containing Amino Acids*, ed. V. P. Kukhar and V. A. Soloshonok, Wiley, New York, 1995.

2 Some recent papers: L. M. McDowell, M. S. Lee, R. A. McKay, K. S. Anderson and J. Schaefer, *Biochemistry*, 1996, **35**, 3328; H. Duewel, E. Daub, V. Robinson and J. F. Honek, *ibid*., 1997, **36**, 3404; I. Ojima, S. D. Kuduk, S. Chakravarty, M. Ourevitch and J. P. Begue, *J. Am. Chem. Soc*., 1997, **119**, 5519; R. A. Komoroski, *Anal. Chem*., 1994, **66**, 1024.

3 T. Umemoto, *Chem. Rev*., 1996, **96**, 1757.

4 V. du Vigneaud, L. F. Audrieth and H. S. Loring, *J. Am. Chem. Soc*., 1930, **52**, 4500; M. D. Armstrong and J. D. Lewis, *J. Org. Chem.*, 1950, **15**, 749; M. J. Brown, P. D. Milano, D. C. Lever, W. W. Epstein and D. C. Poulter, *J. Am. Chem. Soc.*, 1991, **113**, 3176; C. C. Yang, C. K. Marlowe and R. Kania, *ibid.*, 1991, **113**, 3177.

5 J. Fouropulos, Jr., and D. D. DesMarteau, *J. Am. Chem. Soc*., 1982, **104**, 4260.

6 I. A. Koppel, R. W. Taft, F. Anvia, S.-Z. Zhu, L.-Q. Hu, K. Sung, D. D. DesMarteau, L. M. Yagupolski, Y. L. Yagupolski, N. V. Ignatev, N. V. Kondratenko, A. Y. Volkonskii, V. M. Vlasov, R. Notario and P. C. Maria, *J. Am. Chem. Soc*., 1994, **116**, 3047.

7 D. D. DesMarteau and M. Witz, *J. Fluorine Chem.*, 1991, **52**, 7.

8 W. Ying, D. D. DesMarteau and Y. Gotoh, *Tetrahedron*, 1996, **52**, 15.

9 D. D. DesMarteau, *J. Fluorine Chem*., 1995, **72**, 203.

10 From the reaction of **3** with aniline (2 equiv.) in boiling water, diphenylamine was isolated in 30% yield. Only trace amounts are obtained under the same conditions with diphenyliodonium bromide: F. M. Beringer, A. Brierley, M. Drexler, E. M. Gindler and C. C. Lumpkin, *J. Am. Chem. Soc.*, 1953, **75**, 2708.

11 L. A. Carpino, M. Beyermann, H. Wenschuh and M. Bienert, *Acc. Chem. Res.*, 1996, **29**, 268, and refs. therein.

12 S-CF_3CH_2-FMOC-L-Cys-F was reacted with (−)-(*S*)-phenethylamine in water–$NaHCO_3$–CH_2Cl_2.[10] The same reaction was carried out on *S*-CF_3CH_2-Fmoc-(D,L)-Cys-F, prepared from racemic cysteine. *S*-CF_3CH_2-Fmoc-L-Cys-NHCHMePh was a single product by ^{1}H and ^{19}F NMR. *S*-CF_3CH_2-Fmoc-(D,L)-Cys-NHCHMePh was clearly a 1:1 mixture of two compounds [δ_F($CHCl_3$–$CFCl_3$) −66.99, −67.00]. Because the starting material for **6** is only available in the L form, **6** was converted into $N^{\varepsilon}(CF_3CH_2)_2$-$N^{\alpha}$-Fmoc-L-Lys-F, which was reacted separately with (−)-(*S*)- and (+)-(*R*)-phenethylamine. Each amide was identified by NMR. Equal amounts of the two amides were combined, and the mixture showed two compounds by both ^{1}H and ^{19}F NMR [δ_F ($CHCl_3$–$CFCl_3$) −70.83, −70.86].

13 K. Severin, R. Bergs and W. Beck, *Angew. Chem., Int. Ed.*, 1998, **37**, 1086.

14 Ms J. Sayers, NSF-SURP 1997, obtained from 4-aminobutyric acid (GABA) and **1** under the same simple conditions $(CF_3CH_2)_2N(CH_2)_3CO_2CH_2CF_3$ in very high yield (NMR). A non-volatile, easily isolated analog was obtained from GABA phenylethyl ester hydrochloride. The yield of $(CF_3CH_2)_2N(CH_2)_3CO_2C_2H_4Ph$ was 70%, representing more than 80% per alkylation step: D. D. DesMarteau, J. Sayers and V. Montanari, manuscript in preparation.

Received in Corvallis, OR, USA, 27th July 1998; 8/05879B

Stereochemical study on cyclic acetal formation during anodic oxidation of naphthalene derivatives by transformation of chiral alcohol to achiral acetal

Morifumi Fujita,*† Masaki Ohshiba, Shohei Shioyama, Takashi Sugimura* and Akira Tai

Faculty of Science, Himeji Institute of Technology, Kanaji, Kamigori, Ako-gun, Hyogo 678-1297, Japan

A novel stereochemical approach is employed in anodic oxidation of naphthalene derivatives to discriminate the intramolecular radical addition *vs*. intermolecular radical addition paths; the contribution of the latter is revealed to be important, judging from the stereodifferentiating addition of MeOH at C-4 during the anodic oxidation of (1′*S*,3′*R*)-1-(3′-hydroxy-1′-methylbutoxy)-4-methylnaphthalene.

The anodic oxidation of arenes in alkaline MeOH provides oxidative 1,4-addition of the aromatic ring to give acetals or *p*-quinol ethers.[1,2] Swenton *et al*. have revealed that the anodic oxidation proceeds *via* coupling of the arene radical cation with the methoxyl radical (MeO·) generated by the one-electron oxidation of the methoxide anion, followed by nucleophilic addition of a second molecule of MeOH.[3] Introduction of an intramolecular alcoholic function in the substrate through a proper length of linker increases the product yield resulting in cyclic acetal formation on the oxidative product.[3] In this case, there are two possible modes for the coupling of the arene radical cation, *i.e*. with the intramolecular alkoxy radical (Path **A**) or the intermolecular one (Path **B**). Swenton *et al*. proposed that the intramolecular radical coupling is an important path for the anodic oxidation, based on the increase in product yield due to the effective trap of the arene radical cation by the intramolecular alkoxyl radical.[3] However, it is difficult to distinguish between the intramolecular radical coupling path and the intermolecular one using the usual product analyses because these paths give the same product. To discriminate the reaction pathways, we introduce a novel stereochemical approach,‡ named 'chiral eclipse' methodology. The essentials of this stereochemical analysis are as follows (Scheme 1). The intramolecular radical coupling path (Path **A**) gives a *meso* intermediate **3** from the chiral substrate. Therefore, no optically active product is expected in Path **A** because the chirality of the side chain has already disappeared at the time of the addition at C-4. In contrast, the intermolecular coupling path (Path **B**) maintains the chirality of the side chain in the C-4 addition, which is expected to give an optically active product. Here the importance of the intermolecular coupling path (Path **B**) is revealed during the anodic oxidation of naphthalene derivatives having a (1′*S*,3′*R*)-3′-hydroxy-1′-methyl butoxy moiety **1** judging from the result that the optically active alcohol moiety can act as a chiral auxiliary to give a stereodifferentiating product.

Stereochemically pure substrates **1** were prepared in 90–59% *via* the Mitsunobu reaction[4] with the corresponding naphthol and (2*R*,4*R*)-pentane-2,4-diol. The anodic oxidation of **1a** in 1% methanolic KF solution at constant current at a platinum anode§ afforded **2a** in 75% yield at room temperature and 69% yield at −78 °C as a single diastereomer. The two possible products, **2-*si*** or **2-*re***, shown in Fig. 1 are produced by *si*- or *re*-face attack in the intramolecular acetal formation, respectively. The exclusive *si*-face attack of the intramolecular alcohol (**2** = **2-*si***) was proven by the NOE signal between the olefin proton and the methine protons. The diastereoface differentiation may be due to the steric repulsion between the *peri*-proton of the naphthalene core and the cyclic acetal moiety. The chirality of the alcohol moiety of **2** disappears due to the cyclic acetal forming.

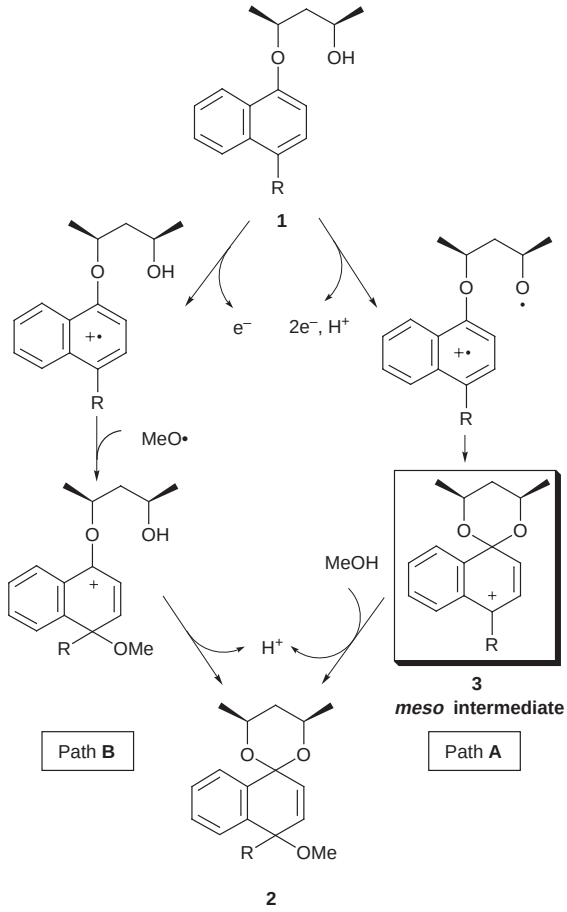

Scheme 1

In this case, the enantiomer ratio of the oxidative product shown in Table 1 directly gives the stereodifferentiation at the C-4 position.

During the anodic oxidation of **1a** at −78 °C, definite π-facial differentiation (67:33) at C-4 was observed, whereas the enantiomer ratio dropped to 53:47 at room temperature. The cyclic acetal **1a** was readily hydrolysed to give the corresponding dienone **4a** in 97% under acidic conditions. The enantiomer ratio of **4a** (67:33) is in good agreement with that of **2a** (67:33),

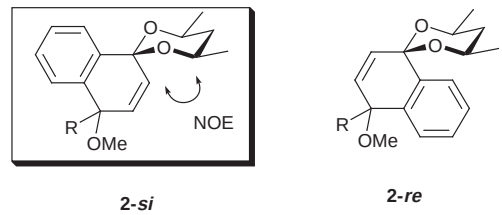

Fig. 1

Table 1 Anodic Oxidation of **1** at −78 °C[a]

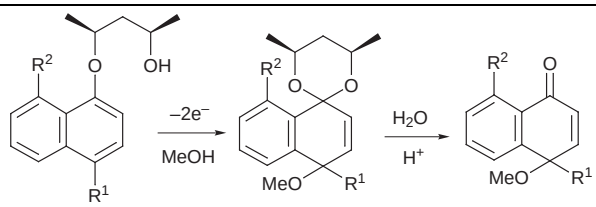

1 **2** **4**

a R^1 = Me, R^2 = H **b** R^1 = Me, R^2 = Me

c R^1 = Et, R^2 = H **d** R^1 = Pr^i, R^2 = H

	Yield[b] (%)	Enatiomer ratio[c]
a	67 (73)	67:33 (53:47)
b	26 (56)	72:28 (53:47)
c	74[d]	57:43[e]
d	59[d]	54:46[e]

[a] The values in parentheses are those obtained at room temperature. [b] Two step yield from **1** to **4**. [c] The values were determined by GC analysis of **4** using a CHROMPACK-Chirasil-DEX CB (i.d. 0.25 mm × 25 m) column. [d] Yield from **1** to **2**. [e] Enantiomer ratio of **2**.

indicating that the hydrolysis proceeds without epimerisation. The stereodifferentiation indicates the significant participation of Path **B** during the anodic oxidation of **1** because in Path **A** the chirality of the linker is eclipsed before the methanolic addition at C-4 resulting in a racemic product. A decrease in the stereodifferentiation was observed when bulky alkyl groups (Et, Pr^i) were introduced at C-4 (**1c**, **d**). The poor stereodifferentiation may be caused by a decrease in the contribution for path **B** due to steric hindrance for the intermolecular MeO· addition at C-4. In contrast, the enantiomer ratio slightly increased to 72:28 in the anodic oxidation of 1,8-dimethyl substituted naphthalene **1b** at −78 °C. The *peri* strain may partially inhibit the intramolecular alkoxyl radical coupling (Path **A**). Thus, the stereodifferentiating addition at C-4 is a general phenomenon during anodic oxidation of **1**, and reflects the contributions of Path **A** and Path **B** to the anodic oxidation mechanism.

As already mentioned, radical addition to the radical cation of the naphthalene derivatives is a key step for the stereodifferentiation during the anodic oxidation as well as the anodic oxidation itself. The regioselectivity for the radical attack at the arene radical cation is strongly influenced by the spin density of the arene radical cation. A high spin density (0.14) is observed at C-4 rather than at C-1 (0.04) in the 4-methylanisole radical cation by EPR measurements.[5,6a] This indicates that radical attack on C-4 is more favorable than on C-1 during the anodic oxidation and supports the importance of the intermolecular radical addition (Path **B**). The intramolecular solvation for arene radical cations has been reported using transient absorption spectra in low polarity media.[6b] The intramolecular alcohol solvates the arene radical cation without attacking it nucleophilically.[6b,7] Such intramolecular association by the chiral alcohol to the arene radical cation may contribute to the stereodifferentiating radical addition at C-4.

This work was partially supported by a Grant-in-Aid for Encouragement of Young Scientists from the Ministry of Education, Science, Sports and Culture, Japan (to M. F.).

Notes and References

† E-mail: fuji@sci.himeji-tech.ac.jp

‡ Recent examples of mechanistic probes using the stereochemical approach are shown in ref. 8. In these cases, the contribution of achiral intermediates was tested using a stereochemical approach.

§ All anodic oxidations were conducted in a single cell at constant current, employing a bulk electrolysis cell set with a circular platinum gauze anode and a platinum wire as the cathode (Bioanalytical System Inc.). Typically, a methanolic solution (40 ml) containing **1** (40 mg) and KF (0.4 g) was deaerated by argon bubbling and electrolysed at 45 mA and 10 V at −78 °C for 135 min.

1 T. Shono, *Electroorganic Chemistry as a New Tool in Organic Synthesis*, Springer-Verlag, Berlin 1984.
2 N. L. Weinberg and B. Belleau, *Tetrahedron*, 1973, **29**, 279; I. Barba, R. Chinchilla and C. Gómez, *Tetrahedron*, 1990, **46**, 7813; A. Nilsson, U. Palmquist, T. Pettersson and A. Ronlán, *J. Chem. Soc., Perkin Trans. 1*, 1978, 708; P. Margaretha and P. Tissot, *Helv. Chim. Acta*, 1975, **58**, 933.
3 M. P. Capparelli, R. E. DeSchepper and J. S. Swenton, *J. Org. Chem.*, 1987, **52**, 4953; M. P. Capparelli, R. S. DeSchepper and J. S. Swenton, *J. Chem. Soc., Chem. Commun.*, 1987, 610; M. G. Dolson and J. S. Swenton, *J. Am. Chem. Soc.*, 1981, **103**, 2361.
4 M. Fujita, Y. Takarada, T. Sugimura and A. Tai, *Chem. Commun.*, 1997, 1631; K. Yamaguchi, T. Sugimura, F. Nishida and A. Tai, *Tetrahedron Lett.*, 1998, **39**, 4521; T. Sugimura, H. Yamada, S. Inoue and A. Tai, *Tetrahedron: Asymmetry*, 1997, **8**, 649.
5 W. T. Dixon and D. Murphy, *J. Chem. Soc., Perkin Trans. 2*, 1976, 1823.
6 (*a*) S. Sankararaman, W. A. Haney and J. K. Kochi, *J. Am. Chem. Soc.*, 1987, **109**, 7824; (*b*) S. Sankararaman, W. A. Haney and J. K. Kochi, *J. Am. Chem. Soc.*, 1987, **109**, 5235.
7 A. Albini, E. Fasani and M. Mella, *Top. Curr. Chem.*, 1993, **168**, 143.
8 B. M. Trost and R. C. Bunt, *J. Am. Chem. Soc.*, 1996, **118**, 235; B. Schwartz and D. G. Drueckhammer, *J. Am. Chem. Soc.*, 1996, **118**, 9826.

Received in Cambridge, UK, 3rd August 1998; 8/06039H

Regioselective alkylation in ionic liquids

Martyn J. Earle,† Paul B. McCormac‡ and Kenneth R. Seddon§

The School of Chemistry, The Queen's University of Belfast, Stranmillis Road, Belfast, Northern Ireland, UK BT9 5AG

The room temperature ionic liquid 1-butyl-3-methylimidazolium hexafluorophosphate, [bmim][PF_6], is used as a 'green' recyclable alternative to dipolar aprotic solvents for the regioselective alkylation at the heteroatom of indole and 2-naphthol.

Efficient alkylation of the ambident nucleophiles indole **1** or 2-naphthol **4** is usually achieved by pre-formation of the ambident indolyl[1] or 2-naphtholate[2] anions and subsequent treatment with alkyl halide. Regioselective alkylation at the heteroatom for these anions is solvent dependant and can be achieved by use of a dipolar aprotic solvent such as DMF.[2,3] The procedure of Heaney and Ley for *N*-alkylation of indoles in DMSO with solid KOH is probably the most convenient method known and obviates the need for strong bases such as NaH or alkyllithiums.[4] However, despite the well known ability of solvents such as DMSO and DMF to accelerate nucleophilic displacements,[5] the relatively high boiling points of these solvents, their thermal instability, considerable odour problems and miscibility with both aqueous and organic phases can make product isolation difficult and solvent recovery almost impossible.

The introduction of air and moisture stable ambient temperature ionic liquids by Wilkes and Zaworotko[6] in 1992 considerably widened the possible applications of ionic liquid systems as solvents and reagents for organic synthesis. Recently room temperature ionic liquids have been reported as solvents for polymerisation,[7] hydrogenation[8] and as catalysts for the Diels–Alder reaction.[9] The ionic liquid [bmim][PF_6] is conveniently prepared,[10] fluid at room temperature, moisture stable and has no detectable vapour pressure. It is an excellent solvent for carbonyl compounds, alkyl halides, alcohols and amines, but is immiscible with saturated hydrocarbon solvents, dialkyl ethers and water. The unique solvating properties of this moisture stable ionic liquid makes it a strong candidate as a recyclable solvent.[11] Our recent interest has been in the area of clean synthesis[12] and as part of a programme to investigate the range of organic reactions possible in ionic liquids, we were interested in the reactions of **1** and **4** with alkyl halides in [bmim][PF_6].

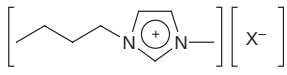

[bmim][PF_6] X = PF_6

[bmim][BF_4] X = BF_4

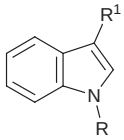

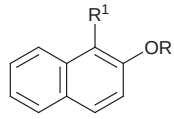

1 R = R^1 = H
2 R = Et, Bu, Me or $PhCH_2$, R^1 = H
3 R = R^1 = Et, Bu, Me or $PhCH_2$

4 R = R^1 = H
5 R = Et, Bu, Me or $PhCH_2$, R^1 = H
6 R = R^1 = Et, Bu, Me or $PhCH_2$

The reaction of **1** with simple alkyl halides at room temperature was examined in [bmim][PF_6] using solid KOH as base; the products were conveniently extracted with Et_2O, and almost exclusive *N*-alkylation to form **2** was seen in all cases. The results for the alkylation of **1** with four typical alkyl halides in this solvent are outlined in Table 1. These reactions were carried out, typically as 10% w/v solutions of **1** in [bmim][PF_6] using 1.3 to 2 equiv. of alkyl halide and 2 equiv. of KOH. Reactions were complete in 2–3 h with almost quantitative extraction of products. The dialkylated products **3** were identified from the proton NMR spectra of the crude extracts and were only observed for the more reactive alkyl halides, $PhCH_2Br$ and MeI. Analogous results were seen for the alkylation of 2-naphthol, **4**, to give predominantly *O*-alkylated products **5** (Table 1). The solvent can be typically recovered by filtering to remove residual insoluble KOH and precipitated potassium halide followed by vacuum drying. The NMR spectra (^1H, ^{13}C, ^{19}F) of recovered solvent indicate no evidence of ionic liquid degradation during the course of the reactions and the recovered solvent has been recycled numerous times with no appreciable decrease in yield or regioselectivity, with only small mechanical losses. The ionic liquid [bmim][PF_6] can truly be compared with classical molecular solvents, with the added advantage of *in situ* generation of anion, and the non-nucleophilic hexafluorophosphate anion avoids problems associated with halide exchange which had been encountered by Brunet and co-workers in their study.[13] Further studies indicate that the related ionic liquid 1-butyl-3-methylimidazolium tetrafluoroborate [bmim][BF_4][14] is also an efficient solvent for alkylation of **1** and **4**.

In conclusion, room temperature ionic liquids are an attractive clean synthetic alternative to classical dipolar aprotic solvents for alkylation of ambident nucleophiles. There are many obvious advantages including simplicity of the methodology, the ease of product isolation, the lack of measurable solvent vapour pressure, the regioselectivity and the potential for recycling. Room temperature ionic liquids are neoteric solvents, and studies are underway to demonstrate their obvious potential as an alternative to classical molecular solvents for organic synthesis.

We are indebted to the EPSRC for funding this research, to the EPSRC and the Royal Academy of Engineering for the award of a Clean Technology Fellowship (to K. R. S.), and to

Table 1 Data for the reaction of indole, **1**, and 2-naphthol, **4**, with a selection of alkyl halides in the room temperature ionic liquid [bmim][PF_6]

Substrate	Alkyl halide	Yield (%)[a]	Products	Ratio[b]
1	EtBr	92	**2**+**3**	> 99 : 1
1	BuBr	93	**2**+**3**	> 99 : 1
1	MeI	91	**2**+**3**	93 : 2
1	BnBr	94	**2**+**3**	95 : 5
4	EtBr	94	**5**+**6**	> 99 : 1
4	BuBr	98	**5**+**6**	> 99 : 1
4	MeI	97	**5**+**6**	97 : 3
4	BnBr	95	**5**+**6**	95 : 5

[a] Isolated yield. [b] The ratio of either **2** : **3** or **5** : **6** was determined by ^1H NMR and gas chromatographic analysis.

Drs John Holbrey and Charles Gordon for assistance and advice.

Notes and References

† E-mail: m.earle@qub.ac.uk
‡ E-mail: p.mccormac@qub.ac.uk
§ E-mail: k.seddon@qub.ac.uk

1 S. Nunomoto, Y. Kawakami, Y. Yamashita, H. Takeuchi and S. Eguichi, *J. Chem. Soc., Perkin Trans. 1*, 1990, 111.
2 N. Kornblum, R. Seltzer and P. Haberfield, *J. Am. Chem. Soc.*, 1963, **85**, 1148.
3 B. Cardillo, G. Casnati, A. Pochini and A. Ricca, *Tetrahedron*, 1967, **23**, 3771.
4 H. Heaney and S. V. Ley, *J. Chem. Soc., Perkin Trans 1*, 1973, 499.
5 J. March, *Advanced Organic Chemistry*, 4th edn., Wiley, New York, 1992.
6 J. S. Wilkes and M. J. Zaworotko, *J. Chem. Soc., Chem. Commun.*, 1992, 965.
7 A. A. K. Abdul-Sada, P. W. Ambler, P. K. G. Hodgson, K. R. Seddon and N. J. Stewart, *World Pat.*, WO 9521871, 1995.
8 Y. Chauvin, L. Mussmann and H. Olivier, *Angew. Chem., Int. Ed. Engl.*, 1995, **34**, 2698.
9 J. Howarth, K. Hanlon, D. Fayne and P. McCormac, *Tetrahedron Lett.*, 1997, **38**, 3097.
10 C. M. Gordon, J. Holbrey, A. R. Kennedy and K. R. Seddon, *J. Mater. Chem.*, in the press.
11 J. G. Huddleston, H. D. Willauer, R. P. Swalloski, A. E. Visser and R. D. Rogers, *Chem. Commun.*, 1998, 1765.
12 K. R. Seddon, *J. Chem. Technol. Biotechnol.*, 1997, **68**, 351.
13 M. Badri, J. J. Brunet and R. Perron, *Tetrahedron Lett.*, 1992, **33**, 4435.
14 P. A. Z. Suarez, J. E. L. Dullius, S. Einloft, R. F. de Souza and J. Dupont, *Polyhedron*, 1996, **15**, 1217.

Received in Liverpool, UK, 7th August 1998; 8/06328A

Enhancement of *Candida antarctica* lipase B enantioselectivity and activity in organic solvents

Marie-Claire Parker,*[a]† Stuart A. Brown,[b] Lindsey Robertson[b] and Nicholas J. Turner[b]

[a] *Department of Chemistry, Joseph Black Building, University of Glasgow, Glasgow, UK G12 8QQ*
[b] *Edinburgh Centre for Protein Technology, Department of Chemistry, University of Edinburgh, King's Buildings, West Mains Road, Edinburgh, UK EH9 3JJ*

The enantioselectivity and catalytic activity of Novozym 435® [*Candida antarctica* lipase B (CALB)] in organic solvents was found to dramatically increase upon the addition of a non-reactive organic base, such as Et_3N, to the reaction system.

It has been shown that the unusual microenvironment of enzymes in organic solvents can affect a number of parameters, including the degree of protein hydration,[1,2] secondary structure,[3] the susceptibility of the protein to inactivation and variations in the ionisation state[4] of side-chain residues. Frequently, these differences have been shown to result in interesting changes in the enzymes, including reversal of substrate specificity and changes in stereoselectivity, although the underlying reasons remain poorly understood.

It is commonly accepted that the best predictor of enzyme catalytic activity in low water organic media is thermodynamic water activity (a_w).[1]‡ Over the past few years although much has been reported on enzyme enantioselectivity in organic media there are as yet no predictive rules available. Crude lipase preparations have proved to be simple and effective biocatalysts for kinetic resolutions, *e.g.* chiral carboxylic acids and alcohols. However, the low purity of these preparations (presence of other lipases and competing hydrolases) can, in specific reactions, lead to low and unpredictable enantioselective behaviour. This effect can be compounded when using organic solvents, due to the effect of different solvent properties on catalytic activity.

The starting point for the work described herein was the lipase (Lipozyme® *Mucor miehei*) catalysed dynamic resolution of 4-substituted oxazol-5(4*H*)-ones, a reaction we have previously employed for the synthesis of enantiomerically pure (*S*)-L-*tert*-leucine.[5] It was previously found that the modest enantioselectivity in toluene (*ca.* 68% ee) could be enhanced (*ca.* 97% ee) by the addition of a catalytic amount of Et_3N to the reaction; the role of Et_3N is not to facilitate racemisation of the substrate.

We decided to investigate this effect in more detail by using a commercially available immobilised lipase,§ Novozym 435 (*Candida antarctica* lipase B[6] (CALB), since a larger substrate range could be tested with this enzyme. The catalytic activity and enantioselectivity of the alcoholysis of (±)-2-phenyl-4-benzyloxazol-5(4*H*)-one **1** using butan-1-ol as the nucleophile (Scheme 1) was monitored¶ under a range of reaction conditions, including controlled water activity. Hydration was controlled by equilibrating‖ enzyme and solvent with the appropriate saturated salt solution[7] of known thermodynamic water activity a_w. Therefore a low a_w system will be one in which the solvent is poorly hydrated and the enzyme, similarly, has a low level of hydration, and at high a_w (*e.g.* 0.97) the solvent is near water saturation and the enzyme is fully hydrated (as would be found in an aqueous system). Table 1 shows the effect of hydration on the initial catalytic rate and enantioselectivity, in three different solvents, n-hexane, toluene and MeCN, either with or without Et_3N.**

It can immediately be seen that the lipase-catalysed reaction is very sensitive to water activity. The addition of a non-reactive organic base,†† Et_3N, to the reaction enhances significantly both the enantioselectivity and catalytic activity of the enzyme. Even low levels of hydration, present in the more nonpolar solvents such as n-hexane and toluene, are detrimental to the overall catalytic performance of CALB. We find that generally for optimum yield and enantioselectivity, both the enzyme and solvent should be rigorously dried prior to addition of Et_3N. We were interested to see if addition of Et_3N to a reaction already in progress and of poor enantioselectivity, could reverse this effect. As can be seen from Fig. 1, the addition of Et_3N after 140 min immediately results in enhanced catalytic rate and enantioselectivity.

In order to examine the generality of the effect of Et_3N we investigated a second reaction, namely the CALB-catalysed

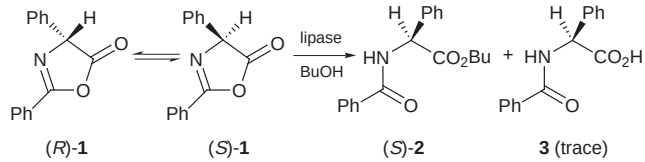

Scheme 1

Table1 Effect of water activity on initial catalytic rate[a,b] and enantiospecificity as a function of hydration, with and without Et_3N

		No Et_3N		Et_3N	
Solvent[c]	a_w	Initial rate/nmol min^{-1} mg^{-1}	Ee (%)	Initial rate/nmol min^{-1} mg^{-1}	Ee (%)
n-hexane	~0 (anhydrous)	26 (± 1.5)	85 (± 3)	30 (± 1.5)	90 (± 3)
n-hexane	0.69	4 (± 0.5)	55 (± 2)	20 (± 1)	87 (± 3)
n-hexane	0.97	1.5 (± 0.15)	30 (± 5)	18 (± 0.9)	80 (± 5)
toluene	~0	15 (± 0.8)	85 (± 4)	27 (± 1.5)	93 (± 3)
toluene	0.22	3	61 (± 6)	17 (± 1)	95 (± 2)
MeCN[d]	~0	15	>99	10	97 (± 2)
MeCN[d]	0.1 (0.5% v/v H_2O)	NR[e]	—	5 (± 0.3)	90 (± 4)
MeCN[d]	0.4 (2% v/v H_2O)	NR[e]	—	NR[e]	—

[a] Initial rate for (*S*)-butyl ester enantiomer **2**. [b] Results reported are the average of three separate measurements. [c] Note ‖. [d] Ref. 8. [e] No reaction.

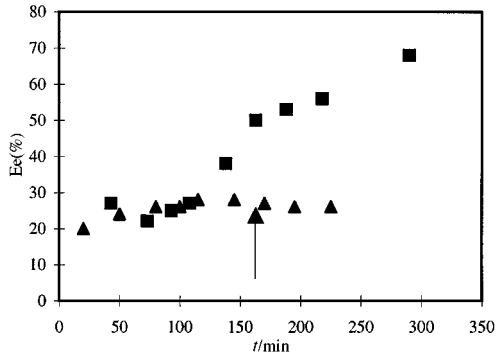

Fig. 1 Effect of Et_3N on ee. Reactions A (▲) and B (■) were carried out under identical conditions (a_w = 0.69). At t = 140 min, 14 mol% Et_3N was added to reaction B (arrow).

reaction between 1-phenylacetoxy-2-methylcyclohexene and butanol yielding 2-methylcyclohexanone and butyl phenylacetate.[9,15] Using n-hexane (a_w = 0) and MeCN (0.5% H_2O, a_w = 0.1) as the solvents, we observed that the addition of Et_3N to the solvent resulted in a dramatic increase in the catalytic activity. An approximate 200-fold increase in activity was observed in MeCN (a_w = 0.1) and a 700-fold one for that in n-hexane (a_w = 0.97). The higher activity found in n-hexane is presumably due to a more intimate contact between the enzyme and Et_3N in a more nonpolar environment. Similarly, the activation effect for (±)-2-phenyl-4-benzyloxazol-5(4*H*)-one ring-opening in MeCN is similar to that described above and is expected to be a result of less Et_3N adsorption to the enzyme in MeCN.

The ability of organic bases to increase the enantioselectivity of lipase-catalysed reactions in water-saturated organic solvents has previously been reported.[10–13] In some cases[11,12] this effect has been attributed to the formation of an ion-pair between the base and any by-product acid. Using electrospray ionisation mass spectrometry (ESI-MS)‡‡ we have detected the formation of carboxylic acid **3** during the course of the oxazolone reaction at intermediate to high water activities (*e.g.* a_w = 0.69–0.97). We have also found that addition of acid **3** to an already hydrated system results in loss of activity, which can be fully recovered upon addition of an organic base, presumably *via* formation of an ion pair. Ion pair formation is observed in both low and high dielectric non-hydrogen bonding solvents such as n-hexane and MeCN. In a high dielectric, non-hydrogen bonding solvent such as MeCN, where the acid was found to be more soluble, we find experimentally that dissolution of acid **3** in n-hexane and MeCN occurs upon addition of Et_3N, thus removing acid from the immediate microenvironment of the enzyme. However, the enhancement of catalytic performance and enantioselectivity for rigorously dried samples, and those of low water activity (a_w < 0.7) where we find no evidence for hydrolysis over the course of the initial rate measurement, cannot be explained in terms of hydrolysis products affecting enantioselectivity, since for an unrelated substrate, an activating effect on the catalytic activity has been demonstrated.

The addition of co-solvents, such as DMF and DMSO, was found to solubilise the acid and thus it was anticipated that they would perform a similar role to Et_3N in removing any acid from the immediate vicinity of the enzyme. Both DMF and DMSO were chosen as additives to the bulk organic solvent (toluene at a_w = 0.22). Although both DMF and DMSO increased the enantioselectivity of the reaction to 85% ee, there was no significant effect on the catalytic rate as found with Et_3N. Since the solvation of the carboxylic acid by these co-solvents occurs by a different mechanism to that of Et_3N, *i.e.* the additives are unable to form ion-pairs, they have limited use in reducing the overall effect.

The role of Et_3N therefore appears to be dual in nature, *i.e.* increasing both the enantioselectivity and catalytic activity of lipase-catalysed reactions. The addition of Et_3N therefore provides an additional strategy for improving the enantioselectivity of lipase-catalysed reactions. We are currently investigating this effect with other lipolytic enzymes.

We are grateful to Boehringer Mannheim, Germany, for the generous gift of lipase samples. The BBSRC is acknowledged for a David Phillips Fellowship (M. C. P.) and a studentship (S. A. B.).

Notes and References

† E-mail: m.parker@chem.gla.ac.uk

‡ The thermodynamic water activity (a_w) describes the mass action effect of water on hydrolytic equilibria and also describes the partitioning of various water phases that can compete for water binding (ref. 1).

§ Polyacrylamide gel electrophoresis of CALB desorbed from the solid support exhibited a single band corresponding to the reported molecular weight of CALB (33 KDa) (ref. 6).

¶ (±)-2-Phenyl-4-benzyloxazol-5(4*H*)-one **1** (0.16 mmol) was placed in a 4 ml screw top vial together with the solvent, (either anhydrous or hydrated), butan-1-ol (0.24 mmol, 1.5 equiv.) CALB (40 mg) and Et_3N (14 mol%). The reaction vial was shaken at 250 rpm on a rotary shaker at 37 °C and the progress and ee (%) of the reaction were monitored by chiral HPLC (Chiralcel-OD, 250 × 4.6 mm, Mallinckrodt Baker, n-hexane–Pr^iOH (90:10 v/v), UV detection λ = 254 nm).

‖ *Candida antarctica* lipase B (CALB) was received as an immobilised preparation (Novozym 435, Boehringer Mannheim, Germany) and was dehydrated over P_2O_5 (at room temp.) for 2–3 days. Rehydration of dried lipase to the desired water activity (a_w) was carried out using saturated salt solutions (equilibration period 48–72 h). (±)-2-Phenyl-4-benzyloxazol-5(4*H*)-one **1** was stored over P_2O_5 at 0 °C; anhydrous solvents were stored over freshly reactivated 3 Å or 4 Å molecular sieves. The water content of dried solvents was measured using Karl Fischer water titration (ref. 15) and found to be < 0.001 wt%. Solvents were hydrated separately from the enzyme using the same water equilibration procedure as described above, approximately 24 h before use.

** Control reactions showed that no detectable ester (as judged by HPLC) was formed in the absence of enzyme, either with or without Et_3N, over a 48 h analysis period.

†† Other organic bases give very similar results to Et_3N, *e.g.* DABCO and lutidine. Insoluble inorganic bases, *e.g.* $KHCO_3$ and K_2CO_3, had no effect and did not result in the high catalytic rate and enantioselectivity observed with the soluble organic bases.

‡‡ Electrospray ionisation mass spectrometry (ESI-MS) and atmospheric chemical ionisation (APCI) were performed on a Micromass Platform II spectrometer (cone voltage 20 V).

1 P. J. Halling, *Enzyme Microb. Technol.*, 1994, **16**, 178.
2 M. C. Parker, A. J. Blacker and B. D. Moore, *Biotechnol. Bioeng.*, 1995, **46**, 452.
3 D. S. Hartsough and K. M. Merz, *J. Am. Chem. Soc.*, 1993, **115**, 6529.
4 E. Zacharis, B. D. Moore and P. J. Halling, *J. Am. Chem. Soc.*, 1997, **119** 12 396.
5 N. J. Turner, J. R. Winterman, R. McCague, J. S. Parratt and S. J. C. Taylor, *Tetrahedron. Lett.*, 1995, **36**, 1113.
6 J. Uppenberg, N. Öhrner, M. Norin, K. Hult, G. J. Kleywegt, S. Patkar, V. Waagen, T. Anthonsen and T. Jones, *Biochemistry*, 1995, **34**, 16 838.
7 G. A. Hutcheon, P. J. Halling and B. D. Moore, in *Methods in Enzymology*: *Lipases Part B*, ed. B. Rubins and E.A. Dennis, Academic Press, NY, 1997, vol. 286, p. 465.
8 J. Gmehling and V. Onken, *Vapour-Liquid Equilibrium Data Collection*, Dechema, Frankfurt, 1977, vol. 1.
9 K. Matsumoto, T. Oishi, T. Nakata, T. Shibata and K. Ohta, *Biocatalysis*, 1994, **9**, 97.
10 B. Berger, C. G. Rabiller, K. Konigsberger, K. Faber and H. Griengl, *Tetrahedron*: *Asymmetry*, 1990, **1**, 541.
11 J. L. L. Rakels, A. J. J. Straathof and J. J. Heijnen, *Tetrahedron*: *Asymmetry*, 1994, **5**, 93.
12 T. Maugard, M. Remaud-Simeon, D. Petre and P. Monsan, *Tetrahedron*, 1997, **53**, 7629.
13 P. Stead, H. Marley, M. Mahmoudian, G. Webb, D. Noble, Y. T. Ip, E. Piga, T. Rossi, S. M. Roberts and M. J. Dawson, *Tetrahedron*: *Asymmetry*, 1996, **7**, 2247.
14 H. A. Laitennen and W. E. Harris, *Chemical Analysis*, 2nd edn, McGraw-Hill, 1975, p. 361.
15 A. J. Carnell, J. Barkley and A. Singh, *Tetrahedron Lett.*, 1997, **38**, 7781.

Received in Liverpool, UK, 10th August 1998; 8/06332J

Catalytic synthesis of 3-vinyl-2,5-dihydrofurans from yne-enes promoted by photochemically activated metal–allenylidene $L_nRu{=}C{=}C{=}CR_2$ complex

Michel Picquet, Christian Bruneau, and Pierre H. Dixneuf†

UMR 6509 CNRS - Université de Rennes, Organométalliques et Catalyse, Campus de Beaulieu, F-35042 Rennes, France

The ruthenium(II)–allenylidene salt [(*p*-cymene)(PCy_3)ClRu=C=C=CPh_2]PF_6 acts as an olefin metathesis catalyst precursor for the yne-ene transformation of the mixed propargylic allyl ethers $HC{\equiv}C{-}CR_2OCH_2CH{=}CH_2$ into 3-vinyl-2,5-dihydrofurans; initial photochemical irradiation efficiently promotes the catalytic activity.

3-Vinyl-2,5-dihydrofurans have potential as Diels–Alder dienes and for access to optically active derivatives *via* asymmetric catalysis.[1] To the best of our knowledge, no direct preparation of these compounds has been reported, whereas a stereoselective route to 3-vinyltetrahydrofuran derivatives from cyclic allylsiloxanes has just been found.[2] However, it appears that the 3-vinyl-2,5-dihydrofuran structure **II** should be reached, in a straightforward way, from oxygenated yne-enes of type **I** *via* catalytic ring closing metathesis (RCM) reaction (Scheme 1). Indeed, since the pioneering work of Katz,[3] carbocycles have been made by RCM reactions using tungsten[3] or chromium[4] carbene catalysts. Recently, neutral 16-electron ruthenium carbenes $(PCy_3)_2Cl_2Ru{=}CHR$ (R = $CH{=}CPh_2$, Ph), which tolerate functional groups, have been shown to efficiently promote access to N- and O-containing heterocycles, *via* ring closing metathesis.[5,6] However, these Ru=CHR complexes appear to be less efficient for the ring closing metathesis of yne-ene derivatives containing a terminal C≡CH bond.[5,7]

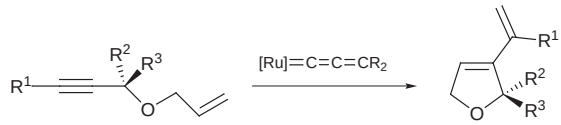

I **II**

Scheme 1

We now report (i) a general method for the preparation of new 3-vinyl-2,5-dihydrofurans of type **II** directly from mixed propargylic allyl ether derivatives **I**, *via* a RCM reaction in the presence of a novel olefin metathesis catalyst, the 18-electron cationic ruthenium allenylidene complex [(arene)(PCy_3)Cl-Ru=C=C=CPh_2]PF_6, which has just been shown to perform the ring closing metathesis of 1,6- to 1,20-dienes,[8] and (ii) that the catalytic species formation is favoured by photochemical activation of the catalyst precursor.

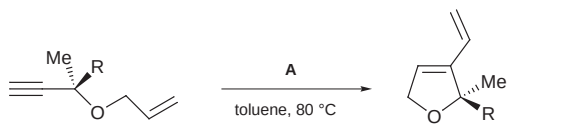

1 R = Ph
2 R = CH_2CHMe_2

8 R = Ph (77%)
9 R = CH_2CHMe_2 (65%)

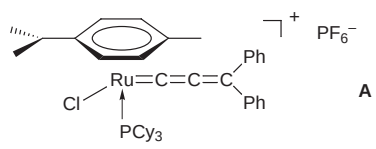

A

Scheme 2

The allyl prop-2-yn-1-yl ethers of type **I** were conveniently prepared from the corresponding prop-2-yn-1-ols on treatment by NaH and allyl bromide in DMF at room temperature (60–97%). The derivatives **1** and **2** were first reacted with 2.5 mol% of [(*p*-cymene)(PCy_3)ClRu=C=C=CPh_2]PF_6 (**A**) in toluene at 80 °C. The conversion was completed after 24 h and 6.5

Table 1 Catalytic synthesis of 3-vinyl-2,5-dihydrofurans **8–14** with photochemically activated ruthenium–allenylidene catalyst **A**[a]

Substrate	Product	Heating period at 80 °C[a]/h	Isolated yield (%)[b]
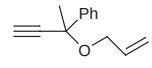 **1**	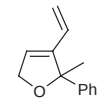 **8**	4	84
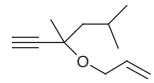 **2**	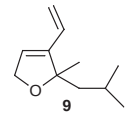 **9**	1	62
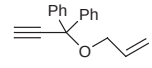 **3**	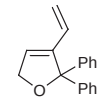 **10**	23	67
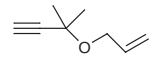 **4**	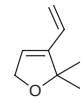 **11**	63[c]	41
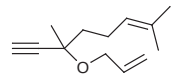 **5**	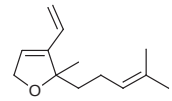 **12**	1	74
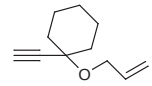 **6**	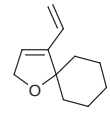 **13**	1	63
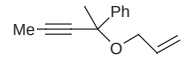 **7**	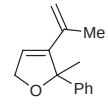 **14**	24	83

[a] Initial UV irradiation (300 nm) at room temperature for 0.5 h in toluene followed by heating at 80 °C until complete conversion of **1–7**. [b] Yields were obtained after distillation under reduced pressure. [c] Reaction performed in refluxing CH_2Cl_2 after irradiation.

h, respectively, and derivatives **8** (77%) and **9** (65%) were obtained as the sole reaction products (Scheme 2).

The 18-electron catalyst precursor is expected to give an active catalytic species after partial decoordination or loss of the arene ligand to generate a highly coordinatively unsaturated ruthenium species. In order to check this hypothesis and in the search for better activity, the previous reaction was performed under UV irradiation [Hg lamp, 300 nm] in order to displace the *p*-cymene ligand, as was suggested for (*p*-cymene)$RuCl_2(PR_3)$.[9] After 0.5 h irradiation at room temperature in toluene followed by thermal reaction at 80 °C for 4 h, the conversion of **1** was completed (*vs*. 24 h at 80 °C previously without initial irradiation) and the 3-vinyl dihydrofuran **8** was obtained in 84% yield. Similarly, the complete conversion of **2** was achieved after only 1 h at 80 °C instead of 6.5 h without irradiation, and **9** was obtained in 62% yield (Table 1).

Preliminary UV irradiation tremendously favours the generation of the active catalytic species as the period of heating at 80 °C was significantly reduced. The allyl ethers **3**–**5** were reacted under the latter conditions and the 3-vinyldihydrofurans **10**–**12** were isolated in 62–84% (Table 1). It is noteworthy that these 3-vinyl-2,5-dihydrofurans are stable in solution at moderate temperature (80 °C) but decompose rapidly when isolated as pure compounds.

The increasing of the steric hindrance at the ether carbon atom C1 slows down the conversion of the ether (**2** > **1** >> **3**). The RCM reaction applied to derivative **6**, easily made from cyclohexanone, led after 1 h at 80 °C to the spirodihydrofuran **13** (63%), and showed reactivity similar to that of the disubstituted derivative **2**. The transformation of compound **7** into the 3-isopropenyldihydrofuran **14** in 83% yield, after irradiation and 24 h of reaction at 80 °C, compared with that of compound **1** (4 h, 84%), indicates that the ring closing metathesis reaction of enynes involving a disubstituted C≡C triple bond is disfavoured. This contrasts with the RCM of yne-enes containing amido or tosylamido functional groups.[5,7] It is noteworthy that the formation of the bis(dihydrofuran) was obtained previously from the disubstituted yne-ene CH_2=$CHCH_2OCH_2C$≡CCH_2OCH_2CH=CH_2 and the L_nRu=CHCH=CPh_2 catalyst.[6]

The above results show the second use of (arene)-Ru=C=C=CR_2 complexes in catalysis.[8] They are not only able to promote non-conjugated diene metathesis, they are also efficient catalysts for the ring closing metathesis of terminal yne-enes. These results bring evidence for the first time that the (arene)Ru=C=C=CR_2 complex **A** can be photochemically activated for improved generation of the active catalytic species and that this catalyst tolerates the presence of a terminal C≡CH bond.

The authors are very grateful to Dr A. Fürstner for creative discussions.

Notes and References

† E-mail: dixneuf@univ-rennes1.fr

1 J. P. Morken, M. T. Didiuk and A. H. Hoveyda, *J. Am. Chem. Soc*., 1993, **115**, 6997; M. T. Didiuk, C. W. Johannes, J. P. Morken and A. H. Hoveyda, *J. Am. Chem. Soc*., 1995, **117**, 7097.
2 C. Meyer and J. Cossy, *Tetrahedron Lett*., 1997, **38**, 7861; J. H. Cassidy, S. P. Marsden and G. Stemp, *Synlett*, 1997, 1411.
3 T. J. Katz and T. M. Sivavec, *J. Am. Chem. Soc*., 1985, **107**, 737; T. M. Sivavec, T. J. Katz, M. Y. Chiang and G. X.-Q. Yang, *Organometallics*, 1989, **8**, 1620.
4 S. Watanuki, N. Ochifuji and M. Mori, *Organometallics*, 1995, **14**, 5062; M. Mori and S. Watanuki, *J. Chem. Soc*., *Chem. Commun*., 1992, 1082.
5 A. Kinoshita and M. Mori, *Synlett*, 1994, 1020; A. Kinoshita and M. Mori, *J. Org. Chem*., 1996, **61**, 8356.
6 S.-H. Kim, N. Bowden and R. H. Grubbs, *J. Am. Chem. Soc*., 1994, **116**, 10801; S.-H. Kim, W. J. Zuercher, N. Bowden and R. H. Grubbs, *J. Org.Chem*., 1996, **61**, 1073.
7 A. G. M. Barrett, S. P. D. Baugh, D. C. Braddock, K. Flack, V. C. Gibson and P. A. Procopiou, *Chem. Commun*., 1997, 1375.
8 A. Fürstner, M. Picquet, C. Bruneau and P. H. Dixneuf, *Chem. Commun*., 1998, 1315.
9 A. Hafner, A. Mühlebach and P. A. van der Schaaf, *Angew. Chem., Int. Ed. Engl*., 1997, **36**, 2121.

Received in Liverpool, UK, 24th July 1998; 8/06005C

Asymmetric cycloadditions of dienes to chloronitroso compounds derived from carbohydrate ketones: syntheses of (−)-physoperuvine and (+)-epibatidine

Adrian Hall,[a] Patrick D. Bailey,[a] David C. Rees[b] and Richard H. Wightman*[a]†

[a] *Department of Chemistry, Heriot-Watt University, UK EH14 4AS*
[b] *Organon Laboratories Ltd., Newhouse, Lanarkshire, UK ML1 5SH*

An α-chloronitroso compound derived from D-xylose undergoes cycloadditions with cyclic dienes to give bicyclic dihydrooxazines of high enantiomeric purity; such adducts were used in a synthesis of (−)-physoperuvine and a formal synthesis of (+)-epibatidine, whilst a pseudoenantiomeric chloronitroso compound is also available from L-sorbose.

There has been considerable interest in recent years in the development of asymmetric versions of the hetero-Diels–Alder cycloaddition[1] of dienes with *C*-nitrosocompounds to form 3,6-dihydro-1,2-oxazines, since the further manipulation of the initial cycloadducts can be used to prepare a wide range of nitrogen-containing organic compounds. Most work has been done using acylnitroso compounds bearing a chiral auxiliary,[2] although the removal of the auxiliary can involve conditions that are not compatible with sensitive functionality. Studies have also been carried out using chiral α-chloronitroso compounds, since in the presence of a nucleophilic solvent solvolysis of the initial cycloadduct occurs to liberate the dihydrooxazine directly. After initial work with steroidal chloronitroso compounds,[3] there has been emphasis on the use of chloronitroso compounds derived from carbohydrate hydroximino lactones.[4,5] We were attracted to the use of chloronitroso compounds derived from readily-available and sterically-rigid carbohydrate ketones; we now report that such systems can give very high degrees of enantioselectivity, whilst also regenerating the auxiliary in high yield and in a form in which it can be easily recycled. We also describe the use of one of our auxiliaries[6] in asymmetric syntheses of two natural products.

Thus, 1,2-*O*-isopropylidene-α-D-xylofuranose,[7] was selectively silylated and then oxidized (PCC, molecular sieves) to give ketone **1** (Scheme 1). Conversion of **1** to its oxime (mixed isomers) and subsequent treatment with *tert*-butyl hypochlorite gave the α-chloronitroso compound **2** (69% overall from D-xylose) as a blue crystalline solid. That chlorination had occurred from the *exo*-face was confirmed by X-ray crystallography, which also indicated the eclipsed nature of the chloronitroso unit[8] (dihedral angle Cl–C–N–O, 0.8°).

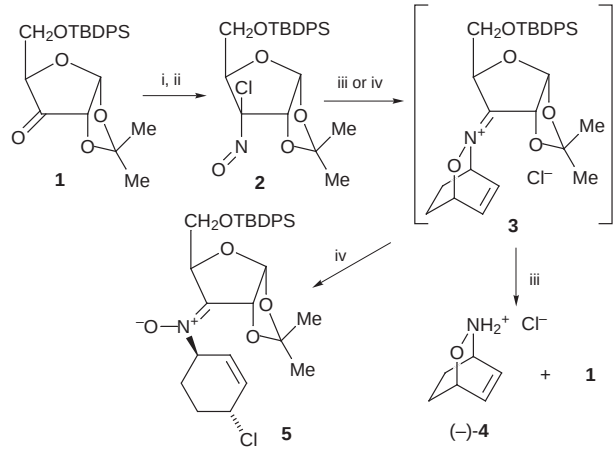

Scheme 1 *Reagents and conditions*: i, $NH_2OH·HCl$, $NaHCO_3$, EtOH–H_2O; ii, Bu^tOCl, CH_2Cl_2; iii, cyclohexa-1,3-diene, $CHCl_3$–Pr^iOH–H_2O (100:100:1), 0 °C; iv, cyclohexa-1,3-diene, $CHCl_3$, 0 °C

Treatment of **2** with cyclohexa-1,3-diene in $CHCl_3$–Pr^iOH containing water (1%) gave the cycloadduct (−)-**4** (94%), together with ketone **1** (95%), which could be recycled. The absolute configuration of (−)-**4** followed from the sign of its optical rotation,[4a,5] and the enantiomeric excess (ee) was shown to be 96% by reaction of (−)-**4** with (+)-camphor-10-sulfonyl chloride and integration of the two pairs of doublets for the diastereotopic protons at C-10 [major isomer from (−)-**4**, δ 2.91 and 3.37; minor isomer from (+)-**4**, δ 2.76 and 3.47].[4a] In contrast, when the reaction of **2** with cyclohexadiene was carried out in a non-nucleophilic and non-coordinating solvent ($CHCl_3$), only the nitrone **5** (69%) was obtained, a result that can be rationalized as occurring by attack of chloride ion on the intermediate iminium ion **3**.‡

Reaction of **2** with cyclopentadiene (Scheme 2) did not give any bicyclic dihydrooxazine under any conditions investigated. Instead, the only product isolated, even in the presence of nucleophilic solvents, was the nitrone **6** (93% in $CHCl_3$), and attempts to divert the course of reaction by addition of silver salts were unsuccessful. The structure of **6**, including the stereochemistry of the C=N double bond, was confirmed by X-ray crystallography. On the other hand, reaction of **2** with cyclohepta-1,3-diene in the presence of water gave only the bicyclic adduct (−)-**7** {$[\alpha]_D$ −11.0 (*c* 1.0, EtOH)} (93%) and ketone **1** (93%). Derivatization of **7** with camphor-10-sulfonyl chloride and analysis by ^1H NMR spectroscopy led to an estimated ee of ⩾96%. The pattern of reactivity shown by **2** as the diene is varied presumably reflects the degree of ring strain present in the intermediate iminium ions (**3** and the equivalent structures). The stereochemistries of (−)-**4** and (−)-**7**, and of **6**, can be rationalized in terms of cycloadditions occurring through *exo*-transition states on the less hindered *si*-face of the nitroso group, away from the isopropylidene unit.

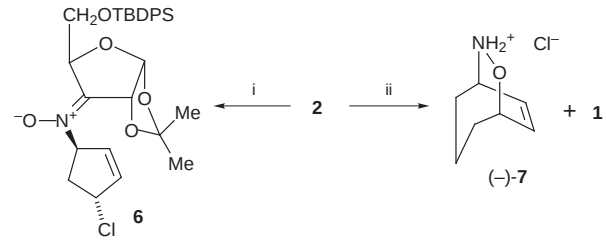

Scheme 2 *Reagents and conditions*: i, cyclopentadiene, $CHCl_3$, room temp; ii, cyclohepta-1,3-diene, $CHCl_3$–Pr^iOH–H_2O (100:100:1), 4 °C

The cycloadduct (−)-**7** was used in an enantioselective synthesis of (−)-(*R*)-physoperuvine [(−)-**13**] (Scheme 3), the *S*-enantiomer of which is the major alkaloid of *Physalis peruviana* Linne.[9] Physoperuvine has been synthesized as a racemate,[10] and in one prior enantioselective synthesis.[11] Reduction of (−)-**7** gave the amino alcohol **8**, (95%) which was converted to the *N*-methyl compound **10** (69% overall) by reduction of the benzyloxycarbonyl derivative **9**. Direct oxida-

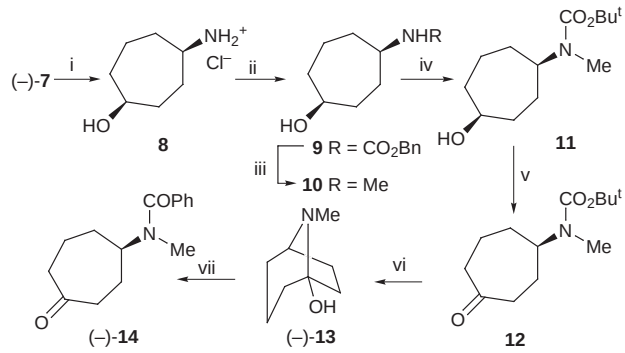

Scheme 3 *Reagents and conditions*: i, H_2, $Pd(OH)_2$/C, MeOH; ii, $ClCO_2Bn$, Na_2CO_3, acetone; iii, $LiAlH_4$, THF, reflux; iv, $(Bu^tOCO)_2O$, $EtNPr^i_2$, CH_2Cl_2; v, PCC, CH_2Cl_2; vi, TFA, then Na_2CO_3 aq; vii, BzCl, pyridine, CH_2Cl_2

tion of **10** with Jones' reagent[10] gave (−)-**13**, but the isolation of the product in good yield was troublesome and the sequence shown in Scheme 3, involving protection of the basic nitrogen, gave (−)-**13** {$[\alpha]_D$ −50.0 (*c* 0.46, CH_2Cl_2)}§ in higher overall yield. Benzoylation of (−)-**13** gave the crystalline *N*-benzoyl derivative (−)-**14**, $[\alpha]_D$ −79.4 (*c* 0.97, CH_2Cl_2) {lit. for the enantiomer, $[\alpha]_D$ +78.0 (*c* 0.44, $CHCl_3$),[11] $[\alpha]_D$ +95.6 (*c* 1.3, $CHCl_3$)[9c]}.

The potent non-opioid analgesic activity shown by (−)-epibatidine [(−)-**17**], isolated from the poison frog *Epipedobates tricolor*, has led to many syntheses,[12] including some enantioselective approaches.[13] The availability of essentially enantiomerically pure cycloadduct (−)-**4** permitted a formal synthesis of (+)-epibatidine [(+)-**17**] (Scheme 4). Reductive cleavage of the N–O bond, and reaction with di-*tert*-butyl dicarbonate gave **15** (67%), and benzoylation of this gave (−)-**16**, mp 78–79 °C, $[\alpha]_D$ −87.6 (*c* 0.89, CH_2Cl_2), enantiomeric with an intermediate {mp 78–79 °C, $[\alpha]_D$ +86.6 (*c* 1.26, CH_2Cl_2)} used, *via ent*-**15**, in Trost and Cook's synthesis of (−)-epibatidine.[13b]

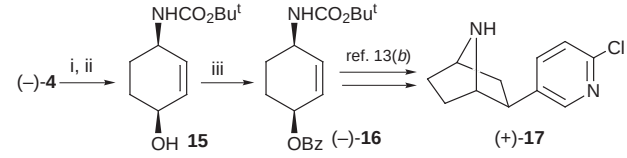

Scheme 4 *Reagents and conditions*: i, Zn, AcOH; ii, $(Bu^tOCO)_2O$, Na_2CO_3, acetone–MeOH; iii, BzCl, DMAP, pyridine, CH_2Cl_2

Although the use of a chiral auxiliary derived from D-xylose leads in both the above syntheses to the enantiomers of the natural products, the commercial availability of L-xylose makes it possible to employ identical chemistry in either enantiomeric series. However, L-xylose is relatively expensive, and so we have prepared (Scheme 5) a chloronitroso compound **20** pseudoenantiomeric with **2** from the cheap L-sorbose, *via* the

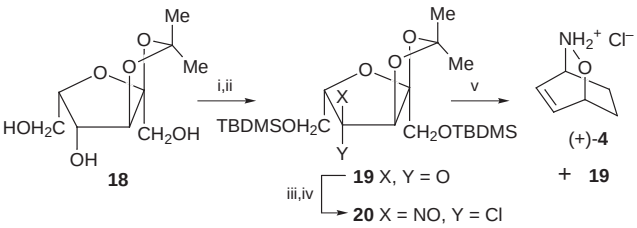

Scheme 5 *Reagents and conditions*: i, TBDMSCl, Et_3N, DMF; ii, PCC, mol. sieves, CH_2Cl_2; iii, $NH_2OH{\cdot}HCl$, $NaHCO_3$, EtOH–H_2O; iv, Bu^tOCl, CH_2Cl_2, 0 °C; v, cyclohexa-1,3-diene, $CHCl_3$–Pr^iOH–H_2O (100:100:1), 0 °C

monoisopropylidene compound **18**,[14] prepared using the same procedure as for the equivalent xylose derivative.[7]

When **20** was treated with cyclohexa-1,3-diene in the presence of water, the cycloadduct (+)-**4** was isolated in 76% yield, together with ketone **19** (86%). The ee of (+)-**4** was estimated as ⩾97% by derivatization with (+)-camphor-10-sulfonyl chloride.[4a] It thus appears that the two ketones **1** and **19** can be used to gain ready access to the two enantiomeric series through cycloadditions of the pseudoenantiomeric chloronitroso compounds **2** and **20**.

We thank the EPRSC for a studentship (A. H.) and for access to the National Mass Spectrometry Service Centre, Organon Laboratories Ltd for additional financial support, and Dr Georgina Rosair for X-ray crystallography.

Notes and References

† E-mail: cherhw@bonaly.hw.ac.uk

‡ The analogous chloronitroso compound derived from di-*O*-isopropylidene-D-glucose behaved very similarly to **2** in the reactions of both Schemes 1 and 2.

§ The specific rotation of physoperuvine does not seem to have been previously reported. Small negative values have been reported for the *hydrochloride* of both natural {$[\alpha]_D$ −0.8 (*c* 1.0, MeOH)} [ref. 9(*b*)] and synthetic {$[\alpha]_D$ −0.98 (*c* 1.28, MeOH)} (ref. 11) *S*-physoperuvine, although a small positive value has also been quoted in a different solvent {$[\alpha]_D$ +1.2 (*c* 1.3, H_2O)} [ref. 9(*a*)]. Our results imply that natural (*S*)-physoperuvine, as the free base, is significantly dextrorotatory.

1 D. L. Boger and S. M. Weinreb, *Hetero-Diels–Alder Methodology in Organic Synthesis*, Academic Press, San Diego, 1987; H. Waldman, *Synthesis*, 1994, 535; J. Streith and A. Defoin, *Synthesis*, 1994, 1107.
2 *e.g.* J. Li, F. Lang and B. Ganem, *J. Org. Chem.*, 1998, **63**, 3403 and references cited therein; A. Ghosh and M. J. Miller, *Tetrahedron Lett.*, 1995, **36**, 6399 and references cited therein; S. F. Martin, M. Hartmann and J. A. Josey, *Tetrahedron Lett.*, 1992, **33**, 3583 and references cited therein; V. Gouverneur, G. Dive and L. Ghosez, *Tetrahedron*: *Asymmetry*, 1991, **2**, 1173; A. Defoin, A. Brouillard-Poichet and J. Streith, *Helv. Chim. Acta*, 1991, **74**, 103; V. Gouverneur and L. Ghosez, *Tetrahedron*: *Asymmetry*, 1990, **1**, 363; A. Miller and G. Procter, *Tetrahedron Lett.*, 1990, **31**, 1043.
3 M. Sabuni, G. Kresze and H. Braun, *Tetrahedron Lett.*, 1984, **25**, 5377.
4 (*a*) H. Braun, H. Felber, G. Kresze, F. P. Schmidtchen, R. Prewo and A. Vasella, *Liebigs Ann. Chem.*, 1993, 261; (*b*) A. Defoin, T. Sifferlen and J. Streith, *Synlett*, 1997, 1294.
5 For amendment of an initially erroneous assignment of absolute configuration to the bicyclic adduct **4** see H. Braun, R. Charles, G. Kresze, M. Sabuni and J. Winkler, *Liebigs Ann. Chem.*, 1987, 1129.
6 For a review on the use of sugar-based auxiliaries, see: P. G. Hultin, M. A. Earle and M. Sudharshan, *Tetrahedron*, 1997, **53**, 14 823.
7 J. Moravková, J. Capková and J. Stanek, *Carbohydr. Res.*, 1994, **263**, 61.
8 A. Gieren and H.-J. Siebels, *Angew. Chem., Int. Ed. Engl.* 1976, **15**, 760.
9 (*a*) M. Sahai and A. B. Ray, *J. Org. Chem.*, 1980, **45**, 3265; (*b*) A. B. Ray, Y. Oshima, H. Hikino and C. Kabuto, *Heterocycles*, 1982, **19**, 1233; (*c*) A. T. McPhail and A. R. Pinder, *Tetrahedron*, 1984, **40**, 1661.
10 D. E. Justice and J. R. Malpass, *J. Chem. Soc., Perkin Trans. 1*, 1994, 2559, and references cited therein.
11 K. Hiroya and K. Ogasawara, *J. Chem. Soc., Chem. Commun.*, 1995, 2205.
12 N. S. Sirisoma and C. R. Johnson, *Tetrahedron Lett.*, 1998, **39**, 2059 and references cited therein; G. M. P. Giblin, C. D. Jones and N. S. Simpkins, *Synlett*, 1997, 589.
13 (*a*) C. Szántay, Z. Kardos-Balogh, I. Moldvai, C. Szántay, Jr., E. Temesvári-Major and G. Blaskó, *Tetrahedron*, 1996, **52**, 11053; (*b*) B. M. Trost and G. R. Cook, *Tetrahedron Lett.*, 1996, **37**, 7485; (*c*) H. Kosugi, M. Abe, R. Hatsuda, H. Uda and M. Kato, *Chem. Commun.*, 1997, 1857; (*d*) S. Aoyagi, R. Tanaka, M. Naruse and C. Kibayashi, *Tetrahedron Lett.*, 1998, **39**, 4513.
14 T. Reichstein and A. Grüssner, *Helv. Chim. Acta*, 1934, **17**, 311.

Received in Liverpool, UK, 7th August 1998; 8/06326E

1,2-Asymmetric induction in the aldol addition reaction of malonate ester enolate to α-alkoxy aldehyde

Shinji Marumoto, Hiroshi Kogen*† and Shunji Naruto

Exploratory Chemistry Research Laboratories, Sankyo Co., Ltd., 2-58, Hiromachi 1-chome, Shinagawa-ku Tokyo, 140-8710 Japan

Stereoselective aldol reactions between the lithium enolate of *tert*-butyl malonate and various α-alkoxy aldehydes in the presence of zinc chloride gave *anti*-1,2-diols in high yields; 2-trityloxypropanal yielded the *syn*-1,2-diol under the same conditions.

The stereoselective aldol reaction represents one of the major challenges of modern synthetic organic chemistry.[1] Many useful methodologies have been reported during the last few decades. For instance, 1,2-asymmetric induction in the aldol reaction of α-alkoxy aldehydes with silyl enol ethers or ketene silyl acetals is well-established.[2] The aldol reaction between α-alkoxy aldehydes and a malonate ester is especially useful for the synthesis of biologically active compounds.[3] For example, our recent synthesis of the neuritogenic agent epolactaene[4] relied exclusively on this operation for the formation of the 1,2-diol. However, Saba *et al*.[5] have been the only ones to report this type of aldol reaction, and the examples are limited. According to their report, when optically active dimenthyl malonate was added to chiral α-alkoxy aldehydes, the *anti* aldol adduct was obtained in ratios from 3:1 to 5:1, even in matched cases. Here we demonstrate simpler and more general methodologies for these aldol reactions which give higher *anti* product stereoselectively.

Initially, we attempted an 1,2-asymmetric aldol reaction between the lithium enolate of *tert*-butyl malonate and 2-benzyloxypropanal **1a**,[6] derived from methyl lactate, at −78 °C (Table 1). When this reaction was carried out without Lewis acid, aldol adduct **4a** was obtained with low diastereoselectivity (60:40, entry 1). However, when we added $MgBr_2$ to coordinate to the carbonyl group, the diastereoselectivity was slightly increased (68:32, entry 2). The reaction was further examined in the presence of various Lewis acids under various conditions.‡ The results are shown in Table 1. High *anti*-selectivity was observed using $ZnCl_2$ (82:18) or $BF_3{\cdot}OEt_2$ (91:9) (entries 4, 5). Moreover, when the reaction was carried out at −98 °C in the presence of $ZnCl_2$, the *anti* aldol adduct was obtained in excellent yield with high stereoselectivity (87:13).

Table 1 Aldol addition reaction of malonate ester enolate to 2-benzyloxypropanal

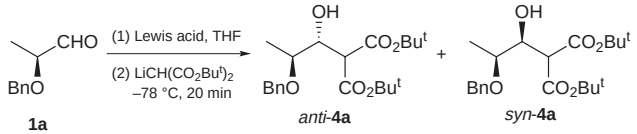

1a *anti*-**4a** *syn*-**4a**

Entry	Lewis acid	Yield (%)	*anti*:*syn*[a,b]
1	None	71[c]	60:40
2	$MgBr_2$	80	68:32
3	$ZnBr_2$	68	73:27
4	$ZnCl_2$	81	82:18
5	$ZnCl_2$	89[d]	87:13
6	$BF_3{\cdot}Et_2O$	52	91:9

[a] Ratios were determined by HPLC analysis of the crude mixture. [b] Stereochemical assignments were secured through deprotection to diol (see note §). [c] Reaction was carried out for 2 h. [d] Reaction was carried out at −98 °C.

In order to further evaluate the effect of the addition process on stereoselectivity, various α-alkoxy aldehydes were examined in this aldol reaction in the presence of $ZnCl_2$ at −78 °C. The results are summarized in Table 2. The stereoselectivity decreased somewhat when a bulky silyl group was used in place of the benzyl group as the protective group (entries 1–3). In contrast, when the alkyl group was changed from methyl to a more bulky isopropyl group (**2a**–**d**) high *anti*-selectivity was obtained using any aldehyde, although the chemical yield was affected by the size of the protective group (entries 4–7). The aldehyde **3a**, derived from mandelic acid, also gave a good result (entry 8).

Table 2 Influence of the substitution of the aldehyde in the aldol reaction in the presence of $ZnCl_2$

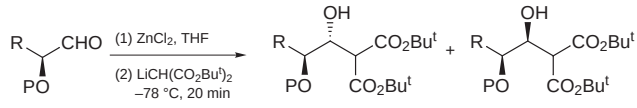

1 R = Me, **2** R = Pr^i, **3** R = Ph — **4** R = Me, **5** R = Pr^i, **6** R = Ph

Entry	Aldehyde	R	P	Yield (%)	*anti*:*syn*[a]
1	**1a**[b]	Me	Bn	81	82:18[c]
2	**1c**[d]	Me	Bu^{t}Ph$_2$Si	92	76:24[e]
3	**1d**[f]	Me	Ph$_3$Si	94	58:42[e]
4	**2a**[g]	Pr^i	Bn	75	97:3[c]
5	**2b**[f]	Pr^i	Bu^{t}Me$_2$Si	(90)[h]	98:2[e]
6	**2c**[i]	Pr^i	Bu^{t}Ph$_2$Si	(39)[h]	97:3[e]
7	**2d**[f]	Pr^i	Ph$_3$Si	(52)[h]	97:3[e]
8	**3a**[j]	Ph	Bn	83	94:6[c]

[a] Stereochemical assignments were secured through deprotection to the diol (see note §). [b] Ref. 6. [c] Ratios were determined by HPLC analysis of the crude mixture. [d] Ref. 7. [e] Ratios were determined by ^{1}H NMR analysis of the crude mixture. [f] Ref. 8. [g] Ref. 9. [h] Figures in parenthesis are the NMR yield. [i] Ref. 10. [j] Ref. 11.

To determine the extent to which the ratio of stereoisomers is affected by the protecting groups on the α-oxygen, we examined 2-trityloxypropanal **1e**[12] under the same conditions (Scheme 1). Surprisingly, the stereoselectivity was reversed and the *syn*-aldol product **4e** was preferred with high selectivity (90:10) in 53% yield (85% yield based on 62% conversion of the aldehyde **5** by ^{1}H NMR analysis). In this case, no aldol product was obtained in the absence of Lewis acid.

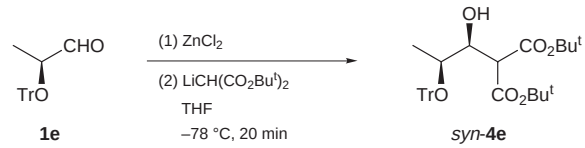

1e *syn*-**4e**

53% (85% conv. yield)

syn : *anti* = 90 : 10

Scheme 1

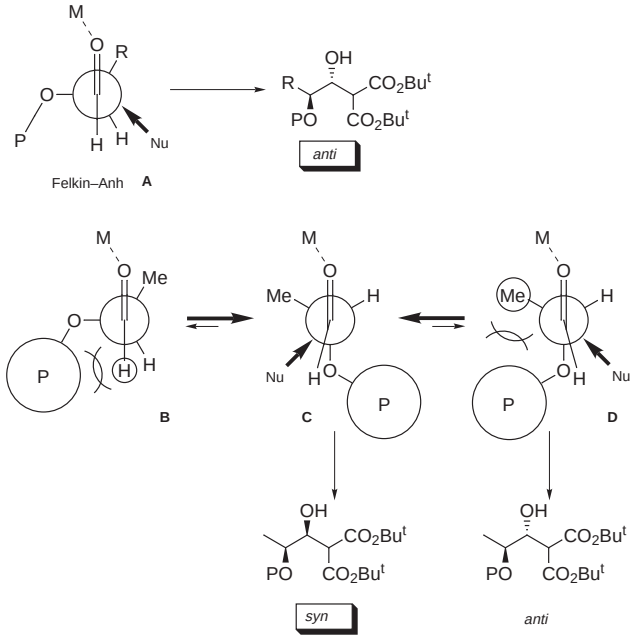

Fig. 1

To explain the reaction mechanism responsible for the observed stereoselectivity, we considered the following. The preferential formation of the *anti*- rather than *syn*-aldol product may be rationalized in terms of the normal Felkin–Anh transition state model[13] **A** described in Fig. 1. On the other hand, the remarkable *syn*-selectivity observed in Scheme 1 could not be explained by this Felkin–Anh transition state model. In this case, we postulate dipolar models **C** and **D**, avoiding steric interaction between the extremely bulky trityl group and aldehyde in model **B**. Because of the steric interaction between the trityl group and the methyl group in model **D**, model **C**, which provides a *syn*-aldol product, is favored over model **D**.

In conclusion, we have demonstrated 1,2-asymmetric induction in the aldol reaction between the lithium enolate of *tert*-butyl malonate and α-alkoxy aldehydes in the presence of a Lewis acid. *Anti*- or *syn*-aldol products were obtained in high yield with high stereoselectivity.

Dedicated to Professor Kenji Koga on the occasion of his 60th birthday.

Notes and References

† E-mail: hkogen@shina.sankyo.co.jp

‡ *General procedure*: To a solution of aldehyde (0.10 mmol) in THF (1 mL) was added zinc chloride (0.5 M in THF, 0.24 ml, 0.12 mmol) at room temperature. The reaction mixture was stirred for 1.5 h and then cooled to −78 °C. A solution of di-*tert*-butyl malonate (34 μl, 0.15 mmol) in THF (1 ml), which was treated with LHMDS (1.0 M in THF, 0.14 ml, 0.14 mmol) at −78 °C for 20 min, was added to the reaction mixture through a cannula. The stirring was continued for another 20 min at this temperature. To the mixture was added saturated aq. NH_4Cl, and the organic material was extracted with Et_2O. The combined organic extracts were dried over anhydrous $MgSO_4$ and concentrated *in vacuo* after filtration. Flash chromatography provided the aldol adduct. In the case of entry 7 in Table 2, the reaction was repeated on a 10 mmol scale. The same result was obtained.

§ The relative stereochemistry of the aldol adducts was determined by deprotection of the major and minor isomers of **1a**, **2a** and **3a** to give the diol and conversion to the corresponding acetonide followed by NOE observations.

1 For a review of stereoselective aldol reactions, see: A. S. Franklin and I. Paterson, *Contemp. Org. Synth.*, 1994, **1**, 317; C. H. Heathcock, in *Comprehensive Organic Synthesis*, ed. B. M. Trost and I. Fleming, Pergamon, Oxford, 1991, vol. 2, p. 181; C. H. Heathcock, in *Asymmetric Synthesis*, ed. J. D. Morrison, Academic Press, New York, 1984, vol. 3, p. 111; D. A. Evans, J. V. Nelson and T. R. Taber, *Top. Stereochem.*, 1982, **13**, 1.
2 C. Gennari, in *Comprehensive Organic Synthesis*, ed. B. M. Trost and I. Fleming, Pergamon, Oxford, 1991, vol. 2, p. 629.
3 J. Yoshimura, *Adv. Carbohydr. Chem. Biochem.*, 1984, **42**, 69.
4 S. Marumoto, H. Kogen and S. Naruto, *J. Org. Chem.*, 1998, **63**, 2068.
5 A. Saba, *Tetrahedron*: *Asymmetry*, 1992, **3**, 371; A. Saba, V. Adovasio and M. Nardelli, *Tetrahedron*: *Asymmetry*, 1992, **3**, 1573.
6 R. E. Ireland, S. Thaisrivongs and P. H. Dussault, *J. Am. Chem. Soc.*, 1988, **110**, 5768.
7 S. K. Massad, L. D. Hawkins and D. C. Baker, *J. Org. Chem.*, 1983, **48**, 5180.
8 Synthesized using the method described in ref. 7.
9 W-R. Li, W. R. Ewing, B. D. Harris and M. M. Joullie, *J. Am. Chem. Soc.*, 1990, **112**, 7659.
10 H. Ina, M. Ito and C. Kibayashi, *J. Org. Chem.*, 1996, **61**, 1023.
11 F. Effenberger, M. Hopf, T. Ziegler and J. Hudelmaeyer, *Chem. Ber.*, 1991, **124**, 1651.
12 K. Mori and H. Kikuchi, *Liebigs. Ann. Chem.*, 1989, 963.
13 N. T. Anh, *Top. Curr. Chem.*, 1980, **88**, 145.

Received in Cambridge, UK, 10th August 1998; 8/06290K

Outstanding effect of SO_2 addition on the rate of carbon oxidation with a Pt catalyst

Junko Oi-Uchisawa,*† Akira Obuchi, Ryuji Enomoto, Atsushi Ogata and Satoshi Kushiyama

Atmospheric Environmental Protection Department, National Institute for Resources and Environment, 16-3 Onogawa, Tsukuba, Ibaraki 305-8569, Japan

Addition of trace SO_2 (*ca*. 8 ppm) to a reactant gas containing NO substantially enhanced the oxidation rate of carbon black mixed with a Pt/SiO_2 catalyst, which is attributed to SO_3 (or H_2SO_4) catalyzing the oxidation of carbon by NO_2.

The emission of soot from diesel engines is a serious environmental problem. Among the many catalysts for soot oxidation that have so far been reported, Pt exhibits high levels of catalytic activity.[1–5] Platinum is thought to promote soot oxidation indirectly, *i.e*. by oxidizing the NO normally coexisting in the exhaust gas into NO_2, which actually oxidizes soot to CO and CO_2. Here we report the effect of adding SO_2 to the reactant gas, which dramatically promoted the oxidation of carbon black.

Platinum (1 wt%) supported on silica gel (Pt/SiO_2) was prepared by impregnating SiO_2 (0.1 to 0.25 mm in diameter, 374 $m^2\ g^{-1}$) with a solution of $Pt(NH_3)_4(OH)_2$, followed by drying, reduction with H_2 at 400 °C and calcination in air at 600 °C. Commercially available carbon black (CB; Nippon Tokai carbon 7350F; primary particle size = 28 nm; specific surface area = 80 $m^2\ g^{-1}$; CHN analysis: C, 97.99; H, 1.12; N, 0.06%; H_2O = 0.58 wt%) was used as model soot. The Pt/SiO_2 catalyst (0.5 g) and CB powder (0.005 g) were simply mixed together with a spatula and placed in the reactor. Mixing in this way results in a 'loose' contact between the catalyst and carbon, which is thought to be close to that found in practical cases.[6] Temperature-programmed reactions (TPRs) were carried out in a tubular quartz reactor. Reactant gases—10% O_2, 7% H_2O, 0 or 1000 ppm NO, 0 to 100 ppm SO_2 and N_2, a composition which is typical of diesel exhaust gas, except for the absence of CO_2—were passed through the mixture of catalyst and CB at a flow rate of 0.5 dm^3 (STP) min^{-1}. The temperature of the reactor was raised from 80 to 700 °C by 10 °C min^{-1}. A non-dispersive IR gas analyzer was used to continuously measure the concentrations of CO and CO_2 emitted by the carbon oxidation. In addition, TPR measurements using an FTIR gas analyzer were separately conducted to measure the concentrations of NO, NO_2 and SO_2 in the product gas.

Fig. 1 shows the effect of the composition of the reactant gas on the CO_2 emission during the TPR. The CO concentration was almost zero in all cases (≤0.8 ppm). In the gas mixture N_2 + O_2 + H_2O [Fig. 1(○)], carbon was not oxidized at all below 500 °C, above which temperature the reaction rate increased abruptly and the oxidation was finished at 675 °C. Platinum had no accelerating effect on the carbon gasification under these conditions, since the TPR result using SiO_2 alone (not shown) was almost the same as that shown in Fig. 1(○). Fig. 1(●) shows the result when 100 ppm SO_2 was added to the reactant gas. Sulfur dioxide had no effect on the oxidation under these conditions. On the other hand, the addition of NO instead of SO_2 brought about an acceleration of carbon oxidation Fig. 1(△). The initial temperature, which we define as the point where the CO_2 concentration exceeds 100 ppm, was about 200 °C lower than that in N_2 + O_2 + H_2O. In the case of SiO_2 alone, such a promotional effect of NO was not observed, but when NO_2 was used instead of NO, the CO_2 emission curve shifted to nearly the same temperature region as Fig. 1(△). These results suggest that NO_2, which is formed by the oxidation of NO over Pt, oxidizes carbon black more strongly than O_2. The effect of NO_2 on soot oxidation has been already reported by several researchers.[4,5,7]

The striking effect of SO_2 was observed when it was further added to N_2 + O_2 + H_2O + NO over the Pt/SiO_2. By adding only 1 ppm of SO_2, the CO_2 emission level at 350 °C increased by 210 ppm [Fig. 1(▲)]. As the concentration of SO_2 was increased, a new peak appeared at around this temperature; when the SO_2 concentration exceeded 23 ppm, CO_2 emission was at its maximum at this temperature [Fig. 1(◇) and (◆)]. The temperature of maximum CO_2 emission was about 300 °C lower than that in the N_2 + O_2 + H_2O mixture and more than 200 °C lower than that in N_2 + O_2 + H_2O + NO. The initial temperature decreased to as low as 250 °C. The CO_2 concentrations at 350 °C in the experiments containing NO were plotted as a function of SO_2 content in the reactant gas (Fig. 2). The CO_2 concentration dramatically increases until the SO_2 content reaches 8 ppm and then almost levels off with further increases in SO_2 content. Such a promotional effect of SO_2 is not observed with SiO_2 alone, even when NO_2 is used instead of NO.

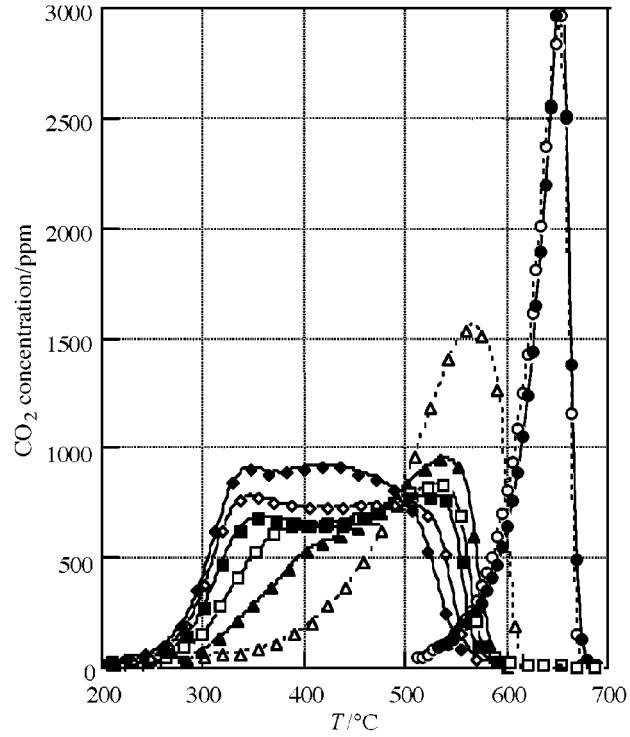

Fig. 1 TPR profiles of Pt/SiO_2 in carbon oxidation. Conditions; catalyst = 0.5 g, carbon = 0.005 g, flow rate = 0.5 $dm^3\ min^{-1}$ (0 °C, 1 atm) (**X** = 10% O_2 + 7% H_2O in N_2, **Y** = 10% O_2 + 7% H_2O + 1000 ppm NO in N_2): (○) **X**, (●) **X** + 100 ppm SO_2, (△) **Y**, (▲) **Y** + 1 ppm SO_2, (□) **Y** + 4 ppm SO_2, (■) **Y** + 8 ppm SO_2, (◇) **Y** + 23 ppm SO_2, (◆) **Y** + 100 ppm SO_2.

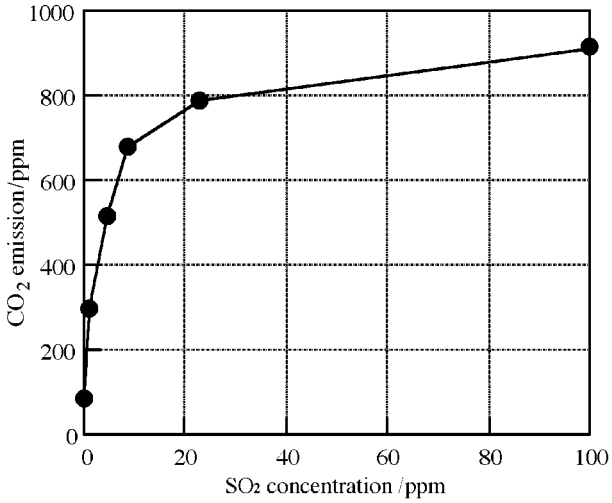

Fig. 2 Effect of the concentration of SO_2 on the activity of Pt/SiO_2 catalyst in carbon oxidation (T = 350 °C). Conditions are as in Fig. 1.

Separate TPR experiments using an FTIR gas analyzer were also carried out under the conditions of 10% O_2, 0.5% H_2O, 1000 ppm NO, 100 ppm SO_2 and N_2. Over Pt/SiO_2, NO starts to be oxidized to NO_2 at 160 °C. The concentration of NO_2 reached a maximum at 330 °C and then decreased in accordance with levels expected from the thermodynamic equilibrium between NO_2, NO and O_2. The concentration of SO_2 in the product gas started to decrease at 165 °C, reached a negligible level between 220 to 500 °C, and then gradually increased in accordance with levels expected from the thermodynamic equilibrium between SO_3, SO_2 and O_2. Evidently, the oxidation of NO into NO_2 and SO_2 into SO_3 (or H_2SO_4 below 300 °C) proceeded over Pt/SiO_2. Incidentally, the oxidation of SO_2 to SO_3 by gaseous NO_2 did not proceed to an observable extent over SiO_2 alone under the conditions of 10% O_2, 0.5% H_2O, 1000 ppm NO_2, 100 ppm SO_2 and N_2. Nitrogen dioxide is regarded as an oxidizer that directly attacks the carbon and turns into NO; the NO may be oxidized to NO_2 over Pt/SiO_2 and reused. On the other hand, the outstanding effect of SO_2 with Pt/SiO_2 only appeared in the presence of NO suggesting that SO_3, produced from SO_2 over Pt, plays a role as a catalyst that accelerates the oxidation of carbon by NO_2.

To confirm this possible role of SO_3 (or H_2SO_4), we tested the effect of NO_2 and H_2SO_4 addition on the carbon oxidation over SiO_2 alone. When 1000 ppm NO_2 and 100 ppm H_2SO_4 were added to the feed containing 10% O_2 + 7% H_2O in N_2, the oxidation was initiated at 280 °C and there were peaks in CO_2 concentration at 380 and 490 °C. By contrast the addition of 100 ppm H_2SO_4 alone did not have any effect on the CO_2 emission rate: the initial and peak temperatures were around 560 and 680 °C, respectively. These results strongly suggest that SO_3 (or H_2SO_4) formed over Pt surfaces catalyzes the oxidation of carbon by NO_2.

Lur'e *et al*.[7] reported that the process of CO_2 formation from the interaction of NO_2 with soot proceeds through the oxidation of active sites on the soot surface, *via* abstraction of oxygen atoms from NO_2, to produce partially oxidized surface species (> C=O) and NO. We suspect that the effect of SO_3 (or H_2SO_4) can be attributed to the enhancement of decomposition of the partially oxidized surface species. It is well known that H_2SO_4 promotes dehydration and decarboxylation of organic compounds.[8] The partially oxidized surface species created by NO_2 may be rather inactive against further oxidation, but can be readily decomposed by a strong acid such as SO_3 or H_2SO_4. After this secondary process, the ability of the carbon surface to be oxidized may be restored.

Notes and References

† E-mail: junko@nire.go.jp

1 G. Neri, L. Bonaccorsi, A. Donato, C. Milone, M. Grazia M. and A. M. Visco, *Appl. Catal. B*, 1997, **11**, 217.
2 H. J. Stein, *Appl. Catal. B*, 1996, **10**, 69.
3 M. Hosoya and M. Shimoda, *Appl. Catal. B*, 1996, **10**, 83.
4 P. Hawker, N. Myers, G. Huthwohl, H. T. Vogel, B. Bates, L. Magnusson and P. Bronnenberg, SAE Technical Paper Series, 970182, 1997.
5 B. J. Cooper, H. J. Jung and J. E. Thoss, *US Pat*. 4902487.
6 J. P. A. Neeft, O. P. Pruissen, M. Makkee and J. A. Moulijn, *Appl. Catal. B*, 1997, **12**, 21
7 B. A. Lur'e and A. V. Mikhno, *Kinet. Catal*., 1997, **38**, 535
8 *Advanced Organic Chemistry, Reactions, Mechanisms and Structure*, 4th edn., ed. J. March, Wiley, New York, p. 389, p. 563, p. 1011

Received in Cambridge, UK, 20th July 1998; 8/05598J

$^{19}F/^{23}Na$ Cross polarization NMR study of hydrofluorocarbon–zeolite binding on zeolite NaY

Kwang Hun Lim and Clare P. Grey*†

Department of Chemistry, SUNY Stony Brook, Stony Brook, NY 11794-3400, USA

$^{19}F/^{23}Na$ Cross polarization (CP) MAS NMR experiments of various asymmetric hydrofluorocarbons (HFCs) such as CF_3CFH_2 (HFC-134a) and CF_2HCFH_2 (HFC-143) adsorbed on zeolite NaY, demonstrate that the hydrogen-containing groups are bound more strongly to the zeolite framework, in the order $CF_3 << CF_2H < CFH_2$; the results help explain the preferential binding of CF_2HCF_2H (HFC-134) over HFC-134a, and hence the effectiveness of basic zeolites in the separation of HFC-134/134a gas mixtures.

The complete phase-out of chlorofluorocarbon (CFC) production in developed countries by the year 2000 has resulted in the development and production of a variety of environmentally-friendly alternatives (the HFCs) for different applications.[1] The syntheses of the HFCs are more complex than the syntheses of the CFCs and unwanted HFC and hydrochlorofluorocarbon isomers are often produced. For example, HFC-134 is a common byproduct in the synthesis of HFC-134a, the replacement for the refrigerant CFC-12 (CF_2Cl_2).[1] Basic molecular sieves have been proposed as a method for separating some of these isomer mixtures.[2] We have, therefore, been applying a variety of NMR and X-ray powder diffraction methods to determine the importance of different interactions in controlling the sorption properties of these gases on faujasite zeolites, and to rationalize trends in separations behavior and HFC reactivity.[3,4] Our previous work on the binding of HFC-134 on zeolite NaY demonstrated that Na-F interactions are very important in these systems, and are strong enough to cause migration of cations from the sodalite cages into the supercage where they can bind to both ends of the HFC molecule.[4]

The efficiency of ^{19}F magnetization transfer in a ^{19}F–^{23}Na CP experiment, from the different ends of the HFC molecule to the sodium cations present in the supercages of the zeolite, has been explored in research described here. The CP efficiency is very sensitive to the offset-frequency of the ^{19}F radio frequency (rf) field: as the offset frequency ($\Delta\nu$) of the rf field (ν_1) is increased, the polarization transfer rate is decreased by a factor $\nu_1^2/(\nu_1^2 + \Delta\nu^2)$.[5] Thus, if the CP experiment is performed with low rf power, the effect of offset-frequency on the transfer rate will be significant. Since the ^{19}F NMR spectra of the asymmetric HFCs show well separated resonances for the different $CF_{3-n}H_n$ groups (for example, the chemical shifts for the CF_3 and CFH_2 groups of HFC-134a are −81 and −246 ppm, respectively), it is possible to study the CP dynamics of the end-groups separately.

Methods used to prepare the samples are identical to those described elsewhere[4] and the samples are labeled *x*HFC/NaY, where *x* indicates the number of HFC molecules per unit cell. The ^{23}Na MAS NMR spectrum of the fully loaded HFC134a/NaY sample ($x \approx 44$–48) at −150 °C is shown in Fig. 1(*a*). The narrow resonance at −7 ppm is assigned to the site I cations of the faujasite structure (in the double six-rings), and the broader resonance centered at −40 ppm contains overlapping resonances from sodium nuclei originally in the site II and I′ positions, in the super and sodalite cages respectively.[4] The narrowing of this resonance, in comparison to that of bare NaY, suggests that some cation migration from site I′ to sites in the supercages may also be occurring on adsorption of HFC-134a.

Variable-temperature ^{19}F MAS NMR was initially performed to confirm that the isotropic motion of the HFCs was frozen out at −150 °C. Rf field strengths of 10–20 and 20–40 kHz were used for ^{23}Na and ^{19}F, respectively, in order to match the Hartmann–Hahn condition for quadrupolar nuclei with non-zero quadrupole coupling constants[5,6] and low rf field strengths and fast spinning speeds were used to help ensure effective ^{23}Na spin-locking.[7]

Fig. 1(*b*) and (*c*) show the $^{19}F \rightarrow ^{23}Na$ CP MAS spectra of the fully-loaded HFC134a/NaY at −150 °C, where the ^{19}F irradiation frequency is placed on the ^{19}F CFH_2 and CF_3 group resonances, respectively. Only one broad ^{23}Na resonance at approximately −40 ppm is observed and the site I resonance is absent, indicating that polarization is only transferred to cations in close proximity to the HFCs. Surprisingly, the CP intensity from the CFH_2 group is much higher than that from the CF_3 group which contains more fluorine spins. In order to investigate this behavior more fully, CP experiments were performed as a function of fluorine irradiation offset: A dramatic decrease in ^{23}Na CP intensity for 32HFC-134a/NaY was observed, as the fluorine irradiation offset $\Delta\nu_1$ is changed from on-resonance for the CFH_2 group (−58 kHz) to on-

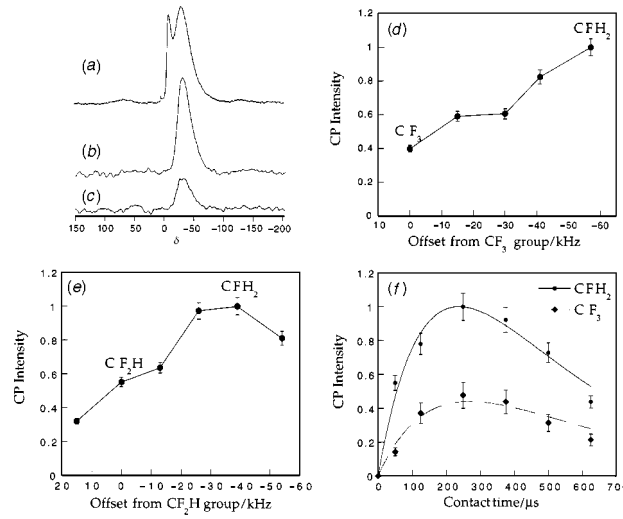

Fig. 1 (*a*) The ^{23}Na MAS NMR spectra of fully-loaded HFC-134a/NaY at −150 °C. Spinning speeds of 10 kHz were used; (*b*) and (*c*): The $^{19}F \rightarrow ^{23}Na$ CP MAS spectra of fully-loaded HFC-134a/NaY at −150 °C. The ^{19}F frequency was placed on resonance for the CFH_2 resonance and CF_3 resonance in (*b*) and (*c*), respectively. Spinning speeds of 9.5 kHz, a 400 μs CP contact time (ct) and an ^{19}F rf field strength, ν_1, of 40 kHz were used, and 1640 FIDs were recorded for each spectrum. $^{19}F \rightarrow ^{23}Na$ CP intensity as a function of fluorine irradiation offset of (*d*) 32HFC-134a/NaY at −150 °C (spinning speed = 9 kHz; ct = 333 μs; ν_1, = 40 kHz) and (*e*) 32HFC-143/NaY at −150 °C (spinning speed = 8 kHz; ct = 250 μs; ν_1 = 20 kHz). (f) 32HFC-134a/NaY at −150 °C, as a function of contact time (ν_1 = 20 kHz). The two curves drawn in (*f*) were obtained with equations for CP intensity given in refs. 11 and 13 (see text). Spectra were acquired with a double-tuned Chemagnetics probe, on a CMX-360 spectrometer with resonance frequencies for ^{19}F and ^{23}Na of 338.7 MHz and 95.2 MHz, respectively. The ^{23}Na chemical shifts reported were referenced to solid NaCl at 0.0 ppm.

resonance for the CF_3 group (0 kHz) [Fig. 1(*d*)]. The same experiment was performed for 32HFC-143/NaY and the CP intensity for on-resonance irradiation of the CFH_2 group was higher than that for the CF_2H group [Fig. (*e*)].

The $^{19}F \rightarrow {}^{23}Na$ CP intensity was studied as a function of the contact time for both samples and the CP curve for HFC-134a is shown in Fig 1(*f*). In order to fit these curves, $T_{1\rho}$ values for the ^{23}Na spins and the ^{19}F in the different groups were all independently measured. The ^{19}F $T_{1\rho}$s (150–300 μs) were much shorter than those for ^{23}Na (*ca.* 600 μs) and are responsible for the relatively rapid decrease in CP intensity for contact times of greater than *ca*. 250 μs. Fits to these curves using the measured $T_{1\rho}$s, using modified versions of expressions given in refs. 5 and 6, demonstrate that the polarization transfer rates ($1/T_{IS}$) are considerably larger for the more hydrogenated groups. For example, using the $T_{1\rho}$ values of 230 ± 5 and 205 ± 5 μs obtained for the CFH_2 and CF_3 and groups of HFC-134a, values of T_{1S} of 480 ± 20 and 1000 ± 50 μs were obtained assuming that each end group is close to only one sodium cation.

Partial charges for the hydrofluorocarbons, calculated with Hartree–Fock methods, are slightly higher for the CFH_2 fluorine in comparison to those found on the CF_3 fluorine atoms of HFC-134a,[8] which should result in an increased Na–F electrostatic interaction. Inelastic neutron scattering and Raman spectroscopy studies of HFC-134 and HFC-134a molecules adsorbed on zeolite NaX have shown that hydrogen bonding to the framework oxygen may also be important.[9] Our ^1H MAS NMR studies of HFC-143 (CFH_2CF_2H) and HFC-134a (CF_3CFH_2) adsorbed on NaY are consistent with this: the ^1H NMR resonance is shifted to higher frequency by 2 ppm on lowering the temperature to −150 °C, suggesting that the hydrogen-containing groups are hydrogen-bonded to the framework oxygens of the zeolite. These results imply that the hydrogen-bonding plays an important role in the binding of the asymmetric HFC molecules. Thus we propose that it is the combination of this hydrogen bonding, and the strong Na–F interaction, that tethers the CFH_2 group tightly to the framework at −150 °C, resulting in efficient fluorine-to-sodium magnetization transfer. The CFH_2 group is more strongly bound than the CF_2H group of HFC-143: again this may be a consequence of the higher partial charge for the CFH_2 group and the potential for more hydrogen bonding.

In conclusion, the double resonance experiments clearly show very different binding for the different end groups of asymmetric HFCs, and demonstrate that the hydrogen-containing groups are bound more strongly to the zeolite framework. The results are consistent with the higher heat of adsorption of CF_2HCF_2H (HFC-134) over HFC-134a,[2] the former containing two hydrogen-containing groups. These findings help provide a fundamental understanding of the role of basic zeolites in the separation of HFC-134/134a gas mixtures. Finally, the NMR results suggest new methods for probing interactions and gas binding in systems involving larger molecules with multiple gas–surface interactions. In these systems, while methods such as calorimetry and adsorption isotherm measurements will provide measures of the average heat of adsorption of the molecule, experiments sensitive to local structure and interactions will be extremely useful in helping to deconvolute the relative importance of the different, sometimes competing, interactions. The CP technique will be particularly applicable when one or more NMR nucleus has a large chemical shift range.

Support from the NSF through an interagency transfer to the US Department of Energy, Office of Basic Energy Sciences is gratefully acknowledged (DE FG02-96ER14681) and for funding to purchase the NMR spectrometer (CHE-9405436). Stimulating conversations with S. M. Auerbach are gratefully acknowledged.

Notes and References

† E-mail: cgrey@sbchem.sunysb.edu

1 L. E. Manzer, *Science*, 1990, **249**, 31; G. Webb and J. Winfield, *Chem. Br*., 1992, **28**, 996; L. E. Manzer and V. N. M. Rao, *Adv. Catal*., 1993, **39**, 329.
2 D. R. Corbin and B. A. Mahler, *U.S. Pat*. 5600040 (July 17, 1995).
3 C. P. Grey and D. R. Corbin, *J. Phys. Chem*., 1995, **99**, 16 821.
4 C. P. Grey, F. I. Poshni, A. F. Gualtieri, P. Norby, J. C. Hanson and D. R. Corbin, *J. Am. Chem. Soc*., 1997, **119**, 1981.
5 M. Mehring, *Principles of High Resolution NMR in Solids*, 2nd edn., 1983, Springer-Verlag, New York.
6 T. H. Walter, G. L. Turner and E. Oldfield, *J. Magn. Reson*., 1988, **76**, 106.
7 A. J. Vega, *J. Magn. Reson*., 1992, **96**, 50.
8 K. K. Irikura and R. R. Cavanagh, personal communication.
9 T. J. Udovic, J. M. Nicol, R. R. Cavanagh, J. J. Rush, M. K. Crawford, C. P. Grey and D. R. Corbin, *Mater. Res. Soc. Symp. Proc*., 1995, **376**, 751.

Received in Corvallis, OR, USA, 15th July 1998; 8/05542D

Phosphorus monoxide as a quadruply bridging ligand: syntheses and X-ray crystal structures of $Ru_5(CO)_{15}(\mu_4\text{-PF})$ and $[H_2NCy_2][Ru_5(CO)_{15}(\mu_4\text{-PO})]$

John H. Yamamoto,[a] Konstantin A. Udachin,[a] Gary D. Enright[a] and Arthur J. Carty*[a,b]†

[a] *Steacie Institute for Molecular Sciences, National Research Council of Canada, 100 Sussex Drive, Ottawa, Ontario, Canada K1A OR6*

[b] *Ottawa-Carleton Chemistry Institute, Department of Chemistry, University of Ottawa, Ottawa, Ontario, Canada K1N 6N5*

The reaction of $Ru_4(CO)_{13}(\mu_3\text{-PNCy}_2)$ 1 with $Ru(CO)_5$ in refluxing hexane yields $Ru_5(CO)_{15}(\mu_4\text{-PNCy}_2)$ 2 in high yield; treatment of 2 with $HBF_4{\cdot}Et_2O$ forms $Ru_5(CO)_{15}(\mu_4\text{-PF})$ 3 which is the first cluster complex to contain a μ_4-fluorophosphinidene ligand, while refluxing 2 with $HBF_4{\cdot}H_2O$ in CH_2Cl_2 yields 3 and the title compound $[Ru_5(CO)_{15}(\mu_4\text{-P=O})][H_2NCy_2]$ 4, an unprecedented example of a cluster complex containing a μ_4-PO ligand.

Phosphorus monoxide (PO) and diphosphorus monoxide (P_2O) are the simplest binary oxides of phosphorus. They have both been spectroscopically characterized in matrices and in molecular beams,[1] but they are not 'reagents in a bottle' since they are unstable with respect to the normal oxides P_4O_6 and P_4O_{10}.

In contrast to nitric oxide, the coordination and organometallic chemistry of PO and P_2O is poorly developed and only recently have methods of synthesizing complexes of these ligands been described.[2–6] To date only two types of coordination modes for phosphorus monoxide are known. Triply bridging μ_3-PO ligands have been trapped or generated in clusters by the direct oxidation of naked phosphide ligands[2,4,5] or by the hydrolytic cleavage of P–N bonds in aminophosphinidene (μ_3-PNR_2) clusters.[3] Examples of terminal, η^1-PO coordination, as in $Mo\{[NC(CD_3)_2Me](C_6H_3Me_2\text{-}3,5)\}_3(\eta^1\text{-P=O})$,[5] have also been described. Doubly and quadruply bonded PO ligands are as yet unknown. In this communication we report the synthesis and structural characterization of an anionic cluster $[Ru_5(CO)_{15}(\mu_4\text{-P=O})]^-$ containing a quadruply bridging phosphorus monoxide ligand. The designed synthesis of this molecule (Scheme 1) also affords the first example known to us of a μ_4-fluorophosphinidene ligand in the neutral cluster $Ru_5(CO)_{15}(\mu_4\text{-PF})$.

We recently described a rational, versatile route to PO ligands which essentially involves the acid promoted substitution of NR_2 groups in aminophosphinidene (μ-PNR_2) ligands by hydroxyl groups followed by deprotonation of the latter by base, as follows:[7]

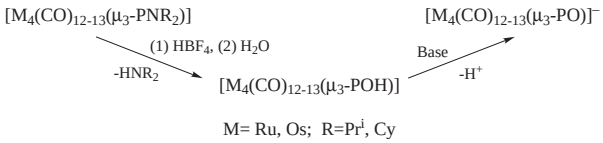

To apply this strategy to the synthesis of a μ_4-PO ligand, we needed a reliable route to a cluster containing a μ_4-PNR_2 ligand. Treatment of $Ru_4(CO)_{13}(\mu_3\text{-PNCy}_2)$[8] **1** (770 mg, 0.78 mmol) in hexane for 8 h with an excess of $Ru(CO)_5$[9] forms $Ru_5(CO)_{15}(\mu_4\text{-PNCy}_2)$ **2**[10] (867 mg, 0.76 mmol) in greater than 95% yield. The cluster **2** consists of a square based pyramid of five ruthenium tricarbonyl groups, with the square face capped by the μ_4-aminophosphinidene ligand.

Reaction of a CH_2Cl_2 solution of **2** (503 mg, 0.51 mmol) with dry $HBF_4{\cdot}OEt_2$ (300 μl) at RT for 3 h afforded $Ru_5(CO)_{15}(\mu_4\text{-PF})$ **3**[11] (503 mg, 0.51 mmol) as green crystals in 96% yield. The ^{19}F and ^{31}P NMR spectra of **3** consist of doublets [$\delta(^{19}F)$ −20.49; $\delta(^{31}P)$ 548.6] with J_{P-F} = 1121 Hz. Since **3** appears to be the first μ_4-PF cluster a single crystal X-ray analysis was carried out.[12] Within the Ru_5 square pyramid (Fig. 1) there are two distinctively different sets of Ru–Ru distances with the bond lengths within the base (Ru–Ru av. 2.9196 Å) being distinctly longer than those to the apical atom Ru(5) (Ru–Ru av. 2.8252 Å). The stereochemistry at the phosphorus atom is that of a flattened square pyramid with a P–F distance of 1.595(2) Å which compares well with a value of 1.58 Å[13] for the axial P–F bonds in PF_5 where the phosphorus atom is also pentacoordinate.

In contrast to the reaction with anhydrous HBF_4, treatment of **2** (57 mg, 0.05 mmol) with an excess of $HBF_4{\cdot}H_2O$ for 6 h gave smaller amounts of **3** (15 mg, 0.01 mmol, 31%) and afforded as the major product $[H_2NCy_2][Ru_5(CO)_{15}(\mu_4\text{-PO})]$ **4** (37 mg, 0.03 mmol, 64%). Spectroscopically, **4**[14] is characterized by a medium strong ν(P=O) band in the infrared spectrum at 1060 cm^{-1} and by a ^{31}P resonance at low field (δ 515). The structure[15] of **4** (Fig. 2) consists of tetrahedral dicyclohexylamino cations packed in the crystal lattice with $[Ru_5(CO)_{15}(\mu_4\text{-PO})]$ cluster anions. In contradistinction with $[H_2N(^iPr_2)][Ru_4(CO)_{12}(\mu_3\text{-PO})]$ there are no significant hydrogen bond interactions between the PO oxygen atom and the cation (PO···HN = 1.75 Å). The geometry of the Ru_5P skeleton resembles that in **3** but the substitution of a PO ligand in **4** for μ_4-PF in **3** causes significant changes in P–X (X = O, F), Ru–P and basal Ru–Ru bond lengths. The P–O distance in **4** [1.516(4) Å] is 0.08 Å shorter than the P–F value [1.595(2) Å] in **3** and is consistent with P=O bond lengths of 1.48–1.52 Å in μ_3-PO clusters.[2–5] However the P–Ru bond lengths in **4** (av. 2.374 Å) are significantly elongated compared to **3** (av. 2.308 Å) and the basal Ru–Ru distances in **4** (av. 2.878 Å) are shorter than in **3**

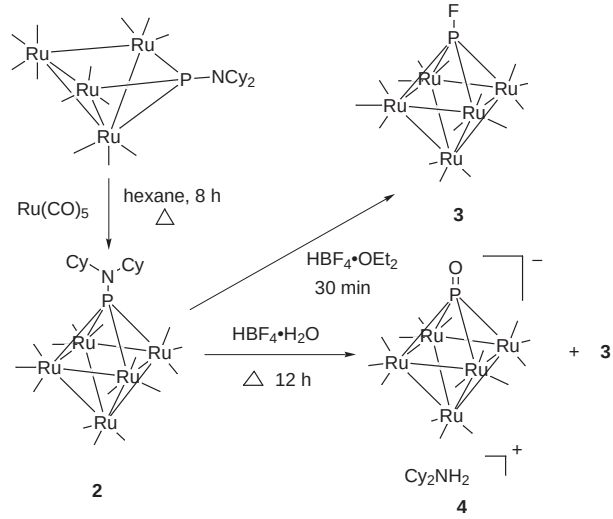

Scheme 1

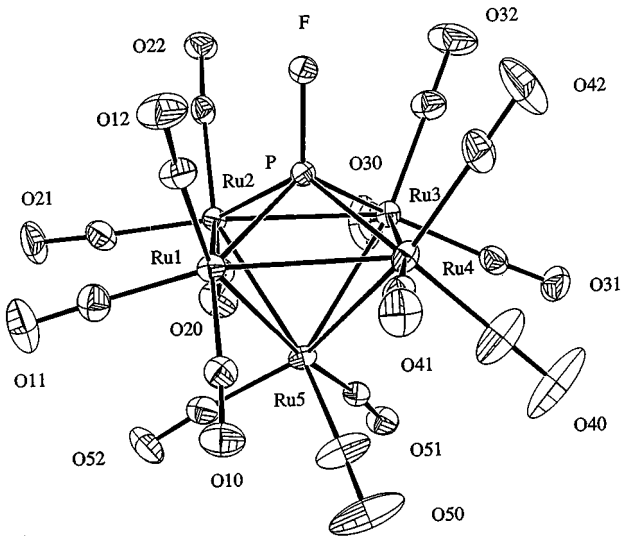

Fig. 1 An ORTEP diagram of $Ru_5(CO)_{15}(\mu_4\text{-PF})$ **3** showing 30% probability thermal ellipsoids. Hydrogen atoms are omitted for clarity. Selected bond lengths not mentioned in the text (Å): Ru(1)–Ru(2) = 2.9558(4), Ru(1)–Ru(4) = 2.9310(4), Ru(2)–Ru(3) = 2.8983(4), Ru(3)–Ru(4) = 2.8932(4), Ru(5)–Ru(3) = 2.8535(4), Ru(1)–Ru(5) = 2.7771(4), Ru(4)–Ru(5) = 2.8432(4), Ru(5)–Ru(2) = 2.8271(4).

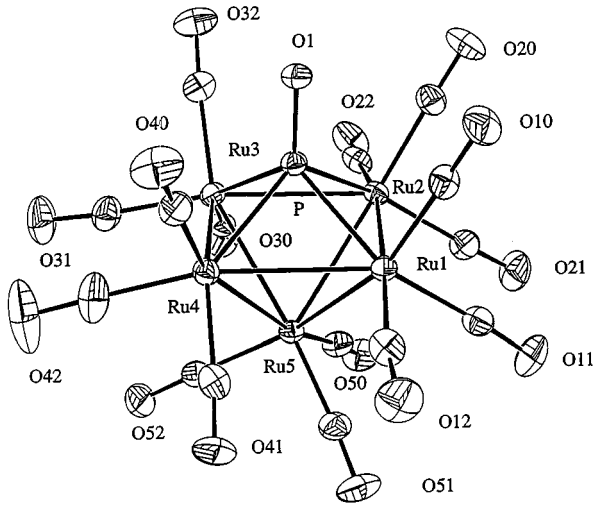

Fig. 2 An ORTEP diagram of $[Ru_5(CO)_{15}(\mu_4\text{-PO})][H_2NCy_2]$ **4** showing 30% probability thermal ellipsoids. Hydrogen atoms and the cation $[H_2N(Cy)_2]$ are omitted for clarity. Selected bond lengths not mentioned in the text (Å): Ru(1)–Ru(2) = 2.850(1), Ru(1)–Ru(4) = 2.876(1), Ru(2)–Ru(3) = 2.893(1), Ru(3)–Ru(4) = 2.908(1), Ru(5)–Ru(3) = 2.908(1), Ru(1)–Ru(5) = 2.836(1), Ru(4)–Ru(5) = 2.803(1), Ru(5)–Ru(2) = 2.843(1).

(av. 2.9196 Å). A simplistic explanation of these facts is that stronger phosphorus bonding to the *exo*-cage oxygen atom weakens cluster phosphorus bonding and strengthens metal–metal bonding.

Although **3** and **4** are obtained in the same reaction of **2** with $HBF_4{\cdot}H_2O$, attempts to directly convert **3** to **4** in the presence of H_2O and HO^- have not been successful.

The synthesis and characterization of a quadruply bridging P=O ligand in **4** adds to the terminal and triply bridging modes now known for this transient ligand. We are currently attempting to expand the range of μ_4-PO complexes and compare the chemistry of these coordinated ligands.

This work was supported by grants from the National Research Council of Canada and the Natural Sciences and Engineering Research Council of Canada (to A. J. C.)

Notes and References

† E-mail: Arthur.Carty@nrc.ca

1 L. Andrews, M. McCluskey, Z. Mielke and R. Withnall, *J. Mol. Struct.*, 1990, **222**, 95.

2 O. J. Scherer, J. Braun, P. Walther, G. Heckmann and G. Wolmershauser, *Angew. Chem., Int. Ed. Engl.*, 1991, **30**, 852.

3 (*a*) J. F. Corrigan, S. Doherty, N. J. Taylor and A. J. Carty, *J. Am. Chem. Soc.*, 1994, **116**, 9799; (*b*) W. Wang, S. Doherty, G. D. Enright, N. J. Taylor and A. J. Carty, *Organometallics*, 1996, **15**, 2770; (*c*) W. Wang and A. J. Carty, *New J. Chem.*, 1997, **21**, 773.

4 (*a*) J. Foerstner, F. Olbrich and H. Butenschon, *Angew. Chem., Int. Ed. Engl.*, 1996, **35**, 1234; (*b*) J. E. Davies, M. C. Klunduk, M. J. Mays, P. R. Raithby, G. P. Shields and P. K. Tompkin, *J. Chem. Soc., Dalton Trans.*, 1997, 715.

5 M. J. A. Johnson, A. L. Odom and C. C. Cummins, *Chem. Commun.*, 1997, 1523.

6 W. Wang, G. D. Enright and A. J. Carty, *J. Am. Chem. Soc.*, 1997, **119**, 12 370.

7 (*a*) W. Wang, G. D. Enright, J. Driediger and A. J. Carty, *J. Organomet. Chem.*, 1997, **461**–**464**, 541; (*b*) J. H. Yamamoto and A. J. Carty, unpublished results.

8 $Ru_4(CO)_{13}PNCy_2$ was synthesized in a manner analogous to that for $Ru_4(CO)_{13}PN(^iPr)_2$ as in ref. 3(*a*) and (*b*).

9 R. Huq, A. J. Poe and S. Chawla, *Inorg. Chim. Acta*, 1980, **38**, 121.

10 Spectral data for $Ru_5(CO)_{13}PN(Cy)_2$ **2**: IR (ν in hexane), 2091 w, 2050 vs, 2031 m, 2000 w, 1989 w cm^{-1}. ^1H NMR (δ in $CDCl_3$), 3.52 (m, 2H), 1.78 (m, 9H), 1.62 (m, 9H), 1.24 (m, 2H). ^{31}P NMR (δ in $CDCl_3$), 490 (s). Anal. Calc. for **2**: C, 28.53, H, 1.95, N, 1.23. Found: C, 28.05, H, 1.85, N, 1.19%.

11 Spectral data for $Ru_5(CO)_{15}PF$ **3**: IR (ν in hexane), 2068 vs, 2039 s, 2024 w, 2004 w cm^{-1}. ^{31}P NMR (δ in $CDCl_3$), 548.6 (d, J_{P-F} = 1121). ^{19}F NMR (δ in $CDCl_3$ *vs.* CF_3COOH), −20.49 (d, J_{P-F} = 1121). Anal. Calc. for **3**: C, 18.47, H, 0.00, N, 0.00. Found: C, 19.20, H, 0.00, N, 0.00%.

12 Crystal data for **3**: green crystals, $Ru_5PO_{15}C_{15}F$, monoclinic, space group $P2_1/n$, a = 9.6072(4), b = 16.7952(7), c = 15.4589(7) Å, β = 100.65(1)°, V = 2451.4(2) Å^3, Z = 4, M = 975.5 D_{calc} = 2.64 mg m^{-3}, μ = 3.15 mm^{-1}, Mo-Kα, λ = 0.70930 Å, T = 123 K, Siemens SMART CCD, crystal size 0.27 × 0.22 × 0.09 mm, $2\theta_{max}$ = 57.5°, 28166 reflections measured, 6349 unique reflections, 5396 observed reflections [$I > 2.5\sigma(I)$], semi-empirical absorption correction. Structure solution by direct methods, refinement on F^2 with anisotropic thermal parameters for all non-hydrogen atoms. Final R and Rw 0.033, 0.031. NRCVAX computer programs. CCDC 182/1001.

13 L. C. Hoskins, *J. Chem. Phys.*, 1965, **42**, 2631.

14 Spectral data for $[Ru_5(CO)_{15}PO][H_2N(Cy)_2]$ **4**: IR (ν in CH_2Cl_2 for CO), 2061 (m), 2044(vs), 2031(m), 2013(s) cm^{-1}. IR (ν in CH_2Cl_2 for PO), 1060 (m) cm^{-1}. ^1H NMR (δ in $CDCl_3$), 6.72 (br s, 2H), 3.06 (m, 2H), 2.00 (d, 4H, J_{H-H} = 11.30), 1.90 (d, 4H, J_{H-H} = 11.61), 1.70 (d, 2H, J_{H-H} = 10.63), 1.45–1.18 (m, 10H). ^{31}P NMR (δ in $CDCl_3$), 515. Anal. Calc. for **4**: C, 28.08, H, 2.09, N, 1.21. Found: C, 27.50, H, 1.62, N, 1.52%.

15 Crystal data for **4**: green crystals, $Ru_5PO_{16}C_{15}{\cdot}NC_{12}H_{24}$, triclinic, space group $P\bar{1}$, a = 10.241(2), b = 12.914(3), c = 30.897(6) Å, α = 91.52(3), β = 99.07(3), γ = 108.18(3)°, V = 3821.4(1) Å^3, Z = 4, M = 1548, D_{calc} = 2.08 mg m^{-3}, μ = 2.04 mm^{-1}, Mo-Kα, λ = 0.70930 Å, $F(000)$ = 2324, T = 123 K, Siemens SMART CCD, crystal size 0.04 × 0.02 × 0.15 mm, $2\theta_{max}$ = 57.5°, 34779 reflections measured, 19259 unique reflections, 19259 observed reflections [$I > 2.5\sigma(I)$], semi-empirical absorption correction. Structure solution by direct methods, refinement on F^2 with anisotropic thermal parameters for all non-hydrogen atoms. Final R and Rw 0.059, 0.093. ShelXNT computer programs. CCDC 182/1001.

Received in Bloomington, IN, USA, 19th June 1998; 8/04648D

Unprecedented luminescence behaviour and structural characterization of a novel class of ruthenium(II) 2,2′-bipyridine complexes with orthometallated aminocarbene ligands

Vivian Wing-Wah Yam,* Ben Wai-Kin Chu and Kung-Kai Cheung

Department of Chemistry, The University of Hong Kong, Pokfulam Road, Hong Kong SAR, People's Republic of China.
E-mail: wwyam@hkucc.hku.hk

Novel luminescent ruthenium(II) bipyridine complexes with orthometallated aminocarbene ligands have been prepared and their photophysical properties studied.

The chemistry of metal σ-acetylide complexes has attracted considerable interest because of the unique properties of the delocalizable π systems. While most studies on ruthenium σ-acetylide complexes were focused on the use of phosphine ligands,[1] corresponding studies on nitrogen donor ligands are relatively rare.[2] In view of the rich photophysical and photochemical behaviour of ruthenium(II) polypyridyl complexes, we have started a program to design and synthesize luminescent organometallic ruthenium(II) σ-acetylide complexes containing polypyridyl ligands. In an attempt to prepare these complexes, we obtained the novel ruthenium(II) orthometallated aminocarbene complexes instead. Here we report the synthesis, characterization, electrochemistry, photophysical behaviour and X-ray crystal structure of this new class of ruthenium(II) orthometallated aminocarbene complexes with 2,2′-bipyridyl ligands, which represents the first of its kind.

Reaction of *cis*-$[Ru(bpy)_2(Me_2CO)_2](OTf)_2$ with phenylacetylene or 4-methoxyphenylacetylene in the presence of sodium ethoxide in ethanol, followed by metathesis reaction using NH_4PF_6 and subsequent recrystallization from MeCN–Et_2O, afforded *cis*-$[Ru(bpy)_2(CO)(\eta\text{-}CH_2Ph)]^+$ **1a**[3] or *cis*-$[Ru(bpy)_2(CO)(\eta\text{-}CH_2C_6H_4OMe)]^+$ **1b** as the PF_6^- salt in reasonable yield; the structure of **1b** was confirmed by X-ray diffraction studies.[4] On the other hand, treatment of *cis*-$[Ru(bpy)_2(Me_2CO)_2](OTf)_2$ with phenylacetylene in the presence of aniline in dry acetone under an inert atmosphere of nitrogen gave a stable orthometallated aminocarbene complex, $[Ru(bpy)_2{=}C(CH_2Ph)NHC_6H_4]^+$ **2a**. Similar reaction with *p*-anisidine in place of aniline gave $[Ru(bpy)_2{=}C(CH_2Ph)NHC_6H_3OMe]^+$ **2b** (Scheme 1).[5–7] The formulation of which were confirmed by satisfactory elemental analyses, FABMS, ^1H NMR and ^{13}C NMR spectroscopy† and the structure of **3b** was further established by X-ray crystallography (Fig. 1).‡

Complex **2b** shows a distorted octahedral structure. The N–Ru–N bond angles subtended by the chelating diimines are 77.0(2) and 77.6(2)°. A C(1)–Ru(1)–C(2) bond angle of 79.5(3)° subtended by the orthometallated *N*-arylcarbene has also been observed. The deviation from the ideal 90° for a regular octahedral geometry is a result of the steric requirement of the bidentate ligands. The bond angles around C(1) are 128.7(5), 116.9(5) and 114.3(6)°, consistent with the sp^2 hybridization of the carbene carbon. The bond distances of Ru(1)–N(1) [2.060(6) Å] and Ru(1)–N(4) [2.058(6) Å] are similar to those reported in other ruthenium(II) polypyridyl complexes (*ca*. 2.05 Å)[8] but those of Ru(1)–N(2) [2.141(5) Å] and Ru(1)–N(3) [2.120(5) Å] are longer than normal. This may be accounted for by the strong *trans* effect of the carbon atoms in the orthometallated *N*-arylcarbene ligand. The Ru(1)–C(2) bond distance [2.047(6) Å] is similar to that observed in other ruthenium(II) complexes with σ-bonded carbon ligands,[9] while the Ru(1)–C(1) bond distance [1.963(7) Å] is shorter than an average Ru–C bond [2.105(5) Å],[9e] which can be ascribed to the presence of Ru–C double bond character.[9f,10] A substantial double-bond character between the heteroatom and the carbene carbon is noticed as the C(1)–N(5) distance [1.318(9) Å] is reduced below that characteristic of a single bond between N and an sp^2 C, typical of Fischer type aminocarbenes (*ca*. 1.31 Å).[10]

The electronic absorption spectra of complexes **2a** and **2b** show moderately intense bands in the visible region which are tentatively assigned as MLCT transitions (Table 1). The intense absorptions in the UV region are assigned as intraligand

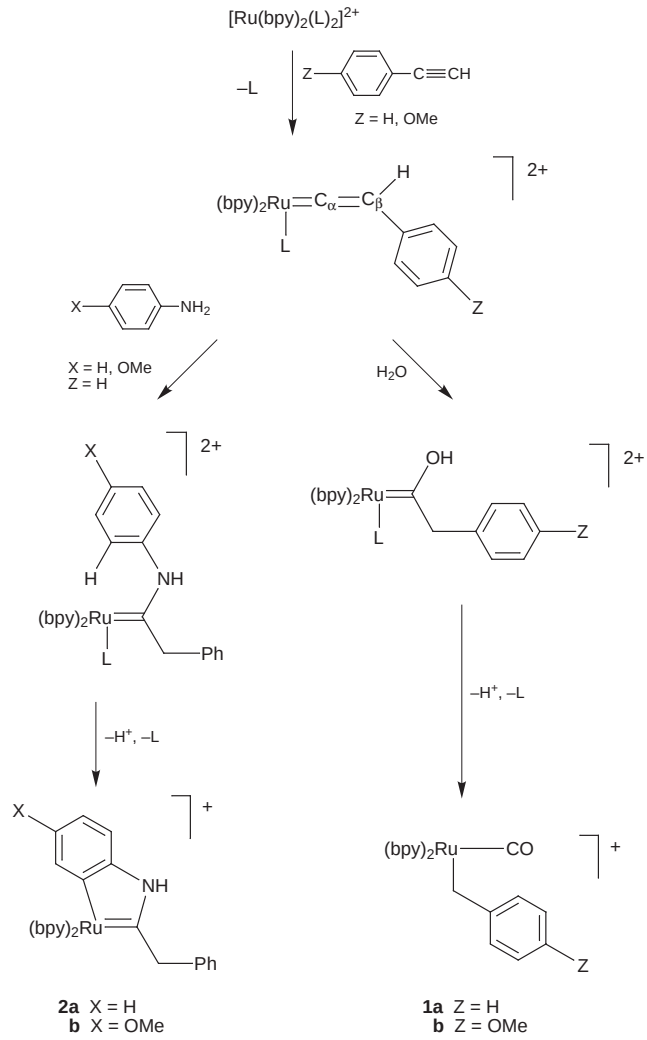

2a X = H
b X = OMe

1a Z = H
b Z = OMe

Scheme 1 Synthetic route to orthometallated ruthenium(II) aminocarbene complexes; L = Me_2CO

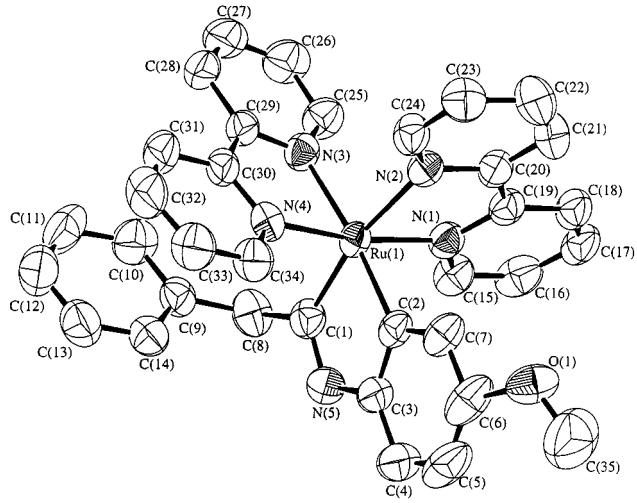

Fig. 1 Perspective drawing of the complex cation **2b** with atomic numbering scheme. Hydrogen atoms have been omitted for clarity. Thermal ellipsoids are shown at the 50% probability levels. Selected bond lengths (Å) and angles (°): Ru(1)–N(1) 2.060(6), Ru(1)–N(2) 2.141(5), Ru(1)–N(3) 2.120(5), Ru(1)–N(4) 2.058(6), Ru(1)–C(1) 1.963(7), Ru(1)–C(2) 2.047(6), C(1)–C(8) 1.514(9), C(8)–C(9) 1.519(10), C(1)–N(5) 1.318(9), C(3)–N(5) 1.426(9); N(1)–Ru(1)–N(2) 77.6(2), N(3)–Ru(1)–N(4) 77.0(2), C(1)–Ru(1)–C(2) 79.5(3), Ru(1)–C(1)–C(8) 128.7(5), C(8)–C(1)–N(5) 114.3(6), Ru(1)–C(1)–N(5) 116.9(5).

Table 1 Photophysical data for complexes **2a** and **2b**

Complex	λ_{abs}/nm (ε/dm^3 mol^{-1} cm^{-1})	Medium	T/K	λ_{em}[a]/nm	τ_0/μs
2a	250 (37 960), 298 (46 400), 370 (11 630), 484 (6230), 572 (6605)	MeCN	298	808	< 0.1
		Solid	298	775	< 0.1
		Solid	77	704	
		Glass[b]	77	742	
2b	250 (37 680), 298 (52 720), 370 (12 645), 482 (6850), 571 (7090)	MeCN	298	813	< 0.1
		Solid	298	767	< 0.1
		Solid	77	701	
		Glass[b]	77	745	

[a] Excitation wavelength at 580 nm. Emission maxima are corrected values. [b] EtOH–MeOH (4 : 1, v/v).

transitions. Excitation of **2a** and **2b** at λ > 350 nm at room temperature produces red luminescence. It is likely that the origin of the emission is ^{3}MLCT in nature, arising from states derived from either a d_π(Ru) → π*(bpy) or a d_π(Ru) → π*(alkylidene) MLCT transition. The close similarity of the absorption and emission characteristics of complexes **2a** and **2b** suggests that the methoxy substituent on the *N*-aryl ring of the aminocarbene unit has relatively little influence on the charge-transfer transition in these complexes.

The redox properties of the complexes **2a** and **2b** are investigated by cyclic voltammetry in acetonitrile using 0.1 mol dm^{-3} NBu_4PF_6 as the supporting electrolyte. Reversible to quasi-reversible reduction couples are observed at −1.66 and −1.89 V *vs*. SCE for **2a** and −1.65 and −1.88 V *vs*. SCE for **2b**; the potentials of which are relatively independent of the scan rate with $\Delta(E_{pa} - E_{pc})$ values of *ca*. 60–90 mV, assigned to the successive reduction of the bipyridine ligand. The relative insensitivity of the reduction potentials to the substituent effect on the aminocarbene unit in **2a** and **2b** further confirms its assignment as bpy-centered reduction. A quasi-reversible oxidation couple is observed at +1.42 V *vs*. SCE for **2b** and an irreversible oxidation wave is noted at E_{pa} = +1.67 V *vs*. SCE for **2a**, which are assigned as metal-centered oxidation. The irreversible nature of the oxidation in **2a** is indicative of the instability of the Ru(III) aminocarbene complex in which the electron-rich methoxy substituent capable of stabilizing the electron-deficient Ru(III) metal center is absent, which may lead to its decomposition.

Further spectroscopic studies to elucidate the nature of the lowest lying excited state are in progress.

V. W.-W. Y. acknowledges financial support from the Research Grants Council and The University of Hong Kong. B. W.-K. C. acknowledges the receipt of a postgraduate studentship, administered by The University of Hong Kong.

Notes and References

† **2a**: Elemental analysis: Calc. for **2a** (found) %: C 54.18 (54.22), H 3.85 (3.56), N 9.30 (9.23); positive FABMS: *m/z* 607 [$M - PF_6$]$^+$; ^{1}H NMR (300 MHz, CD_3CN, 298 K): δ 4.3 (s, 2H, CH_2), 6.2–8.3 (m, 25H, aromatic H), 11.2 (s, 1H, NH); ^{13}C NMR (67.8 MHz, CD_3CN, 298 K): δ 52.71 (CH_2), 113.98–176.58 (aromatic C), 266.01 (Ru=C). **2b** : Elemental analysis: Calc. for **2b** (found) (%): C 57.07 (57.24), H 4.08 (4.08), N 9.51 (9.74); ^{1}H NMR (300 MHz, CD_3CN, 298 K): δ 3.5 (s, 3H, OCH_3), 4.3 (s, 2H, CH_2), 5.8–8.3 (m, 24H, aromatic H), 11.2 (s, 1H, NH); ^{13}C NMR (125.76 MHz, CD_3CN, 298 K): δ 53.25 (OCH_3), 55.70 (CH_2), 105.90–180.09 (aromatic C), 262.70 (Ru=C).

‡ *Crystal data* for **2b** : {$[C_{35}H_{30}ON_5Ru]^+ClO_4^-$}, M_r = 737.18, triclinic, space group $P\bar{1}$ (no. 2), a = 9.398(4), b = 12.843(4), c = 14.994(4) Å, α = 67.74(3), β = 77.36(3), γ = 71.07(3)°, V = 1574(1) Å^3, Z = 2, D_c = 1.555 g cm^{-3}, μ(Mo-Kα) = 6.35 cm^{-1}, F(000) = 752, T = 301 K. Convergence for 436 variable parameters by least-squares refinement on F with $w = 4F_o^2 / \sigma^2(F_o^2)$, where $\sigma^2(F_o^2) = [\sigma^2(I) + (0.018F_o^2)^2]$ for 3911 reflections with $I > 3\sigma(I)$ was reached at R = 0.049 and wR = 0.066 with a goodness-of-fit of 2.75. CCDC 182/1023.

1 See, for example: P. H. Dixneuf, D. Touchard, P. Haquette, N. Pirio and L. Toupet, *Organometallics*, 1993, **12**, 3132; Z. Atherton, C. W. Faulkner, S. L. Ingham, A. K. Kakkar, M. S. Khan, J. Lewis, N. J. Long and P. R. Raithby, *J. Organomet. Chem.*, 1996, **462**, 265; Y. Sun, N. J. Taylor and A. J. Carty, *J. Organomet. Chem.*, 1992, **423**, C43; G. Jia, J. C. Gallucci, A. L. Rheingold, B. S. Haggerty and D. W. Meek, *Organometallics*, 1991, **10**, 3459.

2 See, for example: Y. Degani and T. Willner, *J. Chem. Soc., Chem. Commun.*, 1985, 648; A. M. Echavarren, J. Lopez, A. Santos, A. Romero, J. A. Hermoso and A. Vegas, *Organometallics*, 1991, **10**, 2371; J. Montoya, A. Santos, J. Lopez, A. M. Echavarren, J. Ros and A. Romero, *J. Organomet. Chem.*, 1992, **426**, 383; T. Rappert and A. Yamamoto, *Organometallics*, 1994, **13**, 4984; M. A. Esteruelas, A. Miguel, F. J. Lahoz, A. M. Lopez, E. Onate and L. A. Oro, *Organometallics*, 1994, **13**, 1669; A. Pedersen, M. Tilset, K. Folting and K. G. Caulton, *Organometallics*, 1995, **14**, 875; C. M. Che, S. M. Yang, M. C. W. Chan, K. K. Cheung and S. M. Peng, *Organometallics*, 1997, **16**, 2819; Y. Zhu, O. Clot, M. O. Wolf and G. P. A. Yap, *J. Am. Chem. Soc.*, 1998, **120**, 1812; A. Klose, E. Solari, C. Floriani, S. Geremia and L. Randaccio, *Angew. Chem., Int. Ed. Engl.*, 1998, **37**, 148.

3 T. J. Meyer, B. P. Sullivan, R. B. Smythe and E. M. Kober, *J. Am. Chem. Soc.*, 1982, **104**, 4701.

4 V. W. W. Yam and B. W. K. Chu, unpublished work.

5 C. Bianchini, J. A. Casares, M. Peruzzini, A. Romerosa and F. Zanobini, *J. Am. Chem. Soc.*, 1996, **118**, 4585.

6 M. I. Bruce and A. G. Swincer, *Aust. J. Chem.*, 1980, **33**, 1471.

7 M. I. Bruce, in *Comprehensive Organometallic Chemistry*, Pergamon, Oxford, vol. 7, pp. 350.

8 D. Schomburg, S. Neumann and R. Schmutzler, *J. Chem. Soc., Chem. Commun.*, 1979, 848.

9 See, for example: (*a*) R. J. Doedens and J. A. Moreland, *Inorg. Chem.*, 1976, **15**, 2486; (*b*) U. A. Gregory, S. D. Ibekwe, B. T. Kilbourn and D. R. Russell, *J. Chem. Soc. A*, 1971, 1118; (*c*) J. D. Edwards, R. Goddard, S. A. R. Knox, R. J. McKinney, F. G. A. Stone and P. Woodward, *J. Chem. Soc., Chem. Commun.*, 1975, 828; (*d*) R. J. Sundberg, R. F. Bryan, I. F. Taylor and H. Taube, *J. Am. Chem. Soc.*, 1974, **96**, 381; (*e*) P. B. Hitchcock, M. F. Lappert, P. L. Pye and S. Thomas, *J. Chem. Soc., Dalton Trans.*, 1979, 1929; (*f*) M. F. Lappert, P. B. Hitchcock and P. L. Pye, *J. Chem. Soc., Dalton Trans.*, 1978, 826.

10 F. A. Cotton and C. M. Lukehart, *Progr. Inorg. Chem.*, 1972, **16**, 487.

Received in Cambridge, UK, 20th July 1998; revised manuscript received 15th Setpember 1998; 8/07281G

Synthesis and structural characterization of novel silver(I) complexes of tetradehydro[16]annulene annelated with bicyclo[2.2.2]octene units

Tohru Nishinaga, Tetsu Kawamura and Koichi Komatsu*

Institute for Chemical Research, Kyoto University, Uji, Kyoto 611-0011, Japan. E-mail: komatsu@scl.kyoto-u.ac.jp

The first silver(I) complexes of tetradehydro[16]annulene annelated with bicyclo[2.2.2]octene units were prepared and the incorporation of a silver atom into the cavity center was shown by X-ray crystallography.

The versatility of tribenzotridehydro[12]annulene (**1**) as a ligand in metal complexes was demonstrated by Youngs *et al*.[1] The cavity size of ligand **1** was shown to be suitable for the incorporation of first row transition metals into the cavity center, while the size is too small for a second row transition metal. For example, silver gave only a sandwich complex.[1] Even for a higher homologue, tetrabenzotetradehydro[16]annulene (**2**), there has been no example of incorporation of a second or third row transition metal within its cavity. Only a dicobalt complex has been reported, in which two of the triple bonds are coordinated from the outer side.[2]

Recently we synthesized a series of dehydroannulenes annelated with bicyclo[2.2.2]octene (abbreviated as BCO) including tetradehydro[16]annulene (**3**),[3] which are characterized by a rather low oxidation potential indicative of a raised HOMO level by the annelation of the BCO units.[3] The raised HOMO level should be effective for an interaction between the occupied 2p orbital of the ligand and empty 5s orbital of the silver,[4] which would strengthen the coordination bond by donation from the ligand to the metal.[5] Here we report the synthesis of novel silver-dehydro[16]annulene **3** complexes prepared based on such a rationale.

Annulene **3** was stirred with 1 equiv. of silver(I) triflate (AgOTf) or silver(I) hexafluoroantimonate ($AgSbF_6$) in THF at room temperature for a few days. After concentration of the solution, hexane was added to give precipitates of silver complex **4** (**3**·AgOTf) or **5** (**3**·$AgSbF_6$) both as red powders in 84% or 92% yield respectively. These complexes are stable to air, moisture, and light, in contrast to many silver-alkene, -alkyne, and -arene complexes which are essentially light- or air-sensitive.[6,7]

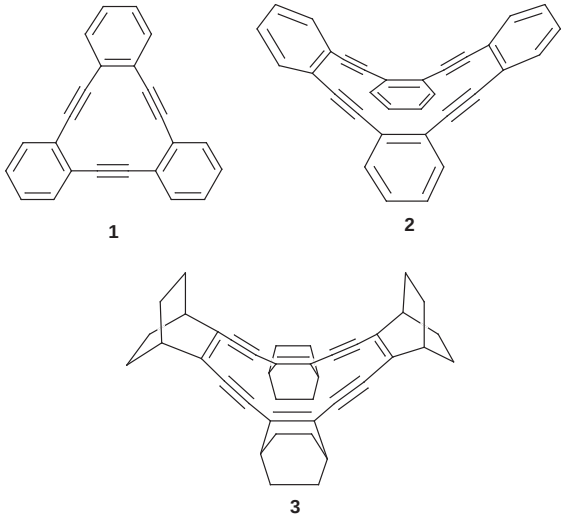

1 **2** **3**

Single crystals of **4** containing 0.5 equiv. hexane and of **5** containing 1 equiv. dichloromethane were obtained and examined by X-ray crystallography.† As shown in Fig. 1, the silver atom is present in the center of the cavity for both complexes and the counter anions are located above the silver atom. The structure of the central ring of the ligand is still tub-like but the folding angles are smaller compared with the X-ray structure of **3**.[3] The shortest distances between the silver and the counter anions, *i.e.* Ag–O in **4** and Ag–F in **5**, were 2.31(1) and 2.67(1) Å respectively. The Ag–O distance is shorter than those (2.36–2.53 Å) in nine reported complexes of AgOTf with arenyl or alkynyl ligands,[7–10] whereas the Ag–F distance is longer than

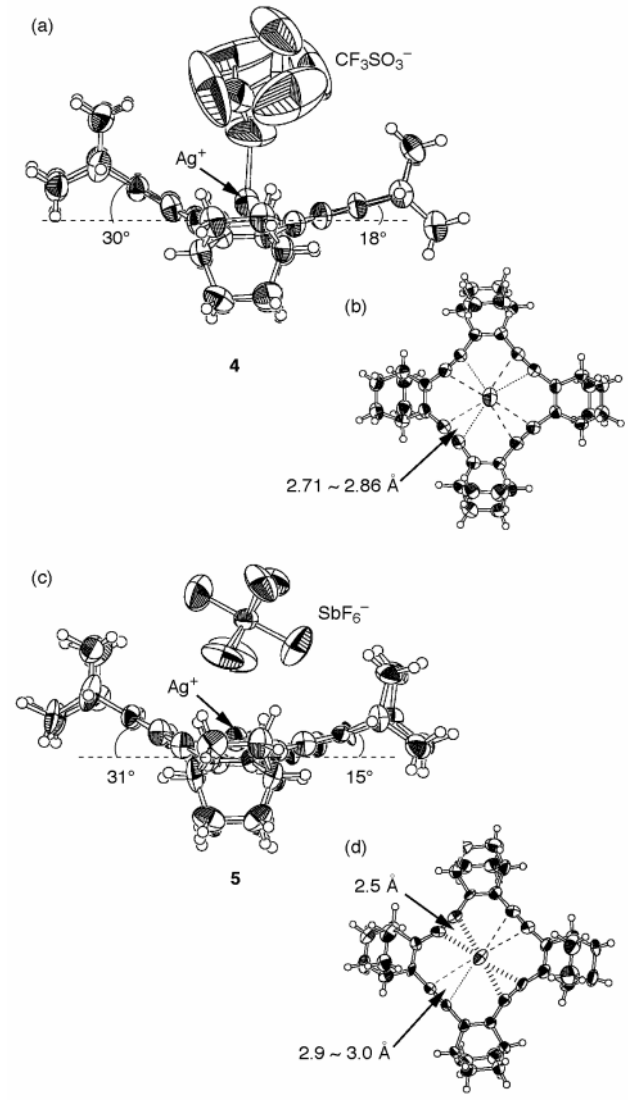

Fig. 1 ORTEP drawing showing (a), (c) side views and (b), (d) top views of **4** and **5**. The counter anions are omitted in the top views for clarity.

Table 1 ^{1}H and ^{13}C NMR spectra for **3–5**

	^{1}H NMR, δ		^{13}C NMR, δ			
Compd.	CH	CH_2	C=C	C≡C	CH	CH_2
3[a]	2.47	1.47 (32H)	132.8	95.4	37.2	25.3
3[b]	2.49	1.54 (16H)	132.5	95.0	36.9	24.9
		1.44 (16H)				
4[a]	2.61	1.55 (32H)	133.4	97.4	36.7	25.1
5[b]	2.64	1.65 (16H)	133.4	98.3	36.5	24.7
		1.44 (16H)				

[a] In $CDCl_3$. [b] In CD_2Cl_2.

the average (2.63 Å) of those (2.54–2.71 Å) in three reported complexes of $AgSbF_6$ with arenyl ligands.[11]

These Ag–anion distances are reflected in the modes of coordination with ligands. The Ag–C(alkyne) distance of complex **4** varies only from 2.714(7) Å to 2.863(7) Å, indicating almost equal coordination with the four acetylene units. On the other hand, the ligand of complex **5** is deformed due to the stronger coordination with a pair of acetylene units which are opposite to each other. The Ag–C distance at the stronger coordination site is 2.52(1)–2.54(1) Å whereas that at the other site is 2.85(2)–3.05(2) Å. Accordingly, the C≡C–C angle for **4** varies only from 170.0(8)° to 174.1(8)°, whereas for **5** the C≡C–C angle is 164(1)–170(1)° at the more strongly coordinated site and 174(1)–178(1)° at the other site.

In order to compare the degree of coordination in **4** and **5**, the Mulliken charge was calculated at the HF/STO-3G level for the silver atoms of AgOTf and $AgSbF_6$ using the X-ray structures with and without the ligand. The charge of silver in the structure with the ligand was calculated to be +0.20 for AgOTf and +0.29 for $AgSbF_6$, while that for the structure without the ligand was +0.50 for AgOTf and +0.77 for $AgSbF_6$. These results indicate that this annulene-type ligand reduces the positive charge on the silver atom and the extent of this reduction is larger for the case of $AgSbF_6$. This type of coordination is presumed to be principally due to the electron donation from the HOMO of the ligand to the LUMO of the metal, and the annelation of the BCO units which raises the HOMO level of the π-system would strengthen this coordination.

The IR spectrum of complex **4** showed that the energy of the C≡C stretching band became weak [2155 cm^{-1} (br)] compared with the free ligand **3** (2251, 2173 cm^{-1}), while the absorption for **5** was too weak to observe. As shown in Table 1, both the ^{1}H and ^{13}C NMR spectra for **4** and **5** also showed slight changes from those of the free ligand. Particularly noteworthy is the downfield shift for the NMR signal for the acetylenic carbon. For the methylene carbon of complexes **4** and **5**, only one NMR signal was observed, indicating that the central ring of the ligand was inverting rapidly on the NMR time scale, like the free ligand **3**.

In summary, we prepared a novel silver complex of tetradehydro[16]annulene annelated with BCO units. This [16]annulene-type ligand was found to have a cavity size suitable for the incorporation of second-row metals, *i.e.* silver, into the center of the ring. Calculated Mulliken charges for the complexes of **4** and **5** indicated that there is considerable electron donation from the ligand to the silver atom.

The present work is supported by Grant-in-Aid from the Ministry of Education, Science, Sports and Culture, Japan. Computation time was provided by the Super Computer Laboratory, Institute for Chemical Research, Kyoto University.

Notes and References

† *Crystal data* for **4**·0.5(C_6H_{14}): $C_{44}H_{47}AgF_3O_3S$, M = 820.78, monoclinic, space group $P2_1/c$, a = 11.780(5), b = 14.766(3), c = 22.502(2) Å, β = 98.79(2)°, V = 3868(1) Å^3, Z = 4, μ(Cu-Kα) = 51.20 cm^{-1}, T = 293 K, for 4265 observed reflections within 2θ = 120.1° and $I > 3.00\sigma(I)$. Data were corrected for absorption (Ψ scan; min., max. correction factors 0.56, 1.00) and Lorentz polarization effects. There is disorder in the trifluoromethyl moiety and two oxygen atoms not directly contacted to the silver atom. The final R value was R = 0.080. For **5**·CH_2Cl_2: $C_{41}H_{42}AgCl_2F_6Sb$, M = 949.30, triclinic, space group $P1$, a = 12.381(3), b = 15.412(4), c = 12.067(3) Å, α = 109.78(2), β = 117.45(2), γ = 84.00(2)°, V = 1919.1(10) Å^3, Z = 2, μ(Cu-Kα) = 114.32 cm^{-1}, T = 293 K, for 2617 observed reflections within 2θ = 120.1° and $I > 3.00\sigma(I)$. Data were corrected for Lorentz polarization effects. The final R value was R = 0.055. CCDC 182/1014.

1 A. Djebli, J. D. Ferrara, C. Tessier-Youngs and W. J. Youngs, *J. Chem. Soc., Chem. Commun.*, 1988, 548; J. D. Ferrara, C. Tessier-Youngs and W. J. Youngs, *J. Am. Chem. Soc.*, 1985, **107**, 6719; J. D. Ferrara, A. A. Tanaka, C. Fierro, C. Tessier-Youngs and W. J. Youngs, *Organometallics*, 1989, **8**, 2089; J. D. Ferrara, C. Tessier-Youngs and W. J. Youngs, *Organometallics*, 1987, **6**, 676; J. D. Ferrara, A. Djebli, C. Tessier-Youngs and W. J. Youngs, *J. Am. Chem. Soc.*, 1988, **110**, 647.
2 D. Solooki, J. D. Bradshaw, C. A. Tessier and W. J. Youngs, *J. Organomet. Chem.*, 1994, **470**, 231.
3 T. Nishinaga, T. Kawamura and K. Komatsu, *J. Org. Chem.*, 1997, **62**, 5354.
4 M. J. S. Dewar, *Bull. Soc. Chim. Fr.*, 1951, **18**, C71.
5 For a review, see A. J. Pearson, *Metallo-organic Chemistry*, Wiley, New York, 1985.
6 J. E. McMurry, G. J. Haley, J. R. Matz, J. C. Clardy and J. Mitchell, *J. Am. Chem. Soc.*, 1986, **108**, 515.
7 J. E. Gano, G. Subramaniam and R. Birnbaum, *J. Org. Chem.*, 1990, **55**, 4760.
8 H. C. Kang, A. W. Hanson, B. Eaton and V. Boekelheide, *J. Am. Chem. Soc.*, 1985, **107**, 1979.
9 R. Gleiter, M. Karcher, D. Kratz, M. L. Ziegler and B. Nuber, *Chem. Ber.*, 1990, **123**, 1461.
10 A. Ikeda and S. Shinkai, *J. Am. Chem. Soc.*, 1994, **116**, 3102; A. Ikeda, H. Tsuzuki and S. Shinkai, *J. Chem. Soc., Perkin Trans. 2*, 1994, 2073.
11 F. R. Heirtzler, H. Hopf, P. G. Jones and P. Bubenitschek, *Chem. Ber.*, 1995, **128**, 1079; P. G. Jones, P. Bubenitschek, F. Heirtzler and H. Hopf, *Acta Crystallogr., Sect. C*, 1996, **52**, 1380; P. G. Jones, F. Heirtzler and H. Hopf, *Acta Crystallogr., Sect. C*, 1996, **52**, 1384.

Received in Cambridge, UK, 24th August 1998; 8/06606J

Acceleration of a hetero-Diels–Alder reaction by cyclic metalloporphyrin trimers

Maurus Marty, Zöe Clyde-Watson, Lance J. Twyman, Moshe Nakash and Jeremy K. M. Sanders*†

Cambridge Centre for Molecular Recognition, University Chemical Laboratory, Lensfield Road, Cambridge, UK CB2 1EW

The hetero-Diels–Alder reaction between a pyridylbutadiene and 3-nitrosopyridine is accelerated by a variety of metalloporphyrin trimers; there is a weak correlation between rate acceleration and product binding strength.

The acceleration of Diels–Alder reactions by artificial receptor molecules is well documented,[1] but there are few systematic studies of how the rate of an intra-cavity reaction can be influenced by fine-tuning the size and flexibility of the host.[2] The examples described so far are special cases of Diels–Alder reactions that have been carefully chosen to match the available hosts, in part because of the synthetic difficulties associated with producing a range of hosts. We now show that the regiospecific hetero-Diels–Alder reaction[3,4] of pyridyl diene **1** with 3-nitrosopyridine **2** to give oxazine **3** (Scheme 1) is a second pericyclic reaction that can be influenced by porphyrin trimer systems such as **5–8**. This cycloaddition is more readily monitored kinetically than our original Diels–Alder reaction as the process is essentially irreversible‡ and forms only a single, fairly robust product. The product has been rearranged to the 1,2-disubstituted pyrrole **4**;[5] if this rearrangement could be induced to occur under conditions compatible with the porphyrin trimers then the possibility of catalytic turnover arises.§

Trimers **5**[6]¶ and **6**[7] each contain three conventional porphyrins while the new[8] heterotrimers **7** and **8** contain one or two dioxoporphyrins respectively. The control (host-free) Diels–Alder reaction between diene **1** and dienophile **2** was monitored by ^{1}H NMR spectroscopy in $CDCl_3$ and in [$^2H_8$]toluene, and showed clean transformation of the starting substrates to the oxazine without significant formation of side products. However, HPLC was the preferred analytical technique for host-accelerated kinetic investigations. In a typical reaction, diene **1**, dienophile **2** and host were mixed in equimolar amounts, each at a concentration of 0.333 mM. The reaction was carried out at 25 °C in CH_2Cl_2 (and also in toluene for trimer **5**) and monitored by HPLC.‖ It proved to be first order with respect to both the diene and dienophile with a rate constant of 3.9×10^{-3} M^{-1}s^{-1} (Table 1). The host-induced rate accelerations (calculated relative to the host-free reaction) for the different hosts are summarised in Table 1.

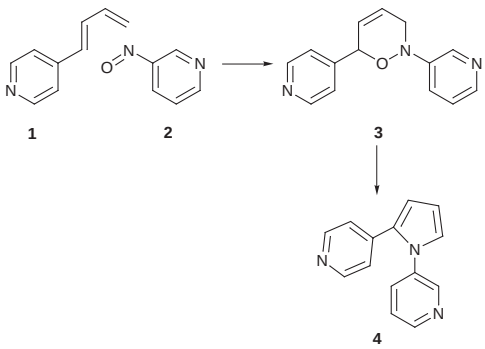

Scheme 1

In order to gauge the affinity of the substrates and product to the various hosts, a series of UV–visible titrations were performed using the established procedure;[9] results for the oxazine product **3** are also summarised in Table 1, together with the effective molarity for binding **3** relative to the two substrates.** For trimer **6**, the values represent an average of all the possible binding interactions to that host (inside/outside for the monodentate substrates, or across acetylene/butadiyne for the bidentate oxazine). Complications arise for the mixed dioxo hosts because pyridine-binding gives no noticeable shift in the Soret band:[8] monitoring the shift of the porphyrin Soret band in these species can thus only yield information about binding interactions at the porphyrin sites and not at the dioxo sites.

In CH_2Cl_2 an acceleration of 1030-fold (relative to the control reaction) was observed for the unsymmetrical host **6**. This is coupled with a particularly high binding affinity of oxazine **3** to **6**, suggesting that the 'product-like' transition state

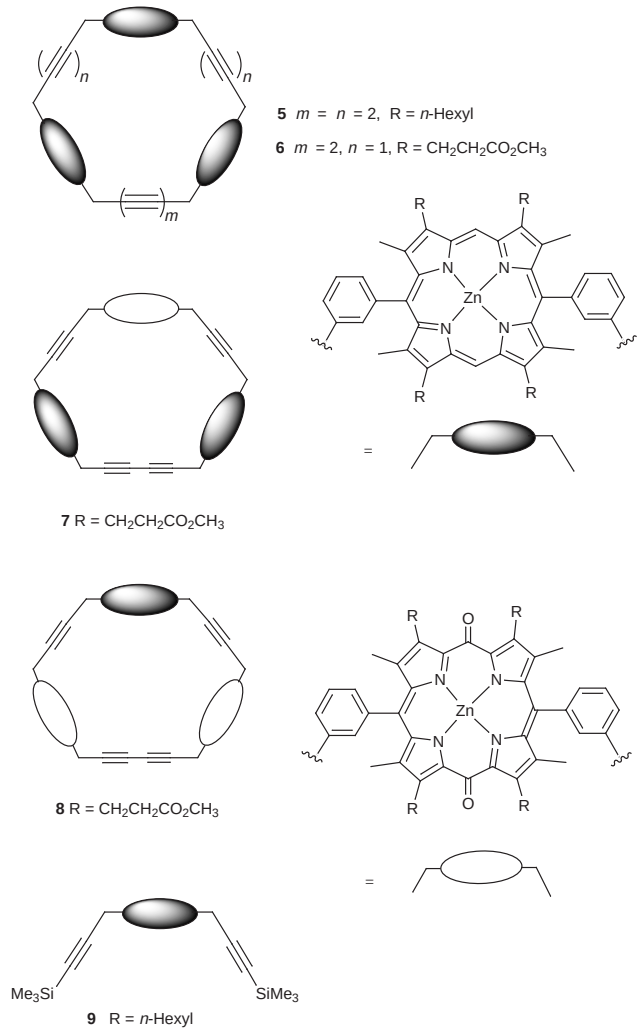

Table 1 Kinetic and equilibrium constant data for formation and binding of **3** with various hosts

Host	Solvent	k/M^{-1} s^{-1}	Rate acceleration (approx.)	Binding constant/M^{-1}	E.M.[a]
Control	CH_2Cl_2	0.0039	—		
Control	PhMe	0.0023	—		
9	CH_2Cl_2	0.0064	2	6.9×10^3	0.0035
9	PhMe	0.0025	1	8.2×10^3	0.0012
5	CH_2Cl_2	1.1	280	7.3×10^6	3
5	PhMe	1.9	830	5.6×10^7	3
6	CH_2Cl_2	4.0	1030	2.3×10^8	13
7	CH_2Cl_2	3.2	820	2.4×10^8	23
8	CH_2Cl_2	2.2	560	1.2×10^8	2

[a] See note **.

for the reaction prefers to bridge the shorter acetylene linker present in this host, rather than the butadiyne link in **5**. Further evidence to support this is obtained from molecular modelling of the oxazine using CERIUS[2] which confirms that the geometry is more complementary to the smaller porphyrin–porphyrin distance. A similar rate acceleration (820-fold) was observed for the mono-dioxo host **7**.

As the magnitude of binding constants and reaction rate constants are likely to display solvent dependence, and as this may subsequently lead to a different rate acceleration, the control reaction and the **5**-host accelerated reaction were also studied in toluene: the 830-fold rate acceleration is significantly higher in toluene than the 280-fold in CH_2Cl_2 (Table 1). The control reaction is 1.7 times faster in CH_2Cl_2 than in toluene, while the host-accelerated reaction is 1.7 times faster in toluene than in CH_2Cl_2 (Table 1). It is possible that in the control reaction the solvent stabilises the Diels–Alder transition state better than the reactants, and that this stabilisation is more significant in CH_2Cl_2 than in toluene, leading to a higher reaction rate in CH_2Cl_2. This is consistent with the observed binding constants being larger in toluene than in CH_2Cl_2.** This stronger binding in toluene will also lead to an increased concentration of the host–substrate reactive complex and to a larger rate enhancement. In addition, it is also possible that the reactants and transition state are not well solvated inside the trimer cavity. In this case, therefore, solvent stabilisation is not as significant as in the control reaction, where the reactive species are not shielded by the host and are easily solvated.

In order to prove that the cycloaddition reaction occurs inside the cavity of the trimeric porphyrin hosts, an inhibition experiment was carried out in which 1 equiv. of oxazine **3** was added to the reaction mixture in the presence of **5**. The resulting rate acceleration is reduced by roughly 20-fold in CH_2Cl_2 and 270-fold in toluene, giving a reaction rate similar to that observed in the presence of porphyrin monomer. Pyrrole **4** is a less effective inhibitor when added to the CH_2Cl_2 or toluene reaction mixture in the presence of **5**: although the initial reaction rate drops to one third of that observed for the **5**-accelerated reaction, complete inhibition does not occur and catalytic turnover is still feasible. The observed decrease is readily explained: if the pyrrole occupies one site inside the cavity, this leaves only two sites to bind the diene and dienophile, decreasing the number of constructive binding possibilities from six to two.

Preliminary results indicate that the hetero-Diels–Alder reaction described is well suited for intra-cavity kinetic studies. Future investigations will focus on initiating the pyrrole formation under conditions compatible with the Diels–Alder cycloaddition, exploring solvent effects, and exploring the influence of changes to the host geometry.

We thank the EPSRC, CIBA Jubiläumsstiftung, British Council, Israel Academy and Ministry of Science, and B'nai B'rith for financial support.

Notes and References

† E-mail: jkms@cam.ac.uk

‡ If the reverse hetero-Diels–Alder reaction were to proceed at a significant rate, a solution of the oxazine would always contain some dienophile **2** which could be trapped by the use of a scavenger. In a control experiment, 10 equiv. of cyclopentadiene were added to a solution of the oxazine in CH_2Cl_2 at 25 °C; after 48 h, ^{1}H NMR analysis showed no evidence for a new adduct.

§ Model building suggests that the intracavity cycloaddition and rearrangement would be even more favourable for 4-nitrosopyridine, but this potential substrate proved too unstable to isolate.

¶ Porphyrins with solubilising *n*-hexyl side chains in place of esters are prepared by the procedure published previously (ref. 6) using the appropriate hexyl-substituted dipyrrole.

‖ Accelerated reactions were initiated by addition of the host and reaction progress was monitored by HPLC (normal phase 8 × 225 mm Spheris S5W column on a HP Series 1050 instrument) or GC (5% dimethyldiphenyl siloxane 25 m × 0.32 mm × 0.25 μm column on a HP GC 5890 Series II instrument). For all the reactions the decrease in concentration of diene and dienophile was monitored. After completion of the host-accelerated reactions a few drops of TFA were added to the reaction mixture to demetallate the porphyrin hosts. The oxazine product is thus released from the cavity and may then be detected by HPLC, confirming that the disappearance of the starting substrates correlates directly with oxazine formation.

** Thermodynamic effective molarity (E.M.) for binding = K(**3**)/[K(**1**)K(**2**)]. In CH_2Cl_2 K(**1**) and K(**2**) are generally *ca* 5×10^3 and 1×10^3 M^{-1} respectively, while in toluene they are around 2–3 times larger.

1 See for example B. Wang and I. O. Sutherland, *Chem. Commun*., 1997, 1495; J. Rebek, Jr. and J. Kang, *Nature*, 1997, **385**, 50; A. D. Hamilton and S. C. Hirst, *J. Am. Chem. Soc*., 1991, **113**, 382; T. R Kelly, V. S. Ekkundi and P. Meghani, *Tetrahedron Lett*., 1990, **31**, 3381; W.-S. Chung, N.-J. Wang, Y.-D. Liu, Y.-J. Leu and M. Y. Chiang, *J. Chem. Soc., Perkin Trans. 2*, 1995, 307.

2 Z. Clyde–Watson, A. Vidal-Ferran, L. J. Twyman, C. J. Walter, D. W. J. McCallien, S. Fanni, N. Bampos, R. S. Wylie and J. K. M. Sanders, *New J. Chem*., 1998, **22**, 493.

3 J. Streith and A. Defoin, *Synthesis*, 1994, 1107; H. Waldman, *Synthesis*, 1994, 535; C. Chapuis, J. Y. de Saint Laumer and M. Marty, *Helv. Chim. Acta*, 1997, **80**, 146; G. Krezse and J. Firl, *Tetrahedron*, 1963, **19**, 1329.

4 For an antibody-catalysed hetero-Diels–Alder reaction, see M. Resmini, A. A. P. Meekel and U. K. Pandit, *J. Chem. Soc., Chem. Commun*., 1995, 571.

5 J. Firl and G. Krezse, *Chem. Ber*., 1966, **99**, 3695; R. M. Rodebaugh and N. H. Cromwell, *Tetrahedron Lett*., 1967, 2859.

6 H. L. Anderson and J. K. M. Sanders, *J. Chem. Soc., Perkin Trans. 1*, 1995, 2223.

7 A. Vidal-Ferran, N. Bampos and J. K. M. Sanders, *Inorg. Chem*., 1997, **36**, 6117.

8 Z. Clyde-Watson, N. Bampos and J. K. M. Sanders, *New J. Chem*., 1998, **22**, in the press.

9 H. L. Anderson, S. Anderson and J. K. M. Sanders, *J. Chem. Soc., Perkin Trans. 1*, 1995, 2231.

Received in Cambridge, UK, 3rd August 1998; 8/06070C

Gel phase MAS ^{1}H NMR as a probe for supramolecular interactions at the solid–liquid interface

Yolanda R. de Miguel,[a] Nick Bampos,[a] K. M. Nalin de Silva,[a] Stephen A. Richards[b] and Jeremy K. M. Sanders*[a]†

[a] *Cambridge Centre for Molecular Recognition, University Chemical Laboratory, Lensfield Road, Cambridge, UK CB2 1EW*
[b] *Glaxo Wellcome Medicines Research Centre, Gunnels Wood Road, Stevenage, UK SG1 2NY*

ArgoGel beads functionalised with mono- and bi-dentate pyridyl ligands give excellent gel phase (MAS) ^{1}H NMR spectra that allow detailed structural characterisation of their non-covalent complexes with metalloporphyrins.

We show here that, in favourable circumstances, gel phase magic angle spinning (MAS) ^{1}H NMR spectroscopy can provide a powerful new tool for probing non-covalent interactions at the solid–liquid interface: such interactions lie at the heart of much of separation science, especially affinity chromatography, and of solid-phase organic synthesis. The recent explosion of polymer-supported chemistry has been accompanied by the development of techniques for coding, tagging and releasing the resulting resin-bound molecules, but there have been few rapid or non-destructive techniques that provide subtle analytical or spatial information for the resin-bound species themselves.[1] Gel phase MAS NMR[2] has recently been applied to structure analysis of molecules attached onto solid supports, and we now demonstrate the potential of this new analytical tool for investigating molecular recognition at interfaces by probing events that occur between polymer-bound pyridyl ligands and a range of porphyrins.

In a conventional solution-state spectrometer, organic solids generally give ^{1}H and ^{13}C NMR resonances with linewidths of 10^4–10^5 Hz due to a combination of strong dipolar interactions and spatial inhomogeneities.[3] If the species of interest is a small molecule attached to a solvent-swollen polystyrene bead *via* a flexible tether, then its molecular mobility can approach that of the solution state. In such circumstances, dipolar interactions are dramatically reduced by averaging and the major line broadening mechanism that remains is the spread of chemical shifts due to spatial inhomogeneities, *i.e.* different effective magnetic fields are experienced by molecules on the inside and outside of a bead or by beads in different parts of the sample tube.[4] This spread of chemical shifts (*ca* 10^3 Hz) can be eliminated by magic angle spinning at relatively low speeds (*ca* 10^3 Hz) in a solution-state spectrometer to give spectra with linewidths that are comparable with small molecules in free solution.

Given our interests in porphyrin-accelerated reactions[5] and in approaches to catalyst discovery that involve selecting potential catalysts *via* strong binding of transition state analogues (TSAs),[6] we wished to investigate the molecular recognition properties of pyridines and TSAs that were covalently bound to polymer beads. Both for the spectroscopic reasons outlined above, and to give maximum molecular accessibility, we chose to attach these ligands to ArgoGel beads: these contain highly flexible PEG chains, grafted to lightly cross-linked polystyrene beads *via* a stable bifurcated linkage, thereby allowing bound molecules to experience a solution-like environment. The attachment of pyridyl ligand **1** onto the beads was performed by deprotonation of the alcohol (Scheme 1) followed by treatment with ArgoGel chloride beads. After reaction, microanalysis suggested complete displacement of chlorine but the nitrogen content was 0.39% instead of the expected 0.59%, highlighting the danger of relying on microanalysis to monitor solid-phase organic reactions. However, after removal of residual broad polymer signals using a CPMG spin-echo sequence,[3] the gel phase MAS ^{1}H NMR spectrum of the beads gave *ca* 1 Hz resolution and allowed direct structural determination of the bound molecules without the need for cleavage [Fig. 1(*a*)].‡ As well as the signals *a*–*e* for **2**, three unexpected signals (*f*, *g* and *h*) were observed. These were assigned to the terminal enol ether by-product **3** resulting from HCl elimination from the resin. Although this is an inconvenient side-product, it proved to be a useful internal standard for binding studies.

Ruthenium porphyrins bind very strongly to pyridine ligands (K *ca* 10^5 M^{-1}),[7] so the pyridyl beads were treated with an excess of ruthenium porphyrin **4**. The dark orange colour of the porphyrin present in the resulting beads did not leach out on washing with a non-coordinating solvent (*e.g.* CH_2Cl_2). After displacement of the solvent molecule in the starting porphyrin, a 1:1 complex had formed on the beads. The CPMG ^{1}H NMR spectrum [Fig. 1(*b*)] showed the characteristic large chemical shift changes experienced by the bound pyridyl ligand due to the porphyrin ring current (Scheme 2); a COSY spectrum confirmed the assignments shown. The CO ligand in the bound complex was evident in a new sharp peak at 1945 cm^{-1} in a spectrum obtained by single bead FT-IR microspectroscopy.[7]

The analogous complex with zinc porphyrin **5** was also prepared. In this case, dark purple beads were obtained which leached porphyrin on washing with CH_2Cl_2. This is not surprising as zinc porphyrins bind relatively weakly (K *ca* 10^3 M^{-1}) to pyridine ligands in solution. The non-spin echo ^{1}H NMR spectrum [Fig. 1(*c*)] of the complex exhibited (superimposed on a broad polymer background) sharp enol ether peaks and two sets of aryl and β signals for the porphyrin itself; these appear to correspond to bound porphyrin within the bead and free porphyrin exchanging with surface-accessible bound porphyrin. The set of inner bound porphyrin signals was assigned by its greater attenuation in a CPMG spectrum [Fig. 1(*d*)]. All the resonances belonging to ligand **2** were broadened beyond detection in this spectrum, presumably due to an exchange process, the details of which are still unclear.

A bipyridyl ligand (which is a TSA for a hetero-Diels–Alder reaction[8] was attached to the resin by the same method as in

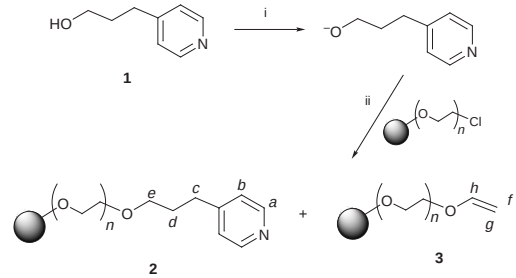

Scheme 1 *Reagents and conditions*: i, NaH, THF, 5 h, room temp.; ii, THF, 45 h, 60 °C

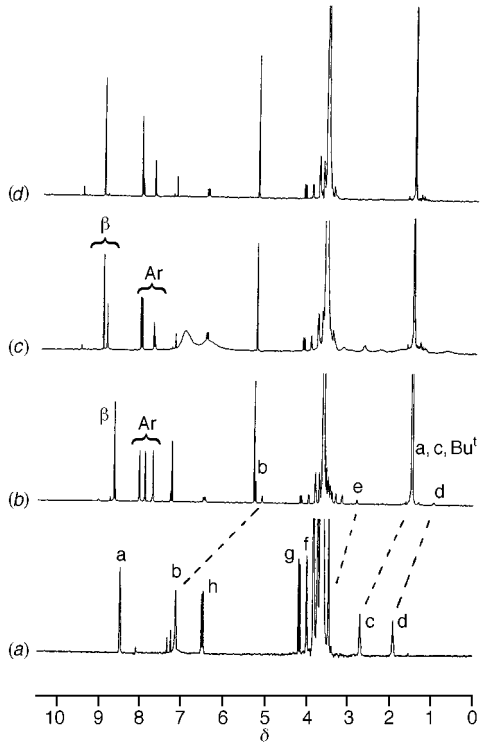

Fig. 1 400 MHz gel phase MAS ^{1}H NMR spectra: (*a*) CPMG spectrum of functionalised beads showing resonances due to **2** and **3**; (*b*) the same beads complexed to porphyrin **4**; (c) non-CPMG spectrum of the beads in (*a*) in the presence of excess porphyrin **5**; (*d*) CPMG spectrum of same sample as in (*c*)

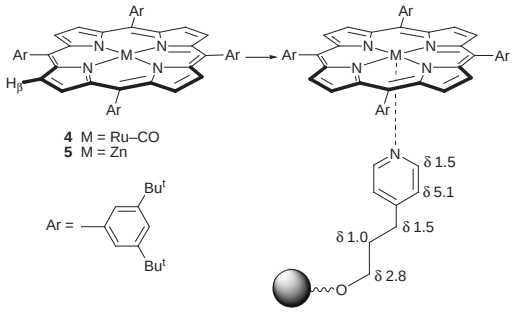

Scheme 2

Scheme 1. The gel phase NMR spectrum of the beads allowed characterisation of the supported bidentate ligand, and again demonstrated formation of enol ether **3**. Treatment of these beads with a flexible porphyrin dimer in CH_2Cl_2 gave the corresponding complex **6** as dark purple beads that did not leach colour on washing, which is consistent with an expected binding constant of more than 10^6 M^{-1}. The one-dimensional and NOESY spectra of these beads allowed assignment of all the bound aromatic resonances of **6** and confirmed that the chemical shifts of ligand and host were essentially identical to the corresponding solution-state complex.

Finally, the bipyridyl beads were treated with our symmetrical Zn_3-butadiyne-linked cyclic porphyrin trimer.[5] Again the bound chemical shifts were as expected, but now all resonances including the enol ether were somewhat broadened. The implication of this result is that overall polymer mobility is reduced, even in chains that are not directly bound to host. We tentatively assign this observation to cross-linking of separate

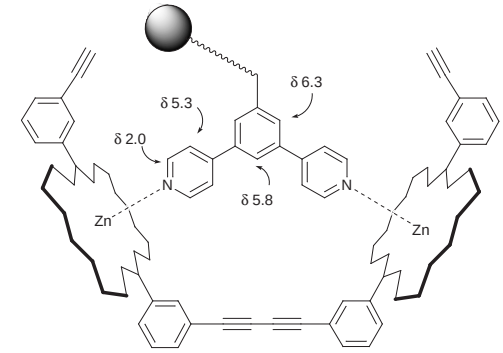

6

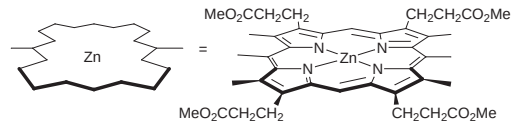

ligand chains *via* binding to the same trimer molecule within bead cavities. As expected, this is reversible: virtually all colour is removed from the beads by addition of the strongly-binding tri-functional ligand tripyridyltriazine.

We have shown that gel phase MAS ^{1}H NMR spectroscopy allows the study of non-covalent interactions between hosts and tethered guests. A wide range of two-dimensional techniques is available, and use of CPMG sequences of variable length should give access to subtle molecular mobility information. Furthermore this powerful technique holds out the prospect of studying the kinetics of molecular penetration into, and exit from, the interior of beads, and of characterising non-covalent cross-linking of ligand chains.

We thank Argonaut Technologies for providing ArgoGel resins and the EPSRC for financial support.

Notes and References

† E-mail: jkms@cam.ac.uk

‡ NMR spectra were acquired at room temperature on a Varian Unity 400 MHz spectrometer using a 'NanoNMR' MAS probe. Sample tubes contained 40 μl of a $CDCl_3$ suspension of beads (*ca*. 1 mg = 0.4 μmol bound molecules), and were spun at 3 kHz. One-dimensional spectra were obtained typically with 32 scans, in *ca* 10 min. The CPMG sequence contained 2000 π-pulses with a repetition time of 2 ms.

1 B. J. Egner and M. Bradley, *Drug Discovery Today*, 1997, **2**, 102; M. A. Gallop and W. L. Fitch, *Curr. Opin. Chem. Biol*., 1997, **1**, 94.
2 M. J. Shapiro and J. R. Wareing, *Curr. Opin. Chem. Biol*., 1998, **2**, 372; P. A. Keifer, *J. Org. Chem*., 1996, **61**, 1558; P. A. Keifer, L. Baltusis, D. M. Rice, A. A. Tymiak and J. N. Shoolery, *J. Magn. Reson., Ser. A*, 1996, **119**, 65.
3 J. K. M. Sanders and B. K. Hunter, *Modern NMR spectroscopy*, 2nd edn., OUP, Oxford, 1993, ch. 8 and 9.
4 R. Quarrell, T. D. W. Claridge, G. W. Weaver and G. Lowe, *Mol. Diversity*, 1996, **1**, 223.
5 Z. Clyde-Watson, A. Vidal-Ferran, L. J. Twyman, C. J. Walter, D. W. J. McCallien, S. Fanni, N. Bampos, R. S. Wylie and J. K. M. Sanders, *New J. Chem*., 1998, **22**, 493.
6 J. K. M. Sanders, *Chem. Eur. J*., 1998, **4**, 1378; S. J. Rowan, P. S. Lukeman, D. J. Reynolds and J. K. M. Sanders, *New J. Chem*., 1998, **22**, 1015.
7 V. Marvaud, A. Vidal-Ferran, S. J. Webb and J. K. M. Sanders, *J. Chem. Soc., Dalton Trans*., 1997, 985.
8 M. Marty, Z. Clyde-Watson, L. J. Twyman, M. Nakash and J. K. M. Sanders, *Chem. Commun*., 1998, 2265.

Received in Cambridge, UK, 3rd August 1998; 8/06034G

Crystal structure of β-MNX (M = Zr, Hf; X = Cl, Br)

Andrew M. Fogg, John S. O. Evans and Dermot O'Hare*

Inorganic Chemistry Laboratory, University of Oxford, South Parks Road, Oxford, UK OX1 3QR. E-mail: dermot.ohare@chem.ox.ac.uk

Superconductivity with critical temperatures of up to 25.5 K has recently been reported for alkali metal intercalates of β-MNX (M = Zr, Hf; X = Cl, Br); we have investigated the structures of these host lattices and found that they are not as reported in the literature but are isostructural with rhombohedral SmSI.

β-ZrNX (X = Cl, Br) was first prepared by Juza and Heners.[1] The crystal structures were reported by Juza and Friedrichsen to consist of a random stacking sequence of hexagonal XZrNNZrX layers leading to cell parameters of $a = b = 2.08$ Å, $c = 9.22$ Å ($a = 3.60$ Å using conventional axes).[2] A second synthetic route to β-ZrNCl *via* chemical vapour transport was reported by Ohashi *et al.* who demonstrated that a supercell with $\sqrt{3}a$ and $3c$ relative to the previous study was required to index their diffraction data though no further structural details were reported.[3]

The intercalation of lithium into β-ZrNCl was first reported by Yamanaka *et al.* in 1984.[4,5] It was subsequently shown that these and other alkali metal intercalates become superconducting below 15 K for doping levels of up to 0.4 mol alkali metal per ZrNCl.[6,7] These compounds represent the first examples of superconducting layered metal nitrides. More recently, β-$Li_{0.48}(THF)_y$HfNCl was shown to undergo a superconducting transition at 25.5 K, the highest of any nitride.[8] Any understanding of these materials will require a correct structural model of both the host lattice and its intercalation compounds. We have thus redetermined the structure of the β-MNX (M = Zr, Hf; X = Cl, Br) host lattices and find the true structure to be different from that generally accepted.

β-MNX (M = Zr, Hf; X = Cl, Br) were synthesised by the reaction of ZrH_2 or Hf with NH_4X followed by crystal growth *via* vapour transport under conditions reported previously.[3,9] Powder X-ray diffraction data for β-ZrNCl, β-ZrNBr and β-HfNCl indicated that in each case the three layer supercell proposed previously was necessary to index the diffraction patterns. Structural studies on β-ZrNCl are complicated by a number of factors relating to its crystal morphology. Firstly, the prevalence of stacking faults along the *c*-axis makes single crystal analysis extremely difficult. These stacking faults are presumably related to the disordered hexagonal cell reported previously.[2] Secondly, the plate-like morphology of the crystals causes preferred orientation to be extreme in microcrystalline samples. Indeed in conventional Bragg–Brentano geometry the preferred orientation is so great that the 00*l* class of reflections are frequently the only ones observed. Attempts to alleviate this problem by grinding and subsequent annealing of the sample resulted in significant loss of crystallinity. In order to obtain suitable data for structural analysis diffraction data were collected in two distinct geometries. The microcrystalline samples were sieved to less than 90 μm and either loaded into a 0.3 mm glass capillary or sprinkled onto a thin Mylar sheet and recorded in transmission geometry on a Siemens D5000 diffractometer using Cu-Kα radiation and a Braun linear position sensitive detector. In this manner data sets were obtained showing either artificially enhanced or diminished 00*l* intensity. The capillary data together with a calculated diffraction pattern based on the reported structural coordinates of the original structure are shown in Fig. 1. The calculated diffraction pattern was produced for a rhombohedral stacking sequence of layers with the layer structure suggested by Juza *et al.* The poor agreement is apparent.

The structure was solved by constructing trial solutions based on ClZrNNZrCl layers with differing stacking sequences and calculating their diffraction patterns within the InsightII software package.[10] The structure showing the closest agreement between the observed and calculated diffraction patterns was found to have rhombohedral symmetry (space group $R\bar{3}m$) and was used as the starting point for a combined Rietveld refinement of both sets of data within the GSAS software suite.[11] The final refinement consisted of 52 parameters (7 structural and 45 instrumental and background) with 3549 data points (9–80° 2θ, step = 0.02°,46 reflections) for the capillary data and 4098 data points (8–90° 2θ, step = 0.02°, 59 reflections) for the flat plate data. Isotropic temperature factors for the Zr and N atoms were constrained to be equal. A refinement in which all the temperature factors were allowed to refine freely led to no improvement in the agreement factors. Convergence was achieved at $\chi^2 = 2.07$, $R_{wp} = 2.40\%$ (capillary), $R_{wp} = 6.40\%$ (flat plate), $R_{wp} = 3.81$ (combined), $R_{F^2} = 16.4$ (capillary) and $R_{F^2} = 16.3\%$ (flat plate) for a rhombohedral cell with $a = 3.6052(1)$, $c = 27.6716(7)$ Å. Whilst these agreement factors are higher than those normally reported, we believe our model to be essentially correct. The diffraction data shown in Fig. 2 illustrate the dramatic effect which preferred orientation can have on the intensities of Bragg reflections of this phase. The structural model reported simultaneously provides a satisfactory fit to both data sets with only a simple March–Dollase type preferred orientation correction.[12,13] For the capillary data, the preferred orientation parameter for the 001 direction is 0.72 and for the flat plate data is 2.14. The atomic coordinates of β-ZrNCl are given in Table 1 and the final Rietveld fits of both sets of data are shown in Fig. 2. Bond valence calculations gave values of 4.51 for Zr, 3.56 for N and 0.96 for Cl.[14,15]

The structure of β-ZrNCl is shown in Fig. 3(a) and it is isostructural with SmSI.[16,17] This structure is known to support intercalation as shown, for example, by the insertion of pyridine into YbOCl.[18] In this structure each Zr atom is seven coordinate in a distorted monocapped octahedral arrangement with three Cl

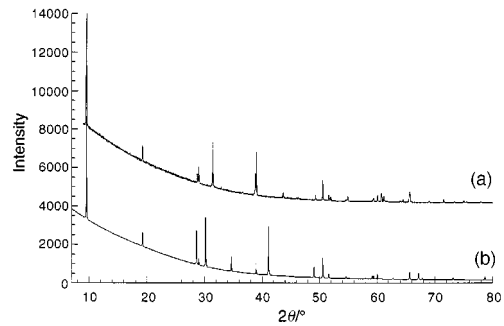

Fig. 1 (a) Powder X-ray diffraction pattern of β-ZrNCl and (b) calculated diffraction pattern based on the fractional coordinates of the original structure

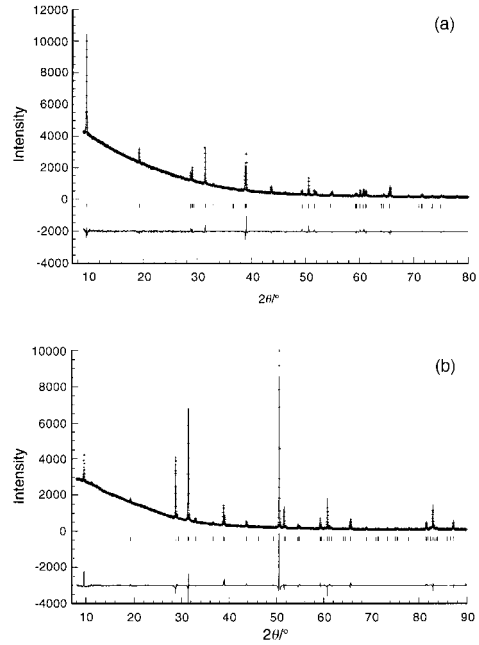

Fig. 2 Final Rietveld fit for β-ZrNCl: (a) capillary data (b) flat plate data; crosses represent the observed data, the solid line is the calculated pattern and the allowed reflection positions and difference profile are shown underneath

Table 1 Fractional atomic coordinates and isotropic thermal parameters for β-ZrNCl (esds in parentheses)

Atom	*x*	*y*	*z*	*U*/Å²
Zr	2/3	1/3	0.7142(1)	0.0080(7)
N	2/3	1/3	0.0425(5)	0.0080(7)
Cl	2/3	1/3	0.4460(2)	0.0117(11)

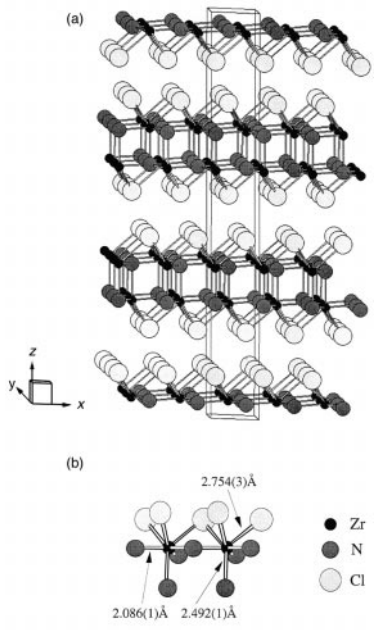

Fig. 3 (a) Structure of β-ZrNCl and (b) local coordination geometry of Zr in β-ZrNCl

atoms at 2.754(3) Å and three N atoms at 2.086(1) Å in a *fac*-arrangement with a fourth capping nitrogen at 2.492(1) Å as shown in Fig. 3(b). The octahedra are distorted by the displacement of the Zr atom from the centre towards the capped N_3 face to such an extent that the Zr and N atoms become essentially coplanar. These monocapped octahedral units are arranged in an edge sharing manner forming the ClZrNNZrCl layer structure. The ClZrNNZrCl layers are held together by van der Waals interactions. Alternatively the structure can be viewed as originating from the NaCl structure in a rhombohedral setting. Removal of alternate layers of cations and replacement of one half of the chloride layers in the sequence ClNNCl gives the β-ZrNCl structure. The vacant Zr layers can then collapse down so that one face of the *fac*-ZrN_3Cl_3 octahedron is capped by an additional N atom. The close relationship between the ZrN slabs in β-ZrNCl and the rock salt structure adopted by ZrN is perhaps of relevance to the superconductivity in the intercalates of β-MNX as the binary nitrides themselves undergo superconducting transitions at 9.05 K (ZrN) and 8.3 K (HfN).[19,20] Perhaps the most significant difference between this structure and the one originally reported is the absence of a short Zr–Zr distance which is instead replaced by the fourth capping N atom.[2,21,22] This Zr–Zr interaction had been thought to play an important role in the superconducting intercalates.

Further confirmation that this is the correct structure can be sought by simulating a structure in DIFFaX in which there is random stacking of the layers.[23] If this model is correct then it should be able to reproduce the data reported by Juza *et al.* This is found to be the case, suggesting that the chemical transport synthesis of Ohashi *et al.* produces a material with the same constituent layers as that produced by Juza, but with significantly enhanced ordering of layer stacking.

Refinement of the structures of β-ZrNBr and β-HfNCl using the same structural model showed that these compounds are indeed isostructural with β-ZrNCl as reported here. Full details of these refinements, the metallocene intercalation chemistry of β-ZrNCl and intercalation of β-ZrNBr will be published elsewhere.

Notes and References

1 R. Juza and J. Heners, *Z. Anorg. Allg. Chem.*, 1964, **332**, 159.
2 R. Juza and H. Friedrichsen, *Z. Anorg. Allg. Chem.*, 1964, **332**, 173.
3 M. Ohashi, S. Yamanaka, M. Sumihara and M. Hattori, *J. Solid State Chem.*, 1988, **75**, 99.
4 S. Yamanaka, M. Ohashi, M. Sumihara and M. Hattori, *Chem. Lett.*, 1984, 1403.
5 M. Ohashi, S. Yamanaka, M. Sumihara and M. Hattori, *J. Inclusion Phenom.*, 1984, **2**, 289.
6 S. Yamanaka, H. Kawaji, K. Hotehama and M. Ohashi, *Adv. Mater.*, 1996, **8**, 771.
7 H. Kawaji, K. Hotehama and S. Yamanaka, *Chem. Mater.*, 1997, **9**, 2127.
8 S. Yamanaka, K. Hotehama and H. Kawaji, *Nature*, 1998, **392**, 580.
9 M. Ohashi, S. Yamanaka and M. Hattori, *J. Solid State Chem.*, 1988, **77**, 342.
10 InsightII Software Package, MSI Simulations Inc., San Diego, 1994.
11 A. C. Larson and R. B. v. Dreele, GSAS—Generalised Structure Analysis System, LA-UR-86-748, Los Alamos National Laboratory, California, 1987.
12 A. March, *Z. Kristallogr.*, 1938, **81**, 285.
13 W. A. Dollase, *J. Appl. Crystallogr.*, 1986, **19**, 267.
14 I. D. Brown and D. Altermatt, *Acta Crystallogr., Sect. B*, 1985, **41**, 244.
15 N. E. Brese and M. O'Keefe, *Acta Crystallogr. Sect. B*, 1991, **47**, 192.
16 N. Savigny, P. Laurelle and J. Flahaut, *Acta Crystallogr., Sect. B*, 1973, **29**, 345.
17 H. P. Beck and C. Strobel, *Z. Anorg. Allg. Chem.*, 1986, **535**, 229.
18 D. A. Odink, K. Song and S. M. Kauzlarich, *Chem. Mater.*, 1992, **4**, 906.
19 B. T. Matthias and J. K. Hulm, *Phys. Rev.*, 1952, **87**, 799.
20 B. W. Roberts, *J. Phys. Chem. Ref. Data*, 1976, **5**, 581.
21 M. Ohashi, T. Shigeta, S. Yamanaka and M. Hattori, *J. Electrochem. Soc.*, 1989, **136**, 1086.
22 P. M. Woodward and T. Vogt, *J. Solid State Chem.*, 1998, **138**, 207.
23 M. M. J. Treacy, J. M. Newsam and M. W. Deem, *Proc. R. Soc. London. A*, 1991, **433**, 499.

Received in Cambridge, UK, 14th August 1998; 8/06415F

Synthesis of carbyne nano-particles by dehydrochlorination of 1,1,1-trichloroethane

Gaoquan Shi†

Department of Chemistry and State Key Laboratory of Coordination Chemistry, Nanjing University, Nanjing 210093, People's Republic of China

Chemical dehydrochlorination of 1,1,1-trichloroethane with anhydrous KOH in the presence of a poly(ethylene glycol) oligomer as phase transfer catalyst leads to the formation of carbyne particles with diameters in the range of 30–50 nm.

Synthesis of carbynes or cumulenic carbons has attracted the attention of many researchers,[1] as we still know much less about this material than about the other carbon polymorphs such as graphite, fullerenes and diamond.[2] Several synthetic routes to carbynes have been developed,[3–5] however, none of them concerned dehydrochlorination of low molecular weight carbon halides. Presented here is a novel chemical approach for synthesizing a carbyne analogue from 1,1,1-trichloroethane.

Carbyne can be prepared by reaction of 1,1,1-trichloroethane with a large amount of anhydrous KOH powder (the molar ratio of the base and the halide should be greater than 5 : 1) in the presence of a poly(ethylene glycol) with molar mass greater than 200 g mol^{-1} as phase transfer catalyst. The reaction can be represented by eqn. (1).

$$n\ CH_3CCl_3 + 3n\ KOH \xrightarrow[20\text{–}30\ ^\circ C,\ 4\ h]{HO(CH_2CH_2O)_mH\ (m\ >\ 3)} \underset{42\%}{-(C\equiv C)_n-} + 3n\ KCl + 3n\ H_2O \quad (1)$$

KOH in excess acts as a water absorbent and removing of water forces the reaction to the right hand. Otherwise, as a large amount of water exist in the system, the reaction produces only 1-chloroacetylene or 1,1-dichloroethylene and no carbon is obtained.

The black powdery carbon obtained by this technique had a particle size of 30–50 nm as shown by its transmission electron micrograph (Fig. 1). Powder X-ray diffraction analysis showed a broad peak at 2θ = 21°, showing the product to be amorphous.

The FT-IR spectrum of the product (Fig. 2) shows no C–Cl bands in the region 520–700 cm^{-1}, indicating extensive dehydrochlorination of the halide. New absorption bands appear in 1600 and 2130 cm^{-1}. They are typical of valence vibrations of carbon–carbon double and triple bonds, respectively.[6,7] The band in the region of 1700 cm^{-1} may be attributed to cumulative double bonds.[8] The very strong band at 1100 cm^{-1} is assigned to the stretching vibration of the C–C bond.[6] Absorption bands typical of valence vibrations of CH_2 were found in the region of 2800–2990 cm^{-1}. No band was observed above 3000 cm^{-1}, which demonstrated that no substitution side reaction was present during the carbonization process.

In the FT-Raman spectrum (Fig. 2) there appears a broad band centered at *ca.* 1900 cm^{-1}, which is attributed to conjugated carbon–carbon triple bonds. A much weaker band centered at *ca.* 1600 cm^{-1} is of 'inner layer' graphite bound by two adjacent graphite planes and the band centered at *ca.* 1400 cm^{-1} is the A_{1g} mode of $D_{6h}{}^4$ symmetry for small graphitic crystallites.[9] The intensity ratio of the 1900 cm^{-1} ($I_{C\equiv C}$) band and 1600 cm^{-1} band (I_{g-C}) is calculated to be 4.0 ± 0.5. There exists no other solid carbon material showing such intense Raman signals for triple-bonded carbon (the $I_{C\equiv C}/I_{g-C}$ of carbynes made *via* other systems was found to be lower than 2.2).[2] The conjugation length of carbyne estimated by the equation developed by Kuzmany *et al.* is *ca.* 15. This value is higher than those of the carbynes reported previously (6–10).[2,4]

While the existence of carbyne has been repeatedly doubted, all the criticisms are not convincing enough to reject the concept of linear carbon allotropes.[10] On the other hand, the FT-IR and FT-Raman spectra results described above provide strong evidence of carbon particles made from 1,1,1-trichloroethane having a polyyne structure with high concentrations of relatively long conjugated triple-bonded carbon sequences.

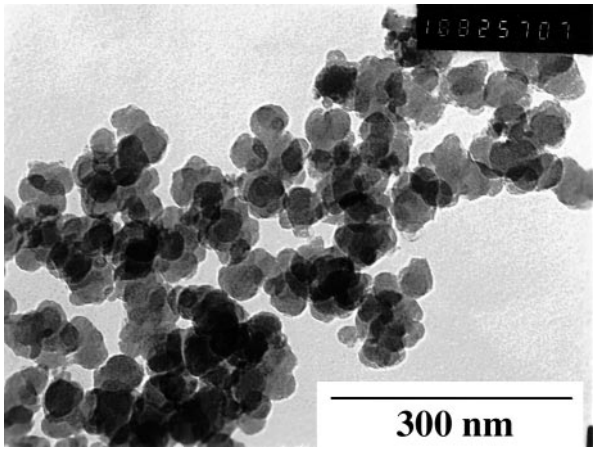

Fig. 1 Transmission electron micrograph of the carbon made from 1,1,1-trichloroethane.

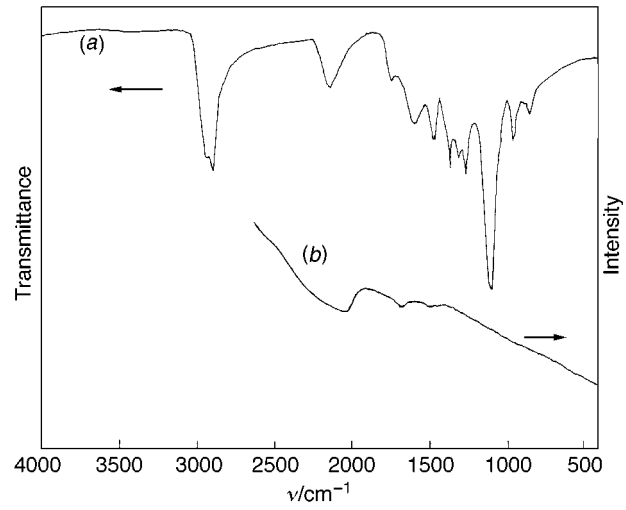

Fig. 2 (*a*) FT-IR and (*b*) FT-Raman spectra of the carbon made from 1,1,1-trichloroethane.

In conclusion, 1,1,1-trichloroethane can be carbonized by anhydrous KOH powder into amorphous carbyne nano-particles. This is the first example of dehydrochlorination of low molecule weight carbon halides into carbynes.

I thank the Natural Science Foundation of China for support of this work (No: 29773019).

Notes and References

† E-mail: hlchen@nju.edu.cn

1 L. Kavan, *Chem. Rev.*, 1997, **97**, 3061.
2 J. Kastner, H. Kuzmany, L. Kavan, F. P. Dousek and J. Küti, *Macromolecules*, 1995, **28**, 344.
3 R. B. Heimann, J. Kleiman and N. M. Salansky, *Carbon*, 1984, **22**, 147; *Nature*, 1983, **306**, 164.
4 M. Kijima, T. Toyabe and H. Shirakawa, *Chem. Commun.*, 1996, 2273.
5 Yu. P. Kadryavtsev, S. Evsyukov, M. Guseva, V. Babaev and V. Khvostov, *Chem. Phys. Carbon*, 1997, **25**, 1.
6 Z. Iqbal, D. M. Ivory, J. S. Szobota, R. L. Elsenbaumer and R. L. Boughman, *Macromolecules*, 1986, **19**, 2992.
7 C. C. Costello and T. J. McCarthy, *Macromolecules*, 1987, **20**, 2819.
8 V. V. Korshak, Yu. P. Kudryavtsev, S. E. Evsyukov, Yu. V. Korshak, V. V. Khvostov, V. G. Babaev and M. B. Guseva, *Makromol. Chem. Phys., Rapid Commun.*, 1988, **9**, 135.
9 H. Nishihara, H. Harada, M. Tateishi, K. Ohashi and K. Aramaki, *J. Chem. Soc., Faraday Trans.*, 1991, **87**, 1187.
10 Yu. P. Kudryavtsev, R. B. Heimann and S. E. Evsyukov, *J. Mater. Sci.*, 1996, **31**, 5557.

Received in Cambridge, UK, 7th July 1998; 8/05244A

A stereoselective and novel approach to the synthesis of 1,3-diols: simple control of diastereoselectivity

Rainer Mahrwald*† and Bilgi Gündogan

Institut für Organische und Bioorganische Chemie der Humboldt-Universität Berlin, Hessische Str. 1-2, D-10115 Berlin, Germany

Complete control of simple diastereoselectivity in the synthesis of 1,3-diols was realized through the use of a one-pot aldol addition and reduction process.

The diastereoselective synthesis of *syn* and *anti* 1,3-diols is currently of considerable interest, as these synthons are frequently found in a variety of polyketide natural products. Those diols with two chemically distinct hydroxy groups are of particular interest, as they are suitable building blocks for further stereoselective transformations. Multistep and more particular syntheses were found in the literature (hydrosilylation[1] or alkylmagnesation[2] of suitable alkenes, oxidative cleavage of double bonds,[3] reductive rearrangement of alkenyl acetals[4]). Moreover there are only a few examples of procedures for synthesising *anti* diols.[5]

Herein, we describe a simple and more general one-pot procedure for the synthesis of both *syn* and *anti* 1,3-diols by the utilization of titanium Lewis acids. Our studies on diastereoselective aldol additions in the presence of titanium Lewis acids have outlined a new series of highly regio-[6] and stereoselective reactions.[6,7] Very recently, we described the stereoselective aldol addition of aldehydes with enolizable aldehydes in the presence of titanium(IV) chloride.[7] The reactions were accomplished with the aid of an amine base. Surprisingly, substituting a titanium(IV) alkoxide as a base resulted in complete reduction of the intermediate β-hydroxy aldehydes when used in a one-pot procedure (Scheme 1).

Importantly, equimolar amounts of titanium(IV) alkoxides were added to a mixture of each starting aldehyde and 1 equiv. titanium(IV) chloride. When using a chloroisopropoxytitanium agent [*i.e.* $ClTi(OPr^i)_3$, $Cl_2Ti(OPr^i)_2$ or $Cl_3Ti(OPr^i)$] in place of both titanium(IV) chloride and the titanium(IV) alkoxide no reactions occurs; neither aldol additions nor reduction processes are observed.‡

Reactions were carried out in toluene or CH_2Cl_2; when using oxygen-containing solvents (Et_2O, THF) this described aldol addition-reduction sequence failed to occur.

The reaction mechanism is thus likely to be very similiar to a Meerwein–Ponndorf reduction. No reduction was observed by using tertiary titanium(IV) alkoxides [*e.g.* titanium(IV) alkoxides derived from from Bu^tOH or BINOL]. Thermodynamic equilibration occurs during the reduction process. The isolated 1,3-diols were formed with a high degree of *anti* selectivity (entries 1–4, Table 1). Similar observations were made in catalytic equilibration processes of hydroxy aldehydes.[7]

Utilizating the $TiCl_4/Ti(OPr^i)_4$ system at low temperature (−78 °C) only equilibration of the formed 3-hydroxy aldehydes is observed, whereas at higher temperatures (0–10 °C) an additional reduction process to the corresponding diols takes place.

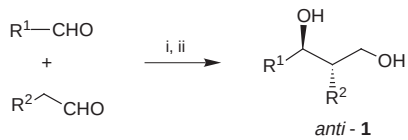

Scheme 1 *Reagents and conditions*: i, $TiCl_4$, CH_2Cl_2, 5 °C; ii, $Ti(OPr^i)_4$

Table 1 Diastereoselective synthesis of 1,3-diols

Entry	R^1	R^2	Method	Compound	Yield[a] (%)	Ratio[b] *syn*/*anti*
1	Ph	Me	A	**1a**[c]	73	9/91
2	Ph	Et	A	**1b**[d]	68	12/88
3	Et	Me	A	**1c**[e]	81	13/87
4	Pr^i	Me	A	**1d**[f]	48	15/85
5	Ph	Me	B	**1a**[c]	81	92/8
6	Ph	Et	B	**1b**[d]	72	90/10
7	Et	Me	B	**1c**[g]	71	86/14
8	Pr^i	Me	B	**1d**[h]	43	92/8

[a] Isolated yields. [b] Determined for the crude products by ^1H and ^{13}C NMR spectroscopy. Method A: $Ti(OPr^i)_4$ was added to a mixture of 1 equiv. of $TiCl_4$ and 1 equiv. of the corresponding starting aldehyde (ref. 5). (Scheme 1). Method B: the β-hydroxy aldehydes were synthesized by a literature procedure (ref. 7). After 16 h, 1 equiv. of $LiAlH_4$ was added to the crude reaction mixture (Scheme 2). [c] Ref. 8. [d] Ref. 2. [e] Ref. 1 and 12. [f] Ref. 11. [g] Ref. 1 and 9. [h] Ref. 10.

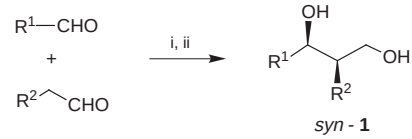

Scheme 2 *Reagents and conditions*: i, $TiCl_4$, base, −78 °C; ii, $LiAlH_4$

Reversal and thus complete control of the simple diastereoselectivity using this one-pot aldol addition-reduction sequence was realized through the synthesis of the corresponding *syn* 1,3-diols. This was achieved by reduction of the crude aldol reaction mixture[7] with $LiAlH_4$. The 1,3-diols thus obtained were isolated with a high degree of *syn* selectivity (see entries 5–8, Table 1 and Scheme 2).

This work was supported by Deutsche Forschungsgemeinschaft and the Fonds der Chemischen Industrie.

Notes and References

† E-mail: rainer = mahrwald@rz.hu-berlin.de

‡ *General procedure* for **1a**: propanal (0.72 ml, 10.0 mmol) and benzaldehyde (1.02 ml, 10.0 mmol) were dissolved in CH_2Cl_2 (20 ml) under inert conditions. $TiCl_4$ (1.1 ml, 10.0 mmol) was added and the solution was cooled to −10 °C. After 30 min at this temperature, $Ti(OPr^i)_4$ (1.5 ml, 5.0 mmol) was carefully added and the solution was stirred for further 16 h at 5 °C, after which water was added (30 ml) and the resulting emulsion filtrated through silica gel–sand. The filtrate was extracted with Et_2O (100 ml) and brine (30 ml) until neutral. The organic layer was separated, dried (Na_2SO_4), fitrated and evaporated *in vacuo*. The pure *anti* 1,3-diol **1a** was separated by flash chromatography using hexane–EtOAc (80:20) as eluent.

1 K. Tamao, T. Nakajima, R. Sumiya, H. Arai, N. Higuchi and Y. Ito, *J. Am. Chem. Soc.*, 1986, **108**, 6090.

2 A. F. Houri, M. T. Didiuk, Z. Xu, N. R. Horan and A. H. Hoveyda, *J. Am. Chem. Soc*., 1993, **115**, 6614.
3 W. R. Roush, K. Ando and A. D. Palkowitz, *J. Am. Chem. Soc*., 1990, **112**, 6348.
4 R. Menicagli, C. Malanga, M. Dell'Innocenti and L. Lardicci, *J. Org. Chem*., 1987, **52**, 5700.
5 H. Sacha, D. Waldmüller and M. Braun, *Chem Ber*., 1994, **127**. 1959 and references cited therein.
6 R. Mahrwald, *Chem. Ber*. 1995, **128**, 919; R. Mahrwald and B. Gündogan, *J. Am. Chem. Soc*., 1998, **120**, 413; R. Mahrwald, *GIT Fachz. Lab*., 1996, **40**, 43.
7 R. Mahrwald and B. Gündogan, *Tetrahedron Lett*., 1997, **38**, 4543; R. Mahrwald, B. Costisella and B. Gündogan, *Synthesis*, 1998, 262.
8 W. R. Roush, K. Ando, D. B. Powers, A. D. Palkowitz and R. J. Haltermann, *J. Am. Chem. Soc*., 1990, **112**, 6339; S. G. Davies, A. J. Edwards, G. B. Evans, and A. A. Mortlock, *Tetrahedron*, 1994, **50**, 6621.
9 C. M. Chan, J. M. Chong and K. Kousha, *Tetrahedron*, 1994, **50**, 2703; R. A. Pilli and K. Z. de Andrade, *Synth. Comm*., 1994, **24**, 233.
10 H. Maehr, R. Yang, L. N. Hong, C. M. Liu, M. H. Hatada and L. J. Torado, *J. Org. Chem*., 1989, **54**, 3816; Y. Mori, M. Asai, J. Kawade and H. Furukawa, *Tetrahedron*, 1995, **51**, 5315.
11 R. O. Duthaler, P. Herold, S. Wyler-Helfer and M. Riedicker, *Helv. Chim. Acta*, 1990, **73**, 659; R. Baker, J. C. Head and C. J. Swain, *J. Chem. Soc., Perkin Trans. 1* 1988, 85; L. Domon, F. Vogeleisen and D. Uguen, *Tetrahedron Lett*., 1996, **37**, 2773.
12 M. Honda, T. Katsuki and M. Yamaguchi, *Tetrahedron Lett*., 1984, **25**, 3857.

Received in Liverpool, UK, 6th August 1998; 8/06222F

Typeset and printed by Black Bear Press Limited, Cambridge, England

Preparation, structure and morphology of polymer supports

David C. Sherrington†

Department of Pure and Applied Chemistry, University of Strathclyde, 295 Cathedral Street, Glasgow, UK G1 1XL

Received (in Cambridge, UK) 19th May 1998, Accepted 18th June 1998

The use of polymer resin beads as an aid to synthesis is becoming an increasingly common feature in both academic and industrial synthesis laboratories. The large majority of users employ materials sourced commercially and adopt or adapt procedures already described in the literature without thinking too deeply about the physico-chemical aspects of the support. Success can be immediate, but more often a learning curve needs to be traversed. The present article seeks to describe the chemistry of synthesising supports and to present a user-friendly description of their key physico-chemical properties. A qualitative and pictorial view of how specific morphologies can be generated, and the relevance of these, is also presented. It is hoped that this insight will be of advantage to users in planning and pursuing their chemistry using polymer supports.

Background

Following the discovery and exploitation of ion exchange resins based on suspension polymerised styrene–divinylbenzene (DVB) beads during the 1950s, an enormous amount of effort was directed towards investigating styrene–DVB sulfonic acid resins as potential heterogeneous catalysts. Patenting activity was extensive and throughout the following decades many key large-scale chemical processes have been established employing sulfonic acid resins as the catalyst.[1,2] These include the manufacture of bisphenol A, isopropyl alcohol, alkylated phenols, branched ethers (petrol organic 'anti-knocks') such as methyl *tert*-butyl ether (MTBE), and a variety of alkyl esters including important (meth)acrylate esters. Despite this, there remains a dearth of knowledge amongst synthetic chemists regarding the usefulness of these polymer-based catalysts.

In 1963 Merrifield took the first step towards introducing polymer-supported chemistry to the wider world of synthesis with the publication of his 'solid phase' peptide synthesis methodology.[3] Notwithstanding this however a more widespread appreciation of the advantages that polymer (and other) supports have to offer to synthesis has only really occurred in the last five years or so, with the explosion in the use of solid phase combinatorial synthetic methodologies,[4,5] spurred on by the need for rapid synthesis and screening of potential lead compounds in drug discovery programmes within the pharmaceutical industry. Increasing familiarity with, and confidence in, the use of polymer resins in solid phase synthesis has stimulated even mainstream organic synthetic groups[6,7] to investigate the prospects of employing polymers as catalyst supports for use, for example, in solution phase combinatorial synthesis. Thus those of us who have been struggling with these systems for many years now find ourselves joined by more illustrious and no doubt more imaginative and skilful colleagues.

Recently the areas of polymer-supported organic reactions[4,8] and polymer-supported catalysts[9,10] have been reviewed from the point of view of the solid phase synthetic chemistry which can be carried out on resins and the reactions that have been catalysed by polymer-supported metal complexes *etc*. The main objective of the present article is to focus on the polymer support itself, and to bring a more informed picture of the molecular structure, porous morphology and physico-chemical nature of the support to hard-pressed users and would-be users of these polymers. The hope is that this insight might explain some of the advantages already experienced in the use of supports and, perhaps more importantly, might help overcome some of the disadvantages or downright failures experienced with attempts to use polymer supports.

Linear polymers

Most polymer supports are based on addition polymers typified by polystyrene, the latter conveniently synthesised from styrene *via* a free radical chain propagation reaction (Fig. 1). Since

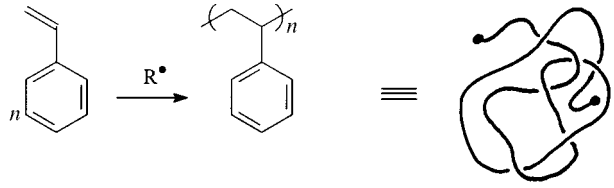

Fig. 1 Polymerisation of styrene to form linear polystyrene, which is a random coil macromolecule.

polystyrene-based supports are particularly widely employed, this is a very convenient model upon which to base a description of the relevant polymer physical chemistry. The principles to be described, however, are widely applicable to other polymer types. Synthetic polymers are generally devoid of any significant secondary or tertiary structure, such as commonly occurs with natural polymers (*e.g.* proteins, DNA), and so individual isolated polymer molecules exist as a random coil typically ~10–20 nm in size, depending upon the molecular weight.[11]

A collection of chemically similar polymer molecules exist as a mass of interpenetrating random coils—not unlike a bowl of spaghetti. In the case of polystyrene in the solid state, at room temperature, individual polymer chains cannot migrate relative to each other, and indeed even rotation about the bonds in the polymer backbone is very inhibited. Only rotation A (Fig. 2) of

Professor D. C. Sherrington graduated from the University of Liverpool with a B.Sc. (Hons) in Chemistry in 1966 and with a Ph.D. in 1969. He was appointed Lecturer at the University of Strathclyde, Department of Pure and Applied Chemistry, in 1971, then Senior Lecturer and Reader, and finally Professor of Polymer Chemistry in 1987. Professor Sherrington has broad interests covering many aspects of polymer chemistry but, in particular, has pioneered the use of polymers as supports for reagents and catalysts in organic chemistry. He has published 220 papers and reviews, and is co-editor of two seminal research texts on polymer-supported species (1981 and 1988). He was international editor of the journal Reactive Polymers *(1987–1996), was elected Fellow of The Royal Society of Edinburgh (1990) and was awarded his D.Sc. (1992) from the University of Liverpool. Finally, he was awarded the RSC/SCI Beilby Medal (1993) for the 'Advancement of Chemistry and its Practice'.*

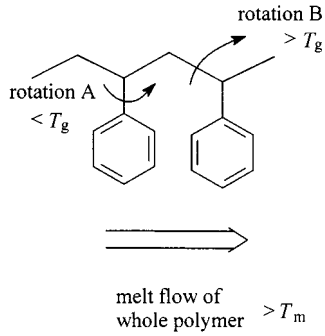

Fig. 2 Molecular motions in polystyrene: T_g = glass transition temperature; T_m = melting point.

the phenyl sidechains occurs freely at room temperature. Overall therefore the polystyrene 'bowl of spaghetti' is essentially frozen at room temperature. Technically the material is said to be below its glass transition temperature, T_g, and the material is amorphous and very glass-like in its general physical nature. The T_g for polystyrene is ~100 °C.[12] Above this temperature free rotation B (Fig. 2) about the bonds of the main chain occurs and the polymer becomes pliable or 'plastic'. The analogy now would be a bowl of 'rubbery spaghetti'. *Complete* movement (translation) of individual polymer chains relative to each is still inhibited until ~250 °C. This is the melting point,[12] T_m, above which polymer chains can flow over and through each other and the polymer becomes a viscous liquid or 'melt' (*i.e.* the 'spaghetti' is now hot and mobile and ready to eat). In the glass-like solid state diffusion of even small non-interacting molecules through solid polystyrene is extremely slow.

Solvation behaviour of polymers

The changes described above brought about by an increase in temperature can also be induced at ambient temperatures by the introduction of small interacting organic solvent molecules. Depending upon the relative strength of the interactions of the solvent–solvent, polymer–polymer, and polymer–solvent molecules, an organic solvent may sorb into polystyrene and allow backbone rotation to occur. This is termed 'plasticisation' and the polymer changes from a glass-like solid material into a soft plastic material. A sorbed solvent may interact even more favourably with the polymer chains, heavily solvate them, and allow them to move apart. Such solvents are called thermodynamically 'good' solvents or 'swelling' solvents (see later). This is the onset of the process of dissolution and if enough of such a solvent is added the individual polymer coils will move completely apart to form an isotropic (uniform) solution in the solvent (Fig. 3). Some solvents interact hardly at all with a given

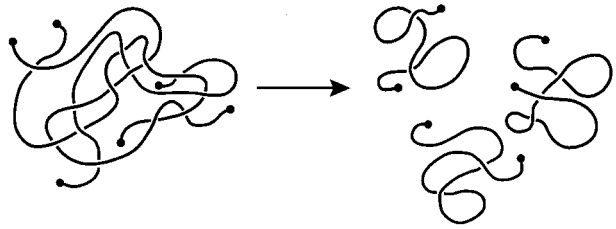

Fig. 3 Dissolution of interpenetrating polymer coils to form independent solvated coils.

polymer and are termed thermodynamically 'bad' solvents, *i.e.* non-solvents, or precipitants. If a polymer is dissolved in a 'good' solvent, and an excess of a 'bad' solvent is added, then the polymer can be precipitated as a solid material. Some typical 'good' solvents and 'bad' solvents for polystyrene are shown in Table 1.

In discussing the compatibility or otherwise of different materials a useful thermodynamic parameter is the solubility parameter δ. This is a measure of the attractive strength between molecules in a material. A solvent and a polymer are likely to be compatible, *i.e.* the solvent is likely to be a 'good' solvent for the polymer, if they have very similar solubility parameters. If the solubility parameters differ, the solvent is likely to be a 'bad' solvent or precipitant for the polymer. The solubility parameter for polystyrene (and copolymers of styrene and divinylbenzene, see later) is ~17–18 $(MPa)^{0.5}$. The corresponding values for a number of 'good' and 'bad' solvents are shown in Table 1.[13] Note that one group of 'bad' solvents has solubility parameters below that of polystyrene, while the other group has values above that of polystyrene.

Soluble polymer supports

In principle therefore soluble linear polymers seem excellent candidates as reaction and catalyst supports, and indeed they have been well-researched in this context.[14] Dilute solutions of linear polymers should allow rapid unimpeded access of reactants and reagents to functional groups on the support, and the recovery and separation of the polymer might be achieved by addition of a suitable precipitant, by micro- or ultra-filtration, and in some cases by thermal cycling. A major disadvantage of linear polymers as supports is that in general they are useful only with solvents in which they will dissolve. If a solvent is used or required, which will not dissolve the polymer, essentially all the advantages of using a linear polymer as a support are lost. In many instances therefore reagents and catalysts are excluded from use, or possible reaction conditions eliminated, simply because a suitable solvent for the polymer and the reaction cannot be found. Furthermore, in practice micro- and ultra-filtration processes are relatively costly and are not convenient, especially for the hard-pressed laboratory organic synthetic chemist, for laboratory automation, or an industrial chemical manufacturer. While precipitation of many polymers by addition of a suitable non-solvent yields a hard granular product which is readily filtered, linear polymers can selectively sorb a 'good' solvent and be precipitated as a sticky mass, impossible to filter. It is also important to realise that linear polymer coils in solution remain isolated from each other only at concentrations below ~1–2 wt%. Above this threshold, polymer coils interact and start to interpenetrate, and at more practical synthetic organic chemical concentrations, say >5 wt%, solutions can become impractically viscous. Bearing in mind that lightly crosslinked polymer networks can be prepared such that they can swell to imbibe >5 times their own mass of solvent (see shortly) and yet remain in a physical form useful for manipulation, the attractiveness of linear polymers as supports is rather limited.

Nevertheless there are situations where linear soluble polymers can be extremely useful and a key factor in this is that chemical reactions performed on such polymers can be

Table 1 Polystyrene solvents and non-solvents solubility parameters δ^a

Good solvents	δ/ $(MPa)^{0.5}$	Bad solvents	$\delta/(MPa)^{0.5}$
Aromatic hydrocarbons		Water	47.9
Benzene	18.8	*Aliphatic alcohols*	
Toluene	18.2	Methanol	29.7
Xylenes	18.0	Ethanol	26.0
Chlorocarbons		2-Ethylhexanol	19.4
1,2-Dichloroethane	20.1	*Aliphatic hydrocarbons*	
Chloroform	19.0	Hexane	14.9
Cyclic ethers		Dodecane	16.2
Tetrahydrofuran	18.6	*Others*	
Dioxane	20.5	Diethyl ether	15.1
		Acetic acid	20.7

[a] δ for polystyrene and styrene–divinylbenzene copolymers is ~17–18 $(MPa)^{0.5}$

monitored by, for example, high resolution solution phase ^{1}H and ^{13}C NMR spectroscopy.[15] Though the resonances due to backbone protons are usually broadened, signals arising from mobile groups in the sidechain are often as sharp as resonances from analogous low molecular weight groups in isotropic solution. Recently, however, considerable advances have also been made in ^{1}H and ^{13}C NMR analysis of crosslinked polymers[16] (see later).

Copolymers and copolymerisation

The introduction of functionality onto a polymer support can often be readily achieved simply by treating the polymer as a structural analogue of a low molecular weight species and then utilising identical chemistry to achieve a desired derivatisation or structural elaboration. Thus polystyrene can be treated as isopropyl benzene and, for example, subjected to electrophilic substitution. An enormous amount of chemistry has been developed using this approach.[1,4,5,17,18] An alternative or complementary approach is to introduce a specific functionality during free radical polymerisation, by utilising a comonomer which already carries the required function, or some precursor group which can subsequently be readily transformed. For example, copolymerisation of styrene and 4-vinylphenyl(diphenyl)phosphine yields polystyrene with pendant triphenylphosphine residues. This approach can be useful in producing a structurally well-defined polymer, for controlling the proportion of functional groups introduced and for providing some information on the distribution of the groups along the polymer chain.

It is important in this context to appreciate that all monomers are not incorporated at the same rate. In a free radical copolymerisation of two vinyl monomers, A and B, the rate at which a given monomer is copolymerised depends on the reactivity of the monomer, the reactivity of the free radical derived from the monomer, and how these two reactivities compare with the corresponding reactivities of the other monomer and its derived radical. These factors are all incorporated in so-called pairs of reactivity ratios, r_A and r_B. Reactivity ratios are determined experimentally and are extensively tabulated[19] for pairs of most common monomers. The values generally fall in the range 0 to 1, but can be much higher in special cases. A low value indicates low reactivity, a high value high reactivity. If two monomers each have a moderate value ($\sim$0.5) then the copolymer they form will have similar composition to that of the comonomer solution. If both monomers have a low value ($\sim$0) then copolymerisation will be slow and a rather regular alternating 1 : 1 copolymer will form, with alternate segments comprised of the different monomer residues. If one reactivity is low ($\sim$0) and the other high ($\sim$1), then the initially formed polymer will be essentially a homopolymer of the most reactive monomer, with extremely low incorporation of the less reactive monomer. In all cases the processes are subject to some statistical distribution and, in addition, in a batch copolymerisation, if the monomers are initially incorporated at different rates the more reactive monomer will be depleted from solution more quickly, and this in turn will start to slow its incorporation. The composition of the copolymer formed will therefore alter with time as polymerisation proceeds (composition drift).

A simple kinetic treatment[20] shows that the copolymer composition, A_{pol}/B_{pol}, is given by eqn. (1),

$$A_{pol}/B_{pol} = \frac{[A](r_A[A]+[B])}{[B](r_B[B]+[A])} \quad (1)$$

where [A] and [B] are the concentrations of the respective comonomers. Knowledge of the r_A and r_B values also allows computation of the mean sequence lengths, S_A and S_B, of A monomer and B monomer segments respectively in the copolymer from eqn. (2).

$$\bar{S}_A = \frac{r_A[A]}{[B]} + 1 \text{ and } \bar{S}_B = \frac{r_B[B]}{[A]} + 1 \quad (2)$$

Thus the reactivity ratios for 4-vinylphenyl(diphenyl)phosphine and styrene are 1.43 and 0.52 respectively, so that the phosphine monomer is considerably the more reactive. For a comonomer mixture of 1:1 therefore the corresponding copolymer composition A_{pol}/B_{pol} will be 1.6, and the values of S_A and S_B, 2.4 and 1.5 respectively. Hence the copolymer formed initially is enriched in phosphine monomer residues and these occur on average in blocks of 2–3 segments. In contrast the reactivity ratios for 4-vinylpyridine and styrene are very similar ($\sim$0.55), so that these comonomers polymerise more or less in a random fashion, with the copolymer backbone composition being controlled essentially by the initial composition of the comonomer mixture. These effects are extremely important, for example, in designing functional copolymers where it is desired to ensure that functional groups are remote from each, and essentially 'site isolated'.[21]

Crosslinked polymers

If styrene is polymerised in a mixture with divinylbenzene (DVB) then the latter becomes a constituent of two polymer chains, effectively linking (crosslinking) the chains together. When all the polymer chains are mutually connected an 'infinite network' is formed (Fig. 4). In our 'bowl of spaghetti' analogy,

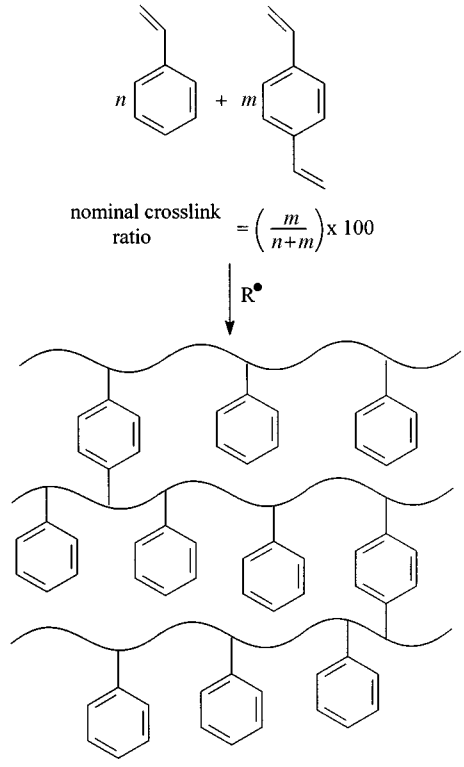

Fig. 4 Polymerisation of styrene and divinylbenzene to form an infinite polymer network.

all the spaghetti strands have been interconnected. Other useful crosslinking monomers are ethylene glycol dimethacrylate (EGDMA) (ethane-1,2-diyl dimethacrylate), trimethylolpropane trimethacrylate (TRIM) [1,1,1-tris(methacryloyloxymethyl)propane] and *N*,*N*-methylenebisacrylamide (MBA). Note that each TRIM residue effectively links three polymer chains together. DVB has three positional isomers (*o*-, *m*- and *p*-) and there are two routinely available commercial grades of DVB, each of which is a complex mixture. There are four major components, *m*- and *p*-DVB, typically in a ratio of $\sim$2 : 1, and *m*- and *p*-ethylstyrene in a similar ratio. In one commercial grade the DVB isomer content is $\sim$50%, and in the other

~80%. Care is therefore required in defining or interpreting the DVB content of crosslinked polymers since this might be quoted as a percentage of technical DVB used to make the polymer, or the figure can be adjusted to reflect only the content of *actual* DVB isomers present. Since for convenience the nominal crosslink ratio or degree of crosslinking of a polymer network is often quoted as the mol% of crosslinker used to prepare the network, defining the actual percentage of DVB isomers employed is more informative since this equates with the nominal crosslink ratio (Fig. 4). Bearing in mind that there is no unambiguous method, and certainly no simple and rapid method, for determining the real crosslink ratio in a polymer network, the nominal figure based on the actual DVB feed is a very useful parameter.

Other structural complications also arise which make defining and measuring the real crosslink ratio even more problematical. Although a defined level of crosslinker can be used to synthesise a polymer matrix there is no guarantee that both vinyl groups of *all* crosslinker molecules will react. Indeed, it is well-known that, particularly when higher levels of DVB are used, a significant number of vinyl groups remain unreacted; indeed these can be exploited as sites for further chemical modification. Much effort has been expended in trying to quantify accurately the levels of residual pendant double bonds, and single pulse excitation (SPE) ^{13}C solid state NMR analysis has recently allowed this.[22] Rather remarkably a crosslinked resin prepared from 100% *p*-divinylbenzene has ~45% of vinyl groups unreacted, *i.e.* the effective crosslink ratio is ~55%. For a resin prepared with the 80% grade of technical DVB, 45% of initial vinyl groups remain, *i.e.* the effective crosslink ratio is ~45%, while for a resin prepared with the 50% grade of technical DVB, ~32% of initial vinyl groups remain, *i.e.* the effective crosslink ratio is ~35%.

During formation of a crosslinked network it is also possible to produce additional (mobile) crosslinks by virtue of spurious entanglements which cannot disassemble (Fig. 5). Generally

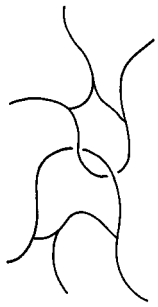

Fig. 5 Permanent entanglement crosslink.

'entanglement crosslinks' increase when the rate or speed of polymerisation is increased. This in turn can be induced by increasing the free radical flux in the polymerisation by increasing the temperature of the reaction and/or the quantity of free radical initiator used. Entanglement crosslinking is also high in a non-agitated polymerisation system, whereas vigorous agitation tends to minimise entanglements. Detecting and quantifying the level of entanglement crosslinking is very difficult.

Further uncertainty in the real level of crosslinking can arise following chemical modification of a polymer network. Some reactions, for example, chloromethylation and sulfonation of polystyrenes, are well known to be accompanied by intramolecular side-reactions which introduce additional crosslinks (Fig. 6) depending upon the conditions used. Again much investigative work has been carried out to try and quantify these reactions and SPE ^{13}C solid state NMR has proved very valuable in the case of the methylene bridging which accompanies chloromethylation.[23] Using the typical conditions to secure essentially quantitative chloromethylation of aromatic

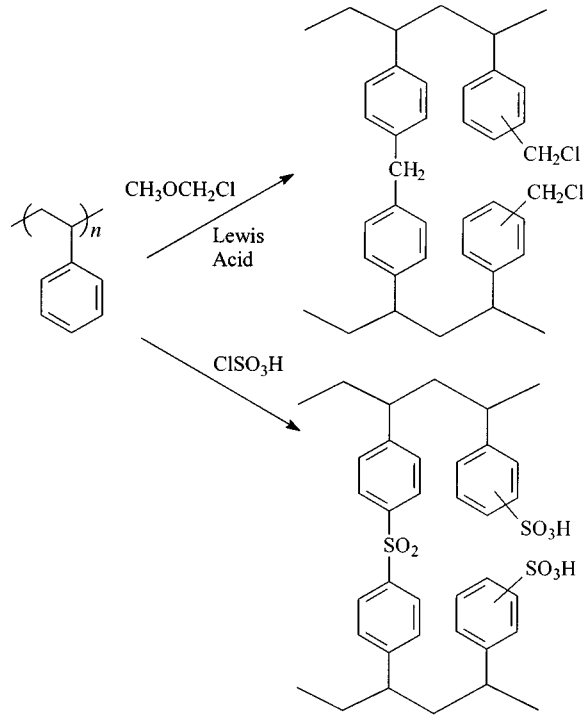

Fig. 6 Secondary crosslinking reactions.

groups in polystyrene resins simultaneously induces ~50% of the aromatic groups to become methylene bridged. While industrial manufacturers of anion exchange resins have learnt to live with, indeed exploit, the methylene bridging side reaction, the discovery of such high levels of these structural units came as a surprise.

Returning to the styrene–DVB copolymerisation, the r_A, r_B values quoted[19] for styrene and *m*-DVB are 0.58 and 0.58, and for styrene and *p*-DVB are 0.26 and 1.2, where the DVB figure refers to the first double bond in the molecule. After this first vinyl group is reacted the now pendant second double bond will assume a reactivity close to that of styrene. In the case of styrene–DVB mixtures these data predict (or imply) that initially the *p*-DVB isomer is incorporated into the copolymer significantly more quickly than styrene (and the *m*-DVB isomer) and that the initially so-formed copolymer is enriched in *p*-DVB residues relative to the composition of the solution phase. The latter becomes progressively more depleted in *p*-DVB and hence its rate of incorporation into the copolymer also falls. These reactivity data therefore predict a copolymer primary structure relatively rich in DVB residues at the start of a chain and somewhat depleted at high chain lengths. The situation however is complex and extensive unpublished data from industrial sources[24] suggest that overall there seems to be a strong tendency for styrene and DVB residues to be incorporated more or less evenly initially to produce a rather regular structure along the backbone tending towards a 1:1 alternating relationship; to some extent this occurs irrespective of the initial styrene–DVB composition of the comonomer solution.

As pointed out earlier, with a divinyl comonomer the polymer formed becomes crosslinked as the second pendant double bond is reacted. Initially this is a local phenomenon with the formation of small volumes of microgel (microgelation) (Fig. 7). Eventually however the mass of growing polymer molecules dissolved in solution becomes crosslinked into one infinite network; the system reaches its 'gel-point'. At the point of macrogelation the comonomer swollen crosslinked polymer mass becomes a monolith soft gel filling the containing vessel (Fig. 7). At this point macroscopic diffusion of molecular compounds in the gel starts to become impaired, with the problem growing more acute as crosslinking increases. Further

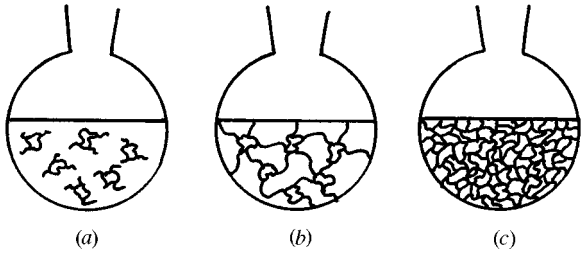

Fig. 7 Polymerisation of a monomer and crosslinker to undergo initially (*a*) microgelation, then (*b*) macrogelation, and finally (*c*) forming a solid glass.

incorporation of comonomers into the crosslinked copolymer becomes less controlled by solution reactivity parameters and more controlled by the composition of the comonomers in the swollen gel, *i.e*. the composition of the copolymer formed tends towards the composition of the comonomers in solution at the gel-point, with formation of a structurally fairly uniform copolymer. If polymerisation is allowed to continue, the liquid comonomers are gradually consumed, the polymer mass becomes increasingly desolvated and finally an amorphous crosslinked glassy monolith is formed in the shape of the containing vessel (Fig. 7). The monolith can be recovered, crushed, solvent extracted and dried to form crosslinked polymer particles or powder with irregular size and shape.

Suspension polymerisation

In practice the size, shape, and often the uniformity of crosslinked polymer particles is vital in most applications. For example, irregularly shaped particles are much more susceptible to mechanical attrition and breakdown to 'fines'. One of the major advantages in using crosslinked polymers as supports is the ease of handling, and robust spherical particles of an appropriate size and size distribution are essential in most applications. The technique of suspension polymerisation allows such particles to be produced fairly readily and highly reproducibly. The methodology is used widely on a laboratory scale but it is also a major large-scale industrial technology as well. Typically a styrene and DVB liquid mixture is dispersed as spherical liquid droplets (the dispersed or non-continuous phase) in a excess of an immiscible water phase (the continuous phase). The styrene–DVB mixture also contains a source of free radicals, the polymerisation initiator, and the aqueous phase generally contains a low level of some dissolved 'suspension stabiliser', a surface active species, often a water-soluble polymer, which helps to maintain the organic monomer droplets separate from each other. The suspension is maintained stable by continuous stirring and the reaction typically heated to ~80 °C for 12 h. During this period the spherical liquid monomer droplets are converted into hard glassy polymer particles, still retaining the spherical symmetry of the original liquid droplets (Fig. 8). The rather attractive 'beads' or 'pearls'

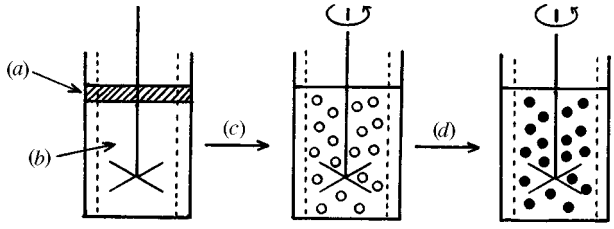

Fig. 8 Schematic representation of suspension polymerisation: (*a*) organic comonomer mixture (with porogen) containing dissolved initiator; (*b*) aqueous continuous phase containing dissolved polymeric suspension stabiliser; (*c*) shearing to form comonomer liquid droplets; (*d*) thermal polymerisation to form solid polymer resin beads.

are referred to as 'resins' (Fig. 9). In the laboratory, when the reaction is complete the resin particles can be collected by

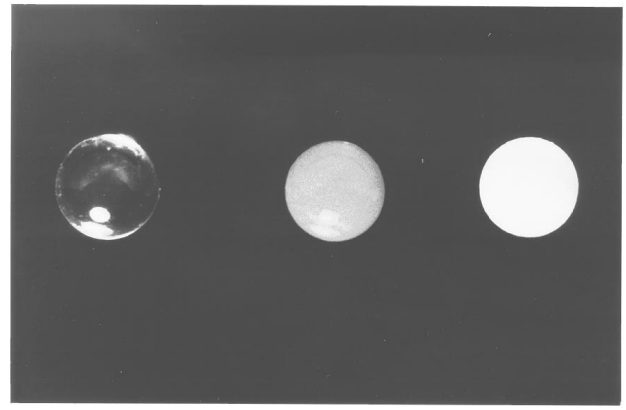

Fig. 9 Optical photograph of (left) gel-type bead, (right) macroporous bead, and (centre) mixed morphology.

filtration and traces of unreacted monomer, initiator and other organic fragments removed by solvent extraction in a Soxhlet, and finally the particles are vacuum dried. Fig. 10 shows the

Fig. 10 Suspension polymerisation reactor, internal volume 1 l, used in the author's laboratory.

type of suspension polymerisation reactor used in the author's laboratory. Further extensive details of suspension polymerisations are available in the literature.[25,26]

Resin morphology

Gel-type resins

When the comonomer mixture in a suspension polymerisation consists only of styrene and DVB (plus the polymerisation initiator) the product generally consists of hard glassy transparent resin beads (see left-hand sample Fig. 9). The percentage

of DVB can be varied in principle from 0–100% but typically for most resin applications the range 0.5–20% is more usual and for combinatorial synthesis resins, 0.5–2%. As described earlier such materials are composed of an amorphous crosslinked infinite network of interpenetrating polymer chains without any fine structure. The polymer chains are in molecular contact with each other, and the resins have very low surface area in the dry state when measured by, for example, N_2 sorption and application of the BET theory, typically less than 10 $m^2\ g^{-1}$ of dry resin. The diffusion of even small molecules through this polymeric glass is very slow indeed. These materials will, however, swell in a 'good' solvent, *e.g.* toluene (*i.e.* a solvent with a solubility parameter similar to that of the polymer), with the percentage swelling typically being inversely related to the DVB content or nominal crosslink ratio. Swelling creates space or 'solvent porosity' within the resin and allows ready access by small molecules to the polymer network. The swelling process itself occurs largely 'from the outside to the interior' and this behaviour has been treated quantitatively using the so-called 'shrinking core' model. In this the polymer network on the geometric exterior of resin beads becomes swollen first, forming an expanded pellicular layer and leaving a central unswollen glassy core. As time goes on the thickness of the swollen layer increases and the central core gradually shrinks and finally disappears (Fig. 11).

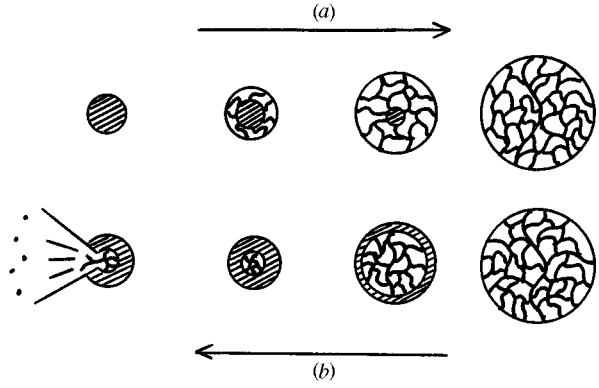

Fig. 11 Solvent response of gel-type resins: (*a*) shrinking glassy core to form an expanded gel in a good solvent; (*b*) contraction of swollen gel on addition to a bad solvent with bursting of resin due to osmotic shock.

Unlike linear polymers (see earlier) even a very 'good' solvent cannot make the individual polymer chains migrate apart because each chain is connected to at least one other by a crosslink—the polymer chains are part of a continuous infinite network. With a very 'good' solvent, the network will swell to its elastic limit, where further expansion is limited by the crosslinks. Note that no swelling occurs with 'bad' solvents for the network, and gel-type resins cannot be exploited in such solvents.

Providing the degree of crosslinking is low, sufficient swelling occurs in appropriate solvents to allow all the network to be penetrated and exploited in chemical reactions. The resultant resin particles, typically ~0.1-1 mm in diameter, have a molecular structure analogous to a ball of rubbery spaghetti, with all spaghetti strands interconnected and the network saturated with free flowing 'sauce'. Very low levels of crosslinker (< 1%) however yield mechanically weak swollen resin networks, easily damaged by shear. On the other hand, highly crosslinked gel-type resin networks, although mechanically stronger, may swell too little even in a very 'good' solvent to allow all the network to be penetrated and exploited.

If a gel-type resin is fully swollen in a 'good' solvent and then introduced into an excess of 'bad' solvent, the solvent types will exchange and the resin starts to shrink. This is the reverse of the swelling process, but again shrinking takes place 'from the outside to the interior'. This can cause very high levels of stress in the resin and if there are any microscopic flaws, *e.g.* cracks, the resin particles can fracture or burst (Fig. 11). The effect is known as osmotic shock, and gel-type resins are only useful if the matrix is able to undergo many cycles of swelling and deswelling without mechanical damage.

With regard to the stepwise synthesis of a complex structure on a gel-type resin, especially when the synthesis is performed under high load conditions (*i.e.* a large proportion of polymer segments are derivatised) it is important to realise that the swelling behaviour of the resin can change enormously as each modification to the resin is made. A very simple example is a chloromethylated polystyrene resin which is highly swollen in toluene and completely collapsed in water. On reaction with trimethylamine to form benzyltrimethylammonium chloride residues the resultant resin is collapsed in toluene yet swollen in water. Such dramatic changes can, for example, give rise to sudden attenuation of reaction and hence low conversion, or can result in the trapping of reagents or by-products. Careful assessment of such possibilities before reaction and an appropriate choice of a (compromise?) solvent or solvent mixtures can be invaluable.

Generally highly swollen gel-type resins are soft and compressible and this can restrict their use in packed columns, particularly on a large scale, when large back pressures can build-up as the resins particles compress into the restricted geometric shape available to them. Many of the above shortcomings can be overcome by the use of macroporous resins.

Macroporous resins

The term 'macroporous' resin is somewhat misleading because its use is not intended to convey anything about the size of pores in a resin. Instead the expression is used simply to indicate a class of resins which have a permanent well-developed porous structure even in the dry state.

If a suspension polymerisation of a styrene–DVB mixture is carried out with the comonomer mixture also containing an appropriate organic solvent (diluent or porogen) at some appropriate level then the internal structure (morphology) of the product resin beads can be very different to that of a gel-type resin. In particular, removal of the solvent or porogen at the end of the polymerisation can leave resin beads which are hard but opaque and with a rough surface which might be visible even with a good optical microscope (see right hand sample, Fig. 9). The polymer matrix is rather heterogeneous or non-uniform. Some areas consist of impenetrable crosslinked and entangled polymer chains, other areas are devoid of polymer. Most importantly, these materials can have much higher surface areas in the dry state (again measured by N_2 BET) than gel-type resins, typically ranging from ~50 to ~1000 $m^2\ g^{-1}$. Unlike gel-type resins these materials do not need to swell in a solvent to allow access to the interior because they possess a permanent porous structure, *i.e.* a permanent network of pores whose dimensions can be manipulated by the precise conditions used in polymerisation. Such materials are called 'macroporous' resins. Providing the surface of the pores is wetted with a compatible solvent, the pore structure can be accessed by essentially all solvents whether categorised as 'good' or 'bad', *e.g.* even water can penetrate macroporous styrene–DVB resins. When a 'good' solvent is contacted with a macroporous resin then as well as filling the pore volume, the solvent may also swell the polymer matrix (*i.e.* the microgel particles—see next section) to some extent. This swelling often occurs rather rapidly because the permanent pore structure gives rapid access to the solvent throughout the whole resin. The swelling (and deswelling) is not restricted in direction 'from the outside to the interior' as with gel-type resins, and no 'shrinking core' effect is manifest. Consequently macroporous resins show much better resistance to osmotic shock.

There is no universally accepted definition of a macroporous resin but in the case of styrene–DVB resins Millar *et al.*[27] suggested that 'The criterion of macroporosity … is that the uptake of cyclohexane in 16 h should not be less than 0.1 $m^2\ g^{-1}$ dry polymer' with cyclohexane falling into the category of a 'bad' solvent for this resin. Recently[28] Millar has suggested the use of *n*-heptane in place of cyclohexane since the latter has a low but finite tendency to sorb into styrene–DVB glassy matrices.

For many years there has been confusion in the literature over the terms 'macroreticular' resins and 'macroporous' resins. A recent patent settlement now allows a clearer definition: a macroreticular resin being one produced in a suspension copolymerisation in which the presence of an appropriate porogen or inert diluent at an appropriate level in the comonomer phase gives rise to phase separation or precipitation of the crosslinked polymer. The resultant isolated dried resin is permanently porous, *i.e.* macroporous, having been produced in this 'macroreticulation process'. The description therefore distinguishes these macroporous species from others where the porosity is created by a different mechanism, *e.g.* gas blowing. The term 'macroreticular' was coined by scientists from Rohm and Haas Co.,[29] although other groups were reporting similar resins around the same time.[27,28,30] In principle, in a suspension polymerisation it is possible to employ a porogen or inert diluent with an appropriate solubility parameter with a particular comonomer composition which does not induce phase separation, or to employ sufficiently low levels of porogen that phase separation does not occur.

Macroporous resins are therefore formed when a porogen is present in the comonomer mixture which causes phase separation of the polymer matrix. At full conversion each polymer bead is composed of a crosslinked polymer phase and a discrete porogen phase, the latter acting as a template for the permanent porous structure of the resin (Fig. 12). Removal of the porogen and drying yields rigid opaque permanently porous beads (see right hand sample, Fig. 9). The point at which phase separation occurs depends upon the nature of the porogen, its compatibility with the incipient polymer matrix and the level at which it is used. These are the key factors that control the fine detail of the resin porous morphology and are discussed in detail in the next section.

In practice the level of crosslinker employed also influences the onset of phase separation and for some commercially produced styrene–DVB resins, the DVB level is adjusted upwards such that even with toluene, a thermodynamically good solvent (for polystyrene) as a porogen, phase separation occurs eventually, since pure poly(DVB) is less compatible with toluene than is polystyrene itself. Thus a matrix prepared from ~25% DVB and ~75% styrene requires ~70% phase volume toluene for phase separation, whereas a mixture with ~80% DVB and ~20% styrene requires only ~30% phase volume of toluene for phase separation as a result of the reduced compatibility arising from the higher DVB level.[24]

It is also worth emphasising that gel-type resins can be made in the presence of a porogen providing the latter is present at a level which does not cause precipitation of the growing polymer. Generally this also requires a low level of crosslinking and the network is formed in a solvent expanded form relative to a normal gel-type species. Hence, for example, a resin prepared with ~5% DVB and ~95% styrene with ~65% phase volume of toluene shows very similar physical characteristics to a normal gel-type resin prepared with ~2% DVB and no toluene present.[31] To some extent therefore the presence of the solvating toluene compensates for the higher level of DVB.

Morphology generation and control

Within each comonomer droplet many polymer molecules begin to grow *via* free radical chain propagation, and indeed with a styrene–DVB mixture these start to crosslink. Initially microgelation occurs but eventually macrogelation of each droplet ensues. In the presence of a porogen sooner or later precipitation of the polymer occurs and this can be before or after macrogelation. Irrespective of this, eventually a well-developed system of microgel particles or microspheres can be detected within each resin bead. These are of approximate spherical symmetry since this represents the form of lowest surface energy. Thus macroporous resin beads (~50–500 μm diameter) are composed of a mass of microgel particles (typically ~1000 Å in diameter) and the molecular structure of an individual microgel particle is very similar to that of a whole gel-type resin bead. To a good approximation therefore a macroporous resin particle can be regarded as comprised of a mass of tiny gel-type particles between which is a complex pore structure or labyrinth of channels (Figs. 13 and 14). The microgel particles are referred to as the 'gel-phase' and the pore structure as the 'pore-phase'. In reality the manner in which the porous morphology develops is very complex, and indeed difficult to study. Further details are available in references 32 and 33, and the references cited therein.

From a practical point of view macroporous resins can be prepared with a wide range of porous structures. These can vary from species with rather low surface area (~50 $m^2\ g^{-1}$ determined by N_2 sorption and application of the BET theory) and a large proportion of macropores (IUPAC definition: micropores < 20 Å; mesopores 20–500 Å; macropores > 500 Å) to species with a very high surface area (~800 $m^2\ g^{-1}$) with a large proportion of micropores. Control of the fine detail of this morphology is exercised by choice of the nature and proportion of the porogen, and the level of crosslinker employed. In particular, controlling the point during polymerisation when phase separation of the polymer network occurs is crucial.

Thus, when a porogen with good compatibility with the polymer network is utilised the network remains fully solvated up to high conversion of monomers into polymer. When phase separation finally occurs the microgel particles are small and discrete, and are swollen with residual monomer and crosslinker. Likewise the separate porogen phase contains unreacted monomer and crosslinker. Further polymerisation in the porogen phase creates additional polymer which acts to fuse microgel particles together; however, relatively low levels of polymer are formed in this way since the conversion of monomer to polymer at the point of phase separation is already rather high. The microgel particles therefore tend to retain their

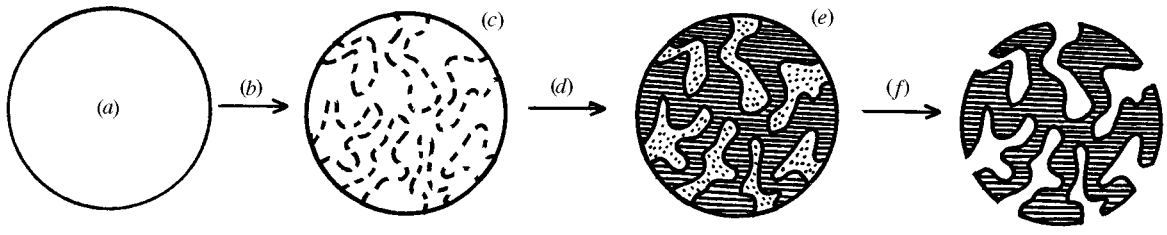

Fig. 12 Action of porogen in forming porous morphology in a macroporous resin: (*a*) monomer, crosslinker and porogen isotropic solution; (*b*) polymerisation; (*c*) polymer network forming; (*d*) porogen and network start to phase separate; (*e*) porogen phase acts as pore template; (*f*) porogen phase removed to yield pores (hatched area = crosslinked polymer; dots = porogen phase).

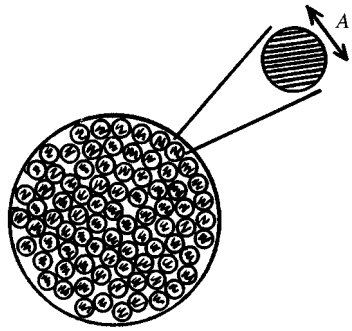

Fig. 13 Enlarged macroporous resin bead showing individual microgel particles (A = 1000 Å).

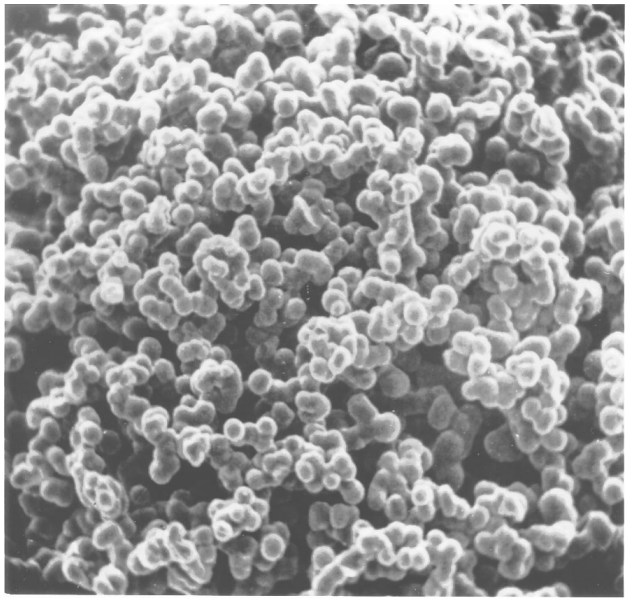

Fig. 14 Scanning electron micrograph of a macroporous resin fracture section (magnification = 5000×).

individual identity and the network of micro- and meso-pores, generated between the microgel particles when first formed, is essentially retained [Fig. 15(*a*)]. Such resins therefore have high

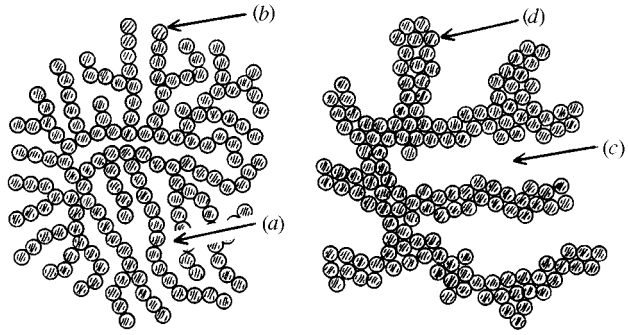

Fig. 15 Connectivity of microgel particles showing formation of small pores (*a*) from a network of interconnecting individual microgel particles (*b*) and large pores (*c*) from a network of fused or aggregated microgel particles (*d*).

surface area and a pore size distribution with a maximum in the micropore/mesopore region. Typically, for styrene–DVB mixtures, porogens such as toluene and xylene are useful in this respect but they must be used with relatively high levels of DVB (> 50%) in order to achieve satisfactory phase separation.

When a porogen is used which induces polymer network phase separation at much lower conversion, then again microgel particles are formed, now swollen with a high level of monomer and crosslinker, and likewise the separate porogen phase contains significant levels of monomer and crosslinker. A great deal more copolymer is therefore formed in the porogen phase after the phase separation process, and this has the effect not only of fusing the microgel particles together, but also causing significant in-filling of small pores between the microgel particles. In an extreme case the individual microgel particles can lose their identity and in scanning electron micrographs large fused *aggregates* of microgel particles can be seen interconnecting to form a labyrinth mainly of macropores, all the micropores having long since been in-filled [Fig. 15(*b*)]. Typically, for styrene–DVB mixtures porogens such as aliphatic hydrocarbons or higher alcohols (*e.g.* 2-ethylhexanol) are useful in this context. Phase separation of styrene-based networks with formation of stable microgel particles occurs readily even with DVB levels down to ~12% and resins are formed with a surface area typically ~50 $m^2 g^{-1}$ and a pore size distribution skewed towards the macropore region. Note that generally the total pore volume is controlled largely by the amount of porogen employed and is less influenced by the nature of the porogen.

Appearance of resin beads

Dry gel-type resin beads appear clear and transparent (or translucent) because the system is an amorphous glassy solid with no discontinuities to allow interaction with visible light and hence scattering and opacity. Various mechanisms can arise giving rise to light scattering. However, for strong scattering some particulate or porous structure is required where the discontinuous features of differing refractive indices have dimensions similar to the dimensions of the wavelength of visible light. The arrays of aggregated microgel particles described above generally are of this size and so macroporous resins prepared with thermodynamically bad porogens are particularly opaque. The microgel particles themselves are usually individually much smaller than the wavelength of light, and so cannot scatter strongly by this mechanism. They can scatter by a less efficient process and so those macroporous species with microgel particles which retain substantially their individual identify (*i.e.* those formed with good porogens and not aggregated) are often less opaque and can even be quite translucent. Depending on the refractive index of the solvent employed all macroporous resins tend to become much less opaque when imbibed with solvent.

Morphology diagram

Putting all the available experimental data together it is possible to generate an idealised morphology or pseudo-phase diagram[27,28,33] defining resin systems in terms of the morphology anticipated from a given type and level of porogen, coupled with the level of crosslinker (Fig. 16). This has been developed for styrene–DVB resins but extensive data now exists for methacrylate resins crosslinked with trimethylolpropane trimethacrylate, and a similar treatment seems possible for this system as well.[34,35] In any event the principles embodied here are more widely applicable. Compositions of polymerising mixtures falling within the macroporous domain yield porous resins whereas those compositions outside this domain yield essentially gel-type or related resins. Thus, for a DVB content of X%, porogen levels below A% do not cause phase separation of the polymer matrix and the network formed is a lightly solvated gel-type which collapses to form a glassy amorphous gel-type resin on drying. For porogen levels between A and B%, phase separation of the polymer network does occur and the dried resins are macroporous types. The total pore volume of the resins increase in going from A to B% and phase separation occurs more quickly as the porogen content increases from A%. The surface area of the so-formed resin therefore falls while the

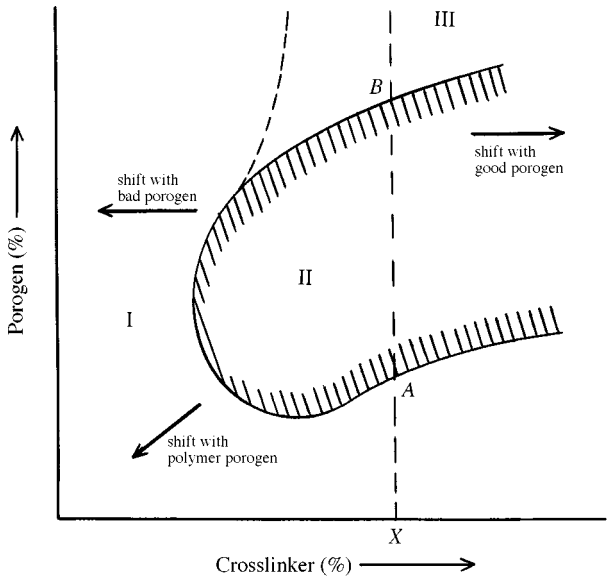

Fig. 16 Resin pseudo-phase diagram: I = gel-type resins; II = macroporous resins; III = microgel powder.

average pore diameter rises. On approaching *B*% porogen the total concentration of polymer formed can become too low for stable beads to be formed (*i.e.* the microgel particles are not well-fused) and above *B*% porogen the microgel particles appear as a fine powder.

Those porogens falling into the category of thermodynamically good solvents push the macroporous domain towards higher crosslink ratios, whereas thermodynamically poor porogens shift the macroporous domain to lower crosslink ratios. A rather interesting and much less studied class of porogens are oligomers or polymers.[28,33] Different polymer types tend to be very incompatible and so rather low levels of a polymer can be employed as a porogen to induce phase separation in polymerisation, with or without a solvent coporogen. The overall trend is to cause phase separation at much lower levels of porogen and at much lower levels of crosslinker. In addition, polymeric porogens tend to create large pores in keeping with the idea that earlier phase separation allows more aggregation of microgel particles and in-filling of small pores.

Bearing in mind that the quantity of initiator, polymerisation temperature and degree of agitation are additional variables that can influence morphology generation, albeit in a less dramatic manner, it is quite clear that these systems are very complex in physico-chemical terms. Not surprisingly therefore the boundary between the formation of a macroporous and an essentially gel-type resin is by no means as sharp as that indicated in Fig. 16. A particularly intriguing regime for styrene–DVB resins is that ~7–12% DVB. Within this range there are polymerisation compositions that can be employed which generate a well-defined macroporous morphology, but the latter is apparently lost on removal of the porogen phase, *i.e.* the pore structure collapses (reversibly) resulting in the formation of a clear glassy amorphous bead.[26,36–38] However, these species are not conventional gel-types since on addition of a suitable solvent the resin re-swells *and* reforms its macroporous morphology. The transparent glassy beads can indeed swell and become opaque, depending on the refractive index of the solvent used. Whether such resins fold and collapse on drying, and the extent to which the pore structure is lost, depends also on the solvent from which drying is undertaken. Though superficially such resins seem to embody the weaknesses of both gel-types and macroporous species, they do offer macroporous morphologies in the swollen state with rather low levels of crosslinker in the microgel particles, and there are applications where this might be a significant advantage.

Composite resin supports

With regard to performing stepwise synthesis of oligopeptides on a support, Merrifield[39] and others settled for very simple gel-type lightly crosslinked polystyrene–DVB beads as optimum. Later, Atherton and Sheppard[40] introduced a more polar *N*,*N*-dimethylacrylamide-based resin, together with an orthogonal protecting group strategy, but again the resin was a gel-type. Rigid macroporous resin beads more suitable for automated use in packed columns, and having greater versatility in terms of use of solvents, gave problems associated with omission of peptide residues, and truncation of peptide growth, probably arising from chemistry taking place in the heavily crosslinked microgel particles. In an attempt to overcome these difficulties two composite supports were developed and commercialised. One employs Kieselguhr as a rigid inorganic primary support, within which is deposited a soft highly swollen polyamide gel and upon which peptide synthesis is performed.[41] The other employs rigid particles of polystyrene in the form of a PolyHIPE®.[42] The latter is a low density (~0.1 g ml^{-1}) macrocellular (~5–10 μm cell diameter) material which allows incorporation of a high level of a soft highly swollen polyamide gel, again the locus for the assembly of peptides. The latter composite functions well in a packed column and offers loading capacities up to ~5 mmol g^{-1}.

More recently those involved in solid phase combinatorial synthesis[5] initiated their work using lightly crosslinked (0.5–2%) gel-type resins developed typically for use with peptide chemistry. These however have been quickly shown to have considerable limitations in terms of both the organic synthetic chemistry that can be carried out on them, and the maximum capacity available. A major limitation in terms of the chemistry is the range of solvents which are capable of swelling styrene–DVB gel-type resins, to the extent that reactions in aliphatic hydrocarbons, alcohols and water are not applicable. A major step forward in this context has been the polystyrene–poly(ethylene glycol) (PEG) composite resin beads developed by Bayer and Rapp[43,44] which form the basis of the TentaGel® range of supports available from Rapp Polymere (Tübingen, Germany) and known also as the 'Rapp resin'. These have a 1–2% crosslinked styrene–DVB resin as their basis, but grafted onto this are long PEG sidechains or 'tentacles' (Fig. 17), the

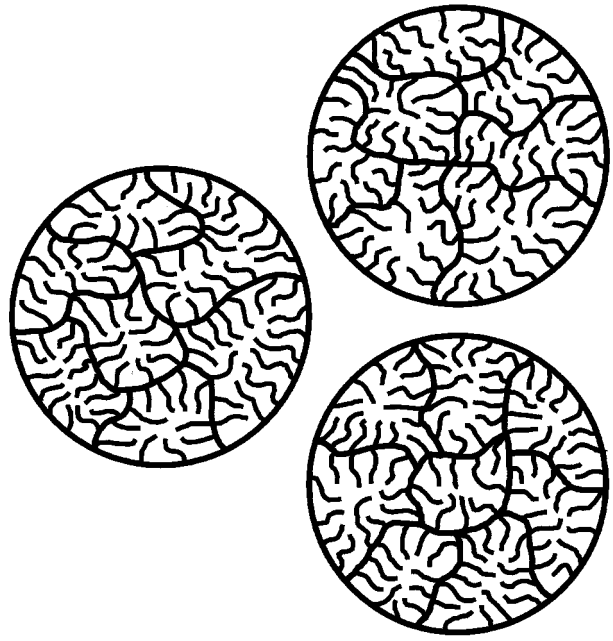

Fig. 17 Tentagel® or Rapp resin showing PEG chains grafted onto gel-type polystyrene–DVB resin; the PEG chains form separate microdomains.

free termini of which are the sites for solid phase synthesis.[45] The materials are unusual and very versatile because of the

broad solvent compatibility range they offer, and also for the high flexibility and accessibility of the functional endgroups. Typically these composites swell 2–4 times in water, alcohols and ether, and 5 times in CH_2Cl_2 and toluene. The PEG chains have a molecular weight of ~3000, and typically the composite comprises ~70 wt% PEG and ~30 wt% crosslinked poly(styrene–DVB).[43] Such high levels of PEG are needed to generate the advantageous broad solvation properties, and unfortunately brings with it some limitations. The composite can therefore be very sticky and difficult to dry; the capacity of the endgroups is necessarily low and so the synthetic capacity of the resin is likewise low. A specific chemical limitation is the benzyl ether linkage between the PEG chains and the polystyrene backbone which can be readily cleaved yielding PEG contamination of products. Some of these problems have been addressed by second generation analogues produced in the USA;[46] in particular it is claimed that the capacity has been improved, and the cleavage problem much reduced. The simple model that synthesis occurs on a long PEG spacer arm from polystyrene is too naive. Undoubtedly in polymer physical chemistry terms these composites represent microphase-separated systems (Fig. 17) in which solid phase synthesis occurs in the microdomains of PEG rather than polystyrene, and both the solvation effects in synthesis and the gel-phase ^{13}C NMR spectroscopy of bound species tend to confirm this.[47]

Thermo-oxidatively stable supports

Polymer supports based on vinyl-type monomers (styrene, methacrylates and acrylamides) have found wide applicability, but a serious limitation is their restricted thermo-oxidative stability. Typically the maximum temperature at which these supports can be operated continuously is currently ~120 °C, although under highly reductive conditions more extreme regimes may be tolerable. Many potentially useful hydrocarbon oxidation catalysts function optimally at higher temperatures under highly oxidative conditions, and there is therefore an opportunity for the development and exploitation of much more thermally stable polymer supports than those routinely available. In this context the use of polyacrylonitrile, polyamides, polysulfones, polyaniline and polysiloxanes has been reported, but these materials have not been produced in the spherical porous particulate form so useful for application in both batch and continuous catalytic processes.

Recently the preparation of spherical particulate forms of polybenzimidazoles,[48] polyimides[49] and polysiloxanes[50] have been reported, and their successful exploitation as supports for alkene transition metal complex oxidation catalysts demonstrated.[51,52] In each case paraffin oil is used as the continuous medium within which droplets of the appropriate polymerisation phase are dispersed using the principles of suspension polymerisation.

For polybenzimidazole (PBI) it is necessary to condense an aromatic tetraamine with an aromatic dicarboxylic acid (Scheme 1) usually in the presence of polyphosphoric acid at ~250 °C.[48] The reaction is difficult to control and reproduce in the laboratory, but samples are now available from a commercial source.[53] Typically the surface area of the dry beads is rather low (~10 $m^2\ g^{-1}$) but remarkably they will sorb ~1 ml of toluene per gram of resin to allow catalyst preparation and exploitation.

The polyimide (PI) species are prepared by condensation of an aromatic dianhydride and an aromatic diamine in a two step process (Scheme 2). Initially polyamide formation occurs at ambient temperature in a solvent such as dimethylacetamide, then imidisation can be induced very conveniently by treatment with acetic anhydride and pyridine at ~65 °C. This dispersion polycondensation *is* conveniently carried out in the laboratory, and functional groups can be introduced by utilising appropriately derivatised diamines into the polymerisation. Using

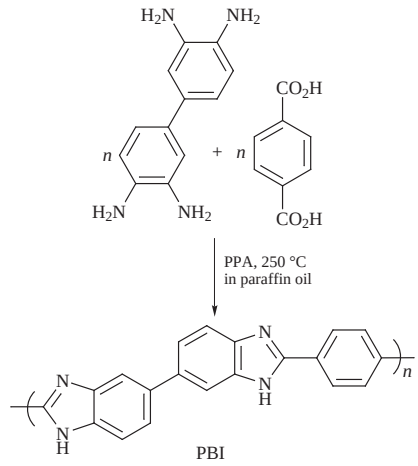

Scheme 1

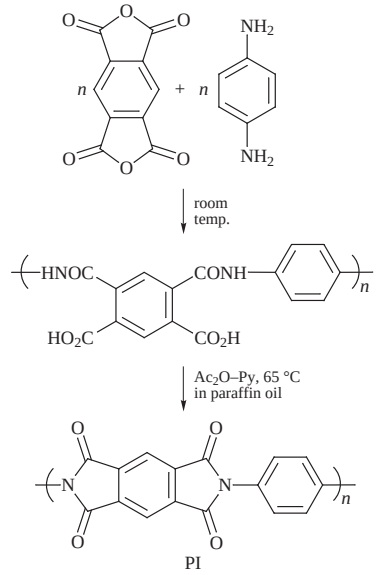

Scheme 2

also a tetraamine as a crosslinker some of the methodology of macroporous resin preparation has been exploited to prepare species with surface area up to ~80 $m^2\ g^{-1}$.[49]

Most recently a similar dispersion methodology has been exploited in producing spherical particulate polysiloxanes.[50] Typically an oligomeric silanol is dispersed with a tetraalkoxysilane and a Sn^{II} catalyst (Scheme 3) in paraffin oil, and the

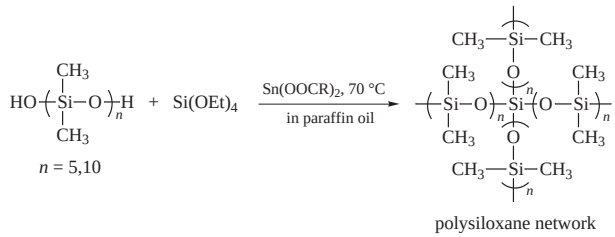

Scheme 3

polycondensation performed at ~70 °C. The highly elastomeric spherical particulate products are most unusual, have essentially no surface area in the dry state, but swell readily in non-polar solvents. While their potential for exploitation is still being explored, the value of PBI and PI particulates as metal complex catalyst supports has already been well-demonstrated. In particular, PBI has been shown to offer highly active, long-lived

and thermo-oxidatively stable Mo-based alkene epoxidation catalysts, perhaps limited only by cost factors. Overall however all of these support species live up to expectation in terms of their thermo-oxidative stability, with thermogravimetric analytical data typically showing little evidence for decomposition in these resins in air below 400 °C.

Technological prospects for polymer supports in synthesis

The two main areas where technological application already exists, and further growth will undoubtedly occur, are polymer-supported catalysts and solid phase combinatorial synthesis and related methodologies. Polystyrene sulfonic acid resins are important industrial catalysts,[1,2] and polymer-supported transition metal complex catalysts are poised to make an important contribution in both the commodity chemicals and speciality fields. A partially Pd^{2+}-exchanged sulfonic acid resin is already used in the B.P. Chemicals Etherol Process[54] in which a mixed C_4 alkane/alkene/diene feedstream is converted in the presence of H_2 and methanol into a mixture of alkanes and branched ethers for direct use in the blending of unleaded petrol. A recently announced methanol carbonylation technology for the production of acetic acid utilises a poly(4-vinylpyridine) resin to immobilise the active Rh catalyst.[55] If ultimately commercialised this will add considerable impetus to the further use of polymer-supported metal complex catalysts. Until recently most polymer-heterogenised versions of asymmetric catalysts have performed rather poorly and, in particular, have given levels of asymmetric induction significantly lower than their homogeneous counterparts.[9,10] We have, however, developed an insoluble branched poly(tartrate ester)[56] with technological potential, since this acts as a very efficient heterogeneous asymmetric ligand in the Sharpless epoxidation of allylic alcohols using $Ti(OR)_4$–*tert*-butylhydroperoxide. Seebach *et al.*[6] have also reported the synthesis of a number of polymer-supported TADDOL ligands and use of these to generate, for example, asymmetric Ti-based Lewis acids. The latter have been shown to function as enantioselective reagents and catalysts in a number of reactions with, in many instances, activity and selectivity very comparable to their homogeneous analogues. Recently also we have developed a number of polymer-supported analogues of Jacobsen's asymmetric alkene epoxidation catalyst with emphasis on ensuring site isolation of the catalyst and pendant attachment of the chiral salen ligand.[57] Scheme 4 shows a typical route we have adopted and in this case the steps in the synthesis can be monitored qualitatively by the obvious colour changes that occur in the resin at each stage (**1**, white; **2**, cream; **3**, pale pink; **4**, sandy yellow; **5** orange; **6**, yellow; **7**, yellow; **8** dark red-brown).‡ The resin catalyst performance compares favourably with the soluble catalyst but is very substrate dependent.

In solid phase combinatorial chemistry primarily gel-type resins have been used as the support, based on experience from solid phase peptide synthesis. However, the more diverse chemistry that must be achieved on supports nowadays is encouraging the use of a broader range of resin morphological variants, and commercial sources of these are becoming available.[46,58]

Automation is also a key factor in combinatorial synthetic methodology, and so scope exists for ingenious development of supports with novel formats to facilitate automation. In this context there is the important concept of inverting the whole solid phase strategy, and carrying out all the combinatorial assembly in solution, by employing an array of supported reagents, catalysts and protecting groups (inverse solid phase combinatorial synthesis). This approach overcomes the major weakness of the normal solid phase method, *i.e.* the limitation in achieving precise molecular structural characterisation at each step of a synthesis. Though magic angle spinning ^{13}C and ^{1}H

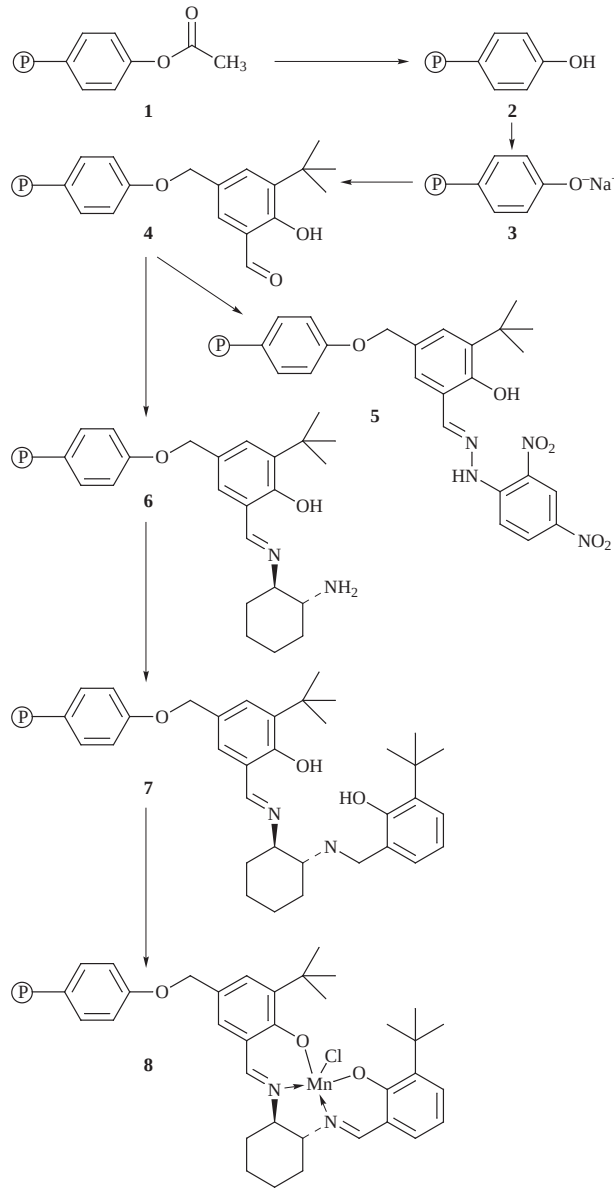

Scheme 4

gel-phase NMR[16] and single bead FTIR, Raman and mass spectral techniques have impinged significantly on this problem, very often the analytical capability still falls far short of that which is achievable with soluble molecules. Interestingly therefore the areas of (inverse) solid phase combinatorial synthesis and polymer-supported catalysts and reagents seem destined to converge and there may be much to be gained by practitioners combing the early literature in this area.[59,60]

Whenever separation problems arise in synthesis, polymer-supported species may have something very positive to offer. These need not involve complex species, *e.g.* poly(4-vinylpyridine)-based resins are useful scavengers of HCl and can avoid the need for aqueous/organic liquid-liquid extractions. The resin is also readily regenerated with aqueous NaOH. At the other extreme, if there is a requirement to trap a particular metal ion from a mixture of ions, then synthesis of a selective chelating ion exchange resin may provide the way forward. A number of groups are also synthesising small libraries of compounds for various applications, and then using a resin-bound specific binding group to 'fish-out' any compound showing a particularly high binding constant.

Not always obvious to the bench/batch chemist are the processing and operational advantages that supported systems can offer. Indeed the option to operate a process under particularly favourably physico-chemical conditions, not acces-

sible when using soluble catalysts, may prove an important driver in the successful application of supported systems. Interestingly, detecting such advantages is not always readily possible until industrial process conditions are probed. So, for those of us committed to this area, a further period of patience and dedication may be required but there is no doubt that the future for polymer-supported synthesis has never been so optimistic.

Acknowledgements

The author acknowledges the skills and efforts of his co-workers over many years that have helped develop the insight expressed in this article. He is also grateful to a number of industry-based colleagues: Dr R. L. Albright (ex Rohm and Haas); Dr J. R. Millar (ex Permutit) and Dr J. Dale (Purolite) for furthering his knowledge of the area.

Notes and references

† E-mail: m.p.a.smith@strath.ac.uk

‡ A photograph of the samples is available on the RSC's web server, http://www.rsc.org/suppdata/cc/1988/2275/, and also forms part of the cover picture of this journal issue.

1 D. C. Sherrington, in *Polymer-supported Reactions in Organic Synthesis*, ed. P. Hodge and D. C. Sherrington, Wiley, Chichester, UK, 1980, ch. 3, p. 157 and references cited therein.
2 H. Widdecke, in *Synthesis and Separations Using Functional Polymers*, ed. D. C. Sherrington and P. Hodge, Wiley, Chichester, UK, 1988, ch. 4, p. 149 and references cited therein.
3 R. B. Merrifield, *J. Am. Chem. Soc.*, 1963, **85**, 2149.
4 F. Balkenhopl, C. von dem Bussche-Hünnefeld, A. Lansky and C. Zechel, *Angew. Chem., Int. Edn., Engl.*, 1996, **35**, 2288.
5 *Combinatorial Peptide and Non-peptide Libraries*, ed. G. Jung, VCH, Weinheim, Germany, 1996.
6 D. Seebach, R. E. Marti and T. Hintermann, *Helv. Chim. Acta*, 1996, **79**, 1710.
7 B. Hinzen and S. V. Ley, *J. Chem.Soc., Perkin Trans. 1*, 1997, 1907; 1988, 1.
8 P. Hodge, *Chem. Soc. Rev.*, 1997, **26**, 417.
9 S. J. Shuttleworth, S. M. Allin and P. K. Sharma, *Synthesis*, 1997, 1217.
10 C. Bolm and A. Gerlach, *Eur. Org. Chem.*, 1998, 21.
11 M. Kurata and Y. Tsunashima, in *Polymer Handbook*, ed. J. Brandrup and E. H. Immergut, Wiley, New York, 3rd edn., 1989, section VII, p. 38.
12 J. F. Rudd, see ref. 11, section V, p. 81.
13 R. A. Orwoll, see ref. 11, section VII, p. 526.
14 D. J. Gravert and K. D. Janda, *Chem. Rev.*, 1997, **97**, 489.
15 H. C. Henderson, D. C. Sherrington and A. Gough, *Polymer*, 1994, **35**, 2867.
16 R. V. Law and D. C. Sherrington, in *Solid State NMR of Polymers*, ed. I. Ando and T. Asakura, Elsevier, The Netherlands, 1998, ch. 15, p. 509.
17 P. Hodge, see ref. 2, ch. 2, p. 43.
18 P. H. H. Hermkens, H. C. J. Ottenheijm and D. Rees, *Tetrahedron*, 1996, **52**, 4527.
19 R. Z. Greenley, see ref. 11, section II, p. 153.
20 M. P. Stevens, *Polymer Chemistry—An Introduction*, 2nd edn., Oxford University Press, Oxford, UK, 1990, ch. 6, p. 221.
21 W. T. Ford, in *Polymeric Reagents and Catalysts*, ed. W. T. Ford, *ACS Symp. Ser.* No. 308, Washington DC, 1986, ch. 11, p. 155.
22 R. V. Law, D. C. Sherrington and C. E. Snape, *Macromolecules*, 1997, **30**, 2868.
23 R. V. Law, D. C. Sherrington, C. E. Snape, I. Ando and H. Korosu, *Ind. Eng. Chem. Res.*, 1995, **35**, 2740.
24 R. L. Albright, personal communication.
25 D. C. Sherrington, see ref. 1, Appendix, p. 469.
26 E. A. Gulke, in *Encyclopedia of Polymer Science and Engineering*, ed. H.F. Mark, N. M. Bikales, C. G. Overberger, G. Menges and J. I. Kroschivitz, 2nd edn., Wiley, New York, vol. 16, 1989, p. 443.
27 J. R. Millar, D. G. Smith, W. E. Marr and T. R. E. Kressman, *J. Chem. Soc.*, 1996, 218.
28 I. M. Abrams and J. R. Millar, *React. Funct. Polym.*, 1997, **35**, 7.
29 R. Kunin, E. Meitzner and N. Bortnick, *J. Am. Chem. Soc.*, 1962, **84**, 305; K. A. Kun and R. Kurin, *J. Polym. Sci., Polym. Lett.*, 1964, **2**, 587; K. A. Kun and R. Kunin, *J. Polym. Sci., Pt I*, 1968, **6**, 2689.
30 J. R. Millar, D. G. Smith and T. R. E. Kressman, *J. Chem. Soc.*, 1965, 304.
31 M. Morrison and D. C. Sherrington, unpublished results.
32 R. L. Albright, *React. Polym.*, 1986, **4**, 155.
33 A. Guyot, see ref. 2, ch. 1, p. 1.
34 J. E. Rosenberg and P. Flodin, *Macromolecules*, 1986, **19**, 1543; 1987, **20**, 1518; 1987, **20**, 1522; A. Schmid and P. Flodin, *Makromol. Chem.*, 1992, **193**, 1579.
35 P. D. Verweij and D. C. Sherrington, *J. Mater. Chem.*, 1991, **1**, 371.
36 J. Gimenez, J. Costa and S. Cervera-March, *Appl. Catal.*, 1987, **31**, 221.
37 Z. Prokop and K. Setinek, *Collect. Czech. Chem. Commun.*, 1974, **79**, 1256.
38 W. Neier, in *Ion Exchange Technology*, ed. D. Naden and M. Streat, Ellis Horwood, Chichester, UK, 1984, p. 361.
39 R. B. Merrifield, *Life During a Golden Age of Peptide Chemistry*, ACS, Washington DC, USA, 1993.
40 E. Atherton and R. C. Sheppard, *Peptides 1974*, ed. Y. Wolman, Halsted Press, NY, 1975, p. 123.
41 E. Atherton, R. C. Sheppard and A. J. Rosevar, *J. Chem. Soc., Chem. Commun.*, 1981, 1151.
42 P. W. Small and D. C. Sherrington, *J. Chem. Soc., Chem. Commun.*, 1989, 1589.
43 E. Bayer, *Angew. Chem., Int. Ed. Engl.*, 1991, **30**, 113.
44 E. Bayer and W. Rapp, GP DE-A3714258 (1988).
45 W. Rapp, see ref. 5, p. 425.
46 Argonaut Technologies Inc., San Carlos, CA 94070, USA - ArgoGel® and ArgoPore® Resins.
47 E. Bayer, K. Albert, H. Willisch, W. Rapp and B. Hemmasi, *Macromolecules*, 1990, **23**, 1937.
48 T. Brock and D. C. Sherrington, *Polymer*, 1992, **33**, 1773.
49 T. Brock, D. C. Sherrington and J. Swindell, *J. Mater. Chem.*, 1994, **4**, 229.
50 K. Alder and D. C. Sherrington, *J. Chem. Soc., Chem. Commun.*, 1998, 131.
51 D. C. Sherrington and M. Miller, *J. Chem. Soc., Perkin Trans. 2*, 1994, 2091.
52 J.-H. Ahn and D. C. Sherrington, *J. Chem. Soc., Chem. Commun.*, 1996, 643; *Macromolecules*, 1996, **29**, 4164.
53 Hoechst-Celanese PBI Aurorez Microporous Beads, Charlotte, NC 28232-2414, USA.
54 B.P. Etherol Process—see *New Catalyst Resins and their Applications*, ed. W. Strüver and R. Wagner, Bayer AG, D-5090 Leverkusen, Germany.
55 See announcement by UOP and Chiyoda, *Eur. Chem. News*, 1997, 26 May–1 June, p. 25.
56 L. Canali, J. K. Kaarjalainen, O. E. O. Hormi and D. C. Sherrington, *J. Chem. Soc., Chem. Commun.*, 1997, 123; J. K. Kaarjalainen, O. E. O. Hormi and D. C. Sherrington, *Tetrahedron: Asymmetry.*, 1998, **9**, 1563.
57 L. Canali, H. Deleuze and D. C. Sherrington, *React. Funct. Polym.*, 1998, in the press; L. Canali, Ph.D. Thesis, University of Strathclyde, Glasgow, 1998, in preparation.
58 Polymer Laboratories Ltd., Church Stretton, SY6 6AX, UK; PL-CMS Resins.
59 A. Akelah and D. C. Sherrington, *Chem. Rev.*, 1981, **81**, 557; *Polymer*, 1983, **24**, 1369.
60 D. C. Bailey and S. H. Langer, *Chem. Rev.*, 1981, **81**, 109.

Paper 8/03757D

ChemComm

Nanoporous silica from amphiphilic block copolymer (ABC) aggregates: control over correlation and architecture of cylindrical pores

Christine G. Göltner,* Beate Berton, Eckart Krämer and Markus Antonietti

Max-Planck-Institute of Colloids and Interfaces, Kantstr. 55, 14513 Teltow/Seehof, Germany.
E-mail: goeltner@mpikg-teltow.mpg.de

Received (in Bath, UK) 20th August 1998, Accepted 9th September 1998

Novel nonionic ABCs are shown to be versatile templates for the sol–gel synthesis of nanoporous silicas, the structure can be fine-tuned by varying the template concentration.

Amphiphilic block copolymers (ABCs), consisting of one hydrophilic and one hydrophobic block, are gaining increasing importance as structure-directing agents in the synthesis of nanoporous ceramic oxides.[1,2] When mixed with water, these polymers undergo aggregation into lyotropic liquid crystalline phases, which are stable over a wide range of composition and temperature. These self-organizing systems, although not mechanically robust in their own right, are well suited as nanotemplates to imprint structure and porosity onto an otherwise dense and amorphous material, such as sol–gel-derived silica.[3–6] ABC templates help to extend the boundaries for pore size, wall thickness and mechanical strength beyond those of previously known nanoporous ceramic oxides.[7,8]

Cylindrical pores represent the closest approximation of one-dimensional cavities, which are of growing importance for a number of topochemical or spectroscopic applications and the generation of anisotropic nanostructured materials. The latter has been elegantly demonstrated by preparing monodisperse carbon nanotubules within nanopores of alumina.[9] Ordered nanoporous arrays were also utilized as tubular membrane separation devices.[10] There is a demand to increase the density of cylindrical pores to a filling factor (*i.e.* volume fraction of the voids) of 0.7 in hexagonally ordered silica to make similar 'nanocapillary' reactors very efficient.

Existing templating routes towards hexagonal porous silica, however versatile they may be, produce defect sites, which are reflected in the physical properties or even reproduced in the secondary cast of the porous material. For example, ABC templates of the poly(butadiene-b-ethylene oxide) (PB–PEO) type were shown recently to be suitable templates for the generation of a rich variety of pore structures in silica.[11] Although these polymers show good solubility in water, their structural polymorphism in these mixtures is such that often wide biphasic ranges occur. This phenomenon increases the number of defect sites over the statistically determined measure.

Therefore, there is a demand for self-organizing templates with a more pronounced tendency to form well ordered phases, which possess a smaller number of defect sites. In this contribution, we present new low-cost, nonionic polymer templates which form superbly stable, homogeneous lyotropic liquid crystalline phases. Such nanocasting media facilitate the control over correlation and architecture by simply varying synthetic parameters during the templating procedure, as opposed to selecting from a library of ABCs.

The results demonstrate the great potential inherent in ABC nanocasting as the method of choice for pore design in ceramic oxides. Poly[(ethylene-co-butylene)-b-(ethylene oxide)] (KLE-3729 and KLE-3736, see Table 1) were obtained from Th. Goldschmidt AG, Essen, Germany, and freeze-dried prior to use.

TMOS was obtained from Aldrich and used as received. HCl (1 M solution from Aldrich) was diluted using distilled water. Sol–gel synthesis of silica in the presence of ABC templates has been described in detail elsewhere.[1] Typically, the ABC (30, 50 or 70 mass% with respect to water) was dissolved in 2 g TMOS before adding 1 g of hydrochloric acid (pH 2). After the hydrolysis had abated, the flask was evacuated for 5–10 min in order to remove methanol, formed during the hydrolysis of TMOS. The birefringent, viscous mixture was then left to polycondense in an open container at 60 °C. The resulting inorganic–organic hybrid materials were calcined at 500 °C (12 h under nitrogen, 16 h under oxygen).

The birefringence of the lyotropic phases was studied between crossed polarizers of an Orthoplan-Pol microscope (Leitz) equipped with a hotstage. Nitrogen sorption measurements were recorded on a Micromeritics Gemini surface analyzer. The sample morphologies were studied with a Zeiss DSM 940 scanning electron microscope operating at an acceleration voltage of 20 kV. Standard TEM investigations were carried out on ground samples. TEM pictures were recorded with a Zeiss EM 912 Omega TEM operating at an acceleration voltage of 120 kV. Optical textures of the ABCs in water revealed that both polymers presented here form lyotropic liquid crystalline phases between 15 and 85% (m/m). Both ABCs show lyotropic phases of normal topology only, as expected from the length ratios of the blocks. This was confirmed by the water-miscibility of the polymer–water phases at all compositions within the phase diagrams.

Sol–gel synthesis of silica in the lyotropic phases of KLEs resulted in homogeneous hybrid materials, which showed no indication of phase separation, as estabished by SEM analysis. The silica monoliths were calcined to completely remove the template.

At low polymer concentrations, casts of spatially non-correlated, cylindrical micelles with low degree of intermicellar order are observed [Fig. 1(a)]. At higher concentrations (50%), these cylinders are closely packed into hexagonal arrays [Fig. 1(b)]. Further increasing the template concentration causes the formation of a lamellar/vesicular structure [Fig. 1(c)], which collapses upon calcination. The deterioration of the lamellar/vesicular structure is expected, as calcination removes the 'scaffolding' ABC template, which keeps individual lamellae apart.

The nitrogen adsorption–desorption isotherms show pronounced hysteresis, making the determination of the pore size distribution by non-imaging methods unreliable. However, the transition from the cylindrical morphologies into a lamellar structure is manifested in the different shape of the nitrogen adsorption-desorption isotherm, with the lamellar sample

Table 1 Physical data of the amphiphilic block copolymers used as templates

ABC	M_n	M_w/M_n	N_A[a]	N_B[a]	Block ratio
KLE-3729	6.6	1.069	68	66	1 : 1
KLE-3736	7.3	1.103	68	82	1 : 1.2

[a] Number of repeat units.

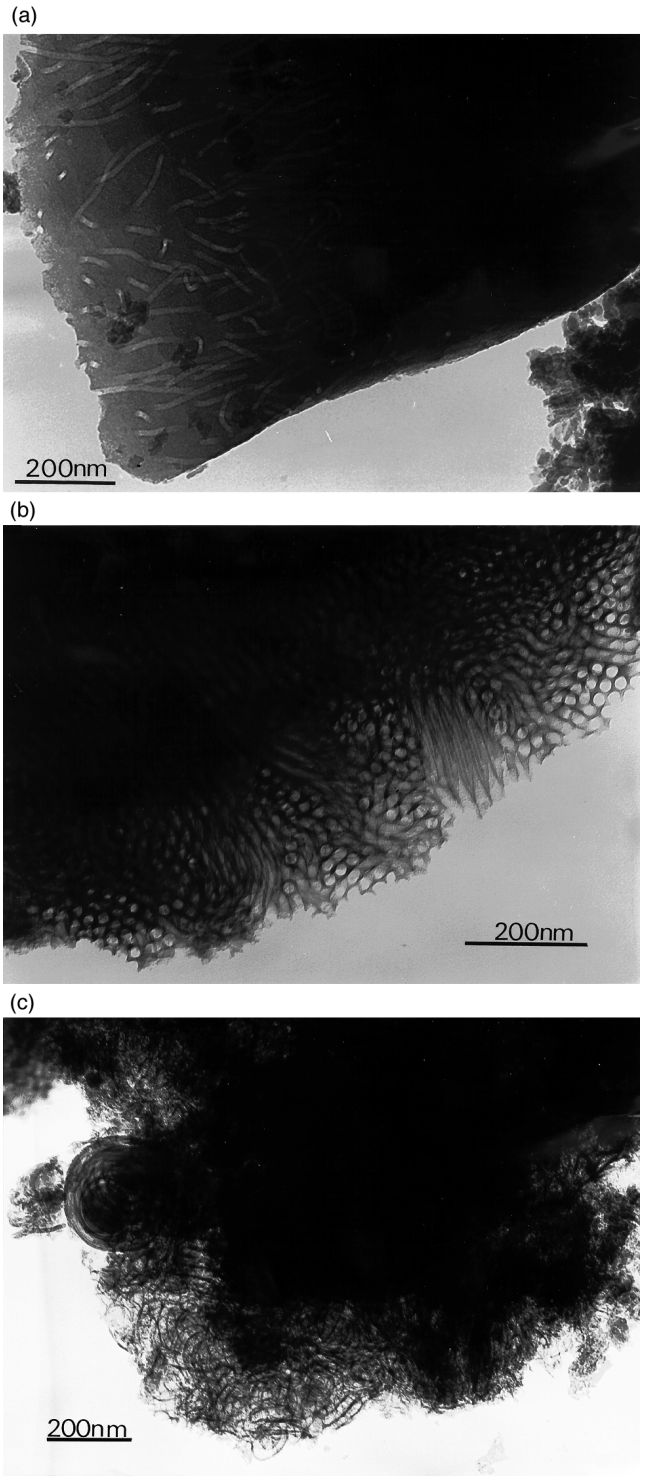

Fig. 1 TEM micrographs of KLE-3729-templated silicas: (a) 30% template (m/m with respect to water): isolated cylinders (diameter 14 nm) display no spatial order with respect to each other and are separated by up to 50 nm thick walls; (b) 50% template: hexagonally packed cylinders (diameter 16 nm, wall thickness 7 nm), (c) 70% template collapsed lamellae and multilamellar vesicles.

lacking distinctive pore condensation. For the cylindrical systems, the specific surface area increases with increasing

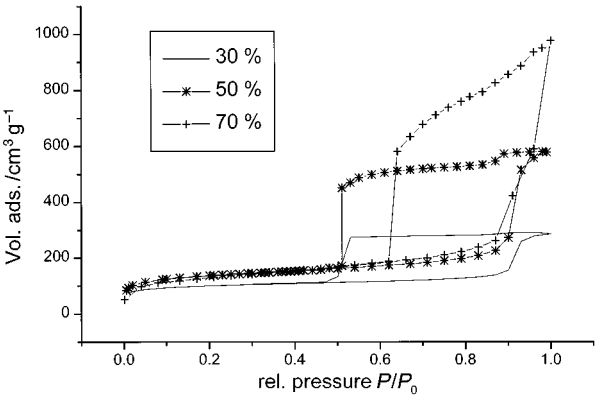

Fig. 2 Nitrogen adsorption–desorption isotherms of KLE-3729-templated silicas depending on the template content: 30% and 50%: typical isotherms showing pore condensation with pronounced hysteresis; 70%: the lamellar/vesicular structure, which is partially collapsed, expectedly does not show distinct pore condensation in the mesopore regime.

template content, demonstrating the contribution of each individual ABC molecule to the overall interface area (Fig. 2).

Amphiphilic block copolymers of the KLE type have proven to be exceptionally well suited for the synthesis of nanoporous silica with cylindrical pore shape. The pore density can be controlled *via* the template content between 30 and 50%. Traversing this concentration regime, isolated cylindrical pores with low spatial correlation evolve into correlated ones with high degree of packing order. Adjusting the pore density and thus the packing order of the cylindrical pores allows control over the pore curvature, as the packing into an hexagonal array automatically goes along with a considerable straightening. Future work will focus on the synthesis of curved and straight nanowires with high aspect ratios. For this purpose, KLE-templated silicas appear to be the most promising candidates presently available.

The authors would like to thank R. Pitschke for graphical work, Th. Goldschmidt AG for generously providing the KLE-type ABCs, the Max-Planck Society and the Deutsche Forschungsgesellschaft (Sfb 1623) for financial support.

Notes and references

1 C. G. Göltner, S. Henke, M. C. Weißenberger and M. Antonietti, *Angew. Chem., Int. Ed. Engl.*, 1998, **37**, 613.
2 D. Zhao, Q. Huo, J. Feng, B. F. Chmelka and G. D. Stucky, *J. Am. Chem. Soc.*, 1998, **120**, 6024.
3 M. C. Weißenberger and C. G. Göltner, *Ber. Bunsen-ges. Phys. Chem.*, 1997, **101**, 1679.
4 E. Krämer, S. Förster, C. Göltner and M. Antonietti, *Langmuir*, 1998, **14**, 2027.
5 G. S. Attard, J. C. Glyde and C. G. Göltner, *Nature*, 1995, **378**, 366.
6 G. S. Attard, M. Edgar and C. G. Göltner, *Acta Mater.*, 1998, **46**, 751.
7 C. G. Göltner and M. Antonietti, *Adv. Mater.*, 1998, **9**, 431.
8 G. D. Stucky *et al.*, *Elsevier Stud. Surf. Sci. Catal.*, 1998, **117**, 1.
9 J. C.Hulteen, J. Jirage and C. R. Martin, *Nature*, 1998, **393**, 346.
10 K. B. Jirage, J. C. Hulteen and C. R. Martin, *Science*, 1997, **278**, 655.
11 C. G. Göltner, B. Berton, E. Krämer and M. Antonietti, *Adv. Mater.*, submitted.

Communication 8/06701E

Synthesis and structure of a novel pentacoordinate organogermanium compound

Yoshito Takeuchi,*[a] Katsumi Tanaka,[a] Keiko Tanaka,[b] Mayumi Ohnishi-Kameyama,[c] Alajos Kálmán[d] and László Párkányi[d]

[a] *Department of Chemistry, Faculty of Science, Kanagawa University, 2946 Tsuchiya, Hiratsuka-shi, Japan 259-1293. E-mail: yoshito@info.kanagawa-u.ac.jp*
[b] *Department of Health Sciences, Kyorin University, 467 Miyashita, Hachioji-sh, Tokyo, Japan, 192-8508*
[c] *Ministry of Agriculture, Forestry and Fisheries, National Food Research Institute, 2-1-2 Kannondai, Tsukuba-shi, Ibaraki, Japan, 305-8642*
[d] *Institute of Chemistry, Chemical Research Center, Hungarian Academy of Sciences, H-1525-Budapest, PO Box 17, Hungary*

Received (in Cambridge, UK) 21st July 1998, Accepted 10th September 1998

Reaction between Bu^tGeCl_3 and mercaptoacetic acid afforded a novel type of pentacoordinate germanium compound *via* $Bu^tGe(SCH_2CO_2H)_3$ which loses one mole of SCH_2CO_2H to afford the pentacoordinate species.

Hypercoordination of organosilicon compounds has been extensively investigated by Corriu and coworkers.[1] Thus, they described a variety of penta-, hexa- or hepta-coordinate silicon compounds where in most cases the donor is a nitrogen moiety (*e.g.* dimethylamino), and the geometrical relation between the silicon and the donor is more or less sterically congested as is the case with 1,8-disubstituted naphthalenes **1**[2] or *o*-substituted tribenzylsilanes **2**.[3,4] They have shown that hypercoordination was also observed for *o*-substituted tribenzylgermanes **3**. We recently reported that, in the related compounds **4** and **5**, the germanium atom is either hexa- or hepta-coordinate although the incipient bonding between germanium and oxygen or sulfur is not very strong.[5]

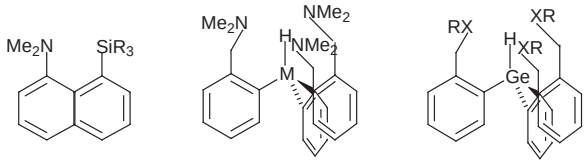

1 **2** M = Si, **3** M = Ge, **4** X = O, **5** X = S

These findings prompted us to examine a further possibility; *i.e.* to observe hypercoordination of germanium atom where the geometrical relation between germanium and the donor atoms is more flexible. Initially we expected that the reaction of *tert*-butyltrichlorgermane (Bu^tGeCl_3) with mercaptoactetic acid ($HSCH_2CO_2H$) (molar ratio 1 : 3) under basic conditions would afford 2,2′,2″-[*tert*-butylgermanetriyltris(thio)]trisacetic acid, $Bu^tGe(SCH_2CO_2H)_3$ which would form heptacoordinate germanium species **6**.

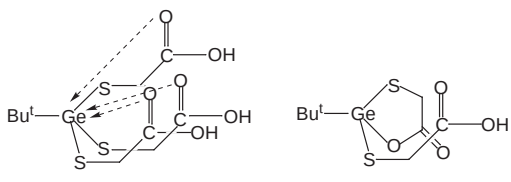

6 **7**

The product, (colorless crystals, mp 152–154 °C from ethyl acetate) corresponds, however, to the molecular formula $C_8H_{14}GeO_4S_2$ [mass spectrum (FBMS): *m*/*z* = 310.9630 $(M + H)^+$; calc. for $C_8H_{14}{}^{72}GeO_4S_2$ = 310.9633], indicating the loss of one mole of $HSCH_2CO_2H$. The product was confirmed by X-ray analysis† as 2-(2-*tert*-butyl-5-oxo-1,3,2-oxathiagermolan-2-ylthio)acetic acid **7**. It is likely that **6** was indeed formed since its yield was substantially decreased when lower amounts (*e.g.* 1 : 2) of mercaptoacetic acid were used. Subsequently an intramolecular nucleophilic substitution takes place on germanium, where one of the $-SCH_2CO_2H$ moieties of **6** acts as a nucleophile while the other is the leaving group to give **7**.

The ORTEP drawing of **7** is shown in Fig. 1, while the molecular packing in crystal is depicted in Fig. 2. The question

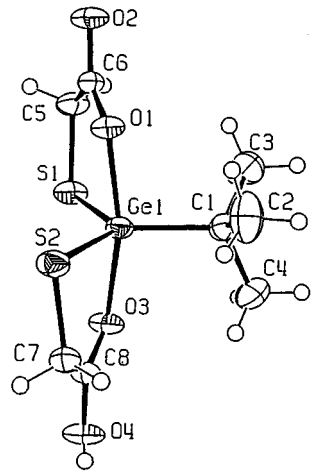

Fig. 1 Molecular structure of **7** showing the atomic labeling. Relevant bond lengths (Å) and angles (°): Ge–C1 1.989(2), Ge–O1 2.045(1), Ge–O3 2.043(1), Ge–S2 2.2143(5), Ge–S1 2.2191(5), S1–C5 1.808(2), S2–C7 1.810(2), O1–C6 1.258(2), O2–C6 1.265(2), O3–C8 1.259(2), O4–C8 1.262(2); C1–Ge–O3 98.89(6), C1–Ge–O1 94.39(6), O3–Ge–O1 166.71(5), C1–Ge–S2 119.73(5), O3–Ge1–S2 86.73(4), O1–Ge1–S2 86.91(4), C1–Ge1–S1 120.05(5), O3–Ge1–S1 86.25(4), O1–Ge1–S1 86.88(4), S2–Ge1–S1 120.19(2), C5–S1–Ge1 97.97(6), C7–S2–Ge1 96.46(6).

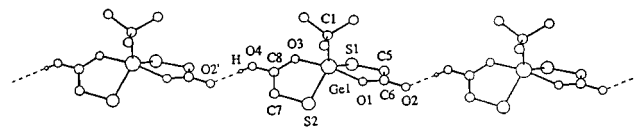

Fig. 2 Molecular packing of **7**. Intermolecular hydrogen bonds are shown by dotted lines. Important distances (Å) and angle (°): O4–H 0.74, H–O2′ 1.73, O4–O2′ 2.453(2); O4–H–O2′ 165.9.

of whether the carbonyl oxygen or the hydroxyl oxygen is coordinated to Ge was resolved by the location of the hydrogen atom which was achieved by refining the analysis.‡ The result shown in Fig. 2 is very conclusive; there is a hydrogen atom between O4 of one molecule and O2 of the adjacent molecule (O2′) to indicate hydrogen bonding in **7** between the CO_2H of one molecule and the lactone carbonyl oxygen of an adjacent molecule. Thus it is the carbonyl oxygen which was coordinated to Ge.

Characteristic points observed for **7** are as follows: (1) The germanium atom is pentacoordinate with trigonal bipyramidal structure. (2) The Ge1–S1, Ge1–S2 and Ge1–C1 bonds are equatorial while the Ge1–O1 and Ge1–O3 bonds are apical with equal length (*ca*. 2.04 Å, a little longer than the standard Ge–O covalent bond length (*ca*. 1.7–1.8 Å). (3) Four atoms, Ge1, S1, S2 and C1 are coplanar with S1, S2 and C1 in a trigonal planar arrangement around Ge. (4) The O1–Ge1–O3 hypercoordinate bond is nearly perpendicular to the S1–S2–C1 plane though the angle (166.7°) slightly deviates from the ideal trigonal bipyramidal structure.

In the case of pentacoordination of group 14 elements, deviation from the ideal trigonal bipyramidal structure is often observed. Thus, Corriu and coworkers[6] reported that the C–Si···N angle of a pentacoordinate compound, 1-(8-dimethylamino)naphthylphenylsilane, is 166.9°.

Altogether it is clear that we obtained a pentacoordinate organogermanium compound where no steric enforcement is involved to enhance the hypercoordination. It should be noted that rotation about the S–CH_2 bond, which should be feasible, would move the CO_2H group far apart from germanium. This in turn appears to suggest that the Ge–O interaction is strong enough to lead to hypercoordination. It should be noted that the solid state, trigonal bipyramidal structure of **7** can be regarded as a model for the intermediate of the S_N2 type reaction on germanium.

The ^1H and ^{13}C NMR spectra of **7** exhibit only one signal for both CH_2 protons and carbonyl carbon nuclei. This can be interpreted only if we assume a rapid equilibrium between two identical pentacoordinate species in solution as indicated below.

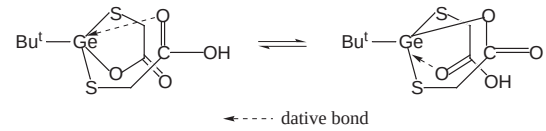

Notes and references

† *Crystal data* for **7**: recrystallized from AcOEt, $C_8H_{14}GeO_4S_2$, M = 310.90, monoclinic, space group *Cc*, a = 7.542(1), b = 18.100(2) c = 9.543(1) Å, β = 111.08(1)°, U = 1215.5(2) Å^3, Z = 4, T = 233 K, D_c = 1.699 Mg m^{-3}, μ = 2.855 mm^{-1}, 9790 reflectons with 2.25 ⩽ θ ⩽ 43.50° were collected on a four-circle diffractometer using graphite-monochromated Mo-Kα radiation. The structure was solved using SHELXS-97 (G. M. Sheldrick, Program for Crystal Strucure Solution, University of Göttingen, Germany, 1997) and refined using SHELXL-97 (G. M. Sheldrick, Program for Crystal Strucure Solution, University of Göttingen, Germany, 1997). $R1$ = 0.034, $wR2$ = 0.0671. CCDC 182/1009

‡ Hydrogen atomic positions were calculated from assumed geometries except H4O that was located in a difference map. Hydrogen atoms were included in structure factor calculations but were not refined. The isotropic displacement parameters of the hydrogen atoms were approximated from the U_{eq} value of the atoms they were bonded to.

1 C. Chuit, R. J. P. Corriu, C. Reyé, and J. C. Young, *Chem. Rev.*, 1993, **93**, 1371.
2 R. J. P. Corriu, M. Nazhar, M. Poirier and G. Royo, *J. Organomet. Chem.*, 1986, **306**, C5.
3 C. Brelière, F. Carré, R. J. P. Corriu and G. Royo, *Organometallics*, 1988, **7**, 1006.
4 C. Brelière, F. Carré, R. J. P. Corriu, G. Royo, M. W. C. Man and J. Lappasset, *Organometallics*, 1984, **13**, 307.
5 Y. Takeuchi, H. Yamamoto, K. Tanaka, K. Ogawa, J. Harada, T. Iwamoto and H. Yuge, *Tetrahedron*, 1998, **54**, 9811.
6 C. Brelière, F. Carré, R. J. P. Corriu, M.. Poirier and G. Royo, *Organometallics*, 1986, **8**, 388.

Communication 8/05709E

A long-lived ^{2}E state for a Cr(III)N_6 amine chromophore at 298 K: [Cr(*fac*-Me_5-D_{3h}tricosaneN_6)]Cl_3†

Kylie N. Brown,[a] Rodney J. Geue,[a] Grainne Moran,[b] Stephen F. Ralph,[c] Hans Riesen[d] and Alan M. Sargeson*[a]

[a] *Research School of Chemistry and the Chemistry Department, Faculty of Science, The Australian National University, Canberra, ACT, 0200, Australia. E-mail: sargeson@rsc.anu.edu.au*
[b] *School of Chemistry, The University of New South Wales, NSW 2052, Australia*
[c] *Department of Chemistry, The University of Wollongong, Northfields Ave, Wollongong, NSW, 2522, Australia*
[d] *School of Chemistry, University College, The University of New South Wales, Australian Defence Force Academy, Canberra ACT 2600, Australia*

Received (in Cambridge, UK) 11th August 1998, Accepted 15th September 1998

The ^{2}E state lifetime of the C_3 ion [Cr(*fac*-Me_5-D_{3h}tricosaneN_6)]$^{3+}$ is 235 μs in H_2O and 1.5 ms in D_2O at 298 K, the longest lifetimes yet reported for a saturated Cr(III)N_6 chromophore at room temperature.

The Cr(III) sarN_6 cage complexes (example shown in **I**) feature surprisingly short ^{2}E lifetimes at 298 K (< 10 ns)[1,2] in comparison with that of the parent [Cr$(NH_3)_6$]$^{3+}$ ion (2.2 μs at 293 K).[3] In contrast, the larger [Cr(*fac*-Me_5-D_{3h}tricosaneN_6)]$^{3+}$ complex (**II**) has a considerably longer ^{2}E lifetime of 235 μs in aqueous solution at the same temperature. This latter complex was obtained recently from the reaction of [Cr$(py)_3Cl_3$] and the free Me_5-tricosaneN_6 ligand in the presence of zinc dust under anaerobic conditions and was characterised by microanalysis, X-ray crystallography, electrochemistry and electronic spectroscopy.[4–6]

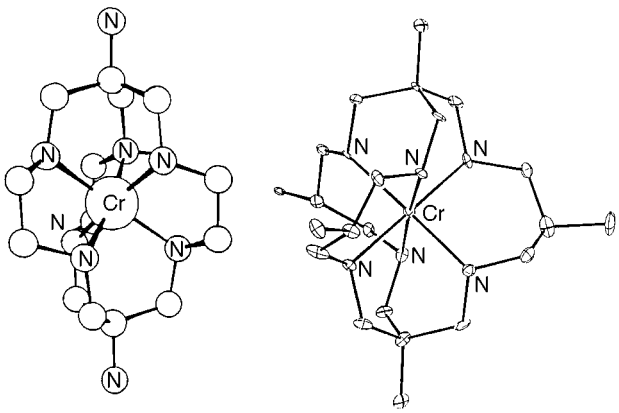

I **II**

Cooling the [Cr(*fac*-Me_5-D_{3h}tricosaneN_6)]$^{3+}$ ion to 77 K merely doubles the ^{2}E lifetime (to 440 μs) and deuteration of the secondary amines extends it to 1.5 ms at 298 K. In contrast, the ^{2}E lifetime for the [Cr(sar)]$^{3+}$ ion increases by ⩾ 10^4-fold upon cooling to 77 K (Fig. 1), to 60 μs, a value consistent with those for a range of related Cr(III) hexaamine complexes.[1,2] Why these apparently similar cage complexes have markedly different photophysical properties needs to be explored.

The rate of excited state relaxation is determined by radiative and non-radiative processes. In the latter instance, electronic energy is dissipated into vibrational energy of the chromophore or the solvent molecules. Photochemical processes such as bond dissociation and redox processes can also contribute to the decay. The Cr(III) cage complexes **I** and **II** have no discernible photochemical ligand dissociation from either the ^{2}E or $^4T_2$ states, unlike the parent [Cr$(NH_3)_6$]$^{3+}$ ion and related di-, tri- and multi-dentate Cr(III)N_6 complexes.[1–4,6–9] It should also be noted that a proposed associative pathway[9–11] is unlikely since the steric constraints of the cage complexes hinder the coordination of a seventh donor group.[1,2] There is also no redox quenching in the presence of a reductant,[4] so it is unlikely that such a process contributes significantly to the ^{2}E decay rate. Back intersystem crossing ($^2E \rightarrow {}^4T_2$) can sometimes provide a deactivation route for Cr(III) complexes; however, the $^4T_2$ state is *ca.* 7000 cm^{-1} higher in energy than the ^{2}E state for both cage complexes. This energy gap is similar to that of other Cr(III) hexaamine complexes where back intersystem crossing has been considered negligible.[8,12–15]

The ^{2}E lifetimes of most saturated amine Cr(III)N_6 complexes lie in the range 60–440 μs in the temperature-independent regime[1,2,8,9,13,15–18] and quantum efficiencies for the luminescence are *ca.* 1%.[1,13,15–17,19] The relaxation rate is thus dominated by non-radiative deactivation, a multiphonon process and as such, strongly dependent on the energy of vibrations accessible in ground and excited states (accepting and promoting modes, respectively). High energy acceptors include N–H stretching modes in this instance and the ^{2}E lifetime dependence on the number of N–H modes in the first coordination sphere has been addressed for a range of Cr(III)N_6 complexes.[17,20] Although deuteration of the coordinated amines increases the lifetime for both cage complexes roughly tenfold at 77 K, the N–H acceptors alone do not account for their very different temperature dependences.

The promoting modes couple the excited state and the ground state and modify the electronic gap by their frequency.[13,21] The population of promoting modes can lead to a strong temperature dependence of the ^{2}E lifetime. In particular, the rapid decrease in the ^{2}E lifetimes from 150 to 200 K for the Cr(III) sar complexes[2] indicates the existence of such an efficient

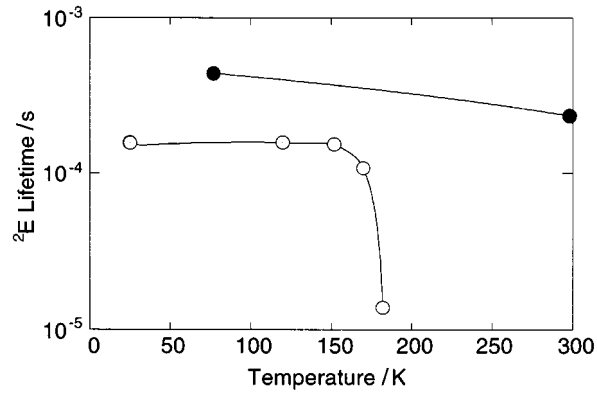

Fig. 1 Temperature dependences of the ^{2}E lifetimes for [Cr(*fac*-Me_5-D_{3h}tricosaneN_6)]Cl_3 (●) and [Cr(sar)]Cl_3 (⊙) in ethylene glycol–water (2 : 1 and 1 : 1, respectively).

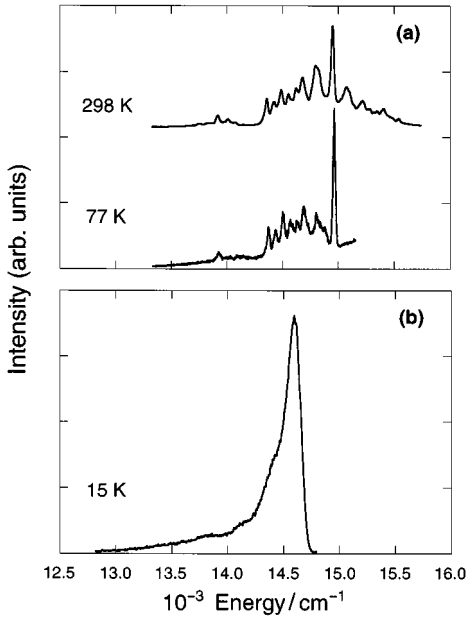

Fig. 2 Emission spectra of (a) [Cr(*fac*-Me_5-D_{3h}tricosaneN_6)]Cl_3 at 298 and 77 K (2 : 1 ethylene glycol–water) and (b) [Cr(sar)]$(CF_3SO_3)_3$ at 15 K (2 : 1 ethylene glycol–water).

promoting mode which becomes thermally activated. In contrast, the lifetime of the [Cr(*fac*-Me_5-D_{3h}tricosaneN_6)]$^{3+}$ ion is decreased only slightly at 298 K, inferring that there is no corresponding and effective promoting mode for this complex.

The 0–0 transition is accompanied by relatively intense vibrational sidelines in the [Cr(*fac*-Me_5-D_{3h}tricosaneN_6)]$^{3+}$ spectrum, characteristic of magnetic dipole-allowed transitions [Fig. 2(a)]. In contrast, the 0–0 transition dominates the emission spectrum of the [Cr(sar)]$^{3+}$ ions [Fig. 2(b)] and the vibrational fine-structure is poorly resolved due to more pronounced inhomogeneous broadening.[22,23] As the N–H interactions for the two types of complexes with the surrounding matrix are likely to be similar, the magnitude of this broadening can be ascribed to the [Cr(sar)]$^{3+}$ ion existing in different conformations. The sar complexes are able to undergo conformational changes such as twisting the ligand caps to change the symmetry from C_3 to D_3. This movement is coupled to other conformational changes involving the alignment of the C–C bond of the ethylenediamine chelate strap with the C_3 axis. The C–C bond may be oblique (*ob*) or parallel (*lel*) to the C_3 axis, giving rise to ob_3, ob_2lel, $oblel_2$ or lel_3 conformations. The same conformational lability is anticipated in the ^{2}E state, since its electronic configuration and thus equilibrium geometry are similar to that of the ground state. The number of effective accepting modes is governed by symmetry and interconversion results in variations in microsymmetry about the Cr(III)N_6 chromophore which induces more accepting modes. It follows that the conformational changes may result in a promoting mode which can be thermally activated.

Conformer interconversion is rather more difficult for the [Cr(*fac*-Me_5-D_{3h}tricosaneN_6)]$^{3+}$ ion. Topological constraints require that cap twisting converts the six-membered chelate rings forming the straps from the stable chair to the less stable skew-boat conformations. The equatorial methyl groups are thereby driven to more axial and less stable positions. Both factors restrict the conformational changes. It is anticipated that the excited state complex also has the same conformational preference and conformational interconversion therefore would not act as a promoting mode in this case. This rigidity may account for the remarkably long ^{2}E state lifetime at 298 K, in contrast to those of the Cr(III) sar complexes. The greater inhomogeneous broadening in the emission spectra of the smaller cage complexes independently supports this argument.

Notes and references

† Abbreviated ligand names used in this paper: *fac*-Me_5-D_{3h}tricosaneN_6: *facial*-1,5,9,13,20-pentamethyl-3,7,11,15,18,22-hexaazabicyclo[7.7.7]tricosane; sar = sarcophagine: 3,6,10,13,16,19-hexaazabicyclo[6.6.6]icosane (see *J. Chem. Soc., Chem. Commun.*, 1994, 1513.

1 P. Comba, A. W. H. Mau and A. M. Sargeson, *J. Phys. Chem.*, 1985, **89**, 394.
2 P. Comba, I. I. Creaser, L. R. Gahan, J. M. Harrowfield, G. A. Lawrance, L. L. Martin, A. W. H. Mau, A. M. Sargeson, W. H. F. Sasse and M. R. Snow, *Inorg. Chem.*, 1986, **25**, 384, and references therein.
3 R. T. Walters and A. W. Adamson, *Acta. Chem. Scand., Sect. A*, 1979, **33**, 53.
4 K. N. Brown, Ph.D. Thesis, Australian National University, 1994.
5 K. N. Brown, D. C. R. Hockless, A. D. Rae, S. R. Ralph, R. J. Geue, A. M. Sargeson, B. Skelton and A. H. White, manuscript in preparation.
6 K. N. Brown, D. C. R. Hockless, S. F. Ralph, H. Riesen, R. Geue and A. M. Sargeson, manuscript in preparation.
7 A. D. Kirk, *Coord. Chem. Rev.*, 1981, **39**, 225, and references therein.
8 N. A. P. Kane-Maguire, K. C. Wallace and D. B. Miller, *Inorg. Chem.*, 1985, **24**, 597.
9 M. W. Perkovic, M. J. Heeg and J. F. Endicott, *Inorg. Chem.*, 1991, **30**, 3140 and references therein.
10 J. F. Endicott, *J. Chem. Ed.*, 1983, **60**, 824 and references therein.
11 J. F. Endicott, T. Ramasami, R. Tamilarasan, R. B. Lessard, C. K. Ryu and G. R. Brubaker, *Coord. Chem. Rev.* 1987, **77**, 1, and references therein.
12 L. S. Forster, *Adv. Photochem.*, 1991, **16**, 215, and references therein.
13 L. S. Forster, *Chem. Rev.*, 1990, **90**, 331, and references therein.
14 T. J. Kemp, *Prog. React. Kinet.*, 1980, **10**, 301 and references therein.
15 A. Ditze and F. Wasgestian, *Ber. Bunsenges. Phys. Chem.*, 1986, **90**, 111.
16 A. Ditze and F. Wasgestian, *J. Phys. Chem.*, 1985, **89**, 426.
17 K. Kühn, F. Wasgestian and H. Kupka, *J. Phys. Chem.*, 1981, **85**, 665 and references therein.
18 P. V. Bernhardt, P. Comba, N. F. Curtis, T. W. Hambley, G. A. Lawrance, M. Maeder and A. Siriwardena, *Inorg. Chem.*, 1990, **29**, 3208 and references therein.
19 K. K. Chatterjee and L. S. Forster, *Spectrochim. Acta.*, 1964, **20**, 1603.
20 L. S. Forster and O. Mønsted, *J. Phys. Chem.*, 1986, **90**, 5131.
21 F. K. Fong, *Theory of Molecular Relaxation. Applications in Chemistry and Biology*, Wiley, New York, 1975.
22 *Topics in Applied Physics: Laser Spectroscopy of Solids*, ed. W. M. Yen and P. M. Selzer, Springer Verlag, New York, 1981, vol. 49 and references therein.
23 H. Riesen, K. N. Brown and A. M. Sargeson, manuscript in preparation.

Communication 8/06321D

$[Mo_9S_8O_{12}(OH)_8(H_2O)_2]^{2-}$: a novel polyoxothiomolybdate with a Mo^{VI} octahedron encapsulated in a reduced Mo^{V} cyclic octanuclear core

Anne Dolbecq, Emmanuel Cadot and Francis Sécheresse*

Institut Lavoisier, UMR C 173 du CNRS, Université de Versailles Saint Quentin, 45 Avenue des Etats Unis, 78035 Versailles, France. E-mail: secheres@chimie.uvsq.fr

Received (in Basel, Switzerland) 13th July 1998, Accepted 8th September 1998

The novel polyoxothioanion $[Mo_9S_8O_{12}(OH)_8(H_2O)_2]^{2-}$ was prepared from the acido-basic condensation of four $\{Mo^{V}_2S_2O_2\}$ building units around a central $\{Mo^{VI}O_6\}$ octahedron, the anion was characterized by X-ray diffraction as a tetramethylammonium salt.

The field of polyoxometalates, although explored for several years, still attracts significant attention,[1] because of its large number of potential applications, especially in the domain of heterogeneous catalysis.[2] We are currently interested in the synthesis of sulfur-containing polyoxoanions, a first step towards the design of sulfur-containing (possibly microporous) three dimensional frameworks. We thus developed a strategy based on the acido-basic condensation of the oxothio building block $\{Mo_2S_2O_2\}$. The efficiency of this method was recently[3] evidenced by the preparation of $[Mo_{12}S_{12}O_{12}(OH)_{12}(H_2O)_6]$, a cyclic oxothio compound prepared from the one-step self-condensation of $[Mo_2S_2O_2]^{2+}$. The condensation reaction was performed by controlled addition of potassium hydroxide to an acidic aqueous solution of the thiocation.† $[Mo_{12}S_{12}O_{12}(OH)_{12}(H_2O)_6]$ appeared to be a convenient starting material for further syntheses because of its ability to regenerate straightforwardly the $\{Mo_2S_2O_2\}$ unit either in acidic solution, as the $[Mo_2S_2O_2(H_2O)_6]^{2+}$ dithiocation,[3] or in basic solution. Indeed, there is strong evidence that $[Mo_{12}S_{12}O_{12}(OH)_{12}(H_2O)_6]$ hydrolyses, at pH > 11, into the dark red, air sensitive, $[Mo_2S_2O_2(OH)_4(H_2O)_2]^{2-}$ dianion.‡ In this way, the condensation of the $\{Mo_2S_2O_2\}$ building blocks occurs when the pH of the solution is lowered. Accordingly, in the absence of any other reactants, the cyclic compound $[Mo_{12}S_{12}O_{12}(OH)_{12}(H_2O)_6]$ is reformed, around pH = 1.5. This procedure is convenient when the reactants are unstable in acidic media; this is the case, for example, for MoO_4^{2-}, which can self condense to give various types of oxoanions.[4]

We thus report here the results of the reaction of MoO_4^{2-} with $[Mo_2S_2O_2(OH)_4(H_2O)_2]^{2-}$, at pH about 5. The synthesis§ is quite straightforward, starting from MoO_4^{2-} and a solution of the dianion. Four building units condense around the central $[MoO_4(H_2O)_2]^{2-}$ anion, which serves as a template, to form the novel polyoxothio anion $[Mo_9S_8O_{12}(OH)_8(H_2O)_2]^{2-}$. This compound has been fully characterized by IR spectroscopy, microanalysis and single crystal X-ray diffraction.¶

The molecular structure of the compound is shown in Fig. 1. The anion has crystallographically imposed inversion symmetry. It can be described as an eight-membered ring encapsulating an $Mo^{VI}O_6$ octahedron. As already observed[3] the $\{Mo_2S_2O_2\}$ unit has a strong tendency to form cyclic arrangements. This eight-membered ring compares well with the one obtained by the condensation of the oxo analog $[Mo_2O_4]^{2+}$ in the presence of oxalic acid.[5] The Mo^{V} atoms have a slightly distorted octahedral coordination: they are connected to a terminal oxygen atom, two hydroxo and two sulfido bridging ligands; the coordination sphere of the Mo centers is completed by a bridging oxygen bound to the central Mo^{VI} atom. The octahedra within the $\{Mo_2S_2O_2\}$ building blocks share edges but they are connected by faces as shown in Fig. 1. Short (*ca.* 2.8 Å) Mo–Mo distances characteristic of a single Mo^{V}–Mo^{V} bond alternate with longer (*ca.* 3.2 Å) Mo–Mo distances within the ring. The inner Mo^{VI} atom is disordered over four positions around the inversion centre, with a 25% occupancy,[6] this disordered Mo atom exhibits a distorted octahedral coordination [Mo–O distances from 1.745(7) to 2.391(7) Å]. In this mixed-valence compound, the electrons are thus strictly localized, as demonstrated by the absence of the blue colour characteristic of electron delocalization in the so-called 'molybdenum blue' species.[4,7]

In conclusion, the synthesis and isolation of the tetramethylammonium salt of the novel polyoxo anion $[Mo_9S_8O_{12}(OH)_8(H_2O)_2]^{2-}$ is straightforward, with a good yield, by simply mixing starting materials which are readily available. The complexity of the anions can be increased by replacing the central MoO_6^{2-} octahedron with a more sophisticated anionic template. The synthesis of $[Mo_9S_8O_{12}(OH)_8(H_2O)_2]^{2-}$ there-

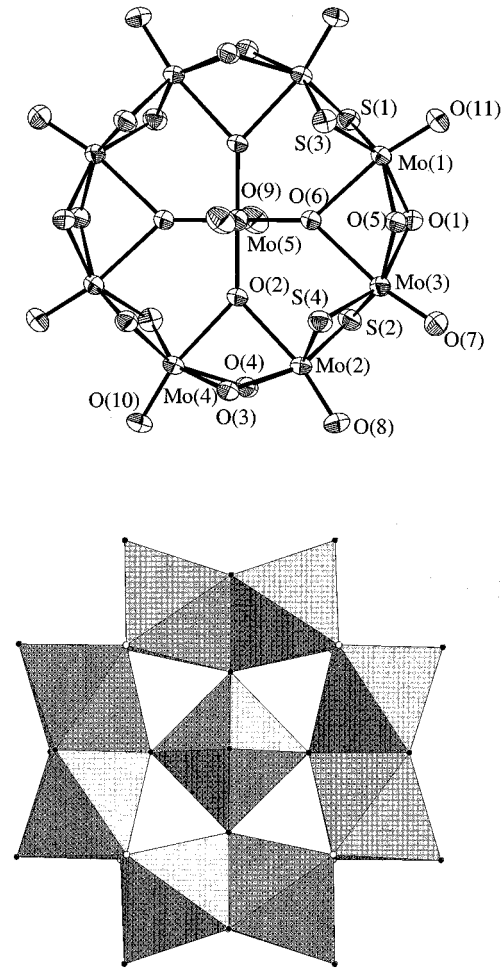

Fig. 1 Molecular structure of the polyoxothioanion $[Mo_9S_8O_{12}(OH)_8(H_2O)_2]^{2-}$. Top: ball-and stick model showing the eight-membered ring and the central $\{MoO_6\}$ octahedra. Thermal ellipsoids are drawn at the 50% probability level. For clarity, the disordered Mo(5) atom has been located at its mean position on the inversion centre, with a mean isotropic factor. Bottom: polyhedral representation showing the connectivity of the building blocks.

fore demonstrates that the acido-basic condensation of the $\{Mo_2S_2O_2\}$ fragments, either starting from an acidic solution or a basic solution, is a promising approach for the preparation of a variety of polyoxothio compounds.

Notes and references

† It should be noted that the crude product, obtained by the synthetic procedure described in ref. 3, before recrystallization has the composition $K_{2.6}(NMe_4)_{0.4}I_3[Mo_{12}S_{12}O_{12}(OH)_{12}(H_2O)_6]\cdot 30H_2O$ as shown by elemental microanalysis: Calc. (Found) C 0.62(1.23); I 12.31(12.13); K 3.29(3.27); Mo 37.23(36.71); N 0.18(0.40); S 12.42(12.72)%.

‡ $[Mo_2S_2O_2(OH)_4(H_2O)_2]^{2-}$ was precipitated as a potassium salt from a 1 M KOH solution, and isolated as a dark red powder. Elemental microanalysis confirmed the molecular formula $K_2[Mo_2S_2O_2(OH)_4(H_2O)_2]\cdot 13H_2O$: Calc. (Found) K 15.85(15.34); Mo 38.88(38.75); S 12.97(13.45)%.

§ As the intermediate $[Mo_2S_2O_2(OH)_4(H_2O)_2]^{2-}$ dianion is sensitive to air oxidation, the synthesis has to be carried out under a constant flow of N_2 gas. 20 ml of 1 M NaOH was first degassed for 10 min and 1 g (0.33 mmol) of $K_{2.6}(NMe_4)_{0.4}I_3[Mo_{12}S_{12}O_{12}(OH)_{12}(H_2O)_6]\cdot 30H_2O$ was added. The solution was stirred vigorously until the yellow powder dissolved to give a dark red solution of the $[Mo_2S_2O_2(OH)_4(H_2O)_2]^{2-}$ dianion. 0.16 g (0.66 mmol) of $Na_2MoO_4\cdot 2H_2O$ was then rapidly added and the pH was adjusted to 4.5 with a solution of 4 M HCl. The precipitation of the polyoxothio anion was achieved by the addition of 0.44 g (4.4 mmol) of $[NMe_4]Cl$ and gave 0.76 g of a thin yellow powder [yield = 86% (based on Mo)]. This powder was collected by filtration, washed with water and ethanol and dried with diethyl ether. IR spectra (KBr pellet, ν/cm^{-1}) gave absorptions at *ca.* 1480s, 1446w, 948s, 830m, 745m, 512s, 415w, 348w. Elemental microanalysis confirmed the molecular formula $[N(CH_3)_4]_2[Mo_9S_8O_{12}(OH)_8(H_2O)_2]\cdot 8H_2O$: Calc. (Found) C 5.46 (5.94); H 2.96 (2.79); Mo 49.09 (48.61); N 1.59 (1.61); S 14.55 (14.26)%. A few single crystals, suitable for X-ray diffraction, were grown in a solution containing only a small amount of tetramethylammonium cations.

¶ *X-Ray crystal structure analysis* for $[N(CH_3)_4]_2[Mo_9S_8O_{12}(OH)_8(H_2O)_2]\cdot 5H_2O$: Intensity data collection was carried out on a yellow crystal of 0.28 × 0.18 × 0.02 mm, with a Siemens SMART three-circle diffractometer equipped with a CCD bidimensional detector, using monochromatized λ(Mo-Kα) = 0.71073 Å. T = 293 K. The absorption correction was based on multiple and symmetry-equivalent reflections in the data set using the SADABS program[8] based on the method of Blessing.[9] *Crystal data* for $C_8H_{24}Mo_9N_2O_{27}S_8$: a = 15.0752(2), b = 12.9951(2), c = 12.6676(1) Å, β = 113.530(1)°, U = 2275.3(5) Å^3, Z = 2, M = 1700.22, D_c = 2.505 g cm^{-3}, monoclinic, space group $P2_1/c$ (no. 14), μ = 28.40 cm^{-1}, index ranges $-12 \leqslant h \leqslant 20$, $-17 \leqslant k \leqslant 17$, $-17 \leqslant l \leqslant 13$; total data 15389; unique data 5817 (R_{int} = 0.037), data with $I_o > 2\sigma(I_o)$ 4419. The structure was solved by direct methods and refined by full matrix least-squares, based on F^2, using the SHELX-TL software package.[10] All non-hydrogen atoms were refined anisotropically except for the disordered molybdenum atom and the water oxygen atoms. No. of variables, 242; final $R(F)$ = 0.040, $wR(F^2)$ = 0.098; GOF 1.08; minimum and maximum peak in difference electron density map −0.96 and 1.57 e Å^{-3}. CCDC 182/1006.

1 See for example the special issues on polyoxometalates of *Chem. Rev.* 1998, **98** and *C. R. Acad. Sci. Paris, Sér. IIc*, 1998.
2 (*a*) *Polyoxometalates: From Platonic Solids to Anti-Retroviral Activity*, ed. M.T. Pope and A. Müller, Kluwer, Dordrecht, 1994, p. 255; (*b*) Y. Yzumi and K. Urabe, *Chem. Lett*., 1981, 663; (*c*) M. Misono, *Catal. Rev. Sci. Eng*., 1987, **29**, 269.
3 E. Cadot, B. Salignac, S. Halut and F. Sécheresse, *Angew. Chem., Int. Ed. Engl.*, 1998, **37**, 611.
4 M. T. Pope, *Heteropoly and Isopoly Oxometalates*, Springer Verlag, New York, 1983.
5 Q. C. Chen, S . Liu and J. Zubieta, *Angew. Chem., Int. Ed. Engl.*, 1988, **27**, 1724.
6 We thank one of the referees for insightful comment on that matter.
7 A. Müller, J. Meyer, E. Krickemeyer and E. Diemann, *Angew. Chem., Int. Ed. Engl.*, 1996, **35**, 1206.
8 G. M. Sheldrick, SADABS, Program for scaling and correction of area detector data, University of Göttingen, Germany, 1997.
9 R. Blessing, *Acta Crystallogr., Sect. A*, 1995, **51**, 33.
10 G. M. Sheldrick, *Acta Crystallogr., Sect A*, 1990, **46**, 467; SHELX-TL version 5.03, Software Package for the Crystal Structure Determination, Siemens Analytical X-ray Instrument Division, Madison, WI, USA, 1994.

Communication 8/05453C

ChemComm

Phosphinocarboxylic acids as building blocks in organometallic crystal engineering. Self-organisation of one-dimensional photoluminescent cyclometallated platinum(II) polymeric structures

Man-Chung Tse, Kung-Kai Cheung, Michael C.-W. Chan and Chi-Ming Che*

Department of Chemistry, The University of Hong Kong, Pokfulam Road, Hong Kong. E-mail: cmche@hkucc.hku.hk

Received (in Cambridge, UK) 20th July 1998, Accepted 15th August 1998

Diphenylphosphinopropanoic acid (Ppa) is utilised for the self-organisation of a luminescent organoplatinum polymeric material, the crystal structure of which features intermolecular hydrogen bonding and π-stacking interactions.

Tertiary phosphines are versatile ligands in coordination and organometallic chemistry, but functional groups which are capable of complementary hydrogen bonding, such as carboxylic acids,[1] are rarely incorporated.[2] Molecular self-assembly employing hydrogen bonding has generated considerable interest in the domain of supramolecular chemistry and molecular recognition.[3] From an organometallic perspective,[4,5] the resultant materials have potential applications in non-linear optics, conductivity and ferromagnetism. The use of π–π stacking interactions in crystal engineering has also been prominent.[6] Their importance is further emphasised by their manifestation, in tandem with hydrogen bonding, in the structures of biological molecules such as DNA and proteins. Our earlier work on cyclometallated-(6-phenyl-2,2′-bipyridine) platinum(II) complexes revealed favourable π–π interactions in solid and solution states.[7] Herein, we describe the employment of diphenylphosphinopropanoic acid[8] (Ppa) as a building block in the supramolecular assembly of an organometallic polymer directed by π-stacking and hydrogen-bonding interactions.

Treatment of Pt(L)Cl [HL = 4-(*p*-tolyl)-6-phenyl-2,2′-bipyridine][7] with Ppa in CH_3CN–H_2O (1 : 1 v/v) at room temperature in the presence of excess NH_4PF_6 yielded [Pt(L)(Ppa)]PF_6 **1** as an orange crystalline solid in 75% yield.† Absorption bands at 1709 and 3448 cm^{-1} in the IR spectrum are assigned to ν(CO) and ν(OH) respectively of the Ppa ligand, while ^{195}Pt satellites (J_{PtP} 3943 Hz) are observed in the ^{31}P NMR spectrum.

The structure of **1** has been determined by X-ray crystallography (Fig. 1).‡ The tridentate cyclometallated ligand L and the phosphine are arranged in a distorted square-planar geometry about the platinum atom. The platinum–nitrogen bond length *trans* to the phenyl group [Pt(1)–N(1) 2.128(8) Å] is noticeably longer than that *trans* to the phosphine ligand [Pt(1)–N(2) 2.018(8) Å]; this is consistent with the greater *trans* influence exerted by the phenyl substituent. The crystal packing in **1** [Fig. 1(b)] reveals hydrogen bonding between two carboxylic acids in adjacent molecules, with clear directionality and short intermolecular contacts [2.65(1) Å] between successive oxygen atoms (O–H···O=C). π-Stacking between the aromatic planes of L (mean 3.68 Å) is more distant than that in [Pt(6-phenyl-2,2′-bipyridine)(PPh_3)]ClO_4 (mean 3.35 Å), although an identical 'head–tail' orientation of the overlapping ligands is evident in both structures.[7] Infinite one-dimensional polymeric zig-zag chains linked by alternating hydrogen-bonding and π–π

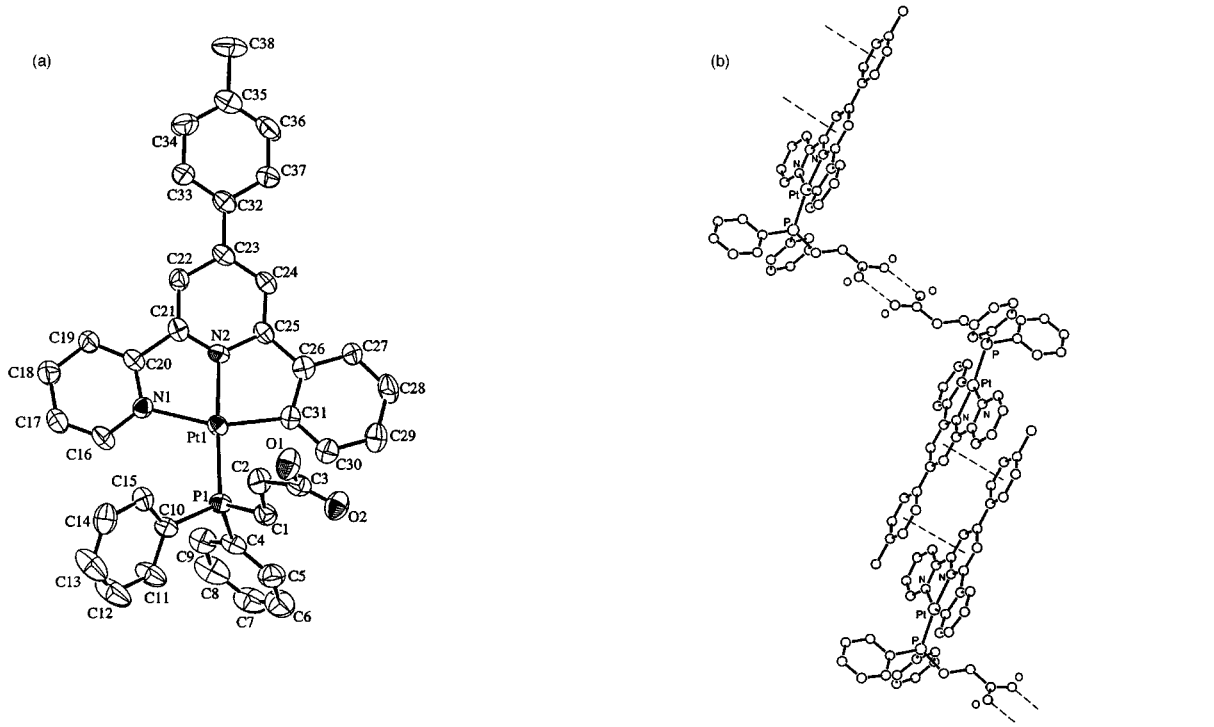

Fig. 1 (a) Perspective view of cation in **1** [40% thermal ellipsoids, all hydrogens are omitted including H(1) attached to O(1)]. Selected bond distances (Å) and angles (°): Pt(1)–P(1) 2.249(3), Pt(1)–N(1) 2.128(8), Pt(1)–N(2) 2.018(8), Pt(1)–C(31) 2.03(1), O(1)–C(3) 1.31(1), O(2)–C(3) 1.21(1), N(1)–Pt(1)–N(2) 76.7(3), N(1)–Pt(1)–C(31) 158.0(4), N(2)–Pt(1)–C(31) 82.1(4), P(1)–Pt(1)–N(2) 172.7(2), O(1)–C(3)–O(2) 124(1). (b) Crystal packing in **1**, showing infinite polymeric zig-zag chains linked by alternating hydrogen-bonding and π–π interactions (anion and all hydrogens are omitted for clarity).

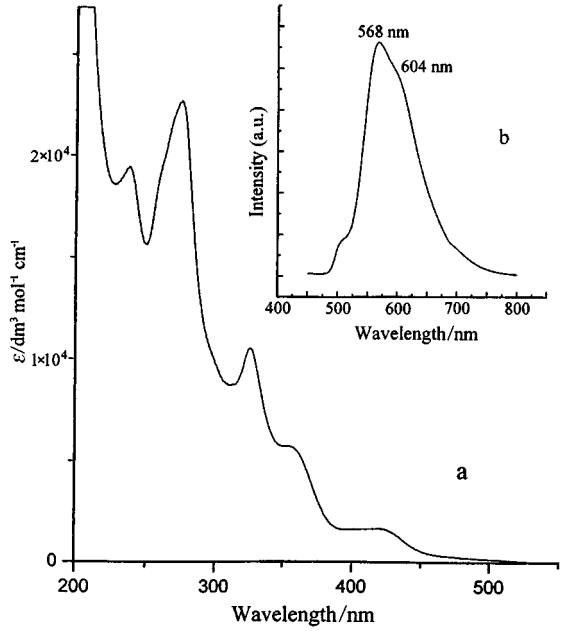

Fig. 2 UV–VIS absorption (a, in CH_3CN) and solid-state emission (b, E_{ex} 350 nm) spectra of **1** at room temperature.

interactions are therefore created. This combination of supramolecular synthons is rarely encountered in coordination compounds.[9]

The absorption spectrum of **1** [Fig. 2(a)] contains a broad low-energy absorption at 430 nm (ε_{max} 1560 dm^3 mol^{-1} cm^{-1}) which is tentatively assigned, like analogous cyclometallated platinum(II) derivatives,[10] to a metal-to-ligand charge transfer (MLCT) transition, namely (5d)Pt→π*(L). Complex **1** exhibits luminescence in solution and in the solid state. Emission at 542 nm in CH_3CN solution at room temperature is similarly ascribed to ^{3}MLCT. The solid-state emission is red-shifted to 568 nm with a shoulder at 604 nm [Fig. 2(b)] and is at a higher energy than the metal–metal-to-ligand charge transfer (MMLCT) emission (630 nm) of $[Pt_2(6\text{-phenyl-2,2′-bipyridine})_2(\mu\text{-dppm})]^{2+}$ which exhibits close intramolecular Pt–Pt contacts [3.270(1) Å].[7] The emission is therefore proposed to originate from ^{3}MLCT accompanied by partial excimeric character. Similar shifts in emission energy have recently been found for transmetallated gold(III) complexes.[11] A blue shift to 528 nm with well-resolved vibronic structure is observed in the frozen state, where the vibrational spacing of 1240 cm^{-1} is comparable to the skeletal stretching of the free ligand L.

Finally, it is pertinent to note that ligation of diphenylphosphinopropanoic acid does not necessitate the formation of complexes with complementary hydrogen bonding in the solid state. The molecular structure of the silver(I) dimer $[(PPh_3)(Ppa)Ag]_2(\mu\text{-Cl})_2$ **2**, synthesised from the reaction of $[AgCl(PPh_3)]_4$ with Ppa, is comprised of bulky peripheral phenyl groups and no hydrogen bonding is apparent.[12] This situation is expected for complexes with congested geometry where possible hydrogen-bonding motifs are segregated and such interactions are precluded. Our future work will exploit phosphinocarboxylic acids as versatile building blocks in transition metal-based crystal engineering.

We acknowledge support from The University of Hong Kong (for a Post-doctoral Fellowship to M. C.-W. C.), the Hong Kong Research Grants Council, and the Croucher Foundation of Hong Kong.

Notes and references

† Satisfactory elemental analysis has been obtained. Selected data for **1**: ^{1}H NMR (CD_3CN): 2.44 (s, 3, Ph*Me*), 2.87–3.22 (m, 4, PC_2H_4), 6.64–8.33 (m, 24, aryl H); ^{31}P NMR (CD_3CN): 18.75 (J_{PtP} 3943 Hz); IR (KBr, cm^{-1}): 1709 ν(CO), 3448 ν(OH).

‡ Crystal data for **1**: $\{[C_{38}H_{32}N_2O_2PtP]PF_6\}$, M = 919.71, triclinic, $P\bar{1}$ (No. 2), a = 9.715(2), b = 20.479(8), c = 9.245(2) Å, α = 101.76(3), β = 95.01(2), γ = 88.46(3)°, V = 1794(1) Å^3, Z = 2, D_c = 1.703 g cm^{-3}, μ(Mo-Kα) = 40.53 cm^{-1}, F(000) = 904, T = 301 K. A yellow crystal of dimensions 0.15 × 0.10 × 0.25 mm was used. A total of 4688 independent reflections were measured on a Rigaku AFC7R diffractometer with graphite monochromatized Mo-Kα radiation (λ = 0.71073 Å) using ω–2θ scans. The structure was solved by Patterson methods and all 51 non-H atoms were refined anisotropically. The H(1) atom bonded to O(1) was located in the difference Fourier map. Convergence for 463 variable parameters by least-squares refinement on F with $w = 4F_o^2/[\sigma^2(I) + (0.024F_o^2)^2]$ for 3954 absorption-corrected (min, max transmission 0.596, 1.000) reflections with $I > 3\sigma(I)$ was reached at R = 0.044 and wR = 0.058. CCDC 182/1015.

1 A. Bader and E. Lindner, *Coord. Chem. Rev*., 1991, **108**, 27.
2 J. M. Forward, Z. Assefa, R. J. Staples and J. P. Fackler Jr., *Inorg. Chem*., 1996, **35**, 16.
3 (*a*) J.-M. Lehn, *Angew. Chem., Int. Ed. Engl*., 1990, **29**, 1304; (*b*) A. D. Burrows, C. W. Chan, M. M. Chowdhry, J. E. McGrady and D. M. P. Mingos, *Chem. Soc. Rev*., 1995, **24**, 329; (*c*) G. M. Whitesides, E. E. Simanek, J. P. Mathias, C. T. Seto, D. N. Chin, M. Mammen and D. M. Gordon, *Acc. Chem. Res.*, 1995, **28**, 37; (*d*) G. R. Desiraju, *Angew. Chem., Int. Ed. Engl*., 1995, **34**, 2311.
4 (*a*) D. Braga, F. Grepioni and G. R. Desiraju, *Chem. Rev.*, 1998, **98**, 1375; (*b*) D. Braga and F. Grepioni, *Chem. Commun*., 1996, 571.
5 (*a*) S. L. James, G. Verspui, A. L. Spek and G. van Koten, *Chem. Commun*., 1996, 1309; (*b*) P. J. Davies, N. Veldman, D. M. Grove, A. L. Spek, B. T. G. Lutz and G. van Koten, *Angew. Chem., Int. Ed. Engl*., 1996, **35**, 1959.
6 (*a*) O. Ermer, *Adv. Mater*., 1991, **3**, 608; (*b*) L. Carlucci, G. Ciani, D. M. Proserpio and A. Sironi, *J. Chem. Soc., Chem. Commun*., 1994, 2755; (*c*) K. A. Hirsch, S. R. Wilson and J. S. Moore, *Chem. Eur. J*., 1997, **3**, 765 and references therein.
7 T. C. Cheung, K. K. Cheung, S. M. Peng and C. M. Che, *J. Chem. Soc., Dalton Trans.*, 1996, 1645.
8 K. Issleib and G. Thomas, *Chem. Ber*., 1960, **93**, 803.
9 M. Munakata, L. P. Wu, M. Yamamoto, T. Kuroda-Sowa and M. Maekawa, *J. Am. Chem. Soc*., 1996, **118**, 3117. For organic analogues, see: (*a*) A. P. Bisson, F. J. Carver, C. A. Hunter and J. P. Waltho, *J. Am. Chem. Soc*., 1994, **116**, 10292; (*b*) F. D. Lewis, J. S. Yang and C. L. Stern, *J. Am. Chem. Soc*., 1996, **118**, 12029; (*c*) P. R. Ashton, A. N. Collins, M. C. T. Fyfe, P. T. Glink, S. Menzer, J. F. Stoddart and D. J. Williams, *Angew. Chem., Int. Ed. Engl*., 1997, **36**, 59. For a structure with alternating auriophilic and hydrogen bonding, see: W. Schneider, A. Bauer and H. Schmidbaur, *Organometallics*, 1996, **15**, 5445.
10 (*a*) V. H. Houlding and V. M. Miskowski, *Coord. Chem. Rev.*, 1991, **111**, 145; (*b*) C. W. Chan, T. F. Lai, C. M. Che and S. M. Peng, *J. Am. Chem. Soc*., 1993, **115**, 11245.
11 K. H. Wong, K. K. Cheung, M. C. W. Chan and C. M. Che, *Organometallics*, 1998, **17**, 3505.
12 M. C. Tse, K. K. Cheung and C. M. Che, unpublished results.

Communication 8/05593I

An artificial receptor for the intermolecular and enantioselective formation of peptide sheets

Frank Eblinger and Hans-Jörg Schneider*†

FR Organische Chemie, Universität des Saarlandes, D 66041 Saarbrücken, Germany

Received (in Cambridge, UK) 22nd July 1998, Accepted 7th September 1998

Peptide strands coupled at the C terminus to bis[*p*-(aminomethyl)phenyl] ether allow in $CHCl_3$ solution association of lipophilic N-protected peptides with hydrogen bonds in the mode of antiparallel β-sheets; the enantioselectivity observed with a phenylalanine derivative is characterized by a binding constant ratio of around 15.

The formation of β-sheets in peptide strands is an important part of protein folding and is of general interest with respect to peptide recognition. Models showing typical β-sheet patterns have until now invariably been formed between *covalently* bound peptide strands with *intramolecular* hydrogen bonds. For the construction of β-sheet patterns Feigel *et al*. used amino acid fragments within macrocycles,[1] whereas in the models of Kemp *et al*.,[2] Kelly *et al*.,[3] Nowick *et al*.,[4] Gellman *et al*.[5] and Ogawa *et al*.,[6] special scaffolds between peptide chains secure a possible intramolecular binding in such hairpin-type structures. In line with our earlier analyses of energetic contributions of hydrogen bonds in such amide-type structures[7] we wanted to measure association constants between separate peptide strands; at the same time we were looking for biomimetic receptors which could distinguish enantiomers on the basis of hydrogen bonds between peptide strands.

Computer aided molecular modelling suggested two peptide strands coupled *via* the *para* positions to a diphenyl ether spacer (or diphenylamine, or diphenylmethane) as suitable host. Such an entity could bind a single strand peptide in the fashion of an antiparallel β-sheet, *e.g*. with two hydrogen bonds per amino acid at each side of the guest molecule (see Fig. 1). In order to avoid steric interference with the spacer the N-terminus of the guest peptide had to bear a formyl group, whereas the C-terminus can in principle take up any amine (or amino acid sequence). The semi-open structure makes this type of receptor a promising starting point for the building-up of longer β-sheets.

As in most other studies[8] relying on hydrogen bonds for complex formation, both host and guest compounds had to be soluble in hydrophobic media such as $CHCl_3$. We tried to achieve this first by introduction of long alkyl chains at the end of the peptide strands. The corresponding derivatives (*e.g*. with R = $C_{15}H_{31}$), however, turned out to be sparingly soluble in $CDCl_3$. Only introduction of the more bulky and spherical adamantyl groups avoid lattice stabilization in the solid state *via* parallel aligned n-alkane chains, and provided materials soluble in $CHCl_3$. Scheme 1 shows the synthesis of the host and guest derivatives; the cleft compound **1** was obtained in 10% overall yield, with $[\alpha]_D^{25}$ = −67.3 (*c* 0.2 M in EtOH) and only one set of ^1H and ^{13}C NMR signals at 400 and 100 MHz, respectively, indicating the absence of racemization. The enantiomers D-**2** and L-**2**, synthesized from commercially available amino acids, show $[\alpha]_D^{25}$ values of −14.7 and +15.2, respectively (*c* 0.2 M in EtOH).

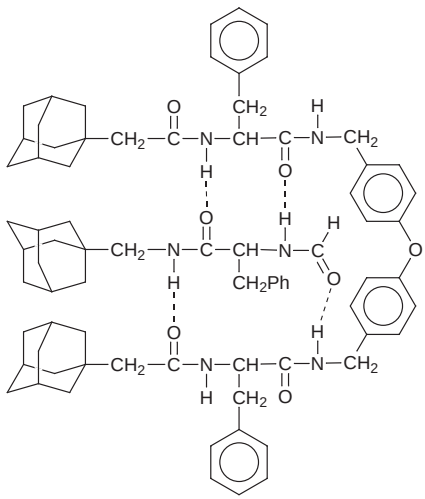

Fig. 1 Antiparallel β-sheet structure of host **1** and guest **2**.

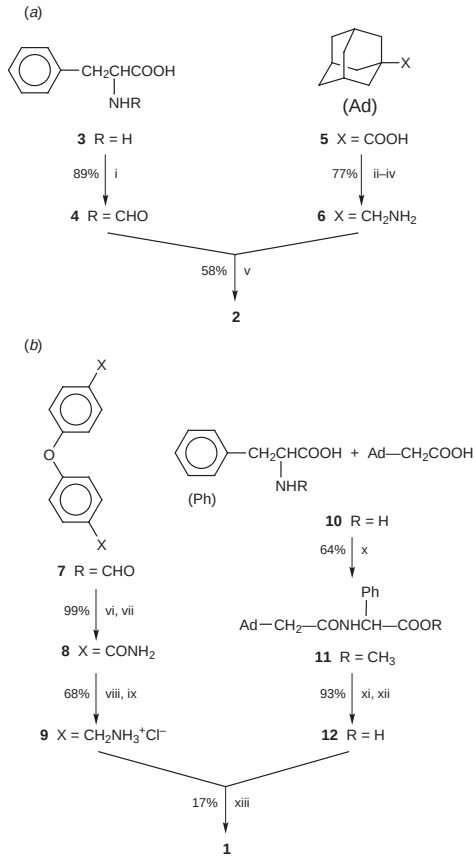

Scheme 1 *Reagents and conditions*: i, HCO_2H, Ac_2O, 278 K; ii, PCl_5; iii, NH_3; iv, BH_3·THF; v, DCC, room temp.; vi, $SOCl_2$; vii, aq, NH_3; viii, BH_3·THF; ix, MeOH, HCl; x, carbonyldiimidazole; xi, NaOH; xii, HCl; xiii, carbonyldiimidazole.

Fig. 2 shows titration curves with host **1** and the enantiomeric guest compounds D-**2** and L-**2**. Whereas the complex with the L-isomer is strong enough to be evaluated *via* non-linear least-squares fitting of the N–H NMR shift change, the complexation constant for the D-isomer can only be obtained from the

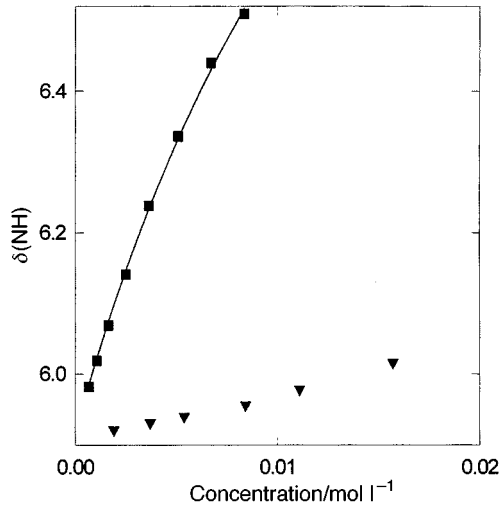

Fig. 2 Titration curves of host **1** with guests (■) L-**2** and (▼) D-**2** in $CDCl_3$ at 298 K. The line represents the best fit.

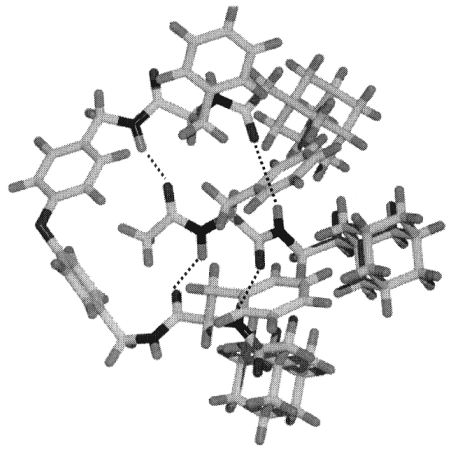

Fig. 3 Quanta/CHARMm minimized structures of the complex of host **1** and guest L-**2**. Hydrogen bonds are marked as dashed bonds.

Table 1 NMR titration results of host **1** and guests D-**2** and L-**2** in $CDCl_3$ at 298 K (The data represent the mean values of two observed N–H signals)

Complex	K/M^{-1}	ΔG/kJ mol^{-1}	CIS (ppm)
1·L-**2**	80 ± 6%	−10.8	1.79
1·D-**2 D**	5 ± 10%	−4.1	(1.79)

observed two N–H shifts of host compound **1** in comparison to the CIS value of 1.8 ppm which is expected for a 100% complex formation. The corresponding CIS for the L-enantiomer complex calculated from the least-squares fit is close to the N–H shielding effects observed in related amide-type associations,[7b] in line with the structure proposed in Fig. 1. The expected downfield shifts of the CH(α) protons could not be evaluated due to small shift changes and/or overlapping with other signals during the titration. Control experiments with related peptide derivatives, also bearing adamantyl groups for solubility reason, showed no self-association in $CHCl_3$; this supports the suggestion that an effective recognition requires hydrogen bonds from *two* sides of the guest as depictet in Fig. 1.

The total binding free energy ΔG (Table 1) for the 'best' isomer L-**2** (11 kJ mol^{-1}) is relatively small in comparison with values observed with related systems, which for $CHCl_3$ as solvent predict up to 5 kJ mol^{-1} per hydrogen bond.[7] The reason for the relatively weak binding might be due to some geometric mismatch, but must be seen primarily as a consequence of unfavourable secondary interactions between donor and acceptor groups. These have been elucidated by Jorgensen *et al*.,[9] and were found to be as large as *e.g*. 2.8 kJ mol^{-1} by systematic analysis of many amide-type associations in $CHCl_3$.[7b]

The degree of chiral discrimination ($\Delta\Delta G \approx 7$ kJ mol^{-1}) compares favourably with the few enantioselective peptide receptors hitherto available.[8a,10] Molecular mechanics calculations (gas phase, $\varepsilon = 3$) using CHARMm[11] shed light on the origin of the observed stereoselectivity: only with the L-isomer does one obtain after energy minimization a structure with the four hydrogen bonds, as depicted in Fig. 3. Minimizations with the D-isomer invariably lead to structures without hydrogen bonds: Unfavourable interactions of the guest (D-**2**) and host benzyl groups lead to deformation of the backbone, preventing the formation of hydrogen bonds. As is often the case, the observed stereoselectivity of association is a consequence of repulsion between groups which are not involved in the formation of non-covalent bonds, and which are remote from the actual binding sites.

Notes and references

† E-mail: ch12hs@rz.uni-sb.de

1 V. Brandmeier, W. H. B. Sauer and M. Feigel, *Helv. Chim. Acta*, 1994, 77, 70; C. Gailer and M. Feigel, *J. Comput. Aided Mol. Des*., 1997, **11**, 273 and references cited therein.
2 D. S. Kemp, B. R. Bowen and C. C. Muendel, *J. Org. Chem*., 1990, **55**, 4650; D. S. Kemp and Z. Q. Li, *Tetrahedron Lett*., 1995, **36**, 4175 and 4179 and references cited therein.
3 J. P. Schneider and J. W. Kelly, *Chem. Rev*., 1995, **95**, 2169; C. L. Nesloney and J. W. Kelly, *J. Am. Chem. Soc*., 1996, **118**, 5836 and references cited therein.
4 J. S. Nowick, E. M. Smith and M. Pairish, *Chem. Soc. Rev*., 1996, **25**, 401; D. L. Holmes, E. M. Smith and J. S. Nowick, *J. Am. Chem. Soc*., 1997, **119**, 7665; J. S. Nowick, M. Pairish, I. Q. Lee, D. L. Holmes and J. W. Ziller, *J. Am. Chem. Soc*., 1997, **119**, 5413; J. S. Nowick and S. Insaf, *J. Am. Chem. Soc*., 1997, **119**, 10903 and references cited therein.
5 R. R. Gardner, L. A. Christianson and S. H. Gellman, *J. Am. Chem. Soc*., 1997, **119**, 5041; H. E. Stanger and S. H. Gellman, *J. Am. Chem. Soc*., 1998, **120**, 4236 and references cited therein.
6 A. B. Gretchikhine and M. Y. Ogawa, *J. Am. Chem. Soc*., 1996, **118**, 1543 and references cited therein.
7 (*a*) H.-J. Schneider, R. K. Juneja and S. Simova, *Chem. Ber*., 1989, **112**, 1211; (*b*) J. Sartorius and H.-J. Schneider, *Chem. Eur. J*., 1996, **2**, 1446; H.-J. Schneider, *Chem. Soc. Rev*., 1994, **22**, 227.
8 (*a*) For a short review see: H.-J. Schneider, *Angew. Chem., Int. Ed. Engl*., 1993, **32**, 848; *Angew. Chem*., 1993, **105**, 890; (*b*) M. Famulok, K. S. Jeong, D. Deslongchamps and J. Jr. Rebek, *Angew. Chem*., 1991, **103**, 880; (*c*) R. Liu and W. C. Still, *Tetrahedron Lett*., 1993, **34**, 2573; (*d*) A. Borchardt and W. C. Still, *J. Am. Chem. Soc*., 1994, **116**, 373; (*e*) J. Dowden, P. D. Edwards and J. D. Kilburn, *Tetrahedron Lett*., 1997, **38**, 1095; (*f*) E. Martinborough, T. M. Denti, P. P. Castro, T. B. Wyman, C. B. Knobler and F. Diederich, *Helv. Chim. Acta*, 1995, **78**, 1037; (*g*) A. Casnati, E. Di Modugno, M. Fabbi, M. Pelizzi, A. Pochini, F. Sansone, G. Tarzia and R. Ungaro, *Bioorg. Med. Chem. Lett*., 1996, **6**, 2699; (*h*) M. Crego, A. Partearroyo, C. Raposo, M. L. Mussons, J. L. Lopez, V. Alcazar and J. R. Moran, *Tetrahedron Lett*., 1994, **35**, 1435 and references cited therein.
9 W. Jorgensen and J. Pranata, *J. Am. Chem. Soc*., 1990, **112**, 2008.
10 S. S. Yoon and C. W. Still, *Tetrahedron Lett*., 1994, **35**, 8557; *J. Am. Chem. Soc*., 1993, **115**, 823 and references cited therein.
11 B. R. Brooks, R. E. Bruccoleri, B. D. Olafson, D. J. States, S. Swaminathan and M. Karplus, *J. Comput. Chem*., 1983, **4**, 187; C. L. Brooks and M. Karplus, *Methods Enzymol*., 1986, **127**, 369; A.T. Brünger and M. Karplus, *Acc. Chem. Res*., 1991, **24**, 54.

Communication 8/05720F

High performance conducting polymer supported oxygen reduction catalysts

Zhigang Qi and Peter G. Pickup*

Department of Chemistry, Memorial University of Newfoundland, St. John's, Newfoundland, Canada A1B 3X7. E-mail: ppickup@morgan.ucs.mun.ca

Received (in Columbia, MO, USA) 6th July 1998, Accepted 23rd September 1998

Conducting poly(3,4-ethylenedioxythiophene)/poly(styrene-4-sulfonate) composites containing Pt catalyst nanoparticles produce currents as high as 0.4 A cm^{-2} at 0.5 V *vs.* NHE for oxygen reduction in gas diffusion electrodes.

Composites consisting of a conducting polymer and a polyanion could be the ideal catalyst supports for proton exchange membrane fuel cells (PEMFC) because they possess both high electronic and proton conductivities as well as being permeable to gases and water. We have reported the chemical deposition of Pt and platinum oxide nanoparticles on a polypyrrole/poly(styrene-4-sulfonate) (PSS) composite, and demonstrated oxygen reduction performances superior to those previously obtained with conducting polymer supported catalysts.[1,2] However, one of the biggest challenges we faced was that the electronic conductivity of the polypyrrole was seriously degraded by the deposition of the catalyst particles under both reducing (formaldehyde, hydrogen, or citrate) and oxidizing conditions (H_2O_2).[1] We found that polyaniline also suffered irreversible conductivity losses when catalysed under similar conditions, and so we turned our attention to poly(3,4-ethylenedioxythiophene) (PEDOT) which is reported to be more stable than polypyrrole under oxidizing conditions[3] and at elevated temperatures.[4] Preliminary results on the chemical synthesis of PEDOT/PSS particles and their use as a catalyst support are reported here. PSS was used as the counter anion during synthesis so that the resulting polymer composite would be a cation (proton) conductor.[5]

Since the EDOT monomer has a low solubility in water (2.1 g l^{-1} at 20 °C) and NaPSS is not soluble in suitable organic solvents, polymerization from solution can only be done under dilute conditions. This is known to lead to conducting polymers with inferior conductivities[6] and this was confirmed in our preliminary experiments. A better approach was to polymerize EDOT from a suspension in NaPSS(aq). In a typical procedure, 0.8 ml of EDOT (7.5 mmol; Bayer) was added to 15 ml of 0.1 M NaPSS (1.5 mmol; Aldrich), and the mixture was stirred vigorously for 30 min. EDOT dispersed much better in 0.1 M NaPSS than in pure water, and this is a key factor in the formation of highly conducting PEDOT/PSS. Upon addition of 15.3 g $Fe(NO_3)_3{\cdot}9H_2O$ (38 mmol) in 5 ml of water, EDOT polymerized immediately leading to a dark blue mixture. A deep blue powder was collected by filtration after 2 h and dried overnight at 50 °C under vaccum. The electronic conductivity of this composite measured with a four-point probe assembly described elsewhere[7] was 9.9 S cm^{-1}. For comparison, the conductivity of carbon black (Vulcan XC-72R) measured similarly was 3.0 S cm^{-1}. After 11 months storage in air, the conductivity of the PEDOT/PSS sample had dropped to 2.2 S cm^{-1}.

Pt deposition (20% by mass) on this PEDOT/PSS composite was then performed in the following way. 0.2010 g PEDOT/PSS and 0.1330 g $H_2PtCl_6{\cdot}xH_2O$ were stirred in 50 ml of aqueous formaldehyde (18%) for 1 h at room temperature. The mixture was then heated to reflux for 1 h, followed by filtration and vacuum drying. A 95% yield of Pt/PEDOT/PSS was obtained. Transmission electron microscopy and X-ray diffraction revealed that this deposition method produces Pt particles on the polymer composite with an average diameter of *ca.* 4 nm.

The electronic conductivity of the catalyzed material was 4.0 S cm^{-1} (Vulcan XC-72R catalyzed with 20% Pt (Electrosynthesis) gave a conductivity of 3.3 S cm^{-1} under the same conditions). Thus PEDOT/PSS is relatively stable to the reducing conditions (formaldehyde) required for Pt decomposition. This is in dramatic contrast to other conducting polymers such as polypyrrole and polyaniline whose conductivities decreased by 3–4 orders of magnitude when refluxed in formaldehyde for 15 min.

After 11 months storage in air, the conductivity of the Pt catalysed PEDOT/PSS sample had dropped to 5 mS cm^{-1}. Other Pt/PEDOT/PSS samples were found to be stable over extended periods when stored in methanol, suggesting that the instability in air is due to overoxidation[8] by O_2 which is activated by the Pt particles. This instability must clearly be overcome before conducting polymer supported catalysts can be considered as viable materials for commercial applications.

Since it has been reported that PEDOT has good stability under oxidizing conditions, we attempted to deposit platinum oxide on PEDOT/PSS *via* the oxidation of $Na_6Pt(SO_3)_4$ by 0.35% H_2O_2.[9] However, we found that the polymer composite was destroyed by the H_2O_2, and only a *ca.* 3% yield of a poorly conducting material was obtained.

A number of Pt catalysed (formaldehyde reduction of H_2PtCl_6) polymer composites were tested for oxygen reduction in a cell[2,7] designed to approximate the conditions in an ambient temperature PEMFC. For comparison, a commercial catalyst (Electrosynthesis; 20% Pt on Vulcan XC-72R carbon black) was tested in the same way. Polarization curves for the catalysed polymers and Pt on XC-72R are shown in Fig. 1. The best Pt/PEDOT/PSS electrode achieved a current density of 0.47 Å cm^{-2} at 0.45 V (*vs.* NHE), which is much better than any previously reported conducting polymer supported system.[2] This electrode gave comparable performance to one with the commercial carbon supported catalyst although a higher Pt

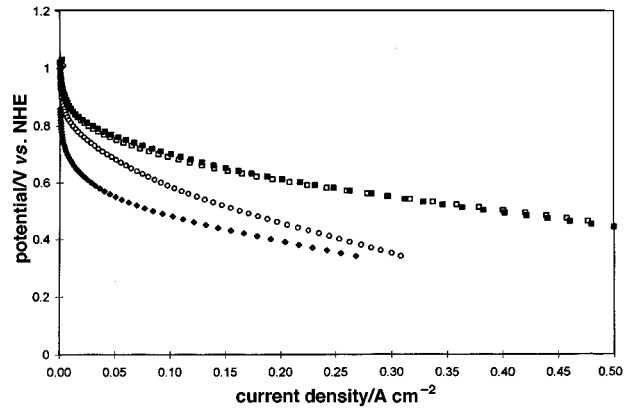

Fig. 1 Polarization curves for oxygen reduction in gas diffusion electrodes at ambient temperature (*ca.* 25 °C). The catalyst was mixed with a PTFE binder and sandwiched between carbon fibre paper exposed to O_2 (1 atm) and a Nafion membrane in contact with 1 M H_2SO_4(aq) containing a reference and counter electrode. (■) Commercial 20% Pt on carbon (0.31 mg Pt cm^{-2}), (□) 37% Pt on PEDOT/PSS prepared at high dilution (0.89 mg Pt cm^{-2}), (○) 19% Pt on PEDOT/PSS prepared at high dilution (0.29 mg Pt cm^{-2}), (◆) 20% Pt on emulsion polymerized PEDOT/PSS (0.40 mg Pt cm^{-2}). Data collected after 2 s at each potential.

loading was required (there was no significant dependence on Pt loading for the commercial catalyst for loadings from 0.2 to 1.0 mg cm^{-1}). Surprisingly, the catalysts prepared with PEDOT/PSS synthesized under dilute conditions performed significantly better than that prepared with the PEDOT/PSS synthesized from an EDOT suspension, despite their lower electronic conductivities (*ca.* 0.3 S cm^{-1}). The active Pt areas and proton conductivities of the two catalysts were similar, suggesting that the different performances are due to different oxygen permeabilities. The factors that determine the activities of Pt/PEDOT/PSS catalysts are under current investigation and will be discussed in detail elsewhere.

The results presented here show that high performance fuel cell catalysts can be prepared with conducting polymer supports. Further optimization can be expected to lead to catalysts that are competitive with the current state of the art in PEMFC catalysts. However, a significant problem that must be overcome is the long term stability of the conducting polymer support in the presence of oxygen and catalytic Pt particles.

This work was supported by the Natural Sciences and Engineering Research Council of Canada and Memorial University. We would also like to thank Mark Lefebvre for making the long term conductivity measurements.

Notes and references

1 Z. Qi and P. G. Pickup, *Chem. Commun.*, 1998, 15.
2 Z. Qi, M. C. Lefebvre and P. G. Pickup, *J. Electroanal. Chem.*, 1998, in press.
3 H. Yamato, M. Ohwa and W. Wernet, *J. Electroanal. Chem.*, 1995, **397**, 163.
4 G. Heywang and F. Jonas, *Adv. Mater.*, 1992, **4**, 116.
5 X. Ren and P. G. Pickup, *J. Phys. Chem.*, 1993, **97**, 5356.
6 J. T. Lei, Z. H. Cai and C. R. Martin, *Synth. Metal.*, 1992, **46**, 53.
7 Z. Qi and P. G. Pickup, *Chem. Mater.*, 1997, **9**, 2934.
8 A. A. Pud, *Synth. Metal*, 1994, **66**, 1.
9 H. G. Petrow and R. J. Allen, *US Pat.* 4 044 193, 1977.

Communication 8/05322G

Analysis of natural abundance deuterium NMR spectra of enantiomers in chiral liquid crystals *via* 2D auto-correlation experiments

Denis Merlet,[a] Bernard Ancian,[b] William Smadja,[a] Jacques Courtieu[a] and Philippe Lesot*[a]†

[a] *Laboratoire de Chimie Structurale Organique, ICMO, URA CNRS 1384, Université de Paris-Sud, 91405 Orsay, France*

[b] *Université Paris VII-Denis Diderot, Département de chimie, 2 Place Jussieu, 75251 Paris cedex 05, France*

Received (in Liverpool, UK) 30th June 1998, Accepted 4th September 1998

Natural abundance deuterium auto-correlation 2D NMR experiments of enantiomers orientated in a chiral polypeptide liquid crystalline solvent (PBLG) are used as a novel analytical tool for the study of chiral solutes.

Enantiomeric analysis *via* NMR spectroscopy is a real challenge for organic chemists.[1–3] In a recent study we have shown the feasibility of visualisation of chiral molecules orientated in the poly(γ-benzyl L-glutamate) (PBLG) liquid crystalline system using proton-decoupled natural abundance deuterium NMR spectroscopy.[4] The proton-decoupled deuterium (^{2}H-{^{1}H}) NMR spectrum of an oriented molecule containing a single deuterium nucleus ($I = 1$) consists of a quadrupolar doublet separated by $\Delta\nu_Q = 3/2(e^2qQ/h)S_{C-D}$, where (e^2qQ/h) is the quadrupole coupling constant and S_{C-D} is the order parameter along the C–D bond.[2,4,5] In a chiral medium the enantiomeric discrimination is observed *via* the measurement of the quadrupolar splitting differences ($\Delta\nu_Q^R - \Delta\nu_Q^S$) and we have shown that the sensitivity of natural abundance deuterium NMR is sufficient to measure the 'Differential Ordering Effects' (DOE) without isotopic enrichment.[4]

In natural abundance deuterium NMR spectroscopy the spectral analysis in an anisotropic medium is simplified due to the absence of residual dipolar couplings between two rare atoms. However, since all deuterons of the chiral solute are simultaneously probed, the spectrum may appear extremely complex for large molecules, due to the excessive overlapping of peaks. In order to illustrate this, the natural abundance ^{2}H-{^{1}H} NMR spectrum of (±)-but-3-en-2-ol dissolved in the PBLG–$CHCl_3$ phase at 301 K is shown in Fig. 1(*a*).‡ The spectrum was recorded at 38.4 MHz using a Bruker AM 250 spectrometer equipped with a 5 mm diameter inverse broadband probe in the unlocked mode.§

In the racemic mixture of but-3-en-2-ol, twelve different chiral isotopomers exist. Consequently, a maximum of 24 peaks (12 doublets), disregarding the solvent doublet, are expected in the natural abundance ^{2}H spectrum, assuming that all deuteron sites are discriminated in a chiral medium. In the experimental 1D spectrum 14 lines of various intensities are clearly observed [Fig. 1(*a*)]. A first analysis of the spectrum based on the chemical shifts allowed us to attribute some of the signals, such as the two quadrupolar doublets for the methyl group (δ 1.19) [Fig. 1(*a*),(*b*)] and the doublet of solvent, which is used as internal reference (δ 7.30) [Fig. 1(*a*),(*g*)]. But we were enable to assign easily the other signals visible in the spectrum. When the assignment problem becomes acute, the use of 2D auto-correlation deuterium NMR experiments is needed in order to attribute the two components of each quadrupolar doublet. A method for the assignment of quadrupolar doublets in perdeuterated liquid crystal molecules was developed many years ago by Emsley and Turner using the pulse sequence $\pi/2 - t_1/2 - \pi/2 - t_1/2 -$ acq.(t_2).[6] However, the analysis of the 2D spectrum is only possible when the deuterons are dipolar coupled, which is not the case in natural abundance ^{2}H-{^{1}H} NMR. In order to resolve specifically the analysis of overcrowded natural abundance deuterium spectra, we propose applying a new 2D pulse sequence developed using the product-operator formalism for spin $I = 1$ nuclei. The basic idea of this sequence is to maximise the intensity of cross peaks which auto-correlate the components of each quadrupolar doublet in the 2D contour plot. This 2D experiment is then complemented by a composite pulse decoupling using the WALTZ-16 sequence to remove the proton–deuterium scalar and dipolar couplings.

The sequence proposed is derived from a COSY experiment in which a π read pulse must be used to transfer coherences in the proper way. In this experiment the diagonal peaks cancel out and only the '*N*-type' cross peaks[7] are observed in the 2D spectrum with a single scan. Disregarding all relaxation terms and phase factors, the expression of the signal during the acquisition period (t_2) is given by eqn. (1).

$$S(t_1,t_2) = e^{[-i(\omega + \pi\Delta\nu_Q)t_1]}.e^{[i(\omega - \pi\Delta\nu_Q)t_2]} + e^{[-i(\omega - \pi\Delta\nu_Q)t_1]}.e^{[i(\omega + \pi\Delta\nu_Q)t_2]} \quad (1)$$

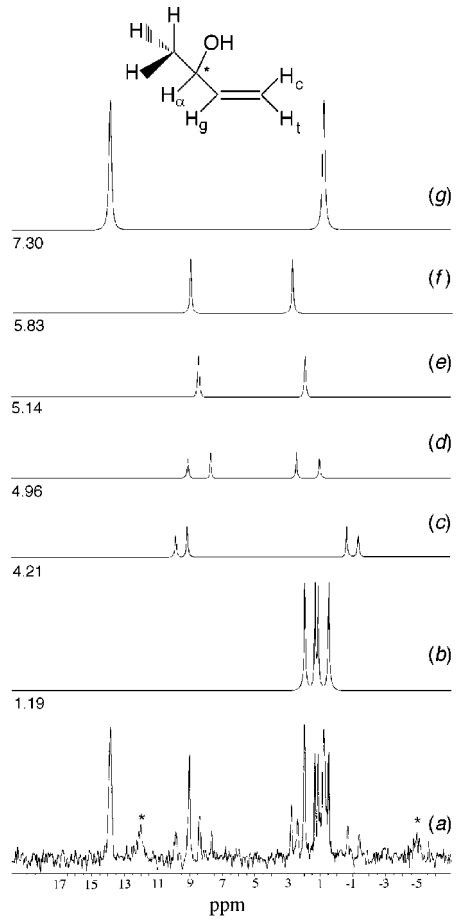

Fig. 1 (*a*) Natural abundance ^{2}H-{^{1}H} NMR spectrum of (±)-but-3-en-2-ol. (*b*)–(*g*) Fitted subspectra of all deuterated isotopomers in the mixture: (*b*) CDH_2, (*c*) D_α, (*d*) D_t, (*e*) D_c, (*f*) D_g and (*g*) $CDCl_3$. The signals of the hydroxy group (*) could not be clearly separated from noise and were not fitted.

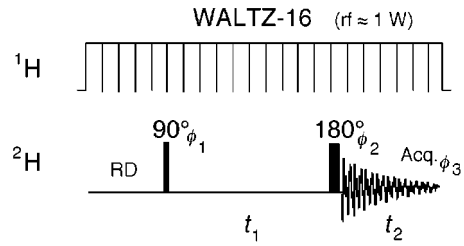

Fig. 2 Schematic diagram of the 2D Q-COSY pulse sequence.

Table 1 Phase cycling[a] of the Q-COSY sequence

ϕ_1	ϕ_2	ϕ_3
x	x	x
x	y	$-x$
x	$-x$	x
x	$-y$	$-x$

[a] The total phase cycling (16 steps) is obtained by applying the CYCLOPS procedure.

The pulse scheme and the phase cycling of the sequence denoted 'Quadrupole-COSY' (Q-COSY) are shown in Fig. 2 and Table 1, respectively. The phase cycling is identical to that used in a classical COSY experiment. As the pulse sequence basically produces a 'pseudo-quadrature' in the F_1 dimension, the 2D spectrum should be displayed in the magnitude mode to avoid the so-called 'phase-twist' lineshape.[7] The analysis of the Q-COSY sequence using the product operator-formalism shows that during the t_2 period only single quantum coherences are different from zero. Thus, this sequence is more sensitive, by a factor of 2, than the sequence of Emsley and Turner.[6] In other words it means that the Q-COSY sequence drives to maximum sensitivity, which is a major advantage for the observation of molecules *via* natural abundance deuterium NMR spectroscopy.

In order to explore the potentialities of the sequence, the natural abundance ^{2}H Q-COSY 2D spectrum of (±)-but-3-en-2-ol dissolved in the PBLG–$CHCl_3$ phase at 301 K was recorded (Fig. 3). The 2D spectrum was obtained using a spectral digitisation of 256 (t_1) × 1024 (t_2) data points, 848 transients per FID were added, leading to a total number of 217088 scans and a total experiment time of around 53 h.¶

As expected, the observation of the cross peaks in the 2D surface enable us to separate all sets of quadrupolar doublets. The comparison with the 1D spectrum recorded under the same conditions then allows us to attribute unambiguously each doublet. Thus, from the 2D contour plot, we can clearly deduce that the peak located at δ9.05 on the 1D spectrum is fortuitously made of three different lines corresponding to three different isotopomers. The same situation arises for the NMR line at δ1.95. These two examples illustrate the usefulness of 2D auto-correlation experiments in enantiomeric analysis *via* natural abundance ^{2}H-{^{1}H} NMR.

From the spectral analysis of the 2D spectrum all the clearly observable quadrupolar doublets in the 1D spectrum could be independently fitted for each isotopomer of mixture as presented in Fig. 1(b)–(g). The analysis shows that only three out of the six possible couples of chiral isotopomers are discriminated, *i.e.* the methyl group, the chiral centre (D_α) and *trans*-position (D_t) in the vinyl group. In addition, because the C–D bonds for the *cis*- and *gem*-deuterons (D_c and D_g) in the vinyl group are more or less parallel, they show a very similar orientation relative to the magnetic field and they must then exhibit the same behaviour relative to the chiral discrimination. In our case the quadrupolar splitting difference between the *cis*- and *gem*-positions is < 3%, and both are not discriminated, thus confirming our spectral assignment.

In conclusion we have demonstrated that natural abundance deuterium 2D auto-correlation experiments with routine magnetic field strengths (5.87 T) and standard NMR instrumentation are feasible and provide crucial information for enantiomeric analysis in chiral liquid crystals. The total experimental time needed to obtain a reasonable signal-to-noise ratio for each deuterium signal on a 250 MHz spectrometer may appear as an important limitation of this technique. However the use of higher magnetic fields will greatly reduce the experimental time.[4] Thus, operating on a 400 MHz spectrometer, only *ca*. 15 h would be needed to reach the same signal-to-noise ratio for (±)-but-3-en-2-ol. Finally, we note that natural abundance deuterium 2D experiments have sensitivities comparable with those of the carbon-13 2D INADEQUATE experiments which are commonly used.[7] Additional studies of the scope of the Q-COSY sequence (sensitivity, resolution improvement and phase sensitive mode) are currently underway. The sequence reported in this study belongs to a new class of 2D auto-correlation experiments for the NMR analysis of spins $I = 1$ in oriented media that we denote 'QUadrupole Ordered SpectroscopY' (QUOSY). Other 2D auto-correlation experiments are currently under development to assess their analytical potential in natural abundance deuterium NMR spectroscopy.

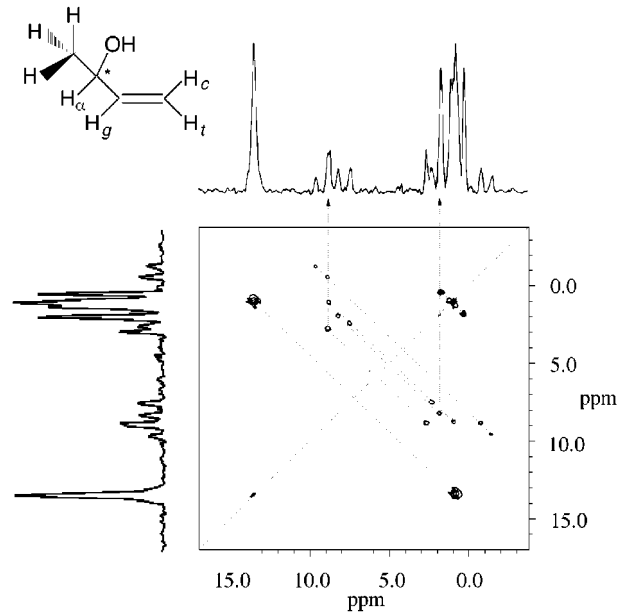

Fig. 3 2D Contour plot of proton-decoupled natural abundance deuterium Q-COSY experiment obtained for (±)-but-3-en-2-ol.

Notes and references

† Corresponding author: E-mail: philesot@icmo.u-psud.fr

‡ *Sample composition* : The NMR sample was made from racemic substrate (100 mg), PBLG (100 mg) with a DP = 854, MW ≈ 188000 (Sigma), and $CHCl_3$ (350 mg). The sample preparation is described in refs. 2–4.

§ *1D Experiment*: The sample was not spun in the field and the temperature was controlled by a BVT 1000 system. The spectrum was recorded using 60° pulses, a 0.5 s recycling delay and 150 000 scans with 1 K data points (around 20 h of experiment time) (see ref. 4). Zero filling to 4 K data points without apodisation was applied. The linewidths of the solute are 3–7 Hz.

¶ *2D experiment*: The recycling delay of the sequence is of 0.75 s. The spectral width in the F_1 and F_2 dimensions is 1500 Hz. A Gaussian filtering in both dimensions ($LB_1 = -4$ Hz, $GB_1 = 20\%$ and $LB_2 = -3$ Hz, $GB_2 = 15\%$) and a symmetrisation procedure were applied.

1 D. Parker, *Chem. Rev.*, 1991, **91**, 1441.
2 I. Canet, J. Courtieu, A. Loewenstein, A. Meddour and J. M. Péchiné, *J. Am. Chem. Soc.*, 1995, **117**, 6520 and references cited therein.
3 A. Meddour, P. Berdagué, A. Hedli, J. Courtieu and P. Lesot, *J. Am. Chem. Soc*., 1997, **119**, 4502.
4 P. Lesot, D. Merlet, A. Loewenstein and J. Courtieu, *Tetrahedron*: *Asymmetry*, 1998, **9**, 1871.
5 J. W. Emsley and J. C. Lindon, *NMR Spectroscopy Using Liquid Crystal Solvents*, Pergamon, Oxford, 1975.
6 J. W. Emsley and D. L. Turner, *Chem. Phys. Lett.*, 1981, **82**, 447.
7 R. R. Ernst, G. Bodenhausen and A. Wokaun, *Principles of Nuclear Magnetic Resonance in One and Two Dimensions*, Clarendon, Oxford, 1987.

Communication 8/05020A

Formation and *in situ* characterization of the first dihydrogen aqua complex: $[Ru(H_2O)_5(H_2)]^{2+}$

Nicolas Aebischer, Urban Frey and André E. Merbach*

Institut de Chimie Minérale et Analytique, Université de Lausanne, BCH-Dorigny, CH-1015 Lausanne, Switzerland. E-mail: andre.merbach@icma.unil.ch

Received (in Basel, Switzerland) 17th July 1998, Accepted 17th September 1998

The product of the reaction between $[Ru(H_2O)_6]^{2+}$ and pressurized H_2 in water is $[Ru(H_2O)_5(H_2)]^{2+}$ whose nature was unambiguously demonstrated by ^1H and ^{17}O NMR and which is the first characterized dihydrogen aqua complex.

$[Ru(H_2O)_6]^{2+}$ **1** is an ideal starting material for the preparation of a great variety of new Ru(II) aqua complexes. For example, the easy reaction of **1** with dissolved gases (CO,[1] N_2[2] and C_2H_4[3]) to form the corresponding $[Ru(H_2O)_5L]^{2+}$ complex is of particular interest for its simplicity and its cleanliness. More interestingly, the dimerization of ethylene catalyzed by **1** in water and under very soft conditions was described.[3] The products of the reaction were identified as different butene isomers, but no indication about the mechanism was given. The existence of a hydride complex may be an intermediate in the reaction pathway. However, no ruthenium(II) aquacomplex containing either a hydride or a dihydrogen ligand has ever been described.

Morris *et al.* proposed a way to predict the stability of a H_2 complex.[4] If a N_2 complex exhibits a stretching frequency, ν_{NN}, in the range 2060–2150 cm^{-1}, the corresponding H_2 complex will be stable *vs.* thermally unstable complexes for $\nu > 2150$ cm^{-1} and hydrides for $\nu < 2060$ cm^{-1}. In the case of $[Ru(H_2O)_5(N_2)]^{2+}$, a ν_{NN} of 2156 cm^{-1} was reported for the solid compound (Nujol mull), and of 2141 cm^{-1} in aqueous solution.[2] These values indicate thus that a dihydrogen complex of limited stability could be prepared but not the hydride complex.

To a 0.1 mol kg^{-1} aqueous solution of $[Ru(H_2O)_6]^{2+}$, prepared in a home-made 10 mm sapphire tube,[5] we applied 4.0 MPa of dihydrogen pressure.† The appearance of only one new peak at −7.68 ppm (beside the peaks of the starting materials) was detected in the ^1H NMR spectra. After 1.5 h, Ru(0) started to deposit on the wall of the tube, probably due to the reduction of the metal by dihydrogen. A new solution was prepared containing $[Ru(H_2O)_6]^{2+}$ (0.110 mol kg^{-1}), toluene-*p*-sulfonic acid (Htos, 0.130 mol kg^{-1}) in 99.95 % D_2O. Subsequently, 3.9 MPa of dihydrogen was applied. After 20 min, beside the signals of the solvent and of the tosylate anion, two singlets at −7.65 and at 4.62 ppm (bound and free dihydrogen) could be observed in the ^1H NMR spectrum. The solution was kept under H_2 pressure for 19 h and shaken from time to time. Then, two 1 : 1 : 1 triplets could be observed [Fig. 1(a)] in addition to the previously mentioned singlets. The first triplet at 4.59 ppm exhibits a coupling constant, $^1J_{HD}$, of 42.8 Hz and is typical of free HD dissolved in bulk water. The second triplet at −7.68 ppm exhibits a $^1J_{HD}$ value of 31.2 Hz and an isotopic shift, $\delta_{HH} - \delta_{HD}$, of +0.023 ppm compared to the signal of bound H–H. The chemical shift as well as the coupling constant of this latter signal are characteristic of a dihydrogen ligand bound to a metal center.[6] No reduction was observed after keeping the solution for three days under H_2 pressure, showing the increased stability of the complex in more acidic medium.

The simplest conceivable dihydrogen complex has the formula $[Ru(H_2O)_5(H_2)]^{2+}$. To verify the formation of such a complex, a new solution was prepared containing $[Ru(H_2O)_6]^{2+}$ (0.0994 mol kg^{-1}) and Htos (0.562 mol kg^{-1}) in 10% oxygen−17 enriched water.‡ Then, 54.0 MPa of dihydrogen pressure was applied to this solution at 297.0 K in a home made high gas-pressure NMR microreactor which assured a constant mixing between the solution and the gas.[7] After 35 min, a singlet at −7.54 ppm was the only new peak in the ^1H NMR spectrum. Simultaneously, the ^{17}O NMR spectrum revealed the appearance of two new peaks at −80.4 and −177.4 ppm beside the signal of bulk water (at 0 ppm) concomitant to the decrease of the Ru(II) hexaqua complex signal at −191.0 ppm [Fig. 1(b)]. The ratio of the integral of the two new peaks is 4.1, with is in very good agreement with the theoretical value of 4 expected for a complex of the formula $[Ru(H_2O_{ax})(H_2O_{eq})_4(H_2)]^{2+}$. The formation reaction of the dihydrogen complex is summarized in eqn. (1), where an estimated value of the equilibrium constant, calculated from the integrals of the ^{17}O NMR signal, is also given.

$$[Ru(H_2O)_6]^{2+} + H_2 \underset{}{\overset{K_{eq} \approx 4 \text{ kg mol}^{-1}}{\rightleftharpoons}} [Ru(H_2O)_5(H_2)]^{2+} \quad (1)$$

An empirical equation has been proposed to calculate the H–D bond distance (in Å) from the $^1J_{HD}$ coupling constant [in Hz, eqn. (2)].[8] With a $^1J_{HD}$ value of 31.2 Hz (*vide supra*), we can

$$d_{H-D} \cong -0.0167\, J_{HD} + 1.42 \quad (2)$$

calculate a H–H bond length of 0.899 Å, only slightly longer than the experimental bond length of free dihydrogen (0.740 Å). This indicates little electron back donation from the metal to the σ* antibonding orbital of the dihydrogen ligand. The main contribution to the Ru–H_2 bond is thus probably an electron donation from the σ orbital of H_2 to the metal. This should cause

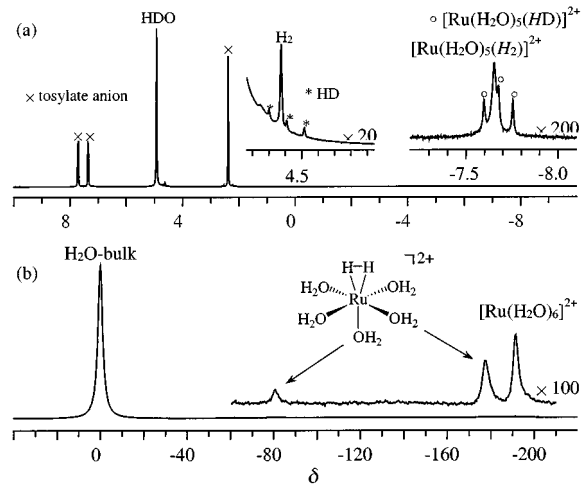

Fig. 1 (a) 400 MHz ^1H NMR spectrum, recorded at 298.4 K, of a solution containing initially $[Ru(H_2O)_6]^{2+}$ (0.110 mol kg^{-1}), toluene-*p*-sulfonic acid (0.130 mol kg^{-1}) in 99.95 % D_2O and kept for 19 h at ambient temperature and under 3.9 MPa of dihydrogen pressure in a 10 mm sapphire tube; (b) 54 MHz ^{17}O NMR spectrum, recorded at 297.0 K, of a solution containing initially $[Ru(H_2O)_6]^{2+}$ (0.099 mol kg^{-1}) and toluene-*p*-sulfonic acid (0.562 mol kg^{-1}) in 10% $H_2{}^{17}O$ and kept for 40 min under 54.0 MPa of dihydrogen pressure at 297.0 K.

an electron depletion of the H–H bond and thus gives an acidic character to the dihydrogen ligand. This may explain the enhanced stability of the dihydrogen complex with the decrease of the pH, possibly by displacing an equilibrium between dihydrogen–hydride complexes [eqn. (3)]. The increase of the

$$[Ru(H_2O)_5(H_2)]^{2+} \underset{+\,H^+}{\overset{-\,H^+}{\rightleftharpoons}} \underset{\text{(intermediate)}}{\{Ru(H_2O)_5(H)^+\}} \underset{-\,D^+}{\overset{+\,D^+}{\rightleftharpoons}} [Ru(H_2O)_5(HD)]^{2+} \qquad (3)$$

acidic character of η^2-coordinated H_2 is in accord with the formation of both bound and free HD molecules observed in the ^{1}H NMR spectra, resulting from an activation of the H–H bound by the metal center.

The longitudinal relaxation time of the ^{1}H NMR signal of bound dihydrogen was also determined at different temperatures by inversion–recovery experiments.§ The T_1 values decreased as a function of the temperature, yet the minimum of the T_1 values was not reached. Nevertheless, all the measured values, < 100 ms, confirm the dihydrogen nature of the ligand. It was shown that dihydrogen ligand has T_1 values < 100 ms but for hydride ligand the value is usually > 350 ms.[6]

The $[Ru(H_2O)_5(H_2)]^{2+}$ complex is the first example of an η^2-dihydrogen complex containing only water as other ligand in the first coordination sphere. There is thus no π-acid ligands to discharge the ruthenium center from some of its electronic density. This situation is similar to the previously reported $[Os(NH_3)_5(H_2)]^{2+}$,[9] and $[Os(NH_3)_4(H_2O)(H_2)]^{2+}$,[10] complexes where, similarly, no π-acid ligands are present in the first shell. However, for these two latter examples, very long relaxation times determined at 20 °C and 400 MHz (T_1 = 345 and 346 ms, respectively) and very small coupling constants ($^1J_{HD}$ = 15.2 and 8.1 Hz, respectively) were reported, indicating long H–H distances. This is due to electron back−donation from the osmium center to the σ* orbital of H_2 causing the elongation of the H–H bond. A similar trend was reported for the complex $[Os(en)_2(H_2)H_2O]^{2+}$, where a dissociative mechanism for the substitution of the water molecule was assigned, with a stabilization of the penta−coordinate intermediate by rearrangement to the dihydride of Os(IV) complex, $[Os(en)_2(H)_2]^{2+}$.[11] In $[Ru(H_2O)_5(H_2)]^{2+}$, the situation is completely different as short relaxation times and large coupling constants were determined. This indicates little π-back-donation to the σ* orbital of H_2. This is a surprising result, as it is well known that Ru(II) aqua complexes bind strongly to π−acid ligands with efficient back-donation from the metal to the ligand which stabilizes the metal center towards oxidation.[12] A similar behavior was reported for $[Ru(H_2O)_5(N_2)]^{2+}$ where it was shown using density functional calculation results that there was no π back-bonding from Ru to N_2, resulting in a weak Ru–N_2 binding energy.[12]

We report here the characterization of the first dihydrogen aquacomplex containing water as the only other ligand. The dihydrogen nature of the ligand was demonstrated by the value of the ^{1}H NMR chemical shift of the bound H_2 signal, by the longitudinal relaxation time, T_1, of this signal and by the characteristic $^1J_{HD}$ value of the coordinated H–D ligand. Moreover, the $[Ru(H_2O_{ax})(H_2O_{eq})_4(H_2)]^{2+}$ structure of the complex was demonstrated by ^{17}O NMR. The activation of the H–H bond was also demonstrated by the appearance in D_2O of the ^{1}H NMR signals of coordinated and free HD molecules. These observations may be of primary importance in understanding the catalytic activity of $[Ru(H_2O)_6]^{2+}$ in the ring opening metathesis polymerisation reaction or in the dimerisation of ethylene. It may also open a new perspective in designing new H_2 activators with very simple chemical structure and efficient catalytic activity in water.

Notes and references

† All the solutions were prepared in a glove box, the solvent was previously degassed using a 20 min argon stream before use and all the observations were carried out under inert atmosphere. For the ^{1}H NMR spectra, the methyl of the toluene-*p*-sulfonic anion signal was taken as a reference at 2.38 ppm.

‡ The solution was kept for half an hour in the glove box to enrich the Ru(II) aquacomplex and reach the isotopic equilibrium. Under these conditions, the half life of the water exchange < 1 min ($k_{ex}^{H_2O}$ = 0.018 s^{-1} at 298 K).[13]

§ The variation as a function of the temperature of the longitudinal relaxation time, T_1, of the signal of H_2 bound in $[Ru(H_2O)_5(H_2)]^{2+}$ were determined on a 400 MHz NMR spectrometer for a solution containing initially $[Ru(H_2O)_6]^{2+}$ (0.101 mol kg^{-1}), toluene-*p*-sulfonic acid (0.598 mol kg^{-1}) and under 5.0 MPa of dihydrogen pressure. The following values were obtained: T_1 (400 MHz) = 55.7 ms (at 296.4 K), 67.1 ms (305.9) and 99.7 ms (321.7).

1 G. Laurenczy, L. Helm, A. Ludi and A. E. Merbach, *Helv. Chim. Acta.*, 1991, **74**, 1236.
2 G. Laurenczy, L. Helm, A. Ludi and A. E. Merbach, *Inorg. Chim. Acta.*, 1991, **189**, 131.
3 G. Laurenczy and A. E. Merbach, *J. Chem. Soc., Chem. Commun.*, 1993, 187.
4 R. H. Morris, K. A. Earl, R. L. Luck, N. J. Lazarowych and A. Sella, *Inorg. Chem.*, 1987, **26**, 2674.
5 T. Cusanelli, U. Frey, D. T. Richens and A. E. Merbach, *J. Am. Chem. Soc.*, 1996, **118**, 5265.
6 G. J. Kubas, *Acc. Chem. Res.*, 1988, **21**, 120.
7 T. Cusanelli, U. Frey, D. Marek and A. E. Merbach, *Spectrosc. Eur.*, 1997, **9**, 22.
8 P. A. Maltby, M. Schlaf, M. Steinbeck, A. J. Lough, R. H. Morris, W. T. Klooster, T. F. Koetzle and R. C. Srivastava, *J. Am. Chem. Soc.*, 1996, **118**, 5396.
9 W. D. Harman and H. Taube, *J. Am. Chem. Soc.*, 1990, **112**, 2261.
10 Z. W. Li and H. Taube, *J. Am. Chem. Soc.*, 1991, **113**, 8946.
11 Z. W. Li and H. Taube, *J. Am. Chem. Soc.*, 1994, **116**, 9506.
12 N. Aebischer, E. Sidorenkova, M. Ravera, G. Laurenczy, D. Osella, J. Weber and A. E. Merbach, *Inorg. Chem.*, 1997, **36**, 6009.
13 I. Rapaport, L. Helm, A. E. Merbach, P. Bernhard and A. Ludi, *Inorg. Chem.*, 1988, **27**, 873.

Communication 8/05579C

An illustration of the expression of cooperative binding energy in arrays of non-covalent interactions

Ben Bardsley and Dudley H. Williams*

Cambridge Centre for Molecular Recognition, University Chemical Laboratory, Lensfield Road, Cambridge, UK CB2 1EW. E-mail: dhw1@cam.ac.uk

Received (in Cambridge, UK) 1st September 1998, Accepted 18th September 1998

An analysis of a thermodynamic cycle for the formation of ligand-bound dimers gives a simple illustration as to how a cooperative binding energy ($\Delta G°_{coop}$) can be expressed over a range of interfaces, rather than at just one of the interfaces within the array.

The phenomenon of cooperativity has been shown to be important in a variety of molecular recognition processes throughout Nature.[1] In such systems, cooperative enhancements to binding are important in conferring relatively large Gibbs free energies of association and also high specificities on binding processes. Different mechanisms for the operation of cooperative binding exist, including conformational changes in the receptors involved, or more subtle structure tightening which may occur without a significant change in receptor conformation.[2–7] This paper gives a simple illustration as to how cooperativity occurring without a significant conformational change can potentially result in large Gibbs free energies of binding and how binding to one part of a receptor can result in the strengthening of binding at other interfaces within that receptor.

In previous work, we have shown that the dimerisation of vancomycin group of antibiotics is cooperative with the binding of ligands (peptides terminating in the sequence –Lys-D-Ala-D-Ala).[8] That is, dimerisation constants are typically greater in the presence of cell wall precursor analogues than in their absence, and ligand binding constants to antibiotic dimers are greater than those to monomers. As a result, dimerisation, with the resultant formation of a tetrameric cooperative array (two ligands binding to an antibiotic dimer), is beneficial to antibacterial activity.[8,9]

Recently, we have identified correlations between the chemical shifts of particular antibiotic protons and the Gibbs free energies of ligand binding ($\Delta G°_{lig}$) and dimerisation ($\Delta G°_{dim}$).[10–12] In both cases, the parameters under consideration (chemical shift) were determined under limiting conditions, *i.e.* antibiotic fully bound by ligand or antibiotic fully dimerised. We have used these monitored proton resonances as microscopic probes of the local tightness of the ligand binding and dimerisation interfaces; when the association constant is large, the resonance related to that interface shows a greater chemical shift change relative to the unassociated state.[11] Using these microscopic probes, we have been able to analyse the interfacial origins of the cooperative binding energy expressed upon formation of a ligand-bound dimer for a number of vancomycin group antibiotics.[12] We describe here a new analysis of this extended cooperative array, based on a thermodynamic cycle, from which it is possible to illustrate in a simple way useful conclusions regarding the expression of cooperative binding energy.

The enhancements to dimerisation and ligand binding resulting from cooperativity can be represented in a thermodynamic cycle showing the formation of a fully ligand-bound dimer from the constituent elements of two antibiotic monomers and two ligand molecules (Fig. 1).[8] There are four binding events occurring in this cycle. The left-hand half of Fig. 1 shows the formation of a fully ligand-bound dimer through the formation of a ligand-free antibiotic dimer followed by the binding of two ligand molecules to that dimer (**A** → **B** → **D**/**E**). The right-hand half of Fig. 1 shows the formation of the same fully ligand-bound dimer, but through the formation of two ligand-bound antibiotic monomers followed by dimerisation of these two monomers (**A** → **C** → **D**/**E**). Two possible scenarios (**D** and **E**) are considered for the formation of the fully ligand-bound dimer. **D** is the hypothetical situation where there is no cooperativity between dimerisation and ligand binding. In this case, there are no net influences on ligand binding due to dimerisation, and *vice versa*, *i.e.* no net influences on dimerisation due to ligand binding. **E** is the situation for the majority of vancomycin group members where dimerisation and ligand binding are cooperative processes, and the resultant Gibbs free energy benefit due to cooperativity is defined as $\Delta G°_{coop}$. We can use this thermodynamic cycle to illustrate the means by which a measured cooperative binding energy can, in theory, be expressed at any of the interfaces within an extended array.

In Fig. 1, the local tightness of the respective ligand binding and dimerisation interfaces (as evidenced from NMR data[11,12]) is represented schematically simply by greater distances between associating entities when the association at that interface is looser. The experimental data show that locally looser interfaces correlate with smaller K_{dim} and K_{lig} (*i.e.* less negative $\Delta G°_{dim}$ and $\Delta G°_{lig}$) values.[11,12] If there is no cooperativity between ligand binding and dimerisation (**D**), then the dimerisation and ligand binding interfaces are antici-

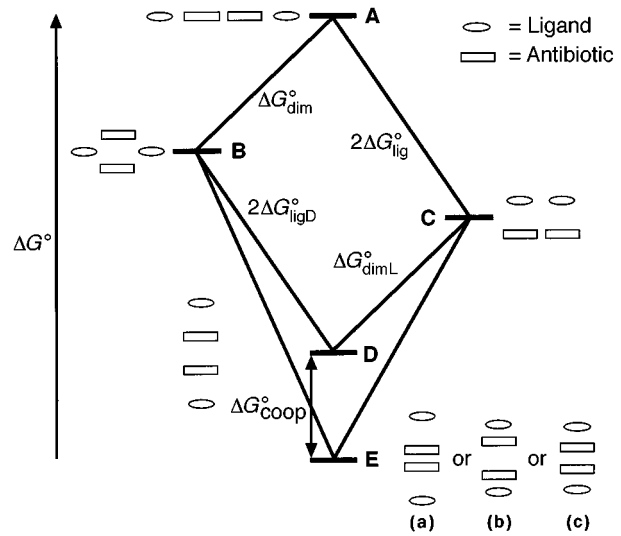

Fig. 1 Schematic thermodynamic cycle showing the formation of a fully ligand-bound antibiotic dimer from the constituent elements of two ligand molecules and two antibiotic monomers (**A**) *via* either a ligand-free antibiotic dimer (**B**) or two ligand-bound antibiotic monomers (**C**). The ligand-bound dimer at (**D**), is formed with no cooperativity between dimerisation and ligand binding. The ligand-bound dimers at (**E**) are formed with a cooperative Gibbs free energy ($\Delta G°_{coop}$) between dimerisation and ligand binding. For the two ligand binding events (**A** → **C** and **B** → **D**/**E**), the Gibbs free energies of binding are multiplied by 2 since each event involves the binding of two ligand molecules. See text for further analysis.

pated to be unchanged from those in **B** and **C**, respectively. If dimerisation and ligand binding are cooperative (**E**), however, then the cooperative binding energy ($\Delta G°_{coop}$) can, in theory, be expressed by tighter binding at either of the two interfaces, *i.e.* at the dimerisation interface and/or at the ligand binding interface.

There are two extreme states to consider for the expression of the cooperative binding energy, $\Delta G°_{coop}$. In **E(a)**, $\Delta G°_{coop}$ is expressed solely at the dimerisation interface and the tightness of the ligand binding interface remains the same as that in **C**. In **E(b)**, $\Delta G°_{coop}$ is expressed solely at the ligand binding interface and the tightness of the dimerisation interface remains the same as that in **B**. In practice, ligand-bound dimers are likely to express cooperative binding energy across both ligand binding and dimerisation interfaces as shown in **E(c)**. However, if we consider one of the extreme cases, *e.g.* **E(a)**, where all the cooperative binding energy is expressed at the dimerisation interface, then $\Delta G°_{coop}$ can still potentially be determined *via* measurement of either of two quantities: the ligand binding constant to dimer (**B** → **E**), or the dimerisation constant of ligand-bound antibiotic (**C** → **E**). For both measurements, $\Delta G°_{coop}$ is the same (**D** → **E**) and can be calculated from the increase in $\Delta G°_{dimL}$ over $\Delta G°_{dim}$, or from the increase in $2\Delta G°_{ligD}$ over $2\Delta G°_{lig}$. It is clear from this that in **E**(**a**), although $\Delta G°_{coop}$ is being expressed solely at the dimerisation interface and there is no increase in the tightness of the ligand binding interface, $2\Delta G°_{ligD}$ will show the same cooperative enhancement over $2\Delta G°_{lig}$ as will $\Delta G°_{dimL}$ over $\Delta G°_{dim}$. The same situation will exist even if $\Delta G°_{coop}$ is expressed solely at the ligand binding interface [**E(b)**]. In this case, although there will be no tightening of the dimer interface, $\Delta G°_{dimL}$ will still show an enhancement of $\Delta G°_{coop}$ over $\Delta G°_{dim}$. Thus, when $\Delta G°_{coop}$ is actually measured, *e.g.* by an increase in $\Delta G°_{dimL}$ over $\Delta G°_{dim}$, it is not possible to say, without further analysis of the complexes formed, at which interface the cooperative binding energy is expressed. (We have recently performed such an analysis of the partitioning of the cooperative Gibbs free energy between the dimerisation and ligand binding interfaces using the chemical shift of a proton at the dimer interface as a probe of interface tightness.[12])

Analogous diagrams would simply illustrate that in any system of weak interactions where there is a cooperative binding energy ($\Delta G°_{coop}$) expressed through the formation of an extended aggregate, then $\Delta G°_{coop}$ can potentially occur at *any* of the interfaces which go to make up that extended array. Also, if cooperativity is observed for a particular binding event in such an extended array, it does not necessarily follow that the bonding at the interface for that particular binding event has been improved.

One consequence of the above discussion is that the size of an extended array (number of non-covalent interactions making up the array) will affect the amount of cooperative binding energy ($\Delta G°_{coop}$) which can potentially be expressed. In the case of a fully ligand-bound antibiotic dimer, $\Delta G°_{coop}$ can be expressed over three binding interfaces whereas, if only one ligand was bound to the dimer, the cooperative binding energy could only be expressed over two binding interfaces. More generally, the greater the number of cooperatively-linked binding interfaces, the greater the scope for cooperative enhancements to binding. It thus follows that the greatest potential for expressing cooperative binding energies that would be expected in Nature are those involving the associations of large arrays of weak interactions, *e.g.* DNA duplexes, ligands binding to proteins.

B. B. thanks the EPSRC for financial support.

Notes and references

1 L. Stryer, *Biochemistry*, Freeman, New York, 3rd edn. 1988, pp. 82, 154–156, 234, 240, 267, 290.
2 N. S. Greenspan, in *Concepts in Chemistry: a contemporary challenge*, ed. D. H. Rouvrey, Research Studies Press Ltd, Taunton, 1997, pp. 383–403.
3 H. Guo and M. Karplus, *J. Phys. Chem.*, 1994, **98**, 7104.
4 M. F. Perutz, *Sci. Am.*, 1978, **239**, 92.
5 G. J. Sharman and M. S. Searle, *J. Am. Chem. Soc.*, 1998, **120**, 5291.
6 P. C. Weber, D. H. Ohlendorf, J. J. Wendoloski and F. R. Salemme, *Science*, 1989, **243**, 85.
7 D. H. Williams and M. S. Westwell, *Chem. Soc. Rev.*, 1998, **27**, 57.
8 J. P. Mackay, U. Gerhard, D. A. Beauregard, M. S. Westwell, M. S. Searle and D. H. Williams, *J. Am. Chem. Soc.*, 1994, **116**, 4581.
9 D. A. Beauregard, D. H. Williams, M. N. Gwynn and D. J. C. Knowles, *Antimicrob. Agents Chemother.*, 1995, **39**, 781.
10 M. S. Searle, G. J. Sharman, P. Groves, B. Benhamu, D. A. Beauregard, M. S. Westwell, R. J. Dancer, A. J. Maguire, A. C. Try and D. H. Williams, *J. Chem. Soc., Perkin Trans. 1*, 1996, 2781.
11 D. H. Williams, B. Bardsley, A. J. Maguire and W. Tsuzuki, *Chem. Biol.*, 1997, **4**, 507.
12 D. H. Williams, A. J. Maguire, W. Tsuzuki and M. S. Westwell, *Science*, 1998, **280**, 711.

Communication 8/06774K

Bis(diphenylphosphino)methane and related ligands as hydrogen bond donors†

Peter G. Jones and Birte Ahrens

Institut für Anorganische und Analytische Chemie, Technical University of Braunschweig, Postfach 3329, 38023 Braunschweig, Germany. E-mail: jones@xray36.anchem.nat.tu-bs.de

Received (in Basel, Switzerland) 26th May 1998, Accepted 15th September 1998

A search of the Cambridge Structural Database reveals that the methylene group of coordinated bis(diphenylphosphino)methane and related ligands can act as a hydrogen bond donor, with H···O distances as short as 2.20 Å; analogous C–H···Cl⁻ interactions are a feature of the packing of dppmSe complexes of silver(I) and gold(I).

Secondary bonding interactions have been the focus of increased interest for several years. The classical hydrogen bond is a well known structural phenomenon; the C–H···O hydrogen bond, at first a controversial postulate, is now accepted as an important factor in determining the nature and stability of solid-state structures.[1] It has been recognised that more acidic C–H groups are likely to provide stronger (shorter) hydrogen bonds, although the inverse correlation between length and strength may not be totally reliable.[1]

It is normal practice in X-ray structure determination to check newly determined structures for possible hydrogen bonds, and indeed this process can now be performed automatically for classical hydrogen bonds.[2] The search for C–H···X interactions is less well integrated into common program systems; correspondingly, it may be assumed that many such interactions fail to be reported. In this Institute, such searches have only recently become routine;[3] we use a default cutoff of 2.6 Å for the H···O distance, although appreciably longer interactions (up to 3 Å) have often been considered genuine hydrogen bonds.

In a recent study of six-membered heterocycles involving the P–CH_2–P unit, we observed some strikingly short intermolecular C–H···O interactions (H···O 2.25, C···O 3.24 Å) involving the methylene group between the phosphorus atoms.[4] This prompted us to re-inspect some of our older structures involving organic phosphorus heterocycles, and we discovered two cases where we had overlooked short intermolecular contacts between the H atoms of a P–CH_2–P unit and keto oxygens (H···O 2.38, 2.29 Å)[5]

Another molecule involving the P–CH_2–P group is the common ligand bis(diphenylphosphino)methane (dppm), $Ph_2PCH_2PPh_2$. The methylene hydrogens of dppm are known to be acidic, particularly in metal complexes; the deprotonated form of the ligand contains an additional donor, the methanide group.[6] It thus seemed likely that dppm complexes might display C–H···O hydrogen bonds.

A search of the Cambridge Structural Database[7] (Oct. 1997 version) was conducted for the fragment P–CH_2–P with an intermolecular H···O contact of < 2.5 Å to any O–C bond. The search was restricted to error-free, ordered structures. Apart from the two structures previously mentioned, a total of 23 structures (all of them complexes or clusters involving dppm or related ligands) with 28 C–H···O substructures were found. The geometry was in all cases acceptably linear (one C–H···O angle of 133°, all others > 143°). The shortest H···O contact was 2.20 Å.

The hydrogen bonds can be classified as follows: M–$CO_{terminal}$···H, 10 cases; M–$CO_{bridging}$···H, 2; $O_{solvent}$···H, 8; O_{anion}···H, 3; ligand C=O···H, 5. In no case were the C–H···O hydrogen bonds mentioned in the original publication; in several cases it was explicitly stated that *no* unusual intermolecular contacts were observed. It should be noted that these relatively few examples represent the shortest such interactions; there are presumably many more with somewhat longer H···O distances.

Although this initial search was restricted to oxygen acceptors, it is clear that other electronegative elements should accept hydrogen bonds from dppm. In view of our interest in coinage metal complexes with selenium ligands,[8] we therefore determined structures of the type $[(dppmSe)_2M]^+Cl^-$ (**1a**, M = Ag, dichloromethane solvate; **1b**, M = Ag, ethanol solvate; **2a**, M = Au, chloroform solvate; **2b**, M = Au, ethanol solvate).‡§ These are the first complexes involving P_2Se_2 coordination at silver(I) and gold(I). The coordination at the metal atoms is distorted tetrahedral; angular distortions arise from the restricted bite of the ligands, but the gold complexes additionally display a major difference in Au–Se bond lengths (0.16 Å in **2b** and 0.30 Å in **2a**; values are given in Figs. 1 and 2). The structure of a two-coordinate gold(I) complex of the same ligand has been reported by Schmidbaur, *et al.*[9] and by chance belongs to the set of 23 compounds discussed above; it displays two C–H···$O_{acetone}$ hydrogen bonds.

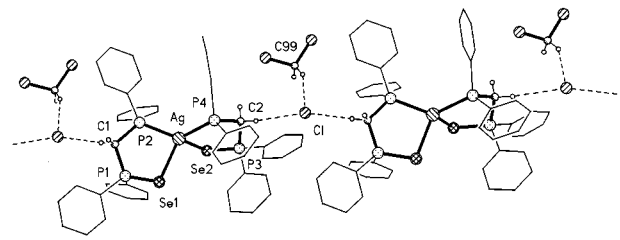

Fig. 1 The structure of **1a** in the crystal. Hydrogen atoms of the phenyl groups are omitted for clarity, radii are arbitrary. Dashed lines represent H bonds. Selected bond lengths (Å) and angles (°): Ag–Se1 2.7086(12), Ag–Se2 2.7749(13), Ag–P2 2.453(3), Ag–P4 2.439(2); bite angles P2–Ag–Se1 92.49(6), P4–Ag–Se2 91.40(6); H···Cl⁻···H 164. The structures of **1b** (isostructural) and **2b** (equivalent packing) are similar to **1a**: **1b** Ag–Se1 2.7179(10), Ag–Se2 2.7643(10), Ag–P2 2.454(2), Ag–P4 2.440(2); P2–Ag–Se1 92.69(5), P4–Ag–Se2 91.64(5); H···Cl⁻···H 159. **2b** Au–Se1 2.9459(12), Au–Se2 2.7891(12), Au–P2 2.306(3), Au–P4 2.319(2); P2–Au–Se1 89.64(7), P4–Au–Se2 91.61(7); H···Cl⁻···H 160.

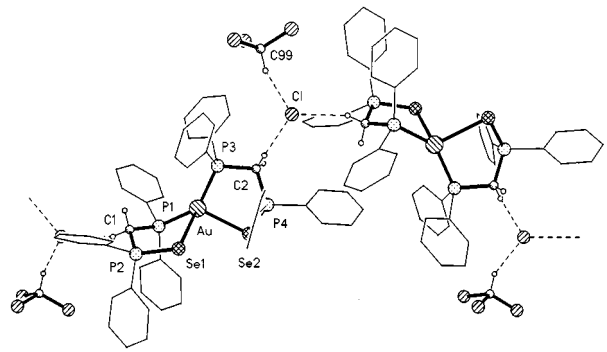

Fig. 2 The structure of **2a** in the crystal. Hydrogen atoms of the phenyl groups are omitted for clarity, radii are arbitrary. Dashed lines represent H bonds. Selected bond lengths (Å) and angles (°): Au–Se1 3.0571(10), Au–Se2 2.7535(9), Au–P1 2.298(2), Au–P3 2.329(2); P1–Au–Se1 83.46(5), P3–Au–Se2 92.65(5), H···Cl⁻···H 112.

Table 1 Hydrogen bond geometry in compounds **1a**,**b**, **2a**,**b**

Compound, H bond	H···Cl⁻/Å	C···Cl⁻/Å	C–H···Cl⁻/°
1a, C–H_{dppm}···Cl⁻	2.87	3.839(9)	168
1a, C–H_{dppm}···Cl⁻	2.61	3.556(9)	160
1a, C–H_{solv}···Cl⁻	2.58	3.467(14)	149
1b, C–H_{dppm}···Cl⁻	2.82	3.779(6)	164
1b, C–H_{dppm}···Cl⁻	2.75	3.705(7)	163
2a, C–H_{dppm}···Cl⁻	2.64	3.576(7)	157
2a, C–H_{dppm}···Cl⁻	2.57	3.535(7)	166
2a, C–H_{solv}···Cl⁻	2.70	3.554(12)	144
2b, C–H_{dppm}···Cl⁻	2.68	3.616(9)	157
2b, C–H_{dppm}···Cl⁻	2.61	3.567(10)	163
2b, O–H_{solv}···Cl⁻		3.042(10)	

All four structures **1a**,**b**, **2a**,**b** display C–H···Cl hydrogen bonds (Table 1), which play a central role in determining the crystal packing. In each structure, the ions are connected into chains (Figs. 1 and 2) by hydrogen bonds C–H_{dppm}···Cl⁻, whereby the chloride accepts two hydrogen bonds. Additionally, there is a C–H_{solv}···Cl⁻ contact from a solvent molecule in **1a** and **2a**, an O···Cl contact involving the ethanol of **2b**, and a similar contact in **1b**, in which however the ethanol is poorly resolved.

A second database search,[7] this time for C–H···Cl contacts, also proved fruitful; a total of 28 hydrogen bonds in 21 structures were found with H···Cl < 2.8 Å and C–H···Cl > 130°. These contacts can be classified as: 14 C–H_{dppm}···Cl_{coord}; 12 C–H_{dppm}···Cl⁻, 2 C–H_{dppm}···$Cl_{(other\ anions)}$. Only one of these contacts was mentioned explicitly as an interaction with dppm in the original publications;[10] it should however be stressed that it was until recently not usual to look for hydrogen bonds involving C–H units. As an example of an unrecognised hydrogen bond, we can again cite our own work; the structure of $[(dppm)_2Au_3Cl_2]^+[(C_6F_5)_3AuCl]^-$ [11] involves a contact C–H_{dppm}···Cl_{anion} with H···Cl 2.70 Å, C–H···Cl 139°.

It may be concluded that coordinated dppm is capable of acting as a C–H···X hydrogen bond donor; in such cases it presumably exerts a significant influence on structure and stability, although to the best of our knowledge this possibility has not previously been discussed in detail. An obvious corollary is that structures of complexes of dppm and related ligands should be routinely screened for such hydrogen bonds.

We thank the Fonds der Chemischen Industrie (Frankfurt) for financial support and Dr C. Thöne for helpful discussions.

Notes and references

† Dedicated to Professor Armand Blaschette on the occasion of his 65th birthday.

‡ Bis[(diphenylphosphino)(diphenylphosphineselenido)methane]silver(I) chloride **1** was obtained from dppmSe and AgCl in 2:1 molar ratio in acetone; after filtration, the product was precipitated in 67% yield with light petroleum. Crystals were grown by diffusion of light petroleum into a solution of **1** in dichloromethane (**1a**) or by diffusion of diethyl ether into a solution of **1** in ethanol (**1b**).

Bis[(diphenylphosphino)(diphenylphosphineselenido)methane]gold(I) chloride **2** was obtained from the reaction of dppmSe with a suspension of (tht)AuCl (tht = tetrahydrothiophene) in 2:1 molar ratio in toluene, followed by precipitation with diethyl ether (yield 66%). Crystals were grown by diffusion of diethyl ether into a solution of **2** in chloroform (**2a**) or ethanol (**2b**).

Satisfactory elemental analyses and consistent NMR spectra (^1H, ^{13}C, ^{31}P, ^{77}Se) were obtained.

§ *X-Ray structure determinations*: data were measured at −100 °C on a Siemens P4 diffractometer using Mo-Kα radiation. Absorption corrections using psi-scans (**2b**: SHELXA[2]). Structures were refined on F^2 using all reflections (program SHELXL-93[2]). Hydrogen atoms were included using a riding model; C–H bond lengths (and H···X contacts) are thus systematically shortened with respect to the true values.

Crystal data: **1a**, **1**·3CH_2Cl_2: $C_{53}H_{50}AgCl_7P_4Se_2$, M = 1324.75, monoclinic, $C2/c$, a = 38.984(7), b = 14.010(2), c = 21.952(4) Å, β = 101.534(12)°, V = 11747(4) Å^3, Z = 8, μ = 2.0 mm^{-1}, 10 989 reflections, 10 260 unique, $wR2$ 0.201, $R1$ 0.066.

1b, **1**·3.5EtOH: $C_{57}H_{65}AgClO_{3.5}P_4Se_2$, M = 1231.21, monoclinic, $C2/c$, a = 39.315(7), b = 14.026(2), c = 22.214(3) Å, β = 100.538(10)°, V = 12 043(3) Å^3, Z = 8, μ = 1.7 mm^{-1}, 21 045 reflections, 10 577 unique, $wR2$ 0.101, $R1$ 0.051.

2a, **2**·2$CHCl_3$: $C_{52}H_{46}AuCl_7P_4Se_2$, M = 1397.80, monoclinic, $P2_1/c$, a = 12.917(2), b = 22.285(3), c = 19.050(3) Å, β = 99.850(10)°, V = 5403.0(13) Å^3, Z = 4, μ = 4.6 mm^{-1}, 14 225 reflections, 9509 unique, $wR2$ 0.108, $R1$ 0.046.

2b, **2**·EtOH: $C_{52}H_{50}AuClOP_4Se_2$, M = 1205.14, orthorhombic, $Pna2_1$, a = 22.425(3), b = 13.713(2), c = 16.035(2) Å, V = 4930.9(11) Å^3, Z = 4, μ = 4.7 mm^{-1}, 11 215 unique reflections, $wR2$ 0.104, $R1$ 0.048. CCDC 182/987.

1 G. R. Desiraju, *Acc. Chem. Res.*, 1996, **29**, 441; T. Steiner, *Chem. Commun.*, 1997, 727; T. Steiner and G. R. Desiraju, *Chem. Commun.*, 1998, 891.

2 SHELXL-97, a program for refining crystal structures. G. M. Sheldrick, Univ. of Göttingen, Germany, 1997. The earlier version SHELXL-93 was used to refine the structures **1a**,**b**, **2a**,**b**.

3 See, for example: D. Henschel, O. Moers, A. Blaschette and P. G. Jones, *Acta Crystallogr., Sect. C*, 1997, **53**, 1877.

4 P. G. Jones and A. Weinkauf, *Acta Crystallogr., Sect. C*, 1998, **54**, in press.

5 I. V. Shevchenko, A. Fischer, P. G. Jones and R. Schmutzler, *Chem. Ber.*, 1992, **125**, 1325; 1247.

6 R. Usón, A. Laguna, M. Laguna, B. R. Manzano, P. G. Jones and G. M. Sheldrick, *J. Chem. Soc., Dalton Trans.*, 1984, 839.

7 F. H. Allen and O. Kennard, *Chem. Des. Autom. News*, 1993, **8**, 31. REFCODES: C–H···O: CERREW, DAMMOT, DISMEX, FELCUU, GIJDAE, JARDEL, JARTOL, JITYUG, JITZAN, KAXYAJ, KIGROH, PAKFEM, PAKFOW, SEJBEO, SINBOG, TETKUY, TIVQUK, TUMLUI, VIVLUH, VUFPAN, ZASCUR, ZOWZOA, ZUXQOY. C–H···Cl: CACPOL, CEYNOJ, DILNIV, DOJKOC, DPMCPD, HEBXUH, JAGNEK, JUMLUY, KIFPUK, KOPRUC, KUKNAF, TAZZID, TUFKEK, TUFKIO, TUPNIB, VOBHID, VUFPAN, YASTAN, YAYSUM, ZUGTOK, ZURGUO.

8 P. G. Jones and C. Thöne, *Acta Crystallogr., Sect. C*, 1992, **48**, 2114, and references therein.

9 H. Schmidbaur, J. Ebner von Eschenbach, O. Kumberger and G. Müller, *Chem. Ber.*, 1990, **123**, 2261.

10 B. R. Sutherland and M. Cowie, *Organometallics*, 1985, **4**, 1637.

11 R. Usón, A. Laguna, M. Laguna, E. Fernández, M. D. Villacampa, P. G. Jones and G. M. Sheldrick, *J. Chem. Soc., Dalton Trans.*, 1983, 1679.

Communication 8/03905D

New sodium organobis(silantriolates)

Bruno Boury,* Francis Carré, Robert J. P. Corriu* and Rosario Nuñez

UMR 5637, CC 007, Université Montpellier II, Sciences et Techniques du Languedoc, 34095 Montpellier Cedex 05, France. E-mail: boury@crit.univ-montp2.fr

Received (in Basel, Switzerland) 3rd June 1998, Accepted 16th September 1998

The sodium salt $(NaO)_3SiC_6H_4Si(ONa)_3$ has been prepared by reaction of the corresponding methoxysilane with an aqueous solution of NaOH and was fully characterized by X-ray crystallographic studies, which indicates the presence of 13 water molecules and one hydroxide group in the crystal structure.

An enormous variety of silicates of general formula SiO_4M_4 is known, based on the different possibilities to associating the basic tetrahedral unit SiO_4 forming linear or cyclic, infinite chains and sheets.[1] By comparison, organosilanolates of general formula $R_xSi(OM)_{4-x}$ (M = group 1 or 2) metal cation are less well known. The preparation of such organosilanolates was first reported by reacting chlorosilane[2] with strong bases, and later, using siloxanes[3] and silanols[4] treated directly with metallic alkali or alkali metal hydroxides. These reaction conditions do not lead to cleavage of the Si–C bond and the organic part remains intact in the silicate. Compounds R_3SiOM (M = Na,[5] K,[6] Cs and Rb[7]) and $R_2SiO_2M_2$ (M = Li and Na[8]) were isolated and fully characterized by crystal X-ray diffraction. More recently, the possibility to prepare siloxanes and silsesquioxanes with silanolate functionalities was demonstrated.[9] Here, we report the synthesis and structural characterization of the first organosilanolate isolated from the reaction of a 1,4-bis-(trialkoxysilyl)benzene with NaOH in aqueous solution.

The growing interest for the elaboration of hybrid materials from molecular precursors led us to investigate the formation of such organosilanolates from precursors of the general formula $(MeO)_3Si–R–Si(OMe)_3$, this type of compound is currently under investigation for the preparation of hybrid materials by sol–gel polycondensation.[10] We were particularly attracted by the possibility to form lamellar or pillared materials and to consider the possibility to organize the organosilanolate molecules through the interaction of ionic Si–O^- groups with the associated cation. We first looked at $(MeO)_3SiC_6H_4Si(OMe)_3$ since the regidity of the phenylene group will favor construction of the corresponding organosilanolate.

The preparation of the sodium salt of $^-O_3SiC_6H_4SiO^-_3$ was carried out in water by treatment of **1** with a slight excess of NaOH (1 : 6.6) [eq. (1)].† The compound obtained after

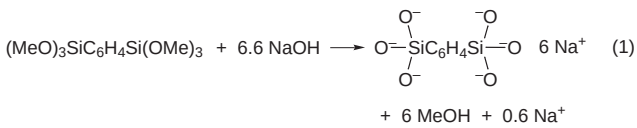

(1)

evaporation of water is a hygroscopic crystalline white powder **2**.‡ Colorless crystals of **3** were isolated from a solution of **2** at 4 °C.† They were poorly stable to air at 25 °C due to loss of water, however, they could be stored for several weeks at −20 °C in a atmosphere saturated in water and this allowed a full characterization by X-ray diffraction crystal structure analysis.§ Fig. 1 shows the ORTEP drawing and important bond lengths and bond angles for **3**.¶ This crystal structure is triclinic and an inversion center is present. In this structure, 13 molecules of water and one hydroxide group are involved in coordination to the sodium cations. The presence of ligated water also results in a high number of strong hydrogen bonds (only some of these are shown is Fig. 1 for clarity, and because the lack of accuracy in the position of some of the hydrogen atoms, prevented location of all of them). The presence of an extended network of strong hydrogen bonds is similar to layered sodium polysilicate hydrates.[11] Another general feature of the sodium phenyl-1,4-bis(silantriolate) packing is the organisation of the phenylene groups which are all parallel to each other and oriented in the same direction, however the interaction between the organic moieties (C_6H_4) are limited since they are surrounded by coordinated Na^+ cations.

In the crystal structure, each silicon atom is bonded to three oxygen atoms and to a carbon atom of the phenyl group. The Si–C bond length of 1.89(8), is typical for such arylsilicon compounds [Si–C_{aryl} (average) 1.88(1) Å]. The geometry around the silicon atom is slightly distorted tetrahedral, one of the three Si-O^- bonds being longer than the other two: Si1–O1 1.679(5) Å, Si1–O2 and Si1–O3 1.605(6)– and 1.609(5) Å, respectively. All these values are typical of Si–O^- bond lengths [≈1.63(4) Å] found in silicates.[12] This distortion is also reflected in the differences between angles O2–Si1–O3 [115.8(3)°] and O3–Si1–O1 [106.6(3)°], both being close to those reported for the sodium trimethylsilanolate trihydrate[5] and sodium silicates.[12] These distortions can be related to the different environment involving the oxygen atoms of the

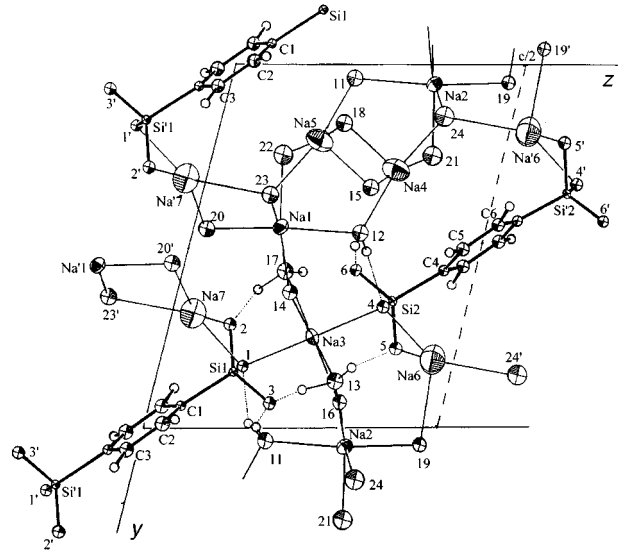

Fig. 1 ORTEP drawing of compound **3**. Select bond distances (Å) and angles (°): Si1–O1 1.679(5), Si1–O2 1.605(6), Si1–O3 1.609(5), Si1–C1 1.887(8), C1–C2 1.389(11), C2–C3 1.396(12), C1–C3 1.402(11), Si2–O4 1.679(5), Si2–O5 1.603(6), Si2–O6 1.601(5), Si2–C4 1.890 C4–C5 1.387(11), C5–C6 1.384(12),. C4–C6 1.397(11), Na1···O17 2.347(6), Na1···O14 2.367(6), Na1···O20 2.399(7), Na1···O22 2.428(7), Na1···O23 2.496(7), Na1···O12 2.582(7), Na3···O14 2.344(6), Na3···O13 2.344(6), Na3···O1 2.491(6), Na3···O4 2.500(6), Na3···O17 2.573(6), Na3···O16 2.576(6), Na4···O12 2.329(7), Na4···O18 2.334(8), Na4···O24 2.363(8), Na4···O15 2.495 Na4···O21 2.603(8), Na6···O5 2.655(8), Na6···O4 2.765(7), Na6···O19 2.774(8), Na6···O24 2.781(8), C1–S1–O1 107.2(3), C1–S1–O1 111.1(3), C1–S1–O3 107.2(3), O1–Si1–O2 108.5(3), O2–Si1–O3 115.8(3), O3–Si1–O1 106.6(3), Si1–C1–C2 123.2(6), Si1–C1–C3 120.8(6), C2–C3–C1 122.1(7).

–SiO_3^{3-} group, especially through their interaction with the sodium atoms.

In the crystal structure of **3**, four kinds of sodium atoms are present, with deficiency coordination number and nature of ligating atoms. Hexacoordination is typical for Na^+ cations in ionic organic structures.[13] In compound **3** some of the sodium atoms are coordinated only to oxygen atoms of water or hydroxide ligands: atoms Na1 and Na2 are hexacoordinated (octahedral geometry) while atoms Na4 and Na5 are pentacoordinated (square pyramidal geometry). For the other Na atoms, interaction with oxygen atoms of the Si-O^- group is observed: Na6 and Na7 are tetracoordinated to two water molecules and to two Si–O^- from the same –SiO_3^{3-} group (tetrahedral geometry) while Na3 is hexacoordinated by water molecules, O13, O14, O16, O17, and by the oxygen atoms O1 and O4 of two Si–O^- of two different phenylene-1,4-bis(silantriolate) anions (octahedral geometry). In addition, some of the ligands are shared between two sodium atom, *e.g.* Na7 shares atom O1 with Na3, as well as Na6 shares O4 and O19 with respectively Na3 and Na2. Similarly, O13 of a water molecule is coordinated to Na3 and Na2.

For the hexa- and penta-coordinated sodium cations, the Na···O interatomic distances are in the range of the Si-O···Na bond lengths (2.303 < d/Å < 2.549 Å) typical of sodium silicates[12] or ionic organosilicate hydrates,[5] and are characteristic of a strong ion-dipole interaction. For sodium atoms in tetrahedral geometry, longer Na···O distances are observed [2.645(8)–2.781(8) Å]. In addition, a distorted tetrahedral arrangement is seen for atoms Na6 and Na7, the O4-Na6-O24 [137.1(3)°] and O1–Na7–O23 [138.0(3)°] angles being much larger than O19–Na6–O24 [92.1(2)°] and O4–Na6–O24 [91.9(2)°]. This distortion can be explained by the participation of the oxygen atoms in ionic interactions and to H bonding.

In conclusion, this type of organobis(silantriolate) species can be easily prepared by treatment of the corresponding organoalkoxysilane with a strong base. Their structure and their crystallization with water present some similarities with mineral and synthetic silicates. Our current investigations of this types of organosilantriolate in our laboratory are mainly directed to the preparation of organized organomineral materials, especially on the role of the cation and the elimination or replacement of water ligands.

Notes and references

† *Typical experimental procedure*: **1**: The synthesis of 1,4-bis(trimethoxysilyl)benzene **1** has been described previously.[14] **2**: To a Schlenk tube containing 1,4-bis(trimethoxysilyl)benzene **1** (2.95 g, $9.28\cdot10^{-3}$ mol) were added 6.6 equiv. of NaOH (2.45 g, $6.12\cdot10^{-2}$ mol.) dissolved in 30 ml of deionized water (pH = 6). The mixture was stirred at room temperature for several hours to obtain a transparent and homogeneous solution. The water was evaporated under reduced pressure at 25 °C to give a crystalline white solid, which was dried *in vacuo* (1 mm Hg) at 25 °C for 16 h to give 6.52 g of compound **2**. **3**: Colorless crystals of **3** (0.51 g) were obtained from a solution of 5 g of **2** in 100 ml of deionized water cooled to 4 °C, at pH = 12.3.

‡ *Selected spectroscopic and analytical data for* **2**: ^{1}H NMR (200 MHz, D_2O, 20 °C): δ7.55 (s, 4H, C_6H_4). FTIR (KBr, cm^{-1}): 3384 ν(H–OH), 3030 ν (C_{ar}-H), 1448, 1131, 1008 ν(Si–O), 880 ν(Si–OH), 778 ν(Si–C).

§ *Crystal data for* **3**: Nonius CAD 4 automated diffractometer, crystal fixed in oil under nitrogen, $C_6H_{31}Na_7O_{20}Si_2$, M_r = 640.4, triclinic, space group $P\bar{1}$ crystal dimensions 0.05 × 0.07 × 0.11 mm, a = 6.265(2), b = 11.949(1), c = 18.844(2) Å, α = 101.594(8), β = 99.56(1), γ = 105.23(1)°, U = 1297.0(4) Å^3, D_c = 1.640 g cm^{-3}, T = 193 K, Z = 2, F = 664, μ(Mo-Kα) = 3.22 cm^{-1}, A^* = 0.55, $2\theta_{max}$ = 44° , R,R_w = 0.0554,0.0586 (statistical weights), N_0 = 1912 observed [$I > 2\sigma(I)$] reflections out of N = 2686 unique, λ(Mo-Kα) = 0.71069 Å The hydrogen atoms of the phenyl groups were placed calculated positions (SHELX-76). After four least-squares refinement cycles with anisotropic thermal parameters for all non-hydrogen atoms some water hydrogen atoms were positioned in a difference Fourier map. These hydrogen atoms were taken in account in the next refinement and Fourier calculations, but their positional parameters were then kept fixed. After six such refinements and difference Fourier maps, the refinement converged to a final R value of 0.0554 (R_w = 0.0586). One of the last peaks searched as a possible hydrogen atom. (on O23) was rejected in view of the unacceptable resulting H–O–H angle value (88°). In the same way, no more than one relevant peak was observed on oxygen atom O22. The list of hydrogen atoms coordinates is available in the supplementary data. Absorption corrections were neglected. Direct methods (SHELXS-86) succeeded in locating the bis-silanolate anion. The other non-hydrogen atoms were located in a Fourier map and two subsequent difference Fourier maps. CCDC 182/1022

¶ Studies have been undertaken to demonstrate if the crystal structure of **3** is representative of the bulk white solid **2**.

1 F. Liebau, *Structural Chemistry of Silicate*, Springer-Verlag, Berlin, 1985.
2 F. S. Kipping, *J. Chem. Soc.*, 1912, **101**, 2108; R. Robinson and F. S. Kipping, *J. Chem. Soc.*, 1912, **101**, 2142; J. A. Meads and F. S. Kipping, *J. Chem. Soc.*, 1914, **105**, 679; J. A. Meads and F. S. Kipping, *J. Chem. Soc*, 1914, **107**, 459.
3 J. F. Hyde, *J. Am. Chem. Soc.*, 1953, **75**, 2166; J. F. Hyde, O. K. Johanson, W. H. Daudt, R. F. Fleming, H. B. Laudenslager and M. P. Roche, *J. Am. Chem. Soc.*, 1953, **75**, 5615; M. B. Fromberg, Y. K. Petrashko, V. D. Vozhova and K. A. Andrianov, *Izv. Akad. Nauk. SSSR, Ser. Khim.*, 1965, **4**, 660.
4 L. H. Sommer, E. W. Pietrusza and F. C. Whitmore, *J. Am. Chem. Soc.*, 1946, **68**, 2282; L. H. Sommer, L. Q. Green and F. C. Whitmore, *J. Am. Chem. Soc.*, 1949, **71**, 3253; W. S. Tatlock and E. G. Rochow, *J. Org. Chem.*, 1952, **17**, 1555.
5 I. L. Dubchak, V. E. Shklover, M. Yu. Antipin, Yu. T. Struchkov, V. M. Kopylov, A. M. Muzafarov, P. L. Prikhodko and A. A. Zhdanov, *J. Struct. Chem.* (*Engl. Transl.*), 1982, **23**, 219; I. L. Dubchak, V. E. Shklover, Y. T. Struchkov, V. M. Kopylov and P. L. Prikhodko, *J. Struct. Chem. (Engl. Transl.)*, 1983, **24**, 218.
6 F. Paver and G. H. Sheldrick, *Acta Crystallogr., Sect. C*, 1993, **C49**, 1283.
7 E. Weiss, K. Hoffmann and H. F. Grützmacher, *Chem. Ber.*, 1970, **13**, 1190.
8 S. Schütte, U. Klingebiel and D. Schmidt-Bäse, *Z. Naturforsch, Teil B*, 1993, **48**, 263.
9 A. Voigt, M. G. Walawalkar, R. Murugavel, H. W. Roesky, E. Parisini and P. Lubini, *Angew. Chem., Int. Ed. Engl.*, 1997, **36**, 2203; F. J. Feher, T. A. Budzichowski and J. W.Ziller, *Inorg. Chem.*, 1997, **36**, 4082.
10 D. A. Loy and K. J. Shea, *Chem. Rev.*, 1995, **95**, 1431; R. J. P. Corriu and D. Leclercq, *Angew. Chem. Int. Ed. Engl.*, 1996, **35**, 1420.
11 W. Schwieger, D. Heidemann and K. H. Bergk, *Rev. Chim. Minér.*, 1985, **22**, 639; A. Brandt, W. Schwieger, and K. H. Bergk, *Rev. Chim. Minér.*, 1987, **25**, 564.
12 W. S. McDonald and D. W. J. Cruickshank, *Acta Crystallogr.*, 1967, **22**, 37.
13 S. Menchetti and O. Sabelly, *Acta Crystallogr., Sect. B*, 1978, **34**, 45; K. T. Wei and D. L. Ward, *Acta Crystallogr., Sect. B.* 1977, **33**, 522.
14 K. J. Shea, D. A. Loy and O. Webster, *J. Am. Chem. Soc.*, 1992, **114**, 6700.

Communication 8/04194F

Convenient synthetic approach towards regioselectively sulfated sugars using limpet and abalone sulfatase-catalyzed desulfation

Hirotaka Uzawa,[a]† Tadashi Toba,[b] Yoshihiro Nishida,[b]‡ Kazukiyo Kobayashi,[b] Norihiko Minoura[a] and Kazuhisa Hiratani[c]

[a] *National Institute of Materials and Chemical Research, 1-1 Higashi, Tsukuba 305-8565, Japan*
[b] *Department of Molecular Design and Engineering, Graduate School of Engineering, Nagoya University, Chikusa-ku, Nagoya 464-8603, Japan*
[c] *National Institute for Advanced Interdisciplinary Research, 1-1-4 Higashi, Tsukuba 305-8562, Japan*

Received (in Cambridge, UK) 27th July 1998, Accepted 1st September 1998

3,6-Disulfated *p*-nitrophenyl β-D-galactopyranoside 3 and 3′,6′-disulfated *p*-nitrophenyl β-lactoside 7, which were regioselectively obtained *via* organotin methodology, were subjected to enzymatic desulfation: limpet and abalone sulfatases (EC 3.1.6.1) hydrolyzed regioselectively the 3- and 3′-sulfate moieties of 3 and 7 to afford 6-monosulfated galactopyranoside 4 and 6′-monosulfated lactoside 8, respectively.

Various sulfated analogues of sialyl Le[a] and Le[x] have been prepared by different groups[1–9] as artificial ligands of the selectin families, which include artificial glycoconjugate polymers and dendrimers carrying sulfated carbohydrates.[10–13] As part of our project to develop biofunctional glycoconjugate polymers able to adsorb certain pathogenic bacteria and their toxins,[14,15] our interests have been directed to regioselectively sulfated sugars as substitutes for natural sialyl oligosaccharides and sulfatides known to bind with various viruses and pathogenic bacteria.[16] Here we report a new chemoenzymatic synthetic approach towards regioselectively sulfated *p*-nitrophenyl (pNP) β-D-galactopyranosides and lactosides.

Regioselective sulfations of carbohydrate molecules reported in recent years may be divided into the following types; chemical methods using stannylated sugars[17] and enzymatic approaches using sulfotransferase for non-sulfated sugar acceptors[18] or glycosyltransferases for sulfated acceptors.[19] Here we describe a convenient synthetic approach using *sulfatases*. Although various types of sulfatases are commercially available at low cost, their utility for chemoenzymatic syntheses has not yet been fully explored. Now we propose a new practical approach which involves introduction of plural sulfates into sugars *via* organotin methodology and then regioselective desulfation with sulfatases. pNP β-D-Galactopyranoside **1** and pNP β-lactoside **5** (Scheme 1) were employed as model compounds to demonstrate our approach. The pNP group is used due to its ready conversion to a *p*-*N*-acryloylaminophenyl group ready for subsequent polymerization.[20,21] Moreover, sulfated galactoses and lactoses are promising ligand candidates for influenza viruses and the other microbes.

The initial chemical approach to **1** and **5** was as follows. Reaction of **1** with Bu_2SnO (1 equiv.) and then SO_3NMe_3 (1 equiv.) gave 3-monosulfated galactoside **2** in 77% yield, while the use of $(Bu_3Sn)_2O$ (0.75 equiv.) and an excess of SO_3NMe_3 (5 equiv.) gave 3,6-disulfated derivative **3** in 97% yield.§ Thus, these chemical methods afforded 3-mono- and 3,6-di-sulfated galactosides in a regioselective manner, while not affording directly the 6-monosulfated galactose **4**. A similar process for **5** using Bu_2SnO (1 equiv.) and then SO_3NMe_3 (1 equiv.) gave selectively 3′-monosulfated pNP β-lactoside **6** (57% isolated yield).¶ Use of Bu_2SnO (3 equiv.) and SO_3NMe_3 (3 equiv.) afforded 3′,6′-disulfated lactoside **7** as the main product (40% yield).‖ Similar reaction of **5** using $(Bu_3Sn)_2O$ instead of Bu_2SnO gave a complex mixture of sulfated products.

The location of sulfate groups in sulfated lactosides **6** and **7** was determined by 2D NMR experiments (^{1}H-^{1}H COSY). The

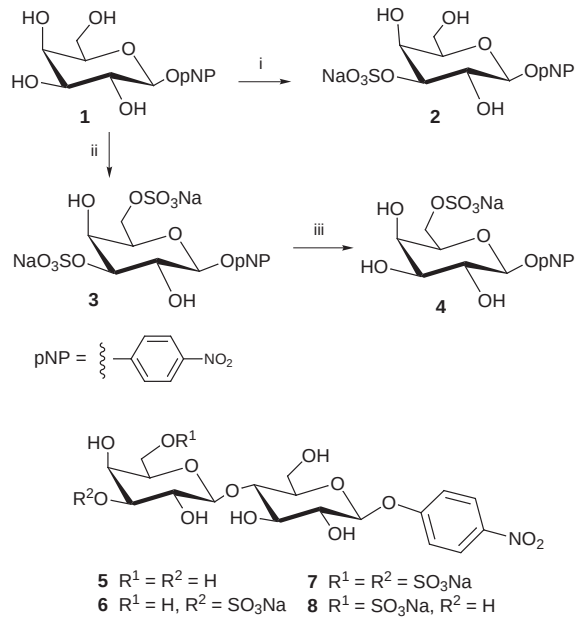

Scheme 1 *Reagents and conditions*: i, Bu_2SnO (azeotropic), SO_3NMe_3, then Dowex Na^+; ii, $(Bu_3Sn)_2O$, (azeotropic), SO_3NMe_3, then Dowex Na^+, 97%; iii, sulfatase, 0.25 M NaOAc–AcOH buffer (pH 6.8), 37 °C, 80%.

signal of H-3′ of a galactose residue (δ 4.32–4.38, dd, *J* 3.0–3.3 and 9.5–9.8 Hz) of **6** and **7** showed downfield shift due to the sulfation at the geminal O-3′, while the H-3 of glucose (δ 3.796 and 3.805, br t, *J* 9.5–9.9 Hz) did not show the corresponding downfield shift. These results showed that the sulfate group was located at O-3′ in the galactosyl residues for both **6** and **7**.

3,6-Disulfated galactoside **3** and 3′,6′-disulfated lactoside **7** were subjected to enzyme-catalyzed desulfation with sulfatases (EC 3.1.6.1) (Table 1).** Three types of commercially available sulfatases were tested, and each of the desulfated products was analyzed by ^{1}H NMR spectroscopy. The enzyme reaction of **3** with snail sulfatase in NaOAc–AcOH buffer (pH 6.8, 37 °C) was completed in 2 days to afford a less polar product. The

Table 1 Regioselectivity of sulfatase-catalyzed desulfation

Substrates	Sulfatases origins[a]	*t*/days[b]	Conversion (%)	Product
3	snail	2	94[c]	**4**
3	abalone	2	> 95[d]	**4**
3	limpet	2	> 95[d]	**4**
7	snail	3	0	—
7	abalone	3	40[c]	**8**
7	limpet	3	> 95[d]	**8**

[a] Commercially available sulfatases from snail (*Helix pomatia*), abalone and limpet (*Patella vulgata*) were used. [b] Typical procedure is shown in footnote ††. [c] Isolated yield. [d] Determined by ^{1}H NMR analysis or TLC.

product was isolated in >90% yield and identified as 6-monosulfated galactoside **4**.†† The 6-sulfated structure could be determined by ^{1}H NMR analysis, *via* comparison of the spectral data with those of **3** and pNP β-D-galactopyranoside **1**. The downfield shift of H-3 (δ 4.484, dd, J = 3.3 and 9.6 Hz for **3**) due to the 3-sulfate could not be observed for **4**, while the downfield shift of the H-6 signals remained. The structure of **4** was further confirmed by an alternative synthesis *via* multiple protections and deprotections. A reference reaction of **3** without the enzyme gave no product. This eliminated the possibility of non-enzymatic hydrolysis. The other two sulfatases (abalone and limpet) showed similar reactivity and regioselectivity. This is the first regioselective desulfation by sulfatases of sulfated sugars bearing more than two sulfate groups in one molecule. 3′,6′-Disulfated lactose **7** showed characteristic behavior towards each of the three enzymes as shown in Table 1; this compound is not a substrate for the snail enzyme, but is an excellent substarte for the limpet enzyme and an acceptable one for the abalone enzyme. The desulfated product of both enzymes could be identified as the 6′-monosulfated lactoside **8**.‡‡ Thus, the sulfatases studied here showed a clear tendency to hydrolyze the 3-sulfate group of galactose and the 3′-sulfate of lactose. This activity can be ascribed to the ability of arylsulfatase A to catalyze desulfation for sulfatides.[22]

In conclusion, we have presented a convenient, regioselective, chemoenzymatic method of sulfating pNP-β-D-galactosides **2**–**4** and pNP-lactosides **6**–**8**. Synthesis and application of glycoconjugate polymers carrying each of these sulfated sugars are in progress and will be reported in due courses.

A part of this study is supported by Funding for the Regional Leading Research Project of Shizuoka Prefecture from the Ministry of Science and Technology of the Japanese Government, and in part by grants from the Ministry of Education, Science, Sports, and Culture, Japan (Priority Areas to K. K.). The authors are also grateful to the Takeda Science Foundation and the Tatematsu Foundation for financial support to Y. N.

Notes and references

† E-mail: uzawa@home.nimc.go.jp
‡ E-mail: nishida@mol.nagoya-u.ac.jp

§ *Synthesis* of **3**. A mixture of **1** (600 mg, 1.99 mmol) and $(Bu_3Sn)_2O$ (0.764 ml, 1.5 mmol) was refluxed in THF–benzene (1:1, 50 ml) for 3 h with continuous azeotropic removal of water. The reaction mixture was concentrated *in vacuo* and the stannylene acetal intermediate treated with SO_3NMe_3 (1.4 g, 0.01 mol) in DMF at 60 °C for 3 h. The reaction mixture was diluted with BnOH (8 ml) and concentrated *in vacuo*. The residue was then purified by sequential column chromatography with sephadex LH-20, ODS and anionic ion exchange resin (Dowex Na^+) to afford 980 mg of **3** (97%). *Selected data* for **3**: δ_H(300 MHz; D_2O) 5.33 (H-1, d, *J* 7.8), 4.48 (H-3, dd, *J* 3.3 and 9.6), 4.43 (H-4, d, *J* 3.3), 4.34–3.93 (m, H-6 and H-6′), 4.01 (H-2, dd, *J* 7.8 and 9.6).

¶ *Synthesis* of **6**. A procedure similar to that used for **1** was performed using **5** (79 mg, 0.17 mmol), Bu_2SnO (43 mg, 0.17 mmol) and SO_3NMe_3 (24 mg, 0.17 mmol) to give **6** (56 mg, 57%). *Selected data* for **6**: δ_H(600 MHz, D_2O) 5.283 (H-1, *J* 7.8), 4.596 (H-1′, *J* 8.1), 4.342 (H-3′, *J* 3.0 and 9.8), 4.297 (H-4′, *J* 3.0), 4.03–3.97 (br d, H-6 of glucose residue, *J* 11.0), 3.89–3.74 (m, H-6, H-6′ and H-6″ of glucose and galactose residues), 3.796 (br t, H-3, *J* 9.5).

‖ *Synthesis* of **7**. A procedure similar to that used for **1** was performed using **5** (79 mg, 0.17 mmol), Bu_2SnO (128 mg, 0.51 mmol) and SO_3NMe_3 (71 mg, 0.51 mmol) to give **7** (53 mg, 40%). *Selected data* for **7**: δ_H(600 MHz, D_2O) 5.313 (H-1, *J* 8.1), 4.629 (H-1′, *J* 7.7), 4.38–4.32 (H-3′, *J* 3.3 and 9.5 and H-4′, *J* 3.3), 4.27–4.20 (H-6 and H-6′ of galactose residue), 4.07–4.02 (br t, H-5′, *J* 6.2), 4.02–3.97 (br d, H-6 of glucose residue, *J* 12.0), 3.805 (br t, H-3, *J* 9.9), 3.90–3.77 (m, H-5).

** Enzymes available from Sigma Co. Ltd. were used without purification. The activities and sources were as followings; snail (*Helix pomatia*), 16.1 units mg^{-1}; abalone (not specified), 23 units mg^{-1}; limpet (*Patella vulgata*), 7.6 units mg^{-1}.

†† *Synthesis* of **4**. A mixture of **3** (80 mg) and sulfatase (from *Helix pomatia*, 5 mg) was dissolved in 0.25 M NaOAc–AcOH buffer (pH 6.8, 2 ml) at 37 °C for 2 days. The reaction mixture was purified by sequential column chromatography with Sephadex LH-20, ODS and anionic ion exchange resin (Dowex Na^+) to give 60 mg (94%) of **4**. *Selected data* for **4**: δ_H(300 MHz, D_2O) 5.17 (H-1, d, *J* 7.3), 4.29–4.17 (H-6 and H-6′, m), 4.07 (H-4, br d, *J* 3.0), 3.87 (H-2, dd, *J* 7.3 and 9.9), 3.82 (H-3, dd, *J* 3.0 and 9.9).

‡‡ *Selected data* for **8**: δ_H(600 MHz, D_2O) 5.304 (H-1, *J* 8.1), 4.506 (H-1′, *J* 7.8), 4.25–4.20 (m, H-6 and H-6′ of galactose residue), 4.03–3.96 [H-4′ (*J* 3.3), H-5′ and H-6 (glucose residue), *J* 12.0], 3.90–3.74 (m, H-5), 3.756 (br t, H-3, *J* 9.0), 3.73–3.66 (m, H-3′ and H-2).

1 T. Suzuki, A. Sometani, Y. Yamazaki, G. Horiike, Y. Mizutani, H. Masuda, M. Yamada, H. Tahara, G. Xu, D. Miyamoto, N. Oku, S. Okada, M. Kiso, A. Hasegawa, T. Ito, Y. Kawaoka and Y. Suzuki, *Biochem. J.*, 1996, **318**, 389.
2 B. K. Brandley, M Kiso, S. Abbas, P. Nikrad, O. Srivastava, C. Foxall, Y. Oda and A. Hasegawa, *Glycobiology*, 1993, **3**, 633.
3 P. J. Green, T. Tamatani. T. Watanabe, M. Miyasaka, A. Hasegawa, M. Kiso, C-T. Yuen, M. S. Stoll and T. Feizi, *Biochem. Biophsy. Res. Commun.*, 1992, **188**, 244.
4 Y.-M. Zhang, A. Brodzki, P. Sinaÿ, F. Uzabiaga and C. Picard, *Carbohydr. Lett.*, 1996, **2**, 67.
5 D. D. Manning, C. R. Bertozzi, N. L. Pohl, S. D. Rosen and L. L. Kiessling, *J. Org. Chem.*, 1995, **60**, 6254.
6 T. V. Zemlyanukhina, N. E.Nifantev, A. S. Shashkov, Y. E. Tsvetkov and N. V. Bovin, *Carbohydr. Lett.*, 1995, **1**, 277.
7 A. Lubineau, J. Le Gallic and R. Lemoine, *J. Chem. Soc., Chem. Commun.*, 1993, 1419.
8 K. C. Nicolaou, N. J. Bockovich and D. R. Carcanague, *J. Am. Chem. Soc.*, 1993, **115**, 8843.
9 C. Galustian, A. M. Lawson, S. Komba, H. Ishida, M. Kiso and T. Feizi, *Biochem. Biophys. Res. Commun.*, 1997, **240**, 748.
10 E. G. Gordon, W. J. Sanders and L. L. Kiessling, *Nature*, 1998, **392**, 30.
11 D. D. Manning, X. Hu, P. Beck and L. L. Kiessling, *J. Am. Chem. Soc.*, 1997, **119**, 3161.
12 R. Roy, W. K. C. Park, D. Zanini, C. Foxall and O. P. Srivastava, *Carbohydr. Lett.*, 1997, **2**, 259.
13 J. Bruning and L. L. Kiessling, *Tetrahedron Lett.*, 1996, **37**, 2907.
14 Y. Nishida, H. Dohi, H. Uzawa and K. Kobayashi, in the press.
15 A. Tuchida, K. Kobayashi, N. Matsubara, T. Muramatsu, T. Suzuki, and Y. Suzuki, unpublished work.
16 O. Fujita and M. Naiki, *Biosci. Bioind.*, 1997, **55**, 181.
17 The use of $(Bu_3Sn)_2O$ and Bu_2SnO were originally reported for selective acylations of sugars, see T. Ogawa and M. Matsui, *Tetrahedron*, 1981, **137**, 2363. For the applications of this method for regioselective sulfations of sugars, see B. Guilbert, N. J. Davis, M. Pearce, R. T. Aplin and S. L. Flitsch, *Tetrahedron*: *Asymmetry*, 1994, **5**, 2163.
18 C.-H. Lin, G.-J. Shen, E. G.-Junceda and C.-H. Wong, *J. Am. Chem. Soc.*, 1995, **117**, 8031.
19 A. Lubineau, C. Auge, N. L. Goff and C. L. Narvor, *Carbohydr. Res.*, 1998, **305**, 501.
20 K. Kobayashi, N. Kakishita, M. Okada, T. Akaike and T. Usui, *J. Carbohydr. Chem.*, 1994, **13**, 753.
21 D. Page and R. Roy, *Glycoconj. J.*, 1997, **14**, 345.
22 R. H. v.-Pal, W. Klein, L. M. v.- Golde and M. L.-Cardozo, *Biochim. Biophys. Acta*, 1990, **1043**, 91.

Communication 8/05830J

A new class of photochromic 1,2-diarylethenes; synthesis and switching properties of bis(3-thienyl)cyclopentenes

Linda N. Lucas, Jan van Esch, Richard M. Kellogg* and Ben L. Feringa*

Department of Organic and Molecular Inorganic Chemistry, University of Groningen, Nijenborgh 4, 9747 AG Groningen, The Netherlands. E-mail: r.m.kellogg@chem.rug.nl; b.l.feringa@chem.rug.nl

Received (in Cambridge, UK) 8th September 1998, Accepted 17th September 1998

A novel synthetic route to diarylethenes fixed in a cyclopentene based on titanium-mediated carbonyl coupling leads to bis(3-thienyl)cyclopentenes that show photochromic behaviour similar to that of known diarylethenes.

Diarylethenes constitute an important class of photochromic molecules, as they are thermally irreversible and show high fatigue resistance,[1] which are promising features for application in optical data storage[2] and as molecular switches.[3,4] The aryl groups are bound to a cycloalkene to prevent *cis–trans* isomerization, which might compete with photocyclization. 1,2-Bisaryl-substituted maleic anhydride,[5] maleimide[6] and perfluorocyclopentene[7] moieties have been employed so far. Each bridging unit has its advantages and disadvantages. Diarylmaleic anhydrides are readily accessible, but are sensitive to acidic conditions and need certain types of aryl derivatives to maintain their photofatigue resistance in the presence of air.[8] Diarylmaleimides are also sensitive to acidic conditions and furthermore show some degradation in the presence of oxygen.[9] Diarylperfluorocyclopentenes exhibit excellent photochromic behaviour, since up to 80 °C they are stable in the presence of air during cyclization, unless strong electron-donating and −withdrawing substituents are introduced at the 5-position of the thiophene ring.[10] Despite these highly attractive properties the expensive and rather volatile starting material octafluorocyclopentene and the low yields commonly found in double substitution reactions of octafluorocyclopentene with lithiated thiophenes are major disadvantages.

Herewith we present a new class of diarylethenes, the dithienylcyclopentenes, and a novel synthetic route to diarylethenes based on titanium-mediated carbonyl coupling. The synthesis can be performed on a large scale from rather cheap starting materials (Scheme 1). We envisioned that an intramolecular McMurry coupling of a bisthienyl substituted 1,3-dicarbonyl compound would be a feasible route to 1,2-dithienylcyclopentenes. Compounds **1–6**† were synthesized starting from 2-methylthiophene, which was chlorinated at the 5-position with NCS in AcOH and benzene, followed by a Friedel–Crafts reaction with $AlCl_3$ and glutaryl chloride at 0 °C. The resulting 1,5-bis(5-chloro-2-methyl-3-thienyl)pentadione was used in a McMurry reaction[11] with $TiCl_3(THF)_3$ and Zn in THF at 40 °C to provide **2a**. Starting from 2,5-dimethylthiophene, **3a** was obtained *via* the same procedure as described above. By using Mg instead of Zn in the McMurry reaction with 1,5-bis(5-chloro-2-methyl-3-thienyl)pentane-1,5-dione, **1a** was obtained.‡ Dialdehyde **4a** was synthesized by double lithiation of **1a** or **2a** followed by quenching with DMF. The conversion of **4a** to **5a** and **6a** was performed according to published procedures.[10,12] Enantiomerically pure (+)-(*R*)-1-phenylethylamine was used in the synthesis of compound **5**.[12] Although the yields in the low-valent titanium coupling step are still modest, this new route provides ready access to a variety of dithienylcyclopentenes.

The photochromic behaviour was followed by both ^1H NMR and UV spectroscopy. Fig. 1 illustrates the change in absorption of a solution of **4a** in benzene upon irradiation at 313 nm. A new absorption band appeared at 583 nm due to formation of the closed form, which has an extended conjugated structure. Table 1 shows the UV–VIS data for the open and closed forms of the new photochromic compounds. Compared to the known diarylethene derivatives the wavelengths at the absorption maxima of the closed forms show a blue shift; only **6b** measured in benzene showed the same absorption maximum in the closed form as was reported earlier for the perfluorocyclopentene analog.[10] The diarylethenes **1a**, **2a** and **3a** turn yellow upon UV irradiation, which is unusual; no diarylethene compounds showing this behaviour have been described in literature. The

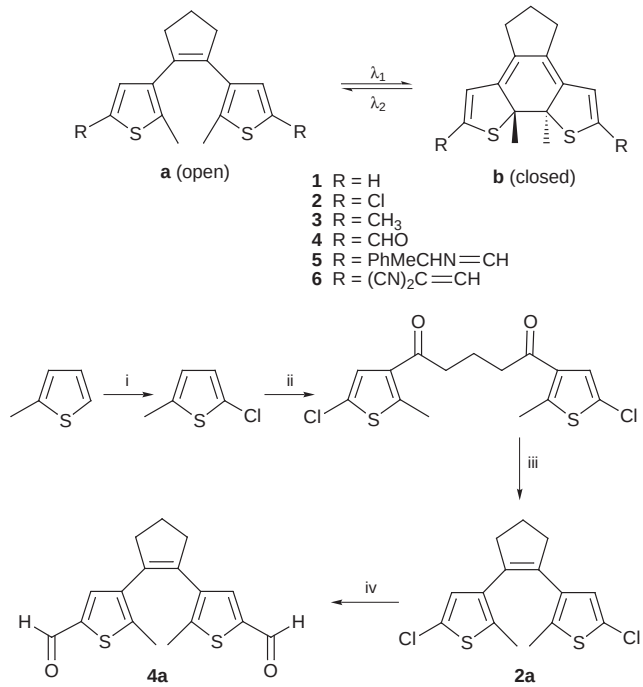

Scheme 1 *Reagents and conditions*: i, NCS, AcOH, benzene, reflux, 80%; ii, $AlCl_3$, glutaryl chloride, CS_2, 0 °C, 94%; iii, $TiCl_3(THF)_3$, Zn, THF, 40 °C, 44%; iv, Bu^nLi, DMF, 39%.

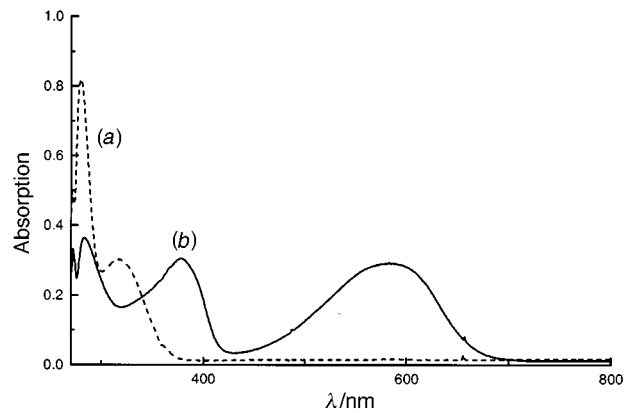

Fig. 1 UV–VIS spectra of **4a** (*a*) before and (*b*) after irradiation for 5 min at 313 nm (2.05×10^{-5} M in benzene).

Table 1 UV–VIS data of the dithienylcyclopentenes

Compound	Solvent	λ_{max}/nm	$\varepsilon/10^3 cm^{-1}$ M^{-1}
1a	hexane	268[a]	10.4
1b	hexane	228	15.7
2a	hexane	240	19.01
2b	hexane	444	1.16
3a	hexane	270[a]	9.5
3b	hexane	220	12.6
4a	benzene	318	14.7
4b	benzene	583	14.3
4a	CH_2Cl_2	317	8.3
4b	CH_2Cl_2	580	6.9
5a	hexane	305[a]	23.5
5b	hexane	557	13.1
6a	benzene	391	41.6
6b	benzene	726	29.8
6a	CH_2Cl_2	395	27.6
6b	CH_2Cl_2	734	20.1

[a] Shoulder.

absorption spectra of compounds **1b** and **3b** show no maxima in the visible region. Therefore diarylethenes **1**–**3** are not suitable for optical switching. Upon photochemical ring closure of **4a**, **5a** (λ = 313 nm) and **6a** (λ = 405 nm), only one methyl signal appeared at high field in their ^{1}H NMR spectra.§ In accordance with the Woodward–Hoffmann rules,[13] we anticipate conrotatory ring closure and a *trans* disposition of the methyl groups.

The half life of the thermal ring opening in benzene at 60 °C of compound **6b** is 4.27 min. Compared to the perfluorocyclopentene analog[10] it shows slower thermal ring opening. Preliminary investigations show that compounds **4b**, **5b** and **6b** are thermally stable under ambient conditions. Finally a number of photochemical bleaching and colouring experiments were performed with compounds **4** and **5**. Dialdehyde **4** showed a ±8% decrease in absorption (UV–VIS) after one cycle, but bisimine derivative **5** performed very well and after ten cycles no degradation was detected. For compounds **1**–**3** it was not possible to perform such switching cycles, because it was impossible to bleach the molecules completely due to a minor difference between the absorption maxima of the open and closed forms of the compounds.

In conclusion a facile synthetic route to a new class of diarylethenes, bis(3-thienyl)cyclopentenes, has been developed. It appears that these bis(3-thienyl)cyclopentenes, which are now readily accessible, show photochromic behaviour, similar to known diarylethenes. Provided the proper substituents are present thermal irreversibility and fatigue resistance are observed. Assessment of the scope of this new methodology and study of applications of these new photochromic compounds is in progress.

Notes and references

† All compounds were fully characterized showing spectroscopic and analytical data in accordance with the structures shown.

‡ Dechlorination occurs during McMurry coupling with low valent titanium prepared using Mg.

§ ^{1}H NMR chemical shift data the CH_3 (thiophene), CH= and CH (thiophene) resonances for the open and closed forms of compounds **4**–**6**: for **4a**: δ 2.04, 9.74, 7.42; for **4b**: δ 2.17, 9.78, 6.72; for **5a**: δ 1.97, 8.25, 6.95; for **5b**: δ 1.94, 8.15, 7.37; for **6a**: δ 2.14, 7.63, 7.40; for **6b**: δ 2.05, 7.43, 6.56.

1 M. Irie and K. Uchida, *Bull. Chem. Soc. Jpn*., 1998, **71**, 985.
2 P. Ball and L. Garwin, *Nature*, 1992, **355**, 761; D. M. Eigler, C. P. Lutz and W. E. Rudge, *Nature*, 1991, **352**, 600; P. Ball, *Designing the Molecular World, Chemistry at the Frontier*, Princeton University Press, Princeton, NJ, 1994, p. 7.
3 G. M. Tsivgoulis and J.-M. Lehn, *Chem. Eur. J*., 1996, **2**, 1399.
4 B. L. Feringa W. F. de Jager and B. de Lange, *Tetrahedron*, 1993, **49**, 8267.
5 M. Irie and M. Mohri, *J. Org. Chem*., 1988, **53**, 803.
6 T. Yamaguchi, K. Uchida and M. Irie, *J. Am. Chem. Soc*., 1997, **119**, 6066.
7 M. Hanazawa, R. Sumiya, Y. Horikawa and M. Irie, *J. Chem. Soc*., *Chem. Commun*., 1992, 206.
8 H. Taniguchi, A. Shinpo, T. Okazaki, F. Matsui and M. Irie, *Nippon Kagaku Kaishi*, 1990, 1138.
9 K. Uchida, Y. Kido, T. Yamaguchi and M. Irie, *Bull. Chem. Soc. Jpn*.,1998, **71**, 1101.
10 S. L. Gilat, S. H. Kawai and J.-M. Lehn, *Chem. Eur. J*., 1995, **1**, 275.
11 A. Fürstner, A. Hupperts, A. Ptock and E. Janssen, *J. Org. Chem*., 1994, **59**, 5215.
12 C. Denekamp and B. L. Feringa, *J. Chem. Soc*., *Perk. Trans. 1*, in the press; C. Denekamp and B. L. Feringa, *Adv. Mater*., in the press.
13 R. B. Woodward and R. Hoffmann, *The Conservation of Orbital Symmetry*, Verlag Chemie, New York, 1970

Communication 8/06998K

Solid state photochemical reaction of achiral *N*-(β,γ-unsaturated carbonyl)thiocarbamate to optically active thiolactone in the chiral crystalline environment

Masami Sakamoto,*[a] Masaki Takahashi,[a] Takeshi Arai,[a] Motoki Shimizu,[a] Kentaro Yamaguchi,[b] Takashi Mino,[a] Shoji Watanabe[a] and Tsutomu Fujita[a]

[a] *Department of Materials Technology, Faculty of Engineering, Chiba University, Yayoi-cho, Inage-ku, Chiba 263-8522, Japan. E-mail: saka@planet.tc.chiba-u.ac.jp*

[b] *Chemical Analysis Center, Chiba University, Yayoi-cho, Inage-ku, Chiba 263-8522, Japan*

Received (in Cambridge, UK) 16th July 1998, Accepted 21st September 1998

_O_-Methyl _N_-(2,2-dimethylbut-3-enoyl)-_N_-phenylthiocarbamate crystallized in the chiral space group $P2_1$, and the solid state photoreaction initiated intramolecular [2+2] thietane formation followed by rearrangement, leading to optically active γ-thiolactone.

Solid state photoreaction provides product selectivity and stereoselectivity compared to reactions that occur in solution due to restriction of molecular movement imposed by the crystal lattice.[1–5] Stereospecific solid state chemical reactions of chiral crystals formed by achiral materials are defined as 'absolute' asymmetric syntheses.[6–11] This asymmetric synthesis must involve two aspects: generating chiral crystals and performing topochemically controlled solid state reactions which yield chiral products. Now we have found a new example of 'absolute' asymmetric synthesis involving the photochemical reaction of an achiral *N*-(β,γ-unsaturated carbonyl)thiocarbamate leading to optically active thiolactone and a unique structure in the crystalline state.

O-Methyl *N*-(β,γ-unsaturated carbonyl)-*N*-phenylthionocarbamates **1a**,**b** were synthesized by acylation of *O*-methyl *N*-phenylthiocarbamate with the corresponding acid chloride in the presence of Et_3N. Recrystallization of **1a** from a hexane yielded colorless crystals; however, single crystals suitable for X-ray crystallographic analysis could not be obtained. On the other hand, thiocarbamate **1b** afforded prismatic single crystals, which were analysed by X-ray crystallography.† It is notable that the conformation of the imide chromophore is *E*,*E*, and remarkably twisted from the ideal imide plane. (Fig. 1) The twist angle of the C(=O)–N moiety is 47.4° and is much greater than that of the C(=S)–N moiety (19.4°).[12] This structure is consistent with the lone pair electrons of the nitrogen atom being conjugated through the thiocarbonyl rather than through a carbonyl group. The phenyl ring is almost orthogonally twisted to the sp^2 nitrogen atom (67°).

Irradiation of a benzene solution of **1a** gave tricyclic thietane, 2,2-dimethyl-5-methoxy-4-phenyl-6-thia-4-azatricyclo-[5.4.$0^{1,7}$.$0^{1,5}$]nonan-3-one **2a**, in 83% yield (Table 1, entry 1). The solid state photolysis also gave racemic **2a** (81%, 80% conversion) (entry 2). The solid state reaction proceeded even at −78 °C (entry 3). The structure of **2a** was determined on the basis of spectroscopic data.

When thiocarbamate **1b** was irradiated in benzene solution, thiolactone **3b** was isolated in 90% yield (entry 4). The solid state photolysis also gave thiolactone **3b** in 85% yield when the reaction conversion was 78% as shown in Table 1, entry 4. The IR spectrum of **3b** showed characteristic absorption due to the thiolactone carbonyl at 1697 cm^{-1} and the C=N bond at 1666 cm^{-1}. The ^1H NMR spectrum showed the absence of an alkenyl group. The ^{13}C NMR spectrum displayed the absence of the signal due to the thiocarbonyl carbon at δ_C 190.8 and exhibited new a sp^3 triplet peaks at δ 30.7 and a doublet at δ 47.7. New singlet peaks derived from the thioester and imino carbons were exhibited at δ 210.7 and 160.7, respectively.

The stereoselective generation of the chiral center is exemplified by the formation of **3b** at the C-4 position {$[\alpha]_D^{20}$ = +8 (*c* 1.0 in $CHCl_3$, 10% ee)} (entry 5). The enantiomeric purity of **3b** was determined by HPLC employing a chiral cell OJ (Daicel Chemical Industry). The solid state photoreaction also proceeded at −78 °C and an optically active compound which showed a better ee value was formed; 20% ee at 84% conversion (entry 6) and 31%ee at 15% conversion (entry 7). The space group of the crystal of **1a** could not be determined because **1a** did not afford single crystals suitable for X-ray crystallography; however, the production of racemic **2a** shows that the crystals are achiral (entries 2 and 3).

A plausible mechanism for the formation of **3** is rationalized on the basis that photolysis of **1** undergoes [2+2] cyclization to thietane **2** and subsequently rearranges to thiolactone **3** (Scheme 1). Ring opening of the initially formed thietane **2** leading to zwitterion **5**, which is facilitated by the lone pair electrons of the nitrogen and oxygen atoms, and subsequent nucleophilic reaction between the thiolate anion and the carbonyl carbon to give **3**.[13] For the tricyclic thietane **2a**, nucleophilic addition of thiolate anion is difficult, because of the conjunction of the

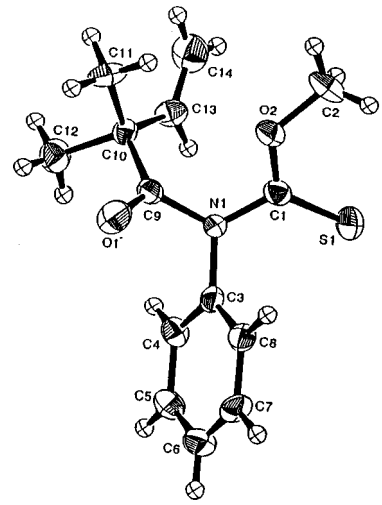

Fig. 1 ORTEP drawing of **1b**. Selected bond lengths (Å) and angles (°); S(1)–C(1) 1.608(6), O(2)–C(1) 1.330(7), N(1)–C(1) 1.355(6), N(1)–C(9) 1.446(7), C(10)–C(13) 1.497(9), O(1)–C(9) 1.201(7), N(1)–C(3) 1.446(7), C(9)–C(10) 1.520(8), C(13)–C(14) 1.301(9), C(1)–N(1)–C(9) 122.6(4), S(1)–C(1)–O(2) 125.6(4), O(2)–C(1)–N(1) 108.6(5), N(1)–C(3)–C(8) 121.3(5), O(1)–C(9)–C(10) 122.0(5), C(9)–C(10)–C(13) 115.5(5), C(10)–C(13)–C(14) 127.2(7), C(1)–N(1)–C(3) 120.8(4), C(3)–N(1)–C(9) 115.5(4), S(1)–C(1)–N(1) 125.7(4), O(1)–C(9)–N(1) 117.5(5), N(1)–C(9)–C(10) 120.1(5), S(1)–C(1)–N(1)–C(9) −168.0(5), O(2)–C(1)–N(1)–C(3) −153.3(5), C(1)–N(1)–C(3)–C(4) −120.6(6), C(8)–C(3)–N(1)–C(9) −105.6(6), O(1)–C(9)–N(1)–C(1) −130.5(6), C(3)–N(1)–C(9)–C(10) −134.8(5).

Table 1 Photochemical reaction of **1** in benzene and the solid state

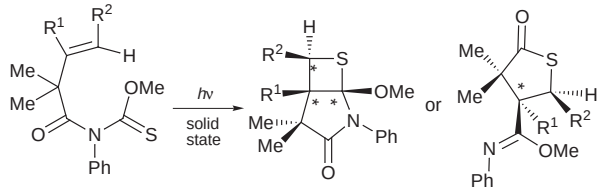

1a $R^1 = R^2 = -(CH_2)_4-$
b $R^1 = R^2 = H$

2a $R^1 = R^2 = -(CH_2)_4-$

3b $R^1 = R^2 = H$ (optically active)

Entry	Substrate	Conditions	*T*/°C	Conversion (%)	Yield (%)[a] **2**	**3**	$[\alpha]_D^{20}$ [b,c]	Ee (%)[c]
1	**1a**	benzene	20	100	83	0	0	0
2	**1a**	solid	0	80	81	0	0	0
3	**1a**	solid	−78	50	85	0	0	0
4	**1b**	benzene	20	100	0	90	0	0
5	**1b**	solid	0	78	0	85	+8	10
6	**1b**	solid	−78	84	0	84	+16	20
7	**1b**	solid	−78	15	0	90	+25	31

[a] Chemical yields are isolated yields and calculated on the basis of consumed thionocarbamates. [b] In units of 10^{-1} deg cm^2 g^{-1}. [c] Of product (either **2** or **3**).

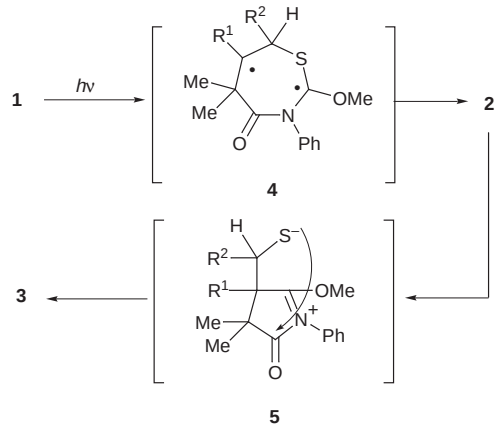

Scheme 1

cyclohexane ring, which results in the formation of stable thietane **2a**.

It is generally accepted that a solid state reaction proceeds with minimum atomic and molecular motion. Therefore, the reactivity is determined the by atomic arrangement, represented by the distances and angles between the reaction sites. From the X-ray structural analysis of the starting thiocarbamate **1b**, the distances between the thiocarbonyl sulfur atom S(1) and the alkenyl carbon C(14) and between the thiocarbonyl carbon C(1) and the alkenyl carbon C(13) are 4.69 and 3.00 Å, respectively (Fig. 1). The fact that the reaction proceeded under these restricted conditions, in which the S(1)···C(14) distance is significantly longer than the sum of the van der Waals radii (3.23 Å), is accounted for by the fact that the initial reactions occurred in a defect in the crystalline lattice, and later reactions occurred in the increasing number of defective regions formed during reaction. Furthermore, two plausible factors are responsible for the relatively low enantiomeric excess of **3b**. One is that the process of cyclization results in increasing numbers of defective regions in the surrounding crystal lattice, in which racemization of the reactant easily takes place. The other is the structural interconversion of the biradical intermediate. If the interconversion of the intermediate seven-membered 1,4-diradical **4** is possible in the space in the crystal lattice or in the increasing number of defective regions where the C–S bond formation took place, it would result in lowering of optical purity.

In conclusion, photoreaction *O*-methyl *N*-(β,γ-unsaturated carbonyl)-*N*-phenylthiocarbamate provides a new example of absolute asymmetric synthesis using a chiral crystalline environment.

Notes and references

† *Crystal data* for **1b**: space group $P2_1$, a = 8.6565(7), b = 9.3990(9), c = 8.9395(6) Å, V = 698.8(1) Å^3, Z = 2, ρ = 1.251 g cm^{-3}, μ(Cu-Kα) = 20.09 cm^{-1}. The structure was solved by direct methods and expanded using Fourier techniques. Final R and R_w were 0.046 and 0.045 for 1194 reflections. CCDC 182/1025.

1 J. R. Scheffer, M. Garcia-Garibay and O. Nalamasu, *Organic Photochemistry*, ed. A. Padwa, Marcel Dekker, New York, Basel, 1987, vol. 8, pp 249–338.
2 J. R. Scheffer and P. R. Pokkuluri, *Photochemistry in Organized and Constrained Media*, ed. V. Ramamurthy, VCH, New York, 1991, pp. 185–246.
3 K. Venkatesan and V. Ramamurthy, *Photochemistry in Organized and Constrained Media*, ed. V. Ramamurthy, VCH, New York, 1991, pp. 133–184.
4 V. Ramamurthy and K. Venkatesan, *Chem. Rev*., 1987, **87**, 433.
5 Y. Ito, *Synthesis*, 1998, 1.
6 M. Sakamoto, N. Hokari, M. Takahashi, T. Fujita, S. Watanabe, I. Iida and T. Nishio, *J. Am. Chem. Soc*., 1993, **115**, 818.
7 L. Addadi and M. Lahav, *Origin of Optical Activity in Nature*, ed. D. C. Walker, Elsevier, New York, 1979; ch. 14.
8 B. S. Green, M. Lahav and D. Rabinovich, *Acc. Chem. Res*., 1979, **69**, 191.
9 F. Toda and S. Soda, *J. Chem. Soc*., *Chem. Commun*., 1987, 1413.
10 M. Vaida, R. Popovitz-Biro, L. Leiserowitz and M. Lahav, *Photochemistry in Organized and Constrained Media*, ed. V. Ramamurthy, VCH, New York, 1991, pp. 248–302.
11 M. Sakamoto, *Chem. Eur. J*., 1997, **3**, 684.
12 Twist angle τ is defined as follows: $\tau = 1/2(\omega_1 + \omega_2)$, where ω_1 and ω_2 are torsion angles S1–C1–N1–C9 and O2–C1–N1–C3 , respectively, for τ of C(=S)–N. Twist angle τ for C(=O)–N is determined in the same manner.
13 M. Sakamoto, K. Obara, T. Fujita, S. Watanabe, T. Nishio and I. Iida, *J. Org. Chem*., 1992, **57**, 3735.

Communication 8/05520C

Impurity annihilation; a strategy for solution phase combinatorial chemistry with minimal purification

Anthony G. M. Barrett,*† Marie L. Smith* and Frederic J. Zecri

Department of Chemistry, Imperial College of Science, Technology and Medicine, London, UK SW7 2AY

Received (in Cambridge, UK) 26th August 1998, Accepted 7th September 1998

The selective annihilation of all contaminants in the solution phase formation of amides or sulfonamides is accomplished by their incorporation into a polyurea and removal by filtration.

Combinatorial chemistry has received much attention of late as an engine for the discovery of new pharmaceuticals, catalysts and materials. Library generation may be accomplished using solid phase organic synthesis or by using conventional solution phase chemistry.[1] There is, however, an unending controversy as to which of the major synthetic strategies for library synthesis is superior. Polymer supported synthesis has the clear advantages of ease of manipulation, the ability to drive reactions to completion by use of excess reagent and isolation of the product by filtration alone. However, many synthetic transformations on solid phase encounter difficulties of analysis and reaction tracking. The development of new reactions on a solid phase is frequently time consuming although once developed they may be used in rapid automated production of libraries. In contrast, the primary advantage of solution phase chemistry is its familiarity to the synthetic chemist. Additionally reactions are generally amenable to easy tracking and analysis. Nonetheless the complicated work-up procedures usually associated with such reactions in solution have been a major hurdle to automation and the use of multi-step sequences. Recently the use of polymer supported scavengers has been described as a method to overcome these problems.[2] Disadvantages include the often slow removal of contaminants and variable quality of the libraries produced. Other strategies include the use of fluorous phase chemistry. Disadvantages here include the lack of fluorinated reagents which often need to be prepared by highly specialised syntheses.[3]

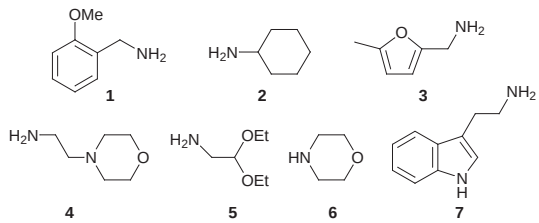

Herein we report a novel method which readily addresses the problem of solution phase library clean-up discussed above. Our approach is based upon the selective annihilation of all contaminants which are then removed by simple filtration as an insoluble product. The procedure is exemplified by the synthesis of amides from the condensation reaction of acid chlorides with amines. Reaction of an acid chloride with excess amine may be used to prepare pure amides in the solution phase without chromatography simply by the polymerisation of the excess amine and filtration (Scheme 1). Co-polymerisation of 1,4-phenylene diisocyanate and pentaethylenehexamine was used to effectively remove the excess amine as a highly insoluble easily filtered polyurea (Table 1).‡ The procedure appears widely applicable with both primary and secondary amines affording the corresponding amides in excellent yield and purity. One caveat is the presence of a second unprotected indole NH function (entry 7, Table 1) which affords none of the desired amide due to its propensity to undergo reaction with 1,4-phenylene diisocyanate and thence to polymer. Sulfonamides may be prepared by the reaction of a sulfonyl chloride with excess amine (Scheme 2 and Table 2).‡ The use of an arenesulfonyl chloride generally gave superior results, both in terms of yield and purity, compared with an alkanesulfonyl chloride.

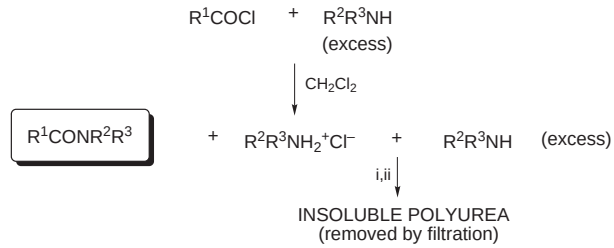

Scheme 1 *Reagents*: i, 1,4-phenylene diisocyanate (excess); ii, pentaethylenehexamine.

Table 1 Formation of amides using impurity annihilation[a]

3,5-$Cl_2C_6H_3COCl$ —(i–iii)→ 3,5-$Cl_2C_6H_3CONR^2R^3$

Entry	Amine	Yield (%)	Purity (%)[b]
1	**1**	92	92
2	**2**	96	99
3	**3**	93	93
4	**4**	90	95
5	**5**	85	98
6	**6**	90	99
7	**7**	0	—

[a] *Reagents*: i, amine (3 equiv.); ii, 1,4-phenylene diisocyanate (6 equiv.); iii, pentaethylenehexamine (2.5 equiv.). [b] Determined by GC–MS and ^{1}H NMR spectroscopy.

Amide and sulfonamide formation may also be accomplished by the reaction of amine with an excess of acyl or sulfonyl chloride, respectively (Scheme 3). Under these circumstances it is necessary to add an excess of poly(vinylpyridine) to capture liberated hydrogen chloride and enable amide or sulfonamide formation to proceed to completion. The excess acyl or sulfonyl chloride is then scavenged by the addition of the polyamine (3

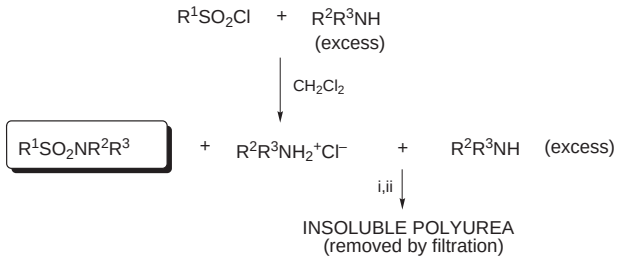

Scheme 2 *Reagents*: i, 1,4-phenylene diisocyanate (excess); ii, pentaethylenehexamine.

Table 2 Formation of sulfonamides using impurity annihilation[a]

(a) R^1 = *p*-Tol
(b) R^1 = Et

Entry	Amine	Yield (%)	Purity (%)[b]
1a	**1**	90	95
1b	**1**	74	81
2a	**2**	79	94
2b	**3**	68	80
3a	**3**	85	89
3b	**3**	64	67
4a	**4**	92	92
4b	**4**	81	57
5a	**5**	97	98
5b	**5**	92	92
6a	**6**	81	92
6b	**6**	80	61

[a] *Reagents*: i, amine (3 equiv.); ii, 1,4-phenylene diisocyanate (6 equiv.); iii, pentaethylenehexamine (2.5 equiv.). [b] Determined by GC–MS and ^{1}H NMR spectroscopy.

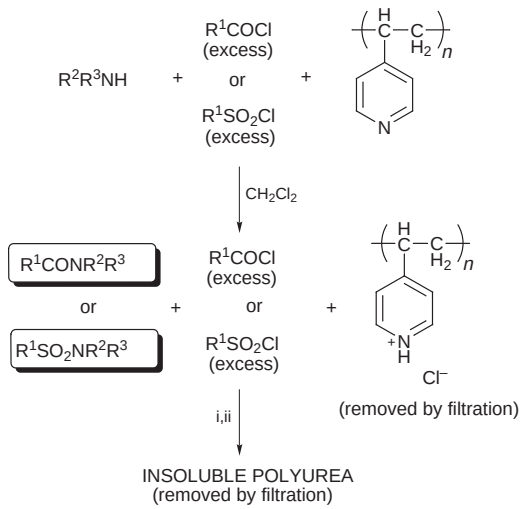

Scheme 3 *Reagents*: i, pentaethylenehexamine (excess); ii, 1,4-phenylene diisocyanate.

Table 3 Formation of sulfonamides and amides using impurity annihilation[a]

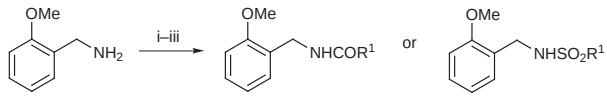

Entry	Chloride	Yield (%)	Purity (%)[b]
1	3,5-$Cl_2C_6H_3COCl$	90	99
2	c-$C_6H_{11}COCl$	98	97
3	2-furylCOCl	95	92
4	4-$MeC_6H_4SO_2Cl$	84	92

[a] *Reagents*: i, chloride (3 equiv.), poly(vinylpyridine); ii, pentaethylenehexamine (3 equiv.); iii, 1,4-phenylene diisocyanate (3 equiv.). [b] Determined by GC–MS and ^{1}H NMR spectroscopy.

equiv.) followed by the addition of the diisocyanate (3 equiv.) to induce polymerisation to the polyurea. Both the polyurea and poly(vinylpyridine) are then simply removed by filtration. Once again excellent yields and purities are obtained (results for various chlorides are listed in Table 3).§ Thus component annihilation is suitable for the removal of either excess electrophilic or nucleophilic components.

In summary, we have developed a method for the efficient 'clean-up' of a number of solution phase reactions that affords the desired products in excellent yields and purities in a reasonable time frame. This methodology has been successfully carried out manually and with the use of automation.¶ Extension of this methodology to the synthesis of esters and for the annihilation of other common reagents‖ will be reported in due course.

We thank RPA and the BBSRC for a studentship (F. J. Z.), Glaxo Wellcome Research Ltd. for their endowment (A. G. M. B.) and the Royal Society for a Dorothy Hodgkin fellowship (M. L. S.).

Notes and references

† E-mail: m.stow@ic.ac.uk

‡ Typical procedure for the formation of amides or sulfonamides using an acid chloride or sulfonylchloride respectively with excess amine: To a solution of the acid chloride or sulfonamide (0.1 mmol) in CH_2Cl_2 (1 ml) was added a solution of the amine (3 equiv.) in CH_2Cl_2 (1 ml). The mixture was stirred at room temperature for 30 min and a solution of 1,4-phenylene diisocyanate (6 equiv.) in CH_2Cl_2 (4 ml) was added. The mixture was stirred at room temperature for 40 min and a solution of pentaethylenehexamine (2.5 equiv.) in CH_2Cl_2 (4 ml) was added. After stirring for 1 h, the heterogeneous mixture was filtered. Evaporation of the solvent under reduced pressure afforded the expected amide in high yield and purity (see Tables 1 and 2 respectively).

§ Typical procedure for the formation of amides or sulfonamides using an amine with excess acid chloride or sulfonyl chloride respectively: To a solution of the amine (0.1 mmol) in CH_2Cl_2 (1 ml) was added a solution of the acid chloride or sulfonyl chloride (3 equiv.) in CH_2Cl_2 (1 ml) and poly(vinylpyridine) (100 mg). The mixture was stirred at room temperature for 30 min when a solution of pentaethylenehexamine (3 equiv.) in CH_2Cl_2 (4 ml) was added. The mixture was stirred at room temperature for 40 min. and a solution of 1,4-phenylene diisocyanate (3 equiv.) in CH_2Cl_2 (4 ml) was added. After stirring for 1 h, the heterogeneous mixture was filtered. Evaporation of the solvent under reduced pressure afforded the expected amide or sulfonamide in high yield and purity (see Table 3).

¶ Automated synthesis was carried out using a Nautilus™ 2400 Organic Synthesizer (Argonaut Technologies, Inc.).

‖ Kurth has recently reported the use of 1,4-phenylene diisocyanate as a convenient reagent for the generation of nitrile oxides from nitroalkanes since the by product urea readily polymerises (see ref. 4).

1 M. A. Gallop, R. W. Barrett, W. J. Dower, S. P. A. Fodor and E. M. Gordon, *J. Med. Chem*., 1994, **37**, 1233; E. M. Gordon, R. W. Barrett, W. J. Dower, S. P. A. Fodor and M. A. Gallop, *J. Med. Chem*., 1994, **37**, 1385; N. K. Terrett, M. Gardner, D. W. Gordon, R. J. Kobylecki and J. Steele, *Tetrahedron*, 1995, **51**, 8135; P. H. H. Hermkens, H. C. J. Ottenheijm and D. C. Rees, *Tetrahedron*, 1996, **52**, 4527; P. H. H. Hermkens, H. C. J. Ottenheijm and D. C. Rees, *Tetrahedron*, 1997, **53**, 5643; S. H. DeWitt and A. W. Czarnik, *Acc. Chem. Res*., 1996, **29**, 114; R. W. Armstrong, A. P. Coombs, P. A. Tempest, S. D. Brown and T. A. Keating, *Acc. Chem. Res*., 1996, **29**, 123; J. A. Ellman, *Acc. Chem. Res*., 1996, **29**, 132; E. M. Gordon, M. A. Gallop and D. V. Patel, *Acc. Chem. Res*., 1996, **29**, 144; F. Balkenhohl, C. von dem Bussche-Hünnefeld, A. Lansky and C. Zechel, *Angew. Chem., Int. Ed. Engl*., 1996, **35**, 2289; K. S. Lam, M. Lebl and V. Krchnák, *Chem. Rev*., 1997, **97**, 411; A. Nefzi, J. M. Ostresh and R. A. Houghton, *Chem. Rev*., 1997, **97**, 449; M. C. Pirrung, *Chem. Rev*., 1997, **97**, 473; D. C. Gravert and K. D. Janda, *Chem. Rev*., 1997, **97**, 489; L. A. Thompson and J. A. Ellman, *Chem. Rev*., 1997, **97**, 555; M. B. Francis, N. S. Finney and E. N. Jacobsen, *J. Am. Chem. Soc*., 1996, **118**, 8983.

2 D. L. Flynn, J. Z. Crich, R. V. Devraj, S. L. Hockerman, J. J. Parlow, M. S. South and S. S. Woodard, *J. Am. Chem. Soc*., 1997, **119**, 4874; J. J. Parlow, D. A. Mischke and S. S. Woodard, *J. Org. Chem*., 1997, **62**, 5908; R. J. Booth and J. C. Hodges, *J. Am. Chem. Soc*., 1997, **119**, 4882; T. A. Keating and R. W. Armstrong, *J. Am. Chem. Soc*., 1996, **118**, 2574; S. W. Kaldor, M. G. Siegel, J. E. Fritz, B. A. Dressman and P. J. Hahn, *Tetrahedron Lett*., 1996, **37**, 7193; K. D. Janda, *J. Org. Chem*., 1998, **63**, 889.

3 D. P. Curran and S. Hadida, *J. Am. Chem. Soc*., 1996, **118**, 2531; D. P. Curran, *Angew. Chem., Int. Ed. Engl*., 1998, **37**, 1175.

4 E. J. Kantorowski, S. P. Brown and M. J. Kurth, *J. Org. Chem*., 1998, **63**, 5272.

Communication 8/06693K

Thermal decomposition of 1-(aminophenyl)-5-*tert*-butyl-4,4-dimethyl-2,6,7-trioxabicyclo[3.2.0]heptanes: unusual O–O bond cleavage competing with normal fragmentation of 1,2-dioxetanes

Masakatsu Matsumoto,* Hiroyuki Murakami and Nobuko Watanabe

Department of Materials Science, Kanagawa University, Tsuchiya, Hiratsuka, Kanagawa 259-12, Japan.
E-mail: matsumo@info.kanagawa-u.ac.jp

Received (in Cambridge, UK) 2nd September 1998, Accepted 21st September 1998

A dioxetane (*ortho*-3a) decomposes thermally to give the normal carbonyl product while dioxetanes (*ortho*-3b–c) decompose at low temperature to afford heterocycles 6 and 7 in high yields.

Thermal decomposition of rather simple 1,2-dioxetanes gives in general two carbonyl products.[1] Charge transfer (CT)-induced decomposition of dioxetanes bearing an electron donor also affords two carbonyl fragments, although its mechanistic aspects and accompanying luminescence should be differentiated from those of simple thermolysis.[2–4] A dioxetane

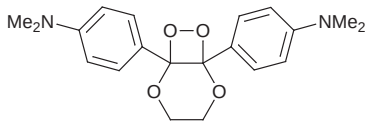

1

bearing *p*-(*N*,*N*-dimethylamino)phenyl groups (**1**) is a typical example of species that undergo CT-induced decomposition.[5] In the course of our investigations on highly efficient chemiluminescent substrates, we found that dioxetanes (*ortho*-**3b–c**) bearing a phenyl substituted with an *N*-methylamino or *N*,*N*-dimethylamino group at the *ortho* position suffer unusual decomposition competing with normal fragmentation, although their unsubstituted *o*-amino (*ortho*-**3a**), *p*-amino (*para*-**3**), and *m*-amino analogues (*meta*-**3**) undergo thermal decomposition to afford normal carbonyl products.

When a dihydrofuran (*para*-**2a**) (100 mg) was irradiated in the presence of catalytic amount of tetraphenylporphin (TPP) in CH_2Cl_2 (10 ml) with a 940 W Na lamp under O_2 atmosphere at 0 °C for 1 h, a dioxetane (*para*-**3a**) bearing a *p*-aminophenyl group† was selectively produced (Scheme 1), although it decomposed considerably during isolation by chromatography (SiO_2) (colorless crystals melted at 83.0 °C, 23% yield). Similar singlet oxygenation of dihydrofurans *para*-**2b** and *para*-**2c** gave dioxetanes *para*-**3b** (*N*-methylamino) and *para*-**3c** (*N*,*N*-dimethylamino),‡ respectively. These dioxetanes (*para*-**3a–c**) decomposed *via* a first-order process to afford the corresponding keto esters (*para*-**4a–c**) exclusively in hot toluene-d_8. The decomposition rates were measured at various temperatures (70–110 °C) in toluene-d_8 and activation parameters for thermolysis of *para*-**3a–c** were estimated as shown in Table 1, where those for dioxetanes bearing a *p*-methoxyphenyl (*para*-**3d**) and a phenyl moiety (**3e**), which were synthesized similarly, are also cited. Table 1 discloses that (i) the thermal susceptibility of *p*-amino derivatives (*para*-**3a–c**) is prominent, (ii) the order of half-life ($t_{1/2}$) (at 25 °C) is *para*-**3c** < *para*-**3b** < *para*-**3a** << *para*-**3d** < **3e**, and (iii) this order is in good agreement with the order of formal oxidation potential of the parent arenes (**5**) corresponding to dioxetanes (*para*-**3a–e**): **5c** < **5b** < **5a** << **5d** < **5e**.[6] These results are consistent with a report on **1** by Schaap[5] and show that CT-induced decomposition takes place most likely for a dioxetane bearing an aryl moiety with low oxidation potential. However, it should be noted that these marked differences in rates of thermal decomposition of *para*-**3** were not observed for *meta*-analogues (*meta*-**3a**, *meta*-**3d**,[7] **3e**): even *meta*-**3a** is very persistent thermally, as shown in Table 1.

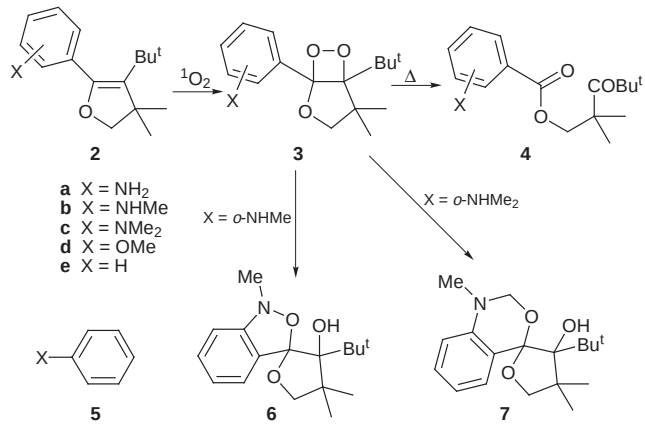

Scheme 1

These facts prompted us to next examine thermolysis of *ortho*-analogues of **3a–c**.

An *o*-aminophenyl moiety was first expected to induce decomposition of dioxetanes (*ortho*-**3a–c**) into **4** similarly to *para*-**3a–c**. A dioxetane bearing an *o*-aminophenyl moiety (*ortho*-**3a**) was synthesized from a dihydrofuran (*ortho*-**2a**) similarly to the case of *para*-**3a** (62% isolated yield). Dioxetane (*ortho*-**3a**) was as unexpectedly stable as its *meta*-analogue (*meta*-**3a**), although it decomposed into the normal product (*ortho*-**4a**) exclusively on heating (see Table 1). The result suggests that the CT from an *o*-aminophenyl moiety most likely occurs far less easily than from a *p*-aminophenyl moiety. The significant difference in ease of CT may be attributed mainly not to electronic factors but to the steric characteristics of the aromatic electron donor: the aryl group for *ortho*-**3a** does not rotate around the C–C bond to the dioxetane ring as freely as that for *para*-**3a** because of steric hindrance by the *o*-amino group.§ This tendency was also observed for the *o*-methoxy derivative (*ortho*-**3d**) which is far more persistent than *para*-**3d**, *meta*-**3d** and the parent dioxetane **3e**.

Singlet oxygenation (−78 °C) of an olefin (*ortho*-**2b**) substituted with an *o*-(*N*-methylamino)phenyl group also gave

Table 1 Activation parameters for the thermolysis of 1-aryl-5-*tert*-butyl-4,4-dimethyl-2,6,7-trioxabicyclo[3.2.0]heptanes **3**[a]

Dioxetane	ΔE_a/kcal mol^{-1}	log *A*	$t_{1/2}$/years at 25 °C	$E_{1/2}$/V[b] of **5**
para-**3a**	28.8	12.6	4.3	0.98
para-**3b**	29.1	13.4	2.0	0.77
para-**3c**	27.7	12.5	1.4	0.73
para-**3d**	30.6	13.4	27	1.76
3e	30.2	12.8	51	2.38
meta-**3a**	29.9	12.7	33	
meta-**3d**	30.2	12.8	50	
ortho-**3a**	30.1	12.9	28	
ortho-**3d**	30.7	12.0	660	

[a] Thermolysis was carried out in toluene-d_8 or in *p*-xylene-d_{10}. [b] Oxidation half-wave potential (ref. 6); solvent system: $R_4N^+ClO_4^-$. (R = Bu or Pr)/MeCN, reference electrode = SCE, working electrode = Pt.

the corresponding dioxetane (*ortho*-**3b**). The thermal decomposition of *ortho*-**3b** exhibited features completely different from those for the dioxetanes described above. On standing for several hours at room temperature in toluene or $CDCl_3$, *ortho*-**3b** changed into an unusual product (**6**) (pale yellow granules melted at 59.0 °C)† without any detectable amount of the normal product (*ortho*-**4b**) expected initially. Dioxetane *ortho*-**3b** decomposed, however, into *ortho*-**4b** in high yield on heating in refluxing toluene. It should be noted that both products **6** and *ortho*-**4b** are thermally stable and do not change into each other upon heating. Thus, we carried out thermolysis of *ortho*-**3b** at various temperatures in toluene-d_8 and measured the product ratio of **6**:*ortho*-**4b**) by 1H NMR spectroscopy: **6**:*ortho*-**4b** = 93:7 at 50 °C, 72:28 at 70 °C, 35:65 at 90 °C, 11:89 at 110 °C. These results suggest that decomposition to *ortho*-**4b** (mode **A**) and unusual decomposition to **6** (mode **B**) take place concurrently in a temperature-dependant manner for dioxetane *ortho*-**3b**.

The decomposition of mode **B** is most likely rationalized by a mechanism similar to the Adam reaction,[9]¶ comprising the intramolecular nucleophilic attack of an *N*-methylamino group at the O–O moiety of the dioxetane and successive O–O bond fission accompanying a proton exchange in an intermediary twitterion (**8**, R^1 = H, R^2 = Me), as illustrated in Scheme 2. Although the proposed mechanism includes multi-step reactions, the decomposition of *ortho*-**3b** to **6** should be essentially a unimolecular reaction as in the pathway to *ortho*-**4b** (mode **A**). Consequently, the product ratio (**6**/*ortho*-**4b**) described above should be equal to the ratio of rate constants (k**B**/k**A**) for the corresponding modes at a given temperature. By plotting log(**6**/*ortho*-**4b**) *vs*. 1/T, we estimated differences in activation energy E_a and log A between modes **A** and **B** as $\Delta E_a = E_a$ (**A**) − E_a (**B**) = 18.9 kcal mol^{-1} and $\Delta \log A = \log A$ (**A**) − $\log A$ (**B**) = 11.7. The result suggests that the mode **B** requires far a lower activation energy and proceeds through a transition state far more highly ordered than mode **A**. As such in the transition state, one can image a structure where the *o*-aminophenyl moiety lies in or near the plane comprising O–C–C shown as **T-1**.

Finally, we attempted to synthesize a dioxetane (*ortho*-**3c**) bearing an *o*-(*N*,*N*-dimethylamino)phenyl moiety. When singlet oxygenation of a dihydrofuran (*ortho*-**2c**) was carried out similarly to the case of *ortho*-**2a** in CH_2Cl_2 at 0 °C, *ortho*-**2c** gave none of the expected dioxetane (*ortho*-**3c**) but gave instead an unprecedented oxygenation product **7** (colorless granules, mp 140.0 °C, 93%)† and a small amount of a keto ester (*ortho*-**4c**) (7%). The low-temperature singlet oxygenation of *ortho*-**2c** gave similar results, so that we could obtain little direct evidence for formation of a dioxetane (*ortho*-**3c**). However, the reaction is reasonably thought to proceed through an unstable dioxetane (*ortho*-**3c**), because both **7** and *ortho*-**4c** are products in which both carbons in the C=C moiety of the starting dihydrofuran (*ortho*-**2c**) are oxygenated. Formation of the unique cyclic aminal **7** is probably attributed to an intramolecular nucleophilic reaction of a dimethylamino group with O–O as in the case of *ortho*-**3b** to **6**; the initially formed zwitterionic intermediate (**8**, R^1, R^2 = Me) may undergo Stevens-like rearrangement[10] to afford **7** as shown in Scheme 2.¶‖

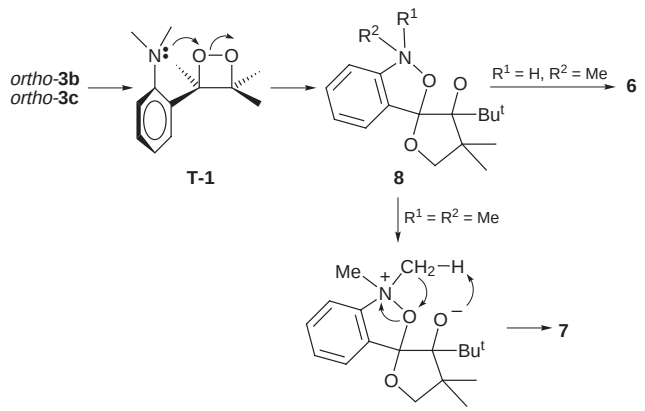

Scheme 2

In conclusion, the present results show that, for dioxetanes bearing a substituted phenyl moiety, a *p*-amino group accelerates significantly decomposition of the dioxetane in the order of H < OMe << NH_2 < NHMe < NMe_2, while *meta*-analogues are insensitive to this substituent effect. On the other hand, *o*-methylamino and *o*-dimethylamino groups cause preferentially unusual decomposition of dioxetane by their intramolecular nucleophilic attack at O–O of the dioxetane, though their unsubstituted amino analogue decomposes to give the normal carbonyl product.

Notes and references

† Structures of all products obtained here were characterized by ^{1}H NMR , ^{13}C NMR, IR, and mass spectral analysis. *Selected data* for **6**: δ_H(400 MHz, $CDCl_3$) 0.92 (s, 9H), 1.22 (s, 3H), 1.54 (s, 3H), 3.14 (s, 3H), 3.72 (qAB, J 7.3, 2H), 4.01 (s, 1H), 6.78 (d, J 7.8, 1H), 7.05 (ddd, J 7.8, 7.3, 1.0, 1H), 7.33 (ddd, J 7.8, 7.3, 1.0, 1H), 7.54 (d, J 7.8, 1H); δ_C(100 MHz, $CDCl_3$) 21.4, 25.7, 28.2, 39.4, 46.7, 47.6, 80.7, 88.4, 110.8, 119.5, 122.3, 127.5, 127.5, 129.8, 151.8. For **7**: δ_H(400 MHz, $CDCl_3$) 0.70 (br s, 9H), 1.19 (s, 3H), 1.50 (s, 3H), 2.86 (s, 3H), 3.73 (qAB, J 7.8, 2H), 4.40 (s, 1H), 4.42 (qAB, J 7.3, 2H), 6.76 (d, J 8.3, 1H), 6.86 (m, 1H), 7.26 (m, 1H), 7.75 (dd, J 7.8, 1.5, 1H); δ_C(100 MHz, $CDCl_3$) 22.7, 26.2, 28.2, 35.1, 40.2, 48.0, 78.5, 79.5, 90.6, 108.0, 112.7, 118.6, 125.2, 129.3, 132.0, 148.9.

‡ Dioxetanes *para*-**3b**,**c** were unstable under the chromatographic conditions, so that the crude *para*-**3b**,**c** including little other than a trace amount of keto ester (*para*-**4b**,**c**) was used without purification for thermolysis.

§ The rate of the CT-induced decomposition of a dioxetane bearing a phenoxide anion as an electron donor has been reported to decrease *via* restriction of rotation of the aromatic ring (ref. 8).

¶ Nucleophilic cleavage of a dioxetane with an aromatic amine is unprecedented, although a *sec*-alkylamine has been reported to cause decomposition of a dioxetane to yield *N*,*N*-dialkyl-*O*-(2-hydroxyethyl)hydroxylamine (Adam reaction) (ref. 9). The possibility cannot be ruled out that the reaction of *ortho*-**3b** to give **6** proceeds by a mechanism including attack of a diradical formed initially by homolytic O–O bond cleavage on an amino group, although *ortho*-**3a** should also give an analogue of **6** by this mechanism. The marked difference in decomposition mode between *ortho*-**3a** and *ortho*-**3b** is most likely attributed to a difference in nucleophilicity between NH_2 and NHMe: the order of nucleophilicity would be NH_2 < NHMe < NMe_2. The thermal instability of *ortho*-**3c** might be also rationalized by the high nucleophilicity of the NMe_2 group.

‖ Nucleophilic attack of a *tert*-alkylamine on a dioxetane has been reported to lead only to normal carbonyl products through Grob fragmentation (ref. 11) of an intermediary zwitterion (ref. 9). For an intramolecular reaction as presented here, a zwitterion such as **8** might, however, cause predominantly Stevens-like rearrangement, because an oxy anion would lie so close to a methyl of the ammonium ion (ON^+Me_2) that the oxy anion is able to easily abstract a methyl proton. The formation of a minor product (*ortho*-**4c**) may be due to Grob fragmentation of **8** and/or direct decomposition of *ortho*-**3c** as in the case of *para*- and *meta*-**3**.

1 A review: C. R. Saha-Moler and W. Adam, *Four-membered Rings with Two Oxygen Atoms* in *Comprehensive Heterocyclic Chemistry II*, ed. A. Padwa, Pergamon, NY, 1996, vol. 1B, pp. 1041–1082.
2 G. B. Schuster, *Acc. Chem. Res*., 1979, **12**, 366.
3 L. H. Catalani and T. Wilson, *J. Am. Chem. Soc*., 1989, **111**, 2633.
4 F. McCapra, *Mechanism in Chemiluminescence and Bioluminescence-Unfinished Business*, in *Bioluminescence and Chemiluminescence*, ed. J. W. Hastings, L. J. Kricka and P. E. Stanley, Wiley, NY, 1996, pp. 7–15.
5 K. A. Zaklika, T. Kissel, A. L. Thayer, P. A. Burns and A. P. Schaap, *Photochem. Photobiol*., 1979, 30, 35; A. P. Schaap, S. D. Gagnon and K. A. Zaklika, *Tetrahedron Lett*., 1982, **23**, 2943.
6 H. Siegerman, *Oxidation and Reduction Half-Wave Potentials of Organic Compounds*, in *Techniques of Electroorganic Synthesis*, ed. N. L. Weinberg, Wiley, NY, 1975, pp. 667–826.
7 M. Matsumoto, N. Watanabe, N. C. Kasuga, F. Hamada and K. Tadokoro, *Tetrahedron Lett*., 1997, **38**, 2863.
8 M. Matsumoto, N. Watanabe, T. Shiono, H. Suganuma and J. Matsubara, *Tetrahedron Lett.*, 1997, **38**, 5825.
9 W. Adam and M. Heil, *J. Am. Chem. Soc*., 1992, **114**, 5591.
10 S. H. Pine, *Org. React*., 1970, **18**, 403.
11 C. A. Grob, *Angew. Chem., Int. Ed. Engl*., 1969, **8**, 535.

Communication 8/06823B

Chloride ion effects on kinetic resolution in Pd-catalysed allylic alkylation

Guy C. Lloyd-Jones* and Susanna C. Stephen

School of Chemistry, Cantock's Close, Bristol, UK BS8 1TS. E-mail: guy.lloyd-jones@bris.ac.uk

Received (in Cambridge, UK) 7th August 1998, Accepted 22nd September 1998

Chloride ion (5 mol%) accelerates and stabilises the oxidative addition of the slow-reacting enantiomer of cyclopentenyl pivaloate to Pd⁰ complexes bearing the Trost modular ligand.

Astute chemical design and serendipity have led to a range of very effective ligands for enantioselective Pd-catalysed allylic alkylation.[1] Cyclic substrates have proven the hardest systems to substitute with high enantiomeric excess (ee) and the modular

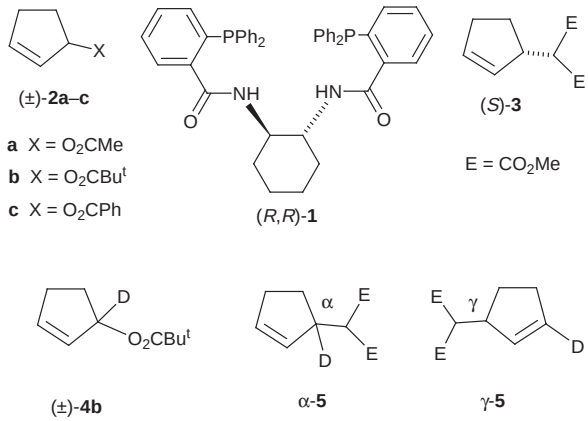

ligand systems of Trost,[2] *e.g.* (*R*,*R*)-**1**, have been almost[3] uniquely successful for this reaction type.

We recently reported a mechanistic study[4] of the 'memory effect'[5] in the '[Pd(*R*,*R*)-**1**]'-catalysed reaction of **2a** with sodio dimethyl malonate ($NaCHE_2$; E = CO_2CH_3) in THF to give (*S*)-**3**. Herein we report on the effect of catalytic chloride ion on the kinetic resolution[6] of **2** and **4** by '[Pd(*R*,*R*)-**1**]'.

Pro-catalysts generated *in situ* from a bidentate ligand (L_2) and $[Pd(allyl)Cl]_2$ are often employed in Pd-catalysed allylic alkylation with $NaCHE_2$. Entry into the catalytic cycle is assumed to proceed *via* alkylation–reduction of $[(L_2)Pd^{II}$-π-allyl][Cl] to generate NaCl, allyl-CHE_2 and '$[Pd(L_2)]$'.[7] Using 2.25 equiv. $NaCHE_2$ and 5 mol% of '[Pd(*R*,*R*)-**1**]' generated *in situ* from (*R*,*R*)-**1** and $[Pd(allyl)Cl]_2$ (**1**/Pd = 3/2) complete conversion of both enantiomers of deuterium labelled pivaloate (±)-**4b** to a mixture of isotopomeric α- and γ-**5** occurs, in THF, within 10 min at room temp. (Table 1, entry 1).

When the reaction was quenched after 5 s, there was evidence of a moderate kinetic resolution ($k_S/k_R \approx 9$): recovered **4b** (25%) was 88% ee (*R*) and α/γ-**5** were obtained in 38% yield.† However, when the '[Pd(*R*,*R*)-**1**]' was generated under chloride-free conditions[8] from $[Pd_2dba_3.CHCl_3]$ (dba = dibenzylideneacetone) or $[Pd(allyl)(MeCN)_2][OTf]$ (**1**/Pd = 3/2) the rate of reaction was reduced and kinetic resolution enhanced. After 10 min, α-**5** and γ-**5** arising exclusively (≥97%) from matched (*S*)-**4b** were obtained in 38–43% yield and mismatched (*R*)-**4b** had been partially resolved (47–51% ee) (Table 1, entry 2). After a further 2 h (*R*)-**4b** was recovered in 28–32% yield and ≥90% ee.‡ There was no racemisation or further conversion[9] of (*R*)-**4b** (despite a large excess of $NaCHE_2$) over a period of 48 h. However, with substoichiometric (0.5 equiv.) $NaCHE_2$ rapid (≤60 s) partial resolution of (±)-**2c** was followed by Pd-catalysed racemisation of remaining (*R*)-**2c** (Fig. 1).

With excess nucleophile, labelled substrates were recovered unscrambled—there was no evidence of the γ-^{2}H isotopomer of (*R*)-**4b** and reaction of (±)-**6b** (95% ^{18}O) afforded (*R*)-**6b** (≥90% ee) and no acyl-^{18}O isotopomer **7b**. These results suggest non-reversible Pd-allyl formation from (*R*)-**4** and (*R*)-**6** under turn-over conditions[10]§ and implicate the nucleophile in the catalyst deactivation process.

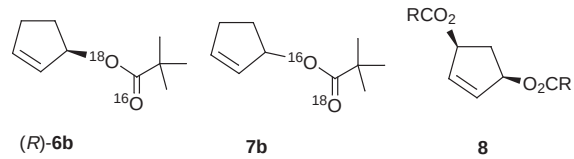

The efficient kinetic resolution of (±)-**4b** by '[Pd-(*R*,*R*)-**1**]' is not in itself surprising—the tight 'chiral pocket'[11] of (*R*,*R*)-**1** is known to effect highly enantioselective (*matched)* ionisation of *meso*-diesters **8**.[2b] More remarkable however, is that 5 mol% chloride ion increases the conversion (not *via* racemisation) of mismatched[12] (*R*)-**4b** (Table 1, compare entries 1 and 2) and inhibits catalyst deactivation. The importance of halide ions, at

Table 1 The effect of chloride on kinetic resolution with Pd^{II} *vs.* Pd^0 catalyst pre-cursors, in THF and CH_2Cl_2

Entry	Pd[a]	Yield (%) (*R*/*S*) (*S*)-α-**5**	(*R*)-γ-**5**	(*R*)-**4b**
1	$[Pd(allyl)Cl]_2$	50 (42:58)	29 (36:64)	0 (—)
2	Pd^{II} [a] or Pd^0 [a]	32 (< 5:95)	11 (> 95:5)	36 (74:26)
3	Pd^{II} [a] + dba[b] + LiCl[c] or Pd^0 [a] + LiCl[c]	33 (< 5:95)	14 (> 95:5)	17–28 (> 95:5)
4	Pd^{II} [a] + LiCl[c]	46 (43:57)	31 (39:61)	0 (—)
5[d]	Pd^{II} [a]	20 (11:89)	5 (66:34)	74 (64:36)
6[d]	$[Pd(allyl)Cl]_2$	60 (33:67)	27 (19:81)	0 (—)

[a] Pd^{II} = $[Pd(allyl)(MeCN)_2][OTf]$; Pd^0 = Pd_2dba_3·$CHCl_3$. [b] 7.5 mol% dba. [c] 5 mol% LiCl. [d] In CH_2Cl_2, 145 min.

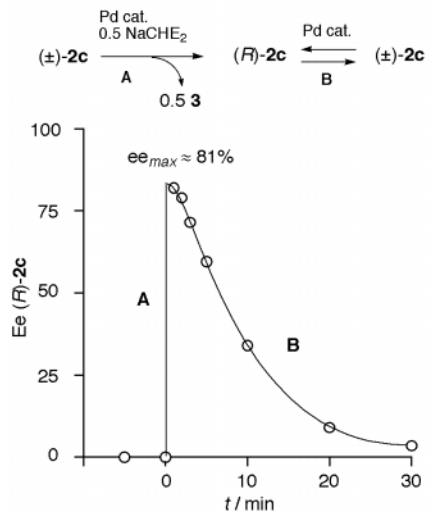

Fig. 1 Kinetic resolution (**A**) then racemisation (**B**) of (±)-**2c** on reaction with 0.5 equiv. $NaCHE_2$, catalysed by chloride-free pro-catalyst generated from 7.5 mol% (*R*,*R*)-**1** and 5 mol% [Pd(allyl)$(MeCN)_2$][OTf].

both the Pd^0 and Pd^{II} oxidation state in cross-coupling and Heck reactions is well documented.[13] However, although a variety of halide effects have been reported in Pd-catalysed allylic substitution[14] these are all mechanistically implicated at the Pd^{II}-π-allyl stage.

To gain further information, we compared the effect of chloride on the selectivity with different pro-catalyst systems in THF. Use of 5 mol% of the Pd^0 pro-catalyst derived from (*R*,*R*)-**1**, [Pd_2dba_3·$CHCl_3$] and LiCl (**1**/Pd/Cl = 3/2/2) resulted in even more effective kinetic resolution giving (*R*)-**4b** (28% yield) in ⩾95% ee in under 10 min (Table 1, entry 3). At this point (*S*)-α-**5** (⩾95% ee) and (*R*)-γ-**5** (⩾90% ee) were derived almost exclusively (> 97%) from matched (*S*)-**4b** and this suggests $k_S/k_R \geqslant 100$.¶ However, complete conversion of residual (*R*)-**4b** to α/γ-**5** occurred in less than 12 h to give α/γ-**5** in 74% yield. Hence the LiCl retarded catalyst deactivation but not kinetic resolution.

With 5 mol% of the Pd^{II} pro-catalyst derived from (*R*,*R*)-**1**, [Pd(allyl)$(MeCN)_2$][OTf] and LiCl (**1**/Pd/Cl = 3/2/2), complete conversion of (±)-**4b** to **5** occurred within 10 min (Table 1, entry 4). When dba (7.5 mol%) was also added to the pro-catalyst mixture, catalysis slowed dramatically and the system behaved similarly to that derived from a Pd^0 source (Table 1, entry 3). When the LiCl was omitted initially but added after 10 min of catalysis, powerful kinetic resolution of (±)-**4b** and catalyst deactivation occurred in the first 10 min and, on addition, the LiCl did not reactivate the catalyst.

The effect of solvent was also briefly studied. In CH_2Cl_2 reactions were slower. There was moderate kinetic resolution (k_S/k_R *ca.* 9) under chloride-(ion)-free conditions (Table 1, entry 5) and a greater 'memory effect' in the presence of 5 mol% chloride (Table 1, entry 6).

Taken together, the results suggest the following: (i) chloride coordination to Pd^0 results in a more reactive and less selective palladate-type catalyst, (ii) palladate formation is disrupted by dba, and (iii) in the absence of chloride and in the presence of $NaCHE_2$, mismatched ionisation of slower reacting (*R*)-**4b** tends to lead to catalyst decomposition.

Generous donations from the Zeneca Strategic Research Fund are gratefully acknowledged. S. C. S thanks the University of Bristol for a Postgraduate Scholarship.

Notes and references

† The deuterium label and stereospecific mechanism allows the distinction of **5** arising from (*R*)- and (*S*)-**4**. Ratios were determined by NMR analysis in C_6D_6 with (+)-Eu(hfc)$_3$: (*S*)-**4b**/(*R*)-**4b** by ^{1}H NMR analysis and (*S*)-α-**5**/(*R*)-γ-**5**/(*R*)-α-**5**/(*S*)-γ-**5** by ^{13}C NMR analysis (see ref. 4).

‡ Analogous results were obtained with (±)-**4a** and (±)-**4c**. Pd-catalysed reaction (5 mol% [(dppf)Pd(allyl)][OTf], THF, 25 °C, 60 s) of the resultant (*R*)-**4a** with 2.25 equiv. $NaCHE_2$ afforded (*R*)-α-**5** and (*S*)-γ-**5** exclusively (> 96%).

§ Reversible ionisation cannot be completely ruled out if a very tight ion-pair {[(**1**)-Pd-(η^x-*c*-C_5H_7)]$^+$[O_2CCMe_3]$^-$} is formed and there is slow relaxation of nucleofuge orientation (*i.e.* equilibration of $^{18}O/^{16}O$) relative to exclusive internal return at the *mismatched* (α) carbon.

¶ For 98% selective conversion of (*S*)-**4b** over (*R*)-**4b** to α/γ-**5** at 43% conversion, $(k_S/k_R)_{calc}$ = 107. This calculation assumes that the slow mismatched ionisation of (*R*)-**4** gives no side products. Thus (k_S/k_R) may be much lower.

1 G. Consiglio and R. M. Waymouth, *Chem. Rev.*, 1989, **89**, 257; C. G. Frost, J. Howarth and J. M. J. Williams, *Tetrahedron: Asymmetry*, 1992, **3**, 1089; B. M. Trost and D. L. Van Vranken, *Chem. Rev.*, 1996, **96,** 395.

2 (*a*) B. M. Trost and R. Radinov, *J. Am. Chem. Soc.*, 1997, **119**, 5962; (*b*) B. M. Trost and D. E. Patterson, *J. Org. Chem.*, 1998, **63**, 1339 and references cited therein.

3 G. Helmchen, S. Kudis, P. Sennhenn and H. Steinhagen, *Pure App. Chem.*, 1997, **69**, 513.

4 G. C. Lloyd-Jones and S. C. Stephen, *Chem. Eur. J.*, 1998, in the press.

5 (*a*) B. M. Trost and R. C. Bunt, *J. Am. Chem. Soc.*, 1996, **118,** 235; (*b*) J.-C. Fiaud and J. L. Malleron, *Tetrahedron Lett.*, 1981, **22**, 1399; (*c*) T. Hayashi, M. Kawatsura and Y. Uozumi, *J. Am. Chem. Soc.*, 1998, **120**, 1681.

6 See *e.g.* H.-J. Gais, H. Eichelmann, N. Spalthoff, F. Gerhards, M. Frank and G. Raabe, *Tetrahedron: Asymmetry*, 1998, **9**, 235; T. Hayashi, A. Yamamoto and Y. Ito, *J. Chem. Soc., Chem. Commun.*, 1986, 1090.

7 J. Tsuji, *Palladium Reagents and Catalysts*, Wiley, Chichester, 1995.

8 The $CHCl_3$ in Pd_2dba_3·$CHCl_3$ can sometimes act as a source of chloride: see O. Loiseleur, P. Meier and A. Pfaltz, *Angew. Chem., Int. Ed. Engl.*, 1996, **35**, 200.

9 Material balance indicates some decomposition of (*R*)-**4b**; *ca.* 25% isolated yield after 2 days but only *ca.* 5% conversion to (*R*)-α- and (*S*)−γ-**5**. We have not been able to detect β-H elimination products: see G. R. Cook and P. S. Shanker, *Tetrahedron Lett.*, 1998, **39**, 4991.

10 For an example of tight/orientated ion-pairing with slow equilibration of $^{18}O/^{16}O$ in a carboxylate, see H. L. Goering, M. M. Pombo and K. D. McMichael, *J. Am. Chem. Soc.*, 1963, **85**, 965.

11 B. M. Trost, *Acc. Chem. Res.*, 1996, **29**, 355.

12 In desymmetrisation reactions of **8**, catalysts derived from [Pd(allyl)Cl]$_2$ gave less satisfactory results than those derived from [Pd_2dba_3.$CHCl_3$]: see ref. 2(*b*).

13 C. Amatore, A. Jutand and A. Suarez, *J. Am. Chem. Soc.*, 1993, **115**, 9531; L. E. Overman and D. J. Poon, *Angew. Chem., Int. Ed. Engl.*, 1997, **36**, 518; W. J. Scott and J. K. Stille, *J. Am. Chem. Soc.*, 1986, **108**, 3033; T. Kamikawa and T. Hayashi, *Tetrahedron Lett.*, 1997, **38**, 7087; K. Rossen, P. J. Pye, A. Maliakal and R. P. Volante, *J. Org. Chem.*, 1997, **62**, 6462.

14 see for example U. Burckhardt, M. Baumann and A. Togni, *Tetrahedron: Asymmetry*, 1997, **8**, 155; M. Kawatsura, Y. Uozomi and T. Hayashi, *Chem. Commun.*, 1998, 217; A. Gogoll, J. Örnebro, H. Grennberg and J.-E. Bäckvall, *J. Am. Chem. Soc.*, 1994, **116**, 3631; ref. 5(*c*).

Communication 8/06324I

Anion-templated formation of a unique inorganic 'super-adamantoid' cage $[Ag_6(triphos)_4(O_3SCF_3)_4]^{2+}$ [triphos = $(PPh_2CH_2)_3CMe$]

Stuart L. James,* D. Michael P. Mingos,* Andrew J. P. White and David J. Williams

Department of Chemistry, Imperial College of Science Technology and Medicine, South Kensington, London, UK SW7 2AY. E-mail: s.l.james@ic.ac.uk; d.mingos@ic.ac.uk

Received (in Basel, Switzerland) 12th August 1998, Accepted 23rd September 1998

In the presence of templating anions, 2 : 3 molar mixtures of triphos and silver(I) cations unexpectedly give novel hexanuclear cages, which result from an unusual '*endo*-methyl' geometry of the triphos ligands.

Multidentate ligands in general tend to promote the formation of metal clusters or aggregates by forming radial metal–ligand bonds which place the metal atoms at the centre of the molecule. For example, 2 : 2 (ligand : metal) diphosphine complexes of silver(I) or copper(I) generally form dinuclear rings shown in Fig. 1(a) and (b), with terminal or bridging anions.[1] Metallocage assembly is receiving increasing attention,[2] and the use of appropriate tripodal phosphines in a 2 : 3 ratio might be expected to give trinuclear cages of the type shown in Fig. 1(c). The only triphos $[MeC(CH_2PPh_2)_3]$ silver(I) complex to be structurally characterised so far is the mononuclear 1 : 1 complex [Ag(triphos)I].[3] Here we report our unexpected observation that a 2 : 3 molar mixture of triphos and silver(I) ions in fact gives a novel hexanuclear cage of formula $[Ag_6(triphos)_4X_4]^{2+}$. The triphosphine ligands assemble with their methyl groups concentrating in the central region of the molecule, and the dative bonds to the complexed phosphino substituents lead to an aggregate of silver ions on the surface. Anions are further complexed to the outside of the cage and appear to play an important templating role.

When solutions of triphos are titrated against a silver(I) salt of an oxo anion [AgX] (X = SO_3CF_3, ClO_4, NO_3) and monitored by $^{31}P\{^1H\}$ NMR spectroscopy, broad featureless signals are seen until a molar ratio of 2 : 3 (triphos : silver) is reached, when only a very sharp pattern with well defined ^{109}Ag–^{31}P and ^{107}Ag–^{31}P coupling is observed. Crystals of the 2 : 3 adduct **1** (X = SO_3CF_3 **1a**, ClO_4 **1b**, NO_3 **1c**)† suitable for X-ray analysis were grown by diffusion of hexane into a tetrachloroethane–acetonitrile solution of the complex.‡ The molecular structure (Fig. 2) is based on a cage of stoichiometry $[Ag_6(triphos)_4(O_3SCF_3)_4]^{2+}$ with approximate *T* symmetry.§ It may be simply represented as a truncated tetrahedron in which the four triphos ligands define the truncated apices and the six silver ions occupy the edges (Fig. 3). The four faces of the cage correspond to fused 18-membered rings each having local C_3 symmetry, containing six phosphorus atoms and three silver(I) centres. Approaching each facial trio of silver(I) atoms is a triflate ion with its oxygen atoms directed inwards. A novel feature is the

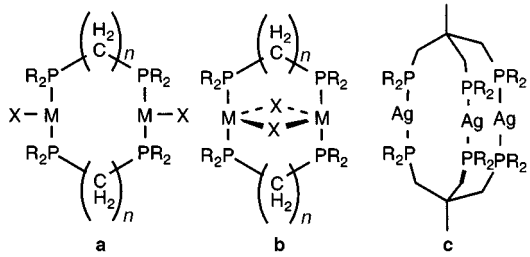

Fig. 1 Macrocyclic diphosphine silver(I) and copper(I) complexes with terminal (a) or bridging (b) anions and postulated trinuclear cages based on triphos ligands (c).

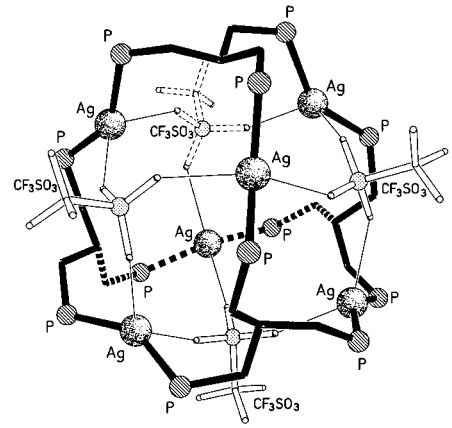

Fig. 2 The central core of complex **1a**. The phenyl and methyl groups on the triphos ligands have been omitted for clarity.

'*endo*-methyl' conformation of the triphos ligands, in which their methyl groups point toward the centre of the cage, leaving only a small cavity of van der Waals radius *ca.* 2.4 Å at the centre. This arrangement differs markedly from the '*exo*-methyl' conformation observed when triphos acts as a face capping ligand.[4] As a consequence, the in-pointing methyls generate an ordered hydrophobic interior and the Ag^+ and $O_3SCF_3^-$ ions form a polar spherical surface.

The average Ag–O distance is 2.66 Å indicating a significant degree of interaction [*cf.* 2.639(4), 2.712(6) and 2.74(2) in $[Ag_2\{\mu\text{-}Ph_2P(CH_2)_6PPh_2\}_2(\mu\text{-}ClO_4)_2]$[1a]]. The resulting geometry at each Ag(I) centre can best be described as distorted tetrahedral, the angles subtended at the two independent metal centres by the phosphorus atoms being 144.6(1) and 147.9(1)°, and by the oxygen atoms 128.2(5) and 126.8(5)° respectively. The O–Ag–O and P–Ag–P planes at each silver ion are essentially orthogonal (between 88 and 90°). The Ag–P

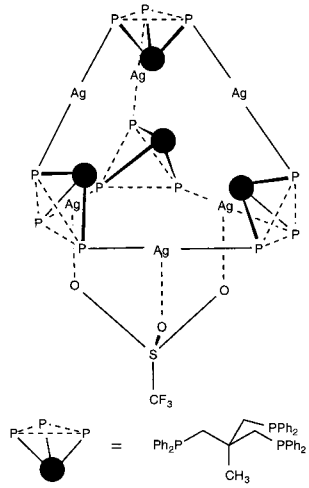

Fig. 3 Truncated tetrahedral representation of complex **1a**.

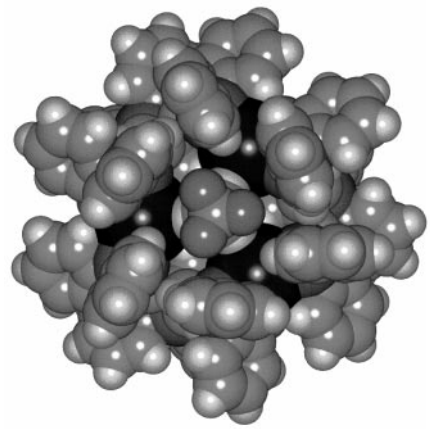

Fig. 4 Space-filling representation of the solid state structure of **1a** viewed along the crystallographic C_3 axis.

distances are in the range 2.405(4)–2.416(4) Å. The ability of triflate to coordinate to the cage is perhaps surprising given the steric bulk of the triphos phenyl substituents. However, the space filling representation of **1a** (Fig. 4) reveals how the phenyl groups are arranged in such a way as to provide channels through which the triflate anions can approach the silver ions. These channels are chiral and could potentially discriminate between enantiomeric anions.

The presence of four faces which are tetrahedrally disposed, each with approximate C_3 symmetry (as in adamantane) but composed of 18-membered rings (*cf.* six-membered as in adamantane) suggests the description 'super-adamantoid' for the cage. In the super-adamantoid cage, bridgehead atoms are replaced by tridentate triphos ligands, and the bridging atoms are replaced by silver ions.

As mentioned above, in solution, sharp ^{31}P NMR spectra are observed at room temperature which indicate chemically equivalent phosphorus atoms. The silver–phosphorus coupling constants $^1J_{^{109}Ag-^{31}P}$ for **1a**–**c** lie in the range 588–561 Hz which is consistent with the silver(I) centres being coordinated to two phosphine groups.[5,6] In addition the, albeit small, variations in chemical shift and silver–phosphorus coupling constants between **1a**, **1b** and **1c** imply that some degree of anion coordination occurs at the silver(I) centres in solution. This is further supported by the ^{19}F NMR spectrum of the triflate complex **1a**, which consists of two singlets at δ −77.9 and −78.6 in a 4 : 2 intensity ratio, as expected for four coordinated and two free triflate anions. On the basis of the closely related NMR spectra of complexes **1a**–**c**, we assume that similar cage structures are formed, at least in solution, for complexes **1b** (X = ClO_4) and **1c** (X = NO_3). By contrast, under similar conditions, a mixture of triphos and $AgBF_4$ gave a solution whose ^{31}P NMR spectrum consisted for the main part (98% of the total intensity) of a broad signal lacking any evidence of ^{109}Ag–^{31}P couplings. The remaining 2% consisted of sharp signals indicative of cage formation. With $AgSbF_6$, only the broad featureless signal was observed. It therefore seems that the less nucleophilic BF_4 and SbF_6 anions are unable to promote the selective formation of the cage structure in solution.

The anion-specific behaviour noted above, *i.e.* selective formation of a rigid cage when X = SO_3CF_3, ClO_4 or NO_3 *vs.* more labile species in which phosphine dissociation occurs on the NMR timescale at room temperature when X = BF_4 or SbF_6, may be related to the μ_3-face-capping coordination mode of the anion in the structure. The anion is required to be tridentate and reasonably nucleophilic. These criteria are satisfied by the O_3SCF_3, ClO_4 and NO_3 anions, but not BF_4^- and SbF_6^-.

In conclusion, complexes **1** have a unique super-adamantoid structure which results from the phosphines adopting a novel tetramer at the centre of the molecule, providing an outer surface which enables the coordination of six silver ions in an octahedral aggregate. This unusual geometry is stabilised by tridentate anions capable of capping the faces of the octahedron.

We would like to thank Dr J. S. Fleming and Mr C.-A. Carraz for obtaining ^{19}F NMR spectra.

Notes and references

† *Experimental*: in a typical preparation, a solution of triphos (70 mg, 0.122 mmol) in tetrachloroethane (4 cm^3) was added to a solution of [AgX] (0.183 mmol) in MeCN (1 cm^3) and the resulting solution layered with hexane to give the product as colourless crystals. ^{31}P NMR (110 MHz, CD_3CN–$CDCl_3$, 4 : 1, 25 °C, 85% H_3PO_4) δ −5.95 ($^1J_{^{109}Ag-^{31}P}$ 588 Hz) **1a**; −4.49 ($^1J_{^{109}Ag-^{31}P}$ 587 Hz) **1b**; −4.75 ($^1J_{^{109}Ag-^{31}P}$ 561 Hz) **1c**. Reactions between triphos and $AgBF_4$ or $AgSbF_6$ were conducted similarly. ^{31}P NMR (110 MHz, CD_3CN–$CDCl_3$, 4 : 1, 25 °C, 85% H_3PO_4); $AgBF_4$: 98% of total intensity is a broad signal from δ −5 to −12, 2% is sharp, with δ −3.67 ($^1J_{^{109}Ag-^{31}P}$ 588 Hz); $AgSbF_6$: broad signal from δ −5 to −12.

‡ *Crystal data* for **1a**: $[(C_{164}H_{156}P_{12}Ag_6)(CF_3SO_3)_4](CF_3SO_3)_2\cdot 6(C_2H_2Cl_4)$, M = 5047.2, rhombohedral, space group $R\bar{3}$ (no. 148), a = 24.454(2), c = 70.832(6) Å, V = 36684(5) Å^3, Z = 6 (the complex has crystallographic C_3 symmetry), D_c = 1.371 g cm^{-3}, μ(Cu-Kα) = 79.5 cm^{-1}, F(000) = 15 192, T = 183 K, clear prisms, 0.53 × 0.53 × 0.37 mm, Siemens P4 rotating anode diffractometer, ω-scans, 11 915 independent reflections. The structure was solved by direct methods and all of the non-hydrogen atoms of the complex and its associated counter-ions were refined anisotropically. The solvent molecules and the remaining counter-ions were found to be highly disordered and could not be resolved. They were thus modelled by the assignment of appropriate partial occupancy atoms to fit the electron density throughout the diffuse area. Refinements were by full matrix least-squares based on F^2 to give R_1 = 0.109, wR_2 = 0.283 for 5962 independent observed absorption corrected [semiempirical based on ψ-scans, max. and min. transmission factors 0.23 and 0.08 respectively] reflections [$|F_o| > 4\sigma(|F_o|)$, $2\theta \leqslant 120°$] and 720 parameters. CCDC 182/1030.

§ The crystallograpic symmetry is C_3 only about an axis passing through one of the triflate anions, though the departures from this symmetry about the other three anions are only slight.

1 (*a*) S. Kitagawa, M. Kondo, S. Kawata, S. Wada, M. Maekawa and M. Munakata, *Inorg. Chem.*, 1995, **34**, 1455; (*b*) E. R. T. Tiekink, *Acta. Crystallogr., Sect. C*, 1990, **46**, 1933; (*c*) D. M. Ho and R. Bau, *Inorg. Chem.*, 1983, **21**, 4073; (*d*) S. P. Neo, Z.-Y. Zhou, T. C. W. Mak and T. S. A. Hor, *ibid.*, 1995, **34**, 520; (*e*) A. F. M. J. van der Ploeg, G. van Koten and A. L. Spek, *ibid.*, 1979, **18**, 1052; (*f*) A. F. M. J. van der Ploeg and G. van Koten, *Inorg. Chim. Acta*, 1981, **51**, 225; (*g*) Y. Ruina, Y. M. Hou, B. Y. Xue, D. M. Wang and D. M. Jin, *Transition Met. Chem.*, 1996, **21**, 28; (*h*) *Acta Crystallogr., Sect. B*, 1976, **32**, 2521; (*i*) F. Caruso, M. Camalli, H. Rimml and L. M. Venanzi, *Inorg. Chem.*, 1995, **34**, 673; (*j*) *J. Org. Chem.*, 1980, **45**, 2995; (*k*) *Inorg. Chim. Acta*, 1997, **69**, 262.

2 R. W. Saalfrank, R. Burak, A. Breit, D. Stalke, R. Hirbstirmer, J. Daub, M. Porsch, E. Bill, M. Muther and A. X. Trautwein, *Angew. Chem., Int. Ed. Engl.*, 1994, **33**, 1621; D. L. Caulder, R. E. Powers, T. N. Parac and K. N. Raymond, *ibid.*, 1998, **37**, 1840; T. Beissel, R. E. Powers and K. N. Raymond, *ibid.*, 1996, **35**, 1084; C. Bruckner, R. E. Powers and K. N. Raymond, *ibid.*, 1998, **37**, 1837; A. J. Amoroso, J. C. Jeffrey, P. L. Jones, J. A. McCleverty, P. Thornton and M. D. Ward, *ibid.*, 1995, **34**, 1443; J. S. Fleming, K. L. V. Mann, C. A. Carraz, E. Psillakis, J. C. Jeffrey, J. A. McCleverty and M. D. Ward, *ibid.*, 1998, **37**, 1279; R. Vilar, D. M. P. Mingos, A. J. P. White and D. J. Williams, *ibid.*, 1998, **37**, 1258.

3 M. Camalli and F. Caruso, *Inorg. Chim. Acta*, 1990, **169**, 189.

4 H. Zimmerman, M. Gomm, E. Kock and J. Ellerman, *Acta Crystallogr., Sect. C*, 1988, **44**, 48; M. R. Churchill, C. H. Lake, W. G. Feighery and J. B. Keister, *Organometallics*, 1991, **10**, 2384.

5 *Methods in Stereochemical Analysis, Volume 8, Phosphorus-31 NMR spectroscopy in Stereochemical Analysis*, ed. J. G. Verkade and L. D. Quin, VCH Publishers Inc., Deerfield Beach, FL, 1987; M. Barrow, H. B. Buergi, M. Camalli, F. Caruso, E. Fischer, L. M. Venanzi and L. Zambonelli, *Inorg. Chem.*, 1983, **22**, 2356.

6 Camalli *et al.* (ref. 3), in broad agreement with our observations, report that reaction between triphos and [AgX] (X = ClO_4 or NO_3) was found to give complexes with silver–phosphorus coupling constants 'higher than expected for complexes of the type AgP_3' (P = phosphine). While noting that definitive structure assignments could not be made, it was postulated that these complexes were two-coordinate with one arm of the triphos ligand non-coordinate. We suggest that they were in fact observing the cages **1b** and **1c** respectively.

Communication 8/06388E

β-Lactam synthetase: implications for β-lactamase evolution

Heather J. McNaughton,[a] Jan E. Thirkettle,[a] Zhihong Zhang,[a] Christopher J. Schofield,*[a]† Susan E. Jensen,[b] Barry Barton[c] and Philip Greaves[c]

[a] *The Oxford Centre for Molecular Sciences, South Parks Road, Oxford, UK OX1 3QY*
[b] *University of Alberta, Edmonton, Alberta, Canada TG6 2E9*
[c] *SmithKline Beecham Pharmaceuticals, Southdownview Way, Worthing, West Sussex, UK BN14 8QH*

Received (in Cambridge, UK) 27th August 1998, Accepted 15th September 1998

A synthetase enzyme catalyses formation of the monocyclic β-lactam ring during clavulanic acid biosynthesis.

The most important inhibitor of serine β-lactamases is clavulanic acid **1**,[1] which is produced by some *Streptomyces spp*.[2] Whilst the central portion (*i.e*. **2** to **3**) of the clavulanic acid **1** biosynthesis pathway is established, significant gaps remain (Scheme 1). Nearing the end of the pathway the process by which the stereochemistry of the ring junction and C-3 positions of clavulanic acid are inverted to give the aldehyde **4** is unknown. At the beginning of the pathway, the intermediates leading to monocyclic β-lactam **2** are unclear. Labelling experiments have demonstrated that likely direct primary metabolic precursors of the 3 and 5-carbon portions of the clavulanic acid skeleton are pyruvate[3,4] and arginine.[5] Further studies have indicated that **5** is an intermediate in the pathway.[6]

Our sequencing studies demonstrated that within the biosynthesis gene cluster[7] of **1** an open reading frame (ORF3) displays a *ca*. 25% sequence identity over 434 of its 513 residues with Asn synthetase B (AS-B), the first 50 amino acids showing no homology. AS-B catalyses the ATP dependent synthesis of Asn from Asp and Gln; *in vitro* Gln can be replaced with NH_3 (Scheme 2).[8] We speculated that the ORF3 gene encoded the enzyme responsible for the conversion of **5** to **2**. Instead of catalysing the intermolecular formation of an amide bond as for AS-B, we envisaged that a synthetase catalysed the cyclisation of **5** to **2**, which in one sense may be viewed as a 'reverse' β-lactamase.

The ORF3 gene was PCR amplified from a cosmid containing the genetic information for the biosynthesis of **1** and sub-cloned into the pET-24a(+) vector,‡ which expressed

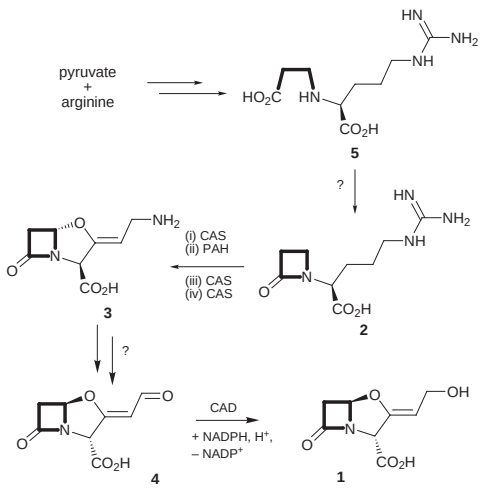

Scheme 1 Outline of the biosynthetic pathway leading to clavulanic acid. CAS = clavaminate acid synthase, PAH = proclavaminate amidinohydrolase, CAD = clavulanic acid dehydrogenase. Each CAS catalysed step is coupled to the conversion of 2-oxoglutarate and dioxygen to succinate.

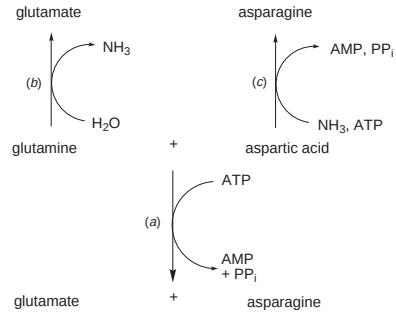

Scheme 2 Reactions catalysed by *E. coli* asparagine synthetase B (AS-B): (*a*) *in vivo* reaction, and (*b*) and (*c*) reactions also catalysed *in vitro*.

native recombinant enzyme in *Escherichia coli* BL21(DE3) at *ca*. 10% of total soluble cell protein. The recombinant ORF3 protein was purified by standard methodologies. N-Terminal sequencing, Western blot, and SDS-PAGE analyses demonstrated the expression and purification of the desired 56 kDa protein.§ Synthetic standards of **5** and **2** were prepared by published methods[9] and used to devise HPLC assays for these compounds. Crude extracts of the recombinant *E. coli* containing the ORF3 gene product and purified protein product were tested for the ability to catalyse the conversion of synthetic **5** to β-lactam **2**. The most sensitive assay involving the derivatisation of guanidino side chains based on the work of Kai *et al*.[10] showed clear conversion of **5** to **2**, when using either crude or purified recombinant protein, but only in the presence of Mg^{2+}, enzyme and ATP. The production of **2** was confirmed by preparative HPLC leading to its isolation. Spectroscopic characterisation of **2** showed it to be identical to the authentic synthetic material [δ_H(500MHz; D_2O) 1.48–1.55 (2H, m, $CH_2CH_2CH_2N$), 1.65–1.73 and 1.76–1.80 (2 × 1H, 2 × m, CH_2CH_2CHN), 2.82–2.89 (2H, m, NCH_2CH_2CO), 3.13 (2H, t, *J* 5, $CH_2CH_2CH_2N$), 3.29–3.31 and 3.35–3.38 (2 × 1H, 2 × m, NCH_2CH_2CO), 3.99 (1H, dd, *J* 5 and 10, $CHCO_2H$); *m/z* (ESI) 229 (MH^+)]. The ORF3 product catalysing the conversion of **5** to **2** was named β-lactam synthetase 1 [BLS (1)].

AS-B possesses an N-terminal cysteine residue and is a member of the family of Ntn (N-terminal nucleophilic) amidotransferases.[11] Studies on AS-B suggest that the N-terminal cysteine attacks the carbonyl of the amide of Gln, in order to increase the nucleophilicity of the amide nitrogen for reaction with the acceptor carbonyl.[12] The β-carboxylate of Asp is activated by reaction with ATP to form β-Asp-AMP and pyrophosphate (PP_i). The timing of nitrogen transfer from the activated glutamine is uncertain, but may proceed *via* a complex to which AMP is still bound **6** or an imide intermediate **7**.[13]

Amongst Ntn enzymes, BLS has an unusual N-terminus lacking an N-terminal cysteine (or serine/threonine), and is probably incapable of activating the nitrogen of the Gln amide for nucleophilic attack. We propose BLS activates the β-amino acid **5** by reaction with ATP to form an acyl adenylate **9** (Scheme 3). Instead of being attacked by Gln this intermediate undergoes cyclisation to **2** and AMP. The N-terminal residue of

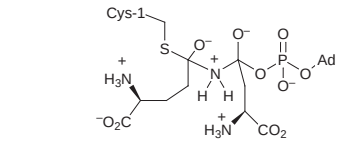

6

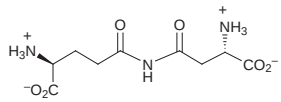

7

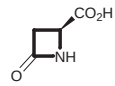

8

BLS is Gly, implying an Ntn type mechanism is not operating in BLS catalysis, unless the N-terminal amino group acts as the general base presumably required to deprotonate the β-amino group of **5**. The proposed BLS mechanism leads to the possibility that the transfer of NH_3 from Gln to Asp during AS-B catalysis also proceeds *via* a β-lactam, **8**. Whatever, the structural and mechanistic relationships between AS-B enzymes and BLS suggest a close evolutionary relationship. Studies aimed at converting AS-B into a β-lactam synthetase and *vice versa* have been initiated.

An open reading frame (*car*A) encoding for an enzyme with sequence similarities to AS-B/BLS has also been found within the biosynthetic gene cluster encoding for enzymes making 1-carbapenem-3-carboxylic acid.[14,15] The particular step catalysed by the CarA enzyme is unknown, but it has been proposed that it catalyses the formation of the β-lactam ring.[15,16] Our results support this proposal, but suggest the CarA enzyme catalyses an ATP/synthetase type reaction rather than a β-lactam cyclisation reaction proceeding *via* a thiol ester intermediate.[17,18]

The only other β-lactam forming enzyme to be so far described is isopenicillin N synthase,[19] which catalyses the oxidation of the peptide L-δ-(α-aminoadipoyl)-L-Cys-D-Val to give isopenicillin N, the first β-lactam formed in the biosynthesis of penicillins. Thus, β-lactam formation during the biosynthesis of clavams, which is driven by the hydrolysis of ATP, occurs *via* a very different mechanism to that during penicillin formation, which is driven by the reduction of dioxygen.

Since AS-B and related enzymes are widespread, and relatively minor modifications of them might lead to BLS type enzymes, BLS activity may have evolved before the less common and seemingly more complex secondary metabolic machinery required for penicillin and cephalosporin biosynthesis. Simple β-lactams such as **8** might have been (and may still be?) present in metabolism before other β-lactams which are more well known because of their antibacterial activity. β-Lactamases may have initially evolved to hydrolyse these monocyclic β-lactams, suggesting they may be ancient enzymes, and it is possible the chromosomal location of some β-lactamase genes reflects this.

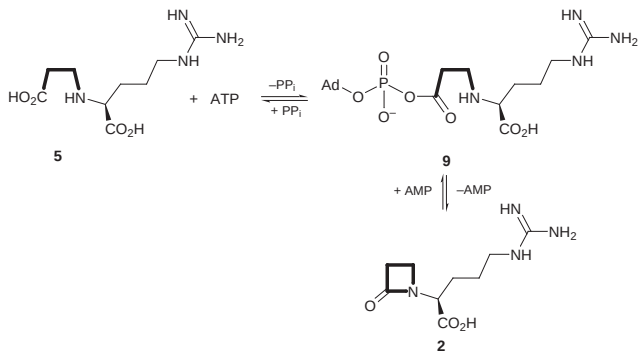

Scheme 3

Analogous modifications of other Ntn enzymes may result in the formation of enzymes catalysing intramolecular cyclisation rather than intermolecular reactions. Thus, for example, modification of Ntn glutamine synthetases would lead to enzymes catalysing the formation of pyroglutamate from glutamate or other γ-lactams from appropriate γ-amino acid precursors.

Note: After acceptance of our manuscript we became aware of the work of Bachmann *et al*.,[20] which also demonstrates that ORF3 encodes for a BLS involved in clavam biosynthesis.

Dedicated to Professor Jack E. Baldwin on the occasion of his 60th birthday.

Notes and references

† E-mail: christopher.schofield@chem.ox.ac.uk

‡ Automated fluorescence DNA sequencing verified the sequence of the first 500bp.

§ Edman degradation of the recombinant protein gave the amino acid sequence GAPVLPAAFGFLASARTGGG, identical with that predicted for the native protein.

1 A. G. Brown, D. Butterworth, M. Cole, G. Hanscomb, J. D. Hood, C. Reading and G. N. Rolinson, *J. Antibiot*., 1976, **29**, 668.
2 For a review see: K. H. Baggaley, A. G. Brown and C. J. Schofield, *Nat. Prod. Rep*., 1997, **14**, 309.
3 J. Pitlik and C. A. Townsend, *Chem. Commun*., 1997, 225.
4 J. E. Thirkettle, J. E. Baldwin, J. Edwards, J. P. Griffin and C. J. Schofield, *Chem. Commun*., 1997, 1025.
5 B. P. Valentine, C. R. Bailey, A. Doherty, J. Morris, S. W. Elson, K. H. Baggaley and N. H. Nicholson, *J. Chem. Soc*., *Chem. Commun*., 1993, 1210.
6 S. W. Elson, K. H. Baggaley, M. Davison, M. Fulston, N. H. Nicolson, G. D. Risbrine and J. W. Tyler, *J. Chem. Soc*., *Chem. Commun*., 1993, 1212.
7 S. E. Jensen, D. C. Alexander, A. S. Paradkar and K. A. Aidoo, *Industrial Organisms, Basic and Applied Molecular Genetics*, American Society for Microbiology, Washington, 1993, p. 169.
8 H. A. Milman and D. A. Cooney, *Biochem. J*., 1979, **181**, 51.
9 J. E. Baldwin, K. D. Merritt, C. J. Schofield, S. W. Elson and K. H. Baggaley, *J. Chem. Soc*., *Chem. Commun*., 1993, 1301.
10 M. Kai, T. Miyazaki, M. Yamaguchi and Y. Ohkura, *J. Chromatogr*., 1983, 268, 417.
11 J. A. Brannigan, G. Dodson, H. Duggleby, P. C. E. Moody, J. L. Smith, D. R. Tomchick and A. G. Murzin, *Nature*, 1995, **378**, 416.
12 S. K. Boehlein, N. G. J. Richards and S. M. Schuster, *J. Biol. Chem*., 1994, **269**, 7450.
13 P. W. Stoker, M. H. O'Leary, S. K. Boehlein, S. M. Schuster and N. G. J. Richards, *Biochemistry*, 1996, **35**, 3024.
14 S. J. McGowan, M. Sebaihia, L. E. Porter, G. S. A. B. Stewart, P. Williams, B. W. Bycroft and G. P. C. Salmond, *Mol. Microbiol*., 1996, **22**, 45.
15 S. J. McGowan, B. W. Bycroft and G. P. C. Salmond, *Trends Microbiol*., 1998, **6**, 203.
16 J. E. Thirkettle, D. Phil. Thesis, University of Oxford, 1997.
17 B. W. Bycroft and C. Maslen, *J. Antibiot*., 1988, **41**, 1231.
18 J. M. Williamson, E. Inamine, K. E. Wilson, A. W. Douglas, J. M. Liesch and G. Albers-Schonberg, *J. Biol. Chem*., 1983, **258**, 10582.
19 P. L. Roach, I. J. Clifton, C. M. H. Hensgens, N. Shibata, C. J. Schofield, J. Hajdu and J. E. Baldwin, *Nature*, 1997, **387**, 827.
20 B. O. Bachmann, R. Li and C. A. Townsend, *Proc. Natl. Acad. Sci. U.S.A*., 1998, **95**, 9082.

Communication 8/06713I

Germanium(II) azides: synthesis and crystal structure of Tp′GeN_3 [Tp′ = hydrotris(3,5-dimethylpyrazol-1-yl)borato]

Alexander C. Filippou,* Peter Portius and Gabriele Kociok-Köhn

Fachinstitut für Anorganische und Allgemeine Chemie, Humboldt-Universität zu Berlin, Hessische Str. 1-2, D-10115 Berlin, Germany. E-mail: filippou@chemie.hu-berlin.de

Received (in Basel, Switzerland) 8th June 1998

The synthesis of the germanium(II) azide Tp′GeN_3 (3) from Tp′GeCl (2) [Tp′ = $HB(3,5\text{-}Me_2pz)_3$] and NaN_3 is reported and the crystal structures of 2 and 3 are compared.

Silicon(IV) and tin(IV) azides have been reported to be versatile reagents in main-group element chemistry[1] and in organic synthesis.[2] In comparison, studies on germanium(IV) azides are still limited[3] and germanium(II) azides are to our knowledge not known, probably due to their propensity to decompose to germanium(IV) nitrides. This has prompted us to carry out the following work describing the synthesis and characterization of the germanium(II) azide Tp′GeN_3 (**3**). **3** was obtained from $GeCl_2$(1,4-dioxane) (**1**)[4] in two steps. In the first step **1** was converted with KTp′ to Tp′GeCl (**2**), which then was treated with NaN_3 to afford selectively **3** (Scheme 1).

Compounds **2** and **3** were isolated as white, slightly air sensitive solids, which are soluble in CH_2Cl_2, moderately soluble in THF and insoluble in pentane, and were fully characterized.† Thus, the IR spectra of **2** and **3** in KBr display the expected absorption bands for the Tp′ ligand. In addition, the azide group in **3** gives rise to two absorptions at 2043 cm^{-1} and 1272 cm^{-1}, which are assigned to the N_3 asymmetric and symmetric stretching vibrations, respectively. The $\nu_{asym}(N_3)$ absorption of **3** appears at lower frequency than that of the germanium(IV) azide Me_3GeN_3 [$\nu_{asym}(N_3)$ = 2103 cm^{-1}][3b] and higher than that of the azide anion [$\nu_{asym}(N_3)$ of $[N(PPh_3)_2]N_3$ in CH_2Cl_2 = 2005 cm^{-1}]. The ^1H and $^{13}C\{^1H\}$ NMR spectra of **2** and **3** display resonances for three equivalent pyrazolyl rings and indicate, taking into consideration the crystal structures of **2** and **3**, that these compounds are fluxional at room temperature.† The activation barrier to the process which equilibrates the pyrazolyl rings is low, since the static structures of **2** and **3** were not observed in CD_2Cl_2 solution even at −83 °C (300 MHz spectrometer).

Compounds **2** and **3** were characterized by X-ray diffraction as shown in Figs. 1 and 2.‡ Single crystals of **2** and **3** were obtained upon diffusion of pentane into a CH_2Cl_2 solution of **2** at ambient temperature and diffusion of an Et_2O–pentane mixture into a THF solution of **3** at −30 °C respectively. Both compounds show a distorted pseudo trigonal bipyramidal coordination geometry around the germanium atom, which is similar to that of related tin(II) compounds.[5] The halogen atom (pseudohalogen) occupies one axial site and the tridentate Tp′ ligand spans the other axial and two equatorial sites. The stereochemically active lone pair at germanium presumably is oriented towards the remaining equatorial vertex. Consequently, the N_{ax}(pz)–Ge–Cl bond angle in **2** [163.15(9)°] and the N_{ax}(pz)–Ge–N_{azide} bond angle in **3** [162.8(2)°] deviate from

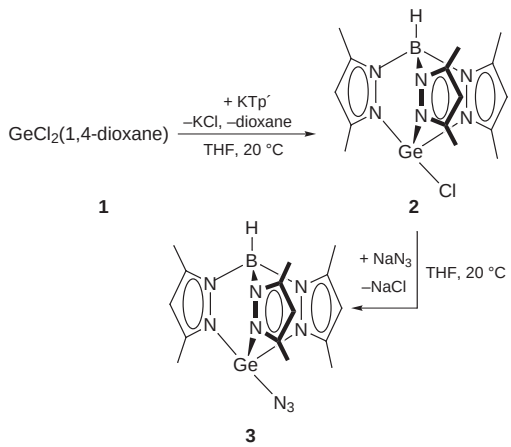

Scheme 1

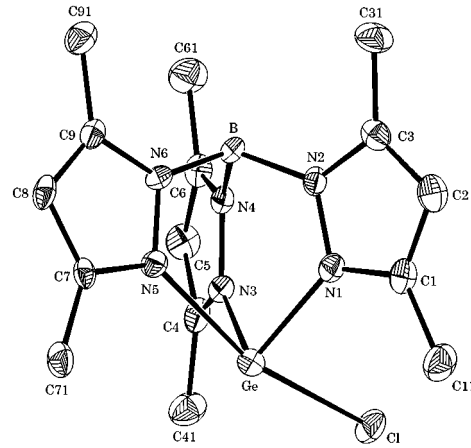

Fig. 1 ZORTEP plot of the molecular structure of **2** with thermal ellipsoids drawn at the 50% probability level. Hydrogen atoms are omitted for clarity. Selected bond lengths (Å) and angles (°): Ge–N(1) 2.023(3), Ge–N(3) 2.013(4), Ge–N(5) 2.379(3), Ge–Cl 2.536(1), N(1)–Ge–N(3) 88.7(1), N(1)–Ge–N(5) 79.9(1), N(3)–Ge–N(5) 79.9(1), Cl–Ge–N(1) 88.4(1), Cl–Ge–N(3) 87.8(1), Cl–Ge–N(5) 163.15(9).

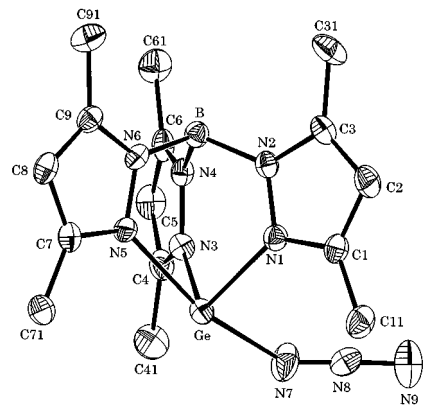

Fig. 2 ZORTEP plot of the molecular structure of **3** with thermal ellipsoids drawn at the 50% probability level. Hydrogen atoms are omitted for clarity. Selected bond lengths (Å) and angles (°): Ge–N(1) 2.034(3), Ge–N(3) 2.013(3), Ge–N(5) 2.297(3), Ge–N(7) 2.262(4), N(7)–N(8) 1.136(5), N(8)–N(9) 1.179(6), N(1)–Ge–N(3) 88.5(1), N(1)–Ge–N(5) 81.9(1), N(3)–Ge–N(5) 80.2(1), N(1)–Ge–N(7) 89.4(1), N(3)–Ge–N(7) 84.8(1), N(5)–Ge–N(7) 162.8(2), Ge–N(7)–N(8) 136.8(3), N(7)–N(8)–N(9) 176.9(5).

180°, the N_{ax}(pz)–Ge–N_{eq}(pz) bond angles are smaller than 90°, and the Ge–N_{ax}(pz) bond [**2**: 2.379(3) Å; **3**: 2.297(3) Å] is considerably longer than the Ge–N_{eq}(pz) bonds [**2**: 2.013(4) and 2.023(3) Å; **3**: 2.013(3) and 2.034(3) Å].[5,6] Striking features of the structures of **2** and **3** are the bonding parameters of the Ge–X groups (X = Cl, N_3). Thus, the Ge–Cl bond of **2** [2.536(1) Å] is considerably longer than those of other germanium(II) chlorides [*e.g.* (C_5Me_5)GeCl: 2.3841(8) Å; $GeCl_2$(1,4-dioxane): 2.265 Å; $GeCl_2$ (g): 2.186(4) Å],[7] and the Ge–N_{azide} bond of **3** [2.262(4) Å] is considerably longer than that of H_3GeN_3 (g) [1.845(6) Å].[3e] Furthermore, the angle at the germanium-bonded nitrogen atom of the azide group is, at 136.8(3)°, larger than those found in covalent main-group element azides, the azide group is almost linear as shown by the angle N(7)–N(8)–N(9) of 176.9(5)°, and the N(7)–N(8) bond is, at 1.136(5) Å, shorter than the N(8)–N(9) bond [1.179(6) Å]. These bonds have lengths between those of a N–N double [1.24 Å] and a N–N triple bond [1.10 Å].[8] All these data let us suggest in valence bond terms a certain contribution of the ionic resonance form [Tp′Ge]$^+$X$^-$ to the Ge–X bond in **2** and **3**.

In conclusion, we have shown that germanium(II) azides can be stabilized using a combination of electronic and steric properties as found in the Tp′ ligand.[9] Preliminary studies show that this concept can be extended also to other ligands providing a valuable access to this interesting class of compounds.

We thank the Deutsche Forschungsgemeinschaft for financial support.

Notes and references

† *Synthesis of* **2**: KTp′ (500 mg, 1.49 mmol) and $GeCl_2$(1,4-dioxane) (344 mg, 1.49 mmol) were weighed into a Schlenk tube and suspended in THF (20 ml). The suspension was stirred for 2 h at room temperature and the solvent was removed *in vacuo*. The residue was treated with CH_2Cl_2 (20 ml) and the solution was filtered through KCl. The filtrate was evaporated to dryness and the residue was washed with pentane (3 × 20 ml) to afford **2** (593 mg, 98%) as a white, microcrystalline solid, 295 °C (decomp. TG–DTA). Anal. Found: C, 44.55; H, 5.59; Cl, 8.79; N, 20.76; $C_{15}H_{22}BClGeN_6$ (405.26) requires: C, 44.46; H, 5.47; Cl, 8.75; N, 20.74%. IR (KBr, cm^{-1}): 2552 [ν(BH)], 1540 [ν(CN)]. ^{1}H NMR (CD_2Cl_2, 300.1 MHz, 298 K): δ 2.39 (s, 9H, CH_3), 2.54 (s, 9H, CH_3), 5.87 (s, 3H, CH). ^{1}H NMR (CD_2Cl_2, 300.1 MHz, 190 K): δ 2.32 (s, 9H, CH_3), 2.49 (s, 9H, CH_3), 5.90 (s, 3H, CH). ^{13}C{^{1}H} NMR (CD_2Cl_2, 75.5 MHz, 298 K): δ 12.2 (*C*CH_3), 12.5 (*C*CH_3), 106.7 (*C*H), 146.2 (*C*CH_3), 150.4 (*C*CH_3). EI-MS (70 eV): *m*/*z* (rel. intensity), 406 (1) [M]$^+$, 405 (2) [M − H]$^+$, 371 (100) [M − Cl]$^+$, 311 (23) [M − 3,5-Me_2pz]$^+$, 275 (9) [M − Cl − 3,5-Me_2pzH]$^+$, 169 (35) [M − Cl − HB(3,5-Me_2pz)$_2$]$^+$, 128 (14) [M − Cl − HB(3,5-Me_2pz)$_2$ − CH_3CN]$^+$. *Synthesis of* **3:** A Schlenk tube was charged with **2** (330 mg, 0.81 mmol) and NaN_3 (98 mg, 1.51 mmol) and the mixture was suspended in THF (30 ml). The suspension was stirred for 8 h at room temperature and the solvent was removed *in vacuo*. The residue was treated with CH_2Cl_2 (20 ml) and the solution was filtered. The filtrate was concentrated *in vacuo* to approximately 1 ml and Et_2O (10 ml) was added. The resulting precipitate was washed with Et_2O (10 ml) and dried *in vacuo* to afford **3** (243 mg, 72%) as a white solid, 216 °C (decomp. TG–DTA). Anal. Found: C, 42.87; H, 5.18; N, 31.01; $C_{15}H_{22}BGeN_9$ (411.80) requires: C, 43.75; H, 5.38; N, 30.61%. IR (KBr, cm^{-1}): 2544 [ν(BH)], 2043 [ν_{asym}(N_3)], 1541 [ν(CN)], 1272 [ν_{sym}(N_3)]. ^{1}H NMR (CD_2Cl_2, 300.1 MHz, 298 K): δ 2.40 (s, 9H, CH_3), 2.46 (s, 9H, CH_3), 5.88 (s, 3H, CH). ^{13}C{^{1}H} NMR (CD_2Cl_2, 75.5 MHz, 298 K): δ 12.3 (*C*CH_3), 12.9 (*C*CH_3), 106.5 (*C*H), 145.6 (*C*CH_3), 149.7 (*C*CH_3). EI-MS (70 eV): *m*/*z* (rel. intensity), 371 (100) [M − N_3]$^+$, 275 (24) [M − N_3 − 3,5-Me_2pzH]$^+$, 169 (33) [M − N_3 − HB(3,5-Me_2pz)$_2$]$^+$, 128 (24) [M − N_3 − HB(3,5-Me_2pz)$_2$ − CH_3CN]$^+$.

‡ *Crystal data*: for **2**: $C_{15}H_{22}BClGeN_6$, M = 405.26, triclinic, space group $P\bar{1}$ (no. 2), a = 7.9795(14), b = 8.683(2), c = 13.350(2) Å, α = 100.860(16), β = 90.781(12), γ = 99.118(16)°, U = 896.0(3) Å^3, Z = 2, D_c = 1.502 g cm^{-3}, μ(Mo-Kα) = 1.803 mm^{-1}, F(000) = 416, λ = 71.073 pm, T = 180 K. A colourless column of dimensions 0.57 × 0.11 × 0.08 mm was used. STOE-STADI4 four circle diffractometer, ω–2θ scan, 3° < 2θ < 50°, 4158 total reflections, 3113 unique. Refinement of the 221 parameters by full-matrix least-squares resulted in R_1 = 0.0448, wR_2 = 0.1128 for $I > 2\sigma(I)$, GOF = 1.034. For **3**: $C_{15}H_{22}BGeN_9$, M = 411.80, monoclinic, space group $P2_1/n$ (no. 14), a = 8.913(3), b = 8.0587(18), c = 25.908(8) Å, β = 96.56(4)°, U = 1848.8(9) Å^3, Z = 4, D_c = 1.480 g cm^{-3}, μ(Mo-Kα) = 1.614 mm^{-1}, F(000) = 848, λ = 71.073 pm, T = 170 K. A colourless prism of dimensions 0.38 × 0.30 × 0.15 mm was used. STOE-IPDS area detector, ϕ-rotation mode 4.7° < 2θ < 52.1°, 12579 total reflections, 3508 unique. Refinement of the 235 parameters by full-matrix least-squares resulted in R_1 = 0.0496, wR_2 = 0.1204 for $I > 2\sigma(I)$, GOF = 1.014. Both structures were solved using the Patterson Method (SHELXS-86) and refined anisotropically *versus* F^2 (SHELXL-97). Hydrogen atoms were placed on calculated positions and refined using a riding model. CCDC 182/1027.

1 (*a*) N. Wiberg, *J. Organomet. Chem.*, 1984, **273**, 141; (*b*) G. Raabe and J. Michl, *Chem. Rev.*, 1985, **85**, 419; (*c*) G. Bertrand, J.-P. Majoral and A. Baceiredo, *Acc. Chem. Res.*, 1986, **19**, 17; (*d*) I. C. Tornieporth-Oetting and T. M. Klapötke, *Angew. Chem.*, 1995, **107**, 559; *Angew. Chem., Int. Ed. Engl.*, 1995, **34**, 511.

2 H. R. Kricheldorf, G. Schwarz and J. Kaschig, *Angew. Chem.*, 1977, **89**, 570; *Angew. Chem., Int. Ed. Engl.*, 1977, **16**, 550.

3 (*a*) W. T. Reichle, *Inorg. Chem.*, 1964, **3**, 402; (*b*) J. S. Thayer and R. West, *Inorg. Chem.*, 1964, **3**, 406; 889; (*c*) I. Ruidisch and M. Schmidt, *J. Organomet. Chem.*, 1964, **1**, 493; (*d*) S. Cradock and E. A. V. Ebsworth, *J. Chem. Soc. A*, 1967, 1226; (*e*) J. D. Murdoch and D. W. H. Rankin, *J. Chem. Soc., Chem. Commun.*, 1972, 748; (*f*) J. E. Drake and R. T. Hemmings, *Can. J. Chem.*, 1973, **51**, 302; (*g*) A. Baceiredo, G. Bertrand and P. Mazerolles, *Tetrahedron Lett.*, 1981, **22**, 2553; (*h*) C. Guimon and G. Pfister-Guillouzo, *Organometallics*, 1987, **6**, 1387; (*i*) T. M. Klapötke and A. Schulz, *Inorg. Chem.*, 1996, **35**, 4995.

4 S. P. Kolesnikov, I. S. Rogozhin and O. M. Nefedov, *Chem. Abstr.*, 1975, **82**, 25328u.

5 (*a*) A. H. Cowley, R. L. Geerts, C. M. Nunn and C. J. Carrano, *J. Organomet. Chem.*, 1988, **341**, C27; (*b*) D. L. Reger, S. J. Knox, M. F. Huff, A. L. Rheingold and B. S. Haggerty, *Inorg. Chem.*, 1991, **30**, 1754.

6 P. C. van der Voorn and R. S. Drago, *J. Am. Chem. Soc.*, 1966, **88**, 3255.

7 J. G. Winter, P. Portius, G. Kociok-Köhn, R. Steck and A. C. Filippou, *Organometallics*, 1998, **17**, 4176, and references therein.

8 T. M. Klapötke, *Chem. Ber.*, 1997, **130**, 443 and references therein.

9 S. Trofimenko, *Chem. Rev.*, 1993, **93**, 943.

Communication 8/07282E

Synthesis and structure of ITQ-9: a new microporous SiO_2 polymorph

Luis A. Villaescusa, Philip A. Barrett and Miguel A. Camblor*

Instituto de Tecnología Química, Avda. Los Naranjos s/n, 46071 Valencia, Spain. E-mail: macamblo@itq.pv.es

Received (in Bath, UK) 20th August 1998, Accepted 22nd September 1998

The new pure silica polymorph ITQ-9 has been synthesised and its structure, comprising medium pore channels and cages, has been solved by direct methods using low resolution powder X ray diffraction data.

Crystalline silica occurs in nature in a small variety of non-porous structural forms. However, it is also possible to synthesise SiO_2 as microporous solids by hydrothermal crystallisation in the presence of organic additives. These additives, which typically remain occluded within the porous silica framework, are called structure directing agents (SDA) and may generally be removed by calcination giving stable, crystalline pure silica polymorphs. A recent viewpoint considers that the role of SDA molecules is to select between different possible silica structures[1] with similar enthalpies of formation.[2] In our opinion, the SDA either kinetically or thermodynamically directs the crystallisation toward a specific phase. When the crystallisation is carried out at near to neutral pH (7–9.5) in the presence of fluoride anions which act as mineralisers, the crystalline silica obtained after calcination generally shows a very high degree of perfection. More specifically, those phases present essentially no Si–O–Si connectivity defects, which are by contrast frequent if the synthesis is carried out in basic medium (with OH^- acting as mineraliser). Owing to the lack of defects the final materials prepared in fluoride aqueous media are very attractive since they show strict hydrophobic properties[3] and a high degree of both short and long range order.[4] We describe here the synthesis of a new crystalline form of SiO_2, denoted ITQ-9 (Instituto de Tecnología Química, no. 9), which possesses a large micropore volume. In addition, we also show that the high degree of crystallographic order presented by this material afforded the resolution of its low symmetry structure by direct methods using low resolution powder X ray diffraction data (PXRD).

Pure silica ITQ-9 has been synthesised using *N*,*N*-dimethyl-6-azonium-1,3,3-trimethylbicyclo(3.2.1)octane (**I**) as SDA. 24.89 g of tetraethylorthosilicate were hydrolysed in 36.65 g of an aqueous solution of this cation in hydroxide form (1.63 moles per 1000 g of solution) under stirring and allowing evaporation of all the ethanol produced plus 16.7 g water. Then, 2.48 g of HF (48% aq.) were added and the thick paste obtained was homogenised by hand stirring before pouring into Teflon lined stainless steel autoclaves. These were heated at 150 °C under slow rotation (60 rpm). After 16 days of heating the contents were filtered, washed and dried. A highly crystalline solid was obtained and its PXRD pattern was indexed as monoclinic, space group *I*2/*m*, *I*2 or *Im*, a = 14.7906, b = 18.1528, c = 7.4547 Å, β = 110.76°. Chemical analysis suggests the chemical formula for as-made ITQ-9 is $[C_{12}H_{24}NF]_2[SiO_2]_{32}$ (based on the unit cell of the calcined material determined in this work, see below) and that the organic SDA is intact within the zeolite.

Calcination in air at 800 °C for 3 hours allows complete removal of the guest species yielding a pure SiO_2 framework with a large micropore volume of 0.21 $cm^3\ g^{-1}$ (determined by the t-plot method from the N_2 adsorption isotherm at 77 K). This framework is essentially free of connectivity defects, as demonstrated by the lack of significant Si(3Si,1OH) resonances near −101 ppm in the ^{29}Si MAS NMR spectrum (Fig. 1, top). The spectrum shows only Si(4Si) resonances in the −107 to −116 ppm chemical shift range. As a consequence of the absence of defects and high short range order there is a high resolution of Si(4Si) sites corresponding to framework Si in at least 6 different crystallographic sites.

After calcination splitting of a number of peaks in the PXRD pattern of ITQ-9 was observed. All the peaks could be indexed as a triclinic cell close to that for the as-prepared material, whilst maintaining the I centering (space group *I*-1). Direct methods using the Sirpow[5] program with Le Bail[6] extracted intensities from the Mprofil[7] program gave no satisfactory solution (a cell content of 32 SiO_2 derived from the density of 1.662 g cm^{-3} determined by pycnometry was used). We thus decided to use the PXRD data of the as-made sample due to its higher monoclinic symmetry. Le Bail extraction and direct methods were repeated as before using space group *I*2/*m* for which a good solution for the framework lacking no Si or O atoms and consisting of a 3D 4-connected net was obtained. Small fragments of organic matter were also found. Hence, the SiO_2 framework obtained for the as-made sample was used, after generation of the additional atomic positions in space group *I*-1, as a starting model for the Rietveld[8] refinement of the calcined triclinic phase, using conventional laboratory PXRD data in the program GSAS[9] with a manually interpolated background together with a pseudo Voigt[10] function to describe the peak shape. Constraints on the Si–O distances were used in the first stages of the refinement and finally removed before the model was refined to convergence. The crystallographic data are summarised in Table 1 and the final atomic positions are

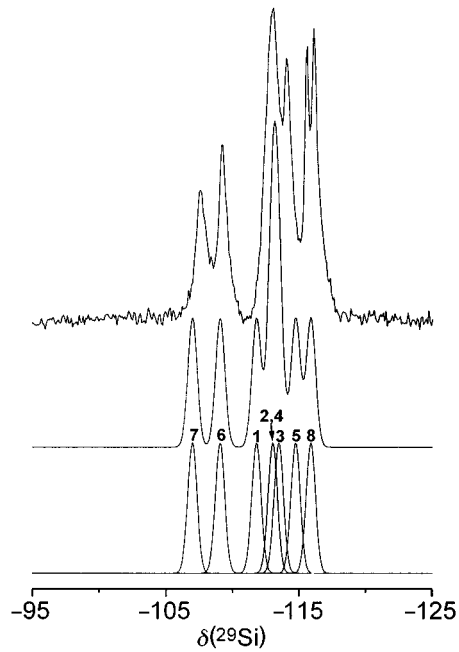

Fig. 1 ^{29}Si MAS NMR (*vs.* TMS) spectrum of calcined pure silica ITQ-9 (top) together with a simulation (middle) obtained by applying the equation of Thomas *et al.*[11] to the average Si–O–Si angles of each Si site in the refined structure (calculated resonances for each individual site are shown at the bottom). Note the absence of Si(3Si,1OH) resonances near −101 ppm and the high resolution of crystallographic sites in the experimental spectrum.

Table 1 Data collection and crystallographic parameters for calcined ITQ-9

Wavelength		Cu-Kα
Temperature/K		298
2θ range/°		5–85 (Range used 15–85)
Step size, 2θ/°		0.01
Count time/s step^{-1}		10 (5–50° 2θ); 40 (50–90° 2θ)
Number of data points		6910
Number of reflections		2527
Number of profile parameters		11
Number of structural parameters		81
Number of constraints		32
Unit cell	*a*/Å	14.7685(13)
	b/Å	18.1793(17)
	c/Å	7.3823(7)
	α/°	89.1402(21)
	β/°	110.6790(26)
	γ/°	90.945(4)
Space group		*I*-1
Residuals	R_{exp}	7.45
	R_{wp}	9.57
	R_p	7.72
	R_b	9.16
	χ^2	1.719

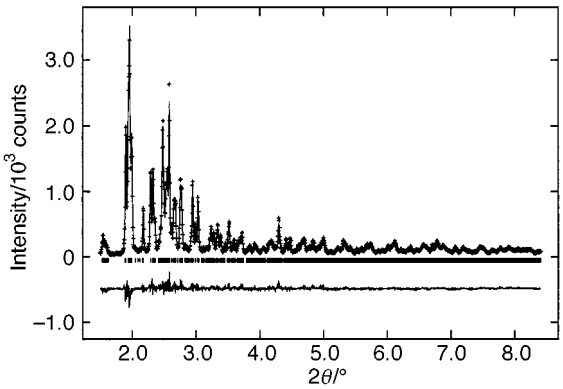

Fig. 2 Rietveld plot for calcined pure SiO_2 ITQ-9: observed data (+), calculated profile (solid line) and difference (lower trace). The tick marks represent the positions of allowed reflections.

available as Electronic Supplementary Information (http://www.rsc.org/suppdata/cc/1998/xxxx), with the final Rietveld plot depicted in Fig. 2. The average Si–O bond length (1.596 Å) and average O–Si–O and Si–O–Si angles (109.4 and 149.9° respectively) are in excellent accord with those expected for zeolite materials. Moreover, simulation of the ^{29}Si MAS NMR spectrum using the average Si–O–Si angles determined by Rietveld refinement for each Si site and the empirical equation of Thomas *et al.*[11] is in excellent agreement with the experimental spectrum (Fig. 1). Energy minimisation calculations using the GULP code[12] together with the potential model of Saunders *et al.*[13] reveal the symmetry lowering to be favourable by *ca.* 5 kJ mol^{-1}.

A projection of the structure of ITQ-9 is presented in Fig. 3. ITQ-9 is a new pure silica polymorph containing one dimensional sinusoidal pores running along [001] with access through ten membered ring windows (10MR windows). The windows are nearly circular in shape and have an average free diameter of around 5.7 Å (assuming the van der Waals radius of O to be 1.35 Å). The maximum and minimum diameters are 6.0 and 5.4 Å, respectively. Between two adjacent 10MR windows there are wider spaces with approximate free dimensions 10.9 Å × 7.4 Å × 4.7 Å. Thus, the pores in essence may be regarded as a one-dimensional arrangement of cages joined through single 10MR windows. In some directions the separation between adjacent pores is a wall with a single O atom (Fig. 3). This and the presence of cages explains the sizeable micropore volume of ITQ-9 (0.21 cm^3 g^{-1}) which is exceedingly large compared to other one-dimensional 10MR (ZSM-23, 0.04 cm^3 g^{-1}), 12MR

Fig. 3 A perspective view of the framework structure of ITQ-9 down [001], showing the nearly circular one-dimensional 10MR pores (average free diameter ≅ 5.7 Å). Large spheres represent tetrahedral Si, while small spheres are two-coordinated O.

(SSZ-24, 0.12 cm^3 g^{-1}) or even 14MR (CIT-5, 0.13 cm^3 g^{-1})[14] zeolites.

Finally, Al can be introduced by direct synthesis into the structure of ITQ-9. The aluminosilicate ITQ-9 presents strong Brønsted acid sites attributed to $[Al(OSi)_4]^-$ framework groups, as revealed by pyridine adsorption and desorption at increasing temperatures monitored by IR spectroscopy. This, together with the large micropore volume of the zeolite, renders ITQ-9 an attractive material for the catalytic transformation of hydrocarbons. Its activity and shape selectivity properties (due to the peculiar pore system encompassing medium sized windows and large cages) are currently under investigation.

The authors gratefully acknowledge financial support by the Spanish CICYT (project MAT97-0723). P. A. B. is grateful to the European Union TMR program for a postdoctoral fellowship.

Notes and references

1 R. F. Lobo, S. I. Zones and M. E. Davis, *J. Inclusion Phenom. Mol. Recognit. Chem.*, 1995, **21**, 47.
2 I. Petrovic, A. Navrotsky, M. E. Davis and S. I. Zones, *Chem. Mater.*, 1993, **5**, 1805.
3 T. Blasco, M. A. Camblor, A. Corma, P. Esteve, J. M. Guil, A. Martínez, J. A. Perdigón-Melón and S. Valencia, *J. Phys. Chem. B*, 1998, **102**, 75.
4 P. A. Barrett, M. A. Camblor, A. Corma, R. H. Jones and L. A. Villaescusa, *J. Phys. Chem.*, 1998, **102**, 4147.
5 A. Atomare, C. Burla, C. Cascarano, C. Cascarino, C. Giacovazzo, A. Gualiardi, G. Polidori and R. M. Canalli, *J. Appl. Crystallogr.*, 1994, **27**, 435.
6 A. Le Bail, *Mater. Res. Bull.*, 1988, **23**, 447.
7 A. D. Murray and A. N. Fitch, Mprofil program for Le Bail decomposition and profile refinement, 1990.
8 H. M. Rietveld, *J. Appl. Crystallogr.*, 1969, **2**, 65.
9 A. Larson and R. B. Von Dreele, GSAS Manual, Los Alamos Report No. LA-UR-86-748, 1986.
10 J. B. Hastings, W. Thomlinson and D. E. Cox, *J. Appl. Crystallogr.*, 1984, **17**, 85.
11 J. M. Thomas, J. Klinowski, S. Ramdas, B. K. Hunter and D. T. B. Tennakoon, *Chem. Phys. Lett.*, 1983, **102**, 158.
12 J. D. Gale, *J. Chem. Soc., Faraday Trans.*, 1997, **93**, 629.
13 M. J. Saunders, M. Leslie and C. R. A. Catlow, *J. Chem. Soc., Chem. Commun.*, 1984, 1271.
14 P. A. Barrett, M. J. Díaz-Cabañas, M. A. Camblor and R. H. Jones, *J. Chem. Soc., Faraday Trans.*, 1998, **94**, 2475.

Communication 8/06696E

meso-η¹-Metalloporphyrins: preparation of palladio- and platinioporphyrins and the crystal structure of 5-[bromo-1,2-bis(diphenylphosphino)-ethanepalladio(II)]-10,20-diphenylporphyrin

Dennis P. Arnold,*[a] Yoshiteru Sakata,[b] Ken-ichi Sugiura[b] and Elizabeth I. Worthington[a]

[a] *Centre for Instrumental and Developmental Chemistry, Queensland University of Technology, G.P.O. Box 2434, Brisbane, Australia 4001. E mail: d.arnold@qut.edu.au*

[b] *The Institute of Scientific and Industrial Research, Osaka University, Mihogaoka 8-1, Ibaraki, Osaka 567-0047, Japan*

Received (in Cambridge, UK) 1st September 1998, Accepted 21st September 1998

***meso*-η¹-Palladio- and platinioporphyrins have been isolated for the first time by means of oxidative addition of bromoporphyrins to Pd(0) and Pt(0) complexes; the X-ray crystal structure of the title complex was determined.**

Palladium-catalysed coupling reactions have been employed by a number of research groups to prepare novel porphyrins. Mercuration/palladation was used by Smith and co-workers to introduce unsaturated substituents into mono-porphyrins,[1] and one of us first applied palladium/phosphine catalysis to the formation of bis(porphyrins).[2] Numerous coupling reactions of the Heck, Suzuki, Sonogashira, and Stille types have since been used to prepare substituted porphyrins and multi-porphyrin arrays linked by alkenes and alkynes, with or without accompanying aryl linkers.[3,4] The most direct entry to this chemistry is *via meso*-haloporphyrins,[4] which are readily prepared in the case of β-unsubstituted porphyrins of the 5,15-diaryl type, such as 5,15-diphenylporphyrin, DPP.[5] For example, 5-bromoDPP and 5-iodoDPP [as the nickel(II) or zinc(II) complexes], couple easily with terminal alkynes, organotin or organozinc compounds, in the presence of Pd(II) or Pd(0) phosphine complexes.[4,6] An essential process in these catalytic cycles appears to be the oxidative addition of the *meso*-carbon-to-halogen bond to a zerovalent palladium precursor. However, until now there were no examples of isolated and characterised *meso*-η¹-palladioporphyrins. Here we report the stoichiometric (rather than catalytic) preparations of a number of such novel organometallic porphyrins, and the single crystal X-ray structure of one example.

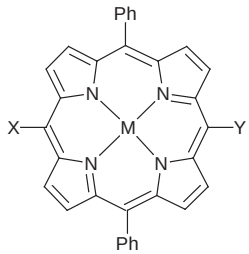

	M	X	Y
1	Ni	H	$Pd(PPh_3)_2Br$
2	H_2	H	$Pd(PPh_3)_2Br$
3	H_2	H	$Pd(AsPh_3)_2Br$
4	Ni	$Pd(PPh_3)_2Br$	$Pd(PPh_3)_2Br$
5	H_2	H	Pd(dppe)Br
6	Ni	H	*cis*-$Pt(PPh_3)_2Br$
7	Ni	H	*trans*-$Pt(PPh_3)_2Br$
8	H_2	H	*cis*-$Pt(PPh_3)_2Br$
9	H_2	H	*trans*-$Pt(PPh_3)_2Br$
10	Ni	$Pd(PPh_3)_2Br$	*trans*-$Pt(PPh_3)_2Br$

The palladioporphyrins **1–5** were prepared by addition of the appropriate stoichiometric amount of palladium(0) precursor [$Pd(PPh_3)_4$ or Pd_2dba_3† + PPh_3, $AsPh_3$, or dppe] to 5-bromoDPP or 5,15-dibromoDPP or the corresponding nickel(II) complexes, in argon-purged toluene at 105 °C. The mono-adducts with the monodentate Group 15 ligands were formed quantitatively within a few minutes, while the double addition to form **4** required 40 minutes heating, and the dppe complex **5** required 8 hours heating. The complexes were readily isolated in high yield by evaporation of the toluene and trituration with ether. The palladioporphyrins are air-stable solids which undergo some Br/Cl exchange when dissolved in chlorinated solvents. We have also extended this chemistry to the analogous *meso*-platinioporphyrins. The addition of $Pt(PPh_3)_3$ to either 5-bromoDPPNi or 5-bromoDPP free-base in refluxing toluene initially leads within about 20 minutes to the *cis* adducts **6** and **8**, respectively, as shown by the characteristic ^1J(PtP) coupling constants in the ^{31}P NMR spectra [*e.g.* for **6**, *J trans* to porphyrin = 1790 Hz, *J trans* to Br = 4250 Hz, ^2J(PP) = 17 Hz]. These initial adducts isomerise over a period of 6 hours to the respective *trans* isomers **7** and **9**. The complexes were characterised by ^{1}H and ^{31}P NMR, electronic absorption, and FAB-mass spectra,‡ and in the case of the diphosphine derivative **5**, by X-ray crystallography.§ For all the Pd complexes except **5**, the ^{31}P NMR spectra showed that the Pd(II) centres have the *trans* geometry.

The crystal structure of **5** comprises two independent molecules in the asymmetric unit. Molecules A and B both display slightly distorted square-planar coordination about the Pd(II) atom, which is η¹-bonded to the *meso*-carbon of a weakly-ruffled porphyrin core (maximum deviation from the 24-atom mean plane = 0.28 Å in molecule A). Molecules A and B differ most markedly in the dihedral angles between the mean planes of the porphyrin and the 10,20-phenyl groups. In molecule A, these angles are 88 and 58°, and in molecule B, 56 and 59°. There is no obvious reason for the unique orthogonality of the phenyl ring in molecule A. Fig. 1 shows the coordination plane of the Pd atom for molecule A. The view from above the porphyrin ring, shown in space-filling form in Fig. 2, indicates how the phenyl groups of the diphosphine ligand shield the face of the porphyrin. This suggests immediately a use for this methodology in the engineering of cavities with tailored shape and hydrophobicity above and below a porphyrin ring, without the typically difficult and tedious synthetic work associated with 'capping' and 'strapping' opposite sides of a porphyrin. Moreover, the use of a chiral diphosphine may offer the intriguing possibility of generating chiral catalytic metalloporphyrins based on the present structural class.

The second insertion of the Pt(0) fragment into 5,15-dibromoDPPNi is so slow that the interesting compound **10** (containing all three members of the nickel triad) could be prepared by addition of $Pt(PPh_3)_3$, heating for 3 hours, followed by addition of Pd_2dba_3/PPh_3, and a further 3 hours heating. A similar but weaker deactivating effect of the Pt(II) fragment was noted by Stang and co-workers in their work on simpler arylene-bridged dipalladium and diplatinum organometallics, examples of which have also recently been reported by Kim *et al.*[7]

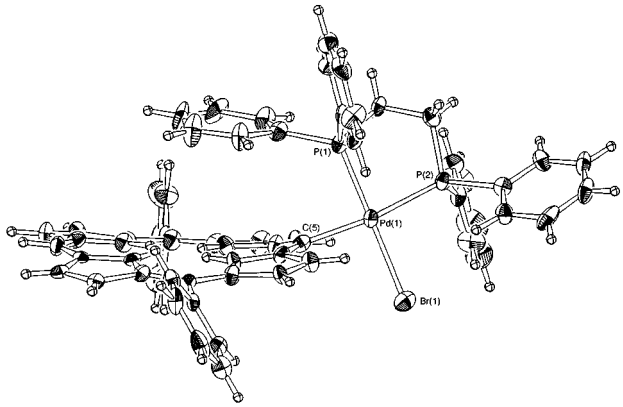

Fig. 1 Molecular structure of **5** (molecule A), showing the Pd coordination plane. Selected bond lengths and angles: Pd(1)–Br(1) 2.469(3), Pd(1)–P(1) 2.240(6), Pd(1)–P(2) 2.327(6), Pd(1)–C(5) 2.05(2) Å; P(1)–Pd(1)–P(2) 85.2(2), Br(1)–Pd(1)–P(2) 96.2(2), Br(1)–Pd(1)–C(5) 91.9(5), P(1)–Pd(1)–C(5) 87.2(6)°.

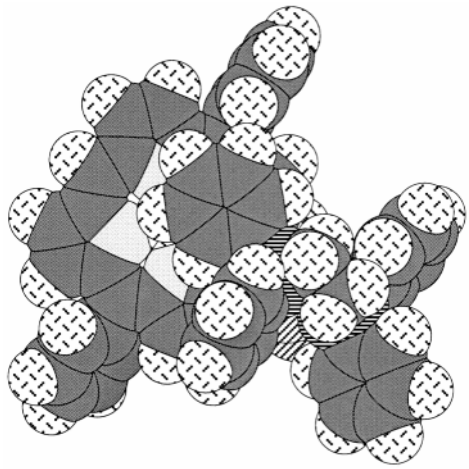

Fig. 2 Space-filling version of the molecular structure of **5**, viewed from normal to the porphyrin plane.

The electronic absorption spectra of our compounds are unexceptional, and the bromobis(phosphine/arsine)metallo moiety exerts a bathochromic effect of similar magnitude to that of a simple bromo substituent. The high polarizability of the heavy metal atoms(s) in direct communication with the porphyrin π-electrons may confer interesting third-order non-linear optical properties on this new class of organometallic compound. We will be exploring their potential applications in this field, as well as in catalysis and for the construction of multi-porphyrin supramolecular arrays.[8]

We thank Q.U.T. for a Special Small Grant, and the Centre for Instrumental and Developmental Chemistry for financial support.

Notes and references

† dba = dibenzylideneacetone (1,5-diphenylpenta-1,4-dien-3-one).

‡ *Spectroscopic data* for **7**: NMR ($CDCl_3$) δ_H 9.52 (s, *meso*-H), 9.51, 8.92, 8.66, 8.21 (all d, β-H), 7.9, 7.65 (m, 10,20-Ph), 7.25, 6.65 (m, PPh); δ_P (*vs.* ext. 85% H_3PO_4) 28.5 [s with ^{195}Pt satellites, J(PtP) 2940 Hz]; UV–VIS (CH_2Cl_2) λ_{max}/nm (log ε) 415 (5.36), 488 sh (3.57), 523 (4.20), 555 sh (3.67); FAB-MS maximum of cluster calc. for $C_{68}H_{49}BrN_4NiP_2Pt$ 1318.16, found 1318.1.

§ *Crystal data* for **5**: $C_{58}H_{45}N_4BrPdP_2$, M_r = 1046.27, monoclinic, space group $P2_1/c$, a = 17.006(6), b = 27.248(8), c = 22.13(1) Å, β = 91.18(5)°, V = 10254(6) Å^3, Z = 8, μ(Mo-Kα) = 12.47 cm^{-1}, D_c = 1.355 g cm^{-3}, T = 232(1) K, R = 0.075, R_w = 0.098 for 7246 reflections with $I > 3\sigma(I)$. CCDC 182/1024.

1 I. K. Morris, K. M. Snow, N. W. Smith and K. M. Smith, *J. Org. Chem.*, 1990, **55**, 1231.
2 D. P. Arnold and L. J. Nitschinsk, *Tetrahedron Lett.*, 1993, **34**, 693.
3 See, for example R. Gauler and N. Risch, *Eur. J. Org. Chem*., 1998, 1193; J.-P. Strachan, S. Gentemann, J. Seth, W. A. Kalsbeck, J. S. Lindsey, D. Holten and D. C. Bocian, *Inorg. Chem.*, 1998, **37**, 1191; R. W. Wagner, T. E. Johnson, F. Li and J. S. Lindsey, *J. Org. Chem*., 1995, **60**, 5266; K. S. Chan, X. Zhou, M. T. Au and C. Y. Tam, *Tetrahedron*, 1995, **51**, 3129; D. P. Arnold and D. A. James, *J. Org. Chem.*, 1997, **62**, 3460.
4 S. G. DiMagno, V. S.-Y. Lin and M. J. Therien, *J. Am. Chem. Soc.*, 1993, **115**, 2513; V. S.-Y. Lin, S. G. DiMagno and M. J. Therien, *Science*, 1994, **264**, 1105; S. G. DiMagno, V. S.-Y. Lin and M. J. Therien, *J. Org. Chem.*, 1993, **58**, 5983.
5 J. S. Manka and D. S. Lawrence, *Tetrahedron Lett*., 1989, **30**, 6989.
6 R. W. Boyle, C. K. Johnson and D. Dolphin, *J. Chem. Soc., Chem. Commun.*, 1995, 527; D. P. Arnold, R. C. Bott, H. Eldridge, F. Elms, G. Smith and M. Zojaji, *Aust. J. Chem.*, 1997, **50**, 495.
7 J. Manna, C. J. Kuehl, J. A. Whiteford and P. J. Stang, *Organometallics*, 1997, **16**, 1897; Y.-J. Kim, S.-W. Song, S.-C. Lee, S.-W. Lee, K. Osakada and T. Yamamoto, *J. Chem. Soc., Dalton Trans.*, 1998, 1775.
8 Sanders and co-workers reported a cyclic trimer comprised of organoplatinum porphyrins in which the platinum atom is linked to the porphyrin *meso* positions by *meta*-ethynylphenyl units, rather than directly as in our compounds: L. G. Mackay, H. L. Anderson and J. K. M. Sanders, *J. Chem. Soc., Perkin Trans. 1*, 1995, 2269.

Communication 8/06769D

A functionalized ruthenium(II)-bis-terpyridine complex as a rod-like luminescent sensor of zinc(II)

Francesco Barigelletti,*[a] Lucia Flamigni,[a] Giuseppe Calogero,[a] Leif Hammarström,[b] Jean-Pierre Sauvage*[c] and Jean-Paul Collin*[c]

[a] *Istituto FRAE-CNR, Via P. Gobetti 101, I-40129 Bologna, Italy*
[b] *Department of Physical Chemistry, University of Uppsala, Box 532, S-75121 Uppsala, Sweden*
[c] *Laboratoire de Chimie Organo-Minérale, Université Louis Pasteur, Faculté de Chimie, 4 Rue Blaise Pascal, F-67008 Strasbourg, France*

Received (in Basel, Switzerland) 12th August 1998, Accepted 23rd September 1998

The nearly non-luminescent ruthenium(II)-terpyridine chromophore, functionalized with an uncoordinated terpyridine fragment, 2, undergoes Zn(II)-induced association leading to a luminescent rod-like 2 : Zn^{2+} : 2 species with a luminescence enhancement factor, EF ⩾ 10.

In the field of transition metal chemistry the assembly of Ru(II), Os(II), and Re(I) complexes to yield polymetallic species is being pursued both for fundamental and practical reasons.[1–4] Examples include (i) the investigation of energy and electron transfer processes in geometrically well defined systems where the metal-based components are held together by covalent bonds,[5–7] (ii) the exploitation of spectroscopic properties (particularly luminescence) for testing the sensing ability of appended groups towards protons, cations, and anions,[1–3] and (iii) the building up of dendritic species comprising tens of metal centres for light-harvesting and energy-collection purposes.[8,9]

An interesting Ru-based chromophore to be employed in such type of assemblies is $[Ru(tpy)_2]^{2+}$ {tpy is 2,2′:6′,2″-terpyridine; Scheme 1 shows the related complex $[(ttp)Ru(ttp)]^{2+}$ **1**, containing the 4′-tolyl-tpy ligand, ttp}.[10] This is because substitution at the 4′ position of tpy allows the construction of geometrically well-defined rod-like rigid species.[11] The luminescence properties of both $[Ru(tpy)_2]^{2+}$ and **1** are rather poor (their room temperature luminescence quantum yield and lifetime in acetonitrile solvent are $\Phi \approx 10^{-5}$ and $\tau < 1 \times 10^{-9}$ s, respectively[10]) but the incorporation of these or related complexes in polynuclear species may result in significant luminescence improvements.[7,12]

By using luminescence spectroscopy we have investigated the properties of acetonitrile–water solutions of the complexes $[(ttp)Ru(tpy\text{-}tpy)]^{2+}$ **2** and $[(ttp)Ru(tpy\text{-}ph\text{-}tpy)]^{2+}$ **3**, Scheme 1,† in the presence of Zn^{2+} [ph = 1,4-phenylene]. We found that Zn^{2+} coordination of the free tpy fragments of **2**[13] is accompanied by a substantial enhancement of luminescence intensity; by contrast no such effect is observable for **3**. Luminescence results are collected in Table 1. In addition we could use luminescence spectroscopy to monitor the formation of the tripartite species, **2** : Zn^{2+} : **2**.

The absorption spectra of **2** and **3** in acetonitrile–water (1 : 1 v/v) display intense absorption bands in the UV region (250–350 nm, $\varepsilon \approx 10^5$ M^{-1} cm^{-1}) and moderately intense bands in the visible region (450–550 nm, $\varepsilon \approx 10^4$ M^{-1} cm^{-1}). The former bands are due to ligand centered (^{1}LC) transitions and those occurring in the visible are due to metal-to-ligand charge-transfer (^{1}MLCT) transitions, of Ru→L electronic configuration.[6,11] Owing to the presence of the uncoordinated tpy fragment in **2** and **3,** addition of Zn^{2+} causes[13] some changes in the absorption features. These changes are only modest in the region of the ligand-centred transitions of both complexes; however, for **2** the longest-wavelength band maximum (MLCT region) undergoes a bathochromic shift from 491 to 498 nm (for **3** the corresponding absorption maximum at 491 nm is not affected by the presence of Zn^{2+}). This indicates that for **2**, the Zn^{2+} ion causes stabilization of the lowest-lying Ru→L CT energy level, which involves the tpy-tpy fragment, Scheme 1. For **3** no such effect is apparent.

The excited states responsible for the luminescence, Table 1, are formally triplet levels of Ru→L CT nature, and involve in

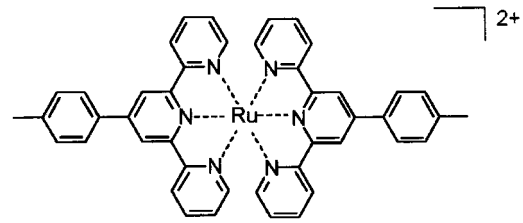

$[(ttp)Ru(ttp)]^{2+}$ **1**

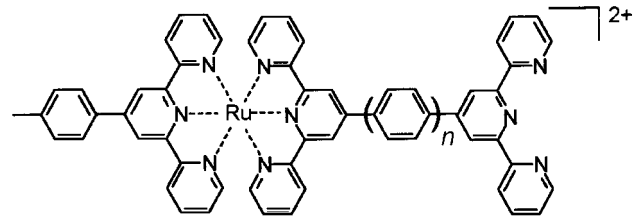

$n = 0$; **2**
$n = 1$; **3**

Scheme 1

Table 1 Luminescence properties[a]

				In the presence of Zn^{2+}[b]		
	λ_{max}[c]/nm	τ/ns	$10^4\Phi$[d]	λ_{max}[c]/nm	τ/ns	$10^4\Phi$[d]
$[(ttp)Ru(ttp)]^{2+}$ (**1**)[e]	640	0.9	0.32			
$[(ttp)Ru(tpy\text{-}tpy)]^{2+}$ (**2**)	660	6.3	1.6	710	84	16
$[(ttp)Ru(tpy\text{-}ph\text{-}tpy)]^{2+}$ (**3**)	648	2.4	0.6	650	3.3	0.9

[a] Room temperature aerated acetonitrile–water (1 : 1 v/v). [b] More than 3 equiv. [c] Band maxima for uncorrected spectra. [d] From corrected spectra. [e] Acetonitrile solvent, ref. 10.

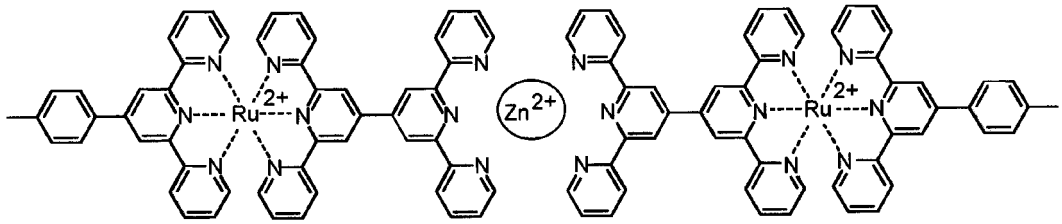

2:Zn^{2+}:2

Scheme 2

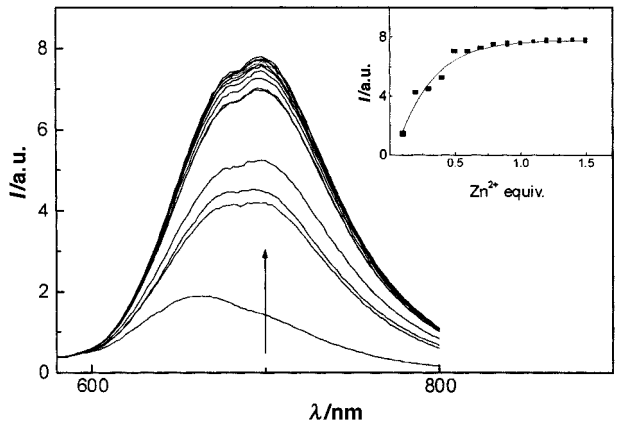

Fig. 1 Luminescence spectrum of complex **2** after Zn^{2+} addition. Excitation wavelength is at 494 nm, where the changes in absorbance intensity are within 5%. The inset shows the luminescence intensity taken at 700 nm *vs.* the added Zn^{2+} equivalents.

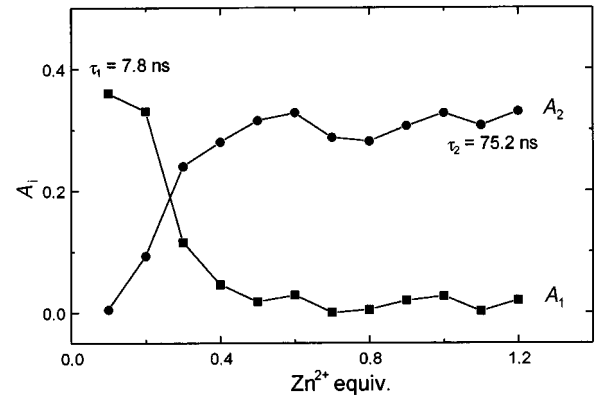

Fig. 2 Changes in the relative amplitudes A_1 and A_2 for the dual luminescence decay of complex **2** (concentration 1×10^{-5} M) upon Zn^{2+} addition. The decays are monitored over the full emission range.

each case the larger size ligand present on either side of the Ru(II) centre, *i.e.* tpy-tpy and tpy-ph-tpy for **2** and **3,** respectively.[10] The luminescence properties gathered in Table 1 indicate that Zn^{2+} remarkably affects the luminescence band maximum, intensity and lifetime for the case of **2**. In contrast, for **3** no substantial changes can be registered. This different behaviour may be understood in terms of the role of the phenylene group in decoupling the Ru-based chromophore and the tpy appended site.[14]

The results of a titration experiment on the luminescence intensity of **2** are illustrated in Fig. 1. For this complex, subsequent additions of Zn^{2+} cause gradual shifts of the band maximum from 660 to 700 nm, with a concomitant increase of the luminescence intensity. The inset of Fig. 1 shows that the change in luminescence intensity at 700 nm *vs.* the Zn^{2+} concentration is consistent with formation of a **2 :** Zn^{2+} **: 2** species.

The same conclusion is supported by the time resolved luminescence properties exhibited upon titration of complex **2** with Zn^{2+}. The luminescence decayed according to a dual exponential law, $I(t) = A_1\exp(-t/\tau_1) + A_2\exp(-t/\tau_2)$, and a global analysis as performed on 12 decay profiles gave τ_1 = 7.8 ns and τ_2 = 75.2 ns, with varying amplitudes (A) depending on the added equivalents of Zn^{2+}, see Fig. 2. Comparison of the results depicted in Fig. 2 with the luminescence properties reported in Table 1 suggests that the two species responsible for the dual exponential behavior are **2** and **2** : Zn^{2+} : **2**. Based on the coordination number of 6 for the Zn(II) centre and on the geometry of the tpy coordination site,[7,13] the **2 :** Zn^{2+} **: 2** complex is most likely linearly arranged with an estimated Ru–Ru distance of 2.2 nm, Scheme 2.

With respect to the starting complex **2**, it is noteworthy that the **2** : Zn^{2+} : **2** complex exhibits improved luminescence properties, EF = 10 (with respect to **2** in neat acetonitrile, EF ≈ 50). This is due to the delocalizing ability of the tpy-tpy ligand[12] combined with the stabilizing effect of the Zn^{2+} centre. Our results, which are in line with those of a recent report on polynuclear complexes where the bridging ligands contain the highly delocalizing ethynyl group,[7] suggest that it is possible to use Ru(II)-terpyridine derivatives both to develop Zn^{2+} luminescent sensors and to construct nanometric rod-like assemblies with tuneable luminescence properties.

Notes and references

† The synthesis and characterization of complexes **1**, **2**, and **3** were described previously.[11] Absorption and luminescence spectra of dilute solutions (≈ 10^{-5} M) in acetonitrile–water (1 : 1 v/v) were recorded with a Perkin Elmer Lambda 5 spectrophotometer and with a Spex Fluorolog II spectrofluorimeter, respectively. Uncorrected luminescence band maxima are used throughout the text. In order to determine corrected band maxima and luminescence quantum yields we followed a procedure described in ref. 12. Luminescence lifetimes were obtained with an IBH single-photon-counting apparatus. The titration experiments were conducted with Gilson P20 Pipetman microburettes by using concentrated solutions (10^{-3} M) of $ZnCl_2$.

1 *Transition Metals in Supramolecular Chemistry*, ed. L. Fabbrizzi and A. Poggi, Kluwer, Dordrecht, 1994.
2 J.-M. Lehn, *Supramolecular Chemistry*, VCH, Weinheim, 1995.
3 A. P. de Silva, H. Q. N. Gunaratne, T. Gunnlaugsson, A. J. M. Huxley, C. P. McCoy, J. Rademacher and T. E. Rice, *Chem. Rev.*, 1997, **97**, 1515.
4 E. C. Constable, *Chem. Commun.*, 1997, 1073.
5 V. Balzani, A. Juris, M. Venturi, S. Campagna and S. Serroni, *Chem. Rev.*, 1996, **96**, 759.
6 F. Barigelletti, L. Flamigni, J.-P. Collin and J.-P. Sauvage, *Chem. Commun.*, 1997, 333.
7 A. Harriman and R. Ziessel, *Chem. Commun.*, 1996, 1707.
8 V. Balzani, S. Campagna, G. Denti, A. Juris, S. Serroni and M. Venturi, *Acc. Chem. Res.*, 1998, **31**, 26.
9 F. Vögtle, *Supramolecular Chemistry*, Wiley, Chichester, 1993.
10 J.-P. Sauvage, J.-P. Collin, J.-C. Chambron, S. Guillerez, C. Coudret, V. Balzani, F. Barigelletti, L. De Cola and L. Flamigni, *Chem. Rev.*, 1994, **94**, 993.
11 F. Barigelletti, L. Flamigni, V. Balzani, J.-P. Sauvage, J.-P. Collin, A. Sour, E. C. Constable and A. M. W. Cargill Thompson, *J. Am. Chem. Soc.*, 1994**, 116**, 7692.
12 L. Hammarström, F. Barigelletti, L. Flamigni, M. T. Indelli, N. Armaroli, G. Calogero, M. Guardigli, A. Sour, J.-P. Collin and J.-P. Sauvage, *J. Phys. Chem. A*, 1997, **101**, 9061.
13 R. H. Holyer, C. D. Hubbard, S. F. A. Kettle and R. G. Wilkins, *Inorg. Chem.*, 1966, **5**, 622.
14 F. Barigelletti, L. Flamigni, M. Guardigli, A. Juris, M. Beley, S. Chodorowski-Kimmes, J.-P. Collin and J.-P. Sauvage, *Inorg. Chem.*, 1996, **35**, 136.

Communication 8/06389C

Macrocyclic polyamine lactam synthesis by diphenyl ether closure of 23-, 24- and 28-membered rings

Simon Carrington,[a] Alan H. Fairlamb[b] and Ian S. Blagbrough*[a]†

[a] *Department of Pharmacy and Pharmacology, University of Bath, Bath, UK BA2 7AY*
[b] *Department of Biochemistry, University of Dundee, Dundee, UK DD1 5EH*

Received (in Cambridge, UK) 26th August 1998, Accepted 10th September 1998

Novel 23-, 24- and 28-membered cyclic polyamine amides (cinnamamides) have been prepared by closure of diphenyl ethers; functionalized conjugates of spermidine and spermine underwent intramolecular aromatic nucleophilic substitution to afford nitro-substituted analogues of cadabicine class (24-membered polyamine lactam) alkaloids.

Polyamines such as triamine spermidine **1** and tetraamine spermine **2** are widely distributed in nature and display a variety of biological activities.[1] Cinnamic acid (3-phenylpropenoic acid) conjugates are commonly isolated as the corresponding *N*-substituted amides from plant sources.[2] Ferulic acid (4-hydroxy-3-methoxycinnamic acid) **3** is found as feruloylputrescine, a conjugate of 1,4-diaminobutane.[3] N^1,N^3-Di-(*E*)-feruloylspermidine **4** has been isolated from *Corylus avellana* L.[3,4] Spermidine conjugates have also been found asymmetrically substituted with both ferulic and caffeic (3,4-dihydroxycinnamic) acids **5**.[3] Maytenine,[5] from *Maytenus chuchuhuasha*, is the unsubstituted dicinnamamide of spermidine **1**. Dicinnamamides of spermine **2** include kukoamine A, a biologically active bis(dihydrocaffeoyl) conjugate.[6,7]

Cyclic polyamine amide containing cinnamamides are less common natural products whose biological activities are largely unknown.[2,8] Spermine **2** containing macrocyclic polyamine lactams include *inter alia* chaenorhine and ephedradine A.[8] Spermidine **1** containing polyamine lactams include codonocarpine **6**, from *Codonocarpus australis*,[9] and capparisinine **7**.[10] Cadabicine **8** is a diphenyl ether 24-membered ring containing spermidine **1**, from *Cadaba farinosa* Forsk. The regiochemical substitution of the diphenyl ether moiety is reversed with respect to the unsymmetrical spermidine moiety in **6** and **7**.[11] We are unaware of a synthesis[2,8] of a cadabicine **8** class alkaloid, although a regiocontrolled synthesis of the *Lunaria* diphenyl ether alkaloid codonocarpine **6** has been reported.[12]

Macrocycles containing diphenyl ethers are of chemical and biological interest as they occur in vancomycin and ristocetin antibiotic families.[13–15] Also, these substitution patterns are found in anti-cancer peptide conjugate RA-VII and ACE inhibitor K-13.[15,16] Macrocyclic polyamine lactams incorporating a diphenyl ether have been prepared using intermolecular Ullmann diaryl ether synthesis followed by lactam formation.[8,12] Herein we report the first design and synthesis of 23-, 24- and 28-membered ring polyamine lactam conjugates that are nitro-substituted analogues of cadabicine **8** class alkaloids.

The required substituted cinnamic acids were prepared from the corresponding benzaldehydes by Knoevenagel condensation.[17,18] Isoferulic acid (3-hydroxy-4-methoxycinnamic acid) **9** was prepared in good yield (92%) under standard conditions starting with malonic acid (EtOH, piperidine, pyridine, 3 h, reflux).[17] 4-Fluorobenzaldehyde was similarly converted into 4-fluorocinnamic acid **10** (85%). Nitration *ortho* to fluorine, in order to activate the final intramolecular nucleophilic substitution (S_NiAr) reaction, achieved with conc. nitric acid, afforded 4-fluoro-3-nitrocinnamic acid **11** (1 h, 0 °C, 72%).

For the 23-membered ring **12**, *N*-(3-aminopropyl)-1,3-diaminopropane was protected with trifluoroacetyl groups on the

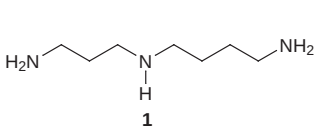

1

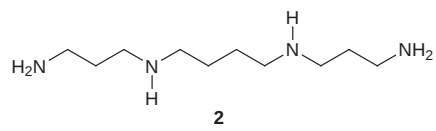

2

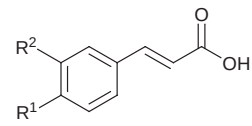

3 R^1 = OH, R^2 = OMe
9 R^1 = OMe, R^2 = OH
10 R^1 = F, R^2 = H
11 R^1 = F, R^2 = NO_2

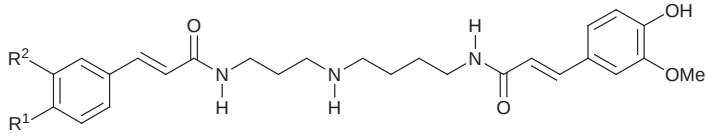

4 R^1 = OH, R^2 = OMe
5 R^1 = OH, R^2 = OH

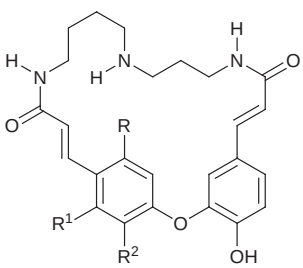

6 R^1 = H, R^2 = OMe
7 R^1 = OMe, R^2 = H

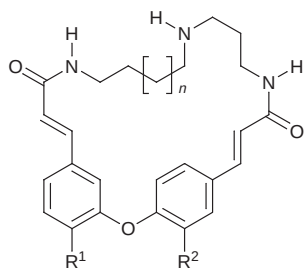

8 *n* = 1, R^1 = OH, R^2 = H
12 *n* = 0, R^1 = OMe, R^2 = NO_2
13 *n* = 1, R^1 = OMe, R^2 = NO_2
14 *n* = 1, R^1 = OH, R^2 = NO_2

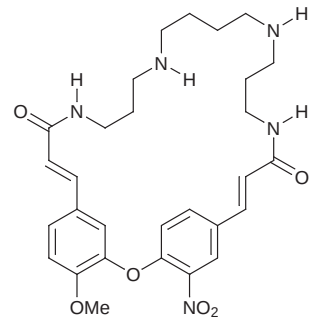

15

primary amino groups (2 equiv. CF_3CO_2Et, THF, 10 min, 25 °C).[19–21] This was followed by immediate Boc protection of the central, secondary amine (Boc_2O, THF, 18 h, 25 °C). Conc. aq. ammonia was added to the solution of tri-protected triamine until the pH was greater than 11 to remove the trifluoroacetyl protecting groups (24 h). Mono-Boc protected amine was isolated and purified by flash column chromatography (15 : 5 : 1, CH_2Cl_2–MeOH–conc. aq. NH_3, v/v/v, R_f 0.13). The cinnamic acid moieties[17,18] were coupled sequentially (first the isoferuloyl **9** then the 4-fluoro-3-nitro **11**) to the primary amines by pre-activation with 2-mercaptothiazoline (2-thiazoline-2-thiol, thiazolidine-2-thione)[5] (DCC, 0.01 equiv. DMAP, CH_2Cl_2, 1 h, 25 °C, followed by filtration to remove the urea). Mono-Boc protected triamine was added to the yellow CH_2Cl_2 solution of the *N*-acylated 2-mercaptothiazoline and the coupling was typically complete after 3 h (*ca*. 50% each acylation). Cyclisation was brought about by stirring with 5 equiv. CsF in anhydrous DMF (18 h) to give 23-membered ring polyamine lactam **12** (79% isolated yield). *O*-Arylation has occurred by intramolecular aromatic nucleophilic substitution (S_NiAr) reaction of *o*-nitro-activated fluoride by the remote phenol.

For the 24-membered ring **14**, spermidine **1** was reacted with formalin to give a hexahydropyrimidine adduct (0.95 equiv. 37% w/w aq. formaldehyde, H_2O, 1 h, 91%) as developed independently by Ganem and Hesse and their co-workers.[22,23] Isoferulic acid **9**[17,18] was coupled to the primary amine of this regioselectively protected spermidine through the 2-mercaptothiazoline activated intermediate (−78 to 25 °C, 55%). After chromatography, this hexahydropyrimidine was deprotected by heating with malonic acid and pyridine (EtOH, reflux, 2 h, 79%).[22] 4-Fluoro-3-nitrocinnamic acid **11** was coupled to the uncovered primary amine and then the secondary amine was protected by a Boc group (1.1 equiv. Boc_2O, MeOH, 18 h, 25 °C, 89%) to afford a linear precursor of cadabicine analogue **13**. Cyclisation was carried out by stirring with 3 equiv. CsF in anhydrous DMF (18 h, 71% isolated yield), final purification by RP-HPLC (5 μm C8 inertpak column eluting with 1:4 aq. TFA (0.1%)–MeOH, v/v, λ = 250 nm). TFA catalysed deprotection (1:1 TFA–CH_2Cl_2, v/v, 45 min, 0 °C, 90%) of the Boc group in diaryl ether **15** was followed by *O*-demethylation with BBr_3 (1.2 equiv., CH_2Cl_2, 3 h, −78 °C) to give 2′-nitrocadabicine **14** in 60% isolated yield.

For the 28-membered ring **15**, spermine **2** was protected in a similar fashion to *N*-(3-aminopropyl)-1,3-diaminopropane *vide supra*. Trifluoroacetyl groups were used to block the two primary amines then two Boc groups were introduced at the secondary amines. Conc. aq. ammonia was used to remove the trifluoroacetyl protecting groups and the N^2,N^3-diBoc spermine was then purified by chromatography. The two cinnamic acid moieties[17,18] were introduced in a stepwise fashion using 2-mercaptothiazoline activation to yield the cyclisation precursor. Cyclisation was carried out in anhydrous DMSO with 3 equiv. K_2CO_3 and 10 equiv. 18-crown-6, the oxygen nucleophilicity was found to be too low without the crown ether. The cyclisation reaction did not proceed to completion at 25 °C (starting material still present after 24 h). However, heating the mixture to 50 °C, in the presence of 18-crown-6, led to complete reaction after 5 h, yielding the desired macrocycle **15** (66%).

The previously proposed mechanism of cyclisation involved bringing the two sites of reaction into proximity by π-orbital stacking interactions between the electron rich guaiacol (2-methoxyphenol) ring and the electron deficient *o*-fluoronitrophenyl ring.[15] However, macrocycle formations of this type have recently been demonstrated to proceed in good yield when the aryl hydroxy group is replaced by an alkyl hydroxy group, proving that such π–π interactions are not necessary for successful cyclisation.[24] As the isolated yields are high, this practical approach by aromatic nucleophilic substitution (intramolecular S_NiAr reaction) should find ready application in the synthesis of natural products and their analogues with particular reference to cyclic spermidine and spermine alkaloids of the codonocarpine **6** and cadabicine **8** classes.

We thank the Department of Pharmacy and Pharmacology, University of Bath, for a studentship (to S. C.). We acknowledge useful discussions with Dr William N. Hunter (University of Dundee), Professor Manfred Hesse (University of Zürich) and Dr Ian S. Haworth (University of Southern California). I. S. B. and I. S. H. are recipients of a NATO grant (CRG 970290). A. H. F. is funded by the Wellcome Trust.

Notes and references

† E-mail: prsisb@bath.ac.uk

1 R. J. Bergeron, *Acc. Chem. Res*., 1986, **19**, 105; I. S. Blagbrough, S. Carrington and A. J. Geall, *Pharm. Sci*., 1997, **3**, 223 and references cited therein.
2 T. A. Smith, J. Negrel and C. R. Bird, *The cinnamic acid amides of di- and polyamines*, in *Advances in Polyamine Research*, ed. U. Bachrach, A. Kaye and R. Chayen, 1983, vol. 4, p. 347; A. Guggisberg and M. Hesse, *The Alkaloids*, Academic Press, 1983, vol. 22, p. 85; A. Guggisberg and M. Hesse, *The Alkaloids*, Academic Press, 1998, vol. 50, p. 219 and references cited therein.
3 B. Meurer, V. Wray, L. Grotjahn, R. Wiermann and D. Strack, *Phytochemistry*, 1986, **25**, 433.
4 A. Husson, R. Besselievre and H.-P. Husson, *Tetrahedron Lett*., 1983, **24**, 1031.
5 Y. Nagao, K. Seno, K. Kawabata, T. Miyasaka, S. Takao and E. Fujita, *Chem. Pharm. Bull*., 1984, **32**, 2687.
6 J. McManis and B. Ganem, *J. Org. Chem*., 1980, **45**, 2041; K. Chantrapromma and B. Ganem, *Tetrahedron Lett*., 1981, **22**, 23; P. Page, S. Burrage, L. Baldock and M. Bradley, *Bioorg. Med. Chem. Lett*., 1998, **8**, 1751.
7 A. H. Fairlamb and A. Cerami, *Annu. Rev. Microbiol*., 1992, **46**, 695; J. A. Ponasik, C. Strickland, C. Faerman, S. Savvides, P. A. Karplus and B. Ganem, *Biochem. J*., 1995, **311**, 371.
8 P. Dätwyler, H. Bosshardt, S. Johne and M. Hesse, *Helv. Chim. Acta*, 1979, **62**, 2712; H. H. Wasserman, R. P. Robinson and C. G. Carter, *J. Am. Chem. Soc*., 1983, **105**, 1697.
9 R. W. Doskotch, A. B. Ray and J. L. Beal, *J. Chem. Soc*., *Chem. Commun*., 1971, 300; R. W. Doskotch, A. B. Ray, W. Kubelka, E. H. Fairchild, C. D. Hufford and J. L. Beal, *Tetrahedron*, 1974, **30**, 3229.
10 V. U. Ahmad, S. Arif, A. U. R. Amber and K. Fizza, *Liebigs Ann. Chem*., 1987, 161.
11 V. U. Ahmad, A. U. R. Amber, S. Arif, M. H. M. Chen and J. Clardy, *Phytochemistry*, 1985, **24**, 2709; V. U. Ahmad, K. Fizza, A. U. R. Amber and S. Arif, *J. Nat. Prod*., 1987, **50**, 1186.
12 M. J. Humora, D. E. Seitz and J. Quick, *Tetrahedron Lett*., 1980, **21**, 3971.
13 D. H. Williams, *Acc. Chem. Res*., 1984, **17**, 364.
14 A. V. Rama Rao, M. K. Gurjar, K. L. Reddy and A. S. Rao, *Chem. Rev*., 1995, **95**, 2135.
15 J. Zhu, *Synlett*, 1997, 133.
16 D. L. Boger, D. Yohannes, J. Zhou and M. A. Patane, *J. Am. Chem. Soc*., 1993, **115**, 3420.
17 F. R. Blase and K. Banerjee, *Synth. Commun*., 1995, **20**, 3187.
18 J. K. Luo, S. L. Castle and R. N. Castle, *J. Heterocycl. Chem*., 1990, **27**, 2047.
19 M. C. O'Sullivan and D. M. Dalrymple, *Tetrahedron Lett*., 1995, **36**, 3451.
20 D. Xu, K. Prasad, O. Repic and T. J. Blacklock, *Tetrahedron Lett*., 1995, **36**, 7357.
21 I. S. Blagbrough and A. J. Geall, *Tetrahedron Lett*., 1998, **39**, 439; A. J. Geall and I. S. Blagbrough, *Tetrahedron Lett*., 1998, **39**, 443.
22 B. Ganem, *Acc. Chem. Res*., 1982, **15**, 290.
23 H. Kühne and M. Hesse, *Helv. Chim. Acta*, 1982, **65**, 1470
24 T. Laïb and J. Zhu, *Tetrahedron Lett*., 1998, **39**, 283.

Communication 8/06688D

Strong intramolecular exchange interactions between nitronyl nitroxide radicals bridged by olefinic spacers

Christophe Stroh,[a] Philippe Turek[b] and Raymond Ziessel*[a]

[a] *Laboratoire de Chimie, d'Électronique et de Photonique Moléculaires, École de Chimie, Polymères et Matériaux (UPRES-A 7008), 1 rue Blaise Pascal, 67008 Strasbourg, France. E-mail: ziessel@chimie.u-strasbg.fr*

[b] *Institut Charles Sadron (UPR 022), Université Louis Pasteur, 6 rue Boussingault, 67083 Strasbourg, France*

Received (in Cambridge, UK) 3rd August 1998, Accepted 25th September 1998

Nitronyl nitroxide radicals bridged by olefinic spacers display strong intramolecular and antiferromagnetic exchange interactions, the magnitude of which depends on the length of the spacer and on steric crowding around the radicaloid subunits.

An essential concern for the development of organic molecular magnetic materials involves minimizing undesired radical–radical interactions whilst promoting efficient exchange coupling along the molecular axis. Because of the inherent difficulty in coupling organic radicals through a bridging framework the use of bis-radicaloid systems has proved less popular than the alternative approach of using transition metals to separate monoradicals.[1] For example, nitronyl nitroxide (NIT) radicals interact only weakly through the π orbitals of an interspersed aromatic spacer because of stereoelectronic inhibition of cross-conjugation[2,3] while directly-linked NIT diradicals exhibit through-space antiferromagnetic coupling.[4] We now report that olefinic spacers promote strong through-bond (TB) interaction between terminal NIT radicals in such a way that complexation to paramagnetic cations might provide novel ferrimagnetic materials.

The deep green diradicals **1**[5] and **2** were synthesised as outlined in Scheme 1.† The all-*trans* conformation of the polyenic skeleton of each diradical was confirmed by X-ray crystallography (Fig. 1).‡ In **1**, the two radicals lie coplanar with the olefinic moiety while the crystal packing shows that the molecules are quasi-isolated with the shortest intermolecular NO···ON distances being > 5 Å. In contrast, the two radical centres in **2** are tilted from coplanarity by 24.9°, due to steric crowding with the neighbouring methyl groups. The crystal packing of **2** reveals relatively short contacts [NO···ON at 3.70 and 3.65 Å, respectively, for OO′ and ON′] between neighbouring molecules within a crystallographic chain [$x + 1$, y, $z + 1$]. Here, the head-to-tail arrangement of the NO subunits, and their relative orientation, are favourable for intermolecular antiferromagnetic interactions. This is indicated by an α angle of 82° for the ON···ƆN and by a β angle of 90° formed between a vector normal to the π* orbitals of the NIT radicals and the N_2O_2 plane.[6]

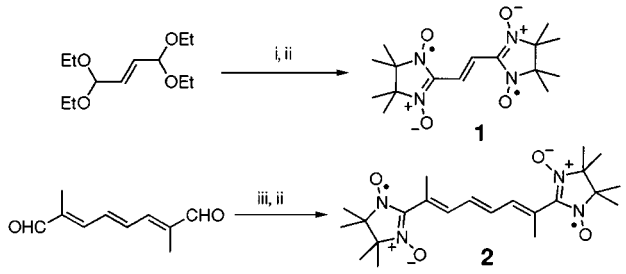

Scheme 1 *Reagents and conditions*: i, MeOH, H_2O, *N*,*N*′-dihydroxy-2,3-diamino-2,3-dimethylbutane sulfate salt, 20 h; ii, $NaIO_4$, H_2O, CH_2Cl_2, 1 h; iii, Benzene, *N*,*N*′-dihydroxy-2,3-diamino-2,3-dimethylbutane, azeotropic distillation, 0.5 h.

The magnetic properties of these two diradicals were studied with a SQUID susceptometer. At 300 K, the product of molar susceptibility and temperature (χT) for both **1** (0.373 emu K mol^{-1}) and **2** (0.613 emu K mol^{-1}) is lower than that expected for two independent spins [0.75 emu K mol^{-1}]. This indicates the predominance of antiferromagnetic interactions. With decreasing temperature, χT for **1** shows a monotonous decrease to zero while a maximum in the susceptibility curve is seen at 75 K for **2** (Fig. 2). The Curie tail observed at low temperature is due to a weak amount (*ca*. 0.1%) of paramagnetic impurities.

In order to avoid intermolecular interactions, compounds **1** and **2** were dispersed in a polystyrene matrix and studied over the 200–300 K temperature range. The χT *vs*. T and the χ *vs*. T plots, respectively, for **1** and **2** display features similar to those found for microcrystalline samples. For **2**, maximal susceptibility is again found around 75 K [inset in Fig. 2(*b*)]. No relevant intermolecular contacts are seen for **1**, such that a good fit of the experimental data was obtained using the Bleaney–Bowers law for an isolated two-spin 1/2 model[7] where the magnetic exchange coupling constant J corresponds to a Hamiltonian of the form $H = -2JS_1S_2$. Here, a large singlet–triplet splitting of $2J/k_B = -469$ K was found, indicating strong TB antiferromagnetic interaction.

In order to fit the susceptibility data for **2**, the Bleaney–Bowers expression for the magnetic susceptibility of a dimer had to be modified by including a mean-field approximation, estimated by a Weiss temperature θ. This describes the average intermolecular interactions throughout the crystal. With respect to **1**, a much weaker TB antiferromagnetic coupling ($2J/k_B = -90$ K) was found, after correction for a mean field temperature of $\theta = -32$ K.

EPR spectra of **1** and **2** were recorded at room temperature in deoxygenated CH_2Cl_2 solutions (*ca*. 5×10^{-5} mol dm^{-3}) and in polystyrene matrices (*ca*. 3.6% w/w). In solution, the EPR

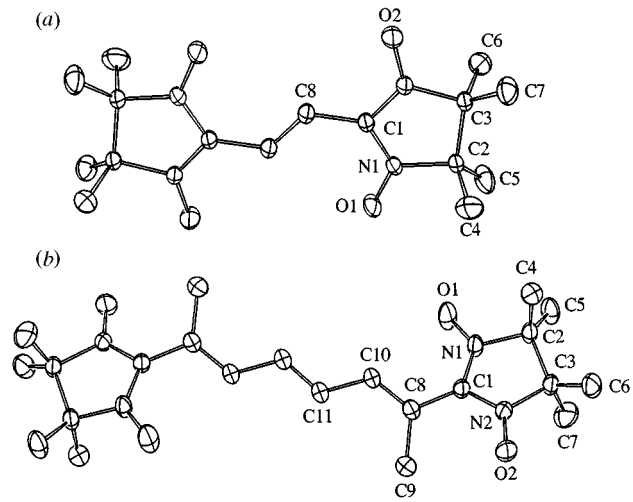

Fig. 1 ORTEP view of a molecular unit of (*a*) **1** and (*b*) **2**.

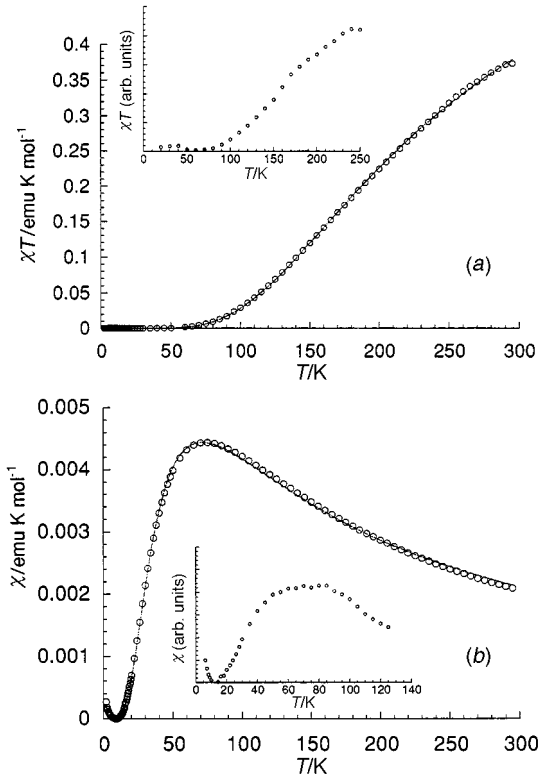

Fig. 2 Temperature dependence of the product of the magnetic susceptibility and temperature (H = 0.5 tesla): (*a*) χT *vs.* T for **1** and (*b*) χ *vs.* T for **2**. The solid line represents the best fit to the experimental data. Insets: χT *vs.* T for **1** and χ *vs.* T for **2** dispersed in a polystyrene matrix.

signal obtained from **2** consists of nine well-separated lines centred at g_{iso} = 2.0065, corresponding to an isotropic hyperfine coupling constant a_N = 3.76 G. This pattern is consistent with strong exchange interaction between a pair of NIT radicals. The solution EPR spectrum of **1** is distorted and centred at g_{iso} = 2.0067, with the observable peaks being separated by *ca*. 3.75 G and lying within the strong exchange limit. In frozen solution, each compound exhibits fine structure (dipolar) lines and a half-field signal (g = *ca*. 4) due to the so-called forbidden (ΔM_S = 2) transitions (Fig. 3).[8] The zero field splitting (ZFS) parameters are estimated as D = 168 G for **1** and D = *ca*. 31 G for **2**, in rough agreement with the values calculated from the crystal structure on the basis of the point dipole approximation (146 < D < 302 G for **1**, and 34 < D < 41 G for **2**).

The experimental data can be well explained by taking into account strong TB antiferromagnetic interaction between the NIT radicals. The geometry and availability of a conductive pathway combine to favour TB interaction rather than through-space exchange. Indeed, the bridging polyenic spacer shows a high propensity for exchange interactions between remote NIT radicals. This is presumably due to efficient orbital overlap between the radicals and the conjugated framework. In this respect, the olefinic spacer is much more effective than aromatic

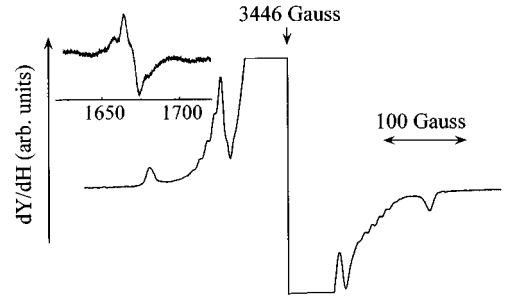

Fig. 3 Fine structured lines observed in the first derivative EPR absorption spectrum (X-band; ν = 9.73 GHz) of **1** dispersed in a polymer matrix and recorded at room temperature. The inset shows the half-field signal.

groups. However, a marked stereoelectronic effect is present in **2**, owing to the presence of methyl substituents at the α position relative to the radicals, which curtails exchange interaction.

In summary, in the absence of steric crowding an olefinic bridge favors a planar diradical in the solid state whose conformation is ideal for TB exchange interaction. This is in marked contrast to bis-NIT coupled directly[4] or *via* aryl spacers. Moreover, the magnetic and electronic properties observed in the crystals are conserved in a diluted polymeric matrix. The pronounced TB interaction inherent in these simple systems might provide access to ferrimagnetic scaffolds by judicious coordination to magnetic metal ions.

Notes and references

† On the basis of spectroscopic evidence, including EI-MS and elemental analysis, the structures of the new compounds were unequivocally authenticated. *Selected data* for **1**: *m/z* 338.2 (M); Found: C, 56.60; H, 7.55; N, 16.37%. For **2**: *m/z* 418.3 (M); Found: C, 62.86; H, 8.05; N, 13.15%.

‡ *Crystal data* for **1**: $C_{16}H_{26}N_4O_4$, monoclinic, space group $P12_1/c$, a = 6.1877(5), b = 11.095(2), c = 13.130(1) Å, β = 99.828(7)°, Z = 2, 1199 independent reflections with $I > 3\sigma(I)$, R = 0.053, R_w = 0.073. For **2**: $C_{22}H_{34}N_4O_4$, monoclinic, space group $P12_1/n$, a = 7.0087(4), b = 16.270(1), c = 10.3874(5) Å, β = 99.244(4)°, Z = 2, 1566 independent reflections with $I > 3\sigma(I)$, R = 0.048 and R_w = 0.076. Collection: MACH3 Nonius diffractometer, Mo-Kα, λ = 0.71073 Å, graphite monochromator, T = 294 K. CCDC 182/1034.

1 *Synthetic Chemistry of Stable Nitroxides*, ed. L. B. Volodarsky, V. A. Reznikov and V. I. Ovcharenko, CRC press, Boca Raton , Florida, USA, 1994.
2 T. Mitsumori, K. Inoue, N. Koga and H. Iwamura, *J. Am. Chem. Soc*., 1995, **117**, 2467 and references cited therein.
3 T. Sugano, M. Tamura and M. Kinoshita, *Synth. Met*., 1993, **55-57**, 3305.
4 F. Alies, D. Luneau, J. Laugier and P. Rey, *J. Phys. Chem*., 1993, **97**, 2922.
5 E. F. Ullman, J. H. Osiecki, D. G. B. Boocock and R. Darcy, *J. Am. Chem. Soc*., 1972, **94**, 7049.
6 A. Caneschi, D. Gatteschi and P. Rey, *Prog. Inorg. Chem*., 1991, **39**, 331.
7 B. Bleaney and K. Bowers, *Proc. R. Soc. Lond*., 1952, **A214**, 451.
8 J. A. Weil, J. R. Bolton and J. E. Wertz, in *Electron Spin Resonance*, Wiley, New York, USA, 1994.

Communication 8/06071A

Stereochemical evidence for elimination–addition and a methylenethioxophosphorane (thiophosphene) intermediate in nucleophilic substitution at the P=S centre of a benzylic phosphonamidothioic chloride

Martin J. P. Harger

Department of Chemistry, The University, Leicester, UK LE1 7RH

Received (in Liverpool, UK) 4th September 1998, Accepted 22nd September 1998

The two diastereoisomers of $ArCH_2P(S)(NMeR^*)Cl$ (Ar = 4-$NO_2C_6H_4$, R* = CHMePh) react with Et_2NH (0.2 mol dm^{-3}) in CH_2Cl_2 to give mixtures of the diastereoisomers of $ArCH_2P(S)(NMeR^*)NEt_2$ in practically the same ratio (54.5 : 45.5 or 53 : 47); such non-stereospecificity points to a thiophosphene intermediate ArCH=P(S)NMeR* as the product-forming species.

Nucleophilic substitution at a phosphoryl (P=O) or thiophosphoryl (P=S) centre generally proceeds by an associative $S_N2(P)$ mechanism with a five-coordinate intermediate or transition-state.[1] An alternative dissociative mechanism, involving elimination–addition (EA) and a transient three coordinate P^V intermediate **2**, is sometimes favoured when the substrate **1**

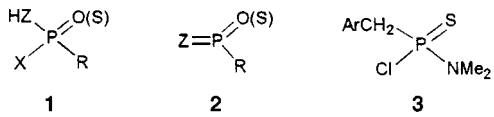

1 **2** **3**

(X = leaving group) has an acidic ligand HZ,[1,2] *i.e.* when Z is an oxygen,[3] sulfur[4] or nitrogen[5] atom. When Z is just a saturated carbon atom however, elimination–addition seems unable to compete with the normal $S_N2(P)$ reaction.[6] An exception may be the benzylic phosphonamidothioic chloride **3**, at least when it is substituted with a nitro group (Ar = 4-$NO_2C_6H_4$).[7] Then it displays remarkably high reactivity towards basic nucleophiles such as Et_2NH, perhaps because the C_α–H bonds are sufficiently acidic for reaction to proceed rapidly by an EA mechanism. To substantiate such a mechanism, and in particular the intermediacy of a three-coordinate methylenethioxophosphorane (thiophosphene) intermediate $[ArCH{=}P(S)NMe_2]$, there is a need of stereochemical information. Working with the individual enantiomers of **3** (Ar = 4-$NO_2C_6H_4$) would present problems, both preparative and analytical, so our attention turned to the related compound **4** (Ar = 4-$NO_2C_6H_4$) (Scheme 1). This is chiral at carbon as well as phosphorus so both substrate and substitution product will exist as diastereoisomers.

The phosphonamidothioic chloride **4** was prepared using 4-nitrobenzylphosphonothioic dichloride $[ArCH_2P(S)Cl_2]$[7] and (*S*)-(−)-PhMeCHNHMe. It is known that benzylic phosphonothioic dichlorides tend to go directly to the diamide when they react with secondary amines,[8] but by keeping the amine concentration low [addition over 5–6 h to a dilute CH_2Cl_2 solution of $ArCH_2P(S)Cl_2$], and having some of the amine hydrochloride (the byproduct of the reaction) present in solution from the outset, the amidic chloride **4** was the major product. Chromatography (silica gel; 15% EtOAc in light petroleum) followed by crystallisation of appropriate fractions afforded pure samples of the two diastereoisomers (**A** and **B**) of **4** [*m*/*z* 370, 368 (M^+, 6%): **A**, mp 108–109 °C, $\delta_P(CDCl_3)$ 90.00; $\delta_H(CDCl_3)$ 3.92 (2H, m, C*H*$_2$Ar), 2.575 (3H, d, J_{PH} 15, N*Me*) and 1.525 (3H, d, J_{HH} 7, CH*Me*Ph); **B**, mp 87–88 °C, $\delta_P(CDCl_3)$ 90.57; $\delta_H(CDCl_3)$ 3.91 (2H, m, C*H*$_2$Ar), 2.61 (3H, d, J_{PH} 15, N*Me*) and 1.30 (3H, d, J_{HH} 7, CH*Me*Ph)].†

The amidic chloride **4** reacted readily with Et_2NH as a dilute solution in CH_2Cl_2, giving the expected diamide product **6** as a mixture of diastereoisomers [$\delta_P(CDCl_3)$ 81.24 and 81.20; $\delta_H(CDCl_3)$ 2.475 and 2.435 (d, J_{PH} 10.5, N*Me*), 1.48 and 0.97 (d, J_{HH} 7, CH*Me*Ph) and 1.135 and 1.015 (t, J_{HH} 7, CH_2*Me*), *m*/*z* 405 (M^+, 15%)]. Whichever diastereoisomer of the substrate was used, the product **6** was obtained as practically the same 54 : 46 mixture having the low-field diastereoisomer (δ_P 81.24; δ_H 2.475, 1.48 and 1.135) in slight excess. As long as the diastereoisomers are configurationally stable under the conditions of reaction, it follows that substitution is non-stereospecific but slightly stereoselective. Such behaviour is not compatible with the normal $S_N2(P)$ mechanism of nucleophilic substitution,[9] but it is entirely reasonable for an EA mechanism in which both diastereoisomers of substrate form the thiophosphene intermediate **5** (Scheme 1). This is planar (trigonal) at phosphorus and can be attacked by Et_2NH at either face (non-stereospecificity), but the two faces are diastereotopic (chirality in NMeR*) so they will not necessarily be attacked with equal ease (diastereoselectivity).

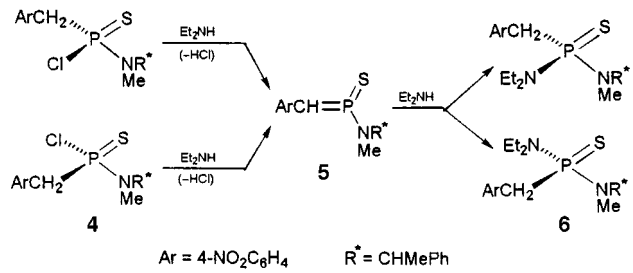

Scheme 1

To assess the stability of the configuration at phosphorus the reactions of the two diastereoisomers of **4** were monitored by ^{31}P NMR spectroscopy, using a 0.2 mol dm^{-3} solution of Et_2NH (large excess) in CH_2Cl_2. In both cases the diastereoisomer composition of the product **6** (*ca.* 54 : 46) remained constant throughout the reaction ($t_{\frac{1}{2}}$ = 35–40 min at 19 °C) and the stereochemical integrity of the substrate was retained (≥95% one diastereoisomer at ≥90% completion).‡ It is therefore certain that non-stereospecificity is an integral part of the process of substitution.

In the course of the NMR experiments it became apparent that the products from the two diastereoisomers of the substrate were in fact not quite identical, the diastereoisomer ratios being 54.5 : 45.5 for **A** and 53 : 47 for **B**. The most obvious explanation is that elimination–addition is not completely dominant, so that a small proportion (1.5%) of the substrate is able to react stereospecifically by the normal $S_N2(P)$ mechanism. This, however, is difficult to reconcile with the behaviour observed using an amine less bulky than Et_2NH. As a base there is not much difference between Et_2NH and Me_2NH but as a nucleophile at a tetrahedral phosphorus centre there is;[10] with $PhP(S)(NMe_2)Cl$, for example, Me_2NH reacts at least a hundred times faster than Et_2NH.[7] If $S_N2(P)$ does compete with the EA

mechanism, it will surely do so much more effectively in the case of Me_2NH. In fact the reaction of **4** with Me_2NH is hardly more stereospecific at all. Using 0.2 mol dm^{-3} Me_2NH in CH_2Cl_2 the diamide product (**6** with Me_2N in place of Et_2N) [*m*/*z* 377 (M^+, 15%)] was formed ($t_{\frac{1}{2}}$ = *ca.* 15 min at 19 °C) with diastereoisomer ratios of 52.5 : 47.5 and 50.5 : 49.5 from **A** and **B** respectively, and again the low-field diastereoisomer [$\delta_P(CDCl_3)$ 85.04; $\delta_H(CDCl_3)$ 2.58 (d, J_{PH} 13, NMe_2), 2.46 (d, J_{PH} 10.5, NMe) and 1.45 (d, J_{HH} 7, CH*Me*Ph)] was formed in slight excess of the other (δ_P 84.97; δ_H 2.41, 2.41 and 0.88).‡ Here too, then, substitution is almost completely non-stereospecific. Any contribution from $S_N2(P)$ must be slight (2%) even with Me_2NH, and with Et_2NH it will surely be negligible. That being so, it seems likely that the reaction of **4** with Et_2NH proceeds entirely by an EA mechanism, with a thiophosphene intermediate, and that slight differences in the composition of the product from the two diastereoisomers are a consequence of the structure of the thiophosphene and/or the environment in which it is formed.§

Notes and references

† The substrate **4** and the products derived from it were fully characterised by NMR (^1H and ^{31}P) and IR spectroscopy, mass spectrometry (EI), and elemental analysis and/or accurate mass measurement.

‡ In CH_2Cl_2 the relative ^{31}P NMR chemical shifts of the two diastereoisomers of the diamide product are reversed (relative to $CDCl_3$) so the product formed in excess appeared at high field [$\delta_P(CH_2Cl_2)$ 80.96 and 81.02 with Et_2NH; 84.71 and 84.82 with Me_2NH].

§ The thiophosphene **5** has a (formal) C–P double bond so (in principle) it exists as *E* and *Z* isomers; these may be formed in differing proportions from the two diastereoisomers of the substrate and react with the nucleophile with differing stereoselectivities. Also, the thiophosphene may be so short-lived that some of it is trapped by the nucleophile before it is able to diffuse away from the chloride ion (or amine hydrochloride) released in the elimination step of the EA mechanism. In these ways the stereochemistry of the product could be influenced by the configuration of the substrate, notwithstanding the planarity at the phosphorus atom of the thiophosphene intermediate.

1 G. R. J. Thatcher and R. Kluger, *Adv. Phys. Org. Chem.*, 1989, **25**, 99; D. M. Perreault and E. V. Anslyn, *Angew. Chem., Int. Ed. Engl.*, 1997, **36**, 433.
2 M. Regitz and G. Mass, *Top. Curr. Chem.*, 1981, **97**, 71.
3 For recent work and references see: E. S. Lightcap and P. A. Frey, *J. Am. Chem. Soc.*, 1992, **114**, 9750; J. M. Friedman, S. Freeman and J. R. Knowles, *J. Am. Chem. Soc.*, 1988, **110**, 1268; L. D. Quin and S. Jankowski, *J. Org. Chem.*, 1994, **59**, 4402.
4 For recent work and references see: P. M. Cullis and R. Misra, *J. Am. Chem. Soc.*, 1991, **113**, 9679; S. P. Harnett and G. Lowe, *J. Chem. Soc., Chem. Commun.*, 1987, 1416. See also L. D. Quin, P. Hermann and S. Jankowski, *J. Org. Chem.*, 1996, **61**, 3944.
5 A. F. Gerrard and N. K. Hamer, *J. Chem. Soc. (B)*, 1968, 539; 1969, 369; S. Freeman and M. J. P. Harger, *J. Chem. Soc., Perkin Trans. 2*, 1988, 81; *J. Chem. Soc., Perkin Trans. 1*, 1988, 2737; M. J. P. Harger, *J. Chem. Soc., Perkin Trans. 2*, 1991, 1057.
6 G. Cevasco and S. Thea, *J. Chem. Soc., Perkin Trans. 1*, 1993, 1103; 1994, 1103.
7 M. P. Coogan and M. J. P. Harger, *J. Chem. Soc., Perkin Trans. 2*, 1994, 2101; M. J. P. Harger and B. T. Hurman, *J. Chem. Res.* (*S*), 1996, 490.
8 M. J. P. Harger, *Tetrahedron Lett.*, 1996, **37**, 8247.
9 R. S. Edmundson, in *Chemistry of Organophosphorus Compounds*, ed. F. R. Hartley, Wiley, Chichester, 1996, vol. 4, ch. 5 and 6.
10 A. Kanavarioti, M. W. Stronach, R. J. Ketner and T. B. Hurley, *J. Org. Chem.*, 1995, **60**, 632.

Communication 8/06926C

Clean catalysis with ionic solvents—phosphonium tosylates for hydroformylation

Nazira Karodia, Steven Guise, Craig Newlands and Jo-Ann Andersen*

School of Chemistry, University of St Andrews, St Andrews, Fife, UK KY16 9ST. E-mail: jma2@st-andrews.ac.uk

Received (in Basel, Switzerland) 10th July 1998, Accepted 7th September 1998

High-melting phosphonium tosylates are synthesised and applied for the first time as solvents in catalytic hydroformylation reactions; variation in the substituents attached to phosphorus can lead to markedly different results; the catalyst systems are non-corrosive, easily manipulated and can readily be recovered and reused.

One of the major problems associated with homogeneous catalysts is that they are difficult to recover at the end of the reaction. Frequently distillation is used as a separation technique, but this is a very energy-intensive process. High-boiling products can remain with the catalyst and lead to catalyst deactivation or product contamination. This problem, especially for expensive and/or toxic precious metal catalyst systems, has precluded their more widespread application in the catalysis industry.

In today's environmentally conscious world, another problem with homogeneous catalysts has emerged, *viz.* many of the solvents traditionally used in transition metal catalysis, such as chlorinated hydrocarbons, acetonitrile, DMF to name but a few, are currently on the 'environmental blacklist'. It is rapidly becoming apparent that the way in which solvents are used in organic synthesis needs rethinking. The way forward may thus be to choose the solvent on environmental grounds and then optimise the reaction in that solvent.[1] In this respect, the use of high-melting ionic solvents (molten salts/ionic liquids) will be highly advantageous if the product(s) can readily be decanted off the stable catalyst system. The advantages of these systems will be manifold: in addition to facilitated catalyst recovery, they may exhibit low viscosity, high thermal and air stability, good electrical conductivity, low vapour pressure and they will readily solubilise the reagents and catalyst. They also exhibit a large 'liquid range', allowing for extensive kinetic control.[2] Room temperature ionic liquids such as alkylimidazolium chloride/$AlCl_3$ have been developed by Seddon and others[2,3] and have been found to function as highly efficient catalytic systems for reactions such as dimerisation and alkylation. However, much less attention has been paid to higher melting ionic solvents such as tetraalkyl ammonium and phosphonium salts. These offer advantages over the room temperature systems in that (i) they are not corrosive and (ii) being solid at room temperature, they are more easily manipulated and product separation is simple, being accomplished by decantation rather than by biphasic extraction. They are also stable to much higher temperatures, thereby enabling more forcing reaction conditions to be applied. We now report our results on the synthesis of tetraalkyl/aryl phosphonium tosylates and their application as solvents in hydroformylation reactions.

Salts **1–4** were synthesised by reaction of the tosylate esters [eqn. (1)] with the appropriate tertiary phosphine [eqn. (2)].

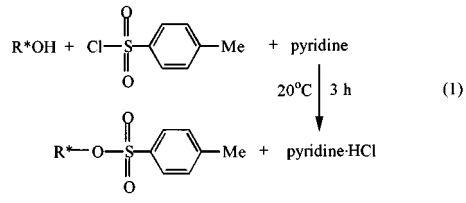

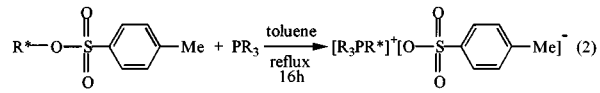

	R	R*
1	Ph	Et
2	Ph	Bu
3	Ph	Octyl
4	Bu	Et

All four salts were fully characterised; selected data are shown in Table 1. They were then applied as solvents in the hydroformylation of hex-1-ene to heptanal (**A**) and 2-methylhexanal (**B**) [eqn. (3)] in the presence of $[Rh_2(OAc)_4]$, both

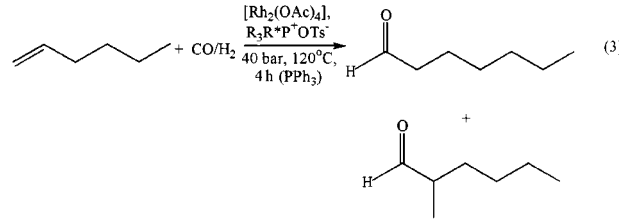

with and without added phosphine ligand. Selected results are shown in Table 2.

In some instances, trace amounts (*ca.* 1–2%) of additional reaction products were observed. The isomerisation products 2-methylhexanal (**B**) and 2-ethylpentanal (**C**) (derived from the isomerisation of hex-1-ene to hex-2-ene and subsequent hydroformylation) were typically present in small amounts. In the case of $Ph_3PBu^+OTs^-$ and $Ph_3POc^+OTs^-$, the corresponding C_5 aldehyde and C_9 aldehyde were observed, respectively. These are most likely to derive from elimination of the bulky alkyl moiety (butyl or octyl) to form the corresponding alkene, analogous to Hoffmann eliminations in ammonium salts. The alkene is then hydroformylated to the corresponding aldehydes (**F**–**J**; see Scheme 1). This elimination process does not occur with $Bu_3PEt^+OTs^-$ or with $Ph_3PEt^+OTs^-$; presumably, in these cases, the ethyl group is small enough to remain bound to the P atom and does not eliminate.

Table 1 Characterisation of phosphonium salts

Salt	Melting point/°C [literature value]	Yield (%)	$\delta(^{31}P)$	ν(P–C)/cm^{-1}
$Ph_3PEt^+OTs^-$; **1**	94–95 [93–94][4]	98	26.6	1460 (P–C_{aryl}); 1380 (P–C_{alkyl})
$Ph_3PBu^+OTs^-$; **2**	116–117 [139–140][4]	98	24.8	1470 (P–C_{aryl}); 1380 (P–C_{alkyl})
$Ph_3POc^+OTs^-$; **3**	70–71	95	26.7	1450 (P–C_{aryl}); 1390 (P–C_{alkyl})
$Bu_3PEt^+OTs^-$; **4**	81–83 [70–78][4]	94	24.6	1380 (P–C_{alkyl})

Table 2 Hydroformylation of hex-1-ene in the presence of phosphonium salts as solvents[a]

Salt	PPh_3	Conversion (%)	Yield (%) A	B	C	Product n : iso ratio (A : [B + C])
1	No	80	29.4	36.0	14.6	1 : 1.3
	Yes	95	55.7	29.8	9.5	1.5 : 1
2	No	96	18.4	34.1	32.3[b]	1 : 4
	Yes	99	20.8	30.2	37.7[b]	1 : 3.2
3	No	49	18.9	22.5	7.6[b]	1 : 1.7
	Yes	100	69.1	25.0	4.9[b]	2.2 : 1
4	No	90	62.6	22.5	4.9	2.5 : 1
	Yes	100	69.3	22.7	7.0	2.2 : 1
1	No[c]	100	65.2	27.4	7.4	1.9 : 1

[a] $[Rh_2(OAc)_4]$, 0.02 g (0.045 mmol); $R_3PR^{*+}OTs^-$, 1.0 g; PPh_3, 0.1 g (0.38 mmol); hex-1-ene, 1.5 ml (12 mmol); 40 bar, 120 °C, 4 h. [b] Trace amounts of elimination products observed. [c] $(Ph_3P)_3Rh(CO)(H)$, 0.085 g (0.093 mmol) added to reaction mixture in place of $[Rh_2(OAc)_4]$.

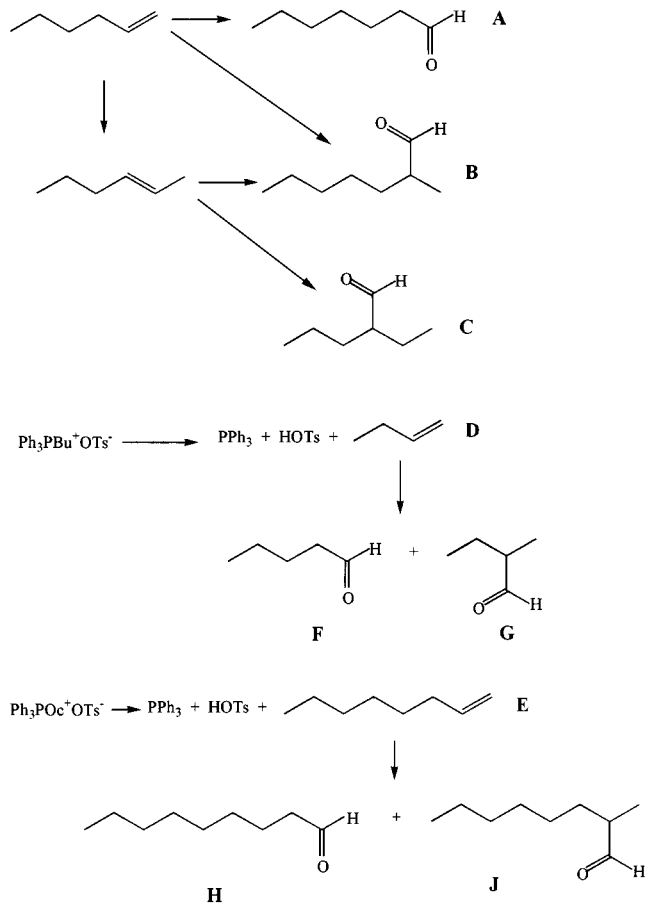

Scheme 1 Hydroformylation of hex-1-ene.

The results in Table 2 indicate that the substituents attached to the central phosphorus atom of the phoshonium salt exert a significant effect on the catalyst performance. With no added phosphine ligand, the conversions range from 66% (for $Ph_3POc^+OTs^-$) to 100% (for $Bu_3PEt^+OTs^-$) and the n : iso ratios range from 2.5 : 1 (for $Bu_3PEt^+OTs^-$) to 1 : 4 (for $Ph_3POc^+OTs^-$). This solvent effect is remarkable and is almost unparalleled in conventional homogeneous catalysis. In addition, our catalyst systems offer the advantage of extremely facile catalyst recovery post-reaction. Upon the addition of excess PPh_3, the catalytic results are very similar to each other (conversions range from 95 to 100% and n : iso ratios range from 1.5 : 1 to 2.2 : 1). We propose that in this case $(Ph_3P)_3Rh(CO)(H)$ forms initially (from $[Rh_2(OAc)_4]$, PPh_3, CO and H_2) and is then the catalytically active species in every reaction. Thus, one would expect very similar results, with only small influences being exerted by the phosphonium solvent.

At the end of the reaction, the reaction mixture was cooled and the liquid organic product was decanted and analysed by GC, GC-MS and NMR. This facile product recovery is the most significant advantage of these systems. The recovered solid was characterised in order to determine that the phosphonium salt had not changed during the course of the reaction, which was indeed the case. The organic products were analysed for rhodium content (by atomic absorption); in all cases, negligible amounts (if any) were observed, indicating that the rhodium catalyst remains within the (crystalline) structure of the solid solvent. These catalyst systems have been re-used several times and gave reproducible results.

Studies are now under way with a larger range of salts, substrates and reaction types to investigate the general applicability of these novel solvents which are analogous to conventional dipolar aprotic solvents but also offer the considerable advantage of facile catalyst recovery and cleaner, efficient catalytic reactions.

We thank the Royal Society of Edinburgh (J. A.), the EPSRC (N. K.) and the Carnegie Trust, University of St Andrews (C. N.).

Notes and references

1 R. A. Sheldon, *ChemTech*, 1994, **3,** 38.
2 K. R. Seddon, Ionic Liquids Review at: http://www.ch.qub.ac.uk/kre/kre.html
3 P. A. Z. Suarez, J. E. L. Dullius, S. Einloft, R. F. de Souza and J. Dupont, *Inorg. Chim. Acta*, 1997, **255**, 207.
4 D. Klamann and P. Weyerstahl, *Chem. Ber.*, 1964, **97**, 2534.

Communication 8/05376F

Stable bis(silyl)nickel complexes with *o*-carboranyl unit: a facile double silylation of alkynes and alkenes

Youngjin Kang,[a] Junghyun Lee,[b] Young Kun Kong,[b] Sang Ook Kang,*[a] and Jaejung Ko*[a]

[a] *Department of Chemistry, Korea University, Chochiwon, Chungnam 339-700, Korea. E-mail: jko@tiger.korea.ac.kr*
[b] *Department of Chemistry, Kyunggi University, Suwon, Kyunggido 440-760, Korea*

Received (in Cambridge, UK) 17th August 1998, Accepted 15th September 1998

The reaction of *o*-bis(dimethylsilyl)carborane with $Ni(PEt_3)_4$ in pentane affords the reactive intermediate, $[o\text{-}(SiMe_2)_2C_2B_{10}H_{10}]Ni(PEt_3)_2$ 2; the facile double silylation of alkynes catalyzed by 2 is reported.

The double silylation of unsaturated organic substrates catalyzed by group 10 metals has been well documented for two decades.[1] Nickel complexes, in particular, provide excellent catalysts for the transformation of silicon-containing linear compounds. Cyclic bis(silyl)nickel complexes have been implicated as important intermediates in the nickel-catalyzed double silylation of arenes,[3] alkynes,[4] alkenes[5] and aldehydes.[6] However, the intermediates have not been isolated due to their instability. We now describe (i) the isolation of the reactive intermediate cyclic bis(silyl)nickel compound with a bulky *o*-carborane unit; (ii) the facile double silylation of alkynes catalyzed by the intermediate under mild conditions; and (iii) the double silylation of alkenes by the stoichiometric reaction with the intermediate.

Addition of 1.2 equiv. of *o*-bis(dimethylsilyl)carborane, prepared from 1,2-$Li_2C_2B_{10}H_{10}$ and 2 equiv. of $SiMe_2ClH$, to $Ni(PEt_3)_4$ in pentane at 25 °C gave a dark red solution, concomitant with the evolution of gas. Standard workup and crystallization from toluene–pentane gave $[o\text{-}(SiMe_2)_2C_2B_{10}H_{10}]Ni(PEt_3)_2$ **2** as a spectroscopically pure, dark red crystalline solid sensitive to air and stable during brief heating to 100–110 °C in 86% yield [eqn. (1)].† The unusual thermal

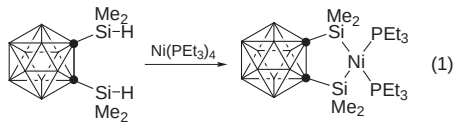

1 **2**

stability of the nickel bis(silyl) compound is attributed to the advantageous properties of the carboranyl unit, including electronic and steric effect.

The ^1H, ^{13}C, ^{31}P and ^{29}Si NMR spectra for **2** support the proposed structure. In particular, the ^{29}Si NMR chemical shift of δ 43.19 as a triplet ($J_{Si-P(cis)}$ 40.11 Hz) resembles the literature value reported for the *cis*-$NiSi_2PC$ complex.[7] The structure of **2** was unambiguously established by a single-crystal X-ray analysis (Fig. 1).‡ Complex **2** has a distorted tetrahedral geometry with the dihedral angle between P(1)–Ni–P(2) and Si(1)–Ni–Si(2) being 86.03°. Such bis(silyl)nickel complexes are rare as indicated by a search of the Cambridge Data Base which revealed only a few previous examples.[8] As expected, the average Ni–Si bond length [2.2424(9) Å] is slightly longer than that of 2.171(3) Å in $[(\mu\text{-}Cl)_2Ni_2(SiCl_3)_4][(CMe_3)_2C_5H_3NH]_2$.[8] The Ni–P bond distance [2.2305(8) Å] is consistent with those observed in other phosphine nickel compounds.[9]

Compound **2** was found to be a good reactive intermediate for the double silylation reaction. The reaction of *o*-bis(dimethylsilyl)carborane **1** with 1-phenylprop-1-yne (1 equiv.) in the presence of a catalytic amount of **2** (0.03 equiv.) for 6 h afforded the double-silylated product **3** in 94% (GC) yield. The reaction was quite sensitive to the reaction conditions. When the same reaction was carried out at higher temperature (70–75 °C), the major component was identified as the acetylene cyclotrimerization product **4** (Scheme 1), which has been characterized by spectroscopic techniques.

When hex-1-yne is employed as a terminal alkyne in the reaction with **1** under the same conditions, the five-membered disilyl ring compound **5** is isolated as a colorless liquid in 71% yield. All the spectral data of **5** was consistent with the proposed formulation.

The reaction of **2** with 1 equiv. of styrene takes place at a higher temperature (80 °C) and affords a moderate yield of the five-membered disilyl ring compound **6** (Scheme 2). A key feature in the ^1H NMR spectrum of **6** includes a singlet at δ 7.71 assigned to the vinyl proton. A characteristic low frequency ^{13}C NMR resonance at δ 139.75 provides evidence for a tethered carbon atom of the two silicon moieties. The structure of **6** has been determined by X-ray crystallography.‡ Such formation of the disilyl ring compound has been observed during the nickel-catalyzed reaction of benzo-disilacyclobutene with styrene.[5] Treatment of **2** with 1 equiv. of 1,1-diphenyl-ethylene in toluene at 80 °C resulted in a brown solution from which the five-membered disilyl ring compound **7** was isolated in a yield of

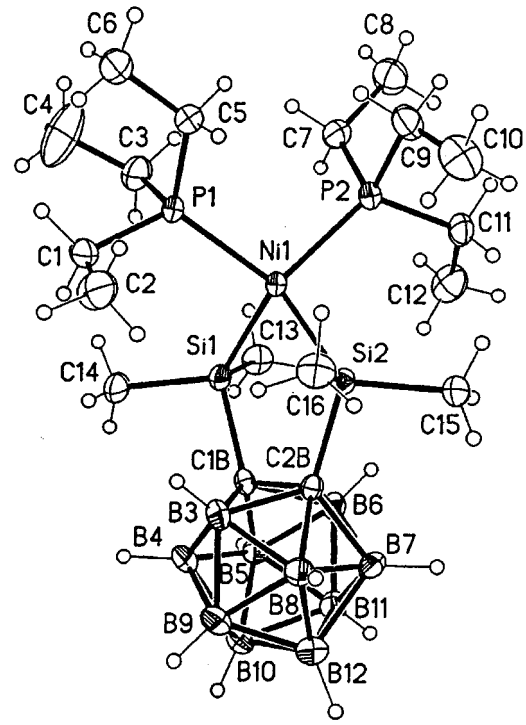

Fig. 1 Molecular structure of **2** showing the atom numbering scheme. Selected distances (Å) and angles (°): Ni(1)–P(1) 2.2265(8), Ni(1)–P(2) 2.2346(8), Ni(1)–Si(1) 2.2371(9), Ni(1)–Si(2) 2.2477(9), Si(1)–C(1B) 1.941(3), Si(2)–C(2B) 1.940(3), C(1B)–C(2B) 1.669(4); P(1)–Ni(1)–P(2) 101.95(3), Si(1)–Ni(1)–Si(2) 83.69(3), P(1)–Ni(1)–Si(1) 96.06(3), P(2)–Ni(1)–Si(1) 140.35(4).

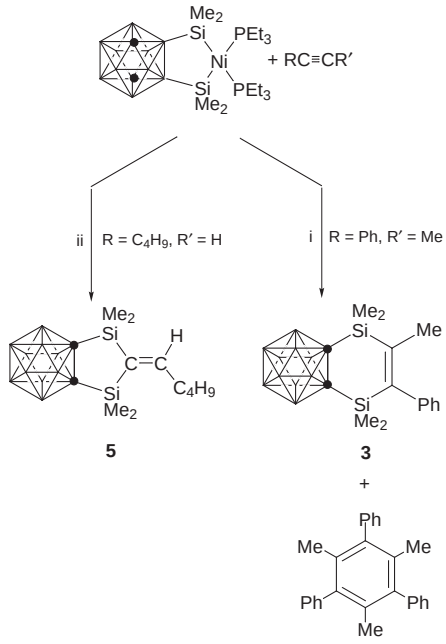

Scheme 1 *Reagents and conditions*: i, PhCCMe (1 equiv.), **1** (1 equiv.), **2** (0.03 equiv.), toluene, 25 °C, 94%; ii, $HCCC_4H_9$ (1 equiv.), **1** (1 equiv.), **2** (0.03 equiv.), toluene, 25 °C, 71%.

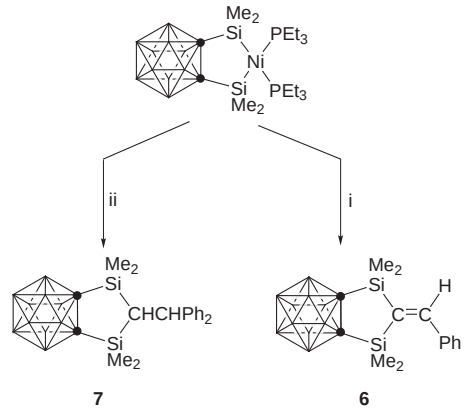

Scheme 2 *Reagents and conditions*: i, $PhCHCH_2$ (1 equiv.), **2** (1 equiv.), toluene, 80 °C, 84%; ii, Ph_2CCH_2 (1 equiv.), **2** (1 equiv.), toluene, 80 °C, 74%.

74%. The formulation of **7** was confirmed by a spectrometric analysis. The mass spectrum of the product showed a molecular ion at *m/z* 440.

Two doublets (δ 3.93, 1.81) in the ^{1}H NMR spectrum of **7** are assigned to the methine protons. A low-frequency ^{13}C NMR resonance at δ 49.87 provides evidence for the tethered carbon atom of the two silicon moieties.

In summary, we have isolated the reactive intermediate, the cyclic bis(silyl) nickel complex, which reacts with unsaturated organic substrates such as an alkyne and alkene, generating a new class of heterocyclic compounds. The intermediate **2** is quite reactive and readily attacked by a variety of organic substrates. This potential has been further exploited in a series of novel chemical transformations with this system.

We are grateful to KOSEF for the generous financial support.

Notes and references

† *Experimental procedure* for **2**: compound **1** (0.48 g, 1.85 mmol) in 20 ml of pentane was added to a stirred solution of $Ni(PEt_3)_4$ (0.98 g, 1.85 mmol) in 20 ml of pentane pentane at −20 °C. The solution was warmed to room temperature for 2 h. The solution was filtered. The residue was dissolved in toluene (20 ml) and this solution was covered with a layer of a pentane (20 ml) at −15 °C. Dark red crystals of **2** formed over a period of several days (0.88 g, 86% yield). ^{1}H NMR (C_6D_6): δ 1.13 (dq, J_{HH} 5.6, J_{HP} 6.4 Hz, CH_2), 0.63 (dt, J_{HH} 5.6 Hz, J_{HP} 14.2 Hz, CH_3), 0.42(s, $SiCH_3$). ^{13}C{^{1}H} NMR (C_6D_6): δ 71.08, 17.05 (d, J_{CP} 16.64 Hz, CH_2), 6.737 (s, CH_3), 4.105 (s, $SiCH_3$). ^{31}P{^{1}H} NMR (C_6D_6) : δ 5.58. ^{29}Si NMR(C_6D_6) : δ 43.19 (t, J_{SiP} 40.11 Hz).

‡ *Crystal data*: **2**: $C_{18}H_{52}B_{10}NiP_2Si_2$, M = 553.53, monoclinic, space group $P2_1/n$, a = 9.4833(6), b = 19.2061(13), c = 16.8724(10) Å, β = 93.029(2), V = 3068.8(3) Å^3, Z = 4, D_c = 1.198 g cm^{-3}, μ(Mo-Kα) = 0.823 mm^{-1}, 6498 reflections observed [$I > 2\sigma(I)$], 298 parameters, largest difference peak 0.401 e Å^{-3}. final R, R_w on [$I > 2\sigma(I)$] data were 0.0545, 0.1072, goodness of fit on F^2 = 1.083.

7: $C_{14}H_{28}B_{10}Si_2$, M = 360.64, monoclinic, space group $P2_1/n$, a = 9.6874(4), b = 18.2763(15), c = 12.7310(7) Å, β = 106.587(4)°, V = 2160.2(2) Å^3, Z = 4, D_c = 1.109 g cm^{-3}, μ(Mo-Kα) = 0.160 mm^{-1}, 4239 reflections observed [$I > 2\sigma(I)$], 255 parameters, largest difference peak 0.243 e Å^3, final R, R_w on [$I > 2\sigma(I)$] data were 0.0506, 0.1316, goodness of fit on F^2 = 0.967. CCDC 182/1017.

1 H. K. Sharma and K. H. Pannell, *Chem. Rev.*, 1995, **95**, 1351; H. Yamashita and M. Tanaka, *Bull. Chem. Soc. Jpn.*, 1995, **68**, 403.
2 M. Ishikawa, J. Ohshita and Y. Ito, *Organometallics*, 1986, **5**, 1518; M. Ishikawa, Y. Nomura, E. Tozaki, A. Kunai and J. Ohshita, *J. Organomet. Chem.*, 1990, **399**, 205.
3 M. Ishikawa, S. Okazaki, A. Naka and H. Sakamoto, *Organometallics*, 1992, **11**, 4135.
4 A. Naka, M. Hayashi, S. Okazaki, A. Kunai and M. Ishikawa, *Organometallics*, 1996, **15**, 1101.
5 M. Ishikawa, S. Okazaki, A. Naka, A. Tachibana, S. Kawauchi and T. Yamabe, *Organometallics*, 1995, **14**, 114.
6 M. Ishikawa, A. Naka, S. Okazaki and H. Sakamoto, *Organometallics*, 1993, **12**, 87.
7 J. Ohshita, Y. Isomura and M. Ishikawa, *Organometallics*, 1989, **8**, 2050.
8 M. M. Brezinski, J. Schneider, L. J. Radonovich and K. J. Klabunde, *Inorg. Chem.*, 1989, **28**, 2414.
9 M. Aresta, C. F. Nobile, V. G. Albano, E. Forni, M. Manassero, *J. Chem. Soc., Chem. Commun.*, 1975, 636.

Communication 8/06457A

TiO_2 photocatalytic reduction of bis(2-dipyridyl)disulfide to 2-mercaptopyridine by H_2O: incorporation effect of nanometer-sized Ag particles

Hiroaki Tada,*[a] Kazuaki Teranishi,[b] Yo-ichi Inubushi[b] and Seishiro Ito[b]

[a] *Environmental Science Research Institute, Kinki University, 3-4-1, Kowakae, Higashi-Osaka, 577-8502, Japan. E-mail: h-tada@apsrv.apch.kindai.ac.jp*

[b] *Department of Applied Chemistry, Faculty of Science and Engineering, Kinki University, 3-4-1, Kowakae, Higashi-Osaka, 577-8502, Japan.*

Received (in Exeter, UK) 27th July 1998, Accepted 25th September 1998

A highly endothermic reduction of bis(2-dipyridyl)disulfide to 2-mercaptopyridine by H_2O selectively proceeds using TiO_2 as a photocatalyst, being significantly enhanced upon incorporation of nanometer-sized Ag particles on TiO_2.

Thiols are the most important of the sulfur containing molecules, owing to their usefulness as starting materials for the syntheses of agrochemicals, pharmaceutical products, petrochemicals, *etc.* Several methods for reducing disulfides to the corresponding thiols use reducing agents, including lithium aluminium hydride, sodium hydride, chromium(II), and triphenylphosphine–H_2O.[1] On the other hand, sulfur compounds frequently have a poisoning effect on transition metal catalysts, which was also observed in the reduction of disulfides to thiols by Pd/charcoal catalyst.[2] Poisoning is generally caused by the high adsorption strength of sulfur compounds for the surface active sites of transition metals. This is the first report on TiO_2 photocatalytic reduction of bis(2-dipyridyl)disulfide (RSSR) to 2-mercaptopyridine (RSH) by H_2O. Particular emphasis was placed on the promoting effect with loading of nanometer-sized Ag particles on TiO_2 (Ag/TiO_2).

TiO_2 and Ag/TiO_2[3] absorb light intensely below 385 nm due to the band gap transition. Nanometer-sized Ag particles have a surface plasmon absorption in the wavelength range $300 < \lambda < 500$ nm.[4] In the spectrum of RSSR, there are two absorption bands above 220 nm, at 233 and 281 nm. Light with $\lambda < 300$ nm was cut off by a Pyrex glass filter and both TiO_2 and Ag were excited by irradiation. When the TiO_2 or Ag/TiO_2 suspension containing RSSR [solvent : H_2O–acetonitrile (99 : 1 v/v)] is irradiated under deaerated conditions, the peak intensities of RSSR weaken concurrently with the appearance of new two bands at 272 and 342 nm, which are in complete agreement with the peak positions of authentic RSH. The production of RSH was also confirmed by HPLC and negligible amounts of by-products were detected. A stoichiometric relation with a ratio of [RSH]/[RSSR] of *ca.* 2 was obtained in the conversion of RSSR to RSH, indicating the selective reduction of RSSR to RSH.

Photoillumination of either Ag/TiO_2 or TiO_2 was required to reduce RSSR. This reaction is thus induced not by Ag photoexcitation but by the band gap transition of TiO_2. During the reaction, a gradual decrease in pH of the solution from 5.8 to 4.8 was observed. A small amount of O_2 was detected in a closed reaction system by gas chromatography. This is probably due to its consumption through the successive reduction by the excited electron and/or the reaction with RSSR. The possibility of the oxidation of acetonitrile, which was added to H_2O in order to dissolve RSSR, was excluded, since no reduction occurred upon using dehydrated acetonitrile as the solvent. From these results above, the overall reaction can be written as eqn. (1).

$$\mathrm{RSSR} + \mathrm{H_2O} \xrightarrow[\mathrm{TiO_2\ or\ Ag/TiO_2}]{h\nu(\lambda > 300\ \mathrm{nm})} 2\mathrm{RSH} + 1/2\mathrm{O_2} \quad \Delta H = +207.9\ \mathrm{kJ\,mol^{-1}} \qquad (1)$$

This highly endothermic reaction may also be attractive from the viewpoint of converting light energy to chemical energy.

Fig. 1 shows time course of the RSH production in the presence of TiO_2 (a) and Ag/TiO_2 (b). The rate of the reaction calculated from the concentration of RSH formed after 100 min illumination (v) is increased by a factor of 5.2 with Ag loading. The continuous formation of RSH for more than 150 min suggests high chemical stability of the Ag deposits under the present conditions. The dependence of v on the amount of Ag loaded ($0 < x < 1$ wt.%) was examined. It was shown that v goes through a maximum near $x = 0.24$ wt.%. A possible explanation for the decrease in v at $x > 0.24$ wt.% is light shielding by Ag. This fact again precludes the possibility of Ag photoinduced reduction of RSSR.

Adsorption isotherms of RSSR on TiO_2 (a) and Ag/TiO_2 (b) were measured at 28.5 ± 0.5 °C. From the analyses of the Langmuir plots, the saturated adsorption amount (Γ_s) and the constant indicative of adsorption strength (β) were calculated to be 1.07×10^{-6} mol g^{-1} and 1.27×10^5 dm^3 mol^{-1} for TiO_2, and 1.92×10^{-5} mol g^{-1} and 1.56×10^6 dm^3 mol^{-1} for Ag/TiO_2. Various self-assembled monolayers (SAMs) of surface active organosulfur compounds such as thiols (R′SH), sulfides (R′SR′) and disulfides (R′SSR′) that adsorb on Ag or Au, owing to the specific interaction of R′S–Ag or R′S–Au, have been a topic in the field of surface science.[5] It has been revealed that R′SSR′ chemisorbs on the surface of Ag(111) or Au(111) *via* S–S bond cleavage.[5] The RS group was previously confirmed by other workers to adsorb on Ag stably without S–C bond fission.[6] The areas occupied by one RS group in the Ag/TiO_2 were calculated to be 6.4 nm^2 group^{-1} for TiO_2 and 0.1 nm^2 group^{-1} for Ag. The corresponding areas for the RS group adsorbed in

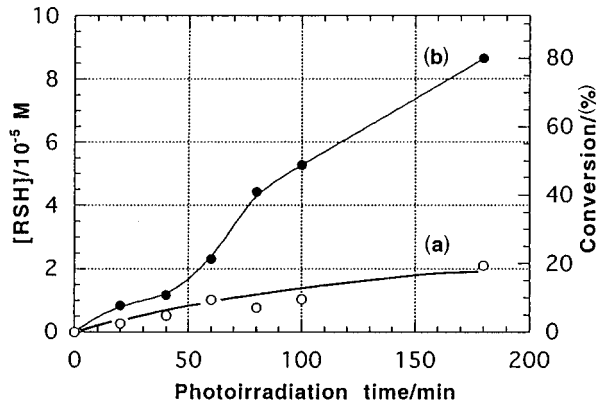

Fig. 1 Time courses of the RSH production in the presence of TiO_2 (a) and Ag/TiO_2 (b). A 5.41×10^{-5} M RSSR solution (50 ml of H_2O–acetonitrile (99 : 1 v/v) was irradiated in the presence of 50 mg TiO_2 or Ag/TiO_2 at 22 ± 1 °C. The light intensity integrated from 320 to 400 nm was 4.62 mW cm^{-2}. Irradiation was commenced after removal of dissolved O_2 by 15 min N_2 bubbling and attainment of adsorption equilibrium by stirring for 1 h in the dark; N_2 bubbling was continued throughout the reaction.

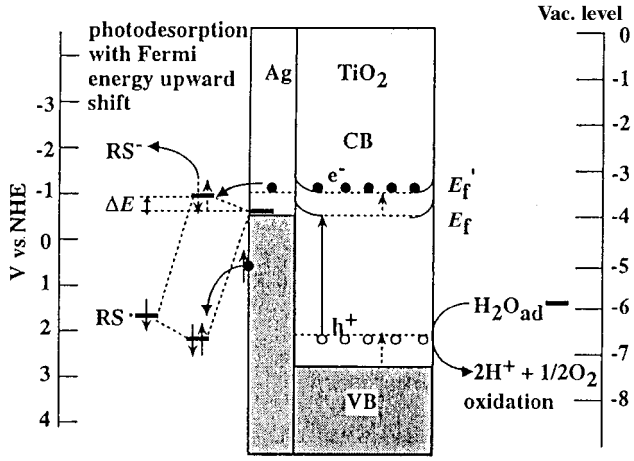

Fig. 2 Energy diagram of the reaction system. The following values were used for its construction: work function of Ag = 4.0 eV;[8] electron energy for the standard hydrogen electrode (SHE) = −4.5 eV *vs.* SHE;[9] flat band potential of TiO_2 at pH 5.5 = −0.45 V from the vacuum level;[10] band gap energy of TiO_2 = 3.2 eV;[10] oxidation potential of H_2O at pH 0 = 1.23 V *vs.* SHE;[10] HOMO of RS· radical = −6.4 eV (this value was obtained from PM3 MO calculations).

the closest packing states were estimated to be *ca.* 0.16 nm^2 $group^{-1}$ for the flat lying orientation and 0.1 nm^2 $group^{-1}$ for the vertical orientation using the PM3 optimized molecular structure. Clearly, the RS groups adsorb on the surface of nanometer-sized Ag particles in a close packed state analogous to those in SAMs, while most of the TiO_2 surface is directly in contact with H_2O.

A plausible reaction mechanism is summarized as follows. In the initial stage of the reaction, selective RSSR adsorption on the surface of Ag accompanied by S–S bond cleavage takes place. Electron–hole pairs are generated by the band gap excitation of TiO_2. Most of the pairs are lost by recombination but a portion of the electrons excited to the conduction band (CB) flow into Ag, while the holes are left in the valence band (VB) of TiO_2. The Schottky barrier at the Ag/TiO_2 interface would assist the charge separation. The hole has enough potential to oxidize H_2O to yield H^+ and O_2. The coupling of H^+ and RS^-, driven to desorb reductively by the excited electron, forms RSH. A similar reductive desorption of *n*-alkanethiols from an Au electrode has been reported by Widrig *et al.*[7] In the TiO_2 system, the reduction of RSSR is thought to proceed in a similar manner as in the Ag/TiO_2 system; however, the alternative reduction site would be surface Ti^{3+} ions. Three factors for reaction enhancement effect of the Ag loading can be proposed. The first is enhanced adsorption of RSSR, the second is the separation of reduction (Ag) and oxidation sites (TiO_2) and the third is that the oxidant (RSSR) and the reductant (H_2O) selectively adsorb on the reduction and oxidation sites, respectively, resulting in a highly selective reaction.

Since the turnover number is calculated to be *ca.* 6.7×10^{14} molecules cm^{-2}, this reaction is qualified to be catalytic. The strangest and most intriguing question raised by this reaction is why RS adsorbed on Ag desorbs from the surface upon irradiation despite its strong adsorption strength as evidenced by the large β value of 1.56×10^6 dm^3 mol^{-1} for Ag/TiO_2. Fig. 2 depicts the energy diagram of the reaction system. A couple of bonding and antibonding orbitals are formed as the result of the interaction between the highest occupied molecular orbital (HOMO) of RS·[11] and an unoccupied molecular orbital (UMO) above the Fermi energy (E_f) of Ag.[12] In the ground state, the bonding orbital is occupied by two electrons, each of which originally belongs to RS· and Ag, respectively, leading to a strong interfacial RS–Ag bond. The contribution of the HOMO of RS· to the bonding orbital is much greater than that of the UMO of Ag. Thus the interfacial bond can approximately be described as RS^-–Ag^+, which is confirmed by XPS measurements of SAMs.[13] On the other hand, in the photoexcitation state, E_f is raised by several hundreds of meV (E_f'),[14] which corresponds to the bonding energy of R′SSR′ on Au (*ca.* 0.5 eV per R′S group).[15] If E_f' exceeds the energy of the interfacial antibonding orbital, it would be occupied by the two electrons from Ag. The destabilizing energy will enable the desorption of RS^- upon illumination, and further the photocatalytic cycle in this reaction. We refer to this as photodesorption with an upward shift of the Fermi energy. Essentially, the electrochemical reductive desorption of *n*-alkanethiol monolayers from Ag and Au electrodes can be interpreted as desorption with an upward shift of the Fermi energy induced by the application of external electric voltage. Widrig *et al.* explained the fact that the reductive desorption from Ag as compared to Au occurs at 0.30 V more negative potential due to the differences in the point of zero charge for the two metals.[7] According to our theory, this can alternatively be attributed to the differences in the work function (Ag = 4.0 ± 0.15 eV, Au = 5.1 ± 0.1 eV),[8] assuming comparable interaction energy (ΔE in Fig. 2).

In conclusion, it has been demonstrated that a highly endothermic reduction of RSSR to RSH by H_2O proceeds selectively and efficiently using Ag/TiO_2 as a photocatalyst. The essential reaction mechanism is presented on the basis of the adsorption and kinetic data. Photodesorption with an upward shift of the Fermi energy is proposed as a key process in the catalytic cycle. This action of Ag/TiO_2 may open up a new field of photocatalytic reactions of heterocompounds, whose thermal catalytic reactions using transition metal catalysts are usually not straightforward due to their poisoning effect.

Support of this work by the ESRI (Kinki University) under the artificial photosynthesis program is gratefully acknowledged.

Notes and references

1 S. Oae, *Organic Chemistry of Sulfur*, Plenum, New York, 1977.
2 T. P. Johnston and R. D. Elliott, *J. Org. Chem.*, 1967, **32**, 2344.
3 TiO_2 particles (anatase, BET surface area = 8.1 m^2 g^{-1}, Ishihara Sangyo Co.) were used. Ag/TiO_2 was prepared according to S.-i. Nishimoto, B. Ohtani, H. Kajiwara and T. Kagiya, *J. Chem. Soc., Faraday Trans. 1*, 1983, **79**, 2685. As particles of < 5 nm were observed to be dispersed on TiO_2 by transmission electron microscopy.
4 T. Ung, M. Giersig, D. Dunstan and P. Mulvaney, *Langmuir*, 1997, **13**, 1773.
5 A. Ulman, *Chem. Rev.*, 1996, **96**, 1533 and references therein.
6 J. Y. Gui, F. Lu, D. A. Stern and A. T. Hubbard, *J. Electroanal. Chem.*, 1990, **292**, 245.
7 C. A. Widrig, C. Chung and M. D. Porter, *J. Electroanal. Chem.*, 1991, **310**, 335.
8 D. E. Eastman, *Phys. Rev. B2*, 1970, 1.
9 F. Lohaman, *Z. Naturforsch., Teil A*, 1967, **22**, 843.
10 M. Graetzel, in *Energy Resources through Photochemistry and Catalysis*, Academic Press, New York, 1983.
11 For R′SH, two types of dissociative adsorption on coinage metals (M) are proposed [eqns. (2) and (3)] (P. E. Laibinis, G. Whitesides, D. L. Allara, Y.-T. Tao, A. N. Parikh and R. G. Nuzzo, *J. Am. Chem. Soc.*, 1991, **113**, 7152).

$$R'SH + M^0 \rightarrow R'S^-–M^I + 1/2\ H_2 \quad (2)$$

$$R'SH + M^I \rightarrow R'S^-–M^I + H^+ \quad (3)$$

In the case of RSSR, homolytic dissociated adosrption appears to be plausible [eqn. (4)].

$$RSSR + 2M^0 \rightarrow 2R'S^-–M^I \quad (4)$$

12 R. Hoffmann, *A Chemist's View of Bonding in Extended Structures*, VCH, New York, 1993.
13 G. K. Jennings and P. E. Labinis, *J. Am. Chem. Soc.*, 1997, **119**, 5208.
14 T. Sakata, T. Kawai and K. Hashimoto, *Chem. Phys. Lett.*, 1982, **88**, 50.
15 J. B. Schlenoff, M. Li and H. Ly, *J. Am. Chem. Soc.*, 1995, **117**, 12 528.

Communication 8/05820B

The first lanthanide-containing helicates self-assembled in water

Mourad Elhabiri,[a] Rosario Scopelliti,[a] Jean-Claude G. Bünzli*[a] and Claude Piguet[b]

[a] *Institute of Inorganic and Analytical Chemistry, BCH, University of Lausanne, CH-1015-Lausanne, Switzerland. E-mail: jean-claude.bunzli@icma.unil.ch*

[b] *Department of Inorganic, Analytical and Applied Chemistry, Sciences II, University of Geneva, CH-1211 Geneva-4, Switzerland*

Received (in Cambridge, UK) 28th August 1998, Accepted 25th September 1998

Triple-stranded bimetallic helicates $[Ln_2(L^C - 2H)_3]$ form in water by a strict self-assembly process and are shown to be thermodynamically very stable (log β_{23} > 26) and luminescent (Ln = Eu).

To cope with the demand for efficient light-converting devices arising from the development of time-resolved fluoroimmunoassays, signalling and luminescent labelling technologies,[1–4] including bimetallic probes which provide two probe signals in one stain, co-ordination chemists have developed several strategies. Among these, self-assembly processes[5] based on the induced fit concept[6] have proved efficient in designing lanthanide building blocks with predetermined structural and physicochemical properties.[7] The ditopic ligand L^A was

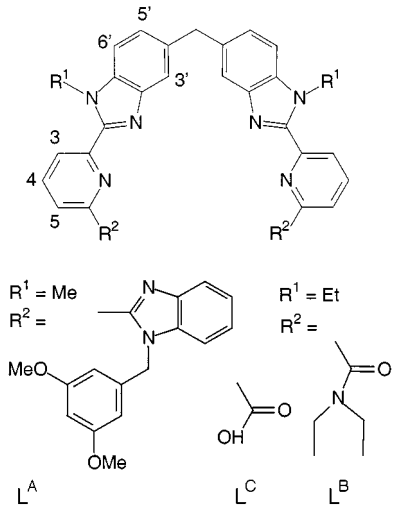

L^A L^C L^B

designed to produce the cationic triple-stranded helicate $[Ln_2(L^A)_3]^{6+}$ by strict self-assembly and the resulting complexes exhibit a large stability in MeCN.[8] The $[Eu_2(L^A)_3]^{6+}$ helicate is, however, only weakly luminescent and is water sensitive, two severe handicaps for its use as a probe. A substantial improvement was achieved upon replacing the terminal benzimidazole groups in L^A by carboxamide binding units in L^B, with a large increase in the Eu-centred luminescence and a good resistance of the triple-stranded helicate $[Eu_2(L^B)_3]^{6+}$ toward hydrolysis in MeCN containing up to 2.5 M water.[9] However, biomedical applications require water soluble probes and, to our knowledge, self-assembly of bimetallic lanthanide-containing edifices in water have only been reported for $[Ln_2L_2]$ supramolecular boxes where L is 2,6-bis[*N*,*N*-bis(carboxymethyl)aminomethyl]-4-benzoylphenol and in which the Ln^{III} cations are linked to each other by an aqua bridge inside the cage.[10] In order to test whether the energetic drive leading to the formation of bimetallic helicates in water is able to compensate the large dehydration enthalpy of the lanthanide aquo-ions, we have introduced two carboxylic acid functions in L^C, which led to the quantitative formation of neutral $[Ln_2(L^C - 2H)_3]$ triple-stranded helicates. These new compounds are thermodynamically highly stable and luminescent (Ln = Eu) and they are the first examples of such structures self-assembled in water.

Ligand L^C was obtained from the hydrolysis of L^B† and the pK_a of the carboxylic groups were determined by potentiometry to be 4.15 ± 0.05 and 7.05 ± 0.05 (0.1 M Et_4NClO_4). ^1H NMR titration of L^C with $Eu(ClO_4)_3 \cdot xH_2O$, in D_2O at pD = 12.74, points to the exclusive formation of a 2 : 3 species (break at $[Eu]/[L^C]$ = 0.64, no hydroxide precipitation before the break point). This speciation is confirmed by spectrophotometric data obtained at pH 7.2 and 298 K in H_2O ($[L^C] = 1.05 \times 10^{-5}$ M, $0 < [Ln] < 1.6 \times 10^{-5}$ M), which can be fitted to eqn. (1) for Ln = La (log β_{23} = 30 ± 1), Eu (26.1 ± 0.4) and Lu (27.3 ± 0.6).‡ Titrations with solutions in MeOH–H_2O 98 : 2 (v/v) yield similar log β_{23} values, 29.6 ± 0.8 (La), 27.8 ± 0.6 (Eu) and 25.9 ± 0.3 (Lu), but data for Eu and Lu have to be fitted to eqns. (1) and (2) with log β_{22} = 21 ± 0.6 (Eu) and 19.1 ± 0.5 (Lu). As a

$$2\ Ln^{3+} + 3\ (L^C - 2H)^{2-} \rightleftharpoons [Ln_2(L^C - 2H)_3] \quad \log \beta_{23} \qquad (1)$$

$$2\ Ln^{3+} + 2\ (L^C - 2H)^{2-} \rightleftharpoons [Ln_2(L^C - 2H)_2]^{2+} \quad \log \beta_{22} \qquad (2)$$

comparison, helicates formed by L^B in aprotic MeCN display log β_{23} values in the range 24–25 and log β_{22} values in the range 19–20.[9] The large thermodynamic stability of the $[Ln_2(L^C - 2H)_3]$ helicates in water is further demonstrated by the partial decomplexation observed in the ^1H NMR spectrum of $[Eu_2(L^C - 2H)_3]$ 3.2×10^{-3} M in D_2O upon adding a 20-fold excess of H_2EDTA^{2-}.

Solid complexes have been isolated for Ln = La, Pr, Nd, Eu, Gd, Tb, Tm, Yb, Lu and crystals suitable for crystallographic investigation were obtained for Eu, Tb and Yb.§ The structure of the Eu-helicate is presented in Fig. 1.¶ The asymmetric unit contains two slightly different neutral bimetallic helicates without imposed crystallographic symmetry but with pseudo-D_3 symmetry, as well as 41 water molecules. Molecule A has an Eu···Eu separation of 8.807(3) Å and features two nine-coordinate Eu^{III} ions with marginally different environments [mean Eu–N distances 2.59(3)/2.62(4) Å, mean Eu–O distances 2.40(2)/2.39(2) Å, ionic radius 1.12(3)/1.13(5) Å]. Molecule B displays a larger Eu···Eu separation, 9.044(3) Å, and co-ordination to carboxylic groups is less symmetrical [mean Eu–N distances 2.60(3)/2.59(5) Å, mean Eu–O distances

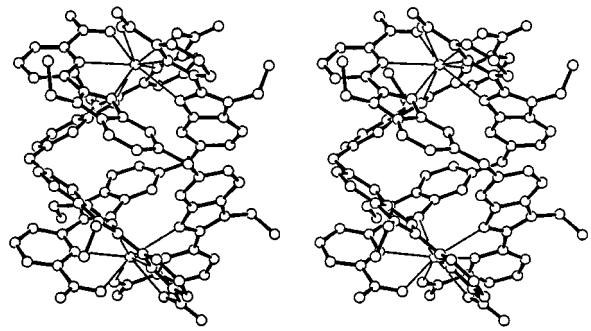

Fig. 1 ORTEP III stereoview of molecule A $[Eu_2(L^C - 2H)_3] \cdot 20.5H_2O$, perpendicular to the pseudo-C_3 axis (upper ion: Eu1A, lower ion: Eu2A).

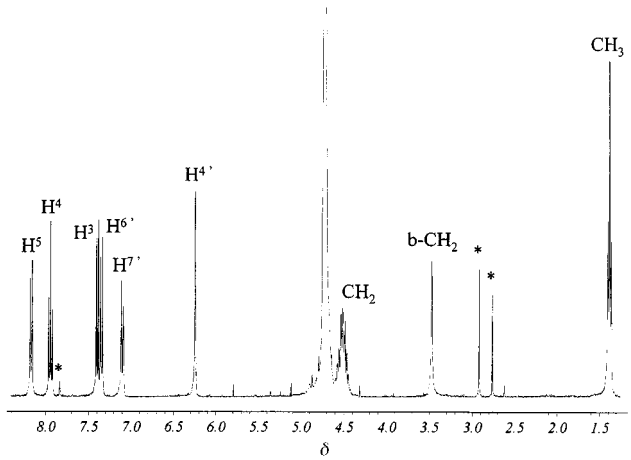

Fig. 2 ^{1}H NMR spectrum of 10^{-4} M $[La_2)L^C - 2H)_3]$ in D_2O at pD = 7 and 303 K, with assignment (b-CH_2: bridging methylene; DMF as internal reference*).

2.40(6)/2.41(4) Å, ionic radius 1.12(5)/1.12(4) Å]. As the pH of the mother liquor is *ca.* 7.5–8.2, a partial protonation of the carboxylic groups associated with the presence of hydroxide counter-anions in the asymmetric unit[11] is not likely especially that the mean C–O distances for coordinated (1.27 Å, A and B) and non-coordinated (1.23 Å, A and 1.24 Å, B) O atoms closely match those found in the tris(dipicolinate)anion.[12] Analysis of the coordination polyhedra[13] of the four different metal ions reveals slightly distorted tricapped trigonal prisms. The facial planes of the two distal tripods defined by the three coordinated O atoms from the carboxylates and the three N atoms from the benzimidazole moieties are almost parallel with mean dihedral angles of 3.4° (A) and 6.8° (B) and the interligand ω_i angles[13,14] are in the ranges 11.1–13.6° (A) and 8.1–14.9° (B) (ideal trigonal prism: 0°). The distances between these facial planes, 3.16 Å (A) and 3.23 Å (B), are substantially shorter than that found in the monometallic tris(dipicolinate) Eu-complex (3.44 Å),[12] pointing to a significant compression along the pseudo C_3 axis. The helical twist of the ligand strands (pitch: 23.7 Å, A and 24.4 Å, B) is achieved through rotation about the methylene C–C bond with interplanar angles between the benzimidazole units in the range 66.5–74.6° (A) and 62.4–72.7° (B). The entire structure is held together by an extensive network of water molecules. Preliminary results on the structure of the Tb and Yb helicates reveal an isotypic series of complexes with Ln^{III} environments comparable to those found for Eu^{III}.

The triple helicate structure is maintained in solution, as demonstrated by the observed ^{1}H NMR spectra in D_2O, which imply the formation of a single, inert and compact complex with D_3 symmetry (Fig. 2).[8,9] A preliminary analysis for the complete Ln series, including separation of the contact and dipolar contributions to the chemical shifts points to an isostructural set of helicates. The $[Ln_2(L^C - 2H)_3]$ complexes display interesting photophysical properties. The quantum yield of the ligand-centred luminescence with respect to quinine sulfate (0.044–0.047 at pH 6.8–12.1 in H_2O) increases 10-fold in the La^{III} and Lu^{III} helicates (0.52 at pH 6.8), while it decreases by a factor 2.5 in the Gd^{III} helicate (0.017 at pH 6.7). The $^1\pi\pi^*$ luminescence disappears in the Eu^{III} and Tb^{III} helicates and the characteristic f–f emission bands are observed. The emission spectrum of the $[Eu_2(L^C - 2H)_3](aq)$ is similar to the solid state spectrum, and the $Eu(^5D_0)$ lifetime of 10^{-8} M solutions amounts to 2.5 ms (H_2O) and 4.6 ms (D_2O). This substantiates the conclusion based on the NMR spectra regarding the solution structure of the helicates and proves that no OH oscillator is interacting directly with the metal ion, the lengthening of the lifetime in D_2O, formally corresponding to an inner-sphere interaction with 0.2 water molecule,[4] can be assigned to second sphere effects.[15] The quantum yield Q^{Eu}_{rel} of the metal-centred luminescence has been measured for solutions in H_2O (pH 7.0) with respect to 10^{-3} M $[Eu(tpy)_3](ClO_4)_3$ in MeCN[9] and is equal to 1.00 (absolute yield: 1.3%), leading to a detection limit of 10^{-9}–10^{-10} M in H_2O and 10^{-10}–10^{-11} M in D_2O. Although Tb^{III} appears to be effectively sensitized by L^C, Q^{Tb}_{rel} is low (0.038) due to an efficient back transfer process which was evidenced by measuring the $Tb(^5D_4)$ lifetime of the helicate between 77 K (2.1 ms) and 270 K (0.05 ms), and which arises from a too close proximity of the $L^C(^3\pi\pi^*)$ and $Tb(^5D_4)$ levels.

In conclusion, strict self-assembly of L^C with Ln^{III} ions in water leads to the formation of a new class of lanthanide carboxylates. The resulting triple-stranded helicates are thermodynamically highly stable and luminescent (Ln = Eu) and the structural control achieved for these architectures is similar to the one provided by pre-organized receptors.

We thank the Swiss National Science Foundation for supporting grants, the Werner Foundation for a grant to C. P. and the Herbette Foundation (Lausanne) for spectroscopic equipment.

Notes and references

†L^C: ^{1}H NMR [$(CD_3)_2SO$]; δ 1.38 (t, *J* 6.59 Hz, ethyl CH_3), 4.20 (s, bridging CH_2), 4.87 (q, *J* 6.55 Hz, ethyl CH_2), 8.10 (d, *J* 6.12 Hz, H^3 or H^5), 8.46 (dd, *J* 7.45/1.76 Hz, H^3 or H^5), 8.14 (t, *J* 7.45 Hz, H^4), 7.64 (s, $H^{4'}$), 7.26 (d, *J* 8.35 Hz, $H^{6'}$), 7.58 (d, *J* 8.35 Hz, $H^{7'}$). ^{13}C NMR [$(CD_3)_2SO$, HSQC]; δ 61.86 (bridging CH_2), 60.54 (CH_2, ethyl), 34.76 (CH_3, ethyl), 158.95 (C^3 or C^5), 144.36 (C^3 or C^5), 145.98 (C^4), 138.24 ($C^{4'}$), 131.10 ($C^{6'}$), 145.12 ($C^{7'}$). ES-MS: *m/z* 547.5 (M + H^+), 588.8 (M + H^+ + MeCN), 607.4 (M + H^+ + MeCN + H_2O). IR (KBr): 1718 (s, C=O), 2931, 2966 (m, aliphatic C–H), 3030, 3066 (w, aromatic C–H), 3421 cm^{-1} (OH). Elemental analysis for $C_{31}H_{26}N_6O_4 \cdot 1.5H_2O$. Calc: C, 64.91; H, 5.10; N, 14.65. Found: C, 65.09; H, 5.15; N 14.70%.

‡ These data correspond to pLn values ($[Ln^{III}]_t = 10^{-6}$ M, $[L^C]_t = 10^{-5}$ M. F. Vögtle, *Supramolecular Chemistry*, Wiley, Chichester, 1991, pp. 92–95) of 11.55 (La), 9.60 (Eu) and 10.19 (Lu).

§ $[Eu(L^C - 2H)_3] \cdot 9H_2O$. Calc. C, 53.36; H, 4.32; N, 11.30. Found: C, 53.20; H, 4.32; N, 12.01%.

¶ $C_{93}H_{72}N_{18}O_{12}Eu_2 \cdot 20.5H_2O$, *M* = 2306.93, monoclinic, space group $P2_1/c$, *a* = 24.808(10), *b* = 36.285(10), *c* = 23.701(10) Å, β = 110.30(3)°, *U* = 20 009(13) Å^3, *Z* = 8, μ = 1.333 mm^{-1}, *T* = 185 K, 93 431 reflections measured, 28 393 independent reflections, 2630 parameters, R_F = 0.0609, wR_2 [$I > 2\sigma(I)$] = 0.1402. CCDC 182/1036.

1 A. P. De Silva, H. Q. N. Gunaratne, T. Gunnlaugsson, A. J. M. Huxley, C. P. McCoy, J. T. Rademacher and T. E. Rice, *Chem. Rev.*, 1997, **97**, 1515.
2 I. Hemmilä, T. Stahlberg and P. Mottram, *Bioanalytical Applications of Labelling Technologies*, Wallac Oy; Turku, 1995.
3 C. H. Evans, *Biochemistry of the Lanthanides*, Plenum, New York, 1990.
4 *Lanthanide Probes in Life, Chemical and Earth Sciences: Theory and Practice*, eds. J.-C. G. Bünzli and G. R. Choppin, Elsevier Science Publ. B. V., Amsterdam, 1989.
5 S. J. Langford and J. F. Stoddart, *Pure Appl. Chem.*, 1996, **68**, 1255.
6 D. E. Koshland Jr., *Angew. Chem. Int. Ed. Engl.*, 1994, **33**, 2375.
7 J.-C. G. Bünzli, S. Petoud, C. Piguet and F. Renaud, *J. Alloys Compds.*, 1997, **249**, 14.
8 C. Piguet, J.-C. G. Bünzli, G. Bernardinelli, G. Hopfgartner and A. F. Williams, *J. Am. Chem. Soc.*, 1993, **115**, 8197.
9 N. Martin, J.-C. G. Bünzli, V. McKee, C. Piguet and G. Hopfgartner, *Inorg. Chem.*, 1998, **37**, 577.
10 M. Latva, P. Makinen, S. Kulmala and K. Haapakka, *J. Chem. Soc., Faraday Trans.*, 1996, **92**, 3321.
11 R. Baggio, M. T. Garland and M. Perec, *Inorg. Chem.*, 1997, **36**, 950.
12 P. A. Brayshaw, J.-C. G. Bünzli, P. Froidevaux, J. M. Harrowfield, Y. Kim and A. N. Sobolev, *Inorg. Chem.*, 1995, **34**, 2068.
13 C. Piguet, J.-C. G. Bünzli, G. Bernardinelli, C. G. Bochet and P. Froidevaux, *J. Chem. Soc., Dalton Trans.*, 1995, 83.
14 F. Renaud, C. Piguet, G. Bernardinelli, J.-C. G. Bünzli and G. Hopfgartner, *Chem. Eur. J.*, 1997, **3**, 1646.
15 R. S. Dickins, D. Parker, A. S. de Sousa and J. A. G. Williams, *Chem. Commun.*, 1996, 697.

Communication 8/06730I

Efficient copper (II)-mediated nuclease activity of *ortho*-quinacridines

Olivier Baudoin, Marie-Paule Teulade-Fichou, Jean-Pierre Vigneron and Jean-Marie Lehn*

Laboratoire de Chimie des Interactions Moléculaires (CNRS UPR 285), Collège de France, 11 place Marcelin Berthelot, 75005 Paris, France. E-mail: lehn@cdf.in2p3.fr

Received (in Basel, Switzerland) 3rd August 1998, Accepted 25th September 1998

The *ortho*-quinacridine compounds OQ_1 and OQ_2 bind strongly to double stranded DNA and effect efficient cleavage in the presence of Cu^{2+} and in the absence of reducing agent; their activity increases further in the presence of hydrogen peroxide.

Artificial metallonucleases have proven to be efficient tools for the footprinting and sequence-specific targeting of nucleic acids.[1] They are composed of a transition or lanthanide metal ion and of a ligand which plays two major roles: it modulates the reactivity of the metal and interacts with the nucleic acid, delivering the reactive metallic species in the vicinity of the sensitive functionnalities of the biopolymer. Among these compounds, copper(II) complexes were found to cleave DNA, most of them in an oxidative manner.[1–3] They usually require high concentrations of the complex and of an external reducing agent (such as dithiothreitol, DTT) to form *in situ* a reactive copper(I) species, two features which may limit their scope for biological applications at the cellular level. A recent article reports the cleavage of double stranded (ds) plasmid DNA by low concentrations of a tambjamine–copper complex; in this case the ligand is acting as an internal reducing agent.[4]

These considerations prompt us to report on results obtained with water-soluble dibenzo[*b*,*j*]phenanthroline (*i.e.* quinacridine) ligands, fused heteroaromatic pentacycles that display a crescent-shaped structure and were designed to present a large overlap area with pairs or triplets of nucleobases. We recently described their synthesis[5] and their ability to stabilise DNA triple helices through putative intercalation.[6] Among them, the *ortho*-quinacridines (OQ) OQ_1 and OQ_2 possess the *ortho*-phenanthroline (OP) substructure, which forms stable copper complexes. Indeed $Cu(OP)_2^{2+}$ is well known for its ability to cleave nucleic acids oxidatively in the presence of a reducing agent, *via* the formation of Cu(I) and subsequently of copper–oxo species.[1,7] At pH 6, OQ_1 and OQ_2 bear respectively two and

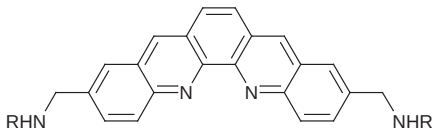

OQ_1, R = $CH_2CH_2CH_3$
OQ_2, R = $(CH_2)_3N(CH_3)_2$

four positive charges located on the ammonium groups of the two side chains.† The ability of OQ to bind to ds DNA was monitored by thermal denaturation experiments and by fluorescence quenching assay[8] (Table 1).

Significant stabilisation of poly(dA.dT)–poly(dA.dT) and efficient displacement of ethidium bromide were observed, indicating that OQ_1 and OQ_2 bind strongly to DNA. OQ_2 was found to be a better DNA ligand than OQ_1 due to its additional positive charges; in addition it seems to have an affinity for DNA comparable to that of the reference compound Hoechst 33258 (stability constant *ca.* 10^7 dm^3 mol^{-1}).[9] Furthermore, the observation of fluorescence contact energy transfer[10] from DNA nucleobases to both dyes gave evidence that intercalation is occurring (data not shown).

Table 1 Interaction of OQ_1 and OQ_2 with Poly(dA.dT)–Poly(dA.dT)

	Ethidium	H33258	OQ_1	OQ_2
ΔT_m[a]/°C	+12	+27	+15	+25.5
C_{50}[b]/μM	—	0.082	0.65	0.081

[a] Variation of the melting temperature of DNA (40 μM in phosphate units) upon addition of the various ligands (6 μM), accuracy ± 1 °C, determined in 30 mM cacodylate buffer (pH 6.0)–10 mM NaCl; the T_m of DNA alone in these conditions was 53.5 °C. [b] Concentration of drug necessary to displace 50% of the DNA-bound ethidium bromide; concentration of DNA 1 μM (in phosphate units) and ethidium 1.26 μM in 30 mM cacodylate buffer (pH 6.0)–10 mM NaCl; the fluorescence emission of ethidium at 595 nm (λ_{exc} = 546 nm) was used to follow this titration.[8]

The ability of OQ to cleave ds plasmid DNA in the presence of Cu^{2+} was then examined (Fig. 1). A slow cleavage was observed (lanes 4–8), with conversion of supercoiled form I to nicked form II at 37 °C over 4 h, in the absence of any reducing agent. In the presence of 100 μM H_2O_2, the nuclease activity of OQ_1–Cu^{2+} and OQ_2–Cu^{2+} was greatly enhanced: Fig. 2 shows a comparison of the cleavage of plasmid DNA (0.4 μg) with low concentrations of OQ or OP (12 μM, [DNA]/[drug] = 10)§ and Cu^{2+} (12 μM), after 5 min incubation at 37 °C, in the absence or presence of 1 mM DTT. In these conditions, all controls were negative including OQ/Cu^{2+} (not shown) and Cu^{2+}/H_2O_2 (lanes 2–3). In the absence of DTT, OQ_1–Cu^{2+} (lane 4) and OQ_2–Cu^{2+} (lane 6) convert effectively form I to forms II (nicked) and III

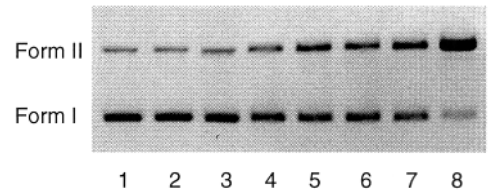

Fig. 1 Cleavage of pUC18 plasmid DNA by OQ_2 in the presence of Cu^{2+}. DNA (0.4 μg) was incubated with OQ_2 in the presence of $CuSO_4$ in 50 mM cacodylate buffer (pH 6.0, total volume 10 μl) at 37 °C and different time. Lane 1, DNA control, 4 h; lane 2, Cu^{2+} 160 μM, 4 h; lane 3, OQ_2 24 μM, 4 h; lanes 4–8, OQ_2 24 μM + Cu^{2+} 160 μM, 15-30-60-120-240 min. OQ_1 exhibited a similar cleavage pattern (data not shown).‡

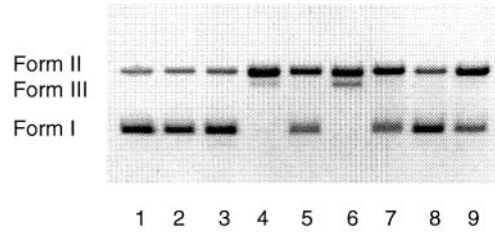

Fig. 2 Cleavage of pUC18 DNA by OQ and OP in the presence of Cu^{2+} and H_2O_2. DNA (0.4 μg) was incubated with the dye in the presence of $CuSO_4$ and H_2O_2 for 5 min at 37 °C in the same buffer as in Fig. 1. Lane 1, DNA control; lane 2, Cu^{2+} 12 μM + H_2O_2 100 μM; lane 3, lane 2 + DTT 1 mM; lane 4, lane 2 + OQ_1 12 μM; lane 5, lane 3 + OQ_1 12 μM; lane 6, lane 2 + OQ_2 12 μM; lane 7, lane 3 + OQ_2 12 μM; lane 8, lane 2 + OP 12 μM; lane 9, lane 3 + OP 12 μM.‡

Table 2 Variation of the absorption maxima of OQ_2 upon addition of Cu^{2+} and H_2O_2[a]

	λ_1	ε_1	λ_2	ε_2	λ_3	ε_3
OQ_2	317	36700	325	34800	—	—
$(OQ_2)Cu^{2+}$	317[b]	29700	328	35400	576	200
$(OQ_2)Cu^{2+}$ + H_2O_2	317[b]	26900	326	29600	577	1400

[a] Wavelength (λ) in nm and molar absorption coefficients (ε) in $dm^3\ mol^{-1}\ cm^{-1}$. Concentration of OQ_2 12 μM in 50 mM cacodylate buffer (pH 6.0); added $CuSO_4$ and H_2O_2 120 μM and 100 μM, respectively. Controls with Cu^{2+} alone (120 μM) and in the presence of H_2O_2 (100 μM) did not show any significant absorption. [b] Present as a shoulder in the major band.

(linear) whereas, as expected, the $(OP)_2Cu^{2+}$ complex (lane 8) does not do so. OQ_2–Cu^{2+} seems more efficient than OQ_1–Cu^{2+} in accordance with the binding affinity of the ligands alone. In presence of DTT, which reduces *in situ* Cu^{2+} to Cu^+, the OP complex becomes active (compare lanes 8 and 9) whereas the activity of the OQ complexes is decreased (lanes 4 to 5 and 6 to 7) though remaining comparable to that of the OP complex. Increasing the time of incubation with OQ_1–Cu^{2+} and OQ_2–Cu^{2+} leads to additional scissions, with increasing percentage of linear form III and appearance of smearing bands.

The efficiency of the DNA cleavage by OQ_2 is dependent on the concentration of copper, with a maximum around 5 equiv. of metal per ligand. A UV titration of OQ_2 by Cu^{2+} indicated the formation of a 1 : 1 complex with a stability constant of 4.7 (in log units). The plateau of the titration is reached at 5 equiv. of Cu^{2+}, in accordance with the copper dependence of the DNA cleavage. The steric hindrance in the vicinity of the two heterocyclic nitrogens prevents a square-planar 1 : 2 Cu^{2+} coordination with OQ_2. Thus a 1 : 1 complex is observed, $(OQ_2)Cu^{2+}$, which is likely the active species responsible for the DNA cleavage. Its relatively weak stability might be ascribed to the effect of the positively charged ammonium linkers of the ligand, which also decreases the basicity of the lone pairs of the heterocyclic nitrogens.[5] By contrast, OP forms a stable square-planar $(OP)_2Cu^{2+}$ complex[11] that is itself unable to cleave DNA. These differences in metal coordination in the $(OQ_2)Cu^{2+}$ and $(OP)_2Cu^{2+}$ complexes might explain the unusual reactivity observed for the former toward DNA. Upon addition of a reducing agent like DTT, the reactive tetrahedral $(OP)_2Cu^+$ is formed *in situ* with subsequent oxidative scission of DNA. The reduced cleavage observed with OQ in these same conditions might be ascribed to the formation of the tetrahedral $(OQ_2)_2Cu^+$ species, which nevertheless retains an activity comparable to that of $(OP)_2Cu^+$ itself.

Table 2 displays the features of the UV spectra of OQ_2 alone and of $(OQ_2)Cu^{2+}$ in the absence and presence of H_2O_2. Upon addition of Cu^{2+} to a solution of OQ_2, a modification of the spectrum is observed with a decrease of the band at 317 nm concomitant to the increase of the band at 325 nm (slightly red-shifted), both bands corresponding to π–π* transitions of the quinacridine moiety; a new band ascribable to d–d transitions of the copper is also emerging at 576 nm. When H_2O_2 is added, a hypochromism of the major band of the ligand (325 nm) is noted along with a hyperchromism of the band at 576 nm, which indicates a strong modification of the metal coordination.

The cleavage of DNA by $(OQ)Cu^{2+}$ complexes and H_2O_2 was inhibited by various radical scavengers: ethanol, thiourea ($HO^\bullet$ scavengers), Tiron ($O_2^{\bullet-}$ scavenger), KI and catalase (H_2O_2 scavengers). These results suggest that the scission mechanism involves the formation of a coordinated peroxide species, with subsequent production of reactive oxygen species that induce oxidative DNA strand scissions. The cleavage in the absence of H_2O_2 (*i.e.* Fig. 1) was not inhibited by reasonable amounts of such scavengers, which does not allow to rule out the intervention of reactive oxygen species.

In conclusion, the $(OQ)Cu^{2+}$ complexes are able to perform an efficient oxidative cleavage of DNA in absence of reducing agent. These new artificial metallonucleases might be interesting lead compounds for the scission of various DNA targets. Further investigations on the reaction mechanism as well as on the structure and sequence selectivity of these reagents are currently underway.

We would like to thank Dr Mireille Fauquet for providing us with generous amounts of pUC18 plasmid and Dr David M. Perrin for helpful discussions.

Notes and references

† All experiments were conducted at pH 6 (cacodylate buffer) where OQ_1 and OQ_2 exist respectively as biprotonated and tetraprotonated species.[5]
‡ All experiments were conducted in the dark in order to avoid photocleavage of DNA by the dyes. Reactions were quenched by adding 1 M KCN and analysed by electrophoresis on 1% agarose gels in 1 M Tris-acetate buffer (80 V, 1 h). The gels were photographed on a UV transilluminator after staining with ethidium bromide.
§ [DNA] in phosphate units.

1 D. S. Sigman, *Acc. Chem. Res.*, 1986, **19**, 180; D. S. Sigman, A. Mazumder and D. M. Perrin, *Chem. Rev.*, 1993, **93**, 2295; G. Pratviel, J. Bernadou and B. Meunier, *Angew. Chem., Int. Ed. Engl.* 1995, **34**, 746; W. K. Pogozelski and T. D. Tullius, *Chem. Rev.* 1998, **98**, 1089; C. J. Burrows and J. G. Muller, *Chem. Rev.* 1998, **98**, 1109.
2 S. Hashimoto, R. Yamashita and Y. Nakamura, *Chem. Lett.*, 1992, 1639; E. L. Hegg and J. N. Burstyn, *Inorg. Chem.*, 1996, **35**, 7474; T. Itoh, H. Hisada, T. Sumiya, M. Hosono, Y. Usui and Y. Fujii, *Chem. Commun.*, 1997, 677.
3 L. A. Basile and J. K. Barton, *J. Am. Chem. Soc.*, 1987, **109**, 7548; G. M. Ehrenfeld, L. O. Rodriguez, S. M. Hecht, C. Chang, V. J. Basus and N. J. Oppenheimer, *Biochemistry*, 1985, **24**, 81; S. Routier, J.-L. Bernier, M. J. Waring, P. Colson, C. Houssier and C. Bailly, *J. Org. Chem.*, 1996, **61**, 2326; F. V. Pamatong, C. A. Detmer, III and J. R. Bocarsly, *J. Am. Chem. Soc.*, 1996, **118**, 5339; D. P. Mack, B. L. Iverson and P. B. Dervan, *J. Am. Chem. Soc.*, 1988, **110**, 7572; M. A. De Rosch and W. C. Trogler, *Inorg. Chem.*, 1990, **29**, 2409; R. Hettich and H.-J. Schneider, *J. Am. Chem. Soc.*, 1997, **119**, 5638.
4 S. Borah, M. S. Melvin, N. Lindquist and R. A. Manderville, *J. Am. Chem. Soc.*, 1998, **120**, 4557.
5 O. Baudoin, M.-P. Teulade-Fichou, J.-P. Vigneron and J.-M. Lehn, *J. Org. Chem.*, 1997, **62**, 5458.
6 O. Baudoin, C. Marchand, M.-P. Teulade-Fichou, J.-P. Vigneron, J.-S. Sun, T. Garestier, C. Hélène and J.-M. Lehn, *Chem. Eur. J.*, 1998, **4**, 1504.
7 J. Gallagher, C.-H. B. Chen, C. Q. Pan, D. M. Perrin, Y.-M. Cho and D. S. Sigman, *Bioconjugate Chem.*, 1996, **7**, 413.
8 B. F. Cain, B. C. Baguley and W. A. Denny, *J. Med. Chem.*, 1978, **21**, 658.
9 S. Frau, J. Bernadou and B. Meunier, *Bull. Soc. Chim. Fr.*, 1996, **133**, 1053.
10 J.-B. Le Pecq and C. Paoletti, *J. Mol. Biol.*, 1967, **27**, 87.
11 R. B. James and R. J. P. Williams, *J. Chem. Soc.*, 1961, 2007.

Communication 8/06095I

A powerful new oxidation agent towards metallic gold powder: *N,N′*-dimethylperhydrodiazepine-2,3-dithione (D) bis(diiodine). Synthesis and X-ray structure of $[AuDI_2]I_3$

Francesco Bigoli,[a] Paola Deplano,*[b] Maria Laura Mercuri,[b] Maria Angela Pellinghelli,[a] Gloria Pintus,[b] Angela Serpe[b] and Emanuele F. Trogu[b]

[a] *Dipartimento di Chimica Generale ed Inorganica, Chimica Analitica, Chimica Fisica, C. S. S. D. CNR, Viale delle Scienze 78, I-43100 Parma, Italy*

[b] *Dipartimento di Chimica e Tecnologie Inorganiche e Metallorganiche, via Ospedale 72, I-09124 Cagliari, Italy. E-mail: deplano@vaxca1.unica.it*

Received (in Basel, Switzerland) 4th August 1998, Accepted 25th September 1998

The oxidation of gold powder by a new safe and powerful oxidising reagent, the bis-diiodine adduct of *N,N′*-dimethylperhydrodiazepine-2,3-dithione (D), to produce $[AuI_2D]I_3$ under ambient conditions is described.

The potential of dihalogen or interhalogen adducts as new oxidising reagents towards elemental metals has been pointed out in recent years by the pioneering work of the McAuliffe group.[1] The used adducts were mainly halogeno-phosphoranes and -thioethers and a variety of complexes with unusual features (for stoichiometries, oxidation numbers and geometries) have been obtained. In particular in the reaction of $Me_3As{\cdot}I_2$ with the noble metal gold, the square-planar $[AuI_3(Me_3As)]$ complex was obtained, while $[AuI_3(Me_3P)_2]$, where gold(III) shows a trigonal-bipyramidal geometry, was produced using $Me_3P{\cdot}I_2$.[2] The importance of these results, apart from their intrinsic interest in the field of inorganic chemistry, lies in the new perspectives opened by these reaction routes in many applications, such as in the recovery of noble metals from exhausted catalysts or in the metal refining industry. In the case of gold, treatments with cyanide are still in use.† The desirable reagents should fulfill the following requirements: they should be inexpensive, easy to handle, non polluting and hopefully also selective. Moreover, it is preferable that they react rapidly.

Based on our extensive past experience in the area of the dihalogen adducts of sulfur and selenium-rich donors, we are now investigating the above mentioned metal activation reaction using the adducts of polyfunctional thione donors.[3] Our working hypothesis is that the proper choice of polyfunctional donors, which can favour the preferred geometry required by the metal undergoing oxidation and give chelation, will add a favourable condition to the spontaneity and selectivity of the oxidation reaction.

Here we present the results obtained using the bis-diiodine adduct of *N,N′*-dimethylperhydrodiazepine-2,3-dithione[4] towards gold. This ligand is a cyclic dithio-oxamide where the two vicinal thioamido groups are suitable to accommodate the square-planar geometry demanded by Au^{III}. The adduct was prepared by mixing the donor and diiodine in a 1 : 2 molar ratio in $CHCl_3$ at room temperature. The orange-brown shiny crystals obtained by slow evaporation were characterized as $D{\cdot}2I_2$. The presence of a strong Raman peak at 146 cm^{-1} assignable to ν(I–I) suggests that the interaction strength in the adduct is medium–strong.[5,6]

The reaction of $D{\cdot}2I_2$ with gold powder is given in Scheme 1. The reaction is performed under mild conditions and without any protection from the air and/or moisture. The solution of the adduct turns from red-orange to red-brown on addition of the metal and after a relatively short time the gold powder disappears. This solution is allowed to stand and the obtained solid is recrystallized from THF–Et_2O giving well-shaped crystals of $[AuDI_2]I_3$. The molecular structure of the cation of

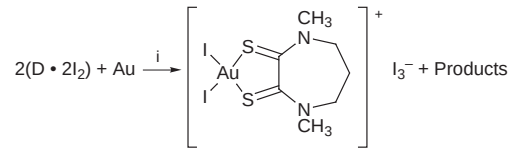

Scheme 1 i, THF, room temperature, 30 min to dissolve 14 mg of gold.

$[AuDI_2]I_3$[7] is shown in Fig. 1. The gold atom has an approximately square-planar configuration [max. dev. −0.037(4) Å for S(1)]. *N,N′*-Dimethylperhydrodiazepine-2,3-dithione acts as an *S,S*-chelating ligand, and bond distances show that electron delocalization does not involve C(1)–C(2).

One of the iodides coordinated to the metal strongly interacts with the anion [I(1)···I(5) (*x*, *y* − 1, *z*) 3.582(2) Å], while the other participates in the formation of chains of monocationic complexes running parallel to *c* by interacting with a sulfur atom of another cation [I(2)···S(1) (*x*, *y*, *z* − 1) 3.790(5) Å].

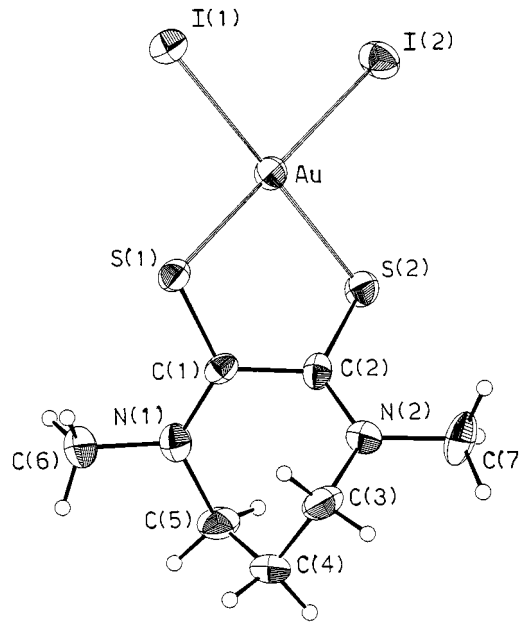

Fig. 1 Molecular structure of $[AuI_2(C_7H_{12}N_2S_2)]^+$. Thermal ellipsoids are drawn at the 30% probability level. Selected bond lengths [Å] and angles [°]: Au–I(1) 2.609(1), Au–I(2) 2.593(2), Au–S(1) 2.351(4), Au–S(2) 2.371(3), S(1)–C(1) 1.672(12), S(2)–C(2) 1.697(13), N(1)–C(1) 1.332(16), N(1)–C(5) 1.484(17), N(1)–C(6) 1.475(17), N(2)–C(2) 1.324(16), N(2)–C(3) 1.455(18), N(2)–C(7) 1.449(17), C(1)–C(2) 1.488(16), C(3)–C(4) 1.51(2), C(4)–C(5) 1.53(2). I(1)–Au–I(2) 92.24(4), I(1)–Au–S(1) 88.07(8), I(2)–Au–S(2) 88.71(9), S(1)–Au–S(2) 90.98(12), C(1)–S(1)–Au 98.3(4), C(2)–S(2)–Au 96.9(4).

The triiodide counterion is asymmetric and essentially linear: I(3)–I(4) 2.863(2), I(4)–I(5) 2.987(2) Å, I(3)–I(4)–I(5) 177.73(5)°. The Raman spectrum in the low frequency range shows peaks at 106s and 138m cm^{-1}, which are assigned to the symmetrical and antisymmetrical stretching of the triiodide units,[5a,b] and peaks at 153s, 166sh cm^{-1} which are likely to be related to the Au–I vibrations.

In conclusion a new oxidation reagent towards the noble metal gold has been synthesized. Since it reacts rapidly under ambient conditions in a one-step reaction and is scarcely polluting, inexpensive and easy to handle, this reagent can be used in practical applications. For the oxidation of noble metals, it represents a significant improvement over the previously reported reagents, $Me_3E{\cdot}I_2$ (E = P, As), which use polluting materials and are impractical since they require strictly anhydrous, anaerobic conditions and long reaction times.

This research was carried out as part of the project 'Materiali Speciali per Tecnologie Avanzate II' supported by the Consiglio Nazionale delle Ricerche (CNR).

Notes and references

† The use of thiourea to accomplish gold dissolution from ore under oxidation conditions avoiding the cyanide process has been reported (see for example R. Schulze, *Ger. Offen. DE*. 3401961 (Cl. C22B3/00) 23 Aug. 1984).

1 N. Bricklebank, S. M. Godfrey, C. A. McAuliffe, A. G. Mackie and R. G. Pritchard, *J. Chem. Soc., Chem. Commun.*, 1992, 944; S. M. Godfrey, C. A. McAuliffe and R. G. Pritchard, *J. Chem. Soc., Dalton Trans.*, 1993, 371 and 2875; S. M.Godfrey, D. G. Kelly, C. A. McAuliffe and R. G. Pritchard, *ibid*., 2053; S. M. Godfrey, C. A. McAuliffe and R. G. Pritchard, *J. Chem. Soc., Chem. Commun.*, 1994, 45; N. Bricklebank, S. M. Godfrey, C. A. McAuliffe and R. G. Pritchard, *J. Chem. Soc., Dalton Trans.*, 1996, 157.

2 S. M. Godfrey, N. Ho, C. A. McAuliffe and R. G. Pritchard, *Angew. Chem., Int. Ed. Engl.*, 1996, **33**, 2344.

3 F. Bigoli, P. Deplano, F. A. Devillanova, V. Lippolis, M. L. Mercuri, M. A. Pellinghelli and E. F. Trogu, *Inorg. Chim. Acta*, 1998, **267**, 115, and references therein.

4 Prepared according to R. Isaksson, T. Liljefors and J. Sandstrom, *J. Chem. Res. (S)*, 1981, 43.

5 (*a*) T. J. Marks, *Ann. NY Acad. Sci*., 1970, **313,** 594; (*b*) J. R. Ferraro, *Coord. Chem. Rev*., 1982, **43,** 205; (*c*) P. Deplano, F. A. Devillanova, J. R. Ferraro, F. Isaia, V. Lippolis and M. L. Mercuri, *Appl. Spectrosc.*, 1992, **46,** 1625; (*d*) F. Bigoli, P. Deplano, M. L. Mercuri, M. A. Pellinghelli, A. Sabatini, E. F. Trogu and A. Vacca, *J. Chem. Soc., Dalton Trans*., 1996, 3583.

6 In fact the strong peak of uncoordinated diiodine (ν = 180 cm^{-1} in solid I_2 [d(I–I) = 2.715 Å, F. van Bolhuis, P. B. Koster and T. Migehelsen, *Acta Crystallogr*., 1967, **23**, 90]) is shifted to lower frequencies upon coordination as a consequence of the lowering of the force constant of the I–I vibration in a CT adduct.

7 Crystal data: $C_7H_{12}AuI_5N_2S_2$, M = 1019.77, crystal dimensions: 0.16 × 0.16 × 0.20 mm, triclinic, space group, $P\bar{1}$, a = 8.204(6), b = 15.994(5), c = 8.080(6) Å, α = 96.68(2), β = 112.40(2), γ = 92.20(2)°, V = 969.6(1.1) $Å^3$, Z = 2, D_c = 3.493 Mg m^{-3}, μ = 15.747 mm^{-1}, F(000) 888; 4249 reflections collected ($3.09 \leqslant \theta \leqslant 27.05°$) at T = 293(2) K, 4249 independent, R_1 = 0.0430 [$I > 2\sigma(I)$], wR_2 = 0.1172(all data), gof = 0.878 for 158 parameters, largest difference peak/hole 1.974/−1.286 e $Å^{-3}$, Data were collected from a Siemens AED diffractometer (graphite-monochromated Mo-Kα radiation, λ = 0.71073 Å) with θ–2θ scan technique. An empirical absorption correction[8] was applied (transmission coefficients: 0.8808, 1.2731). The structure was solved by direct methods using SIR92[9] and refined by full-matrix least-squares against F^2 (SHELXL-97[10]). Anisotropic refinement of all non-H atoms. R values $R_1 = \Sigma||F_o| - |F_c||/\Sigma|F_o|$, $wR_2 = [\Sigma w(F_o^2 - F_c^2)^2/\Sigma w(F_o^2)^2]^{1/2}$.

8 N. Walker and D. Stuart, *Acta Crystallogr., Sect. A*, 1983, **39**, 158.

9 A. Altomare, C. Cascarano, C. Giacovazzo, A. Guagliardi, M. C. Burla, G. Polidori and M. Camalli, *J. Appl. Crystallogr.*, 1994, **27**, 435.

10 G. M. Sheldrick, SHELX-97: Program for Crystal Structure Determination, Universität Göttingen, Germany, 1997.

Communication 8/06158K

ChemComm

Asymmetric synthesis and electrochemical behaviour of a C_2 chiral bisferrocenyl orthoquinone

Ana Gomez Neo, Aurore Gref and Olivier Riant*

Laboratoire des Réactions Organiques Sélectives, ICMO, Université Paris-Sud, 91405 Orsay, France.
E-mail: oliriant@icmo.u-psud.fr

Received (in Cambridge, UK) 4th August 1998, Accepted 25th September 1998

A new chiral bisferrocenyl quinone with C_2 symmetry was prepared by asymmetric synthesis; further condensation with 1,2-diamines led to enantiopure polyaromatic heterocycles into which two ferrocene units are fused.

Due to their unique structural and electronic properties, *o*-benzoquinones[1] and their diimine derivatives have received a great deal of attention as transition metal ligands in coordination chemistry and catalysis.[2] Their 1,2-diketone structure allows the construction of polyaromatic systems *via* various types of condensation reactions. This has led to numerous applications in material sciences[3] and supramolecular chemistry.[4]

We report here the asymmetric synthesis of a new chiral orthoquinone in which two electron-rich ferrocene units are fused. Diastereoselective ortholithiation of enantiopure ferrocenyl acetal (2*S*,4*S*)-**1** by the reported method[5] and further oxidation of the lithio intermediate by iron(III) acetylacetonate led, after removal of the acetal protecting groups, to the chiral bisferrocene bisaldehyde (R_{Fc},R_{Fc})-**2**† in a 70% yield (Scheme 1). Due to the high diastereoselectivity of the deprotonation (98%), only the C_2 symmetric isomer was formed and no *meso* isomer was detected. Pinacolisation of (R_{Fc},R_{Fc})-**2** was efficiently realised by reaction of an excess of SmI_2 in THF and gave a mixture of air sensitive diols which were directly oxidised by MnO_2 in dry $CHCl_3$. After chromatographic purification, the new C_2 symmetric *o*-quinone (R_{Fc},R_{Fc})-**3**‡ was isolated in 55% yield (starting from **2**) and was fully characterised. This deep blue complex proved to be air stable and could be easily prepared on a multigram scale using this procedure.

As a first application, we turned to the condensation of (R_{Fc},R_{Fc})-**3** with various aromatic 1,2-diamines. After optimisation, it was found that condensation of quinone **3** with an excess of 1,2-diaminobenzene in refluxing toluene gave a quantitative yield of the quinoxaline derivative **5a** when freshly activated 4 Å molecular sieves or alumina[6] were used as a dehydrating agent. In the case of adducts **5b**,**c**, longer reaction time were required and optimised yields reached 70% after purification. We found as well that *N*-alkylation of the pyridine nitrogen of adduct **5b** by iodomethane gave a quantitative yield of the stable green pyridinium salt **6**. The structure of the quinoxaline adducts as well as the starting quinone could be unambiguously confirmed by standard ^{1}H and ^{13}C NMR methods as well as HRMS. The electrochemical behaviour of bisferrocene (Fe^{II}, Fe^{II}) complexes such as **3** and **5a** was studied by cyclic voltammetry[7] (Fig. 1). This allowed us to study the stability in solution of the higher oxidation states (Fe^{II}, Fe^{III}) and (Fe^{III}, Fe^{III}). Recording the CV at low sweep rate for **5a** gave two reversible one electron oxidation waves at low potential. In the time scale of the analysis, the mixed valence complex (Fe^{II}, Fe^{III}) is completely stable as well as the corresponding bisferricinium (Fe^{III}, Fe^{III}). As expected, quinone **3** proved to be more difficult to oxidize, showing an increase of +0.34 V for the first oxidation compared to **5a**. The first oxidation wave giving the mixed valence state is reversible at all sweep rates, but the second oxidation wave remains irreversible for sweep rates up to 1000 V s^{-1}, thus showing chemical evolution of the bisferricinium complex. Increasing the sweep rate up to 2000–3000 V s^{-1} shows that this evolution is slow and a life time for the bisferricinum (Fe^{III},Fe^{III}) was evaluated at 3×10^{-2} s. It was also noted that **3** didn't display any reduction wave, in agreement with the electron-rich nature of the carbonyl groups.

We are currently studying the chemistry and the electrochemical behaviour of those enantiopure bimetallic complexes as well as the isolation of the mixed valence complexes.

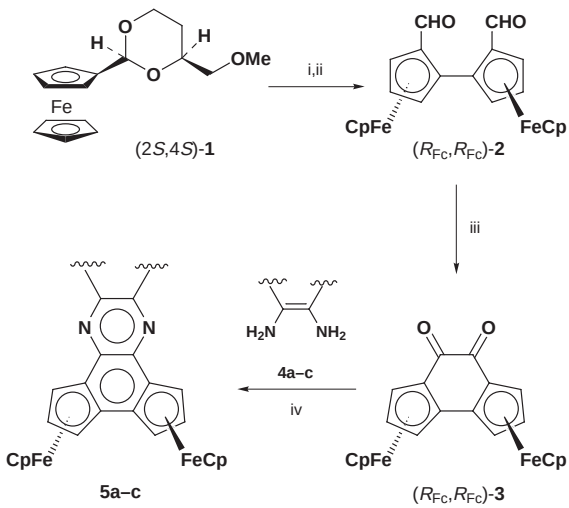

Scheme 1 *Reagents and conditions*: i, Bu^{t}Li (1.1 equiv.), Et_2O, −78 to 25 °C, 1 h, then $Fe(acac)_3$ (1.4 equiv.), 25 °C, 15 h; ii, TsOH, CH_2Cl_2, H_2O, 25 °C, 3 h (70% from **1**); iii, SmI_2 (2.4 equiv.), THF, 25 °C, 15 min, then MnO_2, $CHCl_3$, 25 °C, 30 min (55–60% from **2**); iv, 1,2-diamine (2–3 equiv.), PhMe, 4 Å MS or Al_2O_3, reflux.

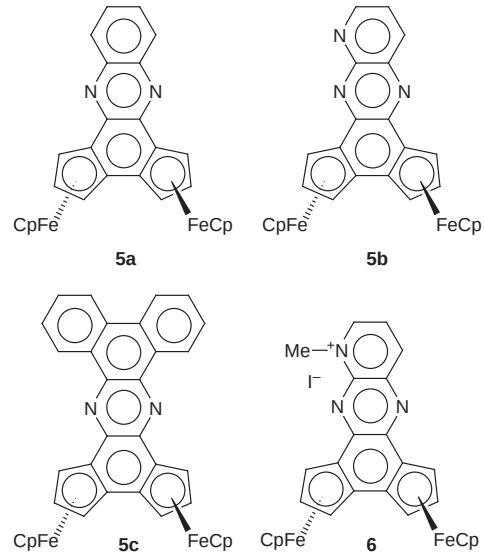

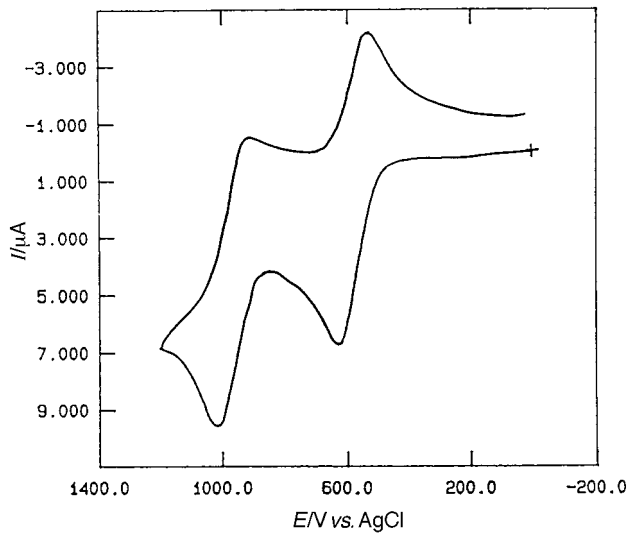

Fig. 1 Cyclic voltammogram of **5a** (2 mM) in 0.1 M Bu_4NBF_4–CH_2Cl_2 at a Pt electrode with a sweep rate of 0.1 V s^{-1}.

We thank CNRS for financial support. One of us (A. G. N.) wishes to thank Universidad de Santiago de Compostela for a grant.

Notes and references

† A multistep synthesis of bisaldehyde **2** was first reported using a resolution step: K. Schlögl and M. Walser, *Monatsh. Chem*., 1969, **100**, 97.

‡ *Synthesis of quinone* **3**: A solution of bisaldehyde **2** (3.33 g, 7.8 mmol) in 30 ml of dry THF was treated under argon with 180 ml of a 0.1 M THF solution of SmI_2 dropwise. After 10 min, the reaction mixture was quenched with aq. NH_4Cl and extracted with Et_2O. After work up, the crude reaction mixture was taken up in 300 ml of $CHCl_3$ and stirred with 30 g of activated MnO_2 for 20 min. Filtration of the reaction mixture on Celite followed by flash chromatography on silica gel (cyclohexane–Et_2O 20:80 to CH_2Cl_2–Et_2O 20:80) delivered the pure quinone **3** as a deep blue solid (1.92 g, 58% yield from **2**).

1 For a review of the chemistry of *o*-quinones, see S. Patai, *The Chemistry of the Quinonoid Compounds*, Wiley, New York, 1988, vol. 2.
2 R. van Asselt, C. J. Elsevier, W. J. J. Smeets, A. L. Speck and R. Benedix, *Recl. Trav. Chim. Pays-Bas*, 1994, **113**, 88; R. Van Asselt and C. Eselvier, *Organometallics*, 1994, **13**, 1972; C. G. Pierpont and C. W. Lange, *Progr. Inorg. Chem*., 1994, **41**, 331.
3 F. E. Arnold, *J. Polym. Sci. A*, 1970, **8**, 2079; J. K. Stille, G. K. Noren and L. Green, *J. Polym. Sci. A*, 1970, **8**, 2245; M. Löffler and A.-D. Schlüter, *Synthesis*, 1994, 75.
4 For recent references, see A. E. Friedman, J.-C. Chambron, J.-P. Sauvage, N. J. Turro and J. K. Barton, *J. Am. Chem. Soc*., 1990, **112**, 4960; K. Wärnmark, J. A. Thomas, O. Heyke and J.-M. Lehn, *Chem. Commun*., 1996, 701 and 2603; J. Borlger, A. Gourdon, E. Ishow and J.-P. Launay, *Inorg. Chem*., 1996, **35**, 2937; M. J. Crossley, L. G. King, I. A. Newsom and C. S. Sheehan, *J. Chem. Soc., Perkin Trans. 1*, 1996, 2675; S. Bodige, A. S. Torres, D. J. Maloney, D. Tate, G. R. Kinsel, A. K. Walker and F. M. MacDonnell, *J. Am. Chem. Soc*., 1997, **119**, 10 364.
5 O. Riant, O. Samuel and H. B. Kagan, *J. Am. Chem. Soc*., 1993, **115**, 5835; O. Riant, O. Samuel, T. Flessner, S. Taudien and H. B. Kagan, *J. Org. Chem*., 1997, **62**, 6733.
6 R. Bosque, C. López, J. Sales and X. Solans, *J. Organomet. Chem*., 1994, **483**, 61.
7 The conditions for cyclic voltammetry have been previously described: A. Gref, P. Diter, D. Guillaneux and H. B. Kagan, *New. J. Chem*., 1997, **21**, 1353.

Communication 8/06543H

ChemComm

Cruciform porphyrin pentamers

M. Graça H. Vicente,* Mark T. Cancilla, Carlito B. Lebrilla and Kevin M. Smith*

Department of Chemistry, University of California, Davis, CA 95616, USA. E-mail: kmsmith@ucdavis.edu

Received (in Corvallis, OR, USA) 14th August 1998, Accepted 25th September 1998

Cruciform porphyrin pentamers 15 and 16 are obtained in good yield by acid-catalyzed tetramerization of Zn^{II}–pyrroloporphyrin 14, followed by oxidation with DDQ; pyrroloporphyrins are in turn obtained from the corresponding pyrrolochlorins by Diels–Alder type reactions of porphyrins involving thermal extrusion of sulfur dioxide from a pyrrole-fused 3-sulfolene.

Syntheses of covalently-linked porphyrin arrays have recently attracted much attention due to their unique photoelectronic properties and potential applications as mimics of light-harvesting in photosynthesis, and as electron/energy transfer moieties in molecular wires.[1–4] A variety of model structures have been reported, mostly containing two or three porphyrin units, either directly coupled,[2] bridged by coplanar aromatic systems,[3] or beta-fused.[4] Coplanar-linked porphyrin arrays are believed to lead to more efficient energy- and electron-transfer superstructures. Recently, a linear beta-fused trimer[4] was prepared from a fused pyrroloporphyrin.[5] Herein we describe the first synthetic route to covalently-linked cruciform pentamer porphyrins, one of which is planar and fully conjugated.

One of our long term objectives is to modify porphyrin macrocycles for use both as dienes and dienophiles. The synthesis and cycloaddition reactions of a pyrrole-fused 3-sulfolene **1** with standard dienophiles were recently reported,[6] and porphyrins have also been shown to react with electron-rich dienes.[7] Thus, when TPP **2** was heated at 240 °C in the presence of an excess of pyrrole **1** and 4 Å molecular sieves, the pyrrolochlorin **3** was produced as a mixture of enantiomers in 20–22% yield. Two minor products are also obtained from this reaction: pyrroloporphyrin **4** (6–10% yield) and isoindoloporphyrin **5** (usually $< 1\%$ due to its ready transformation into further products). Trace amounts of bacteriochlorin were also detected by spectrophotometry. Based on recovered starting material **2**, the yield of products **3–5** was quantitative. Products obtained simply from the dimerization and polymerization of the reactive pyrrolodiene, generated *in situ* from **1**, were also identified by ^{1}H NMR and mass spectrometry. Products **4** and **5** were obtained from pyrrolochlorin **3** by oxidation with *p*-chloranil or DDQ. The Ni^{II} and Zn^{II} complexes of TPP reacted under similar conditions to afford the same products in lower yields due to increased susceptibility toward unwanted oxidation reactions. When the same reaction conditions were applied to octaethylporphyrin **6**, the pyrrolochlorin **7** was obtained in low yield (2–5%). Under the same conditions the iron(III) complex **8** afforded pyrrolochlorin **9** in 6% yield (unoptimized). In contrast, the electron-deficient *meso*-tetra(pentafluorophenyl)porphyrin **10** readily reacted to afford only two products, the pyrrolochlorin **11** (32–39% yield) and the bacteriochlorin **12** (5–10%). When the same reaction was applied to a porphyrin or chlorin bearing a β-vinyl substituent the cycloaddition reaction took place predominantly at the vinyl group. Reactions of pyrrole **1** with functionalized chlorins led to mixtures of products which include bacteriochlorins, isoindolochlorins, and products resulting from addition of another pyrrole to the isoindolochlorin.

All new compounds possessed spectroscopic data in accord with the assigned structures. Pyrrolochlorins **3**, **7**, **9** and **11** possess typical chlorin absorption spectra, with a strong band at λ_{max} 652 nm; pyrroloporphyrin **4** shows an electronic absorption spectrum similar to that of TPP **2**, and isoindoloporphyrin **5** shows a type of rhodo-visible spectrum characteristic of monobenzoporphyrins. Compound **12** (λ_{max} 746 nm) displayed an optical spectrum characteristic of a bacteriochlorin.

Insertion of zinc into pyrroloporphyrin **4** yielded complex **13** in 85–90% yield. The ester function of compound **13** was reduced with $LiAlH_4$ to give alcohol **14** which afforded the crude pentamer **15** after treatment (*e.g.* ref. 8) with acid and

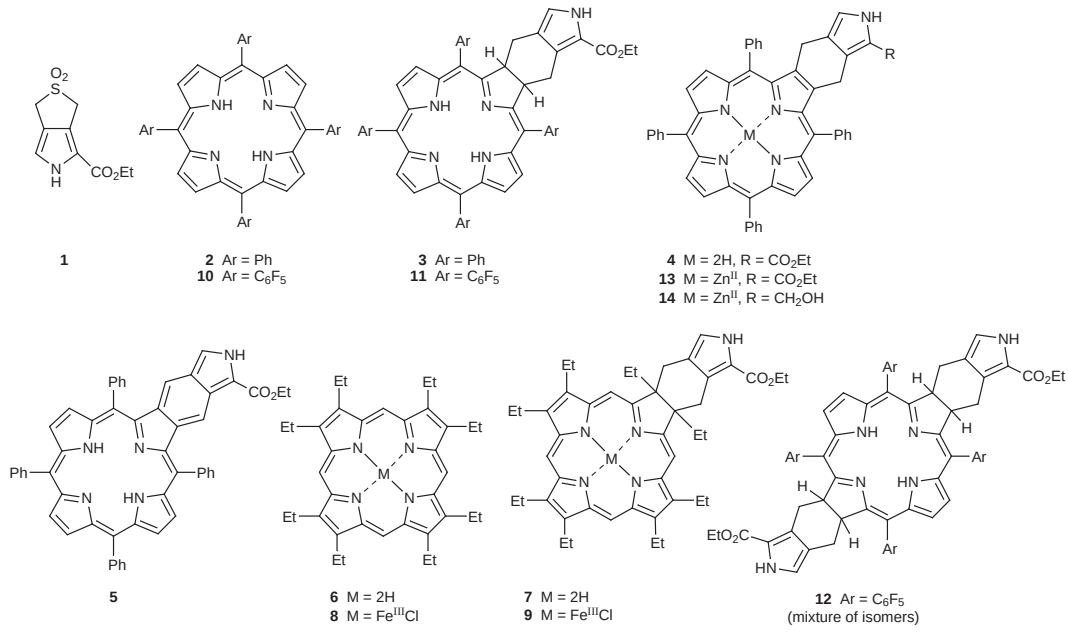

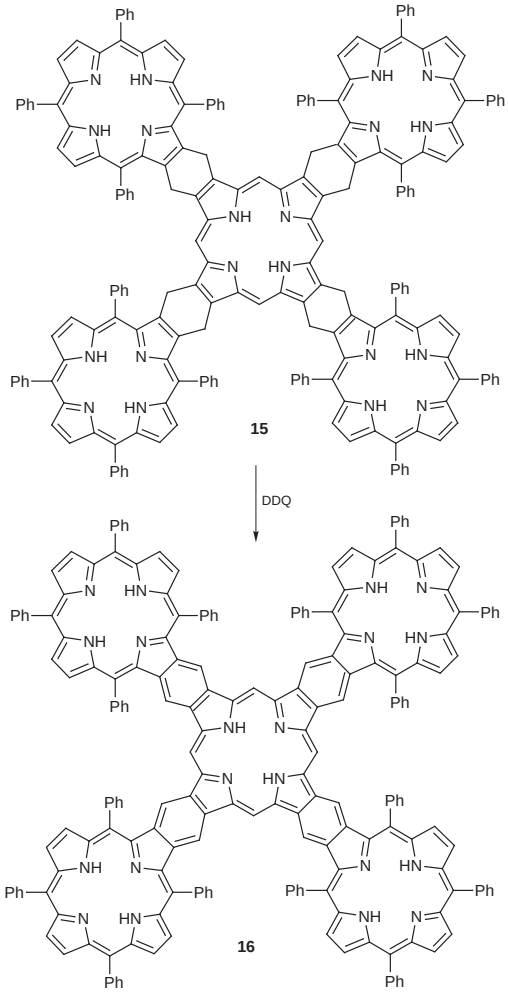

Scheme 1

oxidation with *p*-chloranil. Filtration through Sephadex G-25 resulted in isolation of **15** in 65–75% yield. Mass spectrometry was performed on **15** using matrix-assisted laser desorption ionization (MALDI) with a Fourier transform mass spectrometry (FTMS) analyzer.† This technique has been shown to be highly effective for high resolution MS determinations of large porphyrin compounds.[9] The ^{1}H NMR spectrum of **15** showed only broad bands, even upon addition of TFA, possibly due to aggregation effects of these high molecular-weight molecules. Treatment of pentamer **15** with an excess of DDQ gave the fully conjugated pentamer **16** in quantitative yield (Scheme 1). Compound **16** was also characterized by MALDI-FTMS;† its absorption spectrum showed a long-wavelength band at λ_{max} 774 nm (838 nm in acid). Pentamers **15** and **16** display good solubilities in most organic solvents. The methodology described above offers the opportunity for synthesis of novel heterobimetallic cruciform porphyrin pentamers, and this work is in progress.

This research was supported initially by a grant from JNICT-Portugal (PBIC/C/QUI/2156/95 to MGHV), and subsequently by the National Institutes of Health (HL 22252).

Notes and references

† *Selected data* for **15**: $C_{204}H_{134}N_{20}$ requires 2863.1099; found: 2862.8791 (M^+). For **16**: $C_{204}H_{126}N_{20}$ requires: 2855.0474; found 2854.9263 (M^+).

1 T. E. Clement, D. J. Nurco and K. M. Smith, *Inorg. Chem.*, 1998, **37**, 1150; T. Norsten and N. Branda, *Chem. Commun.*, 1998, 1257; R. N. Warrener, M. R. Johnston and M. J. Gunter, *Synlett*, 1998, 593; G. Zheng, R. K. Pandey, T. P. Forsyth, A. N. Kozyrev, T. J. Dougherty and K. M. Smith, *Tetrahedron Lett.*, 1997, **38**, 2409.

2 R. G. Khoury, L. Jaquinod and K. M. Smith, *Chem. Commun.*, 1997, 1057; A. Osuka and H. Shimidzu, *Angew. Chem., Int. Ed. Engl.*, 1997, **36**, 135; L. Jaquinod, M. O. Senge, R. K. Pandey, T. P. Forsyth and K. M. Smith, *Angew. Chem., Int. Ed. Engl.*, 1996, **35**, 1840.

3 *E.g.* M. J. Crossley and P. L. Burn, *J. Chem. Soc., Chem. Commun.*, 1991, 1569; M. J. Crossley, P. L. Burn, S. J. Langford and J. K. Prashar, *J. Chem. Soc., Chem. Commun.*, 1995, 1921; N. H. Reek, A. E. Rowan, R. de Gelder, T. Beurskens, M. J. Crossley, D. Feyter, F. de Schryver and J. M. Nolte, *Angew. Chem., Int. Ed. Engl.*, 1997, **36**, 361; M. J. Crossley and J. K. Prashar, *Tetrahedron Lett.*, 1997, **38**, 6751; M. J. Crossley, L. J. Govenlock and J. K. Prashar, *J. Chem. Soc., Chem. Commun.*, 1995, 2379.

4 L. Jaquinod, O. Siri, R. G. Khoury and K. M. Smith, *Chem. Commun.*, 1998, 1261.

5 L. Jaquinod, C. Gros, M. M. Olmstead, M. Antolovich and K. M. Smith, *Chem. Commun.*, 1996, 1475; C. P. Gros, L. Jaquinod, R. G. Khoury, M. M. Olmstead and K. M. Smith, *J. Porphyrins Phthalocyanines*, 1997, **1**, 201.

6 M. G. H. Vicente, A. C. Tome, A. Walter and J. A. S. Cavaleiro, *Tetrahedron Lett.*, 1997, **38**, 3639.

7 A. C. Tome, P. S. S. Lacerda, M. G. P. M. S. Neves and J. A. S. Cavaleiro, *Chem. Commun.*, 1997, 1199.

8 N. Ono, H. Kawamura, M. Bougauchi and K. Maruyama, *Tetrahedron*, 1990, **46**, 7483.

9 M. K. Green, C. J. Medforth, C. M. Muzzi, D. J. Nurco, K. M. Shea, K. M. Smith, J. A. Shelnutt and C. B. Lebrilla, *Eur. J. Mass Spectrom.*, 1997, **3**, 439.

Communication 8/06563B

Enantioselective intramolecular cyclizations of prochiral cyclohexanones using chiral lithium amide bases

Jeffrey E. Kropf and Steven M. Weinreb*

Department of Chemistry, The Pennsylvania State University, University Park, Pennsylvania 16802, USA. E-mail: smw@chem.psu.edu

Received (in Corvallis, OR, USA) 31st August 1998, Accepted 25th September 1998

The first examples of intramolecular cyclizations of prochiral cyclohexanones with chiral lithium amide bases have been effected in good yields and enantiomeric ratios.

The use of an amide base and an electrophile to form a carbon–carbon bond at the α-position of a ketone is a fundamental method in organic chemistry. The enantioselective intermolecular version of this reaction, in which a chiral lithium amide base is used with a prochiral ketone, is becoming increasingly widespread.[1–3] As part of an ongoing project in natural product total synthesis, we were interested in applying an intramolecular variation of this chiral alkylation methodology to the preparation of a scalemic intermediate. To the best of our knowledge, this type of enantioselective cyclization has not been previously reported. Here we describe the first examples of the use of chiral lithium amide bases in the enantioselective *intramolecular* deprotonation–alkylation of two prochiral cyclohexanones.

The readily available iodo ketones **1**[7] and **2**[8] which were examined in this methodological study are shown in Scheme 1. The chiral lithium amides used are represented by structures **5**,[9] **6**[10] and **7**.[11] Using published work on intermolecular enantioselective deprotonations of cyclohexanones as a guide, experiments were conducted on cyclization of ketones **1** and **2** to bicyclic systems **3** and **4**, respectively, with amide bases **5**–**7**. Representative results are listed in Table 1.

Initial exploratory experiments were conducted with iodo ketone **1** and amide base **5**. This system leads preferentially to the (*R*,*R*)-enantiomer of **3**.[12,13] This absolute configuration is in accord with published results on deprotonation of simple 4-substituted cyclohexanones with base **5**.[14] Using HMPA as an additive in the intramolecular deprotonation–alkylation of **1** led to bridged ketone **3** in poor to moderate ers (enantiomeric ratios) (entries 1 and 2). These results are in accord with previously reported observations which suggest that HMPA is most effective in inducing high ers with a base that contains one or more internal ligation sites.[1b] However, LiCl has been shown to be a beneficial additive when employing bases either with or without internal ligation sites.[1f] In fact, the best yield and er of (*R*,*R*)-**3** (62% and 87:13, respectively) were achieved using amide **5** along with 2.5 equiv. of LiCl (entry 4).

Cyclization of ketone **1** with amide base **6** led preferentially to the (*S*,*S*)-enantiomer of **3**, whereas base **7** afforded the (*R*,*R*)-enantiomer, although ers were only moderate with both systems (73:27–80:20, entries 5–9). Unlike base **5**, amide base **6** gave

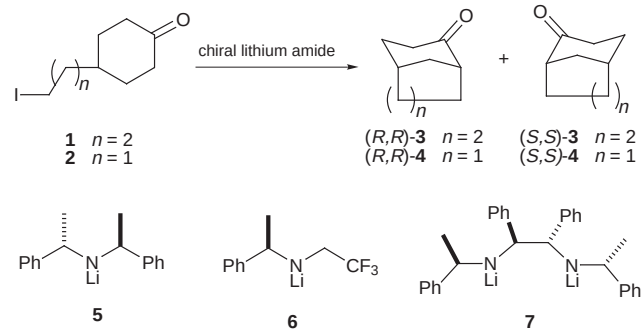

Scheme 1

Table 1 Enantioselective intramolecular cyclization of prochiral cyclohexanones with chiral lithium amides[a]

Entry	Ketone	Lithium amide (equiv.)	Additive (equiv.)	*T*/°C	Product	Yield (%)	Er[b] (*RR*:*SS*)
1	**1**	5 (1.3)	HMPA (2.4) + LiCl (1.3)[c]	−40→room temp.	(*R*,*R*)-**3**	58	59:41
2	**1**	5 (1.3)	HMPA (2.5) + LiCl (1.3)[c]	−50→−10	(*R*,*R*)-**3**	29	82:18
3	**1**	5 (1.3)	LiCl (1.3)[c]	−50→−10	(*R*,*R*)-**3**	44	87:13
4	**1**	5 (1.5)	LiCl (1.0) + LiCl (1.5)[c]	−60→−20	(*R*,*R*)-**3**	62	87:13
5	**1**	6 (1.5)	LiCl (2.0)	−60→−20	(*S*,*S*)-**3**	38	27:73
6	**1**	6 (1.5)	LiCl (1.0)	−60→−20	(*S*,*S*)-**3**	39	22:78
7	**1**	6 (1.5)	LiBr (1.0)	−60→−20	(*S*,*S*)-**3**	42	20:80
8	**1**	7 (1.5)	LiCl (2.0)	−60→−20	(*R*,*R*)-**3**	61	76:24
9	**1**	7 (1.1)	LiCl (1.0)	−60→−20	(*R*,*R*)-**3**	60	76:24
10	**2**	5 (1.5)	LiCl (1.0) + LiCl (1.5)[c]	−60→−20	(*R*,*R*)-**4**	53	79:21
11	**2**	5 (1.05)	LiCl (1.0) + LiCl (1.05)[c]	−80→−40	(*R*,*R*)-**4**	58	90:10
12	**2**	6 (1.5)	LiCl (1.0)	−60→−20	(*S*,*S*)-**4**	61	20:80
13	**2**	6 (1.05)	LiCl (1.0)	−80→−40	(*S*,*S*)-**4**	45	11:89
14	**2**	6 (1.5)	LiCl (1.0)	−80→−40	(*S*,*S*)-**4**	70	10:90
15	**2**	7 (1.1)	LiCl (1.0)	−60→−20	(*R*,*R*)-**4**	57	68:32
16	**2**	7 (1.05)	LiCl (1.0)	−80→−40	(*R*,*R*)-**4**	79	73:27

[a] The experimental procedure for entry 14 is typical: Under an argon atmosphere, a solution of BuLi in hexane (0.30 ml, 1.67 M, 0.502 mmol) was added to a solution of chiral amine (0.102 g, 0.502 mmol) and LiCl (0.014 g, 0.335 mol) in THF (13 ml) at −80 °C affording amide base **6**. The mixture was stirred for 30 min and ketone **2** in THF (0.5 ml) was then added *via* cannula. The solution was allowed to warm to −40 °C and was stirred for 18 h. The reaction mixture was quenched with saturated NH_4Cl (5 ml) and extracted with Et_2O (3 × 15 ml). The organic extracts were sequentially washed with brine (1 × 20 ml), 10% $Na_2S_2O_3$ (1 × 20 ml), 5% HCl (2 × 20 ml) and brine (1 × 20 ml). After drying with Na_2SO_4, and evaporation *in vacuo*, flash chromatography (SiO_2; pentane–Et_2O, 10:1) of the residue gave ketone **4** (0.029 g; 70%). [b] Ers (enantiomeric ratios) were determined by GLC using a chiral Supelco β-DEX 390 column. [c] Formed *in situ* from the hydrochloride salt.

the best results (39% yield and a 78:22 er) when using only 1.0 equiv. of LiCl (entry 6). These results could be improved slightly by substitution of LiBr as the additive in place of LiCl (entry 7). Amide base **7** gave a slightly higher chemical yield of **3** (61%, entry 8) than did amide **6**, but the er was not improved significantly. Thus, of the three bases tested, amide **5** provided the best overall results in cyclization of iodo ketone **1** (entry 4).

As was the case for cyclization of ketone **1**, iodo ketone **2** gave predominantly the (*R*,*R*)-enantiomer of bicyclic ketone **4** with bases **5** and **7**, and the (*S*,*S*)-enantiomer with **6**.[12] Interestingly, the results of the cyclization of ketone **2** were not optimal under the best reaction conditions determined for ketone **1** (*cf*. entries 10, 12 and 15). It was eventually found that of the three bases, lithium amide **6** gave the best results in cyclization of **2** with a 70% yield and a 90:10 er of (*S*,*S*)-**4** using the experimental conditions outlined in entry 14.

In conclusion, we have demonstrated that intramolecular enantioselective cyclizations of prochiral ketones using chiral lithium amide bases are feasible, and can be effected with good ers. The cyclization of ketone **1** was best accomplished to give (*R*,*R*)-**3** in 62% yield and an 87:13 er using lithium amide base **5**, while the cyclization of homologous ketone **2** was effected to afford (*S*,*S*)-**4** in 70% yield and a 90:10 er with amide base **6**. It appears that the chemical yields and ers in these intramolecular cyclizations are highly dependent upon the reaction conditions, base, additive and substrate used, and no obvious trends are evident at this very early stage of development. We are hopeful, however, that with additional work some empirical rules can be devised for this type of enantioselective cyclization.

We are grateful to the National Institutes of Health (CA-34303) for generous financial support. We also thank Professor Xumu Zhang and his research group for help with GLC analyses.

Notes and references

1 (*a*) For reviews, see: K. Koga, *J. Synth. Org. Chem. Jpn*., 1990, **48**, 463; (*b*) P. J. Cox and N. S. Simpkins, *Tetrahedron*: *Asymmetry*, 1991, **2**, 1; (*c*) K. Koga, *Pure Appl. Chem*., 1994, **66**, 1487; (*d*) K. Koga and M. Shindo, *J. Synth. Org. Chem. Jpn*., 1995, **53**, 1021; (*e*) N. S. Simpkins, *Pure Appl. Chem*., 1996, **68**, 691; (*f*) P. O'Brien, *J. Chem. Soc*., *Perkin Trans. 1*, 1998, 1439.

2 The large majority of the work on enantioselective deprotonation of prochiral ketones using chiral lithium amide bases involves trapping the resulting enolates as silyl enol ethers: K. Aoki and K. Koga, *Tetrahedron Lett*., 1997, **38**, 2505; R. Shirai, D. Sato, K. Aoki, M. Tanaka, H. Kawasaki and K. Koga, *Tetrahedron*, 1997, **53**, 5963; H. Chatani, M. Nakajima, H. Kawasaki and K. Koga, *Heterocycles*, 1997, **46**, 53; K. Aoki, K. Tomioka, H. Noguchi and K. Koga, *Tetrahedron*, 1997, **53**, 13 641.

3 In addition, chiral lithium amide bases have beeen successfully used for the enantioselective rearrangement of epoxides (ref. 4), aromatic and benzylic functionalization of aryl chromium complexes (ref. 5), as well as the asymmetric [2,3]-Wittig rearrangement (ref. 6).

4 M. Asami, *J. Synth. Org. Chem. Jpn*., 1996, **54**, 188; D. M. Hodgson, A. R. Gibbs and G. P. Lee, *Tetrahedron*, 1996, **52**, 14 361.

5 R. A. Ewin, A. M. MacLeod, D. A. Price, N. S. Simpkins and A. P. Watt, *J. Chem Soc*., *Perkin Trans. 1*, 1997, 401.

6 S. E. Gibson, P. Ham and G. R. Jefferson, *Chem. Commun*., 1998, 123.

7 Iodo ketone **1** was synthesized from 4-(3-chloropropyl)cyclohexanone (*cf*. A. G. Schultz and J. P. Dittami, *J. Org. Chem*., 1984, **49**, 2615) by a Finkelstein reaction (NaI, acetone, 90%).

8 Iodo ketone **2** was prepared from 4-(2-hydroxyethyl)cyclohexanone (M. A. Ciufolini and N. E. Byrne, *J. Am. Chem. Soc*., 1991, **113**, 8016) using PPh_3 and I_2 (60%).

9 The amine is available commercially as the hydrochloride salt.

10 R. Shirai, K. Aoki, D. Sato, H.-D. Kim, M. Murakata, T. Yasukata and K. Koga, *Chem. Pharm. Bull*., 1994, **42**, 690.

11 K. Bambridge, M. J. Begley and N. S. Simpkins, *Tetrahedron Lett*., 1994, **35**, 3391.

12 The absolute stereochemistry of bicyclic ketones **3** and **4** was determined using the CD Octant rule. For a good discussion, see: E. L. Eliel and S. H. Wilen, *Stereochemistry of Organic Compounds*, Wiley, New York, 1994, p. 1022.

13 Racemic ketone **3** is commercially available. Racemic **4**: E. N. Marvell, D. Sturmer and C. Rowell, *Tetrahedron*, 1966, **22**, 861.

14 K. Sugasawa, M. Shindo, H. Noguchi and K. Koga, *Tetrahedron Lett*., 1996, **37**, 7377.

Communication 8/07052K

Catalytic conversions in water. Part 10.† Aerobic oxidation of terminal olefins to methyl ketones catalysed by water soluble palladium complexes

Gerd-Jan ten Brink, Isabel W. C. E. Arends, Georgios Papadogianakis‡ and Roger A. Sheldon*

Laboratory for Organic Chemistry and Catalysis, Delft University of Technology, Julianalaan 136, 2628 BL Delft, The Netherlands. E-mail: secretariat-ock@stm.tudelft.nl

Received (in Cambridge, UK) 19th August 1998, Accepted 21st September 1998

Water soluble palladium(II) complexes of bidentate diamine ligands, such as bathophenanthroline disulfonate, are stable, recyclable catalysts for the selective aerobic oxidation of terminal olefins to the corresponding alkan-2-ones in a biphasic liquid–liquid system.

The aerobic oxidation of ethylene to acetaldehyde and terminal olefins to the corresponding alkan-2-ones [eqn. (1)–(4)] catalysed by an aqueous solution of palladium(II) and copper(II) salts are collectively known as Wacker oxidations.[1] The function of the copper co-catalyst is to mediate the reoxidation of palladium(0).

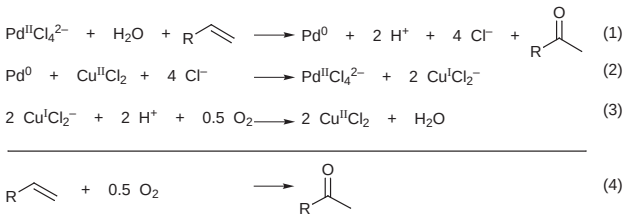

Although commercially successful, this process has several drawbacks. Substantial concentrations of copper salts (*ca.* 1 M) and chlorides (*ca.* 2 M) are added to achieve favourable redox potentials of the Pd^{II}/Pd^0) and Cu^{II}/Cu^{I} couples and to solubilise Cu^{I} as $Cu^{I}Cl_2^-$. Acid (HCl) is required to circumvent clustering of transient atomic palladium. This not only renders the system highly corrosive, but also reduces the catalyst activity, since the rate[2] is inversely proportional to $[H^+]$ and $[Cl^-]^2$. Furthermore, the presence of large amounts of chloride leads to the formation of chlorinated by-products. Hence, much effort has been devoted[1] to the development of alternative co-catalysts, notably the heteropolyacid, $H_3PMo_6V_6O_{40}$, which still requires chloride, albeit in much lower amounts than the conventional Wacker process,[3] and two-component systems involving benzoquinone in combination with iron(II) phthalocyanine[4] or heteropolyacid.[5]

The oxidation of higher olefins introduces additional complications. Rates are much lower owing to their low solubilities in water and raising the temperature results in palladium black formation. Moreover, the products are contaminated with chlorinated by-products and isomerised olefins. Rates can be improved by using water-miscible cosolvents, *e.g.* DMF,[6] or phase transfer catalysis with tetraalkylammonium salts[7] or polyethylene glycols[8] or modified cyclodextrins[9] as inverse phase transfer catalysts. Immobilised catalysts have also been described, *e.g.* palladium-on-vanadium pentoxide,[10] organic polymer-anchored palladium[11] and supported aqueous phase catalysts.[12] However, these systems employ copper/chloride combinations and/or exhibit poor activities and selectivities. There still remains a definite need, therefore, for a system which avoids the use of copper ions, chloride ions and polar organic solvents and which is active, selective and recyclable. We report here a new catalytic system, based on water soluble palladium diamine complexes, which appears to meet these criteria.

Our approach was to stabilise Pd^0 *via* complexation with oxidatively stable (di)amine ligands. In an initial screening we tested ligands **1**–**5** in the oxidation of hex-1-ene at 100 °C.

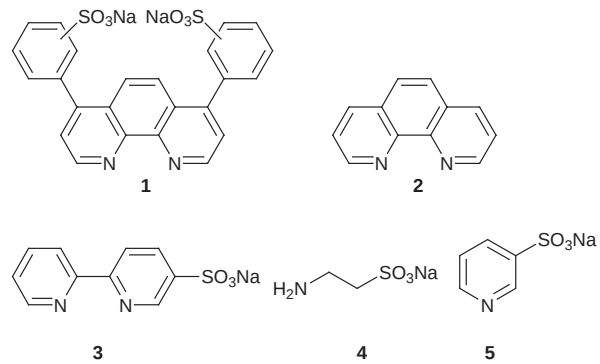

Promising results were observed with the chelating diamines **1**–**3**, while the monodentate ligands **4** and **5** were less effective (Table 1). The best results were observed with bathophenanthroline disulfonate **1**. The catalyst solution was prepared by stirring $Pd(OAc)_2$ (0.0224 g; 0.1 mmol) and **1** (0.0546 g; 0.1 mmol) overnight with 42.5 g of water to afford a clear orange solution. In a typical procedure a 175 ml autoclave was cooled to 0 °C and charged with the catalyst solution, olefin (10 mmol) and internal standard (n-alkane). The autoclave was pressurised with air, heated to 100 °C (30 bar) and kept at this temperature for 10 h. After reaction the autoclave was cooled to 0 °C and depressurised, collecting any volatile material in a liquid nitrogen trap. The mixture was extracted with Et_2O, the extract

Table 1 The palladium catalysed oxidation of olefins[a]

Olefin	Ligand	Olefin conversion (%)	Selectivity to alkanone (%)
Hex-1-ene	**1**	48	99
Hex-1-ene	**2**	42	99
Hex-1-ene	**3**	36	97
Hex-1-ene	**4**	12	40[b]
Hex-1-ene	**5**	2	50[b]
Pent-1-ene	**1**	50	99
Oct-1-ene	**1**	25	99
Cyclopentene	**1**	2	47[c]
Cyclohexene	**1**	2	50[d]
Cyclooctene	**1**	30	100

[a] Conditions: 0.1 mmol $Pd(OAc)_2$, 0.1 mmol ligand, 10 mmol olefin, 10 mmol NaOAc, 10 h at 100 °C and 30 bar in 42.5 g H_2O. [b] Main by-products were hex-2-ene and hex-3-ene. [c] Main by-products were cyclopent-2-en-1-ol and cyclopent-2-en-1-one. [d] Cyclohex-2-en-1-ol, cyclohex-2-en-1-one, benzene and cyclohexane were detected as by-products.

† For Part 9, see G. Verspui, G. Papadogianakis and R. A. Sheldon, *Chem. Commun.*, 1998, 401.

‡ Present address: Laboratory of Industrial Chemistry, Department of Chemistry, University of Athens, Panepistimiopolis - Zogrofou, 15771 Athens, Greece.

Table 2 Recycling of the catalyst[a]

Cycle	Hex-1-ene conversion (%) with NaOAc	Hex-1-ene conversion (%) without NaOAc
1st	48 (99%)	47 (99%)
2nd	44 (96%)	28 (97%)
3rd	40 (95%)	15 (96%)

[a] Conditions as in Table 1, with and without NaOAc (10 mmol).

dried over $MgSO_4$ and analysed by GC using a Varian Star 3400 instrument equipped with a CP Sil 5-CB column (50 m × 0.53 mm).

Under these conditions hex-1-ene underwent 48% conversion to give hexan-2-one in > 99% selectivity. No isomerisation of hex-1-ene and no palladium black formation was observed. Up to 50% conversion (50 turnovers) the rate was independent of [hex-1-ene], indicative of saturation kinetics. Thereafter, the reaction became first order in [hex-1-ene]. When the substrate/catalyst ratio was increased from 100 to 200 the reaction was zero order in hex-1-ene up to 100 turnovers.

Similarly, various terminal and cyclic olefins were oxidised using $Pd(OAc)_2$–**1** under the same conditions (Table 1). Terminal olefins were oxidised selectively, whereas oxidation of cyclopentene and cyclohexene underwent competing allylic oxidation and tended to stop after a few turnovers. At higher temperatures (150 °C) cyclohexene was dehydrogenated into benzene in *ca*. 90% selectivity, in the presence of ionol, as a radical scavenger.

The catalyst could be recycled as is shown in Table 2. The addition of sodium acetate was necessary to stabilise the catalyst. Without NaOAc, formation of palladium black was observed after the second and third cycles. The beneficial effect may be due to preventing the formation of inactive dimers,[13] giant palladium clusters,[14] or even colloidal palladium.[15] Thus, when a solution of the orange complex was heated at 120 °C in the absence of NaOAc the solution became brown–black, indicative of giant cluster or colloidal palladium formation.

In the experiments described in Table 1 stoichiometric amounts of NaOAc were added, but in separate experiments with hex-1-ene it was shown that several equivalents with respect to palladium were sufficient for maintaining stability. The turnover frequency of hex-1-ene was measured as a function of the temperature in the range 70–120 °C. From these data the activation energy was calculated to be 90.2 kJ mol^{-1}. In the presence of sodium acetate the selectivity to hexan-2-one was *ca*. 99% even at 120 °C.

In conclusion, the water soluble bathophenanthroline palladium complex is an effective catalyst for the aerobic oxidation of terminal olefins to the corresponding alkan-2-ones. Catalyst recycling is simple, and due to the absence of $CuCl_2$ and acid, chlorinated and isomerised side products are completely avoided. We are currently investigating the scope of this system, *e.g*. in intramolecular oxypalladation reactions.[16]

Notes and references

1 For recent reviews see: R. Jira, in *Applied Homogeneous Catalysis with Organometallic Compounds*, ed. B. Cornils and W. A. Herrmann, VCH, Weinheim, 1996, pp. 374–393; E. Monflier and A. Mortreux, in *Aqueous Phase Organometallic Catalysis*, ed. B. Cornils and W. A. Herrmann, VCH, Weinheim, 1997, pp. 513–518.

2 I. I. Moiseev, O. G. Levanda and M. N. Vargaftik, *J. Am. Chem. Soc*., 1974, **96**, 1003; P. M. Henry, *Palladium Catalysed Oxidations of Hydrocarbons*, Reidel, Dordrecht, 1980, pp. 41–223.

3 K. I. Matveev, *Kinet. Catal. (Engl. Transl.)*, 1977, **18**, 716; J. H. Grate, D. R. Hamm and S. Mahajan, in *Catalysis of Organic Reactions*, ed. J. Kosak and T. Johnson, Marcel Dekker, Dordrecht, The Netherlands, 1994, pp. 213–264.

4 J.-E. Bäckvall and R. B. Hopkins, *Tetrahedron Lett*., 1988, **29**, 2855; J.-E. Bäckvall, R. B. Hopkins, H. Grennberg, M. M. Mader and A. K. Awasthi, *J. Am. Chem. Soc*., 1990, **112**, 5160.

5 T. Yokata, S. Fujibayashi, Y. Nishiyama, S. Sakaguchi and Y. Ishii, *J. Mol. Catal. A: Chem.*, 1996, **114**, 113.

6 W. H. Clement and C. M. Selwitz, *J. Org. Chem*., 1964, **29**, 241.

7 K. Januszkiewicz and H. Alper, *Tetrahedron Lett*., 1983, **24**, 5159.

8 H. Alper, K. Januszkiewicz and D. J. H. Smith, *Tetrahedron Lett*., 1985, **26**, 2263.

9 E. Monflier, E. Blouet, Y. Barbaux and A. Mortreux, *Angew. Chem.*, 1994, **106**, 2183; E. Monflier, S. Tilloy, E. Blouet, Y. Barbaux and A. Mortreux, *J. Mol. Catal. A: Chem.*, 1996, **109**, 27.

10 A. W. Stobbe-Kreemers, M. Makkee and J. J. F. Scholten, *Appl. Catal. A: Gen.*, 1997, **156**, 219.

11 D. C. Sherrington and H. G. Tang, *J. Catal*., 1993, **142**, 540.

12 J. P. Arhancet, M. E. Davis and B. E. Hanson, *Catal. Lett*., 1991, **11**, 129.

13 S. Wimmer, P. Castan, F. L. Wimmer and N. P. Johnson, *Inorg. Chim. Acta*, 1988, **142**, 13; *J. Chem. Soc., Dalton Trans*., 1989, 403.

14 I. I. Moiseev, in *Catalytic Oxidations: Principles and Applications*, ed. R. A. Sheldon and R. A. van Santen, World Scientific, Singapore, 1995, pp. 203–238 and refs. cited therein; see also G. Schmid, B. Morum and J.-O. Malm, *Angew. Chem*., 1989, **101**, 772; M. Barton and J. P. Atwood, *Coord. Chem. Rev*., 1991, **24**, 43.

15 H. Bönnemann, W. Brijoux, A. S. Tilling and K. Siepen, *Top. Catal*., 1997, **4**, 217.

16 Y. Uozomi, K. Kato and T. Hayashi, *J. Am. Chem. Soc*., 1997, **119**, 5063.

Communication 8/06532B

ChemComm

Investigation of glycerol incorporation into soraphen A

Alison M. Hill,* Jonathan P. Harris and Alexandros P. Siskos

Department of Chemistry, King's College London, Strand, London, UK WC2R 2LS. E-mail: alison.hill@kcl.ac.uk

Received (in Cambridge, UK) 3rd August 1998, Accepted 25th September 1998

Glycerol has been incorporated mid-chain into the polyketide soraphen A 1 at C-3,4 and C-11,12; the *pro*-(*S*)-hydroxymethyl group of glycerol is lost and one of the hydrogens in the *pro*-(*R*)-hydroxymethyl group is retained at C-11 which excludes hydroxymalonate as the immediate precursor to the vicinal methoxy groups at C-11,12.

In polyketide biosynthesis, both the chain starter and extension units are bound *via* thioester linkages to the polyketide synthase (PKS) where condensation takes place. Subsequent condensations occur with the growing acyl chain remaining enzyme bound, until a chain of the correct length is formed. This is released to give the first enzyme free intermediate which can undergo further enzymically catalysed modifications to yield the final product. Acetate and propionate *per se* are not used as the chain extension units, but are activated by carboxylase enzymes to generate malonyl CoA and methylmalonyl CoA, respectively, which undergo a decarboxylative condensation with the enzyme bound acyl chain to add a C_2 or C_3 unit.[1]

The carbon skeleton of the potent antifungal polyketide metabolite, soraphen A **1**, is derived from a benzoyl CoA starter unit, three acetate and three propionate chain extender units and three methionines (Fig. 1);[2] the vicinal hydroxy groups at carbons 3,4 and 11,12 were not labelled by acetate. Unpublished work from Höfle's laboratory has shown that [2-^{13}C]glycerol was incorporated into **1** at carbons 4 and 12.[3] The incorporation of glycerol mid-chain into polyketide metabolites is highly unusual and has been observed in only two other metabolites: leucomycin[4] and concanomycin.[5] It has been postulated in both cases that glycerol is converted to glycolate (or an activated form such as 2-phosphoglycolate) prior to incorporation into the final metabolite. The incorporation of glycolate into geldanamycin[6] has also been observed and it is postulated to be an intermediate in niddamycin biosynthesis,[7] however, it is possible that for all four polyketides, activation of this C_2 unit by a carboxylase enzyme to generate hydroxymalonyl CoA or methoxymalonyl CoA occurs. Here we report the results of preliminary labelling experiments which establishes that the incorporation of glycerol mid-chain into soraphen A is stereospecific and that hydroxymalonate cannot be the immediate precursor for the C_2 unit incorporated at C-11,12.

When [1,3-$^{13}C_2$]glycerol **2a** was administered to the organism,† enhanced signals in the ^{13}C NMR spectrum were observed in the resulting **1** compared with an unlabelled control sample. The feeding experiment resulted in a complex labelling pattern as glycerol had been extensively metabolised through glycolysis, the Krebs cycle and the shikimate pathway. Consequently, enrichments were observed for all the β-positions of acetate-derived carbons, for all positions which originate from propionate, and the phenylalanine-derived carbons C-17, 2′/6′, and 4′ (Fig. 2). Enrichment of the methionine-derived carbon atoms was also observed due to the metabolism of glycerol to *S*-adenosylmethionine *via* serine. The highest level of incorporation of ^{13}C label into **1**, however, was observed at C-3 and 11 (11–15-fold). The feeding experiment with [2-^{13}C]glycerol also gave rise to a complex labelling pattern which was similar but not identical to that obtained by Höfle.[3] The ^{13}C label was incorporated into C-4 and 12 as well as the carboxylate-derived positions of acetate and the phenylalanine-derived carbons 3′/5′ (data not shown). However, the enrichment levels we observed were much higher (*e.g.* 8–13-fold for C-4 and 12, *cf.* 3-fold) and we also observed enrichments of the carboxylate-derived positions of propionate and the phenylalanine-derived carbon 1′ (data not shown).

The above results demonstrated that glycerol was being metabolised *via* glycerate to acetate. Glycerate can also be oxidised to give serine, and subsequently glycine, which is a source of glycolate.[4] Hence, we decided to investigate the possible involvement of glycolate as the C_2 source for the vicinal hydroxy groups at carbons 3,4 and 11,12 by feeding [2-^{13}C]glycine. When [2-^{13}C]glycine was fed to *Sorangium cellulosum*, however, no enhanced signals in the ^{13}C NMR spectrum were observed in the resulting **1** compared with an unlabelled control sample. Labelling studies with [1-^{13}C]glycine and [1-^{13}C]glycolate to investigate leucomycin A biosynthesis resulted in the incorporation of neither precursor into the metabolite, which the authors explained was due to a cell-membrane permeability problem.[4] Hence, it is possible that we have the same problem and that glycolate is still a possible precursor in soraphen A biosynthesis.

To investigate the mechanism of glycerol incorporation into soraphen A further, [$^2H_8$]- and *rac*-, (*R*)- and (*S*)-[1-$^2H_2$]-glycerol‡ were administered to *S. cellulosum* and the resulting **1** analysed by ^{2}H NMR spectroscopy. Deuterium was observed at D-11 and D-14a but it was not incorporated at the same level in all cases (Table 1): the highest percentage incorporation was observed for [$^2H_8$]glycerol and (*R*)-[1-$^2H_2$]glycerol **2b**. The C-3 propionate-derived positions (*i.e.* H-18, 20 and 21) and methionine-derived positions (*i.e.* H-19, 22 and 23) were labelled for the racemic glycerol samples (data not shown) indicating that extensive metabolism had once again occurred.

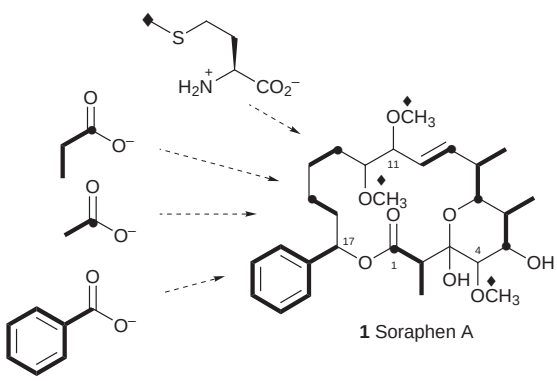

Fig. 1 Biosynthetic origin of soraphen A **1** (ref. 2).

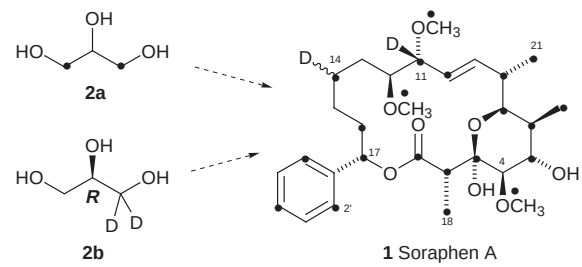

Fig. 2 Incorporation of [1,3-$^{13}C_2$]- and (*R*)-[1-$^2H_2$]-glycerol (**2a** and **2b**) into soraphen A **1**.

Table 1 Incorporation of [$^2H_8$]- and *rac*-, (*R*)- and (*S*)-[1-$^2H_2$]-glycerol into soraphen A **1**

Glycerol	^{2}H Enrichment (%)[a] D-11	D-14
[$^2H_8$]	6.6	2.3
rac-[1-$^2H_2$]	1.5	2.0
(*R*)-[1-$^2H_2$]	5.4	4.3
(*S*)-[1-$^2H_2$]	1.1	0.5

[a] Expressed as % deuterium calculated from natural abundance chloroform signal.

No deuterium was observed at H-4 in **1** from the [$^2H_8$]glycerol feeding experiment, indicating that oxidation at C-2 had taken place before incorporation into H-4. It was not possible to say with certainty that H-12 was not labelled as its signal overlaps with those of H-19 and 23. The incorporation of deuterium at H-11 was 5-fold higher for (*R*)-glycerol compared to its antipode; moreover, incorporation into H-14 was also higher for the (*R*)-enantiomer, demonstrating that this enantiomer was metabolised by the organism in preference to (*S*)-glycerol. Recent experiments conducted with chiral glycerols have shown that (*R*)-glycerol is metabolised in preference to its enantiomer in the biosynthesis of fluoroacetate and 4-fluorothreonine in *Streptomyces cattleya*,[8] and in the biosynthesis of macrophomic acid by the fungus *Macrophoma commelinae*.[9] It is notable that the three different organisms, producing structurally diverse compounds, all metabolise glycerol such that the *pro*-(*R*)-hydroxymethyl group is retained in the metabolite and the *pro*-(*S*)-hydroxymethyl group is lost.

The results from these experiments are consistent with the following observations: the *pro*-(*R*)-hydroxymethyl group is retained and incorporated into **1** at C-3 and 11 [consequently the *pro*-(*S*)-hydroxymethyl group is lost] and C-2 of glycerol is incorporated into C-4 and 12 of **1**. Oxidation of C-2 takes place prior to incorporation into C-4 and possibly also for C-12.

These results raise some interesting questions on how the C_2 unit is incorporated by the soraphen A PKS. Chain extender units, such as malonyl CoA, are attached to the PKS *via* thioester linkages. Clearly, glycerol itself cannot be the immediate precursor in soraphen A biosynthesis. Oxidation of the *pro*-(*S*)-hydroxymethyl group would provide a carboxy group which could be used in the decarboxylative condensation step with the enzyme bound tri- and hepta-ketide intermediates. However, how the *pro*-(*R*)-hydroxymethyl group attaches itself to the PKS is a much more difficult problem. It is possible that glycerol is metabolised to glycolate and then hydroxymalonate (or even methoxymalonate). This mechanism would require oxidation of the *pro*-(*R*)-hydroxymethyl group to a carboxylic acid or coenzyme A thioester, which could then attach to the PKS *via* a thioester linkage. This mechanism is consistent with the ^{13}C labelling experiments, but it would result in complete loss of the deuterium label on the *pro*-(*R*)-hydroxymethyl group, which is inconsistent with the ^{2}H labelling experiments. Hence, while it is possible for the C_2 unit incorporated into C-3,4 of **1** to derive from hydroxy- or methoxy-malonate, retention of the deuterium label at H-11 excludes these precursors as the source for the C_2 unit incorporated at C-11,12. The *pro*-(*R*)-hydroxymethyl group of glycerol must remain as an alcohol (or phosphorylated derivative) or be oxidised to an aldehyde before incorporation into C-11,12; *it cannot be oxidised to a carboxylic acid or coenzyme A thioester*. An alternative, but less likely, explanation is that the *pro*-(*R*)-hydroxymethyl group of glycerol is oxidised to a carbonyl moiety and subsequent reduction, with redelivery of deuterium from a co-factor, results in deuterium enrichment at H-11. Experiments are in progress to further probe the mechanism of glycerol incorporation into soraphen A and to identify a more immediate precursor than glycerol in its biosynthesis. Possible candidates include hydroxypyruvate and glycerate.

Sorangium cellulosum kanamycin resistant wild-type strain M15 was provided by Novartis, Research Triangle Park, North Carolina, USA. We thank Dr T. Schupp (Novartis, Switzerland) for providing Probion S and Mrs J. Hawkes and Mr J. Cobb for NMR support. Deuterium NMR spectra were obtained using the Bruker AMX 400 University of London Intercollegiate Research Service for NMR at King's College. This work was financially supported by funding from King's College, London, The Royal Society, The University of London Central Research Fund and the State Scholarships Foundation (Republic of Greece) (A. P. S.). We thank Dr H. C. Hailes (University College London) for helpful discussions.

Notes and references

† Cultures of a kanamycin resistant strain of *S. cellulosum* (wild-type strain M15) were used in the incorporation experiments. In a typical experiment, production medium G55 (ref. 11) containing 50 g l^{-1} XAD-1180 resin was inoculated with a 9 day old growth medium G51t (ref. 12) culture and isotopically labelled compounds were pulse-fed in duplicate every 48 h between 10 and 16 days post inoculation. [1,3-$^{13}C_2$]-, [2-^{13}C]- and [$^2H_8$]-glycerol (1 g each) and [1-$^2H_2$]-, (*R*)-[1-$^2H_2$]- and (*S*)-[1-$^2H_2$]-glycerol (0.4–0.58 g each) were added as sterile aqueous solutions. The cultures were harvested on day 19 and the resin extracted with Pr^{i}OH. The crude soraphen A was purified by flash chromatography and preparative reverse phase HPLC (C-18) prior to NMR analysis. Typically 30 mg l^{-1} of soraphen A was obtained.

‡ [1-$^2H_2$]Glycerol was made in four steps from solketal: (i) solketal, $KMnO_4$, NaOH; (ii) CH_2N_2 (60% over 2 steps); (iii) $LiAlD_4$ (95%); (iv) AcOH, H_2O, room temp., 16 h (97%). (*R*)- and (*S*)-[1-$^2H_2$]glycerol were made in two steps from methyl isopropylidine-L-glycerate and methyl isopropylidine-D-glycerate, respectively, in 92% yield as above using a modified version of the protocol previously reported (ref. 8); (*R*)-[1-$^2H_2$]solketal, $[\alpha]_D$ +11.2 (*c* 9.4, MeOH) [lit. +15.3 (neat) (ref. 9)] and (*S*)-[1-$^2H_2$]solketal $[\alpha]_D$ −12.4 (*c* 8.7, MeOH) [lit. −14.9 (neat) (ref. 9)]. All three compounds contained 94% deuterium at C-1.

1 D. O'Hagan, *The Polyketide Metabolites*, 1991, Ellis Horwood, Chichester.
2 A. M. Hill and J. P. Harris, unpublished results.
3 N. Bedorf, B. Böhlendorf, D. Schomberg, K. Gerth, H. Reichenbach and G. Höfle, unpublished results.
4 S. Omura, K. Tsuzuki, A. Nakagawa and G. Lukacs, *J. Antibiot*., 1983, **36**, 611.
5 K. U. Bindseil and A. Zeeck, *Helv. Chim. Acta*, 1993, **76**, 150.
6 A. Haber, R. D. Johnson and K. L. Rinehart Jr, *J. Am Chem. Soc*., 1977, **99**, 3541.
7 S. J. Kakavas, L. Katz and D. Stassi, *J. Bacteriol*., 1997, **179**, 7515.
8 J. Nieschalk, J. T. G. Hamilton, C. D. Murphy, D. B. Harper and D. O'Hagan, *Chem. Commun*., 1997, 799.
9 H. Oikawa, K. Yagi, K. Watanabe, M. Honma and A. Ichihara, *Chem. Commun*., 1997, 97.
10 R. E. Hill, A. Iwanow, B. G. Sayer, W. Wysocka and I. D. Spenser, *J. Biol. Chem*., 1987, **262**, 7463.
11 S. Jaoua, S. Neff and T. Schupp, *Plasmid*, 1992, **28**, 157.
12 T. Schupp, C. Toupet, B. Cluzel, S. Neff, S. Hill, J. J. Beck and J. M. Ligon, *J. Bacteriol.*, 1995, **177**, 3673.

Communication 8/06112B

ChemComm

New asymmetric transformation of optically active allene-1,3-dicarboxylate and its application to the formal asymmetric synthesis of (−)-epibatidine

Manabu Node,* Kiyoharu Nishide, Toshio Fujiwara and Shogo Ichihashi

Kyoto Pharmaceutical University, Misasagi, Yamashina, Kyoto, 607-8414, Japan. E-mail: node@mb.kyoto-phu.ac.jp

Received (in Cambridge, UK) 17th August 1998, Accepted 23rd September 1998

A new efficient synthesis of di-(−)-L-menthyl (*R*)-allene-1,3-dicarboxylate [(*R*)-1] involving asymmetric transformation through *epimerization–crystallization* with the assistance of a catalytic amount of Et_3N was developed; the highly *endo*-selective asymmetric Diels–Alder reaction of (*R*)-1 with *N*-Boc-pyrrole for the asymmetric synthesis of 7-*tert*-butoxycarbonyl-7-azabicyclo[2.2.1]heptan-2-one [(−)-6], a synthetic intermediate of (−)-epibatidine, is described.

Allene-1,3-dicarboxylates are useful for [4 + 2] cycloaddition as dienophiles.[1] Kanematsu and his colleagues have reported the highly diastereoselective Diels–Alder reaction of cyclopentadiene with optically active dimenthyl allene-1,3-dicarboxylate **1**, which was prepared by optical resolution using crystallization from a diastereomeric mixture of di-(−)-L-menthyl allene-1,3-dicarboxylates.[2] Naruse and his colleagues recently reported the enantiomeric enrichment of allene-1,3-dicarboxylates by a chiral organoeuropium reagent.[3] For the synthesis of optically active allene, the former method using optical resolution provides a low yield (< 25%), and the latter method has major drawbacks, *i.e*. the need for an equimolar amount of expensive $Eu(hfc)_3$, and the partial decomposition of the substrate due to the long reaction times needed. Therefore, a more efficient method for the preparation of optically active allene-1,3-dicarboxylate is required. Although several crystallization-induced asymmetric transformations by racemization have been reported,[4] the asymmetric transformation of dissymmetric compounds such as allenes has not been examined. We report here a new efficient synthesis of optically active allene-1,3-dicarboxylate by asymmetric transformation through *epimerization–crystallization* with the assistance of a catalytic amount of Et_3N, and its application to the formal total synthesis of (−)-epibatidine using the Diels–Alder reaction as a key step.

Since allene-1,3-dicarboxylate is an excellent Michael acceptor,[5] the epimerization of optically active allene-1,3-dicarboxylate, which was prepared from di-L- or -D-menthyl acetone-1,3-dicarboxylate by a new method[6] using 2-chloro-1,3-dimethylimidazolinium chloride (DMC), as shown in Scheme 1, was examined in the presence of a catalytic amount of Et_3N.

Thus, an optically pure di-(−)-L-menthyl (*R*)-allene-1,3-dicarboxylate [(*R*)-**1**][2] was treated with Et_3N (0.1 equiv.) in an NMR tube to give a diastereomeric mixture of **1** (*R*:*S* = 4:5) within 30 min. This experiment shows that these diastereomers are in equilibrium in the presence of a catalytic amount of Et_3N, as shown in Scheme 2. This result suggests that crystallization-induced asymmetric transformation of **1** would be possible, since the *R* diastereomer formed good crystals.[2a]

To crystallize the *R* diastereomer, a pentane solution of a diastereomeric mixture (*R*:*S* = 4:5) of di-(−)-L-menthyl allene-1,3-dicarboxylate **1** and 0.01 equiv. of Et_3N was kept below −20 °C for 2 days. After removal of the mother liquid, the precipitated crystals were washed with cooled pentane. This crystallization procedure of the mother liquid was repeated twice. Colorless crystalline (*R*)-**1** was obtained in 90% yield (> 98% de). Similarly, the enantiomer (*S*)-**1** was also obtained

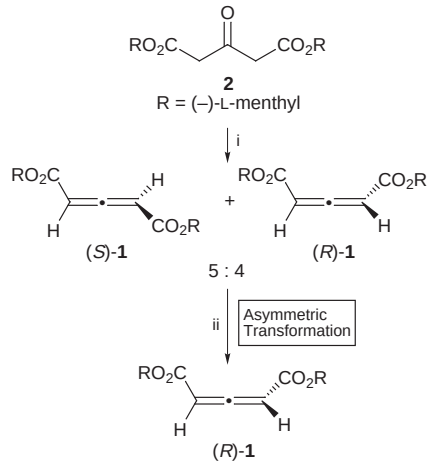

Scheme 1 *Reagents and conditions*: i, DMC, Et_3N, CH_2Cl_2, room temp., 86%; ii, Et_3N (0.01 equiv.), pentane, crystallization (×3), 90%.

by the above asymmetric transformation using (+)-D-menthol as a chiral auxiliary.

Next, we applied di-(−)-L-menthyl (*R*)-allene-1,3-dicarboxylate (*R*)-**1** to an asymmetric synthesis of (−)-epibatidine, which was isolated from the skin of the Ecuadorian poison frog *Epipedobates tricolor*, and possesses a unique 7-azabicyclo-[2.2.1]heptane skeleton and a potent non-opioid analgesic effect.[7] There have been only a few reports[8] on the asymmetric synthesis of (−)-epibatidine, although there have been many reports on its total synthesis.[9,10] We planned the asymmetric synthesis of a synthetic intermediate for (−)-epibatidine using the Diels–Alder reaction of **1** according to Kanematsu *et al*.,[2a] as shown in Scheme 3.

The Diels–Alder reaction of (±)-dimethyl allene-1,3-dicarboxylate with *N*-Boc-pyrrole (10 equiv.) gave almost equimolar amounts of the *endo* and *exo* adducts, both at a low temperature with the assistance of a Lewis acid [$AlCl_3$ (1.2 equiv.), CH_2Cl_2, −78 °C, 12 h, 73%], and at a high temperature[9d] [toluene, 90 °C, 12 h, 89%]. On the other hand, we found that the same reaction of di-L-(−)-menthyl allene-1,3-dicarboxylate (*R*)-**1** with *N*-Boc-pyrrole and $AlCl_3$ in CH_2Cl_2 at −78 °C for 13 h gave the endo adduct (−)-**3** as a sole product in 86% yield. The absolute stereochemistry of the *endo*

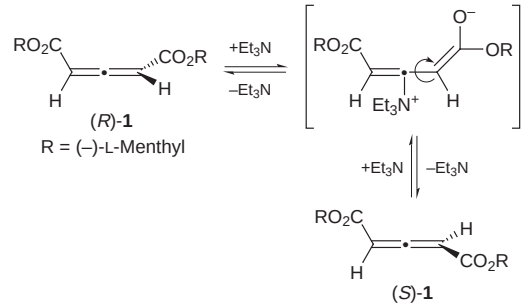

Scheme 2

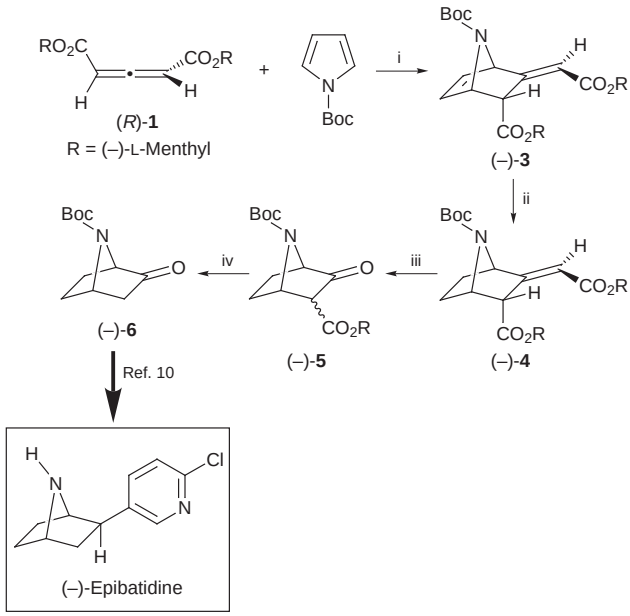

Scheme 3 *Reagents and conditions*: i, $AlCl_3$, CH_2Cl_2, −78 °C, 13 h, 86%; ii, 10% Pd/C, H_2, EtOAc, room temp., 99%; iii, O_3, PPh_3, CH_2Cl_2, −78 °C, 52%; iv, 10% HCl, heat, then Boc_2O, Et_3N, CH_2Cl_2, room temp., 55%.

adduct (−)-**3** was elucidated by an X-ray crystallographic analysis.

The observed significant difference in *endo*/*exo* selectivity between the dimethyl ester and the di-L-(−)-menthyl ester could be explained on the basis of steric repulsion between the *N*-Boc group of the diene and the methyl or menthyl group in the dienophile **1**, based on an X-ray crystallographic analysis.[2a]

The *endo* adduct (−)-**3** was subsequently converted into a synthetic intermediate (−)-**6**[10] for (−)-epibatidine. Thus, regioselective hydrogenation of non-conjugated olefin on (−)-**3** with 10% Pd/C gave the dihydro derivative (−)-**4** quantitatively. After ozonolysis of the remaining double bond, the obtained β-keto ester **5** was subjected to hydrolysis, decarboxylation, and *N*-*tert*-butoxycarbonylation (reprotection of the deprotected secondary amine) to give (−)-**6** in moderate yield; its specific rotation {$[\alpha]_D^{17}$ −74.5 (*c* 1.02, $CHCl_3$), lit.[10a] $[\alpha]_D^{26}$ −75.1 (*c* 1.56, $CHCl_3$)} and spectroscopic data were identical to those in the literature.[10] This transformation constitutes a formal asymmetric synthesis of (−)-epibatidine.

In conclusion, we have developed the first asymmetric transformation of dissymmetric allene-1,3-dicarboxylate through *epimerization* based on addition–elimination with a tertiary amine, and a quite efficient synthesis of (−)-**6** from di-(−)-L-menthyl acetone-1,3-dicarboxylate.

Notes and references

1 For examples: K. A. Parker and S. M. Ruder, *J. Am. Chem. Soc*., 1989, **111**, 5948; M. Yoshida, Y. Hidaka, Y. Nawata, J. M. Rudziñski, E. Osawa and K. Kanematsu, *J. Am. Chem. Soc.*, 1988, **110**, 1232.

2 (*a*) I. Ikeda, K. Honda, E. Osawa, M. Shiro, M. Aso and K. Kanematsu, *J. Org. Chem.*, 1996, **61**, 2031; (*b*) M. Aso, I. Ikeda, T. Kawabe, M. Shiro and K. Kanematsu, *Tetrahedron Lett*., 1992, **33**, 5787; (*c*) I. Ikeda, A. Gondo, M. Shiro and K. Kanematsu, *Heterocycles*, 1993, **36**, 2669.

3 Y. Naruse, H. Watanabe, Y. Ishiyama and T. Yoshida, *J. Org. Chem*., 1997, **62**, 3862; Y. Naruse, H. Watanabe and S. Inagaki, *Tetrahedron: Asymmetry*, 1992, **3**, 603.

4 W.-C. Shieh, J. A. Carlson and G. M. Zaunius, *J. Org. Chem*., 1997, **62**, 8271; J. D. Armstrong, III, K. K. Eng, J. L. Keller, R. M. Purick, F. W. Hartner, Jr., W.-B. Choi, D. Askin and R. P. Volante, *Tetrahedron Lett*., 1994, **35**, 3239; S. K. Boyer, R. A. Pfund, R. E. Portmann, G. H. Sedelmeier and H. F. Wetter, *Helv. Chim. Acta*, 1988, **71**, 337; P. J. Reider, P. Davis, D. L. Hughes and E. J. J. Grabowski, *J. Org. Chem*., 1987, **52**, 955; T. Sohda, K. Mizuno and Y. Kawamatsu, *Chem. Pharm. Bull*., 1984, **32**, 4460; S. Shibata, H. Matsushita, H. Kaneko, M. Noguchi, M. Saburi and S. Yoshikawa, *Heterocycles*, 1981, **16**, 1901; J. C. Clark, G. H. Phillipps and M. R. Steer, *J. Chem. Soc., Perkin Trans. 1*, 1976, 475; M. K. Hargreaves and M. A. Khan, *J. Chem. Soc., Perkin Trans. 1*, 1973, 1204.

5 M. E. Jung, *Comprehensive Organic Synthesis*, ed. B. M. Trost and I. Fleming, Pergamon, Oxford, 1991, vol. 4, pp. 53–58.

6 M. Node, T. Fujiwara, S. Ichihashi and K. Nishide, *Tetrahedron Lett*., 1998, **39**, 6331.

7 T. F. Spande, H. M. Garraffo, M. W. Edwards, H. J. C. Yeh, L. Pannell and J. W. Daly, *J. Am. Chem. Soc*., 1992, **114**, 3475.

8 Asymmetric synthesis of (−)-epibatidine, see: S. Aoyagi, R. Tanaka, M. Naruse and C. Kibayashi, *Tetrahedron Lett*., 1998, **39**, 4513; C. D. Jones, N. S. Simpkins and G. M. P. Giblin, *Tetrahedron Lett*., 1998, **39**, 1023; H. Kosugi, M. Abe, R. Hatsuda, H. Uda and M. Kato, *Chem. Commun*., 1997, 1857; B. M. Trost and G. R. Cook, *Tetrahedron Lett*., 1996, **37**, 7485.

9 For recent synthetic studies on epibatidine, see (*a*) N. S. Sirisoma and C. R. Johnson, *Tetrahedron Lett*., 1998, **39**, 2059; (*b*) M. Ikeda, Y. Kugo, Y. Kondo, T. Yamazaki and T. Sato, *J. Chem. Soc., Perkin Trans. 1*, 1997, 3339; (*c*) G. M. P. Giblin, C. D. Jones and N. S. Simpkins, *Synlett*, 1997, 589; (*d*) N. P. Pavri and M. L. Trudell, *Tetrahedron Lett*., 1997, **38**, 7993; (*e*) S. Singh and G. P. Basmadjian, *Tetrahedron Lett*., 1997, **38**, 6829. Also see the references cited therein.

10 (*a*) D. L. J. Clive and V. S. C. Yeh, *Tetrahedron Lett*., 1998, **39**, 4789; (*b*) S. R. Fletcher, R. Baker, M. S. Chambers, R. H, Herbert, S. C. Hobbs, S. R. Thomas, H. M. Verrier, A. P. Watt and R. G. Ball, *J. Org. Chem*., 1994, **59**, 1771; (*c*) A. Hernández, M. Marcos and H. Rapoport, *J. Org. Chem*., 1995, **60**, 2683; (*d*) J. A. Campbell and H. Rapoport, *J. Org. Chem*., 1996, **61**, 6313; (*e*) E. Albertini, A. Barco, S. Benetti, C. De Risi, G. P. Pollini and V. Zanirato, *Tetrahedron*, 1997, **53**, 17 177.

Communication 8/06477F

An efficient binuclear catalyst for decomposition of formic acid

Yuan Gao,[a] Joshi Kuncheria,[a] Glenn P. A. Yap[b] and Richard J. Puddephatt[a]

[a] *Department of Chemistry, University of Western Ontario, London, Canada N6A 5B7. E-mail: pudd@julian.uwo.ca*
[b] *Department of Chemistry and Biochemistry, University of Windsor, Sunset Drive, Windsor, Canada N9B 3P4*

Received (in Bloomington, IN, USA) 24th July 1998, Accepted 25th September 1998

The complex $[Ru_2(\mu\text{-}CO)(CO)_4(\mu\text{-}dppm)_2]$ is more active than mononuclear ruthenium complexes as a catalyst for decomposition of formic acid to CO_2 and H_2; under conditions of highest activity, a coordinatively unsaturated diruthenium dihydride $[Ru_2H(\mu\text{-}H)(\mu\text{-}CO)(CO)_2(\mu\text{-}dppm)_2]$ is present and can be isolated from solution.

This paper reports the first study of the decomposition of formic acid to hydrogen and carbon dioxide using a locked binuclear catalyst and presents evidence that this is an unusual catalytic reaction in which two metals can act cooperatively to give enhanced activity.† The reversible reaction between HCO_2H and $H_2 + CO_2$ has been the subject of considerable interest, either for catalytic transfer hydrogenation using formic acid or for utilization of CO_2 as a reagent in organic synthesis.[1,2]

The reaction of $[Ru_2(\mu\text{-}CO)(CO)_4(\mu\text{-}dppm)_2]$ **1**,[3] dppm = $Ph_2PCH_2PPh_2$, in acetone (5×10^{-3} M) with formic acid (10^{-1} M) in a closed tube at 20 °C was monitored by NMR. The products were H_2 [$\delta(^1H)$ 4.5] and CO_2 [$\delta(^{13}C)$ 125.8] only and the reaction was complete in 0.3 h, corresponding to a mean turnover rate of *ca.* 70 h^{-1}, and considerably higher activity was observed when the reaction was carried out in an unsealed vessel, for reasons discussed below. The activity is significantly higher than for comparable mononuclear ruthenium complex catalysts: for example, $[RuHBr(CO)(PEt_2Ph)_3]$ gives a turnover rate of *ca.* 4 h^{-1} in refluxing acetic acid (117 °C).[1a]

The high catalytic activity of **1** prompted a more detailed study and some important features of the binuclear catalysis have been elucidated. The catalysis is more efficient in the dipolar aprotic solvent acetone than in solvents such as toluene or dichloromethane. The catalytic reaction is strongly or completely inhibited by the presence of excess CO; in a sealed vessel, CO dissociates from **1** at intermediate stages of reaction and then acts as inhibitor, whereas, in a vessel in which evolved gases sweep CO from the system, this effect cannot occur and so the catalysis is faster. The reaction appears not to be wholly intramolecular since decomposition of either HCO_2D or DCO_2H leads to formation of a mixture of H_2, HD and D_2 rather than HD alone, but the conclusion is weakened by the observation that decomposition of HCO_2H in the presence of D_2 gives both H_2 and HD. The final product mixture from decomposition of HCO_2D or DCO_2H is approximately that expected from statistical considerations ($H_2 : HD : D_2 = 1 : 2 : 1$, determined by MS) but in the very early stages of reaction H_2 is predominant. Under these reaction conditions, there was no evidence for reversibility which would lead to isomerization between HCO_2D and DCO_2H. Decomposition of $H^{13}CO_2H$ gave only H_2 and $^{13}CO_2$, with no free or coordinated ^{13}CO detectable by either IR or ^{13}C NMR.

There were interesting changes in the ruthenium complexes present at various stages of the catalytic reaction and several of these could be isolated or identified spectroscopically. When the reaction was carried out in a sealed tube, the only ruthenium complex present when reaction was complete was unchanged **1** but other complexes were present during catalysis (Scheme 1). The first complex formed at −30 °C was $[Ru_2(\mu\text{-}H)(\mu\text{-}CO)(CO)_4(\mu\text{-}dppm)_2]^+$ **2**, as the formate salt.‡ This complex is formed by protonation of the Ru–Ru bond of **1** and the same cation is formed by protonation with other acids such as $H[BF_4]$.[4] Next to be formed was the cation $[Ru_2(\mu\text{-}HCO_2)(CO)_4(\mu\text{-}dppm)_2]^+$ **3** (also as the formate salt), whose spectroscopic properties‡ are very similar to the known μ-acetate analogue;[4,5] the first formation of H_2 could be detected at this stage. When most formic acid was consumed, two more complexes were formed transiently. The major complex was characterized as $[Ru_2H_2(CO)_4(\mu\text{-}dppm)_2]$ **5**, by the following spectroscopic data.‡[6] In the ^1H NMR spectrum, a hydride resonance at $\delta(^1H)$ −9.25 [qnt, J(PH) 9 Hz] integrated for two protons and a single resonance at $\delta(CH_2P_2)$ 4.6 were observed, in the ^{13}C NMR spectrum a single terminal carbonyl resonance was observed at δ(CO) 196.8, and in the ^{31}P NMR spectrum a singlet was observed at δ(P) 34.3. These data indicate structure **5**, having D_{2h} symmetry; a less symmetrical but fluxional structure is also possible[6] though no change in the NMR spectra was observed at −70 °C. The second transient complex was tentatively identified as $[Ru_2H(HCO_2)(CO)_4(\mu\text{-}dppm)_2]$ **4**.‡ It is characterized in the ^1H NMR by resonances at δ −6.7 (br s, 1H, RuH) and at δ 8.5 (s, 1H, HCO_2), in the ^{13}C NMR (in a reaction using $H^{13}CO_2H$) by δ 165 (s, CH, HCO_2) (the concentration of **4** was never great enough to allow identification of the metal carbonyl resonances even using ^{13}C enriched starting material **1**) and in the ^{31}P NMR by a single resonance at δ 39.8.[5] If structure **4** is correct, it is required to be fluxional in order to give a single resonance in the ^{31}P NMR spectrum.[4] Further

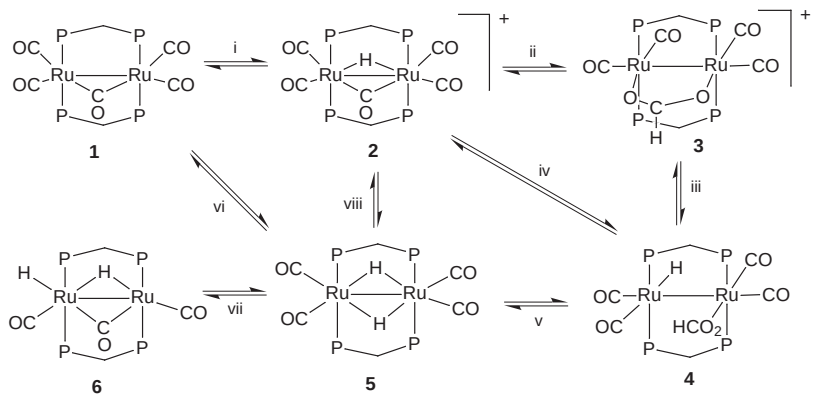

Scheme 1 *Reagents*: i, H^+; ii, HCO_2H, $-H_2$; iii, H_2, $-H^+$; iv, HCO_2^-, −CO; v, $-CO_2$; vi, CO, $-H_2$; viii, −CO; viii, H^+, CO, $-H_2$.

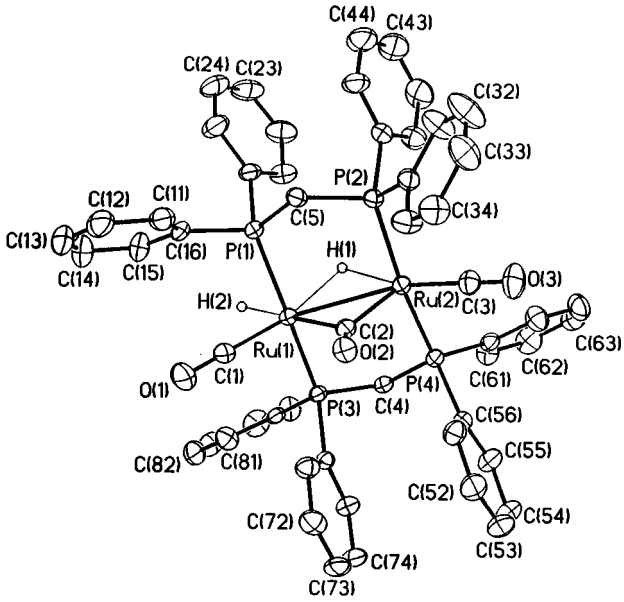

Fig. 1 A view of the structure of $[Ru_2H(\mu\text{-}H)(\mu\text{-}CO)(CO)_2(\mu\text{-}dppm)_2]$. Distances (Å): Ru(1)–Ru(2) 2.8769(5), Ru(1)–C(1) 1.857(5), Ru(1)–C(2) 2.198(5), Ru(2)–C(2) 2.006(4), Ru(2)–C(3) 1.841(5). The hydride H-atoms were located but not refined; approximate distances Ru(1)–H(1) 2.16, Ru(2)–H(1) 2.16, Ru(1)–H(2) 1.66.

study indicated that the concentration of **5** with respect to **2** was pH dependent, since addition of Et_3N led to an increase in the relative concentration of **5**. Overall then, at high $[HCO_2H]$, complex **1** reacted to give **2** and **3** and, as HCO_2H was consumed, the concentrations of these complexes decreased and the transient complexes **4** and **5** appeared, quickly followed by reformation of **1**. These observations are readily rationalized since **5** is expected to be very reactive towards formic acid, and formate probably dissociates easily from **4** in the presence of formic acid to give the less nucleophilic anion $[H(O_2CH)_2]^-$; hence the concentration of these complexes **4** and **5** only builds up to detectable levels when the concentration of formic acid is low.

When the reaction was carried out in an unsealed vessel, the initial reactions were similar but a new complex $[Ru_2H(\mu\text{-}H)(\mu\text{-}CO)(CO)_2(\mu\text{-}dppm)_2]$, **6**, was formed in the later stages rather than **4** or **5**. Complex **6** is a unique example of a coordinatively unsaturated binuclear ruthenium dihydride;[4,6] it could be crystallized from the reaction mixture and was fully characterized by an X-ray structure determination (Fig. 1) as well as by spectroscopic methods.‡ Complex **6** was stable in the solid state but in solution it was stable only in the presence of hydrogen and in the complete absence of oxygen; it reacted rapidly with CO to give **1** with loss of H_2. Clearly, this high reactivity of **6** with CO explains why no **6** is formed when the reaction is carried out in a sealed tube; **6** reacts with one equivalent of CO to give **5** and then with a second equivalent of CO to give **1** and H_2. Solutions containing the coordinatively unsaturated complex **6** were particularly active for further catalytic decomposition of formic acid.

It is interesting to speculate on why the binuclear system described above is so reactive for decomposition of formic acid. The key steps in the initial catalytic reaction are likely to be the overall oxidative addition of formic acid to ruthenium(0) to give a hydrido(formato) complex and then probably a ß-elimination from the formate to give a transient dihydrido(CO_2) complex which ultimately yields H_2 and CO_2. Both of these proposed steps require a vacant coordination site, and the necessary dissociation of two CO ligands is probably easier to accomplish in the binuclear system. There is some independent evidence for CO labilization *cis* to the bridging hydride ligand in complex **2**. Thus, exposure of **2** to ^{13}CO led to carbonyl exchange but the substitution in the terminal carbonyl sites *cis* to the μ-H ligand [$\delta(^{13}C)$ 198.6] was much faster (exchange detected in < 1 h)

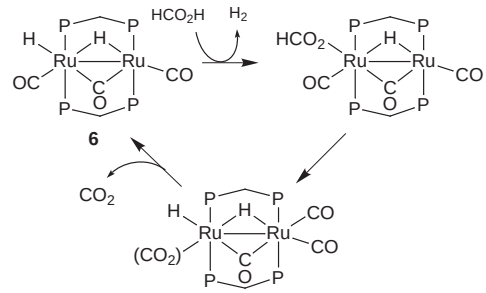

Scheme 2 A possible mechanism of catalysis.

than in the *trans* terminal [$\delta(^{13}C)$ 200.8] or bridging [$\delta(^{13}C)$ 278.6] carbonyl sites (exchange detected after one day).§ While the reactions of Scheme 1 provide a viable route for the catalytic reaction in the presence of CO, the data suggest that CO-deficient complexes, such as **6**, are most active and it is likely that other key intermediates are too short-lived to be detected. A reasonable catalytic cycle involving **6** is shown in Scheme 2.

In summary, this article describes a novel binuclear catalytic system for formic acid decomposition, in which the major ruthenium complexes in solution are dependent on both reaction conditions and the stage of the catalytic reaction. It suggests that binuclear and cluster complexes, especially those that can easily achieve coordinative unsaturation, may have distinct advantages over mononuclear transition metal catalysts for this and related catalytic reactions.[7]

We thank the NSERC (Canada) for financial support.

Notes and references

† Binuclear complexes have been identified in formic acid decomposition previously but were not thought to be involved in the catalytic cycle.[1c]

‡ *Selected spectroscopic data*: **2**: $\delta(^1H)$ −8.9 [qnt, 1H, *J*(PH) 9 Hz, $Ru_2(\mu\text{-}H)$]; $\delta(^{13}C)$ 199, 201 (terminal CO), 278.6 (μ-CO); $\delta(^{31}P)$ 27.8 (dppm). Preliminary X-ray data on the $[BF_4]^-$ salt gives *d*(Ru–Ru) 2.960(3) Å compared to 2.903(2) Å in **1**. **3**: $\delta(^{13}C)$ 188, 206 (terminal CO); 181 (HCO_2); $\delta(^{31}P)$ 30.9 (dppm). **4**: $\delta(^1H)$ −6.7 (m, 1H, RuH), 8.5 (s, 1H, HCO_2); $\delta(^{13}C)$ 165 (HCO_2); $\delta(^{31}P)$ 39.9 (dppm). **5**: $\delta(^1H)$ −9.2 (qnt, 2H, RuH) $\delta(^{13}C)$ 197 (terminal CO); $\delta(^{31}P)$ 34.3 [dppm]. **6**: $\delta(^1H)$ −9.3 [t, 1H, RuH], −9.6 [quint, 1H, $Ru_2(\mu\text{-}H)$]; $\delta(^{31}P)$ = 42.5, 46.5 (m, dppm). *Crystal data* for **6**: monoclinic, space group $P2_1/n$, a = 11.583(1), b = 28.557(3), c = 16.783(2) Å, β = 97.817°, V = 5499(1) Å^3, T = 296 K, μ = 7.1 cm^{-1}, 7115 reflections, R_1 = 0.0466, wR_2 = 0.0918. CCDC 182/1033.

§ The assignments are based on the observation of *J*(CC) coupling between the mutually *trans* bridging and terminal carbonyl ligands in the fully ^{13}CO enriched complex.

1 (*a*) R. S. Coffey, *Chem. Commun.*, 1967, 923; (*b*) S. H. Strauss, K. H. Whitmire and D. F. Shriver, *J. Organomet. Chem.*, 1979, **174**, C59; (*c*) R. S. Paonessa and W. C. Trogler, *J. Am. Chem. Soc.*, 1982, **104**, 3529; (*d*) J.-C. Tsai and K. M. Nicholas, *J. Am. Chem. Soc.*, 1992, **114**, 5117.

2 P. G. Jessop, T. Ikariya and R. Noyori, *Chem. Rev.*, 1995, **95**, 260.

3 J. Kuncheria, H. A. Mirza, H. A. Jenkins, J. J. Vittal and R. J. Puddephatt, *J. Chem. Soc., Dalton Trans.*, 1998, 285; G. M. Ferrence, P. E. Fanwick, C. P. Kubiak and R. J. Haines, *Polyhedron*, 1997, **16**, 1453; H. A. Mirza, J. J. Vittal and R. J. Puddephatt, *Inorg. Chem.*, 1993, **32**, 1327.

4 R. J. Haines, in *Comprehensive Organometallic Chemistry II*, ed. D. F. Shriver and M. I. Bruce, Pergamon, Oxford, 1995, vol. 7, ch. 11; R. W. Hilts, S. J. Sherlock, M. Cowie, E. Singleton and M. M. de V. Steyn, *Inorg. Chem.*, 1990, **29**, 3161.

5 For reversible insertion of CO_2 into Ru–H bonds of mononuclear ruthenium comlexes to give ruthenium formates see for example: M. K. Whittlesey, R. N. Perutz and M. H. Moore, *Organometallics*, 1996, **15**, 5166; G. Jia and D. W. Meek, *Inorg. Chem.*, 1991, **30**, 1953.

6 K. J. Edwards, J. S. Field, R. J. Haines, B. D. Homann, M. W. Stewart, J. Sundermeyer and S. F. Woollam, *J. Chem. Soc., Dalton Trans.*, 1996, 4171.

7 R. D. Adams, *Comprehensive Organometallic Chemistry II*, Pergamon, Oxford, 1995, vol. 10; P. Braunstein and J. Rose, in *Catalysis by Di- and Polynuclear Metal Complexes*, ed. R. D. Adams and F. A. Cotton, Wiley, New York, 1997, p. 346.

Communication 8/05789C

The utility of *N*-methylimidazole and acetonitrile as solvents for the direct reaction of europium with alcohols including the first example of acetonitrile as a μ-η¹ : η¹-bridging ligand

William J. Evans,* Michael A. Greci and Joseph W. Ziller

Department of Chemistry, University of California, Irvine, California 92697-2025, USA. E-mail: wevans@uci.edu

Received (in Corvallis, OR, USA) 13th July 1998, Accepted 23rd September 1998

_N_-Methylimidazole and acetonitrile are suitable solvents for the direct reactions of europium metal with 2,6-$Me_2C_6H_3OH$ and 2,6-$Pr^i_2C_6H_3OH$, which lead to crystallographically characterizable (*N*-methylimidazole)$_3$Eu(μ-$OC_6H_3Me_2$-2,6)$_3$Eu(*N*-methylimidazole)$_2$($OC_6H_3Me_2$-2,6) 1 and [(MeCN)$_2$(2,6-$Pr^i_2C_6H_3O$)Eu]$_2$(μ-$OC_6H_3Me_2$-2,6)$_2$(μ-NCMe) 2, a complex which contains a μ-η¹-acetonitrile ligand.

Owing to the special fluorescent properties of europium,[1] it is desirable to be able to synthetically manipulate this element in a variety of ways in order to optimize its incorporation into devices of practical utility.[2] Syntheses starting from the metal are best since they avoid the preparation of starting materials, such as chlorides or nitrates, require no drying of these materials, and eliminate the possibility of incorporating some of the starting material ligands into the final product. Europium alkoxide and aryloxide complexes, potentially useful in sol-gel processing,[3] can be made by direct reaction of europium with alcohols and phenols in liquid ammonia,[4–6] by reaction of europium with $Hg(C_6F_5)_2$ in phenols,[7] by reaction of europium with Tl(OAr) in THF,[7] and by reaction of europium with Pr^iOH in the presence of Hg^{II} catalysts,[8] but more convenient are the direct reactions of europium solely with liquid alcohols.[9,10] However, the latter route is not as suitable for solid 2,6-dialkylphenols, which provide good ligands for stabilizing and solubilizing europium ions and for making polyeuropium complexes.[4–6,9] We report here that by using *N*-methylimidazole and acetonitrile as solvents, direct reactions of europium with 2,6-dialkylphenols can be achieved to form fully characterizable europium aryloxide complexes. In addition, we report a new type of bonding mode for acetonitrile.

Europium reacts slowly with 2,6-$Me_2C_6H_3OH$ and 2,6-$Pr^i_2C_6H_3OH$ at room temperature in *N*-methylimidazole or acetonitrile to form yellow solutions of paramagnetic divalent europium complexes.† Each 2,6-$R_2C_6H_3OH$ reacts in each solvent, but the R = Me/*N*-methylimidazole and R = Pr^i/MeCN combinations readily provide crystallographically characterizable complexes.‡ (*N*-methylimidazole)$_3$Eu(μ-$OC_6H_3Me_2$-2,6)$_3$Eu(*N*-methylimidazole)$_2$($OC_6H_3Me_2$-2,6) **1** (Fig. 1) and [(MeCN)$_2$(2,6-$Pr^i_2C_6H_3O$)Eu]$_2$(μ-$OC_6H_3Me_2$-2,6)$_2$(μ-NCMe) **2** (Fig. 2).

The bimetallic nature of **1** and the arrangement of the anionic ligands are identical to those reported for (DME)$_2$Eu(μ-$OC_6H_3Me_2$-2,6)$_3$Eu($OC_6H_3Me_2$-2,6)(DME) **3** (DME = 1,2-dimethoxyethane), isolated from a Eu/$HOC_6H_3Me_2$-2,6 liquid ammonia reaction.[4] This unsymmetrical arrangement has also been observed in some calcium and barium alkoxide and siloxide complexes.[11] The structures of **1** and **3** differ in that three *N*-methylimidazole ligands in **1** take the place of two bidentate DME ligands in **3** and hence both europium atoms in **1** are six coordinate, whereas **3** contains one six- and one seven-coordinate europium atom.

Each europium atom in **1** is surrounded by a distorted face sharing bioctahedral arrangement of oxygen and nitrogen donor atoms with the shared face consisting of anionic oxygen atoms. The 2.365(3) Å Eu–O(terminal) and 2.479(3)–2.632(3) Å Eu–O(bridging) bond lengths in **1** are in the range of analogous bond lengths in the literature.[4,12]

Complex **2**, like **1**, is also bimetallic and has a face sharing bioctahedral arrangement of ligand donor atoms. However, its structure differs in that each metal atom has the same set of ligands. Although reactions in liquid ammonia and coordinating solvent yielded structurally similar complexes **1** and **3**, complex **2** is substantially different from the product obtained from europium and $HOC_6H_3Pr^i_2$-2,6 in liquid ammonia, Eu_4(μ-$OC_6H_3Pr^i_2$-2,6)$_4$($OC_6H_3Pr^i_2$-2,6)$_2$(μ_3-OH)$_2$($NCMe_3$)$_6$ **4**.[5] The 2.286(6) and 2.289(5) Eu–O(terminal), 2.438(6), 2.463(5), 2.487(5) and 2.494(6) Eu–O(bridging), and the 2.625(9)–2.667(9) Å Eu–N(terminal) bond lengths in **2** are not unusual for europium(II) aryloxide complexes.[5,12]

The most remarkable feature in **2** is that it contains a μ-η¹ : η¹-acetonitrile ligand, which, to our knowledge, is the first observation of this binding mode for acetonitrile. The 2.847(8) and 2.913(9) Å Eu–N bond lengths of the bridging acetonitrile are longer than the Eu–N(terminal) distances in **2**, as expected.

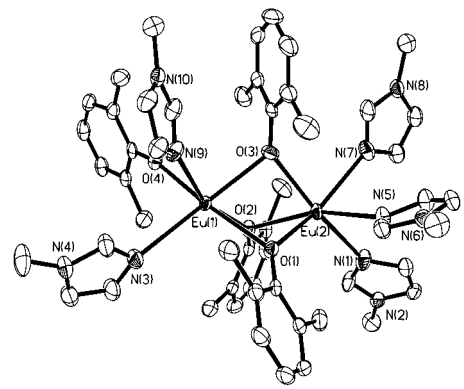

Fig. 1 Plot of $Eu_2(OC_6H_3Me_2$-2,6)$_4$(*N*-methylimidizole)$_5$ **1** with thermal ellipsoids drawn at the 50% probability level and hydrogen atoms omitted for clarity.

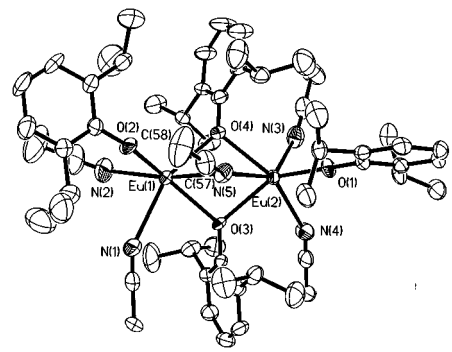

Fig. 2 Thermal ellipsoid plot of $Eu_2(OC_6H_3Pr^i_2$-2,6)$_4$($NCCH_3$)$_5$ **2** with thermal ellipsoids drawn at the 50% probability level and hydrogen atoms omitted for clarity.

The bridging is unsymmetrical with 164.5(8) and 105.0(7)° Eu–N(5)–C(57) angles. This places C(57) closer to Eu(1) than Eu(2), but the 3.391 Å Eu(1)–C(57) distance is too long to constitute a Eu–C bond. Structurally characterized by μ-η^2-acetonitrile ligands have M–C(nitrile) interactions in the range of 1.876(9) to 2.114(7) Å.[13] The Eu(1)–N(5)–Eu(2) angle is 79.9(2)° and the Eu(1)–C(57)–Eu(2) angle is 59.9°. A space filling model of **2** suggests that the μ-η^1 : η^1-nature of this ligand and the inequivalence of the Eu–N(5)–C(57) angles arise because there is only a limited space available for the acetonitrile to fit between the bulky 2,6-diisopropylphenoxide ligands.

The results to date on divalent europium aryloxide chemistry suggest that isolable, crystalline complexes more readily form with either a combination of larger 2,6-dialkyl substituents, such as isopropyl groups, and relatively small ligands, such as acetonitrile, or with a combination of smaller 2,6-dialkyl substituents, such as methyl groups, and larger ligands, such as *N*-methylimidazole or 1,2-dimethoxyethane. Variable binding modes are undoubtedly helpful in accommodating crowded ligand environments and the structure of **2** demonstrates another variation in the binding capacity of acetonitrile.

For support of this research, we thank the Division of Chemical Sciences of the Office of Basic Energy Sciences of the Department of Energy.

Notes and references

† Compounds **1** and **2** are obtained by reaction of europium ingots (typically 5–10 mm in diameter) with $HOC_6H_3Me_2$-2,6 in *N*-methylimidazole or $HOC_6H_3Pr^i_2$-2,6 in acetonitrile, respectively, over 2 days at room temperature followed by centrifugation and recrystallization from the supernatant. Single crystals of complex **2** were isolated in 40% yield from the concentrated acetonitrile solution after several days. Single crystals of complex **1** was isolated from the *N*-methylimidazole solution. However, since the yield was low and the high boiling point of *N*-methylimidazole made solvent removal tedious, an alternate procedure was developed. The direct reaction of europium metal with $HOC_6H_3Me_2$-2,6 in a dilute solution of *N*-methylimidazole (0.5 ml) in toluene (7.0 ml), followed by centrifugation and removal of the toluene under vacuum, forms crystalline **1** in 20% yield, based on reacted Eu. Both **1** and **2** give satisfactory elemental analyses and the effective magnetic moments of 7.5 and 8.0 μ_B for **1** and **2**, respectively, are consistent with Eu^{II}.

‡ *Crystal data* for **1**: $C_{52}H_{66}Eu_2N_{10}O_4$, M = 1199, triclinic, space group $P\bar{1}$, a = 12.142(2), b = 12.763(9), c = 18.906(5) Å, α = 71.60(4), β = 73.718(10), γ = 76.48(3)°, V = 2634.3(20) Å, Z = 2, T = 158 K, μ = 2.412 mm^{-1}, Mo-Kα radiation, graphite monochromator. The raw data were processed with a local version of CARESS. All 9678 data points were corrected for Lorentz and polarization effects and were placed on an approximately absolute scale. All calculations were carried out using the SHELXL program. The structure was solved by direct methods and refined on F^2 by full-matrix least-squares techniques. Hydrogen atoms were included using a riding model. At convergence, $wR2$ = 0.0787 and GOF = 1.036 for 613 variables refined against all 9199 unique data [in comparison, for refinement on F, $R1$ = 0.0282 for those 7984 data with $F > 4.0\sigma(F)$]. For **2**: $C_{58}H_{83}Eu_2N_5O_4$, M = 1218, monoclinic, space group Pn, a = 11.8317(12), b = 21.6202(16), c = 12.9773(13) Å, β = 112.917(7)°, V = 3057.6(5) Å, Z = 2, T = 158 K, μ = 2.077 mm^{-1}, Mo-Kα radiation, graphite monochromator. All 7348 data were collected using a Siemens P4 diffractometer, and handled as described for **1**. All calculations were carried out as described for **1** above and hydrogen atoms were included using a riding model. At convergence, $wR2$ = 0.1141 and GOF = 0.766 for 627 variables refined against all 7348 unique data [in comparison, for refinement on F, $R1$ = 0.0382 for those 6939 data with $F > 4.0\sigma(F)$]. CCDC 182/1031.

1 R. C. Ropp, *Luminescence and the Solid State*, Elsevier, New York, 1991.
2 J. R. McColl and F. C. Palilla, in *Industrial Applications of Rare Earth Elements*, ed. K. A. Gschneidner Jr., *ACS Symp. Ser.*, American Chemical Society, Washington, D.C., 1981, vol. 164, ch. 10; W. A. Thorton, in *Industrial Applications of Rare Earth Elements*, ed. K. A. Gschneidner Jr., *ACS Symp. Ser.*, American Chemical Society, Washington, D.C., 1981, vol. 164, ch. 11; R. C. Ropp, *Studies in Inorganic Chemistry 17, The Chemistry of Artificial Lighting Devices, Lamps, Phosphors and Cathode Ray Tubes*, Elsevier, New York, 1993.
3 D. C. Bradley, R. C. Mehrotra and D. P. Gaur, *Metal Alkoxides*, Academic Press, London, 1978; D. C. Bradley, *Chem. Rev.*, 1989, **89**, 1317; L. G. Hubert-Pfalzgraf, *New J. Chem.*, 1987, **11**, 663.
4 W. J. Evans, W. G. McClelland, M. A. Greci and J. W. Ziller, *Eur. J. Solid State Inorg. Chem.*, 1996, **33**, 145.
5 W. J. Evans, M. A. Greci and J. W. Ziller, *J. Chem. Soc., Dalton Trans.*, 1997, 3035.
6 Yb aryloxides can also be made in this way: B. Cetinkaya, P. B. Hitchcock, M. F. Lappert and R. G. Smith, *J. Chem. Soc., Chem. Commun.*, 1992, 932.
7 G. B. Deacon, T. Feng, P. MacKinnon, R. H. Newham, S. Nickel, B. W. Skelton and A. H. White, *Aust. J. Chem.*, 1993, **46**, 387.
8 L. M. Brown and K. S. Mazdiyasni, *Inorg. Chem.*, 1970, **12**, 2783.
9 W. J. Evans, M. A. Greci and J. W. Ziller, *Inorg. Chem.*, in the press.
10 J. M. Carretas, J. Branco, J. Marçalo, J. C. Waerenborgh, N. Marques and A. Pires de Matos, *J. Alloys Compds.*, 1998, **275**–**277**, 841.
11 K. G. Caulton, M. H. Chisholm, S. R. Drake and W. E. Streib, *Angew. Chem., Int. Ed. Engl.*, 1990, **29**, 1483; S. R. Drake, W. E. Streib, K. Folting, M. H. Chisholm and K. G. Caulton, *Inorg. Chem.*, 1992, **31**, 3205; J. A. Darr, S. R. Drake, M. B. Hursthouse and K. M. A. Malik, *Inorg. Chem.*, 1993, **32**, 5704.
12 G. B. Deacon, C. M. Forsyth, B. M. Gatehouse and P. B. White, *Aust. J. Chem.*, 1990, **43**, 795; J. R. van den Hende, P. B. Hitchcock, S. A. Holmes, M. F. Lappert, W.-P. Leung, T. C. W. Mak and S. Prashar, *J. Chem. Soc., Dalton Trans.*, 1995, 1427.
13 F. A. Cotton and F. E. Kühn, *J. Am. Chem. Soc.*, 1996, **118**, 5826; J. L. Eglin, E. M. Hines, E. Valente and J. D. Zubkowski, *Inorg. Chim. Acta*, 1995, **229**, 113; D. Walther, H. Schönberg, E. Dinjus and J. Sieler, *J. Organomet. Chem.*, 1987, **334**, 377; F. J. G. Alonso, M. G. Sanz, V. Riera, A. A. Abril, A. Tiripiccio and F. Ugozzoli, *Organometallics*, 1992, **11**, 801.

Communication 8/05750H

Novelties of eclectically engineered sulfated zirconia and carbon molecular sieve catalysts in cyclisation of citronellal to isopulegol

G. D. Yadav* and J. J. Nair

Chemical Engineering Division, University Department of Chemical Technology, University of Mumbai (formerly Bombay), Matunga, Mumbai - 400 019, India. E-mail: gdy@udct.ernet.in

Received (in Cambridge, UK), 2nd September 1998, Accepted 28th September 1998

Sulfated zirconia (S-ZrO_2) is a well-known solid superacid catalyst used in various reactions of commercial importance such as isomerisation, alkylation and acylation, nitration, *etc.* The selectivity towards the formation of isopulegol, a potential intermediate in the synthesis of menthol, can be drastically increased by using carbon molecular sieve (CMS) with S-ZrO_2.

Isopulegol is an important intermediate for the manufacture of menthol, used extensively in pharmaceuticals, cosmetics, toothpastes, chewing gum, and other toilet goods as well as in cigarettes.[1] Isopulegol is manufactured from the cyclisation of citronellal. Bogert and Hasselstrom[2] have reported the use of UV in the cyclisation reaction. Activities and selectivities of acid clinoptilolite, mordenite, and faujasite zeolites in the isomerisation of citronellal in n-hexane, chloroform and dichloromethane as solvents have been investigated.[3] The activities of the acidic zeolites for the isomerisation of citronellal were found to be in the following order: HY(max.) > HCC > (clinoptilolite) > HMCP (clinoptilolite + mordenite) > HX at 84 °C in dichloroethane, and the selectivities to isopulegol were HCC (90%) > HMCP (85%) > HY (80%) > HMP (72%) at 80% conversion level. The activity in these studies is related to the total amount of Brønsted acid sites of the catalysts and only a fraction of these sites, located mainly on the external surface of the crystal, were accessible to the reactants due to the diffusional resistance. It was found that the selectivity increases to the isopulegol ether as the accessibility to the acidic centres increases. There are several reports whereby Cu–Cr and Cu–Cr–Mn,[4] tris(triphenylphosphine)rhodium chloride[5] and micellar[6] catalysts have been employed to catalyse the cyclisation reaction. Several Lewis acids as catalyst for the preparation of L-isopulegol from D-citronellal have been used.[7] Dean and Whittaker[8] have studied this reaction with superacids (*e.g.* FSO_3H/SO_2) to observe that the cyclisation follows the same path as the normal acids, yielding isopulegol and neoisopulegol.

We present here the efficacy of a novel shape selective catalyst synergistically produced from sulfated zirconia (S-ZrO_2) and carbon molecular sieve (CMS) in the cyclisation of citronellal to isopulegol. S-ZrO_2 is a very well-known solid superacidic catalyst used in various reactions. The activity of this catalyst is superior to many other solid acid catalysts. But one of the major drawbacks of S-ZrO_2 is that it is not a shape selective catalyst. Hence it cannot be employed in reactions where selectivity is of utmost importance. However, S-ZrO_2 when combined with other materials can produce the desired shape selective catalyst. In this respect, carbon molecular sieve (CMS) can be used in combination with S-ZrO_2 to get a composite shape selective catalyst. The selectivity engineering aspects of catalysts are embodied in this CMS–S-ZrO_2 composite media where one acts as a siever and the inside core as the true catalyst. The isomerisation of citronellal was considered to be interesting in view of the fact that the reaction has been studied by others using zeolites and there are several products generated depending on the type of carbocation and hence on the type and strength of acidic sites.

Zirconium oxychloride, 25% ammonia solution, polyvinyl alcohol, toluene and 98% sulfuric acid were obtained from S.D. Fine Chemicals Ltd. Citronellal containing about 14% isopulegol was obtained from Arofine Industries Ltd.

The catalyst was prepared using the conventional precipitation method.[9] 100 g of zirconium oxychloride were dissolved in distilled water. The solution was then filtered. This solution and 25% aqueous ammonia were added dropwise simultaneously in a beaker with constant stirring while a white precipitate of zirconium hydroxide was obtained at pH 9–10. After complete precipitation it was digested in the vessel for 6 h. The precipitate was filtered through a Buchner funnel and washed thoroughly with distilled water until free of ammonia and chloride ions. The filtered precipitate was dried in an oven at 120 °C for 24 h. The dried catalyst was then crushed to make a fine powder, which was treated with 0.5 M H_2SO_4. 15 ml of 0.5 M H_2SO_4 was required for 1 g of the catalyst. The catalyst so prepared was dried in an oven at 120 °C for 24 h followed by calcination at 230 to 650 °C.

To 10 g of the above prepared catalyst 7.2 ml polyvinyl alcohol (PVA) solution (2 g PVA dissolved in 25 ml distilled water) was added dropwise until it was just wet. It was mixed well to get a uniform coating. It was dried at 100 °C for 1 h and calcined at different temperatures. This catalyst is referred to as S-ZrO_2/CMS catalyst.

In another method, S-ZrO_2 was initially soaked with different solvents such as benzene, cyclohexane, carbon tetrachloride, hexane till wetness. This was coated with the same amount of PVA solution as was done without wetting the catalyst with solvent. These were calcined at different temperatures. Eight different catalysts were prepared as shown in Table 1 where the nomenclature S-ZrO_2/Benzene/CMS refers to S-ZrO_2 soaked with benzene followed by coating with CMS.

All experiments were conducted in a 100 ml fully baffled glass reactor of 5 cm internal diameter. The reactant and solvent were charged to the reactor and the temperature was raised to 95 °C. 0.5 g (2.13×10^{-2} g cm^{-3}) of the desired catalyst was then added to the reactor under constant stirring.

Table 1 Activities of catalysts for cyclisation of citronellal

Catalyst	Time/min	Conversion of citronellal (%)	Selectivity for isopulegol (%)
ZrO_2[230–350]	90	0	—
S-ZrO_2[230–350]	10	96	46
S-ZrO_2[650]	05	95	35
S-ZrO_2[230–350]/CMS	30	91	65
S-ZrO_2[230–350]/Benzene/CMS	20	95	52
S-ZrO_2[230–350]/Cyclohexane/CMS	20	96	61
S-ZrO_2[230–350]/CCl_4/CMS	30	88	53
S-ZrO_2[230–350]/Hexane/CMS	20	95	58

Solvent: toluene = 15 g, reactant: citronellal = 5 g, temperature: 95 °C. Values inside square brackets indicate the calcination temperature.

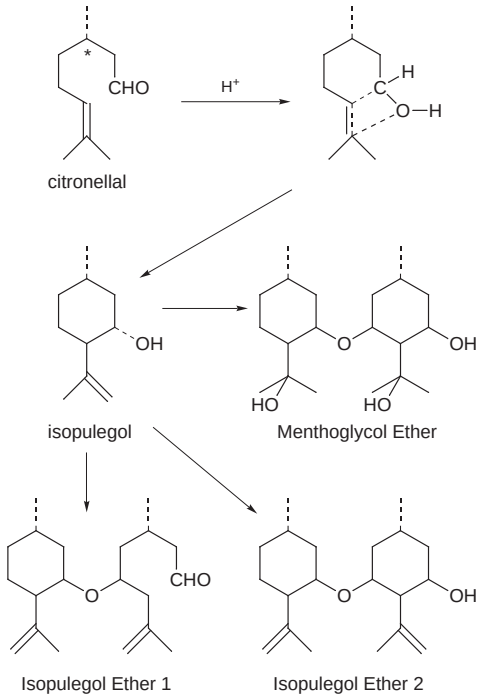

Fig. 1 *trans* addition and cyclisation mechanism.

An initial sample was drawn and the progress of the reaction was monitored on a Perkin Elmer (Model 8500) Gas Chromatograph using an FID detector and coupled with an integrator/plotter. A 2 m × 1/8′ S.S. column of Carbowax with Chromosorb W and 10% C-20M + 2% KOH washed, 80–100 mesh was used. The by-products obtained were predicted, from GC-MS, to be an ether of citronellal–isopulegol (isopulegol ether 1), diisopulegol (isopulegol ether 2) and dimenthoglycol ether (Fig. 1). The mechanism given in Fig. 1 shows the cyclisation of citronellal to isopulegol and the different ethers obtained from isopulegol.[10] There are different stereoisomers of isopulegol.

Table 1 lists the results of the experiments conducted under otherwise similar conditions of mole ratio of reactant and solvent, catalyst loading, speed of agitation and temperature.

It is well established that the formation of isopulegol ether takes place if citronellal is easily accessible to the Brønsted acid sites of the catalyst. Hence, in the case of S-ZrO_2[650] as catalyst, where the calcination temperature is high, the average pore size was found to be 41 Å by nitrogen adsorption isotherm using a Micromeritics surface area analyser (ASAP 2010 Model). When S-ZrO_2[650] was compared with S-ZrO_2[230–350] the selectivity towards the formation of isopulegol was found to increase in the latter. The pore size of S-ZrO_2[230–350] was found to be 28 Å. Hence, even though the Brønsted acidity is expected to be more in case of S-ZrO_2[230–350] as compared to S-ZrO_2[650], which is a Lewis acid catalyst, the pore size is smaller than the latter. This leads to the diffusion controlled formation of isopulegol ether which is kinetically much bulkier than isopulegol and hence the subsequent increase in the formation of the latter. The same reason is true for the decrease in the rate of the reaction. Further, when S-ZrO_2[230–350] is coated with CMS a uniform barrier of pore size 27 Å is obtained. This marginal drop in pore size provides further resistance to the formation of isopulegol ether and hence favour the formation of isopulegol. Also, the external surface of the catalyst which may consist of Brønsted acid sites becomes inaccessible to citronellal which further decreases the formation of isopulegol ether.

In other catalysts used S-ZrO_2[230–350] was initially soaked with different solvents which were immiscible with polyvinyl alcohol solution, before coating with CMS, to prevent the diffusion of polymers into the pores of the catalyst, if any. The initial soaking was not found to be very effective though there was a slight increase in the formation of isopulegol.

S-ZrO_2 modified carbon molecular sieve can be prepared using different polymers as precursors and hence the catalysts can be tailor-made by fine-tuning the pore size according to the requirements. Thus eclectically engineered S-ZrO_2/CMS catalysts lead to much greater selectivity to isopulegol in the cyclisation of citronellal.

Research support from the Department of Science and Technology (DST), Government of India and Darbari Seth Endowment is gratefully acknowledged.

Notes and references

1 J. C. Leffingwell and R. E. Shackelford, *Cosmetics and Perfumery*, 1974, **89,** 69; *Chem. Abstr.*, 1974, **81,** 78 093.
2 M. T. Bogert and T. Hasselstrom, *Synthesis*, 1930, **53**, 4093.
3 M. Fuentes, J. Mograner and De Las Pozas, *Appl. Catal*., 1989, 367.
4 K. Kogami and J. Kumanotani, *Bull. Chem. Soc. Jpn*., 1968, **41**, 2530.
5 K. Sakai and O. Oda, *Tetrahedron Lett*., 1972, 4375.
6 B. C. Clark, S. C. Theresa and A. I. Guillermo, *J. Org. Chem.*, 1984, **49**, 4557.
7 Y. Nakatani and K. Kawashima, *Synthesis*, 1978, 147.
8 C. Dean and D. Whittaker, *J. Chem. Soc., Perkin Trans. 2*, 1990, 1275.
9 P. S. Kumbhar and G. D. Yadav, *Chem. Eng. Sci.*, 1989, **44**, 2535.
10 G. S. Simonsen, '*Terpenes*', vol. I and II, Cambridge University Press, Cambridge, 1931 and 1932.

Communication 8/06815A

An osmium nitrido complex as a π-acid ligand for late transition metals

Thomas J. Crevier, Scott Lovell and James M. Mayer*

Department of Chemistry, Box 351700, University of Washington Seattle, Washington 98195-1700, USA

Received (in Bloomington, IN, USA) 7th July 1998, Accepted 22nd September 1998

The Os(VI) nitrido complex, $TpOs(N)Cl_2$ (1), acts as a π-acid ligand in the cobalt and platinum complexes $CpCo[NOs(Tp)Cl_2]_2$ (2) and $(Me_2S)Cl_2Pt–N{\equiv}Os(Tp)Cl_2$ (3).

Transition metal nitrido complexes $L_nM{\equiv}N$ typically act as nucleophiles, being alkylated or binding to other metals.[1] The two dozen or so known hetero-bimetallic μ-nitrido complexes all involve nucleophilic nitrido complexes and are described as dative adducts $L_nM{\equiv}N{\rightarrow}M'L_m$ (**A**) or metalloimido complexes $L_nM{\overset{\equiv}{=}}N–M'L_m$ (**B**).[2] We have recently prepared an Os(VI) nitrido complex, $TpOs(N)Cl_2$ [**1;** Tp = hydrotris(1-pyrazolyl)borate],[3] that acts as an electrophile. Electrophilic multiply-bonded ligands are less common but such ligands are important in various processes, including atom and group transfers, and dihydroxylation and aminohydroxylation of olefins.[4] Complex **1** is unreactive with protic acids, methyl triflate (MeOTf), $BF_3{\cdot}Et_2O$, and $[Ph_3C][BF_4]$, but it reacts with PPh_3 and carbanions at nitrogen.[3] Despite its lack of reaction with simple electrophiles, we report here that **1** is a good ligand for Co(I) and Pt(II) centers. We propose that the complexes reported herein are a new type of μ-nitrido compound, in which the multiply bonded nitrido fragment is best described as a π acid ligand for the heterometal.

$CpCo(\eta^4\text{-}C_5H_5C_6F_5)$[5] was chosen as a source of the electron-rich CpCo(I) fragment since the η^4-diene should be easily displaced. Indeed, addition of **1** to a benzene solution of $CpCo(\eta^4\text{-}C_5H_5C_6F_5)$ causes an immediate darkening of the solution and precipitation of purple $CpCo[NOs(Tp)Cl_2]_2$ (**2**)† in good yield [eqn. (1)]. NMR data are consistent with a

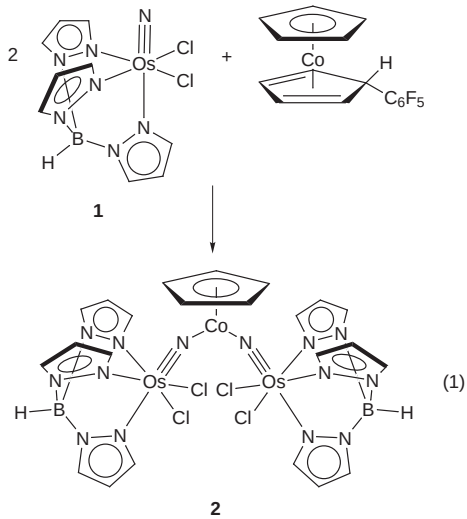

(1)

2

diamagnetic compound with two TpOs fragments per CpCo unit. Slow evaporation of a chloroform solution of **2** forms single crystals suitable for X-ray diffraction.‡ The structure (Fig. 1) shows a two-legged piano stool geometry about the cobalt atom with the two legs being octahedral osmium centers, connected to the cobalt by μ-nitrido ligands. The structure is quite similar to other $CpCoL_2$ complexes, such as $Cp^*Co(CO)_2$.[6] The Co–N–Os angles are essentially linear [171.6(6), 171.8(7)°], which is typical of such μ-nitrido linkages[1a] and indicates sp hybridization at nitrogen. The Os–N

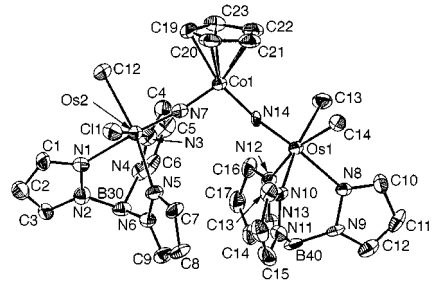

Fig. 1 ORTEP drawing of $CpCo[NOs(Tp)Cl_2]_2$ (**2**), with hydrogen atoms and two $CHCl_3$ of crystallization omitted for clarity. Selected bond lengths (Å) and angles (°): Os(1)–N(14) 1.704(9), Os(2)–N(7) 1.741(10), Co(1)–N(7) 1.696(11), Co(1)–N(14) 1.737(9), Os(2)–N(1) 2.189(11), Os(2)–N(3) 2.054(12), Os(2)–N(5) 2.086(10), Os(1)–N(8) 2.198(10), Os(1)–N(10) 2.070(10), Os(1)–N(12) 2.060(11), Os(1)–N(14)–Co(1) 171.6(6), Os(2)–N(7)–Co(1) 171.8(7), N(7)–Co(1)–N(14) 101.3(5).

distances of 1.704(9) and 1.741(10) Å are indicative of substantial multiple bonding (as is the significant *trans* influence of the nitrido ligand), but these distances are longer than all crystallographically characterized terminal osmium–nitrido bonds (1.525–1.703, av. 1.629 Å).[7] The Co–N bonds are very short [1.696(11) and 1.737(9) Å], much shorter than would be expected for a simple dative interaction. For instance, they are substantially shorter than all reported cobalt–nitrile bonds, which also involve an sp hybridized nitrogen (Co–N 1.883–2.179, av. 1.997 Å).[7] The Co–N bonds in **2** are most similar to those in linear nitrosyl complexes (1.590–1.720, av. 1.658 Å) and are close to cobalt–carbonyl bond lengths (CpCo–CO 1.615–1.782, av. 1.721 Å).[7]

Complex **2** is thermally robust, showing only minor decomposition over two weeks at 75 °C in chloroform solution by ^{1}H NMR. There is no reaction under these conditions with 1 equiv. of PPh_3. Since **1** reacts rapidly with PPh_3, this shows that **2** does not dissociate to **1** at 75 °C. There is also no reaction when a chloroform solution of **2** is heated under 100 Torr of CO at 75 °C for several days.

Complex **1** reacts slowly with $PtCl_2(SMe_2)_2$ in benzene with with loss of Me_2S to give $(Me_2S)Cl_2Pt–N{\equiv}Os(Tp)Cl_2$ (**3**) in good yield [eqn. (2)].† Single crystals of **3** were obtained by

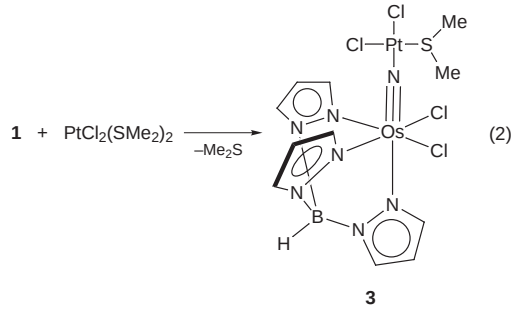

(2)

3

slow evaporation of a benzene solution. The X-ray structure (Fig. 2)‡ shows a molecule of **1** bound to a square planar platinum center. The Pt–N bond of 1.868(8) Å is at the short end of the range of Pt–N bonds in *cis*-dichloroplatinum complexes (1.848–2.371 Å),[7] again closer to those in nitrosyl rather than nitrile complexes. The Os–N bond [1.687(8) Å] is apparently

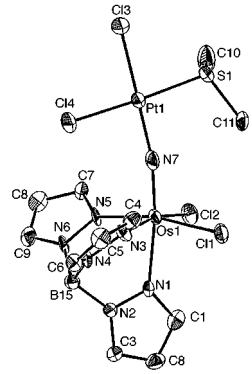

Fig. 2 ORTEP drawing of $(Me_2S)Cl_2Pt{-}N{\equiv}Os(Tp)Cl_2$ (**3**), with hydrogen atoms omitted for clarity. Selected bond lengths (Å) and angles (°): Os(1)–N(7) 1.687(8), Pt(1)–N(7) 1.868(8), Os(1)–N(1) 2.178(7), Os(1)–N(3) 2.071(7), Os(1)–N(5) 2.068(7), Pt(1)–S(1) 2.286(2), Pt(1)–Cl(3) 2.297(2), Pt(1)–Cl(4) 2.317(2), Os(1)–N(7)–Pt(1) 169.2(5).

shorter than those in **2**, although it is presumably slightly longer than in **1**.

The data are most consistent with **1** acting as a π acid ligand in **2** and **3**, as opposed to simply a dative (**A**) or σ only (**B**) ligand. The CpCo(I) fragment forms two legged piano stool structures only with soft and/or π-acid ligands; related CpCo(III) complexes adopt three-legged stool geometries.[8,9] The short Co–N and Pt–N distances and the kinetic inertness of the Co–N bonds are indicative of multiple bond character. The other known platinum μ-nitrido complexes are $(Et_2PhP)_3Cl_2Re{\equiv}N{-}PtCl_2(PEt_3)$,[2d] $(Me_3SiO)_3V{\equiv}N{-}Pt(Me)(PEt_3)_2$,[2a] and three complexes with $[Os(N)O_3]^-$.[10] The first is a labile adduct with dative bonding (resonance form **A**), while the others have N–Pt bond distances [VN–Pt, 2.030(7); O_3OsN–Pt, 2.03(4), 2.040(7), 1.958(7), 2.05(1) Å] which are indicative of single bonding (form **B**) and significantly longer than that in **3**. *Ab initio* DFT calculations on **1** show that the LUMO and LUMO+1 are low-lying Os–N π* orbitals, with significant density at nitrogen.[11] These empty orbitals are quite similar to the π* orbital of CO, the prototypical π acid (Fig. 3).§ The small apparent lengthening of the Os≡N bond in **2** is reminiscent of the small change in the C≡O distance on coordination. This lengthening is smaller if present in **3**, consistent with Pt(II) being a poorer π-donor than Co(I). The bonding in **2** and **3** could alternatively be described as a resonance hybrid of **A** or **B** with a multiple bond form Os=N⇐M′ or Os=N=M′, the latter well known for homonuclear μ-nitrido complexes.[1a]

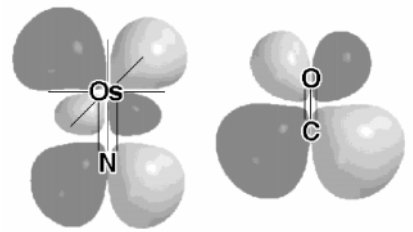

Fig. 3 Calculated LUMOs for **1** and CO.§

The ability of **1** to act as a strong ligand to late transition metals is perhaps surprising in light of its lack of reaction with main group Lewis acids such as $BF_3{\cdot}Et_2O$ and $[Ph_3C][BF_4]$. Complex **1** should be contrasted with the more nucleophilic hydrocarbyl derivatives $TpOs(N)Ph_2$[3a,12] and $CpOs(N)(CH_2SiMe_3)_2$.[2c] The latter forms a BF_3 adduct with $BF_3{\cdot}Et_2O$, is alkylated by MeOTf, and binds to Ag^+ giving a μ-nitrido complex $[Cp(R)_2OsN]_2Ag^+$.[2c] The Ag–N distances [2.15(1), 2.12(2) Å] are 0.27 Å longer than the Pt–N distances in **3**, much larger than the differences in ionic radii (2-coordinate Ag^+, 0.81 Å; 4-coordinate Pt^{2+}, 0.74 Å[13]). $TpOs(N)Ph_2$ does not react with $CpCo(\eta^4\text{-}C_5H_5C_6F_5)$ and an analog of **2** is not observed. The observation that the more nucleophilic osmium nitrides bind more poorly and form longer M–N bonds is not consistent with **1** acting as a simple σ donor ligand (type **A** or **B** bonding). We propose that the osmium nitrido unit in **1** acts as a π-acid ligand as a result of the low lying empty Os–N π* orbitals (Fig. 3). Further studies of **2** and **3**, and preparations of other compounds containing **1** as a ligand, are in progress.

We thank the National Science Foundation for financial support of this research. We also thank Dr B. Bennett for providing results prior to publication, Dr D. Hrovat for assistance in preparing Fig. 3 and Dr K. Goldberg and D. Wick for $PtCl_2(SMe_2)_2$.

Notes and references

† Full preparative, spectroscopic, and calculational details for **1**, **2**, **3**, and $TpOs(NPPh_3)Cl_2$ will be reported in an upcoming full paper. *Selected NMR data*: for **2,** ^{1}H NMR ($CDCl_3$) 5.96 (2H, t), 7.32 (2H, d), 7.49 (2H, d), 6.17 (4H, t), 7.51 (4H, d), 7.55 (4H, d), 5.40 (5H, s); ^{13}C NMR ($CDCl_3$) 107.8, 136.0, 146.0 (pz *trans* to μ-N), 108.5, 137.8, 144.4 (pz *trans* to Cl), 91.2 (Cp). For **3**, ^{1}H NMR ($CDCl_3$) 6.03 (1H, t), 7.42 (1H, d), 7.54 (1H, d), 6.47 (2H, t), 7.75 (2H, d), 8.12 (2H, d), 2.85(6H, s).

‡ Data for both structures were collected on a Nonius KappaCCD with Mo-Kα (λ = 0.71070 Å). *Crystal data*: for **2**·2CH$\underline{C}$l$_3$ at 161 K, $C_{25}H_{27}B_2Cl_{10}Co_1N_{14}Os_2$, M = 1339.06, triclinic, $P\bar{1}$ (no. 2), a = 11.3261(8), b = 14.2844(10), c = 15.3497(10) Å, α = 64.666(5), β = 75.612(5), γ = 68.010(5)°, V = 2069.7(2) Å^3, D_c = 2.149 g cm^{-3}, Z = 2, μ = 72.07 cm^{-1}. Of the 70903 reflections, 7908 unique reflections were used in the final least-squares refinement to yield R = 0.0651 and R_w = 0.1821. For **3** at 161 K, $C_{11}H_{16}B_1Cl_4S_1N_7Pt_1Os_1$, M = 815.26, triclinic, $P\bar{1}$ (no. 2), a = 8.5517(3), b = 10.9693(3), c = 13.2976(3) Å, α = 95.4985(19), β = 92.2917(19), γ = 104.4479(12)°, V = 1199.74(6) Å^3, D_c = 2.257 g cm^{-3}, Z = 2, μ = 116.56 cm^{-1}. Of the 17880 reflections, 4459 unique reflections were used in the final least-squares refinement to yield R = 0.0364 and R_w = 0.1283. CCDC 182/1026.

§ Minor contributions of other atoms to the LUMO in **1** are omitted for the sake of clarity. Full details of the calculations will be published in a forthcoming report.[11]

1 (*a*) K. Dehnicke and J. Strahle, *Angew. Chem., Int. Ed. Engl.*, 1992, **31**, 955; (*b*) W. A. Nugent and J. M. Mayer, *Metal Ligand Multiple Bonds*, Wiley-Interscience, 1988.
2 (*a*) N. M. Doherty and S. C. Critchlow, *J. Am. Chem. Soc.*, 1987, **109**, 7906; (*b*) C. M. Jones and N. M. Doherty, *Polyhedron*, 1995, **14**, 81 and references therein; (*c*) R. W. Marshman, J. M. Shusta, S. R. Wilson and P. A. Shapley, *Organometallics*, 1991, **10**, 1671; (*d*) J. Chatt and B. T. Heaton, *Chem. Commun.*, 1968, 274.
3 (*a*) T. J. Crevier and J. M. Mayer, *J. Am. Chem. Soc.*, 1998, **120**, 5595; (*b*) T. J. Crevier and J. M. Mayer, *Angew. Chem., Int. Ed. Engl.*, 1998, **37**, 1891; (*c*) T. J. Crevier, PhD Thesis, University of Washington, 1998.
4 For leading references, see: (*a*) A. J. DelMonte, J. Haller, K. N. Houk, K. B. Sharpless, D. A. Singleton, T. Strassner and A. A. Thomas, *J. Am. Chem. Soc.*, 1997, **119**, 9907; (*b*) J. Du Bois, C. S. Tomooka, J. Hong and E. M. Carreira, *Acc. Chem. Res.*, 1997, **30**, 364; (*c*) S. N. Brown and J. M. Mayer, *J. Am. Chem. Soc.*, 1996, **118**, 12119.
5 Prepared from Cp_2Co and C_6F_5I. B. K. Bennett, PhD Thesis, University of Utah, Salt Lake City, Utah, 1997.
6 L. R. Byers and L. F. Dahl, *Inorg. Chem.*, 1980, **19**, 277.
7 From the Cambridge Structure Database (January, 1998): F. H. Allen and O. Kennard, *Chem. Des. Automat. News*, 1993, **8**, 31.
8 (*a*) *Comprehensive Organometallic Chemistry*, ed. G. Wilkinson, Pergamon, New York, 1982, vol. 5, pp. 1–276; (*b*) *Comprehensive Organometallic Chemistry II*, ed. G. Wilkinson, Pergamon, New York, 1995, vol. 8, pp. 1–114.
9 R. F. Heck, *Inorg. Chem.*, 1968, **7**, 1513 may report a rare exception.
10 W.-H. Leung, J. L. C. Chim and W.-T. Wong, *J. Chem. Soc., Dalton Trans.*, 1996, 3153; 1997, 3277.
11 D. Hrovat, T. J. Crevier, W. T. Borden and J. M. Mayer, work in progress.
12 J. L. Koch and P. A. Shapley, *Organometallics*, 1997, **16**, 4071.
13 J. E. Huheey, *Inorganic Chemistry*, Harper & Row, New York, 3rd edn., 1983, pp. 73, 75.

Communication 8/05277H

NaB_5C: carbon insertion into a three-dimensional framework of boron octahedra leads to electron-precise cubic carbaborides

Barbara Albert* and Konny Schmitt

Institut für Anorganische Chemie der Rheinischen Friedrich-Wilhelms-Universität, Gerhard-Domagk-Str. 1, 53121 Bonn, Germany. E-mail: albert@snchemie2.chemie.uni-bonn.de

Received (in Cambridge, UK), 8th September 1998, Accepted 29th September 1998

The discussion of whether hexaborides need a minimum electronic stabilisation to exist or not, has now been enriched by the synthesis of NaB_5C, crystallising with the cubic CaB_6 structure.

Carbaborides are solids with an anionic framework consisting of linked boron polyhedra, which are electronically stabilised by the insertion of carbon. The name already indicates a similarity to polyhedral molecules, which are called carbaboranes: substitution of boron by carbon provides electrons which stabilise a certain polyhedral arrangement. Recently, we were able to synthesise a new ternary boron-rich compound, which crystallises in the cubic CaB_6[1] structure type, NaB_5C.

The existence of cubic alkali metal hexaborides has been discussed controversially for a long time. Two compounds, NaB_6[2] and KB_6,[3] have been reported. In an earlier work, we were able to show that 'NaB_6' should actually be described as Na_3B_{20},[4] which does not crystallise in the hexaboride structure type. According to Longuet-Higgins and de V. Roberts,[5] the reason for the instability of cubic hexaborides with monovalent cations is the electronic deficiency of their framework. Following traditional bonding concepts, derived analogous to Lipscomb's model for boron molecules, each B_6 octahedron needs twenty electrons: fourteen intramolecular, to fill the bonding molecular orbitals within the octahedra, plus six intermolecular to satisfy the 2 electron–2 center bond between neighbouring octahedra. This requirement of course is fulfilled for the electron-precise mother compound of the structure type CaB_6, but not for the alkali metal hexaborides, which are low in electrons. On the other hand, similar compounds with excess electrons, like LaB_6, are well known, the extra electron causing their metallic behaviour.

Looking for additional experimental evidence to illuminate the question of bonding and stability of hexaborides, we succeeded in synthesising a new compound. The reaction of a mixture of sodium, boron, and carbon at high temperatures[6] yields a crystalline powder, which contains carbon and shows the typical powder diffraction pattern of cubic hexaborides. The unprecedented combination of these two findings led to the assumption that carbon atoms are statistically distributed at the boron positions in NaB_5C. The substance is black and consists of crystallites similar to cubes and with edge lengths between 0.5 and 1 μm (Fig. 1). Electron energy loss spectroscopy (EELS) at several crystallite fragments proved a boron : carbon ratio of 5 : 1.

The crystal structure of NaB_5C was refined using X-ray powder data and the CaB_6 structure as starting model, boron and carbon sharing the 'framework positions' (Wyckhoff symbol 6f).[7,8] In Fig. 2, the fit between the observed data and the calculated diffraction pattern is shown. As was expected, the

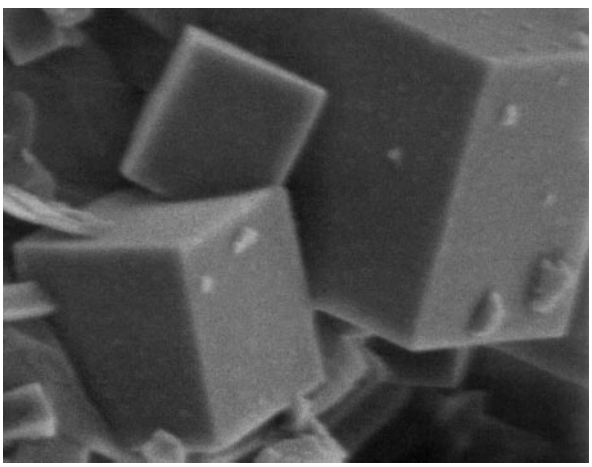

Fig. 1 Scanning electron micrograph of NaB_5C. The length of the edge of the crystallite in the front is 1 μm.

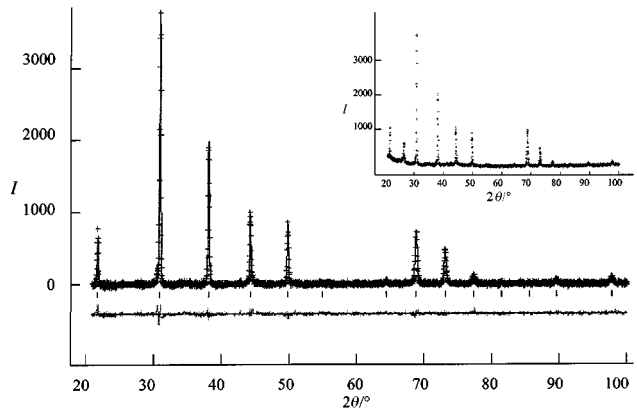

Fig. 2 Observed (+) and calculated (solid line) powder diffraction pattern (corrected for the background) with the difference curve (bottom). The vertical dashes indicate the positions of reflections. The uncorrected data are shown in the insert.

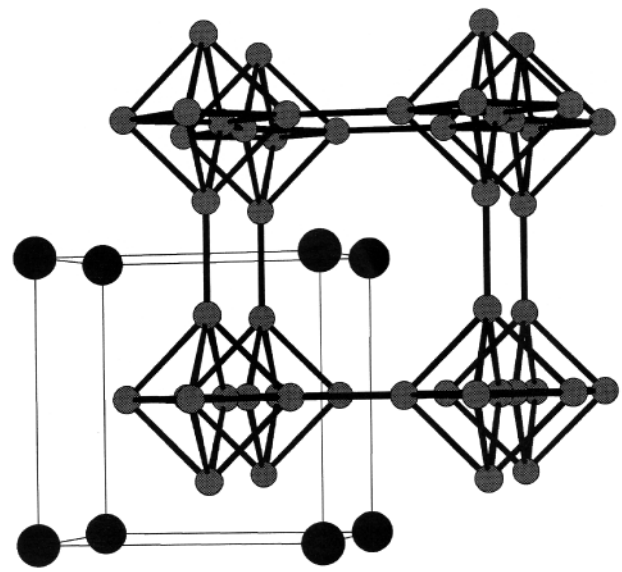

Fig. 3 Section of the structure of NaB_5C (Na: black, B/C: grey).

lattice constant of NaB_5C is smaller (4.09 Å) than the lattice constant which has been predicted for 'NaB_6'[9] (4.16 Å). In addition, we proved the mean B/C–B/C distance to be shorter than the mean B–B distance in hexaborides (1.706 Å in NaB_5C *versus* 1.736 Å in CaB_6[10]). Similar to other boron-rich compounds, the intramolecular bond distances within the octahedra are longer than the distances between them (1.716 Å *versus* 1.665 Å).

In conclusion, the new compound sodium hexa(carbaboride) exhibiting a cubic crystal structure (Fig. 3[11]) contains exactly the amount of carbon atoms in the anionic framework necessary to balance the electron deficiency of a hypothetical binary Na/B compound with a three-dimensional octahedral framework—one carbon atom per octahedron.

We thank Prof. Dr. Johannes Beck, Gieβen, Prof. Dr. Martin Jansen, Stuttgart, Dr. Ulrike Ciesla, Santa Barbara, and Lars-Peter Zenser, Gieβen, for their help. This work was supported by the Land Nordrhein-Westfalen (Lise-Meitner grant for B. A., and Bennigsen-Foerder program) and the Fonds der Chemischen Industrie.

Notes and references

1 M. v. Stackelberg and F. Neumann, *Z. Phys. Chem. B*, 1932, **19**, 314.
2 P. Hagenmuller and R. Naslain, *C. R. Acad. Sci.*, 1963, **257,** 1294.
3 R. Naslain and J. Étourneau, *C. R. Acad. Sci. Ser. C*, 1966, **263**, 484.
4 B. Albert, *Angew. Chem.*, 1998, **110**, 1135; *Angew. Chem., Int. Ed. Engl.*, 1998, **37**, 1117.
5 H. C. Longuet-Higgins and M. de V. Roberts, *Proc. R. Soc. London, Ser. A*, 1954, **224**, 336.
6 Sodium (Merck, Darmstadt, p.a.) was refined by segregation and treated with boron (Chempur, Karlsruhe, 99.9+%) and graphite (Merck, Darmstadt) in a molar ratio of 6 : 5 : 1 at 1050 °C for 2 h in crucibles made of pyrolytic boron nitride, which were sealed in iron crucibles under helium by arc welding. The excess of sodium was removed by distillation at 10^{-2} mbar and 400 °C. The starting materials and products were handled under argon.
7 A. C. Larson and R. B. Von Dreele, Program GSAS, Los Alamos, USA, 1985.
8 Crystal data: NaB_5C, cubic, space group $Pm\bar{3}m$ (221), a = 409.25(1) pm, $V = 68.54 \times 10^6$ pm^3, ρ_{calc} = 2.158 g cm^{-3}, Z = 1, μ = 2.1 mm^{-1}, 17 reflections, 3 refined positional and thermal displacement parameters (the boron and the carbon atom were refined with a common isotropic thermal displacement parameter), R_{wp} = 0.0877, R_p = 0.0677, χ^2 = 1.410 , D_{dw} = 1.496, ρ_{max}/ρ_{min} = 0.854/−0.200 e Å^{-3}. Reflections which stem from a small excess of graphite were cut out of the powder diagram before refinement. Further details of the crystal structure investigation may be obtained from the Fachinformationszentrum Karlsruhe, D-76344 Eggenstein-Leopoldshafen, Germany (e-mail: crysdata@fiz-karlsruhe.de), on quoting the depository number CSD-408930. Data were collected on a Huber powder diffractometer G645, with quartz monochromator, CuKα_1 radiation (λ = 1.54056 Å), flat-plate sample holder, measurement in transmission mode at 20.0(5) °C, 5×10^{-5} mbar, step width 0.006° Θ, measurement range 3–50° Θ. CCDC 182/1040.
9 (*a*) P. Blum and F. Bertaut, *Acta Crystallogr.* 1954, **7**, 81; (*b*) R. Naslain, J. Étourneau and P. Hagenmuller, in *Boron and Refractory Borides*, ed. V. I. Matkovich, Springer, Berlin, 1977, pp 262–292.
10 T. Ito, T. Kasukawa, I. Higashi and Y. Satow, *Proc. 11th Int. Symp. Boron, Borides and Related Compounds*, *JJAP Series*, 1994, **10**, 11.
11 R. Hundt, Program KPLOT, Bonn, Germany, 1979.

Communication 8/06994H

ChemComm

2,3-Methanoamino acid analogs of Arg stabilize secondary structures of a 13 amino acid peptide in aqueous solution

Dongyeol Lim,[a] Destardi Moye-Sherman,[a] Inhye Ham,[a] Song Jin,[a] J. Martin Scholtz[b] and Kevin Burgess*[a]

[a] *Department of Chemistry, Texas A & M University, PO Box 300012, College Station, TX 77842-3012, USA. E-mail: burgess@mail.chem.tamu.edu*

[b] *Department of Medical Biochemistry and Genetics, 440 Reynolds Building, College Station, TX 77843-1114, USA*

Received (in Corvallis, OR, USA) 9th July 1998, Accepted 28th September 1998

Peptidomimetics 1 and 2 of RN24 (an RNase A *C*-peptide analog) in which the Arg$^+$-10 residue is replaced by 2*R*,3*S*-cyclo-Arg′ and by 2*S*,3*S*-cyclo-Arg′, respectively, show less temperature dependence in CD studies than the parent peptide.

The *N*-terminal fragment of RNase A has been adopted as a paradigm for conformational studies of short helical peptides. For instance, CD and NMR studies of a succinimidyl-capped analog of the *C*-peptide, RN24, indicate this 13-mer is *ca*. 50% helical in aqueous buffer at around 3 °C.[1,2] One of the key intramolecular interactions that is thought to stabilize this helical ensemble of conformations is a salt bridge between Glu$^-$-2 and Arg$^+$-10.[3,4] Syntheses of two 2,3-methanoarginine stereoisomers, 2*R*,3*S*-cyclo-Arg′ and 2*S*,3*S*-cyclo-Arg′,[5] gave us a unique opportunity to manipulate the Glu$^-$-2/Arg$^+$-10 interaction by constraining the guanidine functionality to point towards the *C*- and *N*-termini, respectively. Here we report the syntheses of these RN24 peptidomimetics, and CD studies to elucidate their conformational stabilities.

succ-A^{1}E^{2}T^{3}A^{4}A^{5}A^{6}K^{7}F^{8}L^{9}R^{10}A^{11}H^{12}A^{13}-amide RN24

succ-A^{1}E^{2}T^{3}A^{4}A^{5}A^{6}K^{7}F^{8}L^9(*2R,3S*-cyclo-R)^{10}A^{11}H^{12}A^{13}-amide **1**

succ-A^{1}E^{2}T^{3}A^{4}A^{5}A^{6}K^{7}F^{8}L^9(*2S,3S*-cyclo-R)^{10}A^{11}H^{12}A^{13}-amide **2**

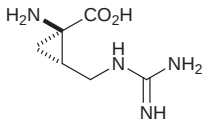

2*R*, 3*S*-cyclo-Arg'
or 2*R*, 3*S*-cyclo-R'

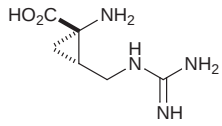

2*S*, 3*S*-cyclo-Arg'
or 2*S*, 3*S*-cyclo-R'

Peptidomimetics **1** and **2** were prepared *via* stepwise couplings of Fmoc-amino acid derivatives[6] on Rink's amide resin[7] using a manual shaker system.[8] Typical conditions and side-chain protecting groups were used. Couplings of natural amino acids were performed by premixing the amino acid with *N*-methylmorpholine, HOBt and PyBOP[9] in DMF. This coupling protocol was modified to incorporate the hindered cyclo-Arg′ residues and the amino acid immediately following (Leu-9). For these couplings, acid fluorides were produced *in situ via* the reagent TFFH (*i.e.* tetramethylfluoroformadinium hexafluorophosphate)[10] with HOAt (1-hydroxy-7-azabenzotriazole)[11] as an activating agent. The coupling to incorporate the cyclo-Arg moieties required only 1 h, whereas the subsequent coupling was more difficult and was run for 12 h. Deprotection of the side chains and cleavage from the resin was performed using TFA and a mixture of scavengers (phenol, ethane-1,2-dithiol and thioanisole). The crude peptide was further purified by preparative RP-HPLC.† Overall yields of isolated materials were in the 10% range giving enough sample for CD studies but not for NMR analysis.

Fig. 1(*a*) compares the CD spectra obtained for RN24, and the peptidomimetics at 3 °C (pH 5.1 buffer, 1 mM in each of sodium citrate, sodium phosphate and sodium borate, was used throughout this study). Peptide/peptidomimetic concentrations were accessed by calibration of the UV absorbance at 212 nm. These data show that the two peptidomimetics adopt helical conformations, but these are less populated than for RN24. With regards to the shape of the spectra, the 2*R*,3*S*-cyclo-Arg′ derivative **1** had an accentuated negative ellipticity at 222 nm relative to a classical α-helix. The other peptidomimetic, **2**, had a CD spectrum with a shape like that of RN24.

Variable temperature CD spectra of the peptidomimetics were particularly informative. The stability of the helical ensemble can be related directly to the change in the helical CD signal with temperature. Relative changes in $[\theta]_{222}$ requires the use of only one peptide solution, thus eliminating the error in the absolute peptide concentration and the variability between peptides. Fig. 1(*b*) is an overlay of five CD spectra for RN24 recorded at 5 °C intervals.‡ The molar ellipticity at 222 nm steadily decreased as the temperature was raised, ultimately corresponding to a *ca*. 40% reduction of the helical character. However, for peptidomimetics **1** and **2** the loss was significantly less over the same temperature range. Estimates for the loss of helical character for these two compounds were 30 and 23%, respectively.

Molecular dynamics simulations of RN24 and the two peptidomimetics was performed. Briefly, CHARMm parameters and coordinates for an ideal α-helix were modified using data sets already developed for the 2,3-methanoarginine analogs.[12] A medium of relative permittivity (ε = 80), and a simulated temperature of 276 K was used throughout. Trajecto-

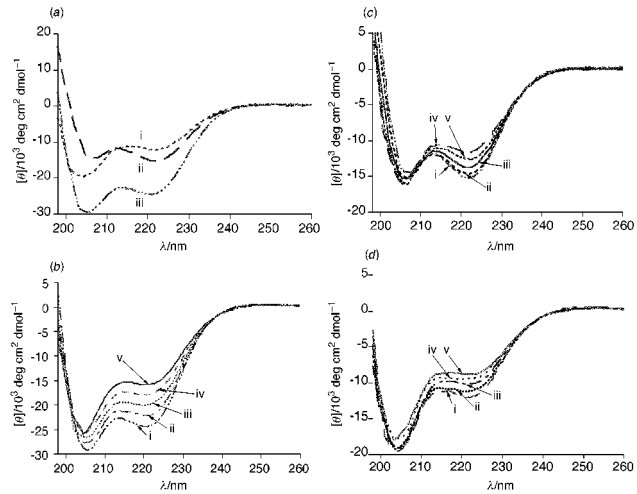

Fig. 1 (*a*) CD of (i) 2*S*,3*S*-cyclo-Arg′ **2**, (ii) 2*R*,3*S*-cyclo-Arg′ **1** and (iii) RN-24. Variable temperature CD of (*b*) RN-24, (*c*) **1** and (*d*) **2** at (i) 3, (ii) 8, (iii) 13, (iv) 18 and (v) 23 °C.

(*a*)

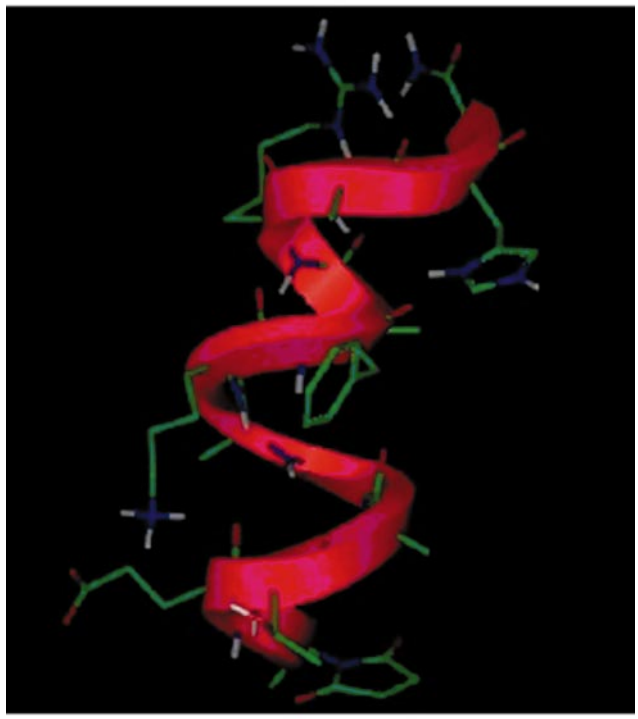

(*b*)

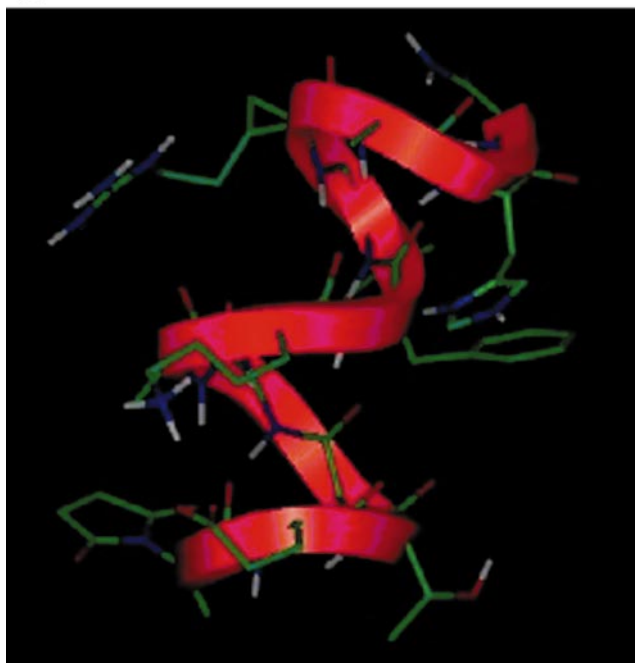

Fig. 2 Illustrative conformers after 200 ps of molecular dynamics for peptidomimetics (*a*) **1** and (*b*) **2**.

ries for the three starting structures sampled over a 200 ps interval showed that helical conformations were maintained for all three compounds throughout the dynamics run; Fig. 2 shows representative snap-shots of peptidomimetics **1** and **2**, respectively. These demonstrate a general trend observed in the molecular simulations, *i.e.* that peptidomimetic **1** tended to favor more tightly wound helical conformers than the 2*S*,3*S*-cyclo-Arg′-containing peptidomimetic **2**.§

In conclusion, we propose that the rigidity of the 2,3-methano analogs of arginine in peptidomimetics **1** and **2** can be used to impart conformational constraints. In this study, CD spectra of peptidomimetics containing these protein amino acids surrogates showed less temperature variations than that of RN24, indicative of a more stable helical structure. We also suggest that these same constraints distort the helical conformations such that atypical CD spectra were observed. The 2*R*,3*S*-cyclo-Arg′-containing peptidomimetic **1** has the Arg-side chain oriented towards the *C*-terminus where it cannot interact with the Glu-2 side-chain [Fig. 2(*a*)]. However, the guanidinium group locked in this orientation reinforces the helix dipole.[13] Conversely, 2*S*,3*S*-cyclo-Arg′ in peptidomimetic **2** presents the same side-chain in such a way that its charge opposes the helix dipole. The guanidinium moiety in this compound is oriented towards the Glu-2 residue, but the salt bridge is disrupted relative to RN24 because the cyclo-Arg′ has one less side chain methylene than natural arginine. The latter two effects result in less perfect helical conformations for peptidomimetic **2** than for **1** [Fig. 2(*b*)]. Other substitutions of 2,3-methanoamino acids into the RNase A *C*-peptide sequence are being investigated in these laboratories.[14]

The authors thank the NIH (GM50772 and DA06554) and The Robert A. Welch Foundation for support, the NIH for a Research Career Development Award, and The Alfred P. Sloan Foundation for a fellowship. D. M. S. thanks NIH for a predoctoral fellowship and TAMU for a Minority Merit Fellowship. J. M. S. is an American Cancer Society Junior Faculty Research Awardee (JFRA-577). We would like to thank Dr Larry Dangott and Ms Jinny Johnson for amino acid analyses, and Mr Jian Zhang for MALDI determinations.

Notes and references

† HPLC conditions: Vydac C18 (22 mm × 25 cm, 10 μm) column with a linear solvent gradient; A = 0.1% TFA in H_2O, B = 0.1% TFA in MeCN; flow rate 6 ml min^{-1}; gradient 5–20% B in A over 60 min. MALDI-MS data: RN24 [M+H_2O], calc. 1455.73, found 1455.91; **1** [M+H_2O], calc. 1454.47, found 1454.80; **2**, calc. 1454.47, found 1454.73.

‡ Concentrations (mM) used in the CD studies as determined by UV analysis at 210 nm: RN24: 1.12×10^{-2}; **1**: 1.14×10^{-2}; **2**: 1.18×10^{-2}.

§ Over the 200 ps period, 200 structures in the dynamics run were sampled; in the latter 100 ps interval, when the structures were adequately equilibrated, nearly all the conformers sampled showed the same fundamental helical characteristics as shown in Fig. 2. This MD experiment was run three times in slightly different ways, and essentially the same results were obtained.

1 K. R. Shoemaker, P. S. Kim, E. J. York, J. M. Stewart and R. L. Baldwin, *Nature*, 1987, **326**, 563.
2 J. J. Osterhout, R. L. Baldwin, E. J. York, J. M. Stewart, H. J. Dyson and P. E. Wright, *Biochemistry*, 1989, **28**, 7059.
3 M. Rico, J. Santoro, F. J. Bermejo, J. Herranz, J. L. Nieto, E. Gallego and M. A. Jiminez, *Biopolymers*, 1986, **25**, 1031.
4 M. Rico, E. Gallego, J. Santoro, F. J. Bermejo, J. L. Nieto and J. Horranz, *Biochem. Biophys. Res. Commun*., 1984, **123**, 757.
5 K. Burgess, D. Lim, K.-K. Ho and C.-Y. Ke, *J. Org. Chem*., 1994, **59**, 2179.
6 E. Atherton and R. C. Sheppard, *Solid Phase Peptide Synthesis, A Practical Approach*, IRL Press, 1989.
7 H. Rink, *Tetrahedron Lett*., 1987, **28**, 3787.
8 J. M. Stewart and J. D. Young, *Solid Phase Peptide Synthesis*, Pierce Chemical Company, 1984.
9 J. Coste, D. Le-Nguyen and B. Castro, *Tetrahedron Lett*., 1990, **31**, 205.
10 L. A. Carpino and A. El-Faham, *J. Am. Chem. Soc*., 1995, **117**, 5401.
11 L. A. Carpino, *J. Am. Chem. Soc*., 1993, **115**, 4397.
12 K. Burgess and D. Lim, *J. Am. Chem. Soc*., 1997, **119**, 9632.
13 D. E. Blagdon and M. Goodman, *Biopolymers*, 1975, **14**, 241.
14 D. Moye-Sherman, S. Jin, I. Ham, D. Y. Lim, J. M. Scholtz and K. Burgess, *J. Am. Chem. Soc*., 1998, **120**, 9435.

Communication 8/05367G

ChemComm

Asymmetric synthesis of 3-phenyl-2,3-methanophenylalanine developed by panning catalysts in a library format

Destardi Moye-Sherman, Mike B. Welch, Joe Reibenspies and Kevin Burgess*

Department of Chemistry, Texas A & M University, PO Box 300012, College Station, TX 77842-3012, USA. E-mail: burgess@mail.chem.tamu.edu

Received (in Corvallis, OR, USA) 10th July 1998, Accepted 28th September 1998

Optimal catalysts for the key cyclopropanation step in a synthesis of the title compound were identified by screening libraries of metal complex–ligand combinations; the synthesis was completed, and a derivative of the final product was crystallized to establish its solid state conformation.

Stereoisomers of 2,3-methanophenylalanine, 'cyclo-Phe', are useful phenylalanine surrogates for syntheses of conformationally constrained peptidomimetics.[1] They impart very specific steric perturbations at the *C*-terminal side or at the *N*-terminal side, depending on the cyclo-Phe isomer selected.[2] For some applications, however, it would be desirable to introduce this type of constraint at the *N*- and *C*-termini *simultaneously*. Consequently, we set about an asymmetric synthesis of 3-phenyl-2,3-methanophenylalanine, '3-Ph-cyclo-Phe'.

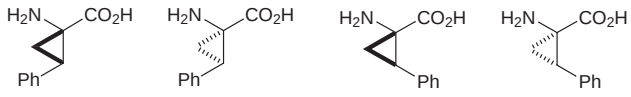

stereoisomers of cyclo-Phe

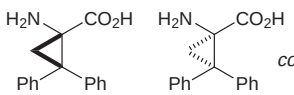

stereoisomers of 3-Ph-cyclo-Phe
constrain N- and C-termini simultaneously

Davies and co-workers have developed remarkably direct and effective syntheses of cyclo-Phe stereoisomers that involve enantio- and regio-selective cyclopropanations of phenylethene.[3] Doyle and co-workers have also shown 1,2-diphenylethene is a good substrate for asymmetric cyclopropanations using phenyl diazoacetate.[4] While it was apparent that the target compound identified above could be obtained using a modification of this approach (Scheme 1), the ideal catalyst for the cyclopropanation step was unknown. We therefore decided to screen some options in a library format.[5–9] This was done by manually weighing and pipetting catalysts and reagents into 24 glass vials set in wells drilled in a cooled aluminium block. Other papers from this laboratory describe the procedure used,[10] but some critical points are given here. All manipulations prior to the analysis were done in a glove box to maintain an inert atmosphere. After the reactions were mostly complete (TLC), the contents of each vial was manually filtered through a silica plug, an internal standard was introduced, and the sample was made up to a standard volume. The analysis was performed using an HPLC instrument equipped with an autosampler and a chiral column (Whelk-O *SS* , Regis Technologies). We estimate this protocol is one or two orders of magnitude faster than a conventional approach wherein a researcher would screen 2–3 reactions at a time.

Several generalities became apparent early in these investigations. First, the weighing errors with respect to the catalyst precursors became significant if the reactions were performed on 10 mg of diazo compound. The test reactions on a plate format were therefore performed on a 50 mg scale, and the important ones were checked on a larger scale. Second, pentane appeared to be the best solvent so this medium was used for all the latter screens. However, this provided a stringent test of reproducibility in these experiments because the data obtained using relatively insoluble catalyst precursors in this very apolar medium were related to the degree of agitation. Small stirrers were used in each well, but we were unable to arrange it so that they all spun smoothly; consequently, some reproducibility issues arose.† Nevertheless, the data obtained from the library screens did indicate promising catalysts for further development.

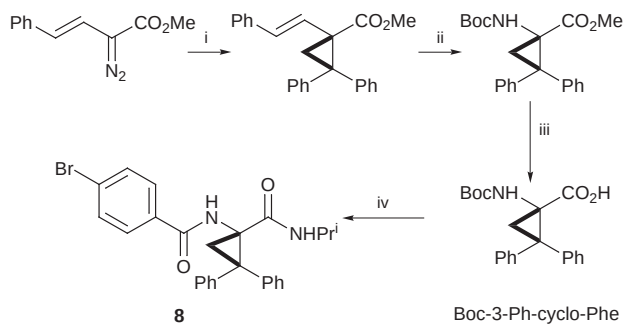

Scheme 1 *Reagents and conditions*: i, 1,1-diphenylethene (5 equiv.), Rh_2(*S*-TBSP)$_4$ (1 mol%), 0 °C, 24 h (86%, 97% ee); ii, cat $RuCl_3$, $NaIO_4$, MeCN–H_2O, CCl_4, 25 °C, 5 h then $(PhO)_2P(O)N_3$, NEt_3, Bu^tOH, reflux, 17 h (90% for 2 steps); iii, LiOH, aq. MeOH, reflux, 4 h (86%); iv, Pr^iNH_2, $Me_2NCFNMe_2{\cdot}PF_6$, CH_2Cl_2, Pr^iNEt_2, 0 °C, 30 min, then 50% TFA in CH_2Cl_2, 0–25 °C, 45 min, then 4-$BrC_6H_4CO_2H$, $Me_2NCFNMe_2{\cdot}PF_6$, CH_2Cl_2, Pr^iNEt_2, 25 °C, 45 min (32% for 3 steps).

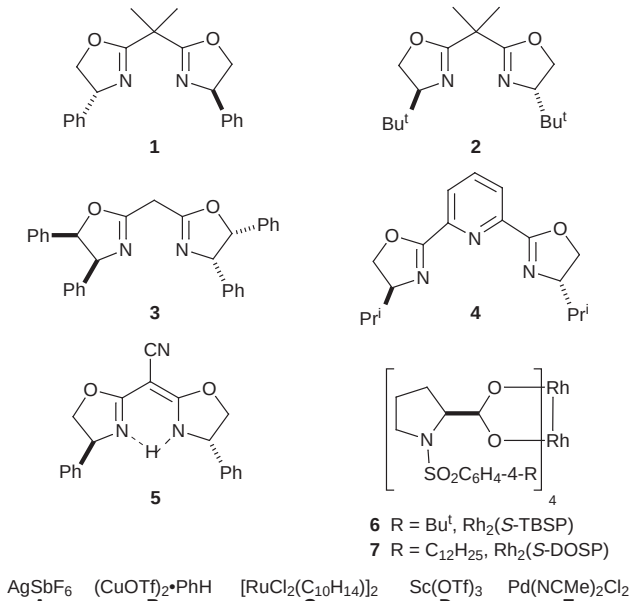

AgSbF$_6$ **A** (CuOTf)$_2$•PhH **B** [RuCl$_2$(C$_{10}$H$_{14}$)]$_2$ **C** Sc(OTf)$_3$ **D** Pd(NCMe)$_2$Cl$_2$ **E**

Several libraries of catalysts were screened to check solvent effects, and metal–ligand combinations/ratios. This data, not shown here, enabled us to bias the screening process in later experiments. Consequently, Fig. 1 refers to a plate screen performed in the latter part of this work.

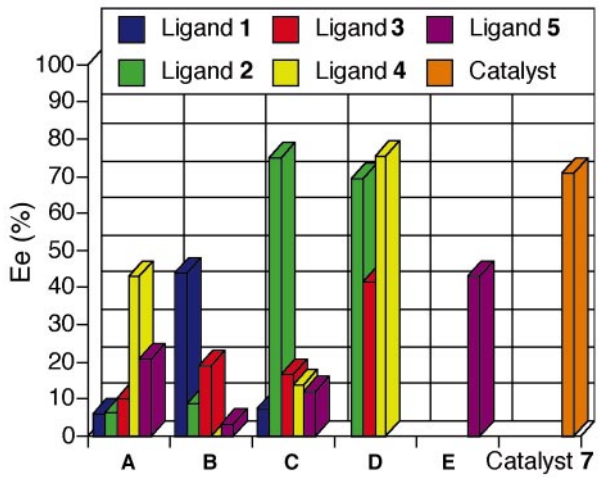

Fig. 1 Enantioselectivity data obtained from a library screen (% yields inset in columns). *Reaction conditions*: 1,2-diphenylethene (5 equiv.), metal (5 mol%), ligand:metal ratio = 1.5:1.0, pentane, 0 °C, 24 h.†

Table 1 Data for catalyst systems tested in conventional way[a]

Entry	Catalyst system	Metal/mol%	Ee (%)[b]	Yield (%)[c]
1[d]	**1B**	5.0	65[e]	62
2[d]	**2A**	5.0	24	2
3	**2B**	5.0	3 (9)	23 (4)[f]
4	**2C**	5.0	> 98 (75)	6 (14)[f]
5	**2D**	5.0	> 98 (69 and 78)	10 (6 and 24)[f]
6[d]	**2D**	5.0	> 98	1
7	**4D**	5.0	86 (75)	9 (16)[f]
8	**6**	10	94	85
9	**6**	5.0	97	88
10	**6**	1.0	97	86
11	**6**	0.1	89	63
12	**7**	1.0	> 98	50

[a] 50 mg scale, pentane, 0 °C, 1,2-diphenylethene (5 equiv.), ligand:metal = 1.5:1.0 for catalysts formed *in situ*. [b] Values in parentheses indicate data obtained in library screen. [c] Isolated yields unless otherwise indicated. [d] Reaction run at 25 °C. [e] > 95% ee after one recrystallization. [f] Measured *vs*. internal standard.

Data given in Fig. 1 and Table 1 indicate that the Davies/McKervey catalysts **6** and **7** were the most useful for the desired transformation. Other combinations gave poor yields and/or enantioselectivities except for the combination of copper triflate with ligand **1**. This gave product with a moderate enantioselectivity and yield, and the product could be crystallized to optical purity. This could be useful in some situations because the latter system, and the Davies/McKervey catalysts **6** and **7**, gave opposite enantiomers of the product.§

The synthesis of Boc-protected 3-Ph-cyclo-Phe was completed as indicated in Scheme 1. Absolute configurations here are assigned by extrapolation of Davies' model for enantioselective cyclopropanations with catalysts like **6** and **7**,[3,11] hence this must be regarded as a prediction rather than an established fact. Finally, a sample of this product was converted into diamide **8**, and single crystals of this material were formed for X-ray diffraction; a Chem3D diagram of the molecular structure is given in Fig. 2.¶ The observed φ,ψ angles (87.7, −152°) do not correspond closely with any idealized turn structure. The conformation seems to be governed by the phenyl rings adopting orientations with their faces beneath the *N*- and *C*-termini, with the *N*- and *C*-amide bonds in pseudo-parallel arrangements below these. Further studies are planned to elucidate less localized effects of 3-phenyl-cyclo-Phe on secondary structures.

K. B. gratefully acknowledges support from NIH (GM50772 and DA06554) and The Robert A. Welch Foundation; and the NIH for a Research Career Development Award, and The Alfred P. Sloan Foundation for a fellowship. D. M. S. thanks NIH for a predoctoral fellowship and TAMU for a Minority Merit Fellowship. We would also like to thank Alex Porte and Mark Powell for helpful discussions.

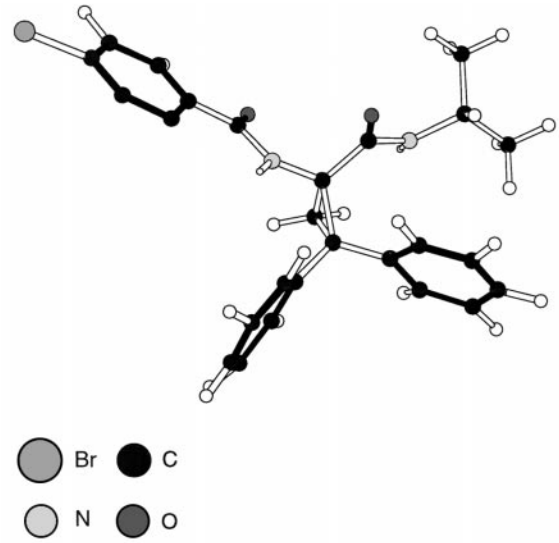

Fig. 2 Chem3D diagram of X-ray structure of 3-Ph-cyclo-Phe diamide.

Notes and references

† Four experiments were repeated on the same plate to check reproducibility in the same library; the worst correspondence of ee values was 26 *vs*. 6%, and the best was 19 *vs*. 18%. Table 1 shows the data obtained from experiments repeated on a larger scale, run in the conventional way. Five data points correspond to experiments that were performed in the plate format. The worst correspondence observed was for entry 5 (98 *vs*. 69% ee). In all five cases the ees obtained when the reactions were repeated on a large scale with efficient stirring were higher than those corresponding to the plate format.

‡ Percent yield for each well measured *vs*. an internal standard (1-acenaphthone): **1A** = 12%; **1B** = 23%; **1C** = 8%; **2A** = 18%; **2B** = 4%; **2C** = 14%; **2D** = 6%; **3A** = 12%; **3B** = 27%; **3C** = 2%; **3D** = 24%; **4A** = 41%; **4B** = 13%; **4C** = 1%; **4D** = 16%; **5A** = 29%; **5B** = 66%; **5C** = 1%; **5E** = 2%; catalyst **7** = 40%.

§ Both enantiomers of $Rh_2(TBSP)_4$ and of $Rh_2(DOSP)_4$ are commercially available from Aldrich, but in each case one is more expensive than the other.

¶ *Crystal data* for **8**: $C_{26}H_{25}N_2O_2Br{\cdot}1/2CH_2Cl_2$, M = 519.8 amu, triclinic, $P\bar{1}$, a = 12.423(3), b = 15.348(3), c = 16.332(3) Å, α = 63.02(2), β = 83.46(2), γ = 67.87(2)°, V = 2564(1) Å^3, Z = 2, T = 193(2) K, μ = 1.35 mm^{-1}, λ = 0.71073 Å, reflections measured: 5045, independent reflections: 4611, extinction coefficient = 0.0004(3), $R(F)$ [$I > 2\sigma(I)$] = 0.0865, $wR(F^2)$ [$I > 2\sigma(I)$] = 0.1118, $S(F^2)$ = 0.953. CCDC 182/1020.

1 C. H. Stammer, *Tetrahedron*, 1990, **46**, 2231.
2 K. Burgess, K.-K. Ho and B. Pal, *J. Am. Chem. Soc*., 1995, **117**, 3808.
3 H. M. L. Davies, P. R. Bruzinski, D. H. Lake, N. Kong and M. J. Fall, *J. Am. Chem. Soc*., 1996, **118**, 6897.
4 M. P. Doyle, Q.-L. Zhou, C. Charnsangavej and M. A. Longoria, *Tetrahedron Lett*., 1996, **37**, 4129.
5 K. Burgess, H.-J. Lim, A. M. Porte and G. A. Sulikowski, *Angew. Chem., Int. Ed. Engl*., 1996, **35**, 220.
6 K. Burgess and A. M. Porte, in *Accelerated Syntheses and Screening of Stereoselective Transition Metal Catalysts*, ed. M. P. Doyle, Greenwich, CT, 1997.
7 S. R. Gilbertson and X. Wang, *Tetrahedron Lett*., 1996, **36**, 6475.
8 M. S. Sigman and E. N. Jacobsen, *J. Am. Chem. Soc*., 1998, **120**, 4901.
9 B. M. Cole, K. D. Shimizu, C. A. Krueger, J. P. A. Harrity, M. L. Snapper and A. H. Hoveyda, *Angew. Chem., Int. Ed. Engl*., 1996, **35**, 1668.
10 A. M. Porte, J. Reibenspies and K. Burgess, *J. Am. Chem. Soc*.,1998, **120**, 9180.
11 H. M. L. Davies, P. R. Bruzinski and M. J. Fall, *Tetrahedron Lett*., 1996, **37**, 4133.

Communication 8/05454A

Crystal structure of an azo dye rotaxane

Sally Anderson,[a] William Clegg[b] and Harry L. Anderson[a]

[a] *Department of Chemistry, University of Oxford, Dyson Perrins Laboratory, South Parks Road, Oxford, UK OX1 3QY. E-mail: harry.anderson@chem.ox.ac.uk*

[b] *Department of Chemistry, University of Newcastle, Newcastle-upon-Tyne, UK NE1 7RU and CCLRC Daresbury Laboratory, Warrington, UK WA4 4AD*

Received (in Liverpool, UK) 20th July 1998, Accepted 28th September 1998

The crystal structure of an anionic azo dye rotaxane shows that the cyclophane embraces the centre of the dye; sodium coordinates to both the dye and the cyclophane, as well as DMSO solvent molecules, resulting in an infinite poly-rotaxane network.

Recently we prepared the first azo dye rotaxanes, by an azo-coupling reaction in water, using hydrophobic binding to ensure that the dye was formed threaded through the cyclophane.[1]

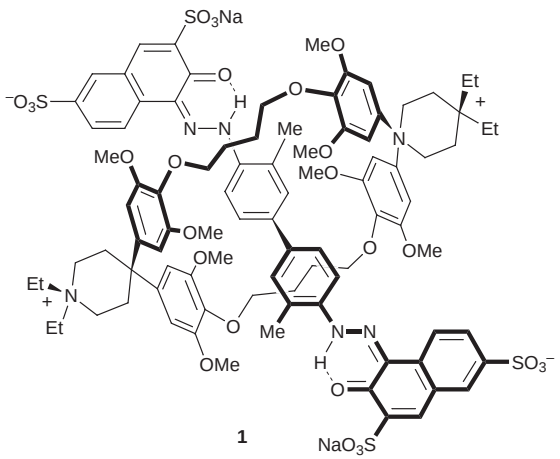

1

Formation of rotaxane encapsulated dyes, such as **1**, allows the environment of the chromophore to be precisely controlled, which may lead to dyes with enhanced chemical and photochemical stability. Here we present the first crystal structure of a rotaxane of this type. Despite the industrial importance of anionic sulfonated naphthalene azo dyes, few crystal structure determinations of these dyes have been reported, which reflects their reluctance to form suitable crystals.[2] The crystal structure of **1** provides valuable insights into the conformational behaviour of both the azo dye and cyclophane components, and shows how these units interact.

Slow diffusion of butanone into a saturated solution of **1** in DMSO and *n*-butanol gave small single crystals suitable for analysis by synchrotron X-ray diffraction at 160 K.† The crystals were highly solvated; six water and five DMSO molecules were located in the asymmetric unit, which contains one rotaxane molecule. **1** crystallises in a centrosymmetric space group P1. The unit cell contains both enantiomeric conformations of the rotaxane. The cyclophane embraces the centre of the dye as shown in Fig. 1. There are no face-to-face stacking π–π interactions between the biphenyl and the cyclophane, but there may be edge-to-face interactions between the four central hydrogens of the biphenyl and the cyclophane aromatic rings (H–centroid distances are 2.87, 3.17, 3.20 and 3.27 Å).[3]

The two ends of the azo dye dumbbell have essentially the same geometry; average bond lengths are shown on Fig. 2. A sodium cation chelates between the β-naphthol oxygen and the

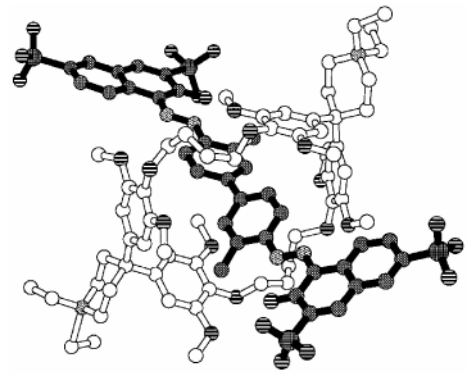

Fig. 1 Molecular structure of rotaxane **1**, not showing solvent molecules, hydrogen atoms and sodium cations.

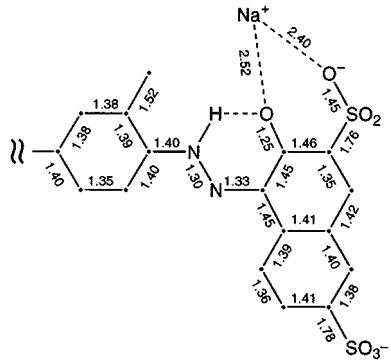

Fig. 2 Average bond lengths (Å) in the azo dye dumbbell componentof **1**.

sulfonate, yet, like most β-naphthol azo dyes,[2a,b,4] this dye is predominantly the hydrogen-bonded hydrazone, rather than azo, tautomer (Scheme 1). This is evident from the short C–O bond (1.25 Å; *cf.* 1.36 Å in PhOH and 1.21 Å in cyclohexanone),[5] short C_α–N bond (1.33 Å; *cf.* 1.24 Å in *E*-azobenzene[6] and 1.39 Å in 1,2-diphenylhydrazine[7]) and long C_α–C_β bond (1.45 Å; *cf.* 1.37 Å in naphthalene[8] and 1.52 Å in cyclohexane[9]).‡ Each half of the dye is approximately planar, with twists of 8.6 and 6.7° about the N–N linkages; the twist about the biphenyl link is 39.8°. The methyl of the tolidine resides near the β-naphthol oxygen, as observed in solution by NMR spectroscopy.[1]

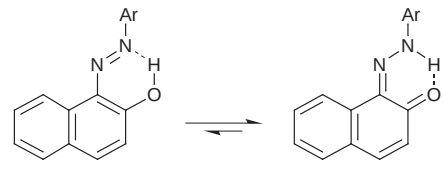

Scheme 1

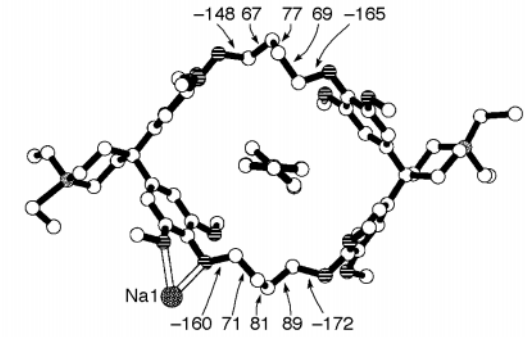

Fig. 3 Structure of the cyclophane component of **1**, showing selected torsion angles (°), viewed down the axis of the biphenyl unit of the dye, which is shown at the centre.

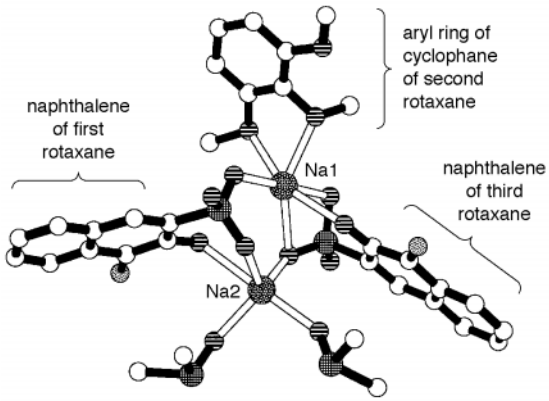

Fig. 4 Two sodium cations coordinate to two anionic dyes; Na1 also binds to the oxygens of the cyclophane of another rotaxane unit, while Na2 binds two DMSO molecules, giving irregular six- and five-coordination geometries.

The conformation of the cyclophane is remarkably convoluted. Both $O(CH_2)_4O$ links are in helical $ag^+g^+g^+a$ conformations, as shown by the torsion angles in Fig. 3. This allows the cyclophane to contract round its guest, which explains how it binds strongly to guests which seem too small to fill the cavity. Three previous crystal structures of cyclophanes of this type have $O(CH_2)_4O$ links with three *anti* and two *gauche* bonds.[10] A sodium cation (Na1) chelates to two *ortho* oxygens on one ring of the cyclophane, twisting it away from the cavity.

Pairs of sodium cations act as a 'glue', binding together the naphthalenes of two separate dyes and a cyclophane of a third rotaxane, as shown in Fig. 4. One sodium cation (Na2) is also coordinated by two DMSO solvent molecules. The Na–O interactions marked in Fig. 4 are in the range 2.24–2.60 Å (mean 2.39 Å); the next shortest Na–O distance is 3.25 Å. Thus the dyes are linked together, generating one-dimensional polymeric strands in the direction of the *a*-axis. Sodium coordination to the cyclophane links these strands together in the *b*-direction, to form double strand ladders. Electrostatic attraction between sulfonates and diethylammonium groups locks these ladders together in the *c*-direction (Fig. 5). Many features of the polyrotaxane network may be unique to this crystal structure, but the conformations of the azo dye and the cyclophane, and the coordination of both components with sodium, are relevant to the behaviour of molecules of this type in solution.

We gratefully acknowledge EPSRC and CCLR for financial support and Dr M. G. Hutchings (BASF, Manchester) for helpful discussion.

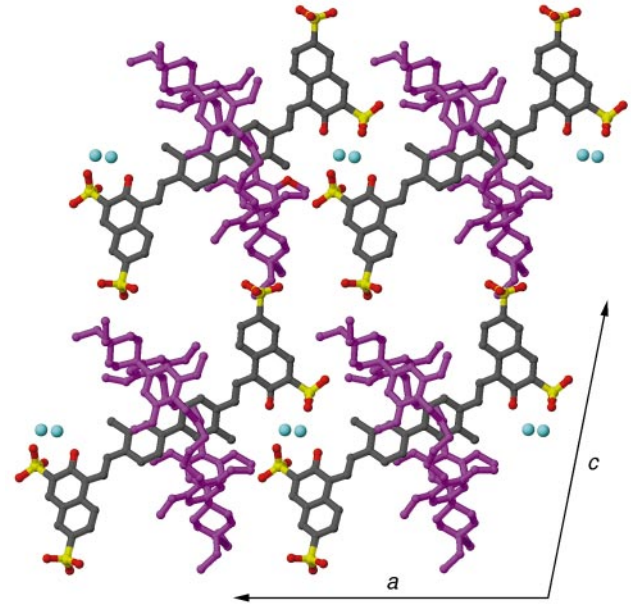

Fig. 5 Packing diagram showing four molecules of **1** in the *ac* plane (Na: blue, O: red, S: yellow and cyclophane: magenta; solvent molecules not shown).

Notes and references

† *Crystal data* for **1**·5DMSO·6H$_2$O: $C_{102}H_{148}N_6Na_2O_{37}S_9$, M = 2384.8, triclinic, space group $P\bar{1}$, a = 17.1896(12), b = 12.3108(14), c = 19.7639(14) Å, α = 100.579(2), β = 101.242(2), γ = 98.719(2)°, U = 6204.7(8) Å^3, Z = 2, λ = 0.6865 Å, μ = 0.25 mm^{-1}, T = 160 K, $R1$ = 0.140 for 12142 'observed reflections' [$F^2 > 2\sigma(F^2)$] and $wR2$ = 0.418 for all 21076 unique reflections (θ < 50°). Disorder in DMSO and water molecules could be only approximately modelled, with the aid of partial occupancies and restraints on geometrical and displacement parameters, and there is residual electron density of up to 1.63 e Å^{-3}. Methods and programs were as described elsewhere (ref. 11). CCDC 182/1039.

‡ Estimated standard deviations in bond lengths and angles involving C, N and O atoms are 0.01–0.02 Å and 0.5–1.0°.

1 S. Anderson, T. D. W. Claridge and H. L. Anderson, *Angew. Chem., Int. Ed. Engl.*, 1997, **36**, 1310.
2 (*a*) W. H. Ojala, L. K. Lu, K. E. Albers, W. B. Gleason, T. I. Richardson, R. E. Lovrien and E. A. Sudbeck, *Acta Crystallogr., Sect. B*, 1994, **50**, 684; (*b*) W. H. Ojala, W. B. Gleason, T. I. Richardson and R. E. Lovrien, *Acta Crystallogr., Sect. C*, 1994, **50**, 1615; (*c*) M. Zenki, T. Shibahara, M. Yamasaki and Y. Kushi, *Anal. Sci.*, 1990, **6**, 153; (*d*) W. H. Ojala, C. R. Ojala and W. B. Gleason, *Antiviral Chem. Chemother.*, 1995, **6**, 25.
3 G. Klebe and F. Diederich, *Philos. Trans. R. Soc. London A*, 1993, **345**, 37.
4 A. Whitaker, *J. Soc. Dyers Colourists*, 1978, **94**, 431.
5 Cambridge Structural Database: D. A. Fletcher, R. F. McMeeking and D. Parkin, *J. Chem. Inf. Comput. Sci.*, 1996, **36**, 746; F. H. Allen and O. Kennard, *Chemical Design Automation News*, 1993, **8**, 31.
6 J. Harada, K. Ogawa and S. Tomoda, *Acta Crystallogr., Sect. B*, 1997, **53**, 662.
7 D. C. Pestana and P. P. Power, *Inorg. Chem.* 1991, **30**, 528.
8 C. P. Brock and J. D. Dunitz, *Acta Crystallogr., Sect. B*, 1982, **38**, 2218.
9 R. Kahn, R. Fourme, D. André and M. Renaud, *Acta Crystallogr., Sect. B*, 1973, **29**, 131.
10 C. Krieger and F. Diederich, *Chem. Ber.*, 1985, **118**, 3620; S. Mattei, P. Seiler, F. Diederich and V. Gramlich, *Helv. Chim. Acta*, 1995, **78**, 1904.
11 W. Clegg, M. R. J. Elsegood, S. J. Teat, C. Redshaw and V. C. Gibson, *J. Chem. Soc., Dalton Trans.*, in the press.

Communication 8/05649H

Novel tellurium halides Te_2Cl_2 and Te_2Br_2

Jarkko Pietikäinen and Risto S. Laitinen

Department of Chemistry, University of Oulu, Linnanmaa, FIN-90570 Oulu, Finland. E-mail: risto.laitinen@oulu.fi

Received (in Basel, Switzerland) 26th May 1998, Accepted 23rd September 1998

Novel Te_2Cl_2 and Te_2Br_2 were prepared by the reaction of Li_2Te and TeX_4 and characterized by mass spectroscopy and ^{125}Te NMR spectroscopy, and by successful syntheses of 1,2-Te_2S_5 and 1,2-Te_2Se_5.

Disulfur and diselenium dihalides are relatively stable[1] and form a useful class of reagents for many synthetic applications. The existence of mixed selenium–sulfur dihalides has also been reported.[1l,2] Here we describe a facile synthesis of Te_2Cl_2 and Te_2Br_2 that have turned out to be surprisingly stable,† though the phase diagrams of the Te–$TeCl_4$ and Te–$TeBr_4$ systems do not give any indications about the existence of Te_2Cl_2 and Te_2Br_2.[4] The closest known tellurium halides of this type are polymeric $(Te_2Cl)_x$, $(Te_3Cl_2)_x$ $(Te_2Br)_x$ and $(Te_2I)_x$.[5]

Te_2Cl_2 and Te_2Br_2 were prepared by reducing elemental tellurium with superhydride and treating the resulting telluride with appropriate tellurium tetrahalogenide [eqn. (1)].‡

$$\mathrm{Te} \xrightarrow{\mathrm{LiBHEt_3}} 1/x\,\mathrm{Te}_x^{2-}$$

$$\mathrm{Te}_x^{2-} + x\mathrm{TeX}_4 \rightarrow x\mathrm{Te}_2\mathrm{X}_2 + 2x\mathrm{X}^- \ (\mathrm{X} = \mathrm{Cl},\ \mathrm{Br}) \quad (1)$$

Ditellurium dichloride was obtained as a yellow liquid, and ditellurium dibromide as an orange–red liquid. Both Te_2Cl_2 and Te_2Br_2 should be stored under an inert atmosphere. Te_2Br_2 however, is stable for hours at room temperature. Te_2Cl_2 is not as stable as Te_2Br_2, but it can also be stored for hours, especially in organic solutions. Chlorinated solvents, however, should be avoided.

Both Te_2Cl_2 and Te_2Br_2 exhibit one major ^{125}Te resonance in their respective NMR spectra (Fig. 1).§ The ^{125}Te chemical shift of Te_2Cl_2 in CS_2 is at 1336 ppm and that of Te_2Br_2 at 1253 ppm. The chemical shift of Te_2Cl_2 in toluene is 1297 ppm.[3] The ^{125}Te chemical shifts of the two species bear a relationship that is expected from the comparison with the ^{77}Se chemical shifts of Se_2Cl_2 and Se_2Br_2.¶ The appearance of only one resonance in the spectra of both compounds indicate an open-chain X–Te–Te–X structure rather than a branched $X_2Te{=}Te$ structure. One minor signal was observed in both spectra (Fig. 1). The chemical shift of this resonance varies (820–880 ppm) and its intensity relative to that of the main resonance increases as a function of time and implies the decomposition of Te_2Cl_2 and Te_2Br_2. We have previously made a tentative assignment of a weak resonance observed at 849 ppm in the S–Se–Te melt at 145 °C to Te_8.[6] It is possible that the decomposition of Te_2X_2 (X = Cl, Br) produces Te_8.‖

The mass spectra of Te_2Cl_2 and Te_2Br_2 are shown in Fig. 2.** The observed isotopic distribution for the molecular ion of Te_2Cl_2 as well as those for its fragments are in a good agreement with the calculated distributions. A reasonable fragmentation that exhibits the expected isotopic distributions could also be deduced in the mass spectrum of Te_2Br_2, though we did not observe the molecular ion.

It is well established that $[Ti(C_5H_5)_2S_5]$ and $[Ti(C_5H_5)_2Se_5]$ react with S_2Cl_2 or Se_2Cl_2 to produce cyclic seven-membered chalcogen compounds (S_7, 1,2-Se_2S_5 and 1,2,3,4,5-Se_5S_2, Se_7, respectively).[7] These titanocene reagents can be used to further verify the identities of Te_2Cl_2 and Te_2Br_2. We present here the preparation of 1,2-Te_2S_5 and 1,2-Te_2Se_5 [eqn. (2)] by treating Te_2Cl_2 with $[Ti(C_5H_5)_2E_5]$ (E = S, Se) in CS_2 in an analogous manner as described previously for 1,2,3,4,5-Se_5S_2.[8]††

$$[\mathrm{Ti}(\mathrm{C_5H_5})_2\mathrm{E_5}] + \mathrm{Te_2X_2} \rightarrow 1,2\text{-}\mathrm{Te_2E_5} + [\mathrm{Ti}(\mathrm{C_5H_5})_2\mathrm{X_2}] \quad (2)$$

Only one ^{125}Te NMR resonance is observed in spectra of both compounds. The signal at 1732 ppm is assigned to 1,2-Te_2S_5 and that at 1724 ppm to 1,2-Te_2Se_5. The latter resonance is

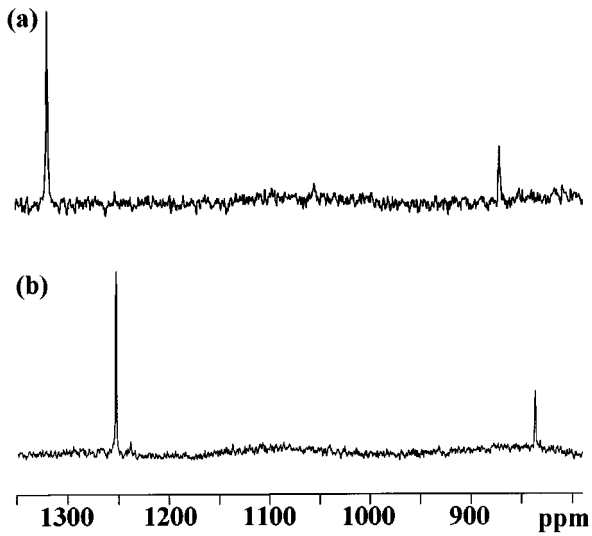

Fig. 1 ^{125}Te NMR spectra of (a) Te_2Cl_2 and (b) Te_2Br_2 in CS_2.

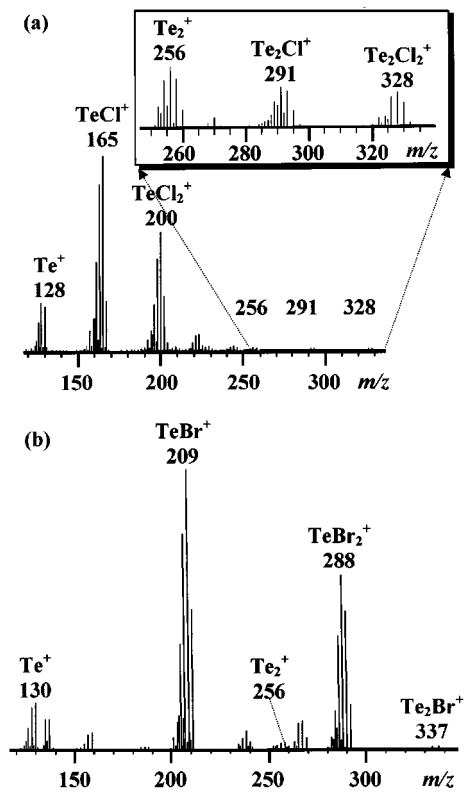

Fig. 2 12 eV mass spectra of (a) Te_2Cl_2 and (b) Te_2Br_2.

expectedly upfield, since selenium is less electronegative than sulfur.[11] The ^{77}Se NMR resonances of 1,2-Te_2Se_5 are 1040, 1019 and 982 ppm (intensity ratio 2 : 1 : 2). These signals are consistent with the ^{77}Se chemical shifts of 1,2,3,4,5-Se_5S_2[12] and imply that 1,2-Te_2Se_5 is also fluxional. It should be noted that Te_2Br_2 is less reactive than Te_2Cl_2.

Financial support from Academy of Finland is gratefully acknowledged.

Notes and references

† Preliminary information on Te_2Cl_2 has been reported previously.[3]

‡ All reactions were carried out under a dry argon atmosphere. $LiBHEt_3$ (15.7 cm^3, 15.7 mmol, 'Super-Hydride' 1 M in THF) and elemental tellurium (1.00 g, 7.84 mmol) were stirred for 15 min under slight warming. The solution was cooled to room temperature and the solution of $TeCl_4$ (2.11 g, 7.84 mmol) or $TeBr_4$ (3.51 g, 7.84 mmol) in 50 cm^3 of THF was added dropwise. The solution was filtered and solvent removed under a dynamic vacuum. The product was dissolved in CS_2 to remove LiX, elemental tellurium, and the unreacted TeX_4 (yields in both cases *ca.* 40% based on the initial amount of TeX_4).

§ The ^{77}Se and ^{125}Te NMR spectra were recorded at 300 K on a Bruker DPX 400 spectrometer (76.311 and 126.241 MHz for ^{77}Se and ^{125}Te, respectively). D_2O was used as an external ^{2}H lock and saturated D_2O solutions of SeO_2 and H_6TeO_6 as external references. The ^{77}Se and ^{125}Te chemical shifts were reported relative to neat Me_2Se and Me_2Te, respectively [$\delta(Me_2Se) = \delta(SeO_2) + 1302.6$; $\delta(Me_2Te) = \delta(H_6TeO_6) + 712$].

¶ The ^{77}Se chemical shift in Se_2Cl_2 is 1271 ppm and that in Se_2Br_2 1171 ppm.[2b]

‖ To test this assignment Te_2Cl_2 was reacted with [$Ti(MeC_5H_4)_2(\mu$-$Te_2)_2Ti(MeC_5H_4)$] (molar ratio 2 : 1) in CS_2. This reaction is expected to form Te_8. We observed a single ^{125}Te resonance at 868 ppm.

** EI-MS mass spectra of Te_2Cl_2 and Te_2Br_2 were recorded using a Kratos MS 80 spectrometer at 12 eV electron energy.

†† 0.26 g of [$Ti(C_5H_5)_2S_5$][9] or 0.44 g of [$Ti(C_5H_5)_2Se_5$][10] (0.77 mmol) was dissolved in 50 cm^3 of CS_2. Te_2Cl_2 (0.25 g; 0.77 mmol) in 10 cm^3 of CS_2 was added into this solution that was subsequently cooled down to −78 °C to precipitate 1,2-Te_2E_5 and [$Ti(C_5H_5)_2Cl_2$]. After filtration and redissolving of [$Ti(C_5H_5)_2Cl_2$] in $CHCl_3$, the remaining product was dried *in vacuo* [yields 0.11 g (34.2%) and 0.31 g (47.6%) for Te_2S_5 and Te_2Se_5, respectively].

1 (*a*) F. Fehér, *Handbuch der Präparative Anorganischen Chemie*, ed. G. Brauer, 3rd edn., Ferdinand Enke Verlag, Stuttgart, 1975, vol. 1, p. 356; (*b*) P. Born, R. Kniep, D. Mootz, M. Hein and B. Krebs, *Z. Naturforsch., Teil B*, 1981, **36**, 1516; (*c*) A. Engelbrecht and F. Sladky, *Adv. Inorg. Chem. Radiochem.*, 1981, **24**, 189; (*d*) R. Steudel, D. Jensen and B. Plinke, *Z. Naturforsch., Teil B*, 1987, **42**, 163; (*e*) A. Haas and H. Willner, *Z. Anorg. Allg. Chem.*, 1979, **454**, 17; (*f*) M. Gopal and J. Milne, *Inorg. Chem.*, 1992, **31**, 4530; (*g*) K. Jug and R. Iffert, *J. Mol. Struct.* (*Theochem*), 1989, **186**, 347; (*h*) H.-J. Mäusle and R. Steudel, *Z. Anorg. Allg. Chem.*, 1980, **463**, 27; (*i*) C. J. Marsden, R. D. Brown and P. D. Godfrey, *J. Chem. Soc., Chem. Commun.*, 1979, 399; (*j*) R. L. Kuczkowski and F. B. Wilson, *J. Am. Chem. Soc.*, 1963, **85**, 2028; (*k*) B. Solouki and H. Bock, *Inorg. Chem.*, 1977, **16**, 665; (*l*) J. Milne and A. J. Williams, *Inorg. Chem.*, 1992, **31**, 4534; (*m*) M. Lamoureux and J. Milne, *Can. J. Chem.*, 1989, **67**, 1936; (*n*) M. Lamoureux and J. Milne, *Polyhedron*, 1990, **9**, 589; (*o*) D. Katryniok and R. Kniep, *Angew. Chem.*, 1980, **92**, 646.

2 (*a*) J. Milne, *J. Chem. Soc., Chem. Commun.*, 1991, 1048; (*b*) J. B. Milne, *Can. J. Chem.*, 1992, **70**, 693; (*c*) R. Steudel, B. Plinke, D. Jensen and F. Baumgart, *Polyhedron*, 1991, **10**, 1037.

3 J. Pietikäinen and R. S. Laitinen, *Phosphorus Sulfur Silicon Relat. Elem.*, 1998, **124**/**125**, 453.

4 A. Rabenau and H. Rau, *Z. Anorg. Allg. Chem.*, 1973, **395**, 273.

5 R. Kniep, D. Mootz and A. Rabenau, *Z. Anorg. Allg. Chem.*, 1976, **422**, 17; R. Kniep, D. Mootz and A. Rabenau, *Angew. Chem.*, 1973, **85**, 504; M. Takeda and N. N. Greenwood, *J. Chem. Soc., Dalton Trans.*, 1976, 631.

6 T. Chivers, R. S. Laitinen, K. J. Schmidt and J. Taavitsainen, *Inorg. Chem.*, 1993, **32**, 337.

7 R. S. Laitinen, P. Pekonen and R. J. Suontamo, *Coord. Chem. Rev.*, 1994, **130**, 1 and references therein.

8 R. Steudel, M. Papavassiliou, E.-M. Strauss and R. Laitinen, *Angew. Chem., Int. Ed. Engl.*, 1986, **25**, 99.

9 A. Shaver and J. M. McCall, *Organometallics*, 1984, **3**, 1823.

10 A. Shaver, J. M. McCall and G. Marmolejo, *Inorg. Synth.*, 1990, **27**, 59.

11 R. S. Laitinen and T. A. Pakkanen, *Inorg. Chem.*, 1987, **26**, 2598.

12 P. Pekonen, Y. Hiltunen, R. S. Laitinen and T. A. Pakkanen, *Inorg. Chem.*, 1990, **29**, 2770.

Communication 8/03907K

A novel route to the preparation of aldehyde end-functionalised oligomers *via* catalytic chain transfer polymerisation

Thomas P. Davis,*[a] Michael D. Zammit,†[a] Johan P.A. Heuts[a] and Keith Moody[b]

[a] *School of Chemical Engineering and Industrial Chemistry, University of New South Wales, Sydney, NSW 2052, Australia. E-mail: t.davis@unsw.edu.au*

[b] *Orica, Newsom St, Ascot Vale, VIC 3032, Australia*

Received (in Cambridge, UK) 15th September 1998, Accepted 30th September 1998

Catalytic chain transfer polymerisation of ethyl α-hydroxymethacrylate with cobaloxime boron fluoride is shown to be an effective route for the production of oligomers with an aldehyde end-functionality.

Catalytic chain transfer polymerisation has proven to be a very efficient technique for molecular weight control in free-radical polymerisation.[1] The catalytic nature of this process and the very high chain transfer constants associated with the used chain transfer agents (*i.e.* certain low spin Co^{II} complexes such as cobaloximes and porphyrins) require only parts per million quantities for a molecular weight reduction by orders of magnitude. Numerous experimental investigations have shown this process to be most efficient for monomers containing an α-methyl group, such as the methacrylate series of monomers.[1,2] Chain transfer constants (*i.e.* the ratio of the chain transfer and the propagation rate coefficients) for cobaloxime boron fluoride

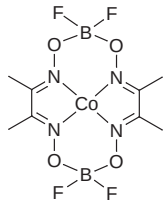

1

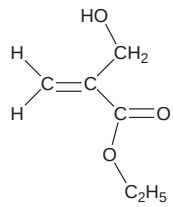

2

1 in methyl methacrylate polymerisation are typically of the order 10^4, whereas they are typically an order of magnitude smaller for styrene (*i.e.* a monomer without an α-methyl group).[2]

The use of catalytic chain transfer agents instead of conventional chain transfer agents such as mercaptans has a further advantage in that it introduces an end-functionality in the form of a terminal double bond, which can subsequently be modified. In the present investigations, our main aim is to introduce a different end-functionality without the need for a post-polymerisation modification. Our target is the acetoacetyl functionality, which has found interesting uses in the field of thermoset coatings chemistry.[3] This functionality can be used for a whole series of crosslinking reactions and Michael additions. Here, we show that this functionality can be introduced by the catalytic chain transfer polymerisation of ethyl α-hydroxymethacrylate **2**, a monomer which belongs to the methacrylate series (and hence should readily undergo the catalytic chain transfer reaction), and whose derived polymeric radical should give the acetoxyacetal functionality *via* a tautomeric rearrangement of the formed enol after the abstraction of a hydrogen atom of the α-hydroxymethyl group (see Scheme 1).

Ethyl α-hydroxymethacrylate **2** was prepared according to the method described by Villieras and Rambaud.[4]‡ It was found that the monomer readily undergoes free-radical polymerisation yielding polymers consisting of approximately 700 monomer units (at 60 °C, [AIBN] = 10^{-2} M) as determined by gel

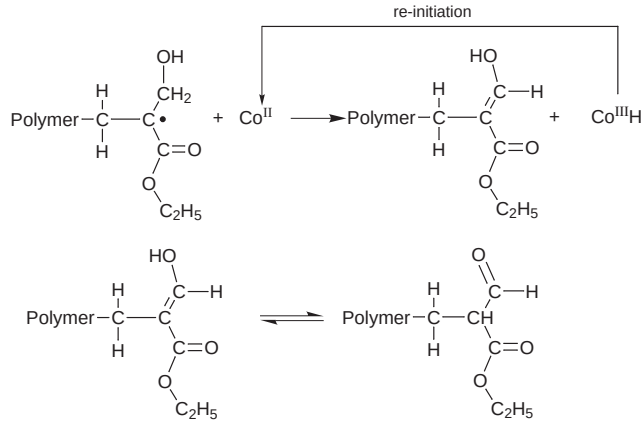

Scheme 1

permeation chromatography using a poly(methyl methacrylate) calibration curve. In order to investigate the catalytic chain transfer behaviour of ethyl α-hydroxymethacrylate with COBF, we estimated its chain transfer constant [with respect to a poly(methyl methacrylate) calibration curve] using the conventional Mayo procedure.[5] In this procedure, the chain transfer constant is determined from the slope of a plot of the reciprocal degree of polymerisation (1/DP) *vs.* the ratio of [chain transfer agent] to [monomer]. In Fig. 1, such a plot is shown for the current system at 60 °C and a chain transfer constant of 700 is found.§ This value, which we expect to be higher once we can use the true Mark–Houwink constants in our molecular weight analysis, clearly indicates that the current monomer is suitable for catalytic chain transfer polymerisation.

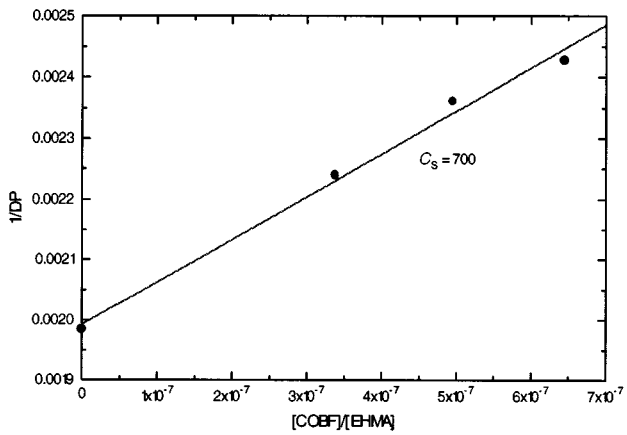

Fig. 1 Mayo plot for the determination of the chain transfer constant (C_S) for COBF in a free-radical polymerisation of ethyl α-hydroxymethacrylate at 60 °C.

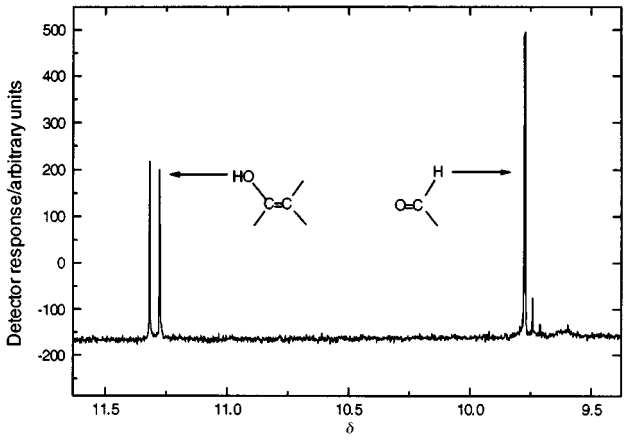

Fig. 2 Expansion of the 300 MHz ^{1}H NMR spectrum of poly(ethyl α-hydroxymethacrylate) in the region between δ 9.5 and 11.5, clearly indicating the presence of aldehyde (δ 9.77) and enol (δ 11.29) endgroups.

The homopolymers obtained *via* catalytic chain transfer polymerisation were analysed using 300 MHz ^{1}H NMR spectroscopy (Bruker ACF 300), and the most interesting region of the obtained NMR spectrum is shown in Fig. 2. The signals that are shown in this figure do not appear in the spectrum of the monomer and can be attributed to the formyl proton (δ9.77) and to enolic hydroxyl protons (δ 11.29). Both signals are characteristic for diketonic systems displaying a keto–enol tautomeric equilibrium.[6] Although further and more detailed NMR studies are required for a more detailed assignment of the signals (*e.g.* whether intramolecular hydrogen bonding occurs),[7] the current results are sufficient proof that the aldehyde end-functionality is indeed formed in significant quantities.

In summary, we have clearly shown that ethyl α-hydroxymethacrylate readily undergoes an effective catalytic chain transfer polymerisation with COBF, and that using this procedure the very useful aldehyde end-functionality is introduced.

We gratefully acknowledge financial support by the Australian Research Council, ICI and Orica, as well as helpful discussions with Professor Mike Gallagher.

Notes and references

† Present address: Dulux Australia, McNaughton Rd, Clayton, VIC 3168, Australia

‡ *Monomer synthesis*. The synthesis route of Villieras and Rambaud was followed exactly, with the only difference that the addition step of the potassium carbonate solution was carried out at 0 °C instead of room termperature. Yield: 75%. δ_H($CDCl_3$, 298 K, 300 MHz) 5.8 and 6.2 (=CH_2), 1.28 (–CH_3), 2.63 (–OH), 4.23 (–CH_2–); ν_{max}(NaCl)/cm^{-1} 1630 (C=C), 1710 (C=O).

§ *Chain transfer constant measurements*. The monomer was purged with high purity nitrogen gas for 1 h prior to use. Two stock solutions were prepared: (i) an initiator stock solution, and (ii) a catalyst stock solution. (i) The initiator solution was prepared by dissolution of approximately 220 mg of AIBN in 45 ml of monomer. (ii) The catalyst stock solution was prepared by dissolution of approximately 3 mg of catalyst into 10 ml of solution (i) and a subsequent 10-fold dilution with solution (i). Four reaction mixtures were then prepared, each containing 4.0 ml of initiator solution and 0, 0.2, 0.3 and 0.4 ml of catalyst stock solution, respectively. At all stages of these preparations, care was taken to exclude oxygen from the reaction mixtures. The reaction ampoules, specially modified for use with standard Schlenck equipment, were further deoxygenated by two freeze-pump-thaw cycles and subsequently placed in a waterbath (thermostatted at 60 °C) for 15 min. Finally the obtained polymer was isolated and molecular weight analysis performed with gel permeation chromatography.

1 T. P. Davis, D. Kukulj, D. M. Haddleton and D. R. Maloney, *Trends Polym. Sci*., 1995, **3**, 365.
2 K. G. Suddaby, D. R. Maloney and D. M. Haddleton, *Macromolecules*, 1997, **30**, 702.
3 F. W. Del Rector, W. W. Blount and D. R. Leonard, *J. Coatings Technol*., 1989, **61**, 31.
4 J. Villieras and M. Rambaud, *Synthesis*, 1982, 924.
5 F. R. Mayo, *J. Am. Chem. Soc*., 1943, **65**, 2324.
6 I. Deutsch and K. Deutsch, *Tetrahedron Lett*., 1966, 1849.
7 L. M. Jackman and S. Sternhell, *Applications of Nuclear Magnetic Resonance Spectroscopy in Organic Chemistry*, 2nd edn, International Series in Organic Chemistry, Pergamon, Oxford, vol. 10, 1978.

Communication 8/07177B

Stable vesicles made from new triple-chain amphiphiles: long-term stability toward leakage of the trapped substances

Yasushi Sumida,[a] Araki Masuyama,[b] Hiroshi Maekawa,[b] Mayuko Takasu,[b] Toshiyuki Kida,[b] Yohji Nakatsuji,[b] Isao Ikeda*[b] and Masatomo Nojima[b]

[a] *Cosmetic Laboratory, Kanebo Corporation, Kotobuki-cho 5-3-28, Odawara, Kanagawa 250-0002, Japan*
[b] *Department of Applied Chemistry, Faculty of Engineering, Osaka University, Yamadaoka 2-1, Suita, Osaka 565-0871, Japan. E-mail: ikeda@chem.eng.osaka-u.ac.jp*

Received (in Cambridge, UK) 4th September 1998, Accepted 29th September 1998

Very stable vesicles, which can keep 5(6)-carboxyfluorescein trapped inside for months, are obtained from triple-chain amphiphiles bearing two carboxylate groups derived from 1-*O*-alkylglycerols.

Numerous endeavours to construct stable liposomes or vesicles have been made. There are two classical approaches to suppressing the leakage of trapped substances: one is the addition of other molecules, such as cholesterol[1] or cholesterol polysaccharides,[2] to bilayer systems, and the other is the introduction of special group(s) or structures into the hydrophobic moiety of the amphiphiles. As examples of the latter, unique amphiphiles bearing polymerisable functional groups[3] or phytanyl moieties[4] in the hydrophobic chains have been reported. It should be noted that most of these specially designed amphiphiles are based on the conventional 'double-chain' structure, like phospholipids.

A series of novel amphiphiles bearing three hydrophobic alkyl chains and two hydrophilic head groups has been designed and prepared previously by the authors' group.[5] It was found that these 'triple-chain' compounds showed a greater ability to lower surface tension and to form micelles at lower concentrations than the corresponding 'double-chain' surfactants bearing two ionic head groups. These results suggest that the three alkyl chains in the molecule can make a positive contribution to the surface-active properties because both the inter- and intramolecular hydrophobic interactions are strengthened compared to those of the corresponding double-chain surfactants.[6] This speculation prompted us to prepare vesicles made from the triple-chain amphiphiles and to compare their ability to suppress the leakage of substances trapped inside with that of vesicles made from conventional phosphatidylcholines.

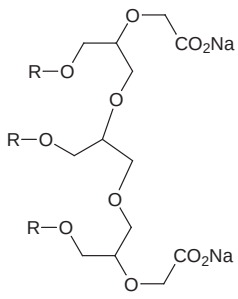

1 R = *n*-$C_{16}H_{33}$

2 R = *n*-$C_{18}H_{37}$

The triple-chain amphiphiles used in this work (**1** and **2**) were bis(carboxylate)s prepared from 1-*O*-alkylglycerols.[5]† Dipalmitoyl- and distearoyl-phosphatidylcholines (DPPC and DSPC, respectively; Nippon Fine Chemical Co., 99.8%) were also used as the reference lipids because these phosphatidylcholines (PCs) bearing saturated acyl chains are known to form relatively stable bilayer membranes at room temperature.[7] Small unilamellar vesicles containing concentrated 5(6)-carboxyfluorescein (CF) in an aqueous buffer solution were prepared by the conventional hydration–sonication method.‡ Fig. 1 shows the released percentage of CF from vesicles made from phospholipids or triple-chain amphiphiles during storage at 40 °C.

Upon comparing the results for the triple-chain amphiphiles with those for the corresponding phospholipids bearing the same number of carbon atoms in one hydrophobic chain (**1** *vs.* DPPC, **2** *vs.* DSPC, respectively), we found that the vesicles made from the triple-chain amphiphiles were much more stable toward the leakage of trapped CF. In particular, vesicles made from **2** released less than 10% of the CF after 12 months under the experimental conditions used in this work. The transition temperatures from the gel state to the liquid crystal state (T_c), measured *via* DSC, of aqueous dispersions of these lipids or amphiphiles are as follows: 45.3 °C (for **1**), 59.3 °C (**2**), 41.1 °C (DPPC) and 56.3 °C (DSPC). In the case of vesicles made from **1** or DPPC, the relatively fast release of trapped CF may be attributed to the high fluidity of the membrane because the T_c of these two compounds is only a little higher than the storage temperature. The large difference in the ability to suppress the leakage between **2** and DSPC, however, cannot be explained by the T_c value.

The microfluidity of the bilayer membrane was estimated by the established method using pyrene as a fluorescent probe.[8] The I_e/I_m ratio (I_e and I_m are fluorescence intensities of the pyrene eximer at 468 nm and the pyrene monomer at 394 nm, respectively) increases as the microfluidity of the hydrophobic phase in the membrane increases. The relation between the I_e/I_m ratio and the measured temperature is shown in Fig. 2. [conditions: amphiphile or lipid (10 mM), pyrene (0.15 mM), 100 mM NaCl, 20 mM Tris-HCl (pH 7.5), excitation at 335 nm]

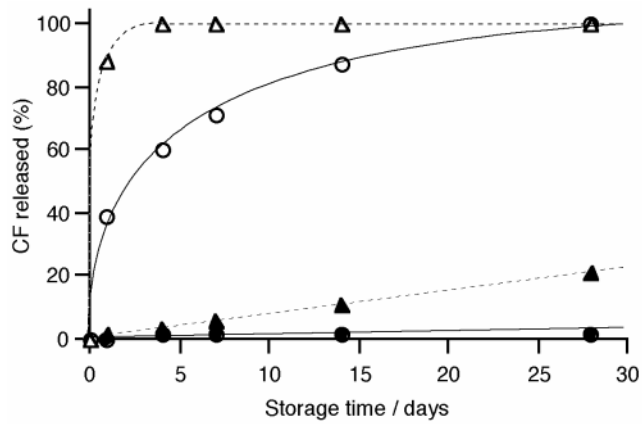

Fig. 1 Release (%) of 5(6)-carboxyfluorescein (CF) trapped inside vesicles of (△) DPPC, (▲) DSPC, (○) **1** and (●) **2** as a function of storage time (days) at 40 °C.

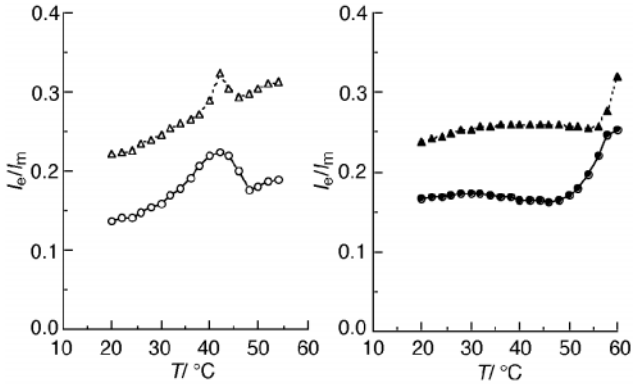

Fig. 2 Effect of temperature on the I_e/I_m ratio of pyrene buried in the membrane of (△) DPPC, (▲) DSPC, (○) **1** and (●) **2** vesicles. Conditions: amphiphile or lipid (10 mM), pyrene (0.15 mM), 100 mM NaCl, 20 mM Tris-HCl (pH 7.5), excitation at 335 nm.

Although the I_e/I_m ratios for **1** and DPPC increased gradually from 30 °C up to about 45 °C, there was very little change in the ratios for **2** and DSPC until 50 °C. These results agree well with the T_c of each compound. It is noteworthy that the I_e/I_m ratio of the triple-chain amphiphile is much lower than that of the corresponding phospholipids bearing the same number of carbons in a hydrophobic chain, meaning lower microfluidity of the membrane made from the triple-chain amphiphiles than that of the phospholipids. In summary, it is possible to say that the long-term stability of vesicles made from **2** toward the leakage of trapped CF may result from the three much more closely packed octadecyl chains in the bilayer of **2**, as compared to other lipids.

Because the triple-chain compounds in this work have two carboxylate groups, vesicles made from these amphiphiles are expected to have some pH-sensitive functions. Detailed investigation of their vesicles under various pH conditions is now in progress.

Notes and references

† The structure and purity of new compounds **1** and **2** were confirmed using the corresponding dimethyl esters because bis(carboxylate) compounds **1** and **2** were hygroscopic. *Selected data* for the dimethyl ester of **1** (R = *n*-$C_{16}H_{33}$), mp 78–79.5 °C (from EtOH); δ_H(400 MHz; $CDCl_3$) 0.88 (t, 9 H), 1.25–1.77 (m, 84 H), 3.40–3.60 (m, 21 H), 3.75 (s, 6 H), 4.35 (m, 4 H); *m/z* (FAB) 1095 [(M+K)$^+$, 100%], 1057 [(M+1)$^+$, 4] (Calc. for $C_{63}H_{124}O_{11}$: C, 71.54; H, 11.81. Found: C, 71.52; H, 11.92%). For the corresponding dimethyl ester of **2** (R = *n*-$C_{18}H_{37}$), mp 80–81 °C (from EtOH); δ_H(400 MHz; $CDCl_3$) 0.88 (t, 9 H), 1.17–1.60 (m, 96 H), 3.34–3.62 (m, 21 H), 3.73 (s, 6 H), 4.33 (m, 4 H); *m/z* (FAB) 1095 [(M+K)$^+$, 100%], 1057 [(M+1)$^+$, 4] (Calc. for $C_{69}H_{136}O_{11}\cdot H_2O$: C, 71.45; H, 11.99. Found: C, 71.55; H, 11.95%).

‡ A film of lipid or amphiphile (40 μmol) was prepared on the inside wall of a test tube by evaporation of its $CHCl_3$ solution and stored in a desiccator overnight under reduced pressure. After addition of 4 ml of a Tris-HCl buffer (20 mM, pH 7.5) containing 100 mM of CF to the test tube, the mixture was vortex-mixed for 10 min and successively sonicated for 5 min at about 10 °C higher than its T_c using a probe-type sonicator under a stream of nitrogen. Small unilamellar vesicles containing trapped CF were separated from untrapped CF by eluting the vesicle dispersion through a Sephadex G-50 gel column with 20 mM Tris-HCl buffer containing 100 mM of NaCl (pH 7.5). The formation of vesicles from compounds **1** and **2** was confirmed by a well-established gel-filtration method (ref. 9). Thus two fractions containing CF were observed in a series of eluates. The first fraction, which was eluted with an excluded volume of the column, indicated the presence of particles including a water phase separated from the outside phase. The second fraction contained a large quantity of untrapped CF only. This was also the case for DPPC and DSPC experiments in this work. The amount of CF released (%) from the vesicles was calculated by means eqn. (1),

$$\text{CF released } \% = (I_x - I_0)/(I_t - I_0) \times 100 \quad (1)$$

where I_0 is the fluorescence intensity of the vesicle suspension containing CF at initial time, I_x is the intensity of the suspension after a definite period of storage, and I_t is the fluorescence intensity after addition of an aqueous solution of Triton X-100 (100 g l^{-1}) to the suspension. The fluorescence intensity at 530 nm was measured at 25 °C using an excitation wavelength at 490 nm.

1 A. Seelig and J. Seelig, *Biochemistry*, 1984, **13**, 4839.
2 J. Sunamoto and K. Iwamoto, in *Therapeutic Drug Carrier Systems*. *2*, CRC Press, Boca Raton, 1985.
3 J. H. Fendler, *Ind. Eng. Chem. Prod. Res. Dev*., 1985, **24**, 107; S. L. Regen, in *Liposomes*: *From Biophysics to Therapeutics*, ed. M. J. Ostro, Marcel Dekker, N. Y., 1987; H. Ringsdorf, B. Schlarb and J. Venzmer, *Angew. Chem*., *Int. Ed. Engl*., 1988, **27**, 114.
4 K. Yamauchi, Y. Sakamoto, A. Moriya, K. Yamada, T. Hosokawa, T. Higuchi and M. Kinoshita, *J. Am. Chem. Soc*., 1990, **112**, 3188; N. Nishikawa, H. Mori and M. Ono, *Chem. Lett*., 1994, 767.
5 Y.-P. Zhu, A. Masuyama, Y. Kirito, M. Okahara and M. J. Rosen, *J. Am. Oil Chem. Soc*., 1992, **69**, 626.
6 Y. Sumida, T. Oki, A. Masuyama, H. Maekawa, M. Nishiura, T. Kida, Y. Nakatsuji, I. Ikeda and M. Nojima, unpublished work.
7 A. Blume, *Biochemistry*, 1983, **22**, 5436.
8 A. K. Soutar, H. J. Pownall, A. S. Hu and L. C. Smith, *Biochemistry*, 1974, **13**, 2828.

Communication 8/06903D

Cyclopenta[*c*]pyrans from 6-oxo-6*H*-1,3,4-oxadiazines†

Manfred Christl,*[a] Notker Bien,[a] Gabriele Bodenschatz,[a] Erich Feineis,[a] Joachim Hegmann,[a] Carola Hofmann,[a] Stefan Mertelmeyer,[a] Joachim Ostheimer,[a] Frank Sammtleben,[a] Susanne Wehner,[a] Eva-Maria Peters,[b] Karl Peters,[b] Matthias Pfeiffer[c] and Dietmar Stalke[c]

[a] *Institut für Organische Chemie, Universität Würzburg, Am Hubland, D-97074 Würzburg, Germany. E-mail: christl@chemie.uni-wuerzburg.de*
[b] *Max-Planck-Institut für Festkörperforschung, Heisenbergstraße 1, D-70569 Stuttgart, Germany*
[c] *Institut für Anorganische Chemie, Universität Würzburg, Am Hubland, D-97074 Würzburg, Germany*

Received (in Liverpool, UK) 15th September 1998, Accepted 29th September 1998

Prepared in a three-step sequence including acid-catalysed cycloaddition of cyclopentadiene to 6-oxo-6*H*-1,3,4-oxadiazines, dehydrogenation with DDQ of the dihydro-α-pyrones formed and reduction of the resulting α-pyrones with DIBAL-H, 1,4-disubstituted cyclopenta[*c*]pyrans are shown to undergo electrophilic substitution; the molecular structures of 1-(4-anisyl)-4-phenylcyclopenta[*c*]pyran and 4-isopropyl-1-phenylcyclopenta[*c*]pyran-7-carbaldehyde have been determined by single crystal X-ray diffraction studies.

Iridoids with a cyclopenta[*c*]pyran skeleton occur widely.[2] For example, plagiolactone **1** is a constituent of the defence secretion produced by the larvae of *Plagiodera versicolora*[3a] and viburtinal **2** was obtained by hydrolysis of the esters

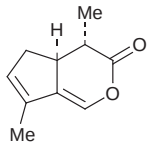

1

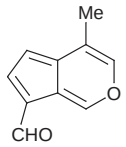

2

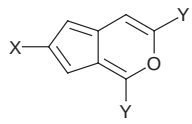

3 X = Y = H
4 X = Bu^t, Y = H
5 X = Bu^t, Y = Ph

extracted from the leaves of *Viburnum tinus*.[4a] One synthesis for each of these compounds is known.[3b,4b]

We report here on a simple route to compounds having the bicyclic systems of **1** and **2** as well as to aldehydes that differ from **2** only by the substituents in the six-membered ring. Hitherto, only three cyclopenta[*c*]pyrans without an acceptor substituent have been described: the parent heterocycle **3**, its *tert*-butyl derivative **4**[5] and its *tert*-butyldiphenyl derivative **5**.[6] No reactions were performed with **3**–**5**. Being 10π-electron systems, they should be aromatic[7] and thus amenable to electrophilic substitution.

The non-catalysed reaction of diphenyl-1,3,4-oxadiazin-6-one **6a** with cyclopentadiene proceeded unsatisfactorily. However, as in the case of norbornene,[8] the presence of TFA led to a strong acceleration of the desired cycloaddition with subsequent formation of the regioisomeric dihydro-α-pyrones **7a** and **8a**. Eleven further oxadiazinones[9] were utilised. Scheme 1 summarises the best results. We had shown previously that the methyl oxooxadiazinecarboxylate **6c** reacts rapidly with cyclopentadiene in the absence of a catalyst.[10] On treatment with triflic acid, the resulting γ-oxoketene now cyclised smoothly to give pure *exo*-**8c**.

The next step was the conversion of **7** and **8** into the α-pyrones **9** and **10**, respectively, with DDQ with yields ranging from 27 (**10c**) to 76% (**9b**/**10b**). In order to improve the yield of

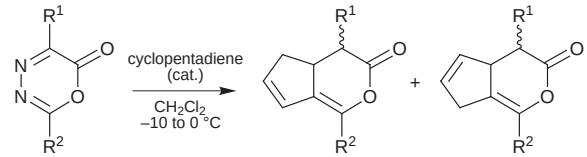

6 **7** **8**

	R^1	R^2	Ratio **7**:**8**	Yield (%)
a	Ph	Ph	8:1	69
b	Ph	4-$MeOC_6H_4$	10:1	73
c	Ph	CO_2Me	<1:>20	80
d	Pr^i	Ph	5:1	84
e	Pr^i	4-ClC_6H_4	>5:<1	85
f	Pr^i	4-$MeOC_6H_4$	>5:<1	80

Scheme 1

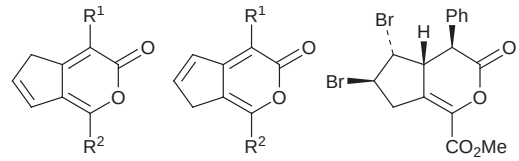

9a–f **10a–d** **11**

10c, we added bromine to **8c** and treated the resulting dibromide **11** with DBU, giving rise to a 1:8 mixture of **9c** and **10c** in 81% overall yield.

To our surprise, the α-pyrones **9** and **10** were directly transformed to the target compounds **12** by DIBAL-H (Scheme 2). The low yield of **12c** has its origin in the attack of the reagent at the ester group. Applying 4 equiv. of DIBAL-H afforded the alcohol **12g** (36% yield). An effect analogous to that of DIBAL-H could be achieved by $AlMe_3$, which converted **9a**/**10a** into the methyldiphenylcyclopenta[*c*]pyran **13** (50%).

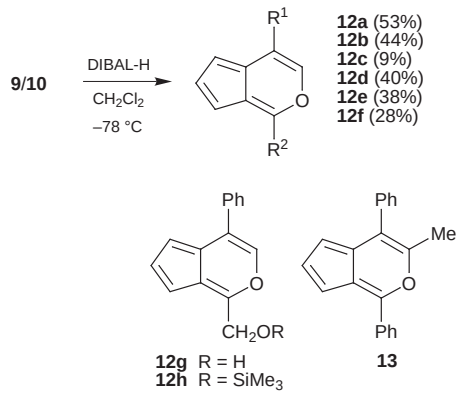

12a (53%)
12b (44%)
12c (9%)
12d (40%)
12e (38%)
12f (28%)

12g R = H
12h R = $SiMe_3$

13

Scheme 2

† Cycloadditions of 6*H*-1,3,4-oxadiazin-6-ones (4,5-diaza-α-pyrones). Part 17. For Part 16, see ref. 1.

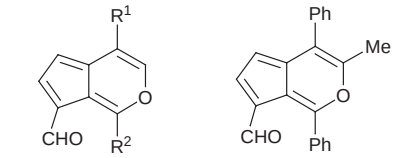

14a,**d**,**e**,**f**

15

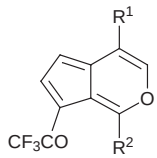

16a,**d**,**g**

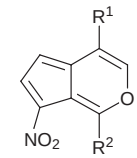

17a,**g**

The availability of compounds **12** and **13** made us try electrophilic substitutions. Formylation with DMF/$POCl_3$ at 0 °C furnished mainly the aldehydes **14** and **15** (61–84%). TFAA/NEt_3 at 20 °C produced the trifluoromethyl ketones **16a**,**d**,**g** (74, 46, 11%). In the case of **16g**, the alcohol **12g** had to be transformed to the TMS ether **12h** prior to trifluoroacetylation. Nitration was achieved with tetranitromethane/Py at 0 °C giving rise to the products **17a**,**g** (56, 38%).

The cyclopenta[*c*]pyrans **12** and **13** are orange to deep red, rather sensitive compounds, which could be purified by chromatography on basic alumina of activity IV. Only the crystalline products (**12a**,**b**,**c**, **13**) were persistent at room temperature, whereas the oils and solutions could only be stored at −30 °C for a short time.

Detailed information on the structures of **12b** and **14d** is provided by X-ray analyses (Fig. 1).‡ The formyl group of **14d** is almost coplanar with the five-membered ring (angle between their best least-squares planes 172°). Astoundingly, the CC bond lengths in the five-membered ring of **14d** hardly differ from those of **12b**. Thus, the distances C(4a)–C(5), C(5)–C(6) and C(6)–C(7) are nearly the same (138.2–139.3 pm) and similar to those of benzene and the corresponding ones of azulene.[11] Also C(4a)–C(7a) and C(7)–C(7a) resemble each other closely (144.5–145.1 pm), but are significantly shorter and longer than the respective bonds of azulene (*ca*. 150 and 140 pm). Unlike its effect in the five-membered ring, the formyl group causes remarkable changes of several bond lengths in the pyran subunit.

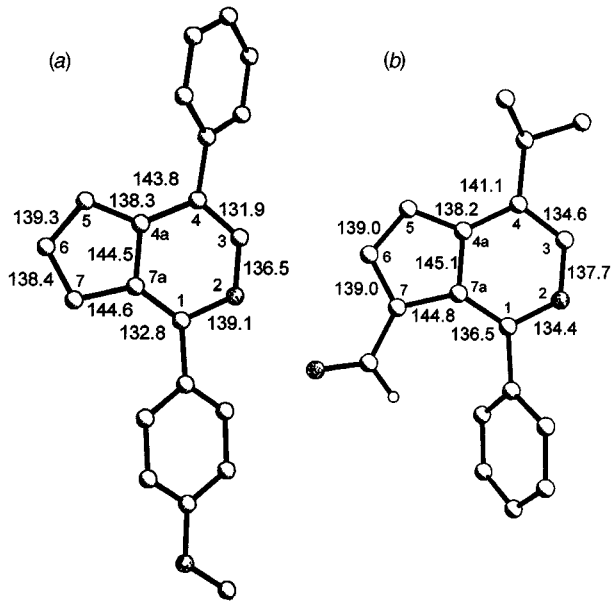

Fig. 1 Molecular structures of (*a*) 1-(4-anisyl)-4-phenylcyclopenta[*c*]pyran **12b** and (*b*) 4-isopropyl-1- phenylcyclopenta[*c*]pyran-7-carbaldehyde **14d**, together with the atomic numbering scheme and some selected bond lengths (pm).

In the UV–VIS spectra (MeCN) of **12a**,**b** and **13** the absorption maxima at longest wavelengths are found at 437–450 nm (log ε 3.13–3.20). As compared to those of **12a** and **13**, the absorptions of the aldehydes **14a** and **15** show hardly any shift in the wavelengths, but an increase of the molar extinction coefficient (log ε 3.73, 3.82). The methyl carboxylate **12c** absorbs at the longest wavelength (490 nm, log ε 2.95).

We thank the Deutsche Forschungsgemeinschaft as well as the Fonds der Chemischen Industrie for financial support, and Degussa AG for gifts of chemicals.

Notes and references

‡ *Crystal data* for **12b**: $C_{21}H_{16}O_2$, M = 300.34, orthorhombic, space group *Pbca*, a = 1269.4(2), b = 735.97(9), c = 3245.4(6) pm, V = 3.0320(8) nm^3, Z = 8, D_c = 1.316 Mg m^{-3}, F(000) = 1264, λ = 71.073 pm, T = 193 K [shock-frozen crystal (0.5 × 0.5 × 0.1 mm) in a drop of oil], μ = 0.084 mm^{-1}. Data were collected on an Enraf-Nonius CAD4 diffractometer using Mo-Kα radiation. A total of 3009 reflections were measured in the scan range of $6.4 \leqslant 2\theta \leqslant 41.7°$, of which 1587 were independent (R_{int} = 0.073). The structure was solved by direct methods (SHELXS-97) and refined by full-matrix least-squares (SHELXL-97). $R1$ = 0.076, $wR2$ (all data) = 0.239.

For **14d**: $C_{18}H_{16}O_2$, M = 264.32, orthorhombic, space group *Pbca*, a = 1555.4(3), b = 969.3(2), c = 1898.0(4) pm, V = 2.862(1) nm^3, Z = 8, D_c = 1.227 Mg m^{-3}, F(000) = 1120, λ = 71.073 pm, T = 293 K, μ = 0.08 mm^{-1}. Crystal size 0.3 × 0.2 × 0.15 mm. Data were collected on a Siemens P4 diffractometer using Mo-Kα radiation. A total of 4663 reflections were measured in the scan range of $3.5 \leqslant 2\theta \leqslant 55.0°$, of which 1534 were independent (R_{int} = 0.051). The structure was solved by direct methods and refined by full-matrix least-squares (SHELXTL PLUS). R = 0.081, R_w = 0.061. CCDC 182/1041.

1 T. T. Tidwell, F. Sammtleben and M. Christl, *J. Chem. Soc., Perkin Trans. 1*, 1998, 2031.
2 L. J. El-Naggar and J. L. Beal, *J. Nat. Prod.*, 1980, **43**, 649; C. A. Boros and F. R. Stermitz, *J. Nat. Prod.*, 1990, **53**, 1055.
3 (*a*) J. Meinwald, T. H. Jones, T. Eisner and K. Hicks, *Proc. Natl. Acad. Sci. U. S. A., 1*977, **74**, 2189; (*b*) J. Meinwald and T. H. Jones, *J. Am. Chem. Soc.*, 1978, **100**, 1883.
4 (*a*) R.-P. Godeau, J.-C. Rossi and I. Fouraste, *Phytochemistry*, 1977, **16**, 604; (*b*) J.-L. Brayer, J.-P. Alazard and C. Thal, *J. Chem. Soc., Chem. Commun.*, 1983, 257.
5 T. Kämpchen, G. Moddelmog, D. Schulz and G. Seitz, *Liebigs Ann. Chem.*, 1988, 855.
6 H. Kato, T. Kobayashi, M. Ciobanu, H. Iga, A. Akutsu and A. Kakehi, *Chem. Commun.*, 1996, 1011; H. Kato, T. Kobayashi, M. Ciobanu and A. Kakehi, *Tetrahedron*, 1997, **53**, 9921.
7 Review on pseudoazulenes: H.-J. Timpe and A. V. El'tsov, *Adv. Heterocycl. Chem.*, 1983, **33**, 185.
8 M. Christl, G. Bodenschatz, E. Feineis, J. Hegmann, G. Hüttner, S. Mertelmeyer, K. Schätzlein and H. Schwarz, *J. Prakt. Chem.*, 1995, **337**, 659.
9 Preparation of the oxadiazinone **6a**: W. Steglich, E. Buschmann, G. Gansen and L. Wilschowitz, *Synthesis*, 1977, 252; the other oxadiazinones **6**, except **6e** (preparation as that of **6d**), have been described in the previous papers of this series.
10 J. Hegmann, E. Ditterich, G. Hüttner, M. Christl, E.-M. Peters, K. Peters and H. G. von Schnering, *Chem. Ber.*, 1992, **125**, 1913.
11 O. Bastiansen and J. L. Derissen, *Acta Chem. Scand.*, 1966, **20**, 1319 and references cited therein.

Communication 8/07233G

Photoinduced non-oxidative coupling of methane over silica-alumina and alumina around room temperature

Yuko Kato,[a] Hisao Yoshida*[a] and Tadashi Hattori[b]

[a] *Department of Applied Chemistry, Graduate School of Engineering, Nagoya University, Nagoya 464-8603, Japan. E-mail: yoshida@apchem.nagoya-u.ac.jp*

[b] *Research Center for Advanced Waste and Emission Management, Nagoya University, Nagoya 464-8603, Japan*

Received (in Cambridge, UK) 2nd September 1998, Accepted 18th September 1998

Around room temperature, photoinduced coupling of methane proceeds without any oxidant molecules on silica-alumina and alumina evacuated at 1073 K; many coupling products in the gaseous phase are obtained from silica-alumina, while most of products on alumina are obtained only through thermal desorption.

The oxidative coupling of methane is an expedient reaction to convert natural gas into useful chemicals. However, it is very difficult to obtain the coupling products in high yield, because oxidation of the coupling products to CO_x proceeds more selectively than the coupling reaction. If the oxidant molecules are removed to avoid complete oxidation, the reaction requires very high temperature[1] and has no practical use. Photoinduced reactions are one of the most available reactions taking place at low temperature where complete oxidation could be minimized. Recently, it was reported that photo-induced coupling of methane proceeded at 373–473 K in the presence of oxygen over TiO_2[2] which is the most widely used photocatalyst. However the selectivity of CO_x was very high and the yield of coupling products was only *ca.* 0.5%. Use of N_2O as oxidant improved the selectivity of coupling products on MgO, but the yield was $< 0.2\%$.[3,4] The possibility of the photoinduced non-oxidative coupling, where no oxidant molecules are employed, was suggested by using transition metal oxides, such as V/SiO_2,[5] TiO_2[6] and Mo/SiO_2.[7] However, the highest yield was only *ca.* 0.007% in the gaseous phase and $< 0.4\%$ even after forced desorption by heating or by admission of water vapor.[7]

Here, we describe that the coupling products are obtained in yields as high as 5% without formation of CO and CO_2 in the non-oxidative coupling of methane over silica-alumina and alumina under photoirradiation. Silica-alumina, which is a member of silica-based materials recently attracting a great deal of attention as a new photocatalyst family,[8–13] was found to be photoactive; it exhibited a characteristic phosphorescence emission spectrum.[9] The photoreactivity of silica-alumina toward gaseous molecules, however, has not been investigated, and the present report is the first in this area.

The silica sample was prepared from $Si(OEt)_4$ by the sol–gel method followed by calcination in dry air at 773 K[14] and its specific surface area was 679 $m^2\ g^{-1}$. The silica-alumina samples, SiO_2–Al_2O_3(L) and SiO_2–Al_2O_3(H), employed were reference catalysts of the Catalysis Society of Japan, JRC-SAL-2 and JRC-SAH-1, respectively.[15,16] The alumina contents were 13.75 and 28.61 mass% and the specific surface areas were 560 and 511 $m^2\ g^{-1}$, respectively.[15,16] The alumina sample was also the JRC sample, JRC-ALO-4 (surface area; 174 $m^2\ g^{-1}$).[15,16]

The reaction tests were carried out in a closed quartz reaction vessel (82 cm^3). The sample (1.0 g) was spread on the flat bottom of vessel (19.6 cm^2), and was treated with 60 Torr (1 Torr = 133 Pa) O_2 for 1 h at 1073 K, followed by evacuation for 1 h at 1073 K. Methane (99.95%) was purified by a vacuum evaporation before use and introduced into the reactor. The initial pressure of methane (100 μmol) in the reactor was 21 Torr and no oxidant molecules were introduced. The sample was irradiated with a 250 W Xe lamp for 18 h. Under photoirradiation, the temperature of the sample bed was measured to be *ca.* 310 K. Products in the gaseous phase were collected with a liquid-N_2 trap and analysed by GC. Then adsorbed products were thermally desorbed by heating (573 K, 15 min), collected, and analysed by GC.

Table 1 shows the product yields in photoinduced non-oxidative coupling of methane, in the absence of gaseous oxidants, over silica, silica-alumina and alumina. Note that in all cases no oxygenates (MeOH, HCHO, CO_2, CO) were detected.

For the empty reactor (run 1), only a trace amount of C_2H_6 was formed upon photoirradiation. On the silica sample (run 2), a small amount of C_2H_6 and C_3H_8 were obtained in the gaseous phase, and a trace amount of C_2H_4 and C_3H_6 were observed as the thermally desorbed products.

Over the silica-alumina samples (runs 3 and 4), the conversions were obviously much higher than that over silica. In the gaseous phase, a large amount of C_2–C_4 alkanes was obtained while smaller amounts of C_2–C_6 alkanes and alkenes were desorbed upon heating. Among the thermally desorbed products, alkenes were the major products. In the dark (in an electric furnace, run 6) at 473 K, no products were detected, clearly indicating that photoirradiation is necessary for the above reaction. On SiO_2–Al_2O_3(L), the total yield reached

Table 1 Results of photoinduced non-oxidative coupling of methane[a]

		Yield of gaseous phase product (C%)[b]				Yield of thermal desorption product at 573 K (C%)[b]								Total
Run	Sample	C_2H_6	C_3H_8	C_4H_{10}	Total	C_2H_4	C_2H_6	C_3H_6	C_3H_8	C_4H_8	C_4H_{10}	C5,6	Total	(C%)[b]
1[c]	—	tr.	0	0	tr.	—	—	—	—	—	—	—	—	tr.
2	SiO_2	0.08	0.01	0	0.09	tr.	0	tr.	0	0	0	0	tr.	0.09
3	SiO_2–Al_2O_3(L)	3.54	0.85	0.14	4.53	0.42	0.01	0.27	0.02	0.20	tr.	0.45	1.37	5.90
4	SiO_2–Al_2O_3(H)	1.82	0.27	0.03	2.12	0.29	0.02	0.24	0.01	0.12	tr.	0.22	0.90	3.02
5	Al_2O_3	0.48	0.02	0	0.50	0.33	2.64	0.03	1.18	0	0.49	0.16	4.83	5.33
6[d]	SiO_2–Al_2O_3(L)	0	0	0	0	0	0	0	0	0	0	0	0	0
7[d]	Al_2O_3	0	0	0	0	0	0	0	0	0	0	0	0	0

[a] Reaction temperature = *ca.* 310 K, reaction time = 18 h, CH_4 = 100 μmol. [b] Based on the initial amount of CH_4. [c] A blank test. [d] Reaction at 473 K without UV-irradiation. tr. = trace.

5.90% and the yield of gaseous phase products reached 4.53%, much higher than those in any other reports on photoinduced coupling of methane.[2–7] It should be noted that no oxidant molecules were introduced in the reaction system and that the temperature of the sample bed, measured by a thermocouple, was only 310 K. The total yield on SiO_2–Al_2O_3(L) was higher than that on SiO_2–Al_2O_3(H). It is reported that SiO_2–Al_2O_3(L) has a larger phosphorescent emission spectrum with fine structure and a clearer peak in its excitation spectrum than SiO_2–Al_2O_3(H). From this result, it is proposed that highly dispersed aluminum species in the silica tetrahedral matrix are responsible for the photoactivity of silica-alumina. In the present case, such species would also play an important role in the photoinduced reaction.

On the alumina sample (run 5), the total yield (5.33%) was as high as that on the silica-alumina sample [SiO_2–Al_2O_3(L)]. Alumina exhibited no activity in the dark (run 7), indicating that photoirradiation is also necessary for the reaction over alumina. However, the feature of reaction on alumina was different from that on silica-alumina; on alumina, the yields of gaseous phase products (C_2H_6 and C_3H_8) were much lower and the most of products were obtained on heating. Among the thermal desorption products, alkanes were dominant on alumina, while they were minor products on silica-alumina.

In conclusion, it was found that the coupling of methane proceeded under photoirradiation on silica-alumina and alumina in the absence of any oxidant molecules. A meaningful amount of coupling products was obtained without the formation of CO and CO_2. Specially, silica-alumina, whose alumina content is lower, exhibited the highest activity without any thermal desorption.

Notes and references

1 L. Guczi, R. A. Van Santen and K. V. Sarma, *Catal. Rev. Sci.-Eng.*, 1996, **38**, 249 and references therein.
2 K. Okabe, K. Sayama, H. Kusama and H. Arakawa, *Chem. Lett.*, 1997, 457.
3 C. Yun, M. Anpo, Y. Mizokoshi and Y. Kubokawa, *Chem. Lett.*, 1980, 799.
4 T. Tashiro, T. Ito and K. Toi, *J. Chem. Soc., Faraday Trans.*, 1990, **86**, 1139.
5 S. L. Kaliaguine, B. N. Shelimov and V. B. Kazansky, *J. Catal.*, 1978, **55**, 384.
6 G. N. Kuzmin, M. V. Knatko and S. V. Kurganov, *React. Kinet. Catal. Lett.*, 1983, **23**, 313.
7 W. Hill, B. N. Shelimov and V. B. Kazansky, *J. Chem. Soc., Faraday Trans. 1*, 1987, **83**, 2381.
8 H. Yoshida, T. Tanaka, S. Matsuo, T. Funabiki and S. Yoshida, *J. Chem. Soc., Chem. Commun.*, 1995, 761.
9 H. Yoshida, T. Tanaka, A. Satsuma, T. Hattori, T. Funabiki and S. Yoshida, *Chem. Commun.*, 1996, 1153.
10 H. Yoshida, T. Tanaka, M. Yamamoto, T. Funabiki and S. Yoshida, *Chem. Commun.*, 1996, 2125.
11 H. Yoshida, K. Kimura, Y. Inaki and T. Hattori, *Chem. Commun.*, 1997, 129.
12 H. Yoshida, T. Tanaka, M. Yamamoto, T. Yoshida, T. Funabiki and S. Yoshida, *J. Catal.*, 1997, **171**, 351.
13 T. Tanaka, S. Matsuo, T. Maeda, H. Yoshida, T. Funabiki and S. Yoshida, *Appl. Surf. Sci.*, 1997, **121**/**122**, 296.
14 S. Yoshida, T. Matsuzaki, T. Kashiwazaki, K. Mori and K. Tarama, *Bull. Chem. Soc., Jpn.*, 1974, **47**, 1564.
15 Y. Murakami, *Stud. Surf. Sci. Catal.*, 1983, **16**, 775.
16 T. Uchijima, *Catalytic Science and Technology*, ed. S. Yoshida, N. Takazawa and T. Ono, Kodansha, VCH, Tokyo, 1991, vol. 1, p. 393.

Communication 8/06825I

Synthesis and structure of the novel heptalithiumtetrarubidium mixed alkoxide peroxide [{($Bu^tOLi)_5(Bu^tORb)_4(Li_2O_2)$·2tmeda}$_\infty$]: twenty-two vertex cage molecules linked by Rb–TMEDA–Rb bridges

William Clegg,[a] Allison M. Drummond,[b] Robert E. Mulvey*[b] and Stephen T. Liddle[a]

[a] *Department of Chemistry, University of Newcastle, Newcastle upon Tyne, UK NE1 7RU*
[b] *Department of Pure and Applied Chemistry, University of Strathclyde, Glasgow, UK G1 1XL. E-mail: r.e.mulvey@strath.ac.uk*

Received (in Cambridge, UK) 10th September 1998, Accepted 30th September 1998

Made by a metal–metal partial exchange reaction involving lithium *tert*-butylamide, rubidium *tert*-butoxide and TMEDA, the title compound represents the first mixed lithium–rubidium organoelement species of its type.

Recent times have witnessed a revival of interest in metal alkoxides. Considerable attention has been paid to them as precursors for the deposition of metal oxides used in the electronics and ceramics industries.[1] Within preparative chemistry, they are best known for their role in two-component superbasic mixtures, typified by 'BuLi·KOBu^t', which often succeed where orthodox alkyllithium reagents fail in difficult proton abstraction applications.[2] Also, the stereochemical rigidity of the Bu^tO^- ligand frequently aids the crystallisation process, thus permitting the gathering of valuable structural information from X-ray crystallographic studies. Recent important crystal structures in this category of $[(C_6H_{11}O^-)_4(Bu^tO^-)_4(Li^+)_4(K^+)_4(KOH)\cdot 5THF]$,[3] $[(Bu^tOLi)_{10}(LiOH)_6]$,[4] $[\{[PhN(H)]_2(Bu^tO)LiNaK\cdot 2TMEDA\}_2]$,[5] and $[\{(cyNLi)_3Sb\}(Bu^tOK)_3\cdot x PhMe]$,[6] respectively give insight into the nature of alkoxide–enolate interactions, the intermediates involved in the hydrolytic degradation of lithium alkoxides, the architecture of an amide–alkoxide model superbase, and the assembling of large polyamidoantimony anionic cage complexes. In earlier work we reported the crystal structure of an octalithium dipotassium mixed oxide alkoxide, which can be formally represented as $[(Bu^tOLi)_6(Bu^tOK)_2(Li_2O)\cdot 2TMEDA]$ **1**.[7] This was prepared by a permutational metal–metal exchange reaction [eqn. (1)], which was incomplete in the sense that a proportion of the potassium *tert*-butoxide reactant molecules remains in the product as part of **1**. We pondered whether this same synthetic strategy applied to rubidium *tert*-butoxide could generate a mixed lithium–rubidium compound, in the knowledge that hitherto no such compound exists in the Cambridge Crystallographic Database.[8] The dearth of studies in organorubidium chemistry generally, flagged in a recent review,[9] provided another incentive for pursuing this topic. As revealed herein, our goal has been realised through the synthesis and crystallographic characterisation of the heptalithiumtetrarubidium mixed alkoxide peroxide $[\{(Bu^tOLi)_5(Bu^tORb)_4(Li_2O_2)\cdot 2TMEDA\}_\infty]$ **2**, the composition, structure, and bonding of which are unprecedented.

$$Bu^tN(H)Li + Bu^tOK \xrightarrow{TMEDA} 1/x[(Bu^tOLi)_6(Bu^tOK)_2(Li_2O)\bullet 2TMEDA] + \text{other products} \quad (1)$$

Standard inert-atmospheric (argon) Schlenk techniques were employed throughout the preparative procedure. Rubidium *tert*-butoxide was pre-prepared as a white powder by a literature method,[10] and subsequently suspended in hexane. To this was added an equimolar amount of $Bu^tN(H)Li$ (in hexane), prepared *in situ* beforehand by lithiation of *tert*-butylamine. The resulting mixture was heated to reflux for 1.5 h, then filtered to remove fine solids leaving a transparent brown solution. Addition of TMEDA (1 mol equivalent) caused the solution to darken. Refrigerating the solution at *ca.* 4 °C for 48 h afforded colourless crystals of **2** [eqn. (2)]. Based on consumption of butoxide molecules the yield obtained was 51%. Satisfactory C, H, Li, N, Rb analyses were obtained. No other product could be crystallised despite prolonged cooling of the solution remaining following removal of **2** (analogous to the situation found with **1**). This is perhaps not surprising since the leftover solutions in containing a mixture of amide (mainly) and butoxide molecules can be likened to a type of superbase, which is a class of compound notoriously difficult to crystallise.

$$Bu^tN(H)Li + Bu^tORb \xrightarrow{TMEDA} 1/x[\{(Bu^tOLi)_5(Bu^tORb)_4(Li_2O_2)\bullet 2TMEDA\}_\infty] + \text{other products} \quad (2)$$

The structure of **2** (Fig. 1)† consists of polynuclear $(Bu^tO)_9(O_2)Li_7Rb_4$ cages (Fig. 2) which link together *via* Rb–TMEDA–Rb bridges. As Fig. 3 shows, this produces polymeric sheets, arranged in layers such that the cages in one sheet run orthogonal to those in the next sheet. The cage possesses exact twofold rotation symmetry about the O(5)···Li(2) axis which bisects the peroxide O(6)–O(6A) bond; the Bu^t group on O(5) is disordered over two orientations. Thus there are three pairs of Li

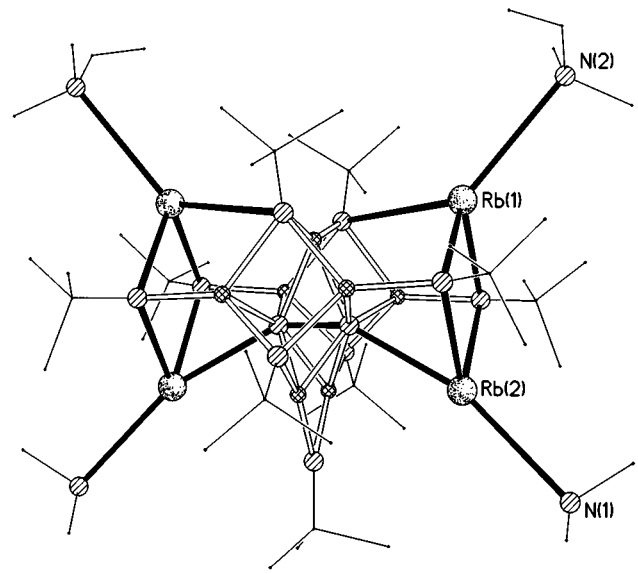

Fig. 1 Double asymmetric unit of **2**. Hydrogen atoms have been omitted for clarity. Selected bond lengths (Å): Rb(1)–N(2) 3.267(7), Rb(2)–N(1) 3.126(7), Rb(1)–O(1) 2.743(5), Rb(1)–O(2) 2.748(5), Rb(1)–O(4) 3.393(5), Rb(2)–O(6) 2.749(4), Rb(2)–O(1) 2.841(5), Rb(2)–O(2) 2.851(5), Li(1)–O(1) 1.873(12), Li(1)–O(3A) 1.944(12), Li(1)–O(4) 2.038(13), Li(1)–O(6) 2.333(11), Li(2)–O(4) 1.844(6), Li(2)–O(6) 1.937(17), Li(3)–O(2) 1.907(13), Li(3)–O(3) 1.934(13), Li(3)–O(4A) 2.101(14), Li(3)–O(6) 2.278(13), Li(4)–O(5) 1.830(14), Li(4)–O(3) 1.876(13), Li(4)–O(6) 1.968(12), Li(4)–O(6A) 1.971(13).

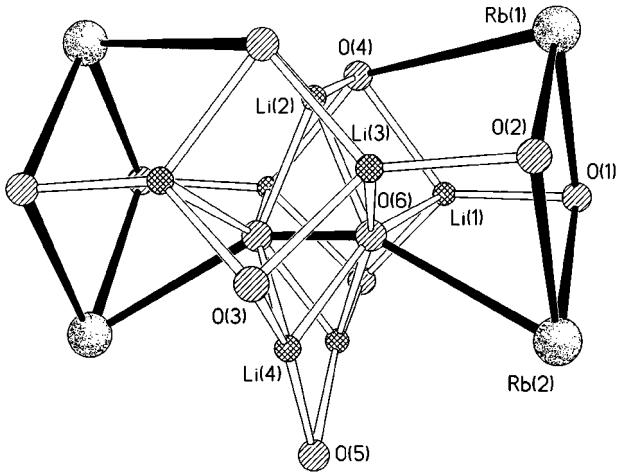

Fig. 2 Twenty-two $O_{11}Li_7Rb_4$ vertex cage core of **2**, with atom labelling.

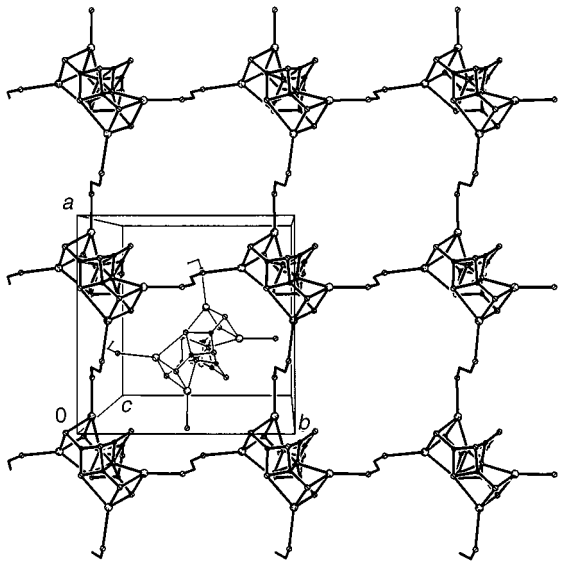

Fig. 3 View showing layer arrangement of polymeric **2**, without Bu^t and TMEDA methyl groups. For clarity, only one cage unit is shown in the further layer.

centres [Li(1), Li(3), Li(4) and their symmetry equivalents] and a unique Li(2), each in a distorted tetrahedral environment; two pairs of distorted tetrahedral Rb centres [Rb(1), Rb(2) with their equivalents]; three pairs of four-coordinate [O(1), O(2), O(3)] and one pair of five-coordinate [O(4)] butoxide O centres and a unique three-coordinate O(5); and a single peroxo unit [O(6)–O(6A)]. The (butoxide) O–Li bond lengths span a wide range [1.830–2.101 Å] reflecting the various coordination numbers involved. This compares with a range of 1.856–2.063 in **1**. Excluding the long O(4)–Rb(1) contact [length 3.393(Å)], the (butoxide) O–Rb bond lengths in **2** have a mean value (2.796 Å) close to that in the $[(Bu^tORb)_4]$ cubane (2.757 Å).[10] To the best of our knowledge, **2** provides the first example of Rb–TMEDA–Rb bridging (mean N–Rb bond length, 3.197 Å), though bridges of this type have long been known for lithium, *e.g.* in $[\{(MeLi)_4{\cdot}2TMEDA\}_\infty]$[11] and $[\{(Bu^nLi)_4{\cdot}TMEDA\}_\infty]$.[12] The peroxo O(6)–O(6A) molecule in **2** is side-on coordinated by Li(2), Li(4) and Li(4A) (mean length, 1.958 Å) forming three OOLi triangles. A similar arrangement exists within the peroxide fragment of the triple-anion structure of $[\{(Me_3SiOLi)_4{\cdot}Li_2O_2{\cdot}(Me_3Si)_2NLi\}{\cdot}2THF]$ [mean peroxo O–Li bond length, 2.002 Å],[13] which coincidentally also contains seven Li centres. Additional end-on coordinations of O(6) and O(6A) in **2** occurs *via* Li(1), Li(3) and Rb(2) (mean lengths: O–Li 2.306 Å, O–Rb 2.749 Å). The O–O bond itself measures 1.541(9) Å, in good agreement with that (1.557 Å) in the aforementioned triple-anion structure. Here the presence of the peroxide molecule demonstrates again the strong oxophilic nature of metal alkoxides, which in **1** manifests itself in the form of oxo (O^{2-}) ions. Peroxide incorporation has also been reported in the barium diketonate $[(thd)_{10}(O_2)(H_2O)_6Ba_6]$ (thd = 2,2,6,6-tetramethylheptane-3,5-dionate),[14] while both peroxo and oxo ions appear in the mixed lithium–magnesium amide $[\{(Me_3Si)_2N\}_4Li_2Mg_2(O_2)_x(O)_y]$.[15] Obviously the mode of formation of such anions is complex and as such, is not yet understood.

Recorded in $[^2H_8]$toluene solution at 300 K, the ^1H NMR (400 MHz) spectrum of **2** exhibits two broad Bu^{t}O resonances centred at 1.25 and 1.44 ppm in an approximate ratio of 5 : 4. The former resonance can be tentatively assigned to the five cage Bu^{t}O$^-$ ligands bound only to Li centres (provided the long O–Rb contacts are disregarded). Significantly, pure Bu^{t}OLi comes at a near-identical chemical shift (1.26 ppm). Likewise, the latter resonance can be assigned to the four cage Bu^{t}O$^-$ ligands bound to mixed Li/Rb centres. Interestingly, the order and chemical shifts of the TMEDA resonances (CH_2, 2.32 ppm; Me, 2.11 ppm) are characteristic of uncoordinated molecules. Hence the implication is that the Li_7Rb_4 cage remains intact, but that the Rb–TMEDA–Rb bridges linking them together in the solid state, cleave in solution. This could explain why **2** is soluble in arene solvents.

In conclusion, we have demonstrated that a metal–metal partial exchange methodology between a rubidium alkoxide and a lithium amide can successfully yield a mixed lithium–rubidium crystalline product, the first of its type. Future work will examine whether the presence of amide ligands is essential for the crystallisation of such novel compositions; or are they accessible by simply mixing together the appropriate homometallic alkoxides?

We thank the EPSRC (for equipment to W. C.) and the University of Strathclyde (for studentship to A. M. D.).

Notes and references

† *Crystal data* for **2**: $C_{48}H_{113}Li_7N_4O_{11}Rb_4$, M = 1312.9, tetragonal, $P4_12_12$, $a = b$ = 14. 7025(14), c = 35.956(4) Å, V = 7772.4(14) Å^3, Z = 4, T = 160 K. The structure was determined from 6844 unique reflections (46913 measured, $\theta \leqslant 25°$, R_{int} = 0.106) and refined[16] to $wR2$ = 0.168 on all F^2 values, conventional R = 0.058 for F values of 5001 reflections with $F_o^2 > 2\sigma(F_o^2)$; 349 parameters, including an absolute structure parameter[17] of 0.002(15); final difference map between +1.00 and −0.41 e Å^{-3}. CCDC 182/1042.

1 D. C. Bradley, *Chem. Rev.*, 1989, **89**, 1317.
2 A. Mordini, in *Advances in Carbanion Chemistry*, ed. V. Snieckus, JAI Press, London, 1992, vol. 1, p. 1.
3 P. G. Williard and G. J. MacEwan, *J. Am. Chem. Soc.*, 1989, **111**, 7671.
4 C. Lambert, F. Hampel, P. v. R. Schleyer, M. G. Davidson and R. Snaith, *J. Organomet. Chem.*, 1995, **487**, 139.
5 F. M. Mackenzie, R. E. Mulvey, W. Clegg and L. Horsburgh, *J. Am. Chem. Soc.*, 1996, **118**, 4721.
6 D. Barr, A. J. Edwards, M. A. Paver, P. R. Raithby, M.-A. Rennie, C. A. Russell and D. S. Wright, *Angew. Chem., Int. Ed. Engl.*, 1995, **34**, 1012.
7 F. M. Mackenzie, R. E. Mulvey, W. Clegg and L. Horsburgh, *Polyhedron*, 1998, **17**, 993.
8 F. H. Allen and O. Kennard, *Chem. Des. Autom. News*, 1993, **8**, 31.
9 R. Snaith, in *Specialist Periodical Reports, Organometallic Chemistry*, the Royal Society of Chemistry, Cambridge, 1998, vol. 26, p. 1.
10 M. H. Chisholm, S. R. Drake, A. A. Naiini and W. E. Streib, *Polyhedron*, 1991, **10**, 337.
11 H. Köster, D. Thoennes and E. Weiss, *J. Organomet. Chem.*, 1978, **160**, 1.
12 N. D. R. Barnett, R. E. Mulvey, W. Clegg and P. A. O'Neil, *J. Am. Chem. Soc.*, 1993, **115**, 1573.
13 C. Drost, C. Jäger, S. Freitag, U. Klingebiel, M. Noltemeyer and G. M. Sheldrick, *Chem. Ber.*, 1994, **127**, 845.
14 A. Drozdov and S. Troyanov, *Polyhedron*, 1996, **15**, 1747.
15 A. R. Kennedy, R. E. Mulvey and R. B. Rowlings, *J. Am. Chem. Soc.*, 1998, **120**, 7816.
16 G. M. Sheldrick, SHELXTL user manual, version 5, Bruker AXS Inc., Madison, WI, 1998.
17 H. D. Flack, *Acta Crystallogr., Sect. A*, 1983, **39**, 876.

Communication 8/07069E

Synthesis, characterization and lectin binding study of carbohydrate functionalized silsesquioxanes

Frank J. Feher,*[a] Kevin D. Wyndham[a] and Daniel J. Knauer*[b]

[a] *Department of Chemistry, University of California, Irvine, California 92697-2025, USA. E-mail: fjfeher@uci.edu*
[b] *Department of Developmental and Cell Biology, University of California, Irvine, California 92697-1450, USA. E-mail: djknauer@uci.edu*

Received (in Bloomington, IN, USA) 21st May 1998, Accepted 25th September 1998

Two carbohydrate-functionalized silsesquioxanes 2 and 3 have been prepared by the reactions of $(H_2NCH_2CH_2CH_2)_8Si_8O_{12}$ 1 with *O*-β-D-galactopyranosyl-(1→4)-D-gluco-1,5-lactone and *O*-α-D-glucopyranosyl-(1→4)-D-gluco-1,5-lactone; the latter (*i.e.* 3) possesses eight maltose-derived substituents and binds with *Concanavalin A*, while the former possesses eight lactose-derived substituents that demonstrates selective binding to the hepatic asialoglycoprotein receptor.

Cell surface carbohydrates play an important role in cell recognition processes and have been implicated in a variety of pathological disorders.[1] In many instances the mechanisms by which these carbohydrates function as signals for cell recognition and subsequent biochemical transformations are not well understood, but the development of new drugs to block undesirable interactions could provide powerful tools for treating or preventing a variety of diseases.[2] One interesting approach for elucidating molecular-level details of recognition phenomena and developing new chemotherapeutics involves the use of polyfunctional molecules as 'scaffolds' to organize structurally well defined assemblies of oligosaccharide units.[3]

Here, we report the first use of polyhedral oligosilsesquioxanes (POSS) as scaffolds for the presentation of multiple carbohydrate units.

We recently introduced the use of $(H_2NCH_2CH_2CH_2)_8Si_8O_{12}$ **1** as a core for dendrimer synthesis[4a] and as a scaffold for the presentation of polypeptide chains.[4b] This water-soluble framework can be prepared *via* neutralization of its octahydrochloride salt, which is obtained in one step (> 35% yield) by the hydrolytic condensation of readily available $H_2NCH_2CH_2CH_2Si(OEt)_3$. Carbohydrate substituents can be attached to the eight amine groups of **1** *via* standard coupling protocols with carbohydrate-derived lactones.[3a–e] For example, the reaction of **1** with *O*-β-D-galactopyranosyl-(1→4)-D-gluco-1,5-lactone affords octagalactose-substituted framework **2**, which is obtained in high yield as a white powder after dialysis against water and precipitation by methanol.† Similarly, the reaction of **1** with *O*-α-D-glucopyranosyl-(1→4)-D-gluco-1,5-lactone produces an excellent yield of **3**, which possesses eight equivalent maltose-derived substituents. The course of these lactone coupling reactions can be conveniently monitored by ^{1}H NMR spectroscopy [$(CD_3)_2SO$] because the chemical shift for the CH_2N group of **1** (δ 2.8) shifts downfield by *ca.* 0.2 ppm upon acylation. The prominent product amide NH resonance at δ 7.7 can also be integrated and used to determine the extent of reaction. Both carbohydrate-functionalized frameworks are stable in solution (water or Me_2SO, 25 °C, 7 days) and elevated temperatures (100 °C) for short durations; both frameworks are also stable in the presence of acids (*e.g.* 1 M HCl or conc. HOAc) and non-nucleophilic bases (*e.g.* DIEA in DMSO).

Both **2** and **3** were characterized by a variety of techniques, including combustion analysis, MALDI-TOF mass spectrometry and multinuclear (^{1}H, ^{13}C, ^{29}Si) NMR spectroscopy [D_2O or $(CD_3)_2SO$]. Assignment of all ^{1}H and ^{13}C resonances

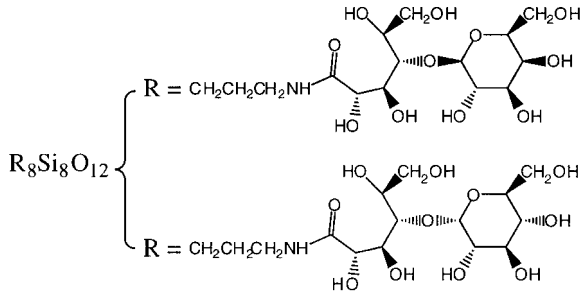

for **2** and **3** could be made on the basis of COSY, HMQC and DEPT experiments, but at concentrations normally required to obtain good signal-to-noise, aggregation of these highly polar frameworks causes marked broadening of many resonances. Dynamic light scattering measurements indicate that aggregation occurs at *ca.* 0.4 mM in water and that aggregates with an effective radius of 100 nm are present at 1.0 mM. The nature of this aggregation is not known, but at 3 mM the ^{29}Si, ^{1}H and ^{13}C spectra [D_2O and $(CD_3)_2SO$] are consistent with two distinct environments (*ca.* 4 : 1) for the pendant groups. The integrated intensities of the featureless resonances attributable to each environment do not appear to change over a concentration range of 1–8 mM and a temperature range of 25–60 °C, but the ratio abruptly changes below 1 mM and is *ca.* 1 : 1 over the concentration range of 0.05–0.5 mM. ^{1}H NMR spectra (D_2O) recorded below 1 mM also exhibit dramatically better resolution with well defined first-order multiplets for the aminopropyl spacers. We suspect that the two different environments are due to restricted rotation about the amide C–N bonds, which can create distinct *cis* and *trans* conformations for the pendant groups. If this is indeed the case, our results are consistent with strong inter- and intra-molecular interactions between pendant carbohydrate groups because *cis–trans* isomerization is slow on the NMR timescale at 25 °C and the *cis*/*trans* ratio changes upon the onset of intermolecular aggregation.

We have explored biological binding affinities of **2** and **3** using the asialoglycoprotein receptor (ASGPR) and *Concanavalin A* (Con A). The ASGPR is an integral mammalian hepatocyte membrane receptor which has selective binding to terminal non-reducing β-D-galactopyranosyl residues and demonstrates increased binding with an increased number of antennary β-D-galactopyranosyl groups.[2,5,6] Early suggestions that enhanced binding to the ASGPR occurs when three galactosyl residues are situated 15, 22, and 25 Å apart and separated by flexible organic spacers (*e.g.* PEG)[7] were supported by observations that three galactose residues tethered to glycerol[6c] or TRIS[2,6a,8] with this approximate spacial relationship exhibit enhanced binding to the ASGPR over mono- or di-valent analogs. Stochastic dynamics calculations[3h] (Macromodel v. 5.5) on **2** show inter-galactose separations comparable to the distances required for enhanced-binding to the ASGPR.

The results from a competitive inhibition study of binding to ASGPR of HepG2 cells are shown in Fig. 1. As illustrated in

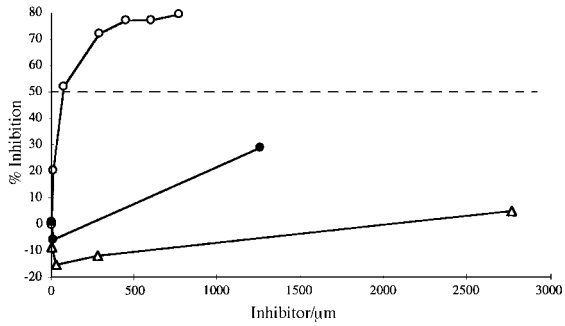

Fig. 1 Competitive inhibition of HepG2-ASGPR mediated uptake of ^{125}I-ASOM (1 μM, 0.5 ml/well) by the hydrochloride salt of **1** (△), **2** (○) and **3** (●) as measured by scintillation counting of the ^{125}I label. The reaction was performed in binding media (0.5 ml/well, pH = 7.4), incubated at 37 °C for 2 h before lysis with 10% SDS (0.5 ml/well). The inhibitory potency (IC_{50}) for unlabelled ASOM was determined to be 0.65 μM from a separate control experiment.

Fig. 1, neither the octahydrochloride of **1** nor the octa-glucose-terminated framework (*i.e.* **3**) substantially inhibit ASGPR-mediated uptake of ^{125}I-labeled Asialoorosomucoid (^{125}I–ASOM) into HepG2 cells (37 °C). In contrast, the octa-β-D-galactose substituted framework (*i.e.* **2**) strongly inhibits uptake of ^{125}I–ASOM. These results are consistent with selective recognition and binding of ASGPR to the β-galactose residues of **2** and no binding to the glucosyl residues of **3** or the ammonium groups of **1**.

It is interesting that the IC_{50} of **2** (57 μM at 37 °C) is comparable to the inhibition potency observed in a similar experiment for a glycerol molecule possessing three pendant lactose residues (IC_{50} = 9.83 μM at 4 °C).[6c] This clearly indicates that the rigid Si_8O_{12} core of **2** does not hinder binding of the galactosyl residues to the ASGPR, and it suggests that each ASGPR is interacting with three of the eight pendant groups from a single molecule of **2**.

The specific binding affinities of **2** and **3** were also assessed using *Concanavalin A* (Con A), which has four domains available for the binding of non-reducing D-glucosyl and D-mannosyl residues. As shown in Fig. 2, mixtures of Con A (35 μM) and **3** at concentrations as low as 7 μM display immediate turbidity and precipitation of a Con A-crosslinked aggregate while there is no significant turbidity when Con A (35 μM) is added to **2** at concentrations as high as 420 μM. These results are consistent with selective recognition and binding of Con A to the D-glucosyl residues of **3** and no binding to the galactosyl residues of **2**. Precipitation of the Con A/**3** aggregate can be reversed by adding D-maltose. The addition of 1.5 mol equiv. of D-maltose leads to a slight decrease in turbidity (*ca.* 25%), but the effect is minor and comparable to the decrease observed upon addition of 75 mol equiv.; complete loss of turbidity occurs upon addition of 750 mol equiv. of D-maltose. These results are similar to results for Con A binding to glycosylated PAMAM dendrimers,[3c,g] a macrocyclic sugar cluster[3a,b] and polystyrene derivatives having pendant oligosaccharides.[3h]

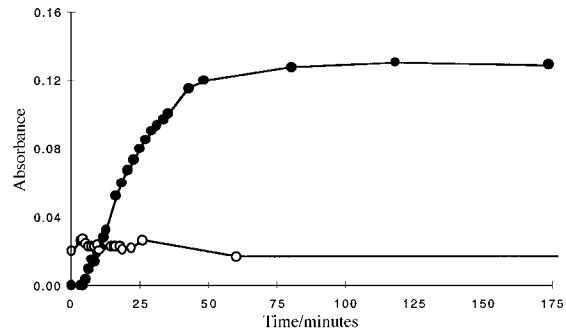

Fig. 2 Interaction of Con A (35 μM) with **2** (420 μM, ○) and **3** (7 μM, ●) as measured by absorbance at 450 nm. The reaction was performed at 25 °C and pH = 7 (0.01 M PBS).

In summary, we have synthesized carbohydrate-functionalized silsesquioxanes that exhibit highly selective and reversible complexation to carbohydrate-binding proteins. In light of the fact that $R_8Si_8O_{12}$ frameworks can be selectively monofunctionalized and subsequently modified to create new $R^1{}_7R^2Si_8O_{12}$ frameworks,[9] these observations have exciting implications for molecular recognition and the design of new site-specific drugs.

These studies were supported by the National Science Foundation (F. J. F.) and the National Institute of Health (D. J. K.). The authors gratefully acknowledge the advice and technical assistance provided by Professors David A. Brant and Charles G. Glabe (UCI), as well as the enthusiastic advice and encouragement provided by Professor A. Richard Chamberlin (UCI) and Dr Mark A. Scialdone (E. I. du Pont de Nemours).

Notes and references

† *Synthesis* of **2**: a solution of **1** (216 mg, 0.245 mmol) in MeOH (3.3 ml) was added to a solution of *O*-β-D-galactopyranosyl-(1→4)-D-glucono-1,5-lactone lactone[3e,5] (1.16 g, 3.41 mmol) in dry Me_2SO (*ca.* 3 ml); the MeOH was immediately removed by stirring under vacuum (25 °C, 0.001 Torr). The solution was stirred under nitrogen (25 °C, 24 h), filtered, and then evaporated (30 °C, 0.01 Torr) to afford a colorless resin, which was dialyzed against H_2O (25 °C, 3 × 4 l) over a period of 24 h. Evaporation (30 °C, 0.01 Torr) of the resulting solution afforded **2** as a spectroscopically pure white powder (472 mg, 53%), which was further purified by reprecipitation from H_2O–MeOH at −30 °C. Yield: 340 mg (40%). ^{1}H NMR [500.0 MHz, 5 mM in $(CD_2)_2SO$, 25 °C]: δ 7.66 (br, NH, 8H), 5.17–3.38 (m, carbohydrate, 168H), 3.10, 3.04 (br, CH_2N, 16H), 1.47 (br, $SiCH_2CH_2$, 16H), 0.56 (br, $SiCH_2$, 16 H). ^{13}C{^{1}H} NMR [125.7 MHz, 5 mM in $(CD_3)_2SO$, 25 °C]: δ 172.36 (s, CO), 104.66 (s, 1′-C), 83.16 (s, 4-C), 75.69, 73.22, 72.00, 71.70, 71.43, 71.17, 70.55, 68.23 (4′-C), 62.34 (s, 6-C), 60.72 (6′-C), 40.89 (br, CH_2N), 22.57 (br, $SiCH_2CH_2$), 8.77 (br, $SiCH_2$). ^{29}Si{^{1}H} NMR (99.38 MHz, 5 mM in D_2O, 25 °C): δ −65.9 (80%), −66.9 (20%). Mass spectrum (MALDI-TOF, DHB-HIQ matrix) *m*/*z* calc. for $C_{120}H_{224}O_{100}N_8Si_8$: $[M + Na]^+$ 3624.1, found 3623.9; $[M - C_{12}H_{19}O_{11} + K]^+$ 3300.95, found 3302.0; $[M - C_{12}H_{19}O_{11} + Na]^+$ 3284.99, found 3284.0; $[M - C_{12}H_{19}O_{11} + H]^+$ 3261.99, found 3262.1. Elemental analysis: found (calc.) for $C_{120}H_{224}O_{100}N_8Si_8{\cdot}3H_2O$: C, 39.63 (39.40), H, 6.15 (6.34), N, 3.05 (3.06).

1 (*a*) T. K. Lindhorst and C. Kieburg, *Angew. Chem., Int. Ed. Engl.*, 1996, **35**, 1953; (*b*) I. A. Wilson and A. E. Clarke, *Carbohydrate–protein interaction*, Springer-Verlag, New York, 1988.
2 A. R. Vaino, W. T. Depew and W. A. Szarek, *Chem. Commun.*, 1997, 1871.
3 (*a*) T. Fujimoto, C. Shimizu, O. Hayashida and Y. Aoyama, *J. Am. Chem. Soc.*, 1997, **119**, 6676; (*b*) T. Fujimoto, C. Shimizu, O. Hayashida and Y. Aoyama, *J. Am. Chem. Soc.*, 1988, **120**, 601; (*c*) K. Aoi, K. Itoh and M. Okada, *Macromolecules*, 1995, **28**, 5391; (*d*) J. Murata, Y. Ohya and T. Ouchi, *Carbohydr. Polym.*, 1997, **32**, 105; (*e*) K. Kobayashi, H. Sumitomo and Y. Ina, *Polym. J.*, 1985, **17**, 567; (*f*) J. Frese, C. H. Wu and G. Y. Wu, *Adv. Drug Delivery Rev.*, 1994, **14**, 137; (*g*) D. Páge and R. Roy, *Bioconjugate Chem.*, 1997, **8**, 714; (*h*) P. R. Ashton, S. E. Boyd, C.L. Brown, N. Jayaraman, S. A. Nepogodiev and J. F. Stoddart, *Chem. Eur. J.*, 1996, **2**, 1115.
4 (*a*) F. J. Feher and K. D. Wyndham, *Chem. Commun.*, 1988, 323.; (*b*) F. J. Feher, K. D. Wyndham, M. A. Scialdone and Y. Hamuro, *Chem. Commun.*, 1998, 1469.
5 T. J. Williams, N. R. Plessas and I. J. Goldstein, *Carbohydr. Res.*, 1978, **67**, C1.
6 (*a*) R. T. Lee, P. Lin and Y. C. Lee, *Biochemistry*, 1984, **23**, 4255; (*b*) J. R. Braun, T. E. Willnow, S. Ishibashi, G. Ashwell and J. Herz, *J. Biol. Chem.*, 1996, **271**, 21 160; (*c*) A. Krebs, W. T. Depew, W. A. Szarek, G. W. Hay and L. J. J. Hronowski, *Carbohydr. Res.*, 1994, **254**, 257.
7 (*a*) Y. C. Lee, R. R. Townsend, M. R. Hardy, J. Lonngren and K. Bock, ed. T. B. Lo, T. Y. Liu and C. H. Li, New York, 1984; (*b*) A. Valentijn, G. A. vanderMarel, L. Sliedregt, T. J. C. vanBerkel, E. A. L. Biessen and J. H. vanBoom, *Tetrahedron*, 1997, **53**, 759.
8 E. A. L. Biessen, D. M. Beuting, H. Roelen, G. A. Vandemarel, J. H. Vanboom and T. J. C. Vanberkel, *J. Med. Chem.*, 1995, **38**, 1538.
9 A. Tsuchida, C. Bolln, F. G. Sernetz, H. Frey and R. Mulhaupt, *Macromolecules*, 1997, **30**, 2818.

Communication 8/06684A

Metal-catalysed multiple boration of ketimines†

Thomas M. Cameron,[a] R. Tom Baker*[a] and Stephen A. Westcott*[b]

[a] *Chemical Science and Technology Division, Los Alamos National Laboratory, MS J514, Los Alamos, NM 87545, USA. E-mail: weg@lanl.gov*

[b] *Department of Chemistry, Mount Allison University, Sackville, NB E4L 1G8, Canada. E-mail: swestcott@mta.ca*

Received (in Bloomington, IN, USA) 24th July 1998, Accepted 17th September 1998

Metal-catalysed addition of $B_2cat'_2$ (cat′ = 4-Bu^t-1,2-$O_2C_6H_3$) to ketimines affords *N*-borylenamines and HBcat′. Analogous catalysed reactions of ketimines with HBcat′ in tetrahydrofuran afford multiply borated products, providing the first examples of metal-catalysed hydroboration of enamines.

Transition metal catalysed diboration of alkenes and alkynes is receiving considerable attention as a convenient and efficient method of generating alkyl- and alkenyl-boronic esters with well defined selectivities.[1] These compounds are valuable substrates for Suzuki coupling,[2] and new developments in this field include the direct synthesis of arylboronic esters from the corresponding aryl halides using diboron compounds[3] or dialkoxyboranes.[4] To date, catalysed diborations have been restricted to functionalizing unsaturated hydrocarbons, with the exception of a recent report by Marder and coworkers describing the 1,4-diboration of α,β-unsaturated ketones.[5] Our interest in aminoboron chemistry prompted us to investigate the diboration of imines. Transition metals can be used to catalyse the hydroboration of imines[6] and we recently found that the corresponding diboration of aldimines provides a direct route to the potent enzyme inhibitors, α-aminoboronic acids.[7,8] In this report we describe the versatility of metal-catalysed boron additions to ketimines which give a variety of novel aminoboronate esters and provide the first examples of metal-catalysed enamine hydroboration.

Reaction of acetophenone-derived imine, PhN=C(CH_3)Ph **1a**, with $B_2cat'_2$ (cat′ = 4-Bu^t-1,2-$O_2C_6H_3$) did not proceed without a catalyst, even at elevated temperatures (90 °C for 1 week).[9] Using 2 mol% $RhCl(PPh_3)_3$ at 25 °C, the reaction produced equal amounts of *N*-borylenamine **2a** and *N*-borylamine **3a**, as ascertained by NMR spectroscopy.[10] These products arise presumably from initial oxidative addition of the diboron compound to the metal center, followed by coordination of the ketimine with subsequent regioselective insertion into the M–B bond. Finally, β-H elimination generates *N*-borylenamine **2a** and 1 equiv. of HBcat′ which can subsequently add to unreacted **1a** to give **3a** (Scheme 1). Similar boration reactions have been observed previously in analogous diboration[1c] and hydroboration[11] reactions of alkenes. Ketimine diborations carried out using a catalytic amount of $Pt(dba)_2$ (dba = dibenzylidene acetone) gave primarily **2a** and HBcat′, as the resulting Pt complex is less effective in catalysing the competitive hydroboration of **1a**. Variation of the steric and electronic properties of the ketimine had a nominal effect on the product distribution as analogous reactions with a variety of ketimines **1b**–**e** gave similar results, as determined by NMR spectroscopy.‡

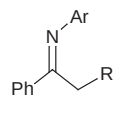

	R	Ar
1a	H	Ph
1b	H	$C_6H_4CF_3$-*p*
1c	H	C_6H_4OMe-*o*
1d	Ph	C_6H_4OMe-*p*
1e	Me	$C_6H_4CF_3$-*p*

In order to obtain evidence for the mechanistic pathway discussed above, we examined the stoichiometric reaction of the unsaturated bis(boryl) complex $RhCl(Bcat')_2(PPh_3)_2$ (generated *in situ* from $RhCl(PPh_3)_3$ and $B_2cat'_2$) with ketimine **1a** and observed quantitative formation of dihydride $RhH_2Cl(PPh_3)_3$[11a,12] along with 2 equiv. of *N*-borylenamine **2a**. This surprising result suggests that intermediate RhHCl(Bcat′)$(PPh_3)_2$,[13] arising from the boration step, reacts with **1a** to give **2a** at a comparable rate to that of the bis(boryl) complex. Previous theoretical studies of metal-catalysed hydroboration indicated that alkene insertion into both M–H and M–B bonds is energetically feasible.[14] Our observation of quantitative formation of *N*-borylenamine indicates that only insertion of ketimine into the M–B bond results in product formation.

These intriguing results prompted us to investigate the metal-catalysed hydroboration of ketimines. Uncatalysed addition of HBcat′ to **1a** in toluene, THF, or chloroform proceeds slowly (days) at 25 °C to give **3a**.[15] Using 2 mol% $RhCl(PPh_3)_3$ in toluene, however, gave a mixture of **2a** and **3a** along with a small amount of the 1,3-diboration product, cat′BN(Ph)CH(Ph)CH_2Bcat′ **4a**, derived from an unprecedented catalysed hydroboration of enamine **2a**. Remarkably, reactions carried out in $CDCl_3$ gave predominantly hydroborated ketimine **3a**, while those in THF afforded predominantly **4a** and the 1,1,3-triboration product, cat′BN(Ph)CH(Ph)CH(Bcat′)$_2$ **5a** in a 3 : 1 ratio.‡ The **4a** : **5a** ratio determined by ^{1}H NMR was confirmed by hydrolysis, which gives elimination products styrene and *E*-vinylboronate ester,[1a] respectively.[16]

Several reactivity trends were observed in the catalysed hydroborations of substituted ketimines.‡ Reaction of the electron poor ketimine, (*p*-$CF_3C_6H_4$)N=C(CH_3)Ph **1b**, with HBcat′ in THF gave more rapid conversion (*cf.* **1a**) of the intermediate enamine and afforded analogous multiply borated amines **4b** and **5b** in a 5 : 1 ratio. The sterically hindered, electron-rich ketimine, (*o*-$MeOC_6H_4$)N=C(CH_3)Ph **1c**, on the other hand, gave primarily enamine **2c** and amine **3c**. Deoxybenzoin-derived imine, (*p*-$MeOC_6H_4$)N=C(CH_2Ph)Ph **1d**, gave both *E*- and *Z*-enamines and only one isomer was hydroborated to a single diastereomer of the 1,3 diboration product **4d**. Steric hindrance also precludes formation of the triborated product and gives rise to Rh-mediated HBcat′ degradation leading to minor

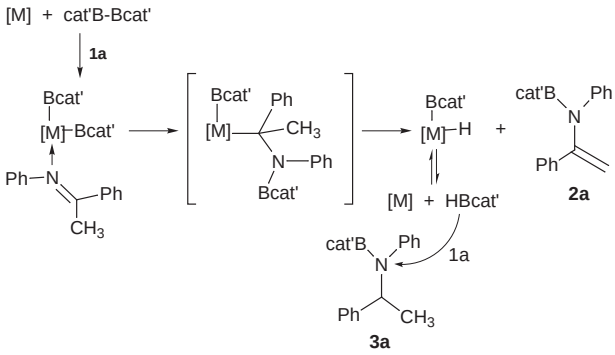

Scheme 1

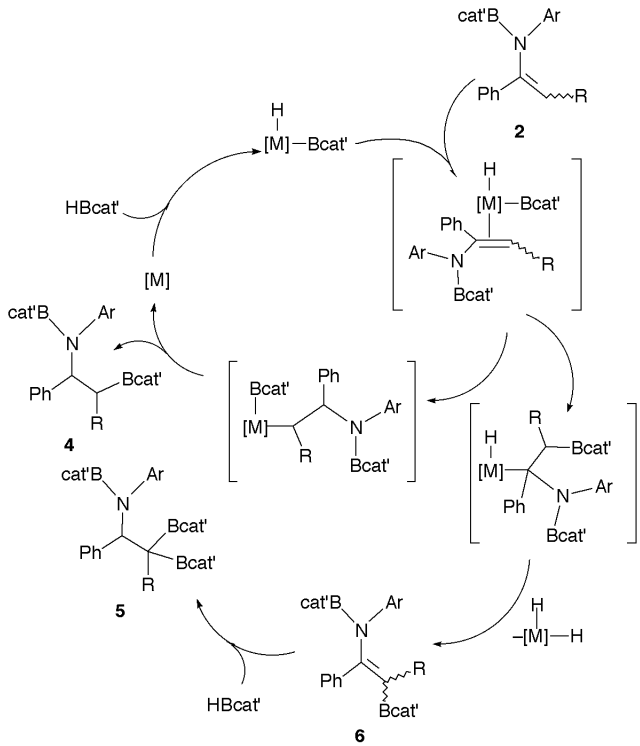

Scheme 2

amounts of aminoborane side-products derived from 'BH_3' addition.[11a] Propiophenone-derived imine, (p-$CF_3C_6H_4$)-N=C(CH_2CH_3)Ph **1e**, is readily converted to isomeric *N*-borylenamines, but subsequent catalysed hydroboration is accompanied by significant HBcat′ degradation.

We propose that formation of the multiply borated products is due to competitive insertion of enamine **2** into M–H and M–B bonds to give **4** and *N*,*C*-diborylenamine **6**; the latter is subsequently hydroborated to **5** (Scheme 2). The enamine hydroboration/boration ratio depends on the substrate, solvent, and catalyst, and further catalyst development is ongoing.

In summary, we have shown that metal-catalysed diboration of ketimines affords *N*-borylenamines and that catalysed hydroboration of these products gives multiply borated amines proposed to result from competing enamine insertion into M–H *vs*. M–B bonds. The first examples of metal-catalysed enamine hydroboration reported herein afford boronate esters which may subsequently be used as substrates to prepare novel functionalized amines. This work is currently in progress.

R. T. B. thanks the Science and Technology Based programs at Los Alamos and S. A. W. thanks the Natural Sciences and Engineering Research Council of Canada.

Notes and references

† Dedicated to Professor Warren R. Roper on the occasion of his 60th birthday.

‡ *Reaction of* **1** *with* $B_2cat'_2$: to a solution of ketimine **1a** (97 mg, 0.5 mmol) dissolved in 0.5 ml of C_6D_6 was added $B_2cat'_2$ (119 mg, 0.5 mmol) and catalyst (2 mol%). The reaction was monitored by ^1H and ^{11}B NMR until **1a** was consumed (*ca.* 48 h). Similar reactions were conducted for **1b**–**e** and faster rates were observed for more electron-rich imines. The ratio of **2**:**3** was 4, 3.3, 2, 1.5, and 6 for **1a**–**e**, respectively. For **1c**, one equiv. of HBcat′ was added to the reaction mixture upon completion in order to cleanly generate **4c** from **2c**.

Reaction of **1** *with* HBcat′: to a solution of ketimine **1a** (40 mg, 0.2 mmol) dissolved in 0.5 ml of [$^2H_8$]THF was added HBcat′ (106 mg, 0.6 mmol) and catalyst (2 mol%). The reaction was monitored by ^1H and ^{11}B NMR until the intermediate *N*-borylenamine **2** was entirely consumed. The ratio of **3**:**4**:**5** was determined by ^1H NMR before and after hydrolysis (see electronic supplementary material for NMR data: http://www.rsc.org./suppdata/cc/1998/2395). Product Ratios for **1a**–**e** + HBcat′ in THF after 4 days at 25 °C: **3a**:**4a**:**5a** = 3:6:2; **2b**:**3b**:**4b**:**5b** = 1:8:12:2; **2c**:**3c**:**4c**:**5c** = 6:8:2:1; **2d**:**3d**:**4d** = 2:5:1; **2e**:**3e**:**4e** = 4:4:1.

1 (*a*) R. T. Baker, J. C. Calabrese, S. A. Westcott, P. Nguyen and T. B. Marder, *J. Am. Chem. Soc.*, 1993, **115**, 4367; (*b*) T. Ishiyama, N. Matsuda, N. Miyaura and A. Suzuki, *J. Am. Chem. Soc.*, 1993, **115**, 11 018; (*c*) R. T. Baker, P. Nguyen, T. B. Marder and S. A. Westcott, *Angew. Chem., Int. Ed. Engl.*, 1995, **34**, 1336; (*d*) C. N. Iverson and M. R. Smith, III, *J. Am. Chem. Soc.*, 1995, **117**, 4403; (*e*) G. Lesley, P. Nguyen, N. J. Taylor, T. B. Marder, A. J. Scott, W. Clegg and N. C. Norman, *Organometallics*, 1996, **15**, 5137; (*f*) C. N. Iverson and M. R. Smith, III, *Organometallics*, 1996, **15**, 5155; (*g*) T. Ishiyama, M. Yamamoto and N. Miyaura, *Chem. Commun.*, 1996, 2073; (*h*) C. N. Iverson and M. R. Smith, III, *Organometallics*, 1997, **16**, 2757; (*i*) T. Ishiyama, M. Yamamoto and N. Miyaura, *Chem. Commun.*, 1997, 689; (*j*) T. Ishiyama, T. Kitano and N. Miyaura, *Tetrahedron Lett.*, 1998, **39**, 2357; (*k*) Q. Cui, D. G. Musaev and K. Morokuma, *Organometallics*, 1997, **16**, 1355; 1998, **17**, 742.

2 S. D. Brown and R. W. Armstrong, *J. Org. Chem.*, 1997, **62**, 6076; N. Miyaura and A. Suzuki, *Chem. Rev.*, 1995, **95**, 2457.

3 T. Ishiyama, M. Murata and N. Miyaura, *J. Org. Chem.*, 1995, **60**, 7508.

4 M. Murata, S. Watanabe and Y. Masuda, *J. Org. Chem.*, 1997, **62**, 6458.

5 Y. G. Lawson, M. J. G. Lesley, T. B. Marder, N. C. Norman and C. R. Rice, *Chem. Commun.*, 1997, 2051.

6 R. T. Baker, J. C. Calabrese and S. A. Westcott, *J. Organomet. Chem.*, 1995, **498**, 109.

7 S. J. Coutts, T. A. Kelly, R. J. Snow, C. A. Kennedy, R. W. Barton, J. Adams, D. A. Krolikowski, D. M. Freeman, S. J. Campbell, J. F. Ksiazek and W. W. Bachovchin, *J. Med. Chem.*, 1996, **39**, 2087; V. Martichonok and J. B. Jones, *J. Am. Chem. Soc.*, 1996, **118**, 950; P. K. Jadhav and H.-W. Man, *J. Org. Chem.*, 1996, **61**, 7951.

8 Metal-catalysed 1,2-diboration of aldimines will be described elsewhere: R. T. Baker, T. M. Cameron and S. A. Westcott, manuscript in preparation.

9 Uncatalysed addition of diboron compounds to aldimines gives stereoselective coupling to C_2-symmetric *N*-boryldiamines: R. T. Baker, T. M. Cameron and S. A. Westcott, unpublished results.

10 NMR data in [$^2H_8$]THF: **2a**: ^1H, δ 7.6–6.8 (ov m, Ph + cat′, 13H), 5.73, 5.42 (s, =CH_2), 1.30 (9H, Bu^t); ^{13}C, δ 148.3 (*C*=CH_2), 149.4, 147.2, 146.4, 144.8, 138.4 (*ipso* of CPh, NPh, and cat′), 129.4, 129.0, 127.5, 123.4 (*o*-, *m*-C of NPh and CPh), 128.9, 124.1 (*p*-C of NPh and CPh), 119.3, 111.4, 110.2 (cat′), 112.5 (=CH_2), 35.4 (Bu^t C), 32.1 (Bu^tCH_3). ^{11}B (90 °C), δ 23.5. **3a**: ^1H, δ 7.6–6.9 (ov m, Ph + cat′, 13H), 5.19 (q, *J* 7, Hz, C*H*Ph), 1.64 (d, *J* 7 Hz, 3H, CH_3), 1.29 (9H, Bu^t); ^{13}C, δ 149.6, 147.5, 146.1, 144.6, 143.6 (*ipso*-C of CPh, NPh and cat′), 129.2, 129.0, 128.9, 127.9 (*o*-, *m*-C of NPh and CPh), 127.7, 126.2 (*p*-C of NPh and CPh), 118.9, 111.1, 109.8 (cat′), 58.4 (CN), 35.3 (Bu^t C), 32.1 (Bu^t CH_3), 20.0 (CH_3); ^{11}B (90 °C), δ 26.3. **4a**: ^1H, δ 7.5–6.8 (ov m, Ph + cat′, 16H), 5.59 ('tr', *J* 8 Hz, C*H*Ph), 2.25 (dd, *J* 16, 8.5 Hz, CH_2B), 2.12 (dd, *J* 16, 8 Hz, CH_2B), 1.30 (9H, Bu^t of NBcat′), 1.27 (9H, Bu^t of CBcat′); ^{13}C, δ 149.6, 149.2, 147.5, 147.0, 146.9, 146.0, 144.6, 143.5 (*ipso*-C of CPh, NPh, NBcat′ and CBcat′), 129.5, 129.2, 129.0, 128.1, (*o*-, *m*-C of NPh and CPh), 127.9, 126.5 (*p*-C of NPh and CPh), 119.9, 118.9, 111.8, 111.1, 110.3, 109.8 (cat′), 60.1 (CN), 35.4, 35.3 (Bu^t C), 32.1 (ov, 6C, Bu^t CH_3), 17.8 (br, CB); ^{11}B (90 °C), δ 35.7 (BC), 20.3 (BN). **5a**: ^1H, δ 7.6–6.9 (ov m, Ph + cat′, 19H), 6.06 (d, *J* 13 Hz, C*H*Ph), 3.17 (d, *J* 13 Hz, CHB_2), 1.32 (9H, Bu^t of NBcat′), 1.26, 1.25 (9H, Bu^t of CBcat′); ^{13}C, δ 62.2 (CN), 18.1 (br, CB).

11 (*a*) K. Burgess, W. A. van der Donk, S. A. Westcott, R. T. Baker, T. B. Marder and J. C. Calabrese, *J. Am. Chem. Soc.*, 1992, **114**, 9350; (*b*) S. A. Westcott, T. B. Marder and R. T. Baker, *Organometallics*, 1993, **12**, 975; (*c*) J. M. Brown and G. C. Lloyd-Jones, *J. Am. Chem. Soc.*, 1994, **116**, 866.

12 M. T. Atlay, L. R. Gahan, K. Kite, K. Moss and G. Read, *J. Mol. Catal.*, 1980, **7**, 31.

13 H. Kono, K. Ito and Y. Nagai, *Chem. Lett.*, 1975, 1095; D. Männig and H. Nöth, *Angew. Chem., Int. Ed. Engl.*, 1985, **24**, 878.

14 D. G. Musaev, A. M. Mebel and K. Morokuma, *J. Am. Chem. Soc.*, 1994, **116**, 10 693; A. E. Dorigo and P. von Rague-Schleyer, *Angew. Chem., Int. Ed. Engl.*, 1995, **34**, 115.

15 A small amount (< 5%) of *N*-borylenamine is also observed in the uncatalysed hydroborations due to HBcat′ reaction with the N–H bond of the enamine tautomer, PhNHCPh=CH_2.

16 Uncatalysed hydroboration of enamines using alkylboranes can be employed to prepare alkenes (after thermal elimination): B. Singaram, C. T. Goralski and G. B. Fisher, *J. Org. Chem.*, 1991, **56**, 5691; G. B. Fisher, C. T. Goralski, L. W. Nicholson and B. Singaram, *Tetrahedron Lett.*, 1993, **34**, 7693.

Communication 8/05792C

The first gold(III) dinuclear cyclometallated derivatives with a single oxo bridge

Maria Agostina Cinellu,[a] Giovanni Minghetti,*[a] Maria Vittoria Pinna,[a] Sergio Stoccoro,[a] Antonio Zucca[a] and Mario Manassero*[b]

[a] *Dipartimento di Chimica, Università di Sassari, Via Vienna 2, I-07100 Sassari, Italy. E-mail: mingh@ssmain.uniss.it*

[b] *Dipartimento di Chimica Strutturale e Stereochimica Inorganica, Università di Milano, Centro CNR, via Venezian 21, I-20133 Milano, Italy. E-mail: m.manassero@csmtbo.mi.cnr.it*

Received (in Basel, Switzerland) 21st July 1998, Accepted 23rd September 1998

The reaction of the gold(III) cyclometallated complexes [Au(L)Cl][BF_4] [L = $N_2C_{10}H_7(CHMeC_6H_4)$-6 1 or $N_2C_{10}H_7(CMe_2C_6H_4)$-6 2, where $N_2C_{10}H_8$ = 2,2′-bipy] with $AgBF_4$ in acetone solution affords the acetonyl derivatives [Au(L){$CH_2C(O)Me$}][BF_4], 3 and 4, and the dinuclear oxo-bridged complexes [$Au_2(L)_2(\mu$-O)][BF_4]$_2$, 5 and 6; the crystal structure of complex 6 gives evidence for an unprecedented unsupported Au–O–Au bridge.

Oxo-bridged units are an important structural feature in the chemistry of early transition metals.[1] These units are also present in the active sites of a number of biological systems such as metalloproteins and metalloenzymes where the μ-oxo bridged moieties are responsible for a wide range of reactions. For this reason the study of synthetic models for these functions has been well developed.[2] In contrast, the chemistry of Group 9–11 late transition metal oxo-complexes has been less investigated[3] despite indications that such complexes may be intermediates in several important catalytic processes.

In a recent paper[4] we have reported the syntheses and characterization of a series of stable gold(III) bis oxo-bridged compelxes with 6-alkyl-2,2′-bipyridines. The crystal structures of *trans*-[$Au_2\{N_2C_{10}H_7(CH_2CMe_3)-6\}_2(\mu$-$O)_2$][$PF_6$]$_2$ and *cis*-[$Au_2\{N_2C_{10}H_7(CHMe_2)-6\}_2(\mu$-$O)_2$][$AuCl_4$][$PF_6$], the first gold(III) oxo-complexes, gave evidence for an $Au_2(\mu$-$O)_2$ core. The reactivity of these species is currently under investigation.

In a preliminary study of the reactivity of a series of gold(III) C,N,N cyclometallated derivatives [Au(L)Cl][BF_4][5] (HL = 6-benzyl- and 6-alkyl-2,2′-bipyridines) we have found that in the presence of $AgBF_4$ these species can activate acetone to give the corresponding acetonyl derivatives [Au(L){$CH_2C(O)$-Me}][BF_4], similar to those described by Vicente *et al.* for C,N cycloaurated complexes and reported to be efficient starting materials for the synthesis of ketones *via* C–C coupling.[6] Now we report that from the reaction of [Au(L)Cl][BF_4] [L = $N_2C_{10}H_7(CHMeC_6H_4)$-6 **1** or $N_2C_{10}H_7(CMe_2C_6H_4)$-6 **2**] with $AgBF_4$ in acetone at room temperature, besides the acetonyl derivatives [Au(L){$CH_2C(O)Me$}][BF_4], **3**† and **4**, dinuclear oxo-bridged complexes [$Au_2(L)_2(\mu$-O)][BF_4]$_2$, **5** and **6**, are formed.‡

To the best of our knowledge, the latter compounds are the first examples of gold(III) oxo-bridged cyclometallated derivatives. The oxo species are likely to result from aqua complexes [Au(L)$(H_2O)]^{2+}$ due to adventitious water. Deprotonation of the most acidic coordinated water molecule should give mononuclear hydroxo intermediates [Au(L)OH]$^+$. An 'oxolation' reaction involving an hydroxo intermediate could give the oxo-bridged species as proposed, *e.g.* in the case of iron(III) oxo complexes.[1]

In the IR spectra a strong absorption at *ca.* 780 cm^{-1} is assigned to the asymmetric stretch of the Au–O–Au moiety by comparison with bent oxo-bridged complexes of other metals.[7] In the FAB mass spectra (positive ions) of compounds **5** and **6** peaks of medium intensity are observed at mass values that correspond to ([M + BF_4]$^+$); in addition, peaks corresponding to the species [Au(L)OH]$^+$ are found in both cases. In the ^{1}H NMR spectrum of complex **5** [$(CD_3)_2CO$ or CD_2Cl_2, room temperature] two sets of signals are observed, as expected due to the presence of diastereomers. In the spectrum of complex **6** (CD_3CN, room temp.) one set of signals is observed, nevertheless a broad signal (at δ 1.4) for the methyl substituents indicates that either rotation about the Au–O bonds or inversion of the six-membered cyclometallated ring are somewhat slowed down. In fact, two well separated singlets at δ 0.85 and 1.88 appear at −40 °C.

The crystal structure of [$Au_2\{N_2C_{10}H_7(CMe_2C_6H_4)-6\}_2(\mu$-O)][$BF_4$]$_2$·MeCN **6**·MeCN, has been determined by single crystal X-ray diffraction.§ It consists of the packing of [$Au_2(L)_2(\mu$-O)]$^{2+}$ cations, BF_4^- anions and MeCN molecules in the molar ratio 1 : 2 : 1 with normal van der Waals contacts. A perspective view of the complex dication is shown in Fig. 1 with selected interatomic distances and angles in the caption. The cation displays an idealized C_2 symmetry, with the twofold axis passing through the oxygen atom and the midpoint of the Au(1)···Au(2) vector. The environments of the two gold atoms are very similar to each other; in particular, corresponding bond lengths involving Au(1) and Au(2) are all coincident within three esds. The two gold atoms are in distorted square-planar coordinations, with Au, O, N and N atoms essentially coplanar [maximum deviations from the respective best planes being +0.009(5) for O and −0.016(1) for Au(1), and +0.004(5) for O and −0.008(1) Å for Au(2)], with C(15) and C(35) lying

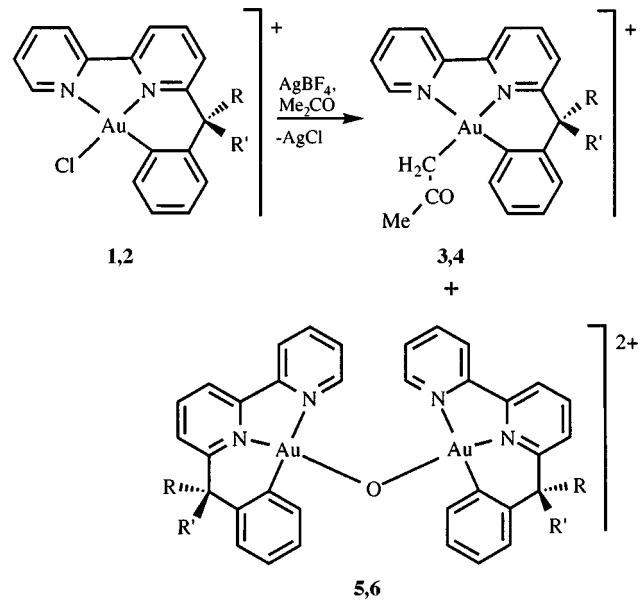

Scheme 1: **1**, **3** and **5**: R = H, R′ = Me; **2**, **4** and **6**: R = R′ = Me.

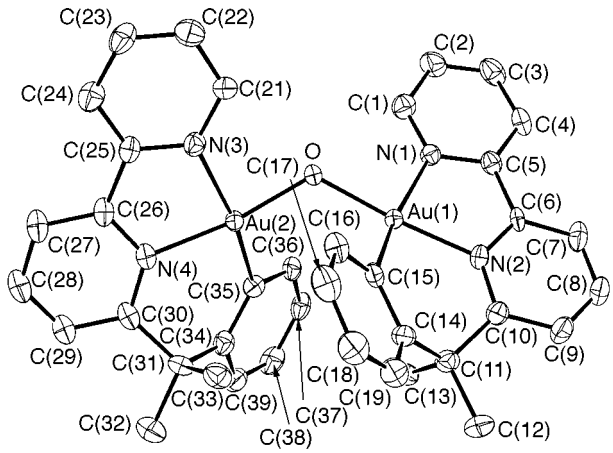

Fig. 1 Perspective view of the complex dication in **6**·MeCN. Selected interatomic distances (Å) and angles (°): Au(1)–O 1.971(5), Au(1)–N(1) 2.103(5), Au(1)–N(2) 2.029(5), Au(1)–C(15) 2.009(6), Au(2)–O 1.956(5), Au(2)–N(3) 2.096(5), Au(2)–N(4) 2.040(5), Au(2)–C(35) 2.009(6), Au(1)···Au(2) 3.422(1), Au(1)–O–Au(2) 121.3(2), O–Au(1)–N(1) 91.9(2), O–Au(1)–N(2) 172.7(2), O–Au(1)–C(15) 94.6(2), N(1)–Au(1)–N(2) 80.9(2), N(1)–Au(1)–C(15) 165.4(2), N(2)–Au(1)–C(15) 92.8(2), O–Au(2)–N(3) 90.5(2), O–Au(2)–N(4) 170.7(2), O–Au(2)–C(35) 96.8(2), N(3)–Au(2)–N(4) 80.3(2), N(3)–Au(2)–C(35) 165.9(2), N(4)–Au(2)–C(35) 92.1(2).

0.487(6) and 0.403(6) Å above these planes. The dihedral angle between these best planes is 58.0(1)°. The distortion is very similar to that found in the cation of complex **2**[5] where atom C(15) is displaced 0.417(6) Å out of the best plane of atoms Au, Cl(1), N(1) and N(2). The present Au(1)–O and Au(2)–O bond lengths, 1.971(5) and 1.956(5) Å, can be compared with the Au–O, 1.976(3), and Au–O′, 1.961(3) Å, distances found in *trans*-$[Au_2\{N_2C_{10}H_7(CH_2CMe_3)\text{-}6\}_2(\mu\text{-}O)_2]^{2+}$,[4] The Au–N and Au–C bond lengths are very similar to the corresponding distances found in **2**, *i.e.* Au–N(1) 2.121(5), Au–N(2) 2.009(4), and Au–C(15) 2.009(6) Å. As previously observed in **2**, in the present cation the six-membered metallacycles are in boat conformations, and one of the hydrogen atoms of the Me groups in pseudo-axial position is rather close to the respective gold atom: Au(1)···H(131) 2.70 and Au(2)···H(331) also 2.70 Å; the corresponding Au···H separation in**2** is 2.62 Å. The Au(1)–O–Au(2) angle is 121.3(2)° and the distance Au(1)···Au(2) 3.422(1) Å, a distance too long to be considered bonding although slightly shorter than the sum of the estimated van der Waals radii (3.60 Å).[8]

We thank the MURST (40%) and CNR for financial support.

Notes and references

† Complex **3** has been described in ref. 5. It was obtained from the reaction of complex **1** with $AgBF_4$ in refluxing acetone; under these conditions complex **5** was not isolated.

‡ Reactions of compounds **1** and **2** with $AgBF_4$: to a solution of **1** (0.289 g, 0.5 mmol) in acetone (20 cm^3) was added a solution of $AgBF_4$ (0.097 g, 0.5 mmol) in acetone (10 cm^3): a precipitate of AgCl was formed immediately. The resulting mixture was stirred for 24 h at room temperature and then filtered off. The solution was evaporated to dryness and the residue was extracted with $CHCl_3$ (3 × 10 cm^3). The filtered chloroform solution was concentrated to small volume and diethyl ether was added to give a whitish precipitate of compound **3** (0.120 g). The residue insoluble in $CHCl_3$ was dissolved in CH_2Cl_2, filtered and concentrated to small volume. Addition of diethyl ether gave a white precipitate of compound **5** (0.080 g).

Compounds **4** and **6** were obtained similarly from **2** (0.222 g, 0.37 mmol). Complex **4** was recrystallized from acetone–diethyl ether to give the analytical sample (0.091 g). At variance with complex **5**, complex **6** is insoluble in acetone so it was abstracted with MeCN from the insoluble product containing AgCl, the filtered solution was concentrated to small volume and diethyl ether added to give a white precipitate of **6** (0.098 g).

§ *Crystal data* for **6**·MeCN: $C_{40}H_{37}Au_2B_2F_8N_5O$, M = 1171.3, monoclinic, space group *Cc* (no. 9) (after refinement), a = 12.744(2), b = 22.309(3), c = 14.062(1) Å, β = 96.72(1)°, U = 3970.4(9) $Å^3$, Z = 4, D_c = 1.959 g cm^{-3}, μ = 74.4 cm^{-1}, $F(000)$ = 2240. Reflections measured 23 557, independent (Friedel pairs not merged) 9339 with R_{int} = 0.033. Empirical absorption correction, SADABS (T_{max} = 1.00, T_{min} = 0.66). Final R_2 (F^2, all reflections) = 0.044, R_{2w} = 0.062, conventional R_1 = 0.032 for 506 parameters. For the inverted structure, final R_2 = 0.047, R_{2w} = 0.071. Siemens SMART CCD area-detector, Mo-Kα radiation (λ = 0.710 73 Å), ω scan mode, θ_{min} = 3°, θ_{max} = 26°. Structure solved by Patterson and Fourier methods and refined by full-matrix least squares with anisotropic thermal parameters for cation and anions. Cation hydrogen atoms placed in calculated positions, acetonitrile hydrogen atoms ignored. Program used was Personal SDP on a PC-486 computer. An attempt to refine the structure in space group *C*2/*c* was unsuccessful (many thermal parameters of cation atoms were non-positive, heavy disorder was introduced for anions and MeCN with occupancy factors of 0.5, final R_1 was 0.12). CCDC 182/1029.

1 B. O. West, *Polyhedron*, 1989, **8**, 219.

2 Some very recent articles: C. E. Dubé, D. W. Wright, S. Pal, P. J. Bonitatebus, Jr. and W. H. Armstrong, *J. Am. Chem. Soc.*, 1998, **120**, 3704; H. Weihe and H. U. Güdel, *J. Am. Chem. Soc.*, 1998, **120**, 2870; E. C. Wilkinson, Y. Dong, Y. Zang, H. Fujii, R. Fraczkiewicz, G. Fraczkiewicz, R. S. Czernuszewicz and L. Que, Jr., *J. Am. Chem. Soc.*, 1998, **120**, 955; T. K. Lal and R. Mukherjee, *Inorg. Chem.*, 1998, **37**, 2373; O. Horner, M. F. Charlot, A. Boussac, E. Anxolabéhère-Mallart, L. Tchertanov, J. Guilhem and J. J. Girerd, *Eur. J. Inorg. Chem.*, 1998, 721; V. Mahadevan, Z. Hou, A. P. Cole, D. E. Root, T. K. Lal, E. I. Solomon and T. D. P. Stack, *J. Am. Chem. Soc.*, 1997, **119**, 11 996; J. E. McGrady and R. Stranger, *J. Am. Chem. Soc.*, 1997, **119**, 8512; C. Kim, Y. Dong and L. Que, Jr., *J. Am. Chem. Soc.*, 1997, **119**, 3635; C. Duboc-Toia, S. Ménage, J. M. Vincent, M. T. Averbuch-Pouchot and M. Fontecave, *Inorg. Chem.*, 1997, **36**, 6148; A. Bérces, *Inorg. Chem.*, 1997, **36**, 4831; N. S. Dean, J. K. Cooper, R. S. Czernuszewicz, D. Ji and C. J. Carrano, *Inorg. Chem.*, 1997, **36**, 2760; H. J. Mok, J. A. Davis, S. Pal, S. K. Mandal and W. H. Armstrong, *Inorg. Chim. Acta*, 1997, **263**, 385; B. H. Ye, X. Y. Li, F. Xue and C. W. Mak, *Chem. Commun.*, 1997, 2407; A. E. M. Boelrijk, T. X. Neenan and J. Reedijk, *J. Chem. Soc., Dalton Trans.*, 1997, 4561; L. Que, Jr., *J. Chem. Soc., Dalton Trans.*, 1997, 3933; A. K. Bhattyacharya, A. B. Mondal and R. Banarjee, *J. Chem. Soc., Dalton Trans.*, 1997, 2351.

3 H. Shan, Y. Yang, A. J. James and P. R. Sharp, *Science*, 1997, **275**, 1460; J. Vicente, M. T. Chicote, R. Guerrero, P. G. Jones and M. C. Ramìrez de Arellano, *Inorg. Chem.*, 1997, **36**, 4438; T. Hosokawa, M. Takano and S. I. Murahashi, *J. Am. Chem. Soc.*, 1996, **118**, 3990; Y. Zhang, R. J. Puddephatt, L. Manojlovic-Muir and K. W. Muir, *Chem. Commun.*, 1996, 2599; H. Schmidbaur, S. Hofreiter and M. Paul, *Nature*, 1995, **377**, 503; K. Angermaier and H. Schmidbaur, *Inorg. Chem.*, 1994, **33**, 2069; Y. Yang, V. Ramamoorthy and P. R. Sharp, *Inorg. Chem.*, 1993, **32**, 1946, and references therein; D. A. Dobbs and R. G. Bergman, *J. Am. Chem. Soc.*, 1993, **115**, 3836; D. Min, R. D. Larsen, K. Emerson and E. H. Abbott, *Inorg. Chem.*, 1990, **29**, 73; W. D. McGhee, T. Foo, F. J. Hollander and R. G. Bergman, *J. Am. Chem. Soc.*, 1988, **110**, 8543; P. Betz and A. Bino, *J. Am. Chem. Soc.*, 1988, **110**, 602; P. R. Sharp and J. R. Flynn, *Inorg. Chem.*, 1987, **26**, 3231, and references therein.

4 M. A. Cinellu, G. Minghetti, M. V. Pinna, S. Stoccoro, A. Zucca, M. Manassero and M. Sansoni, *J. Chem. Soc., Dalton Trans.*, 1998, 1735.

5 M. A. Cinellu, A. Zucca, S. Stoccoro, G. Minghetti, M. Manassero and M. Sansoni, *J. Chem. Soc., Dalton Trans.*, 1996, 4217.

6 J. Vicente, M. D. Bermudez, M. P. Carrillo and P. G. Jones, *Chem. Ber.*, 1996, **129**, 130; J. Vicente, M. D. Bermudez and F. J. Carrion, *Inorg. Chim. Acta*, 1994, **220**, 1; J. Vicente, M. D. Bermudez, F. J. Carrion and P. G. Jones, *J. Chem. Soc., Dalton Trans.*, 1992, 1975, and references therein.

7 G. S. Brownlee, P. Carty, D. N. Cash and A. Walker, *Inorg. Chem.*, 1975, **14**, 323.

8 D. M. P. Mingos, *J. Chem. Soc., Dalton Trans.*, 1996, 561.

Communication 8/05672B

A remarkable Mo catalyst for olefin metathesis: hexagonal mesoporous silica-supported molybdenum oxide (MoO_3/HMS)

Tooru Ookoshi and Makoto Onaka*

Department of Chemistry, College of Arts and Sciences, The University of Tokyo, Komaba, Meguro, Tokyo 153-8902, Japan. E-mail: conaka@komaba.ecc.u-tokyo.ac.jp

Received (in Cambridge, UK) 6th August 1998, Accepted 21st September 1998

Hexagonal mesoporous silica-supported molybdenum oxide exhibits much higher catalytic activity for the metathesis of oct-1-ene in the liquid phase, compared with MoO_3 on normal porous silica and MoO_3 on γ-alumina.

The application of mesoporous materials for various catalysts in organic reactions has been intensively investigated since a Japanese research group[1] and researchers at Mobil Oil[2] independently discovered mesoporous molecular sieves such as FSM-16 and MCM-41 with uniform pore openings in the range 2.0–10.0 nm as well as a tunnel pore structure. For example, acidic FSM-16 containing Al_2O_3 is an effective and recyclable solid acid promoter for *meso*-tetraarylporphyrin synthesis from the corresponding aromatic aldehydes and pyrrole.[3] It has also been shown that titanocene-derived MCM-41 shows high efficiency in the epoxidation of cyclohexene and more bulky cyclic olefins,[4] while *rac*-ethenebis(indenyl)zirconium dichloride-grafted MCM-41 provides highly isotactic polypropenes with a unique spherulite morphology.[5]

Supported molybdenum oxides have received much attention as solid metathesis catalysts because they can be practically used in industrial petrochemical processes such as the Shell higher olefin process for producing detergent-range olefins.[6] Their surface properties and catalytic activity are critically influenced by the oxide support, the surface molybdenum oxide content, the activation conditions, and the oxidation state of the molybdenum species. Supported molybdenum catalysts have generally been prepared in the following ways: (i) by impregnation of the support with molybdate solution;[7] (ii) by treatment of the support with $Mo(CO)_6$;[8] and (iii) by reaction of the support with π-allylmolybdenum compounds.[9]

This paper focuses on hexagonal mesoporous silica (HMS) in terms of developing a new silica support for molybdenum-based olefin metathesis catalysts, and demonstrates that HMS impregnated with molybdenum oxide (MoO_3/HMS) is an efficient catalyst for oct-1-ene metathesis [eqn. (1)].

$$2\ CH_2{=}CH(CH_2)_5CH_3 \xrightarrow{\text{Mo/HMS}} CH_3(CH_2)_5CH{=}CH(CH_2)_5CH_3 + CH_2{=}CH_2 \quad (1)$$

HMS was first prepared from tetraethylorthosilicate (TEOS) and primary amine as a templating agent.[10] The preparation of HMS has several advantages over that of MCM-41: (i) the use of more commercially available primary alkylamines as templating agents in place of expensive alkyltrimethylammonium halides; (ii) the applicability of shorter alkylamines as templating agents; and (iii) easier procedures for sol–gel processing than those for hydrothermal preparations for MCM-41. In work, three HMSs were synthesized by the use of three alkylamines with different alkyl chain lengths (C8, C12, C16).† HMS(C*n*) shall hereafter stand for the HMS obtained using C*n*-alkylamine.

MoO_3-supporting catalysts were prepared by impregnation of the HMSs with molybdate solution.‡ The HMS(C*n*) supports and MoO_3/HMS catalysts were characterized using powder X-ray diffraction and N_2 adsorption. As shown in Table 1, all MoO_3/HMS samples exhibited a single diffraction peak corresponding to a d_{100} spacing of > 3.0 nm,[10] and high BET surface areas of > 800 m^2 g^{-1}, proving that the MoO_3/HMSs were mainly composed of mesopores. No diffraction peaks intrinsic to MoO_3 crystallites were observed, indicating that MoO_3 was finely dispersed on the interior surface of mesoporous HMS.

As a control, MoO_3 was supported on commercially available silica, CARIACT Q-3 (Fuji Silysia Chemical), which has a narrow mesopore-size distribution centered at 3 nm, a specific surface area of 619 m^2 g^{-1}, a pore volume of 0.45 ml g^{-1}, and 75–500 μm particle sizes. The 3.5 and 7 wt% MoO_3/SiO_2 were applied to the metathesis of oct-1-ene in a similar way to MoO_3/HMS.

By the use of 7 wt% MoO_3/SiO_2 (0.15 g) and 3.5 wt% MoO_3/SiO_2 (0.3 g), the metathesis products were scarcely obtained at 323 K, as shown in Fig. 1. Surprisingly, MoO_3-supporting HMS catalysts could induce metathesis of oct-1-ene.§ The catalytic activity is critically dependent on the kind of alkylamine which functioned as templating agent in the formation of HMSs. In particular, MoO_3-supporting HMS(C8) prepared with the aid of octylamine had the highest activity. At the early stage of the metathesis, 7 wt% MoO_3/HMS(C12) and 7 wt% MoO_3/HMS(C16) converted oct-1-ene more rapidly than 7 wt% MoO_3/HMS(C8). However, after this stage on 7 wt% MoO_3/HMS(C12) and 7 wt% MoO_3/HMS(C16), the conversion

Table 1 Structural properties of HMS, MoO_3/HMS, and MoO_3/SiO_2

Mesoporous silica or Mo-supported catalyst	d_{100} Spacing/nm	Surface area/m^2 g^{-1}
HMS(C8)	3.0	1350
7 wt% MoO_3/HMS(C8)	3.0	854
HMS(C12)	3.5	1450
7 wt% MoO_3/HMS(C12)	3.4	1060
HMS(C16)	4.0	1230
7 wt% MoO_3/HMS(C16)	3.5	844
SiO_2[a]	—	619
7 wt% MoO_3/SiO_2[a]	—	514
3.5 wt% MoO_3/SiO_2[a]	—	563

[a] CARIACT Q-3.

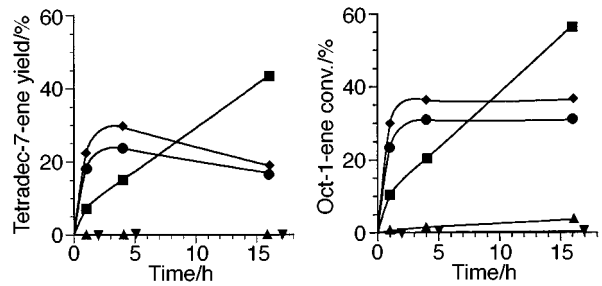

Fig. 1 Metathesis of oct-1-ene on MoO_3/mesoporous silica: ■ 7 wt% MoO_3/HMS(C8). ● 7 wt % MoO_3/HMS(C12), ◆ 7 wt% MoO_3/HMS(C16), ▲ 7 wt% MoO_3/SiO_2 (CARIACT Q-3), ▼ 3.5 wt% MoO_3/SiO_2 (CARIACT Q-3).

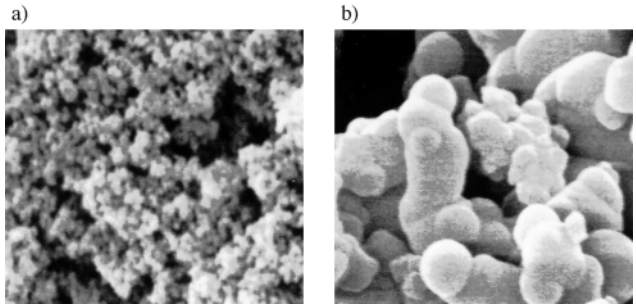

Fig. 2 SEM micrographs of (a) HMS(C8) and (b) HMS(C12) (scale: 30 mm = 1.5 μm).

reached the highest limit owing to the deactivation of the catalysts, and the yield of tetradec-7-ene and the selectivity to tetradec-7-ene decreased [7 wt% MoO_3/HMS(C12), yield: 23% (at 4 h), 17% (at 16 h), selectivity: 75% (at 4 h), 55% (at 16 h); 7 wt% MoO_3/HMS(C16), yield: 29% (at 4 h), 19% (at 16 h), selectivity: 81% (at 4 h), 52% (at 16 h)] due to the fact that the olefinic products gradually decomposed when in contact with the catalysts. In contrast, on 7 wt% MoO_3/HMS(C8), the yield of tetradec-7-ene steadily increased from 14% (at 4 h) to 44% (at 16 h) while maintaining high tetradec-7-ene selectivity [74% (4 h), 77% (at 16 h)], indicating that the metathesis product, tetradec-7-ene,¶ did not undergo further metathesis, polymerization, isomerization, or degradation on the catalyst. In this case, the products other than tetradec-7-ene are mainly highly polymerized products from oct-1-ene.

The SEMs in Fig. 2 of HMS(C8) and HMS(C12) indicate that HMS(C8) is made up of small silica particles of < 50 nm in diameter, while HMS(C12) is spherical silica of 200–700 nm. The shape and size of HMS(C16) (not shown in Fig. 2) are almost the same as those of HMS(C12). Based on the powder X-ray and SEM analysis, HMS(8) has not only smaller pore diameter, but also shorter pore length than HMS(12) and HMS(16). Therefore, it is supposed that at the initial stage of the metathesis (in Fig. 1), MoO_3/HMS(12) and MoO_3/HMS(16) showed higher conversions of oct-1-ene owing to easier passage of the olefin in the wider pores, but MoO_3/HMS(8) was suffering from less deactivation of the Mo sites or less blockage of the pores by polymeric side-products owing to the shorter channel structure, leading to retention of the high yield and high selectivity of the metathesis product.

There are also distinct differences in the catalytic activities on olefin metathesis between MoO_3-supporting HMS and normal silica. Although the reasons why the MoO_3/HMS shows much higher catalytic performance have yet to be elucidated, it is likely that silica with hexagonal channel-type pores is adequate for fixing finely dispersed molybdenum oxides and for stabilizing the molybdenum species in the oxidation state which is essential to the metathesis catalysis. Disordered normal silica could not play such a role.

Silica-supported molybdenum catalysts are normally activated by cocatalysts such as tetraalkyltin[11] or by photoreduction.[12] Neither the presence of such volatile and poisonous cocatalysts nor the photoactivation process is necessary for the MoO_3/HMS system to show high catalytic performance.

MoO_3/HMS(C8) was also compared not only with traditional Al_2O_3-supported[13] molybdenum catalyst (MoO_3/Al_2O_3)[14] but also with MoO_3/Al_2O_3 modified with CoO[14] or K_2O[15] in the metathesis of oct-1-ene at 323 K.[16] In the light of the yield of tetradec-7-ene as well as the selectivity to tetradec-7-ene, 7 wt% MoO_3/HMS(C8) is much superior to 7 wt% MoO_3/Al_2O_3 [yield: 3.8% (at 4 h), 12.5% (at 16 h), selectivity: 35% (at 4 h), 35% (at 16 h)], 7 wt% MoO_3/2 wt% CoO/Al_2O_3 [yield: 4.9% (at 3 h), 3.4% (at 16 h), selectivity: 52% (at 3 h), 27% (at 16 h)], and 7 wt% MoO_3/0.3 wt% K_2O/Al_2O_3 [yield: 3.6% (at 3 h), 4.5% (at 16 h), selectivity: 51% (at 3 h), 51% (at 16 h)].

In conclusion, MoO_3-supporting hexagonal mesoporous silica which was prepared in the sol–gel reaction directed by relatively short alkylamine shows remarkable catalysis in oct-1-ene metathesis in the liquid phase under mild conditions. The interior properties of hexagonal mesoporous silica are quite different from those of normal porous silica and γ-alumina, hence HMSs can be expected to work as effective, new supports for heterogeneous metal-catalyzed reactions.

Notes and references

† Under vigorous stirring, TEOS (100 mmol) was added to a mixture of ethanol (650 mmol), deionized water (3000 mmol) and *n*-octylamine (25 mmol). The resulting mixture was aged by stirring for 48 h at room temperature. Then, the resulting gel was filtered, washed with ethanol, dried *in vacuo* at 393 K, and calcined at 873 K for 4 h in dry air. When *n*-dodecylamine and *n*-hexadecylamine were used as templating agents, the molar compositions of TEOS : amine : EtOH : H_2O were 1.0 : 0.25 : 8.5 : 28.4 and 1.0 : 0.3 : 14 : 23, respectively.

‡ A representative preparation procedure for the 7 wt% MoO_3/HMS catalyst is given: HMS (1.0 g) was kept in contact with saturated steam in a desiccator for 12 h. To the wet HMS was added an aqueous solution (5 ml) of $(NH_4)_6Mo_7O_{24}\cdot 4H_2O$ (0.0923 g). The mixture was stirred gently for 10 min, and dried to almost complete dryness at room temperature under a stream of dry N_2. Five ml of deionized water was added to the supported HMS. The mixture was stirred for 10 min, and exposed again to a N_2 stream reaching almost complete dryness. Then, the catalyst was dried further at 393 K for 2 h under reduced pressure of 1 mmHg.

§ A representative metathesis reaction was performed as follows: the MoO_3/HMS catalyst (0.15 g), which had been predried at 873 K for 2 h in dry air, was weighed and placed in a 20 ml round-bottomed Pyrex flask. The Mo catalyst contained in the flask was again treated at 773 K under reduced pressure of 0.6 mmHg in a tubular electric furnace. After cooling, to the catalyst was added oct-1-ene (3.5 mmol) in dry *n*-heptane (5 ml), and the mixture was stirred at 323 K under a dry N_2 stream. After a specified time, the solid catalyst was filtered off, and the organic products were collected and analyzed by GC using an internal standard of *n*-decane. Tetradec-7-ene was isolated from the organic products through distillation on a Kugelrohr apparatus at 373 K bath temperature under 3 mmHg.

¶ When the distilled products from the metathesis of oct-1-ene on 7 wt% MoO_3/HMS(C8) were oxidatively cleaved upon treatment with $RuCl_3$ and $NaIO_4$, no aldehydes other than heptanal were detected. This result indicates that during the metathesis, no isomerization of the C=C bonds in the olefinic substrates or products took place.

1 T. Yanagisawa, T. Shimizu, K. Kuroda and C. Sato, *Bull. Chem. Soc. Jpn.*, 1990, **63**, 988; S. Inagaki, Y. Fukushima and K. Kuroda, *J. Chem. Soc., Chem. Commun.*, 1993, 680.
2 C. T. Kresge, M. E. Leonowicz, R. J. Roth, J. C. Vartuli and J. B. Beck, *Nature*, 1992, **359**, 710; J. S. Beck, J. C. Vartuli, W. J. Roth, M. E. Leonowicz, C. T. Kresge, K. D. Schmitt, C. T-W. Chu, D. H. Olson, E. W. Sheppard, J. B. Higgins and L. Schlenker, *J. Am. Chem. Soc.*, 1992, **114**, 10 834.
3 T. Shinoda, Y. Izumi and M. Onaka, *J. Chem. Soc., Chem. Commun.*, 1995, 1801.
4 T. Maschmeyer, F. Rey, G. Sankar and J. M. Thomas, *Nature*, 1995, **378**, 159.
5 J. Tudor and D. O'Hare, *Chem. Commun.*, 1997, 603.
6 K. Weissermel and H-J. Arpe, *Industrielle Organische Chemie*, VCH, Weinheim, 4th edn., 1994.
7 T. Sodesawa, E. Ogata and Y. Kamiya, *Bull. Chem. Soc. Jpn.*, 1979, **52**, 1661.
8 R. F. Howe and C. Kemball, *J. Chem. Soc., Faraday Trans. 1*, 1974, **70**, 1153.
9 Y. I. Yermakov, B. N. Kuznetsov and A. N. Startsev, *Kinet. Katal.*, 1974, **15**, 539.
10 P. T. Tanev and T. J. Pinnavaia, *Science*, 1995, **267**, 865.
11 V. I. Bykov, T. A. Butenko, E. S. Finkel'shtein, P. V. Petrovskii and V. M. Vdovin, *Izv. Akad. Nauk SSSR, Ser. Khim.*, 1988, **37**, 1580.
12 B. N. Shelimov, I. V. Elev and V. B. Kazansky, *J. Mol. Catal.*, 1988, **46**, 187.
13 γ-Alumina [N611(N) from Nikki Chemical Co.; specific surface area 181 $m^2\ g^{-1}$, pore volume 0.36 ml g^{-1}] was used.
14 A. Ismayel-Milanovic, J. M. Basset, H. Praliaud, M. Dufaux and L. de Mourgues, *J. Catal.*, 1973, **31**, 408.
15 R. Nakamura, H. Iida and E. Echigoya, *Chem. Lett.*, 1972, 273.
16 Al_2O_3-supported MoO_3 catalysts (0.15 g) were used in the metathesis.

Communication 8/06233A

Bis{(2-diphenylphosphino)phenyl}mercury: a novel bidentate ligand and transfer reagent for the *o*-$C_6H_4PPh_2$ group

Martin A. Bennett,* Maria Contel, David C. R. Hockless and Lee L. Welling

Research School of Chemistry, Australian National University, Canberra, A.C.T. 0200, Australia. E-mail: bennett@rsc.anu.edu.au

Received (in Cambridge, UK), 17th August 1998, Accepted 30th September 1998

The compound [Hg(*o*-$C_6H_4PPh_2$)$_2$] behaves as a *trans*-spanning bidentate ditertiary phosphine in its $PdCl_2$ complex, the two metal atoms being forced into close contact; the palladium(0) complex [Pd{(*o*-$Ph_2PC_6H_4$)$_2$Hg}$_2$] undergoes reductive elimination on heating with formation of the coupled product *o*-$Ph_2PC_6H_4C_6H_4PPh_2$-*o*.

The formation of transition metal complexes containing the four-membered ring M(*o*-$C_6H_4PPh_2$) by *ortho*-metallation (C–H activation) of coordinated triphenylphosphine is well established.[1] In some cases dinuclear or polynuclear species containing bridging *o*-$C_6H_4PPh_2$[2–5] or *o*-$C_6H_4P(Ph)CH_2CH_2PPh_2$[6,7] units can be generated from coordinated PPh_3 or $Ph_2PCH_2CH_2PPh_2$, respectively. Lahuerta *et al*. have reported that the carbon–halogen bonds of *o*-$Ph_2PC_6H_4X$ (X = Cl, Br) can undergo oxidative addition to rhodium(I)[8] and palladium(0)[9] to give *o*-$C_6H_4PPh_2$ complexes of rhodium(III) and palladium(II), and we have shown that *trans*-metallation of *o*-$Ph_2PC_6H_4Li$ provides access to *o*-$C_6H_4PPh_2$ complexes of platinum[10] and gold.[11]

Aryl groups are readily transferred from mercury(II) to both divalent and zerovalent palladium and platinum;[12–14] reactions of this type have been used in the synthesis of cyclometallated N- and O-donor complexes.[15] We wondered if the method could be extended to *o*-$C_6H_4PPh_2$ complexes and report here some preliminary results.

The required bis(aryl)mercury(II), [Hg(*o*-$C_6H_4PPh_2$)$_2$] **1**, is obtained as a colourless solid in 75% yield from the reaction of *o*-$Ph_2PC_6H_4Li$ with $HgCl_2$ in a 2 : 1 molar ratio (Scheme 1).† Use of a 1 : 1 molar ratio gives mainly a poorly soluble, probably polymeric solid [HgCl(*o*-$C_6H_4PPh_2$)]$_n$ **2**, which disproportionates on heating with aqueous–ethanolic KCN to give **1**.

The small magnitude of ^3J(HgP) observed in the ^{31}P and ^{199}Hg NMR spectra of compound **1**‡ indicates that the phosphorus atoms are probably not coordinated; they readily add oxygen, sulfur and BH_3 to give the corresponding dioxide **3**, disulfide **4**, and bis(borane) adduct **5** (Scheme 1), and react with mercuric halides to form dinuclear complexes [HgX_2\{(*o*-$Ph_2PC_6H_4$)$_2$Hg\}] (X = Cl **6a**, Br **6b**) (Scheme 2).†‡ Compound **6a** is more soluble in organic solvents than its isomer **2**.

Coordination *via* phosphorus also takes precedence over aryl group transfer in the reactions of compound **1** with transition metal complexes. Thus, from [$PtCl_2$(cod)] or [$PtR_2(\mu\text{-}SEt_2)]_2$ (R = Me, Ph) colourless platinum(II) complexes of general formula [PtR_2\{(*o*-$Ph_2PC_6H_4$)$_2$Hg\}] (R = Cl **7**, Me **8**, Ph **9**) are obtained, whose Pt–P coupling constants (3624, 1802 and 1592 Hz, respectively) indicate that **1** behaves as a *cis*-bidentate ligand. Complexes **8** and **9** also show well-resolved ^{195}Pt–^{199}Hg coupling in their ^{199}Hg NMR spectra.‡ In contrast, a single-crystal X-ray diffraction study§ of the yellow complex [$PdCl_2$\{(*o*-$Ph_2PC_6H_4$)$_2$Hg\}] **10** isolated as a CH_2Cl_2 solvate from compound **1** and [$PdCl_2(SEt_2)_2$] shows the $PdCl_2$ unit to be coordinated in an only slightly distorted planar array by mutually *trans*-phosphorus atoms (Fig. 1). The coordination geometry about mercury is close to linear and the Pd–P, Pd–Cl and Hg–C distances are normal, but the atomic arrangement imposes a close contact between the metal centres, their separation [2.8797(8) Å] being only slightly greater than the sum of the covalent radii of Pd and Hg (2.77 Å). Similar distances have been reported in platinum(II) complexes that are believed to contain a $Pt^{II}\rightarrow Hg^{II}$ donor interaction,[16] *e.g.* [Pt\{$CH_2C_6H_4P$(*o*-MeC_6H_4)$_2$\}(S_2CNMe)HgI(μ-I)]$_2$ [2.768(1) Å].[17] In its geometrical features ligand **1** resembles ferrocene-1,1′-diylbis(diphenylphosphine), Fe(η^5-$C_5H_4PPh_2$)$_2$ **11**, which behaves as a *trans*-spanning ligand in the complex [Pd(PPh_3)\{(η^5-$C_5H_4PPh_2$)$_2$Fe\}](BF_4)$_2$.[18] In contrast to **1**, however, **11** adopts a *cis*-bidentate mode in its $PdCl_2$ complex.[19]

The initially formed P-donor complexes of ligand **1** can behave as precursors either for coupling or transfer of *o*-$C_6H_4PPh_2$ groups. For example, reaction of [Pd(dba)$_2$] with **1** in a 1 : 2 molar ratio gives an orange, crystalline, trimetallic palladium(0)–mercury(II) complex [Pd\{(*o*-$Ph_2PC_6H_4$)$_2$Hg\}$_2$] **12**, whose precise structure as a solid and in solution remains to

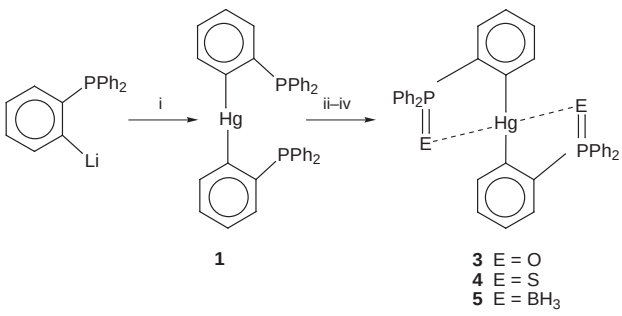

Scheme 1 *Reagents*: i, $HgCl_2$ (0.5 equiv); ii, H_2O_2; iii, S; iv, BH_3SMe_2.

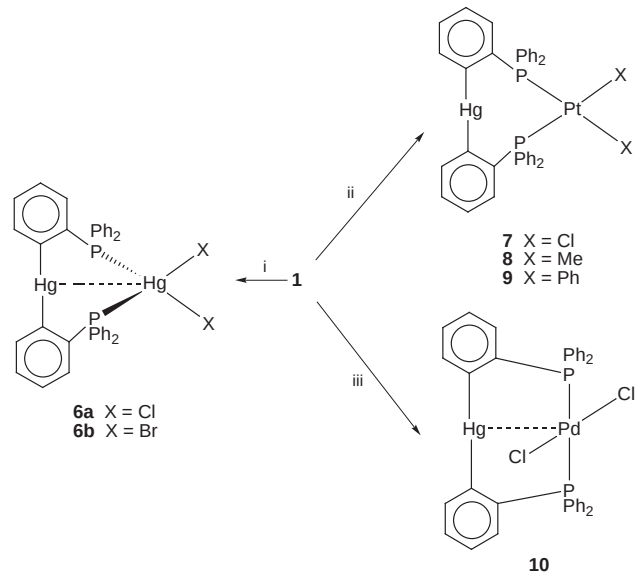

Scheme 2 *Reagents* (1 : 1 ratio in all cases): i, HgX_2 (X = Cl, Br); ii, [PtX_2L_2] (X = Cl, L_2 = cod; X = Me, Ph, L = SEt_2); iii, [$PdCl_2(SEt_2)_2$].

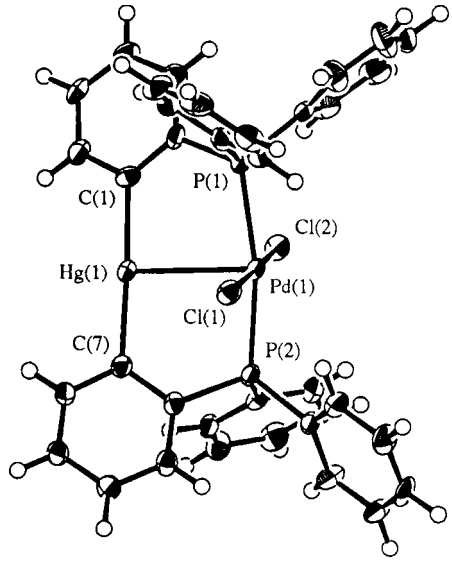

Fig. 1 ORTEP (50%) representation of **10**. Important bond lengths (Å) and angles (°): Pd(1)–Hg(1) 2.8797(8), Pd(1)–Cl(1) 2.308(2), Pd(1)–Cl(2) 2.296(2), Pd(1)–P(1) 2.356(3), Pd(1)–P(2) 2.335(3), Hg(1)–C(1) 2.094(9), Hg(1)–C(7) 2.096(9), C(1)–Hg(1)–C(7) 177.5(4), P(1)–Pd–P(2) 168.45(9), Cl(1)–Pd(1)–Cl(2) 176.75(9).

be established. In refluxing toluene, complex **12** eliminates metallic palladium and mercury, and the coupled product 2,2′-biphenyldiylbis(diphenylphosphine), *o*-$Ph_2PC_6H_4C_6H_4PPh_2$-*o* **13**,[11,20] can be isolated in 60% yield. A similar C–C bond coupling by reductive elimination occurs in the isomerisation of the digold(II) complexes $Au_2X_2(\mu$-*o*-$C_6H_4PPh_2)_2$ (X = Cl, Br, I) and Au_2X_2(*o*-$Ph_2PC_6H_4C_6H_4PPh_2$-*o*),[11] although in this case the ligand remains in the coordination sphere. Reaction of **1** with *trans*-[$PtHCl(PPr^i_3)_2$] in hot toluene gives the monomeric cycloplatinated complex [$PtCl$(*o*-$C_6H_4PPh_2)(PPr^i_3)$] **14**, again with elimination of mercury; the presumed P-donor precursor cannot be detected or isolated.

The coordination chemistry of [Hg(*o*-$C_6H_4PPh_2)_2$] and transfer reactions of *o*-$C_6H_4PPh_2$ to other transition metals are being investigated. We thank the Universidad Pública de Navarra (Spain) for a postdoctoral grant to M. C.

Notes and references

† Data describing full experimental details and analytical data for **12** are available as electronic supplementary information (http://www.rsc.org/suppdata/cc/1998/2401).

‡ *Selected NMR data* for compounds **1–3**, **6a**, **7–10**, **12–14** at 23 °C in CD_2Cl_2, except where stated; $^{31}P\{^1H\}$ NMR spectra at 80.96 MHz, $^{199}Hg\{^1H\}$ NMR spectra at 89.40 MHz referred to neat [$Hg(CH_3)_2$] (**CAUTION**: extremely toxic and volatile); coupling constants in Hz; reported peak multiplicities omit satellites except for the ^{199}Hg resonances of **8** and **9**: **1**: δ_P 0.38 [s, ^3J(HgP) 212], δ_{Hg} [470 t, ^3J(HgP) 214]. **2**: δ_P (DMSO) 29.7 [s, ^1J(HgP) 4798]. **3**: δ_P 31.7 [s, ^3J(HgP) 148], δ_{Hg} −750 [t, ^3J(HgP) 147]. **6a**: δ_P (DMSO) 30.5 [br s, ^1J(HgP) 4835, ^3J(HgP) 554]. **7**: δ_P (DMSO) 15.5 [s, ^1J(PtP) 3624, ^3J(HgP) 320]. **8**: δ_P 24.6 [s, ^1J(PtP) 1802, ^3J(HgP) 241], δ_{Hg} −418 [7-line m, ^3J(HgP) 244, ^4J(HgPt) 220]. **9**: δ_P 18.1 [s, ^1J(PtP) 1592, ^3J(HgP) 264], δ_{Hg} −400 [7-line m, ^3J(HgP) 268, ^4J(HgPt) 280]. **10**: δ_P 19.1 [s, ^3J(HgP) 260], δ_{Hg} −619 [t, ^3J(HgP) 259]. **12**: δ_P (C_6D_6) 14.2 (br s). **13**: δ_P −13.0 (s). **14**: δ_P (C_6D_6) 38.0, −64.8 [ABq, ^2J(PP) 425, ^1J(PtP) 2943, 2064].

§ *Crystal data and data collection parameters for* **10**: $C_{36}H_{28}Cl_2HgP_2Pd\cdot CH_2Cl_2$, M = 985.39, yellow needle, crystal size 0.32 × 0.12 × 0.06 mm, monoclinic, space group $P2_1/c$ (no. 14), a = 11.684(1), b = 25.135(2), c = 12.036(2) Å, β = 93.66(1)°, U = 3527.5(8) Å^3, Z = 4, D_c = 1.855 g cm^{-3}, μ(Cu-Kα) = 151.77 cm^{-1}, F(000) = 1940, analytical absorption correction; 5399 unique data ($2\theta_{max}$ = 120.1°), 4278 with $I > 3\sigma(I)$, R = 0.045, wR = 0.051, GOF = 2.42. CCDC 182/1043.

1 I. Omae, *Coord. Chem. Rev.*, 1980, **32**, 235; *Organometallic Intramolecular-Coordination Compounds*, *J. Organomet. Chem. Library No 18*, Elsevier, 1986, p. 154.
2 C. W. Bradford, R. S. Nyholm, G. J. Gainsford, J. M. Guss, P. R. Ireland and R. Mason, *J. Chem. Soc., Chem. Commun.*, 1972, 87; G. J. Gainsford, J. M. Guss, P. R. Ireland, R. Mason, C. W. Bradford and R. S. Nyholm, *J. Organomet. Chem*., 1972, **40**, C70.
3 M. I. Bruce, G. Shaw and F. G. A. Stone, *J. Chem. Soc., Dalton Trans.*, 1972, 2094.
4 A. K. Chakravarty, F. A. Cotton and D. A. Tocher, *Inorg. Chem.*, 1984, **23**, 4697; A. K. Chakravarty, F. A. Cotton, D. A. Tocher and J. H. Tocher, *Organometallics*, 1985, **4**, 8; F. A. Cotton and K. R. Dunbar, *J. Am. Chem. Soc.*, 1987, **109**, 2199; P. Lahuerta, J. Payá, X. Solans and M. A. Ubeda, *Inorg. Chem.*, 1992, **31**, 385; P. Lahuerta, J. Payá, M. A. Pellinghelli and A. Tiripicchio, *Inorg. Chem.*, 1992, **31**, 1224.
5 M. A. Bennett, D. E. Berry, T. Dirnberger, D. C. R. Hockless and E. Wenger, *J. Chem. Soc., Dalton Trans.*, 1998, 2367.
6 D. P. Arnold, M. A. Bennett, G. M. McLaughlin and G. B. Robertson, *J. Chem. Soc., Chem. Commun.*, 1982, 115.
7 G. Bruno, G. DeMunno, G. Tresoldi, S. Lo Schiavo and P. Piraino, *Inorg. Chem.*, 1992, **31**, 1538.
8 P. Lahuerta, J. Latorre, R. Martinez-Mánez and F. Sanz, *J. Organomet. Chem.*, 1988, **356**, 355.
9 A. M. Arif, F. Estevan, A. García-Bernabé, P. Lahuerta, M. Sanaú and M. A. Ubeda, *Inorg. Chem.*, 1997, **36**, 6472.
10 M. A. Bennett, D. E. Berry, S. K. Bhargava, E. J. Ditzel, G. B. Robertson and A. C. Willis, *J . Chem. Soc., Chem. Commun.*, 1987, 1613.
11 M. A. Bennett, S. K. Bhargava, D. C. R. Hockless, L. L. Welling and A. C. Willis, *J. Am. Chem. Soc.*, 1996, **118**, 10469.
12 R. J. Cross and R. Wardle, *J. Chem. Soc. A*, 1970, 840; G. K. Anderson, *Organometallics*, 1983, **2**, 665.
13 J. Vicente, J. A. Abad, F. Teruel and J. García, *J. Organomet. Chem.*, 1988, **345**, 233, and refs. cited therein.
14 V. I. Sokolov and O. A. Reutov, *Coord. Chem. Rev.*, 1978, **27**, 89.
15 R. J. Cross and N. H. Tennent, *J. Organomet. Chem.*, 1974, **72**, 21; A. F. M. J. van der Ploeg, G. van Koten and K. Vrieze, *J. Organomet. Chem.*, 1981, **222**, 155; E. Wehman, G. van Koten, J. H. Jastrzelski, H. Ossor and M. Pfeffer, *J. Chem. Soc., Dalton Trans.*, 1988, 2975; E. C. Constable, A. M. W. Cargill Thompson, T. A. Leese, D. G. F. Reese and D. A. Tocher, *Inorg. Chim. Acta*, 1991, **182**, 93.
16 A. F. M. J. van der Ploeg, G. van Koten, K. Vrieze, A. L. Spek and A. J. M. Duisenberg, *Organometallics*, 1982, **1**, 1066; M. Krumm, E. Zangrando, L. Randaccio, S. Menzer, A Danzmann, D. Holtenreich and B. Lippert, *Inorg. Chem*., 1993, **32**, 2183.
17 L. R. Falvello, J. Forniés, A. Martin, R. Navarro, V. Sicilia and P. Villarroya, *Inorg. Chem.*, 1997, **36**, 6166.
18 M. Sato, H. Shigeta, M. Sekino and S. Akabori, *J. Organomet. Chem.*, 1993, **458**, 199.
19 T. Hayashi, M. Konishi, Y. Kobori, M. Kumada, T. Higuchi and K. Hirotsu, *J. Am. Chem. Soc.*, 1984, **106**, 158.
20 O. Desponds and M. Schlosser, *J. Organomet. Chem*., 1996, **507**, 257.

Communication 8/06494F

Electrochemical synthesis and structural characterization of the trinuclear copper(I)–copper(II) complex: bis[bis(triphenylphosphine)copper(I)] [bis(thiosalicylate)copper(II)]

Raymond C. Bott,[a] Peter C. Healy*[a] and Dalius S. Sagatys[b]

[a] *School of Science, Griffith University, Brisbane, Queensland 4111 Australia. E-mail: P.Healy@sct.gu.edu.au*
[b] *School of Physical Science, Queensland University of Technology, Brisbane, Queensland, 4000, Australia*

Received (in Cambridge) 2nd September 1998, Accepted 2nd October 1998

A novel, symmetrical trinuclear copper(I)–copper(II) complex, bis[bis(triphenylphosphine)copper(I)][bis(thiosalicylate)copper(II)], [{Cu(PPh$_3$)$_2$}$_2${Cu(C$_7$H$_4$O$_2$S)$_2$}], has been prepared by anodic dissolution of copper into a solution of triphenylphosphine and thiosalicylic acid in acetonitrile and characterized by single crystal X-ray structure determination as its acetonitrile solvate; characterized also is the 1 : 3 copper(I) complex, [tris(triphenylphosphine)(thiosalicylic acid-*S*)copper(I)], formed as an intermediate in the electrosynthesis.

In our ongoing studies on the synthesis, structural and spectroscopic characterization of the adducts of triphenylphosphine with copper(I) carboxylates, [Cu(PPh$_3$)$_n$(O$_2$CR)],[1,2] we have been investigating the feasibility of preparing the compounds by anodic dissolution of copper into an acetonitrile solution of RCO$_2$H and PPh$_3$ with concomitant reduction of the acidic protons to hydrogen gas at a platinum cathode [eqn. (1)].

$$\mathrm{Cu} + n\mathrm{PPh_3} + \mathrm{RCO_2H} \rightarrow [\mathrm{Cu(PPh_3)}_n\mathrm{(O_2CR)}] + 1/2\mathrm{H_2} \quad (1)$$

As part of this work, we recently turned our attention to the reaction with thiosalicylic acid in order to ascertain the effects on the products obtained due to the presence of the thiol group *ortho* to the carboxylic acid. Initial electrolysis† resulted in the deposition of colourless crystalline material which was shown by X-ray structure determination‡ to be the acetonitrile solvated [tris(triphenylphosphine)(thiosalicylic acid-*S*)copper(I)] complex [Cu(PPh$_3$)$_3$(C$_7$H$_5$O$_2$S)]·MeCN **1** with a four-coordinate distorted tetrahedral CuP$_3$S copper coordination sphere (Fig. 1).

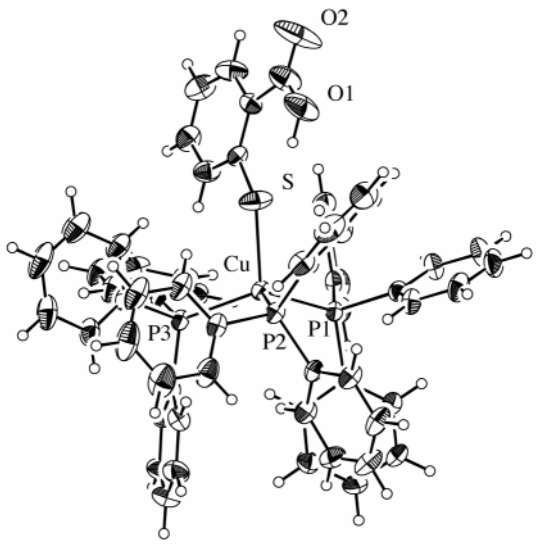

Fig. 1 View of the molecular structure of **1**. Copper coordination sphere: Cu–S 2.369(1), Cu–P(n) 2.367(2), 2.345(2), 2.362(2) Å; S–Cu–P(n) 110.71(7), 96.06(5), 108.94(8)°, P(*n*)–Cu–P(*n* + 1) 109.68(6), 112.02(6), 117.37(5)°. Carboxylate: C–O(*n*) 1.34(1), 1.197(8) Å.

In this complex the carboxylic acid proton forms a strong internal hydrogen bond (O–H···S 1.91 Å) between the oxygen and sulfur atoms. This result is reflected in the IR spectrum of the complex which shows a broad absorption band centred at 2540 cm^{-1} and ascribed to the hydrogen-bonded O–H stretching vibration, together with a moderately strong carbonyl vibration at 1703 cm^{-1}. Continued electrolysis resulted in change in colour of the solution from pale yellow to pale green and then to a darker green during which time crystals of **1** redissolved and new deep green–black crystals slowly formed in their place. The broad absorption band at 2540 cm^{-1} was absent from the IR spectrum of this compound and the band at 1703 cm^{-1} was replaced by two bands at 1620 and 1434 cm^{-1} assignable to asymmetric and symmetric carboxylate stretching vibrations with the difference in wavenumbers indicative of unidentate coordination.[3] This complex was shown by X-ray structure determination to be the acetonitrile solvate of a trinuclear copper(I)–copper(II) complex, bis[bis(triphenylphosphine)copper(I)] [bis(thiosalicylate-*O*, *S*)copper(II)] [{Cu(PPh$_3$)$_2$}$_2${Cu(C$_7$H$_4$O$_2$S)$_2$}]·MeCN **2**. Here we report a description of the structural characteristics of this unusual and interesting compound.

The structure determination shows **2** to crystallize as discrete neutral molecules with one acetonitrile molecule of solvation. Views of the molecule in Figs. 2(a) and 2(b) reveal a symmetrical cylindrical topology built about a central axis defined by the three copper atoms with approximately $D_{\infty h}$ local symmetry. The stoichiometry of the molecule and the coordination geometries about the coppers are consistent with oxidation states of +2 for the central and +1 for the two peripheral coppers. The phenyl groups on the triphenylphosphine and thiosalicylate ligands form a hydrophobic surface to the molecule which encapsulates the P$_2$CuO$_2$CuS$_2$CuP$_2$ core. The respective CuP$_2$, CuO$_2$, CuS$_2$ and CuP$_2$ planes spiral around the central copper axis with dihedral angles that appear to be determined primarily by C–H···π interactions between the phenyl groups [Fig. 2(b)]. The dianionic thiosalicylate ligands coordinate to the central copper(II) atom as bidentate ligands to give a *cis* S$_2$O$_2$ distorted square planar coordination sphere (Fig. 3). The S–Cu–S, O–Cu–O and *cis* S–Cu–O angles range from 86.2(3) to 99.7(1)° while the *trans* S–Cu–O angles are 148.1(2) and 149.0(2)°. The sulfur and oxygen atoms also function as bridging ligands between the copper(II) and copper(I) sites with the Cu(II)–S and Cu(II)–O bonds both *ca.* 0.2 Å shorter than the Cu(I)–S and Cu(I)–O bonds. The PPh$_3$ ligands coordinated to the copper(I) sites each adopt a distorted three-bladed propellor type conformation of the same chirality with each pair of ligands eclipsed with respect to each other and related by an approximate twofold rotation axis bisecting the P–Cu–P angle. We have shown previously that the transition from oxygen donor atoms in [Cu(PPh$_3$)$_2$(O$_2$CPh)] to sulfur donor atoms in the isomorphous [Cu(PPh$_3$)$_2$(S$_2$CPh)] complex results in an increase in the Cu–P distances and a decrease in the P–Cu–P angle, these variations being justified on the grounds of the greater covalency of Cu–S bonds compared to Cu–O bonds.[2] No such trends in the Cu–P bond lengths are apparent for the

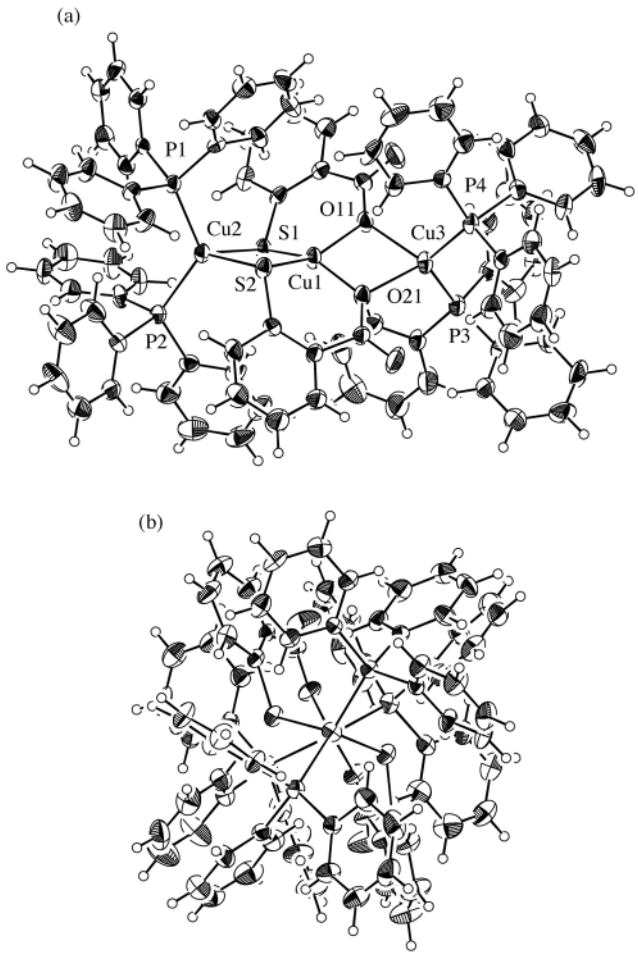

Fig. 2 View of the molecular structure of **2** (a) along and (b) down the Cu···Cu···Cu axis. Copper (II) coordination sphere: Cu(1)–O(*n*1) 1.97(1), 1.94(1) Å, Cu(1)–S(*n*) 2.196(3), 2.208(3) Å, S(1)–Cu(1)–S(2) 99.7(1)°, O(11)–Cu–O(21) 86.2(3)°; S-Cu(1)–O 148.1(2), 149.0(2), 96.4(2) and 93.6(2)°. Copper(I) P_2S_2 coordination sphere: Cu(2)–P(*n*) 2.257(3), 2.258(3), Cu(2)–S(n) 2.451(3), 2.396(3) Å; P(1)–Cu(2)–P(2) 125.0(1)°, S(1)–Cu(2)–S(2) 88.0(1)°. Copper(I) P_2O_2 coordination sphere: Cu(3)–P(n) 2.254(4), 2.229(3) Å, Cu(3)–O(*n*1) 2.20(1), 2.18(1) Å, P(3)–Cu(3)–P(4) 120.4(1)°, O(11)–Cu(3)–O(21) 75.1(2)°. Cu_3 geometry: Cu(1)···Cu(2), 3.159(2), Cu(1)···Cu(3), 3.160(2) Å, Cu(1)–Cu(2)–Cu(3), 178.90(6)°.

present molecule while the P–Cu–P angle of 125.0(1)° for the P_2CuS_2 site is, in fact, greater than the value of 120.4(1)° for the P_2CuO_2 site.

Compound **2** is a new and unusual member of an interesting class of polynuclear adducts between $[M(PPh_3)_2]^+$ (M = Cu, Ag) and anionic metal complexes that were prepared over 20 years ago by Coucouvanis and coworkers by the reaction of $[MX(PPh_3)_2]$ with salts of dianionic metal dithiolate complexes (*e.g.* refs. 4 and 5). The electrochemical synthesis used in the present study provides a new, uncomplicated approach to the preparation of this type of complex with the advantage that prior

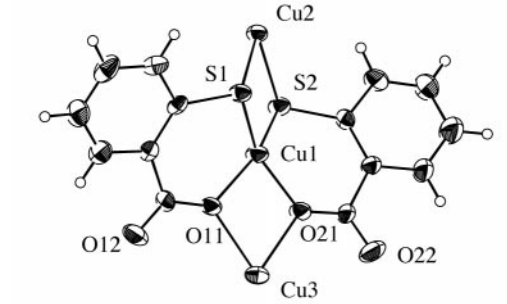

Fig. 3 View of the coordination sphere about the copper(II) atom.

synthesis of the parent dianionic copper(II) complex is not required. In addition, the formation of crystalline products from the reaction mixtures is favoured by the very slow rate of dissolution of the metal as a result of the inherently low concentration of ionic species in the solution.

Notes and references

† *Experimental details*: electrosynthesis. A copper anode and platinum coil cathode were inserted into a solution of 0.154 g (0.001 mol) of thiosalicylic acid (TSA) and 1.05 g (0.004 mol) of triphenylphosphine in 80 ml acetonitrile. Potentiostatic oxidation of the copper anode at 5 V resulted in the colourless solution initially turning a pale and then deeper shade of yellow. After 6–7 h compound **1** crystallized from the solution as large colourless blocky crystals (yield 0.6 g). After electrolysis for *ca.* 15 h, the solution changed to pale green and then to a darker green. During this time some of the crystals of **1** re-dissolved and deep green–black crystalline material (**2**) slowly formed (yield 0.2 g). Repetition of the experiment with PPh_3 to TSA mole ratios ranging from 2 : 1 to 5 : 1 resulted in the synthesis proceeding as above with only variations in the amount of **1** isolated.

Microanalysis: **1.** Found: C, 72.4; H, 5.1; N, 1.3. $C_{63}H_{53}CuNO_2P_3S$ requires C, 72.4; H, 5.1; N, 1.3%. **2.** Found: C, 66.8; H, 4.4; N, 0.5. $C_{88}H_{71}Cu_3O_4NP_4S_2$ requires C, 66.7; H, 4.5; N, 0.9 %.

‡ *Crystal data*: $C_{63}H_{53}CuNO_2P_3S$, **1**: M = 1044.6, triclinic, space group $P\bar{1}$ (C_2^2 no. 2), a = 13.11(1), b = 19.41(3), c = 12.72(1) Å, α = 97.9(1), β = 115.87(5), γ = 104.1(1)°, U = 2713 Å^3, Z = 2, μ (Mo-Kα) = 5.74 cm^{-1}, T = 295 K, N = 9576, N_o [$I > 3\sigma(I)$] = 5006; R = 0.044, R_w = 0.054.

$C_{88}H_{71}Cu_3O_4NP_4S_2$ **2**: M = 1585.2, triclinic, space group $P\bar{1}$, a = 13.017(2), b = 13.642(1), c = 22.475(2) Å, α = 97.915(8), β = 101.929(9), γ = 100.666(4)°, U = 3772 Å^3, Z = 2, μ(Mo-Kα) = 10.3 cm^{-1}, T = 295 K, N = 13257, N_o [$I > 3\sigma(I)$] = 5904; R = 0.061, R_w = 0.045.

§ We thank Karl Byriel, University of Queensland, for collection of the X-ray data set for compound **2**.

1 R. D. Hart, P. C. Healy, G. A. Hope, D. W. Turner and A. H. White, *J. Chem. Soc., Dalton Trans.*, 1994, 773.
2 R. D. Hart, P. C. Healy, M. L. Peake and A. H. White, *Aust. J. Chem.*, 1997, **51**, 67.
3 K. Nakamoto, *Infrared and Raman Spectra of Inorganic and Coordination Compounds*, John Wiley and Sons, 4th edn., New York, 1986.
4 M. L. Caffery and D. Coucouvanis, *J. Inorg. Nucl. Chem.*, 1975, **37**, 2081.
5 F. J. Hollander, Y. L. Ip and D. Coucouvanis, *Inorg. Chem.*, 1976, **15**, 2230.

Communication 8/06813E

Masked allylic zinc reagents

Philip Jones, Nicolas Millot and Paul Knochel*

Fachbereich Chemie der Universität, Hans-Meerwein Strasse, D-35032 Marburg, Germany.
E-mail: knochel@ps1515.chemie.uni-marburg.de

Received (in Liverpool, UK) 29th July 1998, Accepted 22nd September 1998

The preparation of allylic zinc reagents using the fragmentation of sterically hindered tertiary homoallylic alcohols is described

The development and use of allylic organometallic reagents in synthesis has been an underlying theme of modern organic synthesis.[1,2] Despite the plethora of methods currently available for the introduction of allylic moieties into complex molecules several problems remain, most notably that of cross contamination of the product with the Wurtz coupling adduct. Secondly, there are the problems associated with generating stoichiometric amounts of inorganic salts and thirdly, the functionally group tolerance of the reagent due to the highly polar nature of most carbon–metal bonds.

There are several reports in the literature that the addition of allylic organometallics to electrophiles is reversible;[3–6] in particular one report by Miginiac has inspired us.[5a] Therefore it was rationalised that generation of a zinc alkoxide of a sterically hindered tertiary allyl alcohol would result in decomposition to the parent ketone and an allyl zinc reagent, which in the presence of a suitable electrophile could be utilised synthetically. Recently, Nokami has described a related allyl transfer reaction of homoallylic alcohols catalysed by tin(II) triflate which has caused us to disclose our results.[7]

Accordingly a series of tertiary homallylic alcohols **1a**,**b** were prepared. Treatment of the tertiary alcohol bearing two isopropyl groups **1a** first with Bu^{n}Li and then with zinc bromide gave the zinc alkoxide. At room temperature no migration of the allyl group was observed in the presence of benzaldehyde, but after heating at reflux for 6 h the benzylic alcohol **2** could be isolated in 70% yield (Scheme 1). Clearly, as hypothesised the zinc alkoxide had fragmented *in situ* to give an allyl zinc reagent. The reaction could be improved by the addition of a polar co-solvent; after 6 h in a THF–HMPA mixture 98% of the secondary alcohol **2** was observed. Increasing the steric congestion around the zinc alkoxide also resulted in a faster reaction; by using two *tert*-butyl groups **1b** the migration was complete within 1 h at room temperature, resulting in 89% isolated yield of the secondary alcohol **2**.† In both cases, control experiments with lithium and magnesium alkoxides in the absence of zinc salts showed no migration of the allyl group.

Inspired by this reaction the compatibility of these reagents with a range of aldehydes and ketones was investigated (Table 1). Treatment of the zinc alkoxide with heptanal gave dec-1-en-4-ol in 83% yield (entry 1), whilst an α,β-unsaturated aldehyde was also tolerated (entry 2), giving exclusively the 1,2-addition product in 84% yield. In a similar manner, aldehydes bearing an α-substituent reacted well, within 2 h at room temperature, to give the desired allylated product in good yields (entries 3 and 4). Transfer of the allyl group to a ketone required slightly longer reaction times, the reaction usually taking between 2 and 4 h at room temperature to go to completion. Reaction with cyclohexanone gave the allylated adduct in 82% (entry 5), while α,β-unsaturated ketones gave the desired products in reasonable yields (entries 6 and 7). α-Tetralone also reacted well to give the desired material in excellent yield (entry 8).

The reaction is not just limited to carbonyl compounds. It was discovered that nitriles also react well to give β,γ-unsaturated ketones in good yields (Scheme 2). Generation of the zinc alkoxide as previously and addition of the nitrile generates the corresponding imine, which upon hydrolysis liberates the ketones **3a–c** in good yield; both aromatic and enolisable nitriles reacted well.

β,γ-Unsaturated amines can also be prepared using these masked organozinc reagents through reaction with imines (Scheme 3). Addition of Bu^{n}Li and then zinc chloride to a solution of the tertiary allyl alcohol **1b** in THF generates the

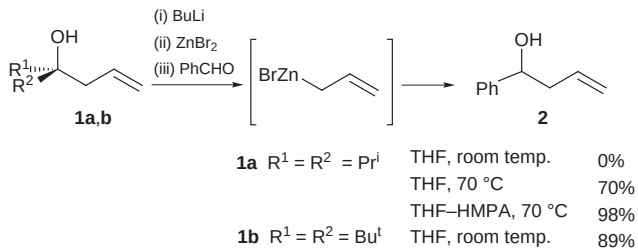

Scheme 1

Table 1 Reaction of masked organozinc reagent **1b** with carbonyl compounds

Entry	Electrophile	Product	Yield (%)[a]
1	$C_6H_{13}CHO$	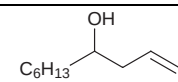	83
2	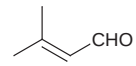	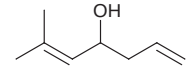	84
3	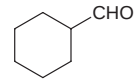	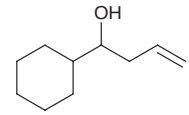	82
4	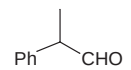	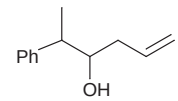	85[b]
5	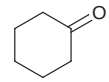	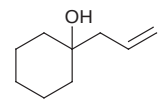	82
6	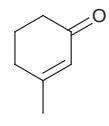	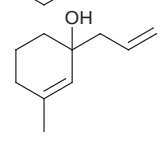	74
7	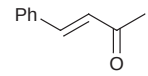	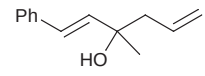	73
8	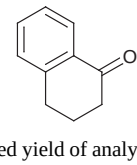	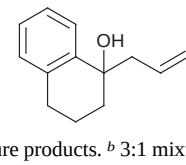	99

[a] Isolated yield of analytically pure products. [b] 3:1 mixture of *erythro*:*threo* isomers.

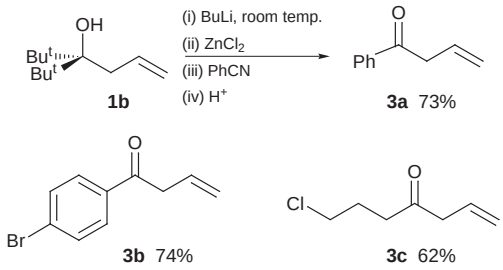

Scheme 2

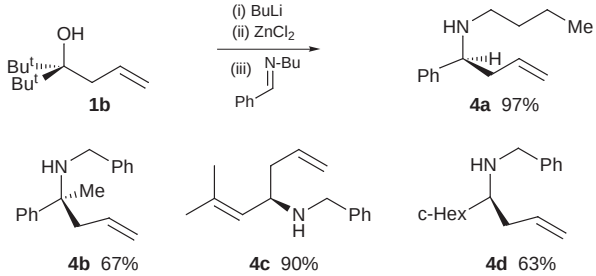

Scheme 3

zinc alkoxide that fragments in a retro-allylation reaction to give the allylzinc reagent *in situ*; in turn this reacts with benzylidenebutylamine to give the secondary amine **4a** in 97% yield. Reaction with benzyl(1-phenylethylidene)amine generates **4b** in 67% yield, whilst the α,β-unsaturated imine, benzyl(3-methylbut-2-enylidene)amine, reacts to give amine **4c** in 90% yield. The α-substituted imine benzyl(cyclohexyl)methyleneamine also reacted in 63% yield to give **4d**.

Carbozincation reactions are also possible using this approach with masked organozinc reagents, indeed reaction of the zinc alkoxide with trimethyl(prop-2-ynyloxy)silane at room temperature gives, within 2 h, the 1,4-diene **5** in 74% yield after hydrolysis (Scheme 4).

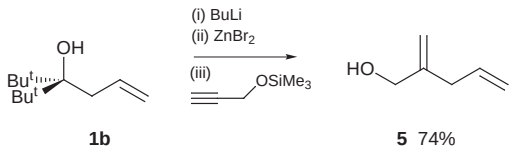

Scheme 4

Although we had eliminated the problems associated with Wurtz coupling, our reagents were not environmentally friendly, generating 1 equiv. of zinc waste; consequently we were delighted to discover that the reaction could be made to function using catalytic amounts of zinc salts—reduction to 50 mol% gave the benzylic alcohol **2** in 95% yield after 6 h, whilst further reductions to 10 mol% gave no loss in efficiency, with the secondary alcohol being isolated in 92%, again within 6 h (Scheme 5). However, all efforts to make the reaction catalytic in base have to date been unsuccessful.

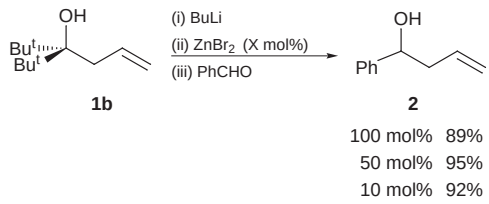

Scheme 5

A further advantage with this concept is the ability of these reagents to tolerate functional groups, in a similar manner to other organozinc reagents.[8] The tertiary alcohols **6** and **7** were

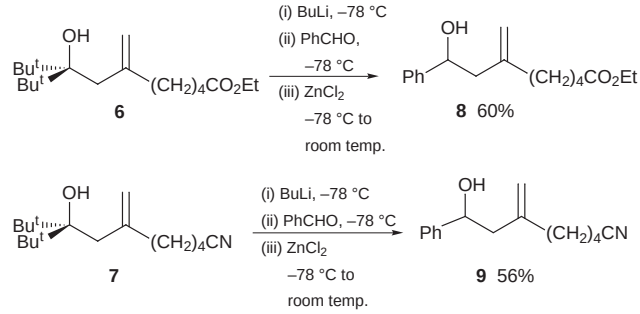

Scheme 6

prepared[9] and treated with BuLi, benzaldehyde and zinc chloride at −78 °C, followed by warming the reaction mixture to room temperature. This gave the desired hydroxy ester **8** and hydroxy nitrile **9** in 60 and 56% yields, respectively.

In summary, we have developed a method for the generation of allylic organozinc reagents by exploiting a retro-addition reaction. This method avoids entirely the problem of Wurtz coupling during formation of the organometallic reagent. The reaction is also very general and addition to a range of electrophiles is possible. The mild conditions associated with this reaction also make it compatible with a range of functional groups and finally the reaction has been shown to be catalytic in zinc salts.[10]

The authors thank the DFG (SFB 260 and Leibniz program) for generous financial support, and the Royal Society for an award (to P. J.) under the European Science Exchange Programme.

Notes and references

† Typical procedure: Preparation of 1-phenylbut-3-en-1-ol **2**: A solution of Bu^{n}Li (2.71 mmol) in pentane (1.40 M, 1.94 ml) was added dropwise over 2 min to a stirred solution of 3-*tert*-butyl-2,2-dimethylhex-5-en-3-ol **1b** (500 mg, 2.71 mmol) in THF (4 ml) at 0 °C under argon. The resulting solution was then stirred for 15 min and a solution of zinc bromide (610 mg, 2.71 mmol) in THF (2 ml) was added, followed by benzaldehyde (275 μl, 2.71 mmol). The reaction was allowed to warm to room temperature and stirred for 1 h. Saturated aq. NH_4Cl solution (15 ml) was added and the resulting mixture was extracted with Et_2O (3 × 15 ml). The combined organic extracts were washed with brine (10 ml), dried and concentrated under reduced pressure to give a crude residue, which was purified by column chromatography on silica using 15% Et_2O–hexanes as eluent to give the desired alcohol **2** (356 mg, 89%) as a colourless oil.

1 W. R. Roush, in *Comprehensive Organic Synthesis*, ed. B. M. Trost, I. Fleming and C. H. Heathcock, Pergamon, Oxford, 1991, vol. 2, pp. 1–53.
2 Y. Yamamoto and N. Asao, *Chem. Rev*., 1993, **93**, 2207.
3 For reaction of Grignard reagents see: R. A. Benkeser and M. P. Siklosi, *J. Org. Chem*., 1976, **41**, 3212; R. A Benkeser, M. P. Siklosi and E. C. Mozdzen, *J. Am. Chem. Soc*., 1978, **100**, 2134; R. A Benkeser, W. G. Young, W. E. Broxterman, D. A. Jones and S. J. Piaseczynski, *J. Am. Chem. Soc*., 1969, **91**, 132; F. Barbot and P. Miginiac, *Bull. Chim. Soc. Fr*., 1977, 113.
4 F. Gerard and P. Miginiac, *Bull. Chim. Soc. Fr*., 1974, 2527; F. Gerard and P. Miginiac, *Bull. Chim. Soc. Fr*., 1974, 1924.
5 (*a*) F. Barbot and P. Miginiac, *Tetrahedron Lett*., 1975, 3829; (*b*) P. Miginiac and C. Bouchoule, *Bull. Chim. Soc. Fr*., 1968, 4675; (*c*) F. Barbot and P. Miginiac, *J. Organomet. Chem*., 1977, **132**, 445.
6 For reversible addition to imines, see A. Bocoum, D. Savoia and A. Umani-Ronchi, *J. Chem. Soc., Chem. Commun*. 1993, 1542.
7 J. Nokami, K. Yoshizane, H. Matsuura and S. Sumida, *J. Am. Chem. Soc*., 1998, **120**, 6609.
8 P. Knochel, J. J. Almena Perea and P. Jones, *Tetrahedron*, 1998, **54**, 8275.
9 These reagents were prepared from 3-*tert*-butyl-2,2,5-trimethylhex-5-en-3-ol by NBS allylic bromination and displacement with the appropriate zinc-copper reagent (ref. 11).
10 A patent has been filed with Chemetall Gmbh (Frankfurt).
11 P. Knochel, M. C. P. Yeh, S. C. Berk and J. Talbert, *J. Org. Chem*., 1988, **53**, 2390.

Communication 8/05952G

Highly diastereoselective reactions using masked allylic zinc reagents

Philip Jones and Paul Knochel*

Fachbereich Chemie der Universität, Hans-Meerwein Strasse, D-35032 Marburg, Germany.
E-mail: knochel@ps1515.chemie.uni-marburg.de

Received (in Liverpool, UK) 29th July 1998, Accepted 22nd September 1998

Substituted allylic organozinc reagents have been prepared using a novel fragmentation reaction; the resulting allylic zinc species are configurationally stable and give excellent regio- and diastereo-selectivities.

We have recently documented an entirely new approach for the generation of allylic zinc reagents based on a retro-allylation, an allylation sequence starting from the sterically hindered tertiary alcohol **1** (Scheme 1).[1,2] Generation of the zinc alkoxide of this homoallylic alcohol results in fragmentation and formation of an allyl zinc reagent **2** *in situ*; this is itself able to react with a range of other electrophiles. This method avoids the problems associated with Wurtz coupling.

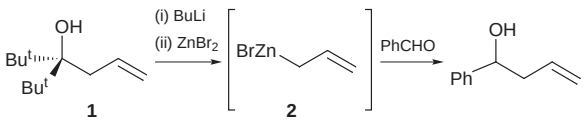

1 **2**

Scheme 1

Substituted allyl zinc reagents had previously been prepared by Tamura from allyl benzoates but with mixed results;[3] we hoped that our mild method would give improved selectivities.

Accordingly, the tertiary alcohol **3** bearing an α-methylallyl group was prepared (Scheme 2).[4] However, we were disappointed to find that upon deprotonation of this material at room temperature with BuLi a rapid isomerisation to the γ-substituted isomer **4** occurred.[5] Undeterred, the deprotonation was attempted at −78 °C, and we were pleased to find no isomerisation. Addition of benzaldehyde followed by a solution of zinc chloride gave within 1 h at −78 °C the benzylic alcohol **5** in 83% isolated yield.† More interestingly, the product was isolated as a 94:6 mixture of *anti*:*syn* diastereomers.[6] This reaction is in stark contrast to the addition of crotylzinc bromide to benzaldehyde, which gives approximately 1:1 mixtures of diastereomers.[7]

Inspired by this reaction, a range of aldehydes were screened (Fig. 1). Reaction of the homoallylic alcohol with cyclohexanecarbaldehyde gave the alcohol **6** in 84% yield, again with the *anti* diastereomer in excess (96:4). Similarly, reaction with 2-butylacrolein gave solely the product of 1,2-addition, giving the homoallylic alcohol **7** in 76% isolated yield as a 97:3 mixture of diastereomers. The reaction with 2-ethylbutyraldehyde and 1-naphthaldehyde gave the expected products **8** and **9** in 86 and 92% yields, respectively; in both cases only the

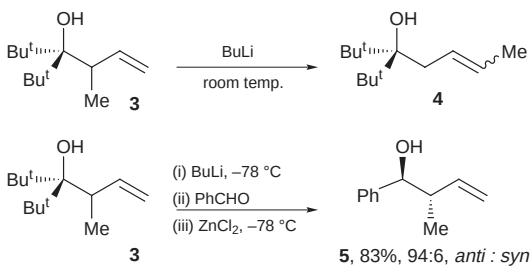

3 **4**

3 **5**, 83%, 94:6, *anti : syn*

Scheme 2

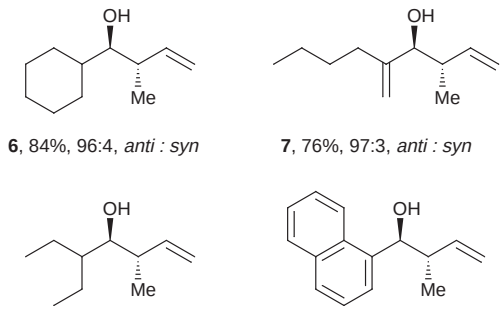

6, 84%, 96:4, *anti : syn* **7**, 76%, 97:3, *anti : syn*

8, 86%, >98:2, *anti : syn* **9**, 92%, >98:2, *anti : syn*

Fig. 1

anti-diastereomer was observed by ^{1}H and ^{13}C NMR spectroscopy. In all cases, none of the γ-substituted product was detected.

Similar results were obtained when we placed other substituents in the α-position. 3-(*tert*-Butyl)-2,2-dimethyl-4-ethylhex-5-en-3-ol **10** was prepared using identical chemistry as used in the preparation of homoallylic alcohol **3**.[4] This too was found to exhibit high levels of *anti*-selectivity. Reaction with BuLi, benzaldehyde and zinc chloride (Scheme 3) gave 2-ethyl-1-phenylbut-3-en-1-ol **11** in 91% as a 91:9 mixture of *anti*:*syn* isomers. Likewise, reaction with cyclohexanecarbaldehyde and 2-ethylbutyraldehyde gave rise to the homoallylic alcohols **12** and **13** in 83 and 81% yields, respectively, both solely as the *anti*-diastereomers.

Further synthetic investigation revealed that a benzyl group could easily be incorporated into the α-position of the homoallylic alcohol (Scheme 4). The precursor was readily prepared form 2, 2-dimethylhex-5-en-3-one **14** by deprotonation with LDA at −78 °C, followed by α-alkylation with BnBr in THF–HMPA in 65% yield. Subsequent reaction with Bu^{t}Li gave the required precursor **15** in 85% yield. As in all previous cases, deprotonation and reaction with benzaldehyde in the presence of zinc chloride gave the desired benzylic alcohol **16** in 89%, again with excellent diastereoselectivity (95:5). Aliphatic aldehydes also reacted well giving the homoallylic alcohols **17** and **18** in 88 and 80% yields, respectively.

Surprised by these results we were interested to investigate the outcome of placing substituents in the γ-position of the

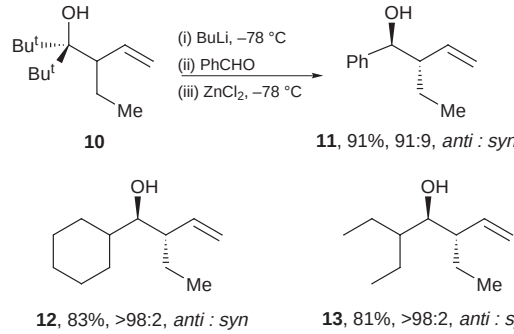

10 **11**, 91%, 91:9, *anti : syn*

12, 83%, >98:2, *anti : syn* **13**, 81%, >98:2, *anti : syn*

Scheme 3

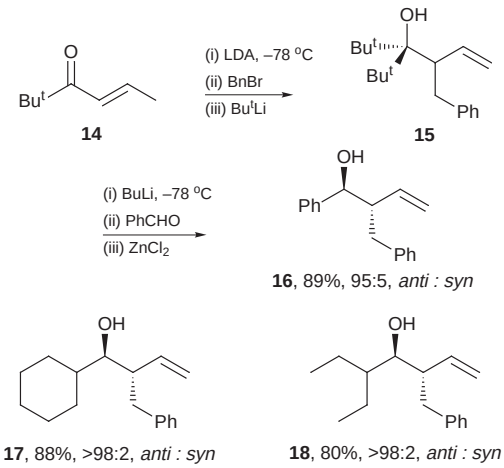

Scheme 4

allylic system. A new synthetic route needed to be adopted and oxirane **19** was prepared and opened with a variety of lithium acetylides to give the homopropargyl compounds **20a**,**b** in reasonable yields (84 and 65%) (Scheme 5). Hydrogenation with palladium on barium sulfate gave the *Z*-isomer **21** quantitatively, whilst treatment with $LiAlH_4$ gave the required *E*-isomer **22**. With these two compounds to hand the migration was investigated. The resulting zinc alkoxides were found to be less reactive. Whereas the α-substituted compounds migrated at −78 °C, these compounds required warming to room temperature before migration could be observed. With **21** migration occurred in 52% yield after 48 h (86% based on recovered starting material) to give the desired homoallylic alcohol **23**, while the *E*-isomer **22** gave the corresponding alcohol **24** in 23% yield after 12 h (87% based on recovered starting material). In both cases the products were isolated as 2:1 mixture of *Z*:*E* isomers. The γ-disubstituted compound **25** was also prepared; however, this compound proved to be stable and no migration was detected.

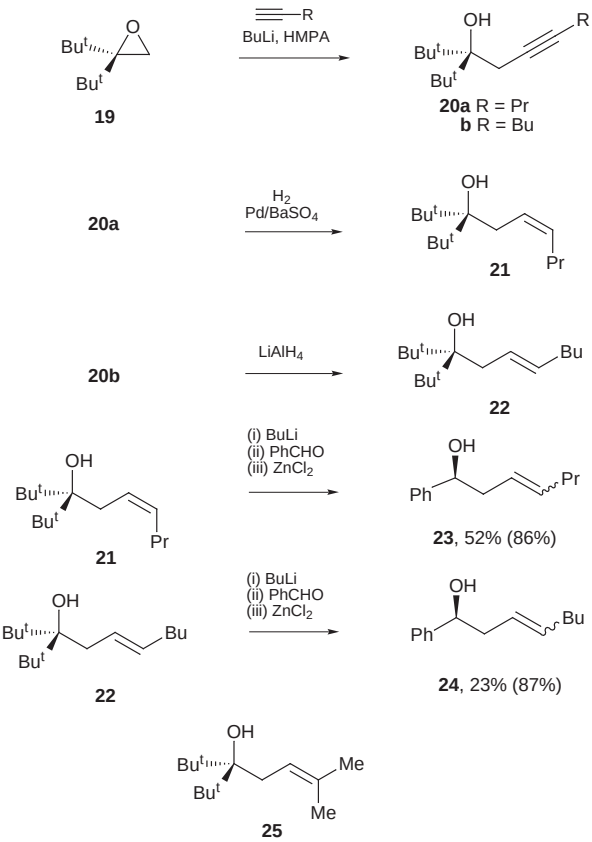

Scheme 5

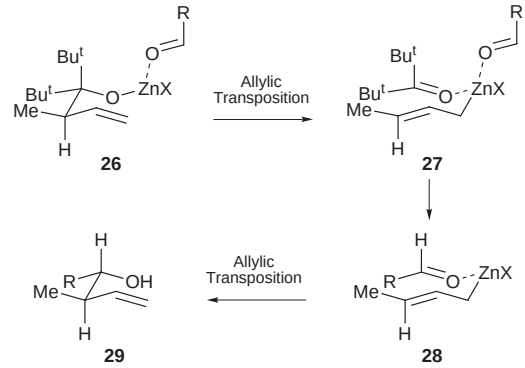

Scheme 6

These results suggest a plausible mechanism involving a double allylic transposition. Generation of the zinc alkoxide of the alcohol **26** results in a cyclic six-membered intermediate where the zinc is complexed to the reacting carbonyl compound (Scheme 6). Allylic transposition gives rise to a crotylzinc reagent **27** complexed to the parent bis(*tert*-butyl) ketone and the reaction partner, the zinc reagent bearing solely a *trans*-configuration. At −78 °C this species is stable and undergoes no isomerisation.[8] Owing to the complexation of the reacting partner with the zinc, a new six-centred intermediate **28** is possible, whereby all the substituents lie in equatorial positions; allylic transposition then gives rise to the product **29**, predominately as the *anti*-diastereomer. This mechanism is supported by the unreactive nature of the γ-substituted isomer, whereby steric congestion prevents the first allylic transposition from occurring.

In summary, we have developed a novel method for the preparation of substituted allylic zinc reagents. This method is extremely selective, giving both excellent regiochemical selectivity and excellent diastereoselectivity. The method is extremely mild and avoids Wurtz coupling products.[9]

The authors thank the DFG (SFB 260 and Leibniz program) for generous financial support, and the Royal Society for an award (to P. J.) under the European Science Exchange Programme.

Notes and references

† Typical procedure: *anti*-2-methyl-1-phenylbut-3-en-1-ol **5**: A solution of BuLi (2.52 mmol) in pentane (1.6 M, 1.58 ml) was added dropwise over 5 min to a stirred solution of 3-*tert*-butyl-2,2,4-trimethylhex-5-en-3-ol (ref. 4) **3** (500 mg, 2.52 mmol) in THF (4 ml) at −78 °C under argon. The resulting solution was then stirred for 15 min and benzaldehyde (256 μl, 2.52 mmol) was added and stirred for a further 15 min; finally a solution of zinc chloride (343 mg, 2.52 mmol) in THF (2 ml) was added over 3 min. The reaction was stirred at −78 °C for 1 h then allowed to warm to room temperature. The reaction was worked up as usual to give a crude residue, which was then purified by column chromatography on silica using 10% Et_2O–light petroleum as eluent to give the desired alcohol (ref. 10) **5** (341 mg, 83%) as a pale yellow oil.

1 Y. Yamamoto and N. Asao, *Chem. Rev*., 1993, **93**, 2207.
2 P. Jones, N. Millot and P. Knochel, *Chem. Commun*., 1998, 2405.
3 M. Shimizu, M. Kimura, S. Tanaka and Y. Tamaru, *Tetrahedron Lett.* 1998, **39**, 609 and references cited therein.
4 R. A. Benkeser, M. P. Siklosi and E. C. Mozdzen, *J. Am. Chem. Soc*., 1978, **100**, 2134.
5 F. Gérard and P. Miginiac, *Bull. Chim. Soc. Fr*., 1974, 2527; F. Barbot and P. Miginiac, *Bull. Chim. Soc. Fr*., 1977, 113.
6 All diastereomeric excesses were determined by ^1H NMR analysis.
7 S. R. Wilson and M. E. Guazzaroni, *J. Org. Chem*., 1989, **54**, 3087.
8 bis (3-Methylallyl)zinc is known to be a rapidly isomerising system at room temperature, hence explaining the 1:1 *anti*:*syn* selectivity in additions to aldehydes. R. Benn, E. G. Hoffmann, H. Lehmkuhl and H. Nehl, *J. Organomet. Chem*., 1978, **146**, 103.
9 A patent has been filed with Chemetall GmbH (Frankfurt).
10 S. Kobayashi and K. Nishio, *J. Org. Chem*., 1994, **59**, 6620.

Communication 8/05953E

Facile oxidation of a carbaporphyrin at the internal carbon atom: synthesis of novel benzo[18]annulene ketals†

Michael J. Hayes, John D. Spence and Timothy D. Lash*

Department of Chemistry, Illinois State University, Normal, Illinois 61790-4160, USA. E-mail: tdlash@ilstu.edu

Received (in Corvallis, OR, USA) 10th August 1998, Accepted 25th September 1998

Treatment of benzocarbaporphyrin 2 with refluxing $FeCl_3$ in $CHCl_3$–alcohol mixtures leads to a remarkably selective oxidation at the interior carbon atom to produce dialkoxy products 5; these species show potentially valuable long wavelength absorptions in their UV–VIS spectra.

The unbounded potential for porphyrins and related macrocycles in novel technological[1] and medicinal applications[2] has lead to widespread interest in the synthesis of related systems such as expanded porphyrins[3] and porphyrin isomers.[4] The recent rediscovery of the '3 + 1' route for porphyrinoid synthesis[5] has allowed the preparation of novel aromatic species where a carbocyclic subunit replaces one of the pyrrolic moieties of the porphyrin macrocycle.[6–9] The first example of a 'carbaporphyrinoid',‡ oxybenzoporphyrin **1**, was first reported

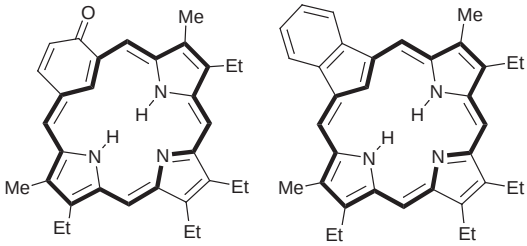

1 **2**

in 1995 and was obtained by the acid catalyzed condensation of a tripyrrane (2,5-bis[2-pyrrolylmethyl]pyrrole) with 4-hydroxyisophthalaldehyde.[6] Several related porphyrinoids were subsequently synthesized by the '3 + 1' approach.[7–9] Perhaps the most captivating of these new aromatic systems are the true carbaporphyrins[7,9] which incorporate a cyclopentadienyl unit instead of the usual pyrrole ring. Benzocarbaporphyrin **2** is particularly easy to synthesize by condensing a tripyrrane with 1,3-diformylindene[7] and thus provides a suitable 'work horse' molecule for further investigations.

In our initial studies on the chemistry of **2**, the possibility of forming metal chelates was explored. However, attempts to isolate stable metal complexes by reacting **2** with various transition metal salts [$Zn(OAc)_2$, $Cu(OAc)_2$, $Ni(OAc)_2$, $FeCl_2$, $CrCl_3$, *etc*.] has so far been unsuccessful. On the other hand, when a solution of **2** in $CHCl_3$ was refluxed with saturated $FeCl_3$ in MeOH, the mixture rapidly turned from a deep brown to a bright green color and a polar green species could be isolated, following chromatography, in high yield.§ No reaction was observed in control experiments in the absence of $FeCl_3$. FAB MS gave an [M + H] ion at *m/z* 560 and confirmed that no Fe^{III} had been incorporated into the structure. The proton NMR spectrum for the green material (Fig. 1) showed an upfield 6H singlet at $\delta -1.32$ while the *meso*-bridge protons were strongly deshielded appearing at δ 9.7 and 10.9. The data were consistent with a dimethyl ketal derivative **3** where the interior carbon

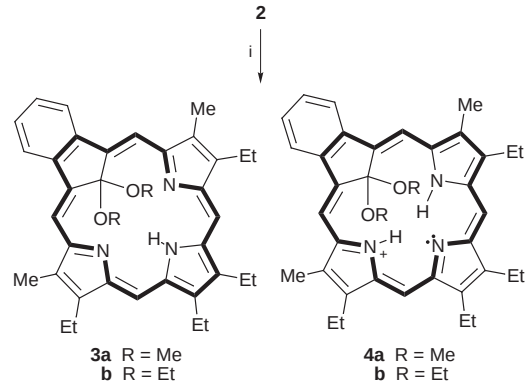

3a R = Me
b R = Et

4a R = Me
b R = Et

Scheme 1

atom has been regioselectively oxidized (Scheme 1). However, a closer examination of the ^{1}H NMR spectrum (Fig. 1) showed that a broad peak near δ 2.15 integrated for 2H and this was assigned to two strongly hydrogen bonded NHs, thereby implying that the isolated compound was in fact a monoprotonated species **4a**. Elemental analysis further confirmed that the isolated material corresponded to the monoHCl salt.§ Additional evidence for the ketal structure was provided by NOE difference proton NMR experiments, and it is particularly noteworthy that the internal NH resonance showed a strong NOE enhancement upon irradiation of the methoxy resonance at $\delta -1.32$. The ^{13}C NMR spectrum for **4a** in $CDCl_3$ confirmed the symmetry of the macrocyclic structure, showing the 19 anticipated carbon resonances. DEPT demonstrated the presence of a quaternary carbon atom at δ 96.9, which is consistent with the presence of an allylic ketal moiety.

We speculate that the regioselectivity for this chemistry may be due to the Fe^{III} being initially coordinated to the three pyrrolic nitrogens and thereby held in proximity to the inner carbon so that oxidation is directed towards this position. The aromaticity of this structure is maintained by reorganizing the 18π electron delocalization pathway through the fused benzene ring (pathway shown in bold) and in this respect **3a** can be

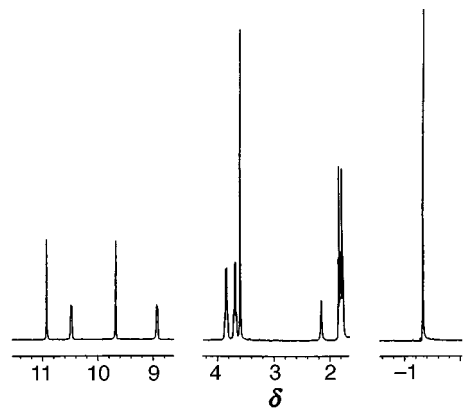

Fig. 1 400 MHz ^{1}H NMR spectrum of benzo[18]annulene **5a** in $CDCl_3$.

† Part 14 of the series 'Conjugated Macrocycles Related to the Porphyrins'. Part 13: T. D. Lash and D. T. Richter, *J. Am. Chem. Soc.*, 1998, **120**, 9965.

considered to be a benzo[18]annulene. Interestingly, benzo-[18]annulene **5** has been shown[10] to have a much reduced

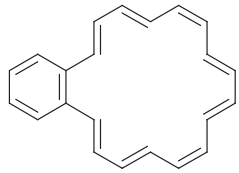

5

diatropic ring current compared to [18]annulene itself (the difference in chemical shift between the inner and outer protons in **5** is < 2 ppm), although this is clearly not the case for the porphyrinoid structure. Protonation is most likely highly favored due to the ability of the aromatic macrocycle to delocalize the positive charge and this factor may also explain the enhanced aromatic character of **4a** compared to benzo-[18]annulene (**5**). The monocation was essentially uneffected by using [$^2H_5$]pyridine as a solvent, although addition of the stronger base Et_3N lead to decomposition possibly due to the instability of the free base **3a**. Reaction of carbaporphyrin **2** with $FeCl_3$ in refluxing EtOH–$CHCl_3$, although significantly slower than for MeOH, gave excellent yields of the diethoxy species **4b**.§

The UV–VIS spectra for **4a** and **4b** showed strong Soret bands near 423 nm, together with strong Q bands in the far red at 748 and 828 nm in the case of **4a** (Fig. 2). Addition of 5% TFA lead to the formation of a new species due to protonation of the remaining nitrogen where the longer wavelength bands underwent a hypsochromic shift (Fig. 2). Porphyrinoids with strong absorption bands in the far visible–near IR are of great current interest and have possible applications in the development of solid state optical devices[1] and as photosensitizers in photodynamic therapy.[2]

The discovery of a straightforward and highly selective method for derivatizing the inner carbon atom of the carbaporphyrin system has great potential for future studies and it should

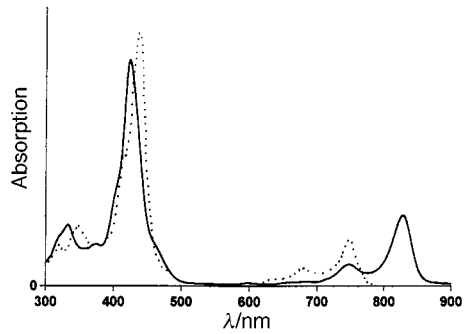

Fig. 2 Electronic absorption spectra of **5a** in $CHCl_3$ (bold line) and dication in 5% TFA–$CHCl_3$ (dotted line).

be possible to fine tune the physical properties of these novel chromophores by selecting other alcohols as reactants (*e.g.* long chain, dendritic). The versatility of this approach will also allow practical applications to be considered.

This work was supported by the National Science Foundation under Grant No. CHE-9732054, the Camille and Henry Dreyfus Scholar/Fellow Program and the Donors of the Petroleum Research Fund, administered by the American Chemical Society.

Notes and references

‡ Carbaporphyrinoids are defined as fully aromatic systems where one or more of the pyrrolyl units of the porphyrin structure have been replaced by a carbocyclic ring.

§ *Selected data* for **5a**: mp 145–147 °C (decomp.); $\lambda_{max}(CHCl_3)$/nm ($\log_{10}$ ε) 333 (4.55), 374 (4.40), 423 (5.12), 5.96 (3.28), 748 (4.10), 828 (4.61); λ_{max}(5% TFA–$CHCl_3$)/nm ($\log_{10}$ ε) 323 (4.37), 348 (4.54), 435 (5.17), 682 (4.06), 748 (4.44); $\delta_H(CDCl_3)$ −1.32 (6H, s, 2 × OCH_3), 1.77 (6H, t), 1.82 (6H, t) (4 × CH_2CH_3), 2.15 (2H, br s, 2 × NH), 3.60 (6H, s, 2 × porphyrin-CH_3), 3.69 (4H, q), 3.84 (4H, q) (4 × porphyrin-CH_2), 8.93 (2H, m) and 10.48 (2H, m) (4 × benzo-H), 9.68 (2H, s) and 10.93 (2H, s) (4 × *meso*-H); $\delta_C(CDCl_3)$ 11.68, 17.29, 18.38, 19.50, 19.60, 47.95, 96.89, 107.37, 112.77, 124.62, 133.24, 135.28, 135.87, 138.63, 139.63, 143.82, 146.01, 147.08, 155.71; HRMS: calc. for $C_{37}H_{42}N_3O_2$ + H: 560.3277. Found: 560.3276. Calc. for $C_{37}H_{42}N_3O_2 \cdot HCl \cdot 0.1CHCl_3$: C, 73.27; H, 6.98; N, 6.91. Found: C, 73.61; H, 7.02; N, 6.97%. This compound consistently analyzed as a partial $CHCl_3$ solvate even after prolonged drying in a vacuum oven. For **5b**: mp 149–151 °C (decomp.); $\lambda_{max}(CHCl_3)$/nm ($\log_{10}$ ε) 332 (4.55), 373 (4.42), 423 (5.11), 594 (3.38), 747 (4.11), 827 (4.65); λ_{max}(5% TFA–$CHCl_3$)/nm ($\log_{10}$ ε) 321 (4.36), 350 (4.54), 436 (5.17), 681 (4.06), 746 (4.43); $\delta_H(CDCl_3)$ −2.35 (6H, t, 2 × OCH_2CH_3), −1.36 (4H, q, 2 × OCH_2CH_3), 1.79 (6H, t), 1.83 (6H, t) (4 × porphyrin-CH_2CH_3), 2.41 (2H, br s, 2 × NH), 3.59 (6H, s, 2 × porphyrin-CH_3), 3.68 (4H, q) and 3.83 (4H, q) (4 × porphyrin-CH_2CH_3), 8.91 (2H, br) and 10.47 (2H, br) (4 × benzo-H), 9.64 (2H, s), 10.90 (2H, s) (4 × *meso*-H); $\delta_C(CDCl_3)$ 11.45, 11.66, 17.29, 18.27, 19.50, 19.58, 56.42, 95.28, 107.12, 112.60, 124.55, 133.11, 134.90, 135.54, 139.30, 139.82, 143.80, 145.74, 146.83, 155.72; HRMS: calc. for $C_{39}H_{46}N_3O_2$ + H: 588.3590. Found: 588.3592. Calc. for $C_{39}H_{46}N_3O_2 \cdot HCl$: C, 75.04; H, 7.43; N, 6.73. Found: C, 74.80; H, 7.49; N, 6.60%.

1 J. Fabian, H. Nakazumi and M. Matsuoka, *Chem. Rev.*, 1992, **92**, 1197.
2 R. Bonnett, *Chem. Soc. Rev.*, 1995, **24**, 19; L. R. Milgrom and S. MacRobert, *Chem. Br.*, 1998, **34** (35), 45.
3 J. Ayub and D. Dolphin, *Chem. Rev.*, 1997, **97**, 2267.
4 E. Vogel, *J. Heterocycl. Chem.* 1996, **33**, 1461.
5 T. D. Lash, *Chem. Eur. J.*, 1996, **2**, 1197.
6 T. D. Lash, *Angew. Chem., Int. Ed. Engl.*, 1995, **34**, 2533. See also, T. D. Lash and S. T. Chaney, *Chem. Eur. J.*, 1996, **2**, 944.
7 T. D. Lash and M. J. Hayes, *Angew. Chem., Int. Ed. Engl.*, 1997, **36**, 840.
8 T. D. Lash and S. T. Chaney, *Tetrahedron Lett.*, 1996, **37**, 8825; T. D. Lash and S. T. Chaney, *Angew. Chem., Int. Ed. Engl.*, 1997, **36**, 839; M. J. Hayes and T. D. Lash, *Chem. Eur. J.*, 1998, **4**, 508.
9 K. Berlin, *Angew. Chem., Int. Ed. Engl.*, 1996, **35**, 1820.
10 U. E. Meissner, A. Gensler and H. A. Staab, *Tetrahedron Lett.*, 1977, **18**, 3.

Communication 8/06394J

Typeset and printed by Black Bear Press Limited, Cambridge, England

Energy transfer, proton transfer and electron transfer reactions within zeolites

V. Ramamurthy,*[a] P. Lakshminarasimhan,[a] Clare P. Grey*[b] and Linda J. Johnston*[c]

[a] *Department of Chemistry, Tulane University, New Orleans, LA 70118, USA. E-mail: murthy@mailhost.tcs.tulane.edu*
[b] *Department of Chemistry, State University of New York, Stony Brook, NY 11794-3400, USA*
[c] *Steacie Institute for Molecular Sciences, National Research Council of Canada, Ottawa, Ontario, Canada K1A 0R6*

Received (in Cambridge, UK) 22nd May 1998, Accepted 26th June 1998

The chemistry of olefins in zeolites illustrates both the potential complexity and utility of zeolites as reaction media. Of particular interest are the changes in product selectivity that result from carrying out oxidation reactions in the constrained space of the zeolite cavity. Since zeolites are capable of promoting proton and electron transfer reactions one needs to be particularly careful in the choice of a zeolite as a reaction medium.

Introduction

Much of our understanding of the reactivity of organic molecules is based on experiments conducted either in the gas phase or in an isotropic liquid phase. Studies conducted in these media have provided empirical rules which help us to predict or rationalize the behavior of moelcules in new environments. Although this has been successful in some cases, it is still difficult to predict the behavior of a molecule enclosed in, for example, a biological matrix or a solid assembly. In part, this is because many interactions between the reactant and the medium are often ignored, since it is not always straightforward to predict the effect of these interactions on chemical reactions. Recognizing the complexity of natural systems, and being inspired by them, chemists have utilized a number of organized media to study, and possibly alter, the behavior of included molecules. Examples of organized media which have been investigated include molecular crystals, inclusion complexes, liquid crystals, micelles and related assemblies such as vesicles, microemulsions and membranes, monolayers, Langmuir–Blodgett films, surfaces (silica, clay and zeolites) and, more recently, natural systems such as proteins and DNA.[1] In this review we are concerned with one such organized/confined medium, namely a zeolite.[2]

In the past, most photochemistry in zeolites has been restricted to reactions of carbonyl systems.[3] The extension of these studies to olefinic systems has demonstrated the complexity of zeolites as reaction media. The chemistry is complicated by both proton and electron transfer processes in which the zeolites themselves participate. This review summarizes a number of studies carried out in our laboratories that demonstrate this complexity of the chemistry. We aim however to show that much of the chemistry can be rationalized by careful characterization of the zeolites and the reaction intermediates by a variety of techniques including MAS NMR and time resolved laser spectroscopy. X and Y zeolites are used as the reaction media.

Structural features of zeolites

Zeolites are inorganic microporous and microcrystalline materials capable of complexing or adsorbing small and medium-sized organic molecules. $[SiO_4]^{4-}$ and $[AlO_4]^{5-}$ tetrahedra form the primary building blocks of zeolites.[2] These tetrahedra are linked by all their corners to form channels and cages or cavities with discrete sizes. The total framework charge of an aluminium-

V. Ramamurthy is the Bernard–Baus Professor of Chemistry at Tulane University in New Orleans. Previously, he was on the faculty at Indian Institute of Science, Bangalore, India (1978–1987) and on the staff of Central Research, DuPont, Wilmington (1987–1994). Following his undergraduate education in India his training in photochemistry was performed under the stewardships of R. S. H. Liu (Univ. Hawaii), P. de Mayo (Univ. Western Ontario) and N. J. Turro (Columbia Univ.) His research interests include the study of molecules in constrained media, solid state photochemisty and catalysis.

Pranatharthiharan Lakshminarasimhan (known as pH) came to USA in 1996 after completing his undergraduate education in India. He obtained a BSc in chemistry (1994) from the University of Madras and a MSc in Chemistry (1996) from the Indian Institute of Technology, Madras. Currently he is working towards a PhD degree at Tulane University and his project involves photochemical studies of organic molecules within zeolites.

Clair P. Grey obtained a BA in Chemistry from the University of Oxford in 1987. Her DPhil studies were carried out with Professors A. K. Cheetham and C. M. Dobson at Oxford. After receiving a DPhil (1991), she spent a year in the University of Nijmegen in Professor W. S. Veeman's Laboratory, as a Royal Society Postdoctoral Fellow, followed by two years as a visiting scientist at DuPont CR&D, Wilmington, Delaware with Dr A. J. Vega. She joined the faculty at SUNY Stony Brook in 1994, as an Assistant Professor, and was promoted to an Associate Professor in 1997. She is the recipient of an NSF National Young Investigator Award (1994), a Cottrell Scholarship (1997), a Dupont Young Professor Award (1977), and Camille and Henry Dreyfus Teacher-Scholar Award (1998) and is currently Alfred P. Sloan Foundation Research Fellow. Her research interests include the use of solid state NMR and diffraction methods to study structure and gas adsorption on catalysts and zeolites, conductivity in ionic conductors, battery materials, and the development and application of new solid-state NMR methodology.

Linda J. Johnston obtained a PhD from the University of Western Ontario, London, Ontario in 1983 under the supervision of Professor P. de Mayo. Following postdoctoral work with Drs K. U. Ingold and J. C. Scaiano she joined the staff at the National Research Council Canada, Ottawa, in 1986. She is currently a senior research officer in the Chemical Biology Program of the Steacie Institute for Molecular Sciences. Research interests include kinetic and mechanistic studies of radical ion chemistry and photochemistry in organized media.

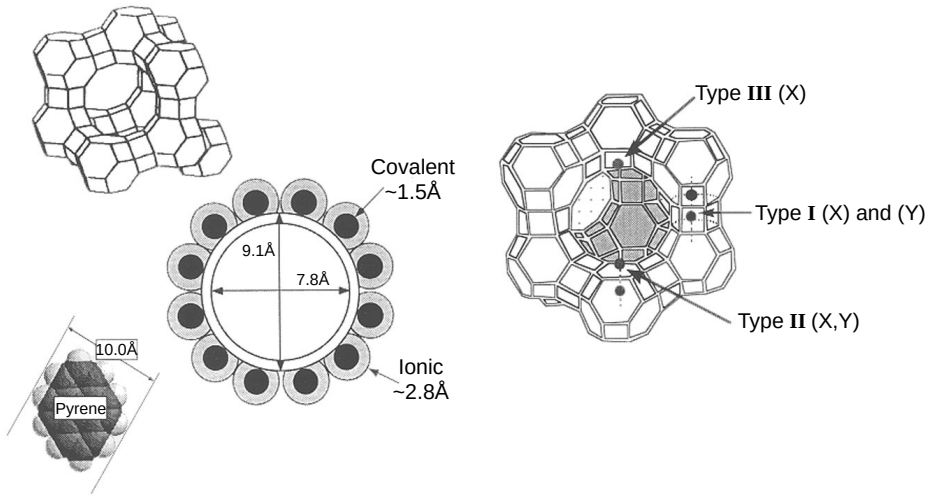

Fig. 1 The basic structural unit of X and Y zeolites. The entrance diameter of a supercage is shown on the left with the dimensions of a guest molecule, pyrene. The cation locations within a supercage are shown in colored circles.

containing zeolite is negative and hence must be balanced by an exchangeable cation, often an alkali or alkaline-earth metal cation. Zeolites can, thus, be represented by the empirical formula $M_{2/n}\cdot Al_2O_3\cdot xSiO_2\cdot yH_2O$, where M are the typically exchangeable cations of valence *n* (typically Na, Ca, Mg, *etc.*), *x* and *y* are integers. The two synthetic forms of faujasite are referred to as zeolite X and Y and have the following typical unit cell composition:

X type $M_{86}(AlO_2)_{86}(SiO_2)_{106}\cdot 264\ H_2O$

Y type $M_{56}(AlO_2)_{56}(SiO_2)_{136}\cdot 253\ H_2O$

where M is a monovalent cation. The faujasite framework has two main cages. The large supercage results from an assembly of the basic units, the 'sodalite cages'. While sodalite cages are too small to accommodate organic moelcules, the spherical supercages are approximately 13 Å in diameter. Access to the supercages is afforded by four 12-membered ring windows about 9 Å in diameter, which are tetrahedrally distributed about the center of the supercages. The supercages thus form a three-dimensional network with each supercage connected to four other supercages through the 12-ring window. The unit cell of X and Y zeolite consists of eight supercages.

The charge-compensating cations are known to occupy at least three different positions in zeolites X and Y.[4] As illustrated in Fig. 1, the first type (site I), with *ca*. 4–8 cations per unit cell, is located in the hexagonal prism faces between the sodalite units. The second type (site II), with 32 ions per unit cell (in both X and Y), is located in the open hexagonal faces. The third type (site III) is only substantially occupied in X zeolite (and CsY) and is located on the walls of the larger cavity. Other sites (II′ and I′) exist in the sodalite cage, but only cations at sites II and III are expected to be readily accessible to the organic molecule adsorbed within a supercage. Note that in certain circumstances substantial rearrangements of these cations can occur, involving migrations of cations between the cages.[5]

Selectivity during singlet oxygen mediated oxidation of alkenes

Singlet oxygen is known to react with electron-rich alkenes *via* a 2 + 2 addition process.[6] When the alkene contains allylic hydrogen atoms, however, the 'ene reaction' is the dominant pathway.[7] Alkenes with more than one distinct allylic hydrogen yield several hydroperoxides (Scheme 1). With a medium such such as a zeoilite, we envisioned that it should be possible to achieve high selectivity during the singlet oxygen ene reaction. The results of this study are presented below, as an example to illustrate the uniqueness, complexities and challenges of zeolites as reaction media.

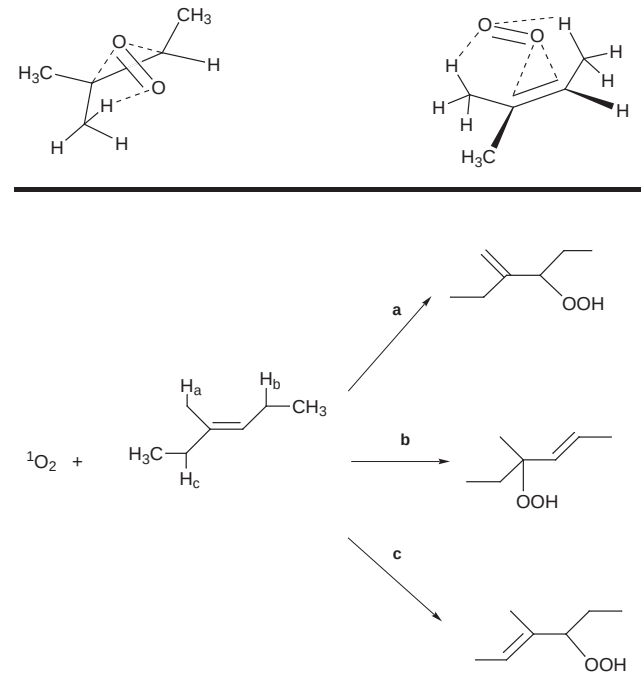

Scheme 1

The generation of singlet oxygen for the subsequent oxidation of alkenes requires assembling three species—oxygen, alkene and a sensitizer—within the internal structure of a zeolite. Monomeric thionin is a useful sensitizer for the generation of singlet oxygen; thionin is easily exchanged into NaY zeolite by stirring the dye with hydrated NaY in water. While the dye, as exchanged, remains in the dimeric form within hydrated NaY, careful dehydration of the zeolite results in a color change.[8] The hydrated dye is violet and upon drying the dye becomes blue. Upon thorough drying, thionin adopts a monomeric structure (Fig. 2) and excitation of a blue zeolite containing monomeric thionin shows an emission from singlet oxygen. Singlet oxygen, thus generated, is capable of undergoing an ene reaction with typical alkenes such as 2,3-dimethylbut-2-ene and 2-methyl-4,4-dimethylpent-2-ene. The product distribution observed with 1,2-dimethylcyclohexene suggests that the hydroperoxides so obtained are not the result of reaction with ground-state triplet oxygen (Scheme 2).[9] These observations confirm that one can generate a reactive singlet oxygen within the confines of a zeolite and set the stage for us

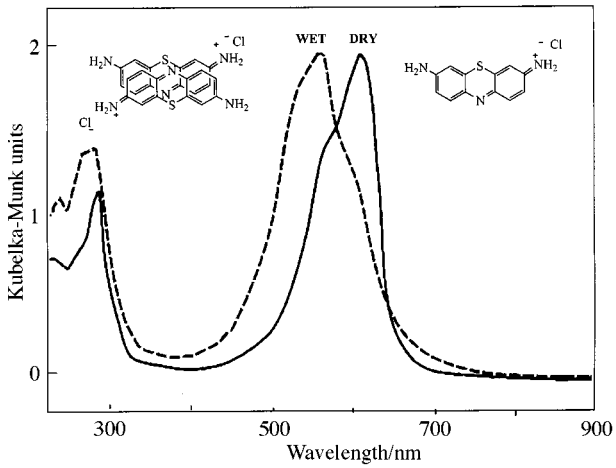

Fig. 2 The diffuse reflectance spectra of thionin included within NaY. The 'dry' and 'wet' samples show different spectra and are differently colored (for colored version of this figure please see http://www.rsc.org./suppdata/cc/1998/2411).

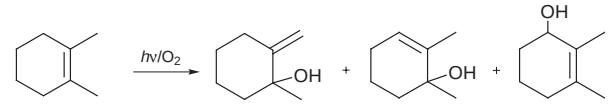

Conditions	Relative Yield (%)		
Rose Bengal / Acetonitrile	89	11	0
Thionin/ NaY/Hexane	90	10	0
Autooxidation	6	39	54

Scheme 2

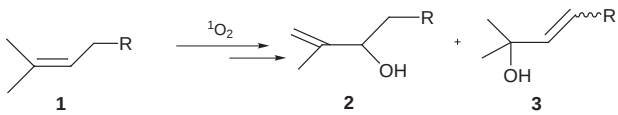

R = CH_3	Relative Yield (%)	
Thionin/CH_3CN	40	60
NaY/Thionin	100	—

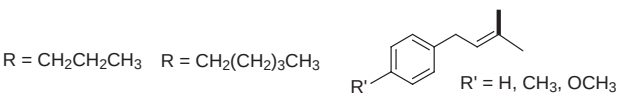

Scheme 3

to explore the initial goal of achieving selectivity during the ene reaction.

A number of alkenes of structure similar to 1-methylpent-2-ene were examined. These alkenes contain two distinct allylic hydrogen atoms and, in an isotropic solution, yield two hydroperoxides with no appreciable selectivity (Scheme 3). Within NaY, a single hydroperoxide is preferentially obtained.[10,11] Similar selectivity was also observed with related alkenes such as the 1-methyl-4-arylbut-2-enes and even more impressive results were obtained with 1-methylcycloalkenes (Scheme 4).[10] These alkenes yield three hydroperoxides in solution with the hydroperoxide resulting from abstraction of the methyl hydrogens formed in the lowest yield. Surprisingly, the minor isomer in solution was obtained in larger amounts within the zeolite. Thus the selectivity is a characteristic of hydroperoxidation of alkenes within zeolites. Product hydroperoxides were isolated in *ca*. 75% yield. Generally alcohols were more easily extracted out of the zeolite than the hydroperoxides. A number of control experiments ensured that the observed selectivity is not an artifact. The yields reported in the schemes are for alcohols.

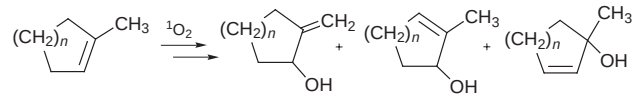

	Relative Yield (%)		
Thionin/CH_3CN	6	45	48
Thionin/NaY/Hexane	100	—	—
Thionin/CH_3CN	10	47	43
Thionin/NaY/Hexane	100	—	—

Scheme 4

The above selectivity is rationalized on the basis of two independent models.[11] In one, the zeolite is postulated to control the conformation of the reactive alkene and, in the other, the zeolite is suggested to polarize the reactive alkene. We wish to emphasize that the above models are only working hypotheses and further experiments are needed (and underway) to identify the origin of selectivity. Formation of both hydroperoxides **2** and **3** from **1** in solution has been rationalized on the basis that singlet oxygen attacks the alkene from the top-right side as shown in Fig. 3 and Scheme 1. In such an approach, the

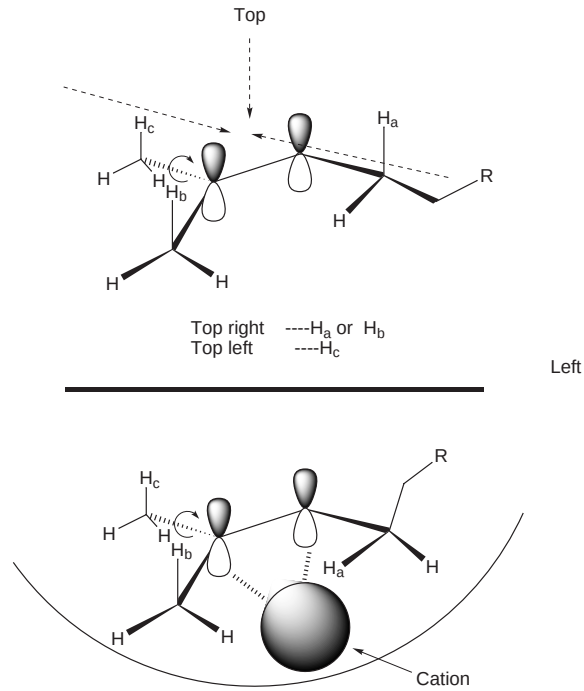

Fig. 3 Cation–alkene interaction within a supercage may control the conformations of allylic hydrogens. For allylic hydrogen abstraction H_a and H_b should be parallel to the π orbital (see top).

transition state is stabilized by secondary interactions between the oxygen and the allylic hydrogens which are situated parallel to the π–p orbitals. In this model, the methyl group on the top-left side (Fig. 3) does not participate in the oxidation process. The results within zeolites clearly suggest that the methylene hydrogens H_a of **1** and **4** (Fig. 3) are not abstracted by the singlet oxygen. While the lack of formation of **3** and **6** within zeolites is an indication that the methylene hydrogens are excluded from the reaction, selective formation of **2** and **5** does not indicate which of the two (or both) methyl groups participates in the oxidation process.

We propose that the R group in the alkene (Fig. 3) plays a crucial role in the type of product(s) formed. While in solution, the most favored conformation places both the methyl and methylene hydrogens in an appropriate geometry for abstraction (Fig. 3), it is quite likely that such a conformation is not favored

within a zeolite. In a supramolecular assembly, one must consider the interactions that arise between the adsorbent/guest and the environment. We speculate that within a zeolite, the alkene will be adsorbed to the surface *via* cation–π interactions. The rotation of the C3–C4 bond may occur under such conditions to relieve the steric strain that develops between the bulky R group and the surface. Such a rotation will place the methylene hydrogens away from the incoming singlet oxygen (Fig. 3), preventing the formation of the tertiary hydroperoxide. The extent of steric repulsion between the surface and the R group may depend on the distance between the group and the surface which, in turn, will be controlled by the size and binding strength of the cation. This model predicts that the selectivity should be directly related to the binding energy of the cation with the alkene; reactions involving larger cations such as Cs^+ ion may be expected to yield lower selectivity than those involving the smaller Na^+ ion.

In the second model, the selectivity is attributed to the polarization of the alkene by the interacting cation. As shown in Fig. 4, when the alkene is asymmetric, the interacting cation

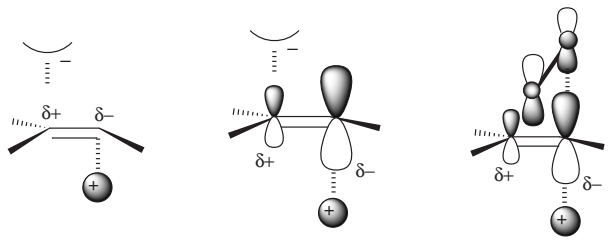

Fig. 4 Cation–alkene interaction may polarize the alkene. Polarization is represented in terms of the size of the orbital.

will be able to polarize the alkene in such a way that the carbon with the greater number of alkyl substituents will bear a partial positive charge (δ+). Singlet oxygen being electrophilic is expected to attack the less substituted electron rich carbon (δ–) and lead to an ene reaction in which the hydrogen abstraction occurs selectively from the alkyl group connected to the δ+ carbon. Polarization of molecules such as pyrene, NO, alkene–oxygen within zeolites has been previously reported.[12,13] In our system, the extent of polarizability will depend on the charge density of the cation. Smaller cations such as Li^+ would be expected to polarize the alkene more effectively than larger cations such as Cs^+. As per this model, selectivity is expected to decrease from Li^+ to Cs^+. Consistent with both the above models, the observed selectivity decreases with the size of the cation (Scheme 5; $Li^+ > Na^+ > K^+ > Rb^+ > Cs^+$).[11]

Both of the above models assume that there is an interaction between the cation and the alkene and that the interaction energy decreases with the size of the cation.[14] ^2H and double resonance NMR studies are in progress to probe the interaction between the adsorbed alkene and the extra-framework cation. Preliminary *ab initio* quantum mechanical calculations performed with several alkenes clearly show a decreasing trend in the binding energy between the cation and the alkene, the smaller cations binding more strongly.[15] Although at pesent we have no direct evidence for interaction between cations and alkenes, we have established the existence of such interactions for aromatics *via* absorption, emission and solid state NMR studies.[16] These cation–aromatic interactions, which involve the π-electrons of aromatics, are well established in the literature.[17]

Extension of the above oxidation studies to alkenes such as limonene gave a complex mixture (Scheme 6).[18] Control experiments revealed that the alkenes themselves undergo rearrangement prior to oxidation. Careful analysis indicated that the very low concentrations of acidic protons that are present in NaY (< 1 per 16 supercages, as determined by NMR and indicator studies described below), a zeolite which is usually considered to be non-acidic, are sufficient to catalyze these rearrangements.[19] Acid catalyzed rearrangement of limonene in solution is well known. In further studies, these very small concentrations of acidic sites were shown to alter the chemistry significantly and to result in a variety of unexpected products that result from the initial protonation of the alkene. We were able to switch off this chemistry, by simply neutralizing the acidic sites with stoichiometric amounts of pyridine. Once these acidic sites are neutralized, oxidation of the alkenes listed in

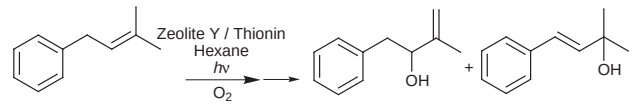

		Relative Yield (%)	
Cation	Cation radius/Å	2°	3°
LiY / Thionin	0.76	100	—
NaY / Thionin	1.02	85	15
RbY / Thionin	1.52	80	20
CsY / Thionin	1.67	66	34

Scheme 5

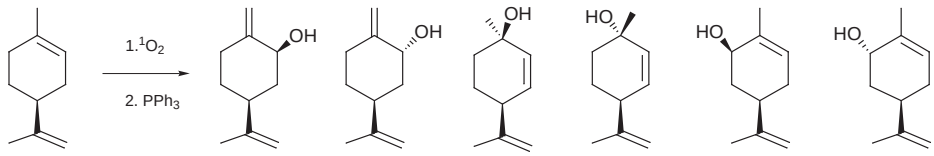

Relative Yield (%)

Conditions	A	B	C	D	E	F
Rose Bengal/ CH_3CN	20	21	34	10	5	10
NaY/Thionin	Rearrangement— Complex mixture					
NaY/Thionin/ Pyridine	Only					

Scheme 6

Scheme 6 can be readily performed without any side reactions.

A fundamental understanding of both the major reaction mechanisms, and the possible side-reactions, clearly requires a detailed study and quantification of the number of acidic and cation sites present in these materials. Details on the characterization of zeolites for Brønsted acidity are presented in the following section.

Probing $M^{2+}Y$, $H^{+}Y$ and $M^{+}Y$ zeolites for Brønsted acidity: implications for reactivity

NMR characterization

One of our laboratories has developed and applied a variety of new solid state double resonance NMR methods to probe the acidic sites present in zeolites and to study gas sorption.[20–24] TRAPDOR NMR methods were used, for example, to probe surface sites which are difficult to observe directly with ^{27}Al MAS NMR methods[20,22,23] since they are associated with large quadrupole coupling constants. Examples include sites of catalytic interest such as the aluminium atoms associated with the Brønsted acid sites in the zeolite [Si–O(H)–Al] and the Lewis acid sites created by dehydroxylation of the framework or by steaming. The TRAPDOR experiment[22,25] exploits the dipolar coupling between nearby nuclei to detect the quadrupolar nuclei (^{27}Al) indirectly. Two experiments are performed: in a ^{1}H–^{27}Al experiment, for example, the first experiment performed is a simple ^{1}H spin-echo. This is referred to as the control experiment. In the second experiment, a ^{1}H spin-echo sequence is again performed, but now the quadrupolar nucleus (in this case ^{27}Al) is irradiated for, typically, the evolution period (τ) of the spin-echo. This is shown schematically in Fig. 5.

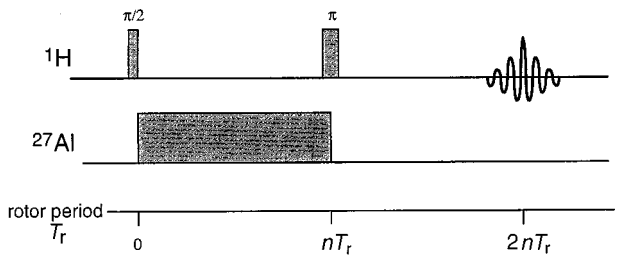

Fig. 5 The ^{1}H–^{27}Al TRAPDOR NMR sequence. An echo is formed at $2nT_r$, where T_r is the rotor period, nT_r is the evolution period, and n is an integer.

Protons nearby to aluminium spins will no longer be completely refocussed, on ^{27}Al irradiation, by the π pulse applied in the middle of this sequence (at nT_r) and their signal, at the echo (at $2nT_r$), will be reduced. This reduction depends on a variety of factors, which include the spinning speeds and ^{27}Al r.f. field strength; more importantly, the loss in signal is extremely sensitive to the ^{1}H–^{27}Al internuclear distance. This fact can be utilized to assign ^{1}H resonances to different aluminium-containing species or to probe proximity between different spins. Lewis acid sites are readily detected on absorption of bases such as trimethylphosphine (TMP) or ^{15}N-labeled monomethylamine: A ^{31}P–^{27}Al or ^{15}N–^{27}Al TRAPDOR NMR experiment is performed and the loss of the ^{31}P or ^{15}N signal at the echo, on ^{27}Al irradiation, indicates that these probe molecules are bound to the Lewis acid site.[24,25]

A simple probe of acidity involves the reaction of trimethylphosphine (TMP) with the Brønsted acid sites [Si–O(H)–Al]:

$$\text{Si–O(H)–Al + TMP} \rightarrow \text{TMPH}^{+} + \text{Si–O–Al}$$

Very different chemical shifts are observed for the TMP molecule and $TMPH^{+}$ cations (at *ca.* −67 and −2 ppm, respectively).[26,23] Since NMR is a quantitative technique, the concentration of Brønsted acid site follows directly from the intensity of the $TMPH^{+}$ resonance. Additional ^{1}H experiments have been performed to ensure that complete reaction of the TMP with the Brønsted acid sites occurred. ^{31}P–^{27}Al TRAPDOR experiments have also been carried out to assign the ^{31}P resonances due to TMP bound to the Lewis acid sites. These methods were applied to characterize HY and CaY.[27,24]

The ^{1}H–^{27}Al TRAPDOR NMR spectra of CaY, calcined in an oven at 500 °C, is shown in Fig. 6. The control experiment, (Fig. 6) obtained without ^{27}Al irradiation, shows a number of

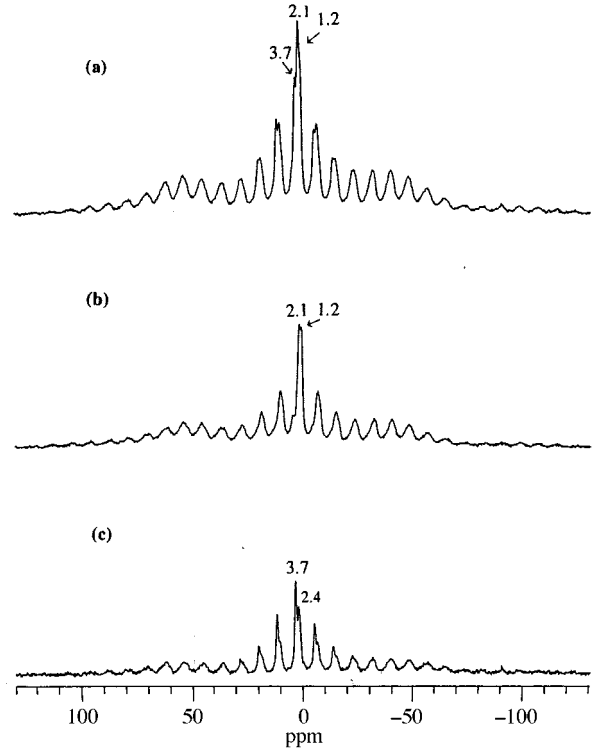

Fig. 6 ^{1}H–^{27}Al TRAPDOR spectra of CaY-500-oven at −500 °C obtained (a) without and (b) with on-resonance ^{27}Al irradiation during τ (τ = 333 μs, spinning speed = 3 kHz; ^{27}Al r.f. field strength = 55 kHz). The difference spectrum [(a) − (b)] is shown in (c). The intensity of (c) has been scaled by a factor of two with respect to (a) and (b).

different resonances at 3.7, 2.1 and 1.2 ppm. The large spinning sideband manifolds result from residual water that is bound to the calcium cations; (b) shows the spectrum obtained on ^{27}Al irradiation. ^{1}H resonances that are observed result from proton species that are distant from aluminium atoms, or that are mobile. The difference spectrum shown in (c) contains resonances from proton spins that are nearby to aluminium. The resonance at 3.7 ppm, due to the Brønsted acid sites [Si–O(H)–Al], is observed clearly in this spectrum, consistent with this. The resonance at 2.4 ppm is due to extra framework aluminium hydroxide species created during activation of the zeolite. The large sideband manifolds are visible in (c) indicating that the water molecules are also tightly bound to the zeolite framework. The resonances at 2.1 and 1.2 ppm are assigned to $CaOH^{+}$ and silanol groups, respectively. The $CaOH^{+}$ groups result from the following reaction, which is well established in CaY zeolites, and is a consequence of the large electrostatic field at the divalent cation:[28]

$$\text{Ca(OH}_2)_n^{2+} \rightarrow \text{CaOH}^{+} + \text{H}^{+} + (n-1)\text{H}_2\text{O}$$

The observation of Brønsted acid resonances at 3.7 ppm is consistent with this. TMP was sorbed on this material to titrate the acid sites and an estimate of *ca.* 16 Brønsted acid sites per unit cell was obtained for this sample by integrating the $TMPH^{+}$ resonance. ^{31}P–^{27}Al TRAPDOR NMR was performed to confirm the lack of Lewis acidity in these samples. Experiments were then carried out for samples activated under a variety of different conditions. CaY activated in an oven at higher temperatures contains less water, but all the other species are

still present. In contrast, CaY activated by slow ramping of the temperature under vacuum to 500, or 600 °C, shows a much lower concentration of Brønsted acid sites (< 1 per unit cell, from TMP titration). Again, no evidence for Lewis acidity was observed.

Similar experiments can be used to quantify the number of Brønsted acid sites in HY zeolites.[24] Typically, the number is less than the predicted amount from the Si/Al ratio, as some dehydroxylation occurs. The ^{1}H MAS NMR spectrum of monomethylamine (MMA) sorbed on an HY sample dehydrated at 400 °C under vacuum is shown in Fig. 7, as a function

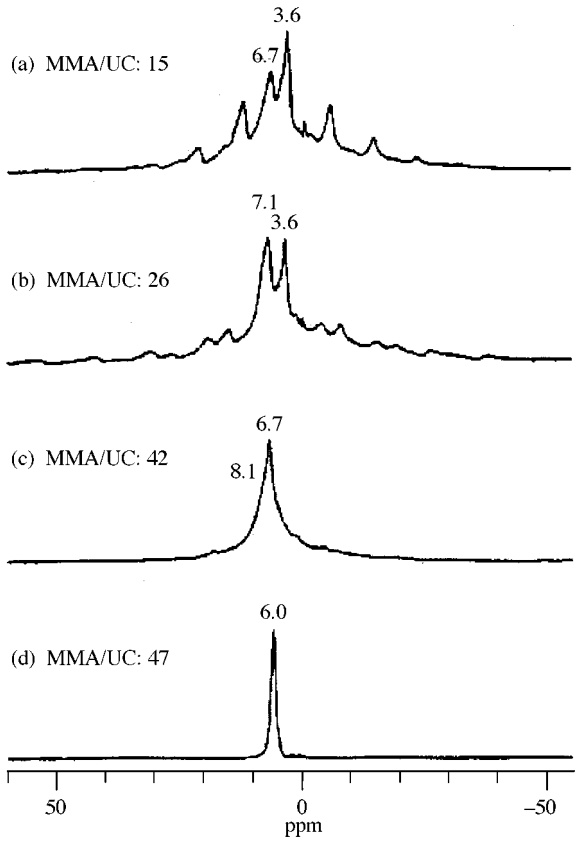

Fig. 7 ^{1}H MAS NMR spectra of [$^2H_3$]monomethyl amine–HY with different loading levels. Loading levels per unit cell are shown on the figure. Spectra were collected at spinning speeds of 3 and 4 kHz for (a) and (b)–(d), respectively. The isotropic resonances are labeled. The small peaks around 0–1 ppm are due to the background signals from the probe head, rotor and inserts. All other resonances are spinning sidebands.

of loading level.[23] Monomethylammonium cations ($MMAH^+$) are formed (resonances at 6.7–8.1 ppm), which at temperatures below −40 °C are rigidly bound to the zeolite framework on the ^{1}H NMR timescale. At loading levels of MMA that exceed the number of Brønsted acid protons (> 42 MMA/u.c.), ^{1}H resonances intermediate in chemical shift between those of MMA (*ca.* 2 ppm) and $MMAH^+$ are observed from species undergoing rapid proton transfer reactions between MMA and $MMAH^+$. This is seen in (d) where a single resonance at 6.0 ppm is observed. Thus a concentration of between 42 and 47 Brønsted acid sites per unit cell is estimated for this sample. The Brønsted acid concentration, as a function of the dehydration temperature, has also been carefully determined from proton spin counting in ref. 29 and our ^{1}H MAS NMR results are consistent with this data. Lewis acid sites created as a result of the dehydroxylation process, are clearly observed on TMP or MMA sorption (with ^{31}P or ^{15}N MAS NMR).[22,23]

The indicator method

As discussed earlier, thermal reactions of alkenes were observed even within alkali-metal ion-exchanged X and Y zeolites, zeolites not traditionally associated with Brønsted acidity. The small concentrations of Brønsted acid sites present in these samples are thought to result from cation deficiencies (*i.e.* a $M^+ : Al^{3+}$ ratio of < 1) caused by the replacement of M^+ by H_3O^+ during ion-exchange or synthesis of the zeolites.[28,30] Quantification of these Brønsted acid sites was critical in order to rationalize the observed chemistry within M^+X and M^+Y zeolites. The materials were initially studied with ^{1}H MAS NMR with similar methods to those described above.[19] ^{1}H MAS NMR spectra of activated NaY showed a very weak resonance at 3.6 ppm which could be tentatively assigned to Brønsted acid sites. Its intensity was, however, extremely small in comparison to the intensity of the residual water and the silanol groups and it was difficult to quantify the numbers of Brønsted acid sites per unit cell. TMP was again sorbed on NaY. The ^{31}P MAS NMR at −150 °C showed a very weak signal at −2 ppm (1/50 times weaker than the main resonance at −60 ppm from weakly bound/physisorbed TMP, for the sample loaded with 26 molecules per unit cell), which was ascribed to $TMPH^+$. From the intensity of this resonance, we estimated that there could be no more than approxiamtely 0.5 Brønsted acid sites per unit cell of NaY. To check the presence of weakly acidic sites, stronger bases such as dimethylamine and methylamine were used as probes for NaY. No evidence for protonation of these probes could be detected with ^{1}H MAS NMR. Note that when these probe molecules were adsorbed in quantities that exceeded the number of Brønsted acid sites, considerable mobility of the probe molecules was typically observed, indicating rapid exchange of the protons between the probe molecules. Although the exchange process can be frozen out at low temperatures such as −150 °C, this mobility complicates the analysis of spectra obtained for samples with very low concentrations of Brønsted acid sites. Based on these studies it was concluded that the number of Brønsted acid sites within NaY was close to, or beyond, the detection limis of NMR. Therefore, we employed a different technique to detect the acidic sites within zeolites. This involved detecting differences in electronic absorption characteristics between protonated and unprotonated forms of a probe molecule.

The success of this technique depended upon finding a dye molecule that would exhibit different colors under acidic and basic conditions and would easily fit within a zeolite. The set of cyanine dyes that we used is listed in Scheme 7.[31] All are brightly colored under basic or neutral conditions and turn colorless under acidic conditions. Two dyes, retinol and retinyl acetate, are blue under acidic conditions but are light yellow under basic/neutral conditions. A preliminary test consisted of monitoring the absorption changes upon addition of a small amount (50 to 200 mg) of an activated zeolite to a standard micromolar hexane solution (5 ml) of the dye. When activated NaY was added to a standard solution of retinol or retinyl acetate, the zeolite immediately turned a dark blue color which persisted for nearly an hour. This observation was interpreted as evidence for the presence of Brønsted acidic sites that are strong enough to protonate retinol and retinyl acetate. When the cyanine dye was added to activated NaY, the bright color of the dye faded and the zeolite remained white. Consistent with this, NaX did not show a positive blue test with either retinol or retinyl acetate or with cyanine dyes. This leads us to conclude that NaX is less acidic than NaY.

The number of Brønsted acid sites was estimated by a conventional titration method. Either *n*-butylamine, diethylamine or pyridine was used as a base to quench the acidic sites present in a zeolite. A typical experiment consisted of stirring a known amount of NaY with varying amounts of the base. After at least 6 h of stirring the indicator dye was added and the visible color change was either observed or recorded. Surprisingly when the base was present in amounts more than 1 per 16 cages retinol and retinyl acetate did not become blue and the cyanine dyes maintained their bright colors. This indicated that no more than one acidic site per 16 supercages (*i.e.* 0.5 H^+ per unit cell)

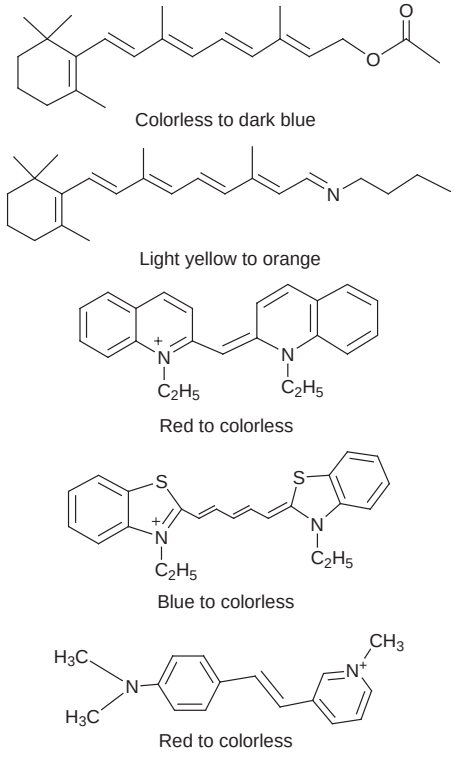

Scheme 7

can be present in NaY. Although this number is small, it is large enough to bring about changes in the structure of guest alkenes *via* a catalytic process.

Careful characterization of CaY, HY, and NaY zeolites has shown that these zeolites contain Brønsted acid sites. Of these HY, as expected, contains the most acidic protons (42–47 per unit cell). This is followed by CaY activated in an oven which contains 16 per unit cell. Even NaY, normally considered to be non-acidic, contain 0.5 protons per unit cell. The acidity of CaY depends on the activation conditions and that of NaY depends on the source. As per our analysis NaX is least acidic. In choosing X and Y zeolites as a reaction media one must be aware of the consequences of the presence of even small numbers of Brønsted acid sites in CaY, HY, and NaY zeolites.[32–34]

Proton transfer reactions within zeolites

In this section the thermal behavior of three alkenes, indene,[35] 4-vinylanisole[36] and 1,1-diarylethylene,[37] within CaY is outlined.[38] In all cases CaY was activated in an oven at 500 °C; activation at 400 °C under vacuum resulted in a less active zeolite. Inclusion of the alkenes in activated CaY gave brightly colored samples that retained their color for several weeks and, in some cases, even months (see http://www.rsc.org/suppdata/cc/1998/2411). For example, 1,1-diphenylethylene gives a green colored zeolite while 4-vinylanisole red–violet and indene dark red. The products isolated, the characterization of the species responsible for the color and a possible mechanism for formation of both the colored species and the final products are described below.

Addition of the activated CaY to a hexane solution of indene resulted in the immediate formation of a dark red color (absorption maximum at 520 nm) that persisted for several months. Extraction of the zeolite with dichloromethane gave products **12–15** (Scheme 8) but, remarkably, did not remove the red color. The red color remained after three months under laboratory conditions and was unaffected by refluxing the zeolite in methanol or water for 24 h or by the addition of dilute HCl. The behavior of vinylanisole was similar to that of indene in that addition of activated CaY to 4-vinylanisole in hexane

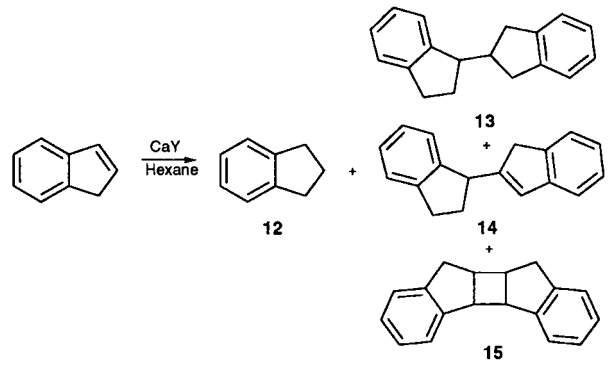

Scheme 8

gave a vibrant red–violet color. The diffuse reflectance spectrum of the solid zeolite consisted of two broad absorptions at 340 and 580 nm (Fig. 8). The 580 nm absorption was not

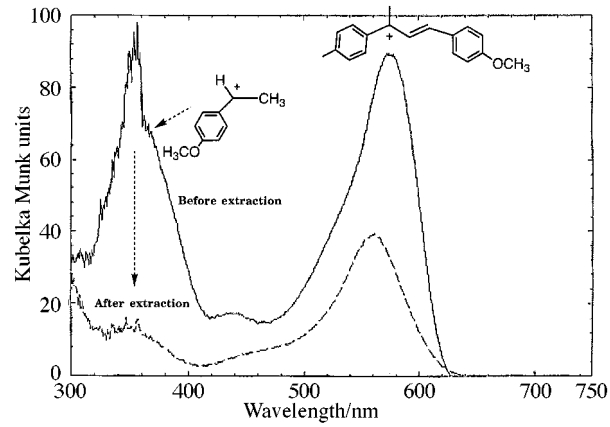

Fig. 8 Diffuse reflectance spectra of 4-vinylanisole included within 500 °C-oven-activated CaY. The sample before extraction shows absorptions due to two independent carbocations. After extraction with dichloromethane, the spectrum is mainly due to the allylic cation (see insert for structure).

removed by any of the extraction procedures noted above for indene. In contrast, extraction of the zeolite with dichloromethane–THF eliminated the 340 nm absorption and gave products **16**–**20** (Scheme 9). The ratio of the products dependent on the loading level of 4-vinylanisole and on the mode of activaiton of CaY. Due to lack of space we will not be going into the details on the relationship between the product distribution and loading level. The 340 nm absorption is attributed to the 4-methoxyphenylethyl cation (see insert in Fig. 8), in good agreement with the literature spectrum for this species in solution.[39] While this cation has a lifetime of only a few microseconds in solution, it is stable for a few days in the zeolite.

Similarly, addition of CaY to a hexane soluton of 1,1-diphenylethylene gave a yellow slurry that turned green and remained so for several days. The diffuse reflectance spectrum (Fig. 9) showed two maxima at 430 and 610 nm. Product extraction (Scheme 10) left a blue zeolite (610 nm). The 430 absorption is attributed to the diphenylmethyl cation, in agreement with the solution spectrum for this species and its independent generation from diphenylethanol in CaY.[40]

The products shown in Schemes 7–9 can be rationalized on the basis of an initial protonation of the olefin by Brønsted acid sites in activated CaY. Detailed H, D isotope studies using D_2O and deuterated extraction solvents were carried out for diphenylethylene and indicated that the first proton comes from acidic sites and the second hydride from the solvent. Scheme 9 illustrates the sequence of reactions that we suggest to explain the formation of the products from 4-vinylanisole; similar schemes can rationalize the products observed for indene and diphenylethylene. A common feature for all three alkenes is the

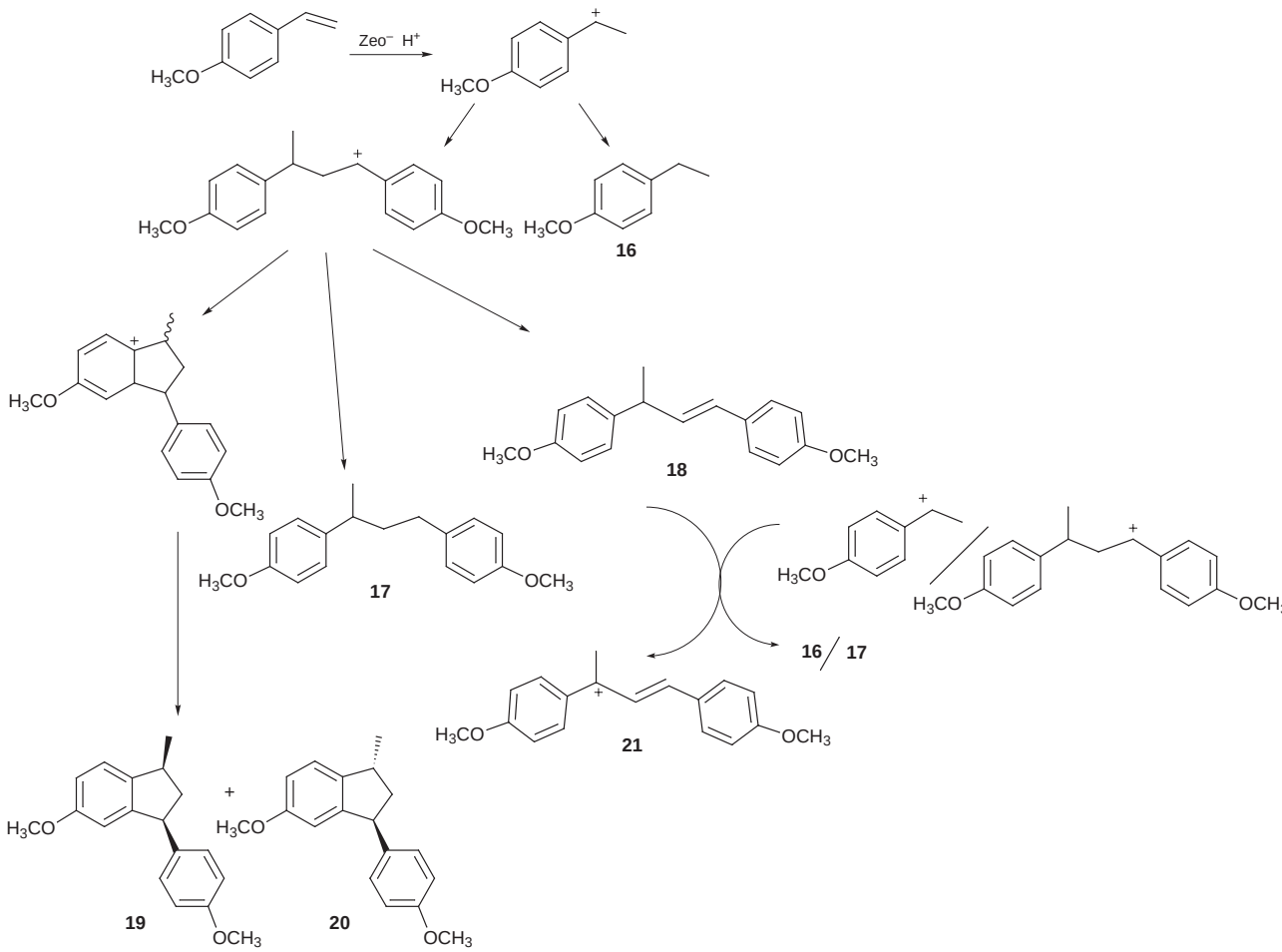

Scheme 9

formation of a strongly colored stable species within CaY. The formation of a red color from indene in the presence of Lewis acids has been reported previously and attributed to carbonium ion **25** (Scheme 11) formed by abstraction of a hydride ion from 2-α-indanylindene **14**.[41] In soluiton, this cation is only stable for a short time, even under an inert atmosphere. We believe that the 520 nm absorption in CaY is due to the same cation, which is indefinitely stable in the zeolite. Similarly, the red–violet color obtained for 4-vinylanisole is assigned to the allylic cation **21** (Scheme 9). This is consistent with the expected absorption for the 1,3-diphenylpropenyl cation and was confirmed by the independent generation of this species from an alcohol precursor.

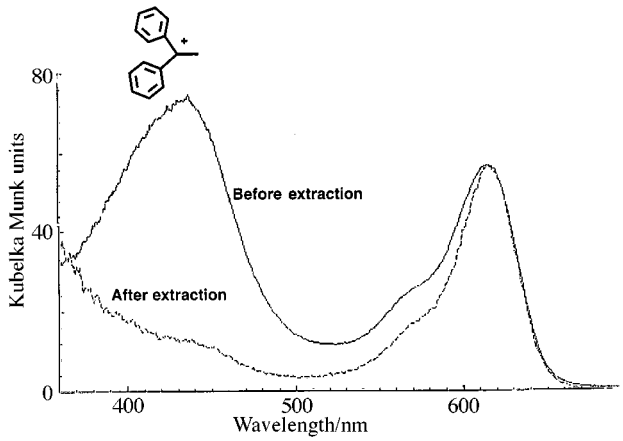

Fig. 9 Diffuse reflectance spectra of diphenylethylene included within 500 °C-oven-activated CaY. The sample before extraction shows absorptions due to two independent carbocations. After extraction with dichloromethane the spectrum is mainly due to an allylic cation.

While there seems to be general agreement in the literature concerning the structure of the persistent cations from indene and 4-vinylanisole, the origin of the blue color (after extraction to remove the yellow component) from diphenylethylene is not yet resolved. A deep blue or green coloration from diphenylethylene in acidic media (both in solution and on silica-alumina surfaces) has been reported previously and several possible explanations have been suggested (Scheme 12).[42,43] One of these is the monomer radical cation, although there are conflicting reports on the solution spectrum of the diphenyl-

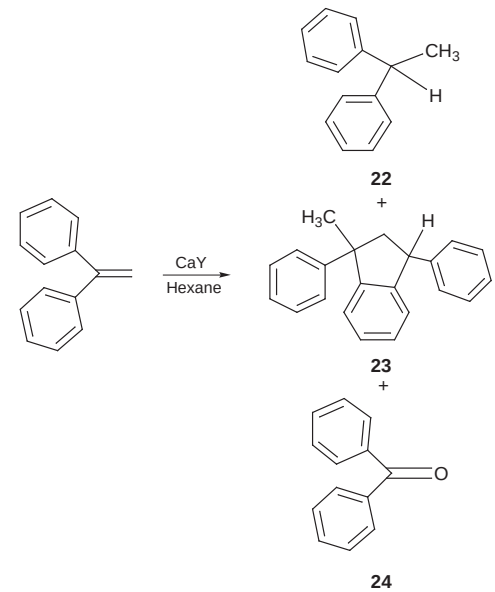

Scheme 10

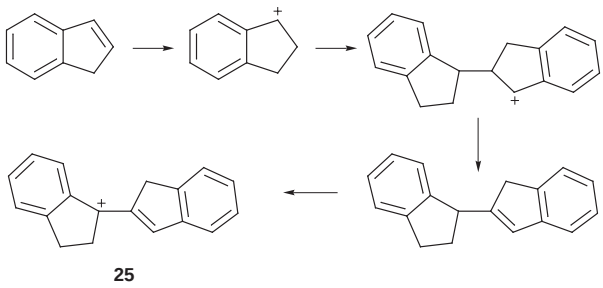

25

Scheme 11

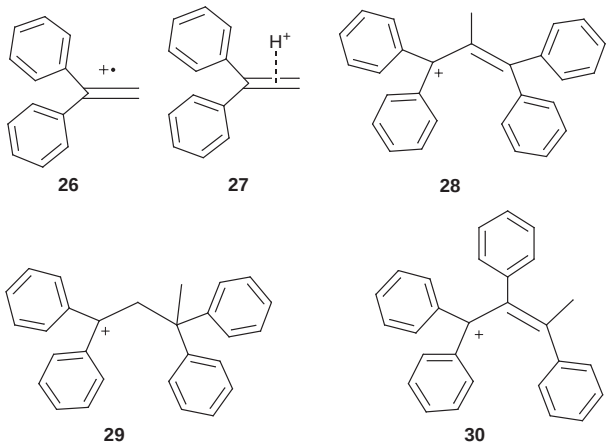

26 27 28

29 30

Scheme 12

ethylene radical cation. Although we have not been able to record the spectrum for this species in solution, we have obtained spectra for two methyl substituted derivatives. Both the 1,1-diphenylprop-1-ene and 1,1-diphenyl-2-methyl-1-ene radical cations have absorption maxima at *ca.* 400 nm with a weak absorption at > 700 nm (Fig. 10). We expect the

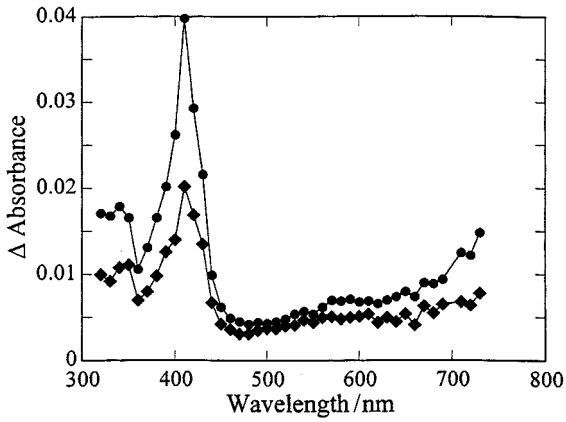

Fig. 10 Transient absorption spectra of the 1,1-diphenyl-2-methylprop-1-ene radical cation generated by 9,10-dicyanoanthracene/biphenyl sensitization in acetonitrile (●, 0.7 μs after laser excitation; ◆, 1.8 μ).

diphenylethylene radical cation to absorb in the same region, making it unlikely that the blue species in CaY is the monomer radical cation. An alternate assignment for the colored species is an olefin–acid π-complex,[42i] although this proposal has not received much experimental support. Others have suggested dimeric cations such as **28** or **29**; of these **29** is less likely to absorb above 600 nm. In fact generation of this species from alkene **32** gave an absorption identical to that of diphenylmethyl cation. Therefore, the original suggestion **28** by Rooney and Hathaway[43] is still one of the most likely structures for the blue colored species; we believe that **30** is also a reasonable possibility.

The difficulty in assigning a structure to the blue species obtained from diphenylethylene arises from the fact that a stable dimeric alkene, that is also a good hydrogen donor, has not been isolated, unlike the results for indene and 4-vinylanisole. As shown in Scheme 13, the only alkene that can be formed from the dimeric cation **31** is **32**, which has no hydrogen that can be easily removed as a hydride. However, alkenes **33** and **34** (Scheme 13) are good hydrogen donors and can give cations **28** and **30** by a similar mechanism to that shown in Schemes 9 and 11. These cations would be expected to absorb above 600 nm. The two alkenes (**33** and **34**) can be formed by rearrangement of **31** to a less stable classical cation **35**. In the absence of other competing processes, even this relatively unlikely rearrangement may occur within a zeolite. In fact if one views **35** as a non-classical phenonium ion (**36** in Scheme 13), rearrangement of **31** to **36** appears feasible. Alkenes **33** and **34** may be formed from **35** *via* migration of either a methyl or phenyl group as illustrated in Scheme 13. Thus, we believe that the colored species formed from diphenylethylene within CaY is either **28** or **30**. We are currently synthesizing precursors of these cations for studies of their absorption spectra within zeolites.

The extraordinary stability of the carbocations **21**, **25** and **28**/**30** derives partly from the π-conjugation with the aromatic substituents. This kinetic stability must be augmented by the highly polar nature of the zeolite supercage. In all these systems, the cations that are generated serve as a counter ion for the zeolite framework and thus become part of the zeolite structure. The unusual ability to stabilize certain carbocations within zeolites has allowed us to handle them as 'normal' laboratory chemicals. For example we have been able to record emission from several of these cations. One such example is provided in Fig. 11. The technique of stabilizing reactive intermediates within the structures of zeolite should allow us characterize, in the future, the excited state properties of reactive intermediates such as carbocations and radical cations.[44]

Electron transfer within zeolites

Electron transfer within zeolites has been the subject of investigation for several decades. Some studies have involved spontaneous electron transfer in which the guest, upon inclusion within an activated zeolite, transfers an electron to the zeolite to form a stable radical cation. Stamires and Turkevich were the first to observe spontaneous electron transfer between the host NH_4^+Y zeolite and the guests 1,1-diphenylethylene, triphenylamine, quinoline, perylene, aniline and *p*-phenylene diamine.[45] We have generated and stabilized radical ions from a number of polyenes and oligomers of thiophenes.[46] For example, when activated Na-ZSM-5 (Si/Al = 23) was stirred with α,ω-diphenylpolyenes (*trans*-stilbene, diphenylbutadiene, diphenylhexatriene, diphenyloctatetraene, diphenyldecapentaene, and diphenyldodecahexaene) in 2,2,4-trimethylpentane, the initially white zoelite and colorless to a pale yellow olefins were transformed into highly colored solid complexes within a few minutes. The samples all exhibited intense EPR signals with *g* values of 2.0028. Diffuse reflectance spectra of these powders (Fig. 12) were identical to the spectra of the radical cations of a few α,ω-diphenylpolyenes reported in the literature.[47] Diffuse reflectance and EPR results favor the conclusion that the colored species formed upon inclusion of α,ω-diphenylpolyenes in Na-ZSM-5 are radical cations. The radical ions thus generated were unusally long lived (several months). The exact nature of the electron acceptor within the zeolite had yet to be unequivocally identified. Although spontaneous generation of radical cations has been established for a number of substrates within Na-ZSM-5 and HY, similar results have not been reported within NaX and NaY zeolites.[48]

In addition to spontaneous electron transfer, relatively long-lived radical cations (lifetimes of milli- to micro-seconds) can be readily generated by direct laser excitation of a variety of aromatic substrates within X and Y zeolites. This phenomenon was orginally reported by Iu and Thomas with NaY and NaX

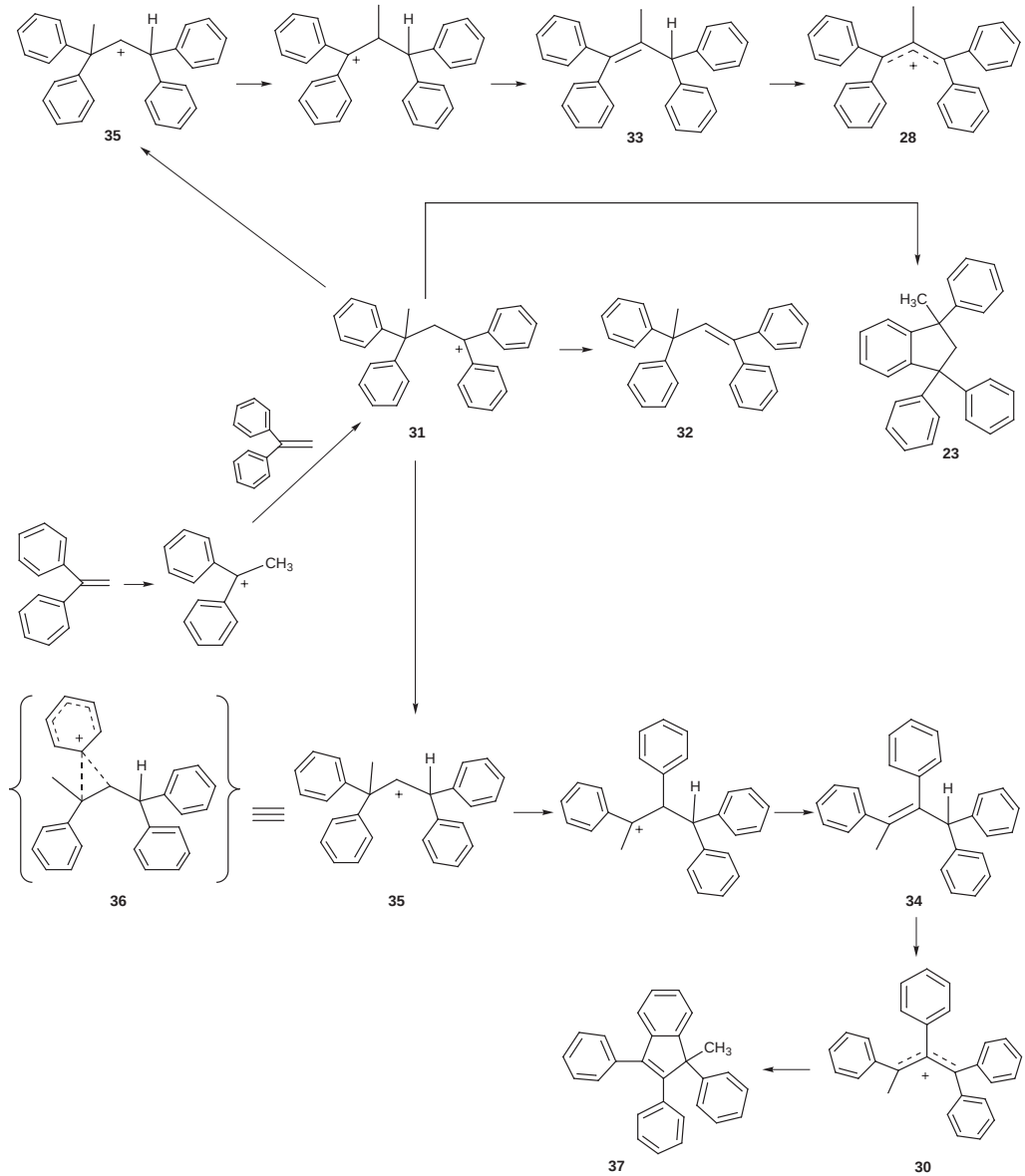

Scheme 13

zeolites as the acceptors and pyrene and anthracene as the donors.[49] Our recent results demonstate that direct excitation of aryl and diarylethylenes in zeolites also leads to radical cation formation, in competition with other excited state decay processes. For example, diffuse reflectance laser flash photolysis of *trans*-stilbene included in NaX zeolite leads to the formation of transient signals assigned to the *trans*-stilbene radical cation (475 nm) and zeolite trapped electrons (Na_4^{3+}, 500 nm).[50,51] The latter can be removed by purging the samples with oxygen, leading to the unambiguous characterizaton of the radical cation. The *trans*-stilbene radical cation was also

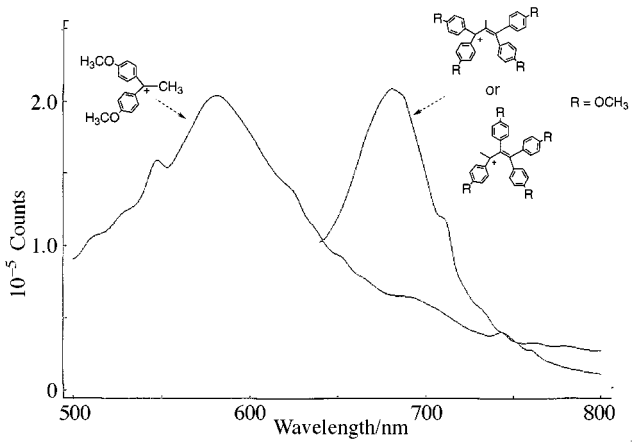

Fig. 11 Fluorescence emission from two cations trapped within CaY. Possible structures of the cations are also shown.

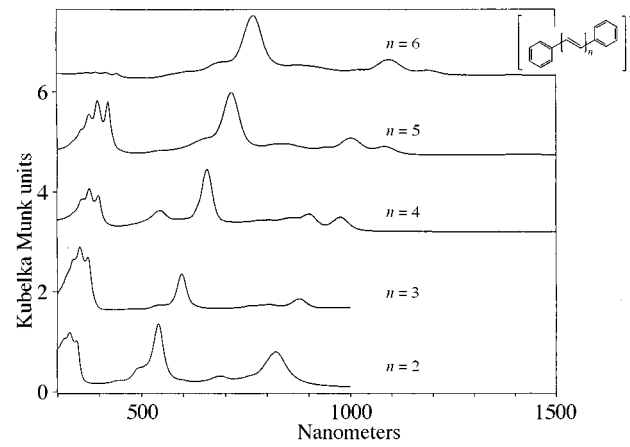

Fig. 12 Diffuse reflectance spectra of α,ω-diphenylpolyenes included within Na-ZSM-5 (Si/Al = 23). The absorption is due to stabilized radical cations of the alkanes.

observed upon excitation of *cis*-stilbene, in addition to weak signals due to photocyclizaton to give dihydrophenanthrene. There was no evidence for the generation of the *cis* radical cation (510 nm). However, a mixture of *cis* and *trans* radical cations was observed upon excitation of the *cis*-stilbene/tetranitromethane charge transfer complex in NaX zeolite, providing evidence that both radical cations were stable with respect to isomerization on the timescale of the laser experiments. Product studies carried out with laser irradiation demonstated that substantial *cis–trans* isomerization of stilbene occured within a few laser pulses. The combined results lead to the conclusion that *cis–trans* isomerization followed by photoionization of *trans*-stilbene was responsible for the observation of the *trans* radical cation upon excitation of *cis*-stilbene. We believe that an alternative possibility of photochemical isomerizaton within the laser pulse is less likely. The less efficient photoionization of *cis*-stilbene was consistent with its shorter singlet lifetime and the fact that it has an additional decay pathway involving photocyclization.

Direct excitation of 4-vinylanisole and *trans*-anethole,[52] as well as several other styrenes,[53] in zeolites also leads to the formation of the respective radical cations. For example, the *tran*-anethole radical cation has two characteristic absorption bands at 620 and 390 nm that agree well with the spectra for the same species in solution. Similar experiments using direct excitation of a number of di(4-methoxyphenyl)ethylenes in NaX zeolites provided evidence for formation of trapped electrons, indicating that photoionization also occurs for these alkenes.[54] However, the yields were considerably lower than for the styrenes, making it difficult to characterize the radical cations.

The products of direct excitation of a hexane slurry of di(4-methoxyphenyl)ethylene included within NaY zeolite are shown in Scheme 14.[55] Interestingly, no products are formed in

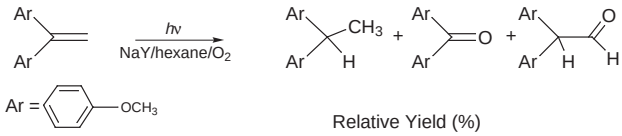

	Relative Yield (%)		
254 nm	73	15	17
300 nm	33	28	37
350 nm	8	41	49
>400 nm	—	49	51
>470 nm	—	49	51
>520 nm	No reaction		

Scheme 14

the absence of oxygen and the nature of the products depends on the excitation wavelength (Scheme 14). The key intermediate in both the reduction and the oxidation processes is believed to be the radical cation of di(4-methoxyphenyl)ethylene. The absorbing species during short and long wavelength excitations are thought to be different: at long wavelength it is in the alkene–oxygen complex and at short wavelength the uncomplexed alkene. The formation of hydrocarbon–oxygen complexes within zeolites had been extensively investigated by Frei *et al*.[56] The diffuse reflectance spectra shown in Fig. 13 indicate that di(4-methoxyphenyl)ethylene forms an oxygen complex when present within NaY. A proposed mechanism for the formation of products upon short and long wavelength excitations is shown in Scheme 15. Under both conditions an electron transfer is thought to be the primary step. During short wavelength excitation the primary electron acceptor is presumed to be the zeolite and during the long wavelength excitation the oxygen complexed to the alkene is likely the electron acceptor. Experiments aimed at a more detailed understanding of these reactions are in progress.

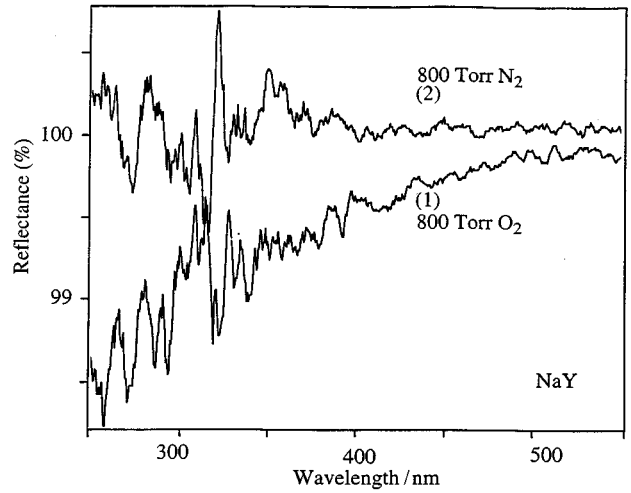

Fig. 13 Diffuse reflectance spectra of 4,4′-dimethoxydiphenylethylene included within NaY. Trace (1) is the difference of spectra taken after and before loading 800 Torr oxygen into the room temperature zeolite. Trace (2) is a control spectrum in which nitrogen was loaded instead of oxygen. Oxygen shows an absorption extending to 500 nm whereas nitrogen shows no such absorption. (We than S. Vasenkov and H. Frei, University of California, Berkeley for recording the spectra for us).

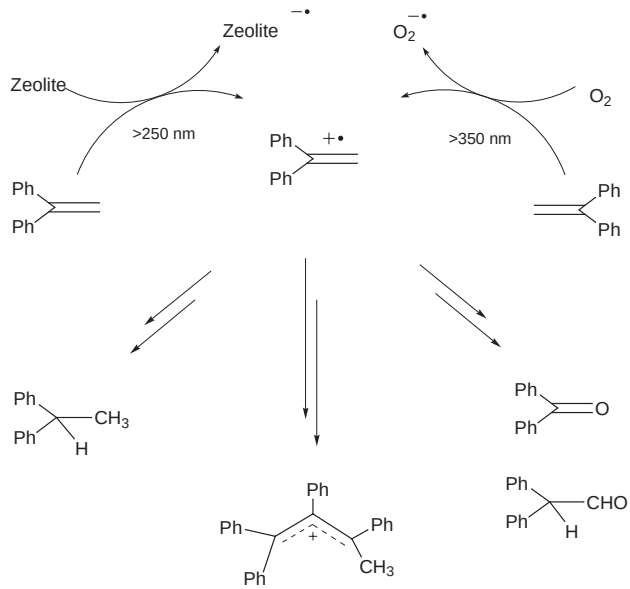

Scheme 15

The stabilization of organic radical cations within zeolites suggests that the confined interior space of a zeolite should provide an ideal environment for carrying out photosensitized electron transfer reactions. This approach has advantages in that one does not require prior preparation of an activated zeolite which may have a relatively small number of active sites as in the spontaneous electron transfer. Photosensitized electron transfer should also be applicable to a wider range of substrates. In addition, the zeolite environment promotes charge separation which is expected to be advantageous, since it will reduce the rate of the back-electron-transfer process that decreases the efficiency of these reactions in solution. We have used the dimerization of arylalkenes to demonstrate the viability of carrying out photoinduced electron transfer reactions for independently loaded sensitizers and alkene donors and to examine the effect of the zeolite environment on the product selectivity. The results obtained for *trans*-anethole using 2,3-dicyanonaphthalene and 9-cyanoanthracene as sensitizers are typical. For example, a combination of steady state and time-resolved fluorescence measurements indicated that the singlet excited state of the sensitizer was quenched by the alkene, predominantly *via* a static mechanism. Diffuse re-

flectance flash photolysis experiments were carried out using 355 nm excitation which excited the sensitizer only. The results demonstrated that the efficient singlet quenching of the sensitizer was accompanied by formation of the *trans*-anethole radical cation (Fig. 14). The latter has a spectrum similar to that

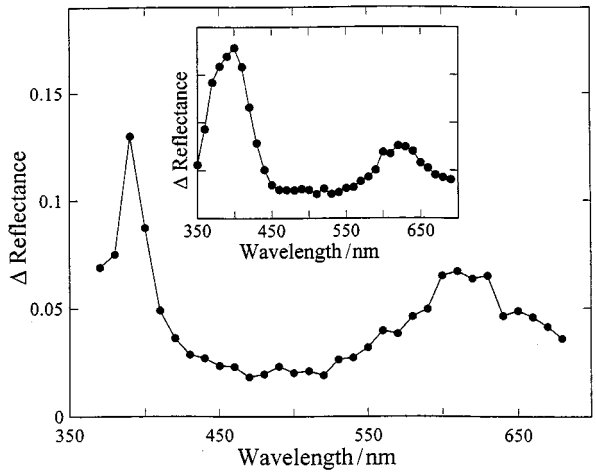

Fig. 14 Transient spectra measured after 355 nm excitation of 2,3-dicyanonaphthalene plus *trans*-anethole in NaX. The inset shows the spectrum obtained by direct 266 nm excitation of *trans*-anethole in NaX.

obtained by direct excitation of *trans*-anethole at 266 nm. The transient spectra also provided evidence for photoionization of the cyanoaromatic sensitizers in competition with electron transfer quenching in the zeolite environment. Efficient electron transfer was observed for 9-cyanoanthracene and 1-cyanonaphthalene sensitizers with *trans*-anethole and 4-vinylanisole, demonstrating the generality of these results. In each case the radical cation was relatively long-lived, illustrating the potential of the zeolite environment for overcoming the limitation of back electron transfer.

The products of the radical cation initiated dimerization of a series of arylalkenes with cyanoaromatic and quinolinium and acridinium sensitizers were examined. The results indicate that the radical cations add to the precursor alkenes to give dimeric products (Scheme 16), as has been observed in solution. In some cases oxidation of the alkenes accompanied dimer formation. A number of control experiments were carried out to ensure that the observed products resulted from sensitization rather than direct photolysis of the alkenes and to ensure that the product ratios did not reflect further reactions of the initial dimers. The product studies demonstrated that radical cation mediated dimerization occurred readily in the zeolite environment and suggested that the radical cations observed in the transient experiments are reactive. The dimer ratios also illustrated some important differences between the soluton and zeolite chemistry. For example, although both *cis*/*syn* and *trans*/*anti* dimers were formed, the zeolite favors the *cis*/*syn* product which has a more spherical shape that is similar to the geometry of the supercage. We believe that this reflects the fact that the more linear *trans*/*anti* isomers are best accommodated in two supercages whereas the *cis*/*syn* dimer can be formed within a single cage and therefore its formation is the more favorable process. It also appears that the zeolite environment is more important in determining the geometry of the dimeric products than the method (direct or sensitized photocycloaddition *vs.* radical ion initiation) used for their generation.

Concluding remarks

The chemistry of alkenes in zeolites illustrates both the potential complexity and utility of zeolites as reaction media. For example, the results discussed above demonstrate that spontaneous thermal proton and electron transfer reactions are

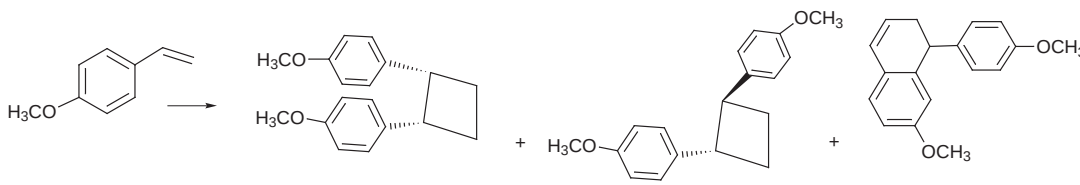

	Relative Yield (%)		
Acetonitrile/PET sensitized	4	90	6
NaX/9-cyanoanthracene	66	26	7

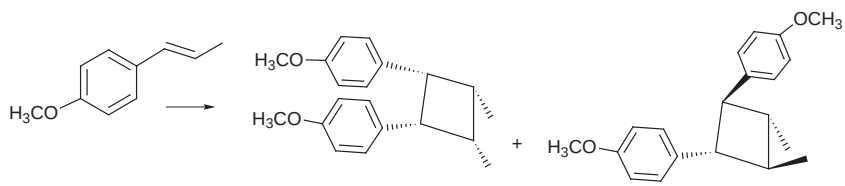

	Relative Yield (%)	
Acetonitrile/PET sensitized	4	96
NaX/9-cyanoanthracene	45	55

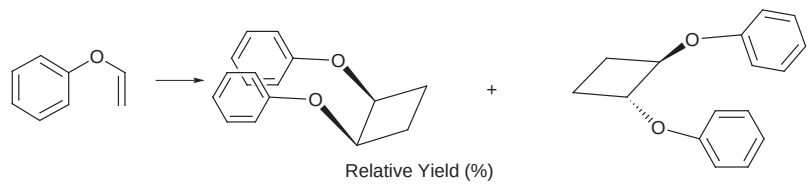

	Relative Yield (%)	
Acetonitrile/PET sensitized	55	45
NaX/9-cyanoanthracene	65	35

Scheme 16

common, particularly for zeolites with relatively large numbers of active sites. NMR studies are particularly useful in correlating the number and type of active sites with the chemistry observed and permit one to select a zeolite and an activation procedure that can be used to tune the chemistry. In cases where the zeolite contains fewer active sites, stable alkenes can undergo a range of photochemical reactions, as demonstrated with the energy transfer sensitized singlet oxygen ene reaction and photoinduced electron transfer reactions that lead to dimeric products. Both examples serve to illustrate the ease with which bimolecular reactions between independently loaded donors and acceptors in zeolites can be carried out. A combination of techniques, including product studies, fluorescence and diffuse reflectance flash photolysis, can provide a detailed picture of the reactive intermediates that lead to the observed chemistry. Of particular interest are the changes in product selectivity that result from carrying out these reactions in the constrained space of the zeolite cavity. The results discussed herein provide an excellent basis for the development of sufficient predictive power that one can tune the behavior of the thermal and photochemical behavior for substrates within zeolites in order to achieve a desired product outcome.

Acknowledgments

V. R. thanks the Division of Chemical Sciences, Office of Basic Energy Sciences, Office of Energy Research, US Department of Energy for generous support of this program and K. Pitchumani, K. J. Thomas, V. Jayathirtha Rao, J. Shailaja, R. J. Robbins and X. Li for their contributions to the work presented here. C. P. G. acknowledges the Donors of the Petroleum Research Fund, administered by the American Chemical Society, and the National Science Foundation National Young Investigator program (DMR-9458017) for support of this research and Hsien-Ming Kao for experimental and intellectual contributions towards the results presented here. L. J. J. thanks L. Brancaleon, D. Brousmiche and P. D. Wood for their contributions to the work presented here.

Notes and References

1 K. Kalyanasundaram, *Photochemistry in Microheterogeneous Systems*, Academic Press, New York, 1987; *Photochemistry in Organized and Constrained Media*, ed. V. Ramamurphy, VCH, New York, 1991.
2 D. W. Breck, *Zeolite Molecular Sieves: Structure, Chemistry and Use*, Wiley, New York, 1974; A. Dyer, *An Introduction to Zeolite Molecular Sieves*, Wiley, Bath, UK, 1988.
3 N. J. Turro and M. Garcia-Garibay in *Photochemistry in Organized and Constrained Media*, ed. V. Ramamurthy, VCH, New York, 1991, p. 1; N. J. Turro, in *Inclusion Phenomena and Molecular Recognition*, ed. J. Atwood, Plenum Press, New York, 1990, p. 289.
4 W. J. Mortier, *Compilation of Extra Framework Sites in Zeolites*, Butterworth Scientific Ltd, Guildford, UK, 1982.
5 C. P. Grey, F. I. Poshni, A. Gualtieri, P. Norby, J. C. Hanson and D. R. Corbin, *J. Am. Chem. Soc.*, 1997, **119**, 1981.
6 *Singlet Oxygen*, ed. H. H. Wasserman and R. W. Murray, Academic Press, New York, 1979; *Singlet Oxygen*, ed. A. A. Frimer, CRC Press: Boca Raton, 1985, vol. 1–4.
7 M. Prein and W. Adam, *Angew Chem., Int. Ed., Engl.*, 1996, **35**, 477.
8 V. Ramamurthy, D. R. Sanderson and D. F. Eaton, *J. Am. Chem. Soc.*, 1993, **115**, 10 438.
9 C. S. Foote, *Acc. Chem. Res.*, 1968, **1**, 104.
10 X. Li and V. Ramamurthy, *J. Am. Chem. Soc.*, 1996, **118**, 10 666.
11 R. Robbins and V. Ramamurthy, *Chem. Commun.*, 1997, 1071.
12 P. H. Kasai and R. J. Bishop, Jr., *J. Am. Chem. Soc.*, 1972, **94**, 5560; P. H. Kasai and R. J. Bishop, Jr., *J. Phys. Chem.*, 1973, **77**, 2308.
13 V. Ramamurthy and D. R. Sanderson, *J. Phys. Chem.*, 1993, **97**, 13 380.
14 R. H. Staley and J. L. Beauchamp, *J. Am. Chem. Soc.*, 1975, **97**, 5920; J. Sunner, K. Nishizawa and P. Kebarle, *J. Phys. Chem.*, 1981, **85**, 1814; C. Schade and P. v. R. Schleyer, *Adv. Organomet. Chem.*, 1987, **27**, 169; W. Setzer and P. v. R. Schleyer, *Adv. Organomet. Chem.*, 1985, **24**, 353.
15 J. Chandrasekar and B. Sunoj, unpublished results; work in progress.
16 V. Ramamurthy, J. V. Caspar, D. F. Eaton, E. W. Kuo and D. R. Corbin, *J. Am. Chem. Soc.*, 1992, **114**, 3882; V. Ramamurthy, J. V. Caspar, D. R. Corbin, B. D. Schlyer and A. H. Maki, *J. Phys. Chem.*, 1990, **94**, 3391; M. A. Hepp, V. Ramamurthy, D. R. Corbin and C. Dybowski, *J. Phys. Chem.*, 1996, **96**, 2629.
17 A. N. Fitch, H. Jobic and A. Renouprez, *J. Phys. Chem.*, 1986, **90**, 1311; A. N. Fitch, H. Jobic and A. Renouprez, *J. Phys. Chem.*, 1986, **90**, 1311; M. Czjzek, T. Vogt and H. Fuess, *Angew. Chem., Int. Ed. Engl.*, 1989, **28**, 770; C. Mellot, M. H. Simonot-Grange, E. Pilverdier, J. P. Bellat and D. Espinat, *Langmuir*, 1995, **11**, 1726; M. Czjzek, T. Vogt and H. Fuess, *Zeolites*, 1992, **12**, 237; C. Kirschhock and H. Fuess, *Zeolites*, 1996, **17**, 381; R. Goyal, A. N. Fitch and H. Jobic, *J. Chem. Soc., Chem. Commun.*, 1990, 1152.
18 R. J. Robbins and V. Ramamurthy, unpublished results.
19 V. Jayathirtha Rao, D. L. Perlstein, R. J. Robbins, P. H. Lakshminarasimhan, H.-M. Kao, C. P. Grey and V. Ramamurthy, *Chem. Commun.*, 1998, 269.
20 C. P. Grey and A. J. Vega, *J. Am. Chem. Soc.*, 1995, **117**, 8232.
21 C. P. Grey and B. S. A. Kumar, *J. Am. Chem. Soc.*, 1995, **117**, 9071.
22 H.-M. Kao and C. P. Grey, *J. Phys. Chem.*, 1996, **100**, 5105.
23 H. M. Kao and C. P. Grey, *Chem. Phys. Let.*, 1996, **259**, 459.
24 H. M. Kao and C. P. Grey, *J. Am. Chem. Soc.*, 1997, **119**, 627.
25 C. P. Grey, A. J. Vega and W. S. Veeman, *J. Chem. Phys.*, 1993, **98**, 7711.
26 W. P. Rothwell, W. Chen and J. H. Lunsford, *J. Am. Chem. Soc.*, 1984, **106**, 2452; J. H. Lunsford, W. P. Rothwell and W. Shen, *J. Am. Chem. Soc.*, 1985, **107**, 1540.
27 H.-M. Kao, C. P. Grey, K. Pitchumani, P. H. Lakshminarasimhan and V. Ramamurthy, *J. Phys. Chem.*, 1998, **102**, 5627.
28 J. W. Ward, *J. Catal*., 1968, **10**, 34.
29 Z. Luz and A. J. Vega, *J. Phys. Chem.*, 1987, **91**, 365.
30 D. W. Breck, *Zeolite Molecular Sieves: Structure, Chemistry and Use*, Wiley, New York, 1974, p. 461.
31 K. J. Thomas and V. Ramamurthy, *Langmuir*, in press.
32 Recently, there have been reports in which photochemical reactions of alkenes in H^+ zeolites have been investigated.[33] However, it has been our experience that alkenes undergo Brønsted acid catalyzed reaction in H^+Y zeolites.[34] Therefore, H^+ zeolites should be avoided as hosts when investigating the photochemical behavior of alkenes.
33 V. Fornes, H. Garcia, M. A. Miranda, F. Mojarrad, M. J. Sabater and N. N. E. Suliman, *Tetrahedron*, 1996, **52**, 7755; M. L. Cano, A. Corma, V. Fornes, H. Garcia, M. A. Miranda, C. Baerlocher and C. Lengauer, *J. Am. Chem. Soc.*, 1996, **118**, 11006; A. Corma, H. Garcia, M. A. Miranda, J. Primo and M. J. Sabater, *J. Am. Chem. Soc*., 1994, **116**, 2276.
34 P. H. Lakshminarasimhan, and V. Ramamurthy, unpublished results; M. Kojima, H. Takeya, Y. Kurovama and S. Oishi, *Chem. Lett.*, 1997, 997.
35 K. Pitchumani and V. Ramamurthy, *Chem. Commun.*, 1996, 2763.
36 V. Jayathirtha Rao, N. Prevost, V. Ramamurthy, M. Kojima and L. J. Johnston, *Chem. Commun.*, 1997, 2209.
37 K. Pitchumani, P. H. Lakshminarasimhan, N. Prevost, D. R. Corbin and V. Ramamurthy, *Chem. Commun*., 1997, 181.
38 K. Pitchumani, A. Joy, N. Prevost and V. Ramamurthy, *Chem. Commun*., 1997, 127; K. Pitchumani, P. H. Lakshminarasimhan, G. Turner, M. G. Bakker, and V. Ramamurthy, *Tetrahedron Lett.*, 1997, 371; K. Pitchumani, D. R. Corbin and V. Ramamurthy, *J. Am. Chem. Soc*., 1996, **118**, 8152.
39 R. A. McClelland, C. Chan, F. Cozens, A. Modro and S. Steenken, *Angew. Chem., Int. Ed. Engl.*, 1991, **30**, 1337.
40 R. A. McCelland, V. M. Kangasabapathy and S. Steenken, *J. Am. Chem. Soc.*, 1988, **110**, 6913; A. Azarani, A. B. Berinstain, L. J. Johnston and S. Kazanis, *J. Photochem. A: Chem.*, 1991, **57**, 175.
41 H. J. Prosser and R. N. Young, *Eur. Polym. J*., 1972, **3**, 879.
42 H. P. Leftin and W. K. Hall, *J. Phys. Chem.*, 1960, **64**, 382; H. P. Leftin, *J. Phys. Chem.*, 1960, **64**, 1714; H. P. Leftin and W. K. Hall, *J. Phys. Chem.*, 1962, **66**, 1457; H. P. Leftin, M. C. Hobson and J. S. Leigh, *J. Phys. Chem.*, 1962, **66**, 1214; J. J. Rooney and R. C. Pink, *Trans. Faraday Soc.*, 1962, 1632; W. K. Hall, *J. Catal.*, 1962, **1**, 53; F. R. Dollish and W. K. Hall, *J. Phys. Chem.*, 1965, **69**, 4402; V. Fornes, H. Garcia, S. Jovanic and V. Marti, *Tetrahedron*, 1997, **53**, 4715; A. Evans, P. M. S. Jones and J. H. Thomas, *J. Chem. Soc.*, 1957, 104.
43 J. J. Rooney and B. J. Hathaway, *J. Catal.*, 1964, **3**, 447.
44 M. K. Boyd, in *Molecular and Supramolecular Photochemistry*, ed. V. Ramamurthy and K. S. Schanze, Marcell Dekker, New York, 1997, vol. 1, p. 147; L. J. Johnston, *Chem. Rev.*, 1993, **93**, 251.
45 D. N. Stamires and J. Turkevich, *J. Am. Chem. Soc.*, 1964, **86**, 749.
46 V. Ramamurthy, J. V. Caspar and D. R. Corbin, *J. Am. Chem. Soc.*, 1991, **113**, 594; J. V. Caspar, V. Ramamurthy and D. R. Corbin, *J. Am. Chem. Soc.*, 1991, **113**, 600.

47 T. Shida and W. H. Hamill, *J. Phys. Chem.*, 1966, **44**, 4372; Y. Yamamoto, T. Aoyama and K. Hayashi, *J. Chem. Soc., Faraday Trans. 1*, 1988, **84**, 2209.
48 X. Liu, K.-K. Iu, J. K. Thomas, H. He and J. Klinowski, *J. Am. Chem. Soc.*, 1994, **116**, 11 811.
49 K. Iu and J. K. Thomas, *J. Phys. Chem.*, 1991, **95**, 506.
50 I. K. Lednev, N. Mathivanan and L. J. Johnston, *J. Phys. Chem.*, 1994, **98**, 11.
51 F. Gessner and J. C. Scaiano, *J. Photochem. Photobiol. A: Chem.*, 1992, **67**, 91.
52 L. Brancaleon, D. Brousmiche, V. J. Rao, L. J. Johnston and V. Ramamurthy, *J. Am. Chem. Soc.*, 1998, **120**, 4926.
53 F. L. Cozens, R. Bogdanova, M. Regimbald, H. Garcia, V. Marti and J. C. Scaiano, *J. Phys. Chem. B*, 1997, **101**, 6921.
54 P. D. Wood and L. J. Johnston, unpublished results.
55 P. Lakshminarasimahn and V. Ramamurthy, unpublished results; work in progress.
56 H. Frei, F. Blatter and H. Sun, *CHEMTECH.*, 1996, **26**, 24.

Paper 8/03871F

Cyclopentadienyl titanium chlorides containing *ortho*-(1-naphthyl)phenoxide ligation

Jonathan S. Vilardo, Matthew G. Thorn, Phillip E. Fanwick and Ian P. Rothwell*

Department of Chemistry, 1393 Brown Building, Purdue University, West Lafayette, IN 47907-1393, USA. E-mail. rothwell@chem.purdue.edu

Received (in Bloomington, IN, USA) 30th June 1998, Accepted 2nd September 1998

A series of mono-cyclopentadiene derivatives of titanium containing *ortho*-(1-naphthyl)phenoxide ligands have been studied; the Ti–Ti distance in the d^1–d^1 species [Cp(Ar-O)Ti(μ-Cl)$_2$Ti(OAr)Cp] is exactly intermediate between that found in paramagnetic [Cp$_2$Ti(μ-Cl)$_2$TiCp$_2$] and diamagnetic [(ArO)$_2$Ti(μ-Cl)$_2$Ti(OAr)$_2$].

Ortho-phenyl phenoxide ligands, *e.g.* **1** (Scheme 1) and **2**, are an important subset of aryloxide ligation that have been used to support inorganic/organometallic chemistry at p-block,[1] d-block[2] and f-element[3] metal centers. Following our successful development of cyclometalation resistant, *e.g.* **3** and **4**, and immune, **5** (Scheme 1) aryloxide ligation[4] we have begun to study the chemistry of potentially chiral *o*-(1-naphthyl)phenoxide ligands. Straightforward synthetic strategies lead to the non-symmetric **6** and symmetric **7** and **8** (Scheme 1, Np = 1-naphthyl).† Both **7** and **8** are produced as a 50/50 mixture of non-chiral *meso* and DL forms. In the case of **7** inter-conversion of the two forms occurs on the NMR timescale with the barrier for naphthyl rotation estimated as 18.0(5) kcal mol^{-1} at 67 °C. Presumably a similar barrier will be present for other *o*-(1-naphthyl)phenols lacking *meta* substituents. In the case of *meta*-phenyl blocked **8** it is possible to isolate the pure, crystalline *meso* form from CH_2Cl_2–heptane and show that inter-conversion in this case requires days at 100 °C.[5] In contrast an adaptation of the chemistry of the late Sir Derek Barton[6] leads to **9** (Scheme 1) which is produced as a single isomer whose subsequent chemistry (below) shows it to be the chiral form.

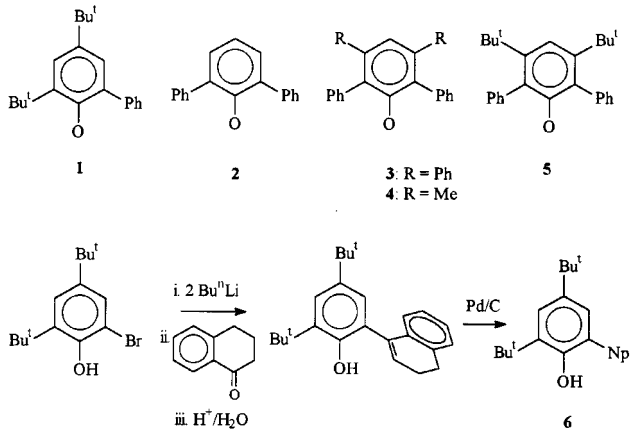

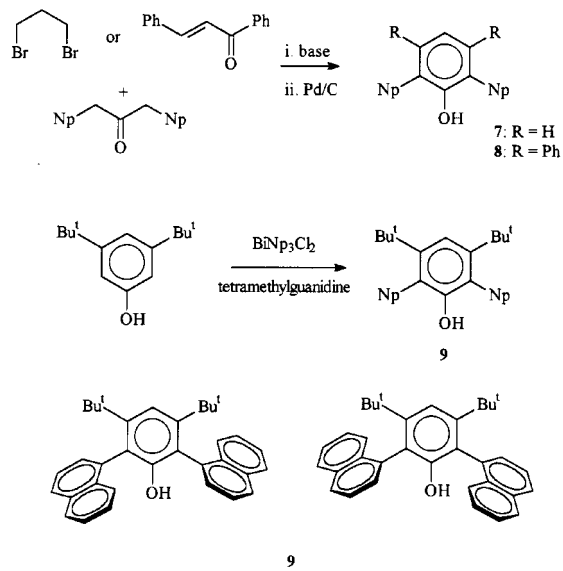

Scheme 1

Reaction of phenols **1**, **4**–**6** and **9** in the presence of pyridine (py) or the lithium salt of **5** with [CpTiCl$_3$] yields the compounds **10**–**12** as orange solids in high yield (Scheme 2). The solid state structure of **12b** (Fig. 1)‡ confirms the chiral nature of the single isomer of phenol **9** generated by the particular method of synthesis. The solution NMR spectroscopic properties of **10**–**12** are as expected with single C_5H_5 resonances and a single set of aryloxide signals in each cause.† In the ^{1}H NMR spectrum of **12b** the C_5H_5 protons resonate at significantly higher field, δ 5.32 compared to the δ 5.6–5.8 region found for the other derivatives. This indicates much greater diamagnetic shielding of adjacent ligand protons and is caused by the presence of the two *ortho*-(1-naphthyl) rings, which are locked in place by the *meta*-*tert*-butyl groups.

Treatment of **10b** with sodium amalgam (1 Na per Ti) leads to a red solution of the dimeric species **13** (Scheme 2). The solid state structure of **13** (Fig. 2)‡ shows a dinuclear compound with a Ti(μ-Cl)$_2$Ti core and terminal aryloxide and Cp groups. The

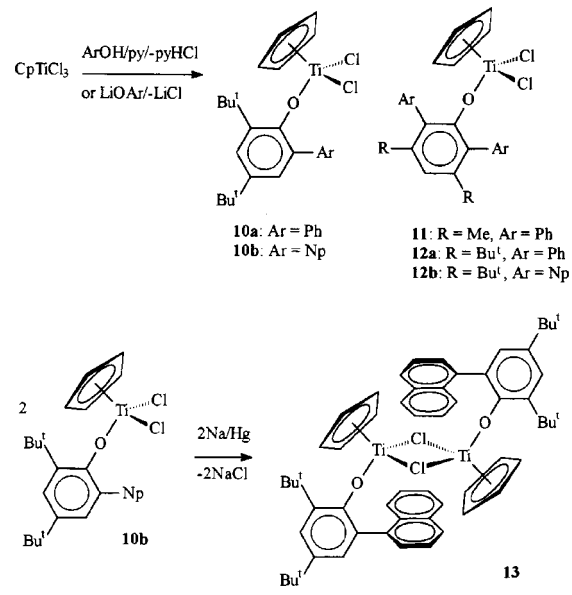

Scheme 2

Table 1 Structural parameters for $[(X)(Y)TiCl_2]$ and $[(X)(Y)Ti(\mu\text{-}Cl)_2Ti(X)(Y)]$; X, Y = Cp or ArO (Np = 1-naphthyl)

Compound	X–Ti–Y/°	Cl–Ti–Cl/°	Ti–Cl/Å	Ti–Ti/Å	Ref.
Cp_2TiCl_2	131	94	2.36 (av.)	—	7
$CpTi(OC_6HNp_2\text{-}2,6\text{-}Bu^t_2\text{-}3,5)_2Cl_2$ **12b**	118	102	2.23 (av.)	—	This work
$Ti(OC_6H_3Ph_2\text{-}2,6)_2Cl_2$	109	113	2.206(1)	—	8
$[Cp_2Ti(\mu\text{-}Cl)]_2$	133	79	2.55 (av.)	3.95 (av.)	9
$[CpTi(OC_6H_2Np\text{-}2\text{-}Bu^t_2\text{-}4,6)(\mu\text{-}Cl)]_2$ **13**	125	115	2.40 (av.)	3.336(1)	This work
$[Ti(OC_6H_3Ph_2\text{-}2,6)_2(\mu\text{-}Cl)]_2$	144	102	2.37 (av.)	2.9827(7)	10

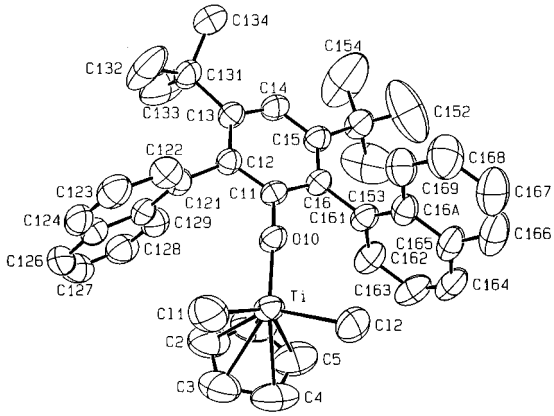

Fig. 1 Molecular structure of **12b** showing the atomic numbering scheme. Selected interatomic distances (Å) and angles (°): Ti–O(10) 1.774(3), Ti–Cl(1) 2.230(2), Ti–Cl(2) 2.244(2); Cl–Ti–Cl 102.36(7), Cp–Ti–O(10) 118.6(2), Ti–O(10)–C(11) 164.1(3).

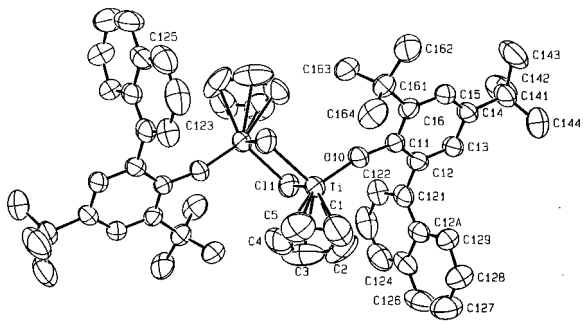

Fig. 2 Molecular structure of **13** showing the atomic numbering scheme. Selected interatomic distances (Å) and angles (°): Ti–Ti 3.336(1), Ti–O(10) 1.817(2), Ti–Cl(1) 2.400(1), 2.406(1); Cl(1)–Ti–Cl(1) 92.07(4), Cp–Ti–O(10) 125.1(3), Ti–O(10)–C(11) 166.7(2).

Cp ligands are arranged in a transoid fashion, with a crystallographic inversion center being present. The molecular structure of **13** is such that each dimeric unit contains two naphthylphenoxides of opposite chirality.

Table 1 collects some structural parameters for selected derivatives of Ti(IV/III), focusing on the effects of replacing Cp ligands by OAr groups. Some trends can be discerned. The Ti–Cl distance decreases significantly in both series of compounds as Cp is replaced by OAr, reflecting an increase in electrophilicity of the metal center. In the tetrahedral Ti(IV) series the Cl–Ti–Cl angle opens up as the corresponding X–Ti–Y angle closes down upon replacement of Cp by OAr.[7,8] The most interesting parameter is the Ti–Ti distances in the d^1–d^1 dimers.[9,10] The 3.95(av.) distance in the Cp_2Ti compounds is consistent with the complete lack of any metal–metal bonding. In contrast the short distance in the diamagnetic bis(aryloxide) is consistent with the presence of a Ti–Ti single bond.[10] In the case of the 'hybrid' paramagnetic species **13**, the Ti–Ti distance is exactly intermediate between the previous two molecules. In this case there is clearly no metal–metal bond present and the observed Ti–Ti distance possibly is purely a consequence of the Ti–Cl distances within the $Ti(\mu\text{-}Cl)_2Ti$ unit.

We thank the National Science Foundation (Grant CHE-9321906) for financial support of this research.

Notes and references

† *Selected spectroscopic data*: aromatic signals unless indicated: ^{1}H NMR (C_6D_6, unless otherwise stated, 30 °C): **6**: ($CDCl_3$) δ 7.00–7.90; 4.82 (s, O*H*); 1.44 (s), 1.32 [s, C(C*H*$_3$)$_3$]. **7**: ($CDCl_3$) δ 6.80–8.20; 4.78 (s), 4.74 (s, O*H*). **8**: ($CDCl_3$) δ 7.00–8.10; 4.95 (s), 4.93 (s, O*H*). **9**: δ 7.9–7.23 (m); 4.15 (s, O*H*); 1.18 [s, C(C*H*$_3$)$_3$]. **10a**: δ 7.22–8.20; 5.60 (s, C_5H_5); 1.67 (s), 1.25 [s, C(C*H*$_3$)$_3$]. **10b**: δ 7.20–7.60; 5.70 (s, C_5H_5); 1.63 (s), 1.27 [s, C(C*H*$_3$)$_3$]. **11**: δ 7.19–7.36; 6.79 (s, *para*-H); 5.78 (s, C_5H_5); 2.03 (s, *meta*-CH_3). **12a**: δ 7.72 (s, *para*-H); 7.30–7.16 (m); 5.91 (s, C_5H_5); 1.23 [s, C(C*H*$_3$)$_3$]. **12b**: δ 7.87 (s, *para*-H); 7.71–7.13 (m); 5.32 (s, C_5H_5); 1.10 [s, C(C*H*$_3$)$_3$]. ^{13}C NMR (C_6D_6, unless otherwise stated, 30 °C): **6**: ($CDCl_3$) δ 149.3 (O–*C*); 123.8–141.8; 35.1, 34.4 [*C*(CH$_3$)$_3$]; 31.7, 29.7 [C(*C*H$_3$)$_3$]. **7**: ($CDCl_3$) δ 150.7, 150.6 (*C*O); 135.1, 135.0, 133.8, 131.95, 131.88, 127.0, 126.93; 131.3, 129.3, 128.4, 128.3, 128.0, 127.8, 126.3, 126.2, 126.0, 125.9, 125.6, 120.3, 120.2. **8**: ($CDCl_3$) δ 151.43, 151.38 (CO); 124.0–141.0. **9**: δ 151.7 (O–*C*); 148.5, 136.2, 133.5, 129.5, 128.1, 128.0, 126.6, 126.1, 125.9, 125.3, 122.8, 118.0, 109.5; 37.2 [*C*(CH$_3$)$_3$]; 32.4 [C(*C*H$_3$)$_3$]. **10a**: δ 165.0 (Ti–O–*C*); 120.6 (C_5H_5); 36.0, 34.7 [*C*(CH$_3$)$_3$]; 31.5, 30.7 [C(*C*H$_3$)$_3$]. **10b**: δ 164.6 (Ti–O–C); 121.1 (C_5H_5); 35.9, 34.7 [*C*(CH$_3$)$_3$]; 31.5, 30.6 [C(*C*H$_3$)$_3$]. **11**: δ 164.3 (Ti–O–*C*); 120.2 (C_5H_5); 20.7 (*meta*-CH_3). **12a**: δ 165.8 (O–*C*); 147.9, 138.5, 132.9, 131.1, 128.5, 127.8, 121.4; 119.8 (C_5H_5); 37.5 [*C*(CH$_3$)$_3$]; 33.0 [C(*C*H$_3$)$_3$]. **12b**: δ 166.2 (O–C); 149.1, 136.6, 135.5, 134.2, 130.4, 128.8, 128.7, 128.3, 127.3, 126.3, 126.1, 125.3, 122.4; 119.6 (C_5H_5); 37.9 [*C*(CH$_3$)$_3$]; 32.8 [C(*C*H$_3$)$_3$].

‡ *Crystal data*: for **12b** at 296 K: $TiCl_2OC_{39}H_{38}$, M = 641.54, space group $P\bar{1}$ (no. 2), a = 10.960(1), b = 11.644(3), c = 15.603(1) Å, α = 71.003(7), β = 104.23(3), γ = 63.402(5)°, V = 1673.5(3) Å^3, D_c = 1.273 g cm^{-3}, Z = 2. Of the 6851 unique reflections collected ($7.69 \leqslant 2\theta \leqslant 62.74°$) with Mo-K$\alpha$ (λ = 0.71073 Å), the 6851 with $F_o^2 > 2\sigma(F_o^2)$ were used in the final least-squares refinement to yield $R(F_o)$ = 0.076 and $R_w(F_o^2)$ = 0.190. For **13** at 296 K: $Ti_2Cl_2O_2C_{58}H_{64}$, M = 959.86, space group $P2_1/n$ (no. 14), a = 12.5923(5), b = 12.7390(6), c = 17.4609(8) Å, β = 109.814(2)°, V = 2635.1(4) Å^3, D_c = 1.210 g cm^{-3}, Z = 2. Of the 6836 unique reflections collected ($5.90 \leqslant 2\theta \leqslant 61.46°$) with Mo-K$\alpha$ (λ = 0.71073 Å), the 6836 with $F_o^2 > 2\sigma(F_o^2)$ were used in the final least-squares refinement to yield $R(F_o)$ = 0.074 and $R_w(F_o^2)$ = 0.169.

1 S. Saito and H. Yamamoto, *Chem. Commun.*, 1997, 1585.
2 I. P. Rothwell, *Chem. Commun.*, 1997, 1331; *Acc. Chem. Res.*, 1988, **21**, 153.
3 D. L. Clark, G. B. Deacon, T. Feng, R. V. Hollis, B. L. Scott, B. W. Skelton, J. G. Watkin and A. H. White, *Chem. Commun.*, 1996, 1729 and references therein.
4 J. S. Vilardo, M. A. Lockwood, L. G. Hanson, J. R. Clark, B. C. Parkin, P. E. Fanwick and I. P. Rothwell, *J. Chem. Soc., Dalton Trans.*, 1997, 3353.
5 For related *ortho*-(2-alkylphenyl)phenols see S. Saito, T. Kano, K. Hatanaka and H. Yamamoto, *J. Org. Chem.*, 1997, **62**, 5651.
6 D. H. R. Barton, D. M. X. Donnelly, P. J. Guiry and J. H. Reibenspies, *J. Chem. Soc., Chem. Commun.*, 1990, 1110; D. H. R. Barton, N. Y. Bhatnagar, J.-C. Blazejewski, B. Charpiot, J.-P. Finet, D. J. Lester, W. B. Motherwell, M. T. B. Papoula and S. P. Stanforth, *J. Chem. Soc., Perkin Trans. 1*, 1985, 2657.
7 A. Clearfield, D. K. Warner, C. H. Saldarriaga-Molina and R. Ropal, *Can. J. Chem.*, 1975, **53**, 1622.
8 J. R. Dilworth, J. Hanich, M. Krestel, J. Beck and J. Strahle, *J. Organomet. Chem.*, 1986, **315**, C9.
9 R. Jungst, D. Sekutowski, J. Davis, M. Luly and G. Stucky, *Inorg. Chem.*, 1977, **7**, 1645.
10 J. E. Hill, P. E. Fenwick and I. P. Rothwell, *Polyhedron*, 1990, **9**, 1617.

Communication 8/05034A

ChemComm

Formation and reactivity of cationic alkyl derivatives of titanium containing *ortho*-(1-naphthyl)phenoxide ligation

Matthew G. Thorn, Jonathan S. Vilardo, Phillip E. Fanwick and Ian P. Rothwell*

Department of Chemistry, 1393 Brown Building, Purdue University, West Lafayette, IN 47907-1393, USA. E-mail: rothwell@chem.purdue.edu

Received (in Bloomington, IN, USA) 14th July 1998, Accepted 2nd September 1998

A series of dimethyl compounds of Ti(IV) have been isolated containing both cyclopentadiene and *ortho*-arylphenoxide ligation; reaction with $[B(C_6F_5)_3]$ generates corresponding cationic methyl species which eliminate methane and form $[Cp(ArO)Ti\{CH_2B(C_6F_5)_2\}(C_6F_5)]$ derivatives.

There is continued research interest in the chemistry of cationic Group 4 metal alkyl compounds.[1] We have recently isolated a series of titanium chloride compounds containing both cyclopentadiene and *o*-arylphenoxide ligation.[2,3] We report here on the structure, dynamics and reactivity of the corresponding neutral and cationic methyl derivatives.[4,5]

Treatment of **1**–**3** with LiMe leads to the corresponding dimethyl compounds **4**–**6** as yellow solids (Scheme 1, Np = 1-naphthyl).† The solid state structure of **4b** is shown in Fig. 1.‡ The Ti–Me distances of 2.076(4) and 2.091(4) Å are intermediate between those reported for $[Cp_2TiMe_2]$,[6] 2.170(2) and 2.181(2) Å, and values of 2.052(2) and 2.069(2) Å found in $[Ti(OC_6H_3Ph_2\text{-}2,6)_2Me_2]$.[7] There is also a corresponding opening up of the Me–Ti–Me angle upon replacing Cp by OAr; *c.f.* 91.3(1)° for $[Cp_2TiMe_2]$, 97.5(2)° in **4b** and 103.9(1)° in $[Ti(OC_6H_3Ph_2\text{-}2,6)_2Me_2]$. In the solution NMR spectra of **4a**, **5** and **6a**, only one signal is present for the Ti–Me groups in the ^{1}H and ^{13}C NMR spectra. This indicates in the case of **4a** that rotation about the Ti–O–Ar bonds is fast on the NMR timescale. In contrast two well-resolved Ti–Me resonances are observed for the *o*-(1-naphthyl) derivatives **4b** and **6b**. In the case of **6b** this is consistent with the presence of the chiral, *dl*-form of the ligand. Variable temperature NMR studies of **4b** show that the two methyl signals remain sharp even at 90 °C (toluene-d_8), indicating slow naphthyl rotation on the NMR timescale at this temperature.

Addition of $[B(C_6F_5)_3]$[8] to **4**,**5** in benzene or toluene solvent leads to the rapid (NMR) formation of the thermally unstable (*vide infra*) cationic **7**,**8**. Variable temperature spectra of these species are highly informative. Low temperature ^{1}H and ^{13}C NMR spectra of **7a** and **8** show a single set of Cp and OAr resonances along with resolved Ti-Me (sharp) and Ti-Me-B (broad) resonances. Spectra obtained for **7a** at ambient temperature show broadening of these methyl signals, but the thermal instability precludes obtaining limiting high temperature spectra. We interpret this broadening as due to exchange of the boron between methyl groups (boron exchange) which is becoming fast on the NMR time scale. For **7b**, two broad methyl signals and a single, sharp Cp resonance are present at room temperature. At −10 °C (toluene-d_8) the Ti-Me and Ti-Me-B signals sharpen up, but there is still only a single Cp resonance. At −30 °C the Cp resonance splits into two signals in the ratio of 80 : 20 representing the two, diastereoisomeric forms. The methyl signals also split into two large, equal intensity signals and one resolvable smaller peak (presumably the second methyl signal is obscured by OAr resonances). We interpret these changes as representing two distinct dynamic processes. The faster process involves exchange between the two diastereoisomers (80 : 20 ratio) of **7b** (Scheme 2) without methyl exchange. This process involves cation–anion dissociation and rearrangement and can only be detected using the chiral *o*-(1-naphthyl)phenoxide. An alternative process for exchange of diastereoisomers would involve naphthyl rotation. However, the variable temperature NMR studies on **4b** and data presented below show that this process is too slow to account for the observed process. The slower process in **7b**, which is also detected for **7a** and **8**, involves Ti-Me/Ti-Me-B exchange. In the case of **7b** this process alone cannot lead to exchange of methyl signals in the NMR spectra. However, when coupled with the faster ion-pair dissociation, it leads to methyl exchange (Scheme 2). Previous work by Marks *et al*. has shown similar dynamics are present in $[Cp'_2Zr(Me)\{MeB(C_6F_5)_3\}]$ species.[8] Based upon the spectra obtained for **7b** we estimate the free energy of activation for ion-pair dissociation to be 12.4(5) kcal mol^{-1} at −25 °C (Cp

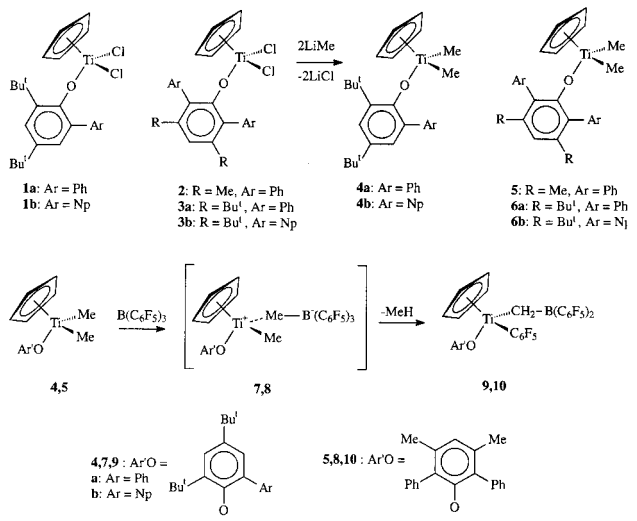

Scheme 1

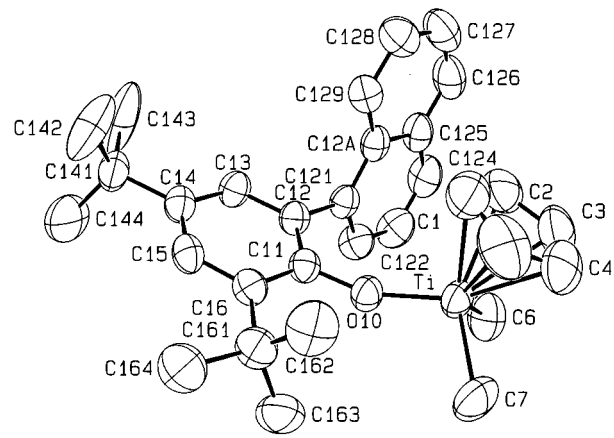

Fig. 1 Molecular structure of **4b** showing the atomic numbering scheme. Selected interatomic distances (Å) and angles (°): Ti–O(10) 1.815(2), Ti–C(6) 2.076(4), Ti–C(7) 2.091(4), C(6)–Ti–C(7) 97.5(2), Cp–Ti–O(10) 123.7(2), Ti–O(10)–C(11) 158.8(2).

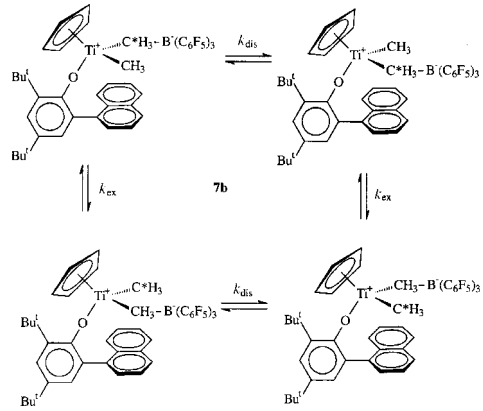

Scheme 2

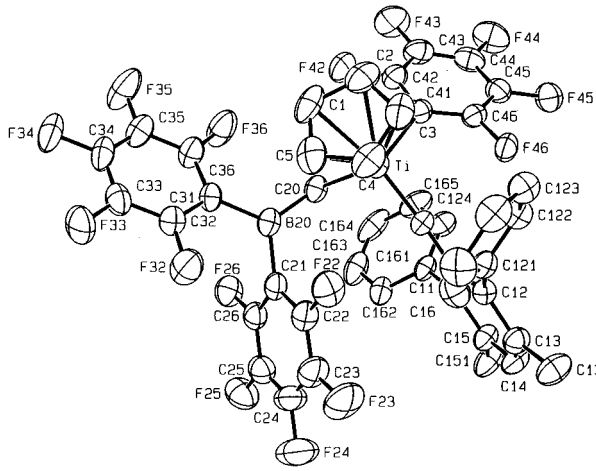

Fig. 2 Molecular structure of **10** showing the atomic numbering scheme. Selected interatomic distances (Å) and angles (°): Ti–O(10) 1.770(2), Ti–C(20) 2.115(2), Ti–C(41) 2.176(2), Cp–Ti–O(10) 126.9(1), C(20)–Ti–C(41) 98.73(8), Ti–O(10)–C(11) 176.2(1).

coalescence temperature at 300 MHz) while that for the methyl exchange is 15.0(5) kcal mol^{-1} at −35 °C.

When monitored by ^{1}H NMR, solutions of **7**,**8** at ambient temperatures over hours eliminate methane and form the neutral species **9**,**10** (Scheme 2). The solid state structure of **10** (Fig. 2) confirms the molecular structure and shows that the boron atom is trigonal planar with no interaction present with the adjacent Ti-C_6F_5 unit.[9] In the ^{1}H NMR spectra of **9a** and **10**, a single set of Cp and OAr resonances are present along with well-resolved diastereotopic Ti-CH_2-B protons. In the case of **9b** containing the chiral *o*-(1-naphthyl) ligand, two sets of sharp NMR signals are present representing a 70 : 30 mixture of the two possible diastereoisomers. The fact that exchange of these isomers is slow on the NMR timescale at ambient temperature confirms that naphthyl rotation cannot account for the observed fluxionality in **7b**.

Notes and references

† *Selected spectroscopic data*: aromatic signals unless indicated: ^{1}H NMR (C_6D_6, 30 °C, unless otherwise stated) **4a**: δ 6.70–7.60; 5.57 (s, C_5H_5); 1.68 (s), 1.32 [s, $C(CH_3)_3$]; 0.85 (s, CH_3). **4b**: δ 7.10–8.00; 5.41 (s, C_5H_5); 1.64 (s), 1.26 [s, $C(CH_3)_3$]; 0.58 (s), 0.15 [s, CH_3]. **5**: δ 7.07–7.29; 6.82 (s, *para*-H); 5.63 (s, C_5H_5); 2.09 (s, *meta*-CH_3); 0.26 (s, Ti-CH_3). **6a**: δ 7.71 (s, *para*-H); 7.31–7.02 (m); 5.75 (s, C_5H_5); 1.29 [s, $C(CH_3)_3$]; 0.10 (s, CH_3). **6b**: δ 7.90 (s, *para*-H); 7.62–7.15 (m); 5.17 (s, C_5H_5); 1.21 [s, $C(CH_3)_3$]; −0.35, −0.81, (s, CH_3). **7a**: δ 6.87–7.45; 5.44 (s, C_5H_5); 1.43 (br, Ti-CH_3); 1.34 (s), 1.19 [s, $C(CH_3)_3$]; 0.90 (br, B-CH_3). (C_7D_8, −10 °C): δ 6.91–7.40; 5.37 (s, C_5H_5); 1.52 (s, Ti-CH_3); 1.32 (s), 1.16 [s, $C(CH_3)_3$]; 0.94 (br, B-CH_3). **7b**: δ 7.05–7.68; 5.36 (s, C_5H_5); 1.32 (s), 1.19 [s, $C(CH_3)_3$]; 0.91 (br, Ti-CH_3); 0.81 (br, B-CH_3). (C_7D_8, −10 °C): δ 6.97–7.68; 5.27 (s, C_5H_5); 1.31 (s), 1.15 [s, $C(CH_3)_3$]; 0.96 (br, Ti-CH_3); 0.77 (br, B-CH_3). ^{1}H NMR (C_7D_8, −30 °C): δ 6.96–7.67; 5.23 (s, C_5H_5-major); 5.14 (s, C_5H_5-minor); 1.31 (s), 1.21 [s, $C(CH_3)_3$]; 0.95 (br, Ti-CH_3-major); 0.76 (br, B-CH_3-major); 0.54 (br, B-CH_3-minor). **8**: δ 6.80–7.32; 6.74 (s, *para*-H); 5.44 (s, C_5H_5); 1.90 (s, *meta*-CH_3); 0.68 (br, Ti-CH_3); 0.53 (br, B-CH_3). (C_7D_8, −20 °C): δ 6.63–7.14; 5.39 (s, C_5H_5); 1.87 (s, *meta*-CH_3); 0.67 (s, Ti-CH_3); 0.46 (br, B-CH_3). **9a**: δ 7.56 (d), 7.13 [d, $^4J(^1H–^1H)$ = 2.5 Hz, *meta*-H]; 6.10 (s, C_5H_5); 4.21 (br), 3.23 (br, Ti-CH_2-B); 1.62 (s), 1.26 [s, $C(CH_3)_3$]. **9b**: δ 6.72–7.86; 6.24 (s), 5.80 (s, C_5H_5); 4.16 (br), 4.14 (br), 3.00 (m, Ti-CH_2-B); 1.60 (s), 1.57 (s), 1.19 (s), 1.15 [s, $C(CH_3)_3$]. **10**: δ 6.85–7.18; 6.68 (s, *para*-H); 5.65 (s, C_5H_5); 3.56 (br), 2.67 (br, Ti-CH_2-B); 1.84 (s, *meta*-CH_3). ^{13}C NMR (C_6D_6, 30 °C) **4a**: δ 160.8 (Ti-O-C); 114.4 (C_5H_5); 58.4, (Ti-CH_3); 35.8, 34.5 [*C*$(CH_3)_3$]; 31.7, 30.5 [C(*C*$H_3)_3$]. **4b**: δ 161.6 (Ti-O-C); 114.1 (C_5H_5); 58.4, 57.8 (Ti-CH_3); 35.8, 34.6 [*C*$(CH_3)_3$]; 31.7, 30.6 [C(*C*$H_3)_3$]. **5**: δ 161.1 (Ti-O-C); 113.7 (C_5H_5); 56.1, (Ti-CH_3); 20.8 (*meta*-CH_3). **6a**: δ 163.0 (O-C); 147.5, 140.8, 132.6, 130.9, 128.3, 126.9, 118.7; 113.5 (C_5H_5); 56.9 (CH_3); 37.4, [*C*$(CH_3)_3$]; 33.1 [C(*C*$H_3)_3$]. **6b**: δ 163.6 (O-C); 152.0, 148.7, 138.9, 135.1, 134.0, 129.7, 126.0, 125.3, 119.9; 113.3 (C_5H_5); 56.5, 56.1 (CH_3); 37.7, [*C*$(CH_3)_3$]; 32.0 [C(*C*$H_3)_3$]. **7a**: δ 163.0 (Ti-O-C); 120.4 (C_5H_5); 113.0 (br, B-CH_3); 77.7 (br, Ti-CH_3); 35.1, 34.4 [*C*$(CH_3)_3$]; 30.8, 29.7 [C(*C*$H_3)_3$]. (C_7D_8, −10 °C): δ 163.2 (Ti-O-C); 120.7 (C_5H_5); 112.9 (br, B-CH_3); 77.4 (s, Ti-CH_3); 35.4, 34.7 [*C*$(CH_3)_3$]; 31.1, 30.0 [C(*C*$H_3)_3$]. **7b**: δ 163.3 (Ti-O-C); 119.9 (C_5H_5); 113.1 (br, B-CH_3); 79.4 (br, Ti-CH_3); 35.1, 34.4 [*C*$(CH_3)_3$]; 30.9, 30.0 [C(*C*$H_3)_3$]. **8**: δ 162.5 (Ti-O-C); 119.3 (C_5H_5); 113.0 (br, B-CH_3); 77.8 (Ti-CH_3); 19.9 (*meta*-CH_3). **9a**: δ 163.7 (Ti-O-C); 119.4 (C_5H_5); 107.1 (br, Ti-CH_2-B); 35.8, 34.7 [*C*$(CH_3)_3$]; 31.4, 30.6 [C(*C*$H_3)_3$]. **9b**: δ 164.4, 164.3 (Ti-O-C); 119.2, 119.0 (C_5H_5); 107.0, 105.5 (br, Ti-CH_2-B); 35.9, 35.8, 34.7, 34.7 [*C*$(CH_3)_3$]; 31.4, 31.4, 30.7, 30.6 [C(*C*$H_3)_3$]. **10**: δ 162.3 (Ti-O-C); 118.1 (C_5H_5); 114.2 (br, Ti-CH_2-B); 20.1 (*meta*-CH_3).

‡ *Crystal data* for **4b** at 296 K: $TiOC_{31}H_{38}$, M = 474.55, space group $P2_1/c$ (no. 14), a = 13.1917(8), b = 11.7251(6), c = 18.788(1) Å, β = 107.115(2)°, V = 2777.4(5) Å^3, D_c = 1.135 g cm^{-3}, Z = 4. Of the 6750 unique reflections collected (4.54 ⩽ 2θ ⩽ 61.36°) with Mo-Kα (λ = 0.71073 Å), the 6750 with $F_o^2 > 2\sigma(F_o^2)$ were used in the final least-squares refinement to yield $R(F_o)$ = 0.064 and $R_w(F_o^2)$ = 0.166. For **10** at 203 K: $TiF_{15}OC_{44}BH_{24}$, M = 912.37, space group $P\bar{1}$ (no. 2), a = 12.2084(5), b = 12.3668(2), c = 13.7876(5) Å, α = 71.440(2), β = 84.811(1), γ = 83.982(2)°, V = 1958.9(2) Å^3, D_c = 1.547 g cm^{-3}, Z = 2. Of the 9835 unique reflections collected (8.00 ⩽ 2θ ⩽ 61.10°) with Mo-Kα (λ = 0.71073 Å), the 9835 with $F_o^2 > 2\sigma(F_o^2)$ were used in the final least-squares refinement to yield $R(F_o)$ = 0.052 and $R_w(F_o^2)$ = 0.126. CCDC 182/996.

1 M. Bochmann, *J. Chem. Soc., Dalton Trans*., 1996, 255; H. H. Brintzinger, D. Fischer, R. Mülhaupt, B. Rieger and R. M. Waymouth, *Angew. Chem., Int. Ed. Engl.*, 1995, **34**, 1143; P. C. Möhring and N. J. Coville, *J.Organomet. Chem*., 1994, **479**, 1; W. Kaminsky, K. Kulper and H. H. Brintzinger, *Angew. Chem., Int. Ed. Engl*., 1985, **24**, 507.

2 J. S. Vilardo, M. G. Thorn, P. E. Fanwick and I. P. Rothwell, *Chem. Commun.*, 1998, 2425.

3 I. M. M. Fussing, D. Pletcher and R. J. Whitby, *J. Organomet. Chem.*, 1994, **470**, 109; K. Nomura, N. Naga, M. Miki, K. Yanagi and A. Imai, *Organometallics*, 1998, **17**, 2152.

4 For related chemistry of perfluorophenoxide derivatives see S. W. Ewart, M. J. Sarsfield, D. Jeremic, T. L. Tremblay, E. F. Williams and M. C. Baird, *Organometallics*, 1998, **17**, 1502; M. J. Sarsfield, S. W. Ewart, T. L. Tremblay, A. W. Roszak and M. C. Baird, *J. Chem. Soc., Dalton Trans.*, 1997, 3097; T. L. Tremblay, S. W. Ewart, M. J. Sarsfield and M. C. Baird, *Chem. Commun.*, 1997, 831.

5 For linked Cp-phenoxide derivatives see Y.-X. Chen, P.-F. Fu, C. L. Stern and T. J. Marks, *Organometallics*, 1997, **16**, 5958.

6 U. Thewalt and T. Wohrle, *J. Organomet. Chem.*, 1994, **464**, C17.

7 P. E. Fanwick, personal communication.

8 X. Yang, C. L. Stern and T. J. Marks, *J. Am. Chem. Soc.*, 1994, **116**, 10015; J. A. Ewen and M. J. Elder, *Chem. Abstr*., 1991, **115**, 136998g; A. G. Massey and A. J. Park, *J. Organomet. Chem.*, 1964, **2**, 245.

9 J. D. Scollard, D. H. McConville and S. J. Rettig, *Organometallics*, 1997, **16**, 1810; R. E. von H. Spence, D. J. Parks, W. E. Piers, M.-A. MacDonald, M. J. Zaworotko and S. J. Rettig, *Angew. Chem., Int. Ed. Engl.*, 1995, **34**, 1230.

Communication 8/05476B

ChemComm

Synthesis and molecular structure of [{$Pd_2(CH_2C_6H_4P(o\text{-tolyl})_2$-κ*C*,*P*)$_2$($\mu_3$-3,5-dmpz-*N*,*N*′,*C*^{4})$_2$Ag(μ-ClO_4)}$_2$] (3,5-dmpz = 3,5-dimethylpyrazolato), a silver derivative showing unprecedented η^1-azolato coordination

Larry R. Falvello, Juan Forniés,* Antonio Martín, Rafael Navarro, Violeta Sicilia and Pablo Villarroya

Departamento de Química Inorgánica, Instituto de Ciencia de Materiales de Aragón, Universidad de Zaragoza-C. S. I. C., 50009 Zaragoza, Spain. E-mail:forniesj@posta.unizar.es

Received (in Cambridge, UK), 29th July 1998, Accepted 29th September 1998

The reaction of [$Pd_2(CH_2C_6H_4P(o\text{-tolyl})_2$-κ*C*,*P*)$_2$($\mu$-3,5-dmpz)$_2$] (1) with $AgClO_4$ renders [{$Pd_2(CH_2C_6H_4P(o\text{-tolyl})_2$-κ*C*,*P*)$_2$($\mu_3$-3,5-dmpz-*N*,*N*′,*C*^{4})$_2$Ag(η^2-μ-ClO_4)}$_2$] (2), a palladium–silver derivative displaying an unprecedented dmpz bridging ligand η^1 bonded to the Ag centers, involving only the C^4 atom of each dmpz ligand.

The chemistry of dimetallic compounds containing two μ-azolato bridging groups has been intensively developed in the last three decades,[1] especially in the case of dirhodium and diiridium derivatives.[2] Studies of these systems have included substitution reactions,[2a,b] oxidative additions,[2c,d] kinetics,[2e,f] electrochemistry,[2g] photochemistry,[2h] hydroformylation reactions[2i] and theoretical studies.[2j] Pyrazolate ligands have a proven ability to hold two metal atoms in close proximity, while permitting a wide range of intermetallic separations. Compounds with two bridging azolato groups show a boat conformation of the central 'M_2N_4' six membered ring. The π-electron rich cleft between the two azolato rings in these molecules offers a potentially interesting site for further complexation (Fig. 1). To our knowledge there has been no previous report of a complex in which a dimetallic 'M_2(μ-azolato)$_2$' moiety uses its π-electron system to accommodate a transition metal cation.

In view of the paucity of dipalladium and diplatinum complexes with μ-azolato bridging groups[3] we decided to explore the synthesis and reactivity of compounds of the type [M_2(C^P)$_2$(μ-L)$_2$] [M = Pd, Pt; C^P = $CH_2C_6H_4P(o\text{-tolyl})_2$; HL = pyrazole (Hpz), 3,5-dimethylpyrazole (H3,5-dmpz)]. The reaction of [Pd_2(C^P)$_2$(μ-3,5-dmpz)$_2$] (**1**)† with $AgClO_4$ renders **2**‡ [eqn. (1)].

$$\underset{\mathbf{1}}{2[Pd_2(C\text{^}P)_2(\mu\text{-}3,5\text{-dmpz})_2]} + 2\,AgClO_4 \rightarrow \underset{\mathbf{2}}{[\{Pd_2(C\text{^}P)_2(\mu_3\text{-}3,5\text{-dmpz-}N,N',C^4)_2Ag(\eta^2\text{-}\mu\text{-}ClO_4)\}_2]} \quad (1)$$

Compound **2**, as has been established by an X-ray study§ (Fig. 2), is formed by two {Pd_2(C^P)$_2$(μ_3-3,5-dmpz-*N*,*N*′,-*C*^{4})$_2$Ag(η^2-μ-ClO_4)} units bridged by two perchlorate groups and related to each other by a crystallographic center of symmetry. Each unit contains a dinuclear palladium fragment 'Pd_2(C^P)$_2$(μ-3,5-dmpz)$_2$' and a silver atom located in the cleft between the two dmpz groups and η^1-bonded to the C^4 atoms of the dmpz ligands.

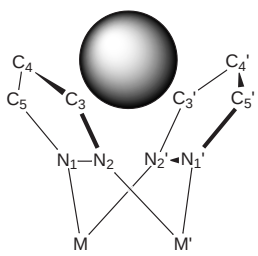

Fig. 1 Schematic diagram showing a guest atom in the cleft formed by the two pyrazolate rings of the moiety [Pd_2(C^P)$_2$(μ-3,5-dmpz)$_2$] .The atom numbering scheme used in the NMR analyses is shown.

The palladium fragment 'Pd_2(C^P)$_2$(μ-3,5-dmpz)$_2$' consists of a typical head to tail dimer with bridged 3,5-dmpz anions, with the usual boatlike conformation of the Pd_2N_4 six-membered metallocycle. The Pd···Pd distance (3.2297(7) Å) is slightly longer than those observed in other Pd (or Pt) complexes with two pyrazolate bridging ligands.[3a–c] The bond distances and angles in the metallocycles in compound **2** are similar to those observed in palladium and platinum compounds

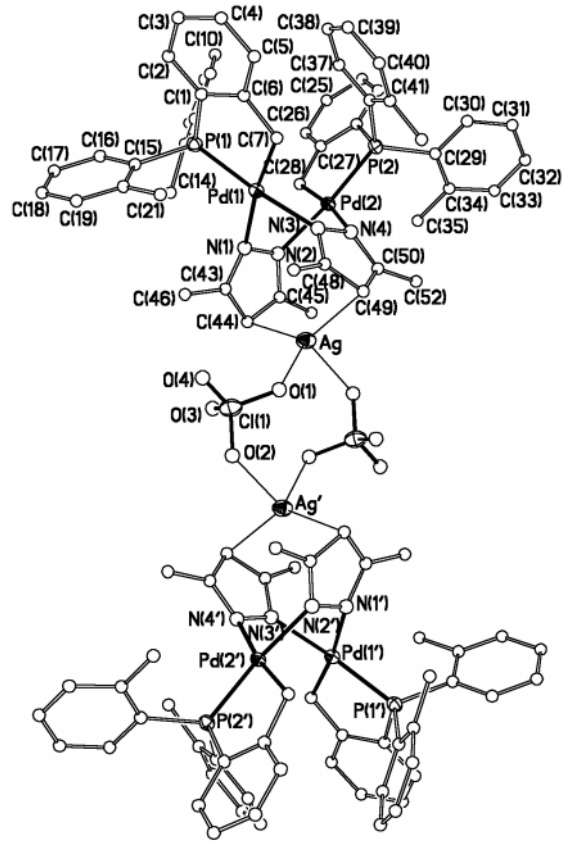

Fig. 2 Molecular structure for compound **2.** Selected bond distances: Pd(1)–C(7) = 2.034(5), Pd(1)–P(1) = 2.2251(13), Pd(2)–C(28) = 2.042(5), Pd(2)–P(2) = 2.2268(13), Pd(1)–N(1) = 2.138(4), Pd(1)–N(3) = 2.097(4), Pd(2)–N(2) = 2.092(4), Pd(2)–N(4) = 2.136(4), Ag–C(44) = 2.410(5), Ag–C(49) = 2.420(5), Ag–O(1) = 2.431(4), Ag–O(2′) = 2.464(4), N(1)–N(2) = 1.371(6), N(1)–C(43) = 1.331(6), C(43)–C(44) = 1.405(7), C(44)–C(45) = 1.410(7), N(2)–C(45) = 1.332(6), N(3)–N(4) = 1.375(6), N(3)–C(48) = 1.342(6), C(48)–C(49) = 1.405(7), C(49)–C(50) = 1.405(7), N(4)–C(50) = 1.330(7) Å. Selected bond angles: Ag–C(44)–C(43) = 94.5(3), Ag–C(44)–C(45) = 89.1(3), Ag–C(49)–C(48) = 86.7(3), Ag–C(49)–C(50) = 95.7(3)°.

containing the same C^P group.[4] The dmpz groups are planar, and the angle between them in each '$Pd_2(C\hat{}P)_2(\mu\text{-}3,5\text{-dmpz})_2$' fragment is 44.8°. Bond lengths and angles around the N and C atoms of the 3,5-dmpz are identical to those observed in other complexes.[3a]

The extraordinary structural feature of this compound is the unprecedented coordination mode of the 3,5-dmpz groups to Ag^+. The silver cation is located in the cleft between, and approximately equidistant from, the two 3,5-dmpz rings at a distance of 2.410(5) Å and 2.420(5) Å from C(44) and C(49) respectively, the C^4 atom of each dmpz ring (Fig. 1). The Ag–C(49) and Ag–C(44) vectors are nearly perpendicular to the corresponding dmpz rings, the angles between the perpendicular to the corresponding rings and the Ag–C^4 bonds being 5.9° [Ag–C(49)] and 4.0° [Ag–C(44)] respectively. The long Ag–C(48) (2.728 Å), Ag–C(50) (2.917 Å), Ag–C(43) (2.883 Å) and Ag–C(45) (2.773 Å) distances seem to exclude any bond interaction between Ag and these atoms. So, both 3,5-dmpz rings seem to be η^1-coordinated [C(44) and C(49)] to the silver atom. The Ag–C bond lengths (*ca.* 2.415 Å) are similar to the shortest values found in Ag–η^1-arene complexes such as $[AgB_{11}CH_{12}\cdot 2C_6H_6]$ [2.400(7) Å],[5a] [Ag(deltaphane)-(O_3SCF_3)] (2.41–2.48 Å),[5b] [Ag{(*Z*)-2,2,5,5-tetramethyl-3,4-diphenylhex-3-ene}(O_3SCF_3)] [2.579(4) Å],[5c] and [indene·$AgClO_4]_2$ [2.47(2) Å],[5d] and are clearly shorter than the Ag–C distances observed in Ag–η^2-arene complexes, such as [Ag(25,26,27,28-tetramethoxycalix(4)arene)$(NO_3\text{-}O,O')$] [2.504(5), 2.643(5), 2.527(5), 2.549(5) Å],[5e] $[\{AuAg(C_6F_5)_2(C_6H_6)_n\}]$ [2.48, 2.50 Å][5f] and [catena(μ-η^4-*rac*(2)(1,5-naphthalino(2)paracyclophane)(μ-perchlorato-*O*,*O*′,*O*″)silver(I)] [2.365, 2.607 Å].[5g]

Finally, the Ag coordination is completed by two Ag–O bonds [Ag–O(1) = 2.431(4), Ag–O(2A) = 2.464(4) Å], one from each of the two bridging ClO_4 groups, in such a way that Ag shows a distorted tetrahedral coordination environment. The Ag–O bond distances are in the range found in complexes with triflate,[5b] nitrate[5e] or for μ-ClO_4 bonded to silver.[6]

As has been mentioned, the bond distances and angles in the dmpz groups in **2** are very similar to those observed in uncomplexed '$M_2L_2(\mu\text{-pz})_2$' compounds, indicating that in spite of the η^1 interaction to the silver centre, the pyrazolato rings maintain their aromaticity. The mass spectrum (FAB^+) of **2** shows the molecular peak for the cation $[Pd_2(C\hat{}P)_2(\mu_3\text{-}3,5\text{-dmpz-}N,N',C^4)_2Ag]^+$ (1119). The sharp ^{31}P, ^1H and ^{13}C NMR signals of **2** at room temperature and their observed shifts with respect to those in the starting material, **1**, indicate that the silver–η^1-dmpz bonds are present in solution. Especially significant are the changes observed in the ^{13}C NMR spectrum of **2** with respect to that of **1**, mainly in the signal due to the C atoms η^1-bonded to silver, the C^4 atom of each dmpz group. For compound **2** it appears at 86.8 ppm, *i.e.*, shifted upfield by 16.34 ppm, and which becomes a multiplet, probably as a consequence of the coupling of the C^4 atoms to the P, ^{107}Ag, and ^{109}Ag nuclei. Due to the poor resolution of this spectrum, no individual values for the coupling constants could be extracted.

Studies of the reactivity of other palladium and platinum pyrazolate complexes towards other Lewis acid metal complexes are in progress.

The authors thank the Dirección General de Enseñanza Superior (Spain) for financial support (Projects PB95-0003-C02-01 and PB95-0792).

Notes and references

† $[Pd_2(C\hat{}P)_2(\mu\text{-}3,5\text{-dmpz})_2]$ (**1**): NMR spectra (RT, CD_2Cl_2) were recorded on either a Varian Unity-300 or a Bruker ARX-300 spectrometer using the standard references: δ_P 35.6 (s); δ_H 5.57 (s, 2H, H^4 3,5-dmpz) 1.68 (s, 6H, 3,5-dmpz), 2.32 (s, 6H, 3,5-dmpz), 2.28 [s, 2H, CH_2 (C^P)], 2.83 [s, 2H, CH_2 (C^P)], 2.87 [s, 6H, Me (C^P)], 1.61 [s, 6H, Me (C^P)]; δ_C 145.7 [d, ^3J(C–P) 3.0 Hz], 147.2 [d, ^3J(C–P) 2.3 Hz, C^3,C^5 (3,5-dmpz)], 103.1 [d, C^4, ^4J(C–P) 3.2 Hz], 14.3 (s, Me, 3,5-dmpz), 12.6 (s, Me, 3,5-dmpz), 28.6 (s, CH_2, C^P), 22.3 [d, ^3J(C–P) 13.8 Hz, Me (C^P)], 21.6 [d, ^3J(C–P) 8.6 Hz, Me (C^P)].

‡ $[\{Pd_2(C\hat{}P)_2(\mu_3\text{-}3,5\text{-dmpz-}N,N',C^4)_2Ag(\eta^2\text{-}\mu\text{-}ClO_4)\}_2]$ (**2**). To a solution of $[Pd_2(C\hat{}P)_2(\mu\text{-}3,5\text{-dmpz})_2]$ (**1**; 0.1136 g, 0.112 mmol) in CH_2Cl_2–OEt_2 (50 : 4 mL) was added $AgClO_4$ (0.0233 g, 0.112 mmol), and the mixture was stirred for 5 h at room temperature. After filtration through Celites, the resulting solution was evaporated to dryness. Upon addition of 15 mL of Et_2O and 2 mL of CH_2Cl_2 a white solid formed immediately, **2** (0.08 g, 58.50%). (Found: C, 51.10; H, 3.96; N, 4.58. $Ag_2C_{104}Cl_2H_{108}N_8O_8P_4Pd_4$ requires C, 51.31; H, 4.47; N, 4.60%). NMR spectra (RT, $CDCl_3$): δ_P 39.1 (s); δ_H 5.52 (s, H^4, 3,5-dmpz), 2.43 (s, Me, 3,5-dmpz), 1.91 (s, Me, 3,5-dmpz), 2.53 [d, ^2J(H–H) 15.0 Hz, CH_2 (C^P)], 3.11 [d, CH_2 (C^P)], 2.74 [s, Me (C^P)], 1.88 [s, Me (C^P)]; δ_C 152.1 (s), 151.7 (s) [C^3, C^5 (3,5-dmpz)], 86.8 [m, C^4 (3,5-dmpz)], 14.6 [s, Me (3,5-dmpz)], 13.2 [s, Me (3,5-dmpz)], 29.0 [s, CH_2 (C^P)], 22.7 [d, ^3J(C–P) 7.2 Hz, Me (C^P)], 22.2 [d, ^3J(C–P) 12.6 Hz, Me (C^P)].

§ *Crystal data* for **2**·CH_2Cl_2·C_5H_{12}: $C_{52}H_{54}AgClN_4O_4P_2Pd_2$·$CH_2Cl_2$·$C_5H_{12}$, M = 1374.12; triclinic, space group $P\bar{1}$ (no. 2), a = 12.686(2), b = 15.050(2), c = 17.349(3) Å, α = 112.190(15), β = 108.53(2), γ = 90.996(15)°, U = 2872.2(7) Å^3, Z = 1, T = 150 K, μ = 1.201 mm^{-1}, graphite monochromated Mo-Kα radiation, λ = 0.71073 Å, yellowish prism with dimensions 0.45 × 0.22 × 0.20 mm, Nonius CAD4 diffractometer, ω scans, data collection range $4 < 2\theta < 50°$, semiempirical absorption correction based on Ψ scans, transmission factors 0.891–0.861, 653 refined parameters with 10049 unique (R_{int} = 0.015) reflections (10547 measured). Full-matrix least-squares refinement of this model against F^2 (program SHELXL-93[7]) converged to final residual indices $R1$ = 0.043, $wR2$ = 0.111. (R factors defined in ref. 7), g.o.f. 1.03. Final difference electron density maps showed six peaks above 1 e Å^{-3} (from 2.68 to 1.35; largest diff. hole −1.45) lying close to the solvent molecules. CCDC 182/1038.

1 (*a*) S. Trofimenko, *Prog. Inorg. Chem.*, 1986, **34**, 115; (*b*) A. P. Sadimenko and S. S. Basson, *Coord. Chem. Rev.*, 1996, **147**, 247; (*c*) G. La Monica and G. A. Ardizzoia, *Prog. Inorg. Chem.*, 1997, **46**, 151; (*d*) J. E. Cosgriff and G. B. Deacon, *Angew. Chem., Int. Ed. Engl.*, 1998, **37**, 286.

2 (*a*) R. Usón, L. A. Oro, M. A. Ciriano, D. Carmona, A. Tiripicchio and M. Tiripicchio-Camellini, *J. Organomet. Chem.*, 1982, **224**, 69; (*b*) C. Tejel, J. M. Villoro, M. A. Ciriano, J. A. López, E. Eguizabal, F. J. Lahoz, V. I. Bakhmutov and L. A. Oro, *Organometallics*, 1996, **15**, 2967; (*c*) D. O. K. Fjeldsted, S. R. Stobart and M. J. Zaworotko, *J. Am. Chem. Soc.*, 1985, **107**, 8258; (*d*) A. Tiripicchio, F. J. Lahoz, L. A. Oro and M. T. Pinillos, *J. Chem. Soc., Chem. Commun.*, 1984, 936; (*e*) R. D. Brost and S. R. Stobart, *Inorg. Chem.*, 1989, **24**, 4308; (*f*) R. D. Brost, D. O. K. Fjeldsted and S. R. Stobart, *J. Chem. Soc., Chem. Commun.*, 1989, 488; (*g*) D. C. Boyd, G. S. Rodman and K. R. Mann, *J. Am. Chem. Soc.*, 1986, **108**, 1779; (*h*) J. L. Marshall, S. R. Stobart and H. B. Gray, *J. Am. Chem. Soc.*, 1984, **106**, 3027; (*i*) C. Claver, P. Kalck, M. Ridmy, A. Thorez, L. A. Oro, M. T. Pinillos, M. C. Apreda, F. H. Cano and C. Foces-Foces, *J. Chem. Soc., Dalton Trans.*, 1988, 1523; (*j*) D. L. Lichtenberger, A. S. Copenhaver, H. B. Gray, J. L. Marshall and M. D. Hopkins, *Inorg. Chem.*, 1988, **27**, 4488.

3 (*a*) V. K. Jain, S. Kannan and E. R. T. Tiekink, *J. Chem. Soc., Dalton Trans.*, 1992, 2231; (*b*) V. K. Jain, S. Kannan and E. R. T. Tiekink, *J. Chem. Soc., Dalton Trans.*, 1993, 3625; (*c*) V. Y. Kukushkin, E. A. Aleksandrova, V. M. Leovac, E. Z. Iveges, V. K. Belsky and V. E. Konovalov, *Polyhedron*, 1992, **11**, 2691; (*d*) V. K. Jain and S. Kannan, *Polyhedron*, 1992, **11**, 27; (*e*) A. Singhal, V. K. Jain and S. Kannan, *J. Organomet. Chem.*, 1993, **447**, 317; (*f*) G. López, J. Ruiz, G. García, J. M. Martí, G. Sánchez and J. García, *J. Organomet. Chem.*, 1991, **412**, 435; (*g*) G. López, J. Ruiz, G. García, C. Vicente, J. Casabó, E. Molins and C. Miravitlles, *Inorg. Chem.*, 1991, **30**, 2605.

4 (*a*) W. A. Herrmann, Ch. Brossmer, K. Öfele, C.-P. Reisinger, T. Priermeier, M. Beller and H. Fischer, *Angew. Chem., Int. Ed. Engl.*, 1995, **34**, 1844; (*b*) L. R. Falvello, J. Forniés, A. Martín, R. Navarro, V. Sicilia and P. Villarroya, *Inorg. Chem.*, 1997, **36**, 6166.

5 (*a*) K. Shelly, D. C. Finster, Y. J. Lee, W. R. Scheidt and C. A. Reed, *J. Am. Chem. Soc.*, 1985, **107**, 5955; (*b*) H. C. Kang, A. W. Hanson, B. Eaton and V. Boekelheide, *J. Am. Chem. Soc.*, 1985, **107**, 1979; (*c*) J. E. Gano, G. Subramaniam and R. Birnbaum, *J. Org. Chem.*, 1990, **55**, 4760; (*d*) P. F. Rodesiler, E. A. Hall Griffith and B. L. Amma, *J. Am. Chem. Soc.*, 1972, 761; (*e*) W. Xu, R. J. Puddephatt, K. W. Muir and A. A. Torabi, *Organometallics*, 1994, **13**, 3054; (*f*) R. Usón, A. Laguna, M. Laguna and B. R. Manzano, *J. Chem. Soc., Dalton Trans.*, 1984, 285; (*g*) H. Schmidbaur, W. Bublack, M. W. Haenel, B. Huber and G. Muller, *Z. Naturforsch. Teil B*, 1988, **43**, 702.

6 (*a*) S. Kitagawa, M. Kondo, S Kawata, S. Wada, M. Maekawa and M. Munakata, *Inorg. Chem.*, 1995, **34**, 1455.

7 G. M. Sheldrick, SHELXL-93, a Program for Crystal Structure Refinement, University of Göttingen, Germany, 1993.

Communication 8/05938A

A highly selective water-soluble dicationic palladium catalyst for the biphasic hydroxycarbonylation of alkenes

Marcel Schreuder Goedheijt, Joost N. H. Reek, Paul C. J. Kamer and Piet W. N. M. van Leeuwen*

Institute for Molecular Chemistry, Department of Inorganic Chemistry, University of Amsterdam, Nieuwe Achtergracht 166, 1018 WV Amsterdam, The Netherlands. E-mail: pwnm@anorg.chem.uva.nl

Received (in Cambridge, UK) 17th August 1998, Accepted 23rd September 1998

The application of a water-soluble diphosphine with a xanthene-type backbone in the biphasic palladium-catalysed hydroxycarbonylation reaction of alkenes leads to the selective formation of carboxylic acids.

Water-soluble organometallic compounds have attracted considerable interest as catalysts.[1] Application of these compounds in two-phase catalysis results in easy separation and recycling of the catalyst.[2]

Various alkenes can be hydroxycarbonylated with carbon monoxide and water using transition metal compounds to yield the corresponding carboxylic acids.[3] Recently, the use of palladium catalysts for the biphasic hydroxycarbonylation of alkenes was reported.[4] The hydroxycarbonylation of alkenes in a two-phase system with the water-soluble palladium catalyst [Pd(TPPTS)$_3$] in the presence of a Brønsted acid as promoter yields carboxylic acids.[4,5] The catalyst predominantly affords carboxylic acids, but in most cases it suffers from low activities and selectivities. Water-soluble bidentate phosphines have been used to form active catalysts for palladium-catalysed alternating copolymerisation, *e.g.* a catalyst formed with the bidentate water-soluble phosphine C_3H_6-1,3-[P(C_6H_4-*m*-$SO_3Na)_2]_2$ (dppp-s) produces polyketone from ethylene and carbon monoxide.[6]

Recently, we developed the water-soluble bidentate diphosphine 2,7-bis(SO_3Na)-Xantphos (**1**) which was successfully applied in the two-phase rhodium-catalysed hydroformylation reaction of alkenes.[7] Here, the highly selective palladium-catalysed formation of carboxylic acids from alkenes and carbon monoxide in the presence of **1** and a Brønsted acid as a cocatalyst will be described.

Complex **2** was prepared by reaction of **1** with $PdCl_2$. Addition of two equivalents of AgOTs (OTs = *p*-$CH_3C_6H_4SO_3^-$) to a solution of **2** resulted in the dicationic palladium complex **3** which was isolated as an orange powder. The $^{31}P\{^1H\}$ NMR spectrum in CD_3OD shows only a singlet at 25.6 ppm which indicates that a *trans* complex is formed exclusively at room temperature.† This is probably due to the large natural bite angle of the xanthene backbone and the coordination of the oxygen atom to the dicationic palladium center.‡ The preferential formation of the *trans* complex, excluding copolymerisation activity which requires a *cis* coordination,[8] prompted us to investigate the applicability of **3** (and **2**) toward the selective formation of carboxylic acids. Indeed, hydroxycarbonylation of ethylene was 100% selective towards the formation of propionic acid without formation of oligomers or copolymers as indicated by ^1H NMR spectroscopy.§ The reaction proceeded at relatively low concentrations of palladium (1.6 mmol l^{-1}). As expected, the activity increased with increasing temperature. The addition of TsOH as a promoter was necessary to stabilise the catalyst as otherwise palladium black is formed during the reaction. The use of propionic acid as the proton donor instead of TsOH gave rise to formation of metallic palladium as well. More strongly coordinating anions stabilise the cationic center which results in a slower reaction and eventually in decomposition of the catalyst at elevated temperatures.[5,6] Run 1 was performed at 95 °C using 50 equivalents of TsOH and a total initial pressure of 30 bar (CO–ethylene = 1 : 1; Table 1). After the reaction very small amounts of palladium metal were formed. The activity (TOF¶ = 133 h^{-1}) increased to 180 h^{-1} when the reaction was carried out at 120 °C (run 2). When an additional equivalent of **1** was added to the catalyst solution an even higher activity was observed (TOF = 304 h^{-1}; run 3). Furthermore, no formation of palladium metal was observed during this run suggesting that the stability of the catalyst system had increased. Lower activities were found when **2** was used as the catalyst (TOF = 218 h^{-1} and 272 h^{-1}; runs 4 and 5) suggesting the higher activity for **3**. Catalysts prepared *in situ* (runs 6 and 7) gave rise to lower rates compared to **3** as well. In this case, the formation of the active catalyst is slower.

In order to investigate the regioselectivity of the catalytic system towards the formation of linear (l) and branched (b) carboxylic acids styrene and propene were also studied as substrates. The hydroxycarbonylation of styrene catalysed by **3** led to a mixture of 2- and 3-phenylpropionic acid (Scheme 2). The l/b ratio of the carboxylic acids was *ca.* 65/35 and a TOF of 40 h^{-1} was observed (run 9). A l/b ratio of *ca.* 70/30 was found when Pd(TPPTS)$_3$ was used as the catalyst (60% selectivity towards the formation of acids). This suggests that **3** does not induce higher selectivity compared to monodentate phosphines.‖ At 70 °C, 30 bar CO pressure and in the presence of 4-*tert*-butylcatechol as a polymerisation inhibitor less thermal polymerisation was observed without any change in activity and l/b ratio.

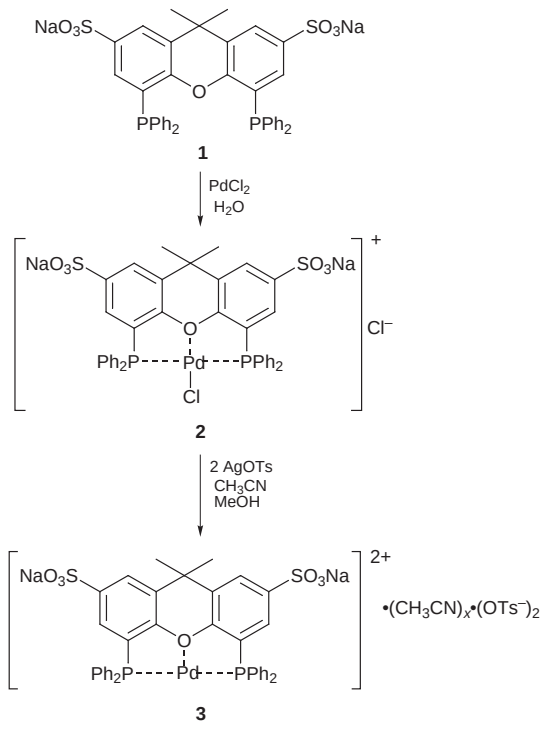

Scheme 1 Synthesis of the cationic palladium complexes **2** and **3**.

Table 1 Palladium-catalysed hydroxycarbonylation of ethylene (**4**), styrene (**5**) and propene (**6**)[a]

Run	Olefin	*p*-$CH_3C_6H_4SO_3H$/ mmol	*T*/°C	*t*/min	l/b	TOF/h^{-1}
1	**4**	0.9	95	180	—	133
2	**4**	0.9	120	180	—	180
3[b]	**4**	0.9	120	180	—	304
4[c]	**4**	0.9	120	180	—	218
5[b,c]	**4**	0.9	120	180	—	272
6[d]	**4**	0.9	120	180	—	266
7[e]	**4**	0.9	120	180	—	259
8	**4**	2.7	120	180	—	260
9[f]	**5**	2.7	95	180	65/35	40
10[g]	**5**	2.7	70	180	65/35	40
11	**6**	0.9	100	180	60/40	55
12	**6**	2.7	120	80	63/37	300
13[h]	**6**	2.7	120	45	65/35	140
14[i]	**6**	2.7	120	60	66/34	76
15	**6**	2.7	120	30	65/35	373
16	**6**	2.7	120	180	63/37	262
17[j]	**6**	2.7	120	180	65/35	163
18[k]	**6**	2.7	120	180	64/36	129

[a] Reaction conditions: 15.8×10^{-3} mmol Pd complex **3**, Brønsted acid, amount of olefin (15 bar of **4** or 9 bar of **6**) without the addition of organic solvent; initial total pressure at RT: 30 bar unless otherwise stated, 10 mL of H_2O. [b] 1 equiv. Xantphos-s added to **3**. [c] Palladium complex **2** was used as precursor. [d] Catalyst prepared *in situ* from $PdCl_2$ and 1 equiv. Xantphos-s. [e] Catalyst prepared *in situ* from $Pd(OAc)_2$ and 1 equiv. Xantphos-s. [f] 35% of polystyrene formed. [g] 4-*tert*-Butylcatechol (5 mmol) was added; 19% of polystyrene formed. [h] pressure **6** = 9 bar; pressure CO = 2 bar at RT. [i] pressure **6** = 9 bar; pressure CO = 1 bar at RT. [j] L/Pd ratio = 2; no formation of palladium black observed. [k] pressure **6** = 4.5 bar.

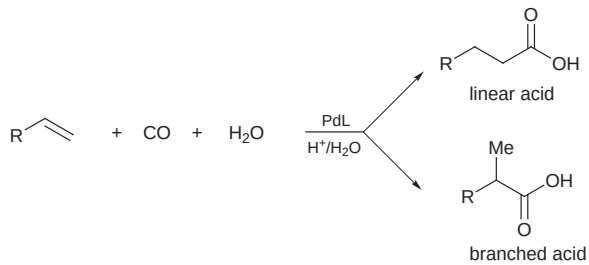

Scheme 2 Palladium-catalysed hydroxycarbonylation of ethylene (**4**; R = H), styrene (**5**; R = Ph) and propene (**6**; R = CH_3) (L = **1**).

Propene was hydroxycarbonylated at higher temperatures (100 °C) than styrene since it is not susceptible to polymerisation (runs 11–17). Under the given reaction conditions (9 bar of propene pressure) no polymer formation was detected, but activities were low (TOF = 55 h^{-1}). At 120 °C the TOF increased significantly [373 h^{-1} after 30 min reaction (run 15) and 262 h^{-1} after 3 h reaction (run 16)]. For the $Pd(TPPTS)_3$ catalyst high rates [TOF = 2507 h^{-1} (15 min); 1307 h^{-1}(30 min)] were observed, but in contrast with our system fast catalyst deactivation was reported.[5] At lower CO pressures the rate decreased and selectivity increased towards the linear acid (runs 13 and 14). At low pressures, the observed rates suggest that the reaction has an approximate first-order dependence on CO and alkene concentrations. Higher ligand to palladium ratios did not improve the selectivity, while a somewhat lower rate was observed (run 17). With a ligand to palladium ratio of 3 (or more) no catalytic activity at all was observed which suggests that a catalytically inactive coordinatively saturated bis-ligand Pd(II) species is formed.

In conclusion, we have shown that the dicationic Pd/Xantphos-s/TsOH system is very effective and 100% selective in the hydroxycarbonylation reaction of alkenes (no traces of oligomeric or polymeric species were observed) towards carboxylic acids. Furthermore, under optimised reaction conditions, no formation of metallic palladium was observed and initial turnover frequencies dropped only slightly within hours indicating that the system is highly stable under the reaction conditions employed. The scope of this useful system is currently under investigation.

We thank the Netherlands Institute for Catalysis Research (NIOK) for financial support.

Notes and references

† *Selected data* for **2**: ^{1}H NMR (CD_3OD): δ 8.32 (s, 2H, ArH), 8.01 (d, J = 7.6 Hz, 2H, ArH), 7.32 (t, J = 5.1 Hz, 8H, ArH), 7.26 (t, J = 5.1 Hz, 8H, ArH), 7.12 (t, J = 5.1 Hz, 4H, ArH), 1.92 (s, 6H, ArH). ^{31}P{^{1}H} NMR (CD_3OD): δ 23.8. (Found: C, 42.2; H, 4.1. Calc. for $C_{39}H_{30}O_7S_2P_2PdCl_2$: C, 42.4; H, 4.2%).For **3**: ^{1}H NMR (CD_3OD; only the dication): δ 8.38 (s, 2H, ArH), 7.42–7.34 (b, 20H, ArH), 6.99 (b, 2H, ArH), 2.03 (s, 6H, CH_3). ^{31}P{^{1}H} NMR (CD_3OD): δ 25.6. (Found: C, 54.5; H, 4.2. Calc. for $C_{53}H_{44}O_{13}S_4P_2Pd\cdot 2(CH_3CN)$: C, 54.0; H, 4.0%).

‡ These type of *trans* complexes were also found in the solid state.

§ *Catalysis:* the appropriate amount of catalyst (15.8 μmol), prepared from **2**, **3** or *in situ* from $PdCl_2$ or $Pd(OAc)_2$ and **1**, was mixed with 0.9 or 2.7 mmol of TsOH. The mixture was charged into a 200 mL stainless steel reaction vessel (ethylene) or a 50 mL Hastelloy C autoclave (styrene and propene) under an atmosphere of argon. Degassed water (10 mL) was added and after five pressurizing–depressurizing cycles with CO, to remove traces of argon/air, the autoclave was pressurized with the appropriate substrates (ethylene and propene) and CO or charged with styrene and pressurized with CO. The contents were heated to the desired temperature and magnetically stirred (840 rpm). After the reaction the autoclave was cooled to room temperature in a ice bath and slowly depressurized. The hydroxycarbonylation products were analysed by ^{1}H NMR (300 MHz, $CDCl_3$).

¶ All TOFs mentioned are average TOFs calculated over the given reaction time.

‖ Since styrene is susceptible to polymerisation, reactions were carried out at lower temperatures (70–95 °C). At 95 °C the selectivity towards carboxylic acids is 65% (35% polystyrene). When no catalyst is present the same amount of polystyrene is formed thermally. The preference for the formation of the linear acid is in contrast with that reported for the $Pd(TPPTS)_3$ catalyst (l/b ratio *ca*. 27/73; TOF = 49 h^{-1}).[5]

1 B. Cornils and W. A. Herrmann, *Aqueous-Phase Organometallic Chemistry—Concepts and Applications*, Wiley-VCH, Weinheim, 1998.
2 E. G. Kuntz, *CHEMTECH*, 1987, **17**, 570.
3 W. Reppe, *Ann. Chem.*, 1953, **582**, 116.
4 S. Tilloy, E. Monflier, F. Bertoux, Y. Castanet and A. Mortreux, *New. J. Chem.*, 1997, **21**, 529.
5 G. Papadogianakis, G. Verspui, L. Maat and R. A. Sheldon, *Catal. Lett.*, 1997, **47**, 43.
6 G. Verspui, G. Papadogianakis and R. A. Sheldon, *Chem. Commun.*, 1998, 401.
7 M. Schreuder Goedheijt, P. C. J. Kamer and P. W. N. M. van Leeuwen, *J. Mol. Catal. A: Chem.*, 1998, **134**, 243.
8 E. Drent, J. A. M. Broekhoven and M. J. Doyle, *J. Organomet. Chem.*, 1991, **417**, 235.

Communication 8/06446F

Novel elimination of hydroxylamine and formation of a nickel tetramer on reactions of glutarodihydroxamic acid with model dinickel hydrolases‡

David A. Brown,*[a] Laurence P. Cuffe,[a] Oliver Deeg,[b] William Errington,[c] Noel J. Fitzpatrick,[a] William K. Glass,[a] Kara Herlihy,[a]† Terence J. Kemp[c] and Hassan Nimir[a]

[a] *Department of Chemistry, University College, Belfield, Dublin 4, Ireland. E-mail: Noel.Fitzpatrick@ucd.ie*
[b] *Erasmus student, University of Wurzburg, Germany*
[c] *Department of Chemistry, University of Warwick, Coventry, UK CV4 7AL*

Received (in Cambridge, UK) 4th September 1998, Accepted 6th October 1998

Reactions of glutarodihydroxamic acid with the hydrolase enzyme urease models, $[Ni_2(\mu\text{-}H_2O)(OAc)_4(tmen)_2]$ and $[Ni_2(OAc)_3(urea)(tmen)_2][OTf]$, lead to novel hydroxylamine elimination and formation of $[Ni_2(OAc)_2\{\mu\text{-}O(N)(OC)_2(CH_2)_3\}(tmen)_2][OTf]$ and the tetramer $[Ni_4(OAc)_2(gluA_2)_2(tmen)_4][OTf]_2$, respectively, both of which are structurally characterised by X-ray crystallography.

Urease is a hydrolytic metalloenzyme[1] which catalyses the hydrolysis of urea and contains a dinickel active site with a Ni–Ni distance of 3.5 Å.[2] Hydroxamic acids inhibit a number of enzymes including urease.[3] The urea complex, $[Ni_2(OAc)_3(urea)(tmen)_2][OTf]$ **A**,[4] reacts rapidly with acetohydroxamic acid (AHA) to give the monobridged hydroxamate complex $[Ni_2(OAc)_2(AA)(urea)(tmen)_2][OTf]$[5] with a very similar structure to that of the acetohydroxamate inhibited C319A variant of *Klebsiella aerogenes* urease.[6] Similarly, reaction of the hydrolase model $[Ni_2(\mu\text{-}H_2O)(OAc)_4(tmen)_2]$ **B**[7] with AHA gives the dibridged complex $[Ni_2(OAc)(AA)_2(tmen)_2][OAc]$.[5] We now report the reactions of **A** and **B** with glutarodihydroxamic acid, $(CH_2)_3(CONHOH)_2$, $gluH_2A_2$, with novel results. **B** reacts rapidly with $gluH_2A_2$ at room temperature in both methanol and dichloromethane in the presence of the triflate ion to give $[Ni_2(OAc)_2\{\mu\text{-}O(N)(OC)_2(CH_2)_3\}(tmen)_2][OTf]$ **I**,§ which contains a deprotonated bridging *N*-hydroxyglutarimide with the deprotonated N–OH oxygen O6 bridging the two divalent nickel ions Ni1 and Ni2 and the two carbonyl oxygens O5 and O7, each coordinated to their respective nickel atoms Ni1 and Ni2 (Fig. 1). Formation of **I** involves the novel elimination of hydroxylamine. We suggest that the two nickel centres in **B** act as Lewis acids polarising both carbonyl groups of $gluH_2A_2$ (**C**, Scheme 1). Subsequent protonation of one nitrogen (**D**, Scheme 1) and attack by the other nucleophilic nitrogen occurs with loss of NH_2OH, ring closure and formation of the tetrahedral intermediate (**E**, Scheme 1) which on deprotonation forms **I**. In this mechanism the dinickel centre probably prearranges the electrophilic and nucleophilic reaction centres similar to the prearrangement of water and urea in urease with the base OH^- formed by deprotonation of a coordinated water molecule replaced by the nitrogen nucleophile. The dinickel centre is essential, since reaction of $gluH_2A_2$ with nickel acetate gives simply $Ni(gluA_2)$ with properties similar to those reported previously for analogous complexes.[8] In contrast, the longer chain dihydroxamic acids, $(CH_2)_n(CONHOH)_2$, n = 4 (adipodihdroxamic acid) and n = 8 (sebacodihydroxamic acid), reacted with **B** to give $[Ni_2(OAc)\{(CH_2)_n(CONHO)_2\}(tmen)_2][X]$, n = 4 **II** and n = 8 **III**, X = OTf or BF_4^-, with no loss of NH_2OH and retention of the characteristic ν(NH) infrared absorption at 3246 cm^{-1}.§ Unfortunately, crystals of **II** and **III** were not suitable for X-ray crystallography, but most likely **II** and **III** are the longer chain analogues of **IV** described below. Molecular modelling calculations, using SPARTAN PM3(tm), predict **I** to be a stable structure for glutardihydroxamic acid but not for the longer chain sebacodihydroxamic acid, confirming the importance of steric factors.

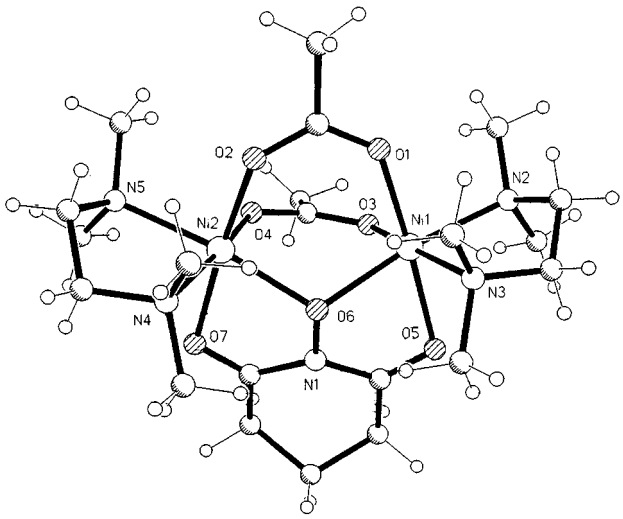

Fig. 1 Molecular structure of the cation of complex **I**. Selected bond distances (Å) and angles(°): Ni1–O6 2.059(2), Ni2–O6 2.040(3), Ni1–O5 2.155(3), Ni2–O7 2.128(3), Ni1–O1 2.019(3), Ni2–O2 2.007(3), O6–Ni1–O5 76.50(10), O7–Ni2–O6 77.97(10), Ni–Ni 3.414(1) and 3.427(1).

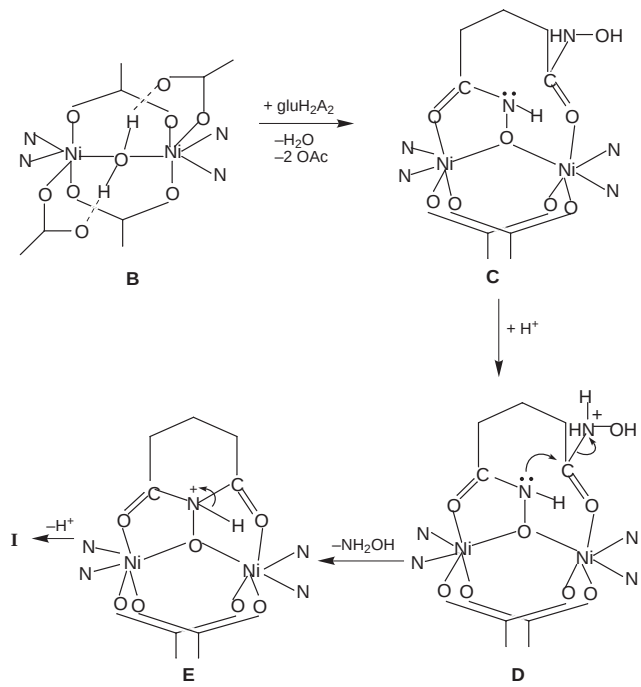

Scheme 1

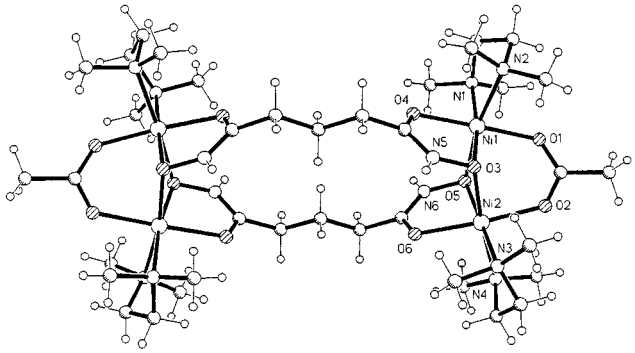

Fig. 2 Molecular structure of the cation of complex **IV**. Selected bond distances (Å) and angles (°): Ni1–O3 2.061(2), Ni2–O3 2.087(2), Ni1–O5 2.121(2), Ni2–O5 2.096(2) Ni1–O4 2.065(2), Ni2–O6 2.062(2), Ni1–Ni2 3.032(1), O4–Ni1–O3 80.27(6), O4–Ni1–O5 97.90(6), O5–Ni1–O3 84.62(6), O5–Ni2–O3 84.62(6).

In contrast to the above reaction of $gluH_2A_2$ with the hydrolase model **B**, reaction with the urease model **A** gives the tetrameric nickel hydroxamate complex **IV**§ $[Ni_4(OAc)_2(gluA_2)_2(tmen)_4][OTf]_2$ (Fig. 2) with accompanying loss of urea. The tetramer contains two sets of nickels atoms Ni1 and Ni2 and their symmetry equivalents, each set bridged by one hydroxamate group of one ligand and one hydroxamate group of the other ligand. As in the corresponding dibridged monohydroxamate (**II** in ref. 5), the deprotonated OH groups O3 and O5 bridge the two nickel centres Ni1 and Ni2, while the carbonyl oxygens O4 and O6 each coordinate to their respective nickel centres Ni1 and Ni2. The bond angles and distances in the dinickel hydroxamate bridges in **IV** and in **II** (ref. 5) are very similar. The structure is duplicated in the other part of the tetramer through the centre of inversion (Fig. 2) with opposite nickel centres, Ni1 and Ni2 being 9.742(1) Å apart. In **I** the Ni–O(bridging) distances Ni2–O6 and Ni1–O6 of 2.040(3) and 2.059(2) Å, respectively, are slightly shorter than the hydroxamate bridging Ni–O distances Ni1–O3 and Ni2–O3 of 2.061(2) and 2.087(2) Å respectively, in the tetramer **IV** (Fig. 2) which may be a factor promoting cyclisation in **I**.

Replacement of bridging water and carboxylates by the deprotonated OH group of the hydroxamic acid is probably part of the driving force of these facile reactions since the resulting bridging oxygen is a feature of all of the complexes which we have studied so far as well as in the dinickel complex containing two salicylhydroxamate bridges.[9] This structural feature also occurs in biological systems such as the acetohydroxamate complex with the C319A variant of urease[6] and the *p*-iodo-D-phenylalanine hydroxamate complex with *Aeromonas proteolytica* aminopeptidase(AAP).[10]

Finally, the displacement of coordinated urea from **A** by $gluH_2A_2$ but not by AHA suggests that inhibition of urease by dihydroxamic acids may also involve displacement of the urea substrate as well as the water molecules (which act as a base source) which is probably the mode of their inhibition by acetohydroxamic acid.

We thank Professor K. Nolan, Royal College of Surgeons in Ireland, for helpful discussions and the EUCOST D8 programme, Project D8/0010/97 for support.

Notes and references

† Present address: Department of Physics, Emory University, Atlanta, GA, USA

‡ Satisfactory microanalyses were obtained for compounds **I**–**IV**. *Preparations* of **I**–**III**: to a solution of **B** (1 mM) in CH_2Cl_2 under nitrogen was added 1 mM of triflate (OTf) (or tetrafluoroborate BF_4^-) and stirred for 1 h followed by 1 mM of $gluH_2A_2$ in methanol. The reaction was monitored by the appearance of IR peaks at 1710, 1750 and 1590 cm^{-1} due to acetic acid and co-ordinated hydroxamate respectively. After work-up, a solution in CH_2Cl_2 was layered with diethyl ether, pentane and 2,2-dimethoxypropane to give blue–green crystals of **I** suitable for X-ray crystallography, **II** and **III** were prepared similarly.

Preparation of **IV**: as for **I**–**III** above but replacing **B** by the urea complex **A** and omitting the addition of triflate ion. Suitable crystals were obtained in this case by vapour diffusion of diethyl ether into a solution of **IV** in methanol/CH_2Cl_2 (1 : 2).

Crystallography: Crystal data: for **I**: $C_{22}H_{44}F_3N_5Ni_2O_{10}S$, M = 745.10, triclinic, space group $P\bar{1}$, a = 10.7655(9), b = 15.7266(13), c = 20.8115(18) Å, α = 73.612(3)°, β = 84.827(3) °, γ = 81.397(3) ° U = 3338.0(5) Å^3 , Z = 4 , λ = 0.71073 Å, μ = 1.262 mm^{-1}. 11303 independent reflections were measured. Final $R1$ = 0.0435 and $wR2$ = 0.1158.

For **IV**: $C_{20}H_{45}F_3N_6Ni_2O_{10}S$, M = 736.10, monoclinic, space group $P2_1/c$, a = 12.4205(7), b = 12.6790(7), c = 20.8914(12) Å, β = 107.1940(10)°, U = 3142.9(3) Å^3 Z = 4 , λ = 0.71073 Å, μ = 1.340 mm^{-1}, 7412 independent reflections were measured. Final $R1$ = 0.0355 and $wR2$ = 0.0867.

Data were collected using a Siemens SMART CCD area-detector diffractometer. Refinement was by full-matrix least squares on F^2 for all data using SHELXL-97.[11] Hydrogen atoms were added at calculated positions and refined using a riding model.

§ Abbreviations: OTf = $CF_3SO_3^-$, OAc = $CH_3CO_2^-$, AHA = acetohydroxamic acid, AA = deprotonated acetohydroxamic acid, $gluH_2A_2$ = glutarodihydroxamic acid, $gluA_2$ = deprotonated glutarodihydroxamic acid.

1 N. Sträter, W. N. Lipscomb, T. Klabunde and B. Krebs, *Angew. Chem. Int. Ed. Engl.*, 1996, **35**, 2024.
2 E. Jabri, M. B. Carr, R. P. Hausinger and P. A. Karplus, *Science*,1995, **268**, 998.
3 H. Kehl, *Chemistry and Biology of Hydroxamic Acids*, ed. S. Karger, Basel, 1982.
4 H. E. Wages, K. L. Taft and S. J. Lippard, *Inorg. Chem.*, 1993, **32**, 4985.
5 M. Arnold, D. A. Brown, O. Deeg, W. Errington, W. Haase, K. Herlihy, T. J. Kemp, H. Nimir and R. Werner, *Inorg. Chem.*, 1998, **37**, 2920.
6 M. A. Pearson, L. O. Michel, R. P. Hausinger and P. A. Karplus, *Biochemistry*, 1997, **36**, 8164.
7 U. Turpeinen, R. Hämäläinen and J. Reedijk, *Polyhedron*, 1987, **6**, 1603.
8 D. A. Brown, N. Ni Choileain, R. Geraty, and J. D. Glennon, *Inorg. Chem.*, 1986, **25**, 3792.
9 A. J. Stemmler, J. W. Kampf, M. L. Kirk and V. L. Pecoraro, *J. Am. Chem. Soc.*, 1995, **117**, 6368.
10 B. Chevrier, H. D'orchymoant, C. Schalk, C. Tarnus and D. Moras, *Eur. J. Biochem.*, 1996, **237**, 393.
11 G. M. Sheldrick, *Shelxl 97, Program for the Refinement of Crystal Structures*, University of Göttingen, Germany, 1997.

Communication 8/06911E

Heterogeneous asymmetric aminohydroxylation of alkenes using a silica gel-supported bis-cinchona alkaloid

Choong Eui Song,*[a] Chun Rim Oh,[a] Sung Woo Lee,[a] Sang-gi Lee,[a] Laetitia Canali[b] and David C. Sherrington[b]

[a] *Division of Applied Science, Korea Institute of Science and Technology, PO Box 131, Cheongryang, Seoul, 130-650, Korea. E-mail: s1673@kistmail.kist.re.kr*

[b] *Department of Pure and Applied Chemistry, University of Strathclyde, Thomas Graham Building, 295 Cathedral Street, Glasgow, UK G1 1XL*

Received (in Cambridge, UK) 7th September 1998, Accepted 5th October 1998

Excellent enantioselectivities of up to > 99% ee have been achieved in the heterogeneous asymmetric aminohydroxylation of *trans*-cinnamate derivatives using silica gel-supported $(QN)_2PHAL$ [SGS-$(QN)_2PHAL$ **1]; the dark brown **1**·Os complex, recovered by simple filtration after reaction, could be reused without any loss of enantioselectivity.**

Highly efficient methods for osmium-catalyzed asymmetric aminohydroxylation (AA) of alkenes in the presence of $(DHQ)_2PHAL$ or $(DHQD)_2PHAL$ ligands have been discovered recently by Sharpless and co-workers.[1] Initially, the catalytic AA reaction exploited TsNClNa (Chloramine-T) as the oxidant/nitrogen source.[1a,b] Subsequently, with the development of new procedures which utilize carbamates-[1d] and amide-derived oxidants,[1e] the substrate scope and selectivity has been greatly improved. The resulting chiral β-amino alcohol group is an important structural element in many biologically active molecules as well as the starting point in the design of many chiral ligands.

Recently, we prepared silica gel-supported $(QN)_2PHAL$ [SGS-$(QN)_2PHAL$ **1**],[2] which with OsO_4 yielded excellent

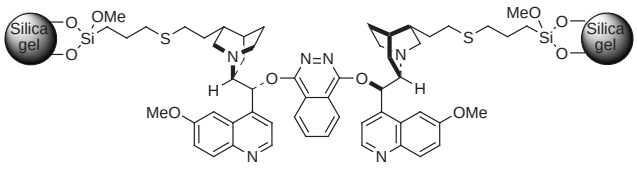

enantioselectivities in asymmetric dihydroxylation of alkenes (> 99% ee for *trans*-stilbene). Moreover the catalytic system, the SGS-$(QN)_2PHAL$ **1**–osmium complex, could be reused after simple filtration without any significant loss of enantioselectivity. UV analysis of the filtrate of the simple mixture of ligand **1** and OsO_4 in $Bu^tOH–H_2O$ (1:1) in several molar ratios (1:1, 2:1, 4:1 *etc*.) showed that the binding affinity of **1** to OsO_4 is much greater than that of the homogeneous analogue $(DHQ)_2PHAL$. No trace amounts of osmium could be found in all filtrates examined. These results encouraged us to examine the efficiency of **1** in the heterogeneous AA reactions. We report here our preliminary findings.

The heterogeneous AA reactions of *trans*-cinnamate derivatives using **1** were carried out either with $EtOCONH_2/Bu^tOCl/NaOH$[1d] or AcNHBr/LiOH[1e] as the oxidant/nitrogen source under the same reaction conditions adopted for the analogous homogeneous process (Scheme 1). The results are summarized in Table 1. The data show that all reactions examined using **1** exhibited excellent enantioselectivities. Generally, the amide-based AA reactions (Table 1, entries 4 and 6) gave higher yields and ees (> 99% ee) than those employing the carbamate-based chemistry (entries 1–3). In particular, the AA reactions at 4 °C with amide as oxidant gave similar chemical yields (71–76%) and ees (> 99% ee) to those obtained in homogeneous AA reactions.[1e] It is noteworthy that when these reactions were carried out at room temperature, the chemical yields were significantly decreased (*ca*. 30–40% yield), whereas the ees were maintained. The reactions always stopped after *ca*. 50% conversion, and the pH of the mixture at the end of the reactions was about 5–6. It is probable that Hoffmann rearrangement[3] of the *N*-bromoacetamide is a significant concurrent reaction at this temperature.

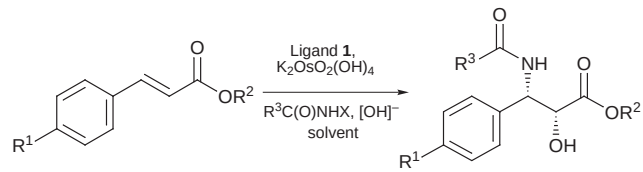

2a R^1 = H, R^2 = Me
b R^1 = OMe, R^2 = Me
c R^1 = NO_2, R^2 = Me
d R^1 = H, R^2 = Pr^i
e R^1 = OMe, R^2 = Pr^i

3a R^1 = H, R^2 = Me, R^3 = OEt
b R^1 = OMe, R^2 = Me, R^3 = OEt
c R^1 = NO_2, R^2 = Me, R^3 = OEt
d R^1 = H, R^2 = Pr^i, R^3 = Me
e R^1 = OMe, R^2 = Pr^i, R^3 = Me

Scheme 1

Table 1 Heterogeneous catalytic AA reaction using SGS-$(QN)_2PHAL$ **1**[a]

Entry	Substrate	Oxidant	Solvent	*t*/h	Yield (%)[b]	Ee (%)[c]	Configuration[c]
1	**2a**	EtOCONClNa	$Pr^iOH–H_2O$	12	40	88	2*R*,3*S*
2	**2b**	EtOCONClNa	$Pr^iOH–H_2O$	12	43	92	2*R*,3*S*
3	**2c**	EtOCONClNa	$CH_3CN–H_2O$	12	52	92	2*R*,3*S*
4	**2d**	AcNBrLi	$Bu^tOH–H_2O$	7	71	> 99	2*R*,3*S*
5[d]	**2d**	AcNBrLi	$Bu^tOH–H_2O$	7	30	> 99	2*R*,3*S*
6	**2e**	AcNBrLi	$Bu^tOH–H_2O$	9	76	> 99	2*R*,3*S*
7[d]	**2e**	AcNBrLi	$Bu^tOH–H_2O$	9	32	> 99	2*R*,3*S*
8[e]	**2e**	AcNBrLi	$Bu^tOH–H_2O$	7	81	> 99	2*R*,3*S*

[a] In all cases 4 mol% $K_2OsO_2(OH)_4$ and 5 mol% ligand were used. The reactions in entries 1–3 were carried out at 10 °C under the same reaction conditions as those reported in ref. 1(*d*). The reactions in entries 4–7 were carried out at 4 °C under the same reaction conditions as those reported in ref. 1(*e*). [b] Isolated yields by column chromatography. [c] The ees and absolute configuration were determined by chiral HPLC analysis.† [d] Reaction was carried out with **1**·Os complex recovered from the reaction in entries 4 and 6 respectively without further addition of $K_2OsO_2(OH)_4$. [e] Reaction was carried out with **1**·Os complex recovered from the reaction in entry 6 with the addition of small amounts of $K_2OsO_2(OH)_4$ (2 mol%).

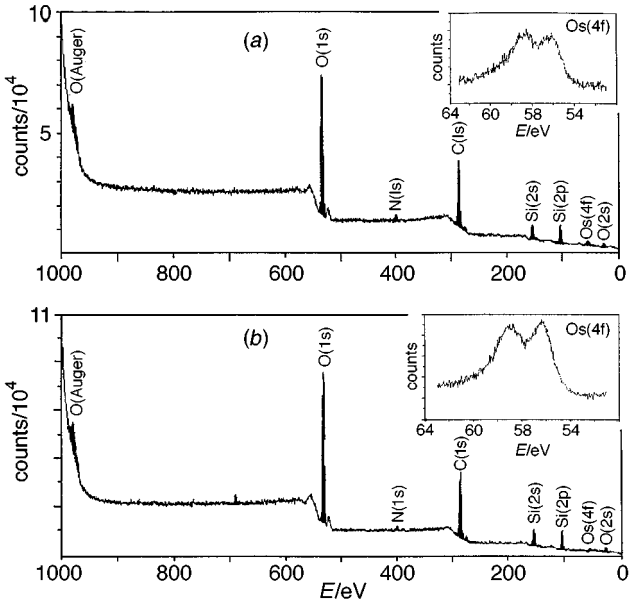

Fig. 1 XPS-spectra of the **1**-Os complex recovered after reaction, entry 4 (a) and entry 6 (b).

The efficiency with which the catalyst can be recycled has also been examined. The dark brown-coloured **1**·Os complex was recovered by simple filtration after each reaction (entries 4 and 6), which is not possible in a homogeneous process. XPS (X-Ray Photoelectron Spectroscopy)-analysis (Fig. 1) of the samples shows clearly that these recovered complexes contain osmium. However, the recovery yields were not high enough ($< 50\%$). The rest of the osmium was obviously lost to the mother liquor. The AA reactions were repeated with these samples without further addition of osmate salt. As shown in entries 5 and 7, the required amino alcohols **3d**,**e** were obtained in 30 and 32% yield with $> 99\%$ ee, respectively. Moreover, the addition of small amounts of osmium to the recovered catalyst regenerated completely the reaction conditions (entry 8). These results indicate the viability of the repetitive use of osmium and the chiral ligand, which is a current intrinsic limitation of catalytic AA and AD reactions.

In conclusion, we have achieved excellent ees for the heterogeneous catalytic AA of alkenes using a silica gel-supported bis-cinchona alkaloid **1**. Moreover, the recovered dark brown-coloured **1**·Os complex can be reused without any loss of enantioselectivity. We have also determined the Os content of this complex by XPS analysis. Further studies are currently in progress to increase the product yield, and the recovery of both the chiral ligand and the osmium.

This research was supported by a grant (MOST 2N17410) from the Ministry of Science and Technology in Korea.

Notes and references

† Determination of enantiomeric excesses: For **3a**: Chiralcel AD, Pr^{i}OH–hexane (10:90), 0.7 ml min^{-1}; 25.0 min (2*R*,3*S*), 29.6 min (2*S*,3*R*). For **3b**: Chiralcel AD, Pr^{i}OH–hexane (10:90), 0.7 ml min^{-1}; 36.1 min (2*R*,3*S*), 54.0 min(2*S*,3*R*). For **3c**: Chiralcel AD, Pr^{i}OH–hexane (10:90), 1 ml min^{-1}; 26.9 min (2*R*,3*S*), 43.2 min (2*S*,3*R*). For **3d**: Chiralcel AD, Pr^{i}OH–hexane (20:80), 1 ml min^{-1}; 6.9 min (2*R*,3*S*), 10.9 min (2*S*,3*R*). For **3e**: Chiralcel AD, Pr^{i}OH–hexane (20:80), 1 ml min^{-1}; 9.6 min (2*R*,3*S*), 16.7 min (2*S*,3*R*).

1 (*a*) G. Li, H. T. Chang and K. B. Sharpless, *Angew. Chem., Int. Ed. Engl.*, 1996, **35**, 451; (*b*) G. Li and K. B. Sharpless, *Acta Chem. Scand.*, 1996, **50**, 649; (*c*) J. Rudolph, P. C. Sennhenn, C. P. Vlaar and K. B. Sharpless, *Angew. Chem., Int. Ed. Engl.*, 1996, **35**, 2810; (*d*) G. Li, H. H. Angert and K. B. Sharpless, *Angew. Chem., Int. Ed. Engl.*, 1996, **35**, 2813; (*e*) M. Bruncko, G. Schlingloff and K. B. Sharpless, *Angew. Chem., Int. Ed. Engl.*, 1997, **36**, 1483; (*f*) K. L. Reddy and K. B. Sharpless, *J. Am. Chem. Soc.*, 1998, **120**, 1207; (*g*) K. L. Reddy, K. R. Dress and K. B. Sharpless, *Tetrahedron Lett.*, 1998, **39**, 3667; (*h*) P. O'Brien, A. O. Simon and D. D. Parker, *Tetrahedron Lett.*, 1998, **39**, 4099.

2 (*a*) C. E. Song, J. W. Yang and H. J. Ha, *Tetrahedron: Asymmetry*, 1997, **8**, 841; (*b*) For the preparation of chiral monomer, C. E. Song, J. W. Yang, H. J. Ha and S. G. Lee, *Tetrahedron: Asymmetry*, 1996, **7**, 645; (*c*) SGS-$(QN)_2$PHAL **1** was prepared as reported in ref. 2(*a*) using silica gel Merck-60 (230–400 mesh) instead of Li Chrosorb SI 60 (Merck, 5 mm). The content of alkaloid in **1** was determined by nitrogen analysis (0.21 mmol of alkaloid per gram).

3 A. W. Hoffmann, *Ber. Dtsch. Chem. Ges.*, 1881, **14**, 2725; E. S. Wallis and J. F. Lane, *Org. React.*, 1967, **3**, 267.

Communication 8/06959J

ChemComm

Alkenyl *O*- and *C*-glycopyranoside homodimerization by olefin metathesis reaction

Romyr Dominique, Sanjoy K. Das and René Roy*

Department of Chemistry, University of Ottawa, Ottawa, K1N 6N5, Canada, Ontario.
E-mail: rroy@science.uottawa.ca

Received (in Cambridge, UK) 28th July 1998, Accepted 5th October 1998

Using ruthenium-catalyzed olefin metathesis, several *O*- and *C*-allyl and *O*-pentenyl D-galactopyranoside and lactoside homodimers were prepared in high yields.

Multivalent neoglycoconjugates have been exhaustively utilized to probe and enhance carbohydrate–protein interactions at the molecular level.[1] Moreover, glycoclusters[2] and dendrimers[3] are also emerging as potential carbohydrate-based therapeutic agents.[4] Several examples exist in which ligand-induced receptor and protein dimerization occurred as a general mechanism for signal transduction.[5] It is conceivable that signal transduction and receptor shedding could also be triggered by carbohydrate oligomers.[6]

Transition metal catalyzed olefin metathesis has gained an important position in organic syntheses in recent years.[7–10]

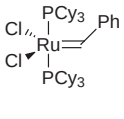

1

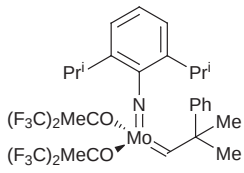

2

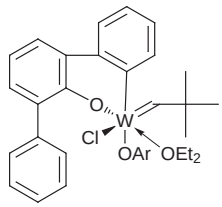

3

Ruthenium carbene complex **1** developed by Grubbs and coworkers[7] and Schrock's molybdenum catalyst **2**[8] are very useful in this respect. Because of its unique properties, high reactivity, stability to air, and remarkable functional group tolerance, benzylidenebis(tricyclohexylphosphine)dichlororuthenium **1** has been chosen as the catalyst of the year. Ruthenium and molybdenum carbenoids have been scarcely used in carbohydrate chemistry.[9] It seemed appealing to apply the olefin metathesis reaction toward the synthesis of carbohydrate homodimers. The only example of carbohydrate homodimerization was reported by Descotes *et al.*[10] in his sugar bolaform syntheses using a tungsten aryloxo complex such as **3**. However, the tungsten-catalyzed alkenyl glycoside homodimerizations were unsuccessful with *O*-allyl glycosides as well as benzyl-protected sugar derivatives. Herein, we report the efficient and high yielding synthesis of some biologically important carbohydrate homodimers starting from either peracetylated or perbenzylated *O*- and *C*-allyl as well as *O*-pentenyl galactopyranosides using ruthenium benzylidene complex **1** (Scheme 1).

Treatment of allyl 2,3,4,6-tetra-*O*-acetyl-α-D-galactopyranoside **4** with 10 mol% of Grubbs' catalyst **1** in refluxing CH_2Cl_2 under a nitrogen atmosphere resulted in the clean formation of homodimer **5** in 92% yield as a mixture of *E* and *Z* stereoisomers in 5:1 molar ratio (Scheme 1).† The only other by-products isolated from these sequential [2+2] cycloaddition and cycloreversion equilibria were the recovered starting material (3%) along with trace amount of cross-metathesis product obtained from the initially released styrene. In order to compare the catalytic activity of Grubbs' catalyst **1** to that of Schrock's catalyst **2**, we repeated the reaction between **4** and 10

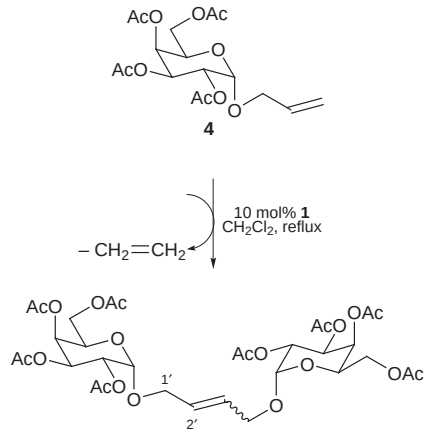

Scheme 1

mol% of **2** in CH_2Cl_2. The reaction, performed under Schlenk conditions, provided the same dimer **5** in 80% yield. Since in both cases the yields were more or less the same, catalyst **1** was preferred because of its operational simplicity.

The ratio of the inseparable *E* and *Z* isomers was determined from analysis of the ^{1}H NMR spectrum of the crude mixture. It is generally accepted that the carbon α to a double bond is more shielded in the *Z* isomer than in the *E* isomer due to the γ effect.[11] So, the empirical relationship $\delta_{\alpha(Z)} < \delta_{\alpha(E)}$ allowed us to determine the relative configuration of the *E* and *Z* stereoisomers. For instance, the ^{13}C NMR spectrum of **5** showed the α carbon of the *Z* isomer at δ 63.5, whereas that of the *E* isomer appeared at δ 67.4 ($\Delta\delta$ 3.9 ppm).

Similarly, olefin metathesis of the corresponding peracetylated β-anomer **6** with 10 mol% of catalyst **1** under the same reaction conditions provided homodimer **7** in 95% yield as a mixture of *E* and *Z* isomers in a 4:1 ratio (Table 1).‡ To further explore the scope of this reaction, *O*-pentenyl β-D-galactopyranoside **8**, allyl β-lactoside **9**, α-*C*-allyl galactopyranoside **10**[12] and β-*C*-allyl galactopyranoside **11**[13] were prepared and reacted with Grubbs' catalyst under the same reaction conditions to give compounds **12–15** respectively. The reactions proceeded successfully with high yields and the results are summarized in Table 1. Then we turned our attention to the synthetically more useful benzyl protected sugars, using allyl 2,3,4,6-tetra-*O*-benzyl-β-D-galactopyranoside **16**. Treatment of **16** with **1** also proceeded smoothly to provide **17** in 76% yield.

In conclusion, Grubbs's ruthenium benzylidene catalyzed olefin metathesis reaction was applied toward the synthesis of polyfunctionalized carbohydrate homodimers for the preparation of potential cross-linkers of biological interest in signal transduction. The reaction is general, high yielding, and compatible with the usual carbohydrate protecting groups. Further work is now in progress to explore the scope of the reaction.

We are thankful to the Natural Sciences and Engineering Research Council of Canada (NSERC) for financial support.

Table 1 Olefin self metathesis of alkenyl *O*- and *C*-glycopyranosides

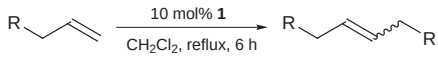

4,6,8–11,16 **5,7,12–15,17**

Entry	Substrate	R	Product (*E*/*Z*)	Yield (%)
1	**4**	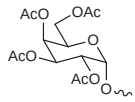	**5** (5/1)	92
2	**6**	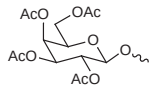	**7** (4/1)	95
3	**8**	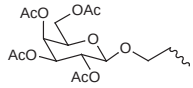	**12** (5/1)	85
4	**9**	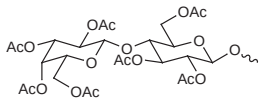	**13** (4/1)	89
5	**10**	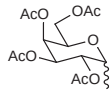	**14** (2/1)	82
6	**11**	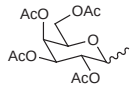	**15** (1/1)	75
7	**16**	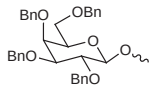	**17** (3/1)	76

Notes and references

† *Typical procedure*: 100 mg (0.148 mmol) of **9** was dissolved in 1 ml of dry CH_2Cl_2. After addition of 6 mg (10 mol%) of catalyst **1**, the resulting purple colored solution was allowed to reflux under N_2 atmosphere for 6 h, to give a black solution which was directly purified by silica gel column chromatography to afford 87.2 mg of **13** (89%) as a solid.

‡ All compounds showed satisfactory NMR (Bruker AMX 500 MHz) and mass spectral data. *Selected data* for **5**: HRMS FAB: calc. for $C_{32}H_{44}O_{20}$ 748.7. Found 749.2 (M + 1), $\delta_H(CDCl_3)$ 5.78 (t, 1 H, *J* 2.8, H-2′, *E* isomer), 5.71 (t, 1H, *J* 3.9, H-2′, *Z* isomer), 5.43 (dd, 1H, *J* 3.4, 1.3, H-4), 5.36–5.30 (m, 1H, H-3), 5.12–5.07 (m, 2H, H-2), 4.22–3.98 (m, 5H, H-1′a, H-1′b, H-5, H-6a, H-6b), 2.11–1.95 (4s, 12 H, 4 ∞ OAc); $\delta_C(CDCl_3)$ 170.3, 170.3, 170.1, 169.9 (C=O), 128.8 (C-2′, *Z* isomer), 128.5 (C-2′, *E* isomer), 95.6 (C-1, *Z* isomer), 95.5 (C-1, *E* isomer), 67.4 (C-1′, *E* isomer), 63.5 (C-1′, *Z* isomer). For **7**: $\delta_H(CDCl_3)$ 5.69 (t, 1H, *J* 2.5, H-2′, *E* isomer), 5.6 (t, 1H, *J* 4.1 Hz, H-2′, *Z* isomer); $\delta_C(CDCl_3)$ 128.6, 64.3 (C-2′ and C-1′ for *Z* isomer), 128.1, 68.7 (C-2′ and C-1′ for *E* isomer). For **12**: $\delta_H(CDCl_3)$ 5.33–5.31 (m, 2H, H-4, H-2′, *E* and *Z*); $\delta_C(CDCl_3)$ 129.9, 28.5 (C-2′ and C-1′ for *E* isomer), 129.4, 23.3 (C-2′ and C-1′ for *Z* isomer). For **14**: $\delta_H(CDCl_3)$ 5.48 (t, 1H, *J* 4.5, H-2′, *Z* isomer), 5.45 (t, 1H, *J* 3.7, H-2′, *E* isomer); $\delta_C(CDCl_3)$ 128.0, 29.9 (C-2′ and C-1′ for *E* isomer), 126.8, 24.8 (C-2′ and C-1′ for *Z* isomer). For **15**: $\delta_H(CDCl_3)$ 5.50–5.45 (m, 1H, H-2′, *E* and *Z* isomer); $\delta_C(CDCl_3)$ 128.5, 35.4 (C-2′ and C-1′ for *E* isomer), 127.3, 30.2 (C-2′ and C-1′ for *Z* isomer).

1 R. Roy, in *Carbohydrate Chemistry*, ed. G. J. Boons, Chapman & Hall, UK, 1998, p. 243; R. Roy, *Curr. Opin. Struct. Biol.*, 1996, **6**, 692; L. L. Kiessling and N. L. Pohl, *Chem. Biol.*, 1996, **3**, 71; N. V. Bovin and H.-J. Gabius, *Chem. Soc. Rev.*, 1995, **24**, 413.

2 Y. C. Lee and R. T. Lee, *Acc. Chem. Res.*, 1995, **28**, 322; A. Lubineau, S. Escher, J. Alais and D. Bonnaffé, *Tetrahedron Lett.*, 1997, **38**, 4087; R. J. Patch, H. Chen and C. R. Pandit, *J. Org. Chem.*, 1997, **62**, 1543; D. Pagé and R. Roy, *Bioorg. Med. Chem. Lett.*, 1996, **6**, 1765; S. A. DeFrees, W. Kosch, W. Way, J. C. Paulson, S. Sabesan, R. L. Halcomb, D.-H. Huang, Y. Ichikawa and C.-H. Wong, *J. Am. Chem. Soc.*, 1995, **117**, 66.

3 R. Roy, *Top. Curr. Chem.*, 1997, **187**, 241; D. Zanini and R. Roy, in *Carbohydrate Mimics*: *Concepts and Methods*, ed. Y. Chapleur, Verlag Chemie, Weinheim, Germany, 1998, p. 385; N. Jayaraman, S. A. Nepogodiev and J. F. Stoddart, *Chem. Eur. J.*, 1997, **3**, 1193.

4 K. J. Yarema and C. R. Bertozzi, *Curr. Opin. Chem. Biol.*, 1998, **2**, 49; R. Roy, in *Carbohydrates in Drug Design*, ed. Z. J. Witczak and K. A. Nieforth, Marcel Dekker, NY, 1997, p. 83.

5 J. A. Wells, *Curr. Opin. Cell Biol.*, 1994, **6**, 163; C.-H. Heldin, *Cell*, 1995, **80**, 213; D. L. Boger and W. Chai, *Tetrahedron*, 1998, **54**, 3955; S. T. Diver and S. L. Schreiber, *J. Am. Chem. Soc.*, 1997, **119**, 5106.

6 P. Velupillai and D. A. Harn, *Proc. Natl. Acad. Sci. U.S.A.*, 1994, **91**, 18; I. Takata, K. Chida, M. R. Gordon, Q. N. Myrvik, M. J. Ricardo, Jr. and L. S. Kucera, *J. Leukocyte Biol.*, 1987, **41**, 248; E. J. Gordon, W. J. Sanders and L. L. Kiessling, *Nature*, 1998, **392**, 30.

7 S. T. Nguyen, R. H. Grubbs and J. W. Ziller, *J. Am. Chem. Soc.*, 1993, **115**, 9858; E. L. Dias, S. T. Nguyen and R. H. Grubbs, *J. Am. Chem. Soc.*, 1997, **119**, 3887; P. Schwab, R. H. Grubbs and J. W. Ziller, *J. Am. Chem. Soc.*, 1996, **118**, 100; M. Schuster and S. Blechert, *Angew. Chem., Int. Engl.*, 1997, **36**, 2036; R. H. Grubbs and S. Chang, *Tetrahedron*, 1998, **54**, 4413; R. H. Grubbs, S. J. Miller and G. C. Fu, *Acc. Chem. Res.*, 1995, **28**, 446.

8 R. R. Schrock, S. J. Murdzek, G. C. Bagan, M. Dimare and M. O'Regan, *J. Am. Chem. Soc.*, 1990, **112**, 3875; G. C. Bagan, J. H. Oskam, H.-N. Cho, L. Y. Park and R. R. Schrock, *J. Am. Chem. Soc.*, 1991, **113**, 6899.

9 For examples in RCM: H. S. Overkleeft and U. K. Pandit, *Tetrahedron Lett.*, 1996, **37**, 547; A. Furstner and T. Muller, *J. Org. Chem.*, 1998, **63**, 424; P. A. Van Hooft, M. A. Leeuwenburgh, H. S. Overkleeft, G. A. Van der Marel, C. A. A. van Boeckel and J. H. van Boom, *Tetrahedron Lett.*, 1998, **39**, 6061; examples in CM: J. Feng, M. Schuster and S. Blechert, *Synlett*, 1997, 129; M. Schuster, N. Lucas and S. Blechert, *Chem. Commun.*, 1997, 823; examples in ROMP: K. H. Mortell, M. Gingras and L. L. Kiessling, *J. Am. Chem. Soc.*, 1994, **116**, 12053; C. Fraser and R. H. Grubbs, *Macromolecules*, 1995, **28**, 7248; K. Nomura and R. R. Schrock, *Macromolecules*, 1996, **29**, 540.

10 G. Descotes, J. Ramza, J.- M. Basset and S. Pagano, *Tetrahedron Lett.*, 1994, **35**, 7379; J. Ramza, G. Descotes, J. M. Basset and A. Mutch, *J. Carbohydr. Chem.*, 1996, **15**, 125.

11 E. Breitmaier and W. Voelter, *Carbon-13 NMR Spectroscopy. High Resolutions Methods and Applications in Organic Chemistry and Biochemistry*, VCH, New York, 1987, pp. 192–195.

12 A. Giannis and K. Sandhoff, *Tetrahedron Lett.*, 1985, **26**, 1479.

13 T. Uchiyama, T. J. Woltering, W. Wong, C. C. Lin, T. Kajimoto, M. Takebayashi, G. W. Schmidt, T. Asakura, M. Noda and C. H. Wong, *Bioorg. Med. Chem.*, 1996, **4**, 1149.

Communication 8/05975F

Rhodium-catalysed direct *ortho* arylation of 2-arylpyridines with arylstannanes *via* C–H activation

Shuichi Oi,* Susumu Fukita and Yoshio Inoue

Department of Materials Chemistry, Graduate School of Engineering, Tohoku University, Sendai 980-8579, Japan. E-mail: oishu@aporg.che.tohoku.ac.jp

Received (in Cambridge, UK) 1st September 1998, Accepted 2nd October 1998

The *ortho* position of the aromatic ring of pyridyl group-substituted aromatic compounds was directly arylated with tetraarylstannanes in the presence of a catalytic amount of a rhodium(I)–phosphine complex.

Transition metal-catalysed cross-coupling reactions of aromatic compounds with arylated typical metal compounds such as Mg, Zn, B, Si and Sn are useful synthetic routes to biaryl compounds.[1] A variety of aromatic compounds such as ArI (Cl, Br), ArOTf, ArOMs, $ArOP(O)(OR)_2$, ArOR, ArSR and ArN_2BF_4 have been used for the cross-coupling reactions with typical arylated metal compounds. These reactions involve C–X bond cleavage [X = halide, OTf, OMs, $OP(O)(OR)_2$, OR, SR and N_2BF_4] *via* the oxidative addition of a low valent transition metal (M) complexes and subsequent transmetalation between the resultant C–M–X species and arylated metal compounds. There has, however, been no report of the cross-coupling reaction between the aromatic C–H bond and organometal compounds. In 1993, Murai *et al*. reported ruthenium-catalysed *ortho* alkylation of acetophenones with terminal alkenes, which represented the first effective catalytic C–C bond formation involving the cleavage of an aryl C–H bond.[2] It is thought that chelation of the acetyl group of acetophenone directs the ruthenium complex to cleave the *ortho* C–H bond. The pyridyl group has also been known to direct transition metal-catalysed C–H bond cleavage of an aromatic ring as in the rhodium-catalysed *ortho* alkylation of pyridylbenzenes with terminal alkenes[3] and ruthenium-catalysed carbonylation with CO and terminal alkenes.[4] We report herein our finding that the *ortho* position of pyridylbenzenes is directly arylated with tetra-arylstannanes in the presence of a catalytic amount of a rhodium(I)–phosphine complex.

Initial work was centered on the reaction of 2-phenylpyridine **1a** with tetraphenylstannane **2a** in the presence of a catalytic amount of various transition metal complexes (Scheme 1). The results are summarized in Table 1. The $[RhCl(C_8H_{14})_2]_2$–PPh_3 catalytic system produced singly phenylated product **3aa** in 24% yield (entry 1). Other phosphine ligands such as PCy_3, $P(OPh)_3$ and dppe were less effective, giving **3aa** in lower yields (entries 2–4). The highest yield was obtained using

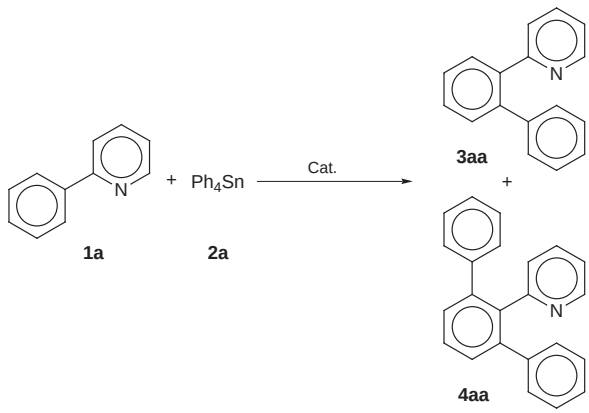

Scheme 1

Table 1 Reaction of **1a** with **2a** in the presence of a catalytic amount of various transition metal complexes[a]

Entry	Catalyst	Yield (%)[b]
1	$[RhCl(C_8H_{14})_2]_2 + 4PPh_3$	24
2	$[RhCl(C_8H_{14})_2]_2 + 4PCy_3$	10
3	$[RhCl(C_8H_{14})_2]_2 + 4P(OPh)_3$	6
4	$[RhCl(C_8H_{14})_2]_2$ + 2dppe	7
5	$RhCl(PPh_3)_3$	29
6	$RhCl(CO)(PPh_3)_2$	5
7	$Pd_2(dba)_3{\cdot}CHCl_3 + 4PPh_3$	0
8	$Pt_2(dba)_3{\cdot}CHCl_3 + 4PPh_3$	0
9	$[IrCl(cod)]_2 + 4PPh_3$	0
10	$Ru_3(CO)_{12} + 6PPh_3$	0

[a] A mixture of **1a** (0.5 mmol), **2a** (0.75 mmol) and metal complexes (10 mol% of **1a**, based on metal) in THF (1.5 ml) was stirred in a sealed vial under N_2 at 120 °C for 20 h. Product was **3aa**. [b] Determined by GLC.

$RhCl(PPh_3)_3$, affording **3aa** in 29% yield (entry 5), while the use of $RhCl(CO)(PPh_3)_2$ gave **3aa** in only 5% yield (entry 6). In these cases, only a trace amount of doubly phenylated product **4aa** was observed. Other low valent transition metal complexes of Pd, Pt, Ir and Ru did not show any catalytic activity (entries 7–10). The reaction of **1a** with **2a** was then carried out in various solvents in the presence of 5 mol% of $RhCl(PPh_3)_3$. The results are summarized in Table 2. The reactions in toluene, THF and MeCN afforded the product **3aa** in low yields of 14, 16 and 12%, respectively, together with a trace amount of **4aa** (entries 1–3). The yield of the products slightly increased using chlorinated alkanes such as $CHCl_3$, 1,2-dichloroethane and 1,1,1-trichloroethane as solvent, affording **3aa** in 32, 37 and 27%, respectively. Surprisingly, 1,1,2,2-tetrachloroethane exhibited a dramatic effect, giving **3aa** and **4aa** in good yields of 65 and 20%, respectively. In this case, trichloroethylene originating from the solvent *via* dehydrochlorination was detected by GLC after the reaction. In order to study the effects of this olefin on the reaction, a small amount (0.25 mmol) of trichloroethylene was added to the reaction of **1a** and **2a** using THF as solvent. This experiment afforded **3aa** and **4aa** in improved yields of 42 and 3%, respectively, compared to the

Table 2 Reaction of **1a** with **2a** in the presence of a catalytic amount of $RhCl(PPh_3)_3$ in various solvents[a]

		Yield (%)[b]	
Entry	Solvent	**3aa**	**4aa**
1	Toluene	14	0
2	THF	16	1
3	MeCN	12	0
4	$CHCl_3$	32	2
5	$ClCH_2CH_2Cl$	37	1
6	$MeCCl_3$	27	1
7	$Cl_2CHCHCl_2$	65 (56)	20 (20)

[a] A mixture of **1a** (0.5 mmol), **2a** (0.5 mmol) and $RhCl(PPh_3)_3$ (5 mol%) in solvent (1.5 ml) was stirred in a sealed vial under N_2 at 120 °C for 20 h. [b] Determined by GLC. Yields in parentheses are for isolated compounds.

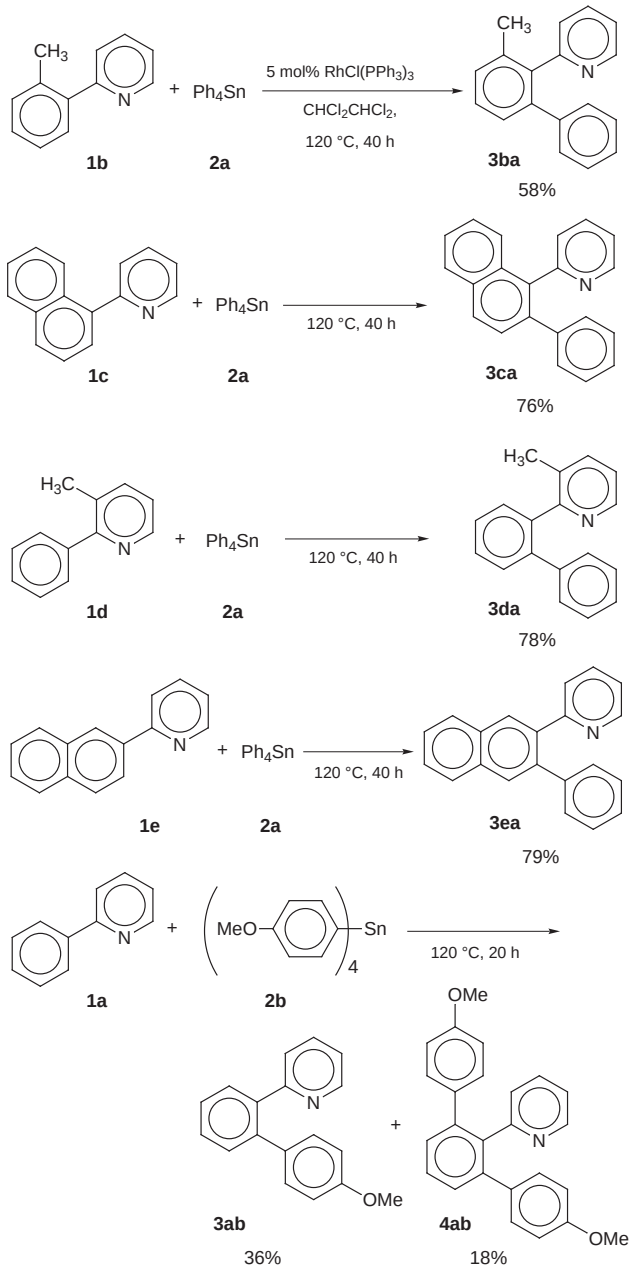

Scheme 2

original yields of 16 and 1% (see Table2, entry 2). Thus the trichloroethylene generated *in situ* during the reaction may partly be responsible for the remarkable effect of 1,1,2,2-tetrachloroethane.

Results for the reactions of other pyridyl-substituted aromatic compounds **1** with arylstannanes **2** in the presence of 5 mol% of $RhCl(PPh_3)_3$ in 1,1,2,2-tetrachloroethane are shown in Scheme 2.†‡ The reactions of **2a** with 2-(2-methylphenyl)pyridine **1b** and 2-(1-naphthyl)pyridine **1c** having only one *ortho* C–H bond on the aromatic ring gave singly phenylated products **3ba** and **3ca**. in good yields. 3-Methyl-2-phenylpyridine **1d** containing two possible reactive *ortho* C–H bonds gave singly phenylated product **3da** in 78% yield selectively. As was described in ref. 3 and 4, the steric interaction between the phenyl group and the methyl group in **3da** prevented the second phenylation. 2-(2-Naphthyl)pyridine **1e** was also phenylated only at the 3-position of the naphthalene ring, affording singly phenylated product **3ea** in 79% yield selectively. In this case, the steric hindrance of the 8-position of the naphthalene ring would prevent phenylation at the 1-position. Tetra(*p*-methoxyphenyl)-stannane **2b** reacted with **1a** affording **3ab** and **4ab** in 36 and 18% yield, respectively.

Although the mechanism of the present reaction is not yet clear, a reaction pathway involving the N atom-directed oxidative addition of the low valent rhodium complex to the *ortho* C–H bond of the phenyl ring followed by phenylation with tetraphenylstannane may be possible.

The reaction reported herein represents the first example of the cross-coupling reaction between aromatic C–H bonds and organometal compounds, and provides a new method for direct arylation of the *ortho* position of pyridyl-substituted aromatic compounds. Further work is now in progress to determine the full scope of this reaction.

Notes and references

† The structures of the compounds **3aa**, **3ba**, **3ca**, **3da**, **3ea**, **3ab**, **4aa** and **4ab** were in a complete accord with the obtained IR, MS, ^1H and ^{13}C NMR and elemental analysis data. The assignment of signals in ^1H and ^{13}C NMR spectra was confirmed by ^1H–^1H COSY and ^1H–^{13}C HMQC spectra.

‡ Typical experimental procedure: A mixture of **1a** (74.2 mg, 0.478 mmol), **2a** (213.5 mg, 0.500 mmol) and $RhCl(PPh_3)_3$ (23.1 mg, 0.025 mmol) in 1,1,2,2-tetrachloroethane (1.5 ml) was stirred in a sealed vial under N_2 at 120 °C for 20 h. The reaction mixture was taken up in $CHCl_3$ and washed with diluted aqueous ammonia and water. After the $CHCl_3$ layer was dried over K_2CO_3, the solvent was evaporated, and then the residue was purified by medium-pressure preparative liquid chromatography (Yamazen Corp., Ultra Pack column, silica gel, 40 μm, 60 Å, 26 × 300 mm) eluting with 3% acetone in $CHCl_3$ to give **3aa** (62.5 mg, 56%) and **4aa** (28.8 mg, 20%). Yields shown in Scheme 2 are for isolated compounds.

1 Reviews: D. W. Knight, in *Comprehensive Organic Synthesis*, ed. B. M. Trost and I. Fleming, Pergamon, London, 1991, vol. 3, pp. 481–520; M. Kumada, *Pure Appl. Chem.*, 1980, **52**, 669; E. Negishi, *Acc. Chem. Res.*, 1982, **15**, 340; N. Miyaura and A. Suzuki, *Chem. Rev.*, 1995, **95**, 2457; T. Hiyama and Y. Hatanaka, *Pure Appl. Chem.*, 1994, **66**, 1471; J. K. Stille, *Angew. Chem., Int. Ed. Engl.*, 1986, **25**, 508; T. N. Mitchell, *Synthesis*, 1992, 803.

2 S. Murai, F. Kakiuchi, S. Sekine, Y. Tanaka, A. Kamatani, M. Sonoda and N. Chatani, *Nature*, 1993, **366**, 529; S. Murai, F. Kakiuchi, S. Sekine, Y. Tanaka, A. Kamatani, M, Sonoda and N. Chatani, *Pure Appl. Chem.*, 1994, **66**, 1527; S. Murai, F. Kakiuchi, S. Sekine, Y. Tanaka, A. Kamatani, M. Sonoda and N. Chatani, *Bull. Chem. Soc. Jpn.*, 1995, **68**, 62; F. Kakiuchu, Y. Tanaka, T. Sato, N. Chatani and S. Murai, *Chem. Lett.*, 1995, 679; F. Kakiuchi, Y. Yamamoto, N. Chatani and S. Murai, *Chem. Lett.*, 1995, 781; M. Sonoda, F. Kakiuchi, N. Chatani and S. Murai, *J. Organomet. Chem.*, 1995, **504**, 151.

3 Y.-G. Lim, Y. H. Kim and J.-B. Kang, *J. Chem. Soc., Chem. Commun.*, 1994, 2267; Y.-G. Lim, J.-B. Kang and Y. H. Kim, *J. Chem. Soc., Perkin Trans. 1*, 1996, 2201.

4 N. Chatani, Y. Ie, F. Kakiuchi and S. Murai, *J. Org. Chem.*, 1997, **62**, 2604.

Communication 8/06790B

Enantioselective Claisen rearrangement of difluorovinyl allyl ethers

Hisanaka Ito, Azusa Sato, Tetsuo Kobayashi and Takeo Taguchi*

Tokyo University of Pharmacy and Life Science, Horinouchi, Hachioji, Tokyo 192-0392, Japan.
E-mail: taguchi@ps.toyaku.ac.jp

Received (in Cambridge, UK) 29th May 1998, Revised manuscript received 5th October 1998, Accepted 5th October 1998

The enantioselective Claisen rearrangement of difluorovinyl allyl ethers was achieved, for the first time, in moderate to good enantioselectivity using a chiral boron reagent as the Lewis acid.

The development of a preparative method for chiral organofluorine compounds is very important in the field of medicinal chemistry.[1] The Claisen rearrangement of difluorovinyl allyl ethers is a powerful tool for the synthesis of β-substituted α,α-difluorocarbonyl compounds.[2] Although enantioselective versions of the Claisen rearrangement have been studied for the construction of chiral molecules,[3] there has been no report dealing with the reaction of difluorovinyl allyl ethers. We recently reported the highly enantioselective aromatic Claisen rearrangement of *o*-allyloxyphenol derivatives mediated by the chiral boron reagent **1**.[4] The efficiency of this system is based on the σ-bond formation of the chiral boron reagent **1**[5] with the phenolic hydroxy group in the substrate and the subsequent coordination of the ethereal oxygen to the boron atom to form a rigid chiral environment in the substrate and to promote the reaction at low temperature. We report herein the application of this system to the enantioselective Claisen rearrangement of difluorovinyl allyl ethers (Scheme 1).

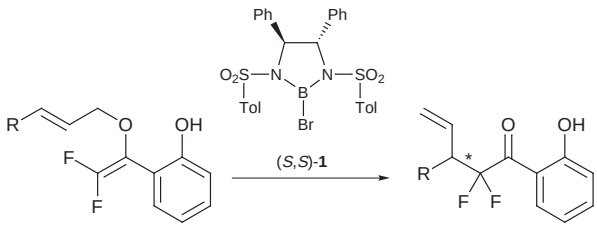

Scheme 1

The substrate **2** having a phenolic hydroxy group was selected, because of the importance of a binding site to the chiral boron reagent **1** in forming a coordinated cyclic intermediate and promoting the reaction. Compound **4a** was prepared from the reaction of 2-methoxymethoxyphenylmagnesium bromide with gaseous trifluoroacetaldehyde generated easily by the reaction of 2 equiv. of trifluoroacetaldehyde ethyl hemiacetal with P_2O_5 at 100 °C, followed by the allylation of the hydroxy group by using 1.2 equiv. of NaH and 1.5 equiv. of (*E*)-1-bromo-3-trimethylsilylprop-2-ene and deprotection under acidic conditions (Scheme 2). Other compounds **4b–d** were also synthesized by the same procedure (32–57% yield). Compound **4** was converted to **2** *via* elimination of fluoride by treatment with 2.5 equiv. of Bu^nLi at −78 to 0 °C in Et_2O. After neutral workup, the vinyl ether **2** was treated with 1.5 equiv. of (*S*,*S*)-**1** in the presence of 1.5 equiv. of Et_3N in CH_2Cl_2 at −78 °C and then the mixture was stirred at ambient temperature to give the rearranged product **3**. The results are summarized in Table 1.

In the chiral boron-mediated Claisen rearrangement, the reaction temperature and enantioselectivity were found to be affected by the configuration of the olefin (*E* or *Z*) and the steric bulkiness of the substituent R at the γ-position. Thus, in the case of **4a** having a TMS substituent, the reaction proceeded at −78 °C to give **3a** with high asymmetric induction (entry 1), while in the reaction of the substrate derived from **4b** having an *E* primary alkyl substituent, a slightly higher temperature was required, giving rise to the product **3b** with moderate selectivity (entry 2).[7] With the *Z* substrate derived from **4c**, the direction of asymmetric induction was opposite to that with *E* substrate **4b** (entry 3).

The absolute stereochemistry of **3d** was determined as shown in Scheme 3. The diastereoselective Claisen rearrangement of **5**

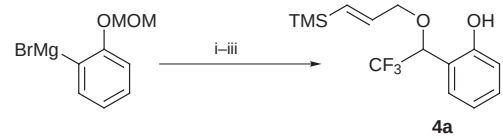

Scheme 2 *Reagents and conditions*: i, trifluoroacetaldehyde generated from its hemiacetal with P_2O_5, THF, 0 °C, 92%; ii, NaH (1.2 equiv.), (*E*)-1-bromo-3-trimethylsilylprop-2-ene, THF–DMF, room temp.; iii, 10% HCl, MeOH, reflux, 31% over 2 steps.

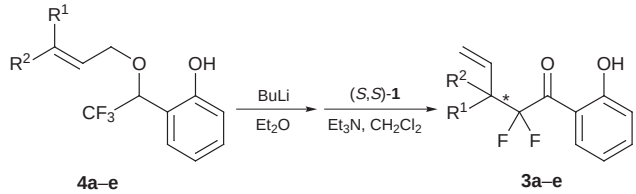

Table 1 The enantioselective Claisen rearrangement of difluorovinyl allyl ethers

Entry	**4**	R^1	R^2	*T*/°C	*t*/h	**3**[a]	Yield (%)[b]	Ee (%)
1	**4a**	H	TMS	−78	3	**3a**	60	85[c]
2	**4b**	H	Pr	−78→−20	5	**3b**	39	41[d]
3	**4c**	Pr	H	−78→−15	5	**3c**	55	55[d]
4	**4d**	Et	H	−78→−15	6	**3d**	58	43[d]
5	**4e**	c-Hex	H	−78→−15	3	**3e**	90	56[d]

[a] Ref. 6. [b] Isolated yield based on **4**. [c] Optical purity determined by HPLC using a Chiralcel OD column. [d] Optical purity was determined by HPLC using a Chiralcel AD column.

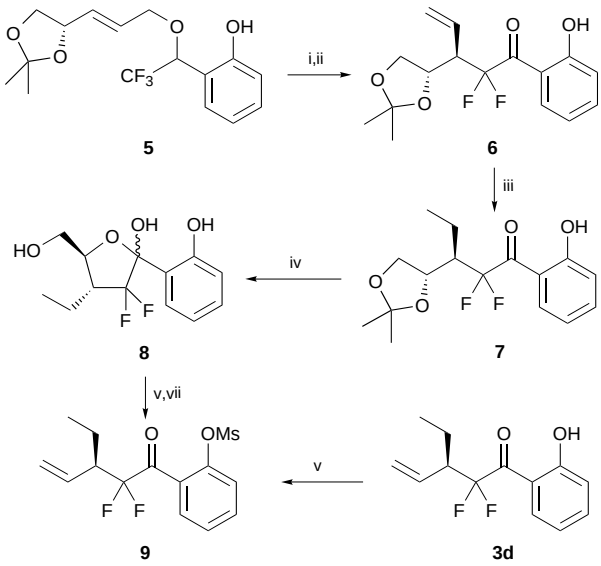

Scheme 3 *Reagents and conditions*: i, Bu^{n}Li, Et_2O; ii, toluene, 70 °C, 47% over 2 steps (5:1); iii, H_2, Pd/C, MeOH, 79%; iv, 10% HCl, THF, 60 °C; v, MsCl, Et_3N, CH_2Cl_2, vi, NaI, butanone, reflux; vii, Zn, AcOH, H_2O–THF, 65% from **7**.

smoothly proceeded to give **6** as a major isomer (47%, 5:1), which has an *R* configuration at the newly formed chiral center.[8] Hydrogenation of the olefin of **6** (79%) and the subsequent deprotection of the acetonide group by acid treatment gave compound **8** as an anomeric mixture. After mesylation of the primary and phenolic hydroxy groups of **8**, the product was converted to the olefin **9** in 65% yield (four steps). The enantioselective Claisen rearrangement product **3d** was also converted to **9** by mesylation. Determination of the absolute stereochemistry of **3d** as *R* configuration could be achieved by comparison of the specific rotation of each compound.

The observed enantioselectivity is possibly explained as shown in Fig. 1. The six-membered intermediate is formed by the attachment of the chiral boron reagent **1** to the phenolic hydroxy group, and the subsequent coordination of the ethereal oxygen to the boron atom. In the case of (*S*,*S*)-**1** and the *Z* isomer of **2**, the *Si* face of the difluorovinyl ether moiety is shielded by

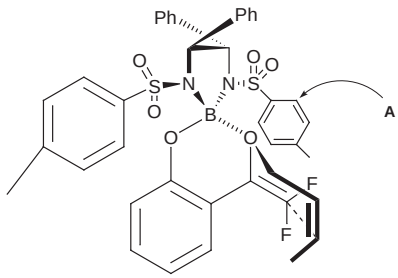

Fig. 1

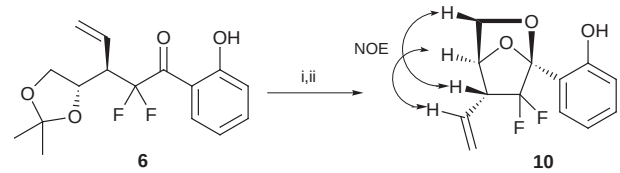

Scheme 4 *Reagents and conditions*: i, 10% HCl, THF, 60 °C; ii, toluene, 100°C, 63% over 2 steps.

the tolylsulfonyl group (**A**), thus the allylic moiety approaches preferably from the *Re* face to avoid steric interaction with **A** in the chair like transition state.

In conclusion, we have demonstrated for the first time enantioselective Claisen rearrangement of difluorovinyl allyl ethers using the chiral boron reagent **1** and the substrate **2** having a phenolic hydroxy group to form an efficient chiral environment.[9]

This work was partially supported by a Grant-in-Aid (No. 09672163) from the Ministry of Education, Science, Sports and Culture, Japan.

Notes and references

1 *Biomedicinal Aspects of Fluorine Chemistry*, ed. R. Filler and Y. Kobayashi, Elsevier Biomedical Press and Kodansha Ltd, 1982; J. T. Welch, *Tetrahedron*, 1987, **43**, 3123; *Organofluorine Compounds in Medicinal Chemistry and Biomedical Applications*, ed. R. Filler, Y. Kobayashi and L. M. Yagupolskii, Elsevier, Amsterdam, 1993.

2 W. B. Metcalf, E. T. Jarvi and J. P. Burkhart, *Tetrahedron Lett*., 1985, **26**, 2861; G.-Q. Shi, Z.-Y. Cao and W.-L. Cai, *Tetrahedron*, 1995, **51**, 5011; G.-Q. Shi and W.-L. Cai, *J. Org. Chem*., 1995, **60**, 6289; H. Greuter, R. W. Lang and A. J. Roman, *Tetrahedron Lett*., 1988, **29**, 3291.

3 K. Maruoka, H. Banno and H. Yamamoto, *J. Am. Chem. Soc*., 1990, **112**, 7791; K. Maruoka, H. Banno and H. Yamamoto, *Tetrahedron*: *Asymmetry*, 1991, **2**, 647; K. Maruoka and H. Yamamoto, *Synlett* 1991, 793; K. Maruoka, S. Saito and H. Yamamoto, *J. Am. Chem. Soc*., 1995, **117**, 1165; E. J. Corey and D.-H. Lee, *J. Am. Chem. Soc*., 1991, **113**, 4026; E. J. Corey and R. S. Kania, *J. Am. Chem. Soc*., 1996, **118**, 1229; U. Kazmaier and A. Krebs, *Angew. Chem., Int. Ed. Engl*., 1995, **34**, 2012; A. Krebs and U. Kazmaier, *Tetrahedron Lett*., 1996, **37**, 7945.

4 H. Ito, A. Sato and T. Taguchi, *Tetrahedron Lett*., 1997, **38**, 4815.

5 E. J. Corey, R. Imwinkelried, S. Pikul and Y.-B. Xiang, *J. Am. Chem. Soc*., 1989, **111**, 5493.

6 Optical rotation ([α]D) was measured in $CHCl_3$ at 26 °C. **3a**: 41.1; **3b**: 18.6; **3c**: −18.3; **3d**: −8.8; **3e**: −20.3.

7 In the absence of Lewis acid, the *E* isomer **2b** smoothly rearranged to **3b** even at room temperature, possibly due to the presence of the phenolic hydroxy group, to form an intramolecular hydrogen bond between the ethereal oxygen.

8 The relative stereochemistry of compound **6** was determined *via* conversions to **10** and a NOESY experiment, as shown in Scheme 4.

9 Regarding the removal of the hydroxyphenyl moiety, we examined some conditions, *i.e*. oxidative degradation of the aromatic ring and cleavage of the carbon–carbon bond of the aryl ketone moiety (Baeyer–Villiger and Schmidt rearrangement). In these experiments, although the aromatic ring was absent from the ^1H NMR analysis of the crude mixture, we were unable to find a clean method for cleavage of the hydroxyphenyl moiety.

Communication 8/07157H

Intramolecular hydrogen bond-promoted C–C bond formation: reaction rate enhancement and regioselective allylation of carbonyl compounds

Hajime Ito, Yasuaki Ujita, Jun-ichi Tateiwa, Motohiro Sonoda and Akira Hosomi*

Department of Chemistry and Graduate School of Chemistry, University of Tsukuba, Tsukuba, Ibaraki 305-8571, Japan. E-mail: hosomi@staff.chem.tsukuba.ac.jp

Received (in Cambridge, UK) 15th September 1998, Accepted 6th October 1998

An intramolecular hydrogen bond promotes rate enhancement in both the allylation and the reduction of carbonyl compounds and also regioselective allylation.

For the design of synthetic reactions, external catalysts or mediators are usually utilized for improving selectivity and mildness of reaction conditions.[1] In the allylation reaction of carbonyl compounds with an allylmetal reagent such as an allylsilane or allyltin, Lewis and Brønsted acid catalysts are often employed for this purpose.[2–4] Usually, the strong acidity of the Lewis or Brønsted acid is needed to complete the reaction. However, the strong acid sometimes causes decomposition of both the allylmetal reagent and the substrate. In order to overcome this drawback, we have introduced an intramolecular hydrogen bond into the substrate to activate the substrate and to stabilize the transition state of the reaction. Although active arguments for the contribution of hydrogen bonds in the transition state of an enzymatic system have been presented, there are fewer reports on the utilization of the stabilization effect of the hydrogen bond in the transition state in C–C bond formation between carbonyl compounds and organometallic reagents.[5,6] To explore the synthetic utility of the hydrogen bond, we focused our attention on the features of the intramolecular hydrogen bond. Its moderate acidity and localization in a specific position in the substrate serve synthetic utility. Here we describe rate enhancement in the allylation and the reduction of a carbonyl group and the regioselective allylation promoted by an intramolecular hydrogen bond.

There are numerous reports on the condensation reaction of an aldehyde with trialkylallyltin promoted by a Lewis or Brønsted acid catalyst.[3–5] The thermal reactions of trialkylallyltin with carbonyl compounds at high temperature or high pressure have also been reported. In our first series of experiments, the activation effect of an intramolecular hydrogen bond in the nucleophilic reaction of organotin compounds was measured at low temperature without the addition of an acid catalyst (Table 1).

Under THF reflux conditions without the addition of a Lewis acid, no adducts were observed for a mixture of tributylallyltin and benzaldehyde, which has no intramolecular hydrogen bond. Although salicylaldehyde **1a** reveals a relatively strong intramolecular hydrogen bond between the hydroxy group and the oxygen atom in the carbonyl group, attempts to afford an allylation product were unsuccessful under the same conditions (entry 1). Introduction of an electron-withdrawing substituent *para* to the hydroxy group provided allylation product **3b** in moderate yield (entry 2). A nitro group *para* to the hydroxy group was most efficient and gave products **3c**,**d** in good yields even at room temperature (entries 3–5). In entry 4, unreacted allyltin was recovered almost quantitatively. Next, in order to clarify the role of the hydroxy group in this reaction, we carried out experiments using carbonyl compounds **1d**,**e** which have no hydrogen bond, and found that such substrates gave no adduct under the same conditions described above (entries 6 and 7). Addition of *p*-nitrophenol was not effective for the allylation

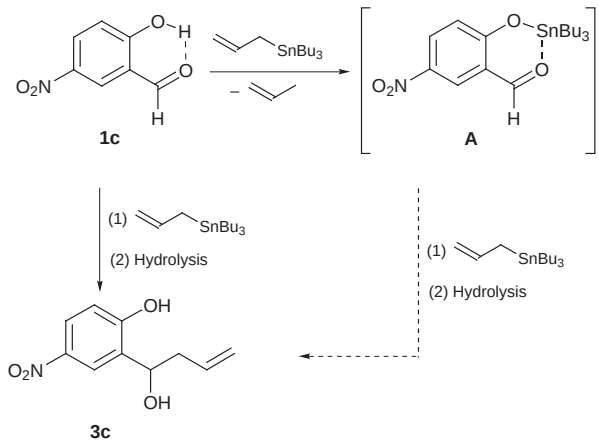

Scheme 1

Table 1 *ortho* Substituent effect in allylation reaction of carbonyl compounds[a]

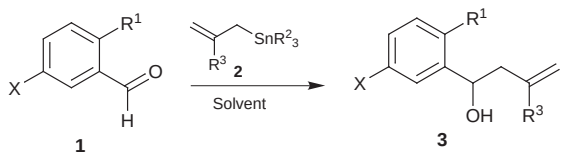

Entry	1	X	R^1	R^2	R^3	*T*/°C	3	Yield (%)
1	**1a**	H	OH	Bu	H	reflux	**3a**	0
2	**1b**	Cl	OH	Bu	H	reflux	**3b**	49
3	**1c**	NO_2	OH	Me	H	room temp.	**3c**	96
4	**1c**	NO_2	OH	Bu	H	room temp.	**3c**	97
5[b]	**1c**	NO_2	OH	Bu	Me	room temp.	**3d**	quant.
6	**1d**	NO_2	H	Bu	Me	room temp.	**3e**	0
7	**1e**	NO_2	OMe	Bu	Me	room temp.	**3f**	0
8[c]	**1d**	NO_2	H	Bu	Me	room temp.	**3g**	8

[a] A mixture of an aldehyde (0.5 mmol) and a trialkylallyltin (1.0 mmol) was stirred in THF (1.0 ml) for 48 h. [b] 1 equiv. of trialkylallyltin was used. [c] 4-Nitrophenol (1.0 equiv.) was added to the reaction.

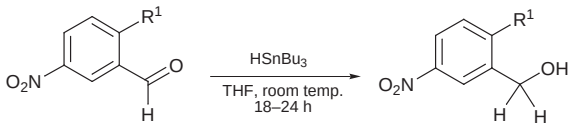

1c R^1 = OH
d R^1 = H
e R^1 = OMe

4a 92%
b 18%
c 12%

Scheme 2

(entry 8). These results clearly show that the hydroxy group of the substrate enhanced the reaction rate of the allylation. In view of the reaction mechanism, two paths are proposed for this rate enhancement (Scheme 1). The first one is that the intramolecular hydrogen bond directly promotes the allylation involving the stabilization of the transition state. In the second path, metalation of the hydroxy group first occurrs to give intermediate **A**. Another nucleophile attacks the carbonyl group of **A** activated by coordination to the internal stannyl group to give the product. The second path is not acceptable on the basis of the experimental result, namely, that 1 equiv. of tributylallyltin is sufficient to complete the reaction. The low reactivity of intermediate **A**, generated *in situ* by the reaction of **1c** with tributyltin methoxide, also suggests the second path can be ruled out.[7,8] These results indicate that the intramolecular hydrogen bond directly promoted the allylation reaction.

The intramolecular hydrogen bond also mediates reduction of carbonyl compounds with tributyltin hydride (Scheme 2). Similar reactivity tendency was also observed in this case. The substrate having an intramolecular hydrogen bond gave reduced product **4a** in good yield.

The immobility of the proton in the hydrogen bond made possible regioselective reaction of a multi-functional compound.[9] An aldehyde which has two carbonyl groups was prepared to examine the selectivity of the allylation.[10] The carbonyl group which is activated by the hydrogen bond was selectively allylated with tributylallyltin (Table 2). The selectivity was very high and minor product **7** was scarcely observed in these cases (entries 1 and 2). Substrates that have no hydrogen bond gave allylated products in poor yield (entries 3 and 4). These results show that an intramolecular hydrogen bond activates a particular functional group in the substrate selectively and stabilizes the transition state to enhance the reaction rate.

In conclusion, a low-acidic intramolecular hydrogen bonding promotes nucleophilic reaction to a carbonyl group. Although the precise mechanism of these reactions involving a low-barrier hydrogen bond (LBHB) is still unclear, this method offers a new tool in organic synthesis.[6]

Financial support for this work is partly provided by Grants-in-Aid for Scientific Research on Priority Areas from the Ministry of Education, Japan, and Pfizer Pharmaceuticals Inc. We thank Dow Corning Toray Silicone Co. Ltd., Chisso Co. Ltd. and Shin-Etsu Chemical Co. Ltd. for a gift of organosilicon compounds.

Table 2 Site selective allylation of carbonyl compounds using an intramolucular hydrogen bond[a]

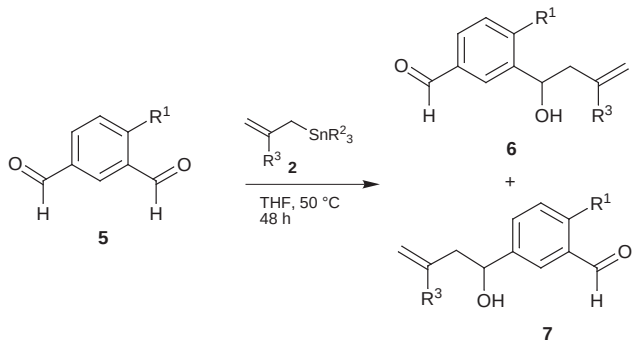

Entry	5	R^1	R^2	R^3	Yield (%)	Ratio 6:7
1	**5a**	OH	Bu	H	95	> 50: < 1
2[b]	**5a**	OH	Bu	Me	99	> 50: < 1
3	**5b**	H	Bu	H	12	—
4	**5c**	OMe	Bu	H	not found	—

[a] A mixture of an aldehyde (0.5 mmol) and a trialkylallyltin (1.0 mmol) was stirred in dry THF (2.0 ml) at 50 °C for 48 h. [b] 5.0 ml of THF was used.

Notes and references

1 S. Shambayati and S. L. Schreiber, in *Comprehensive Organic Synthesis*, ed. B. M. Trost, Pergamon, Oxford, 1991, vol. 1, pp. 283–353.
2 A. Hosomi and H. Sakurai, *Tetrahedron Lett*., 1976, 1295.
3 S, Castellino and D. E. Volk, in *Encyclopedia of Reagents for Organic Synthesis*, ed. L. A. Paquette, Wiley, 1995, vol. 1, pp. 125–128; Y. Yamamoto and N. Asao, *Chem. Rev*., 1993, 2207.
4 V. Gevorgyan, I. Kadota and Y. Yamamoto, *Tetrahedron Lett*., 1993, **34**, 1313; S. E. Denmark, E. J. Weber, T. M. Wilson and T. M. Willson, *Tetrahedron Lett*., 1989, **45**, 1053; A. Yanagisawa, M. Morodome, H. Nakashima and H. Yamamoto, *Synlett*, 1997, 1309: G. Kaur, K. Manju and S. Trehan, *Chem. Commun.*, 1996, 581.
5 T. M. Cokley, P. J. Harvey, R. L. Marshall, A. McCluskey and D. J. Young, *J. Org. Chem*., 1997, **62**, 1961; T. M. Cokley, R. L. Marshall, A. McCluskey and D. J. Young, *Tetrahedron Lett*. 1996, **37**, 1905; N. Asao, A. Noriko, Z. Tan and K. Maruoka, *Synlett*, 1998, 377. After the submission of our paper, condensation reactions between more reactive tetraallyltin species and salicylaldehyde were reported. M. Yasuda, T. Fujibayashi and A. Baba, *J. Org. Chem*., 1998, **63**, 6401.
6 W. W. Cleland and M. M. Kreevoy, *Science*, 1994, **264**, 1887; G. A. Kumar and M. A. McAllister, *J. Am. Chem. Soc*., 1998, **120**, 3159; E. L. Ash, J. L. Sudmeier, E. C. D. Fabo and W. W. Bachovchin, *Science*, 1997, **278**, 1128.
7 After the addition of tributyltin methoxide and the removal of MeOH, the disappearance of **1c** and the appearance of a new set of signals attributed to the quantitative formation of **A** was observed by NMR analysis: δ_H(270 MHz, $CDCl_3$) 0.86 (t, *J* 7.3, 9H), 1.20–1.65 (m, 18H), 8.18 (d, *J* 9.2, 1H), 8.20 (d, *J* 9.2, 3.0, 1H), 8.54 (d, *J* 3.0, 1H), 10.28 (s, 1H).
8 A reaction between **A** and allyltributyltin (1.3 equiv.) in THF for 48 h gave **3c** (11%) and **1c** (82%) at room temperature.
9 S. J. Angyal, P. J. Morris, J. R. Tetaz and J. G. Wilson, *J. Chem. Soc*., 1950, 2141.
10 Similar selectivity was achieved using a Lewis acid catalyst. T. Ooi, D. Uraguchi, N. Kagoshima and M. Maruoka, *J. Am. Chem. Soc*., 1998, **120**, 5327.

Communication 8/07172A

First principles location of the transition state for formation of dimethyl ether in a zeolite

Eric Sandré,[a] Michael C. Payne[a] and Julian D. Gale*[b]

[a] *Cavendish Laboratory (TCM), University of Cambridge, Madingley Road, Cambridge, UK CB3 0HE*
[b] *Department of Chemistry, Imperial College, South Kensington, UK SW7 2AY. E-mail: j.gale@ic.ac.uk*

Received (in Exeter, UK) 12th August 1998, Accepted 6th October 1998

A new transition state searching algorithm has been used to determine the mechanism for methanol condensation to form dimethyl ether within the microporous environment of the zeolite, chabazite, using periodic boundary conditions and density functional theory.

Zeolites are powerful catalytic materials, combining acidity resulting from framework impurities with shape selectivity due to the spatial confines of the microporous environment.[1] Consequently they have found application in many commercial processes and as the variety of framework topologies and dopant ions increases so the possibilities multiply.

Amongst the existing applications of aluminosilicates, the methanol to gasoline reaction[2] is one of the most studied both from an experimental and theoretical perspective. Despite this, there still remain many unanswered questions concerning the precise nature of the role of the zeolite in the reaction mechanism. What is known for certain is that initially methanol condenses to produce dimethyl ether and subsequently hydrocarbons are generated, though it is unclear whether the ether actually lies on the pathway for C–C bond formation or whether it is a competing side reaction.[3]

There are two widely considered mechanisms for the formation of dimethyl ether from methanol in zeolites. In the first mechanism methanol is adsorbed at an acid site and dissociates to produce a framework coordinated methoxy group and water. Although the activation energy for this to occur directly has been shown to be too high, several studies have indicated that the participation of a second methanol lowers the barrier.[4] The second possible mechanism involves the direct S_N2 reaction of one methanol with another. In this scheme, the coordination of one methanol to the acidic hydrogen of a Brønsted acid site leads to weakening of the C–O bond making the methanol more susceptible to nucleophilic attack. The essential difference between the mechanisms is that in the first one the zeolite plays an active chemical role in the pathway, whereas in the second it acts primarily as an acidic solvent. Previous theoretical studies[5,6] have demonstrated that the direct condensation of methanol leads to a sequence of intermediates which are lower in energy and is therefore likely to be the preferred mechanism.

While periodic boundary condition methods have been previously used to study the structure of zeolites and adsorption of molecules within them,[6,7] these studies have not included the location of transition states for *in situ* chemical reactions. Although methods for locating transition states, with or without analytical second derivatives, are well establish for conventional molecular quantum chemistry, particularly when working in internal coordinates, the same is not true for the solid state.

In this work we use for the first time a new refined version of the synchronous transit method in Cartesian space to locate a transition state within a periodic zeolite structure. Here a reaction coordinate is defined—in this case a C–O bond length that is being broken or formed—and a minimisation is performed subject to this distance being constrained through the use of a Lagrange multiplier. Minimisations are performed at two points, one on the reactant and one on the product side. The lower energy point is then moved along the reaction coordinate towards the other point until it is higher in energy, at which stage the process is reversed. At each stage an unconstrained minimisation is performed to ensure that the point is on the correct side of the barrier.

We have used the above approach to locate the transition states for methanol condensation both in the gas phase and within the confines of a microporous environment. As in our previous work[8] we have chosen the zeolite chabazite for the aluminosilicate since the small unit cell of formula $HAlSi_{11}O_{24}$ is computationally tractable and the high symmetry of the purely siliceous material greatly reduces the number of configurational possibilities for the acid site. Furthermore, this system is known to be an active catalyst for the conversion of methanol to dimethyl ether. [9]

All calculations have been performed using planewaves to expand the valence electronic wavefunctions up to a cut-off of 620 eV with the nuclei and core electrons being represented by norm-conserving non-local pseudopotentials.[10] The gradient-corrected density functional of Perdew and Wang (GGA)[11] has been used throughout. Calculations were performed using only the gamma point in the Brillouin zone as this had previously been found to be sufficient. All atoms were allowed to relax freely, except for the distance constraint between the atoms defining the reaction coordinate and the unit cell was held fixed.

When two methanol molecules per acid site are adsorbed in the zeolite the minimum energy configuration has been shown to consist of a methoxonium cation which is hydrogen bonded to an oxygen of the framework, adjacent to aluminium, on one side and to the second methanol on the other.[6] This second methanol is then able to form a hydrogen bond to a more remote oxygen of an Si–O–Si bridge, though dynamical simulations show this interaction to be much weaker.[12] In order for condensation to occur, the second methanol has to first migrate to a configuration which is 61 kJ mol^{-1} higher in energy in which its dipole aligns with that of the methoxonium cation so that the geometry is suitable for nucleophilic attack (Fig. 1).

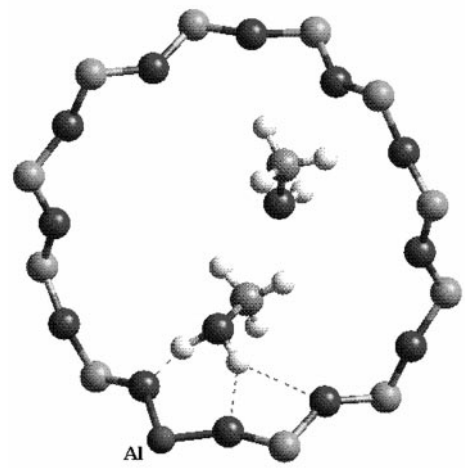

Fig. 1 Reactant configuration for two methanols adsorbed with in chabazite.

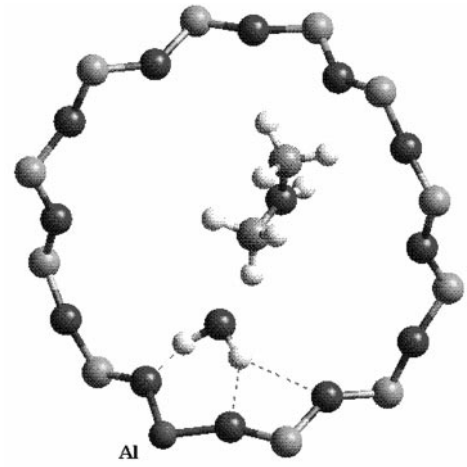

Fig. 2 Initially formed local minimum for the products of methanol condensation, dimethyl ether and water, within the cage of chabazite.

This we take as the reactant configuration for the transition state search.

The arrangement of the products, dimethyl ether and water, as initially formed is shown in Fig. 2. The water molecule remains coordinated to the aluminium defect site in the framework while the dimethyl ether is formed in the protonated state but with no hydrogen bonding possible. Subsequent to this reaction the dimethyl ether can rotate to form a strong hydrogen bond to the water molecule and proton transfer can occur.

For the transition state search, the length of the C–O bond of dimethyl ether which is being formed during the nucleophilic attack is used as the reaction coordinate. The resulting energy profile along the reaction coordinate is illustrated in Fig. 3, the

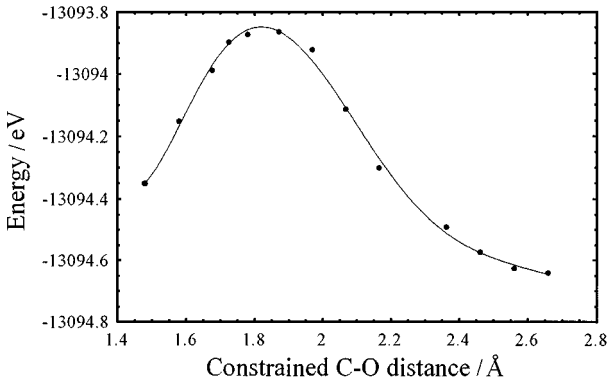

Fig. 3 Plot of energy *versus* constrained C–O distance for the bond being formed in dimethyl ether during methanol condensation within chabazite. Filled circles represent the actual energies, while the solid line is a sixth order polynomial fit to these values.

solid line shows a sixth order polynomial fit and is included as a guide, though it is clear that the shape of the local energy surface is more complex. The transition state occurs quite late when the length of the C–O bond being created has reached a value of 1.8 Å, as compared to the final bond length of 1.45 Å. The local geometry around the carbon at the saddle point is trigonal bipyramidal as would be expected for a true S_N2 mechanism, with the oxygens being approximately equidistant and axial while the CH_3 group has carbenium ion character (Fig. 4).

The predicted activation energy for this process is 71 kJ mol^{-1} when starting from the appropriate minimum energy configuration for two methanol molecules. If the energy required to reach this state is included in the activation energy then the overall value is 132 kJ mol^{-1}. The comparable values for these energetics obtained from previous calculations on gas phase cluster models for zeolites are 89 and 145 kJ mol^{-1}.[5] If we assume that any shift in the values due to differences in basis sets and functionals are small, then we can conclude that the

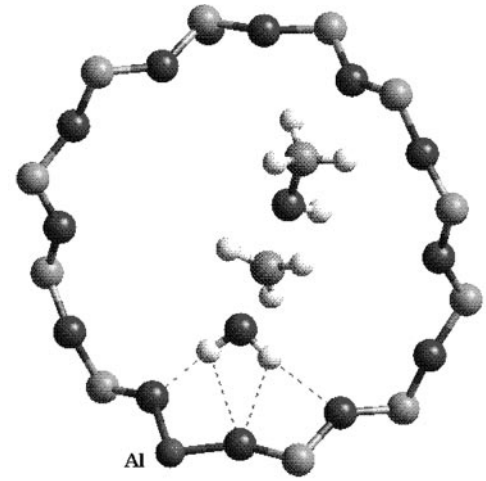

Fig. 4 Transition state structure for conversion of methanol to dimethyl ether.

effect of the full zeolite structure is to lower the activation energy as would be expected. However, given that the reaction occurs with the transition state away from the framework itself this suggests that the primary effect of the zeolite is to act as a polarisable medium which stabilises any charge separation that occurs in the transition state. Significantly, there are no strong directional interactions formed between the activated complex and the zeolite.

In this work we have studied the condensation of methanol to form dimethyl ether and shown that the zeolite catalyses the reaction by acting as a polarisable medium which lowers the energy of charge separation in the transition state. However, the real challenge that lies ahead is to explain the full mechanism of gasoline formation. An advantage of the present method of locating transition states is that no assumption about the reaction pathway is necessary, just a knowledge of the reactants and products. The possibility that there may be multiple minima and transition states between the two chosen configurations can be handled straightforwardly in this way and therefore complex mechanisms may now be determined in combination with a realistic periodic model of a zeolite catalyst.

These calculations were performed on the Hitachi SR2201 located at the University of Cambridge High Performance Computing Facility. J. D. G. acknowledges the support of the Royal Society through a University Research Fellowship.

Notes and references

1 J. M. Thomas, *Philos. Trans. R. Soc. London A*, 1990, **333**, 173.
2 S. L. Meisel, J. P. McCullogh, C. H. Lechthaler and P. B. Weiss, *Chem. Technol.*, 1976, **6**, 86.
3 Y. Ono and T. Mori, *J. Chem. Soc., Faraday Trans. 1*, 1981, **77**, 2209.
4 P. E. Sinclair and C. R. A. Catlow, *J. Chem. Soc., Faraday Trans.*, 1996, **92**, 2099.
5 S. R. Blaszkowski and R. A. van Santen, *J. Am. Chem. Soc.*, 1996, **118**, 5152.
6 R. Shah, J. D. Gale and M. C. Payne, *J. Phys. Chem. B*, 1996, **101**, 4787.
7 E. Nusterer, P. E. Blöch and K. Schwarz, *Angew. Chem. Int. Ed. Engl.*, 1996, **35**, 175.
8 R. Shah, J. D. Gale and M. C. Payne, *J. Phys. Chem.*, 1996, **100**, 11 688.
9 G. P. Tintskaladze, A. R. Nefedova, Z. V. Gryaznova, G. V. Tsitsishvili and M. K. Charkviani, *Zh. Fiz. Khim.*, 1984, **58**, 718.
10 M. C. Payne, M. P. Teter, D. C. Allan, T. A. Arias and J. D. Joannopoulos, *Rev. Mod. Phys.*, 1992, **64**, 1045.
11 J. P. Perdew, in *Electronic Structure of Solids '91*, ed. P. Zeische and H. Eschrig, Akademie Verlag, Berlin, 1991.
12 I. Stich, J. D. Gale, K. Terakura and M. C. Payne, *Chem. Phys. Lett.*, 1998, **283**, 402.

Communication 8/06437G

Oxidative ring contraction of 2-phenyl-1,3-dithiane in ZSM-5: restricted mobility of 1,2-dithiolane radical cations in zeolite channels

Heinz D. Roth,*[a] Kui Shen,[a] Prasad S. Lakkaraju*[b] and Lorenzo Fernández[c]

[a] *Department of Chemistry, Rutgers University, Wright-Rieman Laboratories, New Brunswick, NJ 08854-8087, USA. E-mail: roth@rutchem.rutgers.edu*

[b] *Department of Chemistry, Georgian Court College, Lakewood, NJ 08701, USA. E-mail: lakkaraju@georgian.edu*

[c] *Instituto de Tecnología Química CSIC-UPV, Universidad Politécnica de Valencia, Apartado 22012, 46071 Valencia, Spain*

Received (in Corvallis, OR, USA) 17th June 1998, Accepted 7th October 1998

Incorporation of 2-phenyl-1,3-dithiane 1 into ZSM-5 generated 1,2-dithiolane radical cation $2^{\cdot+}$, the EPR spectrum of which shows an orthorhombic powder pattern (g_1 = 2.0293, g_2 = 2.0193, g_3 = 2.0030); each *g* component showed a 1:4:6:4:1 pattern (a_1 = 10.5, a_2 = 9.3 and a_3 = 9.2 G) due to coupling to four equivalent ^{1}H nuclei, suggesting that the pseudo-axial and −equatorial α-protons undergo conformational equilibration whereas the sulfur centers are held stationary on the EPR time scale.

In the past three decades the structures and properties of zeolites have been extensively studied as prototypes of acidic industrial catalysts.[1–3] In addition, a wide range of organic radical cations have been generated, either spontaneously or upon inclusion of appropriate precursors into zeolites.[4–8] Radical cations generated by this method typically have extended lifetimes and can be studied by conventional spectroscopic techniques. We are interested in zeolite-induced radical cation reactions; our contributions to intra-zeolite chemistry include oxidative deprotonation,[9] dehydrogenation[10] and cyclization.[11]

In a recent study of diphenyl disulfide **3** we observed the EPR spectrum of the 'extended' radical cation $\mathbf{3}^{\cdot+}$,[11] even though this species undergoes rapid conversion to thianthrenium ion $\mathbf{4}^{\cdot+}$ in solution. In an attempt to observe the EPR spectrum of a similarly elusive species, 2-phenyl-1,3-dithiane radical cation $\mathbf{1}^{\cdot+}$, we incorporated **1** into ZSM-5 (Scheme 1). The resulting EPR spectrum supports the conversion of $\mathbf{1}^{\cdot+}$ to $\mathbf{2}^{\cdot+}$ and offers unique insights into the mobility of this radical cation in the zeolite channels.

Incorporation of 2-phenyl-1,3-dithiane **1** into Na-ZSM-5 at room temperature produced an EPR spectrum that can be interpreted as an orthorhombic powder pattern with g_1 = 2.0293, g_2 = 2.0193 and g_3 = 2.0030; each *g* component showed hyperfine coupling (hfc) due to four equivalent protons (1:4:6:4:1 pattern, a_1 = 10.5, a_2 = 9.3 and a_3 = 9.2 G; Fig. 1). The average *g* value, g_{avg} = 2.0172, is in reasonable agreement with the isotropic *g* value, g_{iso} = 2.0183, reported for the radical cation of 1,2-dithiolane, $\mathbf{2}^{\cdot+}$, in solution.[12,13] Likewise, the average hfc observed in the zeolite, a_{avg} = 9.7 G, agrees well with the isotropic coupling constant of 9.75 G reported for $\mathbf{2}^{\cdot+}$ in solution.[12,13] The identity of the species was confirmed by an essentially identical EPR spectrum obtained upon incorporation of an independently synthesized[14] sample of **2** into ZSM-5.

The generation of $\mathbf{2}^{\cdot+}$ by oxidative ring contraction of **1** has precedent in solution; either chemical or electrochemical oxidation of **1** led to the debenzylated, ring-contracted species, $\mathbf{2}^{\cdot+}$.[15–17] In fact, anodic oxidation of dithioacetals has been used to remove the dithiane protecting group of carbonyl compounds. The mechanism for the ring-contraction of dithiane radical cations appears to be understood in general terms.[15–17] This conversion has two principal elements, the formation of an S–S bond and the detachment of the benzyl group. This conversion is formulated typically *via* a disulfide dication.

1,2-Disulfide dications have been observed by fast time-resolved spectroscopy in solution[18] and have been invoked recently in zeolite media.[11] The formation of the S–S bond in the 1,3-dithiane radical cation may favor the second oxidation step. The benzyl function may be removed by two consecutive nucleophilic displacements at the dication.[15–17] In view of the limited diameter of the ZSM-5 channels and the dimensions of **1** and its radical cation and dication, these species should not be accessible to external nucleophiles. Instead, Lewis base sites within the zeolite framework are the likely reagents.

The dynamic behaviour of $\mathbf{2}^{\cdot+}$ in the internal voids of the zeolite is also unusual. The *g* factor anisotropy of $\mathbf{2}^{\cdot+}$ at room temperature indicates that this species is not tumbling or rotating rapidly on the EPR time-scale. On the other hand, the conformational re-orientations ('flickering') of the methylene group (C_4) is still fast, based on the equivalence of the pseudo-axial and −equatorial α-protons at C_3 and C_5. This implies that one or both sulfur centers bearing spin and charge are held rigidly in a potential well or are 'attached' covalently to the zeolite network, whereas the mobility of the trimethylene segment is unaffected by the 'anchoring' of the sulfur centers (Scheme 2). This observation establishes an interesting differ-

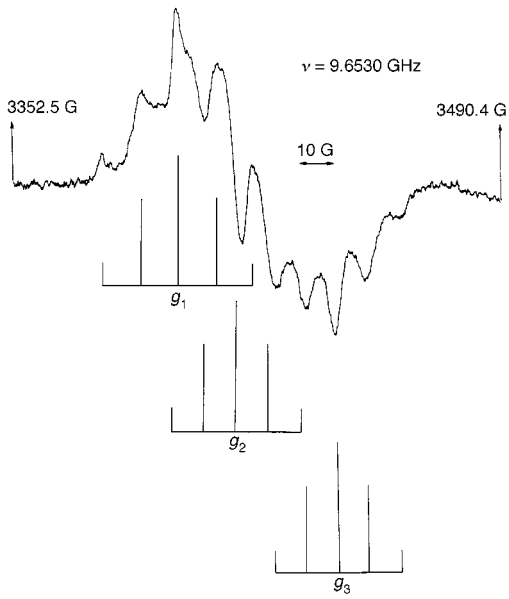

Fig. 1 Room temperature EPR spectrum obtained upon sequestering **1** into ZSM-5. The spectrum is interpreted as an orthorhombic powder pattern with *g* factors g_1 = 2.0293, g_2 = 2.0193 and g_3 = 2.0030, split into 1:4:6:4:1 patterns (a_1 = 10.5, a_2 = 9.3 and a_3 = 9.2 G) due to coupling with four equivalent ^{1}H nuclei. The spectrum is assigned to radical cation $\mathbf{2}^{\cdot+}$.

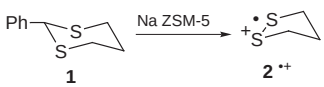

Scheme 1

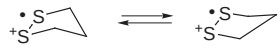

Scheme 2

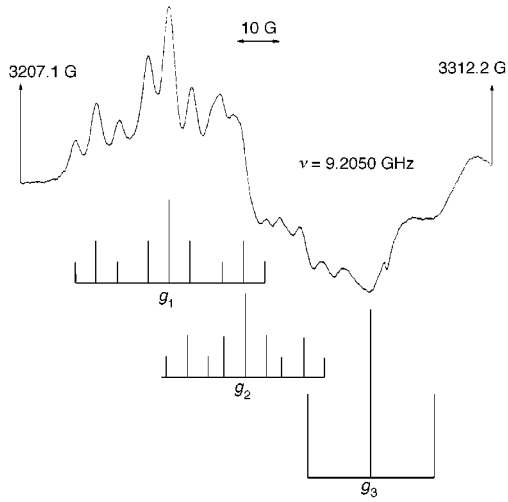

Fig. **2** Low-temperature (77 K) EPR spectrum of $\mathbf{2}^{\cdot+}$, an orthorhombic powder pattern with g_1 = 2.0298, g_2 = 2.0190 and g_3 = 2.0023. Each g component is split into triplet of triplets (interaction with two non-equivalent groups of two ^{1}H nuclei), a_1 = 16.2 and 4.9, a_2 = 13.3 and 4.6 and a_3 = 14.7 G, unresolved.

ence between the dynamicas of $\mathbf{2}^{\cdot+}$ in the zeolite and in solution. In solution, the flickering can be arrested without causing g factor anisotropy;[12,13] in contrast, the zeolite spectrum shows significant g factor anisotropy even when flickering rapidly.

The dynamics of **2** and its radical cation are well-documented in fluid solutions as a function of temperature. The five-membered ring of **2** is slightly twisted around the S–S bond; the sulfur lone pairs are aligned at a dihedral angle of *ca.* 30°.[19] Oxidation of **2** results in a subtle structure change; the sulfur lone pairs (and the S–CH_2 bonds) in $\mathbf{2}^{\cdot+}$ become eclipsed, facilitating the delocalization of spin and charge between the sulfur centers. The planar arrangement of the CH_2–S–S–CH_2 segment forces the bridging methylene group out of plane; a planar structure is a low-lying transition state between two equivalent 'envelope' conformers. At room temperature, the conformers equilibrate rapidly causing the four α-protons to be equivalent (a = 9.75 G, 4H). The inversion slows down with decreasing temperature; the pseudo-axial and −equatorial ^{1}Hs become non-equivalent at 180 K (a = 16.25 G, 2H; a = 3.9 G, 2H).

The low temperature dynamic behavior of $\mathbf{2}^{\cdot+}$ in the zeolite is similar. At 77 K, the flickering of the methylene group is sufficiently slowed to render the α-protons non-equivalent; each g component shows a triplet of triplets (Fig. 2). As in the room temperature spectrum, the splitting is well resolved in the downfield component. However, the g tensor of $\mathbf{2}^{\cdot+}$ remains orthorhombic, similar to that at room temperature.

The severely restricted mobility of $\mathbf{2}^{\cdot+}$ in the zeolite channels was unexpected. Because of its relatively small size (Fig. 3), we had expected $\mathbf{2}^{\cdot+}$ to tumble freely in the zeolite channels. Several radical cations of comparable size showed essentially isotropic spectra; for example, the sharp lines observed for 2,3-dimethylbut-2-ene radical cation in silicalite (a = 11.8 G; 11 of 13 lines are detected) are compatible with essentially free rotation of this radical cation.[20,21] In pentasil zeolites, the corresponding spectra have considerably greater linewidths, apparently due to interaction with the zeolite host and the resulting reduced mobility. Of course, the rotation of bulkier molecules is expected to be hindered; this is confirmed, for example, by the broad(ened) lines observed for anethol radical cation[10] or by the anisotropic (powder type) spectra of iminoxyls in ZSM-5.[9]

Concerning the question of whether the radical cation, $\mathbf{2}^{\cdot+}$, is 'held' in a potential well or covalently linked to the zeolite network, we can exclude the second possibility. The covalent

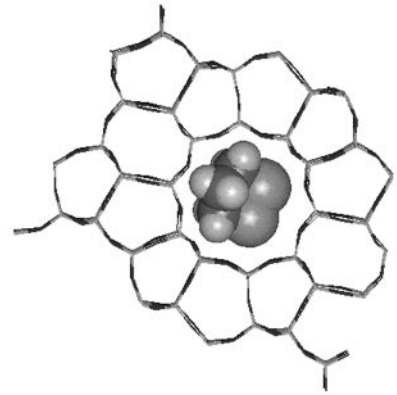

Fig. **3** Molecular modeling visualizing the docking of 1,2-dithiolane radical cation, $\mathbf{2}^{\cdot+}$, optimized at the UHF/6-31G* level of theory, inside the straight channels of ZSM-5.

link would most likely involve bonding of one sulfur atom to the zeolite. The resulting aggregate would be unsymmetrical; its spin density would be localized at the unattached sulfur center, creating a species in which only one CH_2 group is coupled. This is clearly incompatible with the EPR spectrum.

In summary, the formation of 1,2-dithiolane radical cation, $\mathbf{2}^{\cdot+}$, upon inclusion of 2-phenyl-1,3-dithiane, **1**, into Na-ZSM-5 shows several interesting features. The removal of the benzyl function requires nucleophilic displacement; since the intermediate is not accessible to an external nucleophile, Lewis base sites within the zeolite framework are the likely reagent. The orthorhombic g tensor of $\mathbf{2}^{\cdot+}$ in the zeolite indicates that the radical cation is held in a coulombic well within the network of oxygen centers; however, intramolecular processes, such as the ring inversion of the β-methylene group, are unaffected.

Support of this work through grant NSF CHE–9714850 and two NSF equipment grants is gratefully acknowledged.

Notes and references

1 *Zeolite Microporous Solids*: *Synthesis*, *Structure*, *and Reactivity*, ed. E. G. Derouane, F. Lemos, C. Naccache and F. R. Rebeiro, Kluwer, Dordrecht, 1991.
2 Y. Izumi, K. Urabe and M. Onaka, *Zeolite*, *Clay*, *and Heteropoly Acid in Organic Reactions*, Verlag Chemie, Weinheim, 1992.
3 *Radicals on Surfaces*, ed. A. Lund and C. J. Rhodes, Kluwer, Dordrecht, 1995.
4 V. Ramamurthy, C. V. Casper and D. R. Corbin, *J. Am. Chem. Soc*., 1991, **113**, 594.
5 F. R. Chen and J. J. Fripiat, *J. Phys. Chem*., 1992, **96**, 819.
6 C. J. Rhodes, I. D. Reid and E. Roduner, *J. Chem. Soc*., *Chem. Commun*., 1993, 512.
7 E. Roduner, R. Crockett and L. M. Wu, *J. Chem. Soc*., *Faraday Trans*., 1993, **89**, 2101.
8 F. R. Chen and J. J. Fripiat, *J. Phys. Chem*., 1993, **97**, 5796.
9 P. S. Lakkaraju, J. Zhang and H. D. Roth, *J. Phys. Chem*., 1994, **98**, 2722.
10 P. S. Lakkaraju, D. Zhou and H. D. Roth, *Chem. Commun*., 1996, 2605.
11 P. S. Lakkaraju, D. Zhou and H. D. Roth, *J. Chem. Soc*., *Perkin Trans. 2*, 1998, 1119.
12 H. Bock and U. Stein, *Angew. Chem*., *Int. Ed. Engl*., 1980, **19**, 834.
13 H. Bock, U. Stein and A. Semkow, *Chem. Ber*., 1980, **113**, 3208.
14 D. N. Harpp and J. G. Gleason, *J. Org. Chem*., 1970, **35**, 3259.
15 J.-G. Gourcy, G. Jeminet and J. Simonet, *J. Chem. Soc*., *Chem. Commun*., 1974, 634.
16 Q. N. Porter and J. H. P. Utley, *J. Chem. Soc*., *Chem. Commun*., 1978, 255.
17 J.-G. Gourcy, P. Martigny, J. Simonet and G. Jeminet, *Tetrahedron*, 1981, **37**, 1495.
18 M. Bonifacic, K. Schafer, H. Mockel and K.-D. Asmus, *J. Phys. Chem*., 1975, **79**, 1496.
19 T. Schaefer, J. P. Kunkel, R. W. Schurko and G. M. Bernard, *Can. J. Chem*., 1994, **72**, 1722.
20 P. L. Corio and S. Shih, *J. Phys. Chem*., 1971, **75**, 3475.
21 M. V. Barnabas and A. D. Trifunac, *Chem. Phys. Lett*., 1992, **193**, 298.

Communication 8/04593C

Hydrogen-bond recognition of cyclic dipeptides in water

C. Allott,[a] H. Adams,[a] Pablo L. Bernad Jr.,[b] Christopher A. Hunter,*[a]† Carmen Rotger[c] and James A. Thomas[a]

[a] *Krebs Institute for Biomolecular Science, Department of Chemistry, University of Sheffield, Sheffield, UK S3 7HF*
[b] *Instituto Universitario de Quimica, Organometalica Enrique Moles, C/ Julian Claveria s/n, 33071 Oviedo, Spain*
[c] *Department of Chemistry, Universitat de les Illes Balears, 07071 Palma de Mallorca, Spain*

Received (in Cambridge, UK) 24th April 1998, revised manuscript received 9th September 1998, Accepted 11th September 1998

An amide macrocycle with a highly preorganised cavity containing both polar and non-polar recognition sites forms stable complexes with cyclic dipeptides in water *via* amide–amide hydrogen-bonds, NH–π hydrogen-bonds and hydrophobic contacts.

Host–guest systems have been extensively studied in organic solvents and the requirements for designing efficient selective receptors are well-understood.[1] In contrast, the development of comparable systems which function in water has proved much more challenging, because the compounds are not only more difficult to handle, but also more difficult to understand due to the complex behaviour of the solvent. Hydrophobic cavities have been the focus of synthetic recognition systems in water,[2] but there are a limited number of examples where hydrogen-bonding sites have been used in conjunction with hydrophobic binding to provide selective binding in water.[3] It is this arrangement that is the characteristic feature of protein binding pockets which usually have complicated arrays of polar and non-polar sites, and the interplay of their recognition and desolvation properties is one of the factors that makes it difficult to disentangle the complexities of biological recognition.[4] Here we describe a simple synthetic host–guest system which allows us to study this interplay of polar and non-polar binding interactions in water.

The synthesis and recognition properties of **1** have been reported.[5] The water soluble analogue **2** was prepared in the

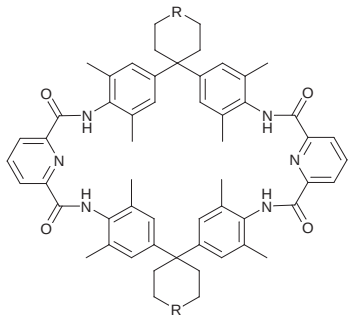

1 R = CH_2
2 R = N^+Me_2 Cl^-

same way. The two quaternary ammonium centres on the receptor periphery were sufficient to confer good water solubility on the macrocyle, and ^{1}H NMR dilution experiments showed no evidence of any aggregation or micelle formation at millimolar concentrations.

Single crystals of **2** suitable for X-ray crystallography of were grown from a water–MeCN mixture.‡ The macrocycle cavity is filled by a cluster of water molecules in the crystal [Fig. 1(*a*)]. Although the waters are within H-bonding distance of each other and sites on the macrocycle (2.8–3.1 Å), partial occupancy and the poor quality of the X-ray data preclude a detailed assignment of the H-bond network. We have previously obtained an X-ray crystal structure of the organic soluble

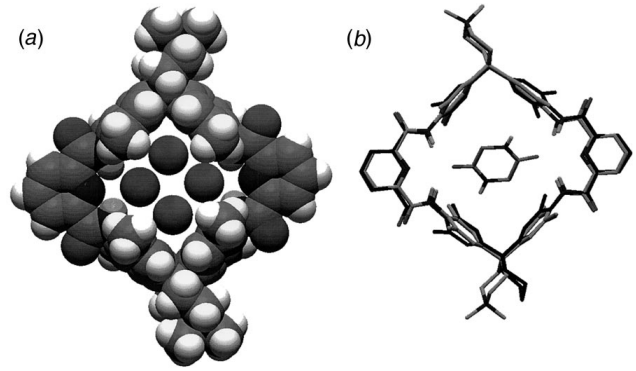

Fig. 1 (*a*) The X-ray crystal structure of **2** showing the positions of the water molecules which solvate the cavity. (*b*) The X-ray crystal structure of **2** superimposed on the X-ray crystal structure of the **1**·**8** complex.

analogue **1** complexed with glycine anhydride **8**,[5] and Fig. 1(*b*) shows this structure superimposed on the structure of **2**. The only difference between the chemical structures of the two macrocycles is the replacement of cyclohexane by quaternised piperidine on the periphery of the macrocycle. The only difference between the conformations of the macrocycles in the two X-ray structures is the orientation of one of these peripheral groups: the geometry of the cavity and arrangement of functional groups is identical, which reflects the high degree of preorganisation conferred on this system by the intramoelcular pyridine–amide hydrogen-bonds.

The recognition properties of the new receptor **2** were investigated by ^{1}H NMR titration experiments in H_2O–D_2O (9 : 1). No detectable changes were observed upon addition of benzoquinone **5** or the diester **7**. The binding constants for the

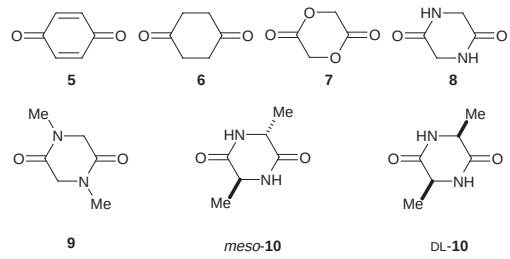

5 **6** **7** **8**

9 *meso*-**10** DL-**10**

other guests investigated are listed in Table 1. The structures of the complexes were determined from the limiting complexation-induced changes in chemical shift and a ROESY experiment for the most stable complex, which is formed with alanine anhydride **10**. The downfield shift for the signal due to the **2** amide protons shows that they form H-bonds with the carbonyl groups of the guests (Table 1). Characteristic upfield shifts are observed for the signals due to CH protons (δ −0.9 to −1.1), the amide protons (δ −0.5) and the methyl protons (δ −0.6 to −0.8) of all the guests which shows these protons are shielded by the aromatic side-walls of the macrocycle on complexation.

Table 1 ^{1}H NMR titration data: association constants and limiting changes in chemical shift for formation of 1 : 1 complexes with macrocycle **2** in water. Data for complexation with macrocycle **1** in $CHCl_3$ are shown for comparison

Guest	K_a/M^{-1} host **2** in water	$\Delta\delta$ (ppm) of **2** amide NH	K_a/M^{-1} host **1** in $CDCl_3$
5	< 5	—	230
6	94 ± 9	+0.1	850
7	< 5	—	340
8	71 ± 8	+0.3	1.0×10^6
9	100 ± 10	+0.1	—
meso-**10**[a]	100 ± 10	+0.7	—
DL-**10**	760 ± 80	+0.5	—

[a] The values for *meso*-**10** were determined by titrating a mixture of DL-**10** and *meso*-**10** into **2**. Using the data obtained previously for DL-**10**, the mixed titration could be analysed in a straightforward manner, because complexation with **2** caused the signals due to DL-**10** and *meso*-**10**, which were initially coincident, to split (these compounds are clearly bound in slightly different geometries inside the macrocycle).

These changes in chemical shift are very similar to those observed for complexation with **1** in $CHCl_3$ and suggest that the structures of all of the complexes are similar to that shown in Fig. 1(*b*).

Cyclohexane-1,4-dione **6**, glycine anhydride **8** and the bis(*N*-methyl) derivative **9** all bind with comparable affinity. We have previously measured the association constants for **1** with guests **5–8** in $CHCl_3$, and the stabilities are all substantially reduced in water, which reflects the increase in solvent competition for the hydrogen-bonding sites (Table 1). However, the selectivity in $CHCl_3$ is quite different from that in water: the association constant for **6** is reduced by an order of magnitude in water; for **5** and **7**, it is at least two orders of magnitude lower, and for **8**, it is four orders of magnitude lower. This trend reflects the relative polarity of the guests and the strength of their interaction with water: more polar guests are more difficult to desolvate in water and are therefore bound weakly. Clearly, decreasing the polarity of the guest should increase binding in water, and we therefore examined three dimethyl derivatives of glycine anhydride. For **9** and *meso*-**10**, there is no increase in affinity, and CPK models suggest that these guests do not fit properly into the cavity. However, the association constant for the other isomer DL-**10** is significantly larger, indicating good shape complementarity which allows additional hydrophobic interactions with the methyl groups to be realised. Intermolecular NOEs observed in a ROESY experiment on the **2**·**10** complex confirm that the **10** methyl groups are close to the aromatic side-walls of the receptor in the complex.

Evidence that NH–π hydrogen-bonds are involved in recognition in this system comes from the rates of exchange of the amide protons with water. H_2O–D_2O (9:1) was used as the solvent, so that we could monitor the amide signals during the NMR titrations. However, this necessitated the use of a solvent suppression sequence which removed the signals due to the amides of **8** and **10**. These protons are in fast exchange with the solvent, but the signals due to the amides of receptor **2** were unaffected by solvent suppression, because they are intramolecularly hydrogen-bonded and exchange slowly with solvent. However during the course of the titration, signals due to the **8** and **10** amide protons appeared and increased in intensity until they reached a similar intensity to the signals due to the host. This implies that complexation of these guests protects the amides from exchange with solvent in the same way as conventional hydrogen-bonds and provides direct evidence for NH–π hydrogen-bonding in these complexes.[5,6]

Thus the functional group interactions responsible for recognition are amide–amide hydrogen-bonds, NH–π hydrogen-bonds and hydrophobic CH–π interactions. Although it is difficult to interpret simplistic binding experiments of this type in terms of individual interaction energies,[6,7] there are some interesting observations to be made in these systems. The association constants for **6** and **8** are very similar: desolvation of **8** is much more difficult than desolvation of **6**, which suggests that either the magnitude of the NH–π interaction in water is comparable to a hydrophobic CH_2–π interaction or that the amide–amide hydrogen-bonds are stronger than the ketone–amide hydrogen-bonds despite the competition with water. Compound **8** is a very polar substrate with very few useful recognition sites for binding in water, and yet **2** is able to complex it with reasonable affinity. The water cluster which solvates **2** presents a polar recognition surface which has a lot of similarities with that of glycine anhydride [Fig. 1(*b*)]. However, the release of these water molecules to bulk solvent on guest complexation is entropically favourable and may be enthalpically favourable for the water which solvates the non-polar part of the receptor.[2a] The most stable complex is formed with DL-alanine anhydride DL-**10**, where hydrophobic interactions with the two methyl groups are responsible for the ten-fold increase the association constant relative to glycine anhydride **8**.

We thank the Lister Institute (C. A. H.), the EPSRC (J. A. T.), the Spanish Government (P. L. B. and C. R.) and the Asturius Government, FICYT (P. L. B.) for funding.

Notes and references

† E-mail: c.hunter@sheffield.ac.uk

‡ *Crystal data* for $C_{60}H_{98}Cl_2N_8O_{18}$; M = 1290.36, crystallises from MeCN–water as long colourless needles; crystal dimensions 0.76 × 0.32 × 0.32 mm, tetragonal, a = 33.6111(15), b = 33.6111(15), c = 13.2959(6) Å, U = 15020.5(12) Å^3, Z = 8, D_c = 1.141 Mg m^{-3}, space group $P4_2/ncm$ (λ = 0.71073 Å), μ(Mo-Kα) = 0.152 mm^{-1}, F(000) = 5536, 59975 reflections, 3879 independent reflections, final R = 0.1611. The crystals were long and fibrous on attempted cleavage. The spots and resolution were very poor, hence the high final R. The complex has C_S symmetry. CCDC 182/1012.

1 *Comprehensive Supramolecular Chemistry*, ed. F. Vogtle, Pergamon, Oxford, vol. 2, 1996.
2 (*a*) S. B. Ferguson, E. M. Sanford, E. M. Seward and F. Diederich, *J. Am. Chem. Soc*., 1991, **113**, 5410; (*b*) S. Mecozzi, A. P. West and D. A. Dougherty, *J. Am. Chem. Soc*., 1996, **118**, 2307.
3 F. Diederich and D. R. Carcanague, *Helv. Chim. Acta*, 1994, **77**, 800; B. Hinzen, P. Seiler and F. Diederich, *Helv. Chim. Acta*, 1996, **79**, 942; (c) V. M. Rotello, E. A. Viani, G. Deslongchamps, B. A. Murray and J. Rebek, *J. Am. Chem. Soc*., 1993, **115**, 797; M. M. Conn, G. Deslongchamps, J. de Mendoza and J. Rebek, *J. Am. Chem. Soc*., 1993, **115**, 3548; Y. Kato, M. M. Conn and J. Rebek, *J. Am. Chem. Soc*., 1994, **116**, 3279; M. Torneiro and W. C. Still, *J. Am. Chem. Soc*., 1995, **117**, 5887.
4 A. R. Fersht and L. Serrano, *Curr. Opin. Struct. Biol*., 1993, **3**, 75.
5 F. J. Carver, C. A. Hunter and R. J. Shannon, *J. Chem. Soc*., *Chem. Commun*., 1994, 1277; H. Adams, F. J. Carver, C. A. Hunter and N. J. Osborne, *Chem. Commun*., 1996, 2529.
6 T. M. Fong, M. A. Cascieri, H. Yu, A. Bansal, C. Swain and C. D. Strader, *Nature*, 1993, **362**, 350; H. Adams, K. D. M. Harris, G. A. Hembury, C. A. Hunter, D. Livingstone and J. F. McCabe, *Chem. Commun*., 1996, 2531.
7 D. H. Williams, B. Bardsley, W. Tsuzuki and A. J. Maguire, *Chem. Biol*., 1997, **4**, 507; H. Adams, F. J. Carver, C. A. Hunter, J. C. Morales and E. M. Seward, *Angew. Chem*., *Int. Ed. Engl*., 1996, **35**, 1542.

Communication 8/07110A

Novel photoinduced aromatization of Hantzsch 1,4-dihydropyridines

Mei-Zhong Jin, Li Yang, Long-Min Wu, You-Cheng Liu and Zhong-Li Liu*

National Laboratory of Applied Organic Chemistry, Lanzhou University, Lanzhou, Gansu 730000, China. E-mail: liuzl@lzu.edu.cn

Received (in Cambridge, UK) 11th September 1998, Accepted 6th October 1998

4-Alkyl- and/or aryl-1,4-dihydro-2,6-dimethylpyridine-3,5-dicarboxylates (Hantzsch 1,4-dihydropyridines) are quantitatively oxidized to the corresponding pyridine derivatives by irradiation in CCl_4 *via* a photoinduced electron transfer mechanism.

A plethora of reagents has been used for oxidation of 1,4-dihydropyridine (DHP) derivatives,[1] a class of model compounds of NADH and drugs for treatment of cardiovascular diseases.[2] Generally, strong inorganic oxidants, such as nitric acid,[3] ceric ammonium nitrate[4] or ferric or cupric nitrates,[5] must be used to accomplish the oxidation. Recent developments include using nitric oxide,[6] pyridinium chlorochromate[7] and clay-supported cupric nitrate accompanied by ultrasound-promotion[8] to improve the efficiency of the aromatization. However, yields are generally moderate and/or tedious work-up procedures are required. We report herein a very convenient, clean and efficient approach for the oxidation of Hantzsch 1,4-dihydropyridines by direct photolysis of the substrate in CCl_4. To the best of our knowledge, this is the first report on photochemical aromatization of Hantzsch 1,4-dihydropyridines (DHPs).

DHP **1** (1 mmol) was dissolved in 25 ml of CCl_4 or CCl_4–MeCN (9:1 v/v) and irradiated with a 250 W high pressure mercury lamp in a Pyrex bottle under argon atmosphere at ambient temperature. After irradiation the solvent was removed under reduced pressure and the corresponding pyridine derivative **2** was obtained in pure form and almost quantitative yield (Scheme 1). One exception is 4-(2-furyl)-DHP **1g** which gave 85% of **2g** together with 13% of de-furyl product **2a**. The results are summarized in Table 1.

It was found that $CHCl_3$ was generated during the reaction, as evidenced by GC, and the solution became acidic after irradiation. Hence there is no doubt that C–Cl bond cleavage takes place during the photolysis. Similar CCl_4- and/or $HCCl_3$-promoted photo-fragmentation reactions have recently been reported from this laboratory[9,10] and by Whitten and co-workers.[11] Therefore, a photoinduced electron transfer mechanism is proposed, as outlined in Scheme 2.

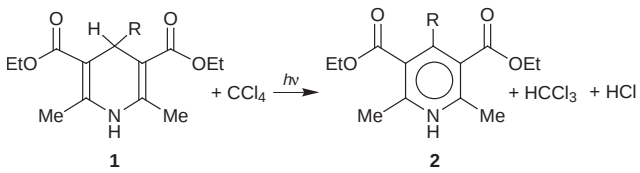

1 **2**

Scheme 1

Table 1 Aromatization of Hantzsch dihydropyridines **1** by direct photolysis in CCl_4

Substrate	R	*t*/h	Product	Conversion (%)	Yield (%)
1a	H	1	**2a**	~100	~100
1b	Me	3	**2b**	~100	~100
1c	Et	3	**2c**	~100	~100
1d	Ph	3	**2d**	~100	~100
1e	*p*-$MeOC_6H_4$	3	**2e**	~100	~100
1f	*p*-ClC_6H_4	3	**2f**	~100	~100
1g	2-furyl	3	**2g**, **2a**	~100	85, 13

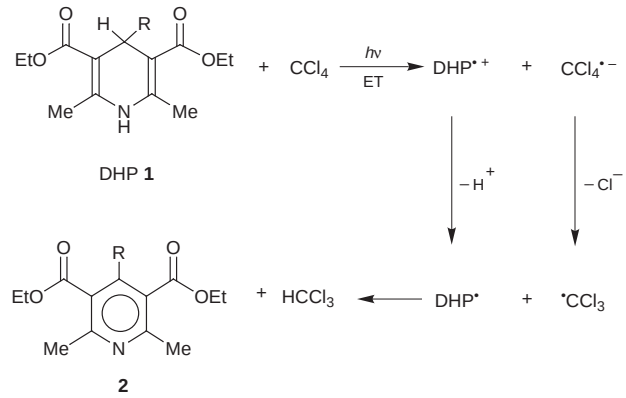

Scheme 2

The critical step in this mechanism is the extremely fast dechlorination of the radical anion of CCl_4. It is well known that alkyl and aryl halides are subject to reductive dissociation upon accepting an electron either electrochemically or photochemically.[12] The lifetime of the radical anion of CCl_4 was reported to be extremely short (less than 10 ps).[13] Therefore, C–Cl bond breaking and electron transfer may even take place concertedly which, in turn, effectively circumvents the back electron transfer and makes the reaction very efficient. Maslak and co-workers[14] have termed unimolecular fragmentation of radical ions as mesolytic cleavage and demonstrated the tremendous facilitation of bond cleavages obtainable from the mesolytic processes. The present reaction involves mesolytic cleavages of both radical anions (aniomesolysis) and radical cations (catiomesolysis), hence, it can be considered as a double mesolytic fragmentation reaction. The aniomesolysis helps to prevent back electron transfer, which enhances the quantum yield of the photolysis, and the catiomesolysis facilitates the deprotonation from DHP. These two effects make the reaction very efficient. This strategy may be applicable to the enhancement of the efficiency of other photoinduced electron transfer reactions. In addition, since no additional oxidant is required other than the solvent CCl_4, and no any waste is produced, this reaction can also be considered as a facile green chemical reaction for the synthesis of pyridine derivatives and may be extended to other synthetic reactions

The authors thank the National Natural Science Foundation of China for financial support.

Notes and references

1 A. Sausins and G. Duburs, *Heterocycles*, 1988, **27**, 291.
2 R. A. Janis and D. J. Triggle, *J. Med. Chem.*, 1983, **26**, 775; E. Wehinger and R. Gross, *Annu. Rep. Med. Chem.*, 1986, **21**, 85.
3 R. H. Boecker and F. P. Guengerich, *J. Med. Chem.*, 1986, **29**, 1596.
4 J. R. Pfister, *Synthesis*, 1990, 689.
5 M. Balogh, I. Hermecz, Z. Meszaros and P. Laszlo, *Helv. Chim. Acta.*, 1984, **67**, 2270.
6 T. Itoh, K. Nagata, Y. Matsuya, M. Miyazaki and A. Ohsawa, *J. Org. Chem.*, 1997, **62**, 3582.
7 J-J. V. Eynde, A. Mayence and A. Maquestiau, *Tetrahedron*, 1992, **48**, 463.

8 A. Maquestiau, A. Mayence and J-J. V. Eynde, *Tetrahedron Lett*., 1991, **32**, 3839.
9 W. Zhang, L. Yang, L. M. Wu, Y. C. Liu and Z. L. Liu, *J. Chem. Soc*., *Perkin Trans. 2*, 1998, 1189.
10 X. Guo, L. Yang, L. M. Wu, Y. C. Liu and Z. L. Liu, *Chin. Chem. Lett*., 1998, **9**, 199.
11 L. Chen, M. S. Farahat, H. Gan, S. Farid and D. G. Whitten, *J. Am. Chem. Soc*., 1995, **117**, 6398; H. Gan, M. A. Kellett, J. W. Leon, L. Kloepper, U. Leinbos, I. R. Gould, S. Farid and D. G. Whitten, *J. Photochem. Photobiol. A*, 1994, **82**, 211.
12 J. Bertran, I.Gallardo, M.Moreno and J.-M. Save'ant, *J. Am. Chem. Soc*., 1992, **114**, 9576.
13 A. Kalamarides, R. W. Marawar, M. A. Durham, B. G. Lindsay, K. A. Smith and F. B. Dunning, *J. Chem. Phys*., 1990, **93**, 4043.
14 P. Maslak and J. N. Narvaez, *Angew. Chem., Int. Ed. Engl*., 1990, **29**, 283; P. Maslak, J. Kula and J. E. Chateauneuf, *J. Am. Chem. Soc*., 1991, **113**, 2304.

Communication 8/07093H

ChemComm

Polymer backbone disassembly: polymerisable templates and vanishing supports in high loading parallel synthesis

Christopher P. Ball, Anthony G. M. Barrett,* Lydie F. Poitout, Marie L. Smith* and Zoë E. Thorn

Department of Chemistry, Imperial College of Science, Technology and Medicine, London, UK SW7 2AY. E-mail: m.stow@ic.ac.uk

Received (in Liverpool, UK) 7th August 1998, Accepted 6th October 1998

In the synthesis of a library of *N*-alkyl-3-aza-8-oxabicyclo[3.2.1]octane-6,7-dimethanol derivatives, prepared from an 7-oxabicyclo[2.2.1]hept-2-ene-5,6-dimethanol derivative *via* ring opening metathesis polymerisation using $Cl_2(Cy_3P)_2Ru{=}CHPh$, selective alkylation, ozonolytic scission of the polymer backbone and reductive alkylation, purification was facilitated by the differential solubility of the polymer intermediates.

The emergence of combinatorial methodologies and parallel syntheses have dramatically accelerated synthetic chemistry and the quest for novel pharmaceuticals and other specialty chemicals.[1] Many state-of-the-art parallel syntheses rely upon polymer-supported procedures in which the substrate is attached to a support throughout a synthetic sequence. Assay is either carried out on the support or following late release. Such supported syntheses are aided by the 'polymer advantage' which allows (i) solid phase reactions to be driven to completion by the addition of excess solution phase reagents which are simply removed by filtration techniques and (ii) the separation of reaction products from the polymer post-cleavage. There is clear merit in maximising substrate loading so that for any given synthesis, sufficient substrate is produced at a minimum resin weight such that compound authentication, bioassay and compound archiving are facilitated. As such there is need to maximise the loadings yet to also facilitate on-support analysis. The use of PEG supports clearly addresses the need for easy solution-based analyses but these supports are not ideal in terms of loadings. On the other hand, the preparation of polymer supported dendritic materials[2] leads to improved loadings yet does not greatly facilitate analysis. The use of insoluble polymers often necessitates the utilisation of time-consuming, non-standard analytical techniques, *e.g.* solid state NMR spectroscopy, in order to determine the character of the polymer-bound substrates.

Herein, we report the concept of polymer backbone disassembly for the preparation of synthetic libraries. In this approach the substrate is also the monomer building block for the polymer. As such the polymer loading should ideally approach quantitative. The polymerisation of an appropriate monomer (starting material) to form an insoluble (or differentially soluble) polymeric material is followed by substrate modification for the introduction of chemical diversity. Finally oxidative disassembly generates the modified monomers which are in fact the small molecules of interest. Polymers derived from ring opening metathesis polymerisation (ROMP)[3] fulfil these criteria and were chosen for initial evaluation in the strategy outlined in Scheme 1. ROMP polymers are, unlike cross-linked polystyrene resins, generally soluble in a range of organic solvents yet insoluble in others. Thus, chemical modifications may be carried out in a homogenous environment thereby avoiding poor solvation which often inhibits reactions carried out with insoluble solid supports. Moreover, reactions may be probed using standard solution phase spectroscopic techniques and the ability to rapidly determine the nature of the attached substrate offers a significant advantage over standard solid-phase organic synthesis. Following synthesis, the ROMP

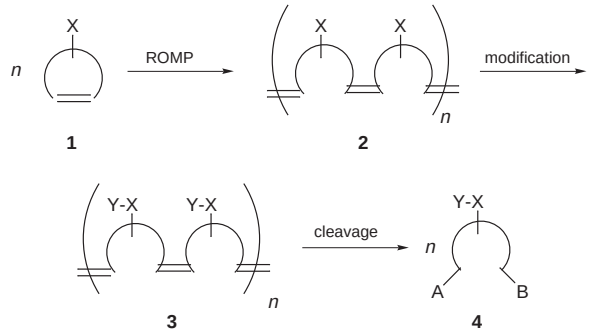

Scheme 1

polymers may be precipitated by the correct choice of solvent to afford solids which can be washed to remove excess reagents. In this respect ROMP polymers show similar behaviour to the PEG polymers recently further developed by Janda *et al*.,[4] after the pioneering work by Bayer, Mutter and Shemyakin.[5]

Norbornene, 7-oxanorbornene and cyclobutene ROMP monomers containing functional groups which are either hydrophilic or hydrophobic in nature are readily available and many offer the opportunity for post-polymerisation chemical modification required for library generation. 7-Oxanorbornene **6** was chosen for initial study as depicted in Scheme 2. The monomer **6** is readily prepared from diol **5** *via* mono-silylation followed by tetrahydropyranyl protection. The use of orthogonal protecting groups[6] allows for a stepwise hydroxy group modification strategy to be utilised in library synthesis. Polymerisation of **6** using the Grubbs catalyst **13**[7] and chain

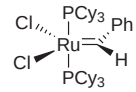

13

termination with ethyl vinyl ether[8] gave polymer **7** as an off-white foam which was most conveniently isolated (90%) following repeated precipitation from 1,2-dichloroethane solution with MeOH. Both ^{1}H and ^{13}C NMR spectra were consistent with polymer **7** having a 1:1 *trans*:*cis* stereochemistry.[8] Selective desilylation of polymer **7** gave the corresponding polyol **8** as a THF-insoluble precipitate which was washed with THF and Et_2O and dried *in vacuo*, whereupon ^{1}H and ^{13}C NMR spectra (acetone-d_6) indicated complete removal of the *tert*-butyldimethylsilyl residues. Alkylation of polymer **8** using MeI or 4-bromobenzyl bromide (R^1X) in the presence of NaH in THF gave the corresponding THF-soluble polymeric ethers **9** which were precipitated from MeOH. In turn, cleavage of the tetrahydropyranyl ether of **9** using TsOH in a MeOH–THF–CH_2Cl_2 (1:2:1) mixture and precipitation from THF followed by further alkylation with MeI or 4-bromobenzyl bromide (R^2X) afforded the polyethers **10** which were isolated in the same way as **9**. All polymers were isolated cleanly and with high recovery.

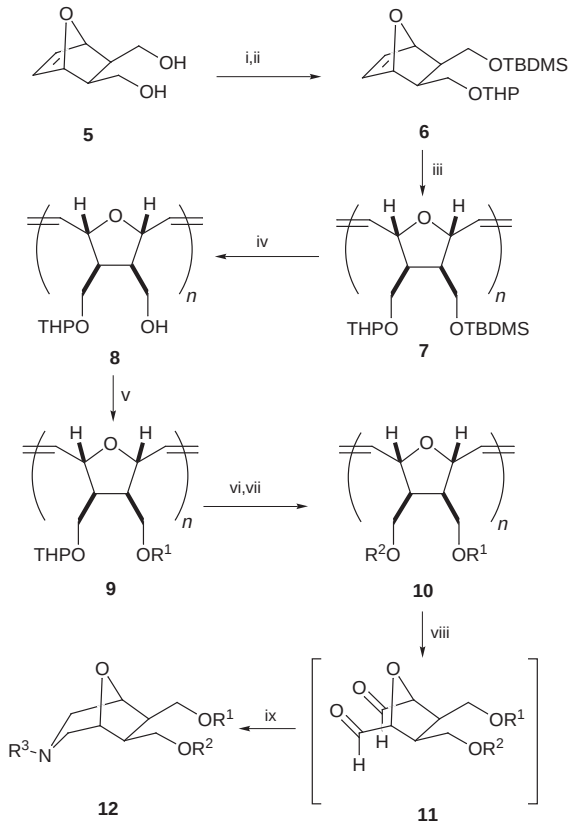

Scheme 2 *Reagents and conditions*: i, NaH, THF, TBDMSCl, 78%; ii, dihydropyran, cat. PPTS, CH_2Cl_2, 92%; iii, **13**, $ClCH_2CH_2Cl$, then $EtOCH{=}CH_2$ quench, 90%; iv, Bu_4NF, THF; v, NaH, THF, R^1X; vi, TsOH, MeOH–THF–CH_2Cl_2 (1:2:1); vii, NaH, THF, R^2X; viii, O_3, CH_2Cl_2, −78 °C, then EtOH, Me_2S; ix, $NaBH(OAc)_3$, R^3NH_2.

The three functionalised polymers **10** were disassembled by ozonolysis with a Me_2S work-up to reveal the corresponding dialdehydes **11** which were not isolated. Direct *in situ* reductive amination[9] with $BnNH_2$, $BuNH_2$ and (cyclohexylmethyl)amine gave the corresponding 3-aza-8-oxabicyclo[3.2.1]octanes **12** in overall yields of around 30% from the starting polymer **7**. The same nine 3-aza-8-oxabicyclo[3.2.1]octane derivatives **12** were prepared from monomer **6** by sequential double deprotection and monoalkylation, ozonolysis and reductive amination. Overall yields in these reactions were comparable (30–40%).

We have demonstrated the utility and advantage of polymer backbone disassembly for the rapid generation of small molecule targets using polymer **7**. Advantages include ease of intermediate purification and facile reaction monitoring. The modification of polymer **7** for library construction with different chemistry is ongoing and will be reported in due course.

We thank Rhône-Poulenc Rorer for the most generous support of our programs on parallel and combinatorial syntheses under the auspices of the TeknoMed project. In addition we thank GlaxoWellcome Research Ltd. for their endowment (to A. G. M. B.), the Royal Society for a Dorothy Hodgkin fellowship (to M. L. S.), the EPSRC for a studentship (to Z. E. T.), Professor Vernon Gibson (for the kind donation of Grubbs catalyst **13**) and the Wolfson Foundation for establishing the Wolfson Centre for Organic Chemistry in Medical Science at Imperial College.

Notes and references

† All new compounds were fully characterised by spectroscopic data and microanalysis and/or high resolution mass spectrometry.

1 N. K. Terrett, M. Gardner, D. W. Gordon, R. J. Kobylecki and J. Steele, *Tetrahedron*, 1995, **51**, 8135; E. M. Gordon, R. W. Barrett, W. J. Dower, S. P. A. Fodor and M. A. Gallop, *J. Med. Chem.*, 1994, **37**, 1385; L. A. Thompson and J. A. Ellman, *Chem. Rev.*, 1996, **96**, 555; J. S. Früchtel and G. Jung, *Angew. Chem., Int. Ed. Engl.*, 1996, **35**, 17; D. J. Gravert and K. D. Janda, *Chem. Rev.*, 1997, **97**, 489.

2 V. Swali, N. J. Wells, G. J. Langley and M. Bradley, *J. Org. Chem.*, 1997, **62**, 4902.

3 V. C. Gibson, *Adv. Mater.*, 1994, **6**, 37; B. M. Novak and R. H. Grubbs, *J. Am. Chem. Soc.*, 1988, **110**, 960; B. M. Novak and R. H. Grubbs *J. Am. Chem. Soc.*, 1988, **110**, 7542; R. H. Schrock, *Acc. Chem. Res.*, 1990, **23**, 158; D. S. Breslow, *Prog. Polym. Sci.*, 1993, **18**, 1141.

4 H. Han, M. M. Wolfe, S. Brenner and K. D. Janda, *Proc. Natl. Acad. Sci. U.S.A.*, 1995, **92**, 6419.

5 M. M. Shemyakin, Y. A. Ovchinnikov, A. A. Kinyushkin and I. V. Kozhevnikova, *Tet. Lett.*, 1965, 2323; M. Mutter and E. Bayer, *Angew. Chem., Int. Ed. Engl.*, 1974, **13**, 88; E. Bayer, I. Gatfield, H. Mutter and M. Mutter, *Tetrahedron*, 1978, **34**, 1829; M. Mutter, *Tetrahedron Lett.*, 1978, **31**, 2839 and 2843.

6 T. W. Greene and P. G. M. Wuts, *Protective Groups in Organic Synthesis*, 2nd edn., Wiley, 1991.

7 P. Schwab, M. B. France, Z. W. Ziller and R. H. Grubbs, *Angew. Chem., Int. Ed. Engl.*, 1995, **34**, 2039.

8 A. D. Benedicto, B. M. Novak and R. H. Grubbs, *Macromolecules*, 1992, **25**, 5893.

9 A. F. Abdel-Magid, C. A. Maryanoff and K. G. Carson, *Tetrahedron Lett.*, 1990, **31**, 5595.

Communication 8/06331A

The structure and energetics of glycine polymorphs based on first principles simulation using density functional theory

C. M. Freeman,[a] J. W. Andzelm,[a] C. S. Ewig,[a] J.-R. Hill[a] and B. Delley[b]

[a] *Molecular Simulations Inc., 9685 Scranton Road, San Diego, CA 92121, USA. E-mail: clive@msi.com*
[b] *Paul Scherrer Institut, Zurich, Badenerstr. 569, CH-8048, Zurich, Switzerland*

Received (in Cambridge, UK) 3rd August 1998, Accepted 2nd October 1998

Density functional theory (DFT) calculations for the crystal structures of polymorphs of the glycine zwitterion are reported; with unit cell parameters constrained at experimentally determined values, energy minimized configurations for three known glycine polymorphs are in good agreement with crystallographically determined structures, and the calculated energies are in qualitative agreement with observed lattice stabilities.

Molecular orbital calculations, employing Hartree–Fock,[1] density functional theory (DFT),[2] or even an appropriate combination of both methods[3] are standard techniques for the structural and energetic description of molecular systems. Significant developments have also recently taken place in the use of first principles methods to represent ionic and covalently bound periodic systems, such as silicon and zeolites, typically employing plane-wave and plane-wave/pseudo-potential approaches.[4–7] However, the simulation of molecular solids using first-principles methods has received considerably less attention[8] and the use of such methods to address the relative energies of crystal polymorphs less still. The lack of suitably refined protocols underlies this comparatively low level of application. Nevertheless, the results presented here show that such calculations are now within the compass of contemporary quantum mechanical methods and computational resources.

To explore the ability of periodic DFT method calculations to describe molecular crystals, calculations were conducted targeting the known polymorphic structures of the glycine zwitterion and using DMol[3].[9–11] The level of theory employed has been shown to be effective in the description of isolated molecules.[12]†

Initial investigations addressed the selection of a suitable quantum mechanical Hamiltonian and basis set. These calculations employed the β-glycine polymorph, which possesses a unit cell containing two symmetry related molecules and a total of 20 atoms.[13] Here results for the BLYP[14–17] functional are summarized. A minimal basis resulted in a 0.34 Å RMS deviation between minimized and observed structures, a double numeric basis (0.33 Å), a double numeric basis with polarization functions on heavy atoms (0.22 Å) and double numeric basis with polarization functions on all atoms (0.21 Å). Of the basis sets sampled then, optimal structural agreement is achieved on full geometry optimization with a so-called double numeric basis set with polarization functions on all atoms (DNP). The DNP basis set has been demonstrated to provide an efficient route to molecular polarizabilities and charge distributions as a result of its reasonable representation of the tail of the wavefunction.[10] However, the ability of this computational approach to describe the relative energetics of polymorphic crystal structures is perhaps of more interest.

To address the calculation of such relative polymorph energies, crystallographically determined structural starting models for α- and γ-glycine were employed.[18,19] As an additional test of the simulation protocol two incorrectly packed arrangements of glycine molecules were used as starting points; S1, containing four molecules in the unit cell dimensions of the α-polymorph, and S2, containing two molecules with cell dimensions of the β-polymorph.

Table 1 The relative BLYP energies, per glycine molecule, of the α-, β- and γ-glycine polymorphs. Also tabulated are the relative energies of hypothetical packing arrangements S1 and S2 and the root mean squared (RMS) displacements between the experimental structure and energy minimized structure

	Polymorph				
	α	β	γ	S1	S2
Energy/kcal mol^{-1}	0.0	2.3	2.0	5.8	15.9
RMS/Å	0.19	0.21	0.30	0.33[a]	1.20[a]

[a] RMS between starting and energy minimized structure.

Energetic results for the systems considered are collected in Table 1. The similarity of the relative energies obtained in the DFT calculations for the α-, β- and γ-polymorphs is mirrored in the experimental observation that all polymorphs are formed at temperatures close to room temperature, with the α-polymorph having the greatest observed stability.[18] The energy differences obtained in the simulations are small and entropic contributions to the lattice stability have not been considered in the present calculations. The inclusion of vibrational entropy would, of course, be possible with increased computation times through calculation of the system's dynamical matrix and appropriate integration of the resulting phonon spectrum. However, the fact that the relative energies of incorrectly packed molecular arrangements S1 and S2 are higher than the observed polymorph energies is of significant interest. For the polar β- and γ-polymorph crystals such a procedure assumes that the macroscopic dipolar energy of the structures is not significant.[20,21] This appears to be a reasonable approximation.[22]

Fig. 1 shows starting structures and optimized structures for each of the polymorphs investigated. Good agreement is

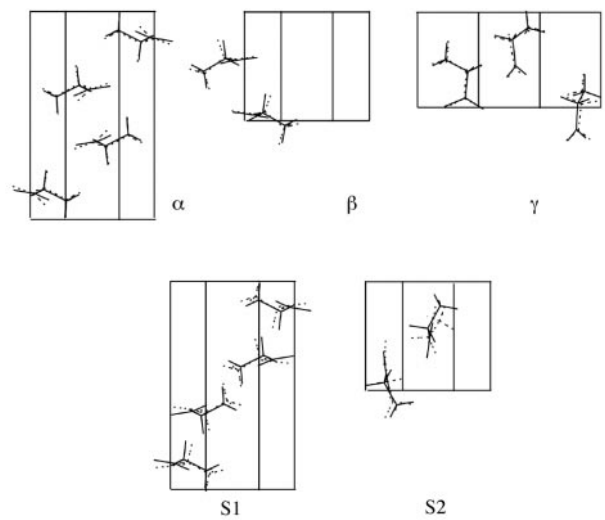

Fig. 1 Structural agreement between energy minimized (dashed line) and experimental structures (solid line) for α-, β- and γ-glycine polymorphs. Hypothetical packing arrangements S1 and S2 (dashed line) show comparison with starting points (solid line).

Table 2 Mulliken (ref. 23) derived partial electronic charges obtained with the BLYP Hamiltonian and DNP basis sets for α-, β- and γ-glycine polymorphs and hypothetical packing arrangements S1 and S2 (molecules 1 and 2). Also tabulated are partial electronic charges for an isolated molecule in the configuration of the unique molecule of the α-glycine polymorph

		Isolated molecule	Polymorph					
			α	β	γ	S1	S2: 1	S2: 2
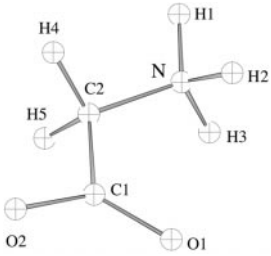	O1	−0.534	−0.640	−0.618	−0.654	−0.630	−0.687	−0.597
	C1	0.401	0.553	0.555	0.546	0.530	0.550	0.514
	N	−0.222	−0.410	−0.456	−0.425	−0.494	−0.410	−0.447
	C2	−0.167	−0.168	−0.185	−0.146	−0.129	−0.185	−0.183
	H1	0.234	0.352	0.356	0.348	0.357	0.269	0.331
	H3	0.258	0.286	0.334	0.293	0.320	0.402	0.329
	H2	0.265	0.344	0.344	0.353	0.351	0.260	0.283
	H5	0.137	0.133	0.149	0.165	0.118	0.149	0.184
	O2	−0.509	−0.650	−0.654	−0.629	−0.622	−0.538	−0.606
	H4	0.137	0.200	0.174	0.147	0.198	0.196	0.184

obtained between simulation and experiment for the known crystal models. The lowest RMS displacement between optimized and experimental structure (0.19 Å) is obtained for the α-polymorph, a structure determined using neutron diffraction data with the lowest crystallographic *R* value of the polymorphs (R = 0.032).[19] The starting geometries of incorrectly packed arrangements, S1 and S2, are altered by the optimization procedure to a greater extent than the observed polymorphs. In neither case do the resulting structures resemble the experimental polymorph structures.

For S1 the structural deviation has an RMS value of 0.33 Å implying that, in this case, energy minimization is able to locate a stationary point in the vicinity of the starting structure. S1 was generated using the unit cell and asymmetric unit of the α-polymorph and applying the symmetry operations of the $P2_1/c$ spacegroup. This procedure yields a packing configuration similar for half the molecules to that of the α-polymorph (spacegroup $P2_1/n$). For S2 larger structural changes are evident in both the RMS displacement (1.2 Å) and in Fig. 1. This polymorph was generated by randomly placing two molecules within the cell of the β-polymorph.

The present calculations employ the experimental unit cell dimensions as a constraint. This reduces computation times through a reduction in the number of variables used to describe the system. However it is important to note that cell parameter data, through indexed powder diffraction patterns, are among the most readily obtained structural information for solid state materials. The current calculations, which focus on the optimization of the geometry within the unit cell, provide valuable information that augments experimental observation and leads to the full description of the crystal.

The magnitudes of partial charges are key to the accuracy of models employing classical mechanics. Table 2 collects the Mulliken[23] charges for each of the atoms of the glycine molecule in the calculations conducted. The calculations are performed within a $P1$ triclinic simulation cell. However, for the α-, β- and γ-polymorphs symmetry is maintained during the optimization, hence charges are reported for a single molecule only. S1 was produced with the $P2_1/c$ spacegroup and also has four equivalent molecules, one of which is listed. For S2, symmetry is not present and charges for both molecules are listed. Interestingly for the experimental polymorphs there is little difference between the atomic partial charges obtained, despite the differences in local environment that each crystal form necessarily imposes on its constituent molecules. For the hypothetical packing arrangements S1 and S2, differing charge distributions are exhibited on several atoms, most notably O1, O2 and N. Also tabulated in Table 2 are gas phase derived atomic charges using the same basis set and Hamiltonian for the structure of the unique molecule of the α-polymorph. The magnitude of charges on oxygen and nitrogen atoms of the isolated molecule are lower than in the crystal structure calculations. The unambiguous definition of atomic partial charges from supplied molecular orbitals is not straightforward.[24,25] In particular Mulliken analysis is sensitive to the choice of basis set. However, these findings, using a particular charge definition method[23] and uniform basis set and calculation type, indicate that the practice of transferring partial charges from gas phase calculations to the condensed phase may lead to an inaccurate description of the charge distribution exhibited by molecules in the crystalline state. Of course, no such ambiguity affects the first-principles calculations where charge density and its variation with environment are both consequences of the molecular orbitals obtained in the solution of the Schrödinger equation.

The calculations demonstrate that energy minimization leading to a determination of the relative energetics of molecular crystals is practical using first principles methods.‡

Notes and references

† The Brillouin zones of the polymorphs were sampled at the Γ point only. A detailed report on the effect of the choice of Hamiltonian and basis set on the structures and energies for molecular solids is in preparation. Geometry optimization (varying all atomic coordinates within the fixed cell) required calculation times of a few days on a single processor of an Origin 200 SGI (180 MHz) workstation.

‡ The computed structures are available from the authors by email.

1 A. Hinchliffe, *Computational Quantum Chemistry*, Wiley, Chichester, 1988.
2 R. G. Parr and W. Yang, *Density Functional Theory of Atoms and Molecules*, OUP, 1989.
3 A. D. Becke, *J. Chem. Phys*., 1993, **98**, 5698.
4 E. Wimmer, *J. Comput.-Aided Mater. Des*., 1993, **1**, 215.
5 F. Haase, J. Sauer and J. Hutter, *Chem. Phys. Lett*., 1997, **266**, 397.
6 R. Shah, J. D. Gale and M. C. Payne, *J. Phys. Chem*., 1997, **B101**, 4787.
7 I. Stich, J. D. Gale, K. Terakura and M. C. Payne, *Chem. Phys. Lett*., 1998, **283**, 402.
8 M. Marchi, J. Hutter and M. Parrinello, *J. Am. Chem. Soc*., 1996, **118**, 7847.
9 B. Delley, *J. Chem. Phys*., 1990, **92**, 508.
10 B. Delley, *J. Phys. Chem*., 1996, **100**, 6107.
11 DMol[3] (Version Cerius[2], 3.5), Molecular Simulations Inc., 9685 Scranton Road, San Diego, CA 92121, USA, 1997.
12 B. B. Laird, R. B. Ross and T. E. Ziegler, *Chemical Applications of Density Functional Theory*, *ACS Symp. Ser. No 629*, ACS, Washington, 1996.
13 Y. Iitaka, *Acta Crystallogr*., 1960, **13**, 35.
14 C. Lee and C. Sosa, *J. Chem. Phys*., 1994, **100**, 9018.
15 C. Lee, W. Yang and R. G. Parr, *Phys. Rev*., 1988, **B37**, 785.
16 R. Colle and D. Salvetti, *Theor. Chim. Acta*, 1975, **37**, 329.
17 A. D. Becke, *Phys. Rev*. 1988, **A38**, 3098.
18 Y. Iitaka, *Acta Crystallogr*., 1961, **14**, 1.
19 P.-G. Jonsson and A. Kvick, *Acta Crystallogr*., 1972, **B28**, 1827.
20 M. W. Deem, J. M. Newsam and S. K. Sinha, *J. Phys. Chem*., 1990, **94**, 8356.
21 J. L. Derissen, P. H. Smit and J. Voogd, *J. Phys. Chem*., 1977, **91**, 1474.
22 B. P. van Eijck and J. Kroon, *J. Phys. Chem. B*, 1997, **B101**, 1096.
23 R. S. Mulliken, *J. Chem. Phys*., 1955, **23**, 1833.
24 K. B. Wiberg and P. R. Rablen, *J. Comput. Chem*., 1993, **14**, 1504.
25 J. Meister and W. H. E. Schwartz, *J. Phys. Chem*., 1994, **98**, 8245.

Communication 8/06102E

ChemComm

Flavin-oligonucleotide conjugates: sequence specific photocleavage of DNA

Christelle Frier,[a] Jean-François Mouscadet,[b] Jean-Luc Décout,*[c] Christian Auclair[b] and Marc Fontecave*[a]

[a] *Laboratoire de Chimie et Biochimie des Centres Redox Biologiques, DBMS-CEA/CNRS/Université J. Fourier, Bat. K, 17 avenue des Martyrs, 38054 Grenoble Cedex 9, France. E-mail: fontecav@cbcrb.ceng.cea.fr*

[b] *CNRS UMR 1772, Institut Gustave Roussy, PRII 39, rue Camille Desmoulins, 94805 Villejuif Cedex, France*

[c] *Laboratoire de Chimie Bioorganique, CNRS EP 811, UFR de Pharmacie, Domaine de la Merci, 38706 La Tronche, France. E-mail: decout@cbcrb.ceng.cea.fr*

Received (in Cambridge, UK) 4th August 1998, Accepted 6th October 1998

A flavin–oligonucleotide conjugate forms a stable triple helix with a double-stranded DNA sequence of HIV-1, and selectively photocleaves it at the 3′-G of a GG doublet located 7 bases away from the flavin position.

Oligonucleotides can be used as selective inhibitors of gene expression.[1] Binding to double-stranded DNA results in short triple helix formation which can block transcription.[2] Moreover, attachment to the oligonucleotide of a reactive group that can irreversibly damage the target DNA in a site-specific fashion should potentiate the inhibitory properties of the oligonucleotide.[2,3]

As a substituent of triple helix forming oligonucleotides (TFOs), flavins such as riboflavin **1** (vitamin B2, Fig. 1) have the advantage of displaying low toxicity and might be activated *in vivo* by diaphorases to produce oxygen species to damage a DNA target.[4] Flavin–TFOs might also be useful tools for *in vitro* studies: riboflavin is one of the most efficient natural photosensitizers, and has previously been shown to induce DNA oxidation[5] and selective RNA cleavage.[6] Upon irradiation, netropsin–flavin conjugates are sequence-specific DNA-cleaving molecules,[7] and flavin–peptide conjugates are able to repair a cyclobutane uracil dimer incorporated into an oligonucleotide.[8] Here, we show that flavin–oligonucleotide conjugates selectively photocleave a double stranded DNA target present in the HIV-1 genome and display original DNA photosensitisation properties.

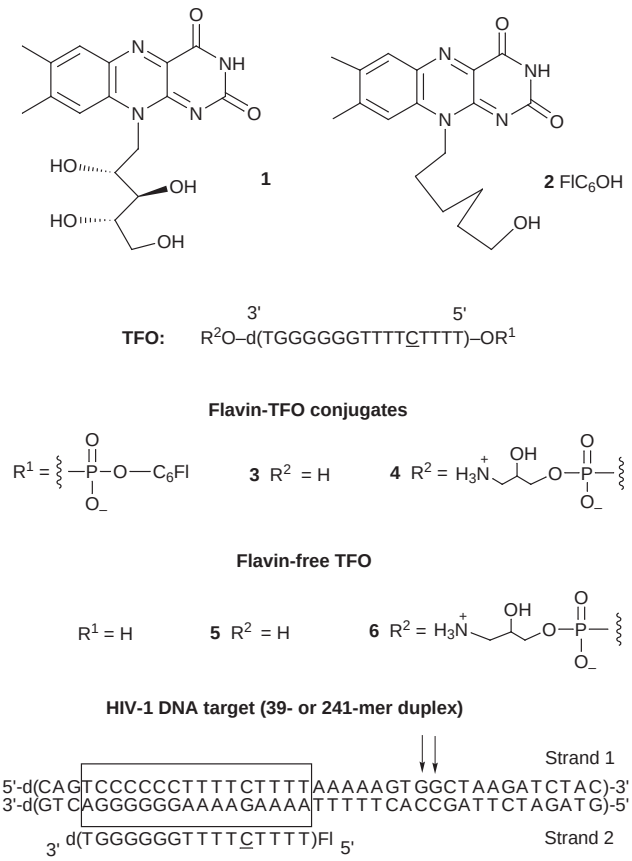

Fig. 1 Structures and sequences (phosphodiester linkages). d(C): 5-methyl-2′-deoxycytidine; DNA target: PPT sequence in a 39 or 241 base pair duplex present in the HIV-1 genome. The arrows indicate the sensitive GG doublet.

The flavin–TFO conjugates **3** and **4** (Fig. 1) were prepared as previously described.[9] The selected 16-mer TFO sequence has been previously shown to allow triple helix formation with duplexes containing the sixteen consecutive bases of the polypurine tract (PPT, Fig. 1) of the HIV-1 genome.[10] The target duplex was obtained from a 241-mer PCR fragment cloned into a pGEM-3Z plasmid. That the triple helix, formed upon hybridisation of the flavin–oligonucleotide conjugate **4** or the corresponding oligonucleotide **6** to the target duplex, was located as predicted was shown from footprinting experiments (data not shown). The protection of the whole PPT sequence of the 241 base pair fragment from hydrolysis by DNase I increased with increased amounts of both oligonucleotides. It should be noted that only the flavin–TFO conjugate **4** gave rise in the absence of irradiation to a large cleavage enhancement selectively at the guanine residue located 7 bases downstream of the triplex-duplex junction. This could be due to a local deformation of the duplex specifically induced by the flavin–TFO.

Triplexes were irradiated for 60 min with UV light and both strands of the target were analyzed by electrophoresis. The observed photocleavage was highly selective as it occurred exclusively on strand 1 and at the closest DNAse I-sensitive GG sequence, located 7 bases downstream of the triplex–duplex junction (Fig. 2, lane 13). No cleavage on strand 2 could be detected in spite of the presence of a GG sextuplet. With the free flavin **2**, alone (lane 7) or in the presence of the flavin-free TFO **6** (lane 11), the photocleavage occured at all G multiplets. No cleavage was observed with the flavin-free TFO (lane 9).

In all cases, irradiation was absolutely required as no reaction occured in the dark (lanes 6, 8, 10, 12). It is interesting to note that the flavin system is very photoreactive; a low intensity light source is able to induce the cleavage (365 nm, 5 mW cm^{-2}, 100 W UV or desk lamp). DNA cleavage was monitored by gel electrophoresis after removal of the major part of spermine by precipitation. Reaction yields were found to depend on the heating time before electrophoresis in the presence of urea (pH 8), suggesting that base damage was heat-labile. Whereas only 25% of the target was cleaved after 3 min heating at 90 °C, the yield was greater than 50% after 30 min heating. Further treatment with 1 M piperidine at 90 °C for 30 min did not increase this yield significantly.

To further characterize the reaction, we used 39-mer oligonucleotides as the target duplex containing the PPT sequence (Fig. 1). Again, a remarkably time- and light-dependent selective cleavage was obtained, with the labile site almost exclusively located at the 3′-guanine of the 5′-GG-3′

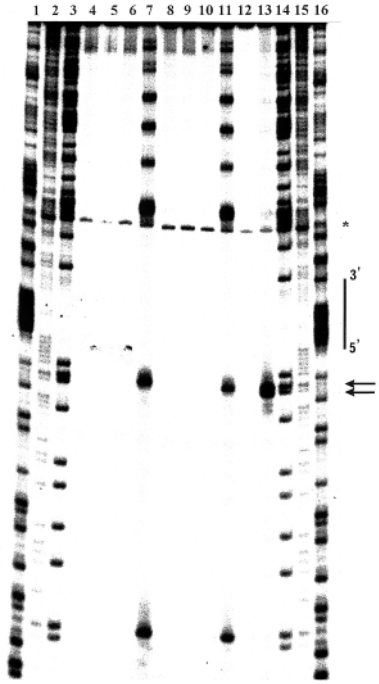

Fig. 2 Phosphoimager picture of a 12% denaturing polyacrylamide gel showing the cleavage products of a 241 base pair duplex DNA target (10 nM, Fig. 1), labeled on strand 1 at the 3′-end, alone (lanes 4,5) or incubated with 10 μM of the flavin **2** (lanes 6,7), the flavin-free TFO **6** (lanes 8,9), both **2** and **6** (lanes 10,11) or the flavin–TFO conjugate **4** (lanes 12, 13). Irradiated samples (lanes 5, 7, 9, 11, 13) are compared to dark samples (lanes 4, 6, 8, 10, 12). Sequencing reactions: T (lanes 1, 16), [G+A] (lanes 2, 15), G (lanes 3, 14). Hybridisation: overnight at room temperature, 20 mM Tris, pH 6.8, 5 mM $MgCl_2$, 0.25 mM spermine, 0.5 μg ml^{-1} of calf thymus DNA; irradiation (365 nm): 1 h at 4 °C, precipitation in EtOH and then heating in urea (7 M, pH 8, 10 mM Tris, 1 mM EDTA) at 90 °C for 5 min. The vertical line shows the presumed position of the flavin–TFO with the flavin moiety at the 5′-end. The arrows show the unique site of damage in the case of **4**. The starting DNA material contained one contaminant (asterisk).

sequence of the target (data not shown). Longer irradiation times also generated a minor amount of cleavage at the 5′-guanine. While alkaline treatment did not significantly affect gel profiles, treatment of the irradiated samples with the enzyme formamidopyrimidine-DNA glycosylase (Fpg) before electrophoresis revealed a second type of damage. The latter, most likely due to the formation of 8-oxo-7,8-dihydro-2′-deoxyguanosine (8-oxodGuo),[11] was detected exclusively at the 5′-guanine of the same sensitive 5′-GG-3′ sequence (data not shown).

Similar results were obtained with the flavin–oligonucleotide conjugate **3**. These results provide the first indication of the potential of flavin–oligonucleotide conjugates as selective DNA photocleaving agents. Cleavage of a viral target occured at only one GG site among 26 G multiplets present in the duplex target (with a total of 111 G). It is likely that the observed DNA damage is the result of electron transfer from guanine to the photoexcited flavin acceptor,[12] in agreement with GG doublets being the most efficient donors.[13] In addition to this high selectivity, this system displays several original features which have yet to be understood: (i) both the 3′- and 5′-G of the GG doublet are damaged while previous studies indicated a higher sensitivity for the 5′-G,[13] and (ii) the reactive doublet is several bases away from the presumed flavin site. Whether the reaction is made possible by a local bending of the HIV DNA in the proximity of the PPT boundary, thus allowing a direct interaction between the flavin and the GG doublet (direct H-abstraction from the sugar or electron transfer), or by a long-range electron transfer[14] is a fascinating question which remains to be elucidated.

We thank Jacques Laval for the gift of Fpg, and financial support from Agence Nationale de la Recherche sur le SIDA (ANRS) is gratefully acknowledged.

Notes and references

1 K. J. Scanlon, Y. Ohta, H. Ishida, H. Kijima, T. Ohkawa, A. Kaminski, J. Tsai, G. Horng and M. Kashani-Sabet, *FASEB J*., 1995, **9**, 1288; W. Roush, *Science*, 1997, **276**, 1192.
2 C. Hélène, *Anticancer Drug Des*., 1991, **6**, 569; N. T. Thuong and C. Hélène, *Angew. Chem., Int. Ed. Engl*., 1993, **32**, 666; M. D. Frank-Kamenetskii and S. M. Mirkin, *Annu. Rev. Biochem*., 1995, **64**, 65.
3 A. S. Boutorine, D. Brault, M. Takasugi, O. Delgado and C. Hélène, *J. Am. Chem. Soc*., 1996, **118**, 9469; P. Bigey, G. Pratviel and B. Meunier, *J. Chem. Soc., Chem. Commun*., 1985, 181. For reviews, see: J. Goodchild, *Bioconjugate Chem*., 1990, **1**, 166; U. Englisch and D. Gauss, *Angew. Chem., Int. Ed. Engl*., 1991, **30**, 613; R. S. Varma, *Synlett*. 1993, 621.
4 P. Gaudu, D. Touati, V. Nivière and M. Fontecave, *J. Biol. Chem*., 1994, **269**, 8182.
5 H. Kasai, Z. Yamaizumi, M. Berger and J. Cadet, *J. Am. Chem. Soc*., 1992, **114**, 9692; K. Ito, S. Inoue, K. Yamamoto and S. Kawanishi, *J. Biol. Chem*., 1993, **268**, 13 221; K. Kino and I. Saito, *J. Am. Chem. Soc*., 1998, **120**, 7373.
6 P. Burgstaller and M. Famulok, *J. Am. Chem. Soc*., 1997, **119**, 1137.
7 M. Bouziane, C. Ketterlé, P. Helissey, P. Herfeld, M. Le Bret, S. Giorgi-Renault and C. Auclair, *Biochemistry*, 1995, **34**, 14051.
8 T. Carell and J. Butenandt, *Angew. Chem., Int. Ed. Engl*., 1997, **36**, 1461.
9 C. Frier, J.-L. Décout and M. Fontecave, *J. Org. Chem*., 1997, **62**, 3520.
10 C. Giovannangéli, M. Rougée, T. Garestier, N. T. Thuong and C. Hélène, *Proc. Natl. Acad. Sci. U.S.A*., 1992, **89**, 8631; P. O. Ilyinski and R. C. Desrosiers, *EMBO J*., 1998, **17**, 3766.
11 J. Tchou, H. Kasai, S. Shibutani, M.-H. Chung, J. Laval, A. P. Grollman and S. Nishimura, *Proc. Natl. Acad. Sci. U.S.A*., 1991, **88**, 4680.
12 J. Cadet, M. Berger, G. W. Buchko, P. C. Joshi, S. Raoul and J.-L. Ravanat, *J. Am. Chem. Soc*., 1994, **116**, 7403; G. W. Buchko, J. Cadet, B. Morin and M. Weinfeld, *Nucleic Acids Res*., 1995, **19**, 3954.
13 H. Sugiyama and I. Saito, *J. Am. Chem. Soc*., 1996, **118**, 7063.
14 U. Diederichsen, *Angew. Chem., Int. Ed. Engl*., 1997, **36**, 2317; R. E. Holmlin, P. J. Dandliker and J. Barton, *Angew. Chem., Int. Ed. Engl*., 1997, **36**, 2714; S. M. Gasper and G. B. Schuster, *J. Am. Chem. Soc*., 1997, **119**, 12 762.

Communication 8/06119J

A novel metalorganic route for the direct and rapid synthesis of monodispersed quantum dots of indium phosphide

Mark Green and Paul O'Brien*

Department of Chemistry, Imperial College of Science Technology and Medicine, South Kensington, London, UK SW7 2AY. E-mail: p.obrien@ic.ac.uk: Fax No., 0171-594-5825

Received (in Cambridge, U.K.) 14th August 1998, Accepted 2nd October 1998

Nanometric particles of InP are readily prepared by the decomposition of the complex $In(PBu^t_2)_3$ at 167 °C in 4-ethylpyridine; the resulting materials show marked quantum confinement effects, and was investigated using optical absorption and photoluminescence spectroscopies, and transmission electron microscopy.

There is considerable current interest in the synthesis of compound semiconductors as isolated particles with dimensions of the order of nanometers.[1] Such materials are small enough to show quantum confinement effect and the electronic properties of the material depend on the size of the particles. The majority of work to date has concerned on II–VI materials[2] which are for many reasons easier to prepare than III–V or II–V semiconductors.[3] Initial attempts to prepare III–V materials focused on the reaction of separate sources in a high boiling point solvents[4] or an electrospray method.[5] However, the properties of the materials were somewhat disappointing. Recently better quality materials have been prepared by thermolysis reactions in TOPO (tri-*n*-octylphosphine oxide), an adaptation of the highly efficient route first described by Murray *et al.* for the preparation of CdSe from dimethylcadmium and tri-*n*-octylphosphine selenide.[2] These methods for III–V TOPO capped quantum dots were initially developed by Micic *et al.*[6,7] and have been further exploited by Alivisatos and co-workers[8,9] and materials with near band edge luminescence have been prepared. However, the methods used fairly ill-defined precursor systems such as an aged solution of $InCl_3$–TOPO in reaction with neat $E(SiMe_3)_3$ (E = As, P). Growth and annealing to form the final crystalline material can take up to a week (at 250 °C) and the resulting product is polydispersed and contaminated with In_2O_3 waste material

We have recently succeeded in using the phosphide compound $[MeCdPBu^t_2]_3$[10] for the preparation of high quality samples of nanocrystalline Cd_3P_2,[11] and have now developed the use of related compounds for the synthesis of III–V materials. We report here, the use of a single molecule precursor in the 'one pot' preparation of nanometric InP quantum dots.

The problems encountered in the synthesis of III–V dots can in part be attributed to covalent nature[3] of the semiconductor and the related effect of strong precursor–solvent interactions. In these systems, nucleation and growth tend to be high temperature processes and temporal separation of the two is difficult, the resulting products are hence often polydispersed and amorphous. The use of a reactive single-source precursor overcomes this problem.

The single source precursor $In(PBu^t_2)_3$ was prepared as described by Jones and coworkers, by reacting $InCl_3$ with 3 equiv. of $LiPBu^t_2$ in hexane.[12] Decomposition to InP was effected by reflux in 4-ethylpyridine (20 ml) for 0.5 h (167 °C, 0.4 g, 0.7 mmol).

$$In(PBu^t_2)_3 \xrightarrow{\text{heat}} \text{Q-InP}$$

Addition of a non-solvent (light petroleum) resulted in flocculation of the InP quantum dots. The powder was then redispersed in either pyridine or 4-ethylpyridine and centrifuged to remove waste material, an optically clear solution of nanoparticles resulted. At this point, addition of excess non-solvent produces a nanodispersed powder of the semiconductor. Electronic spectroscopy of this material showed a band edge of 1.92 eV, as determined by the direct band gap method[13] with an excitonic shoulder at *ca.* 2.72 eV (455 nm), a significant blue shift from the bulk band gap of 1.27 eV.[14] Luminescence spectroscopy shows strong broad near band edge luminescence with λ_{max}. at 2.32 eV (534 nm) (Fig. 1) slightly red shifted from the absorption. Size fractionation has little effect on band edge, indicating the system is highly monodispersed. The sample consists of a large number of relatively monodispersed dots, with an average diameter of 7.24 ± 1.24 nm which is easily observed in TEM experiments (Fig. 2).

This work clearly shows that the use of defined precursors has potential in the preparation of high quality quantum dots. Indeed, the presently reported procedure is both simpler and

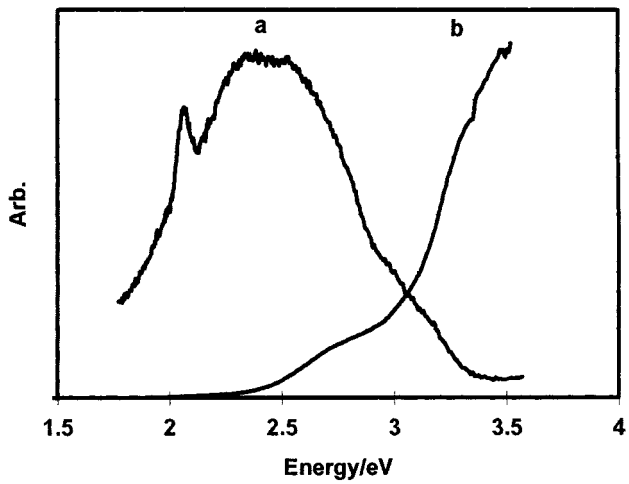

Fig. 1 Luminescence (a) and UV (b) spectra of Q-InP synthesised at 167 °C. Feature at *ca.* 2 eV is a second order excitation (λ_{exc} = 300 nm).

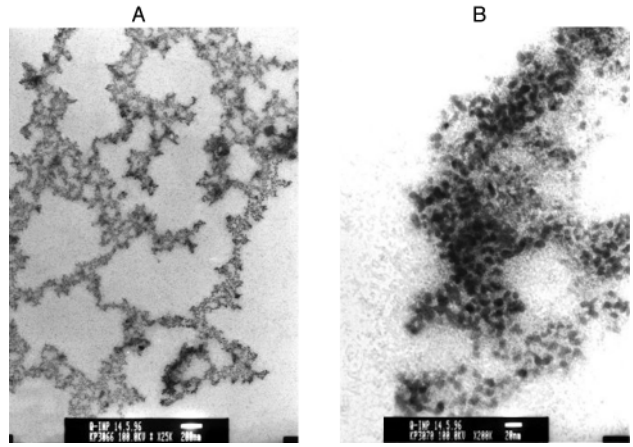

Fig. 2 TEM of Q-InP dispersed on a copper grid: (A) bar = 200 nm, (B) bar = 20 nm.

more rapid than those known to date. Work on other III–V materials is continuing in our laboratory and preliminary results have been obtained which show that organically passivated GaP and InAs can be prepared by related methods.

We thank Keith Pell (Basic Medical Science, QMW, University of London) for TEM and SEM work. Paul O'Brien is the Royal Society Amersham International Research Fellow and the Sumitomo/STS Professor of Materials Chemistry. We thank the EPSRC for grants supporting work on single molecule precursors for quantum dots. M.G. thanks the EPSRC for a studentship and BT for CASE support.

Notes and references

1 M. L. Steigerwald and L. E. Brus, *Acc. Chem. Res.*, 1990, **23**, 183.
2 C. B. Murray, D. J. Norris and M. G. Bawendi, *J. Am.Chem. Soc*., 1993, **115**, 8706
3 J. R. Heathand and J. J. Shiang, *Chem. Soc. Rev*., 1998, **27**, 65.
4 M. A. Olshavsky, A. N. Goldstein and A. P. Alivisatos, *J. Am. Chem. Soc*., 1990, **112**, 9438.
5 O. V. Salata, P. J. Dobson, P. J. Hull and J. L. Hutchinson, *Appl. Phys. Lett.*, 1994, **65**,189.
6 O. I. Micic and Nozik, *J. Lumin*., 1996, **70**, 95.
7 O. I. Micic, C. J. Curtis, K. M. Jones, J. R. Sprague and A. J. Nozik, *J. Phys. Chem*., 1994, *98*, 4966.
8 A. A. Guzelian, U. Banin, A. V. Kadavanich, X. Peng and A. P. Alivisatos, *Appl. Phys. Lett*., 1996, **69,** 1432
9 A. A. Guzelian, J. E. B. Katari, U. Banin, A. V. Kadavanich, X. Peng, A. P. Alivisatos, K. Hamed, E. Juban, R. H. Wolters, C. C. Arnold and J. R. Heath, *J. Phys.Chem*., 1996, **100**, 7212.
10 B. L. Benac, A. H. Cowley, R. A. Jones, C. M. Nunn and T. C. Wright, *J. Am. Chem. Soc.*, 1989, **111**, 4986.
11 M. Green and P. O'Brien, *Adv. Mater*., 1998, **10**, 527.
12 A. M. Arif, B. L. Benac, A. H. Cowley, R. A. Jones, K. B. Kidd and C. M. Nunn, *New. J. Chem*., 1988, 12, 553.
13 J. I. Pankove, *Optical Processes In Semiconductors*, Dover Publication Inc, New York, **1970.**
14 D. R. Lide, *Handbook of Chemistry and Physics*, CRC press, 1997.

Communication 8/06419I

ChemComm

Morphological control of ordered mesoporous silica: formation of fine and rod-like mesoporous powders from completely dissolved aqueous solutions of sodium metasilicate and cationic surfactants

Shoichiro Shio,*[a] Asa Kimura,[a] Michihiro Yamaguchi,[a] Koichi Yoshida[a] and Kazuyuki Kuroda[b]

[a] *Shiseido Basic Research Laboratories, 1050 Nippa-cho, Kohoku-ku, Yokohama-shi, 223-8553, Japan. E-mail: shio_shoichiro@po.shiseido.co.jp*

[b] *Department of Applied Chemistry and Kagami Memorial Laboratory for Materials Science and Technology, Waseda University, Ohkubo-3, Shinjuku-ku, Tokyo 169-8555, Japan*

Received (in Columbia, MO, USA) 1st May 1998, revised manuscript received 18th September 1998, Accepted 23rd September 1998

Fine and rod-like silica-based mesoporous powders with very short diameter and length have been obtained through (1) the complete dissolution of both sodium metasilicate and cationic surfactants and (2) subsequent rapid pH-adjustment for the formation of silica-surfactant mesophase products.

There has been much interest on ordered mesoporous silica molecular sieves because of their large pore sizes with narrow pore size distributions, thermal stability, *etc.*[1–4] It is now apparent that the morphological control as well as handling and texture of mesoporous silica is extremely important in industrial applications. Silica-based mesoporous molecular sieves can be applied to the adsorption and release of moisture and/or lipid components and can be utilized as an adsorbent of perfume, if they are available as minutely sized powders, which is important in the cosmetic industry.

There have been several reports[5–15] which describe methods to control the shape of powders. Rod-like powders were prepared by controlling the surfactant-water content, the concentration of aluminium species, and the condensation rate of silica in the reaction system[7–9] or by bacterial templating.[10] Schacht *et al.* controlled the shape of powders by changing the condensation rate of silica in the phase boundary of O/W emulsion particles and furthermore they obtained individual hexagonal mesoporous silica fibers.[11,12] Precise morphological control of ordered mesoporous powders, in particular, controlling the length of mesopores has not yet been achieved by the procedures described above. The present method is a simple combination of (1) the use of a completely clear solution of both sodium metasilicate and surfactants at low concentrations and (2) rapid pH adjustment (from 13 to 8.5) for the formation of silicate–surfactant mesophase products. Lin *et al.* reported the formation of rod-like mesoporous powders by using a clear surfactant solution and by adjusting the pH value of the final mixture to *ca.* 10 followed by heat treatment at 100 °C for 48 h.[7–9] However, the uniqueness of the present method is the utilization of a clear solution containing both silica species and surfactants and subsequent pH adjustment to 8.5, resulting in instant gel formation, without further heat treatment.

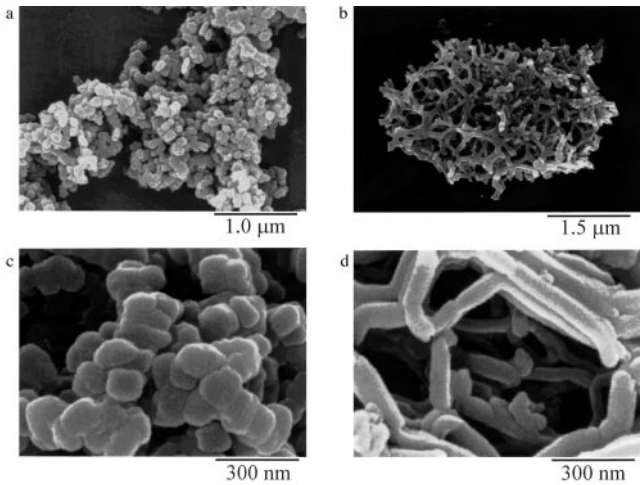

Fig. 1 Field emission scanning electron microscopic (FE-SEM) images of calcined mesoporous powders (Hitachi S-4500, acceleration voltage 15 kV). (a) Fine mesoporous powder (C_{18}-product) (magnification; ×20 000), (b) fine mesoporous powder (C_{18}-product) (magnification; ×100 000), (c) rod-like mesoporous powder (C_{22}-product) (magnification; ×30 000), (d) rod-like mesoporous powder (magnification; ×100 000).

Fine ordered mesoporous powders (C_{18}-product), which have a pore length of *ca.* 100 nm and a particle diameter of *ca.* 100 nm, were synthesized by using stearyltrimethylammonium chloride. Rod-shape ordered mesoporous powders (C_{22}-product), which have a pore length of *ca.* 300 nm and a diameter of *ca.* 50 nm, were also synthesized using behenyltrimethylammonium chloride.

Stearyltrimethylammonium chloride [$C_{18}H_{37}NMe_3Cl$] (STC) (Wako Chemical) and behenyltrimethylammonium chloride [$C_{22}H_{45}NMe_3Cl$] (BTC) (Toho Kagaku) were used in this study. Sodium metasilicate (0.5 mol, Nakarai Tesuku) and STC or BTC (0.1 mol) were dissolved in 1.0 dm^3 deionized water at 70 °C. White precipitates appeared when the pH value of the clear aqueous solution was adjusted to 8.5 by 2 M HCl within 3–5 min at 70 °C. The precipitates after the pH-adjustment were filtered at once, washed five times with water and once with acetone, and dried at room temperature for 12 h. To remove organic materials, the complexes were calcined at 700 °C in air for 5 h.

Powder XRD (JDX 3500 diffractometer) peaks of the C_{18} and the C_{22}-product show four peaks corresponding to (100), (110), (200) and (210) of a hexagonal array, being much broader than those reported for MCM-41 and FSM-16. The *d*-spacings (d_{100}) in the powder XRD patterns of the C_{18}-product before and after calcination were 4.1 and 3.8 nm, respectively. The d_{100} values of the C_{22}-product before and after calcination were 4.8 and 4.3 nm, respectively.

Typical morphologies of the calcined products are shown in Fig. 1. The FE-SEM image at high magnification of the calcined C_{18}-product [Fig. 1(b)] shows fine particles with rounded corners and *ca.* 100 nm diameter.

The morphology of the C_{22}-product is rod-like (*ca.* 50 nm in diameter and 300–500 nm in length) [Fig. 1(d)]. The powders have much shorter diameters and lengths than those of rod-like mesoporous powders reported previously,[7,12] and the rod-like powders formed a 3D-network structure. These results clearly show that the shape of powders can be controlled by a change in alkyl chain lengths of the surfactants.

TEM images (Fig. 2) of the calcined C_{18} and C_{22}-product also clarify the uniqueness of the powders. All the images of the C_{18}-product show ordered mesophases of *ca.* 100 nm in length [Fig. 2(a) and 2(b)]. Because such very short channels reduce the flow time of guest molecules in the mesoporous channels, the C_{18}-product should be an excellent reaction medium for organic substances. The TEM image of the C_{22}-product shows a rod-like shape which has a limited number of channels [Fig. 2(c)].

The N_2-adsorption isotherms (Micromeritics ASAP 2400) of the C_{18} and C_{22}-product showed typical behavior of ordered mesoporous silica. The C_{18} and C_{22}-product have BET specific surface areas of 1050 and 900 $m^2\ g^{-1}$, and pore diameters of 3.0 and 3.5 nm (BJH method), respectively. In addition to the mesopores, the calcined C_{22}-product had a broader range of pore size distribution of 30–100 nm, arising from the 3D network structure of the rods. This finding affords us an additional larger range of pores indicating a short-range hierarchical mesoporous structure. The total pore volumes including mesopores and macropores of the calcined C_{18} and C_{22}-product were 1.3 and 2.8 ml g^{-1}, respectively. Although the specific surface area of the C_{22}-product was a little lower than that of the C_{18}-product, the total pore volume of the C_{22}-product was approximately twice that of the C_{18}-product, which is due to the network formation of rod-like mesoporous powders.

The a_0 values of hexagonal structure [$a_0 = 2d_{100}/\sqrt{3}$] of the calcined C_{18}- and C_{22}-product were 4.4 and 5.0 nm, respectively. The wall thicknesses of these mesoporous materials are estimated from the a_0 values and the pore diameters. Although the calcined C_{22}-product has a different shape from the calcined C_{18}-product, the wall thicknesses for each showed very similar values (*ca.* 1.5 nm). This result suggests that the C_{18} and C_{22}-product were obtained *via* the same formation mechanism.

Because both sodium metasilicate and the surfactants are dissolved completely in water at 70 °C, the surfactants form micelles and silicate ions adhere on them. The shape of surfactant micelles is controlled by several complex factors including (1) the concentration of surfactants, (2) the alkyl chain lengths of surfactants, (3) the concentration of formed salts by adding HCl, and (4) the concentration of silicate species for which the ionic charge varies with pH. Since an increase of the aggregation number of micelles in salt–surfactant solution has been reported,[16] the possible increase of aggregation number (which induces the formation of rod-like micelles) is speculated to be due to silicate ions which can play the role of a salts and the shape of micelles will change from spherical to rod-like. Silicate ions show two condensation steps which depend on the pH of the solution. The first step is the condensation of silicate ions on micelles and the second is the condensation between polymerized silicate species adsorbed on each micelle.[17] The second step gives self-assembled materials with hexagonal structure. Rapid pH adjustment (< 3–5 min) prevents further aggregation of the mesophase, since condensation of silicate ions occurs instantly and uniformly in the solution.

The shape of mesoporous powders is thought to be controlled by the competition between the rate of change in the shape of the surfactant assemblage (from rod-like to spherical by pH adjustment) and the condensation rate of silicate ions during the pH adjustment. If the condensation rate of silicate ions is faster than that of the change in the shape of the surfactant assemblage, the shape of the surfactant does not change markedly, therefore, the shape of the product should conform to the long rod-like shape of the micelles.

Because BTC, with longer alkyl chains, can lead to a longer assembled state relative to STC, the formation of a rod shape of the C_{22}-product is speculated to be due to the faster condensation rate of silicate ions than that of the structural change of the micelles. The same reaction pathways are expected for the system with STC, and the appearance of the C_{18}-product strongly suggests shorter assembled states of STC in aqueous solution.

The authors express their gratitude to Dr N. Ueno (Shiseido Laboratories) for fruitful discussion and his critical reading of this manuscript.

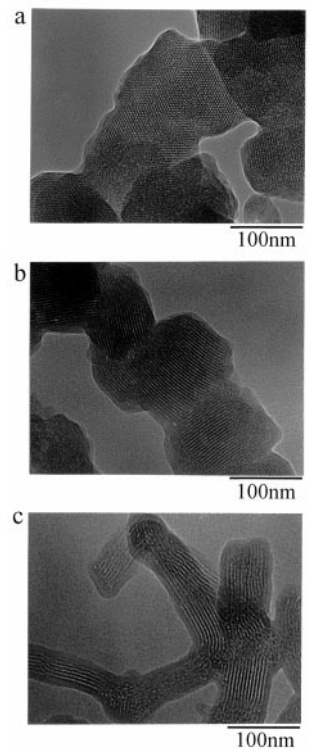

Fig. 2 Transmission electron microscopic (TEM) images of calcined mesoporous powders (Hitachi S-800, 200 kV). (a) Fine mesoporous powder (C_{18}-product) (magnification; ×200 000), (b) fine mesoporous powder (C_{18}-product) (magnification; ×200 000), (c) rod-like mesoporous powder (C_{22}-product) (magnification; ×200 000).

Notes and references

1 C. T. Kresge, M. E. Leonowicz, W. J. Roth, J. C. Vartuli and J. S. Beck, *Nature*, 1992, **359**, 710.
2 J. S. Beck. J. C. Vartuli, W. J. Roth, M. E. Leonowicz, C. T. Kresge, K. D. Schmitt, C. T.-W. Chu, D. H. Olson, E. W. Schlenker, S. B. McCullen, J. B. Higgins and J. L. Schlenker, *J. Am. Chem. Soc.*, 1992, **114**, 10 834.
3 T. Yanagisawa, T. Shimizu, K. Kuroda and C. Kato, *Bull. Chem. Soc. Jpn.*, 1990, **63**, 988.
4 S. Inagaki, Y. Fukusima and K. Kuroda, *J. Chem. Soc., Chem. Commun.*, 1993, 680.
5 H. Yang, N. Coombs and G. A. Ozin, *Nature*, 1997, **386**, 692.
6 H. Yang, N. Coombs and G. A. Ozin, *Adv. Mater.*, 1997, **9**, 811.
7 H.-P. Lin and C.-Y. Mou, *Science*, 1996, **273**, 765.
8 H.-P. Lin, S. Cheng and C.-Y. Mou, *Microporous Mater.*, 1997, **10**, 111.
9 H.-P. Lin, S. Cheng and C.-Y. Mou, *Chem. Mater.*, 1998, **10**, 581.
10 S. A. Davis, S. L. Burkkett, N. H. Mendeison and S. Mann, *Nature*, 1997, **385**, 420.
11 S. Schacht, Q. Hou, I. G. Voigt-Martin, G. D. Stucky and F. Schüth, *Science*, 1996, **273**, 768.
12 Q. Huo, D. Zhao, J. Feng, K. Weston, S. K. Buratto, G. D. Stucky, S. Schacht and F. Schüth, *Adv. Mater.*, 1997, **9**, 974.
13 D. D. Archibald and S. Mann, *Nature*, 1993, **364**, 430.
14 A. Imhot and D. J. Pine, *Nature*, 1997, **389**, 948.
15 M. T. Anderson, J. E. Martin, J. G. Odinek and P. P. Newcomer, *Chem. Mater.*, 1998, **10**, 311.
16 K. Shinoda, N. Yamaguchi and A. Carlsson, *J. Phys. Chem.*, 1989, **93**, 7216.
17 A. Firouzi, D. Kumar, L. M. Bull, T. Besier, P. Sieger, Q. Huo, S. A. Walker, C. Glinka, J. A. Zasadzinski, J. Nicol, D. Margolese, G. D. Stucky and B. F. Chmelka, *Science*, 1995, **267**, 1138.

Communication 8/07424K

An organotemplated vanadium(IV) borate polymer from boric acid 'flux' synthesis, $[H_2en]_4[Hen]_2[V_6B_{22}O_{53}H_8]\cdot 5H_2O$

Ian D. Williams,* Mingmei Wu, Herman H-Y. Sung, X. X. Zhang and Jihong Yu

Departments of Chemistry and Physics, Hong Kong University of Science and Technology, Clear Water Bay, Kowloon, Hong Kong, China. E-mail: chwill@ust.hk

Received (in Cambridge, UK) 28th July 1998, Accepted 25th August 1998

A new 1-D inorganic chain polymer $[H_2en]_4[Hen]_2[V_6B_{22}O_{53}H_8]\cdot 5H_2O$, consisting of $[V_6B_{20}O_{50}H_6]$ cluster subunits linked together through diborate bridges, has been synthesised with high yield and purity by a molten boric acid 'flux' method in which V_2O_5, en and H_3BO_3 (1 : 6 : 25) were heated together at 180 °C for 3 days; the clusters have a central band of six square-pyramidal V^{IV}=O vanadyl groups, which are capped top and bottom by two raft-like polyborate ligands of formula $[B_{10}O_{16}H_3]$.

There has been much recent interest in mixed organic–inorganic materials, especially for the formation of new microporous materials such as metal phosphates.[1,2] For these phosphoric acid is used commonly as a precursor with a variety of basic metal sources and organic templates. Since the discovery of various microporous aluminoborates by Xu and coworkers[3,4] we have been interested in the use of boric acid as a possible reagent in place of phosphoric acid to assist formation of microporous transition-metal borates. Whilst use of H_3PO_4 and H_3BO_3 in tandem can result in the formation of hybrid borate–phosphate phases,[5,6] recently Haushalter *et al.* have shown that hydrothermal reaction of vanadium oxides with boric acid can give rise to novel mixed-valence vanadium borate clusters.[7,8a] Yamase *et al*. have also reported a similar vanadoborate.[8b]

Herein we report that use of molten boric acid as flux can lead to other boron-rich cluster phases and even allow the direct connectivity of such clusters to novel inorganic polymers by additional borate bridges. Furthermore the reaction products are not only different from analogous hydrothermal syntheses, but they are typically of higher purity and yield. This becomes important for strategies in which the formed clusters are to be used as synthetic intermediates.

We find that flux reaction of V_2O_5 with 6 mol equiv. of ethylenediamine (en) and 25 H_3BO_3 at 180 °C for 3 days results in the formation of an off-white crude solid. Removal of the residual boric acid through washing with cold water allows isolation of pale-green block-shaped crystals of **1** as a phase-pure material in *ca.* 75% isolated yield based on V. X-Ray powder diffraction shows three strong peaks of approximately 1 : 2 : 1 intensity ratio with *d*-spacings of 11.2 (200), 10.6 (112) and 10.1 (112)/(004) Å respectively. We have found such peaks in the region of 10 Å *d*-spacing to be characteristic of vanadyl polyborate cluster materials and a useful diagnostic tool.[9]

A single crystal X-ray structure analysis† reveals the structure of **1** to be $[H_2en]_4[Hen]_2[V_6B_{22}O_{53}H_8]\cdot 5H_2O$ consisting of an anionic vanadium polyborate chain polymer, together with $(H_2en)^{2+}$ and $(Hen)^{+}$ counterions and five waters of solvation. The polymer has $[V_6B_{20}O_{50}H_6]$ cluster subunits linked together by linear diborate $[B_2O_3H_2]$ bridges. A portion of the polymer chain is shown in Fig. 1.

The clusters have a central band of six square-pyramidal V^{IV}=O vanadyl groups, which are capped top and bottom by two novel raft-like polyborate ligands of formula $[B_{10}O_{16}H_3]$. The charge and oxidation state of the metals and degree of protonation are often difficult to resolve in such structures, however bond valence sum calculations[10] clearly indicate a charge of V^{4+} for each vanadium centre. The six V=O distances of the asymmetric unit range between 1.607 and 1.618(4) Å and the 24 basal V–O distances from 1.945 to 1.973(4) Å. The pale-green colour is also supportive of the purely V^{IV} formulation and is in contrast with the previous findings of Haushalter and Zubieta of orange, red and dark-green mixed V^{IV}–V^{V} clusters.[7,8] All cluster hydrogens were located in difference Fourier maps and were found to be involved in short [B–OH···O] hydrogen bonds with O···O separations≤2.8 Å. In addition, the formulation of the organic counterions was facilitated by the clear observation of four [N–H···N] hydrogen-bond contacts per asymmetric unit of less than 3.0 Å. This means that both fully protonated and partially protonated ethylenediamines must be present, although there is statistical disorder of the protons on each side of the H-bond double wells.

The toroidal arrangement of square-pyramidal vanadyl groups has each neighboring V atom in an edge-sharing arrangement. All V–V internuclear separations are essentially equivalent and between 3.029 and 3.059(2) Å, indicating there is no significant pairing of V centres to form individual V–V bonds, but rather the contacts are consistent with some weak delocalised metal–metal bonding character, through use of d(*xy*) orbitals. In the crystal structure of **1** all polymer chains run parallel to the *b*-axis; studies are being undertaken to investigate the magnetic behaviour of the polymer.

In addition to the discovery of novel magnetic properties, our original goal was to make new classes of microporous materials. The use of cluster subunits is very attractive in this regard since their large size means that even their close packing must allow for significantly large cavity formation. A number of open-framework molybdenum phosphates with cluster subunits have been reported[11,12] and recently an organically templated Fe-PO was recently synthesised by Lii in which large channels are found since Fe_4 cluster subunits are involved.[13]

Formation of the 1-D polymer **1** is also suggestive that useful materials either for magnetic or porous properties might be formed by connecting metal polyborate clusters together *via* suitable cross linking agents. For this purpose however, a synthetic preparation of the structural building block is necessary. Through modification of the flux conditions, we have now isolated a second compound **2**, which contains the cluster building block from **1.** Thus reaction of V_2O_5 : en : H_3BO_3 in the ratio 1 : 2 : 8 at 180 °C for 3 days affords **2** as pale-green bar-shaped crystals in virtually quantitative yield based on V. From these conditions it is essentially phase-pure based on optical examination and powder X-ray diffraction, for which

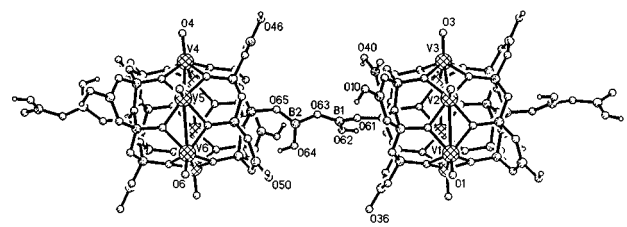

Fig. 1 Structure of **1**, showing a portion of the $[V_6B_{22}O_{53}H_8]_n$ polymer chain.

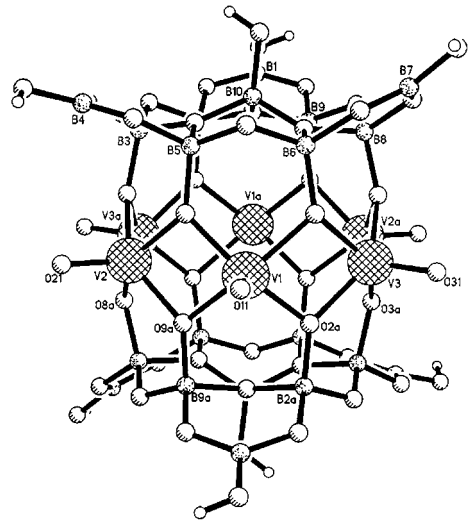

Fig. 2 Side view of the $[V_6B_{20}O_{50}H_8]$ cluster anion of **2**.

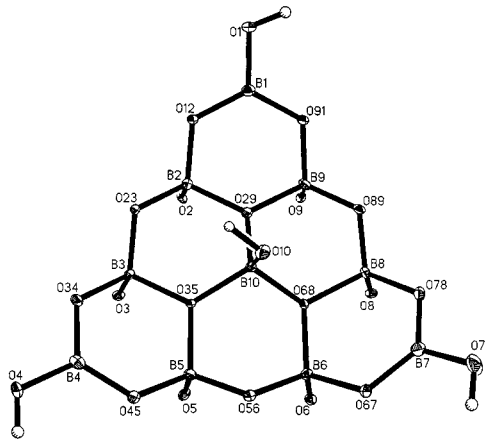

Fig. 3 Raft-like $[B_{10}O_{16}H_4]$ ligand from **2**.

there are 3 different characteristic *d*-spacings of 11.6 (010), 10.6 (001) and 9.8 Å (100)/(101) with an approximate 2 : 1 : 1 intensity ratio.

Single crystal X-ray structure determination† shows **2** to be $[H_2en]_4[V_6B_{20}O_{50}H_8]\cdot 5H_2O$. The structure of the $[V_6B_{20}O_{50}H_8]$ cluster anion of **2** is illustrated in Fig. 2 and its condensed raft-like B_{10} polyborate ligand is shown in Fig. 3. In this case the central boron is terminated by a hydroxy group, rather than being connected to a diborate bridge as in **1**. Boric acid was also used to synthesise the interesting copper polyborate cluster $[Cu_4O\{B_{20}O_{32}(OH)_8\}]^{6-}$ from solution.[14] Although this also has a B_{20} formulation, in this compound the polyborate moiety has an open ring-like structure about a central Cu_4O core.

The crystal structure of **2** is well-ordered and all H-atoms were located in difference Fourier maps. Once more the bond valence sums give V^{4+} for all centres [V=O = 1.605–1.627(2) Å, V–O = 1.932–1.980(2) Å]. The temperature dependent magnetization was measured in a constant applied field of 1 T (MPMS-5S Quantum Design SQUID magnetometer) and indicates that the compound is paramagnetic down to 1.8 K. The calculated moment is 4.03 μ_B per formula unit. This is in contrast to the layer compound $[H_2en][V_2O_5]$ which shows antiferromagnetic coupling between adjacent edge-sharing square pyramidal V^{IV} centres at low temperature.[15] Modelling of the magnetic behaviour is being undertaken, but implies only partial pairing of the six electrons from the d^1 metal centres. We postulate that two electrons are paired in the all-bonding (in-phase) combination of vanadium d(*xy*) orbitals and that the others singly occupy the partially bonding and anti-bonding combinations to give rise to four unpaired electrons and $S = 2$ ground state for the cluster, which may explain the observed magnetic moment. EPR studies will be undertaken to confirm this hypothesis.

Whereas the polymer **1** is practically insoluble in all solvents, (except 1.0 M NaOH which destroys it), the salt **2** is sparingly soluble in hot dmf–water and affords a stable pale-green solution. In this sense it is similar to the large open polyanionic Mo_{154} molybdates and related aggregates.[16] We are now exploring the use of a facile dissolution–precipitation method for synthesis of further hybrid materials from **2**. For example, addition of Ca^{2+} ions to a saturated solution of **2** results in ready precipitation of the calcium salt of the vanadyl cluster as a fine powder.

The advantage of this two-stage synthetic approach is that the complex polyborate cluster can be formed under quite different conditions than are used for its subsequent cross-linking, affording a reasonable degree of design flexibilty. In summary, use of a boric acid flux method can give high yields of phase-pure vanadium borate materials, including both inorganic polymers and discrete cluster compounds. Synthesis of other boron-rich transition-metal phases from the boric acid melt and their potential as synthetic intermediates for formation of microporous materials is under investigation.

The authors wish to thank Mr Alvin Siu for his help with the X-ray work and the Research Grants Council of Hong Kong for financial support. (Grant HKUST 681/96P)

Notes and references

† *Crystal data* for **1**: $C_{12}H_{74}B_{22}N_{12}O_{58}V_6$, monoclinic, *C*2/*c*, T = 218 K, a = 22.602(3), b = 14.181(2), c = 40.225(5) Å, β = 96.22(2)°, V = 12,816(3) Å^3, Z = 8, D_c = 1.93 Mg m^{-3}, μ(Mo-Kα) = 0.98 mm^{-1}, R = 6.20%, wR = 6.95% for 9199 unique observed data to $2\Theta_{max}$ = 53.5°. For **2**: $C_8H_{65}B_{20}N_8O_{58.5}V_6$, triclinic, *P*1, T = 218 K, a = 11.426(2), b = 11.919(2), c = 12.030(2) Å, α = 86.00(2), β = 62.39(2), γ = 77.09(2)°, V = 1413.2(4) Å^3, Z = 1, D_c = 2.03 Mg m^{-3}, μ(Mo-Kα) = 1.10 mm^{-1}, R = 3.96%, wR = 4.29% for 5095 unique observed data to $2\Theta_{max}$ = 55.0°. CCDC 182/990.

1 P. Feng, X. Bu and G. D. Stucky, *Nature*, 1997, **388**, 735.
2 S. Oliver, A. Kuperman and G. A. Ozin, *Angew. Chem., Int. Ed. Engl*., 1998, **37**, 46.
3 J. Wang, S. Feng and R. Xu, *J. Chem. Soc., Chem. Commun*., 1989, 265.
4 J. Yu, R. Xu, Q. Kan, Y. Xu and B. Xu, *J. Mater. Chem*., 1993, **3**, 77.
5 S. Sevov, *Angew. Chem., Int. Ed. Engl*., 1996, **35**, 2630.
6 C. J. Warren, R. C. Haushalter, D. J. Rose and J. Zubieta, *Chem. Mater*., 1997, **9**, 2694.
7 J. T. Rijssenbeek, D. J. Rose, R. C. Haushalter and J. Zubieta, *Angew. Chem., Int. Ed. Engl*., 1997, **36**, 1008.
8 (*a*) C. J. Warren, D. J. Rose, R. C. Haushalter and J. Zubieta, *Inorg. Chem*., 1998, **37**, 1140; (*b*) T. Yamase, M. Suzuki and K. Ohtaka, *J. Chem. Soc., Dalton Trans*., 1997, 2463.
9 M. Wu, H. H-Y. Sung, X. Zhang and I. D. Williams, *J. Solid State Chem*., submitted.
10 I. D. Brown and D. Altermatt, *Acta Crystallogr., Sect. B*, 1985, **41**, 244.
11 R. C. Haushalter, K. G. Strohmaier and F. W. Lai, *Science*, 1989, **246**, 1289.
12 R. C. Haushalter and L. A. Mundi, *Chem. Mater*., 1992, **4**, 31.
13 K-H. Lii and Y-F. Huang, *Chem. Commun*., 1997, 839.
14 G. Heller and J. Pickardt, *Z. Naturforsch., Teil B*, 1985, **40**, 462.
15 Y. Zhang, C. J. O'Connor, A. Clearfield and R. C. Haushalter, *Chem. Mater*., 1996, **8**, 595.
16 A. Müller, E. Krickemeyer, J. Meyer, H. Bögge, F. Peters, W. Plass, E. Diemann, S. Dillinger, F. Nonnenbruch, M. Randerath and C. Menke, *Angew Chem., Int. Ed. Engl*., 1995, **34**, 2122.

Communication 8/05908J

Spectroscopic characterisation of a copper(II) complex of a thioether-substituted phenoxyl radical: a new model for galactose oxidase

Malcolm A. Halcrow,*[a] Li Mei Lindy Chia,[b] Xiaoming Liu,[c] Eric J. L. McInnes,[d] Lesley J. Yellowlees,[c] Frank E. Mabbs[d] and John E. Davies[b]

[a] *School of Chemistry, University of Leeds, Woodhouse Lane, Leeds UK LS2 9JT. E-mail: M.A.Halcrow@chem.leeds.ac.uk*
[b] *Department of Chemistry, University of Cambridge, Lensfield Road, Cambridge, UK CB2 1EW*
[c] *Department of Chemistry, The University of Edinburgh, West Mains Road, Edinburgh, UK EH9 3JJ*
[d] *EPSRC CW EPR Service Centre, Department of Chemistry, University of Manchester, Oxford Road, Manchester, UK M13 9PL*

Received 10th September 1998, Accepted 5th October 1998

The EPR-silent species $[Cu(L^2)(Tp^{Ph})]^+$ exhibits a UV–VIS–NIR spectrum that is very similar to that of active galactose oxidase.

Galactose oxidase ('GOase') is a fungal enzyme that catalyses the oxidation of primary alcohols by molecular oxygen.[1] The active site of GOase contains a $[Cu(His)_2(Tyr)_2(OH_2)]$ centre, in which a basal tyrosinate ligand has been chemically modified by an *ortho*-thioether crosslink formed from a cysteine residue, and is involved in a π-stacking interaction with a neighbouring tryptophan side chain.[2] In active enzyme this modified phenoxide ligand is oxidised to a very long-lived radical,[3] whose oxidation potential is +0.40 V *vs.* NHE (compared to +0.9 V for a 'normal' tyrosine side-chain). We describe here a Cu(II) phenoxide complex containing a thioether-substituted phenoxide ligand, designed as a model for the GOase copper complex, and the spectroscopic characterisation of its Cu(II) phenoxyl oxidation product.

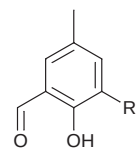

R = H, HL^1
R = SMe, HL^2

2-Hydroxy-3-methylsulfanyl-5-methylbenzaldehyde (HL^2) was prepared from 2-hydroxy-5-methylbenzaldehyde (HL^1)[4] by the method of Wang and Stack.†[5] Complexation of hydrated $Cu(BF_4)_2$ by HL (HL = HL^1, HL^2) and $K[Tp^{Ph}]$ ($[Tp^{Ph}]^-$ = tris-3-phenylpyrazolylborate)[6] in CH_2Cl_2 at room temperature affords dark green solutions, from which deep green microcrystals of $[Cu(L)(Tp^{Ph})]$ ($[L]^-$ = $[L^1]^-$, **1**, $[L]^-$ = $[L^2]^-$, **2**)† can be obtained in 40–45% yield after filtration and addition of a large excess of hexanes. Weakly diffracting single crystals of **2** were grown from toluene–hexanes.‡ The structure shows a square pyramidal Cu(II) centre with a N_3O_2 donor set and unexceptional metric parameters (Fig. 1).

The visible spectra of **1** and **2** in CH_2Cl_2 at 293 K each show a d–d absorption at λ_{max} = 685 nm (ε_{max} = 92–93 dm^3 mol^{-1} cm^{-1}). The X- and Q-band EPR spectra of **1** and **2** in 10 : 1 CH_2Cl_2–toluene solution at 110 K exhibit the $g_{\|} > g_{\perp} > g_e$ pattern expected of a $\{d_{x^2-y^2}\}^1$ or $\{d_{xy}\}^1$ Cu(II) ion (for **1**; $g_{\|}$ = 2.284, $g_{\perp}$ = 2.065, $A_{\|}\{^{63,65}Cu\}$ = 160 G: for **2**; $g_{\|}$ = 2.286, $g_{\perp}$ = 2.065, $A_{\|}\{^{63,65}Cu\}$ = 163 G), only one species being detected in solution for both compounds. These spectra are consistent with **1** and **2** possessing essentially identical tetragonal coordination spheres in CH_2Cl_2. Hence, in this solvent the $[L^2]^-$ ligand in **2** is coordinated *via* both O-donors, with no isomerisation to a form containing O,S-coordinated $[L^2]^-$ taking place. While the lack of observable $A\{^{14}N\}$ couplings for **1** and **2** prevents more detailed EPR studies, we have recently proven that related $[Cu^{II}(L)(Tp^{Ph})]$ (L = bidentate ligand) complexes retain their square-pyramidal solid state geometries upon dissolution in CH_2Cl_2.[7] It is therefore probable that the solution structures of **1** and **2** closely resemble those in the crystal.

The cyclic voltammogram (CV) of **2** in CH_2Cl_2/0.5 M $NBu^n_4PF_6$ at 293 K shows a one-electron couple at $E_{½}$ = +0.53 V *vs.* Fc–Fc$^+$, which is chemically reversible for 10 mV s^{-1} ≤ ν ≤ 1 V s^{-1} and which we assign to a $[L^2]^-/L^{2\cdot}$ oxidation. The observation of a chemically reversible oxidation for coordinated $[L^2]^-$ in **2** is very unusual for a phenoxide without encumbering *tert*-butyl substituents.[8] The CV of **2** also exhibits an irreversible secondary oxidation of variable broadness and intensity centered near E_{pa} = + 0.85 V, which is characteristic of partial adsorption of the initial oxidised species onto the Pt electrode;[9] and an irreversible Cu(II/I) reduction at E_{pc} = −1.29 V with associated daughter peaks at E_{pa} = −0.41 and −0.11 V.

Electrooxidation of **2** in CH_2Cl_2–0.5 M $NBu^n_4PF_6$ at 243 K at a potential corresponding to the **2**/$[\mathbf{2}]^+$ couple yields a brown solution exhibiting only a very weak residual EPR signal from

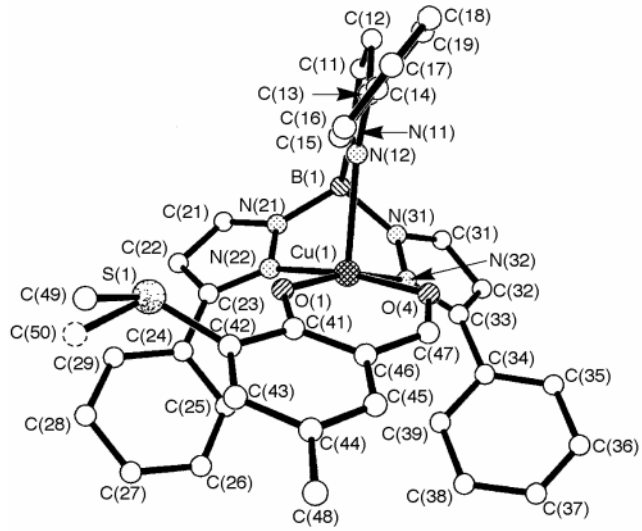

Fig. 1 View of the complex molecule in the crystal of **2**, showing the disordered thioether group. For clarity, all H atoms have been omitted. Selected distances (Å) and angles (°): Cu(1)–N(12) 2.337(6), Cu(1)–N(22) 2.009(6), Cu(1)–N(32) 1.996(7), Cu(1)–O(1) 1.941(7), Cu(1)–O(4) 1.967(5), N(12)–Cu(1)–N(22) 89.7(2), N(12)–Cu(1)–N(32) 90.0(2), N(12)–Cu(1)–O(1) 102.8(2), N(12)–Cu(1)–O(4) 98.7(2), N(22)–Cu(1)–N(32) 87.7(3), N(22)–Cu(1)–O(1) 91.5(3), N(22)–Cu(1)–O(4) 171.3(2), N(32)–Cu(1)–O(1) 167.1(2), N(32)–Cu(1)–O(4) 89.9(2), O(1)–Cu(1)–O(4) 88.9(3).

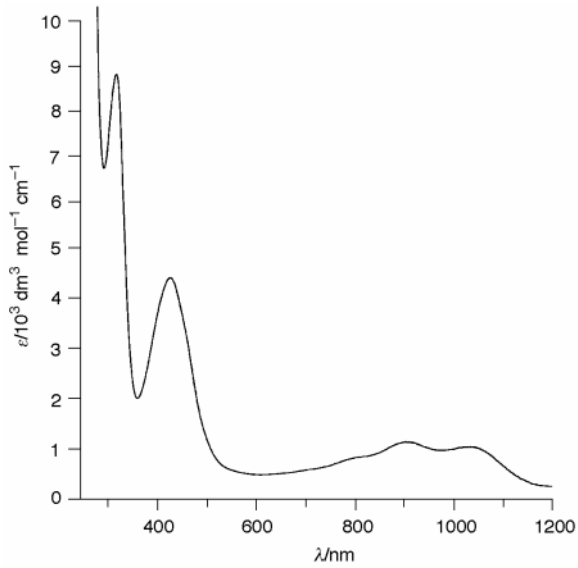

Fig. 2 UV–VIS–NIR spectrum of [**2**]$^+$ in CH_2Cl_2–0.5 M $Bu^n_4NPF_6$ at 243 K.

unreacted **2**. A similar experiment using an optically transparent electrode results in a blue-shift of the $[L^2]^-$-derived absorptions in the UV, and the ingrowth of new peaks in the visible and near-IR regions. The oxidised solution shows λ_{max} = 317 nm ($\varepsilon_{max} \approx 9\,000$ dm^3 mol^{-1} cm^{-1}), 419 (4400), 470 (sh), 725 (sh), 818 (sh), 907 (1200) and 1037 (1100) at 243 K (Fig. 2). Rereduction of this solution at 0 V results in the near-quantitative regeneration of **2**. We ascribe these observations to the generation of an EPR-silent $[Cu^{II}(L^{2\cdot})(Tp^{Ph})]^+$ species [**2**]$^+$. The **2**/[**2**]$^+$ preparative oxidation is not quite reversible, since [**2**]$^+$ decomposes with a half-life of *ca*. 10 h under these conditions; the absorption coefficients quoted above may therefore be slightly underestimated.

Other known Cu(II) phenoxyl complexes, although usually also EPR-silent, give electronic spectra significantly different from [**2**]$^+$, with peaks at λ_{max} = 400–450 nm (ε_{max} = 3000–16 000 dm^3 mol^{-1} cm^{-1}) and 600–680 nm (300–8000).[10] None of these examples contains a thioether side-chain to the phenoxyl ligand, however. Active GOase exhibits two spectroscopic features attributable to the modified tyrosyl radical: a peak at λ_{max} = 444 nm (ε_{max} = 5200 dm^3 mol^{-1} cm^{-1}) and a broad absorption between 600 and 1200 nm, centred at 800 nm (3200) with several low- and high-wavelength shoulders.[11] The similarity of this spectrum to that shown by [**2**]$^+$ (Fig. 2) is striking. The VIS–NIR feature in the spectrum of GOase has been attributed to an inter-ligand charge transfer process between the tyrosyl and tyrosinate ligands.[12] However, the observation of an equivalent broad, structured band for [**2**]$^+$, which lacks a second phenoxide ligand, suggests that $\pi \rightarrow \pi^*$, MLCT and/or LMCT transitions involving the tyrosyl radical should also contribute to this absorption.

The authors thank the Royal Society (M. A. H.), the government of Singapore (L. M. L. C.), the Committee of Vice-Chancellors and Principles (X. L.), the EPSRC, the University of Leeds, the University of Cambridge and the University of Edinburgh for financial support.

Notes and references

† Correct analytical and NMR data were obtained for HL^2. Analytical data for the complexes. **1**: Found: C, 59.7; H, 4.3; N, 11.5; Calc. for $C_{35}H_{29}BCuN_6O_2.CH_2Cl_2$: C, 59.7; H, 4.3; N, 11.6 %. **2**: Found: C, 63.0; H, 4.6; N, 13.4; Calc. for $C_{36}H_{31}BCuN_6O_2S$: C, 63.0; H, 4.6; N, 12.3 %.

‡ *Crystal data* for **2**: $C_{36}H_{31}BCuN_6O_2S$, triclinic, space group $P\bar{1}$, dark green block, 0.30 × 0.25 × 0.20 mm, a = 12.536(8), b = 13.90(2), c = 9.760(4) Å, α = 99.00(7), β = 90.75(4), γ = 102.48(9)°, U = 1638(3) Å^3, Z = 2, T = 150(2) K, μ(Mo-Kα) = 0.773 mm^{-1}; Rigaku AFC7-R diffractometer, 5405 measured reflections, 5126 independent, R_{int} = 0.0941; $R(F)$ = 0.079, $wR(F^2)$ = 0.233, S = 1.076. The thioether methyl C atom of the $[L^2]^-$ ligand was disordered over two sites C(49) and C(50) in a 60:40 occupancy ratio, which were restrained to common S(1)–C(X) and C(42)···C(X) (X = 49, 50) distances of 1.85(1) and 2.77(1) Å, respectively. All non-H atoms except C(49) and C(50) were refined anisotropically. CCDC 182/1047.

1 J. P. Klinman, *Chem. Rev.*, 1996, **96**, 2541.
2 N. Ito, S. E. V. Phillips, C. Stevens, Z. B. Ogel, M. J. McPherson, J. N. Keen, K. D. S. Yadav and P. F. Knowles, *Nature*, 1991, **350**, 87.
3 M. M. Whittaker and J. W. Whittaker, *J. Biol. Chem.*, 1990, **265**, 9610.
4 G. Casiraghi, G. Casnati, G. Pugli, G. Sartori and G. Terenghi, *J. Chem. Soc., Perkin Trans. 1*, 1980, 1862.
5 Y. Wang and T. D. P. Stack, *J. Am. Chem. Soc.*, 1996, **118**, 13 097.
6 D. M. Eichhorn and W. H. Armstrong, *Inorg. Chem.*, 1990, **29**, 3607.
7 M. A. Halcrow, E. J. L. McInnes, F. E. Mabbs, I. J. Scowen, M. McPartlin, H. R. Powell and J. E. Davies, *J. Chem. Soc., Dalton Trans.*, 1997, 4025.
8 A. R. Forrester, J. M. Hay and R. H. Thomson, *Organic Chemistry of Stable Free Radicals*, Academic Press, London, 1968, ch. 7, pp. 281–341.
9 J. L. Stickney, M. P. Soriaga, A. T. Hubbard and S. E. Anderson, *J. Electroanal. Chem. Interfacial. Chem.*, 1981, **125**, 73.
10 D. Zurita, I. Gautier-Luneau, S. Ménage, J.-L. Pierre and E. Saint-Aman, *J. Biol. Inorg. Chem.*, 1997, **2**, 46; J. A. Halfen, B. A. Jadzdzewski, S. Mahaptara, L. M. Berreau, E. C. Wilkinson, L. Que jr. and W. B. Tolman, *J. Am. Chem. Soc.*, 1997, **119**, 8217; J. Müller, T. Weyhermüller, E. Bill, P. Hildenbracht, L. Ould-Moussa, T. Glaser and K. Wieghardt, *Angew. Chem., Int. Ed. Engl.*, 1998, **37**, 616.
11 M. M. Whittaker, P. J. Kersten, N. Nakamura, J. Sanders-Loehr, E. S. Schweizer and J. W. Whittaker, *J. Biol. Chem.*, 1996, **271**, 681.
12 M. L. McGlashen, D. D. Eads, T. G. Spiro and J. W. Whittaker, *J. Phys. Chem.*, 1995, **99**, 4918.

Communication 8/07076H

ChemComm

Alkanes to nitriles and α-iminoesters. Polyoxotungstate photocatalytic radical chain initiation

Zhanmiao Zheng and Craig L. Hill*

Department of Chemistry, Emory University, Atlanta, Georgia 30322, USA. E-mail: chill@emory.edu

Received (in Bloomington, IN, USA) 30th June 1998, Accepted 22nd September 1998

Irradiation of $W_{10}O_{32}^{4-}$ or $PW_{12}O_{40}^{3-}$, alkanes and methyl cyanoformate in CH_3CN solution produces either the corresponding nitriles or α-iminoesters with high selectivity, depending on the temperature, *via* a mechanism involving two roles for the polyoxotungstate.

While a host of C–H bond activation or functionalization methods developed in the last few years have provided a wealth of mechanistic information and some unusual or unprecedented transformations, few of the reactions have been of significant synthetic value. Organometallic systems that activate C–H bonds rarely lead to functionalization and are usually not catalytic in the metal complex,[1–5] while more conventional radical and electrophilic systems usually have selectivity or compatibility difficulties.[4,5] We report here the first catalytic conversion of unactivated C–H bonds to two desirable groups in high selectivity: nitriles and α-imino-acetic acid esters (henceforth iminoesters) *via* polyoxotungstate photocatalysis.[6,7] Nitriles are widely used in synthesis,[8] and α-ketoesters (or acids), readily derived from hydrolysis of the iminoesters, have a rich photochemistry and could be used to render hydrocarbon materials, including polyethylene, sunlight degradable and biodegradable.[9] Nitriles have been generated in moderate to good yields *via* organic radicals generated from conventional precursors (not generated catalytically by alkane C–H bond cleavage), by trapping with *tert*-butylisocyanide,[10] or with aryl and alkylsulfonyl cyanides.[11] Alkanes photolyzed in the presence of ClCN[12] or heated with consumption of considerable conventional radical initiator (10–24 mol% benzoyl peroxide) in the presence of methyl cyanoformate also yield nitriles.[13] The latter reaction forms some iminoester but yields were not given. There appear to be no good routes to iminoesters from unactivated C–H bonds.

Irradiation (λ > 280 nm) of CH_3CN solutions of $W_{10}O_{32}^{4-}$ or $PW_{12}O_{40}^{3-}$ containing one of a variety of alkanes and methyl cyanoformate (MCF) produces the corresponding nitriles at T = 90 °C and iminoesters at T = 22 °C. Significantly, the selectivities for these products and turnovers of the polyoxotungstate vary inversely with the concentration of the polyoxometalate and selectivities approach quantitative values at [polyoxotungstate] < 0.05 mM. Table 1 gives the products from many reactions using 1.5 mM polyoxotungstate, a concentration not optimal for selectivity but one permitting by-product quantification needed for mechanism elucidation. At low [polyoxotungstate], the selectivities for nitriles (high T) and iminoesters (low T) exceed those of all literature reactions. Significantly, as both nitriles and iminoesters are of comparable or lower reactivity than the alkanes themselves, these reactions may be of preparative value. For example, the iminoesters derived from 2,3-dimethylbutane and *cis*-1,2-dimethylcyclohexane were isolated in 59 and 67% yields respectively (at 28 and 61% conversions of alkane).

These and other data discussed below rule out many mechanisms and are consistent with eqn. (1)–(10) for this chemistry. Previous studies (product, kinetics, spectroscopic and others) establish that the oxygen-to-tungsten charge-transfer excited states of polyoxotungstates abstract hydrogen atoms, eqn. (1) and (2).[6,7] The chemoselectivities and regioselectivities exhibited by the products in Table 1 indicate the same dominant C–H bond cleaving species is operable in the presence of MCF: (1) the tertiary/primary (3°/1°) C–H cleavage ratios (> 200 for 2,3-dimethylbutane and *cis*-1,2-dimethylcyclohexane), (2) the lack of reactivity of *tert*-butylbenzene (all primary C–H) and (3) the loss of stereochemistry during functionalization of *cis*-1,2-dimethylcyclohexane. The coupling and disproportionation (alkene only detectable) products in Table 1 are more consistent with radicals than other organic intermediates. Three lines of evidence indicate the title processes, unlike most polyoxotungstate photocatalyzed alkane functionalizations, involve radical chains. First, there is significant inhibition by radical inhibitors. This is seen for production of both reduced polyoxotungstate and organic products. For example, the ratio of rates for production of iminoester from 2,3-dimethylbutane using $W_{10}O_{32}^{4-}$, without and with 2.0 mM hydroquinone (HQ) inhibitor, $k_{\text{no HQ}}/k_{\text{with HQ}}$ > 100. This ratio without and with 2.0 mM 2,6-di-*tert*-butylphenol (BHT), $k_{\text{no BHT}}/k_{\text{with BHT}} = 5.7 \pm 0.2$. For HQ and BHT, respectively, *ca*. 10 and < 2% of the light is absorbed by the inhibitor; the rest by $W_{10}O_{32}^{4-}$. Second, the quantum yields for both nitrile and iminoester reactions exceed 1.0 when [polyoxotungstate] < 0.05 mM. Third, $W_{10}O_{32}^{4-}$ inhibits iminoester formation at high [$W_{10}O_{32}^{4-}$]. In contrast, photocatalytic C–H cleavage by $W_{10}O_{32}^{4-}$ generally exhibits conventional kinetics (reaction first order in $W_{10}O_{32}^{4-}$ and in alkane).[6,7]

Inhibition at high [$W_{10}O_{32}^{4-}$] most likely reflects redox capture of radical by polyoxotungstate.[6]

The two propagation steps, eqn. (3) and (4), both of which are precedented in studies involving conventionally generated radicals,[12] sum to the net reaction for production of iminoester. Several additional experiments establish that the mechanism for nitrile formation is eqn. (1)–(3), (6) and (7) [eqn. (8)–(10) are minor processes]: first, quantification of CO_2 (*via* $BaCO_3$) and CH_4 (*via* GC/TCD) products indicates that [nitrile] ~ [CO_2] ~ [CH_4]; second, when the reactions are run in *N*,*N*-dimethylacetamide (DMA), PhCN, or PhCl *versus* CH_3CN, very little CH_3CN [eqn. (10)] and little or no methyl pyruvate derivatives [eqn. (9)] are formed; third, negligible CH_3CH_3 from coupling of $CH_3\cdot$ is observed in CH_3CN (interestingly [CH_3CH_3]/[CH_4] ~ 1 in DMA). Control experiments demonstrated that reduced

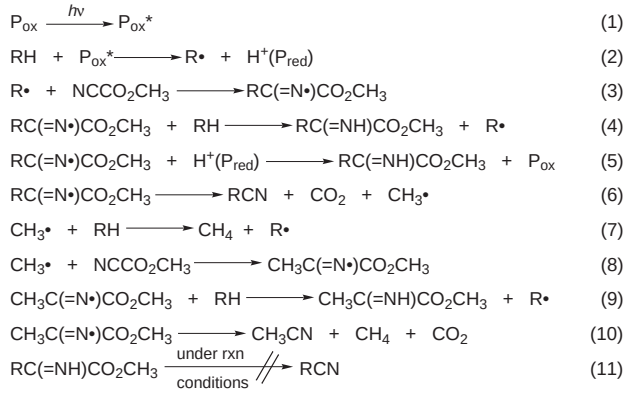

(P_{ox} and P_{red} are oxidised and reduced polyoxotungstate, respectively.)

Table 1 Functionalization of alkanes with methyl cyanoformate *via* polyoxometalate photocatalysis[a]

Polyoxotungstate[b]	Substrate	*t*/h; T/°C[c]	Organic product (%) of detected products[d] (turnovers, based on P_{ox})[e]			
	1		**1a**	**1b**		
$Na_4W_{10}O_{32}$		16; 22	< 1	75 (27)		
$Q_4W_{10}O_{32}$		16; 22	< 1	90 (9.1)		
$Q_3PW_{12}O_{40}$		16; 22	< 1	99 (0.3)		
$Na_4W_{10}O_{32}$		8; 90	78 (11)	6 (0.9)		
$Q_4W_{10}O_{32}$		8; 90	61 (5.3)	21 (1.8)		
	2		**2a**	**2b**	**2c**	
$Na_4W_{10}O_{32}$		16; 22	< 1	51 (8.4)	11 (1.9)	
$Q_4W_{10}O_{32}$		16; 22	< 1	51 (5.6)	< 1	
$Na_4W_{10}O_{32}$		8; 90	78 (20)	3 (0.8)	< 1	
$Q_4W_{10}O_{32}$		8; 90	59 (3.0)	20 (1.0)	< 1	
	3		**3a**	**3b**	**3c**	**3d**
$Na_4W_{10}O_{32}$		16; 22	2 (1.0)	75 (36)	< 1	2 (1.0)
$Q_4W_{10}O_{32}$		16; 22	< 1	80 (25)	< 1	2 (1.9)
$Q_3PW_{12}O_{40}$		16; 22	< 1	50 (0.4)	50 (0.4)	< 1
	4		**4a**	**4b**	**4c**	
$Na_4W_{10}O_{32}$		16; 22	< 1	51 (8.4)	11 (1.9)	
$Q_4W_{10}O_{32}$		16; 22	< 1	51 (5.6)	< 1	
$Na_4W_{10}O_{32}$		8; 90	76 (18)	2 (0.5)	< 1	
$Q_4W_{10}O_{32}$		8; 90	71 (9.2)	16 (2.0)	< 1	
	5		**5a**			
$Na_4W_{10}O_{32}$		8; 90	100 (1.0)			
	6		**6a**			
$Na_4W_{10}O_{32}$		8; 90	100 (0.5)			
	7					
$Na_4W_{10}O_{32}$		8; 90	No reaction			

[a] Acetonitrile solutions of polyoxotungstate (1.5 mM) and alkane (0.5 M) and MCF (0.25 M) were irradiated (550 W medium-pressure Hg lamp; Pyrex filter, $\lambda > 280$ nm). The average conversion (based on MCF) was 15% to simplify product distributions for mechanism elucidation. [b] Q = tetra-*n*-butylammonium. [c] *t* = irradiation time. [d] All new compounds were purified and their compositions and purities (> 98%) confirmed by ^{1}H NMR, high resolution MS, and elemental analysis. Moles of indicated product/moles of total organic products as determined by GC. [e] Turnovers = moles of indicated product/moles of polyoxotungstate.

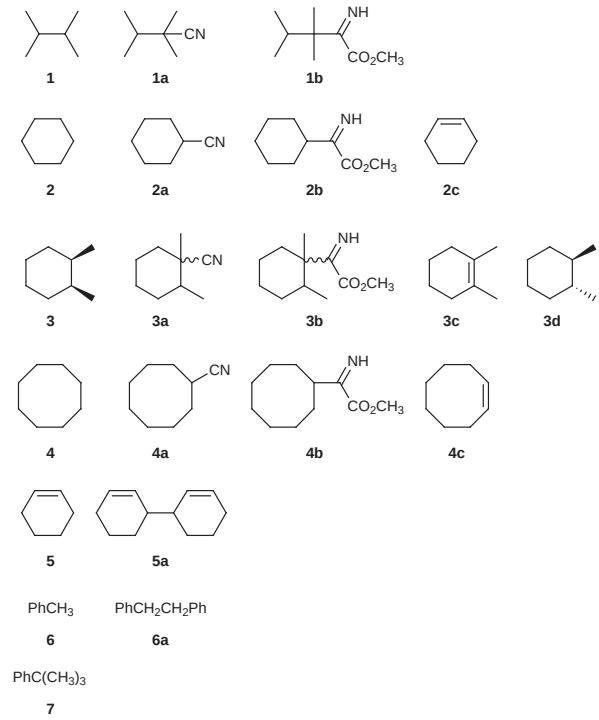

$W_{10}O_{32}^{4-}$ does not react with either MCF (no CN^- is formed) or organic products (iminoester or nitrile). Finally, the yields of iminoester and nitrile correlate strongly (inversely) with each other between 22 and 90 °C, and iminoester does not convert to nitrile under the reaction conditions [eqn. (11) is not operative]. These 2 points suggest that both products derive from a common intermediate, most likely the iminyl radical, $RC(=N\cdot)CO_2CH_3$.

We thank the National Science Foundation (Grant CHE-9412465) for support of this research.

Notes and references

1 B. A. Arndtsen, R. G. Bergman, T. A. Mobley and T. H. Peterson, *Acc. Chem. Res.*, 1995, **28**, 154.
2 R. H. Crabtree, *Chem. Alkanes Cycloalkanes*, 1992, 653.
3 R. H. Crabtree, S. H. Brown, C. A. Muedas, C. Boojamra and R. R. Ferguson, *Chemtech*, 1991, **21**, 634.
4 *Activation and Functionalization of Alkanes*, ed. C. L. Hill, Wiley, New York, 1989, pp. 1–372.
5 *Selective Hydrocarbon Activation: Principles and Progress*, ed. J. A. Davies, P. L. Watson, J. F. Liebman and A. Greenberg, VCH, New York, 1990, pp. 1–568.
6 (*a*) R. F. Renneke and C. L. Hill, *J. Am. Chem. Soc.*, 1988, **110**, 5461; (*b*) R. F. Renneke, M. Pasquali and C. L. Hill, *J. Am. Chem. Soc.*, 1990, **112**, 6585; (*c*) R. F. Renneke, M. Kadkhodayan, M. Pasquali and C. L. Hill, *J. Am. Chem. Soc.*, 1991, **113**, 8357; (*d*) B. S. Jaynes and C. L. Hill, *J. Am. Chem. Soc.*, 1993, **115**, 12212; (*e*) C. L. Hill, *Synlett* 1995, 127.
7 (*a*) T. Yamase and T. Usami, *J. Chem. Soc., Dalton Trans.*, 1988, 183; (*b*) D. Attanasio and L. Suber, *Inorg. Chem.*, 1989, **28**, 3779; (*c*) E. Papaconstantinou, *Chem. Soc. Rev.*, 1989, **18**, 1; (*d*) D. Attanasio, L. Suber and K. Thorslund, *Inorg. Chem.*, 1991, **30**, 590; (*e*) C. Tanielian, *Coord. Chem. Rev*., in press.
8 *Supplement C2: The Chemistry of Triple-Bonded Functional Groups*, ed. S. Patai, Wiley, New York, 1994, vol. 2, pp. 1–1349.
9 (*a*) R. G. Weiss, in *CRC Handbook of Organic Photochemistry and Photobiology*, ed. W. M. Horspool and P.-S. Song, CRC Press, Boca Raton, FL, 1995, ch. 39, pp. 471–483; (*b*) J. Guillet, in *Degradable Polymers*, ed. G. Scott and D. Gilead, Chapman & Hall, London, 1995, ch. 12.
10 G. Stork and P. M. Sher, *J. Am. Chem. Soc.*, 1983, **105**, 6765.
11 D. H. R. Barton, J. C. Jaszberenyi and E. A. Theodorakis, *Tetrahedron*, 1992, **48**, 2613.
12 D. D. Tanner and N. J. Bunce, *J. Am. Chem. Soc.*, 1969, **91**, 3028.
13 D. D. Tanner and P. M. Rahimi, *J. Org. Chem.*, 1979, **44**, 1674.

Communication 8/05036H

Complete rearrangement of a multi-porphyrinic rotaxane by metallation–demetallation of the central coordination site

Myriam Linke, Jean-Claude Chambron, Valérie Heitz, Jean-Pierre Sauvage* and Vincent Semetey

Laboratoire de Chimie Organo-Minérale, UMR 7513 du CNRS, Université Louis Pasteur, Institut Le Bel, 4, rue Blaise Pascal, 67000 Strasbourg, France. E-mail: sauvage@chimie.u-strasbg.fr

Received (in Basel, Switzerland) 22nd July 1998, Accepted 25th September 1998

A new multiporphyrinic [2]rotaxane has been made in which a gold(III) porphyrin is part of the ring; rotation of the string-like fragment within the ring between two diametrically opposed positions is triggered by metallation–demetallation of the central coordination site.

In relation to molecular switches,[1] machines and motors,[2,3] it is of special interest to be able to control at will, amongst other properties, the shape of multicomponent molecular systems. The triggering signal, responsible for the rearrangement of the compound can be photochemical,[4] electrochemical[5] or chemical.[6] Catenanes and rotaxanes are ideally suited for undergoing large amplitude motions under the action of an external stimulus.[7,8]

In the present work, we show that complexing or decomplexing an appropriate metal in a coordination site can bring to close proximity, or spread a long distance apart, given porphyrinic components of the system. The principle is depicted in Fig. 1.

The compound made and studied is a [2]rotaxane in which the string-like fragment bears two zinc(II) porphyrins as blocking groups. The ring through which the string is threaded incorporates a gold(III) porphyrin. It should be noted that these metalloporphyrins are key components of multichromophoric systems undergoing photoinduced electron transfer and proposed as models of given fragments of the photosynthetic reaction centre.[9]

The organic compounds used as intermediates in the synthesis of the [2]rotaxane are represented in Fig. 2. The tetraaryl porphyrin **1** was prepared in 6% yield using pyrrole and a 1 : 1 mixture of the appropriate aldehydes (CF_3CO_2H, in CH_2Cl_2 followed by chloranil treatment[10]). After metallation ($KAuCl_4$) to afford **2** (76%), demethylation (BBr_3) furnished **3** in almost quantitative yield. **5** was obtained by reacting **4**[11] with 2-bromoethanol (K_2CO_3, refluxing DMF) and it was converted to **6** (tosyl chloride, NEt_3, CH_2Cl_2) and subsequently to **7** (NaI, acetone; 30% yield from **4**). Macrocycle **11** was prepared from **3** and **7** (Cs_2CO_3 in DMF, 55 °C; 31% yield). Rotaxane **14** was synthesized following a strategy previously developed in our group for making porphyrin-stoppered rotaxanes.[9] An equimolar mixture of **8**, **11** and $Cu(MeCN)_4^+$ led quantitatively to prerotaxane **12** (not drawn) in which the open chain fragment **8** has been threaded through the ring **11** thanks to the gathering effect of copper(I). The terminal porphyrinic blocking groups of **13** were built from **9**, **10** and **12** (CF_3CO_2H in CH_2Cl_2; chloranil). **14**† was obtained after metallation [$Zn(OAc)_2$] in 13% yield from **8**.

The conformation of **14** is indeed similar to what the drawing of Fig. 3 suggests. In particular, NOE effects measured on $H_{5,6}$ and H_{py} demonstrate unambiguously that a close proximity

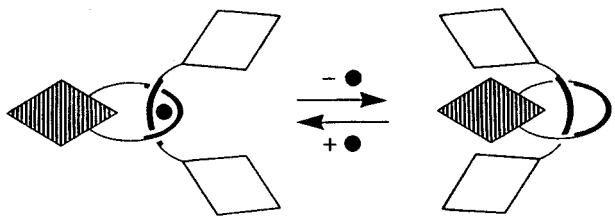

Fig. 1 Control of the mutual arrangement between the gold porphyrin (PAu^+ incorporated in the ring, black diamond) and the zinc porphyrins (PZn end-function of the dumbell, white diamond) by complexation/decomplexation of a metal centre (black circle) within/from the central coordination site. (a) The chemical structure of the two organic constitutive fragments of the rotaxane (ring and thread) is such that, in the complex, the gold porphyrin is remote from the two zinc porphyrins. (b) After removal of the central metal, weak forces may favour an attractive interaction between PAu^+ and the PZn nuclei, leading to a situation in which PAu^+ is pinched between the two PZn units. The interconversion between the situations [(a) and (b)] implies a half-turn rotation of the threaded fragment (axle) within the ring (wheel), the latter being artificially considered as fixed. This motion is reminiscent of the process taking place in the rotary motor of ATP-synthase.[3b]

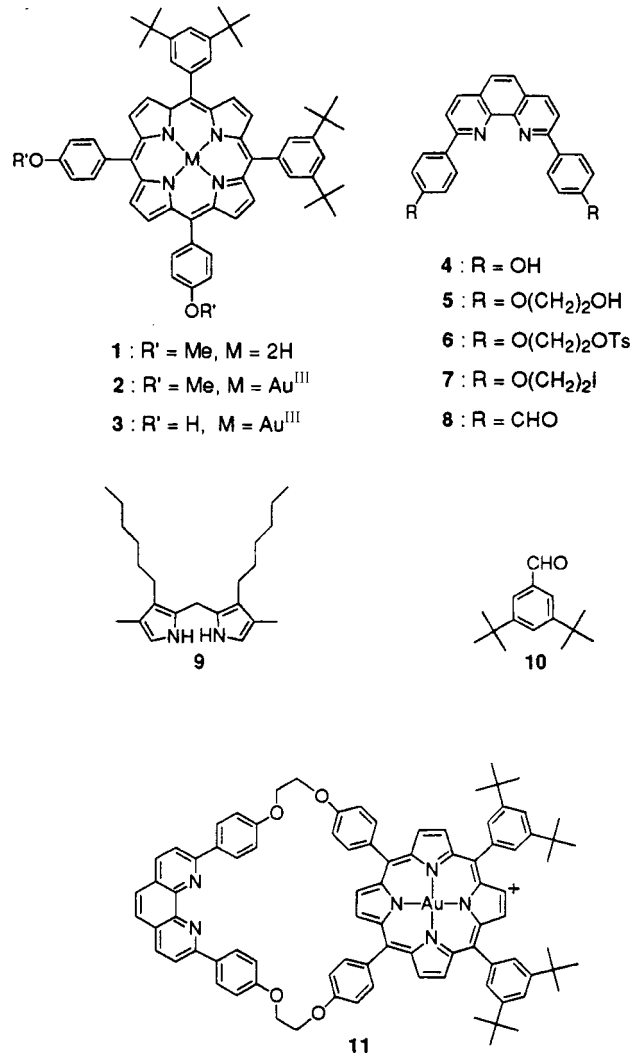

Fig. 2 Intermediates used in the synthesis of the [2]rotaxane.

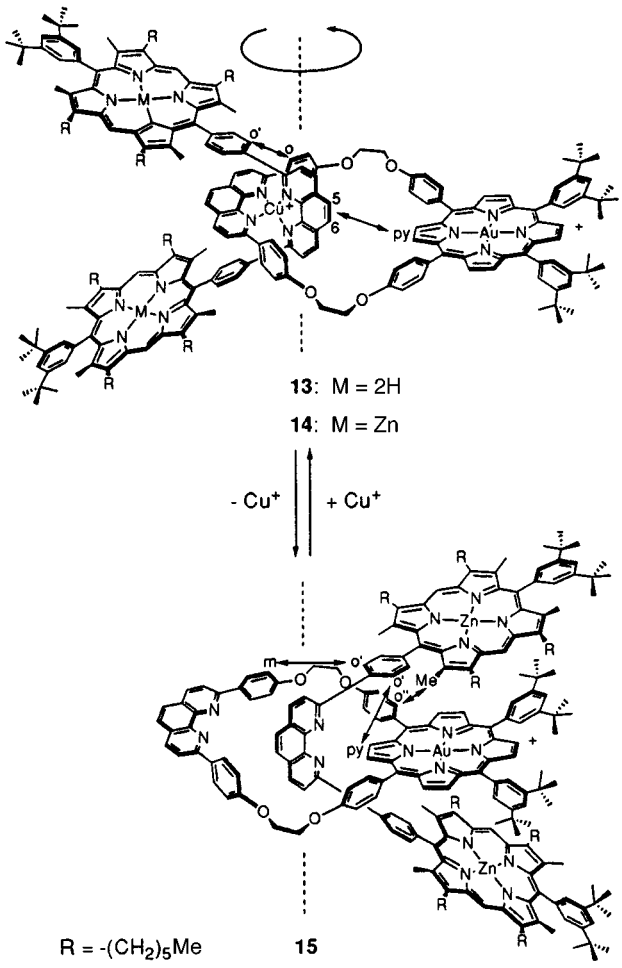

Fig. 3 Metallation–demetallation of the rotaxane induces a complete changeover of the molecule. The most important proton connectivities, as determined by 2D ^{1}H NMR, are indicated by double arrows.

exists between the rear of the 1,10-phenanthroline nucleus belonging to the dumbbell-like fragment and the endocyclic part of the ring-embedded porphyrin. As indicated in Fig. 3, demetallation of **14** affords **15**,† this compound displaying a profoundly modified geometry as compared to **14**. In particular, NOE effects show close proximity between H_m and $H_{o'}$ as well as between H_{py} and $H_{o'}$ and between $H_{o''}$ and H_{Me}, which indicates that the geometry of the molecule is roughly as depicted in Fig. 3.

Space-filling models suggest that within the demetallated rotaxane **15**, free rotation of the 'axle' within the ring can take place. The driving force for bringing PAu^+ between the PZn units, playing the role of two jaws, is certainly related to the extremely different and complementary electronic properties of PAu^+ (electron acceptor) and PZn (electron donor). Very approximate geometrical features can be estimated from the models. Of particular interest are the centre-to-centre (Au···Zn) and the edge-to-edge distances between PAu^+ and PZn. The estimated centre-to-centre separation is *ca.* 19 and *ca.* 7 Å for **14** and **15** respectively. The edge-to-edge distance, which is more relevant to electron transfer, is *ca.* 12 and *ca.* 5 Å for **14** and **15**, although it should be kept in mind that **15** is certainly very flexible, with difficult to estimate interatomic distances. Interestingly, the interconversion between **14** and **15**, although leading to dramatic geometrical changes, is quantitative and reversible. This changeover process can be triggered by other metals such as Ag^+ and Li^+.

We thank the Ministry of Education for a fellowship (to M. L.).

Notes and references

† *Selected data*: **14**: $\delta_H(CD_2Cl_2$, 400 MHz) 10.13 (s, 4H), 9.60 (d, 2H), 9.47 (d, 2H), 9.43 (s, 2H), 9.30 (s, 2H), 8.90 (d, 2H), 8.52 (d, 2H), 8.42 (d, 4H), 8.31 (d, 2H), 8.17 (d, 4H), 8.13 (d, 4H), 8.04 (t, 2H), 7.98 (s, 2H), 7.97 (d, 2H), 7.89 (d, 4H), 7.86 (t, 2H), 7.78 (d, 4H), 7.75 (s, 2H), 7.62 (d, 4H), 7.54 (d, 4H), 6.63 (d, 4H), 4.95 (m, 4H), 4.41 (m, 4H), 3.95 (t, 8H), 3.81 (t, 8H), 2.44 (s, 12H), 2.17 (t, 8H), 2.06 (t, 8H), 1.84 (s, 12H), ≈1.68 (m, 16H), 1.60 (s, 36H), 1.51 (s, 36H), ≈1.50 (m, 16H), ≈1.40 (m, 16H), 0.87 (t, 12H), 0.83 (t, 12H); *m*/*z* (FAB) 3783.6 (M^+); $\lambda(CH_2Cl_2)$/nm 415, 538, 574.

15: $\delta_H(CD_2Cl_2$, 400 MHz) 10.07 (s, 4H), 9.56 (d, 2H), 9.39 (d, 2H), 9.36 (s, 2H), 9.15 (d, 4H), 8.80 (s, 2H), 8.57 (d, 2H), 8.46 (d, 2H), 8.26 (d, 4H), 8.21 (d, 4H), 8.18 (d, 4H), 8.11 (d, 2H), 8.09 (d, 4H), 8.00 (t, 2H), 7.99 (d, 2H), 7.91 (d, 4H), 7.90 (s, 2H), 7.85 (d, 4H), 7.82 (t, 2H), 7.46 (s, 2H), 7.39 (d, 4H), 4.82 (m, 4H), 4.43 (m, 4H), 3.91 (t, 8H), 3.70 (t, 8H), 2.40 (s, 12H), 2.27 (s, 12H), 2.12 (t, 8H), 1.93 (t, 8H), 1.68 (t, 8H), 1.55 (s, 36H), 1.47 (s, 36H), ≈1.40 (m, 16H), ≈1.35 (m, 8H), ≈1.25 (m, 8H), ≈1.20 (m, 8H), 0.85 (t, 12H), 0.72 (t, 12H); *m*/*z* (FAB) 3720.6 (M^+); $\lambda(CH_2Cl_2)$/nm 413, 538, 574.

1 A. P. de Silva, H. Q. N. Gunaratne, T. Gunnlaugsson, A. J. M. Huxley, C. P. McCoy, J. T. Rademacher and T. E. Rice, *Chem. Rev.*, 1997, **97**, 1515; L. Fabbrizzi and A. Poggi, *Chem. Soc. Rev.*, 1995, **197** and references therein.

2 J.-P. Sauvage, *Acc. Chem. Res.*, in press; V. Balzani, M. Gómez-López and J. F. Stoddart, *Acc. Chem. Res.*, in press; D. W. Urry, *Angew. Chem., Int. Ed. Engl.*, 1993, **32**, 819.

3 (*a*) J. Howard, *Nature*, 1997, **389**, 561; (*b*) T. Elston, H. Wang and G. Oster, *Nature*, 1998, **391**, 510 and references therein.

4 S. Shinkai, M. Ishihara, K. Ueda and O. Manabe, *J. Chem. Soc., Chem. Commun.*, 1984, 727; F. Würthner and J. Rebek, Jr., *Angew. Chem., Int. Ed. Engl.*, 1995, **34**, 446.

5 S. Zahn and J. W. Canary, *Angew. Chem., Int. Ed. Engl.*, 1998, **37**, 305; L. Zelikovich, J. Libman and A. Shanzer, *Nature*, 1995, **374**, 790.

6 D. B. Amabilino, C. O. Dietrich-Buchecker, A. Livoreil, Lluïsa Pérez-García, J.-P. Sauvage and J. F. Stoddart, *J. Am. Chem. Soc.*, 1996, **118**, 3905; P. R. Ashton, S. Iqbal, J. F. Stoddart and N. D. Tinker, *Chem. Commun.*, 1996, 479; L. Fabbrizzi, M. Licchelli, P. Pallavicini and L. Parodi, *Angew. Chem., Int. Ed. Engl.*, 1998, **37**, 800.

7 R. A. Bissell, E. Córdova, A. E. Kaifer and J. F. Stoddart, *Nature*, 1994, **369**, 133.

8 A. Livoreil, C. O. Dietrich-Buchecker and J.-P. Sauvage, *J. Am. Chem. Soc.*, 1994, **116**, 9399; A. Livoreil, J.-P. Sauvage, N. Armaroli, V. Balzani, L. Flamigni and B. Venturi, *J. Am. Chem. Soc.*, 1997, **119**, 12 114; J.-P. Collin, P. Gaviña and J.-P. Sauvage, *New J. Chem.*, 1997, **21**, 525.

9 J.-C. Chambron, V. Heitz and J.-P. Sauvage, *J. Am. Chem. Soc.*, 1993, **115**, 12 378; J.-C. Chambron, A. Harriman, V. Heitz and J.-P. Sauvage, *J. Am. Chem. Soc.*, 1993, **115**, 6109; J.-C. Chambron, C. O. Dietrich-Buchecker, V. Heitz, N. Solladié and J.-P. Sauvage, *C. R. Acad. Sci. Paris, Ser. IIb*, 1996, **323**, 483; M. Linke, J.-C. Chambron, V. Heitz and J.-P. Sauvage, *J. Am. Chem. Soc.*, 1997, **119**, 11 329.

10 G. Arsenault, E. Bullock and S. F. MacDonald, *J. Am. Chem. Soc.*, 1960, **82**, 4384; J. S. Lindsey, I. C. Schreiman, H. C. Hsu, P. C. Kearney and A. M. Marguerettaz, *J. Org. Chem.*, 1987, **52**, 827.

11 C. O. Dietrich-Buchecker, J.-P. Sauvage and J.-P. Kintzinger, *Tetrahedron Lett.*, 1983, **24**, 5095; C. O. Dietrich-Buchecker and J.-P. Sauvage, *Tetrahedron*, 1990, **46**, 503.

Communication 8/05746J

Characterisation of agostic interactions by a topological analysis of experimental and theoretical charge densities in [EtTiCl$_3$(dmpe)] [dmpe = 1,2-bis(dimethylphosphino)ethane]

Wolfgang Scherer,*[a] Wolfgang Hieringer,[a] Michael Spiegler,[a] Peter Sirsch,[a] G. Sean McGrady,*[b,c] Anthony J. Downs,[b] Arne Haaland[d] and Bjørn Pedersen[e]

[a] *Anorganisch-chemisches Institut, Technische Universität München, Lichtenbergstraße 4, D-85747 Garching, Germany. E-mail: scherer@zaphod.anorg.chemie.tu-muenchen.de*
[b] *Inorganic Chemistry Laboratory, University of Oxford, South Parks Road, Oxford, UK OX1 3QR*
[c] *Department of Chemistry, King's College London, Strand, London, UK WC2R 2LS*
[d] *Department of Chemistry, University of Oslo, Box 1033 Blindern, N-0315 Oslo, Norway*
[e] *Organisch-chemisches Institut, Technische Universität München, Lichtenbergstraße 4, D-85757 Garching, Germany*

Received (in Cambridge, UK) 31st July 1998, Accepted 5th October 1998

Topological analysis of the experimental and theoretical electron densities in [EtTiCl$_3$(dmpe)] (dmpe = Me$_2$PCH$_2$CH$_2$PMe$_2$) suggests the presence of a (3, −1) bond critical point (CP) between titanium and the β-agostic hydrogen atom; the characteristic curvature in the Ti–C$_\alpha$ bond is proposed as a more general criterion for identifying a β-agostic interaction.

Agostic interactions are of particular interest in organotransition-metal chemistry in view of their potential relevance to important processes like C–H activation. Reliable ways of pinning down these interactions are still at a premium, notwithstanding the numerous examples reported on the basis of structural or spectroscopic measurements or of theoretical studies. Theoretical considerations have lead Popelier and Logothetis (PL) recently to suggest topological analysis of the charge density as a means of identifying agostic interactions.[1] We have tested this hypothesis on a real agostic system by analysing experimental and theoretical electron densities. The ethyltitanium trichloride complex [EtTiCl$_3$(dmpe)] **1** (dmpe = Me$_2$PCH$_2$CH$_2$PMe$_2$) was chosen since its β-agostic interaction has been delineated by a variety of independent techniques.[2]

Long X-ray exposure times hitherto needed for accurate charge density studies have prevented the study of labile organometallic compounds like **1**; with conventional serial data collection techniques using a single scintillation counter, data accumulation may take months. However, Luger and others have demonstrated very recently that charge density studies can be accomplished with exposure times in the order of days using a CCD detector.[3] In our study we have been able to contrive short X-ray exposure times by combining two experiments using a CCD and an imaging plate detector system, both being connected to a rotating anode assembly providing highly intense Mo-Kα radiation. Charge densities were derived from the experimental X-ray data† using the XD program suite[4] based on a standard multipole model as formulated by Hansen and Coppens.[5] Theoretical charge densities were determined by B3LYP DFT calculations[6] using standard basis sets of triple-ζ quality plus polarisation.[7] All such calculations were performed with the Gaussian94 package.[8] The topological analysis of charge densities, based on Bader's 'Atoms In Molecules' (AIM) theory,[9] was effected with the AIMPAC and XD suite.[4,10]

While the geometrical parameters clearly indicate the presence of a β-agostic interaction in **1**: Ti–C 2.1522(9) [2.159], C–C 1.5117(12) [1.518], C$_\beta$–H$_\beta$ 1.13 [1.13], Ti···H$_\beta$ 2.10 [2.12] Å and Ti–C–C 84.5(1) [85.1]° (calculated values in square brackets), no significant charge accumulation between Ti and the C$_\beta$H$_\beta$ unit is evident from the total electron density. More information can be gained from the *gradient vector field* $\nabla\rho(\boldsymbol{r})$ of the calculated and experimental electron density. Hence all bond critical points (CPs)‡ along the bond paths connecting the atoms in **1** can be located [Fig. 1(a,b) and Table 1].

At the bond CP of the C–C bond we determine an electron density ($\rho_{b,calc}$ = 1.616 e Å^{-3}), slightly higher than the corresponding value (1.606 e Å^{-3}) for the C–C bond in ethane or EtTiCl$_3$ **2** (1.576 e Å^{-3}), and significantly lower than that (2.326 e Å^{-3}) for the C=C bond in ethene (Table 1). Since the magnitude of the charge density at the bond CP provides a sensitive measure of the bond strength, one might conclude that the C–C bond order in **1** is only slightly enhanced *vs.* **2**. However, the bond ellipticity parameter (ε)§ of the C–C bond in **1** clearly deviates from zero indicating some double bond character. This accords with the experimental observation of shorter C–C bond lengths in **1** *vs.* **2**,[2] and with the topology of the experimental electron densities (Table 1). Like the C–C bond, the agostic C–H$_\beta$ bond in **1** combines the high electron

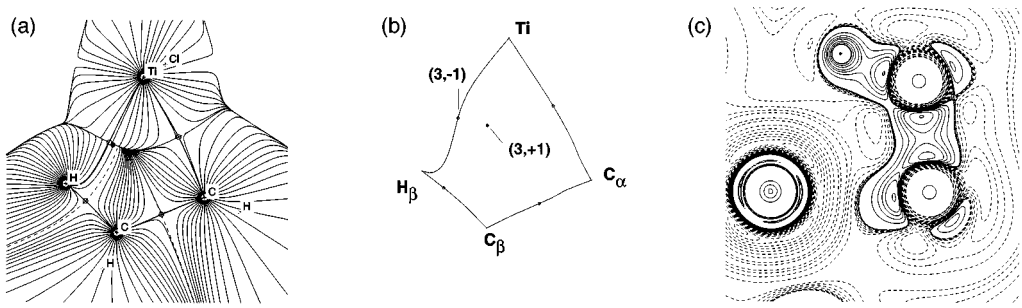

Fig. 1 (a) Calculated gradient vector field $\nabla\rho(\boldsymbol{r})$. Bond CPs are denoted by open circles and the ring CP by a filled circle; nuclei on the molecular plane are denoted by + while the projections of the out-of-plane nuclei are denoted by ÷. Inside the TiC$_\alpha$C$_\beta$H$_\beta$ four-membered ring all gradient paths originate at the (3, +1) ring CP and terminate either at the nuclei or at a (3, −1) bond CP (dashed lines). The gradient vectors linking the (3, −1) bond CP with the atoms constitute the bond paths (thick lines). (b) Bond paths in the TiC$_\alpha$C$_\beta$H$_\beta$ fragment based on experimental charge densities. (c) Experimental-$\nabla^2\rho(\boldsymbol{r})$ function in the TiC$_\alpha$C$_\beta$H$_\beta$ plane (negative values are marked by broken lines).¶

Table 1 Analysis of bond CPs (ρ in e Å^{-3}; ∇^2 in e Å^{-5}; distances in Å, and angles in degrees) in $EtTiCl_3$ and $[EtTiCl_3(dmpe)]$

Unit	Parameter	$EtTiCl_3$ DFT[a]	$EtTiCl_3(dmpe)$ DFT	$EtTiCl_3(dmpe)$ X-Ray
Ti–C_α	Distance	2.042	2.159	2.1522(9)
	ρ_b	0.84	0.63	0.55(3)
	∇^2_b	0.28	1.5	3.09(5)
	ε	0.02	0.06	0.16
C–C	Distance	1.529	1.518	1.5117(12)
	ρ_b	1.58	1.62[b]	1.90(4)[c]
	∇^2_b	−12.1	−12.4[b]	−18.7(1)[c]
	ε	0.04	0.1[b]	0.02[c]
C–H_β[d]	Distance	1.096	1.132	1.132
	ρ_b	1.83	1.67	1.52(5)
	∇^2_b	−21.5	−17.6	−12.6(2)
	ε	0.01	0.0	0.12
Ti···H_β[d]	Distance		2.118	2.096
	ρ_b		0.212	0.17(1)
	∇^2_b		3.3	1.67(1)
	ε		11.28	0.70
ring CP	ρ_r		0.213	0.16(2)
	∇^2_r		3.5	3.00(2)
Ti–C–C	Angle	116.68	85.1	84.5(1)

[a] Geometry optimisations in C_s symmetry. [b] Standard (ρ_b, ∇^2_b, ε) values for ethane and ethene at the same level of theory: 1.606, −13.3, 0.0 and 2.326, −24.906 and 0.34, respectively. [c] Corresponding values of the C–C bond in the dmpe backbone: 1.76(2), −15.42(6), 0.06. [d] β-hydrogen atom in the $TiC_\alpha C_\beta$ plane.

density at the bond critical point ($\rho_{b,calc}$ = 1.67 e Å^{-3}) and the large *negative* value of the Laplacian¶ ($\nabla^2\rho_{b,calc}$ = −17.6 e Å^{-5}) characteristic of covalent bonds [Fig. 1(c)]. The topologies of the Ti–C_α and Ti···H_β interactions are, however, different; in each case the electron density at the bond CP ($\rho_{b,calc}$ = 0.63 and 0.21 e Å^{-3}) is rather low, and the Laplacian ($\nabla^2\rho_{b,calc}$ = 1.5 and 3.3 e Å^{-5}) is *positive*.

Similar topologies were found for the corresponding bonds in the agostic model compound $EtTiCl_2^+$ **3** studied by PL, who invoked an ionic, closed shell Ti···H_β interaction.[1] It would seem better to make the distinction between covalent and ionic bonds on the basis of the wavefunction.[11] Compared with **3**, the β-agostic interaction in **1** is significantly weaker,[2] and closer inspection of the gradient vector field indicates that the Ti···H_β bond CP and the ring CP in **1** are proximal and not very pronounced. The electron densities calculated for the Ti···H_β bond CP and the ring CP inside the $TiC_\alpha C_\beta H_\beta$ fragment are nearly identical, differing not significantly by < 0.001 e Å^{-3}. Simultaneously the negative curvature (λ_2) at the bond CP associated with the axis directed at the ring CP almost vanishes. Thus, the bond and ring CPs almost merge into a singularity in ρ, a phenomenon characteristic of bond fission. This conclusion accords with our experimental findings, showing the gradient path between the ring and the Ti···H_β bond CPs to be extremely flat. We expect therefore that Ti···H bond CPs may not always be found in molecules where the agostic interaction is weaker than in **1**.

However, a further characteristic of the agostic interaction manifests itself in the gradient vector map $\nabla\rho(\boldsymbol{r})$ as significant curvature in the Ti–C_α bond path (Fig. 1a,b). This follows the ridge of maximum charge density between a pair of bonded nuclei, the bond CP of the Ti–C bond is displaced outwards by 0.06 Å from the $TiC_\alpha C_\beta H_\beta$ ring. Such behaviour complies with the conclusions of a previous theoretical study,[2] namely that the M–C_α bonding electrons in **1** are delocalised over the entire ethyl group, reduction of the TiCC valence angle permitting Ti to establish a significant covalent interaction with C_β, and perhaps to a lesser extent with H_β. The consequence is a bent Ti–C_α bond path. Inspection of the Ti–C_α bond path of **1** and all the model agostic systems suggested by PL[1] reveals in every case curvature of the Ti–C_α bond. Moreover, the agostic C_β–H_β bonds are bent away from the metal centre. Thus, the bond CP of the C_β–H_β bond is displaced inside the formal $TiC_\alpha C_\beta H_\beta$ ring, a result in keeping with the calculated C_α–C_β–H_β angle which is always several degrees larger than the normal value (*ca.* 109°).

In conclusion, we have shown that experimental electron densities can be obtained for a labile transition-metal complex using now-standard laboratory technology and near-normal data acquisition times. Some agostic interactions may be identified solely on the basis of charge densities, but the non-linearity of the Ti–C_α bond probably offers a more robust criterion of β-agostic interaction.

Notes and references

† *Crystal data* for $[EtTiCl_3(dmpe)]$: $C_8H_{21}P_2Cl_3Ti$, M = 333.4, red rhombic crystals; monoclinic, space group $P2_1/n$, a = 782.95(2), b = 1611.04(2), c = 1182.16(3) pm, β = 91.613(1)°, V = 1490.54(6) × 10^6 pm^3; T = 105(1) K; Z = 4, $F(000)$ = 688, D_c = 1.495 g cm^{-3}, μ = 13.0 cm^{-1}. 35928 (16334) Bragg reflections with $\sin\theta/\lambda_{max}$ = 1.097 (0.66) Å^{-1} were collected on a kappa-CCD system from Nonius [image plate system from Stoe (IPDS)] with a rotating anode generator (Nonius FR591; Mo-Kα, λ = 0.71073 Å) within 48 (32) h. 13425 (CCD data set) and 3205 (IPDS data set) independent reflections; R_{int} = 0.029 (CCD)/0.025 (IPDS). The deformation density was described by a multipole model in terms of spherical harmonics multiplied by Slater-type radial functions with energy-optimised exponents.[12] The multipole expansion was terminated at the hexadecapolar and dipolar level for the heavy and hydrogen atoms, respectively. The C–H bond distances were constrained to the calculated values. The refinement of 434 parameters against 13241 observed reflections [$F > 3\sigma(F)$] converged to R = 0.027, R_w = 0.037, and a featureless residual $\rho(\boldsymbol{r})$. CCDC 182/1048.

‡ (3, −1)/(3, +1) CPs: two curvatures are negative/positive and ρ is a maximum/minimum at the CP in the plane defined by the axes corresponding to the negative/positive curvatures. ρ is a minimum/maximum at the CP along the third axis which is perpendicular to this plane.

§ The ellipticity ε ($\varepsilon = \lambda_2/\lambda_1 - 1$) of a bond is a measure of the asymmetry between the two principal curvatures (λ_1,λ_2) of ρ at the bond CP perpendicular to the bond.

¶ Values of $\nabla^2\rho(\boldsymbol{r}) < 0$ indicate that charge is locally concentrated at $\boldsymbol{r}$, while positive $\nabla^2\rho(\boldsymbol{r})$ values are characteristic of regions suffering local charge depletion.

1 P. L. A. Popelier and G. Logothetis, *J. Organomet. Chem.*, 1998, **555**, 101.
2 W. Scherer, T. Priermeier, A. Haaland, H. V. Volden, G. S. McGrady, A. J. Downs, R. Boese and D. Bläser, *Organometallics*, 1998, **17**, 4406 and references quoted therein.
3 See for example: T. Koritsanszky, R. Flaig, D. Zobel, H.-G. Krane, W. Morgenroth and P. Luger, *Science*, 1998, **279**, 356; P. Macchi, D. M. Proserpio and A. Sironi, *J. Am. Chem. Soc.*, 1998, **120**, 1447.
4 T. Koritsanszky, S. Howard, P. R. Mallinson, Z. Su, T. Richter and N. K. Hansen, XD—a Computer Program Package for Multipole Refinement and Analysis of Electron Densities from Diffraction Data, Free University of Berlin, 1997.
5 N. K. Hansen and P. Coppens, *Acta Crystallogr., Sect. A*, 1978, **34**, 909.
6 The ED of **1** was discussed on the basis of the B3LYP//BPW91 level of theory.
7 A. J. H. Wachters, *J. Chem. Phys.*, 1970, **52**, 1033; A. D. McLean and G. S. Chandler, *J. Chem. Phys.*, 1980, **72**, 5639; R. Krishnan, J. S. Binkley, R. Seeger and J. A. Pople, *J. Chem. Phys.*, 1980, **72**, 650; A. W. Ehlers, M. Böhme, S. Dapprich, A. Gobbi, A. Höllwarth, V. Jonas, K. F. Köhler, R. Stegmann, A. Veldkamp and G. Frenking, *Chem. Phys. Lett.*, 1993, **208**, 111.
8 M. J. Frisch, G. W. Trucks, H. B. Schlegel, P. M. W. Gill, B. G. Johnson, M. A. Robb, J. R. Cheeseman, T. Keith, G. A. Petersson, J. A. Montgomery, K. Raghavachari, M. A. Al-Laham, V. G. Zakrzewski, J. V. Ortiz, J. B. Foresman, J. Cioslowski, B. B. Stefanov, A. Nanayakkara, M. Challacombe, C. Y. Peng, P. Y. Ayala, W. Chen, M. W. Wong, J. L. Andres, E. S. Replogle, R. Gomperts, R. L. Martin, D. J. Fox, J. S. Binkley, D. J. Defrees, J. Baker, J. P. Stewart, M. Head-Gordon, C. Gonzales and J. A. Pople, Gaussian 94, Revision C.2 and E.2, Gaussian, Inc., Pittsburgh PA, 1995.
9 See, for example: R. F. W. Bader, *Atoms in Molecules: A Quantum Theory*, Clarendon Press, Oxford, 1990.
10 R. F. W. Bader, *Acc. Chem. Res.*, 1985, **18**, 9.
11 J. Cioslowski and S. T. Mixon, *Inorg. Chem.*, 1993, **32**, 3209.
12 E. Clementi and C. Roetti, *At. Data Nucl. Data Tables*, 1974, **14**, 177.

Communication 8/06012F

Preparation of aluminosilicate MCM-41 in desirable forms *via* a novel co-assemble route

Wenyong Lin,[a] Qiang Cai,[a] Wenqin Pang*[a] and Yong Yue[b]

[a] *The Key Laboratory of Inorganic Synthesis and Preparative Chemistry, Department of Chemistry, Jilin University, Changchun, 130023, China. E-mail: inorchem@mail.jlu.edu.cn*

[b] *Wuhan Institute of Physics, The Chinese Academy of Science, Wuhan 430071, China.*

Received (in Cambridge, UK) 6th October 1998, Accepted 6th October 1998

A new alkali-free synthesis system allows us to prepare aluminosilicate MCM-41 directly in a variety of desirable forms: M-AlMCM-41 (M = H, Cu, Zn, Cd, Ni), the solution ion-exchange and subsequent calcination being avoided; the formation is discussed in terms of a co-assemble process.

Aluminosilicate zeolites with desirable cations compensating the framework charge may find wide applications in areas of adsorption, catalysis[1–3] and nanostructure manufacturing.[4–6] To modify the channels/cages of zeolites with suitable cations, various ion-exchange techniques, such as solid-state interaction,[7,8] impregnation,[9] and chemical vapor deposition[10] have been utilized, besides the conventionally used solution ion-exchange method. However, for the recently developed mesoporous molecular sieve MCM-41,[11,12] which has aroused wide interest, successful ion-exchange has only been performed in solution.[6,13–15] This step, however, will cause some structural collapse owing to the weak hydrothermal stability of MCM-41, especially when the exchange level is high.[14] Further, the ion-exchange occurring in solution will inevitably be incomplete because there is always an equilibrium between the ions within the zeolite channels and those in the liquid. In the present report, we describe a novel co-assemble route for the synthesis of MCM-41, which allows for the direct formation of aluminosilicate MCM-41 in a variety of desirable forms, M-AlMCM-41 (M = H, Cu, Zn, Cd, Ni), the solution ion-exchange step thus being avoided. In addition to this, this method offers us a possibility to obtain a deeper understanding into the formation of MCM type materials. We believe, in the present preparation, a co-assemble process occurs, involving surfactant cations, aluminosilicate species and various ammonia coordinated transition metal complex cations: $M(NH_3)_n^{2+}$ (M = Cu, Zn, Cd, Ni, n = 4, 6).

This novel method owes much to the synthesis medium, which involves the substitution of organic weak bases for the conventionally used NaOH or TMAOH, allowing us to introduce desirable inorganic cations without competition of Na^+ or TMA^+. A typical synthesis of Cu-AlMCM-41 was as follows: an ethylamine ($EtNH_2$) solution (70 wt%) was added to a stirred solution containing distilled water, cetyltrimethylammonium bromide (CTAB) and $AlCl_3{\cdot}6H_2O$. Then to the mixture was added a solution prepared by addition of ammonia solution (NH_3 25 wt%) to a $CuCl_2$ solution. After this, tetraethylammonium orthosilicate (TEOS) was added dropwise, leading to a composition of $1.0SiO_2 : xAl_2O_3 : 2.5xCu^{2+} : 20xNH_4OH : 0.14CTAB : 2.4EtNH_2 : 100H_2O$ ($0.01 < x < 0.03$). The reaction mixture was further stirred for 4 h at room temperature before being heated at 110 °C for 4 days. The blue product was recovered by filtration and washed with distilled water until no Cu^{2+} could be detected in the filtrate. After being dried at ambient temperature, the product was heated in air at 600 °C for 7 h, with a heating rate of 1 °C min^{-1} from room temperature to 600 °C. The as-calcined sample was blue. ICP (inductively coupled plasma emission spectroscopy) analysis shows that the Si/Al ratio can be as low as 16, and the Si/Cu ratio as low as 25. Using same procedures, AlMCM-41 can be prepared with other transition metals, such as Zn, Cd and Ni which can form NH_3-coordinated complex cations in a basic medium required for the synthesis. If no metal ion was introduced, the resultant AlMCM-41 can be obtained in its H-form after calcination, the NH_4^+ exchange and subsequent calcination being avoided.

For both the as-synthesized and calcined M-AlMCM-41 (M = H, Cu, Cd, Ni, Zn), XRD shows clear lines characteristic of well defined hexagonal structures. Especially for H-AlMCM-41, an intense main peak (100) with low FWHH and three weak peaks (110), (200), (210) can be clearly resolved, suggesting a highly ordered structure.

To confirm the successful introduction of desirable cations into the exchanging sites of zeolite MCM-41, we immersed the as-calcined sample (typically Cu-AlMCM-41, Si/Al = 16, Si/Cu = 25), in distilled water or $NaNO_3$ aqueous solution (0.05 M), corresponding to a liquid to solid ratio of 200 ml g^{-1}. After stirring for 1 h, the samples were filtered and the fitrate was collected in both cases. For the slurry with distilled water, no copper content was detected, while for the slurry with $NaNO_3$ copper ions could clearly detected. ICP analysis indicates that up to 65% of copper ions can be exchanged after slurrying twice. The exchangeable nature of the copper ions within the AlMCM-41 strongly confirms that the most of the metal ions are located as charge compensating cations. The as-calcined Cu-AlMCM-41 shows clear sharp lines ($g_{\|}$ = 2.34, g = 2.07) in its EPR spectra at both room temperature and −197 °C and the spectra are similar to dehydrated Cu-AlMCM-41 prepared by solution ion-exchange,[13] but different from pure silica MCM-41 containing Cu^{II} ions.[16] Thus the Cu^{II} cations are likely to be mainly in a six-coordinate environment, as for Cu^{II} exchanged into AlMCM-41 in solution.

To our knowledge, the ion exchanging sites of zeolites are usually produced by substituting trivalent Al^{3+} for silicon atoms and the pure silica MCM-41 shows no or very low ion-exchange capacity.[13] In the present case, the successful incorporation of Al^{3+} into the framework of MCM-41 is established by NMR measurements (Bruker MSL-400 spectrometer), as shown in Fig. 1 for H-AlMCM-41 and Cu-AlMCM-41 samples before and after calcination. The as-synthesized samples show only one signal at 51 ppm, corresponding to four-coordinate Al in the framework sites. Upon calcination, a small fraction of aluminium becomes extraframework in nature, as shown by a small peak at −3.5 ppm. The four-coordinate Al^{3+} within the silica framework will be compensated by various extraframework cations. From the synthesis procedure above, it is apparent that the involvement of $EtNH_2$ as the base source renders the synthesis mixture alkali-free. However, of $EtNH_2$ is basic enough (pK_b = 3.25) not only to form MCM-41 but also to dissolve the Al source material and thus Al^{3+} can be incorporated into the framework readily. Other lyotropic organic amines such as dimethylamine and diethylamine are also suitable for this type of preparation. It is this feature of the synthesis that allows us to introduce various cations into the reaction media, and the cations can be occluded within the bulk product and are subsequently located at the charge-balancing

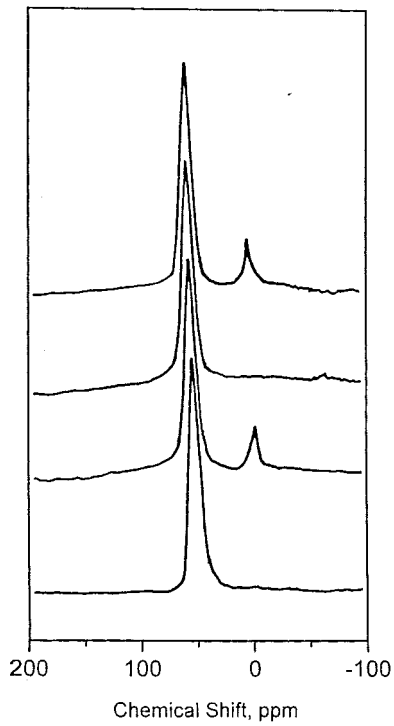

Fig. 1 ^{27}Al MAS NMR spectra of (from bottom to top) as-synthesized H-AlMCM-41, calcined H-AlMCM-41, as-synthesized Cu-AlMCM-41 and calcined Cu-AlMCM-41.

sites upon calcination. On the other hand, ammonia is used to form complex cations with the transition metal ions, preventing them from being precipitated under the basic conditions used.

The occlusion of complex cations within the silicate mesophase may be proposed as a co-assemble process. First, the TEOS molecules are hydrolyzed into oligomeric silicate acids. Then, the surfactant cations (CTA^+) displace the protons of these acids to form inorganic–organic composites, which would further assemble into a periodic mesophase. When the basic conditions are taken into account, the metal cations can also associate with the silicate species by exchanging protons of the silicate acids. As a result, when the cross-linking between the silica leads to solidification of the mesophase the complex cations are occluded within the bulk product. The most likely position of these cations is at the interface between inorganic and organic fractions. Upon calcination to remove the surfactant, the metal complex is decomposed and the remaining metal cations are located at the exchange sites of MCM-41, compensating the negative charge of the aluminosilicate framework. Protonic $EtNH_2$ ($EtNH_3^+$), and NH_3 (NH_4^+) could also be occluded within the as-synthesized MCM-41 at the interface between the surfactant and silicate framework. However, both of these cations can be readily removed by calcination.

Thus, the present co-assemble route offers us not only a convenient route for direct preparation of AlMCM-41 in desirable forms, but is also a potential pathway for encapsulating functional cationic inorganic species within the inorganic–organic interface in a highly dispersed state.

We acknowledge the support of the National Natural Science Foundation of China, the State Key Laboratory of Inorganic Synthesis & Preparative Chemistry of Jilin University and the State Key Laboratory of Crystal of Shandong University.

Notes and references

1 S. Chatterjee, H. L. Greene and J. Y. Park, *J. Catal.* 1992, **138**, 179.
2 W. Grunert, N. W. Hayes, R. W. Joyner, E. S. Shpiro, M. R. H. Siddiqui and G. N. Baeva, *J. Phys. Chem.*, 1994, **98**, 10832.
3 J. Connerton, R. W. Joyner and M. Stockenhuber, *Chem. Commun.*, 1997, 185.
4 M. D. Baker, J. Godber and G. A. Ozin, *J. Phys. Chem.*, 1985, **89**, 2299.
5 G. D. Stucky and J. E. MacDougall, *Science*, 1990, **247**, 669.
6 C.-G. Wu and T. Bein, *Science*, 1994, **264**, 1757.
7 A. V. Kucherov, A. A. Slinkin, *J. Mol. Catal.*, 1994, **90**, 323.
8 H. G. Karge, *Stud. Surf. Sci. Catal.*, 1990, **37**, 1.
9 Y.-Ch. Xie and Y.-Q. Tang, *Adv. Catal.*, 1990, **37**, 1.
10 A. Seidel and B. Boddenberg, *Chem. Phys. Lett.*, 1996, **249**, 117.
11 C. T. Kresge, M. E. Leonowicz, W. J. Roth, J. C. Vartuli and J. S. Beck, *Nature*, 1992, **359**, 710.
12 J. S. Beck, J. C. Vartuli, W. J. Roth, M. E. Leonowicz, C. T. Kresge, K. D. Schmitt, C. T.-U. Chu, D. H. Olson, E. W. Sheppard, S. B. McCullen, J. B. Higgins and J. L. Schlenker, *J. Am. Chem. Soc.*, 1992, **114**, 10834.
13 A. Poppl, M. Harmann and L. Kevan, *J. Phys. Chem.*, 1995, **99**, 17251.
14 J. M. Kim, J. H. Kwak, S. Jun and R. Ryoo, *J. Phys. Chem.*, 1995, **99**, 16742.
15 C. H. Ko and R. Ryoo, *Chem. Commun.*, 1996, 2467.
16 A. Poppl, M. Newhouse and L. Kevan, *J. Phys. Chem.*, 1995, **99**, 10019.

Communication 8/07786J

A rational assembly of a series of exchange coupled linear heterotrinuclear complexes of the type $M_AM_BM_C$ as exemplified by $Fe^{III}Cu^{II}Ni^{II}$, $Fe^{III}Ni^{II}Cu^{II}$ and $Co^{III}Cu^{II}Ni^{II}$

Cláudio Nazari Verani, Thomas Weyhermüller, Eva Rentschler, Eckhard Bill and Phalguni Chaudhuri*

Max-Planck-Institut für Strahlenchemie, PO Box 101365, 54513 Mülheim an der Ruhr, Germany.
E-mail: chaudh@mpi-muelheim.mpg.de

Received (in Basel, Switzerland) 20th August 1998, Accepted 23rd September 1998

A general approach for the rational synthesis of linear trinuclear complexes containing three different metals $M_AM_BM_C$ is described and a member of the series, $Fe^{III}Cu^{II}Ni^{II}$, has been characterized by X-ray crystallography and magnetic susceptibility measurements.

This work stems from our interest in using 'metal oximates' as building blocks for synthesizing hetero- and homopolymetallic complexes containing two,[1] three[2] or four[3] metal centres that constitute a common ground for two areas of current interest, molecular magnetism and metal sites in biology. We have previously demonstrated that using our synthetic strategy it is possible to synthesize a series of complexes of the types $M_AM_BM_A$,[2] $M_AM_BM_BM_A$[4] and $(M_A)_2(\mu_3\text{-}O)_2(M_B)_2$.[3,5] These series are unique and have been proved to be ideal materials for the investigations of exchange mechanism. We describe here a general approach for the rational synthesis of a series of trinuclear complexes containing three different metals $M_AM_BM_C$. To the best of our knowledge these complexes represent the first examples of exchange coupled linear trinuclear complexes containing three different metals. The complexes have been prepared by the general synthetic route shown in Scheme 1. Yields varied between 30% and 50%. Satisfactory analyses (C, H, N, M_A, M_B, M_C) were obtained.

The structure of the complex dication containing the trinuclear core $Fe^{III}Cu^{II}Ni^{II}$, **1**, is shown in Fig. 1.† The coordination geometry of the terminal iron, Fe, is distorted octahedral with three nitrogen atoms, N(1), N(2) and N(3), from the facially coordinated macrocyclic amine, two oxygen atoms, O(1) and O(4), from the oxime ligands and a chloride ion, Cl(1), resulting in the *fac* FeN_3O_2Cl cores. The Fe–O and Fe–N distances are consistent with a d^5 high-spin electron configuration of the Fe centre, as is also evidenced by the Mössbauer spectrum[6] at 80 K, $\delta = 0.45$ mm s^{-1}, $\Delta E_Q = 0.85$ mm s^{-1}. The Fe–Cu–Ni skeleton is almost planar, with an angle Fe–Cu–Ni of 174.0°. The intramolecular separations between the metal centres, Fe···Cu 3.695 Å, Fe···Ni 6.772 Å and Cu···Ni 3.087 Å, are in conformity with the values observed earlier for comparable structures.[2,7] The dihedral angles between the planes FeN(2)N(3)O(1)O(4) and CuN(4)N(7)O(3)O(2), and the latter Cu plane and the Ni plane NiO(3)O(2)N(5)N(6) are 148.5 and 169.4°, respectively.

The geometry of the central Cu(II) centre is square-pyramidal, with the elongated fifth bond (2.43 Å) to axially coordinated oxygen atom O(60) of a methanol molecule. The metrical parameters for the Cu centre are very similar to those of the Cu dimer with the same Schiff-base oxime ligand reported in the literature.[8]

The terminal nickel ion, Ni(II), is coordinated to two azomethine nitrogens, N(5) and N(6), and two bridging phenolate groups, O(2) and O(3), from the Schiff-base oxime ligand. The nickel centre adopts a 6-coordinated environment by interacting with two *trans* axially disposed methanol molecules, O(40) and O(50). The nickel centre is displaced by 0.014 Å from the mean basal plane comprising O(3)O(2)N(5)N(6) atoms toward O(40) or O(50) of a methanol ligand. The equatorial Ni–N and Ni–O (phenoxide) distances are nearly equal, average 2.005(6) Å and 2.025(3) Å, respectively. The Ni–O(methanol) distances are rather long (av. 2.142 Å), as has been observed earlier.[9e] The bridging angles Cu–O(2)–Ni and Cu–O(3)–Ni are equal, 101.6°.

Magnetic data (SQUID) with $H = 2$ T for a polycrystalline sample of FeCuNi, **1**, are displayed in Fig. 2 as μ_{eff} *vs.* *T*. On lowering the temperature μ_{eff} of 6.45 μ_B at 290 K decreases monotonically, approaching a broad minimum around 180 K($\mu_{eff} = 6.40\ \mu_B$) and increases upon further cooling to reach a maximum with a value of 6.91 μ_B at 15 K, which corresponds to the spin-only value for $S = 3$, expected as the ground state for an antiferromagnetically coupled $Fe^{III}Cu^{II}Ni^{II}$ complex. The μ_{eff} *vs.* *T* plot exhibits the expected minimum and indicates an irregular spin-structure[2,9–11] showing a ferromagnetic-like interaction in the temperature range below this minimum. Below 15 K there is a decrease in μ_{eff}, reaching a value of 4.63 μ_B at

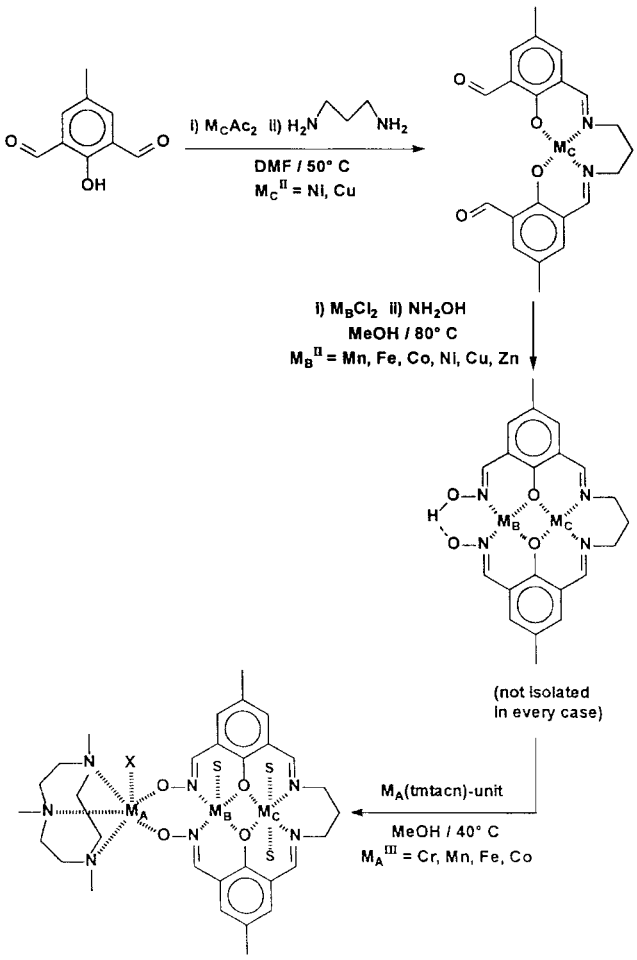

Scheme 1

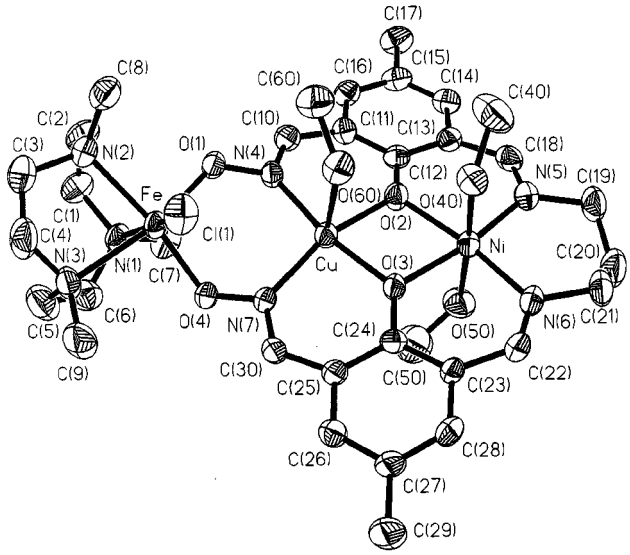

Fig. 1 Structure of the dication $[(tmtacn)Fe(Cl)Cu(CH_3OH)(Schiff\text{-}base\ oxime)Ni(CH_3OH)_2]^{2+}$ with the $Fe^{III}Cu^{II}Ni^{II}$ core. Selected bond lengths (Å): Cu–N(4) 1.951(3), Cu–O(3) 1.956(2), Ni–N(5) 2.000(4), Ni–O(2) 2.025(3), Ni–O(50) 2.137(3), Fe–O(4) 1.916(3), Fe–N(1) 2.211(3), Fe–Cl(1) 2.3383(13).

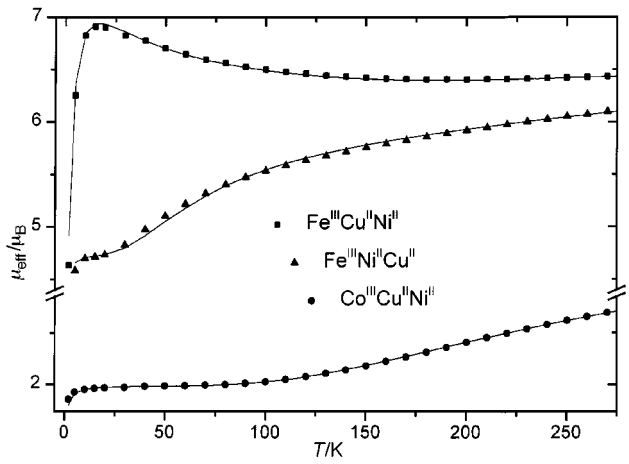

Fig. 2 A plot of μ_{eff} *vs.* T for **1**, **2**, **3**. The solid lines represent the simulations of the experimental data.

2 K; this behaviour might be due to saturation effects or the splitting in the zero-field of the ground state $S_T = 3$. We have confirmed the ground state of $S_T = 3$ by fitting the experimental magnetization curve (7 T) to the Brillouin function for $S = 3$ with $g = 2.075$ in the temperature range 2–290 K. The magnetic interactions operating in this type of linear trinuclear structure result in a ground state of high-spin multiplicity, although the nearest neighbour spin alignments are antiparallel.

A full-matrix diagonalization approach including exchange ($-2JS_1 \cdot S_2$) and Zeeman interactions, together with axial single-ion zero-field interaction (DS_z^2) for the Ni^{II} ion was employed to fit the experimental data. The best fit shown as the solid line in Fig. 2 yields $J_{FeCu} = -19.8\ cm^{-1}$, $J_{CuNi} = -118.6\ cm^{-1}$, $J_{FeNi} = 0$ (fixed), $g_{Ni} = 2.20$ (fixed), $g_{Cu} = 2.10$ (fixed), $g_{Fe} = 2.0$ (fixed), $D = 0$ (fixed).

Our strategy of using 'building blocks' sequentially yields also the isomeric $Fe^{III}Ni^{II}Cu^{II}$, **2**, as is evident by its susceptibility measurements (Fig. 2). The best fit parameters are $J_{FeNi} = -10.6\ cm^{-1}$, $J_{NiCu} = -161.5\ cm^{-1}$, $J_{FeCu} = 0$ (fixed), $g_{Fe} = 2.0$ (fixed), $g_{Ni} = 2.30$ (fixed), $g_{Cu} = 2.10$ (fixed). Thus the exchange interactions in $Fe^{III}Ni^{II}Cu^{II}$, **2**, lead to a different ground state of $S_T = 2$. The exchange interaction between the neighbouring Cu^{II} and Ni^{II} ions in another member of the series, Co^{III}(l.s.)$Cu^{II}Ni^{II}$, **3**, also structurally characterized (data not shown), is of comparable strength, $J_{CuNi} = -125\ cm^{-1}$ (Fig. 2), to that in **1**, $Fe^{III}Cu^{II}Ni^{II}$. The angles Cu–O(phenoxo)–Ni and the distances Cu···Ni are exactly the same in both **1** and **3**, although, in contrast to **1**, the Co–Cu–Ni skeleton is not linear with an angle of 155.6°.

C. N. V. acknowledges thankfully the receipt of a fellowship from DAAD.

Notes and references

† $[C_{33}H_{53}N_7O_8ClFeCuNi](ClO_4)_2 \cdot H_2O$, $M = 1090.3$, monoclinic, space group $P2_1/c$, $a = 14.503(2)$, $b = 16.984(3)$, $c = 19.536(3)$ Å, $\beta = 106.14(3)°$, $V = 4622.4(13)$ Å^3, $Z = 4$, $D_c = 1.567$ g cm^{-3}, $T = 293$ K, $F(000) = 2256$, λ(Mo-Kα) = 0.71073 Å, $\mu = 1.414$ mm^{-1}. Brown black crystal, size 0.40 × 0.32 × 0.30 mm, Nonius Kappa CCD, 21617 reflections collected. Structure solution by using the Siemens SHELXTL-PLUS package (G. M. Sheldrick, Universität Göttingen) from 8831 observed reflections; full-matrix least-squares refinement on F^2, using 7728 reflections and 565 parameters, refinement converged at $R_1 = 0.047$, $R_2 = 0.0895$ (all data). CCDC 182/1032.

1 (*a*) F. Birkelbach, M. Winter, U. Flörke, H.-J. Haupt, C. Butzlaff, M. Lengen, E. Bill, A. X. Trautwein, K. Wieghardt and P. Chaudhuri, *Inorg. Chem.*, 1994, **33**, 3990, and references therein; (*b*) D. Burdinski, F. Birkelbach, M. Gerdan, A. X. Trautwein, K. Wieghardt and P. Chaudhuri, *J. Chem. Soc., Chem. Commun.*, 1995, 963.

2 (*a*) P. Chaudhuri, M. Winter, P. Fleischhauer, W. Haase, U. Flörke and H.-J. Haupt, *J. Chem. Soc., Chem. Commun.*, 1990, 1728; (*b*) D. Burdinski, F. Birkelbach, T. Weyhermüller, U. Flörke, H.-J. Haupt, M. Lengen, A. X. Trautwein, E. Bill, K. Wieghardt and P. Chaudhuri, *Inorg. Chem.*, 1998, **37**, 1009, and references therein.

3 P. Chaudhuri, F. Birkelbach, M. Winter, V. Staemmler, P. Fleischhauer, W. Haase, U. Flörke and H.-J. Haupt, *J. Chem. Soc., Dalton Trans.*, 1994, 2313.

4 C. Krebs, M. Winter, T. Weyhermüller, E. Bill, K. Wieghardt and P. Chaudhuri, *J. Chem. Soc., Chem. Commun.*, 1995, 1913.

5 P. Chaudhuri, M. Winter, P. Fleischhauer, W. Haase, U. Flörke and H.-J. Haupt, *Inorg. Chim. Acta*, 1993, **212**, 241.

6 P. Gütlich, R. Link and A. X. Trautwein, *Mössbauer Spectroscopy and Transition Metal Chemistry*, Springer-Verlag, Berlin, 1978.

7 (*a*) C. J. O'Connor, D. P. Freyberg and E. Sinn, *Inorg. Chem.*, 1979, **18**, 1077; (*b*) R. L. Lintvedt, L. S. Kramer, G. Ranger, P. W. Corfield and M. D. Glick, *Inorg. Chem.*, 1983, **22**, 3580; (*c*) I. Morgenstern-Badarau, M. Rerat, O. Kahn, J. Jaud and J. Galy, *Inorg. Chem.*, 1982, **21**, 3050; (*d*) T. Aono, H. Wada, Y. Aratake, N. Matsumoto, H. Okawa and Y. Matsuda, *J. Chem. Soc., Dalton Trans.*, 1996, 25.

8 E. V. Rybak-Akimova, D. H. Busch, P. K. Kahol, N. Pinto, N. W. Alcock and H. J. Clase, *Inorg. Chem.*, 1997, **36**, 510.

9 (*a*) O. Kahn, *Molecular Magnetism*, VCH Verlagsgesellschaft, Weinheim, 1993; (*b*) O. Kahn, *Adv. Inorg. Chem.*, 1995, **43**, 179; (*c*) *Research Frontiers in Magnetochemistry*, ed. C. J. O'Connor, World Scientific, Singapore, 1993; (*d*) F. Birkelbach, U. Flörke, H.-J. Haupt, C. Butzlaff, A. X. Trautwein, K. Wieghardt and P. Chaudhuri, *Inorg. Chem.*, 1998, **37,** 2000; (*e*) S. Mohanta, K. K. Nanda, L. K. Thompson, U. Flörke and K. Nag, *Inorg. Chem.*, 1998, **37**, 1465, and references therein.

10 Y. Pei, Y. Journaux and O. Kahn, *Inorg. Chem.*, 1988, **27**, 399.

11 P. Chaudhuri, M. Winter, B. P. C. Della Védova, P. Fleischhauer, W. Haase, U. Flörke and H.-J. Haupt, *Inorg. Chem.*, 1991, **30**, 4777.

Communication 8/06575F

ChemComm

Cation flux dependence on carbon chain length in hydraphile channels as assessed by dynamic ^{23}Na NMR methods in phospholipid bilayers

Clare L. Murray and George W. Gokel*

Bioorganic Chemistry Program and Department of Molecular Biology and Pharmacology, Washington University School of Medicine, 660 South Euclid Avenue, Campus Box 8103, St. Louis, MO 63110 USA.
E-mail: ggokel@pharmsun.wustl.edu

Received (in Columbia, MO, USA) 10th August 1998, Accepted 23rd September 1998

The length dependence for the family of tris(macrocycle) channels has been defined by a combination of synthetic and kinetic studies conducted in phospholipid bilayers.

Two modes of cation transport are known to occur *in vivo*: they are designated carrier and channel mechanisms. Both kinds of transport have been studied extensively. The dynamics of carrier transport are generally understood for the limited natural carriers and numerous synthetic ionophores.[1] In the channel mechanism, extensive biophysical and molecular biological studies have defined structural, functional, and selectivity aspects of naturally occurring protein channels.[2] The recent crystal structure of the potassium-selective transmembrane shaker channel has given a view of how the transmembrane helices are positioned within the phospholipid bilayer but mechanistic details in this and other transmembrane proteins remain elusive.[3] The complexity of natural channel compounds has fostered the invention and study of a variety of synthetic model systems that have proved to be more or less successful as ionophores.[4]

We have developed a family of synthetic, transmembrane ionophores based upon crown ethers which have been proved to transport sodium.[5] These compounds consist of three macrocycles connected by hydrocarbon spacers and are terminated by flexible sidechains. We call these compounds 'hydraphiles' in reference to the monster slain by Hercules that had two heads on each neck.[6] The general structure is shown below.

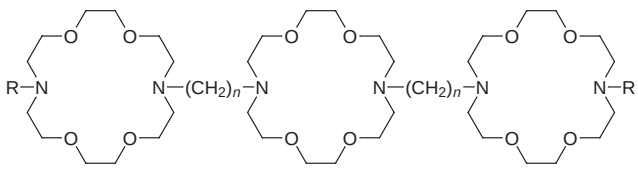

1 *n* = 8, R = benzyl
2 *n* = 10, R = benzyl
3 *n* = 12, R = benzyl
4 *n* = 14, R = benzyl
5 *n* = 16, R = benzyl
6 *n* = 12, R = dansyl

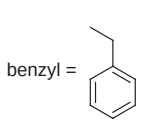

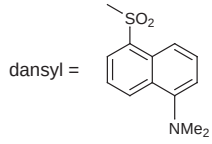

Several of these macrocycle-based channel compounds have been shown by fluorescence methods to transport protons and by dynamic NMR methods to transport alkali metal cations.[5] Considerable evidence has accumulated on the function of these compounds. (1) The central macrocycle is beneficial but not essential for cation transport in the cases where that issue was studied and is probably oriented along the lipid axis in the bilayer. (2) The ionophoretic activity of hydraphiles cannot be explained either by a simple carrier mechanism or by unadorned detergent action.[7] Specifically, neither bis(benzyl)diaza-18-crown-6 nor bis(dodecyl)diaza-18-crown-6 shows any measurable transport in the ^{23}Na NMR experiment. (3) Transport rates generally show a comprehensible structure–activity relationship[5] and follow the Hammett principle.[8] (4) The channel can be blocked by the presence of a hydrogen bond donor attached to the distal macrocycles.[9] In the present work, we wished to gain insight into the structural requirement for spanning the phospholipid membrane's 'hydrocarbon slab.' This insulating portion of the larger bilayer is 30–34 Å across as judged from work reported by Wiener and White[10] and the shaker potassium channel crystal structure.[11] We thus prepared five tris(macrocyclic) hydraphiles that are identical except for the lengths of the spacer chains connecting the central macrocycle to its distal counterpart. It was anticipated that the synthetic channel compounds would show a higher level of cation flux when the length was optimal than when the spacer chains were either too long or too short. In the latter case, a complete shutdown of cation transport was anticipated if the ionophore could not span the insulating regime of the membrane. If the synthetic channel functioned by a carrier mechanism, such a cut-off would not be expected.

Macrocycles **1**–**5** were prepared by a three-step sequence.[12] First, monobenzyldiaza-18-crown-6 ($PhCH_2 < N18N > H$) was prepared either by benzylation of diaza-18-crown-6 or by partial hydrogenolysis of dibenzyldiaza-18-crown-6.[13] Alkylation of $PhCH_2 < N18N > H$ with excess $Br(CH_2)_nBr$ afforded $PhCH_2 < N18N > (CH_2)_nBr$ which was then allowed to react with $H < N18N > H$.[14] Compound **6** was prepared in an analogous fashion except that $H < N18N > H$ was monoalkylated with dansyl chloride rather than benzyl bromide.

Sodium cation flux was measured by using the ^{23}Na NMR-based method of Riddell and co-workers.[15] This technique permits quantitative evaluation of Na^+ transport. The observed rates may be compared with each other and with a standard. Vesicles for the ^{23}Na NMR studies were prepared from phosphatidylcholine (0.14 mmol) and phosphatidylglycerol (0.037 mmol, 4 : 1 w/w). The total Na^+ concentration was adjusted to 100 mM by addition of NaCl. The solutions were buffered using a phosphate buffer held at pH 7.3. The vesicles were prepared by a procedure similar to that described by Papahadjopoulos and Szoka.[16] The preparation used here afforded vesicles having an average diameter of 1750–2000 Å. The total aqueous encapsulation volume in this preparation was 3% as judged by ^{23}Na NMR spectroscopy.

The shift reagent was prepared according to the procedure of Gupta and Gupta[17] from sodium tripolyphosphate and Dy^{3+}. The ^{23}Na NMR chemical shifts were measured as differences between the resonance position in the presence and absence of the Dy^{3+} shift reagent. Compound **6** (standard) or **1**–**5** was incorporated into the vesicles as a CF_3CH_2OH solution ([**1**–**6**] = 5–20 μM). After addition of the subject compound, the samples were agitated and warmed (50–60 °C) for 1 h, cooled to room temperature, and then diluted with D_2O (lock signal) and shift reagent solution. Each solution was allowed to equilibrate for ~1 h before data acquisition. Typically, 240 FID transients were accumulated per data set at 25 °C. The rate results, relative to those determined for **6** (simultaneous with each sample) are recorded in Table 1 and shown graphically in Fig. 1.

The NMR experiment is somewhat complex and we have therefore chosen to normalize the data relative to a simultaneously determined standard (**6**). Transport rates for **6** have

Table 1 Sodium cation transport by tris(macrocycle) ionophores[a]

Cpd.	Structure	Rel. rate[a]
1	$PhCH_2 < N18N > C_8 < N18N > C_8 < N18N > CH_2Ph$	< 2
2	$PhCH_2 < N18N > C_{10} < N18N > C_{10} < N18N > CH_2Ph$	96
3	$PhCH_2 < N18N > C_{12} < N18N > C_{12} < N18N > CH_2Ph$	211[b]
4	$PhCH_2 < N18N > C_{14} < N18N > C_{14} < N18N > CH_2Ph$	201
5	$PhCH_2 < N18N > C_{16} < N18N > C_{16} < N18N > CH_2Ph$	109
6	$Dn < N18N > C_{12} < N18N > C_{12} < N18N > Dn$	100[c]

[a] Rate relative to compound **6**, arbitrarily set at 100. Comparative rates are recorded for 10 μM ionophore concentration. [b] The Na^+ transport rate determined relative to gramicidin (= 100) was 39.[18] [c] The Na^+ transport rate determined relative to gramicidin (= 100) was 23.[19]

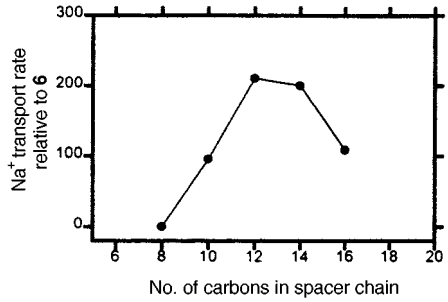

Fig. 1 Na^+ transport *vs.* spacer chain length.

been determined independently more than 10 times and each of the values shown in Table 1 for **1**–**5** represents at least three independent experiments.

Hydraphiles **3** and **6** are both of the form $R < N18N > C_{12} < N18N > C_{12} < N18N > R$ in which R is either benzyl (**3**) or dansyl (**6**). In previous work we noted that the rates for these compounds, relative to gramicidin (= 100), were 39[18] and 23, respectively. The most important observation is that cation flux exhibits clear spacer chain length dependence. Spacer chains having 12 or 14 carbons appear optimal in this system showing relative Na^+ transport rates of 201 and 211, respectively. When the spacer chain length is either increased or decreased by two carbons from the 12–14 range to give **2** or **5**, cation flux is reduced to about half of the previous value. The most striking result, however, is that when the chain length is reduced a further two carbons, $PhCH_2 < N18N > C_8 < N18N > C_8 < N18N > CH_2Ph$ (**1**) proves completely ineffective as an ionophore. Since the hydraphiles are flexible compounds, it seems reasonable that conformational adaptability would still allow function as the chain length increased. If the ionophore must be extended in order to function, the compound must pass a certain size beyond which it simply cannot span enough of the hydrocarbon slab to be functional. This limit appears to have been reached for the octyl spacer chain.

The experimental results presented here resolve two important issues about the hydraphile channel compounds. First, in accord with previous evidence, the carrier mechanism as a possible mode of transport is ruled out. Second, the two-fold changes in transport rates for **2** and **5** compared to **3** or **4** show the sensitivity of this system to dimensional changes of only 4 Å in either direction. This strongly suggests an extended conformation and that the critical membrane span is the insulating hydrocarbon slab rather than the entire phospholipid bilayer.

We thank the NIH for a grant (GM 36262) that supported this work.

Notes and references

1 B. A. Moyer, *Complexation and Transport*, in *Comprehensive Supramolecular Chemistry*, vol. 1, ed. G. W. Gokel, Elsevier Science, Oxford, 1996, p. 377.
2 B. Hille, *Ionic Channels of Excitable Membranes*, 2nd edn., Sinauer Press, Sunderland, MA, 1992; D. G. Nicholls, *Proteins, Transmitters, and Synapses*, vol. 1994, Oxford, Blackwell, 1994; D. J. Aidley and P. R. Stanfield, *Ion Channels: Molecules in Action*, Cambridge University Press, Cambridge 1996.
3 D. A. Doyle, J. M. Cabral, R. A. Pfuetzner, A. Kuo, J. M. Gulbis, S. L. Cohen, B. T. Chait and R. MacKinnon, *Science*, 1998, **280**, 69.
4 G. W. Gokel and O. Murillo, *Acc. Chem. Res.*, 1996, **29**, 425.
5 O. Murillo, S. Watanabe, A. Nakano and G. W. Gokel, *J. Am. Chem. Soc.*, 1995, **117**, 7665.
6 Hydra is defined in *The American Heritage Dictionary* as 'any of several small freshwater polyps of the genus *Hydra* and related genera, having a naked cylindrical body and an oral opening surrounded by tentacles.' This is structurally appropriate to the present systems. The term hydraphile also connotes to us the concept of hydrophilicity. We favor 'hydraphile' over the more cumbersome 'bolaamphiphile' which evokes a vision of random spheres at the ends of swirling and disorganized tethers.
7 O. Murillo, I. Suzuki, E. Abel, C. L. Murray, E. S. Meadows, T. Jin and G. W. Gokel, *J. Am. Chem. Soc.*, 1997, **119**, 5540.
8 O. Murillo, I. Suzuki, E. Abel and G. W. Gokel, *J. Am. Chem. Soc.*, 1996, **118**, 7628.
9 O. Murillo, E. Abel, G. E. M. Maguire and G. W. Gokel, *Chem. Commun.*, 1996, 2147.
10 M. C. Wiener and S. H. White, *Biophys. J.*, 1992, **61**, 434.
11 D. A. Doyle, J. M. Cabral, R. A. Pfuetzner, A. Kuo, J. M. Gulbis, S. L. Cohen, B. T. Chait and R. MacKinnon, *Science*, 1998, **280**, 69.
12 **1**: Anal. calc. for $C_{66}H_{118}O_{12}N_6$: C, 66.74; H, 10.01; N, 7.08%. Found: C, 66.52; H, 9.92; N, 6.98%. **2**: [ESI, $(M + H)^+$] Calc. for $C_{70}H_{126}N_6O_{12}$: 1243.94; Found: 1243.90. **4**: [ESI, $(M + H)^+$] Calc. for $C_{78}H_{143}N_6O_{12}$: 1356.07; Found: 1356.10. **5**: [ESI, $(M + H)^+$] Calc. for $C_{82}H_{151}N_6O_{12}$: 1412.10; Found: 1412.10.
13 F. Cuevas and J. de Mendoza, personal communication, 1998.
14 Compounds **3** (ref. 5) and **6** (ref. 7) were previously reported. The remaining compounds had ^1H NMR, ^{13}C NMR, and high resolution mass spectral data in accord with their structures.
15 F. G. Riddell and M. K. Hayer, *Biochim. Biophys. Acta*, 1985, **817**, 313; D. C. Buster, J. F. Hinton, F. S. Millett and D. C. Shungu, *Biophys. J.*, 1988, **53**, 145; F. G. Riddell, S. Arumugam, P. J. Brophy, B. G. Cox, M. C. H. Payne and T. E. Southon, *J. Am. Chem. Soc.*, 1988, **110**, 734; F. G. Riddell and S. Arumugam, *Biochim. Biophys. Acta*, 1989, **984**, 6; F. G. Riddell and S. J. Tompsett, *Biochim. Biophys. Acta*, 1990, **1024**, 193.
16 D. Papahadjopoulos and F. Szoka, *Proc. Natl. Acad. Sci. USA*, 1978, **75**, 4194.
17 R. Gupta and P. Gupta, *J. Magn. Reson.*, 1982, **47**, 344.
18 In previous work we have used gramicidin as standard. This is described in detail in ref. 5. With increasing experience and confidence, we have adopted a hydraphile as standard because of its greater structural similarity to the compounds under study.
19 E. Abel, G. E. M. Maguire, E. S. Meadows O. Murillo, T. Jin and G. W. Gokel, *J. Am. Chem. Soc.*, 1997, **119**, 9061.

Communication 8/06317F

Diastereoselective cyclopropanation of α,β-unsaturated acetals of a novel camphor-derived chiral auxiliary

Perry T. Kaye* and Warner E. Molema

Department of Chemistry, Rhodes University, Grahamstown, 6140, South Africa. E-mail: chpk@hippo.ru.ac.za

Received (in Cambridge, UK) 3rd September 1998, Accepted 6th October 1998

Reaction of selected α,β-unsaturated aldehydes with phenyl 2,3-dihydroxybornane-10-sulfonate affords acetals which undergo diastereoselective (>99% de) Simmons-Smith cyclopropanation.

The cyclopropyl group occurs in various natural products[1] and, due to its inherent ring strain, finds use as a structural intermediate in synthesis.[2] Barrett and Kasdorf,[3] for example, have exploited the Charette methodology[4] in tandem asymmetric cyclopropanation reactions in the synthesis of a nucleoside containing five cyclopropane units. The Simmons-Smith reaction[5] is commonly used to construct cyclopropane derivatives, and asymmetric applications involving the use of chiral acetals[6] and ketals[7] have been described. We have recently reported[8] moderate diastereoselectivity (40–70% d.e.) in the Simmons-Smith cyclopropanation of α,β-unsaturated acetals, using bornane-2,3-diol as a chiral auxiliary. Increasing steric demand at C-10 of the bornane skeleton was expected to enhance diastereofacial selectivity, and here we report the synthesis and use of phenyl 2-*exo*,3-*exo*-dihydroxybornane-10-sulfonate **4** as a highly efficient chiral auxiliary for the asymmetric cyclopropanation of α,β-unsaturated acetal derivatives.

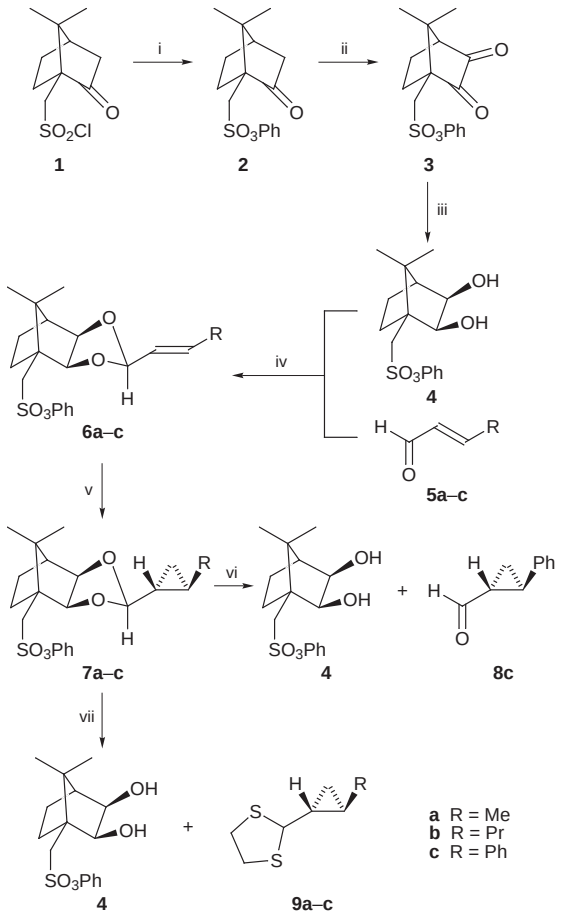

Scheme 1 *Reagents and conditions*: i, PhOH, pyridine; ii, H_2SeO_3, dioxane; iii, $NaBH_4$, MeOH; iv, TsOH, $MgSO_4$, benzene; v, Et_2Zn, CH_2I_2, CH_2Cl_2, −10 °C; vi, (for R = Ph) TsOH, THF–H_2O, reflux, 72 h; vii, $HSCH_2CH_2SH$, TsOH, CH_2Cl_2.

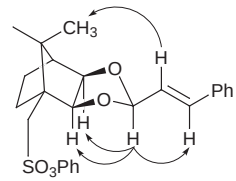

Fig. 1 NOE interactions observed in the NOESY spectrum of the acetal **6c**.

Treatment of (+)-camphor-10-sulfonyl chloride **1** with phenol in pyridine at 0 °C afforded the phenyl ester **2** in 81% yield (Scheme 1), the corresponding camphorquinone **3**† being obtained by subsequent selenous acid (H_2SeO_3) oxidation. Reduction of the diketone **3** with $NaBH_4$ gave the required diol **4**, which was unambiguously characterised by elemental (HRMS) and spectroscopic analysis.‡

Following the procedure developed for the synthesis of bornane-2,3-diol acetals,[8] the diol **4** was condensed with the α,β-unsaturated aldehydes **5a–c** to give the corresponding acetals **6a–c** in 64–74% yield. ^1H and ^{13}C NMR analyses indicated the formation of a single diastereomeric acetal in each case. The presence of heteroatoms and bulky substituents is known to inhibit pseudorotation in 1,3-dioxolane rings[9] and, in the systems studied here, fusion to the rigid bicyclic bornane skeleton is likely to lock the 1,3-dioxolane ring into an envelope conformation. Steric factors are expected to favour formation of the *exo*-acetals—an expectation supported by the NOE interactions observed for the cinnamaldehyde acetal **6c** (Fig. 1) and confirmed by single crystal X-ray analysis of this compound (Fig. 2).§

The Simmons-Smith organozinc reagent exhibits high affinity for ethereal oxygen, and transition state steric demands are considered to be significant.[10] Computer modelling¶ (Fig. 3) clearly indicates the capacity of the phenyl sulfonate moiety to hinder access to the 'front' face of the unsaturated acetals **6a–c**, and initial coordination of the organozinc reagent to the less

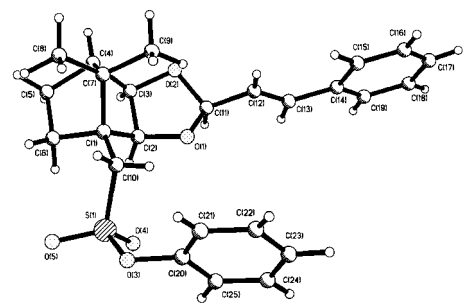

Fig. 2 X-Ray crystal structure of the acetal **6c** at 173 K, showing the crystallographic numbering.

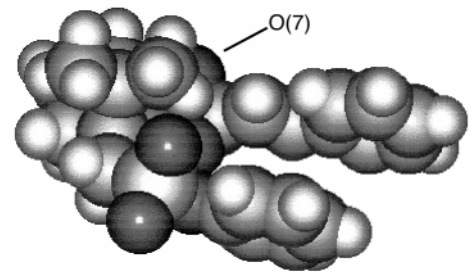

Fig. 3 Computer-modelled space-filling structure of a rotamer of the acetal **6c**, in which the phenyl sulfonate moiety effectively blocks access to one face of the double bond.

hindered acetal oxygen O(7) is predicted to precede methylene delivery from the 'back'.

Cyclopropanation of the acetals **6a–c** was effected by their dropwise addition (as solutions in dry CH_2Cl_2) to a cold, vigorously stirred mixture of Et_2Zn and CH_2I_2 in CH_2Cl_2.[8] Work-up and preparative layer chromatography afforded the cyclopropyl derivatives **7a–c** in good material yield (76–95%) and with complete diastereoselectivity (> 99% de).‖ Confirmation of the predicted stereochemical bias was achieved by hydrolysis of acetal **7c** to afford the known[11] laevorotatory (1*R*, 2*R*)-aldehyde **8c**;** the remarkable resistance of the acetal **7c** to acidic hydrolysis under various conditions is attributed to steric crowding. Release of the chiral auxiliary **4** (in 83–87% yield) from the cyclopropyl derivatives **7a–c** was finally achieved by transthioacetalisation,[12] the corresponding dithiolanes **9a–c** being isolated in 87–92% yield.††

We thank the Foundation for Research and Development (FRD) and Rhodes University for generous financial support, and Dr Leanne Cook (University of the Witwatersrand) for the X-ray crystallographic analysis.

Notes and references

† *Selected data* for **3**: yellow crystals, 48%, mp 78–82 °C (Found: M^+ 322.0846. $C_{16}H_{18}O_5S$ requires *M*, 322.0875).

‡ *Selected data* for **4**: 51%, mp 126–130 °C (from CCl_4) (Found: M^+ 326.1194. $C_{16}H_{22}O_5S$ requires *M*, 326.1188); υ_{max}(KBr)/cm^{-1} 3300 (OH) and 1370 and 1150 (SO_2O); δ_H (400 MHz; $CDCl_3$) 0.84 and 1.14 (6H, 2 × s, 8- and 9-Me), 1.08, 1.49 and 1.76 (4H, 3 × m, 5-CH_2 and 6-CH_2), 1.86 (1H, d, 4-H), 3.05 and 3.21 (2H, 2 × m, 2- and 3-OH), 3.46 (2H, dd, 10-CH_2), 3.88 and 4.16 (2H, 2 × m, 2- and 3-H) and 7.27–7.43 (5H, m, Ar-H); δ_C(100 MHz; $CDCl_3$) 20.8 and 21.9 (C-8 and C-9), 23.7 and 29.4 (C-5 and C-6), 49.1 and 49.4 (C-1 and C-7), 49.8 (C-10), 50.4(C-4), 75.7 and 76.1 (C-2 and C-3) and 122.0, 127.3, 130.0 and 149.1 (Ar-C); *m/z* 308 (**M**−H_2O, 0.001%) and 94 (100).

§ *Crystal data* for **6c**: $C_{25}H_{28}O_5S$, M = 440.53; crystal size 0.36 × 0.18 × 0.08 mm, orthorhombic, space group $P2_12_12_1$; a = 6.8183(4), b = 13.0928(8), c = 25.198(2) Å, V = 2249(2) Å^3, Z = 4, F(000) = 936, D_c = 1.301 g cm^{-3}, μ = 0.178 mm^{-1}. Data collection (Siemens SMART CCD diffractometer; graphite-monochromated Mo-Kα radiation, λ = 0.71070 Å, T = 173 K), ω–2θ scans, 1.62 < θ < 28.26°, 13981 reflections collected (−9 ⩽ h ⩽7, −17 ⩽ k ⩽ 17, −26 ⩽ l ⩽17), 5049 unique with $I > 2\sigma(I)$. Hydrogen atoms were placed in calculated positions and the structure was solved by direct methods using SHELXTL (ref. 13); full-matrix least-squares refinement converged at R_1 = 0.810, wR_2 = 0.1713, GOF = 1.133. Max., min. peaks in final difference map = 0.221, −0.253 e Å^{-1}. CCDC 182/1049.

¶ Using the computer modelling software package, HYPERCHEM®.

‖ As evidenced by both ^{1}H and ^{13}C NMR spectroscopy.

** A solution of the acetal **7c** and PTSA (2 equiv.) in THF–H_2O (5:1) was boiled under reflux for 72 h to afford the aldehyde **8c** (10%), $[\alpha]_D^{26}$ −324 (*c* 0.333, $CHCl_3$), corresponding to (−)-(1*R*,2*R*)-2-phenylcyclopropanecarbaldehyde {$[\alpha]$ −340 (*c* 0.363, $CHCl_3$)} (ref. 11).

†† The cyclopropyl dithiolanes **9a–c** (87–92%) and the diol **4** (83–87%) were obtained from the acetals **7a–c**, following a method described by Caballero *et al*. (ref. 12) and gave satisfactory elemental (HRMS) and spectroscopic analyses. Optical rotation data for the dithiolanes are as follows: **9a**: $[\alpha]_D^{26}$ −35.2 (*c* 0.774, $CHCl_3$); **96**: $[\alpha]_D^{26}$ −18.9 (*c* 2.144, $CHCl_3$); **9c** $[\alpha]_D^{26}$ −88.4 (*c* 1.300, $CHCl_3$).

1 See, for example, A. Mori, I. Arai, H. Yamamoto, H. Nakai and Y. Arai, *Tetrahedron*, 1986, **42**, 6447; A. G. M. Barrett, K. Kasdorf, A. J. P. White and D. J. Williams, *J. Chem. Soc., Chem. Commun*., 1995, 649.
2 H. N. C. Wong, M.-Y. Hon, C.-W. Tse, Y.-C. Yip, J. Tanko and T. Hudlicky, *Chem. Rev*., 1989, **89**, 165.
3 A. G. M. Barrett and K. Kasdorf, *Chem. Commun*., 1996, 325.
4 A. B. Charette and H. Juteau, *J. Am. Chem. Soc*., 1994, **116**, 2651.
5 H. E. Simmons and R. D. Smith, *J. Am. Chem. Soc*., 1958, **80**, 5323.
6 I. Arai, A. Mori and H. Yamamoto, *J. Am. Chem. Soc*., 1985, **107**, 8254; J. Kang, G. J. Lim, S. K. Yoon and M. Y. Kim, *J. Org. Chem*., 1995, **60**, 564.
7 E. A. Mash, S. K. Math and C. J. Flann, *Tetrahedron*, 1989, **45**, 4945.
8 P. T. Kaye and W. E. Molema, *Synth. Commun.*, in press.
9 W. E. Willy, G. Binsch and E. L. Eliel, *J. Am. Chem. Soc*., 1970, **92**, 5394.
10 T. L. Cairns, H. E. Simmons and S. A. Vladuchick, *Org. React*., 1972, **20**, 1.
11 H. Abdallah, R. Cree and R. Carrie, *Tetrahedron Lett*., 1982, **23**, 503.
12 M. Caballero, M. Garcia-Valverde, R. Pedrosa and M. Vicente, *Tetrahedron*: *Asymmetry*, 1996, **7**, 219.
13 G. M. Sheldrick, SHELXTL Ver. 5.03, 1996, Institut für Anorg. Chemie, Göttingen.

Communication 8/06867D

The effect of strain on reactivity: poor leaving groups increase strain-induced inhibition of alkene-forming elimination

Luca Volta and Charles J. M. Stirling*

Department of Chemistry, The University, Sheffield, UK S3 7HF. E-mail: c.stirling@sheffield.ac.uk

Received (in Liverpool, UK) 28th September 1998, Accepted 6th October 1998

Elimination to form a carbon–carbon double bond exocyclic to a cyclopropane ring is inhibited by factors which increase from 1.4 to $10^{4.5}$ as the leaving group becomes poorer; strain induced in the transition structure can amount to some 50% of the enthalpy difference between strained and unstrained products.

The effect of strain on reactivity is a very familiar phenomenon, but one which has only rarely been quantified.[1] In order to quantify the effects of strain on reactivity properly, systems of known and defined strain energy are required (not always a simple matter) and reactions of unambiguous mechanism are also needed (not always a simple matter either). In this connection, earlier work from these laboratories has examined acceleration of 1,2-elimination by incorporation of the leaving group in a strained ring.[2–4] In such cases acceleration results from the release of strain, effectively lowering the energy of the transition structure relative to the starting material. We have also examined the effect of strain in the inhibition of higher order eliminations leading to strained ring products in which the effects of strain are remarkably variable.[5,6] Both situations have been examined theoretically[7,8] and the correlation between theory and practice is good.

We now report on the kinetics of formation of methylenecyclopropanes in activated 1,2-eliminations which reveal the impact of strain as the transition structure changes. The systems we have examined, involving five different leaving groups (Z) are in Table 1, giving rate constants for the unstrained [eqn. (1)] and strained reactions [eqn. (2)] respectively. Making the

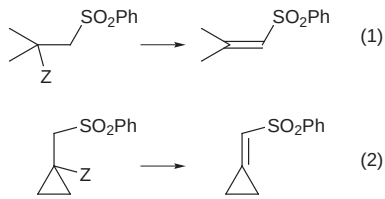

assumption that strain energies are unaffected by substituents, the strain energy difference between substrate and product for the methylenecyclopropane systems of eqn. (2) amounts to 50 kJ mol^{-1}. This is the strain energy difference between cyclopropane and methylenecyclopropane[9] although its origin is under discussion.[10]

The open-chain halides **1** were obtained by homolytic addition of sulfonyl halides to 2-methylpropene.[11] Addition of thiophenol to the alkenyl sulfone **2** gave sulfide **3** which on oxidation gave the bis-sulfone **4** The cyclopropanes were obtained by the routes of Scheme 1. Reactions were run in ethanolic sodium ethoxide to allow direct comparisons with earlier results; the product from the open-chain substrates was the conjugated alkene **2** and non-conjugated alkene **2a**,[12] while the cyclopropanes gave the ethoxy adduct **10** from slow elimination followed by rapid addition to the electrophilic methylenecyclopropane **7**. The unlikely alternative course of direct substitution was ruled out by the piperidine test in which, for example, the bis-sulfone **9** failed to react with piperidine in ethanol (too weakly basic) but reacted rapidly with piperidine in ethanolic sodium ethoxide to give the piperidino derivative **11** (piperidine more nucleophilic than ethoxide).

Reactions were followed by UV spectroscopy for reactions in which the product alkene was detectable and otherwise by GC. Reactions were first order in substrate and first order in base.

Before comment on the impact of strain differentials can be made, it is crucial to be certain of the mechanism of the reactions in each case. Two methods to throw light on the mechanisms have been adopted; the observed rate constants have been compared with the rates of ionisation obtained by interpolation on a Taft plot[13] of $k_{ionisation}$ in ethanolic sodium ethoxide *versus* the inductive constant σ^*. It can be seen that for the leaving groups SO_2Ph, SPh and OMe, the rate constant for ionisation is greater than the elimination rate constant. This points for each case to the $(E1cB)_R$ mechanism, in which a pre-equilibrium with the carbanion is established with the base–solvent system. The rate-determining step in each case, therefore, is the expulsion of the leaving group from the intermediate carbanion. The second procedure was to carry out reactions in EtOD and to examine by ^2H NMR spectroscopy recovered starting material for deuterium incorporation. In all of these cases, starting material had exchanged considerably with the solvent, confirming the conclusions from interpolation. By contrast, with the halogen leaving groups, the observed rate constants in all cases are close to or greater than the interpolated ionisation rate constants and no incorporation of deuterium occurred in exchange experiments. These observations point

Table 1 Elimination to form unstrained and strained alkenes

	Rate constants/mol^{-1} dm^3 s^{-1}				
	Open chain		Cyclopropane		
Z	k_{EtO^-} [a]	$k_{ion.}$ [a,b]	k_{EtO^-} [a]	$k_{ion.}$ [a,b]	k_{rel} unstrained:strained
Br	2.3×10^2	2.3×10^1	3.2×10^2	3.2×10^1	0.7
Cl	7.8×10^1	4.1×10^1	5.5×10^1	5.7×10^1	1.4
SO_2Ph	3.44	8.8×10^2	1.5×10^{-2}	1.2×10^3	230
SPh	6.6×10^{-2}	4.8×10^{-1}	1.0×10^{-5}	6.7×10^{-1}	6000
OMe	4.3×10^{-5} [c]	3.1	1.5×10^{-9} [d]	5.3×10^{-1}	29 000

[a] For reactions in EtONa–EtOH at 25 °C. [b] See text. [c] See ref. 13; [d] By extrapolation from an Arrhenius plot.

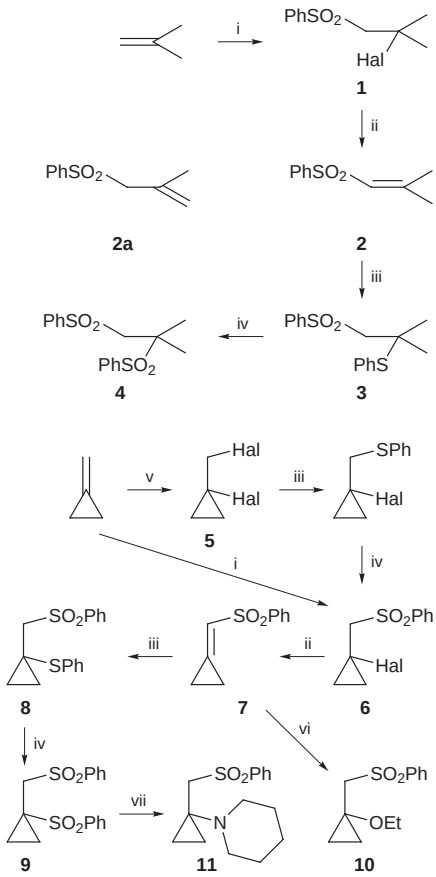

Scheme 1 *Reagents and conditions*: i, $PhSO_2Hal$, AIBN, benzene, 90 °C, 72 h; ii, Et_3N, PhMe; iii, PhSNa, EtOH; iv, H_2O_2, AcOH; v, Hal_2, THF; vi, EtONa, EtOH; vii, EtONa, EtOH, piperidine.

either to the E2 mechanism, in which departure of the leaving group is concerted with β-proton removal, or to the $(E1cB)_I$ mechanism, in which it is not. For the latter mechanism, a close similarity between k_{EtO^-} and $k_{ionisation}$ is to be expected. This is true for the chlorides, but the comparison for the bromides suggests concerted mechanisms.

For 1,2-eliminations, it can reasonably be concluded that the more difficult the leaving group is to expel, the greater is the degree of double-bond character in the transition structure required to expel it. In earlier work[14] we were able to compare accurately the leaving abilities of a series of groups placed β to a sulfonyl-stabilised carbanion. These groups included SO_2Ph, SPh and OMe in descending order of nucleofugality. Nucleofugalities of halide leaving groups could not be assigned because, as in the present work, the reactions did not follow the $(E1cB)_R$ mechanism. Our observation of probable E2 and/or $(E1cB)_I$ mechanisms for the halides mentioned above, suggests higher nucleofugalities for the halogens, as would be expected.

The results of Table 1 show that as the nucleofugality of the leaving group decreases, so the ratio of the reactivities of the unstrained to the strained substrates increases. This reveals a consistent picture in which as the nucleofugality of the leaving group decreases, so the degree of double bond character in the transition structure increases and the additional strain of the double bond exocyclic to the cyclopropane ring is increasingly felt.

This leaves the important question of the extent of strain inhibition in these reactions. In the system with the largest unstrained to strained reactivity ratio, *i.e.* with Z = OMe, the inhibition amounts to a factor of some 29,000 or about 26 kJ mol^{-1} in $\Delta G^{\ddagger}$. This amounts to about 50% of the strain energy difference between strained and unstrained products. When the leaving group is halogen, the unstrained and strained substrates have almost identical reactivities and there appears to be so little double bond character in the transition structure that reactions are little inhibited by formation of a strained alkene product.

We thank the University of Sheffield for the support of this work and Elaine Frary for preliminary experiments.

Notes and references

1 C. J. M. Stirling, *Tetrahedron*, 1985, **41**, 1613.
2 H. A. Earl and C. J. M. Stirling, *J. Chem. Soc., Perkin Trans. 2*, 1987, 1273.
3 D. J. Young and C. J. M. Stirling, *J. Chem. Soc., Perkin Trans. 2*, 1996, 425.
4 S. W. Roberts and C. J. M. Stirling, *J. Chem. Soc., Chem. Commun.*, 1991, 170
5 F. Benedetti and C. J. M. Stirling, *J. Chem. Soc., Perkin Trans. 2*, 1986, 605.
6 S. M. Jeffery and C. J. M. Stirling, *J. Chem. Soc., Perkin Trans. 2*, 1993, 2163.
7 S. M. van der Kerk, J. W. Verhoeven and C. J. M. Stirling, *J. Chem. Soc., Perkin Trans. 2*, 1985, 1355.
8 G. Tonachini, F. Bernardi, H. B. Schlegel and C. J. M. Stirling, *J. Chem. Soc., Perkin Trans. 2*, 1988, 705.
9 J. F. Liebman and A. Greenberg, in *The Chemistry of the Cyclopropyl Group*, ed. Z. Rappoport, Wiley, Chichester, ch. 18, 1987.
10 W. T. G. Johnson and W. T. Borden, *J. Am. Chem. Soc.*, 1997, **119**, 5930.
11 S. Caddick, C. L. Shering and S. N. Woolman, *Chem. Commun.*, 1997, 171.
12 I. Sataty and C. Y. Myers, *Tetrahedron Lett.*, 1974, 4161.
13 P. J. Thomas and C. J. M. Stirling, *J. Chem. Soc., Perkin Trans. 2*, 1977, 1909.
14 D. R. Marshall, P. J. Thomas and C. J. M. Stirling, *J. Chem. Soc., Perkin Trans. 2*, 1977, 1898.

Communication 8/07506I

Synthesis of axially chiral *N,N*-diethyl 2,6-disubstituted benzamides utilizing planar chiral (arene)chromium complexes

Hiroshige Koide[a] and Motokazu Uemura*[a,b]

[a] *Department of Chemistry, Faculty of Integrated Arts and Sciences, Osaka Prefecture University, Sakai, Osaka 599-8531, Japan. E-mail: uemura@ms.cias.osakafu-u.ac.jp*

[b] *Research Institute for Advanced Science and Technology, Osaka Prefecture University, Sakai, Osaka 599-8570, Japan*

Received (in Cambridge, UK) 3rd August 1998, Accepted 28th September 1998

Axially chiral *N,N*-diethyl 2,6-disubstituted benzamides are prepared stereoselectively in an optically active form from a planar chiral (arene)chromium complex.

The tertiary arylamides with 2,6-disubstituents are a class of atropisomeric compounds[1] and the chromatographic separation of some racemates to optically active axial aromatic carboxamides has been achieved by using HPLC on a chiral stationary phase.[2] Clayden and co-workers have reported[3] the synthesis of *diastereomeric* atropisomers by reaction of *N,N*-dialkyl 2-lithio-1-naphthamides with the aldehydes, or reduction of *N,N*-dialkyl-2-acyl-1-naphthamides, or laterally lithiation of *N,N*-dialkyl 2-alkyl-1-naphthamides followed by eletrophilic quenching. The asymmetric deprotonation of *N,N*-dialkyl-1-naphthamides with a combination of butyllithium/(−)-sparteine followed by quenching with alkylhalides giving the axially chiral *N,N*-dialkyl 2-alkyl-1-naphthamides in an optically active form has been recently reported by Beak.[4] However, the optical purity of the axial aromatic carboxamides obtained by this asymmetric deprotonation with the chiral base is moderate. To the best of our knowledge, there is no previous report of asymmetric synthesis of *N,N*-dialkyl 2,6-disubstituted aromatic carboxamides in an *enantiomerically pure form*.

We wish to report the asymmetric synthesis of axially chiral *N,N*-dialkyl 2,6-disubstituted benzamides in an *enantiomerically pure form* by using a planar chiral arene chromium complex.

Both enantiomers of the axially chiral 2-ethyl-6-methylbenzamide were synthesized as shown in Scheme 1. Enantiomerically pure (−)-tricarbonyl(*o*-methylbenzaldehyde)chromium (**1**)[5] was oxidized to the corresponding (−)-methyl benzoate chromium complex **2** ($[\alpha]_D^{26}$ −100.0)† with active manganese dioxide and sodium cyanide in acetic acid and methanol in 85% yield. Conversion of the methyl ester to the corresponding (+)-*N,N*-diethylamide complex **3** ($[\alpha]_D^{26}$ +8.4) was achieved by treatment with lithium diethylamide in THF at −78 °C in 80% yield. Directed *ortho* lithiation[6] of *N,N*-diethyl *o*-methylbenzamide complex **3** with Bu^{t}Li in the presence of TMEDA followed by quenching with ethyl iodide gave the axially chiral (−)-(S_{Ar},S_{ax})[7]-tricarbonyl(*N,N*-diethyl 2-ethyl-6-methylbenzamide)chromium (**4**) ($[\alpha]_D^{25}$ −31.0) in 36% yield, along with 15% yield of tricarbonyl(*N,N*-diethyl 2-propylbenzamide)chromium *via* benzyl methyl lithiation. In this *ortho* lithiation, the *N,N*-diethyl benzamide complex **4** was obtained as a single axially chiral compound without formation of the corresponding (*R*)-axial isomer. The stereochemistry of the axially chiral benzamide complex **4** was determined by X-ray crystallography,‡ and the axial chirality was found to be the (*S*)-configuration in which the diethylamino part was oriented in an *anti*-conformation to the tricarbonylchromium moiety, and the amide carbonyl oxygen is in a *syn*-orientation. The X-ray crystal structure shows that the dihedral angle between the plane of the amide and the aryl ring is approximately perpendicular. The formation of **4** as the single axial isomer by electrophilic quenching of the *ortho*-lithiated intermediate may be attributed to the stereoelectronic repulsion between the tricarbonylchromium and diethylamino fragments. After producing the axially chiral *N,N*-diethyl 2-ethyl-6-methylbenzamide chromium complex **4**, we next investigated an oxidative demetalation giving a chromium free axially chiral *N,N*-diethyl 2-ethyl-6-methylbenzamide. Thus, a solution of (−)-**4** in ether was exposed to sunlight at 0 °C until the yellow color of the solution disappeared. The demetalation product, *N,N*-diethyl 2-ethyl-6-methylbenzamide (**5**) has a positive optical rotation value ($[\alpha]_D^{26}$ +14.0). Similarly, the corresponding axially chiral antipode (−)-*N,N*-diethyl 6-ethyl-2-methylbenzamide (**7**) ($[\alpha]_D^{26}$ −13.0) was obtained from the antipode (+)-tricarbonyl(2-methylbenzaldehyde)chromium (**6**)[5] by following the same reaction sequence. The optical purities of the axial *N,N*-diethyl 2-ethyl-6-methylbenzamides, **5** and **7**, were found to be ~94% ee.[8] However, the optical rotation values of these chromium free axial benzamides slowly decreased on standing at room temperature.

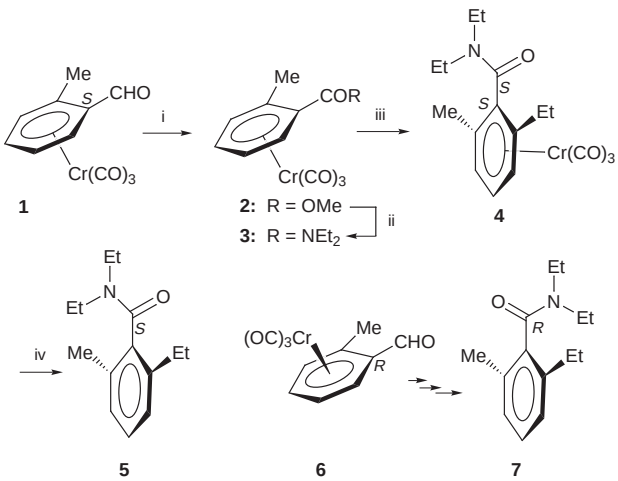

Scheme 1 i, MnO_2, NaCN, AcOH, MeOH, 85%; ii, $LiNEt_2$, THF, −78 °C, 80%; iii, Bu^{t}Li, TMEDA, THF, −78 °C, then EtI, 36%; iv, *hv*, O_2, diethyl ether, 0 °C, 90%.

Since the *N,N*-diethyl 2-ethyl-6-methylbenzamide underwent slow racemization at room temperature,[9] the sterically bulky substituent was next introduced at the *ortho*-position to inhibit the axial isomerization (Scheme 2). The *o*-lithiated intermediate derived from **3** was trapped with acetaldehyde to produce a diastereomeric mixture of **8** at the newly created benzylic center in a ratio of 54 : 46 in 44% yield. The diastereomeric mixture **8** was acetylated, and then treated with triethylaluminium to give tricarbonyl(*N,N*-diethyl 2-methyl-6-isopropylbenzamide)chromium (**9**) ($[\alpha]_D^{24}$ −54.0) *via* a tricarbonylchromium-stabilized benzylic carbocation intermediate[10] in 60% yield. Alternatively, the hydroxide of diastereoisomeric complex **8** was oxidized with acetic anhydride and DMSO to afford acetophenone complex **11** which was further converted to tertiary-alcohol complex **12** ($[\alpha]_D^{25}$ +37.0) by treatment with $MeCeCl_2$

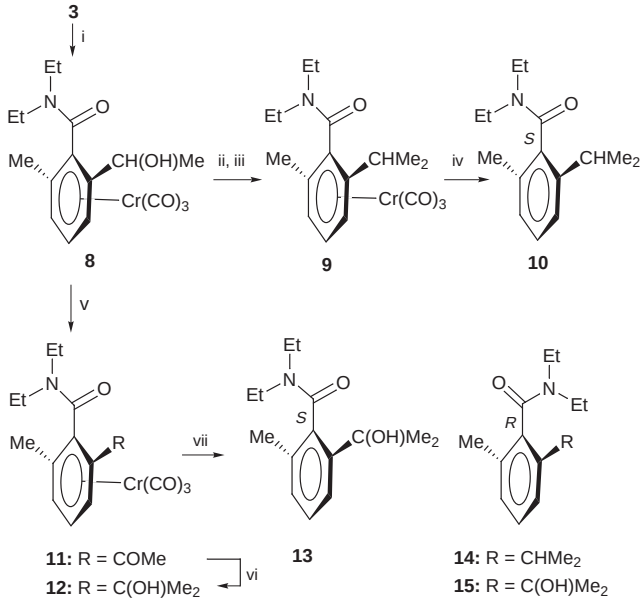

Scheme 2 i, Bu^{s}Li, TMEDA, THF, −78 °C, then MeCHO, 44%; ii, Ac_2O, pyridine, DMAP; iii, Me_3Al, CH_2Cl_2, −78 °C, 60% from **8**; iv, *hν*, O_2, diethyl ether, 0 °C, 98%; v, DMSO, Ac_2O, 88%; vi, $MeCeCl_2$, THF, −78 °C, 94%; vii, *hν*, O_2, diethyl ether, 0 °C, 90%.

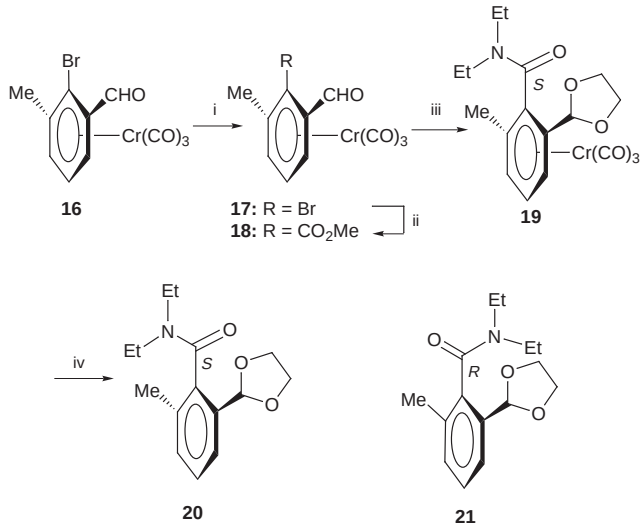

Scheme 3 i, $HO(CH_2)_2OH$, *p*-TsOH, MeCN, $MgSO_4$, 84%; ii, Bu^{n}Li, TMEDA, diethyl ether, then ClCOOMe, 83%; iii, $LiNEt_2$, THF, −78 °C, 60%; iv, *hν*, O_2, diethyl ether, 0 °C, 90%.

in 74% overall yield. These tricarbonylchromium-complexed axially chiral benzamides **9** and **12** gave the (*S*)-axially chiral benzamides **10** ($[\alpha]_D^{23}$ +9.8) and **13** ($[\alpha]_D^{27}$ +63.2) in >99% ee[8] by oxidative demetalation, in which the optical purities of these compounds did not change after prolong standing (36 h) at room temperature. On the other hand, the corresponding (*R*)-axially chiral 2-methyl-6-substituted benzamides **14** ($[\alpha]_D^{23}$ −9.8) and **15** ($[\alpha]_D^{27}$ −63.2) with its optical antipode were prepared from **6** by the same reaction sequence. Thus, axially chiral *N*,*N*-diethyl 2,6-disubstituted benzamides were stereoselectively prepared in enantiomerically pure form by *ortho* lithiation of the planar chiral (benzamide)chromium complex.

Furthermore, the enantiomerically pure axially chiral *N*,*N*-diethyl 2,6-disubstituted benzamide was also stereoselectively prepared by conversion of the methyl ester of planar chiral tricarbonyl(methyl 2,6-disubstituted benzoate)chromium to the diethylamide group as follows (Scheme 3). Thus, the enantiomerically pure (−)-tricarbonyl(2-bromo-3-methylbenzaldehyde)tricarbonylchromium (**16**) ($[\alpha]_D^{27}$ −752.6) was converted to the corresponding tricarbonylchromium complex of methyl 2,6-disubstituted benzoate **18** ($[\alpha]_D^{27}$ −10.4) by usual method. Complex **18** was treated with lithium diethylamide at −78 °C in THF to produce stereoselectively (−)-*N*,*N*-diethyl benzamide **19** ($[\alpha]_D^{25}$ −75.2) with (*S*)-axial configuration as a single isomer in which the stereochemistry was determined by X-ray crystallography.‡ No diastereoisomeric (*R*)-axial benzamide chromium complex was obtained in this reaction. It is reasonable to assume that the sterically bulky diethylamino group approached from the *exo*-side to the tricarbonylchromium moiety. Complex **19** was exposed to sunlight to produce the enantiomerically pure[8] axially chiral benzamide **20** ($[\alpha]_D^{27}$ +33.7). The corresponding (−)-(*R*)-axial benzamide **21** ($[\alpha]_D^{27}$ −33.2) was also prepared from the antipode (+)-(3-methyl-2-bromobenzaldehyde)tricarbonylchromium by the same reaction sequence. This axially chiral compound **20** is stable against axial isomerization at room temperature.

In conclusion, we have demonstrated that axially chiral *N*,*N*-diethyl 2,6-disubstituted benzamides can be prepared with high optical purities by using planar chiral tricarbonyl(arene)chromium complexes.

Partial financial support for this work was provided by a Grant-in-Aid for Scientific Research from the Ministry of Education, Science, Sports and Culture of Japan. We acknowledge the financial support by The Asahi Glass Foundation and Ciba-Geigy Foundation (for Japan).

Notes and references

† All optical rotation values were measured in $CHCl_3$ solution.

‡ *Crystal data* for racemic **4**: empirical formula $C_{17}H_{21}NO_4Cr$, M = 355.35, yellow prismatic, monoclinic, space group $P2_1$, a = 7.363(1), b = 17.4258(7), c = 13.8120(9) Å, β = 96.490(8)°, V = 1760.7(3) Å^3, Z = 4, D_c = 1.340 g cm^{-3}, $F(000)$ = 744.00, μ(CuKα) = 55.12 cm^{-1}, $R(R_W)$ = 0.041 (0.058). A total of 2661 data were collected (using ω scans with 58.58 < 2θ < 59.87°), of which 2443 were unique (R_{int} = 0.014). For racemic **19**: empirical formula $C_{18}H_{21}NO_6Cr$, M = 399.36, yellow prismatic, monoclinic, space group $P2_1/n$, a = 7.487(2), b = 19.806(1), c = 12.905(2) Å, β = 104.93(2)°, V = 1849.0(6) Å^3, Z = 4, D_c = 1.435 g cm^{-3}, $F(000)$ = 832.00, μ(MoKα) = 6.52 cm^{-1}, $R(R_W)$ = 0.039 (0.052), A total of 4559 data were collected (using ω scans with 29.64 < 2θ < 30.00°), of which 4246 were unique (R_{int} = 0.029). CCDC 182/1037.

1 J. H. Ackerman and G. M. Laidlaw, *Tetrahedron Lett.*, 1969, 4487; 1970, 2381; P. M. van Lier, G. H. W. M. Meulendijks and H. M. Buck, *Rec. Trav. Chim. Pays-Bas*, 1983, **102**, 337; M. A. Cuyegkeng and A. Mannschreck, *Chem. Ber.*, 1987, **120**, 803; L. A. M. Bastiaansen, J. A. Kanters, F. H. van der Steen, J. A. C. de Graaf and H. M. Buck, *J. Chem. Soc., Chem. Commun.*, 1986, 536; C. Roussel and U. Berg, *Adv. Heterocycl. Chem.*, 1988, **43**, 173.

2 M. A. Cuyegkeng and A. Mannschreck, *Chem. Ber.*, 1987, **120**, 803; W. H. Pirkle, C. J. Welch and A. J. Zych, *J. Chromatogr.*, 1993, **648**, 101.

3 P. Bowles, J. Clayden and M. Tomkinson, *Tetrahedron Lett.*, 1995, **36**, 9219; J. Clayden, N. Westlund and F. X. Wilson, *Tetrahedron Lett.*, 1996, **37**, 5577; J. Clayden and J. H. Pink, *Tetrahedron Lett.*, 1997, **38**, 2565; J. Clayden, M. Darbyshire, J. H. Pink, N. Westlund and F. X. Wilson, *Tetrahedron Lett.*, 1997, **38**, 8587; J. Clayden, J. H. Pink and S. A. Yasin, *Tetrahedron Lett.*, 1998, **39**, 105.

4 S. Thayumanavan, P. Beak and D. P. Curran, *Tetrahedron Lett.*, 1996, **37**, 2899.

5 Enantiomerically pure compound was obtained by optical resolution of diastereomers obtained from L-valinol; see S. G. Davies and C. L. Goodfellow, *J. Chem. Soc., Perkin Trans. 1*, 1990, 393.

6 V. Snieckus, *Chem. Rev.*, 1990, **90**, 879.

7 First symbol *S* indicates the configuration of the tricarbonylchromium-complexed arene carbon substituted by the diethylamido group, the second *S* shows the axial chirality.

8 The optical purities of axial chiral benzamides were determined by ^{1}H NMR spectroscopy in the presence of chiral shift reagent, Eu(tfc)$_3$.

9 The optical purity of compound **5** decreased with time of standing at room temperature; 86% ee after 6 h, 70% ee after 24 h.

10 M. Uemura, K. Kobayashi, K. Isobe, T. Minami and Y. Hayashi, *J. Org. Chem.*, 1986, **51**, 2859.

Communication 8/06064I

Direct synthesis of heterocyclic $[(RP)_nE]^-$ anions using $[E(NMe_2)_3]$ (E = Sb, As); implications to the mechanism of formation of Zintl compounds

Michael A. Beswick,*[a] Nick Choi,[b] Alexander D. Hopkins,[a] Mary McPartlin,[b] Marta E. G. Mosquera,[a] Paul R. Raithby,[a] Alexander Rothenberger,[a] Dietmar Stalke,[c] Andrew J. Wheatley[a] and Dominic S. Wright*[a]

[a] *Chemistry Department, University of Cambridge, Lensfield Road, Cambridge, UK CB2 1EW. E-mail: dsw1000@cus.cam.ac.uk*

[b] *School of Chemistry, University of North London, London, UK N7 8DB*

[c] *Institut für Anorganische Chemie, Universität Würzburg, Am Hubland, 97074 Würzburg, Germany*

Received (in Cambridge, UK) 23rd September 1998, Accepted 5th October 1998

The low-temperature reactions of $[Sb(NMe_2)_3]$ with $[CyPH_2]$ and [CyPHNa] (1 : 1 : 1 equiv.) and of $[As(NMe_2)_3]$ with [^{t}BuPHLi] (1 : 3 equiv.) in TMEDA–thf [TMEDA = $Me_2NCH_2)_2$] produce [{*cyclo*-$(CyP)_4Sb$}Na·Me_2NH·TMEDA]$_2$ 1 and [{*cyclo*-(^{t}BuP)$_3$As}Li·TMEDA·thf] 2, respectively; at higher temperatures these reactions generate Zintl compounds containing Sb_7^{3-} and As_7^{3-} anions.

In earlier work we showed that a variety of dimethylamido Sb(III) reagents can be employed in the syntheses of a range of stable heterometallic imido cages containing Sb(III) anions (such as $[Sb(NR)_3]^{3-}$ and $[Sb_2(NR)_4]^{2-}$).[1] The reaction of $[Sb(NMe_2)_3]$ with [CyPHLi] (1 : 3 equiv. respectively) gives the Sb(III)/Li complex [{Sb{PCy)$_3$}$_2$Li$_6$·6Me_2NH] (Cy = C_6H_{11}) in which all the Me_2NH produced as a byproduct solvates the six Li^+ cations of the core.[2] Unlike the imido analogue, thermal decomposition of this complex occurs (*ca.* 30–40 °C) to produce the Zintl compound $[Sb_7Li_3·6Me_2NH]$, the product resulting from elimination of the phosphinidene groups (as is illustrated by the isolation of *cyclo*-$[CyP]_4$).[3] This unique phosphinidene coupling reaction (by which molecular cages are converted into molecular alloys) provides the means for the solution deposition of thin photoemissive alkali metal antimonate films[4] from molecular single-source precursors at low temperatures (*i.e.*, an 'alloy paint' approach) rather than using metal vapours.

In order to assess the generality of this approach we decided to investigate a range of reactions of $[E(NMe_2)_3]$ (E = As, Sb) with primary phosphines $[RPH_2]$ and primary phosphido alkali metal complexes (RPHM) (M = Li–Cs) (analogous to those we had used previously for the imido systems[1]). The low-temperature reaction (< 0 °C) of $[Sb(NMe_2)_3]$ with $[CyPH_2]$ (Cy = cyclohexyl) (1 : 1 equiv.) followed by addition of [CyPHNa] (1 equiv.) in the presence of excess TMEDA [= $(Me_2NCH_2)_2$] was performed in order to obtain the heterobimetallic cage [{Sb_2(PCy)$_4$}$_2$$Na_4$], the imido analogue of which ([{Sb_2(NCy)$_4$}$_2$$Na_4$]) was produced under similar conditions using [CyNHNa] and [$CyNH_2$].[5] However, the initial product of this reaction is [{*cyclo*-CyP}$_4$SbNa·TMEDA·Me_2NH]$_2$ **1**,† containing a heterocyclic [{CyP}$_4$Sb]$^-$ anion. Similarly, the low-temperature reaction (*ca.* 25 °C) of [^{t}BuPHLi] with $[As(NMe_2)_3]$ (3 : 1 equiv.) in the presence of TMEDA–thf leads to the direct formation of [{*cyclo*-(^{t}BuP)$_3$As}Li·TMEDA·thf] **2**,† containing a related [{^{t}BuP}$_3$As]$^-$ anion, rather than giving [{As(^{t}Bu)$_3$}$_2$$Li_6$] (*cf.* [{Sb(^{t}Bu)$_3$}$_2$$Li_6$] which is obtained by a similar reaction from $[Sb(NMe_2)_3]$ and [^{t}BuNHLi][6]). At higher temperatures [*ca.* 60 and 110 °C (in toluene), respectively] Zintl compounds containing As_7^{3-} are isolated.† The almost quantitative yields of the latter and the earlier isolation of $[CyP]_4$ from the thermolysis reaction of [{Sb{PCy)$_3$}$_2$Li$_6$·6Me_2NH] to the Zintl compound $[Sb_7Li_3·6Me_2NH]$[3] suggests that elimination of $[RP]_n$ rings from the [{CyP}$_4$Sb]$^-$ and [{^{t}BuP}$_3$As]$^-$ anions of **1** and **2** is a fundamental step in the formation of these Zintl ions. The precise mechanism of this process is still under investigation.

X-Ray crystallographic studies of **1** and **2** were undertaken at low temperature.‡ Complex **1** (Fig. 1) consists of centrosymmetric dimers [{*cyclo*-CyP}$_4$SbNa·TMEDA·Me_2NH]$_2$, in which two heterocyclic [{CyP}$_4$Sb]$^-$ anions are associated by two Na^+ cations. The central Sb_2Na_2 ring has a planar, rhombic shape [Sb(1)–Na(1)–Sb(1a) 87.0(1), Na(1)–Sb(1)–Na(1a) 93.0(1)°], with the pattern of alternating Sb–Na bond lengths [Sb(1)–Na(1) 3.617(4), Sb(1)–Na(1a) 3.229(4) Å] indicating that the two monomer units are only loosely associated (*cf.* estimated 2.98 Å for the Sb–Na bond). Although a similar metallacyclic [(^{t}BuP)$_4$Ni] fragment has been observed in the structure of [{(*cyclo*-^{t}BuP)$_4$Ni}(η^2-^{t}BuP)$_2$],[7] the closest p block relatives to **1** are the neutral heterocycle [SbP(2,4,6-^{t}Bu$_3$C$_6$H$_2$)]$_2$ (composed of a four-membered P_2Sb_2 ring with an endocyclic Sb–Sb bond)[8] and complexes containing the cyclic $[P_5]^-$ anion.[9] Alkali metal Li–Sb bonded complexes have been reported previously;[10] however, **1** is the first containing a Na–Sb bond.

Complex **2** consists of discrete monomers [{*cyclo*-(^{t}BuP)$_3$As}Li·TMEDA·thf], in which a heterocylclic [{*cyclo*-(^{t}BuP)$_3$As}]$^-$ anion is bonded by its anionic centre to a Lewis base solvated Li^+ cation (Fig. 2). The As–Li bond length in **2** [2.62(2) Å] is within the range observed in other complexes of this type (2.46–2.76 Å).[11] The formation of a four-membered P_3As anion in **2**, as opposed to a five-membered unit similar to that found in the related Sb(III) system **1**, may simply result from the smaller covalent radius of As (the shorter As–P bonds being accommodated into a four membered ring unit without inducing excessive strain). The closest relative of **2** is [(^{t}BuP)$_3$As]$_2$, a principal product of the Wurtz coupling reaction

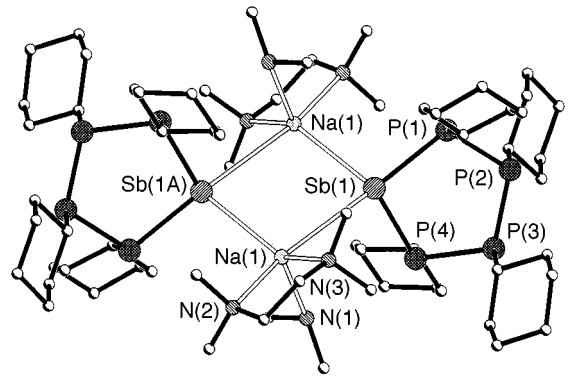

Fig. 1 Molecular structure of **1** with H atoms omitted for clarity. Key bond lengths (Å) and angles (°): Sb(1)–P(4) 2.489(3), Sb(1)–P(1) 2.541(3), P(1)–P(2) 2.192(4), P(2)–P(3) 2.192(4), P(3)–P(4) 2.184(4), Sb(1)–Na(1) 3.617(4), Sb(1)–Na(1a) 3.229(4), Na(1)–N(3) 2.46(1), Na(1)–N(1) 2.49(1), Na(1)–N(2) 2.49(1); P(1)–Sb(1)–P(4) 99.7(1), Sb(1)–P(1)–P(2) 105.7(1), P(3)–P(2)–P(1) 110.9(2), P(4)–P(3)–P(2) 109.4(2), Sb(1)–P(4)–P(3) 105.6(2), Na(1)–Sb(1)–Na(1a) 93.0(1), Sb(1)–Na(1)–Sb(1a) 87.0(1). Symmetry transformations used to generate equivalent atoms $-x + 2$, $-y + 1$, $-z$.

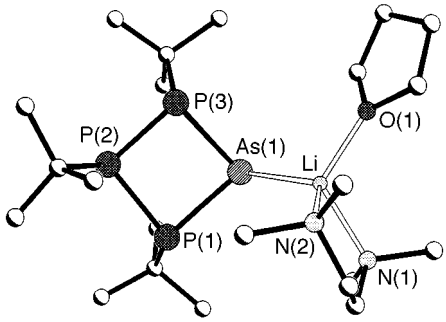

Fig. 2 Molecular structure of **2** with H atoms and the disorder on the thf and TMEDA ligands omitted for clarity. Key bond lengths (Å) and angles (°): As(1)–P(1) 2.333(4), As(1)–P(3) 2.324(3), As(1)–Li 2.62(2), P(1)–P(2) 2.203(4), P(2)–P(3) 2.198(4), Li–N(1,2) av. 2.10, Li–O(1) 1.92(2); P(1)–As(1)–P(3) 85.1(1), P–As–Li av. 107.5, As(1)–P(1)–P(2) 88.2(1), As(1)–P(3)–P(3) 88.5(1), P(1)–P(2)–P(3) 91.4(2).

of $AsCl_3$, $^tBuPCl_2$ and Mg, which consists of two [($^tBuP)_3As$] rings linked by their As centres.[12]

In conclusion, the aforementioned reactions provide direct access to a unique family of group 15 heterocyclic anions (**1** and **2** being the first examples of this type to be characterised). The application of these species as sources of [{RP}$_n$E]$^-$ (E = Sb, As) ligands to other main group and transition metals and the thermolysis of the resulting complexes is an interesting prospect.

We gratefully acknowledge the EPSRC (N. C., A. D. H., M. McP., A. J. W.) the Royal Society (P. R. R., D. S. W.), the Leverhulme Trust (M. A. B.), the Spanish Government (M. E. G. M.), the Gottlieb Daimler- und Karl Benz-Stiftung (A. R.) and Electron Tubes, Ruislip, UK (Case award for A. D. H.) for financial support.

Notes and references

† *Synthesis* of **1**: [Sb(NMe$_2$)$_3$] (5.1 ml, 1.74 mol dm^{-3} in toluene, 8.8 mmol) was added dropwise to a chilled solution of $CyPH_2$ (1.17 ml, 8.8 mmol) in hexane (20 ml). The solution was allowed to warm to room temperature and stirred (10 min). The orange solution produced was transferred by syringe into a chilled (*ca.* −20 °C) solution of [CyPHNa] [prepared *in situ* by the reaction of $PhCH_2Na$ (1.0 g, 8.8 mmol) with $CyPH_2$ (1.17 ml, 8.8 mmol) in hexane (10 ml)–thf (5 ml)]. The reaction mixture was allowed to warm to *ca.* 0 °C. An excess of TMEDA (*ca.* 3.0 ml, 20 mmol) was added and the solution was filtered while cold. Crystallisation at −35 °C (24 h) gave red plates of **1**. Yield 1.1 g (16% on the basis of Sb supplied). Decomp. 75 °C to black solid. ^{1}H NMR (+25 °C, 250 MHz, [$^2H_8$]toluene), δ 1.0–2.0 (overlapping m, 40H, {CyP}$_4$), 2.22 (d, 4H ($^2J_{31_{P-H}}$ *ca.* 6.4 Hz), C(α)-H of {CyP}$_4$), 2.10 (br s, 16H, TMEDA), 2.46 (s, 6H, Me_2NH). Elemental analysis. Calc. C, 50.4; H, 8.8; N, 5.5; P, 16.3. Found: C, 49.0; H, 8.6; N, 5.2; P 15.1%.

Synthesis of **2**: to a stirred, chilled suspension of [LiPH^{t}Bu]$_n$ (6.0 mmol of monomer) in toluene (20 ml) and TMEDA (1.0 ml) was added a solution of [As(NMe$_2$)$_3$] (2.0 mmol, 0.92 cm^3, 2.17 mol dm^{-3} in toluene). The suspension was stirred and gradually allowed to warm to 0 °C, at which stage an orange precipitate was observed. Then thf (20 ml) was added and the mixture stirred for 48 h after which an orange solution (with a fine precipitate) remained. This was filtered off and the solvent reduced to *ca.* 8 ml, the solid produced was redissolved by the addition of thf (*ca.* 1 ml) and storage at −18 °C (12 h) gave orange crystals of **2** suitable for X-ray diffraction studies. Isolated samples of **2** (placed *in vacuo* for *ca.* 15 min, 10^{-1} atm) contain no thf solvate. The following data refer to this material; yield 0.27 g (2% on the basis of As supplied to the reaction); mp. 115 °C to clean orange oil; IR (Nujol), major bands at 1260 m, 1032 s cm^{-1}; ^{1}H NMR (250 MHz, +25 °C, [$^2H_8$]thf), δ 2.39 (s, 4H, CH_2, TMEDA), 2.13 (s, 12H, Me_2N, TMEDA), 1.07 (d, 18H, $^3J_{P-H}$ 11.5 Hz), 1.01 (d, 9H, $J_{31_{P-H}}$ 10.5 Hz); ^{31}P NMR (101.256 MHz, +25 °C, [$^2H_8$]thf; rel. to 80% H_3PO_4–D_2O), δ 7.87 (t), −74.50 (d) (ratio 1 : 2, $^2J_{31_{P-31_P}}$ 179.4 ± 0.8 Hz); Elemental analysis. Calc. C, 46.8; H, 9.3; N, 6.1; P, 20.1. Found: C, 46.0; H, 9.3; N, 7.2; P, 17.6%.

The syntheses and structures of [Sb_7Na_3·3TMEDA·3thf] **3** and [As_7Li_3·3TMEDA]·PhMe **4** (see last ref. 11) obtained in the high temperature reactions will be discussed in a later paper.

‡ *Crystal data*: for **1**: $C_{64}H_{134}N_6Na_2P_8Sb_2$, M = 1525.02, monoclinic, space group $P2_1/n$, a = 11.168(3), b = 22.420(4), c = 16.468(3) Å, β = 92.71(2)°, U = 4118.6(14) Å^3, Z = 2, D_c = 1.230 Mg m^{-3}, λ = 0.71073 Å, T = 223(2) K, μ(Mo-Kα) = 0.859 mm^{-1}. Data were collected on a Siemens P4 diffractometer. The crystal diffracted very weakly at high angle; of a total of 5646 data collected (1.82° ⩽ θ ⩽ 21.00°) 4439 were independent (R_{int} = 0.0532). Relatively high thermal displacement parameters indicated some disorder of the cyclohexyl rings but it was not possible to resolve this. Empirical absorption corrections were applied after initial refinement with isotropic displacement parameters.[13] The structure was solved by direct methods and refined by full-matrix least-squares on F^2 to final values of $R1[F > 4\sigma(F)]$ = 0.069 and $wR2$ = 0.214 (all data);[14] largest peak and hole in the final difference map 0.772 and −0.843 e Å^{-3}.

For **2**: $C_{22}H_{51}AsLiN_2OP_3$, M = 534.42, monoclinic, space group $P2_1/n$, a = 12.238(7), b = 15.574(12), c = 16.27(1), β = 105.23(5)°, U = 2993(4) Å^3, Z = 4, D_c = 1.186 Mg m^{-3}, T = 180(2) K, μ(Mo-Kα) = 1.311 mm^{-1}, F(000) = 1144. Data were collected on a Siemens-Stoe diffractometer using ω–θ scans (3.56 ⩽ θ ⩽ 22.50). Of a total of 7645 reflections, 3900 were independent (R_{int} = 0.1036). The structure was solved using direct methods and refined by full matrix least squares on F^2 to final R indices of $R1$ = 0.086 [$F > 4\sigma(F)$] and $wR2$ = 0.200 (all data);[14] largest peak and hole in the final difference map 1.269 and −0.622 e Å^{-3}. The C atoms of the thf ligand and one of the C atoms of each of the Me_2N groups of the TMEDA were disordered over two sites and were refined with half occupancy. CCDC 182/1045.

1 M. A. Paver, C. A. Russell and D. S. Wright, *Angew. Chem.*, 1995, **107**, 1677; *Angew. Chem., Int. Ed. Engl.*, 1995, **34**, 1545; M. A. Beswick, M. E. G. Mosquera and D. S. Wright, *J. Chem. Soc., Dalton Trans.*, 1998, 2437; M. A. Beswick and D. S. Wright, *Coord. Chem. Rev.*, in press, and references therein.
2 M. A. Beswick, J. M. Goodman, C. A. Harmer, A. D. Hopkins, M. A. Paver, P. R. Raithby, A. E. H. Wheatley and D. S. Wright, *Chem. Commun.*, 1997, 1879.
3 M. A. Beswick, N. Choi, C. N. Harmer, A. D. Hopkins, M. McPartlin and D. S. Wright, *Science*, 1998, **281**, 1500.
4 A. H. Summer, *Photoemission Materials*, R. E. Kruger Publishing Co., 1968.
5 A. Bashall, M. A. Beswick, C. N. Harmer, A. D. Hopkins, M. McPartlin, M. A. Paver, P. R. Raithby and D. S. Wright, *J. Chem. Soc., Dalton Trans.*, 1998, 1389.
6 M. A. Beswick, N. Choi, C. N. Harmer, A. D. Hopkins, M. A. Paver, M. McPartlin, P. R. Raithby, A. Steiner, M. Tombul and D. S. Wright, *Inorg. Chem.*, 1998, **37**, 2177.
7 R. A. Jones, M. H. Seeberger and B. R. Whittlesey, *J. Am. Chem. Soc.*, 1985, **107**, 6424.
8 P. Jutzi, U. Meyer, S. Opiela, M. M. Olmstead and P. P. Power, *Organometallics*, 1990, **9**, 1459.
9 N. Korber and J. Daniels, *J. Chem. Soc., Dalton Trans.*, 1996, 1653; M. Detzel, T. Mohr, O. J. Scherer and G. Wolmershäuser, *Angew. Chem.*, 1994, **106**, 1142; *Angew. Chem., Int. Ed. Engl.*, 1994, **33**, 1110.
10 D. A. Kane and D. S. Wright, unpublished results; G. Becker, A. Münch and C. Witthauer, *Z. Anorg. Allg. Chem.*, 1982, **492**, 15; N. Korber and F. Richter, *Angew. Chem.*, 1997, **109**, 1575; *Angew. Chem., Int. Ed. Engl.*, 1997, **36**, 1512.
11 H. Schumann, E. Palamidis, J. Loebel and J. Pickart, *Organometallics*, 1988, **7**, 1008; G. Becker and C. Whitthauer, *Z. Anorg. Allg. Chem.*, 1982, **492**, 28; A. M. Arif, R. A. Jones and K. B. Kidd, *J. Chem. Soc., Chem. Commun.*, 1986, 1440; R. A. Barlett, H. V. R. Dias, H. Hope, B. D. Murray, M. M. Olmstead and P. P. Power, *J. Am. Chem. Soc.*, 1986, **108**, 6921; M. Driess and H. Pritzkow, *Angew. Chem.*, 1992, **104**, 350; *Angew. Chem., Int. Ed. Engl.*, 1992, **31**, 316; L. Zsolnai, G.Huttner and M. Driess, *Angew. Chem.*, 1993, **105**, 1549; *Angew. Chem., Int. Ed. Engl.*, 1993, **32**, 1439; M. Driess, H. Pritzkow, S. Martin, S. Rell, D. Fenske and G. Baum, *Angew. Chem.*, 1996, **108**, 1064; *Angew. Chem., Int. Ed. Engl.*, 1996, **35**, 986; M. Driess, K. Merz, H. Pritzkow and R. Janoschek, *Angew. Chem.*, 1996, **108**, 2688; *Angew. Chem., Int. Ed. Engl.*, 1996, **35**, 2507.
12 H. Baudler, Y. Aktalay, T. Heinlein and K.-F. Tebbe, *Z. Naturforsch., Teil B*, 1982, **37**, 299.
13 N. Walker, D. Stuart, *Acta Crystallogr., Sect. A*, 1983, **39**, 158.
14 SHELXTL PC version 5.03, Siemens Analytical Instruments, Madison, WI, 1994.

Communication 8/07444E

ChemComm

Molecular structures of 1,12-$B_{12}H_{10}(CO)_2$ and its dihydrate 1,12-$B_{12}H_{10}[C(OH)_2]_2$—a novel bis-carbene complex

Mark A. Fox,* Judith A. K. Howard, Janet M. Moloney and Kenneth Wade*

Chemistry Department, Durham University Science Laboratories, South Road, Durham, UK DH1 3LE. E-mail: m.a.fox@durham.ac.uk

Received (in Cambridge, UK) 4th September 1998, Accepted 5th October 1998

Crystal structures of the dicarbonyl 1,12-$B_{12}H_{10}(CO)_2$ and its hydrated form 1,12-$B_{12}H_{10}(CO_2H_2)_2{\cdot}4H_2O$ show little π-bond character in their B–C bonds but contain significant distortions from the regular B_{12} icosahedron geometry; the hydrate, until now thought to be a hydroxonium salt, contains dihydroxycarbene ('protonated carboxylic acid') ligands $C(OH)_2$.

The three-dimensional aromaticity and π-acidity of polyhedral boranes[1] lends interest to their derivative chemistry when potentially π-bonding ligands are present.[2,3] The dianion $[B_{12}H_{12}]^{2-}$ has particular interest in this connection as it contains the electronically highly delocalized robust B_{12} icosahedron[4] present in tough ceramic materials like elemental boron, boron carbide and metal borides. The I_h symmetry of the dianion is expected to be lowered on attachment of ligands with π bonding potential. We here report structural studies on two neutral complexes 1,12-$B_{12}H_{10}L_2$ in which two opposed hydride ligands of $[B_{12}H_{12}]^{2-}$ are replaced by neutral potentially π-acidic ligands L of a type normally associated with transition metals, namely the carbonyl ligand L = CO or a Fischer carbene ligand L = $C(OH)_2$. The known dicarbonyl $B_{12}H_{10}(CO)_2$ **1**, synthesized from $[B_{12}H_{12}{}^{2-}]$ and CO under high pressure and temperature in low yield,[5,6] had been subjected to a recent photoelectron and theoretical study[7] which suggested it contained single B–C and triple C≡O bonds though this had not been structurally confirmed. The bis(dihydroxycarbene) complex $B_{12}H_{10}[C(OH)_2]_2$ **2**, prepared by us in a neutral hydrated form by hydration of **1**, had hitherto been regarded[5,6,8] as a hydroxonium salt $[H_3O^+]_2[B_{12}H_{10}(CO_2H)_2]^{2-}$ **3** with two carboxylic acid residues CO_2H replacing two hydrogen ligands of $B_{12}H_{12}{}^{2-}$. The hydrate **2** appears to be the first structurally characterized compound with two carbene diol groups. A preliminary potentiometric titration of **2** in water gave pK_a values of 4.2 and 9.0 for loss of the first and second protons respectively.

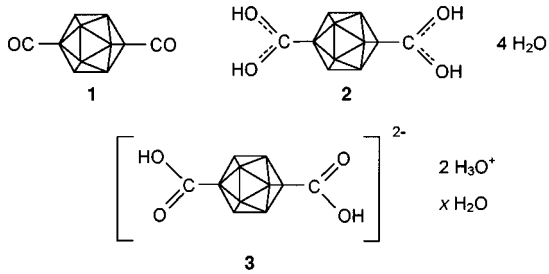

Suitable crystals of $B_{12}H_{10}(CO)_2$ **1** for X-ray crystallography were formed by slow sublimation at 40–50 °C (0.005 mmHg) for 2–3 days. A crystal of the dicarbonyl **1**† was flash-cooled to 100 K and an X-ray diffraction study reveals a well ordered structure in the space group *Cmca*.‡ The molecule has 2/*m* site symmetry, which results in only nine atoms being crystallographically unique. The bond lengths of B–C and C–O and the nearly linear BCO angle in **1** are typical of BCO groups in neutral borane carbonyls.[9] The molecular structure with significant bond lengths and angles is shown in Fig. 1. A crystal of the hydrate $B_{12}H_{10}(CO_2H_2)_2{\cdot}4H_2O$ **2**,§ formed by recrystallization with water, was also flash-cooled to 90 K and shows a well ordered structure in space group *C*2/*c* with two independent water molecules in the asymmetric unit.¶ The hydrate **2** has two carbene diol $C(OH)_2$ groups with identical C–O and O–H bond lengths within experimental error. Fig. 2 shows the molecular structure with significant bond lengths and angles. The supramolecular structure of **2** consists of sheets of cages mediated by water molecules on the (101) plane with hydrogen bond distances (O···H/Å) of 1.73(2) and 1.80(2) between the diol groups and the water molecules, and 1.92(2) and 1.97(2) between the water molecules.

Bond order calculations carried out on the molecular geometries of **1** and **2** using the AM1 program[2] show little π bonding between the borane cluster and the carbonyl groups in **1** and negligible between the cluster and the carbene diol groups

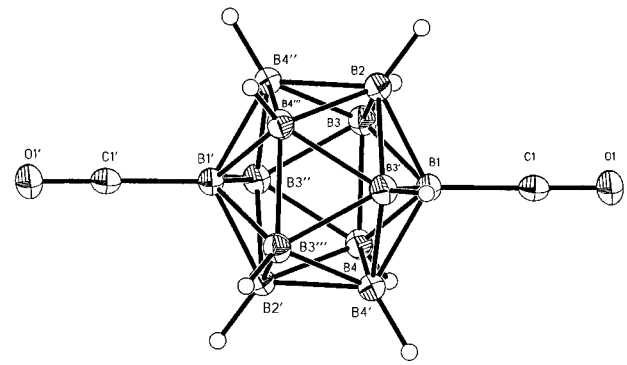

Fig. 1 Molecular structure of **1** (50% ellipsoids). Important interatomic distances (Å) are: O(1)–C(1) 1.119(2), C(1)–B(1) 1.543(2), average B–B distances; polar–tropical 1.768, tropical–tropical 1.824, tropical–tropical′ 1.779. Selected angles (°) O(1)–C(1)–B(1) 179.18(12), C(1)–B(1)–B(2) 117.28(9), C(1)–B(1)–B(3) 118.26(5), C(1)–B(1)–B(4) 119.66(8).

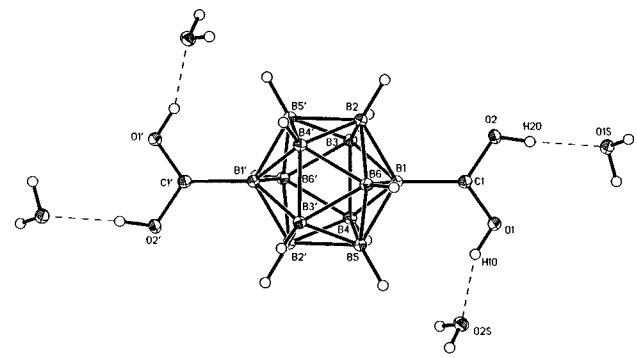

Fig. 2 Crystal structure of **2** (50% ellipsoids). Important interatomic distances (Å) are: O(1)–C(1) 1.289(1), O(2)–C(1) 1.287(1), O(1)–H(10) 0.86(2), O(2)–H(20) 0.84(2), C(1)–B(1) 1.589(1), average B–B distances; polar–tropical 1.779, tropical–tropical 1.801, tropical–tropical′ 1.783. Selected angles (°) C(1)–O(1)–H(10) 116.3(12), C(1)–O(2)–H(20) 110.3(12), O(1)–C(1)–O(2) 114.66(9), O(1)–C(1)–B(1) 125.26(9), O(2)–C(1)–B(1) 120.08(8), C (1)–B(1)–B(2) 119.75(8).

Table 1 Bond lengths and bond orders for B–C and C–O bonds in **1** and **2**

	Bond length (Å)		Total bond order		π-Bond order	
	B–C	C–O	B–C	C–O	B–C	C–O
1	1.543(2)	1.119(2)	0.843	2.422	0.114	1.464
2	1.589(1)	1.287(1)	0.828	1.328	0.064	0.407
		1.289(1)		1.274		0.369

in **2** (Table 1). There is π electron delocalization in all C–O bonds, the carbonyl group bond order is roughly 2.5 in **1** whereas the carbenediol group in **2** has two C–O bond orders of around 1.5 (like those found in symmetrical chelating carboxylates). AM1 calculated Mulliken charges give an overall charge of +0.4 for the carbonyl group in **1** and +0.5 for the diol group in **2**. The molecular structures of **1** and **2** remain largely unchanged in solution as experimental ^{11}B NMR data are in accord with calculated GIAO/NMR data‖ (using the GAUSSIAN94 program) generated from their X-ray geometries.

The distortion of the B_{12} cage geometry in **1** from regular I_h is interesting. If one regards the B_{12} icosahedron as globular, with the substituted boron atoms occupying polar sites, the remainder occupying tropical sites, the dicarbonyl **1** show lengthening of the boron–boron bonds within the tropics, shortening of the bonds linking tropical to polar boron atoms, but little change in the distances linking northern to southern tropical boron atoms (average bond distances shown in the figure captions) compared to $B_{12}H_{12}^{2-}$ (average B–B distance 1.784 Å). The icosahedron is thus squashed from pseudospherical to oblate spheroidal along the polar axis (distances: polar–polar 3.19 Å and tropical–tropical′ 3.45 in **1**, *cf*. 3.39 in $B_{12}H_{12}^{2-}$). Compound **2** and the only other known 1,12-$B_{12}H_{10}L_2$ derivative structurally characterized[10] (L = SMe_2) show similar distortions but these are not as extreme as in **1**.

The remarkably close structural relationship of the substituents in boranes **1** and **2** and in carbocations[11] $MeCO^+$ (C–O 1.110 Å) and $MeC(OH)_2^+$ (C–O 1.273 Å) respectively implies that compounds **1** and **2** can be viewed as neutral main group analogues of bis-carbocations. Further evidence of the close relationship is shown in the ^{13}C NMR peak seen at 200.2 ppm in **2** like those carbene carbons in the carbocations $RC(OH)_2^+$ whose peaks are observed in the 215–190 ppm region.[12] There are parallels of the boranes **1** and **2** with transition metal carbonyl and dioxycarbene $C(OR)_2$ complexes,[13] in which the metal–carbon bonds are always shorter to the carbonyl group than to the dioxycarbene group.

Our findings have implications for other supposed carboxylic acid derivatives of other borane anions. Hydration of the borane dicarbonyls, 1,10-$B_{10}H_8(CO)_2$ and 1,7-$B_{12}H_{10}(CO)_2$, have been reported[5,6] to give carboxylic acids, $[H_3O^+]_2$[1,10-$B_{10}H_8(CO_2H)_2^{2-}$] and $[H_3O^+]_2$[1,7-$B_{12}H_{10}(CO_2H)_2^{2-}$], respectively whereas the related mono-anions, 2-$B_{10}H_9(CO)^-$ and $B_{12}H_{11}(CO)^-$, were reported[14] to produce $[H_3O^+]_2$[2-$B_{10}H_9(CO_2H)^{2-}$] and $[H_3O^+]_2[B_{12}H_{11}(CO_2H)^{2-}]$. Carbenediol groups are probably present in these hydrates. The dicarboxylic acid dianion in **3** is likely to exist in metal salts[6] generated from **2**.

We thank Professor T. R. Spalding (Cork) for discussions and a sample of **1**, Dr R. Kataky for help with the pK_a measurements. We are grateful to EPSRC (M. A. F.) and the Durham University Christopherson fellowship (J. A. K. H.) for financial support.

Notes and references

† *Spectroscopic data* for **1**: ν_{max}/cm^{-1} 2557s (BH); 2209s (CO). δ_C (solvent CD_3CN), 163 (br); δ_B (standard $BF_3{\cdot}Et_2O$), −11.4 (1B, s), −22.4 [5B, d, *J*(BH) 141 Hz], δ_H 1.92 (s, BH).

‡ *Crystal data* for **1**: $C_2H_{10}B_{12}O_2$, *M* = 195.82, orthorhombic, space group *Cmca* (no. 64), *a* = 9.2538(3), *b* = 10.6482(3), *c* = 10.9415(2) Å, *U* = 1078.14(5) Å^3, *Z* = 4, D_c = 1.206 g cm^{-3}, μ = 0.064 mm^{-1}, *F*(000) = 392, *T* = 100(2) K, 653 unique reflections, R_1 = 0.0323 [606 data $I > 2\sigma$(I)], wR_2 = 0.0951 (all data), GOF = 1.101. Hydrogen atoms were refined freely. CCDC 182/1046.

§ *Spectroscopic data* for **2**: ν_{max}/cm^{-1} 3441br s (OH); 2501s (BH); 1651s (CO). δ_C (solvent CD_3CN), 200.2 [1:1:1:1 q, *J*(BC) 87 Hz], δ_B (standard $BF_3{\cdot}Et_2O$), −12.3 (1B, s), −14.4 [5B, d, *J*(BH) = 133 Hz], δ_H 6.19 (12H, brs, 4 H_2O, 4 OH), 1.63 (10H, s, BH).

¶ *Crystal data* for **2**: $C_2H_{22}B_{12}O_8$, *M* = 303.92, monoclinic, space group *C*2/*c* (no. 15), *a* = 13.6298(7), *b* = 7.3018(4), *c* = 15.9244(10) Å, β = 105.720(2)°, *U* = 1525.6(2) Å^3, *Z* = 4, D_c = 1.323 g cm^{-3}, μ = 0.099 mm^{-1}, *F*(000) = 632, *T* = 90(2) *K*, 1749 unique reflections, R_1 = 0.0286 [1591 data $I > 2\sigma(I)$], wR_2 = 0.0814 (all data), GOF = 1.132. Hydrogen atoms were refined freely. CCDC 182/1046.

‖ Calculated GIAO (HF/6-31G*) ^{11}B NMR data for **1**: δ −11.8 (5B), −21.7 (1B); **2**: δ −11.4 (1B), −13.7 (5B).

1 G. A. Olah, G. K. S. Prakash, R. E. Williams, L. E. Field and K. Wade, *Hypercarbon Chemistry*, Wiley, New York, 1987; V. I. Bregadze, *Chem. Rev*., 1992, **92**, 177; B. J. Gimarc and M. Zhao, *Inorg. Chem*., 1996, **35**, 825.

2 For examples see: D. A. Brown, W. Clegg, H. M. Colquhoun, J. A. Daniels, I. R. Stephenson and K. Wade, *J. Chem. Soc., Chem. Commun*, 1987, 889; W. Clegg, R. Coult, M. A. Fox, W. R. Gill and K. Wade, *Polyhedron*, 1992, **11**, 2717; R. C. B. Copley, M. A. Fox, W. R. Gill, J. A. K. Howard, J. A. H. MacBride, R. J. Peace, G. P. Rivers and K. Wade, *Chem. Commun*., 1996, 2033; M. A. Fox, J. A. H. MacBride, R. J. Peace and K. Wade, *J. Chem. Soc., Dalton Trans*., 1998, 401.

3 R. Kivekas, R. Sillanpaa, F. Teixidor, C. Vinas and R. Nunez, *Acta Crystallogr., Sect. C*, 1994, **50**, 2027; D. M. Murphy, D. M. P. Mingos and J. M. Forward, *J. Mater. Chem*., 1993, **3**, 67.

4 P.v.R. Schleyer, G. Subramanian, H. Jiao, K. Najafian and M. Hofmann, *Advances in Boron Chemistry*, ed. W. Siebert, The Royal Society of Chemistry, Cambridge 1997, p. 3.

5 W. H. Knoth, J. C. Sauer, H. C. Miller and E. L. Muetterties, *J. Am. Chem. Soc*., 1964, **86**, 115.

6 W. H. Knoth, J. C. Sauer, J.H. Balthis, H. C. Miller and E. L. Muetterties, *J. Am. Chem. Soc*., 1967, **89**, 4842.

7 P. Brint, B. Sangchakr, M. McGrath, T. R. Spalding and R. J. Suffolk, *Inorg. Chem.*, 1990, **29**, 47.

8 L. D. Hansen, J. A. Partridge, R. M. Izatt and J. J. Christensen, *Inorg. Chem.*,1966, **5**, 569; L. Barton, T. Onak, R. J. Remmel and S. G. Shore, in *Gmelin Handbuch der Anorganischen Chemie*, Borverbindungen 20, Springer-Verlag, Germany, 1979, p. 238; E.L. Muetterties and W. H. Knoth, *Polyhedral Boranes*, Arnold, London, 1968, p. 117; C. E. Housecroft, *Boranes and Metalloboranes*, Wiley, New York, 1990, p.146.

9 S. H. Bauer, *J. Am. Chem. Soc*., 1937, **59**, 1804; W. Gordy, H. Ring and A. B. Burg, *Phys. Rev.*, 1950, **78**, 512; J. Rathke and R. Schaeffer, *Inorg. Chem*., 1974, **13**, 760; J. D. Glore, J. W. Rathke and R. Schaeffer, *Inorg. Chem.*, 1973, **12**, 2175; S. J. Cranson, P. M. Davies, R. Greatrex, D. W. H. Rankin and H. E. Robertson, *J. Chem. Soc., Dalton Trans.*, 1990, 101.

10 E. J. M. Hamilton, G. T. Jordan IV, E. A. Meyers and S. G. Shore, *Inorg. Chem*., 1996, **35**, 5335.

11 G. A. Olah and A. M. White, *J. Am. Chem. Soc.*, 1967, **89**, 3591; J. M. Le Carpentier and R. Weiss, *Acta Crystallogr., Sect. B.*, 1972, **28**, 1421; K. Bartmann and D. Mootz, *Z. Anorg. Allg. Chem.*, 1991, **601**, 31.

12 R. Minkwitz, S. Schneider, M. Seifert and H. Hartl, *Z. Anorg. Allg. Chem*., 1996, **622**, 1404.

13 See for example; M. M. Singh and R. J. Angelici, *Angew. Chem. Int. Ed. Engl*., 1983, **22**, 163; G. L. Miessler, S. Kim, R. A. Jacobson and R. J. Angelici, *Inorg. Chem.*, 1987, **26**, 1690; G. Bondietti, R. Ros, R. Roulet, F. Musso and G. Gervasio, *Inorg. Chim. Acta*, 1993, **213**, 301.

14 K. Shelly, C. B. Knobler and M. F. Hawthorne, *Inorg. Chem*., 1992, **31**, 2889; I. B. Sivaev, V. I. Bregadze and S. Sjoberg, *Russ. Chem. Bull*. (Engl. Transl.), 1998, **47**, 193.

Communication 8/06898D

Direct observation of highly distorted hexa-coordinated aluminium in andalusite by very fast ^{27}Al MAS NMR

João Rocha*

Department of Chemistry, University of Aveiro, 3810 Aveiro, Portugal. E-mail: rocha@dq.ua.pt

Received (in Cambridge, UK) 7th September 1998, Accepted 12th October 1998

Highly distorted hexa-coordinated Al in andalusite can be detected by very fast (> 30 kHz) ^{27}Al magic-angle spinning (MAS) and triple-quantum MAS NMR spectroscopy.

Andalusite is a naturally occurring aluminium silicate named after Andalusia (Spain) where it has been found, and it is one of the three known Al_2SiO_5 polymorphs, the other being sillimanite and kyanite. The crystal structure of andalusite consists of [AlO_6] octahedra forming chains parallel to *c* which are cross-linked by [SiO_4] tetrahedra and [AlO_5] trigonal bipyramids.[1,2] Several studies reporting ^{27}Al magic angle (and variable angle) spinning NMR spectra of andalusite are available.[3,4] ^{27}Al is a half-integer quadrupole (I = 5/2) nucleus and obtaining a good MAS NMR spectrum of andalusite presents a great challenge because all the aluminium nuclei are in highly distorted environments (characterised by large quadrupole coupling constants) and, hence, give very broad peaks.[4] In particular, the [AlO_6] octahedron is so distorted that its ^{27}Al MAS NMR resonance has not previously been observed, even when the sample was spun at 15 kHz.[4] Recently, NMR probes capable of achieving spinning rates of 30–35 kHz became commercially available. Here, we wish to report that the use of such a probe and very fast (> 30 kHz) MAS allows the detection of the broad hexa-coordinated ^{27}Al NMR andalusite resonance. In addition, we also show that by combining very fast MAS and very powerful (> 250 kHz) radiofrequency (rf) fields a ^{27}Al triple-quantum (3Q) MAS NMR spectrum[5] of andalusite can be recorded.

Andalusite from Minas Gerais, Brazil, was characterised by powder X-ray diffraction and ^{29}Si MAS NMR (single peak at δ −79.6). 'Conventional' (single-quantum) ^{27}Al MAS NMR spectra of andalusite recorded at different spinning rates are shown in Fig. 1. In order to obtain meaningful relative signal intensities we have used short (0.6 μs, equivalent to 10^0) and strong rf pulses. The 32.5 kHz MAS spectrum clearly contains two broad resonances centred at δ *ca.* 13 and −110 (with peak singularities at δ −46 and −184), displaying characteristic second-order quadrupole lineshapes. The former has been previously assigned to penta-coordinated aluminium.[3,4] In our 9.4 T magnetic field, the presence of the very broad peak centred at δ *ca.* −110 becomes apparent at MAS rates in excess of 20 kHz, but its lineshape is only well defined at *ca.* 30 kHz. The second-order quadrupole patterns can be simulated to yield the isotropic chemical shifts, δ_{iso}, the quadrupole coupling constants, C_Q, and the asymmetry parameters, η (Fig. 2). The following values are obtained for the penta- and hexa-coordinated Al species, respectively: δ_{iso} 35.5 and 13.0; C_Q = 5.8 and 15.3 MHz; η = 0.69 and 0.08. These quadrupole parameters are in good agreement with previously reported data (C_Q = 5.9 and 15.6 MHz; η = 0.70 and 0.08 for penta- and hexa-coordinated Al, respectively).[3,4,6] The relative intensities of these two Al peaks (the spinning sidebands arising from the m = +1/2 ↔ m = −1/2, central transition hexa-coordinated Al line are included) measured directly from the spectrum are in a 1 : 0.85 ratio, respectively. According to the published crystal structure, this ratio should be 1 : 1 and, thus, NMR slightly underestimates the hexa-coordinated Al population. A more precise estimation of the two Al populations requires the simulation not only of the central transition ^{27}Al MAS NMR spectrum but also of the (±3/2 ↔ ±1/2 and ±5/2 ↔ ±3/2) satellite-transitions spectra. This work is in progress in our laboratory.

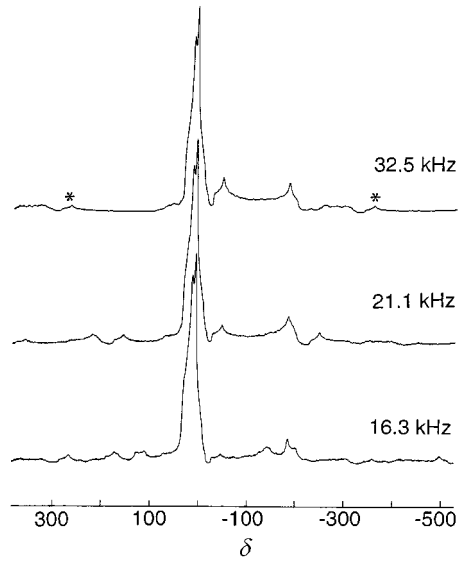

Fig. 1 ^{27}Al MAS NMR spectra of andalusite recorded at 104.3 MHz on a Bruker MSL 400P spectrometer using a Bruker 2.5 mm double-bearing probe, 0.3 s recycle delays, and the spinning rates indicated. Chemical shift reference $[Al(H_2O)_6]^{3+}$. The asterisks denote spinning sidebands arising from the central transition hexa-coordinated Al line.

The large C_Q values of the andalusite Al species make the excitation of ^{27}Al NMR multiple-quantum coherences a very difficult task. We were particularly interested in finding out whether the hexa-coordinated ^{27}Al NMR resonance (with C_Q = 15.3 MHz) could be observed in a triple-quantum experiment. Fig. 3 shows the ^{27}Al 3Q MAS NMR spectrum of andalusite recorded with a very fast sample spinning. The penta-coordinated Al peak is clearly seen and it exhibits an almost undistorted lineshape (inset in Fig. 3). Although very weak, the hexa-coordinated Al resonance is observable. Both peaks (in

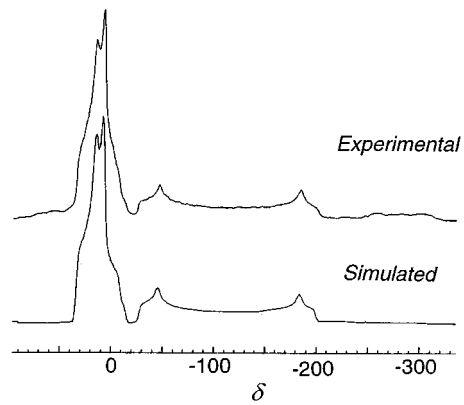

Fig. 2 Experimental and simulated ^{27}Al MAS NMR spectra of andalusite (spinning rate 32.5 kHz).

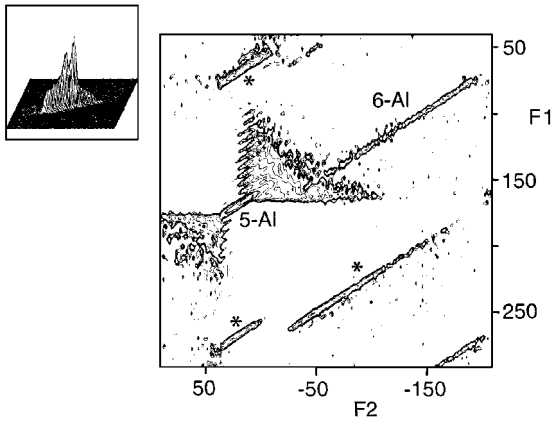

Fig. 3 Unsheared ^{27}Al triple-quantum MAS NMR spectra of andalusite recorded with a rf field amplitude of *ca*. 265 kHz and a spinning rate of 30.2 kHz. 512 data points (864 transients per point) were acquired in the t_1 dimension in increments of 1 μs (or 4.1 μs for the inset spectrum). To produce pure-absorption lineshapes a simple two-pulse sequence was used.[7] The ppm scale was referenced to ν_0 frequency in the ν_2 domain and to $3\nu_0$ in the ν_1 domain (reference $[Al(H_2O)_6]^{3+}$). The inset depicts the penta-coordinated Al resonance. Asterisks denote spinning sidebands along F1.

particular the latter) display strong spinning sidebands along F1.

In the recent past, the use of relatively slow (< 15 kHz) MAS did not allow the detection of Al in highly distorted environments and, thus, the correct quantification of aluminium by NMR was sometimes impossible. ^{27}Al NMR resonances with quadrupole coupling constants in excess of 15 MHz can now be studied with commercially available MAS probes at sample spinning rates of *ca*. 30 kHz. In addition, combining fast MAS and very strong rf fields (> 250 kHz) allows the excitation of ^{27}Al 3Q NMR coherences of highly distorted (C_Q up to *ca*. 15 MHz) Al species.

We acknowledge FEDER and PRAXIS XXI for financial support.

Notes and references

1 C. W. Burnham and M. J. Z. Buerger, *Z. Kristallogr., Kristallgeom., Kristallphys., Kristallchem.*, 1961, **115**, 269.
2 M. T. Vaughn and D. J. Weidner, *Phys. Chem. Miner.*, 1978, **3**, 133.
3 L. B. Alemany and G. W. Kirker, *J. Am. Chem. Soc.*, 1986, **108**, 6158.
4 L. B. Alemany, H. K. C. Timken and I. D. Johnson, *J. Magn. Reson.*, 1988, **80**, 427 and references therein.
5 A. Medek, J. S. Harwood and L. Frydman, *J. Am. Chem. Soc.*, 1995, **117**, 12 779.
6 S. Ghose and T. Tsang, *Am. Mineral.*, 1973, **58**, 749.
7 C. Fernandez, J. P. Amoureux, J. M. Chezeau, L. Delmotte and H. Kessler, *Microporous Mater.*, 1996, **6**, 331.

Communication 8/06939E

A blue electroluminescent molecular device from a tetranucluear zinc(II) compound $[Zn_4O(AID)_6]$ (AID = 7-azaindolate)

Yuguang Ma, Hsiu-Yi Chao, Ying Wu,† S. T. Lee,‡ Wing-Yiu Yu and Chi-Ming Che*

Department of Chemistry, The University of Hong Kong, Pokfulam Road, Hong Kong. E-mail: cmche@hkucc.hku.hk

Received (in Cambridge, UK) 7th July 1998, Accepted 23rd September 1998

A tetranuclear zinc(II) compound with 7-azaindolate (AID) as a bridging ligand exhibits an intense blue emission at 425 nm with a quantum yield of 0.21 in acetonitrile solution at room temperature; a blue-light emitting diode based on the Zn(II) complex as the active emitting layer attains an EL efficiency of 0.25% and brightness of 88 cd m^{-2} at 7.1 V driving voltage with current density of 10 mA cm^{-2}.

The search for new bright blue UV-luminescent metal–ligand compounds is of growing importance in the development of light emitting diode (LED) technology.[1–3] In this regard, polynuclear d^{10} metal complexes are of interest since these compounds are strongly emissive under UV irradiation, and the emission energies can span over a broad spectral range [400–700 nm].[4,5] Previously, we and Peng reported the preparation and crystal structure of a tetranuclear zinc(II) compound $[Zn_4O(AID)_6]$, here denoted as Zn_4, with 7-azaindolate as a bridging ligand.[6] This compound has the following desirable features that enable it to be a good advanced material for blue LED device fabrication: it can be easily prepared and is stable to air and moisture. Our recent studies revealed that it has high thermal stability in air below 400 °C and displays an intense blue photoluminescence with a long lifetime and a high quantum yield at room temperature. The relevant photophysical data are summarised in Table 1. Herein is described a blue LED device with the Zn_4 compound as the active emitting layer.

The Zn_4 compound was prepared by the reaction of zinc(II) acetate with 7-azaindole in methanol, and its crystal structure had already been reported.[6] Schematic representations of the LED devices studied here are shown in Scheme 1. Initially a single-layer LED was fabricated by vacuum deposition of $[Zn_4O(AID)_6]$ (< 200 °C, 2×10^{-6} Torr) onto a glass substrate coated with indium–tin oxide (ITO; sheet resistance 20 Ω □$^{-1}$) to form a thin homogeneous film. The film thickness was found to be 700 Å, and the surface was examined by atomic force microscopy (AFM); the roughness of the surface is 3 nm (RMS amplitude) which is about +4.3% for the film thickness. The surface topology is stable up to 150 °C. The XRD pattern of the Zn_4 thin film revealed a broad peak at 2θ = 15–30°, which contrasts with the sharp peaks at 2θ = 10, 12 and 20° observed for the crystalline powder sample. This indicates that the Zn_4 compound in the vacuum deposited thin film is in an amorphous state. An aluminium cathode (thickness ≈ 2000 Å) was vacuum deposited on top of the Zn_4 film at an evaporation rate of 3–5 Å s^{-1}. The substrate was kept at room temperature during the deposition. The active area of the LED is 2×2 mm^2.

When the single-layer LED was forward biased with the ITO electrode at positive polarity, blue EL was observed. The EL spectrum (Fig. 1) resembles the PL spectrum of the Zn_4 film

Table 1 Photoluminescence data for $[Zn_4O(AID)_6]$ at room temperature

Solvent	λ_{max}/nm	Lifetime/μs	Quantum yield
MeCN	425	0.09	0.21
CH_2Cl_2	427	0.08	0.19
MeCN glass (77 K)	423	0.11	—
solid state	433	0.05	—

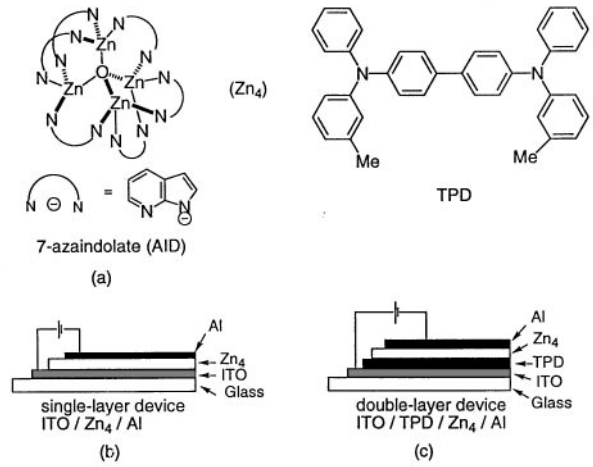

Scheme 1

suggesting that it originates from an excited state of $[Zn_4O(AID)_6]$. However, the brightness of the single-layer device is only 2.5 cd m^{-2} at a driving voltage of 6.5 V and current density of 10 mA cm^{-2}. Because the Zn_4 compound has a high ionisation potential of 5.1 eV [*c.f.* 4.8 eV for tris(8-hydroxyquinolinato)aluminium (Alq_3)], a hole-transport material such as *N*,*N*′-diphenyl-*N*,*N*′-bis(3-methylphenyl)-1,1′-biphenyl-4,4′-diamine (TPD, thickness ≈ 100 Å)[7] was introduced between the emitting Zn_4 and the ITO layers to form a double-layer device as depicted in Scheme 1. The EL brightness and efficiency have thus been greatly enhanced.

Fig. 2 shows the current density–voltage and EL intensity–voltage characteristics of the double-layer LED. When the LED was forward biased with the ITO electrode at positive polarity, blue EL was observed. However, when the device was reverse

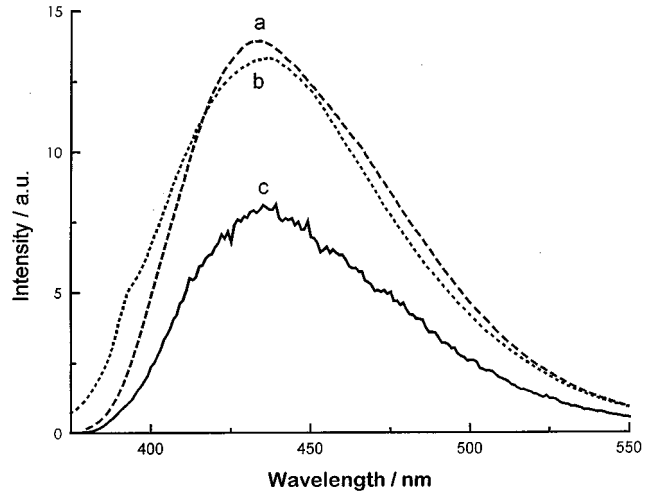

Fig. 1 (a) Solid state photoluminescence spectrum of Zn_4; (b) photoluminescence spectrum of vacuum deposition Zn_4 thin film; (c) electroluminescence spectrum of the single-layer device (ITO/Zn_4/Al).

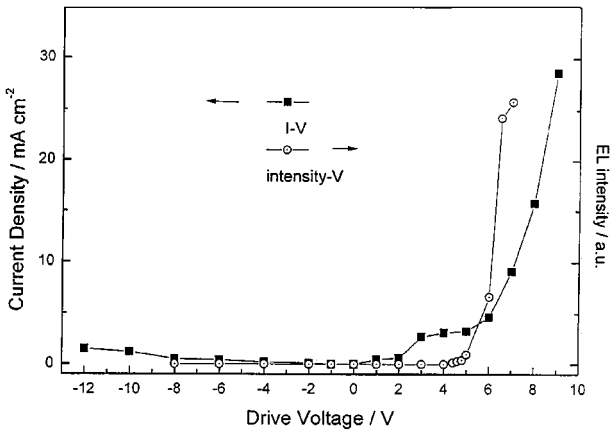

Fig. 2 Current density (*I*)–voltage (*V*) and EL intensity–voltage characteristics.

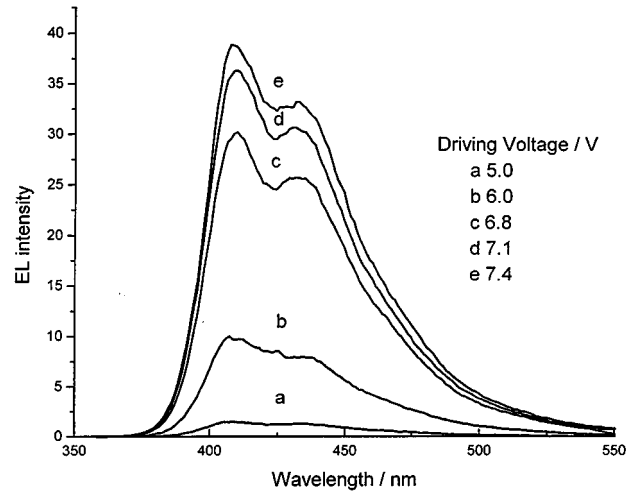

Fig. 3 EL spectra of the double-layer device at various driving voltages.

biased, EL was not observed implying that it is not induced by the dielectric breakthrough of the layer system. The brightness of the device is about 88 cd m^{-2} at a driving voltage of 7.1 V and current density of 10 mA cm^{-2}, and an external EL efficiency of 0.25% (photons per electron) was found, which is 35 times higher than the single-layer device. The double-layer LED shows a rather low turn-on voltage of about 5 V, compared with >12 V usually required for the π-conjugated polymer-based devices.

The EL spectrum of the double-layer LED shows two emission maxima at λ_{em} = 410 and 430 nm (Fig. 3), and this is different from the PL spectrum. We suggest that one of the two emission peaks in the EL spectrum comes from an interface state originating from the TPD and the Zn_4 layers; however, a precise explanation for this emission is not yet known.

Preliminary studies indicated that the present double-layer Zn_4 LED device configuration is stable in open atmosphere. Because of its high thermal stability and high photoluminescence quantum yield, the Zn_4 compound and its related derivatives may provide an alternative to the widely studied Alq_3 compound for future development of LED devices.

We acknowledge support from the University of Hong Kong, the Hong Kong Research Grants Council and the Croucher Foundation.

Notes and references

† Key Laboratory for Supramolecular Structure and Spectroscopy, Jilin University, Changchun 130023.
‡ Present address: Department of Physics and Materials Science, City University of Hong Kong, Tat Chee Avenue, Hong Kong.

1 A. Kraft, A. C. Grimsdale and A. B. Holmes, *Angew. Chem., Int. Ed. Engl.*, 1998, **37**, 402.
2 (*a*) H. J. Brouwer, V. V. Krasnikov, A. Hilberer and G. Hadziioannou, *Adv. Mater.*, 1996, **8**, 935; (*b*) Y. Kim, S. Kwon, D. Yoo, M. F. Rubner and M. S. Wrighton, *Chem. Mater.*, 1997, **9**, 2699.
3 A. Hassan and S. Wang, *Chem. Commun.*, 1998, 211.
4 (*a*) H. Kunkely and A. Vogler, *J. Chem. Soc., Chem. Commun.*, 1990, 1204; (*b*) A. Vogler and P. C. Ford, *Acc. Chem. Res.*, 1993, **26**, 220.
5 (*a*) C.-M. Che, H.-L. Kwong, V. W.-W. Yam and C.-K. Cho, *J. Chem. Soc., Chem. Commun.*, 1989, 855; (*b*) H, Xiao, K.-K. Cheung, C.-X. Guo and C.-M. Che, *J. Chem. Soc., Dalton Trans.*, 1994, 1867; (*c*) B.-C. Tzeng, C.-M. Che and S.-M. Peng, *J. Chem. Soc., Dalton Trans.*, 1996, 1769; (*d*) B.-C, Tzeng, C.-M. Che and S.-M. Peng, *Chem. Commun.*, 1997, 1771.
6 C.-F. Lee, K.-F. Chin, S.-M. Peng and C.-M. Che, *J. Chem. Soc., Dalton Trans.*, 1993, 467.
7 C. W. Tang, S. A. VanSlyke and C. H. Chen, *J. Appl. Phys.*, 1989, **65**, 3610.

Communication 8/05236K

The role of singlet oxygen in the photochemical formation of $C_{60}O$

David I. Schuster,* Phil S. Baran, Russell K. Hatch, Ahsan U. Khan and Stephen R. Wilson

Department of Chemistry, New York University, New York, NY 10003, USA. E-mail: david.schuster@nyu.edu

Received (in Liverpool, UK) 20th August 1998, Accepted 6th October 1998

Ground state C_{60} does not give $C_{60}O$ in the presence of singlet oxygen generated thermally from endoperoxides; evidence is presented that the photochemical formation of $C_{60}O$ from C_{60} proceeds *via* reaction of singlet oxygen with the lowest triplet excited state of C_{60}.

Since its synthesis and characterization in 1992 by Smith *et al*.,[1] several studies on $C_{60}O$ **1** have appeared, showing that oxide **1** can be generated through both thermal[2] and photochemical[1] pathways. Dimethyldioxirane,[2a] ozonolysis,[2b–d,f] MCPBA,[2e] P450 cytochrome models,[2g] and a methyltrioxorhenium–H_2O_2 system[2h] all successfully convert C_{60} to **1**. Oxide **1** can also be

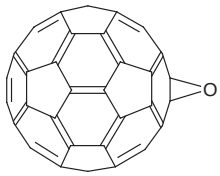

Oxide **1**

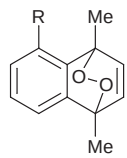

Endoperoxide **2** R = H

3 R = Me

isolated from the byproducts of fullerene synthesis[3a] and by extended irradiation of C_{60} in an oxygen atmosphere.[1] Although much is known about the photophysical and chemical properties of fullerenes, both the thermal and photochemical mechanisms for the formation of fullerene oxides largely remain a mystery.[3]

Foote and co-workers reported in 1991[4] that C_{60} is a very efficient sensitizer for formation of singlet oxygen ($\Phi = 0.96 \pm 0.02$ at 532 nm), and that C_{60} also quenches $^1O_2$, as shown by the shortening of the decay time of $^1O_2$ luminescence at 1270 nm[5] ($k_q = 5 \pm 2 \times 10^5$ M^{-1} s^{-1}).[4] However, no loss of C_{60} or appearance of new products was observed in the presence of oxygen following hundreds of laser pulses,[3b,4] suggesting that $^1O_2$ does not add to ground state C_{60} in solution. We have confirmed that $C_{60}O$ **1** is not formed upon reaction of C_{60} in toluene with $^1O_2$ when the latter is generated *via* the thermolysis of endoperoxides **2** and **3**.[6] Using an authentic sample of oxide **1**, we verified by HPLC analysis[7] that **1**, if formed, could be present in quantities no more than 0.01% of the total amount of C_{60} present in the solution. The presence of $^1O_2$ in this reaction system was verified by monitoring its emission at 1270 nm, which completely disappeared upon addition of β-carotene.[5,8] When cyclohexa-1,3-diene was added to toluene solutions of C_{60} and endoperoxide **2**, the conversion of the diene to its corresponding 1,4-endoperoxide[9] was detected by HPLC,[7] confirming that $^1O_2$ had indeed been generated under these reaction conditions. We also showed that C_{70} as well as several functionalized derivatives of C_{60} were also uneffected by $^1O_2$ generated thermally from endoperoxide **2**, according to HPLC analysis.[7] Juha *et al*. showed some time ago that C_{60} in fullerene–solvent clathrate microcrystallites was unreactive to a stream of chemically generated $^1O_2$.[10]

The question then remains as to the role played by $^1O_2$ in the photochemical formation of **1**. Could an *electronically excited* state of C_{60} lead to $C_{60}O$ by reaction with $^1O_2$? This question was addressed by photoexciting C_{60} in the presence of endoperoxides **2** and **3** as external sources of $^1O_2$. While endoperoxide **2** releases $^1O_2$ readily at temperatures above 0 °C, endoperoxide **3** does not release $^1O_2$ at room temperature.[6a,b] Thus, no emission at 1270 nm was observed from a toluene solution of **3** at room temperature. Thus, we were able to assess the reactivity of photoexcited C_{60} in the presence of two endoperoxides with very different thermal stabilities. In these reactions, 50 equiv. of endoperoxide were added to a 20 mM solution of C_{60} in benzene-d_6. The solutions were thoroughly degassed on a vacuum line by several freeze-pump-thaw cycles, and were then irradiated for 18 h.[11]

In the case of endoperoxide **2**, HPLC analysis revealed the formation of $C_{60}O$ **1** in 10% yield, higher than that (7%) reported from irradiation of C_{60} in an oxygen atmosphere under analogous conditions.[1] We also observed (HPLC) two additional minor products, presumably isomers of $C_{60}O_2$, as well as a brown precipitate, which were previously observed in the direct photooxygenation reaction.[1] The yield of **1** was far lower (2%) using endoperoxide **3**; furthermore, the higher oxidation products were not observed by HPLC in this case.

Thus, not only does the initial presence of $^1O_2$ in the photochemical reaction system increase the yield of fullerene oxide **1**, the absence of $^1O_2$ significantly decreases the efficiency of formation of **1**. This clearly identifies $^1O_2$ as the key species in the mechanism for fullerene oxide formation under photochemical reaction conditions, and suggests that $C_{60}O$ results from reaction of $^1O_2$ (lifetime 24 μs in benzene, 25 μs in toluene)[12] with an excited state of C_{60}. Such a mechanism was previously suggested[10] but no supporting evidence was presented. Given the very short lifetime of the S_1 state of C_{60} (*ca*. 1.2 ns),[13] and the long lifetime of the corresponding T_1 state (variously reported as 40 to 133 μs),[4,14] the triplet excited state is the obvious choice. If **1** were arising from reaction of C_{60} triplets directly with ground state endoperoxide, the yield of **1** should be similar using **2** and **3**. The large disparity in the yields of **1** suggests that this is at best a minor reaction pathway. We therefore conclude that the dominant photochemical pathway to $C_{60}O$ from C_{60} involves the reaction of C_{60} triplet excited states with singlet oxygen.

We are grateful to the National Science Foundation and the Dean's Undergraduate Research Fund, New York University (grant to P. S. B.), for support of this work. We thank Professor N. E. Geactinov for his assistance in providing access to the singlet oxygen apparatus.

Notes and references

1 K. M. Creegan, J. L. Robbins, W. K. Robbins, J. M. Millar, R. D. Sherwood, P. J. Tindall, D. M. Cox, A. B. Smith III, J. P. McCauley Jr., D. R. Jones and R.T. Gallager, *J. Am. Chem. Soc*., 1992, **114**, 1103.

2 (*a*) Y. Elemes, S. K. Silverman, C. Sheu, M. Kao, C. S. Foote, M. M. Alvarez and R. L. Whetten, *Angew. Chem., Int. Ed. Engl*., 1992, **3**, 351; (*b*) J. P. Deng, D. D. Ju, G. R. Her, C. Y. Mou, C. J. Chen, Y. Y. Lin and C.C. Han, *J. Phys. Chem*., 1993, **97**, 11575; (*c*) R. Malhotra, S. Kumar and A. Satyam, *J. Chem. Soc., Chem. Commun*., 1994, 1339; (*d*) J. P. Deng, C. Y. Mou and C. C. Han, *J. Phys. Chem*., 1995, **99**, 14907; (*e*) A. L. Balch, D. A. Costa, B. C. Noll and M. M. Olmstead, *J. Am. Chem. Soc*., 1995, **117**, 8926; (*f*) S. Lebedkin, S. Ballenweg, J. Gross, R. Taylor and W. Krätschmer, *Tetrahedron Lett*., 1995, **28**, 4971; (*g*) T. Hamano, T. Mashino and M. Hirobe, *J. Chem. Soc., Chem. Commun*., 1995, 1537; (*h*) R.W. Murray and K. Iyanar, *Tetrahedron Lett*., 1997, **38**, 335.

3 (*a*) A. Hirsch, *The Chemistry of Fullerenes*, G. Thieme Verlag, Stuttgart, New York, 1994; (*b*) C. S. Foote, *Top. Curr. Chem.*, 1994, **169**, 347; (*c*) D. I. Schuster, *Inter-American Photochemical Society Newsletter*, 1996, **19**, 35.
4 J. W. Arbogast, A. P. Darmanyan, C. S. Foote, Y. Rubin, F. N. Diederich, M. M. Alvarez, S. J. Anz and R. L. Whetten, *J. Phys. Chem.*, 1991, **95**, 11; J. L. Anderson, Y.-Z. An, Y. Rubin and C. S. Foote, *J. Am. Chem. Soc.*, 1994, **116**, 9763.
5 A. U. Khan and M. Kasha, *Proc. Natl. Acad. Sci. U.S.A.*, 1979, **76**, 6047; A. U. Khan, *J. Photochem.*, 1984, **25**, 327; P. R. Ogilby and C. S. Foote, *J. Am. Chem. Soc.*, 1982, **104**, 2069; 1983, **105**, 3423.
6 (*a*) H. H. Wasserman and D. L. Larsen, *J. Chem. Soc., Chem. Commun.*, 1972, 253; (*b*) N. J. Turro, M.-F. Chow and J. Rigaudy, *J. Am. Chem. Soc.*, 1981, **103**, 7218; (*c*) T. Wilson, A. U. Khan and M. M. Mehrotra, *Photochem. Photobiol.*, 1986, **43**, 661.
7 HPLC was performed on a Buckyclutcher-1 column (C. J. Welch and W. H. Pirkle, *J. Chromatogr.*, 1992, **609**, 89); eluent: 70:30 toluene–hexanes; detection 354 nm.
8 Singlet oxygen luminescence at 1270 nm was studied using a previously described ultrasensitive Ge-based near-IR detector: A. U. Khan, *J. Am. Chem. Soc.*, 1981, **103**, 6516; A. U. Khan, *ACS Symp. Ser.*, 1987, **339**, 58.
9 C. Kaneko, A. Sugimoto and S. Tanaka, *Synthesis*, 1974, 876.
10 L. Juha, V. Hamplová, J. Kodymová and O. Spalek, *J. Chem. Soc., Chem. Commun.*, 1994, 2437.
11 The light source was a Hanovia 450 W medium pressure Hg arc lamp cooled by a quartz jacket fitted with a Pyrex filter between the lamp and the inner wall of the jacket.
12 P. B. Merkel and D. R. Kearns, *J. Am. Chem. Soc.*, 1972, **94**, 1029; A. A. Gorman, G. Lovering and M. A. Rodgers, *J. Am. Chem. Soc.*, 1978, **100**, 4527.
13 T. W. Ebbesen, K. Tanigaki and S. Kuroshima, *Chem. Phys. Lett.*, 1991, **181**, 501.
14 M. R. Fraelich and R. B. Weisman, *J. Phys. Chem.*, 1993, **97**, 11 145.

Communication 8/06603E

1,3,2,4-Diselenastannaboretane, a novel selenium-containing four-membered boracycle: synthesis, structure and thermal cycloreversion into a selenoxoborane

Mitsuhiro Ito,[a] Norihiro Tokitoh*[b] and Renji Okazaki[c]

[a] *Department of Chemistry, Graduate School of Science, The University of Tokyo, 7-3-1 Hongo, Bunkyo-ku, Tokyo 113-0033, Japan*
[b] *Institute for Fundamental Research of Organic Chemistry, Kyushu University, 6-10-1 Hakozaki, Higashi-ku, Fukuoka 812-8581, Japan. E-mail: tokitoh@ms.ifoc.kyushu-u.ac.jp*
[c] *Department of Chemical and Biological Sciences, Faculty of Science, Japan Women's University, 2-8-1 Mejirodai, Bunkyo-ku, Tokyo 112-8681, Japan*

Received (in Cambridge, UK) 17th August 1998, Accepted 6th October 1998

Treatment of an overcrowded aryl trihydroborate bearing 2,4,6-tris[bis(trimethylsilyl)methyl]phenyl (Tbt) group with Cp_2TiSe_5 followed by the addition of Ar_2SnCl_2 (Ar = Ph or Mes) and Ph_3P resulted in the isolation of novel selenium-containing four-membered boracycles, 1,3,2,4-diselenastannaboretanes, the thermolysis of which in the presence of 2,3-dimethyl-1,3-butadiene or 2,4,6-tri-*tert*-butylbenzonitrile oxide indicated the formation of a novel class of boron-containing doubly bonded compound, an arylselenoxoborane (Tbt)B=Se.

The chemistry of boracycles containing heavier group 16 elements has been much less investigated than that of the oxygen-containing counterpart such as boroxines [$(RBO)_3$] and other cyclic boronic esters owing to their high sensitivity toward air and moisture.[1] Since a boron atom is known to prefer planar-tricoordinate geometry strongly, small ring compounds containing a boron atom generally have a large ring strain and are quite reactive. Recently, we have reported the synthesis and structures of several stable 1,3,2,4-dithiametallaboretanes, novel sulfur-containing four-membered boracycles, bearing a very bulky and effective steric protecting group, 2,4,6-tris[bis(trimethylsilyl)methyl]phenyl (Tbt) group.[2] We have also described that one of those four-membered ring systems, *i.e.* a 1,3,2,4-dithiastannaboretane derivative, provides us with a new and facile route to the boron–oxygen and boron–sulfur double-bond compounds (oxoborane and thioxoborane, respectively), the synthetic methods to which have, so far, not been well established.[3,4] By contrast, until now there have been very few reports on selenium-containing organoboranes.[5]

Here, we report the synthesis and crystal structure of a kinetically stabilized 1,3,2,4-diselenastannaboretane bearing the Tbt group, a novel selenium-containing four-membered boracycle, together with its thermolysis leading to the formation of an arylselenoxoborane (Tbt)B=Se. Oxoboranes and thioxoboranes are known to be important intermediates in the oxidation or sulfurization of elemental boron or other boron compounds and are widely studied from the viewpoints of theoretical and/or gas-phase chemistry.[6,7] On the other hand, selenoxoboranes, selenium analogues of oxoboranes and thioxoboranes, are thought to be much less stable than oxoboranes and thioxoboranes, and there has been only one report on the gas-phase detection of a chloroselenoxoborane in the reaction of elemental boron with Se_2Cl_2 at 1000 °C.[8] Although the synthesis and structure of 1,3,2,4-diselenadiboretane, a dimer of a selenoxoborane, has already been reported by Nöth and coworkers, no description was given for the intermediary selenoxoborane.[9]

The reaction of an overcrowded trihydroborate **2**, synthesized by the reaction of $(Tbt)B(OMe)_2$ **1** with $LiAlH_4$,[2] with titanocene pentaselenide followed by treatment with Ph_2SnCl_2 gave a novel five-membered boracycle, 1,2,4,3,5-triselenastannaborolane **3**, as yellow crystals in 20% yield from **1** (Scheme 1). Although we have attempted the thermolysis of **3** in the hope of cycloreversion into the selenoxoborane (Tbt)B=Se, no change was observed even at 150 °C in the presence of 2,3-dimethylbuta-1,3-diene as a trapping reagent for a selenoxoborane. We next examined ring contraction of **3** to the 1,3,2,4-diselenastannaboretane by deselenation with Ph_3P. The reaction proceeded smoothly and quantitatively at ambient temperature to give the desired 1,3,2,4-diselenastannaboretane **4**, a novel selenium-containing four-membered boracycle (Scheme 1). Compound **4** showed satisfactory spectral and analytical data, but single crystals suitable for X-ray crystallographic analysis were not obtained owing not only to the low crystallinity but also to its high instability in solution. On the other hand, 2,2-dimesityl-1,3,2,4-diselenastannaboretane **5**, which was prepared from **1** and dichlorodimesitylstannane in 24% yield by a synthetic method similar to that of **4**,[10] gave single crystals suitable for X-ray crystallographic analysis upon recrystallization from 1,2-dimethoxyethane. The crystal structure of **5** is shown in Fig. 1.†

The four-membered ring of **5** is not completely planar with the dihedral angle between planes B(1)–Se(1)–Se(2) and Sn(1)–Se(1)–Se(2) being 13.8° due to the steric repulsion between the Tbt group and one of the mesityl group on the tin atom. The geometry around the central boron atom is found to be perfectly trigonal planar ($\Sigma\angle B = 360°$). The angle between the plane

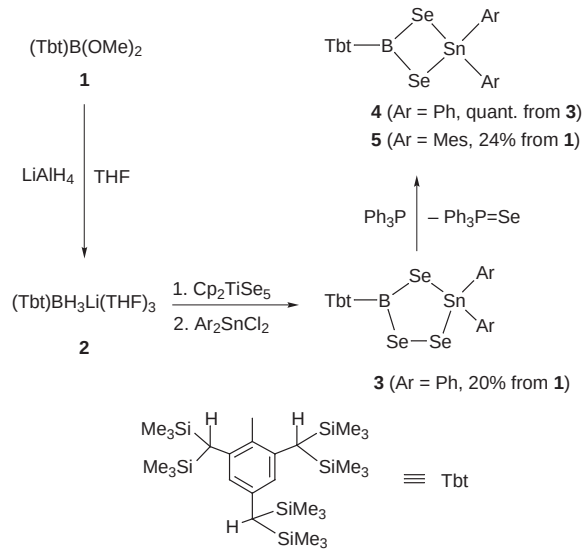

Scheme 1

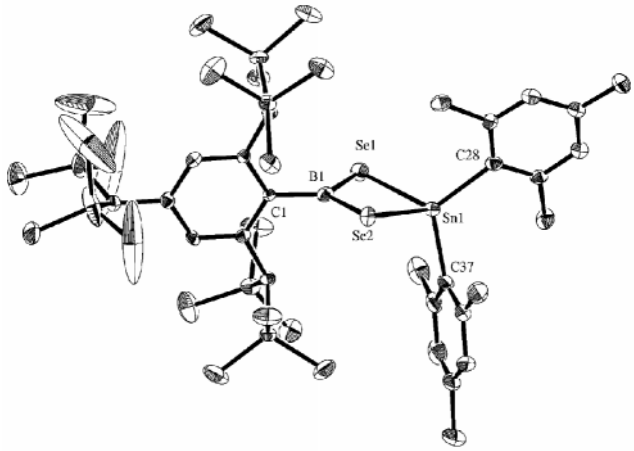

Fig. 1 ORTEP drawing of 2,2-dimesityl-1,3,2,4-diselenastannaboretane **5** with thermal ellipsoid plots (40% probability). Selected bond lengths (Å) and angles (°). B(1)–C(1) 1.557(13), B(1)–Se(1) 1.962(11), B(1)–Se(2) 1.960(10), Se(1)–Sn(1) 2.557(1), Se(2)–Sn(1) 2.566(1), Sn(1)-C(28) 2.149(10), Sn(1)-C(37) 2.127(10), Se(1)–B(1)–Se(2) 114.1(5), Se(1)–B(1)–C(1) 123.2(7), Se(2)–B(1)–C(1) 122.7(8), B(1)–Se(1)–Sn(1) 82.4(3), B(1)–Se(2)–Sn(1) 82.2(4), Se(1)–Sn(1)–Se(2) 79.95(4), C(28)-Sn(1)–C(37) 117.3(3).

defined by B(1)–Se(1)–Se(2) and the aromatic ring plane of the Tbt group is 86.6°, suggesting no conjugative interaction of π-electrons on the Tbt group with the boron atom. These structural features of **5** are similar to those of the 2,2-dimesityl-1,3,2,4-dithiagermaboretane derivative reported by us.[2b]

Since we have already shown that the 2,2-diphenyl-1,3,2,4-dithiastannaboretane derivative, a sulfur-analogue of **4**, acts as a good precursor of a thioxoborane, (Tbt)B=S, on thermolysis,[4] the thermolysis of **4** was also carried out in the expectation that it would dissociate into a boron–selenium double-bonded species (selenoxoborane) (Tbt)B=Se and diphenylstannaneselone.

When a toluene-d_8 solution of **4** and 2,3-dimethylbuta-1,3-diene in a sealed NMR tube was heated at 100 °C for 12 h, the starting material completely disappeared to afford 4,5-dimethyl-1,2-selenaboracyclohex-4-ene **6** (91%) along with the trimer **7** of diphenylstannaneselone **9** (75%) (Scheme 2). The formation of **6** and **7** clearly indicates the initial retro [2+2]cycloaddition of the diselenastannaboretane ring of **4** into the two units, *i.e.* selenoxoborane **8** and diphenylstannaneselone **9**, followed by the [4 + 2]cycloaddition reaction of **8** with co-existing 2,3-dimethylbuta-1,3-diene and the self-trimerization of **9**. To the best of our knowledge, this is the first example of the trapping reaction of a selenoxoborane. Similarly, thermolysis of **4** at 50 °C in the presence of 2,4,6-tri-*tert*-butylbenzonitrile oxide afforded the [3 + 2]cycloadduct of selenoxoborane **10** (59%)† together with **7** (45%). These results show that the selenoxoborane has a double-bond character like oxoborane and thioxoborane previously reported.[3,4]

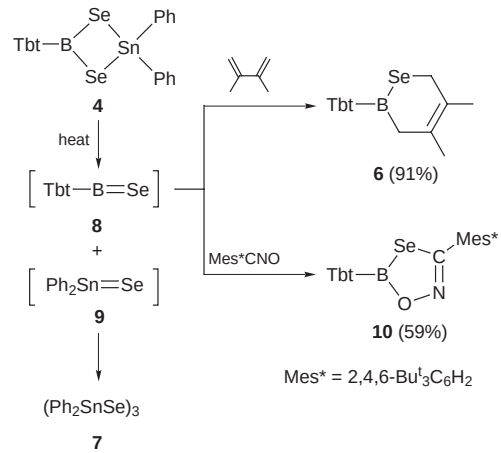

Scheme 2

In summary, we have succeeded in the isolation and crystallographic analysis of the first 1,3,2,4-diselenastannaboretane **4**. Compound **4** undergoes thermal cycloreversion into the overcrowded selenoxoborane (Tbt)B=Se, the formation of which was confirmed by the intermolecular [4+2]cycloaddition reaction with a diene.

This work was partly supported by Grants-in-Aid for Scientific Research (No. 09239208 and 09440216) from the Ministry of Education, Science, Sports, and Culture, Japan. M. I. thanks Research Fellowships of the Japan Society for the Promotion of Science for Young Scientists. We also thank Shin-etsu Chemical and Tosoh Akzo Co., Ltds. for the generous gift of chlorosilanes and alkyllithiums, respectively.

Notes and references

† *Crystallographic data* for **5**: $C_{45}H_{81}BSe_2Si_6Sn$, M = 1087.07, monoclinic, space group $P2_1/n$, a = 21.053(5), b = 13.324(4), c = 21.341(5) Å, β = 91.22(2)°, V = 5634(2) Å^3, Z = 4, D_c = 1.271 g cm^{-3}, T = 173 K, $F(000)$ = 2232.00, yellow prism with dimensions 0.65 × 0.40 × 0.10 mm, μ(Mo-Kα) = 19.00 cm^{-1}, $R(R_w)$ = 0.069(0.075). The intensity data (2θ < 55°) for **1** were collected on a Rigaku AFC7R diffractometer with graphite monochromated Mo-Kα radiation (λ = 0.71069 Å), and 13870 reflections (13517 unique) were measured. The structure of **1** was solved by direct methods with SHELXS-86,[11] expanded using Fourier techniques,[12] and refined by the full-matrix least-squares methods using the TEXSAN crystallographic software package.[13] All the non-hydrogen atoms were refined anisotropically, while the hydrogen atoms were located in the calculated positions. The final cycles of the least square refinement were based on 6066 observed reflections [$I > 3\sigma|I|$] and 497 variable parameters. The maximum and minimum peaks on the final difference Fourier map correspond to 3.48 and −1.04 e$^-$/Å^3, respectively. CCDC 182/1052.

1 C. E. Housecroft, in *Comprehensive Organometallic Chemistry II*, ed. E. W. Abel, F. G. A. Stone and G. Wilkinson, Pergamon Press, Oxford, UK, 1995, vol. 1, ch. 4, p. 129.
2 (*a*) N. Tokitoh, M. Ito and R. Okazaki, *Organometallics*, 1995, **14**, 4460; (*b*) M. Ito, N. Tokitoh and R. Okazaki, *Organometallics*, 1997, **16**, 4314.
3 M. Ito, N. Tokitoh and R. Okazaki, *Tetrahedron Lett.*, 1997, **38**, 4451.
4 N. Tokitoh, M. Ito and R. Okazaki, *Tetrahedron Lett.*, 1996, **37**, 5145.
5 For example: W. Siebert and F. Riegel, *Chem. Ber.*, 1973, **106**, 1012; R. Köster, G. Seidel, R. Boese and B. Wrackmeyer, *Chem. Ber.*, 1988, **121**, 1955; C. D. Habben, *Chem. Ber.*, 1988, **121**, 1967; R. Köster, G. Seidel and M. Yalpani, *Chem. Ber.*, 1989, **122**, 1815; M. Yalpani, R. Boese and R. Köster, *Chem. Ber.*, 1990, **123**, 707; see also ref. 9.
6 (*a*) Gas phase detection of the FBO molecule, see: Y. Kawashima, K. Kawaguchi, Y. Endo and E. Hirota, *J. Chem. Phys.*, 1987, **87**, 2006 and references cited therein; (*b*) for a theoretical study, see: M. T. Nguyen, L. G. Vanquickenborne, M. Sana and G. Leroy, *J. Chem. Phys.*, 1993, **97**, 5224; (*c*) for a review, see: S. H. Bauer, *Chem. Rev.*, 1996, **96**, 1907.
7 R. W. Kirk and P. L. Timms, *Chem. Commun.*, 1967, 18; C. Kirby, H. W. Kroto and M. J. Taylor, *J. Chem. Soc., Chem. Commun.*, 1978, 19; C. Kirby and H. W. Kroto, *J. Mol. Spectrosc.*, 1980, **83**, 1, 130; for a theoretical study, see ref. 6(*b*); for a review, see: H. W. Kroto, *Chem. Soc. Rev.*, 1982, **11**, 435.
8 T. A. Cooper, M. A. King, H. W. Kroto and R. J. Suffolk, *J. Chem. Soc., Chem. Commun.*, 1981, 353.
9 D. Männig, C. K. Narula, H. Nöth and U. Wietelmann, *Chem. Ber.*, 1985, **118**, 3748; E. Hanecker, H. Nöth and U. Wietelmann, *Chem. Ber.*, 1986, **119**, 1904.
10 In this reaction an inseparable mixture of 1,2,4,3,5-triselenastannaboretane and 1,3,2,4-diselenastannaboretane **5** was obtained, to which was added triphenylphosphine without separation.
11 G. M. Sheldrick, SHELXS-86, in *Crystallographic Computing 3*, ed. G. M. Sheldrick, C. Kruger and R. Goddard, Oxford University Press, pp. 175–189.
12 P. T. Beuskens, DIRDIF94. Direct methods for difference structures–an automatic procedure for phase extension and refinement of difference structure factors, Technical Report of the Crystallography Laboratory, University of Nijmegen, The Netherlands.
13 TEXSAN: TEXRAY Structure Analysis Package, Molecular Structure Corporation, 1985.

Communication 8/06478D

C_{60} degrades to $C_{120}O$

Roger Taylor,*[a] Mark P. Barrow[b] and Thomas Drewello[b]

[a] *The Chemistry Laboratory, CPES School, Sussex University, Brighton UK BN1 9QJ. E-mail: R.Taylor@sussex.ac.uk*

[b] *Department of Chemistry, University of Warwick, Coventry, UK CV4 7AL*

Received (in Cambridge, UK) 27th August 1998, Accepted 6th October 1998

At ambient temperature and in the solid state C_{60} degrades to $C_{120}O$ which is present in up to *ca.* 1% concentration in each of thirteen differently sourced samples examined; traces of $C_{120}O_2$ have also been detected.

When pure [60]fullerene was first obtained,[1] it was observed that films which had been left on the surface of a flask for a few days would not redissolve easily, successive extracts being increasingly dilute and more pink in colour relative to the magenta of the pure fullerene.[2] Oxidation was suspected, but further analysis was not possible at that time.

Recently, we have found that completely insoluble products are formed from fullerenes (especially higher fullerenes) on standing.[3,4] These were provisionally described as graphitic due to this insolubility,[3] but more recent work showed that graphitic planes are absent, and moreover, heating KBr discs of them produces matrix-isolated CO_2.[4] Evidently these derivatives contained oxygen, but no further details of the structures could be deduced.

[60]Fullerene, available now from numerous suppliers, comes with a stated purity. Given this assurance, fullerene researchers have had no need to examine the purity of the material. This has not been problematical because purification is usually affected at the derivative stage. Recently however, we found it necessary to check by HPLC (4.6 mm × 25 cm Cosmosil Buckyclutcher column, toluene eluent at 1 ml min^{-1}) the [70]fullerene level in a new batch of [60]fullerene. While the amount of [70]fullerene was virtually undetectable we were surprised to find a significant peak with a retention time of 14.6 min compared with [60]fullerene at 7.4 min, Fig. 1 ([70]fullerene elutes at 11.8 min under these conditions). The retention time was identical to that for an authentic sample[5] of $C_{120}O$ under our conditions. (NB. The retention times for fullerenes and derivatives vary slightly according to the ambient temperature, column condition, and injection volume, and for the above column/eluent/flow have been described[6] as 7.8 and 15.8 min for C_{60} and $C_{120}O$, respectively.) The eluent solution was straw-coloured, and removal of the toluene produced a brown film, which was much less soluble in toluene than either C_{60} or its oxides, further indicating it to be a dimeric species. Examination of twelve commercial samples from various suppliers, and also one of our own dating from 1990, showed that this component is present in *all* of them, with varying concentrations.

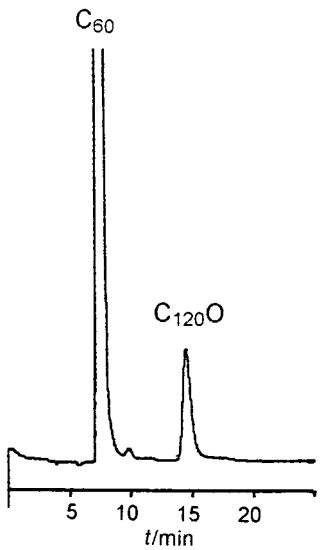

Fig. 1 HPLC of a 1 ml injection of a saturated toluene solution of C_{60}, showing $C_{120}O$ andthe absence of C_{70}.

Although an EI mass spectrum of the component showed just C_{60}, a MALDI-TOF mass spectrum proved it to be $C_{120}O$ (*m/z* 1457), and this was confirmed by comparison of the IR spectrum with that of an authentic sample.[5] The common bands are at 1632m, 1463m, 1456sh, 1429, 1384, 1307, 1218, 1183, 1166, 1101m, 1063, 1033m, 1016sh, 960, 849, 831, 807, 780, 765, 746, 711, 606, 589, 574, 551, 527 and 479 nm. The main bands in our spectrum have also been reported very recently.[7]

It is thus ironic that although various groups have gone to some trouble to prepare and isolate $C_{120}O$,[5,8,9] this was actually unnecessary because it is readily available in the first place, and we have been able to extract multimilligram quantities (which crystallise from carbon disulfide as black needles) from commercial C_{60} The literature preparation method consists of converting C_{60} to $C_{60}O$ which was separated and purified, the two reagents being then heated together for many hours, either in the solid state, or under reflux in 1,2-dichlorobenzene, which results in combination to give $C_{120}O$.

$C_{60}O$, which has been produced by oxidation of [60]fullerene under a variety of conditions *viz.* using photosensitizers,[10] chemically generated singlet oxygen,[11] dimethyldioxirane,[12] iodosobenzene/metal catalysts,[13] methyltrioxorhenium–hydrogen peroxide,[14] ozone,[15] 3-chloroperbenzoic acid,[16] and electrochemistry.[17] It is widely assumed that C_{60} undergoes oxidation to $C_{60}O$ on exposure to air, but we believe this has never been demonstrated. We consider that this does indeed happen, but given that the mono-oxide is strained and predicted to be unstable relative to $C_{120}O$,[18] it is quickly captured by a further C_{60} molecule in a [2 + 2] reaction (Scheme 1) to produce $C_{120}O$.

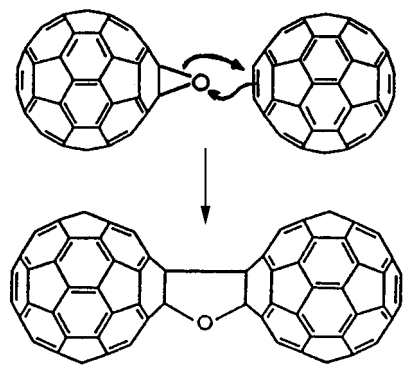

Scheme 1 Conjectured [2 + 2] cycloaddition mechanism for the formation of $C_{120}O$ from C_{60} and $C_{60}O$.

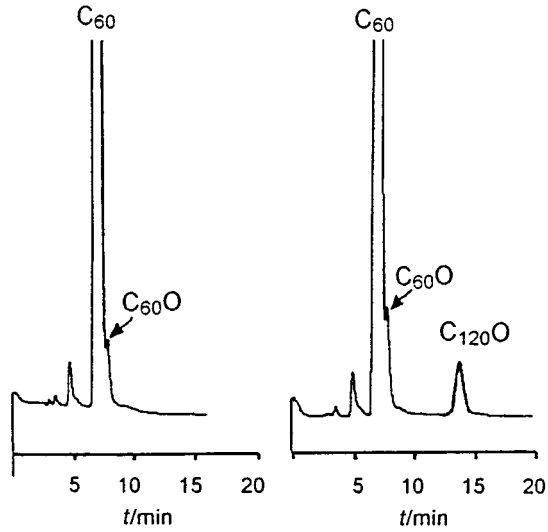

Fig. 2 HPLC traces of saturated toluene solutions (50 μl each) of a C_{60} sample: (a, left) HPLC purified; (b, right) the same material after exposure of the solid to daylight for 40 h.

The possibility that the observed $C_{120}O$ is formed during the arc-discharge process may be discounted since it elutes after [70]fullerene, yet samples in which it is present are entirely free of the latter. Removal of [70]fullerene by chromatographic purification would remove the later-eluting oxide as well. Moreover, given the different separation regimes used by different manufacturers (and none use alumina which was employed to purify our original in-house sample) it would be most surprising that no-one managed to remove any pre-existing $C_{120}O$. In order to provide further information on this point and to confirm our belief that the oxide results from a solid state reaction that occurs at ambient temperature, we exposed a sample of solid HPLC-purified C_{60} to air and daylight for 40 h. Fig. 2(a) and (b) show consecutive HPLC traces for saturated solutions of the solid before and after this exposure. The presence of the $C_{120}O$ peak in the exposed material is apparent, as is the increased intensity of the $C_{60}O$ peak. (The trace of the latter in the purified material arises during the handling and concentration of the HPLC eluent.)

Atmospheric oxidation of [60]fullerene beyond the monoxide stage is likely, giving *e.g.* $C_{60}O_2$ with capture by a further [60]fullerene to give $C_{120}O_2$. Indeed we find evidence of $C_{120}O_2$ in some of the samples, with a peak of retention time under our conditions of 16.9 min, identical to that of an authentic[6] sample. The concentration is however lower than that of $C_{120}O$ despite its formation being energetically more favourable.[18] We believe this is because $C_{60}O$, the $C_{60}O_2$ precursor, is rapidly converted to $C_{120}O$ before further oxidation can occur.

We suggest that $C_{120}O$ may add on further oxygens or $C_{60}O$ molecules (probably remote from the initial addition site, because of steric considerations) to give ultimately a polymer, which is very likely the insoluble oxygen-containing material that we have isolated from various fullerene samples.[3,4] In this connection we find that after a film of HPLC purified C_{60} had stood in daylight during four days, most (*ca.* 70%) would not redissolve readily in toluene (and some not at all). HPLC of the slightly soluble material showed the presence of four components with retention times either similar to, or considerably longer than, the dimeric species described above. This suggests that a mixture of oxygenated dimers and trimers is produced by the more aggressive oxidation, and we hope subsequently to examine these further.

Because the absorption coefficient of $C_{120}O$ is not known (and difficult to measure with any accuracy due to the extremely low solubility in hexane) the percentage present in the examined samples (which varies by a factor of *ca.* 5) is uncertain, but we visually estimate the maximum levels to be around 1%.

These results have consequences. First, they make it difficult to account for the reports[19] that C_{60} has been found to occur naturally. Secondly, the purity levels quoted by suppliers refer to the as-produced material, and are not characteristic of the condition at the time it is used. Thirdly, they make it essential to study the stability of products towards oxidation, if uses are to be found for fullerenes. We know from our own studies that some fullerene derivatives, such as phenylated fullerenes rapidly acquire oxygen on standing,[20] and this may be true for many other derivatives, whilst by contrast, some addends may actually inhibit oxidation. Resolution of this problem must feature amongst the goals of fullerene chemists.

We thank David Box of Dynamic Enterprises Ltd, UK, for providing fullerene samples of different origins.

Notes and references

1 R. Taylor, J. P. Hare, A. K. Abdul-Sada and H. W. Kroto, *J. Chem. Soc., Chem. Commun.*, 1990, 1423.
2 Reported subsequently, (R. Taylor, *Interdisciplinary Science Reviews*, 1992, **17**, 161.)
3 R. Taylor, *Molecular Nanostructures*, eds. H. Kuzmany, J. Fink, M. Nehring and S. Roth, World Scientific, 1998, p. 136.
4 R. Taylor, A. Pénicaud and N. J. Tower, *Chem. Phys. Lett.*, in press.
5 S. Lebedkin, S. Ballenweg, J. Cross, R. Taylor and W. Krätschmer, *Tetrahedron Lett.*, 1995, 4571.
6 A. Gromov, S. Lebedkin, S. Ballenweg, A. G. Avent, R. Taylor and W. Krätschmer, *Chem. Commun.*, 1997, 209.
7 M. Krause, L. Dunsch, G. Siefert, P. W. Fowler, A. Gromov, W. Krätschmer, R. Gutierez, D. Porezag and T. Frauenheim, *J. Chem. Soc., Faraday Trans.*, 1998, **94**, 2287.
8 A. B. Smith, H. Toyuyama, R. M. Strongin, G. T. Furst, W. J. Romanov, B. T. Chait, U. A. Mirza and I. Haller, *J. Am. Chem. Soc.*, 1995, **117,** 9359.
9 A. L. Balch, D. A. Costa, W. R. Fawcett and K. Winkler, *J. Phys. Chem.*, 1996, **100**, 4823.
10 K. M. Creegan, J. L. Robbins, W. K. Robbins, J. M. Millar, R. D. Sherwood, P. J. Tindall, D. M. Cox, J. M. McCauley, D. R. Jones, R. Gallagher and A. B. Smith, *J. Am. Chem. Soc.*, 1992, **114**, 1103; S. W. McElvany, J. H. Callahan, M. M. Ross, L. D. Lamb and D. R. Huffman, *Science*, 1993, **260**, 1632.
11 L. Juha, V. Hamplová, J. Kodymoná and O. Spalek, *J. Chem. Soc., Chem. Commun.*, 1994, 2437.
12 Y. Elemes, S. K. Silverman, C. Sheu, M. Kao, C. S. Foote, M. N. Alvarez and R. Whetten, *Angew. Chem. Intl. Ed. Engl.*, 1992, **31**, 351.
13 T. Hamano, T. Mashino and M. Hiroba, *J. Chem. Soc., Chem. Commun.*, 1995 1537.
14 R. W. Murray and K. Iyanar, *Tetrahedron Lett.*, 1997, **38**, 335.
15 D. Heymann and L. P. F. Chibante, *Recl. Trav. Chim. Pays-Bas*, 1993, **112**, 531, 639; *Chem. Phys. Lett.*, 1993, **207**, 339; R. Malhotra, S. Kumar and A. Satyam, *J. Chem. Soc., Chem. Commun.*, 1994, 1339; J. Deng, C. Mou and C. Han, *J. Phys. Chem.*, 1995, **99**, 14907; J. Deng, D. Ju, G. Her, C. Mou, C. Chen, Y. Lin and C. Han, *J. Phys. Chem.*, 1993, **97**, 11575.
16 T. Nogami, M. Tsuda, T. Ishida, S. Kurono and M. Ohashi, *Fullerene Sci. Technol.*, 1993, **1**, 275; A. L. Balch, D. A. Costa, B. C. Noll and M. M. Olmstead, *J. Am. Chem. Soc.*, 1995, **117**, 8926.
17 W. A. Kalsbeck and H. H. Thorp, *J. Electroanal. Chem.*, 1991, **314**, 363.
18 P. W. Fowler, D. Mitchell, R. Taylor and G. Seifert, *J. Chem. Soc., Perkin Trans. 2*, 1997, 1901.
19 T. K. Daly, P. R. Buseck, P. Williams, and C. F. Lewis, *Science*, 1993, **259**, 1599; D. Heymann, L. P. F. Chibante, W. S. Wolbach, R. R. Brooks and R. E. Smalley, *Science*, 1994, **265**, 645.
20 O. V. Boltalina, J. M. Street and R. Taylor, *Chem. Commun.*, 1998, 1827; A. D. Darwish, P. R. Birkett, G. J. Langley, H. W. Kroto, R. Taylor and D. R. M. Walton, *Fullerene Sci. Technol.*, 1997, **5**, 1667.

Communication 8/06726K

Synthesis of continuous mesoporous silica thin films with three-dimensional accessible pore structures

Dongyuan Zhao,[a,b] Peidong Yang,[a] David I. Margolese,[a] Bradley. F. Chmelka[b,c] and Galen D. Stucky*[a,b]

[a] *Department of Chemistry,* [b] *Materials Research Laboratory and* [c] *Department of Chemical Engineering, University of California, Santa Barbara, California 93106, USA. E-mail: stucky@chem.ucsb.edu*

Received (in Bloomington, IN, USA) 19th June 1998, Accepted 22nd September 1998

Continuous mesoporous silica thin films with three-dimensional (3-D) accessible pore structures (*Pm*3*n*, *P*6$_3$/*mmc* space groups) have been prepared by a dip-coating technique using cationic surfactants as the structure-directing agents in nonaqueous media under acidic conditions.

The integration of hydrogen bonding interaction at the organic/inorganic interface with organic/inorganic domain assembly and the use of sol–gel and emulsion chemistry in acidic media[1–4] has proven to be a general route for the easy processing of ordered mesoporous materials into desired morphologies.[5–11] Mesoporous silica thin films with highly ordered mesostructures have numerous potential applications in catalysis, sensors, separation, and opto-electric devices.[4–11] We have recently described how surfactant and non-aqueous cosolvents can be used to define mesophase structure,[2–4] and to grow 3-D hexagonal mesostructured silica films at solid–liquid and liquid–vapor interface[7] following the film growth procedures described by Yang *et al.*[5] and Aksay *et al.*[6] for 2-D hexagonal mesostructured silica thin films that have 1-D channel structures with the pore channels oriented parallel to the substrate surface. More recently, the formation of continuous supported cubic and 2-D hexagonal mesoporous silica thin films by sol–gel dip-coating using the above acid synthesis procedure[1–3] with addition of ethanol has been reported by Brinker and coworkers;[11] fine tuning of the conditions for film formation yields high quality, pinhole-free films with the desired thickness.[11]

Here we report the formation by dip-coating[11] of continuous, stable mesoporous silica thin films with 3-D accessible pore structures using cationic surfactants. Large-head-group cationic surfactants such as $C_{16}H_{33}N(C_2H_5)_3Br$ (CTEABr) or gemini surfactants such as $C_{18}H_{37}N(CH_3)_2(CH_2)_3N(CH_3)_3Br_2$ ($C_{18\text{-}3\text{-}1}$) can be used as the structure-directing agent. The thin films exhibit highly ordered mesostructures, which can be 3-D cubic (*Pm*3*n* space group) and 3-D hexagonal (*P*6$_3$/*mmc*) structures with high BET surface areas (up to 1500 m^2 g^{-1}) and varying pore sizes (18–25 Å).

The mesoporous silica films were deposited by dip-coating on polished (100)-silicon wafers or glass sheets. The coating solutions were typically prepared by the addition of 0.78 g CTEABr cationic surfactant dissolved in 10 g ethanol (EtOH) to polymeric silica sols made by an acid-catalyzed process with stirring for 1 h at room temperature. The polymeric silica sols were prepared by heating a mixture of 2.08 g tetraethylorthoxysilicane (TEOS), 5.5 g EtOH, 0.5 g water and 0.4 g (0.1 M) HCl at 70 °C for 1 h. To complete the polymerization of the silicate species and to further improve the thermal stability of the film, the as-deposited film was heated at 80 °C in de-ionized water overnight. After drying, the film supported on the silicon wafer was calcined in air at 500 °C for 4 h to remove the organic template.

Generally, supported silica films prepared using cationic surfactants, such as CTEABr, gemini $C_{18\text{-}3\text{-}1}$, and $C_{16}H_{33}N(CH_3)_3Br$ (CTAB), in nonaqueous solutions under acidic conditions are transparent and continuous (see Fig. 1a). The thickness of the film is uniform, and can be varied from 300 nm to several hundred micrometers by changing the coating solution concentration or the coating time.

Fig. 2 shows XRD patterns of as-deposited and calcined supported silica films prepared using cationic surfactants as the structure-directing agent. As-deposited film with CTEABr shows seven well-resolved diffractions peaks in the 2θ range 1–6° (Fig. 2a), suggesting that the as-deposited film has a highly ordered cubic (*Pm*3*n*) mesostructure with a = 84.4 Å. The XRD pattern remains the same as the film is rotated by 180°, suggesting that the film has an isotropic cubic mesostructure.

After calcination, the XRD pattern (Fig. 2b) of the cubic film shows that the cubic mesostructure is preserved with ≈3% shrinkage (a = 81.7 Å). An additional two peaks indexed as (400), (332) are apparent, possibly due to different shrinkage along the 3-D directions. SEM and photomicroscopy images show that the calcined films with thicknesses < 1 μm are not cracked. TEM images recorded along the [100], [210] and [111] orientations of calcined mesoporous silica films prepared using CTEABr surfactant (Fig. 2b–d) show well-ordered 3-D cubic arrays of mesopores and confirm that the silica film has a highly ordered 3-D cubic (*Pm*3*n*) mesostructure after calcination.

N_2 adsorption–desorption isotherms of calcined silica films show type IV curves without the hysteresis loop, a pore size of 20 Å, a pore volume of 0.54 cm^3 g^{-1}, and a BET surface area of 1200 m^2 g^{-1} (Table 1).

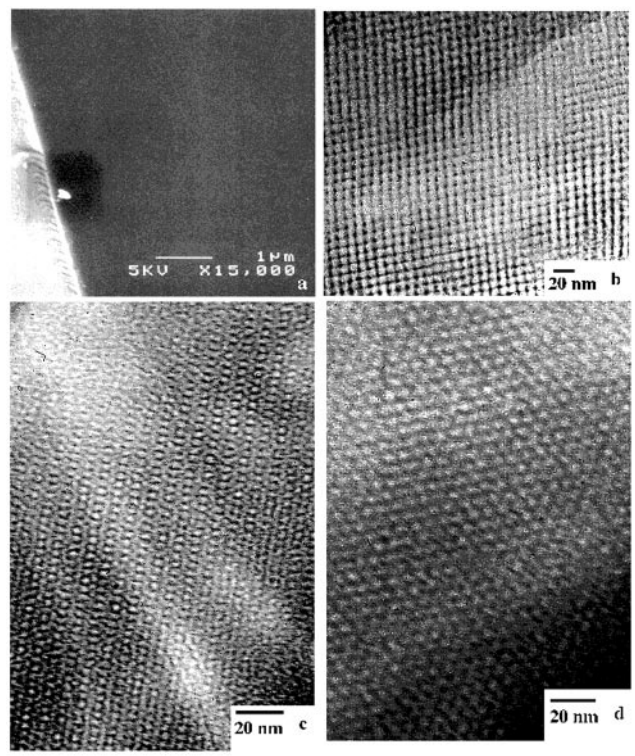

Fig. 1 a, SEM image of as-deposited 3-D cubic mesoporous silica film prepared using CTEABr surfactant. b–d, TEM images of calcined cubic mesoporous silica film with orientations: b, [100] plane; c, [210] plane; and d, [111] plane.

Table 1 Physicochemical properties of mesoporous silica thin films reported in this paper. In each pair with the same surfactant, the second entry was prepared with a high concentration of HCl or a low concentration of surfactant

Surfactant	Phase	Unit cell parameter/Å	Pore size[a]/Å	BET Surface area/m^2 g^{-1}	Pore volume/cm^3 g^{-1}
$C_{16}H_{33}N(C_2H_5)_3Br$	cubic (*Pm*3*n*)	a = 81.7	20	1200	0.54
$C_{16}H_{33}N(C_2H_5)_3Br$	hexagonal (*p*6*mm*)	a = 40.8	18	1080	0.92
$C_{18}H_{37}N(CH_3)_2(CH_2)_3N(CH_3)_3Br_2$	hexagonal ($P6_3/mmc$)	a = 44.7 c = 74.0	24	1500	0.86
$C_{18}H_{37}N(CH_3)_2(CH_2)_3N(CH_3)_3Br_2$	hexagonal (*p*6*mm*)	a = 44.0	25	1160	0.81
$C_{16}H_{33}N(CH_3)_3Br$	hexagonal (*p*6*mm*)	a = 43.9	24	740	0.67
$C_{16}H_{33}N(CH_3)_3Br$	hexagonal (*p*6*mm*)	a = 38.2	19	1490	0.76

[a] After calcination at 500 °C in air, the pore sizes were calculated by using BJH analysis from the adsorption branch of the isotherms.

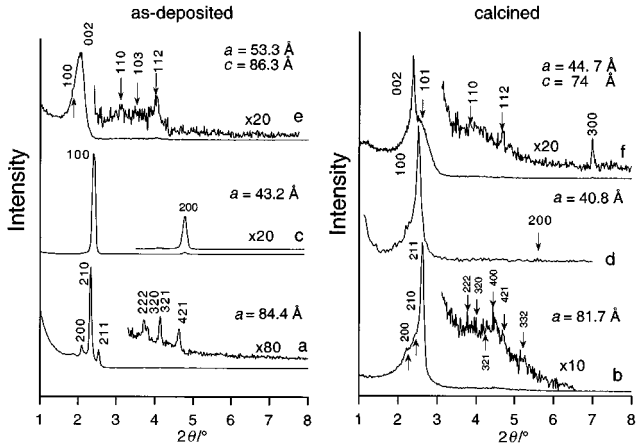

Fig. 2 XRD patterns of a, as-deposited and b, calcined 3-D cubic (*Pm*3*n*) mesoporous silica thin film prepared using CTEABr surfactant; c, as-deposited and d, calcined 2-D hexagonal mesoporous silica thin film prepared using CTEABr surfactant; e, as-deposited and f, calcined 3-D hexagonal mesoporous silica film prepared using gemini $C_{18\text{-}3\text{-}1}$ surfactant.

3-D cubic mesoporous silica thin films can be grown on the substrate over a range of reaction compositions: the ratios can be 1 TEOS : 0.12–0.37 CTEABr : 4.4–8.9 H_2O : 0.0004–0.004 HCl : 10–60 EtOH at room temperature. Unlike aqueous media synthesis [in which CTEABr only favors forming cubic (*Pm*3*n*) silica mesostructures under strongly acidic conditions[1]], in nonaqueous solution, higher concentrations of HCl result in the formation of 2-D hexagonal (*p*6*mm*) silica films confirmed by XRD patterns (Fig. 2c,d) and TEM images. N_2 adsorption measurements show the calcined film to have a pore size of 18 Å, a pore volume of 0.92 cm^3 g^{-1}, and a BET surface area of 1080 m^2 g^{-1} (Table 1).

The 3-D hexagonal mesostructured silica film formed using $C_{18\text{-}3\text{-}1}$ over a range of compositions (1 TEOS : 0.13–0.27 $C_{18\text{-}3\text{-}1}$: 4.4–11 H_2O : 0.0002–0.002 HCl : 10–60 EtOH) at room temperature shows two strong diffraction peaks with *d*-spacings of 46.2 and 43.2 Å, and three weak peaks with *d*-spacings of 30.7, 24.4, 22.5 Å (Fig. 2e). The XRD pattern can be indexed in the 3-D hexagonal space group $P6_3/mmc$ with a = 53.3, c = 86.3 Å. After calcination, the XRD pattern (Fig. 2f) shows four peaks in the 2θ range 1–8°, which can be indexed as (002), (101), (112) and (300). TEM measurements further confirm that the silica film prepared using $C_{18\text{-}3\text{-}1}$ has a highly ordered 3-D hexagonal mesostructure. N_2 adsorption–desorption isotherms show that the calcined films exhibit type IV curves without the hysteresis loop, a narrow pore size distribution at a mean value of 24 Å, and a BET surface area of 1500 m^2 g^{-1} (Table 1).

While in aqueous synthesis, $C_{18\text{-}3\text{-}1}$ surfactant favors formation of only 3-D hexagonal SBA-2,[3] in nonaqueous media lower concentrations of $C_{18\text{-}3\text{-}1}$ surfactant and higher concentrations of HCl yield a hexagonal (*p*6*mm*) oriented silica film with pore channels parallel to the substrate plane. On the other hand, oriented 2-D hexagonal silica films (Table 1) can also be formed through the use of CTAB as the structure-directing agent over a wide range of compositions (1 TEOS : 0.05–0.42 CTAB : 0.8–2 H_2O : 0.0004–0.04 HCl : 10–100 EtOH). The 2-D hexagonal mesostructure is preserved upon changing the concentration of CTAB surfactant and HCl, but the d(100) spacing decreases linearly from 40.8 to 34.5 Å with increase of the concentration of CTAB and HCl. Based on N_2 adsorption measurements, the pore sizes (19–24 Å) of the silica film are also variable with concentration of CTAB and HCl (Table 1). These results suggest that the formation of the silica film occurs with an $S^+X^-I^+$ self-assembly pathway[1] and that CTEABr surfactants have large head group and favor the formation of the 3-D cubic (*Pm*3*n*) mesophase.[3] Higher HCl concentration results in stronger interaction between inorganic and organic species and favors the formation of the 2-D hexagonal mesophase.

This work is supported by the National Science Foundation under grants DMR 95-20971 (GDS) and DMR-9257064 (BFC) and the U.S. Army Research Office under grant DAAH04-96-1-0443. This work made use of MRL Central Facilities supported by the National Science Foundation under Award No. DMR-9632716. B. F. C. is a Camille and Henry Dreyfus Teacher-Scholar and an Alfred P. Sloan Research Fellow.

Notes and references

1 Q. Huo, D. I. Margolese, U. Ciesla, D. G. Demuth, P. Feng, T. E. Gier, P. Sieger, A. Firouzi, B. F. Chmelka, F. Schüth and G. D. Stucky, *Chem. Mater.*, 1994, **6**, 1176; *Nature*, 1994, **368**, 317.
2 S. Schacht, Q. Huo, Voigt-Martinig and G. D. Stucky, *Science*, 1996, **273**, 768.
3 Q. Huo, D. I. Margolese and G. D. Stucky, *Chem. Mater.*, 1996, **8**, 1147; Q. Huo, R. Leon, P. M. Petroff and G. D. Stucky, *Science*, 1995, **268**, 1324.
4 D. Zhao, J. Feng, Q. Huo, N. Melosh, G. H. Fredrickson, B. F. Chmelka and G. D. Stucky, *Science*, 1998, **279**, 548, *J. Am. Chem. Soc.*, 1998, **102**, 6024; D. Zhao, P. Yang, Q. Huo, B. F. Chmelka and G. D. Stucky, *Curr. Opin. Solid State Mater.*, 1998, **3**, 111; Q. Huo, D. Zhao, J. Feng, K. Weston, S. K. Buratto, G. D. Stucky, S. Schacht and F. Schüth, *Adv. Mater.*, 1997, **9**, 974.
5 H. Yang, A. Kuperman, N. Coombs, S. Mamiche-Afara and G. A. Ozin, *Nature*, 1996, **379**, 703; H. Yang, N. Coombs, I. Sokolov and G. A. Ozin, *Nature*, 1996, **381**, 589; H. Yang, N. Coombs, O. Dag, I. Sokolov and G. A. Ozin, *J. Mater. Chem.*, 1997, **7**, 1755.
6 I. A. Aksay, M. Trau, I. Honma, N. Yao, L. Zhou, P. Fenter, P. M. Eisenberger and S. M. Gruner, *Science*, 1996, **273**, 892.
7 S. H. Tolbert, T. E. Schäffer, J. Feng, P. K. Hansma and G. D. Stucky, *Chem. Mater.*, 1997, **9**, 1962.
8 M. Ogawa, *Chem. Commun.*, 1996, 1149; *J. Am. Chem. Soc.*, 1994, **116,** 7941.
9 J. E. Martin, M. T. Anderson, J. G. Odinek and P. P. Newcomer, *Langmuir*, 1997, **13**, 4133.
10 R. Ryoo, C. H. Ko, S. J. Cho and J. M. Kim, *J. Phys. Chem. B*, 1997, **101,** 10610.
11 Y. Lu, R. Ganguli, C. A. Drewien, M. T. Anderson, J. C. Brinker, W. Gong, Y. Guo, H. Soyez, B. Dunn, M. H. Huang and J. I. Zink, *Nature*, 1997, **389**, 364.

Communication 8/04649B

ChemComm

Dendritic hydrogen bonding receptors: enantiomerically pure dendroclefts for the selective recognition of monosaccharides

David K. Smith and François Diederich*

Laboratorium für Organische Chemie, ETH-Zentrum, Universitätstrasse 16, CH-8092 Zürich, Switzerland. E-mail: diederich@org.chem.ethz.ch

Received (in Cambridge, UK) 21st August 1998, Accepted 2nd October 1998

Enantiomerically pure dendritic cleft receptors (dendroclefts) with a 9,9′-spirobi[9*H*-fluorene] core are prepared for the recognition of glucopyranosides by H-bonding in $CDCl_3$; the enantio- and diastereo-selectivities in the complexation processes are modulated by the presence of the dendritic shell.

The development of functional dendrimers is of great current interest.[1] In particular, the dendritic shell can alter the properties of a functional core.[2] Hydrogen-bonding dendritic hosts have been reported, but the branching does not appear to play an active role in modulating guest recognition.[3] In addition chiral recognition inside a dendrimer is as yet unknown, but possesses great scientific and technological potential.[4] Here we report enantiomerically pure dendritic cleft-type receptors (dendroclefts) of first [(−)-**G1**] and second [(−)-**G2**] generation for the chiral recognition of monosaccharide guests *via* H-bonding.

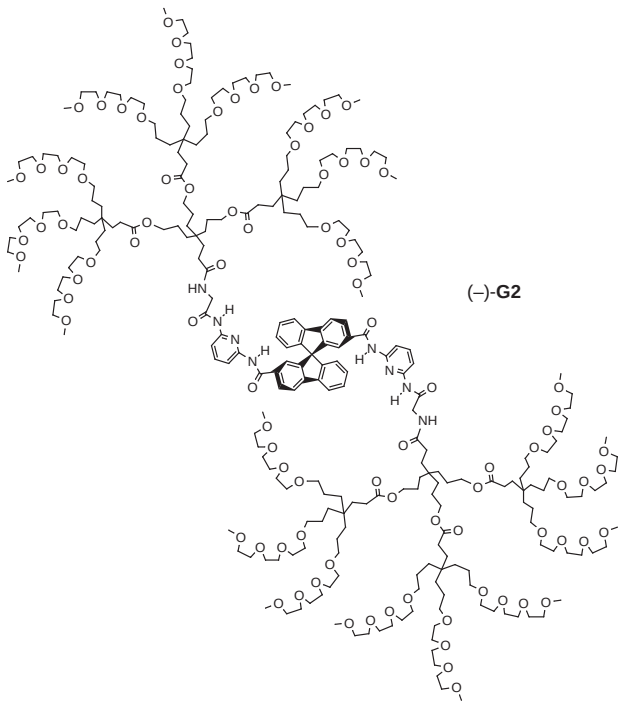

Dendrocleft (−)-**G2** was targeted by the attachment of flexible branches to a rigid, optically pure 9,9′-spirobi[9*H*-fluorene] initiator core bearing 2,6-di(carboxamido)pyridine moieties in the 2,2′-positions.[5] The resulting dendrimer possesses a buried H-bonding cleft suitable for complexing carbohydrate guests.[5,6] Its periphery is functionalised with neutral polyether groups, which provide excellent solubility in a wide range of solvents, including H_2O.

For the synthesis of (−)-**G1** and (−)-**G2** by the convergent approach,[7] the optically active core (−)-**3** was prepared from dicarboxylic acid (−)-(*R*)-**1**[5,8] *via* (−)-**2** and (−)-**G0** (Scheme 1). Attachment of the new dendritic branches **4** or **5**[9] to (−)-**3** provided the optically pure dendroclefts (−)-**G1** and (−)-**G2**, respectively, which were isolated in good yield by preparative gel permeation chromatography {GPC; Biobeads SX-1, CH_2Cl_2 [(−)-**G1**] and THF [(−)-**G2**]}.

Molecular recognition studies were performed by ^{1}H NMR titrations in dry $CDCl_3$ at 298 K using 1-*O*-octyl glucopyranosides (**6–8**) as guests.† Association constants K_a (M^{-1}) and binding free enthalpies $\Delta G°$ (kJ mol^{-1}) for the formed 1:1 complexes are summarized in Table 1. The following conclusions can be drawn.

(i) The complexes formed by the dendroclefts (−)-**G1** and (−)-**G2**, and core (−)-**G0** are of similar strength (K_a between 100 and 600 M^{-1}). Hydrogen bonds between the O-atoms of the sugars and the NH groups of the receptors represent major host–guest interactions in all complexes as evidenced by the large complexation-induced downfield shifts (up to 1.2 ppm at saturation binding) of the NH resonances in the di(carboxamido)pyridine moieties. Apparently, the bulky dendritic shell in (−)-**G1** and (−)-**G2** does not prevent the sugar molecules from penetrating the receptor and interacting with the core H-bonding sites. It is actually quite remarkable that the binding by (−)-**G1** and (−)-**G2** is not weakened by the dendritic shell, which contains a relatively high density of potentially competitive donor oxygen atoms.

(ii) The degree of enantioselectivity in the complexation of the enantiomeric α-glucosides **6** and **7** is reduced upon attachment of the dendritic shells. The difference in stability between diastereoisomeric complexes $\Delta\Delta G°$ decreases from 3.6 kJ mol^{-1} [(−)-**G0**], to 0.8 kJ mol^{-1} [(−)-**G1**], and to 0.5 kJ mol^{-1} [(−)-**G2**].

(iii) On the other hand, the diastereoselectivities of complexation are remarkably enhanced by the presence of the dendritic branches. Thus, the difference in stability between the complexes of the diastereoisomeric guests **7** and **8** increases from 0.7 kJ mol^{-1} [(−)-**G0**], to 1.4 kJ mol^{-1} [(−)-**G1**], and to 2.3 kJ mol^{-1} [(−)-**G2**].

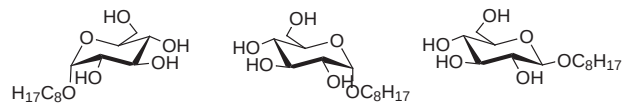

Octyl α-L-glucoside **6** | Octyl α-D-glucoside **7** | Octyl β-D-glucoside **8**

These results indicate that the dendritic shell is controlling the selectivity of complexation at the core, an unprecedented result. There are two plausible reasons for this dendritic modulation of binding selectivity which are currently under investigation. Firstly, the steric demands of the dendritic branching may disfavour certain complexes. Secondly, the oxygen donor atoms in the dendritic shell could participate in the formation of a hydrogen bonding network with the guest, changing the binding selectivity.‡

The use of such dendroclefts as chiroptical sensors[11] is currently under active investigation. Profound changes in the circular dichroism (CD) spectra are observed on addition of the glucopyranoside guests, the response being selective for

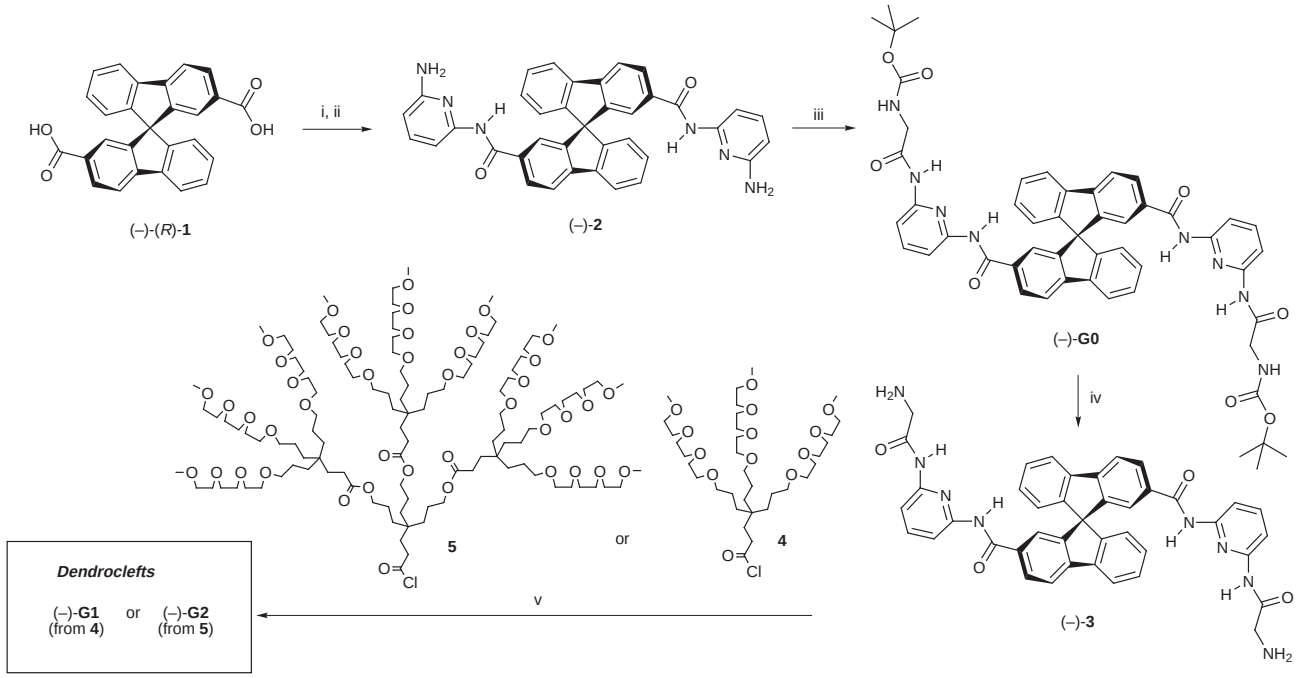

Scheme 1 Synthesis of (−)-**G1** and (−)-**G2**. *Reagents and conditions*: i, $SOCl_2$; ii, 2,6-diaminopyridine, NEt_3, THF, 85%; iii, *N*-Boc-glycine, *O*-(7-azabenzotriazol-1-yl)-1,1,3,3-tetramethyluronium hexafluorophosphate (HATU), NEt_3, THF, 81%; iv, TFA, CH_2Cl_2, 87%; v, NEt_3, DMAP, THF, 40–80%.

Table 1 Association constants K_a and binding free enthalpies $\Delta G°$ for complexes of dendrocleft with glucopyranosides in $CDCl_3$ at 298 K

Host	Guest	K_a/M^{-1}	$\Delta G°$/kJ mol^{-1}
(−)-**G0**	6	100	−11.4
(−)-**G0**	7	425	−15.0
(−)-**G0**	8	570	−15.7
(−)-**G1**	6	160	−12.6
(−)-**G1**	7	225	−13.4
(−)-**G1**	8	390	−14.8
(−)-**G2**	6	170	−12.7
(−)-**G2**	7	205	−13.2
(−)-**G2**	8	520	−15.5

different sugars and different for (−)-**G0** and (−)-**G2**. In addition, the dendritic receptor is readily recycled owing to the very large size difference between host and guest. Gel permeation filtration through a plug of Sephadex gel LH-20 with MeOH as eluent provides quantitative recovery of pure (−)-**G2** from host–guest solutions.

Efforts are now in progress to synthesise dendritic receptors with even more deeply embedded optically active cores. This general approach to dendritic molecular recognition has great potential, both for modelling the buried active sites of sugar binding proteins[12] and for the development of tunable, recyclable receptors and sensors for various analytes.

Support from the ETH Research Council and the Royal Society (E.S.E.P. fellowship to D. K. S) is gratefully acknowledged.

Notes and references

† ^{1}H NMR titrations (300 MHz) were performed at [dendrocleft] = 0.5 mM and [sugar] = 1.25–12.5 mM in $CDCl_3$ de-acidified with K_2CO_3 and dried over 4 Å molecular sieves. The complexation-induced downfield shifts (up to 1.2 ppm at saturation binding) of the resonances of the NH-protons in the dendroclefts were evaluated by nonlinear least-squares curve fitting. Job plot analyses were in agreement with the exclusive formation of 1:1 host–guest complexes. All titrations were repeated with good reproducibility, and the uncertainty in K_a is estimated as ±10%.

‡ The oxygen atoms in the dendritic shell may control the strength and selectivity of binding, as polar additives are well-known to modify sugar recognition in $CDCl_3$ (ref. 10). The core receptor (−)-**G0** was investigated in $CDCl_3$–THF (99:1) to test the effect of intermolecularly added ether (with oxygen donor atoms) on complexation. The association constants for the complexes with **7** and **8** were K_a = 320 and 390 M^{-1}, respectively. Thus, the binding strength was reduced compared to pure $CDCl_3$, as a result of competitive solvation of host and guest by THF molecules. The diastereoselectivity, however, remained low ($\Delta\Delta G°$ = 0.5 kJ mol^{-1}), and it is evident that addition of THF does not induce the same increase in diastereoselectivity as that caused by the dendritic shell.

1 J. Issberner, R. Moors and F. Vögtle, *Angew. Chem., Int. Ed. Engl.*, 1994, **33**, 2413.
2 D. K. Smith and F. Diederich, *Chem. Eur. J.*, 1998, **4**, 1353.
3 G. R. Newkome, B. D. Woosley, E. He, C. N. Moorefield, R. Güther, G. R. Baker, G. H. Escamilla, J. Merrill and H. Luftmann, *Chem. Commun.*, 1996, 2737; S. C. Zimmerman, Y. Wang, P. Bharathi and J. S. Moore, *J. Am. Chem. Soc.*, 1998, **120**, 2172.
4 H. W. I. Peerlings and E. W. Meijer, *Chem. Eur. J.*, 1997, **3**, 1563.
5 (*a*) V. Alcázar and F. Diederich, *Angew. Chem., Int. Ed. Engl.*, 1992, **31**, 1521; (*b*) J. Cuntze, L. Owens, V. Alcázar, P. Seiler and F. Diederich, *Helv. Chim. Acta*, 1995, **78**, 367.
6 (*a*) K. M. Bhattarai, R. P. Bonar-Law, A. P. Davis and B. A. Murray, *J. Chem. Soc., Chem. Commun.*, 1992, 752; (*b*) Y. Kikuchi, Y. Tanaka, S. Sutarto, K. Kobayashi, H. Toi and Y. Aoyama, *J. Am. Chem. Soc.*, 1992, **114**, 10 302; (*c*) M. Inouye, T. Miyake, M. Furusyo and H. Nakazumi, *J. Am. Chem. Soc.*, 1995, **117**, 12 416; (*d*) For a dendrimer which forms covalent boronic esters with monosaccharides in the dendritic branches, see: T. D. James, H. Shinmori, M. Takeuchi and S. Shinkai, *Chem. Commun.*, 1996, 705.
7 C. Hawker and J. M. J. Fréchet, *J. Chem. Soc., Chem. Commun.*, 1990, 1010.
8 The spirobifluorene cleft is *R*-configured in all compounds reported here: P. Lustenberger, E. Martinborough, T. Mordasini Denti and F. Diederich, *J. Chem. Soc., Perkin Trans. 2*, 1998, 747.
9 D. K. Smith, A. Zingg and F. Diederich, in *Supramolecular Science*: *Where it is and where it is going*, ed. R. Ungaro, NATO ASI Series Book, Kluwer, Dordrecht, in the press.
10 R. P. Bonar-Law and J. K. M. Sanders, *J. Am. Chem. Soc.*, 1995, **117**, 259; T. Mizutani, T. Kurahashi, T. Murakami, N. Matsumi and H. Ogoshi, *J. Am. Chem. Soc.*, 1997, **119**, 8991.
11 T. D. James, K. R. A. S. Sandanayake and S. Shinkai, *Angew. Chem., Int. Ed. Engl.*, 1996, **35**, 1911.
12 F. A. Quiocho, *Pure. Appl. Chem.*, 1989, **61**, 1293.

Communication 8/06596I

Isolation of monomeric s-*trans*-acrylic acid as a hydroxy host inclusion crystal showing anomalous C=O stretching absorptions

Fumio Toda,*[a] Koichi Tanaka,[a] Hideko Koshima[a] and Saeed I. Khan[b]

[a] *Department of Applied Chemistry, Faculty of Engineering, Ehime University Matsuyama, Ehime 790-8577, Japan. E-mail: toda@en3.ehime-u.ac.jp*

[b] *Department of Chemistry and Biochemistry, University of California at Los Angeles Los Angeles, California, USA*

Received (in Cambridge, UK) 27th July 1998, Accepted 13th October 1998

The structure of monomeric s-*trans*-acrylic acid, trapped in an inclusion complex with an hydroxy host, was elucidated by X-ray analysis.

Studies of the molecular conformations and rotational isomerism of organic compounds are of fundamental importance in chemical research. There has been especial interest in the conformations and rotamers of simple organic acids which can be studied readily using spectroscopic methods. For example, studies in the gas phase of the simplest organic acid, formic acid

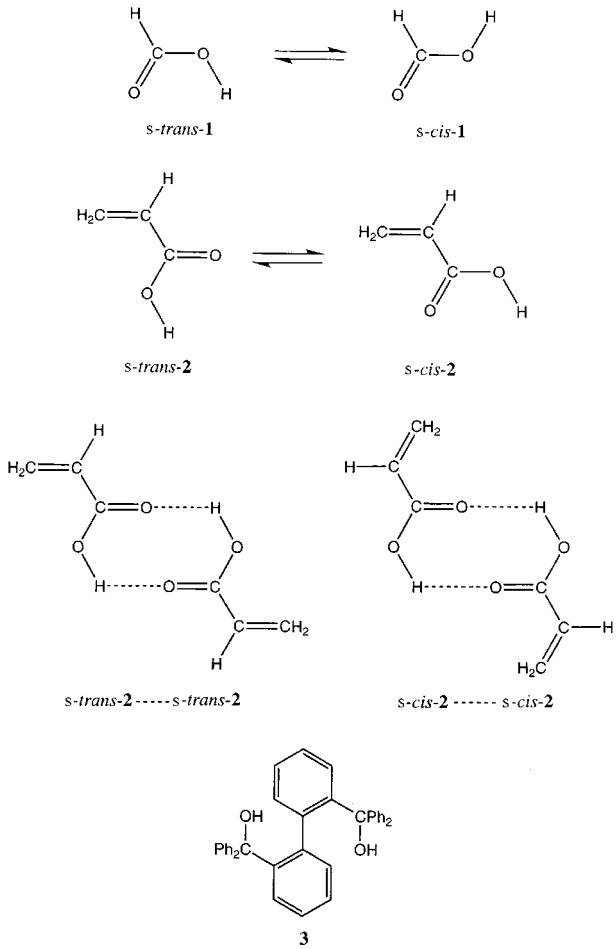

1, show that the s-*trans*-**1** rotamer is the predominant form. This has been characterized by microwave studies,[1–3] electron diffraction,[4–6] and IR spectroscopy.[7,8] Structural studies of s-*trans*-**1** in low temperature matrices have also been accomplished.[9–11] The other rotamer, s-*cis*-**1**, has also been detected by microwave[12,13] and IR spectroscopy.[14] On the other hand in both the liquid and vapor phases of acrylic acid **2**, the cyclic dimer s-*trans*-**2**···s-*trans*-**2** is a major component existing in equilibrium with monomeric **2**.[15] Microwave spectroscopic studies have established that in the vapor phase at low pressures, comparable amounts of s-*cis*-**2** and s-*trans*-**2** coexist with the dimer.[16,17] In the solid state, however, it was demonstrated that **2** exists as two different cyclic dimers, s-*trans*-**2**···s-*trans*-**2** and s-*cis*-**2**···s-*cis*-**2** by IR spectroscopy.[18] Finally, s-*trans*-**2** and s-*cis*-**2** have been identified by IR spectroscopy in a matrix.[19]

Nevertheless, no rotational isomer of **1** or **2** has never been isolated in the pure state. The challenge to isolate a rotational isomer of **2** might be met by using inclusion crystallization with a hydroxy host compound, since this method has been shown to be useful in trapping an unstable rotamer.[20] For example, a nearly eclipsed rotamer of 1,2-dichloroethane (dihedral angle Cl–C–C–Cl = 36°) has been isolated as a host–guest inclusion compound.[21] Finally, we succeeded in isolating s-*trans*-**2** as an inclusion crystal (**4**) with 2,2′-bis(hydroxydiphenylmethyl)-1,1′-biphenyl **3** and studied its conformation by X-ray analysis.

When a solution of **3** (1 g) in **2** (10 g) was kept at room temperature for 1 h, the 2:1 inclusion compound **4** was obtained as colorless needles [0.84 g, 80% yield, mp 130–150 °C (decomp.); Calc. for $C_{79}H_{64}O_6$: C, 85.53; H, 5.81. Found: C, 85.37; H, 5.82%]. The 2:1 molar ratio was determined by elemental analysis and thermogravimetric measurement. X-ray analysis of **4** showed that six molecules of **3** make a cubic cage in which three molecules of **2** are accommodated by formation of a circle (Fig. 1).† The three acrylic acid molecules comprising the circle were found to be disordered over two sites of equal occupancy. In both sites of disorder, three hydrogen bonds between the OH hydrogen of **2** and the OH oxygen of **3** play an important role in constructing the inclusion lattice of **4**. Since the OH hydrogen of **3** does not participate in any hydrogen bond formation, the *ν*OH of **3** in **4** appeared at higher

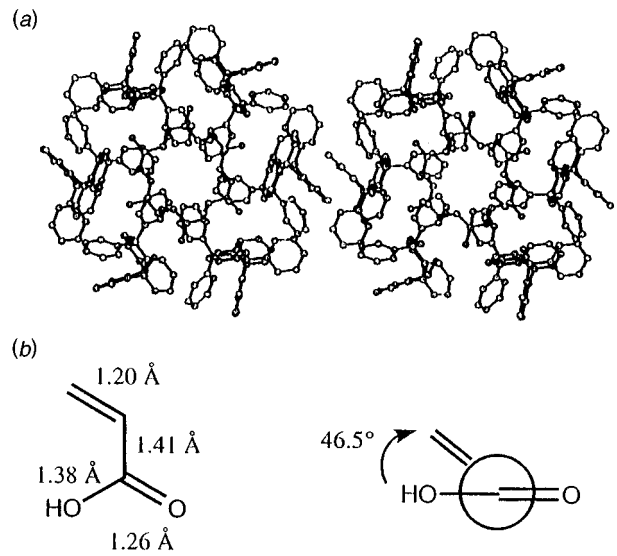

Fig. 1 X-Ray analytical data for **4**: (*a*) stereoview of **4** and (*b*) bond lengths and dihedral angle for s-*trans*-**2** in **4**.

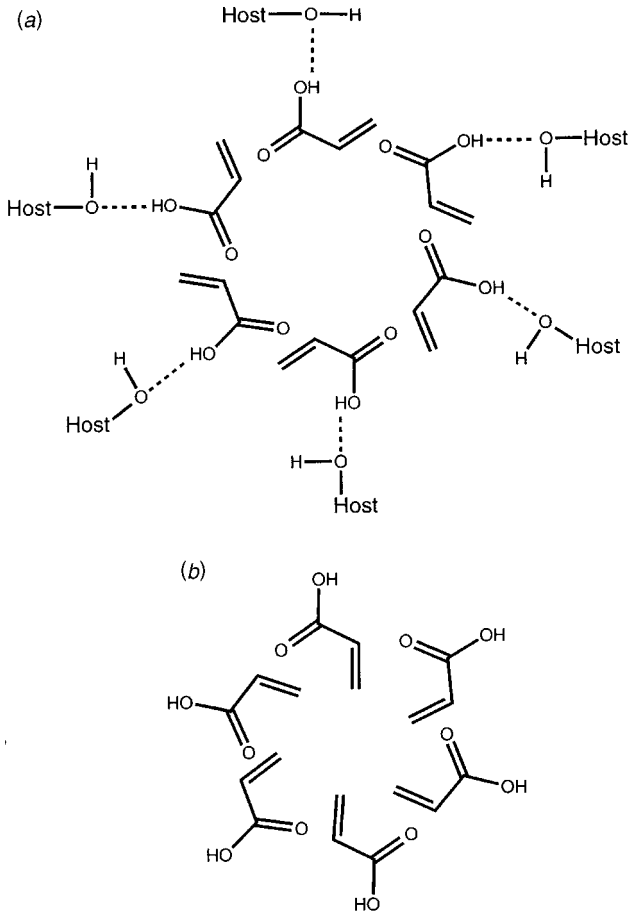

Fig. 2 Schematic drawing: (*a*) a circle of three s-*trans*-**2** molecules in **4** and (*b*) a circle of three s-*cis*-**2** molecules, both involving disorder.

frequency (3290 cm^{-1}) than in pure **3** itself (3230 cm^{-1}). The hydrogen bonds are schematically shown in Fig. 2. It is very clear that **2** exists here as a monomeric form rather than a dimeric one, despite **2** existing as a dimer in the crystalline state at −115 °C.† The formation of the 2:1 inclusion complex in the presence of disorder is analogous to that of **3** combining with acetone molecules in a 2:1 ratio.[22] In the latter case, however, **3** functions as a hydrogen donor and hydrogen bonds between the OH of **3** and C=O of acetone molecule are formed.[22]

This is the first example of the isolation of the monomeric s-*trans* form of **2**, although the dihedral angle between the OH and H_2C=CH groups is a little large (46.5°), as shown in Fig. 1. The C=O and C–OH bonds are also clearly distingishable (Fig. 1). In the small cavity formed by six host molecules of **3**, the dimer of **2** might be too large to be accommodated. The cavity in **4** might also be too small to accommodate **2** in its s-*cis* form. When three s-*cis*-**2** molecules are accommodated to make a similar circle to that of the s-*trans* form, the three vinyl groups are directed inward causing serious steric repulsion, as shown in Fig. 2. Methacrylic acid did not form an inclusion complex with **3** because even if it is included in its s-*trans* form, steric crowding of the methyl groups is significant. These could be the underlying reasons why the monomeric s-*trans*-**2** molecule is isolated.

It is impossible to elucidate the mechanism of the molecular movement of **2** into the cavity, since X-ray analysis can determine only an average situation of molecules, and not their dynamic behavior. However, some speculation on this subject would be worthwhile. For example, the two circles, each consisting of three s-*trans*-**2** molecules (Fig. 1), are interconvertible by either a shift down or up accompanied by a 60° rotation in the plane of the circle. Since an X-ray analysis of **4** at −100 °C gave almost the same result as that obtained at room temperature, such molecular movement would occur quite easily. DSC trace of **4** showed two endotherm peaks at 126 and 255 °C, which correspond to release of the guest and the melting point of the host, respectively. Solid-state ^{13}C CP MAS NMR spectroscopy of **4** showed a broad C=O signal for **2** at δ 169.[23] On the other hand, the ^{13}C NMR spectrum of **4** in $CDCl_3$ showed a sharp C=O signal at δ 170.

It was also found that **2** shows anomalous νOH absorptions in the IR spectrum of **4**. The C=O stretching absorptions are split into three weak bands at 1726, 1699 and 1687 cm^{-1}. Each of these peaks is comparable in strength to those of the νCH=CH_2 absorptions of **2** at 1632 cm^{-1} and of the benzene ring of **3** at 1597 cm^{-1}. This is an unusual phenomenon since acetone in its inclusion complex with **3** showed a normal strong νC=O absorption at 1710 cm^{-1}. In order to know whether this anomalous νC=O absorption appears only in this case or not, some other inclusion compounds with **3** were prepared and their IR spectra studied.

The host **3** formed inclusion compounds with propanoic acid and ethyl acetate in 2:1 ratios. In these inclusion compounds, propanoic acid (1740, 1735, 1818, 1707, 1700 and 1685 cm^{-1}) and ethyl acetate (1704 and 1686 cm^{-1}) showed similar anomalous νC=O absorptions as indicated. In both cases, the νC=O absorptions are split into very weak bands, and the splitting is especially complicated in the case of propanoic acid. Nevertheless, 1:1 inclusion compounds of ethyl acrylate and ethyl propanoate with **3** showed normal strong νC=O bands at 1698 and 1712 cm^{-1}, respectively. These anomalies might not depend on the host:guest molar ratio, since the 2:1 inclusion compound of **3** with acetone also shows normal νC=O absorption.[24] As far as we are aware, such anomalous behavior has not been previously observed. Although the reason for this anomalous behavior is not clear, it is an interesting subject in solid state chemistry[20] and inclusion chemistry, and should be clarified in the future.

Notes and references

† *Crystal data* for **4**: $C_{79}H_{64}O_6$, colorless hexagonal crystals space group *R*3, *a* = 35.27(3), *b* = 35.27(3), *c* = 12.454(9) Å, *V* = 13416(2) $Å^3$, *Z* = 18. Data collection at *T* = 156 K on a Picker (Crystal Logic) with Mo-Kα radiation, 2θ range = 2.4–55.0°, *R* = 0.069, and *Rw* = 0.082. CCDC 182/1007.

1 G. H. Kwei and R. F. Curl Jr., *J. Chem. Phys*, 1960, **32**, 1592.
2 J. Bellet, A. Deldalle, G. Streenbeckeliers and R. Wertheimer, *J. Mol. Struct*., 1971, **9**, 65.
3 R. W. Davis, A. G. Robiette, M. C. L. Gerry, E. Bjanov and G. Winnerwisser, *J. Mol. Spectrosc*., 1980, **81**, 93.
4 J. Karle and L. O. Brockway, *J. Am. Chem. Soc*., 1944, **66**, 574.
5 V. Shomaker and J. M. O'Gorman, *J. Am. Chem. Soc*., 1947, **69**, 2638.
6 I. L. Karle and J. Karle, *J. Chem. Phys*., 1954, **23**, 43.
7 R. C. Millikean and K. S. Ritzer, *J. Chem. Phys*., 1957, **27**, 1305.
8 J. C. Hisatsune and J. Heicklen, *Can. J. Spectrosc*., 1973, **18**, 77.
9 T. Miyazawa and K. S. Pitzer, *J. Chem. Phys*., 1959, **30**, 1076.
10 R. L. Redington, *J. Mol. Spectrosc*., 1977, **65**, 171.
11 J. Lundell, M. Raesaenen and Z. Latajka, *Chem. Phys*., 1994, **189**, 245.
12 W. M. Hocking, *Z. Naturforsch*., 1976, **31A**, 1113.
13 E. Bjarnov and W. M. Hocking, *Z. Naturforsch*., 1978, **33A**, 610.
14 M. Pettersson, J. Lundell, L. Khriachtchev and M. Raesaenen, *J. Am. Chem. Soc*., 1997, **119**, 11 715.
15 W. R. Feairheller Jr. and J. E. Karton, *Spectrochim. Acta, Part A*, 1967, **23**, 2225.
16 K. Bolton, N. L. Owen and J. Sheridan, *Nature*, 1968, **218**, 266.
17 K. Bolton, D. G. Lister and J. Sherida, *J. Chem. Soc., Faraday Trans. 2*, 1974, **70**, 113.
18 J. Uemura and S. Hayashi, *Bull. Inst. Chem. Res., Kyoto Univ*., 1974, **52**, 585.
19 S. Charles, F. C. Cullen, N. L. Owen and G. A. Williams, *J. Mol. Struct*., 1987, **157**, 17.
20 F. Toda, *Acc. Chem. Res*., 1995, **28**, 480.
21 F. Toda, K. Tanaka and R. Kuroda, *Chem. Commun*., 1997, 1227.
22 M. A. Higgs and D. L. Sass, *Acta Crystallogr*., 1963, **16**, 657.
23 The ^{13}C CP MAS NMR spectrum in the solid state was recorded at 75.45 MHz on a JEOL Lambda-300 instrument.
24 F. Toda, A. Kai, R. Toyotaka, W.-H. Yip and T. C. W. Mak, *Chem. Lett*., 1989, 1921.

Communication 8/05845H

Antimony as a symmetrically bridged ligand in a novel neutral complex

Manfred Scheer,*[a] Jan Müller,[a] G. Baum[a] and Marco Häser[b]

[a] *Institute of Inorganic Chemistry, University of Karlsruhe, D-76128 Karlsruhe, Germany. E-mail: mascheer@achibm6.chemie.uni-karlsruhe.de*

[b] *Institute of Physical Chemistry, University of Karlsruhe, D-76128 Karlsruhe, Germany*

Received (in Basel, Switzerland) 20th August 1998, Accepted 13th October 1998

[LW=Sb=WL] 7 (L = $N(CH_2CH_2N(Np))_3$; Np = CH_2CMe_3) is prepared by treatment of [LWCl] 5 with $LiSb(SiMe_3)_2(dme)_n$; the ethylene complex [LWCl(C_2H_4)] 6 is a side product in the synthesis of 5; all complexes are structurally characterised.

Complexes of the general formula [$L_nM{\equiv}E$] (E = P, As) with terminal ligands represent a new class of compounds.[1] With the synthesis and structural characterisation of the phosphido complexes [(Ar′RN)$_3$Mo≡P] (Ar′ = 3,5-$C_6H_3Me_2$, R = $C(CD_3)_2CH_3$) **1**[2] and [$N(CH_2CH_2NSiMe_3)_3M{\equiv}E$] [M = W (**2a**), Mo (**2b**)][3] the speculation about the existence of stable compounds of this class was brought to an end. We have shown that one possibility to synthesise the phosphido complex **2a** is starting from Li[$P(SiMe_3)_2$] according to eqn. (1).[4] Using

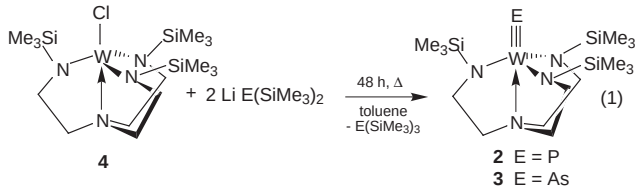

Li[$As(SiMe_3)_2$] in reaction (1), we were also able to synthesise and structurally characterise the arsenido derivative **3**.[4] This raised the possibility of generating complexes with terminal antimonido and bismuthido ligands. The salts Li[$E(SiMe_3)_2$] (E = P, As, Sb, Bi) have been known for a long time for all pnictogen elements,[5] therefore this seems to be a viable route to compounds containing terminal Sb and Bi ligands.

We have found, however, that irrespective of reaction conditions, the conversion between [{$N(CH_2CH_2NSiMe_3)_3$}WCl] **4** and Li[$Sb(SiMe_3)_2(dme)_n$] did not proceed. The steric demand of the $SiMe_3$ groups in complex **4** obviously inhibits the substitution of the Cl atom by the Sb moiety. The use of a sterically less bulky tris(2-amidoethyl)amine ligand should however enable W–Sb bond formation. Herein we report the synthesis and characterisation of [{$N(CH_2CH_2N(Np))_3$}WCl] **5** (Np = $CH_2C(CH_3)_3$) and the reactivity of **5** with Li[$Sb(SiMe_3)_2(dme)_n$].

The reaction of WCl_4(dme) with $Li_3[N(CH_2CH_2N(Np))_3]$ leads to the brown compound [{$N(CH_2CH_2N(Np))_3$}WCl] **5**. A small quantity of the green ethylene complex [{$N(CH_2CH_2N(Np))_2CH_2CH_2NH(Np)$}WCl($\eta^2$-$C_2H_4$)] **6** was also isolated.[6] While complex **5** dissolves well in toluene and is moderately soluble in pentane, compound **6** undergoes decomposition even in solvents of low polarity, resulting in the formation of an insoluble solid which could not be characterised. In the mass spectra of **5** and **6** the peaks for the molecular ions are observed. The ^{1}H NMR spectrum of **5** reveals broad signals at high and low field for the paramagnetic d^2-tungsten complex.†

The source of the ethylene in **6** is uncertain. It is possibly a result of a fragmentation of the tren ligand itself. Schrock and co-workers observed C–N bond cleavage of the ligand framework of a tren complex of tantalum, yielding a N-allyl unit.[7] Moreover, the low yields generally observed in the reactions of chlorotungsten(IV) complexes with tren ligands indicate various side reactions during the synthesis.[8]

In the structure of the trigonal bipyramidal tungsten complex **5** the W–Cl and the W–N_{ax} distances [2.389(2) and 2.179(5) Å] are only slightly shorter than the equivalent distances [2.399(2) and 2.182(6) Å] in the isostructural Me_3Si substituted complex **4**.‡ In **6** (Fig. 1) the W atom exhibits a distorted octahedral coordination geometry.‡ This is one of the few examples where the tetradentate ligand tris(2-amidoethyl)amine does not bind in C_3-symmetrical fashion to a transition metal.[9] This is due to the formation of only two W–N bonds [W–N3 1.964(3), W–N4 2.002(3) Å], whereas N(2) and N(1) coordinate merely with their lone-pair to the tungsten centre [W–N1 2.254(3), W–N2 2.399(3) Å]. The ethylene experiences strong back donation from the d^2 W atom, which is evident from the elongated C–C bond [1.416(6) Å] and short W–C distances of 2.170(4) and 2.175(3) Å. The complex [$W_2(ONp)_6(\eta^2$-$C_2H_4)_2$], in which a bridging ethylene ligand forms a W_2C_2 tetrahedron with the W atoms, shows comparable bond lengths [W–C 2.14(2), C–C 1.45(2) Å].[10]

The reaction of **5** with [$LiSb(SiMe_3)_2(dme)_n$] for 48 h at 110 °C in the dark leads to Sb–W bond formation as shown in eqn. (2). Instead of a terminal antimonido complex, the symmetrically Sb-bridged complex **7** is formed, which is the first neutral Sb-containing example for this class of compounds. Cationic complexes with μ-E_1 ligands for the heavy group 15 elements were described by Huttner and co-workers.[11] Numerous compounds of the form [$L_nM{=}E{=}ML_n$] are known, which contain a symmetrical nitrogen bridge, but not for pnictogens heavier than phosphorus.[12] Stephan and co-workers succeeded in the synthesis of the complex [{Cp_2Zr}$_2$(μ-P)].[13] Cummins and co-workers isolated [{(R′RN)$_3$Mo}$_2$(μ-P)] (R = Ph; R′ = *t*-Bu) at −35 °C as a labile intermediate in the transfer reaction of a terminal P_1 ligand from the phosphido complex **1** to the d^3 complex [(R′RN)$_3$Mo] (R′ = C_6H_5, R = *t*-Bu).[14] It could not be established whether **7** is the result of such an irreversible

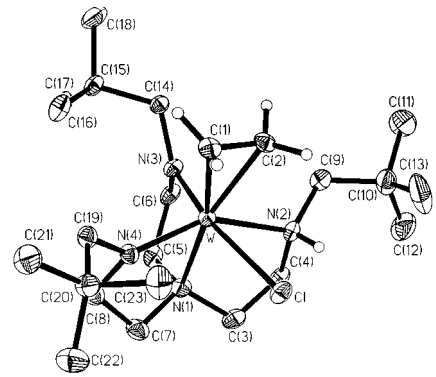

Fig. 1 Molecular structure of **6** (ellipsoids drawn at 30% probability level). Selected bond lengths [Å] and angles [°]: W–Cl 2.5116(12), W–N(1) 2.254(3), W–N(2) 2.399(3), W–N(3) 1.964(3), W–N(4) 2.002(3), C(1)–C(2) 1.416(6), W–C(1) 2.175(3), W–C(2) 2.1704(4), C(1)–W–C(2) 38.0(2), N(1)–W–Cl 94.00(9), N(1)–W–C(1) 165.64(14), N(1)–W–C(2) 156.8 (13), N(1)–W–N(2) 74.28(11), N(1)–W–N(3) 79.69(12), N(1)–W–N(4) 80.41(12), Cl–W–N(2) 74.57(8), Cl–W–N(4) 92.26(10), N(2)–W–N(3) 87.71(12), N(3)–W–N(4) 102.90(14).

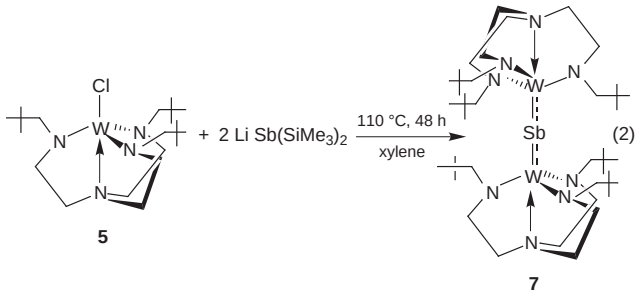

transfer reaction, or after an Sb–W bond formation an intermolecular Me_3SiCl elimination is followed. The M–E–M system of such neutral complexes possesses a $(1\pi_u)^4(1\pi_g)^3$ electron configuration with one unpaired electron. Therefore **7** is a mixed valent W(IV)/W(V) species.

The molecular structure of **7** (Fig. 2) reveals two W-tren units bonded to one Sb atom in a staggered configuration.‡ To the best of our knowledge the Sb–W bond distance of 2.5738(8) Å is the shortest Sb–W bond distance known. The $W–N_{eq}$ bond lengths are consistent with those found in **2** and **3**. The axial W–N(1) bond in **7** is 0.1 Å shorter than the equivalent distance in compounds containing a W≡E triple bond (E = P,[3] As[4]).

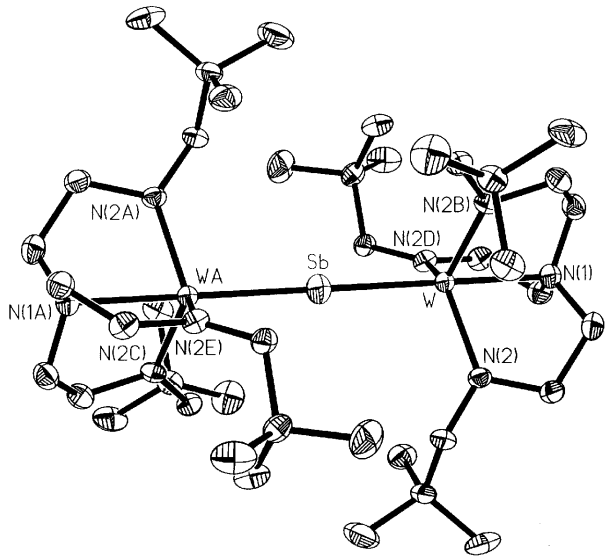

Fig. 2 Molecular structure of **7** (ellipsoids drawn at 30% probability level). Selected bond lengths [Å] and angles [°]: W–Sb 2.5738(8), W–N(1) 2.243(14), W–N(2) 2.000(7), W–Sb–W 180.0, Sb–W–N(1) 180.0, Sb–W–N(2) 101.0(2), N(1)–W–N(2) 79.0(2), N(2)–W–N(2) 116.4(1).

The equilibrium structure of **7** was calculated using the B-P86/SVP approximation.[15] The equal W–Sb bond distances of the paramagnetic compound **7** with respect to an almost linear W–Sb–W framework of 179.6° are 2.612 Å. The experimental distance of the exact linear system in **7** with a centre of inversion at the Sb atom is found to be approximately 0.04 Å shorter. According to the calculations, the corresponding Np-substituted complex with a terminal antimonido ligand possesses a W–Sb bond length of 2.514 Å, an anionic form of complex **7** reveals a W–Sb distance of 2.609 Å.

The results show that a reduction of the steric demand of the R group on the tren ligand leads to novel neutral Sb-bridged complexes. Current work is directed towards the synthesis of such complexes of the other pnictides and towards an optimisation of the size of the substituent R on the tren ligand in order to generate complexes with terminal Sb and Bi ligands.

The authors thank the Deutsche Forschungsgemeinschaft and the Fonds der Chemischen Industrie for financial support.

Notes and references

† Spectroscopic data: **5**: ^{1}H NMR (C_6D_6) δ 9.36 (s, CH_3), −26.1 (b, CH_2), −56.4 (b, CH_2); FI-MS (70 eV, 120 °C) *m*/*z* (%): 573 (100) [M^+]; **6**: FI-MS (10 kV, 120 °C) *m*/*z* (%): 603 (100) [M^+], C,H,N, Calc. for $C_{23}H_{50}ClN_4W$: C 45.89; H 8.37; N 9.31; found: C 45.69; H 8.38; N 9.13; **7**: μ_{eff} (Evan's method, C_6D_8, 300 K) = 2.07 μ_B; EI-MS (70 eV, 180 °C): 1197 (8) [M^+], 660 (91) [$WSbN_4C_{21}H_{45}^+$], 603 (100) [$WSbN_4C_{18}H_{39}^+$].

‡ Crystal structure analyses of **5–7** were performed on a STOE STADI IV (ω-scan mode) diffractometer with Mo-Kα radiation (λ = 0.71073 Å) with empirical absorption corrections (Psi-scans). The structures were solved by direct methods using SHELXS-86,[16a] full-matrix-least-squares refinement on F^2 in SHELXL-93[16b] with anisotropic displacement for non-H atoms. Hydrogen atoms were located in idealized positions and refined isotropically according to the riding model. Crystal structure analysis: **5**: $C_{21}H_{45}ClN_4W$, M = 572.91, monoclinic, space group $P2_1/c$; a = 13.203(3), b = 11.450(2), c = 17.000(3) Å, β = 91.74(3)°, T = 200(2) K, Z = 4, U = 2568.8(9) Å^3, D_c = 1.481 Mg m^{-3}, μ(Mo-Kα) = 46.13 cm^{-1}, F(000) = 1160. A total of 5441 reflections with $3.08 \leqslant 2\theta \leqslant 55.02°$ were collected, of which 5404 were independent and 4048 reflections with $I \geqslant 2\sigma(I)$. Final residuals are R_1 = 0.0370 and wR_2 = 0.1024 and GOF = 1.129 for 253 variables. Residual electron density was found to be between 1.072 and −0.728 e Å^{-3}. **6**: $C_{23}H_{50}ClN_4W$, M = 601.97, monoclinic, space group $P2_1/n$; a = 11.185(2), b = 17.142(3), c = 14.216(3) Å, β = 95.13(3)°, T = 203(2) K, Z = 4, U = 2714.8(9) Å^3, D_c = 1.473 Mg m^{-3}, μ(Mo-Kα) = 43.69 cm^{-1}, F(000) = 1228. A total of 4171 reflections with $3.74 \leqslant 2\theta \leqslant 50.04°$ were collected, of which 4171 were independent and 3835 reflections with $I \geqslant 2\sigma(I)$. Final residuals are R_1 = 0.0240 and wR_2 = 0.0665 and GOF = 1.045 for 271 variables. Residual electron density was found to be between 1.735 and −1.880 e Å^{-3}. **7**: $C_{42}H_{90}N_8SbW_2$, M = 1196.67, trigonal, space group $R\bar{3}$; (no. 148), a = b = 16.409(3), c = 15.669(3) Å, T = 200(2) K, Z = 3, U = 3653.7(12) Å^3, D_c = 1.632 Mg m^{-3}, μ(Mo-Kα) = 52.97 cm^{-1}, F(000) = 1791. A total of 1840 reflections with $3.86 \leqslant 2\theta \leqslant 54.96°$ were collected, of which 1840 were independent and 1555 reflections with $I \geqslant 2\sigma(I)$. Final residuals of R_1 = 0.0470 and wR_2 = 0.1288 and GOF = 1.112 for 83 variables. Residual electron density was found to be between 1.634 and −2.153 e Å^{-3}. CCDC 182/1058.

1 Reviews: M. Scheer, *Angew. Chem.*, 1995, **107**, 2151; *Angew. Chem., Int. Ed. Engl.*, 1995, **34,** 1997; *Coord. Chem. Rev*., 1997, **163**, 271.
2 C. E. Laplaza, W. M. Davis and C. C. Cummins, *Angew. Chem*., 1995, **107**, 2181; *Angew. Chem., Int. Ed. Engl.*, 1995, **34**, 2042.
3 N. Zanetti, R. R. Schrock and W. M. Davis, *Angew. Chem*., 1995, **107**, 2184; *Angew. Chem., Int Ed. Engl*., 1995, **34**, 2044.
4 M. Scheer, J. Müller and M. Häser, *Angew. Chem*., 1996, **108**, 2637; *Angew. Chem., Int. Ed. Engl.*, 1996, **35**, 2492.
5 G. Becker, A. Münch and C. Witthauer, *Z. Anorg. Allg. Chem*., 1982, **492**, 15; G. Becker and C. Witthauer, *Z. Anorg. Allg. Chem*., 1982, **492**, 28; O. Mundt, G. Becker, M. Rössler and C. Witthauer, *Z. Anorg. Allg. Chem*., 1983, **506**, 42.
6 $Li_3[N(CH_2CH_2NNp)_3]$ was synthesised from $N(CH_2CH_2NNp)_3$ with three equivalents of BuLi. The neopentyl-substituted amine is obtained from conversion of tris(2-amionoethyl)amine with pivalinic anhydride and subsequent reaction of the acid amide with $LiAlH_4$. The complex **5** was synthesised according to a modified procedure.[4] **6** crystallises in the form of green crystals along with **5**.
7 J. S. Freundlich, R. R. Schrock and W. M. Davis, *J. Am. Chem. Soc*., 1996, **118**, 3643.
8 Usually the yields are below 15%. Using fluorinated substituents, however, more of the designed product can be obtained.
9 Compare: D. A. Dobbs, R. R. Schrock and W. M. Davis, *Inorg. Chim. Acta*, 1997, **263**, 171.
10 S. T. Chacon, M. H. Chisholm, O. Eisenstein and J. C. Huffmann, *J. Am. Chem. Soc*., 1992, **114**, 8497.
11 A. Strube, G. Huttner and L. Zsolnai, *Angew. Chem*., 1988, **100**, 1586; F. Bringewski, G. Huttner and W. Imhof, *J. Organomet. Chem*., 1993, **448**, C3; S. J. Davies, N. A. Compton, G. Huttner, L. Zsolnai and S. E. Garner, *Chem. Ber*., 1991, **124**, 2731.
12 K. Dehnicke and J. Strähle, *Angew. Chem*., 1992, **104**, 978; *Angew. Chem., Int. Ed. Engl.*, 1992, **32**, 955.
13 M. C. Fermin, J. Ho and D. W. Stephan, *Organometallics*, 1995, **14**, 4247.
14 M. J. A. Johnson, P. M. Lee, A. L. Odom, W. M. Davis and C. C. Cummins, *Angew. Chem.*, 1997, **109**, 110; *Angew. Chem., Int. Ed. Engl.*, 1997, **36**, 87.
15 Structure optimizations were performed using the TURBOMOLE set of programs with the RI-*J* approximation (K. Eichhorn, O. Treutler, H. Öhm, M. Häser and R. Ahlrichs, *Chem. Phys. Lett.*, 1995, **242**, 652). For further details concerning the methods and basis sets, see ref. 4 and citations therein.
16 (*a*) G. M. Sheldrick, SHELXS-86, University of Göttingen, 1986; (*b*) G. M. Sheldrick, SHELXL-93, University of Göttingen, 1993.

Communication 8/06574H

Sigmatropic migrations in cyclononatetraenyl(dipropyl)borane: a combined experimental and computational study

Ilya D. Gridnev,*[a] Peter R. Schreiner,*[b] Mikhail E. Gurskii,[c] Yuri N. Bubnov,[a] Anatoli O. Krasavin[d] and Vadim I. Mstislavski[e]

[a] *A. N. Nesmeyanov Institute of Organoelement Compounds, Vavilova 28, 117813 Moscow, Russia. E-mail: ilh@ineos.ac.ru*
[b] *Institute of Organic Chemistry, University of Göttingen, Tammannstr. 2, D-37077 Göttingen, Germany. E-mail: pschrei@gwdg.de*
[c] *N. D. Zelinsky Institute of Organic Chemistry, Leninsky prosp., 47, Moscow 117913, Russia*
[d] *The Higher Chemical College of the Russian Academy of Sciences, 9 Miusskaya pl., 125047 Moscow, Russia*
[e] *M. V. Lomonosov Moscow State University, Vorob'evy Gory, Moscow, Russia*

Received (in Liverpool, UK) 5th August 1998, Accepted 25th September 1998

Large-ring sigmatropic migrations do not necessarily follow the 'least motion principle' and can only be rationalized by a combination of experimental and computational techniques.

Despite the formulation of the Woodward–Hoffmann rules nearly 30 years ago,[1] the selectivities in sigmatropic migrations in conjugated carbocycles are not easily predictable. The difficulties in rationalizing a particular shift mechanism arise from the neglect of, for instance, orbital coefficients and the 'least motion principle' (LMP), when the Woodward–Hoffmann rules are applied. The possible importance of the LMP is emphasized by the large number of studies on cyclopentadienyl[2] and indenyl[3] derivatives, where mostly [1,5]- and very few [1,3]-sigmatropic migrations are observed. Since [1,5]- and [1,2]-shifts in cyclopentadienyl systems are formally equal, the LMP cannot be probed.[4] To the best of our knowledge, the [1,5]-Sn shifts in triphenyl-[5] and trimethyl-(cycloheptatrienyl)tin[6a] are the only examples violating the LMP.

Our recent studies on cycloheptatrienyl(dialkyl)boron derivatives[6] showed that both orbital *and* distance factors govern the selectivities of sigmatropic migrations. For instance, in the tricarbonyliron complex of cycloheptatrienyl(dipropyl)borane **1** both [1,3]- and [1,7]-B shifts are observed, whereas [1,5]-B shifts were not detected.[6a] This is in accord with orbital control because dialkylboryl groups migrate with inversion of configuration utilizing the unoccupied boron 2*p* atomic orbital (AO).[6b] On the other hand, the [1,7]-B shift is considerably faster than the [1,3]-B shift in **1**;[6a] the [1,7]-B migration is substantially energetically favored in uncomplexed **2**.[6b] Hence, as for the cyclopentadienyl system, the LMP seems to be effective, but could not be differentiated from other effects. We therefore present here a combined experimental and computational study on cyclononatetraenyl(dipropyl)borane **3**, which clearly displays a fast [1,3]-B shift.[7]

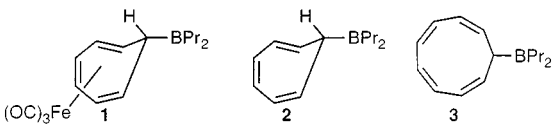

The experimental [1,3]-B shift barrier in **3** is rather low; the ^{1}H NMR data indicate dynamic processes even at −100 °C.[7] Our density functional theory (DFT) computations† show that the *endo*-conformer of **3** (the propyl groups were replaced by methyl groups to speed up the computations) is favored by only 0.3 kcal mol^{-1} over the *exo*-conformer due to overlap between the empty boron 2*p* AO and the π-system of the ring. While the degenerate [1,3] dipropylboryl migration in **3**-all-*cis-endo* could be confirmed computationally, we were unable to localize a [1,3]-B TS for **3**-all-*cis-exo*, despite extensive searches. Instead, we found that **3**-all-*cis-exo* undergoes a [1,2]-B shift to **3a**-mono-*trans-exo* (Scheme 1 and Fig. 1). However, **3**-mono-*trans* is thermodynamically unfavorable by 6.5 kcal mol^{-1} and the [1,2]-B shift is accompanied by a rather high activation barrier (17.3 kcal mol^{-1}; all energies relative to **3**-all-*cis-exo*). Hence, the observed temperature dependence of the NMR spectra and the results of EXSY experiments may be explained by degenerate [1,3]-B shifts in **3**-all-*cis-endo* only.

Although it was impossible to observe the completely averaged ^{13}C NMR spectrum due to the thermal instability of **3**, the spectrum is well resolved at low temperatures (Fig. 2). The pronounced lineshape–temperature dependence in the temperature interval 173–233 K allowed the [1,3]-B shift activation parameters in **3**-all-*cis-endo* to be determined. Lineshape calculations[8] gave: E_a = 6.2 ± 0.5 kcal mol^{-1}, $\Delta_{195\,K}G^{\neq}$ = 8.8 ± 0.1 kcal mol^{-1}; the computed E_a for **3** is 6.6 kcal mol^{-1}.

As we pointed out earlier,[6b] the dialkylboron moiety is partially positively charged; hence, one has to consider the two degenerate LUMOs (schematically depicted in Fig. 3) to determine which migrations are favorable based on orbital phases *and* coefficients. Inversion of configuration is observed for boryl group migrations (*i.e.* a *p*-orbital perpendicular to the plane of the π-system connects the migrating termini). Based on orbital phases only [1,3], [1,5] and [1,9] shifts are symmetry allowed with inversion of configuration in the cyclononatetraenyl system. LUMO 1 indistinguishably only allows for [1,3] and [1,9] shifts, while LUMO 2 permits all three. However, [1,5] migrations are highly unfavorable due to small orbital coefficients. Hence, a clear prediction cannot be made from these considerations.

For direct comparisons, we computed the transition states for [1,*j*]-B sigmatropic migrations in cyclononatetraenyl(dimethyl)borane **3**. As noted above, the E_a for the [1,3]-B shift in **3** agrees very well with the experimental value for **3**. The activation barriers for [1,9]- and [1,3]-B migrations are very

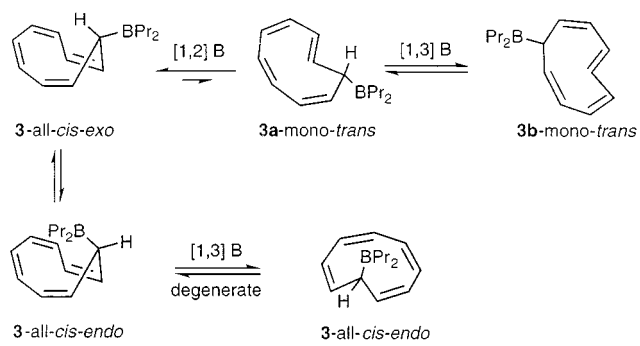

Scheme 1

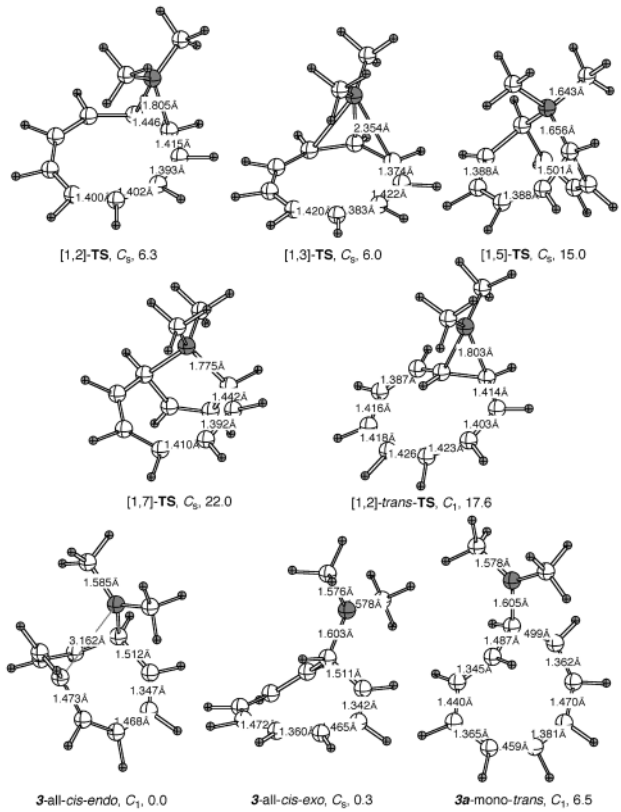

Fig. 1 B3LYP/6-311G*//B3LYP/6-31G* computed ground and transition state structures for dimethylboryl group migrations relative to **3**-all-*cis*-*endo*. Relative energies (ΔH) in kcal mol^{-1}.

similar (within 0.3 kcal mol^{-1}). It should be stressed that in symmetrically conjugated molecules like **3** only the fastest sigmatropic rearrangement can be reliably characterized by NMR analysis. At 188 K and a mixing time of 10 ms, all possible cross-peaks of comparable intensity are observed in the EXSY spectra of **3**. That means that the E_a for the [1,9]-B migration may be only about 1.1 times higher than that for [1,3]-B shifts, in agreement with the computed data. The [1,5] and [1,7] migrations are clearly disfavored by 15.0 and 22.0 kcal mol^{-1}, respectively. They also do not allow the cyclononatetraenyl moiety to become planar and therefore pseudo-Hückel-aromatic in the transition structure.

In summary, we have shown that [1,3]-dialkylboryl shifts in cyclononatetraenyl systems are facile and are slightly favored over [1,2]-shifts. Neither Woodward–Hoffmann rules nor the 'least motion principle' alone can be used for the prediction or rationalization of the migration pathways. Adequate analyses require a combination of dynamic NMR techniques and high-level *ab initio* calculations.

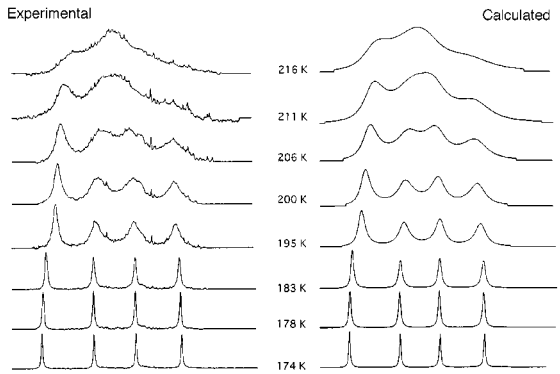

Fig. 2 Temperature-dependent experimental and computed ^{13}C NMR spectra of **3**.

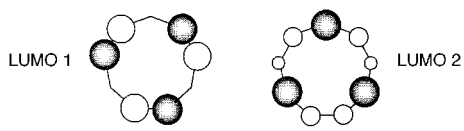

Fig. 3 Simple qualitative presentation of the degenerate Hückel LUMO orbitals for the analysis of allowed suprafacial shifts in conjugated cyclononane systems.

This work was financially supported by the Russian Foundation for Basic Research (Project No. 97-03-32714). An A. v. Humboldt Research Fellowship for I. D. G. is gratefully acknowledged. P. R. S. thanks the Fonds der Chemischen Industrie (Liebig-Fellowship and Sachmittel), the Deutsche Forschungsgemeinschaft, and Professor Armin de Meijere for support. Allotments of computer time from the Höchstleistungsrechenzentrum Jülich as well as the Regional Rechenzentrum Niedersachsen (RRZN Hannover) also are highly appreciated.

Notes and references

† *Computations*: Geometries of all stationary points were optimized using analytical energy gradients (ref. 9, 10). We utilized Becke's three-parameter exchange-correlation functional (ref. 11) including the nonlocal gradient corrections described by Lee–Yang–Parr (LYP) (ref. 12), as implemented in the GAUSSIAN 94 program package (ref. 13). All geometry optimizations were performed with the 6-31G* basis set (ref. 14); stationary structures were characterized by inspecting the updated Hessian matrices. Single point energies were evaluated using a standard 6-311G* basis set (ref. 15); final energies thus refer to B3LYP/6-311+G*//B3LYP/6-31G*. Standard notation is used, *i.e.* // means energy computed at // geometry (ref. 15). Computational results are available as supplementary data: see http://www.rsc.org/suppdata/cc/1998/2507.

1 R. B. Woodward and R. Hoffmann, *Angew. Chem*., 1969, **81**, 797.
2 For reviews see: R. B. Larrabee, *J. Organomet. Chem*., 1974, **74**, 313; C. W. Spangler, *Chem. Rev*., 1976, **76**, 187; P. Jutzi, *Chem. Rev*., 1986, **86**, 983.
3 M. Stradiotto, D. W. Hughes, A. D. Bain, M. A. Brook and M. J. McGlinchey, *Organometallics*, 1997, **16**, 5563 and references cited therein.
4 B. E. Mann, in *Comprehensive Organometallic Chemistry*, ed. G. Wilkinson, Pergamon, Oxford, 1982, vol. 3, pp. 89–125; A. Bonny and S. R. Stobart, *J. Chem. Soc., Dalton Trans*., 1979, 486.
5 R. B. Larrabee, *J. Am.Chem. Soc*,. 1971, **93**, 1510; M. D. Curtis and R. Fink, *J. Organomet. Chem*., 1972, **38**, 299; B. E. Mann, B. F. Taylor, N. A. Taylor, and R. Wood, *J. Organomet. Chem*., 1978, **162**, 137.
6 (*a*) I. D. Gridnev, O. L. Tok, M. E. Gurskii and Y. N. Bubnov, *Chem. Eur. J*., 1996, **2**, 1483; (*b*) I. D. Gridnev, O. L. Tok, N. A. Gridneva, Y. N. Bubnov and P. R. Schreiner, *J. Am. Chem. Soc*., 1998, **120**, 1034.
7 M. E. Gurskii, I. D. Gridnev, A. V. Buevich and Y. N. Bubnov, *Organometallics*, 1994, **13**, 4658.
8 The lineshapes were calculated utilizing a self-written computer program designed for direct iterative search of the activation parameters from the whole set of experimental spectra as proposed by R. Laatikainen, *J. Magn. Res*., 1985, **64**, 375. Iterations were made for two independent NMR operating frequencies (50 and 100 MHz for ^{13}C, Fig. 2; temperature calibration was carried out using a standard calibration sample (4% MeOH in [$^2H_4$]MeOH), providing an approximate accuracy of ±1 K. Temperature coefficients of the chemical shifts were determined by spatial iteration cycles where they were regarded as variable parameters. Linear coefficients were found to be approximately 1 Hz K^{-1} for C-1–4 and 2 Hz K^{-1} for C-5; second order coefficients were less than 0.001 Hz K^{-2}.
9 P. Pulay, in *Modern Theoretical Chemistry*, ed. H. F. Schaefer III, Plenum, New York, 1977, vol. 4, p.153.
10 R. G. Parr and W. Yang, *Density Functional Theory of Atoms and Molecules*, OUP, New York, 1989
11 A. D. Becke, *J. Chem. Phys*., 1993, **98**, 5648.
12 C. Lee, W. Yang and R. G. Parr, *Phys. Rev. B*, 1988, **37**, 785.
13 M. J. Frisch, G. W. Trucks, H. B. Schlegel, P. M. W. Gill, B. G. Johnson, M. A. Robb, J. R. Cheeseman, T. Keith, G. A. Petersson, J. A. Montgomery, K. Raghavachari, M. A. Al-Laham, V. G. Zakrzewski, J. V. Ortiz, J. B. Foresman, C. Y. Peng, P. Y. Ayala, W. Chen, M. W. Wong, J. L. Andres, E. S. Replogle, R. Gomperts, R. L. Martin, D. J. Fox, J. S. Binkley, D. J. Defrees, J. Baker, J. P. Stewart, M. Head-Gordon, C. Gonzalez and J. A. Pople, Gaussian 94, Revision B.3, Gaussian, Inc., Pittsburgh PA, 1995.
14 P. C. Hariharan and J. A. Pople, *Theor. Chim. Acta*, 1973, **28**, 213.
15 W. J. Hehre, L. Radom, P. v. R. Schleyer and J. A. Pople, *Ab Initio Molecular Orbital Theory*, Wiley Interscience, New York, 1986.

Communication 8/06201C

Photochemical reactions of chiral 2,3-dihydro-4(1*H*)-pyridones: asymmetric synthesis of (−)-perhydrohistrionicotoxin

Daniel L. Comins,* Yue-mei Zhang and Xiaoling Zheng

Department of Chemistry, North Carolina State University, Raleigh, North Carolina 27695-8204, USA. E-mail: daniel_comins@ncsu.edu

Received (in Cambridge, UK) 24th September 1998, Accepted 12th October 1998

The first chiral auxiliary-mediated asymmetric synthesis of (−)-perhydrohistrionicotoxin is described.

In an effort to expand the utility of chiral 2,3-dihydro-4(1*H*)-pyridones as synthetic building blocks,[1] we are exploring their annulation using intramolecular [2+2] photocycloaddition reactions.[2] As was first demonstrated by Neier,[3] novel ring systems can be prepared from dihydropyridones using this approach. We were able to demonstrate through model studies that the skeleton of perhydrohistrionicotoxin **1** was accessible using this strategy.[4] Histrionicotoxin **2** is one of the biologically active alkaloids found in the skin secretions of the neotropical frog *Dendrobates histrionicus*.[5] Alkaloids **1** and **2** have been used in

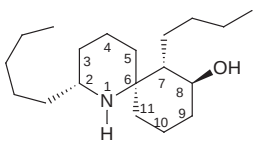

1

perhydrohistrionicotoxin

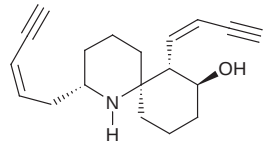

2

histrionicotoxin

studies of the mechanisms involved in transsynaptic transmission of neuromuscular impulses. The biological activity and novel structure of these alkaloids have stimulated numerous synthetic studies.[6] Several racemic and two enantioselective syntheses of **1** have been published. In addition, one asymmetric route to histrionicotoxin **2** has been reported.[6c] The enantioselective routes used enantiopure intermediates prepared by resolution[7] or derived from L-glutamic acid.[6a] Here we report a novel asymmetric synthesis of **1** using a photochemical conversion of an enantiopure 2,3-dihydro-4(1*H*)-pyridone as a key step. The enantiopure dihydropyridone was prepared by an efficient chiral auxiliary-mediated asymmetric synthesis.[1] The synthetic plan called for a stereoselective intramolecular [2+2] cycloaddition of an enantiopure dihydropyridone to set the stereochemistry at C-6 and C-7, and a subsequent cyclobutane ring opening to provide the azaspiroundecane skeleton of **1**.

Reaction of enantiopure 1-acylpyridinium salt **4**, prepared *in situ* from 4-methoxy-3-(triisopropylsilyl)pyridine **3**[8] and the chloroformate of (−)-(1*R*,2*S*,4*R*)-2-(α-cumyl)-4-isopropylcyclohexanol (CPC),[9] with *n*-pentylmagnesium bromide in THF–toluene at −78 °C gave the crude dihydropyridone **5** in 95% yield and 90% de (Scheme 1). Purification by radial PLC (silica gel, EtOAc–hexanes) afforded a 91% yield of pure **5** [mp 75–78 °C; $[\alpha]_D^{23}$ −48.1 (*c* 0.88, $CDCl_3$)]. Treatment of **5** with NaOMe in MeOH followed by aqueous 10% HCl provided dihydropyridone **6** [$[\alpha]_D^{25}$ +353 (*c* 0.18, $CHCl_3$)] in 84% yield, and the chiral auxiliary [(−)-CPC] was recovered in 95% yield. Acylation of **6** with Bu^nLi and $ClCO_2Bn$ gave a 90% yield of enantiopure carbamate **7** [$[\alpha]_D^{23}$ −83.7 (*c* 2.24, $CHCl_3$)]. A side chain was introduced at C-6 of **7** through a 1,4-addition and oxidation sequence. In the presence of TMSCl, copper-mediated conjugate addition of Grignard reagent **8** to **7** provided silyl enol ether **9**. Oxidation of crude **9** with $Pd(OAc)_2$ gave dihydropyridone **10** in 92% overall yield for the two steps.[1c]

The acetal was hydrolyzed and the resulting alcohol was converted to iodide **11** in high yield (84%). The C-4 carbonyl of **11** was protected as the triethylsily enol ether **12**. The synthesis

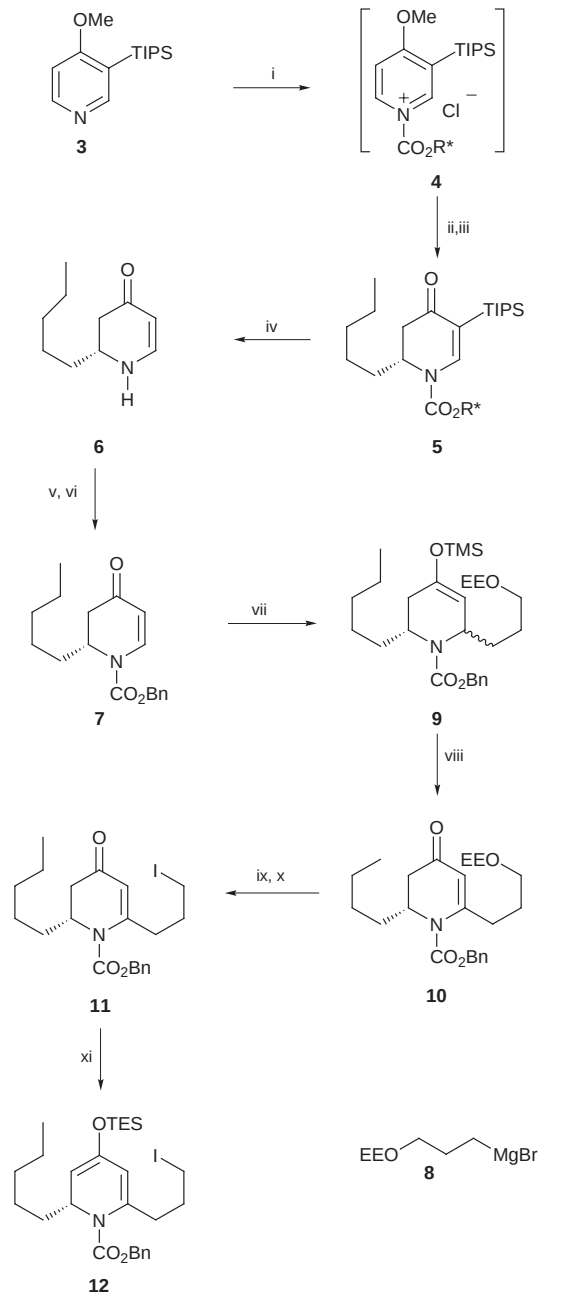

Scheme 1 *Reagents and conditions*: i, $ClCO_2R^*$; ii, $C_5H_{11}MgCl$; iii, H_3O^+; iv, NaOMe, MeOH, then 10% HCl, v, Bu^nLi; vi, $ClCO_2Bn$; vii, **8**, CuBr, TMSCl; viii, $Pd(OAc)_2$, MeCN; ix, oxalic acid; x, NIS, PPh_3; xi, NaHMDS, TESCl.

was continued (Scheme 2) by treatment of crude **12** with the anion of **13**, prepared from the corresponding commercially available aldehyde, to give enone **14** in 94% yield. Protection of the ketone carbonyl using enantiopure bis-TMS ether **15**[10] provided ketal **16** (87%). Since the C-2 substituent of **16** is axial, due to $A^{1,3}$ strain,[11] photocyclization was anticipated to be highly stereoselective for the less hindered olefin face. On photolysis in acetone (460 W Hanovia Hg lamp, 16 min, 5 °C), **16** gave a 79% yield of cycloadduct **17** as the sole isolated product. The (*R*,*R*)-hydrobenzoin ketal of **16** is important for high facial selectivity, for the corresponding ethylene ketal gave only a 7:1 mixture of photoadducts. At this stage of the synthesis, installation of three stereogenic centers with the correct relative and absolute stereochemistry needed for the construction of **1** had been achieved. Treatment of **17** with SmI_2 in THF and DMPU effected cyclobutane ring opening to give spirocyclic ketone **18** in 70% yield, which was converted to a mixture of vinyl triflates **19** (90%) using LiHMDS and *N*-(5-chloro-2-pyridyl)triflimide.[12] Catalytic hydrogenation of this mixture effected vinyl triflate reduction, cleavage of the ketal, and removal of the Z group to provide the known amino ketone **20**[6a] in 81% yield. The synthesis of (−)-perhydrohistrionicotoxin **1** was completed by reduction of **20** with $LiAl(OBu^t)_3H$ according to the procedure of Winkler.[6a] Our synthetic **1** exhibited spectral data in agreement with reported data of authentic material.[5,6] The optical rotation [$[\alpha]_D$ −83.8 (*c* 0.2, CH_2Cl_2)] was also in agreement with literature values [$[\alpha]_D^{22}$ −84.1 (*c* 0.024, CH_2Cl_2); $[\alpha]_D^{22}$ −83.1 (*c* 0.0067, CH_2Cl_2)].[6a]

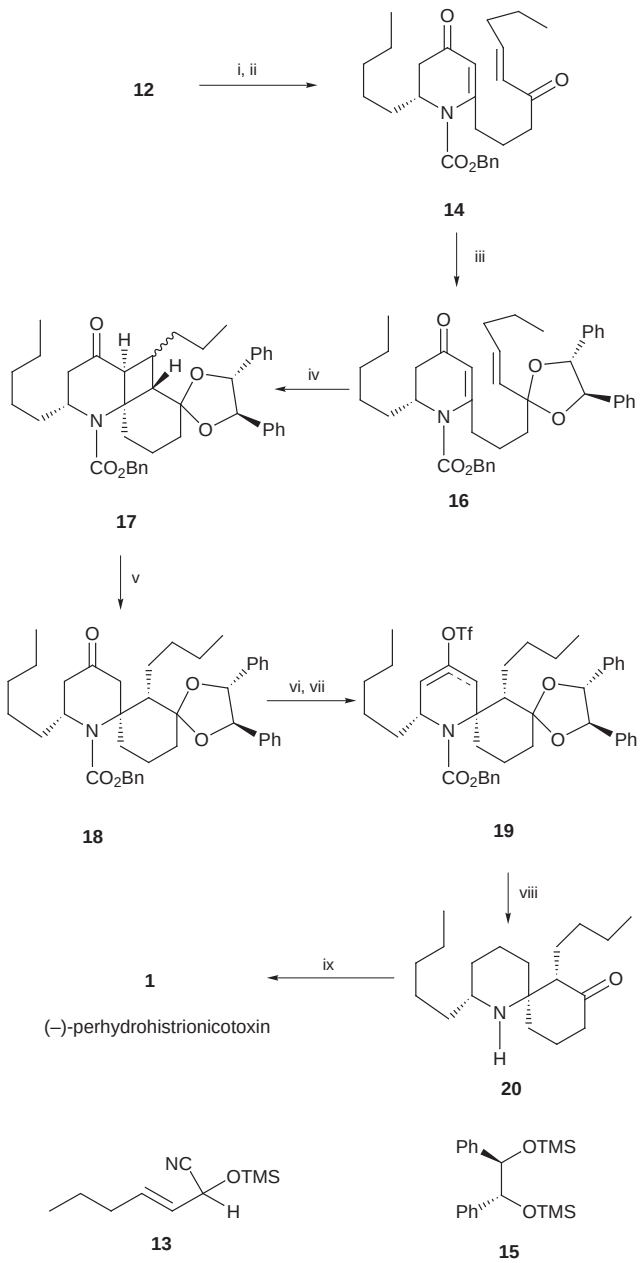

Scheme 2 *Reagents and conditions*: i, **13**, LHMDS, THF; ii, 10% HCl, then 2 M NaOH; iii, **15**, TMSOTf; iv, *hν*, acetone, 5 °C, 16 min; v, SmI_2, THF, DMPU; vi, LHMDS, THF; vii, *N*-(5-chloro-2-pyridyl)triflimide; viii, H_2, $Pd(OH)_2$, Li_2CO_3, EtOH; ix, $LiAl(OBu^t)_3H$.

In summary, the first chiral auxiliary-mediated asymmetric synthesis of (−)-perhydrohistrionicotoxin was accomplished in 15 steps (14% overall yield) with a high degree of stereoselectivity. Key steps include a highly stereoselective intramolecular [2+2] photocyclization of dihydropyridone **16** and a SmI_2-promoted cyclobutane ring opening, which provide the azaspiroundecane skeleton of the alkaloid.

We express appreciation to the National Institutes of Health (Grant GM 34442) and the Petroleum Research Fund (ACS-PRF #28394-AC) for financial support of this research.

Notes and references

† Satisfactory IR, ^1H and ^{13}C NMR spectra, HRMS or microanalyses were obtained for all compounds described.

1 (*a*) D. L. Comins and S. P. Joseph, *Advances in Nitrogen Heterocycles*, ed. C. J. Moody, JAI Press, Greenwich, CT, 1996; vol. 2, pp. 251–294; (*b*) D. L. Comins, S. P. Joseph and X. Chen, *Tetrahedron Lett*., 1995, **36**, 9141; (*c*) D. L. Comins, S. P. Joseph and D. D. Peters, *Tetrahedron Lett*., 1995, **36**, 9449; (*d*) D. L. Comins, S. P. Joseph and Y. Zhang, *Tetrahedron Lett*., 1996, **37**, 793; (*e*) D. L. Comins and L. Guerra-Weltzien, *Tetrahedron Lett*., 1996, **37**, 3807; (*f*) D. L. Comins, X. Chen and S. P. Joseph, *Tetrahedron Lett*., 1996, **37**, 9275; (*g*) D. L. Comins, X. Chen and L. A. Morgan, *J. Org. Chem*., 1997, **62**, 7435; (*h*) D. L. Comins, D. H. LaMunyon and X. Chen, *J. Org. Chem*., 1997, **62**, 8182.

2 D. L. Comins, Y. Lee and P. D. Boyle, *Tetrahedron Lett*., 1998, **39**, 187.

3 P. Guerry and R. Neier, *Chimia*, 1987, **41**, 341; P. Guerry and R. Neier, *J. Chem. Soc., Chem. Commun*., 1989, 1727; P. Guerry, P. Blanco, H. Brodbeck, O. Pasteris and R. Neier, *Helv. Chem. Acta*., 1991, **74**, 163.

4 D. L. Comins and X. Zheng, *J. Chem. Soc., Chem. Commun*., 1994, 2681.

5 J. W. Daly and T. F. Spande, *Alkaloids*: *Chemical and Biological Perspectives*, ed. S. W. Pelletier, Wiley, New York, 1986; vol. 4, ch. 1, pp. 1–274; J. W. Daly, H. M. Garraffo and T. F. Spande, *The Alkaloids*, ed. G. A. Cordell, Academic Press: San Diego, CA, 1993; vol. 43, pp. 185–288.

6 For recent synthetic work and leading references on the histrionicotoxins, see: (*a*) J. D. Winkler and P. M. Hershberger, *J. Am. Chem. Soc*., 1989, **111**, 4852; (*b*) J. J. Venit, M. DiPierro and P. Magnus, *J. Org. Chem*., 1989, **54**, 4298; (*c*) G. Stork and K. Zhao, *J. Am. Chem. Soc*., 1990, **112**, 5875; (*d*) J. Zhu, J. Royer, J.-C. Quirion and H.-P. Husson, *Tetrahedron Lett*., 1991, **32**, 2485; (*e*) C. M. Thompson, *Heterocycles*, 1992, **34**, 979; (*f*) P. Compain, J. Gore and J-M. Vatele, *Tetrahedron Lett*., 1995, **36**, 4063; (*g*) R. W. Fitch and F. A. Luzzio, *Ultrason. Sonochem*., 1997, **4**, 99.

7 K. Takashashi, B. Witkop, A. Brossi, A. M. Maleque and E. X. Albuquerque, *Helv. Chim. Acta*, 1982, **65**, 252.

8 D. L. Comins, S. P. Joseph and R. R. Goehring, *J. Am. Chem. Soc*., 1994, **116**, 4719.

9 D. L. Comins, L. Guerra-Weltzien and J. M. Salvador, *Synlett*, 1994, 972; D. L. Comins and L. Guerra-Weltzien, *Tetrahedron Lett*., 1996, **37**, 3807.

10 C. N. Eid and J. P. Konopelski, *Tetrahedron Lett*., 1991, **32**, 461.

11 For reviews on $A^{1,3}$ strain, see: R. W. Hoffman, *Chem. Rev*., 1989, **89**, 1841; F. Johnson, *Chem. Rev*., 1968, **68**, 375.

12 D. L. Comins and A. Dehghani, *Tetrahedron Lett*., 1992, **33**, 6299; D. L. Comins, A. Dehghani, C. J. Foti and S. P. Joseph, *Org. Synth*. 1996, **74**, 77.

Communication 8/07448H

Conformationally defined piperazine bis(*N*-oxides) bearing amino acid derived side chains

Ian A. O'Neil,* Andrew J. Potter,† J. Mike Southern, Alexander Steiner and James V. Barkley

Robert Robinson Laboratories, Department of Chemistry, University of Liverpool, Crown St, Liverpool, UK L69 7ZD. E-mail: ion@liv.ac.uk

Received (in Cambridge, UK) 4th September 1998, Accepted 7th October 1998

The preparation of a number of piperazine derivatives bearing amino acid substituents on the nitrogen is described; these compounds undergo oxidation with MCPBA to yield bis(*N*-oxides) in which both oxygen atoms are axially orientated and hydrogen bonded to the amide NHs, giving highly defined conformations to the molecules; the structure of the valine derivative (8c) was confirmed by X-ray analysis.

Biological systems rely on polymers, proteins and RNA to carry out the chemical transformations necessary for life. Both proteins and RNA fold into precisely ordered structures which provide a structural framework and the catalytic site for the particular transformation. In addition to their role as catalysts, biopolymers play a central role in the maintenance of structural integrity in living systems. There is great interest in the design and synthesis of polymeric molecules which possess the ability to fold in a discrete and predictable fashion and recently several groups have shown that poly-β-amino acids adopt a stable helical structure.[1] Indeed, Gellman has coined the term 'foldamer' to describe new types of polymeric backbones with well defined and predictable folding properties.

In previous studies we have shown that *N*-alkylated derivatives of proline and pipecolic acid undergo highly diastereoselective oxidations to give tertiary amine oxides that are stabilised by hydrogen bonding (Scheme 1).[2] In most cases these systems are stabilised by the presence of six membered hydrogen bonds between the *N*-oxide oxygen and the amide NH. In addition to their fascinating structural properties, the use of chiral amine oxides as catalysts in a number of synthetically useful transformations has been reported recently.[3]

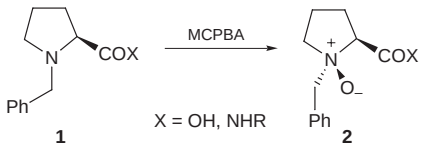

Scheme 1

We considered that we could use this type of hydrogen bonding to enforce a conformational bias on otherwise flexible structures and give them a predictable and specific shape. We were particulary intrigued by the possibility of incorporating α-amino acid residues into the molecule since this would result in a peptide-like compound of defined structure. Earlier work from our group has shown that the oxidation of *N*-benzylpipecolic acid gave the *syn N*-oxide. Interestingly the *N*-oxide adopted an axial orientation in the crystal structure (Scheme 2).

We therefore postulated that attachment of a unit containing a peptide residue possessing an NH residue available for hydrogen bonding, followed by oxidation of both piperazine nitrogens, should yield a bis(*N*-oxide) in which both oxygens were axial and were stabilised by intramolecular hydrogen bonds to the NHs of the peptide chains. The synthesis of such compounds is show in Scheme 3.

† Present address: Ribotargets Ltd, Kett House, 1 Station Road, Cambridge, UK CB1 2JP.

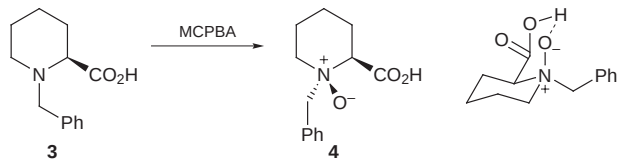

Scheme 2

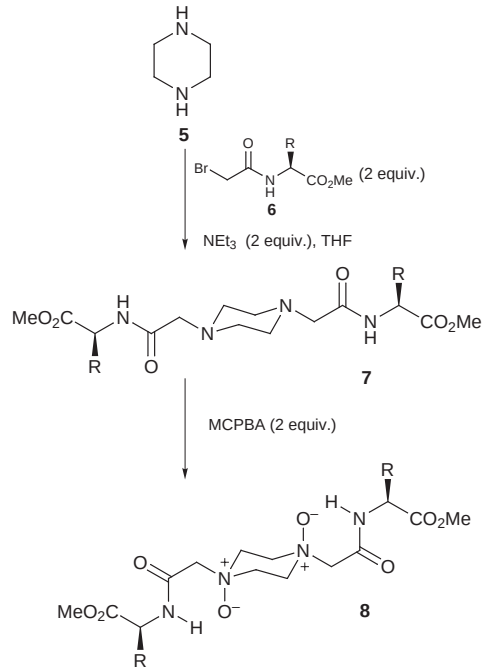

Scheme 3

Piperazine was alkylated on both nitrogens with α-bromo amides derived from a range of α-amino acids using literature procedures.[4] The resulting tertiary amines were treated with 2 equiv. of MCPBA. Clean oxidation was observed and the resulting *N*-oxides were isolated as stable solids. A range of different amino acids was used and the results are summarised in Table 1.

The ^{1}H NMR spectra of the *N*-oxides were highly informative. They showed that the compounds were formed as

Table 1 Synthesis of piperazine bis(*N*-oxides)

		Yield (%)	
Bis(*N*-oxide)	R	*N*-alkylpiperazine	Bis(*N*-oxide)
8a	H	73	63
8b	Me	80	72
8c	Pr^i	67	77
8d	Bu^i	84	74
8e	Ph	79	75
8f	Bn	86	81

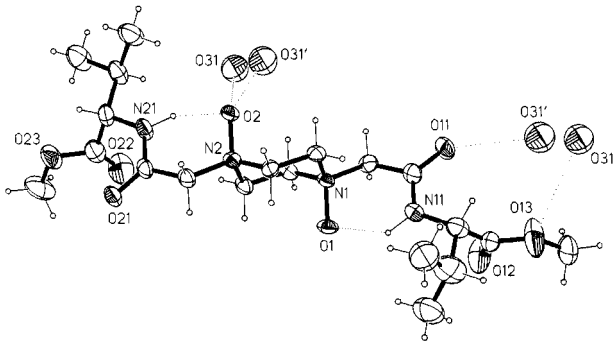

Fig. 1 Crystal structure of **8c** illustrating hydrogen bonding to the disordered water molecule. Thermal ellipsoids set at 50% probability.

single diastereoisomers; in addition the NH signals in $CDCl_3$ appeared as a singlet, which had been shifted downfield by approximately 3.5 ppm in all the compounds after *N*-oxide formation. For example, prior to oxidation, the valine derivative diamine NHs were at δ 7.63; after oxidation they had shifted to δ 11.12, and their chemical shift was found to be concentration independant in $CDCl_3$. The valine derivative gave crystals suitable for X-ray analysis‡ (Fig. 1).

The crystal structure clearly shows that both oxygen atoms are axial and are hydrogen bonded to the NH of the amides. The result is an almost linear molecule of highly defined conformation. N–O bond distances of both *N*-oxide moities are in the same range [N1–O1 1.398(5), N2–O2 1.399(5) Å]. Both hydrogen positions involved in intramolecular hydrogen bonding toward *N*-oxide moieties could be detected in difference Fourier maps and were refined freely. Both show comparable bonding distances [N11–H1 0.97(5), O1···H1 1.82(5), N21–H2 0.93(5), O2···H2 1.84(5) Å]. In addition, intermolecular interactions *via* hydrogen bonding are occuring across a water molecule which is disordered on two positions, resulting in infinite zig-zag-chains throughout the crystal lattice. One of the disordered positions (O31) bridges the amine oxide function O2 with an acyl–O (O13) [O2···O31 2.849(9), O13···O31 3.149(11) Å], while the other position forms a bridge between O2 and an amide–O (O11) [O2···O31′ 2.605(11), O11···O31′ 2.970(11) Å]. In contrast to the above described intramolecular H-bridges, hydrogen postions of the disordered water molecule could not be detected in difference Fourier maps.

In order to establish the range of the hydrogen bonding we prepared the piperazine derivative **10** which bears two amino acid substituents on each of the piperazine nitrogens (Scheme 4). Oxidation proceeded smoothly to give the bis (*N*-oxide) **11**.

NMR analysis of the product clearly showed that only the NHs of the alanine residues were hydrogen bonded to the amine oxide oxygens from their downfield chemical shift from δ 7.02 to 10.50. This specificity allows for fine-tuning of molecular shape.

We are currently examining the incorporation of these units into larger molecular structures and their use as chiral catalysts in a number of synthetic transformations.

We would like to thank the EPSRC and BBSRC for their support of this work (grants GR/K50719 and BO4940). I. O'N. would like to thank The James Black Foundation for continued financial support.

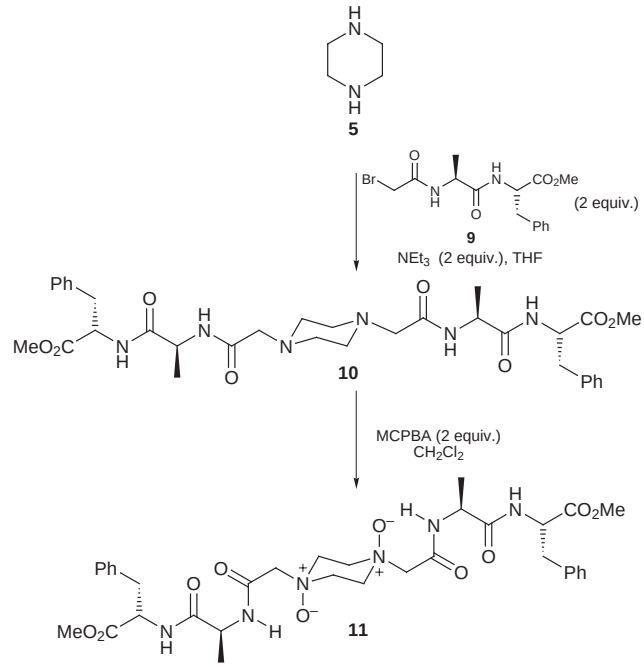

Scheme 4

Notes and references

‡ *Crystal data* for valine derivative: $C_{20}H_{38}N_4O_9$, M = 478.54, monoclinic space group $C2$, a = 25.424(6), b = 5.956(9), c = 16.654(5) Å, α = 100.28(2)°, U = 2481(4) Å^3, Z = 4, D_{calc} = 1.281 g cm^{-3}, μ(Mo-Kα) = 0.101 mm^{-1}. Data were recorded on a Rigaku-AFC6S diffractometer, Mo Kα radiation (λ = 0.71073 Å), T = 153 K, $2\theta_{max}$ = 45°. The structure was solved by direct methods and refined by full-matrix least-squares against F^2 using all data (SHELX97, G. M. Sheldrick, Universität Göttingen, 1997). $R1$ [$I > 2\sigma(I)$] = 0.044, $wR2$ (1813 unique reflections) = 0.117. CCDC 182/1053. The CIF file for the crystal structure is available from the RSC web site: http://www.rsc.org/suppdata/cc/1998/2511

1 D. H. Appella, L. A. Christianson, I. L. Karle, D. R. Powell and S. H. Gellman, *J. Am. Chem. Soc*., 1996, **118**, 13071; D. H. Appella, L. A. Christianson, D. A. Klein, D. R. Powell, X. Huang, J. J. Barchi Jr and S. H. Gellman, *Nature*, 1977, **387**, 381; D. Seebach, M. Overhand, F. N. M. Kuhnle, B. Martinoni, L. Oberer, U. Hommel and H. Widmer, *Helv. Chim. Acta*, 1996, **79**, 913; D. Seebach, P. E. Ciceri, M. Overhand, B. Jaun, D. Rigo, L. Oberer, U. Hommel and H. Widmer, *Helv. Chim. Acta*, 1996, **79**, 2043.

2 I. A. O'Neil, N. D. Miller, J. Peake, J. V. Barkley, C. M. R. Low and S. B. Kalindjian, *Synlett*, 1993, 515; D. Miller, J. V. Barkley, C. M. R. Low and S. B. Kalindjian, *Synlett*, 1995, 617; I. A. O'Neil, N. D. Miller, J. V. Barkley, C. M. R. Low and S. B. Kalindjian, *Synlett*, 1995, 619; I. A. O'Neil, C. D. Turner and S. B. Kalindjian, *Synlett*, 1997, 777; I. A. O'Neil and A. J. Potter, *Tetrahedron Lett*., 1997, **38**, 5731; I. A. O'Neil and A. J. Potter, *Chem. Commun*., 1998, 1487.

3 I. A. O'Neil, C. D. Turner and S. B. Kalindjian, *Synlett*, 1997, 777; M. Nakajima, M. Saito, M. Shiro and S. Hashimoto, *J. Am. Chem. Soc*., 1998, **120**, 6419; M. B. Diana, M. Marchetti and G. Melloni, *Tetrahedron*: *Asymmetry*, 1995, **6**, 1175.

4 R. N. Zuckermann, J. M. Kerr, S. B. H. Kent and W. H. Moos, *J. Am. Chem. Soc*., 1992, **114**, 10646; H. Kessler, *Angew. Chem., Int. Ed. Engl*., 1993, **32**, 543.

Communication 8/06901H

Domain formation in thin films of nonlinear optical side group polymers based on a rigid backbone

Suck-Hyun Lee,* Yong-Seok Kang and Seog-Jeong Song

Department of Applied Chemistry, Ajou University, Suwon, Korea 441-749. E-mail: hyja@madang.ajou.ac.kr

Received (in Cambridge, UK) 17th August 1998, Accepted 12th October 1998

The NLO properties of a *N*-(4-nitrophenyl)-L-prolinol substituted poly(*p*-phenylene terephthalate) polymer are investigated.

Organic polymeric NLO materials are of great interest for practical applications such as electrooptic modulators and switches, due to their fast NLO response time, low cost, ease of fabrication, and large susceptibility. Extensive research efforts have been directed at tailoring organic molecules and their incorporation into polymeric matrices, and substantial progress has been made to reduce their relaxation and improve chromophore loading in the polymer matrix.[1–3] In our studies, we have focussed on rigid chain polymers such as poly(*p*-phenylene terephthalate)s with flexibly attached NLO substituents on the terephthalate moiety. For the pendant chromophore, *N*-(4-nitrophenyl)-L-prolinol was selected. These polymers did not exhibit thermotropic mesophases and the glass transition temperature (T_g) decreased significantly with increasing alkyl tether length, as expected.[4] The present paper deals with domain formation. Most of the results were obtained from the polyester with alkyl tether length of n = 4 (**P4**). The polymer was prepared *via* solution condensation of a chromophore-containing aromatic dicarboxylic acid chloride with hydroquinone in pyridine.[4] The number average molecular weight by gel permeation chromatography was 23,000 in $CHCl_3$ solution based on the polystyrene standard, and the polydispersity of molecular weight (M_w/M_n) was 7.1. The T_g of the polymer was about 68 °C. Polymer films were prepared by spin-coating polymer solutions in tetrachloroethane onto slide glass at 2000–4000 rpm and then treating the slides in a vacuum oven at 60 °C for over 24 h to remove the solvent. Second harmonic generation (SHG) was measured using a Q-switched Nd:YAG laser (1.064 μm) with a pulse repetition rate of 10 Hz. All AFM images were recorded with a Park Scientific Instruments Autoprobe LS, operated in a contact mode.

We studied the surface topographies of the spin coated films before and after corona poling using AFM. The poling was performed in a vertical wire 1 cm above the exposed polymer film. Fig. 1(*a*) shows an AFM scan of the spin coated film (thickness = 2.5 μm). The surface of the thin unpoled film is clean and extremely flat and the root mean squared (rms) roughness value was 2.4 Å. However, this excellent quality film was drastically changed after poling. Fig. 1(*b*) shows an AFM image of the poled film. Numerous mountain-like structures, aligned along the poling direction, were formed during poling. A similar surface morphology of larger size similar to microphase-separated block copolymers[5] was also observed in other samples by optical microscopy [Fig. 1(*c*)]. For the polymer with larger tether length, hills and valleys were also observed but the steepness and curvature decreased and the domains were not well developed compared to the polymer **P4**. As the length of the alkyl side chain increases, the polymer shows decreasing T_g values,[4] suggesting less prominent side chain coupling to the main chain; the growth of domains and their tendency to form would thus decrease. Although the surface topographies of the hills and valleys were characteristic of all the samples, their statistical data were different for each of the samples and preparation conditions studied. Despite the great variations in domain size, the investigated statistical data could be taken as a qualitative indicator of domain size when comparing experimental trends for the samples and poling conditions specified. Fig. 2 shows the growth of domains as a function of poling time obtained from the controlled experiments involving growth after quenching at successive poling times. A high degree of domain growth was achieved at relatively short poling times, and the height of the domains increased only moderately upon further poling. This growth pattern is similar to the two-mode growth in the measured SHG signals, which reached their stable levels after an initial rapid growth. From our data, no apparent differences were observed in the poling dynamics between these domain forming polymers and conventional side group polymers. However, the voltage applied in this study was limited to a relatively low voltage of 6 kV by the onset of film whitening. This whitening or clouding of the film was not associated with chemical degradation of the sample since the spectroscopic analysis did not indicated

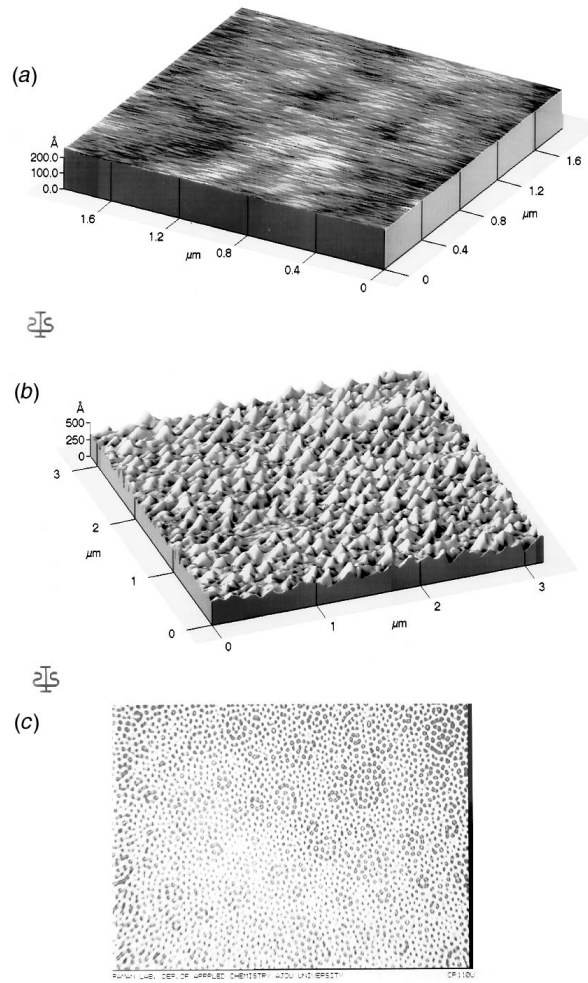

Fig. 1 AFM images for a spin coated film of 2.5 μm thickness (*a*) before and (*b*) after corona poling (92 °C, 5 kV, 15 min). (*c*) An optical micrograph recorded at a different location on the poled film exhibiting larger sizes for the same polymer **P4**.

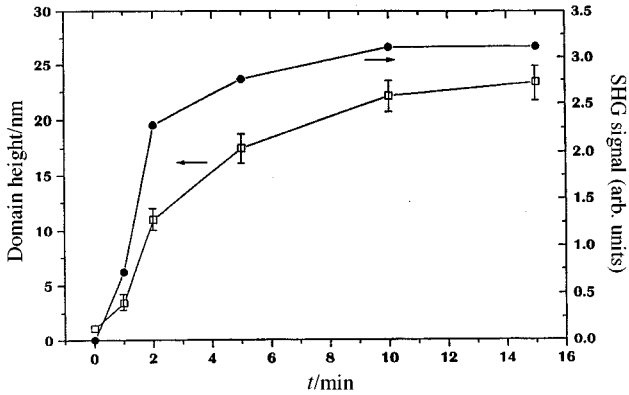

Fig. 2 SHG signal intensity and growth of the domains as a function of poling time measured after quenching at successive poling times at a poling temperature of 75 °C. The error bars were determined by repeating the measurement at five different positions on the same film.

noticeable decomposition at this poling condition. We believe this whitening is due to light scattering by chromophore domains of larger size formed during poling. One related observation for the same film is that relaxation of the SHG signal occurred by the progressive depression on the top of the domains removing the applied poling field. These results suggested that the domain size is apparently correlated with the observed SHG signal intensity.

It is interesting to note that a positive polarity was proven to work with our material much more efficiently than a negative one. When a negative polarity was applied, the observed SHG signal intensity almost vanished. The electric field in this polarity environment causes the axes of dipoles to be directed to the glass substrate, whose barrier effect hinders domain formation. In fact, the domains were not observed by AFM. A possible implication of this polarity effect is that the dipoles in this type of polymers can be oriented to form poled domains in cases where their alignment induced by the electric field facilitates cooperative movement of the rigid main chains. The attempted polings which failed confirmed this. When the corona poling was performed for films on which any barrier layers, including a vacuum deposited metallic electrode, were coated, the resulting SHG response was nearly absent, thus a sandwitch type poling was not adequate. However in cases where the films were corona poled first and then a barrier layer deposited on it, the SHG response remained almost unchanged and its temporal stability was greatly improved. This preliminary result may have important implications for obtaining stable materials for device applications. Design strategies to lock the domain itself would be valuable for improving geometrically the long term stability of second order NLO properties. We have also examined whether the roughened surface or interface had an important role in the measured SHG intensity by double coating the surface of the same polymer as the base film and then remeasuring the SHG intensity. We observed no loss in properties for this sample. This result indicates that the observed SHG should be related to the polar order effect of the chromophores in the domain rather than to the symmetry breaking nature of the roughened surface.

We have measured the SHG response of the samples for angles of incidence between −90 and 90° shortly after poling. The SHG signal of the polymer displayed no fringes, and only one peak indicative of thin sample films compared to the coherence length of the NLO process. In this case it is usual to determine the second order NLO susceptibility d_{33} by the curve fitting method using the intensity equation given by Jerphagnon and Kurtz.[6] We tried to determine d_{33} by fitting the data to the theoretical equation, but the result was not satisfactory and the experimental data systematically deviated from the theoretical values. However, the calculation at a single angle of 58° only resulted in a relatively large value of 50 pm V^{-1} referenced to a value of 0.3 pm V^{-1} for quartz, and the order parameter measured by the UV absorbance ratio was calculated to be 0.58, which to the best of our knowledge is higher than any reported values for poled polymer systems. It is still not clear if the fitting failure is a reflection of morphological changes in the polymeric films after poling. At this stage, it could be speculated that this behaviour is associated with the oriented domains largely formed on the outer surface layer and thus with the efficient second order NLO effect occurred only over a fraction of the film thickness. The SHG intensity against film thickness provides evidence of the inhomogeneous behaviour of chromophore orientations through the film thickness. As the thickness increased, the surface morphology became much rougher as a consequence of the larger sizes of the structure, and the more rugged the surface was, the greater the SHG intensity. However, the SHG intensity did not increase up to the level expected from the l^2 dependence[6] even when the film thickness was far smaller than the coherence length.

We gratefully acknowledge partial funding support from the Korea Science and Engineering Foundation (941-1100-011-2).

Notes and references

1 D. R. Dalton, A. W. Harper, R. Ghosn, W. H. Steier, M. Ziari, H. Fetterman, Y. Shi, R. V. Mustacich, A. K.-Y. Jen and K. J. Shea, *Chem. Mater*., 1995, **7**, 1060.
2 D. M. Burland, R. D. Miller and C. A. Walsh, *Chem. Rev*., 1994, **94**, 31.
3 H. S. Nalwa and S. Miyata, *Nonlinear Optics of Organic Molecules and Polymers*, CRC Press, New York, 1997
4 S. H. Lee, K. C. Lim, J. T. Jeon and S. J. Song, *Bull. Korean Chem. Soc*., 1996, **17**, 11.
5 M. A. Dijk and R. Berg, *Macromolecules*, 1995, **28**, 6773.
6 J. Jerphagnon and S. K. Kurtz, *J. Appl. Phys*., 1970, **41**, 1667.

Communication 8/06495D

Imprinting chiral structures on liquid crystalline elastomers

Craig D. Hasson, Frederick J. Davis and Geoffrey R. Mitchell

Polymer Science Centre, University of Reading, Whiteknights, Reading, UK RG6 6AF.
E-mail: g.r.mitchell@reading.ac.uk

Received (in Cambridge, UK) 28th July 1998, Accepted 13th October 1998

Cross-linking achiral liquid crystalline polymers in the presence of a removable low molecular weight chiral mesogen produces a liquid crystalline elastomer in which a chiral structure has been imprinted.

In 1969 de Gennes published a paper speculating on the properties of a polymer chain lightly cross-linked in a liquid crystalline phase.[1] Using symmetry arguments, he showed that a chiral nematic would give rise to a permanent chirality of the polymer network. The essentials of de Gennes ideas[2] and other theoretical scientists[3,4] concerning nematic liquid crystalline elastomers have been confirmed experimentally,[5,6] however, we believe de Gennes's theory has remained essentially untested to date, probably because of the difficulty of incorporating a polymer backbone into a liquid crystalline phase. Some early work by Tsutsui *et al*.[7,8] attempted to resolve this issue through cross-linking an acrylate polymer in the presence of poly(benzyl-L-glutamate), however it is not clear that this system involved the types of mesogenic interaction originally envisaged by de Gennes. This issue is clearly of some importance in view of the volume of work involving cross-linking in a liquid crystalline solvent.[9] Here we show how low levels of cross-linking can be used to imprint a memory of a chiral mesophase into an elastomer with no imbalance in localised chiral centres.

Scheme 1 shows the principal features of our experiment. An achiral liquid crystalline polymer containing cross-linking sites was mixed with a chiral liquid crystal. The material was then cross-linked in the chiral nematic phase and finally the chiral liquid crystal was removed. Any chiral behaviour would then reflect a memory of the orientation imposed on the sample at the time of cross-linking in the same way that a magnetic[10] or mechanical field[11] imposes a permanent macroscopic order on the sample.

The system used was chosen to give a cholesteric phase with a helical pitch such that the material exhibited the well-known property of selective reflectivity in the visible portion of the electromagnetic spectra.[12] To this end the 4-cyanobenzoate containing acrylate **I**[13] was copolymerised with hydroxyethyl acrylate **II** (6 mol%, introduced to provide sites for cross-linking). This random atactic copolymer exhibited a nematic phase with a nematic–isotropic transition of 128 °C. Solutions were prepared in CH_2Cl_2 (dried over alumina) of this polymer and the chiral cyanobiphenyl **III** (available from Merck as CB15) and films were cast from these solutions onto glass slides

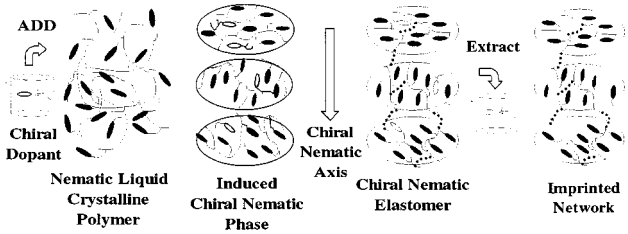

Scheme 1 Description of procedure used to imprint a chiral structure onto a liquid crystalline elastomer: a chiral dopant is added to produce a chiral nematic phase, the polymer is cross-linked and finally the dopant is removed.

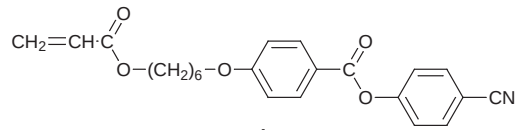

I

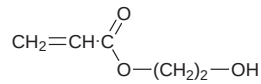

II

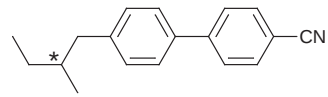

III

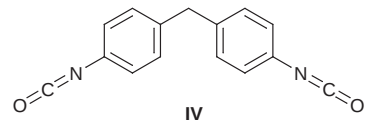

IV

coated with a rubbed film of polyimide. The composition range over which a chiral nematic phase was formed was then determined. It was found that at compositions below *ca*. 60 mol% CB15 a chiral nematic phase could be observed. At lower compositions between *ca*. 20 and 35% CB15 films of the mixture showed selective reflection of visible light. For example, the 30% sample showed a selective reflection at 730 nm at 50 °C and it is this composition which will be used for the subsequent studies. Further films were cast containing the polymer, CB15 and a sufficient quantity of the diisocyanate **IV** to react with all the hydroxy units in the polymer. The solvent was removed at room temperature and the film allowed to dry overnight before heating slowly (2 °C min^{-1}) to the required cross-linking temperature (in this example 50 °C). The sample was held at this temperature for 1 h, whereupon a polyimide sheet was placed on the surface, and 12.5 μm polyimide spacers were used to define the thickness. The material was then cross-linked for 16 days at 50 °C after which time it was found to consist of 72% gel by mass, in line with expectations based on the polydispersity of the sample.[14] The level of cross-linking was light, ~1mol% of the monomer units.

A portion of the elastomer produced from the above procedure was retained for further study, and the remainder of the sample was treated with refluxing acetone to remove both the chiral dopant and any soluble polymer. The extraction process was monitored by UV–visible spectroscopy and as Fig. 1 shows complete removal of both components was achieved after *ca*. 40 min.

The phase behaviour of the materials (*i.e*. mixture, cross-linked elastomer with dopant and cross-linked elastomer with dopant removed) was examined by optical microscopy and UV–visible spectroscopy to probe the pitch of any chiral ordering within the samples. The mixture and the elastomer samples

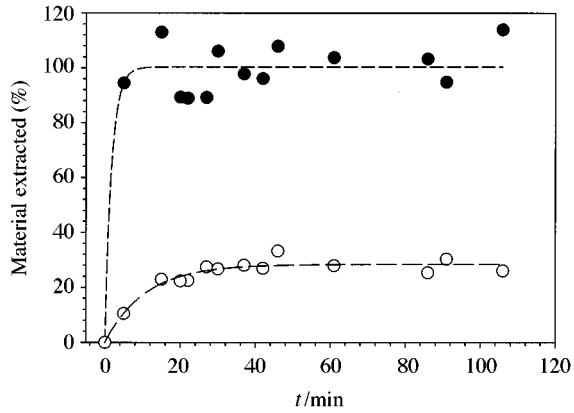

Fig. 1 Plot of the mass of the extracted material (expressed as a mass fraction relative to the initial composition) as a function of the extraction time in refluxing acetone: (●) CB15 and (○) copolymer. The solid lines serve as guides.

cross-linked at 50 °C were visibly coloured, and their absorption spectra are shown in Fig. 2. Clearly, all three samples exhibited a cholesteric reflection, and by implication a chiral nematic phase. In the case of the initial uncross-linked mixture and the cross-linked material in which the dopant was retained, the maximum absorption (λ_{max}) was at 730 nm at 50 °C, although the elastomer showed a much smaller variation of λ_{max} with temperature. Both these materials could be heated reversibly to the isotropic phase, but both passed through a biphasic region on heating in which nematic polymer coexisted with isotropic dopant. For the sample in which the dopant had been removed the maxima in the absorption spectrum moved to a much shorter wavelength, namely 500 nm at 50 °C (if this change were simply due to the presence of the dopant in lower concentrations a shift to higher wavelengths would be expected). Initial measurements suggest that the change in λ_{max} is related in a proportional manner to the change in volume of the sample arising from removal of both dopant and the sol fraction. Interestingly, λ_{max} for this sample remained invariant with temperature until the material became isotropic at 128 °C. On cooling from the isotropic the chiral nematic phase reappeared and an identical absorption spectrum to that initially observed was obtained.

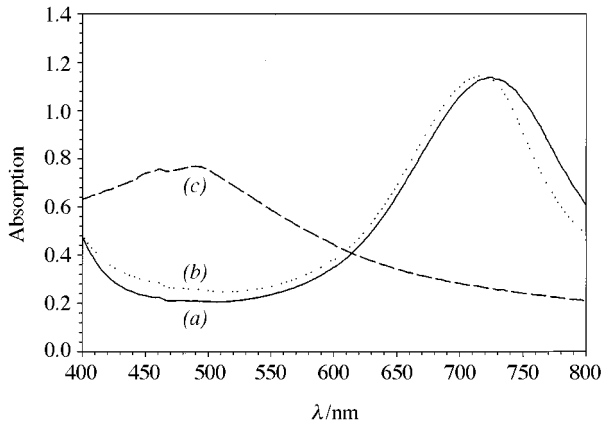

Fig. 2 Absorption spectra obtained from thin films of the liquid crystalline polymers and elastomers studied here: (*a*) mixture, (*b*) elastomer and (*c*) imprinted network. The peaks arise from selective reflection of visible light from the chiral material and are not observed for samples held at temperatures above the clearing point of the polymer.

We have shown that cross-linking an achiral side-chain liquid crystalline polymer in an induced chiral nematic phase results in material which retains a memory of the chirality upon removal of chiral dopant, by virtue of the orientation imposed on the mesogenic side-groups by the chiral nematic phase, and the coupling between the mesogenic side-groups and the polymer backbone. This is a soft imprinting and arises from subtle molecular interactions in contrast to the properties of rigid highly cross-linked networks prepared through photopolymerisation of multifunctional monomers.[9] We believe firstly, these experiments confirm the theory outlined by de Gennes; secondly, this represents a novel route to imprinted materials, not least because of the enhanced behaviour arising from the relatively low levels of cross-linking (for example, they will readily uptake solvent and are not glassy); thirdly this represents a route to materials with new properties which merit further exploration.

This work is supported by the EPSRC. We thank Dr U. Singh of the University of the West Indies for discussions and Merck R&D UK for supplying the chiral dopant CB15.

Notes and references

1 P. G. de Gennes, *Phys. Lett*., 1969, **28A**, 11.
2 P. G. de Gennes, *Compt. Rend. Acad. Sci*., 1975, **B281**, 101.
3 M. Warner, in *Side-Chain Liquid Crystal Polymers*, ed C. B. McArdle, Blackie, New York, 1989.
4 M. Warner and E. M Terentjev, *Progr. Polym. Sci*., 1996, **21**, 853.
5 G. R. Mitchell, P. M. S. Roberts, K. H. Ahn, F. J. Davis, C. D. Hasson, H. Hirschmann and J. A. Pople, *Macromol. Symp*., 1997, **117**, 21.
6 J. Schatzle, W. Kaufold and H. Finkelmann, *Makromol. Chem*., 1989, **190**, 3269; 1991, **192**, 1235.
7 T. Tsutsui, R. Tanaka and T. Tanaka, *J. Polym. Sci., Polym. Lett. Ed*., 1979, **17**, 511,
8 T. Tsutsui and R. Tanaka, *Polymer*, 1981, **22**, 117.
9 See for example, S. M. Kelly, *J. Mater. Chem*., 1995, **5**, 2047.
10 C. H. Legge, F. J. Davis and G. R. Mitchell, *J. Phys. II*, 1991, **1**, 1253.
11 J. Küpfer and H. Finkelmann, *Makromol. Chem., Rapid Commun*., 1991, **12**, 717.
12 P. G. de Gennes and J. Prost, *The Physics of Liquid Crystals*, Clarendon Press, Oxford, 1993, ch. 3.
13 F. J. Davis, A. Gilbert, J. Mann and G. R. Mitchell, *J. Polym Sci.: Polym. Chem*., 1990, **28** 1455.
14 P. M. S. Roberts, G. R. Mitchell and F. J. Davis, *Mol. Cryst. Liq. Cryst., Sect. A*, 1997, **299**, 223.

Communication 8/05891A

Duplex hydrogen bonding promotes intercalation of Cu(T4) in DNA hairpins (Cu(T4) = *meso*-tetrakis(4-(*N*-methylpyridyl))porphyrincopper(II))

Denise K. Crites Tears and David R. McMillin*

Department of Chemistry, Purdue University, West Lafayette, IN 47907-1393, USA. E-mail: mcmillin@purdue.edu

Received (in Bloomington, IN, USA) 3rd August 1998, Accepted 12th October 1998

Inosine-for-guanine replacement in DNA hairpin hosts reveals that the intercalative binding of Cu(T4) depends upon strong hydrogen bonding within the stem.

Water-soluble porphyrin derivatives are of interest for photodynamic therapy,[1,2] as antiviral agents,[3,4] and, in the case of cationic systems, as versatile ligands for DNA-binding studies.[5,6] A wealth of physical data shows that metalated forms lacking axial ligands, such as Cu(T4), intercalate into DNA sequences that are rich in guanine–cytosine (G≡C) base pairs[5,6,7] (H_2(T4) = *meso*-tetrakis(4-(*N*-methylpyridyl))porphyrin). On the other hand, adenine–thymine (A=T) base pairs support external binding in groove regions. A recent report based on DNA hairpin substrates indicated that robust hydrogen bonding within the local B-form structure, not the specific base sequence, promotes intercalative binding.[8] The replacement of a guanine base by inosine provides a strict test of the hypothesis because it is a small perturbation that noticeably impacts the hydrogen bonding within DNA. The effect is to weaken the B-form structure because inosine lacks an NH_2 substituent at its C2 position and can form only two hydrogen bonds with cytosine. The following results show that even one such replacement in a six-base-pair run can dramatically alter the binding of Cu(T4).

The hexadecamers employed all came from the Macromolecular Structure Facility of Purdue University as custom syntheses. In all spectral runs the hairpin-to-copper ratio was 5 : 1. Quantification of the hairpin concentration was possible *via* the absorbance of a denatured sample at 80 °C in conjunction with the ε_{260} values (molar absorptivities at 260 nm) of the component mononucleotides. The extremum in the derivative of the absorbance *versus* temperature profile indicated the melting temperature, T_m. The sequence is normally constant except for residues 3 and 4 and their complements (positions 13 and 14). The two-letter abbreviation identifies the bases in the 3,4 positions:

$$\text{CI} = \begin{matrix}5'\text{-GA}\mathbf{CI}\text{AC}^T\text{T}\\ 3'\text{-CTICTG}_T\text{T}\end{matrix} \qquad \text{AI} = \begin{matrix}5'\text{-GA}\mathbf{AI}\text{AC}^T\text{T}\\ 3'\text{-CTTCTG}_T\text{T}\end{matrix}$$

The data in Table 1 show that replacement of a mid-stem guanine by inosine has a significant impact on the melting temperature and the reaction chemistry of the hairpin. Thus, each replacement reduces the melting temperature by about 12 °C. As a result, the CI, IC and AI hairpins all exhibit about the same T_m, presumably because they have the same number of hydrogen bonds in the stem. As previously reported, the spectral and physical data reveal that Cu(T4) intercalates into the CG hairpin.[8] In contrast, with the CI hairpin all indications point to a complete shift in the mode of binding. More specifically, the weak emission intensity from the latter adduct is a clear sign of an exposed copper center that is subject to axial attack by solvent or basic centers on the surface of the hairpin.[6] Furthermore, in the Soret region the CI adduct shows a small bathochromic shift in the absorption maximum, hyperchromism and an induced CD signal with a positive amplitude—all signs of groove binding.[5,6,9] Similar spectral changes occur in switching from the AG to the AI hairpin except for the inversion in the sign of the induced CD signal (Fig. 1). The remarkable aspect of the AG system is that the loss of just one of fifteen possible hydrogen bonds in the stem drastically alters the binding of Cu(T4).

Regardless of the mode of binding, the DNA must undergo a structural adjustment to accommodate the Cu(T4) ligand because there is no pre-organized binding site. In other words, the uptake of the porphyrin is an induced-fit process. For intercalation, the minimum necessary structural reorganization entails partial unwinding of the double helix and creation of a cavity to house Cu(T4). Even with those modifications, strain is evident,[10,11] and groove binding of Cu(T4) is a competitive phenomenon in DNA hosts containing a short run of A=T base pairs amidst long segments of G≡C steps.[6,12] Groove binding is also disruptive as Cu(T4) cannot conform to the natural contour of DNA. Consequently, uptake occurs with partial melting of the double helix and generation of an appropriate binding pocket.[6,13] Transient Raman studies of Cu(T4) by Nakamoto and co-workers reveal that a run of four consecutive adenine–thiamine (A=T) base pairs suffices to provide the surface area

Table 1 Physical data for Cu(T4) adducts with DNA hairpins[a]

		Absorption		CD		Emission	
Hairpin	T_m/°C	$\Delta\lambda$/nm[b]	%H[c]	λ/nm	$\Delta\varepsilon$/M^{-1} cm^{-1}	λ/nm[d]	I_{rel}[e]
CG	74	10	25	434	−27	434	0.9
CI	50	4	−9	424	16	429	< 0.1
GC[f]	75	8	20	433	−22	432	1.0
IC	50	6	9	432	−13	432	0.2
AG[f]	61	9	25	434	−17	433	0.7
AI	53	5	−5	428	−10	433	0.1
CA[f]	65	7	12	434	−17	433	0.5
CTA[g]	45	10	29	434	−20		0.8

[a] At a hairpin-to-copper ratio of 5 : 1. [b] Bathochromic shift of Soret band from 424 nm. [c] Percent decrease in absorbance at the Soret maximum. [d] Maximum in the excitation spectrum. [e] Relative intensity of the (uncorrected) emission signal. [f] Data from ref. 8. [g] Bulge derivative of CA with unmatched T after C3.

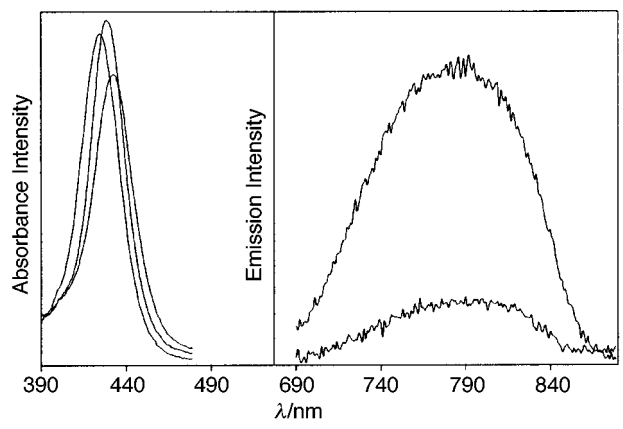

Fig. 1 Absorbance and emission data. Left: in order of decreasing intensity, Soret absorbance of adduct with AI, free Cu(T4), adduct with AG. Right: emissions from adducts with AG (upper) and AI (lower) hairpins.

and/or the flexibility necessary for groove binding.[12] From the standpoint of internalization of the ligand, intercalation and groove binding represent limiting cases of a continuum of possible interactions. Intermediate situations are certainly feasible; for example, an extruded base might stack with an externally bound porphyrin. The adduct with the IC system may, in fact, be some type of an intermediate case. To be sure, the modest hypochromism apparent in the Soret absorption is evidence for some degree of stacking with the DNA bases, and partial protection of the axial coordination positions at copper would explain the definite, albeit weak, emission signal of the adduct.[14] However, classical intercalation does not occur because the emission intensity pales in comparison with that of the GC adduct. More than one type of association may occur because the absorption and excitation maxima do not coincide for the IC or the AI adducts. Yet, the CD spectrum of the latter is clearly not the sum of the signals of a classical groove binder and a classical intercalator.

Though questions remain, the present results provide important insight into the forces influencing the binding of Cu(T4). The main conclusion is that for intercalation of Cu(T4) to occur, a robust hydrogen bonding network must exist within the B-form DNA to compensate for the steric problems posed by the bulky porphyrin. Two predictions follow. One is that the presence of a bulge in the stem may promote intercalative binding by reducing the strain and/or the energy requirement for cavity creation.[15] Indeed, comparisons of the hypochromism and the emission intensity show that Cu(T4) is a more avid intercalator for the CTA hairpin, with the bulge thymine, than the CA control (Table 1). The second prediction is that the mode of binding known as hemiintercalation, which has been observed in the solid,[11] is unlikely to occur in solution, at least in sequences rich in G≡C base pairs. The reason is that hemiintercalation would require base extrusion, but the preservation of hydrogen bonding between bases is, in reality, one of the most important factors that favors internalization over groove binding.

The National Science Foundation supported this research through Grant No. CHE-9726435.

Notes and references

1 B. W. Henderson and T. J. Dougherty, *Photochem. Photobiol.*, 1992, **55**, 145.
2 L. Milgrom and S. MacRobert, *Chem. Br.*, 1998, **34**, 45.
3 D. W. Dixon, L. G. Marzilli and R. F. Shinazi, *Ann. NY Acad. Sci*., 1990, **616**, 511.
4 C. Kasturi and M. S. Platz, *Photochem. Photobiol*., 1992, **56**, 427.
5 R. F. Pasternack and E. J. Gibbs, *Met. Ions Biol. Syst.*, 1996, **33**, 367.
6 D. R. McMillin and K. M. McNett, *Chem. Rev*., 1998, **98**, 1201.
7 K. Ford, K. R. Fox, S. Neidle and M. J. Waring, *Nucleic Acids Res*., 1987, **15**, 2221.
8 M. K. Eggleston, D. K. Crites and D. R. McMillin, *J. Phys. Chem*., 1998, **102**, 5506.
9 R. F. Pasternack, E. J. Gibbs and J. J. Villafranca, *Biochemistry*, 1983, **22**, 2406.
10 R. J. Fiel and B. R. Munson, *Nucleic Acids Res.*, 1980, **8**, 2835.
11 L. A. Lipscomb, F. X. Zhou, S. R. Presnell, R. J. Woo, M. E. Peek, R. R. Plaskon and L. A. Williams, *Biochemistry*, 1996, **35**, 2818.
12 G. D. Strahan, D. Lu, M. Tsuboi and K. Nakamoto, *J. Phys. Chem.*, 1992, **96**, 6450.
13 G. Raner, J. Goodisman and J. C. Dabrowiak, *ACS Symp. Ser.*, American Chemical Society, Washington, D.C., 1989, vol. 402, p. 74.
14 B. P. Hudson, J. Sou, D. J. Berger and D. R. McMillin, *J. Am. Chem. Soc*., 1992, **114**, 8997.
15 L. D. Williams and I. H. Goldberg, *Biochemistry*, 1988, **27**, 3004.

Communication 8/06103C

Dynamic kinetic resolution in the hydrolysis of an α-bromo ester

Matthew M. Jones and Jonathan M. J. Williams*

Department of Chemistry, University of Bath, Claverton Down, Bath, UK BA2 7AY.
E-mail: j.m.j.williams@bath.ac.uk

Received (in Liverpool, UK) 15th September 1998, Accepted 6th October 1998

Bromide can be employed to racemise an α-bromo ester more rapidly than the corresponding acid (carboxylate), and this rate difference has been employed as the basis of a dynamic kinetic resolution reaction.

Dynamic kinetic resolution strategies have been enjoying increasing attention in the last few years.[1] For an ideal dynamic kinetic resolution, the two enantiomers of starting material must react at very different rates. Furthermore, whilst the starting material enantiomers must be in equilibrium, the product must be essentially inert to racemisation. Recent work from this group has described racemisation procedures which strongly favour the starting material.[2]

Herein we report that the racemisation of the α-bromo ester **1** is significantly faster than for the corresponding α-bromo acid **2** under appropriate conditions. Thus, competition experiments between enantiomerically enriched ester **1** and acid **2** show that the ester racemises more quickly (Scheme 1 and Table 1).†

Scheme 1

Table 1 Racemisation of ester **1** and acid **2** with bromides

		Ee of **1** (%)		Ee of **2** (%)	
Bromide	*t*/h	Initial	Final	Initial	Final
KBr	18	38	28	34	34
CsBr	18	80	77	35	35
Bu_4NBr[a]	4	80	0	64	35
Bu_4PBr	18	80	4	33	31
$C_{16}H_{33}P^+Ph_3Br^-$	6	55	5	38	36
Wang polymer-$CH_2P^+Ph_3Br^-$	2	43	0.5	61	58

[a] Performed in H_2O–MeOH (5:1).

We rationalise that the racemisation of the ester **2** occurs *via* S_N2 displacement by bromide (Fig. 1), which is enhanced by the neighbouring carbonyl function (π* C=O). However, under the reaction conditions, the carboxylic acid will be deprotonated, and the carboxylate is less willing to assist the adjacent S_N2

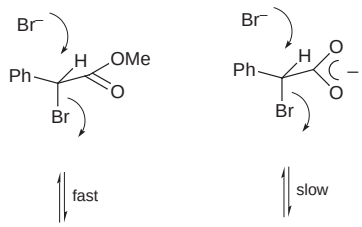

Fig. 1 Preferential racemisation by SN2 bromide displacement of an α-bromo ester.

process. We have not ruled out the possibility that racemisation occurs by simple enolisation, but the racemisation of the ester is not qualitatively dependent on pH (5–8)

The preferred sources of bromide were quaternary ammonium bromides and quaternary phosphonium bromide. In particular, the phosphonium salt produced by heating brominated Wang resin with PPh_3 in toluene for 10 h provided a particularly convenient bromide source.[3] Simple salts such as KBr were significantly less effective for the racemisation of either ester or acid.

We chose to use an enzymatic procedure for the selective hydrolysis of the bromo ester, which has some literature precedent.[4] Thus, ester **1** was hydrolysed by various enzymes in water, using a autotitrater to maintain a constant pH (7.0). A representative selection of these enzymes in a simple kinetic resolution reactions are shown in Scheme 2 and Table 2.

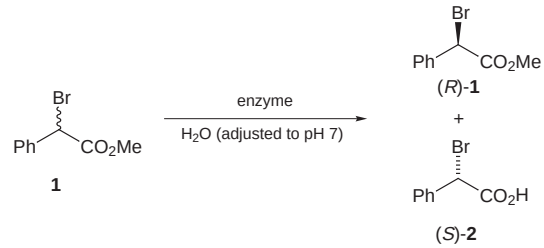

Scheme 2

Table 2 Kinetic resolution of ester **1**[a]

Enzyme	*t*/h	Conversion (%)	Ee of **1** (%)	Ee of **2** (%)
CRL[b]	18	42	69	74
Altus 17[c]	2.5	47	81	80
Altus 20[d]	144	32	51	65

[a] Performed in H_2O. [b] *Candida rugosa* lipase. [c] CLEC-CRL - cross linked enzyme crystal (*Candida rugosa* lipase) [d] CLEC-PCL - cross linked enzyme crystal (*Pseudomonas cepacia* lipase). In this case the *R* enantiomer of acid was formed preferentially.

We favoured the commercially available cross-linked enzyme crystal, Altus 17 (*Candida rugosa* lipase, cross-linked),[5] which provided a fast reaction with reasonably good enantioselectivity in the resolution.

By combining the selective racemisation procedure with simple kinetic resolution, we proceeded to investigate the dynamic kinetic resolution reaction (Scheme 3 and Table 3). Gratifyingly, the combination of the Wang phosphonium

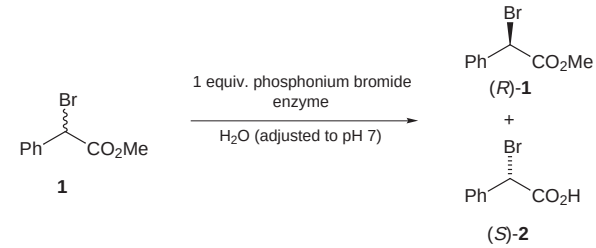

Scheme 3

Table 3 Dynamic kinetic resolution of ester **1**

Bromide	*t*/h	Yield of **2** (%)[a]	Ee of **1** (%)	Ee of **2** (%)
Bu_4PBr	6	26 (30)[b]	26	22
$C_{16}H_{33}P^+Ph_3Br^-$	7	65 (70)	6	68
Wang polymer-$CH_2P^+Ph_3Br^-$	4.5	78 (80)	26	79

[a] Isolated yields. Figures in parentheses are conversions. [b] Performed in H_2O–MeOH (5 : 1).

bromide with Altus-17 afforded an effective dynamic resolution procedure. Thus at 80% conversion, the product **2** was obtained with good enantioselectivity (79% ee, essentially the same as for the simple kinetic resolution). The starting material, although not racemic, was clearly undergoing slow racemisation under the reaction conditions. Presumably the larger phosphonium salts (R^1 = $C_{16}H_{33}$) and the immobilised phosphonium salts are unable to interfere with the immobilised enzyme, which is beneficial in an effective dynamic resolution where both the enzyme and bromide source must co-exist.

In conclusion, we have shown that an α-bromo ester can be successfully racemised in the presence of an α-bromo acid (carboxylate). This provides the basis for a dynamic kinetic resolution procedure using a combination of a hydrolytic enzyme with a source of bromide. Further work extending the range of substrates will shortly be underway.

We are grateful to the EPSRC Clean Technology Unit for a studentship (to M. M. J.) and to the University of Bath for additional support.

Notes and references

† Enantiomeric excess was determined by chiral HPLC. Chiralcel OD, hexane–Pr^iOH–formic acid (240:10:1), 1 ml min^{-1}, methyl ester (**1**): 5.6 min (*R*) and 6.2 min (*S*), acid (**2**): 9.4 min (*R*) and 11.7 min (*S*).

1 S. Caddick and K. Jenkins, *Chem. Soc. Rev*., 1996, 447; R. S. Ward, *Tetrahedron*: *Asymmetry*, 1995, **6**, 1475; H. Stecher and K. Faber, *Synthesis*, 1997, 1.
2 P. M. Dinh, J. A. Howarth, A. R. Hudnott, W. Harris and J. M. J. Williams, *Tetrahedron Lett*., 1996, **37**, 7623; J. V. Allen and J. M. J. Williams, *Tetrahedron Lett*., 1996, **37**, 1859.
3 Brominated Wang resin contains a benzyl bromide function, and was purchased from Novo Biochem. See also; I. Hughes, *Tetrahedron Lett*., 1996, **37**, 7595.
4 For examples, see; P. Kalariitis, R. W. Regenye, J. J. Partridge and D. L. Coffen, *J. Org. Chem*., 1990, **55**, 812; G. Kirchner. M. P. Scollar and A. M. Klibanov, *J. Am. Chem. Soc*., 1985, **107**, 7072; S. K. Dahod, Eur. Pat., 1988, EP257716.
5 CLEC enzymes were purchased from Altus Biologics Inc., 40 Allston St., Cambridge, MA 02139-4211, USA.

Communication 8/07232I

ChemComm

A three-coordinate copper(I)-phenoxide complex that models the reduced form of galactose oxidase

Brian A. Jazdzewski, Victor G. Young, Jr. and William B. Tolman*

Department of Chemistry and Center for Metals in Biocatalysis, University of Minnesota, 207 Pleasant Street SE, Minneapolis, Minnesota 55455, USA. E-mail: tolman@chem.umn.edu

Received (in Bloomington, IN, USA) 28th August 1998, Accepted 12th October 1998

A novel 3-coordinate Cu(I)-phenoxide complex with N-donor supporting ligation was structurally characterized and shown to be highly reactive towards dioxygen, similar to the reduced form of galactose oxidase.

Galactose oxidase (GAO) is a fungal enzyme that couples the 2-electron oxidation of primary alcohols to aldehydes with the reduction of O_2 to H_2O_2.[1] Structural and spectroscopic studies of this enzyme[1,2] and a related system, glyoxal oxidase,[3] have shown that they belong to an important class of metalloproteins that use metal centers and proximal organic radicals together to effect multielectron redox chemistry.[4] In GAO, 2-electron transformations are mediated by a single copper ion coordinated by a cysteine-modified tyrosinate ligand (Y_{272}). A mechanistic picture has emerged from biochemical studies that involves cycling of Cu(I)/Cu(II) and $Y_{272}/Y_{272}^{\bullet}$ redox states (Fig. 1).[1,2,5] The active form (**A**) contains a unique, antiferromagnetically coupled Cu(II)–$Y_{272}^{\bullet}$ pair. After binding of substrate to **A**, proton transfer to a second tyrosinate ligand (Y_{495}) is postulated to occur, followed by an internal 2-electron oxidation (here shown as sequential H atom and electron transfers) to yield the reduced form (**R**). Oxidation of **R** by O_2 yields the important enzyme product H_2O_2 and regenerates the catalytically competent form **A**. While extensive spectroscopic and physicochemical evidence supports the postulated structure of **A**, the proposed formulation for **R** is based solely on an analysis of X-ray absorption near edge and fine structure (XANES and EXAFS) spectroscopic data.[2g] These data show that **R** contains a Cu(I) ion coordinated to 3 or 4 N,O ligands, with the favored coordination number being 3 on the basis of the XANES edge and the average Cu–N,O bond distance from EXAFS of 1.99 Å.

Further understanding of the novel properties and reactivity of the GAO active site has come from synthetic studies, which, among other things, have succeeded in providing well-characterized mononuclear Cu(II)-phenoxyl radical species analogous to **A**.[6] Few examples of monomeric Cu(I)-phenolates that might model deprotonated **R** have been reported,[6g,7] although dicopper(I) complexes with bridging phenolate ligands are relatively common.[8] Of the two monomeric compounds that have been structurally defined by X-ray crystallography, one contains soft, abiological isocyanide coligands.[7a] Sorrell *et al.* published the X-ray structure of a monocopper(I)-phenoxide supported solely by N-donors, but it is 4-coordinate and no O_2 reactivity was reported.[7b] Herein we describe the synthesis and structural characterization of a novel mononuclear Cu(I)-phenoxide complex with a coordination number and coligand complement that closely mimic those proposed for form **R** of GAO. In addition, preliminary reactivity studies show that, like **R**,[5a] the complex is extremely sensitive to oxidation by O_2.

A new sterically hindered, potentially tridentate ligand with one phenolate and two amine donors, 1-(2-hydroxy-3,5-di-*tert*-butylbenzyl)-5-isopropyl-1,5-diazacyclooctane (HL), was prepared by treatment of 1-isopropyl-1,5-diazacyclooctane[9] with 3,5-di-*tert*-butyl-2-hydroxybenzyl bromide[10] and Na_2CO_3 in CH_3CN (Scheme 1).† Attempts to generate a Cu(I) complex by reacting NaL with CuCl or $[Cu(CH_3CN)_4]X$ (X = ClO_4^- or SbF_6^-) under an inert atmosphere in a variety of solvents only led to green mixtures indicative of disproportionation. However, treatment of HL with Cu_xMes_x (x = 2 and 5)[11] in THF under stringent anaerobic conditions followed by precipitation with pentane yielded LCu (**1**) as a white powder (Scheme 1). Combined ^1H and ^{13}C NMR, UV-vis, high resolution MS, and CHN analysis data corroborate the formulation of **1**, which was ultimately confirmed by an X-ray structure on a crystal grown from toluene–pentane (Fig. 2).‡ Only one of the two independent but chemically similar molecules (rotational twins) in the unit cell is shown. A planar T-shaped coordination geometry is adopted by the complex with divergent metal–ligand bond lengths.[12] Thus, one bond is quite long [Cu(1)–N(1) = 2.279(4) Å], one is more typical of Cu(I)–N bonds in 3-coordinate complexes [Cu(1)–N(2) = 1.979(4) Å],[13] and the Cu(I)–phenoxide distance is shorter than any reported previously for such a bond [Cu(1)–O(1) = 1.878(3) Å].[7] Interestingly, the

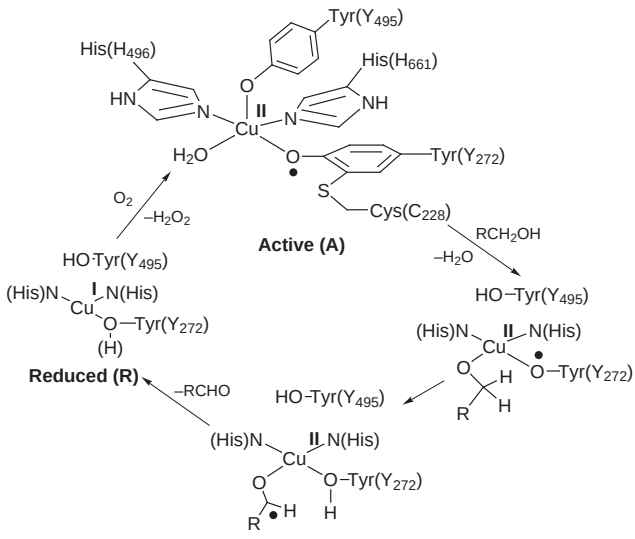

Fig. 1 Proposed mechanism for GAO (adapted from ref. 1).

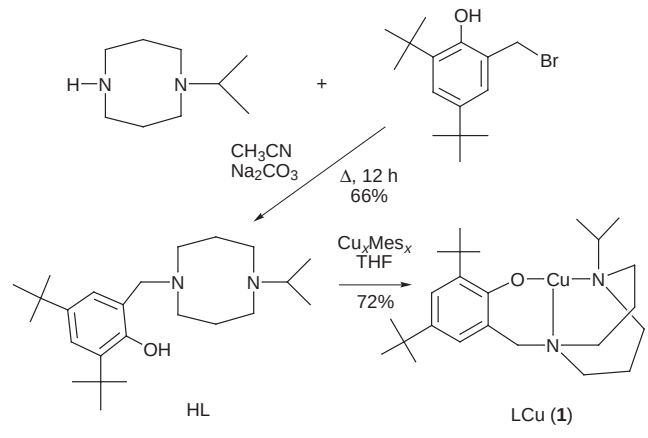

Scheme 1

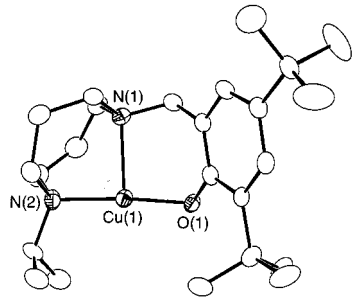

Fig. 2 Drawing of the X-ray crystal structure of LCu (**1**) (only one twin component shown). All ellipsoids are drawn at the 50% probability level. Selected bond lengths (Å) and angles (°): Cu(1)–O(1) 1.878(3), Cu(1)–N(1) 2.279(4), Cu(1)–N(2) 1.979(4), O(1)–Cu(1)–N(1) 96.3(2), O(1)–Cu(1)–N(2) 174.7(2).

average of these three disparate bond distances (2.05 Å) is more typical for 4- rather than 3-coordinate Cu(I) and is slightly greater than the average metal–ligand bond distance in **R** determined by EXAFS analysis (1.99 Å).[2g]

Cyclic voltammetry of **1** in THF with 0.2 M tetrabutylammonium hexafluorophosphate revealed a quasireversible wave with $E_{1/2}$ = −0.10 V *vs*. SCE (scan rate = 100 mV s^{-1}; ΔE_p = 183 mV; $i_{pa} \approx i_{pc}$) and a further irreversible oxidation at +0.32 V.[14] We have been unable to discern whether the quasireversible wave is a 1- or 2-electron process through coulometric measurements due to rapid decomposition of the product of oxidation of **1**. Consistent with a high thermodynamic driving force for oxidation reflected by the negative potential, **1** is extremely air sensitive; room temperature exposure instantly yields a light green solution [λ_{max}/nm (ε/$M^{-1}cm^{-1}$ per copper) 324 (15000), 394 (sh, 800), 656 (250)] of Cu(II) species that we presume is(are) multinuclear on the basis of its(their) EPR silence. By oxygenating a solution of **1** in THF at −72 °C a dark green intermediate was observed [λ_{max}/nm (ε/$M^{-1}cm^{-1}$ per copper) 390 (3800), 418 (3900), 670 (1900); EPR (X-band, 77 K) silent]. This intermediate is short-lived, decaying by a first order process to the aforementioned light green solution at −72 °C with $k = 3.9(1) \times 10^{-3}$ s^{-1} (UV-vis monitoring). Its spectroscopic properties are consistent with a copper-dioxygen adduct [Cu(II)-superoxo or $Cu(II)_2$-peroxo][15] or a Cu(II)-phenoxyl radical species (like **A**),[6a,b,d,e,g,i] all of which would be expected to give rise to low energy CT absorption bands and EPR silence (due to magnetic coupling) and to decay rapidly. Efforts to discern among these possibilities by further characterizing this highly reactive intermediate are ongoing.

In summary, we have prepared and structurally characterized a unique example of a three-coordinate Cu(I)-phenoxide complex supported by N-donors. Its coordination environment and high reactivity with O_2 bear striking similarities to the proposed GAO intermediate **R**. With the aim of gaining insights into the detailed role of **R** in the GAO mechanism, aspects of the reactivity of **1** will be the subject of future studies.[16]

Notes and references

† Characterized by ^1H and ^{13}C NMR, high resolution EI-MS, and CHN analysis.

‡ *Crystal data for* **1:** $C_{24}H_{41}CuN_2O$, M = 437.15, monoclinic, space group $P2_1$, a = 13.3193(2), b = 10.9789(2), c = 16.0969(1) Å, β = 92.349(1)°, V = 2351.89(6) $Å^3$, Z = 4, T = 173 K, μ = 0.944 mm^{-1}. The crystal used for collection was determined to be twinned (twin law −1.0, 0.0, −0.067; 0.0, −1.0, 0.0; 0.0, 0.0, 1.0; Sparks Twinning Programs, Sparks, R. A., Madison, WI, 1977). The rotational twin was modeled by converting the reflection data to the SHELXTL HKLF 5 format using the twin law, the reciprocal metric tensor, and ascending partial-overlap groupings by 0.005 $Å^{-1}$ (7 altogether), by use of the UNTWIN program (V. G. Young, Jr., 1997). Side-by-side comparison of the two twin components (0.49 : 0.21) shows only minor differences in the diazacyclooctane ring conformation, and both molecules appear to be the same enantiomer. The final cycle of full-matrix least-squares refinement (on F^2), based on 7455 reflections ($2.54 < 2\theta < 50.64°$) and 527 variable parameters, with 1 restraint, converged with $R1$ = 0.0482 and $wR2$ = 0.1121. A total of 5515 of the 7455 reflections were either exactly or partially overlapped, and 1950 reflections were considered normal data. Data were collected on a Siemens SMART system and calculations were performed using the SHELXTL-Plus V5.0 suite of programs. CCDC 182/1055.

1 J. W. Whittaker, in *Metalloenzymes Involving Amino Acid Residue and Related Radicals*, ed. H. Sigel and A. Sigel, Marcel Dekker, New York, 1994.

2 (*a*) M. M. Whittaker and J. W. Whittaker, *J. Biol. Chem.*, 1990, **265**, 9610; (*b*) M. L. McGlashen, D. D. Eads, T. G. Spiro and J. W. Whittaker, *J. Phys. Chem.*, 1995, **99**, 4918; (*c*) A. J. Baron, C. Stevens, C. Wilmot, K. D. Seneviratne, V. Blakeley, D. M. Dooley, S. E. V. Phillips, P. F. Knowles and M. J. McPherson, *J. Biol. Chem.*, 1994, **269**, 25095; (*d*) P. F. Knowles, R. D. Brown III, S. H. Koenig, S. Wang, R. A. Scott, M. A. McGuirl, D. E. Brown and D. M. Dooley, *Inorg. Chem.*, 1995, **34**, 3895; (*e*) N. Ito, S. E. V. Phillips, K. D. S. Yadav and P. F. Knowles, *J. Mol. Biol.*, 1994, **238**, 794; (*f*) M. P. Reynolds, A. J. Baron, C. M. Wilmot, E. Vinecombe, C. Stevens, S. E. V. Philips, P. F. Knowles and M. J. McPherson, *J. Biol. Inorg. Chem.*, 1997, **2**, 327; (*g*) K. Clark, J. E. Penner-Hahn, M. Whittaker and J. W. Whittaker, *Biochemistry*, 1994, **33**, 12553.

3 M. M. Whittaker, P. J. Kersten, N. Nakamura, J. Sanders-Loehr, E. S. Schweizer and J. W. Whittaker, *J. Biol. Chem.*, 1996, **271**, 681.

4 J. Stubbe and W. A. van der Donk, *Chem. Rev.*, 1998, **98**, 705.

5 (*a*) M. M. Whittaker, D. P. Ballou and J. W. Whittaker, *Biochemistry*, 1998, **37**, 8426; (*b*) B. P. Branchaud, M. P. Montague-Smith, D. J. Kosman and F. R. McLaren, *J. Am. Chem. Soc.*, 1993, **115**, 798; (*c*) R. M. Wachter, M. P. Montague-Smith and B. P. Branchaud, *J. Am. Chem. Soc.*, 1997, **119**, 7743; (*d*) C. G. Saysell, T. Barna, C. D. Borman, A. J. Baron, M. J. McPherson and A. G. Sykes, *J. Biol. Inorg. Chem.*, 1997, **2**, 702.

6 Selected recent references: (*a*) J. A. Halfen, V. G. Young, Jr. and W. B. Tolman, *Angew. Chem., Int. Ed. Engl.*, 1996, **35**, 1687; (*b*) Y. Wang and T. D. P. Stack, *J. Am. Chem. Soc.*, 1996, **118**, 13097; (*c*) M. M. Whittaker, W. R. Duncan and J. W. Whittaker, *Inorg. Chem.*, 1996, **35**, 382; (*d*) J. A. Halfen, B. A. Jazdzewski, S. Mahapatra, L. M. Berreau, E. C. Wilkinson, L. Que, Jr. and W. B. Tolman, *J. Am. Chem. Soc.*, 1997, **119**, 8217; (*e*) A. Sokolowski, H. Leutbecher, T. Weyhermüller, R. Schnepf, E. Bothe, E. Bill, P. Hildebrandt and K. Wieghardt, *J. Biol. Inorg. Chem.*, 1997, **2**, 444; (*f*) D. Zurita, I. Gautier-Luneau, S. Ménage, J.-L. Pierre and E. Saint-Aman, *J. Biol. Inorg. Chem.*, 1997, **2**, 46; (*g*) Y. Wang, J. L. DuBois, B. Hedman, K. O. Hodgson and T. D. P. Stack, *Science*, 1998, **279**, 537; (*h*) S. Itoh, S. Takayama, R. Arakawa, A. Furuta, M. Komatsu, A. Ishida, S. Takamuku and S. Fukuzumi, *Inorg. Chem.*, 1997, **36**, 1407; (*i*) J. Müller, T. Weyhermüller, E. Bill, P. Hildebrandt, L. Ould-Moussa, T. Glaser and K. Wieghardt, *Angew. Chem., Int. Ed. Engl.*, 1998, **37**, 616.

7 A search of the Cambridge Crystallographic Database (vol. 5.15, April 1998) revealed only two reports of X-ray structures of monomeric Cu(I) phenolates: (*a*) P. Fiaschi, C. Floriani, M. Pasquali, A. Chiesi-Villa and C. Guastini, *J. Chem. Soc., Chem. Commun.*, 1984, 888; (*b*) T. N. Sorrell, A. S. Borovik and C. C. Shen, *Inorg. Chem.*, 1986, **25**, 589.

8 Selected examples: (*a*) R. R. Gagné, R. P. Kreh and J. A. Dodge, *J. Am. Chem. Soc.*, 1979, **101**, 6917; (*b*) T. N. Sorrell and A. S. Borovik, *J. Chem. Soc., Chem. Commun.*, 1984, 1489; (c) T. N. Sorrell, C. C. Shen and C. J. O'Connor, *Inorg. Chem.*, 1987, **26**, 1755; (*d*) K. D. Karlin, R. W. Cruse, Y. Gultneh, A. Farooq, J. C. Hayes and J. Zubieta, *J. Am. Chem. Soc.*, 1987, **109**, 2668.

9 Synthesized *via* a modification of the procedure reported in: R. P. Houser, V. G. Young, Jr. and W. B. Tolman, *J. Am. Chem. Soc.*, 1996, **118**, 11555.

10 A. Sokolowski, J. Müller, T. Weyhermüller, R. Schnepf, P. Hildebrandt, K. Hildenbrand, E. Bothe and K. Wieghardt, *J. Am. Chem. Soc.*, 1997, **119**, 8889.

11 E. M. Meyer, S. Gambarotta, C. Floriani, A. Chiesi-Villa and C. Guastini, *Organometallics*, 1989, **8**, 1067.

12 A similar pattern of divergent bond distances has been seen in another T-shaped Cu(I) complex: J. V. Dagdigian, V. McKee and C. A. Reed, *Inorg. Chem.*, 1982, **21**, 1332.

13 A search of the Cambridge Crystallographic Database (vol. 5.15, April 1998) for Cu–N distances in 3-coordinate Cu complexes gave 161 structures with mean Cu–N = 1.988 Å (standard deviation 0.092 Å).

14 The ferrocene–ferrocenium couple under identical conditions had $E_{1/2}$ = 0.55 V, close to the literature value of 0.56 V: N. G. Connelly and W. E. Geiger, *Chem. Rev.*, 1996, **96**, 877.

15 (*a*) N. Kitajima and Y. Moro-oka, *Chem. Rev.*, 1994, **94**, 737; (*b*) K. D. Karlin, Z. Tyeklár and A. D. Zuberbühler, in *Bioinorganic Catalysis*, ed. J. Reedijk, Marcel Dekker, New York, 1993, pp. 261–315.

16 We thank the NIH (GM47365.), the NSF (NYI Award to W. B. T.), and the Sloan and Camille and Henry Dreyfus Foundations (fellowships to W. B. T.) for funding this research.

Communication 8/06749J

ChemComm

Cationic alkyl aluminium ethylene polymerization catalysts based on monoanionic *N,N,N*-pyridyliminoamide ligands

Michael Bruce, Vernon C. Gibson,* Carl Redshaw, Gregory A. Solan, Andrew J. P. White and David J. Williams

Department of Chemistry, Imperial College, South Kensington, London, UK SW7 2AY. E-mail: V.Gibson@ic.ac.uk

Received (in Cambridge, UK) 13th October 1998

Treatment of the 2,6-bis(imino)pyridines {[2,6-(ArNCR)$_2$C$_5$H$_3$N]} [R = H, Ar = 2,6-*i*-Pr$_2$C$_6$H$_3$ or 2,4,6-Me$_3$C$_6$H$_2$; R = Me, Ar = 2,6-*i*-Pr$_2$C$_6$H$_3$] with AlMe$_3$ at elevated temperature gives, *via* migration of a methyl group to the ligand backbone, the pseudo-five coordinate dimethylaluminium species {2-[ArNCR(Me)],6-(ArNCR)C$_5$H$_3$N}AlMe$_2$ (1a–c); upon treatment with B(C$_6$F$_5$)$_3$, 1a–c cleanly afford the cationic methyl complexes [{2-[ArNCR(Me)],6-(ArNCR)C$_5$H$_3$N}AlMe]$^+$[MeB(C$_6$F$_5$)$_3$]$^-$ (2a–c) which are active for ethylene polymerization.

Neutral aluminium alkyls are well known to act as ethylene oligomerization[1] and polymerization[2] catalysts. However, the potential of cationic aluminium alkyls as catalysts is just emerging. Recent advances by Coles and Jordan[3] have utilised a number of chelating *N,N*-amidinate ligands, *viz.* {RC(NR′)$_2$} (R = Me, R′ = *i*-Pr, Cy; R = *t*-Bu, R′ = *i*-Pr, Cy, SiMe$_3$) which, upon reaction with Me$_3$Al, afford complexes of the form [{RC(NR′)$_2$}AlMe$_2$]. Cationic species are readily generated on further reaction with B(C$_6$F$_5$)$_3$ or [HNMe$_2$Ph][B(C$_6$F$_5$)$_4$], the latter giving amine adducts. In the case of R = *t*-Bu, R′ = *i*-Pr the derived cation [from B(C$_6$F$_5$)$_3$] polymerizes ethylene at ambient temperature, albeit with low activity.

In a separate study, we[4] and Brookhart and coworkers[5] have recently shown that iron and cobalt complexes bearing neutral, 6-electron donor 2,6-bis(imino)pyridine ligands afford exceptionally active polymerization catalysts when activated with methylaluminoxane (MAO). We became interested in extending the range of *N,N,N*-chelate ligands to monoanionic derivatives in which one of the imino groups is transformed into an amido functionality, and nucleophilic attack on the imine carbon using an alkylaluminium reagent offered a convenient approach.[6] The aluminium complexes so-derived can be used to provide a source of free pyridyliminoamine ligands (*via* hydrolysis); details of the synthetic utility of this reaction will be reported elsewhere.[7] Here, we show that the dimethylaluminium complexes bearing such tridentate *N,N,N*-ligands also can be converted cleanly to cationic alkyl derivatives which are active as ethylene polymerization catalysts. The significance of this observation is highlighted by a recent report that bidentate *N,N*-chelate ligand systems can lead to undesirable exchange reactions which thwart the generation of a polymerization-active site.[8]

Reaction of the parent 2,6-bis(imino)pyridines {[2,6-(ArNCR)$_2$C$_5$H$_3$N]} [R = H, Ar = 2,6-*i*-Pr$_2$C$_6$H$_3$ or 2,4,6-Me$_3$C$_6$H$_2$; R = Me, 2,6-*i*-Pr$_2$C$_6$H$_3$] with AlMe$_3$ in refluxing toluene (12 h) results in alkylation of the ligand backbone to give the dimethylaluminium species {2-[ArNCR(Me)],6-(ArNCR)C$_5$H$_3$N}AlMe$_2$ [R = H; Ar = 2,6-*i*-Pr$_2$C$_6$H$_3$ **1a**; R = H; Ar = 2,4,6-Me$_3$C$_6$H$_2$ **1b**; R = Me, Ar = 2,6-*i*-Pr$_2$C$_6$H$_3$ **1c**] in high yield (Scheme 1).†

Crystals of **1b** suitable for an X-ray structure determination were grown from MeCN. The molecular structure‡ of **1b** shows the N(9)–C(9)–py–C(7)–N(7) portion of the ligand to be co-planar to within 0.06 Å (Fig. 1), a geometry very similar to that observed for the closely related bis(imino)pyridine ligand in its iron complex.[4] Here the aluminium atom lies 0.33 Å out of this plane and adopts a severely distorted tetrahedral geometry with

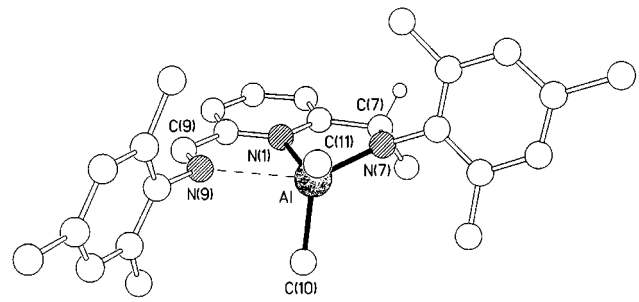

Fig. 1 The molecular structure of **1b**. Selected bond lengths (Å) and angles (°): Al–N(1) 2.029(4), Al–N(7) 1.876(4), Al–N(9) 2.575(4), Al–C(10) 1.990(6), Al–C(11) 1.951(5), C(7)–N(7) 1.444(6), C(9)–N(9) 1.273(5), N(7)–Al–C(11) 103.6(2), N(7)–Al–C(10) 113.8(2), C(11)–Al–C(10) 114.0(3), N(7)–Al–N(1) 81.3(2), C(11)–Al–N(1) 136.0(2), C(10)–Al–N(1) 102.8(2).

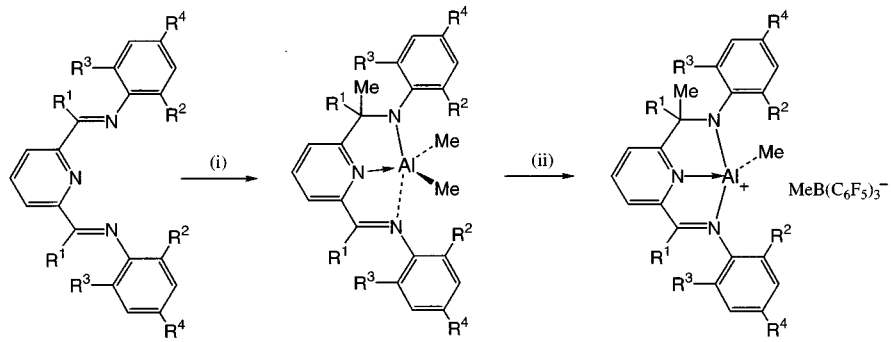

1a R^1 = R^4 = H; R^2 = R^3 = *i*-Pr
1b R^1 = H; R^2 = R^3 = R^4 = Me
1c R^1 = Me; R^2 = R^3 = *i*-Pr; R^4 = H

2a R^1 = R^4 = H; R^2 = R^3 = *i*-Pr
2b R^1 = H; R^2 = R^3 = R^4 = Me
2c R^1 = Me; R^2 = R^3 = *i*-Pr; R^4 = H

Scheme 1 *Reagents and conditions:* (i) AlMe$_3$, toluene, 110 °C, 12 h; (ii) B(C$_6$F$_5$)$_3$, toluene, rt.

Table 1 Results of ethylene polymerization runs with cations **2a–c**

Run[a]	Cation[b]	Yield/g	Activity/ g mol^{-1} h^{-1} bar^{-1}	M_n[c]	M_w[c]	M_w[c]/M_n[c]	M_{pk}[c]
1	**2a**	0.10	80	7800	23 000	2.9	19 000
2	**2b**	0.08	60	5200	33 000	6.3	13 000
3	**2c**	0.15	120	2400	13 000	5.5	9 800

[a] All runs performed in toluene at 5 bar of ethylene, 40 °C, 60 min, using 0.25 mmol of cation. [b] Generated *in situ* from the reaction of equimolar (0.25 mmol) amounts of **1a–c** and $B(C_6F_5)_3$. [c] Determined by GPC at 160 °C.

angles at aluminium ranging between 81.3(2) and 136.0(2)°. There is a slight asymmetry in the Al–Me distances [1.990(6) Å to C(10) and 1.951(5) Å to C(11)] but a more marked difference between the two Al–N bonds, with that to the formally negatively charged nitrogen N(7) being significantly shorter [at 1.876(4) Å] than that to the pyridyl nitrogen [2.029(4) Å]. Perhaps the most interesting feature of the structure is the directing of the imino nitrogen N(9) into the flattened 'basal' face of the tetrahedron—the aluminium atom lies only 0.3 Å out of the N(1)–C(10)–C(11) plane whereas it lies between 0.6 and 0.9 Å out of the other tetrahedral faces. The distance is long at 2.575(4) Å, but bearing in mind the potential for this nitrogen and the pyridyl nitrogen to adopt an *anti* relationship in the absence of a metal ion[7] we believe that this interaction is real and indeed a key feature in the subsequent cation formation in **2**.

The ^{1}H NMR spectra are consistent with the solid-state structures of **1** being maintained in solution. For **1a**, the pyridyl *meta*-protons resonate at δ 8.49 and 7.67 while the coordinated methyl groups appear as singlets at δ −0.67 and −0.89 reflecting the C_1 symmetry of the complex.

The cationic complexes [{2-[ArNCR(Me)],6-(ArNCR)-C_5H_3N}AlMe]$^+$ (**2a–c**) are readily generated on treatment of one equivalent of $[B(C_6F_5)_3]$ in toluene at ambient temperature (Scheme 1).† For example, the ^{1}H NMR spectrum arising from **2a** reveals a sharp singlet at δ −0.70 for the methyl group coordinated to aluminium, while the methyl group coordinated to boron of the $[MeB(C_6F_5)_3]^-$ counter-anion is clearly seen as a broad singlet at δ 0.43. The upfield shift of this resonance is consistent with a free anion[9] and contrasts with the more downfield resonance (δ 1.67) observed by Coles and Jordan in which a B–Me···Al association is invoked.[3]

All the cationic complexes **2a–c** are active for ethylene polymerization (see Table 1) affording solid polyethylene with activities between 80 and 120 g mol^{-1} h^{-1} bar^{-1}. The polymer products in each case are low molecular weight, with M_ws ranging from 33 000 (run 2) to 13 000 (run 3). It is noteworthy that by changing the ligand backbone (otherwise identical) in **2a** from a single methyl group to three methyl groups in **2c** has the effect of reducing the molecular weight by almost half (*cf.* runs 1 and 3).

In a series of experiments on the iron and cobalt catalyst systems, we have shown that the bis(imino)pyridine ligands bonded to iron and cobalt are not attacked by $AlMe_3$ or MAO under the conditions of the polymerization experiment: free bis(imino)pyridine can be isolated in quantitative yield following hydrolytic work-up after the polymerization, *i.e.* no alkylation of the ligand backbone occurs of the type described here.

BP Chemicals Ltd is thanked for financial support. Dr J. Boyle and G. Audley are thanked for NMR and GPC measurements, respectively.

Notes and references

† Satisfactory microanalyses have been obtained. *Selected spectroscopic data:* For **1a**: ^{1}H NMR (CD_2Cl_2, 293 K): δ 8.61 (s, 1H, N=CH), 8.49 [d, 1H, ^3J(HH) 7.6, Py-H_m], 8.15 [app. t, 1H, ^3J(HH) 7.6 Py-H_p], 7.67 [d, 1H, ^3J(HH) 7.6, Py-H_m], −0.67 (s, 3H, AlMe), −0.89 (s, 3H, AlMe). For **1b**: ^{1}H NMR (CD_2Cl_2, 293 K): δ 8.57 (s, 1H, N=CH), 8.30 [d, 1H, ^3J(HH) 7.6, Py-H_m], 8.11 [app. t, 1H, ^3J(HH) 7.6, Py-H_p], 7.68 [d, 1H, ^3J(HH) 7.6, Py-H_m], −0.73 (s, 3H, AlMe), −1.01 (s, 3H, AlMe). For **1c**: ^{1}H NMR (CD_2Cl_2, 293 K): δ 8.31 [app. t, 1H, ^3J(HH) 7.6 Py-H_p], 8.03 [d, 1H, ^3J(HH) 7.6, Py-H_m], 7.78 [d, 1H, ^3J(HH) 7.6, Py-H_m], 2.31 (s, 3H, N=CMe), 1.82 (s, 6H, $NCMe_2$), −0.72 (s, 3H, AlMe), −0.89 (s, 3H, AlMe). For **2a**: ^{1}H NMR (CD_2Cl_2, 293 K): δ 8.68 (s, 1H, N=CH), 8.15 [app. t, 1H, ^3J(HH) 7.6, Py-H_p], 8.17 [d, 1H, ^3J(HH) 7.6, Py-H_m], 8.13 [d, 1H, ^3J(HH) 7.6, Py-H_m], 0.43 (s, 3H, BMe), −0.70 (s, 3H, AlMe). For **2b**: ^{1}H NMR (CD_2Cl_2, 293 K): δ 8.57 (s, 1H, N=CH), 8.33 [app. t, 1H, ^3J(HH) 7.6, Py-H_p], 8.01 [d, 1H, ^3J(HH) 7.6, Py-H_m], 7.98 [d, 1H, ^3J(HH) 7.6, Py-H_m], 4.67 [q, 1H, ^3J(HH) 6.7, C*H*Me], 1.26 (d, 3H, CH*Me*), 0.33 (s, 3H, BMe), −0.85 (s, 3H, AlMe). For **2c**: ^{1}H NMR (CD_2Cl_2, 293 K): δ 8.29 [app. t, 1H, ^3J(HH) 7.6, 7.6, Py-H_p], 8.07 [d, 1H, ^3J(HH) 7.6 Py-H_m], 8.03 [d, 1H, ^3J(HH) 7.6, Py-H_m], 2.30 (s, 3H, N=CMe), 1.79 (s, 6H, $NCMe_2$), 0.40 (s, 3H, BMe), −0.77 (s, 3H, AlMe).

‡ *Crystal data for* **1b**: $C_{28}H_{36}N_3Al$, M = 441.6, triclinic, space group $P\bar{1}$ (no. 2), a = 7.992(2), b = 8.169(1), c = 20.979(3) Å, α = 82.28(1), β = 82.93(2), γ = 71.92(1)°, V = 1285.4(4) Å^3, Z = 2, D_c = 1.141 g cm^{-3}, μ(Cu-Kα) = 8.21 cm^{-1}, F(000) = 476, T = 183 K; orange/red platy needles, 0.23 × 0.17 × 0.03 mm, Siemens P4/RA diffractometer, ω-scans, 3810 independent reflections. The structure was solved by direct methods and the non-hydrogen atoms were refined anisotropically using full matrix least-squares based on F^2 to give R_1 = 0.073, wR_2 = 0.169 for 2432 independent observed reflections [$|F_o| > 4\sigma(|F_o|)$, $2\theta \leqslant 120°$] and 290 parameters. CCDC 182/1059.

1 K. Ziegler, H.-G. Tosel, E. Holzkamp, J. Schneider, M. Söll and W. R. Kroll, *Justus Leibigs Ann. Chem.*, 1960, **629**, 121.
2 H. Martin and H. Bretinger, *Makromol. Chem.*, 1992, **193**, 1283.
3 M. P. Coles and R. F. Jordan, *J. Am. Chem. Soc.*, 1997, **119**, 8125.
4 G. J. P. Britovsek, V. C. Gibson, B. S. Kimberley, P. J. Maddox, S. J. McTavish, G. A. Solan, A. J. P. White and D. J. Williams, *Chem. Commun.*, 1998, 848.
5 B. L. Small, M. Brookhart and M. A. Bennett, *J. Am. Chem. Soc.*, 1998, **120**, 4049.
6 (*a*) J. M. Klerks, D. J. Stufkens, G. van Koten and K. Vrieze, *J. Organomet. Chem.*, 1979, **181**, 271; (*b*) V. C. Gibson, C. Redshaw, A. J. P. White and D. J. Williams, *J. Organomet. Chem.*, 1998, **550**, 453.
7 V. C. Gibson, S. Mastroianni, C. Redshaw, G. A. Solan, A. J. P. White and D. J. Williams, to be submitted.
8 B. Qiani, D. L. Ward and M. R. Smith III, *Organometallics*, 1998, **17**, 3070.
9 X. Yang, C. L. Stern and T. J. Marks, *J. Am. Chem. Soc.*, 1994, **116**, 10015.

Communication 8/07950A

Adsorption of metal cations by hydrous aluminium(III) or iron(III) hydroxide precipitates: enhancement by EDTA and related chelate molecules†

Michael G. Burnett,*[a] Cathy Faharty,[a] Christopher Hardacre,[a] James M. Mallon,[a] R. Mark Ormerod[b] and Graham C. Saunders[a]

[a] *The Questor Centre, Queen's University of Belfast, Belfast, UK BT9 5AG. E-mail: m.burnett@qub.ac.uk*
[b] *Department of Chemistry, University of Keele, Staffordshire, UK*

Received (in Cambridge, UK) 14th August 1998, Accepted 15th October 1998

Stoichiometrically equivalent concentrations of ethylenediaminetetraacetate, EDTA, and of related chelating anions increase the adsorption of *ca*. millimolar concentrations heavy metal aqua-ions on amorphous precipitates of aluminium(III) or iron(III) hydroxide and, although higher concentrations decrease the adsorption, poly-EDTA, a polyelectrolyte containing EDTA functional groups, shows no such decrease.

Inorganic coagulants, such as aluminium(III) or iron(III) salts, are widely used both for cleaning potable water and also for treating a variety of aqueous effluents.[1] The gelatinous metal hydroxide or floc is also used in the treatment of effluents containing heavy metal cations since these are adsorbed[2] by the floc even though they are generally soluble at the pH used. The method is thought to be less successful in the presence of coordinating ligands since these often form soluble metal complexes which are only adsorbed by the floc at pH values[3,4] below those customarily used in water treatment by, for instance, hydrous ferric oxide.[1] However, much of the work in this area is concerned with metal adsorption in sediment or soil so that hydrated aluminium or iron oxides[5] are the absorbents usually studied. Although solutions of EDTA are believed to strip metal cations from soils[6] where they are supposed to be bound by aluminium(III) or iron(III) oxides, EDTA at concentrations comparable to those of the adsorbed metal ions, can increase their adsorption at pH values below 7 through electrostatic binding of the anionic complexes.[5] In this work we have examined the effect of EDTA on heavy metal adsorption during the precipitation of amorphous aluminium or iron hydroxide under conditions typical of those used during effluent treatment. We find that copper, nickel and cadmium show an enhanced cationic adsorption on aluminium hydroxide at pH 7, both separately and when mixed in the same solution. Enhanced adsorption at pH 7 has only been found on an iron(III) floc in the single case of mercury(II). The effect has been studied in more detail for cadmium on aluminium(III) but the similar trends observed in all cases suggest that one theoretical explanation is common to all.

The adsorption experiments were carried out by mixing reagent solutions at a pH of *ca*. 3 and then adjusting the pH to 7 sufficiently slowly to ensure that the final value during processing was 7.000 ± 0.005. The floc and supernatant solution were separated by centrifuging, the floc was redissolved in concentrated nitric acid and then analysed by ICP-AE. A correction was applied in all cases to allow for the adsorbate ions present in the solution which was trapped within the floc gel phase. In some experiments the EDTA present in each phase was estimated spectroscopically at 460 nm by complexation at pH 3 with zirconium(III).

The approach to equilibrium is rapid if all the components are present prior to the adjustment of the pH to 7 but it is slower if, for instance, the floc is formed prior to the addition of EDTA or cadmium. These results resemble the leaching experiments reported[7] previously with a range of hydrous metal oxides. A typical experiment is shown in Fig. 1 for cadmium(II) adsorbed by a floc of aluminium(III). The fraction of cadmium adsorbed decreases progressively with increasing concentration of EDTA as would be expected if the adsorbed ions were being removed from the floc because of the formation of unadsorbed EDTA–metal complexes. However the extrapolated adsorption at zero EDTA is 100% whereas the measured value is 40%. This apparent discontinuity is explained when the experiments are extended to much lower EDTA concentrations, Fig. 2. It is now obvious that the effects of trace amounts of EDTA is to increase the fraction of the metals adsorbed by the floc. The adsorption of the Cd^{2+} in the presence of a stoichiometric equivalent of EDTA increases as the pH rises showing that it occurs at a cationic site despite the anionic character of dissolved $[Cd(edta)]^{2-}$.

The concentration of aluminium found in solution increases with that of EDTA and may be calculated on the basis of the accepted values of the solubility product of aluminium hydroxide and the binding constant of the aluminium–EDTA complex,[8] as shown in Fig. 1.

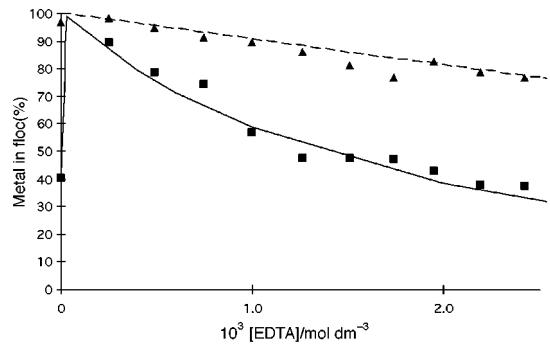

Fig. 1 Effect of EDTA at pH 7, 9.3 mM Al^{3+} and 22.2 μM Cd^{2+}: (■) % Cd(exptl.), (▲) % Al(exptl.), (——) % Cd(calc.), (- - - -) % Al(calc.).

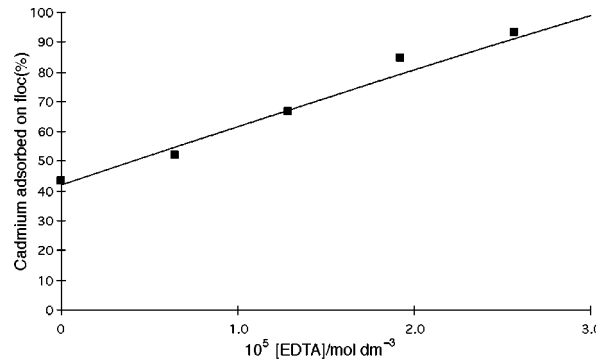

Fig. 2 Effect of low concentrations of EDTA, 12.3 mM Al^{3+} and 29.4 μM Cd^{2+}: (■) % Cd(exptl.), (——) % Cd(calc.).

† A patent has been applied for covering the material presented in this paper, Application No. GB 9817528.4, August 12th, 1998.

It has been found that changes in the EDTA structure do not prevent enhanced metal ion adsorption. Cyclohexylaminetetraacetate and nitrilotriacetate will also promote cadmium retention in aluminium floc although they are much less effective. The enhanced adsorption of cadmium also occurs when the EDTA is in the form of a polyelectrolyte, poly-EDTA, made by the condensation of polyallylamine and ethylenediaminetetraacetic dianhydride.[9] However, although the poly-EDTA enhances adsorption in the same way as does EDTA, the decline in adsorption at higher concentrations shown in Fig. 1 does not occur and the aluminium floc dissolves to a much smaller extent, by 1–2%.

The structure of the species present in the gel phase and in solution have been investigated using EXAFS which reveals the short range order within an amorphous precipitate as well as the corresponding order in the dissolved complexes. The results for cadmium adsorbed on aluminium floc show that the adsorbed metal in the absence of EDTA is identical with the aqua-cation whereas in the presence of EDTA it resembles the dissolved EDTA complex in solution. The compound adsorbed in the gel phase appears to be a six-co-ordinate complex in which the nitrogen or oxygen atoms are present at 0.24 nm from the metal atom. These results suggest that Cd^{2+},edta,Al^{3+} complexation contributes to the binding of cadmium on cationic sites but with only a slight distortion of the normal Cd^{2+},edta complexation found in solution.

The enhanced adsorption and its eventual inhibition by EDTA can be modelled by an equilibrium system provided a suitable adsorption inhibition step is postulated. The adsorption of metal aqua-ions by both aluminium and iron flocs is generally supposed to take place by binding at metal cation exchange sites. Corresponding anion binding sites are also supposed to exist to explain the removal of anions by the same floc.[5] The eventual stripping of the adsorbed metal from the floc is usually attributed to the formation of soluble metal chelates by EDTA. However if a cadmium–edta species is responsible for the enhanced binding, this no longer explains the final desorption stage. The EDTA cannot be operating by combining with the floc adsorption sites since the concentration of the chelate is more than a hundred-fold less than that of the aluminium atoms present. The simplest equilibrium step producing a satisfactory model appears to be the formation of a soluble polynuclear chelate containing both an adsorbent and an adsorbate atom together with at least two EDTA molecules. There is considerable evidence that the formation of polynuclear species is promoted by the presence of organic ligands and solid aluminium hydroxide.[10] Although EDTA complexes of this type have not previously been suggested, polynuclear carboxylate complexes are well known to exist.[11] Equilibria (1)–(7) below reproduce the essential features of our observations and the data in Figs. 1 and 2.

$$Al^{3+} + 3OH^- \rightleftharpoons G_{gel} \quad (1)$$

$$Al^{3+} + edta^{4-} \rightleftharpoons [Al^{3+}(edta^{4-})]^- \quad (2)$$

$$Cd^{2+} + edta^{4-} \rightleftharpoons [Cd^{2+}(edta^{4-})]^{2-} \quad (3)$$

$$H_2O \rightleftharpoons OH^- + H^+ \quad (4)$$

$$G_{gel} + Cd^{2+} \rightleftharpoons [Cd^{2+}(G)]_{gel} + xH^+ \quad (5)$$

$$Cd^{2+} + edta^{4-} + G_{gel} \rightleftharpoons [Cd^{2+}(edta^{4-})(G)]_{gel} + yH^+ \quad (6)$$

$$[Cd^{2+}(edta^{4-})(G)]_{gel} + edta^{4-} \rightleftharpoons [Cd^{2+}(edta^{4-})Al^{3+}(edta^{4-})]^{3-} \quad (7)$$

Gelatinous hydrous aluminium oxide is denoted by G_{gel} and all species subscripted by 'gel' are adsorbed in the floc. The number of adsorbent sites was always greatly in excess of the number of adsorbed species so that the number of sites per gm atom of aluminium could be taken to be constant. The calculated concentration of undissolved aluminium, $[Al^{3+}]_{floc,}$ was therefore assumed in eqns. (5) and (6) to be linearly related by the constant α to the concentration of free adsorption sites per unit volume of solution, Γ,

$$\Gamma = \alpha[Al^{3+}]_{floc}$$

The values for the ionic product of water, the solubility product of aluminium hydroxide and the association constants of EDTA with aluminium and cadmium were taken from the literature[8] and the constants $\alpha K_5/[H^+]^x$, $\alpha K_6/[H^+]^y$ and K_7 were fitted. There was no need to determine x or y since the pH was constant at 7. The theoretical curves in Figs. 1 and 2 were calculated by the iterative solution of the set of equations derived from equilibria (1)–(7). The agreement of experiment and theory shows that the explanation is consistent with observation although further investigation is necessary to establish the structure of the postulated polynuclear soluble species. The same model may also be used successfully to reproduce the effects of pH and the EDTA enhanced metal ion adsorption in other systems.

The fact that enhanced binding may be produced by a chelating polymer without the undesirable side-effects of aluminium and adsorbate solution eventually produced by EDTA suggests that useful new polyelectrolytes may be synthesised which could enhance the flocculative treatment of heavy metal contaminated aqueous wastes.

We thank British Nuclear Fuels plc. for their support, the Daresbury Laboratory for providing X-ray beam time and technical assistance and the Department of Education for Northern Ireland for a CAST award to J. M. M.

Notes and references

1 W. J. Eilbeck and G. Mattock, *Chemical Processes in Waste Water Treatment*, Ellis Horwood, Chichester, 1987.
2 J. A. Davis, *Rev. Mineral.*, 1990, **23**, 777.
3 M. Dario and A. Ledin, *Chem. Speciation Bioavailability*, 1997, **9**, 3.
4 B. Nowack, J. Lützenkirchen, P. Behra and L. Sigg, *Env. Sci. Technol.*, 1996, **30**, 2397.
5 B. Nowack and L. Sigg, *J. Colloid Interface Sci.*, 1996, **177**, 106.
6 Z. B. Li and L. M. Shuman, *Soil Sci.*, 1996, **161**, 226; *Sci. Total Environ.*, 1996, **191**, 95; P. M. Jardine and D. L. Taylor, *Geoderma*, 1995, **67**, 125; D. C. Girvin, P. L. Gassman and H. Bolton, *Soil Sci. Soc. Am. J.*, 1993, **57**, 47.
7 A. L. Bryce, W. A. Kornicker, A. E. Elzerman and S. B. Clark, *Environ. Sci. Technol.*, 1994, **28**, 2353; A. L. Bryce, W. A. Kornicker and A. E. Elzerman, *Environ. Sci. Technol.*, 1995, **29**, 2353.
8 A. Martell and R. Smith, *Critical Stability Constants*, Plenum, New York, 1974.
9 H. Matsuyama, Y. Miyamoto, M. Teramoto and F. Nakashio, *Sep. Sci. Tehnol.*, 1996, **31**, 687; H. Matsuyama, Y. Miyamoto, M. Teramoto, M. Goto and F. Nakashio, *ibid.*, 1996, **31**, 799.
10 G. Furrer, B. Trusch and C. Müller, *Geochim. Cosmochim. Acta*, 1992, **56**, 3831.
11 T. L. Feng, P. L. Urian, M. D. Healy and A. R. Barron, *Inorg. Chem.*, 1990, **29**, 408.

Communication 8/07135G

ChemComm

A hydration-controlled nano-valve in a zeolite?†

David O'Connor,[a] Paul Barnes,*[a] David R. Bates[b] and David F. Lander[b]

[a] *Industrial Materials Group, Department of Crystallography, Birkbeck College, Malet Street, London, UK WC1E 7HX. E-mail: barnes@gordon.cryst.bbk.ac.uk*

[b] *BG plc, Gas Research and Technology Centre, Ashby Road, Loughborough, UK LE11 3GR*

Received (in Bath, UK) 24th July 1998, Accepted 14th October 1998

Ion-exchange and dehydration in clinoptilolite are simulated revealing a novel feature, a hydration-controlled nano-valve, which explains hitherto anomalous behaviour of this important zeolite system.

Clinoptilolite is a naturally occurring and abundant zeolite with ideal formula $Na_6Al_6Si_{30}O_{72}{\cdot}nH_2O$ in the sodium form. It is known for its high cation exchange and water capacity and has been used[1,2] for water purification, animal feed additives, and in the treatment of nuclear waste by adsorption of heavy ions. It also has potential for gas purification, and this was the original interest behind this study: cations in clinoptilolite are known to be mobile in the hydrated state, and therefore the choice of cation and extent of hydration together offer some potential for design in the zeolite's function. One would like to fine-tune the openings within its channels so that one gas molecule is preferentially admitted over another, and be able to exploit this in gas purification through technological processes such as selective temperature/pressure swing adsorption.[3] However it is difficult to predict the ionic behaviour of a given zeolite system: for example, if two different cations are exchanged into a zeolite the resultant behaviour is not necessarily a simple mixture of those of the single cation forms—in other words, the behaviour is non-additive. This is the case with clinoptilolite: its nitrogen uptake, relative to methane, increases significantly[4] away from either the pure Ca- or pure K-form. This anomalous result typifies such non-additivity and requires an explanation that is currently lacking in the literature.

The simulation of a complete ion-exchange process is an ambitious venture requiring an adequate combination of atom potentials and simulation schedule. The exchange route from pure Ca- to a 50 : 50 Ca/K-clinoptilolite was chosen as an ideal prototype for study. The potentials used were obtained from the well characterized universal force-fields of Rappe *et al.*[5] with modifications by Burchardt *et al.*[6] for atom types which occur in zeolite frameworks, together with formal charges for the cations and partial charges for water (Jorgensen[7]), methane (Righini *et al.*[8]) and nitrogen (Murthy *et al.*[9]); cross term parameters for heterogeneous pairs (*e.g.* cation–water) were taken as the geometric mean of the corresponding homonuclear parameters given in these publications.[5,6] The simulation schedule devised (Table 1) was a combination of various Monte-Carlo and molecular dynamics stages with key features: first, the cations are allowed to be mobile, with or without their variable hydration spheres, and frequent total relaxations permit the zeolite framework to respond to this mobility; the repeated simulated annealing ensures that sufficient configurations are explored away from local minima; and the approach used in the ion-exchange (step no. 5) is pragmatic, not attempting to simulate either the thermodynamics or kinetics of the ion-exchange, but purely to obtain reasonable starting configurations for the exchanged state.

As the water content of the Ca-clinoptilolite is increased (stages 2 to 4) the Ca^{2+} cations in the main (10c) channel are progressively hydrated away from the framework oxygens towards the centre of the main channel [Fig. 1(a)]. This (50%) fraction of Ca^{2+} cations then becomes accessible and can be easily exchanged by twice the number of K^+ cations (to preserve charge neutrality) resulting in a hydrated 50 : 50 Ca : K-clinoptilolite [Fig. 1(b)]. After ion-exchange the water continues to play a key role during dehydration, firstly by allowing the newly arrived K^+ cations to gradually approach their eventual destination [Fig. 1(b), (c)]: this gradual exploration is crucial since the simulation fails if this stage is omitted or if the dehydration is performed too rapidly, and this itself reflects a well known feature that zeolite stability is generally very sensitive to mode of dehydration.[11] The water plays a second, more subtle, role during dehydration by mediating the displacement of the K^+ cations to their final (dehydrated) positions [Fig. 1(c), (d)]: the mechanism by which this occurs is that during dehydration the loss of water reduces the effective dielectric medium so that pairs of neighbouring Ca^{2+} cations experience an increasing electrostatic repulsion which is transmitted to the neighbouring K^+ cations. Thus two Ca^{2+} cations, each just inside the minor (8c) side channels, push both K^+ cations by approximately 1.7 Å so that they protrude into the main (10c)

Table 1 Summary of the 7 stages employed in the simulation schedule for modelling hydration, ion-exchange and dehydration of clinoptilolite. The starting framework structure (stage 1) is based on the published structure[10] using an ideal Si : Al ratio of 5 : 1 so that 1 in 6 tetrahedral atoms is an Al; these Al sites are chosen randomly except being subject to Loewenstein's rule.[13] Whereas various initial cation sites can be used for stages 1–4, the crucial insertion in stage 5 has so far only been attempted using positions close to those in the published structure,[10] and as illustrated in Fig. 1(b). Cations and waters can move freely during all simulated annealing (stages 2c, 6a) *and* molecular dynamics (stages 2b, 6b) cycles, whereas the framework atoms move during just the molecular dynamics (stages 2b, 6b) cycles. All stages are taken to the equilibration: Monte-Carlo (stages 2a, 6b) cycles exceed a minimum of 10^6 configurations; molecular dynamics cycles are typically 10^4 steps of 10^{-15} s; simulated annealing cycles are typically 2×10^4 steps of 10^{-15} s, generating an effective annealing temperature range of 300–600 K

Stage	Brief description
1	Start with a suitable clinoptilolite framework structure
2a	A sequence of grand canonical Monte-Carlo (GCMC) simulations at T = 300 K for increasing pressure, in which water molecules are inserted/destroyed within each fixed framework
2b	Molecular dynamics under constant N,P,T for the *whole* system (framework atoms plus waters and cations) for each pressure step
2c	Simulated annealing for mobile water molecules and cations within the fixed framework
3	Loop around steps 2a, 2b, 2c until the final water loading, N, and pressure, P, are achieved
4	Molecular dynamics under constant N,P,T for the whole system (framework atoms plus waters and cations)
5	Removal of least energetically bound Ca^{2+} cations and semi-random insertion of exchange-cations (K^+) up to electrical neutrality
6a	Simulated annealing for the mobile water molecules and cations within the fixed framework
6b	Molecular dynamics under constant N,P,T for the *whole* system: framework atoms plus waters and cations
6b	GCMC (or equivalent) simulations with decreasing pressure
7	Cycle around steps 6b + 6a to complete dehydration (N = 0)

† The term 'valve' is used here to denote adjustable flow in either channel direction.

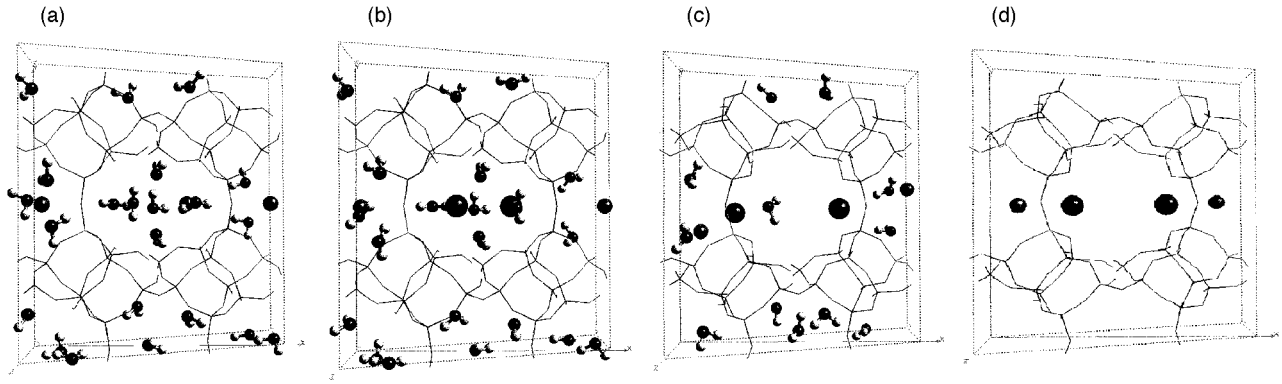

Fig. 1 Computer graphic snapshots obtained during the nano-valve simulation of clinoptilolite: (a) full hydration with the Ca^{2+} cation hydrated away from the framework; (b) a starting configuration after exchange of one Ca^{2+} by two K^+ cations; (c) during dehydration the two K^+ cations approach their framework sites; (d) on complete dehydration the Ca^{2+}–Ca^{2+} repulsion is transmitted to the K^+ cations so that they project into the main (central) 10c channel.

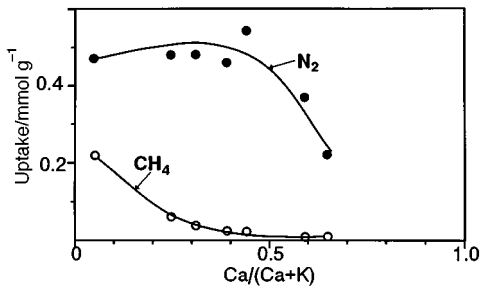

Fig. 2 Dynamic uptake, after 24 seconds exposure of activated clinoptilolite to nitrogen and methane at approximately 1 atmosphere pressure, as a function of the Ca/(Ca + K) ratio. The relative uptake increases significantly away from either the pure potassium (Ca/(Ca + K) = 0) or pure calcium (Ca/Ca + K) = 1) forms. (Data from Robinson *et al.*[4]).

channel reducing its effective diameter from *ca*. 7.2 to 3.8 Å (the actual final Ca–K separations are ~4.3 Å). This lever effect produces a constriction in the main channel which can be described as a 'nano-valve' in the sense that the degree of constriction varies with the degree of dehydration and that the ensuing flow restriction will be down the main channel in the direction of the pressure gradient driving the gas flow; the essential action is illustrated in the graphical abstract.

A difficulty with clinoptilolite is that it is extremely difficult to synthesise, yet the natural form suffers from poor crystallinity. This has prevented[11] a definitive location of cation positions by Rietveld refinement of powder diffraction data as was possible in other studies.[12] However EXAFS spectroscopy is capable of yielding one-dimensional (angle-averaged) information on the local cation environment regardless of specimen crystallinity. Calcium and potassium K-edge EXAFS measurements (Daresbury SRS) on dehydrated Ca : K-clinoptilolite yield average nearest neighbour peaks[11] which are indeed consistent with the nano-valve model described here (the operative Ca^{2+} cation coordinated to 3 framework oxygens (~2.35 Å distance) and K^+ to 4 framework oxygens (~3.0 Å); details and typical plots are available as electronic supplementary information; see http://www.rsc.org/suppdata/cc/1998/2527). However one could conceivably invoke alternative configurations which satisfy these EXAFS-deduced ion coordinations, and therefore some additional confirmation of the nano-valve action is desirable. This has been provided by gas adsorption data (Robinson *et al.*[4]) which show (Fig. 2) that the differential uptake between nitrogen and methane is maximised with the binary cation forms of clinoptilolite. We see from simulations[11] that the diffusion of methane and nitrogen (Table 2) is entirely *via* the main channel of the zeolite, and that methane diffusion is severely restricted relative to nitrogen since the constricted opening of the nano-valve falls in between the kinetic diameters of methane (3.8 Å) and nitrogen (3.0 Å, when axially aligned). Experimental measurements of gas uptake reflect a combination of such kinetic effects with thermodynamic aspects (loading capacity), though kinetic effects would dominate with pressure swing adsorption.

Table 2 Diffusion constants for methane and nitrogen down the main (10c) channel of the single (K^+) and double (50 : 50 Ca^{2+}/K^+) cation forms of clinoptilolite, obtained by *impulse molecular dynamics*. In this method, individual methane or nitrogen molecules are released within the main channel and equilibrated using a 20 ps period of molecular dynamics (individual steps of 10^{-15} s) followed by a further ≥100 ps of molecular dynamics during which the displacement down the channel is traced; the mean diffusion constant is then obtained from the straight line slope of the displacement-squared (*versus* time) plots, of which typical versions have been deposited as electronic supplementary information (see text). One notes that while the absolute values with the Ca/K form are decreased, the relative ratio of nitrogen over methane increases markedly. Diffusion constants are given in units of 10^{-9} m^2 s^{-1}.

Gas	K-clinoptilolite	K/Ca-clinoptilolite
CH_4	0.81	$< 10^{-5}$
N_2	6.48	2.88

In conclusion, this nano-valve, revealed by simulation, explains the anomalous $CH_4 : N_2$ gas adsorption by the binary (Ca/K) cation form of clinoptilolite. It also suggests that the nano-valve might even be continuously controlled by varying the degree of dehydration during calcination of the zeolite. We expect that many other properties (*e.g.* immobilisation in zeolites) might now be similarly predicted provided the effects of water are taken into account.

The authors thank EPSRC, BG plc and the Daresbury SRS.

Notes and references

1 A. Dyer, *Chem. Ind.*, April 1984.
2 L. L. Ames Jnr., *Am. Mineral.*, 1960, **45**, 689.
3 R. T. Yang, *Gas Separation by Adsorption Processes*, Butterworths, Stoneham, MA, 1987.
4 S. C. F. Robinson, M. Morris and D. F. Lander, *Zeolites*, submitted.
5 A. K. Rappé, C. J. Casewit, K. S. Goddard and W. M. Skiff, *J. Am. Chem. Soc.*, 1992, **114**, 10024.
6 E. de Vos Burchardt, V. A. Verheij, H. van Bekkum and B. van der Graaf, *Zeolites*, 1992, **12**, 183.
7 W. L. Jorgensen, *J. Chem. Phys.*, 1983, **79**, 926.
8 R. Righini, K. Maki and M. L. Klein, *Chem. Phys. Lett.*, 1981, **80**, 301.
9 C. S. Murthy, K. Singer, M. L. Klein and I. R. McDonald, *Mol. Phys.*, 1980, **41**, 1387.
10 J. R. Smythe, A. T. Spaid and D. L. Bish, *Am. Mineral.*, 1990, **75**, 522.
11 D. O'Connor, PhD thesis, University of London, 1996.
12 E. Dooryhee, G. N. Greaves, A. T. Steel, R. P. Townsend, S. W. Carr, J. M. Thomas and C. R. A. Catlow, *Faraday Discuss. Chem. Soc.*, 1990, **89**, 119.
13 W. Loewenstein, *Am. Mineral.*, 1954, **39**, 92.

Communication 8/05985C

Equilibria in the $B(C_6F_5)_3$–H_2O system: synthesis and crystal structures of $H_2O{\cdot}B(C_6F_5)_3$ and the anions $[HOB(C_6F_5)_3]^-$ and $[(F_5C_6)_3B(\mu\text{-}OH)B(C_6F_5)_3]^-$

Andreas A. Danopoulos,*[a]† Jane R. Galsworthy,[a] Malcolm L. H. Green,*[a] Sean Cafferkey,[b] Linda H. Doerrer[a] and Michael B. Hursthouse[b]

[a] *Inorganic Chemistry Laboratory, South Parks Road, Oxford, UK OX1 3QR*
[b] *Department of Chemistry, University of Wales, Cardiff, PO Box 912, Cardiff, UK CF1 3TB*

Received (in Basel, Switzerland) 29th June 1998, Accepted 23rd September 1998

Addition of water to the Lewis acid $B(C_6F_5)_3$ gives the neutral compound $H_2O{\cdot}B(C_6F_5)_3{\cdot}2H_2O$ while the reaction between $B(C_6F_6)_3$ and KOH–H_2O in the presence of dibenzo-18-crown-6 gives $[K(dibenzo\text{-}18\text{-}crown\text{-}6)]^+[HOB(C_6F_5)_3]^-$ which crystallises together with the adduct $H_2O{\cdot}B(C_6F_5)_3$; the new binuclear borate anion $[(F_5C_6)_3B(\mu\text{-}OH)B(C_6F_5)_3]^-$ is formed as a salt with the cation $[Ir(\eta^5\text{-}C_5H_5)(C_8H_{12})H]^+$ by addition of H_2O to $B(C_6F_5)_3$ in the presence of $[Ir(\eta^5\text{-}C_5H_5)(C_8H_{12})]$.

Large and very weakly or non-coordinating anions $[BR_4]^-$ [R = 3,5-$(CF_3)_2C_6H_3$, C_6F_5] have recently attracted interest due to their ability to stabilise electrophilic metal cations containing vacant coordination sites.[1a–d] These cations can be generated by interaction of the neutral Lewis acid $B(C_6F_5)_3$ with a zirconium–methyl bond resulting in abstraction of the anionic methyl group and giving the anion $[MeB(C_6F_5)_3]^-$. Apart from the role as a co-catalyst for olefin polymerisation the Lewis and $B(C_6F_5)_3$ has been shown to have a versatile chemistry.[2] Despite the interest in $B(C_6F_5)_3$, however, little is known of its reaction with water. There is a report of the compound $[NHEt_3][HOB(C_6F_5)_3]$[3] and of the platinum complex, $[Pt\{HOB(C_6F_5)_3\}Me(Bu_2bpy)]$ (Bu_2bpy = 4,4′-di-*tert*-butyl-2,2′-bipyridine), which is formed by reaction between $[PtMe_2(Bu_2bpy)]$, $B(C_6F_5)_3$ and H_2O. This latter complex has been structurally characterised and contains the anion $[HOB(C_6F_5)_3]^-$ as a ligand co-ordinated to the platinum centre.[4] Finally, it has been reported that isobutylene and *p*-methylstyrene undergo a 'carbocationic' polymerisation initiated by $B(C_6F_5)_3$ in the presence of water.[5] This implies the presence of acidic protons as reactive species. Herein we report the isolation and full characterisation of three new boron compounds by reactions between $B(C_6F_5)_3$ and H_2O under various conditions which reveal the diverse nature of the $B(C_6F_5)_3$–H_2O system.

Slow evaporation of a $CDCl_3$ solution of $B(C_6F_5)_3$ and several equivalents of water gives colourless crystals of $[H_2O{\cdot}B(C_6F_5)_3]{\cdot}2H_2O$ **1**.[6] An X-ray crystal study reveals that one molecule of water is bound directly to the boron centre, whilst the remaining two water molecules are dispersed throughout the crystal lattice (Fig. 1).‡ All hydrogen atoms have been directly located from the difference map and bond distances indicate hydrogen bonding from the hydrogen atoms in the coordinated water molecule to the oxygen atoms of the remaining two water molecules, as shown in Fig. 1. Variable temperature multinuclear NMR studies of $B(C_6F_5)_3$ in the presence of H_2O shown that in **1** there is a rapid exchange of boron-bound water with the free water molecules.

The existence of **1** and previously reported activity of the $B(C_6F_5)_3$–H_2O system[5] imply the formation of a Lewis acid–base adduct and subsequent ionisation to generate an acidic proton and complementary anion as depicted in Scheme 1.

Further evidence for the formation of the Brønsted acid is provided by the reaction between $B(C_6F_5)_3$ and H_2O in the presence of the 'metal base' $[Ir(\eta^5C_5H_5)(C_8H_{12})]$,[7] which gives the salt $[Ir(\eta^5\text{-}C_5H_5)(C_8H_{12})H][(F_5C_6)_3B(\mu\text{-}OH)B(C_6F_5)_3]$ **2**·2$CHCl_3$, containing the previously unknown binuclear anion, $[(F_5C_6)_3B(\mu\text{-}OH)B(C_6F_5)_3]^-$. The single crystal structure of **2**§ (Fig. 2) shows that there is a large difference of size between the cation and anion. In the anion, the three pentafluorophenyl groups on each boron atom are staggered with respect to each other. The hydroxyl proton is coplanar with the B–O–B unit. The average B–O bond distance of 1.565(1) Å is consistent with other reported B–(μ-OH) bond lengths.[4,8] The B–O–B angle of 139.6(5)° is distinct from those of 144.8(5)° in a diborylcobaltocene complex[8] and 128.2(2)° in $[Pt\{HOB(C_6F_5)_3\}Me(Bu_2bpy)]$.[4]

In the cation, the hydride ligand on iridium is stereochemically active as evidenced by an angle of 20.2° between the Cp ring and the best plane of the coordinating carbon atoms in the cyclooctadiene ligand.

The only previously reported examples of hydroxy-bridged diborates are those prepared using the electrophilic chelates, *cis*-1,2-diborylalkenes[9] or in the coordination sphere of diborylcobaltocene.[8] The cation, $[Ir(\eta^5\text{-}C_5H_5)(C_8H_{12})H]^+$, has previously been synthesised by protonation of the metal base, using strong Brønsted acids such as triflic acid (CF_3SO_3H).[7]

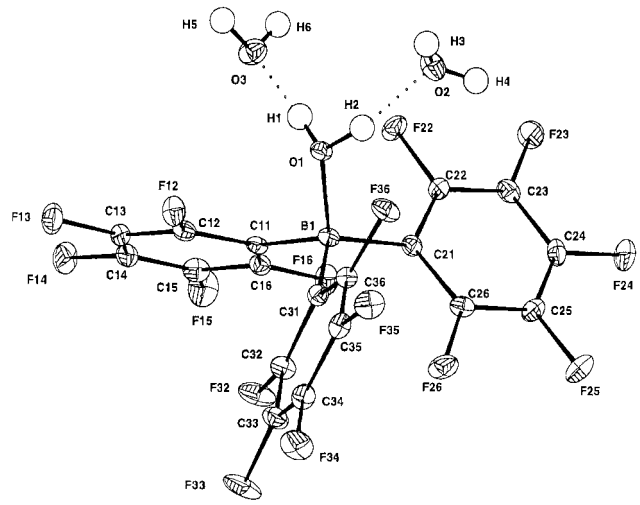

Fig. 1 Asymmetric unit in the crystal structure of **1**·2 H_2O. Selected bond lengths (Å) and angles (°): B(1)–O(1) 1.5769(14), O(1)–H(1) 0.88(2), O(1)–H(2) 0.86(2), O(1)–O(2) 2.572(2), O(1)–O(3) 2.597(2); B(1)–O(1)–H(1) 117.0(14), B(1)–O(1)–H(2) 117.8(12).

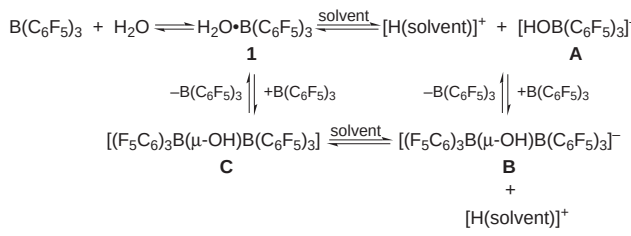

Scheme 1

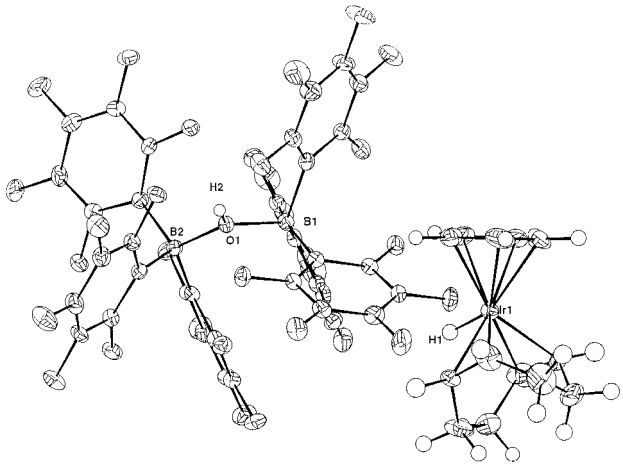

Fig. 2 Cation and anion of **2**. Chloroform molecules have been removed for clarity. Selected bond lengths (Å) and angles (°): Cp_{cent}–Ir(1) 1.867(3), Ir(1)–H(1) 0.7773(19), B(1)–O(1) 1.566(6), B(2)–O(1) 1.564(6), O(1)–H(2) 0.78(6), B–C_{avg} 1.644(8); B(1)–O(1)–B(2) 140.4(4), C–B–Cavg 111(1).

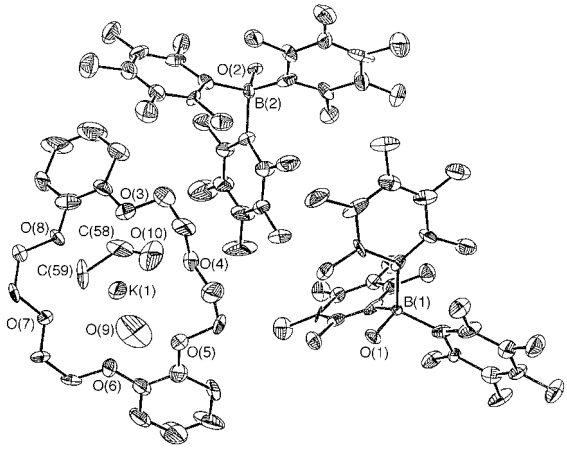

Fig. 3 Asymmetric unit in the crystal structure of **3**. Selected bond lengths (Å) and angles (°): B(1)–O(1) 1.521(10), B(2)–O(2) 1.480(11), B(1)–C 1.606–1.655, B(2)–C 1.583–1.699; C–B(1)–C 105.1–114.3, C–B(2)–C 105.6–113.6.

Formation of an anion with a bridging hydroxide between two $B(C_6F_5)_3$ groups, **B** (Scheme 1), could take place either by binding a second equivalent of $B(C_6F_5)_3$ to the monoborate anion $[HOB(C_6F_5)_3]^-$ **A**, or addition of $B(C_6F_5)_3$ to **1** to form the adduct **C** followed by ionisation to form **B**. The $[HOB(C_6F_5)_3]^-$ anion has been characterised as a ligand,[4] *vide supra*, and we now describe its independent synthesis.

In a further study, $B(C_6F_5)_3$ in a CH_2Cl_2 solution containing dibenzo-18-crown-6 was treated with solid KOH pellets and gave colourless crystals which may be formulated as $\{[H_2O{\cdot}B(C_6F_5)_3]\}\{[K(dibenzo\text{-}18\text{-}crown\text{-}6)]^+[HOB(C_6F_5)_3]^-\}{\cdot}H_2O{\cdot}MeCHO$ **3** (Fig. 3).‡ We assume the acetaldehyde present in the crystal is derived either from reaction of the solvent CH_2Cl_2 with KOH followed by decomposition of the resultant diol or by decomposition of the crown ether under highly basic conditions. There is no interaction of the aldehyde with any of the boron-containing species, although many Lewis base adducts of $B(C_6F_5)_3$ with aldehydes and ketones have been reported.[10] The structure of **3** definitively shows the presence of only one cation and charge balance therefore requires there to be only one monoanion. Hydrogen atoms cannot be located on either of the two $\{OB(C_6F_5)_3\}$ units of **3**, but we can infer that there is one molecule of $[H_2O{\cdot}B(C_6F_5)_3]$ and one of the anion $[HOB(C_6F_5)_3]^-$ present. The larger B–O distance in **3** is not consistent with that of the aqua complex **1** and it is possible that there is some mixing-in of both species at each site, particularly as the aryl ring torsion angles of the two species are equivalent to within a few degrees.

In conclusion, these preliminary studies show that reaction of H_2O with $B(C_6F_5)_3$ gives a stable adduct and that this adduct can coexist with its conjugate base although the factors affecting the equilibrium are not fully understood at present. The formation of mono- or di-borate anions may be a function of cation size or relative metal basicity under the reaction conditions. Further investigations are in progress to elucidate these factors.

We thank the Wilkinson Trust (A. A. D.), the University of Oxford for a Violette and Samuel Glasstone Fellowship (J. R. G.), St. John's College, Oxford (L. H. D.) and the EPSRC for financial support.

Notes and references

† Current address: Department of Chemistry, University of Southampton, Highfield, Southampton, UK SO17 1BJ.

‡ *Crystal data* **1**: $C_{18}H_6BF_{15}O_3$, M_w = 566.02, triclinic, space group *P*t1, a = 9.999(4), b = 10.250(4), c = 10.908(5) Å, α = 90.097(2), β = 103.680(2), γ = 116.27(2)°, V = 966.7(3) Å^3, Z = 2, D_c = 1.94 g cm^{-3}, F(0000) = 544, μ(Mo-$K\alpha$) = 0.220 mm^{-1}. T = 120 K; crystal 0.3 × 0.35 × 0.35 mm; 4494 total reflections, 3442 unique [$I > 3\sigma(I)$, R_{int} = 0.013]; R = 0.0309 and R_w = 0.0380.

2·2$CHCl_3$: $C_{49}H_{19}B_2F_{30}IrO{\cdot}2CHCl_3$, M_w = 1407.17 + 238.74, monoclinic, space group $P2_1/c$, a = 12.070(4), b = 24.789(5), c = 17.341(4) Å, β = 93.547(2)°, V = 5178.5(3) Å^3, Z = 4, D_c = 2.11 gcm^{-3}, F(000) = 2904, μ(Mo-Kα) = 0.303 mm^{-1}. T = 120 K; crystal 0.3 × 0.35 × 0.35 mm; 29 435 total reflections, 8800 unique [$I > 3\sigma(I)$, R_{int} = 0.035]; R = 0.0519, R_w = 0.0589. Hydroxyl and hydride hydrogen atoms located but not refined. Structures of **1** and **2** solved with SIR-92[11] and refined with CRYSTALS.[12,13]

3: $C_{58}H_{33}B_2F_{30}KO_{10}$, M_w = 1520.42, monoclinic, space group $P2_1/c$ (no. 14) a = 12.39(2), b = 33.367(12), c = 13.790(5) Å, β = 97.13(2)°, V = 5659(7) Å^3, Z = 4, D_c = 1.785 g cm^{-3}, F(000) = 3040, μ(Mo-Kα) = 0.248 mm^{-1}. 19 448 data were recorded and merged to give 8392 unique (R_{int} = 0.1365). The structure was solved *via* direct methods (SHELX-93).[14] An absorption correction was applied using DIFABS.[15] The final R, R_w indices [$I > 2\sigma(I)$] were 0.067, 0.099 for 911 parameters (non-hydrogen atoms anisotropic, hydrogen atoms in idealised positions, C–H = 0.96 Å, with U_{iso} tied to U_{eq} of the parent atoms). CCDC 182/1028.

1 (*a*) M. Brookhart, B. Grant and A. F. Volpe, Jr., *Organometallics*, 1992, **11**, 3920; (*b*) K. Seppelt, *Angew. Chem., Int. Ed. Engl.*, 1993, **32**, 1025; (*c*) X. Yang, C. L. Stern and T. J. Marks, *J. Am. Chem. Soc.*, 1991, **113**, 3623; (*d*) M. Bochmann, *J. Chem. Soc., Dalton Trans.*, 1996, 255.

2 See the following articles and references therein: W. E. Piers and T. Chivers, *Chem. Soc. Rev.*, 1997, **26**, 345; A. N. Chernega, A. J. Graham, M. L. H. Green, J. Haggitt, J. Lloyd, C. P. Mehnert, N. Metzler and J. Souter, *J. Chem. Soc., Dalton Trans.*, 1997, 2293; J. R. Galsworthy, J. C. Green, M. L. H. Green and M. Muller, *J. Chem. Soc., Dalton Trans.*, 1998, 15.

3 A. R. Siedle, R. A. Newmark, W. M. Lamanna and J. C. Huffman, *Organometallics*, 1993, **12**, 1491.

4 G. S. Hill, L. Manojlovic-Muir, K. W. Muir and R. J. Puddephatt, *Organometallics*, 1997, **16**, 525.

5 T. D. Shaffer and J. R. Ashbaugh, *J. Polym. Sci. A*, 1997, **35**, 329.

6 $B(C_6F_5)_3{\cdot}3H_2O$ has been mentioned briefly; see footnote in ref. 6.

7 J. R. Sowa, Jr. and R. J. Angelici, *J. Am. Chem. Soc.*, 1991, **113**, 2537.

8 G. E. Herberich, A. Fischer and D. Wiebelhaus, *Organometallics*, 1996, **15**, 3106.

9 R. Koster, G. Seidel, K. Wagner and B. Wrackmeyer, *Chem. Ber.*, 1993, **126**, 305; R. Koster and G. Seidel, *Chem. Ber.*, 1992, **125**, 627.

10 D. J. Parks, W. E. Piers, M. Parvez, R. Atencio and M. J. Zaworotko, *Organometallics*, 1998, **17**, 1369.

11 A. Altomare, G. Cascarano, G. Giacovazzo, A. Guagliardi, M. C. Burla, G. Polidori and M. Camalli, *J. Appl. Crystallogr.*, 1994, **27**, 435.

12 D. J. Watkin, C. K. Prout, J. R. Carruthers and P. W. Betteridge, CRYSTALS Issue 10. Chemical Crystallography Laboratory, Oxford, UK, 1996.

13 D. J. Watkin, C. K. Prout and L. J. Pearce, CAMERON, Chemical Crystallography Laboratory, Oxford, UK, 1996.

14 G. M. Sheldrick, SHELXS-86, Program for Crystal Structure Solution, SHELXTL-93, Program for Crystal Structure Refinement, University of Göttingen, 1986 and 1993.

15 N. P. C. Walker and D. Stuart, *Acta Crystallogr., Sect. A*, 1983, **39**, 158; adapted for FAST geometry by A. Karaulov, University of Wales, Cardiff, 1991.

Communication 8/04918A

Redox-active metal complexes for imaging hypoxic tissues: structure–activity relationships in copper(II) bis(thiosemicarbazone) complexes

Jason L. J. Dearling,[a] Jason S. Lewis,[b] Deborah W. McCarthy,[b] Michael J. Welch[b] and Philip J. Blower*[a]

[a] *Biosciences Dept, University of Kent, Canterbury, UK CT2 7NJ. E-mail: P.J.Blower@ukc.ac.uk*
[b] *Mallinckrodt Institute of Radiology, Washington University School of Medicine, St. Louis, MO 63110, USA*

Received (in Cambridge, UK), 29th July 1998, Accepted 12th October 1998

Reduction potential and lipophilicity of the copper(II) bis(thiosemicarbazone) complexes can be independently controlled by alkylation in the diketone backbone and the N-termini of the ligand, allowing optimisation of radiopharmaceuticals strongly selective for hypoxic tissues.

Hypoxia in tumours can affect the outcome of anti-cancer treatments.[1] Hypoxic malignant tissue is relatively resistant to chemotherapy, and to irradiative therapy because of the lack of oxygen, a potent radiosensitiser. Hypoxia is also associated with other important health problems such as heart disease and stroke. Radiopharmaceuticals for imaging hypoxia have therefore been widely sought in recent years.[2] The current lead compound, ^{18}F-fluoromisonidazole,[3] shows imageable differences between normal and hypoxic tissue, but suffers from slow blood clearance and low tumour-to-muscle ratios.[4]

Copper radionuclides have attracted considerable attention in nuclear medicine because they include isotopes with both diagnostic (Cu-60, Cu-61, Cu-62, Cu-64) and therapeutic (Cu-64, Cu-67) potential. They are becoming increasingly available to the medical community through the use of generator systems and improvements in small cyclotron production.[5] The bis(thiosemicarbazone)s chelate copper(II) to form stable mononuclear, square-planar complexes. These have been investigated for use in anti-cancer chemotherapy,[6] and, in radiolabelled form, as a non-tissue-selective blood perfusion tracer $^{62/64}$Cu(PTSM).[7] The latter complex is capable of rapid entry into cells by passive diffusion as a consequence of its low molecular weight, lipophilicity and planarity.[8] It then becomes trapped intracellularly, regardless of tissue type, probably as a consequence of intracellular reduction to a copper(I) complex.[9] This redox-dependent trapping mechanism may allow, through control of redox potential, synthesis of an analogue that is trapped only in cells that provide a more reducing environment than normal, resulting from the absence of molecular oxygen). This approach could lead to design of imaging agents for hypoxia. Indeed, Cu(ATSM) has demonstrated significant selectivity for hypoxic and ischaemic tissue both *in vitro*[10] and *in vivo*,[10,11] while Cu(PTSM) has little[12] or no[13] selectivity. It has been suggested that the difference in selectivity is due to differences in redox potential.[11] Here we show that both lipophilicity and redox potential can be independently controlled through alkyl substitution at the terminal nitrogen atoms and the diketone backbone, respectively, to give complexes with and without selectivity for hypoxic cells.

We have synthesised a series of thirteen such complexes, with a variety of alkylation patterns. All gave satisfactory elemental analysis and FAB-MS results. The Cu-64-labelled complexes were identified with their non-radioactive analogues by thin-layer radiochromatography. The electrochemistry of the complexes was investigated by cyclic voltammetry using a glassy carbon working electrode in dimethyl sulfoxide containing tetrabutylammonium tetrafluoroborate as support electrolyte. The lipophilicity (log *P*) was determined by octanol extraction of the Cu-64 labelled complexes from water. The labelled complexes were screened for hypoxia selectivity using mammalian cancer cells (EMT6) in a suspension. The hypoxic cell suspension was equilibrated for 1 h with an atmosphere of

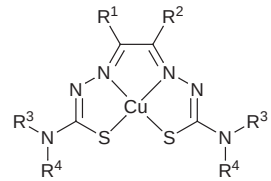

	R^1	R^2	R^3	R^4
GTS	H	H	H	H
GTSM	H	H	CH_3	H
PTS	CH_3	H	H	H
PTSM	CH_3	H	CH_3	H
$PTSM_2$	CH_3	H	CH_3	CH_3
PTSE	CH_3	H	C_2H_5	H
PTSP	CH_3	H	C_6H_5	H
ATS	CH_3	CH_3	H	H
ATSM	CH_3	CH_3	CH_3	H
CTS	C_2H_5	CH_3	H	H
CTSM	C_2H_5	CH_3	CH_3	H
DTS	C_2H_5	C_2H_5	H	H
DTSM	C_2H_5	C_2H_5	CH_3	H

95% N_2–5% CO_2 while the control (normoxic) suspension was similarly equilibrated with 95% air–5% CO_2. The oxygen concentration, measured with a Mettler Toledo 4300 oxygen electrode, in the hypoxic suspension was then below 0.2% (where 100% is the equilibrium concentration under an atmosphere of air). For comparison, the upper limit defining 'radiobiological hypoxia' is 0.66%.[14] Cu-64 complexes were introduced into the suspension at tracer levels, and samples taken at time points over 1 h and centrifuged to isolate the cells. The 'hypoxia selectivity' was determined from the cell uptake ratios at 1 h incubation, and expressed as $\log_{10}$[(% uptake in hypoxic cells)/(% uptake in normoxic cells)]. Thus, hypoxia-selective complexes have positive hypoxia selectivity values while normoxia-selective complexes have negative values.[15]

Fig. 1 shows typical cell uptake *versus* time profiles for two complexes selected to represent hypoxia-selective and normoxia-selective behaviour. The cyclic voltammograms of all the complexes showed a reversible one-electron Cu(II/I) pro-

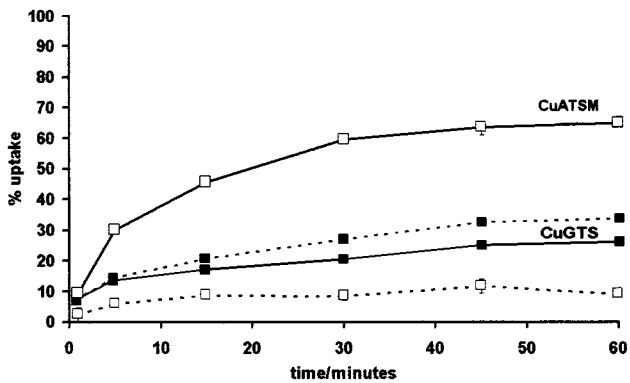

Fig. 1 EMT6 tumour cell uptake profiles selected to typify normoxia-selective (filled squares), and hypoxia-selective (open squares) copper complexes under hypoxic (solid line) and normoxic (broken line) conditions.

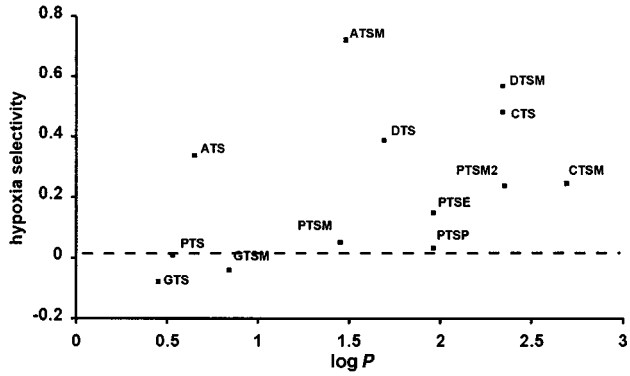

Fig. 2 Plot of hypoxia selectivity (see text for definition) for copper complexes in relation to their lipophilicity values (log *P* octanol/water).

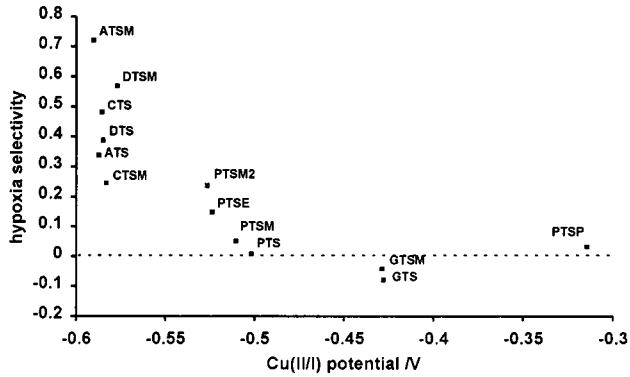

Fig. 3 Plot of hypoxia selectivity (see text for definition) for copper complexes in relation to their Cu(II/I) redox potentials *vs.* Ag/AgCl.

cess. Fig. 2 shows the relationship between lipophilicity (log *P*) and hypoxia selectivity, and Fig. 3 shows the relationship between Cu(II/I) redox potential and hypoxia selectivity.

The inter-relationships between structure, lipophilicity, redox potential and hypoxia selectivity may be summarised as follows. (1) From Fig. 3 it is evident that hypoxia selectivity is strongly dependent on redox potential. (2) On the other hand lipophilic character (Fig. 2), while presumably necessary to allow cell membrane penetration (all of the compounds have log *P* greater than zero), is not an indicator of hypoxia selectivity. (3) The overall number of alkyl groups at positions R^1–R^4 is a poor predictor of redox potential. However, the number in the diketone backbone (R^1 and R^2) is an excellent predictor: complexes with no alkylation at these sites have potentials in the range −0.42 to −0.44 V; those with one alkyl group have potentials in the range −0.50 to −0.53 V; and those with two have potentials in the range −0.57 to −0.59 V. This rule is adhered to by all except the phenyl-substituted complex Cu(PTSP). Alkyl substitution at the N-terminus, on the other hand, does not influence redox potential significantly. (4) Alkyl substitution, either in the complex as a whole or separately in the diketone backbone and N-terminus, is only a very crude predictor of lipophilicity.

These trends support the notion that the redox behaviour of transition metal complexes can be exploited to achieve hypoxia-selective targeting, and that hypoxia selectivity is a function of redox potential in these complexes. Moreover, they provide a basis for designing hypoxia-selective complexes of this type according to redox potential: it appears to be a requirement that the Cu(I/II) redox potential in dimethyl sulfoxide is more negative than −0.57 V *vs.* Ag/AgCl. It might be expected that on shifting the redox potential to much more negative values there will come a point at which the selectivity will diminish again because even hypoxic cells will be incapable of reducing the complexes. This potential is not reached in the present series.

The relationship shown in Fig. 3 suggests that redox potential is not the only factor controlling hypoxia selectivity: although complexes with potentials in the range −0.57 to −0.59 V are all hypoxia selective, they differ in degree of selectivity. Indeed it is to be expected that alkylation pattern would influence selectivity in a complex way through factors such as membrane solubility and steric effects on reaction rates as well as through redox potential. Nevertheless, an appropriate redox potential is the primary requirement for selectivity. The relationship between alkylation pattern and redox potential provides a means of controlling redox potential and lipophilicity separately: R^1 and R^2 can be varied to control redox potential, while R^3 and R^4 can be varied to control lipophilicity and other relevant pharmacokinetic parameters, to produce an ideal radiopharmaceutical for PET imaging of hypoxia.

Many facets of the mechanism of hypoxia-selectivity of these complexes remain to be investigated, including the serum stability[16] of the complexes, whether a single specific intracellular reducing agent is involved, and the reversibility of the trapping in hypoxic cells. Of the complexes investigated here, Cu(ATSM) remains the best candidate in terms of absolute selectivity *in vitro*, and ^{60}Cu(ATSM) is being investigated at the Washington University School of Medicine and Fukai Medical University[17] as an agent for the delineation of hypoxia in humans.

We thank Mr T. A. Perkins for help in producing copper-64 and Mrs E. L. C. Sherman for help with animal cell culture. J. L. J. D. is supported by a studentship and fieldwork grant from the Medical Research Council. We acknowledge the US Dept. of Energy for funding (Grant no. DE-FG02-87ER60512) work undertaken at St. Louis.

Notes and references

1 R. S. Bush, R. D. T. Jenkins, W. E. C. Allt, F. A. Beale, H. Bean, A. J. Dembo and J. F. Pringle, *Br. J. Cancer*, 1978, **37**, Suppl. III, 302.
2 G. R. Cook and I. Fogelman, *Eur. J. Nucl. Med.*, 1998, **25**, 335.
3 G. V. Martin, J. H. Caldwell, M. M. Graham, J. R. Grierson, K. Kroll, M. J. Cowan, T. K. Lewellen, J. S. Rasey, J. J. Casciari and K. A. Krohn, *J. Nucl. Med.*, 1992, **33**, 2202.
4 M. E. Shelton, C. S. Dence, D.-R. Hwang, M. J. Welch and S. R. Bergmann, *J. Nucl. Med.*, 1989, **30**, 351.
5 P. J. Blower, J. S. Lewis and J. Zweit, *Nucl. Med. Biol.*, 1996, **23**, 957; D. W. McCarthy, R. E. Schefer, R. E. Klinkowstein, T. A. Perkins, W. H. Margenau III and M. J. Welch, *J. Nucl. Med.*, 1998, **39**, 234P.
6 D. H. Petering, in *Metal Ions in Biological Systems*, ed. H. Sigel, Marcel Dekker, New York, 1988, p. 197.
7 P. Herrero, J. Markham, C. Weinheimer, C. J. Anderson, M. J. Welch, M. A. Green and S. R. Bergmann, *Circulation*, 1993, **87**, 173.
8 W. K. Subczynski, W. E. Antholine, J. S. Hyde and D. H. Petering, *J. Am. Chem. Soc.*, 1987, **109**, 46.
9 H. Taniuchi, Y. Fujibayashi, H. Okazowa, Y. Yonekura, J. Konishi and A. Yokoyama, *Biol. Pharm. Bull.*, 1995, **18**, 1126.
10 J. S. Lewis, D. W. McCarthy, M. E. Cristel and M. J. Welch, *J. Nucl. Med.*, 1998, **39**, 91P.
11 Y. Fujibayashi, H. Taniuchi, Y. Yonekura, H. Ohtani, J. Konishi and A. Yokoyama, *J. Nucl. Med.*, 1997, **38**, 1155.
12 H. Taniuchi, Y. Fujibayashi, Y. Yonekura, J. Konishi and A. Yokoyama, *J. Nucl. Med.*, 1997, **38**, 1130.
13 M. E. Shelton, M. A. Green, C. J. Mathias, M. J. Welch and S. R. Bergmann, *J. Nucl. Med.*, 1989, **30**, 1843.
14 F. Kallinowski, *Cancer J.*, 1996, **9**, 37.
15 Small amounts of radioactivity (1.8% to 6.0% of total activity) remained in the pellet even in controls without cells, due to binding of tracer to the centrifuge tube. This is not corrected for and will lead to a slight underestimation of selectivity, whether for hypoxic or normoxic cells. Radioactive $CuCl_2$ as a control showed negligible uptake in both hypoxic and normal cells. Cell concentrations in suspensions were 10^6 ml^{-1}. At this level, 50% uptake corresponds to an intracellular-to-extracellular ^{64}Cu concentration ratio of approx. 1900 : 1.
16 C. J. Mathias, S. R. Bergmann and M. A. Green, *Nucl. Med. Biol.*, 1992, **20**, 343.
17 N. Takahashi, Y. Fujibayashi, Y. Yonekura, M. J. Welch, A. Waki, T. Tsuchida, S. Nakamura, N. Sadato, K. Sugimoto, K. Yamamoto and Y. Ishii, *J. Nucl. Med.*, 1998, **39**, 53P.

Communication 8/05957H

Asymmetric Baylis–Hillman reactions: catalysis using a chiral pyrrolizidine base

Anthony G. M. Barrett,* Andrew S. Cook and Akio Kamimura

Department of Chemistry, Imperial College of Science, Technology and Medicine, South Kensington, London, UK SW7 2AY. E-mail: m.stow@ic.ac.uk

Received (in Liverpool, UK) 3rd August 1998, Accepted 16th October 1998

A novel chiral pyrrolizidine base 5 derived from L-proline promotes the Baylis–Hillman reaction of ethyl and methyl vinyl ketones with electron deficient aromatic aldehydes with moderate levels of enantiomeric excess.

The Baylis–Hillman reaction is a convenient process for the preparation of a β-hydroxy-α-methylene ketone, nitrile, ester, *etc*. in one step from an α,β-unsaturated ketone, acrylonitrile or an acrylic ester and an aldehyde.[1] The reaction is mediated by a tertiary amine, and DABCO (diazabicyclo[2.2.2]octane) is the most common catalyst employed. Whilst the Baylis–Hillman reaction of chiral aldehydes or chiral Michael acceptors has been shown to proceed, in some cases, with high diastereoselectivities, the development of chiral catalysts for the Baylis–Hillman reaction is less well developed. Hirama and Markó have respectively reported the use of chiral derivatives of diazabicyclo[2.2.2]octane[2] and of quinidine or cinchonine[3] as enantioselective catalysts. However, these authors observed only modest levels of enantioselectivities (11–47 and 6–45% ee, respectively) and the requirement to use elevated pressures (3–10 Kbar) to ensure acceptable conversions. We have previously published a two step procedure to effect the enantioselective (50–96% ee) Baylis–Hillman reaction of an aldehyde with an α-methylene ketone *via* a tandem Michael addition–aldol reaction of (phenylthio)- or (phenylselenyl)-trimethylsilane catalysed by a chiral borane Lewis acid followed by oxidative elimination.[4] Recently, Soai and co-workers reported the use of (*S*)-BINAP as a catalyst for the enantioselective (9–44% ee) Baylis–Hillman reaction of pyrimidine-5-carbaldehydes with acrylate esters.[5] This work has prompted us to report the use of pyrrolizidine (1-azabicyclo-[3.3.0]heptane) derivatives as alternative chiral catalysts. We considered that such amines may function as efficient catalysts for the Baylis–Hillman reaction on account of their enhanced basicity relative to common tertiary amines[6] and the accessibility of the nitrogen lone pair. We were concerned, in our design, to seek to alleviate the known slow kinetics of the DABCO catalysed Baylis–Hillman reaction.

Swern oxidation of Boc-L-prolinol[7] **1** and direct Wittig homologation gave ester **2**[8] (81%) (Scheme 1). Subsequent hydrogenation over Raney nickel, deprotection of the Boc group, under acidic conditions, and lactamisation gave the pyrrolizidinone[9] **3** (73%). Aldol reaction of lactam **3** with 4-nitrobenzaldehyde in the presence of $BF_3{\cdot}OEt_2$ gave a mixture of four β-hydroxy lactams (94%). The less polar component consisted of a single crystalline diastereoisomer **4**†‡ which was readily isolated in 16% yield. The remaining three diastereoisomers co-chromatographed and were not separable at the lactam oxidation stage. Finally, $BH_3{\cdot}SMe_2$ mediated reduction gave the desired pyrrolizidine **5** which was initially isolated as the robust borane adduct but which could be converted into the free base following sequential reflux with methanolic TsOH and K_2CO_3.

The Baylis–Hillman reaction of ethyl vinyl ketone with 2-nitrobenzaldehyde was examined in MeCN or EtCN solution in the presence of pyrrolizidine **5** (10 mol%) at variable temperatures (−75 to 25 °C). All reactions gave rise to the corresponding β-hydroxy-α-methylene ketone **6** (R^1 = 2-$O_2NC_6H_4$, R^2 = Et) (Table 1) which was formed in variable yield and enantioselectivity.§ The yield of the reaction was significantly improved by cooling and no significant decrease in rate was observed until −50 °C. Leahy has reported unusual temperature dependence on conversions in the DABCO mediated Baylis–Hillman reaction of acrylate esters with aldehydes.[10] Although, the yield of the reaction was optimum at −40 °C, enantioselectivities were superior at higher temperatures with a maximum value at −20 °C (47% ee). Since Aggarwal has reported rate enhancements on the use of lanthanide triflates in the Baylis–Hillman reaction,[11] a series of Lewis acid co-catalysts were examined in the synthesis of **6**. Amongst diverse metal salts examined, those of the alkali metals, in particular sodium, were the most effective additives. A series of aldehydes were allowed to react with ethyl or methyl vinyl ketone in the presence of amine **5** (10 mol%) and 1 M $NaBF_4$ or $NaBPh_4$¶ in MeCN at −20 °C (Table 2). The

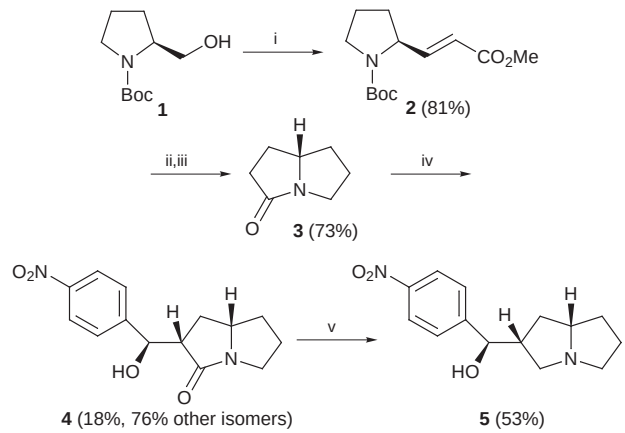

Scheme 1 *Reagents and conditions*: i, Swern oxidation, CH_2Cl_2, then $Ph_3P{=}CHCO_2Me$; ii, Raney Ni, H_2 (40 psi), MeOH; iii, HCl, EtOAc, 0 °C, then NaOMe, MeOH; iv, Lithium 2,2,6,6-tetramethylpiperidide, THF, −78 to −30 °C, then 4-$O_2NC_6H_4CHO$, $BF_3{\cdot}OEt_2$, −78 to −20 °C; v, $BH_3{\cdot}SMe_2$, THF, reflux, then TsOH, MeOH, reflux, then K_2CO_3, MeOH, reflux.

Table 1 Temperature variation in the Baylis–Hillman reaction of 2-nitrobenzaldehyde with ethyl vinyl ketone

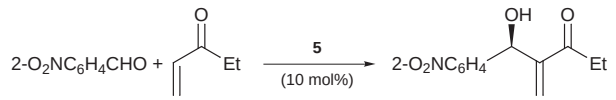

T/°C	Yield (%)	Ee (%)	*t*/d	Solvent
25	27	37	3	MeCN
4	21	42	3	MeCN
−10	57	30	3	MeCN
−20	50	47	2	MeCN
−30	53	31	2	MeCN
−40	93	26	2	MeCN
−75	9[a]	21	3	EtCN

[a] This slow reaction was stopped before reaching completion.

Table 2 Baylis–Hillman reactions of aldehydes with ethyl or methyl vinyl ketones

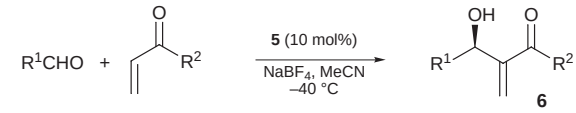

R^1	R^2	Yield (%)	Ee (%)[a]	*t*/h
2-$O_2NC_6H_4$	Et	71	67	18
2-$O_2NC_6H_4$	Me	71	53	18
2-FC_6H_4	Et	31	63	48
2-ClC_6H_4	Et	58	72	14
2-BrC_6H_4	Et	63	71	72
3-$O_2NC_6H_4$	Et	51	37	18
2-Pyridyl	Et	83	21	14
3-Pyridyl	Et	93	49	12
4-Quinolinyl[b]	Et	63	70	18
4-$O_2NC_6H_4$	Et	17	39	48

[a] Determined by HPLC analyses (Chiralcel OD-H and AD). [b] Reaction carried out using $NaBPh_4$ not $NaBF_4$.

corresponding β-hydroxy-α-methylene ketones **6** were isolated in modest to excellent yields (17–93%) and with acceptable levels of enantioselectivity (21–72% ee).‖ The absolute configuration of ketone **6** (R^1 = 2-$O_2NC_6H_4$, R^2 = Me) was determined to be *R* by comparison of the sign of its specific rotation with that of the antipodal ketone.** The absolute stereochemistry of the other β-hydroxy-α-methylene ketones **6** were assigned by analogy since all were laevorotatory. It is reasonable to speculate that the reaction may proceed *via* the intermediate **7** rather than the more sterically congested system **8**. The importance of hydroxy substitution on enhancing the rate

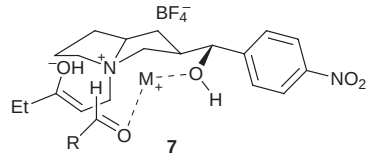

7

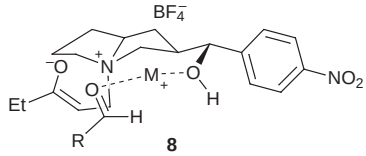

8

of Baylis–Hillman reactions is well known[1] and is exemplified by the fact that 3-hydroxyquinuclidine is a superior catalyst to quinuclidine. Such an effect may also be of significance in both the catalysis by pyrrolizidine **5** and the enhancement of enantioselectivity in the presence of sodium ions. Further studies of this variant of the Baylis–Hillman reaction are now being investigated in our laboratory.

We thank Zeneca, Chiroscience, the EPSRC and the DTI for generous support under the Link Asymmetric Scheme; Glaxo-Wellcome Research Ltd for the most generous endowment (to A. G. M. B.); the Wolfson Foundation for establishing the Wolfson Centre for Organic Chemistry in Medical Science at Imperial College; and George O'Doherty, Oswy Pereira and D. Christopher Braddock for helpful discussions.

Notes and references

† All new compounds were fully authenticated by spectroscopic data and microanalysis and/or HRMS.

‡ The structure of **4** and related β-hydroxy lactams and pyrrolizidines, which were confirmed by X-ray crystallography, will be reported elsewhere.

§ Enantioselectivities of all reactions were determined by HPLC analyses on Chiralcel OD-H and AD columns and, in some cases, by ^{1}H NMR spectroscopy in the presence of the chiral the shift reagent Eu(tfc)$_3$.

¶ For the use of lithium salts to enhance the rate of reactions proceeding *via* ionic intermediates, see ref. 12.

‖ *General experimental procedure* (Table 2, entry 4): **6** (R^1 = 2-ClC_6H_4, R^2 = Et)·$NaBF_4$ (27 mg, 0.25 mmol) followed by 2-chlorobenzaldehyde (26 μl, 0.22 mmol) were added to a stirred suspension of amine **5** (5 mg, 0.019 mmol) in MeCN (0.25 ml) under nitrogen at –40 °C. The reaction mixture was stirred for a further 10 min when ethyl vinyl ketone (19 μl, 0.19 mol) was added and stirring continued for 24 h. The mixture was concentrated *in vacuo* and the residue chromatographed (1:6 EtOAc–hexanes, R_f 0.3) to yield the title compound **6** (R^1 = 2-ClC_6H_4, R^2 = Et) (24.8 mg, 58%) as a colourless oil.

** The absolute stereochemistry of the major adduct **6** (R^1 = 2-$O_2NC_6H_4$, R^2 = Me) was determined by comparison of the sign of the specific rotation with literature data on (4*R*)-4-hydroxy-3-methylene-4-(2-nitrophenyl)butan-2-one, which was prepared by an enantioselective Baylis–Hillman reaction (11–42% ee) and by the partial kinetic resolution of the racemic compound by Sharpless epoxidation using L-(+)-diethyl tartrate (see ref. 2).

1 S. E. Drewes and G. H. P. Roos, *Tetrahedron*, 1988, **44**, 4653; D. Basavaiah, P. D. Rao and R. S. Hyma, *Tetrahedron*, 1996, **52**, 8001; E. Ciganek, *Org. React*., 1997, **51**, 201; L. J. Brzezinski, S. Rafel and J. W. Leahy, *J. Am. Chem. Soc*., 1997, **119**, 4317.
2 T. Oishi, H. Oguri and M. Hirama, *Tetrahedron*: *Asymmetry*, 1995, **6**, 1241.
3 I. E. Markó, P.R. Giles and N. J. Hindley, *Tetrahedron*, 1997, **53**, 1015.
4 A. G. M. Barrett and A. Kamimura, *J. Chem. Soc*., *Chem. Commun*., 1995, 1755.
5 T. Hayase, T. Shibata, K. Soai and Y. Wakatsuki, *Chem. Commun*., 1998, 1271.
6 M. Ikeda, T. Sato and H. Ishibashi, *Heterocycles*, 1988, **27**, 1465; J. Zabicky, in *The Chemistry of Amino Group*, ed. S. Patai, Wiley, London, 1968, p 132.
7 A. F. Spatola, M. K. Anwer, A. L. Rockwell and L. M. Gierasch, *J. Am. Chem. Soc*., 1986, **108**, 825.
8 S. Le Coz, A. Mann, F. Thareau and M. Taddei, *Heterocycles*, 1993, **36**, 2073.
9 R. Grote, A. Zeeck, J. Stümpfel and H. Zähner, *Liebigs Ann. Chem*., 1990, 525.
10 S. Rafel and J. W. Leahy, *J. Org. Chem*., 1997, **62**, 1521.
11 V. K. Aggarwal, G. J. Tarver and R. McCague, *Chem. Commun*., 1996, 2713.
12 P. A. Grieco, *Aldrichim. Acta*, 1991, **24**, 59.

Communication 8/06115G

Application of the chelate enolate Claisen rearrangement to the modification of dipeptides

Uli Kazmaier* and Sabine Maier

Organisch-Chemisches Institut der Universität, Im Neuenheimer Feld 270, 69120 Heidelberg, Germany. E-mail: ck1@popix.urz.uni-heidelberg.de

Received (in Liverpool, UK) 23rd July 1998, Accepted 13th October 1998

Manganese enolates of allylic esters of dipeptides are suitable to undergo Claisen rearrangements, giving rise to unsaturated peptides in excellent yield.

Peptides and cyclopeptides containing unnatural amino acids are quite common in nature, and are often found in marine organisms.[1] Many of these peptides show antibiotic activity,[2] and are therefore highly interesting from a pharmaceutical point of view.[3] For straightforward approaches towards these targets, efficient target screening and optimization of lead structures, flexible synthetic concepts are necessary. In addition to classical peptide coupling of commercially available or synthesized amino acids, the modification of existing peptides is especially suitable for this purpose. These modifications can be carried out in the side chain or directly on the peptide backbone.[4] The great advantage of side chain modifications results from the fact that the chiral center in the newly formed amino acid can be taken over from the precursor amino acid.[5] On the other hand, suitable precursors are necessary. In contrast, achiral glycine subunits can be used for backbone modifications, because the whole side chain is transferred.[6] As reactive intermediates, glycine cation equivalents[7] as well as glycine anions (glycine enolates) can be used.[8] The major drawback of this concept results from the difficulty of controlling the stereochemical outcome of the C–C coupling step.

For quite some time we have been investigating syntheses of γ,δ-unsaturated amino acids.[9] One approach towards these structures is based on a variation of the Claisen rearrangement, proceeding *via* chelated amino acid ester enolates (Scheme 1).[10]

Because of the fixed enolate geometry given by chelation, and the high preference of the Claisen rearrangement for the *chair like* transition state, the *syn* configured rearranged products are formed in a highly stereoselective fashion. If esters of chiral allylic alcohols are used, the corresponding enantiomerically pure amino acids are obtained. [11]

Therefore we were interested to see if it was also possible to transfer this Claisen protocol to peptides, and to use it for backbone modifications. Our early attempts were carried out with zinc enolates, which generally give the best results in the rearrangement of amino acids.[12] But with peptides the yields obtained were modest (20%), although they could be increased (70–80%) by addition of Pd^0 catalysts. However, under these conditions the allylation of the peptide chains proceeds *via* π-allyl–palladium intermediates. This intermolecular process results in significantly lower diastereoselectivities, and also the formation of regioisomers if substituted allylic esters are used. Therefore we undertook an intensive metal tuning to find suitable chelate complexes which undergo Claisen rearrangement without assistance from a palladium catalyst. By far the best results are obtained if manganese salts are used for chelation.[13] We investigated the rearrangement of various esters of dipeptides (Scheme 2) and the results obtained are shown in Table 1.†

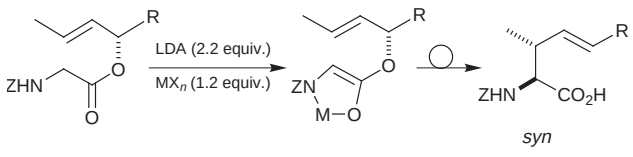

Scheme 1

Independent of the protecting groups (PG) used,‡ the yields obtained with these manganese enolates were always excellent, with both esters of terminal allylic alcohols (entries 1–3) and *trans* configured substituted alcohols (entries 4–11).§ These are especially interesting, because in their rearrangement two new stereogenic centers are formed. Therefore we investigated preferentially the rearrangement of crotyl esters, because the results obtained with these esters in general can be transferred to other *trans* configured esters without problems. In all examples investigated so far, the simple diastereoselectivity of the rearrangement was very high (≥95%) and comparable to the results obtained with amino acids.¶ No significant induced diastereoselectivity was observed. Obviously the *N*-terminal amino acid has no notable influence on the rearrangement. This is also reflected in the high yields obtained, which are also nearly independent on the peptide used.

This protocol is also suitable for the direct introduction of α-alkylated amino acids into peptides (Scheme 3). These derivatives show higher resistances towards proteases, and therefore they are interesting for the development of peptide

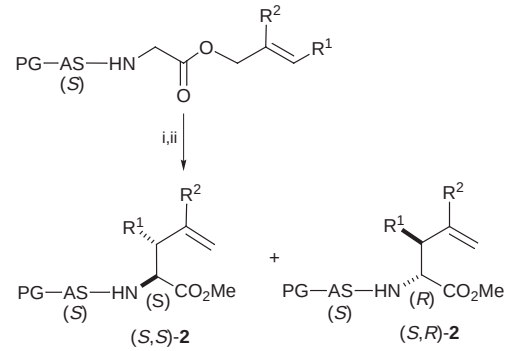

Scheme 2 *Reagents and conditions*: i, LDA (4.0 equiv.), $MnCl_2$ (1.2 equiv.), THF, −78 °C→room temp.; ii, CH_2N_2.

Table 1 Chelate enolate Claisen rearrangement of peptides

Entry	Ester	PG	AS	R^1	R^2	Yield (%)	Selectivity *SS*:*SR*
1	**1a**	Boc	Val	H	Me	88	51:49
2	**1b**	Boc	Phe	H	Me	90	63:37
3	**1c**	Z	Phe	H	Me	88	66:34
4	**1d**	Z	Val	Me	H	92	61:39
5	**1e**	Boc	Val	Me	H	93	37:63
6	**1f**	Boc	Phe	Me	H	93	62:38
7	**1g**	CF_3CO	Phe	Me	H	98	47:53
8	**1h**	Ts	Phe	Me	H	92	35:65
9	**1i**	Ts	Ile	Me	H	83	35:65
10	**1k**	Boc	Met	Me	H	88	33:67
11	**1m**	Boc	Lys(Boc)	Me	H	78	42:58

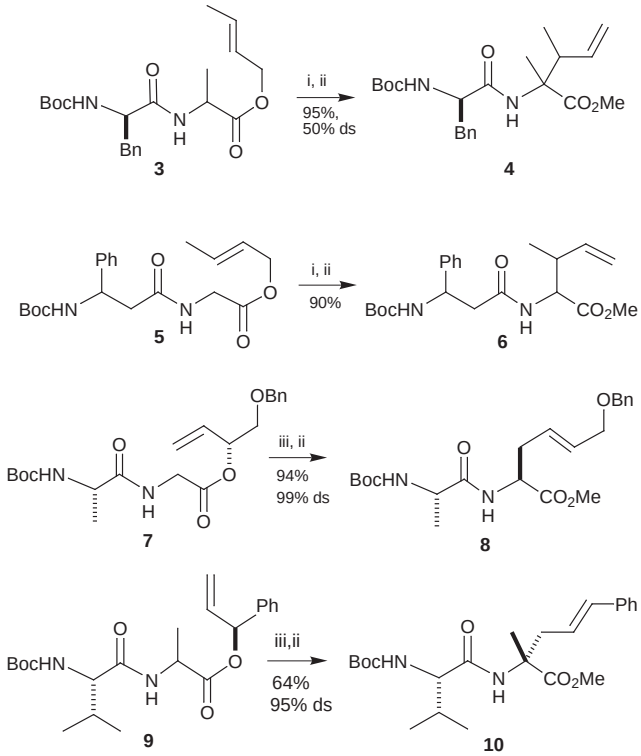

Scheme 3 *Reagents and conditions*: i, LDA (4.0 equiv.), $MnCl_2$ (1.2 equiv.), THF, −78 °C→room temp.; ii, CH_2N_2; iii, LHMDS (4.0 equiv.), $MnCl_2$ (1.2 equiv.), THF, −78 °C→room temp.

based pharmaceuticals.[14] Because of the steric hindrance of these amino acids, their introduction into peptides by classical peptide coupling reactions often causes problems, and therefore special coupling reagents and methods have to be applied.[15] Using the peptide Claisen rearrangement even sterically hindered peptides such as **4** and **10** can be obtained. This procedure is also suitable for the rearrangement of peptides containing β-amino acids (**5**).[16] Since the influence of the adjacent amino acid on the rearrangement can be neglected, this allows for the stereoselective synthesis of peptides if esters of chiral allylic alcohols such as **7** and **9** are used.[17] The corresponding dipeptides **8** and **10** were obtained not only in good to excellent yields but also in a highly diastereoselective fashion.

These unsaturated peptides obtained by backbone modification are suitable substrates for subsequent reactions on the double bond (side chain modifications). These reactions are currently under investigation. We are also looking for chelate complexes which allow chirality transfer from the peptide chain to the new stereogenic center formed during the rearrangement.

Financial support from the Deutsche Forschungsgemeinschaft as well as the Fonds der Chemischen Industrie is gratefully acknowledged.

Notes and references

† General procedure for the peptide Claisen rearrangement: 0.2 mmol of peptide ester **1** was dissolved in 3 ml of THF, before 0.24 mmol of $MnCl_2$ was added. The mixture was cooled to −78 °C. A freshly prepared solution of 0.8 mmol LDA in 2 ml of THF was added slowly and the reaction mixture was allowed to warm to room temperature overnight. The resulting brown solution was hydrolyzed by vigorous stirring with 5 ml 1 M HCl solution, until a clear solution was obtained. After separation of the aqueous layer the rearrangement product was extracted three times with 10 ml of 1 M NaOH solution. The combined basic aqueous layers were acidified with 1 M HCl solution (pH 1) and the peptide was extracted twice with CH_2Cl_2 (15 ml each). After evaporation of the solvent, the crude product was purified by flash chromatography. For analytical purposes the rearrangement products were converted into the corresponding methyl esters with CH_2N_2.

‡ If a trifluoroacetyl group is used as protecting group, LHMDS should be applied instead of LDA.

§ The yields and selectivities obtained with *cis*-configured esters are generally lower, depending on the substituent. This can be explained by an increased rearrangement *via* the *boat like* transition state (ref. 18).

¶ Determined by NMR and/or HPLC analysis

1 *Amino Acids, Peptides and Proteins*, Specialist Periodical Reports, Chemical Society, London.
2 U. Gräfe, *Biochemie der Antibiotika*, Spektrum, Heidelberg, 1992.
3 E. Mutschler, *Arzneimittelwirkungen*, Wissenschaftliche Verlagsgesellschaft, Stuttgart, 1991; A. E. Eberle, *Chimia*, 1991, **45**, 145.
4 D. Seebach, A. K. Beck and A. Studer, in *Modern Synthetic Methods*, ed. B. Ernst and C. Leumann, Verlag Helvetica Chimica Acta/VCH, Basel/Weinheim, 1995, vol. 7, p. 1 and references cited therein.
5 J.-C. Gfeller, A. K. Beck and D. Seebach, *Helv. Chim. Acta*, 1980, **63**, 728; M. J. Dunn, S. Gomez and R. F. W. Jackson, *J. Chem. Soc., Perkin Trans. 1*, 1995, 1639; J. Barluenga, M. A. García-Martín, J. M. González, P. Clapés and G. Valencia, *Chem. Commun.*, 1996, 1505; M. Mezzetti, E. Mincione and R. Saladino, *Chem. Commun.*, 1997, 1063.
6 R. M. Williams, in *Synthesis of Optically Active α-Amino Acids*, Vol. 7 of *Organic Chemistry Series*, ed, J. E. Baldwin and P. D. Magnus, Pergamon, Oxford, 1989.
7 C. J. Easton, I. M. Scharfbillig and E. W. Tan, *Tetrahedron Lett.*, 1988, **29**, 1565; G. Apitz and W. Steglich, *Tetrahedron Lett.*, 1991, **32**, 3163; W. Steglich, M. Jäger, S. Jaroch and P. Zistler, *Pure Appl. Chem.*, 1994, **66**, 2167.
8 Reviews on selective alkylation of peptides: D. Seebach, *Angew. Chem.*, 1988, **100**, 1685; *Angew. Chem., Int. Ed. Engl.*, 1988, **27**, 1624; D. Seebach, *Aldrichim. Acta*, 1992, **25**, 59.
9 Review: U. Kazmaier, *Liebigs Ann./Recl.*, 1997, 285.
10 U. Kazmaier, *Angew. Chem.*, 1994, **106**, 1046; *Angew. Chem., Int. Ed. Engl.*, 1994, **33**, 998.
11 U. Kazmaier and C. Schneider, *Synlett*, 1996, 975; U. Kazmaier and C. Schneider, *Tetrahedron Lett.*, 1998, **39**, 817; U. Kazmaier and C. Schneider, *Synthesis*, 1998, 1321.
12 U. Kazmaier, *J. Org. Chem.*, 1994, **59**, 6667.
13 Reactions of manganese enolates: M. T. Reetz and H. Haning, *Tetrahedron Lett.*, 1993, **34**, 7395; G. Cahiez, K. Chau and P. Cléry, *Tetrahedron Lett.*, 1994, **35**, 3069.
14 C. Toniolo, M. Crisma, S. Pegoraro, G. Valle, G. M. Bonora, E. L. Becker, S. Polinelli, W. H. J. Boesten, H. E. Schoemaker, E. M. Meijer, J. Kamphuis and R. Freer, *Peptide Res.*, 1991, **4**, 66; R. T. Shuman, R. B. Rothenberger, C. S. Campbell, G. F. Smith, D. S. Gifford-Moore, J. W. Paschal and P. D. Gesellchen, *J. Med. Chem.*, 1995, **38**, 4446.
15 C. Palomo, J. M. Aizpurua, R. Urchegui and J. M. Garcia, *J. Chem. Soc., Chem. Commun.*, 1995, 2327; L. A. Carpino, M. Beyermann, H. Wenschuh and M. Bienert, *Acc. Chem. Res.*, 1996, **29**, 268; D. Obrecht, M. Altorfer, C. Lehmann, P. Schönholzer and K. Müller, *J. Org. Chem.*, 1996, **61**, 4080; C. B. Bucher and H. Heimgartner, *Helv. Chim. Acta*, 1996, **79**, 1903; D. H. R. Barton and J. A. Ferreira, *Tetrahedron*, 1996, **52**, 9367.
16 D. Seebach and J. L. Matthews, *Chem. Commun.*, 1997, 2015.
17 Preparation of the chiral alcohols: C. Schneider and U. Kazmaier, *Synthesis*, 1998, 1314.
18 U. Kazmaier, *Tetrahedron*, 1994, **50**, 12895; U. Kazmaier, *J. Org. Chem.*, 1996, **61**, 3694.

Communication 8/05784B

Isostructurality in crystalline oxa-androgens: a case of C–O–H···O and C–H···O interaction mimicry and solid solution formation

Addlagatta Anthony,[a] Mariusz Jaskólski,*[b] Ashwini Nangia*[a] and Gautam R. Desiraju[a]

[a] *School of Chemistry, University of Hyderabad, Hyderabad 500 046, India. E-mail: ansc@uohyd.ernet.in*
[b] *Institute of Bio-organic Chemistry, Polish Academy of Sciences and Department of Crystallography, A. Mickiewicz University, Poznan, Poland*

Received (in Cambridge, UK) 24th August 1998, Accepted 13th October 1998

A C–H···O interaction in 2-oxa-4-androstene-3,17-dione is replaced by a C–O–H···O hydrogen bond in the isostructural 6α-hydroxy analogue, and these compounds form a binary solid solution, showing the similarity of these two crystal structures.

As part of an ongoing study on androgens[1] and their 2-oxa analogues,[2] the crystal structures of 2-oxa-4-androstene-3,17-dione **1**[3] and 6α-hydroxy-2-oxa-4-androstene-3,17-dione

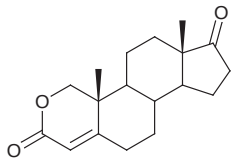

1

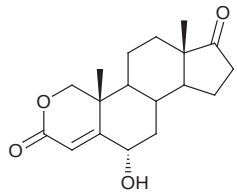

2

2[2] were determined. Crystals of these compounds were obtained from EtOAc–MeOH mixtures. Both these lactones were found to have similar crystal structures. Isostructurality in steroids has been studied previously for compounds that are related by an exchange of functional groups or by epimerisation. Thus, the pairs of compounds gamabufotalin/arenobufagin, cinobufagin/cinobufotalin and digitoxigenin/digirezigenin form solid solutions which are isostructural with the respective individual components while the crystal structures of epimeric 5α- and 5β-androstane-3α,17β-diol are similar, if only to a slightly lesser degree.[4] The conformation of the oxa-steroid skeletons in **1** and **2** are identical.† Accordingly, the crystal structures of **1** and **2** were scrutinised further.‡

Both **1** and **2** adopt the same monoclinic space group, $P2_1$ and the value of the *a*-axis parameter is nearly equal (6.2321 and 6.2214 Å). This is the direction of the hydrogen bond interactions and an inspection of Fig. 1–3 is instructive. In hydroxy lactone **2**, O6–H and C6–H are hydrogen bonded to the lactone carbonyl atom O3 of different screw-axis related molecules, thereby forming chains of alternating O–H···O (1.86 Å) and C–H···O (2.38 Å) hydrogen bonds§ (Fig. 1 and 3). Effectively, O6 behaves as an O–H···O donor and O3 as a bifurcated acceptor. In lactone **1**, the C6 methylene hydrogens are linked to the O3 atom of 2_1-related molecules to give chains of C–H···O hydrogen bonds (2.38 and 2.67 Å) (Fig. 2 and 3). The metrics of these hydrogen bonded chains along [100] in the two structures are given in Fig. 3, from which it is clearly seen that the shorter of the C–H···O hydrogen bonds in**1** behaves as a surrogate of the C–O–H···O bond in**2**. We note that the near equality of the *a*-axis parameter in the two structures allows for the replacement of four links between translationally related O3 atoms in **1** (two weak O···H interactions and two C–H bonds) by five links in **2** (strong O···H interaction, weak O···H interaction, C–H bond, C–O bond and O–H bond).

When a 1:1 mixture of **1** and **2** was crystallised from EtOAc–MeOH, crystals **3**‡ were obtained in the space group $P2_1$ with cell dimensions very similar to those of pure **2**. Structure solution and refinement with partial positional occupancy for O6 yielded a converged model with partial occupancies of 0.28 and 0.720(6) for **1** and **2** respectively, showing that **3** is a binary solid solution.§ While there are examples of equivalence between N–H···O and C–H···O hydrogen bonds in isostructural crystals,[6] the formation of solid solution has not been reported in these cases. Additionally, interaction mimicry between C–O–H···O and C–H···O is a novel occurrence. The present example is therefore unprecedented and offers valuable clues regarding crystal packing in general.

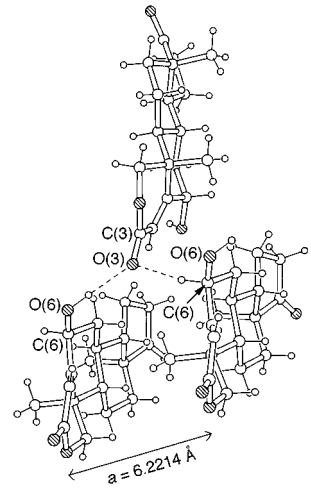

Fig. 1 Hydrogen bonding in hydroxy lactone **2** along [100] to show the O6–H···O3 and C6–H···O3 interactions between 2-related molecules. Oxygen atoms are shaded.

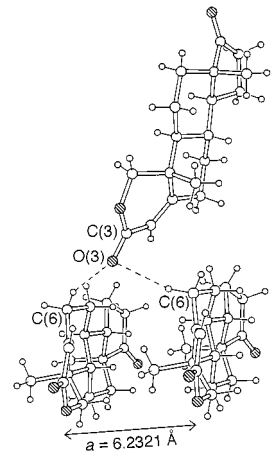

Fig. 2 Hydrogen bonding in lactone **1** along [100] between C6-methylene H-atoms and the carbonyl O3 atom of different 2_1-related molecules. Oxygen atoms are shaded. Notice the identity of *a*-axis and the similarity in hydrogen bonded chains and arrangement of molecules in the structure shown here and in Fig. 1.

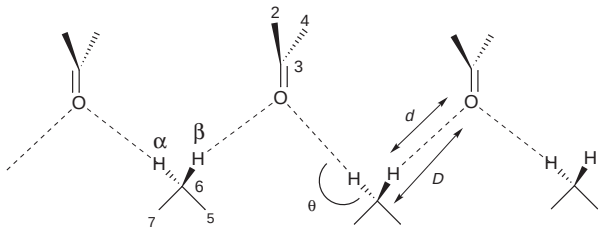

4

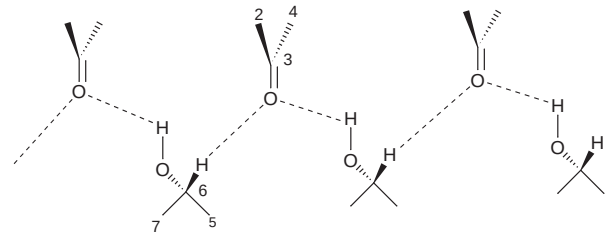

5

Fig. 3 Supramolecular synthons **4** and **5** in the structures of **1** and **2** along [100]. The geometrical parameters (*d*, *D*, *θ*) of the hydrogen bonds with normalised O–H and C–H distances are for **4**: C6–αH···O3: 2.38, 3.381(4) Å, 154° and C6–βH···O3: 2.67, 3.693(4) Å, 157°; **5**: O6–αH···O3: 1.8602(5), 2.831(4) Å, 171° and C6–βH···O3: 2.38 Å, 3.409(4) Å, 158°.α and β refer to the bottom and top faces of the somewhat flattened steroid skeleton.

Firstly, this example shows the equivalence of O–H···O and C–H···O hydrogen bonding and confirms yet again that the structure directing effects of these two interactions can often be the same. It is noteworthy that the C6 H-atoms in Δ^4-steroids are allylic in nature and, as such, activated as C–H donors.[7] Secondly, the formation of a solid solution in such cases is *per se* noteworthy. Binary solid solution formation is the most stringent criterion for isostructurality[8] and occurs here because **1** and **2** have similar overall molecular shapes and also because the hydrogen bonds and recognition patterns in the structure-forming domain, that is along [100], are virtually identical. These patterns are the supramolecular synthons[9] **4** and **5** and they play a significant structural role in all three crystals. Thirdly, the fact that the **3** adopts the structure of **2** rather than that of **1** could be ascribed to the larger size of the OH group compared to the H substituent,[10] while the excess of **2** over **1** in the solid solution might be because of the relative strengths of O–H···O and C–H···O hydrogen bonds in the individual structures.[11] Finally, we note that solid solution formation occurs for this pair of compounds **1** and **2** even though the *b*, *c* and β parameters are significantly different. While the unit cell similarity index Π[8,12] is fortituously close to zero (Π = 0.002), this index could be misleading here. Since the monoclinic axial lengths are quite different (9.926 and 12.050 Å), the other packing features in the crystals, in this case the general coordination arrangements of molecules, are different leading to a degree of isostructurality index,[8,12] I^{21}_{D} of only 75%. Despite this, solid solution formation has been observed leading to the thought that isostructurality along one direction is sufficient to observe mimicry effects,[13] if that direction is important as a structure determinant. The implications of such 'one-dimensional isostructurality' have a bearing on the analysis of similarities in crystal packing that are mediated by robust supramolecular synthons.[14] Such synthons could play an active role during all stages of crystallisation events from nucleation to growth to the final appearance of a single crystal.

We acknowledge Professor U. Wrzeciono and Dr A. Gzella (K. Marcinkowski University of Medical Sciences, Poznan) for X-ray facilities. A. A. thanks CSIR for a fellowship. This research was supported by D. S. T. (SP/S1/G25/91) and in part under the Indo-Polish D.S.T.-K.B.N. exchange scheme (INT/POL/POC/96-98/P22). M. J. thanks H. H. M. I. for support.

Notes and references

† This was determined from an overlay diagram which shows an overall rms deviation of 0.075 Å.

‡ *Crystal data* for **1**: $C_{18}H_{24}O_3$, M = 288.37, mp 185–186 °C, monoclinic, space group $P2_1$, a = 6.2321(3), b = 9.9264(6), c = 12.8120(8) Å, β = 97.079(5)°, V = 786.54(8) Å^3, Z = 2, D_c = 1.218 g cm^{-3}, KM-4 diffractometer, T = 293 K, Cu-Kα, ω–2θ scan mode, 1597 unique reflections, 1434 with $I > 2\sigma(I)$, no absorption corrections. Structure solution and refinement with standard methods (SHELXS86 and SHELX97); H-atoms fixed, final R = 0.0342 (observed), 0.0412 (all), wR = 0.0865 (observed), 0.0919 (all). For **2**: $C_{18}H_{24}O_4$, M = 304.37, mp 244–246 °C, monoclinic, space group $P2_1$, a = 6.2214(7), b = 12.050(1), c = 10.888(1) Å, β = 103.07(1)°, V = 795.10(14) Å^3, Z = 2, D_c = 1.271 g cm^{-3}, KM-4 diffractometer, T = 293 K, Cu-Kα, ω–2θ scan mode, 1514 unique reflections, 1458 with $I > 2\sigma(I)$, no absorption corrections. Structure solution and refinement with standard methods (SHELXS86 and SHELX97); H-atoms fixed, final R = 0.0359 (observed), 0.0378 (all), wR = 0.1013 (observed), 0.1033 (all). For **3**: solid solution of **1** and **2**, $(C_{18}H_{24}O_3)_{0.28}$ + $(C_{18}H_{24}O_4)_{0.72}$, M = 299.89, mp 244–245 °C, monoclinic, space group $P2_1$; a = 6.2246(7), b = 12.014(1), c = 10.915(1) Å, β = 103.09(1)°, V = 795.04(14) Å^3, D_c = 1.252 g cm^{-3}, KM-4 diffractometer, T = 293 K, Cu-Kα, ω–2θ scan mode, 1542 unique reflections, 1497 with $I > 2\sigma(I)$, no absorption corrections. Structure solution and refinement with standard methods (SHELXS86 and SHELX97); H-atoms fixed, final R = 0.0321 (observed), 0.0334 (all), wR = 0.0862 (observed), 0.0880 (all). CCDC 182/1056.

§ The presence of **1** and **2** in single crystals of **3** was further confirmed by IR analysis and their ratio was found to be in the range 3:7 to 4:6 by ^{1}H NMR integration.

1 A. Anthony, M. Jaskólski, A. Nangia and G.R. Desiraju, *Acta Crystallogr*., 1998, **C54**, in the press.
2 A. Nangia and A. Anthony, *Ind. J. Chem*., 1997, **36B**, 1113.
3 A. A. Frimer, J. Hameiri-Buch, S. Ripshtos and P. Gilinsky-Sharon, *Tetrahedron*, 1986, **42**, 5693.
4 G. Argay, A. Kálmán, B. Ribár, S. Vladimirov and D. Zivanov-Stakic, *Acta Crystallogr*., 1987, **C43**, 922; A. Kálmán, G. Argay, D. Zivanov-Stakic, S. Vladimirov and B. Ribár, *Acta Crystallogr*., 1992, **C48**, 812; A. Kálmán, L. Párkányi and G. Argay, *Acta Crystallogr*., 1993, **B49**, 1039.
5 G. R. Desiraju, *Acc. Chem. Res*., 1996, **29**, 441; T. Steiner, *Chem. Commun*., 1997, 727.
6 Z. Berkovitch-Yellin and L. Leiserowitz, *Acta Crystallogr*., 1984, **B40**, 159; T. Steiner, G. Koellner, K. Gessler and W. Saenger, *J. Chem. Soc*., *Chem. Commun*., 1995, 511; L. J. W. Shimon, M. Vaida, L. Addadi, M. Lahav and L. Leiserowitz, *J. Am. Chem. Soc*., 1990, **112**, 6215.
7 V. R. Pedireddi and G. R. Desiraju, *J. Chem. Soc*., *Chem. Commun*., 1992, 988.
8 A. Kálmán, *Adv. Mol. Struct. Res*., 1997, **3**, 189.
9 G. R. Desiraju, *Angew. Chem*., *Int. Ed. Engl*., 1995, **34**, 2311.
10 A. I. Kitaigorodskii, *Molecular Crystals and Molecules*, Academic Press, New York, 1973, pp 108–110.
11 G. A. Jeffrey, *An Introduction to Hydrogen Bonding*, OUP, New York, 1997, p. 12.
12 J. S. Rutherford, *Models Chem*., 1997, **134**, 395.
13 W. Jones, C. R. Theocharis, J. M. Thomas and G. R. Desiraju, *J. Chem. Soc*., *Chem. Commun*., 1983, 1443.
14 A. Nangia and G. R. Desiraju, *Top. Curr. Chem*., 1998, **198**, 57.

Communication 8/06607H

Synthesis of a 1,2-dihydro[60]fullerylglycine derivative by a novel cyclopropane ring opening of a methano[60]fullerene

Glenn A. Burley,[a] Paul A. Keller,*[a] Stephen G. Pyne*[a] and Graham E. Ball[b]

[a] *Department of Chemistry, University of Wollongong, Wollongong, New South Wales, 2522, Australia. E-mail: stephen_pyne@uow.edu.au; paul_keller@uow.edu.au*

[b] *NMR Facility, University of New South Wales, Sydney, New South Wales, 2052, Australia*

Received (in Cambridge, UK) 3rd September 1998, Accepted 14th October 1998

The 1,2-dihydro[60]fullerylgylcine derivative 2 has been prepared by a novel cyclopropane ring opening reaction of the methano[60]fullerene derivative 1.

[60]Fullerenes exhibit a range of interesting biological activities including inhibition of HIV-1 protease,[1] cytotoxicity[2] and the selective cleavage on DNA.[3] Furthermore, the covalent tethering of fullerenes to peptides and proteins has been the goal of a number of studies concerned with the application of fullerene–peptide conjugates to biological problems.[4–8] These conjugates not only enhance the water-solubility of the fullerene and make this molecule more amenable to biological studies, but the fullerene itself can modify the conformation of the tethered peptide and often enhance its biological activity.[6] Such investigations could be greatly enhanced if an α-substituted fulleryl amino acid was available that could be directly incorporated into a peptide sequence. The resulting fulleryl peptides would be expected to have novel secondary structures because of the possibility of π–π and hydrophobic interactions between the peptide and the fullerene surface. Furthermore, these conjugates may have unique biological properties or applications. While a number of fullerylproline derivatives have been prepared[9] the synthesis of an acyclic α-fulleryl amino acid has not been realised. We describe here the synthesis of the 1,2-dihydro[60]fullerylgylcine derivative **2** by a novel ring opening reaction of the methano[60]fullerene derivative **1** (Scheme 1).

Treatment of a solution of [60]fullerene, under Hirsch cyclopropanation conditions,[10] with *tert*-butyl *N*-diphenylmethyleneglycinate, CBr_4 and DBU gave the cyclopropane imino ester **1** in 52% yield after purification by column chromatography. Apart from the signals due to the aryl and *tert*-butyl group (δ 28.3) the ^{13}C NMR spectrum (C_6D_6–CS_2, 1:1) of **1** showed the expected downfield resonances for the sp^2 hybridized carbonyl (δ 162.3) and imine carbons (δ 153.7), 25 sp^2 fullerene carbon resonances (δ 149.3–135.0) and resonances for the quaternary sp^3 carbons at δ 95.0 (C-61), 84.3 (Me_3CO) and 83.8 (C1, C2). The electrospray ionization mass spectrum of **1**, using PhMe–MeCN (30 : 1) as solvent showed a molecular ion at *m/z* 1013. The related ethyl ester **1** (R = Et) could be obtained in 79% yield from C_{60} and ethyl *N*-diphenylmethyleneglycinate. Attempts at the acid hydrolysis (6 M HCl, TFA or TsOH) of **1** (R = Bu^t or Et) have not proven successful and none of the desired cyclopropane amino acid could be isolated.

Reduction of **1** (R = Bu^t) with $NaBH_3CN$ in THF–MeOH at pH 4 gave not the expected reduced imine compound but the novel ring opened 1,2-dihydro[60]fullerylglycine derivative **2** in 44% yield after purification by column chromatography on silica gel. The ring opened structure of **2** was evident from its ^1H NMR (C_6D_6–CS_2, 1:1) spectrum which showed a singlet resonance at δ 6.84 typical of H-2 in a 1-substituted 2-H-C_{60}.[11,12] The structure of **2** was further supported by single proton resonances at δ 5.27 (d, J = 3 Hz, Ph_2CHNH), 4.83 (d, J = 11.7 Hz, H-61) and 3.62 (dd, J = 3, 11.7 Hz, NH). The ^{13}C NMR spectrum of **2** showed 47 sp^2 fullerene resonances in the region δ 154.4–136.2 and resonances for 5 sp^3 carbons in the region δ 83–58. These latter resonances were unequivocally assigned by ^1H–^{13}C NMR correlation experiments (HMBC) as δ 82.8 (Me_3CO), 70.9 (C-61), 68.1 (C-1) , 66.7 (Ph_2CH) and 58.8 (C-2). The two fullerene carbons alpha to C-1 (C-6 and C-9) and C-2 (C-3 and C-12) were observed downfield of the other fullerene resonances and occurred in the region δ 154.4–152.4. Interestingly, C-6 and C-9 and C-3 and C-12 appeared as diastereotopic pairs due to the stereogenicity of C-61 (Fig. 1). The number of different sp^2 fullerene signals suggested that most other fullerene carbons formed diastereotopic pairs.† The assignmements made to individual carbons are shown in Fig. 1. Furthermore, the HMBC experiments confirmed that the 1,2-substituted rather than the 1,4-substituted fullerene had formed.‡

The formation of **2** can be rationalized as occuring by a mechanism similar to that shown in Scheme 1, although this process may not be concerted and the protonation steps may occur at different stages along the reaction pathway. Clearly the driving force for such a ring opening must be stabilization of the incipient C-2 fulleryl carbanion **A** by delocalization over the fullerene ring. Such ring opening of cyclopropane amino esters and acids is known when a β-electron-withdrawing group is

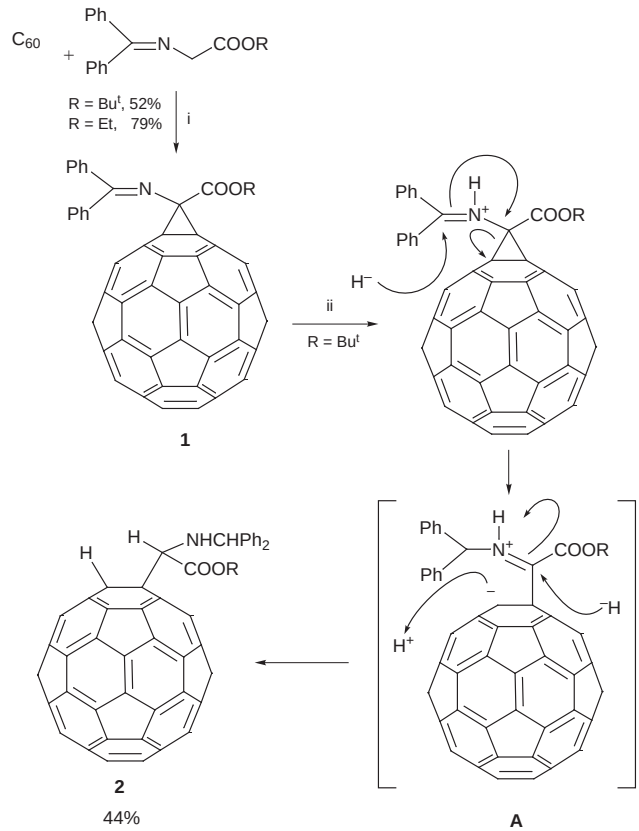

Scheme 1 *Reagents and conditions*: i, DBU, CBr_4, PhCl, room temp.; ii, $NaBH_3CN$, pH 4.

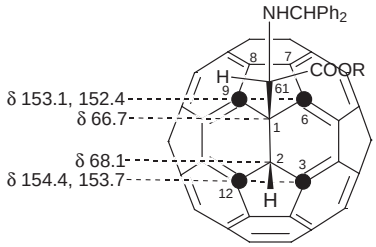

Fig. 1 ^{13}C NMR (C_6D_6–CS_2, 1:1) chemical shifts and assignments for **2** (R = Bu^t).

present on the ring that can stabilize a developing carbanionic centre.[13] The ring opening of fullerene derivatives has been observed before but not on cyclopropane derivatives or under such mild conditions.[14]

In conclusion, we have discovered a novel ring opening reaction of a methano[60]fullerene derivative under reductive conditions that allows the synthesis of 1,2-dihydro[60]fullerylglycine derivatives that would have potential for many interesting biological applications.§

We thank the Australian Research Council for financial support.

Notes and references

† Simple achiral 1-substituted 2-H fullerenes should show 30 different carbons due to their C_s symmetry (ref. 11, 12).

‡ While the structure of **2** was clear from its ^{1}H and ^{13}C NMR and IR spectral data, we have been unable to obtain a useful mass spectrum (ESMS or MALDI) of this compound.

§ To date attempts at the acid hydrolysis of the ester group (6 M HCl, TFA or TsOH) or the hydrogenolysis of the *N*,*N*-diphenylmethylamino group in **2** have not proven successful.

1 S. H. Friedman, D. L. DeCamp, R. P. Sijbesma, G. Srdanov, F. Wudl and G. L. Kenyon, *J. Am. Chem. Soc*., 1993, **115**, 6506; S. W. Friedman, P. S. Ganapathi, Y. Rubin and G. L. Kenyon, *J. Med. Chem*., 1998, **41**, 2424.
2 H. Tokuyama, S. Yamago and E. Nakamura, *J. Am. Chem. Soc*., 1993, **115**, 7918.
3 A. S. Boutorine, H. Tokuyama, M. Takasugi, H. Isobe, E. Nakamura and C. Helene, *Angew. Chem., Int. Ed. Engl*., 1994, **33**, 2462; A. Yi-Zhong, C.-H. B. Chen, J. L. Anderson, D. S. Sigman, C. S. Foote and Y. Ruben, *Tetrahedron*, 1996, **52**, 5179.
4 M. Prato, A. Bianco, M. Maggini, G. Scorrano, C. Toniolo and F. Wudl, *J. Org. Chem*., 1993, **58**, 5578.
5 A. Skiebe and A. Hirsch, *J. Chem. Soc., Chem. Commun*., 1994, 335.
6 C. Toniolo, A. Bianco, M. Maggini, G. Scorrano, M. Prato, M. Marastoni, R. Tomatis, S. Spisani, G. Palu and E. D. Blair, *J. Med. Chem*., 1994, **37**, 4558.
7 A. Bianco, M. Maggini, G. Scorrano, C. Toniolo, G. Marconi, C. Villani and M. Prato, *J. Am. Chem. Soc*., 1996, **118**, 4072.
8 A. Kurz, C. M. Halliwell, J. J. Davis, H. A. O. Hill and G. W. Canters, *Chem. Commun*., 1998, 433.
9 L.-H. Shu, G.-W. Wang, S.-H. Wu, H.-M. Wu and X.-F. Lao, *Tetrahedron Lett*., 1995, **36**, 3871; L. Gan, D. Zhou, C. Luo, H. Tan, C. Huang, M. Lu, J. Pan and Y. Wu, *J. Org. Chem*., 1996, **61**, 1954; A. Bianco, F. Gasparrini, M. Maggini, D. Misiti, A. Polese, M. Prato, G. Scorrano, C. Toniolo, G. Marconi and C. Villani, *J. Am. Chem. Soc*., 1997, **119**, 7550.
10 X. Camps and A. Hirsch, *J. Chem. Soc., Perkin Trans. 1*, 1997, 1595.
11 L. Gan, J, Jiang, W. Zhang, Y. Su, Y. Shi, C. Huang, J. Pan, M. Lu and Y. Wu, *J. Org. Chem*., 1998, **63**, 4240; K.-F. Liou and C.-H. Cheng, *Chem. Commun*., 1996, 1423.
12 C. Siedschlag, H. Luftmann, C. Wolff and J. Mattay, *Tetrahedron*, 1997, **53**, 3587.
13 S. G. Pyne, K. Schafer, B. W. Skelton and A. H. White, *Aust. J. Chem*., 1998, **51**, 127.
14 S. Yamago, A. Takeichi and E. Nakamura, *Synthesis*, 1996, 1380.

Communication 8/06865H

ChemComm

Novel catalysts for thiophene synthesis at lower temperatures

Barry W. L. Southward,*[a] Lance S. Fuller,[b] Graham J. Hutchings,[c] Richard W. Joyner[d] and Russell A. Stewart[b]

[a] *Catalysis Research Centre, Department of Chemistry, University of Reading, Whiteknights, Reading, UK RG6 6AD. E-mail: b.w.l.southward@reading.ac.uk*
[b] *Inspec Fine Chemicals, Four Ashes, Wolverhampton, UK WV10 7BP*
[c] *Department of Chemistry, University of Wales at Cardiff, PO Box 912, Cardiff, UK CF1 3TB*
[d] *Nottingham Trent University, Burton Street, Nottingham, UK NG1 4BU*

Received (in Liverpool, UK) 2nd September 1998, Accepted 16th October 1998

Thiophenes can be synthesised in high yields from the reaction of C_{4+} oxygenates and CS_2 at temperatures 140 °C lower than current industrial catalysts, using novel materials based upon chromium substituted iron oxide hydroxide.

Thiophene derivatives are widely used as raw materials in the production of dyes, agrochemicals and pharmaceuticals.[1] However, in recent years much research has been devoted to their catalytic destruction *via* HDS for obvious environmental reasons.[2] Conversely, the catalytic synthesis of thiophenic systems has received scant attention. Thiophene and alkylthiophenes are currently synthesised on an industrial scale (*ca*. 1000 tonnes p.a.) *via* two processes. The first involves the reaction of C_{4+} alcohols or carbonyls with CS_2 over alkali-promoted chromia alumina.[3] The second is based upon the reaction of an α,β-unsaturated aldehyde with H_2S over alkali/alkaline earth-promoted γ-Al_2O_3.[4] However, the use of alumina-based catalysts results in some disadvantages, chiefly that at the temperatures required to achieve economic yields of product (450–500 °C), cracking reactions occur with resultant losses in yields and premature catalyst deactivation through coke deposition. Hence it is desirable to design a catalyst that can operate at lower temperatures and/or give lower by-product formation. Here we address this problem and present initial data for Cr^{III}-substituted FeOOH, which has been found to be an effective thiophene synthesis catalyst at comparatively low temperatures.

Catalyst synthesis was based upon the method developed by Flanigen *et al*.[5] for the synthesis of Jarosites. This involved dissolving the required molar ratios of Fe^{III} and Cr^{III} sulfates in distilled water at 80 °C. The pH of the resulting solution was adjusted to 4 using aq. NaOH. The slurry formed was then refluxed for 20 h and the solid recovered by vacuum filtration, washed with distilled water and dried (110 °C, 12 h). Samples were then pelleted and sieved (0.6–1.0 mm), prior to testing for thiophene synthesis in a fixed bed microreactor.[6] A typical reaction involved passing a mixed vapour/gas stream of 2-methylbutanol (2MB), CS_2 and N_2 (1:1.5:80 molar ratio) at a total flow rate of 12000 h^{-1} over 1.0 g of catalyst. Product analysis was performed on-line by GC FID analysis with a carbon balance of 98–100% for all data quoted, based upon conversion of the alcohol.

A series of catalysts with increasing Cr content were prepared and tested for their efficacy in the synthesis of 3-methylthiophene (3MT), giving the results shown in Fig. 1 and Table 1. As the Cr concentration increased the yield of 3MT and conversion of alcohol were seen to increase to a maximum at *ca*. 5% Cr (57 mol% 3MT, conversion of 78 mol%), before declining to very low yields at higher Cr levels. The optimum temperature for reaction was found to be 330–350 °C, with typical temperature profile data for the reaction being shown in Table 1. Another obvious advantage of these materials was their very low by-product formation, with only minor levels of alkene formation, presumably *via* dehydration, being observed. Moreover, the proportion of cracked fractions was low and mirrored

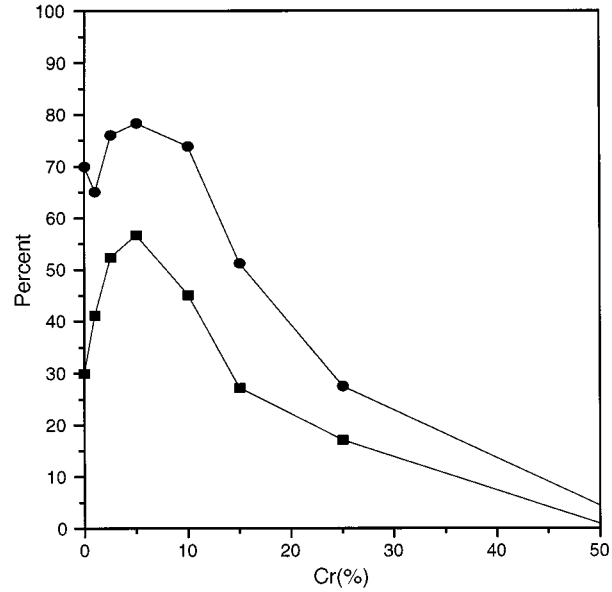

Fig. 1 The effect of Cr loading on the activity and selectivity of catalysts for the synthesis of 3-methylthiophene: (■) 3MT (mol% yield) and (●) 2MB (% conversion). Reaction conditions: 2MB:CS_2:N_2 (1:1.5:80), GHSV = 12000 h^{-1}, all samples taken at optimum temperature of activity (340–360 °C).

Table 1 The effect of Cr content and temperature on catalyst activity.

Cr (%)[a]	Fraction	*T*/°C 300	320	340	360	380	400	420
1	3MT/mol%	22.5	22.0	30.4	35.6	41.2	39.7	29.0
	2MB (% conversion)	44.9	46.8	56.9	61.1	65.1	63.7	49.7
2.5	3MT/mol%	23.1	31.3	52.4	49.1	43.8	35.4	30.2
	2MB (% conversion)	46.7	59.3	76.0	72.7	68.0	58.0	51.7
5	3MT/mol%	36.6	43.8	56.7	43.2	31.6	24.0	23.7
	2MB (% conversion)	55.4	66.4	78.4	64.4	53.8	44.8	45.4
	Thiophene (% conversion)	4.4	5.1	4.4	3.7	3.0	5.3	5.7
	2-Methylbutene (% conversion)	10.2	13.0	15.0	13.6	15.6	13.4	13.6
	Cracked (% conversion)	4.3	4.5	4.4	4.1	3.6	6.2	7.5
10	3MT/mol%	22.0	23.0	31.8	45.1	39.2	31.9	22.8
	2MB (% conversion)	46.6	45.5	58.5	73.9	69.6	60.8	49.6
15	3MT/mol%	24.2	23.6	27.5	27.2	31.1	48.5	66.1
	2MB (% conversion)	40.0	45.9	51.2	50.5	54.5	64.4	79.4
25	3MT/mol%	21.2	16.0	15.6	17.1	28.9	38.0	50.1
	2MB (% conversion)	31.1	26.7	26.5	27.5	40.5	50.2	63.3
50	3MT/mol%	0.4	0.3	0.4	0.6	0.9	1.4	1.9
	2MB (% conversion)	2.0	2.0	2.4	3.1	4.4	6.5	8.6

[a] Nominal Cr loading.

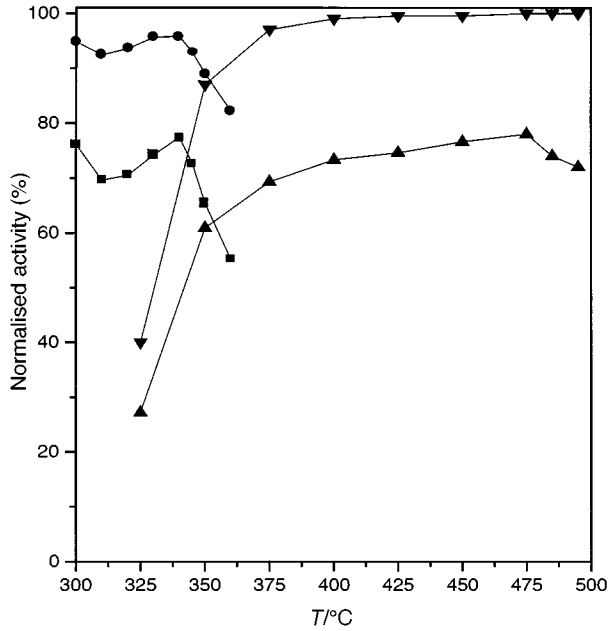

Fig. 2 Comparison of the normalised activities of α-$Fe_{0.95}Cr_{0.05}OOH$ and the current commercial catalyst for the synthesis of 3-methylthiophene: (■) 3MT (FeCrOOH, mol% yield), (●) 2MB (FeCrOOH, % conversion), (▲) 3MT, (▼) 2MB (commercial catalyst, conversion). Reaction conditions: 2MB:CS_2:N_2 (1:1.5:80), GHSV = 12000 h^{-1}, all samples taken after 15 min equilibration at each temperature.

the yield of thiophene, hence this was ascribed to β-methyl cleavage of the alcohol, rather than skeletal cracking as observed with Al_2O_3 based catalysts.

In a further set of experiments the activity of the 5% Cr catalyst (SA 103 m^2g^{-1}) was compared to that of a commercial catalyst (7.5% K_2CO_3 promoted 11% Cr_2O_3 on γ Al_2O_3, SA = 125 m^2 g^{-1}). The results, normalised to surface area, are given in Fig. 2. It is apparent that the commercial catalyst is only active at temperatures > 360 °C, and that temperatures as high as 475 °C are required to attain yields of 75 mol% 3MT, *cf.* 340 °C for the novel 5% Cr catalyst. Moreover, the commercial catalyst gave this optimum yield at a 2-methylbutanol conversion of 99 mol%, *cf.* 95 mol% for the 5% Cr catalyst, reflecting a lower selectivity and a higher formation of potentially deleterious reaction by-products for the commercial catalyst.

The changes in catalytic activity with increasing Cr content (Fig. 1) is not considered to be merely due to variation in surface area. This is confirmed by the similar BET SAs of samples with 0–10% Cr, which were all in the range 100–120 m^2 g^{-1}. However, at higher loadings of Cr, decreases in SA were recorded (15 m^2 g^{-1} for the 49% Cr sample). Hence it is clear that the intrinsic activity of the 5% Cr sample is significantly higher than that of catalysts with higher Cr loadings. Moreover, detailed powder XRD of the samples was performed which indicated that phase changes occurred as a function of Cr concentration. Thus, at 0 < Cr < 2.5% the catalyst was found to comprise of natrojarosite, with traces of α-FeOOH (Goethite) and α-CrOOH (Bracewellite).[7] However, for 3 < Cr < 10%, samples contained only a mixed α-FeOOH/α-CrOOH phase, whilst at Cr > 10% only the presence of a mixed FeCr phase supported on sodium sulfate (Thenardite) was recorded. This latter observation is consistent with the activity displayed by the intermediate Cr (15–25%) loaded samples, which exhibited performance profiles typical of supported oxides.[6] We therefore conclude that the high activities of the low Cr catalysts are related to the presence of a mixed FeOOH/CrOOH phase.

In these initial studies no attempt has been made to optimise catalyst performance by increasing the concentrations or relative proportions of the active phases. However, the data obtained demonstrate the discovery of a new class of catalysts for a lower temperature vapour phase synthesis of thiophenes[8] and may prove to be a starting point for the development of a new generation of industrial catalysts.

We are grateful for the financial support of this work by Synthetic Chemicals Ltd., now Inspec Fine Chemicals Ltd.

Notes and references

1 L. S. Fuller, *Thiophene and Thiophene Derivatives*, in *Kirk-Othmer Encyclopaedia of Chemical Technology*, 4th edn., Wiley, London, 1997, vol. 24, p. 34.
2 R. Prins, V. J. H. de Beer and G. A. Somorjai, *Catal. Rev. Sci. Eng.*, 1989, **31**, 1.
3 N. R. Clark and W. E. Webster, Br. Pat., 1,345,203 (Synthetic Chemicals Ltd.).
4 J. Barrault, M. Guisnet, R. Lucien and R. Maurel, *J. Chem. Res.*, 1978, (*S*) 207; (*M*) 2634 (US Pat. 4,143,052).
5 R. W. Grose and E. M. Flanigen, *Preparation of Catalysts 1*, eds. B. Delmon, P. A. Jacobs and G. Poncelet, Elsevier, Amsterdam, 1976, p. 51.
6 B. W. L. Southward, PhD Thesis, University of Liverpool, 1993.
7 NIST XRD database.
8 B. W. L.Southward, G. J. Hutchings, R. W. Joyner, L. S. Fuller and R. A. Stewart, Eur. Pat. 751,139, 1997.

Communication 8/06829A

Trapping of *n*-butyllithium dimer by a trilithiated derivative of $\{Al[N(H)Bu^t]_3\}_2$

Justin K. Brask,[a] Tristram Chivers*[a] and Glenn P. A. Yap[b]

[a] *Department of Chemistry, University of Calgary, 2500 University Dr. NW, Calgary, Alberta, Canada T2N 1N4. E-mail: chivers@ucalgary.ca*

[b] *Department of Chemistry, University of Ottawa, Ottawa, Ontario, Canada K1N 6N5*

Received (in Bloomington, IN, USA) 10th September 1998, Accepted 19th October 1998

The reaction of $\{Al[N(H)Bu^t]_3\}_2$, obtained as a 1 : 2 mixture of *cis* and *trans* isomers from the addition of $AlCl_3$ to three equiv. $LiN(H)Bu^t$ in diethyl ether, with $LiBu^n$ generates a complex in which a dimeric *n*-butyllithium fragment is trapped by the trilithiated derivative $Li_3Al_2[N(H)Bu^t]_3[NBu^t]_3$.

Current interest in amido derivatives of the Group 13 elements is stimulated primarily by possible applications in materials science.[1–3] Although there has been a recent spate of publications describing homoleptic polyimido anions of p-block elements, *e.g.* $E(NBu^t)_3^{2-}$ (E = Te,[4] Se,[5] S[6]), $Sb(NCH_2CH_2Ph)_3^{3-}$,[7] and $E(NR)_4^{x-}$ (E = S, R = Bu^t, *x* = 2;[8] E = P, R = 1-naphthyl, *x* = 3[9]), no examples of trisimido trianions, $E(NR)_3^{3-}$ (E = Group 13 element, R = alkyl or aryl group) have been reported.

Lithiation has been used to prepare complexes of the type $[R_2AlNLi(thf)_nR']_2$ from $[R_2AlNHR']_2$ (R, R′ = Me, Bu^t or Bu^i, Ph; *n* = 1), although adduct formation is observed for very bulky groups, *e.g.* $Me_2Bu^tAlNH[Li(thf)_3](C_6H_3Pr^i_2\text{-}2,6)$.[10] Nevertheless the trisamido derivatives $[Al(NHR)_3]_n$ (**1a**, R = Pr^i; **1b**, R = Bu^t) are potential precursors of $Al(NR)_3^{3-}$. The isopropyl derivative **1a** is obtained by the reaction of $AlCl_3$ with $LiNHPr^i$ in a 1 : 3 molar ratio in diethyl ether[11] whereas the analogous reaction with $LiNHBu^t$ in *toluene* gives $\{LiAl[N(H)Bu^t]_4\}_2$ rather than **1b**.[1] These observations, and the very recent report of the monomeric complex $Li(thf)Al[N(H)R]_4$ (R = 2,6-$Pr^i_2C_6H_3$),[12] prompt us to describe the formation and structure of the unusual cluster $Li_3Al_2[N(H)Bu^t]_3[NBu^t]_3\cdot(LiBu^n)_2$ (**2**) in attempts to generate $Al(NBu^t)_3^{3-}$. Complex **2** consists of an *unsolvated n*-butyllithium dimer trapped by a trilithiated derivative of **1b**.

Treatment of $LiN(H)Bu^t$ with $AlCl_3$ (3 : 1 molar ratio) in *diethyl ether* gives the dimer **1b** as a *ca.* 1 : 2 mixture of *cis*, **1b′**

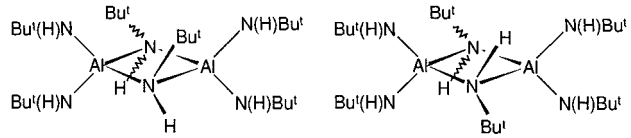

1b′ **1b″**

(C_{2v}), and *trans*, **1b″** (C_{2h}), isomers in 83% yield. The ^1H NMR spectrum of **1b** exhibits three equally intense resonances for **1b′** and two resonances in the ratio 1 : 2 for **1b″**.† The gallium analogue $[Ga(NHBu^t)_3]_2$ has been structurally characterized as the *cis* isomer.[2] The mixture of isomers **1b′** and **1b″** could not be separated by recrystallization.

The reaction of **1b** with six equivalents of $LiBu^n$ in hexane produces the novel cluster $Li_3Al_2[N(H)Bu^t]_3[NBu^t]_3\cdot(LiBu^n)_2$ (**2**). Complex **2** is formed as the major product for stoichiometries ranging from 4 : 1 to 8 : 1, even at reflux, but the optimum yield is obtained when 5 equiv. of $LiBu^n$ are used [eqn. (1)].†

$$5\ LiBu^n + \underset{\textbf{1b}}{\{Al[N(H)Bu^t]_3\}_2} \longrightarrow \underset{\textbf{2}}{Li_3Al_2[N(H)Bu^t]_3[NBu^t]_3\cdot(LiBu^n)_2} + 3\ HBu^n \quad (1)$$

The ^1H NMR spectrum of **2** shows five unique Bu^t environments (1 : 2 : 1 : 1 : 1) at 23 °C which resolve into six equally intense resonances at −20 °C, as well as resonances corresponding to Bu^n groups (Bu^n : Bu^t ~ 1 : 3). These puzzling observations were clarified by a single crystal X-ray structure determination, which revealed an unsolvated complex in which a trilithiated derivative of **1b** is coordinated to the dimer $(LiBu^n)_2$ (Fig. 1).‡ *n*-Butyllithium is hexameric in the solid state if crystallized from a non-coordinating solvent,[13] but the dimer is stabilized by coordination of Li^+ ions to TMEDA.[14] A solvated $(LiBu^n)_2$ moiety has been identified recently in the complex $(Ph_2NLi)[Ph(C_6H_4Li)NLi]_2(LiBu^n)_2(Et_2O)_4$ (**3**),[15] but **2** is unique in incorporating *unsolvated* $(LiBu^n)_2$ with three-coordinate Li^+ ions.

The average Li–C bond length in the puckered Li_2C_2 ring is 2.216(12) Å, *cf.* 2.268 Å for the corresponding distances for **3**.[15] Although the three N–H hydrogens in the trilithiated fragment $Li_3Al_2[N(H)Bu^t]_3[NBu^t]_3$ were not located in the X-ray structural determination, it seems reasonable to associate them with the *three*-coordinate nitrogen atoms N(3), N(4) and N(6). Thus the static structure of **2** contains six inequivalent NBu^t groups consistent with the ^1H NMR spectrum at −20 °C (*vide supra*). However, Li(5) is disordered, with equal occupancies, over two sites in which it is in close contact with either N(1) or N(2). A fluxional process involving Li(5) will give rise to equivalence of the Bu^t groups attached to N(1) and N(2) as observed in the ^1H NMR spectrum at 23 °C. All five Li^+ ions in **2** are three-

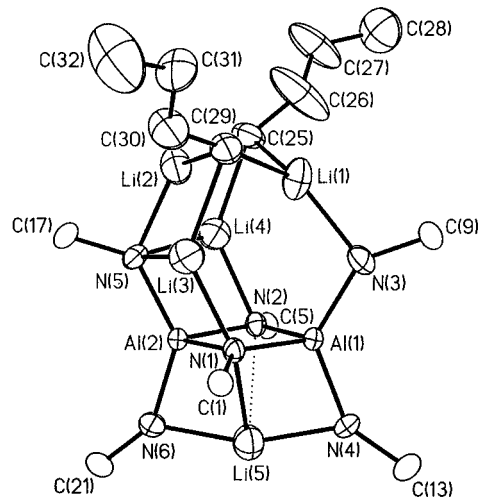

Fig. 1 Molecular structure of $Li_3Al_2[N(H)Bu^t]_3[NBu^t]_3\cdot(LiBu^n)_2$ **2** (30% thermal ellipsoids). For clarity only α-carbon atoms of Bu^t groups are shown and a second, disordered position of Li(5) is omitted. The hydrogen atoms attached to N(3), N(4) and N(6) were not located. Selected bond distances (Å) and angles (°): Li(1)–C(25) 2.262(12), Li(1)–C(29) 2.187(11), Li(1)–N(3) 2.043(12), Li(2)–C(25) 2.181(12), Li(2)–C(29) 2.236(12), Li(2)–N(5) 2.031(12), Li(3)–C(29) 2.238(11), Li(3)–N(1) 2.041(10), Li(3)–N(5) 2.080(11), Li(4)–C(25) 2.157(12), Li(4)–N(2) 2.037(10), Li(4)–N(5) 2.052(11), Li(5)–N(2) 2.303(19), Li(5)–N(4) 2.064(10), Li(5)–N(6) 2.069(11), Al(1)–N(3)–Li(1) 110.3(4), Al(2)–N(5)–Li(2) 127.4(4).

coordinate and the Li–N distances are in the normal range of 2.031(12)–2.075(10) Å with the exception of those involving Li(5) [Li(5)–N(2) = 2.303(19), Li(5)′–N(1) = 2.296(16) Å]. The geometry at aluminium is distorted tetrahedral with NAlN bond angles in the range 87.96(13)–127.90(19)° and 87.14(13)–134.80(17)° for Al(1) and Al(2), respectively. The smallest bond angle (< 90°) is found within the Al_2N_2 ring. The significant difference between the values of N(5)–Al(2)–N(6) and N(3)–Al(1)–N(4) [134.80(17)° *vs*. 127.90(19)°] presumably reflects the coordination of N(5) to Li(3) and Li(4). The Al–N distances [average value = 1.872(4) Å, range 1.833(3)–1.895(3) Å] are comparable to the values found for related lithiated AlN complexes.[10a]

Although LiBu^n has been employed successfully for the dilithiation of the dimer [Bu^{t}N(H)P(μ-NBu^t)]$_2$[16] and the trilithiation of MeSi(NHBu^t)$_3$,[17] the use of alternative metallating reagents will be necessary for the generation of $Al(NR)_3^{3-}$, an isoelectronic analogue of AlO_3^{3-}.

We gratefully acknowledge the NSERC of Canada for financial support and the Killam Memorial Foundation for a fellowship (J. K. B.).

Notes and references

† *Synthesis of* **1b**: A solution of $AlCl_3$ (1.22 g, 9.15 mmol) in diethyl ether (10 mL) was added dropwise to a stirred slurry of LiN(H)Bu^t (2.17 g, 27.4 mmol) in diethyl ether (30 mL) cooled to −78 °C. After 0.5 h at −78 °C the reaction mixture was stirred for a further 1.5 h at 23 °C and subsequently filtered to give a colourless solution. Removal of solvent *in vacuo* yielded white microcrystalline **1b** (1.84 g, 3.78 mmol, 83%); mp 170 °C (decomp.). Anal. calc. for $AlC_{12}H_{30}N_3$: C, 59.22; H, 12.42; N, 17.27. Found: C, 59.24; H, 12.48; N, 17.16%. ^{1}H NMR (C_6D_6, 23 °C, 200 MHz): δ 1.48 (18 H, Bu^t), 1.46 (36 H, Bu^t), 1.37 (18 H, Bu^t), 1.35 (72 H, Bu^t), 1.28 (18 H, Bu^t). ^{27}Al NMR [C_7D_8, 23 °C, 52.12 MHz, $Al(NO_3)_3$ in D_2O]: δ 98.5 ($\Delta\nu_{1/2}$ = 2.08 kHz). IR (KBr, Nujol mulls): 3358 (br) and 3250 (br) cm^{-1} [ν(N–H)]. X-Ray quality crystals (blocks) were obtained in 4 days (23 °C) *via* recrystallization from hexane.

Synthesis of **2**: A 2.5 M solution of LiBu^n in hexanes (2.06 mL, 5.15 mmol) was added dropwise to a stirred solution of **1b** (0.50 g, 1.03 mmol) in hexane (30 mL) cooled to −78 °C. After 0.5 h at −78 °C the reaction mixture was stirred for a further 4 h at 23 °C. Concentration (*ca*. 2 mL) and subsequent cooling (0 °C) of the resulting solution yielded colourless cubes of **2** (0.61 g, 0.97 mmol, 94%); mp 175 °C (decomp.). Anal. calc. for $Al_2C_{32}H_{75}Li_5N_6$: C, 60.75; H, 11.95; N, 13.28. Found: C, 60.14; H, 12.06; N, 13.07%. ^{1}H NMR (C_7D_8, 23 °C, 400 MHz): δ 1.73 [m, 8 H, $CH_2(CH_2)_2CH_3$], 1.50 (9 H, Bu^t), 1.42 (18 H, Bu^t), 1.38 (9 H, Bu^t), 1.34 (9 H, Bu^t), 1.32 (9 H, Bu^t), 1.14 [t, 6 H, $CH_2(CH_2)_2CH_3$], −0.52 [m, 4 H, $CH_2(CH_2)_2CH_3$]. ^{1}H NMR (C_7D_8, −20 °C, 400 MHz): δ 1.73 [m, 8 H, $CH_2(CH_2)_2CH_3$], 1.53 (9 H, Bu^t), 1.43 (9 H, Bu^t), 1.41 (9 H, Bu^t), 1.38 (9 H, Bu^t), 1.35 (9 H, Bu^t), 1.31 (9 H, Bu^t), 1.14 [t, 6 H, $CH_2(CH_2)_2CH_3$], −0.52 [m, 4 H, $CH_2(CH_2)_2CH_3$]. ^{7}Li NMR (C_7D_8, 23 °C, 155.51 MHz, 1 M LiCl in D_2O): δ 0.29 (br), 0.18, −1.16 (approximately 3 : 1 : 1). ^{27}Al NMR [C_7D_8, 23 °C, 52.12 MHz, $Al(NO_3)_3$ in D_2O]: δ 98.0 ($\Delta\nu_{1/2}$ = 762 Hz). IR (KBr, Nujol mulls): 3227 (br) cm^{-1} [ν(N–H)].

‡ *Crystallographic data* for **2**: Colourless cubic crystals of **2** (0.3 × 0.3 × 0.4 mm) were obtained from hexane and mounted on a thin glass fibre. Data were collected on a SMART CCD diffractometer with graphite-monochromated Mo-Kα radiation (0.71073 Å) at 20 °C in the range 1.98° < 2θ < 23.50° (10471 reflections collected, 6241 independent reflections, R_{int} = 0.0457). The structure was solved by direct methods and refinement, based on F^2, was by full-matrix least-squares procedures. All non-hydrogen atoms were refined with anisotropic displacement coefficients. Hydrogen atoms for the Bu^t groups were treated as idealized contributions. Attempts to locate the NH hydrogen atoms were unsuccessful and were ignored. Atomic scattering factors were obtained from the SHELXTL (5.1) program library. $C_{32}H_{75}Al_2Li_5N_6$, M = 632.66, monoclinic, $P2_1/c$, a = 17.872(5), b = 11.472(3), c = 20.606(5) Å, β = 91.896(5)°, V = 4222(2) Å^3, D_c = 1.045 g cm^{-3}, Z = 4, μ = 0.099 mm^{-1}. Refinement converged at $R1$ = 0.0936, $wR2$ = 0.2962. CCDC 182/1063. See http://www.rsc.org/suppdata/cc/1998/2543, for crystallographic files in .cif format.

1 Al: J. S. Silverman, C. J. Carmalt, D. A. Neumayer, A. H. Cowley, B. G. McBurnett and A. Decken, *Polyhedron*, 1998, **17**, 977.
2 Ga: D. A. Atwood, V. O. Atwood, A. H. Cowley, R. A. Jones, J. L. Atwood and S. G. Bott, *Inorg. Chem.*, 1994, **33**, 3251.
3 In: J. Kim, S. G. Bott and D. M. Hoffman, *Inorg. Chem.*, 1998, **37**, 3835.
4 (*a*) T. Chivers, M. Parvez and X. Gao, *Inorg. Chem.*, 1996, **35**, 4336; (*b*), *Angew. Chem., Int. Ed. Engl.*, 1995, **34**, 2549.
5 T. Chivers, M. Parvez and G. Schatte, *Inorg. Chem.*, 1996, **35**, 4094.
6 R. Fleischer, S. Freitag, F. Pauer and D. Stalke, *Angew. Chem., Int. Ed. Engl.*, 1996, **35**, 204.
7 (*a*) M. A. Beswick, N. Choi, C. N. Harmer, A. D. Hopkins, M. McPartlin, M. A. Paver, P. R. Raithby, A. Steiner, M. Tombul and D. S. Wright, *Inorg. Chem.*, 1998, **37**, 2177; (*b*) A. J. Edwards, M. A. Paver, P. R. Raithby, M.-A. Rennie, C. A. Russell and D. S. Wright, *Angew. Chem., Int. Ed. Engl.*, 1994, **33**, 1277.
8 R. Fleischer, A. Rothenberger and D. Stalke, *Angew. Chem., Int. Ed. Engl.*, 1997, **36**, 1105.
9 P. R. Raithby, C. A. Russell, A. Steiner and D. S. Wright, *Angew. Chem., Int. Ed. Engl.*, 1997, **36**, 649.
10 (*a*) D. Rutherford and D. A. Atwood, *J. Am. Chem. Soc.*, 1996, **118**, 11535; (*b*) D. A. Atwood and D. Rutherford, *Organometallics*, 1996, **15**, 436; (*c*) D. A. Atwood and D. Rutherford, *Chem. Commun.*, 1996, 1251.
11 C-C. Chang, M-D. Li, M. Y. Chiang, S-M. Peng, Y. Wang and G-H. Lee, *Inorg. Chem.*, 1997, **36**, 1955. A trimeric structure is proposed on the basis of MS data.
12 M. A. Beswick, N. Choi, C. N. Harmer, M. McPartlin, M. E. G. Mosquera, P. R. Raithby, M. Tombul and D. S. Wright, *Chem. Commun.*, 1998, 1383.
13 T. Kottke and D. Stalke, *Angew. Chem., Int. Ed. Engl.*, 1993, **32**, 580.
14 (*a*) M. A. Nichols and P. G. Williard, *J. Am. Chem. Soc.*, 1993, **115**, 1568; (*b*) D. Hoffmann and D. B. Collum, *J. Am. Chem. Soc.*, 1998, **120**, 5810.
15 R. P. Davies, P. R. Raithby and R. Snaith, *Angew. Chem., Int. Ed. Engl.*, 1997, **36**, 1215.
16 I. Schranz, L. Stahl and R. J. Staples, *Inorg. Chem.*, 1998, **37**, 1493.
17 M. Veith, A. Spaniol, J. Pöhlmann, F. Goss and V. Huch, *Chem. Ber.*, 1993, **126**, 2625.

Communication 8/07081D

ChemComm

Synthesis and structural analysis of an infinite linear coordination network formed by the self-assembly of tetracyanocalix[4]arene ligands and silver cations

Gilles Mislin,[a] Ernest Graf,[a] Mir Wais Hosseini,*[a] André De Cian,[b] Nathalie Kyritsakas[b] and Jean Fischer[b]

[a] *Laboratoire de Chimie de Coordination Organique, UMR CNRS 7513, Université Louis Pasteur, F-67000 Strasbourg, France. E-mail: hosseini@chimie.u-strasbg.fr*

[b] *Laboratoire de Cristallochimie et Chimie Structurale, UMR CNRS 7513, Université Louis Pasteur, F-67000 Strasbourg, France*

Received (in Basel, Switzerland) 23rd September 1998, Accepted 19th October 1998

Using the O-alkylation of the lower rim of the calix[4]arene to impose the 1,3-alternate conformation and the functionalisation of the upper rim to set-up four nitrile groups pointing in a divergent fashion, an *exo*-ligand capable of forming linear coordination networks was obtained; upon self-assembly of the latter and silver cation, a linear coordination polymer was obtained and structurally analysed in the solid state by an X-ray study.

Due to their foreseeable wide scope of applications, coordination polymers which may also be described as molecular networks are currently attracting much attention.[1] In these assemblies, metals in addition to their structural role might also display functional features. The dimensionality (1-, 2- or 3-D networks) as well as the topology (linear, helical) of coordination polymers may be tuned through the interplay between the metal (coordination requirements, *i.e*. coordination number and coordination geometry) and the *exo*-ligand (number of coordination sites and their location, steric control). Many examples of coordination polymers based on bis-monodentate[1,2] bis-bidentate[3,4] and bis-tridentate ligands[5] have been reported. Here we report the synthesis of an *exo*-ligand of the calix[4]arene type bearing four nitrile groups as coordination sites as well as the structural analysis of the free ligand and of its linear Ag^{I}-coordination polymer.

For the formation of molecular networks, the design of *exo*-ligands in which the coordination sites are oriented in a divergent fashion is crucial. Molecular units possessing four coordination sites occupying the apices of a pseudo-tetrahedron may be of interest for construction of linear coordination polymers using metals requiring a tetrahedral coordination geometry. The design of such a ligand may be based on a preorganised backbone offering the possibility of anchoring four coordination sites in an alternating mode below and above its main plane. This aspect was previously demonstrated in the case of mercaptocalix[4]arene derivatives for which in the lower rim the OH groups were replaced by SH moieties.[6] Another design may be based on the use of both the upper and lower rims. Indeed, one may impose the needed 1,3-alternate conformation by proper transformation of all four hydroxy groups, and on the other hand, using *para* positions one may set-up, in a controlled manner, coordination sites. This has been demonstrated in the case of catechol units as the coordination sites.[7] Again, using this strategy, we designed the *exo*-ligand **1** containing four nitrile groups as a building block for the formation of linear coordination polymers. It is worth noting that for ligand **1**, due to the donor effect of oxygen atoms, the binding ability of nitriles is considerably enhanced.

The synthesis of **1** was achieved as follows. The starting material was the *p-tert*-butylcalix[4]arene **2**[8] which after dealkylation in toluene in the presence of phenol and $AlCl_3$ afforded **3** as a mixture of conformers.[9] The O-alkylation of the latter using 2-methoxyethyltosylate in DMF in the presence of Cs_2CO_3 afforded **4** which, after recrystallisation, was shown to adopt the 1,3-alternate conformation.[10] The desired tetracyano compound **1** was obtained after bromination of **4** using NBS in butanone leading to the tetrabromo compound **5** and followed by treatment of the latter by CuCN in *N*-methylpyrrolidone.[11] The structural assignment of **1** was achieved by classical NMR studies as well as by X-ray diffraction† which indeed confirmed the 1,3-alternate conformation (Fig. 1).

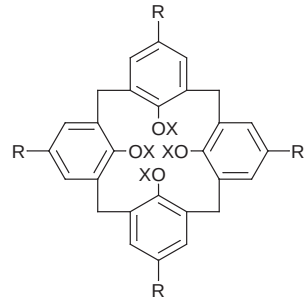

1 R = CN, X = $CH_2CH_2OCH_3$
2 R = $C(CH_3)_3$, X = H
3 R = H, X = H
4 R = H, X = $CH_2CH_2OCH_3$
5 R = Br, X = $CH_2CH_2OCH_3$

The metal cation, Ag^{I}, which is already extensively used for the formation of coordination networks,[12] was chosen because it forms kinetically labile complexes. Furthermore, coordination networks based on the binding of silver by bis-,[13a] tris-[13b] and tetrakis-nitrile[13c] based ligands have been reported. However, Ag^{I} may adopt a wide range of coordination geometries. We have observed linear,[14] trigonal[15] and tetrahedral[4] coordination geometries using pyridine, benzonitrile and bipyridine based ligands respectively.

In principle, for the combination of the ligand **1** and Ag^{I}, one may envisage two types of linear coordination polymers (Fig. 2). The difference between the two possibilities resides in the difference in the coordination geometry around the silver cation. Whereas for the di-coordinated Ag adopting a linear coordination geometry, a 1 : 2 ligand : metal stoichiometry would be obtained, in the case of tetrahedral coordination geometry, a 1 : 1 metal : ligand ratio would be expected.

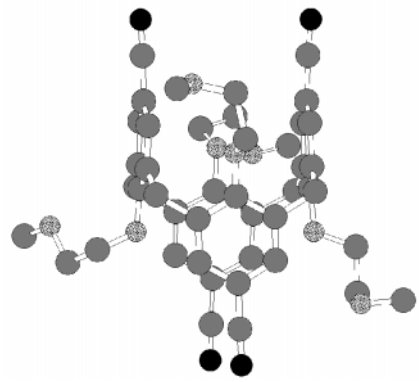

Fig. 1 X-Ray structure of the free ligand **1** adopting the 1,3-alternate conformation. H atoms are not presented for sake of clarity.

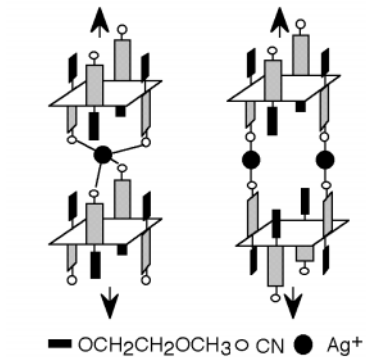

Fig. 2 Schematic representation of two types of linear coordination networks which may be envisaged for the self-assembly of the ligand **1** and Ag^{I} cation adopting tetrahedral- (left) or linear- (right) coordination geometries.

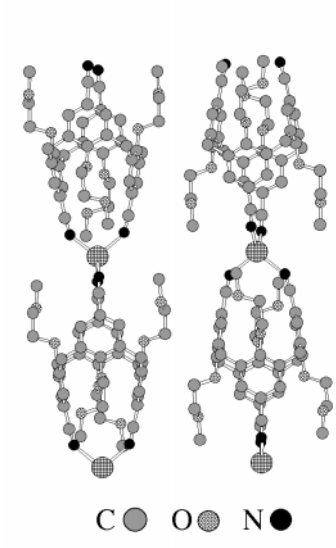

Fig. 3 A portion of the X-ray structure showing fragments of two parallel cationic linear coordination networks obtained by mutual bridging of Ag^{I} cations and ligands **1** (projection down the polymer axis). H atoms, solvent molecules and anions are not presented for sake of clarity.

Upon slow diffusion of a CH_2Cl_2 (1 ml) solution of ligand **1** (5 mg, 6.6×10^{-6} mol) into an EtOH (2 ml) solution of $AgAsF_6$ (20 mg, 6.7×10^{-4} mol) in large excess, a colourless crystalline material was obtained. The analysis of monocrystals by X-ray crystallography‡ revealed the presence of disordered H_2O and EtOH molecules in the lattice. In addition to the solvent molecules the crystal (tetragonal, space group *P*4/*nnc*) was composed of linear coordination polymers and disordered AsF_6 anions. The ligand **1**, as in the absence of Ag^{I} cation (Fig. 1), adopted a 1,3-alternate conformation (Fig. 3). The ether fragments adopted a *gauche* conformation with an OCCO dihedral angle of 73.8°. In order to bind two Ag^{I} cations in the tetrahedral mode of coordination, the calix unit was slightly pinched at the upper rim, *i.e.*, the N···N and O···O distances between nitrogen and oxygen atoms located within the same side of the calix unit were 3.533 and 5.670 Å respectively. The nitrile groups were almost linear with a CCN angle of 176.8° and CN distance of 1.104 Å. The cationic network was formed by mutual bridging between ligands **1** and Ag^{I} cations (Fig. 3). The silver cations were tetrahedrally coordinated to four nitrile groups with the NAgN angle varying from 100.9 to 121.9° (average 106.2°), CNAg angle of *ca.* 144.0° and AgN distance of *ca.* 2.292 Å. The packing of the cationic and anionic components (Fig. 4) showed parallel strands of linear coordination polymers with columns of disordered AsF_6^- anions separated by water molecules.

In conclusion, employing the self-assembly strategy, the formation of a silver coordination network using an *exo*-ligand based on calix[4]arene in the 1,3-alternate conformation and bearing at the upper rim four nitrile groups was achieved. The structure of the infinite network was established by single-crystal X-ray analysis.

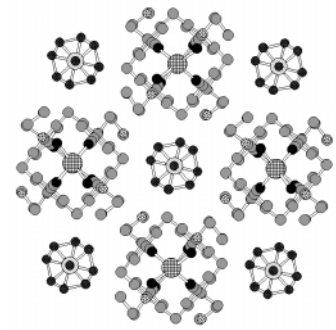

Fig. 4 A portion of the structure showing the packing of the cationic linear coordination networks and AsF_6^- anions (projection normal to the polymer axis). The AsF_6^- anions were found to be disordered. H atoms and solvent molecules (H_2O and EtOH) are not presented for sake of clarity.

Notes and references

† (Colorless, 173 K), $C_{44}H_{44}N_4O_8$, M = 1756.86, orthorhombic, a = 14.8980(3), b = 35.729(1), c = 14.9520(3) Å, U = 7958.8(5) Å^3, Z = 8, space group *Pbca*, D_c = 1.26 g cm^{-3}, Nonius CCD, Mo-Kα, μ = 0.088 mm^{-1}, 3543 data with $I > 3\sigma(I)$, R = 0.045, Rw = 0.056.

‡ (Colorless, 173 K), $C_{44}H_{44}N_4O_8Ag{\cdot}AsF_6{\cdot}2H_2O{\cdot}CH_3CH_2OH$, M = 1135.75, tetragonal, $a = b$ = 14.4450(7), c = 27.129(1) Å, U = 5660.7(7) Å^3, Z = 4, space group *P*4/*nnc*, D_c = 1.33 g cm^{-3}, Nonius CCD, Mo-Kα, μ = 1.001 mm^{-1}, 1078 data with $I > 3\sigma(I)$, R = 0.081, Rw = 0.119. CCDC 182/1062.

1 R. Robson, in *Comprehensive Supramolecular Chemistry*, ed. J. L. Atwood, J. E. D. Davies, D. D. Macnicol and F. Vögtle, Pergamon, Oxford, vol. 6 (ed. D. D. Macnicol, F. Toda and R. Bishop), 1996, p. 733.

2 T. L. Hennigar, D. C. MacQuarrie, P. Losier, R. D. Rogers and M. J. Zaworotko, *Angew. Chem., Int. Ed. Engl*., 1997, **36**, 972.

3 U. Velten and M. Rehahn, *Chem. Commun*., 1996, 2639; S. Decurtins, R. Pellaux, A. Hauser and M. E. von Arx, in *Magnetism: A Supramolecular Function, Vol. C484*, ed. O. Kahn, Kluwer, Dordrecht, 1996, p. 487.

4 C. Kaes, M. W. Hosseini, C. E. F. Rickard, B. W. Skelton and A. White, *Angew. Chem., Int. Ed. Engl*., 1998, **37**, 920

5 E. C. Constable and A. M. W. Cargill Thompson, *J. Chem. Soc., Dalton Trans*., 1992, 3467; M. Ferigo, P. Bonhôte, W. Marty and H. Stoeckli-Evans, *ibid*., 1994, 1549.

6 C. G. Gibs and C. D. Gutsche, *J. Am. Chem. Soc*., 1993, **115**, 5338; X. Delaigue, J. McB. Harrowfield, M. W. Hosseini, A. De Cian, J. Fischer and N. Kyritsakas, *J. Chem. Soc., Chem. Commun*., 1994, 1579; X. Delaigue, M. W. Hosseini, A. De Cian, N. Kyritsakas and J. Fischer, *ibid.*, 1995, 609; X. Delaigue and M. W. Hosseini, *Tetrahedron Lett*., 1993, **34**, 8112.

7 G. Mislin, E. Graf and M. W. Hosseini, *Tetrahedron Lett*., 1996, **37**, 4503.

8 C. D. Gutsche and M. Iqbal, *Org. Synth*., 1989, **68**, 234.

9 C. D. Gutsche and J. A. Levine, *J. Am. Chem. Soc*., 1982, **104**, 2653.

10 W. Verboom, S. Datta, Z. Asfari, S. Harkema and D. N. Reinhoudt, *J. Org. Chem*., 1992, **57**, 5394.

11 M. Conner, V. Janout and S. L. Regen, *J. Org. Chem*., 1992, **57**, 3744.

12 J. Blake, N. R. Champness, S. S. M. Chung, W-S. Li and M. Schröder, *Chem. Commun*., 1997, 1675; M. A. Withersby, A. J. Blake, N. R. Champness, P. Hubberstey, W-S. Li and M. Schröder, *ibid.*, 1997, 2327; M. J. Hannon, C. L. Painting and W. Errington, *ibid.*, 1997, 1805.

13 (*a*) D. Perreault, M. Drouin, A. Michel and P. D. Harvey, *Inorg. Chem*., 1992, **31**, 3688; K. A. Hirsch, S. R. Wilson and J. S. Moore, *ibid.*, 1997, **36**, 2960; K. A. Hirsch, S. R. Wilson and J. S. Moore, *Chem. Eur. J*., 1997, **3**, 765; (*b*) G. B. Gardner, D. Venkataraman, J. S. Moore and S. Lee, *Nature*, 1995, **374**, 792; G. B. Gardner, Y.-H. Kiang, S. Lee, A. Asgaonkar and D. Venkataraman, *J. Am. Chem. Soc*., 1996, **118**, 6946; B. F. Abrahams, S. J. Egan, B. F. Hoskins and R. Robson, *Chem. Commun*., 1996, 1099; (*c*) F.-Q. Liu and T. D. Tilley, *Inorg. Chem*., 1997, **36**, 2090.

14 R. Schneider, M. W. Hosseini, J.-M. Planeix, A. De Cian and J. Fischer, *Chem. Commun*., 1998, 1625.

15 R. Schneider, M. W. Hosseini, J.-M. Planeix, A. De Cian and J. Fischer, unpublished results.

Communication 8/07434H

Catalytic enantioselective ene reactions of imines: a simple approach for the formation of optically active α-amino acids

Sulan Yao, Xiangming Fang and Karl Anker Jørgensen*

Center for Metal Catalyzed Reactions, Department of Chemistry, Aarhus University, DK-8000 Aarhus C, Denmark. E-mail: kaj@kemi.aau.dk

Received (in Cambridge, UK) 15th October 1998, Accepted 21st October 1998

A highly enantioselective ene reaction of readily available tosyl α-imino esters with alkenes catalysed by only 0.1 mol% of chiral $CuPF_6$–BINAP complexes is presented.

The development of asymmetric catalytic reactions has in recent years added a new and very important aspect to chemistry as it allows one to use a small amount of chiral catalysts to form directly optically active compounds.[1]

The ene reaction of alkenes **1** with α-imino esters **2** can give α-amino acids **3** which are among the most fundamental compounds in nature (Scheme 1).

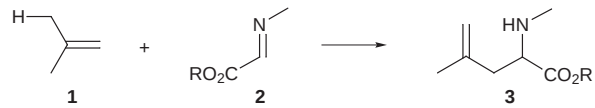

1 **2** **3**

Scheme 1

Within the last decade the asymmetric catalytic addition reactions of carbonyl compounds have been developed to a level where they can be performed with a high degree of stereoselectivity.[2–4] Compared with the highly efficient catalytic enantioselective ene reaction of carbonyl compounds, the related ene reaction of imines has only met with very limited success.[5] The catalytic enantioselective ene reaction of imines has, to the best of our knowledge, not yet been achieved regardless of its potential broad application. One of the problems with this reaction compared with the related reaction of carbonyl compounds is that the imine probably competes with the chiral ligand in coordinating to the Lewis acid and therefore suppresses the chiral information from the ligand.

Recently the first catalytic enantioselective hetero-Diels–Alder reaction,[6] addition of enol silanes[7] and alkylation[8] of α-imino esters **2** have been developed and a recent paper[9] dealing with the catalytic ene reaction of **2** with alkenes prompted us to present our results at the present stage of investigations.

Here we present a highly enantioselective ene reaction of alkenes with tosyl α-imino esters catalysed by chiral $CuPF_6$–BINAP complexes. The strategy behind the catalytic enantioselective ene reaction of α-imino esters is the use of chiral phosphine ligands in combination with copper(I) salts. The chiral phosphine ligands (*R*)-BINAP **4a**, (*R*)-Tol-BINAP **4b**, (*R*,*R*)-DIOP **4c** and (*R*,*R*)-NORPHOS **4d** have been found to be

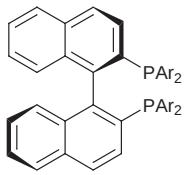

4a Ar = Ph
4b Ar = Tol

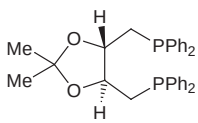

4c

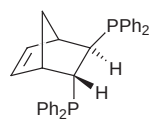

4d

the most promising of the different ligands tested for the ene reaction of α-methylstyrene **1a** with tosyl α-imino ester **2a** in the presence of various Lewis acids. Some representative results are presented in Table 1.

The results for the screening of the various ligands and Lewis acids show that (*R*)-BINAP **4a** and (*R*)-Tol-BINAP **4b** in combination with copper(I) salts catalyse the ene reaction of α-methylstyrene **1a** with tosyl α-imino ester **2a** giving adduct **3a** in good yield and up to 95% ee (Table 1, entries 1–6). The ee of **3a** is counterion-dependent and the highest ees are obtained with PF_6 and ClO_4 as the anions; it is of practical importance that $CuPF_6$ can be used as this Lewis acid is safer, more stable and easier to handle than $CuClO_4$. Changing the catalyst to (*S*)-BINAP–$CuClO_4$ leads to the opposite enantiomer with the same yield and ee. Choosing copper(II) as the Lewis acid in combination with the BINAP ligands leads to a significant reduction in the ee of **3a** (entry 7). The combination of ligand **4b** with other Lewis acids gives only reasonable results in the case of silver(I) (entries 8–12). The application of the chiral ligands (*R*,*R*)-DIOP **4c** and (*R*,*R*)-NORPHOS **4d** leads only to very low yield and ee of **3a** when tested for the ene reaction in combination with $CuPF_6$ as the Lewis acid (entries 13, 14). The results presented in Table 1 are all performed in THF; CH_2Cl_2 can also be used and similarly good results as those presented in entries 1–6 are obtained. The latter solvent has the advantage that the reaction course can easily be monitored by the colour change; the coordination of **2a** to the catalyst complex at the reaction temperature gives a dark purple colour, and when the reaction goes to completion the colour becomes a clear light yellow. We have also tried various chiral bisoxazolines in combination with different Lewis acids but only low to moderate ees were obtained.

The potential and scope of the ene reaction of various alkenes **1a**–**e** with the tosyl α-imino ester **2a** in the presence of (*R*)-Tol-BINAP **4b**–CuX as the catalyst are presented in Table 2.[10]

The results show that both aromatic (**1a**,**b**), cyclic (**1c**,**d**) and simple aliphatic alkenes (**1e**) react with **2a** in the presence of

Table 1 The results for the reaction of α-methylstyrene **1a** with the tosyl α-imino ester **2a** in the presence of the various chiral phosphine ligands **4a**–**d** and Lewis acids (10 mol%) at room temperature in THF

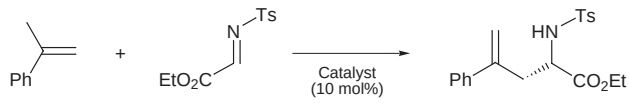

1a **2a** **3a**

Entry	Ligand–metal salt	Yield of **3a**[a] (%)	Ee[b] (%)
1	**4a**–$CuClO_4$	73	93
2	**4b**–$CuClO_4$	75	95
3	**4a**–$CuPF_6$	77	93
4	**4b**–$CuPF_6$	80	95
5	**4a**–CuOTf	58	76
6	**4b**–CuOTf	67	80
7	**4b**–$Cu(OTf)_2$	75	24
8	**4b**–AgOTf	75	73
9	**4b**–$AgClO_4$	72	67
10	**4b**–$AgSbF_6$	63	68
11	**4b**–$Pd(SbF_6)_2$	61	< 5
12	**4b**–$RuArSbF_6$	8	5
13	**4c**–$CuPF_6$	3	< 5
14	**4d**–$CuPF_6$	25	< 5

[a] Isolated yield. [b] Determined by chiral HPLC.

Table 2 The results for the reaction of various alkenes **1a**–**e** with the tosyl α-imino ester **2a** catalysed by (*R*)-Tol-BINAP **4b**–CuX (X = PF_6, ClO_4)[a]

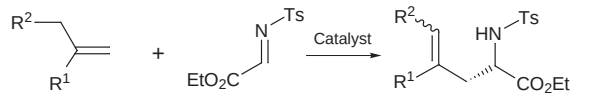

1a R^1 = Ph, R^2 = H
b R^1 = *p*-$MeOC_6H_4$, R^2 = H
c R^1 = R^2 = $(CH_2)_3$
d R^1 = R^2 = $(CH_2)_4$
e R^1 = Me, R^2 = H

2a

3a R^1 = Ph, R^2 = H
b R^1 = *p*-$MeOC_6H_4$, R^2 = H
c R^1 = R^2 = $(CH_2)_3$
d R^1 = R^2 = $(CH_2)_4$
e R^1 = Me, R^2 = H

Entry	Catalyst	1	Load (%)	*T*/°C	*t*/h	Yield[b] (%)	Ee[c] (%)
1[d]	**4b**–$CuClO_4$	**1a**	10	room temp.	18	75	95
2	**4b**–$CuClO_4$	**1a**	10	room temp.	18	85	95
3	**4b**–$CuPF_6$	**1a**	1	−20	38	80	99
4	**4b**–$CuPF_6$	**1a**	0.5	0	22	82	98
5	**4b**–$CuPF_6$	**1a**	0.1	0	24	71	95
6	**4b**–$CuClO_4$	**1b**	1	0	15	81	91
7	**4b**–$CuClO_4$	**1b**	0.1	0	36	80	91
8	**4b**–$CuPF_6$	**1c**	0.5	−20	18	74	92
9	**4b**–$CuPF_6$	**1d**	1	0	60	72	84
10	**4b**–$CuPF_6$	**1e**	2	0	17	49	82
11[e]	**4b**–$CuPF_6$	**1e**	1	0	60	62	78

[a] All reactions were run in CH_2Cl_2 on a 0.4 mmol scale unless otherwise stated. [b] Isolated yield. [c] Determined by chiral HPLC using a Chiralcel OJ or OD column. [d] Solvent THF. [e] The reaction was performed on a 3 mmol scale.

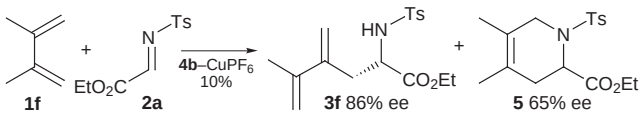

Scheme 2

(*R*)-Tol-BINAP **4b**–CuX (X = PF_6, ClO_4) as the catalyst. For alkene **1a** it appears that the reaction proceeds well using both THF and CH_2Cl_2 as these solvents, giving good yields and high ees of **3a** at room temperature in the presence of 10 mol% of the catalyst (entries 1, 2). Reducing the catalyst loading to 1, 0.5 and even 0.1 mol% causes no significant reduction in the yield of **3a** and even higher enantioselectivities (up to 99%) are obtained (entries 3–5). The *p*-methoxy substituted alkene **1b** reacts in a similar manner with **2a** and an ee of up to 91% is obtained using only 0.1 mol% catalyst loading (entry 7). Methylenecyclopentane **1c** reacts also in a highly enantioselective manner with **2a** with only 0.5 mol% of **4b**–$CuPF_6$ as the catalyst and up to 92% ee is found (entry 8), while methylenecyclohexane **1d** is less reactive and leads to a small reduction in ee compared with **1c** (entry 9). The reaction of isobutylene **1e** with **2a** in the presence of (*R*)-Tol-BINAP **4b**–$CuPF_6$ as the catalyst (entries 10, 11) gives also the corresponding ene product **3e** in reasonable yields and with high ee; the latter reaction can be performed in a gram scale with a catalytic loading of only 1 mol% without affecting the yield and ee. This reaction has been used to assign the absolute stereochemistry of the ene product **3e** as this adduct is easily transformed to the *N*-tosylleucine ethyl ester the stereochemistry of which is found to be *S* by correlation with the same compound prepared from (*S*)-leucine. The absolute stereochemistry of **3e** indicates that the alkene approaches the *si*-face of the tosyl α-imino ester **2a** when coordinated to the catalyst.

2,3-Dimethylbuta-1,3-diene **1f** reacts with the tosyl α-imino ester **2a** in the presence of (*R*)-Tol-BINAP **4b**–$CuPF_6$ (10 mol%) as the catalyst to give both the ene product **3f** and the hetero-Diels–Alder product **5**, with a preference for the latter (**3f**:**5** = 1:9) (Scheme 2). The ee of the ene adduct **3f** was 86% at room temperature, while 65% ee was found for **5**.

We have presented a highly enantioselective ene reaction of alkenes with tosyl α-imino esters catalysed by $CuPF_6$–BINAP complexes. The substrates for this ene reaction are aromatic, cyclic and simple alkenes and the reaction provides a simple method for the preparation of both optically active natural and non-natural α-amino acids; the potential of the ene reaction derives from the fact that it proceeds with only 0.1 mol% of the $CuPF_6$–BINAP catalyst. Work is in progress to develop the reaction further and to understand the mechanism.

Thanks are expressed to the Danish National Science Foundation for financial support.

Notes and references

1 Some recent books dealing with asymmetric catalysis: *Advances in Catalytic Processes*: *Asymmetric Chemical Transformations*, ed. M. Doyle, JAI, Greenwich, CT, 1995, vol. 1; *Catalytic Asymmetric Synthesis*, ed. I. Ojima, VCH, Weinheim, 1993; M. Santelli and J.-M. Pons, *Lewis Acids and Selectivity in Organic Synthesis*, CRC Press, Boca Raton, 1995; *Asymmetric Catalysis in Organic Synthesis*, ed. R. Noyori, Wiley Interscience, New York, 1993; L. F. Tietze and G. Kettschau, *Stereoselective Heterocyclic Synthesis I*, ed. P. Metz, Springer Verlag, Berlin, 1997, vol. 189, pp. 1–120; *Transition Metals for Fine Chemicals and Organic Synthesis*, ed. M. Beller and C. Bolm, Wiley Interscience, UK, 1998.

2 For a general review of eneantioselective ene reactions, see K. Mikami and M. Shimizu, *Chem. Rev*., 1992, **92**, 1021.

3 See also *e.g*. K. Mikami, *Pure Appl. Chem*. 1996, **68**, 639; K. Mauruoka, Y. Hoshino, T. Shirasaka and H. Yamamoto, *Tetrahedron Lett*. 1988, **29**, 3967; D. A. Evans, C. S. Burgey, N. A. Paras and S. W. Tregay, *J. Am. Chem. Soc*., 1998, **120**, 5824.

4 Examples of catalytic enantioselective hetero-Diels–Alder reactions of aldehydes and ketones see *e.g*. K. Maruoka, T. Otoh, T. Shirasaka and H. Yamamoto, *J. Am. Chem. Soc*. 1988, **110**, 310; Q. Gao, K. Ishihara, M. Mouri and H. Yamamoto, *Tetrahedron*, 1994, **50**, 979; G. Keck, X.-Y. Li and D. Krishamurthy, *J. Org. Chem*., 1995, **60**, 5998; Q. Gai, T. Maruyama, M. Mouri and H. Yamamoto, *J. Org. Chem*., 1992, **57**, 1951; M. Bednarski and S. Danishefsky, *J. Am. Chem. Soc*., 1986, **108**, 7060; M. Johannsen and K. A. Jørgensen, *J. Org. Chem*., 1995, **60**, 5757; A. Graven, M. Johannsen and K. A. Jørgensen, *Chem. Commun*., 1996, 3272; S. Yao, M. Johannsen, H. Audrian, R. G. Hazell and K. A. Jørgensen, *J. Am. Chem. Soc*., 1998, **120**, 8599; D. A. Evans and J. S. Johnson, *J. Am. Chem. Soc*., 1998, **120**, 4895; J. Thorhauge, M. Johannsen and K. A. Jørgensen, *Angew. Chem., Int. Ed*., 1998, **37**, 2404

5 Examples of ene reactions of related imines with alkenes are: O. Achmatowicz and M. Pietraszkiewicz, *J. Chem. Soc., Perkin Trans. 1*, 1981, 2680; D. M. Tschan and S. M. Weinreb, *Tetrahedron Lett*., 1982, **23**, 3015; K. Koch, J.-Y. Lin and F. W. Fowler, *Tetrahedron Lett*., 1983, **24**, 1581; D. M. Tschan, E. Turos and S. M. Weinreb, *J. Org. Chem*., 1984, **49**, 5058; S. Hannesian and R.-Y. Yang, *Tetrahedron Lett*., 1996, **30**, 5273.

6 For catalytic enantioselective hetero-Diels–Alder reaction of imines: K. Ishihara, M. Miyata, H. Hattori and Y. Yamamoto, *J. Am. Chem. Soc*., 1994, **116**, 10520; S. Kobayashi, S. Komiyama and H. Ishitani, *Angew. Chem., Int. Ed*., 1998, **37**, 797; S. Yao, M. Johannsen, R. G. Hazell and K. A. Jørgensen, *Angew. Chem., Int. Ed*., 1998, in the press.

7 For catalytic enantioselective addition of enol silyl ethers to imines: E. Hagiwara, A. Fujii and M. Sodeeoka, *J. Am. Chem. Soc*., 1998, **120**, 2474; D. Ferraris, B. Young, T. Dudding and T. Lectka, *J. Am. Chem. Soc*., 1998, **120**, 4548; D. Ferraris, B. Young, C. Cox, W. J. Drury III, T. Dudding and T. Lectka, *J. Org. Chem*., 1998, **63**, 6090.

8 For catalytic enantioselective alkylation of imines: H. Nakamura, K. Nakamura and Y. Yamamoto, *J. Am. Chem. Soc*., 1998, **120**, 4242.

9 W. J. Drury III, D. Ferraris, C. Cox, B. Young and T. Lectka, *J. Am. Chem. Soc*., 1998, in the press.

10 *Experimental procedure*: A 0.008 M solution of the catalyst was prepared by the addition of $CuPF_6$·4MeCN (15 mg, 0.04 mmol) and (*R*)-Tol-BINAP (30 mg, 0.044 mmol) under N_2 to a flame dried Schlenk tube. The mixture was stirred for 1 h under vacuum, freshly distilled CH_2Cl_2 (5 ml) was added with a syringe under N_2 and the light yellow solution was stirred for 1–3 h until it had become absolute homogeneous. Catalytic reaction (1 mol% catalyst): To a flame dried Schlenk tube was added freshly destilled CH_2Cl_2 (1 ml) and an aliquot of the previously prepared catalyst solution (500 μl) under N_2 and stirred for 5 min; then the tosyl α-imino ester **2a** (0.4 mmol) was added at room temp. The dark purple solution was cooled to the desired reaction temperature before the alkene (0.8 mmol) was added. Then the reaction was kept at that temperature until the dark purple colour had changed into a clear yellow solution (10–65 h). After evaporation of the solvent the crude product was purified by flash chromatography (20% EtOAc–pentane) to give the ene adduct.

Communication 8/08019D

Typeset and printed by Black Bear Press Limited, Cambridge, England

A new look at the McMurry reaction

Michel Ephritikhine

Service de Chimie Moléculaire, DSM, DRECAM, CNRS URA 331, CEA Saclay, 91191 Gif sur Yvette, France.
E-mail: ephri@nanga.saclay.cea.fr

Received (in Cambridge, UK) 10th June 1998, Accepted 21st July 1998

The article emphasizes the contradictory features of the McMurry reaction. The historical view shows how the chemists were firmly convinced of the occurrence of pinacolate intermediates and rejected, in spite of some evidence, the alternative pathway *via* carbenoid species. The McMurry reaction continues to find new important applications but suffers from problems of reproducibility. New practical reagents and simplified methods have been developed but rather complicated systems have been designed for obtaining higher selectivities. Recent investigations confirmed that pinacolates would be the precursors to alkenes but also revealed the possible involvement of carbenoid species, putting forward the dual nature of the mechanism of the McMurry reaction.

The huge interest in the McMurry reaction is expressed by the number of accounts devoted to its synthetic applications and, to a lesser extent, its mechanistic aspects;[1–4] an excellent review by Fürstner and Bogdanovic was published in 1996.[4] In this feature article, we would like to focus on the most recent developments but also recall some older facts, placing this field in a distinct perspective.

An historical view

The rich and peculiar history of the McMurry reaction will be more easily assessed after recalling the course of some important events which are not necessarily brought together, without confusion, in the chemist's memory.

In 1972, Sharpless *et al.* reported that ketones and aldehydes could be reductively coupled into alkenes by reaction with WCl_6 and RLi reagents.[5] One year after, two groups discovered that low-valent titanium complexes were also efficient in this coupling process. Tyrlik and Wolochowicz, who used the $TiCl_3$–Mg system, suggested that tetramethylethylene was obtained *via* the carbene species Me_2C:, resulting itself from deoxygenation of acetone. On the other hand, Mukaiyama *et al.* proposed that metallopinacols were intermediates in the reductive coupling of aromatic ketones by means of the $TiCl_4$–Zn system; the mechanism shown in Scheme 1 explained how benzaldehyde and acetophenone were selectively transformed into the corresponding pinacols and alkenes when the reaction was performed in THF at low temperature or in refluxing dioxane.[7] The pinacolate intermediates would be formed either by dimerization of ketyl radicals resulting from one electron transfer from the low-valent metal species to the carbonyl and/or, in the case of the more easily reducible and reactive aromatic ketones, by nucleophilic attack of a ketone dianion to the C=O bond. Therefore, at the very beginning in 1973, two mechanisms were envisaged for the reductive coupling of carbonyl molecules (Scheme 2).

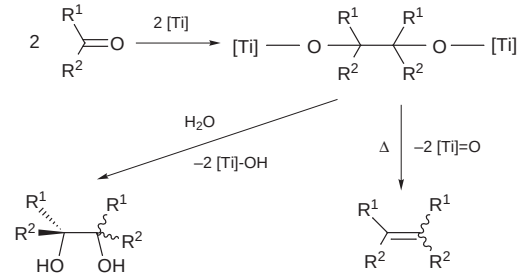

Scheme 1 Reductive coupling of ketones *via* a metallopinacol intermediate.

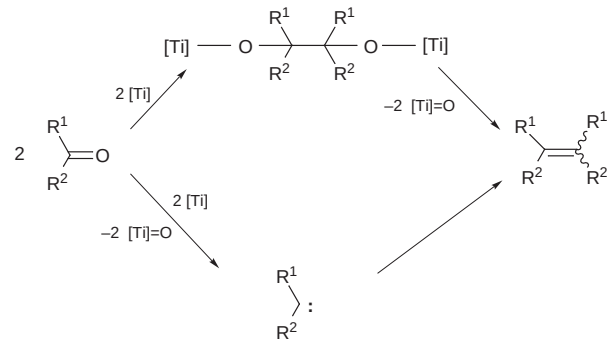

Scheme 2 The two mechanisms proposed in 1973 by Tyrlik and Wolochowicz (bottom) (ref. 6) and by Mukaiyama *et al.* (top) (ref. 7).

In 1974, McMurry and Fleming described a 'new method for the reductive coupling of carbonyls to olefins' with $TiCl_3$ and $LiAlH_4$; they also proposed that pinacolate intermediates were involved in this reaction since pinacols could be isolated as by-products in many cases.[8] The mechanism of Scheme 1 was then rapidly and generally accepted.

Meanwhile, several studies on the reductive coupling of carbonyl compounds to olefins by low-valent molybdenum and tungsten compounds revealed that this reaction involved carbenoid intermediates; the relationship with the alkene metathesis reaction was noted.[9] Such carbene species were detected by Fujiwara *et al.* in 1978,[9] before Bryan and Mayer[10] and Chisholm and co-workers[11,12] isolated in 1990 tungsten oxoalkylidene complexes resulting from reductive cleavage of the ketonic C=O bond. These compounds were found to react further with the ketone to give the olefin at room temperature, presumably *via* a metallaoxetane intermediate, and the mechanism of Scheme 3 could be proposed for the reductive coupling

Michel Ephritikhine obtained his PhD in organic chemistry in 1974 at the University of Paris under the supervision of J. Levisalles. His postdoctoral work with M. L. H. Green in Oxford confirmed his interest in organometallic and inorganic chemistry. From 1976 to 1984, he was in the group of H. Felkin in Gif sur Yvette where he studied the chemistry of rhenium polyhydrides and C–H bond activation of alkanes. In 1984, he joined the Commissariat à l'Energie Atomique in Saclay to work on uranium chemistry. He presently holds the position of Research Director in the CNRS.

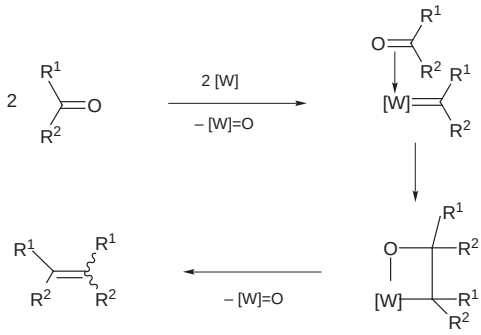

Scheme 3 Reductive coupling of ketones *via* a carbenoid species.

of carbonyl substrates. It is noteworthy that Chisholm *et al.*[12] and Cotton *et al.*[13] also found that low-valent tungsten compounds could react with ketones to give metallopinacols and demonstrated that these latter species were not the source of alkenes.

Amazingly, the belief in the mechanism of Scheme 1 was so strong that another pathway for the titanium catalyzed reaction did not seem conceivable; Chisholm wrote 'superficially, the (W catalyzed) reaction would seem to provide a molecular model for the McMurry reaction...; however, the mechanisms of the two reactions differ'.[12] We note that the reductive coupling of carbonyls into pinacols and alkenes by means of titanium complexes is now called the McMurry reaction; this is justified by the leading role played by McMurry in establishing the reputation of this reaction in organic chemistry.

Recent applications

It is no longer necessary to demonstrate the remarkable efficiency of low-valent titanium compounds for carbon–carbon bond forming; their use in synthesis has been described in detail in previous reviews and only a brief reminder of the main domains of application will be given here, with recent representative examples shown in Fig. 1.

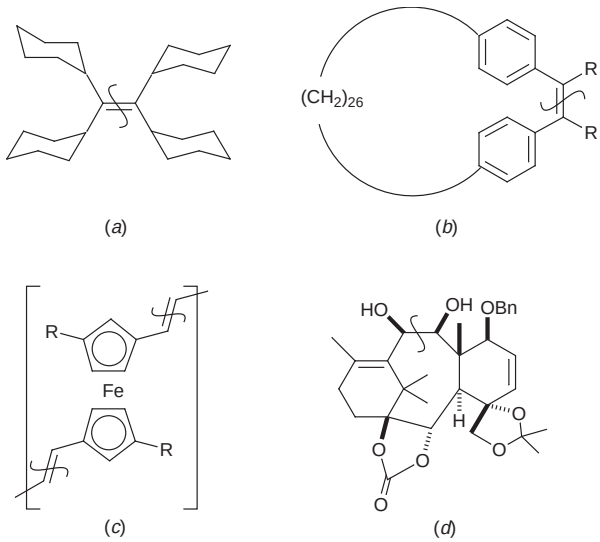

Fig. 1 Examples of compounds obtained by McMurry reactions: (*a*) a strained alkene (ref. 14), (*b*) a macrocycle (ref. 15), (*c*) a polymer (ref. 16) and (*d*) a key intermediate in the synthesis of taxol (ref. 20).

Low-valent titanium compounds served to prepare sterically hindered and/or strained olefins;[14] the driving force of the reaction is the formation of strong titanium–oxygen bonds. Many of these olefins, which exhibit specific physico-chemical properties and have a theoretical interest, could not be prepared by other methods. Also particularly notable is the effectiveness of the McMurry reaction in the synthesis of macrocycles.[15] The exceptional template effect exerted by titanium in intramolecular cyclizations of dicarbonyl molecules allowed the preparation of medium-sized and large rings; the yields are independent of the size of the cycloalkenes. A more recent application of the McMurry reaction was developed in polymer chemistry,[16] with the synthesis of polyvinylene or polypinacol derivatives and the preparation of new monomers with interesting properties.

But above all, it is with its crucial and elegant use in the key steps of numerous syntheses of natural products that the McMurry reaction has known a so great success. After the total synthesis of (+)-compactin and (+)-mevinolin by Clive *et al.*,[17] and the total synthesis of crassin by Dauben *et al.*[18] and McMurry and Dushin,[19] Nicolaou's synthesis of taxol[20] is possibly the most famous synthesis of a natural product which can be prepared with the aid of low-valent titanium compounds.

Very recently, Fürstner and co-workers considerably extended the scope of the conventional McMurry reaction: they found that titanium complexes were valuable auxiliaries for the reductive coupling of acylsilanes[21] and, more notably, the intramolecular cross-coupling reactions of ketones with amides; these substrates were previously reputed unreactive. The chemo- and regio-selective heteroarene synthesis (Scheme 4) represents a new efficient entry to a variety of substituted pyrrole and indole derivatives.[15,22,23]

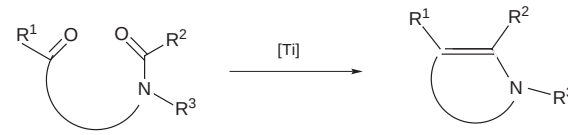

Scheme 4 Reductive coupling of oxo amide molecules.

However, it is also recognized that the McMurry reaction suffers from serious problems of reproducibility, having a bad reputation as being tricky and highly 'co-worker dependent'. The chemist must be aware of the difficulties they will probably encounter in finding the suitable reagent and experimental conditions.

New reagents, new methods

Problems of reproducibility

McMurry reactions are usually carried out in two consecutive steps: reduction of $TiCl_4$ or $TiCl_3$, followed by addition of the carbonyl substrate; this procedure is imperative when the carbonyl compound is not inert towards the reducing agent. Many reducing agents were used: Li, Na, K, KC_8, Mg, Mg(Hg), Zn, Zn(Cu), $LiAlH_4$. This variety does not reflect the chemist's fantasy, but rather the problematic outcome of the reaction. The nature of the titanium reagent, as well as the solvent, temperature and reaction time, have a strong influence on the eventual formation and stereochemistry of the coupling products, diols (*dl* and *meso*) or alkenes (*Z* or *E*); as outlined by Lenoir,[2] a complete rationale for these results has to be found. In attempts to overcome these problems of reproducibility, McMurry himself proposed, after his discovery of the $TiCl_3$–$LiAlH_4$ system (1974),[8] several 'improved procedures' by using the $TiCl_3$–K, $TiCl_3$–Li (1976)[24] and then $TiCl_3$–Zn(Cu) reagents (1978),[25] and finally recommended an 'optimized procedure' with the $TiCl_3(DME)_{1.5}$–Zn(Cu) combination, which 'gave reproducibly high yields in every case it has been used' (1989).[26] The efficacy of this new procedure was illustrated by the coupling of Pr^i_2CO which afforded $Pr^i_2C{=}CPr^i_2$ in 87% yield, instead of 17% by using $TiCl_3$–$LiAlH_4$ and 37% by using $TiCl_3$–Zn(Cu). However, Letcka, a collaborator of McMurry, wrote in 1996, 'McMurry coupling does not always give high yields at the first, or even the second attempt, but with some experience, reproducibly high yields can be attained... We strongly recommend . . . several test couplings on cyclohexanone before venturing a coupling on the more complex

material'.[3] Noteworthily, inferior results were attributed to bad experimental conditions—poor quality reagents or solvents, intrusion of air—rather than a lack of control of the mechanistic course of the reaction.

With the aim of obtaining more efficient reactions and better insights into the mechanisms, new low-valent titanium species have been designed in the last few years, and simplified methods have been developed.

Synthesis of alkenes

After the successful use of titanium graphite, especially in indole synthesis, Fürstner and co-workers reported that reduction of $TiCl_3$ with high surface area sodium gave a highly active titanium species supported on Al_2O_3, NaCl or TiO_2. The titanium–alumina species, which is presumably in the +1 oxidation state, was particularly efficient for the preparation of large cycloalkenes.[21]

Barteau and co-workers found that reductive coupling of aldehydes and ketones could also be carried out as a gas–solid process on the surface of reduced titania;[27–30] the reaction could be performed catalytically in the presence of hydrogen. Such reactions are not in need of strong reducing agents and a reduced oxide catalyst would be cheaper and easier to handle than the usual McMurry reagents in liquid–solid slurries. Moreover, the gas–solid reaction represents a potential route for coating of surfaces by conducting polymers, as suggested by the reductive coupling of *p*-benzoquinone.[28]

For the first time, Fürstner and Hupperts showed that commercially available titanium powder could be used as a McMurry reagent, after destruction of the tightly bound oxide layer by chlorosilane during the activation phase.[15] The Ti–R_3SiCl reagent exerted a strong template effect for macrocyclization reactions. In contrast to other systems which were claimed to produce Ti^0, this reagent was ineffective with aliphatic substrates, thus making chemo- and regio-selective coupling possible. The reaction with the Ti–R_3SiCl reagent could be performed either in two steps, by treating the titanium powder with the chlorosilane prior to addition of the substrate, or by heating all the components together.[15] Such a one-pot procedure, which is reliable when the reducing agent is not strong enough to affect the carbonyl group, had been employed by Mukaiyama with the $TiCl_4$–Zn system[7] and was recently reintroduced by Fürstner *et al.*, with the so called 'instant method'.[23] In fact, Bogdanovic and Bolte found that $TiCl_3$ could be reduced by Zn only if its redox potential has been lowered by co-ordination to the carbonyl substrate and therefore, a two step procedure is superfluous.[31] The simple and convenient 'instant' protocol, which is suitable for conventional McMurry couplings, has been applied to the synthesis of strained indoles.[23] Moreover, the reaction was rendered catalytic in titanium when carried out in the presence of a chlorosilane which reconverted the formed titanium oxychloride into $TiCl_3$.[15]

Synthesis of pinacols

Several works were devoted to the search of low-valent titanium compounds which would be suitable for the synthesis of pinacols with high stereoselectivity; these complexes should allow the McMurry reaction to be stopped at the 1,2-diol stage. Corey *et al.*found in 1976 that aromatic and aliphatic ketones and aldehydes could be coupled into the corresponding pinacols by treatment with $TiCl_4$ and Mg(Hg), at 0 °C in THF; reaction of a cyclic ketone with an excess of acetone gave the unsymmetrical diol.[32] Porta and co-workers reported that pinacols were formed with poor stereoselectivity (*dl*/*meso* = 1.3) by coupling of aromatic carbonyl compounds with aqueous $TiCl_4$ in basic media, but with $TiCl_3$ in anhydrous CH_2Cl_2 the pinacolization was highly diastereoselective (*dl*/*meso* > 100).[33]

Most recent studies revealed that such pinacol coupling reactions could be rendered stereoselective and catalytic with the use of additives and/or modified ligands. Banerji succeeded in stopping the reductive dimerization of acetophenone at the pinacol stage by addition of 10 equiv. of pyridine to the $TiCl_3$–Mg system. Also, in the presence of a stoichiometric amount of a mono- or di-hydroxy auxiliary, pinacols were obtained in higher yields and better stereoselectivity (*dl*/*meso* = *ca*. 4–5); among these additives, catechol was the most interesting for total pinacolization of aromatic carbonyl substrates, even under refluxing conditions.[34]

Ephritikhine reported on the first pinacol coupling reactions catalytic in titanium, by using the $TiCl_4$–Li(Hg) system in the presence of $AlCl_3$; a transmetallation reaction of the titanium pinacolate intermediates with $AlCl_3$ regenerated the precatalyst $TiCl_4$ and gave aluminium diolates which were inert towards the reducing agent and not transformed into the alkene.[35]

Catalytic pinacolization of benzaldehyde was achieved by Nelson with 1% $TiCl_3(THF)_3$ in the presence of Zn and Me_3SiCl. This combination was not effective for the coupling reactions of less electrophilic aldehydes and the diastereoselection was very low, but addition of 5 mol% of Bu^tOH led to a more reactive system which catalyzed the pinacolization of aromatic and aliphatic aldehydes and aryl methyl ketones with *dl*/*meso* ratios ranging from 1.5 to 4.8. Moreover, the stereoselectivity of the homocoupling of aryl aldehydes was substantially enhanced (*dl*/*meso* = 6.7 to 10.1) when 30 mol% of 1,3-diethyl-1,3-diphenylurea was added to the $TiCl_3(THF)_3$–Bu^tOH catalyst.[36]

Pinacol coupling can be affected by organotitanium compounds, as demonstrated by Corey *et al.* with the $CpTiCl_3$–$LiAlH_4$ reagent[32] and then by Handa and Inanaga with the Cp_2TiCl_2–Pr^iMgCl system.[37] Such reactions have known a significant improvement in the last few years. Barden and Schwartz reported that $[Cp_2TiCl]_2$ was able to reductively couple aromatic and α,β-unsaturated aldehydes into 1,2-diols in either anhydrous or aqueous media; the diastereoselectivity was high, with *dl*:*meso* ratios greater than 91:9.[38] Pinacol coupling of aromatic aldehydes was catalyzed by 3 mol% of *rac*-ethylenebis(η^5-indenyltitanium) dichloride in the presence of $MgBr_2$, Me_3SiCl and Zn to give the racemic 1,2-diols in good yield and with excellent diastereoselectivity (*dl*:*meso* > 96:4). These results of Gansäuer are encouraging for the investigation of asymmetric induction using enantiomerically pure metallocene catalysts.[39]

The nature of the active species and intermediates in these pinacol coupling reactions, which are performed with the aid of rather complicated systems, is not known. It is generally proposed that the high stereoselectivity of benzaldehyde or acetophenone coupling is due to the dimerization of ketyl radicals oriented in a manner which minimizes steric interactions between the phenyl groups (Fig. 2).

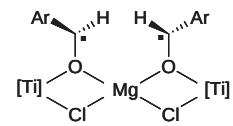

Fig. 2 Proposed intermediate for the diastereoselective coupling of benzaldehyde; [Ti] = Cp_2Ti (ref. 37) or *rac*-ethylenebis(η^5-indenyltitanium) (ref. 39).

New insights into the mechanism

The nature of the active species

As noted above, there was apparently no doubt about the involvement of pinacolate intermediates in the McMurry reaction and the main questions rather concerned the nature of the active species, and in particular its oxidation state. Despite several indications that Ti^{III} or Ti^{II} compounds could effect the

reductive coupling of carbonyl substrates—Corey *et al.* reported in 1976 that $(C_6Me_6)Ti(AlCl_4)_2$ was able to couple acetone and cyclohexanone[32]—it has been long believed that finely divided titanium particles were the active species in McMurry reactions. This assumption was reinforced by the studies of Geise on the $TiCl_3$–M (M = Li, K, Mg) or $TiCl_3$–$LiAlH_4$ systems,[40] but it is now clearly established that the presence of Ti^0 is not a prerequisite for the McMurry reaction.

Barteau found no evidence for the presence of Ti^0 on reduced TiO_2 surfaces active for benzaldehyde coupling; X-ray photoelectron spectroscopy revealed that the active site required for gas–solid reductive coupling is an ensemble of Ti cations in the +1, +2 and +3 oxidation states which collectively effect the four electron reduction.[29]

A decisive contribution to these mechanistic investigations was made by Bogdanovic and Bolte, who identified the nature and mode of action of the active species in some classical McMurry systems.[31] The low-valent titanium species obtained by reduction of $TiCl_3$ with $LiAlH_4$ was shown to be $[HTiCl(THF)_{0.5}]_x$;[41] this titanium hydride reacted with acetophenone to give PhMeC=CMePh and behaved as a strong two electron reductant. In contrast, the $TiCl_2$·LiCl reagent proposed by Eisch *et al.*[42] acted as a one electron reductant in the coupling of PhCOMe. Titanium(II) species were also involved in both the ketone→pinacolate and pinacolate→alkene steps of the reductive coupling of acetophenone with the $TiCl_3$(DME)–Zn(Cu) system; the nucleophilic mechanism proposed for this reaction (Scheme 5) was supported by quantum mechanical calculations.[43] These coupling reactions were shown to proceed by two consecutive steps: formation of the pinacolate intermediates which occurred at room temperature, followed by alkene synthesis at reflux temperature. Their progression was determined after analysis of the products obtained by hydrolysis of aliquots, and occurrence of pinacolate intermediates was inferred from formation of 2,3-diphenylbutane-2,3-diol; however, such intermediates were not observed and characterized. In fact, a very few metallopinacols were isolated from reactions of organic carbonyl substrates with $Cp_2Ti(CO)_2$ or $CpTiX_2$ (X = Cl or Br) and no alkene was obtained from these derivatives.[44]

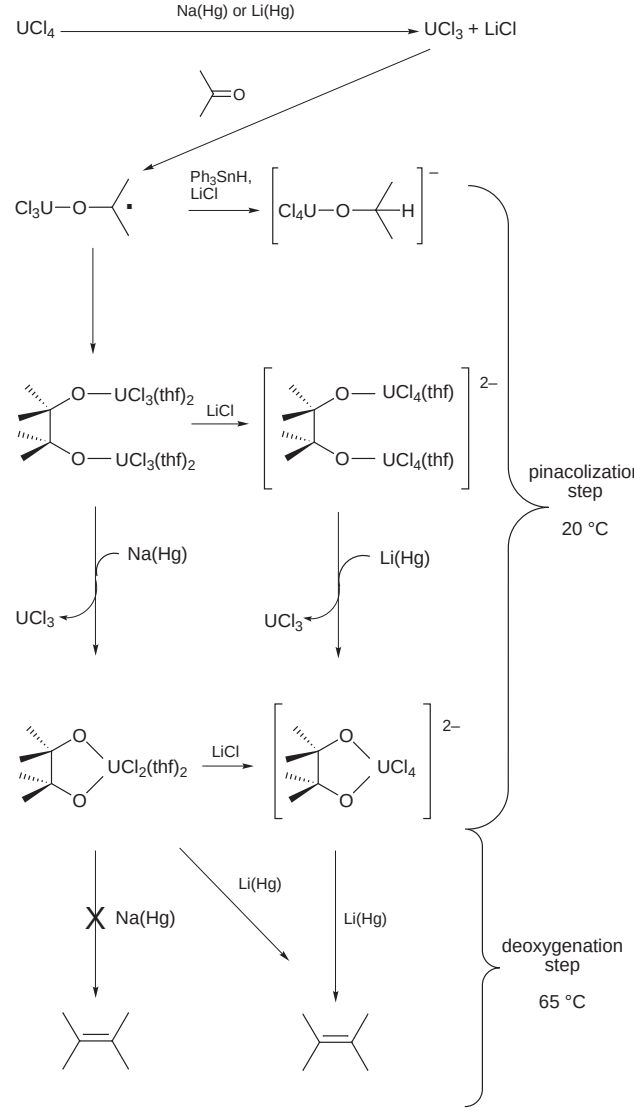

Scheme 6 Metallopinacols isolated from the reductive coupling of acetone with the UCl_4–M(Hg) systems (M = Li or Na).

Characterization of the pinacolate intermediates

Ephritikhine considered the reactions of ketones with the UCl_4–M(Hg) and $TiCl_4$–M(Hg) systems (M = Li or Na). Uranium and titanium complexes exhibit strong similarities in structure and reactivity but uranium compounds have some advantages over their titanium counterparts: they can be easily detected by their highly-shifted paramagnetic NMR signals and they often crystallize with less difficulty. Therefore, the chances of isolating and characterizing the intermediates are greater. The active uranium species in the UCl_4–M(Hg) systems were shown to be in the +3 oxidation state; it was demonstrated by electrochemical studies that reduction of UCl_4 into UCl_4^- was rapidly followed by a chloride ion transfer from UCl_4^- to UCl_4, giving UCl_3 and the anionic U^{IV} complexes $U_2Cl_9^-$ and UCl_5^- which were then reduced at lower potentials.[45]

Reaction of benzophenone with UCl_4 and Na(Hg) afforded successively the mono- and bis-benzopinacolates $UCl_2(O_2C_2Ph_4)$ and $U(O_2C_2Ph_4)_2(THF)_2$; the latter was characterized by its X-ray crystal structure. These compounds gave benzopinacol upon hydrolysis and were transformed into tetraphenylethylene after reduction with Na(Hg).[46] Several metallopinacols were isolated from the reaction of acetone with UCl_4 and M(Hg) (Scheme 6); whatever the amalgam used, the first intermediate was the dinuclear complex $(UCl_3L_2)_2(\mu$-

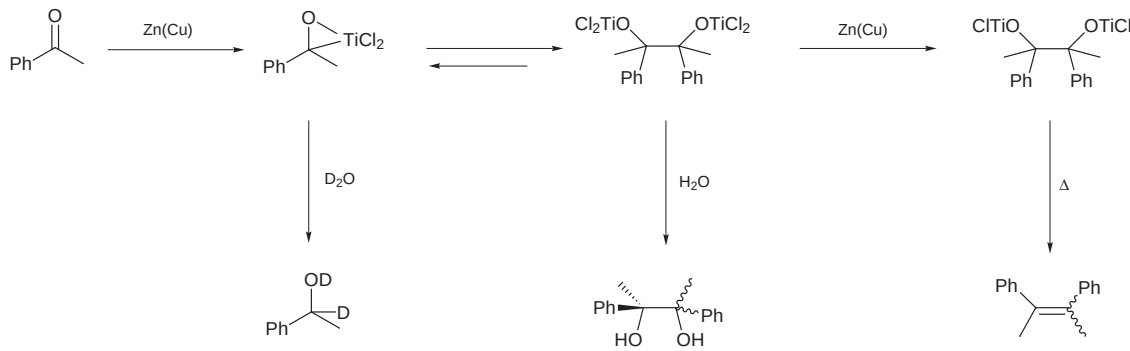

Scheme 5 Proposed mechanism for the reductive coupling of benzophenone with the $TiCl_3$–Zn(Cu) system.

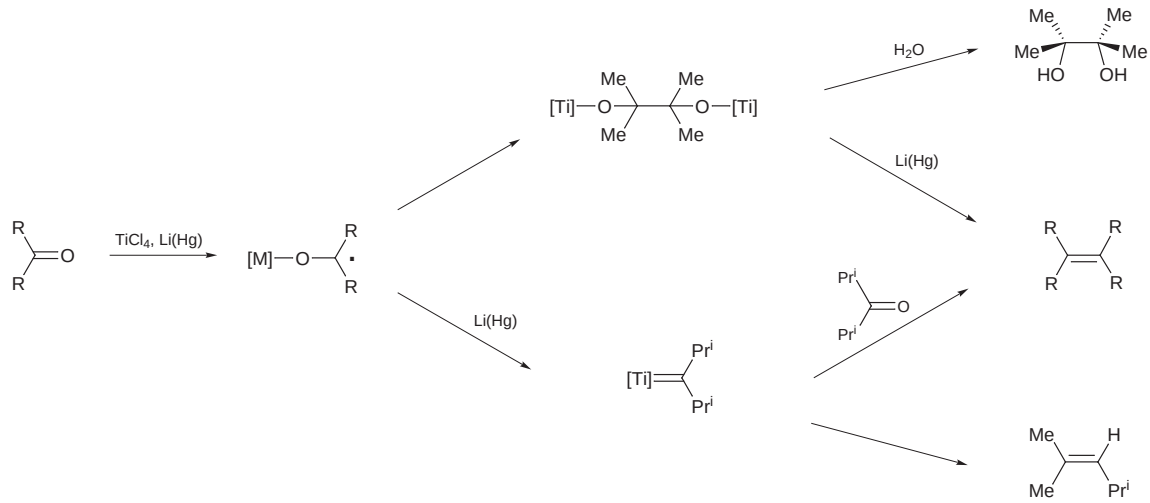

Scheme 7 The distinct mechanisms of the reductive coupling of acetone and diisopropyl ketone with the $TiCl_4$–Li(Hg) system.

$OCMe_2CMe_2O$) (L = THF) resulting from dimerization of the ketyl radical $[Cl_3UOCMe_2]^{\cdot}$; the crystal structure of the adduct with L = $OP(NMe_2)_3$ was determined (see front cover). The structure of the metallopinacols and their eventual transformation into $Me_2C{=}CMe_2$ were found to be strongly influenced by the molar ratio of the reactants, the nature of the reducing agent (M = Na or Li) and of the formed salt (NaCl or LiCl).[47]

Problems of reproducibility

The reductive coupling of acetone with the UCl_4–Li(Hg) system raised the problems of reproducibility. The alkene was formed in almost quantitative yield when the reaction was carried out in two consecutive steps: the pinacolization step at 20 °C and the deoxygenation step at 65 °C. However, it was much less easy, without extensive experience of the UCl_4–Li(Hg) system, to produce the alkene in a reproducible manner using a one pot procedure. This discrepancy could be related to side reactions of the different metallopinacols, which could be avoided only by determining the right time for heating the reaction mixture.[48] It was thus pointed out that, in addition to the quality of the reagents, experimental parameters like reaction time and temperature, which are directly connected to the mechanistic control of the reaction, would constitute major sources of non-reproducibility. These parameters cannot always be easily monitored in an heterogeneous medium.

Evidence of carbenoid intermediates

New facts emerged when Me_2CO was replaced with $Pr^i{}_2CO$ in its reaction with the UCl_4–Li(Hg) or $TiCl_4$–Li(Hg) systems.[49] The only coupling product was then $Pr^i{}_2C{=}CPr^i{}_2$ whereas a large amount of 2,4-dimethylpent-2-ene was formed. Control experiments showed that $Pr^i{}_2C{=}CPr^i{}_2$ did not result from the deoxygenation of pinacolate intermediates; moreover, it was found that $Cl_3TiOCPr^i{}_2CPr^i{}_2OTiCl_3$ was not stable, being readily transformed into a mixture of $TiCl_3$ and $Pr^i{}_2CO$. The facile cleavage of the titanium pinacolates and the absence of pinacol in the product mixture indicated that reductive coupling of $Pr^i{}_2CO$ would not proceed by dimerization of ketyl radicals, whereas formation of 2,4-dimethylpent-2-ene revealed the likely involvement of carbenoid intermediates.

These data put forward the dual nature of the mechanism of these McMurry type reactions (Scheme 7). Contrary to the generally accepted mechanism, metallopinacols are not the only precursors to the alkene; if the ketyl radicals can be effectively coupled into pinacolate intermediates, they can also be reduced and deoxygenated into carbenoid species which provide the alkene after further reaction with the ketone. The course of the reaction, *via* the metallopinacol or the carbenoid intermediates, is largely determined by the steric hindrance of the ketone; the most hindered ketones would follow the carbenoid route because of the difficult coupling of the ketyl radicals, and the reversible cleavage of the pinacolic C–C bond.

Now it seems that some McMurry reactions could be re-examined by considering the possible involvement of carbenoid intermediates. If the formation of 2,4-dimethylpent-2-ene was overlooked in the McMurry reactions of $Pr^i{}_2CO$, cyclohexene was detected among the products of the reductive coupling of cyclohexanone with the $TiCl_3$–K system[40] and the alkenes $RCH{=}CH_2$ (R = Me, Ph) were formed during the coupling of acetone and acetophenone on reduced alumina;[30] these alkenes would indicate the occurrence of carbenes as intermediates, even if such species could not be trapped with usual reagents. Also, Barteau observed that during the coupling of PhCOMe on reduced TiO_2 surfaces, the pinacol product was evolved at much higher temperature than $PhCH{=}CH_2$; this result was interpreted by the formation of pinacolate species at protected sites which are difficult to reduce at low temperature,[30] but it is possible that pinacols and alkenes were produced in parallel rather than sequential processes.[50]

Conclusion

The McMurry reaction represents a versatile transformation which is irreplaceable in organic synthesis. However, the huge interest and great success of this reaction conceal some experimental problems which have to be related to the difficulty in understanding the actual mechanism. Significant progress has obviously been made during the last years in the development of new reagents and methods leading to further interesting applications of low-valent titanium complexes, but these investigations also revealed that the course of the McMurry reaction is more complicated than previously assessed. The structure of the intermediates, pinacolate and/or carbenoid species, is strongly dependent on the nature of the carbonyl substrate, the titanium compound, the reducing agent and the by-products. At each stage of the process, the present intermediates can undergo side reactions which would affect the eventual formation of 1,2-diols or alkenes and give rise to problems of reproducibility. Other important aspects of the mechanism, for example the deoxygenation of the pinacolate intermediates and the role of additives in the stereoselectivity, are even more obscure. No doubt these questions will not discourage chemists, but rather incite them to consider the fascinating McMurry reaction with a more critical view.

Acknowledgments

I thank my colleagues and co-workers, whose names appear in the references, for their valuable contributions to this work.

Notes and references

1 R. G. Dushin, in *Comprehensive Organometallic Chemistry II*, ed. L. S. Hegedus, Pergamon, Oxford, 1995, vol. 12, p. 1071; G. M. Robertson, in *Comprehensive Organic Synthesis*, ed. B. M. Trost, I. Fleming and G. Pattenden, Pergamon, Oxford, 1991, vol. 3, p. 563; Y. Dang and H. J. Geise, *J. Organomet. Chem.*, 1991, **405**, 1; J. E. McMurry, *Chem. Rev.*, 1989, **89**, 1513; C. Betschart and D. Seebach, *Chimia*, 1989, **43**, 39; Y. Dang and H. J. Geise, *Janssen Chim. Acta*, 1989, **7**, 3; 1988, **6**, 3.
2 D. Lenoir, *Synthesis*, 1989, 883.
3 T. Letcka, in *Active Metals. Preparation, Characterization, Applications*, ed. A. Fürstner, VCH, Weinheim, 1996, p. 85.
4 A. Fürstner and B. Bogdanovic, *Angew. Chem., Int. Ed. Engl.*, 1996, **35**, 2442.
5 K. B. Sharpless, M. A. Umbreit, M. T. Nieh and T. C. Flood, *J. Am. Chem. Soc.*, 1972, **94**, 6538.
6 S. Tyrlik and I. Wolochowicz, *Bull. Soc. Chim. Fr.*, 1973, 2147.
7 T. Mukaiyama, T. Sato and J. Hanna, *Chem. Lett.*, 1973, 1041.
8 J. E. McMurry and M. P. Fleming, *J. Am. Chem. Soc.*, 1974, **96**, 4708.
9 Y. Fujiwara, R. Ishikawa, F. Akiyama and S. Teranishi, *J. Org. Chem.*, 1978, **43**, 2477.
10 J. C. Bryan and J. M. Mayer, *J. Am. Chem. Soc.*, 1990, **112**, 2298.
11 M. H. Chisholm, K. Folting and J. A. Klang, *Organometallics*, 1990, **9**, 602.
12 M. H. Chisholm, K. Folting and J. A. Klang, *Organometallics*, 1990, **9**, 607.
13 F. A. Cotton, D. DeMarco, L. R. Falvello and R. A. Walton, *J. Am. Chem. Soc.*, 1982, **104**, 7375.
14 I. Columbus and S. E. Biali, *J. Org. Chem.*, 1994, **59**, 3402.
15 A. Fürstner and A. Hupperts, *J. Am. Chem. Soc.*, 1995, **117**, 4468.
16 T. Itoh, H. Saitoh and S. Iwatsuki, *J. Polym. Sci., Part A: Polym. Chem.*, 1995, **33**, 1589.
17 D. L. J. Clive, K. S. K. Murthy, A. G. W. Wee, J. S. Prasad, G. V. J. da Silva, M. Majewski, P. C. Anderson, C. F. Evans, R. D. Haugen, L. D. Heerze and J. R. Barrie, *J. Am. Chem. Soc.*, 1990, **112**, 3018.
18 W. G. Dauben, T. Z. Wang and R. W. Stephens, *Tetrahedron Lett.*, 1990, 2393.
19 J. E. McMurry and R. G. Dushin, *J. Am. Chem. Soc.*, 1990, **112**, 6942.
20 K. C. Nicolaou, J. J. Liu, Z. Yang, H. Ueno, E. J. Sorensen, C. F. Claiborne, R. K. Guy, C. K. Hwang, M. Nakada and P. G. Nantermet, *J. Am. Chem. Soc.*, 1995, **117**, 634; K. C. Nicolaou, Z. Yang, J. J. Liu, P. G. Nantermet, C. F. Claiborne, J. Renaud, R. K. Guy and K. Shibayama, *J. Am. Chem. Soc.*, 1995, **117**, 645.
21 A. Fürstner and G. Seidel, *Synthesis*, 1995, 63; A. Fürstner, G. Seidel, B. Gabor, C. Kopiske, C. Krüger and R. Mynott, *Tetrahedron*, 1995, **51**, 8875.
22 A. Fürstner, A. Ernst, H. Krauze and A. Ptock, *Tetrahedron*, 1996, **52**, 7329; A. Fürstner, A. Ptock, H. Weintritt, R. Goddard and C. Krüger, *Angew. Chem., Int. Ed. Engl*., 1995, **34**, 678; A. Fürstner, H. Weintritt and A. Hupperts, *J. Org. Chem.*, 1995, **60**, 6637.
23 A. Fürstner, A. Hupperts, A. Ptock and E. Janssen, *J. Org. Chem.*, 1994, **59**, 5215.
24 J. E. McMurry and M. P. Fleming, *J. Org. Chem.*, 1976, **41**, 896; J. E. McMurry and L. R. Krepski, *J. Org. Chem.*, 1976, **41**, 3929.
25 J. E. McMurry, M. P. Fleming, K. L. Kees and L. R. Krepski, *J. Org. Chem.*, 1978, **43**, 3255.
26 J. E. McMurry, T. Letcka and J. G. Rico, *J. Org. Chem.*, 1989, **54**, 3748.
27 M. A. Barteau, *Chem. Rev.*, 1996, **96**, 1413; J. E. Rekoske and M. A. Barteau, *Ind. Eng. Chem. Res.*, 1995, **34**, 2931.
28 H. Idriss and M. A. Barteau, *Langmuir*, 1994, **10**, 3693.
29 H. Idriss, K. G. Pierce and M. A. Barteau, *J. Am. Chem. Soc.*, 1994, **116**, 3063.
30 K. G. Pierce and M. A. Barteau, *J. Org. Chem.*, 1995, **60**, 2405.
31 B. Bogdanovic and A. Bolte, *J. Organomet. Chem.*, 1995, **502**, 109.
32 E. J. Corey, R. L. Danheiser and S. Chandrasekaran, *J. Org. Chem.*, 1976, **41**, 260.
33 A. Clerici and O. Porta, *J. Org. Chem.*, 1985, **50**, 76; A. Clerici, L. Clerici and O. Porta, *Tetrahedron Lett.*, 1996, **37**, 3035.
34 N. Balu, S. K. Nayak and A. Banerji, *J. Am. Chem. Soc.*, 1996, **118**, 5932.
35 O. Maury, C. Villiers and M. Ephritikhine, *New J. Chem.*, 1997, **21**, 137.
36 T. A. Lipski, M. A. Hilfiker and S. G. Nelson, *J. Org. Chem.*, 1997, **62**, 4566.
37 Y. Handa and J. Inanaga, *Tetrahedron Lett.*, 1987, **28**, 5717.
38 M. C. Barden and J. Schwartz, *J. Am. Chem. Soc.*, 1996, **118**, 5484.
39 A. Gansäuer, *Synlett*, 1997, 363.
40 R. Dams, M. Malinowski, I. Westdorp and H. Y. Geise, *J. Org. Chem.*, 1982, **47**, 248.
41 L. E. Aleandri, S. Becke, B. Bogdanovic, D. J. Jones and J. Rozière, *J. Organomet. Chem.*, 1994, **472**, 97.
42 J. J. Eisch, X. Shi and J. Lasota, *Z. Naturforsch., Teil B*, 1995, **50**, 342.
43 M. Stahl, U. Pidun and G. Frenking, *Angew. Chem., Int. Ed. Engl.*, 1997, **36**, 2234.
44 R. S. P. Coutts, P. C. Wailes and R. L. Martin, *J. Organomet.Chem.*, 1973, **50**, 145; J. C. Huffman, K. G. Moloy, J. A. Marsella and K. G. Caulton, *J. Am. Chem. Soc.*, 1980, **102**, 3009; M. Pasquali, C. Floriani, A. Chiesi Villa and C. Guastini, *Inorg. Chem.*, 1981, **20**, 349.
45 O. Maury, M. Ephritikhine, M. Nierlich, M. Lance and E. Samuel, *Inorg. Chim. Acta*, in the press.
46 C. Villiers, R. Adam, M. Lance, M. Nierlich, J. Vigner and M. Ephritikhine, *J. Chem. Soc., Chem. Comm.*, 1991, 1144.
47 O. Maury, C. Villiers and M. Ephritikhine, *Angew. Chem., Int. Ed. Engl.*, 1996, **35**, 1129.
48 M. Ephritikhine, O. Maury, C. Villiers, M. Lance and M. Nierlich, unpublished work.
49 C. Villiers and M. Ephritikhine, *Angew. Chem., Int. Ed. Engl.*, 1997, **36**, 2380.
50 M. A. Barteau, personal communication.

Paper 8/04394I

ChemComm

C–H bond activation and C–N coupling reactions of methylacetylenes and allenes with an imidotitanium complex

Alan Bashall,[a] Philip E. Collier,[b] Lutz H. Gade,*[c]† Mary McPartlin,[a] Philip Mountford*[b]‡ and Dominique J. M. Trösch[c]

[a] *School of Applied Chemistry, University of North London, Holloway Road, London UK, N7 8DB*
[b] *School of Chemistry, University of Nottingham, University Park, Nottingham UK, NG7 2RD*
[c] *Institut für Anorganische Chemie, Universität Würzburg, Am Hubland, 97074 Würzburg, Germany. E-mail: lutz.gade@mail.uni-wuerzburg.de*

Received (in Cambridge, UK) 7th September 1998, Accepted 6th October 1998

Reaction of an imidotitanium complex, stabilized by a tridentate diamidopyridine ligand, with the methyl acetylenes MeC_2Me and MeC_2Ph led to C–H-activation of the substrate and subsequent C–N coupling to give azatitanatetracycles which may be viewed as dimetallated enamines; the same compounds were obtained in reactions with the allenes $Me(H)C{=}C{=}CH_2$ and $Ph(H)C{=}C{=}CH_2$.

We have shown previously that the coordination of the diamidopyridine ligand system developed previously by us[1] to titanium leads to stable monomeric imidotitanium complexes such as **1**.[2] Compound **1** posseses labile pyridine and pyridyl functionalities that, under appropriate reaction conditions, may dissociate to yield an unsaturated and highly reactive imido complex of the type hitherto generally only accessible *via* irreversible thermolysis of certain precursors.[3] The facile accessibility and stability of **1** and its homologues has allowed us to undertake a systematic investigation into their reactivity, in particular C–N coupling with unsaturated hydrocarbons.

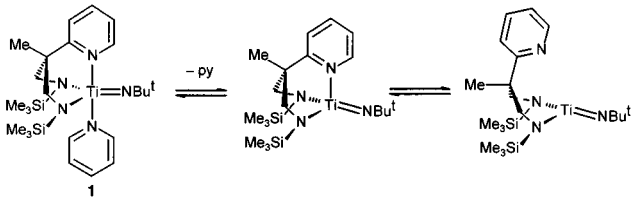

1

Heating compound **1** dissolved in neat but-2-yne or 1-phenylpropyne at 80 °C for 10 days in a sealed tube led to its complete conversion to the novel complexes **2** and **3** (Scheme 1), respectively which were isolated by direct crystallization from the reaction mixture (yields: **2** 73%, **3** 70%).

Neither **2** nor **3** contain the auxiliary pyridine ligand present in the starting material and the ^1H and ^{13}C NMR spectra indicate a transformation of a methyl group of the acetylene substrate.§Thus, new resonances for a metal bound CH_2 group were observed [$\delta(^1H/^{13}C)$ **2**: 1.77/62.4; **3**: 2.03/63.6] as well as those for an olefinic CH unit [$\delta(^1H/^{13}C)$ **2**: 4.76/86.7; **3**: 5.86/96.4]. This led to the formulation of the reaction products as depicted in Scheme 1. Unambiguous evidence for this new structural type was obtained from a single crystal X-ray structure analysis of **2** the result of which is depicted in Figure 1.¶

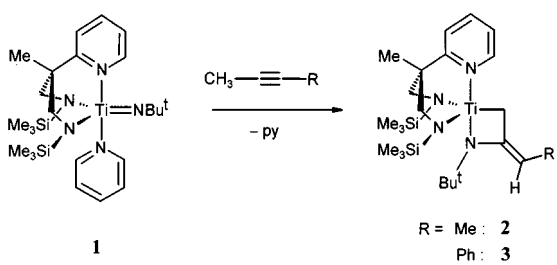

1

Scheme 1

The coordination geometry of the molecule is distorted trigonal bipyramidal. The two amido functions of the tripodal ligand as well as the alkyl C-atom C(45) occupy the equatorial sites while the pyridyl N-atom and the amido-N atom derived from the imido ligand represent the axial ligating atoms. The N(4)–Ti vector is significantly tilted towards the equatorial plane [N(4)–Ti–C(45) 67.6(2)°] as a consequence of the small bite angle of the coordinated chelating metalla-enamine. The bond lengths and interbond angles within the C–N-coupled organic fragment clearly support its interpretation as a metallated enamine with C(45)–C(46) 1.515(9) Å and C(46)–N(4) 1.404(8) Å representing single bonds and C(46)–C(47) 1.338(9) Å being consistent with a C–C-double bond. The {TiN(Bu^t)C(=CHR)CH_2} metalla-azetidine fragment in **2** and **3** is the first crystallographically authenticated example of this structural unit. Related oxo-metallacyclic species (*i.e.* metallaoxetanes) have only recently been fully characterized, namely [Ti(η^5-C_5Me_5)$_2${OC(=CH_2)CH_2}],[4a] [Mo(NBu^t)$_2$-Cl{OC(=CHPPh_3)CPh_2}],[4b] and [Ru(PMe_3)$_4${OC(=CH-Bu^t)CH_2}].[4c] Interestingly, the latter two complexes have a *Z*-configuration for the exocyclic C=C bond, whereas the configuration in **2** and **3** is *E*, presumably due to the steric influence of the N-*tert*-butyl group.

Although the conversion to the reaction products **2** and **3** proceeds slowly it is remarkably selective and could be monitored by ^1H NMR spectroscopy in C_6D_6. The fact that no deuterium was incorporated into the products suggests that the

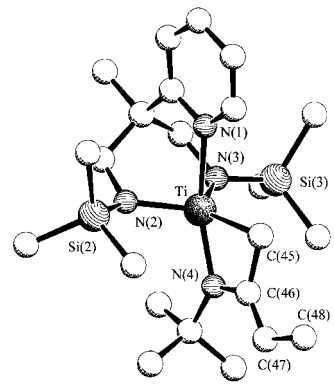

Fig. 1 Molecular structure of [TiL(NBu^t)C(CH_2)CHMe] **2**. Hydrogen atoms are omitted for clarity. Selected bond lengths (Å) and angles (°): Ti–N(3) 1.890(5), Ti–N(2) 1.903(5), Ti–N(4) 1.949(6), Ti–C(45) 2.149(7), Ti–N(1) 2.232(6), N(4)–C(46) 1.404(8), C(45)–C(46) 1.515(9), C(46)–C(47) 1.338(9), C(47)–C(48) 1.532(9), N(3)–Ti–N(2) 110.5(3), N(3)–Ti–N(4) 107.3(3), N(2)–Ti–N(4) 106.3(2), N(3)–Ti–C(45) 121.6(3), N(2)–Ti–C(45) 127.1(3), N(4)–Ti–C(45) 67.6(2), N(3)–Ti–N(1) 86.1(2), N(2)–Ti–N(1) 83.9(2), N(4)–Ti–N(1) 158.3(2), C(45)–Ti–N(1) 90.9(3), C(46)–C(45)–Ti 88.2(4), C(47)–C(46)–N(4) 131.3(7), C(47)–C(46)–C(45) 125.6(7), N(4)–C(46)–C(45) 103.0(6), C(46)–C(47)–C(48) 123.7(8).

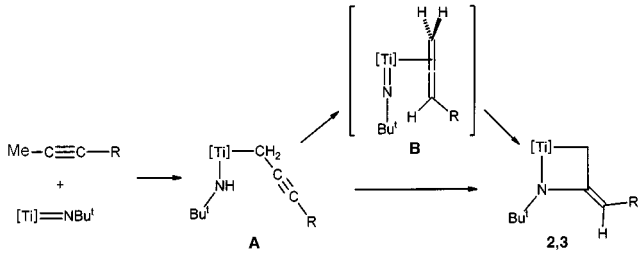

Scheme 2

hydrogen transfer involving the reaction medium does not take place. A reasonable reaction mechanism based on these results is depicted in Scheme 2.

In a first reaction step (formation of intermediate **A**) the Me-group of the methyl acetylene adds across the Ti=NR bond generating an R(H)N-amido ligand and a Ti–alkyl unit.‖ Such C–H bond activation reactions of transiently generated imido compounds have been studied extensively by Wolczanski and others in recent years.[3] In a proposed second step, H atom transfer to an acetylene C-atom leads to the re-formation of the imido unit and a π-bonded allene ligand (**B**).** These fragments couple in the third and final step to give the four-membered azatitanacycle present in **2** and **3**. Supporting evidence for this third step was obtained independently by reacting compound **1** with 1-methylallene and 1-phenylallene, respectively. In both cases the same reaction products (*i.e.* **2** and **3**, respectively) as those described above were obtained (Scheme 3). We would like to point out that, alternatively, intermediate **A** may also be directly converted to the metallacycle.

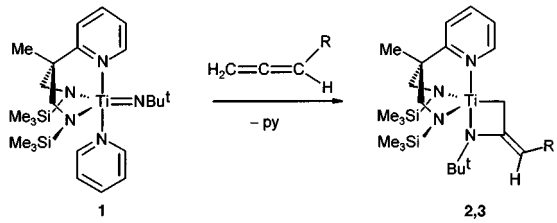

Scheme 3

The reactions of **1** with MeC≡CR and CH_2=C=CHR to form **2** and **3** are the first examples of such transformations in transition metal chemistry. Although reactions of imido complexes with internal alkynes to form metallacycles [L_nM{N(R)C(R)=CR}] are known,[7] no examples of the activation of sp^3 C–H bonds in preference to forming the simple cyclization products have been described.[8] The reaction of **1** with allenes to form a metalla-azetidine is the first fully characterized example of this type for imido complexes, although very recently the reaction of [Ti(η^5-C_5Me_5)$_2$(O)(py)] with allene to form [Ti(η^5-C_5Me_5)$_2${OC(=CH_2)CH_2}] was described.[4a]

In the more general context of organic synthesis *via* organometallics, the remarkable products of a C–N coupling reaction may be viewed as dimetallated enamines. In view of the known chemistry of *mono*-metallated enamines[9] as well as the reactive patterns established for Ti–C units,[10] a rich and varied organic chemistry is expected to derive from these preliminary results.

We acknowledge financial support from the Deutsche Forschungsgemeinschaft, the Fonds der Chemischen Industrie, the Engineering and Physical Science Research Council, the Leverhulme Trust, the DAAD and the British Council. P. M. is The Royal Society of Chemistry Sir Edward Frankland fellow for 1998/99.

Notes and references

† Current address: Institut LeBel, Université Louis Pasteur Strasbourg, 4, rue Blaise Pascal, 67000 Strasbourg, France.

‡ Current address: Inorganic Chemistry Laboratory, South Parks Road, Oxford, UK, OX1 3QR. E-mail: philip.mountford@chemistry.oxford.ac.uk, http://www.chem.ox.ac.uk/researchguide/pmountford.html

§ *Selected spectroscopic data*: **2**: ^{1}H NMR (C_6D_6, 300.1 MHz, 298 K): δ 0.04 [18H, s Si(CH_3)$_3$], 1.00 (3H, s, CH_3), 1.77 (2H, s, CH_2), 1.81[9H, s, NC(CH_3)$_3$], 2.22 [3 H, d, ^2J(HH) 6.3 Hz, CH_3], 3.08 [2H, d, ^2J(HH) 12.8 Hz, CH*H*NSi], 3.70 [2H, d, ^2J(HH) 12.7 Hz, C*H*HNSi], 4.76 [1H, q, ^3J(HH) 6.4 Hz, CH], 6.51 (1H, m, H^5 C_5H_4N), 6.80 [1H, d, ^3J(H^{6}H^5) 7.9 Hz, H^3 C_5H_4N], 7.03 [1H, virtual td H^4 C_6H_4N, ^3J(H^{4}H^5) 7.7 ^3J(H^{4}H^3) 7.9 ^4J(H^{4}H^6) 1.7 Hz], 8.59 (1H, d, ^3J(H^{6}H^5) 5.4 Hz, H^6 C_5H_4N). ^{13}C{^{1}H} NMR (C_6D_6, 75.5 MHz, 298 K): δ 0.06 [Si(CH_3)$_3$], 13.6 (CH_3), 23.3 (CH_3), 30.4 [NC(*C*H$_3$)$_3$], 46.5 [*C*(CH_2NSiMe$_3$)$_2$], 62.4 (CH_2), 56.4 (N*C*Me$_3$), 63.5 (*C*H$_2$NSiMe$_3$), 86.7 (CH), 120.6 (C^3 C_5H_4N), 121.7 (C^5 C_5H_4N), 138.3 (C^4 C_5H_4N), 140.7 [*C*=C(HMe), 145.7 (C^6 C_5H_4N), 159.8 (C^2 C_5H_4N). **3**: ^{1}H NMR (200 MHz, C_6D_6, 295 K): = δ −0.03 (s, 18H, SiMe$_3$), 0.97 (s, 3H, CCH_3), 1.81 (s, 9 H, Bu^t), 2.03 (s, 2 H, CH_2), 3.03 [d, 2H, ^3J(HH) 12.8 Hz, CHHN], 3.71 (d, 2 H, CH*H*N), 5.86 [s, 1 H, C=C*H*(C_6H_5)], 6.50 [ddd, 1H, H^5, C_5H_4N, ^3J(H^{5}H^4) 7.6 ^3J(H^{5}H^6) 5.6 ^3J(H^{5}H^3) 1.2 Hz], 6.76 [dd, 1H, H^3, C_5H_4N, ^3J(H^{3}H^4) 7.9 Hz], 6.95–7.06 (m, 2 H, H^4, C_5H_4N and H^4, C_6H_5), 7.37 (2H, H^{3,5}, C_6H_5), 7.79 (2H, H^{2,6}, C_6H_5), 8.42 (ddd, H^6, C_5H_4N). {^{1}H}^{13}C NMR (50.3 MHz, C_6D_6, 295 K): δ 0.0 [Si(CH_3)$_3$], 23.4 (C*C*H$_3$), 30.6 [NC(*C*H$_3$)$_3$], 47.5 (*C*CH$_3$), 56.2 [N*C*(CH_3)$_3$], 58.0 (*C*H$_2$), 63.6 (*C*H$_2$N), 96.4 [C=*C*H(C_6H_5)], 120.4 (C^3, C_5H_4N), 121.4 (C^4, C_6H_5), 122.0 (C^5, C_5H_4N), 127.9 (C^{2,6}, C_6H_5), 128.3 (C^{3,5}, C_6H_5), 138.7 (C^4, C_5H_4N), 144.23 (C^1, C_6H_5), 145.8 (C^6, C_5H_4N), 147.7 [*C*=CH(C_6H_5)], 159.5 (C^2, C_5H_4N). Correct elemental analyses were obtained for both compounds.

¶ *Crystal data* for [TiL(NBu^t)C(CH_2)CHMe] **2**: $C_{23}H_{44}N_4Si_2Ti$, M = 480.70, monoclinic, space group $C2/c$, a = 28.721(7), b = 10.450(2), c = 18.866(4) A, β = 100.50(2)° V = 5567 A^3, Z = 8, F(000) = 2080, T = 223(2) K, μ = 0.410 mm^{-1}; Siemens P4 diffractometer, 4176 measured data, semi-empirical absorption corrections (ψ-scans, relative T_{max} 0.799 and T_{min} 0.682), 3391 independent reflections, R_{int} = 0.0893, R_1 0.0665, wR_2 = 0.0983 [$I > 2\sigma(I)$], S = 0.0862. Hydrogen atoms were included in calculated positions and anisotropic displacement parameters were assigned to all other atoms. CCDC 182/1050.

‖ Since the reversible addition of alkynes to M=NR or M=O bonds is established, we cannot rule out the reversible aza–titanacyclobutene intermediate prior to C–H activation.[5,6]

** Similar intermediates involving alkenes or alkynes η^2-bound to metal–imido complexes have been proposed previously.[5]

1 S. Friedrich, L. H. Gade, A. J. Edwards and M. McPartlin, *J. Chem. Soc., Dalton Trans.*, 1993, 2861; S. Friedrich, M. Schubart, L. H. Gade, I. J. Scowen, A. J. Edwards and M. McPartlin, *Chem. Ber.*, 1997, **120**, 1751.

2 A. J. Blake, P. E. Collier, L. H. Gade, M. McPartlin, P. Mountford, M. Schubart and I. J. Scowen, *Chem. Commun.*, 1997, 1555.

3 See: J. L. Bennet and P. T. Wolczanski, *J. Am. Chem. Soc.*, 1997, **119**, 10696 and references therein.

4 (*a*) D. J. Schwartz, M. R. Smith and R. A. Andersen, *Organometallics*, 1996, **15**, 1446; (*b*) J. F. Hartwig, R. G. Bergman and R. A. Andersen, *Organometallics*, 1991,**10**, 3344; (*c*) J. Sundermeyer, K. Weber and H. Pritzkow, *Angew. Chem. Int. Ed. Engl.*, 1993, **32**, 731.

5 P. J. Walsh, F. J. Hollander and R. G. Bergman, *J. Am. Chem. Soc.*, 1993, **12**, 3705.

6 J. L. Polse, R. A. Andersen and R. G. Bergman, *J. Am. Chem. Soc.*, 1995, **117**, 5393.

7 For a review of transition metal imido chemistry, see: D. E. Wigley, *Prog. Inorg. Chem.*, 1994, **42**, 239.

8 Thermolysis of [Zr(η^5-C_5Me_5)$_2${OC(Ph)=Ph}] at 150 °C gives an orthometallated (*i.e.* activation of an sp^2-C–H bond) rearrangement product, apparently *via* transient oxo–zirconocene [Zr(η^5-C_5Me_5)$_2$O] and PhC≡CPh: M. J. Carney, P. J. Walsh, F. J. Hollander and R. G. Bergman, *Organometallics*, 1992, **11**, 761.

9 G. Pitacco and E. Valentin, in *The Chemistry of Amino, Nitroso and Nitro Compounds and their derivatives, Part 1*, ed. S. Patai, John Wiley & Sons, Chichester, 1982, p. 623.

10 M. Bochmann, in *Comprehensive Organometallic Chemistry II*, ed. E. W. Abel, F. G. A. Stone and G. Wilkinson Pergamon, Oxford, vol. 4, 1995.

Communication 8/06936K

On intrinsic and extrinsic defect-forming mechanisms determining the disordered structure of 4-iodo-4′-nitrobiphenyl crystals

J. Hulliger* and P. J. Langley

Department of Chemistry and Biochemistry, University of Berne, Freiestrasse 3, CH-3012 Berne, Switzerland. E-mail: juerg.hulliger@iac.unibe.ch

Received (in Cambridge, UK) 4th September 1998, Accepted 12th October 1998

Following up two recent *Chemical Communications* on the structure of the title compound, a theoretical study confirms that the presence of 4,4′-dinitrobiphenyl as an impurity can give rise to disordered crystals, resulting from a chain inversion mechanism.

Recent issues of this journal have contained communications[1,2] on the disordered crystal structure of 4-iodo-4′-nitrobiphenyl (INB), in which the INB molecules pack as parallel and polar ribbons (mm2). From the original viewpoint of designing efficient nonlinear optical (NLO) materials,[1] this type of packing of dipolar entities represents an interesting and relatively seldom case[3] of a material in which all the β_{zzz} axes of the molecular hyperpolarisability β are aligned co-parallel.

The difficulties encountered initially by Sarma *et al*.[1] in obtaining a reliable structural model from X-ray data were resolved more recently by Masciocchi *et al*.[2] and Langley *et al*.[4] through careful sample purification. In interpreting the data of Sarma *et al*., the Milan group[2] identified two possible causes of defect formation in INB: (i) polarity inversion of single ribbons (chains) of INB in the presence of 4,4′-dinitrobiphenyl (DNB) impurity molecules (in analogy to 180° opposed polar macrodomain formation in perhydrotriphenylene inclusion compounds[5]); (ii) two dimensional polytypes, *i.e*. a defect paracrystal composed of many fine grains. The effect of impurity molecules on the NLO characteristics of a host crystal has been demonstrated earlier by Weissbuch *et al*.[6,7] Whilst the mechanisms which permit the favourable creation of such defects at growing crystal faces are mainly well understood,[6,7] the subsequent fates of these faults, and their distribution throughout the structures of the resulting bulk crystals, often remain elusive.

Here we discuss further using energetic arguments the relative likelihood of *intrinsic* (180° orientational disorder) and *extrinsic* [due to DNB and/or 4,4′-diiodobiphenyl (DIB) impurities] defect formation in INB, and the likely true structure of INB which results. Attachment processes during the assembly of INB crystals are driven by the alignment of INB into parallel chains, as well as collinear functional group interactions ($NO_2\cdots$I, I$\cdots$I) between molecules already attached at the {001} surfaces and incoming INB, DNB or DIB molecules (Fig. 1). The total attachment energy E_{att} per molecule in the $+c$ or $-c$ direction contains contributions from lateral and long-range interactions between chains, as well as short-range collinear interactions between the terminal moieties. With respect to the former, we can make a distinction between E_p (parallel) and E_{ap} (antiparallel), that is, the energies corresponding to preferred and defect modes of lateral attachment, respectively (Fig. 1). Values E_{AD} , E_{DD} for the terminal intermolecular interaction energies of isolated, collinear $NO_2\cdots$I (A$\cdots$D) and I$\cdots$I (D$\cdots$D) synthons have been calculated to be -5.7 (3.4 Å) and -2.8 (4.0 Å) kJ mol^{-1}, respectively.[8] The $NO_2\cdots O_2N$ (A$\cdots$A) intermolecular interaction is considered a defect configuration of low occurrence[6,8–9] because a positive interaction energy E_{AA} of $\sim$10 kJ mol^{-1} was estimated for a van der Waals contact of 3.4 Å.[8]

Intrinsic defects, *i.e*. those resulting from 180° orientational disorder during the assembly of a pure INB system, can occur at the growing faces (Fig. 2). For growth along the $+c$ and $-c$ directions, there are two non-degenerate configurations for defect attachments, represented by the energies ΔE_{defect} ($+c$ or $-c$). As a result of a Schottky-type calculation[9] accounting for the molar fraction x of orientational defects, we find that: (i) the temperature of crystal growth can significantly affect the concentration of defects; and (ii) a perfect seed crystal will during growth segregate into two adjacent volumes containing a different number of defects. The ratio of the orientational defects within these two domains can be estimated using the intermolecular interaction energies given above: $x(+c)/x(-c) \cong \exp[(E_{AA} - E_{DD})/RT]$. Since the intermolecular interaction $NO_2\cdots O_2N$ is strongly endothermic, $x(+c)/x(-c)$ is expected to vary between *ca*. 170 and 20 (300–510 K). Continuation of growth along both *c*-directions after defect formation gives rise to one of two different phenomena: *healing* (correction) of the defect or *chain inversion* (Fig. 3). With each phenomenon there are again associated two different energies, corresponding to the two different growth directions $+c$ and $-c$ [see eqn. (1) below].

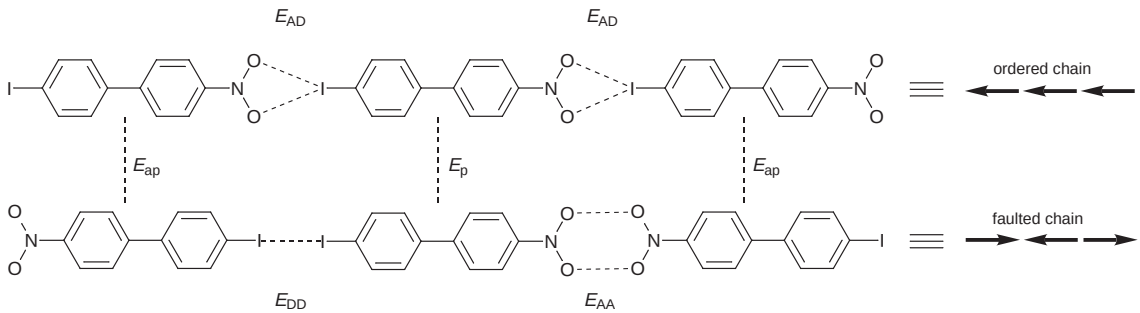

Fig. 1 Model representation of ordered and intrinsically disordered molecular chains of INB. This figure is used to illustrate the interaction energies (positive or negative; represented by dashed lines) under consideration during packing. Definition of interaction energies: $E_p \equiv$ lateral and long-range interactions between molecules (excluding collinear short-range contributions of terminal functional groups) whose dipoles are oriented co-parallel; $E_{ap} \equiv$ same as E_p but between dipoles oriented antiparallel; E_{AD}, E_{DD}, $E_{AA} \equiv$ collinear intermolecular terminal functional group interactions A$\cdots$D, D$\cdots$D, A$\cdots$A, respectively. A and D are defined in the main text. Subsequent figures employ the symbol $\rightarrow$ as a simplified representation of INB, corresponding to the intramolecular dipole orientation $O_2N\rightarrow$I.

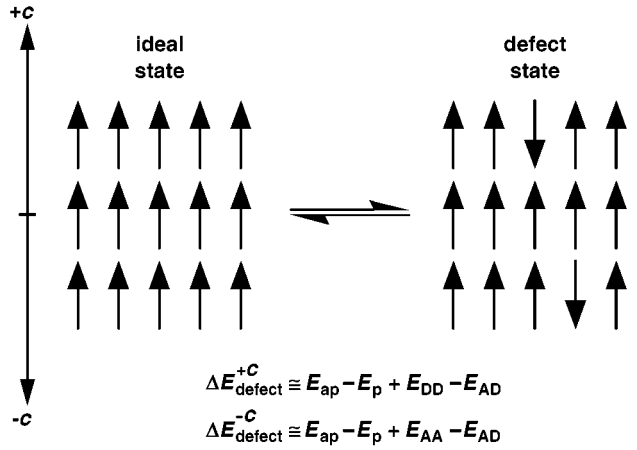

Fig. 2 Intrinsic orientational defect equilibrium at growing faces ($+c$, $-c$) of a polar crystal such as INB.

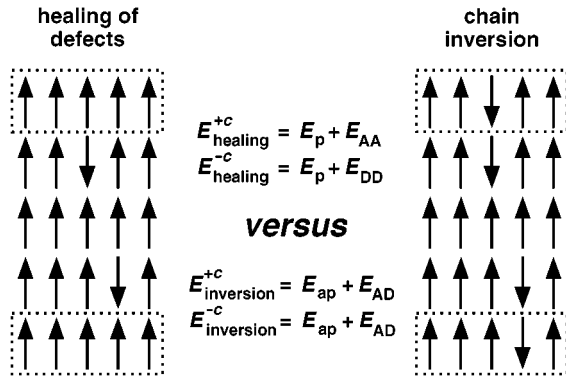

Fig. 3 Healing of defects *versus* chain inversion within the next growth layer after occurrence of primary (intrinsic) defects.

Extrinsic defects can arise due to solid solution formation of INB with DNB or DIB (Fig. 4). In the case of these symmetrically disubstituted components, the preferred mode of incorporation is driven only by the relative strengths of the terminal functional group intermolecular interactions. At an impurity level (in solution) of *ca*. 0.1, both DNB and DIB are incorporated into the growing crystal structure with different degrees of probability with respect to the $+c$ and $-c$ directions. From simplistic energy considerations it can be shown that when healing intrinsic defects, DNB attaches preferentially to defect sites along $-c$ whilst DIB attaches along $+c$. Conversely, when DNB and DIB are the defects themselves, preferred incorporations are along $+c$ and $-c$, respectively (Fig. 4).

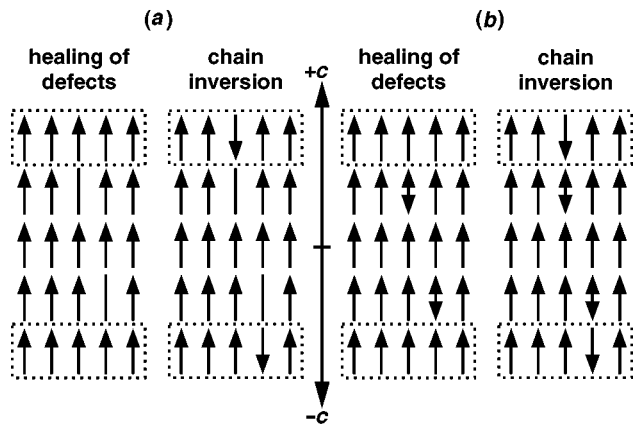

Fig. 4 Influence of DNB (—) or DIB (↔) impurities on subsequent growth layers: (*a*) healing *versus* chain inversion after preferred incorporation of DNB in the $+c$ direction; (*b*) similar scheme for DIB, where in the $-c$ direction favourable induction of a chain inversion may occur.

Which of healing or chain inversion by INB molecules in the next growth layer is the more probable is still, of course, a function of both defect (DNB or DIB) and growth direction ($\pm c$). At x_1(DNB) $\approx$ x_1(DIB), DIB can serve to heal the defects created by DNB and *vice versa*.

In the realistic case reported by Masciocchi *et al.*[2] a more complicated situation arises: preferred attachments of DNB present in the growth medium will occur along $+c$ but healing by INB in the next layer would involve unfavourable $NO_2 \cdots O_2N$ intermolecular interactions. If at this point we allow for an inversion of single chains, the energy $E_{inversion}$ would at each layer have to be lower than the energy of a configuration providing healing by antiparallel attachments (Fig. 4). The corresponding energy difference between is then given by eqn (1).

$$\Delta E(+c, \text{DNB}) \equiv E_{inversion} - E_{healing} \cong -RT\ln x(+c) + 2E_{AD} - E_{AA} - E_{DD} \quad (1)$$

The logarithmic term refers to the concentration of intrinsic defects in pure INB crystals from which an estimate of the unknown difference $E_{ap} - E_p$ has been derived. Using the calculated energy values given above it follows that chain inversion is more stable [$\Delta E(+c) < 0$] as long as the concentration of intrinsic defects in pure INB crystals (300 K) is larger than about 6×10^{-4}. A $wR2$ value of 0.032 (crystal 1 in ref. 2; see also ref. 4) sets an upper limit for $x(+c)$ to a range of a few percent. Although a lower limit cannot be extracted from the present X-ray data, we consider it a reasonable estimate that $x(+c)$ is larger than $\sim 6 \times 10^{-4}$ ($\Delta E_{defect} \leqslant 18.6$ kJ mol^{-1}).

In view of our calculations, we conclude that chain inversion provides a mechanism to continue attachments at sites where preferred intrinsic defects or substitutions by DNB have been formed. Conversely, continuation of attachments at non-preferred sites by DNB is more favoured by healing. Both primary and secondary defect formation contribute to the disordered structure of INB and possibly other structurally similar materials (*i.e.* A,D-disubstituted rod-like molecules). The main conclusion of this work is in agreement with the experimental results and mechanistic proposition given by Masciocchi *et al.*[2] However, the true structure is such that about one half ($+c$) of the crystal volume should show a significant concentration of DNB defects continued by chain inversion, whereas the other half ($-c$) should exhibit diffraction phenomena similar to a well-ordered, monodomain crystal.

We thank Dr O. König (Molecular Simulations Ltd., Cambridge, UK) for the calculated interaction energies. This work has been supported in part by the Swiss National Science Foundation (project no. 21-50828.97).

Notes and references

1 J. A. R. P. Sarma, F. H. Allen, V. J. Hoy, J. A. K. Howard, R. Thaitmattam, K. Biradha and G. R. Desiraju, *Chem. Commun*., 1997, 101.
2 N. Masciocchi. M. Bergamo and A. Sironi, *Chem. Commun*., 1998, 1347.
3 J. Hulliger, P. J. Langley and S. W. Roth, *Cryst. Eng*. (*Suppl. Mater. Res. Bull.*), 1998, in the press.
4 Atomic co-ordinates and geometric parameters *etc*. have been deposited at the Cambridge Structural Database (P. J. Langley, D. Abeln, O. König, J. Hulliger and H.-B. Bürgi, in preparation).
5 J. Hulliger, P. J. Langley, O. König, S. W. Roth, A. Quintel and P. Rechsteiner, *Pure Appl. Opt*., 1998, **7**, 221.
6 I. Weissbuch, M. Lahav, L. Leiserowitz, G. R. Meredith and H. Vanherzeele, *Chem. Mater*., 1989, **1**, 114.
7 I. Weissbuch, R. Popovitz-Biro, M. Lahav and L. Leiserowitz, *Acta Crystallogr*., 1995, **B51**, 115, and references cited therein.
8 Collinear intermolecular interaction energies were calculated by applying the DREIDING 2.2.1 force field. Atomic charges for calculation of the Coulombic interactions were obtained from MOPAC, using the MNDO approximation. Both sets of calculations were performed using Cerius 2 software (Molecular Simulations Ltd., Cambridge, UK).
9 J. Hulliger, *Z. Kristallogr*., 1998, **213**, 441; J. Hulliger, *Z. Kristallogr*, submitted.

Communication 8/06895J

Combinatorial 'library on bead' approach to polymeric materials with vastly enhanced chiral recognition

Peter Murer, Kevin Lewandowski, Frantisek Svec and Jean M. J. Fréchet*

Department of Chemistry, University of California, Berkeley, CA 94720-1460, USA.
E-mail: frechet@cchem.berkeley.edu

Received (in Corvallis, OR, USA) 11th August 1998, Accepted 21st October 1998

A general screening method for enantiomer recognition is introduced for the rapid preparation of novel chiral stationary phases for HPLC in which libraries of mixed chiral selectors are immobilized on polymer beads and the resulting chiral phases tested in the separation of racemic targets followed by deconvolution to afford an optimized separation medium.

Although it is well known that each enantiomer of a chiral compound may exhibit different biological activities, a number of commodity products and fine chemicals, such as drugs, agrochemicals, flavors, fragrances, and pheromones, are currently used in the form of racemic mixtures.[1] Therefore, the general trend is to replace these mixtures with single enantiomers that can be obtained directly, either by an asymmetric synthesis or by the resolution of racemates. In addition, for newly designed drugs, it may be necessary to obtain both enantiomers for pharmacological and toxicological studies. Among the separation techniques, resolution by high-performance liquid chromatography (HPLC) utilizing chiral stationary phases (CSPs) has advanced considerably in the past decade. The preparation of CSPs capable of effective enantiomer recognition is the key to this separation technique. Therefore, many CSPs for HPLC have been prepared and about 100 have been commercialized. Most are derived from various matrix-bound chiral selectors including transition metal complexes,[2] proteins,[3] antibiotics,[4] synthetic polymers and polysaccharides,[5] cyclodextrins and crown ethers,[6] or the π–π donor–acceptor complexes—'brush'-type separation media—pioneered by Pirkle.[7] Given the boundless structural and functional diversity of chiral molecules, no CSP is 'universal' and the separation of new targets may well mandate the development of new optimized complementary CSPs. Our combinatorial methods are aimed at the rapid preparation of tailor-made CSPs designed for a specific racemic solute.

Combinatorial chemistry is a very powerful tool for the preparation of large numbers of related compounds in a short period of time.[8] Today, this approach is a well-established technique used mainly to accelerate the drug discovery process. Combinatorial methods have also recently been used for the discovery of new materials.[9] Attempts to use combinatorial techniques in chromatography have focused on the field of the affinity separations employing the well-known interactions of peptides with target proteins. Typical screening methods have been used to select the most specific affinant with the highest binding constant from libraries of oligopeptides.[10]

We now report a combinatorial approach to the accelerated preparation of highly selective chiral separation media for HPLC based on chemically flexible 'brush'-type chiral selectors. The feasibility of our concept is demonstrated on model systems that involve π-basic selectors since the starting materials for these selectors are readily available in a large variety of chemistries.

Our combinatorial approach involves the attachment of a mixed library of potential selectors to an optimized polymer support[11] followed by on-column screening for enantioselectivity, and deconvolution to identify the single best selector. A small library of amides is prepared by reaction of *N*-Boc-protected L-amino acids with a mixture of aromatic primary amines using an active ester coupling procedure (Scheme 1).† After deprotection of the amino terminus, reaction of the mixed amide library with 5 μm macroporous 4-nitrophenyl carbonate activated poly(2-hydroxyethyl methacrylate-*co*-ethylene dimethacrylate) beads[11] leads to a chiral separation medium (CSP 1) with a multiplicity of polymer-bound selectors. Synthetic polymer beads were used in this study because they provide CSPs with higher selectivities than silica as a result of the elimination of non-specific interactions.[11,12] After packing these beads into a HPLC column, selectivity is assayed by injecting various racemates of chiral targets. Although the use of columns with mixed selectors is normally not recommended for actual enantioseparations[13] it is ideally suited for our combinatorial discovery of optimized selectors.

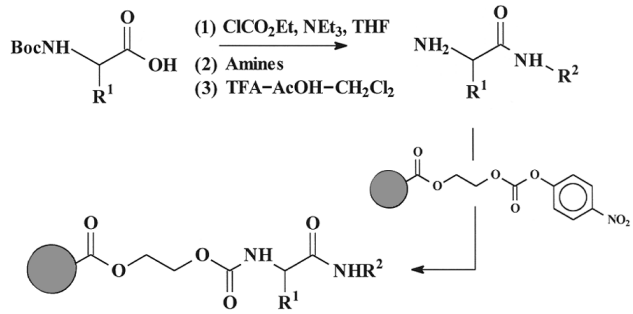

Scheme 1

The feasibility of this 'library-on-bead' approach is demonstrated with a small model library of 36 compounds prepared by reaction of a mixture of three L-amino acids (valine, phenylalanine and proline) with 12 aromatic amines (3,4,5-trimethoxyaniline **1**, 3,5-dimethylaniline **2**, 3-benzyloxyaniline **3**, 5-aminoindane **4**, 4-*tert*-butylaniline **5**, 4-biphenylamine **6**, 1-aminonaphthalene **7**, 4-tritylaniline **8**, 2-aminoanthracene **9**, 2-aminofluorene **10**, 2-aminoanthraquinone **11** and 3-amino-1-phenyl-2-pyrazolin-5-one **12**) (Scheme 2).† Both proline and dimethylaniline are included in the library design since previous work had shown their value in the preparation of efficient CSPs.[11,12,14] Despite the presence of 36 mixed selectors within the same column, CSP 1 separates DL-(3,5-dinitrobenzoyl)leucine diallylamide‡ and other substituted amino acid amides confirming the validity of the mixed selector approach. To determine which of the 36 selectors is the most powerful, a deconvolution process involving the preparation of beads with a progressively smaller number of selectors was used. Separation factors $\alpha = (t_2 - t_0)/(t_1 - t_0)$ where t_0 is the retention time of an unretained compound (column void volume determined using 1,3,5-tri-*tert*-butylbenzene as a marker) and t_1 and t_2 are the retention times of the individual enantiomers were calculated for all the separations to demonstrate the selectivity.

In the next step, each single amino acid was coupled separately with the set of 12 amines resulting in three new polymer-based CSPs (CSP 2–CSP 4). The highest separation factor α of 13.7 was found for the proline-based column while

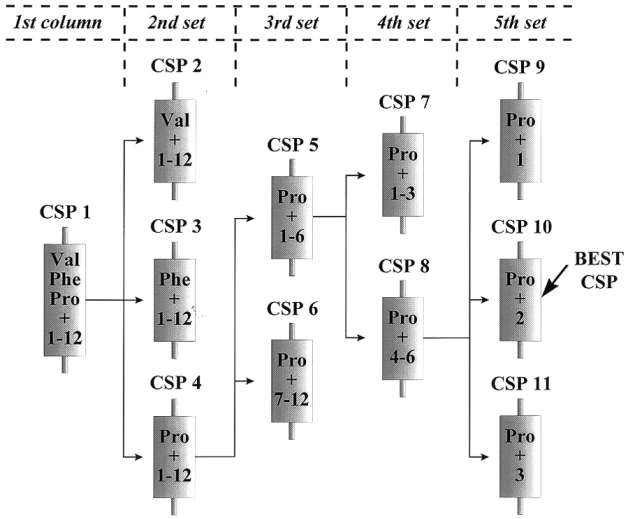

Scheme 2

the α values for the other two columns are close to 5. For the preparation of the third set of columns (CSP 5 and CSP 6), two proline based sub-libraries of selectors were prepared from two six-member groups of amines (**1**–**6** and **7**–**12**) and the respective columns exhibited selectivities of 13.6 and 7.3. In the next step, the six amines present in the more selective column CSP 5 were divided into two groups (**1**–**3** and **4**–**6**) and the columns CSP 7 and CSP 8 exhibited rather high α values of 17.4 and 14.9, respectively. The separation results indicate that both groups of three selectors include at least one with a very high selectivity. CSP 7 that affords somewhat higher selectivity was further deconvoluted. Three columns CSP 9–CSP 11 packed with beads containing only individual selectors were prepared. Although two of these columns (10 and 11) do not exhibit high separation factors (2.5 and 3.6, respectively), an α value of 24.7 was achieved with CSP 9 that features dimethylaniline **2** as a part of the proline selector. The rapid increase in the separation factors reflects not only the improvement in the intrinsic selectivities of the individual selectors, but also the effect of increased loading with more efficient selectors since the overall selector loading determined from nitrogen content remains virtually constant at about 0.7 mmol g^{-1} for all CSPs 1–12. NMR spectra indicate that none of the selectors binds preferentially to the support during the reaction of their mixtures.

A classical 'one column, one selector' approach would require the preparation and testing of 36 CSPs modified with each individual selector. In contrast, our combinatorial scheme documents that the parallelism advantage results in the discovery of a novel highly selective CSP from the same group of 36 selectors using only 11 columns, *i.e.* less than one third. In addition, an unlimited number of racemates may be screened through the various columns. The advantage of the mixed selector column approach becomes even more convincing with much larger sets of selectors. For example, a simple calculation reveals that the use of all 20 natural amino acids with the same 12 amines would lead to a library of 240 selectors that could be deconvoluted using only 17 columns. The question now arises as to what is the highest number of selectors that may be used simultaneously in the first column. It seems that there is no limitation from a chemical point of view. However, in a hypothetical situation in which only a single selector is active and all of the compounds are attached to the beads in equal amounts, the percentage of the active selector in the mixture decreases rapidly and despite its high specific selectivity (separation factor at a loading of 1 mmol g^{-1}), the actual selectivity of a CSP with mixed selectors may be rather small and may even vanish within the limits of experimental errors. Although the sensitivity of the chromatographic screening may somewhat limit this approach, the number of selectors that may be screened in a single column is still impressive. Obviously, the libraries of columns resulting from this approach may be used time and again for the separation of the racemates of a variety of chiral targets.

Funding of this research by the National Institute of General Medical Sciences, National Institutes of Health (GM-44885) is gratefully acknowledged. P. M. thanks the Swiss National Science Foundation for a postdoctoral fellowship.

Notes and references

† The *N-tert*-butoxycarbonyloxy-protected (Boc) amino acids (7.0 mmol) were dissolved in THF (35 ml), cooled and triethylamine (7.0 mmol) and $ClCO_2Et$ (7.0 mmol) were added slowly by syringe. After stirring at −15 °C for 1 h, a cold (−15 °C) mixture of equimolar amounts of the desired aromatic amines (total amount of amines = 7.0 mmol) in THF was admixed. Stirring continued at −15 °C for 1 h and at room temperature overnight. The organic phase was washed, dried over $MgSO_4$ and concentrated to afford the product. This product was dissolved in CH_2Cl_2 cooled to 0 °C, and treated with 1:1 mixture of TFA–AcOH for 12 h. Extraction and drying under high vacuum afforded the deprotected product mixture as a colored solid in near quantitative yield. Integration of the individual ^1H NMR signals for the amide hydrogen atoms of the compounds indicates that all expected products were formed. Et_3N (15 mmol) was added to a slurry of 4-nitrophenyl carbonate-activated poly(2-hydroxyethyl methacrylate-*co*-ethylene dimethacrylate) beads (1.6 g) (ref. 11) in THF at 0 °C. The solution of the selector mixture obtained from the deprotection step in THF was added slowly to this suspension and stirring was continued at room temperature for 3 h and then at 60 °C overnight to afford the chiral stationary phases.

‡ The chiral stationary phases were slurry packed at a constant pressure of 15 MPa into 150 × 4.6 mm i.d. stainless steel columns. Chiral separations were carried out in normal-phase mode using a 1:4 (v/v) hexane–CH_2Cl_2 mixture as the mobile phase.

1 *Chiral Separations, Applications and Technology*, ed. S. Ahuja, ACS, Washington D.C., 1997.
2 V. A. Davankov, *Adv. Chromatogr.*, 1980, **18**, 139.
3 S. Allenmark, B. Bomgren and H. Boren, *J. Chromatogr.*, 1983, **264**, 63.
4 D. W. Armstrong, Y. Tang, S. Chen, Y. Zhou, C. Bagwill and J. R. Chen, *Anal. Chem.*, 1994, **66**, 1473.
5 Y. Okamato and E. Yashima, *Angew. Chem., Int. Ed.*, 1998, **37**, 1021.
6 D. W. Armstrong and W. DeMond, *J. Chromatogr. Sci.*, 1984, **22**, 411.
7 W. H. Pirkle and T. C. Pochapsky, *Chem. Rev.*, 1989, **89**, 347.
8 *Combinatorial Chemistry, Synthesis and Application*, ed. S. R. Wilson and A. W. Czarnik, Wiley, New York, 1997.
9 L. C. Hsieh-Wilson, X.-D. Xiang and P. G. Schultz, *Acc. Chem. Res.*, 1996, **29**, 164.
10 P. Y. Huang and R. G. Carbonell, *Biotechnol. Bioeng.*, 1995, **47**, 288.
11 K. Lewandowski, F. Svec and J. M. J. Fréchet, *Chem. Mater.*, 1998, **10**, 385.
12 Y. Liu, F. Svec, J. M. J. Fréchet and K. N. Juneau, *Anal. Chem.*, 1997, **69**, 61.
13 W. H. Pirkle and C. J. Welch, *J. Chromatogr. A*, 1996, **731**, 322.
14 W. H. Pirkle and P. G. Murray, *J. Chromatogr.*, 1993, **641**, 11.

Communication 8/06397D

Remarkable matrix effect in polymer-supported Jacobsen's alkene epoxidation catalysts

Laetitia Canali,[a] Elaine Cowan,[a] Hervé Deleuze,[b] Colin L. Gibson[a] and David C. Sherrington*[a]

[a] *Department of Pure and Applied Chemistry, Thomas Graham Building, University of Strathclyde, 295 Cathedral Street, Glasgow, UK G1 1XL. E-mail: m.p.a.smith@strath.ac.uk*

[b] *Laboratoire de Chimie Organique et Organometallique, Université Bordeaux I, 33 405 Talence, France*

Received (in Liverpool, UK) 2nd September 1998, Accepted 16th October 1998

Adaptation of the polymer matrix has allowed high enantioselectivity to be achieved for the first time with a polymer-supported chiral Mn^{III}(salen) alkene epoxidation catalyst.

Previous attempts to immobolise Jacobsen's chiral Mn^{III}(salen) asymmetric alkene epoxidation catalyst[1,2] on polymer resins have focussed on copolymerisation of distyryl derivatives of chiral salen ligands, such that the Mn complex formed is essentially localised on a crosslink.[3,4] Perhaps not surprisingly the steric restriction of this system has led to disappointingly low levels of enantiocontrol in epoxidations. Our own first attempt to develop a polymer-supported system was also rather disappointing,[5] but encouraged us to believe that providing the following design criteria could be met, a highly active and selective heterogeneous catalyst should result: (i) the local molecular structure of the Mn complex should mimic precisely the optimum structure of Jacobsen's catalyst; (ii) the complex should be attached by a single flexible linkage to the polymer support to minimise local steric restriction; (iii) the catalyst should be attached to the polymer with sufficiently low loading to maximise site isolation of catalytic centres, hence minimising the possibility of inactive oxo-bridged dimer formation; and (iv) the morphology of the support should be such that no mass transfer limitation arises, with all active sites freely accessible. We now report on the synthesis and application of a number of polymer-supported analogues of Jacobsen's catalyst developed on the basis of the above criteria.

Polymer resin catalysts **P1**–**P5** were synthesised as shown in Scheme 1 to yield Mn complex loadings (calculated from Mn content determined by inductively coupled plasma absorption) of 0.35, 0.17, 0.08, 0.34 and 0.22 mmol g^{-1} respectively. The styrene-based resins used to prepare **P1** and **P2** employed *p*-acetoxystyrene as a functional co-monomer, commercial divinylbenzene (80% DVB grade) as the crosslinker, with styrene itself making up the co-monomer balance. The methacrylate-based resin forming the basis of **P3** likewise used *p*-acetoxystyrene as the functional co-monomer, ethane-1,2-diyl dimethacrylate as the crosslinker, and methyl methacrylate as the co-monomer balance. **P4** was derived from a resin prepared from *p*-hydroxyphenylmaleimide, divinylbenzene and styrene, while **P5** was synthesised from a resin made from 3-methacryloyoxy-2-hydroxybenzaldehyde,[7] ethane-1,2-diyl dimethacrylate and methyl methacrylate. Polymerisation compositions and resin parameters are shown in Table 1. The yields of high quality beads were good and along with subsequent chemical derivatisation confirmed good incorporation of each functional

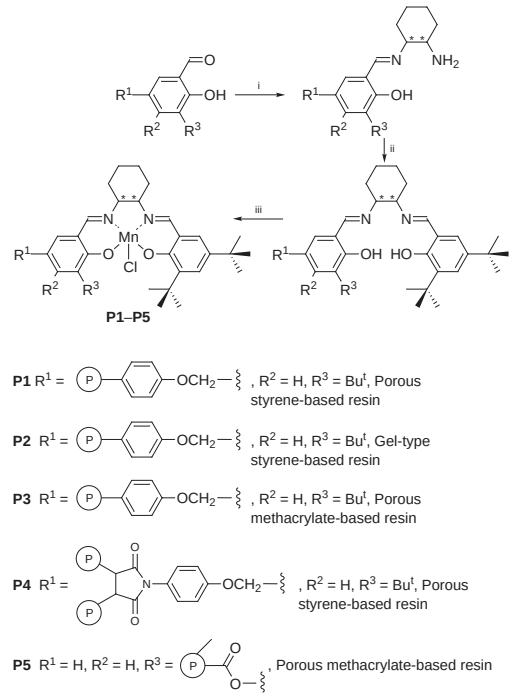

Scheme 1 *Reagents and conditions*: i, (*R*,*R*)-1,2-diaminocyclohexane, CH_2Cl_2, room temp., 12 h; ii, 2,4-di-*tert*-butylsalicylaldehyde (ref. 6); iii, CH_2Cl_2, room temp., 12 h; vi, $Mn(OAc)_2{\cdot}4H_2O$, EtOH, air, reflux, 30 h, then LiCl.

Table 1 Synthesis of resin precursors to polymer catalysts **P1**–**P5**[a]

	Polymerisation conditions				Resin				
Precursor	Cross-linker/ mol%	Co-monomer (%)	Porogen	Monomer: porogen (v/v)	Yield of beads (%)	Bead diameter (% 200–500 μm)	Average pore radius/nm	Surface area/ m^2 g^{-1}	Morphology
P1	1.6[b]	32[c]	—	—	57	39	—	—	Gel-type
P2	24[b]	32[c]	2-Ethylhexan-1-ol	1:1	95	67	5.9[d]	31	Porous
P3	68[e]	13[c]	Toluene	1:1	84	58	0.9[d]	123[f]	Porous
P4	60[b]	20[g]	2-Ethylhexan-1-ol–DMF (7:3, v/v)	1:1	83	80	4.6[d]	227[f]	Porous
P5	30[e]	25[h]	2-Ethylhexan-1-ol–toluene (6:5, v/v)	1:1	73	60	6.5[i]	101[f]	Porous

[a] All polymers made by suspension polymerisation using procedures already reported (ref. 8). [b] DVB. [c] *p*-Acetoxystyrene. [d] from N_2 sorption, BJH method (ref. 9) (Micromeritics Accursorb 2100E). [e] Ethane-1,2-diyl dimethacrylate. [f] From N_2 sorption, BET method (ref. 10). [g] *p*-Hydroxyphenylmaleimide. [h] 3-Methacryloyloxy-2-hydroxybenzaldehyde. [i] Hg intrusion porosimetry (Micromeritics Autopore 9220).

Table 2 Asymmetric epoxidation of 1-phenylcyclohex-1-ene using MCPBA catalysed by polymer-supported chiral Mn^{III}(salen) complex[a]

		Epoxide		
Catalyst	Configuration	Yield (%)[b]	Ee (%)[c]	Configuration[d]
Soluble[e]	*S*,*S*	72	92	(+)-(*R*,*R*)
P1	*R*,*R*	36	61	(−)-(*S*,*S*)
P2	*R*,*R*	47	66	(−)-(*S*,*S*)
P3	*R*,*R*	49	91	(−)-(*S*,*S*)
P4	*R*,*R*	5	5	(−)-(*S*,*S*)
P5	*R*,*R*	5	~0	(−)-(*S*,*S*)

[a] See note †. [b] Determined by GC after 2 h using PhBr as internal standard. [c] Determined by HPLC using Diacel CHIRACEL OJ column (hexane–Pr^iOH, 90:10, as eluent). [d] Absolute configuration confirmed by polarimetry. [e] Jacobsen's catalyst used as supplied from Aldrich.

co-monomer. In the case of the precursors to resin catalysts **P1**–**P3** the acetoxy group was cleaved with NH_2NH_2 and the sodium salt of the liberated phenol reacted with 3-*tert*-butyl-5-chloromethyl-2-hydroxybenzaldehyde.[4] The sodium salt of the phenolic precursor to **P4** was similarly derivatised. In all cases the immobilised salicylaldehyde residues were further elaborated as in Scheme 1. Interim elemental microanalysis of beads at various stages of the catalyst synthesis, and model reactions using 5-bromo-2-hydroxybenzaldehyde instead of the di-*tert*-butyl analogue, confirmed the success of the stepwise synthesis of the catalysts, and indicated typically ⩾90% of salen ligands to be attached pendantly (extensive details will be presented in due course in a full paper[11]). Interestingly the reactions can be monitored superficially by the succession of characteristic colour changes of the beads; acetoxy resin, white; phenolic resin, cream; phenoate resin, pale pink; salicylaldehyde resin, sandy yellow; mono-Schiff-base resin, yellow; salen resin, yellow; Jacobsen resin, dark brown.

Asymmetric epoxidations of 1-phenylcyclohex-1-ene were carried out in CH_2Cl_2 at 0 °C using MCPBA as the oxidant, and NMO as the activator. The conditions employed were typical of those reported in the use of the soluble catalyst.[6] The results obtained are shown in Table 2. In the case of polymer catalysts **P4** and **P5** both the yield and enantiomeric purity of the epoxide product are very low. With **P5** we believe this is so because attachment of the chiral Mn^{III}(salen) complex to the support is *via* the position *ortho* to the phenolic OH on one of the aromatic rings. The synthetic route to this species is facile, cost effective, and offers a highly structurally pure polymer catalyst. We had hoped the local steric restriction might reinforce the enantioselectivity. In practice this seems not to be so, and the local congestion seems so high as to inhibit any significant approach to the Mn centre, let alone an enantiocontrolled one. The poor performance of **P4** is less easily explained. The polymer matrix from which this is derived was synthesised using 60 mol% divinylbenzene crosslinker and 20 mol% *p*-hydroxyphenylmaleimide with a high level of porogen present (Table 1). The porosity characteristics suggest that mass transfer to the interior of this rather heavily crosslinked species should nevertheless be quite good. Since styrene and maleimide display a high tendency to form a 1:1 alternating copolymer structure, despite the modest loading of functional co-monomer, these residues may well therefore be in close proximity to each other in the matrix. Consequently bimolecular deactivating reactions between Mn centres might be encouraged. Since the phenylmaleimide residue is likely to be a rather rigid segment in the matrix backbone, both of these factors seem to have conspired to produce low catalytic activity and selectivity. The performance of the gel-type styrene-based resin **P1** is much better. The enantioselectivity achieved (61% ee) is as good as any previous data in the literature for polymer-supported species of this type, and far better than our earlier attempt with a gel-type resin.[5] In the latter case the polymer catalyst also displayed low activity, suggesting that deactivating dimerisation of the Mn^{III} centres was occurring. With catalyst **P1** the Mn loading level and morphological characteristics are not too different to our earlier gel-type species, but the attachment to the polymer matrix is quite different. Previously the linkage had been *via* an ether group at the position *meta* to the phenolic OH on one of the aromatic groups of the salen.[5] With **P1** the linkage is *via* an oxymethylene at the position *para* to the phenolic OH. Bearing in mind the sensitivity of these chiral salen ligands to the pattern and nature of the substitution on the aromatic rings, this simple change alone may well account for the improved catalytic performance of the gel-type species **P1**. Interestingly, catalyst **P2** is chemically similar to **P1** both in terms of the local structure in and around the catalytic centres, the Mn loading, and in terms of the longer range environment. It differs only in having a (macro)porous morphology rather than a gel-type one. Its dry porosimetry characteristics suggest mass transport should be quite good. Both the activity and enantioselectivity displayed by **P2** are very similar to those of **P1**, and suggest that further manipulations of the morphology of styrene-based resins may not alone offer significant improvement in catalyst activity and selectivity. Catalyst **P3** displays comparable activity to those of **P1** and **P2** under the conditions employed but is significantly more enantioselective (> 90% ee). Indeed the enantiocontrol displayed mirrors that of the soluble catalyst. The experimental ee is significantly higher than that reported to date for any polymer-supported system, and suggests that contrary to earlier findings a practical polymer-supported Jacobsen's catalyst may well be achievable. **P3** is prepared from a heavily crosslinked (macro)porous resin and has rather low loading of Mn sites (0.08 mmol g^{-1}). The dry resin has a good surface area and the porogen employed (toluene) is known to generate rather small pores.[12] Probably of key significance however is that **P3** is derived from a methacrylate-based resin rather than a styrene-based one, although the immediate link to the polymer is *via* a styryl residue. We believe that such a matrix, although macroscopically rigid, has considerably improved local mobility relative to a styrene-based analogue, and of course is of significantly higher polarity. These two factors, coupled with the rather low loading of catalytic sites (0.08 mmol g^{-1}), seem to be key in allowing rapid catalysis and a stereochemical outcome that are essentially analogous to those found with the soluble catalyst.

Notes and references

† Asymmetric epoxidation procedure. Resin beads (0.13 mmol Mn) were poured into a solution containing NMO (15.79 mmol) dissolved in CH_2Cl_2 (25 ml) and evacuated (water pump) for *ca*. 1 min. Phenylcyclohex-1-ene (3.16 mmol) and PhBr (2.04 mmol) were then added and the mixture was cooled to 0 °C. MCPBA (6.32 mmol) was then added in four equal portions over a 2 min period.

1 E. N. Jacobsen, *Asymmetric Catalytic Epoxidation of Unfunctionalised Olefins*, in *Catalytic Asymmetric Synthesis*, ed. I. Ojima, VCH, New York, 1993, p. 159.
2 E. N. Jacobsen, *Transition Metal-Catalysed Oxidations*: *Asymmetric Epoxidations*, in *Comprehensive Organometallic Chemistry II*, ed. E. W. Abel, F. G. A. Stone and E. Wilkinson, Pergamon, New York, 1995, vol. 12, p. 1097.
3 B. B. De, B. B. Lohray and P. K. Dhal, *Tetrahedron Lett*., 1993, **34**, 2371; B. B. De, B. B. Lohray, S. Sivaram and P. K. Dhal, *Macromolecules*, 1994, **27**, 2191; *Tetrahedron*: *Asymmetry*, 1995, **6**, 2105; *J. Polym. Sci*., *Polym. Chem. Ed*., 1997, **35**, 1809.
4 F. Minutolo, D. Pini and P. Salvadori, *Tetrahedron* : *Asymmetry*, 1996, **7**, 2293; F. Minutolo, D. Pini and P. Salvadori, *Tetrahedron Lett*., 1996, **37**, 3375.
5 L. Canali, H. Deleuze and D. C. Sherrington, *React. Funct. Polym*., 1998, in the press.
6 W. Zhang and E. N. Jacobsen, *J. Org. Chem*., 1991, **56**, 2296.
7 Synthesis to be reported. See 4th. Year B.Sc. Report, E. Cowan, University of Strathclyde.
8 P. D. Verweij and D. C. Sherrington, *J. Mater. Chem*., 1991, **1**, 371.
9 E. P. Barrett, L. G. Joyner and P. D. Halinda, *J. Am. Chem. Soc*., 1951, **73**, 373.
10 S. Branauer, P. H. Emmett and E. Teller, *J. Am. Chem. Soc*., 1938, **60**, 309.
11 L. Canali, E. Cowan, H. Deleuze, C. L. Gibson and D. C. Sherrington, unpublished work.
12 D. C. Sherrington, *Chem. Commun*., 1998, 2275.

Communication 8/06841K

ChemComm

Application of Baylis–Hillman methodology in a novel synthesis of quinoline derivatives

Oluwole B. Familoni, Perry T. Kaye* and Phindile J. Klaas

Department of Chemistry, Rhodes University, Grahamstown, 6140, South Africa. E-mail: chpk@hippo.ru.ac.za

Received (in Cambridge, UK) 27th May 1998, Accepted 8th October 1998

Reaction of 2-nitrobenzaldehyde with vinyl carbonyl compounds in the presence of 1,4-diazabicyclo[2.2.2]octane affords Baylis–Hillman products, catalytic reduction of which results in direct cyclisation to quinoline derivatives.

The Baylis–Hillman reaction has been the subject of two recent reviews[1,2] and continues to elicit attention.[3,4] We have demonstrated applications of this reaction in the synthesis of substituted indolizines from pyridine-2-carbaldehydes[5,6] and, in analogous reactions of salicylaldehydes, have uncovered a veritable cascade of transformations involving the formation of chromene and coumarin derivatives.[7,8] Extension of this general methodology to 2-aminobenzaldehydes was expected to provide access to quinoline derivatives.

Numerous quinoline syntheses have been developed,[9] including the Friedlander synthesis (and modifications thereof) in which use is made of 2-aminobenzaldehydes. A limiting factor in the Friedlander methodology, however, is the relative inaccessibility of substituted 2-aminobenzaldehydes. This limitation, coupled with the fact that aldehyde electrophilicity is an important factor in Baylis–Hillman reactions,[10] prompted us to explore the use of 2-nitrobenzaldehyde as an activated alternative to 2-aminobenzaldehyde, subsequent reduction of the nitro group being expected to permit cyclisation *via* the resulting amine. Quinolines have, in fact, been obtained previously in yields of 27–30%, by passing mixtures of 2-nitrobenzaldehyde and various alcohols over a heterogeneous catalyst at elevated temperature (300–320 °C).[11] Here we report preliminary results which clearly illustrate the potential of the Baylis–Hillman approach to quinoline derivatives under remarkably mild conditions.

Treatment of 2-nitrobenzaldehyde **1** with methyl vinyl ketone (MVK) **2a**, methyl acrylate **2b** and ethyl acrylate **2c** in the presence of 1,4-diazabicyclo[2.2.2]octane (DABCO) at, or below, room temperature† afforded the expected Baylis–Hillman products **3a–c** (Scheme 1) in moderate to good yield (68–85%). Several methods of reducing the nitro compounds **3a–c** were examined, the most efficient proving to be catalytic hydrogenation using a 10% palladium on carbon catalyst in EtOH.‡ Reduction of compound **3a** afforded, in 56% yield, a product initially presumed to be 2,3-dimethylquinoline but subsequently identified as the *N*-oxide **4**.§ Hydrogenation of the methyl ester **3b** afforded two cyclised products, *viz*. 3-methyl-2-oxo-1,2,3,4-tetrahydroquinoline **5** (22%) and the 4-hydroxy analogue **6** (59%), the latter as a diastereomeric pair, which could be readily dehydrated (in 70% yield) to the conjugated, achiral 3-methyl-2-quinolinone **7**. The α,β-unsaturated carbonyl moiety in the Baylis–Hillman products **3** is, of course, susceptible to conjugate addition, and treatment of the ethyl ester **3c** with piperidine¶ led to the diastereomers **8**, reduction of which afforded the 2-quinolinone derivative **9**;‖ in this case, cyclisation of the corresponding amino intermediate may only occur *via* acyl substitution. In principle, cyclisation of the reduced, or partially reduced, intermediates may be expected to involve *either* conjugate addition *or* nucleophilic attack at the carbonyl carbon. In practice, the latter path appears to be the dominant, if not exclusive, mode of cyclisation—somewhat surprisingly, given the lack of regioselectivity exhibited by salicylaldehyde analogues.[7,8]

Application of the methodology to the reaction of 2-nitrobenzaldehyde with ethyl vinyl ketone afforded *both* 2-ethyl-3-methylquinoline **10** (25%) *and* the *N*-oxide **11** (31%).

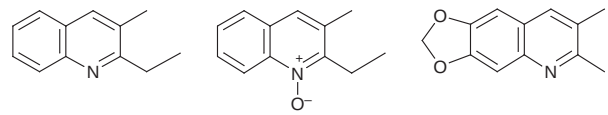

10 **11** **12**

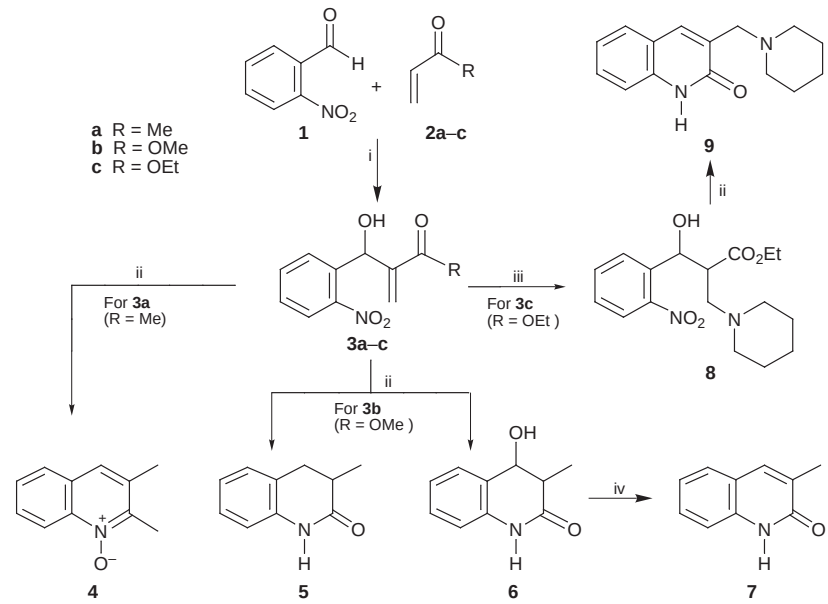

Scheme 1 *Reagents and conditions*: i, DABCO, $CHCl_3$; ii, H_2, Pd-C, EtOH; iii, piperidine, THF; iv, TsOH, toluene, reflux.

Formation of the *N*-oxides **4** and **11** was established, in each case, by FAB MS analysis. Further extension of the procedure to the reaction of methyl vinyl ketone with 6-nitropiperonal gave, amongst other products, the corresponding quinoline **12** (26%).

In summary, application of the Baylis–Hillman reaction to 2-nitrobenzaldehydes provides convenient access to substituted quinoline derivatives which, in turn, constitute useful substrates for further elaboration. The results of ongoing studies, aimed at optimising reaction conditions for the selective formation of the quinolines or their *N*-oxides and exploring the generality of the method, will be reported fully in due course.

We thank the Foundation for Research Development (FRD) and Rhodes University for generous financial support, the University of Lagos, Nigeria, for study leave (to O. B. F.), Dr W. E. Molema for assistance with NMR analysis and Dr L. Fourie (University of Potchefstroom) for FAB MS data.

Notes and references

† In a typical Baylis–Hillman reaction, a solution of 2-nitrobenzaldehyde **1** (5.0 g, 33 mmol), methyl acrylate **2b** (2.95 g, 34.2 mmol) and DABCO (0.18 g, 1.6 mmol) was stirred in a stoppered flask for 3–7 d. [In the case of methyl vinyl ketone **2a**, the reaction was noticeably exothermic; use of CH_2Cl_2 as solvent and cooling the mixture (*ca*. 0 °C) during addition of the reactants resulted in a significantly cleaner product.] The solvent was evaporated *in vacuo* and the residue chromatographed [flash chromatography on silica; elution with hexane–EtOAc (3:1)] to give **3a** (6.78 g; 85%).

‡ Hydrogenation was effected in EtOH at atmospheric pressure using a 10% Pd-C catalyst (wet, Degussa type; as supplied by Aldrich Chemical Co.)

§ *Selected data* for **4**, mp 123–125 °C (Found, by FAB MS, MH^+: 174.09179. Calc. for $C_{11}H_{12}NO^+$, 174.09189.); δ_H(400 MHz; $CDCl_3$) 2.45 (3H, s, 3-Me), 2.68 (3H, s, 2-Me), 7.45 (1H, s, 4-H), 7.51 (1H, t, 6-H), 7.63 (1H, t, 7-H), 7.68 (1H, d, 5-H), 8.68(1H, d, 8-H); δ_C(100 MHz; $CDCl_3$) 14.7 (2-Me), 20.2 (3-Me), 119.6 (C-5), 125.1 (C-4), 127.1 (C-8), 127.7 (C-7), 128.1 (C-4a), 129.2 (C-6), 130.8 (C-3), 139.9 (C-8a), 146.4(C-2)].

¶ A mixture of **2c** (0.5 g), piperidine (0.5 ml) and THF (5 ml) was stirred in a stoppered flask for 24 h. Excess piperidine was evaporated *in vacuo* and the residue was chromatographed [flash chromatography on silica; elution with hexane–EtOAc (2:1)] to give **8** (0.61g, 85%).

‖ Compounds **6**, **8** and **9**, which appear to be new, and the known quinoline derivatives **4**, **5**, **7**, **10–12** were characterised by elemental (high resolution MS) and ^1H and ^{13}C NMR spectroscopic analyses.

1 S. E. Drewes and G. H. P. Roos, *Tetrahedron*, 1988, **44**, 4653.
2 D. Basavaiah, P. Darma Rao and R. S. Hyma, *Tetrahedron*, 1996, **52**, 8001.
3 G. P. Black, F. Dinon, S. Fratucello, P. J. Murphy, M. Nielsen and H. L. Williams, *Tetrahedron Lett*., 1997, **38**, 8561.
4 L. J. Brzezinski, S. Rafel and J. W. Leahy, *Tetrahedron*, 1997, **53**, 16423.
5 M. L. Bode and P. T. Kaye, *J. Chem. Soc*., *Perkin Trans. 1*, 1990, 2612.
6 M. L. Bode and P. T. Kaye, *J. Chem. Soc*., *Perkin Trans. 1*, 1993, 1809.
7 P. T. Kaye and R. S. Robinson, *Synth. Commun*., 1996, **26**, 2085.
8 J. Bacsa, P. T. Kaye and R. S. Robinson, *S. Afr. J. Chem*., 1998, **51**, 47.
9 See, for example, G. Jones, in *Comprehensive Heterocyclic Chemistry*, ed. A. J. Boulton and A. McKillop, Pergamon, Oxford, 1984, vol. 2, p. 395.
10 M. L. Bode and P. T. Kaye, *Tetrahedron Lett*., 1991, **21**, 5611.
11 N. S. Koslov, Y. S. Chumakov and S. I. Kozintsev, *Katal. Sint. Prevrashch. Geterotsikl. Soedin*., 1976, 57 (*Chem. Abstr*., 1978, **88**, 22572).

Communication 8/07827K

ChemComm

Redox-switchable polyester dendrimers incorporating both π-donor (tetrathiafulvalene) and π-acceptor (anthraquinone) groups

Martin R. Bryce,* Pilar de Miguel and Wayne Devonport

Department of Chemistry, University of Durham, Durham, UK DH1 3LE. E-mail: m.r.bryce@durham.ac.uk

Received (in Liverpool, UK) 9th September 1998, Accepted 16th October 1998

The convergent synthesis of $(TTF)_x(AQ)_y$ (TTF = tetrathiafulvalene; AQ = anthraquinone) polyester dendrimers is reported; the molecules undergo clean amphoteric redox behaviour with reversible switching between cationic and anionic states being achieved under electrochemical control; the higher generation system $(TTF)_8(AQ)_4$ displays an intradendrimer charge-transfer interaction in solution.

Dendritic molecules[1] which possess functional groups at the exterior surface and/or embedded within their structure[2] are of current interest. In this context, dendrimers which carry multiple cationic or anionic sites are attracting attention, due to their potential applications as macromolecular polyelectrolytes, catalysts and charge transfer materials. The charged sites may be introduced into the structure in two conceptually different ways: (i) during the synthesis, *e.g.* by using quaternary ammonium linkages,[3] by incorporating transition metals,[4] or by attaching polyanionic surfaces;[5] or (ii) by electrochemical redox processes or chemical doping of a neutral dendrimer which contains redox-active groups.[6] For these systems, the redox centres may behave independently in multi-electron processes (*n* identical non-interacting electroactive centres giving rise to a single *n*-electron wave) or they may interact intra- or inter-molecularly, in which case overlapping or closely-spaced redox waves are observed at different potentials. Representative electron donor groups are ferrocene,[7] metal-(bipyridyl)[8] and tetrathiafulvalene (TTF),[9] while interior anthraquinone (AQ)[10] and peripheral naphthalene diimide[11] groups have been used as electron acceptor units. Dendritic systems containing both strong π-donor and π-acceptor groups covalently bonded into their framework[12] are especially attractive targets as they should possess amphoteric redox properties under electrochemical control,[8b] and may engage in inter- and/or intra-molecular charge-transfer interactions.

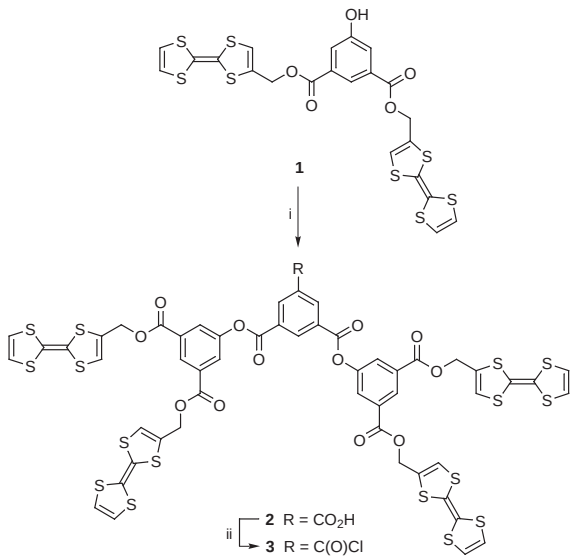

Scheme 1 *Reagents and conditions*: i, benzene-1,3,5-tricarbonyl chloride, DMAP, CH_2Cl_2, 20 °C, silica gel chromatography; ii, oxalyl chloride, toluene 80 °C.

Herein we report the prototype systems **8** and **9** containing both TTF and AQ units, built around a benzene 1,3,5-triester core. The synthesis of the $(TTF)_4$ dendron **3** is shown in Scheme 1.† The reaction of phenol derivative **1**[9a,d] (2.1 equiv.) with benzene-1,3,5-tricarbonyl chloride (1.0 equiv.) in the presence of DMAP as base (CH_2Cl_2, 20 °C) afforded the carboxylic acid derivative **2** (56% yield) after hydrolysis of the unreacted acid chloride group during workup. Reaction of **2** with oxalyl chloride in toluene afforded acid chloride derivative **3** (82% yield). The synthesis of the $(AQ)_2$ reagent **7** is shown in Scheme 2. 2-(Hydroxymethyl)anthraquinone **4** reacted with 5-(*tert*-butyldimethylsiloxy)isophthalic acid **5**[13] using the DMAP-catalysed DCC method[14] to form compound **6** in 55% yield. Attempted desilylation of **6** using TBAF in THF resulted in cleavage of the ester linkages;[15] however, heating a solution of **6** in a mixture of THF–aq. HCl (1 M) gave the alcohol derivative **7** (81% yield) which was only sparingly soluble in most organic

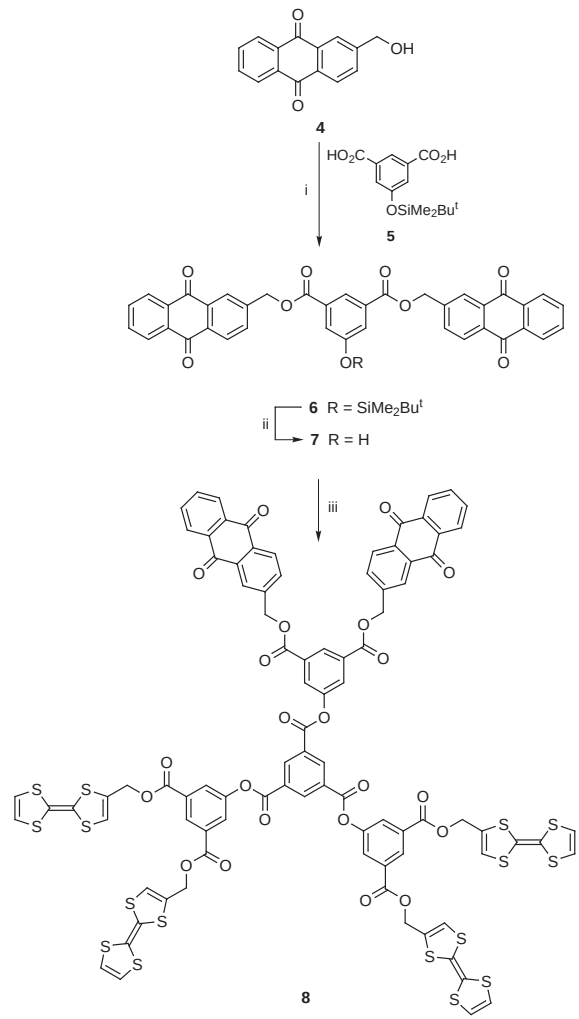

Scheme 2 *Reagents and conditions*: i, DCC, DMAP, CH_2Cl_2, 0–20 °C; ii, HCl (1 M)–THF (7:1 v/v), 50 °C; iii, **3**, DMAP, 1,4-dioxane, reflux.

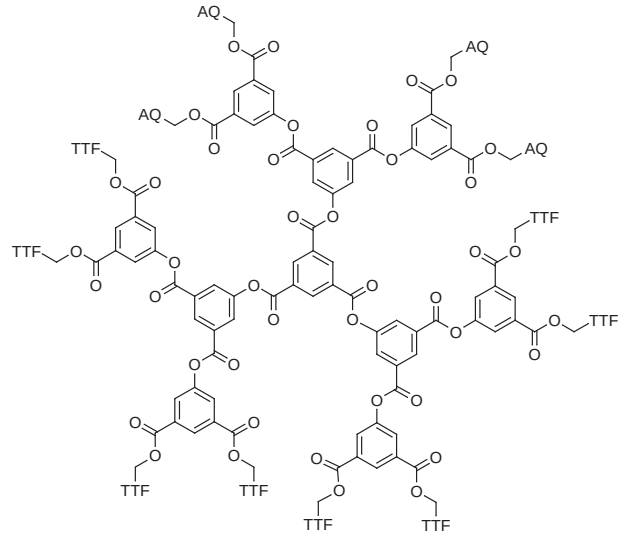

9

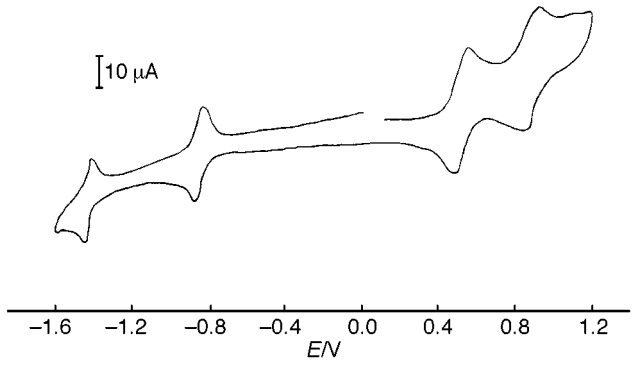

Fig. 1 Cyclic voltammogram of **8** (MeCN, 20 °C, $Bu_4N^+PF_6^-$ electrolyte, Pt electrode, *vs.* Ag/AgCl, scan rate 50 mV s^{-1}).

solvents. Esterification of **7** to afford G1 dendrimer **8** (60% yield, after column chromatography on silica gel) was achieved by reaction with acid chloride derivative **3** in the presence of DMAP in refluxing 1,4-dioxane. Analogous iterative procedures, starting with the known octa-TTF building block,[9d] gave the $(TTF)_8(AQ)_4$ G2 system **9**. Compounds **8** and **9** are soluble in a range of organic solvents (*e.g.* CH_2Cl_2, $CHCl_3$, THF, dichlorobenzene and CS_2): they darken on storage in air, and can be stored for several weeks under vacuum in the dark at 0 °C.

The solution electrochemistry of **8** and **9** has been studied by cyclic voltammetry (CV) in MeCN solution (Fig. 1). Scanning anodically, **8** exhibits two reversible four-electron oxidation waves to form, sequentially, the radical cation and dication of each of the TTF moieties;[16] scanning cathodically, two reversible two-electron waves are observed, corresponding to the reduction of each anthraquinone unit to the radical anion and the dianion.[17] Thus, **8** demonstrates clean amphoteric redox behaviour with reversible switching between the +8, +4, 0, −2 and −4 charged states being achieved. The CV of **9** is very similar (the +16, +8, 0, −4 and −8 states are clearly observed) although the second TTF wave was slightly narrower than the first wave, which was probably due to adsorption phenomena, as observed previously with some higher generation systems.[9d]

An important difference between the G1 and G2 systems **8** and **9** is manifested in their UV–VIS spectra. Compound **9** shows a very weak (ε < 250) broad absorption band in the λ 460–750 nm region in MeCN, which is not present in **8**. The solvent dependency of this band and experiments at various concentrations of **9** suggest that this low energy band arises from intramolecular (rather than intermolecular) π–π charge-transfer from TTF to anthraquinone units. Based on the different redox potentials of these donor and acceptor moieties, the degree of charge-transfer is expected to be small (< 0.1)[18] and that it is observed only in **9** appears to be an interesting consequence of the more densely packed structure of the higher generation molecule.

In summary, an efficient route has been established to polyester 'co-block' dendrimers containing both π-donor and π-acceptor moieties at the periphery. A future direction will be the incorporation into these structures of stronger π-acceptor groups,[18,19] in conjunction with TTF, enabling the study of intramolecular charge-transfer interactions within a dendritic microenvironment. Such materials could find applications in the development of electrooptical switches.

This work was funded by EPSRC (W. D.) and Universidad Complutense de Madrid (P. de. M.).

Notes and references

† All new compounds gave ^1H NMR spectra, mass spectra (FAB or plasma desorption) and analytical data which were entirely consistent with their structures. *Selected data* for **8**: $\delta_H(CDCl_3)$ 9.16 (3 H, s), 8.42 (3 H, t, *J* 1.5), 8.39 (6 H, d, *J* 1.5), 8.22–7.85 (14 H, m), 7.06 (4 H, s), 6.72 (8 H, s), 5.54 (4 H, s) and 5.20 (8 H, s).

1 G. R. Newkome, C. N. Moorefield and F. Vögtle, *Dendritic Molecules*: *Concepts, Synthesis, Perspectives*, VCH, Weinheim, 1996.
2 Reviews: J. Issberner, R. Moors and F. Vögtle, *Angew. Chem., Int. Ed. Engl.*, 1994, **33**, 2413; N. Ardoin and D. Astruc, *Bull. Soc. Chim. Fr.*, 1996, **132**, 875; O. A. Matthias, A. N. Shipway and J. F. Stoddart, *Prog. Polym. Sci.*, 1998, **23**, 1; H.-F. Chow, T. K.-K. Mong, M. F. Nongrum and C-W. Wan, *Tetrahedron*, 1998, **54**, 8543; A. Archut and F. Vögtle, *Chem. Soc. Rev.*, 1998, **27**, 233.
3 K. Rengan and R. Engel, *J. Chem. Soc., Chem. Commun.*, 1992, 757; J.-J. Lee, W. T. Ford and J. A. Moore, *Macromolecules*, 1994, **27**, 4632; P. R. Ashton, K. Shibata, A. N. Shipway and J. F. Stoddart, *Angew. Chem., Int. Ed. Engl.*, 1997, **36**, 2781.
4 S. Achar and J. Puddephat, *J. Chem. Soc., Chem. Commun.*, 1994, 1895.
5 C. J. Hawker, K. L. Wooley and J. M. J. Fréchet, *J. Chem. Soc., Perkin Trans. 1*, 1993, 1287.
6 For a review of redox-active dendrimers see: M. R. Bryce and W. Devonport, in *Advances in Dendritic Macromolecules*, ed. G. R. Newkome, JAI Press, London, 1996, vol. 3, 115.
7 C.-F. Shou and H.-S. Shen, *J. Mater. Chem.*, 1997, **7**, 47.
8 (*a*) S. Serroni, A. Juris, M. Venturi, S. Campagna, I. R. Resino, G. Denti, A. Credi and V. Balzani, *J. Mater. Chem.*, 1997, **7**, 1227; (*b*) V. Balzani, S. Campagna, G. Denti, A. Juris, S. Serroni and M. Venturi, *Accts. Chem. Res.*, 1998, **31**, 26.
9 (*a*) M. R. Bryce, W. Devonport and A. J. Moore, *Angew. Chem., Int. Ed. Engl.*, 1994, **33**, 1761; (*b*) C. Wang, M. R. Bryce, A. S. Batsanov, L. M. Goldenberg and J. A. K. Howard, *J. Mater. Chem.*, 1997, **7**, 1189; (*c*) C. A. Christiansen, L. M. Goldenberg, M. R. Bryce and J. Becher, *Chem. Commun.*, 1998, 509; (*d*) W. Devonport, M. R. Bryce, G. J. Marshallsay, A. J. Moore and L. M. Goldenberg, *J. Mater. Chem.*, 1998, **8**, 1361.
10 V. V. Narayanan, G. R. Newkome, L. A. Echgoyen and E. Pérez-Coredo, *Polym. Prepr.*, 1996, **37**, 419.
11 I. Tabakovic, L. L. Miller, R. G. Duan, D. C. Tully and D. A. Tomalia, *Chem. Mater.*, 1997, **9**, 736.
12 *Cf.* Dipolar dendrimers with cyanophenyl and benzyloxy groups at segmentally-opposed regions have been synthesised: K. L. Wooley, C. J. Hawker and J. M. J. Fréchet, *J. Am. Chem. Soc.*, 1993, **115**, 11496.
13 T. M. Miller, E. W. Kwock and T. X. Neenan, *Macromolecules*, 1992, **25**, 3143.
14 B. Neises and W. Steiglich, *Angew. Chem., Int. Ed. Engl.*, 1978, **17**, 522.
15 *Cf.* S. Hanessian and P. Lavallee, *Can. J. Chem.*, 1975, **53**, 2975.
16 S. Hünig, G. Kiesslich, H. Quast and D. Scheutzow, *Liebigs Ann. Chem.*, 1973, 310.
17 R. Breslow, D. Murayama and D. Drury, *J. Am. Chem. Soc.*, 1974, **96**, 249.
18 V. Kampar and O. Neilands, *Russ. Chem. Rev.*, 1986, **55**, 334.
19 Review: N. Martín, J. L. Segura and C. Seoane, *J. Mater. Chem.*, 1997, **7**, 1661.

Communication 8/07062H

ChemComm

Selective ring opening cross metathesis of cyclopropenone ketal: a one step synthesis of protected divinyl ketones

Mathieu Michaut, Jean-Luc Parrain* and Maurice Santelli*

Laboratoire de Synthèse Organique associé au CNRS, Faculté des Sciences de Saint Jérôme, F-13397 Marseille Cedex 20, France. E-mail: jl.parrain@lso.u-3mrs.fr

Received (in Liverpool, UK) 9th September 1998, Accepted 16th October 1998

Grubbs ruthenium complex efficiently catalyses ring opening cross metathesis of cyclopropenone ketal and terminal olefins to afford 1,4-divinyl ketone ketals in good yields.

Since the Grubbs and Schrock groups described new alkenylidene-ruthenium and -molybdenum catalysts, olefin metathesis has attracted increasing attention.[1] The ring closing metathesis (RCM) reaction using these catalysts has in particular been studied, and syntheses of numerous cyclic structures (from five-membered rings to larger rings) have been reported.[2] In addition, ring opening metathesis of cyclic olefins has been widely used for the realisation of 'living' polymerisation.[3] Recently, the combination of ring opening metathesis (ROM) and selective cross coupling between strained bicyclic olefins and monosubstituted olefins[4,5] has shown another aspect of this powerful reaction which adheres to the 'atom economy' concept.[6] This was cleverly exemplified by Snapper in a very short synthesis of viridiene from bicyclo[3.2.0]heptadiene and butadiene.[4] So far, an identical process starting from cyclopropenes has not been reported, probably because of the steric hindrance of the substituents on the cyclopropenyl ring.[7,8]

In connection with our ongoing interest in the Nazarov cyclisation reaction,[9] an easy access to substituted divinyl ketones was desirable. Considering ring opening cross metathesis promotes selective reaction, we initiated studies on the synthesis of divinyl ketals from cyclopropenone ketals and terminal olefins (Scheme 1).

Following observations of the high reactivity of allylsilanes,[5,10] we initially employed 3 equiv. of allyltrimethylsilane and cyclopropenone propane-1,3-diyl ketal **1**[11] with 1% of Grubbs catalyst [$Cl_2(Cy_3P)_2Ru{=}CHPh$] (≡ [Ru]). The reaction was completed in less than 15 min and led only to the monomeric ring opening cross metathesis product **2i**† in 86% yield. Other possible cross metathesis or self metathesis by-products were not detected. A subsequent attempt was run with an equimolar ratio of the starting products, which provided an identical yield and selectivity for the *E* configuration of the created double bond (*E*:*Z* = 95:5). Moreover, we found that 0.04 mol% of catalyst was sufficient to complete this reaction in 2 h (Scheme 1).

In order to determine the scope and limitations of the reaction, other terminal olefins were reacted under similar conditions. The results are shown in Table 1.‡ With non-functionalized terminal olefins, optimal yields were obtained when benzene was used as solvent. High *E* selectivities were observed in all cases. The reaction was found to be extremely dependant on the substitution on carbon atoms 2 or 3 of the terminal olefins. For example, the reaction between 2-methylhexa-1,5-diene (Table 1, entry 5) and **1** occurred regioselectively on the monosubstituted olefin. On the other hand, methallyltrimethylsilane, 3,3-dimethylbutene or vinyltri-

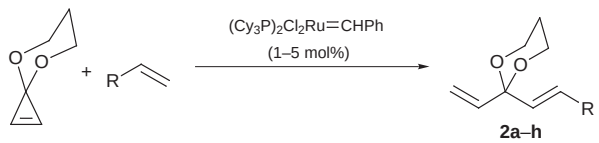

Scheme 1

Table 1 Ring opening cross metathesis of **1** with various olefins

Entry	Alkene	*T*/°C	*t*/h	Product	Yield (%) (*E*:*Z*)
1		room temp.	2	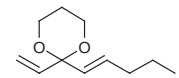 **2a**	83 (87:13)
2		80	0.5	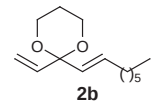 **2b**	79 (86:14)
3		80	2	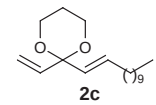 **2c**	69 (82:18)
4	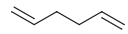	80	3	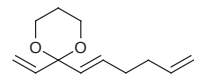 **2d**	32 (86:14)
5	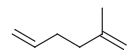	80	2	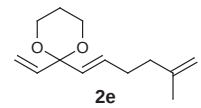 **2e**	76 (85:15)
6	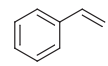	80	5	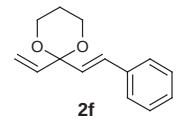 **2f**	86 (96:4)
7[a]		0	2	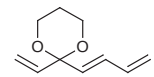 **2g**	28 (80:20)
8	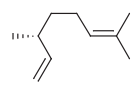	80	5	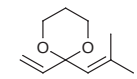 **2h**	52
9		room temp.	0.12	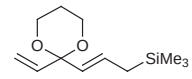 **2i**	86 (95:5)
10		room temp.	3	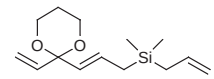 **2j**	52 (95:5)
11[b]	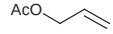	room temp.	1.5	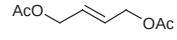	78

[a] Obtained as a separable 30:70 mixture of **2g** and the Diels–Alder adduct derived from **1** and butadiene (norcar-3-en-7-one propane-1,3-diyl ketal). [b] **1** was recovered after work-up.

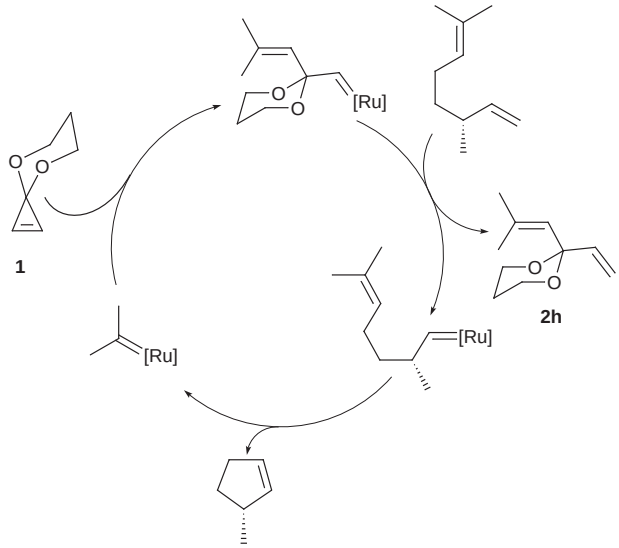

Scheme 2

methylsilane did not give metathesis products. The reaction was also found to be sensitive to electronic effects. With allyl acetate (Table 1, entry 11), no ring opening cross olefin metathesis product was detected. Only the self metathesis reaction took place, affording 1,4-diacetoxybut-2-ene.

In order to introduce a chiral center, we investigated reaction between **1** and the inexpensive (*R*)-citronellene (Table 1, entry 8). Unfortunately, the expected triene was not obtained and, instead, the reaction afforded **2h** (in 52% yield) and 3-methylcyclopentene. To explain this result, which contrasts with the others, we believe that product **2h** is obtained *via* a cascade reaction involving a ring opening cross metathesis[12] associated with a ring closing metathesis (Scheme 2). The above sequence overcomes the limitation imposed by the substitution of olefins and therefore, other 1,6-dienes could be use to introduce a disubstituted alkenyl fragment.

To better understand the reaction mechanism, stoichiometric ROM was performed in $CDCl_3$ at room temperature and examined by ^1H NMR spectroscopy. This experiment showed that cyclopropenone ketal **1** does not react with Grubbs catalyst. As a consequence, an olefin must be present to promote the metathesis reaction. This was illustrated by the reaction performed with styrene (Table 1, entry 6) where the structure of the active species is similar to that of the initial catalyst. Two credible reaction sequences could summarise the catalytic activity.[5,13] Pathway 1 (Scheme 3) utilises substituted alkylidene complex **A**, while the methylene complex **B** displays metathesis activity in pathway 2. A reaction performed with citronellene distinguished between the two mechanistic hypotheses, as the formation of divinyl ketal **2h** as the unique product strongly supports pathway 1. Moreover, we believe that the active catalytic species exhibits a structure different to the starting catalyst. According to the Chauvin mechanism[14] (formation of a metallacyclobutane followed by a cycloreversion process) and following the rational studies of Grubbs,[15] steric reasons could thus largely explain the *E* selectivity.

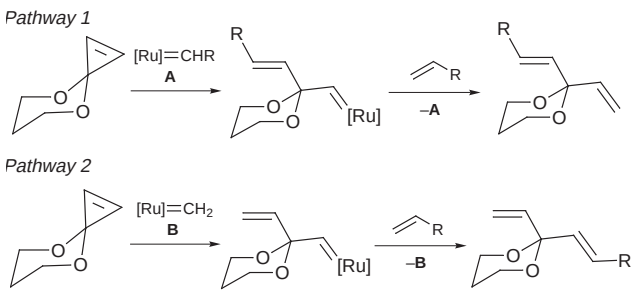

Scheme 3

In conclusion, under Grubbs ruthenium complex catalysis, cyclopropenone ketal reacts with terminal olefins *via* a ring opening cross metathesis reaction to provide selectively protected 1,4-divinyl ketones with a preferential *E* configuration. Studies to extend this reaction to other cyclopropene structures are currently underway and will be reported in due course.

Notes and references

† *Selected data* for *E*-**2i**: δ_H(200 MHz, $CDCl_3$) 5.78 (1H, dt, *J* 17.6, 7.8), 5,75 (1H, dd, *J* 17.6, 10.7), 5.34 (1H, dd, *J* 17.6, 1.9), 5.21 (1H, dd, *J* 17.6, 2), 5.20 (1H, dd, *J* 10.7, 2), 3.90 (4H, m), 1.70 (2H, m), 1.55 (2H, dd, *J* 7.8, 1.9), 0.01 (9H, s); δ_C(50.3 MHz, $CDCl_3$) 139.5, 131.2, 128.1, 115.9, 98.9, 61.1(2C), 26.0, 23.0, −1.7 (3C)

‡ General procedure for the ring opening cross metathesis summarised in Table 1: To a degassed solution of catalyst $Cl_2(Cy_3P)_2Ru$=CHPh (37 mg, 5 mol%) in anhydrous benzene (5 ml) was added a mixture of cyclopropenone ketal **1** (0.1g, 0.9 mmol) and olefin (1.05 mmol) in solution of benzene (3 ml). Then the red solution was heated to reflux. The reaction was checked by GC. After conversion was complete, the solvent was removed under vacuum. The crude product was purified by column chromatography (silica gel deactivated with Et_3N; light petroleum–Et_2O = 9:1). All new compounds were fully characterised spectroscopically.

1 R. H. Grubbs, S. J. Miller and G. C. Fu, *Acc. Chem. Res.*, 1995, **28**, 446; M. Schuster and S. Blechert, *Angew. Chem., Int. Ed. Engl.*, 1997, **36**, 2036; R. H. Grubbs and S. Chang *Tetrahedron*, 1998, **54**, 4413.

2 H. G. Schmalz, *Angew. Chem., Int. Ed. Engl.*, 1995, **34**, 1833; S. K. Armstrong, *J. Chem. Soc., Perkin Trans. 1*, 1998, 371; A. Furstner and T. Muller, *J. Org. Chem.*, 1998, **63**, 424 and references cited therein.

3 G. C. Bazan, E. Khosravi, R. R. Schrock, W. J. Feast, V. C. Gibson, M. B. O'Regan, J. K. Thomas and W. M. Davis, *J. Am. Chem. Soc.*, 1990, **112**, 8378; G. C. Bazan, J. H. Oskam, H. N. Cho, L. Y. Park and R. R. Schrock, *J. Am. Chem. Soc.*, 1991, **113**, 6899; A. W. Stumpf, E. Saive, A. Demonceau and A. F. Noels, *J. Chem. Soc., Chem. Commun.*, 1995,1127

4 M. L. Randall, J. A. Tallarico and M. L. Snapper, *J. Am. Chem. Soc.*, 1995, **117**, 9610.

5 M. F. Schneider, N. Lucas, J. Velder and S. Blechert, *Angew. Chem., Int. Ed. Engl.*, 1997, **36**, 257.

6 B. M. Trost, *Angew. Chem., Int. Ed. Engl.*, 1995, **34**, 259.

7 J. A. Tallarico, M. L. Randall and M. L. Snapper, *Tetrahedron*, 1997, **53**, 16511.

8 P. Schwab, R. H. Grubbs and J. W. Ziller, *J. Am. Chem. Soc.*, 1996, **118**, 100.

9 C. Santelli-Rouvier and M. Santelli, *Synthesis*, 1983, 429.

10 W. E. Crowe, D. R. Goldberg and Z. J. Zhang, *Tetrahedron Lett.*, 1996, **37**, 2117.

11 For minimal steric hindrance we preferred to use the cyclic ketal of cyclopropenone instead of 3,3-dimethoxy- or 3,3-diethoxy-cyclopropene. Compound **1** was prepared from sodium amide and 1,3-dichloropropanone propane-1,3-diyl ketal in ammonia. M. Isaka, S. Ejiri and E. Nakamura, *Tetrahedron*, 1992, **48**, 2045 and references cited therehein.

12 L. R. Sita, *Macromolecules*, 1995, **28**, 656.

13 J. A. Tallarico, P. J. Bonitatebus, Jr. and M. L. Snapper, *J. Am. Chem. Soc.*, 1997, **119**, 7157.

14 J. L. Hérisson and Y. Chauvin, *Makromol. Chem.*, 1970, **141**, 161.

15 E. L. Dias, S. T. Nguyen and R. H. Grubbs, *J. Am. Chem. Soc.*, 1997, **119**, 3887.

Communication 8/07064D

Synthesis, electrochemistry and cyclodextrin binding of novel cobaltocenium-functionalized dendrimers

Blanca González,[a] Carmen M. Casado,[a] Beatriz Alonso,[a] Isabel Cuadrado,*[a] Moisés Morán,*[a] Yun Wang[b] and Angel E. Kaifer*[b]

[a] *Departamento de Química Inorgánica, Facultad de Ciencias, Universidad Autónoma de Madrid, Cantoblanco, 28049-Madrid, Spain*

[b] *Chemistry Department, University of Miami, Coral Gables, FL 33124-0431, USA. E-mail: akaifer@umiami.ir.miami.edu*

Received (in Columbia, MO, USA) 27th July 1998, Accepted 12th October 1998

A series of novel poly(propyleneimine) dendrimers functionalized with 4, 8, 16 and 32 peripheral cobaltocenium subunits were prepared and characterized with a special focus on their electrochemical properties and binding interactions with β-cyclodextrin.

The chemistry of dendrimers[1] continues its fast development as numerous research groups take advantage of dendrimer structural frameworks for a variety of applications.[2] Recently, we have reported[3] on the preparation and properties of dendrimers functionalized with multiple ferrocene sites on their surface and shown that they may act as multisite, redox active guests[3e] for inclusion complexation by cyclodextrins.[4] Here we report the preparation and characterization of four new dendrimers **1**–**4** having 4, 8, 16 and 32 peripheral cobaltocenium subunits. While these positively charged dendrimers are not complexed by β-cyclodextrin (β-CD) in aqueous media, their electrochemical reduction triggers the formation of high molecular weight, multisite inclusion complexes with this host.

The new dendritic macromolecules **1**–**4** were synthesized by condensation reactions of 1-chlorocarbonylcobaltocenium in MeCN with poly(propyleneimine) dendrimers bearing 4, 8, 16 and 32 NH_2 groups respectively, in the presence of Et_3N. After purification by repeated column chromatography (Sephadex LH-20 with MeCN as eluent) all four organometallic dendrimers were isolated as air-stable, yellow (**1** and **2**) or green solids (**3** and **4**). Compounds **1**–**4** are soluble in solvents such as MeCN and DMSO. The structures of the new dendrimers have been straightforwardly established on the basis of ^1H and ^{13}C NMR and IR spectroscopy, MS, and elemental microanalysis.

We have previously reported the voltammetric behavior of cobaltocenium and carboxycobaltocenium in aqueous media as well as their complexation by the host β-CD.[5] We found that the reduced form, cobaltocene, precipitates on the electrode surface giving rise to strong distortions from the wave shape expected for a reversible, one-electron reduction process. The electro-

Table 1 Half-wave potentials measured for the reduction of dendrimers **1**–**4** at 25 °C in several media

	E/V		
Dendrimer	0.1 M $TBA^+PF_6^-$/MeCN[a]	0.1 M NaCl[b]	0.1 M NaCl + excess β-CD[b]
1	−0.75	−0.81	−0.78
2	−0.74	−0.80	−0.77
3	−0.74	−0.78	−0.76
4	−0.73	insoluble	insoluble

[a] Measured by cyclic voltammetry *vs.* SCE. [b] Measured by normal pulse voltammetry against a Ag/AgCl electrode.

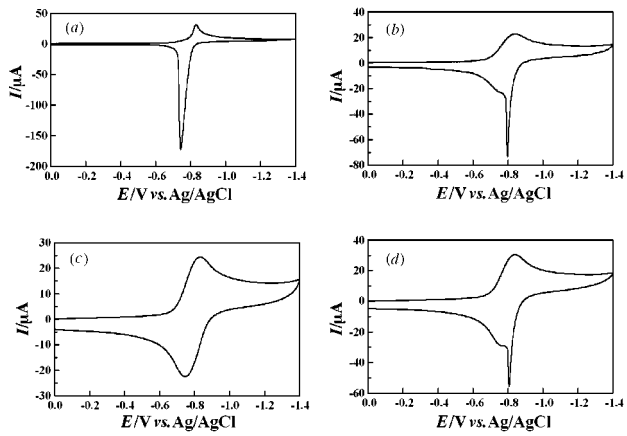

Fig. 1 Cyclic voltammetric behavior on glassy carbon (0.08 cm^2) of a solution containing 0.5 mM **1**, 0.1 M NaCl and (*a*) 0, (*b*) 5.0 and (*c*) 7.0 mM β-CD, and (*d*) 10 mM β-CD + 6.0 mM Fc-N^+Me_3. Scan rate: 0.100 V s^{-1}.

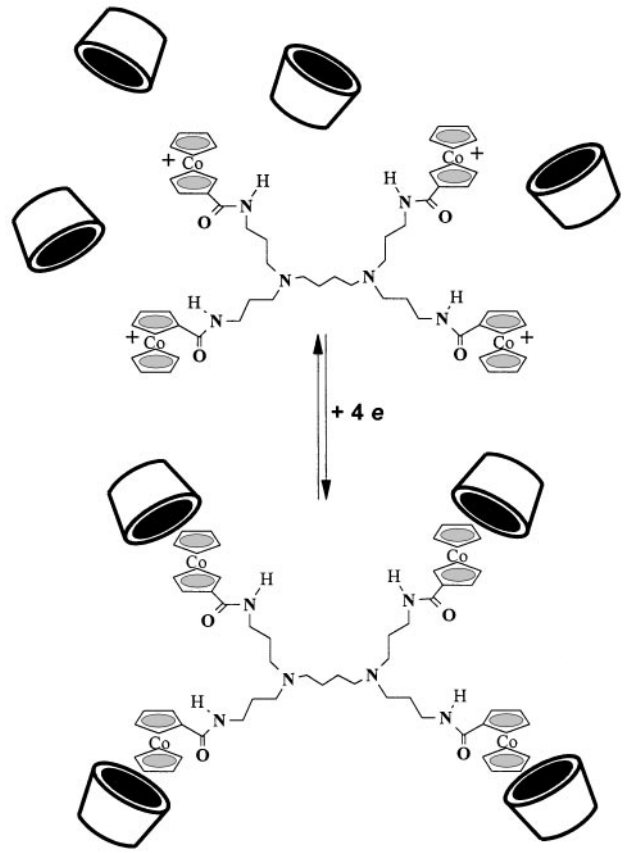

Scheme 1 Electrochemical activation of β-CD binding to dendrimer **1**.

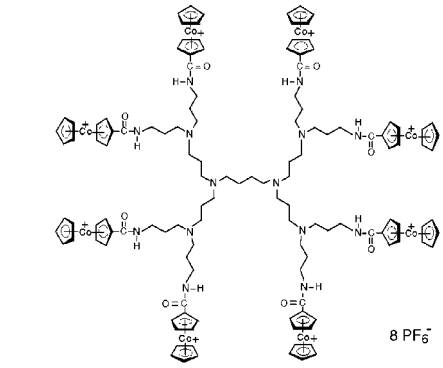

2

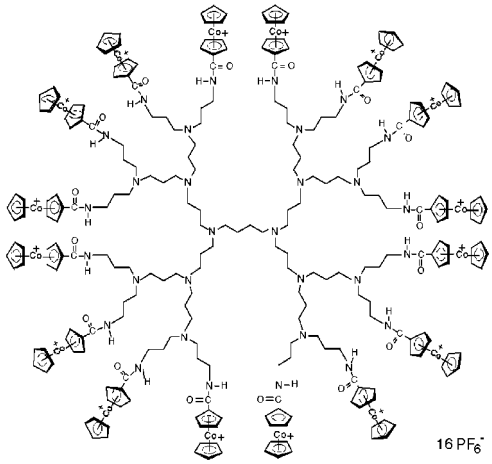

3

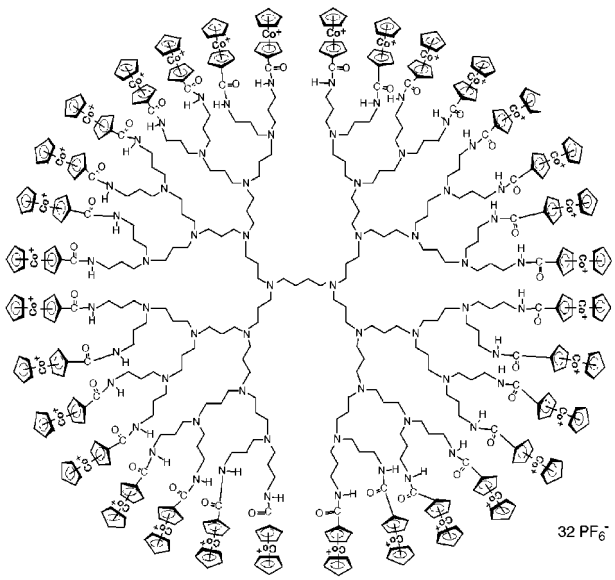

4

chemical behavior of dendrimers **1**–**4** in 0.1 M NaCl is also characterized by the deposition on the electrode surface of their reduced forms, since electrochemical reduction of the peripheral cobaltocenium subunits transforms the highly charged dendrimer structures into very hydrophobic ones. For each dendrimer, all the cobaltocenium subunits are reduced around a single half-wave potential value (see Table 1). A typical cyclic voltammogram is shown in Fig. 1(*a*) (for **1**). Although the cathodic wave departs from the shape expected for a reversible reduction process, the sharp anodic wave clearly reveals the precipitation of the reduced form on the electrode surface. Addition of β-CD to this solution gradually eliminates the sharp anodic spike on the reverse scan [Fig. 1(*b*)]. In the presence of a four-fold excess of host (compared to the total concentration of cobaltocenium subunits in the solution), the cyclic voltammogram exhibits a shape consistent with a fully reversible process [Fig. 1(*c*)]. This finding clearly indicates the solubilization of the reduced form of the dendrimer by formation of inclusion complexes between the peripheral cobaltocene subunits and the freely diffusing β-CD hosts (see Scheme 1). In order to further prove this point, we performed additional experiments with a competing guest [(ferrocenylmethyl)trimethylammonium perchlorate, Fc-$N^+Me_3 \cdot ClO_4^-$]. This ferrocene derivative is an excellent guest for binding by β-CD[6] and competes with the dendrimer cobaltocene centers for the hosts present in the solution. This is confirmed by the voltammogram in Fig. 1(*d*), which shows that the addition of Fc-N^+Me_3 leads to the behavior (sharp anodic peak) associated with the precipitation of the reduced form of **1** on the electrode.

Although dendrimers **2** and **3** are less soluble than **1** in aqueous media (probably due to the hexafluorophosphate counterions) we performed voltammetric experiments with solutions containing 0.05 mM dendrimer and obtained comparable results. Dendrimers **1**–**3** in combination with β-CD constitute a novel type of host–guest system in which the formation of multisite β-CD–dendrimer complexes is driven by the reduction of the dendrimers. These systems afford an example of high molecular weight supramolecular assemblies which undergo association upon 'electrochemical activation' of the guest.

The authors are grateful to the N.S.F. (CHE-9633434), Dirección General de Enseñanza Superior e Investigación Cientiífica (PB97-0001), the IBERDROLA Program for Visiting Professors, NATO (CRG971544), and the U.S.–Spain Joint Committee for Scientific and Technological Cooperation for their generous support of this work. Gifts of cyclodextrins by Cerestar are gratefully acknowledged.

Notes and references

1 D. A. Tomalia and H. D. Durst, *Top. Curr. Chem*., 1993, **165**, 193; C. N. Moorefield and G. R. Newkome, in *Advances in Dendritic Macromolecules*, ed. G. R. Newkome, JAI, Greenwich, CT, 1994, vol. 1, p. 1; J. M. J. Fréchet, *Science*, 1994, **263**, 1710; J. F. G. A. Jansen, E. M. M. de Brabander-van den Berg and E. W. Meijer, *Science*, 1994, **265**, 1226; J. Issberner, R. Moors and J. Vögtle, *Angew. Chem., Int. Ed. Engl*., 1994, **33**, 2413.

2 G. R. Newkome, C. N. Moorefield and F. Vögtle, *Dendritic Molecules*: *Concepts, Synthesis, Perspectives*, VCH, Weinheim, 1996.

3 (*a*) B. Alonso, I. Cuadrado, M. Morán and J. Losada, *J. Chem. Soc., Chem. Commun*., 1994, 2575; (*b*) B. Alonso, M. Morán, C. M. Casado, F. Lobete, J. Losada and I. Cuadrado, *Chem. Mater*., 1995, **7**, 1440; (*c*) I. Cuadrado, M. Morán, J. Losada, C. M. Casado, B. Alonso and F. Lobete, in *Advances in Dendritic Macromolecules*, ed. G. R. Newkome, JAI, Greenwich, CT, 1996, vol. 3, p. 151; (*d*) I. Cuadrado, M. Morán, C. M. Casado, B. Alonso, F. Lobete, B. García, M. Ibisate and J. Losada, *Organometallics*, 1996, **15**, 5278; (*e*) R. Castro, I. Cuadrado, B. Alonso, C. M. Casado, M. Morán and A. E. Kaifer, *J. Am. Chem. Soc*., 1997, **119**, 5760; (*f*) I. Cuadrado, C. M. Casado, B. Alonso, M. Morán, J. Losada and V. Belsjy, *J. Am. Chem. Soc*., 1997, **119**, 7613; (*g*) K. Takada, D. J. Díaz, H. D. Abruña, I. Cuadrado, C. Casado, B. Alonso, M. Morán and J. Losada, *J. Am. Chem. Soc*., 1997, **119**, 10763.

4 For a recent and comprehensive review on cyclodextrins, see: K. A. Connors, *Chem. Rev*., 1997, **97**, 1325.

5 Y. Wang, S. Mendoza and A. E. Kaifer, *Inorg. Chem*., 1998, **37**, 317.

6 R. Isnin, C. Salam and A. E. Kaifer, *J. Org. Chem*., 1991, **56**, 35.

Communication 8/05877F

ChemComm

Stereocontrolled substitution of benzylic ethers complexed to tricarbonylchromium(0)

Domenico Albanese, Susan E. Gibson (née Thomas)* and Ellian Rahimian

Department of Chemistry, Imperial College of Science, Technology and Medicine, South Kensington, London, UK SW7 2AY. E-mail: s.gibson@ic.ac.uk

Received (in Liverpool, UK) 2nd September 1998, Accepted 14th October 1998

The nitrogen nucleophile HN(OH)C(O)OBu^t reacts with non-racemic chiral tricarbonylchromium(0) complexes of benzylic ethers with retention of configuration to provide a novel approach to non-racemic *N*-hydroxycarbamates and amines.

We recently demonstrated that the benzylic methylene group in tricarbonylchromium(0) complexes of benzyl ethers **1** may be functionalised asymmetrically using the non-racemic chiral base **2** (Scheme 1). Deprotonation followed by an electrophilic quench gives the substituted ethers **3** in high yield and enantiomeric excess.[1] Moreover, deprotonation of **3** with the achiral base Bu^{t}Li followed by an electrophilic quench produces the heavily substituted ethers **4** again in good yield and enantiomeric purity.[2] In view of the importance of amines as natural products, pharmaceuticals, and chiral ligands for asymmetric catalysis, we decided to determine whether or not the reliable and robust chemistry used to generate **3** and **4** could be exploited in the synthesis of chiral non-racemic amines. In principle, this could be achieved by nucleophilic substitution using a nitrogen nucleophile, but literature precedent was unpromising: although substitution of α-oxygenated arene tricarbonylchromium(0) complexes with acid/nucleophile combinations *via* a chromium-stabilised carbocation intermediate is well established for carbon, hydrogen, and oxygen nucleophiles,[3] the use of nitrogen nucleophiles is rare and inefficient. Thus, reactions of NH_3, $MeNH_2$ and Me_2NH with benzyl alcohol complexes in the presence of HPF_6 give low yields of substitution products,[4] and although introduction of nitrogen *via* the Ritter reaction works well for complexes of primary benzylic alcohols, it is inefficient for secondary alcohols and fails for tertiary alcohols.[5] We thus report herein that the nitrogen nucleophile *tert*-butyl *N*-hydroxycarbamate facilitates the introduction of nitrogen into α-oxygenated arene tricarbonylchromium(0) complexes **3** and **4** and in doing so provides a novel synthesis of non-racemic chiral *N*-hydroxycarbamates and amines.

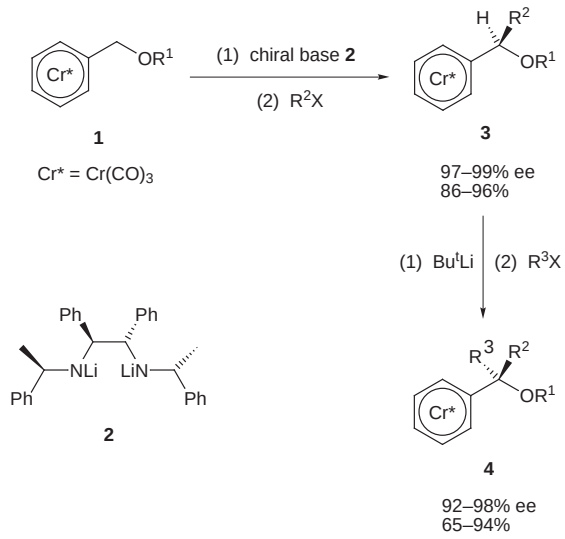

Scheme 1

The first complex to be examined was (*R*)-**5a** (R^1 = H, R^2 = Me),[1] which was synthesised in high enantiomeric purity (99% ee) from the tricarbonylchromium(0) complex of benzyl methyl ether and MeI using the chiral base **2**. Initial reactions of **5a** with a range of nitrogen nucleophiles (*e.g.* RNH_2, R_2NH, $BocNH_2$, BocNHR, BocNHOTBDMS) in the presence of $HBF_4{\cdot}OMe_2$ were disappointing, providing only very low levels of nitrogen incoroporation and complex mixtures of products. In contrast,

Table 1 Addition of HN(OH)C(O)OBu^t to ether complexes **5** and **7**[a]

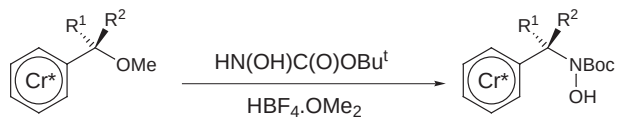

5a–c, 9a,b **6a–c, 10a,b**

Entry	Substrate	R^1	R^2	Ee (%)[b]	$[\alpha]_D$[c]	Product	Yield (%)	Ee (%)[b]	$[\alpha]_D$[c]
1	**5a**	H	Me	99	+53	**6a**	85	99	−68
2	**5b**	H	Et	96	+66	**6b**	53	96	−40
3	**5c**	H	Pr^i	98	+43	**6c**	43	91	+18
4	**9a**	D	Me	99	+53	**10a**	79	88	−53
5	**9b**	Et	Me	99	−10	**10b**	48	80	+6

[a] The experimental procedure for the conversion of **5a** to **6a** (entry 1) is typical: $HBF_4{\cdot}OMe_2$ (0.20 cm^3, 0.26 g, 2.0 mmol) was added dropwise to a yellow solution of **5a** (0.272 g, 1.00 mmol) in CH_2Cl_2 (10 cm^3) at −40 °C under an atmosphere of nitrogen. To the resulting deep blue solution, a precooled solution of HN(OH)C(O)OBu^t (0.532 g, 4.00 mmol) in CH_2Cl_2 (5 cm^3) was added immediately *via* a cannula. The yellow mixture was stirred for 25 min at −40 °C, after which saturated aqueous $NaHCO_3$ (5 cm^3) was added and the mixture allowed to warm to room temperature. Addition of water (5 cm^3), extraction with pentane (3 × 20 cm^3), drying ($MgSO_4$), filtration through Celite and solvent removal *in vacuo* gave a yellow solid. Column chromatography [SiO_2; Et_2O–light petroleum (bp 40–60 °C) 1:5–1:1] gave **6a** as a yellow solid (0.316 g, 85%). [b] Ees measured by HPLC (Chiralcel OD-H); accuracy ±1%. [c] All values measured within the range 20–31 °C (*c* 0.5–1.0) in CH_2Cl_2.

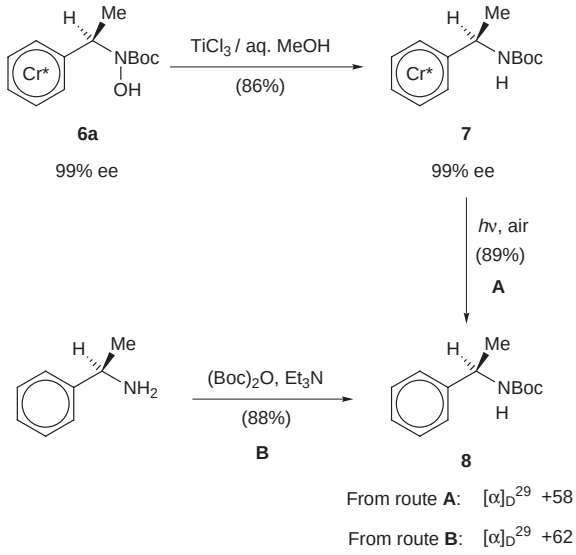

Scheme 2

protonation of **5a** at −40 °C with $HBF_4{\cdot}OMe_2$ followed by addition of commercially available *tert*-butyl *N*-hydroxycarbamate [HN(OH)C(O)OBu^t] gave the nitrogen substitution product **6a** in 85% yield. Moreover the ee of the novel† complex **6a** was measured by chiral HPLC‡ and found to be 99% (Table 1, entry 1).

The absolute configuration of the nitrogen substitution product **6a** was determined by chemical correlation. Reduction of the nitrogen–oxygen bond using $TiCl_3$ in aqueous MeOH[6] proceeded smoothly to give the novel complex **7** without loss of stereochemistry (Scheme 2).§ Oxidative removal of the tricarbonylchromium(0) unit from **7** gave carbamate **8**, the optical rotation of which was essentially identical to a sample prepared from authentic (*R*)-α-methylbenzylamine. Thus the absolute configuration of **6a** is *R* and the conversion of **5a** to **6a** proceeds with retention of configuration, presumably *via* a chromium stabilised carbocation.

In order to probe the effect on the nitrogen substitution reaction of increasing steric hindrance around the benzylic position, complexes **5b**[7] (R^1 = H, R^2 = Et) and **5c**[7] (R^1 = H, R^2 = Pr^i) were prepared and reacted with HN(OH)C(O)OBu^t. The reactions led to the novel products **6b** and **6c** in 53 and 43% yield and 96 and 91% ee respectively (Table 1, entries 2 and 3). Thus increasing steric hindrance leads to notable yield reductions and a small but significant stereochemical leakage. These effects are attributed to a reduced rate of addition of the nitrogen nucleophile to the intermediate carbocation, the increased lifetime of the latter leading to byproducts and rotation about the *ipso* carbon–benzylic carbon bond.

Subsequently, in order to test whether α,α-disubstituted benzylic ethers may be used as substrates in the reaction, complex **9a**[2] and the novel complex **9b** were synthesised from

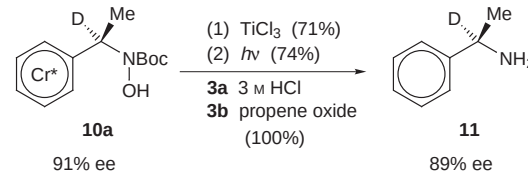

Scheme 3

5a by Bu^{t}Li deprotonation–electrophilic quench sequences.[2] Reaction of **9a** and **9b** with HN(OH)C(O)OBu^t gave the novel complexes **10a** and **10b** in 79 and 48% yield, 88 and 80% ee respectively (Table 1, entries 4 and 5). Thus steric hindrance around the tertiary carbocation generated in the conversion of **9b** to **10b** appears to reduce the rate of nucleophilic attack by HN(OH)C(O)OBu^t allowing significant rotation around the *ipso* carbon–benzylic carbon bond to occur and hence some loss of enantiomeric purity. Finally, the deuterated product **10a** was converted into the labelled amine **11** in good overall yield and without loss of enantiomeric purity (Scheme 3).¶

The authors thank the EPSRC for a studentship (E. R.), and The Accademia Nazionale dei Lincei/The Royal Society for funding a study visit (D. A.) under the auspices of the European Science Exchange Programme.

Notes and references

† The novel complexes **6a–c**, **7**, **9b**, **10a** and **10b** all gave satisfactory spectroscopic (IR, ^{1}H NMR, ^{13}C NMR and low resolution MS) and microanalytical or high resolution MS data.

‡ Racemic products for HPLC analysis were generated by addition of HN(OH)C(O)OBu^t to ether substrates produced by Bu^{t}Li deprotonation–electrophilic quench of the tricarbonylchromium(0) complex of benzyl methyl ether.

§ The ee of **7** was measured by Boc removal, replacement with Z and HPLC analysis (Chiralcel OD-H)

¶ The ee of **11** was measured by derivatisation with 3,5-dinitrobenzoyl chloride and HPLC analysis (Phenomenex - Phase 3014).

1 E. L. M. Cowton, S. E. Gibson (née Thomas), M. J. Schneider and M. H. Smith, *Chem. Commun*., 1996, 839.
2 S. E. Gibson (née Thomas), P. C. V. Potter and M. H. Smith, *Chem. Commun*., 1996, 2757.
3 S. G. Davies and T. D. McCarthy, in *Comprehensive Organometallic Chemistry II*, ed. E.W. Abel, F. G. A. Stone and G. Wilkinson, Pergamon, Oxford, 1995, vol. 12, p. 1048.
4 S. Top, B. Caro and G. Jaouen, *Tetrahedron Lett*., 1978, 787.
5 S. Top and G. Jaouen, *J. Org. Chem*., 1981, **46**, 78.
6 A. Dondoni, S. Franco, F. Merchan, P. Merino and T. Tejero, *Synlett*, 1993, 78; S.-I. Murahashi and Y. Kodera, *Tetrahedron Lett*., 1985, **26**, 4633.
7 The racemic complexes have been reported previously: J. Blagg, S. G. Davies, N. J. Holman, C. A. Laughton and B. E. Mobbs, *J. Chem. Soc., Perkin Trans. 1*, 1986, 1581.

Communication 8/06832A

A novel class of non-chiral banana-shaped liquid crystals with ferroelectric properties

Dong Shen,[a] Siegmar Diele,[b] Ina Wirt[b] and Carsten Tschierske*[a]

[a] *Institut für Organische Chemie der Martin-Luther-Universität Halle-Wittenberg, D-06120 Halle, Kurt-Mothes-Str.2, Germany.. E-mail: coqfx@mlucom6.urz.uni-halle.de*

[b] *Institut für Physikalische Chemie der Martin-Luther-Universität Halle-Wittenberg, D-06108 Halle, Mühlpforte 1, Germany*

Received (in Cambridge, UK) 28th September 1998, Accepted 26th October

The first banana-shaped molecules without Schiff-base units, with broad regions of a ferroelectric switchable liquid crystalline phase and low melting points, have been obtained.

Ferroelectricity, resulting from a spontaneous macroscopic electric polarization, is a property which was first reported by Meyer[1] to occur in a fluid, liquid crystalline phase. Until recently, ferroelectricity in liquid crystals was based on a tilted arrangement of homochiral molecules in layers (*e.g.* smectic C phase) which generates C_{2v} symmetry and allows the occurrence of a spontaneous electric polarization. In recent years such ferroelectric liquid crystals have attracted considerable interest because of their unique switching properties and their technical applications, for example, in fast-switching electrooptical devices.[2] As predicted by theory, ferroelectricity is not restricted to chiral tilted phases.[3–5] In 1996 Niori *et al*.[6] reported on ferroelectricity in a smectic phase formed by bow-shaped ('banana-shaped') non-chiral molecules. Later on, antiferroelectric switching behavior was found for these compounds.[7–9] Not only is the special electrooptical behavior of these non-conventional liquid crystals of interest. These molecules also represent a new subfield of thermotropic liquid crystals, different from the classical types such as calamitic and disc-like mesogens. Up to now, all banana-shaped liquid crystals which exhibit (anti)ferroelectric switching behavior have had a rather uniform structure. They usually comprise 1,3-phenylene bis-benzoates incorporating at least one Schiff-base unit.[6–9] Therefore, a major drawback of these compounds is their limited thermal, hydrolytic and photochemical stability. Furthermore, these special mesophases occur at rather high temperatures. Thus, the design of novel stable and low-melting materials is a topical subject in liquid crystal research.

Here we describe the first banana shaped molecules without Schiff-base units which have a ferroelectric switchable liquid crystalline phase. This was achieved by combination of an angular 3,4′-disubstituted biphenyl central unit with two phenyl benzoate rigid cores *via* ester linkages. Thus the two halves of these banana-shaped molecules are different.

The transition temperatures of the compounds **1–5** are collected in Table 1.† Different mesophases were found depending on the length of the alkyl chains and the temperature. Compounds **1** and **2** with short terminal chains form only one mesophase (M_3). On cooling **1** from the isotropic liquid state at 157 °C batonnets are formed which coalesce into a mosaic-like texture. This texture is identical with that reported for some short chain banana-shaped Schiff-base derivatives,[10] and is designated an X_{B1} phase.‡ A similar texture was also observed by cooling compounds **2–4** from the isotropic liquid.

However, in the case of compound **3** two additional phase transition can be found on further cooling. At 147 °C a nonspecific texture which immediately changes into a gray schlieren texture is formed [see Fig. 2(*a*)]. This mesophase always shows a distinct birefringence and no pseudoisotropic regions can be obtained by shearing. Furthermore, this mesophase has a lower viscosity (comparable to conventional S_A and S_C phases) than the phase M_3. On heating, it directly turns into the isotropic liquid phase at 152 °C without passing the high temperature mesophase. This means that, probably for kinetic reasons, the M_3 phase can only be observed on cooling from the isotropic state. On further cooling, at 86 °C the schlieren texture turns into a mosaic-like texture with a significant increase of the viscosity.

The same trimorphism was also found for **4**, but only the mesophases M_1 and M_2 were detected for the long chain compound **5**. Here, the M_2 phase grows directly from the isotropic liquid as spherulites with a fringe pattern, characteristic of a helical structure [see Fig. 2(*b*)]. This texture is very similar to the texture of the (anti)ferroelectrically switchable mesophase (X_{B2} phase‡) of the banana-shaped Schiff-base derivatives. Slight shearing of the sample gives rise to the same

Table 1 Phase transition temperatures of **1–5**. Abbreviations: Cr = crystalline solid, M_1 = smectic low-temperature mesophase (probably S_G or S_H), M_2 = ferroelectrically switchable mesophase [X_{B2}-phase,‡ probably arrangement shown in Fig. 1(*a*)], M_3 = two-dimensionally ordered (modulated smectic) mesophase [X_{B1}-phase,‡ see arrangement in Fig. 1(*c*)], Iso = isotropic liquid.[a]

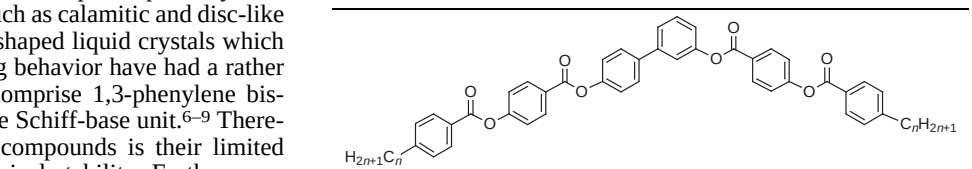

Compound	*n*	T/°C								
1		4 Cr	161					(M_3	157)	Iso
2		6 Cr	119					M_3	158	Iso
3		8 Cr	85	M_1	86	M_2	152			Iso
						(M_2	147	M_3	152	Iso)[a]
4		10[b]		M_1	79	M_2	148			Iso
						(M_2	147	M_3	148	Iso)[a]
5		12[b]		M_1	78	M_2	156			Iso

[a] The phase sequence in parentheses is only observed on cooling (determined by polarizing microscopy). [b] No crystalline phases have been found yet.

(*a*) (*b*) (*c*)

Fig. 1 Selected possible arrangements of banana shaped molecules in their mesophases: (*a*) polar biaxial smectic phases with ferroelectric alignment of the layers, (*b*) antiferroelectric alignment of the layers, and (*c*) modulated layer structure (ribbon phase). The molecules can be arranged perpendicular to the layer plane (S_A-like) or tilted (S_C-like).

(*a*)

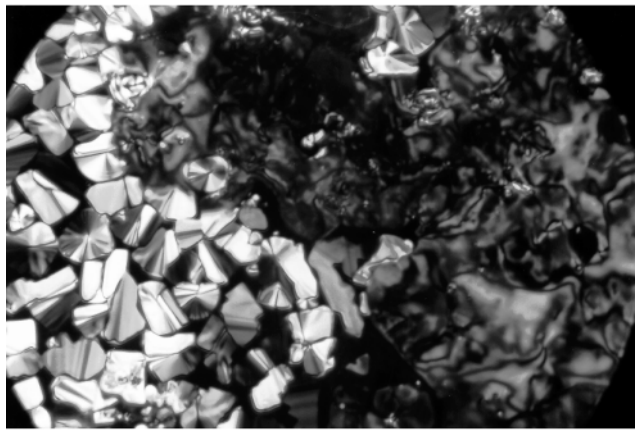

(*b*)

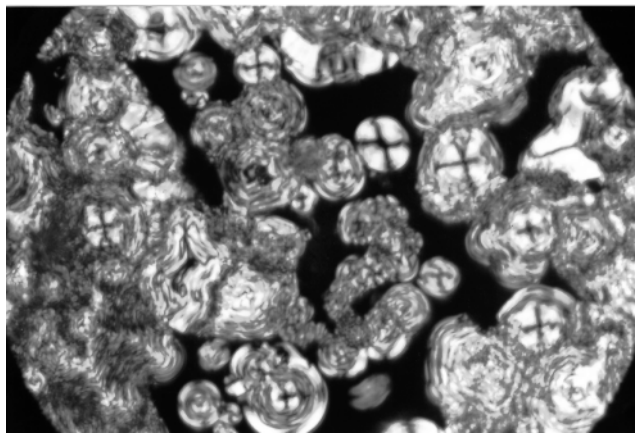

Fig. **2** Optical photomicrographs (crossed polarizers): (*a*) of **3** at the transition from the high temperature mesophase M_3 (left hand side) to the M_2 phase (schlieren-texture at the right hand side) at 147 °C; (*b*) of **5** at the transition from the isotropic liquid to the M_2 phase at 156 °C.

gray schlieren texture as observed for the M_2 phases of **3** and **4**.

X-Ray studies of non-oriented samples of compound **3** have been performed to support the phase characterization. The diffraction pattern of the high temperature phase M_3 (T = 150 °C) shows two reflections with d_1 = 3.24 and d_2 = 2.37 nm, in addition to the diffuse outer scattering. These reflections point to an undulated structure, which is already found in some banana-shaped molecules and is designated as an X_{B1} phase.‡ In the case of compound **1**, monodomains of the M_3 phase were obtained. On the basis of these oriented samples we can deduce a two-dimensional rectangular centered cell for this phase [see Fig. 1(*c*)]. Since the positions of the reflections in the M_3 phase are a linear function of the chain length, the high temperature phases of compounds **1–4** can be assumed to belong to the same type.

The phase transition from the M_3 phase to the M_2 phase is indicated by an alternation of the pattern in the small angle region. The positions of the two reflections fit now the ratio d_1:d_2 = 1:0.5 (d_1 = 2d_2 = 3.74 nm, T = 120 °C), proving a layer structure. The d value is essentially smaller than the length of the molecule (L = 5.0 nm), describing a V-shaped molecule with an angle of about 120° between the two half parts and an all-*trans* conformation of the alkyl chains. This difference leads to a tilt angle of about 41°. However a deviation of the chains from the fully stretched conformation must be assumed, so that the real tilt angle should be smaller than the estimated one. With respect to this preliminary structure the phase under consideration can belong to the type X_{B2} as reported for the Schiff-base derivatives.‡ At further cooling into the low temperature phase M_1 the layer reflections are shifted only a very little, but in the wide angle region several reflections appear. This pattern is maintained down to room temperature. The kind of reflections

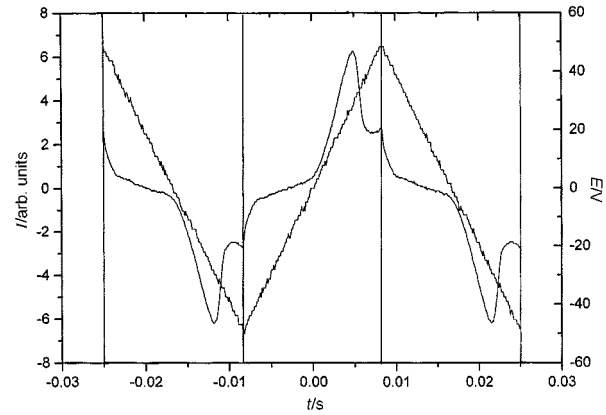

Fig. **3** Switching current response in the M_2 phase of **4** obtained by applying a triangular voltage (±50 V, 30 Hz, 125 °C).

(number, position and intensity) resembles to those of highly ordered smectic phases (S_G or S_H), but further studies are necessary to prove this analogy. Remarkably, after the first melting this compound does not crystallizes again, even after storage for several weeks at room temperature. No crystalline phases have been detected for **4** and **5**.

Preliminary investigations of the switching behavior of the M_2 phase were performed with **4**. The switching current was examined in a 5 μm thick cell by the triangular wave method. Fig. 3 shows the electric response (30 Hz) obtained in the M_2 phase at 125 °C. It can be seen that only one current peak is recorded during a half period, pointing to ferroelectric behavior. This points to the phase structure shown in Fig. 1(*a*), but it should be noted that only a schlieren texture can be obtained between the glass surfaces of the cell. Therefore more detailed electrooptical investigations with uniformly aligned samples are necessary to confirm the precise structures of the switchable mesophases.

This work was supported by the Kultusministerium des Landes Sachsen-Anhalt. We thank C. Lischka (Department of Physical Chemistry, University Halle) for help during the electrooptical investigations.

Notes and references

† The synthesis will be reported in a separate paper, satisfactory C,H analyses and ^{1}H NMR spectra were obtained. *Selected data* for **3**: δ_H(200 MHz, $CDCl_3$, 25 °C, $SiMe_4$) 0.89 (2t, 6H, CH_3), 1.2–1.8 (m, 24H, CH_2), 2.72 (t, *J* 7.7, 4H, Ar-CH_2), 7.2–7.6 (m, 14H, aromatic H), 7.68 (d, *J* 8.6, 2H, aromatic H), 8.14 (d, 4H, *J* 8.2, aromatic H), 8.32 (d, 4H, *J* 8.6, aromatic H).

‡ The nomenclature XB1, XB2 follows the recommendations given at the Workshop 'Banana-Shaped Liquid Crystals: Chirality by Achiral Molecules', December 1997, Berlin.

1 R. B. Meyer, L. Liebert, L. Strzelecki and P. Keller, *J. Phys*., 1975, **36**, L69.
2 N. A. Clark and S. T. Lagerwall, *Appl. Phys. Lett*., 1980, **36**, 899.
3 J. Prost and P. Barois, *J. Chim. Phys*., 1983, **80**, 65.
4 R. G. Petschek and K. M. Wiefling, *Phys. Rev. Lett*., 1987, **59**, 343.
5 R. H. Tredgold, *J. Phys. D*, 1990, **23**, 119.
6 T. Niori, F. Sekine, J. Watanabe, T. Furukawa and H. Takezoe, *J. Mater. Chem*., 1996, **6**, 1231; F. Sekine, Y. Takanashi, T. Niori, J. Watanabe, and H. Takezoe, *Jpn. J. Appl. Phys*., 1997, **36**, L1201.
7 G. Heppke, A. Jakli, D. Krüerke, C. Löhning, D. Lötzsch, S. Paus, S. Rauch and N. K. Sharma, *Abstracts, European Conference on Liquid Crystals*, Zakopane, Poland, 1997, p. 34.
8 W. Weissflog, C. Lischka, I. Benne, T. Scharf, G. Pelzl, S. Diele and H. Kruth, *Proc. SPIE*, 1998, **3319**, 14.
9 D. R. Link, G. Natale, R. Shao, J. E. Maclennan, N. A. Körblova and D. M. Walba, *Science*, 1997, **278**, 1924.
10 J. Watanabe, T. Niori, F. Sekine, T. Furukawa and H. Takezoe, *Jpn. J. Appl. Phys*., 1998, **37**, L139.

Communication 8/07547F

Synthesis of isocyanates from carbamate esters employing boron trichloride

D. C. D. Butler and H. Alper*

Department of Chemistry, University of Ottawa, 10, Marie Curie, Ottawa, Ontario, Canada K1N 6N5

Received (in Corvallis, OR, USA) 17th September 1998, Accepted 21st October 1998

The conversion of carbamate esters to isocyanates and diisocyanates of industrial importance is possible using BCl_3 in the presence of Et_3N; the reaction is simple in execution and work-up, occurring under mild conditions and affording isocyanates in excellent yields.

Presently, isocyanates are manufactured on a commercial scale by reaction of phosgene with amine or amine salt precursors.[1] As restrictions upon the use of very toxic materials such as phosgene and other chlorine-containing compounds within the chemical industry have become more rigorously enforced, there has been increasing interest in developing alternative methods for isocyanate production.[2] One such method (Scheme 1)

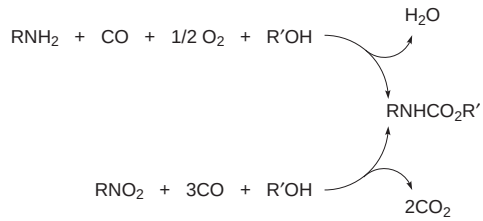

Scheme 1

involves the catalytic production of carbamate esters (by reductive carbonylation of nitro derived compounds,[3] or oxidative carbonylation of amines[4,3b]), dealcoholysis of which gives isocyanates. One of us showed recently that elimination of alcohol from carbamate esters to yield isocyanates can be facilitated using chlorocatecholborane in toluene, in the presence of Et_3N (Scheme 2).[5] This paper demonstrated that the way in which the alcohol product is irreversibly removed from the reaction solution, in the form of an alkyl catecholborate, is pertinent to the significance of this method compared with those which employ the thermal decomposition of carbamate esters, in which recombination of the resulting isocyanate with alcohol is possible.

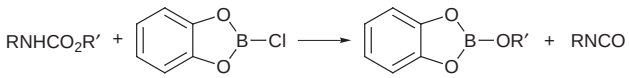

Scheme 2

Having demonstrated the use of chlorocatecholborane in this type of reaction, we reasoned that simple boron halides, BX_3 (X = Cl, Br), may also be active as cheap alternatives. Additionally, it has previously been shown that BX_3 can be generated in the production of benzyl esters by reaction of trialkyl borates with benzylic halides and CO in the presence of catalytic quantities of Pd^0 or Rh^I.[6] This offers the rather attractive option of two concomitant processes achieving commercially valuable ends together with constant recycling of boron.

Boron trihalides are known for their strong Lewis acid character, and for their ability to cleave a wide variety of ethers, acetals and esters under relatively mild conditions.[7] In pursuit of alternative methods of isocyanate production, we now report the results of our work with BBr_3 and BCl_3 in facilitating the conversion of carbamate esters to isocyanates of industrial importance.

Treatment of a carbamate ester with 0.37 equiv. of BCl_3 and 1.1 equiv. of Et_3N, for 30 min in refluxing benzene, afforded the

Table 1 Conversions of carbamate esters to the corresponding isocyanates using BCl_3

Substrate[a]	Product[b]	R	Yield (%)[c]
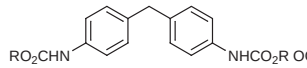	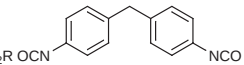	Me Et Pr	87 (72)[d] 93 88
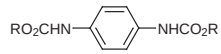	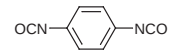	Me Et Pr	90 (79)[d] 100 100
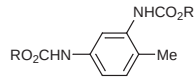	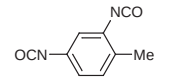	Me Et Pr	92 (70)[d] 90 94
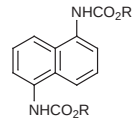	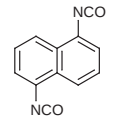	Me Et	98 100
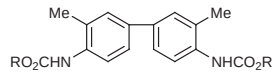	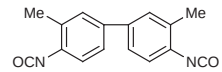	Me Et	91 100
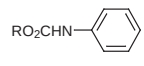	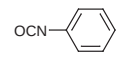	Me Et	93 (57)[d] 94
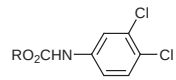	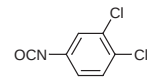	Me Et	87 97
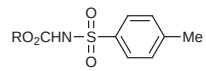	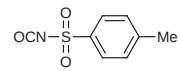	Me Et	92 100
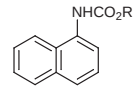	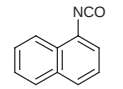	Et	100
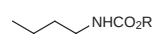	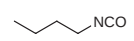	Me Et	71 86
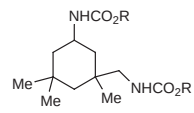	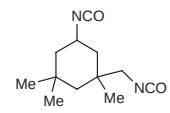	Me[e] Et[e]	73 68
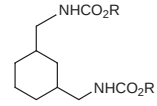	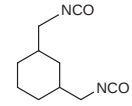	Me[e] Et[e]	68 79

[a] Purities of the carbamate esters were assessed by ^1H NMR analysis and melting points. Reaction conditions: isocyanates: BCl_3 (0.37 equiv.), NEt_3 (1.1 equiv.), refluxing benzene, 0.5 h; diisocyanates: BCl_3 (0.74 equiv.), NEt_3 (2.2 equiv.), refluxing benzene, 0.5 h. [b] Product isocyanates were identified by GC–MS and GC analysis compared with authentic materials. [c] Yields by GC analysis with tetradecane as the internal calibrant. [d] Mixture of *cis* and *trans* isomers. [e] Yields of pure products isolated by vacuum distillation, characterized by ^1H NMR, ^{13}C NMR, IR and MS analysis and by comparison with authentic materials.

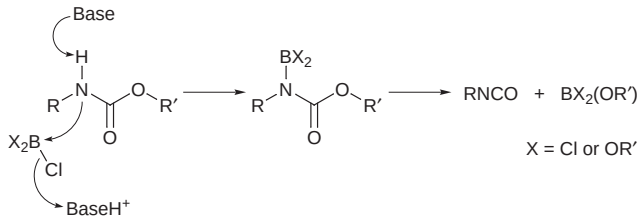

Scheme 3

isocyanate in good yield. In most cases, quantitative or near-quantitative conversion to the product isocyanates was obtained under these relatively mild reaction conditions for a series of aryl, alkyl, alicyclic and tosyl carbamate esters. The reactions were found to be highly selective with only the product isocyanates, partially cleaved carbamate esters (where dicarbamate esters were employed as starting materials), or starting materials being observed in the final solutions. The product isocyanates can usually be easily isolated by evaporation of the solvent and trialkyl borate under reduced pressure followed by vacuum distillation at elevated temperature. For example, toluene-2,4-diyl diisocyanate (TDI), *para*-phenylene diisocyanate (PDI) and 4,4′-methylenebis(phenyl isocyanate) (MDI), which are large-scale raw materials for the manufacture of polyurethane foams,[8] can be isolated as spectroscopically pure materials from their corresponding methyl carbamate esters in 70–79% yield. Toluene-2,4-diyl diisocyanate can also be isolated in good yield from its methyl carbamate ester when the reaction is performed in toluene (65% isolated yield) or hexanes (41% isolated yield). Chlorinated solvents, however, are not suitable media for this reaction. As expected, BCl_3 is converted to trialkyl borate (identifiable by GC–MS), observed after the reaction, consistent with the reaction shown in Scheme 3.

BBr_3, a stronger Lewis acid than BCl_3, was also effective in this reaction, with isocyanate yields being similar to those quoted for BCl_3 in Table 1. However, appreciable amounts of amine were also produced in some cases bringing the selectivity of this reagent into question.

It has previously been shown that PCl_3, and other Lewis acids, can effect the removal of OH from carbamate anions to yield isocyanates by electrophilic, *oxophilic* dehydration.[9] However, we found that PCl_3, when used instead of BCl_3, is capable of less than *ca*. 5% conversion of carbamate esters to isocyanates. Similar yields were attained with $AlCl_3$, and $TiCl_4$ was found to be totally inactive. It is conceivable that PCl_3 can react as an electrophile at nitrogen in this case, and a possible reason for its overall inactivity is the inability to promote cleavage of an alkoxy group from the resulting intermediate.

In conclusion, BCl_3 is an excellent, efficient and economical reagent for the synthesis of mono- and di-isocyantes in high yield.

We are grateful to the Environmental Science and Technology Alliance Canada (ESTAC) for support of this research.

Notes and references

1 P. Braunstein, *Chem. Rev*., 1989, **89**, 1927; G. Ortel, *Polyurethane Handbook*, Hanser, Munich, 1985; H. Twichett, *Chem. Rev*., 1974, **74**, 209.
2 Kirk-Othmer, *Encyclopaedia of Chemical Technology*, 4th edn., Wiley, New York, 1995, vol. 14, p. 902.
3 (*a*) S. J. Skoog and W. L. Gladfelter, *J. Am. Chem. Soc*., 1997, **119**, 11 049; (*b*) A. M. Tafesh and J. Weiguny, *Chem. Rev*., 1996, **96**, 2035; (*c*) P. Wehman, P. C. J. Kamer and P. W. N. M. van Leeuwen, *Chem. Commun*., 1996, 217; (*d*) I. Pri-Bar and J. Schwartz, *J. Org. Chem*., 1995, **60**, 8124; (*e*) V. L. K. Valli and H. Alper, *J. Am. Chem. Soc*., 1993, **115**, 3778 and references cited therein.
4 V. L. K. Valli and H. Alper, *Organometallics*, 1995, **14**. 80; T. W. Leung and B. D. Dombek, *J. Chem. Soc*., *Chem. Commun*., 1992, 205; S. Cenini, M. Pizzotti and C. Crotti, in *Aspects of Homogeneous Catalysis*, ed. R. Ugo, Reidel, Dordrecht, The Netherlands, 1988, vol. 6, p. 97 and references cited therein.
5 V. L. K. Valli and H. Alper,. *J. Org. Chem*., 1995, **60**, 257.
6 H. Alper, H. Hamel, D. J. H. Smith and J. B. Woell, *Tetrahedron Lett*., 1985, **26**, 2273; K. E. Hashem, J. B. Woell and H. Alper, *Tetrahedron Lett*., 1984, **25**, 4879; J. B. Woell and H. Alper, *Tetrahedron Lett*., 1984, **25**, 3791.
7 L. A. Paquette, *Encyclopaedia of Reactants for Organic Synthesis*, Wiley, Chichester, 1995, p 645.
8 Kirk-Othmer, *Encyclopaedia of Chemical Technology*, 4th edn., Wiley, New York, 1997, vol. 24, p. 695.
9 D. Riley, W. D. McGhee and T. Waldman, *ACS Symp. Ser*., 1994, **577**, 122.

Communication 8/07287F

Carbohydrate based IMDA/aldol strategy towards the densely functionalized *trans*-decalin subunit of azadirachtin

Dieter Haag, Xiao-Tao Chen and Bert Fraser-Reid*

Natural Products and Glycotechnology Research Institute Inc, 4118 Swarthmore Road, Durham, NC 27707 USA. E-mail: dglucose@aol.com

Received (in Corvallis OR, USA) 10th August 1998, Accepted 14th October 1998

L-Rhamnal is converted into an hex-2-en-4-ulo *C*-glycopyranoside in which properly configured diastereomeric centers, asymmetric as well as geometric, are developed in the pendant anomeric substitutent *via* a Claisen aldol addition, and the resulting product proceeds *via* an IMDA reaction to provide a highly functionalised terpene AB ring system.

The development of synthetic routes from carbohydrates to densely functionalized carbocycles has been a sustained area of interest in our research group.[1,2] The intramolecular Diels–Alder (IMDA) strategy depicted in Scheme 1[3,4] takes advantage of the preferred β-D-face approach in reactions of pyranosidic 2-ene-4-ones. The desired (*S*)-configuration exists in β-D- and α-L-derivatives, but either may be used since the sugar's C5 stereocenter, whereby D or L is designated, does not survive in the advanced retron **2**. Thus a regioselective Baeyer–Villiger oxidation of **3** permits its ready removal. This simplifying retroanalysis also makes provisions for an array of functional groups such as is found in the clerodane family of terpenes,[5] exemplified by the 'western half' of the azadirachtins **1**.[6] An IMDA approach, based on **4** with appropriate synthons at P, Q, R, S, T and U, for this family of potent pharmacologically active compounds,[7] is therefore desirable.[8]

Dibromination of diacetyl L-rhamnal **5a**, followed by dehydrobromination, gave the 2-bromo glycal **5b** in 72–76% yield (Scheme 2). Danishefsky's version[9] of the Ferrier rearrangement[10] gave a 76% yield of α-L-*C*-glycoside **6a** (along with 19% of the corresponding β-anomer). The acetyl group was replaced by TBDMS and a THF solution of the latter was mixed with 5 equiv. of DMF, and then 6 equiv. of Bu^{t}Li were added slowly (*ca*. 2 h) at −78 °C to furnish, after aqueous work-up, enal **6c** in almost quantitative yield.

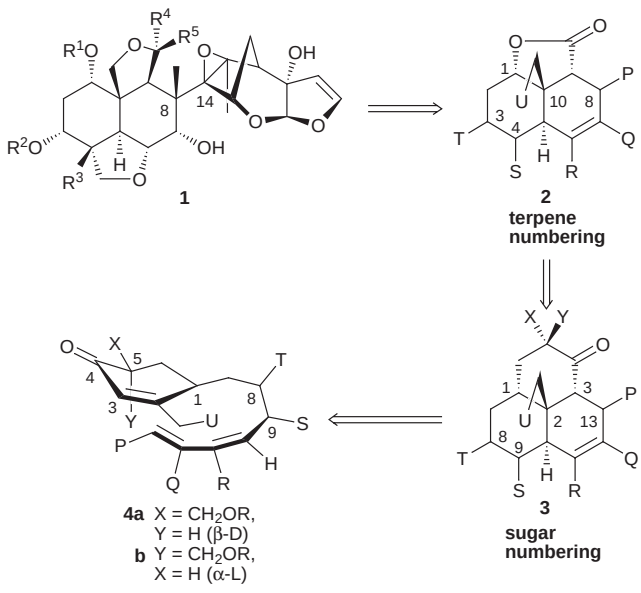

Scheme 1

The *trans*-decalin subunit of azadirachtin **1**, as well as of related terpenoids, invariably possesses hydroxy and carbon substituents at C3 and C4 respectively,[6] positions that correlate with C8 and C9 of the sugar IMDA precursor. These functionalities could conceivably be furnished by an aldol reaction. Accordingly, the aldehyde group of **6c** was first protected by acetalization. Cleavage of the terminal double bond *via* OsO_4 induced dihydroxylation followed by periodate cleavage in two discrete steps, but not in the one-pot Lemieux–Johnson protocol,[11] gave aldehyde **6e** in 85% yield.

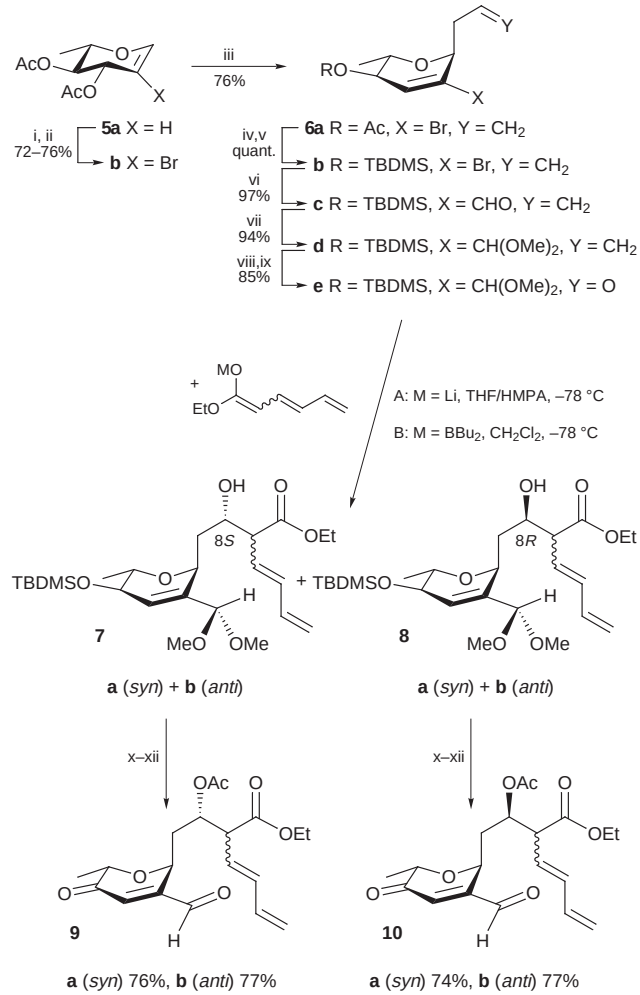

Scheme 2 *Reagents and conditions*: i, Br_2, CH_2Cl_2; ii, A: one-pot, DBU, 76% + 14% of **5a**, or B: work-up, then DBN, toluene–DMSO, 72% + 4% of **5a**; iii, allyltrimethylsilane, $BF_3{\cdot}Et_2O$, CH_2Cl_2, 0 °C to room temp.; iv, NaOMe, MeOH; v, NaH, TBDMSCl, THF; vi, THF, DMF (5.0 equiv.), −78 °C, then Bu^{t}Li (6.0 equiv.); vii, CSA, $Me_2C(OMe)_2$, reflux; viii, NMO, 1% OsO_4, THF–H_2O; ix, $NaIO_4$, THF–H_2O; x, Ac_2O, Py, cat. DMAP, CH_2Cl_2, 0 °C to room temp.; xi, HF·Py, THF, room temp.; xii, PCC, SiO_2, CH_2Cl_2, room temp.

Our next task was to elaborate the anomeric *C*-substituent into the required dienic tether. A Claisen-type aldol addition with ethyl sorbate seemed an ideal approach. Indeed that an 8-hydroxy-9-ethoxycarbonyl addition product had formed was apparent from NMR examination of the crude material. Separation of the four diastereomeric aldol adducts was achieved by (repeated) flash chromatography, and *syn*- and *anti*-configuration were easily distinguished on basis of the coupling constant between the protons attached to C8 and C9 (*syn*: ^3J ~ 5.0 Hz, *anti*: ^3J ~ 9.0 Hz). However, the absolute configuration at C8 and C9 was assigned in retrospect upon isolation of IMDA products **11**–**14** (Table1).

For proof-of-concept, the major component (assigned in retrospect as **7a**, *vide infra*) was acetylated and treatment of the crude material with HF–pyridine in THF for one day at ambient temperature effected desilylation as well as cleavage of the rather acid-sensitive dimethyl acetal. Final activation was accomplished by oxidation with PCC on silica gel to furnish the corresponding aldehyde enone **9a** in 76% yield for the whole four-step sequence. Heating of **5a** in toluene at reflux for 30 h afforded a 23% yield of **11**, the structure being confirmed independently by NMR (Table 1) and X-ray analyses.

Conceivably, the efficiency of the IMDA step, as well as the correct C3 configuration in the resultant product, could both be ensured by fine-tuning the preparative procedures. Thus under conditions A (Scheme 2) variations in the equivalents of enolate, and the duration of the reaction revealed that rapid equilibration was occuring at −78 °C (Table 2). Our studies also showed (*a*) that compounds **7a**+**b**, having the undesired (8*S*)-configuration, were kinetically favored, and (*b*) that the *syn*:*anti* ratios were generally poor. We therefore examined the *syn*-selective protocol of Evans[12] (conditions B) on **6e**, and were rewarded with a 61% yield of **8a**+**b** in an 11:1 ratio.

Steric factors on the tether can substantially affect the course of IMDA reactions.[4,13] We were therefore pleased to see, from the formation of **13** and **14** (Table 1), that the required (*R*)-configuration at C8 of precursors **10a**+**b** presents no obstacle to the success of the IMDA reaction. Conceptually, either configuration at C9 is acceptable in view of the future quaternization at C4 of compounds **13** and **14**. Furthermore, the results in Table 1 suggest that selective formation of the IMDA products may be possible by judicious choice of temperature and duration of the reaction. The bulk of the C8-hydroxy protecting group might also have a salutary effect.

These and other refinements for this IMDA/aldol approach to compounds such as **1** are underway.

We are grateful to Professor A. T. McPhail of Duke University for X-ray structure determination of **14**, and to Dr Ken Henry for insight and helpful suggestions. D. H. thanks the Alexander von Humboldt Foundation for a Feodor Lynen Fellowship. Partial support from the National Institutes of Health (GM 51237) is acknowledged. Dedicated to the memory of Professors H.-D. Scharf and D. H. R. Barton.

Table 1 Influence of the configuration of C8 and C9 in the dienic tether on the course of the IMDA reaction (E = CO_2Et)

IMDA precursor	Conditions	Yield	Product	^3J/Hz
9a	toluene reflux, 30 h	23%	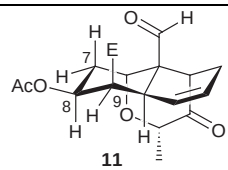 **11**	7,8: 12.4 7',8: 5.0 8,9: 6.0 9,10: 5.6
9b	benzene reflux, 5 h	85%	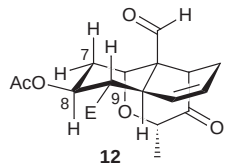 **12**	7,8: 11.5 7',8: 4.7 8,9: 10.6 9,10: 12.6
10a	toluene reflux, 18 h	70%	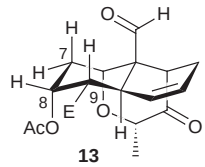 **13**	7,8: 2.9 7',8: 3.8 8,9: 3.6 9,10: 12.6
10b	xylenes reflux, 24 h	44%	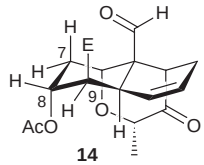 **14**	7,8: 3.2 7',8: 3.8 8,9: 3.1 9,10: 2.6

Table 2 Diastereomeric product distribution in the aldol addition of **9b**

Method	Enolate/ equiv.	*t*/min	Yield (%) **7a**	**7b**	**8a**	**8b**	**7**:**8**	Yield of **6e** (%)
A	2.0	2	29	26	12	12	2.3:1	15
A	2.0	20	24	27	17	11	1.8:1	15
A	2.0	60	24	27	18	11	1.8:1	13
A	4.0	2	35	28	14	13	2.3:1	6
B	2.5	300	29	6	58	5	1:1.8	—

Notes and references

1 B. Fraser-Reid and R. C. Anderson, *Prog. Chem. Org. Nat. Prod.*, 1980, **39**, 1; B. Fraser-Reid and R. Tsang, in *Strategies and Tactics in Organic Synthesis*, ed T. Lindberg, Academic Press, New York, 1989, vol. 2, pp 123–162.
2 J. C. López and B. Fraser-Reid, *Chem. Commun.*, 1997, 2251.
3 R. Tsang and B. Fraser-Reid, *J. Org. Chem.*, 1992, **57**, 1065.
4 J. C. López, A. M. Gómez and B. Fraser-Reid, *J. Chem. Soc., Chem. Commun.*, 1993, 762.
5 I. R. Hanson, *Nat. Prod. Rep.*, 1998, **15**, 93.
6 S. V. Ley, A. A. Denholm and A. Wood, *Nat. Prod. Rep.*, 1993, **10**, 109.
7 M. Jacobson, *Pharmacology and Toxicity of Neem*, in *Focus on Phytochemical Pesticides, The Neem Tree*, ed. J. Jacobson, CRC Press, 1989; vol. 1, p 133.
8 For some examples of synthetic approaches to the azadirachtins, see: S. V. Ley, *Pure Appl. Chem.*, 1994, **66**, 2099; H. Watanabe, T. Watanabe, K. Mori and T. Kitahara, *Tetrahedron Lett.*, 1997, **38**, 4429; N. Konah, J. Ishihara and A. Murai, *Synlett*, 1997, 737.
9 S. J. Danishefsky and J. F. Kerwin Jr., *J. Org. Chem.*, 1982, **47**, 3805.
10 R. J. Ferrier and S. Middleton, *Chem. Rev.*, 1993, **93**, 2779.
11 R. Pappo, D. S. Allen Jr., R. U. Lemieux and W. S. Johnson, *J. Org. Chem.*, 1956, **21**, 478.
12 D. A. Evans, J. V. Nelson, E. Vogel and T. R. Taber, *J. Am. Chem. Soc.*, 1981, **103**, 3099.
13 D. F. Taber, *Intramolecular Diels–Alder and Alder Ene Reactions*, Springer-Verlag, 1984.

Communication 8/06400H

Synthesis and structure of a tetranuclear niobium telluride cuboidal cluster with a central μ_4-O ligand

Vladimir P. Fedin,*[a] Irina V. Kalinina,[a] Alexander V. Virovets,[a] Nina V. Podberezskaya,[a] Ivan S. Neretin[b] and Yuri L. Slovokhotov[b]

[a] *Institute of Inorganic Chemistry, Russian Academy of Sciences, pr. Lavrentjeva 3, Novosibirsk 630090, Russia. E-mail: fedin@che.nsk.su*

[b] *Nesmeyanov Institute of Organoelement Compounds, Russian Academy of Sciences, Moscow 117813, Russia.*

Received (in Basel, Switzerland) 29th July 1998, Accepted 21st September 1998

High-temperature reaction of $NbTe_4$ with KCN at 450 °C and further crystallization from aqueous solution produces an oxygen-centered tetranuclear niobium cubane-type complex, isolated here as $K_6[Nb_4OTe_4(CN)_{12}]\cdot K_2CO_3\cdot KOH\cdot 8H_2O$, and characterized by X-ray crystallography.

Many small clusters of the electron poor transition metals in groups 3 and 4 are stabilized by an interstitial atom, Z,[1] which serves as an electron donor to stabilize metal–metal bonds and/or stabilizes the cluster by the formation of strong M–Z bonds. A few examples of group 5 transition metal cluster complexes, discrete and extended, containing interstitial atoms have been reported, among them $Nb_4OTe_9I_4$,[2] $Nb_6I_{11}H$,[3] $[M_6S_{17}]^{4-}$ (M = Nb, Ta),[4] $[V_4O(edt)_2Cl_8]^{2-}$ (edt = ethane-1,2-dithiolate),[5] $[Nb_4(\mu_4\text{-}O)(\mu\text{-}Cl)_4\{\mu\text{-}(PhC)_4\}_2Cl_4]^{2-}$,[6] Ta_4SiTe_4[7] and $[Nb_6SBr_{17}]^{3-}$.[8]

The metal atoms in the cuboidal cluster complexes $[M_4(\mu_3\text{-}Q)_4L_n]$ (Q = S, Se, Te; L denotes ligating atoms with either neutral or anionic ligands) with four μ_3-Q bridging chalcogenide ligands generally have enough electrons to support metal–metal bond formation. These cluster complexes are known for a wide variety of transition metals, and they appear to be one of the most important common basic structures of small-sized transition metal cluster complexes.[9] So far only one example of a cubane-type niobium compound $Nb_4Se_4I_4$ has been reported.[10] There are as yet no examples of cuboidal clusters M_4ZQ_4 stabilized by an interstitial atom Z.

In the course of our study on the syntheses and reactivities of solid-state molybdenum and tungsten chalcogenides, we recently obtained new cyanocomplexes with cubane-type W_4S_4, W_4Se_4, W_4Te_4 and Mo_4Te_4 cluster cores.[11] Here we report the synthesis and characterization of the first oxygen-centered cubane-type complex $[Nb_4(\mu_4\text{-}O)(\mu_3\text{-}Te)_4(CN)_{12}]^{6-}$. Tetrameric metal complexes which have a $M_4(\mu_4\text{-}O)(\mu\text{-}L)_6$ core are not uncommmon.[2,12] These complexes are known for a wide variety of metals with six μ-bridging ligands, but they are not known for tetranuclear clusters with four μ_3-bridging ligands (cuboidal complexes).

Dark brown crystals of $K_6[Nb_4(\mu_4\text{-}O)(\mu_3\text{-}Te)_4(CN)_{12}]\cdot KOH\cdot K_2CO_3\cdot 8H_2O$ (**1**)† were obtained in moderate yield by high-temperature reaction of $NbTe_4$ with KCN at 450 °C in a sealed ampoule and further crystallization within 5–7 days from aqueous solution. The source of oxygen was presumed to be water/oxygen contamination of the ampoule/reagents. In related studies it has already been reported that it was almost impossible to obtain an oxide-free product even under rigorous oxygen-free/anhydrous conditions.[2,6,12d] Furthermore, hydrolysis and oxidative degradation of KCN may explain the existence of CO_3^{2-} anions in the structure of **1**.

Owing to the presence of H_2O and CO_3^{2-} intense bands were observed in the IR spectra of **1** in KBr or Nujol. The cyanocomplex can be easily identified since it exhibits ν(CN) at 2095 cm^{-1} and also a ν(NbC)/δ(NbCN) band at 410 cm^{-1}.[11b,13] Another band in the low-energy region at 510 cm^{-1} belongs to the asymmetrical vibration of the Nb_4O core.[12c]

The crystal structure of the compound $K_6[Nb_4(\mu_4\text{-}O)(\mu_3\text{-}Te)_4(CN)_{12}]\cdot KOH\cdot K_2CO_3\cdot 8H_2O$ (**1**) contains two independent cluster anions $[Nb_4Te_4(\mu_4\text{-}O)(CN)_{12}]^{6-}$ with similar geometries (one of which is shown in Fig. 1), carbonate anion, some K^+ cations and solvent water.‡ One K^+ and one O form a pair ($K\cdots O$ of 2.7 Å) which is disordered over two positions with site occupancies 0.643(8) and 0.357(8). The overall content of K^+ in the unit cell is 36 (9 per formula unit). The pH of the solution during crystallization was greater than 7 and therefore the carbonate anion must not be protonated (CO_3^{2-}, not HCO_3^-). This means that we have 7 K^+ per cluster anion and oxygen atoms which may be H_2O or OH^-. Quantum chemical calculations on the diamagnetic compound **1** gave a total cluster anion charge of −6 (see below). In accordance with this, we assume that one of the independent oxygen atoms corresponds to OH^- and the remainder to H_2O. It is possible that OH^- corresponds to the oxygen in the disordered pair $K^+\cdots O$, since their observed interatomic distance is close to that which is found for $K^+\cdots OH^-$ in KOH (2.57–2.83 Å[14]).

The cluster anion (Fig. 1) has a structure which is similar to the well-known $[M_4Q_4(CN)_{12}]^{n-}$ cubane-type clusters (M = Mo, W, Re, Q = S, Se, Te[11,13,15]). As usual, the metal and chalcogen atoms form a distorted cube surrounded by 12 terminal CN ligands. The main difference is the presence of a μ_4-oxygen atom in the center of the Nb_4 tetrahedron with Nb–μ_4-O distances at 1.941(7)–1.98(1) Å. The Nb–Nb distances (3.189(2)–3.211(2) Å) are longer than in those compounds which formally possess a Nb–Nb single bond.[16]

Quantum chemistry calculations for the cluster anion $[Nb_4Te_4(CN)_{12}]^{6-}$ were performed with the extended Hückel method using the CACAO program.[17] Frontier orbital energies for **1** reveal a substantial gap (0.54 eV) between the 21e MO and the top of the lower-lying non-bonding block as well as a large (1.62 eV) 21e (HOMO)–18a_1 (LUMO) separation (Fig. 2). The

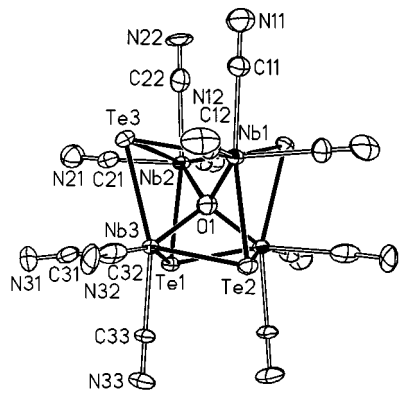

Fig. 1 Anion in **1** (a.d.p. ellipsoids at 50% probability level). All Nb–Nb bonds are omitted for clarity. Some geometrical parameters (Å): Nb–Nb, 3.189(2)–3.211(2), av. 3.202[7]; Nb–μ_4-O, 1.941(7)–1.98(1), av. 1.96[2]; Nb–μ_3-Te, 2.832(2)–2.859(1), av. 2.849[7]; Nb–C, 2.20(2)–2.29(1), av. 2.25[3], C–N, 1.11(2)–1.19(2), av. 1.15[3].

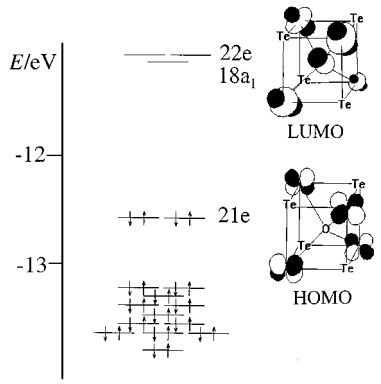

Fig. 2 Extended Hückel MO results for **1**. The corresponding LUMO and HOMO are depicted on the right of the scheme. Only the cluster core Nb_4Te_4O is shown for clarity.

formally non-degenerate $18a_1$ LUMO has both weak Nb–O antibonding and Nb–Nb nonbonding character. The doubly degenerate empty 22e MO, which is very close to $18a_1$ in energy, has a similar bonding pattern. Similarly the degenerate 21e HOMO with a zero contribution of oxygen orbitals is slightly Nb–Nb bonding. The contribution of Te, C and N atomic orbitals in the frontier MOs is negligibly low. According to a bond overlap population analysis Nb–Te bond orders are approximately 1 and Nb–O bond orders are slightly less then 1, generally supporting the model of the centered cubane-like framework tightened with single bonds.

EHMO calculations are in agreement with simple qualitative concepts. Counting oxygen and cyanide as O^{2-} and CN^- and the bridging Te groups as Te^{2-} leads to the formulation $[(Nb^{4+})_4(O^{2-})(Te^{2-})_4(CN^-)_4]^{6-}$, where four electrons are shared by four Nb atoms in the tetrahedral Nb_4 fragment.

Preliminary characterization of the redox behaviour of **1** was performed by cyclic voltammetry (scanning interval: −600 to 1000 mV *vs.* NHE in 0.1 M Na_2SO_4). The oxidation potential occurring at 309 mV has quasi-reversible behaviour. Further oxidation occurring at 900 mV is irreversible.

The authors are grateful to Dr. Davide Proserpio (University of Milano) for the CACAO program package and Dr. M. N. Sokolov for CV experiments. This work was supported by the Russian Foundation for Basic Research (research grants 96-03-33018 and 96-03-32684) and an EU INTAS collaboration (research grant 96-1256).

Notes and references

† *Preparation of* $K_6[Nb_4OTe_4(CN)_{12}]\cdot K_2CO_3\cdot KOH\cdot 8H_2O$ (**1**). $NbTe_4$ was synthesized directly from the elements.[18] A mixture of $NbTe_4$ (2.00 g; 3.31 mmol) and KCN (2.00 g; 30.7 mmol) was heated (450 °C; 48 h) in a sealed Pyrex tube. The product of the reaction was added to 30 ml of water and the mixture was refluxed for 2 h. After filtration, the green-brown solution was allowed to stand at 20 °C for 5–7 days. During this time, the volume was decreased to 3 ml. Dark brown crystals, together with some colourless powder, were isolated by filtration, washed by 60% methanol in order to remove the colourless powder, and dried in air. Yield 0.42 g of $K_6[Nb_4OTe_4(CN)_{12}]\cdot K_2CO_3\cdot KOH\cdot 8H_2O$ (29%). Satisfactory elemental analyses (C, H, N, K, Nb and Te) were obtained. The UV–VIS absorption spectrum of **1** in H_2O gave peak positions [λ/nm (ε/M^{-1} cm^{-1}) per Nb_4] at 450 (1300) and 564 (640). The magnetic susceptibility was measured at 300 K: $\chi_M = -590 \times 10^{-6}$ cm^3 mol^{-1}.

‡ *Crystallography:* a dark brown crystal of $K_6[Nb_4(\mu_3\text{-}Te)_4(\mu_4\text{-}O)(CN)_{12}]\cdot KOH\cdot K_2CO_3\cdot 8H_2O$ (**1**) (0.56 × 0.32 × 0.14 mm) was prepared as described above. X-Ray structural analysis was carried out at room temperature on an Enraf-Nonius CAD4 four-circle diffractometer (MoKα, λ = 0.7107 Å, graphite monochromator, standard techniques). *Crystal data*: $C_{13}H_{17}K_9N_{12}Nb_4O_{13}Te_4$, M = 1783.33, monoclinic, space group $P2_1/m$, a = 12.4688(9), b = 22.658(4), c = 16.318(2) Å, β = 91.584(9)°, U = 4608(1) Å^3, Z = 4, D_c = 2.570 g cm^{-3}. A total of 8724 reflections were collected up to $2\theta_{max}$ = 50°, of which 8316 were unique (R_{int} = 0.0144). Absorption corrections (μ = 4.325 mm^{-1}) were applied by integration from the crystal shape, transmission factors ranging from 0.5629 to 0.2942. The structure was solved by direct methods and refined by full-matrix least-squares on F^2 with an anisotropic approximation using SHELX-97.[19] Hydrogen atoms were not located. One of the potassium cations and one oxygen atom appeared to be disordered. Their occupancy factors were refined together with other parameters. Final R values: $R1$ = 0.0490, $wR2$ = 0.1151 for 5272 $F_o \geqslant 4\sigma(F)$, $R1$ = 0.0823, $wR2$ = 0.1347, GOF = 1.022 for all unique data. CCDC 182/1068. See http://www.rsc.org/suppdata/cc/1998/2579/, for crystallographic files in .cif format.

1 J. D. Corbett, *J. Chem. Soc., Dalton. Trans*., 1996, 575 and references therein.
2 W. Tremel, *J. Chem. Soc., Chem. Commun.*, 1992, 709.
3 A. Simon, *Z. Anorg. Allg. Chem*.,1967, **355**, 311.
4 J. Sola, Y. Do, J. M. Bergand and R. H. Holm, *Inorg. Chem*., 1985, **24**, 1706.
5 J. R. Rambo, J. C. Huffman, G. Christou and O. Eisenstein, *J. Am. Chem. Soc.*, 1989, **111**, 8027.
6 (*a*) F. A. Cotton and M. Shang, *Inorg. Chem.*, 1990, **29**, 2619; (*b*) F. A. Cotton and M. Shang, *J. Am. Chem. Soc*., 1990, **112**, 1584.
7 M. E. Badding and F. J. DiSalvo, *Inorg. Chem*., 1990, **20**, 3952.
8 H. Womelsdorf and H.-J. Meyer, *Angew. Chem., Int. Ed. Engl*., 1994, **33**, 1943.
9 (*a*) A. Müller, *Polyhedron*, 1986, **5**, 323; (*b*) R. H. Holm, *Adv. Inorg. Chem*., 1992, **38**, 1; (*c*) T. Saito, in *Early Transition Metal Clusters with π-Donor Ligands*, ed. M. H. Chisholm, VCH Publishers, New York, 1995, p. 63; (*d*) I. Dance and K. Fisher, *Prog. Inorg. Chem*., 1994, **41**, 637; (*e*) T. Shibahara, *Adv. Inorg. Chem*., 1991, **37**, 143; (*f*) T. Shibahara, *Coord. Chem. Rev*., 1993, **123**, 73; (*g*) L. C. Roof and J. W. Kolis, *Chem. Rev*., 1993, **93**, 1037; (*h*) S. Harris, *Polyhedron*, 1989, **8**, 2843; (*i*) T. Saito, *Adv. Inorg. Chem*., 1996, **44**, 45.
10 V. E. Fedorov, A. V. Mishchenko and V. P. Fedin, *Russ. Chem. Rev.*, 1985, **54**, 408.
11 (*a*) V. P. Fedin, I. V. Kalinina, A. V. Virovets, N. V. Podberezskaya and A. G. Sykes, *Chem. Commun.*, 1998, 237; (*b*) V. P. Fedin, I. V. Kalinina, D. G. Samsonenko, Y. V. Mironov, M. M. Sokolov, S. V. Tkachev, A. V. Virovets, N. V. Podberezskaya, M. R. J. Elsegood, W. Clegg and A. G. Sykes, manuscript in preparation.
12 (*a*) B. O. West, *Polyhedron*, 1989, **8**, 219 and references therein; (*b*) J. Reim, K. Griesar, W. Haase and B. Krebs, *J. Chem. Soc., Dalton. Trans*., 1995, 2649; (*c*) H. Bock, H. tomDieck, H. Pyttlik and M. Schnöller, *Z. Anorg. Allg. Chem*., 1968, **357**, 54; (*d*) F. A. Cotton, X. Feng, P. A. Kibala and R. B. W. Sandor, *J. Am. Chem. Soc*., 1989, **111**, 2148.
13 A. Müller, R. Jostes, W. Eltzner, C.-S. Nie, E. Diemann, H. Bögge, M. Zimmermann, M. Dartmann, U. Reinsh-Vogell, S. Che, S. J. Cyvin and B. N. Cyvin, *Inorg. Chem*., 1985, **24**, 2872.
14 B. Mach, H. Jacobs and W. Schäffer, *Z. Anorg. Allg. Chem*., 1987, **553**, 187.
15 (*a*) A. Müller, E. Krichemeyer, H. Bögge, H. Ratajczak and A. Armatage, *Angew. Chem., Int. Ed. Engl*., 1994, **33**, 770; (*b*) Y. V. Mironov, T. E. Albrecht-Schmitt and J. A. Ibers, *Z. Kristallogr., New Cryst. Struct.*, 1997, **212**, 308.
16 M. Sokolov, A. Virovets, V. Nadolinnyi, K. Hegetschweiler, V. Fedin, N. Podberezskaya and V. Fedorov, *Inorg. Chem*., 1994, **33**, 3503.
17 C. Mealli and D. M. Proserpio, *J. Chem. Educ*., 1990, **67**, 399.
18 A. V. Mischenko, I. V. Yushina and V. E. Fedorov, *Zh. Neorg. Khim*., 1988, **33**, 437.
19 G. M. Sheldrick, SHELX-97 Release 97-2, Göttingen University, Germany, 1997.

Communication 8/05956J

A new strategy for preparing macroporous materials: using a colloidal gas aphron to create an oriented crystal network

R. J. Davey, H. Alison, J. J. Cilliers and J. Garside

Colloids, Crystals and Interfaces Group, Department of Chemical Engineering, UMIST, Manchester, UK M60 1DQ. E-mail: r.j.davey@umist.ac.uk

Received (in Cambridge, UK) 14th September 1998, Accepted 22nd October 1998

We report a simple and generic means of using a static colloidal foam to create a novel porous material, having porosity on the micrometer size scale, that arises from the creation of an oriented crystal network.

The development of materials science over the last decade owes much to our increased understanding of the structural and stereochemical factors which drive molecular recognition[1] processes in the creation of such supramolecular assemblies as crystals,[2] surfactant structures,[3] and colloidal aggregates.[4,5] This progress has been stimulated by the desire to understand and mimic biomineralisation phenomena,[6] to control morphology and polymorphic form of molecular solids,[7] and to synthesise a new generation of functional materials having nanoscale dimensions.[8] One particularly elegant example of this progress has been the discovery that monolayers of amphiphilic molecules at the air/solution interface can be effective in templating nucleation in supersaturated subphases. Thus, for example the control of polymorphic form, crystal size and orientation of calcium carbonate precipitating from aqueous solution have been demonstrated[9] as has[10,11] the catalysed nucleation of α-glycine as {010} pyramids and plates.

The application of this work either for large scale manufacture of particulate products or in the preparation of novel materials has hardly been addressed,[13] largely because it relies on the use of a small scale, static interface between templating monolayer and supersaturated subphase for its viability. In an attempt to demonstrate the potential of this scientific discovery in the preparation of materials we carried out the preliminary experiments reported here in an attempt to make a macroporous material. Control of porosity in the size range 1–100 nm has been demonstrated previously[15,16] but we believe the work reported here to be the first to address porosity in the micrometer size range.

The concept underlying this innovation is that since a foam consists of a high surface area of gas bubbles dispersed in a liquid then, with amphiphilic molecules located at the bubble surfaces, the liquid lamellae separating the bubbles might be used as locations for templated crystallisation. In experiments with single air bubbles in supersaturated glycine solutions we showed previously[12] that, in the presence of an amphiphile chosen to template the nucleation of glycine [*e.g.* (*R*)-leucine[10]] and a surfactant appropriate for stabilising a foam, it was possible to encapsulate a bubble with a crystalline layer of (010) oriented glycine crystals. This oriented nucleation results from the prochiral nature of the {010} faces and their stereochemical relationship to (*R*)-leucine, which segregates at the air/solution interface: it is consistent with earlier reports.[10,11] If this effect could be reproduced throughout the bulk of a stable static foam then it should be possible to utilise such a methodology to create a three dimensional material which has pore sizes corresponding to the bubble size of the foam and a network of solid walls composed of an interconnected array of ordered microcrystals. Such a process is shown schematically in Fig. 1.

In order to realise this concept we first created a colloidal gas aphron. This was achieved following the experimental method of Sebba[13] together with a combination of stabilising surfactant and nucleation inducing template molecules. Thus, for example, a solution of glycine containing 200 μM of either surfactant or a 50 : 50 wt% surfactant/template mixture was prepared at 60 °C and agitated, so as to entrain air, for 15 min at 4500 rpm. This produced a gas aphron with bubble sizes between 10 and 30 μm and 90% volume fraction of air, which under static conditions was stable for *ca.* 1 h. Cooling of this foam then initiated supersaturation and subsequent crystallisation of the glycine. We found that TTAB [$CH_3(CH_2)_{13}N(CH_3)_3Br$] was a particularly effective surfactant for stabilising these aphrons while the hydrophobic α-amino acids (*R*)-leucine and (*R*,*S*)-norleucine were used to template the nucleation at the bubble surface.[11] Control experiments were also carried out in which glycine crystals were prepared by cooling a bulk saturated solution of glycine containing the surfactant mixture. These gave crystals with an (010) plate morphology, as expected from previous work.[10]

When crystallised within the stable aphron containing a templating molecule, glycine was found to nucleate at temperatures between 8 and 15 °C higher than in corresponding bulk solutions (the value depending on the level of supersaturation which varied[12] between 1.01 and 1.20 at 25 °C) indicating that nucleation was catalysed. It was observed that almost no three dimensional growth took place within the bulk solution: glycine crystals grew around and out from the air-solution phase boundaries. This led to the formation of a 'solid foam', consisting of an interconnected glycine crystal network. As crystallisation proceeded a point was reached at which the gas aphron collapsed and liquid drained to the bottom of the sample. This left a 'skeleton' comprising a solid framework of oriented glycine crystals with pore sizes identical to, or slightly larger than, the original aphron bubble sizes. This is seen in

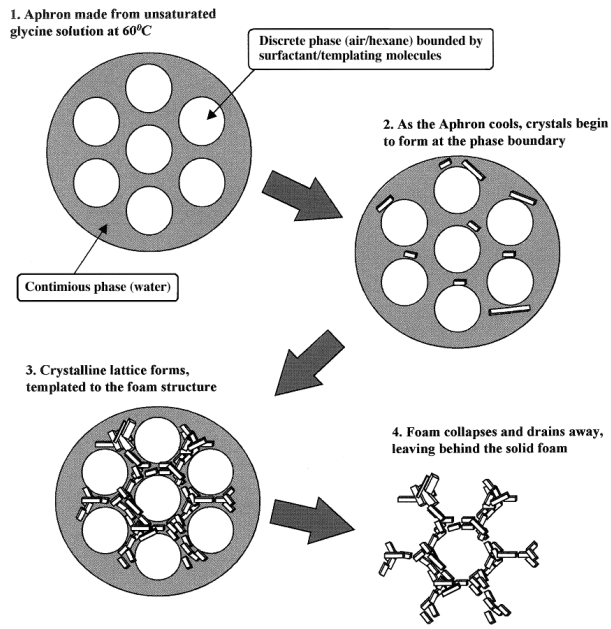

Fig. 1 Schematic depiction of crystallisation in a gas aphron showing the creation of an oriented crystal network and solid foam.

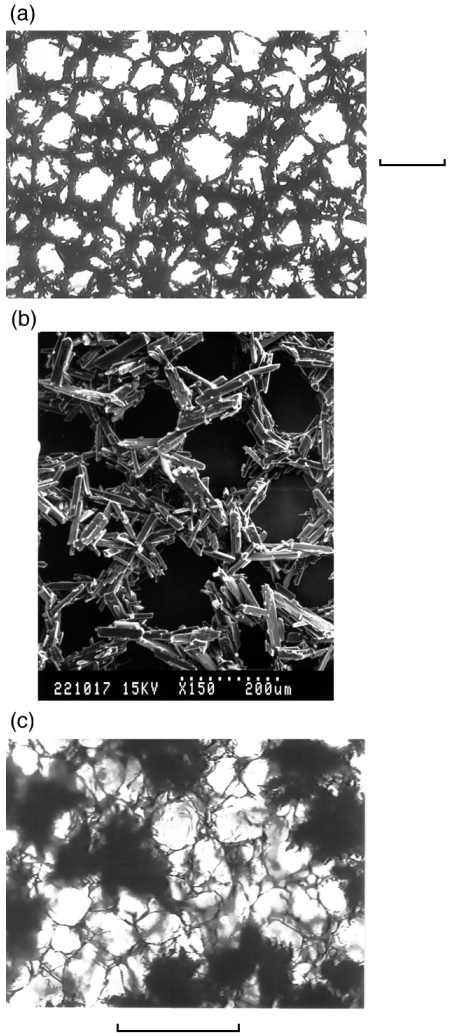

Fig. 2 α-Glycine crystal networks in solid foams prepared from supersaturated aqueous solutions of glycine in a gas aphron using TTAB as a stabilising surfactant and (*R*)-leucine [(a) and (b)] and (*R*,*S*)-norleucine as templating molecules: (a) templated by (*R*)-leucine, an optical micrograph (scale bar 150 μm), (b) templated by (*R*)-leucine, a scanning electron micrograph, (c) templated by (*R*,*S*)-norleucine, and optical micrograph (scale bar 100 μm).

Fig. 2(a), an optical micrograph, and Fig. 2(b), an electron micrograph. Crystals of sizes between 10 and 50 μm are oriented with their (010) facets bounding the pores. Two further observations were evident from the work. Firstly, crystallisation from a stable aphron was not in itself sufficient to create this microstructure: if the templating molecule was not present the oriented nucleation was lost and the foam and crystals collapsed to an unoriented powder. Secondly, when the templating molecule was present as a racemic mixture [(*R*,*S*)-norleucine in this case] not only were crystals templated with (010) orientation but growth was also inhibited in both directions along the *b*-axis yielding thin plate-like crystals. As seen in Fig. 2(c) this again forms a solid foam but now with significantly thinner walls.

It is our belief that this surprisingly simple experimental methodology may now be extended, not only to other solid phases such as fats, waxes, or inorganics but also to employ alternative disperse phases.[14] For example, we performed a preliminary experiment crystallising glycine from aqueous solution in the presence of hexane as the dispersed phase. In this case the size scale of the final crystal network can be reduced since oil drops in the size range 0.1–10 μm may be stabilised and it appears that the oil droplets themselves may be encapsulated by the crystal network. From this we conclude that such structures may have significant potential not in the conventional market place for porous structures, such as catalysis and ceramics but in the equally important arena of formulated products where the crystal network would impose overall structural properties with the release of active components such as agrochemicals, pharmaceuticals or cosmetics, controlled by its porosity, wall thickness and encapsulation properties.

The authors would like to acknowledge the support of EPSRC through its ROPA programme.

Notes and references

1 F. Voegtle, *Supramolecular Chemistry*, John Wiley and Sons, Chichester, 1991.
2 G. Desiraju, *Crystal Engineering*, Materials Science Monographs, 54, Elsevier, Amsterdam, 1989.
3 D. Fennell Evans and H. Wennerstom, *The Colloidal Domain*, VCH Publishers Inc., New York, 1994.
4 R. J. Davey and B. R. Heywood, *First International Particle Technology Forum*, Denver, pub. AICHE, New York, 1994, 362.
5 A. Van Blaaderen, R. Ruel and P. Wiltzius, *Nature*, 1997, **385**, 321.
6 S. Mann, *et al.*, *Science*, 1993, **261**, 1286.
7 R. J. Davey, *et al.*, *J. Am. Chem. Soc.*, 1997, **119**, 1767.
8 J. D. Hopwood and S. Mann, *Chem. Mater.*, 1997, **9**, 1819.
9 S. Mann, *et al.*, *J. Appl. Phys.*, 1991, **24**, 154.
10 I. Weissbuch, *et al.*, *J. Am. Chem. Soc.*, 1988, **110**, 561.
11 E. M. Landau, *et al.*, *J. Am. Chem. Soc.*, 1989, **111**, 1436.
12 B. D. Chen, *et al.*, *J. Am. Chem. Soc.*, 1998, **120**, 1625.
13 F. Sebba, *Foams and Biliquid Foams—Aphrons*, John Wiley and Sons, London, 1987, pp. 63–79.
14 A. Imhof and D. J. Pine, *Nature*, 1997, **389**, 948.

Communication 8/07138A

1,6-Bis(2,4,6-tri-*tert*-butylphenyl)-1,6-dibora-2,5-diaza-hexa-1,5-diine, the first compound containing two B≡N triple bonds

Thomas Albrecht, Gernot Elter and Anton Meller*

Institut für Anorganische Chemie der Universität, Tammannstr. 4, D-37077 Göttingen, Germany. E-mail: punger@gwdg.de

Received (in Cambridge, UK) 21st September 1998, Accepted 21st October 1998

The elimination of hydrogen fluoride from *N*,*N*′-bis[(2,4,6-tri-*tert*-butylphenyl)fluoroboryl]ethylenediamine 1 gives the title compound 2 as a thermally very stable moiety; water is easily added across the B≡N triple bonds.

Iminoboranes R–B≡N–R′[1] and aminoiminoboranes R_2N–B≡N–R′[2] are now quite well known species,[3] particularly due to the work of Paetzold[1] and Nöth.[2] Iminoboranes are kinetically stabilized species and their thermal and hydrolytic stability is dependent upon the steric requirement of the substituents and their resistance against intramolecular chemical attack from the thermodynamically unstable (BN) triple bond. In the past we have studied systematically the stabilization of these moieties by the 2,4,6-tri-*tert*-butylphenyl (supermesityl, Mes*) group.[4,5] If iminoboranes carrying the supermesityl group have the methyl group as the other substituent, their stability against dimerization is retained up to 100 °C. While if the other substituent is ethyl, benzyl, phenyl, *tert*-butyl or trimethylsilyl these iminoboranes will not dimerize, but upon heating will rearrange to give the corresponding benzo[1]borolanes at temperatures between 170 and 350 °C.

Our attempts to prepare a bis(imino)borane by HF-elimination from Mes*BF–NHNH–FBMes*[6] upon treatment with Bu^{t}Li, MeLi or $MN(SiMe_3)_2$ (M = Li, Na) failed. Apparently the two supermesityl groups are too large to permit the necessary approach considering the short bond lengths in the corresponding bis(imino)borane.

By using an ethylene bridge as a spacer to avoid excessive steric interference we have now prepared the first bis(imino)-borane, containing two isolated B≡N triple bonds (Scheme 1).†

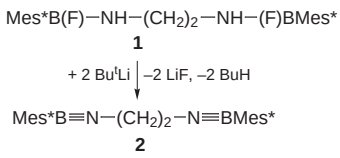

Scheme 1

The bis(imino)borane **2** is thermally stable up to its melting point of 311 °C. It neither dimerizes or oligomerizes nor reacts in an intramolecular fashion to give a benzo[1]borolane derivative. Heating above its melting point, however, delivers several decomposition products, which we could not identify until now. The ^{11}B NMR signal for **2** is at δ 5.9 (for Mes*B≡NMe, δ 5.3[5]) and the IR spectrum shows ν (^{11}BN) = 2020 and ν (^{10}BN) = 2066 cm^{-1}, typical for iminoboranes.[5]

Compound **2** reacts readily with water to yield the corresponding *N*,*N*′-bis[(2,4,6-tri-*tert*-butylphenyl)hydroxyboryl]ethylenediamine derivative **3** (Scheme 2).‡

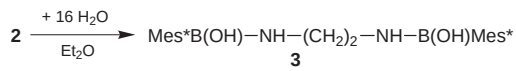

Scheme 2

We are grateful to the Fonds der Chemischen Industrie for financial support of this work.

Notes and references

† Preparative details and selected spectroscopic data for **1** and **2**: All reactions under dry nitrogen. Mes*BF_2 was obtained as described.[4]

1: to 1.2 g (0.02 mol) ethylenediamine dissolved in 100 ml hexane, 17 ml of a solution (23% in hexane) of BuLi (0.04 mol) were added with stirring. The mixture was refluxed for 2 h and then cooled to −15 °C. To the stirred suspension was added 11.8 g (0.04 mol) Mes*BF_2 dissolved in 80 ml hexane and the reaction mixture warmed to ambient temperature and then refluxed (2 h). The solvent was removed under reduced pressure and volatile byproducts removed at 160 °C (0.01 Torr). Sublimation in a three-bulb tube yielded 6.9 g (57%) of yellowish **1**, subl.p 240 °C (0.01 Torr) (air bath temp.). After short path resublimation the mp was 208 °C. $C_{38}H_{64}B_2F_2N_2$ (608.61): satisfactory analytical results. EIMS: *m/z* (%) = 608 (4) $[M]^+$, 551 (3) $[M - CMe_3]^+$, 57 (100).

NMR data: ^{1}H ($CDCl_3$, $SiMe_4$, 250 MHz) δ 1.34 (s, 18H, CMe_3 : 4), 1.43 (d, $^6J_{HF}$ 1.1 Hz, 36H, CMe_3 : 2/6), 3.22 (m, 4H, CH_2), 3.34 (br, d, $^3J_{HF}$ 17.6 Hz, 2H, NH), 7.40 (s, 4H : 3/5); ^{13}C ($CDCl_3$, TMS, 100.6 MHz) δ 31.3 (C*Me*$_3$: 4), 33.0 (d, $^5J_{CF}$ 2.5 Hz, C*Me*$_3$: 2/6), 34.9 (*C*Me$_3$: 4), 37.5 (*C*Me$_3$: 2/6), 41.6 (d, $^3J_{CF}$ 2.1 Hz, CH_2), 121.0 (3/5), 127.5 (br, 1), 149.8 (d, $^5J_{CF}$ 0.6 Hz : 4), 153.6 (d, $^3J_{CF}$ 2.1 Hz : 2/6); ^{11}B ($CDCl_3$, BF_3·OEt_2 ext., 80.25 MHz) δ 33.0; ^{19}F ($CDCl_3$, C_6F_6 int., 188.3 MHz) δ 70.3.

2: to a suspension of 4.0 g (0.0066 mol) of **1** in 70 ml hexane, 9 ml of a 15% solution of Bu^{t}Li in pentane (0.0132 mol) was added dropwise with stirring at 0 °C. The pentane was distilled off and the reaction mixture refluxed for 2 h. The solution was filtered through a pressure funnel, the residue washed with three portions of hexane (20 ml each) and the solvent distilled off under reduced pressure. By short path sublimation in a high vacuum the remainder yields 1.5 g (41%) of colourless **2**; mp 311 °C, subl.p 180 °C (0.0001 Torr) (bath temp.). **2** is only sparingly soluble in organic solvents. $C_{38}H_{62}B_2N_2$ (568.55). Satisfactory elemental analyses were obtained. EIMS: *m/z* (%) = 568 (2) $[M]^+$, 511 (5) $[M - CMe_3]^+$, 284 (100) $[M/2]^+$; FDMS: *m/z* (%) = 568 (100). *NMR data*: ^{1}H ($CDCl_3$, $SiMe_4$, 250 MHz) δ 1.33 (s, 18H, CMe_3 : 4), 1.57 (s, 36H, CMe_3 : 2/6), 3.73 (s, 4H, CH_2), 7.33 (s, 4H : 3/5); ^{13}C ($CDCl_3$, $SiMe_4$, 100.6 MHz) δ 31.3 (C*Me*$_3$: 4), 31.9 (C*Me*$_3$: 2/6), 35.3 (*C*Me$_3$: 4), 36.7 (*C*Me$_3$: 2/6), 44.9 (CH_2), 114.0 (br, 1), 119.6 (3/5), 152.4 (4), 159.1 (2/6); ^{11}B ($CDCl_3$, BF_3·OEt_2 ext., 80.25 MHz) δ 5.9. IR: ν (^{11}BN) = 2020 cm^{-1}, ν (^{10}BN) = 2066 cm^{-1} (in KBr).

‡ Preparative details and selected spectroscopic data for **3**: to a stirred suspension of 2.0 g (0.0035 mol) of **2**, suspended in 30 ml Et_2O was added 1 ml H_2O (0.055 mol, excess). The mixture was refluxed for 2 h and the liquids removed under reduced pressure leaving colourless **3**. Yield: 1.9 g (91%), mp 221 °C; **3** is fairly soluble in THF. $C_{38}H_{66}B_2N_2O_2$ (604.58). Satisfactory elemental analyses were obtained. EIMS: *m/z* (%) = 604 (1) $[M]^+$, 547 (3) $[M - CMe_3]^+$, 302 (15) $[M/2]^+$, 257 (100) $[Mes*BO - Me]^+$. *NMR data:* ^{1}H (THF-d_8, $SiMe_4$, 250 MHz) δ 1.28 (s, 18H, CMe_3 : 4), 1.44 (s, 36H, CMe_3 : 2/6), 3.22 (m, 4H, CH_2), 3.47 (m, br, 2H, NH), 6.46 (d, $^4J_{HH}$ 1.5 Hz, 2H, OH), 7.31 (s, 4H : 3/5); ^{13}C (THF-d_8, $SiMe_4$, 100.6 Hz) δ 31.8 (C*Me*$_3$: 4), 34.0 (C*Me*$_3$: 2/6), 35.4 (*C*Me$_3$: 4), 38.5 (*C*Me$_3$: 2/6), 43.2 (CH_2), 121.4 (3/5), 134.8 (br, 1), 148.7 (4), 153.5 (2/6); ^{11}B (THF-d_8, BF_3·OEt_2 ext., 80.25 MHz) δ 32.7. IR: ν (OH) = 3605 cm^{-1} (in KBr). No dehydration was observed up to the mp.

1 P. Paetzold, *Adv. Inorg. Chem*, 1987, **31**, 123.
2 H. Nöth, *Angew. Chem. Int. Ed. Engl.*, 1988, **27**, 1603.
3 *Gmelin Handbook of Inorganic and Organometallic Chemistry*, 8th edn., 1991, *Boron Compounds 4th Suppl.* Vol. **3a**, pp. 160 and 210.
4 G. Elter, M. Neuhaus, A. Meller and D. Schmidt-Bäse, *J. Organomet. Chem.*, 1990, **381**, 299.
5 G. Elter, M. Geschwentner and A. Meller, *Z. Anorg. Allg. Chem.*, 1993, **619**, 1474.
6 M. Geschwentner, G. Elter and A. Meller, *Z. Naturforsch., Teil B*, 1994, **49**, 459.

Communication 8/07320A

Quantitative gas-phase electrophilicities of the dihalogen molecules XY = F_2, Cl_2, Br_2, BrCl and ClF

A. C. Legon

School of Chemistry, University of Exeter, Stocker Road, Exeter, UK EX4 4QD. E-mail: A.C.Legon@exeter.ac.uk

Received (in Cambridge, UK) 18th September 1998, Accepted 20th October 1998

Intermolecular stretching force constants k_σ determined from the rotational spectra of complexes B···XY, where B is one of the Lewis bases CO, C_2H_2, C_2H_4, HCN, H_2S and NH_3 and XY is a dihalogen F_2, Cl_2, Br_2, BrCl and ClF, are used to establish a quantitative scale of gas-phase electrophilicities E_{XY} of the halogens.

The nature of the initial interaction of homo- or heteronuclear diatomic halogen molecules XY with simple Lewis bases B in chemically reactive mixtures of the two components is a matter of fundamental interest in chemistry.[1] It has recently proved possible to isolate pre-reactive complexes of the type B···XY in gaseous mixtures and then characterise them through their rotational spectra by using a fast-mixing nozzle[2] in combination with a Fourier-transform microwave spectrometer.[3,4] Thereby precise values of several properties of the isolated species B···XY become available, including its angular and radial geometry, the strength of binding (as measured by the intermolecular stretching force constant k_σ), and the extent of electric charge redistribution within XY on complex formation. The efficacy of the fast-mixing nozzle is such that even pre-reactive complexes formed by NH_3, CO, H_2S, C_2H_2 or C_2H_4 with F_2 or ClF can be detected,[5–11] despite the rapid and violent reactions that would attend mixing of the components under normal conditions. Consequently, trends in the properties of B···XY may be identified not only by variation of the Lewis bases over a wide range of types but also by examining complexes with halogens as reactive as fluorine and chlorine monofluoride.

Such an approach has already revealed[12] a remarkable parallelism between the angular geometries of B···XY and B···HX (X,Y = F, Cl or Br). Thus, the pair B···HX and B···XY are isostructural for a given B over the range of XY and HX. This parallelism establishes that some simple rules first proposed for predicting angular geometries of hydrogen-bonded species B···HX,[13,14] and based on simple electrostatic considerations, also apply to the halogen complexes B···XY. The question then arises: Does the parallelism extend to other properties?

Another property of B···HX complexes that was found to vary systematically with B and HX is k_σ, which is the restoring force per unit infinitesimal displacement of the hydrogen bond along its dissociation co-ordinate and, therefore, one measure of the strength of the interaction. In particular, it was discovered[15,16] that k_σ could be partitioned between B and HX to define a nucleophilicity N_B of the proton acceptor region of B and the electrophilicity E_{HX} of HX. The relationship between N_B, E_{HX} and k_σ was established to be[15]

$$k_\sigma = cN_BE_{HX} \quad (1)$$

where c is constant. This empirical equation could be used to predict k_σ of a large number of B···HX from a few N_B and E_{HX} values. For the particular scales of nucleophilicities and electrophilicities chosen, the value c = 0.25 N m^{-1} was appropriate. The advantage of the N_B and E_{HX} thereby established is that they define the propensity of a molecule to interact with either an electrophile or a nucleophile, respectively, in the limit where one molecule probes the other with only minor perturbation, and in isolation in the gas phase. The empirical eqn. (1) has been rationalised on the basis of the electrostatic model of the hydrogen bond elsewhere.[15]

The purpose of this communication is to examine whether the k_σ values of B···XY complexes, where B is CO, C_2H_2, C_2H_4, HCN, H_2S or NH_3 and XY is F_2,Cl_2, Br_2, BrCl or ClF, obey eqn. (1) and, if so, to establish a scale of electrophilicities E_{XY} for halogens and interhalogens. Another aspect of interest is whether a common set of nucleophilicities N_B applies to both the B···HX and B···XY series.

Table 1 displays a matrix of k_σ values for the series of B···XY defined earlier.[5–11,17–32] All values were derived from centrifugal distortion constants D_J or Δ_J established from analyses of rotational spectra, the latter usually observed with the fast-mixing nozzle/FT microwave spectrometer combination. Relationships between k_σ and D_J or Δ_J valid in the quadratic approximation for rigid, unperturbed subunits B and HX or XY have been derived by Millen for complexes of various symmetries.[33]

To test the validity of eqn. (1) for the B···XY in Table 1, the following procedure was used. First, the electrophilicity of BrCl was arbitrarily assigned the value E_{BrCl} = 9.0. Then E_{BrCl} was used with the k_σ values of all but one member of the series B···BrCl and c = 0.25 N m^{-1} to generate the nucleophilicities N_B for the Lewis bases B = CO, C_2H_2, C_2H_4, HCN and H_2S. This approach was not used for N_{NH_3} because there is evidence (see later) that H_3N···BrCl (and H_3N···ClF) involve significant

Table 1 Values of the intermolecular stretching force constant k_σ/N m^{-1} for complexes B···XY[a]

	XY				
B	F_2	Cl_2	Br_2	BrCl	ClF
CO	— (*1.3*)	3.70[b] (*3.6*)	5.13[c](*5.2*)	6.27[d] (*6.3*)	7.02[e] (*6.9*)
C_2H_2	— (*2.0*)	5.61[f] (*5.4*)	— (*7.8*)	9.4[g] (*9.5*)	10.02[h] (*10.3*)
C_2H_4	— (*2.2*)	5.89[i] (*6.0*)	— (*8.7*)	10.5[j] (*10.6*)	10.98[k] (*11.5*)
HCN	2.61[l] (*2.3*)	6.6[m] (*6.2*)	— (*9.1*)	11.09[n] (*11.0*)	12.33[o] (*12.0*)
H_2S	2.36[p] (*2.6*)	6.3[q] (*6.9*)	— (*10.0*)	12.07[r] (*12.1*)	13.34[s] (*13.2*)
NH_3	4.7[t] (*4.7*)	12.71[u] (*12.6*)	18.5[v] (*18.3*)	26.7[w] (*22.3*)	34.3[x] (*24.3*)

[a] Values in italics in parentheses are calculated from the N_B and E_{XY} of Table 2 used in eqn. (1). [b] Ref. 18. [c] Ref. 24. [d] Ref. 26. [e] Ref. 7. [f] Ref. 19. [g] Ref. 27. [h] Ref. 10. [i] Ref. 20. [j] Ref. 28. [k] Ref. 11. [l] Ref. 17. [m] Ref. 21. [n] Ref. 29. [o] Ref. 32. [p] Ref. 6. [q] Ref. 22. [r] Ref. 30. [s] Ref. 8. [t] Ref. 5. [u] Ref. 23. [v] Ref. 25. [w] Ref. 31. [x] Ref. 9.

charge transfer in addition to a simple electrostatic interaction.

Next, the N_B values so generated and recorded in Table 2 were used to establish E_{XY} for XY = F_2, Cl_2, Br_2 and ClF. For example, the appropriate N_B and k_σ pair was substituted into eqn. (1) to give one E_{ClF} value for each member of the series B···ClF. The mean value was then taken. Values of E_{F_2}, E_{Cl_2}, E_{Br_2} and E_{ClF} obtained in this way are included in Table 2 with the set of nucleophilicities N_{CO}, $N_{C_2H_2}$, $N_{C_2H_4}$, N_{HCN}, N_{H_2S} and N_{NH_3}. For the series B···Cl_2, B = NH_3 was not used to give a value of E_{Cl_2}, but instead the mean value of E_{Cl_2} from the remaining members was combined with k_σ of H_3N···Cl_2 to define N_{NH_3}. This approach was preferred because N_{NH_3} could not be satisfactorily obtained from H_3N···BrCl, for reasons alluded to earlier. Likewise, H_3N···ClF was not used in the evaluation of E_{ClF}.

As a check on the procedure, the N_B and E_{XY} of Table 2 were employed in eqn. (1) to generate k_σ for all complexes implied in Table 1. The predicted k_σ, shown in Table 1 in parentheses, are in good agreement with the experimental values when available, except for H_3N···BrCl and H_3N···ClF, whose large k_σ are seriously underestimated. These disagreements can be understood when the electric charge redistribution in the XY subunit, as estimated from the halogen nuclear quadrupole coupling constants, is considered for each member of the series B···Cl_2,[34] B···BrCl[35] and B···ClF.[12] Only a few hundredths of an electronic charge is transferred from X to Y in most complexes except H_3N···BrCl and H_3N···ClF and, in particular, it was shown to be necessary to assume a significant contribution of the ionic structure $[H_3NCl]^+$···F^- in a valence bond description of the latter complex.[9] Presumably a similar assumption is appropriate to the strongly bound H_3N···BrCl[11] but all other B···XY can be understood on the basis of the simple electrostatic model without invoking such charge transfer.[12,34,35]

Some interesting conclusions about B···XY interactions are available by reference to Tables 1 and 2. First, the fact that eqn. (1) applies to the two series of complexes B···HX and B···XY (with exceptions noted) suggests that the intermolecular binding is of a common type in both. For B···HX, the hydrogen bond interaction is well established to be of the simple electrostatic type B··$^{\delta+}$H–X$^{\delta-}$, where $^{\delta+}$H interacts with a nucleophilic region of B.[13,14,36] Presumably, this is also the case for the halogen complexes, with interactions of the type B··$^{\delta+}$X$^{\delta-}$–X$^{\delta+}$ or B··$^{\delta+}$X–Y$^{\delta-}$. It is noteworthy that the order of the electric quadrupole moments of the homonuclear dihalogens is F_2 < Cl_2 < Br_2, while BrCl and ClF have electric dipole moments of similar magnitude.[37] This order of electric moments is consistent with the order F_2 < Cl_2 < Br_2 < BrCl < ClF established here for the electrophilicities E_{XY} of the halogens (see Table 2).

The second conclusion is that, with one exception, the nucleophilicity N_B obtained for each B from the experimental k_σ of Table 1 and eqn. (1) is similar to that established from the B···HX series. The exception is HCN. The N_B and E_{HX} from the B···HX series are included in Table 2 for convenience. Evidently, HCN is a better nucleophile with respect to the hydrogen halides than to dihalogen molecules.

Table 2 Nucleophilicities N_B and electrophilicities E_{XY} of a series of Lewis bases B and dihalogen molecules XY

Nucleophilicities N_B						
B	CO	C_2H_2	C_2H_4	HCN	H_2S	NH_3
This work[a]	2.8	4.2	4.7	4.9	5.4	9.9
Refs. 15 and 16[b]	3.4	5.1	4.7	7.3	4.8	11.5

Electrophilicities E_{XY}[c] or E_{HX}[d]								
XY	F_2	Cl_2	Br_2	BrCl	ClF	HBr	HCl	HF
E_{XY} or E_{HX}	1.9	5.1	7.4	9.0	9.8	4.2	5.0	10.0

[a] Estimated by using the k_σ from Table 1 with eqn. (1) in the manner described in the text. [b] Estimated from the k_σ of a series of B···HX complexes and eqn. (1) (see refs. 15 and 16). [c] This work. [d] Ref. 15.

The author thanks the EPSRC for the award of a Senior Fellowship.

Notes and references

1 See for example, R. S. Mulliken and W. B. Person, *Molecular Complexes, A Lecture and Reprint Volume*, Wiley-Interscience, New York, 1969, ch. 5.
2 A. C. Legon and C. A. Rego, *J. Chem. Soc., Faraday Trans.*, 1990, **86**, 1915.
3 T. J. Balle and W. H. Flygare, *Rev. Sci. Instrum.*, 1981, **52**, 33.
4 A. C. Legon in *Atomic and Molecular Beam Methods*, ed. G. Scoles, Oxford University Press, New York, 1992, vol. 2, ch. 9.
5 H. I. Bloemink, K. Hinds, J. H. Holloway and A. C. Legon, *Chem. Phys. Lett.*, 1995, **245**, 598.
6 G. Cotti, C. M. Evans, J. H. Holloway and A. C. Legon, *Chem. Phys. Lett.*, 1997, **264**, 513.
7 K. Hinds, J. H. Holloway and A. C. Legon, *Chem. Phys. Lett.*, 1995, **242**, 407.
8 H. I. Bloemink, K. Hinds, J. H. Holloway and A. C. Legon, *Chem. Phys. Lett.*, 1995, **242**, 113.
9 H. I. Bloemink, C. M. Evans, J. H. Holloway and A. C. Legon, *Chem. Phys. Lett.*, 1996, **248**, 260.
10 K. Hinds, J. H. Holloway and A. C. Legon, *J. Chem. Soc., Faraday Trans.*, 1996, **92**, 1291.
11 H. I. Bloemink, J. H. Holloway and A. C. Legon, *Chem. Phys. Lett.*, 1996, **250**, 567.
12 A. C. Legon, *Chem. Phys. Lett.*, 1997, **279**, 55.
13 A. C. Legon and D. J. Millen, *Faraday Discuss. Chem. Soc.*, 1982, **73**, 71.
14 A. C. Legon and D. J. Millen, *Chem. Soc. Rev.*, 1987, **16**, 467.
15 A. C. Legon and D. J. Millen, *J. Am. Chem. Soc.*, 1987, **109**, 356.
16 A. C. Legon and D. J. Millen, *J. Chem. Soc., Chem. Commun.*, 1987, 986.
17 S. A. Cooke, G. Cotti, C. M. Evans, J. H. Holloway and A. C. Legon, *Chem. Phys. Lett.*, 1996, **262**, 308.
18 W. Jäger, Y. Xu and M. C. L. Gerry, *J. Phys. Chem.*, 1993, **97**, 3685.
19 H. I. Bloemink, S. A. Cooke, K. Hinds, A. C. Legon and J. C. Thorn, *J. Chem. Soc., Faraday Trans.*, 1995, **91**, 1891.
20 H. I. Bloemink, K. Hinds, A. C. Legon and J. C. Thorn, *Chem. Eur. J.*, 1995, **1**, 17.
21 A. C. Legon and J. C. Thorn, *J. Chem. Soc., Faraday Trans.*, 1993, **89**, 4157.
22 H. I. Bloemink, S. J. Dolling, K. Hinds and A. C. Legon, *J. Chem. Soc., Faraday Trans.*, 1995, **91**, 2059.
23 A. C. Legon, D. G. Lister and J. C. Thorn, *J. Chem. Soc., Faraday Trans.*, 1994, **90**, 3205.
24 E. R. Waclawik, J. M. A. Thumwood, P. W. Fowler, D. G. Lister and A. C. Legon, unpublished observations.
25 H. I. Bloemink and A. C. Legon, *J. Chem. Phys.*, 1995, **103**, 876.
26 S. Blanco, A. C. Legon and J. C. Thorn, *J. Chem. Soc., Faraday Trans.*, 1994, **90**, 1365.
27 H. I. Bloemink, K. Hinds, A. C. Legon and J. C. Thorn, *J. Chem. Soc., Chem. Commun.*, 1994, 1229.
28 H. I. Bloemink, K. Hinds, A. C. Legon and J. C. Thorn, *Angew. Chem., Int. Ed. Engl.*, 1994, **33**, 1512.
29 K. Hinds and A. C. Legon, *Chem. Phys. Lett.*, 1995, **240**, 467.
30 H. I. Bloemink and A. C. Legon, *Chem. Eur. J.*, 1996, **2**, 265.
31 H. I. Bloemink, A. C. Legon and J. C. Thorn, *J. Chem. Soc., Faraday Trans.*, 1995, **91**, 781.
32 K. Hinds, A. C. Legon and J. H. Holloway, *Mol. Phys.*, 1996, **88**, 673.
33 D. J. Millen, *Can. J. Chem.*, 1985, **63**, 1477.
34 A. C. Legon, *Chem. Phys. Lett.*, 1995, **237,** 291.
35 A. C. Legon, *J. Chem. Soc., Faraday Trans.*, 1995, **91**, 1881.
36 A. D. Buckingham and P. W. Fowler, *Can. J. Chem.*, 1985, **63**, 2018.
37 See ref. 5 for a convenient summary of the electric moments of F_2, Cl_2, Br_2, BrCl and ClF.

Communication 8/07288D

ChemComm

Crystalline silica prepared at room temperature from aqueous solution in the presence of intrasilica bioextracts

Carole C. Perry* and Tracey Keeling-Tucker

Department of Chemistry and Physics, The Nottingham Trent University, Clifton Lane, Nottingham, UK NG11 8NS. E-mail: Carole.Perry@ntu.ac.uk

Received (in Bath, UK) 23rd September 1998, Accepted 20th October 1998

Silica, exhibiting crystalline texture has been prepared from aqueous solution at pH *ca.* 7 in the presence of intrasilica biomolecules extracted from the primitive plant *Equisetum telmateia*; some of the silica shows interplanar lattice spacings of 3.5 Å and is present in lath-like objects up to *ca.* 20–30 nm wide and more than 100 nm in length; an electron diffraction pattern obtained from this material also shows interplanar spacings of 3.46, 2.13 and 1.70 Å suggesting that the material might be quartz.

In the field of biomineralization where biological organisms are able to regulate the formation of both crystalline and amorphous composite mineral phases there is much interest in understanding how mineralization occurs.[1] The process requires the concentration of selected elements, the nucleation, growth and moderation of growth of the mineral phase in predefined locations at specific times during the lifetime of a particular organism. Biominerals are usually composite phases containing organic components such as membranes and/or proteins and carbohydrates together with the mineral phase. The relationship between the two is thought to be important in the regulation of mineral composition, crystallographic phase and morphology.[2] The organic phase is largely found external to the mineral phase but low levels (*ca.* 0.03% by weight) of acidic proteinaceous biopolymers can also be found intercalated within the mineral phase, perhaps at crystal domain boundaries.[3] The intercalated biopolymers may have fundamental roles to play in nucleation and/or crystal growth and their presence has also been shown to have dramatic effects on the mechanical properties of crystalline biominerals.[4] For amorphous biominerals such as silica, biopolymers are also found in intramineral locations,[5–7] however, their role in nucleation, particle growth and aggregation remains unclear.

We are interested in extending our understanding of how biosilicas with specific form[8,9] are laid down and additionally we are interested in the preparation of novel silica phases using knowledge gained from the study of biological systems. To this end we have extracted protein-containing biomolecules from intrasilica locations in the branches of *Equisetum telmateia*[5] and used them in the study of silica precipitation at circumneutral pH.† The biopolymer extract used in this study was released by solubilization of the siliceous phase with buffered solutions of HF following treatment of plant materials with a mixture of concentrated nitric and sulfuric acids. The amino acid composition of this extract was rich in serine, glutamine/glutamic acid and glycine and had associated with it a carbohydrate component enriched in glucose and xylose. The 'model' system used to study particulate silica precipitation utilized a catecholato complex of silicon, $K_2[Si(C_6H_4O_2)_3]\cdot xH_2O$ as the source of soluble silicon.[10] At *ca.* physiological pH the complex partially decomposes to yield orthosilicic acid which immediately undergoes polycondensation reactions to relieve any resultant supersaturation.

50 mM solutions of potassium silicon catecholate were used with/without the biopolymer extract at 1% w/w, the pH of the solution was lowered to *ca.* 7.0 by the addition of a predetermined quantity of HCl and the concentrations of orthosilicic acid measured as a function of time by a colorimetric molybdenum blue method.[11] Kinetic analysis of the solution data was carried out in accordance with our previous studies.[12]‡

The effect of the biosilica extracts on both the early oligomerization reactions (*e.g.* the formation of dimers and trimers of orthosilicic acid) and on particle growth by precipitation/dissolution reactions was studied. Electron microscopy studies of the precipitates gave information on the effect of solution additives on nucleation, particle growth and aggregation.

Statistical analysis (students t-test and Mann Whitney U-test)[13] of the kinetic data‡ showed that the addition of 1% w/w of the *Equisetum telmateia* intrasilica extract to the silica oligomerization medium results in a *ca.* 22% increase in the rate of trimer formation (the second reaction in the oligomerization process). The rate constant for the addition of a monomer to an oligomer larger than a trimer is statistically no different for samples including the proteinaceous extract but the rate of removal of monomers from oligomers is reduced by *ca.* 33%. The effect of these changes is to increase the rate at which orthosilicic acid is removed from solution and to reduce the amount of silicon left in solution at the end of the experiment. Fig. 1 shows the increase in the levels of oligomerized silica at all sampling points. Electron microscopy of the precipitated silica shows evidence for aggregates built up from small particles *ca.* 1–2 nm in diameter, much smaller than is expected for the 'blank' system (data not shown, see ref. 10 for an example). Other structures present include ribbon-like (lath-like) objects and curved loops which often show characteristic fringes of *ca.* 3.50 Å. Energy dispersive X-ray analysis of all such areas indicates that the material contains silicon and oxygen.† The ribbon-like structures and loops, Fig. 2(a)–(c), are found in all samples from 1 h after initiation of the precipitation reaction. Samples taken at 48 h after the start of the experiment occasionally exhibit order over distances > 600 nm in length and *ca.* 20–30 nm in width. The images obtained suggest a 'soft' or perhaps 'layered' material (for an example, see ref. 14) but the electron diffraction patterns obtained from some areas with *d*-spacings of 3.46, 2.13 and 1.70 Å are compatible with quartz [PDF 5-490], Fig. 2(d). X-Ray diffraction data could not be obtained from silica collected by centrifugation 7 days after initiation of the reaction (even after an extended scan over 8 h) indicating that the silica sample prepared in the presence of the

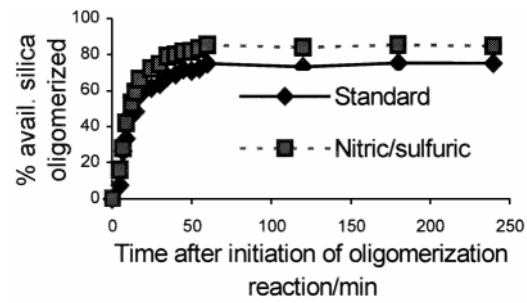

Fig. 1 Plot of % of oligomerized silica (not detectable by the molybdate method) *vs.* time.

biopolymer extract contains only low levels of crystalline material. No additional information was obtained from diffraction studies at low values of 2θ suggesting that the siliceous materials are not mesoporous, lamellar phases.

The presence of the protein-containing extract in the oligomerizing mixture clearly had some effect on nucleation with the formation of (a) smaller particles of silica (the majority of fundamental particles are smaller than 2 nm in diameter as opposed to particles up to 4 nm in diameter for the blank system) and, (b) silica with a crystalline appearance. The presence of the latter material from the earliest analysis point (as assessed by electron microscopy) suggests that this material is formed very early in the reaction profile and is not the result of structural rearrangement with time.

Biopolymers can be removed from the silica precipitated in the 'model' reaction system utilizing the same methods used for their initial production. The levels of proline are decreased and the levels of glycine are *ca*. doubled in the proteinaceous material extracted from the 'model' silica precipitated materials. The amino acid composition of the biopolymer extracts is rich in amino acids known to form β-sheet or β-turn secondary structures. For such structures, the spacing between successive layers is a minimum of 3.5 Å when only glycine is involved but may be 5.7 Å for chains rich in alanine as is found in the silk protein fibroin.[15] It is possible that the observed silica structures are either crystalline silica formed *de novo* from aqueous solution, or more likely, the observed structures are generated by epitaxial matching of the organic and inorganic matrices with the silica structure continuing to develop from the initial biopolymer-controlled nucleation event. It is evident that in the biological environment additional controls must be exerted during the process of silica precipitation in order to prevent the formation of crystalline phases as they are much more difficult to mould into the macroscopic structures produced by living organisms.

Further work will involve identification of the biopolymer component(s) (preliminary studies have shown that the extracts contain both high molecular weight proteins and low molecular weight glycoproteins) which are most effective in the spontaneous generation of crystalline silica structures from supersaturated solutions at room temperature, neutral pH and in the absence of multicharged cations, conditions which would not be expected to yield crystalline silica.[11,16]

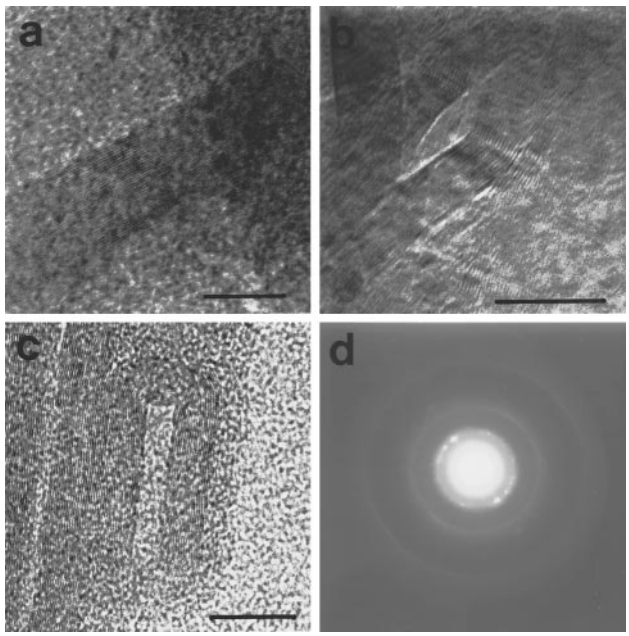

Fig. 2 (a)–(c) Transmission electron microscopy data for unusual silica structures precipitated in the presence of 1% w/w biopolymer extracts. All images shown are from microscope grids prepared by the 'dipping' method. Scale bars represent 10 nm; (d) electron diffraction pattern from (b). Pattern was recorded using a camera length of 100 cm.

Notes and references

† Precipitation experiments were conducted using biopolymer extracts from two separate extractions. The amino acid compositions were measured using an Applied Biosystems 420a amino acid analyser operated by A. C. Willis of the MRC Immunochemistry Unit, Oxford University. For the kinetic measurements, four sample runs were completed for each experiment on the same day using a temperature controlled reaction vessel set at 23 ± 0.1 °C. Samples for electron microscopy studies were taken from parallel experiments by dipping carbon coated formvar covered copper electron microscope grids into the reaction vessel at 1, 4, 24, 48 h and 7 days after the experiment was initiated and allowing the grids to air dry. Samples for electron microscopy were investigated using a JEOL 2010 analytical electron microscope (Link ISIS system) fitted with a LaB_6 filament operating at 200 keV. Magnifications of 200 000 × were necessary to see the lattice fringing present and areas of interest were subjected to energy dispersive X-ray analysis to identify the elements with atomic number ⩾6 present in the sample. A minimum of 10 analyses for each sample area showed that the precipitated material contained Si and O together with traces of K and Cl (N.B. the grids were not washed after sampling by dipping). Crystalline structures as presented in this paper have not been observed by transmission electron microscopy in any of our other model precipitation experiments performed in the presence of a range of singly and multiply charged metal ions, carbohydrates and proteins such as bovine serum albumin, zein, concanavalin A and cytochrome c. Silica samples were also analysed by powder X-ray diffraction; Siemens D500 diffractometer operating in the range 2θ = 1–80° by Professor Mark Weller and Dr Adam Whitehead of Southampton University. The Visual Services Department at The Nottingham Trent University are thanked for printing of the electron micrographs for publication. BBSRC and Crosfield Chemicals are thanked for their funding.

Amino acid composition of bioextract used in the precipitation experiment (mol%); Asx; 8.9, Glx; 15.0, His; 3.5, Lys; 4.94, Arg, 1.54, Ser; 14.24, Thr; 3.91, Tyr; 1.30, Gly; 16.67, Pro; 9.60, Ala; 8.42, Val; 4.07, Leu; 4.3, Ile; 2.64, Phe; 0.98 Amino acid composition of biopolymers extracted from 'model' system precipitated silica (mol%); Asx; 7.56, Glx; 12.3, His; 5.7, Lys; 2.73, Arg, 3.4, Ser; 12.92, Thr; 4.41, Tyr; 2.35, Gly; 30.46, Pro; 4.06, Ala; 6.95, Val; 2.94, Leu; 4.23, Ile; nd, Phe; nd. nd = not detected.

‡ Rate constants:[13] blank system; $k_3 = 4.91 \times 10^{-6}$ mmol^{-2} dm^6 s^{-1}, $k_+ = 5.67 \times 10^{-4}$ s^{-1}, $k_- = 1.19 \times 10^{-5}$ s^{-1}. With 1% biomolecule extracts; $k_3 = 6.29 \times 10^{-6}$ mmol^{-2} dm^6 s^{-1}, $k_+ = 4.73 \times 10^{-4}$ s^{-1}, $k_- = 7.97 \times 10^{-6}$ s^{-1}.

1 *Biomineralization: Chemical and Biochemical Perspectives*, ed. S. Mann, J. Webb and R. J. P. Williams, VCH, Weinheim, 1989.
2 H. Lowenstam and S. Weiner, *On Biomineralization*, OUP, Oxford, 1989.
3 S. Weiner, *J. Exptl. Zool.*, 1985, **234**, 7.
4 A. Berman, J. Hanson, L. Leiserowitz, T. Koetzle, S. Weiner and L. Addadi, *Science*, 1993, **259**, 776.
5 C. C. Harrison (now Perry), *Phytochemistry*, 1996, **41**, 37.
6 N. Kröger, G. Lehmann, R. Rachel and M. Sumper, *Eur. J. Biochem.*, 1997, **250**, 99.
7 K. Shimizu, J. Cha, G. D. Stucky and D. E. Morse, *Proc. Natl. Acad. Sci.*, 1998, **95**, 6234.
8 C. C. Perry, in *Biomineralization: Chemical and Biochemical Perspectives*, ed. S. Mann, J. Webb and R. J. P. Williams, VCH, Weinheim, 1989, p. 223.
9 C. W. Li and B. E. Volcani, *Philos. Trans. R. Soc. London Sect. B*, 1984, **304**, 519.
10 C. C. Perry and Y. Lu, *J. Chem. Soc., Faraday Trans.* 1992, **88**, 2915.
11 R. K. Iler, *The Chemistry of Silica*, Wiley-Interscience, 1979.
12 C. C. Harrison (now Perry) and N. Loton, *J. Chem. Soc., Faraday Trans.*, 1995, **91**, 4287.
13 G. C. Miller and G. N. Miller, *Significant Tests in Statistics for Analytical Chemistry*, Ellis Horwood, 3rd edn., 1993.
14 Y. Rosenfeld Hacohen, E. Grunbaum, R. Tenne, J. Sloan and J. L. Hutchison, *Nature*, 1998, **395**, 336.
15 R. E. Marsh, R. B. Corey and L. Pauling, *Biochim. Biophys. Acta*, 1955, **16**, 1.
16 H. Harder and W. Flehmig, *Geochim. Cosmochim. Acta*, 1970, **34**, 295.

Communication 8/07404F

EPR study of platinum supported on NaY

Thorsten Schmauke, Einar Möller and Emil Roduner*

Institut für Physikalische Chemie, Universität Stuttgart, Pfaffenwaldring 55, D-70550, Germany. Tel: +49 711 685 4490; Fax: +49 711 685 4495. E-mail: roduner@indigo01.chemie.uni-stuttgart.de

Received (in Bristol, UK) 1st July 1998, Accepted 26th October 1998

Pt/NaY was prepared by the aqueous ion-exchange method and investigated by EPR spectroscopy. After reduction with H_2 using a static system, an orthorhombic EPR signal was observed with g_1 = 2.531, g_2 = 2.322, g_3 = 2.062, coaxial with the hyperfine components a_1 = 64.9 G, a_2 = 74.6 G, a_3 = 72.6 G; this signal is assigned to Pt^+ ions. Typical cation sites for location in the supercages are excluded for symmetry reasons.

Hetereogenous catalysts consisting of transition metal ions or small clusters supported on zeolites play a key role in important petrochemical reactions.[1] Since the activity and the selectivity of catalytic reactions depend on the size of clusters, characterization of the size, location, electronic and atomic structure by techniques such as TEM, EXAFS, XRD, XPS, TPR, TPD, H_2 chemisorption, ^{129}Xe NMR, IR or electron paramagnetic resonance (EPR) is indispensable. EPR has been shown to be an important tool for the characterization of many transition metals in zeolites.[2] In many cases it is possible to distinguish between different oxidation states, coordination numbers, complex symmetries and crystal field strengths. It is of importance for a further understanding of heterogenous catalysis to observe changes of the catalytically active transition metal centers during reactions. The site determines the accessibility by reacting molecules. In view of the importance of Pt on zeolites it is surprising that there have been no publications of EPR studies until today.

Samples were prepared *via* ion-exchange at 343 K over 48 h by dropwise addition of 0.003 M $[Pt(NH_3)_4]Cl_2$ solution to NaY slurry, resulting in a Pt loading of 4%. The exchanged zeolite was filtered, washed with deionized water in order to remove Cl^- ions, and dried at 296 K in air. Calcination was conducted by heating Pt/NaY from room temperature to 563 K at 0.5 K min^{-1} in flowing O_2 (270 ml min^{-1} g^{-1}), and holding at 563 K for 3 h. After this treatment platinum is located as PtO in the supercages of Y zeolite as has been shown using X-ray methods, electron microscopy and gas adsorption.[3,4] The zeolite was pumped at 523 K to remove water, and reduction was performed by heating from 296 K to 563 K at 0.5 K min^{-1} in a closed EPR tube with different molar ratios of Pt : H_2 (1 : 3 or 1 : 6), and holding at the final temperature for 6 h. X-Band EPR spectra were recorded on a Bruker EMX spectrometer in the temperature range 4 K to 150 K in H_2 atmosphere.

For reduction at a molar ratio of Pt : H_2 = 1 : 6, no EPR spectrum is observed. For a molar ratio Pt : H_2 = 1 : 3, the EPR spectrum at 4 K shows overlapping signals (Fig. 1). The spin concentration corresponds to about 0.5% of the total Pt loading. The main signal is orthorhombic with resolved ^{195}Pt hyperfine splitting (natural abundance 33.8%, $I = \frac{1}{2}$). Simulation[5] yields the spin Hamiltonian parameters g_1 = 2.531, g_2 = 2.322, g_3 = 2.062, a_1 = 64.9 G, a_2 = 74.6 G, a_3 = 72.6 G with coaxial *g*- and *a*-tensors. The orthorhombic symmetry allows us to exclude the possibility that the species is located at a typical cation site,[6] since axial symmetry should be expected for these sites. Going to higher temperatures, the lines broaden and the intensity decreases. Above 100 K only a very weak and broad spectrum is observed. This behavior may be caused by dynamic effects, for example by jump exchange of the observed species between different sites. At this point we have no explanation for the remaining minor features, which are superimposed mainly on the central line.

Several EPR spectra of formal Pt(I) complex compounds with organic ligands have been described.[7] The general sequence of *g*-values in all these spectra is $g_1 > g_2 \approx g_e >> g_3$, and the authors assign them to Pt^+, in contrast to expectation since for a d^9 system all *g*-values should be larger than g_e due to spin–orbit coupling.[8] Other authors[9] assume that during electrochemical preparation of these complexes a reduction of the organic ligands occurs, leading to species which are better described as $Pt^{II}(L^-)$ than as $Pt^I(L)$. The present case is different since a reduction of the zeolite lattice is more difficult than a reduction of unsaturated organic ligands. Indeed, *g*-values in the sequence $g_1 > g_2 > g_3 > g_e$ indicate the presence of platinum in the formal oxidation state of +1. For Pt^{3+} ions (d^7) $g_i > g_e$ is expected as well as for all ions with a more than half filled d-shell. Since we used an excess of hydrogen for the reduction of PtO it is unlikely that Pt^{3+} is formed.

Axial EPR spectra of Pt^+ ions with spin Hamiltonians characterized by $g_\parallel$ = 3.29, $g_\perp$ = 2.261, $a_\parallel \leqslant$ 10 G and $a_\perp$ = 229 G for an Ar matrix and $g_\parallel$ = 3.13, $g_\perp$ = 2.214, $a_\parallel \leqslant$ 10 G and $a_\perp$ = 311 G for a Kr matrix were reported.[10] Compared with the observed platinum species in Y zeolite, the *g*-anisotropy of Pt^+ was larger in the rare gas matrices because of the weaker crystal field.

The ^{195}Pt hyperfine splitting of about 70 G in NaY is equivalent to an s-orbital contribution of 0.6%, which is similar to the 1.4% for Pt^+ in Ar and 1.9% in Kr matrices.[10] The formation of Pt clusters during reduction is a well known process,[12] but based on the isotropic hyperfine coupling constant[11] of about 12000 G for Pt^0 a much higher s-character is expected for neutral clusters. We therefore exclude the possibility that the spectrum observed here represents clusters. The contribution of d-orbitals of Pt^+ in rare gas matrices is 54% for Ar and 76% for Kr.[10] The observed d-orbital contribution for Pt^+/NaY is only about 2%, possibly because of the contribution of excited p-orbitals.[10,13,14] Another possibility is the delocalization of spin density to ligands since the d-orbital contribution is smaller by about a factor 30 for Pt^+ in NaY than for Pt^+ in rare gas matrices. On the other hand, the high *g*-value allows us to exclude the possibility that the radical is localized on oxygen since $O^{\cdot-}$ or $O_2^{\cdot-}$ have *g*-values near g_e.[15,16] A more attractive interpretation is based on the assumption that one (or two) of the

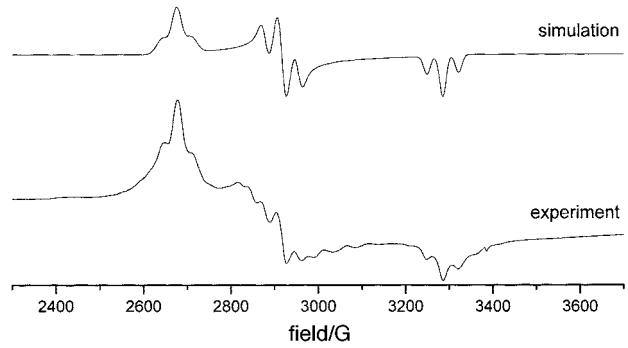

Fig. 1 Simulation and X-band EPR spectrum of Pt/NaY observed at 4 K.

hyperfine components is of negative sign, which is experimentally not distinguishable. This leads to near-zero s-character and somewhere of the order of 36% d-character, which is much closer to the results reported for Pt^+/Ar, and also compatible with the high g-values.

The present results introduce a new, non-invasive tool for the characterization of one of the most important catalysts. Further EPR experiments aiming at a better understanding of reaction mechanisms of heterogenous catalysis on Pt exchanged zeolites are in progress. This includes other preparation conditions and examinations of further zeolites which lead to Pt cations located at different sites, for example in sodalite cages,[3,4] and consequently to other environments which can be studied by EPR. Adsorption of organic compounds or oxidation may lead to the disappearance of the observed EPR signals, and perhaps to the appearance of other EPR active species. ESEEM experiments may give more detailed information about the nature of ligands around the observed species.

We thank M. Munzarová for valuable comments.

Notes and references

1 B. C. Gates, J. R. Katzer and G. C. A. Schuit, *Chemistry of Catalytic Processes*, McGraw Hill, New York, 1979.
2 L. Kevan, *Electron Spin Reson. B*, 1991, **12**, 99.
3 P. Gallezot, *Catal. Rev*., 1979, **20**, 121.
4 E. J. Creyrton, A. C. T. van Duin, J. C. Jansen, P. J. Kooyman, H. W. Zandbergen and H. van Bekkum, *J. Chem. Soc., Faraday Trans.*, 1996, **92**, 4637.
5 Simfonia Version 1.25, Bruker EPR simulation program based on perturbation theory.
6 H. Klein, C. Kirschhock and H. Fuess, *J. Phys. Chem.*, 1994, **98**, 12 345.
7 R. J. Klinger, J. C. Huffman and J. K. Kochi, *J. Am. Chem. Soc.*, 1982, **104**, 2147.
8 K. Dyrek and M. Che, *Chem. Rev.*, 1997, **97**, 305.
9 P. S. Braterman, J. I. Song, F. M. Wimmer, S. Wimmer, W. Kaim, A. Klein and R. D. Peacock, *Inorg. Chem.*, 1992, **31**, 5084.
10 R. J. Van Zee and W. Weltner Jr., *Chem. Phys. Lett.*, 1997, **266**, 403.
11 W. M. H. Sachtler and A. Y. Stakheev, *Catal. Today*, 1992, **12**, 283.
12 A. Weil, J. R. Bolton and J. E. Wertz, *Electron Paramagnetic Resonance*, John Wiley & Sons, New York, 1994.
13 N. Rösch, A. Görling, D. E. Ellis and H. Schmidbaur, *Angew. Chem., Int. Ed. Engl.*, 1989, **28**, 1357.
14 C. P. Keijzers and E. De Boer, *J. Chem. Phys.*,1972, **57**, 1277.
15 R. B. Clarkson and S. McClellan, *J. Catal.*, 1980, **61**, 551.
16 C. Daul, H. Fischer, J. R. Morton, K. F. Preston and A. v. Zelewsky, *Landolt-Börnstein, Group II: Atomic and Molecular Physics Volume 9a, Magnetic Properties of Free Radicals*, ed. H. Fischer, K.-H. Hellwege, Springer-Verlag, Heidelberg, 1977.

Communication 8/05409F

$[(silox)_2ReO]_2$ (silox = $^tBu_3SiO$) contains a Re≡Re bond and terminal oxo ligands

Richard E. Douthwaite, Peter T. Wolczanski* and Erika Merschrod

Cornell University, Baker Laboratory, Department of Chemistry, Ithaca, New York, USA 14853. E-mail: ptw2@cornell.edu

Received (in Bloomington, IN, USA) 14th September 1998, Revised manuscript received 19th October 1998. Accepted 23rd October 1998

The preference for terminal rather than bridging {*i.e.* $[(silox)_2Re]_2(\mu\text{-}O)_2$} oxo ligands in C_2 $(silox)_2(O)Re{\equiv}Re(O)(silox)_2$ is electronic, not steric, in origin.

Use of the bulky siloxide $^tBuSiO^-$ (silox) ligand has enabled investigations of several low coordinate, monomeric complexes of groups 4–6,[1–4] but metal–metal bond formation cannot always be averted. $[(silox)_2MH_2]_2$ (M^{IV} = Nb, Ta)[5] dimers form upon reduction of $(silox)_2MCl_3$ under H_2 when M^V trihydride derivatives were expected, and while sterically protected $(silox)_2W{=}N^tBu$,[4] an unusual three-coordinate W^{IV} derivative, was isolable, a less hindered W^{III} environment encouraged triple-bond formation, *i.e.* $(silox)_2XW{\equiv}WX(silox)_2$ (X = Cl, H, Me, Et).[6] Attempts to extend the theme of low-coordination to Re[7] have instead resulted in the synthesis of C_2 $(silox)_2(O)Re{\equiv}Re(O)(silox)_2$, whose terminal oxo groups are an apparent oddity.

In contrast to metatheses within groups 4–6, treatments of various rhenium chlorides with Na(silox) were ineffective. Utilization of Tl(silox), prepared *via* metathesis of Hsilox with TlOEt, mitigated some of the undesired redox processes. Addition of Tl(silox) to $ReCl_3(PEt_3)_3$[8] (100 °C, 12 h, C_6H_6) afforded orange $(silox)ReCl_2(PEt_3)_2$ **1** (60%), and a similar treatment (100 °C, 2 d, C_6H_6) of Cl_4ReL_2 (L = THT,[9] THF)[10] gave the blue, trigonal bipyramidal (X-ray) Re^V complex, $(silox)_3ReCl_2$ **2** (33%) upon chromatographic work-up in air. Metathesis of Re_3Cl_9 with 3 equiv. Tl(silox) (100 °C, 12 h, C_6H_6) provided dark green, C_s (X-ray) $[(silox)ReCl]_3(\mu\text{-}Cl)_3$ **3** (85%); further incorporation of silox into **1–3** could not be effected.

Treatment of *cis*-$ReOCl_3(PEt_3)_2$[11] with 3 equiv. of Tl(silox) afforded orange $(silox)_2(O)Re{\equiv}Re(O)(silox)_2$ **4** [eq (1)] in moderate yield (38%) after extensive trituration with hydro-

$$cis\text{-}ReOCl_3(PEt_3)_2 + 3\ Tl(silox) \xrightarrow[\text{benzene, -3 TlCl}]{\text{160 °C, 3 d}} \underset{\mathbf{4}}{(silox)_2(O)Re{\equiv}Re(O)(silox)_2} + \ldots. \quad (1)$$

carbons and crystallization from THF. Two singlets in its ^1H NMR spectrum suggested C_2 symmetry, and IR spectroscopy revealed a moderate band at 944 cm^{-1} tentatively assigned to ν(ReO). An X-ray diffraction study of **4** confirmed the molecular C_2 symmetry, terminal oxo and silox ligands, and distorted tetrahedral geometry about each Re (Fig. 1). Inter-silox angles O1–Re1–O4 [124.9(2)°] and O2–Re2–O3 [123.1(2)°] are significantly splayed due to a steric interaction. While O4–Re1–Re2 110.8(2)° and O3–Re2–Re1 112.5(2)° are relatively normal, they contrast with O1–Re1–Re2 [92.8(2)°] and O2–Re2–Re1 [93.0(2)°], which cant toward more open space between the silox and oxo groups. The d(Re≡Re) of 2.3593(6) Å is long compared to common Re^{II} d^5–d^5 ($\sigma^2\pi^4\delta^2\delta^{*2}$) triple bonds and related C_2 ditungsten species.[12] The Re–oxo bond lengths of 1.690(5) and 1.729(6) Å are slightly longer than average, but most comparisons are with oxo ligands on higher valent derivatives,[13,14] where shorter bonds are expected. Two Re-silox distances are normal [d(Re1–O1) = 1.822(5), d(Re2–O2) = 1.819(5) Å], while the remaining Re1–O4 [1.875(6) Å] and Re2–O3 [1.909(6) Å] linkages are quite long due to the respective *trans*-influences of the O6 and O5 oxo groups transmitted through the Re≡Re bond.

$(silox)_2(O)Re{\equiv}Re(O)(silox)_2$ **4** was remarkably inert toward simple donors (*e.g.* CO, py, alkenes), reducing agents (*e.g.* H_2, Me_3SiH), common oxidants (*e.g.* I_2, $BrCH_2CH_2Br$, pyO, Me_3NO, H_2CCH_2O, N_2O) and heterocumulenes (*e.g.* CS_2, PhN=C=O), and reacted with a few substrates or reagents (*e.g.* $PhPH_2$, Na/Hg, O_2) to give mixtures. Terminal rhenium–oxo bonds have been noted to be strong and inert in mononuclear complexes [*cf.* $(MeC_2Me)_2RReO$],[14] yet aggregation *via* μ-oxo formation is common.[15] Since **4** could have adopted a $[(silox)_2Re]_2(\mu\text{-}O)_2$ **5** configuration without undue steric strain {*cf.* $[(silox)_2W]_2(\mu\text{-}CMe)_2$},[16] calculations were employed to assess the terminal oxo electronic structure preference.

Fig. 2 illustrates truncated extended Hückel MO diagrams for the model complex $(HO)_2(O)Re{\equiv}Re(O)(OH)_2$ **4′**, which was given the structural parameters of **4** and adjusted to be C_2, and $[(HO)_2Re]_2(\mu\text{-}O)_2$ **5′**, whose optimized geometry [*e.g.* d(ReRe) ≒ 2.53 Å, d(Re–O_b) = 1.94 Å] was determined from density functional theory (DFT). The EHMO calculations revealed **5′** to be *ca.* 4 eV less stable than the observed **4′** system, with a very small HOMO–LUMO gap of *ca.* 0.5 eV. The extreme discrepancy in total energy is due to a tremendous increase of Re–O and Re–Re π* character realized in the three highest occupied orbitals of **5′**. In the unbridged geometry **4′**, the Re≡Re bond is comprised of the usual σ- and two π-bonding orbitals,[17] and while the d^3 fragment MOs have a significant amount of Re–O π*-character, it is largely dissipated upon forming the

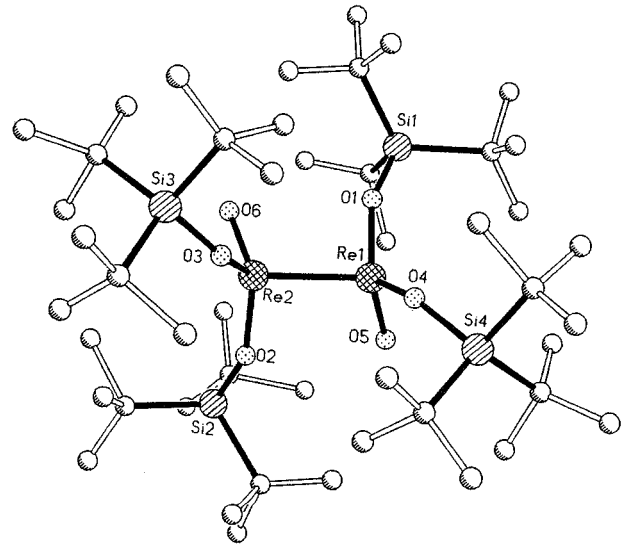

Fig. 1 Molecular view of $(silox)_2(O)Re{\equiv}Re(O)(silox)_2$ **4**. Selected (see text) interatomic distances (Å) and angles (°): Si1–O1 1.629(5), Si2–O2 1.637(5), Si3–O3 1.704(6), Si4–O4 1.728(6); O1–Re1–O5 112.4(2), O4–Re1–O5 109.8(2), O2–Re2–O6 115.9(2), O3–Re2–O6 104.6(3), O5–Re1–Re2 104.9(2), O6–Re2–Re1 106.4(2), Re1–O1–Si1 156.9(4), Re1–O4–Si4 146.7(4), Re2–O2–Si2 153.3(4), Re2–O3–Si3 149.4(4).

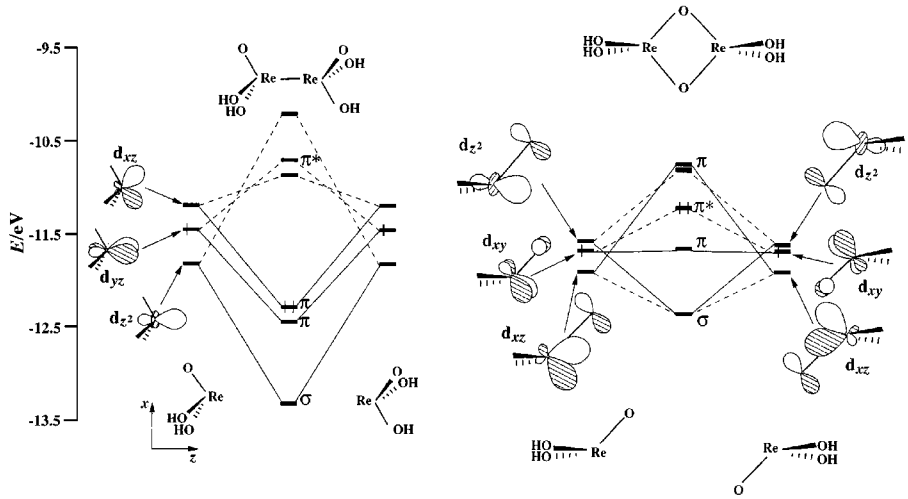

Fig. 2 Truncated MO diagrams for $(HO)_2(O)Re{\equiv}Re(O)(OH)_2$ **4′** and $[(HO)_2Re]_2(\mu{-}O)_2$ **5′**, modeling $(silox)_2(O)Re{\equiv}Re(O)(silox)_2$ **4** and hypothetical $[(silox)_2Re]_2(\mu{-}O)_2$ **5**, respectively.

metal–metal bond. In the μ-oxo version **5′**, dimerization of the $(HO)_2ReO$ fragments affords a Re–Re σ-bonding (σ) orbital that is principally d_{z^2} and a Re–Re π-bonding (π) orbital based on d_{xy}, but both have significant Re–O π* character, and the latter is rendered virtually non-bonding relative to the fragment MOs. Another Re–Re π-bonding orbital derived from d_{xz} contains so much Re–O π* character that it is destabilized relative to a Re–Re π* orbital that is populated instead. The net $\sigma^2\pi^2\pi^{*2}$ ordering describes a single Re–Re bond, and an assessment of the core orbitals (not shown) indicates that the Re–O antibonding π-interactions are not compensated enough by the two additional Re–O σ-interactions. Interestingly, the calculated minimum energy configuration of **4′** does not have a classical ethane-like geometry,[17] but optimizes with an HO–Re–Re angle near 90°, as in the crystal structure of **4**.

The cylindrical symmetry accorded the terminal oxos in **4** permits four significant π-bonds, whereas disruption of virtually all Re–O π-bonding in the bridged form is poorly balanced by additional σ-interactions; the terminal oxo structural preference of **4** is electronic in character. Thermodynamic preferences of $[(EtC_2Et)_2(O)Re]_2$ over $[(EtC_2Et)_2Re](\mu\text{-}O)(\mu\text{-}EtC_2Et)[Re(O)(EtC_2Et)]$,[18] and $(RO)_2(^tBuC{\equiv})Re = Re(\equiv C\text{-}^tBu)(OR)_2$[19] over μ-alkylidyne bridged forms, may be similarly ascribed. In compounds that lack additional terminal π-donors, or contain two less electrons {*e.g.* d^2-d^2 $[(Me_3SiCH_2)_2Re]_2(\mu\text{-}CSiMe_3)_2$},[20] the bridged form of multiple metal–ligand bond may prevail.[15]

Financial support from the National Science Foundation (CHE-9528914), Cornell University and The English-Speaking Union, for a Lindemann Trust Fellowship (R. E. D.), is gratefully acknowledged. We thank Ana-Rita Mayol and Emil Lobkovsky for experimental assistance, and Chase A. Munson for the initial calculations.

Notes and references

Selected analytical data: **1** (C_6D_6), δ_H δ1.58 (12 H, br q, CH_2), 7.00 (18 H, br t, CH_3), 8.07 (27 H, s, ^{t}Bu); δ_C δ10.31 (CH_2), 48.78 (CMe_3), 112.81 [$C(CH_3)_3$], 121.44 (CH_3). Anal. Calc. for $C_{24}H_{57}OSiP_2Cl_2Re$, C, 40.7, H, 8.1. Found: C, 40.8, H, 8.3%. **2** (C_6D_6), δ_H 6.70 (br, ^{t}Bu); δ_C 44.64 [$C(CH_3)_3$], 167.30 (CMe_3); UV–VIS (CH_2Cl_2) 700 nm (ε = 50 dm^3 mol^{-1} cm^{-1}), 577 [170, e″($^3A_2'$) → e′($^3A_2''$)], 345 (3100), 283 (5900). Anal. Calc. for $C_{36}H_{81}O_3Si_3Cl_2Re$, C, 47.9, H, 9.0. Found C, 47.6, H, 8.6%. **3** (C_6D_6), δ_H 1.12 (27 H, s, ^{t}Bu), 1.17 (54 H, s, ^{t}Bu); δ_C 22.51 (CMe_3), 23.56 (2xCMe_3), 30.37 [$C(CH_3)_3$], 30.62 [2x$C(CH_3)_3$]. Anal. Calc. for $C_{36}H_{81}O_3Si_3Cl_6Re_3$: C, 30.5; H, 5.7. Found: C, 31.1; H, 5.9%. **4** (C_6D_6), δ_H 1.26 (s, ^{t}Bu), 1.30 (s, ^{t}Bu); δ_C 24.20 (CMe_3), 24.86 (CMe_3), 30.74 [$C(CH_3)_3$], 30.79 [$C(CH_3)_3$]. Anal. Calc. for $C_{48}H_{108}O_6Si_4Re_2$: C, 46.6; H, 9.1. Found: C, 45.5, H, 8.6%.

Crystallographic data: **4**. 4 THF, $C_{64}H_{140}O_{10}Re_2Si_4$, M = 1554.58, D_c = 1.500 g cm^{-3}, μ = 3.66 mm^{-1}; orthorhombic, space group $Pca2_1$, a = 22.927(5), b = 12.552(3), c = 23.922(5) Å, U = 6844(2) Å^3, Z = 4, T = 293(2) K, 2923 independent reflections, R_1 = 0.1024, GOF(F^2) = 1.085% CCDC 182/1073.

References

1 P. T. Wolczanski, *Polyhedron*, 1995, **14**, 3335.
2 K. J. Covert, D. R. Neithamer, M. C. Zonnevylle, R. E. LaPointe, C. P. Schaller and P. T. Wolczanski, *Inorg. Chem.* 1991, **30**, 2494; K. J. Covert, P. T. Wolczanski, S. A. Hill, S.A. and P. J. Krusic, *Inorg. Chem.*; 1992, **31**, 66; K. J. Covert, A.-R. Mayol and P. T. Wolczanski, *Inorg. Chim. Acta*, 1997, **263**, 263.
3 J. B. Bonanno, T. P. Henry, D. R. Neithamer, P. T. Wolczanski and E. B. Lobkovsky, *J. Am. Chem. Soc.*, 1996, **118**, 5132; J. B. Bonanno, P. T. Wolczanski and E. B. Lobkovsky, *J. Am. Chem. Soc.*, 1994, **116**, 11 159; D. R. Neithamer, R. E. LaPointe, R. A. Wheeler, D. S. Richeson, G. D. Van Duyne and P. T. Wolczanski, *J. Am. Chem. Soc.* 1989, **111**, 9056-9072.
4 D. F. Eppley, P. T. Wolczanski and G. D. Van Duyne, *Angew. Chem., Int. Ed. Engl.*, 1991, **30**, 584.
5 R. E. LaPointe and P. T. Wolczanski, *J. Am. Chem. Soc.* 1986, **108**, 3535; R. L. Miller, R. Toreki, R. E. LaPointe, P. T. Wolczanski, G. D. Van Duyne and D. C. Roe, *J. Am. Chem. Soc.*, 1993, **115**, 5570.
6 R. L. Miller, K. A. Lawler, J. L. Bennett and P. T. Wolczanski, *Inorg. Chem.* 1996, **35**, 3242; R. L. Miller, P. T. Wolczanski and A. L. Rheingold, *J. Am. Chem. Soc.*, 1993, **115**, 10 422.
7 M. Weidenbruck, C. Pierrard and H. Pesel, *Z. Naturforsch., Teil B*, 1978, **33**, 1468.
8 G. W. Parshall, *Inorg. Synth.*, 1965, **17**, 111.
9 I. M. Gardener, M. A. Bruck, P. A. Wexler and D. E. Wigley, *Inorg. Chem.* 1989, **28**, 3688.
10 E. A. Allen, N. P. Johnson, D. T. Resevear and W. Wilkinson, *J. Chem. Soc. A*, 1969, 788.
11 J. Chatt, J. D. Garforth, N. P. Johnson and G. A. Rowe, *J. Chem. Soc.*, 1964, 601; J. Chatt and G. A. Rowe, *J. Chem. Soc.* 1962, 4019.
12 F. A. Cotton and R. A. Walton, *Multiple Bonds Between Metal Atoms*, Oxford University Press, New York, 2nd edn., 1993.
13 W. A. Nugent and J. M. Mayer, *Metal–Ligand Multiple Bonds*, Wiley Interscience, New York, 1988.
14 E. Spaltenstein, T. K. G. Erikson, S. C. Critchlow and J. M. Mayer, *J. Am. Chem. Soc.*, 1989, **111**, 617.
15 D. M. Hoffman, *Comprehensive Organometallic Chemistry*, ed. E. W. Abel, F. G. R. Stone and G. Wilkinson, Pergamon, Exeter, UK, 1995, vol. 6, pp 231–235.; K. P. Gable, F. A. Zhuravlev and A. F. T. Yokochi, *Chem. Commun.*, 1998, 799 and references therein.
16 R. L. Miller, Ph.D. Thesis, Cornell University, 1993.
17 A. Dedieu, T. A. Albright and R. Hoffmann, *J. Am. Chem. Soc.*, 1979, **111**, 3141; M. H. Chisholm, D. L. Clark, M. J. Hampden-Smith and D. M. Hoffman, *Angew Chem. Int. Ed. Engl.*, 1989, **28**, 432.
18 E. Spaltenstein and J. M. Mayer, *J. Am. Chem. Soc.*, 1991, **113**, 7744.
19 R. Toreki, R. R. Schrock and M. G. Vale, *J. Am. Chem. Soc.* 1991, **113**, 3610.
20 M. Bochmann, G. Wilkinson, A. M. R. Galas, M. B. Hursthouse and K. M. A. Malik, *J. Chem. Soc., Dalton Trans.*, 1980, 1797.

Communication 8/08306A

ChemComm

Decarboxylation of an α-amino acid coordinated to cobalt(III): kinetic stabilisation and molecular structure of a Co–C–N three-membered ring incorporated into a cobalt(III) macrocyclic ligand complex†‡

Deborah M. Tonei, Lisa-Jane Baker, Penelope J. Brothers, George R. Clark and David C. Ware*

Department of Chemistry, The University of Auckland, Private Bag 92019, Auckland, New Zealand. E-mail: d.ware@auckland.ac.nz

Received (in Cambridge, UK) 22nd September 1998, Accepted 28th October 1998

Photochemically-induced decarboxylation of a cobalt(III) cyclam complex bearing two coordinated *N*-carboxymethyl pendant arms results in kinetic stabilisation of the resulting aminoalkyl three-membered Co–C–N ring, which has been characterised by an X-ray crystal structure determination.

Cobalt(III) complexes containing chelated amino acids have been subjected to intense investigation, with most attention being paid to α-amino acid complexes. They have been used as activating and protecting groups in peptide synthesis, and they undergo a variety of useful reactions, many of which cannot be achieved with non-complexed α-amino acids.[1] These include alkylation at the α-carbon, imine formation, and condensation, oxidation and decarboxylation reactions.

The mechanism proposed for the photochemical decarboxylation of cobalt amino acid complexes involves, in sequence, excitation into the LMCT band, homolytic cleavage of the cobalt–oxygen bond, loss of carbon dioxide and recombination to produce a new cobalt(III)–carbon bond as part of a chelating aminoalkyl group (Scheme 1).[2,3] When the substrate contains a β-amino acid the resulting aminoalkyl group comprises a four-membered Co–C–C–N ring [Scheme 1(a)], and several such examples have been structurally characterised.[4] However, the corresponding three-membered rings that would result from decarboxylation of a chelated α-amino acid ligand [Scheme 1(b)] have proved to be more elusive.[2] In just one case, the use of the π-acids bipyridine or phenanthroline as the ancillary ligands on cobalt led to isolable products containing three-membered Co–C–N rings.[5] The compound resulting from the decarboxylation of the glycinato ligand in $[Co(gly)(bipy)_2]^{2+}$ was characterised by crystallography. Although the hydrogen atoms in the cobalt aminoalkyl moiety were not located and the structural and spectroscopic data were not fully reconciled, this structure did serve to demonstrate the formation of a three-membered ring by a decarboxylation reaction.

We have investigated kinetic stabilisation of the Co–C–N three-membered ring. As part of our interest in reactions of ligands coordinated to cobalt(III) we have prepared complexes of macrocyclic and acyclic hexadentate ligands bearing pendant coordinated α-amino acid groups.[6,7] They are ideal substrates for investigation of decarboxylation reactions, as the resulting aminoalkyl group would be appended to a macrocyclic ligand. One such candidate is $[Co(1,4\text{-bcc})]ClO_4$ (1,4-bcc = 1,4-bis-(carboxymethyl)cyclam) which contains a cyclam-based tetra-azamacrocycle bearing two *N*-carboxymethyl substituents.[7] An aqueous solution containing $[Co(1,4\text{-bcc})]ClO_4$ was irradiated for 120 minutes at 0 °C, resulting in a colour change from pink to pale orange. The product was purified by ion exchange chromatography, isolated as the salt $[Co(L^1)]BPh_4$, and characterised by elemental analysis, cyclic voltammetry, UV-visible, ^1H and $^{13}C\{^1H\}$ NMR spectroscopy and an X-ray crystal structure determination.§ The complex contains a substituted cyclam macrocycle bearing one intact *N*-carboxymethyl arm, but loss of CO_2 from the other *N*-carboxymethyl group results in a three-membered ring containing a cobalt σ-alkyl group (Scheme 2).

The molecular structure of the $[Co(L^1)]^+$ cation is shown in Fig. 1. The four nitrogens of the cyclam ring remain coordinated in the equatorial plane and the axial sites are occupied by an oxygen of the one remaining *N*-carboxymethyl group and the newly formed σ-bonded CH_2 group. The presence of the strained three-membered Co–C–N ring results in very irregular geometry around the cobalt atom, as exemplified by the O(1)–Co–C(13) and N(1)–Co–C(13) angles. The C(13)–N(1) bond length is shorter than the other C–N bond lengths in this complex but is still within the range observed for a C–N single bond (1.47 Å).[8] Both hydrogen atoms on C(13) were located crystallographically. The C(1)–N(1)–C(10) and H(13A)–C(13)–H(13B) angles of 110.4(2)° and 108(3)°, respectively, indicate sp^3 hybridization at N(1) and C(13).

Relative to the precursor $[Co(1,4\text{-bcc})]^+$, the lengthening of the Co–O(1) bond,[4] the shift of the d–d bands in the UV-visible spectrum[9] and the more negative reduction potential observed by cyclic voltammetry[7] are all consistent with the presence of the strong-field σ-bonded alkyl ligand in $[Co(L^1)]^+$. The cation has C_1 symmetry and the $^{13}C\{^1H\}$ NMR spectrum exhibits a unique signal for each of the 13 carbon atoms.

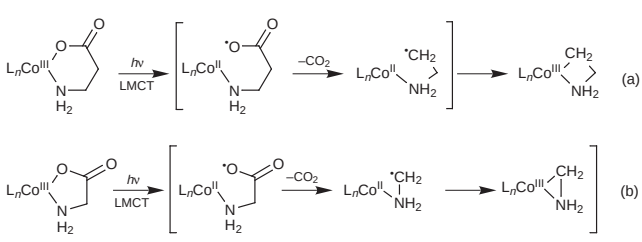

Scheme 1

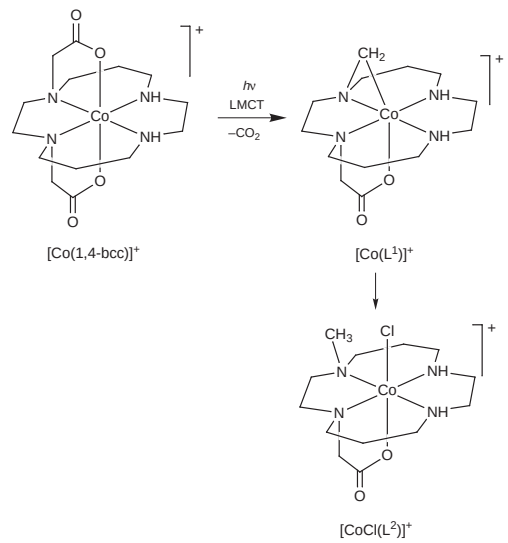

Scheme 2

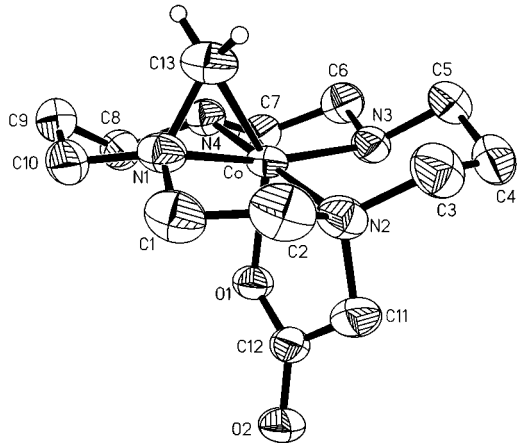

Fig. 1 Molecular structure of $[Co(L^1)]BPh_4$. Selected bond lengths (Å) and angles (°): Co–O(1) 1.993(2), Co–N(1) 1.920(2), Co–N(2) 1.993(2), Co–N(3) 1.987(2), Co–N(4) 1.961(2), Co–C(13) 1.980(3), C(13)–N(1) 1.447(4), C(13)–H(13A) 0.93(4), C(13)–H(13B) 0.96(4), O(1)–Co–C(13) 143.90(12), N(1)–Co–C(13) 43.52(12), Co–N(1)–C(13) 70.44(17), Co–C(13)–N(1) 66.06(15), O(1)–Co–N(1) 100.54(9).

Only two other structurally characterised examples of a Co–CH_2–NR_2 ring have been reported, both incorporated into a polydentate ligand, although they were prepared by quite different routes to that reported here.[10,11] In one of these examples, the ring was formed by C–H activation of an N–CH_3 group incorporated in a tetraaza macrocycle.[11] We observe the complementary reaction to this, wherein $[Co(L^1)]BPh_4$ undergoes Co–CH_2 bond cleavage upon heating in aqueous dilute HCl. The product, $[CoCl(L^2)]^+$, was characterised by an X-ray crystal structure determination§ and contains a chloro ligand *trans* to the N-carboxymethyl pendant arm and an N–CH_3 group derived from the CH_2 group (Scheme 2).

$[Co(L^1)]^+$ arises from the decarboxylation of a coordinated α-amino acid. Its successful isolation is attributed to the fact that the nitrogen atoms of the α-amino acid moieties in the $[Co(1,4\text{-bcc})]^+$ precursor are attached to a macrocyclic ligand, resulting in kinetic stabilisation of the aminoalkyl three-membered ring. This complements the earlier report concerning the photochemical decarboxylation of $[Co(gly)(bipy)_2]^{2+}$ in which stabilisation of the Co–C–N three-membered ring in the product has been attributed to the presence of the π-acid bipyridine ligands.[2] Our result is general and we have isolated further examples of Co–C–N three-membered rings resulting from photochemical decarboxylation of cobalt(III) complexes containing coordinated α-amino acid groups incorporated into other macrocyclic ligands.

D. M. T. is grateful to The University of Auckland for the award of a doctoral scholarship.

Notes and references

† This paper is dedicated to our colleague and friend Professor Warren Roper on the occasion of his 60th birthday.

‡ See http://www.rsc.org/suppdata/cc/1998/2593/, for experimental data for the complexes reported in this communication.

§ *Crystal data:* $[Co(L^1)]BPh_4 \cdot p$-xylene: Crystals were grown from acetonitrile–*p*-xylene. $C_{49}H_{59}BCoN_4O_2$, M = 805.74, monoclinic, space group $P2_1/n$, a = 14.8555(5), b = 17.4488(6), c = 17.2455(6) Å, β = 110.2770(10)°, U = 4193.2(2) Å^3, $F(000)$ = 1716, D_c = 1.276 g cm^{-3}, Z = 4, μ(Mo-Kα, λ = 0.71073 Å) = 0.454 mm^{-1}. Intensity data were collected to a θ limit of 26° on a Siemens 'SMART' diffractometer[12] at 203(2) K and corrected for absorption.[13] The structure was solved from Patterson and heavy-atom electron density maps[14] and refined by full-matrix least-squares analysis on F^2 employing SHELXL93.[15] All non-hydrogen atoms were allowed to assume anisotropic motion. The two hydrogen atoms on C(13) were located and individually refined. Other hydrogens were placed in calculated positions and refined using a riding model. Refinement converged to 0.0504 (R_w = 0.1356) for 6384 reflections for which $I > 2\sigma(I)$.

$[CoCl(L^2)]ClO_4$ (see http://www.rsc.org/suppdata/cc/1998/2593/, for molecular structure (Figure S1)): Crystals were grown from aqueous solution. $C_{13}H_{27}Cl_2CoN_4O_6$, M = 465.22, triclinic, space group $P\bar{1}$, a = 8.456(2), b = 9.689(3), c = 12.161(6) Å, α = 90.95(3), β = 109.51(3), γ = 96.09°, U = 932.4(6) Å^3, $F(000)$ = 480, D_c = 1.650 g cm^{-3}, Z = 2, μ(Mo-Kα, λ = 0.71069) = 1.245 mm^{-1}. Intensity data were collected to a θ limit of 25° on an Enraf-Nonius CAD-4 diffractometer[16] at 292(2) K and corrected for absorption.[17] Structure solution as above. The riding model was used for all hydrogens. Refinement converged to 0.0571 (R_w = 0.1546) for 2561 reflections for which $I > 2\sigma(I)$. CCDC 182/1072. See http://www.rsc.org/suppdata/cc/1998/2593/, for crystallographic files in .cif format.

1 J. M. Harrowfield, A. M. Sargeson and P. O. Whimp, *Inorg. Chem.*, 1991, **30**, 1792.
2 A. L. Poznyak and V. I. Pavlovski, *Angew. Chem., Int. Ed. Engl.*, 1988, **27**, 773.
3 E. Natarajan and P. Natarajan, *Inorg. Chem.*, 1992, **31**, 1215.
4 H. Kawaguchi, M. Yoshida, T. Yonemura, T. Ama, K. Okamoto and T. Yasui, *Bull. Chem. Soc. Jpn.*, 1995, **68**, 874; A. L. Poznyak, V. I. Pawlowski, L. M. Schkolnikowa, N. M. Djatlowa and A. B. Iljuchin, *J. Organomet. Chem.*, 1986, **314**, C59; A. V. Gasparyan, L. M. Shkol'nikova, V. K. Bel'skii, A. L. Poznyak, V. E. Stel'mashok and N. M. Dyatlova, *Koord. Khim.*, 1987, **13**, 1710; L. M. Shkol'nikova, A. V. Gasparyan, V. K. Bel'skii, V. E. Stel'mashok, A. L. Poznyak and N. M. Dyatlova, *Koord. Khim.*, 1987, **13**, 823.
5 A. L. Poznyak, V. I. Pavlovski, E. B. Chuklanova, T. N. Polynova and M. A. Porai-Koshits, *Monatsh. Chem.*, 1982, **113**, 561; E. B. Chuklanova, T. N. Polynova, M. A. Porai-Koshits, A. L. Poznyak and V. I. Pavlovskii, *Koord. Khim.*, 1988, **14**, 103.
6 P. J. Brothers, G. R. Clark, H. R. Palmer and D. C. Ware, *Inorg. Chem.*, 1997, **37**, 5470.
7 D. C. Ware, D. M. Tonei, L-J. Baker, P. J. Brothers and G. R. Clark, *Chem. Commun.*, 1996, 1303.
8 J. A. Huheey, E. A. Keiter and R. L. Keiter, *Inorganic Chemistry*, Harper Collins, New York, 2nd edn., 1993, p. A-30.
9 M. P. Granchi and B. E. Douglas, *Inorg. Nucl. Chem. Lett.*, 1978, **14**, 23.
10 S. M. Polson, L. Hansen and L. G. Marzilli, *J. Am. Chem. Soc.*, 1996, **118**, 4804.
11 C.-K. Poon, W.-K. Wan and S. S. T. Liao, *J. Chem. Soc., Dalton Trans.*, 1977, 1247.
12 SMART & SAINT, Siemens Analytical Instruments Inc., Madison, Wisconsin, USA, 1994.
13 R. H. Blessing, *Acta Crystallogr., Sect. A*, 1995, **51**, 33.
14 G. M. Sheldrick, SHELXS-97, Program for the Solution of Crystal Structures, Universität Göttingen, Germany, 1990; SHELXTL, Siemens Analytical Instruments Inc., Madison, Wisconsin, USA, 1994.
15 G. M. Sheldrick, SHELXL-93, Program for the Refinement of Crystal Structures, Universität Göttingen, Germany, 1997.
16 Enraf-Nonius, CAD-4 Software, Delft, The Netherlands, 1989.
17 A. C. T. North, D. C. Phillips and F. S. Matthews, *Acta Crystallogr., Sect. A*, 1968, **24**, 351.

Communication 8/07365A

Microwave activation of electrochemical processes at microelectrodes

Richard G. Compton, Barry A. Coles and Frank Marken*

Physical and Theoretical Chemistry Laboratory, Oxford University, UK OX1 3QZ.
E-mail: Frank@physchem.ox.ac.uk

Received (in Exeter, UK) 17th August 1998, Accepted 26th October 1998

Electrochemical experiments at platinum microdisc electrodes are shown to be possible in an environment of intense microwave radiation and a considerable current enhancement observed for the ferrocyanide/ferricyanide redox couple in aqueous 1 M KCl is shown to be Faradaic in nature consistent with a rapid heating effect causing the temperature in the liquid phase at the electrode/solution interface to locally superheat.

By combining the use of a source of activation with the range of known electrochemical methodology new types of experiments and in some cases novel applications of electrochemistry, *e.g.* in photoelectrochemistry and in sonoelectrochemistry, have been developed. The interaction of microwave radiation with electrochemical systems, that is with redox and chemical processes at solid/liquid and liquid/liquid interfaces, is to date unexplored, although the interest in microwave enhanced chemistry[1] and the use of microwave radiation and microwave technology have become widespread over the recent decades. The use of *low* power microwave radiation in electrochemical systems is of considerable importance in areas of research such as *in-situ* electrochemical EPR[2] (typically X-band, 9.5 GHz) and microwave reflectance characterisation[3] of semi-conducting electrodes. The activation of the electrochemical system due to absorption of microwave radiation can in these cases usually be ignored due to the rather low intensities involved. However, microwave radiation is known to interact not only with molecules in the gas phase but also with condensed materials and interfaces with sufficient dielectric loss, ε'',[4] and may therefore be employed to activate an electrochemical system.

An 800 W, 2.45 GHz domestic multi-mode microwave oven has been modified† to supply constant power or pulsed microwave radiation of variable power and to allow an electrochemical cell to be inserted into a high intensity region. In Fig. 1 a schematic drawing of the experimental arrangement is shown. In Fig. 2(a)–(c) voltammograms for the one electron oxidation of 2 mM $Fe(CN)_6^{4-}$ at a 25 μm diameter Pt disc electrode in aqueous 1 M KCl are shown. The observed limiting current, I_{lim} = 6.4 nA, is slightly higher than that expected for the known diffusion coefficient, $D(Fe(CN)_6^{4-}) = 0.63 \times 10^{-9}$ $m^2\ s^{-1}$,[5] presumably due to micro-electrode imperfection. The expression for quasi-steady-state voltammetry at a microdisc

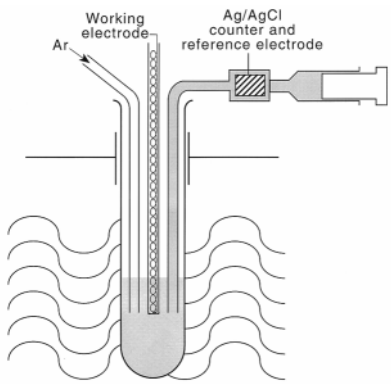

Fig. 1 Schematic representation of the electrochemical cell used for experiments in the presence of microwave radiation.

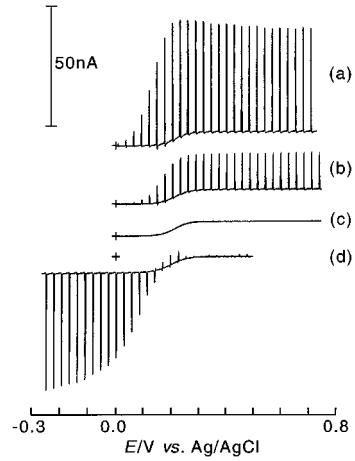

Fig. 2 Voltammograms obtained for (a)–(c) the oxidation of 2 mM $Fe(CN)_6^{4-}$ and (d) the reduction of 2 mM $Fe(CN)_6^{3-}$ in aqueous 1 M KCl at a 25 μm diameter Pt disc electrode and with a scan rate of 10 mV s^{-1}; 0.6 s microwave pulses with (a) and (d) 24 W and (b) 16 W microwave intensity.

electrode[6] has been shown to be $I_{lim} = 4nFDcr$. In this expression n denotes the number of electrons transferred per molecule, F, the Faraday constant, c, the concentration, and r, the radius of the electrode. Pulsed microwave radiation can be seen to induce current pulses which are superimposed on the quasi-steady-state current response.

In Fig. 2(a) the effect of 24 W (absorbed microwave power, see Table 1) microwave pulses of 0.6 s duration is shown. Current pulses are observed at potentials well negative of those of the current response in the absence of microwave radiation. The equilibrium potential for the $Fe(CN)_6^{4-/3-}$ redox couple is known to be affected by the temperature and data for the equilibrium potential–temperature dependence determined in the same cell over a 70 °C range and with the temperature of the reference electrode kept constant at 25 °C suggest a linear dependence with $dE/dT = -1.53$ mV K^{-1} consistent with published data.[7] Therefore at higher temperature the current response for the oxidation of $Fe(CN)_6^{4-}$ is expected to occur at a more negative potential in qualitative agreement with the

Table 1 The rate of microwave heating of 5 cm^3 water or aqueous solution in the electrochemical cell placed in a high intensity area of the modified microwave oven

	Pure water		1 M aqueous KCl	
Microwave power level	Rate of heating/ K s^{-1}	Absorbed energy[a]/W	Rate of heating/ K s^{-1}	Absorbed energy[a]/W
A	0.15	4	0.26	7
B	0.40	10	1.0	24
C	0.77	18	1.7	41
D	1.1	28	3.4	83
E	1.8	43	4.7	113

[a] Calculation based on a calibration procedure in which joule heating with a resistor is used to induce a temperature change.

Table 2 The temperature measured potentiometrically after *ca.* 0.2 s in a solution of 5 mM $Fe(CN)_6^{4-}$, 5 mM $Fe(CN)_6^{3-}$, and 1 M KCl at a 25 μm diameter Pt disc electrode when a 0.6 s pulse of microwave radiation is applied

Microwave pulse intensity/W	7	16	24	33
Temperature/°C	60 ± 6	87 ± 9	120 ± 12	150 ± 15

experimental observation [Fig. 2(a)]. From the current trace in Fig. 2(a) it can be concluded that the temperature of the bulk solution is not significantly affected by the pulsed microwave radiation. The current immediately returns to the expected value, I_{lim}, after each microwave pulse. The rate of heating observed independently in an experiment monitoring the bulk solution temperature was 1 K s^{-1} for the 24 W microwave intensity setting (see Table 1). Therefore it appears to be possible that the intensity of the microwave radiation is considerably higher at the electrode/solution interface compared to the average intensity experienced by the solution phase. A lower microwave intensity of 16 W induces a smaller current response as shown in Fig. 2(b). More importantly, microwave pulses of 24 W intensity applied to the reduction process of 2 mM $Fe(CN)_6^{3-}$ in 1 M KCl at a 25 μm diameter Pt disc electrode [Fig. 2(d)] also induce current jumps superimposed on the quasi-steady-state voltammetric response with complementary features. The cathodic current increases by a similar factor compared to the increase of the anodic current [Fig. 2(a)] and the shift of the half wave potential towards more negative potentials upon irradiation with microwaves is apparent. From this observation and from the linear dependence of both the quasi-steady-state current and the microwave enhanced current on the concentration of the redox reagent it can be concluded that the observed current for the $Fe(CN)_6^{4-/3-}$ redox couple in 1 M KCl in the presence of microwave radiation is purely *Faradaic*.

In order to achieve a more quantitative description of the heat pulse induced by microwave radiation at the electrode/solution interface the temperature can be estimated potentiometrically based on the equilibrium potential for a solution of 5 mM $Fe(CN)_6^{4-}$, 5 mM $Fe(CN)_6^{3-}$, and 1 M KCl under zero current condition. This measurement allows the temperature at the electrode/solution interface to be measured simultaneously with applying microwave pulses and data for the observed trend are given in Table 2. These data are valid only for the 25 μm diameter Pt disc electrode and cell geometry used in this set of experiments. However, the data suggest an approximately linear dependence of the microwave intensity absorbed by the bulk solution and the heating induced by the microwave radiation focused by the micro-electrode. Further, for short periods of time superheating of the solution phase can be observed.

The diameter of the working electrode also is a crucial factor in determining the magnitude of the heating effect. In experiments with a 50 μm diameter Pt disc electrode higher microwave intensities were required in order to give similar temperature jumps compared to those observed at the 25 μm diameter Pt disc electrodes. In experiments conducted with a 1 mm diameter Pt disc electrode the heating effect remained negligible even at the highest microwave intensity settings. In general, the temperature measured at the electrode strongly depends on (i) the microwave intensity, (ii) the cell geometry and positioning of the electrode, (iii) the type of solvent and solute used and produced during the course of the electrode reaction. The use of organic solvent systems is possible and the parameter characterising the microwave absorption has been shown to be the dielectric loss.[4]

The 0.6 s pulse which has been employed in the experiments shown in Fig. 2 is sufficient for thermal equilibrium to be achieved, at least locally at the electrode surface. With the knowledge of the approximate temperature at the electrode/solution interface it is possible to calculate the mass transport limited current based on the temperature dependence of the diffusion coefficient of $Fe(CN)_6^{4-}$. The limiting current observed for the oxidation of 2 mM $Fe(CN)_6^{4-}$ in 1 M KCl shows an Arrhenius type increase consistent with an activation energy of 14.3 kJ mol^{-1} and in agreement with Walden's rule[8] and literature data.[5] The expected mass transport controlled limiting current for the oxidation of 2 mM $Fe(CN)_6^{4-}$ at 120 °C can be calculated to I_{lim} = 26 nA. In the corresponding voltammogram [Fig. 2(a)] the observed limiting current is 50 nA and therefore higher. For a temperature of 90 °C the limiting current for the oxidation of 2 mM $Fe(CN)_6^{4-}$ is expected to be 18 nA which is slightly lower than the experimentally observed current in the presence of microwave radiation of 20 nA [Fig. 2(b)]. Therefore under conditions employed in Fig. 2 the temperature jump induces a current response with transient characteristics especially for very large temperature jumps. Further indications for the non-steady-state behaviour are the microwave induced *anodic* current in Fig. 2(d) at 0.22 V *vs*. Ag/AgCl for the reduction of $Fe(CN)_6^{3-}$ and the maximum observed at 0.24 V *vs*. Ag/AgCl for the microwave induced current associated with the oxidation of $Fe(CN)_6^{4-}$ [Fig. 2(a)].

The time scale for a steady-state current to be achieved at a microdisc electrode within ε% has been shown[9] to be approximately $t_\varepsilon = 10^4 r^2/\pi^3 \varepsilon^2 D$. In this expression the time t_ε is related to the electrode radius, r, and the diffusion coefficient, D. For a microdisc electrode of 25 μm diameter the expected time scale for the transient current to settle within 5% of the steady-state current is in the order of 2 s. Therefore the time scale for current transient after a temperature jump is expected to be larger compared to the time scale needed for the temperature to settle.

It has been shown both that microwave activation is an interesting new tool for enhancing and controlling processes in electrochemical systems and that electrochemical detection may be employed for microwave induced chemical processes.

Notes and references

† The intensity distribution in a Panasonic NN-3456 multi-mode microwave oven with modified electric power supply and fitted with a water load was mapped. A hole through the cavity wall extended by a 14.7 mm inner diameter brass tube, 50 mm long, which acted as a waveguide below cutoff, allowed a 1.41 cm diameter electrochemical cell to be inserted into a high intensity region (Fig. 1). A special working electrode design with a range of Pt disc electrodes of 25, 50, and 1000 μm diameter sealed into glass was used to prevent both radiation from escaping through the inlet and sparking. The lead-out from the micro-electrode was in the form of a helix made by winding 0.19 mm diameter platinum wire on a 0.46 mm diameter mandrel with 28 turns per cm. A test with a radiation meter (Apollo XI microwave monitor, Apollo Ltd.) confirmed this design to act as a filter and to stop microwave radiation from being conducted out of the cavity. In electrochemical experiments an Autolab PGSTAT 20 system (Eco Chemie, NL) was used for recording voltammetric and microwave intensity data. Reagents of analytical grade purity and demineralised water of conductivity not less than 18 MΩ cm were used. If not stated otherwise experiments were conducted under an inert atmosphere of argon and at a temperature of 25 ± 2 °C.

1 *Microwave-Enhanced Chemistry*, ed. H. M. Kingston and S. J. Haswell, The American Chemical Society, Washington, 1997.
2 R. G. Compton and A. M. Waller, in *Spectroelectrochemistry: Theory and Practice*, ed. R. J. Gale, Plenum Press, New York, 1988, p. 349.
3 See for example G. Schlichthörl, E. A. Ponomarev and L. M. Peter, *J. Electrochem. Soc*., 1995, **142**, 3062.
4 See for example C. Gabriel, S. Gabriel, E. H. Grant, B. S. J. Halstead and D. M. P. Mingos, *Chem. Soc. Rev*., 1998, **27**, 213.
5 R. V. Bucur, A. Bartes and V. Mecea, *Electrochim. Acta*, 1978, **23**, 641.
6 K. B. Oldham and J. C. Myland, *Fundamentals of Electrochemical Science*, Academic Press, New York, 1994.
7 See for example T. Zerihun and P. Gründler, *J. Electroanal. Chem*., 1996, **404**, 243.
8 P. W. Atkins, *Physical Chemistry*, 5th edition, Oxford University Press, Oxford, 1994.
9 C. G. Zoski, *J. Electroanal. Chem*., 1990, **296**, 317.

Communication 8/06511J

ChemComm

Dramatic increase of the DNA cleavage activity of Cu(Clip-phen) by fixing the bridging linker on the C^3 position of the phenanthroline units

Marguerite Pitié, Brigitte Sudres and Bernard Meunier*

Laboratoire de Chimie de Coordination du CNRS, 205 route de Narbonne, 31077 Toulouse cedex 4, France. E-mail: bmeunier@lcc.toulouse.fr

Received (in Cambridge, UK) 7th October 1998, Accepted 28th October 1998

The synthesis of a new ligand with two phenanthrolines bridged on their C^3 carbon by a serinol is reported; Cu(3-Clip-phen) cleaves DNA more efficiently than the parent Cu(2-Clip-phen) bridged on the C^2 carbon.

The redox activity of cuprous complexes of 1,10-phenanthroline (phen) is well known as artificial nuclease. They are able to realise single-strand cleavages of DNA in the presence of H_2O_2 by oxidative attack on deoxyribose units from the minor groove of DNA.[1,2] $Cu^I(phen)_2$ is significantly more reactive[3] than $Cu^I(phen)$ but the association constant for the second phenanthroline ligand is only $10^{5.5}$ dm^3 mol^{-1} which is too low for a biological use at submicromolar concentrations of these complexes.[4] For this reason, we have recently prepared Clip-phen (renamed 2-Clip-phen in the present study, Scheme 1) with two phenanthroline entities linked *via* their C^2 carbon by a short flexible arm in order to favor the 2 : 1 phen–Cu stoichiometry.[5] In the presence of a reductant and air, we observed an increase of DNA cleavage activity on ΦX174 by a factor two for Cu(2-Clip-phen) compared to $Cu(phen)_2$. In addition, the serinol bridge between the two phenanthrolines of 2-Clip-phen allowed further functionalisation on its primary amino group with different possible vectors (polyamines, intercalators, oligonucleotides) in order to increase or to modulate the binding domain of these DNA cleavers. So, the attachment of the natural polyamine spermine (a minor groove binder) to 2-Clip-phen afforded a new conjugate with enhanced nuclease efficiency.[6]

The bridging serinol was fixed on the C^2 carbon of phen units in 2-Clip-phen, near the chelating nitrogen atoms, in order to decrease the length between the two phen entities. But, having in mind that this substitution on C^2 carbon has been observed to disactivate the DNA cleavage activity of Cu–phen complexes,[1,7] we decided to prepare a new bis-chelating ligand, 3-Clip-phen, with the serinol bridge between the C^3 carbons of phen units. The 3-position is known to have fewer effects on redox activity[4] and may also allow the use of a small bridge like serinol between the two phen units in order to favor a mononuclear Clip-phen complex $[Cu^{II}(Clip\text{-}phen)]^{2+}$. However the C^3 monosubstitution of the phen ligand, which limits steric constraints for DNA interactions and for conformational changes during the reduction of Cu^{II} to Cu^I, has been little studied although a conjugate of acridine on the C^3 carbon of phen has been described to cleave DNA.[8]

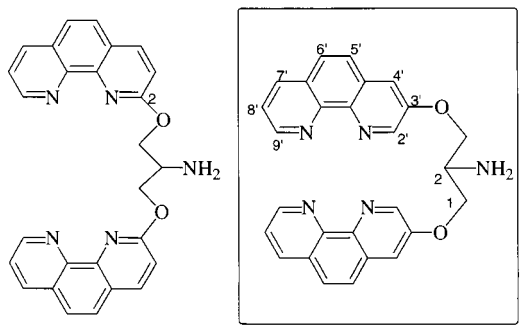

Scheme 1 Structures of 2-Clip-phen and 3-Clip-phen. Numbering corresponds to NMR assignments.

The synthetic strategy used to prepare 3-Clip-phen was based on the synthesis of the 2-Clip-phen parent compound. Two equivalents of halogenated phenanthroline (600 mg, 2.3 mmol of 3-bromophenanthroline prepared according to ref. 9) and one equivalent of serinol (109 mg, 1.18 mmol) were stirred for 24 h in dry DMF (14 mL) in presence of 9 equivalents of NaH (423 mg, 10.5 mmol of a 60% dispersion in mineral oil). At 0 °C, 2-Clip-phen was obtained in good yield, but 3-Br-phen gave only 4% of 3-Clip-phen under the same conditions. The low reactivity of 3-Br-phen for nucleophilic aromatic substitution required warming of the reaction mixture.[10] Unfortunately the quantitative reduction of 3-Br-phen by NaH at 80 °C forced us to choose intermediate heating conditions at 50 °C. Under these conditions 3-Clip-phen was only obtained in 27% yield after purification [addition of ethanol and water in the reaction mixture in order to destroy the excess of NaH, then extraction with chloroform, precipitation with hexane to remove unreacted 3-Br-phen and phen and a neutral alumina column ($CHCl_3$ with 0–5% of methanol)].†

3-Clip-phen was metallated with one equivalent of $CuCl_2$ and its DNA cleavage activity was compared to that of $[Cu(2\text{-}Clip\text{-}phen)]Cl_2$. Relaxation of supercoiled ΦX174 DNA (form I) into relaxed circular (form II) and linear (form III) conformations was used to quantify the relative cleavage efficiency of these copper complexes. The nuclease activity of these Cu(II) complexes (1 μM) was initiated by addition of 5 mM mercaptopropionic acid (MPA) in the presence of air. Fig. 1 summarises the results obtained.‡

As expected, no degradation of DNA was observed in the absence of reductant. The comparison of lanes 4 and 5 shows that Cu(3-Clip-phen) complex exhibited a significantly higher activity than Cu(2-Clip-phen) since all form I disappeared, to give forms II and III (50% of the starting material) and a smear (corresponding to multifragmented DNA), whereas form I was

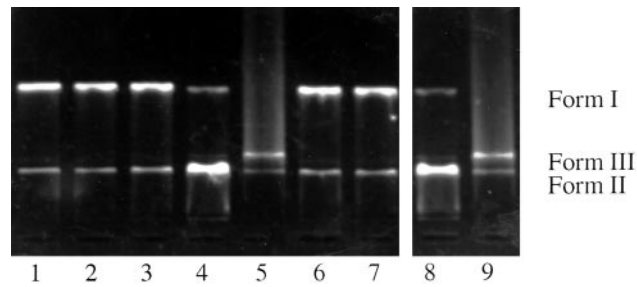

Fig. 1 Comparison of ΦX174 cleavage efficiency between 2-Clip-phen and 3-Clip-phen in the presence of $CuCl_2$ and 5 mM MPA. Lane 1: control DNA. Lane 2: 1 μM 2-Clip-phen and $CuCl_2$ without MPA. Lane 3: 1 μM 3-Clip-phen and $CuCl_2$ without MPA. Lane 4: 1 μM 2-Clip-phen and $CuCl_2$. Lane 5: 1 μM 3-Clip-phen and $CuCl_2$. Lane 6: control DNA with 5 mM MPA. Lane 7: control DNA with 1 μM $CuCl_2$ and 5 mM MPA. Lane 8: 1 μM 2-Clip-phen and 2 μM $CuCl_2$. Lane 9: 1 μM 3-Clip-phen and 2 μM $CuCl_2$.

still present for the same concentration of Cu(2-Clip-phen) under identical conditions. Assuming a non-specific single-strand cleavage of the DNA double-helix, as previously observed for Cu(2-Clip-phen),[6] the number of single-strand breaks per ΦX174 DNA molecule was calculated according to ref. 11. Cu(3-Clip-phen) gave 32 ± 4 single strand breaks per ΦX174 DNA compared with 1.4 ± 0.2 for Cu(2-Clip-phen). The comparison of lanes 5 and 9 shows also that Cu(3-Clip-phen) gave the same number of single strand breaks when metallated by 1 equivalent of copper salt [1 Cu for 2 phen entities, corresponding to a Cu(3-Clip-phen) complex] or 2 equivalents of copper salt [1 Cu per phen entity, corresponding to a putative Cu_2(3-Clip-phen) compound] as expected for a ligand able to chelate the same copper ion with its two phen subunits.

In order to understand this high DNA cleavage activity of Cu(3-Clip-phen), work on interactions of the complex with DNA are in progress. New conjugates of 3-Clip-phen with DNA binders are also in preparation in order to increase the nuclease activity of this promising new family of DNA cleavers.

Dr Jean-Pierre Sauvage (Université Louis Pasteur, Strasbourg) is gratefully acknowledged by the authors for fruitful discussions on phenanthroline reactivity which initiated the preparation of 3-Clip-phen.

Notes and references

† 3-Clip-phen has been characterised by ^{1}H NMR (250 MHz, $CDCl_3$) δ 9.14 (dd, 2H, *J* 4.3, 1.7 Hz, H9′), 8.96 (d, 2H, *J* 2.9 Hz, H2′), 8.20 (dd, 2H, *J* 8.1 and 1.7 Hz, H8′), 7.78 and 7.72 (AX, 2H, *J* 8.9 Hz, H5′, H6′), 7.60 (d, 2H, *J* 2.9 Hz, H4′), 7.56 (dd, 2H, *J* 8.1, 4.3 Hz, H7′), 4.36 (m, 4H, H1), 3.82 (q, 1H, *J* 5.4 Hz, H2); MS (CDI, NH_3): *m*/*z* (%) = 448 (M + H, 100), 268 (14.0), 252 (22.7), 197 (75.9); UV–VIS (MeOH) λ_{max}/nm (ε/dm^3 mol^{-1} cm^{-1}): 240 (59 500), 272 (44 100), 294 (23 900, sh), 314 (8200, sh), 328 (5700), 344 (3800). Anal. Calc. for $C_{27}H_{21}N_5O_2 \cdot 4\ H_2O$: C, 62.42; H, 5.63; N, 13.48. Found: C, 62.38; H, 5.09; N, 13.66%.

‡ Complexes were prepared as 1 mM solutions in DMF–water (2 : 3) then diluted to 4 μM with water prior to the addition of 5–10 μL of a solution of supercoiled ΦX174 DNA (7 nM, 40 μM in bp) in 80 mM sodium phosphate buffer (pH 7.2), 100 mM NaCl and 20 mM $MgCl_2$. After 30 min at room temperature, DNA cleavage was initiated by addition of 5 μL of a 20 mM aquous solution of mercaptopropionic acid and incubated at 37 °C for 1 h prior to being loaded on a 0.8% agarose gel containing 1 μg mL^{-1} of ethidium bromide. Bands were located by UV light, photographed and quantified by microdensity. The correction coefficient 1.47 was used for the decrease in stainability of form I DNA *versus* forms II and III.[12]

1 D. S. Sigman, A. Mazumder and D. M. Perrin, *Chem. Rev.*, 1993, **93**, 2295.
2 G. Pratviel, J. Bernadou and B. Meunier, *Adv. Inorg. Chem.*, 1998, **45**, 251.
3 J. M. Veal, K. Merchant and R. L. Rill, *Nucleic Acids Res.*, 1991, **19**, 3383.
4 B. R. James and R. J. P. Williams, *J. Chem. Soc.*, 1961, 2007.
5 M. Pitié and B. Meunier, *Inorg. Chem.*, 1998, **37**, 3486.
6 M. Pitié and B. Meunier, *Bioconjugate Chem.*, 1998, **9**, 604.
7 J. Gallagher, C. B. Chen, C. Q. Pan, D. M. Perrin, Y. Cho and D. S. Sigman, *Bioconjugate Chem.*, 1996, **7**, 413; T. B. Thederan, M. D. Kuwabara, T. A. Larsen and D. S. Sigman, *J. Am. Chem. Soc.*, 1989, **111**, 4941.
8 F. C. K. Chiu, R. T. C. Brownlee, K. Mitchell and D. R. Phillips, *Bioorg. Med. Chem. Lett.*, 1994, **4**, 2721.
9 D. Tzalis, Y. Tor, S. Failla and J. S. Siegel, *Tetrahedron Lett.*, 1995, **36**, 3489.
10 D. Tzalis and Y. Tor, *Angew. Chem., Int. Ed. Engl.*, 1997, **36**, 2666 and references therein.
11 R. P. Hertzberg and P. B. Dervan, *Biochemistry*, 1984, **23**, 3934.
12 J. Bernadou, G. Pratviel, F. Bennis, M. Girardet and B. Meunier, *Biochemistry*, 1989, **28**, 7268.

Communication 8/07807F

Supramolecular cation of an acyclic polyether: potassium(pentaethylene glycol) in a molecular conducting nickel dithiolate salt

Tomoyuki Akutagawa,*[a,b] Yu-ichiro Nezu,[b] Tatuso Hasegawa,[a,b] Ken-ichi Sugiura,[c] Takayoshi Nakamura,*[a,b] Tamotsu Inabe,[d] Yoshiteru Sakata[c] and Allan E. Underhill[e]

[a] *Research Institute for Electronic Science, Hokkaido University, Sapporo 060-0812, Japan. E-mail takuta@imd.es.hokudai.ac.jp*
[b] *Graduate School of Environmental Earth Science, Hokkaido University, Sapporo 060-0810, Japan*
[c] *Institute of Scientific and Industrial Research, Osaka University, Osaka 567-0047, Japan*
[d] *Department of Chemistry, Faculty of Science, Hokkaido University, Sapporo 060-0810, Japan*
[e] *Department of Chemistry, University of Wales, Bangor, Gwynedd, UK LL57 3UW*

Received (in Cambridge, UK) 25th September 1998, Accepted 19th October 1998

The X-ray structural analysis of the title compound revealed the formation of segregated [Ni(dmit)$_2$] (dmit = 2-thioxo-1,3-dithiol-4,5-dithiolate) columns and dimeric K$^+_2$[PEG]$_2$ (PEG = pentaethylene glycol) supramolecular cations in the crystal; the interaction between K$^+$ and acyclic PEG was found to be weaker that that between K$^+$ and cyclic polyether 18-crown-6.

Composite organic polymer electrolytes are promising candidates for applications in high energy density electrochemical batteries.[1] Polyethylene oxide (PEO) derivatives especially have been extensively examined as non-crystalline polymeric ion-conducting materials. The crystal structure of a uniaxially oriented PEO–NaI ionic conductor has been reported previously.[2] The structure of a single crystal of PEO as an ion-transport environment has not been reported. The classification of the nature of the coordination in PEO–ion moieties will assist in the construction of organic crystalline ionic conductors.

Organic π-molecular systems have a tendency to form a one-dimensional columnar stack structure, in which electrons can move along the stack through overlap of the π-systems.[3] We have been attempting to construct electron–ion hybrid conducting systems based on crystalline molecular conductors, and have reported the formation of supramolecular cation (SC$^+$) structures within organic conductors.[4] For example, a typical cation complex of a cyclic polyether, K$^+$(18-crown-6), can be incorporated into a highly conducting [Ni(dmit)$_2$] (dmit = 2-thioxo-1,3-dithiol-4,5-dithiolate) salt as K$^+$(18-crown-6)[Ni(dmit)$_2$]$_3$ with a room temperature conductivity (σ_{RT}) of 0.08 S cm^{-1}.[5] We report here the incorporation of a cation complex of an acyclic polyether as a new SC$^+$ unit in a [Ni(dmit)$_2$] organic conductor, in which the potassium cation is included within the cyclic pentaethylene glycol (PEG) (Scheme 1).

Single crystals of K$^+$(PEG)[Ni(dmit)$_2$]$_3$ were prepared by the electrocrystallization method.† The unit cell contains three crystallographically independent [Ni(dmit)$_2$] units **A–C** and one K$^+$(PEG) unit. A segregated non-uniform [Ni(dmit)$_2$] column is observed with the stacking order of **A–C–B** along the *c*-axis; the molecular planes of [Ni(dmit)$_2$] are nearly parallel to the *ab*-plane (Fig. 1). Each [Ni(dmit)$_2$] molecule is connected by side-by-side S···S interactions, forming a layer structure within the *ac*-plane, and the K$^+$(PEG) units exist in the interlayer space. The plane of K$^+$(PEG) is inclined at 45° to the *b*-axis. A weak interatomic contact is found between the terminal sulfur of [Ni(dmit)$_2$] **C** and K$^+$(PEG), K$^+$···S(30) = 3.282(7) Å. This distance is *ca*. 0.15 Å longer than the sum of the van der Waals radius of S and the ionic radius of K$^+$.[6]

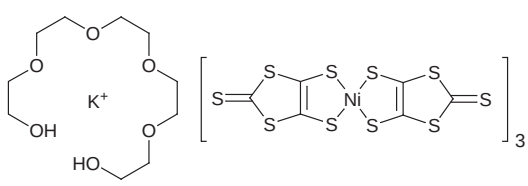

K$^+$(PEG)[Ni(dmit)$_2$]$_3$

Scheme 1

The mean interplanar distances of [Ni(dmit)$_2$] within a column are 3.50 (**A–B**), 3.65 (**A–C**), and 3.45 Å (**B–C**) with overlap modes of slipped metal–ring (**A–B**), metal–metal (**A–C**), and metal–ring (**B–C**) types, respectively [Fig. 1(b)]. A

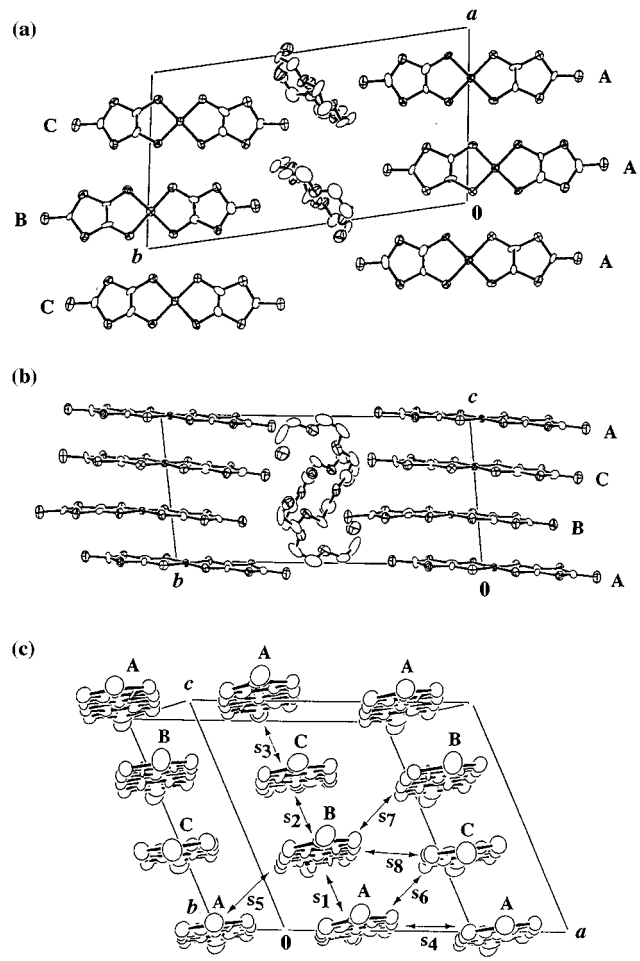

Fig. 1 Crystal structure of K$^+$(PEG)[Ni(dmit)$_2$]$_3$, (a) viewed along the *c*-axis, (b) along the *a*-axis. (c) [Ni(dmit)$_2$] layer viewed along the long axis of [Ni(dmit)$_2$] together with the numbering scheme of overlap integrals (s_1–s_8).

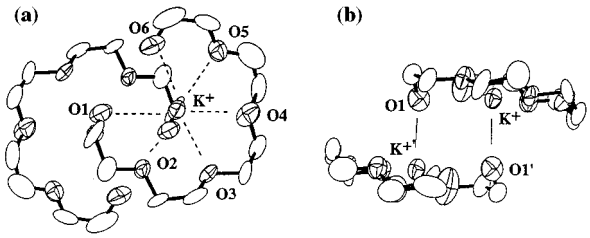

Fig. 2 Supramolecular cation (SC^+) unit of $K^+_2(PEG)_2$, (a) viewed along the perpendicular direction to the K^+(PEG) plane, (b) side view of K^+(PEG) dimer with the oxygen atom numbering scheme. Primes indicate atoms generated by passing through the inversion center. Dashed and solid lines indicate the $K^+\cdots O$ interactions.

similar trimer structure was also observed in K^+(18-crown-6)[Ni(dmit)$_2$]$_3$ with an **A–B–A** stacking arrangement. Fig. 1(c) shows the intermolecular interactions within the [Ni(dmit)$_2$] layer viewed along the long axis of [Ni(dmit)$_2$]. The overlap integrals (s_1–s_8 × 10^{-3}) were obtained by using extended Hückel molecular orbital calculatons.[7] Since the **A–B** interaction (s_1 = 19.07) is significantly larger than **A–C** (s_2 = −1.05) and **B–C** (s_3 = 2.47), the [Ni(dmit)$_2$] column mainly consists of **A–B** dimers and weakly interacting **C** molecules between the **A–B** dimers in the order –(**A–B**)–**C**–(**A–B**)–. In the case of K^+(18-crown-6)[Ni(dmit)$_2$]$_3$, the intratrimer *s* value (s_{intra} = 15.3) indicated the formation of tightly bounded **A–B–A** trimers within the column. By replacing the SC^+ unit of the cyclic [K^+(18-crown-6)] with the acyclic [K^+(PEG)], the stacking mode of [Ni(dmit)$_2$] within the column is changed from the trimer to the dimer.

Within the *ab*-plane, the [Ni(dmit)$_2$] molecules form a sheet-like structure of –**A–A–A–** and –**B–C–B–** arrangements along the *a*-axis [Fig. 1(a)]. Owing to the symmetry of the LUMO of [Ni(dmit)$_2$], the interstack interactions along the *a*-axis are small (s_4 = 0.10 and s_8 = 0.20), resulting in weak interactions within the sheets. The interactions along the $a + c$ direction (s_5 = 0.50, s_6 = 0.86, and s_7 = −0.33) also do not effectively increase the interstack interactions.

Fig. 2 shows the SC^+ unit viewed along the orthogonal [Fig. 2(a)] and parallel [Fig. 2(b)] directions to the molecular plane of K^+(PEG). The SC^+ unit has two K^+(PEG) units which are related by the inversion center, and are connected by two axial K^+ (K^+)$\cdots$O1′ (O1) interactions [solid lines in Fig. 2(b)] to form a dimerized $K^+_2(PEG)_2$ supramolecular cation. The K^+ is coordinated by six PEG oxygen atoms [dashed lines: $K^+\cdots$O1 = 3.00(1), $K^+\cdots$O2 = 2.90(1), $K^+\cdots$O3 = 2.81(1), $K^+\cdots$O4 = 2.86(1), $K^+\cdots$O5 = 2.90(1), $K^+\cdots$O6 = 2.77(2) Å] and an axial oxygen of another PEG unit [solid lines: $K^+\cdots$O1 = 2.86(2) Å]. The average $K^+\cdots$O distance within the PEG unit (2.87 Å) is in the same range as the sum of the van der Waals radius of oxygen and the ionic radius of K^+ (2.85 Å). In the case of K^+(18-crown-6), the average $K^+\cdots$O distance (2.804 Å) is*ca*. 0.07 Å shorter than that in the acyclic K^+(PEG) system, indicating a weaker cation binding ability of the acyclic polyether relative to the corresponding cyclic one due to the *macrocyclic effect*.[8] The weaker cation binding ability (10 000×) should be more appropriate to ionic conductivity in the solid.

The K^+(PEG)[Ni(dmit)$_2$]$_3$ salt showed semiconducting behavior over the temperature range 150–300 K, which is consistent with the non-uniform dimerized stack of [Ni(dmit)$_2$]. Fig. 3 shows the log(resistivity/Ω cm) *vs*. T^{-1}/K^{-1} plots of (i) K^+(PEG)[Ni(dmit)$_2$]$_3$ and (ii) K^+(18-crown-6)[Ni(dmit)$_2$]$_3$.[5] The room temperature conductivity (σ_{RT} = 0.001 S cm^{-1}) is two orders of magnitude lower that that of K^+(18-crown-6)[Ni(dmit)$_2$]$_3$ (σ_{RT} = 0.08 S cm^{-1}). The activation energy E_a (0.17 eV) of the acyclic system is intermediate in range between the high (0.28 eV) and low (0.12 eV) temperature semiconducting phases of K^+(18-crown-6)[Ni(dmit)$_2$]$_3$.

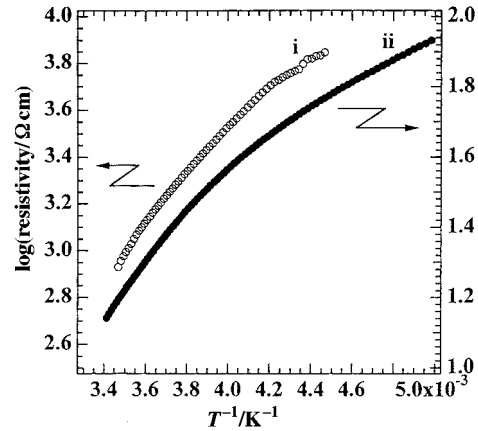

Fig. 3 Log(resistivity/Ω cm) *vs*. T^{-1}/K^{-1} plots of (i) K^+(PEG)[Ni(dmit)$_2$]$_3$ (○) and (ii) K^+(18-crown-6)[Ni(dmit)$_2$]$_3$ (●).

In conclusion, the supramolecular cation of acyclic K^+(PEG) has been incorporated into the electrically conducting [Ni(dmit)$_2$] salt. The coordination ability of PEG to K^+ is smaller that that of 18-crown-6 due to the loss of macrocyclic effect, which helps to construct the ion-conducting field within the crystalline solid. Attempts to insert shorter or longer polyethylene glycol chains into the conducting [Ni(dmit)$_2$] salts are now in progress to construct ion-conducting paths.

This work was partly supported by a Grant-in-Aid for Science Research from the Ministry of Education, Science, Sports, and Culture of Japan.

Notes and references

† The constant current (1.5 μA) electrocrystallization of (*n*-Bu$_4$N)[Ni(dmit)$_2$] (19.6 mg), $KClO_4$ (42.3 mg), and PEG (140 mg) in acetonitrile (18 ml) gave black-plate single crystals. The crystal data are as follows: $C_{28}H_{20}O_6S_{30}Ni_3K$, M = 1629.5, crystal dimensions 0.75 × 0.25 × 0.02 mm^3, Rigaku AFC-7R diffractometer, Mo-Kα radiation (λ = 0.71069 Å), triclinic, space group $P\bar{1}$ (no. 2), a = 12.700(5), b = 21.826(5), c = 11.166(7) Å, α = 91.40(3), β = 113.54(3), γ = 99.14(3)°, U = 2788(2) Å^3, T = 298 K, Z = 2, D_c = 1.941 g cm^{-3}, $F(000)$ = 1638.0, μ(Mo-Kα) 22.41 cm^{-1}, Lorentz polarization and absorption corrections applied, 13374 reflections measured, 12797 independent reflections, 4391 reflections with $I > 3.00\sigma(I)$ used in refinement. Calculations were performed using teXsan crystallographic software packages with refinements based on F. Weighting scheme employed: $w = 1/\sigma^2(F_o)$. Solution by direct methods: non-hydrogen atoms refined anisotropically, and no refinement of hydrogen atoms. $(\Delta\rho)_{max}$ = 1.22 e Å^{-3}, $(\Delta\rho)_{min}$ = −0.97 e Å^{-3}, R = 0.080, R' = 0.083. CCDC 182/1061.

1 (*a*) P. V. Wright, *Br. Polym. J*., 1975, **319**, 137; (*b*) M. A. Ratner and D. F. Shriver, *Chem. Soc. Rev*., 1988, **88**, 109.
2 Y. Chatani and S. Okamura, *Polymer*, 1987, **28**, 1815.
3 D. O. Cowan, *New Aspects of Organic Chemistry*, ed. Z. Yoshida, T. Shiba and Y. Oshiro, *Proc. 4th Int. Kyoto Conf.*, Kodansha Ltd, Tokyo, 1989.
4 (*a*) T. Akutagawa, T. Nakamura, A. E. Underhill and T. Inabe, *J. Mater. Chem*., 1997, **7**, 135; (*b*) T. Akutagawa, T. Nakamura, A. E. Underhill and T. Inabe, *Synth. Met*., 1997, **86**, 1961; (*c*) T. Nakamura, T. Akutagawa, K. Honda, A. E. Underhill, A. T. Coomber and R. H. Friend, *Nature*, 1998, **394**, 159.
5 T. Akutagawa, T. Nakamura, T. Inabe, K. Sugiura, Y. Sakata and A. E. Underhill, unpublished results.
6 A. Bondi, *J. Phys. Chem*., 1964, **68**, 441.
7 (*a*) T. Mori, A. Kobayashi, Y. Sasaki, H. Kobayashi, G. Saito and H. Inokuchi, *Bull. Chem. Soc. Jpn*., 1984, **57**, 627; (*b*) R. H. Summerville and R. J. Hoffmann, *J. Am. Chem. Soc*., 1976, **98**, 7240.
8 (*a*) D. K. Cabbiness and D. W. Margerum, *J. Am. Chem. Soc*., 1969, **91**, 6540; (*b*) R. D. Hancock and A. E. Martell, *Comments Inorg. Chem*., 1988, **6**, 237.

Communication 8/07474G

Visible light-induced desulfurization technique for light oil

Yasuhiro Shiraishi,[a] Yasuto Taki,[a] Takayuki Hirai*[a] and Isao Komasawa[ab]

[a] *Department of Chemical Science and Engineering, Graduate School of Engineering Science, Osaka University, Machikaneyama-cho 1-3, Toyonaka, Osaka 560-8531, Japan. E-mail: hirai@cheng.es.osaka-u.ac.jp*

[b] *Research Center for Photoenergetics of Organic Materials, Osaka University, Machikaneyama-cho 1-3, Toyonaka, Osaka 560-8531, Japan*

Received (in Cambridge, UK) 25th August 1998, Accepted 26th October 1998

A visible light-induced desulfurization process for light oil, effected by electron-transfer photooxygenation and liquid–liquid extraction, allows the deep desulfurization of light oil under moderate conditions and without hydrogen.

The desulfurization of light oil has become one of the urgent problems of the world.[1] In order to protect against environmental contamination, the sulfur level in diesel fuels is presently limited to 0.05 wt% in Japan and Europe, and this will certainly be tightened in the near future. The current technology of hydrodesulfurization (HDS), when adopted on an industrial scale, can desulfurize aliphatic and acyclic sulfur-containing compounds adequately. The above process, however, when treating dibenzothiophene and its derivatives (DBTs),[2–4] apparently fails to reach the new specifications imposed by recent Clean Air Regulations. Thus, to produce light oil containing a very low level sulfur requires inevitably rather severe conditions. For the development of an energy-saving desulfurization process, a new approach is needed which isn't limited to the conventional HDS method.

As reported by Berthou and Vignier,[5] DBTs in spilled crude oil are sunlight-photooxidized to DBT sulfoxide (DBT-O) and DBT sulfone (DBT-O_2) in sea water. These sulfur-oxygenated DBTs are highly polarized and are water-soluble. The application of this photochemical oxidation to desulfurization has been realized in our previous studies, using oil–water[6,7] and oil–polar solvent[8] two-phase systems, and in which the desulfurization of light oil to a sulfur content of less than 0.05 wt% has been achieved successfully. However, UV irradiation was found to be essential to oxidize DBTs and desulfurization hardly progressed at wavelength of $\lambda > 400$ nm.

Electron-transfer type photosensitizers, such as cyano-substituted anthracene, differ from the usual energy-transfer type photosensitizers, and act as the anode by absorbing the wavelength of light equivalent to their lowest excitation energy. The sulfur-containing compounds, having the free electron on the S atom, are thought to be readily one-electron oxidized by this type of photosensitizer. In this work, we consider such a photoprocess applied to the indirect photooxygenation of DBTs and thus to the desulfurization of DBTs in light oil.

A schematic electron-transfer process between 9,10-dicyanoanthracene (DCA) and DBT in MeCN is shown in Fig. 1. DCA has a relatively low reduction potential and can be excited at wavelengths greater than 400 nm. DCA exhibits a strong, blue fluorescence in both polar and non-polar solvents. This blue fluorescence is quenched by adding DBT with the rate constant of $k_{q,\,DBT} = 1.75 \times 10^{10}$ L mol^{-1} s^{-1}, and a yellow fluorescence is then exhibited. Exciplex emission is observed only in non-polar solvents, and not in MeCN and MeOH; this suggests that dissociation of the ion pairs occurs only in the most polar solvents.

An MeCN solution containing DBT and DCA was irradiated to visible light of wavelength $\lambda > 400$ nm (main emission peak: 406 nm), generated by a high-pressure mercury lamp with a 3 wt% $NaNO_2$ solution filter.[9] As shown in Fig. 2, only in MeCN were the corresponding sulfoxide (DBT-O) and sulfone (DBT-O_2) photogenerated at high yield, whereas no reaction was

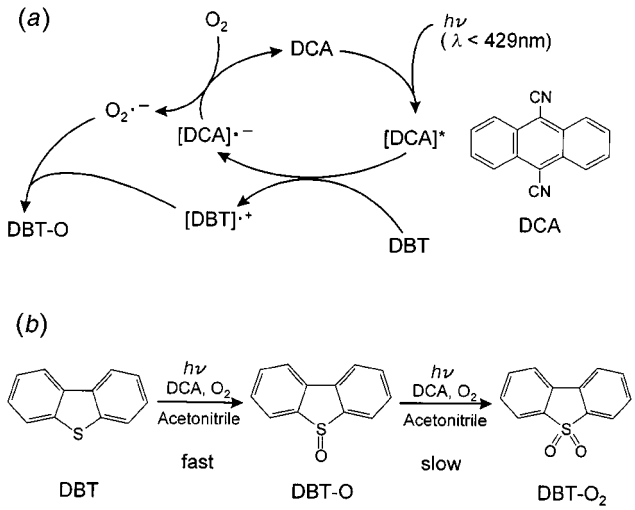

Fig. 1 (*a*) Electron-transfer process occurring in MeCN between DCA, DBT and oxygen. (*b*) Schematic representation of the reaction route of DBT by DCA sensitized photooxygenation.

observed in protic solvents such as MeOH and Pr^{i}OH or in non-polar solvents. This behavior is expected for a process proceeding *via* an intermediate ion pair, since such a pair will be too poorly solvated in non-polar solvents to be separated. Other photosensitizers such as *p*-benzoquinone or 1-cyanonaphthalene are not applicable to this process, since the oxidation potential of the former is lower than the reduction potential for O_2 and the latter is excited at wavelength shorter than 320 nm. These findings suggest that DCA is the most suitable photosensitizer for the photooxygenation of DBT, which seems to proceed *via* the three steps shown schematically in Fig. 1. These are (i) photoexcitation of DCA, (ii) one-electron oxidation of DBT and one-electron reduction of O_2 (generation of superoxide ion $O_2^{\cdot -}$) and (iii) combination of radical ion pairs (DBT$^{\cdot +}$

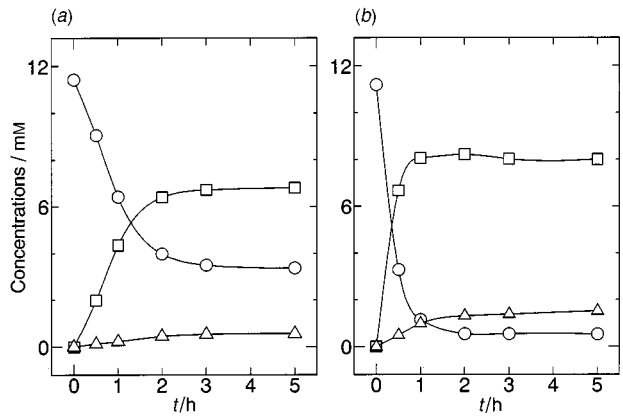

Fig. 2 Time-course variation for the concentrations of (○) DBT, (□) DBT-O and (△) DBT-O_2 by DCA photosensitized reaction in MeCN. The initial concentrations of DCA are (*a*) 0.02 and (*b*) 0.1 mM.

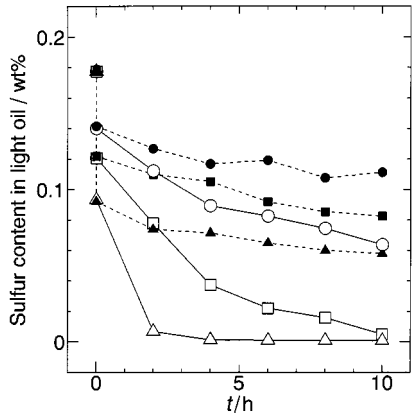

Fig. 3 Time-course variation of sulfur content in light oil for differing solution volume ratios: MeCN:light oil = (○,●) 1:1, (□,■) 3:1 and (△,▲) 7:1; filled symbols = without DCA, open symbols = with DCA.

and $O_2^{\cdot -}$). In alcoholic solvents, the oxygenation seems to be prevented, owing to the shorter lifetime for $O_2^{\cdot -}$. Bacciochi *et al.*[10] have suggested the C–S cleavage mechanism for the electron-transfer reaction of benzyl phenyl sulfide, but DBT gave only the S oxidation product, as mentioned in the case of diphenyl sulfide.[11] This is attributable to a stabilization of the C–S bond of DBT by thiophenic heterocycles. The rate of DBT oxidation decreased with photoirradiation time, as shown in Fig. 2(*a*), since the DBT-O formed also quenches the DCA fluorescence ($k_{q,\,DBT\text{-}O} = 7.37 \times 10^9$ L mol^{-1} s^{-1}) and competitive electron-transfer occurs. This problem can be solved by adding a larger quantity of DCA [Fig. 2(*b*)]. The two photoproducts of DBT, DBT-O and DBT-O_2, are both highly polarized and insoluble in non-polar light oil.[12] Thus the process has potential for the desulfurization of light oil.

The above photoprocess was applied to the desulfurization of light oil containing ca. 0.18 wt% sulfur, which is below the previous regulation in Japan (0.2 wt%). Light oil (50–200 ml) and MeCN (200–350 ml) saturated with DCA were introduced into the reaction vessel at MeCN:light oil volume ratios of 1:1, 3:1 or 7:1 v/v. The solutions were photoirradiated using a high-pressure mercury lamp with a 3 wt% $NaNO_2$ solution filter, combined with air bubbling at atmospheric pressure.

Certain quantities of DBTs from the light oil in the light oil–MeCN two-phase system transfer into the MeCN phase, together with other aromatics. The photoirradiation of the two-phase system thus causes the oxidation of the DBTs in the MeCN, resulting in the successive removal of the DBTs from the light oil phase.[8] Fig. 3 shows the effect of the addition of DCA on the time-course variation of the sulfur content in the light oil, with respect also to variations in the MeCN:light oil volume ratio. The data points, at an irradiation time of zero, show the distribution equilibria for the sulfur contents in the two-phase systems. Without DCA, the sulfur content was reduced only slightly, since the light oil contains three-ring aromatics which absorb visible light only weakly. The reduction rate for the sulfur content was enhanced drastically however by the addition of DCA. For an MeCN:light oil volume ratio of 3:1, 2 h of irradiation decreased the sulfur level to 0.05 wt%, and 10 h of irradiation decreased the value to 0.005 wt%, which is the value presently strictly legislated in Sweden. Light oil containing such a low sulfur level has not been achieved so far by the HDS method, even under severe operating conditions at 673 K.[3] Thus, the present method is applicable as an energy-saving deep desulfurization process to meet with the newest regulation for sulfur content in light oil, and requires only air bubbling and irradiation with visible light, avoiding the use of hydrogen and high pressure.

The present study thus describes a novel desulfurization process for light oil, effected by the combination of electron-transfer photooxygenation and liquid–liquid extraction using an oil–MeCN two-phase system. This could be developed as a desulfurization process utilizing solar irradiation as a light source. Work is in progress to develop the overall process, including a method for subsequent recovery of DCA from the resulting solutions.

The authors are grateful for financial support in the form of a Grant-in-Aid for Scientific Research (No. 09555237) from the Ministry of Education, Science, Sports and Culture, Japan, and by The Foundation of Sanyo Broadcasting (for T. H.)

Notes and references

1 B. Lee, *J. Air Waste Manage. Assoc*., 1990, **41**, 16.
2 M. Houalla, D. H. Broderick, A. V. Sapre, N. K. Nag, V. H. J. De Beer, B. C. Gates and H. Kwart, *J. Catal*., 1980, **61**, 523.
3 T. Kabe, A. Ishihara and H. Tajima, *Ind. Eng. Chem. Res*., 1992, **31**, 1577.
4 A. Amorelli, Y. D. Amos, C. P. Halsig, J. J. Kosman, R. J. Jonker, M. De Wind and J. Vrieling, *Hydrocarbon Process*., 1992, **June**, 93.
5 F. Berthou and V. Vignier, *Int. J. Environ. Chem*., 1986, **27**, 81.
6 T. Hirai, K. Ogawa and I. Komasawa, *Ind. Eng. Chem. Res*., 1996, **35**, 576.
7 T. Hirai, Y. Shiraishi, K. Ogawa and I. Komasawa, *Ind. Eng. Chem. Res*., 1997, **36**, 533.
8 Y. Shiraishi, T. Hirai and I. Komasawa, *Ind. Eng. Chem. Res*., 1998, **37**, 203.
9 J. G. Carbart and J. N. Pitts, Jr., *Photochemistry*, Wiley, New York, 1968, p. 737.
10 E. Bacciochi, C. Crescenzi and O. Lanzalunga, *Tetrahedron*, 1997, **53**, 4469.
11 J. Eriksen, C. S. Foote and T. L. Parker, *J. Am. Chem. Soc*., 1977, **99**, 6455.
12 J. Bundt, W. Herbel and H. Steinhart, *J. High Resolut. Chromatogr*., 1992, **15**, 682.

Communication 8/06658B

The fixation and reduction of dinitrogen using lanthanides: praseodymium and neodymium *meso*-octaethylporphyrinogen–dinitrogen complexes

Elisa Campazzi, Euro Solari, Carlo Floriani* and Rosario Scopelliti

Institut de Chimie Minérale et Analytique, BCH, Université de Lausanne, CH-1015 Lausanne, Switzerland. Phone: +41 (21) 692 39 02; Fax: +41 (21) 692 39 05. E-mail: carlo.floriani@icma.unil.ch

Received (in Basel, Switzerland) 23rd September, Accepted 26th October 1998

The *meso*-octaethylporphyrinogen–sodium–lanthanide complexes, [{(η^5 : η^1 : η^5: η^1-Et_8N_4)M}Na$(thf)_2$], in the presence of Na metal and under a nitrogen atmosphere, fix and reduce dinitrogen to the $[N_2]^{2-}$ anion, as shown by the isolation of the dinuclear complexes containing the [M(μ-η^2 : η^2-N_2)M] moiety [M = Pr, Nd].

Lanthanide metals can be particularly appropriate in the exploitation of the electron-rich nature of the *meso*-octaalkylporphyrinogen tetraanion. The ligand in turn can provide between 8 and 24 electrons as it adapts the bonding mode of each pyrrolyl anion from η^1 to η^5 based on the requirements of the metal.[1,2] The unique nature of this ligand, which has been recently widely explored in early transition metal organometallic chemistry, centers on its ability to function in a bifunctional manner[1,2] when bonded to acid metals, and through its peculiar redox chemistry.[3] These properties seem to be particularly suitable for exploring the reactivity of lanthanide–porphyrinogen complexes towards dinitrogen. Surprisingly, only one dinitrogen–lanthanide derivative is known for samarium.[4]

Herein we report dinitrogen complexes of Pr and Nd. The synthesis of the unknown starting compounds **3** and **4** has been carried out according to the sequence in Scheme 1. Owing to the potential complication of using lithium, which could eventually reduce N_2,[4b] all preparations and subsequent reactions involved the use of sodium.

Complexes **3**† (light-yellow crystals) and **4**† (light-blue crystals) can occur either in the monomeric or dimeric form, depending on the solvent used during their crystallization. The bonding mode of the lanthanide ion and the sodium cation has been proved by an X-ray analysis on **4**. Complexes **3** and **4** were reduced in THF under a nitrogen atmosphere with sodium, in the presence of small amounts of naphthalene and led to the yellow, **5**,‡ and green, **6**,‡ microcrystalline solids, respectively. Two different solid state forms of the N_2 derivatives have been obtained, depending on the crystallization solvents. Thus, complexes **5** and **6**, when recrystallized from dimethoxyethane (DME) and dioxane, gave **7**‡ and **8**,‡ respectively.

The structures of **7**§ and **8**§ are shown in Figs. 1 and 2 along with selected structural parameters. In both compounds, the porphyrinogen is η^5 : η^1 : η^5 : η^1 bonded[1,2] to the lanthanide ion. Both compounds show two sodium cations η^1 : η^3 bonded to the porphyrinogen and complete their hexacoordination with DME in **7** or two dioxane molecules in **8**. Two additional sodium cations function as countercations in **7**, while in **8** they interact with N_2. The N–N axis is perpendicular to the lanthanide–lanthanide direction, displaying a μ-η^2 : η^2 bonding mode.[4a,5] In both compounds **7** and **8**, unlike in [{(η^5-$C_5Me_5)_2$Sm}$_2$(μ-η^2 : η^2-N_2)][4a] [N–N, 1.088(12) Å] or [{UN($CH_2CH_2NSiBu^tMe_2)_3$}$_2$(μ-η^2 : η^2-N_2)] [N–N, 1.109(7) Å] the N–N distance is in good agreement with a bielectronic reduction of N_2.[6] The magnetic moments at 298 K of the complexes **3** and **5**, **4** and **6**, are very close [μ_{eff} = 3.53, **3**; 3.44, **5**; 3.29, **4**; 3.18 μ_B, **6**] and they remain constant over a wide range of temperature (50–320 K). These results allows the assignment of the +III oxidation state to all metal ions in **3–6**, and rules out any significant coupling between the two paramagnetic centres. In compounds **7** and **8** the lanthanide–N distances are relatively short and comparable to those of amido derivatives.[7] The rather short Na–N(N_2) distances support the interaction of the alkali cation with an anionic form of N_2. Unlike in [{(η^5-$C_5Me_5)_2$Sm}$_2$(μ-η^2 : η^2-N_2)] or in [{UN($CH_2CH_2NSiBu^tMe_2)_3$}$_2$(μ-η^2 : η^2-N_2)], no loss of N_2 was observed, though complexes **5–8** were kept under vacuum for a rather long time. Dinitrogen was evolved from **5**

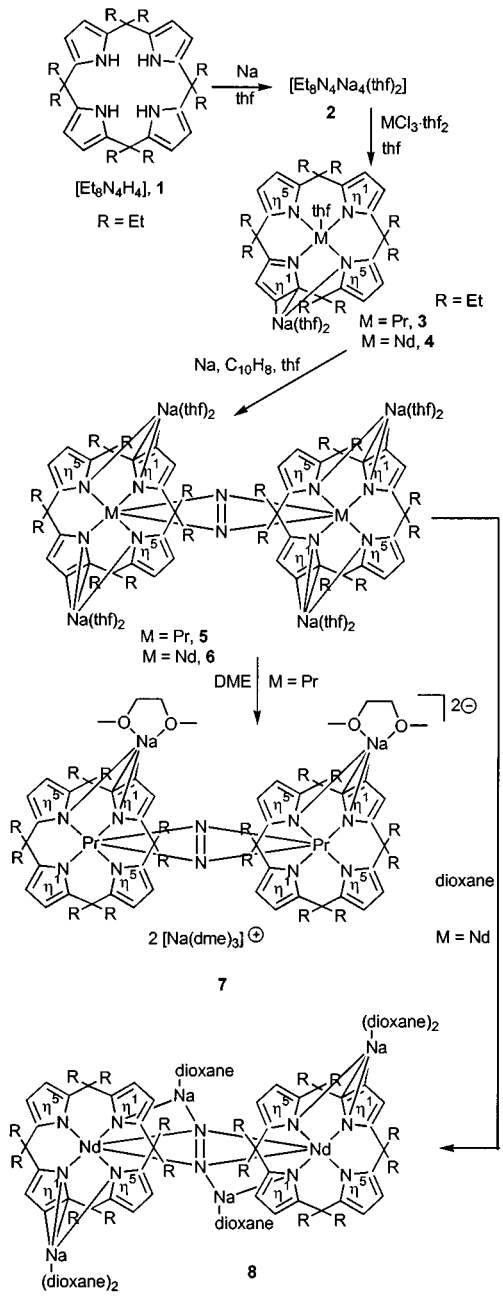

Scheme 1

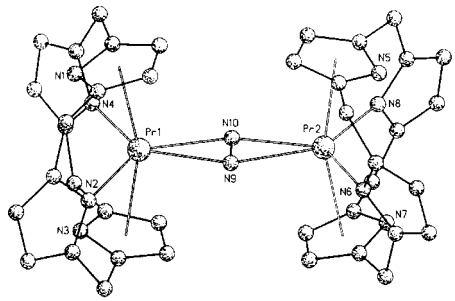

Fig. 1 An XP drawing of complex **7**. Selected bond distances (Å): Pr(1)–η^5(Pyr)$_{av}$ 2.605(6), Pr(1)–η^1(Pyr)$_{av}$ 2.579(5), Pr(1)–N(9) 2.475(5), Pr(1)–N(10) 2.414(5), Pr(2)–η^5(Pyr)$_{av}$ 2.604(6), Pr(2)–η^1(Pyr)$_{av}$ 2.576(5), Pr(2)–N(9) 2.455(5), Pr(2)–N(10) 2.425(4), N(9)–N(10) 1.254(7). η^5(Pyr)$_{av}$ indicates the centroid of the pyrrolyl anion.¶

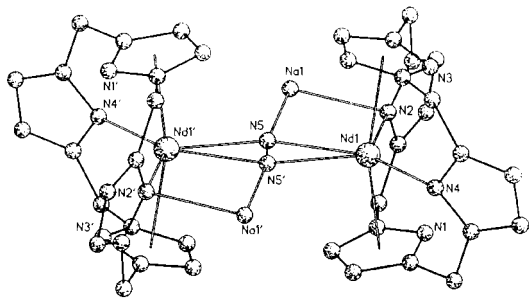

Fig. 2 An XP drawing of complex **8**. Selected bond distances (Å): Nd(1)–η^5(Pyr)$_{av}$ 2.562(5), Nd(1)–η^1(Pyr)$_{av}$ 2.550(4), Nd(1)–N(5) 2.511(4), Nd(1)–N(5′) 2.508(4), Na(1)–N(5) 2.308(4), Na(1)–η^1(Pyr)$_{av}$ 2.433(4), N(5)–N(5′) 1.234(8). Prime denotes a transformation of $-x$, $1-y$, $-z$. η^5(Pyr)$_{av}$ indicates the centroid of the pyrrolyl anion.¶

and **6** in the expected amount only after oxidation with I_2. The present report deals with some important issues and in particular the use of an electron-rich ligand like porphyrinogen and its role in the fixation of dinitrogen in a reduced form bound to lanthanides like Pr and Nd, which are generally difficult to reduce.

Notes and references

† *Procedures for* **3** *and* **4**: [$PrCl_3$·thf$_2$] (11.2 g, 28.6 mmol) was added to a light-yellow solution of **2** (22.3 g, 28.9 mmol) in THF (600 cm³). The resulting yellow-green suspension was kept stirring for 12 h at room temperature. The solid, mainly NaCl, was filtered off and the resulting solution evaporated to dryness. The yellow solid was recrystallized from THF–pentane (18.2 g, 75%). (Found: C, 62.63; H, 7.67; N, 6.71. $C_{44}H_{64}N_4NaPrO_2$ requires C, 62.55; H, 7.63; N, 6.63%). Complex **4** was obtained following the same procedure. (Found: C, 62.22; H, 7.36; N, 6.66. $C_{44}H_{64}N_4NaNdO_2$ requires C, 62.30; H, 7.60; N, 6.61%).

‡ *Procedures for* **5**–**8**: Na metal (0.21 g, 9.26 mmol) and naphthalene (0.30 g, 2.31 mmol) were added to a THF (200 cm³) suspension of **3** (6.51 g, 7.70 mmol) in a 3 dm³ flask. Stirring gave a red solution after 2 h and was continued for 24 h. Standing for 2 more days resulted in a yellow microcrystalline solid. The amount of solid was increased by partial evaporation of THF until 70 cm³ and addition of pentane (100 cm³) (5.8 g, 73%). (Found: C, 60.81; H, 7.60; N, 6.91. $C_{104}H_{160}N_{10}Na_4Nd_2O_8$ requires C, 60.87; H, 7.86; N, 6.86%). The reaction of **5** (1.44 mmol) in THF (100 mL) with I_2 (4.33 mmol) gave N_2 (1.39 mmol). Complex **5** recrystallized from DME gave crystals of **7** suitable for X-ray analysis. The synthesis of **6**, obtained as green crystals, was carried out following the procedure reported for **5**. (Found: C, 60.51; H, 7.95; N, 6.95. $C_{104}H_{160}N_{10}Na_4Nd_2O_8$ requires C, 60.67; H, 7.83; N, 6.80%). Oxidation of **6** (1.43 mmol) with I_2 in THF evolved 1.34 mmol of N_2. The recrystallization of **6** from dioxane gave crystals of **8**, analyzed by X-ray diffraction.

§ *Crystal data* for **7**: $C_{104}H_{176}N_{10}Na_4O_{16}Pr_2$, M = 2196.33, monoclinic, space group $P2_1/c$, a = 20.1877(14), b = 19.2513(14), c = 29.745(2) Å, β = 94.134(6)°, V = 11529.8(14) Å³, Z = 4, D_c = 1.265 g cm^{-3}, F(000) = 4640, λ(Mo-Kα) = 0.71073 Å, μ = 0.912 mm^{-1}; crystal dimensions 0.51 × 0.44 × 0.53. Diffraction data were collected on a KUMA CCD at 173 K. For 16219 observed reflections [$I > 2\sigma(I)$] the conventional R is 0.0687 ($wR2$ = 0.1668 for 22661 independent reflections). *Crystal data* for **8**: $C_{124}H_{200}N_{10}Na_4Nd_2O_{26}$, M = 2627.38, monoclinic, space group $P2_1/c$, a = 12.908(3), b = 15.537(2), c = 32.885(9) Å, β = 94.02(2)°, V = 6579(3) Å³, Z = 2, D_c = 1.326 g cm^{-3}, F(000) = 2772, λ(Mo-Kα) = 0.71070 Å, μ = 0.865 mm^{-1}; crystal dimensions 0.40 × 0.38 × 0.27. Diffraction data were collected on a mar345 area detector at 173 K. For 8471 observed reflections [$I > 2\sigma(I)$] the conventional R is 0.0546 ($wR2$ = 0.1623 for 10692 independent reflections). CCDC 182/1065. See http://www.rsc.org/suppdata/cc/1998/2603, for crystallographic files in .cif format.

¶ *meso*-Ethyl groups and sodium cations bonded to the periphery of porphyrinogen have been omitted for clarity.

1 D. Jacoby, C. Floriani, A. Chiesi-Villa and C. Rizzoli, *J. Chem. Soc., Chem. Commun.*, 1991, 790; *J. Am. Chem. Soc.*, 1993, **115**, 3595; D. Jacoby, S. Isoz, C. Floriani, A. Chiesi-Villa and C. Rizzoli, *J. Am. Chem. Soc.*, 1995, **117**, 2793; C. Floriani, in *Stereoselective Reactions of Metal-Activated Molecules*, ed. H. Werner and J. Sundermeyer, Vieweg, Wiesbaden, 1995, pp. 97–106; S. De Angelis, E. Solari, A. Chiesi-Villa and C. Rizzoli, *Organometallics*, 1995, **14**, 4505; D. Jacoby, S. Isoz, C. Floriani, K. Schenk, A. Chiesi-Villa and C. Rizzoli, *Organometallics*, 1995, **14**, 4816; S. Isoz, C. Floriani, K. Schenk, A. Chiesi-Villa and C. Rizzoli, *Organometallics*, 1996, **15**, 337; G. Solari, E. Solari, A. Chiesi-Villa and C. Rizzoli, *Organometallics*, 1997, **16**, 508.

2 C. Floriani, *Pure Appl. Chem.*, 1996, **68**, 1.

3 S. De Angelis, E. Solari, A. Chiesi-Villa and C. Rizzoli, *J. Am. Chem. Soc.*, 1994, **116**, 5691; *J. Am. Chem. Soc.*, 1994, **116**, 5702; C. Floriani, *Chem. Commun.*, 1996, 1257.

4 Two reports appeared on Sm–N_2 chemistry, the first one (a) containing a true N_2 bridging two samarium ions, the second one (b) containing the Li_4N_2 unit within two samarium ions: (a) W. J. Evans, T. A. Ulibarri and J. W. Ziller, *J. Am. Chem. Soc.*, 1988, **110**, 6877; (b) J. Jubb and S. Gambarotta, *J. Am. Chem. Soc.*, 1994, **116**, 4477.

5 The unusual μ-η^2 : η^2 bonding mode has been found also in a U(III) derivative: P. Roussel and P. Scott, *J. Am. Chem. Soc.*, 1998, **120**, 1070.

6 R. Ferguson, E. Solari, C. Floriani, D. Osella, M. Ravera, N. Re, A. Chiesi-Villa and C. Rizzoli, *J. Am. Chem. Soc.*, 1997, **119**, 10104 and references therein; C. E. Laplaza, M. J. A. Johnson, J. C. Peters, A. L. Odom, E. Kim, C. C. Cummins, G. N. George and I. J. Pickering, *J. Am. Chem. Soc.*, 1996, **118**, 8623 and references therein; A. Zanotti-Gerosa, E. Solari, L. Giannini, C. Floriani, A. Chiesi-Villa and C. Rizzoli, *J. Am. Chem. Soc.*, 1998, **120**, 437.

7 M. F. Lappert, P. P. Power, A. R. Sanger and R. C. Srivastava, *Metal and Metalloid Amides. Synthesis, Structures and Physical Properties*, Ellis Horwood, Chichester, UK, 1980, ch. 8.

Communication 8/07405D

A new cinchona-modified platinum catalyst for the enantioselective hydrogenation of pyruvate: the structure of the 1:1 alkaloid–reactant complex

Mihály Bartók,*[ab] Károly Felföldi,[a] Béla Török[b] and Tibor Bartók[c]

[a] *Department of Organic Chemistry and*
[b] *Organic Catalysis Research Group of the Hungarian Academy of Sciences, József Attila University, H-6720 Szeged, Dóm tér 8, Hungary. E-mail: bartok@chem.u-szeged.hu*
[c] *Analytical Laboratory of Cereal Research Institute, PO Box 391, H-6701 Szeged, Hungary*

Received (in Liverpool, UK) 8th September 1998, Accepted 26th October 1998

The hydrogenation of ethyl pyruvate to (*S*)-ethyl lactate (up to 70% ee) over a Pt/Al_2O_3 catalyst using α-isocinchonine as a modifier strongly supports the structure of the intermediate complex [cinchona alkaloid (open conformer)–pyruvate 1:1 complex] of this type of reactions.

As is well known, one of the most important fields in contemporary chemical research is the preparation of chiral compounds. The potential of asymmetric catalytic processes is especially high, since in this way large amounts of chiral products can be prepared using catalytic amounts of chiral modifier.[1,2] As a result of industrial and economical requirements the major aim is to develop heterogeneous catalytic asymmetric syntheses.[3–6] In this respect, the hydrogenation of pyruvates is one of the most frequently studied reactions.[7,8] After optimization 95[9]–97% ee[10] was achieved over Pt/Al_2O_3 catalyst using cinchonidine (CD) as the modifier in the preparation of (*R*)-ethyl lactate and 90%[11] ee using cinchonine (CN) for (*S*)-ethyl lactate (Scheme 1).

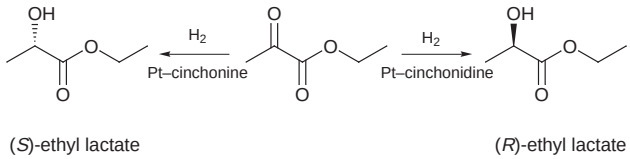

Scheme 1

Since pyruvate hydrogenation is one of the two[12,13] good ee producing heterogeneous chiral hydrogenations (α-keto esters,[12] β-keto esters and 1,3-diketones[13]), extensive efforts have been made to gain insight into the mechanism. Many mechanistic details of the pyruvate hydrogenation are known, however, there is no agreement concerning the structure of the intermediate (CD–pyruvate 1:1 complex) responsible for chirality. The intermediate complexes (depending on the reaction conditions) published recently are summarized in Fig. 1.

As shown, there is no significant conceptional difference between the structures in each groups [group I: Fig. 1(*a*),[14] (*b*),[15] (*c*),[16] (*f*);[17] group II: (*d*),[18] (*e*)[19]]. The CD in all intermediates in group I is in the 'open' conformation, while in group II it is in the 'closed'conformation. Between the two groups, however, there is a huge difference. The intermediates belonging to group I are anchored to the surface of the platinum catalyst by a multicenter π-bond from the quinoline skeleton and the conjugated σπ systems of pyruvate. In contrast, the structures belonging to group II are already formed in the solution and the complex most likely adsorbs through the conjugated σπ system of the substrate and the non-bonding electron pairs of the quinoline nitrogen due to the so-called 'shielding effect'. It has been clearly proven[7,8,15] that the conformation of the modifier plays a determining role in the chiral induction.

Here we provide new information about the structure of the intermediate complex and experimental proof of whether the 'closed' conformation of the cinchona alkaloids is necessary for chiral induction. For this reason, two cinchona alkaloids, CN and α-isocinchonine (ICN) were selected as chiral modifiers.

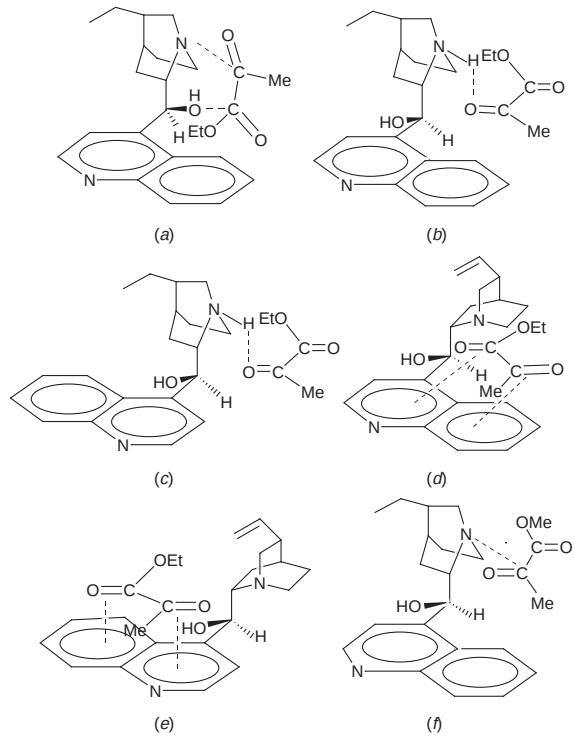

Fig. 1 The structures of the cinchonidine–ethyl pyruvate intermediate complexes.

Although the mechanistic proposals mentioned above are related to the platinum–CD system,[7,8,14,17,18] there is no reason to assume that when using CN the mechanism should be basically different.[11,12,15] Fig. 2 illustrates the most stable

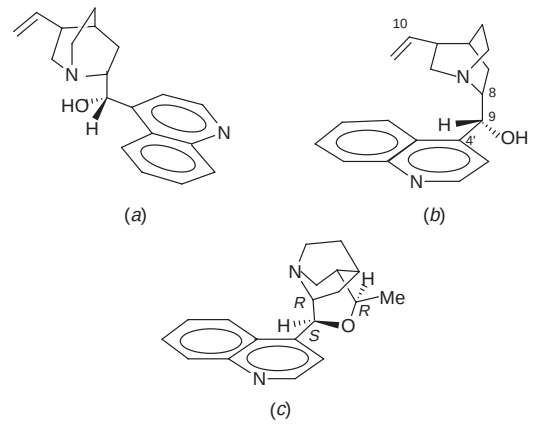

Fig. 2 The conformations of cinchonine [(*a*) 'open' conformer, (*b*) 'closed' conformer] and (*c*) α-isocinchonine.

Table 1 Enantioselective hydrogenation of ethyl pyruvate over a 5% Pt/Al_2O_3 catalyst (Engelhard 4759) in AcOH at room temperature [50 mg of catalyst (as received), 5 mg of modifier, 5 ml of solvent and 0.25 ml of ethyl pyruvate][a]

Modifier	H_2 pressure/bar	Conversion (%)	Ee (%) (configuration)
CD	1	100	80 (*R*)
CD	50	100	90 (*R*)
CN	1	95	72 (*S*)
CN	50	98	67 (*S*)
ICN	1	94	67 (*S*)
ICN	50	98	69 (*S*)

[a] Analysis: ee (%) = 100{[*R*] − [*S*] (or [*S*] − [*R*])}/([*R*] + [*S*]), chiral GC (HP 5890 GC-FID, 30 m long Lipodex-A column), HPLC-MS (HP1090 Ser.II HPLC-HP5989B MS with an HP5987A ES interface).

conformations of CN [Fig 2(*a*)] and ICN [Fig. 2(*c*)] alkaloids suggested and verified by combined NMR and X-ray analysis and molecular mechanical calculations.[20–22] Conformational changes in CN are possible by rotation along the C(4′)–C(9) and C(8)–C(9) bonds. [It should be noted that in the case of flat adsorption of the quinoline skeleton on platinum, as already pointed out,[17,23] the C(4′)–C(9) rotation is hindered.] To realize our aim mentioned above, ICN was selected because it cannot rotate around C(8)–C(9). It is also known that ICN exists only in '*anti*-open' conformation.[22]

The enantioselective hydrogenation of ethyl pyruvate (EtPy) was performed either in a conventional atmospheric hydrogenation apparatus or in a Berghof Bar 45 autoclave at room temperature (25 °C). The results are shown in Table 1.

As the HPLC–ESMS measurements revealed, the ICN modifier did not revert back to CN, *i.e*. the cyclic ether structure remained stable during the hydrogenations. As the results clearly show the ICN modifier of fixed conformation showed practically the same performance (conversion, ee) as CN during the hydrogenations.

The proposed intermediate complex of the chiral hydrogenation carried out in the presence of ICN is illustrated in Fig. 3. It should be mentioned that only the existence of the '*anti*-open' conformer was proven in solution;[22] the formation of the '*syn*-open' conformer during the adsorption cannot be excluded.

These experimental data strongly support the existence of the structures in Fig.1(*b*) and (*c*) when working under acidic conditions. Further measurements are necessary, however, to distinguish between the two structures. Although the reaction conditions are not fully optimized in the case of CN and ICN it is unambiguously proven that the formation of a cinchona alkaloids(closed)–EtPy complex is not a precondition for chiral induction. On the other hand, extensive studies with respect to cinchona-modified pyruvate hydrogenation in AcOH, accompanied by the present results, strongly supports the 1:1 adsorptive interaction model[7,8] of Baiker, Blaser and co-workers. In neutral solvents, the recently revised mechanistic proposal by Wells[17] and co-workers seems most likely.

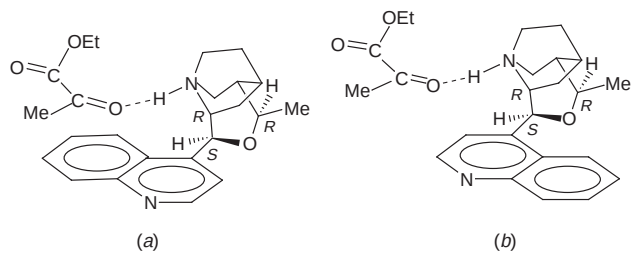

Fig. 3 The structures of α-isocinchonine–ethyl pyruvate intermediate complexes [(*a*) '*anti*-open' complex, (*b*) '*syn*-open' complex].

Our results obtained with ICN suggest further mechanistic studies of cinchona-modified asymmetric syntheses utilising other cinchona alkaloids of rigid conformation. The results of this work provide further proof of our earlier statement[24] that the conformation of the reactants is of crucial importance in determining the selectivity of metal-catalyzed transformations.

Financial support by the Hungarian National Science Foundation (OTKA Grant T016109) and the Hungarian Academy of Sciences (AKP 97-4 2,4) is highly appreciated. Our most sincere thanks are due to Dr J. Thiel (A. Miczkiewicz University, Poznan, Poland) for the donation of the α-isocinchonine sample used to start these investigations.

Notes and references

1 *Catalytic Asymmetric Synthesis*, ed. I. Ojima, VCH, Weinheim, 1993.
2 R. Noyori, *Asyymmetric Catalysis in Organic Chemistry*, Wiley, New York, 1994.
3 H. U. Blaser, *Tetrahedron*: *Asymmetry*, 1991, **2**, 935.
4 H. U. Blaser and M. Müller, *Stud. Surf. Sci. Catal*., 1991, **59**, 73.
5 R. A. Sheldon, *Chirotechnology*, Marcel Decker, New York, 1993.
6 *Chiral Reactions in Heterogeneous Catalysis*, ed. G. Jannes and V. Dubois, Plenum, New York and London, 1995.
7 A. Baiker, *J. Mol. Catal. A*: *Chem*., 1997, **115**, 473 and references cited therein.
8 H. U. Blaser, H. P. Jalett, M. Müller and M. Studer, *Catal. Today*, 1997, **37**, 441 and references cited therein.
9 H. U. Blaser and H. P. Jalett, *J. Mol. Catal*., 1991, **68**, 215.
10 B. Török, K. Felföldi, G. Szakonyi, K. Balázsik and M. Bartók, *Catal. Lett*., 1998, **52**, 81.
11 M. Schürch, T. Heinz, R. Aeschimann, T. Mallatt, A. Pfaltz and A. Baiker, *J. Catal*., 1998, **173**, 187.
12 Y. Orito, S. Imai and S. Niva, *J. Chem. Soc. Jpn*., 1979, 1118.
13 K. Ito, T. Harada, A. Tai and Y. Izumi, *Chem. Lett*., 1979, 1049.
14 R. L. Augustine and S. K. Tanielyan, *J. Mol. Catal. A*: *Chem*., 1996, **112**, 93.
15 A. Baiker and H. U. Blaser, *Handbook of Heterogeneous Catalysis*, ed. G. Ertl, H. Knözinger and J. Weitkamp, Wiley-VCH, Weinheim, 1997, vol. 5, p. 2422.
16 H. U. Blaser, H. P. Jalett, M. Garland, M. Studer, H. Thies and A. Wirth-Tijani, *J. Catal*., 1998, **173**, 282.
17 K. E. Simons, P. A. Meheux, S. P. Griffiths, I. M. Sutherland, P. Johnston, P. B. Wells, A. F. Carley, M. K. Rajumon, M. W. Roberts and A. Ibbotson, *Recl. Trav. Chim. Pays-Bas*, 1994, **113**, 465.
18 J. L. Margitfalvi, M. Hegedűs and E. Tfirst, *Stud. Surf. Sci. Catal*., 1996, **101**, 241.
19 J. L. Margitfalvi, E. Tfirst, M. Hegedűs and E. Tálas, *17th Conference on Catalysis of Organic Reactions*, ed. F. E. Herkes, New Orleans, L. A., March 29–April 2, 1998, Pre-Prints, Poster 5.
20 G. D. H. Dijkstra, R. M. Kellogg, H. Wynberg, J. S. Svendsen, I. Marko and K. B. Sharpless, *J. Am. Chem. Soc*., 1989, **111**, 8069.
21 G. D. H. Dijkstra, R. M. Kellogg and H. Wynberg, *J. Org. Chem*., 1990, **55**, 6121.
22 J. Thiel and P. Fiedorow, *J. Mol. Struct*., 1997, **405**, 219.
23 G. Bond and P. B. Wells, *J. Catal*., 1994, **150**, 329.
24 M. Bartók, Á. Molnár and J. Apjok, *J. Catal*., 1985, **95**, 605.

Communication 8/07039C

Calix[4]arenes with perfluorinated alcoholic functions at the upper rim: a new class of neutral anion receptors

N. Pelizzi, A. Casnati and R. Ungaro*

Dipartimento di Chimica Organica e Industriale dell'Università, Viale delle Scienze, 43100-Parma, Italy. E-mail: ungaro@ipruniv.cce.unipr.it

Received (in Liverpool, UK) 2nd September 1998, Accepted 22nd October 1998

Two or four perfluorinated alcoholic functions were successfully introduced at the upper rim of calix[4]arenes, affording a new type of neutral receptor for anion recognition; preliminary binding studies indicate that the difunctionalized receptors 3a and 3b are selective for Y-shaped carboxylate ions over spherical anions which are, on the contrary, more efficiently bound by the tetraalcohol 6.

Compared with cation complexation, anion recognition represents a less explored area of research, in spite of the important role played by anionic species both in chemistry and biology. However, very recently interest in this field has grown and several new hosts which specifically recognize anions have been synthesized.[1] Most of the organic synthetic receptors for anions are charged species[2] or contain a metal center which directly coordinates to the anion[3] or increases the binding ability of other functional groups.[3] Nevertheless, neutral hosts which complex anions *via* hydrogen bonding are known.[4] So far mainly amides[5] and (thio)ureas[6] or a combination of the two[7] have been used as hydrogen bonding donor groups for the synthesis of electroneutral organic receptors. These groups have also been linked to calixarenes, at either the upper or lower rim, for the synthesis of selective anion receptors. It is well known that perfluoro alcohols are very good anion solvating agents,[8] and that they can affect the kinetics of chemical processes by specific anion solvation.[9] Moreover Pirkle *et al*. used chiral fluoro alcohols as chiral solvating agents and were able to determine the enantiomeric compositions of chiral Lewis bases.[10] Surprisingly, nobody has exploited so far the fluoro alcohol function as a binding site in the design of more complex receptors for anions and polar organic molecules.

We explored the possibility of introducing two or four fluoro alcohol functions at the upper rim of calix[4]arenes blocked in the cone conformation, and report here our successful synthetic results together with some preliminary anion binding properties of the new ligands synthesized.

The difunctionalized anion receptors **3a**,**b** are obtained by two different methods (Scheme 1). Method A exploits the known procedure reported in the literature for the synthesis of simple fluoro ketones.[11] The reaction of the dibromotetrapropoxycalix[4]arene **1**[6b] with Bu^{t}Li in dry THF gives the diketone **2** in 18% yield. The subsequent reduction of **2** with $NaBH_4$ in dry MeOH gives the fluorinated calix[4]arene dialcohol **3** as 1:1 mixture of **3a** (*RR, SS* racemic mixture) and **3b** (*RS, SR meso*). Better yields (85%) are obtained by Method B, reacting the tetrapropoxy calix[4]arene dialdehyde **4**[12] with trifluoromethyltrimethylsilane in the presence of a catalytic amount of TBAF.[13] The two diastereoisomers **3a** (racemic mixture) and **3b** (*meso*) can be separated by column chromatography (SiO_2, hexane–EtOAc 9:1) and their structure assigned by NMR analysis in $CDCl_3$.† The racemic mixture **3a** and the *meso* compound **3b** are easily distinguished by the multiplicity of the signals of the unsubstituted aromatic nuclei; **3a** presents a C_2 axis and gives three doublets of doublets, while **3b** has a symmetry plane and generates two doublets and two triplets.

Since it has been shown that calixarenes bearing strong hydrogen bonding groups like (thio)urea[14] form in apolar solvents dimeric molecular capsules we have studied solvent

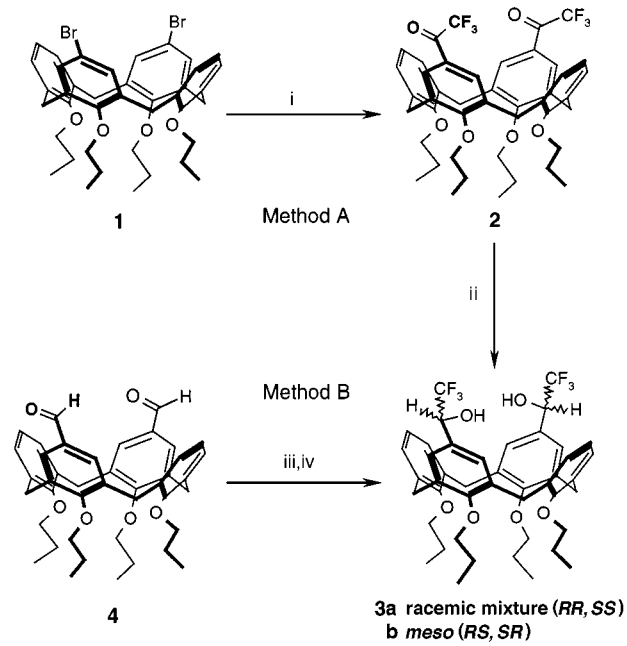

Scheme 1 *Reagents and conditions*: i, Bu^{t}Li, CF_3CO_2Et, THF, −80 °C; ii, $NaBH_4$, MeOH; iii, CF_3SiMe_3, TBAF, THF; iv, 4 M HCl.

effects on **3a** and **3b**. The independency upon diluition of NMR spectra in $CDCl_3$ and the osmometric determination of the molecular weight indicate that there are no *inter*molecular hydrogen bonds and that **3a**,**b** are monomeric in solution. However a significant conformational rearrangement is observed in the ^1H NMR spectra of the diastereomeric mixture passing from $CDCl_3$ to [$^2H_6$]DMSO: the hydrogens *ortho* to the trifluoromethyl alcohol give signals between δ 6.2 and 6.6 in $CDCl_3$, whereas they are shifted to between δ 7.1 and 7.3 in [$^2H_6$]DMSO. On the contrary the signals of the unsubstituted aromatic rings, which are between δ 6.8 and 7.1 in $CDCl_3$, shift to the region between δ 6.0 and 6.7 in [$^2H_6$]DMSO. This behaviour is due to two different pinched cone conformations adopted in $CDCl_3$ and in [$^2H_6$]DMSO (Fig. 1). In $CDCl_3$ the upfield shift of the aromatic hydrogens of the nuclei bearing the fluorinated alcohols indicates that an intramolecular hydrogen bond is present between the two OH groups which keeps these

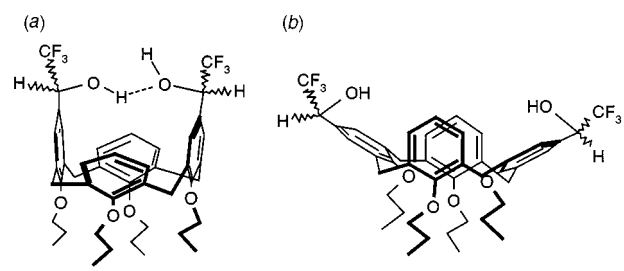

Fig. 1 The two pinched cone conformations adopted by **3a**,**b** in (*a*) $CDCl_3$ and (*b*) [$^2H_6$]DMSO.

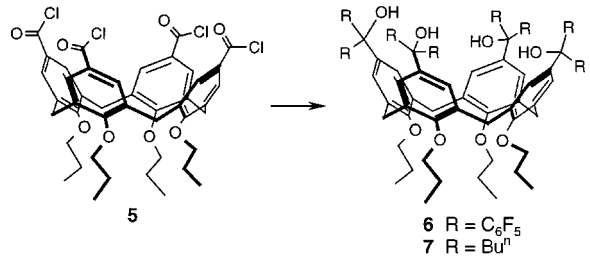

Scheme 2 *Reagents and conditions*: i, RI, Li.

two functionalized aromatics in the shielding cone of the other two. On the contrary in [$^2H_6$]DMSO the intramolecular hydrogen bonding is prevented by solvation and the calixarene adopts a piched cone conformation where the unsubstituted aromatic rings are in the shielding cone of the other two.

We have also synthesized the calix[4]arene derivative **6** (Scheme 2), which bears four perfluorinated alcoholic functions at the upper rim, by reacting the tetraacyl chloride **5**[15] with C_6F_5I and lithium in dry Et_2O (yield 15%)† and, for comparison, compound **7** (yield 95%).†

Preliminary binding studies using titration NMR experiments‡ reveal that both receptors are able to complex anions in $CDCl_3$. Difunctionalized receptors **3a** and **3b** show selectivity in the recognition of carboxylate over spherical anions with the racemic compound **3a** binding acetate anion (K_{ass} = 435 M^{-1}) more efficiently than the *meso* compound **3b** (K_{ass} = 200 M^{-1}). Also in the case of a chiral guest like the anion of *N*-lauroyl-L-phenylalanine we have observed a stronger association of the racemic compound **3a** (K_{ass} = 165 M^{-1}) with respect to the *meso* compound **3b** (K_{ass} = 40 M^{-1}), the latter probably giving rise to unfavorable steric interactions. On the other hand the tetrafunctionalized receptor **6** binds spherical anions such as bromide (K_{ass} = 480 M^{-1}) more efficiently than acetate anion (K_{ass} = 90 M^{-1}). Although these data may be negatively affected by the presence of intramolecular hydrogen bonding, a comparison with the data reported in the literature for the interactions between anions and other hydrogen bonding donor groups[5,16] seems to indicate that the strength of the interaction between the perfluorinated alcoholic functions and anions is smaller than that of the same anions with urea or sulfonamide groups, but comparable with carboxamides. The importance of the perfluorinated groups for anion binding is however indicated by the fact that compound **7** shows no interaction with either bromide and acetate anions under the same conditions.

We are currently working on the synthesis of more rigid calixarene receptors in order to avoid intramolecular hydrogen bonding.

This research was supported by MURST (Supramolecular Devices Project) and by CNR. We also thank C. I. M. (Centro Interdipartimentale Misure) for the use of NMR and mass spectrometry instruments.

Notes and references

† All new compounds were characterized by ^{1}H (300 MHz) and ^{13}C NMR (75 MHz) spectroscopy, CI mass spectrometry, IR spectroscopy and melting point. *Selected data* for **3a** (*RR*, *SS* racemic mixture): mp 99–102 °C; δ_H($CDCl_3$) 0.93 (t, 6H, *J* 7.4, $OCH_2CH_2CH_3$), 1.06 (t, 6H, *J* 7.5, $OCH_2CH_2CH_3$), 1.86–2.01 (m, 8H, $OCH_2CH_2CH_3$), 3.16 (d, 2H, *J* 13.3, $ArCH_{eq}Ar$), 3.18 (d, 2H, *J* 13.3, $ArCH_{eq}Ar$), 3.74 (t, 4H, *J* 7.1, $OCH_2CH_2CH_3$), 3.99 (t, 4H, *J* 7.6, $OCH_2CH_2CH_3$), 4.42 [q, 2H, *J* 6.6, $ArCH(OH)CF_3$], 4.45 (d, 2H, *J* 13.3, $ArCH_{ax}Ar$), 4.46 (d, 2H, *J* 13.3, $ArCH_{ax}Ar$), 6.31 (d, 2H, *J* 2.0, ArH), 6.58 (d, 2H, *J* 2.0, ArH), 6.81 (dd, 2H, *J* 7.4, ArH), 6.93 (dd, 2H, *J* 7.4, *J* 2.0, ArH) and 6.95 (dd, 2H, *J* 7.4, 2.0, ArH); δ_C($CDCl_3$) 9.7, 10.3 (q, $OCH_2CH_2CH_3$), 22.7, 23.1 (t, $OCH_2CH_2CH_3$), 30.6, 30.7 (t, $ArCH_2Ar$), 72.2 [qd, *J* 30, $ArCH(OH)CF_3$], 76.3, 76.9 (t, $OCH_2CH_2CH_3$), 122.1 (s, Ar *para*), 123.9 (q, *J* 275, CF_3), 125.1 (d, ArH *para*), 128.0, 128.4, 128.7 (d, Ar *meta*), 133.7, 134.4, 135.6 (s, ArH *ortho*) and 156.7, 156.8 (s, Ar *ipso*); *m/z* (CI) 789 (90, M), 771 (100, M − H_2O) and 751 (80, M − $2H_2O$). For **3b** (*RS*, *SR meso*): mp 105–107 °C; δ_C($CDCl_3$) 0.92 (t, 6H, *J* 7.3, $OCH_2CH_2CH_3$), 1.07 (t, 6H, *J* 7.3, $OCH_2CH_2CH_3$), 1.84–2.01 (m, 8H, $OCH_2CH_2CH_3$), 3.15 (d, 2H, *J* 13.3, $ArCH_{eq}Ar$), 3.19 (d, 2H, *J* 13.3, $ArCH_{eq}Ar$), 3.73 (t, 4H, *J* 7.0, $OCH_2CH_2CH_3$), 4.00 (t, 4H, *J* 8.7, $OCH_2CH_2CH_3$), 4.43 [q, 2H, *J* 6.6, $ArCH(OH)CF_3$], 4.46 (d, 4H, *J* 13.3, $ArCH_{ax}Ar$), 6.22 (d, 2H, *J* 2.0, ArH), 6.55 (d, 2H, *J* 2.0, ArH), 6.84 (t, 1H, *J* 7.2, ArH), 6.85 (t, 1H, *J* 7.2, ArH), 6.98 (d, 2H, *J* 7.2, ArH) and 7.1 (d, 2H, *J* 7.2, ArH); δ_C($CDCl_3$) 9.8, 10.5 (q, $OCH_2CH_2CH_3$), 22.8, 23.3 (t, $OCH_2CH_2CH_3$), 30.7, 30.9 (t, $ArCH_2Ar$), 72.2 [qd, *J* 33, $ArCH(OH)CF_3$], 76.4, 77.1 (t, $OCH_2CH_2CH_3$), 122.1, 122.2 (s, Ar *para*), 123.9 (q, *J* 285, CF_3), 125.1 (d, ArH *para*), 127.6, 128.7, 128.9 (d, Ar *meta*), 133.6, 134.2, 135.9 (s, ArH *ortho*) and 156.7, 157.0, 157.2 (s, Ar *ipso*); *m/z* (CI) 789 (100, M), 771 (95, M − H_2O) and 751 (65, M − $2H_2O$). For **6**: Yield 15%; mp 168–170 °C; δ_H($CDCl_3$) 1.02 (t, 12H, *J* 7.5, $OCH_2CH_2CH_3$), 1.92–1.99 (m, 8H, $OCH_2CH_2CH_3$), 3.15 (d, 4H, *J* 13.0, $ArCH_{eq}Ar$), 3.90 (br s, 4H, OH), 3.95 (t, 8H, *J* 7.6, $OCH_2CH_2CH_3$), 4.52 (d, 4H, *J* 13.0, $ArCH_{ax}Ar$) and 6.64 (s, 8H, ArH); δ_C($CDCl_3$) 10.1 (q, $OCH_2CH_2CH_3$), 22.9 (t, $OCH_2CH_2CH_3$), 31.3 (t, $ArCH_2Ar$), 77.8 (t, $OCH_2CH_2CH_3$), 118.0 (s, Ph *ipso*), 126.1 (d, Ar *meta*), 134.4 (s, Ar *ortho*), 135.9 (s, Ar *para*), 137.6 (d, J_{CF} 241, Ph *meta*), 141.0 (d, J_{CF} 240, Ph *para*), 144.6 (d, J_{CF} 241, Ph *ortho*) and 156.9 (s, Ar *ipso*); *m/z* (CI) 2040 (50, M) and 2022 (100, M − H_2O). For **7**: Yield 95%; mp 103–104 °C; δ_H($CDCl_3$) 0.85 (t, 24H, *J* 7.2, $CH_2CH_2CH_2CH_3$), 0.98 (t, 12H, *J* 7.4, $OCH_2CH_2CH_3$), 1.20–1.24 (m, 16H, $CH_2CH_2CH_2CH_3$), 1.53–1.64 (m, 16H, $CH_2CH_2CH_2CH_3$), 1.86-2.0 (m, 16H, $CH_2CH_2CH_2CH_3$), 1.94 (m, 8H, *J* 7.4, $OCH_2CH_2CH_3$), 3.13 (d, 4H, *J* 12.8, $ArCH_{eq}Ar$), 3.85 (t, 8H, *J* 6.9, $OCH_2CH_2CH_3$), 4.44 (d, 4H, *J* 12.8, $ArCH_{ax}Ar$) and 6.73 (s, 8H, ArH); δ_C($CDCl_3$) 10.2 (q, $OCH_2CH_2CH_3$), 14.0 (q, $CH_2CH_2CH_2CH_3$), 23.1 (t, $OCH_2CH_2CH_3$), 25.8 (t, $CH_2CH_2CH_2CH_3$), 31.4 (t, $ArCH_2Ar$), 39.7 (t, $CH_2CH_2CH_2CH_3$), 75.5 (t, $OCH_2CH_2CH_3$), 76.5 (t, *C*OH), 125.0 (s, Ar *meta*), 134.0 (d, Ar *para*), 140.7 (s, Ar *ortho*) and 154.9 (s, Ar *ipso*); *m/z* (CI) 1090 (100, M − $4H_2O$+H).

‡ Association constants (K_{ass}) were determined by ^{1}H NMR titration experiments in $CDCl_3$; stock solutions of host and guest in $CDCl_3$ at different concentrations were prepared and mixed together in the NMR tube in various molar ratios. ^{1}H NMR spectra were recorded at 300 K and the chemical shift of some protons were plotted *versus* guest concentration. Non-linear regression analyses allowed the determination of K_{ass} (accuracy ±10%).

1 *Supramolecular Chemistry of Anions*, ed. A. Bianchi, K. Bowman-James, E. Garcia-España, Wiley, New York, 1997; P. D. Beer and P. Schmitt, *Curr. Opin. Chem. Biol*., 1997, **1** , 475; F. P. Schmidtchen and M. Berger, *Chem. Rev*., 1997, **97**, 1609; M. M. G. Antonisse and D. N. Reinhoudt, *Chem. Commun*., 1998, 443.
2 B. Dietrich, T. M. Fyles, J. M. Lehn, L. G. Pease and D. L. Fyles, *J. Chem. Soc*., *Chem. Commun*., 1978, 934.
3 P. D. Beer, *Chem. Commun*., 1996, 689; M. P. Hughes and B. D. Smith, *J. Org. Chem*., 1997, **62**, 4492.
4 P. Bühlmann, S. Nishizawa, K. P. Xiao and Y. Umezawa, *Tetrahedron Lett*., 1997, **53**, 1647.
5 For a recent Review Article on amides in anion recognition, see I. Stibor, D. S. M. Hafeed, P. Lhoták, J. Hodacová, J. Koca and M. Cajan, *Gazz. Chim. Ital*., 1997, **127**, 673; B. R. Cameron and S. J. Loeb, *Chem. Commun*., 1997, 573.
6 (*a*) J. Scheerder, M. Fochi, J. F. J. Engbersen and D. N. Reinhoudt, *J. Org. Chem*., 1994, **59**, 7815; (*b*) A. Casnati, M. Fochi, P. Minari, A. Pochini, M. Reggiani, R. Ungaro and D. N. Reinhoudt, *Gazz. Chim. Ital*., 1996, **126**, 99; (*c*) N. Pelizzi, A. Casnati, A. Friggeri and R. Ungaro, *J. Chem. Soc*., *Perkin Trans. 2*, 1998, 1307.
7 M. Fe de la Torre, S. Gonzales, E. G. Campos, M. L. Mussons, J. R. Moran and M. Cruz Caballero, *Tetrahedron Lett*., 1997, **38**, 8591.
8 C. Reichardt, *Solvents and Solvent Effects in Organic Chemistry*, VCH, Weinheim, 1988.
9 F. L. Schadt, P. v.R. Schleyer and T. W. Bentley, *Tetrahedron Lett*., 1974, **27**, 2335.
10 W. H. Pirkle, R. L. Muntz and I. C. Paul, *J. Am. Chem. Soc*., 1971, **93**, 2817; W. H. Pirkle and P. L. Rinaldi, *J. Org. Chem*., 1977, **42**, 3217.
11 X. Creary, *J. Org. Chem*., 1987, **52**, 5026; L. S. Chen, G. J. Chen and C. Tamborski, *J. Fluorine Chem*., 1981, **18**, 117.
12 A. Dondoni, A. Marra, M. −C. Scherrmann, A. Casnati, F. Sansone and R. Ungaro, *Chem. Eur. J*., 1997, **3**, 1774.
13 R. Krishanamurti, D. R. Bellew and G. K. S. Prakash, *J. Org. Chem*., 1991, **56**, 984; G. K. S. Prakash and A. K. Yudin, *Chem. Rev*., 1997, **97**, 757.
14 J. Scheerder, R. Vreekamp, J. F. J. Engbersen, W. Verboom, J. P. M. van Duynhoven and D. N. Reinhoudt, *J. Org. Chem*., 1996, **61**, 3476; O. Mogck, E. F. Paulus, V. Böhmer, I. Thondorf and W. Vogt, *Chem. Commun*., 1996, 2533.
15 F. Sansone, S. Barboso, A. Casnati, M. Fabbi, A. Pochini, F. Ugozzoli and R. Ungaro, *Eur. J. Org. Chem*. 1998, 897.
16 T. R. Kelly and M. H. Kim, *J. Am. Chem. Soc*., 1994, **116**, 7072; P. J. Smith, H. V. Reddington and C. Wilcox, *Tetrahedron Lett*., 1992, **33**, 6085.

Communication 8/06837B

The selective catalytic oxidation of silanes to silanols with H_2O_2 activated by the Ti-beta zeolite

Waldemar Adam,[a] Hermenegildo Garcia,[b] Catherine M. Mitchell,[a] Chantu R. Saha-Möller[a] and Oliver Weichold*[a]

[a] *Institut für Organische Chemie der Universität Würzburg, Am Hubland, D-97074 Würzburg, Germany. E-mail: adam@chemie.uni-wuerzburg.de*
[b] *Instituto de Tecnología de Quimica, UPV-CSIC, Avda de los Naranjos s/n, E-46071 Valencia, Spain*

Received (in Liverpool, UK) 23rd September 1998, Accepted 26th October 1998

Ti-beta catalyses the oxidation of small- and medium-sized silanes to the corresponding silanols by aqueous (30%) H_2O_2 as oxygen donor with high conversions and excellent selectivity (no disiloxane).

Although organosilanols have been of continual interest since their discovery,[1] only a limited number of methods for their selective preparation are available. Sterically exposed silanols are especially problematic as they readily dimerize with traces of acid or base to the disiloxanes. Therefore, the commonly used method, *i.e.* the hydrolysis of chlorosilanes,[2] is only applicable for sterically encumbered derivatives. Currently one of the best methods of making silanols is the oxidation of silanes with dioxiranes,[3] but the disadvantage is that this reagent is used stoichiometrically. Catalytic Si–H insertions have also been reported for nickel, palladium, chromium, rhodium, and copper complexes,[4] but these reactions are either limited to special substrates or produce disiloxanes in high amounts.

Recently we developed the first *selective* metal-catalysed Si–H insertion by using the methyltrioxorhenium/urea–H_2O_2 adduct (MTO/UHP) oxidant[5] and proposed that the observed selectivity derives from oxidation in the urea channels (host–guest chemistry), which suppresses the subsequent dimerization of the silanol to the disiloxane. Since the redox molecular sieves TS-1 and Ti-beta are known to catalyse efficiently a variety of oxidations by H_2O_2,[6–9] it was of interest to explore whether such Ti-doped zeolites could serve as catalyst as well as host for the selective oxyfunctionalisation of silanes without disiloxane formation. Indeed, that this is the case is demonstrated herein for Ti-beta, which effectively catalyses the selective oxidation of silanes to silanols by H_2O_2. Most conveniently, our titanium zeolite-catalysed Si–H insertions [eqn. (1)] may be conducted at room temperature with H_2O_2, an environmentally benign oxygen source since its reduction product is water.

$$\underset{\textbf{1a–f}}{R^1R^2R^3SiH} \xrightarrow[\text{MeCN, 20 °C, 24}]{\text{Ti zeolite, } H_2O_2} \underset{\textbf{2a–f}}{R^1R^2R^3SiOH} + \underset{\textbf{3a–f}}{[R^1R^2R^3Si]_2O} \quad (1)$$

The Ti-beta samples used throughout this study were provided by Professor A. Corma, Valencia, Spain, with a Ti content of 2 wt% (as TiO_2) and an aluminium content of 0.29 wt%, and were cation-exchanged by 0.16 M aq. NaOAc. In a typical experiment, the substrate (*ca*. 330 μmol) was dissolved in 1 ml of MeCN, 1.1 equiv. of H_2O_2 (85% or 30% aq. solution) was added while stirring, followed by 30–50 mg of titanium catalyst. The slurry was stirred at ambient temperature (*ca*. 20 °C) for 24 h, subsequently the zeolite was removed by means of a membrane filter (millipore HV, 0.45 μm pore size) and washed three times with 2 ml of acetone. The product mixture was analysed by capillary gas chromatography (Fisons HRGC 5160 Mega Serie, 30-m HP-5 capillary column, FID) and the products were identified by comparing the GC retention times with authentic samples. Conversions and mass balances were calculated relative to an internal standard (Table 1).

Table 1 Conversions, mass balances and product selectivities of the oxidation of silanes **1** to silanols **2** by titanium catalysts

Entry	Substrate	Catalyst	Oxygen source	Conversion[a] (%)	Mass balance[a] (%)	Selectivity[b] **2**:**3**
1	$EtMe_2SiH$ **1a**	Ti-beta	85% H_2O_2	95	68	> 99:1
2	$PrMe_2SiH$ **1b**	Ti-beta	85% H_2O_2	80	87	> 99:1
3	Bu^tMe_2SiH **1c**	Ti-beta	85% H_2O_2	85	63	> 99:1
4	$PhMe_2SiH$ **1d**	TS-1	85% H_2O_2	traces	86	> 99:1
5	$PhMe_2SiH$ **1d**	Ti-beta	85% H_2O_2	58	> 99	> 99:1
6	$PhMe_2SiH$ **1d**	Ti-beta	30% H_2O_2	61	> 99	> 99:1
7	$PhMe_2SiH$ **1d**	Ti-beta[c]	30% H_2O_2	> 99	89	> 99:1
8	$PhMe_2SiH$ **1d**	Ti-beta (calc.)	85% H_2O_2	48	72	59:41
9	$PhMe_2SiH$ **1d**	Ti-beta[d]	85% H_2O_2	35	80	85:15
10	$PhMe_2SiH$ **1d**	$Ti(OPr^i)_4$[e]	*t*BuOOH	38	74	39:61
11	Et_3SiH **1e**	Ti-beta	85% H_2O_2	74	71	> 99:1
12	Et_3SiH **1e**	Ti-beta	30% H_2O_2	75	74	> 99:1
13	(+)-Me(α-Np)PhSiH (*S*)-**1f**	Ti-beta	85% H_2O_2	—	> 99	—

[a] Entries 1,2: determined by ^1H NMR spectroscopy directly on the crude reaction mixture, error ±5% of the stated values; entries 3–10: mass balances and conversions were determined by gas chromatography against an internal standard, error ±1% of the stated values; conditions for **2a**: 35 °C (8 min)→[30 °C min^{-1}]→100 °C (1 min)→[30 °C min^{-1}]→160 °C (2 min), flow 0.5 kg cm^{-2}, against toluene; for **2b**: 40 °C (7 min)→[30 °C min^{-1}]→100 °C (2 min)→[30 °C min^{-1}]→150 °C (5 min)→[30 °C min^{-1}]→240 °C (1 min), flow 0.5 kg cm^{-2}, against ethylbenzene; for **2c**: 35 °C (14 min)→[30 °C min^{-1}]→240 °C (5 min), flow 1.0 kg cm^{-2}, against toluene; for **2d**: 80 °C (4 min)→[30 °C min^{-1}]→130 °C (1 min)→[30 °C min^{-1}]→240 °C (1 min), flow 0.4 kg cm^{-2}, against *n*-hexadecane; for **2e**: 40 °C (3 min)→[30 °C min^{-1}]→100 °C (1 min)→[30 °C min^{-1}]→160 °C (1 min), flow 1.2 kg cm^{-2}, against *n*-dodecane; entry 13: determined by HPLC analysis with Chiralcel® OD-H column with *n*-hexane–Pr^iOH (9:1) as eluent and dimethyl isophthalate as internal standard, error ±2% of the stated value. [b] Selectivities were determined by gas chromatography under the conditions and with the internal standards specified in footnote *a*, error ±1% of the stated values. [c] Recycled catalyst. [d] Catalyst was stirred for 24 h with 1 equiv. H_2O_2 in MeCN and recycled as described. [e] In the presence of diethyl L-tartrate.

For our studies, two titanium-doped zeolites were used, namely TS-1 (5.3 × 5.6 Å)[10] and Ti-beta-Na (6.4 × 7.6 Å).[10] Control experiments showed that no reaction occurred in the absence of the titanium zeolite. This clearly indicates that the oxidative species requires the titanium metal for the activation of H_2O_2 and that direct oxidation of the silane by H_2O_2 does not take place. For comparison with a homogeneous Ti^{IV} catalyst, we employed the well-known $Ti(OPr^i)_4$/Bu^tOOH oxidant.

When Ti-beta was used as oxidation catalyst, good to excellent conversions of the silanes **1a–e** to the corresponding silanols **2a–e** were obtained (Table 1, entries 1–3,5–7,11,12). In contrast, the conversion of the model substrate **1d** with the homogeneous system was lower by 20% (entry 10 compared to entries 5,6). Notably, the silane **1f** is not oxidised because it is sterically too encumbered to enter the zeolite channels (entry 13). Steric hindrance is also the reason why the silane **1d** is not oxidised when the TS-1 zeolite is employed as catalyst (entry 4). The latter results provide unequivocal evidence that these oxidations take place inside the zeolite and not on the outer surface. In addition, if any oxidation of the silanes were to occur on the outer surface of the zeolite, significant amounts of the corresponding disiloxane products should have been formed, in analogy to the Si–H insertion in solution with $Ti(OPr^i)_4$/Bu^tOOH (entry 10).

A major advantage of the Ti-beta/oxidant system for the transformation of silanes to silanols is the fact that excellent product ratios of silanol *versus* disiloxane were obtained for all the silanes studied. This is in stark contrast to the silanol/disiloxane product distributions which have been observed in most previous studies.[4] A further benefit is the fact that the 85% aq. H_2O_2 solution may be substituted by 35% aq. H_2O_2 solution without any loss of selectivity and reactivity (entry 5 *vs*. 6 and entry 11 *vs*. 12).

Since the inorganic framework of the zeolite is quite resistant to oxidative degradation, it was of interest to explore the possibility of catalyst recycling. Indeed, we found that the Ti-beta zeolite may be re-used several times by heating the filtered catalyst at 240 °C for several hours. Interestingly, the recycled catalyst showed even higher catalytic activity (entry 7). It is known that calcination reduces the coordination number of the lattice-bound titanium[11] from 5 or 6 to 4, and thus it seemed likely that the increase in activity is due to the loss of coordinated water; thus more activated sites for H_2O_2 are generated. However, an independently calcinated (*ca*. 500 °C) sample of Ti-beta did not show enhanced catalytic activity (entry 8); moreover, a lower silanol selectivity was observed (59:41). Furthermore, when a sample of Ti-beta was stirred in MeCN with 1 equiv. H_2O_2 for 24 h and recycled as described above, a moderate silanol selectivity (entry 9) was obtained. We propose that the increased catalytic activity is due to *in situ* silylation of free OH groups in the zeolite lattice. The beneficial effect of silylation on the enhancement of catalytic activity has previously been reported for Ti-MCM-41[12] and was assigned to a change to a less polar zeolite interior. The lower silanol selectivity in entries 8 and 9 might be caused by a higher zeolite acidity due to loss of coordination water on calcination, which would promote silanol dimerisation.

Recently, a peracid-type transition-state structure for the Ti-beta-catalysed epoxidation of chiral allylic alcohols with H_2O_2 has been assessed.[8] In analogy, we propose also for the Si–H insertion a five-membered ring peracid-type geometry, as shown in Fig. 1.

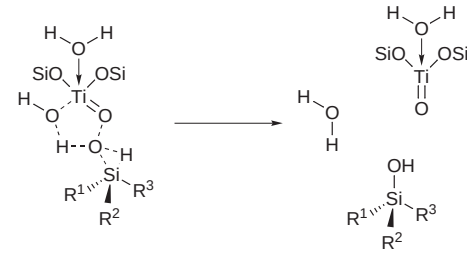

Fig. 1 Proposed transition-state structure for the titanium-catalysed Si–H oxidation.

In conclusion, the well-known Ti-beta/H_2O_2 oxidant is an excellent system for the catalytic conversion of silanes selectively into silanols. This catalytic oxidation takes place inside the zeolite channels and the observed selectivity (no disiloxane) is due to prevention of the dimerization of the silanol.

The authors thank the Deutsche Forschungsgemeinschaft (SFB 347 'Selektive Reaktionen Metall-aktivierter Moleküle'), the Bayerische Forschungsstiftung (Bayerischer Forschungsverbund Katalyse - FORKAT), and the Fonds der Chemischen Industrie for generous financial assistance. A gift of Ti-beta-Na zeolite from Professor A. Corma is greatly appreciated.

Notes and references

1 A. Ladenburg, *Chem. Ber*., 1871, **4**, 901.
2 E. G. Rochow and W. F. Gilliam, *J. Am. Chem. Soc*., 1941, **63**, 798; R. O. Sauer, *J. Am. Chem. Soc*., 1944, **66**, 1707.
3 W. Adam, R. Mello and R. Curci, *Angew. Chem., Int. Ed. Engl*., 1990, **29**, 890.
4 L. H. Sommer, J. E. Lyons, *J. Am. Chem. Soc*., 1969, **91**, 7061; E. Matarasso-Tchiroukhine, *J. Chem. Soc., Chem. Commun*., 1990, 681; C. Egger and U. Schubert, *Z. Naturforsch., Teil B*, 1991, **46**, 783; U. Schubert and C. Lorenz, *Inorg. Chem*., 1997, **36**, 1258.
5 W. Adam, C. M. Mitchell, C. R. Saha-Möller and O. Weichold, *J. Am. Chem. Soc*., submitted.
6 A. Corma, M. A. Camblor, P. Esteve, A. Martínez and S. Valencia, *J. Catal*., 1994, **145**, 151.
7 I. W. C. E. Arends, R. A. Sheldon, M. Wallau and U. Schuchardt, *Angew. Chem., Int. Ed. Engl*., 1997, **36**, 1144.
8 W. Adam, A. Corma, T. I. Reddy and M. Renz, *J. Org. Chem*., 1997, **62**, 3631.
9 P. Kumar, R. Kumar and P. Pandey, *Synlett*, 1995, 289; T. I. Reddy and R. S. Varma, *Chem. Commun*., 1997, 471.
10 E. Höft, H. Kosslick, R. Fricke and H.-J. Hamann, *J. Prakt. Chem*., 1996, **338**, 1; M. A. Camblor, A. Corma, A. Martínez and J. Pérez-Pariente, *J. Chem. Soc., Chem. Commun*., 1992, 589; M. A. Camblor, A. Corma and J. Pérez-Pariente, *Zeolites*, 1993, **13**, 82.
11 T. Blasco, M. A. Camblor, A. Corma and J. Pérez Pariente, *J. Am. Chem. Soc*., 1993, **115**, 11806.
12 T. Tatsumi, K.A. Koyano and N. Igarashi, *Chem. Commun*., 1998, 325.

Communication 8/07442I

New efficient synthesis of phosphonofluorodithioates ROP(S)(S$^-$)F and their structural analogues

Izabela Tworowska and Wojciech Dąbkowski*

Centre of Molecular and Macromolecular Studies, Polish Academy of Sciences, 90–363 Łódź, Sienkiewicza 112, Poland. E-mail: wdabkow@bilbo.cbmm.lodz.pl

Received (in Liverpool, UK) 7th September 1998, Accepted 26th October 1998

The title compounds 3 are formed in very high yield from a one-pot sequential reaction of 1,3,2-dithiaphospholane P^{III} derivatives 1, which are transformed into the corresponding P^{IV} compounds 2 by addition of elemental sulfur and finally into fluoridodithioates 3 by TBAF.

Phosphorus dithioacids play an important role as reagents, ligands and stereochemical probes in ^{31}P NMR spectroscopy.[1] Dithioacids containing a fluorine ligand attached directly to the phosphorus atom are rare.[2] The method of choice for the preparation of simple phosphonofluoridodithioates is not applicable for the preparation of phosphonofluoridodithioate monoesters derived from natural products. Unlike for nucleoside phosphonofluoridate[3a–c] or phosphonofluoridothioate[3d] monoesters, there is only one synthetic method available for the preparation of nucleoside phosphonofluoridodithioate monoesters.[3e] Stawinski and Bollmark have devised a synthesis of nucleoside phosphonofluoridodithioate monoesters *via* oxidation of nucleoside phosphonodithioate with I_2 in pyridine in the presence of TMSCl, followed by addition of triethylamine trishydrofluoride (TAF) to give the nucleoside phosphonofluoridodithioate.[3e]

The importance of phosphoro-fluorine compounds in pure and applied chemistry stimulated our interest in the synthesis of phosphorus dithioacids with P–F bonds. Our studies on the synthesis of phosphonodithioates from 3′-thiothymidine by anhydro-ring opening of 2,3′-anhydrothymidine[4] required an efficient synthesis of *O*,*O*-disubstituted phosphonodithioic acids. We now disclose a novel synthesis of the title compounds **3** containing a wide variety of substituents attached to the phosphorus center (Scheme 1). Our method is based on 1,3,2-dithiaphospholane derivatives **1** which are readily available from ethane-1,2-dithiol and an appropriate P^{III} compound.

The protocol we have developed involves two consecutive reactions carried out in one pot: sulfurization of compound **1** to form compound **2** and finally the reaction with TBAF to open the dithiaphospholane ring with spontaneous elimination of ethylene sulfide and formation of the desired acid **3** (Scheme 1). The roots of this approach are derived from methodology described by Stec.[5]

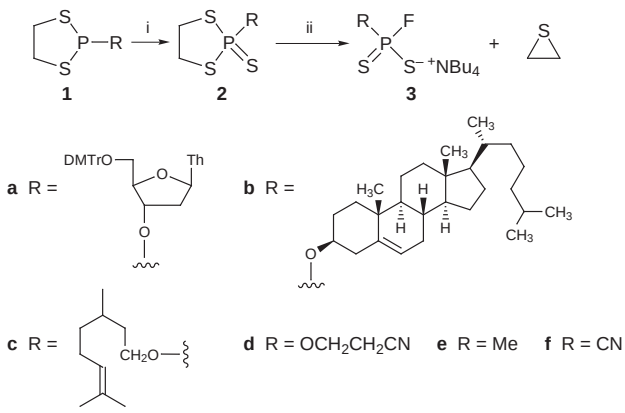

Scheme 1 *Reagents and conditions*: i, S_8, benzene; ii, TBAF, THF.

To illustrate the power and versality of this strategy several examples are presented which include the fluoro dithioacids **3** containing alkyl and alkoxyl (nucleosidyloxy) moieties attached to the phosphorus center. The first example comes from nucleotide chemistry (Scheme 1).† The compounds **1a** and **2a** have been prepared according to the modified procedure of Okruszek and Olesiak.[5b] The condesation of **1** (R = NPr$^i_2$) with 5′-dimethoxytritylthymidine was performed in the presence of TMSCl yielding **1a** in very high yield.[6]†

According to this method *O*-cholesteryl phosphonofluoridodithioate **3b** was obtained in quantitative yield (Scheme 1).‡ 2-Cholesteryloxy-2-thioxo-1,3,2-dithiaphospholane **2b** was the first prepared by Stec and coworkers.[7]

An analogous synthetic pathway led to **3c**§ starting from **1c** (Scheme 1). Synthesis of the 2-citronellyloxy-1,3,2-dithiaphospholane **1c** was achieved by the coupling of **1** (R = NPr$^i_2$) with citronellol in the presence of TMSCl as activator.[6]

The phosphonofluoridodithioate **3d**¶ can be conveniently prepared from **1d**, which is readily available from **1** (R = NPr$^i_2$) *via* condensation with 2-cyanoethanol in the presence of TMSCl. Compound **1d** was transformed into **2d**¶. Ring opening with TBAF gave the dithioacid **1d** (Scheme 1) which, after removal in the presence of Et_3N of the 2-cyanoethyl group, gave the phosphonofluoridodithioic acid **4** [δ_P($CDCl_3$) 67.50(d); δ_F($CDCl_3$) −0.42 (d, $J_{P–F}$ = 1108.96)].

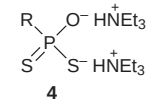

4

The methylphosphonofluoridodithioate **3e**‖ was prepared from compound **1e**[8] (Scheme 1). The preparation of the latter involves the condensation of ethane-1,2-dithiol with methyl(dichloro)phosphine.

The same strategy allowed us to prepare a novel inorganic structure, the cyanophosphonofluoridodithioate **3f**** (Scheme 1). The cyano derivative **1f** was prepared by the reaction **1** (R = Cl) with trimethylsilyl cyanide.

In summary we have developed a novel, efficient and general method for the synthesis of phosphonofluorodithioates **3**. Yields of the final products are very good, exceeding 95%. They show high stability at ambient temperature and can be conveniently converted into free acids by the action of toluene-*p*-sulfonic acid. Acids **3** are strong nucleophiles and thus serve as useful precursors to a wide variety of hitherto unknown functionalized heteroatom systems and ligands. The new route leading to phosphonofluorodithioic acids **3** described here is noteworthy in its flexibility. It can also be extended to analogues of **2** containing a P=Se group.

This work was supported by the German–Polish project (POI-211-96).

Notes and references

† The solvents were reagent grade and were distilled and dried by conventional methods before use. NMR spectra were recorded on a Bruker AC200 spectrometer (^{31}P 81.014 MHz, H_3PO_4 external standard; ^{19}F

188.15 MHz, $CFCl_3$). The compounds **1a** and **2a** were prepared according to the modified procedure of Okruszek and Olesiak [ref. 5(*b*)]. *Typical procedure* for **1** (R = NPr^i_2): A solution of $Pr^i_2NPCl_2$ (10 mmol) in dry THF (10 ml) was added dropwise at room temperature under a nitrogen atomosphere to the solution of ethane-1,2-dithiol (10 mmol) and Et_3N (20 mmol) in dry THF (50 ml) with stirring for 2 h. After 2 h, $Et_3N{\cdot}HCl$ was filtered off and the filtrate evaporated *in vacuo*. The residue was distilled under reduced pressure.

For **1a**: A solution of 5′-DMTr-thymidine (10 mmol) in dry THF (10 ml) was added dropwise at room temperature under a nitrogen atmosphere to a solution of **1** (R = NPr^i_2) (10 mmol) and TMSCl (0.6 mmol) in dry THF (20 ml). After 1 h the mixture was evaporated *in vacuo* and the residue was purified by column chromatography [$\delta_P(CDCl_3)$ 150.67].

For **2a**: To a solution of **1a** in THF was added elemental sulfur, and the mixture was stirred overnight at room temperature. The solvent was evaporated and the residue was chromatographed using acetone–CH_2Cl_2 as eluent to give pure **2a** [$\delta_P(CDCl_3)$ 122.65].

For **3a**: To a solution of **2a** (10 mmol) in dry THF was added a solution of TBAF (11 mmol) in THF at room temperature. After 1 h the mixture was evaporated *in vacuo* and the residue was purified by column chromatography [$\delta_P(CDCl_3)$ 119.64 (d); $\delta_F(CDCl_3)$ −4.92 (d, J_{PF} 1103.74)].

‡ *Selected data* for **1b**: $\delta_P(CDCl_3)$ 147.24. For **2b** $\delta_P(CDCl_3)$ 118.33. For **3b**: $\delta_P(CDCl_3)$ 118.65 (d); $\delta_F(CDCl_3)$ −3.36 (d, J_{PF} 1096.38). Compounds **1b**, **2b** and **3b** were prepared according to the procedure described in note †.

§ *Selected data* for **1c**: $\delta_P(CDCl_3)$ 142.75. For **2c**: $\delta P(CDCl_3)$ 120.53. For **3c** $\delta_P(CDCl_3)$ 120.24 (d); $\delta_F(CDCl_3)$ −8.53 (d, J_{PF} 1094.22). Compounds **1c**, **2c** and **3c** were prepared according to the procedure described in note †.

¶ *Selected data* for **1d**: $\delta_P(CDCl_3)$ 150.19. For **2d**: $\delta_P(CDCl_3)$ 123.34. For **3d**: $\delta_P(CDCl_3)$ 120.84 (d); $\delta_F(CDCl_3)$ −6.07 (d, J_{PF} 1096.30). Compounds **1d**, **2d** and **3d** were prepared according to the procedure described in note †.

‖ *Selected data* for **1e**: $\delta_P(CDCl_3)$ 42.78. Compound **1e** was prepared as described by Peake *et al.* (ref. 7). For **2e**: $\delta_P(CDCl_3)$ 90.58. For **3e**: $\delta_P(CDCl_3)$ 129.8 (d); $\delta_F(CDCl_3)$ −25.55 (d). Compounds **2e** and **3e** were prepared according to the procedure described in note †.

** *Selected data* for **1f**: $\delta_P(CDCl_3)$ 10.71. Compound **1f** was prepared by the reaction of **1** (R = Cl) with TMSCN. For **2f**: $\delta_P(CDCl_3)$ 108.0. For **3f**: $\delta_P(CDCl_3)$ 60.18 (d), $\delta_F(CDCl_3)$ −41.01 (d, J_{PF} 1070.1). Compounds **2f** and **3f** were prepared according to the procedure described in note †. For **2f**, the sulfurization procedure using B_2S_3 is superior to that employing elemental sulfur.

1 M. Potrzebowski and J. Michalski, *^{31}P High Resolution Solid State NMR Studies of Thiophosphooroorganic Compounds*, in *Phosphorus-31 NMR Spectral Properties in Compound Characterization and Structural Analysis*, ed. Quin and J. G. Verkade, VCH, Weinheim, 1994, pp. 413–426.

2 H. W. Roesky, *Chem. Ber.*, 1968, **101**, 3679; R. K. Harris, *J. Chem. Soc., Dalton Trans.*, 1972, 1590; E. Fluck, R. Schimdt and W. Haubold, *Phosphorus Sulfur*, 1978, **5**, 141.

3 (*a*) R. Wittmann, *Chem. Ber.*, 1963, **96**, 771; (*b*) Netherlands Patent 6,516,242 (July 28, 1996); *Chem. Abstr.*, 1967, **66**, 11162j; (*c*) C. Sund and J. Chattopadhyaya, *Tetrahedron*, 1989, **45**, 7523; (*d*) W. Dąbkowski and I. Tworowska, *Chem. Lett.*, 1995, 727; (*e*) J. Stawinski and M. Bollmark, *Tetrahedron Lett.*, 1996, **37**, 5739; (*f*) K. Misiura, D. Szymanowicz and W. J. Stec, *Chem. Commun.*, 1998, 515.

4 W. Dąbkowski, M. Michalska and I. Tworowska, *Chem. Commun.*, 1998, 427.

5 (*a*) A. Okruszek, A. Sierzchała, M. Sochacki and W. J. Stec, *Tetrahedron Lett.*, 1992, **33**, 7585; (*b*) A. Okruszek and M. Olesiak, *J. Med. Chem.*, 1994, **37**, 3850; (*c*) A. Okruszek, A. Sierzehala, K. L. Fearon and W. J. Stec, *J. Org. Chem.*, 1995, **60**, 6998; (*d*) A. Okruszek, M. Olesiak, D. Krajewska and W. J. Stec, *J. Org. Chem.*, 1997, **62**, 2269.

6 W. Dąbkowski, I. Tworowska, J. Michalski and F. Cramer, *Chem. Commun.*, 1997, 877.

7 J. Błaszczyk, M. Wieczorek, A. Okruszek, A. Sierzchała and W. J. Stec, *J. Chem. Crystallogr.*, 1996, **26**, 33.

8 S. C. Peake, M. Fild, R. Schmutzler, R. K. Harris, J. M. Nichols and R. G. Rees, *J. Chem. Soc., Perkin Trans. 2*, 1972, 380.

Communication 8/07029F

ChemComm

A significant effect of anion binding ureas on the product ratio in the palladium(II)-catalyzed hydrocarbonylation of alkenes

Jan Scheele, Peter Timmerman and David N. Reinhoudt*

Laboratory of Supramolecular Chemistry and Technology, University of Twente, PO Box 217, 7500 AE Enschede, The Netherlands. E-mail: smct@ct.utwente.nl

Received (in Cambridge, UK) 27th August 1998, Accepted 21st October 1998

Hydrogen bonding of urea derivatives to the anionic ligands X of (dppp)PdX_2 catalysts significantly increases the hydroacylation of cyclopentene relative to the hydroformylation, most probably due to a decreased coordination strength of the anionic ligands.

Transition metal complexes are important homogeneous catalysts for alkene polymerization[1] and alkene/CO copolymerization reactions.[2] In the L_2PdX_2-catalyzed hydrocarbonylation of alkenes with synthesis gas (CO/H_2) either aldehydes (hydroformylation), ketones (hydroacylation), or polyketones (copolymerization) are formed. The type of reaction is determined mainly by the coordination strength of the anionic ligands X in L_2PdX_2.[3] Only Pd^{II} catalysts with weakly coordinating anions (*e.g.* X = TFA) show sufficient activity in such hydrocarbonylation reactions. These catalysts are prepared by anion metathesis reactions of L_2PdX_2 with the corresponding silver salt (X = Cl)[4] or Brønsted acid (X = OAc).[5] Alternatively, strong Lewis acids like methylalumoxane (MAO)[6] or $SnCl_2$[7] are added.

Our group has developed a variety of anion receptors based on multiple hydrogen bonding to (sulfon)amides[8] or (thio)ureas,[9] or coordination to a Lewis acidic uranyl center.[10] These anion receptors have been applied for anion-selective sensors (CHEMFETs)[11] and in membrane transport studies. Recently, we have described the catalytic activity of anion receptors in acyl transfer reactions.[12]

Here we show that *N*,*N*′-disubstituted urea derivatives **1**–**5**

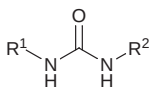

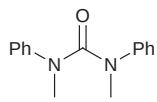

6

1 $R^1 = R^2 = Ph$
2 $R^1 = p\text{-}F_3CC_6H_4$, $R^2 = Ph$
3 $R^1 = R^2 = p\text{-}F_3CC_6H_4$
4 $R^1 = Bu^n$, $R^2 = Ph$
5 $R^1 = R^2 = Bu^n$

significantly influence the performance of the (dppp)PdX_2 catalyst [dppp = 1,3-bis(diphenylphosphino)propane] in hydrocarbonylation reactions. The effect is attributed to the interaction[13] of the acidic urea protons with the counterions (X = OAc, TFA, OTs) leading to a decrease in their coordination strength. There are reports of hydrogen bonding to the anionic ligands of transition metal complexes in the solid state.[14] To the best of our knowledge this is the first report in which hydrogen bonding to the anionic ligands of a homogeneous catalyst alters the product ratio of the reaction.[15]

As a model reaction we used the Pd^{II}-catalyzed hydrocarbonylation of cyclopentene with synthesis gas in anisole.† The mechanism for this reaction[3] is depicted in Scheme 1. Hydride **8** is formed by reaction of precatalyst (dppp)PdX_2 with H_2. The rate of the subsequent exchange reaction of cyclopentene for X depends strongly on the coordination strength of the counterion to the Pd center.[4,16] Migratory insertion gives the σ-alkyl–Pd complex **9** and consecutive CO insertion yields the acyl–Pd intermediate **10**. The formation of **10** from **8** is monitored by the turnover number of CO (TON_{CO}), *i.e.* the number of CO insertions per Pd center. Intermediate **10** can react further in two different ways, either giving cyclopentanecarbaldehyde **11** or yielding one of the ketones **13**–**15** after insertion of a second molecule of cyclopentene. In all cases **8** is regenerated either by β-elimination or by oxidative addition of HX to the Pd^0 complex formed.

The selectivity for ketones increases from 14 to 98% reflecting the decrease in coordination strength of the anionic ligands X in the series of (dppp)PdX_2 (X = TFA, OMs, OTs, OTf, entries 1–4 in Table 1) with $6.0 \times 10^2 < TON_{CO} < 9.2 \times 10^2$ mol (mol Pd)$^{-1}$ h^{-1}. With (dppp)Pd$(OAc)_2$ (entry 5) the TON_{CO} is reduced to 0.2×10^2 mol (mol Pd)$^{-1}$ h^{-1} because of the stronger coordinating acetate, and the selectivity for ketones is 24%. Weaker coordinating anions may enhance the (intrinsic) electrophilicity of the Pd^{II} center and, of course, these anions are more easily displaced from the (fourth) coordination site which facilitates the formation of intermediates **10** (increased TON_{CO}) and **12** (increased selectivity for ketones).

We found that in the presence of 0.6 mol% [7.5 equiv. with respect to the (dppp)Pd$(TFA)_2$ catalyst] of *N*,*N*′-diphenylurea **1** the selectivity for ketones increases from 14 to 25% (entry 6 in Table 1), whereas the TON_{CO} increases from 6.0×10^2 to 7.8×10^2 mol (mol Pd)$^{-1}$ h^{-1}.‡ With 0.6 mol% of the urea derivatives **2** and **3**, containing either one or two electron-withdrawing substituents at the phenyl rings that will increase the anion affinity of the urea moiety,[17] the selectivity for ketones shows a sharp increase from 14 to 49 and 61%, respectively (entries 7 and 8). In both cases the TON_{CO} is similar to that in the presence of urea **1**. Both *N*-butyl-*N*′-phenylurea **4** and *N*,*N*′-dibutylurea **5** do not significantly change the selectivity for ketones (entries 9 and 10), which is in accordance with the much lower acidity and anion binding strength of (di)alkyl ureas compared to diaryl ureas.[18]

The altered selectivities of the catalyst upon addition of diarylureas **1** or **3** were also observed for the catalysts

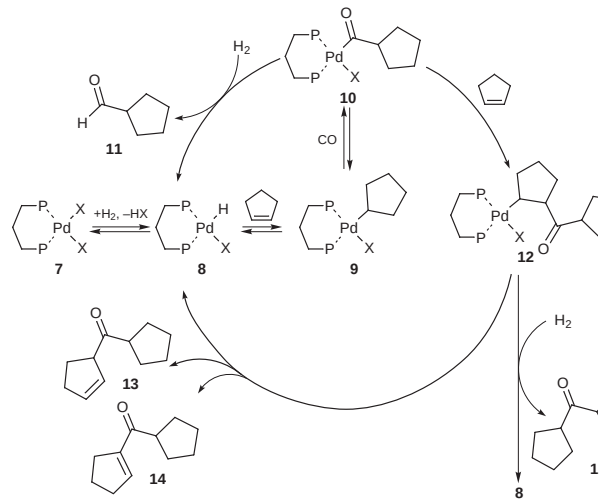

Scheme 1 Catalytic cycle for the Pd^{II}-catalyzed hydrocarbonylation of cyclopentene.

Table 1 Selectivity for ketones and turnover number for the hydrocarbonylation of cyclopentene with CO and H_2 in the presence of urea derivatives **1**–**6**[a]

Entry	Anion	Receptor[b]	Selectivity (%)[c]	$TON_{CO}/10^2$ mol (mol Pd)$^{-1}$ h^{-1} [d]
1	OTf	—	98	8.7
2	OTs	—	54	8.2
3	OMs	—	41	9.2
4	TFA	—	14	6.0
5	OAc	—	24	0.2
6	TFA	**1**	25	7.8
7	TFA	**2**	49	7.8
8	TFA	**3**	61	8.3
9	TFA	**4**	16	5.9
10	TFA	**5**	10	5.1
11	OAc	**1**	45	0.4
12	OAc	**3**	80	0.4
13	OTs[e]	**1**	82	7.0
14	OTs	**3**	95	10
15	TFA	**6**	14	6.4
16	TFA[f]	**6**	12	5.8
17	OAc	**6**	25	0.3
18	OTs	**6**	51	9.6

[a] Cyclopentene (5 ml), anisole (10 ml), (dppp)PdX_2 (0.08 mol%), 110 °C, 80 bar (CO:H_2 = 1:1), analysis by GC FID, integrals were not corrected for sensitivities. [b] 7.5 equiv. cocatalyst compared to Pd catalyst. [c] Percentage of hydroacylation products (**13–15**) of the total amount of products formed, accuracy ±2%. [d] Turnover number of CO determined as the sum of TONs of all products **11**, **13**, **14** and **15**; accuracy ±5% (see note ¶). [e] 10 equiv. cocatalyst **5**. [f] 13 equiv. cocatalyst **6**.

(dppp)Pd(OAc)$_2$ (entries 11 and 12) and (dppp)Pd(OTs)$_2$ (entries 13 and 14). In both cases the stronger anion binding urea **3** causes the largest change in the selectivity for ketones, *i.e.* from 24 to 80% for (dppp)Pd(OAc)$_2$ and from 54 to 95% for (dppp)Pd(OTs)$_2$. The TON_{CO} is enhanced from 0.2×10^2 to 0.4×10^2 and from 8.2×10^2 to 10×10^2 mol (mol Pd)$^{-1}$ h^{-1}, respectively. These results suggest that the observed increase in ketone formation is the result of complexation of the anionic ligands by the urea derivatives **1**–**3** *via* hydrogen bonding which decreases the coordination strength of the counterions to the Pd center.

Experiments carried out in the presence of a large excess of tetrasubstituted urea **6**, which is unable to bind anions *via* hydrogen bonding, show that neither the selectivity for ketones nor the TON_{CO} is affected to a significant extent (entries 15–18 in Table 1). This excludes the possibility that the observed effect is due to coordination of the urea carbonyl to the Pd center or to a change in the polarity of the reaction medium.§

Our results show that hydrogen bond formation to the anionic ligands X of (dppp)Pd catalysts can significantly change the selectivity of the catalyst in the hydrocarbonylation of cyclopentene with synthesis gas. Addition of *N*,*N*′-diarylureas **1**–**3** strongly favours hydroacylation with respect to hydroformylation. The maximum effect is observed with the stronger anion binding urea **3**.

We thank the Shell Research & Technology Centre, Amsterdam, for financial support and Professor Dr E. Drent and Dr W. P. Mul for helpful discussions.

Notes and references

† *Experimental procedure*: Hydrocarbonylation experiments were performed in a 100 ml autoclave at 110 °C. 10 ml anisole, 5 ml cyclopentene, 0.08 mol% of (dppp)PdX_2 catalyst, and urea cocatalyst were brought under a H_2 atmosphere whereafter the autoclave was pressurized with 40 bar CO and 40 bar H_2. After a reaction time of 20 h the autoclave was cooled down and the gas (pressure drop < 15 bar) was vented off. The products were analysed by GC FID (CPSIL-5, 50 m).

‡ The amount of added *N*,*N*′-diphenylurea **1** correlates well with the selectivity for ketones formed in the reaction and the TON_{CO}. With varying amounts (2–18 equiv.) of **1** as cocatalyst in the (dppp)Pd(TFA)$_2$ catalyzed reaction both the selectivity for ketones and the TON_{CO} are increased. A maximum of 37% and 8.9×10^2 mol (mol Pd)$^{-1}$ h^{-1} was reached with 1.5 mol% (18 equiv.) of **1** (limited by the solubility of **1** in the reaction medium).

§ Additional evidence for hydrogen bond formation of **1**–**5** to the anionic ligands X of (dppe)PdX_2 (X = Cl, TFA, OTs) was obtained by IR, ^{1}H and ^{31}P NMR spectroscopic studies in $CDCl_3$ at room temperature (ref. 19). Addition of 2 equiv. (dppe)$PdCl_2$ to an 1 mM solution of *N*,*N*′-diphenylurea **1** (free N–H vibration at 3422 cm^{-1}) gave rise to an additional N–H stretch frequency at 3330 cm^{-1} in the FT–IR spectrum. The ^{1}H NMR spectra of ureas **1**–**5** show in all cases downfield shifts ($0.40 > \Delta\delta > 0.15$ ppm) for the urea proton signals upon addition of 1 equiv. of (dppp)PdX_2, which is indicative for hydrogen bond formation. Furthermore the ^{31}P NMR resonances of the (dppe)PdX_2 complexes shift over 1 ppm downfield upon addition of 2 equiv. of **1**. Similar downfield shifting of the ^{31}P NMR resonances is also observed upon weakening of the coordination strength of the anions of (dppe)PdX_2 (X = TFA: δ 63.1; X = OTs: δ 69.9). In contrast to this the addition of 1,3-dimethyl-1,3-diphenylurea **6** to the Pd complexes did not induce any significant shift of the ^{31}P NMR resonances.

¶ The TONs based on conversion of cyclopentene ($TON_=$).can easily be calculated from Table 1 according to $TON_= = TON_{CO} \times (1 +$ selectivity).

1 H. H. Brintzinger, D. Fisher, R. Mülhaupt, B. Rieger and R. M. Waymouth, *Angew. Chem., Int. Ed. Engl.*, 1995, **34**, 1143; P. Margl, L. Deng and T. Ziegler, *Organometallics*, 1998, **17**, 933.

2 E. Drent, Eur. Pat. Appl. 121,965 A2, 1984; E. Drent, J. A. M. van Broekhoven and M. J. Doyle, *J. Organomet. Chem.*, 1991, **417**, 235; A. Sen, *Adv. Polym. Sci.*, 1986, **73/74**, 125.

3 E. Drent and P. H. M. Budzelaar, *Chem. Rev.*, 1996, **96**, 663; C. Pisano and G. Consiglio, *Gazz. Chim. Ital.*, 1994, **124**, 393.

4 A. Yamamoto, *J. Organomet. Chem.*, 1995, **500**, 337.

5 E. Drent, *Pure Appl. Chem.*, 1990, **62**, 661.

6 L. K. Johnson, C. M. Killian and M. Brookhart, *J. Am. Chem. Soc.*, 1995, **117**, 6415.

7 F. Agbossou, J. F. Carpentier and A. Mortreux, *Chem. Rev.*, 1995, **95**, 2485.

8 S. Valiyaveettil, J. F. J. Engbersen, W. Verboom and D. N. Reinhoudt, *Angew. Chem., Int. Ed. Engl.*, 1993, **32**, 900.

9 J. Scheerder, J. P. M. van Duynhoven, J. F. J. Engbersen and D. N. Reinhoudt, *Angew. Chem., Int. Ed. Engl.*, 1996, **35**, 1090.

10 D. M. Rudkevich, Z. Brzozka, M. J. Palys, W. P. R. V. Stauthamer, G. J. van Hummel, S. M. Franken, S. Harkema, J. F. J. Engbersen and D. N. Reinhoudt, *J. Am. Chem. Soc.*, 1994, **116**, 4341.

11 M. M. G. Antonisse, B. H. M. Snellink-Ruël, J. F. J. Engbersen and D. N. Reinhoudt, *J. Chem Soc., Perkin Trans. 2*, 1998, 773.

12 V. van Axel Castelli, R. Cacciapaglia, G. Chiosis, F. C. J. M. van Veggel, L. Mandolini and D. N. Reinhoudt, *Inorg. Chim. Acta*, 1996, **246**, 1.

13 Ureas are known to bind to a variety of (delocalized) anions *via* hydrogen bonding. E. Fan, S. A. Van Arman, S. Kincaid and A. D. Hamilton, *J. Am. Chem. Soc.*, 1993, **115**, 369.

14 van Koten, *Angew. Chem., Int. Ed. Engl.*, 1996, **35**, 1959;K. Biradha and G. R. Desiraju, *Organometallics*, 1996, **15**, 1284; E. S. Shubina, N. V. Belkova and L. M. Epstein, *J. Organomet. Chem.* 1997, **536–537**, 17; F. Grepioni, G. Cojazzi, S. M. Draper, N. Scully and D. Braga, *Organometallics*, 1998, **17**, 296.

15 The influence of thiourea on the palladium catalyzed reaction of terminal alkynes has been reported. However, this effect is attributed to coordination of the thiocarbonyl moiety to the Pd center and not to hydrogen bonding. B. Gabriele, G. Salerno, M. Costa and G. P. Chiusoli, *J. Organomet. Chem.* 1995, **503**, 21.

16 G. P. C. M. Dekker, C. J. Elsevier, K. Vrieze, P. W. N. M. van Leeuwen and C. F. Roobeek, *J. Organomet. Chem.*, 1992, **430**, 357.

17 C. S. Wilcox, E. Kim, D. Romano, L. H. Kuo, A. L. Burt and D. P. Curran, *Tetrahedron*, 1995, **51**, 621.

18 S. Nishizawa, P. Bühlmann, K. P. Xiao and Y. Umezawa, *Anal. Chim. Acta*, 1998, **358**, 35.

19 Chloroform has approximately the same solvation strength as anisole. Y. Marcus, *Ion Solvation*, Wiley, New York, 1985.

Communication 8/06722H

ChemComm

Synthesis of cross-conjugated trienes by dimerization of allenes with palladium-phenol catalyst

Mieko Arisawa, Takumichi Sugihara† and Masahiko Yamaguchi*

Faculty of Pharmaceutical Sciences, Tohoku University, Aoba, Sendai 980-8578, Japan.
E-mail: yama@mail.pharm.tohoku.ac.jp

Received (in Cambridge, UK) 28th September 1998, Accepted 26th October 1998

Cross-conjugated trienes were synthesized by dimerization of monosubstituted allenes in the presence of a catalyst system consisted of $Pd_2(dba)_3$, *p*-nitrophenol, and P(*p*-Tol)$_3$.

Cross-conjugated trienes have attracted considerable interest in polymer chemistry[1] and theoretical chemistry[2] as well as in synthetic chemistry, and various methods have been developed for the preparation of the parent 3-methylenepenta-1,4-diene and its derivatives.[3] Although catalytic dimerization of substituted allenes can directly provide such trienes, an effective method has as yet not been developed. The dimerization reaction of 3-methylbuta-1,2-diene was reported to give 2,5-dimethyl-3,4-bismethylenehex-1-ene, which was promoted by a stoichiometric amount of a nickel(0) complex.[4] The reaction, however, gave a very low yield of the cross-conjugated triene when other allenes were employed. Although palladium complexes are known to catalyze dimerization of propa-1,2-diene in the presence of water or amine giving hydroxylated or aminated 2,3-dimethylbuta-2,3-diene,[5] the method was not applied to the synthesis of cross-conjugated trienes. Described here is an efficient synthesis of the trienes by catalytic dimerization of monosubstituted allenes, alka-1,2-dienes. A novel combination of $Pd_2(dba)_3$ (dba = dibenzylideneacetone), *p*-nitrophenol, and P(*p*-Tol)$_3$ was employed for the catalyst.

When undeca-1,2-diene **1** was treated with $Pd_2(dba)_3$ (5 mol%), P(*p*-Tol)$_3$ (15 mol%) and *p*-nitrophenol (10 mol%) in refluxing THF for 12 h, (9*E*,12*E*)-10-methyl-11-methyleneicosa-9,12-diene **2** was obtained in quantitative yield (Table 1, entry 5). The structure including the stereochemistry was determined unambiguously by spectroscopic methods. Added phenol played an important role, and no reaction took place in its absence (entry 1). This reaction was effectively promoted by phenol possessing an electron-withdrawing group (*p*-nitrophenol) while the yield of **2** decreased when phenol, alkylphenol, or methoxyphenol was used (entries 2–4). Considerable amounts of adducts **3** or **4** derived from **2** and the phenols were formed in the latter cases. Since AcOH also promoted the reaction (entry 10), phenol appeared to function as the Brønsted acid.[6] The dimerization reaction did not occur with sodium phenoxide or tributyltin phenoxide. Use of P(*p*-Tol)$_3$ was also essential, and the reaction was retarded by the introduction of electron-withdrawing substituents on the aromatic ring (entry 7). Bidentate phosphines gave 1,3-diene without forming the dimeric product (entries 8 and 9).

The dimerization reaction of other methylene-substituted allenes under the above reaction conditions proceeded stereoselectively to give the cross-conjugated (*E*,*E*)-trienes in quantitative yields (Table 2). With this catalyst system, a product–catalyst ratio of 1000:1 could be reached (entry 2). Dimerization of a methyne substituted allene, 1-cyclohexylpropa-1,2-diene, was sluggish, although the stereoselectivity was retained (entry 8).

† Present address: Faculty of Pharmaceutical Sciences, Tokushima Bunri University, Yamashiro-cho, Tokushima 770-8514, Japan.

When **1** was dimerized in the presence of 1.0 equiv. of AcOD (> 99 atom% D) or *p*-$NO_2C_6H_4OD$ (76 atom% D), the dimer **2**-*d* was obtained in 78% yield (79 atom% D) and 93% (56

Table 1 Effect of phenol and phosphine on the allene dimerization

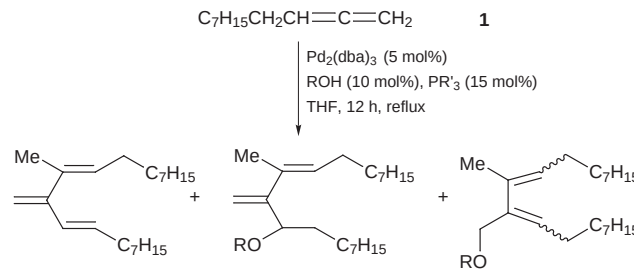

Entry	R	R′	Yield (%) **2**	recovered **1**	**3** and/or **4**
1	none	*p*-Tol	—	95	—
2	*p*-$MeOC_6H_4$	*p*-Tol	60	18	10
3	*p*-Tol	*p*-Tol	54	7	9
4	Ph	*p*-Tol	91	—	4
5	*p*-$NO_2C_6H_4$	*p*-Tol	96	—	—
6	*p*-$NO_2C_6H_4$	Ph	89	—	—
7	*p*-$NO_2C_6H_4$	*p*-ClC_6H_4	57	20	—
8	*p*-$NO_2C_6H_4$	dppe[a]	—	42	—[b]
9	*p*-$NO_2C_6H_4$	dppf[c]	—	—	—[d]
10	Ac	*p*-Tol	74	—	—

[a] 1,2-Diphenylphosphinoethane. [b] Undeca-1,3-diene was obtaiend in 36% yield. [c] 1,1′-Bis(diphenylphosphino)ferrocene. [d] Undeca-1,3-diene was obtained in 71% yield.

Table 2 Synthesis of cross-conjugated trienes by the allene dimerization reaction

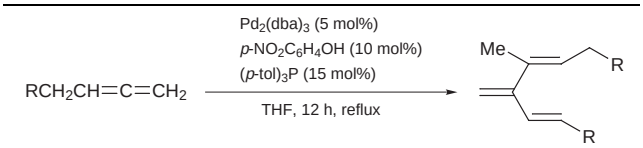

Entry	Allene	Yield (%)
1	$C_7H_{15}CH_2CH_2$=C=CH_2	96
2	$C_7H_{15}CH_2CH$=C=CH_2	99[a]
3	$C_5H_{11}CH_2CH$=C=CH_2	96
4	$Bu^tMe_2SiOCH_2CH_2CH$=C=CH_2	96
5	$Bu^tMe_2SiO(CH_2)_2CH_2CH$=C=$CH_2$	89
6	$PhCH_2CH$=C=CH_2	93
7	$PhCH_2CH_2CH$=C=CH_2	99
8	*c*-$C_6H_{11}CH$=C=CH_2	36[b]

[a] The reaction was carried out using 5 mmol of **1** in the presence of 0.1 mol% of $Pd_2(dba)_3$, 0.3 mol% of P(*p*-Tol)$_3$ and 0.2 mol% of *p*-nitrophenol. [b] Starting material was recoverd in 32% yield.

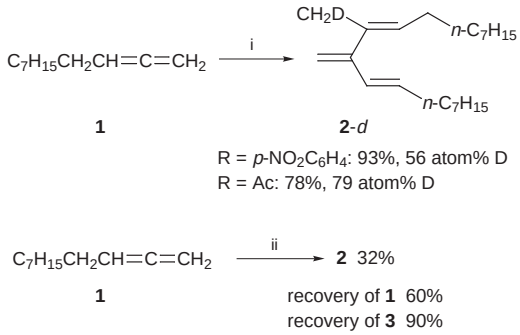

Scheme 1 *Reagents and conditions*: i, $Pd_2(dba)_3$ (5 mol%), P(p-Tol)$_3$ (15 mol%), ROD (100 mol%), THF, reflux, 12 h; ii, $Pd_2(dba)_3$ (5 mol%), P(p-Tol)$_3$ (15 mol%), **3** (R = p-Tol) (10 mol%), THF, reflux, 12 h.

atom% D) yield, respectively (Scheme 1). A ^{2}H NMR experiment revealed deuteration at the methyl group. A considerable part of the proton was thus introduced from the external proton source. In order to know the role of the adducts **3** and **4** in the reaction, the dimerization of **1** was conducted in the presence of a catalytic amount of **3** (R = p-Tol) instead of p-nitrophenol. After reacting for 12 h, only 32% yield of the dimer **2** was obtained with **1** recovered in 60% yield. Approximately 90% of the adduct **3** (R = p-Tol) was also recovered unchanged. The result, compared to that of Table 1, entry 3, indicated that the formation of **3** and **4** was not the major process of the present catalytic reaction.

Although the dimerization reactions of propa-1,2-diene and 3-methylbuta-1,2-diene was studied to some extent,[4,5] the mechanism still remained unclear. Based on our experiments and the results of the $(R_3P)_3Ni$-promoted stoichiometric dimerization reaction of 3-methylbuta-1,2-diene, the following working hypothesis was presented (Scheme 2). Since the nickel reaction took place *via* a nickelacycle,[4] it may be likely that the present palladium-catalyzed dimerization involved a palladacycle.[7] The reductive elimination with concomitant proton transfer from the δ-carbon atom to the α′-carbon atom gave the cross-conjugated triene. Our deuteration experiments showed that the δ-proton in the palladacycle was not transferred

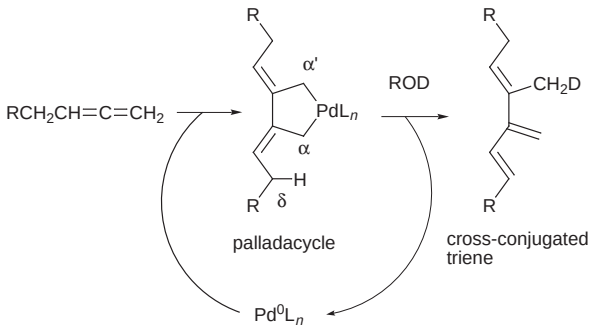

Scheme 2

intramolecularly. The process appeared to be catalyzed by phenol.

Polymerization of the cross-conjugated trienes obtained in the present study was also examined. Triene **2** was treated with $SnCl_4$ and Bu^{t}Cl in CH_2Cl_2 at −50 °C for 1 min.[8] After aqueous workup and purification by gel permeation chromatography, soluble polymer was obtained in 30% yield (M_n = 1.9 × 10^4, M_w/M_n = 1.93). Use of protic acid (H_2SO_4, $HClO_4$, TfOH) gave insoluble materials. The cationic conditions turned out to be suitable for the polymerization of **2**, and radical conditions (AIBN, 80 °C), anion treatment (Bu^{n}Li or Bu^{t}Li, THF, −78 °C) or thermal treatment (80 °C, 24 h, under argon or oxygen) gave low molecular weight oligomers.

The dimerization reaction of **1** is representative. Under an argon atmosphere, a mixture of $Pd_2(dba)_3$ (45.7 mg, 5 mol%), P(p-Tol)$_3$ (45.6 mg, 15 mol%), **1** (152 mg, 1.0 mmol) and p-nitrophenol (13.9 mg, 10 mol%) in THF (5 ml) was heated at reflux for 12 h. THF was then removed under reduce pressure, and the residue was purified by flash chromatography (hexane) over silica gel giving **2** (145.9 mg, 96%).

The authors thank Professor Tokuji Miyashita (Institute for Chemical Reaction Sciences, Tohoku University) for obtaining M_w and M_n values for the polymer. This work was supported by grants from the Japan Society of Promotion of Science (RFTF 97P00302) and the Ministry of Education, Science, and Culture, Japan.

Notes and references

1 For example, W. J. Bailey, J. Economy and M. E. Hermes, *J. Org. Chem*., 1962, **27**, 3295; R. C. Blume, U.S. Pat. 3,860,669; *Chem. Abstr*., 1975, **82**, 172295j; U.S. Pat. 3,912,702; *Chem. Abstr*., 1976, **84**, 18546b.

2 For example, U. Fleischer, W. Kutzelnigg, P. Lazzeretti and V. Mühlenkamp, *J. Am. Chem. Soc*., 1994, **116**, 5298.

3 A review: H. Hopf, *Angew. Chem*., *Int. Ed. Engl*., 1984, **23**, 948. Also see for examples, S. Kanemasa, H. Sakoh, E. Wada, and O. Tsuge, *Bull. Chem. Soc. Jpn*., 1986, **59**, 1869; G. Kaupp, H. Frey and G. Behmann, *Chem. Ber*., 1988, **121**, 2127; J. I. G. Cadogan, S. Cradock, S, Gillam and I. Gosney, *J. Chem. Soc*., *Chem. Commun*., 1991, 114; W. S. Trahanovsky and K. A. Koeplinger, *J. Org. Chem*., 1992, **57**, 4711.

4 M. Englert, P. W. Jolly and G. Wilke, *Angew. Chem*., *Int. Ed. Engl*., 1972, **11**, 136; D. J. Pasto, N.-Z. Huang and C. W. Eigenbrot, *J. Am. Chem. Soc*., 1985, **107**, 3160; D. J. Pasto and N.-Z. Huang, *Organometallics*, 1985, **4**, 1386.

5 D. R. Coulson, *J. Org. Chem*., 1973, **38**, 1483; Y. Inoue, Y. Ohtsuka and H. Hashimoto, *Bull. Chem. Soc. Jpn*., 1984, **57**, 3345.

6 Yamamoto recently reported a Pd–acetic acid catalyst. M. Al-Masum, M, Meguro and Y. Yamamoto, *Tetrahedron Lett*., 1997, **38**, 6071; S. Kamijo, M. Al-Masum and Y. Yamamoto, *Tetrahedron Lett*., 1998, **39**, 691.

7 Treatment of propa-1,2-diene with a Pd^0 complex was reported to give dimeric π-allylpalladium. M. S. Lupin, J. Powell and B. L. Shaw, *J. Chem. Soc. A*, 1966, 1687. The compound could be another candidate for the intermediate of the present reaction.

8 See the following for a related system using PhCHClMe/$SnCl_4$: T. Higashimura, Y. Ishihama and M. Sawamoto, *Macromolecules*, 1993, **26**, 744.

Communication 8/07527A

On the cyclization mechanism of squalene: a ring expansion process of the five-membered D-ring intermediate

Tsutomu Sato,[a] Takamasa Abe[b] and Tsutomu Hoshino*[ab]

[a] *Graduate School of Science and Technology, and*
[b] *Department of Applied Biological Chemistry, Faculty of Agriculture, Niigata University, Ikarashi, Niigata 950-2181, Japan. E-mail: hoshitsu @agr.niigata-u.ac.jp*

Received (in Cambridge, UK) 7th September 1998, Accepted 26th October 1998

Site-directed mutagenesis experiments with W169F, W169H and W489F for the squalene-hopene cyclase, and the formation of 10 possessing the five-membered D-ring and a tetrahydrofuran moiety as the enzyme product of the analogue 8 with a hydroxy group, strongly suggest that a ring expansion reaction from the five- to the six-membered ring is responsible for the D-ring formation of hopene.

The cyclization of squalene **1** into pentacyclic triterpenes, hop-22(29)-ene **2** and hopan-22-ol **3**, is an outstanding reaction from the point of view of both stereo- and regio-chemical specificity, with the formation of five new carbon–carbon bonds and nine new chiral centers.[1] Oxidosqualene also undergoes the polyolefin cyclization analogous to squalene.[1] Recent progress on the two cyclases of squalene and oxidosqualene has spurred mechanistic studies of the polycyclization reactions. Squalene-hopene cyclase (SHC) is believed to fold the linear molecule **1** into an all pre-chair conformation **1a** inside the enzyme cavity, leading to **2** and **3** through the generation of a series of carbocation intermediates (Scheme 1).[2] Scheme 1 also shows that the C- and D-rings are formed by anti-Markovnikov closures. Site-directed mutagenesis experiments of SHC revealed that both D-376 and D-377 were crucial for the catalysis.[3] Recently, an X-ray analysis of *Alicyclobacillus acidocaldarius* SHC has been reported.[4] We have independently succeeded in an overexpression of the SHC and reported the first identification of the tryptophan residues 169 and 489 as components of the active sites; substitution of these tryptophans with valine and leucine by point mutations resulted in complete loss of the enzyme activity.[5] Here, we report that mutants of W169F, W169H and W489F produce the normal cyclization products **2** and **3** together with an abnormal tetracyclic product **4** consisting of a 6/6/6/5-fused ring system, the formation of **4** being in agreement with the Markovnikov rule. This finding leads us to propose that a ring expansion reaction is involved in the D-ring formation of **2** and **3**.

Cell-free homogenates of the mutants prepared by site-directed mutagenesis were incubated with **1** at optimal temperatures (45 °C for W169F and W169H, and 53 °C for W489F). The wild-type has a catalytic optimum at 60 °C and pH 6.0.[3,5] A large scale incubation of **1** (150 mg) for 16 h with a cell-free extract from a 6 l culture of W169F afforded **2**, **3** and **4** (an oil) (100.5, 10 and 6 mg, respectively) after the separation with a SiO_2 column (hexane–EtOAc). The incubation of other mutants conducted with the same quantities of **1** and cell-free extracts as for W169F gave the following isolated yields: for mutant W169H: **2** (73.5 mg), **3** (6.3 mg) and **4** (33.0 mg), and for mutant W489F: **2** (36.8 mg), **3** (3.3 mg) and **4** (9.8 mg). Detailed 2D NMR analyses[6] revealed that **4** had a dammarene skeleton with an exomethylene group, but the 17-side chain had an α-orientation (17-*epi*-dammarene). No other product was detected in the reaction mixtures except for recovered **1**.

Concomitant production of **4** together with the two normal products **2** and **3** indicates that a common intermediate **5** is being produced during the polyolefin cyclization process (Scheme 2). Formation of the dammarene cation **5** having a 6/6/6/5-fused ring system is thermodynamically favored by Markovnikov control. Proton elimination from the methyl group would give **4** [path (*b*)], while the ring expansion process from a five- to six-membered D-ring would give the hopanyl C22-cation **7** *via* a disfavored anti-Markovnikov C-17 cation **6** [path (*a*)], the latter being formed after the ring expansion of **5** has been processed. The ring expansion competes with the deprotonation. Steric factors also favor the formation of **5**; given that the cyclization reaction proceeds by adopting a pre-chair conformation **1a** for the D-ring construction, greater repulsion would occur due to the 1, 3-diaxial arrangement between the two methyls at the 15- and 19-positions (squalene numbering), thus resulting in the less hindered conformation **1b**.

A similar ring expansion has been proposed for the C-ring formation in lanosterol biosynthesis, based on the trapping of

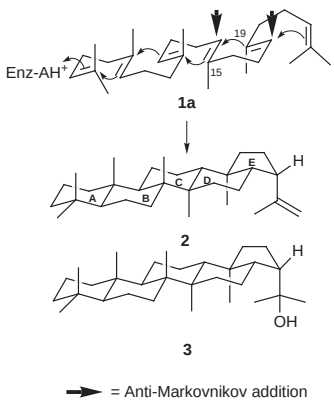

Scheme 1

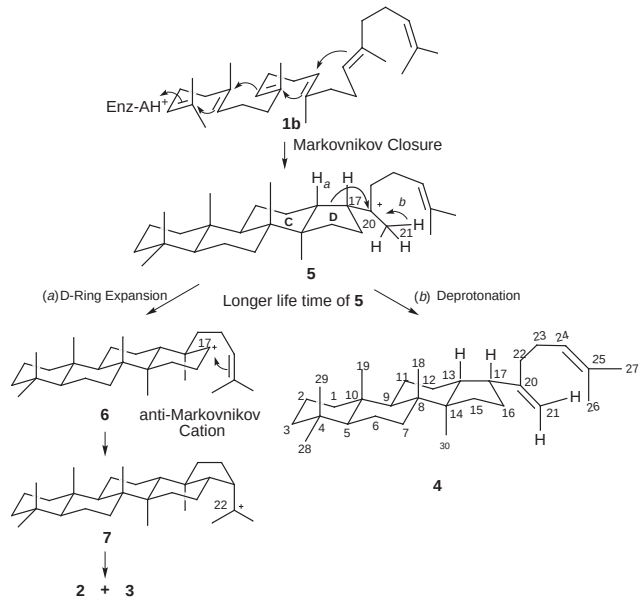

Scheme 2

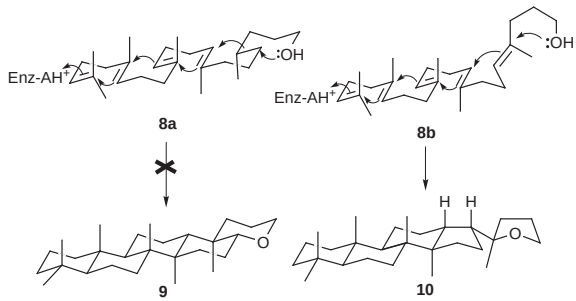

Scheme 3

the five-membered C-ring intermediate (a 6/6/5-fused ring) from incubation experiments with substrate analogues.[7] Incubation of the squalene analogue **8** (C_{27}-OH), prepared *via* treatment of H_5IO_6 with 2,3-oxidosqualene followed by reduction with $LiAlH_4$, with the wild-type SHC afforded **10**[6] almost quantitatively (Scheme 3). Compound **9** and other products were not detected. Formation of **10** strongly supported the suggestion that the cyclization reaction proceeded *via* the prefolded **8b** (like **1b**), but not through **8a** (like **1a**), and also gave unequivocal evidence for the involvement of a discrete metastable C-20 carbocation intermediate like **5** prior to the ring expansion and further cyclization; the hydroxy group would have attacked the tertiary C-20 cation thus produced due to its highly nucleophilic nature, resulting in the formation of a tetrahydrofuran ring in **10**. A dammarene cation similar to **5** was postulated for the cyclization mechanism of 2,3-dihydrosqualene[8] and 29-methylidene-2,3-oxidosqualene[9] by SHC.

Since the mutants of W169V and W489L were completely inactive,[5] it appears that the tight binding to **1** comes from the aromatic ring residue, not from the hydrophobic aliphatic residues of SHC. To date, cation–π interactions induced by aromatic moieties, resulting in the carbocation stabilization, have been proposed for the catalysis and/or acceleration of the polycyclization reaction.[10] Kinetic values for the mutants were compared with that of the wild-type.[11] For the mutant W169F, K_m increased 17-fold, but V_{max} remained unchanged. On the other hand, for the mutant W489F, K_m increased 5.5-fold, but V_{max} was only 14% of the wild type. These kinetic results imply that the W169 would bind to **1** rather than stabilizing the carbocation, while W489 may exhibit both binding and cation stabilization, and also suggest that the higher electron density of the π-electrons, the greater affinity to **1**. The looser binding of the phenylalanine or histidine residues to **1**, near the D-ring, in the mutant SHCs would lead to the longer lifetime of **5**, as inferred from the thermodynamic and steric preferences. Compared to W169F, W169H significantly increased the amount of **4** 5.5-fold; the histidine residue may abstract a proton from the 21-methyl [path (*b*)], indicating that the position of W169 in the cavity may possibly be close to the 21-methyl of **5**, but further evidence is required to confirm this.

Notes and references

1 I. Abe, M. Rohmer and G. D. Prestwich, *Chem. Rev*., 1993, **93**, 2189.
2 G. Ourisson, M. Rohmer and K. Poralla, *Annu. Rev. Microbiol*., 1987, **41**, 301.
3 C. Feil, R. Sussmuth, G. Jung and K. Poralla, *Eur. J. Biochem*., 1996, **242**, 51.
4 K. U. Wendt, K. Poralla and G. E. Schulz, *Science*, 1997, **277**, 1811.
5 T. Sato, Y. Kanai and T. Hoshino, *Biosci. Biotechnol. Biochem*., 1998, **62**, 407.
6 All the HRMS (EI) and NMR (H-H COSY 45, HOHAHA, NOESY, DEPT, HMQC and HMBC) spectra were consistent with the proposed structures of **4** and **10**.
7 E. J. Corey and H. Cheng, *Tetrahedron Lett*., 1996, **37**, 2709; E. J. Corey, S. C. Virgil, H. Cheng, C. H. Baker, S. P. T. Matsuda, V. Singh and S. Sarshar, *J. Am. Chem. Soc*., 1995, **117**, 11 819; T. Hoshino and Y. Sakai, *Chem. Commun*., 1998, 1591.
8 I. Abe and M. Rohmer, *J. Chem. Soc., Perkin Trans. 1*, 1994, 783.
9 I. Abe, T. Dang, Y. F. Zheng, B. A. Madden, C. Fei, K. Poralla and G. D. Prestwich, *J. Am. Chem. Soc*., 1997, **119**, 11 333.
10 K. Poralla, *Bioorg. Med. Chem. Lett*., 1994, **4**, 285; I. Abe and G. D. Prestwich, *Proc. Natl. Acad. Sci. U.S.A*., 1995, **92**, 9274; D. A. Dougherty, *Science*, 1996, **271**, 163.
11 The mutations gave a lowering of the optimal temperature, but no change with pH. Reactions with 5 μg of purified SHC were conducted at 30 °C and pH 6.0 for 1 h; thermal denaturation of the SHCs was not found. The kinetic values of K_m and V_{max} were determined from Lineweaver–Burk plots as follows: K_ms: 16.7, 277, 280 and 92 μM; and V_{max}s: 0.09, 0.078, 0.045 and 0.017 nmol min^{-1} μg^{-1}, respectively, for the wild-type, W169F, W169H and W489F.

Communication 8/06948D

Synthesis of novel 'supercharged' analogues of pyrophosphoric acid

Xiaohai Liu, Harry Adams, and G. Michael Blackburn*

Krebs Institute, Department of Chemistry, University of Sheffield, Brook Hill, Sheffield, UK S3 7HF. E-mail: g.m.blackburn@sheffield.ac.uk

Received (in Liverpool, UK) 11th September 1998, Accepted 26th October 1998

Syntheses of two novel halomethanetriyltrisphosphonic acids are based on an improved preparation of methanetriyltrisphosphonic acid: pK_as for their second acidic dissociations show they are 'supercharged' relative to pyrophosphoric acid, PP_i, while X-ray crystallographic analysis of fluoromethanetriyltrisphosphonic acid establishes its isosteric character relative to PP_i.

Many of the functions of ATP in cellular chemistry have been explored by nucleotide analogues containing phosphonate moieties stable to hydrolysis.[1] By contrast, the dinucleoside 5′,5″-polyphosphates, also a ubiquitous component of all cells, have biological functions that are not yet adequately understood,[2] although some of them (*e.g.* Ap_5A,[3] Ap_5U,[4] Ap_5dT[5]) have proved valuable as transition state mimics for investigation of a range of kinases and show that multiplicity of anionic charge is a major factor in protein affinity. We[6] and others[7] have generated a variety of analogues of ATP and of diadenosine 5′,5″-polyphosphates, Ap_nA, designed to resist specific or general enzymatic hydrolysis, some of which have shown promising therapeutic activity.[8] In an ongoing programme to synthesise analogues of nucleotides with enhanced affinity for receptors[9] and better charge correlation with transition states for selected kinases,[10] we have developed new organophosphorus mimics of pyrophosphoric acid by the substitution of the carbon of methylenebisphosphonic acid by anionic functions. These species should have additional anionic charge relative to simple methylenebisphosphonates and also when incorporated into ATP and Ap_nA analogues.

We envisaged that methanetriyltrisphosphonic acid **3b** and its α-chloro **5** and α-fluoro **7** derivatives would best fulfil this specification, firstly because the introduction of a third ionizable phosphonate (PO_3H_2) group into methylenebisphosphonic acid **1** would be expected to deliver additional anionic charge at physiological pH and secondly because it has been well-established that α-halogenation can enhance the acidity of an alkylphosphonic acid while retaining the stability of its P–C bond to enzymatic cleavage.[11] Since the published procedure[12] for the preparation of hexaethyl methanetriyltrisphosphonate proved of uncertain utility in our hands, we developed[9] an independent multi-step route to this compound, but this gave only low yields of **3b**. We here describe a significantly improved synthesis of methanetriyltrisphosphonic acid and its esters using a modification of Gross's original procedure[12] on which we have established the preparation of novel chloro- and fluoro-methanetriyltrisphosphonic acids. Their physical properties and X-ray structure analysis demonstrate that they are 'supercharged' analogues of pyrophosphoric acid having isosteric character relative to pyrophosphate.

Tetraisopropyl methylenebisphosphonate **1** was reacted with diethyl chlorophosphite in the presence of NaHMDS (in contrast to NaH) (Scheme 1).[12] The reaction quickly reached equilibrium when 4 equiv. of diethyl chlorophosphite and NaHMDS were used to drive the equilibrium towards product **2**. Intermediate **2** was found to be unstable during either acidic (AcOH quench) or basic (sat. $NaHCO_3$ quench) work-up and decomposed to give starting material **1**. Therefore, it was oxidised *in situ* with iodine in pyridine–THF–water to give the desired product **3a** in 72% yield.[13] This provides a significant

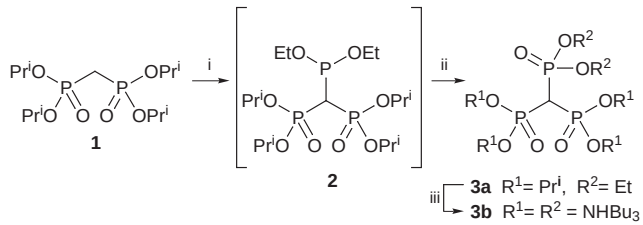

Scheme 1 *Reagents and conditions*: i, NaHMDS, $(EtO)_2PCl$, toluene, room temp.; ii, 0.5 M I_2 solution in Py–THF–H_2O (40:9:1); iii, Me_3SiBr, CH_2Cl_2, reflux overnight, then MeOH, Bu_3N.

improvement for the general synthesis of esters of methanetriyltrisphosphonic acid. When **3a** was heated with TMSBr[14] in CH_2Cl_2 overnight at reflux, methanetriyltrisphosphonic acid was isolated in 98% yield as its tris(tributylammonium) salt **3b** following solvolysis in the presence tri-*n*-butylamine. This product was converted quantitatively into its trisodium salt by precipitation from MeOH with NaI solution (0.5 M in acetone).

Chloromethanetriyltrisphosphonate ester **4** was obtained in 97% yield after treatment of the methanetriyltrisphosphonate ester **3a** with NaOCl solution (Scheme 2).[15] Deprotection of the ester functions was achieved by refluxing with TMSBr and tri-*n*-butylamine in CH_2Cl_2 in 98% yield. (The addition of 1.5 equiv. of base was necessary for clean deprotection of **4** to avoid loss of phosphoric acid from the product **5**, which we observed under acidic conditions, as has been noted elsewhere[16]).

Fluoromethanetriyltrisphosphonate **6** was prepared from **3a** in 77% yield using perchloryl fluoride[17] at −78 °C in the presence of NaHMDS. Substituting *N*-fluorobis(benzene)-sulfonimide for $FClO_3$ gave no product even at room temperature. Presumably this is a consequence of the extreme steric hindrance to electrophilic substitution at the central carbon in **3a**.

Deprotection of **6** was effected in quantitative yield under the conditions used for **4** and the structure of product **7** (as its trisodium salt) confirmed by X-ray crystallography (Fig. 1). From the X-ray crystallographic data of fluoromethanetriyltrisphosphonate, it is clear that the P–C–P geometry (both the P–C bond distance and the P–C–P bond angle)[18] is close to that in

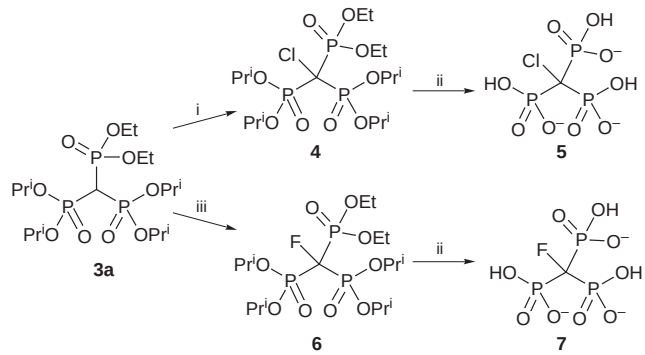

Scheme 2 *Reagents and conditions*: i, 4–20% NaOCl, $NaHCO_3$, 0 °C, 1.5 h; ii, TMSBr, Bu_3N, CH_2Cl_2, reflux overnight; iii, $FClO_3$, NaHMDS, THF, −75 °C.

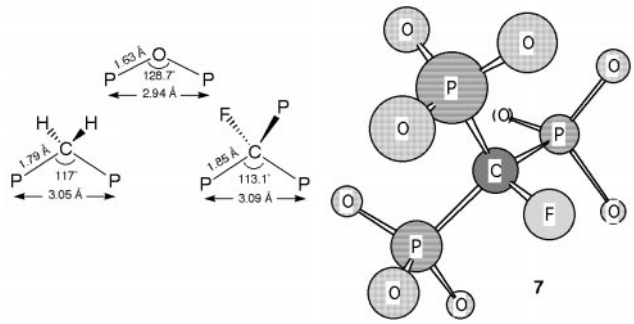

Fig. **1** A comparison of bond angles and bond distances in pyrophosphate, methylenebisphosphonate and fluoromethanetriyltrisphosphonate salts (left) and the X-ray crystallographic structure of the trisodium salt of **7** (right).

methylenebisphosphonate salts[7,19] while the overall phosphorus–phosphorus separation is very close to that observed for methylenebisphosphonate and pyrophosphate salts, largely as a result of compensation between a smaller P–C–P angle and longer P–C bonds (Fig. 1). The crystal lattice of **7** can be considered as a layered structure where one face of the anion coordinates to the sodium ion layer whilst the other face interacts *via* hydrogen bonding to the next anionic layer. This is illustrated in the packing diagram (Fig. 2).

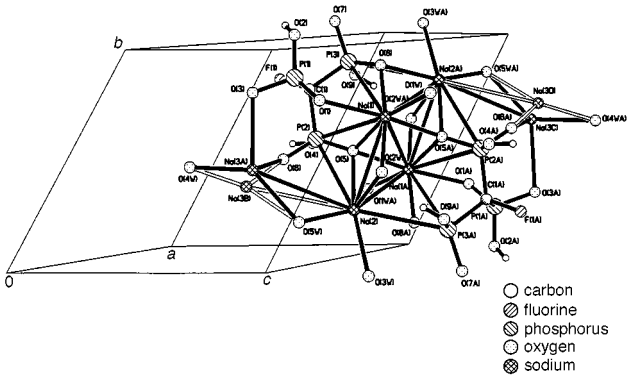

Fig. **2** Crystal packing diagram for **7** illustrating the layered structure and the intermolecular interactions described in the text.

The pK_as of these methanetriyltrisphosphonic acid analogues together with those for α-sulfonylmethylenebisphosphonic acid and α-carboxymethylenebisphosphonic acid[9] were measured under physiological conditions (37 °C, 0.152 M NaCl), which called for deconvolution of titration curves for multiple overlapping pK_as. The ionic state of these trisphosphonates calculated for pH 7.0 (Table 1) show clearly that all five species are 'supercharged' at physiological pH. Methanetriyl-, chloromethanetriyl- and fluoromethanetriyl-trisphosphonic acids have at least one more negative charge than pyrophosphate at pH 7.0. By comparison, α-sulfonylmethylenebisphosphonic acid[9] has a charge of 3.71 minus and α-carboxymethylenebisphosphonic acid[9] 3.3 minus at pH 7.0. It is to be expected that this charge differential will be maintained or enhanced in analogues of ATP and Ap$_n$A containing these trisphosphonates, thereby underpinning the investigation of the role of anionic charge in nucleotide binding to enzymes and receptors.

Table 1 Ionisation constants for polyphosphonic acids determined in the range 3.5 < pH < 10.5 at 37 °C and 0.152 M NaCl

Entry	pK_a3	pK_a4	pK_a5	Net charge at pH 7.0
Pyrophosphoric acid	6.6	9.4	—	2.72
Methanetriyltrisphosphonic acid **3b**	—[a]	6.46	9.90	3.77
Chloromethanetriyltrisphosphonic acid **5**	—[a]	5.92	9.08	3.92
Fluoromethanetriyltrisphosphonic acid **7**	—[a]	5.77	8.86	3.95
α-Sulfonylmethylenebisphosphonic acid[b]	—[a]	6.61	10.57	3.71
α-Carboxymethylenebisphosphonic acid[b]	—[a]	7.24	10.11	3.35

[a] The first three ionisation constants were too low to be accessed in the pK_a titrations employed. pH titration curves were deconvoluted for multiple overlapping pK_a values using a programme written for an Apple Macintosh computer. [b] Ref. 9.

Syntheses of such supercharged analogues of ATP and of Ap$_n$As, determination of their physical characteristics, and studies on protein binding is under active investigation. These results also identify these trisphosphonic acids as strong candidate ligands for calcium ion ligation and as potential bone affinity agents.

We gratefully acknowledge financial support from BBSRC (ROPA/MOLO4558).

Notes and references

1 R. Engel, *The Role of Phosphonates in Living Systems*, ed. R. L. Hildebrand, CRC Press, Boca Raton, 1983, pp. 97–138.
2 G. M. Blackburn, M-J. Guo and A. G. McLennan, *Ap$_4$A and Other Dinucleoside Polyphosphates*, ed. A. G. McLennan, CRC Press, Boca Raton, 1992, pp. 305–32.
3 G. E. Lienhard and I. I. Secemski, *J. Biol. Chem*., 1973, **248**, 1121; C. W. Muller and G. E. Schulz, *J. Mol. Biol*., 1992, **224**,159.
4 K. Scheffzek, W. Kliche, L. Wiesmuller and J. Reinstein, *Biochemistry*, 1996, **35**, 9716.
5 A. Lavie, M. Konrad, R. Brundiers, R. S. Goody, I. Schlichtling and J. Reinstein, *Biochemistry*, 1998, **37**, 3677.
6 G. M. Blackburn, M-J. Guo, S. P. Langston and G. E. Taylor, *Tetrahedron Lett*., 1990, **31**, 5637; G. M. Blackburn and M-J. Guo, *Tetrahedron Lett*., 1990, **31**, 4371.
7 R. G. Yount, D. Babcock, W. Ballantyne and D. Ojala, *Biochemistry*, 1971, **10**, 2484; M. Saddy, A. Valleix, L. Lebeau and C. Mioskowski, *J. Org. Chem*., 1995, **60**, 3685.
8 B. E. Crack, C. E. Pollard, M. W. Beukers, S. M. Roberts, S. F. Hunt and A. H. Ingall, *Br. J. Pharmacol*., 1995, **114**, 475; R. G. Humphries, W. Tomlinson, J. A. Clegg, A. H. Ingall, N. D. Kindon and P. Leff, *Br. J. Pharmacol*., 1995, **115**, 1110; B. K. Kim, P. C. Zamecnik, G. Taylor, M-J. Guo and G. M. Blackburn, *Proc. Natl. Acad. Sci. U.S.A*., 1992, **89**, 11 056; S. W. Chan, S. J. Gallo, B. K. Kim, M-J. Guo, G. M. Blackburn and P. C. Zamecnik, *Proc. Natl. Acad. Sci. U.S.A*., 1997, **94**, 4034.
9 X. Liu, X-R. Zhang and G. M. Blackburn, *Chem. Commun*., 1997, 87.
10 D. M. Williams, D. L. Jakeman, J. S. Vyle, M. P. Williamson and G. M. Blackburn, *Bioorg. Med. Chem. Lett*., 1998, **8**, 2603.
11 G. M. Blackburn, D. A. England and F. Kolkmann, *J. Chem. Soc*., *Chem. Commun*., 1981, 930.
12 H. Gross, B. Costisella, S. Ozegowski and I. Keitel, *Phosphorus Sulfur Silicon*, 1993, **83**, 203.
13 *Selected data* for **3a**: $C_{17}H_{40}O_9P_3$ $[M+H]^+$, 481.1877 (calc. 481.1885); $\delta_H(CDCl_3)$ 5.03–4.75 (4 H, m), 4.35–4.10 (4 H, m), 3.12 (1 H, q, J 24.9) and 1,45–1.30 (30 H, m); $\delta_P(CDCl_3)$ 15.22 (t, *J* 36.89) and 12.81 (d, *J* 36.89).
14 C. E. McKenna, M. R. Higa, N. H. Cheung and M-C. McKenna, *Tetrahedron Lett*., 1977, 155.
15 O. T. Quimby, J. D. Curry, D. A. Nicholson, J. B. Prentice and C. H. Roy, *J. Organomet. Chem*., 1968, **13**, 199.
16 H. Gross, I. Keitel, B. Costisella and C. E. McKenna, *Phosphorus Sulfur Silicon*, 1991, **61**, 177.
17 M. R. C. Gerstenberger and A. Haas, *Angew. Chem*., *Int. Ed. Engl*., 1981, **20**, 647; M. Schlosser and G. Heinz, *Chem. Ber*., 1969, **102**, 1944.
18 *Crystal data* for **7**: $CH_3FNa_3O_9P_3{\cdot}5H_2O$, *M* = 429.99, triclinic $P\bar{1}$ (C^1_i, No.2), *a* = 8.761(7), *b* = 9.190(7), *c* = 10.096(7) Å, α = 68.07(6), β = 74.71(7), γ = 62.90(5)°, *V* = 666.9(9) Å^3, *Z* = 2, D_c = 2.141 mg m^{-3}, *T* = 293 K, *R*1 = 0.0577, *wR*2 = 0.1651, No. of unique reflections = 2305, Radiation source = Mo-Kα (λ = 0.71073 Å). The values given for bond lengths, bond angles, and P–P distance are the average of the values observed. CCDC 182/1067. See http://www.rsc.org/suppdata/cc/1998/2619 for a crystallographic file in .cif format.
19 K. H. Scheit, *Nucleotide Analogs*, Wiley, New York, 1980, pp. 100–101.

Communication 8/07162D

Efficient synthesis of β-substituted α-chloro enones by rhodium(II)-catalyzed reactions of cyclic diazodicarbonyl compounds with acid chlorides

Yong Rok Lee* and Jung Yup Suk

School of Chemical Engineering and Technology, College of Engineering, Yeungnam University, Kyongsan, 712-749, Korea. E-mail: yrlee@ynucc.yeungnam.ac.kr

Received (in Cambridge, UK) 8th September 1998, Accepted 26th October 1998

An efficient synthesis of α-chloro α,β-enones is achieved by rhodium(II)-catalyzed reaction of cyclic diazodicarbonyl compounds with a variety of acid chlorides in good yield.

α-Halo enones have been widely used as valuable and versatile intermediates in the synthesis of α-carbon substituted enones[1] and biologically active natural products.[2] There are many convenient methods available for the preparation of α-bromo and α-iodo enones.[3] However, these procedures are not suitable for the preparation of α-chloro enones. α-Chloro enones are typically prepared by an addition–elimination reaction of enones with PhSCl,[4] ring opening of dichlorocyclopropane with aq. AcOH,[5] and oxidative chlorination of enones with HCl/MCPBA/DMF.[6] Although several methods for the synthesis of these compounds have been developed, their synthetic exploitation has been limited by the difficulties in handing the required strong acidic conditions, and side reactions involving over-oxidation. The necessity for overcoming these serious problems has prompted a search for new methods for the preparation of α-chloro enones.

We have been interested in rhodium-catalyzed reactions of diazodicarbonyl compounds with several substrates.[7] Recently, the rhodium-catalyzed reaction of diazocarbonyl compounds with furans, pyrroles, alkynes and nitriles has been widely studied by several groups.[8] However, the rhodium-catalyzed reaction of diazocarbonyl compounds with acid halides has not been investigated. We report here a new and efficient synthesis of β-substituted α-chloro enones utilizing rhodium(II)-catalyzed reactions of cyclic diazodicarbonyl compounds with a variety of acid chlorides.

The strategy that we have developed begins with the reaction of cyclic diazodicarbonyl compounds **1–5** and acid chlorides (ten-fold excess), which serve as a solvent and a reactant, in the presence of 1 mol% of $Rh_2(OAc)_4$, as shown in Scheme 1.

Treatment of 2-diazocyclohexane-1,3-dione **1** with AcCl at room temperature for 3 h gave the 3-acetoxy-2-chlorocyclohex-2-enone **6** in 81% yield, without a trace of expected 1,3-dioxole

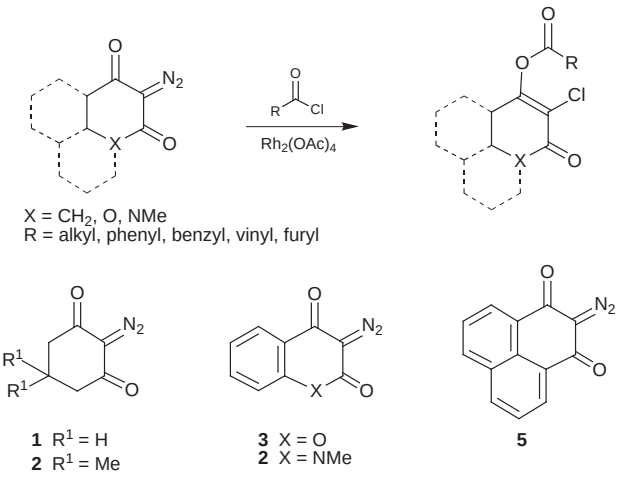

Scheme 1

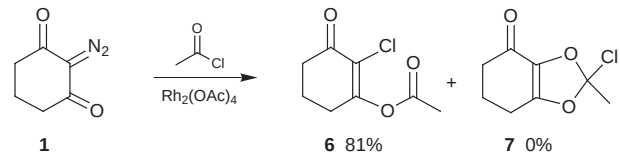

Scheme 2

7 (Scheme 2).[9] Support for the structural assignment comes from spectroscopic analysis. The enone **6** is identified by the IR carbonyl absorptions of the enone at 1693 cm^{-1} and the vinyl ester at 1777 cm^{-1}, and the ^1H NMR peak of the methyl group of the vinyl acetate as a singlet at δ 2.26. Further support for the structural assignment of **6** is obtained from its ^{13}C NMR spectrum, which clearly shows the expected eight carbons, including the two carbonyl carbons of the enone at δ 191.31 and the vinyl ester at δ 166.15.

Reaction of diazodicarbonyl compounds **1** and **2** with a range

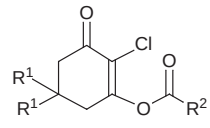

8	R^1 = H, R^2 = Pr	96%
9	R^1 = H, R^2 = Ph	35%
10	R^1 = Me, R^2 = Pr	92%
11	R^1 = Me, R^2 = Bn	71%
12	R^1 = Me, R^2 = (*E*)-prop-1-enyl	70%
13	R^1 = Me, R^2 = 2-furyl	20%

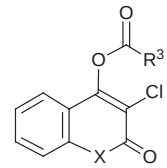

14	R^3 = Me, X = O	35%
15	R^3 = Et, X = NMe	70%

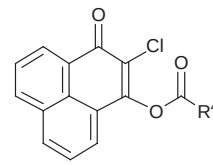

16	R^4 = Et	74%
17	R^4 = Pr	74%

of acid chlorides gave compounds **8–13**. In all cases, only a single product was seen. In particular, reaction of diazodicarbonyl compound **2** with crotonyl chloride gave the enone **12** in 70% yield. In this reaction, no addition product to the C=C bond could be detected. Reaction of diazodicarbonyl compounds **2** and **3** with acid chlorides such as PhCOCl, 2-furoyl chloride and AcCl gave the expected enone **9** (35%), **13** (20%) and **14** (35%) in low yields. This is likely to be due to the instability of products. Importantly, our result is in clear contrast to that of Alonso who reported that the copper(II)-catalyzed reaction of acyclic methyl 2-diazo-3-oxobutyrate with carbonyl compounds such as aldehydes or ketones afforded 1,3-dioxole adducts in moderate yields.[9]

In order to extend the utility of this methodology, reactions of more complex diazodicarbonyl compounds **3–5** with acid chlorides were examined. In these cases, only a single product was also detected. In particular, there is no direct precedent for Rh^{II}-catalyzed reactions of diazodicarbonyl compounds **3–5**

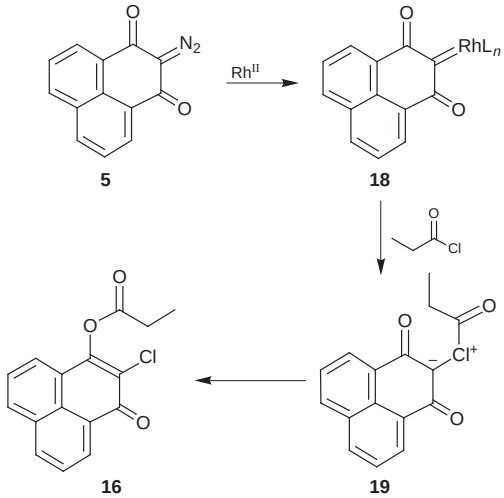

Scheme 3

with other substrates such as alkenes, alkynes, furans, and carbonyl compounds, so it is noteworthy that reaction of **3–5** with acid chlorides give the α-chloro enone **14–17** in 35–74% yields.

Although the exact mechanism of the reaction is still not clear, it is best described as shown in Scheme 3. The diazodicarbonyl compound **5** first gives a carbenoid **18** (or a carbene) by displacement of nitrogen by $Rh_2(OAc)_4$. Nucleophilic addition of acid chloride to the electrophilic carbenoid **18** yields an ylide **19**, which subsequently undergoes intramolecular nucleophilic addition of oxygen to the carbonyl group and the cleavage of the acyl–Cl bond to give product **16**.

In conclusion, rhodium-catalyzed reaction of cyclic diazodicarbonyl compounds with a variety of acid chlorides offers a simple and facile method for the synthesis of α-chloro α,β-unsaturated ketones. Further application of this reaction will be investigated, and is now in progress in our laboratory.

This work was supported by the Korea Science and Engineering Foundation (981-0303-016-2).

Notes and references

† *Selected data* for **6**: δ_H(300 MHz, $CDCl_3$) 2.67 (2H, t, *J* 6.2), 2.59 (2H, dd, *J* 6.1, 5.1), 2.26 (3H, s), 2.06 (2H, m); δ_C(75 MHz, $CDCl_3$) 191.31, 166.15, 164.31, 121.97, 37.21, 29.84, 20.58, 20.13; ν_{max}(neat)/cm^{-1} 2959, 1777, 1693, 1630, 1427, 1371, 1352, 1281, 1169, 1065, 1007, 968, 912, 873, 845. For **12**: mp 59–60 °C; δ_H(300 MHz, $CDCl_3$) 7.18 (1H, m), 5.95 (1H, d, *J* 15.5), 2.58 (2H, s), 2.46 (2H, s), 1.95 (3H, d, *J* 7.0), 1.11 (6H, s); ν_{max}(neat)/cm^{-1} 3370, 2962, 2878, 1742, 1694, 1653, 1624, 1460, 1443, 1414, 1372, 1343, 1314, 1296, 1283, 1196, 1150, 1098, 1026, 1009, 970, 945, 833, 750. For **14**: mp 167–168 °C; δ_H(300 MHz, $CDCl_3$) 7.59 (1H, dd, *J* 8.2, 7.5), 7.49 (1H, d, *J* 7.8), 7.39 (1H, d, *J* 8.2), 7.34 (1H, dd, *J* 7.8, 7.5), 2.49 (3H, s); ν_{max}(neat)/cm^{-1} 3109, 3071, 3045, 1784, 1730, 1620, 1566, 1493, 1453, 1356, 1281, 1200, 1173, 1138, 1090, 1038, 1015, 1001, 903, 777 734. For **15**: mp 134–135 °C; δ_H(300 MHz, $CDCl_3$) 7.61 (1H, dd, *J* 8.2, 7.2), 7.58 (1H, d, *J* 7.3), 7.41 (1H, d, *J* 8.2), 7.28 (1H, dd, *J* 7.3, 7.2), 3.79 (3H, s), 2.79 (2H, q, *J* 7.5), 1.36 (3H, t, *J* 7.5); ν_{max}(neat)/cm^{-1} 2988, 2946, 2922, 1772, 1653, 1624, 1601, 1501, 1306, 1182, 1113, 1074, 1001, 972, 882, 866. For **16**: mp 146–147 °C; δ_H(300 MHz, $CDCl_3$) 8.69 (1H, d, *J* 7.5), 8.21 (1H, d, *J* 8.0), 8.30 (1H, d, *J* 8.3), 7.84 (1H, d, *J* 7.4), 7.76 (1H, dd, *J* 8.0, 7.6), 7.61 (1H, dd, *J* 8.3, 7.4); ν_{max}(neat)/cm^{-1} 2963, 2932, 2874, 1765, 1647, 1577, 1404, 1377, 1323, 1300, 1211, 1182, 1148, 1122, 1063, 965,842, 820, 777.

1 L. S. Liebeskind and J. Wang, *Tetrahedron Lett*., 1990, **31**, 4293; E. Negishi, Z. R. Owczarczyk and D. R. Swanson, *Tetrahedron Lett*., 1991, **32**, 4453; M. Kabat, J. Kiegiel, N. Cohen, K. Toth, P. M. Wovkulich and M. R. Uskokovic, *Tetrahedron Lett*., 1991, **32**, 2343; C. R. Johnson, J. P. Adams, M. P. Braun and C. B. W. Senanayake, *Tetrahedron Lett*., 1992, **33**, 919.

2 C. R. Johnson and M. P. Braun, *J. Am. Chem. Soc*., 1993, **115**, 11 014; C. R. Johnson, L. S. Harikrishnan and A. Golebiowski, *Tetrahedron Lett*., 1994, **35**, 7735; C. R. Johnson, J. P. Adams and M. A. Collins, *J. Chem. Soc., Perkin Trans. 1*, 1993, 1.

3 P. Bovonsombat, G. J. Angara and E. McNelis, *Tetrahedron Lett*., 1994, **35**, 6787; C. R. Johnson, J. P. Adams, M. P. Braun, C. B. W. Senanayake, P. M. Wovkulich and M. R. Uskokovic, *Tetrahedron Lett*., 1992, **33**, 917; C.-K. Sha and S.-J. Huang, *Tetrahedron Lett*., 1995, **36**, 6927; J. P. Whang, S. G. Yang and Y. H. Kim, *Chem. Commun*., 1997, 1355; K. Matsuo, S. Ishida and Y. Takuno, *Chem. Pharm. Bull*., 1994, **42**, 1149.

4 S. V. Ley and A. J. Whittle, *Tetrahedron Lett*., 1981, **22**, 3301.

5 G. Stork and V. Nair, *J. Am. Chem. Soc*., 1979, **101**, 1315.

6 K. M. Kim, K. H. Chung, J. N. Kim and E. K. Ryu, *Synthesis*, 1993, 283.

7 Y. R. Lee and J. Y. Suk, *Heterocycles*, 1998, **48**, 875; Y. R. Lee, *Tetrahedron*, 1995, **51**, 3087; Y. R. Lee and A. Morehead, Jr., *Tetrahedron*, 1995, **51**, 4909.

8 M. P. Doyle, M. A. Mckervey and T. Ye, *Modern Catalytic Methods for Organic Synthesis with Diazo Compounds*: *from Cyclopropanes to Ylides*, Wiley, New York, 1997; T. Ye and M. A. Mckervey, *Chem. Rev*., 1994, **94**, 1091; A. Padwa, *Acc. Chem. Res*., 1991, **24**, 22; M. C. Pirrung, J. Zhang and A. T. McPhail, *J. Org. Chem*., 1991, **56**, 6269; R. D. Connell, M. Tebbe, P. Helquist and B. Akermark, *Tetrahedron Lett*., 1986, **27**, 5559.

9 M. E. Alonso and A. W. Chitty, *Tetrahedron Lett*., 1981, **22**, 4181; M. E. Alonso, M. C. Garcia and A. W. Chitty, *J. Org. Chem*., 1985, **50**, 3445.

Communication 8/06993J

Synthesis of stable monomeric iridium(0) and iridium(−1) complexes

Souâd Boulmaâz,[a] Marina Mlakar,[b] Sandra Loss,[a] Hartmut Schönberg,[a] Stephan Deblon,[a] Michael Wörle,[a] Reinhard Nesper[a] and Hansjörg Grützmacher*[a]

[a] *ETH Zentrum, Laboratorium für Anorganische Chemie, Universitätsstr. 6, CH-8092 Zürich, Switzerland. E-mail: gruetz@inorg.chem.ethz.ch*

[b] *Centre for Marine Research-Zagreb, Rudjer Boskovic Institute, 10001 Zagreb, Croatia*

Received (in Cambridge, UK) 7th October 1998, Accepted 30th October 1998

Using the tropp^{Ph} ligand 1, stable monomeric d^8-Ir^{+I}, d^9-Ir^0 and d^{10}-Ir^{-I} complexes could be isolated and structurally characterized; in all complexes, the metal centre lies within a coordination sphere intermediate between a square plane and a tetrahedron.

Upon stepwise reduction of a square planar d^8-metal complex, electrons are filled into metal–ligand antibonding orbitals, which eventually will lead to structural distortion towards a tetrahedron.[1] Qualitative MO-arguments indicate, that strong σ-donors will induce a preference for a tetrahedral structure while π-acceptor ligands may give rise to a more square planar structure. In line with these predictions pioneering electrochemical and EPR studies by Pilloni *et al.*[2] and Orsini and Geiger[3] showed that while d^9-[Rh(cod)$_2$] and d^9-[Rh{P(OR)$_3$}$_4$] probably have almost planar structures, [Rh(PPh$_3$)$_4$] is likely to have a tetrahedral co-ordination.

Using the new ligand (dibenzo[*a*,*d*]cycloheptene-5-yl)diphenylphosphine **1** (dibenzo*trop*ylidenyl *p*hosphine = tropp^{Ph}, the superscript indicates substituents bonded to phosphorus),[4,5] we were able to isolate a series of stable mononuclear [Ir(tropp^{Ph})$_2$] complexes were the metal centre formally adopts a d^8, d^9, and d^{10} valence electron configuration.

Thus, we prepared the lemon yellow pentacoordinated chloro iridium complex [Ir(tropp^{Ph})$_2$Cl] **3** and the orange–red tetracoordinated complex [Ir(tropp^{Ph})$_2$]$^+$ PF$_6^-$ **4** using standard synthetic methods as shown in Scheme 1. Both the neutral complex **3** and the cationic species **4** are easily reduced by lithium or sodium metal in thf to give the deep green paramagnetic iridium(0) complex **5** (μ_{eff} = 1.7 μ_B). Further reduction with sodium metal leads to the diamagnetic burgundy red iridate complex [Na(thf)$_6$]$^+$ [Ir(tropp^{Ph})$_2$]$^-$ **6**. A comproportionation reaction between **6** and **4** is the preferred synthetic method for radical **5**, which is isolated in almost quantitative yield because of its low solubility.†

X-Ray structural studies‡ for **4**, **5** and **6** show structural changes caused by the stepwise addition of two electrons without changing either the number or the coordination mode of the metal bound ligands.[6]

The structures of the d^8-Ir cation **4** and that of d^9-**5** are remarkably similar and are superimposed in Fig. 1. In both compounds two phosphorus centres of each tropp^{Ph} ligand are coordinated in *trans*-positions at the iridium centre. The Ir–P and Ir–C distances (see Table 1) lie within the expected range.

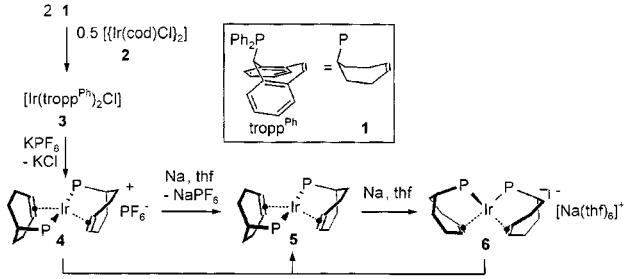

Scheme 1

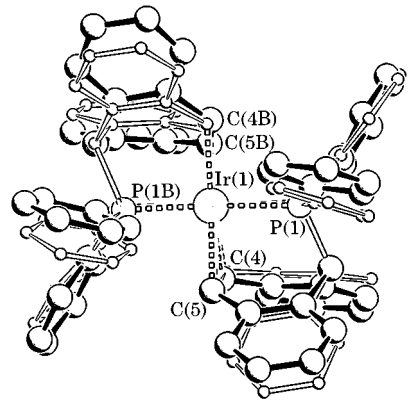

Fig. 1 Overlaid molecular structures of cation **4** (filled lines) and radical **5** (unfilled lines). Selected bond lengths and angles are given in Table 1.

Table 1 Selected bond lengths (Å), bond angles (°) and interplane angles φ (°) of **4**, **5** and **6**

	Ir–P	Ir–C4/C4A	Ir–C5/C5A	C4/C4A–C5/5A	α/°	β/°	φ
4	2.308(3)	2.18(1)	2.19(1)	1.42(2)	169.7(1)	143.5(5)	38.0
5	2.272(3)	2.21(1)	2.15(1)	1.46(2)	165.5(1)	149.4(5)	33.8
6	2.241(1)	2.171(6)	2.127(6)	1.472(9)	98.5(7)	101.0(4)	50.6

The iridium centres deviate significantly from square planar arrangements even in the cation for which planar coordination is expected.[7] Also, the P–Ir–P angles α [**4**: 169.7(1)°; **5**: 165.5(1)°] and (•)–Ir–P angles β [**4**: 143.5(5)°; **5**: 149.5(5)°; (•) = midpoint of the coordinated C=C unit] deviate significantly from 180°. Furthermore, the interplane angles φ (**4**: 38°; **5**: 34°) between the intersections of the P–M–(•) planes show this distortion. A plot of the structure of the iridate anion of [Na(thf)$_6$]$^+$ [Ir(tropp^{Ph})$_2$]$^-$ **6** is shown in Fig. 2.

Both phosphorus centres now occupy mutually *cis*-positions in the distorted coordination sphere which remains intermediate

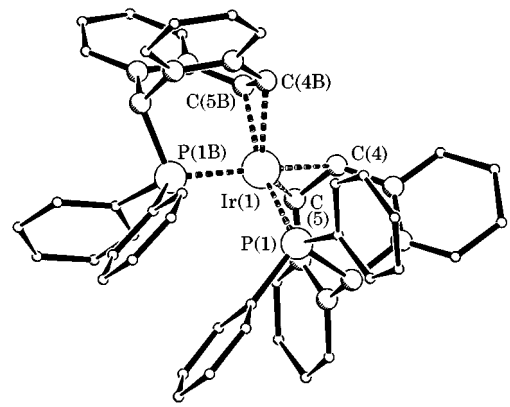

Fig. 2 Molecular structure of the anion of **6.** Selected bond lengths and angles are given in Table 1.

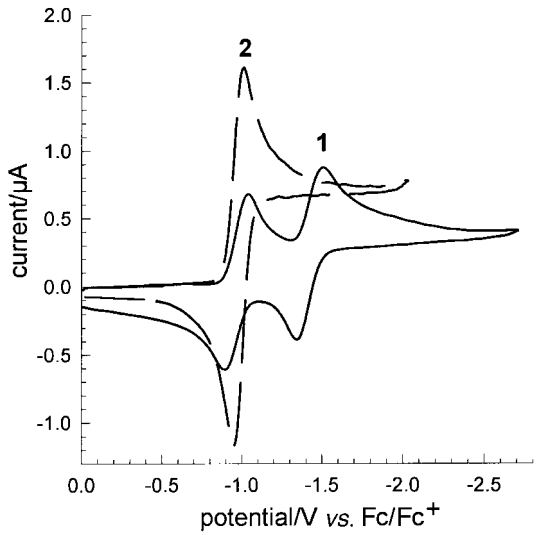

Fig. 3 Cyclic voltammogram of **4** in th–$Bu^n_4NPF_6$ electrolyte (trace 1) or MeCN–$Bu^n_4NPF_6$ electrolyte (trace 2); 298 K, 100 mV s^{-1}; Pt working electrode (0.785 mm^2/ Pt counter electrode/ Ag reference electrode, ferrocene as internal standard for calibration (+0.352 V *vs*. Ag/AgCl).

between a square plane and a tetrahedron (φ = 50.6°). Selected structural data are also listed in Table 1. The Ir–P and Ir–C bond distances do not show significant changes with the formal metal oxidation state in $[Ir(tropp^{Ph})_2]^{+1/0/-1}$ complexes. A slight lengthening of the co-ordinated C=C bond [C4–C5 1.42(2) Å in **4** *vs*. 1.472(9) Å in **6**] indicates increasing metal to ligand d–p(π)-back-donation. Hence, the only significant change is found in the interplane angle φ which changes by about 15° towards a more tetrahedral structure when d^8-**4** and d^9-**5** ($\varphi \approx 36°$) are transformed into d^{10}-**6** ($\varphi \approx 51°$). Note that both centro-symmetric planar structures (φ = 0°) or tetrahedral structures (φ = 84°) are found in $[M(tropp^{Ph})_2]^n$ complexes for M = Rh, n = +1, or Co, n = 0, respectively.[5,8] Hence, the structural features of the iridium complexes described in this work are not merely caused by steric requirements of the ligand. The Ir^{+1}/Ir^0 and Ir^0/Ir^{-1} redox couples are shifted to remarkably low potentials. The cyclic voltammogram of **4** in a $Bu^n_4NPF_6$–THF (trace 1) and $Bu^n_4NPF_6$–MeCN electrolyte (trace 2) is shown in Fig. 3.

While in thf the Ir^{+I}/Ir^0 and Ir^0/Ir^{-I} redox couples ($E^1_{\frac{1}{2}}$ = −0.97 V, ΔE = 149 mV; $E^2_{\frac{1}{2}}$ = −1.426 V; ΔE = 165 mV) appear separately, proving an overall stepwise EE mechanism, a further cathodic shift of the second wave is observed in MeCN leading to only one two-electron wave at $E^{1,2}_{\frac{1}{2}}$ = −0.982 V (ΔE = 91.4 mV).[9] It will be now interesting to study the application of tropp type complexes in electrocatalytic cycles running over four formal oxidation states at the metal centre (*i.e.* Ir^{+III}–Ir^{-I}).

This work was supported by the Swiss Science Foundation. S. D. thanks the Gottlieb Daimler and Carl-Benz Foundation, S. L. the DAAD for a grant.

Notes and references

† $[Ir(tropp^{Ph})_2Cl]$ **3**: $tropp^{Ph}$ **1** (2.29 g, 6.074 mmol) and $[Ir(cod)Cl]_2$ **2** (1.02 g, 1,52 mmol) were dissolved in toluene (50 ml). The resulting yellow solution was stirred for 2 h at *ca*. 70 °C. Compound **3** crystallised overnight at room temp. to give a lemon yellow powder, 2.8 g (94.0%). ^{1}H NMR ($CDCl_3$, 300 MHz, 25 °C, TMS) δ 5.03 (t, J_{PH} 3.5 Hz, 2H, CHP), 4.10 (m, 2H, CH=CH), 3.45 (q, $^3J_{HH+PH}$ 3.4 Hz, 2H, CH=CH); ^{31}P NMR ($CDCl_3$, 81 MHz) δ 48.15 (s); ^{13}C NMR ($CDCl_3$, 75.43 MHz, 25 °C): δ 49.9 (m, CHP), 48.7 (s, CH=CH), 43.9 (s, CH=CH). $[Ir(tropp^{Ph})_2]^+PF_6^-$**4**: KPF_6 (130 mg, 0.706 mmol) was added to a solution of **3** (700 mg, 0.714 mmol) in 10 ml thf. The reaction mixture was stirred for 4 h at room temp. forming an orange–red suspension. Precipitates were filtered off and washed with thf until only colourless KCl remained. The filtrate was concentrated to *ca*. 5 ml and was layered with toluene. Compound **5** crystallized as orange–red crystals (760 mg, 97.7%). ^{1}H NMR (CD_2Cl_2, 300 MHz, 25 °C, TMS) δ 5.89 (t, J_{PH} 3.7Hz, 2H, CHP), 5.37 (t, 2H, $^3J_{HH+PH}$ 3.3 Hz, 4H, CH=CH); ^{31}P NMR (CD_2Cl_2, 81 MHz, 25 °C) δ 71.44 (s); ^{13}C NMR (CD_2Cl_2, 75.43 MHz, 25 °C) δ 68.9 (s, CH=CH), 49.5 (t, J_{CP} = 13.4 Hz CHP). UV–VIS: λ_{max} = 444 nm. $[Na(thf)_6][Ir(tropp^{Ph})_2]$ **6**: sodium (30.0 mg, 1.3 mmol) was added to a solution of **2** (500 mg, 0.51 mmol) in 10 ml thf and the reaction mixture was stirred for 48 h at room temp. The resulting deep red solution was filtered from the precipitate which was washed several times with thf until only colourless NaCl remained. The combined thf extracts were concentrated to 3 ml and were layered with *n*-hexane (5 ml). Compound **6** crystallized as deep red crystals (690 mg, 96.6%). ^{1}H NMR (thf-d_8, 300 MHz, 25 °C, TMS) δ 4.56 (d, J_{HP} 9.5 Hz, 2H, CHP), 4.03 (m, 2H, CH=CH), 2.14 (m, 2H, CH=CH); ^{31}P NMR (thf-d_8, 81 MHz) δ 82.7 (s); ^{13}C NMR (thf d_8, 75.43 MHz, 25 °C) δ 54.3 (m, CHP), 44.7 (m, CH=CH), 44.2 (m, CH=CH). UV–VIS: λ_{max} = 450 nm. $[Ir(tropp^{Ph})_2]$ **5**: **3** (500 mg, 0.51 mmol) and **6** (714 mg, 0.51 mmol) were dissolved in thf (15 ml) and stirred for 2 h at room temp. The resulting deep green solution was separated from the precipitate. The latter was treated as before and the combined thf extracts were reduced to 10 ml and layered with *n*-hexane (5 ml). Compound **5** crystallized as black crystals (750 mg, 77.8%). UV–VIS: λ_{max} = 592 nm.

‡ *Crystal data:* **4**·1.5thf: monoclinic, space group $P2_1/n$; a = 13.382(2), b = 30.666(5), c = 15.611(2) Å, β = 108.913(1)°, V = 6060.5(16) Å^3; Z = 4, Mo Kα radiation, $2\theta_{max}$ = 46.5°. 29467 reflections, 8718 independent (R_{int} = 0.0981); direct methods; full-matrix least-squares refinement (based on F^2) with SHELXTL (Version 5.0); R_1 = 0.0639, wR_2 = 0.1471 (based on F^2) for 715 parameters and 5487 reflections with $I > 2\sigma(I)$. **5**: twinned black needles. By cutting larger crystals into smaller pieces, we obtained a crystal, where one twin individium was dominant. The diffraction pattern of this crystal could be indexed by neglecting weak reflections of the smaller twin component and the structure could be solved successfully. Nevertheless, occasional overlapping of reflections of the twin components affects the accuracy of the structure refinement as well as the resulting *R*-values. Monoclinic, space group $P2_1/n$, a = 20.544(3), b = 9.359(1), c = 22.179(3) Å, β = 101.44(1)°; V = 4179.7(11) Å^3; Z = 4, Mo Kα radiation, $2\theta_{max}$ = 49.4°. 19535 reflections, 7092 independent (R_{int} = 0.0543); direct methods; full-matrix least-squares refinement (based on F^2) with SHELXTL (Version 5.0); R_1 = 0.0683, wR_2 = 0.1614 (based on F^2) for 514 parameters and 5328 reflections with $I > 2\sigma(I)$. **6**: orthorhombic, space group *Pcca*; a = 23.777(4), b = 12.679(2), c = 23.819(4) Å; V = 7199.1(6) Å^3; Z = 4, Mo Kα radiation, $2\theta_{max}$ = 55°. 37241 reflections, 7626 independent ($R_{int.}$ = 0.0939); direct methods; full-matrix least-squares refinement (based on F^2) with SHELXTL (Version 5.0); R_1 = 0.0467, wR_2 = 0.0969 (based on F^2) for 422 parameters and 3927 reflections with $I > 2\sigma(I)$. All non-hydrogen atoms were refined anisotropically, hydrogen atoms were refined on calculated positions using the riding model. In **4**, PF_6 and thf were refined as rigid bodies. In **5**, anisotropic displacement factors were restrained using SIMU and ISOR (see SHELX-97 manual, W.S. Sheldrick, Göttingen University). CCDC 182/1078. See http://www.rsc.org/suppdata/cc/1998/2623/for crystallographic files in .cif format.

1 E. A. Halevi and R. Knorr, *Angew. Chem.*, 1982, **94**, 307; *Angew. Chem., Int. Ed. Engl.*, 1982, **21**, 288.
2 G. Pilloni, G. Zotti and S. Zecchin, *J. Organomet. Chem.*, 1986, **317**, 357 and references therein.
3 J. Orsini and W. E. Geiger, *J. Elektroanal., Chem.*, 1995, **380**, 83 and references therein.
4 J. Thomaier, S. Boulmaâz, H. Schönberg, H. Rueegger H. Hillebrecht, H. Pritzkow and H. Grützmacher *New J. Chem.*, 1998, in press.
5 H. Schönberg, S. Boulmaâz, M. Wörle, L. Liesum, A. Schweiger and H. Grützmacher, *Angew. Chem.*, 1998, **110**, 1492; *Angew. Chem., Int. Ed. Engl.*, 1998, **37**, 1423.
6 See multi-electron reduction/oxidation of arene complexes were the hapticity of the ligands changes: Ch. Elschenbroich and A. Salzer, *Organometallchemie*, Teubner, Stuttgart, 1988, p. 366; W. J. Browyer, J. W. Merkert, W. E. Geiger and A. L. Rheingold, *Organometallics*, 1989, **8**, 191; W. J. Browyer and W. E. Geiger, *J. Am. Chem. Soc.*, 1985, **107**, 5657.
7 For tetrahedrally distorted d^8-Rh complexes see: H. Schumann, M. Heisler and J. Pickardt, *Chem. Ber*. 1977, **110**, 1020; R. L. Harlow, S. A. Westcott, D. L. Thorn and R. T. Baker, *Inorg. Chem.*, 1992, **31**, 323 and references therein.
8 S. Deblon, H. Schönberg, H. Grützmacher and S. Loss, unpublished work.
9 For the analysis of formally two electron processes see, for example: D. T. Pierce and W. E. Geiger, *J. Am. Chem. Soc.*, 1992, **114**, 6063; K. Hinkelmann and J. Heinze, *Ber. Bunsenges. Phys. Chem.* 1987, **91**, 243.

Communication 8/07804A

Bond energy of complexes of neon with aromatic molecules: rotational spectrum and dynamics of pyridine–neon

Assimo Maris, Walther Caminati* and Paolo G. Favero

Dipartimento di Chimica 'G. Ciamician', Università di Bologna, Via Selmi 2, I-40126 Bologna, Italy. E-mail: caminati@unibo.it

Received (in Exeter, UK) 18th September 1998, Accepted 30th October 1998

The equilibrium configuration of the very weakly bonded pyridine···Ne complex has been deduced from its free jet millimeter-wave spectrum; the three van der Waals motions have approximated fundamentals in the range 19–31 cm^{-1} and the dissociation energy has been estimated to be 1.1 kJ mol^{-1}.

At very low pressures and temperatures, conditions similar to those of interstellar space, rare gases (RG) form stable adducts with various molecules.[1] It can be questionable if these processes are real chemistry, but we will see that the difference with respect to 'normal' chemistry is quantitative rather than qualitative. The combination of supersonic expansion with spectroscopic techniques[2] has allowed an extensive investigation of the chemistry of these adducts.

Jet cooled rotationally resolved spectra supply the most detailed information on the dynamics (and thus on the binding energy) of the van der Waals motions: the measured distortion from a rigid rotor behaviour is in fact mainly due to the van der Waals vibrations (see for example refs. 3–6).

Taking into account the van der Waals complexes between a RG atom and an aromatic ring molecule investigated with such techniques, about twenty complexes involve an Ar atom while only one (benzene–Ne[7]) involves a Ne atom.[1] This is likely to be due to the lower interaction energy of Ne.

Most of these studies have generally been performed with pulsed molecular beam microwave Fourier transform, as for example benzene–RG[7,8] (RG = Ne, Ar, Kr, Xe) and pyridine–RG[9,10] (RG = Ar, Kr). Recently a direct absorption technique, free jet millimeter-wave absorption spectroscopy, has also been applied to the investigation of such complexes, as, for example, pyrimidine–Ar[6] and pyridazine–Ar.[11]

Here we report the rotational spectrum of pyridine–neon (PYR-Ne), investigated with the latter technique. Fig. 1 shows PYR–Ne, PYR, the switching of the principal axes upon formation of the adduct, and the van der Waals structural parameters.

The Stark and pulse modulated free jet absorption millimeter-wave spectrometer used in this study has already been described elsewhere.[12] The complex was formed by flowing neon at a pressure of *ca.* 1.5 bar over the sample at room temperature, and expanding the mixture through a pulsed nozzle (repetition rate 5 Hz) with a diameter of 0.35 mm, reaching an estimated 'rotational' temperature of *ca.* 7–8 K. Neon (99.995%) was supplied by Linde, and pyridine by Aldrich. The accuracy of the frequency measurements is about 0.05 MHz.

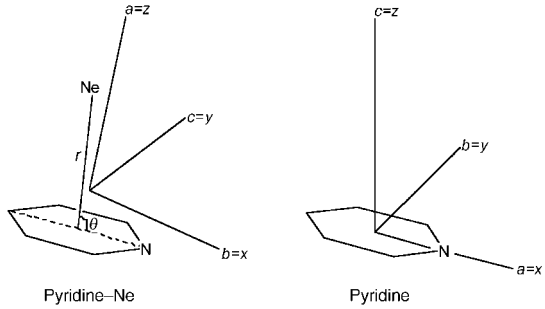

Fig. 1 Geometry and principal axes system in PYR···Ne and PYR.

The first estimate of the rotational constants of PYR–Ne has been based on a model similar to that of Fig. 1, with Ne positioned 3.4 Å above the PYR plane, along the perpendicular to the center of mass (c.m.), and with the r_0 geometry of PYR as in the isolated molecule.[13] The spectrum has been assigned and the 43 measured transitions (available upon the authors) have been fitted with Watson's 'S' reduced Hamiltonian (I^r representation).[14] Quartic and sextic centrifugal distortion parameters where required to fit the spectrum, in accord with the large amplitude inherent in the Ne motions. Only μ_b-type transitions have been observed. Owing to the low value of the μ_a-dipole component and to the high J values involved, μ_a-type transitions were too much weak to be detected with our spectrometer. Table 1 collects the determined parameters.

The three translational motions of the isolated Ne are replaced by three low energy vibrational modes upon formation of the complex. Because of the low energy and large amplitude of these van der Waals motions, which bring Coriolis coupling contributes to the moments of inertia, usual methods for structure determination supply poor results. Here we will apply a method which takes into account these effects. One of the van der Waals motions can be considered the stretching between the two centers of mass of the two constituent molecules, while the remaining ones can be thought of as two internal rotations of Ne around PYR.

The stretching (radial part of the Ne motions) can be, in a first approximation, isolated from the other motions. For asymmetric top complexes in which the stretching coordinate is near-parallel to the inertial a-axis the stretching force constant (k_s) can be estimated by approximating the complex to a molecule made of two rigid parts, by using equations of the type:[3]

$$k_s = 16\,\pi^4\,(\mu_D\,R_{CM})^2\,[4B_D^4 + 4C_D^4 - (B_D - C_D)^2(B_D + C_D)^2]/(hD_J) \qquad (1)$$

The subscript D denotes a dimer quantity, μ_D is the pseudo diatomic reduced mass, R_{CM} is the distance between the centers of mass of the monomers (3.386 Å for PYR–Ne), and D_J is the centrifugal distortion constant. k_s, the corresponding harmonic stretching fundamental (ν_s), the dissociation energy (E_B) and the equilibrium distance of Ne (r_e) from the center of mass of PRM are reported in Table 2, and compared to the correspond-

Table 1 Spectroscopic constants of pyridine–Ne (S-reduction, I^r-representation)

A/MHz	3011.42(7)[a]	d_1/kHz	−0.55(1)
B/MHz	1876.40(7)	d_2/kHz	−0.029(2)
C/MHz	1858.03(7)	H_J/Hz	−1.8(3)
D_J/kHz	20.3(2)	H_{JK}/Hz	−20.3(9)
D_{JK}/kHz	90.7(6)	H_{KJ}/Hz	62(1)
D_K/kHz	−105.2(2)	H_K/Hz	−38.9(4)
N^b	43	σ^c/MHz	0.11

[a] Errors in parenthesis are expressed in units of the last digit. [b] Number of transitions in the fit. [c] Standard deviation of the fit.

Table 2 Parameters describing the van der Waals motions, geometry and dissociation energy for PYR–Ne and PYR–Ar

	PYR–Ne	PYR–Ar[a]		PYR–Ne	PYR–Ar[a]
k_s/N m^{-1}	0.92	3.05	ν_Y/cm^{-1}	19.9	34.5
k_X/N m^{-1}	0.12	0.39	X_e[b]/Å	0.245	0.298
k_Y/N m^{-1}	0.12	0.38	r_e[b]/Å	3.316	3.485
ν_s/cm^{-1}	31.1	44.2	ϕ_e[b]/°	4.2	4.9
ν_X/cm^{-1}	19.6	34.1	E_B/cm^{-1}	90	259

[a] From ref. 4. [b] The equilibrium position of the noble gas is shifted in the direction from the center of mass of the ring towards the nitrogen atom, forming an angle ϕ_e (= 90 − θ of Fig. 1) with the perpendicular to the ring.

ing values for the related complex PYR–Ar.[4] E_B and r_e have been adjusted within a Lennard-Jones type potential in such a way to reproduce ν_s and $(B + C)_0$. A one-dimensional flexible model[15] has been used to calculate rotational and vibrational energy levels. Fig. 2 shows the Lennard-Jones potential energy curves for PYR–Ne and PYR–Ar.

As to the two Ne internal rotations their effects are reflected either in the anomalous high values of the Δ_{JK} and Δ_K centrifugal distortion parameters, as outlined in several of the complexes of aromatic molecules with rare gases (see, *e.g.* refs. 4, 5, 11), and in the negative changes of the planar moments of inertia M_{xx} and M_{yy} (Fig. 1) in going from isolated PYR to PYR–Ne. The procedure to extract the bends van der Waals potential energy parameters from centrifugal distortion is rather complex for low symmetry complexes as PYR–Ne. For this reason we extracted this information for the C_s symmetry PYR–Ne complex from the ΔM_{xx} and ΔM_{yy} values of Table 3. The planar moments of inertia are defined and related to the rotational constants through eqn (2):

$$M_{aa} = \Sigma_i m_i a_i^2 = h/(16\pi^2)\,(-1/A + 1/B + 1/C),\ etc. \quad (2)$$

They represent the mass extension along the principal axes. Their shifts on going from the isolated molecule to the complex (Fig. 1) are shown in Table 3 for the PYR/PYR–Ne and PYR/PYR–Ar systems. Owing to the axis switching upon formation of the complexes the more consistent quantities ΔM_{xx}, ΔM_{yy} and ΔM_{zz} (Fig. 1) are reported there. The smaller value of ΔM_{zz} for PYR–Ne is in accord with the fact that Ne is lighter than Ar, and closer to the ring center of mass. By contrast, it is difficult, at first sight, to understand the negative value of ΔM_{yy}, and why this value for PYR–Ne is more negative than that of PYR–Ar. A rather simple interpretation of this effect has been given for pyrimidine–Ar,[6] in terms of mass dispersion and vibrational Coriolis couplings associated with the two bendings. The two motions are considered local harmonic oscillations on one side of the ring, by a model that describes the A′ type mode in the *xz* plane by the displacement *X* and the A″ type displacement in the *y* direction by *Y*:

$$V(X,Y) = (1/2)\,[k_x\,(X - X_e)^2 + k_y Y^2] \quad (3)$$

where X_e is the displacement, within the symmetry plane, of the neon atom from the *z* axis at equilibrium. The calculations were

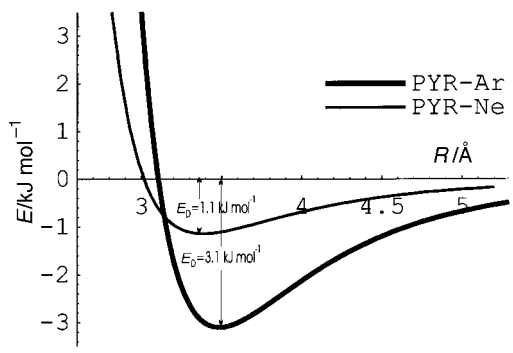

Fig. 2 Lennard-Jones potential energy diagrams for the dissociation of PYR···Ne and PYR···Ar.

Table 3 Shifts of planar moments of inertia (in uÅ^2) in going from the isolated molecule to the complex for PYR–Ne and PYR–Ar

	PYR→PYR–Ne	PYR→PYR–Ar[a]
ΔM_{xx}	−1.838	−1.081
ΔM_{yy}	−1.123	−0.697
ΔM_{zz}	186.775	335.404

[a] From data of refs. 12 and 13.

made by using the two-dimensional version of the above mentioned flexible model,[15] resolving the range (−2.0 Å, +2.0 Å) into 21 mesh points for each of the *X* and *Y* displacements. X_e, k_x, and k_y have been adjusted in order to reproduce ΔM_{xx} and ΔM_{yy}. Since the two pieces of data do not allow one to estimate more than two of the three parameters, we assumed $k_x = k_y$, a condition nearly fulfilled for this kind of complexes.[4] The results are shown in Table 2. Although $X_e = \pm 0.245$ Å was obtained, a comparison with other complexes[4,6] suggests the minus rather than the plus sign and yields $X_e = -0.245$ Å, which means that the vertical on the ring plane passing through the equilibrium position of the neon atom, at 3.316 Å above the ring plane, is tilted by about 4.2° from the center of mass of the ring towards the nitrogen atom. The 'equilibrium' values discussed above refer to the limit situation without van der Waals vibrations, but with half a quantum of each ring vibrations. Despite the fact that Ne is much lighter than Ar, the bend vibrational fundamental frequencies of 19.6 and 19.9 cm^{-1}, are considerably lower than the values of 34.1 and 34.5 cm^{-1} for PYR–Ar,[4] indicating that PYR–Ne is much floppier than PYR–Ar (see Table 2 for a comprehensive comparison).

As a conclusion we can remark that Ne has a binding energy to aromatic molecules which is about 1/3 of that of Ar, and about two–three orders of magnitude smaller of that of normal chemical bonds.

We thank Mr A. Millemaggi for technical help, and the Ministero dell'Università e della Ricerca Scientifica e Tecnologica, and the CNR for financial support.

Notes and references

1 S. E. Novick, *Bibliography of Rotational Spectra of Weakly Bound Complexes*, 1998, available at http://www.wesleyan.edu/chem/bios/vdw.html.
2 J. B. Anderson, R. P. Andres and J. B. Fenn, *Adv. Chem. Phys.* 1966, **10**, 275.
3 D. J. Millen, *Can. J. Chem.*, 1985, **63**, 1477; W. G. Read, E. J. Campbell and G. Henderson, *J. Chem. Phys.*, 1983, **78**, 3501.
4 R. P. A. Bettens, R. M. Spycher and A. Bauder, *Mol. Phys.*, 1995, **86**, 487.
5 J. Makarewicz and A. Bauder, *Mol. Phys.*, 1995, **84**, 853.
6 W. Caminati, S. Melandri, P. G. Favero and R. Meyer, *Chem. Phys. Lett.*, 1997, **268**, 393.
7 Th. Brupbacher and A. Bauder, *Chem. Phys. Lett.*, 1990, **173**, 435; Th. Brupbacher, J. Makarewicz and A. Bauder, *J. Chem. Phys.*, 1994, **101**, 9736.
8 E. Arunan, T. Emilsson and H. S. Gutowsky, *J. Chem. Phys.*, 1994, **101**, 861.
9 T. D. Klots, T. Emilsson, R. S. Ruoff and H. S. Gutowsky, *J. Phys. Chem.*, 1989, **93**, 1255.
10 R. M. Spycher, D. Petiprez, F. L. Bettens and A. Bauder, *J. Phys. Chem.*, 1994, **98**, 11863.
11 W. Caminati, A. Millemaggi, P. G. Favero and J. Makarewicz, *J. Phys. Chem.*, 1997, **101**, 9272.
12 S. Melandri, W. Caminati, L. B. Favero, A. Millemaggi and P. G. Favero, *J. Mol. Struct.*, 1995, **352/353**, 253; S. Melandri, G. Maccaferri, A. Maris, A. Millemaggi, W. Caminati and P. G. Favero, *Chem. Phys. Lett.*, 1996, **261**, 267.
13 F. Mata, M. J. Quintana and G. O. Sørensen, *J. Mol. Struct.*, 1977, **42**, 1.
14 J. K. G. Watson, in *Vibrational Spectra and Structure*, ed. J. R. Durig, Elsevier, New York/Amsterdam, 1977, pp. 1–89.
15 R. Meyer, *J. Mol. Spectrosc.*, 1979, **76**, 266.

Communication 8/07289B

Synthesis and structural characterisation of platinum silasesquioxane complexes

Hendrikus C. L. Abbenhuis,*[a] Andrew D. Burrows,*[b] Huub Kooijman,[c] Martin Lutz,[c] Mark T. Palmer,[b] Rutger A. van Santen[a] and Anthony L. Spek[c]

[a] *Schuit Institute of Catalysis, Eindhoven University of Technology, PO Box 513, 5600 MB Eindhoven, The Netherlands. E-mail: H.C.L.Abbenhuis@tue.nl*

[b] *Dept. of Chemistry, University of Bath, Claverton Down, Bath, UK BA2 7AY. E-mail: a.d.burrows@bath.ac.uk*

[c] *Bijvoet Centre for Biomolecular Research, Crystal and Structural Chemistry, Utrecht University, Padualaan 8, 3584 CH Utrecht, The Netherlands*

Received (in Cambridge, UK) 19th October 1998

The reaction of partially condensed silasesquioxanes of the type $[R^1{}_7Si_7O_9(OH)_2(OR^2)]$ (R^1 = *c*-C_5H_9, *c*-C_6H_{11}; R^2 = H, $SiMe_3$) with either $[Pt(dppe)(CO_3)]$ or $[Pt(dppe)Cl_2]/Ag_2O$ leads to the formation of $[R^1{}_7Si_7O_9(OR^2)O_2Pt(dppe)]$, crystallographically characterised for R^1 = *c*-C_5H_9; R^2 = $SiMe_3$, providing unprecedented routes to late transition metal silasesquioxane complexes.

Currently, metallasilasesquioxanes are considered as the best soluble models for silica-supported transition metal species and an increasing number of examples of *early* transition metal compounds based on these ligands is being reported.[1] In contrast, metallasilasesquioxanes involving *late* transition metals are considerably rarer, and to date no such examples of mononuclear platinum group complexes have been characterised crystallographically. Transmetallation reactions have briefly been reported to give platinum silasesquioxane complexes,[1] though no experimental details were published and the reported transmetallations suffer from requiring the use of thallium or tetraalkylstibonium intermediates. Here we detail two simple routes to platinum silasesquioxane complexes and present the first example of an X-ray single crystal structure of a mononuclear platinum metal silasesquioxane complex.

Platinum silasesquioxane complexes can be conveniently prepared (Scheme 1) by utilising the reactivity of the acidic silasesquioxane silanol groups[2] with the carbonate functionality in $[Pt(dppe)(CO_3)]$ [dppe = bis(diphenylphosphino)ethane].[3] In all cases the reactions are slow with full conversion only occurring after several days, but yields are good with no by-products observed.† $^{31}P\{^1H\}$ NMR spectroscopy provides a useful method for following the reactions, and resonances for the silasesquioxane derivatives **3** and **4** occur in all cases upfield and with larger ^1J(PPt) coupling constants than for $[Pt(dppe)(CO_3)]$.‡ Both chemical shifts and ^1J(PPt) coupling constants for **3** and **4** fall within a narrow range [δ between 26 and 28, referenced to external 85% phosphoric acid, and ^1J(PPt) between 3730 and 3780 Hz]. The chemical shifts are similar to those reported previously for $[Pt(dppe)(OSiMe_3)_2]$ [δ 27.1, ^1J(PPt) 3595][4] and $[Pt(dppe)(OMe)_2]$ [δ 28.5, ^1J(PPt) 3342][5] though the coupling constant is somewhat larger, reflecting the lower *trans* influence of the silasesquioxane. The reactivity of $[Pt(dppe)(CO_3)]$ is in marked contrast to that of $[Pt(PPh_3)_2(CO_3)]$, for which no reaction with **1** was observed after several days. A similar pattern was observed in the reaction of these platinum carbonates with ethane-1,2-diol, for which the equilibrium constant was approximately 27 times greater for $[Pt(dppe)(CO_3)]$ than for $[Pt(PPh_3)_2(CO_3)]$.[6]

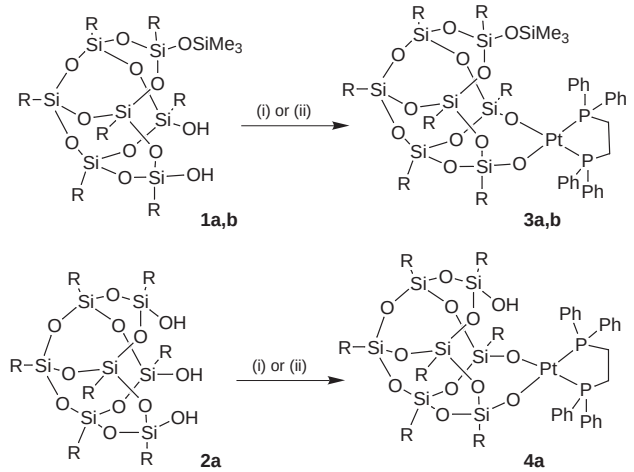

Scheme 1 (i) $[Pt(dppe)CO_3)]$, CH_2Cl_2; (ii) $[Pt(dppe)Cl_2]$, Ag_2O, CH_2Cl_2, Δ (**a**, R = *c*-C_5H_9; **b**, R = *c*-C_6H_{11}).

A second useful preparative route utilises the reaction of the silasesquioxane silanol groups with the chlorides on $[Pt(dppe)Cl_2]$ in refluxing dichloromethane in the presence of the base silver(I) oxide.[7] Again the reaction is slow, though more general than the carbonate route as it allows $PMePh_2$ analogues of **3** and **4** to be prepared.

Single crystals of complex **3a** were grown from the slow diffusion of acetonitrile into a toluene solution, and the molecular structure is shown in Fig. 1.§ The co-ordination geometry around the platinum centre is distorted square planar,

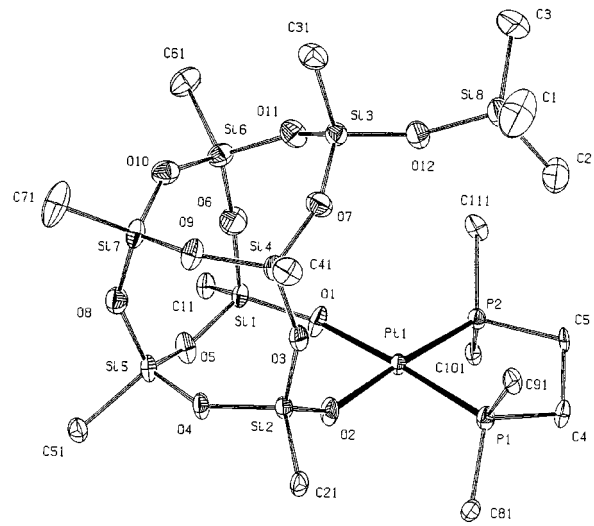

Fig. 1 Perspective ORTEP plot of **3a**. For clarity, thermal ellipsoids are shown at 50% probability; no H and only C attached to Si and P are shown. Selected interatomic distances (Å) and interbond angles (°) are: Pt–O(1) 2.031(6), Pt–O(2) 2.036(4), Pt–P(1) 2.195(2), Pt–P(2) 2.204(2), Si(1)–O(1) 1.573(6), Si(2)–O(2) 1.566(6), other Si–O 1.597(7)–1.647(7), O(1)–Pt–O(2) 90.3(2), O(2)–Pt–P(1) 90.2(2), P(1)–Pt–P(2) 86.90(8), P(2)–Pt–O(1) 92.5(2), Pt–O(1)–Si(1) 146.2(4), Pt–O(2)–Si(2) 148.3(4), Si(3)–O(12)–Si(8) 152.8(5), other Si–O–Si 140–170.

with *cis* angles ranging from 86.9 to 92.5°. The Pt–O and Pt–P distances compare well with those found in the isoelectronic compound [Pt(dppe)$(OCH_3)_2$] [Pt–P = 2.222(3), 2.228(3) Å, Pt–O = 2.037(7), 2.041(7) Å][5] with the slight shortening of the Pt–P bonds in complex **3a** with respect to [Pt(dppe)$(OCH_3)_2$] again consistent with the lower *trans* influence of the silasesquioxane. The Si–O distances in the platinum siloxy functions [Si(1)–O(1) = 1.573(6) Å; Si(2)–O(2) = 1.566(6) Å] are significantly shorter than those present in the silasesquioxane skeleton [1.597–1.647 Å; typical 1.63 Å], while in the silasesquioxane silanol **1a**, these distances are 1.619(7) and 1.616(7) Å (*vide infra*). This bond shortening may be ascribed to the absence of electron donation of the oxygen lone pairs to the electron rich platinum centre which will lead to a stronger Si–O bond by enhanced electron donation to silicon; this effect is absent or the reverse in high oxidation state early transition metal silasesquioxanes.[8]

In order to make a better evaluation of the structural features of the silasesquioxane unit present in **3a**, we determined the molecular structure of the silasesquioxane disilanol **1a** (Fig. 2); single crystals were prepared by allowing acetonitrile to diffuse slowly into a toluene solution of **1a**.§ This disilanol was found to be a monomeric compound that crystallises into two distinct isomers that differ mainly by the orientations of the, highly disordered, cyclopentyl units. Although the quality of the structure determination is poor ($R1$ = 0.1423), the conformation of the Si/O skeleton of **1a** can be discussed with regard to that present in **3a**. Such a comparison reveals that the Si/O skeletons of both compounds are remarkably similar. For instance, the intramolecular distance of the ligating oxygen atoms O(1) and O(2) in **3a** is 2.88(1) Å *versus* 2.67(1) Å in **1a**, while the intramolecular distance Si(1)–Si(3) in **3a**, which can be considered as a measure for the binding cavity, of 5.22(1) Å is virtually equal to that of 5.21(1) Å measured in **1a**. As a result, one might conclude that the silasesquioxane diol is ideally preorganised for co-ordination to a Pt(II) centre following deprotonation.

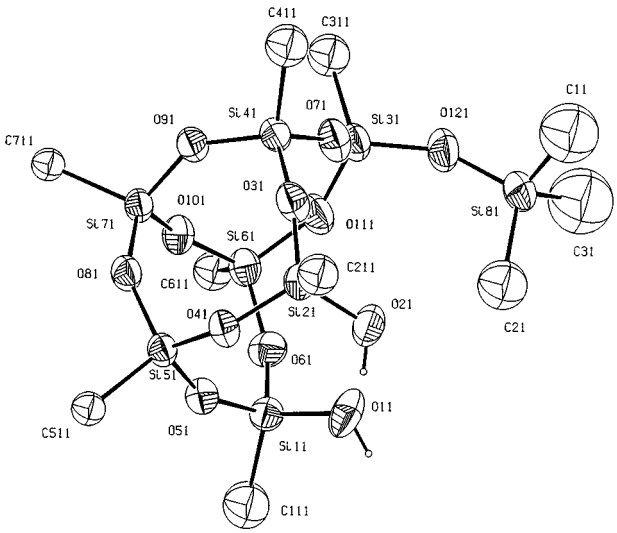

Fig. 2 Perspective ORTEP plot of one of the independent molecules of **1a**. For clarity, thermal ellipsoids are shown at 50% probability; no H and only C attached to Si are shown. Selected interatomic distances (Å) and interbond angles (°) are: Si(11)–O(11) 1.650(8), Si(21)–O(21) 1.619(8), other Si–O 1.579(10)–1.650(8), Si–O–Si 149–156.

We are currently investigating the reactivity of the hydroxyl group in **4** and those of the known silasesquioxane tetrasilanol (c-$C_7H_{13})_6Si_6O_7(OH)_4$[9] with a view to preparing bimetallic metallasilasesquioxanes.

H. C. L. A. thanks the Royal Netherlands Academy of Arts and Sciences (KNAW) for a fellowship. This work was supported in part (A. L. S., M. L.) by the Netherlands Foundation for Chemical Research (SON) with financial aid from the Netherlands Organisation for Scientific Research (NWO). The British Council and NWO are thanked for financial support to HCLA and ADB (Grant JRP313).

Notes and references

† A typical preparation (**3a**): Silasesquioxane **1a** (294 mg, 0.304 mmol) was added to a solution of [Pt(dppe)(CO_3)] (200 mg, 0.306 mmol) in dichloromethane (20 cm^3) and the mixture stirred at room temperature (typically 7 days). The solvent was removed under reduced pressure, the crude solid washed with acetonitrile, and recrystallised from toluene–acetonitrile to give colourless crystals of **3a** (90% yield). (Anal. Found: C, 49.8; H, 6.25%; $C_{62}H_{96}Si_8O_{12}P_2Pt$ requires C, 49.8; H, 6.41%). Silasesquioxane silanols **1b** and **2a** were prepared according to ref. 2 and 9, respectively. The new silasesquioxane **1a** was prepared by an identical method as reported for **1b** starting from 17.0 g of **2a**, 25 mL of Et_3N and 2.20 mL of Me_3SiCl to give 13.6 g (75%) of **1a;** ^{1}H NMR (400 MHz, $CDCl_3$, 25 °C) δ 4.22 (s, 2H, SiOH), 1.76–1.48 (m, 56H, C_5H_9), 1.49 (m, 7H, C_5H_9), 0.16 (s, 9H, $SiMe_3$). ^{13}C{^{1}H} NMR (75 MHz, $CDCl_3$, 25 °C) δ 27.6–27.0 (CH_2), 23.7, 22.7, 22.4, 22.3, 22.1 (1 : 2 : 2 : 1 : 1 for CH), 1.7 ($SiMe_3$).

‡ *Selected spectroscopic data*: **3a**: ^{1}H NMR (400 MHz, $CDCl_3$, 25 °C) δ 8.06 (dq, 8H, Ph), 7.50 (t, 4H, Ph), 7.43 (m, 8H, Ph), 2.14 (m, 4H, $P(CH_2)_2P$), 1.72 (m, 12H, C_5H_9), 1.50 (m, 28H, C_5H_9), 1.27 (m, 4H, C_5H_9), 1.12 (m, 12H, C_5H_9), 0.92 (m, 3H, C_5H_9), 0.81 (m, 2H, C_5H_9), 0.54 (m, 2H, C_5H_9), −0.29 (s, 9H, $SiMe_3$). ^{13}C{^{1}H} NMR (100 MHz, $CDCl_3$, 25 °C) δ 28.7 (CH_2P), 28.5–26.4 (other CH_2), 25.1, 24.2, 23.2, 23.0 (2 : 3 : 1 : 1 for CH), 1.0 ($SiMe_3$). ^{29}Si{^{1}H} NMR (79 MHz, CH_2Cl_2, 0.02 M Cr(acac)$_3$, 25 °C) δ 6.0 ($SiMe_3$), −65.1, −66.3, −66.6, −68.7 (1 : 1 : 2 : 3). ^{31}P{^{1}H} NMR (162 MHz, $CDCl_3$, 25 °C) δ 27.1 [^1J(PPt) = 3773 Hz]. FAB-MS 1539 $[M + H]^+$. **4a**: ^{1}H NMR (400 MHz, $CDCl_3$, 25 °C) δ 8.0 (m, 8H, Ph), 7.5 (m, 12H, Ph), 2.2 (m, 4H, $P(CH_2)_2P$), 1.9–0.8 (m, 63H, C_6H_9). ^{13}C{^{1}H} NMR (100 MHz, $CDCl_3$, 25 °C) δ 29 (CH_2P), 28.6–26.7 (other CH_2), 25.10, 23.22, 23.11, 22.69, 22.60 (2 : 2 : 1 : 1 : 1 for CH). ^{31}P{^{1}H} NMR (162 MHz, $CDCl_3$, 25 °C) δ 26.7 [^1J(PPt) = 3730 Hz].

§ *Crystal data* for **3a**: $C_{64}H_{96}Si_8P_2O_{12}Pt{\cdot}C_2H_3N$, M_r = 1580.22, orthorhombic, space group *Pccn* (no. 56) with a = 47.997(4), b = 13.9845(11), c = 21.803(2) Å, V = 14634(2) Å^3, D_c = 1.434 g cm^{-3}, Z = 8, F(000) = 6544, μ(Mo-Kα) = 2.15 mm^{-1}, 13789 reflections measured, 12902 independent, (1.0° < θ < 25.00°, ω scan, T = 150 K, Mo-Kα radiation, graphite monochromator, λ = 0.71073 Å). Hydrogen atoms were included in the refinement at calculated positions riding on their carrier atoms. Refinement of 812 parameters converged at a final $wR2$ value of 0.1439, $R1$ = 0.0525 [for 7517 reflections with $F_o > 4\sigma(F_o)$], S = 1.111. *Crystal data* for **1a**: $C_{38}H_{74}Si_8O_{12}$, M_r = 947.69, triclinic, space group $P\bar{1}$ (no. 2) with a = 14.5232(12), b = 15.7325(8), c = 23.4701(15) Å, α = 102.358(5), β = 97.036(6), γ = 92.941(5)°, V = 5182.2(6) Å^3, D_c = 1.215 g cm^{-3}, Z = 4, F(000) = 2040, μ(Mo-Kα) = 0.259 mm^{-1}, 17993 reflections measured, 17304 independent, (0.9° < θ < 25.34°). Data collection performed as described for compound **3a**. The reference reflections displayed a decay of 2%. Refinement of 669 parameters converged at a final $wR2$ value of 0.4489, $R1$ = 0.1423 [for 7874 reflections with $F_o > 4\sigma(F_o)$]. CCDC 182/1064. See http://www.rsc.org/suppdata/cc/1998/2627/, for crystallographic files in .cif format.

1 F. J. Feher and T. A. Budzichowski, *Polyhedron*, 1995, **14**, 3239; J.-C. Liu, S. R. Wilson, J. R. Shapley and F. J. Feher, *Inorg. Chem*., 1990, **29**, 5138.
2 F. J. Feher, D. A. Newman and J. F. Walzer, *J. Am. Chem. Soc.*, 1989, **111**, 1741.
3 A. D. Burrows, D. M. P. Mingos, S. E. Lawrence, A. J. P. White and D. J. Williams, *J. Chem. Soc., Dalton Trans*., 1997, 1295.
4 M. A. Andrews and G. L. Gould, *Organometallics*, 1991, **10**, 387.
5 H. E. Bryndza, J. C. Calabrese, M. Marsi, D. C. Roe, W. Tam and J. E. Bercaw, *J. Am. Chem. Soc*., 1986, **108**, 4805.
6 M. A. Andrews, E. J. Voss, G. L. Gould, W. T. Klooster and T. F. Koetzle, *J. Am. Chem. Soc*., 1994, **116**, 5730.
7 R. D. W. Kemmitt, S. Mason, J. Fawcett and D. R. Russell, *J. Chem. Soc., Dalton Trans*., 1992, 1165; A. D. Burrows, D. M. P. Mingos, A. J. P. White and D. J. Williams, *J. Chem. Soc., Dalton Trans*., 1996, 149.
8 F. J. Feher, *J. Am. Chem. Soc*., 1986, **108**, 3850, F. J. Feher and R. L. Blanski, *J. Chem. Soc., Chem. Commun*., 1990, 1614; M. Crocker, R. H. M. Herold and A. G. Orpen, *Chem. Commun*., 1997, 2411.
9 F. J. Feher, T. A. Budzichowski, R. L. Blanski, K. J. Weller and J. W. Ziller, *Organometallics*, 1991, **10**, 2526.

Communication 8/08130A

ChemComm

Synthesis of alkenyl-substituted cyclic enol ethers by catalytic ring-closing metathesis of alkynyl ethers

J. Stephen Clark,*[a] Graham P. Trevitt,[a] Dean Boyall[a] and Blanda Stammen[b]

[a] *School of Chemistry, University of Nottingham, University Park, Nottingham, UK NG7 2RD. E-mail: j.s.clark@nottingham.ac.uk*
[b] *Discovery Chemistry, Pfizer Central Research, Sandwich, Kent, UK CT13 9NJ*

Received (in Cambridge, UK) 2nd October 1998, Accepted 28th October 1998

Ring-closing enyne metathesis can be used to prepare alkenyl-substituted six- and seven-membered cyclic enol ethers in moderate to good yield.

Over the past two decades, fused polycyclic ether natural products, such as the brevetoxins and the ciguatoxins,[1] have attracted considerable attention because of their fascinating structures and potent biological activities.[2] Many of the natural products of this type possess arrays of *trans*-fused six- and seven-membered cyclic ethers, as exemplified by gambierol.[3]

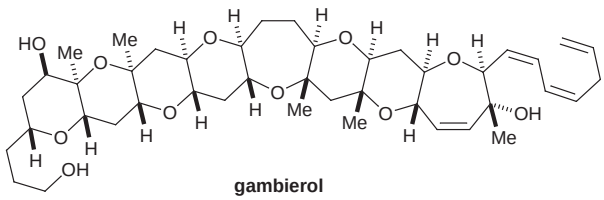

gambierol

Recently, we[4] and others[5] have found that ring-closing metathesis reactions offer a powerful and general approach to the synthesis of cyclic ether sub-units found in the brevetoxins and ciguatoxins. We have demonstrated that the sequence of ring-closing metathesis[6] and hydroboration can be used to prepare six- and seven-membered cyclic ethers[4a] and that ring-closing metathesis of allylic ethers[4b] can be used to prepare eight- and nine-membered cyclic ethers in excellent yield.

In connection with our continuing studies directed towards the synthesis of the brevetoxins and the ciguatoxins, we became interested in exploiting ring-closing enyne metathesis reactions to complement the enol ether and allylic ether ring-closing metathesis reactions that we have already developed.[4] Our interest in the use of ring-closing enyne metathesis reactions was stimulated by recent promising reports from the groups of Murai,[7] Mori,[8] and Barrett and Gibson[9] who have described the preparation of carbocycles and nitrogen heterocycles using ruthenium-catalysed enyne metathesis reactions.

The general strategy for the preparation of sub-units of the brevetoxins and ciguatoxins using a ring-closing enyne metathesis reaction is shown in Scheme 1. We envisaged subjecting a suitably functionalised alkynyl ether **1** to a ruthenium-catalysed ring-closing metathesis reaction to obtain the alkenyl-substituted enol ether **2**. Elaboration of this product (R^3 = H) by hydroboration or by reaction with $^1O_2$ and hydrogenation of the resulting cyclic peroxide,[10] would provide the diol **3**. Application of the same reactions to the vinylsilane-substituted cyclic enol ether **2** (R^3 = SiR_3) would afford the vinyl-substituted cyclic ether **4** by Peterson elimination of the resulting β-hydroxy silane.[11] The pendant vinyl group of this compound would then provide scope for construction of an additional cyclic ether by a subsequent ring-closing metathesis reaction.

We wanted to ascertain whether alkynyl ethers would undergo reaction with the Grubbs catalyst, $Cl_2Ru(PCy_3)_2$-CHPh,[12] in contrast to enol ethers, which were unreactive to this catalyst or the metal alkylidenes generated from it. We also wanted to determine whether terminal alkynyl ethers would

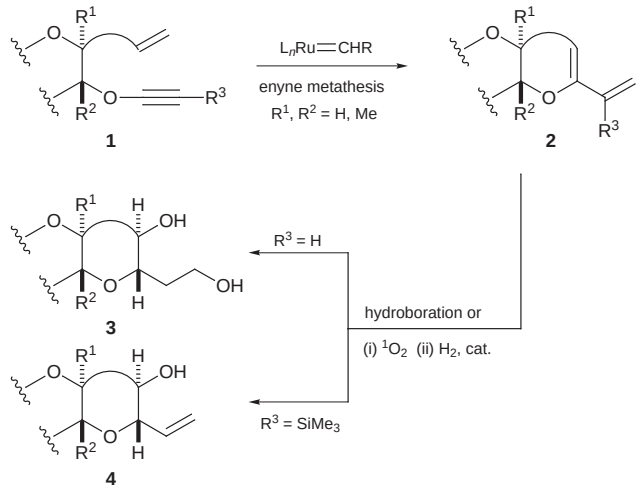

Scheme 1

undergo efficient ring-closing metathesis because there was evidence to suggest that terminal alkynes are not generally good substrates for this reaction.[8,9]

The alkynyl ethers required for our study were prepared from the alcohols **5a** and **5b**, which are readily available from (*R*)-2,3-*O*-isopropylideneglyceraldehyde (Scheme 2).[4b,13] The cyclisation substrates **7a** and **7b** were prepared by an adaptation of Greene's method for the synthesis of alkynyl ethers.[14] This method involves deprotonation of an alcohol with KH and reaction of the resulting alkoxide with Cl_2C=CHCl to give a mixture of dichloro enol ethers that are then converted to the required alkynyl ether by treatment with *n*-butyllithium.[14] Greene has demonstrated that this sequence of reactions can be performed in a one-pot fashion without isolation and purification of the intermediate dichloro enol ethers, and that it can be used to convert hindered secondary alcohols into alkynyl ethers.

Initially, we used Greene's one-pot procedure to convert the alcohols **5a** and **5b** to the required alkynyl ethers **7a** and **7b**. However, only modest yields of the products were obtained, so we opted to isolate the dichloro enol ethers produced upon reaction of Cl_2C=CH_2 with the sodium alkoxides generated from the alcohols **5a** and **5b**. Enol ether formation proceeded in reasonable yield and the products **6a** and **6b** were isolated as stable crystalline solids. Treatment of these dichloro enol ethers with *n*-butyllithium provided the alkynyl ethers **7a** and **7b** in very high yield. The yields over two steps, including isolation of the intermediate dichloro enol ethers, were only marginally lower those obtained by Greene when he used his one-pot procedure for the preparation of related systems.[14]

Having prepared the ethers **7a** and **7b**, we then obtained the other substrates of interest by alkylation of these terminal alkynes. Thus, the substrates **8a** and **8b** were prepared by deprotonation of the alkynyl ethers **7a** and **7b** followed treatment with methyl iodide, and the silyl-substituted alkynyl

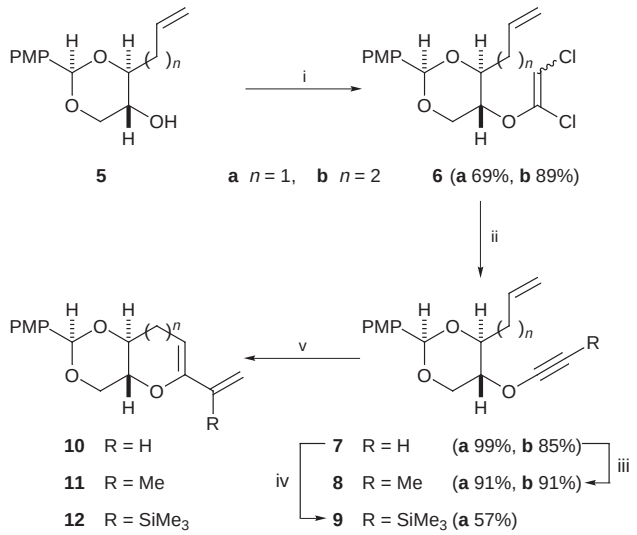

Scheme 2 *Reagents and conditions*: i, NaH, THF, rt, then $CHClCCl_2$ (3 equiv.), −50 °C→rt; ii, *n*-BuLi, Et_2O, −78 °C→rt; iii, *n*-BuLi, DMPU, −78 °C, Et_2O, then MeI, −10 °C→rt; iv, *n*-BuLi, Me_3SiCl, Et_2O, −78 °C→rt; v, $Cl_2Ru(PCy_3)_2CHPh$ (10 mol%), CH_2CH_2 (10 min), CH_2Cl_2, rt or reflux, 4 h or 14 h.

ether **9a** was prepared by deprotonation of the alkyne **7a** and reaction of the resulting anion with trimethylsilyl chloride.

The ring-closing metathesis reactions of the alkynyl ethers **7**–**9** were explored (Scheme 2). Treatment of each substrate with the Grubbs catalyst, $Cl_2Ru(PCy_3)_2CHPh$,[12] in CH_2Cl_2 at reflux led to successful ring-closing metathesis and afforded the alkenyl-substituted cyclic enol ethers **10**–**12** (Table 1).† The highest yields for the ring-closing enyne metathesis reaction were obtained upon cyclisation of the alkynyl ethers **7a** and **8a** to give the six-membered cyclic enol ethers **10a** and **11a**. Interestingly, the terminal alkynyl ether **7a** underwent efficient cyclisation, although a higher yield was obtained upon reaction of the substrate **8a**, containing a non-terminal alkyne. The silyl-substituted alkynyl ether **9a** also underwent cyclisation, but in low yield; it is likely that the poor yield for this reaction can be attributed to the steric bulk of trimethylsilyl substituent.[8a]

The ring-closing enyne metathesis reactions to produce seven-membered cyclic enol ethers proved to be less successful than those to produce the alkenyl-substituted dihydropyrans. The reactions were slow, and prolonged reaction times were required for complete reaction. There was little difference between the yield obtained upon cyclisation of the terminal alkynyl ether **7b** to give the diene **10b** and that obtained upon cyclisation of the methyl-substituted substrate **8b** to give the diene **11b**.

In all the enyne metathesis reactions, the ruthenium catalyst was 'pre-activated' by the passage of ethene through the solution of the catalyst prior to addition of the substrate, and reactions were then performed under an atmosphere of ethene. Inferior yields were obtained upon cyclisation of the substrates **7b** and **8b** when the reactions were performed in the absence of ethene.

Table 1 Results of ring-closing enyne metathesis reactions of the alkynyl ethers **7**–**9** catalysed by $Cl_2Ru(PCy_3)_2CHPh$ (10 mol%)

Substrate	Reaction time/h	Product	Yield (%)[a]
7a	4[b]	**10a**	65
7b	14[c]	**10b**	33
8a	4[b]	**11a**	77
8b	14[c]	**11b**	27
9a	4[b]	**12a**	20

[a] Yield of isolated product after chromatography on silica gel. [b] Reaction performed in CH_2Cl_2 at reflux. [c] Reaction performed in CH_2Cl_2 at room temperature.

Our results show that ring-closing metathesis of alkynyl ethers can be used to prepare alkenyl-substituted cyclic enol ethers. Although the yields of seven-membered cyclic enol ethers were low, we have demonstrated that the reaction is a synthetically viable one for the preparation of alkenyl dihydropyrans in good yield. We have also shown that the Grubbs catalyst, $Cl_2Ru(PCy_3)_2CHPh$,[12] can be used for ring-closing enyne metathesis of alkynyl ethers, which contrasts with the lack of reactivity exhibited by this catalyst towards related enol ethers.[4a,15]

The cyclic ethers **10a** and **10b** are potentially useful enantiomerically pure chiral building-blocks for the synthesis of sub-units of the brevetoxins and ciguatoxins. The elaboration of these compounds (*e.g.* **2**→**3**) is currently under investigation, and the results of these studies will be reported in due course.

We thank the Engineering and Physical Sciences Research Council for the award of a CASE Studentship (to D. B.) and the University of Nottingham for financial support.

Notes and references

† Typical procedure for the ring-closing enyne metathesis of the substrates **7**–**9**: The catalyst, $Cl_2Ru(PCy_3)_2CHPh$ (38 mg, 0.045 mmol, 10 mol%), was dissolved in dry CH_2Cl_2 (60 mL) and a stream of ethene passed through the solution for 10 min (the solution turned from purple to orange in colour). A solution of the alkyne (0.45 mmol) in dry CH_2Cl_2 (5 mL) was added by cannula to the solution of the catalyst under an atmosphere of ethene at room temperature. The flask was then washed with further CH_2Cl_2 (3 mL) and this was added to the reaction mixture. The mixture was then stirred under a static atmosphere of ethene at reflux (4 h) or room temperature (21 h). On completion of the reaction, the solvent was then removed *in vacuo* and the residual material was purified by flash column chromatography on silica gel (hexane–Et_2O, 4:1 with 1% triethylamine) to afford the product as a colourless solid.

1 For a review of marine polycyclic ether toxins, see T. Yasumoto and M. Murata, *Chem. Rev.*, 1993, **93**, 1897.
2 For recent syntheses of brevetoxins A and B, see K. C. Nicolaou, *Angew. Chem., Int. Ed. Engl.*, 1996, **35**, 589; K. C. Nicolaou, Z. Yang, G.-Q. Shi, J. L. Gunzner, K. A. Agrios and P. Gärtner, *Nature*, 1998, **392**, 264.
3 M. Satake, M. Murata and T. Yasumoto, *J. Am. Chem. Soc.*, 1993, **115**, 361.
4 (*a*) J. S. Clark and J. G. Kettle, *Tetrahedron Lett.*, 1997, **38**, 123; (*b*) J. S. Clark and J. G. Kettle, *Tetrahedron Lett.*, 1997, **38**, 127.
5 K. C. Nicolaou, M. H. D. Postema and C. F. Claiborne, *J. Am. Chem. Soc.*, 1996, **118**, 1565; T. Oishi, Y. Nagumo and M. Hirama, *Synlett*, 1997, 980; M. Delgado and J. D. Martín, *Tetrahedron Lett.*, 1997, **38**, 6299; M. T. Crimmins and A. L. Choy, *J. Org. Chem.*, 1997, **62**, 7548.
6 For recent reviews concerning ring-closing metathesis, see R. H. Grubbs, S. J. Miller and G. C. Fu, *Acc. Chem. Res.* 1995, **28**, 446; H.-G. Schmalz, *Angew. Chem., Int. Ed. Engl.*, 1995, **34**, 1833; M. Schuster and S. Blechert, *Angew. Chem., Int. Ed. Engl.*, 1997, **36**, 2036; S. K. Armstrong, *J. Chem. Soc., Perkin Trans. 1*, 1998, 371; R. H. Grubbs and S. Chang, *Tetrahedron*, 1998, **54**, 4413.
7 N. Chatani, T. Morimoto, T. Muto and S. Murai, *J. Am. Chem. Soc.*, 1994, **116**, 6049.
8 (*a*) A. Kinoshita and M. Mori, *Synlett*, 1994, 1020; (*b*) A. Kinoshita and M. Mori, *J. Org. Chem.*, 1996, **61**, 8356; (*c*) A. Kinoshita and M. Mori, *Heterocycles*, 1997, **46**, 287.
9 A. G. M. Barrett, S. P. D. Baugh, D. C. Braddock, K. Flack, V. C. Gibson and P. A. Procopiou, *Chem. Commun.*, 1997, 1375.
10 For the functionalisation of a closely related system by this procedure, see E. Alvarez, M. Rico, R. M. Rodríguez, D. Zurita and J. D. Martín, *Tetrahedron Lett.*, 1992, **33**, 3385.
11 E. W. Colvin, *Silicon in Organic Synthesis*, Butterworths, London, 1981, ch. 12, pp. 142–164.
12 P. Schwab, M. B. France, J. W. Ziller and R. H. Grubbs, *Angew. Chem., Int. Ed. Engl.*, 1995, **34**, 2039.
13 J. Mulzer and A. Angermann, *Tetrahedron Lett.*, 1983, **24**, 2843; J. Jurczak, S. Pikul and T. Bauer, *Tetrahedron*, 1986, **42**, 447.
14 A. Moyano, F. Charbonnier and A. E. Greene, *J. Org. Chem.*, 1987, **52**, 2919.
15 O. Fujimura, G. C. Fu and R. H. Grubbs, *J. Org. Chem.*, 1994, **59**, 4029.

Communication 8/07667G

ChemComm

Difluorotoluene, a thymine isostere, does not hydrogen bond after all

Xue Wang and K. N. Houk*

Department of Chemistry and Biochemistry, University of California, Los Angeles, CA 90095, USA. E-mail: houk@chem.ucla.edu

Received (in Corvallis, OR, USA) 26th June 1998, Revised Manuscript Received 20th October 1998, Accepted 21st October 1998

The lack of significant hydrogen bonding by 2,4-difluorotoluene, an isostere of thymine, is confirmed by *ab initio* calculations and force field modelling of nucleic acids.

Watson–Crick base-pairing is the information code which directs replication, transcription and translation.[1] Base-pairing is produced by hydrogen-bonding which stabilizes the DNA double helical structure.[2] The free energy differences between matched and mismatched base pairs in aqueous solution are estimated to be in the range of 0.2 to 0.4 kcal mol^{-1} for terminal base pairs[3] and 1 to 3 kcal mol^{-1} for internal base pairs.[4] In 1988, Echols and Goodman noted that the energy difference between hydrogen bonding of matched and mismatched terminal pairs is insufficient to account for the remarkably high fidelity of Watson–Crick base pairing in DNA replication by the DNA polymerase (10^4 to 10^5).[5] It was proposed that the geometry of the complex between the template and substrate on DNA polymerase was more important than hydrogen bonding in controlling polymerase fidelity.

In 1994, Kool and co-workers proposed that there is no significant hydrogen bonding between adenine (**A**) and the

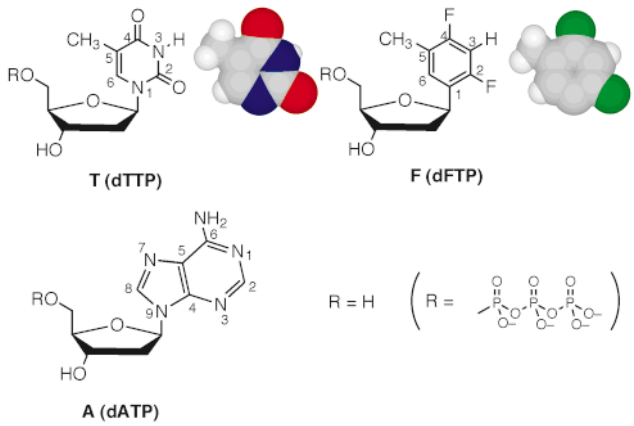

thymine (**T**) isostere, **F**.[6] Nevertheless, numerous studies now show that **F** can be readily incorporated in place of **T** by DNA polymerase.[7] In **F**, fluorines replace oxygens, and carbons replace nitrogens. Much evidence has been amassed in accord with the idea. ^{1}H NMR and X-ray data indicated that **F** does not H-bond with natural nucleotides in solution.[8] Single nucleotide insertion and 'running start' experiments demonstrated that **F** expressed similar selectivity to **T** during the replication of a DNA strand in the presence of Klenow fragment (KF) of *Escherichia coli* DNA polymerase.[7] The geometry of the reaction complex, not hydrogen bonding, seems of principal importance in the fidelity of the DNA polymerase.

However, Evans and Seddon proposed that the hydrogen bonding between **A** and **F** still plays an important role in DNA replication even with templates containing **F**.[9] In their communication, *ab initio* RHF/6-31G**, semi-empirical AM1 and PM3 calculations were presented which reveal large dipole moments of the methyl derivative of 2,4-difluorotoluene **1** (1.86 D) in comparison to H_2O (1.82 D). They suggested that the polar nature of 2,4-difluorotoluene is important for hydrogen bonding and hence, DNA replication. They reported the electrostatic potential surfaces of **1** and N^1-methylthymine **2** [Fig. 1(*a*)]. These are clearly similar, suggesting that **F** mimics the shape, the charge distribution and hydrogen-bonding patterns of **T** [Fig. 1(*b*)]. Evans and Seddon supported the 'status quo' concerning the major role of hydrogen-bonding on replication fidelity, even with **F**.

We have reinvestigated these issues with quantum mechanics and molecular mechanics, to test the ability of hydrogen-bonding by **F** and the potential role in base-pairing interactions in DNA.

It is well known that fluorinated olefins and aromatic compounds are poor hydrogen bond acceptors. Fluorine has a greater electronegativity and lower polarizability than oxygen, which renders it a much poorer hydrogen bond acceptor. At the MP2/TZV++(3d,1f,1p) level of theory, vinyl C(sp^2)–F forms hydrogen bonds with water with a strength of only 1.5 kcal mol^{-1}, significantly lower than typical hydrogen bonds of 5 to 10 kcal mol^{-1}.[10] **F** contains two aromatic C(sp^2)–F moieties. The hydrogen bonding strength of **F** with water should be even less.

We recomputed **1** and **2** with semi-empirical PM3, *ab initio* RHF/3-21G and RHF/6-31G** calculations.[11] At the RHF/6-31G** level, the electrostatic charges of fluorines in **1** are both 0.21, and the dipole moment of **1** is 1.90 D. The electrostatic charges of the oxygens in **2** are both 0.61, and the dipole moment of **2** is 4.83 D. The dipole moment of the water molecule has also been calculated using the RHF/6-31G** method for comparison, giving a value of 2.15 D. In spite of the representation displayed in Fig. 1(*a*), the fluorines of **F** and oxygens of **T** have significantly different electrostatic charges. The electrostatic potential range used in the published pictorial representation for **1** is from −19 to +27 electron per atomic unit, while it is from −46 to +51 electron per atomic unit for **2**.

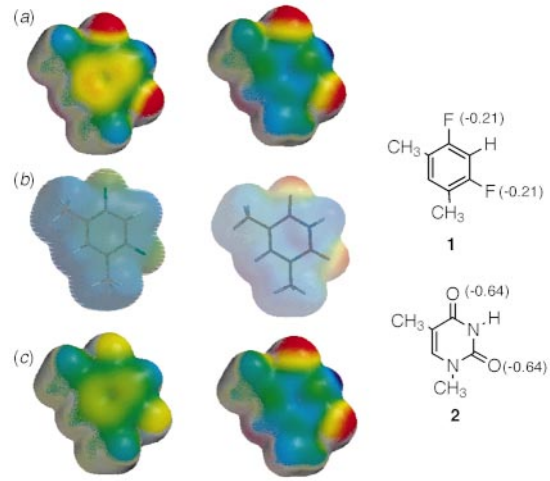

Fig. 1 The electrostatic potential surfaces of **1** and **2**: (*a*) as presented in ref. 9 [the range of electrostatic potential shown in thymine is from red (−46.0) to blue (+50.5) and in difluorotoluene is from red (−19.0) to blue (+27.3); the units are electrons per atomic unit), (*b*) PM3 model and (*c*) RHF/6-31G** model [both (*b*) and (*c*) using the same potential range (−46.1 to +50.5 from red to blue for RHF) for both structures from our calculations; the units are electrons per atomic unit and charges are given in parenthesis].

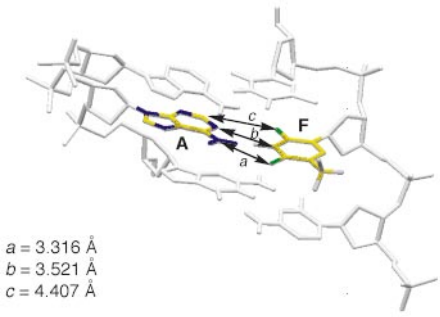

Fig. 2 Molecular modelling shows no obvious hydrogen bonding of **F** with **A**.

Because of this, the color pictures in Fig. 1(*a*) provide the incorrect impression that the electrostatic potentials are very similar. When plotted on the same color scale [Fig. 1(*b*),(*c*)], it is obvious that the electrostatic potential range of **1** is much more limited than that of **2**. Hydrogen bonds involving **F** will be very weak, perhaps impossible to detect in solution. Indeed, this is the conclusion of Kool *et al*. based upon experimental data.[8] The dipole moment of **1** is also significantly smaller than **2**, even smaller than H_2O. Since replication experiments are performed in aqueous solution, DNA strands are solvated. Hydrogen bonding between **F** and **A** is not competitive with hydrogen bonding between solvent water molecules and **A**, even if **F** can weakly complex with **A** in the gas phase.

Since the Evans–Seddon paper, others have tested the ideas computationally.[12,13] Meyer and Sühnel did calculations on **F**–**A** and **T**–**A** complexes using the RHF, B3LYP and MP2 methods and the 6-31G** basis set.[12] Without zero point correction, the complexation energy for **T**–**A** is 11.7 kcal mol^{-1}, significantly larger than the complexation energy for **F**–**A** (−3.8 kcal mol^{-1}).

However, in aqueous solvent, the loosely complexed **F**–**A** is readily dissociated. Santhosh and Mishra did calculations on **F**–**A** and **T**–**A** systems in a solvent cavity model (PCM) at the 4-31G level with AM1 geometries.[13] The complexation energy of **F**–**A** becomes repulsive (3.5 kcal mol^{-1}) in aqueous media, while it is attractive for the **T**–**A** complex (−11.1 kcal mol^{-1}). The best distance for fluorine of **F** and nitrogen of **A** is 3.533 Å (calculated from their graph), significantly longer than that of **T**–**A** (3.0 Å). We performed RHF/6-31G* optimizations and SCI-PCM solvent cavity model calculations on **F**–**A** and **T**–**A** as well. With RHF/6-31G* optimized geometries, and SCI-PCM solvation calculations at the RHF/6-31G* level, the energy difference between **F**–**A** and uncomplexed **A** and **F** is −1.4 kcal mol^{-1}. This means that the **F**–**A** complex becomes repulsive in aqueous solution, as Santhosh and Mishra showed.[13] The complexation energy for **T**–**A** in water is computed to be −5.2 kcal mol^{-1}. **F** does not hydrogen bond with **A** in aqueous solution.

We have also modelled the polydeoxynucleotides containing **F**–**A** or **T**–**A** complexes. The AMBER* force field was employed in these calculations.[14] The charges on the oxygens in **T** are −0.47 and −0.53, respectively, and the charges on the fluorines in **F** are both −0.25. A strand of 3-nt DNA is shown in Fig. 2. Whereas the distances between O^4 of **T** and NH_2 of **A**, and between N^3 of **T** and N^1 of **A**, are computed to be 2.832 and 2.851 Å respectively, the distance between F^4 of **F** and NH_2 of **A** is 3.316 Å, and the distance between C^3 of **F** and N^1 of **A** is 3.521 Å. These are 0.484–0.670 Å longer, a clear indication of the absence of hydrogen-bonding in the small DNA oligomer. Importantly, the distance between N^3 of **T** and N^1 of **A** calculated with the AMBER* force field (2.851 Å) is close to those measured from high resolution DNA X-ray structures (2.82 ± 0.07 Å),[12] and the distance between F^4 of **F** and N^1 of **A** calculated with the AMBER* force field (3.521 Å) is close to the value obtained from RHF/4-31G//AM1 calculations by Santhosh and Mishra (3.533 Å).[13]

Force field calculations of a 12-nt DNA fragment with the GB/SA* solvation model[15] also show that there is no hydrogen-bonding between **F** and **A** (Fig. 3). In DNA double helices, the

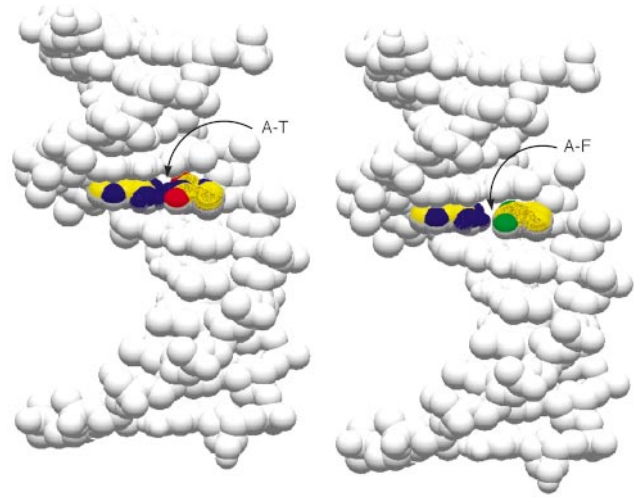

Fig. 3 The structure of 12-nt DNA with **A**–**T** or **A**–**F** base pairs.

base pairs adjacent to **F**–**A** are strongly hydrogen bonded. This, along with π-stacking to **F** and **A**, keeps the **F**–**A** base pair from separating. Aqueous solvation also keeps DNA strands tightly coiled. Even with the assistance from neighboring base pairs, the **F**–**A** hydrogen bonding distances are still 0.6–0.7 Å longer than those of **T**–**A**. All evidence suggests that there is no hydrogen bonding between **F** and **A**. However, the π-stacking and the shape of the whole DNA strands are not distorted significantly with **F** in place of **T**. As a nearly perfect isostere, **F** should be able to fit into the DNA template-polymerase-substrate complex without disturbing the structure.

The experimental and theoretical studies support the conclusion of Kool *et al*. that the hydrogen bonding of **F**–**A** is very unlikely to play an important role in DNA replication. Geometrical effects must account for the high fidelity of DNA replication in the presence of polymerase.

Notes and references

1 J. D. Watson and F. H. C. Crick, *Nature*, 1953, **171**, 737.
2 G. C. Pimentel and A. L. McClellan, *The Hydrogen Bond*, Freeman, San Francisco, 1960; G. A. Jeffrey and W. Saenger, *Hydrogen Bonding in Biological Structures*, Springer-Verlag, New York, 1991; G. A. Jeffrey, *An Introduction to Hydrogen Bonding*, Oxford, New York, 1997.
3 J. Petruska, M. F. Goodman, M. S. Boosalis, L. C. Sowers and C. Cheong, *Proc. Natl. Acad. Sci. U.S.A.*, 1988, **85**, 6252.
4 L. A. Loeb and T. A. Kunkel, *Annu. Rev. Biochem.*, 1982, **52**, 429.
5 H. Echols and M. F. Goodman, *Annu. Rev. Biochem.*, 1991, **60**, 477; M. F. Goodman, *Proc. Natl. Acad. Sci. U.S.A.*, 1997, **94**, 10 493.
6 B. A. Schweitzer and E. T. Kool, *J. Org. Chem.*, 1994, **59**, 7238.
7 R. X.-F. Ren, B. A. Schweitzer, C. J. Sheils and E. T. Kool, *Angew. Chem., Int. Ed. Engl.*, 1996, **35**, 743; S. Moran, R. X.-F. Ren, C. J. Sheils, S. Rumney and E. T. Kool, *Nucleic Acid Res.*, 1996, **24**, 2044; R. X.-F. Ren, N. C. Chaudhuri, P. L. Paris, S. Rumney and E. T. Kool, *J. Am. Chem. Soc.*, 1996, **118**, 7671; K. M. Guckian, B. A. Schweitzer, R. X.-F. Ren, C. J. Sheils, P. L. Paris, D. C. Tahmassebi and E. T. Kool, *J. Am. Chem. Soc.*, 1996, **118**, 8182; S. Moran, R. X.-F. Ren, S. Rumney IV and E. T. Kool, *J. Am. Chem. Soc.*, 1997, **119**, 2056; S. Moran, R. X.-F. Ren and E. T. Kool, *Proc. Natl. Acad. Sci. U.S.A.*, 1997, **94**, 10 506; D. Liu, S. Moran and E. T. Kool, *Chem. Biochem.*, 1997, **4**, 919.
8 B. A. Schweitzer and E. T. Kool, *J. Am. Chem. Soc.*, 1995, **117**, 1863; K. M. Guckian and E. T. Kool, *Angew. Chem., Int. Ed.*, 1998, **36**, 2825.
9 T. A. Evans and K. R. Seddon, *Chem. Commun.*, 1997, 2023.
10 J. A. K. Howard, V. J. Hoy, D. O'Hagan and G. T. Smith, *Tetrahedron*, 1996, **52**, 12 613.
11 SPARTAN Version 4.0, Wavefunction, Inc., 18401 Von Karman Ave., #370, Irvine, CA 92715, USA.
12 M. Meyer and J. Sühnel, *J. Biomol. Struct. Dynamics*, 1997, **15**, 619.
13 C. Santhosh and P. C. Mishra, *Int. J. Quantum Chem.*, 1998, **68**, 351.
14 F. Mohamadi, N. G. J. Richards, W. C. Guida, R. Liskamp, M. Lipton, C. Canfield, G. Chang, T. Hendrickson and W. C. Still, *J. Comput. Chem.*, 1990, **11**, 440.
15 D. Qiu, P. S. Shenkin, F. P. Hollinger and W. C. Still, *J. Phys. Chem.*, 1997, **101**, 3005.

Communication 8/07425I

ChemComm

Nitrile functionalised pendant-arm derivatives of [9]aneN$_3$ as new multidentate ligands for inorganic crystal engineering ([9]aneN$_3$ = 1,4,7-triazacyclononane)

Lorenzo Tei, Vito Lippolis, Alexander J. Blake, Paul A. Cooke and Martin Schröder*

School of Chemistry, The University of Nottingham, University Park, Nottingham, UK NG7 2RD. E-mail: m.schroder@nottingham.ac.uk

Received (in Cambridge, UK) 23rd September 1998, Accepted 12th October 1998

Functionalised pendant-arm derivatives of [9]aneN$_3$ have been used as building blocks for the synthesis of inorganic multi-dimensional networks in the presence of Ag^I.

Crystal engineering and the design of solid-state architectures have become areas of increasing interest over recent years.[1–4] Initially, attention was focused mainly upon the use of supramolecular contacts (particularly hydrogen bonding and π–π interactions) between suitable organic molecules to generate multi-dimensional arrays and networks.[1–3] More recently, the design of three-dimensional inorganic coordination polymers has become a rapidly expanding area[4,5] with transition metal ions such as Cu^I and Ag^I and multidentate ligands derived from 4,4′-bipy being used as building blocks for different network topologies and structural motifs.[6–8] Although subtle factors such as π–π interactions between ligand units and/or the nature of the anion may have profound effects on the topology of the cationic coordination array, the design and synthesis of new multidentate ligands that can be used as building blocks for the construction of desired solid-state architecture is still the major target.

Functionalised pendant arm derivatives of aza-crown ether macrocycles have long been used as ligands for producing complexes of low nuclearity and of high kinetic and thermodynamic stability, with the coordinated transition-metal ion(s) adopting specific coordination and redox properties which make them relevant as models for metallobiosites or catalytic reagents.[9,10] The pendant groups are carefully chosen and are often attached to the macrocyclic framework to give endocyclic complexes. However, functionalised pendant arms have not been previously intentionally attached onto aza-crown ether rings for the purpose of assembling a multidentate ligand to be used in the construction of three-dimensional exocyclic solid-state architectures.

We report herein the synthesis† and coordination properties of the new ligands L^1 and L^2 with Ag^I. We argued that nitrile functionalised pendant arms would prevent these polydentate

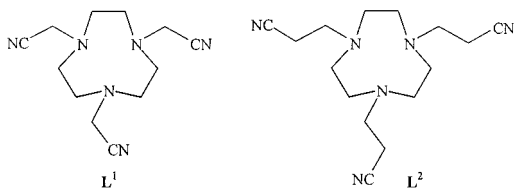

ligands from encapsulating tetrahedral metal centres (Ag^I, Cu^I) or forming sandwich complexes with them, but would promote the formation of multinuclear or polymeric compounds.

Reaction of L^1 with 1 molar equivalent of $AgPF_6$ in MeCN at room temperature gives colourless plate crystals following partial removal of the solvent and diffusion of Et_2O vapour into the remaining solution. A single crystal X-ray determination‡ confirms the product to be a three-dimensional polymer, $\{[Ag(L^1)](PF_6)\}_\infty$ **1**. Each Ag^I ion is coordinated to six N-donors in a distorted octahedral coordination geometry, with one face taken up by the three N-donors of the triaza ring [Ag–N 2.523(4)–2.547(4) Å]. The remaining three positions are occupied by the N-donors of nitrile groups belonging to three different molecules of $[Ag(L^1)]^+$ [Ag–N 2.311(4)–2.486(4) Å] (Figs. 1 and 2). A three-dimensional inorganic network is therefore formed in which each molecule of L^1 is a node linked to four different Ag^I centres (Fig. 2) and each Ag^I ion represents a six-connected junction *via* NCH_2CN linkers to six other Ag^I ions in the overall 3D single network. Six-connected single networks at Ag^I consisting of a cationic frame linked by molecular rods are very rare in the literature, the only reported example being the complex $[Ag(pyz)_3]SbF_6$ which is topologically related to the structures of ReO_3 or Prussian blue.[7c]

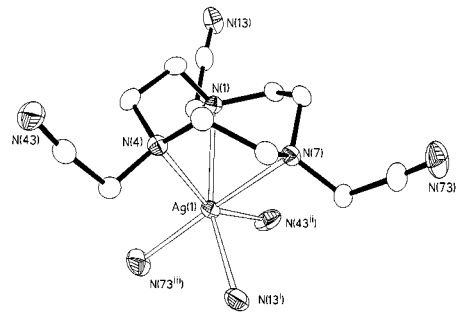

Fig. 1 View of the coordination sphere around the Ag^I ion in the $[Ag(L^1)]^+$ cation with numbering scheme adopted. The nitrogen atoms N(13^i), N(43^{ii}) and N(73^{iii}) belong to three different symmetry related molecules of L^1 [i = $x+1/2, -y+3/2, z-1/2$; ii = $x-1/2, -y+3/2, z-1/2$; iii = $-x+1/2, y+1/2, -z+1/2$]. Hydrogen atoms are omitted for clarity and displacement parameters are drawn at 50% probability.

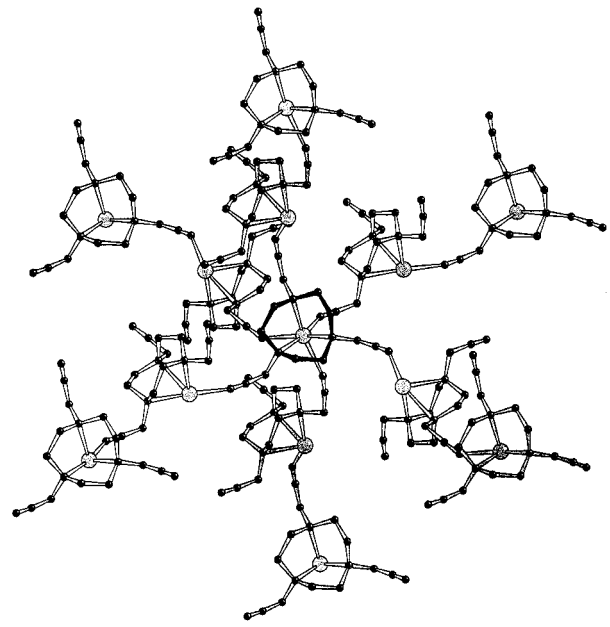

Fig. 2 View of part of the $\{[Ag(L^1)]^+\}_\infty$ three-dimensional polymer. Counter-anions are omitted for clarity and chains running through the structure are distinguished by the colour of their bonds.

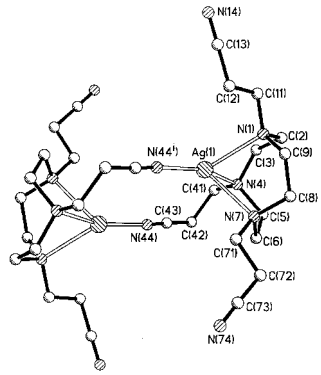

Fig. 3 View of the $[Ag_2(L^2)_2]^{2+}$ dinuclear cation with numbering scheme adopted. Hydrogen atoms are omitted for clarity. Symmetry operation i = $-x+1, -y+1, -z$.

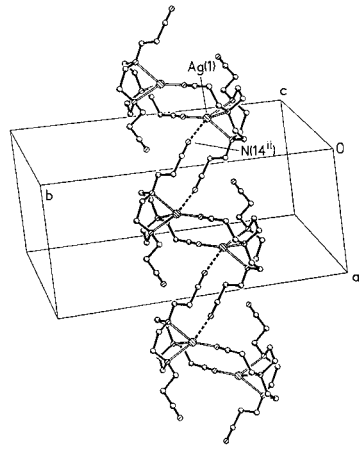

Fig. 4 Packing diagram for the $\{[Ag_2(L^2)_2]^{2+}\}_\infty$ polymeric chain. Counter-anions are omitted for clarity. Symmetry operation ii = $-x+2, -y+1, -z$.

Using the same synthetic procedure as for **1**, colourless crystals were obtained from the reaction of L^2 with $AgBF_4$ in 1:1 molar ratio in MeCN. Although analytical and mass spectroscopic data for the product were consistent with the stoichiometry $[Ag(L^2)]BF_4$, a single crystal structure determination was undertaken to ascertain the ligation and nuclearity of the complex. The structure confirms the product to be a one-dimensional zigzag polymer, $\{[Ag_2(L^2)_2](BF_4)_2\}_\infty$ **2** in which the repeating unit is the binuclear complex cation $[Ag_2(L^2)_2]^{2+}$ which lies across a crystallographic inversion centre (Fig. 3). Each Ag^I ion in the binuclear fragment is coordinated to four N-donors in a distorted tetrahedral geometry with N–Ag–N angles ranging from 74.0(2) [N(4)–Ag(1)–N(7)] to 159.1(2)° [N(4)–Ag(1)–N(44^i), i = $-x+1, -y+1, -z$] and Ag–N bond distances from 2.192(6) [Ag(1)–N(44^i)] to 2.504(5) Å [Ag(1)–N(7)]. Three out of four N-donors are provided by the [9]aneN_3 framework of a molecule of L^2 and the fourth, which completes the coordination sphere around the metal centre, belongs to the nitrile group of a pendant arm of the symmetry related $[Ag(L^2)]^+$ unit (Fig. 3). One of the remaining two pendant arms of L^2 interacts with a Ag^I centre of an inversion-related $[Ag_2(L^2)_2]^{2+}$ binuclear fragment [Ag(1)–N(14^{ii}) 2.779(7) Å, ii = $-x+2, -y+1, -z$] to give an infinite zigzag polymer along the *a* axis (Fig. 4). Thus, simply altering the pendant arm length, from C_2 in L^1 to C_3 in L^2, affords a different network motif for the resultant coordination polymer.

The work described herein represents the first attempt to use properly designed functionalised pendant-arm derivatives of aza crown ethers as building blocks for the synthesis of extended inorganic architectures. We have also shown that the potential of this type of ligand can be increased further by the fine-control over the nature of the resulting inorganic network offered by varying the length of the pendant arms.

We thank the EPSRC for financial support.

Notes and References

† The ligands L^1 and L^2 were prepared in 53 and 95% yield, respectively, starting from [9]aneN_3·3HBr and [9]aneN_3, respectively, according to procedures adapted from the literature.[11] L^1: Found (calc. for $C_{12}H_{18}N_6$): C, 58.2 (58.5); H, 7.6 (7.4); N, 34.0 (34.1%); ^{1}H NMR ($CDCl_3$, 298 K, 300 MHz), δ 2.85 (12H, s), 3.59 (6H, s); ^{13}C NMR ($CDCl_3$, 298 K, 75 MHz), δ 54.12, 46.49, 116.14. L^2: Found (calc. for $C_{15}H_{24}N_6$): C, 61.80 (62.50); H, 8.22 (8.33); N, 28.88 (29.17%); ^{1}H NMR ($CDCl_3$, 298 K, 300 MHz), δ 2.44 (6H, t, *J* 6.67 Hz, CH_2CN), 2.79 (12H, s), 2.86 (6H, t, *J* 6.62 Hz, NCH_2CH_2CN); ^{13}C NMR ($CDCl_3$, 298 K, 75 MHz), δ 17.06, 54.06, 55.71, 119.26.

‡ Stoe Stadi-4 four-circle diffractometer, Mo-Kα radiation, ω–θ scans, θ_{max} = 25°. Both structures were solved using direct methods[12] and all non-H atoms were located using subsequent difference Fourier methods.[13] Hydrogen atoms were placed in calculated positions and thereafter allowed to ride on their parent atoms.

Crystal data: $\{[AgL^1](PF_6)\}_\infty$ **1**: $C_{12}H_{18}AgF_6N_6P$, M = 499.16, monoclinic, space group $P2_1/n$ (no. 14), a = 10.652(9), b = 15.400(9), c = 10.924(6)Å, β = 92.14(6)°, U = 1791(2)Å^3, T = 150(2) K, Z = 4, D_c = 1.851 g cm^{-3}, μ(Mo-Kα) = 1.283 mm^{-1}. At final convergence R_1 [$I \geqslant 2\sigma(I)$] = 0.0364, wR_2 (all data) = 0.0976 for 247 refined parameters, S = 1.08, $(\Delta/\sigma)_{max}$ = 0.025, $\Delta\rho_{max, min}$ = 0.97, −1.02 e Å^{-3}.

$\{[Ag_2(L^2)_2](BF_4)_2\}_\infty$ **2**: $C_{15}H_{24}AgBF_4N_6$, M = 483.08, monoclinic, space group $P2_1/n$ (no. 14), a = 9.7157(7), b = 22.949(2), c = 10.1326(6)Å, β = 116.892(6)°, U = 2014.9(3)Å^3, T = 298(2) K, Z = 4, D_c = 1.592 g cm^{-3}, μ(Mo-Kα) = 1.048 mm^{-1}. At final convergent R_1[$I \geqslant 2\sigma(I)$] = 0.0546, wR_2 (all data) = 0.1246 for 261 refined parameters, S = 1.17, $(\Delta/\sigma)_{max}$ = 0.070, $\Delta\rho_{max, min}$ = 0.79, −0.56 e Å^{-3}. CCDC 182/1054.

1 G. R. Desiraju, in *Crystal Engineering: Design of Organic Solids*, Elsevier, Amsterdam, 1989.
2 *The Crystal as a Supramolecular Entity*, ed. G. R. Desiraju, Wiley, 1995.
3 G. R. Desiraju, *Angew. Chem., Int. Ed. Engl*., 1995, **34**, 2311.
4 B. F. Hoskins, R. Robson and D. A. Slizys, *Angew. Chem., Int. Ed. Engl*., 1997, **36**, 2752; N. R. Champness and M. Schröder, *Curr. Opin. Solid State Mater. Chem*., 1998, **3**, 419.
5 S. R. Batten and R. Robson, *Angew. Chem., Int. Ed. Engl*., 1998, **37**, 1460.
6 A. J. Blake, N. R. Champness, A. N. Khlobystov, D. A. Lemenovskii, W.-S. Li and M. Schröder, *Chem. Commun*., 1997, 1339, 2027; A. J. Blake, N. R. Champness, S. S. M. Chung, W.-S. Li and M. Schröder, *Chem. Commun*., 1997, 1675; M. A. Withersby, A. J. Blake, N. R. Champness, P. Hubberstey, W.-S. Li and M. Schröder, *Angew. Chem., Int. Ed. Engl*., 1997, **36**, 2327.
7 (*a*) M. Fujita, Y. J. Kwon, S. Washizu and K. Ogura, *J. Am. Chem. Soc*., 1994, **116**, 1151; (*b*) L. R. MacGillary, S. Subramanian and M. J. Zaworotko, *J. Chem. Soc., Chem. Commun*., 1994, 1325; (*c*) L. Carlucci, G. Ciani, D. M. Proserpio and A. Sironi, *Angew. Chem., Int. Ed. Engl*., 1995, **34**, 1895; (*d*) *J. Chem. Soc., Dalton Trans*., 1997, 1801; (*e*) L. Carlucci, G. Ciani, P. Macchi and M. D. Proserpio, *Chem. Commun*., 1998, 1837.
8 P. Losier and M. J. Zaworotko, *Angew. Chem., Int. Ed. Engl*., 1996, **35**, 2779; T. L. Hennigar, D. C. Macquarrie, P. Losier, R. D. Rogers and M. J. Zaworotko, *Angew. Chem., Int. Ed. Engl*., 1997, **36**, 972; M. Fujita, O. Sasakhi, K. Watanabe, K. Ogura and K. Yamaguchi, *New. J. Chem*., 1998, **22**, 189; O. M. Yaghi and G. Li, *Angew. Chem., Int. Ed. Engl*., 1995, **34**, 207.
9 P. V. Bernhardt and G. A. Lawrence, *Coord. Chem. Rev*., 1990, **104**, 297; P. Chaudhuri and K. Wieghardt, *Prog. Inorg. Chem*., 1987, **35**, 329.
10 F. H. Fry, B. Graham, L. Spiccia, D. C. R. Hockless and E. R. T. Tiekink, *J. Chem. Soc., Dalton Trans*., 1997, 827 and references therein; S. J. Brudenell, L. Spiccia, A. M. Bond, P. Comba and D. C. R. Hockless, *Inorg. Chem*., 1998, **37**, 3705.
11 D. G. Fortier and A. McAuley, *Inorg. Chem*., 1989, **28**, 655; L. R. Gaham, G. A. Lawrence and A. M. Sargeson, *Aust. J. Chem*., 1982, **35**, 1119.
12 G. M. Sheldrick, SHELXS-97, *Acta Crystallogr., Sect. A*, 1990, **46**, 467.
13 G. M. Sheldrick, SHELXL-97, University of Göttingen, Germany, 1997.

Communication 8/07409G

A new chiral ligand for the Fe–Lewis acid catalysed asymmetric Diels–Alder reaction

Marion E. Bruin and E. Peter Kündig*

Département de Chimie Organique, Université de Genève 30 Quai Ernest Ansermet, CH-1211 Genève 4, Switzerland. E-mail: peter.kundig@chiorg.unige.ch

Received (in Basel, Switzerland) 17th August 1998, Accepted 23rd October 1998

The readily accessible enantiopure hydrobenzoin forms the backbone of the new bidentate ligand BIPHOP-F that is shown here to provide the chiral environment for a highly enantioselective Fe–Lewis acid catalysed Diels–Alder reaction between α,β-enals and dienes.

The high versatility of the Diels–Alder reaction in the synthesis of six-membered ring compounds and the potential for the control of up to four stereogenic centres make this transformation one of the key reactions in organic synthesis. Lewis acid catalysis has further enhanced its scope. Recent focus in this area has been on the use of chiral Lewis acids as catalysts and both main group and transition metal Lewis acids have yielded impressive results.[1,2]

Our earlier report in this area centred on the chiral Cp iron(II) Lewis acid **1** containing the electron poor C_2-symmetric

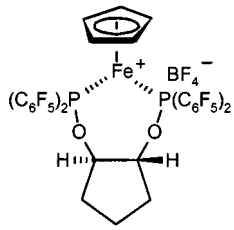

(*R*,*R*)-**1**

bidentate phosphorus ligand CYCLOP-F derived from *trans*-cyclopentane-1,2-diol **2**.[2a,3a] While both enantiomers of **2** are available by diastereoselective synthesis[3b] or enzymatic resolution,[4] the synthesis of **2** in larger quantities is time consuming and costly.

We here report on the new ligand BIPHOP-F (**4**) and on its use in the Fe–Lewis acid catalysed Diels–Alder reaction. Models suggested that hydrobenzoin **3** would be a good candidate for replacement of the cyclopentanediol backbone. As diol **3** is readily synthesised *via* Sharpless dihydroxylation,[5] we were surprised to find that its previous use in the synthesis of bidentate phosphorous ligands is limited to a single report.[6]

Ligand **4**† was prepared in near quantitative yield by reaction of (*R*,*R*)- or (*S*,*S*)-hydrobenzoin [(*R*,*R*)-**3** or (*S*,*S*)-**3**] with *bis*(pentafluorophenyl)phosphorus bromide[7] in the presence of triethylamine. The Lewis acid catalyst **6** was obtained by photolytic ligand exchange in [$CpFe(CO)_2Me$] followed by protolytic demethylation of complex **5**[2a] (Scheme 1). The unsaturated Fe complex **6** was trapped *in situ* with either acetonitrile, acrolein, or benzaldehyde to give, after precipitation with hexane, complexes **7a**–**c**, respectively.

Complex **7a** is stable and is readily characterised. The acetonitrile ligand is strongly bound and the complex does not exhibit catalytic activity towards the Diels–Alder reaction between enals and dienes. Complexes **7b** and **7c** are stable at ambient temperature in the solid state and can be weighed out in air without degradation. In CH_2Cl_2 solution, the aldehyde ligands in **7b** and **7c** are labile and in the absence of excess free aldehyde, the complexes slowly decompose at temperatures above −20 °C. Both **7a** and **7b** can be used as precatalysts in Diels–Alder reactions between α,β-enals and dienes (Table 1). 2,6-Di-*tert*-butylpyridine was added to scavenge residual acid impurities that adversely affected enantioselectivities. We subsequently found that 2,6-dimethylpyridine was equally efficient.

The results in Table 1 show that *exo/endo* ratios, yields, and enantiomeric excess obtained matched, and in some cases slightly exceeded, those realised with catalyst **1**. Increasing the quantity of diene led to a faster reaction and to higher yields but in some cases, *e.g.* the reactions between cyclopentadiene and acrolein or α-bromoacrolein, resulted in a drop of enantioselectivity. This presumably is due to the competitive uncatalysed background reaction. The sense of asymmetric induction observed is the same for both Lewis acids **1** and **6**. Indeed, the chiral catalyst sites are very similar. Fig. 1‡ shows the chiral pocket of the catalysts **6** and **1**[2a] and the postulated position of methacrolein in the transition state assembly.§ The diene approaches the alkene C_α-*si*-face of the *s*-trans conformer of the coordinated enal. The *re*-face is shielded by a pentafluorophenyl ring of the ligand and the ligand backbone.

In summary, the new C_2-symmetric bidentate phosphorus ligand BIPHOP-F **4** derived from (*R*,*R*)- or (*S*,*S*)-hydrobenzoin **3** described here proved to be an effective ligand in the Fe^{II}

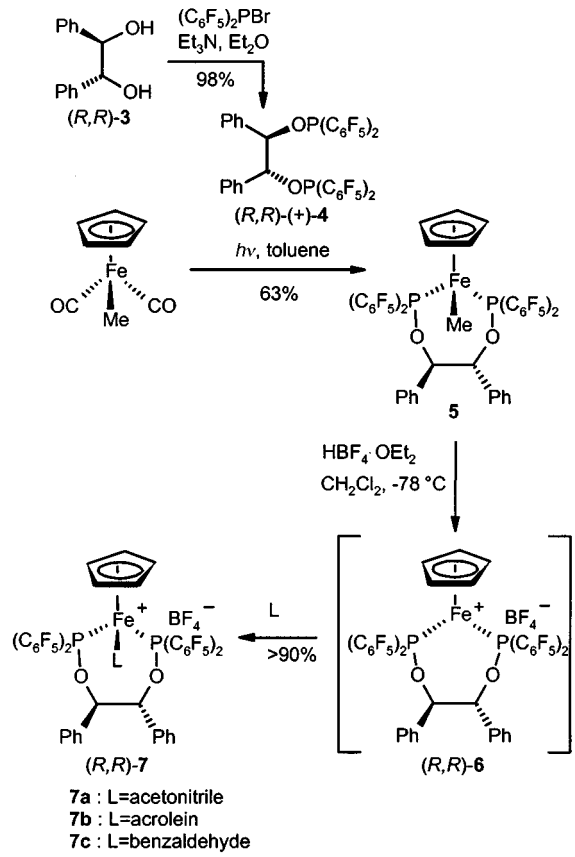

Scheme 1

Table 1 Diels–Alder reactions with complex **7b**[a]

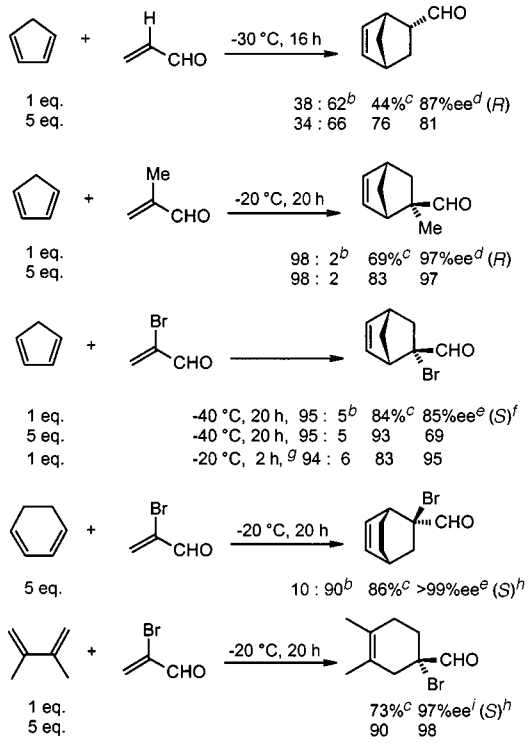

[a] The Diels–Alder reactions were carried out in freshly distilled CH_2Cl_2 (1 M solution) with 5 mol% precatalyst **7b** and 5 mol% of 2,6-di-*tert*-butylpyridine or 2,6-dimethylpyridine. Analogous results were obtained with **7c**. [b] *exo/endo* Ratio. [c] Isolated yield after flash-chromatography. [d] The ee was determined by GC analysis of the diasteromeric acetals obtained by reaction with (2*R*,4*R*)-pentanediol.[8] The absolute configuration was assigned by comparing the sign of $[\alpha]_D^{20}$ with literature values.[8,9] [e] The enantiomeric excess was determined from the ^{1}H NMR spectrum in the presence of the chiral shift reagent Eu(hfc)$_3$. [f] The absolute configuration was assigned by comparison with literature data.[10] [g] Slow addition of the diene (1 h). [h] The absolute configuration assigned is based on the presumption of attack of the enal C_α-*si*-face (same as in the first three examples in the Table). [i] The enantiomeric excess was determined by GC analysis on a chiral column (MN FS-Lipodex E).

catalysed asymmetric Diels–Alder reaction of α,β-enals with dienes and its ease of synthesis merits attention for other applications in asymmetric catalysis.

We thank the Swiss National Science Foundation for support of this work. (SNSF grants 20-045291.95 and 20-52478.97). We also thank Ms Maria Mayor Lopez and Professor Jacques Weber for carrying out computational studies on the catalysts.

Notes and references

† (*S*,*S*)-**4**: mp (toluene): 124 °C. $[\alpha]_D^{20}$ −82 (CH_2Cl_2, *c* = 2.31).^{1}H NMR (C_6D_6, 400 MHz): δ 6.89–6.82 (m, 4H, *o*-H_{arom}), 6.81–6.68 (m, 6H, *m*,*p*-H_{arom}), 5.23–5.17 (m, 2H, CHOP). ^{31}P NMR (C_6D_6, 162 MHz): δ 87.2 (p, *J* 40 Hz). IR (CH_2Cl_2): 1640m, 1517s, 1480s, 1380m, 1290m, 1202w, 1143w, 1091s, 980s, 919w, 882w, 800w, 638w, 585w. Elemental analysis: Calc. for $C_{38}H_{20}F_{20}O_2P_2$: C, 48.43; H, 1.28. Found: C, 48.37, H, 1.60%.

‡ The site of **1** was taken from the X-ray structure of $[(\eta^5\text{-}C_5H_5)Fe(MeCN)(CYCLOP\text{-}F)][PF_6]$.[2a] The site of **6** was modelled from the X-ray structure of the complex $[(\eta^5\text{-}C_5H_4CF_3)Fe(Me)(BIPHOP\text{-}F)]$ (**8**). The synthesis of **8** and the X-ray structure determination will be reported in a forthcoming full paper.

§ Based on accommodation of methacrolein in the chiral pocket with geometry optimization by molecular mechanics (MM+) and EHMO. Details will be reported in a forthcoming full paper.

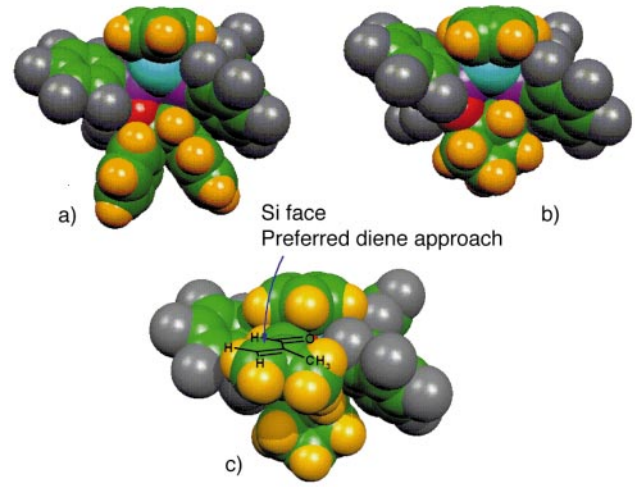

Fig. 1 (a) Coordination site of catalyst (*R*,*R*)-**6**, (b) coordination site of catalyst (*R*,*R*)-**1** and (*c*) catalyst (*R*,*R*)-**1** + methacrolein. The diene approach to the methacrolein C_α-*si*-face is indicated by the arrow.‡

1 For recent reviews, see: K. Narasaka, *Synthesis*, 1991, 1; H. B. Kagan and O. Riant, *Chem. Rev.*, 1992, **92**, 1007; U. Pindur, G. Lutz and C. Otto, *Chem. Rev.*, 1993, **93**, 741; E. J. Corey and A. Guzman-Perez, *Angew. Chem. Int. Ed. Engl.*, 1998, **37**, 389.

2 For asymmetric Diels–Alder reactions catalysed by chiral Cp– and arene–transition metal Lewis acids, see: (*a*) E. P. Kündig, B. Bourdin and G. Bernardinelli, *Angew. Chem., Int. Ed. Engl.*, 1994, **33**, 1856; (*b*) D. Carmona, C. Cativiela, R. García-Correas, F. J. Lahoz, M. P. Lamata, J. A. López, M. P. López-Ram de Víu, L. A. Oro, E. San José and F. Viguri, *Chem. Commun.*, 1996, 1247; (*c*) D. L. Davies, J. Fawcett, S. A. Garratt and D. R. Russell, *Chem. Commun.*, 1997, 1351; (*d*) D. Carmona, C. Cativiela, S. Elipe, F. J. Lahoz, M. P. Lamata, M. P. López-Ram de Víu, L. A. Oro, C. Vega and F. Viguri, *Chem. Commun.*, 1997, 2351; (*e*) A. J. Davenport, D. L. Davies, J. Fawcett, S. A. Garratt, L. Lad and D. R. Russell, *Chem. Commun.*, 1997, 2347.

3 (*a*) E. P. Kündig, C. Dupré, B. Bourdin, A. Cunningham Jr. and D. Pons, *Helv. Chim. Acta*, 1994, **77**, 421; (*b*) A. F. Cunningham Jr. and E. P. Kündig, *J. Org. Chem.*, 1988, **53**, 1823.

4 R. Seemayer and M. P. Schneider, *J. Chem. Soc., Chem. Commun.*, 1991, 49.

5 K. B. Sharpless, W. Amberg, Y. L. Bennani, G. A. Crispino, J. Hartung, K.-S. Jeong, H.-L. Kwong, K. Morikawa, Z.-M. Wang, D. Xu and X.-L. Zhang, *J. Org. Chem.*, 1992, **57**, 2768; Z.-M. Wang and K. B. Sharpless, *J. Org. Chem.*, 1994, **59**, 8302.

6 M. Kawashima and R. Hirata, *Kankyo Kagaku Sentaa Kk. Jpn. Kokai Tokkyo Koho JP*, 66,345,789, 1994. *Chem. Abstr.*, 1995, **123**, 33385r.

7 M. Fild, O. Glemser and I. Hollenberg, *Z. Naturforsch Teil B*, 1966, **21**, 920; R. Ali and K. B. Dillon, *J. Chem. Soc., Dalton Trans.*, 1990, 2593.

8 K. Furuta, S. Shimizu, Y. Miwa and H. Yamamoto, *J. Org. Chem.*, 1989, **54**, 1481.

9 S. Hashimoto, N. Komeshima and K. Koga, *J. Chem. Soc., Chem. Commun.*, 1979, 437.

10 E. J. Corey and T.-P. Loh, *J. Am. Chem. Soc.*, 1991, **113**, 8966; L. A. Paquette, C. W. Doecke, F. R. Kearney, A. F. Drake and S. F. Mason, *J. Am. Chem. Soc.*, 1980, **102**, 7228.

Communication 8/06445H

ChemComm

2,2′-Bi-1,6-naphthyridine metal complexes: a new ligand and a novel 2 × 2 inclined interpenetration of (4,4) nets or formation of helicoidal chains†

He-Ping Wu,[a] Christoph Janiak,*[a] Lars Uehlin,[a] Peter Klüfers[b] and Peter Mayer[b]

[a] *Institut für Anorganische und Analytische Chemie, Universität Freiburg, Albertstr. 21, D-79104 Freiburg, Germany. E-mail. janiak@uni-freiburg.de*

[b] *Institut für Anorganische Chemie, Universität Karlsruhe, Kaiserstr. 12, D-76131 Karlsruhe, Germany*

Received (in Cambridge, UK) 28th September 1998, Accepted 29th October 1998

Cobalt(II), zinc(II) and cadmium(II) salts react with the new spacer ligand 2,2′-bi-1,6-naphthyridine 1 to give 2D-planar (4,4) frameworks which interpenetrate such that each grid window of each sheet has two other sheets passing through it with all sheets being equivalent whereas copper(I) tetrafluoroborate and 1 form a 2_1-helicoidal chain with neigboring chains interlocking through an aromatic π–π interaction.

The synthesis of interpenetrating nets and the elucidation of the factors leading to a periodic entanglement is an area of increasing interest.[1] Many interpenetrating structures were obtained from attempts to create porous solid bases on metal coordination polymers.[2] As nature tends to avoid vacuum, identical copies of the frameworks with large openings interpenetrate to fill this empty space rather than to create a single network.[3] In the design of metal–ligand networks rigid and multidentate ligands with pyridine groups feature prominently as building blocks.[4] In our study of functionalized 2,2′-bipyridine-type ligands[5] we look here at the self-assembly process of the new spacer 2,2′-bi-1,6-naphthyridine **1**[6] with various metal salts.

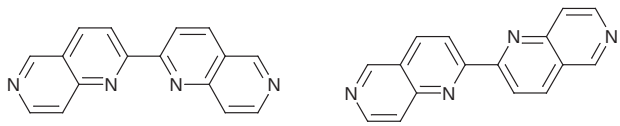

s-cis *s-trans* conformation

1

The choice of functionalized 2,2′-bipyridine building blocks stems from the aim to supply functional groups within the inner walls of a porous coordination polymer as is schematically depicted in **2**. Such functionalities should eventually interact with organic guest molecules, *e.g.* through hydrogen bonding, or allow for the anchoring of additional metal ions.

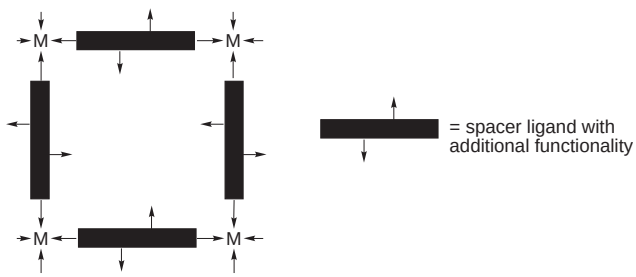

2

Spacer **1** reacts with cobalt chloride, zinc or cadmium perchlorate in the presence of a slight excess of KSCN in water–ethanol (1 : 1) to give well formed crystals in yields of 50% and above. The products were investigated by single crystal X-ray analysis† and correspond to the formula $^2_\infty$[M(NCS)$_2$(μ-**1**)$_2$] (M = Co, Zn, Cd) (matching the C,H,N analytical data‡). The three M(II) compounds are isostructural. The binaphthyridine ligand assumes the *s-trans* conformation and bridges between the metal centers. Four ligands of **1** are arranged around the metal in a square-planar fashion and two *trans* (nitrogen-bound) isothiocyanato ligands complete the octahedral metal coordination sphere. The bonded metal–**1** arrangement leads to planar (4,4) nets. Fig. 1 shows an individual metal–ligand grid. The bridged metal–metal distances along the edges of the parallelograms are around 15.76–16.05 Å and the distances along the shorter and longer diagonals are 21.44–21.95 and 23.10–23.43 Å, respectively, depending on the metal. The 2D framework from Fig. 1 is interpenetrated in an inclined mode[1] by symmetry related, identical sheets to give an interlocked 3D structure. The manner of interpenetration is such that each window of each grid has parts of two other sheets passing through it, which we would like to call a 2 × 2 interpenetration (Figs. 2 and 3). It was surprising at first that the rings were large enough and the binaphthyridine rods slim enough to allow the passage of two sheets, when considering the van der Waals surfaces of the aromatic system and the NCS group. A space-

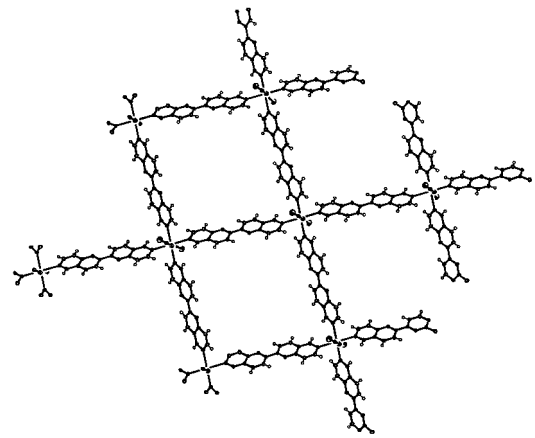

Fig. 1 View of a section of the planar individual metal–ligand network in $^2_\infty$[M(NCS)$_2$(μ-**1**)$_2$] (M = Co, Zn, Cd).

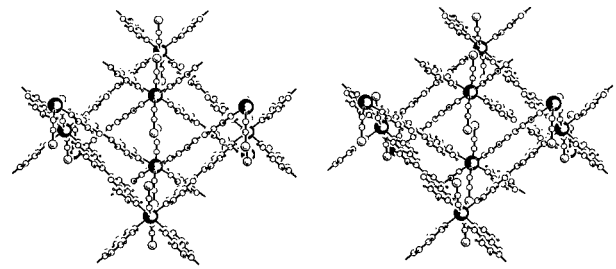

Fig. 2 Stereoview along *b* of the interpenetration of parts of two sheets through a grid window in $^2_\infty$[M(NCS)$_2$(μ-**1**)$_2$] (M = Co, Zn, Cd).

† Dedicated to Professor Dr Bernt Krebs on the occasion of his 60th birthday.

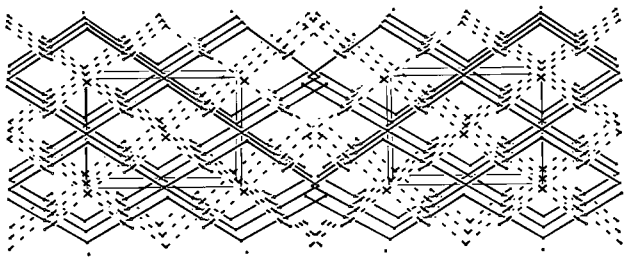

Fig. 3 Stereoview along *c* of the schematic framework of $^{2}_{\infty}$[M(NCS)$_2$(μ-**1**)$_2$] (M = Co, Zn, Cd), with only the metal center and the central C–C unit of the binaphthyridine moiety shown. Sheets of different inclination are drawn with solid or dashed lines, respectively.

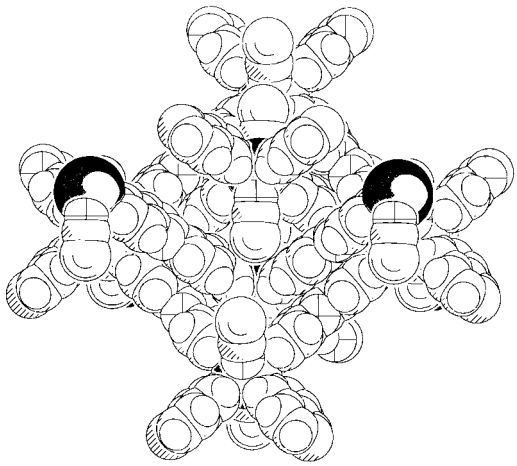

Fig. 4 Space-filling drawing of the interpenetration of parts of two sheets through a grid window in $^{2}_{\infty}$[M(NCS)$_2$(μ-**1**)$_2$] (M = Co, Zn, Cd).

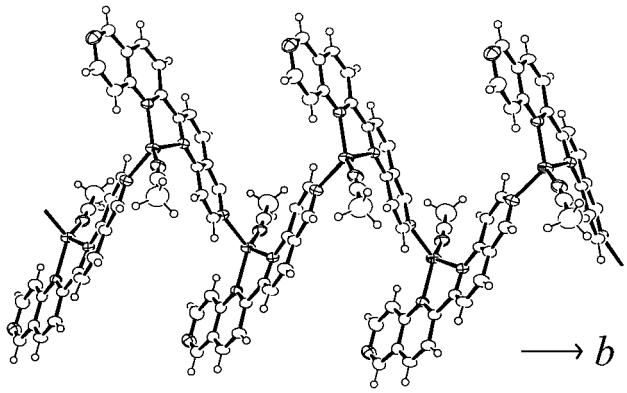

Fig. 5 Section of the 2_1-helical coordination polymer of $^{1}_{\infty}$[Cu(MeCN)(μ-**1**)]BF_4·0.5CH_2Cl_2. Anion and solvent molecule have been omitted for clarity.

filling model then illustrated the close π–π contact of the naphthyridine moieties (Fig. 4). The knots or metal centers of the intersecting networks do not lie within the plane of the pierced ring but above and below. The nets run either parallel to the (021) or to the (02 − 1) plane. The inclination of the sheets is almost perpendicular, the angle ranges from 92.9° for the cobalt to 93.7° for the cadmium grids. A similar mode of interpenetration was so far only reported in the structure of [Cd(py)$_2${Ag(CN)$_2$}$_2$],[7] for the more common type of a 1 × 1 interpenetration in (4,4) square grid sheets, the structure of $^{2}_{\infty}$[M(4,4′-bipy)$_2$]SiF_6 (M = Zn, Cd) is a typical example.[8]

The anellated arene substituents in the α position to the bipyridine nitrogen donor atoms prevent the chelating coordination of two or three ligands of **1** with its bipyridine unit in an octahedral complex. A bipyridine selectivity in **1** (cuproin group) can, however, be expected towards copper(I). An X-ray study† revealed that the reaction of **1** with [Cu(MeCN)$_4$]BF_4 in MeCN–CH_2Cl_2 led to a compound of formula $^{1}_{\infty}$[Cu(MeCN)(μ-**1**)]BF_4·0.5CH_2Cl_2. A 1D-coordination polymer (Fig. 5) originates from the chelation of the copper center by **1** in its *s-cis* conformation together with the bridging action of the ligand to the next metal through one of its exodentate nitrogen donors. The distorted tetrahedral coordination sphere at copper is completed by an acetonitrile ligand. The copper–ligand strand assumes a helicoidal conformation following a 2_1 screw axis. The neighboring parallel strands are of opposite helicity and interlock (interdigitate) through π–π interactions of the extended aromatic binaphthyridine system.

We acknowledge the support by the Humboldt Foundation (fellowship for H.-P. W.), the Fonds der Chemischen Industrie, the DFG, and the graduate college 'Unpaired Electrons'.

Notes and references

† *Crystal data*: $^{2}_{\infty}$[Co(NCS)$_2$(μ-**1**)$_2$], orthorhombic, space group *Cmca*, *a* = 21.4385(17), *b* = 15.918(1), *c* = 8.3683(5) Å, *V* = 2855.8(3) Å^3, *Z* = 4, D_c = 1.6087, final *R*, *wR* values 0.0321, 0.0744 for 1334 independent reflections with $I > 2\sigma(I)$.

$^{2}_{\infty}$[Zn(NCS)$_2$(μ-**1**)$_2$], orthorhombic, space group *Cmca*, *a* = 21.5003(19), *b* = 15.925(1), *c* = 8.3967(5) Å, *V* = 2875.0(4) Å^3, *Z* = 4, D_c = 1.6129, final *R*, *wR* values 0.0269, 0.0744 for 1555 independent reflections with $I > 2\sigma(I)$.

$^{2}_{\infty}$[Cd(NCS)$_2$(μ-**1**)$_2$], orthorhombic, space group *Cmca*, *a* = 21.9537(13), *b* = 16.027(1), *c* = 8.5477(5) Å, *V* = 3007.5(3) Å^3, *Z* = 4, D_c = 1.6457, final *R*, *wR* values 0.0235, 0.0606 for 1679 independent reflections with $I > 2\sigma(I)$.

$^{1}_{\infty}$[Cu(MeCN)(μ-**1**)]BF_4·0.5CH_2Cl_2, monoclinic, space group *C*2/*c*, *a* = 22.4063(16), *b* = 8.1045(4), *c* = 22.5896(18) Å, *V* = 4029.8(5) Å^3, *Z* = 8, D_c = 1.624(2), final *R*, *wR* values 0.0358, 0.0797 for 2754 independent reflections with $I > 2\sigma(I)$.

Data collection by the ω-scan method, Mo-Kα radiation (λ = 0.71073), graphite monochromator, at 200 K on a STOE IPDS diffractometer. Structure solution by direct methods (SHELXS-97)[9] and refined by full-matrix least-squares on F^2 (SHELXL-97);[9] all non-hydrogen positions found and refined with anisotropic temperature factors. Graphics were obtained with ORTEP3 and PLUTON for Windows.[10] CCDC 182/1024. See http://www.rsc.org/suppdata/cc/1998/2637/ for crystallographic files in .cif format.

‡ *Elemental analyses*: $^{2}_{\infty}$[Co(NCS)$_2$(μ-**1**)$_2$] calc. C 59.04, H 2.89, N 20.26; found C 58.68, H 2.92, N 20.22%. $^{2}_{\infty}$[Zn(NCS)$_2$(μ-**1**)$_2$] calc. C 58.49, H 2.89, N 20.06; found C 58.16, H 2.81, N 20.00%. $^{2}_{\infty}$[Cd(NCS)$_2$(μ-**1**)$_2$] calc. C 54.81, H 2.68, N 18.81; found C 54.95, H 2.74, N 19.10%. $^{1}_{\infty}$[Cu(MeCN)(μ-**1**)]BF_4·0.5CH_2Cl_2 calc. C 35.96, H 2.03, N 11.10; found C 35.77, H 2.18, N 11.08%.

1 S. R. Batten and R. Robson, *Angew. Chem., Int. Ed. Engl.*, 1998, **37**, 1460.
2 C. Janiak, *Angew. Chem., Int. Ed. Engl.*, 1997, **36**, 1431; O. M. Yaghi, H. Li, C. Davis, D. Richardson and T. L. Groy, *Acc. Chem. Res.*, 1998, **31**, 474.
3 P. Losier and M. J. Zaworotko, *Angew. Chem., Int. Ed. Engl.*, 1996, **35**, 2779; O. M. Yaghi and G. Li, *Angew. Chem. Int. Ed.*, 1995, **34**, 207; D. Venkatarman, S. Lee, J. Zhang and J. S. Moore, *Nature*, 1994, **371**, 591.
4 L. Carlucci, G. Ciani, P. Macchi and D. M. Proserpio, *Chem. Commun.*, 1998, 1837; L. R. MacGillivray, R. H. Groeneman and J. L. Atwood, *J. Am. Chem. Soc.*, 1998, **120**, 2676; A. J. Blake, N. R. Champness, A. Khlobystov, D. A. Lemenovskii, W.-S. Li and M. Schröder, *Chem. Commun.*, 1997, 2027; C. Janiak, L. Uehlin, H.-P. Wu, P. Klüfers, H. Piotrowski and T. G. Scharmann, *Inorg. Chem.*, submitted.
5 H.-P. Wu, C. Janiak, G. Rheinwald and H. Lang, *J. Chem. Soc., Dalton Trans.*, publication (8/07450J).
6 C. Janiak, L. Uehlin and S. Deblon, unpublished work.
7 T. Soma and T. Iwamoto, *Mol. Cryst. Liq. Cryst.*, 1996, **276**, 19; *J. Inclusion Phenom. Mol. Recognit. Chem.*, 1996, **26**, 161.
8 R. W. Gable, B. F. Hoskins and R. Robson, *J. Chem. Soc., Chem. Commun.*, 1990, 1677.
9 G. M. Sheldrick, Programs for Crystal Structure Analysis, University of Göttingen, Germany 1997.
10 M. N. Burnett and C. K. Johnson, *ORTEP-III*: Oak Ridge Thermal Ellipsoid Plot Program for Crystal Structure Illustrations, Oak Ridge National Laboratory Report ORNL-6895, 1996. PLATON/PLUTON97: A. L. Spek, *Acta Crystallogr., Sect. A*, 1990, **46**, C34. Windows versions: L. J. Farrugia, *J. Appl. Crystallogr.* 1997, **30**, 565.

Communication 8/07522K

ChemComm

Formal stereoselective synthesis of (±)-akagerine

M.-Lluïsa Bennasar,* Bernat Vidal, Bilal A. Sufi and Joan Bosch*

Laboratory of Organic Chemistry, Faculty of Pharmacy, University of Barcelona, Barcelona 08028, Spain. E-mail: jbosch@farmacia.far.ub.es

Received (in Cambridge, UK) 9th October 1998, Accepted 30th October 1998

A stereoselective synthesis of pentacyclic dilactam 1, a known precursor of the indole alkaloid akagerine, involving addition of the enolate of 1-acetylindole 2 to 3-acetyl-2-fluoropyridinium salt 3, cyclization of the resultant 1,4-dihydropyridine, elaboration of the (*E*)-ethylidene substituent and closure of the C ring by Pummerer reaction, is reported.

Akagerine is a tetracyclic indole alkaloid isolated in 1975 from *Strychnos usambarensis*[1] and later from several *Strychnos* species.[2] This Corynanthean[3] alkaloid has a peculiar skeleton lacking the characteristic piperidine (D) ring and containing an additional link between N-1 and C-17 (biogenetic numbering);[4] consequently, it incorporates a perhydroazepine ring fused to a tetrahydro-β-carboline unit. Akagerine has received little attention from the synthetic standpoint: only one total synthesis in the racemic series *via* dilactam **1**[5] (Scheme 1) and one enantioselective synthesis of (−)-akagerine[6] through a completely different route have been reported to date.

We present here a short, stereoselective route to pentacyclic dilactam **1**. Our approach takes advantage of our previously developed methodology for the synthesis of bridged indole alkaloids, based on the addition of indole-containing enolates to *N*-alkyl-3-acylpyridinium salts, with subsequent acid-promoted cyclization of the resultant 1,4-dihydropyridine.[7] Taking into account the easy hydrolysis of the C–F bond in 2-fluoropyridines,[8] we thought that the use of a pyridinium salt bearing a fluorine atom at the 2-position in the above two-step sequence would lead to a bridged tetracyclic intermediate embodying the required 2-piperidone moiety present in **1**. On the other hand, the closure of the C ring would be effected by electrophilic cyclization of a thionium ion generated by Pummerer rearrangement,[9] taking advantage of the functionalized two-carbon substituent present at the piperidone nitrogen.

The synthetic sequence is outlined in Scheme 2. Thus, reaction of the enolate derived from 1-acetylindole **2** with 3-acetyl-2-fluoropyridinium salt **3** gave (25%) 1,4-dihydropyridine **4**,[10] which underwent cyclization (58% yield) upon the indole 2-position with concomitant cleavage of the C–F bond by treatment with TsOH in the presence of LiI.[11] The spectroscopic data of the resulting tetracyclic lactam **5**[12] clearly showed that the acetyl carbonyl group was in an enolized form, presumably with a *Z* double bond configuration.

The elaboration of the C-20 (*E*)-ethylidene double bond was effected in a stereoselective fashion by conversion of the 1-hydroxyethylidene group of **5** into the corresponding triflate, followed by Pd^0 catalyzed reduction with Bu_3SnH.[13] Following this protocol **6** was obtained in 45% overall yield from **5**.

MCPBA oxidation of tetracyclic sulfide **6** gave the corresponding sulfoxide (mixture of stereoisomers), which smoothly underwent Pummerer rearrangement with TFAA in CH_2Cl_2 in the presence of 2,6-di(*tert*-butyl)pyridine at room temperature.[14] When the presumed acyloxy sulfide intermediate was refluxed in CH_2Cl_2 the desired pentacyclic sulfide **7** (a single diastereomer, undetermined configuration at C-6) was obtained in 71% overall yield from **6**.

Finally, desulfurization of **7** with Bu_3SnH–AIBN gave the desired pentacyclic dilactam **1** in 72% yield. The ^1H NMR data of **1** are in agreement with those previously reported.[5,15] Taking into account the previous work by Winterfeldt,[5] the synthesis of **1** represents a formal total synthesis of (±)-akagerine.

Financial support from the DGICYT, Spain (project PB94-0214) is gratefully acknowledged. Thanks are also due to the

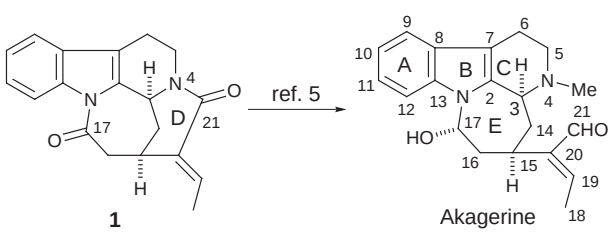

Scheme 1

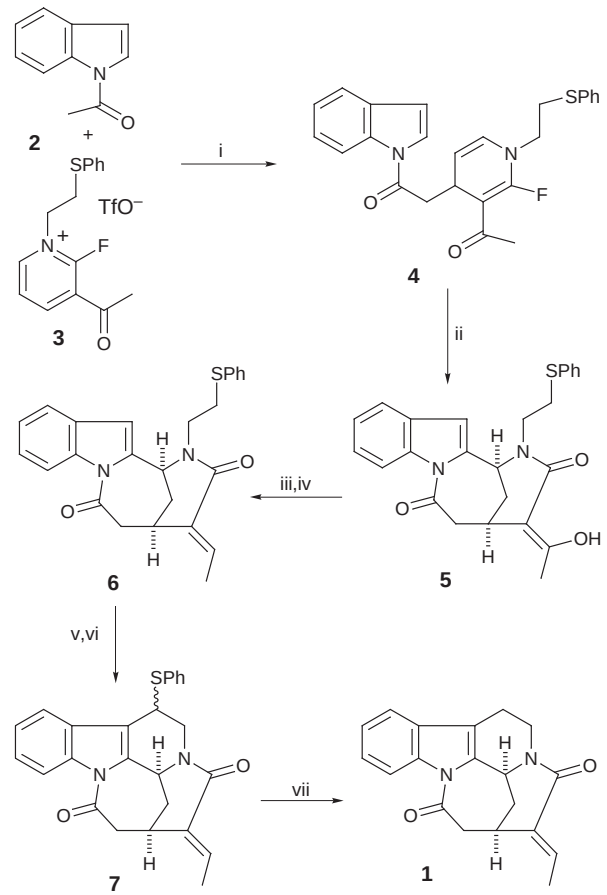

Scheme 2 *Reagents and conditions*: i, LDA, THF, −30 °C, 1.5 h; ii, C_6H_6, TsOH, MeOH, LiI, room temp., 2 h; iii, Tf_2O, 1,8-bis(dimethylamino)naphthalene, −30 to −10 °C, 1 h; iv, Bu_3SnH, $Pd(Ph_3P)_4$, LiCl, THF, reflux, 1 h; v, MCPBA, CH_2Cl_2, −70 °C, 30 min; vi, TFAA, 2,6-di(*tert*-butyl)pyridine, CH_2Cl_2, room temp., 30 min, then reflux, 1.5 h; vii, Bu_3SnH, AIBN, benzene, reflux, 1 h.

‘Comissionat per a Universitat i Recerca’ (Generalitat de Catalunya) for Grant 1997SGR0018.

Notes and references

1 L. Angenot, O. Dideberg and L. Dupont, *Tetrahedron Lett*., 1975, 1357.
2 G. Massiot and C. Delaude, in *The Alkaloids*, ed. A. Brossi, Academic Press, San Diego, 1988, vol. 34, pp. 211–329.
3 M. V. Kisakürek, A. J. M. Leeuwenberg and M. Hesse, in *Alkaloids*: *Chemical and Biological Perspectives*, ed. S. W. Pelletier, Wiley, New York, 1983, vol. 1, pp. 211–376.
4 J. Le Men and W. I. Taylor, *Experientia*, 1965, **21**, 508.
5 W. Benson and E. Winterfeldt, *Angew. Chem., Int. Ed. Engl*., 1979, 862; W. Benson and E. Winterfeldt, *Heterocycles*, 1981, **15**, 935.
6 B. Danieli, G. Lesma, M. Mauro, G. Palmisano and D. Passarella, *J. Org. Chem*., 1995, **60**, 2506.
7 For a review, see: J. Bosch and M.-L. Bennasar, *Synlett*, 1995, 587.
8 P. Rocca, C. Cochennec, F. Marsais, L. Thomas-dit-Dumont, M. Mallet, A. Godard and G. Quéguiner, *J. Org. Chem*., 1993, **58**, 7832; D. L. Comins and J. K. Saha, *Tetrahedron Lett*., 1995, **36**, 7995.
9 For a review, see: A. Padwa, D. E. Gunn, Jr. and M. H. Osterhout, *Synthesis*, 1997, 1353 and references cited therein.
10 All yields are from material purified by column chromatography. Satisfactory spectral, analytical and/or HRMS data were obtained for all new compounds.
11 M.-L. Bennasar, J.-M. Jiménez, B. A. Sufi and J. Bosch, *Tetrahedron Lett*., 1996, **37**, 7653.
12 *Selected data* for **5**: δ_H(300 MHz, $CDCl_3$) 2.09 (s, 3H, 18-H), 2.32 (dm, *J* 14, 1H, 14-H), 2.44 (m, 1H, 14-H), 2.81 (m, 1H, 5-H), 2.96 (br d, *J* 12.8, 1H, 16-H), 3.15 (m, 4H, 6-H, 15-H, 16-H), 3.60 (m, 1H, 5-H), 4.80 (d, *J* 5.1, 1H, 3-H), 6.16 (s, 1H, 7-H), 7.26–7.33 (m, 7H, Ar), 7.42 (d, *J* 7.6, 1H, 9-H), 8.13 (d, *J* 8.2, 1H, 12-H); δ_C(75 MHz, $CDCl_3$) 18.4 (C-18), 29.3 (C-15), 30.7 (C-6), 32.3 (C-14), 44.4 (C-5), 47.7 (C-16), 56.9 (C-3), 96.7 (C-20), 112.5 (C-7), 115.5 (C-12), 120.6 (C-9), 123.7 (C-10), 125.8 (C-11), 126.3 (Ph), 129.2 (Ph), 129.5 (C-8), 135.0 (Ph), 135.2 (C-2), 138.4 (C-13), 168.9 (C-19), 171.7, 172.7 (C-17, C-21).
13 K. Ritter, *Synthesis*, 1993, 735.
14 K. Cardwell, B. Hewitt, M. Ladlow and P. Magnus, *J. Am. Chem. Soc*., 1988, **110**, 2242.
15 *Selected data* for **1**: δ_C(75 MHz, $CDCl_3$) 14.3 (C-18), 20.0 (C-6), 27.6 (C-15), 27.3 (C-14), 42.4 (C-5), 47.0 (C-16), 51.9 (C-3), 115.2 (C-12), 117.8 (C-9), 120.1 (C-7), 123.9 (C-10), 125.2 (C-11), 132.6 (C-20), 135.8 (C-2), 136.8 (C-13), 138.1 (C-19), 166.1 (C-21), 172.1 (C-17).

Communication 8/07868H

ChemComm

Double diastereocontrol in the synthesis of enantiomerically pure polyoxamic acid

Laurence M. Harwood* and Sarah M. Robertson

Department of Chemistry, University of Reading, Whiteknights, Reading, UK RG6 6AD.
E-mail: l.m.harwood@reading.ac.uk

Received (in Liverpool, UK) 24th September 1998, Accepted 26th October 1998

Polyoxamic acid 4 is prepared by a short and efficient process involving diastereochemically matched cycloaddition of 5-(*S*)-phenylmorpholin-2-one 1 with (*S*)-glyceraldehyde acetonide 2, followed by sequential hydrolysis and hydrogenolysis of the adduct.

We have demonstrated the use of 5-(*S*)-phenylmorpholin-2-one **1**† as a chiral template in the rapid, diastereo- and enantiocontrolled synthesis of β-hydroxy-α-amino acids.[1] In this process, the chiral azomethine ylide intermediate generated by condensation with an aldehyde is trapped by excess of the aldehyde to furnish a cycloadduct which can be subsequently dismantled to lead to *threo*-(2*S*, 3*R*)-configured products of high stereochemical integrity (Scheme 1).

In the cycloaddition step, stereochemical discrimination arises from the chiral azomethine ylide reacting with an achiral aldehyde dipolarophile. Utilizing a chiral aldehyde in such a reaction therefore poses the question as to whether there might be diastereochemical 'match' or 'mismatch' in either the ylide generation step or the cycloaddition step between the chiral reacting partners.

We now report an efficient synthesis of polyoxamic acid **4**,[2] the unique polyhydroxyamino acid constituting the side chain moiety of the antifungal polyoxin antibiotics.[3] The key conversion in our synthesis involves reaction of 5-(*S*)-phenylmorpholin-2-one **1** with excess (*S*)-glyceraldehyde acetonide **2** (obtained from commercially available 5,6-*O*-isopropylidene-L-gulono-1,4-lactone.[4]) in refluxing toluene with removal of water.‡ It would appear that this combination of starting materials leads to matched diastereocontrol as close examination of the crude product mixture isolated from reaction between (*S*)-**2** with 5-(*S*)-phenylmorpholin-2-one **1** indicated the presence of only a single product. This could be isolated in 53% yield and showed spectroscopic features consistent with those expected of a cycloadduct resulting from highly diastereoselective reaction of two equivalents of (*S*)-**2** with (*S*)-**1**.

By analogy with our earlier rationale for stereocontrol in both ylide generation and trapping steps, cycloaddition of the aldehyde dipolarophile to the *E*-isomer of the azomethine ylide from the face opposite the 5-phenyl substituent would be predicted to furnish cycloadduct **3** (Scheme 2).[1]

Although a solid, crystals of sufficient quality for X-ray structural analysis could not be obtained. A combination of 2-dimensional ^{1}H NMR and NOE difference studies supported the predicted stereochemical outcome of the cycloaddition step, enhancements of signals corresponding to H_2 and $H_{3\beta}$ on irradiating H_7 proving diagnostic of their mutual *syn*-relationship, but the stereochemistry at C-9 remained unresolved.‡

Final confirmation of the stereochemical outcome of the ylide generation and trapping sequence came by conversion of **3** to polyoxamic acid as its natural (2*S*,3*S*,4*S*) enantiomer. Treatment of the cycloadduct with aqueous methanolic HCl gave the deketalized methyl ester which was not isolated but subjected immediately to hydrogenolysis (H_2, Pearlman's catalyst, aq. MeOH, TFA) leading to the isolation of a homogeneous material in 95% overall yield with a specific rotation $[\alpha]_D^{24}$ +2.4 (*c* 1.0, H_2O), [lit.,[2d] +2.2 (*c* 1.0, H_2O)] and spectroscopic data identical with those of authentic polyoxamic acid **4** (Scheme 3).§ In the same manner, the non-natural enantiomer

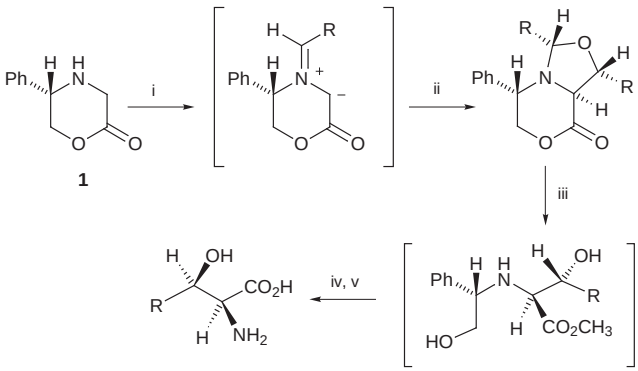

Scheme 1 *Reagents and conditions*: i, RCHO, solvent, reflux; ii, RCHO (excess); iii, 1 M HCl, MeOH, reflux; iv, H_2 (5 atm), $Pd(OH)_2$/C, TFA (1 equiv.), aq. MeOH; v, basic ion-exchange resin.

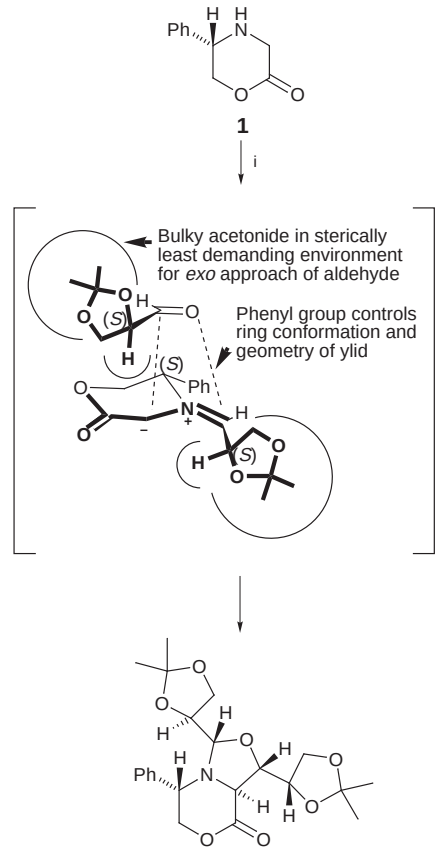

Scheme 2 *Reagents and conditions*: i, (*S*)-glyceraldehyde acetonide **2** (3 equiv.), toluene, reflux.

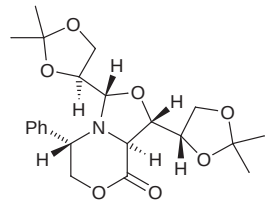

3

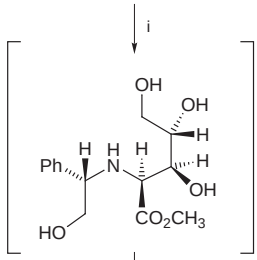

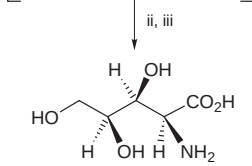

(+)–polyoxamic acid

4

Scheme 3 *Reagents and conditions*: i, 1 M HCl, MeOH, reflux; ii, H_2 (5 atm), $Pd(OH)_2/C$, TFA (1 equiv.), aq. MeOH; iii, basic ion-exchange resin.

of polyoxamic acid was obtained by reacting (*R*)-glyceraldehyde acetonide (prepared by oxidative cleavage of 1,2:5,6-di-*O*-isopropylidene-D-mannitol[5]) with (*R*)-**1**, followed by sequential degradation of the cycloadduct. Pure *ent*-polyoxamic acid was isolated in excess of 50% yield over the whole sequence, with a specific rotation, $[\alpha]_D^{24}$ −2.5 (*c* 1.0, H_2O).

Having successfully prepared polyoxamic acid and its enantiomer it was decided to investigate the synthesis of diastereoisomers by employing the alternative combination of reactant enantiomers. However, under the same conditions as before, reaction of 5-(*S*)-phenylmorpholin-2-one **1** with (*R*)-**2** resulted in a product mixture consisting of roughly equal quantities of three products which were found to be diastereoisomers of **3** by spectroscopic analysis. Unfortunately none could be isolated with sufficient purity to permit definitive structural assignment, nor was it possible to separate the deprotected acids at the ultimate stage of the synthetic route. However, the observation of three cycloadducts indicates diastereochemical mismatch in more than one element of the ylide generation and trapping sequence, be it reactant ylide geometry, diastereofacial control or *exo*/*endo* approach of the dipolarophile.

In conclusion, we have demonstrated that diastereochemically matched and mismatched reactions can occur in the generation and trapping of azomethine ylides in which both starting materials are chiral and have established a rapid diastereocontrolled synthesis of polyoxamic acid *via* a diastereochemically matched reaction of 5-(*S*)-phenylmorpholin-2-one with (*S*)-glyceraldehyde acetonide. We are currently investigating the scope of this process and applying it to the synthesis of other enantiomerically pure β-hydroxy-α-amino acids with additional stereogenic centres.

We thank the University of Reading for postgraduate support under the R.E.T.F. framework (to S. M. R).

Notes and references

† We use the trivial morpholin-2-one nomenclature to describe the 2,3,5,6-tetrahydro-*4H*-oxazin-2-one ring system.

‡ *Cycloaddition procedure*: Freshly prepared aldehyde **2** (780 mg, 6 mmol, 3 equiv.) was added to a solution of the morpholin-2-one **1** (177 mg, 1 mmol, 1 equiv.) in dry toluene (60 ml) and the reaction mixture heated to reflux for 48 h under nitrogen with a Soxhlet extractor containing activated 3Å sieves. Solvent was removed *in vacuo* to yield a pale yellow oil which solidified on cooling. Column chromatography, eluting with Et_2O–light petroleum (1:4) and recrystallisation from Et_2O furnished **3** as colourless fine needles (220 mg, 53%), mp 199–202 °C ($C_{22}H_{29}NO_7$ requires C, 63.0; H, 7.00; N, 3.3. Found C, 62.8; H, 6.85; N, 3.2%); ν_{max}(KBr)/cm^{-1} 1737; δ_H(250 MHz, $CDCl_3$) 7.47–7.33 (m, 5H), 4.47 (t, *J* 11.3, 1H), 4.44 (d, *J* 9.0, 1H), 4.42 (ddd, *J* 8.9, 6.4, 2.3, 1H), 4.32 (d, *J* 8.0, 1H), 4.27 (dd, *J* 11.3, 3.1, 1H), 4.18 (dd, *J* 9.0, 2.3, 1H), 4.10–4.02 (m, 3H), 3.99 (dd, *J* 11.3, 3.1, 1H), (3.91 (t, *J* 8.9, 1H), 3.84 (dd, *J* 8.7, 4.2, 1H), 1.40 (s, 6H), 1.26 (s, 3H) and 1.07 (s, 3H); NOE H7→H2 (4.0%)→H3β (3.8%)→H10 (1.2%); δ_C(100 MHz, $CDCl_3$) 167.4, 135.3, 129.2, 128.9, 128.6, 109.9, 109.3, 96.6, 74.3, 74.1, 73.3, 66.2, 66.0, 60.1, 59.3, 26.3, 26.2, 25.4 and 24.8; *m*/*z* (CI) 420 (MH^+); $[\alpha]_D^{25}$ +23.2 (*c* 1.0, $CHCl_3$).

§ *Preparation of polyoxamic acid*: To a solution of cycloadduct **3** (0.2 mmol) in MeOH (4 ml) was added 1 M HCl (1 ml) and the reaction mixture heated to reflux under nitrogen for 1 h. The solvent was removed *in vacuo* and the residue transferred to a Fischer–Porter bottle. TFA (15 μl), Pearlman's catalyst (70 mg), MeOH (3 ml) and water (0.3 ml) were added, the solution degassed and subjected to hydrogen at 5 atm. for 48 h. Catalyst was removed by centrifugation, the solvent removed *in vacuo* and the crude mixture purified on a Dowex® basic ion-exchange column to yield **4** as a colourless powder (31 mg, 95%), mp 152–154 °C (decomp.) (lit., 165–170 °C,[2d] 162–168 °C[2g]). Spectroscopic data as in ref. 2(*c*); $[\alpha]_D^{24}$ +2.4 (*c* 1.0, H_2O), [lit.,[2d] +2.2 (*c* 1.0, H_2O)]; *ent*-**4** $[\alpha]_D^{24}$ −2.5 (*c* 1.0, H_2O). We thank Professor R. F. W. Jackson for providing copies of ^1H and ^{13}C NMR spectra of polyoxamic acid.

1 L. M. Harwood, J. Macro, D. J. Watkin, C. E. Williams and L. F. Wong, *Tetrahedron*: *Asymmetry*, 1992, **3**, 1127; D. A. Alker, G. Hamblett, L. M. Harwood, S. M. Robertson and C. E. Williams, *Tetrahedron*, 1998, **54**, 6089.

2 For recent synthetic approaches to polyoxamic acid and derivatives, see: (*a*) A. Dondoni, S. Franco, F. L. Merchàn, P. Merino and T. Tejero, *Tetrahedron Lett*., 1993, **34**, 5479; (*b*) R. F. W. Jackson , N. J. Palmer and M. J. Wythes, *J. Chem. Soc*., *Chem. Commun*., 1994, 95; (*c*) R. F. W. Jackson, N. J. Palmer, M. J. Wythes, W. Clegg and M. R. J. Elsegood, *J. Org*. *Chem*., 1995, **60**, 6431; (*d*) B. M. Trost, A. C. Krueger, R. C. Bunt and J. Zambrano, *J. Am*. *Chem*. *Soc*., 1996, **118**, 6520; (*e*) S. H. Kang and H-W. Choi, *Chem*. *Commun*., 1996, 1521; (*f*) G. Casiraghi, G. Rassu, P. Spanu and L. Pinna, *Tetrahedron Lett*., 1994, **35**, 2423; (*g*) A. K. Saksena, R. G. Lovey, V. M. Girijavallabhan, A. K. Ganguly and A. T. McPhail, *J. Org*. *Chem*., 1986, **51**, 5024.

3 K. Isono, K. Asahi and S. Suzuki, *J. Am*. *Chem*. *Soc*., 1969, **91**, 7490.

4 C. Hubschwerlen, *Synthesis*, 1986, 962; C. Hubschwerlen, J-L. Speclin and J. Higelin, *Org*. *Synth*., 1995, **72**, 1.

5 J. Mann, N. K. Partlett and A. Thomas, *J. Chem*. *Res*. (*S*), 1987, 369.

Communication 8/07471B

The biosynthesis of pramanicin: intact incorporation of serine and absolute configuration of the antibiotic

Petar Duspara, Stephen I. Jenkins, Donald W. Hughes and Paul H. M. Harrison*

Department of Chemistry, McMaster University, 1280 Main Street West, Hamilton, Ontario, L8S 4M1, Canada. E-mail: pharriso@mcmaster.ca

Received (in Corvallis, OR, USA) 21st September 1998, Accepted 21st October 1998

Biosynthetic incorporation of isotopically labelled serines into pramanicin 1 in *Stagonospora* sp. ATCC 74235 shows that L-serine is incorporated as an intact entity with all four bonds to the α-carbon retained; thus 1 is assigned the 5*S* absolute configuration.

We have recently described the biosynthesis of pramanicin[1] **1** (Scheme 1) in *Stagonospora* sp. ATCC 74235.[2] Eight acetate units combine in the 'head-to-tail' manner typical of fatty acids and polyketides[3] prior to cyclization with the three-carbon precursor corresponding to carbon atoms 4 to 6 in **1**. The resulting putative tetradeca-2,4-dienoyltetramic acid[1] is then presumably further modified to furnish **1**. We demonstrated that incorporation of DL-[1-^{13}C]serine proceeded very efficiently: only C-4 of **1** was labelled, suggesting that serine is the direct amino acid precursor of **1**. However, serine can be converted to a number of metabolites *in vivo*, and we thus sought further evidence for the proposed intact incorporation of a serine entity into **1**. We also wished to establish which enantiomer of serine is utilised in the biosynthetic pathway and to correlate these results with the as yet unknown absolute configuration of pramanicin. Experiments directed toward these issues are described herein.

Cultures of *Stagonospora* sp. ATCC 74235 were grown,† precursors were added, and pramanicin was isolated as described previously.[1,2] Incorporations of L-[2,3,3-$^{2}H_3$]serine, L-[1,2,3-$^{13}C_3$,^{15}N]serine, and the separated D- and L-enantiomers of [2-^{2}H,3-^{13}C]serine‡ furnished samples of pramanicin **2–5**, respectively (Scheme 2).

Pramanicin **2** derived from L-[2,3,3-$^{2}H_3$]serine exhibits two resonances in the ^{2}H{^{1}H} NMR spectrum in MeOH. One signal corresponds in chemical shift to one of the two diastereotopic protons at C-6 (δ 3.79), which is well separated from other resonances in the proton NMR spectrum. The other deuterium signal, somewhat larger than the first, correlates with the proton chemical shift of the other C-6 proton and to that of H-5; these two resonances are close in proton chemical shift (δ 3.55 and 3.49, respectively), and the breadth of the signals in the deuterium NMR spectrum precluded their resolution. These resonances remained unresolved in acetone, but the spectrum in DMSO, where the difference in shift between the two protons is larger,[2] did exhibit a clear shoulder, most notably when the sample was heated to 85 °C to reduce viscosity and enhance ^{2}H relaxation. Nonetheless, we sought to clarify this result, and thus **2** was converted to the mono-pivaloyl derivative **6** (pivaloyl chloride, TEA, 70 °C, 30 min, Scheme 2). In the proton NMR spectrum of **6**, the two C-6 protons are shifted downfield by 0.58 and 0.51 ppm, relative to **1**, while H-5 gives a unique resonance which is shifted downfield by only 0.13 ppm. The deuterium NMR spectrum of **6** exhibited three resonances, corresponding to the two H-6 (δ 4.30 and 4.00), and the H-5 (δ 3.55) resonances [Fig. 1(A)].§ However, the D-5 signal intensity was significantly weaker than either of the D-6 resonances, and integration showed that only about 0.5 deuterons were present at this site.

These results clearly show that L-serine is a viable precursor to pramanicin: a strong deuterium signal was observed although the precise incorporation could not be measured in this experiment. Further, there is no cryptic oxidation state change at C-3 of serine since both of the diastereotopic deuterons at this position are incorporated. The retention of some deuterium at C-5, derived from H-2 of serine, is most readily explained by direct incorporation of the L-enantiomer. The observed loss of deuterium would arise from an incidental, reversible process which results in net exchange of the α-proton. This solvent exchange could conceivably be accomplished by the action of a serine racemase;[9,10] a transaminase (to interconvert serine and 3-hydroxypyruvate);[9] serine hydroxymethyl transferase (SHMT), which interconverts serine with glycine and methylene-tetrahydrofolate (CH_2-THF);[9,11] or any of several enzymes which catalyse β-elimination or β-replacement reactions on serine or its derivatives.[9] Extensive investigations of amino acid racemases [whether double-base or pyridoxal phosphate (PLP) dependent] have shown that this process invariably occurs with substantial or complete loss of the substrate α-proton.[10] However, the PLP-dependent SHMT catalyses several processes, including racemisation of alanine and the exchange of both the prochiral α-protons of glycine, and thus this enzyme could possibly lead to deuterium-labelled D-serine which could then be incorporated into **1**.

To resolve these issues, we next incorporated L-[1,2,3-$^{13}C_3$,^{15}N]serine. Analysis of the extensive coupling pattern [Fig. 1(B)] in the ^{13}C{^{1}H} NMR spectrum of the derived pramanicin **3** showed the labelling pattern of [4,5,6-$^{13}C_3$,^{15}N]pramanicin, derived from an intact serine molecule, along with the [6-^{13}C]- and [4,5-$^{13}C_2$,^{15}N]-iso-

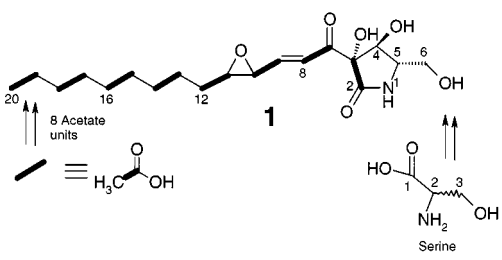

Scheme 1

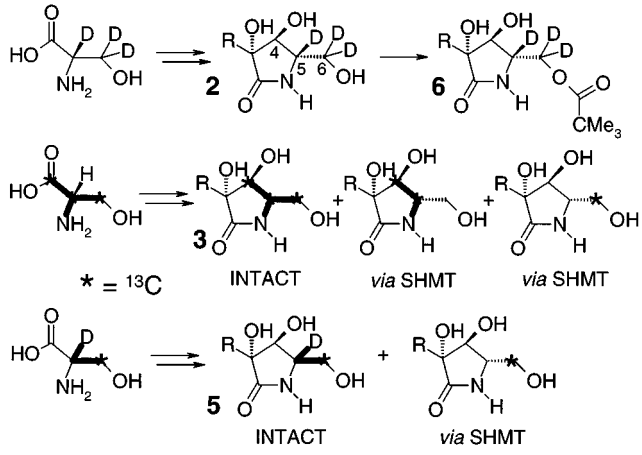

Scheme 2

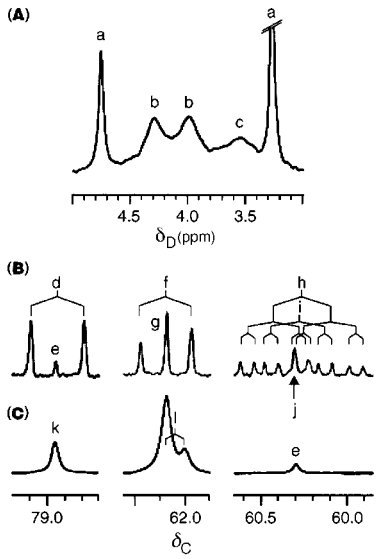

Fig. 1 (A) $^{2}H\{^{1}H\}$ NMR spectrum of 6-pivaloylpramanicin **6** derived from L-[2,3,3-$^{2}H_3$]serine: (a) natural abundance signals from MeOH solvent; (b) diastereotopic deuterons at C-6; (c) 5-D. (B), (C) Partial $^{13}C\{^{1}H\}$ NMR spectra of pramanicin **1** derived from (B) L-[1,2,3-$^{13}C_3$,^{15}N]serine and (C) L-[2-^{2}H,3-^{13}C]serine mixed with DL-[1-^{13}C]serine. Left: C-4; centre: C-6; right: C-5. For complete assignments, see ref. 1,2. Traces in (B) have the same scaling for both axes, as do those in (C), but (B) and (C) have different natural abundance peak heights. (d) $^{1}J_{^{13}C\text{-}4\text{-}^{13}C\text{-}5}$ = 38 Hz; (e) natural abundance signal; (f) $^{1}J_{^{13}C\text{-}5\text{-}^{13}C\text{-}6}$ = 40 Hz; (g) enriched singlet from action of SHMT on labelled CH_2—THF and unlabelled glycine; (h) coupled signals from [4,5,6-$^{13}C_3$,^{15}N]pramanicin from an intact serine unit, $^{1}J_{^{13}C\text{-}4\text{-}^{15}N}$ = 10 Hz; (i) signals for [4,5-$^{13}C_2$,^{15}N]pramanicin from action of SHMT on unlabelled CH_2—THF and labelled glycine; (j) natural abundance signal plus coupled component; (k) enhanced singlet from [1-^{13}C]serine; (l) β-deuterium isotope shift, $\Delta\delta$ 74 ppb.

topomers. The ^{15}N NMR spectrum showed only a coupled signal,¶ so all molecules labelled at C-2 are attached to ^{15}N and all enriched ^{15}N atoms are adjacent to ^{13}C. Thus there is no detectable action of either transaminase or serine β-elimination enzymes *en route* to **1**. However, SHMT is present in this microbial strain, and gives rise to the two non-intact isotopomers *via* cleavage of serine to [^{13}C]CH_2-THF and [$^{13}C_2$,^{15}N]glycine, followed by re-condensation of each fragment with the corresponding unlabelled partner. Nonetheless, the observation of substantial intact incorporation shows that SHMT is not required for the biosynthesis of **1** from serine. The results also exclude biosynthetic mechanisms in which the polyketide component is produced as an amide, and subsequent condensation with an α-keto acid leads to **1**.

When the L-enantiomer of [2-^{2}H,3-^{13}C]serine was mixed with DL-[1-^{13}C]serine (32 mol%) as internal standard and incorporated into **1**, C-4 and C-6 [18 and 82%, respectively, of total ^{13}C incorporated, Fig. 1(C)] were labelled with carbon-13, and the C-6 resonance exhibited a shifted signal ($\Delta\delta$ 74 ppb, 28% of total C-6 enrichment) due to a β-deuterium isotope shift. The corresponding D-[2-^{2}H,3-^{13}C]serine similarly mixed with DL-[1-^{13}C]serine gave product labelled with carbon-13 only at the control site, C-4.‖ Thus, the D-enantiomer is not a significant precursor for **1**, while the C-3:C-2:H-2 unit of L-serine is partially incorporated in an intact manner into C-6:C-5:H-5 of **1**. The remaining enrichment of the C-6 signal without concomitant incorporation of deuterium can be accounted for by the reversible action of SHMT.

In summary, L-serine is the true biosynthetic precursor for **1**, and is converted with all four atoms which are attached to the α-carbon atom retained. SHMT is not required in the pathway. These results are completely consistent with the proposed route to **1** *via* an acyltetramic acid.[1] The simplest conclusion is that the absolute configuration of pramanicin at C-5 is the same as that of L-serine, *i.e.* 5*S*; the remaining chiral centres in the tetramic acid moiety of **1** are then defined by the work of Schwartz *et al.*,[2] who determined the relative configurations of C-3 to C-5. The absolute configuration of the *trans*-epoxide remains undetermined. There is no evidence for racemisation of L-serine, or epimerisation of other biosynthetic intermediates in the pathway to **1**, which would lead to the opposite configuration of **1**, *i.e.* 5*R*. Although this possibility cannot be rigorously excluded by these or indeed by other whole-cell isotope labelling experiments, it would require the action of an enzyme which alters the configuration yet proceeds with substantial retention of the α-proton; there is little precedent for such an activity.[10] Further work on the pathway to the polyketide moiety of **1**, as well as the X-ray crystal structure of **1**, will be described shortly.

Financial support by the Natural Sciences and Engineering Research Council of Canada is gratefully acknowledged. Part of this work was undertaken through the Co-operative Education Program, Hamilton-Wentworth Catholic District School Board, St. Jean de Brébeuf High School, Hamilton.

Notes and references

† *Stagonospora* was cultured in liquid medium LCM (100 ml in 500 ml Erlenmeyer flasks). Labelled serines (12–20 mg per culture flask) were added as sterile solutions in water at 24 h intervals over days 2–6. After 7 days, work-up as previously described gave *ca*. 10 mg of **1** per flask.

‡ The samples of D- and L-[2-^{2}H,3-^{13}C]serine were prepared from DL-[3-^{13}C]serine using the pyridoxal-dependent exchange of the α-proton in D_2O as described for [2-^{2}H]serine by Miles and McPhie (ref. 4), using some of the modifications of de Kroon *et al*. (ref. 5), as well as those of Townsend *et al*. (ref. 6), who prepared [2-^{3}H,1-^{14}C]serines; some minor modifications designed to conserve the yield based on labelled serine were also used. For the same reason, the resolution method of Velluz *et al*. (ref. 7) as modified by Gorissen *et al*. (ref. 8) was used in preference to the multi-step chemical and enzymatic resolution used by the former workers. All new compounds and isotopomers gave satisfactory spectral data; for serine hydrochlorides, $[\alpha]_D^{30}$: D, −9.0 ± 0.5; L, +10.0 ± 0.5 (*c* 1, H_2O).

§ The measured shifts in the deuterium NMR spectrum are 0.005–0.006 ppm upfield of those in the proton spectrum; this can be ascribed to the method of referencing the two spectra. Proton spectra in CD_3OD are referenced to C*H*D$_2$OD at δ 3.30, while the deuterium spectra in CH_3OH are referenced to natural abundance CH_2*D*OH; the observed solvent nuclei thus experience different isotope shifts.

¶ The ^{15}N NMR spectrum was recorded in DMSO-d_6, using polarisation transfer by the INEPT sequence: δ −256.4 relative to CH_3NO_2 at δ 0 (lit.[2] −229.1, converted from a different external standard), dd ($^{1}J_{^{15}N\text{-}^{1}H}$ 93 Hz, lit.[2] 92 Hz, $^{1}J_{^{15}N\text{-}^{13}C}$ 9 Hz).

‖ A small enhancement (0.14%) at C-6 was observed; this may however be accounted for by traces of the L-enantiomer present in the sample (< 2% required).

1 P. Harrison, D. W. Hughes and R. W. Riddoch, *Chem. Commun*., 1998, 273.
2 R. E. Schwartz, G. L. Helms, E. A. Bolessa, K. E. Wilson, R. A. Giacobbe, J. S. Tkacz, G. F. Bills, J. M. Liesch, D. L. Zink, J. E. Curotto, B. Pramanik and J. C. Onishi, *Tetrahedron*, 1994, **50**, 1675.
3 For recent reviews, see: B. J. Rawlings, *Nat. Prod. Rep*., 1997, **14**, 335; 1997, **14**, 523; 1998, **15**, 275.
4 E. W. Miles and P. McPhie, *J. Biol. Chem*., 1974, **249**, 2852.
5 A. I. P. M. de Kroon, J. W. Timmermans, J. A. Killian and B. de Kruijff, *Chem. Phys. Lipids*, 1990, **54**, 33.
6 C. A. Townsend, A. M. Brown and L. T. Nguyen, *J. Am. Chem. Soc*., 1983, **105**, 919.
7 L. Velluz, G. Amiard and R. Heymes, *Bull. Soc. Chim. Fr*., 1954, 1015.
8 H. Gorissen, C. van der Maesen, A. Mockel, G. Journee and V. Libert, in *Synthesis and Applications of Isotopically Labelled Compounds 1991*, ed. E. Buncel and G.W. Kabalka, Elsevier, New York, 1992, pp. 588–591.
9 For PLP-dependent enzymes, see: C. Walsh, *Enzymatic Reaction Mechanisms*, W. H. Freeman, New York, 1977; *Vitamin B6, Pyridoxal Phosphate* in *Coenzymes and Cofactors*, ed. D. Dolphin, R. Poulson and O. Avramovi, Wiley, New York, 1986, vol. 1.
10 For a recent review, see: M. E. Tanner and G. L. Kenyon, in *Comprehensive Biological Catalysis*, Academic Press, San Diego, London, 1998, vol. 2, pp. 7–41.
11 For reviews of SHMT, see: L. Schirch, *Adv. Enzymol. Relat. Areas Mol. Biol*., 1982, **53**, 83; R. G. Matthews and J. T. Drummond, *Chem. Rev*., 1990, **90**, 1275.

Communication 8/07401A

Synthesis and chemoselective activation of phenyl 3,5-di-*O*-benzyl-2-*O*,4-*C*-methylene-1-thio-β-D-ribofuranoside: a key synthon towards α-LNA

Poul Nielsen[a] and Jesper Wengel*[b]

[a] *Department of Chemistry, Odense University, DK-5230 Odense M, Denmark*
[b] *Center for Synthetic Bioorganic Chemistry, Department of Chemistry, University of Copenhagen, Universitetsparken 5, DK-2100 Copenhagen, Denmark. E-mail: wengel@kiku.dk*

Received (in Cambridge, UK) 2nd September 1998, Accepted 27th October 1998

A bicyclic thiofuranoside (phenyl 3,5-di-*O*-benzyl-2-*O*,4-*C*-methylene-β-D-ribofuranoside) was efficiently synthesized and introduced as the key synthon in a method for convergent synthesis of α- and β-LNA nucleosides; acid-induced ring-opening reactions of the corresponding bicyclic methyl furanoside are also described.

In the search for an ideal nucleic acid mimic, intensive research towards conformationally restricted oligonucleotide analogues has been carried out during the last years.[1] We have recently introduced LNA (Locked Nucleic Acid) as a novel class of preorganized oligonucleotide analogues showing very interesting properties.[2–4]† In our initial synthetic approaches, monomeric β-configurated LNA nucleosides (*e.g.* the thymine derivative **13**, 5-methyl-2′-*O*,4′-*C*-methyleneuridine or (1*S*,3*R*,4*R*,7*S*)-7-hydroxy-1-hydroxymethyl-3-(thymin-1-yl)-2,5-dioxabicyclo[2.2.1]heptane, Scheme 2) were synthesized by stereoselective condensation of appropriately protected 4-*C*-hydroxymethyl-1,2-di-*O*-acetyl furanoses with silylated nucleobases and subsequent base-induced ring-closure and deprotection;[2,3] linear syntheses of LNA nucleosides have also been accomplished.[5–7] Here, a novel synthetic strategy is introduced, involving the use of a bicyclic carbohydrate precursor for nucleobase coupling reactions thus revealing the first synthesis of α-configurated LNA nucleosides. Our interest in these α-anomers, and in α-LNA, was stimulated by reports that α-DNA, in comparison with β-DNA, forms a more stable duplex with complementary RNA.[8,9]

The protected 4-*C*-hydroxymethyl furanose **1** was synthesized according to the known method[3,10] and converted to the methanesulfonate **2** in 99% yield (Scheme 1). This compound was treated with HCl in MeOH–H_2O (7 : 1 v/v) to give the anomeric mixture of methyl furanosides **3** in 95% yield. Treatment with NaH gave the two isomeric bicyclic methyl furanosides **4** and **5** in 60 and 30% yield, respectively. The structures of the two products were verified using NMR experiments. Thus, mutual NOE contacts between H-1, H-2 and H-3 verified the α-configuration of **5** and the absence of NOE contacts between H-1 and H-3 verified the β-configuration of **4**. The coupling constants $^3J_{H1,H2}$ and $^3J_{H2,H3}$ were in both cases extremely small (~ 0 Hz) confirming the bicyclo[2.2.1]heptane structures. An attempt to use these bicyclic methyl furanosides as precursors for synthesis of LNA nucleosides failed. Thus, coupling of thymine to furanoside **4** using a modified Vorbrüggen methodology[11] [*N*,*O*-bis(trimethylsilyl)acetamide (BSA) and Me_3SiOTf in MeCN] afforded in 59% yield one major product which was assigned as the ring-opened derivative **6** existing as a mixture of diastereoisomers.[12] The considerable ring strain in the bicyclic structure is a plausible explanation for the favouring of the Lewis acid mediated ring-opening reaction over the cleavage of the anomeric bond.

As an attempt to overcome this problem, better leaving groups were introduced at the anomeric position (Scheme 1 and 2). In order to obtain a mixture of 1′-*O*-acetyl derivatives, methyl furanoside **4** (and/or **5**) was treated with 80% aq. AcOH to give a deprotected intermediate, which was subsequently acetylated. The latter reaction was slow and problematic giving a major product in only 23% yield, which was assigned as the pure β-anomer **7**. NMR spectra of the deprotected intermediate showed distinctive aldehyde signals suggesting ring strain and the predominance of the monocyclic intermediate **4a** to be responsible for the slow and low-yielding conversion to furanose **7**. Summarizing, the strategies depicted in Scheme 1 are not convenient for synthesis of the bicyclic nucleosides.

Thioglycosides have been intensively investigated for glycosylation reactions due to their ability to react with sulfur-specific electrophiles, thereby creating sulfonium cations readily displaced as leaving groups.[13,14] In the case of phenyl thioglycosides, there have been reports of nucleobase coupling reactions yielding natural as well as modified nucleosides.[15,16]

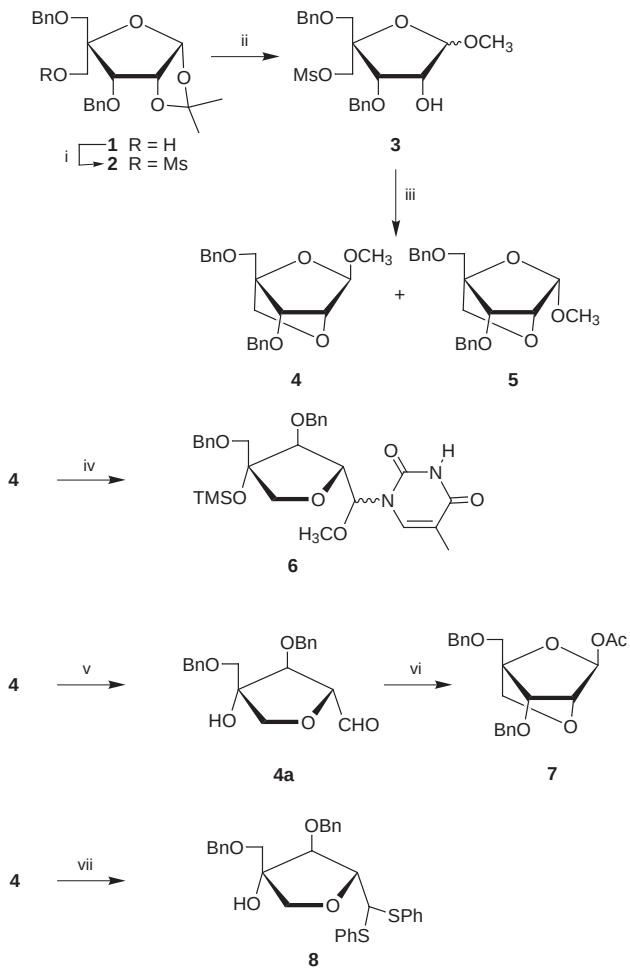

Scheme 1 *Reagents and conditions*: i, MsCl, pyridine; ii, 20% HCl in MeOH, H_2O; iii, NaH, DMF; iv, thymine, BSA, Me_3SiOTf, MeCN; v, 80% AcOH; vi, Ac_2O, pyridine; vii, Me_3SiSPh, Me_3SiOTf, CH_2Cl_2.

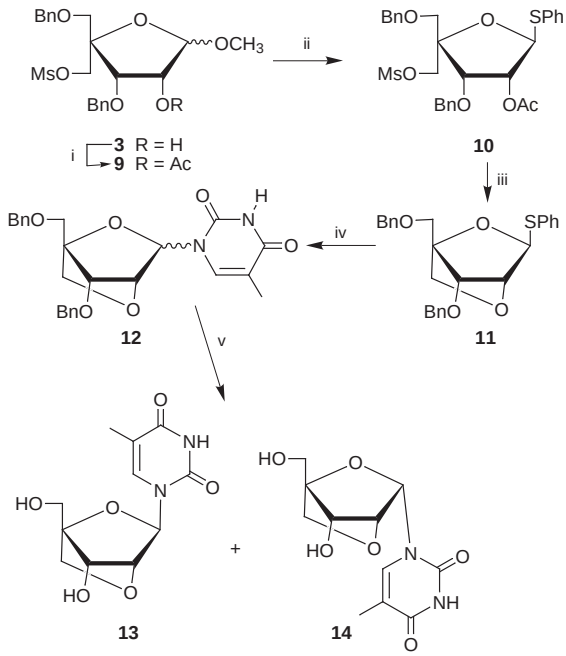

Scheme 2 *Reagents and conditions*: i, Ac_2O, pyridine; ii, Me_3SiSPh, Me_3SiOTf, CH_2Cl_2; iii, NH_3, MeOH, then NaH, DMF; iv, thymine, HMDS, then NBS, **11**, 4 Å molecular sieves, CH_2Cl_2; v, H_2, $Pd(OH)_2$/C, EtOH, CH_2Cl_2.

Furthermore, oxidized phenylsulfenyl glycosides have been used in glycosylations[17] and in nucleobase coupling reactions.[18,19] Thioglycosides have been obtained from *O*-glycosides,[13] but treatment of the bicyclic methyl furanoside **4** with Me_3SiSPh and Me_3SiOTf[13] gave the ring-opened dithioacetal derivative **8** in 61% yield (Scheme 1). However, after protection of the methyl furanoside **3** to give 2′-*O*-acetyl derivative **9** in 97% yield (Scheme 2), the β-thiofuranoside **10** was obtained in 66% yield using Me_3SiSPh and Me_3SiOTf (25% of starting material **9** was recovered). Only trace of the α-anomer of **10** was detected due to the expected anchimeric assistance from the 2′-*O*-acetyl group. The acetyl group was removed with methanolic ammonia and direct ring-closure was very efficiently performed using NaH affording phenyl 3,5-di-*O*-benzyl-2-*O*,4-*C*-methylene-β-D-ribofuranoside **11**‡ in 95% yield.

Condensation of the bicyclic phenyl thiofuranoside **11** with silylated thymine[20] using NBS as a thiophilic activator[13,16] gave an inseparable mixture of anomeric nucleosides **12** (α:β ~ 2:1) in 61% yield (or 100% yield based on the recovery of 39% starting material). This mixture was directly deprotected by hydrogenation to give the known β-LNA nucleoside **13** and its α-LNA nucleoside analogue **14**§ (in preliminary yields of 12 and 25%, respectively). The expected bicyclic structure of **14** was verified by mass spectrometry and NMR spectroscopy which revealed, as for **13**,[2,3,5] negligible $^3J_{H1',H2'}$ and $^3J_{H2',H3'}$ coupling constants (~0 Hz). Importantly, no ring-opening reactions were detected using this nucleobase coupling method taking advantage of the chemoselective cleavage of the anomeric bond by NBS.

A general bicyclic thioglycoside synthon **11** for nucleobase coupling reactions has been efficiently synthesized. The applicability of thiofuranoside **11** has been demonstrated by the synthesis of the known β-LNA nucleoside **13** and the first α-LNA nucleoside **14**, and analogous thioglycosides may prove useful for convergent syntheses of other constrained bicyclic nucleoside derivatives. The general use of **11** as a precursor for synthesis of α- and β-LNA nucleosides is currently under investigation.

The Danish Natural Science Research Council, The Danish Technical Research Council and Exiqon A/S, Denmark, are thanked for financial support.

Notes and references

† LNA is defined as an oligonucleotide (analogue) containing one or more monomeric LNA nucleosides. These LNA monomers are preorganized in a 3′-*endo* conformation as shown by X-ray crystallography (see ref. 5) and NMR studies (see ref. 2 and 3).

‡ *Selected data* for **11**: $\delta_H(CDCl_3)$ 7.46–7.26 (15 H, m, Bn, SPh), 5.35 (1 H, s, H-1), 4.68–4.56 (4 H, m, Bn), 4.31 (1 H, s, H-2), 4.10 (1 H, s, H-3), 4.09 (1 H, d, *J* 7.3, H-5′), 3.93 (1 H, d, *J* 7.8, H-5′), 3.79 (2 H, m, H-5); $\delta_C(CDCl_3)$ 138.03, 137.45, 133.42, 132.36, 129.19, 128.55, 128.46, 128.05, 127.84, 127.83, 127.76 (Bn, SPh), 89.96 (C-1), 87.18 (C-4), 79.71 (C-2), 79.40 (C-3), 73.64 (Bn), 73.23 (C-5′), 72.30 (Bn), 66.31 (C-5); *m*/*z* (FAB) 435 (M + H), 457 (M + Na) (Found: C, 71.76; H, 6.18; $C_{26}H_{26}O_4S$ requires C, 71.86; H, 6.03%).

§ *Selected data* for **14**: $\delta_H(CD_3OD)$ 7.78 (1 H, d, *J* 1.3, H-6), 5.88 (1 H, s, H-1′), 4.38 (1 H, s, H-2′), 4.34 (1 H, s, H-3′), 4.08–3.69 (4 H, m, H-5′, H-5″), 1.92 (3 H, d, *J* 1.2, CH_3); $\delta_C(CD_3OD)$ 138.00 (C-6), 110.08 (C-5), 92.49, 89.01 (C-4′, C-1′), 80.89, 74.27, 73.33 (C-2′, C-3′, C-5′), 59.29 (C-5″), 12.53 (CH_3); *m*/*z* (EI) 270 (M^+, 100%).

1 P. Herdewijn, *Liebigs Ann.*, 1996, 1337.
2 S. K. Singh, P. Nielsen, A. A. Koshkin and J. Wengel, *Chem. Commun.*, 1998, 455.
3 A. A. Koshkin, S. K. Singh, P. Nielsen, V. K. Rajwanshi, R. Kumar, M. Meldgaard, C. E. Olsen and J. Wengel, *Tetrahedron*, 1998, **54**, 3607.
4 S. K. Singh and J. Wengel, *Chem. Commun.*, 1998, 1247.
5 S. Obika, D. Nanbu, Y. Hari, K. Morio, Y. In, T. Ishida and T. Imanishi, *Tetrahedron Lett.*, 1997, **38**, 8735.
6 A. A. Koshkin, V. K. Rajwanshi and J. Wengel, *Tetrahedron Lett.*, 1998, **39**, 4381.
7 S. Obika, D. Nanbu, Y. Hari, J. Andoh, K. Morio, T. Doi and T. Imanishi, *Tetrahedron Lett.*, 1998, **39**, 5401.
8 N. T. Thuong, U. Asseline, V. Roig, M. Takasugi and C. Hélène, *Proc. Natl. Acad. Sci. U.S.A.*, 1987, **84**, 5129.
9 C. Gagnor, J.-R. Bertrand, S. Thenet, M. Lemaitre, F. Morvan, B. Rayner, C. Malvy, B. Lebleu, J.-L. Imbach and C. Paoletti, *Nucleic Acids Res.*, 1987, **15**, 10419.
10 T. Waga, T. Nishizaki, I. Miyakawa, H. Ohrui and H. Meguro, *Biosci. Biotechnol. Biochem.*, 1993, **57**, 1433.
11 H. Vorbrüggen, K. Krolikiewicz and B. Bennua, *Chem. Ber.*, 1981, **114**, 1234.
12 A similar ring-opening has been observed when coupling monocyclic methyl furanosides: P. T. Jørgensen, E. B. Pedersen and C. Nielsen, *Synthesis*, 1992, 1299.
13 K. C. Nicolaou, S. P. Seitz and D. P. Papahatjis, *J. Am. Chem. Soc.*, 1983, **105**, 2430.
14 P. Fügedi, P. J. Garegg, H. Lönn and T. Norberg, *Glycoconjugate J.*, 1987, **4**, 97.
15 L. J. Wilson, M. W. Hager, Y. A. El-Kattan and D. C. Liotta, *Synthesis*, 1995, 1465.
16 H. Sugimura, K. Osumi, T. Yamazaki and T. Yamaya, *Tetrahedron Lett.*, 1991, **32**, 1813.
17 D. Kahne, S. Walker, Y. Cheng and D. J. Van Engen, *J. Am. Chem. Soc.*, 1989, **111**, 6881.
18 L. Chanteloup and J.-M. Beau, *Tetrahedron Lett.*, 1992, **33**, 5347.
19 A. De Mesmaeker, C. Lesueur, M.-O. Bévièrre, A. Waldner, V. Fritsch and R. M. Wolf, *Angew. Chem., Int. Ed. Engl.*, 1996, **35**, 2790.
20 E. Wittenburg, *Chem. Ber.*, 1966, **99**, 2380.

Communication 8/06817H

ChemComm

$La_{0.9}Sr_{0.1}Ga_{0.8}Mn_{0.2}O_{2.85}$: a new oxide ion conductor

V. Thangadurai, A. K. Shukla and J. Gopalakrishnan*

Solid State and Structural Chemistry Unit, Indian Institute of Science, Bangalore 560 012, India.
E-mail: gopal@sscu.iisc.ernet.in

Received (in Cambridge, UK) 28th September 1998, Accepted 3rd November 1998

Isovalent substitution of Mn(II) for Mg(II) in the oxide ion conductor, $La_{0.9}Sr_{0.1}Ga_{0.8}Mg_{0.2}O_{2.85}$, yields a new oxide ion conductor which exhibits an ionic conductivity (σ = 4.6 × 10^{-2} S cm^{-1} at 800 °C) that is comparable to the conductivity of the Mg(II) analogue; interestingly, the Mn(II) oxide has a lower activation energy for conduction (E_a = 0.47 eV) than the Mg(II) oxide.

The strontium- and magnesium-substituted lanthanum gallate perovskite, $La_{0.9}Sr_{0.1}Ga_{0.8}Mg_{0.2}O_{3-z}$ **I**, first reported by Ishihara *et al.*[1] has turned out to be an excellent oxide ion conductor[2] that promises to replace yttria-stabilized zirconia (YSZ) in solid oxide fuel cells (SOFCs) operating at relatively low temperatures (600–800 °C).[3,4] Besides providing an optimal concentration of oxide ion vacancies, the exact role of strontium and magnesium toward the high oxide ion conductivity of phase **I** is unclear at present. While it is known[1,5] that substitution of other cations (such as Ca, Ba, lanthanides) for La/Sr adversely affects the ionic conductivity of **I**, the effect of other divalent cations substituting for Mg(II) in **I** has, to our knowledge, not been investigated.† We considered that Mn(II) would be an effective replacement for Mg(II) in **I**, in view of its size‡ and stability under reducing conditions. Also a Mn(II)-derivative of **I** is likely to have a better compatibility as electrolyte material in SOFCs using $La_{1-x}Sr_xMnO_3$ (LSM) as cathode material.[6] Accordingly, we investigated Mn(II)-substituted derivatives of **I** having the general formula, $La_{1-x}Sr_xGa_{1-y}Mn_yO_{3-z}$ **II**, for several values of x and y. Since Mn(II) is not stable under the normal synthetic conditions employed for the preparation of **I**, we developed a special route for the synthesis of members of **II** that involves preparation of a higher valent Mn perovskite first, followed by its subsequent reduction to the Mn(II) phase in hydrogen. Stabilization of lower/unusual oxidation states of transition metals under reducing conditions has been reported for several perovskite-related oxides.[7] Typical examples are stabilization of Ni(I) in $LaNiO_2$, $YSr_5Ni_3O_8$ and $LaSrCr_xNi_{1-x}O_{4-y}$.

Our results, which are reported here, show that the Mn(II)-derivative of **I** is indeed an excellent oxide ion conductor whose conductivity (σ = 4.6 × 10^{-2} S cm^{-1} at 800 °C) is comparable to that of **I**, but with a lower activation energy E_a for conduction (E_a = 0.47 eV).

$La_{1-x}Sr_xGa_{1-y}Mn_yO_z$ **II** oxides were prepared for various values of x and y between $0 < x, y \leqslant 0.2$ by reacting dry La_2O_3, $SrCO_3$, Ga_2O_3 and $MnC_2O_4{\cdot}2H_2O$ in the required proportions at 1100 °C (12 h), 1400 °C (12 h) and 1450 °C (36 h) in air, with intermittent grindings. At the last stage, the samples were made into pellets (0.9 cm diameter and *ca.* 0.2 cm height) suitable for electrical conductivity measurements. Powder X-ray diffraction (XRD) patterns (Siemens-D5005 X-ray diffractometer, Cu-Kα radiation) revealed formation of nearly single-phase perovskite-like materials for x = 0.1; y = 0.2 (**IIa**) (Fig. 1) and x = 0.2; y = 0.2 (**IIb**). All the major reflections could be indexed on a rhombohedral perovskite cell, excepting the weak ones at $d \approx$ 3.15 and 2.98 Å. These impurity reflections, which are likely due to La_4SrO_7, are weaker in **IIa** than in **IIb** indicating that the composition of **IIa** is closer to a single-phase perovskite than **IIb**. This observation is consistent with the formation of a single-phase perovskite in the Mg(II) system for the composition $La_{0.9}Sr_{0.1}Ga_{0.8}Mg_{0.2}O_{2.85}$.[1,8–10]

Considering that manganese in these oxides would be in a higher oxidation state, we investigated reduction of **IIa** and **IIb** in a thermogravimetric (TG) balance (Cahn TG-131 system) in flowing hydrogen (10 ml min^{-1}). Reduction occurs in two stages (*ca.* 250 and 500 °C) with weight losses of 0.30 and 0.15% respectively. These weight losses are consistent with the compositions $La_{0.9}Sr_{0.1}Ga_{0.8}Mn_{0.2}O_{2.92}$ for **IIa** and $La_{0.9}Sr_{0.1}Ga_{0.8}Mn_{0.2}O_{2.85}$ for **IIIa**, where the oxidation state of manganese is Mn(II). The reduced sample (**IIIa**) is oxidized in air back to the original stoichiometry in a single step around 200 °C. Accordingly, the average oxidation state of manganese in the precursor oxide **IIa** is 2.7+, which would correspond to the formula $La_{0.9}Sr_{0.1}Ga^{III}_{0.8}Mn^{III}_{0.14}Mn^{II}_{0.06}O_{2.92}$. Powder XRD patterns show that the reduced materials retain the rhombohedral perovskite structure,§ albeit with a slight increase in the unit cell parameters (Table 1), that is consistent with the reduction of Mn(III) to Mn(II).

Ionic conductivity of both as-prepared (**IIa** and **IIb**) and hydrogen-reduced samples (**IIIa** and **IIIb**) was measured on sintered pellets coated with gold paste. Impedance data were obtained in air (as-prepared samples) or in flowing argon (reduced samples) at 100 Hz–15 MHz and 60–800 °C employing a HP4194A Impedance/Gain-Phase Analyzer interfaced with an IBM-PC. For each sample, measurement was made for at least two heating and cooling cycles. Impedance plots at low temperatures could be resolved into two semicircles corresponding to the bulk and grain-boundary contribu-

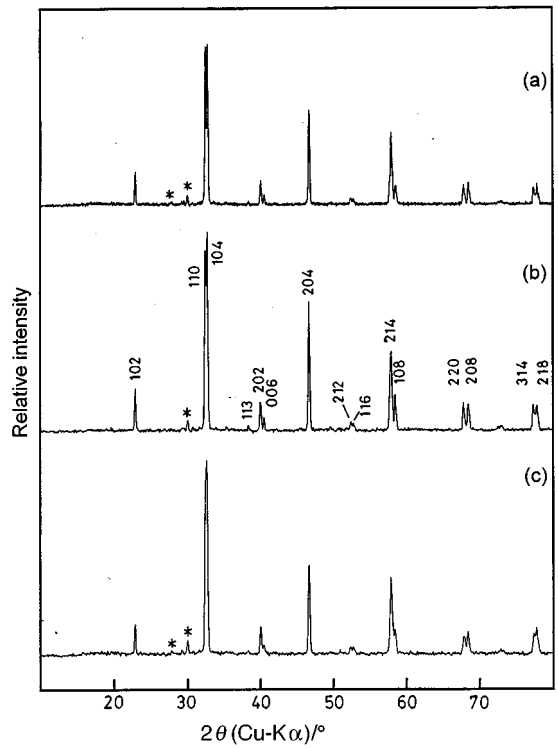

Fig. 1 Powder XRD patterns (Cu-Kα) of (a) $La_{0.9}Sr_{0.1}Ga_{0.8}Mn_{0.2}O_{2.92}$ **IIa**, (b) $La_{0.9}Sr_{0.1}Ga_{0.8}Mn_{0.2}O_{2.85}$ **IIIa** (reduction product of **IIa**) and (c) $La_{0.8}Sr_{0.2}Ga_{0.8}Mn_{0.2}O_{2.80}$ **IIIb**. Reflections due to impurity phase are marked by asterisks.

Table 1 Chemical composition, lattice parameters and ionic conductivity data for $La_{1-x}Sr_xGa_{1-y}Mn_yO_z$ perovskites[a]

Composition	Lattice parameters[b]			$\sigma_{800\ °C}$/S cm^{-1}	E_a[c]/(eV)
	a/Å	c/Å	V/Å^3		
$La_{0.9}Sr_{0.1}Ga_{0.8}Mn_{0.2}O_{2.85}$ (**IIIa**)	5.524(2)	13.360(7)	353.0(2)	4.60×10^{-2}	0.47
$La_{0.8}Sr_{0.2}Ga_{0.8}Mn_{0.2}O_{2.80}$ (**IIIb**)	5.525(1)	13.381(1)	353.7(1)	3.00×10^{-2}	0.57
$La_{0.9}Sr_{0.1}Ga_{0.8}Mn_{0.2}O_{2.92}$ (**IIa**)	5.518(1)	13.335(4)	351.6(2)	3.03×10^{-2}	0.38
$La_{0.9}Sr_{0.1}Ga_{0.8}Mg_{0.2}O_{2.85}$ (**I**)		[d]	358.14[e]	1.00×10^{-1}	1.07[f]

[a] For comparison, the data for $La_{0.9}Sr_{0.1}Ga_{0.8}Mg_{0.2}O_{2.85}$ **I** are also included. [b] Rhombohedral lattice parameters are given for the hexagonal setting. [c] 60–800 °C. [d] The lattice parameters of **I** are a = 7.816, b = 5.539, c = 5.515 Å, β = 90.06° (ref. 10). [e] Equivalent volume. [f] Data taken from ref. 2.

tions to the resistivity. We have uniformly obtained the conductivity from the low-frequency intercept of the impedance plots, that includes both bulk and grain-boundary contributions. Accordingly, the values quoted here would correspond to a lower estimate of the actual conductivity of the samples.

The Arrhenius plots of the conductivity of the **III**-series of oxides are shown in Fig. 2. The conductivity (σ) at 800 °C and the activation energy (E_a) values obtained from the Arrhenius plots are given in Table 1. We see that among the samples investigated, sample **IIIa**, which is the Mn(II) analog of the well known oxide ion conductor, $La_{0.9}Sr_{0.1}Ga_{0.8}Mg_{0.2}O_{2.85}$, shows the highest conductivity of 4.6×10^{-2} S cm^{-1} at 800 °C. The corresponding conductivity for the Mg(II) oxide[2] is *ca.* 1.0×10^{-1} S cm^{-1} at 800 °C. The E_a value for the Mn(II) derivative (0.47 eV) is however significantly lower than the corresponding E_a for the Mg(II) oxide[2] (1.07 eV). Accordingly, we see that isovalent substitution of Mn(II) for Mg(II) in the oxide ion conductor, $La_{0.9}Sr_{0.1}Ga_{0.8}Mg_{0.2}O_{2.85}$, produces a new oxide ion conductor whose conductivity is of the same order of magnitude as the Mg(II) parent oxide, but lowers the activation energy E_a. Interestingly, as-prepared samples (**IIa** and **IIb**) where manganese occurs in a mixed-valent state [Mn(II)/(III)] also exhibit considerable conductivity. Both ionic as well as electronic contributions to the conductivity most likely exist in these phases.

We have investigated the oxygen partial pressure dependence of the conductivity of the sample **IIIa**. The results show a slight increase in the conductivity at higher oxygen pressures [$p(O_2) > 10^{-8}$ atm], indicating the appearance of a p-type electronic contribution. We therefore believe that the conduction of the Mn(II) oxide reported here would be purely ionic only at low oxygen partial pressures [$p(O_2) < 10^{-10}$ atm].

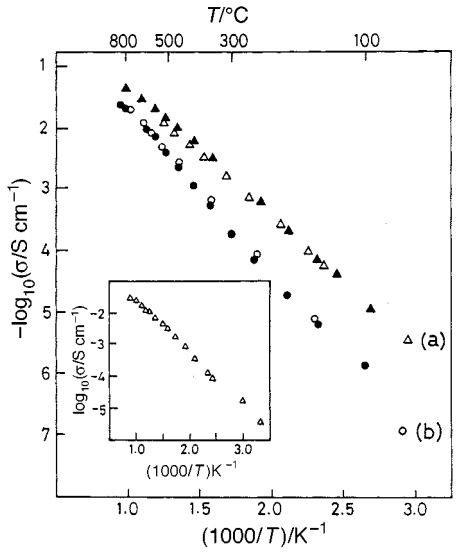

Fig. 2 Arrhenius plots for the electrical conductivity of (a) $La_{0.9}Sr_{0.1}Ga_{0.8}Mn_{0.2}O_{2.85}$ **IIIa** and (b) $La_{0.8}Sr_{0.2}Ga_{0.8}Mn_{0.2}O_{2.80}$ **IIIb**. Closed and open data points correspond to second heating and cooling cycles respectively. The data for sample **IIa** are shown in the insert.

In conclusion, we have shown that isovalent substitution of Mn(II) for Mg(II) in 'the most promising oxide ion conductor', $La_{0.9}Sr_{0.1}Ga_{0.8}Mg_{0.2}O_{2.85}$ **I** yields a new oxide ion conductor exhibiting a comparable conductivity with a lower activation energy. The present work suggests that substitution of other divalent cations such as Co(II), Ni(II), Zn(II) and Cd(II) in **I** is worthy of exploration, especially to understand the role of ionic radius and electronic configuration in determining σ and E_a.

We thank the Indo–French Centre for the Promotion of Advanced Research, New Delhi and the Department of Science and Technology, Government of India for financial support of this work. V. T. thanks the Council of Scientific and Industrial Research, New Delhi, for the award of a research fellowship.

Notes and references

† After the present work was completed, we came to know that the Fe- and Cr-substituted derivatives of **I** have recently been investigated: R. T. Baker, B. Gharbage and F. M. B. Marques, *J. Eur. Ceram. Soc.*, 1998, **18**, 105.

‡ The effective ionic radii of Mn(II) and Mg(II) in octahedral coordination are 0.83 and 0.72 Å respectively. Mn(II), like Mg(II), is known to accept octahedral coordination in oxides; see R. D. Shannon, *Acta Crystallogr., Sect. A*, 1976, **32**, 751.

§ Unlike the Mg(II) oxide **I**, which crystallizes in an orthorhombic[7] (*Pnma*) perovskite structure [with a slight distortion to monoclinic (*I*2/*a*) symmetry[9]], the Mn(II) analog reported here adopts a rhombohedral ($R\bar{3}m$) perovskite structure.

1 T. Ishihara, H. Matsuda and Y. Takita, *J. Am. Chem. Soc.*, 1994, **116**, 3801.
2 M. Feng and J. B. Goodenough, *Eur. J. Solid State Inorg. Chem.*, 1994, **31**, 663.
3 T. Ishihara, H. Minami, H. Matsuda, H. Nishiguchi and Y. Takita, *Chem. Commun.*, 1996, 929.
4 K. Huang, M. Feng, J. B. Goodenough and C. Milliken, *J. Electrochem. Soc.*, 1997, **144**, 3620.
5 T. Ishihara, H. Matsuda and Y. Takita, *Solid State Ionics*, 1995, **79**, 147.
6 K. Huang, M. Feng, J. B. Goodenough and M. Schmerling, *J. Electrochem. Soc.*, 1996, **143**, 3630.
7 M. Crespin, P. Levitz and L. Gatineau, *J. Chem. Soc., Faraday Trans.*, 1983, **79**, 1181; M. James and J. P. Attfield, *J. Chem. Soc., Chem. Commun.*, 1994, 1185; J. E. Millburn and M. J. Rosseinsky, *Chem. Mater.*, 1997, **9**, 511.
8 J. Drennan, V. Zelizko, D. Hay, F. T. Ciacchi, S. Rajendran and S. P. S. Badwal, *J. Mater. Chem.*, 1997, **7**, 79.
9 P. R. Slater, J. T. S. Irvine, T. Ishihara and Y. Takita, *Solid State Ionics*, 1998, **107**, 319.
10 P. R. Slater, J. T. S. Irvine, T. Ishihara and Y. Takita, *J. Solid State Chem.*, 1998, **139**, 135.

Communication 8/07529H

Influence of hemicyanine dye structures on spectral properties of their supramolecular complexes with amylose

William B. Heuer,[a] H. S. Lee[b] and Oh-Kil Kim*[c]

[a] *Chemistry Department, US Naval Academy, Annapolis, MD 21402-5026, USA*
[b] *Division of Materials Science, Brookhaven National Laboratory, Upton NY 11973, USA*
[c] *Chemistry Division, Code 6120, Naval Research Laboratory, Washington D.C. 20375-5342, USA. E-mail: okkim@ccf..nrl.navy.mil*

Received (in Columbia, MO, USA) 30th June 1998, Revised Manuscript Received 14th October 1998, Accepted 22nd October 1998

Hemicyanine chromophores bearing long-chain alkyl substitutents on the donor and/or acceptor ends have been prepared, and absorption and emission spectra of their supramolecular complexes with amylose have been studied in order to relate them to their supramolecular structures.

We have developed a novel strategy[1] based on supramolecular complexation of alkyl-substituted hemicyanine dyes (guest) by amylose (host). This not only prevents chromophore aggregation but also provides many added advantages such as improved thermal stability[2] and enhanced hyperpolarizabilty.[3] The unique feature of this system is the development of a supramolecular self-poling[4] in solution-cast thin films.

Since the guest dye fluoresces strongly in the inclusion,[1,5,6] the dye itself can be utilized as a probe to monitor the binding interaction with the host amylose, depending on external conditions such as temperature (thermochromism).[7] Hemicyanine dyes have also been studied as potential voltage-sensitive probes in biomembranes.[8,9] The dyes exhibit a negative solvatochromism,[10,11] in that spectral shifts of absorption and fluorescence, in response to the solvent polarity, occur to the blue and to the red, respectively. However, in lipid membranes, their spectral behavior is reversed, exhibiting a further blue-shift beyond the absorption in water. This is interpreted to be due to the differential solvation of the chromophore oriented in a lipid bilayer.[12] Here we discuss spectral properties of the supramolecular chromophores (which are uniaxially oriented in the host cavity) when they (dyes **1** and **2**) are mono-functionally

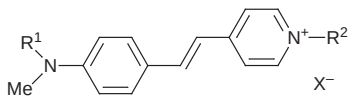

1 R^1 = Me, R^2 = $C_{16}H_{33}$, X = Br
2 R^1 = $C_{16}H_{33}$, R^2 = Me, X = I
3 R^1 = R^2 = $C_{16}H_{33}$, X = Br

derived by blocking one of the sensing partners (amino head and pyridinium tail) with a long alkyl chain and retaining (deactivating) it inside the cavity, thereby allowing the other unit to function for polar sensing. In this respect, one of the present hemicyanine–amylose supramolecules, which contains dye **2**, can be regarded as a model of the dye probe imbedded in the lipid bilayer. Spectral results are compared to demonstrate how the chromophore structure is reflected in the sensing activity of their supramolecular complex.

Visible absorption and emission spectra of dyes **1**–**3** in various DMSO–water mixtures (without amylose) reveal significantly different aggregation tendencies. While dye **1** exhibits negligible aggregation even at Φ_{DMSO} = 0.2, spectral data indicate that aggregation (*ca*. 420 nm) of dyes **2** and **3** occurs below Φ_{DMSO} = 0.55 and 0.75, respectively. This suggests that for the fixed alkyl chain length, substitution at the amine end of the chromophore (relative to the pyridinium end) has a greater influence on the overall hydrophobic character of the molecule.

The spectral properties of dyes **1**–**3** in DMSO-rich mixtures ($\Phi_{DMSO} \geqslant 0.75$) containing amylose† are nearly identical to those of comparable mixtures without amylose, since no inclusion (only free dye state) occurs even in the presence of amylose. However, significant differences due to the presence of amylose are observed as the Φ_{DMSO} of the solvent mixture is decreased. In particular, a dramatic enhancement of fluorescent emission (Fig. 1) is observed at $\Phi_{DMSO} \approx 0.6$ for all three dyes, indicative of supramolecular confinement of the chromophore by the helical amylose.[3] The greater fluorescence enhancement due to the inclusion complexation of dyes **2** and **3** relative to **1** presumably reflects stronger binding of more hydrophobic amino residue by amylose. For all three dyes, the full inclusion of amylose is attained at $\Phi_{DMSO} \approx 0.5$, as evidenced by the

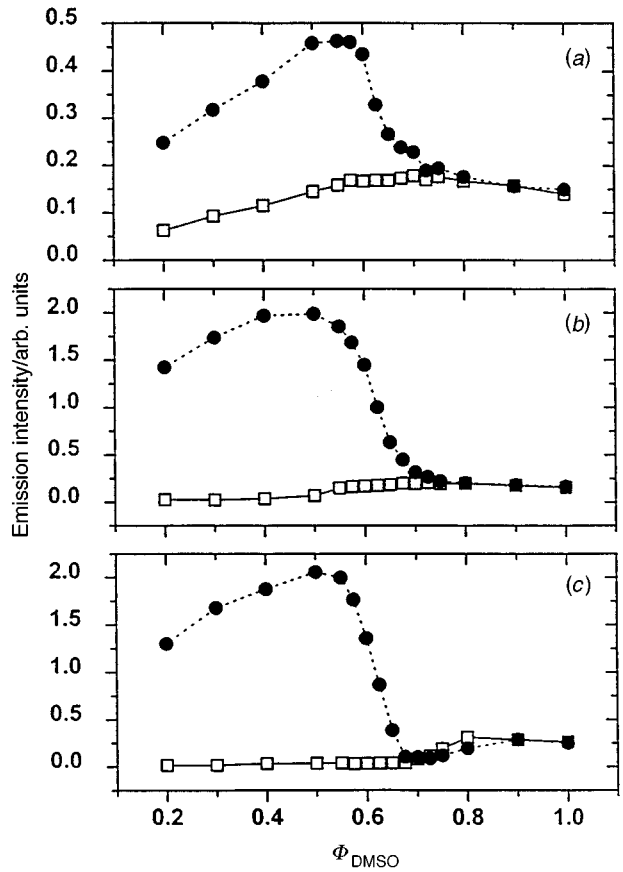

Fig. 1 Integrated fluorescence intensity (480–760 nm) *vs*. Φ_{DMSO} (volume fraction of DMSO) for dyes **1**–**3** in DMSO–H_2O mixtures with (●) and without (□) added amylose: (*a*) dye **1**, (*b*) dye **2** and (*c*) dye **3**. [Dye] = 1.5 × 10^{-5} M in all cases, and [Amylose] = 1.0 × 10^{-3} M for solutions containing amylose. Excitation wavelength = 425 nm.

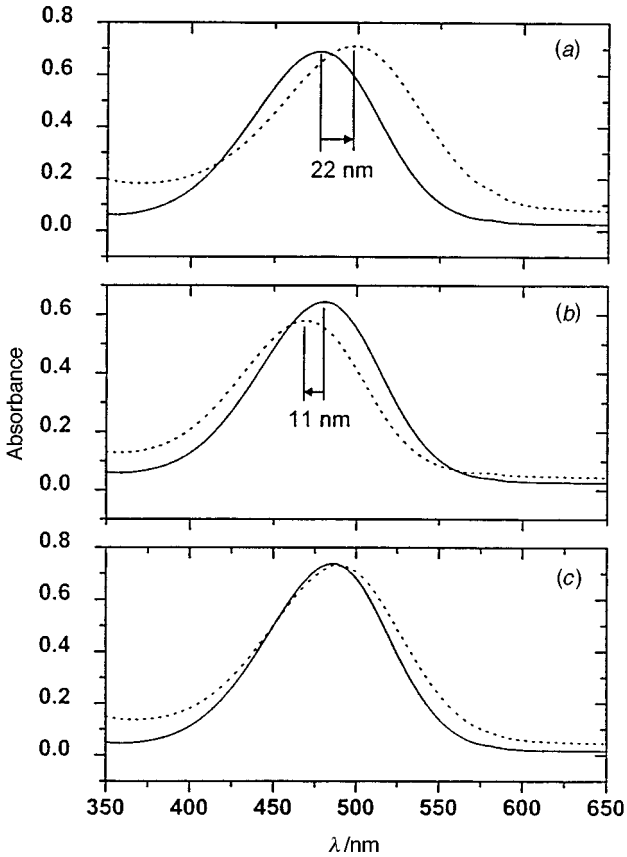

Fig. 2 Visible spectra of dyes **1**–**3** in the free state (—) compared with those of their inclusion complexes (···): (*a*) dye **1**, (*b*) dye **2** and (c) dye **3**. Free dye spectra were recorded at Φ_{DMSO} = 0.90. Spectra of included dyes were recorded at Φ_{DMSO} = 0.50, [amylose] = 1.0×10^{-3} M and [dye] = 1.5×10^{-5} M in all cases.

maximum fluorescence emission‡ of the supramolecular complex. The gradual decrease in emission intensity of the included dye in water-rich mixtures ($\Phi_{DMSO} < 0.50$) is not due to the separation of the dye from the amylose inclusion. It can be therefore attributed, as previously suggested,[3] to conformational changes (*i.e.* swelling) of the amylose helix induced by increasing the solvent polarity of the medium.

The characteristic free dye absorption (at *ca.* 475 nm) of dyes **1**–**3** undergoes a spectral shift (Fig. 2) upon complexation with amylose. This is associated with the difference in intramolecular charge-transfer (ICT) transitions between the free dye state and the inclusion state. The ICT band-shifts due to the complexation of the dyes (**1**–**3**), which are determined by comparing visible spectra of each dye in the fully-included and free (unincluded) states, differ in both magnitude and direction, depending on the dye structure. In view of the fluorescence results (*vide supra*), a fully-included dye can be represented by the spectra recorded at Φ_{DMSO} = 0.5 in the presence of amylose. However, it is difficult for dyes **2** and **3** to represent the free dye state in the spectra recorded under identical solvent condition (Φ_{DMSO} = 0.5), due to aggregation of the dyes. Alternatively, the free state of each dye can be best represented by its spectrum recorded at Φ_{DMSO} = 0.90, where no aggregation occurs even in the presence of amylose (mentioned above).

Thus, as shown in Fig. 2, complexation of dye **1** induces a 22 nm red-shift, but a 11 nm blue-shift is observed upon the complexation of dye **2** under comparable conditions. In contrast, the visible λ_{max} for the inclusion state of dye **3** is red-shifted by only 3 nm relative to the free dye. For dye **1**, the position of the alkyl substituent ensures that the charged pyridinium group resides completely within the nonpolar host cavity in the inclusion state. Exclusion of the pyridinium moiety from solvent contact results in the red-shift in visible absorption of the included dye relative to the free dye in this case. In contrast, inclusion of dye **2** confines the alkyl-substituted amino donor in the host cavity, while the pyridinium cation end resides near the edge of the host, being in contact with the bulk solvent polarity. This situation leads to a blue shifting of the absorption band. The common feature in both cases is that the local environment of the sensing units (amino donor and pyridinium acceptor) is differentiated by inclusion formation. Unlike the case of dyes **1** and **2**, both the donor and acceptor moieties of dye **3** are confined in the same environment in the inclusion. This situation seems to have little influence on the ICT in the excited state, leading to a negligible spectral shift.

In solutions of non-inclusion free dye, both the donor-head and acceptor-tail of dye molecules are exposed to a homogeneous environment. The fact that hemicyanine dyes exhibit negative solvatochromism (blue-shift of λ_{max} with increasing solvent polarity)[10,11,13] and that charge-shift occurs in the chromophore by excitation, suggests that the ground state is more stable than the excited state, and that the pyridinium cation in the ground state has a greater influence on the spectral shift relative to the neutral amino donor in the excited state. The opposite spectral shifts of the supramolecules can therefore be interpreted as being due to the fact that, when the pyridinium cation is exposed to a polar environment (dye **2** case), the ground state has a stronger influence on ICT, whereas when it is disposed in a nonpolar environment (dye **1** case), the excited state has a stronger influence on ICT. Accordingly, the spectral behavior of the present amylose–hemicyanine supramolecular complex bearing dye **2** shows a close resemblance of the membrane-embedded case, *i.e.* blue shifts in both absorption and fluorescence spectra relative to the free molecular state.

In summary, the direction of absorption band-shift upon inclusion of amphiphilic hemicyanine dyes by amylose has been related to the dye structure. This is interpreted in terms of the difference in local environments surrounding the sensing units of the chromophore in the inclusion. The charged pyridinium (acceptor) group, being more strongly influenced by the environmental polarity, plays a dominant role in determining the ICT band shift.

We gratefully acknowledge partial support from ONR, DARPA/ETO and AFOSR (to O. K. K.), as well as the support of the Naval Academy Research Council and ONR grant N0001497WR20008 (to W. B. H.).

Notes and references

† A low molecular weight (4500 D) amylose (Aldrich) was used for a 1:1 complexation (ref. 1) with the dyes, except for dye **3** with which a 2:1 complexation seems to be more favorable.

‡ The emission band shift due to the inclusion is significant and the direction of the shift depends on the dye structure; the shift of dye **1** is to the red and that of dye **2** to the blue. A minor band shift occurs between different Φ_{DMSO} regions.

1 O.-K. Kim and L.-S. Choi, *Langmuir*, 1994, **10**, 2842.
2 S.-F. Lau, A. J. Sosnowik, L.-S. Choi, J. H. Callahan and O.-K. Kim, *J. Thermal Anal.*, 1996, **46**, 1081.
3 K. Clays, G. Olbrechts, T. Munters, A. Persoons, O.-K. Kim and L.-S. Choi, *Chem. Phys. Lett.*, 1998, **293**, 337.
4 O.-K. Kim, L.-S. Choi, H.-Y. Zhang, X.-H. He and Y.-H. Shih, *J. Am. Chem. Soc.*, 1996, **118**, 12 220.
5 Y. Hui, J. C. Russel and D. G. Whitten, *J. Am Chem. Soc.*, 1983, **105**, 1374.
6 Y. Hui and W. Zou, in *Frontiers in Supramolecular Organic Chemistry and Photochemistry*, ed. H.-J. Schneider and H. Duerr, VCH, Weinheim, 1991, pp. 203–221.
7 L.-S. Choi and O.-K. Kim, *Macromolecules*, in press.
8 L. M. Loew, L. B. Cohen, B. M. Salzberg, A. L. Obaid and F. Bezanilla, *Biophys. J.*, 1985, **47**, 71.
9 H. Ephardt and P. Fromherz, *J. Phys. Chem.*, 1993, **97**, 4540.
10 P. Fromherz, *J. Phys. Chem.*, 1995, **99**, 7188.
11 U. Narang, C. F. Zhao, J. D. Bhawalkar, F. V. Bright and P. N. Prasad, *J. Phys. Chem.*, 1996, **100**, 4521.
12 L. M. Loew, L. Simpson, A. Hassner and V. Alexanian, *J. Am. Chem. Soc.*, 1979, **101**, 5439.
13 C. Reichardt, *Solvent and Solvent Effects in Organic Chemistry*, VCH, Weinheim, 1990.

Communication 8/08359B

Enantiomerically pure 1,3,2-dioxaborolanes: new reagents for the hydroboration of alkynes

Joachim E. A. Luithle, Jörg Pietruszka* and Andreas Witt

Institut für Organische Chemie, Universität Stuttgart, Pfaffenwaldring 55, D-70569 Stuttgart, Germany. E-mail: joerg.pietruszka@po.uni-stuttgart.de

Received (in Liverpool, UK) 14th September 1998, Accepted 26th October 1998

Stable, enantiomerically pure alkenylboronic esters 2 are conveniently prepared by direct hydroboration employing the new 1,3,2-dioxaborolane 4; their highly diastereoselective cyclopropanation can be achieved.

Alkyl- and alkenyl-boronic esters are versatile intermediates in organic syntheses, readily available *via* several well established routes.[1] Arguably, the direct hydroborations of alkenes and alkynes using either catechol-[2] or pinacolborane[3] are the most straightforward method to accomplish their preparation. However, the products are frequently water-sensitive[2] or thermolabile[4] and as such they are not always easy to handle, purify and store. Recently, we reported on the high stability of boronates formed by the condensation of alkenylboronic acids with diol **1**,[5] which was conveniently synthesized from dimethyl tartrate.[6] The cyclopropanation of alkenylboronic ester **2** with CH_2N_2 (Pd^{II} catalyzed) was a high yielding process giving readily separable cyclopropylboronic esters **3**, albeit the diastereomeric ratio was low.[5]

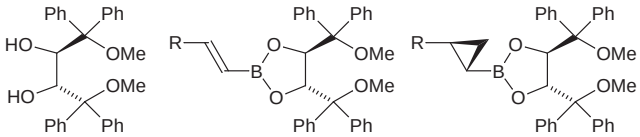

1 **2** **3**

In order to improve the overall efficiency of these reactions, we were not only interested in increasing the selectivity of the cyclopropanation, but especially in omitting the somewhat laborious sequence of alkyne hydroboration, hydrolysis and condensation to give **2**.[3,7] In addition, boroxine formation[5b,8] and their sluggish reaction with diol **1** made us look for alternatives. We envisaged a direct hydroboration with a chiral hydroborating reagent. Although several attempts to make use of, for example, pinanediol failed in the past,[3,9] we were encouraged by the findings of Knochel *et al*. who utilized pinacolborane under exceptionally mild conditions.[3]

The preparation of the hydroborating reagent **4** was straightforward (Table 1). On the other hand, hydroboration of alkyne **5** with **4** did not occur either at room temperature, or in refluxing CH_2Cl_2. After hydrolysis, 1-hydroxy-1,3,2-dioxaborolane **6** was the only isolated product, whose structure was unequivocally determined by X-ray crystallography† after recrystallization from MeOH (formation of ester **7**; Fig. 1). It was established that the desired hydroboration could be achieved to give **2** by heating the alkyne **5** with **4** neat at higher temperature (120 °C).‡ The stable alkenylboronic ester **2a** was directly crystallized† from the reaction mixture (Fig. 2). Only traces of a regioisomer (< 1%) could be detected. It proved advantageous to use two equivalents of alkynes in cases where the starting materials, *e.g*. **5b**,**c**, have relatively low boiling points and consequently the reaction temperatures needed to be decreased (90 °C). This was probably also the reason for the failure of all attempts to hydroborate 3,3-dimethylbutyne **5d**. Protected propargyl alcohols are valuable starting materials that were also successfully employed in this sequence. Both, *tert*-butyldiphenylsilyl (TBDPS) and *tert*-butyldimethylsilyl (TBDMS) protected alcohols **5e**,**f** gave microanalytically pure esters **2e**,**f** in good yield (66–83%). Increasing the reaction temperature, which is compatible with high-boiling compounds like **5g**, not only decreased the reaction time, but also allowed for better yields.

Table 1 Synthesis of highly stable alkenylboronic esters **2** *via* direct hydroboration using the new reagent **4**

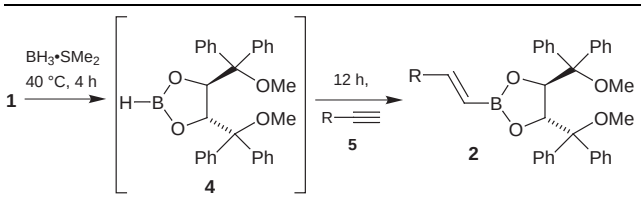

Compound	R	*T*/°C	Yield of **2** (%)
a	Ph	120	82
b	n-C_5H_{11}	90	68
c	Bu^n	90	70
d	Bu^t	40–90	—
e	$TBDPSOCH_2$	120	66
f	$TBDMSOCH_2$	120	70
g	$TBDPSO(CH_2)_3$	135	83

The following experiments proved that this method is rather general. (1*R*,2*R*,3*S*,5*R*)-Pinanediol[9] and (*R*)-1,1,2-triphenyl-

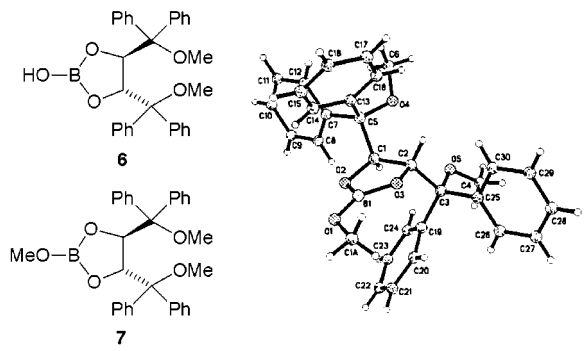

6

7

Fig. **1** Molecular structure of **7**, obtained after hydrolysis of reagent **4** (furnishing **6**) and recrystallization from MeOH.

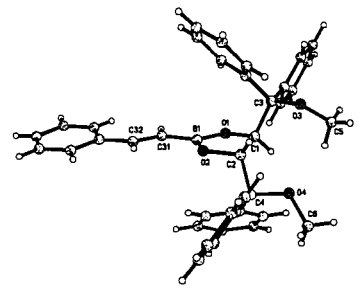

Fig. **2** Molecular structure of **2a**.

ethane-1,2-diol[10] furnished the corresponding alkenylboronic esters **8** and **9** in good yield (81 and 67%), respectively. Diastereoselective cyclopropanation using CH_2N_2 and $Pd(OAc)_2$ yielding cyclopropanes **10** and **11** was also possible (> 95%), however, the diastereomeric ratio was relatively low (Fig. 2; major diastereomers shown).§ Furthermore, we observed that ester **11** slowly hydrolyzes on silica. While cyclopropane **10** is perfectly stable under these conditions, separation of diastereomers cannot yet be achieved. Under the same, now optimized conditions (0 °C, slow addition and 5–10 mol% catalyst), we obtained cyclopropanes **3a** and **3b** in superior selectivity (86:14 and 93:7) as white solids that were easily separable from their diastereomers (> 95%).

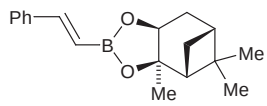

8
(120 °C, 81%)

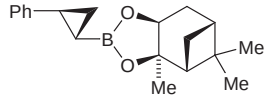

10
dr 63:37

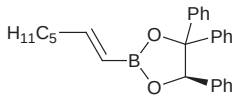

9
(120 °C, 67%)

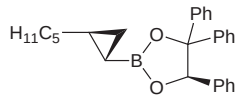

11
dr 60:40

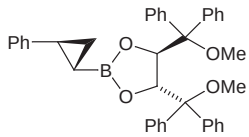

3a
dr 86:14

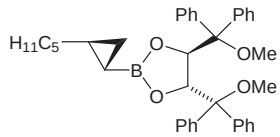

3b
dr 93:7

The reason for the good selectivity is not well understood. Examining the X-ray structures of compounds **2a** and **7** (Fig. 1 and 2), it is obvious that the conformation of the 1,3,2-dioxaborolane rings with the bulky substituents is in both cases very similar, efficiently blocking three quadrants. This should also be true for the reactive conformation and consequently one face of attack should be favoured.

In summary, we have demonstrated that direct hydroboration with chiral hydroborating reagents leads to enantiomerically pure, highly stable alkenylboronic esters. These building blocks should prove versatile for a plethora of further transformations, *e.g*. cycloaddition reactions. We have shown that cyclopropanation can easily be achieved in excellent yield and good diastereomeric ratio. This short sequence furnishing enantiomerically pure cyclopropylboronic esters should allow access to a variety of different stereochemically homogeneous 1,2-disubstituted cyclopropanes utilizing the vast synthetic potential of boronic esters.[1,5]

Financial support by the Fonds der Chemischen Industrie (doctoral fellowship for J. E. A. L. and Liebig fellowship for J. P.) and the Deutschen Forschungsgemeinschaft (fellowship for J. P.) is gratefully acknowledged. We also thank the Institut für Organische Chemie der Universität Stuttgart (Professor Dr F. Effenberger and Professor Dr V. Jäger), Dr W. Frey for performing the X-ray crystal structure analyses, and Degussa AG (Hanau) and Boehringer Ingelheim KG (Biberach) for their ongoing support.

Notes and references

† *Crystal data* for **2a**: $C_{38}H_{35}BO_4$, M_r = 566.5, colourless, crystal size 0.7 × 0.4 × 0.2 mm, a = 10.031(2), b = 16.714(3), c = 18.736(2) Å, U = 3142.0(6) Å^3, T = 293 K, orthorhombic, space group $P2_12_12_1$, Z = 4, D_c = 1.197 mg m^{-3}, μ = 0.076 mm^{-1}. 2807 measured reflections, 2807 independent reflections. Refined by full-matrix least-squares on F^2 for all data weights to R = 0.057, wR = 0.094, S = 1.067, H atoms riding, max. shift/error 0.001, residual ρ_{max} = 0.117 e Å^{-3}.

For **7**: $C_{31}H_{31}BO_5$, M_r = 494.4, colourless, crystal size 0.5 × 0.5 × 0.35 mm, a = 11.839(2), b = 8.6176(9), c = 13.7172(11) Å, β = 110.526(8)°, U = 1310.7(3) Å^3, T = 293 K, monoclinic, space group $P2_1$, Z = 2, D_c = 1.253 mg m^{-3}, μ = 0.083 mm^{-1}. 3197 measured reflections, 3054 independent reflections. Refined by full-matrix least-squares on F^2 for all data weights to R = 0.050, wR = 0.095, S = 1.043, H atoms riding, max. shift/error 0.001, residual ρ_{max} = 0.216 e Å^{-3}. CCDC 182/1066.

‡ Procedure for alkenylboronic ester **2a** is representative: Diol **2** (4.55 g, 10.0 mmol) was carefully dried at 50 °C under reduced pressure for 1 h. Under an atmosphere of nitrogen, CH_2Cl_2 (5 cm^3) was added and the solution cooled to 0 °C. $BH_3{\cdot}SMe_2$ (1.2 cm^3, 12 mmol, 10 M in SMe_2) was added dropwise with vigorous stirring, followed by refluxing the mixture for 4 h. The solvent was removed, the reagent cooled to 0 °C and alkyne **5a** (2.2 cm^3, 20 mmol) slowly added. The flask was closed with a septum, slowly heated to 120 °C and kept at this temperature for 12 h. After cooling to room temperature usual work-up and purification under standard conditions followed [ref. 5(*a*)]. Alternatively, the product **2a** could be directly crystallized (MeOH–light petroleum) from the resulting oil, furnishing a colourless solid (1.90 g, 3.40 mmol, 34%). From the remaining mother liquor additional product **2a** (2.70 g, 4.80 mmol, 48%) was obtained after chromatography (silica, eluent: Et_2O–pentane, 1:6). All spectra were in agreement with published data [ref. 5(*a*)].

§ Diastereomeric ratios of cyclopropylboronic esters were determined by ^{1}H NMR analysis using a Bruker ARX-500 spectrometer. Conversion to cyclopropanols with known configuration allowed the unambiguous stereochemical assignment of the cyclopropanes [ref. 5(*a*)].

1 For general reviews on the syntheses of organoboranes and their applications in organic syntheses: D. S. Matteson, *Stereodirected Synthesis with Organoboranes*, ed. K. Hafner, C. W. Rees, B. M. Trost, J.-M. Lehn and P. von Ragué Schleyer, Springer-Verlag, Heidelberg, 1995; A. Pelter, K. Smith and H. C. Brown, *Borane Reagents*, Academic Press, London, 1988; H. C. Brown, G. W. Kramer, A. B. Levy and M. M. Midland, *Organic Synthesis via Boranes*, Wiley, New York, 1975; D. S. Matteson, *The Chemistry of the Metal–Carbon Bond*, ed. F. Hartley and S. Patai, Wiley, Chichester, 1987, vol. 4, ch. 3; H. C. Brown, E. Negishi and M. Zaidlewicz, *Comprehensive Organometallic Chemistry*: *Organoborane Compounds in Organic Synthesis*, ed. G. Wilkinson, F. G. A. Stone and E. W. Abel, Pergamon, Oxford, 1982, vol. 7; H. C. Brown and P. K. Jadhav, *Asymmetric Synthesis*: *Asymmetric Hydroboration*, ed. J. D. Morrison, Academic Press, Orlando, Florida, 1983, vol. 2.

2 H. C. Brown and S. K. Gupta, *J. Am. Chem. Soc*., 1971, **93**, 1816; H. C. Brown and S. K. Gupta, *J. Am. Chem. Soc*., 1972, **94**, 4370; H. C. Brown and S. K. Gupta, *J. Am. Chem. Soc*., 1975, **97**, 5249; H. C. Brown and J. Chandrasekharan, *J. Org. Chem*., 1983, **48**, 5080.

3 C. E. Tucker, J. Davidson and P. Knochel, *J. Org. Chem*., 1992, **57**, 3482.

4 D. S. Matteson, *J. Am. Chem. Soc*., 1960, **82**, 4228; D. S. Matteson and G. D. Schaumberg, *J. Org. Chem*., 1966, **31**, 726.

5 (*a*) J. E. A. Luithle and J. Pietruszka, *Liebigs Ann./Recl*., 1997, 2297; other diastereoselective cyclopropanations using enantiomerically pure alkenylboronic esters: (*b*) T. Imai, H. Mineta and S. Nishida, *J. Org. Chem*., 1990, **55**, 4986; (*c*) J. Pietruszka and M. Widenmeyer, *Synlett* 1997, 977; racemic cycloproppylboronic esters: (*d*) S.-M. Zhou, Y.-L. Yan and M.-Z. Deng, *Synlett* 1998, 198; (*e*) Z. Wang and M.-Z. Deng, *J. Chem. Soc., Perkin Trans. 1*, 1996, 2663; (*f*) J. P. Hildebrand and S. P. Marsden, *Synlett* 1996, 893; (*g*) P. Fontani, B. Carboni, M. Vaultier and G. Maas, *Synthesis* 1991, 605; (*h*) P. Fontani, B. Carboni, M. Vaultier and R. Carrié, *Tetrahedron Lett*., 1989, **30**, 4815; (*i*) R. L. Danheiser and A. C. Savoca, *J. Org. Chem*., 1985, **50**, 2401; (*j*) Y. N. Bubnov, O. A. Nesmeyanova, T. Y. Rudashevskaya, B. M. Mikhailov and B. A. Kazansky, *Tetrahedron Lett*., 1971, 2153.

6 K. Nakayama and J. D. Rainier, *Tetrahedron*, 1990, **46**, 4165.

7 H. C. Brown and J. B. Campbell Jr., *J. Org. Chem*., 1980, **45**, 389; H. C. Brown, N. G. Bhat and V. Somayaji, *Organometallics* 1983, **2**, 1311.

8 NMR experiments and mass spectrometric investigations established the trimeric nature. These compounds do not react directly with diol **1**, but must first be stirred with 1 equiv. of water in Et_2O before refluxing in the presence of molecular sieves to yield the alkenylboronic ester **2**.

9 D. S. Matteson, K. M. Sadhu and M. L. Peterson, *J. Am. Chem. Soc*., 1986, **108**, 810; D. S. Matteson, P. K. Jesthi and K. M. Sadhu, *Organometallics*, 1984, **3**, 128; R. Ray and D. S. Matteson, *J. Indian Chem. Soc*., 1982, **59**, 119.

10 R. Devant, U. Mahler and M. Braun, *Chem. Ber*., 1988, **121**, 397.

Communication 8/07163B

Dynamics of water molecules in a templated aluminophosphate: molecular dynamics simulation of inelastic neutron scattering spectra

A. J. Ramirez-Cuesta,[a,b] P. C. H. Mitchell,*[a] A. P. Wilkinson,[c] S. F. Parker[d] and P. Mark Rodger[a]

[a] *Department of Chemistry, University of Reading, Reading, UK RG6 6AD. E-mail: scsmitch@reading.ac.uk*
[b] *Departamento de Fisica, Universidad Nacional de San Luis, 5700 San Luis, Argentina*
[c] *School of Chemistry and Biochemistry, Georgia Institute of Technology, Atlanta, Georgia 30332-0400, USA*
[d] *Rutherford Appleton Laboratory, Chilton, Didcot, Oxon, UK OX11 0QX*

Received (in Cambridge, UK) 29th September 1998, Accepted 30th October 1998

In the templated aluminophosphate, DL-$[Co(en)_3]Al_3(PO_4)_4{\cdot}3H_2O$, the water molecules mediate the template–layer interaction: through a molecular dynamics simulation of the water molecule dynamics we have assigned the librational modes of water in the inelastic neutron scattering spectrum to motions of water molecules in three different environments.

In chemical self-assembly molecular sub-units spontaneously form supramolecular frameworks. For zeolites and microporous aluminium phosphates self-assembly is achieved using organic molecules and coordination compounds as structure directing templates.[1] Recently the use of chiral cobalt complexes in directed synthesis of layered aluminophosphates (ALPOs) has been described. One such ALPO is DL-$[Co(en)_3]Al_3(PO_4)_4{\cdot}3H_2O$,† which consists of ALPO layers with $[Co(en)_3]^{3+}$ cations and water molecules in the interlayer region.[2] We are currently investigating the nature of the interactions between the templating cations, the water molecules and the ALPO layers. A question of current interest is whether the interlayer water molecules have a structural role. Water is known to play an important role in biological self assembly, for example by stabilising biopolymer conformations through hydrogen bonding:[3] may water similarly mediate interaction between the templating $[Co(en)_3]^{3+}$ cation and the ALPO layer? Although X-ray crystallography located the oxygen atoms of the interlayer water molecules in our templated ALPO the positions of the hydrogen atoms could only be inferred. We now describe how a combination of inelastic neutron scattering (INS) and molecular dynamics (MD) simulations has revealed the location and hydrogen bonding interactions of the water molecules. The water molecules, which have a structural role in the interlayer region, occupy three different sites.

INS spectra of the templated ALPO, DL-$[Co(en)_3]Al_3(PO_4)_4{\cdot}3H_2O$, and the templating complex, $[Co(en)_3]Cl_3$, both hydrated ($2H_2O$) and anhydrous, were recorded on the TFXA spectrometer at the Rutherford Appleton Laboratory ISIS facility.[4] The compounds (10 g) in aluminium foil sachets were measured at 20 K over energy transfers in the range 16–4000 cm^{-1}. Molecular dynamics calculations were carried out on the templated compound using the program DL_POLY.[5] Initial coordinates were taken from the X-ray crystal structure.[1] The force-field for interactions within the ALPO layers was adapted from van Beest *et al.*[6–8] while for the templating cation, $[Co(en)_3]^{3+}$, we used Lennard-Jones (12–6) atomic potentials with CHARMM parameters[9] supplemented with partial charges calculated using DGauss; water was modelled with the SPC potential.[10] Previously we had validated this force-field in simulations of $[Co(tn)_3]Al_3(PO_4)_4{\cdot}2H_2O$.[11]†

We focus on the librational motions of the water molecules, which occur in the region 250–1000 cm^{-1}. The calculated density of states, $G(\omega)$, was obtained as the Fourier transform of the auto-correlation function $\langle \boldsymbol{v}_a(0){\cdot}\boldsymbol{v}_a(t)\rangle$ of velocities $\boldsymbol{v}_a(t)$ for atoms α,

$$G(\omega) = \frac{1}{N}\sum_{\alpha}\frac{1}{2\pi}\int_{-\infty}^{\infty} e^{-i\omega t}\langle \boldsymbol{v}_\alpha(0)\cdot\boldsymbol{v}_\alpha(t)\rangle \mathrm{d}t$$

where ω is frequency.[12] Experimentally, the density of states is weighted by the scattering cross sections of the atoms and so is completely dominated by hydrogen atom motions; thus calculations of $G(\omega)$ are reported only for α = hydrogen.

The INS spectra of DL-$[Co(en)_3]Al_3(PO_4)_4{\cdot}3H_2O$, $[Co(en)_3]Cl_3$ and $[Co(en)_3]Cl_3{\cdot}2H_2O$ are shown in Fig. 1. The main features of these spectra arise from H atoms, associated with either ethylenediamine ligands or water molecules. Bands arising from ethylenediamine, Fig. 1, were found to be coincident in all three spectra. Thus the experimental spectrum for water in the hydrated AlPO was obtained by subtracting the $[Co(en)_3]Cl_3$ spectrum from the templated ALPO, DL-$[Co(en)_3]Al_3(PO_4)_4{\cdot}3H_2O$ (with intensities normalised to the ethylenediamine peak at 320 cm^{-1}). This spectrum is presented in Fig. 2 along with a smoothed spectrum obtained by Gaussian deconvolution of the experimental difference spectrum; peak positions are listed in Table 1.

In Fig. 2 we also show the vibrational density of states for water calculated from our molecular dynamics simulations. There is a good correlation between the experimental and calculated spectra. Both exhibit one broad and three sharp peaks, and the positions of the latter are in good agreement. The main discrepancy is that the broad peak is harder to resolve in the experimental spectrum, and this subsequently affects the comparison of relative intensities, so it has been considered as a single feature. We conclude that the simulations reproduce the essential features of the experiment, and so enable a more detailed assignment of these peaks from the simulated motions of the water molecules.

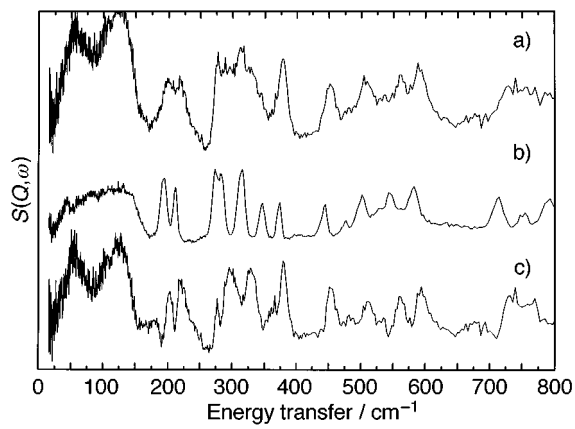

Fig. 1 Experimental INS spectra, (a) templated ALPO DL-$[Co(en)_3]Al_3(PO_4)_4{\cdot}3H_2O$, (b) dehydrated template $[Co(en)_3]Cl_3$ and (c) the hydrated template $[Co(en)_3]Cl_3{\cdot}2H_2O$.

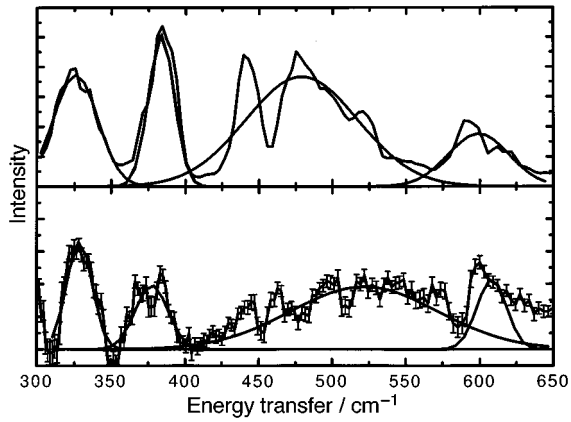

Fig. 2 Calculated (top) and experimental (bottom) difference spectra in the 300–650 cm^{-1} region. Gaussians are indicated to show the four major peaks.

Table 1 Experimental and calculated INS frequencies and relative intensities for $300 < \omega < 650$ cm^{-1}. Peak intensities have also been decomposed into contributions from the three principal librational modes, see Fig. 3

Experiment		Simulation				
				Fractional contribution to intensity[a]		
Frequency/ cm^{-1}	Relative intensity[a]	Frequency/ cm^{-1}	Relative intensity[a]	ω_x	ω_y	ω_z
328	0.16	326	0.19	0.00	0.05	0.95
376	0.13	387	0.18	0.24	0.04	0.72
400–575	0.51	420–550	0.50	0.34	0.02	0.64
599	0.20	599	0.13	1.00	0.00	0.00

[a] Integrated area under the peak.

To obtain a detailed assignment of the water frequencies, the calculated spectrum has been decomposed into contributions from librations about the three principal molecular axes (defined in Fig. 3). From Table 1 it can be seen that the density of states is dominated by librations around the *x* and *z* axes, with no intensity in the *y*-axis librations. All three components do exhibit three separate peaks, indicating three distinct environments for the water molecules. The main features of the broad peak exhibit a more complex structure in the experiment as well as in the simulation.

Our simulation of the structure of DL-$[Co(en)_3]Al_3(PO_4)_4 \cdot 3H_2O$ in comparison with the INS spectrum has revealed three different environments for the three water molecules. By combining our analysis of the experimental INS spectrum and molecular dynamics simulations we are able to locate the water molecules, in particular the hydrogen atoms, in a way not possible from the X-ray structure alone. These results now open up the possibility of identifying how water mediated interactions between the AlPO layers and the templating cation determine the structure of the layered solid.

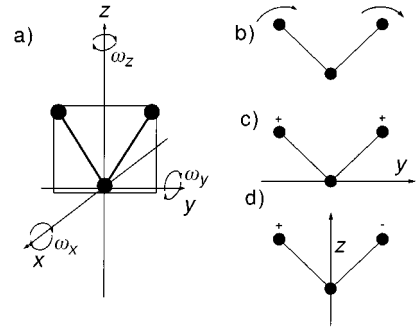

Fig. 3 Three principal rotational/librational modes for water.

We thank EPSRC for financial support under grant GR/K90463 and for allocation of computing time on the J90 Cray supercomputer at the CCLRC Atlas Centre (P. C. H. M.). We thank J. Kruger for the preparation of the AlPO sample.

Notes and references

† Abbreviations: en = 1,2-diaminoethane, tn = 1,3-diaminopropane.

1 M. E. Davis and R. F. Lobo, *Chem. Mater.*, 1992, **4**, 756; D. A. Bruce, A. P. Wilkinson, M. G. White and A. Bertrand, *Chem. Commun.*, 1995, 2059.
2 K. Morgan, G. Gainsford and N. Milestone, *Chem. Commun.*, 1995, 425.
3 L. J. Barbour, G. W. Orr and J. L. Atwood, *Nature*, 1998, **393**, 671.
4 J. Penfold and J. Tomkinson, Rutherford Appleton Laboratory Report, RAL-86-019, 1986.
5 T. R. Forester and W. Smith; DL_Poly User Manual, CCLRC, Daresbury Laboratory, version 2.0, 1995.
6 B. W. H. van Beest, G. J. Kramer and R. A. van Santen, *Phys. Rev. Lett.*, 1990, **64**, 1955.
7 G. J. Kramer, N. P. Farragher, B. W. H. van Beest and R. A. van Santen, *Phys. Rev. B*, 1991, **43**, 5068 and references therein.
8 N. Henson, A. Cheetham and J. Gale, *Chem. Mater.*, 1996, **8**, 664.
9 *Quanta*, Parameter Handbook, Molecular Simulations, release 3.3, 1992.
10 H. J. C. Berendsen, J. P. M. Postma, W. F. van Gunsteren and J. Hermans, in *Intermolecular Forces*, ed. B. Pullman, Reidel, Dordrecht, 1981, p. 331.
11 A. J. Ramirez-Cuesta, P. C. H. Mitchell and P. M. Rodger, *J. Chem. Soc., Faraday Trans.*, 1998, **94**, 2249.
12 A. J. Dianoux, G. R. Kneller, J. L. Sauvajol and J. C. Smith, *J. Chem. Phys.*, 1993, **99**, 5586; A. J. Dianoux, J. L. Sauvajol, G. R. Kneller and J. C. Smith, *J. Non-cryst. Solids*, 1994, 472; G. R. Kneller, W. Doster, M. Settles, S. Cussack and J. C. Smith, *J. Chem. Phys.*, 1992, **97**, 8864; L. van Hove, *Phys. Rev.*, 1954, **95**, 249; *Physica*, 1958, **24**, 404.

Communication 8/07575A

ChemComm

Electroactive dendritic π-conjugated oligothienylenevinylenes

Isabelle Jestin, Eric Levillain and Jean Roncali*

Ingénierie Moléculaire et Matériaux Organiques, CNRS UMR 6501, Université d'Angers, 2 Bd Lavoisier, 49045 Angers, France. E-mail: jean.roncali@univ-angers.fr

Received (in Cambridge, UK) 7th October 1998, Accepted 30th October 1998

Electroactive π-conjugated oligothienylenevinylenes end-capped with dendritic branches of generation one to three have been synthesized.

Thienylenevinylene oligomers (*n*TVs) have recently emerged as a new class of extensively π-conjugated systems.[1] Whereas at a molecular level *n*TVs are interesting models of molecular wires, they also open interesting potentialities as advanced materials for electronic and photonic applications. Progress in these areas implies a supramolecular control of interchain interactions in order to develop at will either compact materials with high electron mobility or, in contrast, single molecular wires.

We report here the synthesis of monodisperse electroactive *n*TVs end-capped with dendritic chains[2] and preliminary results on their electrochemical behavior. Previous examples of incorporation of linear π-conjugated systems within dendritic structures involved dendrimers with poly(*p*-phenylene)[3] and oligotriacetylenes[4] cores.

In order to analyze the effect of progressive steric shielding of the *n*TV system, Fréchet type dendrons[5] of generation 1, 2 and 3 have been attached at both ends of a tetrathienylenevinylene (4TV) derived from 3,4-dihexylthiophene to afford the target compounds **1–3**. While the construction of dendrons from 1-trifluoromethyl-4-bromomethylbenzene **5** is based on the Fréchet type convergent approach,[5] the originality of our strategy lies in the conversion of each generation of dendron into a phosphonate (**Gn-W**) with final assembly of the target system *via* a two-fold Wittig–Horner olefination of dialdehyde **4** with phosphonates **G1-W**, **G2-W** and **G3-W** (Scheme 1).

Reaction between **5** and 3,5-dihydroxybenzyl alcohol in the presence of K_2CO_3 and 18-crown-6 afforded the benzylic alcohol of the first generation (**G1-OH**) which was then converted into the bromomethyl derivative (**G1-Br**) by reaction with PBr_3. Repetition of the procedure followed by re-crystallization at each step gave successively **G2-Br** and **G3-Br** in high yields. Reaction of **G1-Br** and **G2-Br** with diethyl phosphite in the presence of NaH led to phosphonates **G1-W** and **G2-W** while **G3-W** was prepared by reaction of **G3-Br** with phosphite (yields ⩾ 90%). Compounds **1–3** were obtained in 50–60% yield by double Wittig–Horner olefination of dialdehyde **4** with phosphonates **G*n*-W**. The target compounds were fully characterized by ^1H and ^{13}C NMR analyses, elemental analyses, FAB and MALDI-TOF mass spectroscopies.†

Compounds **1–3** exhibit identical UV–VIS spectra with λ_{max} at 542 nm and ε_{max} = 100000. Owing to the extension of the conjugation length by the grafting of two styryl groups, these values are larger than those for the 4TV core and are close to those for 6TV.[1] All spectra exhibit a well-resolved vibronic fine structure which indicates that the increase of **G*n*** does not alter the planarity and rigidity of the π-conjugated backbone.

Compounds **1–3** show identical cyclic voltammograms (CV) with two reversible one-electron oxidation waves corresponding to the formation of the cation radical and dication at redox potentials $E°_1$and $E°_2$ of 0.53 and 0.65 V (Fig. 1). Both $E°_1$and $E°_2$ values were fully independent of **G*n***. Furthermore, the linear dependence of the intensity of the first anodic peak of compound **3** *vs*. the square root of scan rate between 25 and 5000 mV s^{-1} shows that the charge-transfer process between

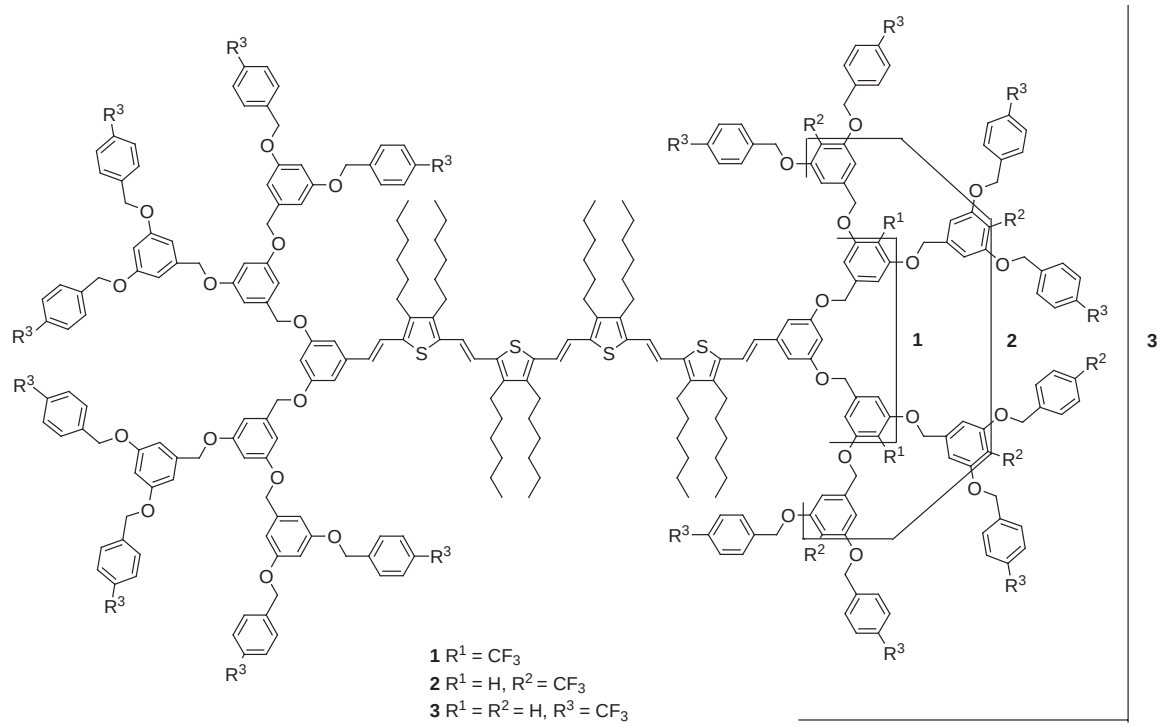

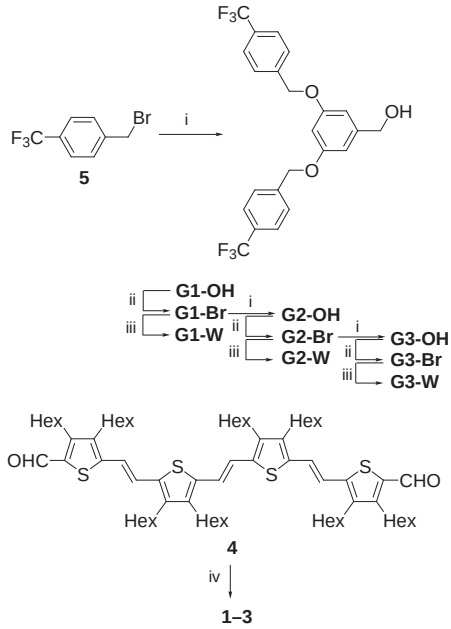

Scheme 1 *Reagents and conditions*: i, 3,5-dihydroxybenzyl alcohol, K_2CO_3, 18-crown-6, acetone; ii, PBr_3, toluene; iii, **G1-W**, **G2-W**, $HPO(OEt)_2$, NaH, THF, **G3-W**, $P(OEt)_3$, reflux; iv, **Gn-W**, Bu^tOK, THF.

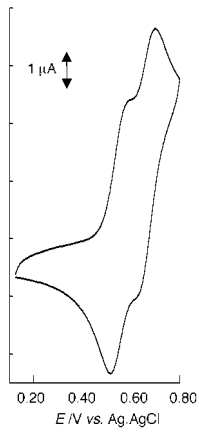

Fig. 1 Cyclic voltammogram for **3** (10^{-4} M) in 0.5 M Bu_4NPF_6/CH_2Cl_2, Pt electrodes, scan rate 100 mV s^{-1}.

the electrode and the core electrophore is not subject to kinetic limitation. This behavior contrasts with that of redox active metal centers encapsulated in dentridic structures for which the increase of **G*n*** leads to a progressive decrease of the reversibility of the oxidation and/or reduction process and to a positive and/or negative shift of the corresponding potential.[6] The independence of the electroactivity of the π-conjugated system on **G*n*** observed here may be related to the length of the electrophore which prevents complete steric burial within the dendritic structure. We also observed that the $E°_1$ value for **3** was independent of substrate concentration in the range of 5 10^{-5} to 5 10^{-3} M. This result is consistent with an absence of follow-up reaction of the cation radical such as formation of a π-dimer;[7] however, this hypothesis needs further confirmation.

Work is now underway to extend this approach to longer *n*TVs and to analyze in more detail the effects of the dendritic branches on inter-chain interactions.

Notes and references

† *Selected data* for **3**: Mp 201 °C; $\delta_H(CDCl_3)$ 7.61 (d, 32H, ^3J 8.2), 7.50 (d, 32H, ^3J 8.1), 7.19 (d, 2H, ^3J 15.7), 7.02–6.98 (m, 6H), 6.78 (d, 2H, ^3J 15.5, 2), 6.72 (d, 4H, ^4J 2.1), 6.68 (d, 8H, ^4J 2.0), 6.67 (d, 16H, ^4J 2.1), 6.53–6.50 (m, 14H), 5.07 (s, 32H), 4.96 (s, 24H), 2.58 (m, 16H), 1.56–1.29 (m, 64H), 0.94–0.86 (m, 24H); *m/z* (MALDI-TOF) 5344.56 (M + 2) [Calc. (found): C, 66.39 (66.96); H, 5.25 (5.20); F, 16.85 (17.06); S, 2.32% (2.40%)].

1 E. Elandaloussi, P. Frère, P. Richomme, J. Orduna, J. Garin and J. Roncali, *J. Am. Chem. Soc*., 1997, **119**, 10774; I. Jestin, P. Frère, P. Blanchard and J. Roncali, *Angew. Chem., Int. Ed*., 1998, **37**, 942; I. Jestin, P. Frère, E. Levillain, N. Mercier, D. Stievenard and J. Roncali, *J. Am. Chem. Soc*., 1998, **120**, 8150.

2 G. R. Newcome, C.N. Moorefield and F. Vögtle, *Dendritic Molecules, Concepts Synthesis, Perspectives*, VCH, Weinheim, New York 1996; D.A. Tomalia, A.M. Naylor and W.A. Goddard, *Angew. Chem., Int. Ed. Engl*., 1990, **29**, 138

3 B. Karakaya, W. Claussen, K. Gessler, W. Saenger and A.-Dieter Schlüter, *J. Am. Chem. Soc*., 1997, **119**, 3296.

4 A. P. H. J. Schenning, R. E. Martin, M. Ito, F. Diederich, C. Boudon, J. P. Gisselbrecht and M. Gross, *Chem. Commun*., 1998, 1013.

5 C. J. Hawker and J. M. J Fréchet, *J. Am. Chem. Soc*., 1990. **112**, 7638.

6 P. J. Dandliker, F. Diederich, M. Gross, C. B. Knobler, A. Louati and E. M. Sandford, *Angew. Chem., Int. Ed. Engl*., 1994, **33**, 1739.; G. R. Newkome, R. Güther, C. N. Moorefield, F. Cardullo, L. Echegoyen, E. Pérez-Cordero and H. Luftmann, *Angew. Chem., Int. Ed. Engl*., 1995, **34**, 2023; C. B. Gorman, B. L. Parkhurst, W. Y. Su and K.-Y. Chen, *J. Am. Chem. Soc*., 1997, **119**, 1141.

7 M. G. Hill, K. R. Mann, L. L. Miller and J. F. Penneau, *J. Am. Chem. Soc*., 1992, **114**, 2728; P. Bäuerle, U. Segelbacher, A. Maier and M. Mehring, *J. Am. Chem. Soc*., 1993, **115**, 10217; P. Hapiot, P. Audebert, K. Monnier, J. M. Pernaut and P. Garcia, *Chem. Mater*., 1994, **6**, 1549.

Communication 8/07810F

ChemComm

The first solid-phase synthesis of oligothiophenes

Patrick R. L. Malenfant and Jean M. J. Fréchet*

Department of Chemistry, University of California, Berkeley, CA 94720-1460, USA.
E-mail: frechet@cchem.berkeley.edu

Received (in Cambridge, UK) 10th September 1998, Accepted 19th October 1998

The solid-phase synthesis of asymmetric oligothiophenes on a chloromethylated macroporous resin, using an alternating sequence of bromination and Stille coupling reactions, has been used to afford oligomers up to the pentamer in excellent yield and purity.

Polythiophenes[1] and the related oligothiophenes[2] have received considerable attention due to their interesting optical and electronic properties, as well as their high environmental stability both in the neutral and oxidized state. Unfortunately, the coupling reactions used to prepare oligothiophenes (*i.e.* Kumada, Stille, Suzuki and Negishi)[3] are plagued by undesirable side-reactions such as homocoupling and loss of functionalization, thus making the purification and isolation of pure oligomers in high yield a difficult task. The pioneering work of Merrifield in the area of solid-phase synthesis has provided the synthetic chemist with a powerful tool for the rapid and frequently automated synthesis of oligomeric organic compounds.[4] Solid-phase synthesis is ideal for multi-step syntheses[4–6] since the isolation of intermediates is not required, and rapid purification is easily achieved by simply washing impurities and excess reagents away from the insoluble polymeric support.

Most of the published work employing organometallic cross-coupling reactions on solid supports has focused on one-step syntheses leading to simple bis-aryl or vinyl-aryl compounds.[7] Palladium mediated cross-couplings such as the Heck, Stille and Suzuki reactions have become increasingly important for the solid-phase synthesis of clinically useful compounds.[8] Recently, palladium catalyzed cross-coupling reactions have been employed[9] independently by Moore and Tour to prepare phenylacetylene oligomers on solid support. Herein, we report the first solid phase synthesis of oligothiophenes in which an alternating sequence of bromination and Stille coupling reactions provides an efficient, high-yielding synthesis of oligothiophenes from the dimer to the pentamer with excellent purity.

The solid phase synthesis is depicted in Scheme 1. The 2,2′-bithiophene-5-carboxylic acid moiety **1** was bound to a macroporous Merrifield-type chloromethylated resin using a standard nucleophilic displacement of the resin's benzylic chloride in DMF.[10] While gel resins, in their swollen state, are generally more reactive than their macroporous counterparts, the latter have a more rigid structure with permanent pores that allows their use in almost any solvent and may facilitate reactions involving ionic or sparingly soluble species. Therefore, the high crosslink density/constant-porosity of the macroporous resin is expected to render it less susceptible to both fouling by low solubility by-products and potential side reactions such as homocoupling that may accompany the coupling step. Such side-reactions would increase the cross-linking of a gel resin, limiting both swelling and reaction conversion, while also reducing the ability to wash out any trapped impurities. The use of a macroporous resin also allows relatively high resin loadings while minimizing[10b,11] the potential for the site–site interactions that would lead to attachment to multiple sites.[12] A macroporous resin, Argopore-Cl, with Merrifield-type $ClCH_2$ functionality at a loading level of 1.03 mequiv. Cl g^{-1} met our needs. The extent of loading of **1** determined by cleavage of the dimer from the support using NaOMe in THF was 0.73 mequiv. g^{-1} suggesting that 84% of the sites of the starting resin had been functionalized to **2**. The coupling step itself was readily monitored by FT-IR spectroscopy as the CH_2Cl peak at 1265 cm^{-1} disappeared while a new peak at 1712 cm^{-1} corresponding to the bound bithiophene ester **2** appeared. Bromination of **2** at the terminal α-position using excess NBS in DMF, followed by coupling to 2-(trimethylstannyl)-4-octylthiophene[13] using $Pd(PPh_3)_2Cl_2$ in DMF as the catalyst afforded the resin-bound trimer **4**. A systematic study involving the coupling step followed by cleavage and quantitative analysis of the product showed that a minimum of 4 equiv. of stannane is required to maximize the conversion of the dimer bromide **3** to the trimer. The monobromination of **4** to the trimer bromide **5** using NBS in DMF was only accomplished in high yield when a stoichiometric amount of NBS was used. The use of an excess of NBS leads to a dibromination product, as confirmed by EI-MS and HPLC analysis of the product isolated after cleavage from the resin. ^{1}H NMR analysis of the cleaved product suggests that the second bromine atom is introduced into the thiophene ring and not at the allylic position of the octyl chain. Attempts at monitoring the bromination on solid support by FT-IR proved fruitless as bands characteristic

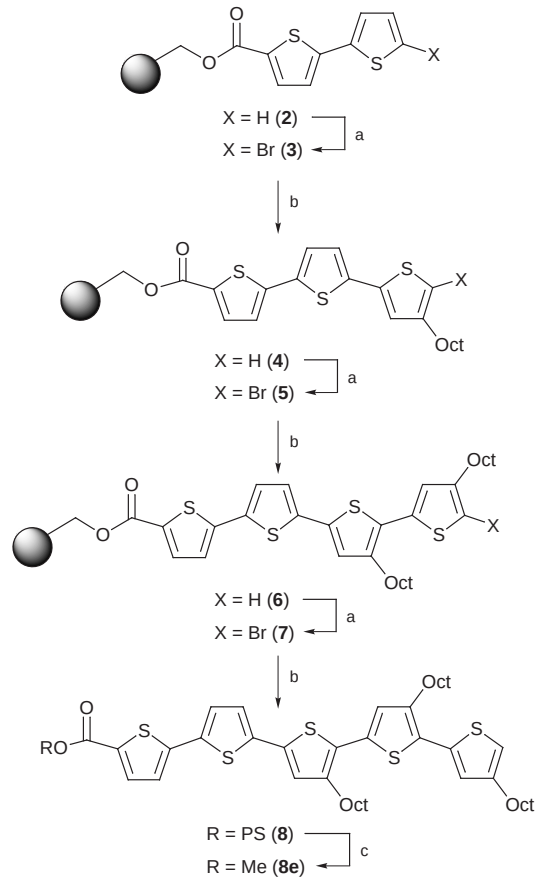

Scheme 1 *Reagents and conditions*: a, NBS, DMF, room temp.; b, 2-(trimethylstannyl)-4-octylthiophene, $Pd(PPh_3)_2Cl_2$, DMF, 80 °C; c, NaOMe, THF, reflux, 1 h, then MeI, 18-C-6, reflux, 3 h.

Table 1. Purity and yield of methyl ester oligothiophenes cleaved from the resin

Entry	Oligomer	HPLC purity[a] (% yield)
1	Dimer **2e**	98
2	Dimer bromide **3e**	97
3	Trimer **4e**	95
4	Trimer bromide **5e**	95
5	Tetramer **6e**	93
6	Tetramer bromide **7e**	95
7	Pentamer **8e**	89 (90)[b]

[a] Reverse phase HPLC analysis was performed by UV–VIS spectroscopy at 254 nm using THF–ACN as the eluant. [b] The acid/ester cleavage product was converted exclusively to the ester *in situ* by treatment with 18-C-6 and MeI. Loading of the linker was determined by cleavage (0.73 mequiv. g^{-1}). Yield of **8e** (from **2**) is based on the theoretical loading of **8** (0.486 mequiv. g^{-1}) itself calculated assuming quantitative conversion at every step from **2** to **8**.

of the transformations are located in the fingerprint region and thus overlap with strong resin background absorbance. Reaction of trimer bromide **5** with 2-(trimethylstannyl)-4-octylthiophene in DMF using $Pd(PPh_3)_2Cl_2$ as the catalyst afforded the resin-bound tetramer **6**. A final iteration involving successive activation and coupling steps finally afforded the resin bound pentamer **8**. All of the above reactions were performed without stirring since the Argopore macroporous resins are very fragile and are readily ground to a fine powder if magnetic stirring is used. Destruction of the resin beads makes handling difficult and leads to losses since resin fragments can make their way through the filter during work-up.

Cleavage from the resin can be accomplished at any stage in the synthesis, using NaOMe in THF,[10c] to afford the cleaved oligomer as a mixture of the methyl ester and a lesser amount of the sodium carboxylate product. In typical control experiments, 100–200 mg aliquots of the resins were subjected to cleavage and the resulting methyl ester dissolved in CH_2Cl_2 was isolated by filtration through silica prior to analysis by reverse phase HPLC. Entries 1–7 in Table 1 represent a sequence in which the synthesis of the pentamer was monitored at each step through HPLC analysis of the cleaved ester products. Although this HPLC analysis only allows an evaluation of the purity of the cleaved ester product, our findings clearly suggest that all reactions reached a high level of conversion. To accurately measure the yield of pentamer **8e,** the cleaved product mixture (ester and carboxylate) was treated with MeI under phase transfer conditions with 18-crown-6 to ensure conversion of the sodium carboxylate fraction to its methyl ester derivative. This transformation is conveniently accomplished directly as part of the cleavage step even while the resin is still present. After washing the resin with THF, CH_2Cl_2 and MeOH, concentration of the organic phase *in vacuo*, and filtration of the CH_2Cl_2 solution through a short silica plug, pentamer **8e** was isolated in 90% yield and in high purity as assessed by HPLC, ^1H NMR and elemental analysis.[14] This high yield of pentamer is remarkable considering that both the activation and coupling steps are susceptible to side reactions and that no purification, other than a simple filtration, was done after each of the six steps.

Oligothiophene syntheses are notorious for the need of extensive chromatographic purification and the *ease* of purification with the solid-phase protocol is clearly an advantage over the traditional solution phase purification methods. This solid-phase synthesis approach, affording easy access to oligomeric materials, complements our recently demonstrated[13] solution-phase fragment coupling approach in which brominated asymmetric building blocks can be used to prepare longer symmetric oligothiophenes in a single step. Finally, it should be noted that cleavage from the resin affords oligomers with a functional handle that may be exploited later to attach the oligomers to a variety of substrates in order to exploit their intrinsic properties or to impart such properties as enhanced solubility and/or novel optical and electronic properties.[13]

Financial support of this research by the AFOSR MURI program and partial support by NSF (DMR- 9796106) is gratefully acknowledged. Stimulating discussions with Dr Lambertus Groenendaal and the gift of Argopore-Cl resin from Argonaut Technologies Inc. are also acknowledged with thanks.

Notes and References

1 T. A. Skotheim, *Handbook of Conducting Polymers*, 2nd edn., ed. J. R. Reynolds and R. L. Elsenbaumer, Marcel Dekker, New York, 1997; R. D. McCullough, *Adv. Mater*., 1998, **10**, 93.

2 J. M. Tour, *Chem. Rev*., 1996, **96**, 537; J. Roncali, *Chem. Rev*., 1997, **97**, 173; 1992, **92**, 711; P. Bäuerle, in *Electronic Materials: The Oligomer Approach*, ed. G. Wegner and K. Müllen, VCH, Weinheim, 1997, ch. 2, pp. 105–197.

3 J. Nakayama, T. Konishi and M. Hoshino, *Heterocycles*, 1988, **27**, 1731; G. Barbarella, A. Bongini and M. Zambianchi, *Macromolecules*, 1994, **27**, 3039; D. Delabouglise, M. Hmyene, G. Horowitz, A. Yassar and F. Garnier, *Adv. Mater*., 1992, **4**, 107; G. Bidan, A. De Nicola, V. Enée and S. Guillerez, *Chem. Mater*., 1998, **10**, 1052.

4 R. B. Merrifield, *J. Am. Chem. Soc.*, 1963, **85**, 2149; G. R. Marshall, R. B. Merrifield, in *Biochemical Aspects of Reactions on Solid Supports*, ed. G. R. Stark, Academic Press, New York, 1971, ch. 3, pp. 111–169; *Polymer-Supported Reactions in Organic Synthesis*, ed. P. Hodge and D. C. Sherrington, Wiley, New York, 1979.

5 J. M. J. Fréchet, *Polymer-supported Synthesis of Oligosaccharides*, in *Polymer-Supported Reactions in Organic Synthesis*, ed. P. Hodge and D. C. Sherrington, Wiley, New York, 1979, pp. 407–434; J. M. J. Fréchet, *Tetrahedron*, 1981, **37**, 663; J. Y. Roberge, X. Beebe and S. J. Danishefsky, *J. Am. Chem. Soc.*, 1998, **120**, 3915.

6 *Special Issue: Combinatorial Chemistry*, ed. A. W. Czarnik and J. A. Ellman; *Acc. Chem. Res.*, 1996, **29**, 112; J. S Früchtel and G. Jung, *Angew. Chem., Int. Ed. Engl.*, 1996, **35**, 17; P. H. H. Hermkens, H. C. J. Ottenheijm and D. Rees, *Tetrahedron*, 1996, **52**, 4527.

7 S. Wendeborn, S. Berteina, W. K.-D. Brill and A. De Mesmaeker, *Synlett*, 1998, 671 and references therein; S. Berteina, S. Wendeborn, W. K.-D. Brill and A. De Mesmaeker, *Synlett*, 1998, 676.

8 M. J. Plunkett and J. A. Ellman, *J. Am. Chem. Soc*., 1995, **117**, 3306; B. J. Backes, J. A. Ellman, *J. Am. Chem. Soc*., 1994, **116**, 11 171; C. J. Andres, D. L. Whitehouse and M. S. Deshpande, *Curr. Opin. Chem. Biol.*, 1998, **2**, 353.

9 (*a*) J. K. Young, J. C. Nelson and J. S. Moore, *J. Am. Chem. Soc*., 1994, **116**, 10 841; (*b*) J. C. Nelson, J. K. Young and J. S. Moore, *J. Org. Chem*., 1996, **61**, 8160; (*c*) L. Jones II, J. S. Schumm and J. M. Tour, *J. Org. Chem*.,1997, **62**, 1388.

10 (*a*) B. F. Gisin, *Helv Chim. Acta.*, 1973, **56**, 1476; (*b*) M. J. Farrall and J. M. J. Fréchet, *J. Am. Chem. Soc.*, 1978, **100**, 7998; (*c*) R. Frenette and R. W. Friesen, *Tetrahedron Lett.*, 1994, **35**, 9177.

11 J. M. J. Fréchet, E. Bald and F. Svec, *React. Polym.*, 1982, **1**, 21.

12 J. I. Crowley and H. Rapoport, *Acc. Chem. Res*., 1976, **9**, 135; L. T. Scott, J. Rebek, I.. Ovsyanko and C. L. Sims, *J. Am. Chem. Soc.*, 1977, **99**, 625.

13 P. R. L. Malenfant, L. Groenendaal and J. M. J. Fréchet, *J. Am. Chem. Soc.*, 1998, **120**, 10 990.

14 Methyl 4″,4‴,4⁗-trioctyl-2,2′:5′,2″:5″,2‴:5‴,2⁗:5⁗,2⁗′-quinquethiophene-5-carboxylate (**8e**): 0.1903 g of **8** (theory: 0.486 mequiv. g^{-1} or 0.092 mmol) afforded 67.3 mg (0.083 mmol) of **8e** in a yield of 90%. Mp 49 °C (DSC); $\lambda_{max}(CHCl_3)$/nm 422; υ(KBr)/cm^{-1} 3095, 3069, 2953, 2924, 2851, 1710, 957, 934, 847, 822, 805, 786, 745; δ(500 MHz, $CDCl_3$) 7.70 (d, *J* 3.9, 1H), 7.18 (d, *J* 3.8, 1H), 7.12 (d, *J* 3.9, 1H), 7.07 (d, *J* 3.8, 1H), 7.02 (s, 1H), 6.97 (2 d, 2H), 6.90 (s, 1H), 3.89 (s, 3H), 2.75 (2 t, *J* 8.0, 4H), 2.61 (t, *J* 7.7, 2H), 1.66 (m, 6H), 1.49–1.14 (m, 30H), 0.88 (m, *J* 6.8, 9H); δ_C(125 MHz, $CDCl_3$) 162.45, 143.92, 143.69, 140.32, 139.63, 137.97, 135.35, 134.72, 134.33, 133.90, 133.19, 131.29, 131.16, 130.55, 128.66, 127.22, 127.15, 125.98, 124.21, 123.68, 120.10, 52.20, 31.88, 30.57, 30.49, 30.47, 30.43, 29.55, 29.54, 29.45, 29.43, 29.42, 29.40, 29.35, 29.27, 22.67, 14.10; HRMS (FAB) calc. for $C_{46}H_{62}O_2S_5$ 806.3353; found 806.3349 (Calc. for $C_{46}H_{62}O_2S_5$: C, 68.44; H, 7.74; S, 19.86. Found: C, 68.60; H, 8.00; S, 19.63%).

Communication 8/07091A

Solvent control in the formation of mononuclear and dinuclear double-helical silver(I)-2,2′:6′,2″-terpyridine complexes

Gerhard Baum,[b] Edwin C. Constable,*[a] Dieter Fenske[b] Catherine E. Housecroft[a] and Torsten Kulke[a]

[a] *Institut für Anorganische Chemie, Spitalstrasse 51, CH-4056 Basel, Switzerland. E-mail: constable@ubaclu.unibas.ch*

[b] *Institut für Anorganische Chemie, Universität Karlsruhe (TH), Engesserstraße, 76128 Karlsruhe, Germany*

Received (in Cambridge, UK) 17th September 1998, Accepted 2nd November 1998

The coordination behaviour of chiral 2,2′:6′,2″-terpyridines with silver(I) is solvent dependent; in acetonitrile, mononuclear [Ag(L)(MeCN)]$^+$ complexes are formed, whereas in less coordinating solvents such as methanol or nitromethane, solid state tetranuclear bis(double helices) [{Ag_2L_2}$_2$]$^{4+}$ are obtained.

It is well established that oligopyridines and related ligands form helicates with a variety of metal centres.[1–3] Although copper(I) forms dinuclear double-helicates with 2,2′:6′,2″-terpyridines (tpy),[4,5] we have been unable to isolate analogous silver(I) species.[6] To date, the only oligopyridine system for which solution equilibria between {ML}$_n$ species have been established involves 2,2′:6′,2″:6″,2‴:6‴,2⁗-quinquepyridines and cobalt(II).[7] In the course of our studies on chiral helicates[5,8] we have revisited the 2,2′:6′,2″–terpyridine–silver(I) system and now show that both mononuclear and dinuclear double-helical species may be isolated and that the equilibrium between mono- and dinuclear species is solvent dependent.

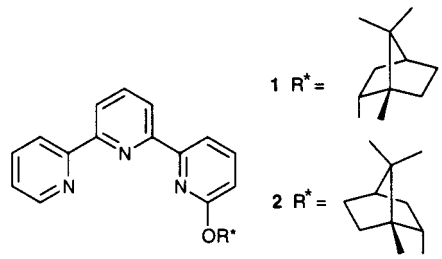

The chiral ligands 1*S*-(−)-**1** and 1*R*-(+)-**2** (L)[8] reacted with Ag(O_2CMe) in MeOH to give colourless solutions from which white solids were precipitated by the addition of [NH_4][PF_6]. Both solutions and solids were photosensitive and turned yellow and then brown upon several hours exposure to sunlight. The electrospray mass spectra of these solids in MeOH or MeCOMe exhibited peaks assigned to {AgL}, {AgL_2} and {$Ag_2L_2(PF_6)$} whereas in acetonitrile, predominantly mononuclear species were observed. Recrystallisation from MeOH, $MeNO_2$ or MeCN gave solids with a 1 : 1 ratio of silver to L but which were qualitatively and quantitatively different. The ^{1}H NMR spectra of solutions of these solids were solvent dependent, although identical spectra were obtained in a given solvent for both crude and recrystallised materials. Reversible changes occurred upon adding CD_3CN to CD_3OD solutions. The magnitude of these changes suggested that different chemical species might be present in solvents of varying donor ability and the spectra in acetonitrile resembled those of the known [Ag(tpy)(MeCN)]$^+$.[6]

The ligands are chiral and CD spectroscopy proved useful. In [Ag(L)(MeCN)]$^+$, the only source of chirality is the ligand and the CD spectra of MeCN solutions of any of the solids are compatible with this formulation; the spectra exhibit $\Delta\varepsilon$ values of ± 2 mol^{-1} l cm^{-1} {$[\alpha]_D$ (MeCN) = ± 60°, $[M]_D$ (MeCN) = ± 420°}, similar to those of the free ligands and with equal and opposite responses for **1** and **2** compounds. We have previously shown that related dicopper(I) double helicates are formed with good diastereoselectivity for the *P* or *M* helicates and have CD responses with characteristic bands at 320 nm allowing the assignment of *P* or *M* helical chirality.[5,8,9] Solutions in MeOH or $MeNO_2$ of the crystals obtained from $MeNO_2$ showed equal and opposite responses at 329 nm {$\Delta\varepsilon$ ± 20 mol^{-1} l cm^{-1}; $[\alpha]_D$ = ± 200°; $[M]_D$ = ± 2530°} for the compounds derived from **1** and **2**; addition of MeCN to the MeOH solution resulted in a decrease in the CD response and eventually the development of the same spectrum as observed for pure MeCN solutions (Fig. 1). Similar changes were observed upon adding MeOH to MeCN solutions. On the basis of these observations we propose the formation of mononuclear [Ag(L)(MeCN)]$^+$ species in MeCN but of double-helical complexes in $MeNO_2$ and MeOH; the sign of the CD response at 329 nm[5,8,10] and the observation of only a single solution species by NMR in MeOH suggest diastereoselective formation of *M*-[Ag_2(**1**)$_2$]$^{2+}$ and *P*-[Ag_2(**2**)$_2$]$^{2+}$.

The recrystallisation of silver(I) complexes of simple 2,2′:6′,2″-terpyridines from MeCN leads to solvento species [Ag(L)(MeCN)]$^+$ [6] and this proved also to be the case with **1**. Fig. 2(a) shows the molecular structure of one of the two mononuclear [Ag(**1**)(MeCN)]$^+$ cations present in [Ag(**1**)(MeCN)][PF_6]·Et_2O. The silver is four coordinate and bonded to the three nitrogen donors of **1** and an acetonitrile molecule; the coordination geometry is distorted square planar and the silver lies 0.13–0.15 Å out of the plane defined by the three tpy nitrogen donors and the acetonitrile nitrogen donor lies 0.51–0.66 Å from this plane. The planar cations are stacked within the lattice [Fig. 2(b)] with a zigzag arrangement of silver centres (Ag···Ag = 5.277, 5.577 Å) resulting in efficient π-stacking of the tpy domains. The zigzag structure results in π-bonding interactions between silver and the central ring of the tpy in the adjacent cations to give a sandwich structure (Ag···centroid, 3.646, 3.514 Å).

X-Ray quality crystals of the product formed in $MeNO_2$ were obtained by the diffusion of Et_2O into an MeCOMe solution. The crystal structure of one of the cations found in the solid state

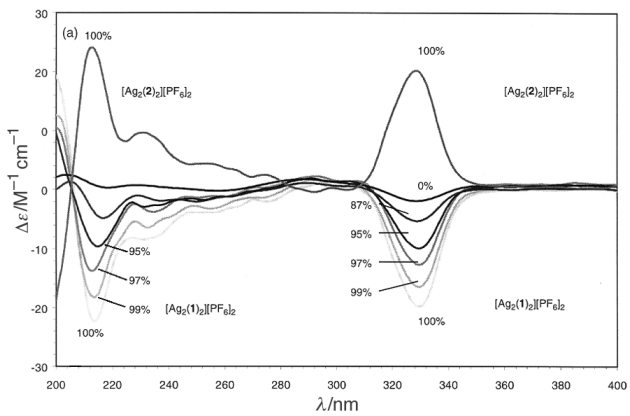

Fig. 1 CD spectra of MeOH solutions of the complexes formed with **2** and **1** and the effect of adding MeCN to the complex with **1**.

in the compound $[Ag_2(\mathbf{1})_2][PF_6]_2\cdot$MeCOMe is presented in Fig. 3. Firstly, a disilver head-to-head double helicate is present with Ag···Ag distances of 2.914–2.940 Å. Each silver is effectively two coordinate with short Ag–N bonds (2.146–2.616 Å) to terminal pyridine rings of each of two ligands and two longer Ag···N contacts to the central rings (3.1–3.2 Å). However, the structure is rather more complex; each of the double helicates forms a short (3.107, 3.156 Å) tail-to-tail Ag···Ag contact with a second dinuclear unit to give a tetranuclear unit. Each of the dinuclear subunits possesses the same helical chirality (both *M* in the case of Fig. 3). The tail-to-tail arrangement results in π-stacking of the terminal pyridine rings of the two dinuclear subunits (3.669–3.783 Å).

As discussed above, solution measurements indicated diastereoselective formation of *M*-$[Ag_2(\mathbf{1})_2]^{2+}$ and *P*-$[Ag_2(\mathbf{2})_2]^{2+}$ helicates; however, in the solid state, there are two tetranuclear

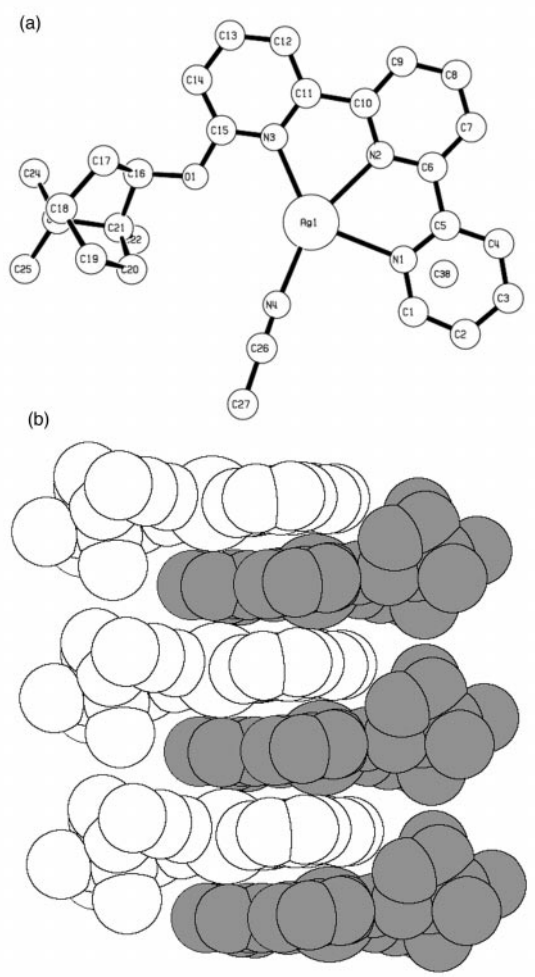

Fig. 2 (a) One of the $[Ag(\mathbf{1})(MeCN)]^+$ cations and (b) the packing of cations in the lattice of $[Ag(\mathbf{1})(MeCN)][PF_6]\cdot Et_2O$. H-atoms omitted for clarity.

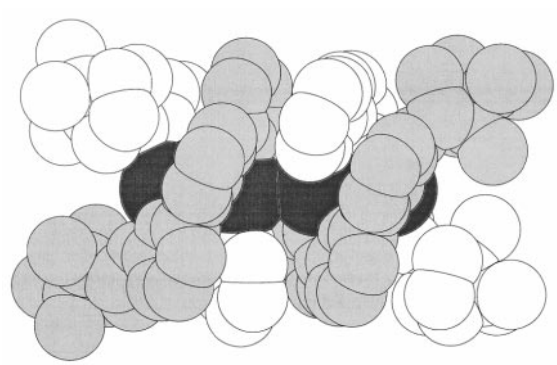

Fig. 3 The structure of the tetranuclear *M*,*M*-$[Ag_2(\mathbf{1})_2]^{2+}$ cation in $[Ag_2(\mathbf{1})_2][PF_6]_2\cdot$MeCOMe. H-atoms omitted for clarity.

units within the lattice, one of which has two *P* and the other two *M* helicates as dinuclear subunits–a diastereomeric excess of 0%! This illustrates the subtlety of the interactions controlling stereoselectivity in helicates. Although the formation of the tetranuclear units can be understood in terms of the favourable stacking and Ag···Ag interactions, the formation of both*P* and *M* helices in the solid state (but not in solution) is unexpected. A similar observation has been reported for mononuclear complexes[10] and it appears to be a consequence of a low energy barrier for the interconversion of diastereomers combined with crystal packing effects of the same order as the energy difference between the diastereomers. There are no short contacts between chiral substituents of adjacent tetranuclear subunits.

In conclusion, we have now established that silver(I) behaves in a similar manner to copper(I) and forms double helical complexes with tpy ligands. However, the tendency for the formation of Ag···Ag interactions results in a subsequent aggregation process to give tetranuclear species.

We should like to thank the Schweizerischer Nationalfonds zur Förderung der wissenschaftlichen Forschung and the University of Basel for support.

Notes and references

‡ *Crystal data*: for $C_{31}H_{40}AgF_6N_4O_2P$, M = 753.52, triclinic, space group $P\bar{1}$ (no. 1), a = 7.1000(10), b = 12.170(2), c = 19.907(5) Å, α = 106.09(2), β = 90.72(2), γ = 93.40(2)°, U = 1649.1(6) Å^3, θ range 3.2–28.1°), Z = 2, D_c = 1.518 Mg m^3, Mo-Kα radiation (λ = 0.710 73 Å), μ(Mo-Kα) = 7.3 cm^{-1}, F(000) = 772, T = 173 K, 11 593 independent reflections [11 008, $I > 2.0\sigma(I)$]. Refinement converged at a final R = 0.0264, 0.0282 (all data) $wR2$ = 0.0696, 0.0716 (all data). Minimum and maximum final electron density 0.51 and 0.24 e Å^3.

For $C_{26.5}H_{30}AgF_6N_3O_{1.5}P$, M = 667.38, monoclinic, space group $P2$, (no. 4), a = 13.831(3), b = 33.071(6), c = 25.147(6) Å, β = 91.34(2), U = 11 499(4) Å^3, θ range 2.1–26.0°, Z = 16, D_c = 1.542 Mg m^3, Mo-Kα radiation (λ = 0.710 73 Å), μ(Mo-Kα) = 8.22 cm^{-1}, F(000) = 5408, T = 183 K, 55 171 independent reflections [39 367, $I > 2.0\sigma(I)$]. Refinement converged at a final R = 0.0492 , 0.0694 (all data), $wR2$ = 0.1278, 0.1403 (all data). Minimum and maximum final electron density 0.493 and 0.840 e Å^3.

Data collected were measured on a STOE IPDS Image Plate diffractometer; structure solution SHELXL-97, SHELXS-97. CCDC 182/1080. See http://rsc.org/suppdata/cc/1998/2659/for crystallographic files in .cif format.

1 E. C. Constable. in *Comprehensive Supramolecular Chemistry*, ed. J.-M. Lehn. Pergamon, Oxford, 1996, vol. 9, p. 213.
2 C. Piguet, G. Bernardinelli and G. Hopfgartner, *Chem. Rev.*, 1997, **97**, 2005.
3 E. C. Constable, *Tetrahedron*, 1992, **48**, 10 013; *Prog. Inorg. Chem.*, 1994, **42**, 67.
4 K. T. Potts, M. Keshavarz-K, F. S. Tham, H. D. Abruna and C. Arana, *Inorg. Chem.*, 1993, **32**, 4450; E. C. Constable, A. J. Edwards, M. J. Hannon and P. R. Raithby, *J. Chem. Soc., Chem. Commun.*, 1994, 1991.
5 E. C. Constable, T. Kulke, M. Neuburger and M. Zehnder, *Chem. Commun.*, 1997, 489.
6 E. C. Constable, A. J. Edwards, G. R. Haire, M. J. Hannon and P. R. Raithby, *Polyhedron*, 1998, **17**, 243.
7 E. C. Constable, J. V. Walker, D. A. Tocher and M. A. M. Daniels, *J. Chem. Soc., Chem. Commun.*, 1992, 768; E. C. Constable and J. V. Walker, *J. Chem. Soc., Chem. Commun.*, 1992, 884; E. C. Constable, M. A. M. Daniels, M. G. B. Drew, D. A. Tocher, J. V. Walker and P. D. Wood, *J. Chem. Soc., Dalton Trans.*, 1993, 1947; E. C. Constable, A. J. Edwards, P. R. Raithby and J. V. Walker, *Angew. Chem., Int. Ed. Engl.*, 1993, **32**, 1465; *New J. Chem.*, 1998, **22**, 219.
8 E. C. Constable, T. Kulke, M. Neuburger and M. Zehnder, *New J. Chem.*, 1997, **21**, 633, 1091; G. Baum, E. C. Constable, D. Fenske and T. Kulke, *Chem. Commun.*, 1997, 2043; *Inorg. Chem. Commun.*, 1998, **1**, 80.
9 M. Ziegler and A. von Zelewsky, *Coord. Chem. Rev.*, in press.
10 P. Biscarini, R. Franca and R. Kuroda, *Inorg. Chem.*, 1995, *34*, 4618.

Communication 8/07254J

ChemComm

Divergent assembly of a starburst tetracosacobalt compound

Edwin C. Constable,* Oliver Eich, Catherine E. Housecroft* and Lesley A. Johnston

Institut für Anorganische Chemie, Universität Basel, Spitalstrasse 51, CH-4056 Basel, Switzerland.
E-mail: housecroft@ubaclu.unibas.ch

Received (in Cambridge, UK) 8th October 1998, Accepted 30th October 1998

The syntheses of $C[\{p\text{-}C_6H_4C{\equiv}C\}_nH]_4$ (n = 1,2,3) and their reactions with $Co_2(CO)_8$ have led to the formation of starburst molecules with rigid, cluster-containing arms; up to twelve cluster units have been incorporated.

We are currently developing synthetic strategies for the preparation of monodispersed dendritic and starburst molecules containing metal centres,[1–3] with a view to developing novel materials. Here, we report initial studies on the synthesis of metal-rich species containing low oxidation state carbonyl clusters with precise spatial distribution. We hope to use molecules of this type, which exhibit distinct onion-like shells of 'organic' and 'inorganic' components, for the formation of metal oxide nanospheres with precise dimensions.

Very recently, there has been active interest in the use of multifunctional alkynes containing 1,3,5-triethynylbenzene

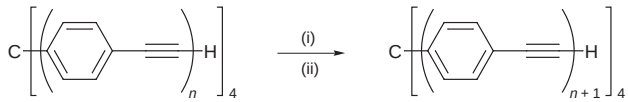

1 n = 1
2 n = 2

2 n = 1
3 n = 2

Scheme 1 *Reagents and conditions*: i, *p*-$IC_6H_4C{\equiv}CSiMe_3$; ii, NaOH (aq).

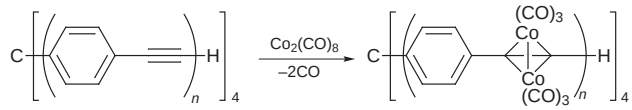

1 n = 1
2 n = 2
3 n = 3

4 n = 1
5 n = 2
6 n = 3

Scheme 2

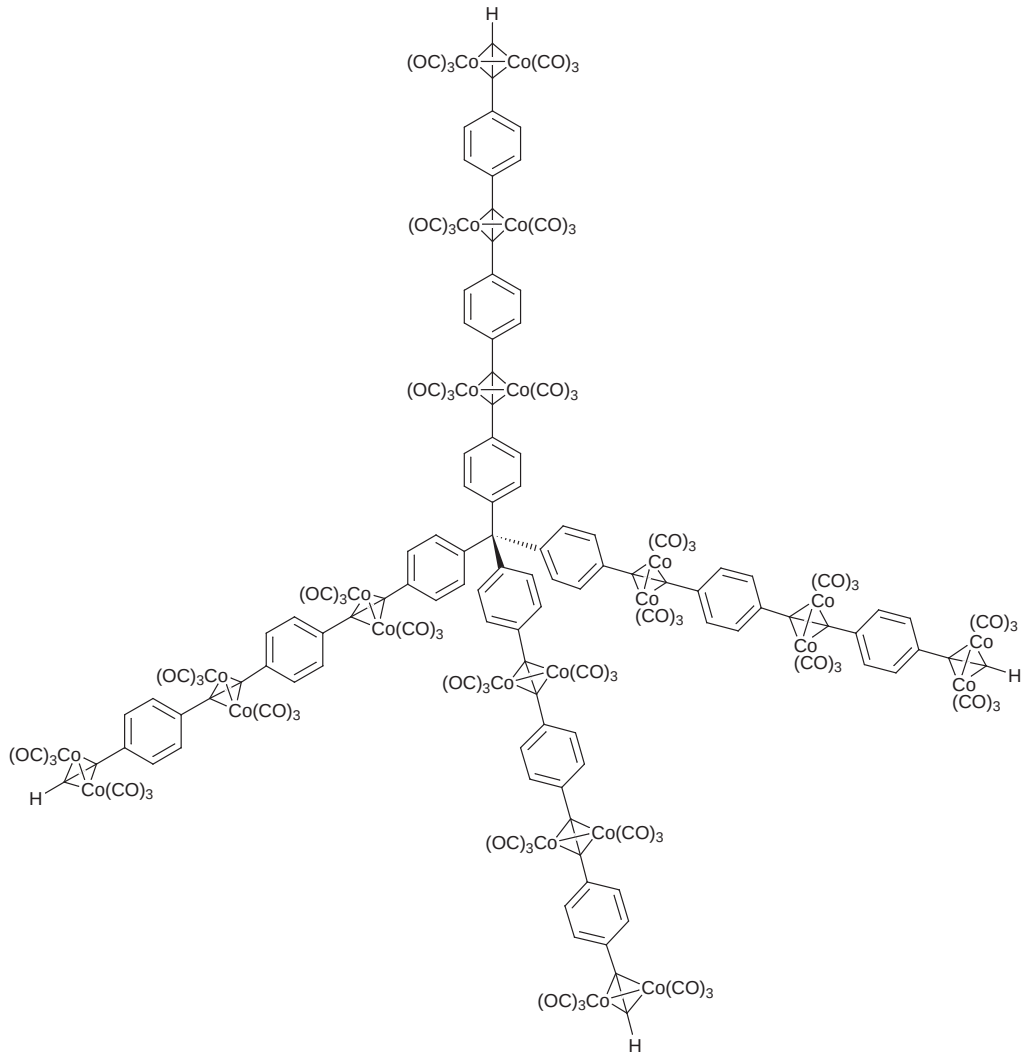

Fig. 1 Proposed structure of compound **6**.

cores as building blocks for starburst systems.[4–7] Here, we focus on multifunctional alkynes radiating from a tetrahedral carbon centre; the compound $C(p\text{-}C_6H_4I)_4$[8] has previously been recognised as a precursor for the assembly of nanostructures such as organometallic tripodaphyrins.[9,10] We report here the reaction of alkynes **1**–**3**, (prepared by a divergent strategy), with dicobalt octacarbonyl to give starburst molecules **4**–**6** which possess rigid, cluster-containing arms. The synthetic procedure may be extended to allow the incorporation of any desired number of alkyne substituents. Reactions between alkynes and $Co_2(CO)_8$ are well established, and provide a useful means of entry into this novel area.[11–13] More recently, Diederich and coworkers have shown that cyclic systems containing $\{C_2Co_2(CO)_6\}$ units are stabilised with respect to the corresponding polyalkynes.[14,15]

Compound **1** was prepared as previously reported,[8–10] and reaction of **1** with an excess of $Co_2(CO)_8$ gave **4** as a brown solid in 46% isolated yield after chromatographic purification.† The IR spectrum showed the expected absorptions in the carbonyl region. In the ^{1}H NMR spectrum, the change in the chemical shift of the alkyne proton from δ 3.06 in **1** to δ 6.37 in **4** was consistent with the incorporation of the RC≡CH group into a $Co_2(CO)_6$(RCCH) cluster unit. Both the ^{1}H and ^{13}C NMR spectra were in accord with a symmetrical product, *i.e.* reaction of all four alkyne functionalities with $Co_2(CO)_8$ and this was supported by the observation in the MALDI-TOF mass spectrum of a parent ion corresponding to **4**.

Systematic growth of each polyyne chain from the carbon core of **1** was achieved‡ by sequential divergent reaction as shown in Scheme 1. Compounds **2** and **3** were characterised by NMR spectroscopy and mass spectrometry. Reaction of each alkyne generation with an excess of $Co_2(CO)_8$ (Scheme 2) gave moderately good yields of compounds **5** and **6**.§ The spectroscopic data for **5** and **6**, and mass spectrometric data for **6** (no parent ion could be obtained for **5**) were fully in accord with cluster formation at each of the alkyne functionalities of the respective precursors. ^{13}C NMR chemical shift correlations across the series of compounds **1**–**6** provided additional support for their formulation. A schematic representation of compound **6** is given in Fig. 1. In going from **3** to **6**, each carbon incorporated into a Co_2C_2-cluster core undergoes a change in local geometry and the C_{ring}–$C_{cluster}$–$C_{cluster}$–C_{ring} is no longer linear. Crystallographic determinations of [1,4-$\{Co_2(CO)_6CHC\}_2C_6H_4$][16] and $[Co_2(CO)_6C_2Ph_2]$[17] show the C_{ring}–$C_{cluster}$–$C_{cluster}$ angles to be *ca.* 140°. We estimate from molecular modelling studies that the radius of compound **6** is in the range 1.6–2 nm.

We are currently extending these studies to higher generations and to the oxidative degradation of the compounds.

This work was supported by the Schweizerischer Nationalfonds zur Förderung der wissenschaftlichen Forschung, the University of Sydney (Eleanor Sophia Wood Travel Scholarship, L. A. J.), and the University of Basel. We thank Dr W. Amrein (ETH, Zürich) for obtaining mass spectrometric data for **4**.

Notes and references

† **4**: Alkyne **1** (19 mg, 0.046 mmol) and $Co_2(CO)_8$ (94 mg, 0.27 mmol) were stirred in CH_2Cl_2 (or acetone) for 1 h, the solvent removed, and the residue purified by column chromatography [SiO_2, hexane:CH_2Cl_2 (1 : 1)] to give a dark brown solid (33 mg, 46%). IR ($CHCl_3$, cm^{-1}) ν_{CO} 2092s, 2057vs, 2027vs. ^{1}H NMR (300 MHz, $CDCl_3$) δ 7.44 (d, 8H, *J* 8.1 Hz), 7.22 (d, 8H, *J* 8.1 Hz), 6.37 (s, 4H); ^{13}C NMR (101 MHz, $CDCl_3$) δ 199.4 (CO), 145.8, 135.5, 131.4, 129.5, 89.5 ($C_{cluster}$), 73.0 ($C_{cluster}$), 64.9 (C_{quat}); MS (MALDI-TOF) *m/z* 1532 $[M - CO]^+$.

‡ **2**: Alkyne **1** (83 mg, 0.20 mmol), *p*-$IC_6H_4C{\equiv}CSiMe_3$ (251 mg, 0.837 mmol), CuI (15 mg, 0.080 mmol) and $[(PPh_3)_2PdCl_2]$ (56 mg, 0.080 mmol) were stirred in dry, degassed NEt_3 (10 ml) under argon for 42 h at 41 °C. Chromatographic work-up [alumina, hexane–CH_2Cl_2 (4 : 1)] gave the TMS-protected intermediate as a yellow crystalline solid; it was dissolved in THF (30 ml), and 1 M NaOH (30 ml) added; the solution was stirred for 1 h at room temperature. Water was added and after extraction with CH_2Cl_2, the residue was purified by column chromatography [SiO_2, hexane–CH_2Cl_2 (1:1)] to give a yellow crystalline product (107 mg, 66 %). ^{1}H NMR (250 MHz, $CDCl_3$) δ 7.47–7.43 (m, 24H), 7.20 (d, 8H, *J* 8.3 Hz), 3.18 (s, 4H); ^{13}C NMR (63 MHz, $CDCl_3$) δ 146.1, 132.1, 131.5, 131.2, 130.9, 123.6, 122.0, 121.1, 90.9 (C_{alkyne}), 89.3 (C_{alkyne}), 83.3 (C_{alkyne}), 78.9 (C_{alkyne}), 65.0 (C_{quat}); MS (MALDI-TOF) *m/z* 816 $[M]^+$, 614 $[M - 2C_6H_4CCH]^+$, 413 $[M - 4C_6H_4CCH]^+$.

3: Alkyne **2** (47 mg, 0.058 mmol), *p*-$IC_6H_4C{\equiv}CSiMe_3$ (72.5 mg, 0.242 mmol), CuI (4.4 mg, 0.023 mmol) and $[(PPh_3)_2PdCl_2]$ (16.2 mg, 0.023 mmol) were stirred in dry, degassed NEt_3 (5 ml) under argon for 12 h at 35 °C. Work-up similar to that for **2** gave a white crystalline solid (37 mg, 53 %). ^{1}H NMR (250 MHz, $CDCl_3$) δ 7.50–7.44 (m, 40H), 7.22 (d, 8H, *J* 8.3 Hz), 3.18 (s, 4H); ^{13}C NMR (75 MHz, $CDCl_3$) δ 146.1, 132.1, 131.6, 131.5, 131.2, 130.9, 123.5, 123.3, 122.1, 121.2, 91.0 (C_{alkyne}), 90.9 (C_{alkyne}), 90.7 (C_{alkyne}), 89.6 (C_{alkyne}), 83.2 (C_{alkyne}), 79.0 (C_{alkyne}), 65.0 (C_{quat}); MS (MALDI-TOF) 1217 $[M]^+$, 915 $[M - \{C_6H_4C_2\}_3H]^+$, 613 $[M - 2\{C_6H_4C_2\}_3H]^+$.

§ **5** and **6**: As for **4**. Isolated yields of **5** and **6** were 26 and 45% respectively. **5**: IR ($CHCl_3$, cm^{-1}) ν_{CO} 2089s, 2057vs, 2028vs. ^{1}H NMR (250 MHz, $CDCl_3$) δ 7.60–7.29 (m, 32H), 6.39 (s, 4H); ^{13}C NMR (75 MHz, $CDCl_3$) δ 199.1 (CO), 145.7, 138.4, 137.3, 136.3, 131.6, 130.6, 129.6, 128.5, 91.7 ($C_{cluster}$), 91.3 ($C_{cluster}$), 89.1 ($C_{cluster}$), 72.8 ($C_{cluster}$), 65.0 (C_{quat}). **6**: IR (KBr pellet, cm^{-1}) ν_{CO} 2090s, 2052vs, 2020vs. ^{1}H NMR (300 MHz, $CDCl_3$) δ 7.61–7.31 (m, 48H), 6.40 (s, 4H); ^{13}C NMR (75 MHz, $CDCl_3$) δ 199.1 (CO), 145.7, 138.3, 138.1, 137.4, 136.3, 131.7, 130.7, 129.8, 129.7, 129.6, 128.6, 91.7 ($C_{cluster}$), 91.6 ($C_{cluster}$), 91.4 ($C_{cluster}$), 91.3 ($C_{cluster}$), 89.1 ($C_{cluster}$), 72.9 ($C_{cluster}$), 65.0 (C_{quat}); MS (MALDI-TOF) *m/z* 4653 $[M]^+$.

1 E. C. Constable, *Chem. Commun.*, 1997, 1073.
2 E. C. Constable, C. E. Housecroft, M. Cattalini and D. Phillips, *New J. Chem.*, 1998, 193.
3 E. C. Constable and C. E. Housecroft, in *Self-assembly in Synthetic Chemistry*, ed. J. D. Wuest, Kluwer Academic Press, Dordrecht, in press.
4 H. Werner, P. Bachmann, M. Laubender and O. Gevert, *Eur. J. Inorg. Chem.*, 1998, 1217.
5 S. Leininger, P. J. Stang and S. Huang, *Organometallics*, 1998, **17**, 3981.
6 M. Uno and P. H. Dixneuf, *Angew. Chem. Int. Ed. Engl.*, 1998, **37**, 1714.
7 N. J. Long, A. J. Martin, F. F. de Biani and P. Zanello, *J. Chem. Soc., Dalton Trans.*, 1998, 2017.
8 M. Simard, D. Su and J. D. Wuest, *J. Am. Chem. Soc.* 1991, **113**, 4696.
9 O. Mongin and A. Gossauer, *Tetrahedron Lett.*, 1996, **37**, 3825.
10 O. Mongin and A. Gossauer, *Tetrahedron*, 1997, **53**, 6835.
11 H. Greenfield, H. W. Sternberg, R. A. Friedel, J. H. Wotiz, R. Markby and I. Wender, *J. Am. Chem. Soc.*, 1956, **78,** 120.
12 R. D. W. Kemmitt and D. R. Russell in *Comprehensive Organometallic Chemistry*, ed. E. W. Abel, F. G. A. Stone and G. Wilkinson, Pergamon, Oxford, 1982, vol. 5, p. 1.
13 R. L. Sweany in *Comprehensive Organometallic Chemistry II*, ed. E. W. Abel, F. G. A. Stone and G. Wilkinson, Pergamon, Oxford, 1995, vol. 8, p. 1.
14 Y. Rubin, C. B. Knobler and F. Diederich, *J. Am. Chem. Soc.*, 1989, **112**, 4966.
15 *Modern Acetylene Chemistry*, ed. P. J. Stang and F. Diederich, Wiley-VCH, Weinheim, 1995.
16 C. E. Housecroft, B. F. G. Johnson, M. S. Khan, J. Lewis, P. R. Raithby, M. E. Robson and D. A. Wilkinson, *J. Chem. Soc., Dalton Trans.*, 1992, 3171.
17 D. Gregson and J. A. K. Howard, *Acta Crystallogr., Sect. C*, 1983, **39**, 1024.

Communication 8/07838F

ChemComm
FEATURE ARTICLE

Stereocontrolled synthesis and reactivity of sugar acetylenes

Minoru Isobe,† Rena Nishizawa, Seijiro Hosokawa and Toshio Nishikawa

Laboratory of Organic Chemistry, School of Bioagricultural Sciences, Nagoya University, Chikusa, Nagoya 464-8601, Japan. E-mail: isobem@agr.nagoya-u.ac.jp

Received (in Cambridge, UK) 29th June 1998, Accepted 17th August 1998

C-Glycosidation is of great significance in the organic synthesis of optically active materials, since it allows the introduction of carbon chains to sugar chirons and the use of sugar nuclei as a chiral pool as well as a carbon source. Silylacetylenes are sufficiently reactive to form 'sugar acetylenes' for the selective introduction of various acetylenic groups in an *alpha-axial* manner at the anomeric position of D-hexopyranose rings. 1,4-*Anti* induction, on the other hand, gives a different stereochemical outcome in the case of C-glycosidation of pentopyranose glycals. The mechanism of these reactions includes oxonium cation intermediates in which stereoelectronic and/or steric factors drive the direction of the incoming silylacetylene. Bis-C-glycosidation allows the introduction of sugars at both ends of some bis(trimethylsilyl)acetylenes. A 2,3-dideoxyglucose derivative provides the corresponding C-1 α-acetylenic compounds, which would increase the scope of C-glycosidation with silylacetylenes. In sugar acetylenes, the alkynyl group at the anomeric position of a pyranose ring is epimerized *via* a hexacarbonyldicobalt complex by treatment with trifluoromethanesulfonic acid. The three steps—cobalt complexation, acidic transformation and decomplexation—afford overall epimerization and thus one can obtain either the α- or β-alkynyl C-glycoside as desired. Ring opening of a dihydropyran derivative using Nicholas-type cation intermediates is also part of this study. Several sets of decomplexation conditions for *endo*-type acetylene–cobalt complexes provide various olefins possessing potential utility for synthesis. These methodologies have been utilized for the synthesis of polyoxygenated natural products and derivatives.

Introduction

In target-orientated synthesis, continuous efforts have provided organic chemistry with a considerable number of new synthetic methodologies. These include new concepts for multistep syntheses that achieve the desired target in a more straightforward manner. Syntheses of optically active natural products have posed many problems despite there being numerous methodologies available to the organic chemist. Sugars have been used as chirons as well as carbon sources in many organic syntheses.[1] The induction of one or more stereogenic centers onto a side chain extending from a sugar ring is another application which has attracted much attention.[2] We have designed and developed C-glycosidation (alkynylation) as a key reaction for the introduction of a carbon chain onto sugars. Those alkynylated compounds are called 'sugar acetylenes' for short,[3] and they have been applied to syntheses of natural products such as tautomycin[4] and ciguatoxin.[5]

Professor Minoru Isobe was born in Nagoya, educated in Nagoya and found his academic position in Nagoya University. He received his PhD degree with Professor Toshio Goto (silkworm diapause hormone) in 1973, and moved to Columbia University in New York as a postdoctoral researcher under the guidance of Professor Gilbert Stork (Prostaglandin F_2a). He was appointed an Associate Professor (1975–1991) in Professor Goto's group after Dr Yoshito Kishi left for Harvard University, and then Professor of Organic Chemistry (1991). His synthetic interests have mostly focused on the total synthesis of natural products, such as vernolepin, maytansine, okadaic acid, tautomycin and allo-yohimbane, and he is currently involved in the total synthesis of tetrodotoxin, ciguatoxin etc. *He has expanded his interests in bioorganic chemistry into the fields of bioluminescence, insect diapause, protein phosphatase inhibitors* etc. *and into those mechanistic elucidation processes including the counter proteins. He has received awards from the Agricultural Chemical Society for young chemists in 1980 and from the Society of Synthetic Organic Chemistry, Japan in 1996. He is currently a project leader at JSPS-RFTF.*

Rena Nishizawa was born in Osaka, Japan, in 1974. She received her BS degree from Nagoya University in 1997 and is currently an MS student under the supervision of Professor Minoru Isobe at the School of Bioagricultural Sciences of Nagoya University, involved in the study on the chemistry of C-glycosidation.

Dr Seijiro Hosokawa was born in Kurashiki, Japan, in 1968. He received his BS and MS degrees from Hokkaido University under the supervision of Professor Haruhisa Shirahama, and his PhD from Nagoya University under the supervision of Professor Minoru Isobe in 1996. After a year of postdoctoral research at Nagoya University and an additional one year at the Scripps Research Institute under the supervision of Professor K. C. Nicolaou, he became an Assistant Professor of Chemistry in 1998 in the Faculty of Pharmaceutical Sciences, Science University of Tokyo. His research interests include organic synthesis and bioorganic chemistry.

Dr Toshio Nishikawa was born in Nagano, Japan, in 1962. He received his BS degree in 1985 from Shizuoka University under the direction of Professor Daisuke Uemura and his MS degree in 1987 from Nagoya University. After spending time as a research associate at the research institute of the Sapporo Brewery Company (1987–1988), he returned to Nagoya University and received his PhD in 1995 from the same University under the supervision of Professor Minoru Isobe. Currently he is an Assistant Professor in the School of Bioagricultural Sciences at Nagoya University. His research interests include the development of new synthetic methods and the organic synthesis of nitrogen-containing natural products for the elucidation of biological problems.

C-Glycosidation with silylacetylene

During the course of our synthetic studies on okadaic acid,[6] an oxygenated marine natural product, we used the Hosomi–Sakurai reaction for the coupling of allyltrimethylsilane and tri-*O*-acetyl-D-glucal to prepare one of the starting materials.[7] We came across with a similar C-glycosidation under acidic conditions with silylacetylenes instead of allylsilane (R = $SiMe_3$).[8] The stereoselectivity of this reaction is excellent, giving only the α-acetylene, and is better than that in the allylsilane case (α:β = 96:4). C-Glycosidation with silylacetylenes allows a wide variety of substituents on the other end of the acetylene, and the resulting alkynylated sugar derivatives are of great potential utility as starting materials for natural product synthesis in optically active form.[9] Examples with different substituents are listed in Table 1.[8–10] In the reaction, R

Table 1 Alkynylation of tri-*O*-acetyl-D-glucal with silylacetylenes

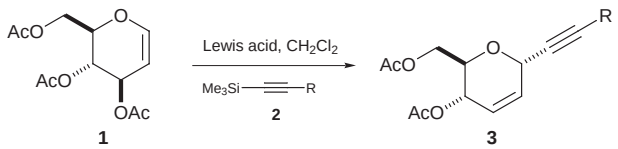

Entry	R	Lewis acid	*T*/°C	Yield (%)
1	H	$TiCl_4$	0	0
2	Me	$SnCl_4$	−15	99
3	$SiMe_3$	$TiCl_4$	−20	75
4	$SiMe_3$	$SnCl_4$	−20	99
5	Bu^n	$TiCl_4$	−20	68
6	CH_2SPh	$TiCl_4$	−20	15
7	CH_2OAc	$TiCl_4$	−20	0
8	$(CH_2)_2OAc$	$TiCl_4$	−20	22
9	$(CH_2)_3OAc$	$TiCl_4$	−20	36
10	$(CH_2)_4OAc$	$TiCl_4$	−20	59

has to be larger than Me to afford alkynylation in reasonably good yield. The yield with R = H (entry 1) is almost 0%.[10a] On the other hand, the stronger Lewis acid $SnCl_4$ seems to work better than $TiCl_4$ in the case of R = $SiMe_3$ (entries 3 and 4). When R is a methylene group with an OAc moiety at the terminal position, *e.g.* the reaction with prop-2-ynyl acetate (entry 7), no alkynylated product is given. The yields of products increase with the higher homologous acetates (entry 8–10). This is due to the moderating effect of the methylene group(s) on the OAc moiety, which destabilizes the cationic transition state. These results suggest that the mechanism of this alkynylation reaction involves cationic charge development at the 2′-carbon in the transition state. In case of the phenylthio group (R = SPh, discussed later), the product is unstable with the stronger acids, and high yield is observed only with milder Lewis acid such as $BF_3{\cdot}OEt_2$; the nucleophilicity of (phenylthio)silylacetylene is high enough to yield the phenylthioethynylation product in good yield.[11]

Possible mechanism of C-glycosidation and proof of stereochemistry

This C-glycosidation includes eliminative formation of the enonium ion (as shown in Scheme 1) to which silylacetylene can coordinate from the α side. The stereochemistry should largely be determined by the coordination between two π-electron orbitals of the onium and acetylene groups, while the stereoelectronic control allows the α-pseudo-axial orbital to make the bond, as shown in Fig. 1.

In 2,3,4,6-tetra-*O*-acetyl-D-glucal the C-glycosidation took place in a similar fashion to that in the tri-*O*-acetyl-D-glucal cases above with silylacetylenes (Scheme 2).[9] In this particular reaction, as shown in **8** and **9** (Scheme 3), the primary products are all unstable under the work-up conditions and/or silica gel chromatography. The reaction mixture is immediately subjected to hydride reduction ($NaBH_4$ and $CeCl_3$ in MeOH; or $LiAlH_4$, < −40 °C), in which the reagent accelerates elimination of the 4-OAc group (**8**) and then attacks the resultant ketone from opposite side of the *axially* oriented α-alkynyl group, thus giving a 2α-hydroxy group.

Incidentally, reduction with $LiAlH_4$ at higher temperature (*ca*. 0 to −10 °C) is usually followed by hydroalumination of the acetylene **8**, resulting in the formation of *trans* olefin **10**. The acetylene group in **3** can be partially reduced into *cis* olefin **11** with diimide (Fig. 2). These partial reduction products give NOEs in their NMR spectra between H-5 and H-1′ to prove the

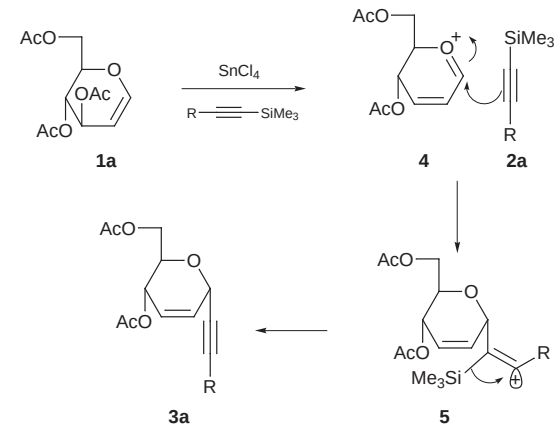

Scheme 1

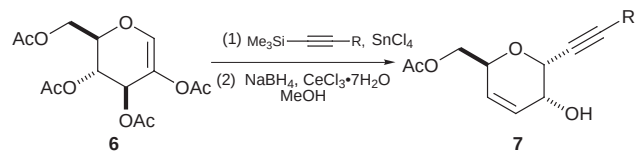

Scheme 2

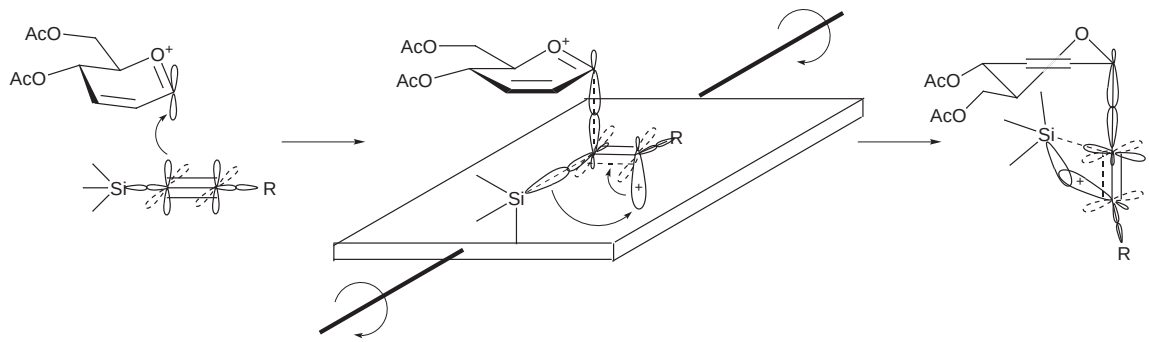

Fig. 1

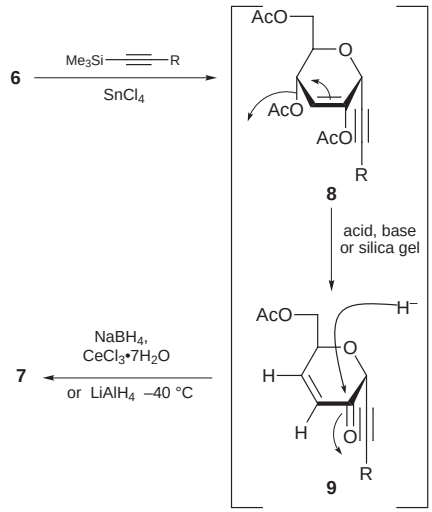

Scheme 3

α stereochemistry of the original acetylene (Fig. 2).[9] Hydrosilylation of the benzylidene acetylene **21** (in Scheme 4) also gives two products (**12a** and **13a**), providing further evidence for the stereochemistry; thus, similar NOEs are observed. These benzylidene compounds have the bulky olefinic group in the α axial position in **12** or the α equatorial position in **13**, the latter showing an NOE between H-1 and H-4 due to the boat conformation of the tetrahydropyran ring.

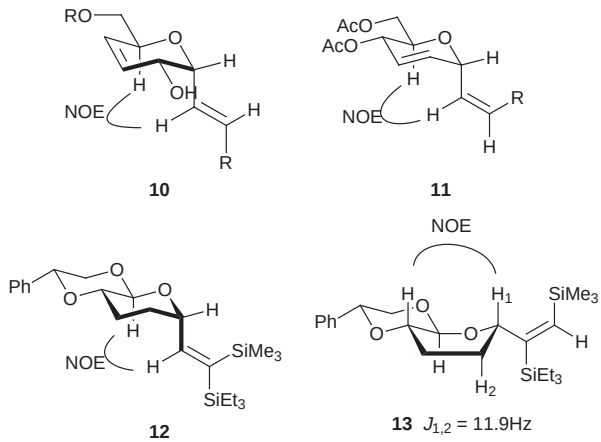

Fig. 2

Expansion of C-glycosidation to similar systems

In Table 2 other examples of C-glycosidation of 2,3-dideoxyglucose derivative **14** with silylacetylene are shown. The acetylation of the glycoside is critical to provide the C-1 leaving group which generates the oxonium ion, with which silyl acetylenes can react to form the α sugar acetylene. Scheme 4 illustrates the preparation of these compounds in order to prove the stereochemistry, and includes C-glycosidation of the saturated pyran ring. In this case the C-1 OAc group in **14** is necessary to provide a good leaving group, to generate the oxonium cation **17** to which the silylacetylene coordinates. After conversion to the corresponding 4,6-benzylidene derivative **21**, its acetylene group was subjected to hydrosilylation to provide a mixture of regioisomers **12a** and **13a**.[12]

Table 2 C-glycosidation of 2,3-dideoxyglucose derivative **14** with silylacetylene **15**

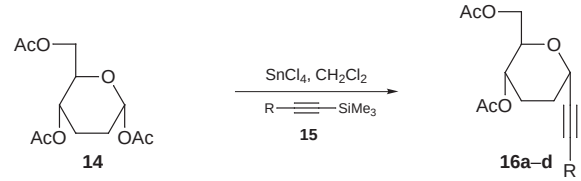

Entry	Alkyne	R	*T*/°C	Product	Yield (%)
1	**15a**	$SiMe_3$	0	**16a**	73
2	**15b**	$C{\equiv}CSiMe_3$	0	**16b**	71
3	**15c**	(*Z*)-CH=CHCl	0	**16c**	83
4	**15d**	(*Z*)-CH=CHC≡$CSiMe_3$	−78	**16d**	35

Sugars at both ends of an acetylene

In the C-glycosidation of silylacetylenes with glucal type compounds, both of the examples in Schemes 1 and 2 afford different sugar products (R = $SiMe_3$) bearing trimethylsilylacetylene moieties, respectively. But these silylacetylenes do not react further with another equivalent of glycal. This lack of reactivity is observed for prop-2-ynyl acetate (entry 7, Table 1); thus no double C-glycosidation product was obtained in this particular case, presumably due to the presence of an electron-

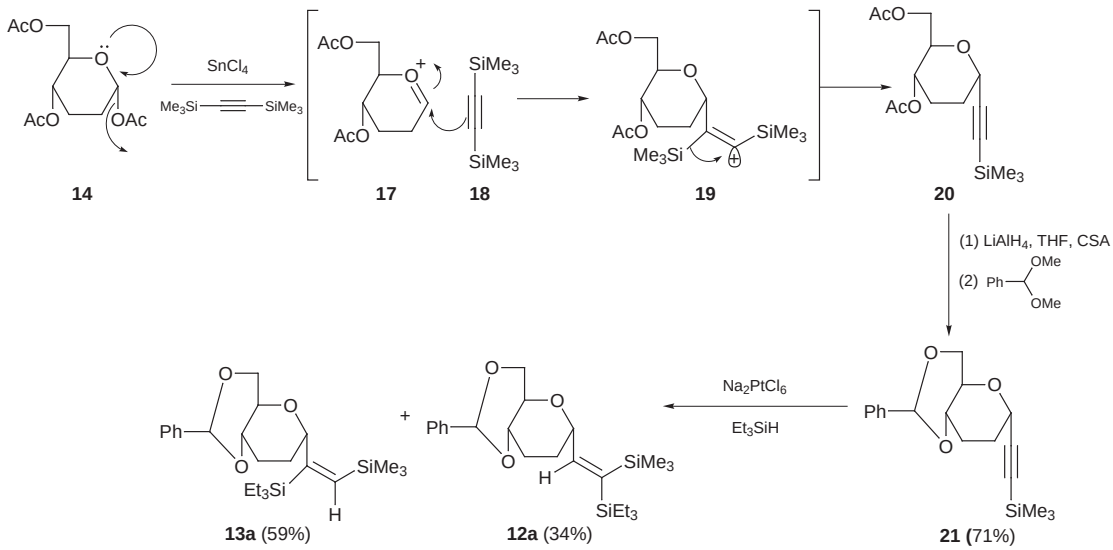

Scheme 4

withdrawing oxygen atom at the properglic position, that destabilizes the cationic intermediates. However, further examination of some other reactions provided several good examples of double C-glycosidation between two glycals and bis(silylacetylene)s connected by longer carbon chains. Scheme 5(*a*) and (*b*) show the first examples of disilylacetylenes with sugar rings to both ends. The reaction process is stepwise, providing first mono- and then di-glycosidation products. This fact suggests that the second C-glycosidation is slower than the first,[13] and that it is possible to attach two different kinds of sugar ring, as in Scheme 5(*b*) and (*d*). The silylacetylene moieties can also form the ends of endiyne compounds [Scheme 5(*c*) and (*d*)].

Phenylthioacetylenes

Higher reactivity is observed for silylacetylenes carrying a phenylthio group at the other end. The reagent 1-trimethylsilyl-2-phenylthioacetylene is prepared from the lithium salt of ethynyltrimethylsilane and *S*-phenyl benzenethiosulfonate.[14] In this case high yields are obtained with a weaker Lewis acid catalyst such as $BF_3{\cdot}OEt_2$ by stirring for 20 min in MeCN. In Scheme 6(*a*) and (*b*)[12,15] are demonstrated the first two examples, with quantitative formation of the phenylthioacetylenes. Similar C-glycosidations are possible from *O*-glycosides [Scheme 6(*c*)–(*e*)].[4b,15,16] Most of these examples give high yields with 1-trimethylsilyl-2-phenylthioacetylene in the presence of $BF_3{\cdot}OEt_2$. Mechanistically, the phenylthio group can provide electrons which help develope cationic charge at the adjacent carbon in the transition state of the C-glycosidation. The product, a phenylthioacetylenic sugar, does not react further with $BF_3{\cdot}OEt_2$, but does with $SnCl_4$. The yields dramatically drop with stronger Lewis acid catalyst (such as $SnCl_4$ or $TiCl_4$) and/or by prolonging the reaction period.

Other interesting examples

Nicolaou *et al*. reported a similar example of silylacetylene addition to methylated glucal acetate [**34** in Scheme 7(*a*)].[17] Williams demonstrated that bromide (in **36** and **38**) is a better leaving group, using an alkynyltin species and zinc chloride as the Lewis acid catalyst [Scheme 7(*b*) and (*c*)].[18] They reported high α selectivity with hexose (**37**), but variable selectivity with pentofuranose (**39**). Recently Veyrieres described the reaction of 2-deoxy-2-azido-1-bromo compound **40** with an alkynyltin species in the presence of silver tetrafluoroborate catalyst [Scheme 7(*d*)].[19] Martin found that the selectivity of the

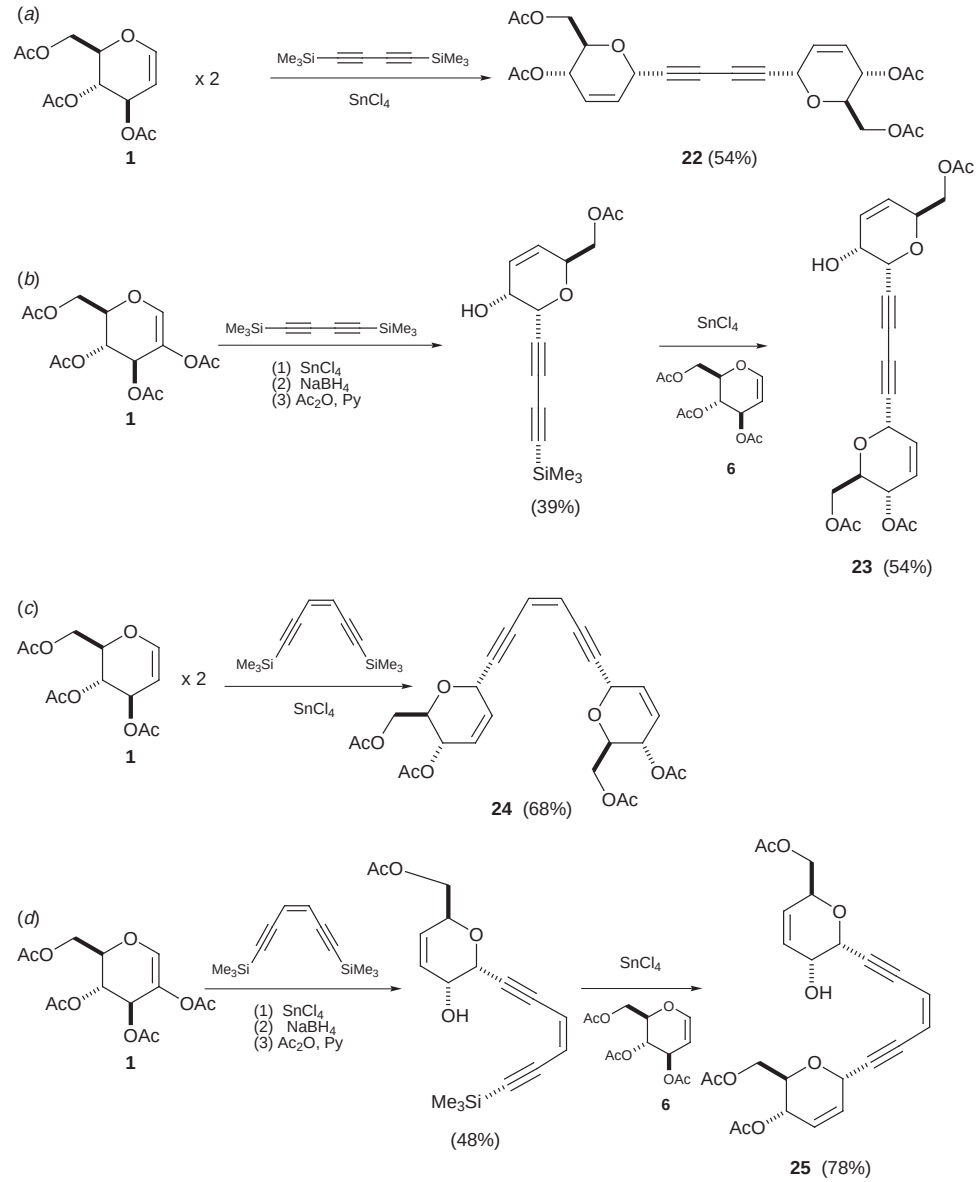

Scheme 5

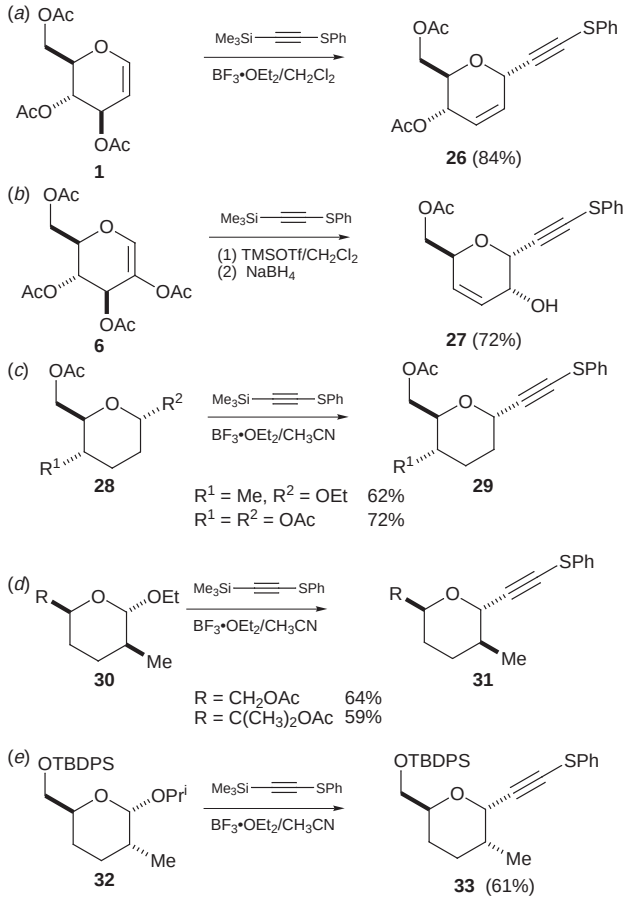

Scheme 6

reaction of (±)-1-formyl-2-alkoxypentopyranose with various silylacetylenes varied with the substituent on the other end of the acetylene moiety; thus, 1,2-*syn* and 1,2-*anti* selectivities were observed as shown in Scheme 7(*e*).[20]

1,4-*anti* Selectivity of silylacetylene to pentopyranoside

We expanded the *C*-glycosidation reaction to pentopyranose derivatives such as di-*O*-acetyl-D-xylal **45** and di-*O*-acetyl-L-arabinal **47** during the course of synthetic studies on the ABC segment of ciguatoxin (CTX, see compounds **109**–**111**), a polyether marine natural product.[21] This glycosidation provides a single stereoisomer.[22] During the CTX synthesis, this stereogenic center is destroyed and is thus not significant in the above mentioned synthesis (we did not even determine whether the stereochemistry was α or β at first). Recently, the stereochemical induction turned out to be in striking contrast to the previous cases. Namely, tri-*O*-acetyl-D-glucal **1** and bis-trimethylsilylacetylene react in the presence of a Lewis acid in a highly stereospecific manner to give exclusively the α-axial orientation in the product **3**.[9] The examples of silylacetylene addition to hexopyranoglycals occur under various acidic conditions but they all produce only the α-acetylene products with 1,4-*syn* selectivities higher than 95%. On the other hand, similar addition of silylacetylene to pentopyranoglycal diacetates (such as **45** and **47**) and dipivalates (**51** and **56**) affords the opposite results; thus, 1,4-*anti* stereochemistry is observed with the exclusive products **46**, **48**, **49**, **50**, **53**, **55**, **57** and **58** in the pentopyranose cases as shown in Table 3. Various nucleophiles add to the same pentopyranose glycals to afford similar results.[23]

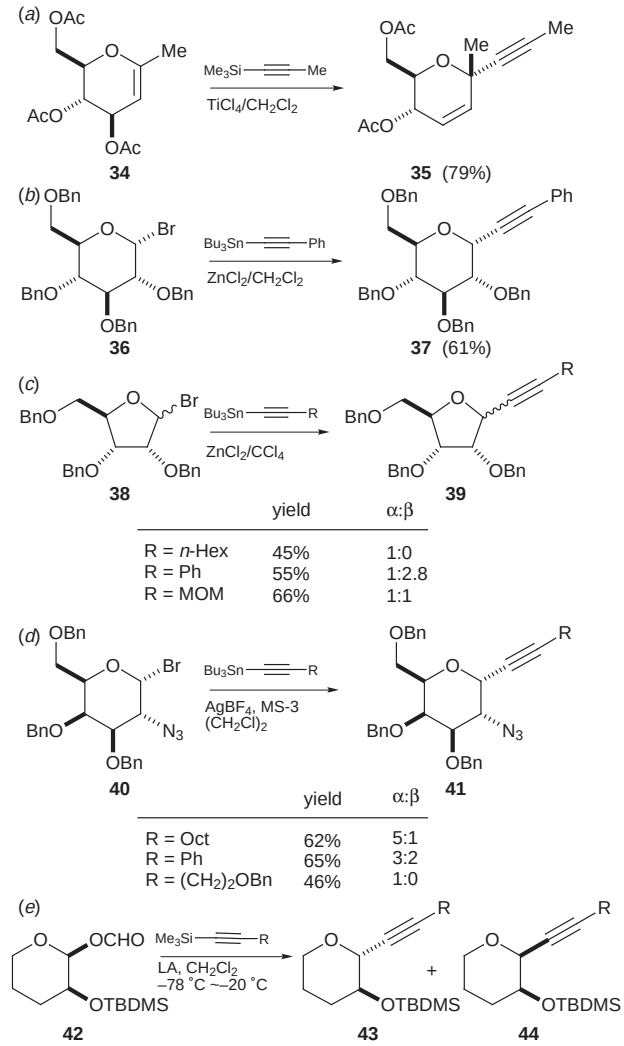

	LA	yield (%)	**43** : **44**
R = H	$TiCl_4$	60	0 : 100
R = H	$SnCl_4$	73	0 : 100
R = $SiMe_3$	$TiCl_4$	74	66 : 34
R = $SiMe_3$	$SnCl_4$	68	80 : 20
R = Me	$TiCl_4$	81	70 : 30
R = Me	$SnCl_4$	67	100 : 0
R = Pr	$TiCl_4$	66	80 : 20
R = Pr	$SnCl_4$	72	90 : 10
R = Ph	$TiCl_4$	64	80 : 20
R = Ph	$SnCl_4$	71	95 : 5

Scheme 7

Application of the Hosomi–Sakurai reaction to this system provides the 1,4-*anti* products [Scheme 8(*a*) and (*b*)]. The reaction of a vinylsilyl ether with **45** also affords a 1,4-*anti* product **61** [Scheme 8(*c*)]. An oxygen nucleophile (propan-2-ol) mainly yields a 1,4-*anti* product, although the *syn*:*anti* selectivity was 25:75 [Scheme 8(*d*)].[23]

Stereochemical control

Miljkovic *et al*. reported a 1,4-position stabilization effect for the oxocarbenium intermediate in a hydrolysis of pentopyranoside[24] [Scheme 9(*a*)]; thus, the benzyloxy group of **63** (R = Bn) sits in an axial orientation [**64**(**4*ax***) in Fig. 3] to stabilize the oxocarbenium ion through space rather than in an equatorial position **64**(**4*eq***). On the other hand, an acyloxy group such as an acetyl group provided no stabilizing or even destabilizing

Table 3 1,4-*anti* Selecvtivity in the reaction of silylacetylene with pentopyranoside

Entry	Glycal	Nucleophile	Lewis acid (conditions)	Major product	Yield (%)
1	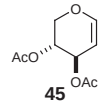 **45**		$TiCl_4$ –40 ~ –15 °C 2 h	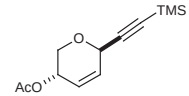 **46**	73
2	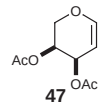 **47**		$TiCl_4$ –40 ~ –15 °C 2 h	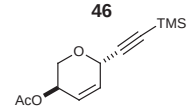 **48**	97
3	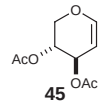 **45**		$TiCl_4$ –40 ~ –15 °C 2 h	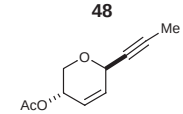 **49**	99
4	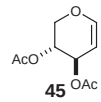 **45**		$BF_3{\bullet}OEt_2$ 0 °C 15 min	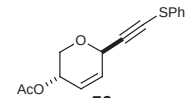 **50**	88
5	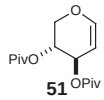 **51**	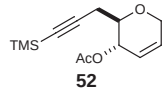 **52**	$TiCl_4$ –20 °C 2 h	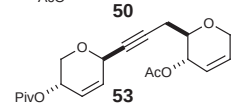 **53**	87
6	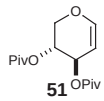 **51**	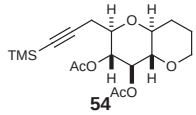 **54**	$SnCl_4$ –20 °C 40 min	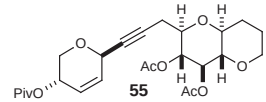 **55**	96
7	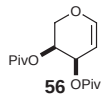 **56**	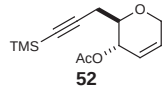 **52**	$TiCl_4$ –20 °C 2 h	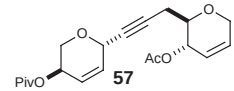 **57**	54
8	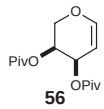 **56**	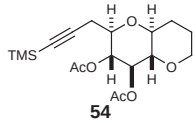 **54**	$SnCl_4$ –20 °C 2 h	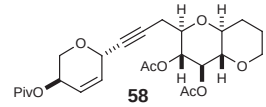 **58**	83

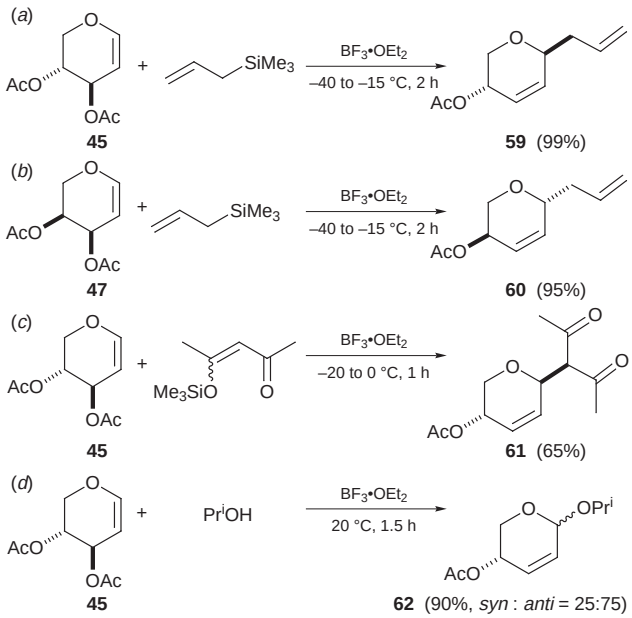

Scheme 8

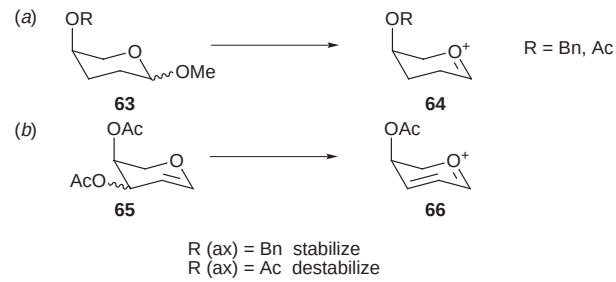

Scheme 9

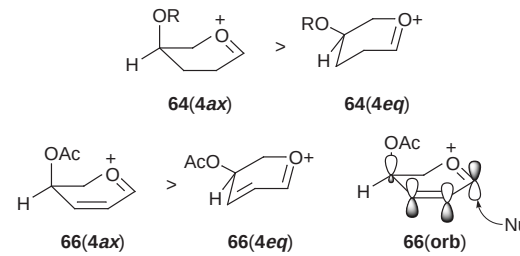

Fig. 3

effect during the hydrolysis. A similar explanation might be possible in the enoxocarbenium ion **66** formed during pentose C-glycosidation [Scheme 9(*b*)]. The suggestion that the reaction proceeds *via* **66**(**4*ax***) and not **66**(**4*eq***) would explain the 1,4-*anti* orientation, because the nucleophile silylacetylene would approach from the α side (*anti* to the acetoxy group). An alternative explanation may be due to orbital interaction; thus, the axially orientated 4β-acetoxy group reduces the electron density in the π-electron lobe at C-2 in the β-face, making the *anti*-lobe at C-1 more reactive [**66**(**orb**)]. We must await further experimental results before deciding which mechanism is operative.

These results prompted us to do mixing experiments with glucal and galactal derivatives (Scheme 10) in our laboratory to

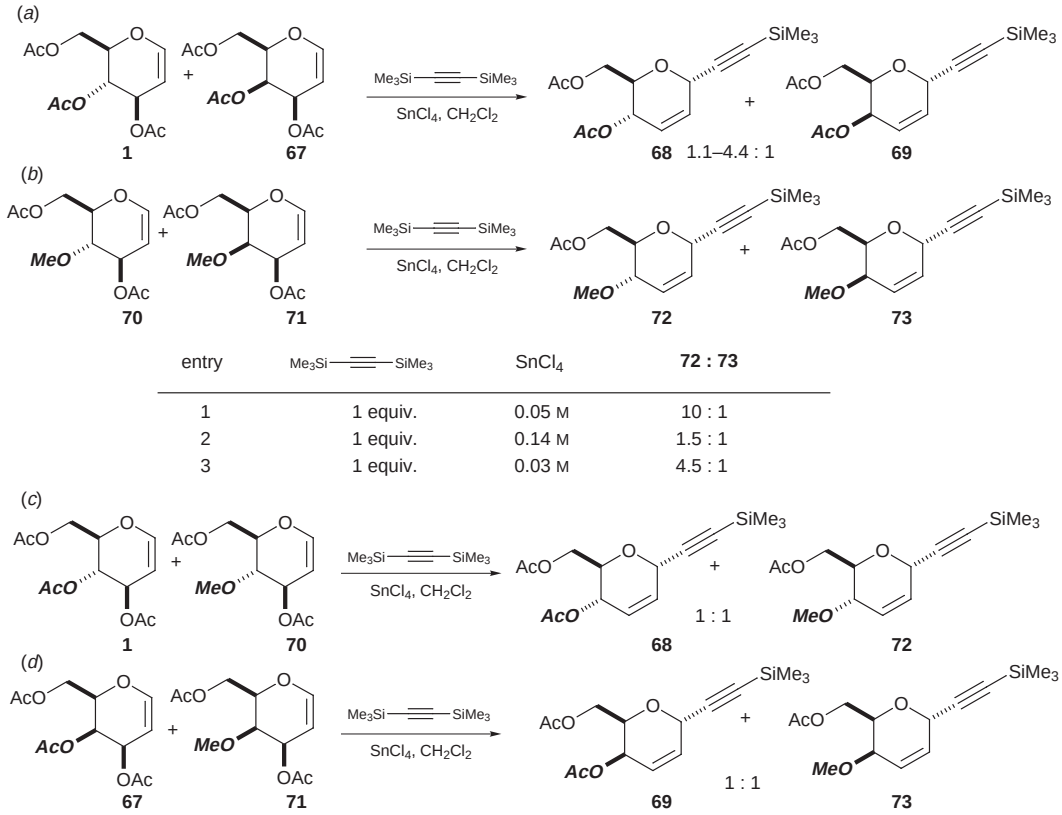

Scheme 10

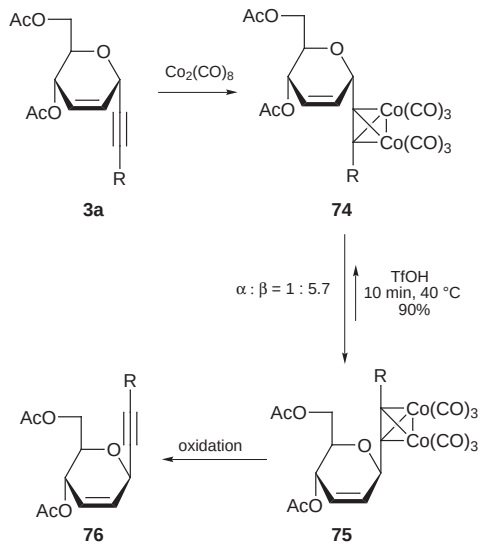

Scheme 11

determine the relative rates of C-glycosidation in pentopyranose systems, to thus avoid conformational problems. Glucals always give higher yields than galactals in C-glycosidations, even with the reaction being interrupted after only a short reaction time [Scheme 10(*a*) and (*b*)]. When mixtures of the 4-acetoxy and 4-methoxy substituted glucals or galactals were subjected to the C-glycosidation conditions [Scheme 10(*c*) and (*d*)], the ratio of the products was 1:1. These results for the bond formation process are striking different to those of the hydrolysis case, although similar oxocarbenium ions are involved. The mechanism and kinetics of these C-glycosidations need to be studied further.

Epimerization of the C-1 alkynyl group on the pyranose ring using an acetylenehexacarbonyldicobalt complex

The stereoselectivity of these C-glycosidations with silylacetylenes exclusively leads to products with the α-axial orientation. If an epimerization were possible which gave products with β orientation, this methodology would be more useful, giving access to both α and β configurations. Nicholas reported that complexation of an alkynyl group with octacarbonyldicobalt provides a hexacarbonyldicobalt complex which stabilizes the carbocation at the proparglic position.[25] Application of the Nicholas reaction to α-sugar acetylenes under acidic conditions would give the thermodynamically more stable β-equatorial isomer at equilibrium under the reaction conditions.[26] In fact the overall process including cobalt complexation, acid epimerization and oxidative decomplexation can take place as illustrated in Scheme 11. Reagents often used for the decomplexation include *N*-methylmorpholine *N*-oxide, cerium(IV) ammonium nitrate, ferric nitrate, iodine *etc*. Among these oxidants, iodine reacts very fast even at 0 °C to finish the reaction in 36 min, providing the acetylene in quantitative yield even with large excess of iodine. Often the last two steps can be carried out in one pot.

Examples of epimerization of the α sugar acetylenes into β ones are shown in Scheme 12(*a*) and (*b*), in which the 2,3-dehydro ring systems are involved with different acetylene cobalt complexes. The ratios of equilibration in these cases are 1:4–6, rather low values which may be due to the single pairs of 1,3-diaxial interactions since they have an energy difference of only *ca*. 1 kcal mol^{-1}. The saturated ring system in Scheme 12(*c*) gives a higher ratio (1:19) due to three pairs of 1,3-diaxial interactions (Fig. 4). The ratios vary in Scheme 12(*d*) which includes 3,4-en-2-ol system; the ratios increase in accordance with the size of the alkoxy substituents. The major cause in this case may be due to 1,2-strain, as shown in Fig. 5.[26]

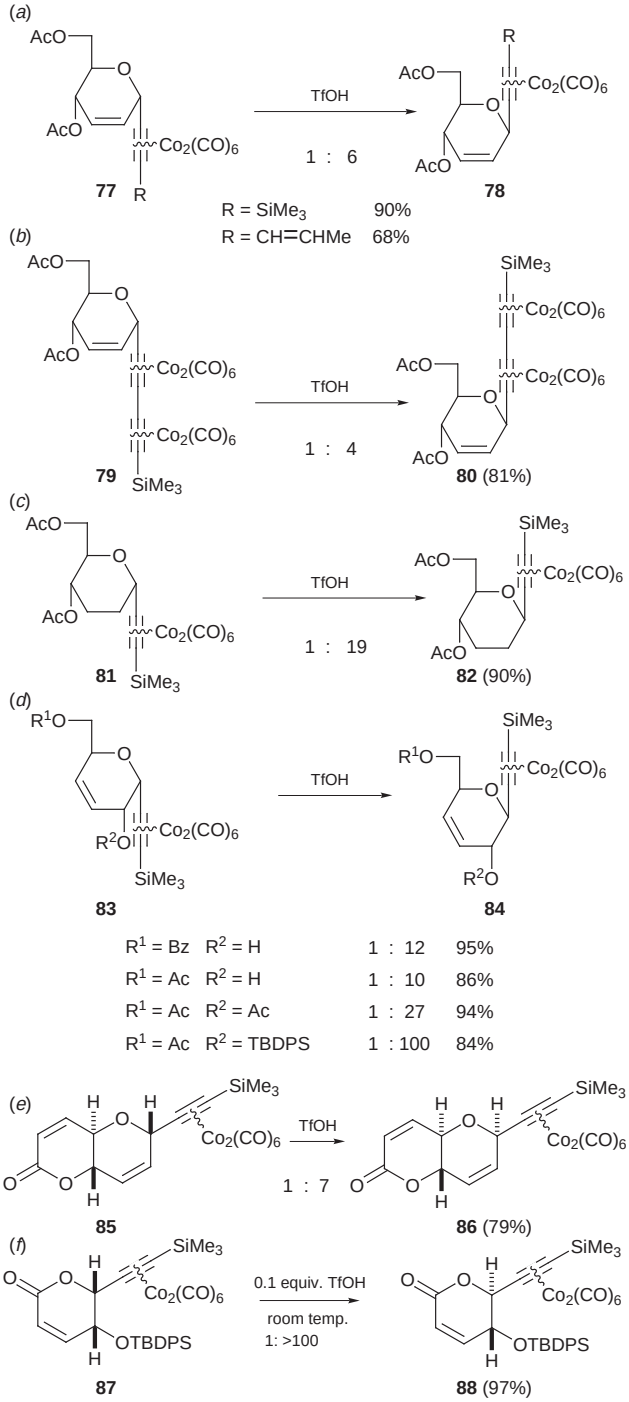

Scheme 12

Conformational preferences are not the only necessary factors for a high equilibrium ratio for the acetylene cobalt complex. The bicyclic example shown in Scheme 12(*e*) may have a rigid ring system, but the important thermodynamic factor is once again a single 1,3-diaxial interaction, resulting in a 1:7 ratio. Evidences of this 1,2-strain is clearly demonstrated in Scheme 12(*f*), where the ring system does not have the carbon corresponding to C-6. A Nicholas reaction makes the epimerization possible.[26]

Opening of the pyranose ring and re-cyclization

The above epimerization *via* the cation intermediate is an important characteristic of the cobalt complex in sugar acetylenes. The same cation intermediate is potentially applicable to medium ether ring formation and other useful protocols. Oxepane ring formation from six-membered ether precursors is usually impractical due to thermodynamic constraints. In Scheme 13, oxepene **89** is planned to cyclize from **92** *via* the cation **90** derived from the sugar acetylene hexacarbonyldicobalt complex **91**. The overall reaction is shown in Scheme 14; opening of the ring of the 3,4-unsaturated glucose derivative **83** takes place under acetolysis conditions (TfOH in Ac_2O at −40 °C) for a few hours to provide **93** as a diastereomeric mixture at the C-3 position. The *cis* olefinic compound **93** is decomplexed (**94**) and further manipulated *via* the protecting groups of the hydroxy moieties (**95**), cyclizing into the corresponding oxepene compound **96**. Decomplexation gives **97**, which has *syn-trans* stereochemistry.[27]

Ring opening also takes place with the 2,3-unsaturated system, as shown in Scheme 15. In this case, acid treatment of **98** generates the enoxocarbenium ion at the anomeric position (original sugar numbering C-1) and epimerization is followed by ring opening (**99**). The process is different from the above cases with 3,4-double bonds because the *cis*-2,3-unsaturated system has the cation at the allylic position, which can equilibrate into the more stable *trans* allylic cation, resulting in the acetylation of the 7-hydroxy group. If this occurs, one can make produce a spontaneous ring-recyclization by positioning a nucleophilic hydroxy group at the other side of the acetylene hexacarbonyldicobalt group.

Scheme 16 illustrates this plan; the substrate, unsaturated six-membered **101**, should transform into **104** *via* the cation intermediates **102**, in which the *cis* allylic cation at the C-1 position can equilibrate to the more stable *trans* allylic cation **103**. The latter cannot re-cyclize back to **101** and waits for the addition of the hydroxy group on the other side to afford **104** with various ring sizes, such as seven-, eight-, nine- and ten-membered rings, depending upon the number of methylenes.

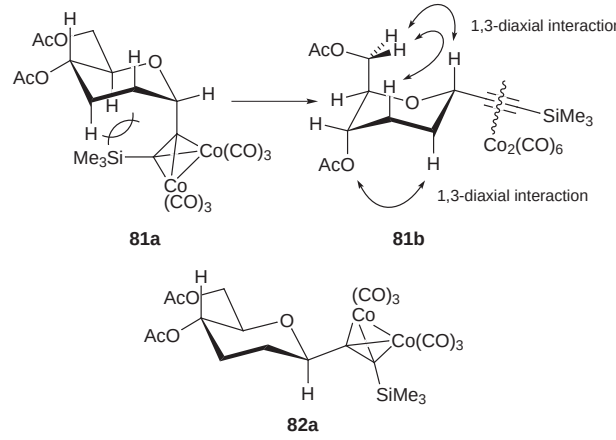

Fig. 4

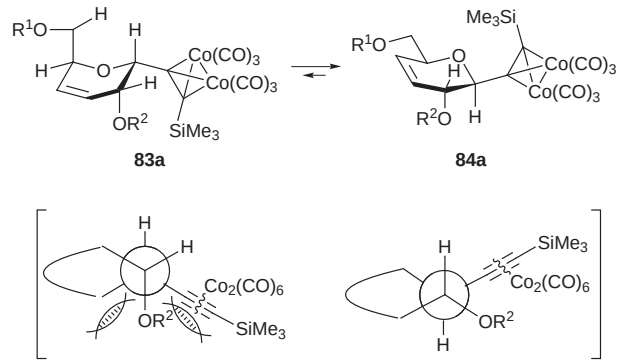

Fig. 5

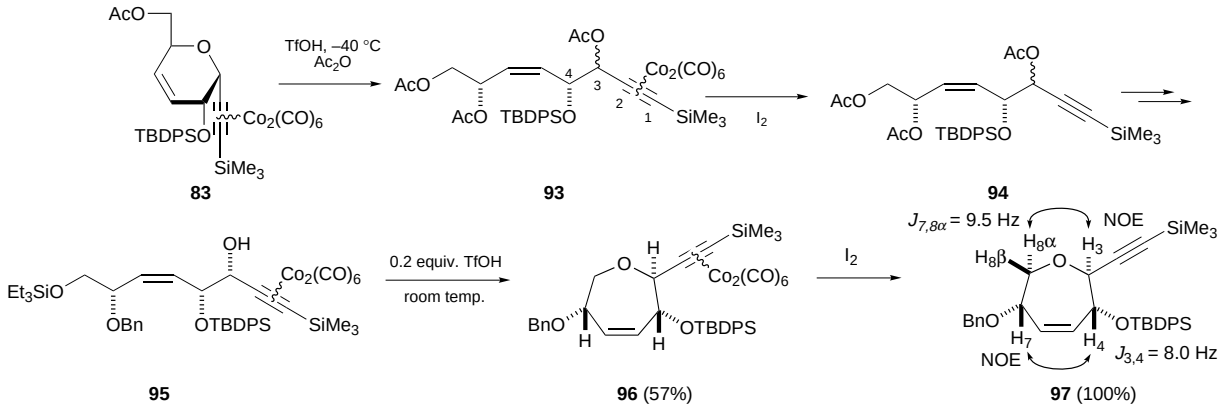

83 **93** **94**

95 **96** (57%) **97** (100%)

Scheme 14

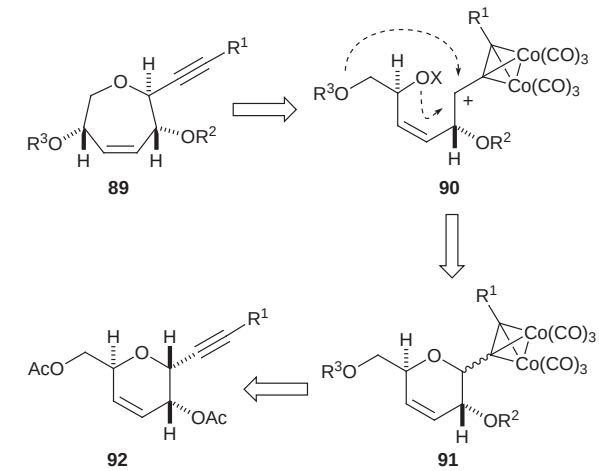

89 **90** **92** **91**

Scheme 13

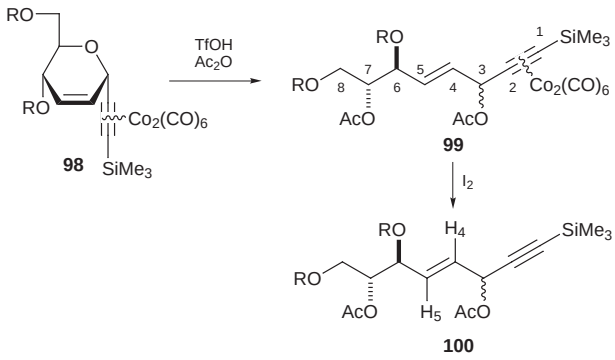

98 **99** **100**

Scheme 15

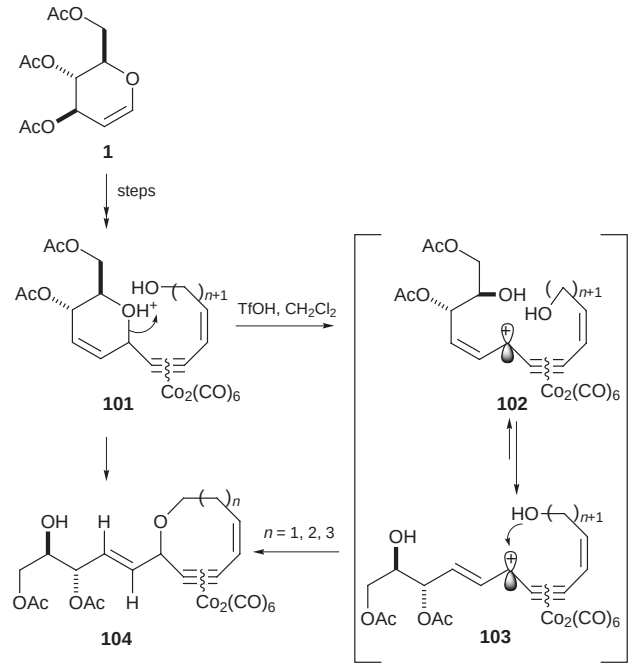

1 **101** **102** **104** **103**

Scheme 16

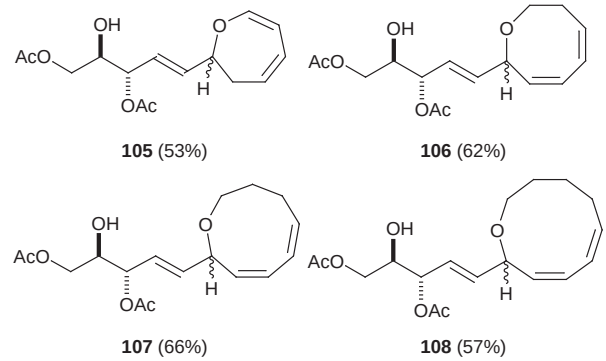

105 (53%) **106** (62%)

107 (66%) **108** (57%)

The multistep sequence of reactions (**1**→**101**) includes C-glycosidation with silylacetylene, and Pd-catalyzed ene–yne coupling with the *cis* vinyl iodide to provide the precursor **101**.[5]

The resulting ring compounds (**104**) are a new type of acetylene cobalt complex with the complex inside the ring system; thus, the *endo*-complex cannot be decomplexed under oxidative conditions as for the *exo*-complex. Finally, Rh-C was found to be effective for the synthesis of the decomplexed dienes **105**–**108** under high pressure H_2.[5] The carbons corresponding to the original acetylene complex end up as the olefinic carbons (except for the double bond transposition in the seven-membered system). Incidentally, the rhodium catalyst thus formed during the decomplexation of hexacarbonyldicobalt fulfils the reductive function of the cobalt complex into olefins, but did not reduce the double bonds under the reaction conditions.

Application to ciguatoxin synthesis

Above methodologies have been developed for application to the synthesis of ciguatoxin and gambiertoxins, potent toxins causing marine ciguatera poisoning. When this synthesis was started, the absolute configuration and part of the relative

configuration had not been determined. Recently, Yasumoto reported that the absolute configuration of ciguatoxin is that of the opposite enantiomer.[21] Various side chains are attached to the 5 position of the A-ring, such as a 1,3-diene or 1-en-3,4-diol. We have demonstrated the synthesis of the AB(C) ring system with three possible side chains (**109**–**111**).[23] The synthesis of one of these compounds is shown in Scheme 17. The silylacetylene moiety was attached to the bicyclic compound **54**, which added to D-xylal **51** to afford the coupling product *anti*-acetylene as a single stereoisomer **55**. The cobalt complex of **55** was treated with pivalic anhydride in the presence of TfOH to afford the *trans* olefin (**112**). This was followed by hydrolysis of the acetate protecting group to give the hydroxy group (**113**) and then by a second treatment with acid to provide the tricyclic compound (**115**) together with some isomeric compound (**114**). Decomplexation of the *endo*-cobalt complex was achieved to give **111** using Wilkinson's catalyst under the high pressure hydrogen atmosphere.[5,23]

Novel reductive decomplexation of acetylene hexacarbonyldicobalt complex

Acetylene hexacarbonyldicobalt complexes[28] have mostly been used for the protection of triple bonds as well as for C–C bond

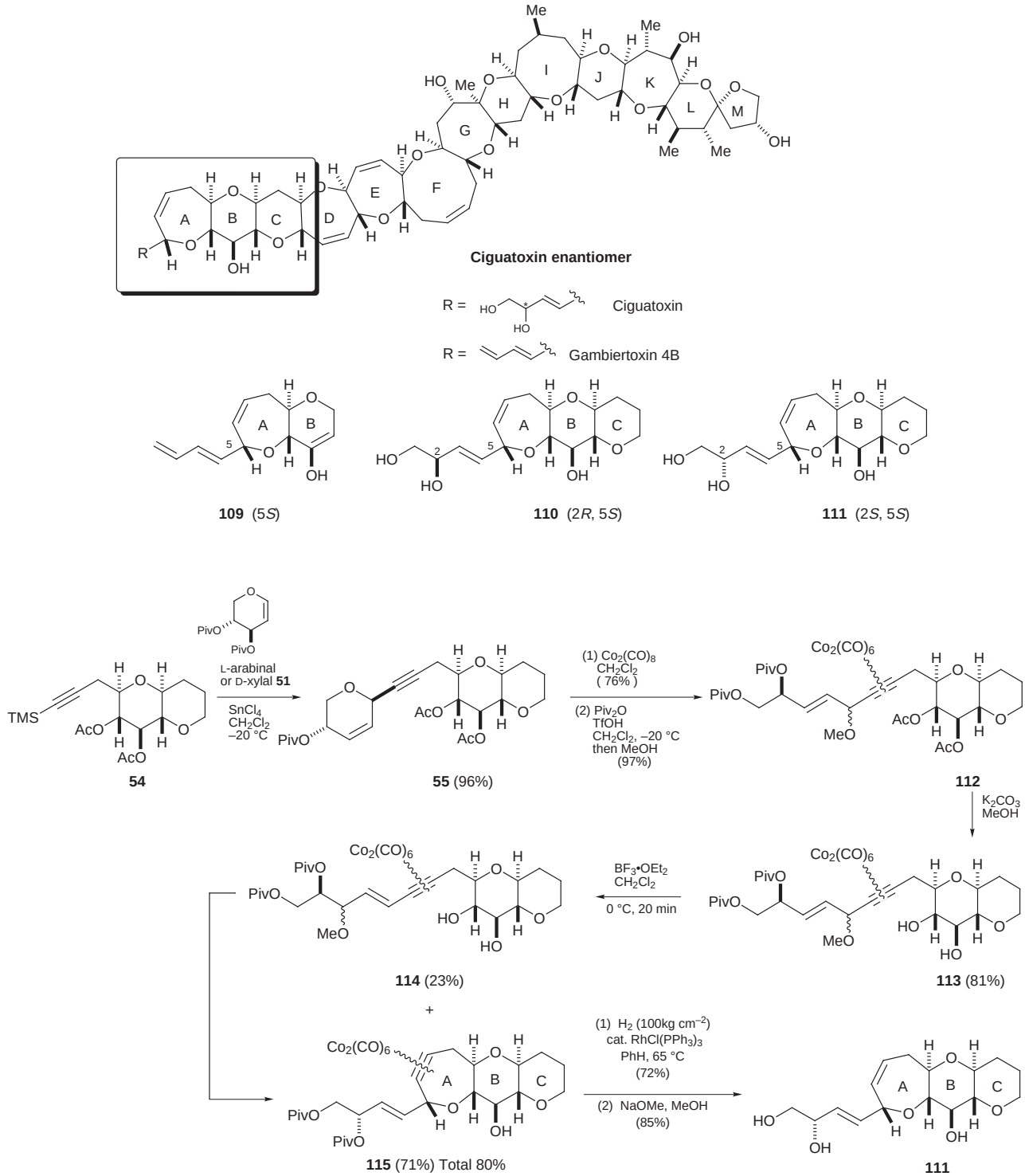

Scheme 17

and C–O bond formation reactions,[23,29] and thus they have been applied to natural product syntheses.[30] The most common decomplexation is an oxidative procedure leading to the original triple bond, but this is limited to the exocyclic cases as discussed previously. In endocyclic complexes only decomplexation under high pressure hydrogen using a Rh catalyst provides olefinic cyclic ethers.[5,23] Recently Kuwajima reported a Birch reduction for such decomplexation.[31] Here we describe two additional decomplexation protocols applicable to either *exo*- or *endo*-cyclic acetylene cobalt complexes, as shown in Scheme 18.[32]

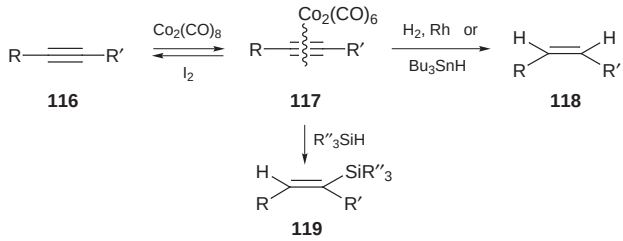

116 **117** **118** **119**

Scheme 18

The new method is applicable to either *endo*- or *exo*-complexes to provide simple *cis*-olefins (with tri-*n*-butyltin hydride) or *cis*-vinyl silanes (with trialkylsilanes or triarylsilanes) at the original position of the acetylene (Scheme 18). Various examples using SnH are shown in Table 4. A simple terminal acetylene–dicobalt complex is converted to a terminal olefin (entry 1). Two examples of *exo*-complexes gave *cis*-olefins (entries 2 and 3). *endo*-Complexes of seven- and nine-membered rings are also shown (entries 4–7). Of particular interest is the bis(hexacarbonyldicobalt) complex of the nine-membered ring, which is only able to decomplex under these conditions, since using rhodium under high pressure conditions failed to give the diene.[32] This method was applied to the synthesis of ABC fragment **109** of gambiertoxin.[33]

Table 4 Decomplexation of acetylene hexacarbonyldicobalt with Bu^n_3SnH

Entry	Substrate	Product	Yield (%)
1	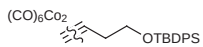 **120**	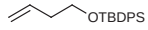 **121**	60
2	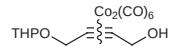 **122**	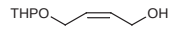 **123**	64
3	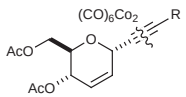 **124** R = H **74** R = $SiMe_3$	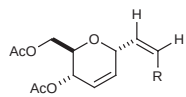 **125** **11**	55 64
4	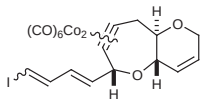 **127**	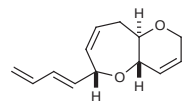 **128**	81
5	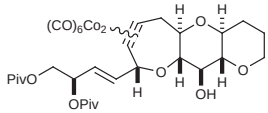 **129**	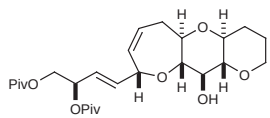 **110**	82
6	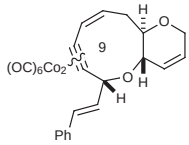 **130**	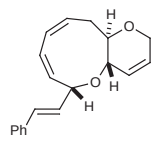 **131**	61
7	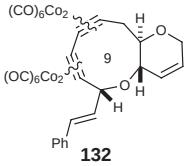 **132**	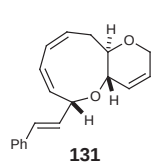 **131**	35

Table 5 Decomplexation of acetylene hexacarbonyldicobalt with R_3SiH

Entry	Substrate	Silane/solvent	Product (% yield, ratio)
1	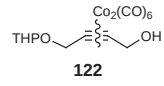 **122**	Et_3SiH C_6H_6	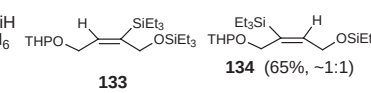 **133** **134** (65%, ~1:1)
2	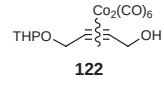 **122**	Ph_3SiH C_6H_6	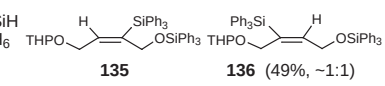 **135** **136** (49%, ~1:1)
3	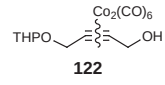 **122**	Ph_3SiH C_6H_6–EtOH	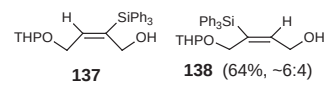 **137** **138** (64%, ~6:4)
4	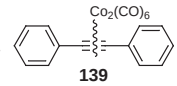 **139**	Et_3SiH C_6H_6	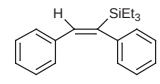 **140** (78%)
5	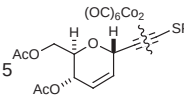 **141**	Et_3SiH C_6H_6	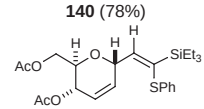 **142** (87%)
6	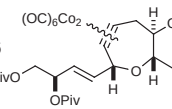 **143**	Et_3SiH C_6H_6	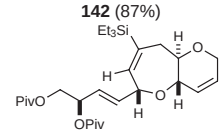 **144** (74%)

Similarly the acetylene hexacarbonyldicobalt *endo* or *exo* complexes can be converted into the corresponding *cis*-vinylsilanes. In entries 1 and 2 in Table 5, alcohol (**122**) is converted using triethyl- or triphenyl-silanes into *cis*-vinylsilanes as the silyl ethers. When this reaction is carried out in EtOH–benzene, the corresponding alcohols (**137**, **138**) are obtained in free form. A symmetric precursor (**139**) affords a single product (**140**). A sterically unequal acetylene **141** is converted into a single hydrosilation product (**142**). The *endo* complex **143** also gives a single product (**144**) in which the silyl group is situated away from the neighboring substituent. Thus, the hydrosilylation of cobalt complexes becomes synthetically very useful.

Summary

This review describes new aspects of sugar acetylenes, including their preparation (C-glycosidation with silylacetylene), epimerization and medium ring re-cyclization *via* acetylene hexacarbonyldicobalt complexes. Expansion of these synthetic concepts demonstrates some applicability to the synthesis of ciguatoxin. New reactions have been developed for decomplexation of the cobalt acetylene complexes, particularly for both the *endo*- and *exo*-complexes. This chemistry will further develop towards better synthetic methods for natural product synthesis.

Acknowledgments

This review is a summary of recent studies largely achieved in our laboratory. The authors are gratefully indebted to Dr Yoshiyasu Ichikawa, Mr Takahiro Tsukiyama, Dr Shigeyoshi Tanaka, Dr Jiang Ymin, Dr Steven Peters and Dr Chavie Yenjai for participating in the above experiments and/or the earlier stages of the program. Miss R. Saeeng, Mr T. Liu and Mr K. Kira are thanked for contributing to related chemistry. Dr V. Rukachaisirikul, Dr T. Franz and Mrs Jianmin Li are thanked for their help in the preparation of this manuscript. This research was financially supported by a Grant-in-Aid for Scientific Research from the Ministry of Education, Science, Sports, and Culture of Japan, JSPS-RFTF program, and scholarships from the Hitachi International Foundation, JSPS and Monbusho.

Notes and references

1 *Total Synthesis of Natural Products*: *The 'Chiron' Approach*, Stephen Hanessian, Pergamon, Oxford, 1983.
2 M. Isobe, M. Kitamura and T. Goto, *Chem. Lett*., 1982, 1907; M. Kitamura, M. Isobe, Y. Ichikawa and T. Goto, *J. Org. Chem*., 1984, **49**, 3517; M. Kitamura, M. Isobe, Y. Ichikawa and T. Goto, *J. Am. Chem. Soc*., 1984, **106**, 3252.
3 M. Isobe, *Yukigousei Kagaku Kyoukaishi*, 1994, **52**, 968.
4 (*a*) Y. Ichikawa, K. Tsuboi, Y. Jiang, A. Naganawa and M. Isobe, *Tetrahedron Lett*., 1995, **36**, 7101; (*b*) Y. Jiang and M. Isobe, *Tetrahedron*, 1996, **52**, 2877; (*c*) K. Tsuboi, Y. Ichikawa, Y. Jiang, A. Naganawa and M. Isobe, *Tetrahedron*, 1997, **53**, 5123.
5 M. Isobe, C. Yenjai and S. Tanaka, *Synlett*, 1994, 916; C. Yenjai and M. Isobe, *Tetrahedron*, 1998, **54**, 2509.
6 M. Isobe, Y. Ichikawa and T. Goto, *Tetrahedron Lett*., 1986, **27**, 963; M. Isobe, Y. Ichikawa, D.-L, Bai, H. Masaki and T. Goto, *Tetrahedron*, 1987, **43**, 4767.
7 S. Danishefsky and J. F. Kerwin, *J. Org. Chem*., 1982, **47**, 3803.
8 Y. Ichikawa, M. Isobe, M. Konobe and T. Goto, *Carbohydr. Res*., 1987, **171**, 193.
9 T. Tsukiyama and M. Isobe, *Tetrahedron Lett*., 1992, **33**, 7911.
10 (*a*) Data are partly taken from the Masters Thesis of M. Konobe, Nagoya University (1988); (*b*) T. Nishikawa and M. Isobe, unpublished results.
11 Very recently we have found that trimethylsilyl(propargyl)silane can only react with OTBDPS protection, thus avoiding coordination to $SnCl_4$ due to its steric bulkiness. R. Saeeng and M. Isobe, unpublished results.
12 Data are partly taken from the Master Thesis of T. Tsukiyama, Nagoya University, 1992.
13 T. Tsukiyama, S. C. Peters and M. Isobe, *Synlett*, 1993, 413.
14 A. Herunsalee, M. Isobe, Y. Fukuda and T. Goto, *Synlett*, 1990, 701.
15 M. Isobe, and Y. Jiang, *Tetrahedron Lett*., 1995, **36**, 567.
16 Y. Jiang, Y. Ichikawa and M. Isobe, *Tetrahedron*, 1997, **53**, 5103; K. Tsuboi, Y. Ichikawa and M. Isobe, *Synlett*, 1997, 713.
17 K. C. Nicolaou, C. K. Hwang and M. E. Duggan, *J. Chem. Soc., Chem. Commun*., 1986, 925.
18 D. Zhai, W. Zhai and R. M. Williams, *J. Am. Chem Soc*., 1988, **110**, 2501.
19 C. Leteux and A. Veyrieres, *J. Chem. Soc., Perkin Trans. 1*, 1994, 2647.
20 E. Alvarez, R. Perez, M. Rico, R. M Rodriguez, M. C. Suarez and J. D. Martin, *Synlett*, 1996, 1082.
21 M. Stake, A. Morohashi, H. Oguri, T. Oishi, M. Hirama, N. Harada and T. Yasumoto, *J. Am. Chem. Soc*., 1997, **119**, 11 325.
22 S. Hosokawa, B. Kirschbaum and M. Isobe, *Tetrahedron Lett*., 1998, **39**, 1917.
23 S. Hosokawa and M, Isobe, *Synlett*, 1995, 1179; S. Hosokawa and M. Isobe, *Synlett*, 1996, 351; M. Isobe, S. Hosokawa and K. Kira, *Chem. Lett*., 1996, 473.
24 M. Miljkovic, D. Yeaglley, P. Deslongchamps and Y. L. Dory, *J. Org. Chem*., 1997, **62**, 7597.
25 K. M. Nicholas, *Acc. Chem. Res*., 1987, **20**, 207 and references cited therein.
26 S. Tanaka, T. Tsukiyama and M. Isobe, *Tetrahedron Lett*., 1993, **34**, 5757; S. Tanaka and M. Isobe, *Tetrahedron*, 1994, **50**, 5633.
27 S. Tanaka and M. Isobe, *Tetrahedron Lett*., 1994, **35**, 7801; S. Tanaka, N. Tatsuta, O, Yamashita and M. Isobe, *Tetrahedron*, 1994, **50**, 12 883; S. Tanaka and M. Isobe, *Synthesis*, 1995, 859.
28 H. Greenfield, H. W. Sternberg, R. A. Friedel, J. Wotiz, R. Markby and I. Wender, *J. Am. Chem. Soc*., 1956, **78**, 120.
29 A. V. Muehldorf, A. Guzman-Perez and A. F. Kluge, *Tetrahedron Lett*., 1994, **35**, 8755; S. L. Schreiber, M. T. Klimas and T. Sammakia, *J. Am. Chem. Soc*., 1987, **109**, 5749.
30 M. Saha, B, Baphy and K. M. Nicholas, *Tetrahedron Lett*., 1986, **27**, 915; P. J. Harrington, *Transition Metals in Total Synthesis*, Wiley, New York, 1990, pp. 241–301; T. F. Jamison, S. Shambayati, W. E. Crowe and S. L. Schreiber, *J. Am. Chem. Soc*., 1994, **116**, 5505; C. Mukai, O. Kataoka and M. Hanaoka, *J. Org. Chem*., 1995, **60**, 5910.
31 T. Nakamura, T, Matsui, K. Tanino and I. Kuwajima, *J. Org. Chem*., 1997, **62**, 3032.
32 S. Hosokawa and M. Isobe, *Tetrahedron Lett*., 1998, **39**, 2609.
33 S. Hosokawa and M. Isobe, unpublished results.

Paper 8/04940H

Ruthenium-mediated amidation of saturated C–H bonds and crystal structure of a bis(tosyl)amidoruthenium(III) complex of 1,4,7-trimethyl-1,4,7-triazacyclononane

Sze-Man Au, Suo-Bo Zhang, Wai-Hong Fung, Wing-Yiu Yu, Chi-Ming Che* and Kung-Kai Cheung

Department of Chemistry, The University of Hong Kong, Pokfulam Road, Hong Kong. E-mail: cmche@hkucc.hku.hk

Received (in Cambridge, UK) 28th August 1998, Accepted 16th October 1998

A bis(tosyl)amidoruthenium(III) complex of 1,4,7-trimethyl-1,4,7-triazacyclononane (Me_3tacn) is prepared, and its crystal structure revealed the two tosylamido ligands in a *cis* configuration; the '[Ru^{III}(Me_3tacn)$(NHTs)_2$(OH)] + Ag(I) or PhINTs' protocol can effect amidation of saturated C–H bonds, and an electrophilic tosylimidoruthenium intermediate is implicated based on Hammett correlation studies and trapping experiments.

Amidation of saturated C–H bonds is an appealing route to amides and amines.[1] To our knowledge, only a handful of catalytic systems involving [*N*-(toluene-*p*-sulfonyl)imino]phenyliodinane (PhINTs) as a nitrogen source have been reported for this transformation,[2] and a highly reactive metal tosylimido (M=NTs) species is usually postulated to be the active intermediate. To date, few M=NTs complexes are known to react with saturated C–H bonds.[3] We reason that those M=NTs species capable of acting on saturated C–H bonds would be highly oxidizing and react readily with organic solvents rendering their isolation and/or investigation difficult. A way to tackle this problem would be to prepare structurally characterized metal–tosylamido complexes. Through proton-coupled oxidations, either chemically[4] or electrochemically,[5] it may be feasible to *in situ* generate and study the highly reactive M=NTs species from its tosylamido precursor. Herein is described the first tosylamidoruthenium(III) complex that can mediate amidation of saturated C–H bonds.

[Ru^{III}(Me_3tacn)$(NHTs)_2$(OH)] (**1**; Me_3tacn = 1,4,7-trimethyl-1,4,7-triazacyclononane) was prepared by reacting [(Me_3tacn)$Ru^{III}Cl_3$][6] (0.1 g, 0.26 mmol) with TsNHNa (0.4 g, 2.1 mmol) in methanol (20 cm^3) at room temperature for 3 hours and was isolated as a yellow crystalline solid.† Magnetic susceptibility measurement gave μ_{eff} = 1.8 μ_B, consistent with a Ru(III) formulation. The infrared spectrum of **1** shows the N–H stretch at 3400 cm^{-1}. Fig. 1 shows the structure of complex **1** established by X-ray crystallography.‡ The two tosylamido ligands are in a *cis* configuration [N–Ru–N bond angle = 80.4(2)°]. The Ru^{III}–N(tosylamido) distances of 2.072(5) and 2.140(5) Å are in between the related values of 2.025(1) Å in [Ru^{IV}(Por)(NHTs)(pz)] (Por = porphyrinato ligand; pz = pyrazolate)[7] and 2.21(1) Å in [Ru^{II}(Et_2dtc)$(PPh_3)_2$(CO)(NH-$SO_2C_6H_2Pr^i_3$-2,4,6)] (Et_2dtc = *N*,*N*′-diethyldithiocarbamate).[8] The observed Ru–OH distance of 1.947(4) Å is comparable to the related value of 1.904(2) Å found for [Ru^{III}(N_2O_2)($O-H_2$)(OH)]$(ClO_4)_2$ (N_2O_2 = 6,7,8,9,10,11,17,18-octahydro-6,10-dimethyl-5*H*-dibenzo[*e*,*n*][1,4,8,12]dioxadiazacyclopentadecine).[9] The Ru–N–S angles of 144.3(3)° and 132.3(3)° suggest that the nitrogen atom is sp^2 hybridized.

We found that addition of weakly oxidizing $AgClO_4$ to **1** in acetonitrile gave a red species (λ_{max} = 480 nm), which would react with PPh_3 to produce TsN=PPh_3 and [Ru^{II}(Me_3tacn)-$(MeCN)_3$]$(ClO_4)_2$ quantitatively. Likewise, other oxidants such as PhI$(OAc)_2$ and $(CPh_3)(PF_6)$ are equally effective for this transformation. On the other hand, (1-cyclohexenyloxy)trimethylsilane was found to be converted to α-*N*-tosylaminocyclohexanone§ under '**1** + $AgClO_4$' conditions comparable to the related transformations by the '[(L)Mn^V≡N] + $(CF_3CO)_2O$' (L = Schiff base)[10*a*] and 'Cu(I) + PhINTs'[10*b*] systems. These findings imply that a reactive Ru=NTs species might have been generated upon chemical oxidation of **1** presumably *via* oxidative deprotonation of the coordinated amido ligands. Although attempts to isolate and characterize the Ru=NTs species of Me_3tacn have proved futile, the '**1** + Ag(I)' protocol was found to carry out facile C–H amidation of allylic and aromatic hydrocarbons to afford the corresponding tosylamides (RNHTs).

When cyclohexene (1 mmol) was treated with **1** (0.16 mmol) and $AgClO_4$ (0.2 mmol) in acetonitrile (5 cm^3), a red solution resulted. The red color slowly disappeared upon stirring for 3 h at room temperature to form a yellow to brown solution with metallic silver deposited at the bottom of the reaction vessel. After GLC analysis, allylic toluene-*p*-sulfonamide was produced in 63% yield based on the Ru complex (Table 1). Ethylbenzene, cumeme, indane and tetralin also reacted similarly to afford the corresponding benzyl tosylamide derivatives in 41–75% yield. It is noteworthy that adamantane can also be converted to 1-adamantane tosylamide selectively in 59% yield by the **1**/$AgClO_4$/MeCN system. In all cases, $TsNH_2$ was detected as well, and the 'RNHTs + $TsNH_2$' production reached a total of 200% for two tosylamido moieties per ruthenium complex.

The effect of *para*-substituents (*p*-Y-$C_6H_4CH_2CH_3$; Y = MeO, Me, H, F, Cl) on the amidation of ethylbenzene by employing **1**/$AgClO_4$ conditions has been studied. The relative rates (k_{rel}) were established under competitive conditions where equimolar amounts of ethylbenzene and its substituted derivative were used. We found that both electron-donating and -withdrawing substituents can promote the reaction, and a straight line (R = 0.99) results using Jiang's σ_{JJ}•[11] and

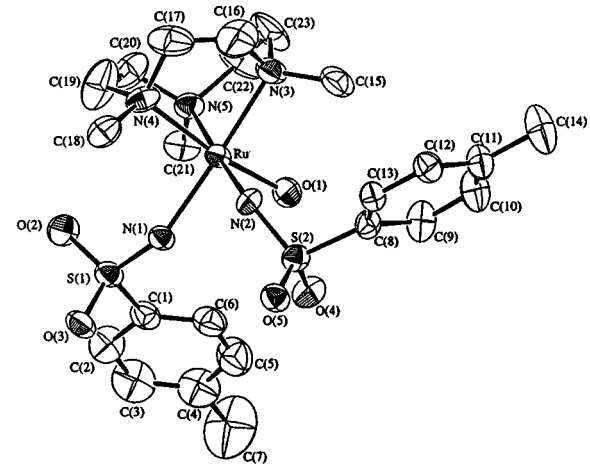

Fig. 1 Molecular structure of [Ru^{III}(Me_3tacn)$(NHTs)_2$(OH)] and atom-numbering scheme. Significant bond distances (Å) and angles (°): Ru–N(1) 2.072(5), Ru–N(2) 2.134(5), Ru–O(1) 1.949(4), Ru–N(3) 2.131(5), Ru–N(4) 2.190(5), Ru–N(5) 2.129(5), N(1)–S(1) 1.549(5), N(2)–S(2) 1.566(5); N(1)–Ru–N(2) 80.2(2), O(1)–Ru–N(2) 92.0(2), O(1)–Ru–N(1) 96.2, O(1)–Ru–N(3) 90.7(2), N(2)–Ru–N(4) 96.5(2), N(1)–Ru–N(5) 102.6(2), Ru–N(1)–S(1) 144.6(3), Ru–N(2)–S(2) 132.5(3).

Table 1 Ruthenium amidation of saturated C–H bonds

			'**1** + Ag(I)'	'**1** + PhINTs'
Entry	Substrate	Product	Yield (%)[a,b]	Yield (%); turnover number[c,d]
1		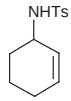	63	52; 29
2		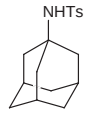	59	50; 25
3	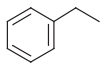	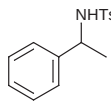	75	72; 48
4	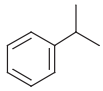	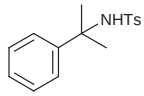	41	30; 23
5	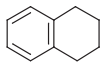	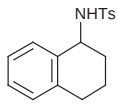	60	49; 25
6		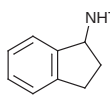	52	45; 25
7	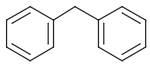	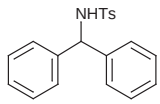	65	55; 37

[a] Reaction conditions: to an acetonitrile suspension (5 cm^3) containing hydrocarbon substrate (1 mmol) and **1** (0.16 mmol) was added $AgClO_4$ (0.2 mmol); the resulting red solution was stirred for 3 h at room temperature. Aliquots were analyzed by GLC for product identification and quantification. [b] Yields are based on the amount of Ru complex used. [c] Reaction conditions: an acetonitrile mixture (10 cm^3) of hydrocarbon substrate (1 mmol) and **1** (2 mol%) was treated with PhINTs (6 mmol), and the reddish brown solution was stirred at room temperature for 12 h. After rotary evaporation to dryness, the amide product was extracted with diethyl ether. Aliquots were taken from the organic extracts and analyzed by GLC for product identification and quantification. [d] Yields are based on the amount of PhI formed.

Hammett σ^+ substituent constants, and $\rho_{JJ}\bullet$ = +0.85 and ρ^+ = −0.67 ($|\rho_{JJ}\bullet/\rho^+|$ = 1.27) are obtained (Fig. 2). The correlation suggests that the ruthenium-mediated amidation reaction should involve a benzylic radical intermediate produced by H-atom abstraction of ethylbenzene. The negative ρ^+ value is indicative of an electrophilic nature of the active ruthenium species. The results of the correlation studies and the trapping experiments imply that a highly oxidizing Ru=NTs species was generated upon oxidation of complex **1**.

The amidation reaction can become catalytic when PhINTs was utilized as the terminal nitrogen source and **1** as the catalyst in acetonitrile at room temperature (see Table 1). The reaction of hydrocarbon substrates with PhINTs in the presence of 2 mol% of **1** in acetonitrile afforded the corresponding amides in moderate to good yields. Up to 75 turnovers could be achieved for the amidation of ethylbenzene when a lower catalyst loading (**1** : PhINTs : ethylbenzene = 1 : 100 : 200) was employed.

We acknowledge support from The University of Hong Kong and The Hong Kong Research Grants Council.

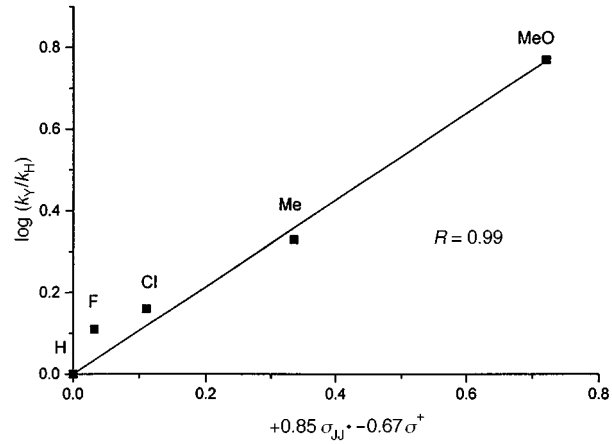

Fig. 2 Dual-parameter Hammett correlation studies for the ruthenium-mediated amidation of *para*-substituted ethylbenzenes.

Notes and references

† Characterization data for **1**. UV–VIS [λ_{max}/nm (log ε_{max}/dm^3 mol^{-1} cm^{-1})] (CH_3CN): 222 (4.26), 286 (3.59), 400 (3.35). Infrared (Nujol mull)/cm^{-1}: 3400 (ν_{N-H}). FAB-MS: *m*/*z* 613 $[M - OH]^+$, 460 $[M - NHTs]^+$, 443 $[M - OH - NHTs]^+$. Anal. Calc. for $C_{23}H_{38}N_5O_5RuS_2$: C, 43.87; H, 6.08; N, 11.12. Found: C, 43.9; H, 6.09; N, 11.15%.

‡ Crystal data for **1**: $C_{23}H_{38}N_5O_5RuS_2$, *M* = 629.77, monoclinic, space group $P2_1/n$ (no. 14), crystal dimensions 0.25 × 0.20 × 0.10 mm, *a* = 12.129(2), *b* = 15.696(3), *c* = 16.202(3) Å, β = 108.49(2)°, *U* = 2976.1(10) $Å^3$, *Z* = 4, D_c = 1.405 g cm^{-3}, μ = 7.06 cm^{-1}, *F*(000) = 1308. Intensity data were collected at 301 K on a MAR diffractometer with graphite monochromatized Mo-Kα radiation (λ = 0.71073 Å). A total of 5144 unique reflections were obtained from a total of 26480 reflections (R_{int} = 0.058) and 2741 with $I > 3\sigma(I)$ were used in the structural analysis; *R* = 0.047, R_w = 0.051 with a goodness-of-fit of 1.62. The final Fourier difference map showed residual extrema in the range 0.90 to 0.46 e $Å^{-3}$. CCDC 182/1060. See http://www.rsc.org/suppdata/cc/1998/2677 for crystallographic files in .cif format.

§ α-*N*-Tosylaminocyclohexanone: yield = 48%, see also ref. 10(*b*).

1 C. J. Moody, in *Comprehensive Organic Synthesis*, ed. B. M. Trost and I. Fleming, Pergamon, Oxford, 1991, vol. 7, p. 21; M. Johannsen and K. A. Jørgensen, *Chem. Rev*., 1998, **98**, 1689.
2 (*a*) R. Breslow and S. H. Gellman, *J. Chem. Soc., Chem. Commun*., 1982, 1400; (*b*) J. P. Mahy, G. Bedi, P. Battioni and D. Mansuy, *Tetrahedron Lett*., 1988, **29**, 1927; (*c*) I. Nägeli, C. Baud, G. Bernardinelli, Y. Jacquier, M. Moran and P. Müller, *Helv. Chim. Acta*, 1997, **80**, 1087.
3 Some highly electrophilic trialkylsilylimido complexes of early transition metals (*e.g.* Ti^{IV}, Zr^{IV} and Ta^{V}) are known to activate saturated C–H bonds, see: C. C. Cummins, S. M. Baxter and P. T. Wolczanski, *J. Am. Chem. Soc*., 1988, **110**, 8731; C. P. Schaller and P. T. Wolczanski, *Inorg. Chem.*, 1993, **32**, 131; J. L. Bennet and P. T. Wolczanski, *J. Am. Chem. Soc.*, 1994, **116**, 2179.
4 J. P. Pérez, P. S. White, M. Brookhart and J. L. Templeton, *Inorg. Chem*., 1994, **33**, 6050.
5 K.-Y. Wong, C.-M. Che, C.-K. Li, W.-H. Chiu, Z.-Y. Zhou and T. C.-W. Mak, *J. Chem. Soc., Chem. Commun*., 1992, 754; W.-H. Chiu, K.-K. Cheung and C.-M. Che, *J. Chem. Soc., Chem. Commun*., 1995, 441; W.-H. Chiu, S.-M. Peng and C.-M. Che, *Inorg. Chem*., 1996, **35**, 3369.
6 P. Neubold, B. D. Bedora, K. Wieghardt and J. Weiss, *Inorg. Chem*., 1989, **28**, 459.
7 S.-M. Au, W.-H. Fung, M.-C. Cheng, C.-M. Che and S.-M. Peng, *Chem. Commun.*, 1997, 1655.
8 W.-H. Leung, M.-C. Wu, J. L.-C. Chim and W.-T. Wong, *Inorg. Chem*., 1996, **35**, 4801.
9 C.-K. Li, C.-M. Che, W.-F. Tong and T.-F. Lai, *J. Chem. Soc., Dalton Trans*., 1992, 813.
10 (*a*) J. Du Bois, C. S. Tomooka, J. Hong and E. M. Carreira, *Acc. Chem. Res*., 1997, **30**, 364; (*b*) D. A. Evans, M. M. Faul and M. T. Bilodeau, *J. Am. Chem. Soc*., 1994, **116**, 2742.
11 X.-K. Jiang, *Acc. Chem. Res*., 1997, **30**, 283.

Communication 8/08048H

ChemComm

Catalytic benzene coupling on caesium/nanoporous carbon catalysts

Mark G. Stevens,[a] Keith M. Sellers,[a] Shekhar Subramoney[b] and Henry C. Foley*[a]

[a] *Center for Catalytic Science and Technology, Department of Chemical Engineering, University of Delaware, Colburn Laboratory, Academy Street, Newark, Delaware 19716, USA. E-mail: foley@che.udel.edu*
[b] *Du Pont Company, Experimental Station, PO Box 80228, Wilmington, Delaware 19880-0228, USA*

Received (in Bloomington, IN, USA) 24th August 1998, Accepted 19th October 1998

Caesium/nanoporous carbon materials have a very high affinity for hydrogen, breaking the extremely energetic C–H bond in benzene and promoting its condensation to biphenyl, opening a new class of chemical reactions to heterogeneous catalysis.

Graphite intercalation compounds of alkali metals have been extensively studied[1] and shown to have very high affinity for hydrogen. The compound $C_{24}K$ promotes deuterium exchange with methane[2] and hydrocarbons having acidity equal to or greater than that of benzene.[3] Béguin and Setton[4] found C_8K could condense benzene to biphenyl at 298 K. However, these materials are pyrophoric, have relatively low surface area, and exfoliate at reaction temperature.[5] In a previous paper[6] we revealed caesium entrapped in high-surface-area ($\sim$1000 $m^2\ g^{-1}$) nanoporous carbon is an excellent catalyst for double-bond migration in olefins but, unlike alkali-metal graphite intercalation compounds, is not pyrophoric and is thermally stable towards desorption up to 773 K.

By preparing nanoporous carbon (NPC) from poly(furfuryl alcohol)–poly(ethylene glycol) mixtures[7–10] we obtain chemically inert solids that contain nanopores,[7,8] with sizes distributed around 0.5 nm, and transport pores[11] with sizes distributed around 10 nm that allow access to catalytic sites contained by the nanopores.[12] Since caesium's atomic diameter (0.48 nm covalent) is close to the mean nanopore size of the NPC, the vapor of elemental caesium is rapidly and strongly adsorbed.[6] By this means we have produced materials containing up to 42% caesium by weight.

Through magnetic-susceptibility measurements and electron-paramagnetic-resonance spectroscopy studies[6] of these Cs/NPC materials, we have shown them to contain unpaired electrons. Significantly, an identical *g* factor value of 2.0026 was obtained† both for the free radicals in the carbon precursor, as well as those present in material loaded with 15% Cs by weight. The *g*-shift is roughly proportional to the mean spin–orbit coupling constant, which in the case of caesium should be large. The EPR data, however, are not indicative of such an effect. Instead the *g*-value demonstrates that caesium's orbitals do not participate; hence, the electrons from caesium are donated to the carbon. These two facts, along with their demonstrated ability to promote the double-bond migration in olefins,[6] suggest that the Cs/NPC materials should have an affinity for hydrogen similar to, or higher than, their purely graphitic analogues. In 1976, at least two studies[3,4] found that potassium graphite would couple benzene to biphenyl. Béguin and Setton[4] found that a proton donor/acceptor solvent (THF) was required to promote the reaction and that water was required to extract the biphenyl product from the alkali-metal graphite. Matsuzaki and coworkers[13] performed a detailed study of the polymerization of benzene over alkali-metal graphite compounds. Based on a series of experiments, they proposed a polymerization mechanism: two benzene radical anions $C_6H_6^{\cdot -}$ form, then couple and lose dihydrogen forming $C_{12}H_{10}^{2-}$ the dianion of biphenyl, a species they observed by Raman spectroscopy. This dianion loses an electron to produce the biphenyl radical anion, $C_{12}H_{10}^{\cdot -}$, which reacts with another benzene radical anion to propagate the chain and to produce polyphenyl. Finally, caesium metal alone, when reacted with benzene in THF and then washed with water, yielded 1,1′,4,4′-tetrahydrobiphenyl.[14]

In our study, batch reactions‡ of benzene over a 10% Cs/NPC produced biphenyl and terphenyl products. Fig. 1 displays results of several experiments at various temperatures. From these data the apparent first-order activation energy can be calculated as 34 kJ mol^{-1}, indicating a coupling-limited, free-radical reaction or that the reaction is taking place in the internal diffusion limited regime. Table 1 displays the typical carbon selectivity. Gas chromatography measurements of the vapor phase over the products confirmed the presence of hydrogen. Control experiments using pure NPC produced no detectable biphenyl. Finally, long-term experiments (8 g benzene reacted over 0.5 g 10% Cs/NPC at 450 °C for 72 hours)confirmed the catalytic nature of the reaction, by acheiving over 5 turnovers, based on the *total* molar caesium content.

To confirm the catalyst is not some form of caesium metal that has leached into the liquid phase, we performed a second set of experiments (Table 2), in which benzene was converted to biphenyl in the vapor phase. A mixture of benzene in argon (5 mol%) was circulated over the catalyst at 450 °C and 2 bar.§ By means of a continuous separation built into this recirculating reactor, nearly 100% selectivity to biphenyl was achieved at

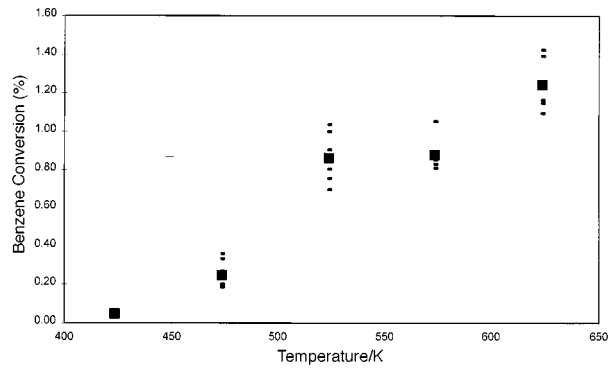

Fig. 1 In each experiment 8 g benzene was reacted for three hours over 0.5 g of a 10% Cs by weight catalyst: (−) indicates individual experiments, (■) indicates average for a given temperature.

Table 1 Average carbon selectivity of reaction at 1–3% conversion of benzene

Product	Carbon selectivity (%)
Biphenyl	75
o-Terphenyl	4
m-Terphenyl	7
p-Terphenyl	14

Table 2 Results of vapor-phase study

Benzene charge/ml	Catalyst/ g	Cs^0 in catalyst (%)	Benzene conversion (%)	Cs° turnovers	Time/ h
100	1.5	15.0	2.40	20.43	96
50	1.0	14.9	2.60	16.70	72
50	1.1	15.8	2.75	15.15	72
50	1.0	0.0	0.00	—	96

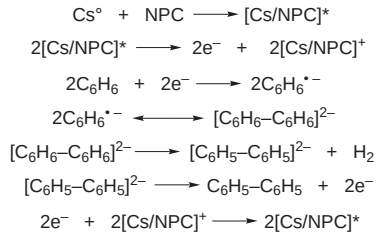

Scheme 1 Plausible catalytic mechanism.

near 2.5% benzene conversion. In this manner 29.8 mmol of benzene were converted to biphenyl in 96 hours over 1.46 mmol of caesium supported on NPC. This amounts to more than 20 turnovers based upon the *total* molar caesium content of the catalyst. The experiment was repeated twice with essentially the same result. Again, a control experiment using pure NPC did not produce detectable levels of biphenyl.

Since Cs/NPC can facilitate the breaking of the C–H bond in benzene (460 kJ mol^{-1}), we conclude that the metal provides, through its powerful electropositive nature, the electrons necessary to initiate the process. The carbon mediates the reaction by acting as the electron repository, stabilizing the intermediate radical anions. In the mechanism proposed by Matsuzaki and coworkers,[13] hydrogen and electron transfer are critical steps. The carbon may aid in these steps by promoting the net redox chemistry. Protons generated in the reaction can couple to produce dihydrogen with the carbon supplying the electrons to mediate the process. Additionally, the electron exchange between neutral benzene and the radical anion is facile ($E_a \approx 12$ kJ mol^{-1}),[15] and the carbon may stabilize the intermediate radical anions produced in this chemistry, making the net chemistry catalytic rather than stoichiometric. A plausible catalytic mechanism is shown in Scheme 1. Since the EPR measurements indicate caesium promotes its electron into the local carbon structure, in essence NPC acts as a macro radical anion that may be thought of as [Cs^+/$NPC^{\cdot -}$]. From this vantage point we can begin to see why the material may be so able to promote demanding redox chemistry.

Finally, we have previously shown that caesium, when loaded at high ratios (2/1 Cs^0/C w/w), promotes the rearrangement of the amorphous NPC to nanotubes, polyhedra and other crystalline structures;[16] transmission electron microscopy¶ of the catalyst before and after benzene treatment indicates that approximately 5% (by volume) of the carbon has transformed to ordered structures. This limited conversion of the amorphous NPC as compared to previous work[16] may be attributed to the combined effects of lower caesium content and the competitive reaction with benzene. In conclusion, since the phenyl radical anion is extremely difficult to produce and especially considering that deuterium exchange with methane has been shown,[2] these results indicate an entirely new class of radical chemistry may be open to heterogeneous-catalytic exploration in the future.

Notes and references

† EPR experiments were performed on a Bruker ER-200D electron-paramagnetic-resonance analyzer at 298 K. The authors wish to thank Dr. Paul Krusic and Mr. Steven Hill of the DuPont Company for their assistance with these measurements.

‡ Batch reactions were performed in a stainless-steel, 'tubing-bomb' reactor (2.54 cm o.d., 1.77 cm i.d. 15 cm long, capped with a hex nut and plug, internal volume: 12 cm^3). Catalyst and benzene were loaded in an argon-atmosphere glove box. Extreme care was taken to eliminate air and water contamination of the experiment. The reactor was sealed with a titanium gasket, removed from the glove box and placed in a fluidized sand bath maintained at the reaction temperature. After the desired reaction time was reached, the reactor was quenched in water and the products were analyzed by gas chromatography, confirmed by mass spectrometry.

§ A recirculating vaporizer/condenser reactor was constructed for the experiments. Catalyst was loaded in an argon atmosphere glove box. Extreme care was taken to eliminate air and water contamination of the experiment. Argon cycled through the system at 1500 sccm in the following order: bubbled through a temperature controlled (298 K) vessel containing 100 ml of benzene that was dried and deoxygenated over molecular sieves and lithium ribbon; the benzene rich (5 mol%) argon passed through a flow controller, a diaphragm pump and to the catalyst bed; the stream was heated to 723 K and flowed through the catalyst bed (1.5 g of catalyst containing 15% by weight Cs, 0.025 s per pass contact time); the reacted stream then returned to the bottom of the benzene vessel in which the biphenyl was trapped due to its low vapor pressure (0.005 bar at 298 K) to repeat the cycle. Products were analyzed by gas chromatography. No terphenyl was detected.

¶ The control (untreated catalyst) and benzene treated samples were prepared for transmission electron microscopic (TEM) studies by depositing them dry on carbon-coated Cu TEM grids. The grids were examined in a JEOL 2000FX S/TEM fitted with a Noran energy dispersive spectroscopic elemental analyzer. The control sample consisted of disordered appearing carbon with the Cs dispersed uniformly throughout the support. While we were not able to image individual particles of Cs on the carbon support, elemental analysis confirmed the presence of Cs everywhere in the sample. The used catalyst appeared similar to the control sample in microstructure as well as elemental composition with the Cs dispersed uniformly throughout the support. However, we observed a small fraction of the carbon to have ordered to graphitic nanoparticles and microscopic sheets of graphitic/turbostratic carbon during the benzene reaction process. No Cs was detected in these ordered pockets of carbon. Based on the TEM analysis, we estimate the amount of ordered carbon in the benzene-treated sample to be approximately 5% on a volume basis.

1 N. Bartlet and B. W. McQuillan, in *Intercalation Chemistry*, ed. M. S. Whittingham and A. J. Jacobson, Academic Press, New York, 1982, pp. 19–50 and references therein.
2 M. Ichikawa, K. Kawase and K. Tamaru, *J. Chem. Soc., Chem. Commun.*, 1972, 177.
3 J. M. Lalancette and R. Roussel, *Can. J. Chem.*, 1976, **54**, 2110.
4 F. Beguin and R. Setton, *J. Chem. Soc., Chem. Commun.*, 1976**,** 611.
5 F. J. Salzano and S. Aronson, *J. Chem. Phys.*, 1966, **45**, 6.
6 M. G. Stevens and H. C. Foley, *Chem. Commun.*, 1997**,** 519.
7 H. C. Foley, *Microporous Mater*., 1995, **4**, 407.
8 H. C. Foley, M. S. Kane and J. F. Goellner, in *Access in Nanoporous Materials*, ed. T. J. Pinnavaia and M. F. Thorpe, Plenum, New York, 1995.
9 D. S. Lafyatis, J. Tong and H. C. Foley, *Ind. Eng. Chem. Res.*, 1994**, 30**, 865.
10 R. K. Mariwala and H. C. Foley, *Ind. Eng. Chem. Res.*, 1994**, 33**, 607.
11 D. S. Lafayatis, J. Tung and H. C. Foley, *Ind. Eng. Chem. Res.*, 1991**, 30**, 865.
12 M. S. Kane, L. C. Kao, R. Mariwala, D. F. Hilscher and H. C. Foley, *Ind. Eng. Chem. Res.*, 1996, **35**, 3319.
13 S. Matsuzaki, M. Taniguchi and M. Sano, *Synth. Met.*, 1986, **16**, 343.
14 E. Grovenstein, T. H. Longfield and D. E. Quest, *J. Am. Chem. Soc.*, 1977, **99**, 2801.
15 G. Malinoski and W. H. Bruning, *J. Am. Chem. Soc.*, 1967, **89**, 5063.
16 M. G. Stevens, S. Subramoney and H. C. Foley, *Chem. Phys. Lett.*, 1998, in press.

Communication 8/06604C

Modulation of iron reduction potential by deprotonation at a remote site

Riccardo F. Carina,[a] Ludovica Verzegnassi,[a] Gérald Bernardinelli[b] and Alan F. Williams*[a]

[a] *Department of Inorganic, Analytical and Applied Chemistry, University of Geneva, 30 quai Ernest Ansermet, CH 1211 Genève 4, Switzerland. E-mail: Alan.Williams@chiam.unige.ch*

[b] *Laboratory of X-ray Crystallography, University of Geneva, 24 quai Ernest Ansermet, CH 1211 Genève 4, Switzerland*

Received (in Basel, Switzerland) 21st September 1998, Accepted 2nd November 1998

Remote site deprotonation of a coordinated imidazole ligand switches the reduction potential of coordinated iron over a narrow pH range from +0.920 to −0.460 V.

A fundamental concept of coordination chemistry is that ligand type may favour one oxidation state of a metal over another. Thus π-acceptor ligands such as CO and PF_3 stabilise low oxidation states, whereas high oxidation states are favored by π-donor ligands such as fluoride or anionic oxygen donors. Implicit in this concept is the idea that chemical modification of the ligand may change its ligating properties, and thereby modify the reduction potential of the metal to which it is coordinated. Protonation or deprotonation of the ligand at a site remote from the metal–ligand bond is a simple, reversible method of modification, and in this communication we show how the deprotonation of a coordinated imidazole ligand can influence dramatically the redox potential of iron bound to the ligand as well as influencing the spin state.

Ligand **1** in acetonitrile forms the complex $[Fe(\mathbf{1})_2]^{2+}$ expected by analogy with the related benzimidazole ligand **2**

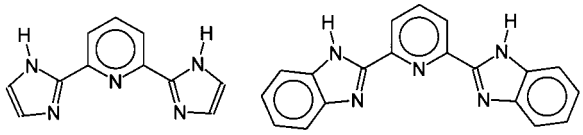

1 **2**

whose complexes with iron(II) have been studied previously.[1–3] The dark red complex† showed a strong MLCT band in methanol at 520 nm (ε = 5900 l mol^{-1} cm^{-1}). Upon treatment with Bu^{t}OK in methanol under nitrogen the solution became dark purple and showed the red shift and increase in intensity previously observed[1,2] for $[Fe(\mathbf{2})_2]^{2+}$ upon deprotonation; at the end points corresponding to $[Fe(\mathbf{1} - H)_2]$ the MLCT was at 536 nm (ε = 6220 l mol^{-1} cm^{-1}) and for $[Fe(\mathbf{1} - 2H)_2]^{2-}$ 538 nm (ε = 7620 l mol^{-1} cm^{-1}). Admission of air to the basic solution or addition of base in presence of oxygen gave a sky blue solution showing two weaker bands at 588 nm (ε = 870 l mol^{-1} cm^{-1}) and 730 nm (ε = 790 l mol^{-1} cm^{-1}) typical of low spin iron(III) coordinated by a diimine,[4] and no Fe(II) MLCT. The blue complex could be isolated as a sodium salt‡ either from the iron(II) complex after treatment with base or by reaction of $FeCl_3$ with **1** in presence of base. Elemental analysis and ESMS confirmed the presence of iron(III), and X-ray crystallography§ showed the expected pseudo-octahedral structure of the deprotonated complex $[Fe(\mathbf{1} - 2H)_2]^-$ (Fig. 1) and showed only slightly shorter Fe–N bond lengths [Fe–N_{py} 1.920(6) Å, Fe–N_{imid} 1.935(7) Å] than those observed for $[Fe(\mathbf{2})_2]^{2+}$.[2]

Since iron(II) coordinated to unsaturated nitrogen heterocyclic ligands is generally very hard to oxidise, the observation of spontaneous oxidation by air was surprising, especially since $[Fe(\mathbf{2})_2]^{2+}$ is not oxidised in base. Cyclic voltammetry studies in acetonitrile (glassy carbon electrode, 0.1 M NEt_4ClO_4 electrolyte , scan rate 200 mV s^{-1}) showed a reversible Fe^{III}–Fe^{II} wave at +0.920 mV *vs.* NHE for $[Fe(\mathbf{1})_2]^{2+}$, typical for an iron(II)–diimine complex. Upon deprotonation however, the Fe^{III}–Fe^{II} wave shifted to −0.460 mV for $[Fe(\mathbf{1} - 2H)_2]^-$ confirming the dramatic shift in redox potential, and explaining the observed sensitivity to oxidation by air. Reaction of iron(III) with two equivalents of **1** gave a yellow solution which darkened on standing as a result of reduction to $[Fe(\mathbf{1})_2]^{2+}$. No complex $[Fe(\mathbf{1})_2]^{3+}$ could be isolated, but a complex analysing as $[Fe(\mathbf{1})Cl_3]$ analogous to that formed by **2**[1] could be isolated.

Magnetic moments measured in methanol solution by the Evans method showed $[Fe(\mathbf{1})_2]^{2+}$ to have spin crossover behaviour analogous to $[Fe(\mathbf{2})_2]^{2+}$ [1,3] with a room temperature value of μ_{eff} = 3.6 μ_B, falling close to zero at 200 K. The change in UV–VIS spectrum of $[Fe(\mathbf{1})_2]^{2+}$ upon deprotonation at room temperature is consistent with the transition to a fully low spin state. $[Fe(\mathbf{1} - 2H)_2]^-$ in methanol gave μ_{eff} = 1.92 μ_B consistent with low spin Fe(III), while a solution of stoichiometric composition $[Fe(\mathbf{1})_2]^{3+}$ gave μ_{eff} = 6.3 μ_B, indicating high spin Fe(III). It is thus possible to switch the spin states by pH changes.

Deprotonation of coordinated imidazole at the pyrrolic hydrogen has been reported on many occasions[5] and often results in the imidazolate acting as a bridging ligand with formation of binuclear species.[6] For **1** − 2H this is impossible as a result of steric hindrance from the pyridyl moiety, but the basic nature of the deprotonated nitrogens is shown by the strong hydrogen bonds formed between N3 and N5 and the water molecules bound to sodium in $[Fe(\mathbf{1} - 2H)_2][Na-$

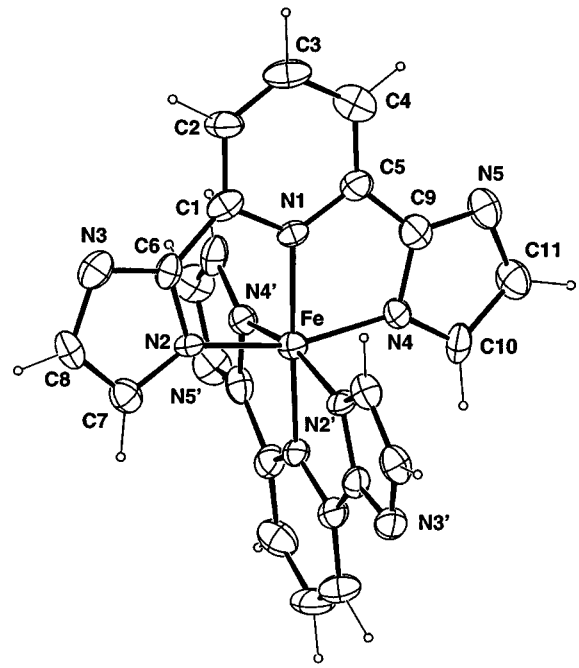

Fig. 1 Structure of the $[Fe(\mathbf{1} - 2H)_2]^-$ ion. A crystallographic twofold axis passes through the iron atom perpendicular to the pyridine–pyridine axis. Ellipsoids are shown at the 40% probability level.

$(H_2O)_4]_{0.5}[Na(MeCN)_4(THF)_2]_{0.5}$ [distances N···O 2.78(1) and 2.81(1) Å]. Potentiometric titration of a solution of $[Fe(\mathbf{1})_2]^{2+}$ [DMF–H_2O (4 : 1), I = 0.1 M KNO_3, in presence of air] with KOH showed the loss of four protons with pK values (estimated by a least squares fitting of the titration curve) of 8.19(5), 8.67(7), 9.86(10) and 9.92(9). These values should be interpreted with some caution since oxidation probably occurs before dissociation of all the protons. After removal of two protons the spectrum of the mixture is very similar to a superposition of the spectra of $[Fe(\mathbf{1})_2]^{2+}$ and $[Fe(\mathbf{1} - 2H)_2]^{-}$.The p$K_a$s are close to those previously reported for imidazole bound to Fe(II).[5]

We have found no reference to the effect of imidazole deprotonation upon redox potential in the literature. Although we would intuitively expect that the progressive introduction of negative charge onto the ligand would favour the higher oxidation state, the magnitude of the effect, some 1380 mV, is much greater than we anticipated. Haga *et al.* have studied the effect of deprotonation of coordinated benzimidazole ligands in ruthenium and osmium complexes[7] and has shown a shift of the reduction potential to more negative values upon deprotonation of *ca.* 300 mV per proton. This is broadly consistent with the effect observed here for the removal of four protons. It is of course well known that deprotonated pyrrolic ligands such as porphyrins and phthalocyanines allow stabilisation of iron(III) in a low spin state.

In conclusion, we have shown that it is possible to switch the redox potential of the iron(III)/iron(II) couple from strongly oxidising to strongly reducing over a limited range of pH (between 8 and 10). There is consequently a strong coupling between electron and proton transfer: proton loss from the ligand is followed by electron loss from iron(II), and proton capture by the ligand makes the iron(III) oxidising. We believe that this may be significant for biological oxygen chemistry, where reduction of dioxygen is accompanied by proton transfer to the dioxygen moiety, and oxidation of water requires concomitant deprotonation. It is to be noted that in many oxygen-reducing enzymes, iron is coordinated by imidazole ligands from histidine residues,[8] while in photosystem II the manganese ions are equally thought to have imidazole in the coordination sphere.[9] In such systems deprotonation of the imidazole might allow the attainment of a high oxidation state for manganese; proton transfer from coordinated water to the imidazole would then raise the oxidation potential of the metal to a degree where oxidation of the coordinated oxygen would be possible. Experiments to test this hypothesis are in progress. Finally, we may note that the protonation–deprotonation equilibrium also switches the spin state of the iron, and the affinity of the ligand for the metal, notably in the Fe(III) state.

Notes and references

† A solution of **1**[10] (58 mg, 275 μmol) in a minimum of MeCN was added to a solution of $Fe(ClO_4)_2·6H_2O$ (50 mg, 138 μmol) in a minimum of MeCN. The red solution was evaporated to dryness, the solid dissolved in 2 ml of MeCN and diethyl ether was slowly diffused into the solution. Orange–red crystals, 85 mg (122 μmol, yield 88%) of $[Fe(\mathbf{1})_2](ClO_4)_2·H_2O$. ESMS: *m/z* 576.8 $\{[Fe(\mathbf{1})_2](ClO_4)^+\}$ (5%), 259.2 $\{[Fe(\mathbf{1})_2](MeCN)^{2+}\}$ (70%), 238.7 $\{Fe(\mathbf{1})_2]^{2+}\}$ (100%). Calc. for $C_{22}H_{20}N_{10}Cl_2O_9Fe$: C, 38.01; N, 20.15; H, 2.90. Found: C, 38.35; N, 20.52; H, 3.08%.

‡ To a solution of $[Fe(\mathbf{1})_2](ClO_4)_2·H_2O$ (43 mg, 63 μmol) in 3 ml MeOH were added, slowly and under vigorous stirring, 2.42 ml of a freshly prepared NaOH solution (0.102 M in MeOH, 252 μmol), then the solution was filtered over Celite. The blue solution was evaporated to dryness, the solid dissolved in 6 ml of MeCN and some drops of MeOH and THF slowly diffused into the solution. Blue crystals were separated and dried to give 29 mg (48 μmol, yield 78%) of $Na[Fe(\mathbf{1} - 2H)_2]·(H_2O)_2·THF$ ESMS: *m/z* 474.1 $\{[Fe(\mathbf{1} - 2H)_2]^{-1}\}$ (100%). Calc. for $C_{26}H_{26}N_{10}O_3FeNa$: C, 51.58; N, 23.14; H, 4.33. Found: C, 51.74; N, 23.53; H = 4.64%.

§ *Crystal data*: $[Fe(\mathbf{1} - 2H)_2][Na(H_2O)_4]_{0.5}[Na(MeCN)_4(THF)_2]_{0.5}$, M = 343.7, tetragonal, space group $P4\bar{2}_1/c_1$, a = 13.3185(5), c = 19.455(1) Å, V = 3451.0(3) Å^3, T = 200 K, Z = 4, μ(Cu-Kα) = 4.039 mm^{-1}, 1661 observed reflections $[|F_o| > 4\sigma_0(F_o)]$, R = 0.051, R_w = 0.046. CCDC 182/1079. See http://rsc.org/suppdata/cc/1998/2681/for crystallographic files in .cif format.

1 A. W. Addison, S. Burman, C. G. Wahlgren, O. A. Rajan, T. M. Rowe and E. Sinn, *J. Chem. Soc., Dalton Trans.*, 1987, 2621.
2 S. Rüttimann, C. M. Moreau, A. F. Williams, G. Bernardinelli and A. W. Addison, *Polyhedron*, 1992, **6**, 635.
3 W. Linert, M. Konecny and F. Renz, *J. Chem. Soc., Dalton Trans.*, 1994, 1523.
4 G. M. Bryant and J. E. Ferguson, *Aust. J. Chem.*, 1971, **24**, 275.
5 R. J. Sundberg and R. B. Martin, *Chem. Rev.*, 1974, **74**, 471; R. K. Boggess and R. B. Martin, *Inorg. Chem.*, 1974, **13**, 1525.
6 See, for example: P. V. Bernhardt, G. A. Lawrence and N. J. Curtis, *Polyhedron*, 1992, **6**, 1347; C. Piguet, B. Bocquet, E. Müller and A. F. Williams, *Helv. Chim. Acta*, 1989, **72**, 323; N. Matsumoto, Y. Mizguchi, G. Mago, S. Eguchi, H. Miyasaka, T. Nakashima and J.-P. Tuchagues, *Angew. Chem., Int. Ed. Engl.*, 1997, **36**, 1860.
7 M. Haga, T. Ano, K. Kano and S. Yamabe, *Inorg. Chem.*, 1991, **30**, 3483; M. Haga, M. M. Ali, S. Koseki, K. Fujimoto, A. Yoshimura, K. Nozaki, T. Ohno, K. Nakajima and D. J. Stufkens, *Ibid.*, 1996, **35**, 3335, M. Haga, M. M. Ali and R. Arakawa, *Angew. Chem., Int. Ed. Engl.*, 1996, **35**, 76.
8 P. Nordlund, B-M. Sjöberg and H. Eklund, *Nature*, 1990, **345**, 593; A. C. Rosenzweig, C. A. Frederick, S. J. Lippard and P. Nordlund, *Nature*, 1993, **366**, 537.
9 V. K. Yachandra, V. J. DeRose, M. J. Latimer, I. Mukerji, K. Sauer and M. P. Klein, *Science*, 1993, **260**, 675.
10 R. F. Carina, G. Bernardinelli and A. F. Williams, *Angew. Chem., Int. Ed. Engl.*, 1993, **32**, 1463.

Communication 8/07321J

Photoreductive dechlorination of chlorinated benzene derivatives catalyzed by ZnS nanocrystallites

Yuji Wada,[a] Hengbo Yin,[b] Takayuki Kitamura[a] and Shozo Yanagida*[a]

[a] *Material and Life Science, Graduate School of Engineering, Osaka University, Suita, Osaka 565-0871, Japan*
[b] *Department of Chemical Engineering, Shenyang Institute of Chemical Technology, Shengyang, China*

Received (in Cambridge, UK) 3rd August 1998, Accepted 28th October 1998

ZnS nanocrystallites effectively enhanced photo-reduction of chlorinated benzene derivatives in the presence of triethylamine as a sacrificial electron donor under UV irradiation (λ > 300 nm), leading to selective and stepwise dechlorination to give benzene at the final stage.

Photochemical detoxification of halogenated compounds, such as PCB, dioxin, and DDT, has been attracting much attention because this can be regarded as a promising process to eliminate C–Cl bonds under environmentally relevant and mild conditions. In particular, TiO_2-catalyzed photoprocesses involving oxidation and reduction in aqueous systems have been extensively investigated.[1] In such systems, however, photooxidation proceeds through the formation of hydroxyl radical (HO•), leading to unavoidable formation of unknown photoproducts especially from polychlorinated compounds.[2,3] Further, the rate of such photodegradation often slows in the case of polychlorinated compounds because they are electron-deficient molecules, *i.e*. their oxidation potentials are very positive in nature, showing resistance to the electrophilic attack of HO•.[4] Therefore, reductive processes with semiconductors should be investigated practically for the purpose of detoxification of chemicals.[5,6]

In this paper, we show that photoreduction induces selective dehalogenation of chlorinated benzene derivatives, providing more favorable dehalogenation processes than the photooxidative ones. In particular, ZnS nanocrystallites stabilized in *N*,*N*-dimethylformamide (DMF)[7] catalyze photoreduction of chlorinated benzene derivatives, leading to their step-wise dechlorination under UV-irradiation at ambient temperature.

A DMF solution of ZnS nanocrystallites was prepared by the reaction of $Zn(ClO_4)_2$ with H_2S under cooling with ice and water as described elsewhere.[7] Photoreactions were carried out under cooling with water by UV irradiation of a DMF solution (2 ml) containing a substrate (25 mM), ZnS nanocrystallites (2.5 mM in diatomic concentration as ZnS) and triethylamine (TEA, 1 M) in a Pyrex glass tube using a 500 W high pressure mercury lamp. The reaction mixtures were analyzed by gas chromatography with a fused silica capillary column (HiCap-CBP20, 25 m × 0.2 mm, Shimadzu) using dodecane as an internal standard.

Fig. 1 shows time conversion plots of the photoreaction of 1,4-dichlorobenzene. The concentration of 1,4-dichlorobenzene decreased during irradiation with and without ZnS nanocrystallites. However, the rate of the conversion in the presence of ZnS nanocrystallites was twice that at the beginning and several times faster at the later stages than that in the absence of ZnS crystallites. In parallel with the consumption of 1,4-dichlorobenzene the formation of chlorobenzene was observed and benzene was formed at the final stage, *i.e*. after the induction period of 1 h with the decreased rate of formation of chlorobenzene, indicating that 1,4-dichlorobenzene is dechlorinated successively to benzene through chlorobenzene. Hydrogen was formed competitively but in a small amount (2–3 μmol in 5 h) in the presence of ZnS nanocrystallites. No other byproducts, such as biphenyl derivatives and chlorophenol, were detected by GC analysis, showing a consistent material balance between the consumed substrate and the products.

The dechlorination proceeded at a relatively high rate even without ZnS nanocrystallites. The absorption spectrum measured for the mixture of 1,4-dichlorobenzene and TEA showed the appearance of a shoulder at the long wavelength edge of the absorption of 1,4-dichlorobenzene, suggesting the formation of the exciplex between the two compounds. The formation of the exciplex should contribute to the photochemical dechlorination without the catalyst.[8,9] On the other hand, the photocatalytic dechlorination in the presence of ZnS nanocrystallites should mainly proceed through the excitation of ZnS, since ZnS nanocrystallites absorb most light in this region when they are present in the system.

In our earlier report, ZnS nanocrystallites prepared in DMF act as a photocatalyst for the two-electron reduction of CO_2 to HCOOH or CO in the presence of triethylamine.[7] The photogenerated electrons on ZnS nanocrystallites possess such a high reducing power (< -2.2 V *vs*. SCE) that the substrates are subject to successive two-electron reduction, causing the stepwise dechlorination. This fact suggests that the anion radicals first formed should be readily dechlorinated to the radicals, which may undergo further reduction and protonation. The electrons can be supplied by photooxidation of TEA. The resulting TEA^{+}• works as a proton source giving $[Et_2NHCHCH_3]$• which can also function as a good electron source in the system.[7]

In Table 1 are listed the conversions and the product distributions for the photodechlorination of various chlorobenzene derivatives observed in the presence of ZnS nanocrystallites with their reduction potentials.[10,11] The distribution of the products observed for the reactions of polychlorobenzenes well confirmed the successive and stepwise dechlorination reactions. For example, in the reaction of 1,2,3,4-tetrachlorobenzene, 1,2,4-trichlorobenzene formed preferentially is dechlorinated at the 2 position giving 1,4-di-

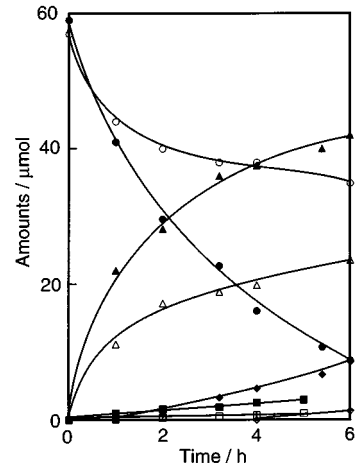

Fig. 1 Time profile of the photocatalytic dechlorination of 1,4-dichlorobenzene by ZnS nanocrystallites. In the presence of ZnS: 1,4-dichlorobenzene (●), chlorobenzene (▲), benzene (◆), hydrogen (■); in the absence of ZnS: 1,4-dichlorobenzene (○), chlorobenzene (△), benzene (◇), hydrogen (□).

Table 1 Dechlorination of various chlorobenzenes by ZnS–DMF[a]

Substrate[b]	E_{red}[c]/V *vs.* SCE	t[d]/h	Conv.[e] (%)	Composition of reaction products/mol%							
				ben	m	1,2-di	1,3-di	1,4-di	1,2,3-tri	1,2,4-tri	tetra
m	−2.44	4.2	31	32	69	—	—	—	—	—	—
1,2-di	−2.22	4.0	59	4.3	64	41	—	—	—	—	—
1,3-di	−2.20	4.0	56	2.9	58	—	44	—	—	—	—
1,4-di	−2.20	4.0	73	7.9	64	—	—	27	—	—	—
1,2,3-tri	−1.96	3.9	90	Trace	36	34	21	0	10	—	—
1,2,4-tri	−2.00	5.0	69	Trace	15	4.0	9	39	—	31	—
tetra	−1.76	4.0	75	Trace	1.6	1.6	2	7.8	6.9	44	25

[a] Reaction solution containing substrate (25 mM), TEA (1 M) and ZnS (2.5 mM) in DMF was irradiated with UV light (λ > 300 nm) under N_2. Abbreviations: ben, benzene; m, chlorobenzene; 1,4-di-, 1,4-dichlorobenzene; 1,3-di, 1,3-dichlorobenzene; 1,2-di, 1,2-dichlorobenzene; 1,2,3-tri, 1,2,3-trichlorobenzene; 1,2,4-tri, 1,2,4-trichlorobenzene; tetra, 1,2,3,4-tetrachlorobenzene. [b] Starting substrates. [c] From ref. 9 and 10; measured in DMSO solution containing TEABr (0.1 M) as electrolyte. [d] Irradiation time. [e] Conversion of substrates.

chlorobenzene as the predominant product in the isomers of dichlorobenzene, and is further dechlorinated to benzene through chlorobenzene.

The order of the photocatalytic dechlorination rates was 1,2,3-trichlorobenzene > 1,4-dichlorobenzene > 1,2,3,4-tetrachlorobenzene > 1,2,4-trichlorobenzene ≈ 1,3-dichlorobenzene ≈ 1,2-dichlorobenzene >> chlorobenzene. This order is roughly explained by the order of the redox potentials shown in Table 1, in other words, ease of reduction of the substrates.

In conclusion, the reduction of polychlorobenzene photocatalyzed by ZnS nanocrystallites gives selective and successive dechlorination without formation of any unidentified byproducts containing chlorine atoms. This photoreduction should provide a new strategy for detoxification of hazardous chlorinated aromatics under minimum-energy conditions.

This work was partly supported by Grants-in-Aid for Scientific Research from the Ministry of Education, Science, Sports, and Culture of Japan (Nos. 09490023, 09218236).

Notes and references

1 D. Cesareo, A. D. Domenico, S. Marchini and L. Passerini in *Homogeneous and Heterogeneous Photocatalysis*, ed. E. Pelizzetti and N. Serpone, D. Reidel Publishing Co., Dordrecht, 1985, vol. 174, p. 593; B. G. Oliver and J. H. Carey, *ibid.*, p. 629; D. F. Ollis, *ibid.*, p. 651.
2 J. Theurich, M. Lindner and D. W. Bahnemann, *Langmuir*, 1996, **12**, 6368.
3 D. Mas, P. Pichat and C. Guillard, *Res. Chem. Intermed.*, 1997, **23**, 275.
4 Y. Wada, M. Taira, D. Zheng and S. Yanagida, *New J. Chem.*, 1994, **18**, 589.
5 W. Choi and M. R. Hoffmann, *Environ. Sci. Technol.*, 1995, **29**, 1646.
6 D. C. Schmelling, K. A. Gray and P. V. Kamat, *Environ. Sci. Technol.*, 1996, **30**, 2547.
7 M. Kanemoto, H. Hosokawa, Y. Wada, K. Murakoshi, S. Yanagida, T. Sakata, H. Mori, M. Ishikawa and H. Kobayashi, *J. Chem. Soc., Faraday Trans.*, 1996, **92**, 2401.
8 M. Ohashi, K. Tsujimoto and K. Seki, *J. Chem. Soc., Chem. Commun.*, 1973, 384.
9 N. J. Bruce, S. Saffe and L. O. Ruzo, *J. Chem. Soc., Perkin Trans. 1*, 1975, 1607.
10 S. O. Farwell, F. A. Beland and R. D. Geer, *Electroanal. Chem., Interfacial Electrochem.*, 1975, **61**, 303.
11 J. W. Sease, F. G. Burton and S. L. Nickol, *J. Am. Chem. Soc.*, 1968, **90**, 2595.

Communication 8/06035E

Stabilization of the merocyanine form of photochromic compounds in fluoro alcohols is due to a hydrogen bond

Takayuki Suzuki, Fu-Tyan Lin, Satyam Priyadashy and Stephen G. Weber*

Department of Chemistry, University of Pittsburgh, Pittsburgh, Pennsylvania 5260, USA. E-mail: sweber+@pitt.edu

Received (in Columbia, MO, USA) 10th August 1998, Accepted 3rd November 1998

Fluoroalcohols [1,1,1,3,3,3-hexafluoropropan-2-ol (HFP), 2,2,2-trifluoroethanol (TFE) and 2-fluoroethanol (FE)], acting as Lewis acids, stabilize the π-conjugated, colored merocyanine forms of spiropyran and spirooxazine photochromic compounds as metal ions do.

We[1] and others[2] have been interested in the interactions of metal ions with photochromic compounds such as spiropyrans, spironaphthoxazines, and chromenes for potential applications in optical switching, memory and sensors. In these photochromic compounds, light is used to cleave a single C–O bond in the pyran or oxazine ring (so-called closed form) which results in the creation of a relatively more polar species (so-called open or merocyanine form). Metals influence this process by associating with this now electron-rich oxygen atom in the open form. It has been reported that 1,1,1,3,3,3-hexafluoropropan-2-ol (HFP) stabilizes the merocyanine form of polymer-bound nitrospiropyran through a general effect of the solvent's 'polarity'.[3] We wondered if HFP and other fluoro alcohols[4] known as good H-bond donors could stabilize the open form of spirooxazines in particular, and other similar photochromics in general, and if so, do they work as the metal ions do, through a specific Lewis acid/Lewis base interaction?

Compound **1**, 1,3-dihydro-5-methoxy-1,3,3-trimethylspiro-

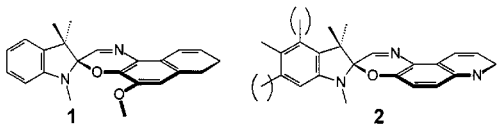

1 **2**

[2*H*-indole-2,3′-[3*H*]naphtho[2,1-*b*][1,4]oxazine] is purple at room temperature at equilibrium without photolysis in HFP-*d* (2 atom% ^{1}H on the hydroxy group). ^{1}H NMR integration shows that about 50% of **1** exists in the open form(s) **1′**. ^{1}H ROESY spectra for these solutions have cross peaks between the solvent hydroxy proton and the *N*-methyl protons in **1**. There is also a cross peak between the solvent hydroxy proton and the methoxy methyl in the merocyanine form of the molecule **1′**. There is evidence for both so-called TTC[5] and TTT isomers of **1′**; cross peaks are indicated as arrows in Fig. 1.

Compound **2** (1,3,3-trimethyl 5,6-dimethylspiro[2*H*-indole-2,3′-[3*H*]pyrido[3,2-*f*][1,4]benzoxazine][6]) also opens to the merocyanine form(s) **2′** in fluoro alcohols. Compound **2′** comprises 70 mol% in HFP, 15 mol% in TFE, 9 mol% in FE, and 2 mol% in EtOH in the dark. A TFE-d_3 (5 atom% ^{1}H) solution containing **2** is also purple at equilibrium at room temperature, although it is only about 15% open form. A signal is observed between the hydroxy proton of TFE and the 2′-proton of **2′** (ring proton *ortho* to the oxygen) in the ^{1}H NOESY spectrum. Furthermore, the resonance of the hydroxy proton of TFE is deshielded (δ 5.4) in comparison to pure TFE (δ 5.2) as shown in Fig. 2. When the solution is irradiated with UV (300–400 nm) light, the resonance becomes more deshielded (Fig. 2). We infer that TFE interacts with **2′** *via* an H-bond to the oxygen with rapid exchange on the NMR time scale (500 MHz). Additionally, we note a signal between the *N*-methyl protons at the indole group and the imine proton for **2′** in the ^{1}H NOESY spectrum, while there are no signals between the imine proton and the geminal methyl protons, nor are there signals between the imine proton and the 2′-proton; thus, for **2′**, TTC is the only isomer in TFE. In a solution of **2** in HFP, which is 70% ring-opened, there are several cross peaks (^{1}H ROESY) indicating the presence of both the TTC and TTT isomers. The cross peaks are illustrated schematically in Fig. 3. There is also a cross peak between the solvent hydroxy proton and the open-form *N*-methyl protons, once again indicating a possible H-bond to the former oxazine ring oxygen. If, as implied in the ^{1}H NMR studies, the stability of the open forms is due to H-bonding, there should be additional manifestations of the H-bond on the properties and spectroscopy of the compounds.

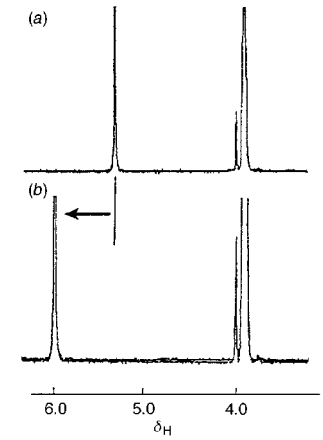

Fig. 2 ^{1}H NMR spectra (500 MHz) of the hydroxy proton of (*a*) TFE equilibrated in the dark, and (*b*) the same solution measured after irradiation with UV light. The TFE-d_3 solution contains **2**/**2′** (15 mM) and TFE (0.5 mM).

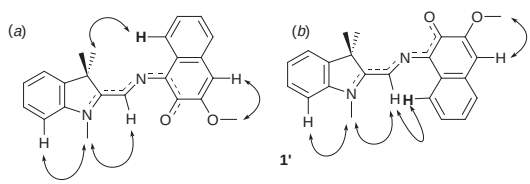

Fig. 1 (*a*) TTC and (*b*) TTT merocyanines **1′**. Cross peaks in the ^{1}H ROESY spectrum used to assign the structure are shown as curved arrows. The cross peaks of the bold H atoms are particularly diagnostic.

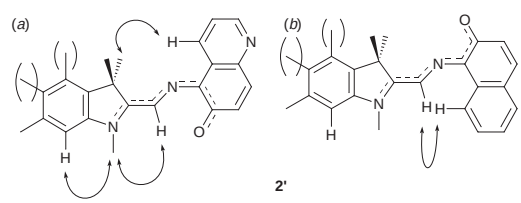

Fig. 3 (*a*) TTC and (*b*) TTT merocyanines **2′**. Cross peaks in the ^{1}H ROESY spectrum used to assign the structure are shown as curved arrows.

By perturbing a solution of **2**/**2′** in TFE with the appropriate wavelength range of light, excess **2** or **2′** can be formed. Both time courses can be analyzed as first order reactions within the temperature range of 15–40 °C (Fig. 4). Both activation energies are equal (25 ± 1 kcal mol^{-1} **2**→**2′**, 25 ± 1 kcal mol^{-1} **2′**→**2**), so the resulting difference is the enthalpy difference between **2** and **2′** which is 0 ± 1.4 kcal mol^{-1}. Typical values for similar molecules are *ca.* 4 kcal mol^{-1} in most solvents, from the non-polar benzene and toluene to the polar EtOH and MeCN.[7] The difference of 4 kcal mol^{-1} is consistent with the enthalpy of an H-bond in general[8] and with those between TFE and various acceptors in noncompetetive solvents[9] in particular.

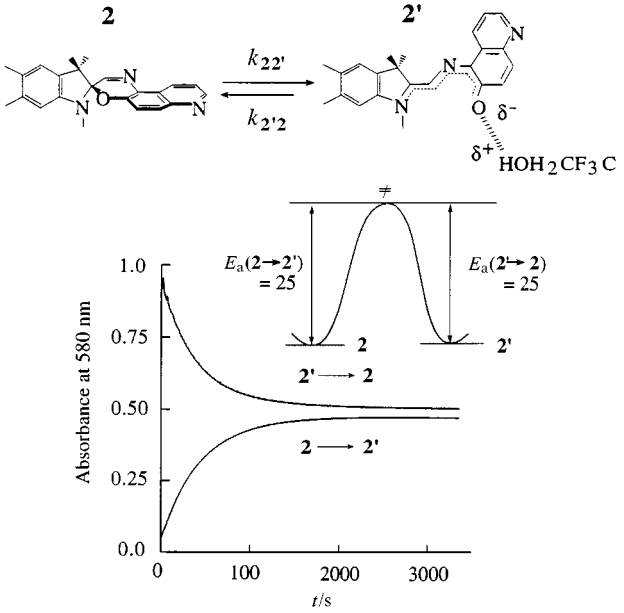

Fig. 4 Kinetics of the opening and closing reactions of **2**/**2′** in TFE (0.7 mM) at 22 °C. Activation energies are in kcal mol^{-1}.

If there is a specific H-bond formed as hypothesized, then there should be a shift in the λ_{max} of the long wavelength band of the merocyanine.[6] In common solvents, the long wavelength band of the merocyanine is weakly solvatochromic (*e.g.* λ_{max} in toluene, MeCN and MeOH for **2′** is 602 nm, EtOH, 605 nm, ethylene glycol and 3-methyloxazolidin-2-one, 610 nm). However, in the fluoro alcohols there is considerable solvatochromism (λ_{max} values: HFP, 534 nm; TFE, 582 nm; FE, 590 nm). The values of $E_T(30)$ as a benchmark for the strength of hydrogen-bond donation and polarity of the fluoro alcohols are also in the order HFP > TFE > FE [$E_T(30)$: 63.3, 59.8, 55.5 respectively].[4f] Furthermore, there is a good correlation between the energy of the long wavelength band of the merocyanine and the logarithm of the equilibrium constants (estimated as [**2′**]/[**2**] from the NMR data). Thus, changes in the energy of the ground state, through solvent H-bonding to the oxygen, influence the spectroscopy and the equilibrium consistently.

We have performed *ab initio* calculations[13,14] on all the solvent molecules and the solute **2′**. We also performed preliminary calculations on the H-bonded complexes at the semiempirical quantum level using PM3 parameterization. Full geometry optimizations of the complexes with the solvents HFP, TFE and FE were performed. The calculated H-bond distance between the O of the **2′** carbonyl and the H of the hydroxy hydrogen of the solvent are 1.7729, 1.818 and 1.820 Å for HFP, TFE and FE, respectively. The calculations support the observed order in the effectiveness of the fluoro alcohols in stabilizing the merocyanine form. Theory also shows very little change in the O–H bond distances in the fluoro alcohols (difference: complex-free solvent (Å) HFP: 0.014, TFE: 0.0163, FE: 0.0058).

Finally, we note that the behavior in the Lewis acid solvents differs dramatically from the behavior in the weak Brönsted acid, glacial acetic acid (AA). A sample of **2**/**2′** in AA, after a considerable time, yields a band at 420 nm. This solution is not photoactive. The band at 420 nm arises from protonated **2′** with TTT geometry [Fig. 3(*b*)].[1b] When a quantity of Et_3N equivalent to the AA is added to the solution, the band due to the protonated form disappears. There is no significant absorbance in the visible region. Illumination with UV light yields a transient absorption peak at 610 nm, which is characteristic of **2′** in polar solvents.

The Lewis acid Zn^{II} causes the ring opening reaction **2**⟶**2′**. The complex is stable, as is the solvate of HFP. The visible wavelength is 538 nm, between that of HFP and TFE solutions. Thus, the original hypothesis that Lewis acids of different sorts similarly influence the structure and properties of the photochromic species is confirmed.

We are grateful to Dr Barry van Gemert and Mr David Knowles at PPG, Inc., Chemicals Division, for providing **1** and **2**. This work was supported by the Office of Naval Research and the National Science Foundation (CHE-9710213).

Notes and references

1 (*a*) M. T. Stauffer, D. B. Knowles, C. Brennan, L. Funderburk, F.-T. Lin and S. G. Weber, *Chem. Commun*., 1997, 287; (*b*) M. J. Preigh, F. Lin, K. Z. Ismail and S. G. Weber, *J. Chem. Soc., Chem. Commun*., 1995, 2091.

2 J. D. Winkler, C. M. Bowen and V. Michelet, *J. Am. Chem. Soc*., 1998, **120**, 3237 and references cited therein.

3 (*a*) F. Ciardelli, D. Fabbri, O. Pieroni and A. Fissi, *J. Am. Chem. Soc*., 1989, **111**, 3470; (*b*) A. Fissi, O. Pieroni, F. Ciardelli, D. Fabbri, G. Ruggeri and K. Umezawa, *Biopolymers*, 1993, **33**, 1505.

4 (*a*) K. F. Purcell and S. T. Wilson, *J. Mol. Spectrosc*., 1967, **24**, 468; (*b*) A. D. Sherry and K. F. Purcell, *J. Phys. Chem*, 1970, **74**, 3535; (*c*) K. F. Purcell, J. A. Stikeleather and S. D. Brunk, *J. Am.Chem. Soc*., 1969, **91**, 4019; (*d*) Y. Marcus, *Chem. Soc. Rev*., 1993, **22**, 409; (*e*) M. J. Kamlet, J.-L. M. Abboud, M. H. Abraham and R. W. Taft, *J. Org. Chem*., 1983, **48**, 2877; (*f*) C. Reichardt, *Chem. Rev*., 1994, **94**, 2319.

5 This shorthand nomenclature reflects the *transoid* or *cisoid* orientation about the partial double bonds between the former spiro carbon and the naphthalene ring.

6 The synthesis generates about 50% each of the 1,3,3-trimethyl 5,6-dimethyl compound and 1,3,3-trimethyl 4,5-dimethyl compound. Such mixtures are not distinguishable as mixtures except by NMR spectroscopy. For example, first order processes fit a single exponential, and UV–VIS spectra do not show extra bands or shoulders compared to analogous compounds with no methyl substituents on the aromatic portion of the indole ring (positions 4, 5, 6 and 7).

7 J. B. Jr. Flannery, *J. Am. Chem. Soc*., 1968, **90**, 5660; N. Y. C. Chu, *Can. J. Chem*., 1983, **61**, 300; S. Keum, M. Hur, P. M. Kazmaier and E. Buncel, *Can. J. Chem*., 1991, **69**, 1940.

8 M. D. Joesten and L. J. Schaad, *Hydrogen Bonding*, Marcel Dekker, New York, 1974; S. N. Vinogradov and R. H. Linnell, *Hydrogen Bonding*, Van Nostrand Reinhold, New York, 1971; G. A. Jeffrey and Y. Yeon, *Acta Crystallogr*., 1986, **B42**, 410.

9 L. Eberson, M. P. Hartshorn, O. Persson and F. Radner, *Chem. Commun*., 1996, 2105.

10 A full geometry optimization was carried out at the RHF level using the 6-31G* basis set with the GAUSSIAN94 package: GAUSSIAN 94, Revision D.4, M. J. Frisch, G. W. Trucks, H. B. Schlegel, P. M. W. Gill, B. G. Johnson, M. A. Robb, J. R. Cheeseman, T. Keith, G. A. Petersson, J. A. Montgomery, K. Raghavachari, M. A. Al-Laham, V. G. Zakrzewski, J. V. Ortiz, J. B. Foresman, J. Cioslowski, B. B. Stefanov, A. Nanayakkara, M. Challacombe, C. Y. Peng, P. Y. Ayala, W. Chen, M. W. Wong, J. L. Andres, E. S. Replogle, R. Gomperts, R. L. Martin, D. J. Fox, J. S. Binkley, D. J. Defrees, J. Baker, J. P. Stewart, M. Head-Gordon, C. Gonzalez, and J. A. Pople, Gaussian, Inc., Pittsburgh PA, 1995.

11 Y. J. Chang and E. W. Castner, Jr. *J. Phys. Chem*., 1996, **100**, 2684; W. J. Hehre, L. Radom, P. v. R. Schelyer and J. A. Pople, *Ab Initio Molecular Orbital Theory*, Wiley, New York, 1986.

Communication 8/06316H

ChemComm

Synthesis and characterisation of a novel microporous niobium silicate catalyst

João Rocha,*[a] Paula Brandão,[a] Andreas Phillippou[b] and Michael W. Anderson[b]

[a] *Department of Chemistry, University of Aveiro, 3810 Aveiro, Portugal. E-mail: ROCHA@DQ.UA.PT*
[b] *Department of Chemistry, UMIST, PO Box 88, Manchester, UK M60 1QD*

Received (in Cambridge, UK) 26th October 1998, Accepted 6th November 1998

The synthesis and characterisation of a novel microporous niobium silicate (AM-11), an excellent catalysts for the conversion of alcohols, are reported.

Recently, the synthesis of microporous framework titanium silicates, displaying zeolite-type properties and containing Ti(IV) usually in octahedral coordination, has attracted much interest.[1–4] As a natural extension of this work, we have embarked on a systematic study aimed at preparing novel microporous zirconium[5] and niobium[6] silicates. Here we report the synthesis and structural characterisation of a novel microporous niobium silicate denoted AM-11 (Aveiro-Manchester microporous solid no. 11).

AM-11 was prepared in Teflon-lined autoclaves under static hydrothermal conditions. An alkaline solution was made by mixing 1.27 g tetraethylorthosilicate (Aldrich), 2.40 g ethanol, 6.40 g H_2O, 1.68 g NaOH (Merck) and 0.53 g NaF (Aldrich). A second solution was made by mixing 20.0 g H_2O, 3.00 g oxalic acid (Panreac), 1.00 g niobium oxalate (Niobium Products) and stirred overnight. These two solutions were combined, seeded with 0.1 g ETS-4[1] and stirred thoroughly. The pH (after a 1 : 100 water dilution) was adjusted to 10.2 by adding an ammonia solution (25%, Merck). The gel, with a composition 1.0 Na_2O : 1.0 SiO_2 : 0.15 Nb_2O_5 : 240 H_2O, was autoclaved for 15 days at 200 °C. The crystalline product was filtered off, washed with distilled water and dried at ambient temperature, the final product being an off-white microcrystalline powder.

AM-11 samples were characterised by powder X-ray diffraction (XRD), scanning electron microscopy (SEM), ^{93}Nb, ^{29}Si and ^{23}Na magic-angle spinning nuclear magnetic resonance (MAS NMR), Raman spectroscopy, thermogravimetry (TG), adsorption isotherms and catalytic tests.

SEM (not shown) reveals that AM-11 crystals are needles *ca.* 10 μm in length. Energy dispersive absorption of X-rays yields Si/Nb and Na/Nb molar ratios of *ca.* 4.6 and 0.3, respectively.

The total AM-11 mass loss between 30 and 700 °C is *ca.* 16.5%. Two stages of dehydration are observed (not shown): between 30 and 270 °C the solid loses *ca.* 10.5% while between 270 and 700 °C the mass loss is *ca.* 6%. The adsorption behaviour of AM-11 was investigated in order to assess the porosity of the material. Nitrogen and methanol adsorption isotherms are both type I with maximum uptakes of *ca.* 0.15 and 0.11 g g^{-1}, respectively. Although the material is microporous, the propane uptake was found to be negligible suggesting a very small pore size. However, ethanol, *n*-propanol and 2-methylpropan-1-ol have uptakes of *ca.* 0.6–0.7 g g^{-1} at $P/P^0 = 0.5$. This conflicting behaviour may originate in the polarity of the sorbate.

The powder XRD pattern of AM-11 is shown in Fig. 1, while the *d*-spacings and intensities of the main reflections are collected in Table 1. Peak intensities were altered by changing the method of sample preparation indicating the occurrence of preferred orientation effects. *In situ* powder XRD patterns recorded under vacuum at temperatures up to 650 °C (not shown) are similar to the pattern given by the parent hydrated material. The water in AM-11 is zeolitic and its removal is not permanent. This was confirmed by first heating a sample at 650 °C and then keeping it, for several hours, in contact with air at room temperature. The powder XRD patterns and TG curves of the parent and calcined hydrated materials were found to be identical.

The ^{29}Si MAS NMR spectrum of AM-11 [Fig. 2(*a*)] displays a resonance at δ −95.6, a group of (at least) three overlapping peaks at δ −105.5, *ca.* −106.7 and −108.1 and a sharp signal at δ −111.1. The attribution of these resonances is difficult because, to the best of our knowledge, no systematic study is available on the relationship between the ^{29}Si NMR chemical shift and the number of niobium polyhedra coordinating a given silicon tetrahedron. Our previous study on synthetic analogues of the mineral nenadkevichite, containing framework niobium,[6] suggests that this relationship may be similar to that found for titanium silicates where a systematic downfield chemical shift is observed when increasing numbers of titanium polyhedra coordinate a given silicon tetrahedron.[7] We assign the peak at δ −111.1 to Si(4 Si, 0 Nb) environments. The resonances at δ −105.5, *ca.* −106.7 and −108.1 are tentatively assigned to Si(4 Si, 0 Nb) or Si(3 Si, 1 Nb) environments,[3] while that at δ −95.6 is attributed to Si(3 Si, 1 Nb) or Si(2 Si, 2 Nb) sites.

The central-transition ^{93}Nb MAS NMR spectrum [Fig. 2(*b*)] of AM-11 contains a broad (full-width at half maximum, FWHM, *ca.* 127 ppm) resonance centred at δ −100 relatively to solid Nb_2O_5 (the other peaks are spinning sidebands). Considering the few ^{93}Nb NMR spectra reported for niobium

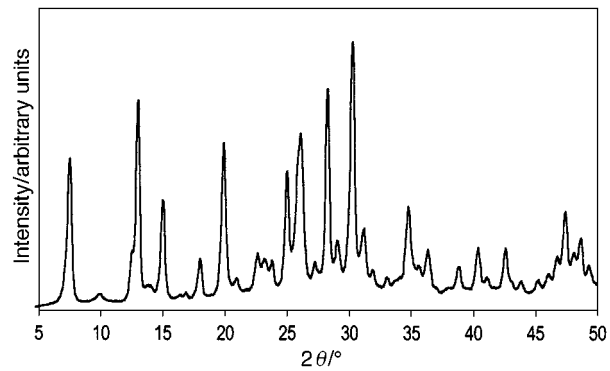

Fig. 1 Powder XRD pattern of AM-11.

Table 1 Powder XRD data of AM-11

d/Å	I/I_0	*d*/Å	I/I_0
11.861	64	3.421	63
8.964	4	3.279	7
7.114	14	3.165	85
6.841	80	3.080	15
6.489	3	2.959	100
6.337	3	2.873	23
5.923	34	2.810	7
4.941	15	2.715	5
4.474	61	2.584	36
4.243	6	2.523	8
3.940	17	2.475	18
3.860	6	2.323	12
3.827	8	2.237	20
3.750	12	2.198	6
3.571	43	2.125	20

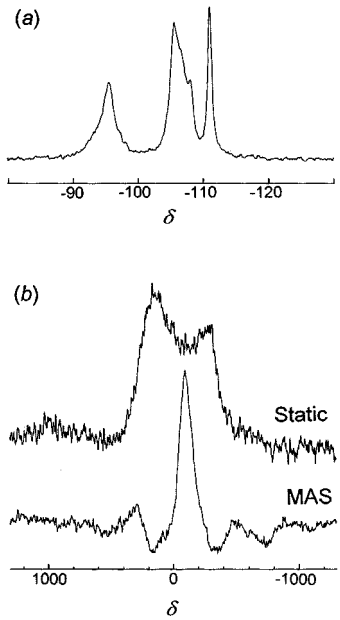

Fig. 2 (*a*) ^{29}Si MAS, (*b*) ^{93}Nb MAS and static NMR spectra of AM-11, recorded at 79.50 and 97.84 MHz on a Bruker MSL 400P spectrometer using spinning rates of 5 and 32 kHz, respectively.

Table 2 Conversions and product distributions (wt%) of isopropanol and *tert*-butanol over AM-11[a]

	Isopropanol[b]	*tert*-butanol[c]
Conversion	99.9	99.9
Propene	85.7	
Acetone	14.2	
Isobutene		98.9
C_5–C_9		1.0

[a] Catalyst activation at T = 400 °C and P = 1 atm for 3 h. [b,c] P = 1 atm, WHSV = 2 h^{-1}, TOS = 60 min; [b] T = 350 °C, Ar carrier gas flow 10 ml min^{-1}; [c] T = 250 °C, Ar carrier gas flow 30 ml min^{-1}.

silicates containing hexa-coordinated niobium which give resonances at *ca.* δ 0,[6] this value is slightly shifted to low frequency. This may be due to a large quadrupole coupling constant, (simulation of the static spectrum in Fig. 2(*b*) indicates a rather large value, in excess of 26 MHz) which results in a significant low-frequency shift. The FWHM of the static spectrum is *ca.* 640 ppm. Hence, MAS narrows the NMR resonance by a factor of five. Now, when second-order quadrupole effects dominate, MAS only narrows the peaks by a factor of *ca.* 3.6. We conclude that other line broadening mechanisms, such as chemical shift anisotropy and dipolar interactions are in operation.

The central-transition ^{23}Na MAS NMR spectrum of AM-11 (not shown) contains a broad peak centred at δ −6 with a faint shoulder at *ca.* δ −12 (relatively to aqueous NaCl).

The Raman spectrum of AM-11 (not shown) displays a main, strong and sharp, band at 687 cm^{-1} and several fainter bands in the range 100–300 cm^{-1}. The former peak is typical of NbO_6 octahedra in porous niobium silicates: the synthetic analogues of nenadkevichite give a similar peak at 668 cm^{-1} and weak bands at 100–300 cm^{-1}.[6]

A preliminary charcterisation of the acid–base properties of AM-11 was performed by means of isopropanol conversion, a probe reaction which is tailored for both acidity and basicity.[8] The main products of this catalytic process are propene and acetone resulting from acid dehydration and base-catalysed dehydrogenation respectively. The product distributions are given in Table 2 and indicate that this material exhibits both acidic and basic active sites in its as-synthesised form. Further studies of the catalytic properties of AM-11 were carried out using *tert*-butanol. From the results given in Table 2, it is apparent that AM-11 dehydrates *tert*-butanol to isobutene with remarkably high activity and selectivity. This finding coupled with the large pore volume of this material point to its potential in catalysis. Moreover, conventional ion-exchange experiments may enhance both its basic and acidic properties.

In conclusion, we report the synthesis and characterisation of AM-11, a novel microporous niobium silicate which is a promising catalyst for the dehydration of alcohols. Work is in progress in order to solve the crystal structure of this material.

This work was supported by PRAXIS XXI and FEDER.

Notes and references

1 M. W. Anderson, O. Terasaki, T. Ohsuna, A. Phillippou, S. P. Mackay, A. Ferreira, J. Rocha and S. Lidin, *Nature*, 1994, **367**, 347.
2 M. W. Anderson, O. Terasaki, O. Ohsuna, P. J. O'Malley, A. Phillippou, S. P. MacKay, A. Ferreira, J. Rocha and S. Lidin, *Philos. Mag. B*, 1995, **71**, 813.
3 Z. Lin, J. Rocha, P. Brandão, A. Ferreira, A. P. Esculcas, J. D. Pedrosa de Jesus and M. W. Anderson, *J. Phys. Chem. B*, 1997, **101**, 7114.
4 M. S. Dadachov, J. Rocha, A. Ferreira, Z. Lin and M. W. Anderson, *Chem. Commun.*, 1997, 2371.
5 J. Rocha, P. Ferreira, Z. Lin, J. R. Agger and M. W. Anderson, *Chem. Commun.*, 1998, 1269.
6 J. Rocha, P. Brandão, Z. Lin, A. Ferreira and M. W. Anderson, *J. Phys. Chem.*, 1996, **100**, 14 978.
7 M. L. Balmer, B. C. Bunker, L. Q. Wang, C. H. F. Peden and Y. Su, *J. Phys. Chem. B*, 1997, **101**, 9170.
8 P. E. Hathaway and M. E. Davies, *J. Catal.*, 1989, **116**, 263.

Communication 8/08264B

ChemComm

Fast and selective homogeneous hydrogenation with nickel(II) phosphane catalysts

Ingrid M. Angulo, Alexander M. Kluwer and Elisabeth Bouwman*

Leiden Institute of Chemistry, Gorlaeus Laboratories, Leiden University, PO Box 9502, 2300 RA Leiden, The Netherlands. E-mail: bouwman@chem.leidenuniv.nl

Received (in Cambridge, UK) 25th September 1998, Accepted 28th October 1998

Nickel(II) phosphane complexes are able to hydrogenate oct-1-ene to *n*-octane with high turnover numbers and high selectivities at low temperature and moderate pressure.

From recent research it is known that the active site of the enzyme hydrogenase contains nickel.[1] This enzyme, present in some bacteria, activates molecular hydrogen at atmospheric pressure and room temperature. However, although nickel is widely used as a heterogeneous catalyst for hydrogenation reactions (Raney nickel), homogeneous hydrogenation catalysts containing nickel are scarcely found in the literature.[2] Yet, homogeneous nickel catalysts are known for related reactions like isomerisation, oligomerisation, polymerisation, hydrosilylation and hydrocyanation.[3]

Herein we report on a novel *homogeneous in situ* nickel catalyst for the hydrogenation of linear olefins. In this research nickel(II) acetate in combination with several diphosphane ligands was tested on catalytic activity in the hydrogenation of oct-1-ene (Scheme 1).

In our search for homogeneous nickel hydrogenation catalysts, initially nickel(II) salts in the absence of any ligands were tested. Nickel(II) acetate, without addition of ligand, showed some hydrogenation activity at a reaction temperature of 373 K. It has been reported that nickel(II) acetate in methanol in reductive reaction conditions at elevated temperatures may form colloidal nickel,[4] which is an active, but heterogeneous hydrogenation catalyst. The presence of a black precipitate in the reaction mixture after the hydrogenation reaction at 373 K indicates that also in this case some colloidal nickel was formed. However, this hydrogenation activity drops to zero when the reaction temperature is lowered to 323 K; even after 20 h no hydrogenation activity was observed and no colloidal nickel was formed.

Subsequently, some didentate phosphane ligands were added to nickel(II) acetate, to investigate their influence on catalytic activity.† The results of the hydrogenation reactions are presented in Table 1.

Initially, two simple phosphane ligands, dppe and dppp (for abbreviations see Scheme 1), were used (Table 1, entries 1 and 2). Whereas nickel(II) acetate alone shows some hydrogenation activity at 373 K (probably heterogeneous), the presence of dppe or dppp leads to an unreactive complex. When dppe or dppp is added to the green nickel(II) acetate solution, almost immediately a yellow complex is formed. The fact that the colour of this solution does not change during the hydrogenation experiment and that no black precipitate is observed, indicates that the phosphane ligands prevent the formation of colloidal nickel. As the simple phosphane ligands dppe and dppp did not lead to active hydrogenation catalysts, it was decided to use some more complex phosphane ligands, and methoxyphenyl and cyclohexyl derivatives were selected (Scheme 1).

$R_2P(CH_2)_nPR_2$

Ligand[a]	R	*n*
dppe	Ph	2
dppp	Ph	3
dcpe	*c*-C_6H_{11}	2
dcpp	*c*-C_6H_{11}	3
o-MeO-dppe	*o*-$MeOC_6H_4$	2
o-MeO-dppp	*o*-$MeOC_6H_4$	3
m-MeO-dppe	*m*-$MeOC_6H_4$	2
m-MeO-dppp	*m*-$MeOC_6H_4$	3
p-MeO-dppp	*p*-$MeOC_6H_4$	3

Scheme 1 Structure of the ligands. dppe = 1,2-bis(diphenylphosphino)-ethane, dppp = 1,3-bis(diphenylphosphino)propane, dcpe = 1,2-bis(dicyclohexylphosphino)ethane, dcpp = 1,3-bis(dicyclohexylphosphino)propane, *o*-MeO-dppe = 1,2-bis(di-*ortho*-methoxyphenylphosphino)ethane, *o*-MeO-dppp = 1,3-bis(di-*ortho*-methoxyphenylphosphino)propane, *m*-MeO-dppe = 1,2-bis(di-*meta*-methoxyphenylphosphino)ethane, *m*-MeO-dppp = 1,3-bis(di-*meta*-methoxyphenylphosphino)propane, *p*-MeO-dppp = 1,3-bis(di-*para*-methoxyphenylphosphino)propane.

First, *o*-MeO-dppe was tested in combination with nickel(II) acetate for hydrogenation activity at 373 K in methanol. The formed catalytic species was very active, so that within 15 min, all the oct-1-ene had reacted. Therefore the hydrogenation reaction was performed at a lower temperature of 323 K (Table 1, entry 3). After 1 h the reaction mixture contained, besides *n*-octane and unreacted oct-1-ene, also some isomerisation products, mainly *cis*- and *trans*-oct-2-ene. The propane-bridged analogue *o*-MeO-dppp was also tested on hydrogenation activity in combination with nickel(II) acetate (Table 1, entry 4). With this ligand the activity is increased to 350 turnovers h^{-1}. Furthermore, when ethanol is used as the solvent the activity increased further to 410 turnovers h^{-1} (Table 1, entry 5).

Application of the cyclohexyl ligand dcpe leads to a very active catalyst (Table 1, entry 6). The reaction temperature had to be lowered even further, to 298 K, to be able to follow the reaction course. Even at this low temperature a high turnover number of 460 after 1 h was reached. In contrast to the results obtained with the *ortho*-methoxy ligands the propane-bridged analogue dcpp leads to a somewhat less active catalyst with 350 turnovers h^{-1} (Table 1, entry 7).

In order to establish the homogeneity of the catalysts, the catalytic activity as a function of the amount of catalyst was determined. Only in the case of a homogeneous catalyst is the activity expected to be directly proportional to the catalyst concentration. We performed this test with the *in situ* catalyst formed with nickel(II) acetate and *o*-MeO-dppe; we found that

Table 1 Nickel-catalysed hydrogenation of oct-1-ene[a]†

Entry	Ligand	TON[b]	*T*/K	Solvent
1	dppe	0	373	EtOH
2	dppp	0	373	EtOH
3	*o*-MeO-dppe	220	323	MeOH
4	*o*-MeO-dppp	350	323	MeOH
5	*o*-MeO-dppp	410	323	EtOH
6	dcpe	460	298	MeOH
7	dcpp	350	298	MeOH
8	*m*-MeO-dppe	0	373	MeOH
9	*m*-MeO-dppp	0	373	EtOH
10	*p*-MeO-dppp	0	373	EtOH

[a] *Reaction conditions*: oct-1-ene/Ni = 500, Ni/ligand = 1, [Ni] = 0.005 M, *t* = 1 h, $p(H_2)$ = 50 bar. [b] Turnover number in mol *n*-octane per mol $Ni(OAc)_2$ after 1 h.

the activity of the catalyst increased linearly (correlation coefficient = 0.997) with the catalyst concentration. It is possible that the reaction conditions, dihydrogen, electron-rich phosphine plus an alcohol solvent, can cause reduction of nickel, leading to a heterogeneous catalyst, but even when a non-coordinating, electron-rich phosphine, such as tris(*ortho*-methoxyphenyl)phosphine, is used under identical reaction conditions, no hydrogenation activity is observed. These results, in combination with the observation that pure nickel(II) acetate does not lead to an active catalyst under the reaction conditions, lead to conclusion that genuine homogeneous catalysts are observed here.

The positive effect of the *ortho*-methoxyphenyl and the cyclohexyl groups in the diphosphane ligands on the hydrogenation activity compared to dppe and dppp could be due to either steric or electronic effects. Both the *ortho*-methoxyphenyl group and the cyclohexyl group are weaker π-acceptors than a simple phenyl group. As a consequence the basicity of the phosphorus atoms in the corresponding diphosphane ligands is higher, which will influence the electrophilic nature of the nickel(II) ion. This extra electron density at the metal increases its ability to interact with dihydrogen. Furthermore, *ortho*-methoxyphenyl and cyclohexyl groups are much more bulky than the phenyl group.

In an initial attempt to separate electronic from steric effects of the methoxyphenyl group the *meta* and *para* analogues of these phosphane ligands were also tested for hydrogenation activity in combination with nickel(II) acetate (Table 1, entries 8, 9 and 10). None of the formed complexes showed any hydrogenation activity even at higher reaction temperatures. Only some isomerisation was observed in the case of *p*-MeO-dppp. This indicates that the positive effect of the *ortho*-methoxyphenyl groups on the hydrogenation activity is predominantly steric. It is known that the ligands dppe and dppp can form bis(ligand) complexes with nickel such as in $[Ni(dppe)_2][NO_3]_2$.[5] A positive influence because of steric properties may be explained by a lower probability of the formation of inactive bis(ligand) complexes with the bulkier *ortho*-methoxyphenyl- or cyclohexyl-derived ligands. So far, no X-ray structures of bis(ligand) complexes containing the *ortho*-methoxyphenyl and the cyclohexyl groups in the diphosphane ligands have been reported.

It is assumed that the catalytic cycle for isomerisation at least partly coincides with that of the hydrogenation reaction. With some of the catalysts reported here, a considerable amount of the oct-1-ene is initially isomerised; However, over time the amount of these internal olefins also decreases suggesting that either the catalyst is able to hydrogenate these or isomerisation back to the terminal olefin occurs. Further investigations will concentrate on elucidating the mechanism of the hydrogenation reaction and isomerisation, with these nickel catalysts by variation of the substituents on the phosphane ligand and by changing the reaction conditions.

In conclusion, novel truly homogeneous nickel containing hydrogenation catalysts are described, which show faster and more selective catalytic activity compared to known homogeneous nickel containing hydrogenation catalysts.[2] In the future, a further improved nickel catalyst may replace the more expensive rhodium and ruthenium catalysts which are currently used. Even enantioselective nickel hydrogenation catalysis complexes can be envisaged.

This research has been financially supported by the Council for Chemical Sciences of the Netherlands Organization for Scientific Research (CNWO). We thank Dr J. Reedijk and Dr E. Drent for fruitful discussions. Shell International Chemicals B. V. kindly provided some phosphane samples.

Notes and references

† In a typical experiment, 0.1 mmol nickel(II) acetate tetrahydrate and 0.1 mmol of the ligand were mixed in 20 ml of dry solvent for 10 min at room temperature under an argon atmosphere. For *o*-MeO-dppe or *p*-MeO-dppp mixing was performed at elevated temperatures and/or for prolonged times, until the ligand was completely dissolved. Solutions containing ligands *o*-MeO-dppp, *m*-MeO-dppe or *m*-MeO-dppp had to be refluxed for 5 h. Then, 50 mmol of oct-1-ene was added to the yellow–orange solution and mixing continued for 5 min. The mixture was transferred into the autoclave, under oxygen-free conditions, and a hydrogen pressure of 50 bar applied. The reaction was initiated by heating the autoclave to the desired temperature. Samples were taken every 15 min over 1 h and were analysed using gas chromatography.

1 R. Cammack, in *Bioinorganic Catalysis*, ed. J. Reedijk, Marcel Dekker Inc., New York, 1993, ch. 7.
2 E. A. Emken, E. N. Frankel and R. O. Butterfield, *J. Oil Am. Chem. Soc.*, 1965, **43**, 14; H. Itatani and J. C. Bailar, Jr., *J. Am. Chem. Soc.*, 1967, **89**, 1600; P. Abley and F. J. McQuillin, *Gen. Discuss. Faraday Soc.*, 1968, **46**, 31; G. Henrici-Olivé and S. Olivé *J. Mol. Catal.*, 1975/76, **1**, 121; T. Thangaraj, S. Vancheesan, J. Rajaram and J. C. Kuriacose, *Indian J. Chem., Sect. A*, 1980, **19**, 404; D. Chatterjee, H. C. Bajaj, S. B. Halligudi and K. N.Bhatt, *J. Mol. Catal.*, 1993, **84**, L1.
3 *Applied Homogeneous Catalysis with Organometallic Compounds*, ed. B. Cornils and W. A. Herrmann, VCH Publishers, New York, 1996, Sections 2.3, 2.4, 2.5 and 3.2.14.
4 C. Kelber, *Ber.*, 1917, **50**, 1509.
5 A. F. Williams, *Acta Crystallogr., Sect. C*, 1989, **45**, 1002.

Communication 8/07497F

ChemComm

Practical radical cyclisations leading to the construction of near-stereopure quaternary carbon stereogenic centres

Raymond McCague,[a] Robin G. Pritchard,[b] Richard J. Stoodley*[b] and Douglas S. Williamson[b]

[a] *Chirotech Technology Ltd., Cambridge Science Park, Milton Road, Cambridge, UK CB4 4WE*
[b] *Department of Chemistry, UMIST, PO Box 88, Manchester, UK M60 1QD. E-mail: richard.stoodley@umist.ac.uk*

Received (in Liverpool, UK) 12th October 1998, Accepted 2nd November 1998

The 2,3,4,6-tetra-*O*-acetyl-β-D-glucopyranosyl auxiliary is effective in directing bromopropargyloxy additions to the olefinic bonds of vinylogous esters/carbonates; in the presence of AIBN and 1-ethylpiperidinium hypophosphite, the adducts undergo highly stereoselective reductive radical cyclisations in which quaternary carbon stereogenic centres are generated.

The control of the absolute stereochemical outcome of reactions that generate quaternary carbon stereogenic centres is an important requirement in synthesis which is receiving much attention.[1] For radical methodology to provide a contribution, it is necessary to effect stereoselective additions of tertiary carbon radicals to carbon-based radical acceptors or of carbon radicals to tertiary olefinic acceptors. The ability to direct such radical additions by the use of temporarily attached auxiliaries† would offer notable synthetic versatility. To date, however, very few examples of such processes have been reported.[2]

Recently, we have shown that vinylogous esters/carbonates bearing the 2,3,4,6-tetra-*O*-acetyl-β-D-glucopyranosyl auxiliary react with NBS and primary alcohols with excellent regioselectivity, high *anti* stereoselectivity and reasonable facial selectivity.[3] For example, in reactions involving PrOH, the olefins **1a–c** gave rise to *ca*. 6:1 mixtures of the bromopropoxy derivatives **2a–c** and **3a–c** (Scheme 1), from which the major products **2a–c** could be isolated in near-stereopure states and satisfactory yields by fractional crystallisation. Seeking to stereoselectively replace the bromine atoms by functional carbon substituents, we have studied the radical reactivity of bromides of type **4**. We now report our findings.

As outlined in Scheme 2, it was envisaged that, in the presence of a radical reducing agent, bromides of type **4** would afford tertiary radicals of type **5** which would undergo 5-*exo*-*dig* cyclisations and acceptance of hydrogen atoms to give products of types **6** and/or **7**. In an initial experiment, it was found that the vinylogous ester **1a** was converted into a 4:1 mixture of the requisite bromide **4a** and a diastereomer by the action of NBS and propargyl alcohol; fractional crystallisation provided **4a**,‡ mp 169–170 °C, $[\alpha]_D$ −68 (*c* 0.54, CH_2Cl_2), in 54% yield. When heated in toluene under reflux with AIBN and Bu_3SnH, **4a** was transformed into one major product (35% yield after chromatography and crystallisation), mp 94–95 °C, $[\alpha]_D$ −23 (*c* 0.25, CH_2Cl_2), that clearly possessed the structure **6a** or **7a** on the basis of its analytical and spectral properties.

That the radical cyclisation product possessed the stereostructure **6a** was established by an X-ray crystallographic analysis of a derivative. Thus, catalytic hydrogenation (H_2, 5% Pd–C, EtOAc) afforded a 3:1 mixture of dihydro derivatives, from which the major diastereomer, mp 151–152 °C, $[\alpha]_D$ +40 (*c* 0.25, CH_2Cl_2), was isolated by fractional crystallisation. The product possessed the stereostructure **8** on the basis of the X-ray analysis§ (Fig. 1). Clearly, the radical **5a** had undergone a reductive cyclisation to give **6a** rather than **7a**. Moreover, there was a preference for hydrogen addition to **6a** to occur *syn* to the acyl group. Finally, the presumed stereochemical outcome of the initial bromopropargyloxylation reaction was substantiated.

Numerous attempts were made to improve the efficiency of the **4a**→**6a** transformation and to avoid the handling of toxic tin-based reagents. The use of AIBN and tris(trimethylsilyl)-silane[4] in toluene under reflux provided a cleaner raw product but chromatography was still required to remove impurities; **6a** was then isolated in 65% yield. However the best result was achieved when **4a** was heated with AIBN and 1-ethylpiperidinium hypophosphite[5] in toluene under reflux; the crude product, obtained in essentially quantitative yield after work-up, was very largely **6a**.

The effectiveness of the overall technology was demonstrated further by its application to the vinylogous ester **1b**. Thus, subjection of **1b** to the action of NBS and propargyl alcohol gave **4b**‡ (47% yield after crystallisation), mp 133–134 °C, $[\alpha]_D$ −82 (*c* 0.25, CH_2Cl_2), which underwent the hypophosphite-induced reductive radical cyclisation to give largely **6b** almost quantitatively; crystallisation provided **6b**,‡¶ mp 133–134 °C, $[\alpha]_D$ −28 (*c* 0.28, CH_2Cl_2), in 61% yield.

The excellent stereoselectivity observed in the aforecited radical cyclisations can be accommodated by an extension of a stereoinduction model proposed by Giese.[6] Thus, it is envisaged that the cyclisation occurs by way of the conformer **9** in which the acetal hydrogen atom is *syn* to the olefinic bond of the delocalised radical. A prediction of this model is that the stereochemical outcome is determined solely by the acetal configuration and that the auxiliary plays no direct role in the stereoinduction process.

The vinylogous ester **10a**‖ was converted into the acetylenic bromide *rac*-**11a**‡ (73% yield after chromatography) which

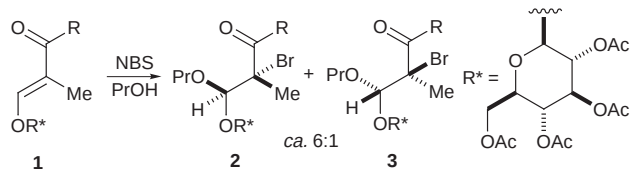

Scheme 1

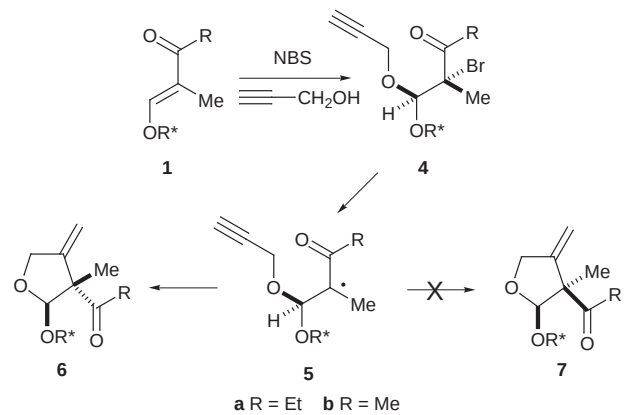

Scheme 2

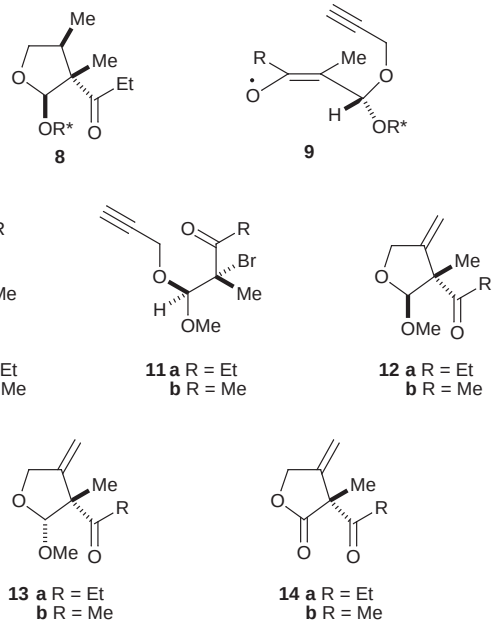

underwent radical cyclisation to give compound *rac*-**12a**‡ (77% yield after chromatography) [a comparative NOE difference spectroscopic study on *rac*-**12a** and *rac*-**13a** (obtained by equilibration of *rac*-**12a** using TsOH and MeOH) left little doubt about the stereochemical assignments]. Similarly, **11b**‡ (obtained in 78% yield after chromatography by bromopropargyloxylation of **10b**‖) afforded *rac*-**12b**‡ (74% yield after chromatography). Clearly, the configuration of the acetal stereocentre of the reactants *rac*-**11a** and *rac*-**11b** determines the configuration of the quaternary carbon stereocentre of the products *rac*-**12a** and *rac*-**12b**, providing strong support for the stereoinduction model **9**.

To complete the study, it was appropriate to remove the sugar auxiliary from **6a** and **6b** and to determine the enantiomeric purities of the products. In preliminary experiments, it was shown that *rac*-**12a** and *rac*-**12b** could be oxidised (CrO_3, H_2SO_4, Me_2CO, ultrasound)[7] to the γ-lactones *rac*-**14a** and *rac*-**14b**,** the enantiomers of which were separable by GC.††

Under methanolysis conditions (TsOH, MeOH), **6a** was transformed into a 1:1 mixture of the methoxy derivatives **12a** and **13a**‡ (84% yield after chromatography), $[\alpha]_D$ −110 (*c* 0.16, CH_2Cl_2), whereas **6b** afforded a 3:1 mixture of the methoxy derivatives **12b** and **13b**‡ (79% yield after chromatography), $[\alpha]_D$ −142 (*c* 0.30, CH_2Cl_2). Following Jones' oxidation of the mixtures, the γ-lactones **14a** and **14b**** were isolated, each with 96% ee. Since the ee analyses were conducted on products that had been obtained from raw samples of **6a** and **6b**, it is clear that the hypophosphite-induced radical cyclisations displayed excellent stereoselectivities; moreover, the diastereomeric purities of the precursors **4a** and **4b** were high. When a crystallised sample of **6b** was employed, the derived γ-lactone **14b** possessed an ee of >99%.

The aforecited findings are significant in the following respects. In the presence of AIBN, 1-ethylpiperidinium hypophosphite offers marked advantages over Bu_3SnH or tris(trimethylsilyl)silane in effecting 5-*exo*-*dig* reductive radical cyclisations‡‡ of acetylenic bromides. The high stereoselectivities observed in the radical cyclisations are striking; they can be accommodated by a simple stereoinduction model dictated by allylic strain considerations. As well as providing a further illustration of the versatility of vinylogous esters/carbonates of type **1** in asymmetric synthesis, the technology enables units featuring quaternary carbon stereogenic centres with three functional arms to be assembled in multigram quantities.

We thank the DTI and EPSRC for subsidisation of a studentship (to D. S. W.) under the Link Asymmetric Synthesis Programme. We are also grateful to P. D. Tiffin for relevant preliminary studies and to Dr G. Potter for helpful advice.

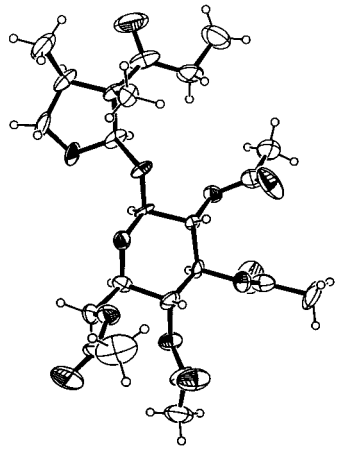

Fig. 1 Molecular structure of **8**.

Notes and references

† For examples of the use of chiral auxiliaries in radical reactions, see ref. 8.

‡ This compound displayed analytical and spectral properties that supported its assigned structure.

§ *Crystal data* for **8**: $C_{23}H_{34}O_{12}$, M = 502.5, monoclinic, space group $P2_1$, a = 6.425(6), b = 23.566(7), c = 17.545(7) Å, β = 90.36(4)°, Z = 4 (2 molecules per asymmetric unit), D_c = 1.256 g cm^{-3}, $F(000)$ = 1072, μ(Mo–Kα) = 1.05 cm^{-1}, crystal size 0.30 × 0.25 × 0.25 mm. A total of 4328 reflections were measured, 4315 of which were unique (R_{int} = 0.067), on a Siemens R3m/V diffractometer using the $\omega/2\theta$ scan method (λ = 0.71073 Å) at 293(2) K. The structure was solved by direct methods and refined by full-matrix least-squares based on F^2, with all non-hydrogen atoms anisotropic and hydrogen atoms constrained in calculated positions. The final cycle converged to R = 0.1280 and wR^2 = 0.2431. CCDC 182/1081. The crystallographic data is available as a .cif file; see http://www.rsc.org/suppdata/cc/1998/2691

¶ A solution of **4b** (5.61 g, 10 mmol), 1-ethylpiperidinium hypophosphite (8.99 g, 50 mmol) and AIBN (0.34 g, 2.0 mmol) in toluene (150 cm^3) was heated under reflux for 1 h. The resulting olive-green mixture was concentrated and the residue was dissolved in CH_2Cl_2. The solution was filtered through a pad of Celite and the filtrate washed with water (×2) and brine. Evaporation of the dried ($MgSO_4$) organic phase left a white solid (5.05 g) which was largely **6b**. After crystallisation from Pr^{i}OH, **6b** (2.99 g, 61%) was isolated in a pure state.

‖ Compounds **10a** and **10b** were prepared by methylation (MeOTs, Me_2SO) of the corresponding sodium enolates [obtained by the method of Kaushal *et al*. (ref. 9)].

** The yields of these products were low (10–18%).

†† The enantiomers were separated on a Chiraldex γ-cyclodextrin trifluoroacetyl column (heated from 100 to 160 °C at a rate of 1.5 °C min^{-1}).

‡‡ This appears to be the first report of the use of 1-ethylpiperidinium hypophosphite to effect such reactions.

1 S. F. Martin, *Tetrahedron*, 1980, **36**, 419; K. Fuji, *Chem. Rev*., 1993, **93**, 2037; E. J. Corey and A. Guzman–Perez, *Angew. Chem., Int. Ed*., 1998, **37**, 388.
2 M.–Y. Chen, J.–M. Fang, Y.–M. Tsai and R.–L. Yeh, *J. Chem. Soc., Chem. Commun*., 1991, 1603; P. A. Zoretic, X. Weng, C. K. Biggers, M. S. Biggers, M. L. Caspar and D. G. Davis, *Tetrahedron Lett*., 1992, **33**, 2637; B. B. Snider and Q. Zhang, *Tetrahedron Lett*., 1992, **33**, 5921; Q. Zhang, R. M. Mohan, L. Cook, S. Kazanis, D. Peisach, B. M. Foxman and B. B. Snider, *J. Org. Chem*., 1993, **58**, 7640.
3 M. S. Idris, D. S. Larsen, A. Schofield, R. J. Stoodley and P. D. Tiffin, *Tetrahedron Lett*., 1995, **36**, 3251.
4 C. Chatgilialoglu, *Chem. Rev*., 1995, **95**, 1229.
5 D. H. R. Barton, D. O. Jang and J. C. Jaszberenyi, *J. Org. Chem*., 1993, **58**, 6838.
6 B. Giese, M. Bulliard and H.-G. Zeitz, *Synlett*, 1991, 425.
7 A. Srikrishna, S. Nagaraju and G. V. R. Sharma, *J. Chem. Soc., Chem. Commun*., 1993, 285.
8 D. P. Curran, N. A. Porter and B. Giese, *Stereochemistry of Radical Reactions*, VCH, Weinheim, 1996, ch. 5.
9 R. Kaushal, S. Sovani and S. S. Deshapande, *J. Indian Chem. Soc*., 1942, **19**, 107.

Communication 8/07930G

ChemComm

Experimental evidence of partially rate limiting ion-pair interconversion in a base catalyzed 1,3-proton transfer reaction

Anita Hussénius,* Olle Matsson and Göran Bergson

Institute of Chemistry, Uppsala University, Box 531, S-751 21 Uppsala, Sweden. E-mail: anitah@kemi.uu.se

Received (in Liverpool, UK) 7th October 1998, Accepted 26th October 1998

The relative rates for interconversion and reprotonation of the ion-pair intermediates are of the same order of magnitude in the piperidine catalyzed 'degenerate' rearrangement of 1,3-dimethylindene, as investigated using ^{1}H and ^{2}H NMR spectroscopy by letting the 1,3-hydron transfer reaction compete with isotope (^{1}H/^{2}H) exchange.

Many organic and biochemical reactions involve the transfer of a proton from a carbon acid to a base. Hydrogen bonded carbanions have been postulated as intermediates in essentially all hydron transfer reactions from carbon acids.[1] Therefore, mechanistic interpretations of observed phenomena such as kinetic isotope effects and enantioselectivities require detailed knowledge of processes involving carbanion ion pairs. The simple example shown in Scheme 1 illustrates this point (the 'degeneracy' of this rearrangement reduces the number of different rate constants, thus simplifying the kinetic analysis). Application of the steady-state approximation to the two reactive ion-pair intermediates gives the relation [eqn. (1)]

$$k = k_1/[2 + (k_{-1}/k_{12})] \quad (1)$$

between the phenomenological rate constant k (which can be determined experimentally) for this 1,3-proton transfer reaction, and the mechanistic rate constants, k_1, k_{-1} and k_{12}. If and only if the interconversion of the ion pairs (k_{12}) is much faster than collapse back to a covalent entity (k_{-1}), can observed effects on k be discussed straightforwardly in terms of the proton abstraction step (k_1). Thus, it is of great importance to know the magnitude of the rate constant ratio (k_{-1}/k_{12}).

Arguments for rapid interconversion ($k_{12} >> k_{-1}$) of the intermediates arise from the fact that no covalent bonds are formed or broken in this process, making it plausible that the ammonium ion, once formed, should be able to slide between the 1- and 3-positions with very low activation energy. Evidence for the existence of two ion-pair intermediates not in equilibrium with each other has, however, been presented by Ahlberg and Thibblin.[2,3] Thus, the assumption of rapid interconversion of ion pairs has to be tested, if possible, for each specific system.

Herein, we report on an experimental investigation aimed at retrieving information about the relative rates referred to above. The crucial point is that the 1,3-hydron transfer is allowed to compete with isotopic exchange of the 'mobile' hydron mediated by ammonium ion rotation within the ion pair.[4–6] Our system (Scheme 2) mimics the simple case given in Scheme 1. 1,3-Dimethylindene, in which a trideuteriomethyl group is substituted for one of the methyl groups, was used as a substrate. The CD_3 group served only as a label making it possible to distinguish between the 1- and 3-positions and to follow the time evolution of the concentrations of all four species (**I**–**IV**) by ^{1}H and ^{2}H NMR spectroscopy. The expected small secondary isotope effects due to this labelling can be neglected

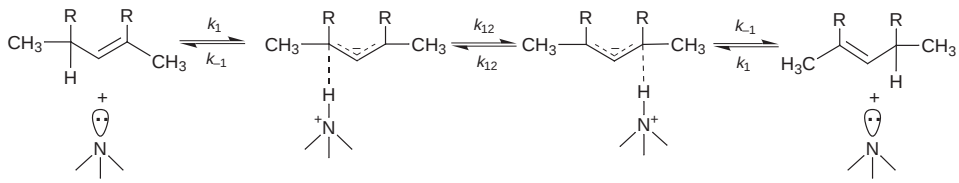

Scheme 1

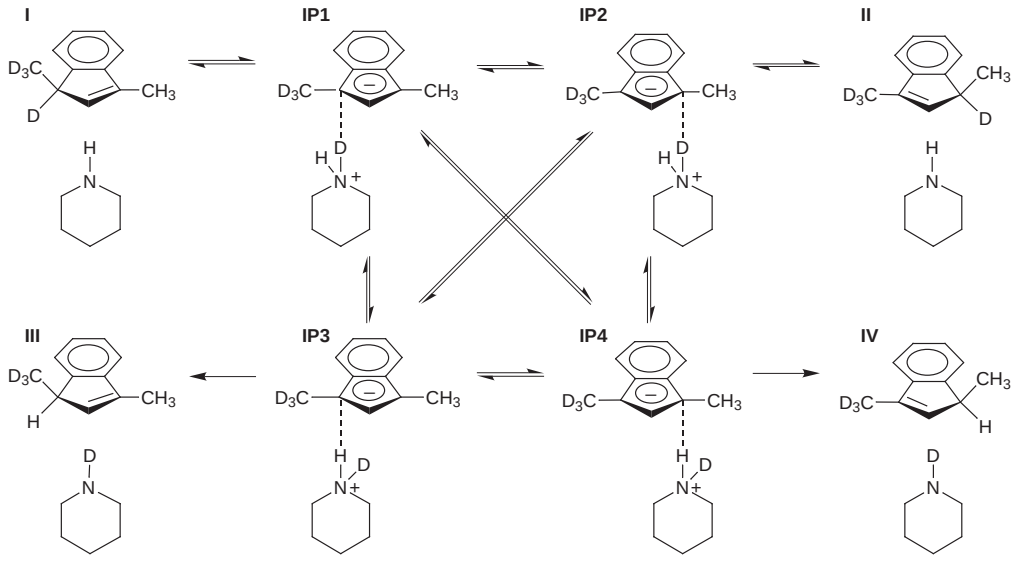

Scheme 2

in the present context. The reaction was run in benzene solution and the secondary amine piperidine was used as base-catalyst and (^{1}H/^{2}H) −exchange agent. If the substrate is deuteriated in the C1 position, the use of protic base results in incorporation of protium in the dimethylindene due to rotation of the ammonium ion within the ion pair. If the base is used in large excess, the ^{1}H/^{2}H exchange is practically irreversible. The kinetics of this protium incorporation, in the 1- and 3-positions respectively, provides a measure of the relative rates of ion-pair equilibration and collapse.

In Scheme 2 a mechanistic model for our system is depicted. Starting at the upper left corner, the amine abstracts a deuteron from 1,3-dimethylindene **I** and an ion-pair intermediate **IP1** is formed. Either the hydron transfer proceeds, *via* interconversion to the ion pair **IP2**, to the rearranged product **II** without deuterium/protium exchange, or a new ion pair **IP3** is formed through ammonium ion rotation (a direct route from **IP2** to **IP4** cannot be excluded, but the presence of such a route does not influence our conclusions). Now, the ion pairs **IP3** and **IP4** can interconvert, just as **IP1** and **IP2**. If the ion-pair interconversion is much faster than collapse, the two exchange products **III** and **IV** will appear in equal amounts (or more precisely in the ratio 1.04, which is the magnitude of the secondary equilibrium isotope effect, determined as the average from several kinetic experiments) from the very start of the reaction. On the other hand, if these products, **III** and **IV**, appear in unequal amounts, the assumption of fast ion-pair interconversion is not valid. Thus, by studying the kinetics of formation of the exchange products **III** and **IV**, information can be obtained regarding the relative rates of ion-pair interconversion and ion-pair collapse.

The present kinetic data have been obtained from ^{1}H and ^{2}H NMR spectra of quenched and concentrated samples, taken at regular time intervals from the reaction mixture. The experiments were performed in benzene solution at 20 °C. The secondary amine piperidine was used as base catalyst, in an excess of 45–50 equiv. of the substrate concentration. The use of a large excess of base permits the ^{1}H/^{2}H exchange reaction, to a good approximation, to be regarded as irreversible. In principle it is possible to start from either of the four different isotopically substituted 1,3-dimethylindenes but all kinetic experiments reported here have started from the substrate 1-[^{2}H$_3$]methyl-3-methyl[1-^{2}H]indene[7–9] and protic piperidine.

In the kinetic procedure, the isotopically substituted 1,3-dimethylindene (70–100 mg) was weighed into a calibrated 10 ml volumetric flask. A stock solution of piperidine in benzene was prepared in a volumetric flask which was then sealed with a tight PTFE septum and a screwcap. Both flasks were thermostatted at 20.00 °C. The temperature was measured with a calibrated mercury thermometer with an absolute accuracy of 0.02 °C. The temperature did not deviate more than 0.02 °C from the average value during the kinetic runs and was thus 20.00 ± 0.04 °C. Base solution was withdrawn by means of a nitrogen flushed syringe and the 10 ml flask was filled to the mark. A clock was started when half of the base solution had been added. The flask was sealed with a septum and a screwcap and was then rapidly shaken and replaced in the thermostat bath. Samples (1–1.5 ml) were taken at regular time intervals. The reaction was quenched with 2–3 ml of 5 M HCl, which was cooled to at least −10 °C. The organic phase was separated and washed with brine and distilled water. The solution was concentrated by evaporation and ^{2}H NMR spectra were recorded. Residual solvent was removed at reduced pressure, the residue was dissolved in C^{2}HCl$_3$ (Ciba-Geigy, > 99.9 atom% ^{2}H) and finally the ^{1}H NMR spectra were recorded. When the pure substrate was subjected to the work-up conditions it was recovered unchanged.

The samples of the quenched reaction contain four different isotopically substituted 1,3-dimethylindenes resulting from rearrangement and exchange reactions (see Scheme 2). There are three signals of interest in the NMR spectra: the signal at δ 1.28 from the methyl group at the C1 position of the indene ring system, the signal at δ 2.13 from the methyl group at the C3-position, and the signal at δ 3.40 from the protium (deuterium) at C1. Computer resolution of the ^{1}H signals at δ 1.28 was performed using a curve fitting routine, to be able to solve for the four unknown concentrations. The signal at this shift consists of a doublet from **IV**, a singlet from **II** (see Scheme 2) and also a signal from traces of protium in the trideuteriomethyl group at the 1-position. Utilizing computer resolution the ^{1}H NMR spectrum is, in principle, sufficient for determination of the content of each species. The ^{2}H NMR spectra have been recorded in order to allow for a double check of the relative concentrations.

Table 1 Relative concentrations[a] of the four 1,3-dimethylindenes in the reaction mixture at different tmies, in a piperidine[b] catalyzed rearrangement/exchange experiment starting from 1-[^{2}H$_3$]methyl-3-methyl[1-^{2}H]indene **I** in benzene at 20 °C

t/s	**I**	**II**	**III**	**IV**	**III/IV**
0	0.988	—	0.012	—	—
1835	0.819	0.0237	0.104	0.0527	1.97
1690	0.718	0.0367	0.143	0.103	1.39
5400	0.643	0.0370	0.175	0.145	1.21
7200	0.586	0.0312	0.202	0.181	1.12
12600	0.428	0.0338	0.270	0.268	1.01
∞	0.0102	0.00990	0.497	0.483	1.03

[a] The total concentration of substrate was 0.0677 M. The concentration is normalized to 1 in the table. [b] [Piperidine] = 3.149 M.

In Table 1 the results from a typical kinetic experiment are displayed. In the beginning of the experiment (18% reaction) the isotopically exchanged indene **III**, produced by collapse of **IP3**, appear in the reaction mixture in a concentration almost twice as high as that of indene **IV**, produced from **IP4** ([**III**]/[**IV**] = 1.97). The concentration ratio of the exchanged indenes then gradually decreases towards the secondary equilibrium isotope effect (for simplicity, the reversible piperidine catalyzed rearrangement between **III** and **IV** has been omitted from Scheme 2). The conclusion is thus that the assumption of fast ion-pair equilibration is not valid for the system studied. This is in accordance with recently published theoretical calculations for a similar rearrangement.[10] In that study it was found that the relevant activation barriers were dependent of the structure of the catalyzing base as well as on the solvent. A full account including a detailed kinetic analysis of the present reaction system will be published in due course.

Notes and references

1 D. J. Cram, *Fundamentals of Carbanion Chemistry*, Academic Press, New York 1965, pp. 86–103.
2 A. Thibblin, S. Bengtsson and P. Ahlberg, *J. Chem. Soc., Perkin Trans. 2*, 1977, 1569.
3 A. Thibblin, *Chem. Scr.*, 1983, **22**, 182.
4 D. J. Cram and R. Gosser, *J. Am. Chem. Soc.*, 1963, **85**, 3890.
5 D. J. Cram and R. Gosser, *J. Am. Chem. Soc.*, 1964, **86**, 2950, 5445 and 5457.
6 G. Bergson and L. Ohlsson, *Acta Chem. Scand.*, 1967, **21**, 1353.
7 L. Ohlsson, I. Wallmark and G. Bergson, *Acta Chem. Scand.*, 1966, **20**, 750.
8 C. F. H. Allen and F. W. Sprangler, *Org. Synth.*, 1955, **Coll. Vol. 3**, 377.
9 G. Bergson, O. Matsson and S. Sjöberg, *Chem. Scr.*, 1977, **11**, 25.
10 M. Agback, S. Lunell, A. Hussénius and O. Matsson, *Acta Chem. Scand.*, 1998, **52**, 541.

Communication 8/07798C

ChemComm

A new redox-tunable near-IR dye based on a trinuclear ruthenium(II) complex of hexahydroxytriphenylene

Anita M. Barthram, Rosemary L. Cleary, Ralph Kowallick and Michael D. Ward*

School of Chemistry, University of Bristol, Cantock's Close, Bristol, UK BS8 1TS. E-mail: mike.ward@bristol.ac.uk

Received (in Cambridge, UK) 8th October 1998, Accepted 10th November 1998

The complex $[\{Ru(bipy)_2\}_3(\mu^3\text{-}L)]^{3+}$ (H_6L = hexahydroxytriphenylene), in which the tris-dioxolene bridging ligand is formally in the tris-semiquinone oxidation state [sq,sq,sq], undergoes three reversible ligand-centred oxidations to the [q,q,q] state (q = quinone); it exhibits very strong NIR absorption arising from Ru → L charge transfer whose maximum wavelength may be tuned over a wide range according to oxidation state.

Compounds which absorb light strongly in the near IR (NIR) region of the spectrum have numerous potential applications, including (i) optical data storage devices, in which reading and writing is performed by diode lasers; (ii) Q-switching of lasers, whereby continuous low-energy output in the NIR region is converted to very short, intense bursts; and (iii) photodynamic therapy, which takes advantage of the relative transparency of living tissue to NIR radiation.[1] Prominent examples of such compounds include nickel(II)–dithiolene complexes[2] and extended quinones.[3] If the strong NIR absorption is not permanent but may be switched on by some external perturbation, then the compound is of additional interest as a switchable electrochromic dye; such compounds are relatively rare.[4]

The simple complex $[Ru(bipy)_2(sq)]^+$ (bipy = 2,2′-bipyridine; sq = 1,2-benzosemiquinone monoanion) is of potential interest in this regard, having a NIR transition at about 900 nm (ε *ca.* 10^4 dm^3 mol^{-1} cm^{-1}) arising from a $Ru[d_\pi] \rightarrow sq(\pi^*)$ MLCT process.[5] It undergoes ligand-centred redox behaviour, being oxidised to $[Ru(bipy)_2(q)]^{2+}$ (q = 1,2-benzoquinone) and reduced to $[Ru(bipy)_2(cat)]$ (cat = catecholate dianion), in both of which forms this NIR transition is absent.[5] We have recently been interested in the electrochemical and spectroscopic properties of dinuclear complexes in which two such Ru(II) fragments are linked by bridging ligands containing two dioxolene termini.[6] We describe here the synthesis, electrochemical and UV–VIS–NIR properties of $[\{Ru(bipy)_2\}_3(\mu\text{–}L)]^{n+}$ (**1**$^{n+}$, n = 3–6) in which three such redox-active Ru(II) fragments are linked in a triangular array by the bridging ligand hexahydroxytriphenylene (H_6L).[7] Spectroelectrochemical analysis in four oxidation states reveals an exceptionally strong absorbance in the NIR region which may be tuned over a wide range according to oxidation state.

Reaction of hexahydroxytriphenylene[7] with 3 equiv. of $[Ru(bipy)_2(OH_2)_2]^{2+}$ (ref. 8) in refluxing ethanol–water–KOH at reflux in air for 2 h, followed by precipitation of the complex with NH_4PF_6 and chromatographic purification (alumina; CH_2Cl_2–MeOH, 19 : 1 v/v), afforded in 50% yield $[\mathbf{1}][PF_6]_3$ (Scheme 1) as a black solid. Characterisation was on the basis of FAB mass spectrometry [*m/z* 1848 {70%, $M - PF_6$}, 1703 {100%, $M - 2PF_6$}] and a satisfactory elemental analysis. The +3 charge implies that each of the three dioxolene fragments is in the semiquinone oxidation level (denoted sq-sq-sq) following synthesis in air, which is to be expected.[5,6] Individual $\{Ru(bipy)_2(sq)\}^+$ units have one unpaired electron on the semiquinone ligand, but when two such units are linked in a *para* substitution pattern by a suitable conjugated bridge, the two electrons pair up to give diamagnetic dinuclear complexes with formation of an additional π-bond resulting in a quinonoidal bridging ligand.[6] In $[\mathbf{1}]^{3+}$ any two of the semiquinone sites can be spin-paired, resulting in a monoradical.†

Cyclic and square-wave voltammetry of $[\mathbf{1}][PF_6]_3$ was performed in MeCN. If each dioxolene site showed the expected cat/sq and sq/q interconversions characteristic of mononuclear $[Ru(bipy)_2(sq)]^+$ then we would expect to see six redox processes linking seven oxidation states of the bridging ligand ranging from [cat,cat,cat] to [q,q,q]. Six waves were indeed observed, whose potentials (from a square-wave voltammogram) are +0.66, +0.36, −0.03, −0.43, −0.70 and −0.97 V *vs.* ferrocene–ferrocenium. The approximately constant and quite substantial spacing between these redox potentials is to be expected given the proximity of the dioxolene sites to one another.[6] Of these six processes only the first four appeared fully reversible (equal cathodic and anodic peak currents, ΔE_p 60–80 mV) by cyclic voltammetry using a Pt-wire working electrode (Fig. 1); the two processes at most negative potentials showed stripping peaks on the return waves, characteristic of absorption on the Pt electrode surface after generation of the [cat,sq,sq] and more reduced oxidation states. Despite this it is apparent that all seven oxidation states are in principle accessible.

We therefore subjected $[\mathbf{1}][PF_6]_3$ to a spectroelectrochemical study in an OTTLE cell (MeCN, −30 °C) spanning the oxidation states sq,sq,sq (**1**$^{3+}$), sq,sq,q (**1**$^{4+}$), sq,q,q (**1**$^{5+}$) and q,q,q (**1**$^{6+}$). For all three interconversions clean isosbestic points

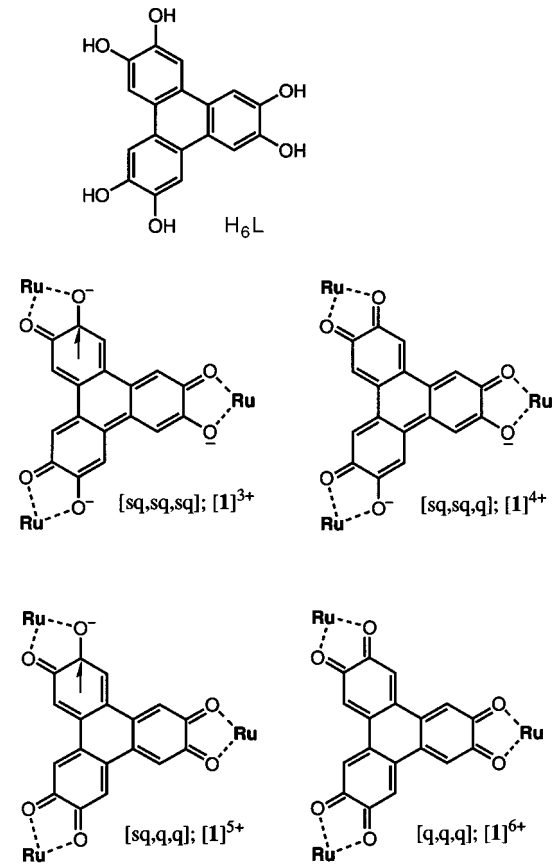

Scheme 1 Ru ≡ $\{Ru(bipy)_2\}^{2+}$.

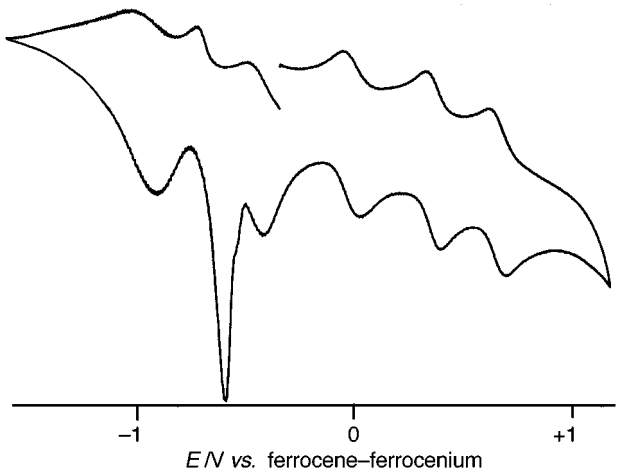

Fig. 1 Cyclic voltammogram of $[\mathbf{1}]^{3+}$ in MeCN, showing the stepwise interconversions between the [cat,cat,cat] and [q,q,q] states of the bridging ligand. Only the three most positive processes, from [sq,sq,sq] to [q,q,q], are fully reversible at a Pt electrode.

were observed, and after the final oxidation to $[\mathbf{1}]^{6+}$, re-reduction regenerated exactly the spectrum of the starting $[\mathbf{1}]^{3+}$. The results (Fig. 2) show that (i) the redox chemistry is indeed ligand-centred, and (ii) the complex has exceptionally strong absorption in the near-IR region whose absorption maximum varies monotonically with oxidation state. It is helpful to recall that for mononuclear $[Ru(bipy)_2(sq)]^+$, the MLCT transition at 900 nm shifts to *ca.* 640 nm on oxidation to $[Ru(bipy)_2(q)]^{2+}$.[5] For $[\mathbf{1}]^{3+}$, the MLCT transition involving the delocalised [sq,sq,sq] bridging ligand occurs at 1170 nm (ε = 40 000 $dm^3\ mol^{-1}\ cm^{-1}$). As the ligand is oxidised in steps to the [sq,sq, q], then [sq,q,q] and finally [q,q,q] oxidation states this absorption maximum moves in steps to 1083 (ε = 74 000), 909

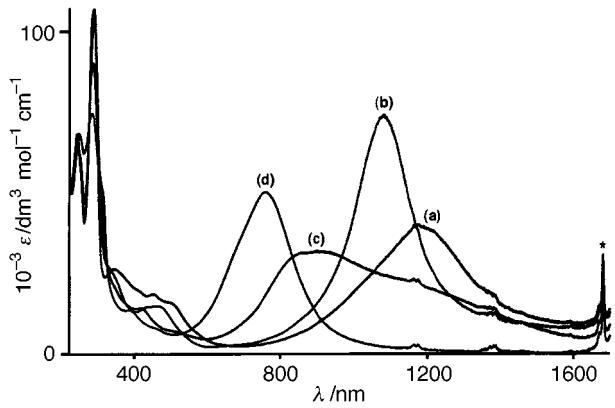

Fig. 2 Electronic spectra of (a) $[\mathbf{1}]^{3+}$, (b) $[\mathbf{1}]^{4+}$, (c) $[\mathbf{1}]^{5+}$ and (d) $[\mathbf{1}]^{6+}$ (MeCN, −30 °C); * denotes a solvent-based IR overtone.

(ε = 32 000) and finally 759 nm (ε = 50 000 $dm^3\ mol^{-1}\ cm^{-1}$). The 'mixed-valence' [sq,sq,q] and [sq,q,q] states must therefore be delocalised, because a single transition at a 'weighted average' position occurs in each case rather than two separate transitions characteristic of distinct sq and q sites in the bridging ligand. These transitions are remarkably intense and broad: the absorption coefficients of 32 000–74 000 $dm^3\ mol^{-1}\ cm^{-1}$ are comparable to those of commercially useful NIR dyes,[1,2] and the lower-energy three transitions have long low-energy tails (extending to 1700 nm and over) such that in these oxidation states the molecule is effectively a panchromatic NIR absorber. This complex therefore shows an unusual combination of very strong NIR absorbance and tunability of the absorption maximum over a wide range using four readily accessible oxidation states.

We thank the EPSRC for Ph.D. studentships (A. M. B. and R. L. C.).

Notes and references

† That $[\mathbf{1}][PF_6]_3$ is a monoradical and not a triradical was confirmed both experimentally and theoretically. An EPR spectrum (frozen MeCN solution, 77 K) has a near-symmetric signal at g = 2.017 characteristic of a semiquinone-based monoradical with no evidence for Δm_s = 2 or Δm_s = 3 transitions. A MOPAC calculation on $[L]^{3-}$ in the [sq,sq,sq] state showed that the three frontier orbitals involved in conversion between the [cat,cat,cat] and [q,q,q] states are non-degenerate, such that the [sq,sq,sq] state (as well as the [sq,q,q] and [sq,cat,cat] states) are monoradicals, whilst the others are diamagnetic, as in Scheme 1.

1 M. Emmelius, G. Pawlowski and H. W. Vollmann, *Angew. Chem., Int. Ed. Engl.*, 1989, **28**, 1445; J. Fabian and R. Zahradnik, *Angew. Chem., Int. Ed. Engl.*, 1989, **28**, 677; J. Fabian, H. Nakazumi and M. Matsuoka, *Chem. Rev.*, 1992, **92**, 1197.
2 U. T. Mueller-Westerhof, B. Vance and D. I. Yoon, *Tetrahedron*, 1991, **47**, 909; F. Bigoli, P. Deplano, M. L. Mercuri, M. A. Pellinghelli, G. Pintus, E. F. Trogu, G. Zonnedda, H. H. Wang and J. M. Williams, *Inorg. Chim. Acta*, 1998, **273**, 175; H. Shiozaki, H. Kakazumi, Y. Nakado and T. Kitao, *Chem. Lett.*, 1987, 2393.
3 K. Takahashi, A. Gunji, K. Yanagi and M. Miki, *J. Org. Chem.*, 1996, **61**, 4784.
4 K. Yoshida, N. Oga, M. Kadota, Y. Ogasahara and Y. Kubo, *J. Chem. Soc., Chem. Commun.*, 1992, 1114; Y. Kubo, *J. Chem. Soc., Perkin Trans. 1*, 1994, 2521; S.-M. Lee, M. Marcaccio, J. A. McCleverty and M. D. Ward, *Chem. Mater.*, in press.
5 M. Haga, E. S. Dodsworth, and A. B. P. Lever, *Inorg. Chem.*, 1986, **25**, 447.
6 L. F. Joulié, E. Schatz, M. D. Ward, F. Weber and L. J. Yellowlees, *J. Chem. Soc., Dalton Trans.*, 1994, 799; A. M. Barthram, R. L. Cleary, J. C. Jeffery, S. M. Couchman and M. D. Ward, *Inorg. Chim. Acta*, 1998, **267**, 1.
7 H. Naarmann, M. Hanack and R. Mattmer, *Synthesis*, 1994, 477; D. R. Beattie, P. Hindmarsh, J. W. Goodby, S. D. Haslan and R. M. Richardson, *J. Mater. Chem.*, 1992, **2**, 1261.
8 J. C. Jeffery, D. J. Liard and M. D. Ward, *J. Chem. Soc., Dalton Trans.*, 1996, 879.

Communication 8/07835A

Synthesis of a ferrocene bridged cyclam: a new redox-active macrocycle and the structure of a nickel(II) complex with strongly coupled metal centers

Herbert Plenio* and Clemens Aberle

Institut für Anorganische und Analytische Chemie, Albertstr. 21, 79104 Freiburg, Germany. E-mail: plenio@uni-freiburg.de

Received (in Basel, Switzerland) 16th September 1998, Accepted 30th October 1998

The reaction of 1,1′-ferrocene-bis(methylenepyridinium) with 1,4,8,11-tetraazacyclotetradecane-5,12-dione followed by reduction of the product with $LiAlH_4$ results in a ferrocene bridged cyclam, which is a very efficient redox-switch for transition metal ions due to the short iron-to-metal ion distances.

Cyclam (1,4,8,11-tetraazacyclotetradecane) and its numerous derivatives are among the most important macrocyclic ligands;[1] its coordination chemistry is well explored[2] and a number of cyclam–metal complexes are catalytically active.[3]

We were interested in synthesizing a ferrocene-bridged cyclam, since we anticipated that this would result in short distances between the ferrocene iron and any metal ion coordinated within the tetraaza-macrocycle. Consequently the interactions between the different metal centers are expected to be very strong and redox reactions at the ferrocene should have a pronounced effect on the properties of cyclam and those of the metal ions coordinated by it. This should add a new dimension to the coordination chemistry of cyclam and allow the design of new molecules for the electrochemical sensing of transition metal cations[4] and anions,[5] redox-switched catalysis,[6] the redox-switched bonding of metal ions[7] and biomimetic chemistry.[8]

However, partially substituted cyclams are less easily available and only recently a very convenient synthesis utilizing 1,4,8,11-tetraazacyclotetradecane-5,12-dione was presented by Guilard and coworkers.[9] In order to generate the ferrocene bridged cyclam, 1,1′-ferrocene-bis(methylenepyridinium) was reacted with 1,4,8,11-tetraazacyclotetradecane-5,12-dione in refluxing acetonitrile (Scheme 1).† After chromatographic work-up two main products were isolated: the 1 + 1-addition product (yield *ca.* 50%), the 2 + 2-addition product (yield *ca.* 24%) and a small amount of 3 + 3-product (*ca.* 5%). The total yields and the ratios of the different oligomers depended on the concentration of the reactants in the reaction mixture and it is possible to raise the amount of the 2 + 2- and 3 + 3-product significantly by decreasing the amount of solvent. Ferrocene-cyclam **1** can be synthesized in 86% yield from the initial 1 + 1-product by reduction with $LiAlH_4$. The 2 + 2-product can also be reduced in this manner resulting in the respective cofacial bis(ferrocene-cyclam) **2**.

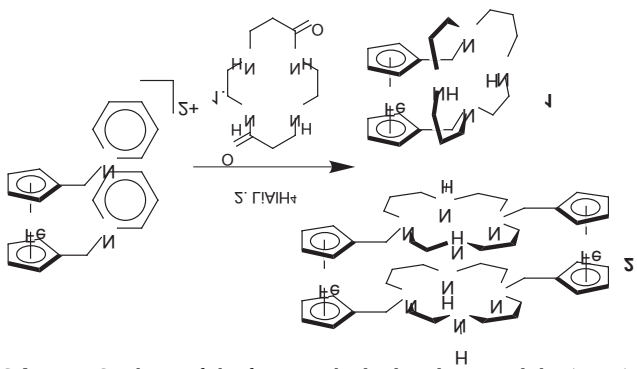

Scheme 1 Synthesis of the ferrocene bridged cyclam **1** and the (2 + 2)-addition product **2**.

Initially we were interested in the electrochemical properties of the ferrocene-cyclam and its transition metal complexes. Table 1 lists redox data obtained by cyclic voltammetry in acetonitrile from which it is obvious that the magnitude of the redox shifts and hence the redox-switching effect per single metal ion is enormous, when for example compared to the $\Delta E_{½}$ values of related ferrocenyl-substituted cyclams[10,11] ($\Delta E_{½}$ < 100 mV) and is significantly larger than those of aminoferrocene metal complexes synthesized by us.[12]

To better understand the coordinating properties of **1** as well as the origin of the extremely large redox shifts we attempted to crystallize a metal complex of this ligand and were successful with $Ni(CF_3SO_3)_2$ (Fig. 1).‡ In the crystal, nickel is coordinated in the center of the tetraazamacrocycle in a square-planar environment, which is only slightly distorted, even though the oxygen atom of an acetone molecule displays a weak contact to Ni^{2+} [Ni1–O2 320.8(9) pm]. This square-planar geometry also appears to be present in solution as evidenced by the diamagnetic nature of the complex in acetonitrile. The stereo-

Table 1 Electrochemical data of **1** and transition metal complexes as determined by cyclic voltammetry in MeCN using NBu_4PF_6 as supporting electrolyte *vs.* cobaltocene ($E_{½}$ = −0.94 V) or ferrocene ($E_{½}$ = +0.40 V) reference

	$E_{½}$/V(Fe^{II}–Fe^{III})	$\Delta E_{½}$/mV
1	+0.33	—
1·$Co(CF_3SO_3)_2$	+0.69	+360
1·$Ni(CF_3SO_3)_2$	+0.71	+380
1·$Cu(CF_3SO_3)_2$	+0.74	+410
1·$Zn(CF_3SO_3)_2$	+0.80	+470

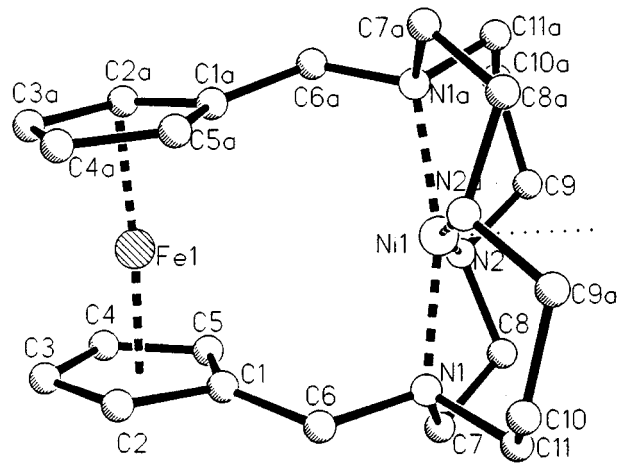

Fig. 1 Crystal structure of **1**·$Ni(CF_3SO_3)_2$ (acetone molecule, counter ions and hydrogen atoms omitted for clarity). Important bond lengths, interatomic distances (pm) and bond angles (°): Ni–N1 195.9(4), Ni–N2 194.8(5), Fe1–Ni1 385.4(8), N1–Ni–N1a 166.1(3), N2–Ni–N2a 162.4(3), N1–Ni–N2a 95.1(2), N1–Ni–N2 87.0(2).

chemistry of **1**·Ni(CF_3SO_3)$_2$ in the solid state is *trans*-I according to the Bosnich classification[13] and consequently both N–H vectors point approximately towards the ferrocene. Another unusual feature of this crystal structure is the rather short distance between iron and nickel [385.4(8) pm] and this can easily explain why upon Ni^{2+}-coordination the iron redox potentials are perturbed drastically. The above mentioned distance might be too long to account for a significant interaction (other than electrostatic) between the metals, but it once again raises the question about the possibility of bonding interactions between the iron in ferrocene and metal cations.[14] The fact that the ferrocene HOMO is predominantly localized on iron has nurtured speculation about donor–acceptor type interactions between the ferrocene iron and other metal ions. Investigations of metal ion complexes of ferrocene-cyclam **1** could provide a more conclusive answer to this question. The geometry of the ferrocene unit itself is essentially unremarkable though not ideal as evidenced by the small tilt (6.4°) of the respective planes of the two cyclopentadienyl rings; a more significant distortion is observed in the methylene groups (C6, C6a) which deviate from the respective cyclopentadienyl plane by 10.5°.

In conclusion this communication offers a simple two step synthesis of a redox-active cyclam ligand in which, owing to the intimate coupling of the metal centers, redox reactions at the ferrocene will strongly alter the coordination characteristics of the ligand.

Notes and references

† *Synthesis of ferrocene cyclam*. **A.** 1,1′-ferrocene-bis(methylenepyridinium) chloride tosylate (5.12 g, 9.02 mmol), 1,4,8,11-tetraazacyclotetradecane-5,12-dione (2.06 g, 9.02 mmol) and Na_2CO_3 (7.0 g) were added to acetonitrile (300 mL) and heated under reflux for 60 h. The cold reaction mixture was filtered and the filtrate evaporated to dryness. The residue was purified by chromatography ($CHCl_3$–MeOH = 10 : 1) to yield ferrocene–cyclamdione (2.0 g, 50%), 2 + 2-product (0.94 g, 24%) and 3 + 3-product (*ca*. 0.20 g, 5%). EIMS: 438 (M^+); ^{1}H NMR ($CDCl_3$) δ 2.11–2.29 (m, 6H), 2.58–3.36 (m, 10H), 3.82–4.08 (m, 12H), 8.97 (s, NH), 9.02 (s, NH). **B**. Ferrocene–cyclamdione (4.4 g, 10 mmol) was dissolved in a mixture of thf (100 mL) and $CHCl_3$ (200 mL). To the ice-cooled solution was added $LiAlH_4$ (7.6 g, 200 mmol) and stirring continued for 48 h. After careful hydrolysis of excess $LiAlH_4$ with water (70 mL), 15% aq. NaOH (200 mL) were added and the product extracted with $CHCl_3$. The organic layer was separated, dried over $MgSO_4$, filtered and the filtrate evaporated to dryness. The residue was purified by chromatography (MeOH–Et_2NH = 10 : 1) to yield 3.5 g (86%) of **1**. ^{1}H NMR ($CDCl_3$) δ 1.40 (d, 14 Hz, 2H), 1.85 (d, 12 Hz, 2H), 2.14 (d, 11 Hz, 4H), 2.46–2.95 (m, 14H), 3.22 (td, 7 Hz, 3 Hz, 2H), 3.73 (s, 2H), 3.93–4.08 (m, 10H). ^{13}C NMR ($CDCl_3$) δ 25.64, 47.02, 51.55, 53.40, 53.49, 58.20, 65.37, 65.76, 67.40, 70.26, 88.35. All compounds have been characterized by elemental analysis and NMR spectroscopy.

‡ *Crystal data for* **1**: $C_{27}H_{40}F_6FeN_4NiO_7S_2$, M = 825.3, T = 293 K, tetragonal space group $P4_32_12$, $a = b$ = 10.5735(15), c = 30.251(6) Å, V = 3382.0(10) Å^3, Z = 4, D_c = 1.621 g cm^{-3}, F (000) = 1704, μ(Mo-Kα) = 1.19 mm^{-1}, θ-range: 2.7–25.97°, reflections (collected/unique): 3524, 3137, refinement: full matrix least squares on F^2, data–parameters: 3137/219, final R-indices [$I > 2\sigma(I)$]: $R1$ = 0.0452, $wR2$ = 0.110, largest diff. peak and hole: +0.419, −0.370 e Å^{-3}. The structure was solved and refined using the SHELX-97 program suite.[15] CCDC 182/1077. See http://www.rsc.org/suppdata/cc/1998/2697 for crystallographic files in .cif format.

1 L. F. Lindoy, *The Chemistry of Macrocyclic Ligand Complexes*, Cambridge University Press, Melbourne, 1989.
2 M. Lachkar, R. Guilard, A. Atmani, A. deCian, J. Fischer and R. Weiss, *Inorg. Chem*., 1998, **37**, 1575; M. R. Oberholzer, M. Neuburger, M. Zehnder and T. A. Kaden, *Helv. Chim. Acta*, 1995, **78**, 505; J. R. Röper and H. Elias, *Inorg. Chem*., 1992, **31**, 1202 and references therein.
3 E. Fujita, J. Haff, R. Sanzenbacher and H. Elias, *Inorg. Chem*., 1994, **33**, 4627; G. Pozzi, M. Cavazzini, S. Quici and S. Fontana, *Tetrahedron Lett*., 1997, **38**, 7605.
4 J. M. Lloris, R. Martínez-Máñez, T. Pardo, J. Soto and M. E. Padilla-Tosta, *J. Chem. Soc., Dalton Trans*., 1998, 2635.
5 P. D. Beer, *Acc. Chem. Res*., 1998, **31**, 71.
6 A. M. Allgeier and C. A. Mirkin, *Angew. Chem*., 1998, **37**, 937; *Angew. Chem., Int. Ed*., 1998, **37**, 894.
7 H. Plenio and C. Aberle, *Organometallics*, 1997, **16**, 5950.
8 H. Plenio and C. Aberle, *Angew. Chem*., 1998, **110**, 1467; *Angew. Chem., Int. Ed.*, 1998, **37**, 1397.
9 F. Rabiet, F. Denat and R. Guilard, *Synth. Commun*., 1997, **27**, 979.
10 M. J. L. Tendero, A. Benito, J. Cano, J. M. Lloris, R. Martínez-Máñez, J. Soto, A. J. Edwards, P. R. Raithby and M. A. Rennie, *J. Chem. Soc., Chem. Commun*., 1995, 1643.
11 G. DeSantis, L. Fabrizzi, M. Licchelli, C. Mangano, P. Pallavicini and A. Poggi, *Inorg. Chem*., 1993, **32**, 854.
12 H. Plenio and D. Burth, *Organometallics*, 1996, **15**, 4054.
13 B. Bosnich, C. K. Poon and M. L. Tobe, *Inorg. Chem*., 1965, **8**, 1102.
14 H. Plenio and R. Diodone, *J. Organomet. Chem*., 1995, **492**, 73 and references therein.
15 G. M. Sheldrick, SHELX−97, A Program Suite for the Solution and Refinement of Crystal Structures, University of Göttingen, 1997.

Communication 8/07240J

Iron complexes of the $N(CH_2CH_2S)_3^{3-}$ ligand; a paramagnetic, trigonal bipyramidal Fe(II) CO complex as a chelate ligand

Sian C. Davies, David L. Hughes, Raymond L. Richards and J. Roger Sanders

Nitrogen Fixation Laboratory, John Innes Centre, Colney Lane, Norwich, UK NR4 7UH.
E-mail: ray.richards@bbsrc.ac.uk

Received (in Cambridge, UK) 1st October 1998, Accepted 6th November 1998

The paramagnetic complex anions $[Fe(NS_3)Cl]^-$ [NS_3 = $N(CH_2CH_2S)_3^{3-}$] and$[Fe(NS_3)(CO)]^-$ have been prepared and structurally characterised; with $FeCl_2$, $[Fe(NS_3)(CO)]^-$ gives the structurally characterised, linear, paramagnetic cluster complex $[Fe\{Fe(NS_3)(CO)\text{-}S,S'\}_2]$.

A number of metal sites in enzymes carry three sulfur-donor ligands. These include the low-spin Fe centre of nitrile hydratase,[1] which is bound to three cysteine sulfur and two amide nitrogen atoms, and the cofactor of molybdenum nitrogenase, FeMoco, an $MoFe_7S_9$ cluster in which the six central iron atoms are each coordinated by three sulfides.[2] The Mo atom in FeMoco is coordinated by three sulfides as well as two oxygens from homocitrate and one histidine nitrogen[2] and it is thought that the vanadium atom in vanadium nitrogenase[3] and one iron atom in the 'iron-only' nitrogenase[4] are in similar environments. We are particularly interested in models for the trigonally S-coordinated Fe centres in the central portion of FeMoco and the S_3-coordinated Mo, V or Fe centres at the histidine end of nitrogenase cofactor clusters. Following our investigation of the nitrogen chemistry of vanadium coordinating the tetradentate tripodal ligand $N(CH_2CH_2S)_3^{3-}$ (NS_3),[5] we report iron chemistry of this ligand which, because its ligation involves three sulfur atoms, relates to the metal environments in the enzymes mentioned above. In the course of this work we have discovered a novel, paramagnetic carbonyl complex of iron which acts as a chelate ligand, as described below.

The starting point of our iron chemistry is the Fe(III) complex anion $[FeCl(NS_3)]^-$ **1**, obtained as shown in Scheme 1, which on reduction under CO gives the Fe(II) anion $[Fe(NS_3)(CO)]^-$ **2**. The NEt_4 salts of **1** and **2** {also the vanadium complex $NEt_4[VCl(NS_3)]$[5]} are isostructural; in both structures, the anion lies disordered about a crystallographic mirror plane.† Figs. 1 and 2 show the iron atoms to have trigonal bipyramidal geometry. In the solid state, both complexes are paramagnetic, The NEt_4 salt of **1** has μ_{eff} = 5.87 μ_B, S = 5/2. Mössbauer data at 77 K, (rel. natural Fe), are; isomer shift (IS) 0.37 mm s^{-1} and quadrupole splitting (QS) 1.00 mm s^{-1}. The NEt_4 salt of **2** has μ_{eff} = 2.79 μ_B, S = 1; IS = 0.22, QS 0.99 mm s^{-1}. Comparison of the anions in Figs. 1 and 2 shows that in the carbonyl **2** the Fe–N distance [2.035(8) Å] and the average Fe–S distance [2.278(3) Å] are shorter than the corresponding distances in the chloride **1** [2.273(3) and 2.316(2) Å respectively], despite the higher formal oxidation state of the metal in **1**. This is probably a consequence of the higher spin state of **1** and electron withdrawal by CO in **2**, and results in a relative distortion of the trithiolate ligand; the mean S–Fe–N angle contracts from 87.8(1)° in **2** to 83.6(2)° in **1**.

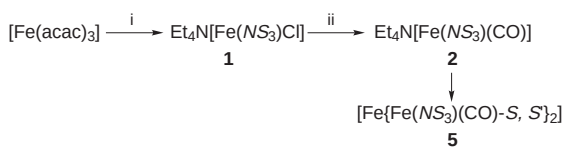

Scheme 1 *Reagents and conditions*: i, $N(SH)_3$ + Et_4NCl in MeCN; ii, Na/CO in MeCN; iii, $FeCl_2$ (0.5 mol ratio) in MeCN or Me_2SO.

Paramagnetic CO complexes of iron are extremely rare and as far as we are aware only two other examples, $K[Fe\{N(CH_2CONPr^i)_3\}(CO)]$[6] **3** and $Et_4N[Fe\{P[C_6H_3S\text{-}2(Ph\text{-}3)]_3\}(CO)]$[7] **4**, are known. Both have similar magnetic and Mössbauer properties to those of **2** but both have ν(CO) at 1940 cm^{-1}, a notably higher frequency than that of **2** (1885 cm^{-1}). Evidently the $FeNS_3^-$ site in **2** is more electron releasing to CO than are the corresponding iron sites in **3** and **4**.

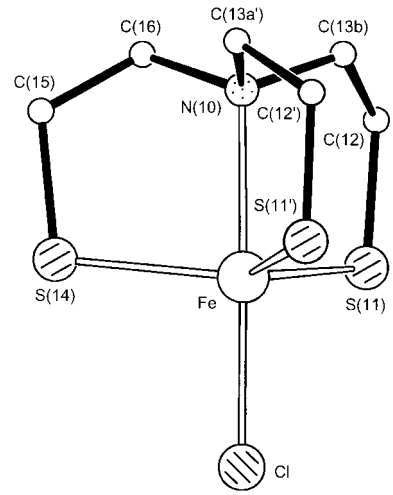

Fig. 1 The molecular structure of anion **1**. The disorder about the mirror symmetry plane is not shown; the atoms C(13a′), C(13b) and C(16) have half occupancy of the sites shown. Selected molecular dimensions: Fe–N(10) 2.273(3), Fe–Cl 2.3120(14), Fe–S(11) 2.3143(9), Fe–S(14) 2.3193(12) Å; N(10)–Fe–Cl 179.00(9), N(10)–Fe–S(average) 83.6(2)°.

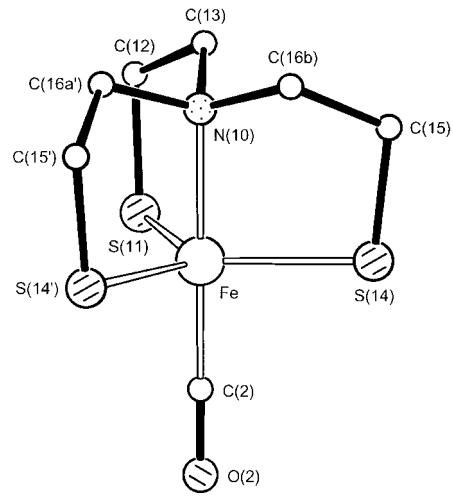

Fig. 2 The molecular structure of anion **2** which has disorder similar to that described in Fig. 1. Selected molecular dimensions: Fe–N(10) 2.035(8), Fe–C(2) 1.720(14), C(2)–O(2) 1.154(14), Fe–S(11) 2.281(3), Fe–S(14) 2.272(2) Å; N(10)–Fe–C(2) 179.7(5), N(10)–Fe–S(av.) 87.8(1)°.

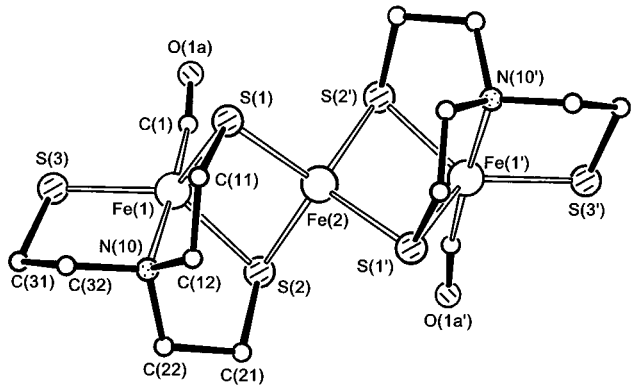

Fig. 3 The molecular structure of **5**, viewed down the twofold symmetry axis through Fe(2). Selected molecular dimensions: Fe(1)–N(10) 2.052(3), Fe(1)–C(1) 1.765(4), C(1)–O(1a) 1.13(1) (major component in disordered carbonyl group), C(1)-O(1b) 1.22(2), Fe(1)–S(1) 2.2677(10), Fe(1)–S(2) 2.2563(10), Fe(1)–S(3) 2.2139(9), Fe(2)–S(1) 2.2774(9), Fe(2)–S(2) 2.2928(10), Fe(1)···Fe(2) 2.6663(5) Å; N(10)–Fe(1)–C(1) 175.67(13), N(10)–Fe(1)–S(av.) 88.1(3), Fe(1)–S(1)–Fe(2) 71.84(3), Fe(1)–S(2)–Fe(2) 71.76(3), S(1)–Fe(1)–S(2) 107.79(3), S(1)–Fe(2)–S(2) 106.21(3), S(1)–Fe(2)–S(2') 105.93(3), S(1)–Fe(2)–S(1') 121.89(6), S(2)–Fe(2)–S(2') 110.50(6)°.

The latter sites are sterically hindered and **3** and **4** are made by CO addition to trigonal pyramidal iron-complex precursors. We have not been able to isolate the monomeric precursor to **2**, $[Fe(NS_3)]^-$. Instead, we obtain as yet uncharacterised products which appear to be multinuclear, probably because sulfur acts as a bridging group in them. However, the bridging ability of its sulfur ligands allows **2** itself to function as a ligand in a controlled way. Thus treatment of **2** with $FeCl_2$ (Scheme 1) affords the novel green, paramagnetic, linear Fe_3S_4 carbonyl cluster $[Fe\{Fe(NS_3)(CO)\text{-}S,S'\}_2]$ **5** [ν(CO) 1937 cm^{-1}. Mössbauer consistent with two different iron(II) sites: IS = 0.60, QS = 1.96 (intensity 1); IS = 0.22, QS = 1.17 mm s^{-1} (intensity 2)].

The structure of **5** (Fig. 3)† shows that this complex is made up from two trigonal bipyramidal $Fe(NS_3)(CO)$ units, each of which bridges through two of its sulfur atoms to a central Fe, which thus has distorted tetrahedral geometry and lies on a crystallographic twofold symmetry axis. Within the $Fe(NS_3)$-(CO) units, the Fe-S distances involving the four bridging S atoms are 2.256(1) and 2.268(1)Å, but those to the non-bridging S atoms are shorter [2.214(1) Å]. The Fe-S distances about the central Fe are 2.277(1) Å and 2.293(1) Å. All the iron atoms can be regarded as formally in oxidation state two, but solid **5** has μ_{eff} = 1.54 μ_B per molecule at 20 °C showing considerable electron coupling. The molecule is disordered with two distinct sites for the O atoms of the CO ligands; the C–O distances are 1.131(12) and 1.22(2) Å, with corresponding Fe–C–O angles of 168.8(6) and 161.4(9)°.

We note that the C–O stretching frequencies in the IR spectra of **2** (1885 cm^{-1}) and **5** (1937 cm^{-1}) are in the region of several frequencies observed in stopped-flow FTIR studies of CO complexes of *Klebsiella pneumoniae* nitrogenase (1880, 1906, 1936 and 1958 cm^{-1}).[8]

We also point out that treatment of the NEt_4 salt of **1** with NaN_3 gives $NEt_4[Fe(NS_3)N_3]$, which has relevance to azide inhibition of the iron site in nitrile hydratase.[1] This and other complexes of inhibitors of nitrile hydratase are under investigation, although MeCN appears to bind very weakly to the $FeNS_3^-$ site.

The shape of our iron cluster is reminiscent of those of the linear trinuclear complexes $[Et_4N]_3[Fe_3S_4(SPh)_4]$[9] and $[Et_4N]_3[VFe_2S_4Cl_4]$.[10] We anticipate in our future work that **2** and related complex anions such as $[Fe(NS_3)(CNR)]^-$ will function as ligands to allow assembly of a range of multinuclear complexes of iron with other metals. Already, we have obtained the analogue of **5**, $[Fe_3(NS_3)_2(CNC_6H_{11})_2]$, [from $Fe(acac)_3$, NS_3H_3, and CNC_6H_{11},[11] and $[Fe_2Co(NS_3)_2(CO)_2]$ (by use of $CoCl_2$ in place of $FeCl_2$ in step iii of Scheme 1).

We thank the BBSRC for support of this work and Dr D. J. Evans for Mössbauer spectroscopic measurements.

Notes and references

† *Crystal data*: NEt_4 salt of **1**: $C_{14}H_{32}ClN_2S_3Fe$, M = 415.9, orthorhombic, space group *Pbcm* (no. 57), a = 8.7922(9), b = 14.3189(11), c = 15.9028(14) Å, V = 2002.1(3) Å^3. Z = 4, D_c = 1.38 g cm^{-3}, F(000) = 884, μ(Mo-Kα) = 1.196 mm^{-1}, T = 293(2) K, λ(Mo-Kα) = 0.71069 Å.

Crystals are black, irregular, hexagonal prisms. One, *ca.* 0.60 × 0.45 × 0.27 mm mounted on a glass fibre; photographic examination; Enraf-Nonius CAD4 diffractometer (with monochromated radiation) for accurate cell parameters (25 reflections, θ = 10–11°, each centred in four orientations) and diffraction intensities (2504 unique reflections to θ_{max} = 28°, 1870 'observed' with $I > 2\sigma_I$). Structure determined by automated Patterson routines;[12] refined (on F_o^2) by full-matrix least-squares methods[13] to wR_2 = 0.167 and R_1 = 0.064 for all 2504 reflections weighted $w = 1 / [\sigma^2(F_o^2) + (0.1034P)^2 + 0.48P]$ where $P = (F_o^2 + 2F_c^2) / 3$.

For the NEt_4 salt of **2**: $C_{15}H_{32}N_2OS_3Fe$, M = 408.5, orthorhombic, space group *Pbcm*, a = 8.8530(7), b = 14.1800(11), c = 15.869(2) Å, V = 1992.1(3) Å^3. Z = 4, D_c = 1.36 g cm^{-3}, F(000) = 872, μ(Mo-Kα) = 1.07 mm^{-1}, T = 293 K, λ(Mo-Kα) = 0.71069 Å. The crystal is a deep bluish-green needle, *ca.* 0.50 × 0.12 × 0.11 mm; 1111 unique reflections to θ_{max} = 21°, 678 'observed'. Structure refined to wR_2 = 0.170 and R_1 = 0.089 for all 1111 reflections weighted $w = 1 / [\sigma^2(F_o^2) + (0.0919P)^2]$.

For **5**: $C_{14}H_{24}N_2O_2S_6Fe_3$, M = 612.26, tetragonal, space group $I4_1cd$, (no.110) $a = b$ = 13.5324(4), c = 24.499(2) Å, V = 4486.2(3) Å^3. Z = 8, D_c = 1.81 g cm^{-3}, F(000) = 2496, μ(Mo-Kα) = 2.49 mm^{-1}, T = 293 K, λ(Mo-Kα) = 0.71069 Å. Crystal is a black, irregular dodecahedron, *ca.* 0.28 × 0.24 × 0.24 mm; 1668 unique reflections to θ_{max} = 30.0°, 1453 'observed'. Structure refined to wR_2 = 0.046 and R_1 = 0.029 for all 1668 reflections weighted $w = 1 / [\sigma^2(F_o^2) + (0.0066P)^2]$. CCDC 182/1083.

1 W. Huang, J. Jia, J. Cummings, M. Nelson, G. Schneider and Y. Lunqvist, *Structure*, 1997, **5**, 691; J. J. Ellison, A. Nienstedt, S. C. Shoner, D. Barnhart, J. A. Cowen and J. A. Kovacs, *J. Am. Chem. Soc*., 1998, **120**, 5691.
2 D. C. Rees, M. K. Chan and J. Kim, *Adv. Inorg. Chem*., 1993, **40**, 89.
3 R. R. Eady, *Adv. Inorg. Chem*., 1991, **36**, 77.
4 R. N. Pau, in '*Biology and Biochemistry of Nitrogen Fixation*', ed. M. J. Dilworth and A. R. Glenn, Elsevier, Oxford, 1991, p 37.
5 S. C. Davies, D. L. Hughes, Z. Janas, L. Jerzykiewicz, R. L. Richards, J. R. Sanders and P. Sobota, *Chem. Commun*.,1997, 1261.
6 M. Ray, A. P. Golombek, M. P. Hendrich, V. G. Young, Jr. and A. S. Borovik, *J. Am. Chem. Soc*., 1996, **118**, 6084.
7 D. H. Nguyen, H-F. Hsu, M. Millar, S. A. Koch, C. Achim, E. L. Bominaar and E. Münck, *J. Am. Chem. Soc*., 1996, **118**, 8963.
8 S. J. George, G. A. Ashby, C. W. Wharton and R. N. F. Thorneley, *J. Am. Chem. Soc.*, 1997, **119**, 6450.
9 K. S. Hagen, A. D. Watson and R. H. Holm, *J. Am. Chem. Soc*., 1983, **105**, 3905; R. H. Holm, *Adv. Inorg. Chem.*, 1992, **38**, 1 and references therein.
10 Y. Do, E. D. Simhon and R. H. Holm, *Inorg. Chem*., 1985, **24**, 4635.
11 J. R. Dilworth, L. Cooper, R. L. Richards and J. R. Sanders, unpublished work.
12 G. M. Sheldrick, *Acta Crystallogr., Sect. A*, 1990 **46**, 467.
13 G. M. Sheldrick, SHELXL - Program for crystal structure refinement, University of Göttingen, 1993.

Communication 8/07655C

Acetaldehyde hydration by zinc–hydroxo complexes: coordination number expansion during catalysis

Xiaodong Xu, Ajay R. Lajmi and James W. Canary*

Department of Chemistry, New York University, New York, NY 10003, USA. E-mail: james.canary@NYU.edu

Received (in Bloomington, IN, USA) 17th August 1998, Accepted 6th November 1998

The complexes [Zn(tren)(OH)]$^+$ and [Cd(Me$_6$tren)(OH)]$^+$ are excellent catalysts for the hydration of acetaldehyde while the closely related complex [Zn(Me$_6$tren)(OH)]$^+$ does not catalyze the reaction, consistent with the notion that zinc ions require the ability to accommodate expanded coordination numbers in hydrolytic reactions such as those catalyzed by the enzyme carbonic anhydrase.

Carbonic anhydrases are widely occurring Zn(II) metalloenzymes that catalyze the interconversion of CO_2 and HCO_3^-. The catalytic zinc ion in human carbonic anhydrase II is ligated by three histidine residues and a water molecule in its resting state. Most detailed mechanisms postulated for carbonic anhydrases[1] require expansion of the coordination sphere of the zinc ion from four to five (or six) during the catalytic cycle for addition of zinc-bound hydroxide to the CO_2 with concomitant polarization of the carbonyl group by zinc, and for associative displacement of the bicarbonate product by water.[2] Higher coordination number intermediates are suggested by crystallographic analyses,[3,4] but little functional data is available that bears on the significance of this issue. In this paper, we test the hypothesis that zinc ions require coordination number increases in hydrolysis catalytic cycles, specifically the hydrolysis reaction of acetaldehyde catalyzed by zinc complexes of the synthetic ligands tris(2-aminoethyl)amine (tren) and tris(2-dimethylaminoethyl)amine (Me$_6$tren).

The hydration of acetaldehyde is catalyzed by carbonic anhydrase and has also been studied extensively with several synthetic catalysts and buffers.[5,6] A plot of log(k_{cat}) *vs.* pK_a (k_{cat} = dk_{obs}/d[ZnL]) yields a linear relationship suggesting that the mechanism of the reaction is simple nucleophilic attack upon the carbonyl. A simplified mechanistic scheme for the reaction is shown in Scheme 1, with the zinc-hydroxo form of the catalyst shown as the catalytically active species. Associative exchange is generally observed for substitution reactions of zinc complexes of these ligands;[7] formation of intermediate **3** requires an expanded coordination sphere.

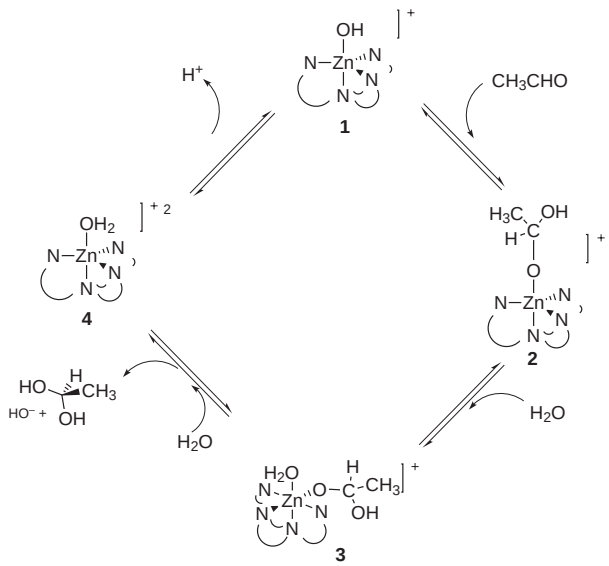

Scheme 1 Proposed mechanism for hydration of acetaldehyde catalyzed by Zn(II) or Cd(II) complexes.

The ligands tren and Me$_6$tren offer an opportunity to examine this question since zinc complexes of tren can form six-coordinate complexes but those of Me$_6$tren cannot. In five-coordinate complexes, both ligands adopt a C_3-symmetric conformation [Fig. 1(a)].[8] However, in six-coordinate complexes, tren adopts a C_σ conformation [Fig. 1(b)] that is sterically inaccessible to Me$_6$tren due to the steric hindrance caused by the bulky dimethylamino substituents. A search of the Cambridge Structural Database[9] yielded over 20 structures of tetradentate complexes of Me$_6$tren, all of which showed the ligand in a C_3-conformation while tren complexes showed both five-coordinate (C_3) and six-coordinate (C_σ) complexes. Thus the zinc ion in [Zn(Me$_6$tren)(OH)]$^+$ should be limited to

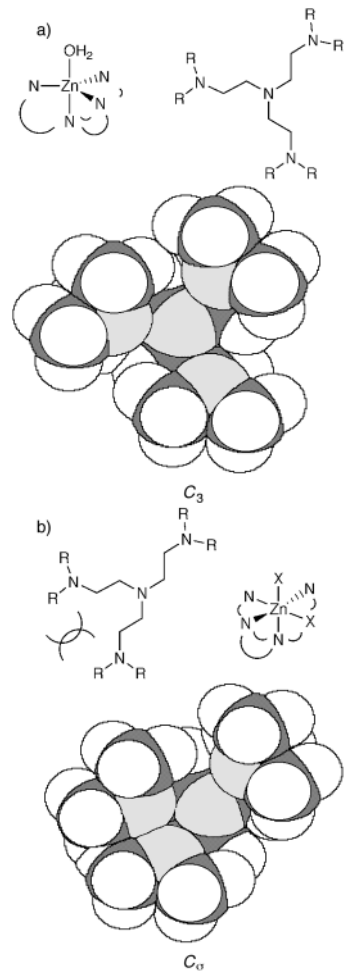

Fig. 1 C_3 (a) and C_σ (b) conformations observed for penta-coordination and hexa-coordination. Steric hindrance in Me$_6$tren precludes hexa-coordination.

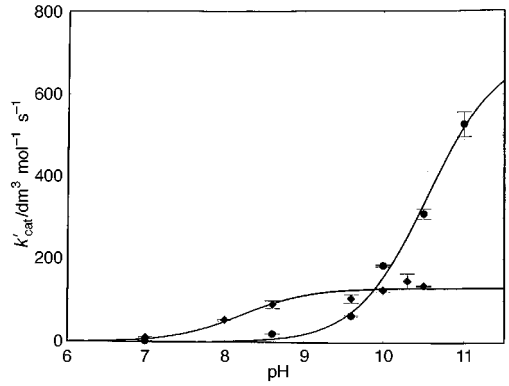

Fig. 2 pH–rate profiles for $[Zn(tren)(OH)]^+$ (●) and $[Cd(Me_6tren)(OH)]^+$ (◆).

maximal five-coordination while in $[Zn(tren)(OH)]^+$ six-coordination should be readily achievable. Thus, intermediate **3** should be accessible only for the tren complex, and the Me_6tren complex should not catalyze the reaction.

The hydration rate of acetaldehyde in aqueous solution was determined using stopped flow UV–VIS detection, monitoring the decrease of the carbonyl band at 278 nm. The solution used in this work was 10% aq. MeCN {0 °C, 0.1 M $NaClO_4$; $[CH_3CHO]$ = 36 mM, $[[Zn(L)(OH)]^+]$ = 0.25–5 mM}.[5,10] The results are shown in Fig. 2, where each data point represents 3–5 experiments at different catalyst concentrations, each run in triplicate; The line is a non-linear least-squares fit of $k'_{obs} = k_{cat}\chi_{[Zn(L)OH]^+}$ where $\chi_{[Zn(L)OH]^+}$ is the mole fraction of catalytically active species. The observed pH–rate profile for $[Zn(tren)(OH)]^+$ reveals a point of inflection at pH 10.5 similar to the published pK_a.[11] The log(k_{cat}) is 2.84, consistent with that predicted from the Brønsted analysis (2.9).[6] However, for the complex $[Zn(Me_6tren)(OH)]^+$, no catalysis was observed even though it should be easily seen under these conditions [predicted log(k_{cat}) = 2.0].

It was reasoned that although the hydration reaction is not catalyzed by $[Zn(Me_6tren)(OH)]^+$, it should be catalyzed by $[Cd(Me_6tren)(OH)]^+$ complex since the Cd(II) ion may have an expanded coordination number due to its large ionic radius.[8] The observed pH–rate profile is shown in Fig. 2. The pK_a value from curve fitting is 8.2 which compares favorably with that determined by pH titration.[12] The log(k_{cat}) is 2.12 as expected from the Brønsted relationship discussed above.

Based on the available data, the most likely explanation for the inactivity of $[Zn(Me_6tren)(OH)]^+$ is the inability of water to displace the hydrated acetaldehyde intermediate due to the steric bulkiness of the ligand that prevents hexa-coordination of the Zn(II) ion. Formation of **2** should not be hindered by the methyl groups in Me_6tren as indicated by examination of models and calculations of heats of formation (Spartan: MNDO)[13] of **2** and various similar compounds that failed to show any significant steric interaction between the atoms of the acetaldehyde and the ligand.

It is widely believed that one reason that enzymes maintain low coordination numbers to catalytic zinc ions is to increase the acidity of the zinc-bound water molecule.[14–16] The implication of the present study is that zinc ions involved in hydrolytic reactions require access to an expanded coordination sphere for catalyst turnover. This requirement may be an additional reason for the frequent observation of four-coordinate zinc ions in crystal structures of resting state enzyme active sites, and higher coordination numbers in corresponding enzyme-inhibitor complexes.

We thank the National Institutes of Health (GM 49170) for support of this work.

Notes and references

1 J. N. Earnhardt and D. N. Silverman, in *Comprehensive Biological Catalysis*, ed. M. Sinnott, Academic Press, San Diego, 1998, vol. 1, p. 483.
2 Z. Liljas, K. Håkansson, B. H. Jonsson and Y. Xue, *Eur. J. Biochem.*, 1994, **219**, 1.
3 K. Håkansson and A. Wehnert, *J. Mol. Biol.*, 1992, **228**, 1212.
4 Y. Xue, A. Liljas, B.-H. Jonsson and S. Lindskog, *Proteins: Struc., Funct., Genet.*, 1993, **17**, 93.
5 P. Woolley, *Nature*, 1975, **258**, 677.
6 P. Woolley, *J. Chem. Soc., Perkin Trans. 2*, 1977, 318.
7 S. F. Lincoln, A. M. Hounslow and J. H. Coates, *Inorg. Chim. Acta*, 1983, **77**, L7.
8 C. S. Allen, C.-L. Chuang, M. Cornebise and J. W. Canary, *Inorg. Chim. Acta*, 1995, **239**, 29.
9 F. H. Allen and O Kennard, *Chem. Des. Automat. News*, 1993, **8**, 31.
10 E. Kimura, T. Shiota, T. Koike, M. Shiro and M. Kodama, *J. Am. Chem. Soc.*, 1990, **112**, 5805.
11 J. W. Canary, J. Xu, J. M. Castagnetto, D. Rentzeperis and L. A. Marky, *J. Am. Chem. Soc.*, 1995, **117**, 11 545.
12 G. Anderegg and V. Gramlich, *Helv. Chim. Acta*, 1994, **77**, 685.
13 Spartan 4.0: Wavefunction, Inc., 18401 Von Karman Ave., Ste. 370, Irvine, CA 92612.
14 L. Banci, I. Bertini, C. Luchinat and J. M. Moratal, in *Enzymatic and Model Carboxylation and Reduction Reactions for Carbon Dioxide Utilization*, ed. M. Aresta and J. V. Schloss, Kluwer Academic Publishers, Dordrecht, 1990, p. 181.
15 U. Hartmann, R. Gregorzik and H. Vahrenkamp, *Chem. Ber.*, 1994, **127**, 2123.
16 A. Looney, R. Han, K. McNeill and G. Parkin, *J. Am. Chem. Soc.*, 1993, **115**, 4690.

Communication 8/06440G

Solution and soluble polymer syntheses of 3-aminoimidazoline-2,4-diones

Juyoung Yoon,† Chang-Woo Cho, Hyunsoo Han and Kim D. Janda*

Department of Chemistry, The Scripps Research Institute and The Skaggs Institute for Chemical Biology, 10550 N. Torrey Pines Road, La Jolla, CA 92037, USA. E-mail: kdjanda@scripps.edu

Received (in Corvallis, OR, USA) 9th September 1998, Accepted 6th November 1998

3-Aminoimidazoline-2,4-dione derivatives have been synthesized from a combination of α- and aza-amino acids by both solution phase and soluble polymer supported approaches; this soluble polymer methodology combines clean product isolation with recycling of the original matrix.

Molecular diversity based on combinatorial organic synthesis is now being used for rapid lead generation in both drug discovery and the development of biologically active compounds with potential therapeutic value.[1] Recently, solid-phase synthesis of heterocycles bearing one or more nitrogen atoms such as diketopiperazines,[2] diazines,[3] and hydantoins[4] has received considerable attention due to their medicinal importance. Hence, development of strategies for the mixture/parallel synthesis of additional heterocyclic structures either in solution or on a polymer support is of key interest.

The synthesis and structure assignment of hexahydro-1,2,4-triazine-3,6-dione **2**, isomeric with 3-aminoimidazoline-2,4-dione **1**, has been rather cryptic for over 30 years.[5–7] It has been demonstrated[6,7] that a hexahydro-1,2,4-triazine-3,6-dione could be prepared by the reaction of *N*-[*N*-(phenylthiocarbonyl)glycyl]-*N*′-(benzyloxycarbonyl)hydrazine with lead acetate.[8] A similar cyclization of ethyl semicarbazinoacetate [$H_2NNHC(O)NHCH_2CO_2Et$] with NaOEt[9] was discovered to lead to **1** rather than **2**. A more recent attempt[10] to synthesize 1,2,4-triazine-3,6-diones by the reaction of hydrazine with α-lactams gave mainly **1**.[11] If **1** or **2** could be made in a controlled

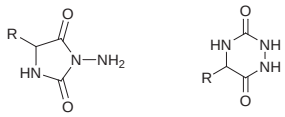

1 **2**

fashion they should make interesting targets for combinatorial synthesis/drug discovery as they are structurally rigid, possess ample hydrogen donor/acceptor functionality and contain two points for diversity generation. Herein we describe our synthetic approach to 3-aminoimidazoline-2,4-diones **1**, our application of this strategy to a soluble polymer support, and our ability to design a methodology that allows regeneration of the resin.

As detailed *vide supra* examples relating to the controlled syntheses of 3-aminoimidazoline-2,4-dione derivatives have been sparse. In 1985, a concise one step synthesis from α-amino acids and *tert*-butyl carbazate was reported by Lalezari,[12] however, this report also detailed a major problem with this synthetic tack which induced racemization of the product. To avoid this unwanted racemization, our solution phase approach utilized Et_3N or Pr^i_2NH at room temperature for the cyclization step, allowing optical activity‡ to be preserved.

As shown in Scheme 1, *N*-benzyloxycarbonyl protected amino acids were used as convenient starting materials in the solution phase synthesis. Thus, protected amino acids were coupled with our previously described Boc-protected aza-amino acids[13] using DCC and DMAP in typically 95% yield.

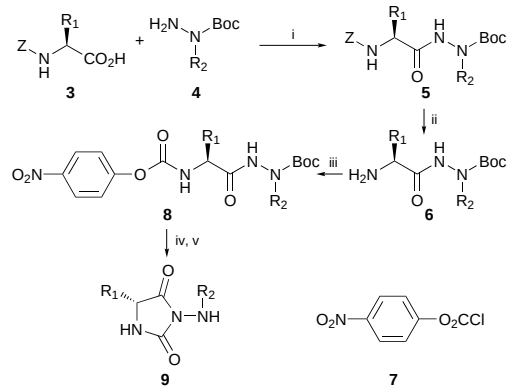

Scheme 1 *Reagents and conditions*: i, DCC, DMAP; ii, H_2/Pd-C; iii, **7** (1.1 equiv.), Et_3N (1.1 equiv.); iv, TFA–CH_2Cl_2 (1:1 v/v); v, dilution, Et_3N (1.1 equiv.).

After removal of the benzyloxycarbonyl (Z) group, nitrophenyl chloroformate was introduced to generate an activated intermediate for the cyclization reaction. Removal of the Boc group was performed using TFA–CH_2Cl_2 (1:1), followed by cyclization in Et_3N–CH_2Cl_2 (1:100 v/v) at 25 °C, and the desired unracemized 3-aminoimidazoline-2,4-diones **9** were obtained in approximately 75% yield.

With a sound solution phase strategy in hand we extended our methodology to a soluble polymer supported synthesis. In this scenario linear homopolymer [polyethylene glycol monomethyl ether (MeO-PEG)] served as our carrier for polymer synthesis and purification. We have demonstrated the advantages of using liquid phase synthesis through the construction of both peptide/small molecule combinatorial libraries[14] and as a reagent/catalyst support.[15]

Linker **10** was prepared *via* the oxidation of 4-(*tert*-butoxy)benzaldehyde with Ag_2O. This acid was coupled to MeO-PEG5000-amine and upon deprotection with TFA gave phenol **11** which was now ready for the first diversity step coupling (Scheme 2). The amino acid was introduced in the form of isocyanate **12**[16] and this building block was attached to **11** granting **13**; the second point of diversity, Boc-aza-amino acid **4** was added to deprotected **13** providing PEG-**14**. It should be stressed that the unique physical properties of the MeO-PEG homopolymer allowed each coupling/deprotection reaction to be purified by precipitation of the modified homopolymer. Furthermore, reaction progress was conveniently monitored by ^1H and ^{13}C NMR spectroscopy. Finally, after removal of the Boc group, **14** could be base-cyclized and thus cleaved from the support generating a variety of 3-aminoimidazoline-2,4-diones in greater than 90% purity and in 62–80% yield (Table 1). The structures of the products were confirmed by ^1H, ^{13}C NMR and FAB mass as well as IR spectroscopy.§ For example, ^1H NMR analysis of **9d** in [$^2H_6$]DMSO clearly shows a doublet at δ 2.49 for NCH_3 and a quartet for NH at δ 5.43. Also, all of the compounds showed distinct peaks in their IR spectra at 1775 and 1725 cm^{-1} which is indicative of a 3-aminoimidazoline-2,4-dione structure.[5] Lastly, it was possible to regenerate PEG-**11** and reapply this material in another round of synthesis. This was accomplished by simple treatment of the isolated reaction PEG-**11** with 1 M NaOH which in effect removed any previous

† Present address: Department of Chemistry, Silla University, 1-1 San, Kwaebop-dong, Sasang-gu, Pusan, 617-736 Korea.

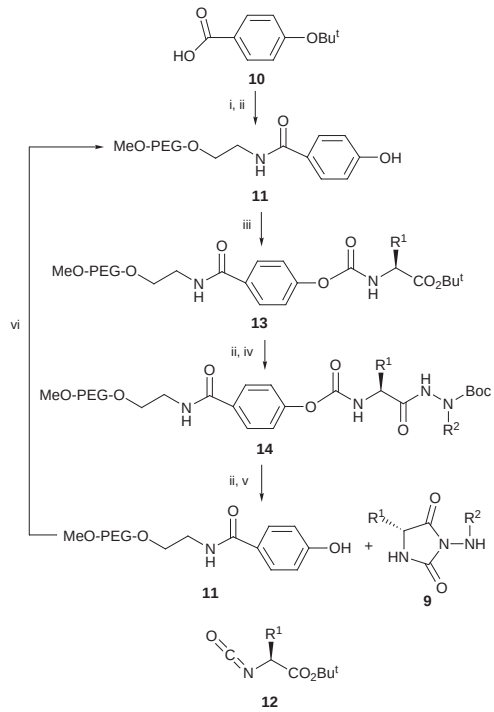

Scheme 2 *Reagents and conditions*: i, MeO-PEG-$CH_2CH_2NH_2$, DCC, DMAP; ii, TFA–CH_2Cl_2 (1:1 v/v); iii, **12**, Et_3N; iv, **4**, DCC; v, dilution, Pr^i_2NEt (1.1 equiv.), vi, 1 M NaOH.

Table 1 3-Aminoimidazoline-2,4-diones generated *via* Scheme 2

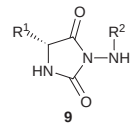

Compound	R^1	R^2	Yield (%)[a]
9a	H	Me	62
9b	Me	Me	73
9c	Pr^i	Me	75
9d	Bu^s	Me	78
9e	Bn	Me	80
9f	Bn	*p*-$MeOC_6H_4CH_2$	78
9g	Bn	Bu^i	74
9h	Me	H	60
9j	Bu^i	H	67
9k	Bn	H	67

[a] Yields are based on the conversion of **11** to **9** and are isolated yields.

materials that had accumulated during the synthesis of **9**. We could use this PEG-**11** again without any significant reduction in loading or yield, which was confirmed by ^{1}H NMR analysis.

In conclusion, we have shown both solution and liquid phase methodologies for the controlled stepwise synthesis of 3-aminoimidazoline-2,4-diones. In our strategy we have provided a method that allows for the incorporation of two points of diversity which can be drawn from a large pool of building blocks. Finally, our approach allows for polymer regeneration and its reuse.

Financial support of this research by the Skaggs Institute for Chemical Biology and NIH GM56154 is gratefully acknowledged. C.-W. C. wishes to thank Korea Science and Engineering Foundation (KOSEF) for a postdoctoral fellowship. We also thank Professor R. V. Hoffman for many helpful discussions.

Notes and references

‡ Optical rotation values for **9b**,**c**,**e**–**g**,**j** are reported in their characterization data (see below). In the case of **9b**, there was no significant change in its optical rotation value after a first and second recrystallization from EtOH. This supports our assumption that there was no sign of racemization in our synthetic scheme. {before recrystallization: $[\alpha]_D^{24}$ −39.0 (*c* 1.06, MeOH), after first recrystallization: $[\alpha]_D^{24}$ −38.8 (*c* 1.06, MeOH), after second recrystallization: $[\alpha]_D^{24}$ −40.3 (*c* 1.04, MeOH)}

§ *Selected data* for **9a**: mp 189–191 °C; δ_H([$^2H_6$]DMSO, 400 MHz) 8.00 (br s, 1H), 5.40 (br s,1H), 3.87 (d, 2H), 2.51 (d, 3H); δ_C([$^2H_6$]DMSO, 101 MHz) 169.8, 156.5, 44.5, 36.9; ν($CHCl_3$)/cm^{-1} 3024, 1772, 1724, 1211; HRMS [FAB, (M + 1)$^+$]: calc. 130.0617, found 130.1612. For **9b**: mp 182–185 °C; δ_H(CD_3OD, 400 MHz) 3.99 (q, 1H), 2.55 (s, 3H), 1.27 (d, 3H); δ_C(CD_3OD, 101 MHz) 172.5, 155.1, 50.1, 34.9, 14.8; ν($CHCl_3$)/cm^{-1} 3006, 1768, 1724, 1214; HRMS [FAB, (M + 1)$^+$]: calc. 144.0773, found 144.0766; $[\alpha]_D^{24}$ −39.0 (*c* 1.06, MeOH). For **9c**: mp 138–140 °C; δ_H($CDCl_3$, 400 MHz) 6.73 (br s, 1H), 4.32 (br s, 1H), 3.90 (d, 1H), 2.72 (s, 3H), 2.23 (m, 1H), 1.04 (d, 3H), 0.91 (d, 3H); δ_C($CDCl_3$, 101 MHz) 171.3, 156.9, 60.9, 38.0, 30.2, 18.6, 15.9; ν($CHCl_3$)/cm^{-1} 3024, 1774, 1718, 1208; HRMS [FAB, (M + Na)$^+$]: calc. 194.0905, found 194.0914; $[\alpha]_D^{24}$ −73.0 (*c* 0.69, $CHCl_3$). For **9d**: δ_H(DMSO, 400 MHz) 8.17 (s, 1H), 5.53 (q, 1H), 3.97 (d, 1H), 2.49 (d, 3H), 1.77 (m, 1H), 1.18–1.34 (m, 2H), 0.90 (d, 3H), 0.84 (t, 3H); δ_C(CD_3OD, 101 MHz) 169.6, 154.2, 57.3, 34.3, 33.6, 20.8, 11.2, 8.0; ν($CHCl_3$)/cm^{-1} 3024, 2986, 1774, 1718, 1214; HRMS [FAB, (M+1)$^+$]: calc. 186.1242, found 186.1239. For **9e**: mp 210–213 °C; δ_H($CDCl_3$, 400 MHz) 7.30 (m, 5H), 5.45 (br s, 1H), 4.26 (q, 1H), 4.23 (m, 1H), 3.28 (dd, 1H), 2.90 (dd, 1H), 2.58 (d, 3H) ; δ_C($CDCl_3$, 101 MHz) 170.6, 155.5, 134.6, 129.4, 128.9, 127.6, 61.0, 56.9, 37.8; ν($CHCl_3$)/cm^{-1} 3011, 1762, 1724, 1227; HRMS [FAB, (M + 1)$^+$]: calc. 220.1086, found 220.1094; $[\alpha]_D^{24}$ −63.9 (*c* 0.39, MeOH). For **9f**: mp 125–128 °C; δ_H($CDCl_3$, 400 MHz) 7.30 (m, 5H), 7.16 (d, 2H), 6.86 (d, 2H), 5.24 (s, 1H), 4.35 (br s, 1H), 4.15 (m, 1H), 3.95 (d, 2H), 3.78 (s, 3H), 3.23 (dd, 1H), 2.69 (dd, 1H); δ_C($CDCl_3$, 101 MHz) 170.6, 159.4, 155.6, 134.9, 130.7, 129.3, 128.9, 127.7, 127.5, 113.8, 56.9, 55.2, 53.9, 37.8; ν($CHCl_3$)/cm^{-1} 3011, 1755, 1737, 1215; HRMS [FAB, (M + Na)$^+$]: calc. 348.1324, found 348.1335; $[\alpha]_D^{24}$ −76.0 (*c* 0.42, MeOH). For **9g**: δ_H($CDCl_3$, 400 MHz) 7.28 (m, 5H), 6.21 (s, 1H), 4.26 (q, 1H), 4.21 (m, 1H), 3.21 (dd, 1H), 2.94 (dd, 1H) 2.53 (t, 2H), 1.55 (m, 1H), 0.90 (d, 3H); δ_C($CDCl_3$, 101 MHz) 170.9, 156.1, 134.5, 129.5, 128.8, 127.5, 58.4, 56.8, 37.5, 26.6, 20.3; ν($CHCl_3$)/cm^{-1} 3440, 3023, 1774, 1731, 1214; HRMS [FAB, (M+H)$^+$]: calc. 262.1556, found 262.1563; $[\alpha]_D^{24}$ −66.7 (*c* 0.59, MeOH). For **9h**: mp 134–136 °C; δ_H(CD_3OD, 400 MHz) 3.99 (q, 1H), 1.26 (d, 3H); δ_C(CD_3OD, 101 MHz) 173.1, 156, 50.1 14.9; ν($CHCl_3$)/cm^{-1} 3021, 1784, 1726, 1208; HRMS [FAB, (M + 1)$^+$]: calc. 130.0616, found 130.0612. For **9j**: mp 150–153 °C; δ_H(CD_3OD, 400 MHz) 3.95 (m, 1H), 1.71 (m, 1H), 1.54 (m, 1H), 1.39 (m, 1H), 0.84 (d, 6H); δ_C(CD_3OD, 101 MHz) 171.3, 154.7, 51.3, 37.9, 21.6, 19.4, 17.1; ν($CHCl_3$)/cm^{-1} 3023, 1793, 1724, 1208; HRMS [FAB, (M + 1)$^+$]: calc. 172.1086, found 172.1080; $[\alpha]_D^{24}$ −78.1 (*c* 0.64, MeOH). For **9k**: mp 201–203 °C; δ_H(CD_3OD, 400 MHz) 7.16 (m, 5H), 4.23 (m, 1H), 3.03 (dd, 1H), 2.89 (dd, 1H); HRMS [FAB, (M + 1)$^+$]: calc. 206.0930, found 206.0924.

1 *Molecular Diversity and Combinatorial Chemistry*, ed. I. M. Chaiken and K. D. Janda, American Chemical Society, Washington DC, 1996; L. A. Thompson and J. A. Ellman, *Chem. Rev*., 1996, **96**, 555; M. A. Gallop, R. W. Barrett, W. J. Dower, S. P. A. Fodor and E. M. Gordon, *J. Med. Chem*., 1994, **37**, 1233.
2 A. K. Szardenings, T. S. Burkoth, H. H. Lu, D. W. Tien and D. A. Campbell, *Tetrahedron*, 1997, **53**, 6573; D. W. Gordon, J. Steele, *Bioorg. Med. Chem. Lett*., 1995, **5**, 47.
3 J. S. Panek and B. Zhu, *Tetrahedron Lett*., 1996, **37**, 8151.
4 J. Matthews and R. A. Rivero, *J. Org. Chem*., 1997, **62**, 6090; S. W. Kim, S. Y. Ahn, J. S. Koh, J. H. Lee, S. Ro and H. Y. Cho, *Tetrahedron Lett*., 1997, **38**, 460.
5 J. Gut, A. Novocek and P. Fiedler, *Collect. Czech. Chem. Commun*., 1968, **33**, 2087.
6 J. G. Dain, Doctoral Dissertation, Duquesne University, 1970, *Diss. Abstr. Int. B*, 1971, **32**, 160; *Chem. Abstr*., 1972, **76**, 3807.
7 T. J. Schwan and T. J. Sanford, *J. Heterocycl. Chem*., 1979, **16**, 1655.
8 A. Lindemann, N. H. Khan and K. Hoffman, *J. Am. Chem. Soc*., 1952, **74**, 476.
9 J. Gante and W. Lautsch, *Chem. Ber*., 1964, **97**, 994.
10 R. V. Hoffman and N. K. Nayyar, *J. Org. Chem*., 1995, **60**, 5992.
11 Professor R.V. Hoffman, Personal communication.
12 I. Lalezari, *J. Heterocycl. Chem*., 1985, **22**, 741.
13 H. Han and K. D. Janda, *J. Am. Chem. Soc*., 1996, **118**, 2539.
14 D. J. Gravert and K. D. Janda, *Chem. Rev*., 1997, **97**, 489.
15 P. Wentworth Jr., A. M. Vandersteen and K. D. Janda, *Chem Commun*., 1997, 759; H. Han and K. D. Janda, *Angew. Chem., Int. Ed. Engl*., 1997, **36**, 1731; H. Han and K. D. Janda, *J. Am. Chem. Soc*., 1996, **118**, 7632; H. Han and K. D. Janda, *Tetrahedron Lett*., 1997, **38**, 1527.
16 Isocyanates **12** were prepared from *tert*-butyl amino acids and triphosgene. See S. Goldschmidt and M. Wick, *Liebigs Ann. Chem*., 1952, **575**, 217 for this preparation.

Communication 8/07067I

Iron-catalyzed allylic amination by nitroorganics

Radhey S. Srivastava† and Kenneth M. Nicholas*

Department of Chemistry and Biochemistry, University of Oklahoma, Norman, OK 73019, USA. E-mail: knicholas@ou.edu

Received (in Corvallis, OR, USA) 15th September 1998, Accepted 28th October 1998

$[CpFe(CO)_2]_2$ catalyzes the reaction of nitroaromatics with olefins under CO to produce allyl amines regioselectively; a coordinated organonitrogen species is implicated as the active aminating agent.

In contrast to oxygenation, synthetically useful methods for the direct introduction of nitrogen into hydrocarbons (nitrogenation) are few. Metal-mediated nitrogenation reactions have been receiving increasing attention, as evidenced by recent reports of metal-catalyzed aziridinations[1] and hydroaminations[2] of olefins, both of which involve addition to the double bond. Processes for the direct *allylic* nitrogenation of hydrocarbons, which could expand the scope of the commercially important ammoxidation of propylene to acrylonitrile,[3] also hold considerable appeal. Recent efforts in this laboratory and others have led to the development of Mo-[4] and Fe-catalyzed[5] reactions of olefins with aryl hydroxylamines, which provide *N*-aryl-*N*-allyl amines in generally moderate yields and with excellent regioselectivity. A novel azodioxide–iron complex has been implicated as the active aminating agent in the allylic aminations catalyzed by iron salts.[5b]

In order to enhance the synthetic utility of metal-catalyzed allylic aminations and to further explore the reactivity of coordinated organonitrogen species, we have been interested in the use of more readily available prospective aminating agents, including amines[6] and, here, nitroorganics. The metal-catalyzed reactions of nitroarenes and CO can produce various useful organonitrogen compounds, including amines, urethanes, ureas and isocyanates.[7] We now report the discovery of a new allylic amination system, which employs nitroarenes as aminating

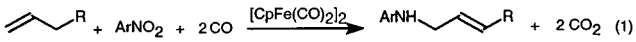

agents and inexpensive $[CpFe(CO)_2]_2$ as the catalyst [eqn. (1)]. Initial experiments indicate that this system is distinct, both mechanistically and chemoselectively, from the recently reported $Ru_3(CO)_{12}$/(α-diimine)-catalyzed system for allylic amination.[8]

The reactions of olefins with nitroarenes catalyzed by $[CpFe(CO)_2]_2$ (5 mol%) were carried out in dioxane at 150–180 °C under 50–75 atm of CO.‡ Representative results for a number of olefins and nitro compounds are summarized in Table 1. The desired allyl amines were the only olefin-derived products detected, generally constituting 75–95% of the volatile N-containing products; *N*,*N*-diaryl ureas are the principal byproducts.§ The yield of allyl amine depends markedly on the structure of both the olefin and the nitro compound. Among the small set of test olefins 1,1-disubstituted derivatives were aminated most efficiently (entries 1,2) while 1,2-disubstituted, trisubstituted and terminal olefins were aminated less efficiently (entries 3–5). With unsymmetrical alkenes (entries 1–5) single regioisomers were obtained which are derived from introduction of nitrogen at the less-substituted vinylic carbon with double bond transposition, characteristic of ene reactions.[9] Probing the structure/reactivity correlation of the nitroarene component with α-methylstyrene (AMS) as the substrate (entries 1, 6–9), nitrobenzene gave a nearly quantitative yield, nitroarenes bearing electron-withdrawing groups gave moderate yields, and nitroanisole afforded a poor yield of the corresponding allyl amine.

Initial screening experiments demonstrated that the dinuclear **1** is the most active among several related complexes tested as amination catalysts. In the reaction of nitrobenzene with AMS (dioxane, 160 °C, 70 atm CO) neither bimetallic $Cp_2Mo_2(CO)_4$ nor other mono-iron complexes, *e.g.* $Fe(CO)_5$, $CpFe(CO)_2Br$ or $CpFe(CO)_2(THF)^+$, produced appreciable quantities of allyl amine. However, a 52% yield of the allyl amine from AMS was obtained using $CpFe(CO)_2(\eta^1\text{-allyl})$ (**2**, 5 mol%) as (pre)-catalyst. The documented ability of the two active (pre)-catalysts, **1** and **2**, to generate the $CpFe(CO)_2$ radical[10,11] suggests that this species may be involved in the catalytic mechanism.

Given the unprecedented catalytic activity of **1** and the distinctive regioselectivity of the amination reaction several experiments were conducted to probe the nature of the actual aminating species. Firstly, evidence was gathered indicating that two potential reactive free organonitrogen species are not involved. Nitrosobenzene, an established enophile,[12] was excluded as an intermediate since the amination of AMS by nitrobenzene proceeded cleanly in the presence of the PhNO-trapping agent, 2,3-dimethylbutadiene [eqn. (2)],[13] with none of the corresponding hetero-Diels–Alder adduct being produced.¶

Table 1 Allylic amination by nitroarenes catalyzed by $[CpFe(CO)_2]_2$

Entry	Alkene	Nitroarene	Allylamine	Yield[a,b] (%)
1		$PhNO_2$		92
2		$PhNO_2$	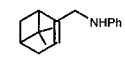	64
3		$PhNO_2$	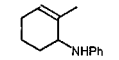	27
4	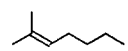	$PhNO_2$	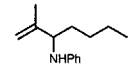	10
5		$PhNO_2$	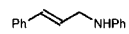	13
6		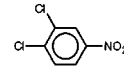	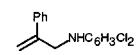	54[c]
7		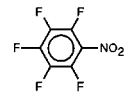	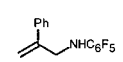	57[c]
8		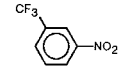	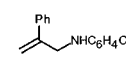	52[c]
9		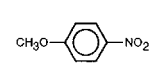	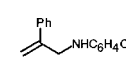	2[c]

[a] GC yield, naphthalene standard. [b] New compounds were isolated and characterized spectroscopically. [c] Isolated yield.

† Present address: Department of Chemistry, University of Southwestern Louisiana, Lafayette, LA 70504, USA.

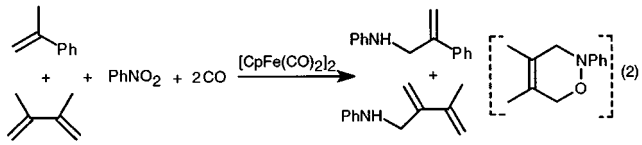

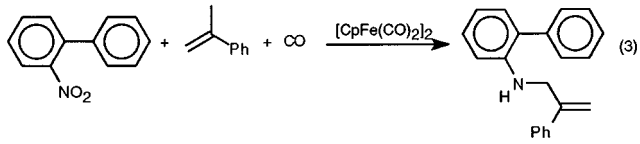

Similarly, amination of AMS by 2-nitrobiphenyl afforded the corresponding *N*-biphenyl-*N*-allyl amine exclusively [eqn. (3)], but no detectable carbazole, the established product of intramolecular nitrene trapping.[14] Together these results suggest that a coordinated organonitrogen species serves as the active aminating agent in the reactions catalyzed by **1**.

More direct information on the iron species involved in the catalytic reaction was obtained by examining a dark red paramagnetic compound **3** which can be isolated from the stoichiometric reaction of **1** with nitrobenzene in the absence of olefin (dioxane, 100 °C, 75 atm CO, Scheme 1). Although we have not yet established the structure of **3**,‖ this compound appears to be catalytically relevant since it both stoichiometrically (in the absence of nitrobenzene) and catalytically (in the presence of nitrobenzene) efficiently aminates AMS (dioxane, 160 °C, 60 atm CO, TON *ca*. 8). Moreover, **3** aminates AMS in the presence of the nitrosobenzene trap, 2,3-dimethylbutadiene, again suggesting that the nitrogen fragment is transferred in the coordination sphere of the metal.

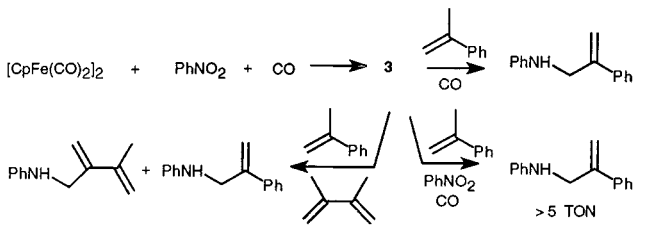

Scheme 1

In summary, $[CpFe(CO)_2]_2$ has been found to be an effective catalyst for the regioselective allylic amination of olefins by nitroarenes. It is significant that iron-catalyzed reactions involving nitroorganics and CO are rare.[15] Moreover, the differing chemoselectivity and trapping results between the present system and the $Ru_3(CO)_{12}$/α-diimine-catalyzed aminations[8]** suggests the involvement of distinctly different active aminating agents. Further insight into the mechanism of this new catalytic amination process, including the nature of the active iron species involved, awaits the results of studies in progress.

We are grateful for support provided by the National Science Foundation (CHE 9610277). We also thank Professors F. Ragaini and S. Cenini (Milan) for discussions and communication of their recent results prior to publication.

Notes and references

‡ *General procedure*: $[CpFe(CO)_2]_2$ (0.15 mmol), nitrobenzene (2.9 mmol), olefin (3.8 mmol) and dioxane (10 ml) were placed in the glass liner of a stainless steel autoclave under nitrogen. The autoclave was charged with CO (900–1000 psi) and then heated at 160–180 °C for 22–24 h, during which time aliquots were withdrawn *via* dip tube for GC analysis. The autoclave was cooled, the solution was transferred into a Schlenk tube, and the volatiles were removed *in vacuo*. The residue was triturated with light petroleum–Et_2O. The insoluble residue contained the *N*,*N*-diaryl ureas. The extracts were chromatographed on silica gel using light petroleum–Et_2O as eluent to afford the allyl amine. New compounds were characterized by NMR and MS analysis.

§ Small amounts of aryl amine (1–20%), azoarene (1–5%), and azoxyarene (1–5%) were also detected by GC–MS analysis. Non-volatile *N*,*N*-diaryl urea by-products were isolated by crystallization/chromatography.

¶ The hetero-Diels–Alder adduct was shown to be stable under the conditions of the catalytic reaction.

‖ *Selected data* for **3**: ν_{max}(KBr)/cm^{-1} 2033 and 1965; EPR (CH_2Cl_2)/G 3525 (bs); *m*/*z* (FAB) 628, 471, 396, 342, 288, 195; the elemental analysis of **3**, while indicating the presence of C, H, N and Fe, suggests contamination by an organic impurity.

** In the $Ru_3(CO)_{12}$/diimine-catalyzed reactions, aryl amines are the major byproducts (ref. 8) and amination in the presence of dimethylbutadiene affords substantial quantities of the hetero-Diels–Alder adduct. F. Ragaini and S. Cenini, personal communication, 1998.

1 E. W. Svastits, J. H. Dawson, R. Breslow and S. H. Gellman, *J. Am. Chem. Soc*., 1985, **107**, 6427; J. P. Mahy, G. Bedi, P. Battioni and D. Mansuy, *New J. Chem*., 1989, **13**, 651; K. J. O'Conner, S.-J. Wey and C. J. Burrows, *Tetrahedron Lett*., 1992, **33**, 1001; D. A. Evans, M. M. Faul, M. T. Bilodeau, B. A. Anderson and D. M. Barnes, *J. Am. Chem. Soc*., 1993, **115**, 5328; R. E. Lowenthal and S. Masamune, *Tetrahedron Lett*., 1991, **32**, 7373; Z. Li, R. W. Quan and E. N. Jacobsen, *J. Am. Chem. Soc*., 1995, **117**, 5889; R. S. Atkinson, J. Fawcett and P. J. Williams, *Tetrahedron Lett*., 1995, **36**, 3241; K. Noda, N. Hosoya and R. Irie, *Synlett*, 1993, **7**, 469; P. J. Perez, M. Brookhart and J. L. Templeton, *Organometallics*, 1993, **12**, 261.

2 M. R. Gagne, C. L. Stern and T. J. Marks, *J. Am. Chem. Soc*., 1992, **114**, 275; M. R. Gagne and T. J. Marks, *J. Am. Chem. Soc*., 1989, **111**, 4108; Y. Li and T. J. Marks, *Organometallics*, 1996, **15**, 3770; M. A. Giardello, V. P. Conticello, L. Brard, M. R. Gagne and T. J. Marks, *J. Am. Chem. Soc*., 1994, **116**, 10241.

3 Review: R. K. Grasselli, *J. Chem. Ed*., 1986, **63**, 216; P. Arthur and B. C. Pratt, US Pat. 2,571,099, 1951; W. C. Drinkard and R. V. Lindsay, US Pat. 3,496,215, 1970.

4 L. S. Liebeskind, K. B. Sharpless, R. D. Wilson and J. A. Ibers, *J. Am. Chem. Soc*., 1978, **100**, 7061; D. A. Muccigrosso, S. E. Jacobson, P. A. Apgar and F. Mares, *J. Am. Chem. Soc*., 1978, **100**, 7063; A. Srivastava, Y. Ma, R. Pankayatselvan, W. Dinges and K. M. Nicholas, *J. Chem. Soc., Chem. Commun*., 1992, 853; M. Johannsen, K. A. Jorgensen, *J. Org. Chem*., 1994, **59**, 214; R. S. Srivastava and K. M. Nicholas, *J. Org. Chem*., 1994, **59**, 5365.

5 (*a*) R. S. Srivastava and K. M. Nicholas, *Tetrahedron Lett*., 1994, **35**, 8739; (*b*) R.S. Srivastava, M. A. Khan and K. M. Nicholas, *J. Am. Chem. Soc*., 1996, **118**, 3311; (*c*) R. S. Srivastava and K. M. Nicholas, *J. Am. Chem. Soc*., 1997, **119**, 3302; (*d*) M. Johannsen and K. A. Jorgensen, *J. Org. Chem*., 1994, **59**, 214; (*e*) M. Johannsen and K. A. Jorgensen, *J. Org. Chem*., 1995, **60**, 5979.

6 R. S. Srivastava and K. M. Nicholas, *Chem. Commun*., 1996, 2335.

7 Review: S. Cenini and F. Ragaini, *Catalytic Reductive Carbonylation of Organic Nitro Compounds*, Kluwer, Dordrecht, 1997; A. Bassoli, B. Rindone, S. Tollari, S. Cenini and C. Crotti, *J. Mol. Catal*., 1990, **60**, 155; S. J. Skoog and W. L. Gladfelter, *J. Am. Chem. Soc*., 1997, **119**, 11049.

8 S. Cenini, F. Ragaini, S. Tollari and D. Paone, *J. Am. Chem. Soc*., 1996, **118**, 11964.

9 Reviews: W. Oppolzer and V. Snieckus, *Angew. Chem., Int. Ed. Engl*., 1978, **17**, 476; H. M. R. Hoffmann, *Angew. Chem., Int. Ed. Engl*., 1969, **8**, 556; B. Snider, *Acc. Chem. Res*., 1980, **13**, 426.

10 T. H. Whitesides and J. Shelly, *J. Organomet. Chem*., 1975, **92**, 215; A. Hudson, M. F. Lappert and B. K. Nicholson, *J. Chem. Soc., Dalton Trans*, 1977, 551.

11 M.-T. Lee, P. S. Waterman, R. H. Magnuson, R. E. Meirowitz, A. Prock and W. P. Giering, *Organometallics*, 1998, **7**, 2146.

12 G. T. Knight, *J. Chem. Soc., Chem. Commun*., 1970, **1016**; R. E. Banks, R. N. Haszeldine and P. J. Miller, *Tetrahedron Lett*., 1970, **4417**; G. E. Keck, R. R. Webb and J. B. Yates, *Tetrahedron*, 1981, **37**, 4007.

13 E. C. Taylor, C.-P. Tseng and J. B. Rampal, *J. Org. Chem*., 1982, **47**, 552.

14 R. J. Sundberg, M. Brenner, S. R. Suter and B. P. Das, *Tetrahedron Lett*., 1970, 2715; R. J. Sundberg and R. W. Heintzelmen, *J. Org. Chem*., 1974, **39**, 2546.

15 H. Alper and K. E. Hashem, *J. Am. Chem. Soc*., 1981, **103**, 6514 (→ carbamates); K. Cann, T. Cole, W. Sleigir and R. Pettit, *J. Am. Chem. Soc*., 1978, **100**, 3969 (→ anilines); J.E. Kmiecik, *J. Org. Chem*., 1965, **30**, 2014 (→ azoarenes).

Communication 8/07248E

ChemComm

Preparation of a silica-supported peroxycarboxylic acid and its use in the epoxidation of alkenes†

Jacob A. Elings, Rachida Ait-Meddour, James H. Clark* and Duncan J. Macquarrie

Green Chemistry Group, Department of Chemistry, University of York, Heslington, York, UK YO1 5DD. E-mail: jhc1@york.ac.uk

Received (in Cambridge, UK) 28th September 1998, Accepted 3rd November 1998

A new solid peroxyacid based on organically modified silica has been prepared and successfully applied to the epoxidation of alkenes.

Peroxyacids are active straightforward epoxidation reagents with wide application.[2] They do not require catalysts and are often excellent epoxidation reagents for unfunctionalised alkenes. Their use in epoxidation, however, is disputed because of the requirement of at least stoichiometric amounts in the reaction, resulting in the production of large amounts of acid waste. Although recycling of these acids to peroxyacids is possible by treatment with hydrogen peroxide in the presence of concentrated acids, this is normally not attractive for present-day homogeneous processes. An additional problem is that some types of the more active peroxyacids are not stable and therefore unsafe for use on a large scale. Because of these drawbacks the use of peroxyacids is not popular in industry.[3] The use of heterogeneous peroxyacids can deliver important improvements with respect to workup, recycling and stability. Heterogenisation of peroxyacids has, however, scarcely been studied and in the literature only a few examples are known where peroxyacids were supported on polystyrene resins.[4–8] Although these polymer-supported peroxyacids are active epoxidation reagents, their performance is poor due to the electron-releasing effect of the polymer backbone and their need for swelling. Furthermore, the close contact of easy oxidisable polymer backbones with strongly oxidative peroxyacids can potentially be dangerous (explosive). We now report a novel robust heterogeneous peroxyacid based on chemically modified silica, which is an active, selective and effective reagent for alkene epoxidation.

The preparation of the silica-supported peroxyacid is summarised in Scheme 1. The preparation of the cyanoethyl silica was partially based on a previously reported sol-gel method for MCM-type silicas.[9] Typically, tetraethyl orthosilicate (TEOS, 20.4 g, 98 mmol) and 2-cyanoethyltriethoxysilane (CETS, 21.3 g, 98 mmol) were added, separately, to a mechanically stirred mixture of ethanol (104 ml), water (106 ml) and *n*-dodecylamine (10 g, 54 mmol) at room temperature. A milky solution was rapidly formed, followed by precipitation. The stirring was continued for 21 h, yielding a thick white suspension. This was filtered and *n*-dodecylamine was removed by heating the solid at reflux in absolute ethanol (200 ml) for 3 h. This extraction was repeated three times. The solid was then dried in a vacuum oven at 95 °C for one night, yielding 15.2 g of a fine white solid (CN-silica). The CN-silica (10.0 g) was hydrolysed by heating it in 50% (v/v) aqueous sulfuric acid at 150 °C for 3 h. After cooling to room temperature, the silica was filtered and washed with an excess of water. Drying in a vacuum oven at 95 °C for one night afforded 10.3 g of COOH-silica. To 1 g of the COOH-silica were successively added methanesulfonic acid (3.0 g, 31 mmol) and hydrogen peroxide (70 wt% aqueous solution, 1.75 g, 36 mmol). This mixture was stirred at room temperature for 5 h. After this, the mixture was combined with 50 ml of water and filtered. The residue was thoroughly washed with an excess of water. The COOOH-silica (**1**) obtained was dried in a desiccator over KOH under vacuum for one night. Approximately 0.25 g of this desiccator-dried material was used to determine the number of peroxyacid groups by reductive titration with 0.1 M aq. $Na_2S_2O_3$ in the presence of I^-. Similarly prepared were **2** (ratio CETS:TEOS = 1:2) and **3** [3-cyanopropyltriethoxysilane (CPTS) instead of CETS, ratio CPTS:TEOS = 1:1].

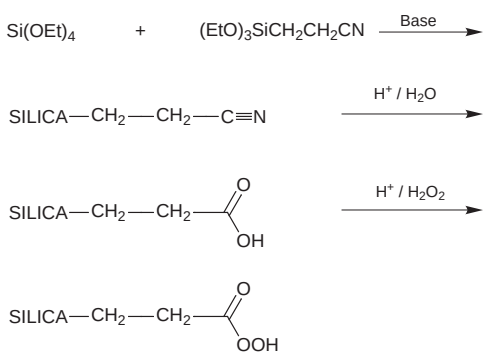

Scheme 1

The epoxidation of *cis*-cyclooctene and cyclohexene to their corresponding oxides was carried out as follows. To a solution of the alkene (4 mmol) in 50 ml $CHCl_3$ was added the remaining part of the desiccator-dried COOOH-silica (0.75 g). This mixture was stirred at 30 °C for 24 h, after which it was filtered. The silica residue was washed with 25 ml $CHCl_3$. The combined filtrates were analysed by GC using 1,4-dichlorobenzene as an internal standard.

Table 1 shows that the treatment of the COOH-silicas with hydrogen peroxide in the presence of an acid resulted in materials containing peroxy groups. We confirmed that these were really supported peroxyacids by checking a blank silica. When a silica comprising TEOS only was treated in a similar way with hydrogen peroxide, no oxidation activity was found, which rules out the possibility of physically adsorbed hydrogen peroxide as the active reagent. Comparison of the peroxyacid loadings of **1** and **2** shows an interesting phenomenon. Despite the fact that the relative number of CETS groups in the synthesis of **2** was decreased by a factor 2 with respect to that of **1**, this resulted only in a reduction of the number of peroxyacid groups

Table 1 Epoxidation of *cis*-cyclooctene with silica-supported peroxyacids

Silica	**1**	**2**	**3**
Number peroxyacids/mmol g^{-1}	3.54	2.88	3.31
Specific surface area/m^2 g^{-1} [a]	426	1080	597
Conversion *cis*-cyclooctene (%)	55	57	62
Selectivity to cyclooctene oxide (%)	100	88	96
Efficiency of oxygen transfer (%)[b]	81	87	91

[a] Determined for the parent COOH–silica using the BET isotherm with dinitrogen as adsorbate. [b] 100 × (mmol epoxide formed)/(mmol COOOH groups per g dried silica × exact amount COOOH-silica).

† See ref. 1

Table 2 Reagent recyclability in the epoxidation of cyclohexene with COOOH-silica **2**

Cycle	Number peroxyacids/mmol g^{-1}	Conversion (%)	Selectivity (%)	Efficiency of oxygen transfer (%)
0	2.95	57	77	81
1[a]	2.97	55	77	76

[a] The spent reagent of cycle 0 was removed by filtration, washed with $CHCl_3$, dried and subsequently regenerated. The amounts of reactant used in the regeneration process and epoxidation were adapted to the amount of spent reagent which remained after its recovery.

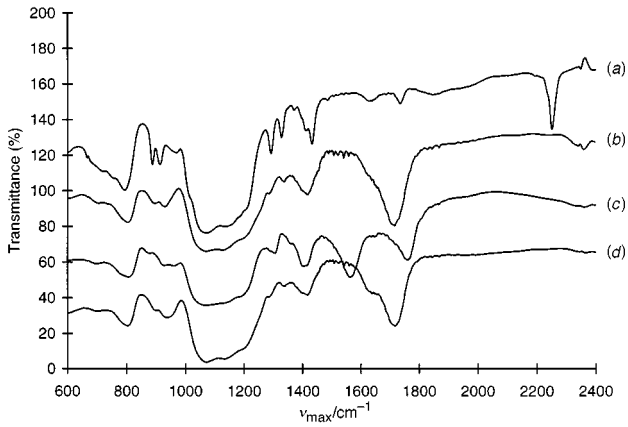

Fig. 1 DRIFT spectra of silica-supported peroxyacid **1** and its precursors: (*a*) CN-silica, (*b*) COOH-silica, (*c*) COOOH-silica **1** and (*d*) spent COOOH-silica.

in the final product by a factor of 1.2. This result may indicate a better accessibility of the carboxylic groups in the precursor of **2**, which is supported by its higher surface area.

Fig. 1 shows the DRIFT spectra of COOOH-silica **1** and its precursors. The precursors display the expected bands for CN (2252 cm^{-1}) and COOH (1715 cm^{-1}), respectively. Conversion of the COOH group into its corresponding peracid resulted, as expected,[2] in a shift of the band for the carbonyl group to higher frequencies (1760 cm^{-1}) and a spectrum consistent with that found for peracetic acid.[10] Interestingly, DRIFT also shows that the supported peroxyacid is converted into its parent acid during the epoxidation process (and neutralisation of the unreacted groups by reductive titration). This indicates that recycling is in principle possible.

Tables 1 and 2 show that the new COOOH-silicas were capable of epoxidising *cis*-cyclooctene and cyclohexene with high to excellent selectivities. In neither of the cases could by-products be detected by GC. Table 2 also shows that by giving spent COOOH-silica **2** another treatment with hydrogen peroxide/methanesulfonic acid, we managed to fully recycle the former number of peroxy groups, resulting in a silica which was still capable of epoxidising cyclohexene. Comparison of the oxygen transfer efficiencies of the silica materials with known polymer systems shows that the silica materials were much more effective in their transfer of oxygen to *cis*-cyclooctene. For example, Harrison and Hodge found for their polymer-supported peroxyacid (loading 3.5–4.0 mmol g^{-1}) a maximum efficiency of 48% only.[6] Despite the fact that we used an excess of alkene in our epoxidation experiments, the peroxy oxygens were not fully transferred to the substrate. Although decomposition of the supported peroxyacids may be responsible for the loss of oxygens (reminiscent of epoxidation with conventional peroxyacids[2]), we found in the case of **1**, by reductive titration of spent material, that the 'missing oxygens' could mainly be attributed to unreacted peroxyacid groups, indicating the presence of groups inaccessible to the alkene.

The new peroxyacid reagents have several important characteristics including loadings and activities which approach those found for conventional homogeneous peroxyacids (*e.g.* 70% MCPBA $\approx$ 4 mmol g^{-1}). Also, these materials appear to be stable under anhydrous conditions at room temperature (no loss in activity on drying and on storing the dry material over at least 24 h). We are currently optimising the performance of above mentioned supported peroxyacids. For this purpose, the effect of solvent and temperature will be studied in detail. Preliminary results show that epoxidation of a range of alkenes can be achieved using the new solid peroxyacid, that these materials are also effective in benign solvents such as EtOAc and that the oxygen transfer efficiencies can be further enhanced by fine-tuning of the silica synthesis and porosity.

We are grateful to the European Commission for a TMR Marie Curie Grant (to J. A. E.), to the Royal Academy of Engineering/EPSRC for a Clean Technology Fellowship (to J. H. C.) and the Royal Society for a University Research Fellowship (to D. J. M.).

Notes and references

1 UK Patent applied for.
2 D. Swern, in *Organic Peroxides*, ed. D. Swern, Wiley, New York, vol. 2, 1971.
3 R. A. Sheldon, in *Applied Homogeneous Catalysis with Organometallic Compounds*, ed. B. Cornils and W. A. Hermann, VCH, Weinheim, 1996, vol. 1, pp. 411–423.
4 C. R. Harrison and P. Hodge, *J. Chem. Soc., Chem. Commun.*, 1974, 1009.
5 J. M. J. Fréchet and K. E. Haque, *Macromolecules*, 1975, **8**, 130.
6 C. R. Harrison and P. Hodge, *J. Chem. Soc., Perkin Trans. 1*, 1976, 605.
7 C. R. Harrison and P. Hodge, *J. Chem. Soc., Perkin Trans. 1*, 1976, 2252.
8 C. W. Jefford and G. Bernardinelli, *Tetrahedron Lett.*, 1985, **26**, 615.
9 D. J. Macquarrie, *Chem. Commun.*, 1996, 1961.
10 *The Aldrich Library of FT-IR Spectra, Edition I*, Aldrich, Milwaukee, 1985.

Communication 8/07517D

α-Carbonyl radical cyclization approach toward spiro[4.4]nonene: total synthesis of dimethyl gloiosiphone A

Chin-Kang Sha* and Wen-Yueh Ho

Department of Chemistry, National Tsing Hua University, Hsinchu 300, Taiwan, ROC.
E-mail: cksha@chem.nthu.edu.tw

Received (in Cambridge, UK) 2nd November 1998, Accepted 9th November 1998

The total synthesis of dimethyl gloiosiphone A 2 was achieved *via* an α-carbonyl radical spirocyclization.

Gloiosiphone A **1** and its dimethyl derivative **2** were isolated from red marine algae *Gloiosiphonia verticillaris*.[1] Crude lipid collections of *Gloiosiphonia verticillaris* were found to exhibit profound antimicrobial activity against several *Staphylococcus*,

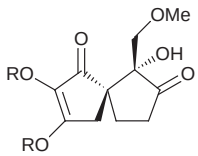

1 R = H
2 R = Me

Bacillus and *Salmonella* species. Since the causative agent **1** was not stable enough for isolation, the crude collections were treated with CH_2N_2 to furnish the more stable dimethyl derivative **2**.

Compounds **1** and **2** comprise a new structural class featuring a highly oxygenated spiro[4.4]nonene system. Due to their potential antimicrobial activity and novel molecular skeleton, these compounds are challenging synthetic targets. The first total synthesis of dimethyl gloiosiphone A **2** has been achieved recently by Paquette's group.[2] As an extension of our work on the α-carbonyl radical cyclization reaction,[3] we report herein the total synthesis of **2** using an α-carbonyl radical cyclization as the key step. The retrosynthetic analysis is outlined in Scheme 1. The spirononene structure in **2** could be produced by an α-carbonyl radical cyclization followed by appropriate oxidation (**4**⟶**3**). The radical precursor iodo ketone **4** would be generated according to our method[4] from **5**, which in turn could be prepared from cyclopentanone **6** according to Yamashita's procedure.[5]

Treatment of cyclopentanone **6** with *N*,*N*-dimethylhydrazine in the presence of TFA as catalyst furnished hydrazone **7** (Scheme 2). Deprotonation of **7** with Bu^{n}Li at 0 °C followed by alkylation with 5-iodopent-1-yne and hydrolysis yielded the required ketone **5**. Ketone **5** was sequentially treated with HMDS/TMSI and NaI/MCPBA in THF to afford iodo ketone **4**.

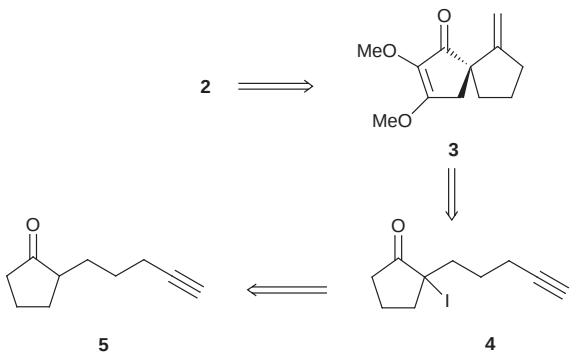

Scheme 1

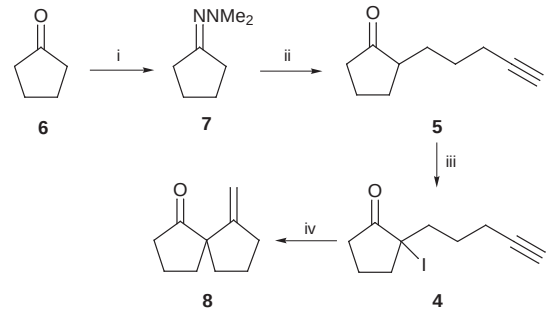

Scheme 2 *Reagents and conditions*: i, H_2NNMe_2, 90%; ii, Bu^{n}Li, 0 °C, 5-iodopent-1-yne, then 10% HCl, 1 h, 80%; iii, HMDS, TMSI, CH_2Cl_2, then NaI, MCPBA, THF, 82%; iv, $(Bu_3Sn)_2$ (0.1 equiv.), sun lamp, C_6H_6, 1.5 h, then Bu_3SnH (1.05 equiv.), AIBN, C_6H_6, 87%.

Treatment of **4** with Bu_3SnH under standard conditions furnished the required spirocyclic compound **8** in 50% yield. To improve the yield, an atom transfer radical reaction was adopted.[6] Thus, irradiation of a benzene solution of ketone **4** at reflux with a sun lamp in the presence of $(Bu_3Sn)_2$ (0.1 equiv.) followed by reduction of the resulting vinyl iodide with Bu_3SnH (1.05 equiv.) using AIBN as initiator furnished spiro compound **8** in 87% overall yield.

We then focused our attention on the introduction of enol ether moieties into **8**. First, iodo ketone **9** was generated from **8** by the same method used for the transformation of **5**⟶**4** (Scheme 3).[3] The iodo ketone **9** was then converted into unsaturated ketone **10** *via* a modified version of Sato's method.[7] Accordingly, **9** was oxidized with DMSO at 70 °C followed by addition of I_2 (1 equiv.) to provide **10**.

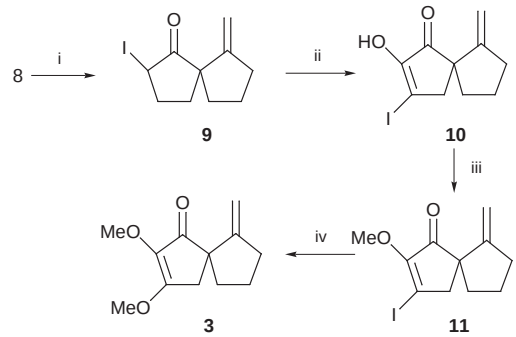

Scheme 3 *Reagents and conditions*: i, HMDS, TMSI, CH_2Cl_2, then NaI, MCPBA, THF, 82%; ii, DMSO, I_2, 86%; iii, NaH, MeI, DMF, 95%; iv, NaOMe (10 equiv.), MeOH, 92%.

Compound **10** was subsequently methylated with NaH and MeI to give methoxy iodo enone **11**. Nucleophilic displacement of iodide in **11** with NaOMe then furnished dimethoxy enone **3**.

Allylic oxidation of **3** with SeO_2 gave diketone **12** (60%) (Scheme 4). Treatment of **12** with a catalytic amount of OsO_4 with NMO as the co-oxidant gave dihydroxy ketone **13**. Finally, selective methylation of the primary alcohol with dimethyl sulfate in presence of excess K_2CO_3 (10 equiv.) afforded

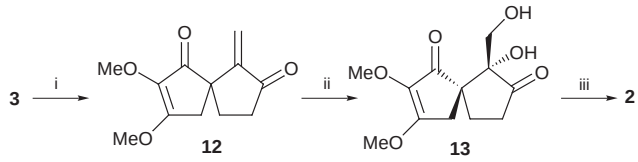

Scheme 4 *Reagents and conditions*: i, SeO_2, dioxane, reflux, 60%; ii, OsO_4, NMO, Bu^{t}OH, THF, H_2O, 87%; iii, K_2CO_3 (10 equiv.), Me_2SO_4, 75%.

dimethyl gloiosiphone A **2**. All spectral data for **2** are in good agreement with those reported in the literature.[1,2]

In summary, a total synthesis of dimethyl gloiosiphone A **2** has been accomplished in a stereoselective manner in which an α-carbonyl radical cyclization reaction was employed to facilitate the construction of the key spiro[4.4]nonene skeleton. Application of this versatile α-carbonyl radical cyclization methodology toward the total synthesis of more complex natural products is under current investigation.

We thank the National Science Council of the Republic of China for financial support (NSC87-2113-M-007-043).

Notes and references

1 J. L. Chen, M. F. Moghaddam and W. H. Gerwick, *J. Nat. Prod*., 1993, **56**, 1205.
2 L. A. Paquette, C. F. Sturino and P. Doussot, *J. Am. Chem. Soc*., 1996, **118**, 9456; C. F. Sturino, P. Doussot and L. A. Paquette, *Tetrahedron*, 1997, **53**, 8913.
3 C.-K. Sha, C.-Y. Shen, T.-S. Jean, R.-T. Chiu and W.-H. Tseng, *Tetrahedron Lett*., 1993, **34**, 7641; C.-K. Sha, R.-T. Chiu, C.-F. Yang, N.-T. Yao, W.-H. Tseng, F.-L. Liao and S.-L. Wang, *J. Am. Chem. Soc*., 1997, **119**, 4130; C.-K. Sha, K. C. Santhosh and S.-H. Lih, *J. Org. Chem*., 1998, **63**, 2699.
4 C.-K. Sha, T.-S. Jean and D.-C. Wang, *Tetrahedron Lett*., 1990, **31**, 3745.
5 T. Mino, S. Masuda, M. Nishio and M. Yamashita. *J. Org. Chem*., 1997, **62**, 2633.
6 D. P. Curran, *Synthesis*, 1988, 417 and 489; D. P. Curran, in *Free Radicals in Synthesis and Biology*, ed. F. Minisci, Kluwer, Dordrecht, 1988, p. 37.
7 K. Sato, Y. Kojima and H. H. Sato, *J. Org. Chem*., 1970, **35**, 2374.

Communication 8/08455F

Molecular design of thermotropic liquid crystalline polyhydroxy amphiphiles exhibiting columnar and cubic mesophases of the normal type

Konstanze Borisch,[a] Carsten Tschierske,*[a] Petra Göring[b] and Siegmar Diele[b]

[a] *Institute of Organic Chemistry, University Halle, Kurt-Mothes-Str. 2, D-06120 Halle, Germany. E-mail: coqfx@mlucom6.urz.uni-halle.de*

[b] *Institute of Physical Chemistry, University Halle, Mühlpforte 1, D-06099 Halle, Germany*

Received (in Cambridge, UK) 26th October 1998, Accepted 5th November 1998

The phase sequence Col_{h1}–Cub_{V1}–S_A–Col_{h2}–Cub_{I2}, which represents a major part of the theoretical lyotropic phase diagram of detergent solvent systems, was realized for the first time in a binary mixture of two thermotropic amphiphilic liquid crystals without any solvent.

The molecular self-organization of amphiphilic molecules in aqueous systems with formation of micelles and lyotropic mesophases is a well known phenomenon.[1] Different types of lyomesophases can be detected depending on the amphiphile structure,[2] the concentration and the temperature. Beside the layer-like lamellar phase (L_α, smectic A: S_A) other mesophases consisting of curved aggregates occur. Cylindrical aggregates organize into hexagonal columnar phases (H, Col_h) and globular or non-globular spheroids can build cubic mesophases (discontinuous cubic phases, Cub_I). Another type of cubic mesophase consisting of two mutually interwoven networks of branched cylinders (bicontinuous cubic mesophases, Cub_V) occurs at the transitions between smectic and columnar phases. For each of the non-lamellar mesophases two different types are possible. Normal phases (type 1) have the stronger cohesive forces located in the continuum surrounding the aggregates. In the reversed (or inverse) phases (type 2) they are located inside the aggregates.

Many amphiphilic molecules can form not only lyotropic phases in aqueous systems, but also thermotropic mesophases as pure materials.[3] In particular, amphiphilic polyhydroxy compounds[3] and carbohydrate derivatives can have a wide variety of different thermotropic mesophases.[4] The formation of large dynamic hydrogen bonding networks between the hydroxy groups and the micro-segregation of the hydrophilic and the lipophilic parts of the individual molecules into separate regions are important driving forces for their self-organization. The kind of mesophase formed depends on the temperature and the chemical structure of the amphiphiles. Double chain compounds usually form columnar mesophases (Col_{h2}) or bicontinuous cubic mesophases (Cub_{V2}). Amphiphiles with three long aliphatic chains, such as **1** (see Fig. 1), can form micellar cubic mesophases built up from spheroidic closed micelles (Cub_{I2}).[5,6] Because the stronger cohesive forces (hydrogen bonding) are located inside the aggregates surrounded by the flexible alkyl chains the thermomesophases of these molecules are similar to the reversed lyotropic mesophases of detergent solvent systems. Interestingly, most non-lamellar thermomesophases of pure amphiphiles belong to the reversed type.† In particular, the concept of taper-shaped molecules[7] is based on this type of molecular organization.

Therefore we set out to design novel amphiphilic polyhydroxy compounds which can organize to thermotropic mesophases which represent analogues of normal lyotropic systems. Their aggregates should consist of micro-segregated lipophilic cores surrounded by polar shell regions providing cohesive forces *via* dynamic hydrogen bonding. To achieve this, we have synthesized the amphiphilic molecule **2**‡ consisting of two large hydrophilic polyhydroxy units and a single lipophilic chain connected *via* an aromatic linking unit (**2**, Fig. 1).

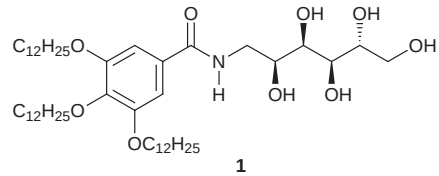

1

Cr 94 °C Cub_{I2} 227 °C Iso

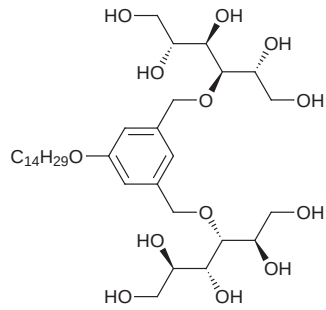

2

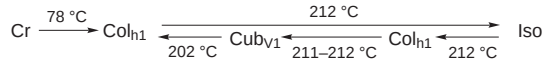

Fig. 1 Thermotropic phase transitions of **1** and **2**. The transition temperatures of **2** from the Col_{h1} phase to the Cub_{V1} phase depend on the cooling rate. Abbreviations: Cr = crystalline solid; Col_{h1} = normal hexagonal columnar phase,; Cub_{V1} = normal bicontinuous cubic phase; Cub_{I2} = reversed discontinuous cubic mesophase; Iso = isotropic liquid state.

Compound **2** was studied by polarizing microscopy and X-ray diffraction. On heating, the material melts at 78 °C into a birefringend mesophase with a non-specific texture. This mesophase turns into the isotropic liquid state at 212 °C. On cooling from the isotropic melt the formation of a spherulitic texture can be observed at the same temperature. Immediately after its occurrence optically isotropic domains appear and rapidly coalesce to a highly viscous optically isotropic phase. On further cooling a mosaic-like texture occurs at 202 °C. On re-heating this texture remains without changes up to the isotropization temperature at 212 °C. The X-ray diffraction pattern of this birefringent phase is characterized by three sharp reflexes in the small angle region and a diffuse scattering in the wide angle region. The ratio of the positions of the small angle reflections is $1:3^{1/2}:2$, proving a hexagonal two-dimensional lattice with a hexagonal lattice parameter of a_{hex} = 4.66 nm at T = 80 °C and a_{hex} = 4.49 nm at T = 180 °C (hexagonal columnar mesophase). The diameter of the columns (*ca.* 4.5 nm) is in good agreement with a radial arrangement of the molecules (L = 3.0 nm in their most extended conformation) in cylinders with the fluid alkyl chains assembled in their centers. The number of molecules which should be arranged on average in the cross-section of a 0.45 nm thick slice of the columns is about 8.§

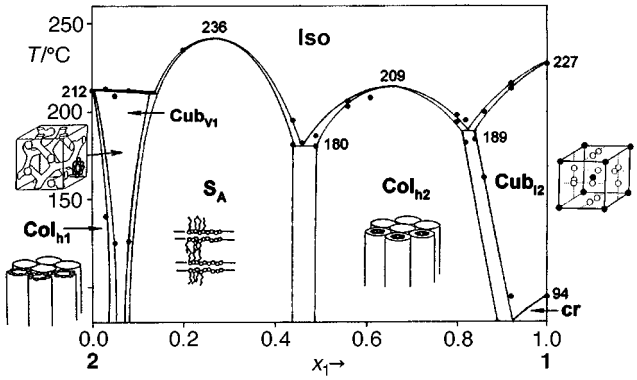

Fig. 2 Phase diagram of the binary system **1/2**. The transition temperatures observed in the heating scans (polarizing microscopy) are shown. In the cooling scans a Cub_{V1}/Col_{hl} dimorphism is found for the pure compound **2** (Fig. 1) and the Cub_{V1}–Col_{h1} transition is shifted to lower temperatures and lower concentrations of **1**. A *Ia3d* cubic lattice is shown as an example for the bicontinuous Cub_{V1} phase (the cylinders are filled with the alkyl chains). The Cub_{I2} phase is described in ref. 5(*c*),(*d*). Abbreviations: S_A = smectic A phase, Col_{h2} = reversed hexagonal columnar phase. Other abbreviations, see Fig 1.

The optically isotropic mesophase should be a cubic mesophase as indicated by the optical isotropy, the high viscosity and the cornered phase boundaries which occurring during its growth. Proof of this using X-ray scattering was not possible because of the high temperatures required. Remarkably the cubic mesophase is only formed on cooling the sample from the isotropic liquid state after passing the small range of a columnar mesophase. It seems that the cubic phase is the thermodynamical stable phase in the temperature range between 202 and 212 °C, however the formation of this three-dimensionally ordered mesophase is hindered for kinetic reasons, and its formation from the columnar phase is more strongly hindered in the heating cycles.¶

The normal type of the mesophases of **2** was proven by means of miscibility experiments.[5b,d] The phase diagram of **2** with the triple chain amphiphile **1**[5b] is shown in Fig. 2. In the contact regions of the hexagonal columnar mesophase of **2** with the reversed micellar cubic phase (Cub_{I2}) of **1**, the columnar phase of **2** is lost and is completely replaced by the cubic mesophase. In a concentration range between X_1 = 0.1 and 0.4 a broad region of a smectic A layer structure is found. The stability of this mesophase is significantly higher than those of the mesophases of the pure compounds. Upon a further increase of the content of **1** a second columnar mesophase is induced. Because the interface curvature changes continuously from left to right, the induced columnar phase which is intermediate between the S_A and the reversed micellar Cub_{I2} phase should be a reversed columnar phase (Coh_{h2}). Thus, in the contact region between **2** and **1**, five different mesophases can be observed:‖ Col_{h1}–Cub_{V1}–S_A–Col_{h2}–Cub_{I2}. This sequence represents a major part of the theoretical lyotropic phase diagram of detergent solvent systems, which was realized for the first time in a binary system of two different amphiphiles in the absence of any solvent and is a proof of the normal type of the mesophases of **2**. Thus, with exception of normal cubic mesophases consisting of spheroidic closed micelles (Cub_{I1}) all the main mesophase types found in lyotropic systems were successfully realized as their thermotropic closed analogues.‖

This work was supported by the Deutsche Forschungsgemeinschaft and the Fonds der Chemischen Industrie.

Notes and references

† The first amphiphilic compound which could have a normal (probably bicontinuous) cubic mesophase was recently reported (ref. 8), furthermore some polysaccharides with cubic or columnar mesophases have been described (ref. 9); however, no experimental proof of the normal type phase structure was given in these references.

‡ Synthesized by etherification of 3,5-bisbromomethyl-1-tetradecyloxybenzene (obtained by reduction of methyl 3,5-tetradecyloxybenzene-1,3-dicarboxylate with $LiAlH_4$, followed by treatment with PBr_3) and 1,2:5,6-di-*O*-isopropylidene-D-mannitol (NaH in DMF) followed by deprotection (10% HCl in MeOH). Expected C, H analyses, mass and ^1H and ^{13}C NMR spectra were obtained: δ_H(400 MHz, DMSO-d_6, 27 °C, $SiMe_4$) 0.83 (t, 3 H, *J* 6, CH_3), 1.22–1.38 (m, 22 H, CH_2), 1.65–1.69 (m, 2 H, CH_2), 3.31–3.67 (m, 16 H, C*H*$_2$OH, C*H*OH, CH_2OC*H*), 3.91 (t, 2H, *J* 7, OCH_2), 4.18 (d, 2H, *J* 7, OH), 4.30 (t, 2H, *J* 6, OH), 4.45 (t, 2H, *J* 6, OH), 4.50–4.59 (m, 8H, OH, C*H*$_2$OCH), 6.81 (s, 3H, aromatic H); δ_C(126 MHz, DMSO-d_6, 30 °C, $SiMe_4$) 13.9 (CH_3), 22.0, 25.5, 28.6, 28.7, 28.8, 28.9, 29.0, 31.2 (CH_2), 67.3 (OCH_2), 64.0, 63.0 (*C*H_2OH), 70.4, 71.0, 71.1, 77.9 (*C*HOH, CH_2O*C*H), 73.0 (*C*H_2OCH) 158.5, 140.5, 118.4, 112.2 (aromatic C); *m*/*z* (ESI-MS) 701 ([M + Na]$^+$, 100%).

§ $n = (a_{hex}^2/2)h(N_A/M)\rho$ with ρ = 1 g cm-3, N_A = Avogadro constant, *M* = molecular mass, *h* = 0.45 nm (diffuse scattering in the wide angle region of the X-ray pattern).

¶ No prolonged heating is possible at these temperatures due to decomposition.

‖ As in other binary mixtures of amphiphilic polyhydroxy compounds [ref. 5(*b*)] no reversed bicontinuous cubic mesophase (Cub_{V2}) could be detected between the S_A phase and the reversed Col_{h2} phase, although the reason for this is not yet clear. However, this phase was realized with other polyhydroxy amphiphiles [ref. 5(*b*),(*d*)].

1 G. J. T. Tiddy, *Phys. Rep.*, 1988, **57**, 1; J. M. Seddon and R. H. Templer, in *Handbook of Biological Physics*, ed R. Lipowsky and E. Sackmann, Elsevier, Amsterdam, 1995, vol. 1, p. 97.
2 J. N. Israelachvili, D. J. Mitchell and B. W. Ninham, *J. Chem. Soc., Faraday Trans. 2*, 1976, **72**, 1525.
3 C. Tschierske, *Progr. Polym. Sci.*, 1996, **21**, 775.
4 Reviews: J. W. Goodby, *Mol. Cryst. Liq. Cryst.*, 1984, **110**, 205; G. A. Jeffrey, *Acc. Chem. Res.*, 1986, **12**, 179; G. A. Jeffrey and L. M. Wingert, *Liq. Cryst.*, 1992, **12**, 179; H. Prade, R. Miethchen and V. Vill, *J. Prakt Chem.* 1995, **337**, 427.
5 (*a*) K. Borisch, S. Diele, P. Göring and C. Tschierske, *Chem. Commun.*, 1996, 237; (*b*) K. Borisch, S. Diele, P. Göring, H. Müller and C. Tschierske, *Liq. Cryst.*, 1997, **22**, 427; (*c*) K. Borisch, S. Diele, P. Göring, H. Kresse and C. Tschierske, *Angew. Chem.*, 1997, **109**, 2188; *Angew. Chem., Int. Ed Engl.*, 1997, **36**, 2087; (*d*) K. Borisch, S. Diele, P. Göring, H. Kresse and C. Tschierske, *J. Mater. Chem.*, 1998, **8**, 529.
6 Columnar and cubic mesophases of dendrimers: V. S. K. Balagurusamy, G. Ungar, V. Percec and G. Johansson, *J. Am. Chem. Soc.*, 1997, **119**, 1539.
7 A. Eckert, B. Kohne and K. Praefcke, *Z. Naturforsch*, 1988, **43b**, 878; G. Lattermann and G. Staufer, *Liq. Cryst.*, 1989, **4**, 347; K. Praefcke, B. Kohne, W. Stephan and P. Marquardt, *Chimia*, 1989, **43**, 380; K. Praefcke, P. Marquardt, B. Kohne and W. Stephan, *J. Carbohydr. Chem.*, 1991, **10**, 539; V. Percec, D. Tomazos, J. Heck, H. Blackwell and G. Ungar, *J. Chem. Soc., Perkin Trans. 2*, 1994, 31.
8 V. Vill, T. Böcker, J. Thiem and F. Fischer, *Liq. Cryst.*, 1989, **6**, 349.
9 V. Vill, *Habilitationsschrift*, Hamburg, 1997, p. 35.

Communication 8/08271E

ChemComm

A formal synthesis of both atropenantiomers of desertorin C

Rekha V. Kyasnoor and Melvyn V. Sargent*

Department of Chemistry, University of Western Australia, Nedlands, Western Australia, 6907, Australia. E-mail: mvs@chem.uwa.edu.au

Received (in Cambridge, UK) 20th October 1998, Accepted 6th November 1998

Asymmetric synthesis of both enantiomers of 1,1′-(2′,4-dihydroxy-6,6′-dimethoxy-2,4′-dimethylbiphenyl-3,3′-diyl)-bisethanone allows the formal synthesis of both enantiomers of 4,4′,7,7′-tetramethoxy-5,5′-dimethyl-6,8′- bicoumarin (desertorin C).

The desertorins A **1**, B **2** and C **3** are a family of unsymmetrical coumarin dimers of fungal origin which are optically active on account of restricted rotation about their stereogenic axes.[1]

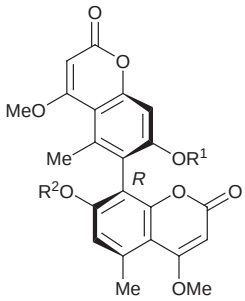

1 $R^1 = R^2 = H$
2 $R^1 = H$, $R^2 = Me$
3 $R^1 = R^2 = Me$
4 $R^1 = R^2 = Bz$

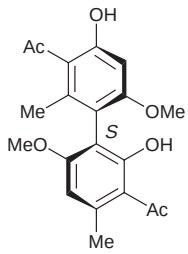

5

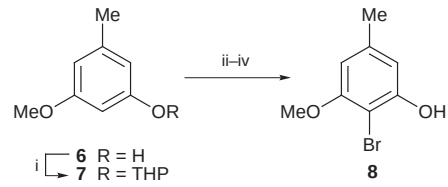

Scheme 1 *Reagents and conditions*: i, TsOH, dihydropyran, THF, 0 °C, 20 h; ii, BuLi, Ar, THF, TMEDA, 25 °C, 4 h; iii, $BrCF_2CF_2Br$, 25 °C, 1 h; iv, H^+, H_2O.

Methylation of both desertorins A and B provides desertorin C which on base hydrolysis yields the diketone **5**.[1] We have previously synthesized desertorin C in racemic form using the (±)-diketone **5** as the key intermediate.[2] Subsequently the absolute configuration of the desertorins was established as *R* by an X-ray crystal structure determination of the bis-bromobenzoate **4**.[3] We now describe a synthetic approach to both enantiomers of desertorin C.

O-Methylorcinol **6** (Scheme 1) was protected as its tetrahydropyranyl ether **7** which on lithiation and subsequent treatment with 1,2-dibromotetrafluoroethane and acidic work-up gave the bromophenol **8**,[4] mp 71–72 °C, in 60% overall yield. Mitsunobu reaction (Scheme 2) between this bromo-

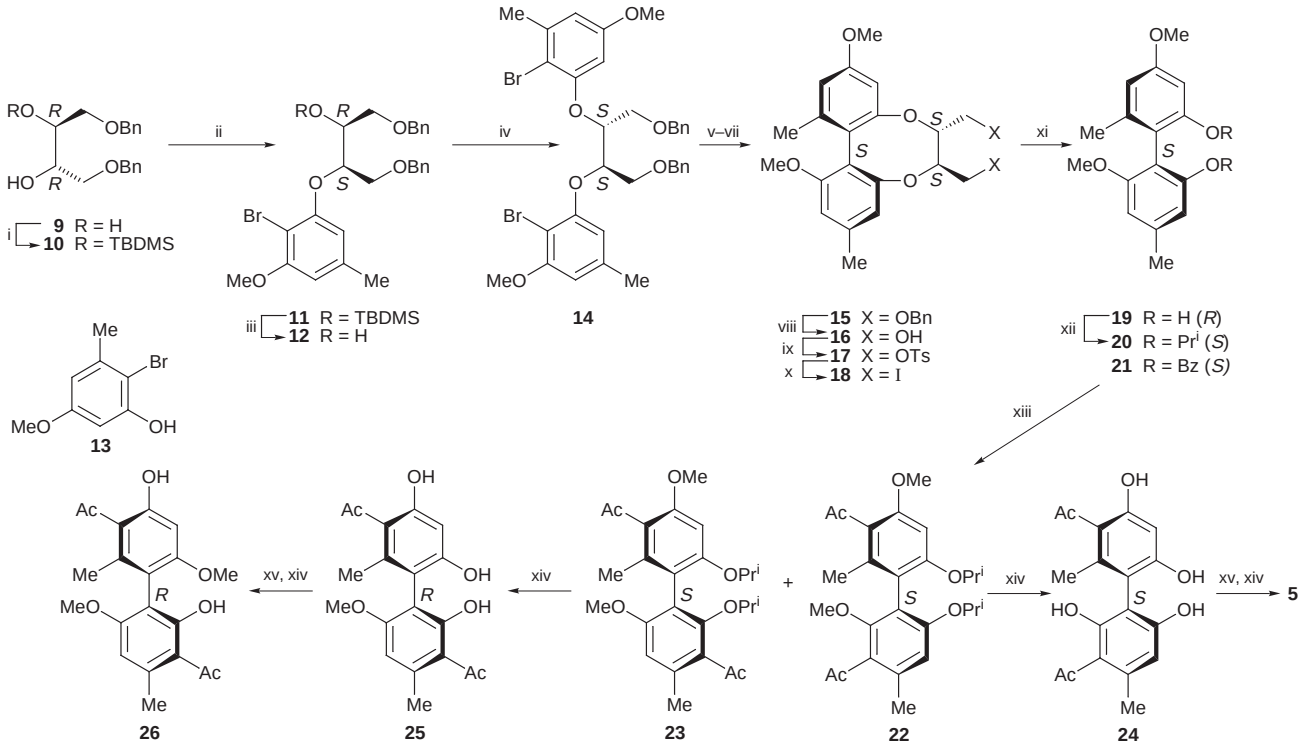

Scheme 2 *Reagents and conditions*: i, TBDMSCl, imidazole, DMF, 25 °C, 15 h, 76%; ii, **8**, Bu_3P, DEAD, THF, 25 °C, 24 h; iii, Bu_4NF, THF, 25 °C, 1 h; iv, **13**, Bu_3P, DEAD, THF, 25 °C, 48 h; v, BuLi, Ar,THF, −78 °C, 1 h; vi, CuCN, TMEDA, −78 to −40 °C, 15 min; vii, O_2, −78 °C, 3 h; viii, H_2, Pd/C, EtAc, 94%; ix, TsCl, C_5H_5N, 0 °C, 7 h, 78%; x, NaI, Me_2CO, reflux, 5 h, 91%; xi, Zn, EtOH, reflux, 1 h, 80%; xii, Pr^iBr, K_2CO_3, DMF, 45 °C, 48 h, 68%; xiii, TFAA, AcOH, CH_2Cl_2, 25 °C, 7h, 69%; xiv, BCl_3, CH_2Cl_2, 0 °C, 2 h; xv, MeI, K_2CO_3, DMF, 40 °C, 15 h.

phenol **8** and the mono(*tert*-butyldimethylsilyl)ether **10** of 1,4-di-*O*-benzyl-L-threitol **9**[5] gave the ether **11** (68%) which on deprotection afforded the alcohol **12** (90%). This alcohol was caused to react in another Mitsunobu reaction with the bromophenol **13**.[6] The resultant D-threitol derivative **14**, mp 54–56 °C (45%), was subjected sequentially to lithiation, copper(I) cyanide and dry oxygen after the manner of Lipschutz *et al*.,[7] which gave the cyclized product **15** (40%). Deprotection was achieved by hydrogenolytic debenzylation and tosylation of the resultant diol **16**. The tosylate **17** was converted into the iodide **18**, mp 155–157 °C, which on reductive elimination with activated zinc supplied the diol **19**, mp 134–136 °C, $[\alpha]_D^{20}$ −27 (*c* 0.67, $CHCl_3$).

In order for the intramolecular coupling **14**→**15** to occur the aryloxy substituents in the intermediate higher order cyanocuprate[7] are predicted to adopt, on account of the anomeric effect, the *gauche* conformation depicted in Fig. 1. Hence the axial configuration of the intermediate cyclic compound **15** is *S* and that of the diol **19** is *R*. The diol appeared to be enantiomerically pure since it was not resolved on HPLC on two chiral columns[8] nor did the ^1H and ^{19}F NMR spectra of the derived Mosher diester show the presence of the other enantiomer even in the presence of a lanthanide shift reagent. The CD spectrum (MeCN) of the derived dibenzoate **21** showed exciton splitting centred at λ 226 nm with a positive first Cotton effect (λ 237 nm, $\Delta\varepsilon$ 24.3) and a negative second effect (λ 215 nm, $\Delta\varepsilon$ −9.0) in keeping with the *R* configuration of the diol **19**.[9]

Since *O*-methylorcinol **6** undergoes *C*-monoacetylation at both positions *ortho* to the hydroxy group, the diol **19** was isopropylated and the resultant ether **20** was acetylated with AcOH and TFAA, which supplied an inseparable mixture of the diketones **22** and **23**. Selective dealkylation of this mixture with BCl_3 yielded the tetrol **24** (30%), mp 198–200 °C, $[\alpha]_D^{20}$ 32.8 (*c* 0.86, Me_2CO), $\delta_{OH}(CDCl_3)$ 8.46, 8.54, 11.80 and 13.42, and the triol **25** (35%), mp 120 °C decomp., $[\alpha]_D^{20}$ −61.0 (*c* 1.05, Me_2CO), $\delta_{OH}(CDCl_3)$ 8.36, 11.87 and 12.45. Methylation and selective demethylation of the tetrol **24** gave the (*S*)-diketone **5** (69%), mp 147–149 °C (lit.,[1] 149–150 °C), $[\alpha]_D^{20}$ 34.0 (*c* 0.94, Me_2CO),[10] which had previously been obtained by basic hydrolysis of desertorin C.[1] The (*R*)-diketone **26** (82%), mp 145–146 °C, $[\alpha]_D^{20}$ −53.0 (*c* 0.80, Me_2CO),[11] was obtained in a similar fashion from the triol **25**. Since the racemic diketone has been converted into desertorin C this constitutes a formal synthesis of both of the enantiomers of this metabolite.

Both the synthetic diketone **5** and the degradation product **5** appear to have undergone some racemisation, the former presumably at the tetrol stage, and the latter under the harsh conditions of the hydrolysis.

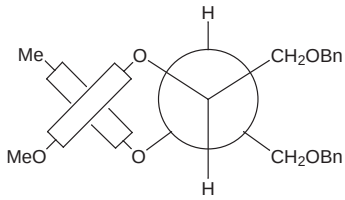

Fig. 1 Newman projection along the 2,3-bond of the D-threitol **14** in the conformation for the coupling reaction leading to **15**.

Notes and references

1 K. Nozawa, H. Seyea, S. Nakajima, S. Udagawa and K. Kawai, *J. Chem. Soc., Perkin Trans. 1*, 1987, 1735.
2 M. A. Rizzacasa and M. V. Sargent, *J. Chem. Soc., Perkin Trans. 1*, 1988, 2425.
3 K. Kawai, M. Shiro and K. Nozawa, *J. Chem. Res.*, 1995, 701.
4 G. I. Feutrill and R. N. Mirrington, *Aust. J. Chem.*, 1972, **25**, 1719.
5 E. A. Mash, K. A. Nelson, E. V. Densen and S. B. Hemperly, *Org. Synth.*, 1993, **Coll. Vol. VIII**, 155.
6 J. R. Cannon, T. M. Cresp, B. W. Metcalf, M. V. Sargent, G. Vinciguerra and J. A. Elix, *J. Chem. Soc.* (*C*), 1971, 3495.
7 B. H. Lipschutz, F. Kayser and Z.-P. Lui, *Angew. Chem., Int. Ed. Engl.*, 1994, **33**, 1842.
8 Pirkle type 1A and Chiralpak OT (+).
9 N. Harada and K. Nakanishi, *Circular Dichroic Spectroscopy*: *Exciton Coupling in Organic Spectrochemistry*, University Science Books, Mill Valley, 1983.
10 CD spectra: Degradation product λ(MeOH)/nm 227 and 270 ($\Delta\varepsilon$ 7.7 and −6.5). Synthetic product λ(MeCN)/nm 196, 216, 231, 275, 296 and 340 ($\Delta\varepsilon$ 10.4, −31.8, 18.3, −9.0, 3.8 and 1.9). The racemic diketone was not resolved on HPLC nor was its ^1H NMR spectrum resolved in the presence of (*S*)-1-(anthracen-9-yl)-2,2,2-trifluoroethanol.
11 CD spectrum: λ(MeCN)/nm 196, 216, 230, 276, 295 and 335 ($\Delta\varepsilon$ −19.8, 52.7, −33.5, 14.7, −7.5 and −5.2).

Communication 8/08146H

Vicinal diamination of 1,4-dihydropyridines

Rodolfo Lavilla,* Rakesh Kumar, Oscar Coll, Carme Masdeu and Joan Bosch

Laboratory of Organic Chemistry, Faculty of Pharmacy, University of Barcelona, 08028 Barcelona, Spain. E-mail: lavilla@farmacia.far.ub.es

Received (in Liverpool, UK) 6th October 1998, Accepted 10th November 1998

Electrophilic interaction of iodine with *N*-alkyl-1,4-dihydropyridines 1 in the presence of secondary amines stereoselectively leads to the corresponding *trans*-2,3-diamino-1,2,3,4-tetrahydropyridines 2 in satisfactory yields (79–94%); the method allows the synthesis of piperidine, pyrrolidine, morpholine and piperazine derivatives.

Continuing our research on the development of new transformations of 1,4-dihydropyridines,[1] we have recently described some 'non-biomimetic' oxidations of these compounds, in which the normal production of the corresponding pyridinium salt is avoided.[2–4] As a consequence, several unusual transformations of these heterocyclic systems have emerged as useful synthetic tools. For instance, the oxidative addition of halonium ions (*N*-halosuccinimide or related alkoxyhalogenations) was investigated, and the method was successful for the preparation of 2-substituted 3-halo-1,2,3,4-tetrahydropyridines, which, in turn, may be considered as valuable synthetic intermediates.[3] In these reactions, we observed the formation of some byproducts, arising from the nucleophilic trapping of the iminium ion produced in the interaction of the enamine moiety with the halogenating agent. We reasoned that the use of nitrogenated species in these processes would result in the formation of interesting tetrahydropyridines bearing amino substituents at positions 2 and 3 (Scheme 1).[5]

The use of amines as nucleophiles in this type of transformation is normally avoided,[6,7] because of the easy oxidation of the nitrogen atom or its coordination with the electrophile. We felt, however, that this process could be dramatically reduced due to the high reactivity of the enamine moiety present in dihydropyridines **1**, which may rapidly attack the halogen to form a 3-halo-3,4-dihydropyridinium ion. In good agreement with our expectations, when dihydropyridine **1a**[8] was treated in THF solution with iodine (3.5 equiv.) in the presence of an excess of pyrrolidine, the 2,3-diaminotetrahydropyridine **2a**† was stereoselectively formed in 87% yield (Scheme 2 and Table 1).‡ The stereochemistry of the addition was ascertained by NMR methods (including homo- and hetero-correlation techniques). The small H^2–H^3 coupling constant observed suggests a *trans* relationship between the two pyrrolidine groups and a major conformation in which these substituents are axial (it should be noted that in a tetrahydropyridine ring such a substitution pattern displays no serious 1,3-diaxial interactions).

The formation of **2a**§ could be rationalized by considering the initial formation of a *trans*-2-amino-3-iodotetrahydropyridine, which would undergo an internal nucleophilic substitution reaction followed by a stereoselective ring opening of the resulting aziridinium ion promoted by a second equivalent of the secondary amine.[9]

The reaction seems to be quite general, and works well with different alkyl groups at the dihydropyridine nitrogen (methyl and benzyl) and electron-withdrawing groups at the 3 position (methoxycarbonyl and cyano). Several cyclic secondary amines¶ were tested, including pyrrolidine, piperidine, morpholine and *N*-methylpiperazine, and the corresponding *trans* vicinal diamines were isolated in good yields. It should be noted that the diamination of olefins usually involves multistep sequences and/or the use of expensive organometallic reagents. The yields were slightly improved by adding solid Na_2CO_3 to the reaction mixture, but efforts to reduce the amount of iodine and/or secondary amine to stochiometric amounts resulted in decreased yields, even after longer reaction times.

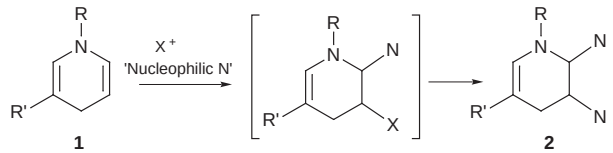

Scheme 1

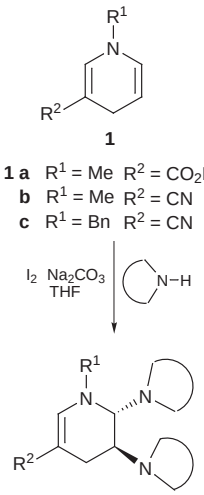

Scheme 2

This remarkable process is also suitable for the formation of cyclic adducts. Thus, when **1a** was allowed to react with iodine in the presence of *N*,*N*′-dimethylethylenediamine, the bicyclic adduct **3** was obtained (80% yield) as a slightly unstable oil, probably as a mixture of two isomers. Column chromatography (SiO_2, elution with CH_2Cl_2–EtOAc) allowed the purification of the major component. The stereochemistry of the ring fusion in

Table 1 Vicinal diamination reactions from dihydropyridines **1**

Entry	Dihydropyridine	Secondary amine	Product	Yield (%)
1	**1a**	pyrrolidine	**2a**	87
2	**1a**	piperidine	**2b**	90
3	**1b**	pyrrolidine	**2c**	94
4	**1b**	piperidine	**2d**	89
5	**1b**	morpholine	**2e**	84
6	**1c**	pyrrolidine	**2f**	79
7	**1c**	1-methylpiperazine	**2g**	86
8	**1a**	$MeNH(CH_2)_2NHMe$	**3**	80

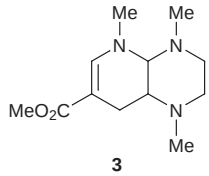

3

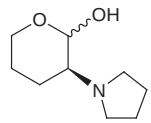

4

the major isomer was determined to be *cis*,‖ as the coupling constant between the ring fusion hydrogens is small (J < 1 Hz; a *trans*-decalin type fusion would result in a much larger coupling constant). This was confirmed by NOE and NOESY experiments. The difference with respect to the previous acyclic systems (where only *trans* products **2** were obtained) may reflect the fact that, in the present case, the intramolecular nucleophilic attack in the initially formed *trans*-2-amino-3-iodotetrahydropyridine takes place faster from the remaining secondary amino group to form the more stable 6-membered ring. Alternatively, an aziridinium intermediate could undergo ring-opening to give a 3-amino-3,4-dihydropyridinium cation, which could be intramolecularly trapped by the remaining secondary amino group.

The use of this methodology with enol ethers was tested next, and when 3,4-dihydro-2*H*-pyran was treated with iodine and pyrrolidine, an unstable compound was obtained (presumably the corresponding 2,3-diaminotetrahydropyran), which decomposed during column chromatography to furnish the hemiacetal **4**** (27%, non-optimized yield) as an anomeric mixture.[10] It is worth mentioning that cyclohexene failed to yield significant amounts of the corresponding addition product[11] on treatment with iodine and pyrrolidine under the usual reaction conditions, thus suggesting that only electron-rich olefins are good substrates for this kind of oxidative additions.

In summary, we have described a new 'non-biomimetic' oxidation of 1,4-dihydropyridines that allows the vicinal diamination of these substrates in an efficient and stereocontrolled manner.

This work was supported by the DGICYT, Spain (project PB94-0214). Thanks are also due to the Comissionat per Universitats i Recerca (Generalitat de Catalunya) for Grant SGR97-00018. O. C. and R. K. thank the 'Ministerio de Educación y Cultura', Spain, for fellowships.

Notes and references

† All new compounds were characterized by ^{1}H and ^{13}C NMR, IR, UV, MS and HRMS or elemental analysis.

‡ *General procedure* for oxidative diamination reactions. A solution of iodine (3.5 mmol) in THF (50 ml) was added dropwise under N_2 atmosphere to a stirred suspension of dihydropyridine **1** (1 mmol), secondary amine (25 mmol), and Na_2CO_3 (95 mmol) in THF (50 ml) kept at 0 °C, and stirring was continued at room temperature until no dihydropyridine is detected by TLC (usually 1–3 h). Water (150 ml) was added, and the mixture was extracted with EtOAc (3 × 75 ml). The combined organic extracts were washed with aq. $Na_2S_2O_3$ solution (100 ml, 0.5 M) and brine (100 ml), and dried (Na_2SO_4). The solvent was removed under reduced pressure, and the residue was purified by column chromatography (SiO_2, elution with CH_2Cl_2–EtOAc) to yield pure 2,3-diaminotetrahydropyridines.

§ *Selected data* for **2a**: δ_H 7.39 (s, 1H, H-6), 3.66 (s, 3H, OCH_3), 3.57 (br s, 1H, H-2), 3.09 (s, 3H, NCH_3), 2.59 (m, 10H), 2.30 (m, J 16.8, 4.4, 1.4, 1H, H-4), 1.75 (m, 8H); δ_C 168.4 (CO), 144.9 (C-6), 93.1 (C-5), 78.0 (C-2), 58.4 (C-3), 51.8 (OCH_3), 50.1, 50.0, 43.2 (NCH_3), 22.9, 22.8, 20.5 (C-4).

¶ The use of primary amines (pentylamine, hexylamine, methylamine) resulted in complex reaction mixtures, from which the desired products, as well as the corresponding aziridines, were detected in trace amounts.

‖ *Selected data* for *cis*-**3**: δ_H 7.23 (s, 1H, H-6), 3.61 (s, 3H, OCH_3), 3.13 (br s, 1H, H-4a), 2.99 (s, 3H, NCH_3), 2.86 (m, 1H, H-8a), 2.76 (m, 2H), 2.43–2.19 (m, 4H), 2.38 (s, 3H, NCH_3), 2.22 (s, 3H, NCH_3); δ_C 168.0 (CO), 144.3 (C-6), 94.4 (C-7), 78.6 (C-4*a*), 56.1 (C-8*a*), 50.6 (OCH_3), 47.3, 42.2, 42.0, 41.9, 24.7 (C-8).

** *Selected data* for **4** (major anomer): δ_H 5.16 (d, J 3.3, 1H, H-2), 3.91 (m, 1H, H-6), 3.53 (m, 1H, H-6), 2.57 (m, 4H), 2.26 (m, 1H, H-3), 1.80–1.60 (m, 9H); δ_C (data for the major anomer) 91.4 (C-2), 64.1 (C-6), 58.9 (C-3), 50.9, 24.1 (C-5), 23.6, 23.0 (C-4).

1 For a review on the chemistry of dihydropyridines, see: D. M. Stout and A. I. Meyers, *Chem. Rev*., 1982, **82**, 223.
2 R. Lavilla, F. Gullón, X. Barón and J. Bosch, *Chem. Commun*., 1997, 213.
3 R. Lavilla, O. Coll, R. Kumar and J. Bosch, *J. Org. Chem*., 1998, **63**, 2728.
4 R. Lavilla, O. Coll, M. Nicolàs and J. Bosch, *Tetrahedron Lett*., 1998, **39**, 5089.
5 For the aziridination of 1,4-dihydropyridines, see: B. K. Warren and E. E. Knaus, *J. Med. Chem*., 1981, **24**, 462. For a review on the chemistry of aminals, see: L. Duhamel, in *The Chemistry of Functional Groups, Supplement F*, Part 2, ed. S. Patai, Wiley, New York, 1982, p. 849.
6 For a general review of olefin amination reactions promoted by electrophiles, see: M. Orena, in *Methods of Organic Chemistry, Stereoselective Synthesis*, ed. G. Helmchen, R. W. Hoffmann, J. Mulzer and E. Schaumann, Thieme, Stuttgart, 1996, vol. 9. p. 5291. Also see: J. Rodriguez and J.-P. Dulcère, *Synthesis*, 1993, 1177.
7 Only intramolecular haloamination of olefins is relevant in synthesis: D. R. Williams, D. L. Brown and J. M. Benbow, *J. Am. Chem. Soc*., 1989, **111**, 1923; S. R. Wilson, S. R. Sawicki and J. C. Huffman, *J. Org. Chem*., 1981, **46**, 3887; I. Monkovic, T. T. Conway, H. Wong, Y. G. Perron, I. J. Pachter and B. Belleau, *J. Am. Chem. Soc*., 1973, **95**, 7910; D. Tanner, M. Sellén and J. E. Bäckvall, *J. Org. Chem*., 1989, **54**, 3374; W. R. Bowman, D. L. Clark and R. J. Marmon, *Tetrahedron*, 1994, **50**, 1275.
8 For the preparation of *N*-alkyl-1,4-dihydropyridines, see: M. E. Brewster, A. Simay, K. Czako, D. Winwood, H. Farag and N. Bodor, *J. Org. Chem*., 1989, **54**, 3721.
9 For a related regio- and stereo-selective ring opening of aziridinium ions, see: S. E. de Sousa and P. O'Brien, *Tetrahedron Lett*., 1997, **38**, 4885.
10 For a recent and effective method to carry out this transformation, see: J. Du Bois, C. S. Tomooka, J. Hong and E. M. Carreira, *J. Am. Chem. Soc*., 1997, **119**, 3179. Also see: M. Sunose, K. M. Anderson, A. G. Orpen, T. Gallagher and S. J. F. Macdonald, *Tetrahedron Lett*., in the press.
11 E. J. Corey, S. Sarshar, M. D. Azimioara, R. C. Newbold and M. C. Noe, *J. Am. Chem. Soc*., 1996, **118**, 7851.

Communication 8/07776B

Methylation of zinc bound thiolates; a model for cobalamine independent methionine synthase

Udo Brand, Michael Rombach and Heinrich Vahrenkamp*

Institut für Anorganische und Analytische Chemie, Universität Freiburg, Albertstr. 21, D-79104 Freiburg, Germany. E-mail: vahrenka@uni-freiburg.de

Received (in Basel, Switzerland) 21st September 1998, Accepted 10th November 1998

Pyrazolylborate–zinc–thiolate complexes react under mild conditions with methyl iodide, dimethylsulfate and trimethylsulfonium iodide, liberating the corresponding methyl thioethers; the driving force for these reactions lies in the high nucleophilicity of the zinc-bound thiolates and the low donor quality of thioethers toward zinc.

Methylation of thiols is an essential biological process,[1] being required *inter alia* for the biosynthesis of methionine or during DNA repair by the Ada protein. It is becoming evident that zinc plays an important rôle in this process,[2] being involved catalytically in Ada,[3] cobalamine independent methionine synthase,[4] or methanol–CoM–methyltransferase.[5] A common source of the methyl group is methyltetrahydrofolate, in the form of a methylammonium cation. Frequently methylcobalamine is the methyl group transfer agent, but in the world of plants which lacks vitamin B_{12} the methylating enzyme catalyzes the direct alkyl transfer from the methyl source to the thiol.

Model studies involving zinc complexes were published by Walker and Lippard[6] [reactions of $Zn(SPh)_4^{2-}$, $LZn(SPh)_3^-$ or $L_2Zn(SPh)_2$ with trimethyl phosphate] and by Darensbourg and coworkers[7] [reactions of a solvated tetradentate-N_2S_2 zinc complex with iodomethane and dibromopropane]. In the former case it was concluded that the thiolate dissociates from zinc prior to alkylation, and in the latter case the intermediate replacement of a thiolate ligand by a solvent molecule could not be ruled out. We now present evidence for the intramolecular alkylation of zinc bound thiolates and show how the ligand environment of zinc as well as the nature of the thiolates and the methylating agents affect the group transfer reactions.

Based on the proposal[8] that in cobalamine independent methionine synthase the reacting thiol homocysteine is activated as a protein–zinc–thiolate in a neutral or monoanionic L_3Zn–SR complex, we chose again substituted pyrazolylborates Tp* to mimic the protein L_3 environment, thereby ensuring that the Tp*Zn thiolates are uncharged and that the zinc ion is encapsulated by the 3-substituents of the Tp* ligands. Complexes **1** and **2** were used as model compounds. Such complexes form spontaneously from the corresponding Tp*Zn–OH complexes (our 'enzyme models')[9] and thiols at neutral pH,[10] as verified here for **1a** and **1b**. **2a** and **2b**, whose corresponding $Tp^{Me,Me}Zn$–OH complex is unstable, were prepared from $Tp^{Me,Me}Zn$–Cl and the sodium thiolates.†

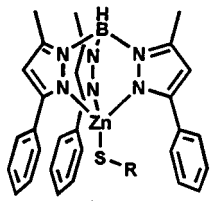

L^1Zn–SR

1a: R = Et

1b: R = CH_2Ph

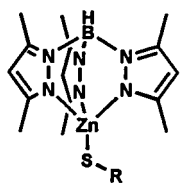

L^2Zn–SR

2a: R = Et

2b: R = CH_2Ph

All four complexes **1** and **2** reacted with methyl iodide in a 1:1 ratio in chloroform at room temperature according to eqn. (1).‡ There can be no doubt that the methylations occur at

$$LZn-SR + MeX \longrightarrow LZn-X + MeSR \qquad (1)$$

the zinc bound thiolates, the main pieces of evidence being the non-polar reaction conditions and the fact that cationic Tp*Zn•L complexes can exist only in the presence of very good donor ligands and only in the absence of even weakly coordinating anions.[11] It was verified that the free thiols do not react with methyl iodide under the given reaction conditions. Furthermore, the intermediate existence of free thiolates was deemed unlikely by an exchange experiment: replacement of SEt^- in **1a** by SCH_2Ph^- to form **1b**‡ is about 20 times slower than methylation of SEt in **1a** under the same conditions. Preliminary kinetic data indicate that, as expected, the reactions are bimolecular. Surprisingly, the reactions of **1a** and **1b** are about ten times faster than those of **2a** and **2b**. This indicates that the higher hydrophobicity around zinc in complexes **1** due to encapsulation by the phenyl groups outweighs their lower accessibility due to steric hindrance by the same phenyl groups as a rate-determining factor. An important part of the driving force for these reactions must be ascribed to the poor donor quality of the resulting thioethers toward zinc. It is extremely unlikely that they would form the above-mentioned cationic Tp*Zn–L complexes, and we are actually not aware of any structurally characterized zinc complex with a monodentate thioether ligand.

Methylation reactions according to eqn. (1) were also achieved with dimethylsulfate in chloroform.‡ Although dimethylsulfate is known to be a stronger methylating agent than methyl iodide, it did not react faster here. This is further evidence for the intramolecular nature of these methylations: in a four-center Zn–S/C–X transition state of a bimolecular reaction there is more driving force to proceed *via* a soft–soft interaction (Zn–I) than *via* a soft–hard interaction (Zn–OSO_2OMe). In line with this the related Tp*Zn–OSO_2Me complexes[11] were found to be difficult to handle. $Tp^{Ph,Me}Zn$–OSO_2OMe has so far been characterized only in solution, and instead of $Tp^{Me,Me}Zn$–OSO_2OMe the complex $(Tp^{Me,Me})_2Zn$ was isolated, which is a known dismutation product of unstable $Tp^{Me,Me}Zn$–X complexes.[12]

In an attempt to apply more 'natural' methylating agents, complex **1a** was treated with trimethylsulfonium iodide as a model for the biological methyl donor *S*-adenosyl methionine[4] and with *N*-methylpyridinium iodide as a model for methyltetrahydrofolate. These reactions required higher temperatures and the more polar solvent acetonitrile for the ionic reagents. A clean methylation was achieved with trimethylsulfonium iodide, leaving $Tp^{Ph,Me}Zn$–I. The *N*-methylpyridinium reagent did not transfer a methyl group. When the more electrophilic reagent 2-bromo-*N*-methylpyridinium iodide was used its bromide substituent was replaced by the ethylthio group according to eqn. (2). Thus the zinc bound thiolate of **1a** is a strong enough nucleophile to attack halopyridinium systems. In

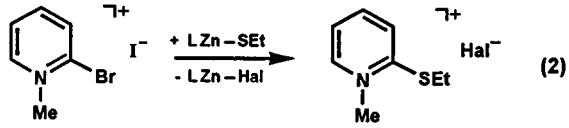

this case the remaining zinc species was a mixture of $Tp^{Ph,Me}Zn$–Br and $Tp^{Ph,Me}Zn$–I.‡

The methylation reactions reported here are the closest representations of their biological models yet, specifically of cobalamine independent methionine synthase. The precursors of the Tp*Zn thiolate complexes, the Tp*Zn hydroxide complexes which exist at neutral pH and which may represent the resting enzymes, incorporate the thiols spontaneously with liberation of H_2O, *i.e.* without pH effects. The thiolate complexes react with neutral and ionic methylation reagents in a sterically restricted situation reminiscent of that in the enzymes. An important factor driving the reactions must be the high nucleophilicity of the zinc bound thiolate groups, as we previously found for the zinc bound hydroxide in analogous Tp*Zn–OH complexes.[9,13] Coupled with the low donor strength of thioethers toward zinc, again analogous to the leaving tendency of H_2O from $[Tp^*Zn–OH_2]^+$, this makes the methylation reactions facile and rapid.

At this stage of the investigation we see two challenges. One concerns the choice of alkylating agents which should be closer relatives of methyltetrahydrofolate or *S*-adenosyl methionine. The other concerns the testing of a mechanistic implication of the intramolecular alkylations by methyl iodide. A four-center transition state Zn–O/E–O has been found likely for hydrolytic cleavages of $R_nE(O)$–X substrates by Tp*Zn–OH.[14] If an analogous Zn–S/C–I transition state is implied for the reactions between Tp*Zn–SR and CH_3–I, then this corresponds to front-side attack of the nucleophile at the C-I unit which means retention of configuration at carbon. A mechanistic investigation is indicated which should answer this question as well as that of possible ionic intermediates of the methylation reactions.

This work was supported by the Deutsche Forschungsgemeinschaft.

Notes and references

† The constitution of Tp*Zn–SR complexes has been established by structure determinations of $Tp^{tBu,Me}$Zn-SEt[9a] and $Tp^{Cum,Me}$Zn–SPh.[10c] The new species **1** and **2** were characterized by analyses, spectra and a structure determination of **2a**.

‡ On the millimolar scale the methylations by methyl iodide take 1–2 h for **1a**, **b** and about 1 day for **2a**, **b**. The quantitative nature of the methylation reactions and the identity of the resulting thioethers were ascertained by NMR. In those cases where Tp*Zn–Hal or Tp^*_2Zn complexes resulted these were isolated by crystallization and identified by comparing their spectra with data from the literature. The reaction between **1a** and an excess of $[N(PPh_3)_2][SCH_2Ph]$ leads to *ca*. 10% of **1b** after 3 days and takes weeks to reach equilibrium.

1 R. G. Matthews and J. T. Drummond, *Chem. Rev.*, 1990, **90**, 1275.
2 R. G. Matthews and C. W. Goulding, *Curr. Opin. Chem. Biol.*, 1997, **1**, 332.
3 L. C. Myers, M. P. Terranova, A. E. Ferentz, G. Wagner and G. L. Verdine, *Science*, 1993, **261**, 1164.
4 J. C. Gonzales, K. Peariso, J. E. Penner-Hahn and R. G. Matthews, *Biochemistry*, 1996, **35**, 12 228.
5 K. Sauer and R. K. Thauer, *Eur. J. Biochem.*, 1997, **249**, 280.
6 J. J. Wilker and S. J. Lippard, *Inorg. Chem.*, 1997, **36**, 969.
7 C. A. Grapperhaus, T. Tuntulani, J. H. Reibenspies and M. Y. Darensbourg, *Inorg. Chem.*, 1998, **37**, 4052.
8 K. Peariso, C. W. Goulding, S. Huang, R. G. Matthews and J. E. Penner-Hahn, *J. Am. Chem. Soc.*, 1998, **120**, 8410.
9 (*a*) R. Alsfasser, M. Ruf, S. Trofimenko and H. Vahrenkamp, *Chem. Ber.*, 1993, **126**, 703; (*b*) M. Ruf, K. Weis and H. Vahrenkamp, *J. Chem. Soc., Chem. Commun.*, 1994, 135; (*c*) K. Weis and H. Vahrenkamp, *Inorg. Chem.*, 1997, **36**, 5589.
10 (*a*) M. Ruf and H. Vahrenkamp, *Inorg. Chem.*,1996, **35**, 6571; (*b*) M. Ruf, R. Burth, K. Weis and H. Vahrenkamp, *Chem. Ber.*, 1996, **129**, 1251; (*c*) R. Burth and H. Vahrenkamp, *Z. Anorg. Allg. Chem.*, 1998, **624**, 381.
11 T. Brandsch, F. A. Schell, K. Weis, M. Ruf, B. Müller and H. Vahrenkamp, *Chem. Ber.*, 1997, **130**, 283.
12 A. Looney, R. Han, I. B. Gorell, M. Cornebise, K. Yoon, G. Parkin and A. L. Rheingold, *Organometallics*, 1995, **14**, 274.
13 (*a*) M. Ruf and H. Vahrenkamp, *Chem. Ber.*, 1996, **129**, 1025; (*b*) K. Weis, M. Rombach, M. Ruf and H. Vahrenkamp, *Eur. J. Inorg. Chem.*, 1998, 263.
14 M. Rombach, C. Maurer, K. Weis, E. Keller and H. Vahrenkamp, *Chem. Eur. J.*, in the press.

Communication 8/07326K

The electrochemistry of tetramesityldisilene, $Mes_2Si{=}SiMes_2$

Zeng-Rong Zhang,[a] James Y. Becker*[a] and Robert C. West[b]

[a] *Department of Chemistry, Ben-Gurion University of the Negev, Beer-Sheva 84105, Israel. E-mail: becker@bgumail.bgu.ac.il*

[b] *Department of Chemistry, University of Wisconsin, Madison, WI 53706, USA*

Received (in Cambridge, UK) 22nd October1998, Accepted 4th November 1998

The outcome of the controlled potential oxidation and reduction of a disilene, tetramesityldisilene (TMDS), indicates that the main silicon containing products involve only one silicon atom and have the general structure $Mes_2SiX(Y)$, X and Y being H, OH or F.

A great deal of progress has been made in disilene chemistry since the isolation of the first stable disilene in 1981.[1] Advances in the chemistry of stable (and marginally stable) disilenes are described in a recent review,[2] and several other reviews covering Si=Si double bonds have been published.[3–6] The disilenes are far more reactive than their alkene counterparts. Even though the stable disilenes are sterically hindered, they are remarkably reactive toward many electrophilic and nucleophilic reagents, providing a complex and elaborate chemistry of the Si=Si double bond.[2–6]

Information in the literature on the electrochemical behavior of disilenes is very limited. To the best of our knowledge, the only published work related to cyclic voltammetry measurements.[7] All tetraaryl- and dialkyldiaryl-disilenes investigated exhibited one irreversible oxidation wave and one irreversible reduction wave. The oxidation potentials were similar (0.4–0.5 V *vs.* SCE), indicating that the highest occupied molecular orbital (HOMO) of each species lies at approximately the same energy level. However, their reduction potentials were found to be dependent on the substitution pattern, −2.0 to −2.2 V for tetraaryldisilenes and about −2.6 V (*vs.* SCE) for dialkyldiaryldisilenes. These results indicate that the lowest unoccupied molecular orbital (LUMO) of tetraaryldisilenes is lower in energy than the LUMO of dialkyldiaryldisilenes,

The present communication reports for the first time results of the controlled potential electrolysis of a disilene. Tetramesityldisilene, $Me_2Si{=}SiMes_2$ (TMDS) was studied by both anodic oxidation and cathodic reduction. The products obtained upon electrochemical oxidation of TMDS in MeCN using Bu_4NPF_6 as the supporting electrolyte are shown in Fig. 1. Interestingly, all of the detected products contain only one silicon atom. It seems that the anodic process invovles the cleavage of both the π and σ bonds. This behavior is remarkably different from what has been observed by chemical oxidation.

For example, reactions of disilenes with the single-oxygen transfer agents N_2O or azoxybenzene[8] give three-membered rings of type **I**. Disilenes react with oxygen[8,9] of the air to give compounds **I** and/or 1,2-disiladioxetanes **II**; the latter undergo rearrangement to cyclodisiloxanes **III** in a subsequent step.[10]

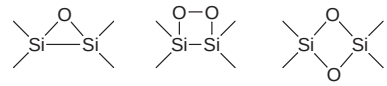

I **II** **III**

Upon comparing the results described in Table 1, column A (in THF) with those in column B (in MeCN), in both cases, the same six products were formed (**1**–**6**), but the ratio of products which contain fluorine atoms (**1**–**3**) to those without fluorine atoms (**4**–**6**) is higher in MeCN. When the electrolyte was changed from Bu_4NPF_6–MeCN (column B) to Et_4NBF_4–MeCN (column C), only five products were obtained (**1**–**5**), the fluorinated ones becoming even more predominant. In Bu_4NClO_4–MeCN solution (column D), the reaction became more selective to yield three products only, **4**–**6**. Upon changing the Pt anode material (column C) to glassy carbon (column E), leavng all other conditions the same, the reaction became somewhat less selective and yielded more non-fluorinated products at the expense of the fluorinated ones. Evidently, the preferred products in THF or in the presence of ClO_4^- are **5** and **6**, whereas **3** is favored in the presence of BF_4^-. The above results indicate that solvent, electrolyte and anode material all play a role in the product outcome upon electrochemical oxidation of tetramesityldisilene.

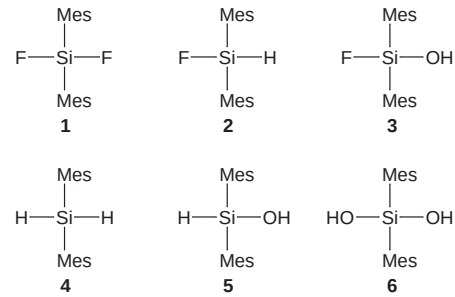

Fig. 1 Molecular structures of products obtained by anodic oxidation of TMDS.

Table 1 Product distribution from electrochemical oxidation of TMDS[11]

	Yield (%)[a]					
Product	A	B	C	D	E	Mass spectrum (EI) (*m/z*)
1	5	21	27	—	11	304(M^+), 289(100%), 184, 120
2	6	26	11	—	13	286(M^+), 271, 166, 120(100%)
3	15	17	40	—	36	302(M^+), 287, 182, 120(100%)
4	13	17	5	13	11	268(M^+), 253, 148(100%), 120
5	25	13	15	26	19	284(M^+), 269, 164, 120(100%)
6	36	6	—	52	10	300(M^+), 285, 180(100%), 120

[a] Yields reported are relative and estimated by GLC. A, Electrolyte solution 0.1 mol l^{-1} Bu_4NPF_6–THF; working electrode: Pt. B, Electrolyte solution: 0.1 mol l^{-1} Bu_4NPF_6–MeCN; working electrode: Pt. C, Electrolyte solution: 0.1 mol l^{-1} Et_4NBF_4–MeCN; working electrode: Pt. D, Electrolyte solution: 0.1 mol l^{-1} Bu_4NClO_4–MeCN; working electrode: Pt. E, Electrolyte solution: 0.1 mol l^{-1} Et_4NBF_4–MeCN; working electrode: glassy carbon.

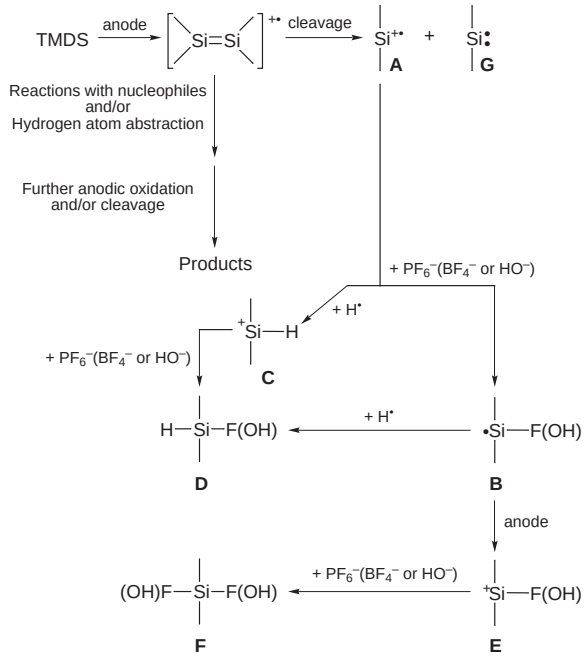

Scheme 1 Mechanism for the electrochemical oxidation of TMDS.

A plausible mechanism which accounts for the formation of all products in the electrochemical oxidation process is outlined in the over simplified Scheme 1. The initially formed unstable radical cation from TMDS is a highly reactive species and could undergo a number of different reactions, *i.e.* reactions with nucleophiles, abstraction of hydrogen atoms, cleavage, *etc*. For example, the direct cleavage may lead to a radical cation **A** and silylene **G**. The radical cation **A** may undergo an attack by PF_6^- (BF_4^- or HO^-) anion to form the radical **B**, or abstract a hydrogen atom (from solvent or electrolyte) to generate a silylenium cation **C**, followed by a chemical reaction with a nucleophile to yield **D** (products **2** and **5**). Intermediate **B** could undergo further anodic oxidation to the cation **E**, or abstract a hydrogen atom from its surroundings to generate **D**. Cation **E** may react with PF_6^- (BF_4^- or HO^-) anion to form **F** (products **1**, **3** and **6**). It is noteworthy that the formation of some of the products outlined in Fig. 1, as well as **4**, could also originate from silylene **G**.

Results of the controlled potential electrochemical reduction[12] of TMDS in both THF and acetonitrile are shown in Scheme 2. A major product found was mesitylene. As in the anodic process, the silicon products (except for compound **8**) contain only one silicon atom, probably due to fragmentation of the initial electrochemically generated anion radical. The same four products (**1**, **2**, **7** and **8**) were obtained both in THF and MeCN. However, an additional product, **4**, was detected in THF.

Surprisingly, some of the products (**1**, **2** and **4**) observed by the electrochemical reduction process are identical to those obtained by the anodic oxidation. Therefore, it is reasonable to suggest that these products could stem from the same intermediate, which might be generated in both types of reactions. Attempts to trap such intermediate and characterize its nature are underway,

The electrochemical reduction of TMDS in MeCN–Bu_4NClO_4 (0.1 mol l^{-1}) solution was also attempted. The GLC chromatogram indicated the formation of a very complex mixture of products (> 20 peaks!), which has yet to be analysed, among which Mes_2SiH_2 and $Mes_2Si(H)(OH)$ could be detected.

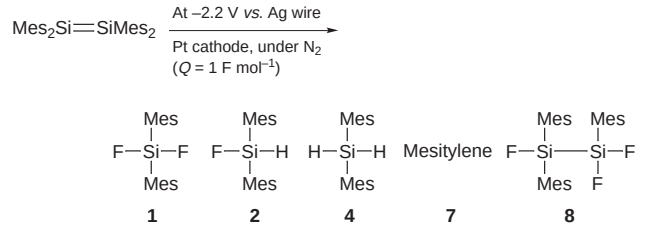

	A: 0.1 mol l^{-1} Bu_4NPF_6–THF	**B**: 0.1 mol l^{-1} Bu_4NPF_6–MeCN
1	9%	31%
2	18%	25%
4	20%	—
7	47%	35%
8	6%	9%

Scheme 2 Results of cathodic reduction of TMDS.

The authors are thankful to the Israel Science Foundation for supporting this research through a grant.

Notes and references

1 R. West, M. J. Fink and J. Michl, *Science*, 1981, **214**, 1343.
2 R. Okazaki and R. West, *Adv. Organomet. Chem.*, 1996, **39**, 231.
3 G. Raabe and J. Michl, *Chem. Rev.*, 1985, **85**, 419; G. Raabe and J. Michl in *The Chemistry of Organic Silicon Compounds*, ed. S. Patai and Z. Rappoport, Wiley, New York, 1989, pp. 1015–1142.
4 R. West, *Angew. Chem., Int. Ed. Engl.*, 1987, **26**, 1201; R. West, in *The Chemistry of Inorganic Ring Systems*, ed. R. Steudel, Elsevier, Amsterdam, Netherlands, 1992, pp. 35–50.
5 T. Tsumuraya, S. A. Batcheller and S. Masamune, *Angew. Chem., Int. Ed. Engl.*, 1991, **30**, 902.
6 M. Weidenbruch, *Coord. Chem. Rev.*, 1994, **130**, 275.
7 B. D. Shepherd and R. West, *Chem. Lett.*, 1988, 183.
8 H. B. Yokelson, A. J. Millevolte, G. R. Gillette and R. West, *J. Am. Chem. Soc.*, 1987, **109**, 6865.
9 H. B. Yokelson, A. J. Millevolte, B. R. Adams and R. West, *J. Am. Chem. Soc.*, 1987, **109**, 4116; K. L. McKillop, G. R. Gillette, D. R. Powell and R. West, *J. Am. Chem. Soc.*, 1992, **114**, 5203.
10 H. Watanabe, K. Takeuchi, K. Nakajima, Y. Nagai and M. Goto, *Chem. Lett.*, 1988, 1343; A. J. Millevolte, D. R. Powell S. G. Johnson and R. West, *Organometallics*, 1992, **11**, 1091.
11 All experiments were carried out in a drybox ([H_2O] < 1 ppm; [O_2] < 1 ppm), employing controlled potential electrolysis (on Pt) in an 'H' type two-compartment cell and pulsing from 0 to 0.5 V (*vs.* Ag wire) every 0.5 s. Typically, the working compartment contained 0.1–0.2 mmol of disilene dissolved in 25 ml solution. Electricity consumption is *ca.* 1 F mol^{-1}. Solvents MeCN and THF were distilled over P_2O_5 and benzophenone/Na, respectively. All electrolytes were dried under vacuum (*ca.* 30 mmHg) at 105 °C for 48 h. HRMS results for MH^+: Found (calc. for M). **1**: 305.1547 (305.1547 for $C_{18}H_{23}F_2Si$); **2**: 287.1620 (287.1640 for $C_{18}H_{24}FSi$); **3**: 303.1590 (303.1595 for $C_{18}H_{24}FOSi$); **4**: 269.1733 (269.1745 for $C_{18}H_{25}Si$); **5**: 285.1500 (285.1694 for $C_{18}H_{25}OSi$); **6**: 301.1420 (301.1643 for $C_{18}H_{25}O_2Si$); **7**: 120.0910 (120.0948 for C_9H_{12}); **8**: 470.2155 (470.2120 for $C_{27}H_{33}F_3Si_2$).
12 The chemical reduction of sterically congested disilenes by alkali metals has not been studied. Formation of disilene anion radicals is reported to result from reductions of the corresponding dichlorodisilenes by alkali metals,[13] but to the best of our knowledge there is no report on the nature of products obtained by reaction/decomposition of this type of anion radical.
13 M. Weidenbruch, K. Kramer, A. Schafer and J. K. Blum, *Chem. Ber.*, 1985, **118**, 107; M. Weidenbruch, K. Kramer, K. Peters and H. G. von Schnering, *Z. Naturforsch., Teil B*, 1985, **40**, 601.

Communication 8/08198K

Detection of a novel intermediate in the addition of thiols to osmium carbonyl clusters

Keranio Kiriakidou,[a] Maria Rosaria Plutino,[a] Fabio Prestopino,[a,b] Magda Monari,[b] Maria Johansson,[a] Lars I. Elding,[a] Esteve Valls,[c] Roberto Gobetto,[c] Silvio Aime[c] and Ebbe Nordlander*[a]

[a] *Inorganic Chemistry 1, Chemical Center, Lund University, Box 124, S-221 00 Lund, Sweden. E-mail: Ebbe.Nordlander@inorg.lu.se*
[b] *Dipartimento di Chimica "G.Ciamician", Università di Bologna, via Selmi 2, 40124 Bologna, Italy*
[c] *Dipartimento di Chimica I.F.M., Università di Torino, Via P. Giuria 7, 10125 Torino, Italy. E-mail: aime@silver.ch.unito.it*

Received (in Cambridge, UK) 16th September 1998, Accepted 29th October 1998

Spectroscopic studies of the reaction of $[Os_3(CO)_{11}MeCN)]$ with *para*-thiocresol to form $[Os_3(\mu\text{-}H)(CO)_{10}(\mu\text{-}SC_6H_4Me\text{-}p)]$ indicate that the reaction proceeds *via* a two-step consecutive process involving the intermediate $[Os_3(CO)_{11}(MeC_6H_4SH\text{-}p)]$, in which there is an agostic Os–H–S interaction.

Hydrodesulfurization (HDS) processes are used to remove sulfur from organosulfur compounds in fossil fuels.[1] These catalytic processes are subject to intensive investigation because of the widespread use of HDS and its economic and environmental importance. Although structures of the active components of HDS catalysts have been proposed,[1] the exact nature of the interaction between sulfur-containing hydrocarbons and the catalyst(s), and the mechanism of the catalytic reaction(s), have not been elucidated.

Friend *et al*.[2] have studied the adsorption and desulfurization of thiols on Mo(110) surfaces. The cleavage of the sulfur–hydrogen bond to form a metal-bound thiolate has been found to be rapid whereas the cleavage of the carbon–sulfur bond appears to be the rate-limiting step. Several metal complexes containing sulfur ligands have been synthesized as both structural and functional models for HDS processes.[3] We are currently studying whether it is possible to monitor the initial coordination of thiols to polynuclear metal complexes and to relate these phenomena to HDS processes.[4] Here we wish to describe how the reaction between $[Os_3(CO)_{11}(MeCN)]$ **1** and *para*-thiocresol proceeds *via* the intermediate $[Os_3(CO)_{11}(MeC_6H_4SH\text{-}p)]$ **2** to form the final product $[Os_3(\mu\text{-}H)(CO)_{10}(\mu\text{-}SC_6H_4Me\text{-}p)]$ **3**. The intermediate (**2**) is proposed to contain an agostic Os–H–S interaction; to our knowledge, this is the first example of an agostic interaction involving a thiol hydrogen.

Two resonances could be detected at high field when the reaction of stoichiometric equivalents of **1** and *para*-thiocresol was monitored by ^{1}H NMR at ambient temperature. Fig. 1(a) shows the variation of the intensities of the two signals with time. There is a relatively rapid build-up of the resonance at δ −4.81 followed by a slower decay of the intensity of this signal, while there is a gradual build-up of the signal at higher field. This implies that the resonance at lower field is due to an intermediate which is gradually converted to the final product with a resonance at δ −17.00. The high-field resonance may be ascribed to the bridging hydride of the final product **3**† by comparison to previously known $[Os_3(\mu\text{-}H)(CO)_{10}(\mu\text{-}SR)]$ clusters.[4,5] The shift of the second resonance occurs at lower field than may be expected for a hydride coordinated to a triosmium cluster;[6] the signal is assigned to the thiol hydrogen and it is suggested that the shift arises from an agostic interaction of this hydrogen with one of the osmium atoms. The T_1 relaxation times for the two signals are similar, although not identical, being 2.08 s for the intermediate **2** and 4.37 s for the final species **3**. Greater discrepancies in relaxation times for the two signals have been observed for the same type of reaction involving other thiols.[7]

It was possible to slow down the above reaction so that the intermediate was the predominant species by mixing the reactants and rapidly cooling the solution to −60 °C; at this temperature, **2** was found to be stable for several hours. A ^{13}C NMR spectrum‡ of a carbon-13 enriched sample of **2** at −60 °C showed that the intermediate possesses eleven carbonyls, consistent with the proposed formula $[Os_3(CO)_{11}(MeC_6H_4SH\text{-}p)]$. On the basis of the ^{13}C–^{13}C and ^{13}C–^{1}H coupling pattern, several ^{13}CO resonances have been assigned. Moreover, a 2D-EXSY experiment showed that all CO ligands (except one at δ 171.54) exchange pair-wise, suggesting the possible occurrence

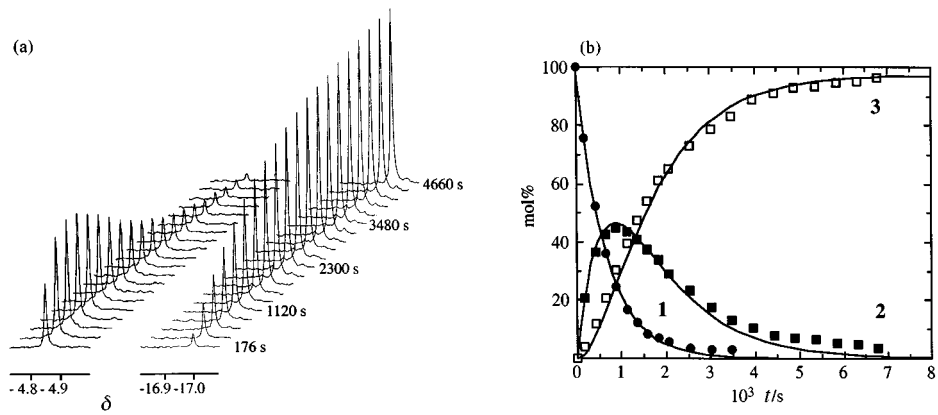

Fig. 1(a) ^{1}H NMR signal variations *vs.* time for compounds **2** and **3** in the reaction of **1** with RSH (t_s = 236 s; RSH = *para*-thiocreosol; [**1**] = 0.012 M; [RSH] = 0.053 M; [MeCN] = 0.054 M; solvent = $CDCl_3$; T = 295.2 K). (b) Time dependence of the concentrations of the species **1**–**3**.

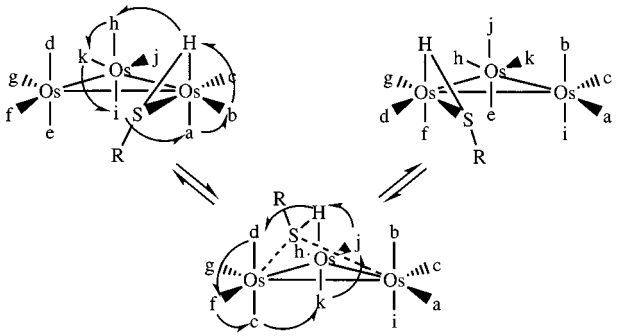

Scheme 1 Proposed fluxional mechanism for ligand exchange in the intermediate $[Os_3(CO)_{11}(MeC_6H_4SH\text{-}p)]$ **2**. This mechanism is in agreement with the following pairwise exchange for all carbonyls except k, which stays in the same magnetic environment: a ↔ f, b ↔ d, c ↔ g, e ↔ i, h ↔ j.

of a sliding motion of the thiol moiety on the surface of the cluster accompanied by two successive, one-step-only, merry-go-round processes as depicted in Scheme 1. This exchange process is reminiscent of that observed in the enantiomerization of $[Os_3H(\mu\text{-}H)(CO)_{11}]$.[6] Further (indirect) evidence for an agostic Os–H–S interaction could be derived from the reaction of **1** with PhSeH which proceeds *via* an intermediate with a characteristic ^{1}H NMR resonance at δ −5.4. This resonance contains satellites due to ^{1}H–^{77}Se coupling and the value of the coupling constant is unusually low ($^1J_{SeH}$ = 38.1 Hz), which is consistent with elongation of the Se–H bond.

The kinetics of the reaction of **1** with *para*-thiocresol were measured by UV–VIS, IR and NMR spectroscopy. Two consecutive reactions were observed in dichloromethane at 298.2 K. Analysis of the changes of the IR and ^{1}H NMR spectra during the course of the reaction showed that the processes under study involve fast thiol addition to **1** and subsequent slow cleavage of the S–H bond with concomitant dissociation of a carbonyl ligand to yield the final product [eqn. (1)].

$$\mathbf{1} + \mathrm{RSH} \xrightarrow[-\mathrm{MeCN}]{k_{obs1}} \underset{\mathbf{2}}{[Os_3(CO)_{11}(RSH)]} \xrightarrow[-\mathrm{CO}]{k_{obs2}} \mathbf{3} \quad (1)$$

The first step could be observed by rapid-mixing UV–VIS spectroscopy in the range 300–480 nm and the kinetics of the two steps were studied spectrophotometrically at different ligand concentrations under pseudo-first-order conditions. The observed rate constants, k_{obs1} = (1.52 ± 0.1) × 10^{-2} s^{-1} and k_{obs2} = (1.09 ± 0.08) × 10^{-3} s^{-1}, were found to be independent of ligand concentration. On the other hand, studies carried out in the presence of different concentrations of free acetonitrile indicated consecutive processes. Immediately after mixing the reactants, the ^{1}H NMR spectra showed the presence of resonances belonging to the starting cluster **1**, the intermediate **2** and the final product **3**. The concentrations of the three species were evaluated from the integrals of the signals at δ 2.72 for C*H*$_3$CN in **1** and of the agostic hydrogen (**2**) and hydride (**3**) resonances [*cf.* Fig 1(a)]. The time dependence of the concentrations for the three species is shown in Fig. 1(b).

The dissociative natures of the transition states for both steps are confirmed by the fact that (i) both rate constants are independent of ligand concentration, (ii) the activation parameters§ obtained from the temperature dependence of k_{obs1} and k_{obs2} [*cf.* eqn. (1)] are consistent with a dissociative process, and (iii) in the first step, the displacement of the acetonitrile by the sulfur donor ligands is retarded by the addition of the free leaving group; a plot of the rate constants for the *para*-thiocreosol at different acetonitrile concentrations shows saturation, with a curvilinear dependence on the concentration of the entering thiol. Scheme 2 shows the overall mechanism proposed for these reactions. The first step is a reversible dissociation of acetonitrile from **1**, to give a labile and coordinatively unsatured intermediate, '$[Os_3(CO)_{11}]$', which

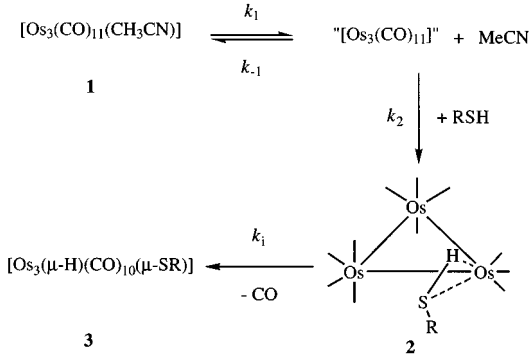

Scheme 2 Proposed mechanism for the formation of $[Os_3(\mu\text{-}H)(CO)_{10}(\mu\text{-}SC_6H_4Me\text{-}p)]$ **3** *via* the intermediate $[Os_3(CO)_{11}(MeC_6H_4SH\text{-}p)]$ **2**.

undergoes either acetonitrile addition to form the starting cluster or thiol addition to form the intermediate $[Os_3(CO)_{11}(RSH)]$ **2**. The latter loses carbon monoxide to form the final compound $[Os_3(\mu\text{-}H)(CO)_{10}(\mu\text{-}SC_6H_4Me\text{-}p)]$ **3**.¶ The mechanism depicted in Scheme 2 appears to be general. Thus far, similar kinetics and the same type of intermediate have been detected for all thiols that we have reacted with $[Os_3(CO)_{11}(NCMe)]$, including ethanethiol, *ortho*- and *meta*-thiocresol, 2-naphthalenethiol and *tert*-butylthiol.[7]

This research has been supported by grants from the Swedish Natural Science Research Council (to L. I. E. and E. N.), the Consiglio Nazionale delle Ricerche (to M. M and S. A.), the European Union (TMR Network Metal Clusters in Catalysis and Organic Synthesis - MECATSYN, to E. N and S. A.; a postdoctoral Human Capital and Mobility (HCM) fellowship to M. R. P.) and the Metal Cluster network of the European Science Foundation (travel grant to F. P.). We are indebted to Dr Jason King for assistance with the NMR measurements.

Notes and references

† *Selected spectroscopic data* for **3**: ^{1}H NMR (CD_2Cl_2, 300 MHz) δ 7.19–7.05 (m, 4H), 2.35 (s, 3H), −17.00 (s, 1H); IR (hexane) ν_{CO}/cm^{-1} 2108w, 2067s, 2057m, 2024s 2016m, 2002m, 1990w, 1983w; FABMS *m/z* 976 (M^+). The molecular structure of **3** has been determined by X-ray crystallography.[7]

‡ ^{13}C NMR ($CDCl_3$) δ 181.83 ($^2J_{CC}$ 37.2 Hz), 180.90 ($^2J_{CH}$ 27.5 Hz), 180.31 ($^2J_{CC}$ 35.1 Hz), 179.84 ($^2J_{CC}$ 37.2 Hz), 179.42 ($^2J_{CH}$ 6.5 Hz), 177.29 ($^2J_{CC}$ 35.1 Hz), 175.71, 171.54, 170.95, 169.96 ($^2J_{CH}$ 6.5 Hz), 159.99.

§ k_{obs1}: $\Delta H^‡$ = 98 ± 2 kJ mol^{-1}, $\Delta S^‡$ = 48 ± 7 J K^{-1} mol^{-1}; k_{obs2}: $\Delta H^‡$ = 90 ± 2 kJ mol^{-1}, $\Delta S^‡$ = 2 ± 8 J K^{-1} mol^{-1}.

¶ The experimental data were fitted by the following equation:

$$k_{obs1} = a[\mathrm{RSH}]/(b[\mathrm{MeCN}] + [\mathrm{RSH}])$$

The rate laws for the two steps of the mechanism depicted in Scheme 2 are:

$$k_{obs1} = k_1[\mathrm{RSH}]/(k_{-1}/k_2[\mathrm{MeCN}] + [\mathrm{RSH}]);\ k_{obs2} = k_i$$

The calculated parameters *a* and *b* can be related to the rate constants as $a = k_1 = (1.46 \pm 0.04) \times 10^{-2}$ s^{-1} and $b = k_{-1}/k_2 = (0.591 \pm 0.06)$.

1 H. Topsøe, B. S. Clausen and F. E. Massoth, *Catalysis-Science and Technology*, ed. J. R. Anderson and M. Boudart, Springer-Verlag, Berlin, 1996, vol. 11, p. 114.
2 C. M. Friend and D. A. Chen, *Polyhedron*, 1997, **16**, 3165; C. M. Friend, *Sci. Am.*, 1993, **268**, 74; C. M. Friend and J. T. Roberts, *Acc. Chem. Res.*, 1988, **21**, 394.
3 R. J. Angelici, *Polyhedron*, 1997, **16**, 3073.
4 M. Monari, R. Pfeiffer, U. Rudsander and E. Nordlander, *Inorg. Chim. Acta*, 1996, **247**, 131.
5 E. G. Bryan, B. F. G. Johnson and J. Lewis, *J. Chem. Soc., Dalton Trans.*, 1977, 1328.
6 S. Aime, W. Dastru', R. Gobetto and A. J. Arce, *Organometallics*, 1994, **13**, 3737.
7 K. Kiriakidou, M. R. Plutino, F. Prestopino, M. Monari, L. I. Elding, E. Valls, R. Gobetto, S. Aime and E. Nordlander, unpublished results.

Communication 8/07222A

$CsFeSiO_4$: a maximum iron content zeotype

Paul F. Henry and Mark T. Weller*

Chemistry Department, University of Southampton, Highfield, Southampton, UK SO17 1BJ. Tel and Fax No. 00 44 1703 593592. E-mail: mtw@soton.ac.uk

Received (in Bath, UK) 21st September 1998, Accepted 9th November 1998

The alkali-metal iron silicate, $CsFeSiO_4$, has been synthesised, using a gel decomposition method followed by high temperature annealing, and shown to adopt the zeolite ABW structure constructed from alternating FeO_4 and SiO_4 tetrahedra surrounding caesium.

Substitution of iron into zeolitic frameworks using hydrothermal methods has been investigated by several groups[1–5] but with limited success due to the difficulty of attaining purely tetrahedral Fe(III) in an aqueous environment. Levels of tetrahedral iron that can be incorporated into the framework, replacing aluminium, are generally restricted to a few percent and octahedral iron species often block the zeolite pores. The main motivation behind substitution of transition metal centres (particularly Fe, Co, Mn and Cr) into frameworks lies in the attempt to build selective redox catalysts by utilising the channels inherent within zeolite structures. A secondary idea is the possibility of producing new pigments by incorporating coloured species into frameworks rather than intercalating coloured species into the channels within frameworks.[6–9]

Some complex tetrahedra based iron silcate materials have been previously reported in the literature: $KFeSiO_4$ exists in three forms,[10] α-$KFeSiO_4$ is orthorhombic but of unknown structure, β-$KFeSiO_4$ adopts the stuffed tridymite structure and γ-$KFeSiO_4$ has the kaliophilite structure. Studies into the K_2O-Fe_2O_3-SiO_2 phase field[11,12] have also shown the existence of iron leucite, $KFeSi_2O_6$, and iron feldspar, $KFeSi_3O_8$, which show analogous polymorphism with their corresponding aluminium compounds.

A polycrystalline sample of $CsFeSiO_4$ was prepared as follows. Stoichiometric quantities of LUDOX (40% by weight SiO_2 in water, Aldrich) and $Fe(NO_3)_3{\cdot}9H_2O$ (99.9%, Aldrich) were dissolved in 50 ml of 2M HNO_3. A 1.5-fold excess of $CsCO_3$ (99.9%, BDH) was then added to the solution; excess was added to compensate for the high volatility of caesium salts at the intermediate temperatures used in the experimental procedure. 100 ml ethanol was added under constant stirring followed by 10 ml of .880 ammonia solution, added dropwise. A brown spongy material was seen to precipitate from the solution as the ammonia was added, which partially redissolved on addition of further ammonia solution. The mixture was heated to dryness over a period of 12 h. The resultant solid was then partially decomposed in an alumina crucible at a temperature of 250 °C for a further 12 h. The brown powder obtained was thoroughly ground and heated for a further 16 h at 600 °C, then 850 °C and finally 1000 °C. After each heat treatment a powder X-ray diffraction (PXD) pattern was collected, using a D5000 Siemens diffractometer (Cu-Kα_1 radiation) operating in reflection geometry. The annealing at 1000 °C was repeated until there was no observable change in the powder diffraction pattern. The final product was found to be mustard yellow in colour. Data, for Rietveld analysis using the GSAS suite of programs,[13] were obtained over 16 h for the 2θ range 10–110° using a step size of 0.02°.

The initial PXD pattern collected from $CsFeSiO_4$ after annealing at 600 °C was found to contain no discernible Bragg reflections. The PXD pattern collected after annealing at 850 °C showed a new phase to be present, although the diffraction pattern was very weak. Repeated annealing at 1000 °C gave a crystalline material with sharp Bragg reflections, which were indexed on an orthorhombic unit cell using the PC program TREOR90.[14] Comparison of the PXD pattern with that simulated for a material adopting the zeolite ABW structure with the calculated lattice parameters gave very good agreement. No evidence of leucite or feldspar type impurities were found in the pattern.

Full Rietveld analysis was then performed using the structure of the known ABW material $LiAlSiO_4$[15] as the starting model but with iron on the aluminium position and caesium replacing lithium. In this model the silicon and aluminium positions are distinct, *i.e.* the framework is ordered with alternating tetrahedral ions in accordance with Loewenstein's rule.[16] The framework was refined, subject to some hard and soft constraints; these constraints are necessary due to the in-

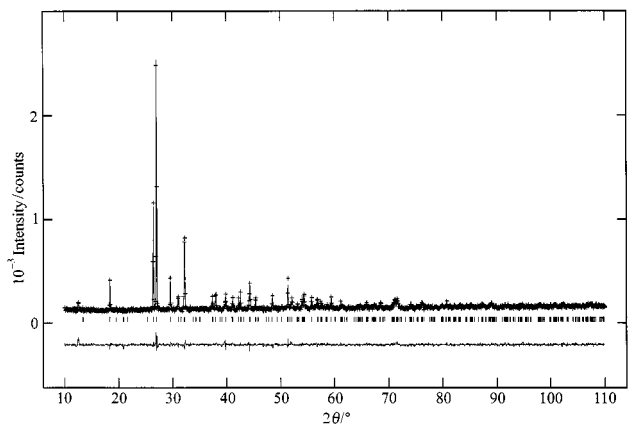

Fig. 1 Final Rietveld refinement profile of $CsFeSiO_4$. The observed data are crosses, the calculated pattern a solid line, the tick marks show the allowed reflections and the lower line is the difference plot; R_{wp} = 6.85%, R_p = 5.24%, R_e = 5.63% and $R_{F^{**}2}$ = 13.52% for 355 observations.

Table 1 Atomic coordinates for $CsFeSiO_4$

Atom	Site	x	y	z	Occupancy	U_i/U_e ×100
Cs	4*a*	0.2021(4)	0.495(5)	0.5009(9)	1.013(10)	3.44(14)
Si	4*a*	0.082(5)	−0.018(19)	0.193(3)	1.0	2.30(28)
Fe	4*a*	0.417(3)	−0.021(13)	0.314(2)	1.0	2.30(28)
O1	4*a*	0.092(3)	0.007(13)	0.014(2)	1.0	4.8(6)
O2	4*a*	−0.007(10)	−0.246(9)	0.261(10)	1.0	4.8(6)
O3	4*a*	0.019(9)	0.232(10)	0.262(10)	1.0	4.8(6)
O4	4*a*	0.229(3)	−0.077(8)	0.276(6)	1.0	4.8(6)

Table 2 Cell and space group information

	$CsFeSiO_4$
Space group	$Pc2_1n$
a/Å	9.5858(4)
b/Å	5.5538(3)
c/Å	9.0476(4)
V/Å^3	481.67(4)
Z	4

sensitivity of the technique for a caesium containing material. The thermal factors of the oxygen sites were constrained to be identical, as were those of the silicon and iron sites. The Si–O and Fe–O bond lengths were refined with a soft constraint (standard deviation of 0.005 Å) at 1.625 and 1.825 Å respectively. The refinement converged smoothly to give the excellent final profile fit illustrated in Fig. 1. Atomic data and cell data are given in Tables 1 and 2. Refinement was also attempted using the disordered framework ABW model of $CsAlTiO_4$[17] in the space group *Imma* but this gave much poorer profile fit parameters and was discarded. The refined structure is constructed of alternating SiO_4 and FeO_4 vertex linked tetrahedra with the alkali-metal cation occupying the large 8-ring cavities parallel to the crystallographic *b*-axis. Channels also exist along the *a*-direction (4-rings) and *c*-direction (6-rings) as illustrated in Fig. 2.

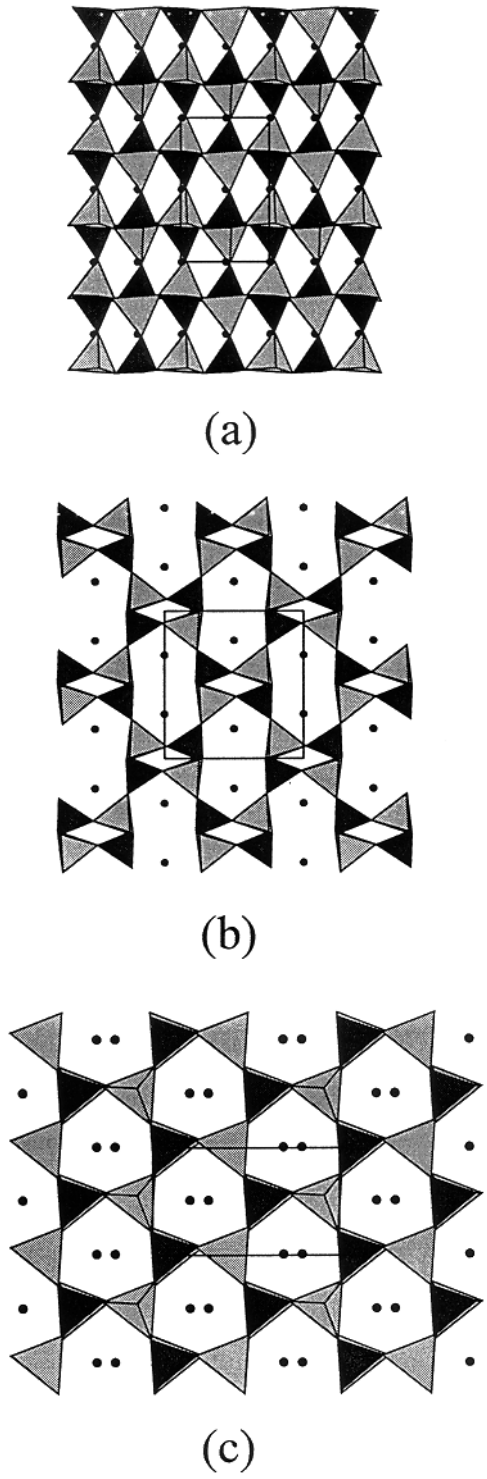

Fig. 2 Representations of the structure of $CsFeSiO_4$ along (a) [100], (b) [010] and (c) [001] illustrating the channels. Dark tetrahedra represent SiO_4, light tetrahedra represent FeO_4 and the black spheres are caesium.

The stability of the product material to moisture was studied by stirring in deionised water for 3 days at 45 °C. Residual water content was measured by thermogravimetric analysis (TGA) using an STA1500 TGA/DSC. Elemental analysis was carried out using a JEOL JSM-6400 SEM equipped with a TRACOR series II energy dispersive X-ray analysis system. TGA showed the as-made material to contain no residual water. Attempts were made to hydrate the material by exposure to water vapour for 3 days but subsequent TGA measurements showed no weight loss up to 1000 °C indicating no water uptake. The material was also found to be air and moisture stable. EDAX on $CsFeSiO_4$ showed the ratio of Cs : Fe : Si to be approximately 1 : 1 : 1 in accordance with that expected for an ABW product stoichiometry.

Further, $AFeTiO_4$ (A = Cs, Rb) have been synthesised using the same experimental technique as dark brown powders. Rietveld analysis on $CsFeTiO_4$ using powder X-ray data show this material also adopts the zeolite ABW structure and TGA reveals no residual water within the structure. Attempts to synthesise the germanium analogues have met with limited success. Further structural characterisation of materials using powder neutron diffraction data is planned to investigate the framework ordering in detail.

$CsSiFeO_4$, with a structure based on alternating FeO_4^{5-} and SiO_4^{4-} tetrahedra, is the first framework material having the maximum level of iron in a zeotype. The ability to incorporate such high levels of iron is a result of templating at high temperatures using caesium rather than in aqueous solution where six coordinate iron is unavoidable and influences the nature of the zeolite product.

The financial support of EPSRC is gratefully acknowledged.

Notes and references

1 D. W. Lewis, C. R. A. Catlow, G. Sankar and S. W. Carr, *J. Phys. Chem.*, 1995, **99**, 2377.
2 R. B. Borade and A. Clearfield, *Chem. Commun.*, 1996, 2267.
3 D. Mazza and M. L. Borlera, *Powder Diffraction*, 1997, **12**, 87.
4 P. N. Joshi, S. V. Awate and V. P. Shiralkar, *J. Phys. Chem.*, 1993, **97**, 9749.
5 D. E. W. Vaughan, K. G. Strohmaier, I. J. Pickering and G. N. George, *Solid State Ionics*, 1992, **53**–**56**, 1282.
6 M. T. Weller and K. E. Howarth, *J. Chem. Soc., Chem. Commun.*, 1991, 373.
7 J. B. Guimet, *Bull. Soc. Enc. Ind. Nat.*, 1828, **27**, 346.
8 C. G. Gmelin, *Bull. Soc. Enc. Ind. Nat.*, 1828, **27**, 216.
9 W. Depmeier, H. Schmid, N. Setter and M. L. Werk, *Acta Crystallogr., Sect. C*, 1987, **43**, 2251.
10 J. J. Bentzen, *J. Am. Ceramic Soc.*, 1983, **66**, 475.
11 G. T. Faust, *Am. Mineral.*, 1936, **21**, 735.
12 G. T. Faust, *Schweiz. Mineral. Petrogr. Mitt.*, 1963, **43**, 165.
13 A. C. Larson and R. B. Von Dreele, General Structure Analysis System, Los Alomos National Laboratory LAUR86-748, 1994.
14 P. E. Werner, L. Eriksson and M. Westdahl, *J. Appl. Crystallogr.*, 1985, **18**, 367.
15 I. S. Kerr, *Z. Kristallogr.*, 1974, **139**, 186.
16 W. Loewenstein and M. Lowenstein, *Am. Mineral.*, 1954, **39**, 92.
17 B. M. Gatehouse, *Acta Crystallogr. Sect. C*, 1989, **45**, 1674.

Communication 8/07741J

Plasmacatalytic low-temperature conversion of NO_x to N_2 by ammonium-loaded zeolites in a dielectric barrier discharge

H. Miessner,*[a] R. Rudolph[a] and K.-P. Francke[b]

[a] Institut für Umwelttechnologien GmbH and [b] Gesellschaft zur Förderung der naturwissenschaftlich-technischen Forschung e.V., Rudower Chaussee 5, D-12489 Berlin, Germany. E-mail: info@iut-berlin.com

Received (in Cambridge, UK) 28th September 1998, Accepted 13th November 1998

The direct application of a silent electrical discharge on an ammonium-loaded zeolite as catalyst to remove NO in excess oxygen results in a synergetic improvement of NO_x abatement at temperatures below 373 K.

The selective catalytic reduction (SCR) of NO using the addition of reductants like NH_3, urea, hydrocarbons, alcohols, *etc*. has been studied intensively as a potential method to remove NO_x from exhaust gases with excess oxygen.[1] Depending on the type of catalysts and the reductant used, SCR is effective in a temperature range between 450 and 900 K.

In a recent publication, Richter *et al*.[2,3] have described a catalytic low-temperature conversion of NO_x to N_2 using NH_4^+ ions fixed in zeolites as reductant. NO is converted in these systems to N_2 in excess oxygen even at temperatures as low as 373 K. The intermediate oxidation of NO to NO_2 is believed to be the key step limiting the reaction rate of the reaction sequence. As we will show here, the abatement of NO in oxygen excess can be significantly enhanced further by applying a silent electrical discharge immediately on the ammonium-loaded zeolite as catalysts.

For the experiments a reactor was used that enables a dielectric barrier discharge (DBD) directly on the catalyst bed. A glass tube as dielectric is surrounded by a copper grid as ground electrode and contains an inner electrode, which consists of a rod with equidistant steel discs leaving a gap to the glass tube of 0.5 mm. Between these discs the catalyst can be positioned. As catalyst, a mordenite with a Si : Al ratio of 11 was used in the ammonium form. The mordenite has been shown to be effective in the low temperature conversion of NO_x, but also other zeolites (*e.g.* Y, ZSM-5) could be used.[2,3] The electric discharge was initiated by a high-voltage pulse generator with 20 kV peak voltage, 20 μs rise time and a repetition rate up to 115 Hz. The gas composition (NO, NO_2, N_2O, HNO_x) was determined by an FTIR spectrometer equipped with a long-path (20 m) gas cell (Perkin Elmer) and a NO_x-analyser (ECO-Physics). The energy deposited into the discharge was determined by integrating the voltage–charge traces monitored with a digitising oscilloscope (Tektronics TDS 520 C).

Fig. 1 shows the dependence of the conversion of 500 ppm NO in N_2–O_2 (5 vol%) on the applied energy both with and without the catalyst. Without the NH_4-mordenite, NO is partly removed by reactions with the active species from the electric discharge, but at the same time NO_2 is formed and the overall NO_x concentration remains nearly constant. Using the catalyst alone, part of the NO is removed already without an electric discharge. This is due to the reaction described by Richter *et al*.[3] and also by adsorption phenomena at 343 K. At 373 K *ca.* 400 ppm and at 423 K 450 ppm NO remain in the gas phase without electric discharge. Applying additionally the DBD, a complete conversion of NO without the formation of a significant amount of NO_2 was observed. For comparison it should be noted that the energy input of 20 W h m^{-3} is equivalent to an adiabatic temperature increase of *ca.* 70 K.

The conversion of NO to N_2 strongly depends on the oxygen concentration in the gas. Fig. 2 shows this dependence again with and without NH_4-mordenite as catalyst. Whereas the conversion without catalyst declines with increasing oxygen concentration (the NO is converted to NO_2 *vide supra*), the behaviour in the presence of NH_4-mordenite is just the opposite: The conversion strongly increases with the oxygen content. This is in line with the proposal[3] of the intermediate oxidation of NO to NO_2 as the rate limiting step in the reaction mechanism. The electric discharge obviously promotes this intermediate NO-oxidation, resulting in an enhanced overall reaction rate.

To analyse the influence of the electric discharge in more detail, the local position of the catalyst was varied in order to have the discharge in front of, behind and directly on the catalyst bed. Fig. 3 shows the effect of these combinations on

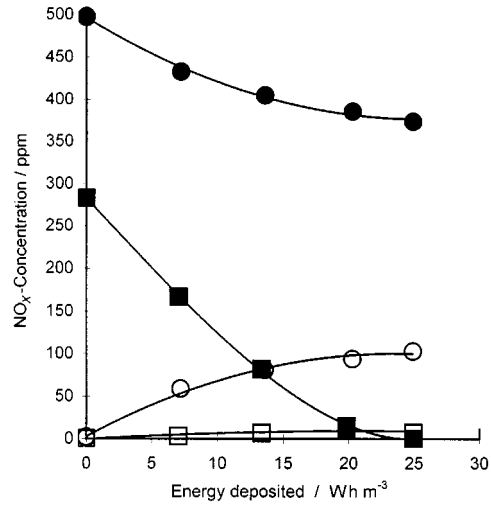

Fig. 1 NO_x concentration after conversion of 500 ppm NO in N_2–O_2 (5 vol%) with (■ : NO, □ : NO_2) and without (● : NO, ○ : NO_2) NH_4-mordenite as catalyst at 343 K and GSHV = 3000 h^{-1}.

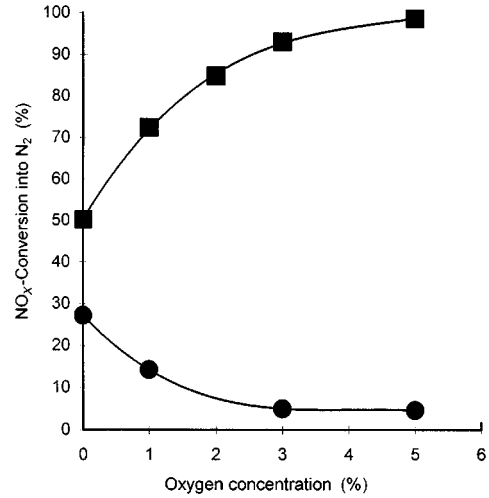

Fig. 2 Conversion of 500 ppm NO into N_2 at DBD (25 W h m^{-3}) without (●) and with (■) NH_4-mordenite as catalyst at 343 K and GSHV = 3000 h^{-1}.

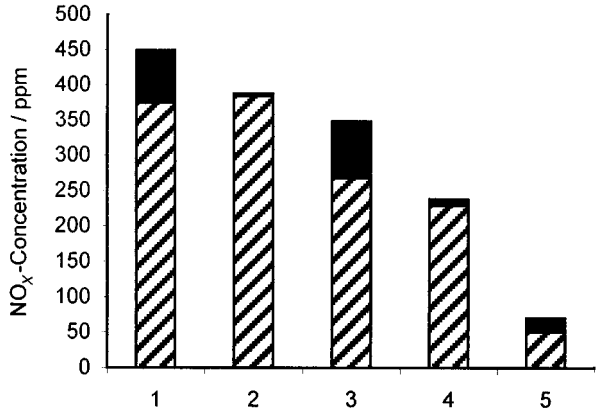

Fig. 3 NO_x concentration after conversion of 500 ppm NO in N_2–O_2 (2 vol%): DBD, without catalyst (1); with NH_4-mordenite, no DBD (2); DBD behind the catalyst (3); DBD in front of the catalyst (4); DBD over the catalyst (*in situ*) (5). Conditions at the catalyst: 343 K, GSHV = 3000 h^{-1}, DBD: *ca*. 25 W h m^{-3}, NO: hatched, NO_2: black.

the NO_x concentration. The application of the DBD behind the catalyst (column 3) converts a part of the remaining NO to NO_2 as should be expected (*cf*. column 2). If the DBD is applied in front of the catalyst, the NO_2 formed in the electric discharge (*cf*. column 1) is converted by the catalyst to nitrogen (column 4). Finally, the *in situ* application of the discharge directly on the catalyst bed results in a synergetic increase of the NO conversion to a degree much higher than the sum of the individual effects (column 5).

This synergy can be explained by the interaction of discharge-induced plasmachemical reactions with the catalysis on the zeolite. A silent electrical discharge in an oxygen-containing gas mixture produces mainly oxygen radicals as active species.[4] Atomic oxygen leads to fast oxidation by the three body reaction (1). In case of the discharge alone without any catalyst, NO removal is limited because of back-reaction (2) and only a part of NO can be converted to NO_2 (Fig. 3, columns 1 and 3). In the presence of NH_4-zeolite, however, NO_2 is removed from the gas stream by the fast catalytic reaction (3),[3] thus preventing the undesirable back conversion (2) of NO_2 to NO.

$$NO + O + M \rightarrow NO_2 + M \quad (1)$$

$$NO_2 + O \rightarrow NO + O_2 \quad (2)$$

$$NO + NO_2 + 2\ NH_3 \rightarrow 2N_2 + 3H_2O \quad (3)$$

The ammonia bonded to the zeolite is consumed during the reaction with NO_x, leaving the zeolite in the H-form. To maintain the catalytic activity, the zeolite has to be reloaded from time to time with gaseous NH_3 or by ion exchange. Initial experiments have demonstrated that this can be done without loss of activity.

The authors thank M. Richter and R. Eckelt (Berlin) for helpful discussions and for supplying the sample of the NH_4-mordenite. Prof. Dr. J. Leonhardt (Berlin) is acknowledged for his encouragement of the work and for useful discussions. The Bundesministerium für Bildung, Wissenschaft, Forschung und Technologie (BMBF) is acknowledged for financial support (13N7178).

Notes and references

1 For recent reviews, see for example: R. Burch, *Pure Appl. Chem.*, 1996, **68**, 377 or A. Fritz and V. Pitchon, *Appl. Catal. B: Environ.*, 1997, **13**, 1.
2 M. Richter, B. Parlitz, R. Eckelt and R. Fricke, *Chem. Commun.*, 1997, 383.
3 M. Richter, R. Eckelt, B. Parlitz and R. Fricke, *Appl. Catal. B: Environ.*, 1998, **15**, 129.
4 B. Eliasson, M. Hirth and U. Kogelschatz, *J. Phys. D: Appl. Phys.*, 1987, **20**, 1421.

Communication 8/07546H

ChemComm

Remarkable stabilization of the anionic semiquinone radical of 6-azaflavin by hydrogen bonding with a receptor in chloroform

Takeshi Kajiki,[a] Hideki Moriya,[a] Shin-ichi Kondo,[a] Tatsuya Nabeshima[b] and Yumihiko Yano*[a]

[a] *Department of Chemistry, Gunma University, Kiryu, Gunma 376-8515, Japan. E-mail: yano@chem.gunma-u.ac.jp*
[b] *Department of Chemistry, University of Tsukuba, Tsukuba, Ibaraki 305-8571, Japan*

Received (in Cambridge, UK) 5th October 1998, Accepted 29th October 1998

An anionic semiquinone radical of 6-azaflavin (6-AzaFl) was found to be stabilized by hydrogen bonding of a melamine derivative bearing an *N*-phenylguanidinium ion in $CHCl_3$, but not by the correponding *N*-unsubstituted guanidinium ion.

Flavin conenzymes such as FMN and FAD exhibit diverse functions through interactions with apoproteins, in which hydrogen bondings play important roles in the regulation of redox prperties.[1] Flavin semiquinone radicals are known to be stable when bound to apoproteins, whereas non-bound semiquinone radicals are unstable due to disproportionation.[2] Yoneda *et al*. reported that the anionic semiquinone radical of flavin 6-carboxylate is stabilized by intramolecular hydrogen bonding of the 6-CO_2H group at the N(5) position even in aqueous solution.[3] This suggests that the hydrogen bonding to the N(5) position is essential for stabilization of an anionic semiquinone radical of flavin. This was tested by employing 6-AzaFl and a melamine derivative bearing an *N*-phenylguanidinium ion **1** in $CHCl_3$. We report herein that receptor **1** is able to stabilize the anionic semiquinone radical of 6-AzaFl in $CHCl_3$, whereas receptor **2** is unable to stabilize it.

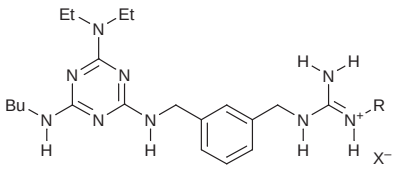

1 R = Ph, X = I
2 R = H, X = ClO_4

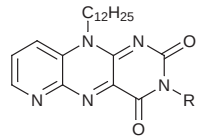

6-AzaFl R = H
6-Aza-MeFl R = Me

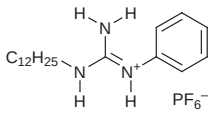

3

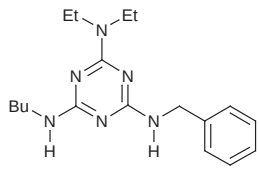

4

Receptor **1** was prepared by reaction of 2-butylamino-4-diethylamino-6-(3-aminomethyl-benzylamino)-*s*-triazine[4] with *S*-methyl-*N*-phenylisothiouronium iodide[5] in EtOH, and **3** was prepared from dodecylamine and *S*-methyl-*N*-phenylisothiouronium iodide, followed by counteranion exchange with KPF_6.† The pK_a value of the guanidinium hydrogen of **1** was determined to be 10.7 by spectroscopic pH titration at 280 nm in buffer solutions containing 20% MeCN,‡ which is considered to be lower than that of **2** by at least 1–2 pK_a units.[6]§ The binding constant of 6-AzaFl·**1** was determined spectrophotometrically [K = (5.3 ± 0.3) × 10^3 dm^3 mol^{-1} in $CHCl_3$] as described previously.[4] Despite of more acidic guanidinium hydrogen of **1**, the K value of 6-AzaFl·**1** is smaller than that of 6-AzaFl·**2** [K = (1.4 ± 0.1) × 10^5 dm^3 mol^{-1} in $CHCl_3$].[4] This requires an explanation, since a more acidic H-donor is known to give a larger binding constant for H-bonded complexation.[7] The thermodynamic parameters for the complex formation (ΔH and $T\Delta S_{298}$: −27 and −6.0 kJ mol^{-1} for 6-AzaFl·**1**; −34 and −5.0 kJ mol^{-1} for 6-AzaFl·**2**)¶ indicated that the complex formation is mainly controlled by the enthalpy term. The ^{1}H NMR study of the complexes implied steric hindrance for complexation of 6-AzaFl and **1**. Namely, as shown in Fig. 1, the larger upfield shifts of C(7)-H of 6-AzaFl upon addition of **1** rather than **2** suggest that C(7)-H is situated in a position close enough to feel the ring current of the *N*-phenyl ring of **1** due to the steric hindrance between C(7)-H and the *ortho*-H of the *N*-phenyl ring.

Redox potentials of 6-AzaFl were determined by cyclic voltammetry in CH_2Cl_2.[8]‖ In the absence of the receptors, 6-AzaFl showed a reversible redox couple ($E_{1/2}$ = −971 mV *vs*. ferrocene/ferrcenium). Upon increasing the concentration of the receptors, the redox potentials shifted in a positive direction in both receptors, finally leading to fixed potentials; $E_{1/2}$ = −738 mV for **1** (5 equiv.), and −767 mV for **2** (3 equiv.). The shifts of the potentials due to the receptors ($\Delta E_{1/2}$) are 233 mV for **1** and 204 mV for **2**, corresponding to stabilization of the 6-AzaFl radical anion by 22 and 20 kJ mol^{-1}, respectively. It should be noted that the cyclic voltammogram of 6-Aza-MeFl was not affected by addition of **1**.

Formation of a semiquinone radical of 6-AzaFl was detected spectrophotometrically by employing the oxidation of dithiothreitol (DTT) in $CHCl_3$ under anaerobic conditions as shown in Fig. 2. In the presence of **2** or a mixture of **3** (K = 180 ± 2 dm^3 mol^{-1}) and **4** (K = 150 ± 6 dm^3 mol^{-1}),[4] the absorption spectrum of 6-AzaFl [Fig. 2(*a*)] was changed to that of 2e-reduced 6-AzaFl [Fig. 2(*b*)]. On the other hand, in the presence of **1**, the spectrum shown in Fig. 2(*c*) was observed, suggesting formation of the anionic semiquinone radical of 6-AzaFl,[2,9] which was confirmed to be stable for at least 48 h. With a large

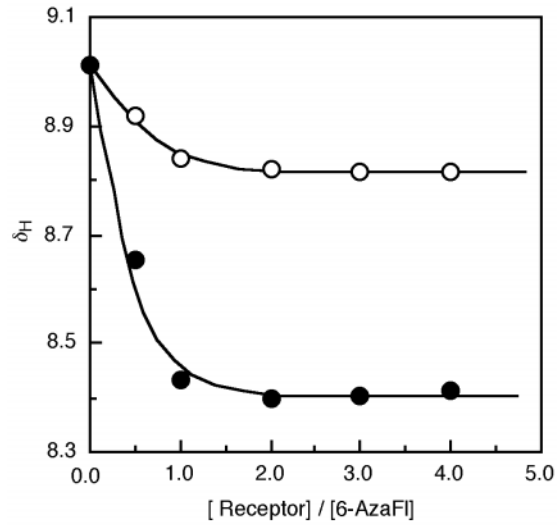

Fig. 1 Changes of chemical shifts of C(7)H in $CDCl_3$ upon addition of the receptors at 25 °C: (●) **1**, (○) **2**.

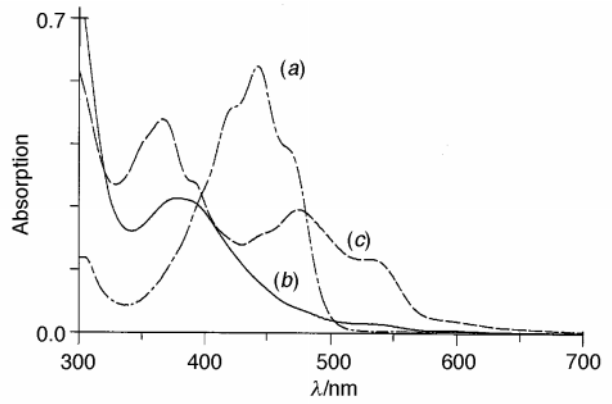

Fig. 2 Absorption spectra of 6-AzaFl in the reaction with DTT. [6-AzaFl] = 5.0×10^{-5} mol dm^{-3}, [DTT] = [Bu_3N] = 5.0×10^{-4} mol dm^{-3} in the presence of **1** or **2** (1.0×10^{-4} mol dm^{-3}) in $CHCl_3$ at 25 °C under N_2; (*a*) oxidized form, (*b*) reduced form, and (*c*) anionic semiquinone radical.

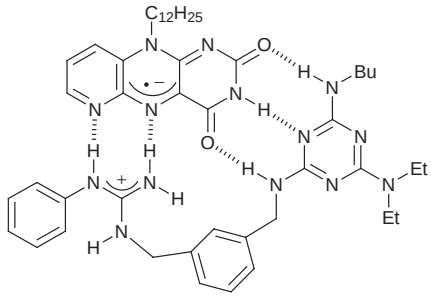

Fig. 3 Structure of 6-AzaFl$^{\cdot-}$ **1**.

excess of DTT, the spectrum shown in Fig. 2(*c*) changed to that shown in Fig. 2(*b*). The spectrum shown in Fig. 2(*b*) was found to give that in Fig. 2(*c*) after O_2 bubbling only with the receptor **1**, suggesting formation of the radical by coproportionation of reduced 6-AzaFl and oxidized 6-AzaFl, or direct electron transfer from the reduced 6-AzaFl to O_2.[2b] Plots of the amount of the anion radical (absorption at 525 nm) *vs*. [**1**] allowed us to calculate the binding constant as 7.7×10^5 dm^3 mol^{-1} which is much larger than that of 6-AzaFl·**1** due to stronger hydrogen acceptability of the anionic radical (6-AzaFl$^{\cdot-}$) as shown in Fig. 3.

Formation of 6-AzaFl radical anion in the presence of **1** was also confirmed by EPR spectroscopy in $CHCl_3$ under anaerobic conditions (Fig. 4). Although hyperfine lines could not be obtained, a *g* value of 2.0040 is in reasonable agreement with those obtained for other flavin radicals.

In summary, we have demonstrated that the acidity of a H-donor of a receptor molecule plays a crucial role in the stabilization of the anionic semiquinone radical of 6-azaflavin. This is the first example showing that intermolecular hydrogen bonds are able to stabilize the anionic semiquinone radical. The receptor molecule could be regarded as an apoprotein model. Furthermore the present results are of use for understanding the functional groups at the active sites of flavoenzymes which give a stable anionic semiquinone radical.

This work was supported in part by a Grant-in-Aid for Scientific Research from the Ministry of Education, Science, Sports and Culture of Japan.

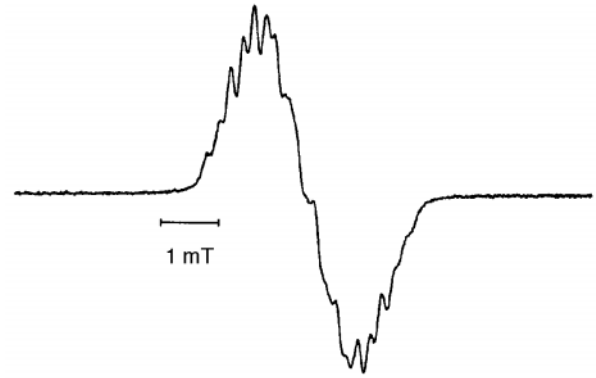

Fig. 4 EPR spectrum of the radical generated by reaction of 6-AzaFl (5.0×10^{-3} mol dm^{-3}) with DTT (5.0×10^{-3} mol dm^{-3}) and Bu_3N (5.0×10^{-3} mol dm^{-3}) in the presence of **1** (5.0×10^{-3} mol dm^{-3}) in $CHCl_3$ at 25 °C under N_2.

Notes and references

† Compound **1**: Yield 54%, mp 178–179 °C (EtOH–diethyl ether). Satisfactory elemental analyses and ^{1}H NMR data were obtained. Compound **3**: Yield 70%, mp 63–65 °C. Receptors **2** and **4**, and 6-azaflavins were supplied from our previous study (ref. 4).

‡ MeCN was added to improve the solubility of **1**.

§ The pK_a for **2** could not be determined by spectroscopic pH titration because of the lack of noticeable absorption changes, but was estimated to be 12–13 (ref. 6).

¶ The thermodynamic parameters were calculated from the following data: 6-AzaFl·**1**; 9.1×10^3 dm^3 mol^{-1} (10 °C), 4.2×10^3 (20), 3.9×10^3 (30), 2.8×10^3 (40). 6-AzaFl·**2**; 1.5×10^5 dm^3 mol^{-1}(20 °C), 1.1×10^5 (30), 7.2×10^4 (40), 5.0×10^4 (50).

‖ To compare the potentials, we used conditions similar to those of ref. 8. [6-AzaFl] = 1.0×10^{-3} mol dm^{-3}, [$Bu_4N^+ClO_4^-$] = 0.1 mol dm^{-3}, 25 °C. Scan rate: 100 mV s^{-1}.

1 R. M. Burnett, G. D. Darling, S. Kendal, M. E. LwQuesen, S. G. Mayhew, W. W. Smith and M. L. Ludig, *J. Biol. Chem*., 1974, **149**, 4383; V. Massey and P. Hemmerich, *Biochem. Soc. Trans*., 1980, **8**, 246; V. Massey, *FASEB*., 1995, **9**, 473.

2 (*a*) D. E. Edmondson and G. Tollin, *Top. Curr. Chem*., 1983, **108**, 109; (*b*) F. Müller, *Chemistry and Biochemistry of Flavoenzymes*, ed. F. Müller, CRC Press, Boston, 1991, vol. 1, p. 23.

3 T. Akiyama, F. Simeno, M. Murakami and F. Yoneda, *J. Am. Chem. Soc*., 1992, **114**, 6613.

4 N. Tamura, T. Kajiki, T. Nabeshima and Y. Yano, *J. Chem. Soc*., *Chem. Commun*., 1994, 2583.

5 C. R. Rasmussen, F. J. Villani, Jr., L. E. Weaner, B. E. Reynolds, A. R. Hood, L. R. Hecker, S. O. Nortey, A. Hanslin, M. J. Costanzo, E. T. Powell and A. J. Molinari, *Synthesis*, 1988, 456; C. R. Rasmussen, F. J. Villani, Jr., B. E. Reynolds, J. N. Plampin, A. R. Hood, L. R. Hecker, S. O. Nortey, A. Hanslin, M. J. Costanzo, R. M. Howse Jr. and A. J. Molinari, *Synthesis*, 1988, 460.

6 C. H. Hannon and E. V. Anslyn, *Bioorganic Chemistry Frontiers*; Springer-Verlag, Berlin, 1993, Vol. 3, p. 193; D. D. Perrin, *Dissociation Constants of Organic Bases in Aqueous Solution*, Butterworths, London, 1965, p. 445.

7 C. S.Wilcox, E. Kim, D. Romanos, L. H. Kuo, A. L. Burt and D. P. Curran, *Tetrahedron*, 1995, **51**, 621; J. DeFord, F. Chu and E. V. Anslyn, *Tetrahedron Lett*., 1996, **37**, 1925; C-T. Chu and J. S. Siegel, *J. Am. Chem. Soc*., 1994,**116**, 5959; K. M. Neder and H. W. Whitlock, Jr., *J. Am. Chem. Soc*., 1990, **112**, 9412.

8 E. Breinlinger, A. Niemz and V. M. Rottelo, *J. Am. Chem. Soc*., 1995, **117**, 5379.

9 V. Massey and G. Palmer, *Biochemistry*, 1966, **10**, 3181; D. J. Steenkamp and M. Gallup, *J. Biol. Chem*., 1978, **253**, 4086.

Communication 8/07737A

Synthesis and X-ray structure of a complex containing two (η^3-allyl)Mo^{II} units bridged by $Mo^{VI}O_4^{2-}$ and exhibiting an unusual type of aggregation

Cornelia Borgmann, Christian Limberg* and László Zsolnai

Universität Heidelberg, Anorganisch-Chemisches Institut, Im Neuenheimer Feld 270, D-69120 Heidelberg, Germany. E-mail: Limberg@sun0.urz.uni-heidelberg.de

Received (in Basel, Switzerland) 3rd July 1998, Accepted 26th October 1998

Treatment of the $[Mo(\eta^3\text{-}C_3H_4Me)(bipy)(CO)_2(Me_2CO)]^+$ cation with an aqueous MoO_4^{2-} solution enabled the first structural characterisation of an (η^3-allyl)MoO complex, which aggregates to a dimer showing Mo=O···H–C contacts in the solid state.

Organotransition-metal chalcogenide complexes are noteworthy in representing a link between solid, more or less ionic, metal chalcogenides and low-valent molecular organometallic systems.[1] Despite the potential importance of organomolybdenum oxo systems containing molybdenum in the highest oxidation states +5 and +6 as catalytic intermediates in industrial processes,[2] there are known as yet few model complexes of this sort.

One example of heterogeneous catalysis where such species might play a significant role entails the oxidation of propene to acrolein using MoO_3/Bi_2O_3 as the catalyst and this has gained considerable technical importance. Nontheless, the reaction mechanism has remained for the most part speculative. The results of their experiments on isotopic enrichment lead Grasselli and Burrington to suggest the intermediate formation of symmetric π-allyl complexes (or the chemisorption of delocalised allyl radicals) to Mo centres of the catalyst's surface.[3] Furthermore recent investigations suggest that in heterogeneous oxidation catalyses where Mo-oxides are employed the oxygen atoms found in the organic oxidation products have their origin in previously *bridging* positions.[4]

So far there are no compounds existent in the literature which could be regarded as functional models for the oxo molybdenum π-allyl surface intermediates under discussion. Only few allyl molybdenum compounds containing ligands with oxygen donor functions of any kind have been synthesised and characterised structurally,[5] and none of those bear the terminal or bridging O^{2-} ligands characteristic to the catalyst.

We have shown that complexes with (η^3-allyl)Mo units in oxygen-rich coordination spheres containing RO^- ligands (R = Me, H) can be obtained if cationic complexes with labile ligands are employed as starting materials.[6] Making use of the same principles we have now achieved for the first time the synthesis and structural characterisation of an allyl–Mo complex containing an O^{2-} link to another Mo centre.

The interface reaction of a $[Mo(\eta^3\text{-}C_3H_4Me)(bipy)(CO)_2(Me_2CO)]BF_4$ **1** solution in acetone—prepared by treatment of $[Mo(\eta^3\text{-}C_3H_4Me)(bipy)(CO)_2Cl]$ with $AgBF_4$ as established for the corresponding $\eta^3\text{-}C_3H_5$ complex[7]—with a solution of Na_2MoO_4 in water leads to the precipitation of a crystalline maroon solid insoluble in all common organic solvents. However, its elemental analysis suggested the composition $[\{Mo(\eta^3\text{-}C_3H_4Me)(bipy)(CO)_2\}_2(\mu\text{-}MoO_4)]$ **2**† which had been aimed at (Scheme 1).

An X-ray diffraction analysis‡ of a single crystal yielded the structure shown in Fig. 1, which clearly proves the presence of an O–MoO_2–O moiety bridging two $Mo(\eta^3\text{-}C_3H_4Me)(bipy)(CO)_2$ units. One of the latter [Mo(3/4)] was disordered through a rotation by 0.5° around the Mo(1)–O(2) axis and in Fig. 1 for clarity only the Mo(4) fragment is shown. The Mo(3/4)–O(2) and Mo(2)–O(1) distances [2.092(3) and 2.107(3) Å] lie within a range characteristic for bonds of the molybdate unit

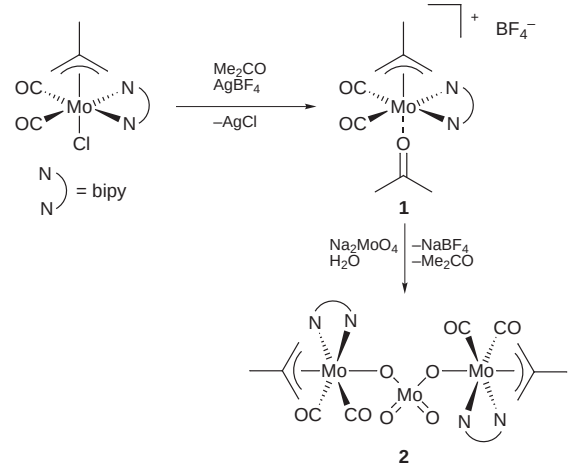

Scheme 1

to other Mo centres (2.02–2.15 Å)[8] indicating a real bonding situation rather than a weak coordination of the MoO_4^{2-} unit. The Mo(1)–O(1/2) bridging distances [1.795(3) and 1.797(2) Å] are also typical (1.75–1.85 Å) and the angles found within the central unit of **2** are all very close to the perfect tetrahedral angle. However, if just the solid state structure of the *individual* molecule is considered it does seem surprising that the two organometallic fragments coordinated to the MoO_4^{2-} unit are not oriented symmetrically with respect to the latter: Mo(1/2/4) and O(1/2) are almost in a plane intersecting the C(13)–Mo(2)–C(15) angle while the corresponding C(55)–Mo(4)–C(53) angle of the other subunit escapes intersection by a rotation of this fragment by *ca.* 90° around the Mo(4)–O(2) bond.

An explanation can be found if the structure as a whole is considered: As obvious from Fig. 2 the molecules can pack very efficiently through an internal rotation as described and this

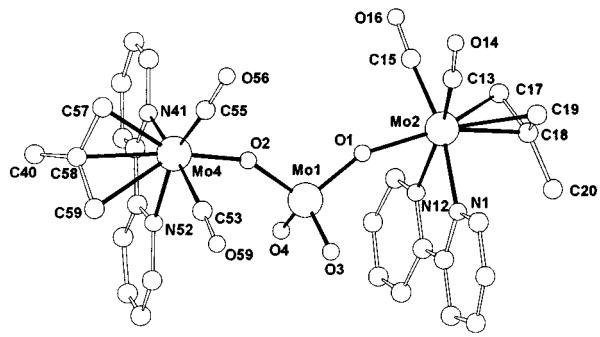

Fig. 1 Structural representation of $[\{Mo(\eta^3\text{-}C_3H_4Me)(bipy)(CO)_2\}_2(\mu\text{-}MoO_4)]$ **2**. Selected bond lengths (Å) and angles (°): Mo(1)–O(3) 1.731(3), Mo(1)–O(4) 1.739(3), Mo(1)–O(1) 1.795(3), Mo(1)–O(2) 1.797(3), Mo(2)–O(1) 2.107(3), Mo(3/4)–O(2) 2.092(4); Mo(1)–O(1)–Mo(2) 156.8(2), Mo(1)–O(2)–Mo(3/4) 150.8(2), O(3)–Mo(1)–Mo(4) 107.6(2), OC–Mo(2)–CO 78.7(2), OC–Mo(3/4)–CO 76.2(5); averaged distances and angles: Mo(2)–C_{meso} 2.243(4), Mo(2)–C_{term} 2.323(5), Mo–N 2.254(9), Mo–CO 1.97(1), OC–Mo–N_{trans} 168.9(5), OC–Mo–N_{cis} 104.1(5).

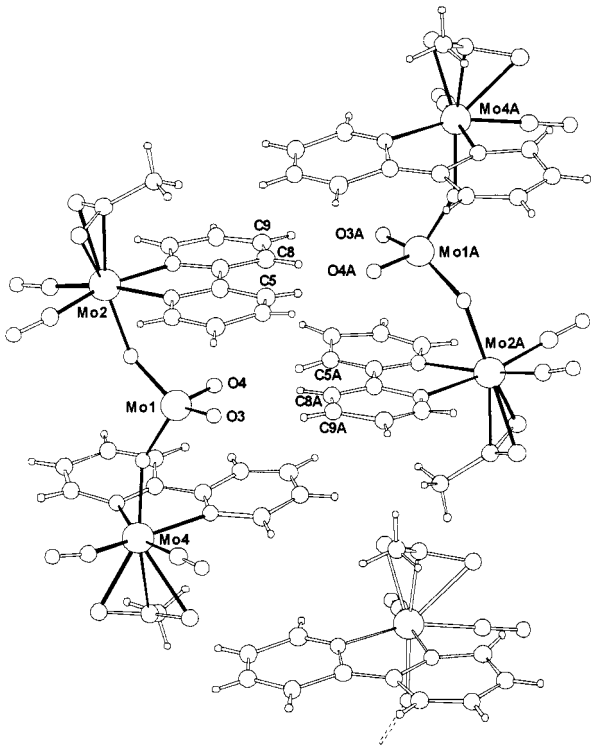

Fig. 2 Structural arrangement of the molecules of **2** in the unit cell. Selected bond lengths (Å): O(3)–C(9A) 3.180, O(3)–C(8A) 3.279, O(4)–C(5A) 3.213, O(4)–C(8A) 3.421.

leads to symmetric dimeric aggregates. These show very short Mo=O···C distances suggesting that there are intermolecular contacts between the protons of the bipy ligands and the Mo=O groups (compare Fig. 2 where the calculated H positions are shown; the Mo=O···H distances were calculated to lie between 2.39 and 2.77 Å). Of course the short C–H···O=Mo distances neither have to be indicative of attractive interactions,[9] nor is the presence of the corresponding contacts necessary to explain the structural features observed, so that attention now focused on the Mo=O bonds. The Mo=O bond lengths in d^0 molybdenum dioxo complexes usually fall in a narrow range and are not strongly effected by the nature of the other ligands at the metal.[10] It has been shown, though, that *classical* H-bridging to a $HNEt_4^+$ cation[8c] can selectively lengthen one of two Mo=O bonds in a MoO_2 unit by *ca.* 0.03 Å. The Mo=O distances observed in **2** [1.731(3) and 1.739(3) Å] are certainly located at the 'tail' of the d(Mo=O) distribution and have to be described as long, which may support the idea of attractive interactions.

Complex **2** is EPR silent and magnetic measurements showed it to be diamagnetic at room temperature, which suggests the presence of a hitherto unknown Mo^{II}–O–Mo^{VI}–O–Mo^{II} unit. Few compounds possessing two oxo bridged Mo centres differing in their oxidation states by *two* are known. An organometallic representative involving a bridging MoO_4^{2-} unit, too, is the complex $[(Cp^{Me}{}_2Mo^{IV})_2(\mu\text{-}Mo^{VI}O_4)_2]$.[8a] In **2** the difference in oxidation states amounts to *four*, which is unusual and had to find an explanation in the redox potentials of the two subunits. Indeed—probably due to the strongly π-accepting ligands—the $[Mo^{II}(\eta^3\text{-}C_3H_4Me)(bipy)(CO)_2(Me_2CO)]^+$ cation showed a reversible oxidation wave at a potential as high as 0.88 V (*vs.* SCE), which cannot be reached by molybdate[11] and this fact allowed the isolation of **2**.

The molybdate complex reported here contains π-allyl–Mo fragments which are bonded *via* 'pure' oxygen bridges to Mo^{VI} centres also providing Mo^{VI}=O groups in close proximity. It therefore already meets some of the requirements to serve as a structural model complex for surface intermediates during molybdenum oxide catalysed propene oxidation. However, other important features like the high oxidation states of all metal centres are still missing so that **2** is not suitable to simulate the properties of these intermediates. Methallyl radicals are released at 193 °C but no oxidation or allyl shift occurs, probably due to the large intramolecular separation of the coordinated allyl ligands from the oxo groups.

C. L. is grateful to the Deutsche Forschungsgemeinschaft for a scholarship and C. B. acknowledges financial support through the Landesgraduiertenförderung Baden-Württemberg. We also wish to thank Professor Dr G. Huttner for his generous support.

Notes and references

† 0.389 g (2 mmol) of $AgBF_4$ in 15 ml acetone were added to a suspension of 0.798 g (2 mmol) of $[Mo(\eta^3\text{-}C_3H_4Me)(bipy)(CO)_2Cl]$ in 30 ml of acetone *via* cannula. After 20 min of stirring the AgCl precipitated was removed by filtering and the filtrate overlayered by a solution of 0.492 g (2 mmol) $Na_2MoO_4{\cdot}H_2O$ in a mixture of 10 ml of deoxygenated water and 15 ml of acetone. At the interface crystals suitable for X-ray diffraction grew within 24 h. If the solution is stirred **2** precipitates immediately and almost quantitatively. The precipitate is washed with water and thf and dried *in vacuo*. Yield: 0.84 g (0.9 mmol, 95%). Anal. Calc. for $C_{32}H_{30}Mo_3N_4O_8$: C, 43.35; H, 3.41; N, 6.35. Found: C, 43.50; H, 3.56; N 6.14%. Characteristic bands in the IR spectrum (KBr/cm^{-1}): 1934s [ν(CO)], 1851s [ν(CO)], 914w, 876s, 838vs (br), 805s (sh), 734m [all ν(Mo–O) and ν(Mo=O)].

‡ *Crystal structure* data for **2**·0.5 Me_2CO: $C_{33.5}H_{33}N_4Mo_3O_{8.5}$, M_r = 915.46, triclinic, space group $P\bar{1}$, Z = 2, a = 10.700(2), b = 13.361(3), c = 13.654(3) Å, α = 71.98(3), β = 83.48(3), γ = 69.02(3)°, V = 1733.20 Å^3, 3.4 < 2θ < 54°, Mo-Kα radiation, λ = 0.71073 Å, ω-scan, T = 200 K, μ = 1.126 mm^{-1}, D_c = 1.754 g cm^{-3}, measured 15768, independent 6904, and observed reflections 4892, criterion: $I > 2\sigma(I)$, structure solved by direct methods (program: SHELXS-97), refined *versus* F^2 (program: SHELXL-97) with anisotropic temperature factors for all non-hydrogen atoms, 519 refined parameters with R = 0.039, residual electron density (max./min.): 0.698/−0.837 e Å^{-3}. CCDC 182/1069. See http://www.rsc.org/suppdata/cc/1998/2729/ for crystallographic data in .cif format.

1 F. Bottomley and L. Sutin, *Adv. Organomet. Chem.*, 1988, **28**, 339.
2 J. Sundermeyer, *Angew. Chem.*, 1993, **105**, 1195; *Angew. Chem., Int. Ed. Engl.*, 1993, **32**, 1144.
3 R. K. Grasselli and J. D. Burrington, *Adv. Catal.*, 1981, **30**, 133; G. W. Keulks, L. D. Krenzke and T. M. Notermann, *Adv. Catal.*, 1978, **27**, 183; R. K. Grasselli and J. D. Burrington, *Ind. Engl. Chem. Prod. Res. Dev.*, 1984, **23**, 394.
4 T. Ono, N. Ogata and Y. Mijaryo, *J. Catal.*, 1996, **161**, 78; T. Ono, H. Numata and N. Ogata, *J. Mol. Catal.*, 1996, **105**, 31.
5 M. G. B. Drew and G. F. Griffin, *Acta Crystallogr., Sect. B*, 1979, **35**, 3036; M. S. Kralik, J. P. Hutchinson and R. D. Ernst, *J. Am. Chem. Soc.*, 1985, **107**, 8296; F. Dawans, J. Dewailly, J. Meunier-Piret and P. Piret, *J. Organomet. Chem.*, 1974, **76**, 53; S. J. Rettig, A. Storr and J. Trotter, *Can. J. Chem.*, 1988, **66**, 97; V. S. Joshi, V. K. Kale, K. M. Sathe, A. Sarkar, S. S. Tavale and C. G. Suresh, *Organometallics*, 1991, **10**, 2898; J. W. Faller, J. T. Nguyen, W. Ellis and M. R. Mazzieri, *Organometallics*, 1993, **12**, 1434; N. J. Christensen, P. Legzdins, J. Trotter and V. C. Yee, *Organometallics*, 1991, **10**, 4021; K. R. Breakell, S. J. Rettig, A. Storr and J. Trotter, *Can. J. Chem.*, 1979, **57**, 139; D. Mohr, H. Wienand and M. L. Ziegler, *J. Organomet. Chem.*, 1977, **134**, 281; S. K. Chowdhury, V. S. Joshi, A. G. Samuel, V. G. Puranik, S. S. Tavale and A. Sarker, *Organometallics*, 1994, **13**, 4092; W. Kläui, A. Müller, W. Eberspach, R. Boese and I. Goldberg, *J. Am. Chem. Soc.*, 1987, **109**, 164; these references include ligands R_2O, RO^-, OH^-, [P]–O^-, [S]–O^- but not RCO_2^-.
6 C. Borgmann, C. Limberg, H. Pritzkow, L. Zsolnai and E. Kaifer, *J. Organomet. Chem.*, 1998, accepted.
7 P. Powell, *J. Organomet. Chem.*, 1977, **129**, 175.
8 (*a*) K. Prout and J.-C. Daran, *Acta Crystallogr., Sect. B*, 1978, **34**, 3586; (*b*) G. Schoettel, J. Kress, J. Fischer and J. A. Osborn, *J. Chem. Soc., Chem. Commun.*, 1988, 914; (*c*) D. Attanasio, V. Fares and P. Imperatori, *J. Chem. Soc., Chem. Commun.*, 1986, 1476; (*d*) T. C. Hsieh and J. Zubieta, *Inorg. Chem.*, 1985, **24**, 1287; (*e*) T. C. Hsieh, S. N. Shaikh and J. Zubieta, *Inorg. Chem.*, 1987, **26**, 4079.
9 D. Braga, F. Grepioni, E. Tagliavini, J. J. Novoa and F. Mota, *New. J. Chem.*, 1998, 755.
10 J. M. Mayer, *Inorg. Chem.*, 1988, **27**, 3899.
11 *Gmelin Handbook of Inorganic Chemistry*, Springer Verlag, Heidelberg, 8th edn., 1988, pp. 135.

Communication 8/05154B

ChemComm

Monolayer of metallo-supramolecular complexes

Tim Salditt,*[a] Qingrui An,[a] Anton Plech,[a] Christian Eschbaumer[b] and Ulrich S. Schubert*[b]

[a] *Sektion Physik der Ludwig-Maximilians-Universität München, Geschwister-Scholl-Platz 1, D-80539 München, Germany. E-mail: tim@lspserver.roentgen.physic.uni-muenchen.de*

[b] *Lehrstuhl für Makromolekulare Stoffe, Technische Universität München, Lichtenbergstr. 4, D-85747 Garching, Germany. E-mail: schubert@makroserv.tech.chemie.tu-muenchen.de*

Received (in Bath, UK) 8th October 1998, Accepted 10th November 1998

Self-assembled thin films of metallo-supramolecular complexes were prepared and characterized by synchrotron based X-ray reflectivity and fluorescence techniques.

In recent years, layer-by-layer self-assembly has become a very useful technique as an easy and inexpensive method for the preparation of functional thin films.[1] Monolayers and multilayers containing *e.g*. organics, polymers or nanoparticles have been prepared providing a potential approach towards advanced materials or devices with molecularly engineered properties.[2] However, to date, this method has not been used for the defined arrangement of special functional supramolecular units with nanometer dimensions into ordered molecular architectures on surfaces.[3] Here, we report the successful extension of the self-assembly technique to such metallo-supramolecular systems.

We used metal–ligand interactions as non-covalent forces to assemble well-ordered metallo-supramolecular architectures. Such metal coordination arrays ([1 × 1] or [2 × 2] grid-type architectures) based on transition metal ions with octahedral coordination and terpyridine or 4,6-bis(6′-(2′,2″-bipyridyl))-pyrimidine ligands were found to present interesting electronic, magnetic, and structural properties, such as electronic interactions between the metal centers and antiferromagnetic transitions at low temperatures.[4,5] These complexes are formed by spontaneous self-assembly of the corresponding ligands and suitable metal ions such as Co(II), Cd(II), Zn(II) or Hg(II) (see Fig. 1 for [2 × 2] grids). Besides the design and synthesis of 'isolated' grid units, the ordered and stable arrangement of such metallo-supramolecular architectures on surfaces or thin films is of special interest. Two approaches were recently described: (a) hydroxy-terminated grids could be organized on a water trough using the Langmuir–Blodgett (LB) technique and transferred onto substrates;[6] (b) unfunctionalized ligands were self-assembled in the presence of metal ions at the air–water interface.[7] However, both methods are rather complicated and not applicable for larger areas. We used the self-assembly into thin monomolecular films by adsorption onto polyelectrolyte covered substrates. As model systems for the film growth we chose the [1 × 1] Zn(II) and [2 × 2] Cd(II) complexes (Fig.1).†

First we prepared a thin cushion of polyelectrolytes onto a glass or silicon substrate using poly(ethyleneimine) hydrochloride (PEI) followed by the adsorption of a layer of poly(styrenesulfonate) (PSS) which reversed the surface density (Fig. 2).‡ In the next step the supramolecular units were adsorbed on the PSS layer. Owing to the counterions used the complexes were not soluble in water. However, the procedure could be also performed in acetone.§

To characterize the obtained layers we performed both specular and non-specular X-ray reflectivity measurements:¶ Examples of the reflectivity profiles are displayed in Fig. 3 as a function of vertical momentum transfer q_z after normalization by the Fresnel reflectivity $R_F(q_z)$. The response is proportional to the squared Fourier transform of the density gradient along the interface normal[8] and hence reflects the vertical film structure. The three data sets are shifted by arbitrary factors for clarity and correspond to films composed of the polyelectrolyte layers PSS/PEI/Si (a) without any metal complexes, (b) with [1 × 1] Zn complexes, and (c) with [2 × 2] Cd complexes adsorbed on top. The spacing of the minima is given by the inverse $2p/d$ of the total layer thickness d, yielding (a) d = 30 Å, (b) 46 Å and (c) 66 Å, respectively. Note the large thickness increase when [2 × 2] Cd grids are adsorbed, indicating an upright position of the grids (see Fig. 2). The observed differences in the oscillation amplitude reflects the different density contrasts and interfacial widths. The most pronounced fringes in Fig. 3(b) indicate particularly well defined interfaces for the adsorbed [1 × 1] Zn complexes. A more complete data analysis will be presented elsewhere.[9] Similar curves have been measured with [1 × 1] Cu(II), [1 × 1] Hg(II) and [1 × 1] Cd(II) adsorbed onto the polyelectrolytes. From the typical mass densities of the adsorbed [1 × 1] metal complexes, molecular

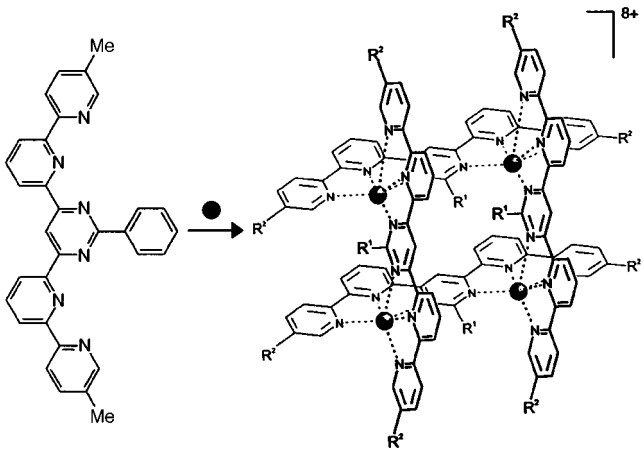

Fig. 1 Schematic representation of the *bis*-terdentate ligands leading to the formation of the [2 × 2] grid type complexes $[Cd_4L_4]^{8+}$ (R^1 = Ph, R^2 = Me). The terpyridine ligand (5,5″-dimethyl-2,2′:6′,2″-terpyridine) and the complexes are not shown.

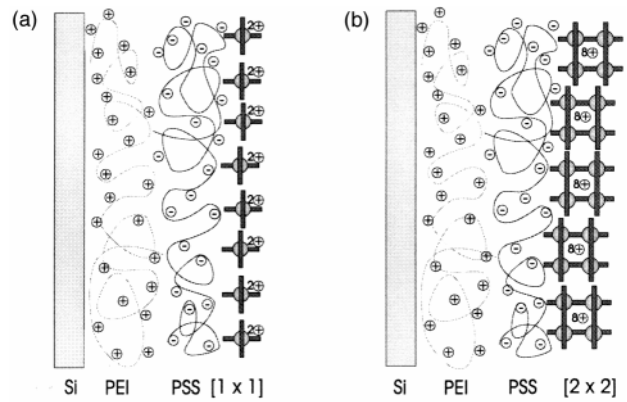

Fig. 2 Schematic drawing illustrating the build-up of the complex layers: (a) [1 × 1] metal grids; (b) [2 × 2] metal grids. Si, PEI and PSS refer to silicon substrate, poly(ethyleneimine) and poly(styrene-4-sulfonate), respectively. The filled circles denote the metal ions.

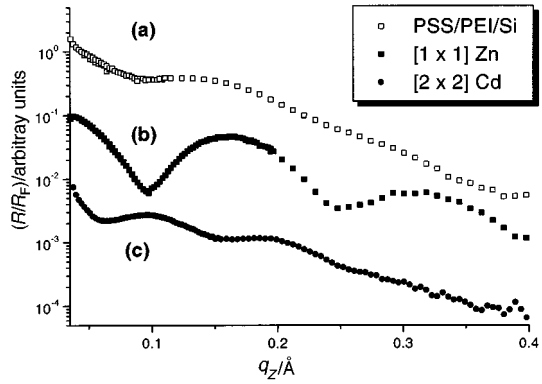

Fig. 3 Typical X-ray reflectivity profiles $R(q_z)/R_F(q_z)$ of the self-assembled films after normalization by the Fresnel reflectivity $R_F(q_z)$. The three data sets are shifted by arbitrary factors for clarity and correspond to films composed of the polyelectrolyte layers PSS/PEI/Si (a) without any metal complexes, (b) with [1 × 1] Zn complexes, and (c) with [2 × 2] Cd complexes adsorbed on top. The curves reflect the laterally averaged density profiles of the film along the interface normal (see text). The total film thickness can be derived directly from the spacing of the minima.

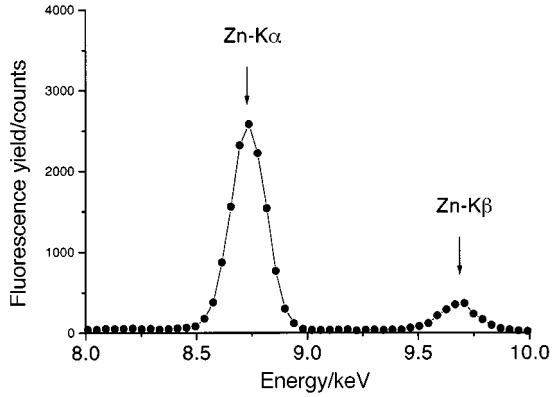

Fig. 4 The successful adsorption of complexes is evidenced most directly by the measured X-ray fluorescence. Typical spectra of monomolecular layers are collected on the time scale of a few min. For the case of [1 × 1] Zn the corresponding Kα and Kβ emission lines are observed.

volumes of *ca*. 1700 Å^3 can be inferred, yielding a mean intermolecular distance of *ca*. 11 Å. This value is in good agreement with the metal–metal distance in the crystals indicating an essentially closed packed complex layer.[10] Furthermore, to investigate the lateral structural parameters of the complex layer (two-dimensional order) we performed grazing incidence X-ray diffraction on the [2 × 2] Cd complexes. However, as yet, we could not find a long-range ordering within the layer.‖

Simultaneously to the specular reflectivity, the X-ray fluorescence of the metal ions in the complexes adsorbed on the surface has been measured.** X-Ray fluorescence under grazing incidence has been shown to be a very powerful tool of surface chemical analysis. By means of the characteristic fluorescence energies (Kα and Kβ lines for Co, Cu, Zn, Lα for Hg) excitable at an incident energy of 12.5 keV, this provides the most direct proof of the complex adsorption. Moreover, the variation of the fluorescence yield with α_i contains quantitative information on the position and width of the metal distribution with respect to the substrate. A typical curve of the energy dispersive spectrum for the [1 × 1] Zn complex is shown in Fig. 4.

At this stage, we use the data as additional, unequivocal proof that the complexes of different types have been adsorbed. Except for the peaks of the corresponding elements the spectra were clean, indicating no contamination of other transition metals or cross-contamination in sample preparation.

The present results demonstrate a simple entry to an ordered arrangement of metallo-supramolecular systems on surfaces. Using X-ray reflectivity we could establish the controlled adsorption of one layer of metal complexes onto a PSS/PEI substrate. Furthermore, the structures of the films have been characterized by synchrotron based X-ray reflectivity and fluorescence techniques. The layer-by-layer adsorption method together with the described analytical techniques opens new avenues for the construction of novel metallo-supramolecular thin film materials which could find potential applications in the preparation of various optical, electronic, or magnetic devices.

This study was supported by the Bayerisches Staatsministerium für Unterricht, Kultus, Wissenschaft und Kunst, the Fonds der Chemischen Industrie and the Deutsche Forschungsgemeinschaft (DFG).

Notes and references

† The ligands were synthesized and characterized as described elsewhere.[4–6] The reaction of suitable quantities of the ligands and the corresponding metal acetates in refluxing methanol or water exclusively leads to the formation of the monomolecular or tetranuclear complexes (isolated as PF_6 salts and recrystallized twice from acetone–ether).

‡ The silicon or glass substrates were washed extensively in trichloroethylene, methanol, and Millipore water followed by treatment with 5 M KOH (glass) and a saturated KOH solution in ethanol (silicon), respectively, for 1 min. Subsequently, they were washed with water. All samples were then kept in a 0.5% solution of poly(ethyeneimine) hydrochloride (PEI) for 20 min. Then the samples were rinsed in water followed by adsorption of a layer of poly(styrenesulfonate) (PSS) in a 3 mg ml^{-1} solution of PSS in water. The samples were again washed with water.

§ The metal complexes were adsorbed on the PSS layer by immersing the samples in 0.5 mg ml^{-1} solutions of the complexes in acetone for *ca*. 20 min and subsequent rinsing in acetone and water before drying (acetone did not destroy the polyelectrolyte layers, as shown by *ex situ* and *in situ* measurements).

¶ X-Ray experiments were carried out at the D4 bending magnet station of the storage ring DORIS at HASYLAB/DESY with a monochromatic X-ray beam of 12.5 keV. Typically, the reflectivity can be recorded over eight orders of magnitude, after correction for diffuse scattering background.

‖ The surface diffuse scattering (non-specular scattering) has been measured both in the plane of incidence and out of the plane of incidence.

** The X-ray fluorescence under grazing angles was recorded simultaneously with the reflectivity measurements. The detector was placed at 90° opposite the sample surface at a distance of a few centimeters.

1 A. Ulman, *An Introduction to Ultrathin Organic Films: From Langmuir–Blodgett to Self-Assembly*, Harcourt Brace Janovitch, Boston, 1991; G. A. Ozin, *Adv. Mater*. 1992, **4**, 612; S. Mann, *J. Mater. Chem*., 1995, **5**, 935.

2 G. Decher and J.-D. Hong, *Ber. Bunsenges. Phys. Chem*., 1991, **95**, 1430; Y. Lvov, G. Decher and H. Möhwald, *Langmuir* 1993, **9**, 481; J. Fendler, in *Thin Films, Vol 20, Organic Thin Films and Surfaces: Directions for the Nineties*, ed. A. Ulman, Academic Press, 1995, p. 11; Y. Sun, E. Hao, X. Zhang, B. Yang, M. Gao and J. Shen, *Chem. Commun*., 1998, 2381.

3 J.-M. Lehn, *Supramolecular Chemistry–Concepts and Perspectives*, VCH, Weinheim, Germany, 1995.

4 G. S. Hanan, U. S. Schubert, D. Volkmer, E. Riviere, J.-M. Lehn, N. Kyritsakas and J. Fischer, *Can. J. Chem.*, 1997, **75**, 169; G. S. Hanan, D. Volkmer, U.S. Schubert, J.-M. Lehn, G. Baum and D. Fenske, *Angew. Chem.*, 1997, **109**, 1929; *Angew. Chem., Int. Ed. Engl*., 1997, **36**, 1842; U. S. Schubert, C. H. Weidl and J.-M. Lehn, *Des. Monom. Polym.*, 1999, **2**, in press; U. S. Schubert, C. H. Weidl and C. Eschbaumer, submitted.

5 O. Waldmann, J. Hassmann, P. Müller, G. S. Hanan, D. Volkmer, U. S. Schubert and J.-M. Lehn, *Phys. Rev. Lett.*, 1997, **78**, 3390; O.Waldmann, J. Hassmann, P. Müller, D. Volkmer, U. S. Schubert and J.-M. Lehn, *Phys. Rev. B*, 1998, **58**, 3277.

6 U. S. Schubert, J.-M. Lehn, J. Hassmann, C. Y. Hahn, N. Hallschmidt and P. Müller, in *Functional Polymers*, ed. A. O. Patil, D. N. Schulz and B. M. Novak, *ACS Symp. Ser.* 1998, **704**, 248.

7 I. Weissbuch, P. N. W. Baxter, S. Cohen, H. Cohen, K. Kjaer, P. B. Howes, J. Als-Nielsen, G. S. Hanan, U. S. Schubert, J.-M. Lehn, L. Leiserowitz and M. Lahav, *J. Am. Chem. Soc*., 1998, **120**, 4850.

8 T. P. Russel, *Mater. Sci. Rep.*, 1990, **5**, 171.

9 Q. An, T. Salditt, J. Peisl, C. Eschbaumer, C. H. Weidl and U. S. Schubert, in preparation.

10 See, for example: E. C. Constable, *Adv. Inorg. Chem. Radiochem*., 1986, **30**, 69.

Communication 8/08163H

ChemComm

Hydrothermal assembly and structural characterisation of one- and two-dimensional organic/inorganic hybrid materials constructed from diphosphopentamolybdate(VI) clusters and $\{Cu(en)\}^{2+}$ complex groups

Jianjiang Lu, Yan Xu,* Ngoh K. Goh and Lian S. Chia

Division of Chemistry, School of Science, Nanyang Technological University, Singapore 259756, Republic of Singapore. E-mail: xuy@nievax.nie.ac.sg

Received (in Cambridge, UK) 30th September 1998, Accepted 10th November 1998

Three novel low-dimensional organic/inorganic hybrid materials, assembled hydrothermally, are constructed from diphosphopentamolybdate(VI) clusters linked through $\{Cu(en)\}^{2+}$ groups; the initial Mo/Cu and Mo/en ratios and the use of F^- ions control the connectivity between the phosphomolybdate clusters and $\{Cu(en)\}^{2+}$ groups, and hence the dimensionality of the solid architectures.

Self-assembly of inorganic molecular precursors in a quest for supramolecular chemistry is one of the highly recognised areas of chemical research. The significant contemporary interest in the transition polyoxometalate–phosphorus based solid materials[1–5] reflects their diverse applications in the areas such as catalysis, sorption and molecular electronics.[6–9] These solids are noted not only for their rich chemical reactivity and structural complexity, but for their unique capability of allowing a variety of chemical reactions to take place in the intracrystalline region. It is evident that chemically robust clusters of polyoxometalates can be assembled through charge compensating cations forming extended structures, though the mechanism by which the assembly is organised remains elusive. A popular strategy in the realisation of materials engineering involves combined applications of hydrothermal synthesis method and structure-directing templates. The feasibility of this strategy can be demonstrated by the advancement in porous materials[10] and the development of low-dimensional and microporous transition metal phosphates.[2–5]

The chemistry of polyoxomolybdate–phosphorus has been extensively studied due to their inherent potential for the development of supramolecular chemistry.[11] The recent success in the hydrothermal assembly of low-dimensional and microporous heteropolymolybdate-based hybrid materials using transition metal coordination complexes suggests a novel approach towards rational synthesis of metal oxide/organic solids.[12] As a continuation of our effort in the hydrothermal assembly of polyoxomolybdate(VI)-based solid materials,[13] we seek to explore the assembly of phosphomolybdates in the presence of Cu^{2+} and en under the influence of a F^- switch. Here, we report the hydrothermal synthesis and structural characterisation of three novel one- and two-dimensional hybrid solids, $[H_2en]_2[\{Cu(en)(OH_2)\}Mo_5P_2O_{23}]\cdot 4H_2O$ **1**, $[H_2en][\{Cu(en)_2\}Mo_5P_2O_{22}(OH_2)]\cdot 2H_2O$ **2** and $[\{Cu(en)(Hen)\}_2Mo_5P_2O_{23}]\cdot 3H_2O$ **3**.

Solids **1**-**3** were synthesised from the hydrothermal reactions of $MoO_3\cdot H_2O$, H_3PO_4, $CuSO_4\cdot 5H_2O$, en, H_2O with and without the use of F^- ions at 160 °C for 72 h.† The concentration of F^- ions in the initial mixtures was found to be critical for the synthesis of **1**. Solid **2** was obtained from similar reaction mixtures to **1** in the absence of F^- ions. Solid **3** was obtained from reaction mixtures containing much higher Cu^{2+} and en concentrations in comparison to those of **1** and **2**. *In situ* PXRD studies‡ showed that the crystal structures of solids **1**-**3** remained intact until *ca.* 400 °C. The synthesis of the three solids is sensitive to the specific reaction conditions such as the Mo/Cu and Mo/en ratios, suggesting a kinetically controlled crystallisation mechanism.

The structure of $[H_2en]_2[\{Cu(en)(OH_2)\}Mo_5P_2O_{23}]\cdot 4H_2O$ **1**§ is constructed from linking of the $[Mo_5P_2O_{23}]^{6-}$ clusters and $\{Cu(en)(OH_2)O_2\}^{2+}$ square pyramids into spiral-shaped chains of $[\{Cu(en)(OH_2)\}Mo_5P_2O_{23}]^{4-}$ as shown in Fig. 1. The geometry of the $[Mo_5P_2O_{23}]^{6-}$ cluster[11] can be described as a ring of five distorted MoO_6 octahedra with two PO_4 tetrahedra capped on each side. Two adjacent $[Mo_5P_2O_{23}]^{6-}$ clusters are connected through a $\{Cu(en)(OH_2)\}^{2+}$ unit *via* corner-sharing interactions of the type PO–Cu with Cu–O 1.949(5), 2.014(5) Å. The copper site is defined by two nitrogen donors from an en molecule, two *cis*-oxo groups from two adjacent $[Mo_5P_2O_{23}]^{6-}$ clusters and one oxygen donor from a H_2O molecule. The axial Cu–O bond [Cu-OH_2 2.432(7) Å] is considerably longer than the equatorial Cu–O bonds [Cu–O 1.949(5), 2.014(5) Å] owning to Jahn–Teller distortion. The $[\{Cu(en)(OH_2)\}Mo_5P_2O_{23}]^{4-}$ chains align in parallel and are packed such that each chain is circumscribed by two groups of four alike chains, which are related by a *pseudo* 4-fold axis, giving rise to an elongated cylindrical unit. As a result, pseudo-one-dimensional channels are formed that are filled with the charge-compensating Hen_2^{2+} cations.

Modifying the reaction mixture of **1** by reducing the F^- ion content leads to the co-crystallisation of solids **1** and **2**. Monophasic crystals of **2** are produced by removing F^- ions from the reaction mixtures. Examination of the structure of $[H_2en][\{Cu(en)_2\}Mo_5P_2O_{22}(OH_2)]\cdot 2H_2O$ **2**§ reveals that it consists of the $[Mo_5P_2O_{22}(OH_2)]^{4-}$ clusters[11] linked through the $\{Cu(en)_2O_2\}^{2+}$ octahedra into a virtual one-dimensional chain of $[\{Cu(en)_2\}Mo_5P_2O_{22}(OH_2)]^{2-}$ as shown in Fig. 2. Each $[Mo_5P_2O_{22}(OH_2)]^{4-}$ cluster is connected to two $\{Cu(en)_2O_2\}^{2+}$ octahedra through the two terminal oxo groups of a common MoO_6 octahedron forming weak interactions of the type Cu–OMo with Cu–O 2.490(6), 2.503(6) Å. The two axial Cu–O bonds of the $\{Cu(en)_2O_2\}^{2+}$ octahedron are, as expected, elongated. The adjacent chains of $[\{Cu(en)_2\}Mo_5P_2O_{22}(OH_2)]^{2-}$ are in close contact forming pseudo-two-dimensional layers through weak interactions of the type P···O 3.325(6) Å as shown in Fig. 2. The striking differences between the structures of **1** and **2** lie in (i) the number of en molecules

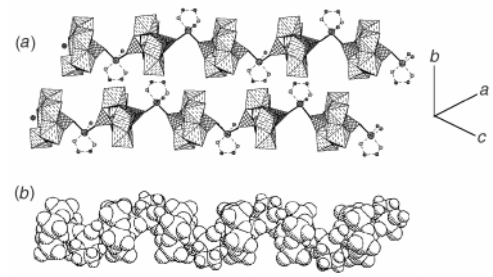

Fig. 1 (a) A polyhedral and ball-and-stick packing view of the $\{[Cu(en)(OH_2)\}Mo_5P_2O_{23}]^{4-}$ chains of **1** showing the connectivity between the $[Mo_5P_2O_{23}]^{6-}$ clusters and $\{Cu(en)(OH_2)O_2\}^{2+}$ square pyramids and orientation of the chains. Octahedra and tetrahedra represent Mo and P atoms respectively. Cu atoms are shown by large ahtched circles. (b) The space-filling plot of the spiral-shaped chains of **1**.

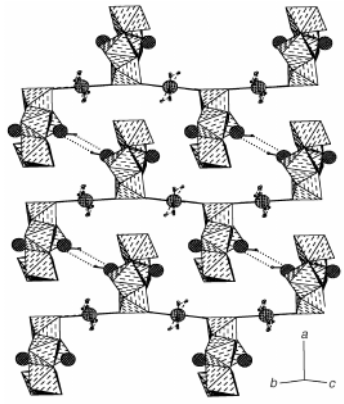

Fig. 2 A polyhedral and ball-and-stick representation of **2** showing (i) the connectivity between the $[Mo_5P_2O_{22}(OH_2)]^{4-}$ clusters and $\{Cu(en)_2O_2\}^{2+}$ octahedra; (ii) the packing and orientation of the $[\{Cu(en)_2\}Mo_5P_2O_{22}(OH_2)]^{2-}$ chains and the pseudo-layers formed as a result of interchain interactions. Octahedra represent Mo atoms. P and Cu atoms are shown by large heavy-crossed and heavy-shaded circles.

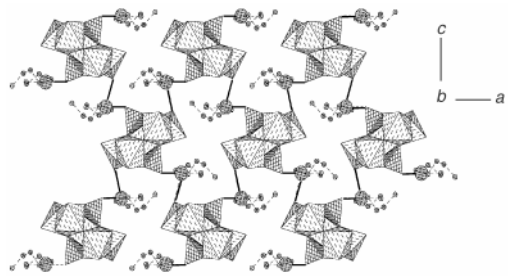

Fig. 3 A polyhedral and ball-and-stick representation of the $[\{Cu(en)(Hen)\}_2Mo_5P_2O_{23}]$ layer of **3** showing the connectivity between the $[Mo_5P_2O_{23}]^{6-}$ clusters and $\{Cu(en)(Hen)O_2\}^{3+}$ square pyramids and the 12-membered rings. Octahedral and tetrahedra represent Mo and P atoms respectively. Cu atoms are shown by large dotted circles.

participated in forming $\{Cu(en)\}^{2+}$ building blocks and (ii) the connectivity between $[Mo_5P_2O_{23}]^{6-}$ clusters and $\{Cu(en)\}^{2+}$ groups, namely, PO–Cu in **1** and MoO–Cu in **2**. The packing of chains gives rise to an elongated cylindrical unit in **1** and pseudo-layers in **2**. We believe that the strong coordination effect of F^- ions plays a role in controlling the reaction between Cu^{2+} center and the N donors of en molecules, and between Cu^{2+} center and the O donors of $[Mo_5P_2O_{23}]^{6-}$ clusters or H_2O molecules.

The solid architectures of **1** and **2** provide examples of different ways of connecting $[Mo_5P_2O_{23}]^{6-}$ clusters and $\{Cu(en)\}^{2+}$ groups. It suggests that further condensation of $[Mo_5P_2O_{23}]^{6-}$ clusters into higher dimensional solids through the linkage of $\{Cu(en)\}^{2-}$ groups could be feasible. Reducing the initial Mo/Cu and Mo/en ratios results in the successful crystallisation of solid **3**. The structure of $[\{Cu(en)(Hen)\}_2Mo_5P_2O_{23}]\cdot 3H_2O$ **3**§ is constructed from $[Mo_5P_2O_{23}]^{6-}$ clusters[11] linked through $\{Cu(en)(Hen)\}^{3+}$ groups into two-dimensional layers of $[\{Cu(en)(Hen)\}_2Mo_5P_2O_{23}]$ as shown in Fig. 3. Each $[Mo_5P_2O_{23}]^{6-}$ cluster is bonded to four $\{Cu(en)(Hen)\}^{3+}$ groups through two PO_4 tetrahedra and two MoO_6 octahedra forming two pairs of covalent interactions of the types Cu–OP and Cu–OMo with Cu–O 1.952(2), 2.557(2) Å respectively. The Cu^{2+} center of $\{Cu(en)(Hen)O_2\}^{3+}$ square pyramid receives contributions from three nitrogen donors belonging to one and half en molecules, one oxygen donor from a PO_4 unit and one oxygen donor from a MoO_6 unit with Cu–N 1.991(3), 2.011(3), 2.020(3) Å and Cu–O 1.952(2), 2.557(2) Å. This results in the 12-membered rings ($Mo_4P_4Cu_4$) of the $[\{Cu(en)(Hen)\}_2Mo_5P_2O_{23}]$ layers of **3**. Adjacent $[\{Cu(en)(Hen)\}_2Mo_5P_2O_{23}]$ layers are separated by H_2O molecules with small interlamellar separation owing to the presence of extensive network of H-bonds. The coexistence of Cu–OP and Cu–OMo linkages plays a critical role in constructing the layer structure of **3** which contrast strikingly to the Cu–OP and Cu–OMo linkages in building up the chain structures of **1** and **2** respectively.

The successful isolation of solids **1**–**3** provides novel examples of assembling phosphomolybdate clusters through the templating effects of $\{Cu(en)\}^{2+}$ groups for design of composite oxide materials. It demonstrates that the use of hydrothermal techniques is essential for the realisation of materials design. The dimensionality of solid architectures is, to certain degree, tailorable while the key leading to the success lies on the kinetic aspect of assembly process. While the mineralising mechanism of F^- ions remains debatable, its critical role in constructing solid architectures is manifest. The present study reveals the rich hydrothermal chemistry of the phosphomolybdate–Cu–en system and the structural versatility evolving from altering reaction kinetics. This highlights the feasibility of engineering metal–organoamine–phosphomolybdate solids with potentially interesting and useful properties.

We thank Nanyang Technological University, Singapore, for financial support (Grant: RP 17/97XY).

Notes and references

† *Synthesis*: hydrothermal reactions were performed in PTFE-lined stainless steel autoclave reactors (22 mL). Mole ratios of $MoO_3\cdot H_2O$, H_3PO_4 (85 mass%), $CuSO_4\cdot 5H_2O$, en, H_2O, F^- are 3 : 4 : : 2.3 : 500 : 13.3 for **1**, 4.3 : 6.4 : 1 : 3.4 : 1730 : 0 for **2** and 1 : 2.3 : 1.8 : 3.8 : 460 : 0 for **3**.

‡ *Powder XRD data*: *in situ* PXRD patterns were collected on a Siemens D5005 diffractometer with graphite-monochromated Cu-Kα radiation (λ = 1.5418 Å). Heating was conducted in the temperature range RT–1000 °C under vacuum.

§ *Crystal data*: $C_6H_{38}N_6CuMo_5P_2O_{28}$ **1**: M_w = 1247.60, monoclinic, space group *Cc*. a = 14.821(3), b = 14.419(3), c = 16.132(5) Å, β = 109.087(5)°, V = 3258.0(14) Å^3, Z = 4, D_c = 2.544 g cm^{-3}, μ = 2.716 mm^{-1}, T = 296 K. R_1 = 0.0267 for 3222 reflections. $C_6H_{32}N_6CuMo_5P_2O_{25}$ **2**: M_w = 1193.56, triclinic, space group $P\bar{1}$. a = 10.6813(14), b = 11.176(2), c = 12.852(2) Å, α = 75.568(13), β = 89.297(6), γ = 86.545(8) °, V = 1483.1(4) Å^3, Z = 2, D_c = 2.673 g cm^{-3}, μ = 2.969 mm^{-1}, T = 296 K. R_1 = 0.0496 for 5138 reflections. $C_4H_{20}N_4CuMo_{2.5}PO_{13}$ **3**: M_w = 666.60, orthorhombic, space group *Ibca*. a = 11.478(4), b = 39.171(8), c = 15.226(6) Å, V = 6845(4) Å^3, Z = 16, D_c = 2.587 g cm^{-3}, μ = 3.190 mm^{-1}, T = 296 K. R_1 = 0.0246 for 3006 reflections. The structures were solved by direct methods and refined using full-matrix least squares on F^2 using SHELXTL. The H_2O molecules of **2** and the C and N atoms of the en molecules of **2** and **3** are disordered. CCDC 182/1089. See http://www.rsc.org/suppdata/cc/1998/2733/ for crystallographic files in .cif format.

1 G. Cao and T. Mallouk, *Inorg. Chem.*, 1991, **30**, 1434 and references therein.
2 R. Haushalter and L. Mundi, *Chem. Mater.*, 1992, **4**, 31 and references therein.
3 P. Feng, X. Bu, S. Tolbert and G. Stucky, *J. Am. Chem. Soc*., 1997, **119**, 2497.
4 V. Soghomonian, Q. Chen, R. Haushalter and J. Zubieta, *Chem. Mater.*, 1993, **5**, 1595; P. Zapf, R. Haushalter and J. Zubieta, *Chem. Mater.*, 1997, **9**, 2019.
5 T. Gier and G. Stucky, *Nature*, 1991, **349**, 508.
6 P. Cox, *Transition Metal Oxides*, Clarendon Press, UK, 1995.
7 A. Cheetham, *Science*, 1994, **264** and references therein.
8 V. Day and W. Klemperer, *Science*, 1985, **228**, 533.
9 M. Pope, *Heteropoly and Isopoly Oxometalates*, Springer, New York, 1983.
10 S. Wilson, T. Cannan, E. Flanigen, B. Lok and C. Messina, *ACS Symp. Ser*., 1983, **218**, 79; Q. Huo, D. Margolene and G. Stucky, *Chem. Mater.*, 1996, **8**, 1147.
11 M. Lowe, J. Lockhart, G. Forsyth, W. Clegg and K. Fraser, *J. Chem. Soc. Dalton Trans.*, 1995, **1**, 145 and references therein.
12 J. Debord, R. Haushalter, L. Meyer, D. Rose, P. Zapf and J. Zubieta, *Inorg. Chim. Acta.*, 1997, **256**, 165; D. Hagrman, P. Zapf and J. Zubieta, *Chem. Commun.*, 1998, 1283.
13 Y. Xu, L. An and L. Koh, *Chem. Mater.*, 1996, **8**, 814; J. Lu, Y. Xu, N. Goh and L. Chia, *Chem. Commun.*, 1998, 1709; J. Lu and Y. Xu, *Chem. Mater.*, 1998, in press.

Communication 8/07617K

ChemComm

Aromatic inclusion within a neutral cavity-containing rectangular grid

Ryan H. Groeneman, Leonard R. MacGillivray and Jerry L. Atwood*

Department of Chemistry, University of Missouri-Columbia, Columbia, MO 65211, USA.
E-mail: atwoodj@missouri.edu

Received (in Cambridge, UK) 5th October 1998, Accepted 9th November 1998

Reaction of $CoCl_2·6H_2O$ with pyrazine and disodium terephthalate in water results in the formation of a neutral cavity-containing rectangular grid, $[Co(pyz)(terph)(H_2O)_2]$, which includes a tightly bound aromatic as a guest; classification of these frameworks also provides targets for chemical synthesis.

In a recent report, we demonstrated the one-pot synthesis of a cationic cavity-containing rectangular grid, $[M(4,4'\text{-bipy})(pyca)(H_2O)_2]^+$ **1** [where M = Co(II) or Cd(II); 4,4′-bipy = 4,4′-bipyridine; pyca = pyridine-4-carboxylate], which self-assembles in the solid state to form stacked layers.[1] The stacking exhibited by this framework yielded interconnected microchannels which include highly disordered neutral (*i.e.* solvent H_2O) and charged (*i.e.* NO_3^- ions) guest species. In this contribution, we now extend the chemistry of these materials to neutral frameworks and demonstrate, for the first time, the ability of a cavity-containing rectangular grid, $[Co(pyz)(terph)(H_2O)_2]$ **2** (where pyz = pyrazine, terph = 1,4-benzenedicarboxylate), to include an aromatic (*i.e.* pyz) as a guest. We also demonstrate that it is possible to classify these and related square grids based on simple charge considerations which we anticipate will aid in the synthesis and sorting of these compounds as new members of each family continue to emerge.

There are, in principle, only four ways in which either a cationic or neutral rectangular grid may be constructed using a M^{2+} ion (M = transition metal) (Table 1).† In the first case, both bridging ligands, in terms of charge, must be neutral. In the second case, one bridging ligand must possess a − 1 charge. In the third case, both bridging ligands must possess a − 1 charge. Finally, in the fourth case, one bridging ligand must possess a − 2 charge. In each case, either a square planar or octahedral metal center may be employed for the assembly process. In this study, an example of case 4, which is based upon an octahedral metal center, is presented. Notably, for a square grid, there are only two ways in which such a framework may be constructed. Either the bridging ligand must possess a − 1 charge or be neutral. This latter observation is due to the fact that only a single bridging ligand may be used to construct a square grid framework.

When a hot, aqueous solution (5 mL) of $CoCl_2·6H_2O$ (238 mg, 1.0 mmol) was added to a hot, aqueous solution (4 mL) of pyrazine (160 mg, 2.0 mmol) and disodium terephthalate (210 mg, 1.0 mmol) according to eqn (1), crystals of **2**·pyz suitable for X-ray analysis formed, after cooling, within a period of approximately 1 week (yield 16.2 %, single product). The formulation of **2**·pyz was confirmed by single-crystal X-ray analysis‡ and thermogravimetric analysis.

$$CoCl_2·6H_2O + 2\ pyz + Na_2(terph) \rightarrow \mathbf{2}·pyz \qquad (1)$$

A view depicting the metal ion coordination in **2** is shown in Fig. 1. In a similar way to **1**,[1] the metal center is coordinated to two *trans* μ-pyz ligands, two *trans* μ-terph ions, and two *trans* water molecules that form a slightly distorted octahedral coordination environment. As a result, a cavity-containing rectangular grid has formed. Unlike **1**, however, the anion possesses a −2 charge and the framework is therefore neutral. Notably, the grids lie parallel to the crystallographic *ab* plane and exhibit intragrid M···M separations of 7.2× 11.3 Å across each pyz ligand and terph ion, respectively. In a similar way to **1**, the anion participates in two O–H···O hydrogen bonds with two coordinated water molecules [O···O 2.683(2) Å] such that the carboxylate moieties of the ligand lie approximately orthogonal to the MN_2O_2 plane.

Table 1 Summary of rectangular grids

Case	Metal[a]	Ligand I	Ligand II	Ref.
1	M^{2+}	Neutral	Neutral	2
2	M^{2+}	−1	Neutral	1
3	M^{2+}	−1	−1	–
4	M^{2+}	−2	Neutral	3, this study

[a] Square planar or octahedral transition metal center.

As shown in Fig. 2, the bridging ligands of **2** have generated a cavity with dimensions suitable to accommodate a molecule of pyz. The included guest, which, in contrast to **1**,[1] is well ordered, participates in π-π interactions (centroid···centroid 3.34 Å) and C–H···N hydrogen bonds§ (C···N 3.34 Å) with the anion and bridging pyz ligand, respectively. Although aromatic guest inclusion has been demonstrated in discrete[7,8] and infinite square assemblies,[9,10] these observations illustrate, for the first time, the ability of a rectangular framework to host an aromatic guest.

A view depicting the extended structure of **2** is shown in Fig. 3. As in **1**[1] and $Cu(4,4'\text{-bipy})(pyz)(H_2O)_2(PF_6)_2$ **3**,[2] the grids self-assemble in the solid state such that they form stacked layers. Notably, the grids of **2** interact by way of O–H···O hydrogen bonds [O···O 2.808(3) Å], which involve coordinated water molecules and carboxylate moieties of the terph ion, such that adjacent layers lie offset. This, in turn, generates guest-

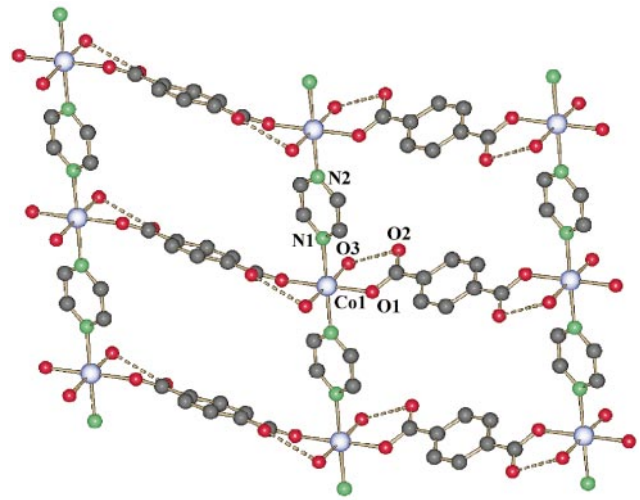

Fig. 1 A view of **2** depicting the coordination environment around the Co(II) metal centres. Selected interatomic distances (Å): Co(1)–O(1) 2.059(2), Co(1)–O(3) 2.121(2), Co(1)–N(1) 2.190(3), Co(1)–N(2) 2.163(3), O(2)···O(3) 2.683(2). All bond distances are within expected ranges. The guest has been omitted for clarity.

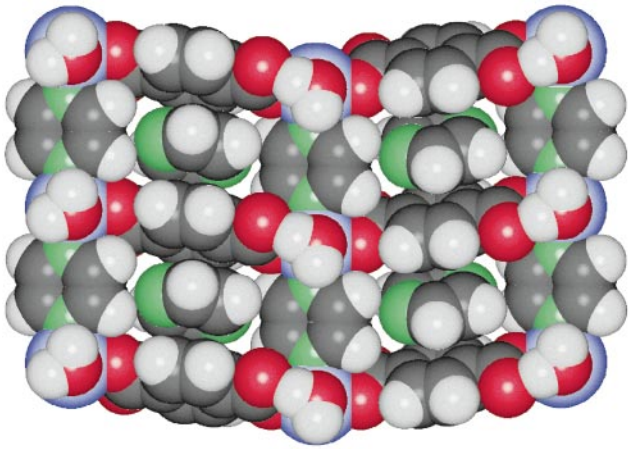

Fig. 2 A space-filling model of **2**·pyz. The guest is held within the cavity by a combination of π–π interactions and C–H···N hydrogen bonds.

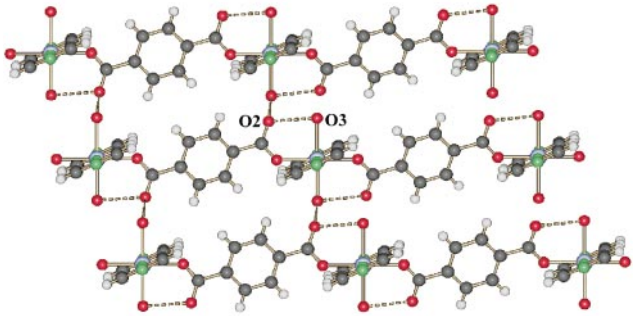

Fig. 3 A view depicting the O–H···O hydrogen bonds [O(2)···O(3) 2.808(3) Å] which occur between the stacked layers of **2**.

filled microchannels which run in an oblique direction with respect to the layers. Interestingly, thermal analysis of **2**·pyz reveals that, in contrast to **1**, the guest is tightly bound within the lattice. The TGA trace displays a rapid weight loss of 20.0% (calculated 19.1%), from 107 to 252 °C, which corresponds to one molecule of pyz.§ The resulting material, [Co(pyz)(terph)(H_2O)$_2$], then slowly decomposes with loss of pyz and the terph ion to yield the metal oxide.

The results reported herein illustrate the utility of using the process of self-assembly for the construction of *multi*-component host–guest architecture. By selecting appropriately functionalized components, we have shown that it is possible to extend the chemistry of rectangular grids involving bridging pyridines/diazines and carboxylate moieties to neutral frameworks. Considering the relatively small number of cavity-containing rectangular frameworks which have been synthesized to date (Table 1), it also now possible to target certain grids, for chemical synthesis, which have not yet been constructed (*e.g.* case 3), in which case members of each family may display similar properties. We are also currently exploring further inclusion properties of **2**, with a view to determine whether other aromatic guest molecules can be isolated within the framework.

We are grateful for funding from the National Science Foundation (NSF) and the Natural Sciences and Engineering Research Council of Canada (NSERC) for a doctoral scholarship (L. R. M.).

Notes and references

† To place our results in the context of those obtained to date, we limit our discussion to M^{2+} ions (M = transition metal) and exclude anionic frameworks.

‡ *Crystal data* for **2**·pyz: monoclinic, space group *C*2/*c*, a = 11.415(1), b = 7.161(1), c = 20.585(2), β = 96.189(2), U = 1682.8(3) Å^3, D_c = 1.66 g cm^{-3}, Mo-Kα radiation (λ = 0.71070 Å) for Z = 4. Least-squares refinement based on 1496 reflections with $I_{net} > 2.0\sigma(I_{net})$ (out of 1835 unique reflections) led to a final value of R = 0.039. Aromatic hydrogen atoms were placed by modeling the moieties as rigid groups with idealized geometry, maximizing the sum of the electron density at the calculated hydrogen positions. Structure solution was accomplished with the aid of SHELXS-86[4] and refinement was conducted using SHELXL93[5] locally implemented on a Pentium-based IBM compatible computer. CCDC 182/1084.

§ For comparison, **1** exhibits an initial weight loss at 25 °C. Similar square-based systems have been shown to exhibit initial guest weight losses below 70 °C.[10–12]

1 L. R. MacGillivray, R. H. Groeneman and J. L. Atwood, *J. Am. Chem. Soc.*, 1998, **120**, 2676.
2 M.-L. Tong, X.-M. Chen, X.-L. Yu and T. C. W. Mak, *J. Chem. Soc., Dalton Trans.*, 1998, 5.
3 S. Kawata, S. Kitagawa, M. Kondo, I. Furuchi and M. Munakata, *Angew. Chem., Int. Ed. Engl.*, 1994, **33**, 1759.
4 G. M. Sheldrick, *Acta. Crystallogr., Sect. A*, 1990, **46**, 467.
5 G. M. Sheldrick, SHELXL93, University of Göttingen, Germany, 1993.
6 G. R. Desiraju, *Acc. Chem. Res.*, 1996, **29**, 441.
7 M. Fujita, J. Yazaki and K. Ogura, *Tetrahedron Lett.* 1991, **32**, 5589.
8 P. N. W. Baxter, J.-M. Lehn, B. O. Kneisel and D. Fenske, *Chem. Commun.* 1997, 2231.
9 M. Fujita, Y. J. Kwon, S. Washizu and K. Ogura, *J. Am. Chem. Soc.*, 1994, **116**, 1151.
10 O. M. Yaghi, L. Hailian and T. L. Groy, *Inorg. Chem.* 1997, **36**, 4292.
11 J. Lu, T. Paliwala, S. C. Lim, C. Yu., T. Niu and A. J. Jacobson, *Inorg. Chem.*, 1997, **36**, 923.
12 P. Losier and M. J. Zaworotko, *Angew. Chem., Int. Ed. Engl.*, 1996, **35**, 2779.

Communication 8/07738J

The nature of the interaction of molecular fluorine and Lewis bases B from a comparison of the properties of B···F_2 and B···HF

A. C. Legon

School of Chemistry, University of Exeter, Stocker Road, Exeter, UK EX4 4QD E-mail: a.c.legon@exeter.ac.uk

Received (in Cambridge, UK) 7th October 1998, Accepted 4th November 1998

Comparison of angular geometries, radial geometries and intermolecular stretching force constants k_σ of the two series of complexes B···F_2 and B···HF, where B is H_2S, HCN, CH_3CN, H_2O, $(CH_2)_2O$ or NH_3, allows conclusions about the nature of the interaction in B···F_2 and the shape of the F atom in F_2.

The reactivity of elemental fluorine is legendary. It results from the ease with which the F–F bond is broken, coupled with the great strength of the bonds E–F (E = H,C or N) that are formed. Hence, the reactions of F_2 with many simple compounds are highly exothermic. Once sufficient concentrations of F atoms have been produced, presumably initially at surfaces and then through the temperature rise as the reaction begins, self-acceleration sets in through chain processes. Explosions can then result. But what of the interactions of the difluorine molecule F_2 itself with other molecules B when the possibility of reactions proceeding through fluorine atoms is precluded?

We have recently demonstrated that, by using a simple device, the complexes B···F_2 formed by simple Lewis bases B with F_2 may be isolated and characterised before any chemical reaction can occur.[1–6] The device is called a fast-mixing nozzle.[7] It consists of a pair of concentric, coterminal tubes of circular cross section that issue into the evacuated Fabry–Pérot cavity of a Fourier-transform microwave spectrometer.[8] The inner tube is a glass capillary of 0.3 mm internal diameter but the outer is constructed from Teflon. A dilute mixture of F_2 in argon is pulsed *via* a solenoid valve down the outer tube while the pure Lewis base B is flowed continuously into the vacuum chamber through the glass capillary. The coaxial gas flows undergo adiabatic expansion as they emerge from the tubes and so molecules of B and F_2 meet only when F_2 is moving away from surfaces at rate of *ca.* 5×10^4 cm s^{-1}, which is the terminal speed of the gas pulse for argon as carrier gas.[8] Complexes B···F_2 so formed are rapidly cooled to their lowest rotational and vibrational energy states and achieve collisionless expansion in *ca.* 10 μs. Thereafter, the complexes are effectively frozen and no chemical reaction is possible. The B···F_2 can then be characterised through their rotational spectrum in the relatively long period before the gas encounters a vessel wall, *etc*.

Analysis of the rotational spectrum of B···F_2 leads to details of the radial and angular geometry and to the strength of the interaction, as discussed elsewhere for complexes B···HX.[9] Sufficient B···F_2 have now been characterised to allow general conclusions about the nature of the interaction of F_2 with simple Lewis bases B. Table 1 summarises the radial and angular geometries of the six complexes B···F_2[1–6] and the six analogous hydrogen-bonded complexes B···HF,[10–16] where B is H_2S, HCN, CH_3CN, H_2O, $(CH_2)_2O$ or NH_3. Also included in Table 1 are the intermolecular stretching force constants k_σ. These are available from the centrifugal distortion constants D_J or Δ_J for weakly bound complexes in the quadratic approximation with the assumption of rigid, unperturbed subunits B and F_2 by using expressions developed by Millen[17] and provides one measure of the strength of the B–F_2 interaction.

Several general points emerge from Table 1. First, the angular geometries of the pair B···F_2/B···HF are isomorphous for a given B. The detailed similarity within the pair for H_2O···XF (X = F or H), for H_2S···XF and for $(CH_2)_2O$···XF, in each of which the geometry is not dictated by the symmetry of B, is remarkable. Although both H_2O···F_2 and H_2O···HF are

Table 1 Comparison of properties of complexes B···F_2 and B···HF

	Angular geometry		r(Z···F)/Å			k_σ/N m^{-1}	
B	Type	Details (ϕ/°)	B···F_2	B···HF	σ(Z)+σ(F)[a]/Å	B···F_2	B···HF
H_2S	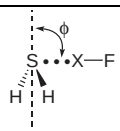	X = F ϕ = 113(5)[b] X = H ϕ = 91[c]	3.20(1)[b]	3.249[c]	3.20	2.36(4)[b]	12(2)[d]
HCN	HCN···X–F	$C_{\infty v}$(X = F and H)[e,f]	2.803(3)[e]	2.805(1)[f]	2.85	2.61(1)[e]	18.26(5)[f]
CH_3CN	CH_3CN···X–F	C_{3v}(X = F and H)[g,h]	2.748(3)[g]	2.751(1)[h]	2.85	1.49(1)[g]	19.83(5)[h]
H_2O	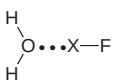	Effectively planar, C_{2v}(X = F and H)[i,j]	2.719(4)[i]	2.684(16)[k]	2.75	3.63(7)[i]	25(2)[l]
$(CH_2)_2O$	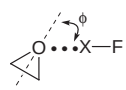	X = F ϕ = 76(4)[m] X = H ϕ = 72.0(2)[n]	2.63(6)[m]	2.629(5)[n]	2.75	—[o]	—[o]
NH_3	H_3N···XF	C_{3v}(X = F and H)[p,q]	2.708(7)[p]	2.71[q]	2.85	4.70(3)[p]	32.8[q]

[a] Sum of van der Waals radii from ref. 26; σ(N) = 1.50 Å, σ(O) = 1.40 Å, σ(S) = 1.85 Å σ(F) = 1.35 Å. [b] Ref. 5. [c] Ref. 10. [d] Ref. 11. [e] Ref. 3. [f] Ref. 12. [g] Ref. 2. [h] Ref. 13. [i] Ref. 4. [j] Ref. 14 and 18; [k] Refitted to rotational constants of $H_2{}^{16}O$···HF, $H_2{}^{18}O$···HF, $D_2{}^{16}O$···DF from ref. 14. [l] Calculated from Δ_J of ref. 15 by method of ref. 17. [m] Ref. 6. [n] Ref. 16. [o] Expressions in ref. 17 are not appropriate to calculation of k_σ from Δ_J for molecules of this geometry. [p] Ref. 1. [q] Calculated from B_0 or D_J values communicated to the author by B. J. Howard and P. R. R. Langridge-Smith (unpublished).

recorded as effectively planar, $H_2O\cdots HF$ has been shown[18] to have a small potential energy barrier (126 cm^{-1}) to the planar C_{2v} conformation that separates the two equivalent equilibrium geometries of C_s symmetry having a pyramidal configuration at O. The top of the barrier lies only slightly above the zero-point energy level and the vibrational wavefunctions have C_{2v} symmetry. In view of the much weaker bond in $H_2O\cdots F_2$, it is likely that the barrier in this species is even lower. This interpretation is reinforced by the fact that a low-lying vibrational satellite attributed to internal rotation of the H_2S subunit is observed in $H_2S\cdots F_2$ but not in $H_2S\cdots HF$, which is rigidly pyramidal.

Secondly, we note from Table 1 that the k_σ for the $B\cdots F_2$ are smaller than those of the $B\cdots HF$ by a factor of 6 to 8. Indeed, the $B\cdots F_2$ are so weak that their k_σ values are closer to those of $B\cdots Ar$ complexes. For example, k_σ = 3.6(4) N m^{-1} and 2.18 N m^{-1} for oxirane$\cdots F_2$[6] and oxirane$\cdots$Ar,[19] respectively.

Thirdly, the distance $r(Z\cdots F)$ from the acceptor atom Z in B to the nearest F atom is almost identical within a given pair $B\cdots F_2$/$B\cdots HF$.

What explanation can be offered for these observations? The behaviour of the $B\cdots HF$ complexes was interpreted[20,21] on the basis of a simple electrostatic interaction of B and HF, *i.e.* between unperturbed electric charge distributions. The angular geometries of $B\cdots HF$ were first rationalised[20] on the basis of the simple rule which states that in the equilibrium geometry the axis of the HF molecule coincides with the axis of a non-bonding electron pair on the acceptor atom Z in forming a hydrogen bond with B. This rule was subsequently given a quantitative basis by a simple electrostatic model.[22] The variations of the k_σ in $B\cdots HF$ complexes has also been interpreted in terms of an electrostatic interaction.[23]

The results in Table 1 suggest a similar approach for $B\cdots F_2$. In that case, the fact that the leading term in the Taylor series expansion of the electric charge distribution of F_2, namely its electric quadrupole moment Q = 2.76 × 10^{-40} C m^2, is very small[24] while HF has an electric dipole moment[25] μ = 1.8265 D (6.0925 × 10^{-30} C m) ensures that the interaction $B\cdots{}^{\delta+}F\overset{\delta-}{\delta+}F^{\delta+}$ will be much weaker than in $B\cdots{}^{\delta+}H\text{–}F^{\delta-}$. This is borne out by the k_σ values of Table 1. Moreover, the nearly spherical F_2 electric charge distribution explains why the magnitudes of k_σ for $B\cdots F_2$ are like those of $B\cdots Ar$. Presumably, the London dispersion interaction is more significant for $B\cdots F_2$ than for $B\cdots HF$, for which the preponderant contribution is electrostatic. In some ways F_2 behaves like its united atom Ar in complexes with B.

Evidently, the electrostatic part of the energy of interaction in $B\cdots F_2$ is still definitive of the angular geometry and hence the latter is of the same form for a given pair $B\cdots F_2$/$B\cdots HF$. Nevertheless, the weaker electrostatic term in the $B\cdots F_2$ is consistent with a lower barrier to internal rotation of the H_2S subunit in $H_2S\cdots F_2$ than in $H_2S\cdots HF$.

Given that the $B\cdots F_2$ interaction is weak, it seems likely that the distance $r(Z\cdots F)$ will be determined by the sum of the van der Waals radii $\sigma(Z)$ and $\sigma(F)$ of the atoms Z and F. Values of $\sigma(Z) + \sigma(F)$ generated from Pauling's radii[26] are given in Table 1. If a range of 0.05 Å is assigned to the Pauling radii, the $r(Z\cdots F)$ for both $B\cdots F_2$ and $B\cdots HF$ are identical with the sum $\sigma(Z) + \sigma(F)$, since the mean difference $\Delta r = \{\sigma(Z) + \sigma(F)\} - r(Z\cdots F)$ is only 0.07(6) for the $B\cdots F_2$ and 0.09(4) for the $B\cdots HF$. It was suggested earlier[22] that the distance $r(Z\cdots F)$ in hydrogen-bonded complexes can be taken as the sum of the van der Waals radii of Z and F, in view of the lack of a repulsive electron shell for the nearly bare proton $^{\delta+}H$ in HF. This is illustrated graphically in Fig. 1, in which the netted spheres of appropriate van der Waals radius drawn on the O and F atoms in the scale diagrams of $H_2O\cdots F_2$ and $H_2O\cdots HF$ just touch in each case.

The fact that Δr is effectively zero for $B\cdots F_2$ suggests that F_2 may not be 'snub-nosed' in the sense that Cl_2 is, *i.e.* that the van der Waals radius along the axis is not shorter than the value perpendicular to it. For several $B\cdots Cl_2$, the mean value of Δr is found to be *ca.* 0.5 Å. *Ab initio* calculations of the type[27] used to establish the anisotropy of the van der Waals radius of Cl_2 would settle this.

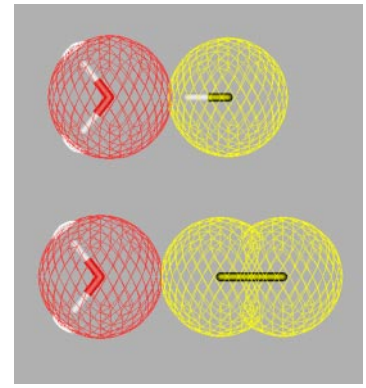

Fig. 1 Stick models of $H_2O\cdots HF$ (upper) and $H_2O\cdots F_2$ (lower) drawn to scale, with the experimental intermolecular separations $r(Z\cdots F)$ given in Table 1. The nets are spheres having the appropriate van der Waals radii (red for oxygen, yellow for fluorine, white for hydrogen). The sphere for the H of HF is not drawn, for the reason discussed in the text. For convenience, both molecules are depicted as planar. Note that the van der Waals spheres of oxygen and the inner fluorine atom just touch in each case.

The author thanks the EPSRC for the award of a Senior Fellowship.

Notes and references

1 H.I. Bloemink, K. Hinds, J. H. Holloway and A. C. Legon, *Chem. Phys. Lett.*, 1995, **245**, 598.
2 S. A. Cooke, G. Cotti, C. M. Evans, J. H. Holloway and A. C. Legon, *Chem. Phys. Lett.*, 1996, **260**, 388.
3 S. A. Cooke, G. Cotti, C. M. Evans, J. H. Holloway and A. C. Legon, *Chem. Phys. Lett.*, 1996, **262**, 308.
4 S. A. Cooke, G. Cotti, J. H. Holloway and A. C. Legon, *Angew, Chem., Int. Ed. Engl.*, 1997, **36**, 129.
5 G. Cotti, C. M. Evans, J. H. Holloway and A. C. Legon, *Chem. Phys. Lett.*, 1997, **264**, 513.
6 C. M. Evans, J. H. Holloway and A. C. Legon, *Chem. Phys. Lett.*, 1997, **267**, 281.
7 A. C. Legon and C. A. Rego, *J. Chem. Soc., Faraday Trans.*,1990, **86**, 1915.
8 T. J. Balle and W. H. Flygare, *Rev. Sci. Instrum.*, 1981, **52**, 33.
9 A. C. Legon, *Chem. Soc. Rev.*, 1990, **19**, 197.
10 R. Viswanathan and T. R. Dyke, *J. Chem. Phys*, 1982, **77**, 1166.
11 L. C. Willoughby, A. J. Fillery-Travis and A. C. Legon, *J. Chem. Phys.*, 1984, **81**, 20.
12 A. C. Legon, D. J. Millen and L. C. Willoughby, *Proc. R. Soc. London Ser. A*, 1985, **401**, 327.
13 P. Cope, D. J. Millen, L. C. Willoughby and A. C. Legon, *J. Chem. Soc., Faraday Trans. 2*, 1986, **82**, 1197.
14 J. W. Bevan, Z. Kisiel, A. C. Legon, D. J. Millen and S. C. Rogers, *Proc. R. Soc. London Ser. A*, 1980, **372**, 441.
15 G. Cazzoli, P. G. Favero, D. G. Lister, A. C. Legon, D. J. Millen and Z. Kisiel, *Chem. Phys. Lett.*, 1985, **117**, 543.
16 A. C. Legon, A. L. Wallwork and D. J. Millen, *Chem. Phys. Lett.*, 1991, **178**, 279.
17 D. J. Millen, *Can. J. Chem.*, 1985, **63**, 1477.
18 Z. Kisiel, A. C. Legon and D. J. Millen, *Proc. R. Soc. London Ser. A*, 1982, **381**, 419.
19 R. A. Collins, A. C. Legon and D. J. Millen, *J. Mol. Struct.*, 1986, **135**, 435.
20 A. C. Legon and D. J. Millen, *Faraday. Discuss. Chem. Soc.*, 1982, **73**, 71.
21 A. C. Legon and D. J. Millen, *Chem. Soc. Rev.*, 1987, **16**, 467.
22 A. D. Buckingham and P. W. Fowler, *Can. J. Chem.*, 1985, **63**, 2018.
23 A. C. Legon and D. J. Millen, *J. Am. Chem. Soc.*, 1987, **109**, 356.
24 S. Peebles, P. W. Fowler and A. C. Legon, unpublished calculations.
25 J. S. Muenter and W. Klemperer, *J. Chem. Phys.*, 1970, **52**, 6033.
26 L. Pauling, *The Nature of the Chemical Bond*, Cornell University Press, Ithaca, NY 1960, ch.7, pp. 258–264.
27 S. A. Peebles, P. W. Fowler and A. C. Legon, *Chem. Phys. Lett.*, 1995, **240**, 130.

Communication 8/07791F

Templated formation of multi-porphyrin assemblies resembling a molecular universal joint

Martin R. Johnston,[a] Maxwell J. Gunter[b] and Ronald N. Warrener*[a]

[a] *Centre for Molecular Architecture, Central Queensland University, Rockhampton, Queensland, 4702, Australia. E-mail: r.warrener@cqu.edu.au*

[b] *Department of Chemistry, University of New England, Armidale, NSW, 2351, Australia*

Received (in Cambridge, UK) 21st September 1998, Accepted 13th November 1998

The rigid bis-porphyrinic host 2 forms 1:1 complexes with rigid 5,15-bis(4-pyridyl)porphyrins and both 1:1 and 2:1 complexes with tetrapyridylporphyrin 4, with the latter complex providing a new example of a self-assembled system containing an enclosed molecular environment.

Strategies for self-assembly are receiving increasing attention for the construction of multichromophoric supramolecular arrays involving porphyrins.[1] In particular, metal ion co-ordination utilising ligation of the metallated porphyrin nucleus has proven efficient for positioning photoactive components.[2,3] Systems exerting co-operativity between two or more non-covalent interactions provide access to self-assembled arrays with increased stability compared to systems relying on a single interaction alone.[3] The construction of such porphyrinic arrays is a key to the development of synthetic models which mimic the manner in which nature assembles the photoactive components within the photosynthetic apparatus and produces charge separation in high quantum yield.[4]

Here, we show that the rigid bis-porphyrin **2** can react with rigid dipyridyl porphyrins to form 1:1 complexes, and that the tetrapyridylporphyrin component **4** can form both 1:1 and 2:1 complexes;† the latter porphyrin array **7** has a shape and mobility reminiscent of a universal joint.‡ While such a structure is novel and aesthetically intriguing, its value is conceptual; it may have interesting photophysical properties and its formation suggests similar methodologies for the assembly of other large covalent capsules.

Molecular modelling (AM1) revealed that a self-assembled host–guest arrangement between bis-porphyrin **2** and rigid dipyridyl rod **3** or tetrapyridyl rod **4** should be feasible, based on the following dimensions: a porphyrin centre-to-centre distance in **2** of 22 Å (Fig. 1); pyridine N–N distances in 5,15-dipyridyl substituted porphyrins **3** and **4** of 15.7 and 15.5 Å, respectively; and an average zinc porphyrin to pyridyl bond distance of 2.2 Å.[7]

Mixing equimolar amounts of rigid bis-porphyrin **2** [formed from **1**[8] by treatment with $Zn(OAc)_2$ in CH_2Cl_2–MeOH] and dipyridyl porphyrin rod **3**§ ($CDCl_3$ or CD_2Cl_2) resulted in the formation of a 1:1 complex **5** (C_{2v}). Examination by ^{1}H NMR spectroscopy revealed sharp resonances for **3** complexed on the inside of **2** in which the resonances for **2** were slightly broadened. Such broadening has been observed previously in complexation studies involving **3**,[9] and in both cases these signals were sharpened by cooling the solution to 263 K or below.

The α- and β-pyridyl resonances of **3** within **5** are drastically affected by the host porphyrin system's magnetic anisotropy, shifting upfield by 5.74 and 1.66 ppm respectively. In contrast, the proton resonances of the fused carbocyclic framework in **5** are only slightly affected by the guest porphyrin (*ca.* $\Delta\delta$ 0.14). Such large pyridyl shifts are indicative of coordination of the bis-pyridyl porphyrin guest with the bis-zinc porphyrin host.[3]

UV spectroscopic titrations carried out in CH_2Cl_2 at 298 K (424 and 433 nm) yielded a Job plot with a maximum at $x = 0.5$, confirming the 1:1 stoichiometry of complexation in **5**. Analysis of the titration data by non-linear least-squares revealed an empirical association constant of *ca.* 10^8 M^{-1}. This association constant is considerably stronger than that observed for pyridine itself with a zinc porphyrin precursor (10^4 M^{-1}) indicating strong chelation within **5**.

When the dipyridylporphyrin guest was replaced by the tetrapyridylporphyrin **4**,[10] the ^{1}H NMR spectrum at 303 K for a 1:1 mixture of host **2** and guest **4** in $CDCl_3$ revealed sharp

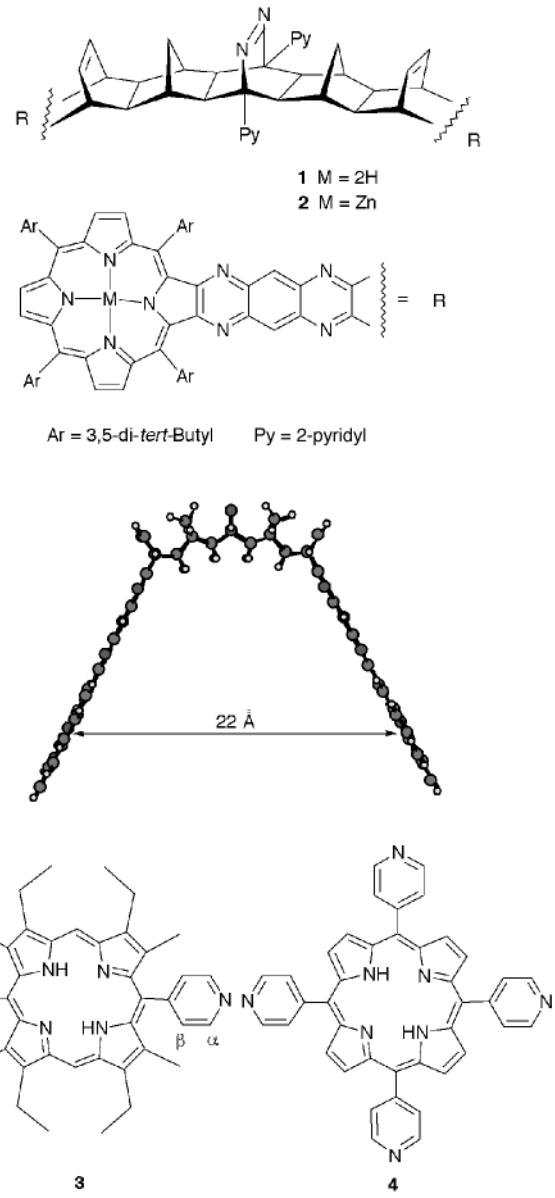

Fig. 1 Molecular modelling of the skeletal backbone of **1** reveals the overall U-type geometry.

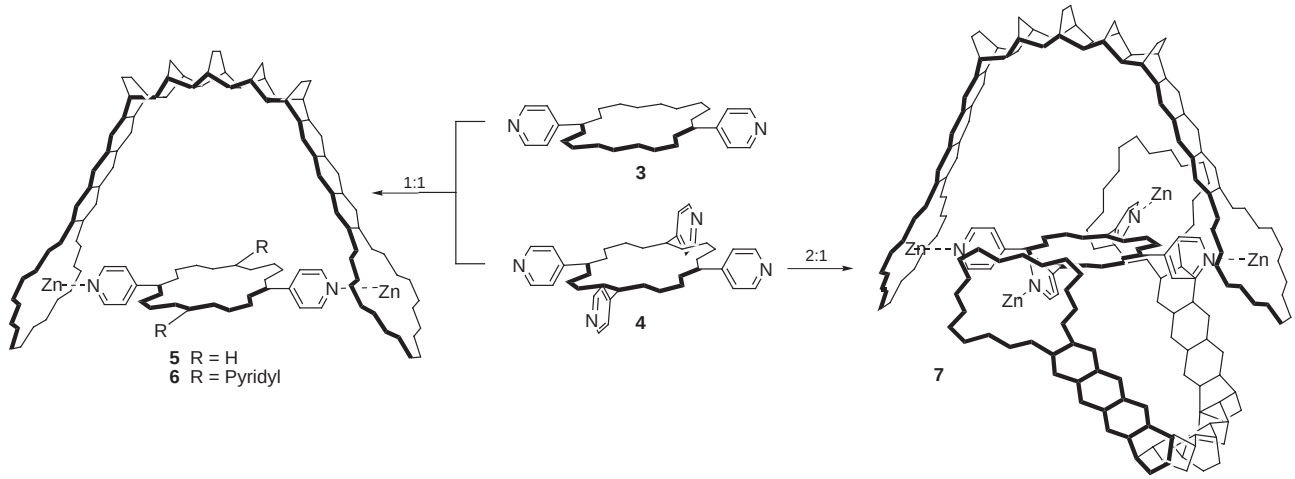

Scheme 1

resonances for **2** and, surprisingly, only a single resonance for **4**, the pyrrole NH (δ −3.77, $\Delta\delta$ −0.89 ppm). The resonances for the protons of the norbornyl backbone of cavity molecule **2** are again only slightly affected by the addition of **4** (*ca*. $\Delta\delta$ 0.04 ppm), but the fact that those on the inside face of the backbone are most affected is consistent with the formation of an internal 1:1 complex. Cooling this solution to 233 K produced a new set of proton resonances where the resonances for α- and β-protons of **4** now reflect their new complexed environment. Two unique sets of resonances for the pyridyl ring protons were observed with the most shielded set occurring at δ 3.19 ($\Delta\delta$ −5.9 ppm) and 6.35 ($\Delta\delta$ −1.8 ppm).

The second set of pyridyl ring protons for **4** in the 1:1 complex **6** are less shielded (*viz*. α $\Delta\delta$ −0.2 ppm, β $\Delta\delta$ −0.49 ppm) from the resonances of uncomplexed **4** and this smaller shift is consistent with the uncoordinated pyridyl groups being in a complexed environment such as **6**. Saturation transfer experiments revealed that the two sets of pyridyl ring proton resonances undergo rapid exchange. The above data support **4** being complexed within the cavity of **2** yet with an uncoordinated environment for the second set of pyridyl rings, as illustrated in Scheme 1. The formation of the 1:1 complex in solution is consistent with electrospray mass spectrometry of the complex, which yielded peaks for **6** (*m/z* 1837 $[M + 2H]^{2+}$).

We were intrigued by the possibility of encapsulating the tetratopic guest **4** within two of the ditopic host units **2**. ^{1}H NMR examination at 303 K of a solution containing a 2:1 ratio of **2** to **4** revealed a similar situation to the 1:1 case, *i.e*. complete absence of any resonances for **4** except for the pyrrole NH resonance (δ −4.05 $\Delta\delta$ −1.17 ppm) and small but significant changes for the resonances of **2** (*ca*. $\Delta\delta$ 0.09 ppm). Cooling the solution to 233 K again yielded new resonances derived from guest **4**, *i.e*. two sets of resonances for the pyridyl protons of **4**, but now both sets of resonances indicate porphyrin coordination ($\Delta\delta$ α −5.76, −6.17 and β −1.67, −2.99 ppm). Furthermore, two resonances were observed for the β-pyrrole resonances of **4** in **7** compared to a single resonance for uncomplexed **4**.

We interpret these data as follows. The two α- and β-pyridyl proton resonances are a result of the assymmetry enforced by the horizontal and rotationally rigid positioning of **4** within **7**. The two β-pyrrole resonances can result from either of two effects, (a) the formation of a distorted complex (Scheme 1) where the complexation of the second equivalent of **2** is forced to adopt an eccentric position owing to the steric interactions between the *tert*-butyl substituents on the porphyrin subunits¶ and where the subunits are reciprocating slowly on the NMR timescale, or (b) the result of slow NH tautomerism in the central free-base porphyrin unit, with fast exchange between the two possible eccentric conformations of **7**.‖ We also note that free-base **2** shows evidence of NH tautomerism at similar low temperatures. In either case, the result is an intriguing arrangement resembling a molecular scale mechanical universal joint.

The concept of organising two host molecules around a central template has been successfully employed by others to create enclosed molecular environments.[5,6] The ability of **2** to act as a host for other porphyrinic guests opens the way for non-covalent positioning of photoactive components and such studies are underway in our laboratories.

Notes and references

† Crossley *et al*. have recently reported the first 2:1 complex involving the self-assembly of rigid bisporphyrins (2 equiv.) using a flexible tetratopic amine (ref. 5).

‡ This complex also bears some resemblance to the topology of the Rebek 'ball-like' molecules, although the latter assemble independently of guest inclusion in contrast to the templated assembly described here (ref. 6).

§ The synthesis of the dipyridylporphyrin rod **3** was achieved by the acid-catalysed condensation of 3,3′-diethyl-4,4′-dimethyldipyrromethane and pyridine-4-carbaldehyde followed by oxidation with chloranil (ref. 9).

¶ Such an off-centre arrangement is also supported by molecular modelling.

‖ We thank the referee for suggesting this alternative. Experiments are currently underway to differentiate between (a) and (b).

1 M. D. Ward, *Chem. Soc. Rev*., 1997, 365.
2 D. B. Amabilino and J. P. Sauvage, *New J. Chem*., 1998, 395 and references cited therein.
3 H. L. Anderson, C. A. Hunter and J. K. M. Sanders, *J. Chem. Soc*., *Chem. Commun*., 1989, 226; H. L. Anderson, S. Anderson and J. K. M. Sanders, *J. Chem. Soc*., *Perkin Trans. 1*, 1995, 2231; H. L. Anderson, *Inorg. Chem*., 1994, **33**, 972; X. Chi, A. J. Guerin, R. A. Haycock, C. A. Hunter and L. D. Sarson, *J. Chem. Soc*., *Chem. Commun*., 1995, 2567; C. A. Hunter, R. K. and Hyde, *Angew. Chem*., *Int. Ed. Engl*., 1996, **35**, 1936; E. Alessio, M. Macchi, S. Heath and L. G. Marzilli, *Chem. Commun*., 1996, 1411.
4 M. R. Wasielewski, *Chem. Rev*. 1992, **92**, 435; V. Balzani and F. Scandola, *Supramolecular Photochemistry*, Ellis Horwood, Avon, 1991; H. Kurreck and M. Huber, *Angew. Chem*., *Int. Ed. Engl*., 1995, **34**, 849.
5 J. N. Reek, A. P. H. L. Schenning, A. W. Bosman, E. W. Meijer and M. J. Crossley, *Chem. Commun*., 1998, 11.
6 J. P. Sauvage, *New J. Chem*., 1985, **9**, 299; C. Valdes, U. P. Spitz, L. M. Toledo, S. W. Kubik and J. Rebek, *J. Am. Chem. Soc*., 1995, **117**, 12733.
7 S. Anderson, H. L. Anderson, A. Bashall, M. McPartlin and J. K. M. Sanders, *Angew. Chem*., *Int. Ed. Engl*., 1995, **34**, 1096.
8 R. N. Warrener, M. R. Johnston and M. J. Gunter, *Synlett*, 1998, 593.
9 H. L. Anderson, C. A. Hunter and J. K. M. Sanders, *J. Chem. Soc*., *Chem. Commun*., 1989, 226; H. L. Anderson, C. A. Hunter, M. N. Meah and J. K. M. Sanders, *J. Am. Chem. Soc*., 1990, **112**, 5780.
10 F. R. Longo, M. G. Finarelli and J. B. Kim, *J. Heterocycl. Chem*., 1969, **6**, 927; A. Adler, F. R. Longo, J. D. Finarelli, J. Goldmacher, J. Assour and L. Korsakoff, *J. Org. Chem*., 1967, **32**, 476.

Communication 8/07339B

ChemComm

A strong-base induced [4+2] cycloaddition of homophthalic anhydrides with enolizable enones: a direct and efficient synthesis of *peri*-hydroxy aromatic compounds

Namakkal G. Ramesh, Kiyosei Iio, Akiko Okajima, Shuji Akai and Yasuyuki Kita*

Graduate School of Pharmaceutical Sciences, Osaka University, 1-6, Yamada-oka, Suita, Osaka 565-0871, Japan. E-mail: kita@phs.osaka-u.ac.jp

Received (in Cambridge, UK) 11th September 1998, Accepted 28th October 1998

A direct and efficient synthesis of *peri*-hydroxy aromatic compounds *via* a strong-base induced [4+2] cycloaddition of homophthalic anhydrides with α-phenylsulfinyl enolizable enones has been accomplished.

In the past two decades, considerable effort has been devoted to the synthesis of biologically important polycyclic *peri*-hydroxy aromatic compounds which include anthracyclines,[1] fredericamycin A,[2] granaticin,[3] bostrycin,[4] olivin[5] and other polycyclic antibiotics. Among the methods known for the construction of the key *peri*-hydroxy aromatic frameworks,[6] the strong-base induced [4+2] cycloaddition reaction of homophthalic anhydrides to dienophiles[7] continues to dominate, due to the generality and efficiency of the reaction as well as ready accessibility of the starting materials. An added advantage is the direct synthesis of *peri*-hydroxy compounds in a single step. The applicability of this methodology has already been realized in the total synthesis of a variety of natural products such as anthracyclines,[1i,8] galtamycinone[9] and dynemicin A.[10] However, all these examples utilize non-enolizable dienophiles such as quinone-type compounds or α,β-unsaturated esters.[7b] On the other hand, the strong-base induced reaction of homophthalic anhydride with enolizable enones such as cyclohex-2-en-1-one or its β-substituted derivatives did not give any of the cycloaddition products[7b] although in some cases the expected product was obtained in low yield.[11] This is probably due to extensive enolization under the basic reaction condition, which might in turn retard the cycloaddition step.

Since the discovery of this reaction by us in 1982,[7a] we have been engaged in developing its variants and utilizing this methodology for the synthesis of natural compounds. We have now extended this reaction to enolizable enones. We reasoned that the aforesaid problem could be readily overcome by the introduction of a suitable functional group at the α-position of the enone moiety which should be electron deficient in order to increase dienophilicity and should also behave as a leaving group, to provide directly the *peri*-hydroxy aromatic compounds.

A number of functional groups such as Br, SPh, S(O)Ph, SO_2Ph were considered and among them, the sulfinyl group, which fulfils the above-mentioned criteria, was found to be the substituent of choice. Here we report an efficient, strong-base induced [4+2] cycloaddition of various homophthalic anhydrides with α-sulfinyl substituted enones providing directly the *peri*-hydroxy aromatic compounds in moderate to good yields.

The homophthalic anhydrides **1a**–**d** were prepared according to the reported method.[7] The strong-base induced reaction of homophthalic anhydride **1a** with 2-phenylsulfinylcyclopent-2-en-1-one **2a** was investigated in detail in order to optimize the reaction conditions. Similar to our earlier work,[7d] we have found that NaH is more suitable than other bases (Bu^{t}OK, LDA *etc*.). As can be seen from Table 1, among the various sets of reaction conditions tried, use of 1.1 equiv. of NaH in refluxing dioxane was adjudged the best, affording after acylation the *peri*-hydroxy compound as its acetate **3a** in good yield. In a typical experiment, to a slurry of NaH in dry dioxane was added a solution of homophtahlic anhydride **1a** in dioxane. The resulting slurry was stirred at room temperature for 30 min and then for 20 min each at 80 °C and 120 °C (bath temperature). Enone **2a** was then added and the reaction mixture was stirred for 20 min., cooled, quenched with aq. NH_4Cl and extracted with EtOAc. The crude reaction mixture, after evaporation of the solvent, was treated with Ac_2O and pyridine and left overnight at room temperature. Column chromatography afforded the *peri*-hydroxy aromatic compound as its acetate **3a**. Subsequently, all the reactions were performed using the same conditions, except for the final reaction time.

This base catalyzed [4+2] cycloaddition reaction was found to be general for a range of substituted homophthalic anhydrides **1a**–**d** as well as with different sulfinyl substituted enones **2a**–**e**, including that having an acetal functional group, affording the respective products in moderate to good yields (Table 2). Noteworthy is the success of the reaction with acyclic enone **2e**, which is a rewarding result given the report that no reaction was observed between homophthalic anhydride and methyl but-2-enoate.[11a] It is highly relevant that the reactions of homophthalic anhydrides **1a** and **1b** with cyclohex-2-en-1-one and cyclopent-2-en-1-one were not successful. The reactions under identical conditions resulted only in complex mixtures and no useful product could be isolated, indicating the possibility of a base-induced enolization in these cases. Thus, it is clearly evident that the sulfinyl group present at the α-position of the enone moiety plays an important role in directing the course of the reaction. Furthermore, the highlight of the reaction is the rapid *syn*-elimination of the phenylsulfinyl moiety under the reaction conditions, a unique characteristic of this functional group,[7d] providing directly the *peri*-hydroxy aromatic compounds in a single step. The advantages of the sulfinyl group are emphasized by the fact that the strong-base induced reaction of homophthalic anhydride with 2-bromocyclohex-2-en-1-one was not successful. Reaction of **1a** with 2-bromocyclohex-2-en-1-one, under identical conditions for 7 h, afforded after acylation acetate **3e** in only 7% yield with the recovery of a large amount of unreacted bromocyclohexenone. Use of an additional equivalent of base (2.2 equiv.) in order to bring about the *trans*-elimination of HBr from a possible non-aromatized cycloadduct, did not lead to any significant improvement in the yield. The reaction afforded, after 3 h, the acetate **3e** in only 10% yield.

Table 1 Reaction of homophthalic anhydride **1a** with the enone **2a** in the presence of NaH under various conditions

Entry	Solvent	*T*/°C	Time	Yield of **3a**[a] (%)
1	THF	room temp.	25 h	20
2	THF	reflux	15 min	41
3	1,2-diethoxyethane	reflux	20 min	45
4	1,4-dioxane	reflux	20 min	62

[a] Isolated yields after column chromatography

Table 2 NaH induced [4+2] cycloaddition reaction of various homophthalic anhydrides **1** with different sulfinyl substituted enones **2** in refluxing dioxane

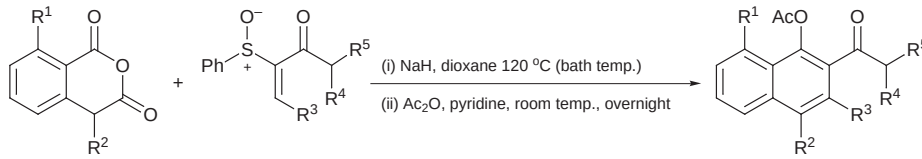

1a–d **2a–e** **3a–n**

	Homophthalic anhydride			Dienophile					Product	
Entry	**1**	R^1	R^2	**2**	R^3	R^4	R^5	*t*/min	**3**	Yield (%)[a]
1	**1a**	H	H	**2a**		$-CH_2-$	H	20	**3a**	62
2	**1b**	H	SPh	**2a**		$-CH_2-$	H	20	**3b**	58
3	**1c**	H	OMe	**2a**		$-CH_2-$	H	20	**3c**	59
4	**1d**	OBn	H	**2a**		$-CH_2-$	H	20	**3d**	56
5	**1a**	H	H	**2b**		$-(CH_2)_2-$	H	20	**3e**	70
6	**1b**	H	SPh	**2b**		$-(CH_2)_2-$	H	20	**3f**	58
7	**1c**	H	OMe	**2b**		$-(CH_2)_2-$	H	20	**3g**	62
8	**1a**	H	H	**2c**		$-(CH_2)_3-$	H	20	**3h**	60
9	**1b**	H	SPh	**2c**		$-(CH_2)_3-$	H	20	**3i**	52
10	**1a**	H	H	**2d**		$-(CH_2)_2-$	$(CH_2)_2X$[b]	20	**3j**	63
11	**1b**	H	SPh	**2d**		$-(CH_2)_2-$	$(CH_2)_2X$[b]	20	**3k**	57
12	**1a**	H	H	**2e**[c]	Ph	H	H	90	**3l**	49
13	**1b**	H	SPh	**2e**[c]	Ph	H	H	180	**3m**	48
14	**1c**	H	OMe	**2e**[c]	Ph	H	H	210	**3n**	41

[a] Isolated yields after column chromatography. [b] X = 1,3-dioxan-2-yl. [c] *E*:*Z* = *ca.* 6:1 mixture.

The generality and efficiency of the reaction, ready availability of the starting materials coupled with the unique activating as well as leaving ability of the sulfinyl group renders this method an attractive one for the synthesis of *peri*-hydroxy aromatic compounds using enolizable enones. The application of this methodology for the synthesis of natural products is in progress and will be reported in a forthcoming paper.

This work was supported by a Grant-in-Aid for Scientific Research from the Ministry of Education, Science and Culture, Japan (08245101) and Special Coordination funds of the Science and Technology Agency of Japanese Govrnment. We are grateful to the Japan Society for the Promotion of Science for a postdoctoral fellowship to N. G. R.

Notes and references

1 (*a*) R. H. Thompson, *Naturally Occurring Quinones*, Academic Press, New York, 1971; (*b*) F. Arcamone, *Topics in Antibiotics Chemistry*, ed. P. G. Sammes, Halstead Press, New York, 1978, vol.2; (*c*) S. T. Crooke and S. D. Reich, *Anthracyclines*: *Current Status and New Developments*, Academic Press, New York, 1980; (*d*) F. Arcamone, *Med. Res. Rev*., 1984, **4**, 153; (*e*) P. T. Gallagher, *Contemp. Org. Synth*., 1996, **3**, 433; (*f*) S. Terashima, *J. Synth. Org. Chem. Jpn*., 1982, **40**, 20; (*g*) M. J. Broadhurst, C. H. Hassall and G. J. Thomas, *Chem. Ind*. (*London*), 1985, 106; (*h*) K. Krohn, *Angew. Chem., Int. Ed. Engl*., 1986, **25**, 790; (*i*) Y. Tamura and Y. Kita, *J. Synth. Org. Chem. Jpn*., 1988, **46**, 205; (*j*) K. Krohn, *Tetrahedron*, 1990, **46**, 291.

2 D. L. Boger, O. Hüter, K. Mbiya and M. Zhang, *J. Am. Chem. Soc*., 1995, **117**, 11839 and references cited therein.

3 K. Nomura, K. Okazaki, K. Hori and E. Yoshii, *J. Am. Chem. Soc*., 1987, **109**, 3402.

4 D. S. Larsen and R. J. Stoodley, *Tetrahedron*, 1990, **46**, 4711 and references cited therein.

5 W. R. Rousch, M. R. Michaelides, D. F. Tai, B. M. Lesur, W. K. M. Chong and D. J. Harris, *J. Am. Chem. Soc*., 1989, **111**, 2984 and references cited therein.

6 N. J. Broom and P. G. Sammes, *J. Chem. Soc., Chem. Commun*., 1978, 162; G. A. Kraus and H. Sugimoto, *Tetrahedron Lett*., 1978, 2263; F. M. Hauser and R. P. Rhee, *J. Org. Chem*., 1979, **101**, 178; J. H. Dodd and S. M. Weinreb, *Tetrahedron Lett*., 1979, 3593; J.-P. Gesson, J.-C. Jacquesy and B. Renoux, *Tetrahedron*, 1984, **40**, 4743; G. A. Kraus and B. S. Fulton, *Tetrahedron*, 1984, **40**, 4777; K. A. Parker and E. L. Tallman, *Tetrahedron*, 1984, **40**, 4781; D. L. Boger and I. C. Jacobson, *J. Org. Chem*., 1991, **56**, 2115.

7 (*a*) Y. Tamura, A. Wada, M. Sasho, K. Fukunaga, H. Maeda and Y. Kita, *J. Org. Chem*., 1982, **47**, 4376; (*b*)Y. Tamura, M. Sasho, K. Nakagawa, T. Tsugoshi and Y. Kita, *J. Org. Chem*., 1984, **49**, 473; (*c*) Y. Tamura, M. Sasho, S. Akai, H. Kishimoto, J. Sekihachi and Y. Kita, *Chem. Pharm. Bull*., 1987, **35**, 1405; (*d*)Y. Kita, K. Iio, A. Okajima, Y. Takeda, K. Kawaguchi, B. A. Whelan and S. Akai, *Synlett*, 1998, 292 and references cited therein.

8 F. Matsuda, M. Kawasaki, M. Ohsaki, K. Yamada and S. Terashima *Tetrahedron*, 1988, **44**, 5745; J.-F. Lavallee, R. Rej, M. Courchesne, D. Nguyen and G. Attardo, *Tetrahedron Lett*., 1993, **34**, 3519; M. Kirihara and Y. Kita, *Heterocycles*, 1997, **46**, 705.

9 T. Matsumoto, H. Yamaguchi and K. Suzuki, *Synlett*, 1996, 433.

10 M. D. Shair, T. Y. Yoon, K. K. Mosny, T. C. Chou and S. J. Danishefsky, *J. Am. Chem. Soc*., 1996, **118**, 9509.

11 (*a*) Y. S. Rho, S. H. Park, Y. J. Kwon, J. H. Yoo and I. H. Cho, *Bull. Korean Chem. Soc*., 1996, **17**, 944; (*b*) D. Mal, N. K. Hazra, K. V. S. N. Murthy and G. Majumdar, *Synlett*, 1995, 1239; (*c*) A. P. Marchand, P. Annapurna, W. H. Watson and A. Nagl, *J. Chem. Soc., Chem. Commun*., 1989, 281.

Communication 8/07095D

ChemComm

Synthesis of extended α,α′-oligo(silylthiophenes) by cerium(IV) oxidative coupling reactions

Ali H. Mustafa and Michael K. Shepherd*

School of Biological and Applied Sciences, University of North London, UK N7 8DB. E-mail: m.shepherd@unl.ac.uk

Received (in Liverpool, UK) 21st August 1998, Accepted 9th November 1998

Cerium(IV) oxidative dimerisations of 4,4′-bis(trimethylsilyl)-2,2′:5′,2″-terthiophene and the quaterthienyl analogue 1c gave the corresponding sexi- and octi-thiophenes; the latter have been used to prepare α-linked hexadecithiophene and tetracosithiophene derivatives.

The extreme insolubility of extended oligothiophenes renders purification and spectral analysis increasingly difficult for unsubstituted systems containing more than six α-linked thiophene units. Only two literature citations can be found for oligomers beyond octithiophene, namely decithiophene, obtained by electrochemical oxidation of quinquithiophene and characterised by absorption spectra in the solid state,[1] and dodecithiophene, identified as an impurity in crude samples of octithiophene by mass spectroscopy.[2] Oligo(alkylthiophenes) bearing long-chain β-substituents are much more soluble, and derivatives containing up to sixteen rings have been characterised.[3–5] The longest of these, an octadodecylhexadecithiophene, was obtained in 19% yield after coupling of the corresponding lithiooctithiophene with $CuCl_2$.[5] We reasoned that silylated oligomers should be soluble enough to aid purification and, *via* electrophilic displacement of silicon, subsequently afford straightforward access to the unsubstituted analogues and other derivatives required for physical studies. We describe here our results to date, culminating in the isolation of the twentyfour-ring dodecakis(trimethylsilyl)tetracosithiophene **4d**, the longest oligomer yet reported.

We obtained β,β-disilylated thiophenes **1b–e**† by the $NiCl_2$(dppp)-catalysed couplings[6] of 2 equiv. of the Grignard reagent prepared from 2-bromo-4-trimethylsilylthiophene‡ with 2,5-dibromothiophene, 5,5′-dibromo-2,2′-bithiophene, 5,5′-dibromo-2,2′:5′,2″-terthiophene and 5,5‴-dibromo-2,2′:5′,2″:5″,2‴-quaterthiophene,‡ respectively. The yields increase on moving from **1b** to the quinquithienyl **1d**, but the very low solubility of both the sexithienyl **1e** and the dibromoquaterthienyl precursor rendered this route impractical for the preparation of oligomers containing more than five rings.

To circumvent this problem we turned our attention to coupling the readily-soluble quaterthienyl **1c**. We were encouraged by the observation that aged thin-layer chromatograms of **1c** showed progressive formation of a lower R_f component on re-elution. This was attributed (and subsequently confirmed by comparison with pure samples) to photo-oxidation of **1c** to the dimer **4a** on the silica surface. A reaction of **1c** with ceric ammonium nitrate gave moderate yields (*ca.* 15%) of **4a**, the major product being 3,4‴-bis(trimethylsilyl)-5-nitro-2,2′:5′,2″:5″,2‴-quaterthiophene (43%). When using ceric ammonium sulfate as the oxidising agent the octithiophene **4a** was isolated in up to 66% yield,§ with varying amounts of the dodecithiophene **4b** (4–7%) and hexadecithiophene **4c** (0.5–2%) as byproducts (Scheme 1). The high yield of dimer obtained under these conditions is surprising, bearing in mind that oxidation potentials for these systems should be inversely related to the size of the oligomer.[6,7] Cerium(IV) sulfate oxidations were more rapid, but the relative proportions of **4b**,**c** and other higher molecular weight products increased with respect to **4a**. The oligomers **4a–c** are bright yellow crystalline solids which exhibit intense greenish fluorescence in dilute solution. The UV–VIS absorption spectra show only a small bathochromic shift on moving from **1c** (λ_{max} 389 nm) to **4c** (λ_{max} 419 nm), in contrast to the n-dodecyl derivatives,[5] which move from yellow (λ_{max} 379 nm) to violet (λ_{max} 464 nm) along the same sequence. In our series, the closer proximity of the bulky silyl substituents to the point of coupling presumably leads to a higher degree of twisting about every fourth α,α′-linkage, reducing through-conjugation. This may be fortuitous—levelling the oxidation potentials of these systems and hence suppressing their tendency to polymerise.

Coupling of the terthiophene **1b** under conditions as described above gave the sexithiophene **3a** (48% yield) and the nonithiophene **3b** (11%) as major products,¶ along with higher oligomers. This reaction proved more sluggish than that above, probably as a consequence of the higher energy of the terthienyl cation radical intermediate. A reaction of 4-trimethylsilyl-2,2′:5′,2″-terthiophene resulted in coupling in even lower yield

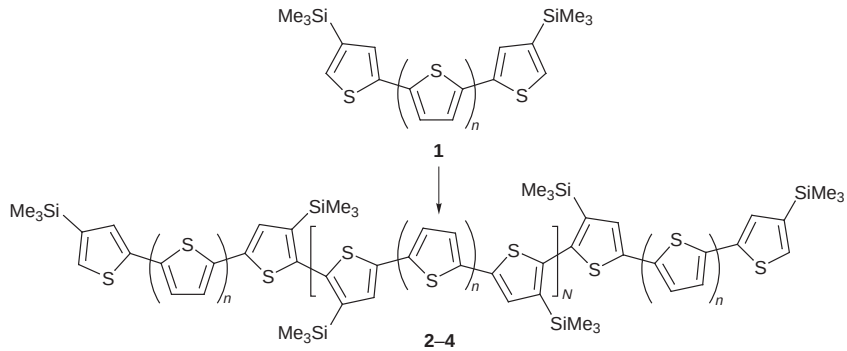

1a *n* = 0
b *n* = 1 (42%)
c *n* = 2 (83%)
d *n* = 3 (94%)
e *n* = 4 (8%)

2 *n* = 0, *N* = 0
3a *n* = 1, *N* = 0
b *n* = 1, *N* = 1

4a *n* = 2, *N* = 0
b *n* = 2, *N* = 1
c *n* = 2, *N* = 2
d *n* = 2, *N* = 4
e *n* = 2, *N* = 6

Scheme 1

(8%), between the two α-positions adjacent to the β-silyl group; the sexithiophene **1e** and its 4,3‴-disilyl isomer were not detected. These observations are in line with a recent study on the stabilising effect of progressive β-methylation on cation radicals derived from 5,5′-dimethyl-2,2′-bithiophene.[8] Attempts to dimerise 4,4′-bis(trimethylsilyl)-2,2′-bithiophene **1a** to **2** in like manner resulted in quantitative recovery of the starting material.

The octithiophene **4a** oligomerised on reaction with cerium(IV) sulfate in 1,2-dichloroethane at room temperature to give the sexadecithiophene **4c** (35% yield), the tetracosithiophene **4d** (11%), and a mixture of higher oligomers (*ca*. 20%) after column chromatography on silica. The dotriacontithiophene **4e** appears to be the major constituent of the residue, corroborated by TLC studies of dimerisation attempts using **4c**, but we have not yet been able to isolate pure samples. The relative insolubility of the higher oligomers of **4** has prevented preparative separation by chromatography, while the more soluble analogues **3** are not satisfactorily resolved beyond **3b**. We anticipate that replacement of either or both trimethylsilyl substituents in **1c** by more lipophilic alkylsilyl groups should circumvent this problem and ultimately, *via* protodesilylation, enable preparation of the parent systems. Preliminary studies indicate that compounds **3a** and **4a** give quantitative yields of analytically pure sexithiophene and octithiophene respectively, on treatment with TFA in CH_2Cl_2.

Notes and references

† New compounds have been characterised by spectroscopic and microanalytical data.

‡ Prepared by bromination of the appropriate disilyl derivative: NBS, aq. THF, 0 °C.

§ Preparation of **4a**: Finely ground cerium ammonium sulfate (10.5 g) was added in portions over *ca*. 6 h to a stirred solution of **1c** (3.0 g) in C_6H_6 (40 cm^3). The resulting suspension was stirred at room temperature for *ca*. 30 h, the solvent removed under reduced pressure, and the solid residue extracted with pentane (100 cm^3). The extract was chromatographed directly on silica (the column should be shielded from light) eluting with pentane to give unreacted **1c** (0.72 g). Further eulution with 4% CH_2Cl_2 in pentane gave **4a** (1.87 g, 62%, 82% based on consumed **1c**), bright yellow crystals, mp 147–149 °C (Found: C, 55.9; H, 5.3. $C_{44}H_{50}S_8Si_4$ requires C, 55.8; H, 5.3%); δ_H(250 MHz, $CDCl_3$) 7.29 (2 H, d, α-H, A,H-rings), 7.20 (2 H, d, β-H, A,H-rings), 7.13 (2 H, s, D,E-rings), 7.08 (8 H, m, B,C,F,G-rings), 0.29 (18 H, s, $SiMe_3$, A,H-rings), 0.17 (18 H, s, $SiMe_3$, D,E-rings); δ_C 130.8, 129.3, 128.3, 124.7, 124.6, 124.3, 124.2 (C-H), 143.7, 143.2, 140.6, 137.9, 137.8, 136.4, 136.1, 135.8, 135.6 (quaternary carbons), 0.6, −0.7 (CH_3); *m/z* (LSI) 947 $(M + 1)^+$ (100%). Further gradient elution up to 25% CH_2Cl_2 in pentane gave **4b** (125 mg, 4%), followed by **4c** (14 mg, 0.5%) and a mixture of higher oligomers (15 mg).

¶ The yields for coupling reactions of **1b** and **4a** have not been optimised, and do not take into account recovery of the precursors.

1 Z. Xu, D. Fichou, G. Horowitz and F. Garnier, *J. Electroanal. Chem. Intrafacial Electrochem*., 1989, **267**, 339.
2 D. Fichou, M. Teulade-Fichou, G. Horowitz and F. Demanze, *Adv. Mater*., 1997, **9**, 75.
3 W. ten Hoeve, H. Wynberg, E. E. Havinga and E. W. Meijer, *J. Am. Chem. Soc*., 1991, **113**, 5887.
4 M. Sato and M. Hiroi, *Chem. Lett*., 1994, 985.
5 P. Bäuerle, T. Fischer, B. Bidlingmeir, A. Stabel and J. P. Rabe, *Angew. Chem., Int. Ed. Engl*., 1995, **34**, 303.
6 D. D. Cunningham, L. Laguren-Davidson, H. B. Mark, C. Van Pham and H. Zimmer, *J. Chem. Soc., Chem. Commun*., 1987, 1021.
7 P. Bäuerle, U. Segelbacher, A. Maier and M. Mehring, *J. Am. Chem. Soc*., 1993, **115**, 10217.
8 G. Engelmann, G. Kossmehl, J. Heinze, P. Tschuncky, W. Jugelt and H-P. Welzel, *J. Chem. Soc., Perkin Trans. 2*, 1998, 169.

Communication 8/06600K

Reductive intramolecular cyclization of α-bromo silyl ethers mediated by samarium diiodide

H. S. Park, I. S. Lee, D. W. Kwon and Y. H. Kim*

Department of Chemistry, Korea Advanced Institute of Science and Technology, Taejon 305 - 701 Korea. E-mail:kimyh@sorak.kaist.ac.kr

Received (in Cambridge, UK) 5th October 1998, Accepted 12th November 1998

A new SmI_2-promoted intramolecular reductive cyclization of β-(α-bromo siloxy) carbonyl compounds is reported.

In the last decade, SmI_2 has become one of the most developed reagents in organic synthesis due to the oxophilicity of samarium metal and its powerful one election donor reactivity with various functional groups.[1] Reductions, reductive cyclizations or coupling reactions using SmI_2 have been intensively studied. In particular, intramolecular reductive cyclizations have brought noticeable results in the formation of highly functionalized carbocycles[1,2] and heterocycles.[1,3] Barbier type reactions,[1c,4] Reformatsky type reactions,[1c,5] pinacolic coupling reactions[1c,6] and ketone-olefin coupling reactions[1b,c,7] have been investigated for intramolecular reductive cyclization. Aryl radical cyclization,[8] halide induced cyclization,[1b,c,9] and sequence cyclization[1a,10] have also been reported. Of these reactions, Barbier type reactions give excellent results for cyclization with high stereoselectivity.[1c]

Intramolecular cyclizations of β-(α-bromo siloxy) alkenes or alkynes or vinyl bromo siloxy derivatives *via* a free radical process by treatment with Bu_3SnH gave various useful cyclic silyl ethers[11] with high degrees of regio-, chemo- and stereoselectivity; the reaction products are potentially useful intermediates which can be converted to triols by Tamao oxidation.[12]

Although many attempts have been made to construct functionalized carbocycles or heterocycles by ring closure of a ketyl radical or anion with a ketene or alkyne, there is no reported example of radical or anion cyclization of β-(α-bromo siloxy) carbonyl derivatives mediated by SmI_2. Matsuda and co-workers examined cyclization of β-(α-bromo siloxy) carbonyl derivatives in sugar moieties, and demonstrated that no cyclization occurred.[13]

We were intrigued by the possibility of another Barbier type reaction, this time with β-(α-bromo siloxy) carbonyl substrates using SmI_2. The β-(α- bromo siloxy) carbonyl substrates were prepared *via* two steps as shown in Scheme 1. The ketones were condensed with aldehydes or ketones under typical aldol conditions.[14] For the preparation of α-substituted aldol products, Bu^n_2BOTf was used and the *erythro* product was obtained as the major product. The resulting β-hydroxy ketone was treated with bromomethyl(dimethyl)chlorosilane in the presence of pyridine at 0 °C to provide the desired product **1** in excellent yields as shown in Scheme 1. Their structures were identified by ^1H and ^{13}C NMR and mass spectroscopy.

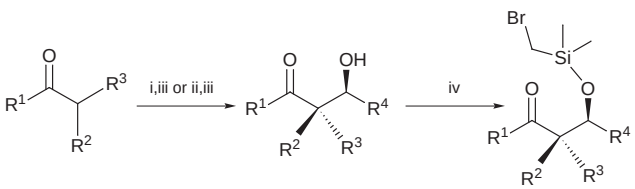

Scheme 1 *Reagents and conditions*: i, LDA, THF, −78 °C; ii, Bu^n_2BOTf, Pr^i_2NEt, THF, −78 °C; iii, R^4CHO, −78 °C; iv, $ClMe_2SiCH_2Br$, pyridine, CH_2Cl_2, 0 °C.

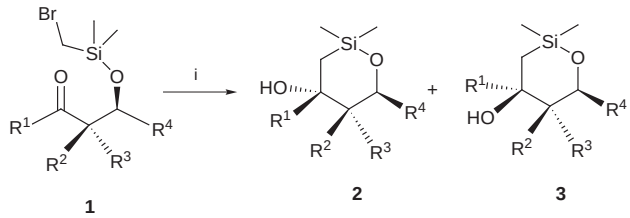

Scheme 2 *Reagents and conditions*: i, SmI_2 (2 equiv.), HMPA (4 equiv.), THF, −78 °C.

Here we describe a new intramolecular reductive cyclizations of β-(α-bromo siloxy) carbonyl compounds **1** with SmI_2 in the presence of HMPA to **2**, as shown in Scheme 2.

In order to generalize the cyclization of β-(α-bromo siloxy) carbonyl substrates, both acyclic (**1a–j**) and cyclic substrates (**1k–n**) were subjected to the cyclizations under the optimized reaction conditions [SmI_2 (2.2 equiv.), HMPA (4 equiv.), THF, −78 °C]. The results obtained are summarized in Table 1.

Formation of two stereoisomers is possible; one is the *syn* isomer, which has the R^3 and OH groups pointing in the same direction, and the other is *anti* isomer, which has the R^3 and OH groups pointing in opposite directions. As a result the *syn* isomer **2** was obtained together with trace amount of the *anti* isomer **3**. The configuration of **2** (**2f**) was identified by ^1H and ^{13}C NMR and NOE experiments (Fig. 1) and mass spectroscopy. The *syn* isomer conformation obtained could be explained by steric hindrance in the transition state. In the four possible transition states, conformation **A** seems to be the most favorable due to steric effects, as suggested by Molander.[9]

In the absence of HMPA, the yield of **2** is low and desilylated aldol products were obtained as the major product. *Erythro* or *threo* cyclohexanone substrates gave the corresponding *erythro* or *threo* products respectively in good yields. The substrate **1d** gave the desired cyclized product **2d** (44%) together with olefin

Table 1 Cyclization of siloxy derivatives using SmI_2[a]

Substrate	R^2	R^1	R^3	R^4	*t*/min	Ratio **2**:**3**	Yield (%)[b]
1a	H	Ph	H	Et	10	> 99:1	61
1b	H	Ph	H	Pr	15	> 99:1	75
1c	H	Me	H	Pr	30	> 99:1	72
1d	H	Pr^i	H	Pr	30	> 99:1	44[c]
1e	H	Me	H	c-Hex	30	> 99:1	57
1f	Me	Et	H	Ph	30	95:5	65 (15)[d]
1g	Me	Et	K	Pr	30	90:10	67
1h	Me	Et	H	Bu^t	30	95:5	62
1i	Me	Ph	H	H	15	92:8	71
1j	Me	Ph	H	Ph	10	95:5	35
1k	$-(CH_2)_4-$		H	Ph	10	> 99:1	74
1l	H		$-(CH_2)_4-$	Ph	10	> 99:1	69
1m	$-(CH_2)_3-$		H	Ph	10	> 99:1	80
1n	$-(CH_2)_3-$		H	Et	30	> 99:1	63

[a] All reactions were carried out using SmI_2 (2.2 equiv.) in THF and HMPA (4 equiv.) at −78 °C. [b] Isolated yields. [c] Eliminated olefin was obtained in *ca.* 20% yield. [d] The reaction was carried out in the absence of HMPA.

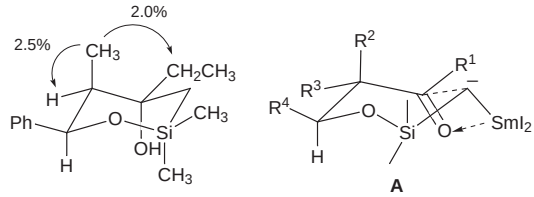

Fig. **1** NOE correlations of β-hydroxy cyclic silyl ether.

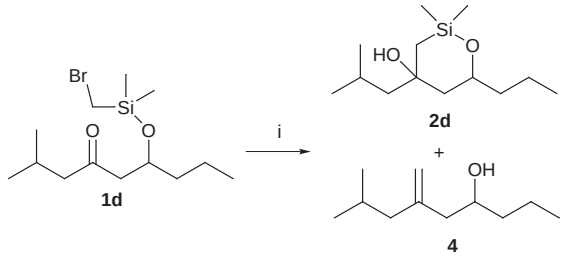

Scheme 3 *Reagents and conditions*: i, SmI_2 (2.2 equiv.), HMPA (4 equiv.), THF, −78 °C.

4 (20%) which is formed by elimination of the siloxy moiety as shown in Scheme 3.

In the reaction mechanism, there are two possible process; a radical–radical coupling process and a samarium Grignard-type anion process (Scheme 4). In the radical–radical coupling reaction, 2 equiv. of SmI_2 generates both a ketyl radical and an alkyl radical which couple each other. On the other hand, the organosamarium Grignard-type species, which could be generated from an alkyl radical by one more electron transfer from SmI_2, could add to the carbonyl group. Since the reactivity of primary alkyl bromides with SmI_2 is higher than that of carbonyl groups, it can be considered that the organosamarium Grignard-type process is more favorable.

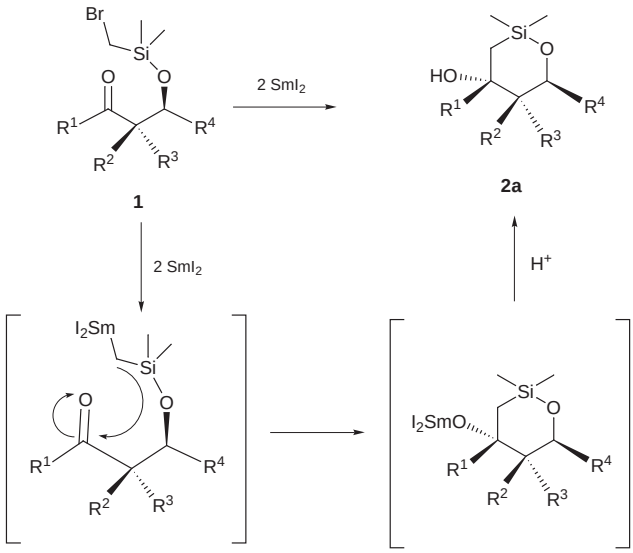

Scheme 4

The α-effect of the silicon moiety may also help to promote the organosamarium pathway. Most of the reactions gave the reduced aldol products in *ca*. 20% yield as a side product. Formation of the aldol side product also supports the organosamarium pathway. If the reaction occurs *via* a diradical pathway, the carbonyl moiety might be reduced to a β-OH moiety. However, only the desilylated aldol products (up to 20%) were obtained and confirmed.

The authors acknowledge the financial support of the Korea Research Foundation.

Notes and references

1 (*a*) G. A. Molander and C. R. Harris, *Tetrahedron*, 1998, **55**, 3321; (*b*) G. A. Molander and C. R. Harris, *Chem. Rev*., 1996, **96**, 307; (*c*) G. A. Molander, *Chem. Rev*., 1992, **92**, 29; B. M. Trost, *Comprehensive of Organic Synthesis*, 1991, vol. 1, p. 235; (*d*) J. A. Soderquist, *Aldrichchim. Acta*., 1991, **24**, 15; (*e*) H. B. Kagan and J. L. Namy, *Tetrahedron*, 1986, **42**, 6573.

2 G. A. Molander and C. R. Harris, *J. Org. Chem*., 1997, **62**, 2944; G. A. Molander and C. del Pozo, *J. Org. Chem*.,1997, **62**, 2935; G. A. Molander and C. R. Harris, *J. Org. Chem*., 1997, **62**, 7418; C. F. Sturino and A. G. Fallis, *J. Am. Chem. Soc*., 1995, **116**, 7447; Z. Zhou and S. M. Bennett, *Tetrahedron Lett*., 1997, 1153.

3 D. C. Ha, C. S. Yun and E. Yu, *Tetrahedron Lett*., 1996, **37**, 2577; J. E. Baldwin and M. G. Moloney, *Tetrahedron*, 1994, **50**, 9411; J. M. Aurreoechea and M. S. Spizua, *Heterocycles*, 1994, **37**, 223; S. I. Fukuzawa and T. Tsuchimoto, *Synlett*, 1993, 803.

4 G. A. Molander and C. R. Harris, *J. Am. Chem. Soc*., 1997, **117**, 3705; G. A. Molander and J. A. Mckie, *J. Org. Chem*., 1991, **56**, 4112.

5 G. A. Molander, J. B. Etter and L. S. Harry, *J. Am. Chem. Soc*., 1991, **113**, 8036.

6 M. Carpiatero, A. F. Mayorals and C. Jaramillo, *J. Org. Chem*., 1997, **62**, 1916; T. Wirth, *Angew. Chem., Int. Ed. Engl*., 1996, **35**, 61; J. L. Chiara, W. Cabri and S. Hanessian, *Tetrahedron Lett*., 1991, **32**, 1125.

7 G. A. Molander and C. L. Pozo Losada, *J. Org. Chem*., 1997, **62**, 2935; M. K. Schwarbe and R. P. Little, *Synth. Commun*., 1997, **27**, 837; G. A. Molander and S. R. Shakya, *J. Org. Chem*., 1996, **61**, 5885; T. K. Sarkar and S. K. Nancy, *Tetrahedron Lett*., 1996, **37**, 5195.

8 J. M. Arrecoechea, A. Arricta and F. P. Cossio, *J. Org. Chem*., 1997, **62**, 1125; M. Murakami, M. Hayashi, Y. Ito, F. Pallemer, J. Collin and H. B. Kagan, *Appl. Organomet. Chem*., 1995, **9**, 385; D. P. Curran and M. J. Totleben, *J. Am. Chem. Soc*., 1992, **114**, 6050; D. P. Curran and P. Wipf, *J. Org. Chem*., 1992, **57**, 1740.

9 Z. Zhou, D. Larouche and S. M. Bemelt, *Tetrahedron*, 1995, **51**, 11623; C. F. Stariro and A. G. Fallis, *J. Am. Chem. Soc*., 1994, **116**, 7447; G. A. Molander and J. A. Mckie, *J. Org. Chem*., 1993, **58**, 7126.

10 T. Skrydstrup, *Angew. Chem., Int. Ed. Engl*., 1997, **36**, 345.

11 S. Bogen, M. Journet, and M. Malacria, *Synth. Commun*., 1994, **24**, 1215; M. Journet, W. Smadja and M. Malacria, *Synlett*, 1991, 320; M. Koreeda and L. G. Hanmann, *J. Am. Chem. Soc*., 1990, **112**, 8175; K. Tamao, K. Maeda, T. Yamaguchi and Y. Ito, *J. Am. Chem. Soc*., 1989, **111**, 4984.

12 K. Tamao, N. Ishida, T. Tanaka and M. Kumada, *Organometallics*, 1983, **2**, 1694. The product **1l** was smoothly converted into the triols in 70% yield *via* Tamao oxidation. The structure was determined by ^{1}H NMR and EI mass spectroscopy (*m/z* 236, 85%).

13 S. Ichikawa, S. Shuto, N. Minakawa and A. Matsuda, *J. Org. Chem*., 1997, **62**, 1368.

14 D. A. Evans, E. Vogel and J. V. Nelson, *J. Am. Chem. Soc*., 1979, **101**, 6120.

Communication 8/07736C

Synthesis and characterization of a novel bipolar polymer for light-emitting diodes

Yunqi Liu, Hong Ma and Alex K-Y. Jen*

Department of Chemistry, Northeastern University, 360 Huntington Avenue, Boston, Massachusetts 02115, USA. E-mail: ajen@lynx.neu.edu

Received (in Cambridge, UK) 14th October 1998, Accepted 10th October 1998

A novel bipolar light-emitting polymer containing both efficient hole and electron injecting/transporting segments exhibiting high thermal stability (T_d = 445 °C), good electrochemical reversibility, excellent thin film-forming and light-emitting properties (bright yellow emission, a rectification ratio greater than 10^5 and a low turn-on voltage of 3.7 V) is reported.

For most of the conjugated polymers that are reported in the literature, the hole injection/transport is more favorable than the electron injection/transport due to the electron-richness of the π-conjugated systems. To facilitate the electron injection, metals with low work functions, such as calcium and magnesium, have been used as cathodes. However, the stability of the resulting devices is severely compensated for by the sensitivity of these metals to both oxygen and moisture. To circumvent these problems, several approaches have been utilized, such as synthesizing highly electron-affinitive polymers,[1] inserting an additional electron injecting/transporting layer between the emitter and the cathode[2] and blending small molecules into the polymer matrix.[3] Although some success has been achieved, several deficiencies are associated with these methods. For example, more tedious and complex multilayer structures were needed to offset the poor hole injection of the highly electron-affinitive polymers for achieving high device efficiency. In addition, phase separation often occurs when the dopant concentration is high. Recently, Bao *et al*.[4] reported the results of light-emitting polymers containing both electron and hole transporting moieties that achieved efficient device performance. Thus, it is desirable to design and synthesize a bipolar polymer that possesses both a hole injecting/transporting segment and an electron-affinitive segment in order to enhance the charge injecting/transporting ability. Polyquinolines (PQs) are a class of heteroaromatic polymers that possess excellent thermal stability, good thin film processibility, high electron affinity and unique nonlinear optical properties.[5,6] A blue electroluminescent (EL) device using a fluorinated polyquinoline (PQ-100) as the emitting layer has been reported that possessed a very high turn-on voltage (50 V) due to difficulties achieving efficient/balanced charge injection.[7] On the other hand, tetraphenyldiaminobiphenyl (TPD) has been widely used as an excellent hole-transport material in fabricating small molecule EL devices.[8] In the hope of combining both the blue light-emitting and good electron-affinitive properties of the bisquinoline and the efficient hole-injecting/transporting properties of the TPD into a single bipolar material to enhance the overall performance of an EL device, we have copolymerized these two functional moieties *via* a nucleophilic replacement reaction/polycondensation. Here we report the excellent thermal, electrochemical and EL results obtained from this polymer.

The synthesis of the copolymer (TPD-PQE) is outlined in Scheme 1. Compound **1** was synthesized (80% yield) from 4,4′-diamino-3,3′-dibenzoyldiphenyl ether and 4-fluoroacetophenone.[9] Compound **2** was synthesized (50% yield) from the modified Buchwald coupling reaction[10,11] between 4-anisidine and 4,4′-dibromobiphenyl in the presence of tris(dibenzylideneacetone)dipalladium [$Pd_2(dba)_3$], 1,1′-bis(diphenylphosphino)ferrocene (dppf) and NaOBu^t, followed by the addition of 1-bromo-4-butylbenzene and additional NaOBu^t. Compound **3** was obtained (72% yield) from **2** by a demethylation reaction.[12] Polymerization between **1** and **3** was carried out in the presence of K_2CO_3 in a NMP–toluene solvent mixture.[13] The resulting viscous polymer solution was precipitated into MeOH, followed by Soxhlet extraction with MeOH to afford polymer **4** (78% yield). The chemical structures of monomers and polymer were confirmed by ^{1}H NMR and elemental analyses.

TPD-PQE was a pale-grey fibrous solid. As a result of the two n-butyl groups attached on the TPD moiety, the TPD-PQE was readily soluble in common organic solvents, such as $CHCl_3$, THF and cyclopentanone. The weight average molecular weight (M_w = 58400 with a polydispersity index of 5.76) was determined by gel permeation chromatography using THF as eluent and polystyrene as standard.

The thermal properties of TPD-PQE were determined by thermal gravimetric analysis (TGA) and differential scanning

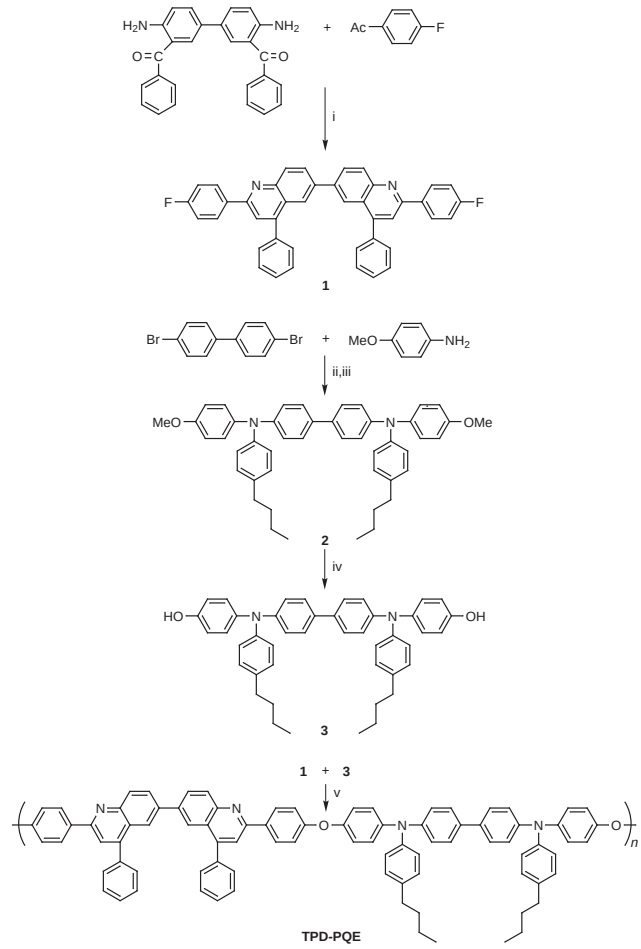

Scheme 1 *Reagents and conditions*: i, conc. H_2SO_4, AcOH; ii, $Pd_2(dba)_3$, dppf, toluene, NaOBu^t, 90 °C; iii, 4-BrC_6H_4Bu, NaOBu^t; iv, $BBr_3{\cdot}SMe_2$, $ClCH_2CH_2Cl$; v, K_2CO_3, toluene, NMP.

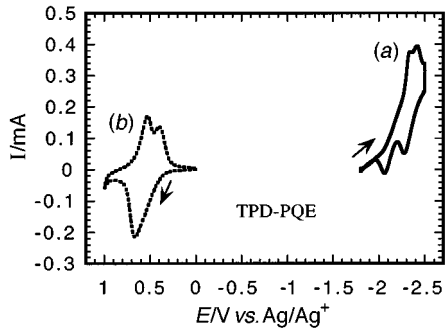

Fig. 1 Cyclic voltammetry of TPD-PQE spun-coated on ITO glass in an MeCN solution of TBAP (0.1 M) at a scan rate of 40 mV s^{-1}: (*a*) reduction and (*b*) oxidation.

calometry (DSC). The TPD-PQE possessed excellent thermal stability with a glass transition temperature (T_g) of 196 °C, and a T_d (onset of the decomposition temperature) of 445 °C.

The energy levels of TPD-PQE were investigated by cyclic voltammetry (CV). A thin film of the polymer was spin-coated onto pre-cleaned indium-tin-oxide (ITO) glass as a working electrode (~3 cm^2) from a cyclopentanone solution (concentration ~ 3 mg ml^{-1}). The reference and counter electrodes were Ag/Ag^+ (non-aqueous) and Pt gauze, respectively. The experiment was carried out under nitrogen with tetrabutylammonium perchlorate in anhydrous MeCN (TBAP, 0.1 M) as the supporting electrolyte. A typical CV curve is shown in Fig. 1. Two redox-active moieties were revealed for the copolymers. It is worth pointing out that the oxidative (*p*-doping) process was highly reversible and the reductive (*n*-doping) process was quasi-reversible for TPD-PQE. As a matter of fact, such a bipolar ability is beneficial to the performance of LEDs. The energy values of the lowest unoccupied molecular orbital (LUMO) and the highest occupied molecular orbital (HOMO) for TPD-PQE were calculated using the ferrocence (FOC) value of −4.8 eV below the vacuum level.[14] The onset potentials of oxidation and reduction of TPD-PQE (Fig. 1) were determined as +0.39 and −2.07 V *vs.* Ag/Ag^+, corresponding to +0.27 and −2.19 V *vs.* FOC (EFOC = 0.12 V *vs.* Ag/Ag^+). Thus, the HOMO and LUMO levels and the HOMO–LUMO gap should be −5.07, −2.61 and 2.46 eV, respectively. The optical E_g calculated from the onset (426 nm) of the UV–VIS absorption spectra of the spin-coated films for TPD-PQE was 2.91 eV.

To fabricate LED devices, copper phthalocyanine (CuPc), tris(8-hydroxyquinoline)aluminium (Alq_3) and Al layers were evaporated in a vacuum (10^{-6} Torr). Thin films of poly(9-vinylcarbazole) (PVK) and TPD-PQE were spin-coated from a 1,2-dichloroethane solution and from a $CHCl_3$ solution, which were filtered through a 0.2 μ Teflon filter before spin-coating. Three types of LEDs with the structure of ITO/CuPc/TPD-PQE/Al (**A**), ITO/PVK/TPD-PQE/Alq_3/Al (**B**) and ITO/TPD-PQE/Alq_3/Al (**C**) were employed in this study. The thickness of the TPD-PQE was the same (~35 nm) for all three types of LEDs, while the thickness of CuPc, PVK, Alq_3 and Al were ~35, ~40, ~50 and ~100 nm, respectively. The active area of the resulting devices was 7.07 mm^2. All of the fabrication processes

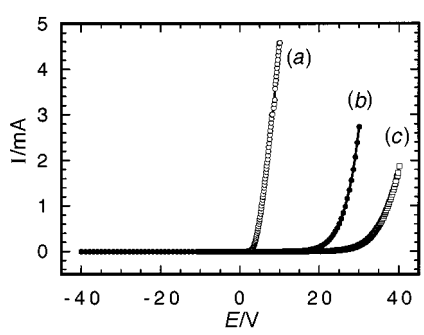

Fig. 2 Current–voltage characteristic for the light emitting devices. (*a*) ITO/CuPc/TPD-PQE/Al **A**, (*b*) ITO/PVK/TPD-PQE/Alq3/Al **B** and (*c*) ITO/TPD-PQE/Alq3/Al **C**.

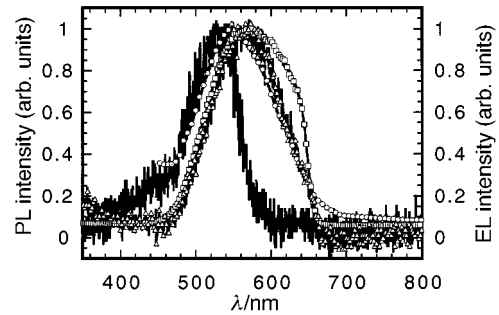

Fig. 3 (○) Photoluminescence spectrum of TPD-PQE and electroluminescence spectra of (—) ITO/CuPc/TPD-PQE/Al **A**, (□) ITO/PVK/TPD-PQE/Alq3/Al **B** and (△) ITO/TPD-PQE/Alq3/Al **C**.

(except for vacuum evaporation) and measurements were performed in air and at room temperature.

Fig. 2 shows the current–voltage characteristics of the LEDs. Excellent diode behavior was found for these devices. The turn-on voltage and rectification ratio were determined to be 3.7 V, and 5.1×10^4 (at 4.5 V) for **A**, 21.0 V and 4.2×10^5 (at 30.0 V) for **B**, and 30.1 V and 6.0×10^4 (at 36.0 V) for **C**, respectively. It is worth noting that, for these devices using PVK or CuPc as hole injecting/transporting layers, the turn-on voltages were decreased, while using Alq_3 as an electron injecting/transporting layer, the turn-on voltages were increased. This indicated that the TPD-PQE polymer has a good electron injecting/transporting ability. When the hole injecting/transporting (PVK or CuPc) layers were introduced, the overall charge injection/transport of the devices were balanced, which led to the decrease of the turn-on voltages.

Fig. 3 shows the photoluminescence (PL) spectrum of a TPD-PQE film and EL spectra of the LEDs. The PL spectrum of TPD-PQE had an emission peak at 547 nm when it was excited at 366 nm. The EL spectrum from device **A** is blue-shifted (λ_{max} = 530 nm) compared to the PL spectrum of the TPD-PQE. In particular, its long wavelength side became much steeper. This was due to partial absorption by CuPc in the 520–680 nm region.[15] The shape of the EL spectrum from device **C** is similar to the PL spetrum of TPD-PQE, however, it is red-shifted to 568 nm. In the case of device **B**, the EL emission shows a peak at 570 nm with a shoulder at ~620 nm. The shoulder is probably due to emission from aggregates of carbazole groups.[19] Bright light emission can clearly be seen under room light at forward bias for all three types of LEDs.

In conclusion, a bipolar copolymer was synthesized and characterized. This polymer showed high thermal stability, good electrochemical reversibility and excellent thin film-forming ability. In addition, very good LED performance was obtained with a low turn-on voltage, high rectification ratio, and bright light emission.

Notes and references

1 N. C. Greenham, S. C. Moratti, D. D. C. Bradley, R. H. Friend and A. B. Holmes, *Nature*, 1993, **365**, 628.
2 R. Brown, D. D. C. Bradley, P. L. J. Burn, H. Burroughes, R. H. Friend, N. Greenham and A. Kraft, *Appl. Phys. Lett.*, 1992, **61**, 2793.
3 Zhang, H. V. Seggern, B. Kraabel, H. W. Schmidt and A. J. Heeger, *Synth. Met.*, 1995, **72**, 185.
4 H. Peng, Z. N. Bao and M. E. Galvin, *Chem. Mater.*, 1998, **10**, 2086.
5 Zhang, A. S. Shetty and S. A. Jenekhe, *Acta Polym.*, 1998, **49**, 52.
6 A. K-Y. Jen, X. M. Wu and H. Ma, *Chem. Mater.*, 1998, **10**, 471.
7 D. Parker, Q. Pei and M. Marrocco, *Appl. Phys. Lett.*, 1994, **65**, 1272.
8 A. VanSlyke and C. W. Tang, US Pat., 1991, 5,061,569.
9 A. Fehnel, *J. Org. Chem.*, 1966, **31**, 2899.
10 S. Thayumanavan, S. Barlow and S. R. Marder, *Chem. Mater.*, 1997, **9**, 3231.
11 J. P. Wolfe and S. L. Buchwald, *J. Org. Chem.*, 1996, **61**, 1113.
12 G. Williard and C. B. Fryhle, *Tetrahedron Lett.*, 1980, **21**, 3731.
13 L. Hedrick and J. W. Labadie, *Macromolecules*, 1990, **23**, 1561.
14 J. Pommerehne, H. Vestweber, W. Guss, R. F. Mahrt, H. Bassler, M. Porsch and J. Daub, *Adv. Mater.*, 1995, **7**, 551.
15 Q. Liu, M. S. Liu, X. C. Li and A. K-Y. Jen, *Chem. Mater.*, in the press.

Communication 8/07975G

ChemComm

Catalytic asymmetric allylic transfer reaction: (4-trimethylsilylbut-2-ynyl)stannane as a new reagent leading to the enantioselective synthesis of dienyl alcohols

Chan-Mo Yu,*[a] Sook-Kyung Yoon,[ab] Seung-Joo Lee,[a] Jae-Young Lee[a] and Sung Soo Kim[b]

[a] *Department of Chemistry and Institute of Basic Science, Sungkyunkwan University, Suwon 440-746, Korea. E-mail: cmyu@chem.skku.ac.kr*

[b] *Division of Medicinal Chemistry, Korea Research Institute of Chemical Technology, Daejeon 305-600, Korea*

Received (in Cambridge, UK) 13th October 1998, Accepted 16th November 1998

Catalytic enantioselective addition of (4-trimethylsilylbut-2-ynyl)tributylstannane to aldehydes provides trimethylsilylmethylallenyl alcohols in high enantioselectivity which can be converted with a second electrophile to the corresponding dienyl alcohols.

There is considerable interest in the development of catalytic process utilizing chiral Lewis acids to realize efficient and practical asymmetric syntheses.[1] In previous studies, we have demonstrated that the utilization of molecular synergetic reagents for catalytic asymmetric allylic transfer reactions resulted in not only a significant increase in the reaction rate but also a reduced dosage of chiral catalyst. Our approach involves the use of BINOL–Ti^{IV} complex as a chiral promoter along with Et_2BSPr^i or Me_3SiSPr^i as an accelerating synergetic reagent that has recently shown to provide highly enantioselective versions of allylic transfer reactions of achiral aldehydes such as allylation,[2] propargylation[3] and allenylation.[4] The efficiency of this protocol in terms of enantioselectivity and catalytic ability has encouraged us to apply the extension of this method to more versatile systems which would expand the scope and utility of allylic transfer reactions.[5] Described herein is an extension of the molecular accelerating strategy aimed at finding new reagents and realizing useful and practical ways to advance new levels of asymmetric synthesis. In this study we focus on the addition of a bifunctional reagent to an aldehyde and subsequent attack by a electrophile to form dienyl alcohols. The realization of an efficient method in this reaction should be valuable because many useful functional group transformations can be foreseen for chiral alcohols.[6] In the present research, the following observations were made: (i) (4-trimethylsilylbut-2-ynyl)stannane is effective as a new reagent; (ii) dramatic solvent effects are observed when using $PhCF_3$; (iii) the efficient chemical transformation of homoallenylsilane into dienyl alcohols.

Our initial studies began with 1,4-bis(tributylstannyl)but-2-yne **1** as the allylic transfer reagent, which was prepared from the reaction of Bu_3SnLi (2 equiv.) with 1,4-dichlorobut-2-yne at −78 °C in THF.[7] The chiral catalyst, BINOL–Ti^{IV} complex **3**, was prepared by the reaction of (*S*)-BINOL (BINOL = 2,2′-dihydroxy-1,1′-binaphthol) and $Ti(OPr^i)_4$ (2:1) in the presence of 4 Å molecular sieves at 25 °C for 2 h.[8] Initial reactions of **1** and **2** in the presence of chiral catalyst **3** afforded none of the adduct **5** under various conditions. Fortunately, this lack of reactivity was overcome by introducing synergetic reagent Et_2BSPr^i **4**. Treatment of **1** with **2** (R = $PhCH_2CH_2$) and then **4** in the presence of **3** (10 mol%) at −20 °C for 20 h in CH_2Cl_2 afforded **5** along with undesired **6** in 58% combined yield in a ratio of 2:1 as judged by 500 MHz ^1H NMR analysis of the crude product (Scheme 1). Treatment of **5** with 10% HCl in THF cleanly gave dienyl alcohol **6** without loss of optical purity. Using heptanal as substrate under the same conditions, similar results were obtained but the formation of dienyl alcohol **6** still remained a problem. However, attempts at further conversion with benzaldehyde gave very poor results (< 10% conversion, at −20 °C for 36 h).

The formation of dienyl alcohol **6** from **5** was attributed to the acidic reaction media (Pr^iOH with Ti^{IV} species).† We speculated that the limited scope of the reaction and the side reaction with **1** can be solved by introducing the relatively less bulky and more stable silyl substituent instead of the stannyl group at C-4 on **1**. The new reagent **7**, a crucial compound in the present research, was prepared from propargyltrimethylsilane by the following sequences. Lithiation of propargylsilane with BuLi in THF (−78 °C, 1 h) followed by addition of paraformaldehyde (−78 to −20 °C, 2 h) gave (4-hydroxybut-2-ynyl)silane in 74% yield after distillation.[9] Treatment of (4-hydroxybut-2-ynyl)silane with BuLi at −78 °C for 1 h in THF followed by reaction with TsCl at −78 °C for 1 h and then −20 °C for 2 h gave the corresponding tosylate which used in the next reaction without isolation. Subsequent treatment of the tosylate with Bu_3SnLi at −78 °C for 2 h afforded **7**. Final purification of **7** was effected by distillation (75–82% yield, bp 121–122 °C at 0.4 mmHg).‡ Initial experiments on the allylic transfer reaction of **7** with various aldehydes promoted by **3** along with **4** under similar conditions (−20 °C for 18–24 h in CH_2Cl_2) afforded encouraging but marginal results. Although no or trace amounts (> 30:1) of dienyl alcohols **6** were produced during the reaction, the product yields for **8** ranged from 39 to 72% with 83–92% ee, as indicated in Table 1. After exploring numerous sets of conditions, we were delighted to find that the use of α,α,α-trifluorotoluene ($PhCF_3$) as solvent led to the best results in terms of chemical yields and enantioselectivities.[10] Under optimal conditions, the allylic transfer reaction was carried out according to the following procedure: The red–brown mixture of (*S*)-BINOL–Ti^{IV} complex (10 mol%) was cooled to −20 °C, and **2** (R = $PhCH_2CH_2$) was added. To this mixture was added dropwise **7** (1.2 equiv.) in $PhCF_3$ followed by **4** (1.2 equiv.) in $PhCF_3$ using a gas-tight syringe *via* a syringe pump over 1 h along the wall of the flask while keeping the temperature below −20 °C. After 18 h at −20 °C, the mixture was quenched by the addition of a saturated aqueous $NaHCO_3$. After work up, chromatography on Et_3N treated silica gel gave **8** (R = $PhCH_2CH_2$) in 78% yield with 97% ee. Additional experiments with various aldehydes were carried out and representative

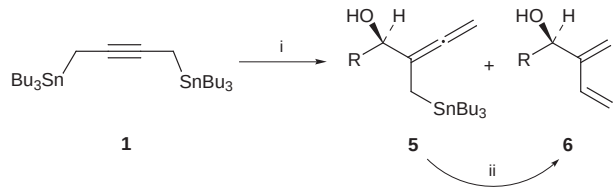

Scheme 1 *Reagents and conditions*: i, RCHO **2**, (*S*)-BINOL–Ti^{IV} **3** (10 mol%), Et_2BSPr^i **4**, −20 °C, 20 h, CH_2Cl_2 [R = $PhCH_2CH_2$, 58% (68:32), 91% ee; R = C_6H_{13}, 55% (57:43), 88% ee]; ii, 10% aq. HCl, 0 °C, 2 h, THF.

Table 1 Allylic transfer reactions of **7** with achiral aldehydes[ab]

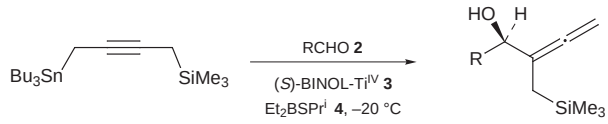

7 **8**

Entry	R	Solvent	*t*/h	Yield (%)[c]	Ee (%)[d]
1	$PhCH_2CH_2$	CH_2Cl_2	18	62	92
2	$PhCH_2CH_2$	$PhCF_3$	18	78	97
3	C_6H_{13}	CH_2Cl_2	18	60	90
4	C_6H_{13}	$PhCF_3$	18	83	97
5	Ph	CH_2Cl_2	24	39	84
6	Ph	$PhCF_3$	24	54	91
7	$Me_3SiC{\equiv}C$	CH_2Cl_2	24	50	83
8	$Me_3SiC{\equiv}C$	$PhCF_3$	24	62	88

[a] All reactions were carried out at −20 °C in indicated solvent. [b] BINOL:Ti(OPr^i)$_4$ = 2:1 (10 mol%). [c] Yields refer to isolated and purified products. [d] Ees were determined by preparation of (+)-MTPA ester derivatives, analysis by 500 MHz ^{1}H NMR spectroscopy, and comparison with corresponding diastereomers which were prepared from (*R*)-BINOL-Ti^{IV}.

results are summarised in Table 1. It is noteworthy that the formation of bis-allylated diol was not detected. Also, reduced dosage of chiral catalyst **3** (5 mol%) resulted in diminished chemical yield and longer reaction time (**2**, R = $PhCH_2CH_2$, −20 °C, 36 h, 34%).

The absolute configuration of the predominating enantiomer of the adducts **8** was unambiguously established after conversion to **6** by comparison of their specific rotations with that of known alcohols.[11] The absolute sense of the asymmetric induction parallels previous observations on catalytic allylations that employed the (*S*)-BINOL–Ti^{IV} catalyst.[2–4]

The adducts **8** are readily amenable to further conversion with electrophiles to give the useful synthetic intermediates, dienyl alcohols, with retention of enantiopurity, as described in Scheme 2. For example, the alcohol **6** was obtained from the reaction of **8** (R = $PhCH_2CH_2$) with acidic media in 78% isolated yield (a 4:1 mixture of aqueous HF and HCl at 0 °C in THF). Treatment of **8** (R = $PhCH_2CH_2$) with bromine (1.1 equiv.) in the presence of pyridine (5 equiv.) in CH_2Cl_2 at −78 °C for 1 h afforded **9** along with the corresponding silyl ether (less than 10%) which was readily desilylated with Bu_4NF in THF (over all 71% yield).

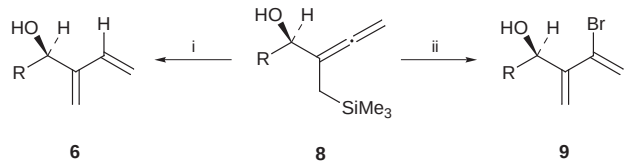

6 **8** **9**

Scheme 2 *Reagents and conditions*: i, aq. HF/HCl (4:1), 0 °C, THF (R = $PhCH_2CH_2$, 78%; R = C_6H_{13}, 81%; R = Ph, 68%); ii, Br_2 (1.1 equiv.), pyridine (5 equiv.), −78 °C, 1 h, CH_2Cl_2, then TBAF, THF (R = $PhCH_2CH_2$, 71%; R = C_6H_{13}, 74%).

In summary, this paper describes a new bifunctional reagent for the catalytic asymmetric allylic transfer reaction in a very general and efficient way which promises to be widely applicable. We believe that the products can serve as synthetic intermediates for the synthesis of chiral substances by selective functional group transformations.

Generous financial support of this research by grants from the Ministry of Education (BSRI 97-3420) and the Korea Science and Engineering Foundation (KOSEF 97-0501-02-01-3) is gratefully acknowledged.

Notes and references

† Removal of Pr^{i}OH under reduced pressure after formation of catalyst resulted in significantly diminished chemical yields. Also, according to the results of control experiments under identical conditions except for the use of aldehyde, we did not observe formation of any buta-2,3-dienylstannane from **1**.

‡ Compound **7** was prepared in quantity, purified by distillation, and is stable to storage, whereas compound **1** could not be distilled and is somewhat unstable to storage at −20 °C over more than a week.

1 General discussions on chiral Lewis acids: R. Noyori, *Asymmetric Catalysis in Organic Synthesis*, Wiley, New York, 1994, pp. 255–297; K. Maruoka and H. Yamamoto, in *Catalytic Asymmetric Synthesis*, ed. I. Ojima, VCH, New York, 1993, pp. 413–440; K. Mikami in *Advances in Catalytic Process*, ed. M. P. Doyle, JAI Press, Greenwich, 1995, pp. 1–44.
2 C.-M. Yu, H.-S. Choi, W.-H. Jung, H.-J. Kim and J. Shin, *Chem. Commun*., 1997, 761; C.-M. Yu, H.-S. Choi, W.-H. Jung and S.-S. Lee, *Tetrahedron Lett*., 1996, **37**, 7095.
3 C.-M. Yu, S.-K. Yoon, H.-S. Choi and K. Baek, *Chem. Commun*., 1997, 763; C.-M. Yu, H.-S. Choi, S.-K. Yoon and W.-H. Jung, *Synlett*, 1997, 889.
4 C.-M. Yu, S.-K. Yoon, K. Baek and J.-Y. Lee, *Angew. Chem*., 1998, **110**, 2504; *Angew. Chem., Int. Ed*., 1998, **37**, 2392.
5 For reviews, see: Y. Yamamoto and N. Asao, *Chem. Rev*., 1993, **93**, 2207; D. Hoppe, W. R. Roush and E. J. Thomas, in *Stereoselective Synthesis, Vol. 3*, ed. G. Helmchen, R. W. Hoffmann, J. Mulzer and E. Schaumann, Thieme, Stuttgart, 1996, pp. 1357–1602; M. Santell and J.-M. Pons, *Lewis Acids and Selectivity in Organic Chemistry*, CRC Press, New York, 1996, pp. 91–18; J. A. Marshall, *Chem. Rev*., 1996, **96**, 31.
6 For example, see: B. M. Trost and H. Urabe, *J. Am. Chem. Soc*., 1990, **112**, 4982.
7 H. J. Reich, I. L. Reich, K. E. Yelm, J. E. Holladay and D. Gschneidner, *J. Am. Chem. Soc*., 1993, **115**, 6625; H. J. Reich, K. E. Yelm and I. L. Reich, *J. Org. Chem*., 1984, **49**, 3438.
8 G. E. Keck, K. H. Tarbet and L. S. Geraci, *J. Am. Chem. Soc*., 1993, **115**, 8467; G. E. Keck and D. Krishnamurthy, *J. Am. Chem. Soc*., 1995, **117**, 2363; G. E. Keck and D. Krishnamurthy, *Org. Synth*., 1997, **75**, 12.
9 H. Mastalerz, *J. Org. Chem*., 1984, **49**, 4092.
10 A. Ogawa and D. P. Curran, *J. Org. Chem*., 1997, **62**, 450.
11 For the dienylboration using stoichiometric homoallenylborane, see: R. Soundararajan, G. Li and H. C. Brown, *J. Org. Chem*., 1996, **61**, 100.

Communication 8/07940D

Ab initio structure determination of norbornene from powder diffraction data using molecular packing analysis method

Jinrong Min, Jordi Benet-Buchholz and Roland Boese*

Institut für Anorganische Chemie, Universität-GH Essen, D-45117 Essen, Germany.
E-mail: boese@structchem.uni-essen.de

Received (in Cambridge, UK) 8th October 1998, Accepted 17th November 1998

The previously unknown crystal structre of the low temperature ordered phase of norbornene was solved from a set of powder diffraction data with severe preferred orientation collected on a laboratory X-ray diffractometer by first predicting the starting model by means of molecular packing analysis method, which was then refined against the experimental data by means of Rietveld method.

Norbornene, bicyclo[2.2.1]-2-heptene, belongs to a family of compounds which have a globular molecular shape, form orientational disordered plastic crystals and undergo phase transitions from high temperature disorderd phases to low temperature ordered phases. During the phase transition, plastic crystals usually shatter and it is very difficult to obtain single crystals from the ordered phases. For norbornane (C_7H_{12}),[1] the crystal structure of the low temperature ordered phase was solved by model building due to the special geometrical arrangement of molecules in the unit cell and refined against high-resolution synchrotron powder diffraction data. For norbornadiene (C_7H_8),[2] the crystal structure of the low temperature ordered phase was solved from single crystal grown by means of the *in situ* technique[3] from solution. This technique, however, failed so far for norbornene.

There is currently a major renaissance in the use of powder diffraction techniques for determining crystal structures at atomic resolution.[4] In this paper, we report the crystal structure of the low temperature ordered phase of norbornene (commercial product) solved from powder diffraction data at 105 K on an ordinary laboratory X-ray diffractometer (Siemens D5000, 7° position-sensitive detector, curved graphite monochromator and Cu-Kα_1 radiation). The structure only exists in an ordered form at low temperatures. The sample was sealed inside a capillary (d = 0.3 mm) and data were collected in steps of 0.0166° from 10.40 to 110.40° in 2θ, counting time 200 s per step. Indexing based on a monoclinic unit cell (TREOR90[5]) and refinement of unit cell dimensions with the whole pattern gave: a = 7.6011(7), b = 8.5985(8), c = 8.7290(8) Å, β = 97.313(3°), V = 565.87(9) Å^3. Systematic absences suggested that the possible space group was $P2_1/c$, although $P2_1$, $P2$, Pc, $P2/c$ could not be excluded for sure in the beginning. $P2/m$, Pm and $P2_1/m$ are excluded from symmetry considerations.

The sample has severe preferred orientation and contains a little impurity of the hexagonal high temperature disordered phase because not all of the sample has transformed into the ordered phase when cooling through the phase transition point at 145.3 K.[6] Preferred orientation, a well known problem that can seriously undermine structure solution attempts, is present in this sample. Therefore, the conventional structure determination method[7] did not succeed in this case, and we turned to molecular packing analysis method.[8] We first predicted structure models by molecular packing analysis method in possible space groups, simulated the diffraction patterns which were then compared to the experimental pattern. Subsequent Rietveld refinement[9] led to a final model.

The only inputs required by molecular packing analysis method are the molecular structure and an intermolecular force field. This method is used to predict the structure of crystals or molecular clusters by energy minimization, based on a variety of published force fields or a user-defined force field. The intermolecular or nonbonded energy of the molecular assembly is represented by a pairwise sum over atoms in different molecules. Crystal lattice sums are accurately evaluated using the accelerated convergence method.[10] The structural variables considered by the program are the rotations and translations of several molecules, and selected internal rotations. Molecules may be related by space group symmetry operations. In our case, we constructed the molecular structure from norbornadiene.[2] The energy minimization was implemented using the fixed unit cell dimensions and on different possible space groups. Rotation and translation parameters of the independent molecule were allowed to vary, while the symmetry-related molecules moved in a dependent way. We just considered the VDW energy term, because Coulomb energy is insignificant for this compound. The final minimized energies are listed in Table 1. From this table, we can see that $P2_1/c$ has the lowest packing energy. These predicted models were used to simulate the powder diffraction patterns, which are shown in Fig. 1. From this figure, we can exclude the space groups $P2$, $P2_1$, and Pc. When we tried to refine the structure in $P2/c$, it did not

Table 1 Molecular packing energies of the low temperature ordered phase of norbornene assuming different space groups at fixed cell dimensions

Space group	$P2_1/c$	$P2/c$	Pc	$P2_1$	$P2$
Packing energy/kJ mol^{-1}	−56.2	−43.9	−32.7	−19.1	22.4

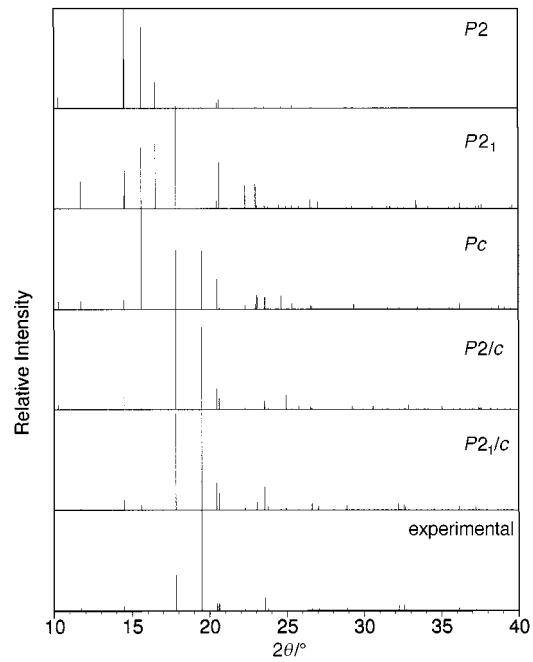

Fig. 1 Simulated powder diffraction patterns from predicted models by molecular packing analysis method on different space groups.

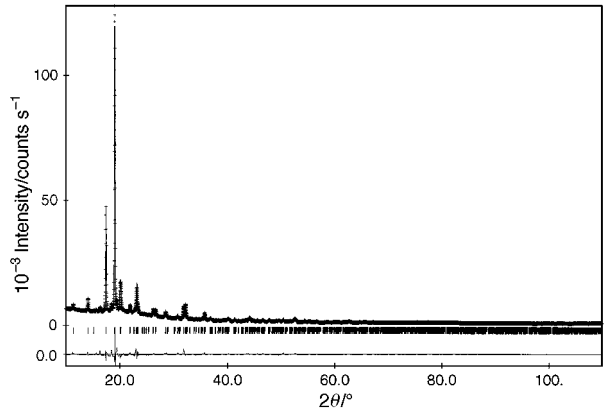

Fig. 2 Observed (plus marked line), calculated (solid line) and difference patterns (at the bottom) for the low temperature ordered phase of norbornene at 105 K. The short vertical lines mark the positions of possible Brag reflections.

converge. Therefore, we can conclude that the correct space group of the low temperature phase of norbornene is $P2_1/c$.

The atomic coordinates of the model predicted by molecular packing analysis method were input into the Rietveld refinement program FULLPROF.[11] A pseudo-Voigt profile function was selected to describe the diffraction peak profiles. After some cycles of refinement, the difference pattern between the observed and calculated patterns shows obvious preferred orientation along [111], which was modelled using Marsh–Dollase function.[12] At the beginning of refinement, only the positions of the carbon atoms were refined with an overall isotropic thermal parameter and without any constraints on the bond distances. After some cycles, one C–C bond became remarkably shorter than the other C–C bonds, indicating its

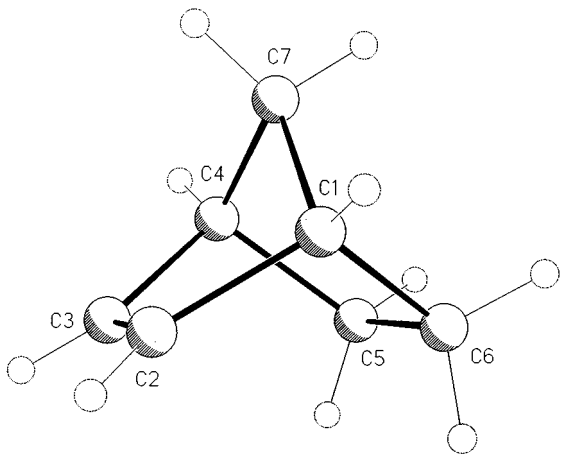

Fig. 3 Molcular structure of low temperature ordered phase of norbornene.

double bond characteristic. The positions of the hydrogen atoms were generated using the SHELXTL utilities XP[13] on the ideal positions after each cycle of refinement of carbon atoms. Fig. 2 shows the Rietveld refinement pattern. The remarkably good fit between the observed and calculated patterns supports the structure model.[14] Fig. 3 shows the molecular structure of the low temperature ordered phase of norbornene.

In summary, from the successful structure determination of norbornene, we wish to encourage the scientific community to exploit the structural information which can be readily obtained from powder diffraction data with inhouse techniques.

We gratefully acknowledge financial support by the Fonds der Chemischen Industrie. One of the authours (J. M.) is supported by the Alexander von Humboldt-Stiftung as a Humboldt fellow.

Notes and references

1 A. N. Fitch and H. Jobic, *J. Chem. Soc., Chem. Commun.*, 1993, 1516.
2 J. Benet-Buchholz, T. Haumann and R. Boese, *Chem. Commun.*, 1998, 2003.
3 R. Boese and M. Nussbaumer, in *Organic crystal chemistry*, ed. E. W. Jones, Oxford University Press, Oxford, UK, 1994, p. 20; V. R. Thalladi, H.-C. Weiss, D. Bläser, R. Boese, A. Nangia and G. R. Desiraju, *J. Am. Chem. Soc.*, 1998, **120**, 8702.
4 K. D. M. Harris and M. Tremayne, *Chem. Mater.*, 1996, **8**, 2554; K. Shankland, W. I. F. David and T. Csoka, *Z. Kristallogr.*, 1997, **212**, 550.
5 P.-E. Werner, L. Eriksson and M. Westdahl, *J. Appl. Crystallogr.*, 1985, **18**, 367.
6 The DSC investigation was performed on DuPont 9900 controlled by program General V2.2A, heating rate 2 °C min^{-1}.
7 The general procedure for the conventional method is: extracting structure factor amplitudes; structure solution (direct methods or patterson method), Fourier recycling and refinement by single crystal method; and finish with Rietveld refinement.
8 D. E. Williams, Program mpa/mpg, Molecular Packing Analysis/ Molecular Packing Graphics. Department of Chemistry, University of Louisville, Louisville, KY 40292, USA.
9 H. M. Rietveld, *J. Appl. Crystallogr.*, 1969, **2**, 65.
10 D. E. Williams, *Acta Crystallogr., Sect. A*, 1971, **27**, 452.
11 J. Rodriguez-Carvajal, in *Collected Abstracts of Powder Diffraction Meeting*, Toulouse, France, July 1990, p. 127.
12 W. A. Dollase, *J. Appl. Crystallogr.*, 1986, **19**, 267.
13 Siemens Analytical X-ray Instruments, Inc., 1994, Ver. 5.03.
14 *Crystal data* for norbornene at 105 K: C_7H_{10}, M = 94.16, monoclinic, space group $P2_1/c$, a = 7.6011(7), b = 8.5985(8), c = 8.7290(8) Å, β = 97.313(3)°, V = 565.87(9) $Å^3$, Z = 4, D_c = 1.105 g cm^{-3}. Overall isotropic thermal parameter B = 3.2(1) $Å^2$. Final Rietveld refinement converted to R_p = 4.66%, R_{wp} = 6.48%, R_b = 10.0%, R_{exp} = 2.00%, χ^2 = 10.5 for 35 variables and 715 reflections distributed over 6025 profile points. Bond lengths (Å): C(1)–C(2) 1.524(1), C(3)–C(4) 1.522(1), C(2)–C(3) 1.334(1), C(4)–C(5) 1.563(1), C(1)–C(6) 1.562(1), C(5)–C(6) 1.557(1), C(1)–C(7) 1.547(1), C(4)–C(7) 1.545(1). See http://www.rsc.org/suppdata/cc/1999/2751/ for listing of bond lengths and angles and atomic coordinates.

Communication 8/07829G

ChemComm

The determination of gaseous molecular density using a hybrid vapour sensor

Marcus J. Swann, Andrew Glidle, Li Cui, John R. Barker and Jonathan M. Cooper*

Department of Electronics and Electrical Engineering, University of Glasgow, Glasgow, Scotland, UK G12 8QQ. E-mail: jmcooper@elec.gla.ac.uk

Received (in Exeter, UK) 19th October 1998, Accepted 9th November 1998

The simultaneous responses from a conductance sensor and a gravimetric quartz crystal sensor can be combined as a hybrid measurement which yields the analyte vapour's molecular density.

The measurement of odours is of importance in the monitoring of industrial, bio-agricultural and environment processes. Traditionally analytical methods, including gas chromatographic mass spectrometry[1] or optical measurements,[2] have made use of inherent physical characteristics of the vapour. In other gas sensing systems, such as electronic noses,[3–5] where the instrumentation and methodology may be more simple, there is often a lack of detailed mechanistic knowledge as to what determines the sensor response. As a consequence, one of the greatest challenges in artificial olfaction is the development of a convenient sensor technology where the analytical response results from an intrinsic molecular signature or property of the gas. Here, we show how a hybrid device, comprising a conductimetric and gravimetric sensor pair, can, through the simple ratioing of their responses, determine the molecular density of one or more vapour(s). The method that we propose has an advantage over existing olfactory techniques in that it generates quantitative physical information describing the gas composition (analogous to, for example, an IR stretch).

Much work on the development of electronic noses[3–9] has focused on two distinct sensing methods, namely, conductivity measurements based on chemoresistors[3–5] and the (mass sensitive) quartz crystal microbalance (QCM).[6–9] In both technologies, a transducing element is coated with a membrane, which may be either an organic polymer, an inorganic oxide, or simply a functionalised self assembled monolayer.[3–9] Responses are measured, either by an increase in mass (as is the case for a QCM), or by a change in electrical resistance (exemplified by the chemoresistor) due to the interaction of the gas with the overlayer. A notable difference, however, between the two systems is the common use of non-conducting overlayers in QCM sensors, and of conducting polymers or metal oxides in the chemoresistor systems.

Both the QCM[9–11] and conductimetric techniques[3–5] have been expanded to utilise arrays of different sensors. Consequently, commercial instruments have exploited signal processing as a means of producing an olfactory image and hence identifying the composition of an unknown vapour stream.[12]

A recent innovation has resulted in the manufacture of conductimetric sensors, fabricated using a dispersion of carbon-black[13] or any other finely divided conducting material[14] in a non-conducting polymer (so forming a conducting membrane). Sorbtion of a vapour into such a composite matrix causes a change in the electrical resistance by influencing the length of percolation paths between conducting particles within the polymer film. A consequence of this methodology for sensor fabrication has been to greatly extend the variety of polymers and deposition methods which can be used in these sensor systems. Additionally, by using these composites, interpretation of the measured resistance changes becomes simplified through the finding that changes in conductivity are linear with the (single component) vapour phase concentration[13] (below the percolation threshold). Importantly, it has been proposed[13,14] that the resistance change is proportional to the change in polymer-composite's volume, due to swelling.

In producing our sensors, we have exploited the possibility of measuring resistance changes in thin films of carbon black composite materials at a conductimetric sensor, on exposure to a range of vapours (due to changes in the polymer-volume) whilst simultaneously determining increases in mass at a similarly coated QCM (due to vapour sorbtion). Thus, we have developed a device which is capable of determining the molecular density of an odour (as a vapour's mass divided by its volume). This measurement, which can be determined by ratioing the voltage outputs from the QCM and the conductimetric sensor pair using a simple potential divider, provides a straightforward method to obtain an intrinsic physical signature of a gaseous species.

In the series of experiments described below, conductimetric sensors (Fig. 1, left) were fabricated as interdigitated electrodes with gap sizes of either 20 or 40 μm and an effective length of 10 cm. These electrodes have the advantage that they can be functionalised by spin coating (2000 rpm) or by an ink jet printer, from a solution containing both dissolved polymer and a carbon-black dispersion. The gravimetric (QCM) sensors (Fig. 1, right) were 10 MHz AT cut quartz crystals (ICM Co., Oklahoma, USA) and were spin coated using a solution of the polymer alone. Typical coating solutions contained 200 mg poly(ethylene oxide) (Aldrich) with/or without 50 mg carbon black (Cabot Co., Bilerica, USA), in 10 g of chloroform.

Vapours were passed over the sensor pair using a regulated flow system enabling the simultaneous measurement of QCM and conductimetric responses. Fig. 2 shows the changes in frequency and resistance of the QCM and interdigitated sensors

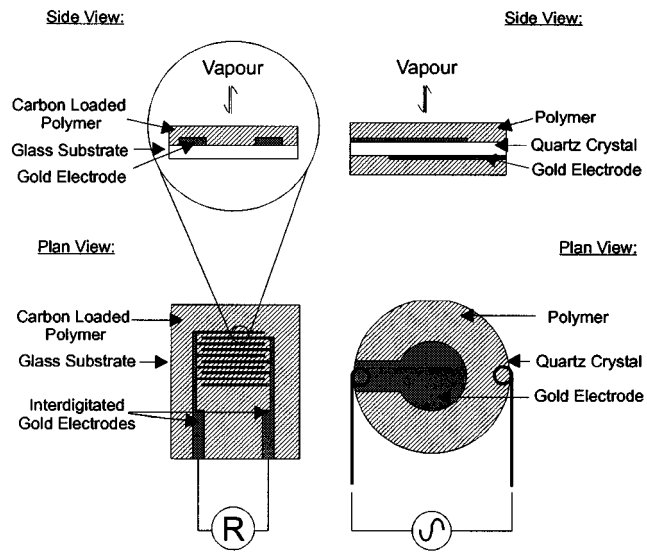

Fig. 1 Schematic diagram of the two sensor types. The conductimetric sensor (left) is a molecular volume sensitive transducer, consisting of two interdigitated electrodes. The quartz crystal microbalance (right) is a mass sensitive transducer, based on the change in resonant frequency of a quartz crystal.

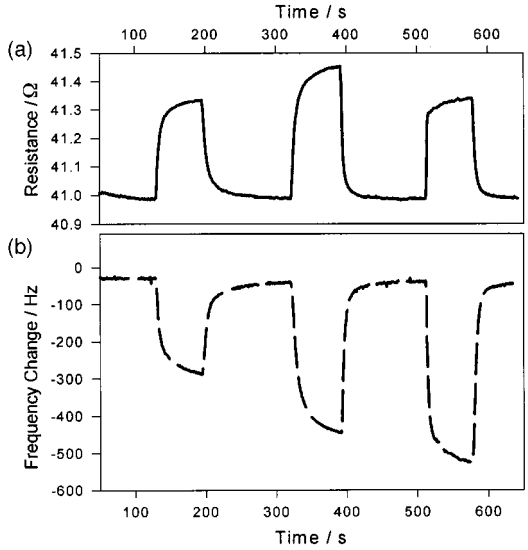

Fig. 2 Response of poly(ethylene oxide) coated (a) conductimetric and (b) QCM sensors to *n*-hexane (13 mmHg), water (9 mmHg) and chloroform (6 mmHg) in nitrogen as a function of time. Between exposure to vapour samples, the sensors were purged with dry nitrogen.

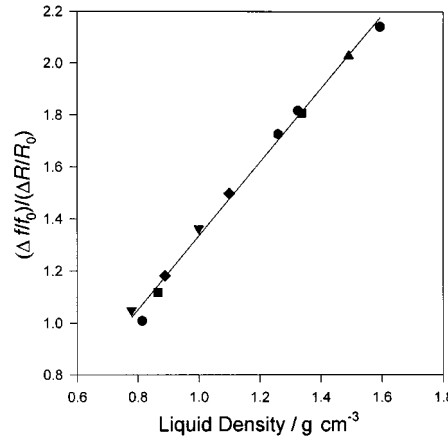

Fig. 3 A plot of $[(\Delta f/\Delta f_0)/(\Delta R/R_0)]$ *vs.* the vapour's liquid density for a range of different solvents, where f_0 is the film's dry mass, and R_0 is its initial resistance. The solvents were cyclohexane (ρ = 0.779 g cm^{-3}), hexanol (0.814), toluene (0.865), THF (0.889), water (1.00), deuterium oxide (1.10), dichloroethanene (1.26), dichloromethane (1.33), trichloroethane (1.338), chloroform (1.49) and carbon tetrachloride (1.59). The straight line is a linear regression fit to the data, (r^2 = 0.99).

on exposure to vapours of *n*-hexane, water and chloroform (at different selected, partial pressures). As can be seen, chloroform gives the largest frequency (mass) change for the given resistance change, and hexane the smallest. Although the rate of change of the response of the sensors is different for each vapour, the time dependent responses of a conductimetric and QCM sensor pair follow each other closely. Indeed, division of the temporal responses from each of the sensors in the pair is linear for a given gas, indicating that the output of the hybrid device is constant for different amounts of sorbed vapour (the actual amount of sorbed vapour can still be determined from the individual conductimetric, or gravimetric responses).

Confirmation that the sorbtion of gas does lead to a volume change in the sensing layer, as proposed by others,[13,14] has been investigated by simple neutron and X-ray reflectivity experiments (not detailed here) showing that thin films of polymers swell to as much as 150% of their original thickness on exposure to suitable vapours.

To demonstrate the independence of the ratio of conductimetric to gravimetric responses, with amount of sorbed vapour, we measured the percentage frequency change and percentage resistance change for different vapour pressures of dichloromethane (9.2 mm–138 mm Hg). The relationship is linear over the concentration range studied, although the non-zero intercept obtained from an unconstrained best fit line may reflect the influence of the bath gas (N_2) on polymer swelling.

To examine the hypothesis that the sorbed species' molecular density can be calculated from a simultaneous measurement dependent on the volume change in the conductance sensor and a corresponding gravimetric measurement, we investigated a hybrid device's response to a variety of vapours generated from volatile liquids. Fig. 3 illustrates the ratio of gravimetric change to the polymer volume increase by showing the ratio of QCM frequency change to interdigitated electrode resistance change as a function of the density of the sorbed vapour. To demonstrate that the hybrid sensor response was independent of vapour–polymer interactions, the odours were chosen in order to be representative of hydrophobic, hydrophilic, polar, non-polar, and isotopically substituted molecules. The wide range of liquid densities covered by these species (0.78–1.59 g cm^{-3}) further emphasises the versatile nature of the methodology in monitoring different vapours, including light hydrocarbon gases and heavier halogenated species. Ultimately, these techniques may be extended to (volatile) metal complexes (*e.g.* UF_6).

In conclusion, we have shown that by combining carbon-black loaded polymer conductimetric and QCM sensors, we can greatly augment the information obtained when compared with the use of either one sensor material, or one measurement system alone. This simplicity of signal processing is not found in current array based conductimetric electronic noses, owing to the numerous factors influencing conductivity mechanisms in, for example, the family of poly(pyrroles).[12] Although QCM and chemoresistance measurements have previously been made simultaneously,[15,16] giving responses which are linear with respect to the amount of (single component) vapour species adsorbed, the magnitude and sign of their proportionality coefficients are not readily related to the molecular species involved. This clearly contrasts with the novel sensor configuration that we have demonstrated here.

The authors wish to thank both MAFF and The Leverhulme Trust for supporting this work.

Notes and references

1 R. Mariaca and J. O. Bosset, *Lait*, 1997, **77**, 13.
2 K. Villberg, A. Veijanen, I. Gustafsson and K. Wickstrom, *J. Chromatr. A*, 1997, **791**, 213.
3 J. W. Gardner, M. Craven, C. Dow and E. L. Hines, *Meas. Sci. Technol.*, 1998, **9**, 120.
4 P. S. Barker, J. R. Chen, N. E. Agbor, A. P. Monkman, P. Mars and M. C. Petty, *Sens. Actuators B*, 1994, **17**, 143.
5 J. V. Hatfield, P. Neaves, P. J. Hicks, K. Persaud and P. Travers, *Sens. Actuators B: Chem.*, 1994, **18**, 221.
6 G. Sauerbrey, *Z. Phys.*, 1959, **155**, 206.
7 G. H. King, *Anal. Chem.*, 1964, **36**, 1735.
8 D. S. Ballantine Jr., R. M. White, S. J. Martin, A. J. Ricco, G. C. Frye, H. Wohltjen, R. M. White and E. T. Zellers, *Acoustic Wave Sensors*, Academic Press, San Diego, 1997, ISBN:0-12-077460-7.
9 J. W. Grate and M. H. Abraham, *Sens. Actuators B*, 1991, **3**, 85.
10 A. Hierlemann, U. Weimar, G. Kraus, G. Gauglitz and W. Gopel, *Sens. Mater.*, 1995, **7**, 179.
11 Z. Deng, D. C. Stone and M. Thompson, *Analyst*, 1996, **121**, 671.
12 T. N. Nagle, R. Gutierrez-Osuna and S. S. Schiffman, *IEEE Spectrum*, 1998, **9**, 22.
13 M. C. Lonergan, E. J. Severin, B. J. Doleman, S. A. Beaber, R. H. Grubbs and N. S. Lewis, *Chem. Mater.*, 1996, **8**, 2298.
14 E. J. Severin, B. J. Doleman, R. D. Sanner, M. C. Lonergan, R. H. Grubbs and N. S. Lewis, *Abstracts of Papers of ACS*, 1997, vol. **213**, 35-BTEC.
15 J. M. Slater and E. J. Watt, *Analyst*, 1991, **116**, 1125.
16 K. Nigorikawa, Y. Kunugi, Y. Harima and K. Yamashita, *J. Electroanal. Chem.*, 1995, **396**, 563.

Communication 8/08060G

The synergetic effect of cobalt and indium in ferrierite catalysts for selective catalytic reduction of nitric oxide with methane

B. Sulikowski,*[a] J. Janas,[a] J. Haber,*[a] A. Kubacka,[a] Z. Olejniczak[b] and E. Wloch[a]

[a] *Institute of Catalysis and Surface Chemistry, Polish Academy of Sciences, Niezapominajek 1, 30-239 Kraków, Poland. E-mail: ncsuliko@cyf-kr.edu.pl; nchaber@cyf-kr.edu.pl*

[b] *Institute of Nuclear Physics, Radzikowskiego 152,31-342 Kraków, Poland*

Received (in Cambridge, UK) 27th October 1998, Accepted 17th November 1998

A pronounced synergetic effect was found in the title reaction when indium and cobalt ions were present simultaneously in zeolite ferrierite.

A number of catalysts have been tested in the SCR of NO_x, including mixed oxides, supported metals and zeolites of different compositions.[1] While the SCR of NO with olefins proceeds usually smoothly on zeolite catalysts,[2] it is much more difficult to perform the title reaction using methane, a very stable molecule, and to achieve the reduction of NO while preventing total oxidation of the organic molecule by oxygen. Li and Armor showed that methane can be successfully used as a reductant of NO on Co^{2+}, Mn^{2+} and Ni^{2+}-exchanged ferrierites.[3] Ga and In/H-ZSM-5 were active catalysts in the title reaction.[4] Indium oxide supported on TiO_2–ZrO_2 showed significant activity for reduction of NO with propene, but not with methane, ethene, propane or alcohols.[5] We wish to report on the characterization and performance of Co^{2+} and/or In^{3+} containing ferrierite in the SCR of NO with CH_4, in the presence of excess oxygen.

Ferrierite was synthesized hydrothermally by using pyrrolidine (pyr) or piperidine (pip) and Ludox AS-40. The gels having compositions of (10–12) SiO_2 : (4.8–7.0) pyr : (0.48–0.64) NaOH : 1.0 Al_2O_3 : (380–460) H_2O and (11–12) SiO_2 : (4.0–6.0) pip : (6.5–7.5) NaOH : 1.0 Al_2O_3 : (160–220) H_2O have been homogenized for few hours and allowed to crystallize in the Teflon-lined stainless-steel autoclaves under autogenous pressure for 2–13 days at 160–200 °C. After calcination at 550 °C ferrierite was ion-exchanged with ammonium acetate (twice) and transformed into the hydrogen form (H-FER) by calcination. The Si/Al ratio of H-FER (I) was 6.1 and BET (Ar) = 335.7 $m^2\ g^{-1}$; for H-FER (II) the Si/Al ratio was 7.8 and BET = 321.1 $m^2\ g^{-1}$, respectively. XRD showed both samples contained pure ferrierite phase (no mordenite or other phases were present).

^{29}Si MAS NMR spectra of both hydrogen forms were typical for pure ferrierite phase,[6] giving three signals at −108.2, −113.6 and −117.5 ppm. A fourth weak signal was found at −102.7 ppm. ^{27}Al MAS NMR revealed that aluminium in all the samples is present in tetrahedral positions. More detailed discussion of silicon and aluminium NMR spectra of ferrierites will be given elsewhere.

H-FER was modified further by Co(II) and In(III) ions using standard and solid-state ion exchange (s.s.i.e.) procedures.[7] Cobalt acetate (Merck, p.a.) was mixed with H-FER (I) in an agate mortar and calcined in air (heating rate 50 °C h^{-1}) at 550 °C for 2.5 h to yield Co-FER (I) with Co/Al molar ratio of 0.27. The sample In-FER (1) was obtained by ion exchange from indium nitrate solution at pH = 2.1, washed, dried and calcined in air at 550 °C for 2 h (In/Al = 0.12). Another catalyst was prepared by grounding zeolite and indium(III) oxide, heating in He to 400 °C and reducing with hydrogen at this temperature for 2 h. The sample was cooled down to ambient temperature in the He flow to give In-FER (2) with In/Al = 0.99. Finally, Co,In-FER was prepared from the Co-FER (I) sample by applying the additional s.s.i.e. procedure. Thus Co-FER (I) was ground with In_2O_3, heated in the helium flow to 400 °C, reduced with hydrogen for 2 h and cooled to room temperature in He. The catalyst labelled Co,In-FER had Co/Al = 0.27 and In/Al = 0.23.

The catalytic tests were performed in the continuous flow microreactor connected on-line with a gas chromatograph, at GHSV = 10 000 h^{-1}. All the data in Tables 1–3 are related to steady-state conditions. After these conditions were established (*ca.* 2 h) no measurable loss of catalysts activity was observed up to two days on stream (except H-FER).

The selective catalytic reduction (SCR) of NO by a hydrocarbon molecule (here methane) in the presence of oxygen proceeds according to eqn. (1):

$$2\ NO + CH_4 + O_2 \rightarrow N_2 + CO_2 + 2\ H_2O \quad (1)$$

In addition to reaction (1), at least two other parallel processes can be envisaged. First, the hydrocarbon can be fully oxidized by the molecular oxygen [eqn. (2)]:

$$CH_4 + 2\ O_2 \rightarrow CO_2 + 2\ H_2O \quad (2)$$

Second, NO can be oxidized to NO_2 instead of being reduced [eqn. (3)]:

$$NO + 1/2\ O_2 \rightarrow NO_2 \quad (3)$$

Table 1 A comparison of the selective catalytic reduction (SCR) of NO on indium forms of ferrierite. The oxidation of NO to NO_2 without methane in the feed is also shown (*O*)[a]

	In-FER (1)			In-FER (2)		
T_R/°C	*X*	*Y*	*O*	*X*	*Y*	*O*
250	24.4	tr.	17.0	6.3	4.7	0
300	28.0	3.1	21.4	14.4	8.1	18.9
350	23.9	4.2	19.5	8.9	11.3	8.1
400	21.6	8.2	15.0	4.1	14.2	6.4
450	28.3	15.7	12.7	2.3	32.2	0
500	39.4	24.8	9.5	4.9	50.1	0
525	40.5	38.6	9.4			

[a] Reaction conditions: NO = 1000 ppm, CH_4 = 2000 ppm, O_2 = 4%, H_2O = 2500 ppm; GHSV = 10 000 h^{-1}; *X* = conversion of NO (mol%), *Y* = conversion of methane (mol%) in the presence of NO, *O* = oxidation of NO to NO_2 (mol%) in the absence of methane.

Table 2 Selective catalytic reduction of NO on the hydrogen and cobalt forms of ferrierite, in the presence of methane and oxygen; reaction conditions as in Table 1

	H-FER (II)			Co-FER (I)		
T_R/°C	*X*	*Y*	*O*	*X*	*Y*	*O*
250	21.3	tr.	23.1			
300	19.8	2.3	27.4	~2	7.5	10.2
350	10.7	3.8	17.2	10.8	11.7	42.1
400	1.0	5.0	8.1	37.2	10.7	50.1
450	0	6.1	1.3	40.9	20.7	28.2
500	2.6	9.3	0	45.1	42.6	13.0
525				44.7	66.6	3.6

Table 3 Selective catalytic conversion of NO on Co,In-ferrierite, in the presence of methane and oxygen. Reaction conditions as in Table 1

	Co,In-FER		
T_R/°C	*X*	*Y*	*O*
300	20.0	4.1	19.8
350	61.3	14.6	42.7
400	91.7	29.3	43.3
425	98.4	42.0	34.4
450	97.6	52.9	27.3
475	95.5	63.0	
500	91.5	87.0	15.5

Third, the partial reduction of NO to N_2O may proceed. However, in the presence of methane and ethene the yield of N_2O was low (up to 5%). Accordingly, the following three reactions have been studied on ferrierite-based catalysts: (i) the SCR of NO; (ii) the oxidation of NO to NO_2 in the absence of methane; and (iii) the combustion of CH_4 to CO_2 and H_2O (without NO in the feed).

On pure hydrogen form of ferrierite the conversion (*X*) of NO at 250–300 °C was *ca.* 20% (Table 2). However, the zeolite loses its activity relatively quickly (< 1 h on stream). Moreover, the conversion of NO decreases sharply with the temperature. Above 400 °C the solid becomes essentially inactive. In the absence of CH_4 the oxidation of NO to NO_2 proceeds at low temperatures and above 450 °C is negligible (Table 2, column *O*).

The activity of the catalysts containing indium shows much more pronounced conversion in the temperature range 250–350 °C (Table 1). Contrary to the H-FER sample, the oxidation of NO to NO_2 was observed on In-FER (1) in the whole temperature range studied, up to 525 °C. However, under the SCR conditions, the oxidation of NO prevails only at temperature 200–250 °C, while above 350 °C the SCR of NO was the main process. The conversion level of NO does not exceed *ca.* 40% at 500–525 °C. The sample In-FER (2) is much less active; the oxidation of NO to NO_2 above 350 °C becomes negligible, while the total conversion of NO is nearly the same as found for H-FER. Finally, the oxidation of methane on this catalyst rises quickly with the temperature. As is seen from Table 1, no simple parallelism exists between the ability of catalysts to oxidize CH_4 and its performance in the SCR of NO.

The activity of pure Co-FER (I) under the same conditions is similar to the In-FER (1) sample. The catalyst shows an ability to oxidize NO (Table 2, column *O*). Thus summarizing, moderate conversions of NO have been obtained on the catalysts containing either cobalt or indium cations in the zeolite matrix [In-FER (1), Co-FER (I)].

We have found, however, that when cobalt and indium ions were present simultaneously in ferrierite, a very significant synergetic effect was observed. The conversion of NO increases sharply from 20 to 98% in the temperature range 300–425 °C (Table 3, column *X*). It is also remarkable that on Co,In-FER no NO_2 was found in the effluents above 300 °C. As the conversion of methane reveals, at 300–425 °C the SCR of NO proceeds predominantly. This is confirmed further by a very low combustion of methane in the absence of NO (for example, combustion of CH_4 without NO was < 1% at 300 °C and 6% at 400 °C). Above 400 °C the competition between reactions (1) and (2) becomes more important. As a result the combustion of methane by molecular oxygen increases with temperature. We note, however, that even at 500 °C methane is still able to reduce NO. Another interesting feature of the Co,In ferrierite is low yield of N_2O, decreasing continuously from 5.6% at 350 °C to 0% at 500 °C.

The activity of Co,In-FER catalyst was measured for comparison purposes using ethene in the stream instead of methane. The results are summarized in Fig. 1. Surprisingly, the conversion of NO is lower at high temperatures when using ethene as the reductant. Moreover, high (> 90%) conversion of NO on the Co,In-FER catalyst in the presence of methane was observed in a broader range (400–500 °C). Two remarkable features of our catalyst formulation are seen: (i) higher activity at high temperatures when using methane as the reductant; and (ii) still high activity in the de-NOx process with ethene. Typical behaviour of other zeolite catalysts investigated by us (mordenite and ZSM-5) was different: high activity in the presence of ethene and *lower* when using methane.[8]

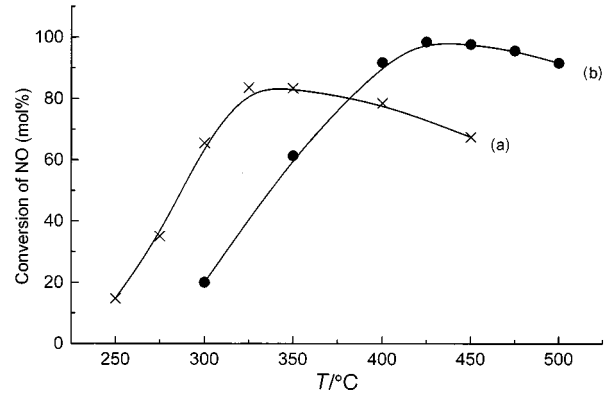

Fig. 1 Conversion of NO (mol%) on the Co,In-FER in the presence of ethene (a) and methane (b).

Finally, it is interesting to speculate on the surface species, as revealed in Co,In-FER by ESCA. We found the following concentrations of the catalyst components—Si : Al : O : In : Co = 0.261 : 0.045 : 0.647 : 0.031 : 0.016. The Si/Al ratio was 5.8 (in bulk, 6.1 was found by atomic absorption). Analysis of cobalt species gave Co(II) : Co(III) = 0.99. Upon heating to 400 °C, concentration of In and Co on the surface decreases to 0.023 and 0.013, respectively. This is in a very good agreement with higher initial activity of the catalyst (75.2% at 300 °C) in comparison with 65.5% steady-state value reached after 2 h on stream. Distribution of Co ions in crystals is very homogeneous, as seen by comparing Co/(Si+Al) = 0.038 (bulk) and 0.036 (surface). Contrary to this, even after heating at 400 °C the surface of ferrierite is enriched with indium oxide species [In/(Si+Al) = 0.064 (surface) and 0.033 (bulk)], at variance with the case demonstrated for large crystals of H-ZSM-5.[9]

We are grateful to Dr. Jerzy Stoch for ESCA analysis. We thank the State Committee for Scientific Research (KBN), Warsaw, for support (grants no. 2P 303 053 07 and no. 2 P03B 077 13).

Notes and references

1 F. P. Boer, L. L. Hegedus, T. R. Gouker and K. P. Zak, *CHEMTECH*, 1990, 312.
2 T. Tabata, H. Ohtsuka, M. Kokitsu and O. Okada, *Bull. Chem. Soc. Jpn.*, 1995, **68**, 1905.
3 Y. Li and J. N. Armor, *Appl. Catal. B*, 1993, **3**, L1; *J. Catal.*, 1994, **150**, 376.
4 E. Kikuchi, M. Ogura, N. Aratani, Y. Sugiura, S. Hiromoto and K. Yogo, *Catal. Today*, 1996, **27**, 35.
5 Y. Kintaichi, M. Haneda, M. Inaba and H. Hamada, *Catal. Lett.*, 1997, **48**, 121.
6 R. E. Morris, S. J. Weigel, N. J. Henson, L. M. Bull, M. T. Janicke, B. F. Chmelka and A. K. Cheetham, *J. Am. Chem. Soc.*, 1994, **116**, 11 849.
7 B. Sulikowski, *Heterogeneous Chem. Rev.*, 1996, **3**, 203; B. Sulikowski, J. Find, H. G. Karge and D. Herein, *Zeolites*, 1997, **19**, 395.
8 B. Sulikowski, J. Haber, J. Janas, A. Kubacka and E. Wloch, *Pol. Pat. App.* P 316266, 1996.
9 V. Kanazirev, V. Valtchev and M. P. Tarassov, *J. Chem. Soc., Chem. Commun.*, 1994, 1043.

Communication 8/08314B

ChemComm

1,2-Bis(4,4′-dipyridinium)ethane: a versatile dication for the formation of [2]rotaxanes with dibenzo-24-crown-8 ether

Stephen J. Loeb* and James A. Wisner

School of Physical Sciences, Chemistry & Biochemistry, University of Windsor, Windsor, Ontario, Canada N9B 3P4. Fax: + (519) 973-7098. E-mail: loeb@uwindsor.ca

Received (in Cambridge, UK) 24th September 1998, Accepted 9th November 1998

The 1,2-bis(4,4′-dipyridinium)ethane dication threads through dibenzo-24-crown ether (DB24C8) to form a [2]pseudorotaxane which is easily stoppered to form [2]rotaxanes either by alkylation or coordination of a transition metal complex.

To date, most [2]rotaxanes involving crown ethers have been templated by either the stacking interactions between π-electron rich and π-electron poor aromatic rings[1] or hydrogen bonding between secondary dialkylammonium ions and crown ether oxygen atoms.[2] We have recently demonstrated that various 1,2-bis(pyridinium)ethane dications **1a**–**d** will thread through the 24-membered crown ethers 24C8, B24C8 and DB24C8 to form [2]pseudorotaxanes in which the major templating forces are $N^+\cdots O$ and C–H···O interactions.[3] By adding various substituents (X) to the 4-position of the pyridinium ring, it was possible to prepare a series of interlocked molecules containing DB24C8 with K_a values ranging from 105 $dm^3\ mol^{-1}$ for **1a** to 1200 $dm^3\ mol^{-1}$ for **1d** in MeCN solution.

We have now turned our attention to converting these [2]pseudorotaxanes into permanently interlocked [2]rotaxanes. Our strategy was to prepare an appropriate 1,2-bis(pyridinium)ethane dication which could form a stable [2]pseudorotaxane and be easily stoppered to form a [2]rotaxane. In a straightforward variation of our previous work, these criteria were met by using 4,4′-bipyridinium units; X = 4-pyridine, **1e**.[4] The 1:1 interaction of **1e** with DB24C8 resulted in formation of the [2]pseudorotaxane **2** (Scheme 1) as identified by ^1H NMR spectroscopy, ESI-MS and an association constant of 920 $dm^3\ mol^{-1}$ measured at 298 K in MeCN. Spectroscopic data are consistent with binding *via* $N^+\cdots O$ interactions, C–H···O hydrogen bonds and π-stacking analogous to that found in solution for **1a**–**d** and in the solid state, by X-ray crystallography, for **1d** (X = CO_2Et).[3]

Two routes were used to convert the [2]pseudorotaxane **2** to a permanently interlocked [2]rotaxane. First, **2** was alkylated at the terminal, pyridine nitrogen atoms with bulky *tert*-butylbenzyl groups by vigorously stirring a two-phase $MeNO_2$–saturated $NaBF_4(aq)$ solution containing 1 equiv. of **1e**, 6 equiv. of *tert*-butylbenzyl chloride and 3 equiv. of DB24C8. The [2]rotaxane **3** was isolated in 46% yield by extraction of the product into CH_2Cl_2 (Scheme 2). Significant *downfield* shifts (ppm) for α^+ (0.34) and $^+NCH_2$ (0.33) protons were indicative of C-H···O hydrogen bonding to crown ether O-atoms and *upfield* shifts were observed for the α (0.03), β (0.28), β^+ (0.27) and crown aromatic protons (0.26, 0.50) indicating π-stacking between the catechol and bipyridinium aromatic rings. An X-ray crystal structure determination† of **3** verified the nature of the interaction and an ORTEP diagram is shown in Fig. 1.

The [2]rotaxane, **3** exhibits $N^+\cdots O$ interactions ranging from 3.41 to 4.50 Å and eight C–H···O hydrogen bonds with C···O distances in the range 3.18–3.69 Å. The orange colour of the solid material is consistent with charge transfer interactions between the normally colourless crown ether and dipyridinium fragments. The S-shaped conformation of the dibenzo-24-crown ether molecule allows this π-stacking phenomenon to occur through both *intra*molecular and *inter*molecular interactions as shown in Fig 2.

In a metal–ligand, self-assembly reaction, the [2]pseudorotaxane **2** was used as a ligand and stoppered with organopalladium fragments to form the metallo-[2]rotaxane **4**. This was done by simply mixing 1 equiv. of **1e**, with 2 equiv. of $[Pd\{C_6H_3(PhSCH_2)_2\}(MeCN)]BF_4$ and 3 equiv. of DB24C8 in MeCN solution. The ^1H NMR spectrum of this solution showed that the [2]rotaxane **4** was formed in quantitative yield. As for **3**, significant *downfield* shifts for α^+ (0.41) and NCH_2 (0.38) protons were observed indicative of C–H···O hydrogen bonding to crown ether O-atoms, while *upfield* shifts were observed for the α (0.24), β (0.32), β^+ (0.38) and crown aromatic protons (0.31, 0.58) indicating π-stacking between the two sets of

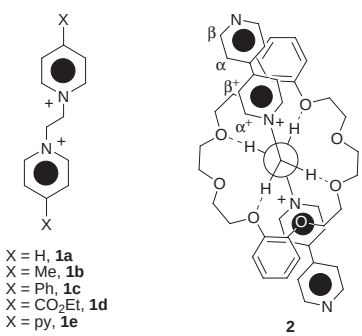

Scheme 1 Formation of [2]pseudorotaxane **2** from the 1,2-bis(4,4′-dipyridinium)ethane dication **1e** and DB24C8. **2** is viewed along the $^+NCH_2CH_2N^+$ vector in a Newman type projection emphasizing four of the stabilizing C–H···O interactions.

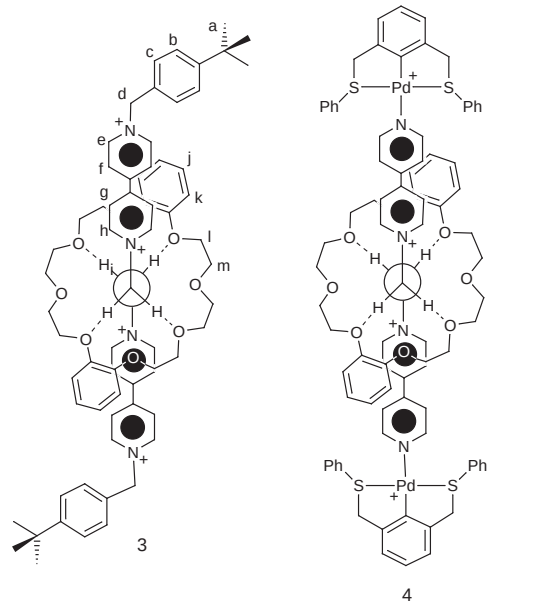

Scheme 2 [2]Rotaxanes can be formed from **2** by adding 'stopper' groups.

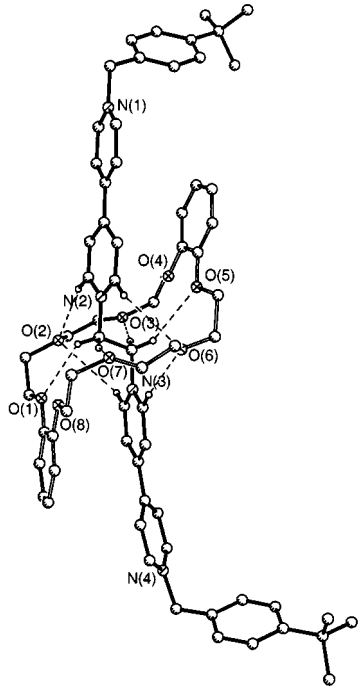

Fig. 1 An ORTEP diagram of the [2]rotaxane **3** showing the basic numbering scheme. $N(2)^{+}\cdots O$ distances; O(1) 4.52, O(2) 3.79, O(3) 3.93, O(4) 3.41, O(5) 3.55, O(6) 4.06, O(7) 3.80, O(8) 4.50 Å. $N(3)^{+}\ldots O$ distances; O(1) 3.43, O(2) 3.97, O(3) 4.05, O(4) 4.68, O(5) 4.64, O(6) 3.74, O(7) 4.22, O(8) 3.65 Å. C–H···O bonds: C(19)···O(2) 3.33, C(20)···O(6) 3.62, C(24)···O(2) 3.69, C(28)···O(6) 3.18, C(22)···O(1) 3.29, C(22)···O(7) 3.27, C(23)···O(3) 3.24, C(23)···O(5) 3.54 Å.

aromatic rings. An X-ray crystal structure determination of **4** verified the nature of the interaction and an ORTEP diagram is shown in Fig. 3.

The [2]rotaxane, **4** shows a series of $N^{+}\cdots O$ interactions ranging from 3.51 to 4.90 Å and eight C–H···O hydrogen bonds with C···O distances in the range 3.18–3.62 Å. The SPh rings of the metal fragment do not interact with the rest of the molecule. The organopalladium fragment is large enough to prevent unthreading and acts as a stopper in the designed manner.

The ability of the 1,2-bis(4,4′-dipyridinium) dication to form [2]rotaxanes using simple synthetic methodologies demonstrates that this component has the potential to be an important building block for the construction of more complex mechanically linked systems such as [2+*n*]rotaxanes, molecular necklaces[5] [*n*]MN and [*n*]catenanes.

We thank the Natural Sciences and Engineering Council of Canada for financial support of this research.

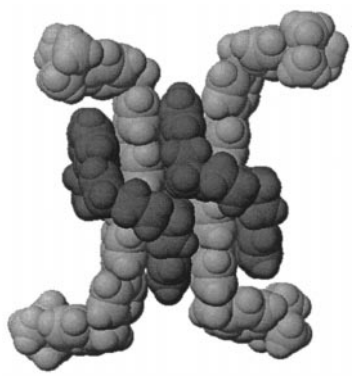

Fig. 2 A space-filling model showing the packing of two adjacent molecules of **3** in the unit cell.

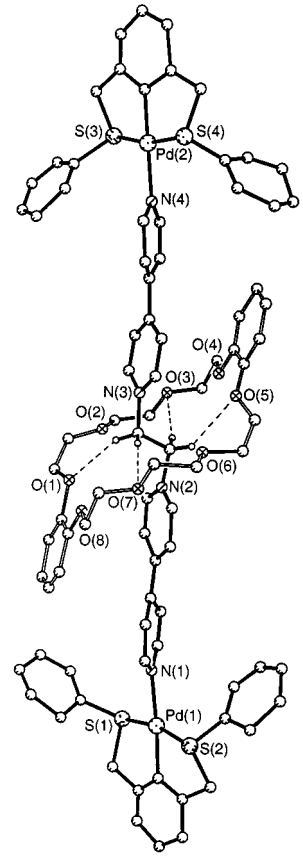

Fig. 3 An ORTEP diagram of the metal-capped [2]rotaxane **4** showing the basic numbering scheme. $N(2)^{+}\cdots O$ distances; O(1) 3.51, O(2) 3.78, O(3) 4.51, O(4) 4.85, O(5) 4.64, O(6) 3.80, O(7) 3.92, O(8) 3.55 Å. $N(3)^{+}\cdots O$ distances; O(1) 4.47, O(2) 3.68, O(3) 3.87, O(4) 3.54, O(5) 3.58, O(6) 3.86, O(7) 4.48, O(8) 4.90 Å. C–H···O bonds: C(28)···O(2) 3.31, C(29)···O(6) 3.28, C(33)···O(2) 3.18, C(37)···O(6) 3.42, C(31)···O(3) 3.62, C(31)···O(5) 3.44, C(32)···O(1) 3.44, C(32)···O(7) 3.51 Å.

Notes and references

† *Crystal data*: for **3**: $C_{68}H_{82}B_4F_{16}N_4O_8$, M = 1430.62, triclinic, space group $P\bar{1}$, a = 13.9669(3), b = 17.0627(3), c = 17.0640(3) Å, α = 86.686(1), β = 80.281(1), γ = 75.390(1)°, U = 3878.1(1) Å^3, T = 293(2) K, Z = 2, μ = 0.104 mm^{-1}, 9521 independent reflections (R_{int} = 0.0293), $R1$ = 0.1297, $wR2$ = 0.3690 ($I > 2\sigma I$), $R1$ = 0.1847, $wR2$ = 0.4310 (all data), Goodness-of-fit (F^2) = 0.908.

For **4**: $C_{86}H_{86}B_4F_{16}N_4O_8Pd_2S_4$, M = 1991.87, monoclinic, space group Pc, a = 17.8929(3), b = 14.3181(2), c = 19.4361(3) Å, β = 116.800(1)°, U = 4444.5(1) Å^3, T = 298(2) K, Z = 2, μ = 0.589 mm^{-1}, 11604 independent reflections (R_{int} = 0.0500), $R1$ = 0.0569, $wR2$ = 0.1198 ($I > 2\sigma I$), $R1$ = 0.0977, $wR2$ = 0.1431 (all data), Goodness-of-fit (F^2) = 0.974. Data were collected on a Siemens SMART CCD instrument and solutions performed using the SHELXTL 5.03 Program Library for Structure and Solution and Molecular Graphics, Siemens Analytical Instrument Division, Madison, WI, USA, 1995. CCDC 182/1085. See http://www.rsc.org/suppdata/cc/1998/2757/ for crystallographic files in .cif format.

1 D. B. Amabilino and J. F. Stoddart, *Chem. Rev*. 1995, **95**, 2725 and references therein; D. Philp and J. F. Stoddart, *Angew. Chem.*, 1996, **108**, 1242; *Angew. Chem., Int. Ed. Engl.*, 1996 **35**, 1154 and references therein.

2 P. R. Ashton, P. T. Glink, J. F. Stoddart, P. A. Tasker, A. J. P. White and D. J. Williams, *Chem. Eur. J.* 1996**, 2**, 729.

3 S. J. Loeb and J. A. Wisner, *Angew. Chem.* 1998, **110**, 3010; *Angew. Chem., Int. Ed. Engl*., 1998, **37**, 2838.

4 M. I. Attalla, N. S. McAlpine and L. A. Summers, *Z. Naturforsch., Teil B*, 1984, **39**, 74.

5 D. Whang and K. Kim, *J. Am. Chem. Soc.* 1997, **119**, 451; D. Whang, K-M. Park, J. Heo, P. Ashton and K. Kim, *J. Am. Chem. Soc.* 1998, **120**, 4899.

Communication 8/07449F

Synthesis of 2-deoxy and 2,6-dideoxy glycosides under neutral conditions in $LiClO_4/Et_2O$ mixtures

Heidrun Schene and Herbert Waldmann*

Universität Karlsruhe, Institut für Organische Chemie, Richard-Willstätter-Allee 2, D-76128 Karlsruhe, Germany. E-mail: waldmann@ochhades.chemie.uni-karlsruhe.de

Received (in Cambridge, UK) 5th October 1998, Accepted 6th November 1998

Glycosides of 2-deoxy and 2,6-dideoxy carbohydrates were built up in high yields and with high stereoselectivity in 0.1 M $LiClO_4/Et_2O$ mixtures; the glycosidations proceed under neutral conditions and without need for an additional promoter such as a strong Lewis acid, a heavy metal salt or an alkylating reagent.

2-Deoxy and 2,6-dideoxy glycosides are important substructures of antitumor drugs, antibiotics active against Gram-positive bacteria and drugs used in the treatment of cardiac insufficiency. Owing to this biological relevance the development of methods for the efficient and stereoselective construction of deoxyglycosidic linkages is of great relevance to organic synthesis, medicinal and bioorganic chemistry.[1] In comparison to the synthesis of other glycosides this problem is particularly challenging, since 2-deoxy glycosides are more acid-labile. Furthermore no stereodirecting neighboring group adjacent to the anomeric center is available that may direct the steric course of the glycosidation reaction. To circumvent these problems for deoxy glycoside synthesis, mostly electrophile-mediated addition of acceptor alcohols to the double bond of glycals followed by reductive removal of the C-2 substituents introduced into this position is employed.[2] Alternatively, glycosyl donors with 2-substituents acting as a neighboring group[3] or 1,2-anhydropyranoses[4] are used followed by reductive removal of the 2-substituent. Clearly, the application of direct methods for the efficient construction of 2-deoxy and 2,6-dideoxy glycosides is highly desirable.[5] These transformations should proceed under very mild and preferably neutral conditions without the use of strong Lewis acids or other promoters such as toxic and expensive heavy metal salts. We now report that trichloroacetimidates and fluorides of 2-deoxy and 2,6-dideoxy carbohydrates are activated under neutral conditions in solutions of $LiClO_4$ in Et_2O to give the correspondig deoxyglycosides with pronounced stereoselectivity and in high yields (Scheme 1).[6]

If benzyl-protected 2-deoxyglucosyl trichloroacetatimidate **1**[7] was treated with 6-O-deprotected benzylated glucoside **5a** in Glycosides of 2-deoxy and 2,6-dideoxy carbohydrates were built up in high yields and with high stereoselectivity in 0.1 M $LiClO_4/Et_2O$ mixtures; the glycosidations proceed under neutral conditions and without need for an additional promoter such as a strong Lewis acid, a heavy metal salt or an alkylating reagent.solutions of metal perchlorates in different solvents, the desired disaccharide **11** was formed smoothly. A brief survey of the reaction conditions (solvent, metal perchlorate, other metal salts, concentration of the salt) revealed that the best results were recorded in 0.1 M $LiClO_4$ in Et_2O. Under these conditions the desired glycoside was formed in 89% yield with a slight preference for the α-anomer (Table 1, entry 1). At lower or higher perchlorate concentration (0.03–0.5 M), in CH_2Cl_2, toluene or MeCN and in the presence of $Ba(ClO_4)_2$, $Zn(ClO_4)_2$ or $Mg(ClO_4)_2$, the yield was lower and the α/β selectivity remained almost unchanged. $LiClO_4$ could be replaced by $Li(NTf)_2$,[8] $LiBF_4$ or $LiPF_6$; however in the presence of these salts the results were not improved. Also the β-imidate corresponding to **1** gave inferior yields and the α/β selectivity remained unchanged. Therefore, all further reactions were conducted with the α-anomer **1** in 0.1 M $LiClO_4/Et_2O$ solutions.

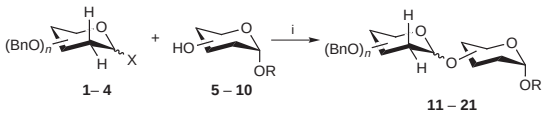

Scheme 1 *Reagents and conditions*: i, 0.1 M $LiClO_4$, 4 Å molecular sieves, solvent, room temp.

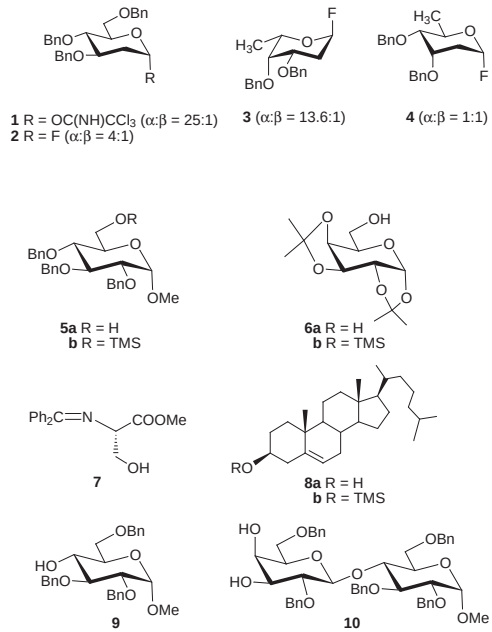

Table 1 Results of the glycosylation reactions in $LiClO_4/Et_2O$ mixtures employing 2-deoxy and 2,6-dideoxyglycosyl donors **1–4** and glycosyl acceptors **5–10** to give glycosides **11–21**

Entry	Glycosyl donor	Glycosyl acceptor	Product	Yield (%)[a]	Anomeric ratio (α : β)[b]
1	**1**	**5a**	**11**	89	1.5 : 1
2	**1**	**6a**	**12**	91[c]	2 : 1
3	**1**	**7**	**13**	57[d]	2.4 : 1
4	**1**	**8a**	**14**	78	1 : 1
5	**1**	**9**	**15**	37	only α
6	**2**	**5a**	**11**	65	13.4 : 1
7	**2**	**6a**	**12**	49	6 : 1
8	**2**	**8**	**14**	31	11.3 : 1
9	**3**	**5b**	**16**	49	8.1 : 1
10	**3**	**6b**	**17**	75	12.7 : 1
11	**3**	**8b**	**18**	66	only α
12	**3**	**10**	**19**	33	only α
13	**4**	**5b**	**20**	52	1 : 1.3
14	**4**	**6b**	**21**	61	9.5 : 1

[a] All glycosides were chromatographically purified and identified by ^1H NMR spectroscopy (250, 400 or 500 MHz). [b] Determined by integration of the relevant signals in the ^1H NMR spectra of the anomeric mixtures after chromatographic purification. [c] 0.15 M $LiClO_4$. [d] In CH_2Cl_2.

Under these gentle conditions glycosyl donor **1** reacts with galactose derivative **6a**, serine imine **7** and cholesterol **8a** to give the desired glycosides **12–14** in high yields, while glucosyl disaccharide **15** is obtained with lower yield (Table 1, entries 1–5). Thus 2-deoxyglycosyl imidate **1** is efficiently activated in the absence of a strong Lewis acid. The rate-accelerating effect of this reaction medium may be attributed to the ability of $LiClO_4/Et_2O$ solutions to stabilize polar or ionic transition states or intermediates like glycosyl cations.[6,9]

Although with imidate **1** the desired glycosides were formed in high yields the stereoselectivity remained low (Table 1, entries 1–4, see, however, entry 5). Therefore other glycosyl donors were investigated. Whereas use of the diethyl phosphite analogous to **1** did not improve this situation, 2-deoxyglycosyl fluoride **2** led to significantly higher anomer ratios. Glycosyl donor **2** is also activated in 1 M $LiClO_4$ in Et_2O under very mild conditions and reacts with selectively deprotected glucose **5a**, galactose **6a** and cholesterol **8a** to give glycosides **11**, **12** and **14** in useful yields. However, in these cases the α-anomers are formed with ratios ranging from 6:1 to 13.4:1 (Table 1, entries 6–8). Thus, by means of this method 2-deoxyglycosides can be constructed under very gentle conditions and with pronounced stereoselectivity.

In order to extend the scope of this very mild method, glycosylation of 2,6-dideoxy carbohydrates was investigated. Since in the case of 2-deoxyglucose the glycosyl fluoride had shown the most advantageous results, deoxy-L-fucosyl fluoride **3** and D-digitoxosyl fluoride **4** were prepared[7] and subjected to the glycosidation reactions.† As glycosyl acceptors silyl ethers **5b**, **6b** and **8b** were employed to facilitate the reactions by formation of the very stable Si–F bond. Lactose derivative **10** was used to investigate if regioselectivity can be achieved. Upon treatment of benzyl-protected 2-deoxyfucosyl fluoride with glucose derivative **5b**, galactosyl acceptor **6b**, cholesteryl silyl ether **8b** and lactose derivative **10** in 0.1 M $LiClO_4$ in Et_2O, glycosides **16–19** were smoothly formed in moderate to high yields. In all cases the anomer ratio was gratifyingly high (Table 1, entries 9–12). Whereas the glucose and the galactose disaccharides were obtained with α/β ratios of 8.1 to 12.7, cholesteryl glycoside **18**‡ and trisaccharide **19** were formed with complete α-selectivity. Furthermore, the glycosylation of lactose acceptor **10** proceeded with complete regioselectivity to deliver exclusively the 4′-deoxyfucosyl trisaccharide. Thus, under these reaction conditions glycosides of 2-deoxy-L-fucose can be prepared with high selectivity and the method is applicable to the construction of oligosaccharides.

D-Digitoxosyl fluoride **4** reacted with glucosyl and galactosyl silyl ethers **5b** and **6b** under the mild conditions provided by the $LiClO_4/Et_2O$ systems to give the corresponding disaccharides **20** and **21** in satisfying yields (Table 1, entries 13 and 14). Whereas with glucose acceptor **5b** the anomers were formed in nearly a 1:1 ratio, for galactose disaccharide **21** a high α/β ratio was once more recorded.

In conclusion the results detailed above demonstrate that in 0.1 M $LiClO_4/Et_2O$ mixtures glycosides of 2-deoxy and 2,6-dideoxy carbohydrates are formed in useful yields and with high stereoselectivity. The glycosidation reactions proceed under neutral conditions and without need for an additional promoter usually applied in glycoside synthesis, *i.e.* a strong Lewis acid, a heavy metal salt or an alkylating reagent.

This research was supported by the Deutsche Forschungsgemeinschaft and the Fonds der Chemischen Industrie.

Notes and references

† *General procedure* for the glycosydations with the fluorides **2**, **3** and **4** as donors. Pulverized, freshly activated molecular sieves (4 Å) (70 mg), $LiClO_4$ or $Ba(ClO_4)_2$ (0.2 mmol) and acceptor (0.2 mmol) were stirred in Et_2O, CH_2Cl_2 or MeCN (1 ml) for 30 min under argon. To this suspension was added a solution of the donor (0.1 mmol) in the same solvent (1 ml). In the case of acceptors without a TMS group, CsF (0.1 mmol) was used as an acid scavenger. After stirring for 3 d (2 d with the donors **3** and **4**) at room temperature, the reaction mixture was diluted with CH_2Cl_2 (50 ml), filtered and washed with water. The organic layer was dried over Na_2SO_4 and concentrated *in vacuo*. The crude product was purified by flash chromatography.

‡ *Selected data* for **18**: This compound was purified by flash chromatography with EtOAc–hexane (1% NEt_3) 1:8→1:4→1:2. White solid; mp 109 °C; R_f: 0.66 (EtOAc–hexane 1/2); $[\alpha]_D$ −72.2 (*c* 1.0, $CHCl_3$); δ_H(500 MHz, $CDCl_3$) 0.67 (s, 3H), 0.85–1.57 (m, 33H), 1.15 (d, $J_{5,6}$ 6.5, 3H, 6-CH_3), 1.76–1.84 (m, 3H), 1.93–2.01 (m, 3H, 2′-H, 2H Chol), 2.17–2.21 (m, 2H, 2-H), 2.32 (dd, *J* 3.0, 13.2, 1H), 3.41–3.44 (m, 1H), 3.61 (s, 1H, 4-H), 3.87 (q, $J_{5,6}$ 6.6, 1H, 5-H), 3.94–3.96 (m, 1H, 3-H), 4.59–4.64 (m, 2H, OCH_2Ph), 4.69, 4.96 (2d, J_{gem} 11.8, 2H, OCH_2Ph), 5.11 (d, $J_{1,2}$ 3.3, 1H, 1-H), 5.32 (d, *J* 4.8, 1H), 7.24–7.39 (m, 10H, Ph*H*).

1 J. Thiem and W. Klaffke, *Top. Curr. Chem*., 1990, **154**, 285; K. Toshima and K. Tatsuta, *Chem. Rev*., 1993, **93**, 1503.

2 For recent references see: J. Thiem and W. Klaffke, *J. Org. Chem*., 1989, **54**, 2006; S. Sabesan and S. Neira, *J. Org. Chem*., 1991, **56**, 5468; K. Suzuki, G. A. Sulikowski, R. W. Friesen and S. J. Danishefsky, *J. Am. Chem. Soc*., 1990, **112**, 8895; H. Mereyala, V. R. Kulkarni, D. Ravi, G. V. M. Sharma, B. Venkateswara Rao and G. B. Reddy, *Tetrahedron Lett*., 1992, **48**, 545; K. Toshima, S. Mukaiyma, Y. Nozaki, H. Inokuchi, M. Nakata and K Tatsuta, *J. Am. Chem. Soc*., 1994, **116**, 9042;

3 For recent references see: J. Thiem, M. Gerken and K. Bock, *Liebigs Ann. Chem*., 1983, 462; Y. Ito and T. Ogawa, *Tetrahedron Lett*., 1990, **46**, 89; K. Toshima, Y. Nozaki and K. Tatsuta, *Tetrahedron Lett*., 1991, **32**, 6887; R. Preuss and R. R. Schmidt, *Synthesis*, 1988, 694; S. Hashimoto, Y. Yanagiya, T. Honda and S. Ikegami, *Chem. Lett*., 1992, 1511.

4 J. Gervay and S. Danishefsky, *J. Org. Chem*., 1991, **56**, 5448.

5 Recent references: application of the Koenigs–Knorr reaction in the direct synthesis of 2-deoxy glycosides employing the insoluble silver silicate: (*a*) J. Thiem and S. Köpper, *Tetrahedron*, 1990, **46**, 133; (*b*) R. W. Binkley, *J. Carbohydr. Chem*., 1990,**9**, 507; application of glycosyl phosphoramidites and phosphites for the direct synthesis of 2-deoxy glycosides: (*c*) H. Li, M. Chem and K. Zhao, *Tetrahedron Lett*., 1997, **38**, 6143; (*d*) S. Hashimoto, A. Sano, H. Sakamoto, M. Nakajima, Y Yanagiya and S. Ikegami, *Synlett*, 1995, 1271; application of glycosyl sulfoxides for the direct synthesis of 2-deoxy glycosides: (*e*) S.-H. Kim, D. Augeri, D. Yang and D. Kahne, *J. Am. Chem. Soc*., 1994, **116**, 1766; application of gylcosyl fluorides for the direct synthesis of 2-deoxy glycosides: (*f*) J. Junnmann, I. Lundt and J. Thiem, *Liebigs Ann. Chem*., 1991, 759.

6 H. Waldmann, G. Böhm, U. Schmid and H. Röttele, *Angew. Chem*., 1994, **106**, 2024; *Angew. Chem., Int. Ed. Engl*., 1994, **33**, 1944; G. Böhm and H. Waldmann, *Tetrahedron Lett*., 1995, **36**, 3843; G. Böhm and H. Waldmann, *Liebigs. Ann. Chem*., 1996, 613 and 621; U. Schmid and H. Waldmann, *Chem. Eur. J*., 1998, **4**, 494; H. Schene and H. Waldmann, *Eur. J. Org. Chem*., 1998, 1227.

7 α-Configured glucosyl trichloroacetimidate **1** was synthesized by treatment of 3,4,6-tri-*O*-benzyl-2-deoxyglucose with NaH and Cl_3CCN in CH_2Cl_2 according to the general procedure described by R. R. Schmidt, J. Michel and M. Roos, *Liebigs Ann. Chem*., 1984, 1343. The corresponding β-anomer was obtained by employing K_2CO_3 as base. In both cases the yield was quantitative. Glycosyl fluorides **2–4** were obtained in quantitative yield by treatment of the corresponding 1-*O*-deprotected benzylated carbohydrates with diethylamino sulfur trifluoride (DAST) in CH_2Cl_2 according to the general procedure (W. Rosenbrook, Jr., D. A. Riley and P. A. Lartey, *Tetrahedron Lett*., 1985, **26**, 3).

8 S. T. Handy, P. A. Grieco, C. Mineur and L. Ghosez, *Synlett* 1995, 565; R. Tamion, C. Mineur and L. Ghosez, *Tetrahedron Lett*., 1995, **36**, 8977.

9 P. A. Grieco, *Aldrichim. Acta*, 1991, **24**, 59; H. Waldmann, *Angew. Chem*., 1991, **103**, 1335; *Angew. Chem., Int. Ed. Engl*., 1991, **30**, 1306; U. Schmid and H. Waldmann, in *Organic Synthesis Highlights III*, ed. J. Mulzer and H. Waldmann, Wiley-VCH, Weinheim, 1997, pp. 205–210

Communication 8/07734G

ChemComm

Are vinylidenes possible intermediates in thermal rearrangements of substituted cyclopropenes? A theoretical study†

Norman Goldberg* and Wilhelm Graf von der Schulenburg

Institute of Organic Chemistry, Technical University Braunschweig, Hagenring 30, D-38106 Braunschweig, Germany. E-mail: n.goldberg@tu-bs.de

Received (in Liverpool, UK) 11th September 1998, Accepted 17th November 1998

The thermally induced ring-opening reactions of substituted cyclopropenes to the corresponding vinylidenes have been investigated computationally; the alkyl-substituted singlet vinylidenes have been found to lie in potential wells of 7–11 kcal mol^{-1} (DFT calculations; 1 kcal = 4.184 kJ).

Vinylidenes, unsaturated carbenes of the type $R_2C{=}C{:}$, have received a great deal of attention during recent years. They have been postulated as reactive intermediates in organic reactions[1] and the simplest member of this family of compounds, $H_2C{=}C{:}$, was characterised by mass spectrometry[2] and negative ion photoelectron spectroscopy[3] of the corresponding vinylidene anion, $H_2C{=}C^{-\cdot}$. These experimental as well as several theoretical studies[4] demonstrate that the singlet vinylidene, $H_2C{=}C{:}$, lies in a very shallow potential energy well and readily rearranges to acetylene on the picosecond time scale.[3b] Thus, the observation of a vinylidene species in the mass spectrometric studies was attributed to a long-lived, excited triplet species.

Another experimental entry into the chemistry of vinylidenes was predicted by Yoshimine and co-workers[4b] in a theoretical study on the thermal ring opening of cyclopropene. Based upon their calculations, the authors proposed that cyclopropene may not only rearrange to propyne *via* a homolytic bond cleavage to vinyl carbene and subsequent hydrogen migration (as previously assumed[5]), but that methylvinylidene also constitutes an energetically viable intermediate. Recent experimental studies on the pyrolysis of substituted cyclopropenes[6] have furnished the first experimental evidence for the involvement of vinylidene carbenes as intermediates in the thermal rearrangements of highly strained cyclopropenes. Hopf *et al.*[6d] found that isomeric cyclopropenes can be thermally interconverted and proposed that the common intermediates in these reactions are vinylidenes. However, to the best of our knowledge the only singlet vinylidene that has been successfully trapped and characterized is difluorovinylidene, $F_2C{=}C{:}$, which was recently observed by matrix isolation and theoretical studies.[7]

These interesting experimental results have prompted us to investigate the possible intermediates in the thermal isomerizations (Scheme 1) of a number of substituted cyclopropenes [Structures **1**, **3** and **4**, where R = R′ = H (**1a**, **3a**, **4a**), R = H, R′ = CH_3 (**1b**–**4b**) and R = R′ = CH_3 (**1c**–**4c**)] by means of

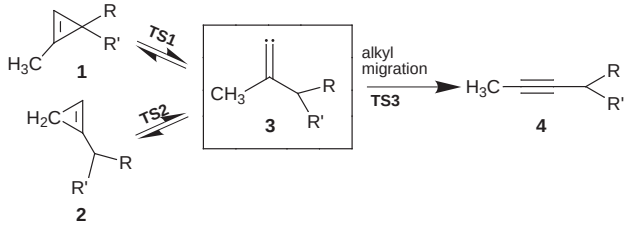

Scheme 1 Thermally induced formation of vinylidenes (**3**) from cyclopropenes (**1** and **2**) and alkyne formation (**4**) *via* alkyl migration.

† Details of the theoretical study are available from the RSC web page, see http://www.rsc.org/suppdata/cc/1998/2761

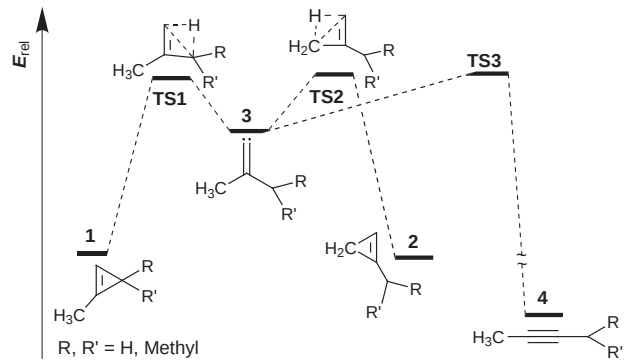

Fig. 1 Schematic singlet potential energy surface of alkyl-substituted cyclopropenes (**1**, **2**), vinylidenes (**3**), alkynes (**4**) and transition states (**TS1**,**TS2** and **TS3**).

hybrid density-functional (B3LYP) and *ab initio* (CCSD(T)) methods.[8]

A schematic potential energy surface for the important pathways leading to vinylidenes and the subsequent formation of alkynes upon alkyl migration is shown in Fig. 1. Formation of the corresponding vinylidenes occurs *via* a transition state involving the simultaneous breaking of a bond and a hydrogen shift, which for the reverse reaction is best described as an intramolecular insertion of the vinylidene carbene into the C–H bond (Fig. 2). Both types of substituted cyclopropenes, **1** and **2**, thus give rise to identical vinylidenes.

Our theoretical results (Table 1) indicate that the alkyl-substituted vinylidenes **3a**–**c** are all intermediates in the ring-opening reactions of alkylcyclopropenes (**1a**–**c** and **2a**–**c**). In the case of dimethylvinylidene **3a**, the symmetry-allowed 1,2-migration of a methyl group (**TS3a**) (with retention of its configuration), lies 11.1 kcal mol^{-1} above the vinylidene, while the transition state for the cyclization reaction (**TS1a**) giving

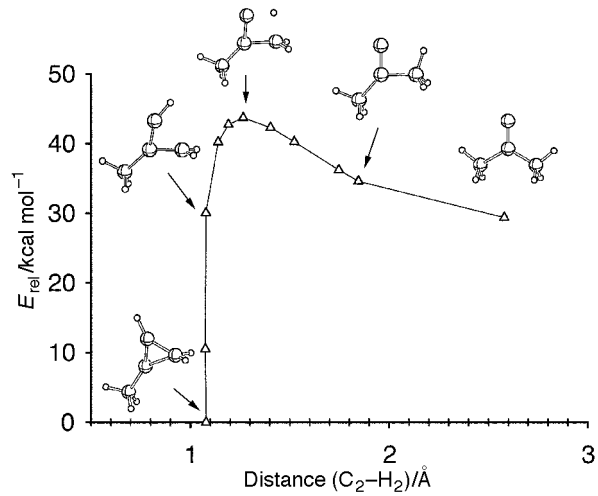

Fig. 2 Intrinsic reaction coordinate (IRC) for the formation of dimethylvinylidene (**3a**) from 1-methylcyclopropene (**1a**) *via* **TS1a** (B3LYP/6-31G*).

Table 1 Relative energies [in kcal mol^{-1}; B3LYP/6-311+G(2d,p) and CCSD(T)/6-31G(d) level of theory] of alkylvinylidenes (**3a–c**) with respect to their cyclopropene precursors (**1a–c** and **2b**,**c**), their connecting transition states (**TS1a–c** and **TS2b**,**c**) and the transition states for the alkyl migrations leading to alkynes (**TS3a–c**)

	1a		**3a**	**TS1a**		**TS3a**	
B3LYP	−25.9		0.0	12.5		11.1	
CCSD(T)	−29.2		0.0	15.0		13.0	
	1b	**2b**	**3b**	**TS1b**	**TS2b**	**TS3b-Me**	**TS3b-Et**
B3LYP	−28.4	−26.0	0.0	9.4	12.5	11.3	9.6
CCSD(T)	−29.1	−26.6	0.0	12.3	15.4	13.8	12.0
	1c	**2c**	**3c**	**TS1c**	**TS2c**	**TS3c-Me**	**TS3c-Pr^i**
B3LYP	−30.4	−26.3	0.0	7.3	12.5	10.9	9.7
CCSD(T)	−31.3	−27.1	0.0	9.8	15.1	13.1	11.1

rise to the 1-methylcyclopropene is 12.5 kcal mol^{-1} higher in energy (all B3LYP results). The lowest exit channel for ethylmethylvinylidene **3b** lies 9.4 kcal mol^{-1} above the vinylidene and the lowest isomerization pathway of methylisopropylvinylidene **3c** requires 7.3 kcal mol^{-1}. Thus all three investigated vinylidenes correspond to minima on their energy surfaces, substantiating the proposal that these reactive species are indeed common intermediates in the isomerization of cyclopropenes.[6d]

Overall, the good correlation of *ab initio* and density-functional results lends confidence to the quality of our thermochemical predictions. Further support for the reliability of the B3LYP data comes from comparison of these results with experimentally determined activation energies. The average deviation of the calculated barrier heights from the experimentally obtained values for the cyclopropene-to-vinylidene transition states **TS1b–c** and **TS2b–c**[6d,9] is found to be 2.4 kcal mol^{-1} at the B3LYP/6-31G* level and 0.1 kcal mol^{-1} at the B3LYP/6-311+G(2d,p) level. The results of the B3LYP/6-311+G(2d,p) calculations lie within the experimental error bars. This means that, given an average experimental error of 0.4 kcal mol^{-1},[6d,9] the relative error in the B3LYP/6-311+G(2d,p) must be smaller than 0.5 kcal mol^{-1}. The deviation of the *ab initio* results [CCSD(T)/6-31G*] from the experimental values is about 3.5 kcal mol^{-1}. Similar excellent agreement between activation energies obtained with the B3LYP method and experimental values has recently been noted for [3,3]-sigmatropic rearrangements.[10]

The experimentally observed formation of alkynes from vinylidenes involves a rate-affecting alkyl migration. With unsymmetrically substituted vinylidenes (**3b–c**) either a methyl (**TS3b-Me** and **TS3c-Me**) or an alkyl (**TS3b-Et** and **TS3c-Pr^i**) migration can occur. The calculations show that alkyl migration **TS3b-Et** and **TS3c-Pr^i** is preferred over the methyl shift (**TS3b-Me** and **TS3c-Me**), although the differences in the activation energies for these processes are small [ΔE_a(B3LYP) = 1.7 and 1.2 kcal mol^{-1}, respectively]. This agrees with experimental results from the pyrolysis of ^{13}C-labelled cyclopropenes **1b** and **1c**,[6e] where the ratio of **TS3b-Et** and **TS3b-Me** is found to be 3:1 and of **TS3c-Pr^i** and **TS3c-Me** is 1.4:1. The reasons for these small energetic differences, although difficult to pinpoint, most likely result from a combination of hyperconjugation, which stabilizes the three-centre two-electron bonds in these transition states, and steric effects, leading to a destabilization of the TS for the migration of higher substituted alkyl groups.

We have also investigated the homolytic bond-cleavage that gives rise to vinyl carbenes (**5a** and **5b**) (Scheme 2). Although

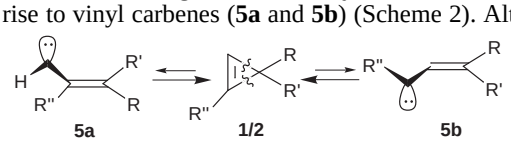

Scheme 2

this reaction is in some cases energetically preferred over vinylidene formation, it leads to an energetic dead end.[11] Subsequent hydrogen shifts of these vinyl carbenes that would lead to the corresponding allenes or dienes are all found to lie higher in energy than the corresponding vinylidene pathways and the transition states for the direct formation of alkynes from these conjugated carbenes all lie approximately 20 kcal mol^{-1} above the transition states for the alkyne formation from the corresponding vinylidenes.

These findings agree well with the experimentally observed product distributions in the pyrolysis of various cyclopropenes where the main decomposition channel was found to lead to alkynes.[6a–d,9]

The theoretical results support the proposed mechanistic pathway for the thermal ring-opening of highly strained cyclopropenes, and demonstrate that alkyl-substituted singlet vinylidenes correspond to intermediates that lie in potential energy wells deep enough to allow their characterization by spectroscopic methods. Experiments aimed at further characterisation of these interesting sub-valent carbon species thus seem promising. In contrast to previous assumptions, our theoretical investigations indicate that vinyl carbenes are not intermediates in the formation of alkynes from cyclopropenes.

N. G. kindly thanks Professor H. Hopf for his continuing support and interest in our work and the DFG for a fellowship.

Notes and references

1 P. J. Stang, *Chem. Rev*., 1978, **78**, 383.
2 D. Sülzle and H. Schwarz, *Chem. Phys. Lett*., 1989, **156**, 397.
3 (*a*) S. M. Burnett, A. E. Stevens, C. S. Feigerle and W. C. Lineberger, *Chem. Phys. Lett*., 1983, **100**, 124; (*b*) K. M. Ervin, J. Ho and W. C. Lineberger, *J. Phys. Chem*., 1989, **91**, 5975.
4 (*a*) J. T. Carrington, L. M. Hubbard, H. F. Schaefer, III and W. H. Miller, *J. Am. Chem. Soc*., 1984, **80**, 4347; (*b*) M. Yoshimine, J. Pacansky and N. Honjou, *J. Am. Chem. Soc*., 1989, **111**, 4198; (*c*) G. Vacek, J. R. Thomas, B. J. DeLeeuw, Y. Yamaguchi and H. F. Schaefer, III, *J. Chem. Phys*., 1993, **98**, 4766; (*d*) G. Vacek, J. R. Thomas, B. D. DeLeeuw and H. F. Schaefer, III, *J. Chem. Phys*., 1994, **100**, 4969.
5 R. Srinivasan, *J. Chem. Soc*., *Chem. Commun*., 1971, 1041.
6 (*a*) H. Hopf, G. Wachholz and R. Walsh, *Chem. Ber*., 1985, **118**, 3579; (*b*) H. Hopf, A. Plagens and R. Walsh, *J. Chem. Soc*., *Chem. Commun*., 1994, 421; (*c*) I. R. Likhotvorik, R. D. Brown and J. M. Jones, *J. Am. Chem. Soc*., 1994, **116**, 6175; (*d*) H. Hopf, W. Graf von der Schulenburg and R. Walsh, *Angew. Chem*., *Int. Ed. Engl*., 1997, **36**, 381; (*e*) W. Graf von der Schulenburg, H. Hopf and R. Walsh, *Angew. Chem*., in press.
7 J. Breidung, H. Bürger, C. Kötting, R. Kopitzky, W. Sander, M. Senzlober, W. Thiel and H. Willner, *Angew. Chem*., *Int. Ed. Engl*., 1997, **36**, 1983.
8 Gaussian 94 (Revision E4), M. J. Frisch, G. W. Trucks, H. B. Schlegel, P. M. W. Gill, B. G. Johnson, M. A. Robb, J. R. Cheeseman, T. Keith, G. A. Petersson, J. A. Montgomery, K. Raghavachari, M. A. Al-Laham, V. G. Zakrzewski, J. V. Ortiz, J. B. Foresman, J. Cioslowski, B. B. Stefanov, A. Nanayakkara, M. Challacombe, C. Y. Peng, P. Y. Ayala, W. Chen, M. W. Wong, J. L. Andres, E. S. Replogle, R. Gomperts, R. L. Martin, D. J. Fox, J. S. Binkley, D. J. Defrees, J. Baker, J. P. Stewart, M. Head-Gordon, C. Gonzalez and J. A. Pople, Gaussian Inc., Pittsburgh PA, 1995. All structures were optimized at the B3LYP/6-311+G(2d,p) level of theory, characterized by frequency calculations and are zero-point energy corrected. In the case of homolytic bond cleavage reactions unrestricted calculations were carried out. CCSD(T)/6-31G* energies correspond to single-point calculations of the B3LYP/6-311+G(2d,p) structures. These energies were corrected with the zero-point energies obtained at the B3LYP/6-311+G(2d,p) level. For all transition structures IRC calculations were performed.
9 H. Hopf, W. Graf von der Schulenburg and R. Walsh, in preparation.
10 K. A. Black, S. Wilsey and K. N. Houk, *J. Am. Chem. Soc*., 1998, **120**, 5622.
11 Nevertheless this pathway is responsible for the thermal racemization of optically pure cyclopropenes (E. J. York, W. Dittmar, J. R. Stevenson and R. G. Bergman, *J. Am. Chem. Soc*., 1973, **95**, 5680). Bergman and co-workers reported an E_a of 32.6 kcal mol^{-1} for the racemization of 1,3-diethylcyclopropene. We find that the lowest E_a values for formation of vinylcarbenes from cyclopropenes **1b** and **2b** are 31.4 and 33.7 kcal mol^{-1}, respectively (B3LYP).

Communication 8/07120I

Stereoselective sulfoxidation of α-mannopyranosyl thioglycosides: the *exo*-anomeric effect in action

David Crich,*[a] Jan Mataka,[a] Sanxing Sun,[a] K.-C. Lam,[b] Arnold L. Rheingold[b] and Donald J. Wink[a]

[a] *Department of Chemistry, University of Illinois at Chicago, 845 West Taylor Street, Chicago, IL 60607-7061, USA. E-mail: dcrich@uic.edu*

[b] *Department of Chemistry and Biochemistry, University of Delaware, Academy Street, Newark, DE 19716, USA*

Received (in Corvallis, OR, USA) 29th May 1998, Accepted 10th November 1998

As a consequence of the *exo*-anomeric effect, and in contrast to their β-anomers, α-thioglycosides undergo stereoselective oxidation to give very predominantly the *R*-sulfoxides, as revealed by X-ray crystallography.

The sulfoxide method is a very powerful tool for the formation of glycosidic linkages to even very sterically hindered, unreactive glycosyl acceptors.[1–3] In most of the work described in the literature β-thioglycosides are oxidized to mixtures of sulfoxides,[3–5] which are used as such in the coupling reaction. In contrast, we have noted that a range of differentially protected α-mannopyranosyl thioglycosides are oxidized with excellent stereoselectivity to give essentially diastereomerically pure sulfoxides. These may then be employed productively in the efficient synthesis of β-mannopyranosides.[6–9] We now report the configuration of three α-mannopyranosyl sulfoxides, as determined by X-ray crystallography and chemical correlation, and discuss a possible reason for the stereoselectivity.

Initially, we noted that thioglycoside **1** was oxidized stereoselectively by magnesium monoperoxyphthalate (MMPP) in aqueous THF to give a single sulfoxide **8** in excellent yield, but were unable to assign configuration.[10] Similar results were obtained with MCPBA in CH_2Cl_2. Subsequently, the same phenomenon was observed with thioglycosides **2**–**7** and **15**–**17**, giving the corresponding sulfoxides **9**–**14** and **18**–**20**.[6–9,11,12] In view of the mechanism of the stereoselective β-mannosylation process,[9] in which the sulfoxide simply serves as a convenient precursor to the actual glycosylating species, the α-mannosyl triflate, the configuration at sulfur is of no consequence. However, curiosity dictated that we seek the origins of this unanticipated stereoselective sulfoxidation. Eventually, we were rewarded by the growth of single crystals of **20** (mp 109–111 °C) suitable for X-ray crystallographic analysis from EtOH solution. In due course the configuration at sulfur was revealed to be *R* (Fig. 1).

In an attempt to obtain an isomeric sulfoxide, **16** was oxidized with $NaIO_4$ and with Oxone, but in each case only **19** was obtained. It was therefore apparent that the stereoselectivity was not a function of the reagent and, for example, hydrogen bonding to the ring oxygen. We next submitted thioglycoside **21** to oxidation with MCPBA and again were rewarded by the formation of one major sulfoxide (> 10:1). Crystals suitable for X-ray analysis were again obtained (mp 190 °C, EtOH) and the structure consequently revealed to be **22** (Fig. 2), with the same configuration at sulfur as **20**. Again, a diverse range of oxidants provided the same major sulfoxide. Treatment of **22** with NaH and then BnBr in THF provided sulfoxide **10**, albeit in only 35% yield, so fixing its configuration at sulfur as *R*. Thus, we have established that three of the eleven sulfoxides in question have the same *R*-configuration and see no reason to doubt that the remainder follow the pattern.

In view of the range of different oxidants and solvents employed, each giving the same result, we conclude that the stereoselectivity of the oxidation is dictated predominantly by

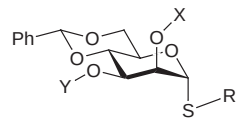

1 R = Et, X = TBDMS, Y = Bn
2 R = Et, X = TMS, Y = Bn
3 R = Et, X = Y = Bn
4 R = Ph, X = Y = Bn
5 R = Et, X = Y = allyl
6 R = Et, X = allyl, Y = Bn
7 R = Ph, X = Y = Me

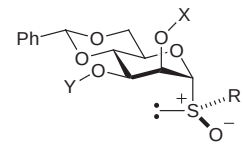

8 R = Et, X = TBDMS, Y = Bn
9 R = Et, X = TMS, Y = Bn
10 R = Et, X = Y = Bn
11 R = Ph, X = Y = Bn
12 R = Et, X = Y = allyl
13 R = Et, X = allyl, Y = Bn
14 R = Ph, X = Y = Me

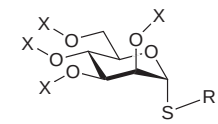

15 R = Et, X = Bn
16 R = Ph, X = Me

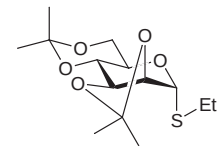

17

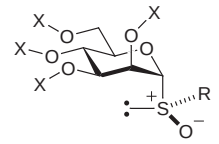

18 R = Et, X = Bn
19 R = Ph, X = Me

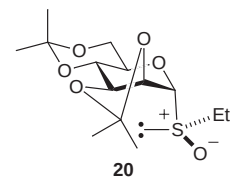

20

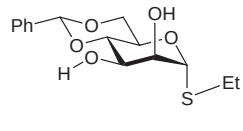

21

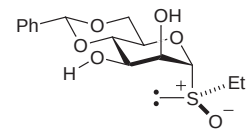

22

steric effects[13] and the conformation imposed on the thioglycosides by the *exo*-anomeric effect.[14–16] Thus, as seen from the Newman projection in Fig 3, in the conformation imposed by the *exo*-anomeric effect the *pro-R* lone pair of the α-thioglycosides is exposed to attack. On the other hand oxidation of the *pro-S* lone pair would be substantially hindered by the pyranose ring, and especially by the axial hydrogens, H-3 and H-5. In the case of the β-thioglycosides, the two lone pairs are less sterically differentiated and mixtures of sulfoxides result.

Finally, we note that the two crystalline sulfoxides both adopt the same conformation (Fig. 1 and 2) about the C1–S bond, which roughly mirrors that imposed on the original thioglyco-

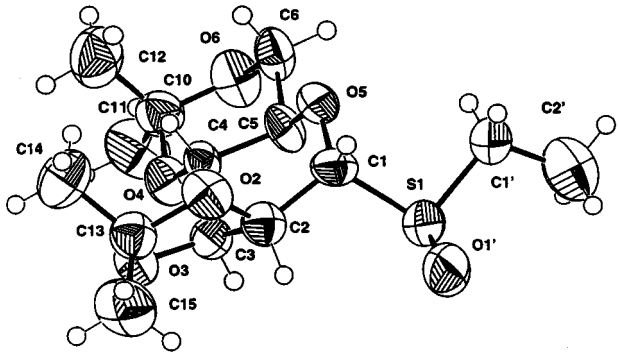

Fig. **1** Structure of **20** showing crystallographic numbering scheme adopted.

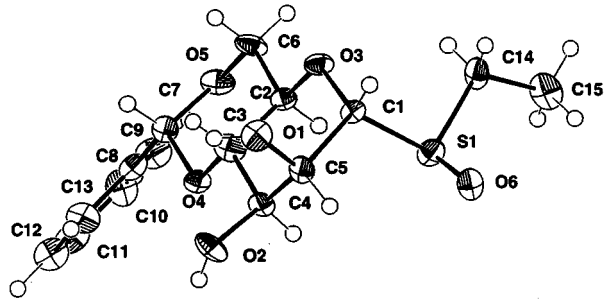

Fig. **2** Structure of **22** showing crystallographic numbering scheme adopted.

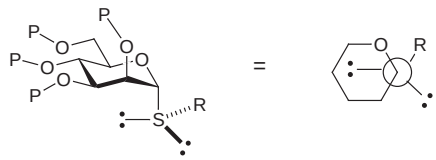

P = protecting group or H

Fig. **3**

sides by the *exo*-anomeric effect. However, in this instance, it seems likely that this is more a consequence of minimization of repulsion between the C1–O5 and S–O dipoles.[17]

We thank the NSF (CHE 9625256 and NIH GM57335) for partial support of this work.

Notes and references

1 R. Liang, L. Yan, J. Loebach, M. Ge, Y. Uozumi, K. Sekanina, N. Horan, J. Gildersleeve, C. Thompson, A. Smith, K. Biswas, W. C. Still and D. Kahne, *Science*, 1996, **274**, 1520.
2 D. Kahne, S. Walker, Y. Cheng and D. V. Engen, *J. Am. Chem. Soc*., 1989, **111**, 6881.
3 L. Yan and D. Kahne, *J. Am. Chem. Soc*., 1996, **118**, 9239.
4 R. Kakarla, R. G. Dulina, N. T. Hatzenbuhler, Y. W. Hui and M. J. Sofia, *J. Org. Chem*., 1996, **61**, 8347.
5 However, we note that the two unprotected β-galactosyl phenyl sulfoxides are hydrolyzed at different rates by aqueous TfOH, presumably due to differential intramolecular hydrogen bonding interactions: N. Khiar, I. Alonso, N. Rodriguez, A. Fernandez-Mayorales, J. Jimenez-Barbero, O. Nieto, F. Cano, C. Foces-Foces and M. Martin-Lomas, *Tetrahedron Lett*., 1997, **38**, 8267.
6 D. Crich and S. Sun, *Tetrahedron*, 1998, **54**, 8321.
7 D. Crich and S. Sun, *J. Org. Chem*., 1996, **61**, 4506.
8 D. Crich and S. Sun, *J. Org. Chem*., 1997, **62**, 1198.
9 D. Crich and S. Sun, *J. Am. Chem. Soc*., 1997, **119**, 11217.
10 D. Crich, S. Sun and J. Brunckova, *J. Org. Chem*., 1996, **61**, 605.
11 D. Crich and Z. Dai, *Tetrahedron Lett*., 1998, **53**, 1681.
12 A further, unassigned example of diastereoselective sulfoxidation of an α-mannosyl thioglycoside: G. Stork and J. J. La Clair, *J. Am. Chem. Soc*., 1996, **118**, 247.
13 C. R. Johnson and D. McCants, *J. Am. Chem. Soc*., 1965, **87**, 1109.
14 E. Juaristi and G. Cuevas, *The Anomeric Effect*, CRC Press, Boca Raton, 1995.
15 P. Deslongchamps, *Stereoelectronic Effects in Organic Chemistry*, Pergamon, Oxford, 1983.
16 A. J. Kirby, *The Anomeric Effect and Related Stereoelectronic Effects at Oxygen*, Springer-Verlag, Berlin, 1983.
17 *Crystal data* for **20**: $C_{14}H_{24}O_6S$, M = 320.39, monoclinic, a = 11.282(7), b = 9.766(10), c = 15.555(12) Å, β = 99.73(6)°, V = 1689(2) Å^3; $P2_1$, Z = 4 (two independent molecules per asymmetric unit), μ = 0.22 mm^{-1}. Of 3381 reflections measured at room temperature, 3163 independent reflections were used in refinement on F^2. Final agreement factors for 390 least-squares parameters for 1887 data with $I > 2\sigma(I)$ (with values for all independent reflections in parentheses): R = 0.0412 (0.0830), R_w = 0.0984 (0.1217), GOF = 1.032 (1.131). For **22**: $C_{15}H_{20}O_6S$, M = 328.37, monoclinic, a = 5.1509(2), b = 12.9187(4), c = 11.4762(5), β = 95.554(2)°, V = 760.07(8) Å^3, $P2_1$, Z = 2. μ = 0.24 mm^{-1}. Of 2613 reflections measured at T = 173 K, there were 1718 independent reflections used in refinement against F^2 with 1551 having $I > 2\sigma(I)$. Final agreement factors for 199 least-squares parameters (with values for all independent reflections in parentheses): R = 0.0864 (0.1039), $wR2$ = 0.2847 (0.2582), GOF = 2.415 (2.414). CCDC 182/1088. The crystallographic data is available as a .cif file: see http://www.rsc.org/suppdata/cc/1998/2763/

Communication 8/04126A

Enantioselective palladium catalyzed allylic substitution with chiral thioether derivatives of ferrocenyl-oxazoline and the role of planar chirality in this reaction

Shu-Li You, Yong-Gui Zhou, Xue-Long Hou and Li-Xin Dai*

Laboratory of Organometallic Chemistry, Shanghai Institute of Organic Chemistry, Chinese Academy of Sciences, 354 Fenglin Lu, Shanghai 200032, China. E-mail: dailx@pub.sioc.ac.cn

Received (in Cambridge, UK) 26th October, 1998 Accepted 12th November 1998

A series of chiral thioether dervatives of ferrocenyl-oxazolines, prepared with diastereoselectivities > 95 : 5, have been shown to be highly efficient catalysts for a palladium catalyzed allylic substitution reaction, with enantioselectivity of 81–98% ee, and the role of planar chirality in these ligands was also discussed.

In the past few years, palladium catalyzed allylic substitutions[1] have been used extensively in asymmetric carbon–carbon bond formation to provide chemo-, regio-, diastereo-, and enantioselectivity.[2] A variety of chiral ligands have been studied. In addition to the widely used phosphine or phosphite ligands, sulfur–nitrogen ligands have recently been proved to be successful.[3] For example, Williams explored thioether of phenyloxazoline ligands for the palladium catalyzed allylic substitution,[13a,b] good to excellent enantioselectivities were obtained. Other groups also showed the high enantioselectivity obtained with this type of N,S-bidentate ligand. Recently, planar chiral bidentate ligands have been successfully applied in many asymmetric reactions. The work of Fu and coworkers showed that the single planar chiral bidentate ligands were highly efficient catalysts for several asymmetric reactions.[4] In conjunction with our group's interest on asymmetric sulfonium ylide reaction[5] and transfer hydrogenation with planar chiral ferrocene derivatives[6] as ligands, we disclose a preliminary result of our studies on the synthesis of chiral thioether derivatives of ferrocenyl-oxazoline and application in palladium catalyzed allylic substitution. The role of planar chirality in this reaction was also studied.

Recently, Ahn *et al.* have reported an efficient diastereoselective synthesis of chiral oxazolinylferrocene compounds.[7] According to Ahn's method and our own experience, a series of chiral thioether derivatives of ferrocenyl-oxazoline were synthesized as follows: oxazolinylferrocene **2** was treated with *n*-BuLi and equimolar amount of TMEDA in Et_2O at −78 °C for 2 h (Scheme 1), the resulting mixture quenched with electrophiles (Me_3SiCl, $PhSO_2SR'$ or R'SSR'), then usual work-up to give the pure products. The diastereoselectivities of **3** and **5** determined by 300 MHz ^1H NMR were > 95 : 5.

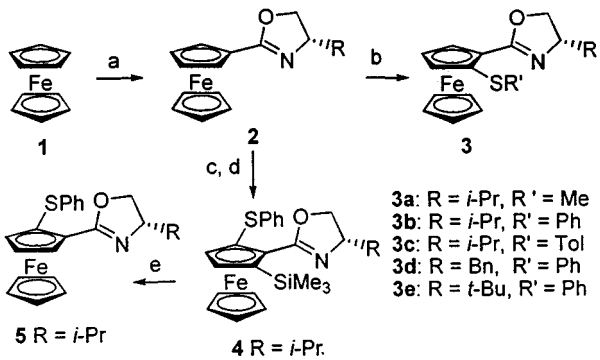

Scheme 1 *Reagents and conditions*: a, See refs. 7–9; b, (1) *n*-BuLi, TMEDA, Et_2O −78 °C, 2 h; (2) $PhSO_2SMe$ or R'SSR' 67–91%; c, (1) *n*-BuLi, TMEDA, Et_2O, −78 °C, 2 h; (2) TMSCl 93%; d, (1) *n*-BuLi, Et_2O, −78 °C, 2 h; (2) PhSSPh 70%; e, TBAF, THF, reflux, 6 h 88%.

To assay the effectiveness of ligands and other factors in palladium catalyzed alylic substitution, we chose the usual test reaction, the reaction of 1,3-diphenylprop-2-enyl acetate with the nucleophile derived from dimethyl malonate. Conditions A [$NaCH(CO_2Me)_2$, THF, r.t.] or B [$CH_2(CO_2Me)_2$, BSA, LiOAc, DCM, r.t.] were used in the reaction (Scheme 2).

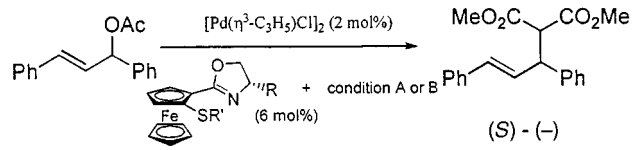

Scheme 2 Condition A: $NaCH(CO_2Me)_2$, THF, r.t. Condition B; $CH_2(CO_2Me)_2$, BSA [*N*,*O*-Bis(trimethyl)acetamide], LiOAc, CH_2Cl_2, r.t.

First, we investigated the effect of different salts on reaction yields and enantioselectivies under condition B with the catalyst derived from **3c** and $[Pd(\eta^3\text{-}C_3H_5)Cl]_2$. The results are summarized in Table 1, and it was found that ee values did not change in the presence of the salts listed in Table 1 (88.1–89.9%), but that the reaction time varied significantly (3–48 h). In view of the reaction time, yield and ee value, the lithium acetate (Table 1, entry 4) was used throughout this work.

Using the above conditions, a variety of ligands and conditions in the palladium catalyzed asymmetric allylic substitutions are summarized in Table 2. The sense of enantioinduction was determined by HPLC and confirmed by specific rotation of the product methyl-2-carbomethoxy-3,5-diphenylpent-4-enolate[10] and was found to be *S* in all cases. Comparing conditions A and B, we obtained higher enantioselectivities with the latter, which is consistent with most literature reports.[1,2] From entries 1–6 we found that ligands **3b** and **3c** are superior to **3a**. The chiral thioether of ferrocenyl-oxazolines derived from different amino alcohols show different effectiveness for enantioselectivities. The results showed that R = *t*-Bu (entries 9,10) is superior to R = *i*-Pr (entries 3,4) or Bn (entries 7,8). Entry 11 showed that the palladium complex with ligand **4** could mediate the allylic substitution reaction

Table 1 Asymmetric palladium catalyzed allylic substitution with different salts under condition B[a]

Entry	Salt	*t*/h	Yield (%)[b]	Ee (%)[c]
1	None	5	98	88.4 (*S*)
2	KOAc	48	96	88.1 (*S*)
3	NaOAc	48	85	88.2 (*S*)
4	LiOAc	3	98	89.9 (*S*)
5	Cs_2CO_3	5	98	89.4 (*S*)

[a] Reaction conditions: 2 mol% $[Pd(\eta^3\text{–}C_3H_5)Cl]_2$, 6 mol% **3c**, 3 mol% salt, 300 mol% $CH_2(CO_2Me)_2$, 300 mol% BSA. [b] Isolated yield based on the 1,3-diphenylprop-2-enyl acetate. [c] Determined by HPLC (chiralcel OJ column). [d] Absolute configuration of product was assigned through comparison of the sign of specific rotations with the literature data.[10]

Table 2 Asymmetric palladium catalyzed allylic substitution with different ligands

Entry	Ligand	Reaction condition	*t*/h	Yield (%)[a]	Ee (%)[b]
1	**3a**	A	1	98	73.9 (*S*)
2	**3a**	B	3	98	81.9 (*S*)
3	**3b**	A	2	98	84.0 (*S*)
4	**3b**	B	3	98	89.4(*S*)
5	**3c**	A	2	98	83.9 (*S*)
6	**3c**	B	3	98	89.9 (*S*)
7	**3d**	A	2	98	81.1 (*S*)
8	**3d**	B	5	98	87.8 (*S*)
9	**3e**	A	12	98	95.6(*S*)
10	**3e**	B	10	98	98.0 (*S*)
11	**4**	B	3	98	75.3 (*S*)
12	**5**	B	3	98	90.4 (*S*)

[a] Isolated yield based on the 1,3-diphenylprop-2-enyl acetate. [b] Determined by HPLC (chiralcel OJ column). [c] Absolute configuration of product was assigned through comparison of the sign of specific rotations with the literautre data.[10]

smoothly, while the bulkier trimethylsilyl group may decrease the enantioselectivity of the product.

Compared with the palladium complexes of chiral thioethers of phenyloxazoline ligands reported by Williams,[3a] the palladium complexes with chiral thioethers of ferrocenyl–oxazolines are more efficient. The allylic substitution reaction catalyzed by the latter under our conditions is much faster and gives almost quantitative yields.

In order to investigate the effect of planar chirality on the absolute configuration and enantioselectivity of this reaction, diastereoisomer **5** was also synthesized, and subjected to palladium catalyzed allylic substitution. Under essentially similar conditions (condition B), a similar enantioselectivity (89.4% in entry 4 *vs.* 90.4% in entry 12, Table 2) and the same absolute configuration was obtained. It seems that the absolute configuration is governed mainly by the central chirality of the oxazoline ring. (It seems that planar chirality plays a much less important role in palladium catalyzed allylic substitution.) This phenomenon was also found in our previous work on ruthenium-catalyzed asymmetric transfer hydrogenation with ferrocene derived catalysts.[6]

In order to further clarify the role of the planar chirality in this reaction, we may remove the central chirality on the oxazoline ring. For this purpose, the single planar chiral thioether of ferrocenyl-oxazoline (**8**) was designed and synthesized[11] (Scheme 3). Ligand **8** was subjected to palladium catalyzed allylic substitution under essential similar conditions as above (condition B) but only 8.5% ee was obtained and the absolute configuration is *R*. This result can explain why diastereosiomer

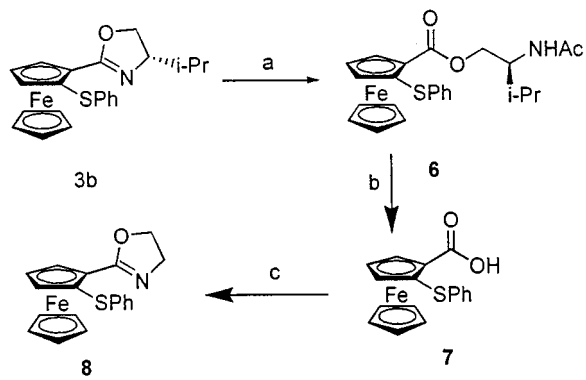

Scheme 3 *Reagents and conditions*: a, (1) TFA, H_2O, Na_2SO_4, THF; (2) Ac_2O, Py, CH_2Cl_2, 88%; b, (1) 2.5 M NaOH (aq), THF, 55 °C (2) H_3O^+, 85%; c, (1) $(ClCO)_2$, $NH_2(CH_2)_2OH$, Et_3N, CH_2Cl_2, (2) TsCl, Et_3N, DMAP, CH_2Cl_2, 63%.

Table 3 Asymmetric palladium catalyzed allylic substitution with **3** and **9**

Entry	Ligand	Condition[b]	*t*/h	Yield (%)	Ee (%)[c]
1	**9a**[a]	A'	36	91	78
2	**3b**	A	2	98	84.0
3	**9a**[a]	B'	36	96	90
4	**3b**	B	3	98	89.4
5	**9b**[a]	B'	96	92	96
6	**3e**	B	12	98	98.0

[a] 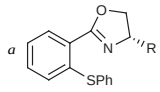 **9a**: R = *i*-Pr; **9b**: R = *t*-Bu. [b] Condition A': $[Pd(\eta^3\text{-}C_3H_5)Cl]_2$ (2.5 mol%), 9 (10 mol%), $NaCH(CO_2Me)_2$, THF, 20 °C. Condition B': $[Pd(\eta^3\text{-}C_3H_5)Cl]_2$ (2.5 mol%), 9 (10 mol%), KOAc (3 mol%), BSA, $CH_2(CO_2Me)_2$,CH_2Cl_2, 20 °C. [c] Absolute configuration of product was *S* for all cases.

5 achieved only a little higher ee than ligand **3b** (90.4% entry 12 *vs.* 89.4% entry 4 in Table 2); the planar chirality matched the central chirality in **5** for the oxazoline ring whereas they are mismatched in ligand **3**. The ee obtained with ligand **8** was low but did have an influence in this asymmetric allylic substitution reaction. Furthermore, it is noteworthy to compare the reaction rate of the reaction catalyzed by **3** with the counterpart of the thioether of phenyloxazoline **9** (Table 3). For all the reactions catalyzed by **9**, the rates are much slower than those of the ferrocene derivatives.[12]

Financial support from the National Foundation of China (29790127) and Chinese Academy of Sciences is gratefully acknowledged.

Notes and references

1 Reviews: C. G. Frost, J. Howarth and J. M. J. Williams, *Tetrahedron: Asymmetry*, 1992, **3**, 1089; B. M. Trost and D. L. Van Vranken, *Chem. Rev.*, 1996, **96**, 395; G. Consiglio and R. M. Waymouth, *Chem. Rev.*, 1989, **89**, 257; S. A. Godleski, in *Comprehensive Organic Synthesis*, ed. B. H. Trost, Pergamon Press, Oxford, 1991, vol. 4, p. 585.

2 Recent examples: B. M. Trost and R. C. Bunt, *Angew. Chem. Int. Ed. Engl*, 1996, **35**, 99; B. M. Trost and F. D. Toste, *J. Am. Chem. Soc.*, 1998, **120**, 815; B. M. Trost and D. E. Patterson, *J. Org. Chem.*, 1998, **63**, 1339.

3 (*a*) G. J. Dawson, C. G. Frost, C. J. Martin and J. M. J. Williams, *Tetrahedron Lett.*, 1993, **34**, 7793; (*b*) J. V. Allen, J. F. Bower and J. M. J. Williams, *Tetrahedron Asymmetry*, 1994, **5**, 1895; (*c*) J. V. Allen, S. J. Coote, G. J. Dawson, C. G. Frost, C. J. Martin and J. M. J. Williams, *J. Chem. Soc., Perkin Trans. 1*, 1994, 2065; (*d*) K. Boogwick, P. S. Pregosin and G. Trabesinger, *Organometallics*, 1998, **17**, 3254 (*e*) B. Koning, A. Meetsma and R. M. Kellogg, *J. Org. Chem.*, 1998, **63**, 5533, and references therein.

4 J. C. Ruble, J. Tweddell and G. C. Fu, *J. Org. Chem.*, 1998, **63**, 2794; S. Qiao and G. C. Fu, *J. Org. Chem.*, 1998, **63**, 4168.

5 A. H. Li, L. X. Dai, X. L. Hou, Y. Z. Huang and F. W. Li, *J. Org. Chem.*, 1996, **61**, 489; A. H. Li, Y. G. Zhou, L. X. Dai, X. L. Hou, L. J. Xia and L. Lin, *Angew. Chem., Int. Ed. Engl.*, 1997, **36**, 1317.

6 X.-D. Du, L.-X. Dai, X.-L. Hou, L.-J. Xia and M.-H. Tang, *Chin. J. Chem.*, 1998, **16**, 90.

7 K. H. Ahn, C.-W. Cho, H.-H. Beak, J. Park and S. Lee, *J. Org. Chem.*, 1996, **61**, 4937.

8 C. J. Richards, T. Damalidia, D. E. Habbis and M. B. Hursthouse, *Synlett.*, 1995, 74.

9 P. J. Graham, R. V. Lindsey, G. W. Parshall, M. L. Peterson and G. M. Whitman, *J. Am. Chem. Soc.*, 1957, **79**, 3416.

10 P. Wimmer and M. Widhalm, *Tetrahedron: Asymmetry*, 1995, **6**, 657.

11 A. M. Warshawsky and A. I. Meyers, *J. Am. Chem. Soc.*, 1990, **112**, 8090; T. D. Nelson and A. I. Meyers, *J. Org. Chem.*, 1994, **59**, 2655; W. B. Zhang, T. Kido, Y. Nakatsuji and I. Ikeda, *Tetrahedron Lett.*, 1996, **37**, 7995.

12 We also noticed a similar rate enhancing effect in the asymmetric transfer hydrogenation of ketones catalyzed by ruthenium complexes with phosphinoferrocenyloxozolines (ref. 6).

Communication 8/08267G

Theoretical search for new ferromagnetically coupled transition metal complexes

Eliseo Ruiz,*[a] Santiago Alvarez[a] and Pere Alemany[b]

[a] *Departament de Química Inorgànica, Universitat de Barcelona, Diagonal 647, 08028 Barcelona, Spain. E-mail: eliseo@linus.qui.ub.es*

[b] *Departament de Química Física,Universitat de Barcelona, Diagonal 647, 08028 Barcelona, Spain*

Received (in Cambridge, UK) 14th October 1998, Accepted 9th November 1998

Computational methods based on the density functional theory have been employed in the search for new ferromagnetic molecules and several compounds are predicted to exhibit stronger ferromagnetic coupling than the known hydroxo-bridged complexes, especially remarkable is the very strong coupling predicted for oxo-bridged Cu(II) or Ni(II) dimers.

One of the strategies applied to obtain new materials with interesting magnetic properties consists of increasing their structural dimensionality by combining binuclear building blocks to form chains, layers or tridimensional networks.[1] The choice of binuclear transition metal building blocks with different exchange coupling patterns opens up a number of possibilities in this area.[2] Hence, the magnetic behavior of a variety of such compounds has been explored during the last decades[3] with the aim of designing molecular magnets or molecule-based magnets. However, the large number of known antiferromagnetic complexes is in sharp contrast with the paucity of ferromagnetic systems. Up to now, the search for ferromagnetic coupling in binuclear transition metal complexes has been based on the synthesis of heteronucler complexes with strictly orthogonal singly-occupied molecular orbitals (SOMOs) or of complexes with accidentally degenerate SOMOs. Theoretical studies are therefore of great help in establishing the factors that lead to such accidental degeneracy in a given compound.

In recent work[4,5] we have shown the ability of hybrid density functional-Hartree–Fock methods to provide good numerical estimates of the exchange coupling constant J (defined in the Heisenberg hamiltonian $H = -JS_1S_2$) by using the B3LYP method[6] implemented in the GAUSSIAN package,[7] combined with a modified broken-symmetry approach.[8] The excellent results obtained so far prompted us to apply such methodology in search for new complexes with ferromagnetic behavior. A reasonable starting point for this search is to chemically modify Cu(II) systems already known to behave ferromagnetically, such as the hydroxo- or the end-on azido-bridged complexes. In particular, the hydrogen atom of the hydroxo bridging group offers a wider choice for chemical substitution. For hydroxo-bridged Cu(II) binuclear complexes, a classical correlation between the experimental exchange constant and the Cu–O–Cu bond angle θ indicates that those complexes are antiferromagnetic for $\theta > 98°$, but ferromagnetic for smaller angles.[9] In our previous work, we have shown that for these complexes the out-of-plane shift (τ) of the hydrogen atoms on the bridge also plays a crucial role in determining the magnetic behavior, since the ferromagnetic coupling increases with τ.[4,5]

We started by analyzing the influence of the substituent at the oxygen atom on the value of J, using the model compounds $[(NH_3)_2Cu(\mu\text{-}OR)_2Cu(NH_3)_2]$ **1**, with the bond angles θ and τ fixed at 101 and 0°, respectively. From now on we will refer to this particular structure as geometry **A**. In spite of the antiferromagnetic character found for the hydroxo-bridged complexes with this structure, we compare the calculated value of J with that of the hydroxo derivative with the same geometry as a criterion for selecting the best candidates. The calculated exchange constants for the different models with geometry **A**[10] are presented in Table 1, together with an indication of the pertinent structural data for the related compounds found in the Cambridge Structural Database (CSD).[11] From the calculated values of J some conclusions can be drawn: (1) all the alkoxo- and phenoxo-bridged complexes show stronger antiferromagnetic coupling than the hydroxo-bridged ones, in agreement with the experimental results. (2) For the methoxo-bridged compounds, substitution of the hydrogen atoms by alkyl groups weakens the antiferromagnetic coupling. (3) In general, the larger the electronegativity of the substituent, the stronger the antiferromagnetic coupling (*i.e.*, the values of $-J$ appear in the order OF > OCR_3 > OH ≈ OBR_3 > $OSiR_3$ ≈ $OGeR_3$ > $OAlR_3$ > OLi), although there are a few exceptions to this rule. The effect of substituents at a distance of two bonds cannot be rationalized according to the same electronegativity criterion, as seen for the two R groups in $OSiR_3$ and $OGeR_3$.

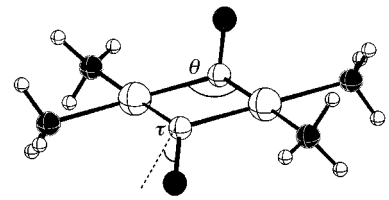

Table 1 Calculated coupling constants (cm^{-1}) for $[(NH_3)_2Cu(\mu\text{-}OR)_2Cu(NH_3)_2]^{n+}$ with structure **1** (n = 0, OR = O, OSO_3, OBR_3 and $OAlR_3$; n = 4 for OR = OPy; n = 2 for all other OR) in geometries **A** (θ = 101°, τ = 0°) and **B** (θ = 96°, τ = 50°)

	J_{calc}					
R	**A**	**B**	N^a	θ/°	τ/°	J_{exp}
F	−1855		0			
Me	−778		14	98–104	2–48	
BH_3	−687	+273	0			
Et	−669		31	96–105	2–44	−1064/−65
Bu^t	−617		2	102–103	22–29	
Ph	−587		36	96–105	0–33	−852/−166
Py	−675		15	104–110	3–26	−855/−242
H	−493	−46	15	94–105	0–62	−509/+172
GeH_3	−331	+5	0			
SiH_3	−278	+19	0			
$Ge(OH)_3$	−259	−36	0			
COMe	−230	−75	11	95–107	4–24	
NO_2	−221	−58	1	106	13	
$Si(OH)_3$	−202	−14	0			
$Al(OH)_3$	−134	+137	0			
SO_3	−108	+60	1	103	9	
SOMe	+8	−104	1	105	46	
Li	+100	+331	0			
—	+989	+782	0			

[a] The experimental structural data have been obtained with the help of the CSD.[11] The number (N) indicates the structures with planar Cu_2O_2 rings. An all electron double-ζ basis has been employed in the calculations.[12]

Since the angles θ and τ adopted in the model structure **A** are not expected to favor ferromagnetism, we selected the least antiferromagnetic or most ferromagnetic compounds for further exploration with a structure more likely to favor ferromagnetism. For them, a second set of calculations was performed with θ and τ fixed at 96 and 50°, respectively (geometry **B**), and the calculated coupling constants are also presented in Table 1. In practically all cases, the new geometry results in a decrease of the antiferromagnetic contribution, as expected for the smaller energy gap of the SOMOs obtained by reducing θ while simultaneously increasing τ.[13] The exceptions (O and $OSOCH_3$) should be attributed to the fact that the energy ordering of the SOMOs is inverted in these compounds. As a consequence, the energy gap between these two orbitals increases with the Cu–O–Cu bond angle and a stronger antiferromagnetic contribution results.[4] From the calculated exchange coupling constants, one can conclude that the sulfato and OX bridges with X = Li, BR_3, AlR_3, SiR_3 or GeR_3 could yield ferromagnetic complexes. Especially remarkable is the fact that the OBH_3-bridged compound is made much more ferromagnetic upon changing its geometry from **A** to **B**. However, we could only detect one case of a related complex in the literature, having an OB(R)=O bridge and quite large Cu–O distances. In summary, our results indicate that copper(II) binuclear complexes bridged by oxygen bonded to an electropositive atom, such as an alkali, alkaline-earth, group 13 or group 15 element, are good candidates to present a strong ferromagnetic coupling. Notice that our prediction of ferromagnetic systems is based on a particular set of structural parameters (θ = 96° and τ = 50°). Thus, we are investigating whether such structures are energetically feasible for the selected compounds by optimizing model structures of increasing complexity. Preliminary results show that the selected systems adopt structures close to that corresponding to geometry **B** and a strong ferromagnetic coupling should be expected.

A particularly surprising result is the exceptionally strong ferromagnetic coupling constants obtained for the oxo-bridged complex of copper (+989 and +782 cm^{-1} for geometries **A** and **B**, respectively), as compared to the largest values reported in the literature for azido- and hydroxo-bridged complexes (+170 and +172 cm^{-1}, respectively).[14,15] To obtain a more realistic model of an oxo-bridged complex, we have repeated the calculations adding an NH_3 ligand in the fifth coordination position of each copper atom, whereupon the calculated exchange constant for geometry **B** is reduced to +661 cm^{-1}, exhibiting still a very strong ferromagnetic character, comparable to the calculated value (+685 cm^{-1}) for the optimized structure of the penta-coordinate copper model. In agreement with the Hay–Thibeault–Hoffmann model,[13] all the oxo-bridged model calculations reveal a near-degeneracy of the two SOMOs. Unfortunately, no oxo-bridged Cu(II) complexes have been described in the literature to the best of our knowledge. An indication of the ability of the oxo bridge to induce ferromagnetic coupling is provided by the μ-aqua–μ-oxo complex described by Chaudhuri *et al.*,[16] which is tautomeric to the corresponding bis(μ-hydroxo) complex. The latter presents a coupling constant of −90 cm^{-1} whereas the former shows a ferromagnetic behavior with a singlet–triplet gap of +74 cm^{-1}. Recently, Root *et al.* reported the structure of a trinuclear complex containing a Cu_3O_2 core with two Cu(II) and one Cu(III) ion showing a singlet–triplet gap of +14 cm^{-1}.[17]

Similar bis (μ-oxo) complexes with transition metals other than copper have been described, mainly with manganese[18,19] and iron.[20] In sharp contrast to our theoretical prediction for copper, these complexes show antiferromagnetic coupling. To verify our predictions against the experimental data for Mn and Fe, we have studied the dependence of **J** on the angle θ for the model complex $[(NH_3)_4M(\mu\text{-}O)_2M(NH_3)_4]$, where M = Cu, Ni or Mn. The results, represented in Fig. 1, show a parabollic dependence of J on θ, with the maximum value of J appearing at smaller angles in the order Mn > Ni > Cu, similar to that we previously found for the end-on azido-bridged complexes.[21]

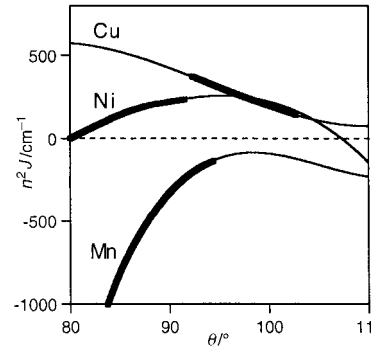

Fig. 1 Total exchange constants (n^2J, where n is the number of unpaired electrons per metal atom) for bis μ-oxo complexes of Cu(II), Ni(II) and Mn(II) as a function of the bridging angle θ. The outlined parts of the curves correspond to those geometries within 3 kcal mol^{-1} of the calculated energy minima (1 cal = 4.184 J).

The main difference is that for the azido complexes ferromagnetic coupling is found for the three metals while the oxo-bridged Mn(II) complexes show antiferromagnetic behavior, consistent with the available experimental data for the d^5 Fe(III) oxo-bridged complex.[20] The values of the optimized θ angles are also different for the two bridges with the same metal. Thus, for the end-on azido complexes the order Mn > Ni > Cu was found for such angle, whereas for the oxo-bridged complexes the largest value is that for Cu. As a conclusion, Ni(II) and Cu(II) complexes with an oxo bridge or with electropositive substituents at the bridging oxygen constitute interesting synthetic goals for new potentially ferromagnetic systems.

Financial support was provided by DGES (project PB95-0848-C02) and CIRIT (grant 1995SGR-00421). Computing resources allocated at CESCA are also acknowledged.

Notes and references

1 G. De Munno, M. Julve, F. Lloret, J. Faus, M. Verdaguer and A. Caneschi, *Inorg. Chem.*, 1995, **34**, 157.
2 G. Viau, M. G. Lombardi, G. De Munno, M. Julve, F. Lloret, J. Faus, A. Caneschi and J. M. Clemente-Juan, *Chem. Commun.*, 1997, 1196.
3 O. Kahn, *Molecular Magnetism*, VCH Publishers, 1993.
4 E. Ruiz, P. Alemany, S. Alvarez and J. Cano, *J. Am. Chem. Soc.*, 1997, **119**, 1297.
5 E. Ruiz, P. Alemany, S. Alvarez and J. Cano, *Inorg. Chem.*, 1997, **36**, 3683.
6 A. D. Becke, *J. Chem. Phys.*, 1993, **98**, 5648.
7 GAUSSIAN94 computer code, M. J. Frisch *et al.*, Pittsburgh, PA, 1994.
8 L. Noodleman and D. A. Case, *Adv. Inorg. Chem.*, 1992, **38**, 423.
9 V. H. Crawford, H. W. Richardson, J. R. Wasson, D. J. Hodgson and W. E. Hatfield, *Inorg. Chem.*, 1976, **15**, 2107.
10 The following structural parameters were used for the model calculations: Cu–O = 2.0 Å, Cu–N = 2.0 Å, N–H = 109.5°, Ni–O = 2.05 Å, Ni–N = 2.10 Å, Mn–O = 2.30 Å.
11 F. H. Allen and O. Kennard, *Chem. Des. Automat. News*, 1993, **8**, 31.
12 A. Schaefer, H. Horn and R. Ahlrichs, *J. Chem. Phys.*, 1992, **97**, 2571.
13 P. J. Hay, J. C. Thibeault and R. Hoffmann, *J. Am. Chem. Soc.*, 1975, **97**, 4884.
14 S. S. Tandon, L. K. Thompson, M. E. Manuel and J. N. Bridson, *Inorg. Chem.*, 1994, **33**, 5555.
15 R. J. Majeste and E. A. Meyers, *J. Phys. Chem.*, 1970, **74**, 3497.
16 P. Chaudhuri, D. Ventur, K. Wieghardt, E.-M. Peters and A. Simon, *Angew. Chem., Int. Ed. Engl.*, 1985, **24**, 57.
17 D. E. Root, M. J. Henson, T. Machonkin, P. Mukherjee, T. D. P. Stack and E. I. Solomon, *J. Am. Chem. Soc.*, 1998, **120**, 4982.
18 E. Libby, R. J. Webb, W. E. Streib, K. Folting, J. C. Huffman, D. N. Hendrickson and G. Christou, *Inorg. Chem.*, 1994, **28**, 4037.
19 N. Kitajima, U. P. Singh, H. Amagai, M. Osawa and Y. Moro-oka, *J. Am. Chem. Soc.*, 1991, **113**, 7757.
20 Y. Zang, Y. Dong, L. Que Jr., K. Kauffmann and E. Münck, *J. Am. Chem. Soc.*, 1995, **117**, 1169.
21 E. Ruiz, P. Alemany, S. Alvarez and J. Cano, *J. Am. Chem. Soc.*, 1998, **120**, 11 122.

Communication 8/07973K

Inhibitors of DNA polymerase β from *Schoepfia californica*

Jie Chen, Yu-Huan Zhang, Li-Kai Wang, Steven J. Sucheck, Angela M. Snow and Sidney M. Hecht*

Departments of Chemistry and Biology, University of Virginia, Charlottesville, Virginia 22901, USA. E-mail: sidhecht@virginia.edu

Received (in Corvallis, OR, USA) 8th September 1998, Accepted 18th November 1998

Fractionation of a hexane extract prepared from the plant *Schoepfia californica* was carried out by bioassay guided fractionation, affording five inhibitors of DNA polymerase β; four of these were shown to be anacardic acid and structurally related derivatives, while the fifth was oleic acid.

In addition to their role in DNA replication, at least three eukaryotic DNA polymerases participate in the repair of damaged DNA.[1] Given that elements in our environment such as sunlight and pollution provide a steady source of DNA damage, the repair of damaged DNA must be essential to maintain cell viability.[2] There is, however, at least one context in which DNA damage repair is not beneficial, namely following the clinical administration of antitumor agents that function by damaging DNA. The repair of DNA damage inflicted by these agents on cancer cells must mitigate their therapeutic potency.

DNA polymerase β is believed to have primary responsibility for supporting short patch DNA base excision repair.[3–5] This pathway has specifically been implicated in the repair of DNA damage caused by agents such as *cis*-platinum, bleomycin and neocarzinostatin.[3,4,6–8] To identify non-toxic compounds that can block the function of DNA polymerase β selectively, and which may thereby be able to potentiate the action of anticancer agents such as bleomycin, we have surveyed plant extracts for naturally occurring inhibitors of polymerase β.[9] Presently we describe five natural inhibitory principles from *Schoepfia californica* that can potentiate the action of bleomycin and *cis*-platinum.

A hexane extract prepared from the twigs, leaves and fruit of *Schoepfia californica* was partitioned between hexane and MeOH; the hexane phase contained most of the polymerase β inhibitory activity. Successive bioassay-guided fractionations on two silica gel columns and then by preparative silica gel TLC afforded an active fraction that effected 94% inhibition of polymerase β function at 5 μg ml^{-1} *vs.* 38% inhibition for the initial extract.† Fractionation (C_8 column, 80% MeOH) then afforded pure compounds **1–5**; all were obtained as colorless needles except **3**, which was a colorless oil.

The structures were determined by spectroscopic analysis. Compound **1** was found to have a molecular ion at *m/z* 374.2822, establishing the molecular formula as $C_{24}H_{38}O_3$. The ^{13}C NMR spectrum of **1** displayed six resonances (δ 110.31, 115.87, 122.74, 135.38, 147.76 and 163.65) assigned to an aromatic ring and a resonance at δ 175.67 assigned to a carboxylate carbon, thus accounting for five of the six units of unsaturation implied by the molecular formula. The presence of three aromatic resonances in the ^{1}H NMR spectrum at δ 6.77 (d, *J* 7.5), 6.87 (d, *J* 7.5) and 7.36 (dd, *J* 7.5, 7.5) indicated that the aromatic ring was trisubstituted; the multiplicities of the proton resonances were consistent with a 1,2,3-trisubstituted benzenoid system.‡

The chemical shift of the carboxylate at δ 175.67 was typical of a carboxylate attached to an aromatic ring; the downfield shift of the aromatic H at δ 7.36 (dd) suggested the *para* relationship of this H to the carboxylate moiety. That the remaining O atom was present as part of a phenolic substituent was suggested by the downfield shift of one ring carbon (δ 163.65). The *ortho* relationship of this OH to the ring carboxylate was supported by the upfield shift of the ring C atom (δ 110.31), consistent with the known (δ 12.7) shielding effect of *ortho* phenolic OH groups.[15]

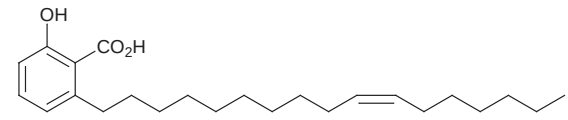

1

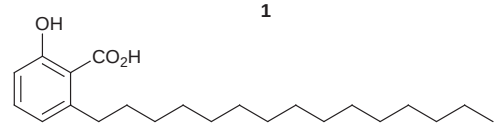

2

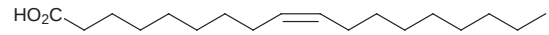

3

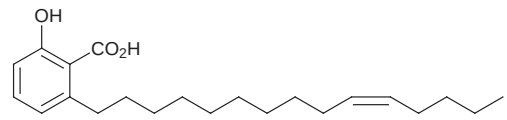

4

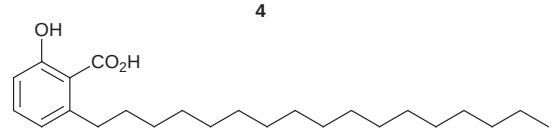

5

These data suggested that **1** was a 6-substituted salicylic acid; the ^{1}H and ^{13}C NMR spectra were consistent with an unbranched alkyl substituent containing a single double bond. The double bond configuration was assigned as *cis* based on the ^{13}C NMR resonances of the allylic carbon atoms.[16] Determination of the olefin position was made by modification of published procedures.[17]

The structure assigned to **1** was confirmed by chemical synthesis, as outlined in Scheme 1. Ethyl 2-hydroxy-6-methylbenzoate **6**[18] was protected as the corresponding MEM ether[19] and the ethyl ester was saponified, affording carboxylic acid derivative **7** as colorless prisms (71% yield). Treatment of **7** with LDA (2 equiv., THF), followed by admixture of (9*Z*)-hexadec-9-enyl bromide at 0 °C,[20] afforded homologated salicylic acid derivative **8** (68% yield). MEM deprotection[19] provided **1**[14] as colorless needles (80% yield). The synthetic and naturally derived samples were found to be identical as judged by their behavior on silica gel TLC, and by their identical ^{1}H and ^{13}C NMR and mass spectra, as well as their equal abilities to inhibit DNA polymerase β (*vide infra*).

Compounds **2**, **4**, and **5** were found to have spectroscopic properties most similar to **1**. The structures were assigned in the same fashion as for **1**, a process facilitated by previous reports

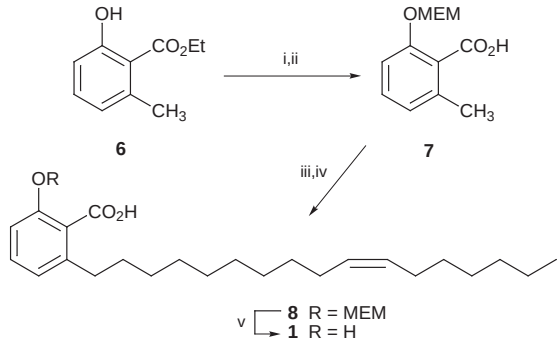

Scheme 1 *Reagents and conditions*: i, MEMCl, Pr^i_2NEt; ii, Bu^tOK, 61% over 2 steps; iii, LDA; iv, (9*Z*)-hexadec-9-enyl bromide, 68% over 2 steps; v, $ZnBr_2$, 80%.

of each of these compounds.[21] Verification of the structure assignments was accomplished by total chemical synthesis of each. The mass spectrum of **3** contained a molecular ion having *m/z* 282. The ^1H and ^{13}C NMR spectra of **3** were found to be identical with those of oleic acid.[13]

The activities of **1**–**5** as inhibitors of DNA polymerase β are shown in Table 1. Compound **1** exhibited an IC_{50} of 1.4 μM in the absence of bovine serum albumin (BSA). BSA reduced the IC_{50} to 9 μM, undoubtedly reflecting the binding of **1** to this (basic) protein. Unsaturated analogues **1** and **4** were found to have the greatest potencies in the presence of BSA (9 and 19 μM, respectively), and to be reproducibly more active than saturated derivatives **2** and **5**. Oleic acid, which is a simple fatty acid, was active only at significantly higher concentration. Methylation of the phenol or carboxylic acid moieties essentially eliminated inhibitory activity as did conversion of the carboxylate of **5** to the respective carboxamide, demonstrating that the anacardic acids are specific inhibitors rather than simple denaturants.§

Table 1 Inhibition of rat liver DNA polymerase by **1**–**5** and structurally related compounds[a]

Compound	IC_{50}/μM
1	1.4[b]
1	9
2	30
3	72
4	19
5	25

[a] Determined as described in footnote †. [b] Determined in the absence of bovine serum albumin.

Compound **1** and a few structurally related species were evaluated in more detail as DNA polymerase β inhibitors. In both short and long term mammalian cell culture, these compounds potentiated the action of DNA damaging agents such as bleomycin (Table 2) and *cis*-platinum, and inhibited bleomycin-induced unscheduled DNA synthesis. They also blocked DNA polymerase β-mediated gap filling of a DNA duplex substrate.[12] Thus specific inhibitors of DNA polymerase β may well be able to potentiate the effects of the DNA damage caused by clinically used antitumor agents that function at this locus.

Table 2 Potentiation of the cytotoxicity of bleomycin (BLM) by **1**[a]

Compounds present	Viable cells (% of control)
—	100
50 μM BLM	96
50 μM **1**	98
50 μM BLM + 50 μM **1**	68

[a] P388D, cells were cultured in suspension in the presence of the test compounds for 6 h, then assessed for viability by trypan blue exclusion staining.

We thank Ms Shelley Starck, University of Virginia, for biochemical evaluation of these agents and Dr Mark Hemling, SmithKline Beecham Pharmaceuticals, for the high resolution mass spectrometry data. We thank Dr Akio Matsukage, Aichi Cancer Center Research Institute, Nagoya, for providing us with a source of cloned rat DNA polymerase β. This work was supported by NIH Research Grant CA50771 from the National Cancer Institute.

Notes and references

† Inhibition of polymerase β was assayed in 62.5 mM ammediol buffer, pH 8.6, containing 10 mM $MgCl_2$, 1 mM dithiothreitol, 50 μg ml^{-1} of BSA, 6.25 μM deoxynucleotide triphosphates including [^{3}H]thymidine triphosphate and 12.5 μg of DNase I-treated calf thymus DNA. The reactions were initiated with 0.2 μg of rat liver DNA polymerase β (ref. 10,11), incubated at 37 °C for 1 h, and monitored as described (ref. 12).

‡ The assignments of the H3, H4 and H5 resonances in the NMR spectra of **1**, **2**, **4** and **5** were further supported by HMQC spectroscopy. The spectra also proved useful for assigning proton and carbon resonances in the aliphatic substituents of **1–5**, used in combination with the full ^{13}C NMR assignments of a number of common fatty acids (ref. 13) and the ^{1}H-coupled ^{13}C NMR spectra of several compounds structurally related to **1**, **2**, **4** and **5** (ref. 14).

§ Also determined was the selectivity of inhibition. A number of derivatives were found to be essentially inactive as inhibitors of calf thymus DNA topoisomerase I, AMV reverse transcriptase, DNA polymerase I (Klenow fragment) and restriction endonuclease *Hin*dIII at concentrations at which those compounds strongly inhibited DNA polymerase β.

1 See, *e.g.* T. S.-F. Wang, *Annu. Rev. Biochem.*, 1991, **60**, 513; Y. Matsumoto and K. Kim, *Science*, 1995, **269**, 699; A. Sancar, *Annu. Rev. Biochem.*, 1996, **65**, 43.
2 B. N. Ames, M. K. Shigenaga and T. M. Hagen, *Proc. Natl. Acad. Sci. U.S.A.*, 1993, **90**, 7915.
3 M. R. Miller and D. N. Chinault, *J. Biol. Chem.*, 1982, **257**, 10204.
4 J. A. DiGiuseppe and S. L. Dresler, *Biochemistry*, 1989, **28**, 9515.
5 R. K. Singhal, R. Prasad and S. H. Wilson, *J. Biol. Chem.*, 1995, **270**, 949.
6 S. Seki and T. Oda, *Carcinogensis*, 1988, **9**, 2239.
7 A. J. Fornace, Jr., B. Zmudzka, M. C. Hollander and S. H. Wilson, *Mol. Cell. Biol.*, 1989, **9**, 851.
8 J.-S. Hoffmann, M.-J. Pillaire, G. Maga, V. Podust, U. Hübscher and G. Villani, *Proc. Natl. Acad. Sci. U.S.A.*, 1995, **92**, 5356.
9 Polymerase β inhibitors of moderate potency have been reported, although none has been used to potentiate the action of DNA damaging antitumor agents. See K. Ono, H. Nakane and M. Fukushima, *Eur. J. Biochem.*, 1988, **172**, 349; Y. Mizushina, H. Yagi, N. Tanaka, T. Kurosawa, H. Seto, K. Katsumi, M. Onoue, H. Ishida, A. Iseki, T. Nara, K. Morohashi, T. Horie, Y. Onomura, M. Narusawa, N. Aoyagi, K. Takami, M. Yamaoka, Y. Inoue, A. Matsukage, S. Yoshida and K. Sakaguchi, *J. Antibiot.*, 1996, **49**, 491; H.-D. Sun, S.-X. Qiu, L.-Z. Lin, Z.-Y. Wang, Z.-W. Lin, T. Pengsuparp, J. M. Pezzuto, H. H. S. Fong, G. A. Cordell and N. R. Farnsworth, *J. Nat. Prod.*, 1996, **59**, 525; H. Ishiyama, M. Ishibashi, A. Ogawa, S. Yoshida and J. Kobayashi, *J. Org. Chem.*, 1997, **62**, 3831; N. Tanaka, A. Kitamura, Y. Mizushina, F. Sugawa and K. Sakaguchi, *J. Nat. Prod.*, 1998, **61**, 193.
10 T. Date, M. Yamaguchi, F. Hirose, Y. Nishimoto, K. Tanihara and A. Matsukage, *Biochemistry*, 1988, **27**, 2983.
11 S. G. Widen, P. Kedar and S. H. Wilson, *J. Biol. Chem.*, 1988, **263**, 16992.
12 A. M. Snow, Ph.D. Thesis, University of Virginia, 1995.
13 J. G. Batchelor, R. J. Cushley and J. H. Prestegard, *J. Org. Chem.*, 1974, **39**, 1698.
14 H. Itokawa, N. Totsuka, K. Nakahara, K. Takeya, J.-P. Lepoittevin and Y. L. Asakawa, *Chem. Pharm. Bull.*, 1987, **35**, 3016.
15 D. F. Ewig, *Org. Magn. Reson.*, 1979, **12**, 499.
16 See, *e.g.* F. D. Gustone, M. R. Pollard, C. M. Scrimgeour and H. S. Vedanayagam, *Chem. Phys. Lipids*, 1977, **18**, 115; J. W. deHaan and L. J. M. de Ven, *Org. Magn. Reson.*, 1979, **5**, 147; R. Rossi, A. Carpita, M. G. Quirici and C. A. Varacini, *Tetrahedron*, 1982, **38**, 639.
17 See *e.g.* J. R. Barr, R. T. Scannell and K. Yamaguchi, *J. Org. Chem.*, 1989, **54**, 494.
18 F. M. Hauser and S. A. Pogany, *Synthesis*, 1980, 814.
19 E. J. Corey, J.-L. Gras and P. Ulrich, *Tetrahedron Lett.*, 1976, **11**, 809.
20 P. L. Creger, *J. Am. Chem. Soc.*, 1970, **92**, 1396. The bromide itself was accessible from the corresponding commercially available alcohol by treatment with Ph_3PBr_2 (P. E. Sonnet, *Synth. Commun.*, 1976, **6**, 21).
21 See, *e.g.* Y. Yamagiwa, K. Ohashi, Y. Sakamoto, S. Hirakawa, T. Kamikawa and I. Kubo, *Tetrahedron*, 1987, **43**, 3387; R. Zehnter and H. Gerlach, *Liebigs Ann.*, **1995**, 2209.

Communication 8/07053I

ChemComm

A unique mode of molecular recognition in palladium(II) metallacrown ethers

Dale C. Smith, Jr., Charles H. Lake and Gary M. Gray

Department of Chemistry, University of Albama at Birmingham, Birmingham, AL 35294, USA. E-mail: gmgray@uab.edu

Received (in Bloomington, IN, USA) 15th September 1998, Accepted 26th October 1998

Metallacrown ethers of the type $[PdX_2\{Ph_2P(CH_2CH_2O)_4CH_2CH_2PPh_2\text{-}P,P'\}]_m$ (X = Cl, I) exhibit a unique and reversible mode of molecular recognition in which PdX_2 units are incorporated into the metallacrown ether ring *via* a ring-expansion reaction to form dimetallacrown ethers.

Molecular receptors are of interest as chemical sensors, catalysts and models for complex biochemical receptors.[1] Recently, molecules with multiple receptor sites have received considerable attention. The multiple receptor sites can give rise to unusual catalytic properties[2] or allow the molecules to function as highly selective sensors.[3]

Metallacrown ethers are a class of molecular receptors with both crown ether- and transition metal-receptor sites.[4,5] We now report that the metallacrown ether $[PdCl_2\{PPh_2(CH_2CH_2O)_4CH_2CH_2PPh_2\text{-}P,P'\}]_m$, **1**,[6] exhibits a unique mode of molecular recognition in which the metallacrown ether ring is expanded by the incorporation of a $PdCl_2$ moiety. The product of this reaction is the first reported example of a dimetallacrown ether.

In a typical experiment, the metallacrown ether $[PdCl_2\{PPh_2(CH_2CH_2O)_4CH_2CH_2PPh_2\text{-}P,P'\}]_m$ **1**, which is mixture of *cis*- and *trans*-monomers and cyclic *n*-mers,[6] is reacted with either $[PdCl_2(PhCN)_2]$ or $PdCl_2$. This reaction is rapid with soluble palladium salts, *i.e.* $PdCl_2$ in acetonitrile or $[PdCl_2(PhCN)_2]$ in dichloromethane, but takes place even when the palladium salt is insoluble, *i.e.* $PdCl_2$ in chloroform. Both reactions give high yields of the dimetallacrown ether $[Pd_2Cl_2(\mu\text{-}Cl)_2\{PPh_2(CH_2CH_2O)_4CH_2CH_2PPh_2\text{-}P,P'\}]_m$, **2**, (Scheme 1). A similar reaction of **1** with either $[PdCl_2(PhCN)_2]$ or $PdCl_2$ and excess NaI in an acetonitrile–dichloromethane mixture gives a high yield of the dimetallacrown ether $[Pd_2I_2(\mu\text{-}I)_2\{PPh_2(CH_2CH_2O)_4CH_2CH_2PPh_2\text{-}P,P'\}]_m$, **3**. The latter reaction is of interest because it demonstrates that it is possible to exchange the anion in the dimetallacrown ether without exchanging the cation.

Comparison of the rates of $PdCl_2$ binding by **1** and $[PdCl_2(PPh_2Et)_2]$ **4**[7] in chloroform-*d* solutions clearly demonstrates the importance of the metallacrown ether receptor in **1**. After 20 h at ambient temperature, **1** is completely converted into **2**. In contrast, after 20 h at ambient temperature, only 10.5% of **4** is converted into the corresponding dinuclear palladium complex, $[Pd_2Cl_4(PPh_2Et)_2]$.

The binding of $PdCl_2$ by the metallacrown ether, **1**, is strong and reversible. It is not possible to remove the $PdCl_2$ from **2** by extracting chloroform-*d* solutions of **2** with 0.5 M aqueous HCl solutions. However, the $PdCl_2$ can be completely removed from **2** *via* chromatography, with the $PdCl_2$ remaining on the silica and **1** eluting from the column.

Chloroform-*d* solutions of **2** and **3** contain multiple resonances in their $^{31}P\{^1H\}$ NMR spectra (Fig. 1) indicating that these complexes, like **1**, exhibit both geometrical and monomer/*n*-mer equilibria in solution.[6] The major resonance in the $^{31}P\{^1H\}$ NMR spectrum of **2** is assigned to the monomeric *syn*-dimetallacrown ether **2b** while the minor resonances are assigned to *n*-meric dimetallacrown ethers **2a**. This assignment is supported by the decrease in ratio of the major resonance **2b** to the minor resonance **2a** both as the concentration increases (8.0/1 at 0.0175 M *versus* 4.3/1 at 0.0350 M) and as the

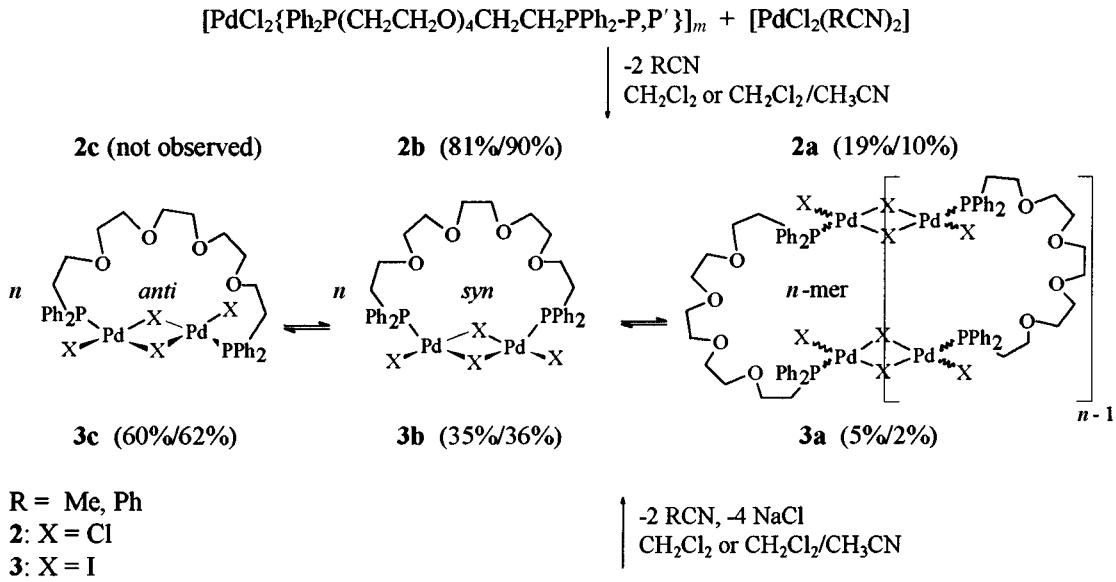

Scheme 1 Proposed equilibria for the dimetallacrown ethers. The relative species percentages were determined by integration of the quantitative $^{31}P\{^1H\}$ NMR spectra and are given for both 0.0350 M and 0.0175 M solutions of **2** in chloroform-*d* and for both 0.0350 M and 0.0175 M solutions of **3** in (1 : 1) dichloromethane/chloroform-*d* at 295 K.

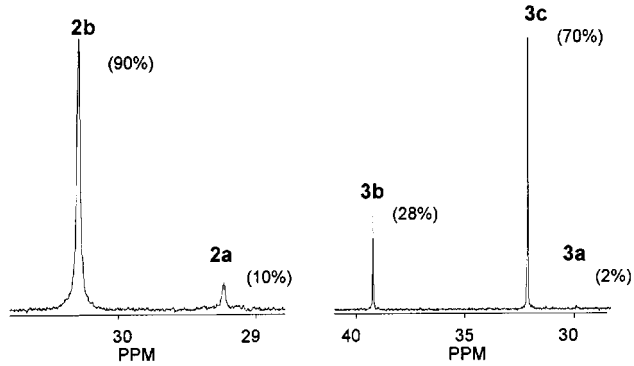

Fig. 1 $^{31}P\{^{1}H\}$ NMR spectra of 0.0175 M solutions of the dimetallacrown ethers, **2** and **3**, in chloroform-*d* at 295 K. {Spectral parameters: $^{31}P\{^{1}H\}$, 121.498 MHz, number of scans 256, line broadening 1.0 Hz, sweep width 2439.02 Hz, 30° inverse gated pulse, pulse delay 30 sec}.

temperature decreases (11.3/1 for a 0.0175 M solution at 331 K *versus* 8.0/1 for a 0.0175 M solution at 295 K).[8] The assignment of **2b** as the *syn* isomer is based on the similarity of the chemical shift of its $^{31}P\{^{1}H\}$ NMR resonance to those of *syn*-$Pd_2Cl_4L_2$ (L = monodentate phosphine) complexes.[9]

The major resonance in the $^{31}P\{^{1}H\}$ NMR spectrum of **3** is assigned to the monomeric *anti*-dimetallacrown ether **3c**, and the minor resonance is assigned to the *syn*-dimetallacrown ether **3b** (Fig. 1). This assignment is supported by the increase in the ratio of the major resonance **3c** to the minor resonance **3b** as the polarity of the solvent decreases (1.8/1 in a 1 : 1 dichloromethane–chloroform mixture *versus* 2.4/1 in chloroform). The very small, upfield resonances **3a** appear to be due to *n*-meric

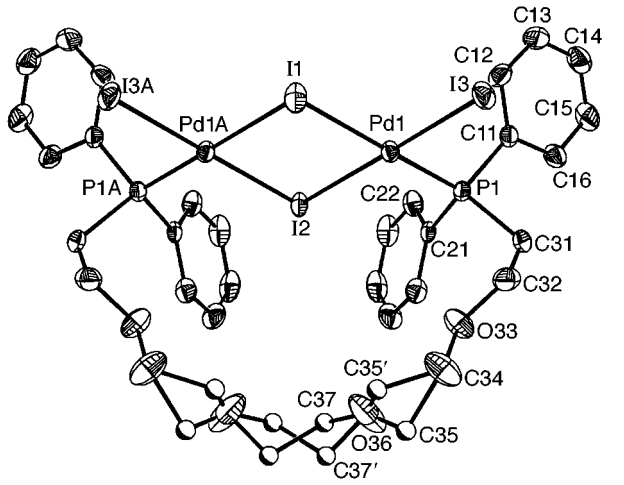

Fig. 2 Molecular structure of **3c**. For clarity the hydrogen atoms are removed, and the complete molecule (two asymmetric units) is shown. Selected bond lengths [Å] and angles [°]: Pd1–I1 2.667(1), Pd1–I2 2.602(1), Pd1–I3 2.598(1), Pd1–P1 2.264(2), P1–C11 1.822(7), P1–C21 1.819(6), P1–C31 1.815(7); I1–Pd1–I2 84.0(1), I1–Pd1–I3 91.3(1), I2–Pd1–I3 173.9(1), I1–Pd1–P1 177.4(1), I2–Pd1–P1 94.7(1), I3–Pd1–P1 90.1(1), Pd1–I1–Pd1A 94.3(1), Pd1–I2–Pd1A 97.4(1), Pd1–P1–C11 115.1(2), Pd1–P1–C21 113.6(2).

dimetallacrown ethers. The very different behavior of **2** and **3** in solution demonstrates that the halide ligand has a surprising effect on both the isomerization and *n*-merization equilibria in dimetallacrown ethers.

The X-ray crystal structure of **3c**,[10] shown in Fig. 2, suggests that this dimetallacrown ether could have quite different receptor properties from those of the previously reported metallacrown ethers, *cis*-[$PtCl_2\{PPh_2(CH_2CH_2O)_4$-$CH_2CH_2PPh_2$-P,P′}], **5**, and *trans*-[$Mo(CO)_4\{PPh_2(CH_2$-$CH_2O)_4CH_2CH_2PPh_2$-P,P′}], **6**.[4d,4e] The average cross-ring oxygen–oxygen distance in **3c** (O33–O36A and O33A–O36, 5.27 Å), which provides a measure of the ring size, is intermediate between that in **5** (4.66 Å) and that in **6** (5.87 Å).[4d,4e] The angle of intercept between the least squares planes through the ether oxygens (O33, O36, O33A, O36A) and that containing the Pd_2I_2 fragment is 42° in **3c**. In contrast, the angle between the least squares planes through the ether oxygens and the $PtCl_2$ center in **5** is 60°. The smaller angle means that an alkali metal cation in the dimetallacrown ether receptor site would be in closer proximity to the transition metal center in **3c** (the distance from the centroid of the four ether oxygens to Pd1 is 4.984 Å). A bifunctional molecule, such as CO, could easily coordinate to both the Pd and the alkali metal cation in the dimetallacrown ether.

Notes and references

1 B. R. Cameron, S. S. Corrent and S. J. Loeb, *Angew. Chem., Int. Ed. Engl.*, 1995, **34**, 23; W. van Veggel, F. V. J. M. Verboom and D. N. Reinhoudt, *Chem. Rev.*, 1994, **94**, 279; L. F. Lindoy, *The Chemistry of Macrocyclic Ligand Complexes*, Cambridge University Press, Cambridge, UK, 1989, pp. 1–273.

2 S. J. McLain and F. J. Waller, *US Pat.*, 1984, 4,432,904.

3 A. P. de Silva, H. Q. Gunaratne and C. P. McCoy, *J. Am. Chem. Soc.*, 1997, **119**, 7891.

4 (*a*) C. H. Duffey, C. H. Lake and G. M. Gray, *Organometallics*, 1998, **17**, 3550; (*b*) P. J. Stang, D. H. Cao, K. Chen, G. M. Gray, D. C. Muddiman and R. D. Smith, *J. Am. Chem. Soc.*, 1997, **119**, 5163; (*c*) G. M. Gray, F. P. Fish and C. H. Duffey, *Inorg. Chim. Acta*, 1996, **246**, 229; (*d*) G. M. Gray, *Comments. Inorg. Chem.*, 1995, **17**, 95; (*e*) G. M. Gray and C. H. Duffey, *Organometallics*, 1995, **14**, 238; (*f*) G. M. Gray and C. H. Duffey, *Organometallics*, 1995, **14**, 245; (*g*) A. Varshney, M. Webster and G. M. Gray, *Inorg. Chem.*, 1992, **31**, 2580; (*h*) A. Varshney and G. M. Gray, *Inorg. Chem.*, 1991, **30**, 1748.

5 J. Powell, M. R. Gregg, A. Kuksis, C. J. May and S. J. Smith, *Organometallics*, 1989, **8**, 2918; J. Powell, A. Kuskis, C. J. May, P. E. Meindl and S. J. Smith, *Organometallics*, 1989, **8**, 2933.

6 D. C. Smith, Jr. and G. M. Gray, *Inorg. Chem.*, 1998, **37**, 1791.

7 W. J. Louch and D. R. Eaton, *Inorg. Chim. Acta.*, 1978, **30**, 243.

8 H. Sawada, *Thermodynamics of Polymerization*, Marcel Dekker, Inc., New York, NY, 1976, pp. 153–205.

9 S. O. Grim and R. L. Kelter, *Inorg. Chim. Act.*, 1970, **4**, 56.

10 Crystallograpic data: Formula, $C_{34}H_{28}O_4I_4P_2Pd_2$; M = 1282.9; orthorhombic, a = 17.2007(28), b = 24.7961(40), c = 9.5467(20) Å, V = 4072(2) Å^3; T = 297 K; *Pnma*, Z = 4; μ = 4.028 mm^{-1}; refl. meas. = 7278, ind. refl. = 2734 (R_{int} = 3.09%); R = 4.16, R_w = 5.33 (all data). Crystallographic data for **3c** have been deposited with the Cambridge Crystallographic Data Centre as supplementary publication No. CCDC-101344. CCDC 182/1070.

Communication 8/07170E